JOURNAL OF AGRICULTURAL AND FOOD CHEMISTRY

Editorial

pubs.acs.org/JAFC

New Features and Expanded Coverage for *Journal of Agricultural and Food Chemistry*

Publishing in *JAFC* has never been more inviting. With ACS Publications Division support and the support of the Divisions of Agrochemicals and Agricultural and Food chemistry, in 2013 the *Journal* launched two ***Research Article of the Year*** awards, one slanted toward agrochemicals and the other toward food chemistry. It was difficult to decide on the winners, but with so many excellent candidates from 2012 published manuscripts two were chosen. In the Agrochemical category, award winners were John Grabber, Dino Ress, and John Ralph for "Identifying New Lignin Bioengineering Targets: Impact of Epicatechin, Quercetin Glycoside, and Gallate Derivatives on the Lignification and Fermentation of Maize Cell Walls" (*J. Agric. Food Chem.* **2012**, *60* (20), 5152−5160). In the Food Chemistry category, authors Caroline Hellfritsch, Anne Brockhoff, Frauke Stähler, Wolfgang Meyerhof, and Thomas Hofmann received the award for "Human Psychometric and Taste Receptor Responses to Steviol Glycosides" (*J. Agric. Food Chem.* **2012**, *60* (27), 6782−6793). Both Research Articles of the Year were the topics of presentations made at the National Meeting of the American Chemical Society in Indianapolis, by corresponding authors John Grabber and Thomas Hoffman (Figure 1).

Figure 1. JAFC Managing Editor Matt Hotze (left) and Editor Jim Seiber (right) congratulate 2013 Research Article of the Year Lectureship awardees John Grabber (left middle) and Thomas Hofmann (right middle) during their lecture session at the Fall ACS National Meeting in Indianapolis in September 2013.

JAFC also launched a **new category, Targeted Metabolomics Applied to Agriculture and Food** (for details, see the author guidelines at http://pubs.acs.org/page/jafcau/submission/authors.html). Associate Editors Peter Schieberle and Russ Molyneux and I will describe the new category in an upcoming Perspective (in process), which includes the prospects for this exciting new field and its many applications in agricultural and food chemistry. Metabolomics is one of the new endeavors that is cross disciplinary in scope and can involve biotechnology, analytical chemistry, sensory science, toxicology, nutrition, and many other fields important to *JAFC*. As the Perspective states, "*JAFC* will limit the section on Targeted Metabolomics to those manuscripts that at least attempt to characterize the differing compounds in order to draw substantive conclusions, for example, on pathways or mechanisms of formation or modification."[1]

Got something new and exciting that can be described in 2000 words and 4 graphics or less? Then check out the new **Letters category** launched in September 2013 and also described at the author guidelines link, above. Letters are being accepted that are brief, timely, and urgent. The first Letters submissions are undergoing peer review and are expected to be published as JAMs and ASAP soon.

Two other *JAFC* categories have enjoyed significant growth in numbers of publications received and published in 2013. Reviews and Perspectives, both standing categories for several years, had their best years ever, with 10 Perspectives and 45 Reviews published as of this writing. Table 1 lists the Perspectives published in 2013. Our hats-off to the authors who responded to the call for manuscripts, or volunteered topics themselves, and to several of our Associate Editors (Russ Molyneux played a major role) and Managing Editor Matt Hotze for stimulating the pipeline in these two categories.

We have also been active with new **ACS Selects** (formerly called Virtual Issues) covering the fields of **gut microbiota** and the **health implications of nanotechnology** in agricultural and food chemistry. Our guest editors for the Microbiota issue, Associate Editors Francisco Tomás-Barberán and Yoshinori Mine, worked with Managing Editor Matt Hotze to select manuscripts published during 2011−2013 that best represented the field from the *JAFC* perspective, and then worked with an international cadre of authors to publish additional new content on this topic.

Similarly, Guest Editor Hongda Chen, National Program Leader for USDA-ARS, worked with editors from four ACS journals (*JAFC*, *ACS Nano*, *ES&T*, and *ACS Sustainable Chemistry and Engineering*), to assemble a consensus choice of representative manuscripts published in the fast developing field of **nanotechnology**. This new ACS Selects will roll out soon. You can view all of the ACS Selects/Virtual Issues that *JAFC* has participated in at the JAFC Selects webpage (http://pubs.acs.org/page/jafcau/vi/index.html)

Continually refreshed with new science and new features, it is no surprise that *JAFC* retained its leadership as **the most cited journal in three ISI categories**, Agriculture, Applied Chemistry, and Food Science and Technology. The journal is blessed with an outstanding group of **Associate Editors (Hanne Christine Bertram, Zhen-Yu Chen, John W. Finley, Chi-Tang Ho, Yoshinori Mine, Russell J. Molyneux, Peter**

Published: January 8, 2014

ACS Publications © 2014 American Chemical Society

dx.doi.org/10.1021/jf405286v | *J. Agric. Food Chem.* 2014, 62, 1−3

Table 1. Perspectives Published in *JAFC* during 2013

Can an Increase in Celiac Disease Be Attributed to an Increase in the Gluten Content of Wheat as a Consequence of Wheat Breeding?
D. D. Kasarda
J. Agric. Food Chem. 61 (6), 1155−1159

Safety Assessment and Caloric Value of Partially Hydrolyzed Guar Gum
J. W. Finley, A. Soto-Vaca, J. Heimbach, T. P. Rao, L. R. Juneja, J. Slavin, G. C. Fahey
J. Agric. Food Chem. 61 (8), 1904−1913

Perspectives on Communicating Risks of Chemicals
K. Armbrust, M. Burns, A. N. Crossan, D. A. Fischhoff, L. E. Hammond, J. J. Johnston, I. Kennedy, M. T. Rose, J. N. Seiber, K. Solomon
J. Agric. Food Chem. 61 (20), 4676−4691

Methods for Comparing Data across Differently Designed Agronomic Studies: Examples of Different Meta-analysis Methods Used to Compare Relative Composition of Plant Foods Grown Using Organic or Conventional Production Methods and a Protocol for a Systematic Review
K. Brandt, D. Średnicka-Tober, M. Barański, R. Sanderson, C. Leifert, C. J. Seal
J. Agric. Food Chem. 61 (30), 7173−7180

Compositional Analysis of GM Crops: Key Issues and Future Needs
O. Hoekenga, J. Srinivasan, G. Barry, A. Bartholomaeus
Special Issue: Safety of GM Crops: Compositional Analysis
J. Agric. Food Chem. 61 (35), 8248−8253

A Look at Product Development with Genetically Modified Crops: Examples from Maize
R. H. Mumm
Special Issue: Safety of GM Crops: Compositional Analysis
J. Agric. Food Chem. 61 (35), 8254−8259

Bringing a Transgenic Crop to Market: Where Compositional Analysis Fits
L. S. Privalle, N. Gillikin, C. Wandelt
Special Issue: Safety of GM Crops: Compositional Analysis
J. Agric. Food Chem. 61 (35), 8260−8266

Unintended Compositional Changes in Genetically Modified (GM) Crops: 20 Years of Research
R. A. Herman W. D. Price
DOI: 10.1021/jf400135r
Special Issue: Human Health and Transgenic Crops
J. Agric. Food Chem. 61 (48), 11695−11701

Mapping the Scientific Research on Wine and Health (2001−2011)
J. L. Aleixandre, J. L. Aleixandre-Tudo, M. Bolaños, R. Aleixandre-Benavent
J. Agric. Food Chem. 61 (49), 11871−11880

Targeted Metabolomics, a New Section in the *Journal of Agricultural and Food Chemistry* (JAFC)
J. N. Seiber, R. J. Molyneux, P. Schieberle
J. Agric. Food Chem. 61, DOI: 10.1021/jf4046254

Schieberle, **Takayuki Shibamoto**, **Veronika Somoza**, **Francisco Tomás-Barberán**, **Elizabeth Waters**, and **Liangli (Lucy) Yu**) and strong support from ACS Publications Division and the ACS technical divisions of Agricultural and Food Chemistry and Agrochemicals.

We take this opportunity to congratulate Associate Editor Taka Shibamoto for receiving the Award for the Advancement of Application of Agricultural and Food Chemistry from the Division of Agricultural and Food Chemistry of the ACS at the Indianapolis meeting (Figure 2.) Professor Shibamoto has identified Maillard browning reaction chemicals in several foods and beverages. Recently, we had occasion to congratulate another strong supporter of *JAFC*, Lucy Sun Hwang, at a symposium held in her honor during the 2013 International Society for Nutraceuticals and Functional Foods (ISNFF) in Taipei, Taiwan, in November. Lucy has been a strong advocate for agricultural and food chemistry in Asia and worldwide (Figure 3). Also in 2013, I had the opportunity to serve as

Figure 2. Associate Editor Takayuki Shibamoto received the 2013 Award for the Advancement of Application of Agricultural and Food Chemistry from the Division of Agricultural and Food chemistry of ACS at the Indianapolis meeting.

Figure 3. The *Journal* salutes the distinguished Career of Professor Lucy Hwang (left middle) at the Annual Conference of the International Society For Nutraceuticals and Functional Foods, held November 5−9, 2013, in Taipei, Taiwan. Associate Editors Chi-Tang Ho (right middle), who made the presentation on behalf of the *Journal*, Associate Editor Zhen-yu Chen (far right), and Advisory Board member Gow-Chen Yen (far left) are pictured.

Thematic Chair for the ACS National Meeting in New Orleans, Louisiana, under the theme banner of "Energy and Food". Almost half the divisions organized symposia within the theme. Associate Editor Peter Schieberle gave an excellent plenary address titled "Chemistry of food flavors: simply pleasure or beyond?", and Associate Editor John Finley arranged a symposium on "The Interconnected World of Energy, Food and Water."

This was also a year filled with travel by several of us to attend **international meetings** on several continents. Some of the meetings we attended will culminate in manuscript clusters, cutting edge Research Articles or Letters, Perspectives, and Reviews published in issues of *JAFC*. It is important for the *Journal* to be represented at meetings such as these, where a broad cross section of new authors can be encouraged to publish their best work in *JAFC*. Over the past year we have had the opportunity to publish work presented at six meetings as symposium clusters in special issues— Advances in Food Allergen Detection, IX Italian Congress of Food Chemistry, Florida Pesticide Residue Workshop 2012, Safety of GM Crops: Compositional Analysis, ISMR11 − 100 Years of the Maillard Reaction, and Human Health and Transgenic Crops. An upcoming meeting of particular note is the **13th IUPAC Congress of Pesticide Chemistry**—Crop, Environment, and Public Health Protection Technologies for a Changing World, to be cosponsored by IUPAC and ACS AGRO and held August 10−14, 2014, in San Francisco, California, in conjunction with the Fall National Meeting of the ACS. I look forward to seeing many of you at these meetings.

On behalf of the *JAFC* team, our Associate Editors, Editorial Advisory Board members, ACS staff, and editorial assistants, I take this opportunity to thank all of our authors and reviewers (a list of our 2013 reviewers follows this editorial) and editorial staff who contributed to our successes in 2013. I extend our **best wishes for a successful, healthy and prosperous 2014!**

Jim Seiber, Editor

AUTHOR INFORMATION

Notes

Views expressed in this editorial are those of the author and not necessarily the views of the ACS.

REFERENCES

(1) Seiber, J. N.; Molyneux, R. J.; Schieberle, P. Targeted metabolomics: a new section in the *Journal of Agricultural and Food Chemistry*. *J. Agric. Food Chem.* **2013**, DOI: 10.1021/jf4046254.

JOURNAL OF AGRICULTURAL AND FOOD CHEMISTRY

EDITORIAL

pubs.acs.org/JAFC

REVIEWER LIST 2013

The Editor and Associate Editors gratefully acknowledge the following scientists for reviewing manuscripts during 2013. Many of these individuals reviewed several manuscripts. We thank all of the reviewers for their contributions of time and talent. Note: this list reflects reviews received between November 13, 2012, and November 10, 2013.

Kjersti Aaby
J. J. Aaron
Jawad Aarrouf
Antonio Abad-Fuentes
Javier Abadía
Soleiman Abbasi
Soheir Abd El-Rahman
Elsayed M. Abdelaal
Ahmed M. Abdel-Salam
Azlina Abdul Hamid
Lukman Bola Abdulra'uf
Keiko Abe
Naoki Abe
Maher Abou Hachem
Veronika Abram
Pilar A. Abrodo
Lutfi Abu-Elheiga
Lilian Elizabeth Abugoch
Cesare Accinelli
Bradley Ackermann
Manuel Acosta
Reiko Adachi
Shuji Adachi
Gerhard Adam
Ernest Adeghate
Adeleke A. Adeniyi
N. P. Aditya
Muhammad Adnan
Marielle Adrian
Evelyn Adu-Kwarteng
Guido Aerts
Ohad Afik
Gopalakrishna AG
Giovanni Agati
Gabriel Agbor Agbor
Eduardo Agosin
Renu Agrawal
Reginald Agu
Claudio Lima Aguiar
Véronique Aguié
Julio C. Aguilar-Cordero
Yolanda Aguilera
Ingrid Aguiló-Aguayo
Vivek Ahluwalia
Dong U. Ahn
Joong-Hoon Ahn
Jungoh Ahn
Behzad Ahvazi
Mohammed Aider
Diego Airado-Rodríguez
Olusegun J. Ajayi
Mitsugu Akagawa
M. Humayoun Akhtar
Fatma Akinci Yildirim
Hiroshi Akiyama
Jaap Akkerdaas
Casimir C. Akoh
Ozlem Akpinar
Abdurrahman Aktumsek
Sayuri Akuzawa
Cesarettin Alasalvar
Katherine T. Alben
Klaus Albert
Silvia María Albillos
Lutz Alder
Ricardo Bicca Alencastro
Begona Alfaro
Elena Algar
W. Russ Algar
Jafar Al-Hakkak
Andrea Aliboni
Hoehuri Alkadi
Ana Allende
Jeremy D. Allison
Agostinho Almiro Almeida
Luis Almela
Eva Almenar
Gonzalo L. Alonso
Jose Luis Alonso
Rosa Maria Alonso-Salces
Eman Al-Sayed
Fadwa Al-Taher
Rotimi Aluko
Rotimi E. Aluko
Ana M. Álvarez-Fernández
Renato Amadò
Haru Amagase
Yoshiaki Amakura
Per Åman
Sandra Amann
Edna Regina Amante
Joana S. Amaral
Ryszard Amarowicz
Antonella Amicucci
Lourdes Amigo
Nikolaus Amrhein
Elpiniki G. Amvrazi
Mohamed Analla
Pon Velayutham Anandh Babu
Carmen Rafaela Ancin-Azpilicueta
Gaby Andersen
Henrik Jorgen Andersen
Wendy Cook Andersen
David Anderson
James V. Anderson
Olin D. Anderson
Richard A. Anderson
José Paulo Andrade
Juan E. Andrade
Paula B. Andrade
Peter R. Andreana
Cristina Andrés-Lacueva
Donato Andueza
Roberto Anedda
Skelte G. Anema
Monica Anese
Laura Anfossi
Riccardo Angelini
Maria De Angelis
Franca Angerosa
Alberto Angioni
Michael J. Angove
Tadeusz Aniszewski
Fabiana Antognoni
Andrea Antonelli
Farooq Anwar
Takayoshi Aoki
Reşat Apak
Constatin Apetrei
Michael Appell
Eugenio Aprea
Farrukh Aqil
Nadia Mohamed Said Arafa
Hirofumi Arai
Panagiotis Arapitsas
Michel Mozeika Araújo
Vicent Arbona
Douglas D. Archbold
Anna Ardevol
Ardiansyah Ardiansyah
Nurit Argov-Argaman
Dimitris S. Argyropoulos
Covadonga Arias
Manuel Arias-Estevez
Tsutomu Arie
Katsuhiko Ariga
Toyohiko Ariga
Keizo Arihara
Jiro Arima
Sakae Arimoto-Kobayashi
Ana C. M. Arisi
Kaoru Ariyama
Bahram Arjmandi
Marco Arlorio
Kevin Armbrust
Monica Armenteros
Daniel W. Armstrong
John Thor Arnason
Nils Arneborg
Susan D. Arntfield
Luis Arola
Naveen Arora
Daniel Arrieta-Baez
Giorgio Arrigoni
Javier Arrizon
Francisco Teodoro Arroyo
Teresa Arroyo
Nasima Arshad
Derya Arslan
Idris Arslan
Jacques Artaud
William E. Artz
Joseph Arul
Yoshinori Asakawa
Tomiko Asakura
Tadao Asami
Abdeslam Asehraou
Robert E. Asenstorfer
Muhammad Asgher
Gavin Ash
Hitoshi Ashida
Vincent M. Asiago
Ruhan Askin Uzel
Ahmad Asoodeh
Sandra Assis Aparecida Assis
Iciar Astiasaran
Linda S. Aston
Thierry Astruc
Athar Ata
Ebru Ates
Sergio G. Atienza
Sabrine Attia
Christophe Aubert
Santiago Pedro Aubourg
Anne-Marie Aucour
Cyril Auger
Anna-Marja Aura
Rossella Avallone
Giuseppina Avantaggiato
Pinarosa Avato
J. Fernando Ayala-Zavala
Faik Ahmet Ayaz
Nuran Aydemir

Published: January 08, 2014

ACS Publications © 2014 American Chemical Society

Belen Ayestaran Iturbe
Maria Jose Ayora-Cañada
Arash Azarfar
Ricardo Antunes Azevedo
Margarita Aznar
Andre Baby
Sabulal Baby
Benoit Bach
Tomasz Baczek
Thomas M. Badger
Vladimir Badmaev
Hyung Hee Baek
Bojlul Bahar
Theeshan Bahorun
Hua Bai
Naisheng Bai
Antonietta Baiano
Roberto Baigorri
Clifton Baile
William A. Bailey
Mikhail Yurievich Balakshin
M. S. Balathanigaimani
Mercè Balcells
Susanne Baldermann
Vincent Balter
Narcisa Bandarra
Brian Bandy
Punam Bandyopadhyay
Vassya S. Bankova
Jie Bao
Jinsong Bao
Li Bao
Paula Baptista
Malgorzata Baranska
Ana Paulina Barba De La Rosa
Coral Barbas
William E. Barbeau
Reyes Barbera
Laura Bardi
Andersson Barison
Allen Barker
Jose Barluenga
Laurent Barnavon
Biancamaria Baroli
María Verónica Baroni
Jaione Barrenetxe
Diane Marie Barrett
António S. Barros
Frederico Barros
Helena Barros
Veronique J. Barthet
John P. Bartley
Begoña Bartolome
Eduardo Bárzana
Ugur Basaran
Altaf Halim Basta
Juan Antonio Giménez Bastida
Maria Lourdes Bastos
Max Batenburg
Irineu Batista
Graeme D. Batten
Paola Battilani
Maurizio Battino
Stefan Bauer
Biljana Stevan Bauer Petrovska
Sabine Baumgartner
Ana-Belen Bautista-Ortin
Luigi Bavaresco
Banu Bayram
Laurent Bazinet
Scott R. Bean
Ivana Beara
Adilson Beatriz
John J. Beck
Thomas Becker
Diane M. Beckles
Manfred Beckmann
Jules Beekwilder
George B. Beestman
Timothy H. Begley
Mohammad Behbahani
Ross C. Beier
Donald Clarence Beitz
M. Belewu
Nacer Bellaloui
François Bellemare
Andrea Bellincontro
Luis A. Bello-Perez
Josefina Belloque
Federica Belluti
Peter S. Belton
Simona Belviso
Ronald Belyea
James Noble BeMiller
Abdellah Benachour
Obdulio Benavente-Garcia
Justin Garfield Bendall
Alessandra Bendini
Daniel Ben-Ghedalia
Soottawat Benjakul
Rodney M. Bennett
Micaela Benzi
Alexander Berestetskiy
Enrico Bergamaschi
Bryan W. Berger
Monique Berger
Ralf Günter Berger
Peter Bergquist
Mark A. Berhow
César I. Beristain
Maria Dolores Bermejo
Pilar Bermejo-Barrera
José Bernal
Matthew W. Bernart
Stéphane Bernillon
Roberta Bernini
Houda Berrada
Davide Bertelli
Yves Bertheau
Franz Berthiller
Lorenzo Bertin
Pietro Bertino
Eric Bertoft
Hanne C. Bertram
Loic Bertrand
Matthias Besler
Noelia Betoret Valls
Don Betowski
Karen Bett-Garber
Jordan F. Betz
Joseph M. Betz
A. Bevilacqua
Dejan Bezbradica
Ranilson S. Bezerra
Sandeep D. Bhale
M. M. Srinivas Bharath
Bilal Ahmad Bhat
Saleem Bhat
Anjan Bhattacharyya
Shobhana Bhide
Prasanta C. Bhowmik
Kaishun Bi
Yanlan Bi
Dobroslawa Bialonska
Carlo Bicchi
Jacek Bielawski
Peter Biely
Martin Biendl
Catherine Billaud
Andrew Billin
Keren A. Bindon
Linda Bisson
Denis Blache
Barbara A. Blackwell
Cinta Blade
Maria Blanco
Ralf Harald Blank
Sonia Blasioli
Georgios Blekas
Christophe Bliard
Eric Block
Elke Bloem
Ramune Bobinaite
Otilia Bobis
Steve Craig Bobzin
Ulrike Böcker
Marie Bodinier
Volker Boehm
Johanna Bogen
Paolo Bogoni
Torsten Bohn
Jen Bohon
Eduardo Boido
Georgios Bokias
Silvia Bolado
Nanthi Bolan
Imre Boldizsár
Bradley Warren Bolling
Joseph Martin Bollinger Jr.
Ivana Bonaccorsi
Pamela L. Boner
Laetitia M. Bonnaillie
Jean-Louis Bonnemain
Estelle Bonnin
Francesco Bonomi
Monica Bononi
Josep Serra Bonvehí
Graham Bonwick
Squire J. Booker
Melike Bor
Marai H. Borawska
Nicolas Bordenave
Matteo Bordiga
Alessandra Bordoni
Rosivaldo Santos Borges
Eva Borghesi
Rafael Borneo
Katalin Böröczky
Claudio Dario Borsarelli
Alan David Borthwick
Emanuele Boselli
Paul Kenneth Boss
Chellampillai Bothiraja
Mohamed Bouaziz
Renaud Boulanger
Leslie D. Bourquin
Sedat Bozari
Mara Elga Medeiros Braga
Gianfranco Brambilla
Luca Brambilla
Rob G. V. Bramley
Ferdinando Branca
Adriano Brandelli
David L. Brandon
Kirsten Brandt
Satinder K. Brar
Annett Braune
Frederique Bravin
Laura Bravo
Lothar Brecker
Andreas Breidbach
Andrew P. Breksa III
Manuel Brenes
William Edward Brewer
Kristof Brijs
Ana Briones Perez
Michel Britten
Kevin Brix
Peter Briza
Stefania Brocca
Andre Brodkorb
N. Broekaert
Kerensa Broersen
Hermann Broll
Richard H. Bromilow
Allan Fraser Brown
Daren Brown
Eleanor M. Brown
Hans Brückner
Katrina Brudzynski
Werner Brueller
Roque Bru-Martínez
Eva María Brun
Philip D. Brune
Markus Brunnbauer
Kurt Brunner
Gosta Brunow
Jennifer Lynn Brzezinski
Le Bu
Franz Bucar
Ken A. Buckle
Roman Buckow
Jurga Budiene
Grazyna Budryn
Rosalind Ann Bueckert
Mark Buecking
María Pilar Buera
Andrea Buettner
John A. Bumpus
Mirko Bunzel
Carmen Burbano
Iva Burešová
Joanna Burger
Maksim A. Burkin
Betty Burri
Kerstin Martha Mensien Burseg
Britt M. Burton-Freeman
Claus Buschmann
Rodney J. Bushway
Mark Busman
Jesus H. Busto
Ronald G. Buttery
Peter Butz

dx.doi.org/10.1021/jf405539n |J. Agric. Food Chem. 2014, 62, 4–21

Christian Butzke
William Craig Byrdwell
Michal Bystrzejewski
Youngjae Byun
Maria Fiorenza Caboni
Pierluigi Caboni
Carmen Cabrera
Gustavo Cabrera
Francisco Cabrera-Chávez
Maria Joao Cabrita
F. Cacciola
Estrella Cadahía
Keith R. Cadwallader
Bettina Caemmerer
Thomas Michael Cahill
Kezhou Cai
Liming Cai
Yizhong Cai
Yong Cai
Zhonghua Cai
G. P. Cairns
Céline Cakir-Kiefer
Carole Calas-Blanchard
Ana María Calderón De La Barca
Sonia Calligaris
Antonis C. Calokerinos
Elizabeth M. Calvey
Malick Camara
José Sousa Câmara
Luiz Claudio Cameron
Randall G. Cameron
Federica Camin
Luigi Campanella
Natalia Campillo
Francisco A. P. Campos
Nafiz Oncu Can
Joan-Miquel Canals
Jaclyn Canas
Paul F. Cancalon
Juliana Cancino
Alan A. G. Candlish
Ramon Canela-Garayoa
Joaquin Canizares
Maud Cansell
Maria J. Cantalejo
Celia Maria Cantin
Emma Cantos-Villar
Charles Lowell Cantrell
Charles L. Cantrell
Aocheng Cao
Heping Cao
Min-Jie Cao
Ping Cao
Rihui Cao
Shifeng Cao
Song Cao
Tiesen Cao
Xiufang Cao
Esra Capanoglu
Francesco Caponio
Francesco Capozzi
Jack C. Cappozzo
Lorenzo Caputi
Denise Cara
Jose V. Carbonell
Ángel A. Carbonell-Barrachina
Marie-Annette Carbonneau
Marcella L. Card
Anaberta Cardador-Martinez
Barbara Cardazzo
Mireille Cardinal
Daniel R. Cardoso
Daniel Rodrigues Cardoso
Susana Maria Cardoso
Andrea Caridi
Reinhold Carle
Celia R Carlini
Urrea Carlos
Maria C. Carpinella
Alegría Carrasco-Pancorbo
Catalina Carrasco-Pozo
Francisco M. Carrau
Elena Cartea
Chris Carter
Florbela Carvalheiro
Susana Casal
Isidre Casals
Paula Casati
Osvaldo Cascone
E. Casero
Luca Casettari
Edoardo Casiglia
Angélica Castaño
Jose Maria Castellano
Massimo Castellari
Maria Antonietta Castiglione Morelli
Patrice Castignolles
Noelia Castillo Muñoz
Laurence Castle
Raffaello Castoria
Inar Alves Castro
Remedios Castro Mejías
Cristiano Casucci
Tommaso R.I. Cataldi
Dinnella Caterina
Ivana Cavoski
Greg Cawthray
Mehmet Fatih Cengiz
Ana M. Cenzano
Ruth Cerda Belmares
Mar Cerdán
Christoph Cerny
Miguel A. Cerqueira
Lorenzo Cerretani
Arturo Cert
Attilio Cesáro
Carlos L. Cespedes
Carlos Leonardo Cespedes-Acuna
Brigitte Chabbert
Radhouane Chaffai
Thauming Cham
Jamshidkhan Chamani
Janice Chambers
C. Kevin Chambliss
Narong Chamkasem
Danny Chan
Kung-Chi Chan
Wan Chan
Arun Chandrashekar
Chen-Tien Chang
Chi-I Chang
Fang-Rong Chang
Hsueh-Wei Chang
Ke Liang Bruce Chang
Pahn-Shick Chang
Perng-Kuang Chang
Shang-Tzen Chang
Shu-Wei Chang
Sue-Joan Chang
Tsong-Min Chang
Tsu-Chung Chang
Yuan-Shiun Chang
Yuhua Chang
Yu-Jia Chang
Helene Chanvrier
Pei-Dawn Lee Chao
Yun-Peng Chao
Veronique Chaplain
Denis Charlebois
Denys Charles
Johannes Charlier
Stefan Chassaing
Bruce M. Chassy
Subhasish Chatterjee
Dereck Chatterton
Sharmila Chattopadhyay
Chi Fai Chau
Chi-Fai Chau
Dharam Paul Chaudhary
Abdul Shakoor Chaudhry
Lim Chaw Jiang
C. T. Che
Seronei Chelulei Cheison
Bing Huei Chen
Bingcan Chen
C. S. Chen
Chang-Jun Chen
Chia-Yang Chen
Ching-Hsein Chen
Ching-San Chen
Chun-Jen Chen
C.-Y. Oliver Chen
Daofeng Chen
Feng Chen
Fengping Chen
Fu-An Chen
Guo Chen
Guoying Chen
Hauh-Jyun Candy Chen
Hongping Chen
Hongwei Chen
Hsien-Jung Chen
Huadong Chen
Hu-biao Chen
Hui Chen
Jian Chen
Jian-Ye Chen
Jie Chen
Jih-Jung Chen
Jiluan Chen
Jinghhua Chen
Kai Chen
Kuan-Chou Chen
Lanzhen Chen
Lei Chen
Li Chen
Liming Chen
Ming-Hsuan Chen
Ming-Ju Chen
Pei Chen
Po Ting Chen
Qing-Xi Chen
Qinhua Chen
Shaohua Chen
Shao-Nong Chen
Shiguo Chen
Su Chen
Tianfeng Chen
Wansheng Chen
Wei-Jen Chen
Xiaoli Chen
Xiaoyan Chen
Xiaozhuo Chen
Xiguang Chen
Xin Chen
Xingguo Chen
Yanyi Chen
Yeming Chen
Yen-Lin Chen
Yi-Chen Chen
YiWen Chen
Yong Chen
Yue-Hwa Chen
Yu-Kuo Chen
Yung-Hsiang Chen
Zhao Chen
Zhen-Yu Chen
Christopher H. K. Cheng
Hsueh-Ling Cheng
Juei-Tang Cheng
Kuan-Chen Cheng
Kun Cheng
Luisa W. Cheng
Zhihong Cheng
Zhiliang Cheng
Ling-Zhi Cheong
Irene Chetschik
Peter C. K. Cheung
Francois Chevalier
Veronique Cheynier
Chung-Jen Chiang
Meng Tsan Chiang
Wen-Dee Chiang
Emma Chiavaro
Kazuhiro Chiba
Ravindra Nath Chibbar
Naveen Chikthimmah
Koo B. Chin
Antonia P. Chiou
Robin Y.-Y. Chiou
Kleopatra Chira
Marco Chisari
David Chitwood
Chung Y. Cho
Il Kyu Cho
Jean-Marc Chobert
Dong-Hwan Choe
Chang Won Choi
Hyung-Kyoon Choi
Sang-Won Choi
Sung-Seen Choi
Woo-Jung Choi
Young Hae Choi
Kiattawee Choowongkomon
Harish M. Chopade
Kanwaljit Chopra
Chang-Hung Chou
Jyh-Ching Chou
Shen-Chieh Chou

Efterpi Christaki
Paul Christakopoulos
Philippe Christen
Kathrine Bisgaard Christensen
Lars Porskjær Christensen
Soren Brogger Christensen
Philip Christenson
Monika Christmann
Norbert Christoph
Ching-Liang Chu
Khim Hoong Chu
Pak-Sin Chu
Xiaogang Chu
Yung-Lin Chu
Chia-Chi Chuang
Show-Mei Chuang
Pin Ju Chueh
Donghwa Chung
Hau Yin Chung
Hyung-Wook Chung
Ill-Min Chung
Jing-Gung Chung
Myong-Soo Chung
Namhyun Chung
Shin-Kyo Chung
Si-Yin Chung
Stephen Wai Cheung Chung
Sung Hyun Chung
Charng-Cherng Chyau
M. Ciani
Salvatore Ciappellano
M. Antonietta Ciardiello
Margit Cichna-Markl
Zuzana Ciesarova
Alejandro Cifuentes
Blaz Cigic
Clara Cilindre
Antonio Cilla
Giuseppe Cirillo
Sedat Citak
Debra Arwood Clare
Andrew C. Clark
David Alan Clark
Robert Daniel Clark
Morten R. Clausen
Gary Clayton
Alain Clement
Alfonso Clemente
Andrew J. Clifford
Michael N. Clifford
Isabelle Coats
Joel R. Coats
Mehmet Coelhan
Elisabete Coelho
Seth Cohen
Manuel A. Coimbra
Mateja Colaric Bajc
Mary Florence Cole
Isidro Gonzalez Collado
Sonia Collin
Stuart G. Collins
Mark W. Collison
Luiz Alberto Colnago
Emilie Combet
Elena Comelli
Ramon Companyó
Enma Conde
Celia Conesa
Sean D. Conklin
Michael A. Conlon
Michael J. Considine
Roberto Consonni
Giovanna Contarini
Lanfranco Conte
Pellegrino Conte
María del Mar Contreras
Attilio Converti
Daniel Cook
Dave J. Cook
Robert Graham Cooks
Janine M. Cooney
Mauro Coppa
Juan-José R. Coque
Thibaud Coradin
Philippe Corbisier
Lucimara Mach Cortes Cordeiro
Roger Corder
Renzo Cordera
Chiara Cordero
Paul Cordero
Harold Corke
Danilo Corradini
Milena Corredig
Manuela Correia
Nieves Corzo
Fernanda Cosme
Joana Costa
Silvia M. B. Costa
Ana Maria Costa Freitas
Greg L. Cote
Michael A. Cotta
Geoffrey Cottenet
John Coupland
Eric Courot
Francis Courtois
Daniel Cozzolino
David J. Craik
Benedikt Cramer
Todd Crawford
Rebecca Creamer
Mauro Andrea Cremonini
Colin Crews
Kevin D. Croft
Thomas Croguennec
Timothy R. Croley
Jean-Claude Crouzet
Alan Crozier
Stephen J. Crozier
Rui Cruz
Carmen Cuadrado
Osman Cubuk
Rosa Paula Odejar Cuevas
Jian Dong Cui
Catherine Culver
Paolo Curir
Elena Curti
Larry Curtis
Gustavo Andres Curutchet
Malgorzata Renata Cyran
Andreas Czepa
Michael Czerny
Zsuzsanna Czibulya
Jaroslaw Czubinski
Agata Czyżowska
Renato D'Ovido
Cag da Camara
Fernando Batista Da Costa
Neil C. Da Costa
Edson Luiz da Silva
Maria Fátima das Graças Fernandes Da Silva
Roberta Claro da Silva
Abdelali Daddaoua
Arnon Dag
Maria Daglia
Jungui Dai
Zhiyuan Dai
Photis Dais
Chiara Dall'Asta
Trine Kastrup Dalsgaard
Robert G. Dambergs
Stefano D'Amico
Ji Dan
Martin Danaher
Olivier Dangles
Sven Dänicke
James R. Daniel
John C. Danilewicz
Dennis Dannehl
Dirk Dannenberger
Alessandro D'Annibale
Philippe Darriet
Mukul Das
Prasanta Kumar Das
Undurti N. Das
Arsalan Daudi
Alberto Davalos
Mark W. Davey
Tomas Davidek
Howard V. Davies
Kevin Davies
Noel W. Davies
Cindy Davis
Mark Franklin Davis
Michael R. Davis
Corinna Dawid
Julie Dawson
Li Day
Fabian Millar Dayrit
Godwin Basil D'Cunha
Begoña de Ancos
Dalene de Beer
Marthe de Boevre
Johannes de Bruijn
Vincenzo de Feo Sr.
Julius W. de Folter
Victor de Freitas
Annalisa de Girolamo
Denis De Keukeleire
André de Kok
José Pedro de la Cruz
Miguel de la Guardia
Raul de la Rosa
Roberto de la Torre Roche
F. X. C. de las Heras
Anthony John de Lucca
Elvira Gonzalez de Mejia
Bruno de Meulenaer
Luiz Fernando Cappa de Oliveira
Sonia de Pascual-Teresa
M. Paz de Peña
Mertxe de Renobales
Theo C. de Rijk
Eva De Rijke
Sarah De Saeger
Rodrigo Octavio Mendonça Alves de Souza
Nunziatina De Tommasi
André J. de Villiers
Melgardt de Villiers
Ric C. H. de Vos
Lisa L. Dean
Manisha Deb Mandal
Eric A. Decker
Jiri Dedina
Wanchai De-Eknamkul
Gisela H. Degen
Andreas Degenhardt
Fien Degryse
Mark A. Dekeyser
Daniele Del Buono
Luigi Del Giudice
Ana Del Olmo
Raquel Del Pino-García
Daniele Del Rio
Jose Carlos Del Rio
Jose Antonio Del Rio
Manuel del Valle
Philippe Delahaut
Kevin Delaney
Jan A. Delcour
Cristina Delgado-Andrade
Franciso Delgado-Vargas
Eduardo Santiago Dellacassa
Marina DellaGreca
Dominique Delmas
Nestor Jorge Delorenzi
Stephen Richard Delwiche
Tigst Demeke
Fatih Demirci
Qian Deng
Shuguang Deng
Yiqun Deng
Z. Deng
Ze-yuan Deng
Nikolai D. Denkov
Yves Desjardins
Aurelien Desmarchelier
Frédéric Destaillats
Vicenta Devesa
Mathias Devreese
Ralph Dewey
Guy D'Hallewin
Preeti Dhar
Karaj Singh Dhillon
Rong Di
Ernesto Di Maio
Corrado Di Natale
Fabio Di Nocera
Attilio Di Pietro
Angela Di Pinto
Francesco Di Renzo
Jinling Diao
Daniel Anthony Dias
Olga Diaz

dx.doi.org/10.1021/jf405539n |J. Agric. Food Chem. 2014, 62, 4–21

Rocio I. Diaz de la Garza
Marta E. Diaz-Garcia
Eric Dickinson
John Didzbalis
Horst Diehl
William Diehl-Jones
Helmut Dietrich
Joseph Dietrich
Jason Dietz
Lubbert Dijkhuizen
Ming-Wu Ding
Yousong Ding
Yunjie Ding
Yuping Ding
Irene Dini
Harun-Diraman
Michael Dobres
Thierry Doco
Daniel R. Doerge
Mahmut Doğan
Zeynep Banu Doganlar
Piero Dolara
Gregory G. Dolnikowski
Valentina Fernandes Domingues
Herminia Dominguez
Jose M. Dominguez
Zhou Jing Dong
Hasan Ḧuseyin Donmez
Francesco Donsì
Sonia Dopico-García
Gregory Doran
Emmie Dornez
Michael Dowd
Patrick F. Dowd
Chang Hu Bae
K. Ghimire Bimal
René Draaisma
Silvina R. Drago
Mary Anne Drake
William Mason Draper
Elena Dreassi
Darcy R. Driedger
Stephan Drusch
Changwen Du
Ming Du
Maret Du Toit
Wessel Johannes Du Toit
Changqing Duan
Jingjing Duan
Xuewu Duan
Yong-Ping Duan
Yuanyuan Duan
Juan Duarte
Maria Fatima Duarte
N. K. Dubey
Vikash Kumar Dubey
Christian Dubos
Paul-Henri Ducrot
Julien Ducruet
Montserrat Duenas
Tammy R. Dugas
Stephen O. Duke
Marc-Emmanuel Dumas
Marie-Josée Dumont
Valery Dumont
Andreas Dunkel
Kerryn Dunse
Kwaku Gyebi Duodu
Daniel M. Dupont
Marcello Duranti
Prem Dureja
Robert Durst
Jens Duus
Chandradhar Dwivedi
Gary A. Dykes
Susan E. Ebeler
Merete Edelenbos
Klaus Eder
Indika Edirisinghe
Thomas Efferth
P. Eganathan
David Ehret
Arnold Eilert
Gerhard Eisenbrand
Brian David Eitzer
Chima Ejikeme
Meike Eklund
Jenny Ekman
Hesham El-Beshbishy
Anna Maria Eleuteri
Pedro Elez-Martinez
Ryan J. Elias
Fred Joseph Eller III
Sabine Ellinger
Christopher T. Elliott
Stephen John Elmore
Gordon Michael Elsey
Ali Elshafei
Kaveh Emami
Karl-Heinz Engel
Ulrich H. Engelhardt
Toshiki Enomoto
Jordi Eras
Tomas Erban
Helmut Erbersdobler
John W. Erdman
John Erdman, Jr.
Ingrid Ericson Jogsten
Hüseyin Erten
Felix F. Escher
M. Teresa Escribano-Bailon
Ana Escudero
Asim Esen
Carl Emil Aae Eskildsen
Juan C. Espín
Montserrat Espiñeira
Anunciación Espinosa Mansilla
Judith Dolores Espinoza-Perez
Richard Espley
Nour-Eddine Es-Safi
Melanie Esselen
Mario Estévez
Yuzuru Eto
E. Etxeberria
D. Evan Evans
Antonio Evidente
Alice Ewert
Graham Terence Eyres
Hiroshi Ezura
María Paula Fabani
George C. Fahey Jr.
Jed W. Fahey
Mark L. Failla
Oskar Faix
Robert John Falconer
Maria L. Faleiro
James F. Faller
Eli Fallik
Elena Falqué
Peihong Fan
Titan S. Fan
Wenlai Fan
Anne Laure Fanciulino
Binghu Fang
F. Fang
Jian-Min Fang
Tony J. Fang
Wei Huan Fang
Yulin Fang
Zhenglai Fang
Martín Leandro Fanzone
Franco Faoro
Adriana Farah
Mir Ali Farajzadeh
A. Fardet
Ali Reza Fardin-Kia
Clara Fares
Ana Paula Farinha
Linda Farmer
Sebastian Farnaud
Rosaura Farré
Harold M. Farrell Jr.
Elisa Fasoli
Majekodunmi Oladeji Fatope
Cameron Faustman
Federico Federici
Bruno Fedrizzi
Peter Felker
John Fellman
Chris Fellows
Fengqin Feng
J. Feng
Jianguo Feng
Shengyu Feng
Tao Feng
Yi Feng
M. A. Fernandez
Victoria Fernandez
Brígida Fernández De Simón
Jesus Dionisio Fernández-Bayo
Juan Fernández-Bolaños
Avelina Fernandez-Garcia
Alberto Fernandez-Gutierrez
Roberto Fernandez-Lafuente
Miguel A. Fernandez-Muino
María-Soledad Fernández-Pachón
Alessandra Ferrandino
Osvaldo Ferrarese-Filho
Isabel C. F. R. Ferreira
Isabel M. P. L. V. O. Ferreira
Leonardo Cesar Ferreira
Susana Ferreira
Vicente Ferreira
Evelina G. Ferrer
Federico Ferreres
Mario G. Ferruzzi
Dimitrios Fessas
Michael Festing
A. G. Fett-Neto
Luciano Fietto
Ana Cristina Silva Figueiredo
John Weldon Finley
John Westcott Finley
Antonio Fiorentino
Dennis Fiorini
Joan G. Fischer
Ian Denis Fisk
Montserrat Fitó
Richard J. Fitzgerald
Riccardo Flamini
Mary T. Fletcher
Dimitrios John Fletouris
Swaran Flora
Monica Flores
Rolando Flores
Giovanni Floris
Terence Lee Fodey
Péter Fodor
Vincenzo Fogliano
Ariel R. Fontana
Debora Fontanini
Malcolm Donald Elder Forbes
Paul Ford
Fabio Forlani
W. Alison Forster
Torgils Fossen
Krishna L. Foster
Kylie D. Foster
Milica Fotirić Akšić
Imogen Foubert
Glen P. Fox
Daniela Fracassetti
Cesar G. Fraga
Pilar Francino
David Francis
Leigh Francis
Octávio L. Franco
M. Teresa Frangipane
Damian Conrad Frank
Jan Frank
Oliver Frank
Stephanie Frank
Knut Franke
Edwin N. Frankel
Chlodwig Franz
Alessio Frassoldati
Alessandra Fratianni
Felix Frauendorfer
Giuseppe Fregapane
Xavier C. Frette
Carl Frey
Juana Frias
Kristina Fricke
Joel Mitchel Friedman
Mendel Friedman
Helge Fritsch
Kevin Fritshe
Jona Ines Fritz
María José Frutos
Derek Fry
Ming-Lai Fu
Shu-Ling Fu
Yu-Jie Fu
Anthea Fudge

E. Patrick Fuerst
Ko Fujimori
Naoko Fujita
Shuji Fujita
Koji Fukui
Kenji Fukunaga
Eiichiro Fukusaki
Kazuhiko Fukushima
Claudia Maria Furlan
Takeshi Furuta
Ana San Maria Gabriel
Jerzy Gaca
Giova Gadda
Giovanni Gadda
Stefan Gafner
Valerie Gagnaire
Anna Gajda
E. Gajewska
Roberta Galarini
Dimitrios Galaris
Simon Galas
Gianni Galaverna
Maria Teresa Galceran
Teresa Galeano-Díaz
Rudolf Galensa
Lourdes Gallardo-Guerrero
Claudio Galli
Sophie Gallier
Blanca Gallo
Vito Gallo
Lorenzo Gallus
Christophe Claude Galopin
Julio Galvez
Andrea Catalina Galvis-Sánchez
Giorgio Gambino
Angelita Gambuti
Chee-Yuen Gan
Jay J. Gan
Fernando Gandía-Herrero
Beatriz Gandul Rojas
Michael G. Gänzle
Hongwei Gao
Hong-Wen Gao
Hui-yuan Gao
Jin-Ming Gao
Wenyuan Gao
Wen-Yun Gao
Gaizka Garai-Ibabe
Leif Alexander Garbe
Eric A. E. Garber
Carlos Garcia
Maria Alejandra Garcia
Guadalupe Garcia Llatas
Virginia Garcia-Canas
María Teresa García-Conesa
Hugo García-Galindo
Teresa Garcia-Gasca
Diego Luis Garcia-Gonzalez
Silverio García-Lara
José María García-Mina
Juan F. Garcia-Reyes
Cristina Garcia-Viguera
Rocio Garcia-Villalba
Teresa Garde-Cerdán
Dale R. Gardner
Gary M. Gardner
Antonio Garrido-Fernández
Sherry Garris
Gil Garrote
Klaus Gase
Mattia Gasperotti
Klaus Gassenmeier
Giuseppe Gattuso
Valerie Gaudin
Paola Gauffin Cano
R. Gavara
Igor Gavin
Terrence Gavin
Marija Gavrovic-Jankulovic
Urszula Gawlik-Dziki
Gabriella Gazzani
Wentzel Ca Gelderblom
Pierre Gelinas
Goran Gellerstedt
Steven Gendel
Zeng Chao Geng
Maria I. Genovese
Carla Gentile
Alessandra Gentili
Zhang Genyi
Milen Ivanov Georgiev
Constantinos A. Georgiou
Jared Quinton Gerlach
Hernâni Gerós
Ioannis Gerothanassis
Zev Gerstl
Jan M. C. Geuns
Martin Geyer
Ashraf Ghanem
Greg Gharst
Alireza Ghassempour
Sue Ghazala
Remy Ghidossi
Giovanna Ghirlanda
Marc Ghislain
Amit K. Ghosh
Banibrata Ghosh
Ilias Giannenas
Valentina Gianotti
Donna Gibson
Michael J. Gidley
Thomas Giersch
Martin Gierus
Maria Isabel Gil
Alexis Romain Gilbert
Robert G. Gilbert
Edward Gilding
Angel Gil-Izquierdo
Brendon Gill
Chris I. R. Gill
Robert J. Gilliom
Rosa M. Giner
Idit Ginzberg
Camilla Giovannini
Amadeo Gironés-Vilaplana
Albert W. Girotti
Paolo Giudici
Arne Glabasnia
Raymond Philip Glahn
Michael Glei
Gregory M. Glenn
Kevin Challon Glenn
P. Glibowski
Marcus A. Glomb
Julie M. Goddard
Tzonka Godjevargova
Danica Erin Goggin
Kheng-Lim Goh
Koen Goiris
Elmas Gök
Hakan Goker
Vural Gökmen
N. Gokoglu
José Anchieta Gomes Neto
Aurelio Gómez-Cadenas
Ana Maria Gómez-Caravaca
Agustina Gomez-Hens
Encarna Gomez-Plaza
Luís M. Gonçalves
Deming Gong
Yuansheng Gong
Maria Gonzales
Maria Jose Gonzalez
Ramon Gonzalez
Álvaro Sebastián González
Ana María González Paramás
Azucena González-Coloma
Cristina González-Fernández
M. Carmen Gonzalez-Mas
Cynthia L. Goodman
Richard E. Goodman
Madhuban Gopal
T. Gopinandhan
Fernando Gordillo-Delgado
André Gordon
Michael H. Gordon
Sherald H. Gordon
Shela Gorinstein
Stanislava Gorjanovic
Sylwia Gorlach
Irina Goryacheva
Vikram Suryaprakash Gota
Marijan Gotić
Tetsuhisa Goto
Katherine T. Gottschall-Pass
Pere Gou
Luis Goya
Anju Goyal
Aymeric Goyer
Franco Gozzo
Mary H. Grace
Fernando Granado-Lorencio
Pablo Granitto
Michael Granvogl
Benoit Graulet
David A. Gray
Robert A. Graybosch
Anna Grazia Mignani
Heather Green
M. Scott Greer
Paola Grenni
Peter M. Gresshoff
Gordon Wayne Gribble
Casey C. Grimm
Konrad Grob
Jude W. Grosser
Maria Victoria Eiras Grossmann
Carlos R. F. Grosso
Clara Grosso
Christian W. Gruber
Michael Grusak
Wieslaw I. Gruszecki
Frank Gu
Liwei Gu
Zhenxin Gu
Hongxia Guan
Stefano Guandalini
Michael Guarnieri
Muralikrishna Gudipati
Miguel Gueimonde
Catherine Guerin-Dubiard
Angel Guerrero
Nicoletta Guerrieri
Luís F. Guido
Jose Luis Guil Guerrero
María D. Guillén
Claude Guillou
Hardeep Singh Gujral
Elzbieta Gujska
İlhami Gülçin
Atilla Gulec
Maria Gullino
Yusuf Ziya Gunata Sr.
Changjiang Guo
Zheng Guo
Zhiyong Guo
Sumit Gupta
Ozan Gurbuz
Brian Guthrie
Fanny Guyomarch
Sylvain Guyot
Jorge Luis Guzman Mar
Tae Youl Ha
Yeong Lae Ha
Ilka Haase
Norbert Haase
Mary Hadley
Guido R. M. M. Haenen
Rahman Md. Hafizur
Bruno Hagenbuch
Ann E. Hagerman
Beverley A. Hale
Nigel George Halford
Clifford Hall III
Tim Hall
Ewelina Hallmann
Dietmar Haltrich
Kenji Hamase
Yasunori Hamauzu
Matthias Hamburger
Karyn L. Hamilton
Earl G. Hammond
Daniela Hampel
Gerd Hamscher
Abdallah Hamze
Bo Han
Dong-Wook Han
Jaehong Han
Jaejoon Han
Lujia Han
Qian Han

dx.doi.org/10.1021/jf405539n |J. Agric. Food Chem. 2014, 62, 4–21

Quan-Bin Han
Yifan Han
Ales Hanc
John Travers Hancock
Akihiro Handa
Sara M. Handy
Yong D. Hang
Stephan Hann
Abdelali Hannoufa
Christophe Hano
Jens Hansen-Moller
Liping Hao
Xiaojiang Hao
Zhigang Hao
Hideaki Hara
Hiroshi Hara
Kazutomo Haraguchi
Mamoru Haratake
Sanaz Haratifar
James F. Harbertson
Katrin Harms
Juan Francisco Haro
Gregory S. Harper
George G. Harrigan
Keith Harris
Philip J. Harris
M. Harrison
Rogers Emughedi Harry-O'kuru
Richard M. Hartshorn
Omar R. Harvey
Gesa Haseleu
Jovin Hasjim
Neuza Mariko Aymoto Hassimotto
Tomohisa Hasunuma
Ronald D. Hatfield
Hajime Hatta
Ryota Hattori
Emmanuel Hatzakis
Efimia Hatzidimitriou
Rachel Hauser-Davis
Palatasa Havea
Michael J. Havey
John Havlin
G. E. Hawkes
Nobuyuki Hayashi
Saeed A. Hayek
Heiko Hayen
Lynn Haynes
El Akrem Hayouni
Douglas G. Hayward
Jan Hazebroek
Stanley L. Hazen
Guangyuan He
Hai-Lun He
Hong-Ping He
Hongwu He
Jian He
Kan He
Limin He
Qinghua He
Rong-Rong He
Xiangjiu He
Xu-Sheng He
Ying He
David Heber
Vincent Robert Hebert
Mette S. Hedemann
Mikael S. Hedenqvist
Mikael Hedenqvist
Sam Heenan
Heidi Heidi Goenaga-Infante
Mark Heiman
Daniela Heimler
I. Marina Heinonen
Anja Heins
Elke Heiss
Jarkko Kalevi Hellström
Gregg Henderson
Suzanne Hendrich
Matt Hengel
Thomas Henle
Kristin Hennig
Geneive Elizabeth Henry
Cynthia A. Henson
Andrea Henze
Thomas J. Herald
Markus Herderich
Francisco José Heredia
Miguel Hererro
Rod A. Herman
Anne-Marie Hermansson
Isidro Hermosín-Gutiérrez
Manuel Hernandez-Cordoba
Blanca Hernández-Ledesma
María Dolores Hernando Guil
Dolores Hernanz Vila
Tomas Herraiz
Ana Herrero
C. Herrero Latorre
Joseph Hershenhorn
John L. Hess
Stéphanie Heuskin
Hildegarde Heymann
Muneaki Hidaka
Francisco J. Hidalgo
Miki Hiemori-Kondo
Christopher P. Higgins
Camilla Hill
Heidi Hill
Helen Hill
Herbert H. Hill, Jr.
Mihaela Hillebrand
Florentine Hilty
Max Hincke
Wade Hines
Joerg Hinrichs
Makoto Hirako
Chi-Tang Ho
Hung-Yao Ho
I-Pin Ho
Yuan-Soon Ho
Yuh-Shan Ho
Rodrigo B. Hoff
Angela Hoffman
Karin Hoffmann-Sommergruber
Thomas Hofmann
Petra Hogger
Barbara Hohn
Lee Hoi Seon
Askild Lorentz Holck
Aline Holder
David Holding
Peter C. H. Hollman
David Holm
Thomas Holzhauser
Jungil Hong
Mee Young Hong
Yan Hong
Young-Shick Hong
Yeoh Beng Hoong
Antony M. Hooper
Dallas Hoover
Helene Hopfer
Marcin Horbowicz
Fumihiko Horio
Damaso Hornero-Mendez
Daniela Horvat
Carl Hoseney
Atsushi Hoshino
Keizo Hosokawa
Masashi Hosokawa
Arland T. Hotchkiss
De-Xing Hou
Qingxi Hou
Wen-Chi Hou
Xiaolin Hou
Todd A. Houston
Siew Eng How
Luke R. Howard
Amy Howell
Kate Howell
Geza Hrazdina
Milan Hruby
Rong-Hong Hsieh
Yih-Shou Hsieh
Yue-Ie Hsing
Cheng-Chim Hsu
Cheng-Kuang Hsu
Shi-lan Hsu
Bin Hu
Bing Hu
Dan-Ning Hu
Dingfei Hu
Jiye Hu
Jun Hu
Miao-Lin Hu
Ming Hu
Peng Hu
Qiuhui Hu
Shengjun Hu
Xinzhong Hu
Zhi-Bin Hu
Zhoujian Hu
Chiung Hui Huang
Dejian Huang
Fang Huang
Fenghong Huang
Guan-Jhong Huang
Hsiu-Chen Huang
Huazhang Huang
Hui-Chun Huang
Jianbin Huang
Jinhai Huang
Jirong Huang
Kexuan Huang
Luqi Huang
Nan Huang
Qingchun Huang
Qingrong Huang
T. C Huang
Wuyang Huang
Xirong Huang
Yang Huang
Yu Huang
Yuming Huang
Machteld Huber
Christian W. Huck
Jan-Carlos Hufnagel
David John Huggins
Michael F. Hughes
Jowita Humin
Hans-Ulrich Humpf
William Hunter
Thom Huppertz
Elton Hurlow
Andrew Hursthouse
Carin A. Huset
Faris Karim Hussain
Søren Husted
Kevin Huvaere
Bang Yeon Hwang
Chin-Fa Hwang
Geum-Sook Hwang
Stefania Iametti
Elena Ibañez
Maria Ibanyez
Hisham R. Ibrahim
Salam A. Ibrahim
Vassiliki Iconomidou
Savarimuthu Ignacimuthu
Takashi Iimure
Tsuyoshi Ikeda
Julius Kwagh-Har Ikya
Nebojsa Ilic
Yoshihiro Imahori
Masaki Imai
Shinsuke Imai
Jee-Young Imm
U. Immer
Harvey E. Indyk
Donald Ingram
John Ingram
Gabbriella Innocenti
Kuniyo Inouye
Maria Iorizzi
Richard Ipsen
Gabriela Irazoqui
Kazuhiro Irie
Florin-Dan Irimie
Marcello Iriti
José Hipólito Isaza Martínez
Mamoru Isemura
Yasuyuki Ishida
Teturo Ishii
Emy Luiza Ishii-Iwamoto
Hiroya Ishikawa
Shin-ichi Ishikawa
Tsutomu Ishikawa
Ciro Isidoro
Md. Tofazzal Islam
Amin Ismail
Baraem Ismail
Murray Bruce Isman
Shirou Itagaki
Hideyuki Ito
Tomohiro Itoh
Wayne T. Iwaoka
María Izquierdo-Pulido
Nicolai David Jablonowski
Ayanna Jackson

Brian P. Jackson
Lauren Jackson
Mike Jackson
Scott Harding Jackson
Doris M. Jacobs
Charlotte Jacobsen
Jacek Jaczynski
Arunakaran Jagadeesan
Margaretha Jagerstad
Ramon Jaime
Vikas Jaitak
Lidija Jakobek
Judit Jakus
Mahbubul Alam Foizul Jalal
Delano James
Kuo-Ching Jan
Jay-lin Jane
Jeandre Jaques
Robert L. Jarret
Eila P. Järvenpää
Jordane Jasniewski
Aneta Jastrzębska
Chamila Jayasinghe
Jae-Young Je
Legault Jean
Philippe Jeandet
Piotr Jedziniak
Peter M. Jeffers
David William Jeffery
Elizabeth Hutt Jeffery
Jennifer Jeffery
Henryk H. Jelen
G. Ronald Jenkins
Ida Johanne Jensen
Sidsel Jensen
Igor Jerkovic
Gerold Jerz
Flemming Jessen
Marimuthu Jeya
Rajesh Jha
Jin-Woo Jhoo
Baoping Ji
Junfeng Ji
Jun-yuan Ji
Yewei Ji
Wenjie Jian
Aimin Jiang
Bo Jiang
Deshou Jiang
Dingxin Jiang
Jianxin Jiang
Jinqing Jiang
Shann-Tzong Jiang
Xuntian Jiang
Yuanrong Jiang
Yue Ming Jiang
Zhi-Hong Jiang
Zongyong Jiang
Zheng Ji-lu
Ana Jimenez-Araujo
Antonio Jimenez-Escrig
Jose C. Jimenez-Lopez
Rodrigo Jiménez-Saiz
Fen Jin
Mingjie Jin
Peng Jin
Qingzhe Jin
Shigeki Jin
Zhendong Jin
Zhuang Jin
Chuanyong Jing
Hao Jing
Leopold Frieda Jirovetz
Cheorun Jo
Daniel Joel
Anna Jofré
Katja Salomon Johansen
Eva Johansson
Yoko Shibuya Johnson
John J. Johnston
Deanna Jones
Julie Jones
Russell L. Jones
William Paul Jones
Tammy L. Jones-Lepp
Sisse Jongberg
Arjan Jonker
Seong Soo Joo
Etienne Jooken
Juana Dolores Jorda
António M. Jordão
Bodil Jørgensen
Elizabeth Joubert
Daniel Joulain
Michael Jourdes
M. Emilia Juan
Rong-Huay Juang
Luis Juliá
Mira Jun
Xie Jun
Mun Yhung Jung
Colette Jungas
Alois Jungbauer
Jerzy Juskiewicz
Lesław Juszczak
John A. Juvik
Piotr Kachlicki
Roohollah Torabi Kachosoangi
Nina Kacjan Marsic
Rassoul Kadkhodaee
Pawel Kafarski
Shinzo Kagabu
Isabelle Ann Kagan
Norihiko Kageyama
Melanie Kah
Yoichi Kainoh
Josef Kaiser
Mitali Kakran
Vladimir I. Kalinin
Heikki Kallio
Stamatina Kallithraka
Wilhelmina Kalt
Willy Kalt
Curtis Mbulanyumba Kalua
Yasutomi Kamei
Alaa Kamel
Shigehiro Kamitori
Tetsuro Kamiya
Alexander A. Kamnev
Kazuki Kanazawa
Satoshi Kaneco
Hirotaka Kaneda
Rensuke Kanekatsu
Hideo Kaneko
Shu Kaneko
Byoung-Cheorl Kang
Jeong-Hun Kang
Jonghoon Kang
Young-Hee Kang
Kurunthachalam Kannan
Joseph Kanner
Ming-Ching Kao
Virginie Noutchogoue Kapchie
Romain Kapel
Sudhir Kapoor
Haralabos Karantonis
Thomas Karbowiak
Ehsan Karimi
Reijo Karjalainen
John Karlik
David S. Karpovich
Peter Karuso
Naoya Kasai
Donald D. Kasarda
Sashi G. Kasimsetty
Hiroyuki Kataoka
Shigeru Katayama
Atsushi Kato
Masaya Kato
Norihisa Kato
Diksha Kaushik
Nat N. V. Kav
Nickolas G. Kavallieratos
Jun Kawabata
Yasushi Kawagoe
Yoshichika Kawai
Shin-ichi Kayano
Figen Kaymak-Ertekin
A. P. Polycarpe Kayodé
Shaoyong Ke
Michael Keenan
Panagiotis Kefalas
J. Kehoe
Jaap Keijer
Hasim Kelebek
Alan L. Kelly
Mitch Kelly
Sabine Kemmlein
Belinda Kemp
James A. Kennedy
Garry Kerch
Philip G. Kerr
William L. Kerr
Serhat Keser
Emre Keskin
Agnes Keszler
Young Soo Keum
Michael Keusgen
Claire Kevers
Abdul Latif Khan
Avik Khan
Deena Khan
Khalil Khan
Ruhul A. Khan
Farhath Khanum
Rabie Khattab
Baharullah Khattak
Ashot Khrimian
V. A. Khripach
Johannes Kiefl
Arie K. Kies
Manfred Kietzmann
Hiroe Kikuzaki
Michelle Kilcoyne
Paul Andrew Kilmartin
Beom Seok Kim
Chong-Tai Kim
Chul Ho Kim
Gil-Hah Kim
Hakryul Kim
Hanseong Kim
Hye Jung Kim
Hyeung-Rak Kim
Hyoun-Ju Kim
Hyun-Jin Kim
In Seon Kim
Jang-Eok Kim
Jeong-Han Kim
Ji Yeon Kim
Junheon Kim
Kyung Hyun Kim
MeeKyung Kim
Se-Jae Kim
Somi Kim
Sung Hoon Kim
Sung Y. Kim
Yangha Kim
Young-Min Kim
Youngmok Kim
Young-Suk Kim
Martin Kimanya
Ken-ichi Kimura
Makoto Kimura
Tobias Kind
Jerry W. King
Joan M. King
Beatriz King-Diaz
A. Douglas Kinghorn
Vassilis Kiosseoglou
Nese Kirimer
Apostolos Kiritsakis
Lara Kirsch
Taro Kishida
Anna K. Kiss
Seiya Kitamura
Yoshie Kitamura
David Kitts
S. Kivatinitz
Arthur L. Klatsky
Erich Kleinpeter
Gijs Kleter
Sappasith Klomklao
James Levi Klotz
Holger Knapp
Allan Ray Knight
Dietmar Knopp
Robert Knott
John Paul Knox
Knud Erik Bach Knudsen
Ching-Huai Ko
Jiunn Liang Ko
Yuan-Tih Ko
Kazunori Koba
Kenji Kobata
Fumiyuki Kobayashi
Robert Kobelski
Matthias Koch
Jan P. Kochansky
Sunil Kochhar
Gabor Kocsy
Hiroyuki Kodama
Terry Koerner
P. Köhler
Peter Köhler
Ralf Köhler
Noriko Kohyama
Marja E. Koivunen
Shosuke Kojo

Vanja Kokol
Sabina Galus Kokoszka
Sevgi Kolaylı
Andeas Kolb
Joanna Kolodziejczyk-Czepas
Michalis Komaitis
Marina Komrakova
Izabela Konczak
Chang-Suk Kong
Chuihua Kong
I. Kong
Lingtian Kong
Lingyi Kong
Tao Kong
Xiangzhen Kong
Tetsuya Konishi
Yasuko Kawamura Konishi
Yutaka Konishi
Kunihiko Konno
Michael George Kontominas
Rai S. Kookana
John L. Koontz
Stef J. Koppelman
Randall A. Kopper
Thomas Koppmann
Dean Adam Kopsell
Figen Korel
Samira Ibrahim Korfali
Mojca Korosec
Shigenobu Koseki
Takuya Koseki
Agnieszka Kosińska
Iztok Joze Kosir
William C. Koskinen
Tatjana Košmerl
Georgina Kosturkova
M. Kostyukovsky
Eiichi Kotake-Nara
Yiannis Kourkoutas
Tayeb Koussa
Georgios Koutsidis
Jozef Kovacik
Martin F. Kovacs Jr.
Jennifer A Kovacs-Nolan
Janine Kowalczyk
P. Kowalski
Naoto Koyama
Stanislav Kracmar
Jaroslav A. Kralovec
Gerhard E. Krammer
Maria Kratchanova
Dietmar Krautwurst
Carsten Krebs
Ivan Kreft
Jan-Ulrich Kreft
Johanna Kreissl
Dario Kremer
Robert Kremer
Ulrich Krings
Hari Bhupathi Krishnan
Manonmani Haravey Krishnan
Eleana Kristo
Woravimol Krittaphol
Lothar Wilfried Kroh
Dana A. Krueger
Alexander J. Krynitsky
Vlastimil Kuban
Marta Kucharska
Annette Kuehn
Omer Irfan Kufrevioglu
Jan Kuhlmann
Shirley Kuhnen
Nikolai Kuhnert
Arnis Kuksis
Jozef Kula
Ulrich Kulozik
S. Kumagai
Dhirendra Kumar
Rajesh Kumar
Vineet Kumar
Shigenori Kumazawa
Alina Kunicka
Chia-Feng Kuo
Ching-Chuan Kuo
Jen Min Kuo
Min-Liang Kuo
Ping-Chung Kuo
Po-Lin Kuo
Sheng-Chu Kuo
Tzong-Fu Kuo
Yao-Haur Kuo
Michael Kurantz
Hiroshi Kurihara
Keisuke Kurita
Sudarshan Tanaji Kurwadkar
Miyako Kusano
Martin Kussmann
Markus Küsters
Barbara Kusznierewicz
Frantisek Kvasnicka
M. Kverka
Dong-Yeul Kwon
Hyung-Jin Kwon
Joong Ho Kwon
Oran Kwon
Petri Kylli
John Marcus Labavitch
Dirk W. Lachenmeier
Jaromir Lachman
Markus Lacorn
Mita Lad
G. S. Ladics
Michael R. Ladisch
Helle N. Lærke
Domenico Lafiandra
M. Jesús Lagarda
Gaetano Laghetti
Bert Lagrain
Ching-Shu Lai
Furao Lai
Oi-Ming Lai
William Laing
Franco Maria Lajolo
Hanne Lakkenborg Kristensen
Santosh P. Lall
C. Lamacchia
Fernand Lambein
Joshua D. Lambert
Milena Lambri
Anna-Maija Lampi
Rosa M. Lamuela-Raventós
Roman Lang
Bernd Markus Lange
Wenjian Lao
I. Lara
Isabel Lara Ayala
Pablo Antonio Lara-Martín
Cynthia K. Larive
María Angélica Larraín
Mar Larrosa
Flemming Hofmann Larsen
Mette Larsen
Steve Larsen
Barbara Lata
Elci Latif
Sajid Latif
Vincenzo Lattanzio
Anja Kaarina Lätti
Gladys O. Latunde-Dada
V. Felipe Laurie
Vera Lavelli
Tao Le
Thao T. Le
Bruno Le Bizec
Jean-Luc Le Quere
Canh Le Tien
Vincent Lebot
Blanca Hernandez Ledesma
Gerard Ledoigt
David R. Ledoux
Bao-Hong Lee
Byong H. Lee
Chan Lee
Chao-Ying Lee Lee
Chen-Chen Lee
Chihoon Lee
Ching-Kuo Lee
Choong Hwan Lee
Dae-Hee Lee
Dongho Lee
Hoi-Seon Lee
Hyeon Gyu Lee
Jiyoung Lee
Jong Hun Lee
Joonhee Lee
Jung Hoon Lee
Jung-Bum Lee
Jungmin Lee
Kung-Ta Lee
Kuo-Kau Lee
Kwang Youl Lee
Kwang-Geun Lee
Meng-Shiou Lee
Mi Kyeong Lee
Ming-Fen Lee
Moon Kyu Lee
Sang Guei Lee
Sang Kook Lee
Sanghyun Lee
Seong Hun Lee
Sung-Eun Lee
Sung-Ho Lee
Tzu-Tai Lee
Viola Lee
Wen-Sen Lee
Woo Song Lee
Michele Lees
Patricia Marie Legler
Katharina Lehmann
Steven J. Lehotay
Pekka Lehtonen
Hongtao Lei
Xingen Lei
Erich Leitner
Paul Lemieux
Ann T. Lemley
D. Lemos
Robert Willis Lencki
Marcello Salvatore Lenucci
Wai Fun Leong
Maria Leontowicz
Hrvoje Lepedus
Sittiwat Lertsiri
Uri Lesmes
Gene E. Lester
Alexander Kai-Man Leung
Ping Chung Leung
Carol E. Levin
Grazyna Lewandowicz
Jakob Ley
Aifeng Li
Can-Peng Li
Cheng Hao Li
Chunyang Li
Deqiang Li
Faqiang Li
Fengqin Li
Genxi Li
Gongke Li
Guoliang Li
Guolin Li
Hai-Hang Li
Hui Li
Hui-Jing Li
Jianfa Li
Jianhong Li
Jiebing Li
Jing Li
Ke Li
Laura Li
Liqing Li
Liya Li
Peiwu Li
Pengcheng Li
Qing Xiao Li
Quanhong Li
Rong Li
Shaoping Li
Sheng-Hong Li
Shiming Li
Si-Quan Li
Ti Li
Tingqiang Li
Wei Li
Weifen Li
Wen-Hong Li
Xiang Li
Xiaoxi Li
Yanling Li
Yao-Qun Li
Yong-Qiang Li
Yu Li
Yue Li
Zaigui Li
Zheng Li
Zheng-Ming Li
Zhong Li
Jerzy Lisek
Chia-Hua Liang
Hao Liang
Jianfen Liang

Jin Liang
Juan Boo Liang
Yu-Chih Liang
Yue Liang
Yuerong Liang
Yalin Liao
Pao-Chi Liao
Yu-Cai Liao
Erica Liberto
Eunice Chi Yu Li-Chan
Gérard Liger-Belair
Chong-Kuei Lii
Mary Ann Lila
Cathrine Lillo
Loong-Tak Lim
Soon Sung Lim
Nanteetip Limpeanchob
Amy Hui-Mei Lin
Cheng-Wen Lin
Chi-Chen Lin
Chih-Cheng Lin
Chih-Li Lin
Chun-Ching Lin
Da-Gin Lin
Daohui Lin
Doung-Liang Lin
Fu-Pang Lin
Jianming Na Lin
Jin-Ming Lin
Jin-Yuarn Lin
Jun Lin
Jun-Fang Lin
Kunde Lin
Li-Yun Lin
Longze Lin
Lu Lin
Mengshi Lin
Tsai-Yun Lin
Wenhan Lin
Wun-Yuan Lin
Xucong Lin
Yaw-Huei Lin
Yun-Lian Lin
Yu-Wei Lin
Andrew B. Lindstrom
Sandra Lindstrom
Wee Suk Ling
Wenhua Ling
Henk Lingeman
Susanne Lischka
John H. Litchfield
Aiping Liu
Baolin Liu
Bao-Sheng Liu
Bo Liu
Chan-Min Liu
Cheng-Kung Liu
Chengmei Liu
Chenguang Liu
Chuan-Fu Liu
Dasen Liu
Donghong Liu
Dongting Liu
Fengquan Liu
Hongbing Liu
Hongsheng Liu
Huijun Liu
Jiaren Liu
Ji-Kai Liu
Jing-Bo Liu
Jingfu Liu
Junqiu Liu
Kuan-Ju Liu
Kwang Hyeon Liu
Kwang-Hyeon Liu
Mai Li Liu
Mingzhu Liu
Ning Liu
Pengfei Liu
Pinghua Liu
Qiaoquan Liu
Rutao Liu
Shang-Zhong Liu
Shing-Hwa Liu
Xiangfei Liu
Xiaofei Liu
Xinghai Liu
Yanhong Liu
Yonghong Liu
Yun Liu
Yung-Chuan Liu
Zai-Qun Liu
Zhaoyin Liu
Zhiqian Liu
Zhiqiang Liu
Peng Liua
Chi-Chu Lo
Chih-Kang Lo
Chih-Yu Lo
Y. Martin Lo
Yi-Chen Lo
Angela Roberta Lo Piero
Consuelo Lobato-Calleros
Wayne Loescher
Amy Logan
A. R. Logesh
M. Lohmus
Jack J. Lohne
Monica Rosa Loizzo
B. R. Lokesh
Francesco Longobardi
Colin Longstaff
Katja Loos
Richard LoPachin
Lucia Maria Xavier Lopes
Norberto Peporine Lopes
Christelle Lopez
Sergio Lopez
María Dolores López
Agustin Lopez Munguia
Gracia López-Carballo
Rosina Lopez-Fandino
Luis Javier López-Giraldo
Jose Manuel Lopez-Nicolas
Jose Eugenio Lopez-Periago
Cristina López-Vázquez
Axel Lorentz
Jose Manuel Lorenzo
Natalia Loscos
Ilario Losito
Jack N. Losso
Blas Lotina-Hennsen
Hong-Xiang Lou
Lili Lou
S. N. Lou
Yonggen Lou
Simon M. Loveday
David P. Lovell
Douglas W. Lowman
José Daniel Lozada Ramírez
Changming Lu
Cheng-Ping Lu
Fachuang Lu
Jian Lu
Jun Lu
Qing-Yi Lu
Weiying Lu
Xiaonan Lu
Yanhua Lu
Yingqing Lu
Aldo Di Luccia
Juan J. Lucena
Luigi Lucini
Juan Maria Luco
Edward C. Lulai
Jianmei Luo
Shaojun Luo
Wenhong Luo
Yaguang Luo
Yangchao Luo
Zhigang Luo
Zisheng Luo
María Dolores Luque De Castro
Sue Lurie
John W. Lyga
Graham Henry Lyons
Ching Yung Ma
Dongying Ma
Hao Ma
Lena Ma
Yibing Ma
Yueming Ma
Zhongjun Ma
Herve Macarie
Ruth S. MacDonald
Wade Mace
Maria Ligia Rodrigues Macedo
Alan Robert Mackie
Lucia Maddau
Jens Mäder
Ronald L. Madl
Fernando Madrid
Hiroshi Maeda
Osamu Maeda
Stefan Maertlbauer
Rodrigo Maestre
Isabel Mafra
Ruben M. Maggio
Kanjana Mahattanatawee
Pamela Anne Maher
Giuseppe Maiani
Pitchaon Maisuthisakul
Małgorzata Anna Majcher
Soumyajit Majumdar
Tapas K. Makar
Yoshio Makino
Antonios M. Makris
Alexandra Malachova
Marian Kjellevold Malde
Julia Maldonado-Valderrama
Soheila J. Maleki
Ashok Kumar Malik
Veronika Mall
Eligio Malusá
Joao Malva
Jan Malyszko
Stefano Mammi
Gianfranco Mamone
Ricky Y. K. Man
Claudine Manach
Ileana Manduteanu
Jordi Manes
Alfonso Mangoni
Audronė Mankevičienė
Caterina Manna
Luisa Mannina
Anna Katharine Mansfield
Fani Mantzouridou
Paloma Manzanares
Jianwei Mao
Zhengwei Mao
Takashi Maoka
Sameer A. S. Mapari
Angel Maquieira
Chris M. Maragos
Matteo Marangon
Alejandro Gregorio Marangoni
Marcelo Maraschin
Stéphanie Marchand
R. Marchant
Andrea Marchetti
Eric Marchioni
Massimo F. Marcone
Ombretta Marconi
Maria Carla Marcotullio
Norma E. Marcovich
Pauline Marcq
Maria Cristina Marcucci Ribeiro
Benedetta Margiotta
Alicia Marín
Nebojsa S. Marinković
A. Mariod
Lilian Regina Barros Mariutti
Julie Louise Markham
Doris Marko
Nelson Marmiroli
José Carlos Marques
William D. Marshall
Stefan Martens
François-Pierre J. Martin
Keith R. Martin
J. M. Martina
Olga Martin-Belloso
Kalyani Martinelango
Juan A. Martinez
Rafael Gimenez Martinez
Vicente Martinez
Guillermo Martinez Avila
Maria del Carmen Martinez
Enrique Martínez Force
Ramon Martinez-Mañez
Domingo Martinez-Romero Sr.

dx.doi.org/10.1021/jf405539n |J. Agric. Food Chem. 2014, 62, 4–21

Silvana Martini
Maria João Martins
Susana Martins
I. Martinussen
Maria Jesus Martin-Valero
Erwin Märtlbauer
J. Martucci
Cesare Marucchini
Nobuyuki Maruyama
Gorji Marzban
Stéfania Masci
Joseph H. Massey
Taro Masuda
Toshiya Masuda
Shigeki Masunaga
Rachel Mata
Kristen E. Matak
Kanyand Matand
Raquel Mateos
Inmaculada Mateos-Aparicio
U. Matern
M. L. Mateus
Nuno Mateus
Hiroshi Matsufuji
Kenji Matsui
Toshiro Matsui
Hikaru Matsumoto
Kinzo Matsumoto
Hiroaki Matsuo
Makoto Matsushita
James Mattheis
James C. Matthews
Paul Matthews
Fulvio Mattivi
Luiz H. C. Mattoso
Lisa J. Mauer
Ronald Maul
Ana Luísa Maulvault
Thomas P. Mawhinney
Carl A. Maxwell
Florian Mayer
Eugene Mazzola
Melinda C. Mccann
Thu McCann
Shaunna McCauley
David Julian McClements
Anna Mcclung
Laura L. Mcconnell
Susan Patricia McCormick
Gordon J. McDougall
Tony Kevin Mcghie
William McGlynn
Robert J. McGorrin
Susan O. McGuire
Marla McIntosh
Ken Mcmillin
Mary Ellen P. Mcnally
Jacqui M. McRae
Sharifudin Md. Shaarani
Giuseppe Meca
Mauro Mecozzi
Jand Venes Rolim Medeiros
Jheem D. Medh
Isabel Medina
Kumudini M. Meepagala
Laila Meija
Michael Meitinger
Ghozlene Mekhloufi
Antonio J. Meléndez-Martínez
Matthias F. Melzig
Pedro Mena
Rogerio O. Mendes
Menghsiao Meng
Qingxiang Meng
Carolin Menzel
Adriana Zerlotti Mercadante
Josep Vicent Mercader
Julien Mercier
Lucio Merlini
Marta Mesías
Frédéric Mestdagh
Ákos Mesterházy
Montse Mestres
Montserrat Mestres
Manfred Metzler
Stamatios F. Mexis
Michael Meyer
Samia-Mezouari
Raffaele Mezzenga
Bruno Mezzetti
Ján A. Miernyk
Graça Miguel
Luka D. Mihajlovic
Jorn D. Mikkelsen
Rene Mikkelsen
Kirsi Susanna Mikkonen
Emmanuel Mikros
Jegor Miladinovic
Fermin I. Milagro
Paul E. Milbury
Magdalena Milczarek
Eleana Miliou
Jasminka Milivojevic
Jocelyn G. Millar
A. Raymond Miller
Glenn Miller
J. David Miller
Kenneth B. Miller
Reinhard Miller
Tanja Mimmo
Yoshinori Mine
Warren Michael Miner-Williams
R. A. W. Mines
Piotr Minkiewicz
Susana Patricia Miranda
Hamed Mirhosseini
M. Miriani
Sidney S. Mirvish
Takumi Misaka
Petra Mischnick
Yael G. Mishael
Avinash Mishra
Sumit Mishra
Alyson Elayne Mitchell
John S. Mitchell
Pranabendu Mitra
Kamila Mitrowska
Hisashi Miyagawa
Makoto Miyahara
Shiro Miyake
Shigeo Miyao
Hitoshi Miyazaki
Kouji Miyazaki
Takuro Miyazaki
Teruo Miyazawa
Norio Miyoshi
Takaharu Mizutani
Ce-Hui Mo
Huanbiao Mo
William Moar
Ali I. Mohamed
Norhaizan Mohd Esa
Mohd Hazim Mohd Yusop
Guerfel Mokhtar
Bill Molin
Ana M. Molina López
Joachim Molkentin
Peter Molnar
Ibolya Molnár-Perl
Philip Molyneux
Russell John Molyneux
M. Monfreda
Efigenia Montalvo-Gonzalez
Fernando Montanes
Alfredo Montaño
Naim Montazeri
Jin Kim Montclare
Fanny Monteil-Rivera
Cinzia Montemurro
Maria Da Conceição Branco Silva Mendonça Montenegro
Angel Montoya
Carlos Montoya
Hyo-Bang Moon
Jae-Hak Moon
Joon-Kwan Moon
Tae Wha Moon
Amram Mor
Lidia Moraes
Simone Morais
Fermin Morales
Francisco Morales
Francisco J. Morales
Juan C. Morales
M. Lourdes Morales
Maria Teresa Morales
Paloma Moran
Carmen Moraru
Antonio Morata
Robert A. Moreau
Antonio Moreda-Piñeiro
Jorge Moreda-Piñeiro
Ricardo F. A. Moreira
Michael J. Morello
Diego A. Moreno
F. Javier Moreno
Maria Angeles Moreno
Maria Victoria Moreno Arribas
Antonio Moreno Herrera
M. Victoria Moreno-Arribas
Eduardo Moreno-Jiménez
Cédric Moretton
David E. Morgan
Jeffrey N. Morgan
Diego P. Morgavi
Kenji Mori
Ágnes M. Móricz
Toshio Morikawa
Masanori Morimoto
Kyoji Morita
Tatsuya Morita
Vincenzo Morra
Douglas Morrison
Mohamed A. Morsy
David N. Mortimer
Monica Mosca
Jill K. Moser
Gretchen Mosher
Magdi Mossoba
M. E. Mostafa
Mary O'Connell Motherway
Maria José Motilva
Donald S. Mottram
R. I. Moustafine
Paraskevi Moutsatsou
Emmanuel Moyse
Xindong Mu
Irene Mueller-Harvey
Michio Muguruma
Alister D. Muir
Eric S. Muise
Kazuo Mukai
Hasan Mukthar
Maurizio Mulas
Bill Mullen
Christo Muller
Josef Müller
Christopher A. Mullin
Luc Multigner
Rita H. Mumm
William R. Mundy
Sakthivel Muniyan
Edvani Curti Muniz
Sergi Munne-Bosch
Rosario Muñoz
Kesav Muntha
Akira Murakami
Koji Muramoto
Masatsune Murata
Takahisa Murata
Michael Murkovic
Kaeko Murota
Kotamballi Chidambara Murthy
Marilena Musci
Koenraad Muylaert
Kyung Myung
Altafhusain B. Nadaf
Ryoji Nagai
Masaya Nagao
Ram H. Nagaraj
Kornél Nagy
Seung-Yeol Nah
R. Naidoo
Muraleedharan Gopalan Nair
Bai Naisheng
L. Najafian
Hugo Nájera
Seiji Nakagame
Yoshiaki Nakagawa
Hiromitsu Nakajima
Kazuhiko Nakamura
Kozo Nakamura
Soichiro Nakamura

Yoshimasa Nakamura
Akimasa Nakano
Woranan Nakbanpote
Myung Hee Nam
Michio Namikoshi
Komeine Nantanga
Alessandra Napolitano
Kazuhiro Nara
Mirella Nardini
J. Roberto Oliveira Nascimento
Robert J. Nash
Norbert Nass
Atef M. K. Nassar
Senthil Natesan
Françoise Nau
Luciano Navarini
Duroy A. Navarre
Jose L. Navarro
Daniele Naviglio
Jan Nawrot
Naila Naz
Bhagyalakshmi Neelwarne
Timothy L. Negley
Giuseppina Negri
Sybille Neidhart
Gerry Neilsen
Andrew Peter Neilson
Tze Loon Neoh
Francoise Nepveu
Cristina Nerin
Anil Narayan Netravali
Susanne Neugart
Ken Ng
Nhuan Nghiem
Thanh Dong Nguyen
Hui Ni
Michael T. Nickerson
Shaoping Nie
Dennis Nielsen
Jette Nielsen
Kristian Fog Nielsen
Piritta Niemi
Ludwig Niessen
Pedro M. Nieto
Biljana Nigovic
Etsuo Niki
Maria Nikolantonaki
Lars L. Nilsson
Mathias Nilsson
Dilara Nilufer-Erdil
Li Ning
Sansey Nishibe
Naoko Nishizawa
Shoko Nishizono
N. Nitin
Chiara Nitride
Fuge Niu
Wenze Niu
Yuge Niu
Masha Y. Niv
Hong Kyoon No
Boguslaw Nocek
Koji Noge
Ana Rita Araujo Nogueira
Cassana Seimi Nomura
H. Nonaka
Martijn W. J. Noort
Simone Noremberg
Toshio Norikura
Ivana Novak
Vittorino Novello
Maria J. Nozal
Hajime Nozawa
Nikoletta Ntalli
Roberto Nucci
Clara Nudel
Karin Nuernberg
Fernando Milheiro Nunes
Marco T. Nunez
Estrella Nuñez-Delicado
Bangun Prajanto Nusantoro
Laura Nyström
James H. Oard
Hirotaka Obana
D. Obenland
A. Oberholster
Hassan K. Obied
Elías Obreque-Slier
Nora M. O'Brien
Peter J. O'Brien
Isabel Odriozola-Serrano
Itzhak Ofek
Masahiro Ogawa
Yasumitsu Ogra
Nives Ogrinc
Deok-Kun Oh
Myung Sook Oh
Seikwan Oh
Tomokazu Ohnuma
Daisaku Ohta
Yuichi Oishi
Yoshinori Okada
Keiki Okazaki
Wieslaw Oleszek
Hans-Werner Olfs
Cornelius Olieman
Bonastre Oliete
Cláudio Oliveira
Joana Oliveira
Jose T. A. Oliveira
Alberto de Jesus Oliveros Bastidas
Velimatti Ollilainen
Begona Olmedilla-Alonso
Michalis Omirou
Gemma Oms-Oliu
Roberta Onori
B. Dave Oomah
Elizabeth I. Opara
José Orantes Bermejo
Greg Organ
José de Jesús Ornelas-Paz
George González Ortega
Natividad Ortega
Frank Theodore Orthoefer
Luis Ortiz
Carmen Ortiz Mellet
Alicia Ortiz Moreno
Joaquín A. Ortuño
M. J. Oruna
Jesus Osada
B. Osborne
James Osborne
Tatsuya Oshima
Coralia Osorio Roa
Juan Osorno
Henrik Ostdal
Jan Oszmienski
León Felipe Otálvaro
Patricia I. Oteiza
Norihiro Otsubo
Yuzuru Otsuka
Herbert Otteneder
Don E. Otter
Shiyi Ou
Zheng Ouyang
Janel Elizabeth Owens
Özgül Özdestan
Yoshihiro Ozeki
Peggy Ozias-Akins
Yoshihisa Ozoe
Fernando Pablos
Deborah Pacetti
Helena Pachon
Maurizio Paci
Severina Pacifico
Graciela Wild Padua
Paulina Pająk
Marimuthu Palanisamy
Gopinadhan Paliyath
Alberto Palliotti
Peter T. Palmer
Carlo Alberto Palmerini
Lluís Palou
'Afa K. Palu
Baoliang Pan
Canping Pan
Cheol-Ho Pan
Chorng-Liang Pan
James L. Pan
Min-Hsiung Pan
Tai-Long Pan
Tzu-Ming Pan
Xiangqing Shawn Pan
Xuejun Pan
Daniel G. Panaccione
Sagar S. Pandit
Min Pang
Dimitrios Papachristos
Vassiliki Papadimitriou
Emmanouil H. Papaioannou
Adele Papetti
Sharon K. Papiernik
Juan Carlos Parajo
Efstathia Paramera
Adamantini Paraskevopoulou
José Emilio Pardo
Miguel Angel Pardo
Alberto Pardossi
Octavio Paredes-Lopez
Lucia Pareja
Rangan Parimalan
Hwangseo Park
Il-Kwon Park
Jae B. Park
Ki Hun Park
Kye Won Park
Kyechung Park
Sang Un Park
Seung-Chun Park
Sunghyouk Park
Yeonhwa Park
Yong-Doo Park
Jane K. Parker
Kirk L. Parkin
Hamendra Singh Parmar
Virinder Singh Parmar
Giovanni Parolari
Wendy Parr
Roberto Parra-Saldivar
Jason G. Parsons
Riitta Partanen
Angelika Paschke
David S. Pasco
Sonia Pascual-Teresa
Perfecto Paseiro
Giulio Pasinetti
Antonella Pasqualone
Sabina Passamonti
Alberto Passi
Edgar Pastene
Barbara Pastuszewska
Gabor Patonay
David Ian Pattison
E. Patyra
Luz Maria Paucar-Menacho
Anneleen Pauly
Roman Pavela
Elke Pawelzik
Mark J. Payne
Florastina Payton-Stewart
Manuel Pazos
Frederick Grant Pearce
M. Soledade C. Pedras
Maria Angeles Pedreno
Franco Pedreschi
Ronald B. Pegg
Renjun Pei
Shi-Chun Pei
Yanxi Pei
Richard Peigler
Jaroslav Pejchal
Jacob Pekar
Federica Pellati
Alvaro Pena-Neira
Chi-Chung Peng
Chiung-Chi Peng
Chiung-Huei Peng
Dungeng Peng
Hung-Sheng Peng
Kou-Cheng Peng
Robert Y. Peng
Xin-wen Peng
Rosane M. Peralta
Ana Luisa Pereira
Edenir Rodrigues Pereira-Filho
Gemma Perello
António Manuel Peres
Cidalia Peres
Ana Gracia Perez
Montse Perez
Cesar Perez-Alonso
Maria Carmen Perez-Camino
Francisco Jose Perez-Cano
Jose Ricardo Perez-Correa
Antonio Pérez-Gálvez

Jara Pérez-Jiménez
Cristina Perez-Ternero
María Jesús Periago
Nebojsa Perisic
Matthew Permenter
Javier Sanchez Perona
J. P. Peros
Enzo Perri
Daniel Perrone
Irena Perucka
Gene Pesti
James Pestka
Paul Herbert Peterman
Arnd Petersen
Mikael Agerlin Petersen
Devin G. Peterson
Robert K. Peterson
Carmen L. O. Petkowicz
Marian Petre
Goffredo Petrone
Katia Petroni
Rita Petrucci
Michael Petz
Andreas D. Peuke
Marie-Agnès Peyron
Stéphane Peyron
Kim-Yen Phan-Thien
Brian Phillippy
Katherine M. Phillips
Melissa Phillips
Surapon Piboonpocanun
Anna Lisa Piccinelli
Federica Piccirilli
Clara Piccirillo
Eran Pichersky
Jana Pickova
Yolanda Pico
Adeline Picot
Angela Rosa Piergiovanni
Luciano Piergiovanni
Amedeo Pietri
Lukasz N. Pietrzak
Antonio Piga
Vieno Piironen
Jana Pika
Gustavo Pimentel
Fernando Pina
Samantha Pinho
Jorge Antonio Pino
Glaucia Maria Ferreira Pinto
Rui Climaco Pinto
Roberto Pinton
Filippo Pirisi
Monika Pischetsrieder
Mariusz Piskula
Paola Pittia
María Isabel Pividori
Consuelo Pizarro
Roberto Pizzala
Rosa Pizzano
Steven M. Plakas
Joana M. Planas
Pierluigi Plastina
Lucía Plaza
Merichel Plaza
Patricia Plaza-Bolaños
Stavros Plessas
Lynda Podhorniak
Anna Podsędek
Norberto Pogna
Pawel Pohl
Luigi Poisson
Krzysztof Polewski
M. G. Polissiou
Federico Pomar Barbeito
Céline Poncet-Legrand
Alexandre Pons
Colin Frank Poole
Ron Porat
John R. Porter
Todd D. Porter
María P. Portillo
Andrea Porzel
Nebojsa Potkonjak
Thomas L. Potter
Nina Aagaard Poulsen
Joseph Robert Powers
Marta Prado
Habibur Rahman Pramanik
K. Nagendra Prasad
Paul David Prenzler
Neil P. J. Price
Carlos Priminho Pirovani
Witoon Prinyawiwatkul
Ronald L. Prior
Laura S. Privalle
Smriti Priya
Andrew Proctor
Nicholas William Proschogo
Yunqiao Pu
Rosa Puchades
Vladimir Puchart
María Cecilia Puppo
W. Ronald Purdum
Stig Purup
Lesley Putman
Raymond A. Putnam
Young-Hee Pyo
Krystyna Pyrzynska
Guangyan Qi
Phoebe X. Qi
Wei Qi
Chuanfan Qian
Kun Qian
Michael C. Qian
Xuhong Qian
Bo Qin
Ruijun Qin
Zhaohai Qin
Hong Qing
Jian Qiu
Jing Qiu
Ning Qiu
Xi Qiu
Le-Qing Qu
Ron Qu
Xiaogang Qu
Jesus Alberto Quezada-Gallo
Stephane Quideau
Daniel Quinn
Ted K. Raab
Victor Raboy
Juliana Neves Rodrigues Ract
Jeanne I. Rader
Blaga Radovanovic
Andrea Raffaelli
Arthur Jonas Ragauskas
Sivakumar Raghavan
Raghu Rajasekaran
Anoosh Rakhshandeh
Randeep Rakwal
Jean-Philippe Ral
Mohamed Fawzy Ramadan
B. Ramakrishnan
Ayyalusamy Ramamoorthy
Ranjith Ramanathan
Ravikumara Neralakere Ramanna
Daniel Ramon
Fernando Ramos
Maria Joäo Ramos
Sonia Ramos
Gurinder Jit Randhawa
Archna Rani
A. G. Appu Rao
Qinchun Rao
S. L. N. Rao
Gabriela Rapeanu
Paolo Rapisarda
Hava Rappoport
Peter Have Rasmussen
Reuven Rasooly
Luca Rastrelli
Bakhtiyor Rasulev
Khanok Ratanakhanokchai
R. George Ratcliffe
Gabriela Ratz
Doris Rauhut
Saroat Rawdkuen
Harshadrai M. Rawel
Dorothea F. K. Rawn
Ashish Rawson
Sierra Rayne
Marilyn Rayner
Isidra Recio
Rita Redaelli
Begoña Redruello
Clare Helen Redshaw
Jess D. Reed
Vivienne E. Reeve
Carlos Regalado
Klaas Reglitz
Jorge Regueiro
Sophie Marie Réhault-Godbert
Manuel Joaquín Reigosa
Renate Reimschuessel
Salette Reis
Di-Feng Ren
Guixing Ren
Yulin Ren
Catherine M. G. C. Renard
Zed Rengel
Fabiano Reniero
Teresa Requena
Martin Resano
Patrizia Restani
Eugenio Revilla
Wim Paul Reybroeck
Caue Ribeiro
Henelyta S. Ribeiro
Alejandra Ribera
Jorge Manuel Ricardo-Da-Silva
Clifford Paul Rice
Claire Richard
Schwen Richard
Florence Richard-Forget
Mark P. Richards
Elke Richling
Daniel J. Ricks
C. W. Rico
Cyren M. Rico
William P. Ridley
Klaus Riediger
Michael Riediker
Pier Giorgio Righetti
Agnes M. Rimando
Gerald Rimbach
James M. Rini
Jose Luis Rios
Sara J. Risch
Alberto Ritieni
Nuria Rius
R. Rivera-Madrid
Sandra Rivero
S.I. Rizvi
George P. Rizzi
Angela Maria Rizzo
Anna Rizzolo
Damon B. Robb
Katherine Robbins
C. Robert
Sue A. Roberts
Thomas Hugh Roberts
James A. Robertson
Jim Robertson
Richard John Robins
Simon P. Robinson
John F. Robyt
Martin Röder
Maria J. Rodrigo
Miguel Machado Rodrigues
Begonia Rodriguez
César Rodríguez
Francisco Rodríguez
Jose Miguel Rodríguez Mellado
Juan Miguel Rodriguez Patino
Luis Miguel Rodríguez-Alcalá
Delia B. Rodriguez-Amaya
Juan José Rodríguez-Bencomo
Javier-Germán Rodríguez-Carpena
Guillermo Rodríguez-Gutiérrez
Guadalupe Carmen Rodriguez-Jimenes
Ana Rodriguez-Mateos
Sonia Rodriguez-Sanchez
Rogelio Rodríguez-Sotres
M. A. Rogers
Peter John Rogers
Gu Seob Roh

dx.doi.org/10.1021/jf405539n |J. Agric. Food Chem. 2014, 62, 4–21

Barbara Rohm
Sascha Rohn
Manuel Roig
Ana Maria Rojas
Valérie Rolland
Luca Rolle
Judith M.Rollinger
Gianfranco Romanazzi
Hernán Mauricio Romero
Maria-Paz Romero
Roberto Romero-Gonzalez
Felicidad Ronda Balbas
Xingmin Rong
Martin Ronis
William Rooney
Yrjö H. Roos
Maria Emília Rosa
Charlita Rosal
Gaspar Ros-Berruezo
Devin Jerrold Rose
Martin Rose
Marianna Roselli
Moshe Rosenberg
Kurt Rosentrater
Alastair Ross
Mark M. Ross
Samir A. Ross
Ranieri Rossi
Carmen Rossini
Andreas Rossmann
Christophe Rothan
Giuseppe Leonardo Rotino
Jean-Max Rouanet
Maryse Rouelle
Russell Rouseff
Ioannis G. Roussis
Kenneth H. Roux
Molay Roy
Nicolas Rozes
Zhenhua Ruan
Antonio Ruano
Malte Rubach
Giuseppe Ruberto
Mónica Rubilar
Patrizia Rubiolo
Ángela Rubio-Moraga
Robert B. Rucker
Alisa Rudnitskaya
Ricardo Rueda
José A. Rufián-Henares
Antonieta Ruiz
David Ruiz
Juan Manuel Ruiz
Maria Luisa Ruiz del Castillo
Kimmo Rumpunen
Prithy Rupa
Pilar Rupérez
Gian Luigi Russo
Mario Vincenzo Russo
Nino Russo
Shane Mcartney Rutherfurd
Michael Rychlik
Mojmir Rychtera
Jong Hoon Ryu
Cristina M. Sabliov
Gianattilio Sacchi
Gavin L. Sacks
Nermin Abdel Hamid Sadik
Buket Sahin
Stefan Sahlstrom
Atsushi Sakai
Shohei Sakuda
Michihiko Sakurai
E. Salas
Joaquín J. Salas
Carlos Edmundo Salas Bravo
Mohammad Saleem
Mahmoud Saleh
Ione Salgado
Pablo R. Salgado
Kevin J. Saliba
M. Rosario Salinas
Juha-Pekka Salminen
Jean Michel Salmon
Salvatore Salomone
Serafina Salvati
Sabine Sampels
Roberto Samperi
Fernanda San Martin
Ana Sanches-Silva
Lourdes Sánchez
María-Teresa Sánchez
Alberto Sánchez Arribas
María Jesús Sánchez-Martín
Concepción Sánchez-Moreno
Eva Sanchez-Palomo
Raquel Sánchez-Pérez
Amandeep K. Sandhu
Pilar Sandin-España
Georgina Sandoval
Pat Sandra
Shengmin Sang
Jurmkwan Sangsuwan
Sindhuja Sankaran
Léa Silvia Sant'Ana
Anderson de Souza Sant'Ana
Rogelio Santiago
Ana Cristina Santos
Celestino Santos-Buelga
Carlos Sanz
Teresa Sanz
Michael S. Saporito
Jorge A. Saraiva
Gautam Sarath
P. S. Saravana
Ujjal Sarkar
Lucas Sartori
Leonie A. Sarubbo
Yasuto Sasaki
Gary John Sassano
Jutamaad Satayavivad
Shridhar Krishna Sathe
Akira Sato
Kenji Sato
Kiyotaka Sato
Mayumi Sato
Ryuichiro Sato
Rie Satoh
Tomomi Satoh
Pawel Satora
Kiyoshi Satouchi
Hideo Satsu
Tulasi Satyanarayana
Cédric Saucier
Luc Saulnier
James A. Saunders
Fulgencio Saura-Calixto
Marc E. Savard
Brett Savary
Akiyoshi Sawabe
Sonia Guadalupe Sáyago-Ayerdi
Sedat Sayar
Christine H. Scaman
Matteo Scampicchio
Alessio Scarafoni
Marina Scarpa
Karola Schaefer
Oliver Schafer
Sebastian Schaffer
K. M. Schaich
Kevin Schalinske
Alexander G. Schauss
Nils Helge Schebb
Jodi Scheffler
Catherine H. Schein
Roberta Schiavone
Andreas Schieber
Birgitt Schieberle
Peter Schieberle
Elisabetta Schievano
Jurgen Schiller
Mark Wesley Schilling
Alberto Schiraldi
Kristin Schirmer
Hedwig Schlichtherle-Cerny
Peter Schmid
Shelly J. Schmidt
Christophe Schmitt
Bernd Schneider
Claus Schneider
Marilyn Schneider
Carola Schoenknecht
Peter Francis Scholl
Margit Schollenberger
Elke Scholten
Kevin K. Schrader
Lukas Schreiber
Monika Schreiner
Jan Schripsema
Peter Schröder
Jessica Schuett
Kevin Albert Schug
Christian Schuh
David Jay Schultz
Hartwig Schulz
Vera Schulzova
Julia Schumann
Claude Schummer
Wilfried G. Schwab
Wolfgang Schwack
Axel Schwekendiek
Giampiero Scortichini
Ian Melville Scott
Nicola J. A. Scott
Natividad Sebastià
Rabiha Seboussi
Nehir El Sedef
Navindra P. Seeram
Christoph Seger
D. Seglina
Vegard Herman Segtnan
Verena Seidl-Seiboth
Ines Sellami
Serkan Selli
Gordon W. Selling
María V. Selma
Mrinal Kumar Sengupta
Thomas Senn
Scott Allen Senseman
Enrique Sentandreu
Miguel Angel Sentandreu
Mauro Serafini
Jolanta Sereikaite
Kjell Sergeant
Lucrezia Sergio
Sergio O. Serna-Saldivar
Maria Serrano
Maurizio Servili
Evodia Setati
Cynthia Elina Setiawan
T. Seto
A. Mark Settles
William N. Setzer
Steven John Severtson
Stefano Sforza
Elisabetta Sgarbi
Cristina Sgherri
Amita Shah
Fereidoon Shahidi
Guomin Shan
Dale L. Shaner
Adarsh Shanker Shanker
Bing Shao
Xi Shao
Anurag Sharma
Ashok K. Sharma
Om Sharma
Yogesh C. Sharma
Neil Shay
Dzmitry Shcharbin
Lee-Yan Sheen
Barry J. Shelp
Chwan-Li Shen
Jianzhong Shen
Li Shen
Lirong Shen
Qi Shen
Qun Shen
Rui-Ling Shen
Zheng-Wu Shen
Zhiping Shen
Jiping Sheng
Jiali Shentu
Gordon Seymour Shephard
Robert Sheridan
Fuu Sheu
Joen Rong Sheu
Jyh-Horng Sheu
Ming-Thau Sheu
Peter R. Shewry
Ainong Shi
Guoyue Shi
Haiming Shi
Jian-Gong Shi
John Shi
Linqi Shi
Shu Yun Shi
Xianglin Shi
Zugui Shi

Chyuan-Yuan Shiau
Takayuki Shibamoto
Youn Young Shim
Tomoya Shimbata
Ken Daniel Shimizu
Kosuke Shimizu
Kayoko Shimoi
Takeshi Shimosato
Makoto Shimoyamada
Daniel Shin
Eui-Cheol Shin
Takuro Shinano
Kazutoshi Shindo
Hiroshi Shinmoto
Takahiro Shiotsuki
Paul R. Shipley
Nobuya Shirai
Artiwan Shotipruk
Prachand Shrestha
Qing-Yao Shu
Barbara Shukitt Hale
Li Shun-Xing
Tatsiana G. Shutava
Andriy A. Sibirny
Barbara Siegmund
Bert John Siemens
Joice Sifuentes dos Santos
Vandna Sikand
Parames C. Sil
Angela Silva
Carlos Peres Silva
Dilson Silva
Fatima Regina Mena Barreto Silva
Tomé S. Silva
Damaris Silveira
Armando Jorge Domingues Silvestre
Jesus Simal-Gandara
Bela Simandi
Blake A. Simmons
Ryan R. Simon
Antonio Simon-Fuentes
Breda Simonovska
Sebnem Simsek
Andrew J. Sinclair
Anand Singh
Daljit Singh
Harminder Pal Singh
Narpinder Singh
Pravin Kumar Singh
Raushan Singh
Zora Singh
Maxim Sinkevich
Patricia Sinnecker
Jussi Sipila
Egle Machado de Almeida Siqueira
Timothy W. Sirk
Ryszard Siuda
Malin E. Sjöö
Maria Skalkam
Alexios-Leandros Skaltsounis
Mojca Škerget
Leif H. Skibsted
Andre G. Skirtach
Michele M. Skopec
Louise Slade
Ana Slatnar
Joanne L. Slavin
Margaret Slavin
Thomas L. Slewinski
Rune Slimestad
Bogdan A. Slominski
Jens J. Sloth
Carolyn Marie Slupsky
Alan J. Slusarenko
Guy Smagghe
Matthew Smallwood
Joseph L. Smilanick
Alison G. Smith
Darrin Lee Smith
David J. Smith
J. Scott Smith
Paul A. Smith
Philip C. Smith
Rachelle Smith
Richard Lee Smith Jr.
Nicholas Harrer Snow
Anatoly Petrovich Sobolev
Victor S. Sobolev
Carmen Socaciu
Rafel Socias i Company
Miguel A. Sogorb
O. S. Samuel Sojinu
Romana Sokolova
Francisco Solano
Michele Solfrizzo
Alexei E. Solovchenko
Jamorn Somana
Veronika Somoza
Bao-An Song
Huanlu Song
Shili Song
Xiao Yan Song
Yeongok Song
YiHu Song
Sanjeev Soni
Patricio Anibal Sorichetti
Theodore G. Sotiroudis
Herlinda Soto-Valdez
A. Sourianarayanane
Ferda Soyer
Mustafa Soylak
Julian E. Spallholz
Giuseppe Spano
Thomas C. Sparks
Francesca Sparvoli
Carmela Spatafora
Karl Speer
Giorgia Spigno
Michael B. Sporn
Apostolos Spyros
Nair Sreejayan
I. Srianta
Krishnapura Srinivasan
Rajendra Prasad Srivastava
Marc Stadler
Richard Herman Stadler
Dan Staerk
Jan Stagsted
Elisabeth Stahl-Biskup
Angelique Stalmach
Stephen B. Stanfill
Ruth E. Stark
Timo D. Stark
Christian Starkenmann
Evangelia Stefanoudaki-Kartzouraki
Marina Stefova
Bryan L. Stegelmeier
Peter Stehle
Hans H. Stein
Martin Steinhaus
Petra Steinhaus
Havard Steinshamn
Nicole R. Stendell-Hollis
Gladys L. Stephenson
Sokratis Stergiadis
Philip C. Stevenson
Graham G. Stewart
Markus Stieger
Michael Roy Stiff
Matteo Stocchero
Helga Stopper
Gary D. Strahan
Hanna Strandler
Mark J. Strynar
Gerald Stuebiger
Cecil Stushnoff
Hartmut Stützel
Haijia Su
Ming-Jai Su
Rongxin Su
Yi-Cheng Su
Yongchao Su
Zheng-Yuan Su
Michihiro Sugano
Kent Dennis Sugden
Yukihiro Sugimoto
Manickam Sugumaran
Hyung Joo Suh
Michael Sullivan
Michael Sulyok
Michele Suman
Surendranath P. Suman
Mark W. Sumarah
Carmine Summo
Baoshan Sun
Chuanxin Sun
Han-Dong Sun
Jian Sun
Jianghao Sun
Luyi Sun
Qingjie Sun
Run-Cang Sun
Shao-Long Sun
Weizheng Sun
Xiulan Sun
Yong Sun
Yuanxia Sun
Ulrik Kræmer Sundekilde
Leena Suntornsuk
Worapot Suntornsuk
Panuwat Suppakul
Jeonghee Surh
Vipa Surojanametakul
Joaquin Surra
Phiriyatorn Suwanmala
Jinya Suzuki
Tatsuro Suzuki
Joy E. Swanson
Stuart Swanston
Mark Sykes
A. Synytsya
Shiau Sy-Yu
Y. T. Szeto
Aleksandra Barbara Szydłowska-Czerniak
Amani Taamalli
Raphael Tabacchi
Nurhayat Tabanca
Louisa Tabatabai
Maria Tabernero
Zeynep Tacer-Caba
Hirofumi Tachibana
Paola Taddei
Motoyuki Tagashira
Davide Tagliazucchi
Umeo Takahama
Koretaro Takahashi
Makoto Takahashi
Yoko Takahashi
Tsujita Takahiro
Tomoyuki Takaku
Yoshiaki Takaya
Gary R. Takeoka
Hirosato Takikawa
Elad Tako
Miklós Takó
Kiyoshi Takoi
Stephen T. Talcott
S. P. Tallury
Tarja Tamminen
Hitoshi Tamura
Tsunenobu Tamura
Chin Ping Tan
Fa-Jui Tan
Takashi Tanaka
Takuji Tanaka
Bo Tang
Chuan-He Tang
Feng-Yao Tang
Guangwen Tang
Lei Tang
Mingliang Tang
Qi-zhu Tang
Wenping Tang
Ya-Jie Tang
Zhiyong Tang
Akiyoshi Taniguchi
Masaru Tanokura
Sherry Ann Tanumihardjo
Anna L. Tan-Wilson
J. Tao
Yongsheng Tao
Anita Tarbuk
Hirokazu Tarui
Marko Tapio Tarvainen
Maria Tasioula-Margari
Akira Tateishi
Fernando Tateo
Bernhard Tauscher
Aldo Tava
John R. N. Taylor
Larry Thomas Taylor
Mark A. Taylor
P. Taylor
Steven L. Taylor
Saad Tayyab
John R. Teasdale
A. Tecante
Doriana Tedesco
Pierre-Louis Teissedre
Bárbara Teixeira
Gustavo H. Teixeira
Noelia Tena

dx.doi.org/10.1021/jf405539n |J. Agric. Food Chem. 2014, 62, 4–21

Torstein Tengs
Maija Tenkanen
Paula Tennant
Gian Carlo Tenore
Mircea Teodorescu
Norihiko Terahara
Junji Terao
Masanori Terasaki
Masaaki Terashima
Roberto Terzano
Valeria Terzi
Luisa Tesoriere
Nishanth Tharayil
Dil Thavarajah
Jay J. Thelen
Katerina Theodoridou
Piyada Thipyapong
Nikolaos S. Thomaidis
Muthumani Thomas
Jean-Pierre Thomé
Tom S. Thompson
Jasmine Thorkildsen
Ulf Thrane
De Run Tian
He Tian
Lining Tian
Yaoqi Tian
Yuan Tian
Rohan V. Tikekar
Alain Tissier
Michel Tissut
Joanne K. Tobacman
Aldo Todaro
Setsuko Todoriki
Peter M. A. Toivonen
Francisco Tomás-Barberán
Patrick L.Tomco
Motohiro Tomizawa
Alan E. Tonelli
Changlun Tong
Rosanna Toniolo
Ondulla Tyvette Toomer
Ed Topp
Aleksandra M. Torbica
Fatih Törnük
Carolina Andrea Torres
Josep Lluis Torres
Patricia Torres
Bohn Torsten
Baldwyn Torto
Milena Martelli Tosi
Janet C. Tou
K. Toyoda
Andreas Tredoux
Brent Trela
Dieter Treutter
Marco Trevisan
David Edward Tribe
Domenico Trombetta
Ana M. Troncoso
Jurij Trontelj
Michele Trotta
Mary Wat Trucksess
Antonio-Jose Trujillo
Van-Den Truong
Chia-Wen Tsai
Guo-Jane Tsai
Li-Yu Tsai
Pijen Tsai
Tung-Hu Tsai
Ying-Chieh Tsai
Karl W. K. Tsim
Maria Z. Tsimidou
Apollinaire Tsopmo
Satoru Tsuchikawa
Koichiro Tsuchiya
Takanori Tsuda
Tsuyoshi Tsuduki
Kazunobu Tsumura
Youying Tu
Yunfei Tu
Zheng Tu
Aurelia Tubaro
Franco Tubaro
Carlo I. G. Tuberoso
Ludmila Tuckova
Jose Tudela Serrano
Artemio Zabala Tulio
Rosa Tundis
Siriporn Tuntipopipat
Kieran M. Tuohy
Giovanni Mario Turchini
Katarzyna Turnau
Allison Turner
Sherri B. Turnipseed
Maciej Turowski
Cynthia Tyburczy
Bor-Show Tzang
Jason T. C. Tzen
Cornelius E. Uboh
Katsumi Uchiyama
Esra Uckun
Chibuike C. Udenigwe
Maurizio Ugliano
Silvio Uhlig
Franz Ulberth
Abul H. J. Ullah
Detlef Ulrich
Kaoru Umehara
Takashi Umemura
Tadasu Urashima
Laurent Urban
Pier Paolo Urgeghe
Hiroko Ushio
Ewald Usleber
Anatolii Usov
Hiroshi Uyama
Patrizia Vaccino
Cristina Maria Valcu
M. Valdivia-López
Vasilij Valenčič
Daniela Valensin
Patrícia Valentão
Katerina Valentová
Daniel Valero
Edelmira Valero
Fernando Vallejo
Ludovico Valli
Josep Valls
Victoriano Valpuesta
Antonio Valverde
Henk Van As
Richard B. Van Breemen
Marie-Rose Van Calsteren
Fred R. Van De Voort
Hans Van den Brink
Wim Van den Ende
H. J. Van den Top
Justin Van der Hooft
Erik Van Der Linden
Grishja Van der Veer
Jeroen Peter Van Dijk
Thien Van Do
John Van Duynhoven
Jeanette Van Emon
Leo J. L. D. Van Griensven
J. David Van Horn
Isabelle Van Leuven
Ronald Van Ree
Jairam Vanamala
Adrian Vanbeek
Rob Vandebriel
Lynn Vanhaecke
Kimberly Vanhees
Gordon Van't Slot
Joao Varela
Patroklos Vareltzis
Prasad S. Variyar
Todor Vasiljevic
Joaquin Velasco
Edwin J. A. Veldhuizen
William Keith Vencill
Carmen Venegas
Lakshmanan Venkatachalam
Yeldur P. Venkatesh
Petras Rimantas Venskutonis
John R. Vercellotti
Paula Veríssimo
Mahendra Kumar Verma
Martina Vermathen
Aude Vernhet
Rob Verpoorte
Andrea Versari
Antonella Verzera
Vaclav Vetvicka
Glauce Barros Viana
Ariel Roberto Vicente
Stefania Vichi
Stefanie Vichi
Margarida C. Vieira
Natalie Vigier
Michel H. Vignes
Mar Vilanova
Mar Villamiel
Débora Villaño
Adriana Villanueva-Carvajal
Jaime Villaverde
Juan José Villaverde
P. Villeneuve
Marco Vincenti
Simone Vincenzi
Marcus Vinje
Joe A. Vinson
Franca Viola
Jesui Vergilio Visentainer
Shipra Vishnoi
Francesco Visioli
Paola Vitaglione
Sara Vitalini
Sauro Vittori
Vittoria Vittoria
Goran T. Vladisavljevic
Johann Vollmann
Jitraporn Vongsvivut
Christoph Von-Holst
Kenneth A. Voss
Urska Vrhovsek
Pia Maarit Vuorela
Koji Wada
Tais Aleriana Lucon Wagemaker
Kristiina Wahala
Hans-Ulrich Waiblinger
Yuhya Wakasa
Toshiyuki Wakimoto
K. Z. Walker
Michelle Walker
Michael H. Walter
Rosemary L. Walzem
Xiaochun Wan
Janitha P. D. Wanasundara
Bao-Lei Wang
Bin-Gui Wang
Bor-Sen Wang
Chaoyang Wang
Chau-Jong Wang
Chengjun Wang
Chen-Ya Wang
Chin-Kun Wang
Daoquan Wang
Dayong Wang
Fa Yuan Wang
Guang Wang
Hsiao-Chi Wang
Hui-Min Wang
Jia-Kun Wang
Jian Wang
Jianhua Wang
Jiansheng Wang
Jia-Sheng Wang
Juan Fei Wang
Jun Wang
Kejian Wang
Kun Wang
L. Wang
L. S. Wang
Lisa Wang
Ming Li Wang
Mingfu Wang
Ming-Hua Wang
Peng Wang
Ping Wang
Qi Wang
Qiang Wang
Qin Wang
Qing Min Wang
Qingmin Wang
Qing-Min Wang
Qiquan Wang
Selina C. Wang
Sheng-Yang Wang
Shuo Wang
Steven S.-S. Wang
Tao Wang
Thomas T. Y. Wang
Tian Wang
Wence Wang
Wen-Xiong Wang
Wenyi Wang
Xiaoyong Wang
Xingguo Wang
Ya-Jane Wang
Yanbo Wang
Yanji Wang

dx.doi.org/10.1021/jf405539n |J. Agric. Food Chem. 2014, 62, 4–21

Yi Wang
Ying-Jan Wang
Yong-Hua Wang
Youwei Wang
Yu Wang
Yuhong Wang
Yuh-Tai Wang
Yuxi Wang
Yuxia Wang
Zhao Mei Wang
Zheng Ming Wang
Zhouping Wang
Zhuanhua Wang
Ali Abbas Wani
Akira Wanikawa
Frederick Warren
Benedikt Warth
Andrzej Wasik
Eiki Watanabe
Fumio Watanabe
Mitsuru Watanabe
Naoharu Watanabe
Tatsuo Watanabe
Toshihiro Watanabe
Yomi Watanabe
Ramida Watanapokasin
Andrew L. Waterhouse
Geoffrey Ivan Neil Waterhouse
Deborah M. Waters
C. B. Watkins
Bernhard Watzl
Tzong-Der Way
Deepthi Weerasinghe
Teresa A. Wehner
J. Bernhard Wehr
Cunxu Wei
Guor-Jien Wei
Hao Wei
Yimin Wei
Yingjie Wei
Zhaojun Wei
Ulrike Weiler
Paul J. Weimer
Randy Alan Weintraub
Richard G. Weiss
Robert Welch
David Weldon
Frank Welle
Nikolaus Wellner
Bei Wen
Zhiyou Wen
Brian Bor-Chun Weng
Chia-Jui Weng
Ching-Feng Weng
Meng-Shih Weng
Wolfgang Wenzel
Uwe Wenzel
Ian Wesley
Leslie George West
Leslie Ann Weston
David Wetzel
Bruce D. Whitaker
Brittany L. White
Jason C. White
Ralph Whitehead
Andrew K. Whittaker
Harry Wichers
Macdonald Wick
Margaret E. Wickham-St. Germain
Wieslaw Wiczkowski
Wilbur Warren Widmer
Hilde Henny Wijngaard
Lars Wiking
Frank Will
Michael P. Williamson
Ron B. H. Wills
Karl A. Wilson
Zdeněk Wimmer
Chris Winefield
Chris Winkel
Carl K. Winter
Peter Winterhalter
Renger F. Witkamp
Ute Wittstock
Ken Witwer
Ursula Woelwer-Rieck
Kolanowski Wojciech
Aneta Wojdylo
Walter J. Wolf
Charlene Wolf-Hall
Dominic W. S. Wong
Jon W. Wong
Ka Hing Wong
Po-Keung Wong
Yiu-chung Wong
Sugunya Wongpornchai
Sun-Hee Woo
Bruce Wood
Delilah F. Wood
Philip A. Wood
Jan Byron Wooten
Amanda J. Wright
Katarzyna Wrobel
Ronald E. Wrolstad
Aibo Wu
Changlong Wu
Chieh-Hsi Wu
Chi-Hao Wu
Chih-Chung Wu
Chin-San Wu
ChunFu Wu
Gang Wu
Gang Wu
Hai-Qiang Wu
Hou Wu
Huifeng Wu
Hui-Ming Wu
James Swi-Bea Wu
Jiang-Ping Wu
Jianping Wu
Jiu-Lin Wu
Jun Wu
Jyh-Horng Wu
Li-Chen Wu
Liming Wu
Longhua Wu
Ming-Chang Wu
Ming-Jiuan Wu
Qing-Li Wu
She-Ching Wu
Shengjun Wu
ShiBiao Wu
Shih-Hsiung Wu
Shuai Wu
Tong Tony Wu
Wei Wu
Xianli Wu
Yanbing Wu
Yang-Chang Wu
Yongjiang Wu
Yongning Wu
Ziyun Wu
Matthias Wuest
Daniel A. Wunderlin
David S. Wunschel
Rimo Xi
Zhen Xi
Shuqin Xia
Xiaodong Xia
Wensheng Xiang
Hang Xiao
Hui Xiao
Jianbo Xiao
Jun-Song Xiao
Kai Xiao
Zou Xiao-Bo
Guoxiang Xie
Jiahua Xie
Jianping Xie
M. Y. Xie
Mei-Lin Xie
Meng-Xia Xie
Ming-Yong Xie
Ruliang Xie
Zhuohong Xie
Jiaying Xin
Huabin Xing
Youling L. Xiong
Bin Xu
Changmou Xu
Chunlin Xu
Feng Xu
Ganrong Xu
Han-Hong Xu
Jian-guo Xu
Jie Xu
Jiliu Xu
Jimmy Xu
Juan Xu
Lu Xu
Ming Xu
Peng Xu
Wen Tao Xu
Xiaoyong Xu
Xuebing Xu
Yan Xu
Yixiang Xu
Zhimin Xu
Richeng Xuan
Bingzhong Xue
Changhu Xue
Yemin Xue
Kimiko Yabe
Rickey Y. Yada
Jay Kant Yadav
Jhillu Singh Yadav
Haruyo Yagi
Betsy Jean Yakes
Kit L.Yam
Noriko Yamabe
Montarop Yamabhai
Haruki Yamada
M. Yamamori
Masayuki Yamasaki
Chunyan Yan
Hongyuan Yan
Pei-Sheng Yan
Ru Yan
Xiaojing Yan
Yanchun Yan
Yeong-Yu Yan
Yue-Ming Yan
Yasemen Yanar
Baoru Yang
Chung S. Yang
Deng-Jye Yang
Guang Yang
Guang-Fu Yang
Hsin-Ling Yang
Hsueh-Hui Yang
Huqing Yang
John J. Yang
Jun Yang
Ling Yang
Litao Yang
Paul Yang
Shyh-Chyun Yang
Sung Jae Yang
T. Yang
Tiankui Yang
W. Z. Yang
Wenzhu Yang
Xiao-Quan Yang
Xinling Yang
Yaling Yang
Yiqi Yang
Yuechao Yang
Zhen Yang
Zhenfeng Yang
Zhi Min Yang
Zhi-Hong Yang
Bin Yao
Chih-Jung Yao
Linxing Yao
Muhammad Yasin
Midori Yasuda
Akio Yasuhara
Akemi Yasui
Varoujan Antranik Yaylayan
Christian C. Yde
Aiqian Ye
Bang-Ce Ye
Lin Ye
Michael Ye
Min Ye
Peng Ye
Wen-Cai Ye
Yang Ye
M. C. Yebra
An-I Yeh
Chi-Tai Yeh
Chuan-Mei Yeh
Shu-Lan Yeh
Ahmet Yemenicioglu
Gow-Chin Yen
Jui-Hung Yen
Mao-Hsiung Yen
Siok-Koon Yeo
Chahan Yeretzian
Ramesh R. Yettella
Mahmut Yildiz
Murat Yilmaztekin
Daqiang Yin
Mei-Chin Yin
Ping Yin
Robert A. Yokley
Katsuhiko Yokoi
Kazushige Yokota
Tomoya Yokoyama
Koichi Yoneyama
Hiromi Yoshida
Hiroo Yoshida

dx.doi.org/10.1021/jf405539n |J. Agric. Food Chem. 2014, 62, 4–21

Kumi Yoshida
Munehiro Yoshida
Tadashi Yoshihashi
Tohru Yoshimura
Mari Yotsu-Yamashita
Min You
Wendy Marie Young
Bi Yu
Bin Yu
Guanping Yu
Hailong Yu
Jianqing Yu
Jinsheng Yu
Liangli (Lucy) Yu
Long Yu
Mingrui Yu
Peiqiang Yu
Rina Yu
Rongmin Yu
Shujuan Yu
Youwei Yu
Zhiling Yu
Gwo Fang Yuan
Jian-Ping Yuan
Qipeng Yuan
Tao Yuan
Tong-Qi Yuan
Yang Yuan
Ying-Jin Yuan
Onder Yumrutas
Felipe Yunta
María del Mar Yust
Dimitrios Zabaras
Ioannis Zabetakis
Lorenzo Zacarias
Pilar Zafrilla
Fernando Zamora
Rosario Zamora
Emanuela Zanardi
Severino Zara
Vincenzo Zara
Sotirios G. Zarogiannis
Luis Zea
Qendrim Zebeli
Reinhard Zeleny
Cheng-Ming Zeng
Mingyong Zeng
Teng Zeng
Jürgen Zentek
Edgar Zenteno
Giuseppe Zeppa
Hua-Min Zhai
Bo Zhang
Boce Zhang
Caiqiao Zhang
Chao-Xian Zhang
Chiqian Zhang
Dabing Zhang
Genyi Zhang
Guodong Zhang
Guo-Lin Zhang
Guowen Zhang
Haixia Zhang
Hanqi Zhang
Hui Zhang
Jian-Ping Zhang
John Zhang
Kai Zhang
Mingwei Zhang
Qing-He Zhang
Qun-Lin Zhang
Suxia Zhang
Taiying Zhang
Tao Zhang
Xiaoguang Zhang
Xiao-Lian Zhang
Xiaoming Zhang
Xiaoqing Zhang
Xuewu Zhang
Xumin Zhang
Xunli Zhang
Yanjun Zhang
Ying Zhang
Youwei Zhang
Yu Zhang
Yu-Zhu Zhang
Zhanyuan Zhang
Zhe Zhang
Zhiping Zhang
ZunJian Zhang
Dayun Zhao
Feng-Qi Zhao
Guanghua Zhao
Guohua Zhao
Haifeng Zhao
Hengqiang Zhao
Hongwei Zhao
Jian Zhao
Jincai Zhao
Mouming Zhao
Ning Zhao
Ping Zhao
Guangyong Zhao
Wei-Guang Zhao
Wei-Jun Zhao
Xinrui Zhao
Yanyun Zhao
Yunfeng Zhao
Yuqing Zhao
Guodong Zheng
Jie Zheng
Jolene Zheng
M. H. Zheng
Minghui Zheng
Wenjie Zheng
Yonghua Zheng
Yongquan Zheng
Zuoxing Zheng
Fan Zhijin
Xu Zhixiang
Fang Zhong
Lin-Xin Zhong
Na Zhong
Qixin Zhong
Shian Zhong
Ying Zhong
Ailing Zhou
Anguo Zhou
Dongmei Zhou
Hai-Chao Zhou
Jie Zhou
Jinjin Zhou
June Zhou
Kequan Zhou
Meixue Zhou
Ming Zhou
Ping Zhou
Xiao-Qiu Zhou
Y. H. Zhou
Zhiqin Zhou
Biao Zhu
Caiping Zhu
Guonian Zhu
Hongjun Zhu
JunYong Zhu
Li-Jia Zhu
Wei Zhu
Weiming Zhu
Weiyun Zhu
Xuntao Zhu
Yingting Zhu
Zaifang Zhu
Zhengxi Zhu
Zhichen Zhu
Guoqiang Zhuang
Shiwen Zhuang
Shulin Zhuang
Christian Zidorn
Diego Cunha Zied
Gregory R. Ziegler
Danuta Zielinska
Henryk Zielinski
Benno Zimmermann
Ouliana Ziouzenkova
Svetlana Zivanovic
Otmar Zoller
Holger Zorn
Long Zou
Xiao-Qing Zou
Xiaoyong Zou
Yunfan Zou
Petr Zuman
Rommy Zuniga
Yuegang Zuo

dx.doi.org/10.1021/jf405539n |J. Agric. Food Chem. 2014, 62, 4–21

JOURNAL OF AGRICULTURAL AND FOOD CHEMISTRY

Perspective

pubs.acs.org/JAFC

Targeted Metabolomics: a New Section in the *Journal of Agricultural and Food Chemistry*

James N. Seiber,[†] Russell J. Molyneux,[§] and Peter Schieberle*[,#]

[†]4143 Meyer Hall, Department of Environmental Toxicology, University of California, Davis, California 95616, United States

[§]Daniel K. Inouye College of Pharmacy of Hawaii at Hilo, 34 Rainbow Drive, Hilo, Hawaii 96720, United States

[#]Deutsche Forschungsanstalt für Lebensmittelchemie, Lise-Meitner-Straße 34, 85354 Freising, Germany

Starting in 2013, *JAFC* initiated a new section "Targeted Metabolomics Applied to Agriculture and Food" for manuscripts describing applications of metabolomics related to research topics in agriculture, food, and nutrition, in particular, metabolite-targeted analysis and progress in the development of analytical platforms for metabolomics methodologies. This description was expanded somewhat in the Journal's Scope, Policy, and Instructions for authors (revised April 2013) with the additional statement:

"A metabolome is the complete quantitative set of small molecules (metabolites) in a biological system, i.e., a food, which varies continuously with time. Also metabonomics studies, focused on changes in a given metabolome, e.g., induced by environmental conditions or diseases, fall into this category. Metabolic profiling or metabolomics fingerprinting correlated with multivariate or data-mining methods are acceptable, if presented in a targeted way".

This Perspective is meant to further explain the types of studies/topics that might fall within the scope of the new targeted metabolomics section of the *Journal of Agricultural and Food Chemistry* and to encourage authors to submit manuscripts to this section of *JAFC*.

Due to the rapid development in the sensitivity and/or selectivity of analytical equipment, such as NMR, GC×GC-MS, or LC-MS (i.e., UHPLC-Q-TOF) as well as the option to handle large data sets by new software, metabolomics has developed and expanded largely in the past 15 years. A symposium, "Applications of Metabolomics in Agriculture", was held at the American Chemical Society Spring meeting in 2005 covering information to that date, and a Perspective was subsequently published summarizing the content of the symposium, which included papers on understanding metabolic pathways, food and environmental safety, and nutrition, diet, and health.[1] The Perspective particularly pointed out the challenges and opportunities which lay ahead for this exciting field.

Metabolomics is a very promising approach of the postgenomics era aimed at facilitating our understanding of the dynamics of biochemical composition within living systems. It is fundamental to understanding systems biology in its efforts to integrate DNA, RNA, protein, and metabolite analyses in phenotypic, morphological, clinical, food, and other biological contexts. Metabolomics can also be quite useful as a guide to optimizing trait development in agricultural products[2] or in improving food-processing conditions by comparing changes in the food's metabolome.[3] The analytical tools of most use in metabolomics (NMR spectroscopy, mass spectrometry, and others) can yield massive data sets when following changes in the metabolome of often hundreds of metabolites simultaneously over time, for example, in relation to nutritional status, environmental changes, etc. Thus, it provides a more complete picture of composition than generally seen with traditional plant biochemistry and natural product analyses.

The literature differentiates between two concepts of metabolomics: untargeted and targeted methodologies.[4] Untargeted methods are intended to analyze as many compounds as possible of the entire set of chemical compounds in a given sample, that is, a food at different stages of fermentation/processing or a body fluid after ingestion of a certain diet, including unknowns. Usually the raw data on the analyzed set of molecules occurring in a minimum of two samples are compared and, after data alignment, compounds occurring in one of the samples are visualized by application of bioinformatics approaches, that is, dedicated software. The untargeted approach is, thus, unbiased and tries to differentiate/compare samples by statistical means, that is, chemometrics, to find discriminant metabolites whether the structure was known or is unknown. It must, however, be kept in mind that the set of compounds analyzed depends on several parameters, in particular, on the conditions of compound isolation from the insoluble matrix. Furthermore, a sufficient number of samples must have been analyzed to allow statistical calculations.[5] In contrast, targeted metabolomic approaches aim at measuring defined groups of previously identified metabolites that are biochemically relevant. The targeted approach is designed to first confirm the structures of specific compounds by using reference compounds or reliable library data, and the "targeted" marker metabolites are then commonly compared on the basis of quantitative results, including concentration changes over time or condition. The number of analytes considered is usually high in both approaches, although target approaches must be limited to compounds representing, for example, food quality or that are markers of a biological phenomenon. A recent paper explains well the term metabolomics and the differences between a targeted and an untargeted approach.[4]

Nevertheless, there is a close relationship between the two approaches, because an untargeted approach should be done first to show differences in the set of analytes in the samples under investigation, that is, to help annotate those compounds

Received: October 15, 2013
Revised: December 5, 2013
Accepted: December 9, 2013
Published: December 20, 2013

ACS Publications © 2013 American Chemical Society

dx.doi.org/10.1021/jf4046254 | *J. Agric. Food Chem.* 2014, 62, 22−23

that are likely to be most relevant to addressing the research plan or question. If marker compounds are pinpointed from such "untargeted" comparisons, a library search must follow to establish whether a compound is already known. This process is commonly known as dereplication.[6,7] If the structure is not yet described, the study must then be focused on the identification and quantitation of the marker compounds according to standards set forth in previous *JAFC* perspectives.[8,9] However, whereas in conventional studies these standards require complete identification of compounds under investigation, it is obvious that in a targeted metabolomics study, dealing with tens or hundreds of compounds, it is almost impossible to conform to such requirements. Nevertheless, when claims are made for specific compounds as metabolic markers, such compounds should be fully characterized. In an ideal situation this will require that both NMR and MS techniques be concurrently applied (together with others that might be definitive), because the former tends to lack sensitivity and the latter, selectivity.

Researchers who follow an untargeted approach are strongly encouraged to undertake further characterization of those compounds showing differences in given samples. *JAFC* will limit the section on targeted metabolomics to those manuscripts that at least attempt to characterize the differing compounds to draw substantive conclusions, for example, on pathways or mechanisms of formation or modification. An untargeted approach alone is primarily descriptive and may not be driven by a scientific concept and experimental design and, therefore, generally will not fall within *JAFC*'s scope. Because *JAFC* is primarily a chemistry journal, it is important for authors to include in their manuscripts examples of their spectroscopic/spectrometric data sets, so that readers can evaluate the ability of the techniques to discriminate between the numerous compounds that may be present.

JAFC has already published a number of good examples translating the metabolomics approach into food chemistry, which illustrate the breadth and depth of this field.[1,3,10−14] Also, guidelines for minimum standards in conducting metabolomics studies published by, for example, the Metabolomics Standard Initiative (MSI) or the COSMOS (Coordination of Standards in Metabolomics), should be consulted.[15,16]

With the boundaries defined in this Perspective, we leave it to authors, reviewers, and readers of the Journal to populate and comment on the development of targeted metabolomics applicable to agricultural and food chemistry.

AUTHOR INFORMATION

Corresponding Author

*(P.S.) Phone: +49 8161 712932. Fax: +49 8161 71 2970. E-mail: peter.schieberle@ch.tum.de.

Notes

The authors declare no competing financial interest.

REFERENCES

(1) Dixon, R. A.; Gang, D. R.; Charlton, A. J.; Fiehn, O.; Kuiper, H. A.; Reynolds, T. L.; Tjeerdema, R. S.; Jeffery, E. H.; German, J. B.; Ridley, W. P.; Seiber, J. N. Applications of metabolomics in agriculture. *J. Agric. Food Chem.* **2006**, *54*, 8984−8994.

(2) Catchpole, G. S.; Beckmann, M.; Enot, D. P.; Mondhe, M.; Zywicki, B.; Taylor, J.; Hardy, N.; Smith, A.; King, R. D.; Kell, D. B.; Fiehn, O.; Draper, J. Hierarchical metabolomics demonstrates substantial compositional similarity between genetically modified and conventional potato crops. *Proc. Natl. Acad. Sci. U.S.A.* **2005**, *102*, 14458−14462.

(3) Beleggia, R.; Platani, C.; Papa, R.; Di Chio, A.; Barros, E.; Mashaba, C.; Wirth, J.; Fammartino, A.; Sautter, C.; Conner, S.; Rauscher, J.; Stewart, D.; Cativelli, L. Metabolomics and food processing: from semolina to pasta. *J. Agric. Food Chem.* **2011**, *59*, 9366−9377.

(4) Patti, G. J.; Yanes, O.; Siuzdak, G. Metabolomics: the apogee of the omics trilogy. *Nat. Rev., Mol. Cell Biol.* **2012**, *13*, 263−269.

(5) Goodacre, R.; Broadhurst, D.; Smilde, A. K.; Kristal, B. S.; Baker, J. D.; Beger, R.; Bessant, C.; Connor, S.; Capuani, G.; Craig, A.; Ebbels, T.; Kell, D. B.; Manetti, C.; Newton, J.; Paternostro, G.; Somorjai, R.; Sjöström, M.; Trygg, J.; Wulfert, F. Proposed minimum reporting standards for data analysis in metabolomics. *Metabolomics* **2007**, *3*, 231−241.

(6) Cordell, G. A.; Shin, Y. G. Finding the needle in the haystack. The dereplication of natural products extracts. *Pure Appl. Chem.* **1999**, *71*, 1089−1094.

(7) Bradshaw, J.; Butina, D.; Dunn, A. J.; Green, R. H.; Hajek, M.; Jones, M. M.; Lindon, J. C.; Sidebottom, P. J. A. Rapid and facile method for the dereplication of purified natural extracts. *J. Nat Prod.* **2001**, *64*, 1541−1544.

(8) Molyneux, R. J.; Schieberle, P. Compound identification: a *Journal of Agricultural and Food Chemistry* perspective. *J. Agric. Food Chem.* **2007**, *55*, 4625−4629.

(9) Schieberle, P.; Molyneux, R. J. Quantitation of sensory-active and bioactive constituents in food: a *Journal of Agricultural and Food Chemistry* perspective. *J. Agric. Food Chem* **2012**, *60*, 2404−2408.

(10) Intelman, D.; Haseleu, G.; Dunkel, A.; Lagemann, A.; Stephan, A.; Hofmann, T. Comprehensive sensomics analysis of hop-derived bitter compounds during storage of beer. *J. Agric. Food .Chem.* **2011**, *59*, 1939−1953.

(11) Vrhovsek, U.; Masuero, D.; Gasperotti, M.; Franceschi, P.; Caputi, L.; Viola, R.; Mattivi, F. A versatile targeted metabolomics method for the rapid quantification of multiple classes of phenolics in fruits and beverages. *J. Agric. Food Chem.* **2012**, *60*, 8831−8840.

(12) Kim, H.-J.; Park, K.-J.; Lim, J.-H. Metabolomic analysis of phenolic compounds in buckwheat (*Fagopyrum esculentum* M.) sprouts treated with methyl jasmonate. *J. Agric. Food Chem.* **2011**, *59*, 5707−5713.

(13) Hanhinva, K.; Rogachev, I.; Aura, A.-M.; Aharoni, A.; Poutanen, K.; Mykkänen, H. Qualitative characterization of benzoxazinoid derivatives in whole grain rye and wheat by LC-MS metabolite profiling. *J. Agric. Food Chem.* **2011**, *59*, 921−927.

(14) Kiefl, J.; Pollner, G.; Schieberle, P. Sensomics analysis of key hazelnut odorants (*Corylus avellana* L. 'Tonda Gentile') using comprehensive two-dimensional gas chromatography in combination with time-of-flight mass spectrometry (GC×GC-TOF-MS). *J. Agric. Food Chem.* **2013**, *61*, 5226−5235.

(15) Fiehn, O.; Wohlgemuth, G.; Scholz, M.; Kind, T.; Lee, D. Y.; Lu, Y.; Moon, S.; Nikolau, B. Quality control for plant metabolomics: reporting MSI-Compliant studies. *Plant J.* **2008**, *53*, 691−704.

(16) Salek, R. M.; Steinbeck, C.; Viant, M. R.; Goodacre, R.; Dunn, W. B. The role of reporting standards for metabolite annotation and identification in metabolomics studies. *Gigascience* **2013**, *2*, 13−14.

JOURNAL OF AGRICULTURAL AND FOOD CHEMISTRY

Letter

pubs.acs.org/JAFC

Volunteer Stratification Is More Relevant than Technological Treatment in Orange Juice Flavanone Bioavailability

ABSTRACT: The effect of two technological treatments on orange juice flavanone bioavailability in humans was assessed. Processing affected flavanone solubility and particle size of the cloud. Volunteers were stratified in high, medium, and low urinary excretion capabilities. Flavanones from high-pressure homogenized juice showed better absorption than those of conventional pasteurized juice in high excretors. These differences were not observed in medium and low excretors. High flavanone excretors took advantage of the high-pressure homogenization juice attributes (smaller cloud particle size) and showed an improved absorption/excretion. Stratification of the individuals by their excretion capability is more relevant than technological treatments in terms of flavanone bioavailability. This stratification should be considered in clinical studies with citrus juices and extracts as it could explain the large interindividual variability that is often observed.

KEYWORDS: *bioavailability, flavanones, orange juice, technological treatments, volunteer stratification*

INTRODUCTION

Hydrostatic high pressure and pulsed electric fields have consolidated as alternatives to conventional citrus processing, as these mild treatments produce juices with quality characteristics similar to those of fresh juice.[1] Although the impact of these novel technologies on orange juice bioactives has been studied,[2] their effect on flavanone bioavailability in humans has not been studied to the same extent.

Conventional processing leads to flavanone precipitation from the soluble fraction to the cloud.[3] As flavanone solubility is a key factor for their bioavailability,[4] there is an interest in developing new technologies that increase orange juice flavanone solubility. High-pressure homogenization with moderate heat treatment is able to reduce orange juice particle size (micrometer scale), leading to microsuspensions of the cloud that might increase flavanone bioavailability.[5]

The systemic health effects of citrus flavanones depend on their absorption. Hesperidin is not absorbed in the small intestine, and it reaches the colon, where it is hydrolyzed by gut microbiota to release hesperetin that is then absorbed.[4,6] Depending on the gut bacterial composition of the different volunteers, they can have different levels of rhamnosidase activity and therefore different capabilities to absorb and excrete hesperetin.[7,8] Due to the large interindividual variability in flavanone absorption and excretion, a previous stratification of volunteers by their absorption/excretion capability was suggested to be desirable in nutritional studies.[4]

The aim of this study was to evaluate the effect of the high-pressure homogenization versus conventional pasteurization on citrus juice flavanone bioavailability in humans. This will be assessed by taking into account the stratification of volunteers in different flavanone absorption/excretion levels.

MATERIALS AND METHODS

Orange Juices. Fruits from a *Citrus* hybrid between mandarin and sweet orange (*Citrus sinensis* L. var. 'Ortanique') were harvested at optimal maturity index during the season 2011−2012 from an orchard located in Lliria (Valencia, Spain) and kept at 8 °C before being processed. Fresh hand-squeezed juice was prepared using a hand-squeezer (Braun MPZ22, Madrid, Spain) and then was filtered using a 2 mm steel sieve. The juice was immediately consumed after preparation. High-pressure homogenized (HPH) juice was previously tempered at 31 °C in a steam-jacketed kettle and homogenized at 150 MPa in a high-pressure homogenizer (NS3015H model, GEA Niro Soavi S.p.A., Parma, Italy). During homogenization, the juice was heated at 68 °C for 10 s, and when it reached the outlet section of the system, it was immediately cooled at 7 °C in a plate heat-exchanger (model junior, APV Ibérica S. A., Madrid, Spain). Samples were bottled also in 1 L glass jars with twist-off lids (both previously sterilized with fluent steam). Conventional pasteurization (CP) of samples was carried out using a plate heat-exchanger (model Junior, APV Ibérica S.A) fed at 1 L/min, where the juice was heated at 92 °C for 40 s and finally cooled at 7 °C, and aseptically bottled in 1 L glass jars with twist-off lids (both were previously sterilized with fluent steam).

Qualitative and Quantitative Analyses of Juice Flavanones. These were carried out as reported previously by HPLC-DAD-MS.[4] The different flavanones were quantified as hesperidin.

Volunteer Stratification and Intervention Study. Volunteers' (n = 18) flavanone absorption/excretion capability after the intake of orange juice had been characterized in previous studies.[4] All volunteers had a consistent behavior over the past two years regarding their individual capability for flavanone excretion after orange juice consumption. High, medium, and low excretors were identified. High (flavanone excretion values >10% of the ingested flavanones), medium (excretion values between 5 and 10%), and low excretors (excretion values < 5%) were characterized. A crossover study (10 males and 8 females; 20−50 years old) was carried out as reported previously.[4] The volunteers ingested 400 mL of the juices. Flavanone intake was quoted as hesperetin and naringenin equivalents.

Analysis of Flavanone Metabolites in Urine. Volunteers collected 24 h urine, and samples were stored and processed as reported previously.[4] Phase II metabolites of flavanones were identified and quantified by a UPLC 1290 Infinity series (Agilent Technologies) equipped with a triple-quadrupole mass spectrometer (6460 Jet Stream series, Agilent Technologies).

A Poroshell 120 C18 column (100 × 3.0 mm i.d., 2.7 μm) (Agilent, Palo Alto, CA, USA) was used at room temperature, and the injected volume was 3 μL. Gradient elution was carried out using water/formic acid (99:1, v/v) and acetonitrile at a constant flow rate of 0.5 mL/min. The gradient used was [t (min), % acetonitrile v/v] (0, 1), (10, 40), (12, 90), and (15, 1).

The optimum mass spectrometer parameters for detection of hesperetin and naringenin aglycones, hesperetin 7- and 3′-glucuronide,

Received: November 3, 2013
Revised: December 15, 2013
Accepted: December 17, 2013
Published: December 17, 2013

ACS Publications © 2013 American Chemical Society

Table 1. Flavanone Content of the Orange Juices[a]

	fresh			homogenized (HPH)			pasteurized (CP)		
flavanone	soluble	cloud	total	soluble	cloud	total	soluble	cloud	total
naringenin-7-rutinoside-4′-glucoside	0.31 (0.01)[b]	nd		0.62 (0.02)	nd		0.51 (0.02)	0.11 (0.01)	
hesperetin-7-rutinoside-3′-glucoside	0.51 (0.02)	nd		1.43 (0.04)	0.11 (0.01)		1.43 (0.04)	0.12 (0.01)	
naringenin-7-rutinoside	3.32 (0.04)	0.11 (0.01)		9.04 (0.12)	1.93 (0.02)		8.92 (0.06)	2.33 (0.04)	
hesperetin-7-rutinoside	8.63 (0.11)	0.32 (0.01)		10.72 (0.13)	13.61 (0.14)		10.64 (0.09)	16.01 (0.06)	
naringenin-4′-methyl-7-rutinoside	0.92 (0.01)	nd		1.84 (0.04)	1.21 (0.02)		1.61 (0.03)	1.54 (0.02)	
total	13.69 (0.05)^{C}	0.43 (0.01)^{C}	14.12 (0.05)^{C}	23.54 (0.07)^{A}	16.86 (0.05)^{B}	40.40 (0.05)^{B}	23.09 (0.05)^{A}	20.08 (0.05)^{A}	43.17 (0.05)^{A}

[a]Values are expressed as mg/100 mL. [b]Standard deviation (n = 3). Means followed by the same letter are not significantly different according to Duncan's test (P < 0.05).

naringenin 7- and 4′-glucuronide, and hesperetin 7- and 3′-sulfate (50 μM) were optimized, connecting directly the column to the Jet Stream. Pure standards were synthesized by Villapharma (Murcia, Spain).

Source parameters were as follows: capillary voltage, −3500 V; charging potential, −500 V; nebulizer pressure, 40 (psi); auxiliary gas, heated to 275 °C and introduced at a flow rate of pure nitrogen, 9 L/min. The multiple reaction monitoring (MRM) method monitored five transitions for each analysis: hesperetin, m/z 301→164; hesperetin glucuronide, m/z 477→301; hesperetin diglucuronide, m/z 653→(477)→301; hesperetin sulfoglucuronide, m/z 557→(477)→301; hesperetin sulfate, m/z 381→301, with a dwell time for each transition of 8 ms. Concentrations of hesperetin diglucuronide and hesperetin sulfoglucuronide metabolites were estimated by synthesized hesperetin glucuronide calibration curves (20, 10, 5, 2.5, 1 μM). For naringenin, metabolites were as follows: naringenin, m/z 271→113; naringenin glucuronide, m/z 447→271; naringenin diglucuronide, m/z 623→(447)→271; naringenin sulfoglucuronide, m/z 527→(447)→271; naringenin sulfate, m/z 351→271, with a dwell time for each transition of 8 ms. Concentrations of naringenin diglucuronide and naringenin sulfoglucuronide metabolites were estimated by synthesized naringenin glucuronide calibration curves (20, 10, 5, 2.5, 1 μM).

Limits of quantification (LOQs) were 80, 50/80, and 40/50 nM for hesperetin, hesperetin 7- and 3′-glucuronides, and hesperetin 7- and 3′-sulfates, respectively. Limits of detection (LODs) were 30, 20/30, and 15/20 nM, respectively. In the case of naringenin metabolites, LOQs were 30 and 70/500 nM for naringenin and naringenin 7- and 4′-glucuronides, and LODs were 10 and 20/200 nM, respectively.

The intraday repeatability of the UPLC-QqQ method was assessed from 10 consecutive chromatographic runs using a standard solution with 2.5 μM of every standard in MeOH/0.1% (v/v) formic acid. The interday repeatability of the method was assessed by analyzing the same standard solution for two consecutive days. The relative standard deviation (RSD) for peak area was in the range of 0.5−4.7% in the intraday test and 1.3−3.5% in the case of the interday test. Finally, an analysis of variance (ANOVA) was carried out, and means were separated by Duncan's test (P < 0.05%).

RESULTS AND DISCUSSION

Table 1 shows that both pasteurized (CP) and homogenized (HPH) juices had similar flavanone contents with slight differences in the soluble and cloud fractions. The particle size, however, was much smaller in the homogenized juice (Figure 1). The flavanone content of fresh hand-squeezed orange juice was considerably lower than those of thermally processed juices, consistent with the milder extraction process and the lack of a cloud fraction in the fresh juice. However, flavanones were mainly in the soluble phase.

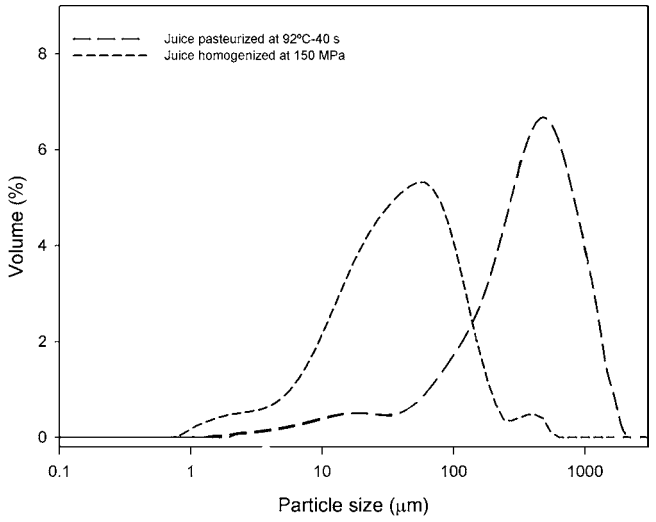

Figure 1. Representative particle size distribution of citrus juices produced by conventional pasteurization (CP) and high-pressure homogenization (HPH).

After juice intake, either hesperetin 7-sulfate or 7-glucuronide was the most abundant urinary metabolites. Their isomers in the 3′-position were found in lower concentrations (between 2 and 5 times). Hesperetin sulfoglucuronide and hesperetin diglucuronide were minor metabolites. The same trend was found for naringenin metabolites.

Volunteers were stratified after the intake of fresh orange juice, and high excretors showed mean excretion values of 15% of the flavanone intake; medium excretors, 9%; and low excretors, 3%, after fresh juice intake (Figure 2).

Homogenization and pasteurization led to a decrease in the percentage of ingested flavanones that were excreted with regard to hand-squeezed juice (Table 2; Figure 2A). This decrease was not observed when only the soluble flavanones were considered.

The total excretion percentage of fresh hand-squeezed orange juice reached mean values of 8.1 and 11.0% for hesperetin and naringenin, respectively (Table 2). Those values were in the range of previous papers.[9,10]

High flavanone excretors showed no significant differences in flavanone excretion (% ingested dose) after the intake of fresh

dx.doi.org/10.1021/jf4048989 | J. Agric. Food Chem. 2014, 62, 24−27

Table 2. Flavanone (Hesperetin and Naringenin) Excretion after the Intake of Fresh, Homogenized, and Pasteurized Citrus Juices and Stratification of Volunteers by Their Excretion Capabilities (High, Medium, and Low Excretors)[a]

		fresh	homogenized (HPH)	pasteurized (CP)
ingested dose (mg equivalents hesperetin)		18.8	51.6	56.2
ingested soluble dose (mg hesperetin)		18.2	24.2	24.0
all excretors	excreted equivalents (mg)	1.5 (±0.3)A	2.5 (±0.6)A	1.9 (±0.3)A
	total excreted equivalents 24 h (%)	8.1 (±1.4)A	4.8 (±1.1)B	3.3 (±0.5)B
	relative % of the soluble intake	8.4 (±1.5)A	10.1 (±2.4)A	7.7 (±1.1)A
high excretors[b]	excreted equivalents (mg)	2.8 (±0.4)Ba	6.3 (±0.8)A	3.0 (±0.5)B
	total excreted equivalents 24 h (%)	14.8 (±2.0)Aa	12.2 (±1.6)Aa	5.4 (±0.8)Ba
	relative % of the soluble intake	15.3 (±2.1)Ba	26.0 (±3.4)Aa	12.6 (±1.9)Ba
medium excretors[c]	excreted equivalents (mg)	1.7 (±0.2)Ab	2.0 (±0.6)Ab	2.1 (±0.3)Ab
	total excreted equivalents 24 h (%)	9.0 (±1.3)Ab	3.9 (±1.1)Bb	3.7 (±0.6)Bb
	relative % of the soluble intake	9.3 (±1.4)Ab	8.4 (±2.3)Ab	8.8 (±1.3)Ab
low excretors[d]	excreted equivalents (mg)	0.5 (±0.1)Ac	0.7 (±0.2)Ac	1.0 (±0.2)Ac
	total excreted equivalents 24 h (%)	2.9 (±0.5)Ac	1.3 (±0.4)Bc	1.7 (±0.3)Bc
	relative % of the soluble intake	3.0 (±0.5)Ac	2.9 (±0.9)Ac	4.0 (±0.8)Ac
		fresh	homogenized (HPH)	pasteurized (CP)
ingested dose (mg equivalents naringenin)		7.0	21.9	22.5
ingested soluble dose (mg naringenin)		6.8	18.3	17.9
all excretors	excreted equivalents (mg)	0.8 (±0.1)B	1.7 (±0.4)A	1.5 (±0.3)A
	total excreted equivalents 24 h (%)	11.0 (±1.8)A	7.7 (±1.9)B	6.7 (±1.2)B
	relative % of the soluble intake	11.4 (±1.9)A	9.3 (±2.3)A	8.5 (±1.6)A
high excretors[b]	excreted equivalents (mg)	1.4 (±0.1)Ba	4.6 (±0.9)Aa	3.1 (±0.8)Aa
	total excreted equivalents 24 h (%)	19.9 (±1.6)Aa	20.8 (±4.0)Aa	14.7 (±2.8)Aa
	relative % of the soluble intake	20.5 (±1.7)Aa	24.9 (±4.8)Aa	18.4 (±3.5)Aa
medium excretors[c]	excreted equivalents (mg)	1.0 (±0.1)Ab	1.1 (±0.1)Ab	1.5 (±0.2)Ab
	total excreted equivalents 24 h (%)	14.2 (±2.1)Ab	5.1 (±0.6)Bb	6.6 (±0.9)Bb
	relative % of the soluble intake	14.6 (±2.1)Ab	8.6 (±2.5)Bb	10.2 (±2.4)Bb
low excretors[d]	excreted equivalents (mg)	0.3 (±0.2)Bc	0.7 (±0.2)Ac	0.7 (±0.1)Ac
	total excreted equivalents 24 h (%)	5.0 (±2.5)Ac	3.2 (±1.0)Ac	2.9 (±0.5)Ac
	relative % of the soluble intake	5.1 (±2.6)Ac	3.8 (±1.2)Ac	3.6 (±0.6)Ac

[a]Values are mean (n = 18) ± standard errors. Means followed by the same capital letter within a row are not significantly different according to Duncan's test ($P < 0.05$). Means followed by the same lower case letter within a column are not significantly different according to Duncan's test ($P < 0.05$). [b]n = 4. [c]n = 7. [d]n = 7.

hand-squeezed orange juice and that of HPH juices, whereas differences with fresh juice persisted for both medium and low excretors (Figure 2B). High excretors must have a gut microbiota very active in releasing hesperetin from hesperidin, and therefore they take advantage of the smaller cloud particle size in the HPH juice with more hesperidin available to interact with the gut bacteria than in pasteurized juice. Meanwhile, the lower levels of the appropriate microbiota to hydrolyze rutinosides in the medium and low excretors did not allow enhanced flavanone bioavailability when the flavanone accessibility was improved, and no significant differences between HPH and pasteurized juices were found (Figure 2).

Although pasteurized juice showed the lowest absorption and excretion rates, high excretors were able to maximize flavanone absorption up to 49 and 57% higher than those of the low excretors for both hesperetin and naringenin, respectively (Table 2).

The results show that high flavanone excretors have the appropriate microbiota and the intestinal transporters necessary to efficiently absorb and excrete flavanones after orange juice intake and can better benefit from improvements in flavanone solubility and accessibility than low excretors who do not respond in the same way.

The amounts of hesperetin glycosides present in the soluble fraction of the three juices obtained were quite similar, ranging between 9.1 mg/100 mL for fresh hand-squeezed and 12.1 for the HPH juice (Table 1). Thus, the relative urinary excretion expressed as percentage of the soluble intake was calculated. This ranged for all excretors from 7.7% for the pasteurized juice to 10.1% for the homogenized juice with no statistically significant differences among treatments (Table 2). The same trend was found for naringenin equivalents present in the soluble fraction. Therefore, the intake of similar amounts of soluble flavanones leads to similar relative urinary excretion of metabolites. However, significant differences in excretion were found when volunteers were stratified for their excretion capabilities. Thus, the differences observed for flavanone excretion after the intake of HPH and CP juices by high excretors clearly indicated that other juice characteristics, such as particle size, can also be relevant for absorption in addition

dx.doi.org/10.1021/jf4048989 | J. Agric. Food Chem. 2014, 62, 24−27

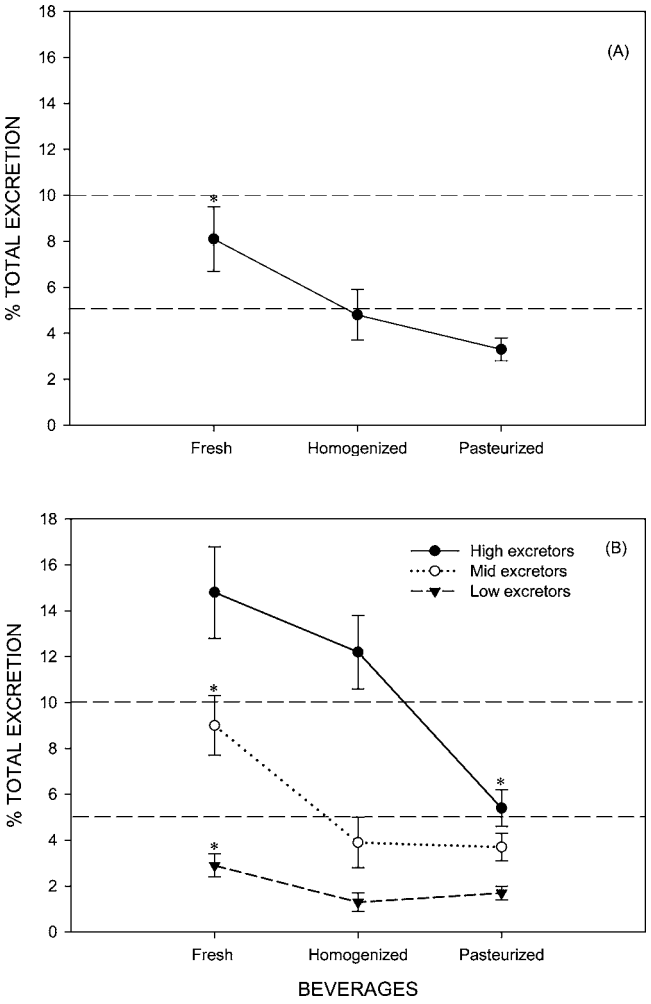

Figure 2. Urinary excretion of hesperetin after the intake of juices produced by different technological treatments in volunteers stratified as high, medium, and low excretors: (A) mean values for all volunteers (n = 18); (B) stratification in high (n = 4), medium (n = 7), and low (n = 7) excretors. Error bars are standard errors. Values are percentage of the total hesperetin intake excreted in urine. *, $p < 0.05$, significantly different according to Duncan's test.

to flavanone solubility, in agreement with previous results on carotenoid bioavailability.[11]

These results suggest that volunteer stratification for flavanone excretion should be considered in future studies to evaluate the bioavailability and health effects of citrus flavanones.

María Tomás-Navarro[†]
Fernando Vallejo*[,†]
Enrique Sentandreu[§]
Jose L. Navarro[§]
Francisco A. Tomás-Barberán[†]
[†]Quality, Safety and Bioactivity of Plant Foods, Food Science and Technology Department, CEBAS-CSIC, Campus de Espinardo, 30100 Murcia, Spain
[§]IATA-CSIC, Agustín Escardino 7, 46980 Paterna, Valencia, Spain

AUTHOR INFORMATION

Corresponding Author
*(F.V.) E-mail: fvallejo@cebas.csic.es. Phone: +34 968 396 374.

Funding
This work has been supported by Projects CSD2007-00063 (Fun-C-Food; Consolider Ingenio 2010) and Fundación Séneca (grupo de excelencia GERM 06 04486).

Notes
The authors declare no competing financial interest.

REFERENCES

(1) Sánchez-Moreno, C.; Plaza, L.; Elez-Martínez, P.; De Ancos, B.; Martín-Belloso, O.; Cano, M. P. Impact of high pressure and pulsed electric fields on bioactive compounds and antioxidant activity of orange juice in comparison with traditional thermal processing. *J. Agric. Food Chem.* **2005**, *53*, 4403−4409.

(2) Sanchez-Moreno, C.; Plaza, L.; De Ancos, B.; Cano, M. P. Effect of high-pressure processing on health-promoting attributes of freshly squeezed orange juice (*Citrus sinensis* L.) during chilled storage. *Eur. Food Res. Technol.* **2003**, *216*, 18−22.

(3) Baker, R. A.; Cameron, R. G. Clouds of *Citrus* juices and juice drinks. *Food Technol.* **1999**, *53*, 64−69.

(4) Vallejo, F.; Larrosa, M.; Escudero, E.; Zafrilla, M. P.; Cerdá, B.; Boza, J.; García-Conesa, M. T.; Espín, J. C.; Tomás-Barberán, F. A. The concentration and solubility of flavanones in orange beverages affect their bioavailability in humans. *J. Agric. Food Chem.* **2010**, *58*, 6516−6524.

(5) Sentandreu, E.; Gurrea, M. D.; Betoret, N.; Navarro, J. L. Changes in orange juice characteristics due to homogenization and centrifugation. *J. Food Eng.* **2011**, *105*, 241−245.

(6) Mullen, W.; Archeveque, M. A.; Edwards, C. A.; Matsumoto, H.; Crozier, A. Bioavailability and metabolism of orange juice flavanones in humans: impact of a full-fat yogurt. *J. Agric. Food Chem.* **2008**, *56*, 11157−11164.

(7) Gonzalez-Barrio, R.; Trindade, L. M.; Manzanares, P.; De Graaff, L. H.; Tomas-Barberan, F. A.; Espin, J. C. Production of bioavailable flavonoid glucosides in fruit juices and green tea by use of fungal α-L-rhamnosidases. *J. Agric. Food Chem.* **2004**, *52*, 6136−6142.

(8) Scalbert, A.; Williamson, G. Dietary intake and bioavailability of polyphenols. *J. Nutr.* **2000**, *130*, 2073S−2085S.

(9) Nielsen, I. L. F.; Chee, W. S. S.; Poulsen, L.; Offord-Cavin, E.; Rasmussen, S. E.; Frederiksen, H.; Enslen, M.; Barron, D.; Horcajada, M. N.; Williamson, G. Bioavailability is improved by enzymatic modification of the citrus flavonoid hesperidin in humans: a randomized, double-blind, crossover trial. *J. Nutr.* **2006**, *136*, 404−408.

(10) Borges, G.; Mullen, W.; Mullen, A.; Lean, M.; Roberts, S.; Crozier, A. Bioavailability of multiple components following acute ingestion of a polyphenol-rich juice drink. *Mol. Nutr. Food Res.* **2010**, *54*, S268−S277.

(11) Stinco, C. M.; Fernández-Vázquez, R.; Escudero-Gilete, M. L.; Heredia, F. J.; Meléndez-Martínez, A. J.; Vicario, I. M. Effect of orange juice's processing on the color, particle size, and bioaccessibility of carotenoids. *J. Agric. Food Chem.* **2012**, *60*, 1447−1455.

JOURNAL OF AGRICULTURAL AND FOOD CHEMISTRY

Article

pubs.acs.org/JAFC

Occurrence of Alk(en)ylresorcinols in the Fruits of Two Mango (*Mangifera indica* L.) Cultivars during On-Tree Maturation and Postharvest Storage

Stefanie Kienzle,[†] Reinhold Carle,[†] Pittaya Sruamsiri,[§] Carola Tosta,[†] and Sybille Neidhart*[,†]

[†]Institute of Food Science and Biotechnology, Chair of Plant Foodstuff Technology, Hohenheim University, Garbenstrasse 25, 70599 Stuttgart, Germany

[§]Department of Crop Science and Natural Resources, Faculty of Agriculture, Chiang Mai University, Chiang Mai 50200, Thailand

Supporting Information

ABSTRACT: Regarding their relevance for the fungal resistance of mangoes in long supply chains, the alk(en)ylresorcinols (AR) were quantitated in peel and mesocarp throughout storage (27 days, 14 °C, ethylene absorption). The 12 'Chok Anan' and 11 'Nam Dokmai #4' lots picked between 83 and 115 days after full bloom (DAFB) had different harvest maturity indices. The development of dry matter and fruit growth indicated physiological maturity ~100 DAFB. During storage, all fruits ripened slowly, mostly until over-ripeness and visible decay. The total AR contents always ranged at 73 ± 4.5 and 6.4 ± 0.7 mg hg^{-1} of 'Chok Anan' and 'Nam Dokmai #4' peel dry weight, respectively, but only at 6.7 ± 0.7 and 0.9 ± 0.1 mg hg^{-1} for the corresponding mesocarp ($P \leq 0.05$). These narrow concentration ranges were contradictory to the decreasing fungal resistance. Accordingly, the alk(en)ylresorcinols have not been a deciding factor for the fungal resistance.

KEYWORDS: *alk(en)ylresorcinols, Mangifera indica, maturation, peel, plant resistance, postharvest handling*

INTRODUCTION

Prevalent plant diseases in mango crops such as anthracnose and black spot disease, which are caused by *Colletotrichum gloeosporioides* (Penz.) Penz. & Sacch. and *Alternaria alternata* (Fr.) Keissl., respectively, remain quiescent after fungal infection of the fruit on the tree until the onset of ripening after harvest.[1] The diseases are controlled by preharvest application of fungicides and postharvest hot-water dipping baths, which may include added fungicides. Consideration of the natural defense system might contribute to avoiding the use of fungicides, which are unacceptable in some destination areas.[1] Among the antimicrobial compounds of the mango fruit,[2,3] alk(en)ylresorcinols[4] (AR) are thought to restrain the development of anthracnose and *Alternaria* rot[5,6] and may be an alternative to synthetic fungicides.[7,8] Termination of fungal quiescence by the onset of fruit ripeness coincided with a significant decline of the AR contents in the peel.[1,5,6,9] Cultivar-specific resistance to anthracnose and infections by *A. alternata* were related to the AR contents of the mango peel[5,9] and more recently to those of the mango sap.[10]

The AR presumably play different roles as barrier-forming allelochemicals and phytoanticipins[11] in a mango-specific plant defense system.[12] The latter involves a longitudinal multilayered network of branching resin ducts in the outer region of the mango pericarp with a cultivar-specific mean number of ducts per cross-section area that has been correlated with the resistance to fruit flies.[13] This network of resin ducts pervades the fruit and thus also occurs in the inner mesocarp regions and the base.[14] Epithelial cells secreting the lipophilic sap fraction,[15] which displays cultivar-specific profiles of monoterpenes[16] as bioactive ingredients[17] besides AR,[10] were distinguished from those releasing a mucilaginous sap fraction.[18] This hydrophilic fraction contains several enzymes[19] as typical defense proteins,[12] especially a laccase-type polyphenol oxidase (PPO)[20,21] and peroxidase (POD).[21] Conventionally, the commercial harvest time is before the onset of mango ripening on the tree, when sap flow is still occurring.[22] Because the abscission zone of mangoes is penetrated by two separate duct systems (i.e., that of the fruit and that of the stalk),[14] irritant sap spurting and oozing from the abscission point may cause sapburn, which is prevented in fresh-fruit marketing by postharvest desapping of the fruit.[10]

Being phenolic lipids, the AR consist of a resorcinol moiety that is linked to an alk(en)yl chain, by analogy with the catechol-based urushiols of other Anacardiaceae species.[23] The chain varies in length, mostly between C_{15} and C_{19}, and in the degree of unsaturation. Among a range of AR homologues in *Mangifera indica* L., heptadecenyl- ($C_{17:1}$), heptadecadienyl- ($C_{17:2}$), and pentadecylresorcinol ($C_{15:0}$) are prevalent.[9,10,24−26] Due to their amphiphilic nature,[27] their numerous biological activities, for example, antimicrobial, antiparasitic, anticancer, anti-inflammatory, and cytotoxic properties, chiefly involve effects on the structure and function of membranes as well as the interaction with proteins, including effects on membrane-related enzyme activities.[23,28] Via the analogous interaction with cytoplasmic membranes of epidermal cells, the AR of mangoes act as haptens, causing allergic contact dermatitis after sensitization. Cross-sensitivity between AR and urushiols may occur,[24,29] but the resorcinol moiety of AR needs initial hydroxylation for subsequent *o*-quinone formation.[23]

Received: January 23, 2013
Revised: November 26, 2013
Accepted: November 28, 2013
Published: December 18, 2013

ACS Publications © 2013 American Chemical Society

Consistent with a notable susceptibility of 'Nam Dokmai' fruit to anthracnose,[7,30] extremely low AR contents had been reported for this cultivar.[9,10,26] With regard to the suitability of 'Chok Anan'[31] and 'Nam Dokmai #4'[32] fruit for long supply chains, we have recently described the impacts of different maturity stages at harvest on the properties of the mangoes during postharvest storage for up to 27 days at 14 °C under ethylene absorption. Apart from their different sensitivities to chilling injury[33] and the preferential distribution channels,[34,35] the two cultivars differed in their characteristic harvest maturity criteria and in their suitability for storage.[31,32] In the present follow-up study, the AR profiles were specified for both the peel and the mesocarp of these fruits[31,32] as a function of harvest time, maturity stage at harvest, and postharvest quality and ripeness during cold fruit storage, respectively. The aim was to identify the relevance of the AR for the shelf life of the fruit in long supply chains concerning options for their control by appropriate timing.

MATERIALS AND METHODS

Plant Material. As detailed previously,[31,32] fresh 'Chok Anan' (C) and 'Nam Dokmai #4' (N) mango fruits (*M. indica* L.) were obtained from research orchards in Mae Jo and San Sai (northern Thailand), respectively, during the main harvest season in April−May 2008. For both cultivars, the usual commercial harvest time (UCH) is ∼100 days after full bloom (DAFB) in this region.[31,36] Picking of the fruit every 6 days around the expected UCH of each cultivar resulted in five harvest days between 83 and 107 DAFB for 'Chok Anan' (C1−C5, Figure 1) and between 91 and 115 DAFB for 'Nam Dokmai #4' (N1−N5), respectively.[31,32] Each time, ∼300 fruits were picked from 10 trees at different positions within the canopy. To specify their maturation times on the tree, the average DAFB until each of the 10 harvest dates was estimated, because DAFB-precise harvest of individual fruits would have required tagging of the flowers and continuous evaluation of the field temperature. After their transportation to Chiang Mai University under passive-air cooling, they were washed to remove leaked sap. To minimize sap exudation during transport and subsequent sapburn during storage,[14,22] the fruits had been severed ∼10 cm above the stem end of the pedicel, which was cut back to 1 cm just before washing. Being nonuniform batches, the fruits of each harvest day were sorted into two or three categories *A*−*C* (Figure 1) according to their peel color that was rated visually, on the basis of the RHS color chart.[31,32] Because the measured peel color varied significantly within each category across the harvest period in similar ranges as it did across the three categories on each harvest day, the 12 'Chok Anan' and 11 'Nam Dokmai #4' fruit lots that resulted from the five harvest dates per cultivar were explored as individual variants of specific harvest maturity (C1*A*−C5*C* and N1*A*−N5*C*, respectively; Figure 1).[31,32]

The fruits of each variant were stored in cardboard boxes for up to 27 days at 14 °C and 50−60% relative humidity (RH) in the presence of ethylene absorbers ($KMnO_4$) to delay ripening (Figure 1).[31,32] Rotten fruits were removed immediately. To complete the previously reported characterization of the variants after 1, 10 ± 1, 18 ± 1, and 27 days of storage[31,32] by AR analyses, three fruits without visible defects were manually peeled per variant with a stainless steel mango peeler on each of those days for the sampling of peel and mesocarp (Figure 1). The latter was cut into cubes (∼1 cm^3). The strip-shaped peel samples (∼1−2 mm thickness) represented the skin plus residual pulp, which was attached to the skin after fruit peeling. For the AR analyses, these peel and mesocarp samples were ultrarapidly frozen in liquid nitrogen, freeze-dried, vacuum-packed in polyethylene pouches, and stored at −80 °C until airfreight transport (∼ −40 °C) to Hohenheim University. There, the freeze-dried samples were pulverized in a laboratory blender (Waring, Torrington, CT, USA) after immersion into liquid nitrogen. The powders were vacuum-packed in polyethylene pouches and stored (−20 °C) until analysis.

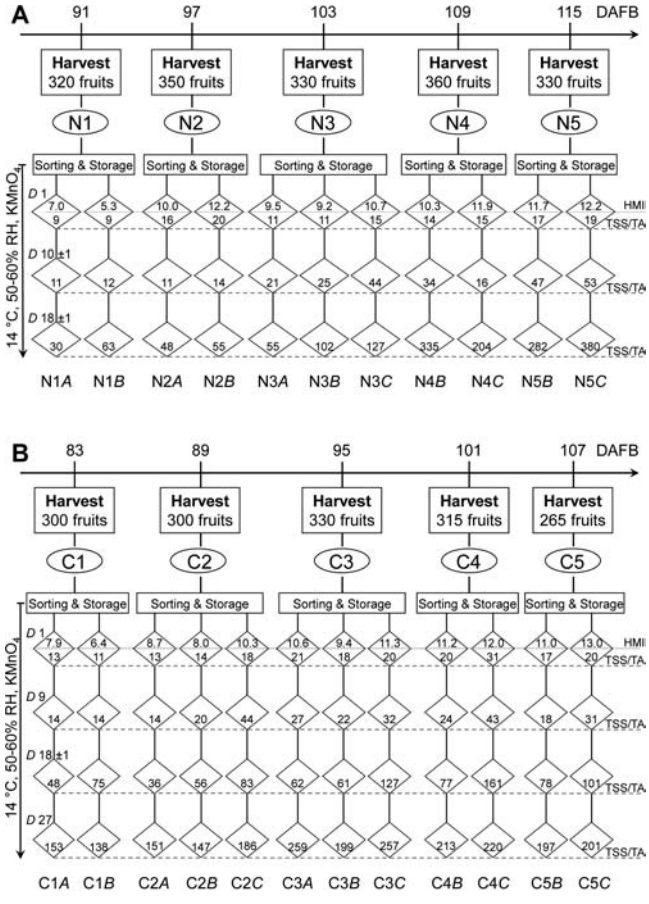

Figure 1. Experimental design, based on (**A**) 'Nam Dokmai #4' (N) and (**B**) 'Chok Anan' (C) fruits that were picked on five days between 91 and 115 days and between 83 and 107 days after full bloom (DAFB), respectively. Sorting of the fruits of each batch (N1−N5, C1−C5) into the categories *A*−*C* directly after the harvest yielded the variants N1*A*−N5*C* and C1*A*−C1*C*, respectively, which were immediately stored at 14 °C (50−60% RH, $KMnO_4$).[31,32] Each variant was composed of 110−180 fruits for 'Nam Dokmai #4' and 57−213 for 'Chok Anan'. On several days (*D*) of storage (rhombs), aliquots of each variant were used for the analysis of alk(en)-ylresorcinols and a range of attributes reported earlier,[31,32] such as the reproduced sugar/acid ratios (TSS/TA), which rose disproportionately with increasing fruit ripeness. On day 1, each variant was also specified by the harvest maturity index (HMI, Tables 4 and 5), which rose with increasing maturity.

Sample Preparation for the Analysis of Alk(en)ylresorcinols. Alk(en)ylresorcinol extraction from the pulverized peel was performed in duplicate. The method of Knödler et al.[25] was slightly modified to facilitate the procedure. Aliquots of 2.5 g of peel powder were extracted with 50 mL of dichloromethane in a capped 100 mL glass bottle by continuous stirring at room temperature for 1 h under a N_2 atmosphere. Centrifugation[25] was replaced by filtration through a Büchner funnel with filter paper no. 4 (Whatman, Maidstone, UK) to separate the solids from the crude extract. The residue was extracted with 50 mL of dichloromethane for 30 min.[26] Evaporation of the combined filtrates in vacuo at 30 °C left a residue that was dissolved in 10 mL of dichloromethane. Its solid-phase extraction (SPE) on polyamide (2 g, 0.05−0.16 mm; Carl Roth, Karlsruhe, Germany), filled in Econo-Pac columns (Bio-Rad, Munich, Germany), followed, after the sorbent had successively been conditioned with 20 mL of methanol and 25 mL of dichloromethane. The peel extract was applied to the column, the latter was washed with 25 mL of dichloromethane, and the AR were recovered by elution with 50 mL of methanol. After evaporation of the eluate in vacuo (30 °C), the dried residue was

dx.doi.org/10.1021/jf4028552 | J. Agric. Food Chem. 2014, 62, 28−40

Table 1. UV Spectra and APcI(+)-MS^n Fragmentation Patterns of 5-Alk(en)ylresorcinol Homologues That Were Quantitated in both the Peel and Mesocarp of 'Chok Anan' and 'Nam Dokmai #4' Mango Fruits

peak	RT[a] (min)	alkyl group (R)[c]	CF[b]	HPLC-DAD UV spectrum λ_{max} (nm)	$[M + H]^+$ m/z	HPLC/APcI(+)-MS^n m/z (% base peak)
alk(en)ylresorcinols found in the mango samples						
1	11.6	$C_{17:3}$	0.98276	205, 275, 280	343	MS^2[343]: 163 (100), 123 (67), 177 (31), 149 (14), 137 (10), 191 (7)
2	12.7	$C_{15:1}$	0.99375	202, 275, 280	319	MS^2[319]: 123 (100)
3	14.4	$C_{17:2}$	0.98851	213, 275, 280	345	MS^2[345]: 123 (100), 163 (33), 177 (20), 137 (12), 149 (9)
4	17.2	$C_{15:0}$	1	208, 275, 280	321	MS^2[321]: 111 (100)
5	18.1	$C_{17:1}$	0.99425	211, 275, 280	347	MS^2[347]: 123 (100)
6	20.1	$C_{19:2}$	1.06897	202, 275, 280	373	MS^2[373]: 123 (100), 163 (16), 137 (14), 177 (11), 261 (3), 275 (2)
7	23.4	$C_{17:0}$	1	202, 275, 280	349	MS^2[349]: 111 (100), 123 (7)
8	24.3	$C_{19:1}$	1.07471	202, 275, 280	375	MS^2[375]: 123 (100)
reference standards (S)						
S1	17.0	$C_{15:0}$	1	208, 275, 280	321	MS^2[321]: 111 (100)
S2	23.1	$C_{17:0}$	1	214, 275, 280	349	MS^2[349]: 111 (100)

[a]RT, retention time (Figure 2). [b]CF, molecular weight correction factor. [c]R: $C_{15:0}$, pentadecyl; $C_{15:1}$, pentadecenyl; $C_{17:0}$, heptadecyl; $C_{17:1}$ heptadecenyl; $C_{17:2}$, heptadecadienyl; $C_{17:3}$, heptadecatrienyl; $C_{19:1}$, nonadecenyl; $C_{19:2}$, nonadecadienyl.

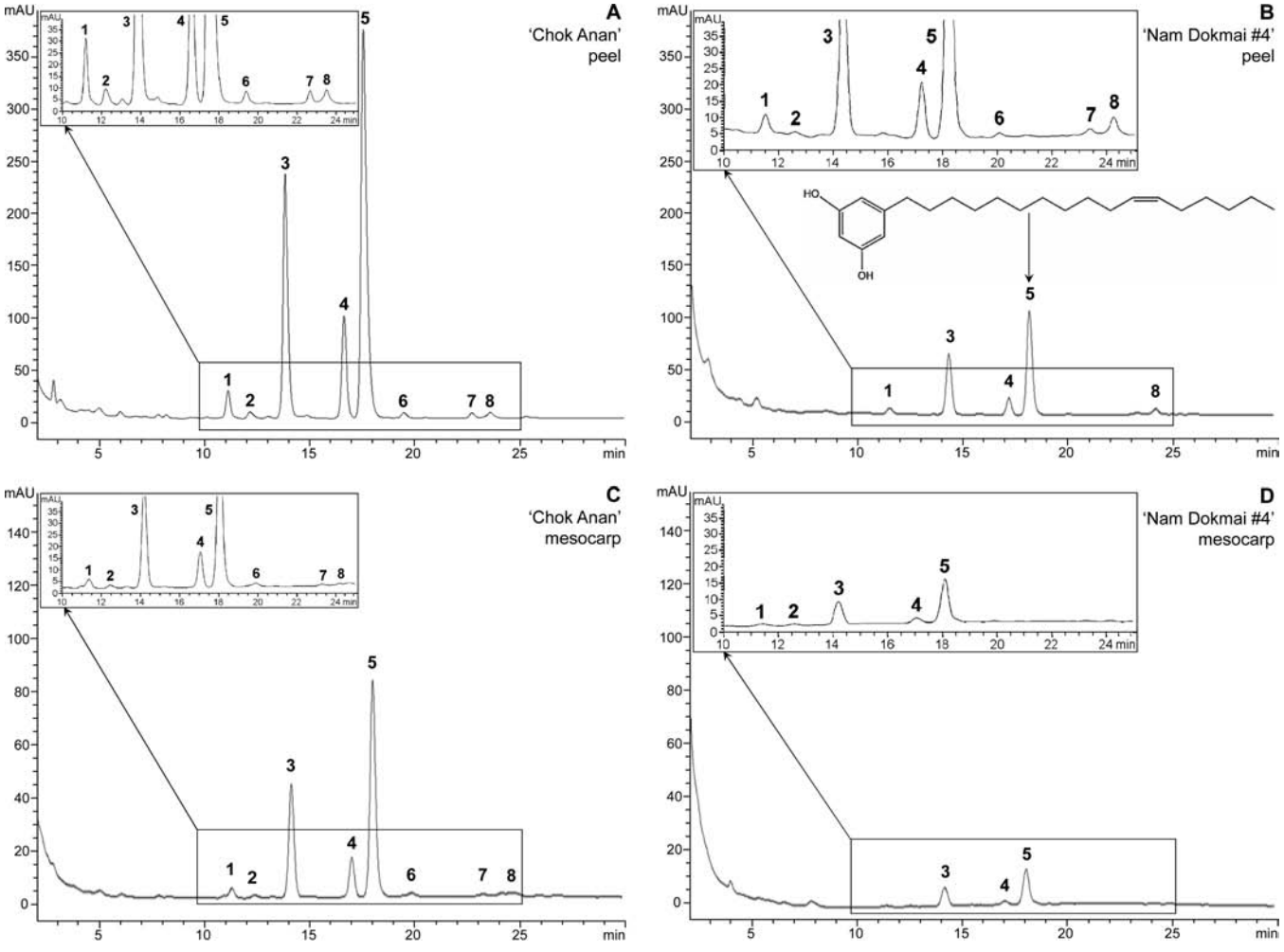

Figure 2. HPLC fingerprints of the alk(en)ylresorcinols of mango fruit at 275 nm: (**A**) 'Chok Anan' peel (injection volume v = 10 μL); (**B**) 'Nam Dokmai #4' peel (v = 25 μL); (**C**) 'Chok Anan' mesocarp (v = 25 μL); (**D**) 'Nam Dokmai #4' mesocarp (v = 75 μL). For peak assignments, cf. Table 1.

dissolved in 0.5 mL of methanol and membrane-filtered (0.45 μm) into vials for HPLC and LC-MS analyses, respectively.[25]

The mesocarp powder was initially extracted in the same way to identify the AR homologue profile by LC-MS analysis. Because only the three major AR homologues **3**–**5** (Table 1) were quantifiable in the pulp (cf. Figure 2), a simpler and faster method without SPE and the hazardous dichloromethane was developed for the AR quantitation in the pulp samples. Comparative application of both extraction methods to two or three pulp samples of each cultivar showed no significant effects on the analytical results ($P \leq 0.05$; data not shown).

dx.doi.org/10.1021/jf4028552 | J. Agric. Food Chem. 2014, 62, 28–40

The carotenoids, which were present in the crude mesocarp extract without SPE on polyamide, did not interfere with the quantifiable AR compounds **3**–**5** during HPLC analysis. Only the quantitation of the minor compounds **6**–**8** (Table 1), traces of which were otherwise maximally detectable in the pulp, would have been affected by coelution of a few of the carotenoids. Hence, the mesocarp powder was finally analyzed in duplicate by extracting each aliquot (2.5 g) with 50 mL of ethyl acetate in a capped 100 mL glass bottle by continuous stirring at room temperature for 1 h under a N_2 atmosphere. The extract was filtered through a Büchner funnel with Whatman filter paper no. 4. The residue was extracted with 50 mL of ethyl acetate (30 min). Evaporation of the combined filtrates to dryness in vacuo (30 °C) left a residue that was dissolved in methanol (0.5 mL) and membrane-filtered (0.45 μm) into vials for HPLC analysis.

HPLC and LC-MS Analyses of Alk(en)ylresorcinols. Each extract was analyzed by the injection of 10–75 μL into a HPLC system described elsewhere.[25] The AR were separated on a 150 mm × 3.0 mm i.d., 3 μm, C18 Aqua column (Phenomenex, Torrance, CA, USA) with a 4.0 mm × 2.0 mm i.d. C18 ODS guard column. Gradient elution at 25 °C and a flow rate of 0.6 mL min^{-1} involved the eluents A (100% redistilled water) and B (100% methanol). To remove the chlorophylls of pigment-containing extracts from the column completely, the gradient program of Knödler et al.[25] was amended as follows: from 17 to 9% A (20 min), 9% A isocratic (10 min), from 9 to 0% A (5 min), 0% A isocratic (15 min), from 0 to 17% A (0.1 min), 17% A (5 min). The total run time was 55 min. Detection of the AR was at 275 nm, while their UV–vis spectra were recorded in the range of 200–600 nm.

The same HPLC system was connected to an Esquire 3000+ ion trap mass spectrometer with an APcI source (Bruker, Bremen, Germany) for the LC-MS analyses, which were performed as detailed elsewhere.[25] The AR of the extracts were separated under the HPLC conditions described above. Positive ion mass spectra of the column eluate were recorded in the range of m/z 100–500.[25] Nitrogen served as the drying gas at a flow rate of 5 L min^{-1} and as the nebulizing gas at a pressure of 65 psi.

By analogy with Knödler et al.,[25] the individual compounds were identified by their retention times and their UV and mass spectra. The AR contents in the peel of each cultivar and in 'Chok Anan' pulp were calculated from linear seven-point calibration curves of the respective reference standards (5–1000 mg L^{-1} for 5-pentadecylresorcinol; 10–2100 mg L^{-1} for 5-heptadecylresorcinol) at 275 nm. Due to the very low alk(en)ylresorcinol contents of 'Nam Dokmai #4' pulp, five-point calibration curves of 5-pentadecylresorcinol (0.78–78 mg L^{-1}) and 5-heptadecylresorcinol (0.75–75 mg L^{-1}), respectively, were used for those samples. Because no reference standards were available for the unsaturated compounds, the calibration curve of the corresponding saturated standard substance was used in these cases, together with a molecular weight correction factor (CF; Table 1).[37] The contents of 5-nonadecenyl- and 5-nonadecadienylresorcinols were analogously obtained from the calibration curve of 5-heptadecylresorcinol. The two reference standards (HPLC purity ≥ 95%; S1 and S2 in Table 1) were from Sigma-Aldrich (St. Louis, MO, USA). All reagents and solvents were of analytical or HPLC grade (VWR, Darmstadt, Germany).

Statistical Analyses. Multiple pairwise comparisons of means (Tukey's tests), using SAS 9.1 (SAS Institute, Cary, NC, USA), yielded the significant differences between the variants ($P \leq 0.05$).

RESULTS AND DISCUSSION

Characteristic Alk(en)ylresorcinol Homologues in Mango Peel and Pulp. Because the available reference standards included only 5-pentadecylresorcinol (S1: $C_{15:0}$) and 5-heptadecylresorcinol (S2: $C_{17:0}$), the identity of the alk(en)ylresorcinol homologues occurring in the peel and mesocarp of both cultivars had to first be confirmed by HPLC-DAD-MS^n (Table 1). For this purpose, two or three samples of peel and pulp, respectively, were examined per cultivar. Purification of their dichloromethane extracts by solid-phase extraction excluded potential interference of coextracted carotenoids. The UV spectrum of each alk(en)ylresorcinol homologue showed the typical absorbance maxima of the 1,3-dihydroxybenzene chromophore at 275 and 280 nm (Table 1). By the presence of the latter maximum as a shoulder of the first one, the AR were clearly distinguishable from alkylcatechols.[38]

Eight alk(en)ylresorcinol homologues were found in all peel samples (Figure 2A,B) and in 'Chok Anan' mesocarp (Figure 2C), but only five of them in the pulp of 'Nam Dokmai #4' fruit (Figure 2D). Regardless of the cultivar and the part of the fruit, the main compound (Figure 2) was confirmed[9,10,24–26] to be 5-heptadecenylresorcinol (**5**; $C_{17:1}$), producing a $[M + H]^+$ ion of m/z 347 (Table 1). The second most important one was 5-heptadecadienylresorcinol (**3**; $C_{17:2}$; m/z 345). Oka et al.[24] had isolated the two AR from mango peel to describe their contact allergenic activities. After localization of the double bonds by 1D and 2D NMR, Knödler et al.[28] assigned their structures to 5-(11′*Z*-heptadecenyl)resorcinol and 5-(8′*Z*,11′*Z*-heptadecadienyl)resorcinol, respectively. The third major compound (Figure 2) was again[26] 5-pentadecylresorcinol (**4**; $C_{15:0}$; m/z 321) that yielded a stable fragment at m/z 111 (Table 1) due to protonation of the aromatic system. The latter is typical of saturated AR.[25] In addition, compound **4** had the same characteristics that the reference standard S1 revealed for the $C_{15:0}$ homologue (Table 1). Unlike 'Chok Anan' mesocarp, 'Nam Dokmai #4' pulp contained only traces of **4** (Figure 2D).

The other alk(en)ylresorcinol homologues were the minor compounds **1**, **2**, and **6**–**8** (Table 1). Quantitation of all five was feasible only for 'Chok Anan' peel (Figure 2A). The quantifiable minor alk(en)ylresorcinol homologues of 'Nam Dokmai #4' peel were restricted to **1** and **8**, because those samples contained merely traces of **2**, **6**, and **7** (Figure 2B). In all of the mesocarp samples, none of the minor compounds could be quantitated, because only traces of them were found, either for all five ('Chok Anan', Figure 2C) or simply for **1** and **2** ('Nam Dokmai #4', Figure 2D). The minor compounds included the second saturated alk(en)ylresorcinol homologue. Consistent with Knödler et al.,[25] it occurred in a number of samples (Figure 2) and proved to be 5-heptadecylresorcinol (**7**; $C_{17:0}$; m/z 349). Its identity was confirmed by the reference standard S2 (Table 1). The monounsaturated minor compounds were 5-pentadecenylresorcinol (**2**; $C_{15:1}$) and 5-nonadecenylresorcinol (**8**; $C_{19:1}$), which implicated $[M + H]^+$ ions of m/z 319 and 375, respectively. Like the main compound **5** ($C_{17:1}$), they showed a single characteristic fragment at m/z 123 (Table 1) due to the formation of the 1,3-dihydroxytropylium ion by β-cleavage of the alkyl chain.[25] In contrast to the saturated and monounsaturated alk(en)ylresorcinol homologues, the di- and polyunsaturated ones (**1**, **3**, **6**; Table 1) chiefly yielded product ions at m/z 123, 137, 149, 163, and 177 in the MS^2 experiment. As detailed elsewhere,[25] this overall indicated unsaturated hydrocarbon chains for the major compound **3** ($C_{17:2}$) mentioned above and the minor compounds **1** and **6**. The latter two were 5-heptadecatrienylresorcinol ($C_{17:3}$; m/z 343) and 5-nonadecadienylresorcinol ($C_{19:2}$; m/z 373), respectively (Table 1).

On the whole, the same three major and five minor alk(en)ylresorcinol homologues that were reported earlier for the peel and pulp of other cultivars[26] were also found in these two varieties. However, the minor compounds of their pulp were unquantifiable ('Chok Anan') or, for the majority of them, even undetectable ('Nam Dokmai #4').

Alk(en)ylresorcinol Contents Observed after Different Harvest Times. Because the sap flow is known to vary with

the stage of maturation at harvest,[7,22] the occurrence of AR in the sap[10] might suggest analogous changes in the alk(en)ylresorcinol contents of the fruit. To test this hypothesis, the alk(en)ylresorcinol contents found 1 day after harvest were to be related to the fruit development stages observed at harvest between 83 and 115 DAFB (Tables 2 and 3). The 11 'Nam Dokmai #4' (N1*A*−N5*C*; Table 2) and the 12 'Chok Anan' fruit variants (C1*A*−C5*C*; Table 3), which were distinguished per cultivar by their on-tree maturation periods (DAFB) plus the assigned category *A*−*C* (Figure 1), also differed in the dry matter (DM) of the pulp[31,32] and in the fruit mass (Tables 2 and 3), which were recorded 1 day after harvest and on the picking day, respectively. Local experience had shown that the fruit in this growing region can generally be expected to be fully mature ∼100 DAFB, being the usual commercial harvest time (UCH).[31,36] Accordingly, the seed development as well as fruit growth and the accumulation of dry matter should be completed then, being a prerequisite for the full potential of subsequent ripening. Consequently, physiological maturity may be identified retrospectively by the onset of the plateau levels that fruit size and dry matter should have reached within the constraints of the surrounding conditions.[8] DM had thus been recommended as a maturity indicator to distinguish mature from immature fruit.[39]

For the 'Nam Dokmai #4' fruit, the growth phase ended ∼97 DAFB (N2) according to the DM plateau shown by all variants picked 97−115 DAFB (N2−N5) (Table 2).[32] The fruit mass increased from the first (N1, 91 DAFB; 268−270 g) to the last harvest (N5, 115 DAFB; 349−353 g), but the differences were insignificant between 97 and 109 DAFB (N2−N4; 291−307 g) (Table 2). The mass of the N1 fruit was equal to the relatively small size reported by Vásquez-Caicedo et al.[34] for ripe fruit of this cultivar (271 g), but the cited value might also be due to the influence of the fruit load of the tree. A decrease by 0.14 g for every extra fruit was stated for 'Kensington Pride' mangoes.[40]

Because the development of the 'Chok Anan' fruit on the tree was overall less uniform (in terms of peel color[32] and fruit mass), the stage of physiological maturity was less evident. The fruit masses of the 'Chok Anan' variants tended to increase from 179 g (C1*A*) 83 DAFB to 277 g (C5*C*) 107 DAFB (Table 3). However, the fruits of each harvest day greatly varied in size, which always rose from category *A* to *C* (Table 3). Within each of the categories *B* and *C*, the fruit size was constant for 'Chok Anan' between 95 and 107 DAFB (C3−C5). In addition, these latter seven variants and a few of the C2 lots (89 DAFB) presented a constant maximal DM (19−23 g hg^{-1}; Table 3).[31] The end of the 'Chok Anan' growth phase was thus deemed to be 95 DAFB (C3). Similarly, an increase in fruit size from 227 to 239 g between 84 and 100 DAFB[41] and an average fruit mass of 275 g at the ripe stage[34] were reported earlier for 'Chok Anan' fruit of the study area, whereas fruits below 200 g are usually considered unmarketable.[42]

For both cultivars, the end of the growth phase 95−97 DAFB (N2, C3) was thus indeed just before the estimated UCH (100 DAFB), which was just before the 'Nam Dokmai #4' harvest N3 (103 DAFB) and coincided with C4 (101 DAFB) for 'Chok Anan'. However, ethylene production was not yet detectable 1 day after harvest for any of the 23 variants.[31,32]

According to the alk(en)ylresorcinol levels of the peel ($c_{AR,p}$) 1 day after harvest, the variants of each cultivar could be separated into two $c_{AR,p}$ classes that clearly depended on the harvest time. For the peel of 'Chok Anan' fruit that was already picked 83−101 DAFB (C1−C4; i.e., until UCH), $c_{AR,p}$ usually amounted to 67−88 mg hg^{-1} of dry weight (DW). By contrast, the peel of the two C5 variants, which were picked last (107 DAFB; i.e., clearly after UCH), showed $c_{AR,p}$ levels of merely 51−58 mg hg^{-1} (Table 3). Only variant C2*C* (fruit of the category *C* from the harvest C2 89 DAFB) insignificantly differed in the $c_{AR,p}$ from the two C5 variants (C5*B*, C5*C*). On average, the peel of the 10 'Chok Anan' variants forming the C1−C4 group had a $c_{AR,p}$ of 76 ± 8.9 mg hg^{-1} of DW (Table 3). It significantly differed ($P \leq 0.05$) from that of the C5 group (55 ± 5.5 mg hg^{-1}). However, compared to the 95% confidence interval (CI) of the mean for the former group (±6.4 mg hg^{-1}), that of the latter was high (±49 mg hg^{-1}).

For 'Nam Dokmai #4' peel, $c_{AR,p}$ (Table 2) reached only ∼one-ninth of the contents in 'Chok Anan' peel. Approximately until UCH, elevated $c_{AR,p}$ levels of 8.4−11.4 mg hg^{-1} of DW occurred between 91 and 97 DAFB (N1−N2; Table 2). Again, the fruit picked afterward (N3−N5, 103−115 DAFB) showed lower alk(en)ylresorcinol contents (3.3−7.6 mg hg^{-1}). Almost all last-mentioned 'Nam Dokmai #4' variants significantly differed from the first group ($P \leq 0.05$). The $c_{AR,p}$ group mean amounted to 9.4 ± 2.2 mg hg^{-1} of DW for the "until-UCH" group N1−N2, but dropped to the significantly ($P \leq 0.05$) lower average of 5.8 ± 1.3 mg hg^{-1} for the "post-UCH" group N3−N5 (Table 2). These ranges were met by the alk(en)ylresorcinol levels, which were reported for peel of the same cultivar by Knödler et al.[26] (79.33 mg kg^{-1} of DW) and Hassan et al.[9] (∼10−19 μg g^{-1} of FW; i.e., ∼5.0−9.5 mg hg^{-1} of DW, assuming 20% DM). Desapping, which was applied by Hassan et al.,[9] might lower the alk(en)ylresorcinol contents due to losses via the released resin. However, the data presented in Tables 2 and 3 referred to peel samples that were obtained without desapping of the fruit. They suggested that the $c_{AR,p}$ levels significantly fell after UCH.

Thus, cultivar-specific "until-UCH" ranges above ∼8 and ∼60 mg hg^{-1} of DW for the peel of 'Nam Dokmai #4' and 'Chok Anan', respectively, could be distinguished from "post-UCH" ranges below that limit. The time when the $c_{AR,p}$ drop was noticed (N3, 103 DAFB; C5, 107 DAFB) corresponded to the stage 3−6 days after UCH (i.e., 6−12 days after the onset of the DM and fruit mass plateaus 95−97 DAFB; Tables 2 and 3). However, because the fruit was picked only every 6 days, the significant decline of $c_{AR,p}$ might already have started up to 5 days earlier.

Nevertheless, the total alk(en)ylresorcinol contents of the mesocarp ($c_{AR,m}$) ranged rather uniformly at 0.6−1.6 mg hg^{-1} of DW around a grand mean of 1.0 ± 0.2 mg hg^{-1} for all 'Nam Dokmai #4' variants (Table 2) and at 5.5−9.8 mg hg^{-1} of DW around an average of 7.5 ± 1.0 mg hg^{-1} for all 'Chok Anan' lots (Table 3), regardless of the on-tree maturation time (91−115 and 83−107 DAFB, respectively). Consideration of DM resulted in the equivalent alk(en)ylresorcinol contents of the fresh mesocarp ($c_{AR,fm}$), being 0.1−0.3 mg hg^{-1} of fresh weight (FW) for 'Nam Dokmai #4' (Table 2) and 0.9−2.3 mg hg^{-1} for 'Chok Anan' (Table 3). The levels reported by Droby et al.[6] (1.5−2.1 mg hg^{-1} of FW) and Knödler et al.[26] (2.6−18.7 mg hg^{-1} of DW) for the pulp of various cultivars were comparable to those of 'Chok Anan' flesh. On a dry weight basis, the alk(en)ylresorcinol amounts in the pulp represented only ∼$^1/_{10}$ of the total AR contents in the peel (Tables 2 and 3), as already implied in Figure 2 for each cultivar.

Alk(en)ylresorcinol Contents of Fruits Differing in Harvest Maturity. Because the physiological maturity had been ascribed to the stages 95−97 DAFB (N2, C3) within the 24 days of examined on-tree maturation up to 115 DAFB, a clearer distinction of individual harvest maturity stages was of interest with respect to beginning ripening on the tree and its

Table 2. 'Nam Dokmai #4' Mango Fruits (Variants N1*A*–N5*C*)[a] Harvested after Different Maturation Times on the Tree (Days after Full Bloom, DAFB): Fruit Size, Peel and Mesocarp Portions of the Fresh Fruit, as well as the Total Alk(en)ylresorcinol (AR) Contents of the Peel and Mesocarp, Respectively, 1 Day after Harvest

harvest day/batch no.:	N1		N2		N3			N4		N5	
DAFB:	91		97		103			109		115	
category:	*A*	*B*	*A*	*B*	*A*	*B*	*C*	*B*	*C*	*B*	*C*
fruit variant:	N1*A*	N1*B*	N2*A*	N2*B*	N3*A*	N3*B*	N3C	N4*B*	N4C	N5*B*	N5C
dry matter, DM (g hg^{-1}) [32]	14.1	14.6	18.3	18.8	20.0	19.5	19.0	18.3	18.6	18.7	19.1
fruit size (fresh mass),[b,c] *m* (g)	268 ± 6 d	270 ± 7 d	299 ± 6 c	291 ± 6 c	303 ± 7 bc	322 ± 6 b	303 ± 6 bc	303 ± 6 bc	307 ± 7 bc	353 ± 7 a	349 ± 7 a
pulp and peel portions of the fresh fruit[b,d]											
mesocarp: w_m (g hg^{-1} fruit)	77.3 ± 0.7 b	81.0 ± 0.7 ab	79.7 ± 0.5 ab	79.3 ± 1.0 ab	81.1 ± 2.3 ab	80.3 ± 0.5 ab	80.8 ± 0.8 ab	83.7 ± 0.3 a	82.3 ± 0.5 a	83.2 ± 0.5 a	83.2 ± 0.5 a
peel: w_p (g hg^{-1} fruit)	12.7 ± 0.5 ab	11.3 ± 0.3 abc	12.9 ± 0.4 ab	13.3 ± 0.3 a	10.9 ± 1.9 abc	11.8 ± 0.3 abc	11.1 ± 0.3 abc	9.9 ± 0.2 bc	10.2 ± 0.4 abc	9.8 ± 0.5 bc	9.2 ± 0.1 c
total alk(en)ylresorcinol contents of the mesocarp[b,e]											
$c_{AR,m}$ (mg hg^{-1} DW)	1.0 ± 0.1 bcd	0.8 ± 0.02 cd	0.9 ± 0.1 bcd	0.8 ± 0.05 cd	0.8 ± 0.1 bcd	1.1 ± 0.01 bc	1.0 ± 0.1 bcd	0.7 ± 0.1 cd	0.6 ± 0.02 d	1.3 ± 0.1 ab	1.6 ± 0.2 a
$c_{AR,fm}$ (mg hg^{-1} FW)	0.14	0.12	0.17	0.14	0.17	0.22	0.19	0.14	0.11	0.24	0.31
total alk(en)ylresorcinol contents of the peel[f]											
$c_{AR,p}$ (mg hg^{-1} DW)[b]	9.0 ± 0.4 b	8.4 ± 0.3 bc	8.6 ± 0.7 b	11.4 ± 0.3 a	7.6 ± 0.4 bcd	4.9 ± 0.3 ef	6.6 ± 0.1 cde	3.3 ± 0.04 f	6.0 ± 0.5 de	5.4 ± 0.1 e	6.5 ± 0.03 cde
$c_{AR,p}$ group mean ± SD (±95% CI) (mg hg^{-1} DW)	group N1–N2 (n = 4): 9.4 ± 1.4 (±2.2)				group N3–N5 (n = 7): 5.8 ± 1.4 (±1.3)						

[a]The fruits of the batches N1–N5 were harvested on five different days between 91 and 115 DAFB and sorted into the categories *A*–*C* according to their peel color to obtain the 11 fruit variants N1*A*–N5*C* (Figure 1A) having the previously reported dry matter contents (DM) in the mesocarp.[32] [b]Mean ± standard error. Values with different letters horizontally (a–f) were significantly different ($P \leq 0.05$) due to maturity (harvest time and category). [c]*m*, mean of the masses of 100 fresh fruits that were weighed (±0.01) per variant on the harvest day. [d]w_p and w_m, average mass percentages of peel and mesocarp, respectively, for n = 5 fresh fruits 1 day after harvest. [e]$c_{AR,m}$ and $c_{AR,fm}$, AR content of the mesocarp per dry weight (DW) and per fresh weight (FW), respectively. The grand mean ± standard deviation (±confidence interval, $P \leq 0.05$) was 1.0 ± 0.3 mg hg^{-1} DW (±0.2 mg hg^{-1}) for $c_{AR,m}$ of the 11 variants and 0.18 ± 0.06 mg hg^{-1} FW (±0.04 mg hg^{-1}) for their $c_{AR,fm}$. [f]$c_{AR,p}$, AR content of the peel per dry weight, including the group means with standard deviation (SD) and confidence interval ($P \leq 0.05$) (95% CI) for the variant groups N1–N2 and N3–N5 comprising n = 4 and 7 variants, respectively.

dx.doi.org/10.1021/jf4028552 | J. Agric. Food Chem. 2014, 62, 28–40

Table 3. 'Chok Anan' Mango Fruits (Variants C1*A*–C5*C*)[a] Harvested after Different Maturation Times on the Tree (Days after Full Bloom, DAFB): Fruit Size, Peel and Mesocarp Portions of the Fresh Fruit, as well as the Total Alk(en)ylresorcinol (AR) Contents of the Peel and Mesocarp, Respectively, 1 Day after Harvest

harvest day/batch no.:	C1		C2			C3			C4		C5	
DAFB:	83		89			95			101		107	
category:	*A*	*B*	*A*	*B*	*C*	*A*	*B*	*C*	*B*	*C*	*B*	*C*
fruit variant:	C1*A*	C1*B*	C2*A*	C2*B*	C2*C*	C3*A*	C3*B*	C3*C*	C4*B*	C4*C*	C5*B*	C5*C*
dry matter, DM (g hg^{-1}) [31]	16.6	15.5	18.7	15.5	18.7	22.4	18.6	21.9	23.0	19.9	18.6	21.9
fruit size (fresh mass), *m* (g)[b,c]	179 ± 3 f	283 ± 5 a	200 ± 5 e	239 ± 5 d	244 ± 5 cd	241 ± 8 d	260 ± 7 bc	273 ± 8 ab	238 ± 5 d	270 ± 5 ab	244 ± 7 cd	277 ± 6 ab
pulp and peel portions of the fresh fruit[b,d]												
mesocarp: w_m (g hg^{-1} fruit)	75.8 ± 0.7 e	76.5 ± 0.5 de	77.1 ± 0.5 cde	79.8 ± 1.4 bc	79.0 ± 1.4 bcd	77.4 ± 0.9 cde	80.7 ± 0.7 ab	82.6 ± 0.9 a	78.4 ± 0.7 bcde	78.3 ± 0.7 bcde	78.5 ± 1.2 bcde	77.2 ± 0.9 cde
peel: w_p (g hg^{-1} fruit)	14.2 ± 0.2 a	13.6 ± 0.3 ab	12.4 ± 0.6 bc	12.2 ± 0.7 bc	13.3 ± 0.6 ab	11.2 ± 0.1 cd	10.0 ± 0.4 de	9.4 ± 0.5 e	12.2 ± 0.3 bc	12.4 ± 0.5 bc	12.3 ± 0.5 bc	12.7 ± 0.5 b
total alk(en)ylresorcinol contents of the mesocarp[b,e]												
$c_{AR,m}$ (mg hg^{-1} DW)	5.5 ± 0.1 d	7.6 ± 0.3 bc	5.5 ± 0.02 d	7.8 ± 0.1 ab	7.8 ± 0.5 ab	9.0 ± 0.5 ab	5.7 ± 0.2 cd	8.9 ± 0.4 ab	9.8 ± 0.5 a	9.8 ± 0.3 a	7.2 ± 0.1 bcd	5.7 ± 0.7 cd
$c_{AR,fm}$ (mg hg^{-1} FW)	0.9	1.2	1.0	1.2	1.5	2.0	1.1	1.9	2.3	1.9	1.3	1.2
total alk(en)ylresorcinol contents of the peel[f]												
$c_{AR,p}$ (mg hg^{-1} DW)[b]	74.5 ± 0.3 bc	74.7 ± 1.6 bc	67.1 ± 2.3 cde	73.4 ± 4.6 bcd	61.3 ± 2.3 def	84.1 ± 2.9 ab	74.3 ± 1.9 bc	88.4 ± 0.8 a	88.0 ± 2.8 a	69.3 ± 1.4 cde	50.6 ± 1.4 f	58.4 ± 1.9 ef
$c_{AR,p}$ group mean ± SD (±95% CI) (mg hg^{-1} DW)	group C1–C4 (n = 10): 75.5 ± 8.9 (±6.4)										group C5 (n = 2): 54.5 ± 5.5 (±49.1)	

[a]The fruits of the batches C1–C5 were harvested on five different days between 83 and 107 DAFB and sorted into the categories *A*–*C* according to their peel color to obtain the 12 fruit variants C1*A*–C5*C* (Figure 1B) having the previously reported dry matter contents (DM) in the mesocarp.[31] [b]Mean ± standard error. Values with different letters horizontally (a–f) were significantly different ($P \leq 0.05$) due to maturity (harvest time and category). [c]*m*, mean of the fresh masses of 57–100 fruits that were weighed (±0.01) per variant on the harvest day. [d]w_p and w_m, average mass percentages of peel and mesocarp, respectively, for n = 5 fresh fruits 1 day after harvest. [e]$c_{AR,m}$ and $c_{AR,fm}$, AR content of the mesocarp per dry weight (DW) and per fresh weight (FW), respectively. The grand mean ± standard deviation (±confidence interval, $P \leq 0.05$) was 7.5 ± 1.6 mg hg^{-1} DW (±1.0 mg hg^{-1}) for $c_{AR,m}$ of the 12 variants and 1.5 ± 0.5 mg hg^{-1} FW (±0.3 mg hg^{-1}) for their $c_{AR,fm}$. [f]$c_{AR,p}$, AR content of the peel per dry weight, including the group means with standard deviation (SD) and confidence interval ($P \leq 0.05$) (95% CI) for the variant groups C1–C4 and C5 comprising n = 10 and 2 variants, respectively.

dx.doi.org/10.1021/jf4028552 | J. Agric. Food Chem. 2014, 62, 28–40

Table 4. Harvest Maturity Index (HMI)[a] Indicating the Maturity of 'Nam Dokmai #4' Mango Fruits (Variants N1*A*−N5*C*, Figure 1A) 1 Day after Harvest According to the Previously Reported Results[32] of Principal Component Analysis for Principal Component 1 (PC1)[b]

harvest day/batch no.:	N1		N2		N3			N4		N5	
days after full bloom (DAFB):	91		97		103			109		115	
category:	*A*	*B*	*A*	*B*	*A*	*B*	*C*	*B*	*C*	*B*	*C*
fruit variant:	N1*A*	N1*B*	N2*A*	N2*B*	N3*A*	N3*B*	N3*C*	N4*B*	N4*C*	N5*B*	N5*C*
TA (g hg^{-1})[32c]	1.09	1.09	0.65	0.55	0.87	0.81	0.65	0.71	0.71	0.62	0.56
PC1 score ($S_{PC1,N}$)[32c]	2.96	4.74	−0.03	−2.21	0.54	0.81	−0.71	−0.25	−1.93	−1.73	−2.18
HMI (= $-S_{PC1,N}$ + 10)	7.0	5.3	10.0	12.2	9.5	9.2	10.7	10.3	11.9	11.7	12.2

[a]Similar HMI values indicated similar maturity stages among the 11 variants specified in Table 2. The variants comprising the most mature fruits 1 day after harvest were identified by the maximal HMI. [b]PC1 accounting for 54.6% of the variance represented the maturity on the first day (14 °C) after harvest by combining the contributions of the following mesocarp attributes *x* (Pearson correlation coefficients between PC1 and *x* in parentheses; $P \leq 0.05$, *; $P \leq 0.01$, **; $P \leq 0.001$, ***; $P \leq 0.0001$, ****):[32] contents of titratable acids (0.94****), chlorophyll *b* (0.85**), total soluble solids (−0.79**), dry matter (−0.77**), chlorophyll *a* (0.67*), and all-*trans*-*β*-carotene (−0.63*), as well as mesocarp firmness (0.28) and mesocarp color, the latter in terms of the CIE hue angle (0.89***) and chroma (−0.60*). [c]For the most relevant attribute (TA, mesocarp contents of titratable acids) and for the PC1 scores ($S_{PC1,N}$) converted into the HMI, the values stated earlier[32] are indicated.

Table 5. Harvest Maturity Index (HMI)[a] Indicating the Maturity of 'Chok Anan' Mango Fruits (Variants C1*A*−C5*C*, Figure 1B) 1 Day after Harvest According to the Previously Reported Results[31] of Principal Component Analysis for Principal Component 1 (PC1)[b]

harvest day/batch no.:	C1		C2			C3			C4		C5	
days after full bloom (DAFB):	83		89			95			101		107	
category:	*A*	*B*	*A*	*B*	*C*	*A*	*B*	*C*	*B*	*C*	*B*	*C*
fruit variant:	C1*A*	C1*B*	C2*A*	C2*B*	C2*C*	C3*A*	C3*B*	C3*C*	C4*B*	C4*C*	C5*B*	C5*C*
TA (g hg^{-1})[31c]	0.70	0.90	0.64	0.62	0.49	0.47	0.50	0.52	0.52	0.39	0.48	0.39
PC1 score ($S_{PC1,C}$)[31c]	−2.12	−3.57	−1.32	−1.96	0.34	0.64	−0.58	1.34	1.20	2.04	1.03	2.97
HMI (= $S_{PC1,C}$ + 10)	7.9	6.4	8.7	8.0	10.3	10.6	9.4	11.3	11.2	12.0	11.0	13.0

[a]Similar HMI values indicated similar maturity stages among the 12 variants specified in Table 3. The variants comprising the most mature fruits 1 day after harvest were identified by the maximal HMI. [b]PC1 accounting for 41.4% of the variance represented the maturity on the first day (14 °C) after harvest by combining the contributions of the following mesocarp attributes *x* (Pearson correlation coefficients between PC1 and *x* in parentheses; $P \leq 0.05$, *; $P \leq 0.01$, **; $P \leq 0.001$, ***; $P \leq 0.0001$, ****):[31] contents of titratable acids (−0.92****), dry matter (0.83***), all-*trans*-*β*-carotene (0.62*), chlorophyll *b* (−0.47), chlorophyll *a* (−0.15), and total soluble solids (0.14), as well as mesocarp firmness (−0.47) and mesocarp color, the latter in terms of the yellow (b^*_m; 0.88***) and green (a^*_m; 0.74**) CIE values. [c]For the most relevant attribute (TA, mesocarp contents of titratable acids) and for the PC1 scores ($S_{PC1,C}$) converted into the HMI, the values stated earlier[31] are indicated.

possible impact on the alk(en)ylresorcinol contents. As detailed earlier,[31,32] the 11 'Nam Dokmai #4' and the 12 'Chok Anan' variants had been examined regarding similar maturity stages 1 day after harvest by principal component analysis (PCA) on the basis of characteristic pulp attributes (cf. footnotes of Tables 4 and 5). The effect of the maturity stage at this point was represented by the first principal component (PC1).[31,32] The content of titratable acids (TA) always contributed most to PC1, while low TA levels indicated advanced stages of maturity (Tables 4 and 5).[31,32] Whereas DM and the fruit mass were useful to estimate the point of full physiological maturity (Tables 2 and 3), TA and other pulp attributes had turned out to be even more relevant to distinguish the maturity stages 1 day after harvest by PC1 (Tables 4 and 5).[31,32] Because the PC1 score of a fruit variant ($S_{PC1,N}$ for 'Nam Dokmai #4'; $S_{PC1,C}$ for 'Chok Anan') thus characterized the maturity stage of that variant best,[31,32] it was converted into a cultivar-specific harvest maturity index (HMI) > 0 (Tables 4 and 5) to compare the variants of each cultivar more conveniently.

As already suggested by the TA contents that greatly varied within ranges of 0.55−1.09 g hg^{-1} for 'Nam Dokmai #4' (Table 4) and 0.39−0.9 g hg^{-1} for 'Chok Anan' (Table 5), the 11−12 variants of each cultivar had proven to differ widely in their maturity stages 1 day after harvest.[31,32] For each cultivar, the HMI roughly doubled from the least mature to the most mature variant (Tables 4 and 5). Due to the uneven development of the fruits, the variants, which corresponded to different categories *A*−*C* on a particular harvest day, differed in their maturity stages, especially in the case of 'Chok Anan'. However, all variants that were harvested after they had reached full maturity (N2−N5, 97−115 DAFB; C3−C5, 95−107 DAFB) displayed quite similar HMI levels (≥73% of the maximal HMI).

Most importantly, the variants of the above "post-UCH" groups with reduced alk(en)ylresorcinol contents of the peel (N3−N5, Table 2; C5, Table 3) and the fully mature N2 and C4 variants that were harvested just before the $c_{AR,p}$ drop had almost identical HMI values. Moreover, the marked changes of the mesocarp,[31,32] which were expressed by the increasing HMI (Tables 4 and 5), had no impact on the overall constant alk(en)ylresorcinol contents of the pulp ($c_{AR,m}$, Tables 2 and 3). The alk(en)ylresorcinol contents were thus independent of the mesocarp changes[31,32] that were associated with the maturation on the tree according to the fruit analyses 1 day after harvest. As discussed above, the two $c_{AR,p}$ classes of each cultivar on day 1 rather suggested an effect of the harvest time, which appeared to be related to the point of completed seed development.

Despite the great quantitative AR differences between the two cultivars, the fruits always displayed similar ratios of peel mass to mesocarp mass (Tables 2 and 3). Consequently, $c_{AR,p}$ was not influenced by the peel percentage of the fruit. The peel uniformly constituted 11.2 ± 1.4 and 12.2 ± 1.4 g hg^{-1} of the fruit mass for 'Nam Dokmai #4' and 'Chok Anan', respectively

dx.doi.org/10.1021/jf4028552 | J. Agric. Food Chem. 2014, 62, 28−40

(Tables 2 and 3), regardless of the on-tree maturation time and the maturity stage 1 day after harvest. It has to be taken into account that the peel consists of the fruit skin and adhering pulp. Together with the layer of the main vascular bundles, mesocarp firmness thus affects the peel thickness, which is chiefly defined by the ability of being peeled easily. The uniform peel percentages were consistent with the firmness that was reported earlier for the mesocarp of the fruit 1 day after harvest.[31,32] It also varied only slightly among all the variants of each cultivar, although the most mature variants N5*C* and C5*C* always proved to be the softest fruits within the narrow firmness ranges.[31,32]

Alk(en)ylresorcinol Contents Observed during Low-Temperature Fruit Storage. The findings of Droby et al.[5] regarding an AR drop from fungitoxic to nontoxic levels at adequate fruit ripeness after postharvest ripening may suggest that refrigeration can improve the AR retention during long-distance transports due to minimized respiration and ripening. In the cited study,[5] the total AR contents of the peel ($C_{17:1}$, $C_{15:0}$) insignificantly varied around 202 ± 13 μg g^{-1} of FW (~101 ± 6.5 mg hg^{-1} of DW, assuming 20% DM) within a period of 55 days before and 12 days after harvest for 'Tommy Atkins' fruit, which had been inoculated with *A. alternata* spores after picking. The authors noted a dramatic development of black spot symptoms at the ripe stage after 17 days, when the total alk(en)ylresorcinol content of the peel dropped by 50% to 103 μg g^{-1} of FW (~52 mg hg^{-1} of DW).[5] Alk(en)ylresorcinol contents in the latter order of magnitude were also shown by the 'Chok Anan' variants picked last (C5*B*/*C*, Table 3), but already 1 day after harvest. For noninoculated fruit of different varieties, Droby et al.[5] found 154−232 μg g^{-1} of FW (~77−116 mg hg^{-1} of DW) in the peel at the green-mature stage at harvest, but only 74−125 μg g^{-1} of FW (~37−63 mg hg^{-1} of DW) at the ripe stage, when disease symptoms developed in inoculated fruit after postharvest ripening. Such low alk(en)ylresorcinol levels (76 μg g^{-1} of FW) were also shown by the peel of ripe 'Tommy Atkins' fruit after ripening on the tree.[5] Hassan et al.[9] observed a significant postharvest drop of the predominant 5-*n*-heptadecenylresorcinol only between the "harvest" and the "sprung" stages.

By contrast, the 11 'Nam Dokmai #4' and 12 'Chok Anan' variants were not exposed to ripening conditions after the harvest, but stored at 14 °C (Figure 1) to test the above hypothesis by mimicking basic conditions of long supply chains. However, the application of ethylene absorbers and the minimum temperature, which was also tolerated by green-mature fruit without chilling injury, did not preclude slow ripening during storage, even though the ripening rates differed among the variants, as detailed earlier.[31,32] Accordingly, the TA contents always declined significantly, in addition to parallel softening and an increase in the total soluble solids (TSS), all-*trans*-β-carotene, and mesocarp yellowness (b^*_m).[31,32] As previously shown by multivariate analyses for each cultivar,[31,32] the quality that was reached by a few of the variants after a short time (e.g., N5*B*/*C* after 10 ± 1 days)[32] was also shown by others after longer storage (e.g., N2*A*/*B* after 18 ± 1 days).[32] The ripening rate of each variant could be described by the characteristic development of well-established ripeness indicators,[31,32] such as the disproportionately rising sugar/acid ratio (TSS/TA) and the postharvest ripeness index (RPI_{KS}),[43] which declines linearly after a possible lag phase. These two variables are compiled in the Supporting Information for the 'Nam Dokmai #4' (Table S1) and the 'Chok Anan' (Table S2) variants to compare the AR contents found after different storage times with the particular ripeness of each sample. A total increase of TSS/TA from 9 to 380 for 'Nam Dokmai #4' within 18 ± 1 days and from 11 to 259 for 'Chok Anan' within 27 days, while the RPI_{KS} overall declined from 11 to 3.4 and 4.3, respectively, indicated marked changes in ripeness.[31,32] In total, the 33 'Nam Dokmai #4' and 48 'Chok Anan' lots of all the sampling days represented a great number of different ripeness stages (Tables S1 and S2).

Unacceptably high TSS/TA ratios ≥102 indicated over-ripeness or decay on day 18 ± 1 for N3*B*/*C* and all N4−N5 variants (Table S1), which were previously deemed to be semi-fast-ripening and fast-ripening, respectively, and together constituted >50% of the 'Nam Dokmai #4' variants.[32] After this storage time, microbial spoilage of individual fruits had been observed among those variants.[32] For this cultivar, postharvest storage with parallel AR analysis was thus only feasible until that time. For 'Chok Anan', the variants comprising fruit of category *C* showed this fast-ripening behavior (C2/3/4/5*C*, Table S2), whereas over-ripeness and notable decay of individual fruits were noted on day 27 for all 12 variants.[31] However, the variants that were harvested as soon as their pulp had adopted predefined values for a range of key attributes just before UCH ripened only moderately during storage[31,32] and thus proved to be most suitable for long supply chains. These were the two 'Chok Anan' variants C2*A* and C2*B* that were picked 89 DAFB (Table 3) at a stage of mesocarp attributes,[31] which corresponded to a HMI of ~8−9 (Table 5). For 'Nam Dokmai #4', such storage behavior was shown by N2*A* and N2*B*[32] that were harvested 97 DAFB (Table 2). The storage behavior of this cultivar depended on the on-tree maturation time rather than on the HMI-related pulp properties.[32] One day after harvest, the variants N2*A* and N2*B* even had HMI levels (~10−12) in the upper range (Table 4).

Despite the great changes in fruit ripeness, the total AR contents of peel ($c_{AR,p}$) and mesocarp ($c_{AR,m}$) always varied within ranges, which were already found 1 day after harvest (Tables S1 and S2). They were not correlated with the ripeness indicators. The Pearson correlation coefficients between $c_{AR,p}$ and RPI_{KS}, for example, were only 0.23 for 'Nam Dokmai #4' (n = 33) and −0.15 for 'Chok Anan'(n = 48).

For the aforesaid "until-UCH" group of 'Nam Dokmai #4' (N1−N2), the elevated mean AR content of the peel 1 day after harvest (9.4 ± 2.2 mg hg^{-1} of DW, Table 2) significantly fell by 38% during storage to an average level of 5.8 ± 0.9 mg hg^{-1} for the days 10−18 ($P \leq 0.05$). This decline seemed to correspond to the AR drop by 50% that was mentioned above for 'Tommy Atkins' peel after 12 days of ripening at 20 °C.[5] After 10−18 days, the four N1−N2 variants thus showed the same mean $c_{AR,p}$ level that was found for the seven variants of the "post-UCH" group (N3−N5) both 1 day after harvest (5.8 ± 1.3 mg hg^{-1}, Table 2) and throughout storage (6.2 ± 1.2 mg hg^{-1} for days 10−18), despite the deviant behavior of variant N4*B* (Table S1). However, the apparent outlier N4*B* implied that $c_{AR,p}$ of 'Nam Dokmai #4' peel actually varied around a grand mean of 6.4 ± 0.7 mg hg^{-1} ($P \leq 0.05$) within the total postharvest storage time (Table 6). In the large "until-UCH" group of 'Chok Anan' (C1−C4) comprising 10 variants, the elevated $c_{AR,p}$ mean 1 day after harvest (76 ± 6.4 mg hg^{-1} of DW, Table 3) did not change during storage (73 ± 6.2 mg hg^{-1} for days 9−27). The $c_{AR,p}$ means of the two "post-UCH" variants C5*B*/*C* after 1 (55 ± 49 mg hg^{-1}, Table 3) and 9−27 days (74 ± 18 mg hg^{-1}) were not distinguishable from each other in view of the small number of variants in this group.

dx.doi.org/10.1021/jf4028552 | J. Agric. Food Chem. 2014, 62, 28−40

Table 6. Average Total Alk(en)ylresorcinol Contents[a] of Peel ($c_{AR,p}$) and Mesocarp ($c_{AR,m}$) throughout Storage (14 °C) of 'Nam Dokmai #4' and 'Chok Anan' Mango Fruits

	'Nam Dokmai #4' (variants N1A–N5C on days 1–18 ± 1 of storage; n = 33 samples)[b]					'Chok Anan' (variants C1A–C5C on days 1–27 of storage; n = 48 samples)[b]				
	mean	SD[c]	95% CI[d]	minimum	maximum	mean	SD[c]	95% CI[d]	minimum	maximum
peel: $c_{AR,p}$ (mg hg^{-1} DW)	6.4	2.0	0.7	2.8	11.4	72.9	15.4	4.5	44.9	109.6
mesocarp: $c_{AR,m}$ (mg hg^{-1} DW)	0.9	0.4	0.1	0.4	1.7	6.7	2.6	0.7	2.2	12.8

[a]Contents in mg hg^{-1} of dry weight (DW). [b]For the data of the individual samples, cf. the Supporting Information. [c]SD, standard deviation. [d]95% CI, confidence interval ($P \leq 0.05$).

Table 7. Alk(en)ylresorcinol Patterns[a] of Peel and Mesocarp throughout Storage (14 °C) of 'Nam Dokmai #4' and 'Chok Anan' Mango Fruits

	'Nam Dokmai #4' (variants N1A–N5C on days 1–18 ± 1 of storage; n = 33 samples)[b]					'Chok Anan' (variants C1A–C5C on days 1–27 of storage; n = 48 samples)[b]				
	mean	SD[c]	95% CI[c]	minimum	maximum	mean	SD[c]	95% CI[c]	minimum	maximum
homologues in the peel (%)										
$C_{17:1}$ **5**	56.4	2.1	0.8	50.3	61.6	54.4	1.0	0.3	51.8	56.5
$C_{17:2}$ **3**	29.8	1.5	0.5	26.2	32.3	28.9	0.5	0.2	27.5	30.0
$C_{15:0}$ **4**	8.0	0.8	0.3	6.8	10.7	11.0	0.9	0.3	9.7	13.1
Σ major compounds	94.3					94.3				
	(6.0 ± 0.7 mg hg^{-1} DW)[d]					(68.7 ± 4.2 mg hg^{-1} DW)[d]				
$C_{19:1}$ **8**	3.5	2.5	0.9	tr	11.4	0.9	0.2	0.1	0.5	1.6
$C_{17:3}$ **1**	2.2	1.3	0.5	tr	5.8	2.9	0.2	0.1	2.4	3.4
$C_{15:1}$ **2**	tr[e]					1.0	0.1	0.02	0.8	1.2
$C_{17:0}$ **7**	tr					0.5	0.1	0.03	0.2	0.7
$C_{19:2}$ **6**	tr					0.5	0.1	0.03	0.2	0.7
Σ minor compounds	5.7					5.7				
	(0.4 ± 0.1 mg hg^{-1} DW)[d]					(4.2 ± 0.3 mg hg^{-1} DW)[d]				
homologues in the mesocarp[f] (%)										
$C_{17:1}$ **5**	67.2	3.6	1.3	62.5	80.8	60.8	1.5	0.4	56.4	63.5
$C_{17:2}$ **3**	32.8	3.6	1.3	19.2	37.5	29.3	0.9	0.3	26.7	31.3
$C_{15:0}$ **4**	tr					9.9	1.7	0.5	7.5	15.2

[a]Alk(en)ylresorcinol homologues **1**–**8** (cf. Table 1 and Figure 2) in % of the total content in peel and mesocarp respectively. [b]For the data of the individual samples, cf. the Supporting Information. [c]SD, standard deviation; 95% CI, confidence interval ($P \leq 0.05$). [d]Mean content ± 95% CI (DW, dry weight). [e]tr, traces. [f]In the mango mesocarp, only traces of the minor compounds were found (Figure 2).

On the whole, it proved debatable whether the harvest time (Tables 2 and 3) and the ripeness stage[5,9] have causal effects on the postharvest alk(en)ylresorcinol levels in the peel during the low-temperature storage. Even for the peel of over-ripe 'Chok Anan' fruits, no postharvest drop of $c_{AR,p}$ to non-fungicidal levels[1,5] was observed. The findings rather suggested a variation of $c_{AR,p}$ around a grand mean of 73 ± 4.5 mg hg^{-1} ($P \leq 0.05$) for 'Chok Anan' peel between harvest and day 27 of storage (Table 6).

Concurrently, the alk(en)ylresorcinol levels in the mesocarp of this cultivar ranged around 6.7 ± 0.7 mg hg^{-1} of DW (Table 6), regardless of the harvest time or the period of low-temperature storage. The analogous average content of 'Nam Dokmai #4' mesocarp (0.9 ± 0.1 mg hg^{-1} of DW, Table 6) confirmed an earlier report for 'Nam Dokmai' pulp (0.496 mg hg^{-1}).[26] Although the peel was richer in AR, there was no stage at which 'Nam Dokmai #4' peel reached the alk(en)ylresorcinol levels that had been deemed fungitoxic.[5]

Cultivar-Specific Alk(en)ylresorcinol Profiles. The alk(en)ylresorcinol pattern that was found 1 day after harvest for all variants per cultivar remained unchanged during storage (Tables S1 and S2 of the Supporting Information). On average, the homologue profile in 'Chok Anan' peel thus comprised 54% $C_{17:1}$, 29% $C_{17:2}$, 11% $C_{15:0}$, 2.9% $C_{17:3}$, 1.0% $C_{15:1}$, 0.9% $C_{19:1}$, 0.5% $C_{17:0}$, and 0.5% $C_{19:2}$ (Table 7). Consistent with the ~11 times lower $c_{AR,p}$ mean of 'Nam Dokmai #4' peel compared to that of 'Chok Anan' peel (Table 6), the number of quantifiable compounds (**1**, **3**–**5**, and **8**; Table 1) was also smaller. The portions of the homologues $C_{17:1}$ (56%), $C_{17:2}$ (30%), $C_{15:0}$ (8.0%), $C_{19:1}$ (3.5%), and $C_{17:3}$ (2.2%) (Table 7) were similar to those stated earlier for the peel of this cultivar,[26] except for the compounds $C_{15:1}$ (**2**), $C_{17:0}$ (**7**), and $C_{19:2}$ (**6**), which could not be quantitated in the present study (Figure 2B). The three major homologues ($C_{17:1}$, $C_{17:2}$, and $C_{15:0}$) uniformly constituted 94.3% of the AR amount in the peel for each cultivar (Table 7). Their peel AR patterns differed most in the portion of compound **8** ($C_{19:1}$), which was the prevailing minor homologue in 'Nam Dokmai #4' peel (Table 7).

On the whole, the relative homologue composition in the peel was comparable to the profiles of several other cultivars,[26] chiefly in terms of the major compounds that were considered exclusively in some studies.[5,9,24] Accordingly, the variety had little influence. Solely for some Chinese cultivars, the $C_{17:2}$ portions slightly exceeded those of $C_{17:1}$, which was otherwise prevailing.[26] However, the location and seasonal conditions of cultivation and postharvest procedures such as desapping had turned out to be further influencing factors.[9,10] Nonetheless, the large number of data in the Supporting Information, which are summarized in Table 7, showed that the alk(en)ylresorcinol profile was independent of the maturity stage.

dx.doi.org/10.1021/jf4028552 | J. Agric. Food Chem. 2014, 62, 28–40

In the 'Chok Anan' pulp, the relative portions of the alk(en)ylresorcinol homologues $C_{17:2}$ (29%) and $C_{15:0}$ (9.9%) were almost equal to the respective percentages in the peel (Table 7). Only the $C_{17:1}$ portions of the mesocarp AR (61% for 'Chok Anan', 67% for 'Nam Dokmai #4') exceeded those of the peel (54 and 56%, respectively) because the latter were lower in favor of the quantifiable minor compounds.

Relevance of the Alk(en)ylresorcinol Contents for the Mango Defense System. The high similarity of the AR profiles among the cultivars, especially regarding the major homologues (Table 7), was consistent with the concept of a mango-specific defense system.[12,26] Differences chiefly existed in the average alk(en)ylresorcinol levels (Table 6) and in the profiles of minor compounds (Table 7), but both cultivars had equal mass percentages of peel (Tables 2 and 3). The variety showing an overall higher susceptibility to ripening and decay during low-temperature storage[32] had extremely low alk(en)ylresorcinol contents (Table 6).

The strikingly narrow ranges within which the alk(en)ylresorcinol contents of peel and pulp varied per cultivar regardless of maturity and ripeness (Table 6) supported the assumed role of the amphiphilic AR as phytoanticipins,[11] which occur in the biphasic sap[10] of a defense system that is based on resin ducts.[12] These resin ducts act as a reservoir and routes for the fast transport of preformed defense compounds to the points of attack, where the phytoanticipins are efficacious due to transiently high local concentrations.[12] Hence, the functionality of such compounds does not require their accumulation until reaching fungitoxic contents[5] in the peel and pulp. Consistent with the prevalence of the resin ducts in the exocarp,[13,14] 7−11 times higher AR contents occurred in the peel compared to the pulp (Table 6).

Although the sap itself was not isolated and analyzed, the findings of Tables 2−7 must be ascribed to the AR of the sap that was included in the samples. This was mainly suggested by the scarce average contents in the peel and pulp of 'Nam Dokmai #4' (Table 6). As shown by Hassan et al.,[10] the alk(en)ylresorcinol content of 'Nam Dokmai' sap[10] was ∼10 times higher than in the peel of this cultivar[9] and met the fungicidal levels stated earlier for the peel of other cultivars,[5] although it was much lower compared to the sap of AR-rich varieties.[10] Due to the temporary local accumulation at the site of attack as a result of the fast sap transport via the resin ducts, the production of small amounts of defense substances is already enough.[12] According to Konno,[12] resin-duct-based defense is deemed most effective against tiny herbivores, which may be coated completely by the released sap and faced with particularly high concentrations relative to their own size. Likewise, the sap with its concentrated membrane-active AR severely irritates the skin locally,[20,22] but the pulp, containing the sap and its AR in a highly diluted form, can usually be eaten by mango-sensitive people suffering from contact dermatitis, if someone else peels the fruit.[29] Because the strongest binding to proteins had been stated for AR with C_{19} chains,[23] the notable percentage of the $C_{19:1}$ homologue among the minor AR compounds in 'Nam Dokmai #4' may slightly contribute to compensate the scarce total amounts (Tables 6 and 7) through a specific affinity to enzyme proteins.

Consistent with the mobility of the sap and possible defense-related local concentration changes, the alk(en)ylresorcinol contents of the peel ($c_{AR,p}$) were not correlated with those of the pulp ($c_{AR,m}$; Tables S1 and S2). The resin ducts in the mesocarp might have served as a reservoir. According to Joel,[13] the thickness of the layer containing 90% of the ducts in the outer portion of the peel significantly differed between resistant and susceptible cultivars, but no correlation between peel thickness and the resistance of the fruit to fruit flies or between the thickness of the peel and that of the duct layer was observed.

The significantly lower alk(en)ylresorcinol contents, which were noted 1 day after harvest within the narrow concentration range of each cultivar for the peel of the fruit picked after UCH (Tables 2 and 3) or for other peel samples after some time of postharvest ripening,[5,9] might have been caused by a gradually decreasing sap production, sinking sap mobility in the resin ducts, and/or stronger multiple attack by pathogens after UCH.[7,12,22] Kumpoun et al.[7] obtained the maximum amount of the alk(en)ylresorcinol-containing lipophilic sap fraction from 'Mahajanaka' fruit, when the latter was picked at the commercial harvest time (98−105 DAFB). When on-tree maturation was extended for up to 126 DAFB, the total amount of sap released from the harvested fruit and the lipophilic fraction declined continuously.[7]

The alk(en)ylresorcinol production appeared to be influenced by the complex interaction of various environmental factors,[9,10] which may include the UV-light-induced resistance to diseases[44] such as anthracnose.[8,10] Furthermore, the activities of various sap enzymes, including PPO and POD, were shown to change during maturation[19] and ripening.[20] However, according to the Tables S1 and S2 of the Supporting Information, maturity and ripeness had no impact on the AR amounts, which could not prevent the occurrence of anthracnose symptoms in the over-ripe fruits of each cultivar after long low-temperature storage.[31,32] Indeed, the effectiveness of the defense system at this low temperature might be different from that during usual postharvest ripening, which was covered by other AR studies.[5,9] For example, peeling-associated injury was reported to induce notable AR accumulation in the outermost flesh layers, when the peeled fruit was left at ≥15 °C, but not ≤10 °C.[6] As detailed earlier for the variants studied,[31,32] the slow ripening during storage at 14 °C until over-ripeness (Tables S1 and S2) and decay involved chlorophyll degradation to undetectable levels, but only a poor development of the pulp color and the carotenoids. Similarly, the low temperature might have delayed or prevented any changes in the sap composition during storage,[45,46] or it may have affected physical sap properties,[12] such as its flow properties.[22] Altogether, this suggests a follow-up study of the cultivar-specific appearance of the resin duct system[13] together with the parallel examination of the other sap components in addition to the AR.

In conclusion, the AR proved to be present in the peel and the pulp within narrow concentration ranges that were typical of the cultivar and the part of the fruit, but independent of maturity and ripeness. As supported by the cited findings, the observed occurrence of the AR in peel and pulp could be explained by the presence of AR in the sap portions contained therein. The previously recommended harvest just before UCH involved the best protection of the fruit during storage due to moderate ripening at low temperature,[31,32] but the natural AR reserves proved irrelevant for the storage behavior and could not prevent the decay of over-ripe fruits. In view of their activity toward membranes and proteins,[23,28] the AR thus appear to be involved in protection against anthracnose, but in a complex way together with other factors of the sap-based defense system.

■ ASSOCIATED CONTENT

Supporting Information

Two supplemental tables showing the total alk(en)ylresorcinol contents and the homologue profiles in both the peel and the mesocarp on different days of postharvest storage at 14 °C as a function of the ripeness indicators of the fruit for 'Nam Dokmai #4' (Table S1) and 'Chok Anan' mangoes (Table S2). This material is available free of charge via the Internet at http://pubs.acs.org.

■ AUTHOR INFORMATION

Corresponding Author

*(S.N.) Phone: +49(0)711 459 22317. Fax: +49(0)711 459 24110. E-mail: sybille.neidhart@uni-hohenheim.de.

Funding

As part of the Special Research Program "Sustainable Land Use and Rural Development in Mountainous Regions of Southeast Asia" (The Uplands Program), this research was funded by Deutsche Forschungsgemeinschaft (DFG), Bonn, Germany: Project SFB 564-E2.3.

Notes

The authors declare no competing financial interest.

■ ABBREVIATIONS USED

AR, alk(en)ylresorcinols; $c_{AR,m}$, AR content of the mesocarp; $c_{AR,p}$, AR content of the peel; CI, 95% confidence interval; CF, molecular weight correction factor; DAFB, days after full bloom; DM, dry matter; DW, dry weight; FW, fresh weight; HMI, harvest maturity index; PC(A), principal component (analysis); POD, peroxidase; PPO, polyphenol oxidase; RH, relative humidity; RPI_{KS}, postharvest ripeness index; $S_{PC1,N}$ and $S_{PC1,C}$, principal component 1 score of a 'Nam Dokmai #4' and a 'Chok Anan' variant, respectively; SPE, solid-phase extraction; TA, content of titratable acids; TSS, total soluble solids; TSS/TA, sugar/acid ratio; UCH, usual commercial harvest (time)

■ REFERENCES

(1) Prusky, D.; Kobiler, I.; Miyara, I.; Alkan, N. Fruit diseases. In *The Mango: Botany, Production and Uses*, 2nd ed.; Litz, R. E., Ed.; CAB International: Wallingford, UK, 2009; pp 210−230.

(2) Negi, P. S.; Saby John, K.; Prasada Rao, U. J. S. Antimicrobial activity of mango sap. *Eur. Food Res. Technol.* **2002**, *214*, 327−330.

(3) Engels, C.; Weiss, A.; Carle, R.; Schmidt, H.; Schieber, A.; Gänzle, M. G. Effects of gallotannin treatment on attachment, growth, and survival of *Escherichia coli* O157:H7 and *Listeria monocytogenes* on spinach and lettuce. *Eur. Food Res. Technol.* **2012**, *234*, 1081−1090.

(4) Cojocaru, M.; Droby, S.; Glotter, E.; Goldman, A.; Gottlieb, H. E.; Jacoby, B.; Prusky, D. 5-(12-Heptadecenyl)-resorcinol, the major component of the antifungal activity in the peel of mango fruit. *Phytochemistry* **1986**, *25*, 1093−1095.

(5) Droby, S.; Prusky, D.; Jacoby, B.; Goldman, A. Presence of antifungal compounds in the peel of mango fruits and their relation to latent infections of *Alternaria alternata*. *Physiol. Mol. Plant Pathol.* **1986**, *29*, 173−183.

(6) Droby, S.; Prusky, D.; Jacoby, B.; Goldman, A. Induction of antifungal resorcinols in flesh of unripe mango fruits and its relation of latent infection by *Alternaria alternata*. *Physiol. Mol. Plant Pathol.* **1987**, *30*, 285−292.

(7) Kumpoun, W.; Uthaibutra, J.; Boonyakiat, D. Antifungal compound content in mango latex at different maturity stages. *Acta Hortic.* **2008**, *804*, 303−308.

(8) Johnson, G. I.; Hofman, P. J. Postharvest technology and quarantine treatments. In *The Mango: Botany, Production and Uses*, 2nd ed.; Litz, R. E., Ed.; CAB International: Wallingford, UK, 2009; pp 529−605.

(9) Hassan, M. K.; Dann, E. K.; Irving, D. E.; Coates, L. M. Concentrations of constitutive alk(en)ylresorcinols in peel of commercial mango varieties and resistance to postharvest anthracnose. *Physiol. Mol. Plant Pathol.* **2007**, *71*, 158−165.

(10) Hassan, M. K.; Irving, D. E.; Dann, E. K.; Coates, L. M.; Hofman, P. J. Sap properties and alk(en)ylresorcinol concentrations in Australian-grown mangoes. *Ann. Appl. Biol.* **2009**, *154*, 419−427.

(11) Baerson, S. R.; Schröder, J.; Cook, D.; Rimando, A. M.; Pan, Z.; Dayan, F. E.; Noonan, B. P.; Duke, S. O. Alkylresorcinol biosynthesis in plants. New insights from an ancient enzyme family? *Plant Signal. Behav.* **2010**, *5*, 1286−1289.

(12) Konno, K. Plant latex and other exudates as plant defense systems: roles of various defense chemicals and proteins contained therein. *Phytochemistry* **2011**, *72*, 1510−1530.

(13) Joel, D. M. Resin ducts in the mango fruit: a defence system. *J. Exp. Bot.* **1980**, *31*, 1707−1718.

(14) Joel, D. M. The duct systems of the base and stalk of the mango fruit. *Bot. Gaz.* **1981**, *142*, 329−333.

(15) Joel, D. M.; Fahn, A. Ultrastructure of the resin ducts of *Mangifera indica* L. (Anacardiaceae). 2. Resin secretion in the primary stem ducts. *Ann. Bot.* **1980**, *46*, 779−783.

(16) Saby John, K.; Jagan Mohan Rao, L.; Bhat, S. G.; Prasada Rao, U. J. S. Characterization of aroma components of sap from different Indian mango varieties. *Phytochemistry* **1999**, *52*, 891−894.

(17) Loveys, B. R.; Robinson, S. P.; Brophy, J. J.; Chacko, E. K. Mango sapburn: components of fruit sap and their role in causing skin damage. *Aust. J. Plant Physiol.* **1992**, *19*, 449−457.

(18) Joel, D. M.; Fahn, A. Ultrastructure of the resin ducts of *Mangifera indica* L. (Anacardiaceae). 3. Secretion of the protein-polysaccharide mucilage in the fruit. *Ann. Bot.* **1980**, *46*, 785−790.

(19) Saby John, K.; Bhat, S. G.; Prasada Rao, U. J. S. Biochemical characterization of sap (latex) of a few Indian mango varieties. *Phytochemistry* **2003**, *62*, 13−19.

(20) Robinson, S. P.; Loveys, B. R.; Chacko, E. K. Polyphenol oxidase enzymes in the sap and skin of mango fruit. *Aust. J. Plant Physiol.* **1993**, *20*, 99−107.

(21) Saby John, K.; Bhat, S. G.; Prasada Rao, U. J. S. Isolation and partial characterization of phenol oxidases from *Mangifera indica* L. sap (latex). *J. Mol. Catal. B* **2011**, *68*, 30−36.

(22) Brown, B. I.; Wells, I. A.; Murray, C. F. Factors affecting the incidence and severity of mango sapburn and its control. *ASEAN Food J.* **1986**, *2*, 127−132.

(23) Kozubek, A.; Tyman, J. H. P. Bioactive phenolic lipids. In *Studies in Natural Products Chemistry*, 1st ed.; Atta-ur-Rahman, Ed.; Elsevier: Amsterdam, The Netherlands, 2005; Vol. 30, pp 111−190.

(24) Oka, K.; Saito, F.; Yasuhara, T.; Sugimoto, A. A study of cross-reactions between mango contact allergens and urushiol. *Contact Dermatitis* **2004**, *51*, 292−296.

(25) Knödler, M.; Berardini, N.; Kammerer, D. R.; Carle, R.; Schieber, A. Characterization of major and minor alk(en)ylresorcinols from mango (*Mangifera indica* L.) peels by high-performance liquid chromatography/atmospheric pressure chemical ionization mass spectrometry. *Rapid Commun. Mass Spectrom.* **2007**, *21*, 945−951.

(26) Knödler, M.; Reisenhauer, K.; Schieber, A.; Carle, R. Quantitative determination of allergenic 5-alk(en)ylresorcinols in mango (*Mangifera indica* L.) peels, pulp and fruit products by HPLC-DAD. *J. Agric. Food Chem.* **2009**, *57*, 3639−3644.

(27) Kozubek, A.; Tyman, J. H. P. Resorcinolic lipids, the natural non-isoprenoid phenolic amphiphiles and their biological activity. *Chem. Rev.* **1999**, *99*, 1−25.

(28) Knödler, M.; Conrad, J.; Wenzig, E. M.; Bauer, R.; Lacorn, M.; Carle, R.; Schieber, A. Anti-inflammatory 5-(11′*Z*-heptadecenyl)- and 5-(8′*Z*,11′*Z*-heptadecadienyl)-resorcinols from mango (*Mangifera indica* L.) peels. *Phytochemistry* **2008**, *69*, 988−993.

(29) Weinstein, S.; Bassiri-Tehrani, S.; Cohen, D. E. Allergic contact dermatitis to mango flesh. *Int. J. Dermatol.* **2004**, *43*, 195−196.

(30) Dinh, S.-Q.; Sangchote, S. Infection of *Colletotrichum gloeosporioides* on mango fruit and its resistance. *Agricultural Science Journal* **2002**, *33*, 68−70.
(31) Kienzle, S.; Sruamsiri, P.; Carle, R.; Sirisakulwat, S.; Spreer, W.; Neidhart, S. Harvest maturity specification for mango fruit (*Mangifera indica* L. 'Chok Anan') in regard to long supply chains. *Postharvest Biol. Technol.* **2011**, *61*, 41−55.
(32) Kienzle, S.; Carle, R.; Sruamsiri, P.; Sirisakulwat, S.; Spreer, W.; Neidhart, S. Harvest maturity detection for 'Nam Dokmai #4' mango fruit (*Mangifera indica* L.) in consideration of long supply chains. *Postharvest Biol. Technol.* **2012**, *72*, 64−75.
(33) Chidtragool, S.; Ketsa, S.; Bowen, J.; Ferguson, I. B.; van Doorn, W. G. Chilling injury in mango fruit peel: Cultivar differences are related to the activity of phenylalanine ammonia lyase. *Postharvest Biol. Technol.* **2011**, *62*, 59−63.
(34) Vásquez-Caicedo, A. L.; Neidhart, S.; Pathomrungsiyounggul, P.; Wiriyacharee, P.; Chattrakul, A.; Sruamsiri, P.; Manochai, P.; Bangerth, F.; Carle, R. Physical, chemical and sensory properties of 9 Thai mango cultivars and evaluation of their technological and nutritional potential. International Symposium, *"Sustaining Food Security and Managing Natural Resources in Southeast Asia: Challenges for the 21st Century"*, Jan 8−11, 2002, Chiang Mai, Thailand; https://www.uni-hohenheim.de/fileadmin/einrichtungen/sfb564/events/uplands2002/Full-Pap-S3B-3_Vasquez.pdf (accessed Dec 30, 2012).
(35) Mahayothee, B.; Neidhart, S.; Mühlbauer, W.; Carle, R. Effects of calcium carbide and 2-chloroethylphosphonic acid on fruit quality of Thai mangoes under various postharvest ripening regimes. *Eur. J. Hortic. Sci.* **2007**, *72*, 171−178.
(36) Plant Varieties Protection Division. *Plant Germplasm Database: Mango*; Ministry of Agriculture and Cooperative, Department of Agriculture: Bangkok, Thailand, 2001; Vol. 1, pp 76, 90.
(37) Chandra, A.; Rana, J.; Li, Y. Separation, identification, quantification, and method validation of anthocyanins in botanical supplement raw materials by HPLC and HPLC-MS. *J. Agric. Food Chem.* **2001**, *49*, 3515−3521.
(38) Draper, W. M.; Wijekoon, D.; McKinney, M.; Behniwal, P.; Perera, S. K.; Flessel, C. P. Atmospheric pressure ionization LV-MS-MS determination of urushiol congeners. *J. Agric. Food Chem.* **2002**, *50*, 1852−1858.
(39) Saranwong, S.; Sornsrivichai, J.; Kawano, S. Prediction of ripe-stage eating quality of mango fruit from its harvest quality measured nondestructively by near infrared spectroscopy. *Postharvest Biol. Technol.* **2004**, *31*, 137−145.
(40) Bally, I. S. E.; Harris, M. A.; Foster, S. Yield comparisons and cropping patterns of Kensington Pride mango selections. *Aust. J. Exp. Agric.* **2002**, *42*, 1009−1015.
(41) Spreer, W.; Müller, J. Estimating the mass of mango fruits (*Mangifera indica*, cv. Chok Anan) from its geometric dimensions by optical measurement. *Comput. Electron. Agric.* **2011**, *75*, 125−131.
(42) Spreer, W.; Nagle, M.; Neidhart, S.; Carle, R.; Ongprasert, S.; Müller, J. Effect of regulated deficit irrigation and partial rootzone drying on the quality of mango fruits (*Mangifera indica* L., cv. 'Chok Anan'). *Agric. Water Manage.* **2007**, *88*, 173−180.
(43) Vásquez-Caicedo, A. L.; Heller, A.; Neidhart, S.; Carle, R. Chromoplast morphology and β-carotene accumulation during postharvest ripening of mango cv. 'Tommy Atkins'. *J. Agric. Food Chem.* **2006**, *54*, 5769−5776.
(44) Wilson, C. L.; Ghaouth, A. E.; Chalutz, E.; Droby, S.; Stevens, C.; Lu, J. Y.; Khan, V.; Arul, J. Potential of induced resistance to control postharvest diseases of fruits and vegetables. *Plant Dis.* **1994**, *78*, 837−844.
(45) Lalel, H. J. D.; Singh, Z.; Tan, S. C. Ripening temperatures influence biosynthesis of aroma volatile compounds in 'Kensington Pride' mango fruit. *J. Hortic. Sci. Biotechnol.* **2004**, *79*, 146−157.
(46) Pandit, S. S.; Kulkarni, R. S.; Giri, A. P.; Köllner, T. G.; Degenhardt, J.; Gershenzon, J.; Gupta, V. S. Expression profiling of various genes during the fruit development and ripening of mango. *Plant Physiol. Biochem.* **2010**, *48*, 426−433.

JOURNAL OF AGRICULTURAL AND FOOD CHEMISTRY

Article

pubs.acs.org/JAFC

Effect of Cultivation Practices on the β-Glucan Content of *Agaricus subrufescens* Basidiocarps

Diego Cunha Zied,*[,†] Arturo Pardo Giménez,[‡] Jose Emilio Pardo González,[§] Eustáquio Souza Dias,[#] Maiara Andrade Carvalho,[#] and Marli Teixeira de Almeida Minhoni[⊥]

[†]Faculdades Integradas de Bauru (FIB), Rua Rodolfina Dias Domingues 11, Jardim Ferraz, 17056-100 Bauru, SP, Brazil

[‡]Centro de Investigación, Experimentación y Servicios del Champiñón (CIES), C/Peñicas s/n, Apartado 63, 16220 Quintanar del Rey, Cuenca, Spain

[§]Escuela Técnica Superior de Ingenieros Agrónomos, Universidad de Castilla-La Mancha (UCLM), Campus Universitario s/n, 02071 Albacete, Spain

[#]Departamento de Biologia, Universidade Federal de Lavras (UFLA), CP 3037, 37200-000 Lavras, MG, Brazil

[⊥]Faculdade de Ciências Agronômicas, Universidade Estadual Paulista (FCA/UNESP), Rua José Barbosa de Barros 1780, 18610-307 Botucatu, SP, Brazil

ABSTRACT: The present work aimed to assess the effect of the following treatments on the medicinal potential (β-glucan content) and agronomical performance (yield) of *Agaricus subrufescens*: five different fungal strains, three cultivation substrates (compost), four casing layers, and four cultivation environments. Two experiments were performed, and the results indicate that the greatest contribution to the variation in β-glucan content was the strain (35.8%), followed by the casing layer (34.5%), the cultivation environment (15.7%), and the type of compost (9.9%). On the other hand the variation in yield was affected most by the cultivation environment (82.1%), followed by the strain (81.3%), casing layer (49.1%), and compost type (15.2%). These findings underscore the importance of developing a production protocol that employs specific cultivation practices for improving mushroom yield as well as β-glucan content.

KEYWORDS: *almond mushroom, medicinal potential, strain, compost, yield*

INTRODUCTION

The incidence of cancer is gradually increasing, and more types of diseases associated with cancer are reported each year.[1] In addition to radiotherapy and chemotherapy, immunotherapy and biotherapy are also regarded as important tools for cancer treatment.[2]

Immunotherapy and biotherapy include several different approaches, such as biological response modifiers, cytosines, lymphocyte transplant, and genetic therapy, along with the use of medicinal plants and alternative medicines, such as mushrooms.[3] Clinical trials for these therapies continue to be widely performed, and there is increasing evidence to support the efficacy of these approaches; however, the underlying mechanisms remain poorly understood.[1,4,5]

Agaricus subrufescens, which is synonymous with *Agaricus blazei* ss. Heinemann and *Agaricus braziliensis*, is a basidiomycete fungus commonly referred to as "almond mushroom" or "medicinal mushroom". Its medicinal properties (namely, tumor-inhibitory activity) have been attributed to the presence of β-glucan polysaccharides.[6]

There is some controversy in the literature regarding the medicinal substances present in *A. subrufescens*. Camelini et al.[7] reported that the quality of the extracts depends on the chemical composition of the mushrooms and the β-glucan content, in particular. Other chemical components, such as steroids,[8,9] lectin,[10] and several polysaccharides,[1] have also been extensively studied.

Although the scientific community is increasingly concerned with the identification of the active substances present in mushrooms with medicinal properties, important agronomical and physiological characteristics have been overlooked. These factors are critical in production processes, and they may influence the chemical characteristics of mushrooms.

Eira[11] highlighted the importance of using samples of registered origin for experimental procedures. The same publication further described how factors such as cultivation conditions, substrate composition, and the strain used may interfere with the results. In other words, the results obtained using generic samples of unregistered origin are not conclusive. Accordingly, factors such as these should be controlled in any experiment that aims to compare the nutritional and functional properties of *A. subrufescens*.

In a study comparing the basidiocarp β-glucan contents of field and greenhouse mushrooms from Brazil and greenhouse mushrooms from Japan, Park et al.[12] observed lower β-glucan contents for *A. blazei* mushrooms grown in greenhouses (7.6 ± 2.8 g 100 g^{-1} mushroom dry weight grown in Japan and 8.4 ± 0.9 g 100 g^{-1} mushroom dry weight grown in Brazil) than for those grown in the field (10.1 ± 2.1 g 100 g^{-1} mushroom dry

Received: August 14, 2013
Revised: November 29, 2013
Accepted: December 5, 2013
Published: December 5, 2013

ACS Publications © 2013 American Chemical Society

weight). However, the authors did not indicate whether all of the basidiocarps analyzed were of the same strain.

Firenzuoli et al.[13] previously noted the lack of studies with data for specific cultivation characteristics, as well as the agronomical and physiological behavior of *A. blazei* strains used in pharmacological, biochemical, and medicinal research.

The cultivation practices used for *A. subrufescens* in Brazil derive from the practices used for *A. bisporus* production and incorporate some of the management techniques from recently published studies.[14−17] At a national and international level, there is still no cultivation protocol or guide that addresses how certain practices influence the presence of active substances in harvested mushrooms and the agronomical performance of *A. subrufescens* as well as how the cultivation of this species may be rendered viable and sustainable.

In the present study, two experiments were performed to assess how various cultivation practices (different strains, compost materials, casing layers, and cultivation environments) affect the final β-glucan content of the cultivated basidiocarps and agronomical outcomes (yield, number and weight of basidiocarps, precociousness, and time to first harvest).

MATERIALS AND METHODS

Two experiments were performed. The first experiment tested the effect of different strains and compost formulations. The strains and formulations that yielded the best results in the first experiment were subsequently used in the second experiment, which assessed the effect of different casing layers and cultivation environments.

Spawn. For the first experiment, five commercial *A. subrufescens* strains that have been deposited at the Mycotec of the Módulo de Cogumelo FCA/UNESP were used. The main characteristics of the strains are listed in Table 1. Strain ABL 99/30 was selected for the second experiment. The spawns used in both experiments were produced according to the methodology described by Zied et al.[18]

Composting (Phases I and II). The three composts used in the first experiment were produced according to the "traditional" composting method. Phase I (26 days total) consisted of 7 days of prewetting and 19 days of fermentation. The composts were turned six times. Phase II of composting lasted 9 days (8 h at 59 ± 1 °C pasteurization and 8 days at 47 ± 2 °C conditioning). The three composts were prepared simultaneously. The materials used on each compost and their chemical composition at the end of phase II are listed in Table 2. The initial C/N ratio of the compost at the moment the pile was set up was previously calculated for 33-37/1.

The compost containing sugar cane bagasse and oat straw was used for the second experiment and produced in the same manner as described for the first experiment. At the end of phase II, the chemical characteristics of the compost were as follows: 1.66% N content, 0.45% P_2O_5, 0.26% K_2O, 5.53% Ca, 0.23% Mg, 0.98% S, 65% organic matter (OM), 36.2% C, 300 mg kg^{-1} Na, 10 mg kg^{-1} Cu, 3300 mg kg^{-1} Fe, 128 mg kg^{-1} Mn, 28 mg kg^{-1} Zn, a C/N ratio of 22/1, and a pH of 6.83.

Compost Inoculation and Spawn Run. In both experiments, the respective strains were mixed with the composts after pasteurization and conditioning and were then placed into plastic boxes containing 12 kg of compost and 120 g of spawn. The composts were subsequently incubated for 21 days in the dark in a climate-controlled chamber with a compost temperature of 28 ± 1 °C, at 75 ± 5% relative humidity, and without ventilation. The spawn growth of the strains during this period was periodically monitored, and the cultures were checked for compost contamination by mold and other microorganisms.

Casing Layer. In the first experiment, a mix of soil and charcoal (4:1, v/v) was used. Calcitic lime was added for pH correction, followed by pasteurization for 12 h at 58 °C. When the mycelia were fully developed, the compost was pressed and leveled to facilitate the addition of the casing layer to a height of 5 cm. A 12.5 L volume of

Table 1. Strain Code; Collection Year, City, State, and Country; and General Characteristics of the Strains Used in the Present Study

code	collection year	collection city, state, country	general characteristics
ABL 99/28	1999	Botucatu, São Paulo, Brazil	strain deposited at the Mycotec of the Mushroom Module; characterized by its medium size, strong texture, and average to low yield
ABL 99/30	1999	Piedade, São Paulo, Brazil	commercial mushroom strain from the Atushi group; characterized by its medium to small size, strong texture, high yield and precociousness, reduced time to first harvest (±38 days), and slightly low fructification temperature (±25 °C)
ABL 03/44	2003	Lençóis Paulista, São Paulo, Brazil	commercial mushroom strain from Fazenda Santa Fé; characterized by its medium size, strong texture, reduced time to first harvest (±40 days), and average to high yield
ABL 04/49	2004	São José do Rio Preto, São Paulo, Brazil	commercial mushroom strain from the producer Goto; characterized by its medium to large size, strong texture, average to high yield, and high production temperature (±28 °C)
ABL 06/59	2006	Brasília, Federal District, Brazil	commercial mushroom strain from the Brasmicel Co.; characterized by its large size, moderate texture, high precociousness, reduced time to first harvest (±39 days), and low yield; it is highly susceptible to attacks by *Verticillium fungicola* and *Mycogone perniciosa*

dx.doi.org/10.1021/jf403584g | J. Agric. Food Chem. 2014, 62, 41−49

Table 2. Materials Used in the Formulation of Composts 1, 2, and 3 and Their Respective Chemical Characteristics at the End of Phase II of Composting[a]

	dry weight (kg)									
compost	sugar cane bagasse	oat	Massai	Aruana	soybean meal	urea	ammonium sulfate	simple superphosphate	gypsum	calcitic lime
1	141	0	130	0	9.2	2	1.5	4	15	25
2	141	130	0	0	9.2	2.5	2.4	4	15	25
3	141	0	0	131	9.2	1	1	4	15	25

	chemical characteristics														
	%								mg kg^{-1} dry matter						
compost	N	P_2O_5	K_2O	Ca	Mg	S	OM	C	Na	Cu	Fe	Mn	Zn	C/N	pH
1	1.81	1	1.09	5.15	0.48	1.36	64	35.6	440	0	500	260	20	20:1	6.25
2	1.76	0.66	1.04	5.44	0.48	1.26	68	37.8	440	0	400	160	18	21:1	7.04
3	1.6	0.64	1.31	5.20	1.68	1.40	65	36.2	1160	172	400	306	212	23:1	6.94

[a]Composts: substrates prepared with 1, sugar cane bagasse (*Saccharum officinarum*) and Massai straw (*Panicum maximum* cv. Massai); 2, sugar cane bagasse (*S. officinarum*) and oat straw (*Avena sativa*); and 3, sugar cane bagasse (*S. officinarum*) and Aruana straw (*P. maximum* cv. Aruana).

Table 3. Physicochemical Properties of the Casing Layers Used in the Present Study

	chemical characteristics[a]															
		%							mg kg^{-1} dry matter				μs cm^{-1}		WHC	
casing layer[b]	pH	OM	P	H + Al	K	Ca	Mg	SB	CEC	V	Fe	Mn	EC	g cm^{-3} De	saturated	0.006 MPa
S + CH	6.8	9	4	10	1.1	64	3	68	78	88	5	0.6	190.7	1.12	0.48	0.20
S + CF	6.7	52	19	11	1.7	135	17	154	164	94	13	2.5	492.0	0.86	0.58	0.22
S + PB	7.1	31	6	9	2.1	163	8	173	182	95	5	0.6	104.5	0.84	0.62	0.25
S + PM	7.3	45	22	10	3.2	183	10	196	206	96	10	0.8	367.8	0.81	0.72	0.26

[a]OM, organic matter; SB, sum of bases; CEC, cationic exchange capacity; EC, electrical conductivity; De, total density; WHC, water-holding capacity. [b]S, soil; CH, charcoal; CF, coconut fiber; PM, peat moss; PB, pine bark.

Table 4. Performance of Environmental Variables under the Different Cultivations

	air temperature (°C)			compost temperature (°C)			relative humidity (%)			light intensity (20000 lx)		
cultivation environment[a]	max	min	av	max	min	av	max	min	av	max	min	av
CC	30.1	16.3	25.9	29.0	17.5	25.0	100	90	97	35	35	35
GDF	41.2	16.7	24.2	30.5	17.7	21.0	100	35	60.8	23	0	11.5
GMF	46.9	17.2	27.6	33.4	18.2	24.3	100	37	54.3	1390	0	695
GTF	55.3	17.0	30.6	38.3	17.9	29.6	100	32	48.7	2990	0	1495
av	43.3	16.8	27.0	32.8	17.8	24.9	100	48.5	65.2	1110	0	560

[a]CC, climate-controlled chamber; GDF, greenhouse with Duplalon film; GMF, greenhouse with milky film; GTF, greenhouse with transparent film; av, average.

casing was added to each plastic box containing 12 kg of compost. The boxes were placed in a greenhouse (with a low-density polyethylene milky plastic film 150 μm thick; E.L.V. Leitoso, Electro Plastic, São Paulo, Brazil) with partial control of temperature, relative humidity, and aeration. During the cultivation, the air temperature ranged from 10 to 40 °C, the compost temperature ranged from 18 to 32 °C, and the relative humidity was between 35 and 100%.

In the second experiment, four casing layers were used: soil + charcoal (4:1, v/v), soil + coconut fiber (4:1, v/v), soil + composted pine bark (4:1, v/v), and soil + sphagnum peat moss. The soil used was the same as in the first experiment. Prior to the addition of the casing layer, calcitic lime was added to the soil, which was subsequently wetted and mixed with the organic materials (charcoal, coconut fiber, composted pine bark, and sphagnum peat). The main physicochemical properties of the casing layers are listed in Table 3.

After homogenization, the casing layers were pasteurized and placed over the compost as described for the first experiment. The boxes containing the four casing layers were then placed under four different cultivation environments: a climate-controlled chamber (length × width × height: 12 × 2.3 × 2.3 m) (Model Dalsem Mushrooms Container, Horst, The Netherlands); an experimental greenhouse (length × width × height: 8 × 4 × 2.5 m) with a low-density polyethylene Duplalon double-sided (black/white) plastic film 120 μm thick (E.P.B. Estufa Preto e Branco, Electro Plastic, São Paulo, Brazil); an experimental greenhouse (length × width × height: 8 × 4 × 2.5 m) with a low-density polyethylene milky plastic film 150 μm thick (E.L.V. Leitoso, Electro Plastic); and an experimental greenhouse (length × width × height: 8 × 4 × 2.5 m) with a low-density polyethylene transparent plastic film 150 μm thick (E.L.V. Difusor M36, Electro Plastic).

Primordial Induction. In the first experiment, the primordial induction occurred naturally, according to the weather conditions of the day or week. The total production time was 120 days, with some primordial growth observed after 21 days. Depending on the strain and compost used, the number of harvest flushes during cultivation ranged from two (strain ABL 99/30 inoculated on compost 1) to seven (strain ABL 03/44 inoculated on compost 3).

In the second experiment, the environmental conditions varied for each cultivation environment (compost and air temperatures, relative humidity, and light intensity). The environmental conditions during production for the different cultivation environments are listed in Table 4.

In all three greenhouse environments (Duplalon, milky, and transparent plastic film), the primordial induction occurred naturally, according to the weather conditions of the day or week. In the climate-controlled chamber, the environmental variables (temperature, relative

dx.doi.org/10.1021/jf403584g | J. Agric. Food Chem. 2014, 62, 41−49

Table 5. Agronomical Performance of *A. subrufescens* and the Basidiocarp β-Glucan Content According to the Type of Compost and Fungal Strain Used

compost[a]	strain				
	ABL 99/28	ABL 99/30	ABL 03/44	ABL 04/49	ABL 06/59
Yield (%)					
1	10.76 a AB[b]	15.34 a A	12.89 a A	11.59 a AB	2.9 a B
2	7.97 a B	20.37 a A	9.83 a B	10.09 a B	3.66 a B
3	5.45 a B	16.13 a A	9.01 a AB	10.18 a AB	1.9 a B
CV[e] (%)			64		
MSD[f]		7.46[c]		8.71[d]	
av[g] (%)			9.81		
Number of Basidiocarps (u)					
1	74.62 a AB	119.07 a A	99.08 a AB	85.53 a AB	18.51 a B
2	61.01 a B	154.92 a A	74.67 a AB	77.50 a AB	15.75 a B
3	47.87 a AB	128.71 a A	73.66 a AB	67.37 a AB	8.87 a B
CV (%)			80.47		
MSD		70.13[c]		81.86[d]	
av (u)			73.35		
Basidiocarp Weight (g)					
1	17.72 a A	18.48 a A	14.95 a A	17.62 a A	19.55 a A
2	18.02 a A	16.78 a A	19.48 a A	16.60 a A	22.25 a A
3	19.54 a A	13.91 a A	14.84 a A	18.63 a A	22.55 a A
CV (%)			37.65		
MSD		8.08[c]		9.43[d]	
av (g)			18.07		
Precociousness (%)					
1	33.32 a B	57.71 a AB	33.06 a B	46.94 a B	100 a A
2	29.69 a B	63.68 a AB	40.11 a B	37.95 a B	100 a A
3	28.89 a B	59.86 a AB	24.65 a B	57.86 a AB	98.52 a A
CV (%)			56.84		
MSD		36.37[c]		42.46[d]	
av (%)			53.85		
Time to First Harvest (Days)					
1	42.19 a A	39.60 a A	46.18 b A	47.15 a A	39.16 a A
2	40.80 a AB	36.92 a A	34.67 a A	45.26 a B	39.15 a AB
3	55.60 b B	39.54 a A	39.22 a A	44.29 a A	38.85 a A
CV (%)			10.9		
MSD		6.94[c]		8.12[d]	
av (days)			41.91		
β-Glucan (g 100 g^{-1} Mushroom Dry Weight)					
1	4.73 a A	4.63 a A	4.01 b A	5.95 a A	7.79 a A
2	3.45 a A	5.10 a A	4.86 b A	3.62 a A	6.81 a A
3	3.04 a B	5.46 a AB	9.67 a A	4.83 a AB	3.90 a B
CV (%)			44.37		
MSD		4.64[c]		5.45[d]	
av (g 100^{-1})			5.19		

[a]Composts: substrates prepared with 1, sugar cane bagasse (*Saccharum officinarum*) and Massai straw (*Panicum maximum* cv. Massai); 2, sugar cane bagasse (*S. officinarum*) and oat straw (*Avena sativa*); and 3, sugar cane bagasse (*S. officinarum*) and Aruana straw (*P. maximum* cv. Aruana). [b]Lower case letters compare results within the same column, and upper case letters compare results within the same row according to Tukey's test ($P \leq 0.05$). [c]Minimum significant difference for values within the same column (compost comparison). [d]Minimum significant difference for values within the same row (strain comparison). [e]CV, coefficient of variation. [f]MSD, minimum significant difference. [g]av, average.

humidity, and aeration) were manipulated according to the methodology described by Zied and Minhoni[19] to control the production and to obtain five flushes.

The total production time was 120 days, with some primordial growth observed after 21 days, in the climate-controlled chamber and in the greenhouses with Duplalon or milky plastic film. Depending on the casing layer and cultivation environment used, the number of harvest flushes during cultivation ranged from two (casing layer with charcoal grown in a greenhouse with Duplalon plastic film) to five (casing layer with charcoal grown in the climate-controlled chamber).

Harvest. The basidiocarps were harvested manually, followed by the scraping of the bottom of the stalk to remove casing layer residues. The analysis was subsequently performed to quantify yield, time to first harvest, precociousness, basidiocarp weight, and the number of basidiocarps.

Experimental Design. For the first experiment, a double-factorial design was used, with five *A. subrufescens* strains (ABL 99/28, 99/30, 03/44, 04/49, and 06/59) and three composts (Massai and sugar cane bagasse, oat straw and sugar cane bagasse, and Aruana straw and sugar cane bagasse) in a completely randomized design. A double-factorial design was also used for the second experiment, with four casing layers

dx.doi.org/10.1021/jf403584g | J. Agric. Food Chem. 2014, 62, 41−49

Figure 1. Yield (%) and β-glucan content (g 100 g^{-1} mushroom dry weight) for the five fungal strains, three composts, four casing layers, and four cultivation environments tested.

(soil + charcoal, soil + coconut fiber, soil + composted pine bark, and soil + sphagnum peat moss) and four cultivation environments (climate-controlled chamber, experimental greenhouse with Duplalon plastic film, experimental greenhouse with milky plastic film, and experimental greenhouse with transparent plastic film) in a completely randomized design. For both experiments, eight replicates were performed for each treatment, with each replicate consisting of a box containing 12 kg of compost.

Analyzed Variables. The following data were measured and analyzed as previously described by Pardo et al.,[20] and Zied et al.:[16] yield (basidiocarp fresh weight divided by the compost fresh weight multiplied by 100 and expressed as a percentage); the number of basidiocarps (count of the harvested basidiocarps); basidiocarp weight (basidiocarp fresh weight divided by the number of basidiocarps, expressed in grams); precociousness (yield over the first half of the total harvest time divided by the yield over the total harvest time multiplied by 100 and expressed as a percentage); and time to first harvest (number of days between casing and harvesting of the first flush). The β-glucan content of the basidiocarps was determined using the methodology of the Foundation of Japanese Food Analysis Center[21] and the modifications proposed by Prosky et al.[22] as described by Park et al.[12]

Statistical Analyses. The means of each variable analyzed were compared using Tukey's test ($p \leq 0.05$) and SAS JMP software. Sigma Stat 3.5 software was used to calculate linear correlations among the values for yield, number, and weight of basidiocarps, precociousness, time to first harvest, and basidiocarp β-glucan content.

RESULTS AND DISCUSSION

Experiment 1. The ABL 99/30 strain had the highest yield and number of mushrooms, whereas the ABL 06/59 strain had the lowest yield and number (Table 5). However, the mushrooms of the ABL 06/59 strain had greater weights (not statistically significant). One possible explanation for this finding is that yield was positively correlated with the number of basidiocarps (r = 0.993) and negatively correlated with basidiocarp weight (r = −0.742). When analyzed separately, the type of compost used had no effect on the yield or the number of mushrooms produced.

These results are in contrast with the findings of González Matute et al.,[23] who observed an effect of substrate composition on yield. The authors used sunflower seed hulls, spent compost, vermiculite compost, peat moss, and brewery waste, with C/N ratios between 40:1 and 71:1.

Although correlations between the yield and the number and weight of basidiocarps were observed, basidiocarp weight was not significantly different among the various strains or composts. The lack of statistical significance was due to the high coefficients of variation obtained for yield (64%), the number of basidiocarps (80.47%), and basidiocarp weight (37.65%).

The average values of the yield and number of basidiocarps for strains ABL 99/30, 03/44, and 04/49 were higher than the

dx.doi.org/10.1021/jf403584g | J. Agric. Food Chem. 2014, 62, 41−49

Table 6. Agronomical Performance of *A. subrufescens* and the Basidiocarp β-Glucan Content According to the Type of Casing Layer and Cultivation Environment Used

	cultivation environment			
casing layer (4:1, v/v)	climate-controlled chamber	greenhouse with Duplalon film	greenhouse with milky film	greenhouse with transparent film
		Yield (%)		
soil + charcoal	14.72 A a[a]	3.63 A b	6.10 A b	5.03 A b
soil + coconut fiber	12.71 A a	0.35 B b	0.87 C b	1.45 B b
soil + pine bark	15.37 A a	3.94 A b	4.32 BA b	5.53 A b
soil + peat moss	13.60 A a	2.00 AB b	2.11 CB b	1.04 B b
CV[d] (%)		73		
MSD[e]		3.25[b]		3.1[c]
av[f] (%)		5.7		
		Number of Basidiocarps (u)		
soil + charcoal	137.28 AB a	34.14 A b	68. 57 A b	43.66 AB b
soil + coconut fiber	174.54 A a	1.75 A b	35.85 AB b	52.14 A b
soil + pine bark	97.85 B a	37.85 A b	4.15 B b	8.65 B b
soil + peat moss	120.14 B a	21.14 A b	13.85 B b	9.20 B b
CV (%)		91.3		
MSD		43.37[b]		58.23[c]
av (u)		53.19		
		Basidiocarp Weight (g)		
soil + charcoal	13.71 A a	13.62 B a	11.61 B a	15.70 A a
soil + coconut fiber	11.77 A b	27.85 A a	16.02 B a	15.23 A ab
soil + pine bark	15.96 A b	13.33 B b	33.52 A a	24.25 A ab
soil + peat moss	14.11 A a	17.38 AB a	19.91 B a	21.74 A a
CV (%)		64.21		
MSD		13.31[b]		12.72[c]
av (g)		17.85		
		Precociousness (%)		
soil + charcoal	72.30 a A	84.29 a A	67.87 a A	65.58 a A
soil + coconut fiber	42.71 a A	71.00 a A	63.61 a A	64.36 a A
soil + pine bark	61.75 a A	93.00 a A	75.03 a A	69.73 a A
soil + peat moss	56.94 a A	68.78 a A	67.75 a A	66.21 a A
CV (%)		36.07		
MSD		36.98[b]		34.18[c]
av (%)		71.74		
		Time to First Harvest (Days)		
soil + charcoal	37.1 B a	34.7 A a	30.2 A a	33.5 A a
soil + coconut fiber	38.49 B a	40.84 A a	38.36 AB a	41.34 A a
soil + pine bark	23.4 A a	36.4 A b	42.9 B b	38.7 A b
soil + peat moss	37.6 B a	34.7 A a	34.7 AB a	41.2 A a
CV (%)		17.34		
MSD		10.54[b]		10.51[c]
av (days)		36.53		
		β-Glucan (g 100 g^{-1} Mushroom Dry Weight)		
soil + charcoal	5.17 A a	3.97 A a	3.75 A a	6.62 A a
soil + coconut fiber	2.51 A a	6.01 A a	6.65 A a	2.03 A a
soil + pine bark	4.86 A a	4.20 A a	3.68 A a	4.71 A a
soil + peat moss	9.07 A a	7.01 A a	5.37 A a	4.38 A a
CV (%)		71.28		
MSD		7.3[b]		5.2[c]
av (g 100 g^{-1})		4.99		

[a]Upper case letters compare results within the same column, and lower case letters compare results within the same row according to Tukey's test ($P \leq 0.05$). [b]Minimum significant difference for values within the same column (casing layer comparison). [c]Minimum significant difference for values within the same row (cultivation environment comparison). [d]CV, coefficient of variation. [e]MSD, minimum significant difference. [f]av, average.

overall average for all of the treatments (9.81% and 73.35 u). The average basidiocarp weight values for strains ABL 99/29 and 06/59 were higher than the overall average for all of the treatments (18.07 g).

In a study analyzing three different composts and two strains, Kopytowski Filho[24] observed no significant differences in yield for the interaction of the two factors (i.e., compost versus strain). However, when the two factors were analyzed separately, ABL 99/30 was found to have a higher yield than ABL 04/49, and the use of organic compost was found to have a higher yield than synthetic and semisynthetic composts.

dx.doi.org/10.1021/jf403584g | J. Agric. Food Chem. 2014, 62, 41−49

In the present study, strains ABL 06/59 and 99/30 had the highest values of precociousness, which were markedly higher than the overall average for all treatments (53.85%). These values indicate that for these two strains, most of the production occurred during the first 47 days of harvest following primordial formation. It should be noted that precociousness values were positively correlated with basidiocarp weight (0.835), indicating that under the tested conditions, the mushrooms produced during the first half of the cultivation cycle had higher weights.

Zied et al.,[25] studied Tifton (T)- and oat (O)-based composts and the following casing layers: acrylamide gel (gel), soil + coal (c), and soybean meal supplement (s). They reported the following precociousness values: Tgel (75%) > Oc (61%) > Ogel (58%) > Os (57%) > Ts (53%) > Tc (51%). In another study using strain ABL 04/49,[25] a higher precociousness value was obtained than that observed in the present study for the same strain cultivated with oat-based compost and soil + charcoal casing (37.95%). This discrepancy may reflect differences in the environmental conditions in a given week or month.

The shortest times until the first harvest were observed for strains ABL 99/30, 03/44, and 06/59 regardless of the type of compost used, with the following exception: the time until first harvest increased when strain ABL 03/44 was grown with Massai straw and sugar cane bagasse. The type of compost used also influenced the time to first harvest. In addition to reducing the values of yield and precociousness, the application of Aruana straw and sugar cane bagasse compost to strain ABL 99/28 increased the time to first harvest.

The basidiocarp β-glucan content was not affected by the yield, the number of basidiocarps, basidiocarp weight, precociousness, or the time to first harvest. However, the β-glucan content was affected by the strain and the type of compost used. For example, significant differences in β-glucan content were observed when strains ABL 99/30, 03/44, and 04/49 were grown with Aruana straw and sugar cane bagasse compost.

The average β-glucan content observed for the tested treatments (5.19 g 100 g^{-1} mushroom dry weight) can be used to establish an acceptable level of β-glucan in basidiocarps for export. The strain alone is responsible for 35.8% of the variation in the β-glucan values, whereas the type of compost used is responsible for 9.9% of the variation (Figure 1). Thus, the strain used is of the utmost importance, and it should be selected in accordance with the type of raw material used in the compost.

Wang et al.[26] tested six different substrate formulations for the production of *A. blazei*, with the final N contents of the compost ranging between 1.2 and 1.55%. The authors used asparagus straw, cottonseed hull, cow manure, soybean cake, and gypsum as the raw materials for the compost production and did not find any significant differences in the final polysaccharide content of the basidiocarps.[26]

Experiment 2. The highest yield values were obtained in the climate-controlled chamber (Table 6) and were not affected by the type of casing layer used (Tukey, $\leq$0.05). However, the type of casing layer had a significant effect on yield in the greenhouses with partial climate control regardless of the type of plastic film used. The more open casings (soil + charcoal and soil + composted pine bark) resulted in a higher yield.

When the different casing layers and cultivation environments were compared, a positive correlation between yield and the number of basidiocarps (r = 0.81) and a negative correlation between the number of harvested basidiocarps and respective unit weights (r = −0.695) were observed. No correlations were observed for precociousness, time to first harvest, or basidiocarp β-glucan content.

Similar results were reported by Zied et al.,[18] who observed that the number of harvested basidiocarps was negatively correlated with the water-holding capacity of the casing layer and positively correlated with the total density and porosity of the casing layer. Pardo et al.[27] reported that a porous casing layer resulted in an earlier first flush for *A. bisporus* and an increased number of mushrooms, albeit with reduced weight.

The treatments that resulted in a higher yield also resulted in a higher number of harvested basidiocarps and reduced weight. The only treatment for which this trend was not observed was the soil + pine bark casing layer in the climate-controlled chamber. In this case, a significantly higher weight was observed (Tukey's test at a 5% significance level). These findings indicate that factors such as porosity are less important in the casing layer material in a controlled environment.

The environmental variables resulted in lower yields in the greenhouses with plastic films (Table 4). Zied and Minhoni[19] previously recommended 27 ± 2 °C compost temperature, 25 ± 2 °C air temperature, and 90 ± 2% relative humidity during the initial 12 days following the addition of the casing layer and during the intervals between flushes. For primordial induction, the compost temperature should be lowered to 20 ± 2 °C, the air temperature to 18 ± 2 °C, and the relative humidity to 85 ± 2%.

No statistically significant differences in precociousness were observed, although the values observed were higher than those observed in the first experiment. Precociousness exceeded 50% during the first half of the harvest period in approximately 93% of the recorded cases (Table 6), which indicates a more concentrated cultivation during the first days of growth. This result may permit shorter cultivation cycles, especially for the following combinations: soil + charcoal/climate-controlled chamber, soil + charcoal/greenhouse with Duplalon film, soil + composted pine bark/greenhouse with Duplalon film, and soil + composted pine bark/greenhouse with milky film.

It should be noted that casing layers with higher porosity and lower water-holding capacity (soil + charcoal and soil + pine bark) have been associated with precociousness. For instance, Colauto et al.[17] observed that casing layers with high porosity (lime schist and Santa Catarina peat) had a higher biological efficiency than less porous casing layers (soil + coal and São Paulo peat).

The soil + pine bark casing layer in the climate-controlled chamber and the soil + charcoal casing layer in the greenhouse with milky film resulted in the shortest times to first harvest. The only casing layer that significantly affected the time to first harvest in relation to a particular cultivation environment was soil + pine bark under greenhouse conditions, which resulted in a later first flush.

The basidiocarp β-glucan content was not significantly affected by the type of casing layer or cultivation environment. This finding is in contrast with the results of Park et al.,[12] for a study comparing the basidiocarp β-glucan content of mushrooms grown in Brazil and Japan. They compared field-grown and greenhouse mushrooms that were produced in Brazil with mushrooms produced in greenhouses in Japan and found that *A. blazei* grown in greenhouses had lower β-glucan contents (7.6 ± 2.8 g 100 g^{-1} mushroom dry weight grown in Japan and

8.4 ± 0.9 g 100 g^{-1} mushroom dry weight grown in Brazil) than *A. blazei* grown in the field (10.1 ± 2.1 g 100 g^{-1} mushroom dry weight). The differences from the present study in terms of the β-glucan content may reflect differences in the types of compost and the strains used.

The average values of β-glucan content obtained in the present study for the tested treatments (4.99 g 100 g^{-1} mushroom dry weight) can be used to establish an acceptable level of β-glucan in basidiocarps. The casing layer and cultivation environment were responsible for 34.5 and 15.7%, respectively, of the variation in β-glucan content (Figure 1). Thus, the choice of casing layer is important for producing basidiocarps with desired physical characteristics.

Production Protocol. The spatial variability of the β-glucan content and yield as affected by the tested factors (fungal strain, compost, casing layer, and cultivation environment) are presented in Figure 1. These values may be used as indicators for the adoption of production practices and the creation of a protocol of good cultivation practices that can be used by producers wishing to export *A. subrufescens*.

The factor with the greatest contribution to the variation in β-glucan content was the strain (35.8%), followed by the casing layer (34.5%), the cultivation environment (15.7%), and the type of compost (9.9%). The variation in yield was affected most by the cultivation environment (82.1%), followed by the strain (81.3%), casing layer (49.1%), and compost type (15.2%).

The present findings indicate that standard values can be set to 5 g 100 g^{-1} mushroom dry weight for β-glucan content and 10% for yield. The following cultivation practices are also proposed:

- Strains ABL 99/30, ABL 03/44, and ABL 04/49 should be used because of their good agronomical performance and reasonable β-glucan contents.
- Compost prepared from sugar cane bagasse and wheat or Massai straw can be used by Brazilian growers. An adequate formulation of the substrate is of central importance in obtaining high yields, as balanced compost (C/N ratio of 33−37:1) minimizes variation in the yield and β-glucan content.
- The casing layer is determinant of the yield and β-glucan content of basidiocarps, which varied greatly in the present study depending on the treatments used. The casing layer should be selected according to the desired physical characteristics of the harvested basidiocarps (e.g., number and weight of basidiocarps). At the same time, the use of pine bark and charcoal as a supplement to the soil is recommended due to the low cost of these materials in Brazil (1:4, v/v).
- The cultivation environment is another determinant of yield. The large variation in yield throughout the year caused by seasonal weather changes is one of the main reasons growers abandon commercial cultivation. Cultivation in climate-controlled chambers is therefore recommended because it is not affected by variations in external environmental conditions and does not directly influence the β-glucan content of the harvested basidiocarps.

AUTHOR INFORMATION

Corresponding Author

*(D.C.Z.) Phone: + 55 14 2109-6200. Fax: + 55 14 2109-6202. E-mail: dczied@gmail.com.

Funding

We are grateful to the Foundation for Research Support of the State of Minas Gerais (FAPEMIG − CAG/BPD 00081-11) and the Foundation for Research Support of the State of São Paulo (FAPESP − 2012/15101-4) for their financial support.

Notes

The authors declare no competing financial interest.

REFERENCES

(1) Ohno, N.; Furukama, M.; Miura, N. N.; Adachi, Y.; Motoi, M.; Yadomae, T. Antitumor β-glucan from the cultured fruit body of *Agaricus blazei*. *Biol. Pharm. Bull.* **2001**, *24* (7), 820−828.

(2) Sone, S. Clinical oncology. *Ann. Oncol.* **1999**, *5*, 475−493.

(3) Suzuki, T. Soluble mannan and β-glucan inhibit the uptake of *Malassezia furfur* by human monocytic cell line, THP-1. *FEMS Immunol. Med. Micol.* **1998**, *21*, 223−230.

(4) Mohagheghpour, N.; Dawson, M.; Hobbs, P.; Judd, A.; Winant, R.; Dousman, L.; Waldeck, N.; Hokama, L.; Tuse, D.; Kos, F. Glucans as immunological adjuvants. *Adv. Exp. Med. Biol.* **1995**, *383*, 13−22.

(5) Rios-Hernandez, M.; Dos-Santos, N. J.; Cardoso, S.; Bello-Garciga, J. L.; Pedroso, M. Immunopharmacological studies of β-1,3-glucan. *Arch. Med. Res.* **1994**, *25*, 179−180.

(6) Zied, D. C.; Pardo Gonzalez, J. E.; Pardo Giménez, A.; Minhoni, M. T. A. Características generales, producción y comercialización de *Agaricus blazei* (Murrill) ss. Heinemann (*A. brasiliensis*): una nueva alternativa de cultivo de hongo en España. In *Jornadas Tecnicas del cChampiñon y Otros Hongo Cultivados en Castilla-La Mancha*; CIESC: Cuenca, Spain, 2012; pp 55−76.

(7) Camelini, C. M.; Maraschin, M.; Mendonça, M. M.; Zucco, C.; Ferreira, A. G.; Tavares, L. A. Structural characterization of β-glucans of *Agaricus Braziliensis* in different stages of fruiting body maturity and their use in nutraceutical products. *Biotechnol. Lett.* **2005**, *27*, 1295−1299.

(8) Osaki, Y.; Kato, T.; Yamamoto, K.; Okubo, J.; Miyazaki, T. Antimutagenic and bactericidal substances in the fruit body of a Basidiomycete *Agaricus blazei* Jun-17. *Yakugaku Zasshi* **1994**, *114*, 342−350.

(9) Takaku, T.; Kimura, Y.; Okuda, H. Isolation of an antitumor compound from *Agaricus blazei* Murrill and its mechanism of action. *J. Nutr.* **2001**, *131*, 1409−1413.

(10) Kawagishi, H.; Inagaki, R.; Kanao, T.; Mizuno, T.; Shimura, K.; Ito, H.; Hagiwara, T.; Nakamura, T. Fractionation and antitumor activity of the water-insoluble residue of *Agaricus blazei* fruiting bodies. *Carbohydr. Res.* **1989**, *186*, 267−273.

(11) Eira, A. F. *Cultivo do Cogumelo Medicinal Agaricus blazei (Murrill) ss. Heinemann*; Ed.a Aprenda Fácil: Viçosa, Minas Gerais, Brazil, 2003; pp 398.

(12) Park, Y. K.; Ikegaki, M.; Alencar, S. M.; Aguiar, C. L. Determinação da concentração de β-glucano em cogumelos *Agaricus blazei* Murril por método enzimático. *Cienc. Tecnol. Aliment.* **2003**, *23* (3), 312−316.

(13) Firenzuoli, F.; Gori, L.; Lombardo, G. The medicinal mushroom *Agaricus blazei* Murrill: review of literature and pharmaco-toxicological problems. *eCAM* **2007**, *5* (1), 3−15.

(14) Kopytowski Filho, J.; Minhoni, M. T. A. C/N ratio on yield of *Agaricus blazei* Murrill ss. Heinemann. *Mushroom Sci.* **2004**, *16*, 213−220.

(15) Silva, V. A.; Souza Dias, E.; Valle, R. H. P.; Silva, R.; Schwan, R. F.; Moreira, G. F. Isolamento e identificação de bactérias presentes nos solos de cobertura utilizados no cultivo do cogumelo *Agaricus blazei* Murrill. *Cienc. Agrotec.* **2007**, *31*, 1364−1373.

(16) Zied, D. C.; Minhoni, M. T. A.; Kopytowski Filho, J.; Andrade, M. C. N. Production of *Agaricus blazei* ss. Heinemann (*A. braziliensis*) on different casing layers and environments. *World J. Microbiol. Biotechnol.* **2010**, *26*, 1857−1863.

(17) Colauto, N. B.; Silveira, A. R.; Eira, A. F.; Linde, G. A. Alternative to peat for *Agaricus braziliensis* yield. *Bioresour. Technol.* **2010**, *101*, 712−716.

(18) Zied, D. C.; Minhoni, M. T. A.; Kopytowski Filho, J.; Barbosa, L.; Andrade, M. C. N. Medicinal mushroom growth as affected by non-axenic casing soil. *Pedosphere* **2011**, *21* (2), 146−153.
(19) Zied, D. C.; Minhoni, M. T. A. Influência do ambiente de cultivo na produção do cogumelo *Agaricus blazei* ss. Heinemann (*A. brasiliensis*). *Energia Agric.* **2009**, *24*, 17−36.
(20) Pardo Giménez, A.; Zied, D. C.; Pardo Gonzalez, J. E. Utilización de compost agotado de champiñón como Capa de coberturas en nuevos ciclos de producción. *Pesqui. Agropecu. Bras.* **2010**, *45*, 1164−1171.
(21) Foundation of Japanese Food Analysis Center. No 398040072-001 52-1, Yoyogi-Machi, Shibuya-Ku, Tokyo, 1980; pp 52.
(22) Prosky, L.; Asp, N. G.; Schweizer, T. F.; DeVries, J. W.; Furda, I. Determination of insoluble, soluble, and total dietary fiber in foods and food products: interlaboratory study. *J. Assoc. Off. Anal. Chem.* **1988**, *71*, 1017−1023.
(23) González Matute, R.; Figlas, D.; Curvetto, N. *Agaricus blazei* production on non-composted substrate based on sunflower seed hulls and spent oyster mushroom substrate. *World J. Microbiol. Biotechnol.* **2011**, *27* (6), 1331−1339.
(24) Kopytowski Filho, J. *Produtividade e eficiência biológica de Agaricus blazei (Murrill) Heinemann, em diferentes condições de cultivo*. Ph.D. thesis, FCA/UNESP, Botucatu, São Paulo, 2006; pp 134.
(25) Zied, D. C.; Minhoni, M. T. A.; Kopytowski Filho, J.; Arruda, D. P.; Andrade, M. C. N. Production of *Agaricus blazei* ss. Heinemann (*A. braziliensis*) in function of different casing layers and composts. *Inci* **2009**, *34*, 437−442.
(26) Wang, Q.; Li, B. B.; Li, H.; Han, J. R. Yield, dry matter and polysaccharide content of the mushroom *Agaricus blazei* produced on asparagus straw substrate. *Sci. Hortic.* **2010**, *125*, 16−18.
(27) Pardo, A.; De Juan, J. A.; Pardo, J. E. Performance of composted vine shoots as a peat alternative in casing materials for mushroom cultivation. *J. Food Agric. Environ.* **2003**, *1* (2), 209−214.

JOURNAL OF AGRICULTURAL AND FOOD CHEMISTRY

Article

pubs.acs.org/JAFC

Reduced Herbicide Leaching by in Situ Adsorption of Herbicide–Micelle Formulations to Soils

Haim Katz[†] and Yael G. Mishael*

Department of Soil and Water Sciences, The Robert H. Smith Faculty of Agriculture, Food and Environment, Hebrew University of Jerusalem, Rehovot 76100, Israel

ABSTRACT: Aiming to reduce herbicide leaching, "in situ" adsorption of herbicide–micelle formulations to soils was explored. Sulfentrazone or metolachlor were solubilized in cationic micelles, and these herbicide–micelle formulations were applied to sandy and alluvial soils. Sulfentrazone adsorption to the soils was negligible; however, its adsorption via its solubilization in micelles and their adsorption to the soil was significant and in good agreement with the Freundlich and Langmuir models. Adsorption of solubilized herbicide to the sandy soil was higher than to the alluvial soil. The low ratio between the surfactant concentration and the cation exchange capacity (CEC) of the alluvial soil brought upon micelle decomposition and reduction in herbicide adsorption. Therefore, an optimized ratio between surfactant and soil CEC was chosen to maximize herbicide retention. Even upon adding relatively low loadings of surfactant (0.075–0.3% w/w soil), herbicide leaching through the soils was significantly reduced (2–5-fold) in comparison with the commercial formulations.

KEYWORDS: *reduced leaching, slow release formulations, surfactants, sulfentrazone, metolachlor*

INTRODUCTION

Herbicides provide substantial agronomic and economic benefits. However, introducing bioactive molecules to the environment poses environmental issues including their leaching and surface migration, which may cause soil, surface, and groundwater contamination.[1,2] Furthermore, migration and leaching reduce herbicide concentration at the topsoil which reduces weed control efficacy. Herbicide leaching in the soil is governed by several factors, such as soil characteristics, chemophysical properties of herbicides, the effect of climatic conditions, and tillage methods.[1,3]

In the current study the extensive leaching of sulfentrazone and metolachlor, which have been detected in groundwater,[4−6] is addressed. Sulfentrazone (water solubility of ∼280 ppm) is an anionic herbicide (pK_a = 6.56), its mobility enhances with the increase in soil pH, and its adsorption to the soil especially at alkaline pHs is negligible.[7] Metolachlor, although nonionic, is relatively soluble in water (490 ppm),[8] and its sorption to soils is considered not high.[9]

The main approaches to reduce herbicide leaching are herbicide dose optimization, site specific weed management, and nonchemical weed control such as mechanical and thermal. Another approach widely pursued in the past few decades is developing slow release formulations,[10−33] many of which are based on organically modified clay minerals[10,12,15−17,19,24,26−35] including organoclays,[11,15,16,19,31,32,34,36] polymer–clays,[23,24,29,30,33] and micelle–clays.[20,25,28,35] Several of these formulations were tested and found to reduce leaching through soil columns; however, their preparation is inefficient since it entails large water volumes, loss of active ingredient, drying, grinding the formulation and resuspending the powdered formulations, etc.

Therefore, an alternative approach of in situ formation of organo–clay sorbents for herbicide retention, by adding the organic cations to the soil, was developed.[37−39] A few studies have reported the enhanced adsorption of herbicides (and other organic contaminants) in soils treated with surfactants.[40−42] However, these reports did not include leaching studies nor did they address herbicide solubilization in micelles, since surfactant concentrations were below the critical micelle concentration (CMC).

The phenomenon of solubilization, increasing the solubility of an insoluble or poorly soluble organic substance in a surfactant solution, has been widely studied for many decades and is well-established in different fields such as medicine, cosmetics, detergency, and environment.[43−48] For example, studies on soil remediation by "enhanced pump and treat" have addressed the issue of surfactant concentration below and above their CMC and indicated that upon formation of micelles in the solution pollutant mobility was enhanced.[49,50]

In previous studies on micelle–clay slow release formulations,[25,26,35] we demonstrated that herbicides (sulfumeturon and sulfosulfuron) adsorption to the clay is enhanced when the surfactant is adsorbed as micelles (vs monomers). In a later study we described the mechanism of sulfentrazone and metolachlor solubilization in octadecyltrimethylammonium (ODTMA) micelles and characterized the herbicide–micelle adsorption to the clay. The percent of active ingredient (sulfentrazone and metolachlor) in clay formulations based on solubilization of the active ingredient in micelles is 4-fold higher than in organo–clay formulations.[11]

These clay based formulations have been tested and found to reduce leaching through soil columns; however, their application in the field is problematic due to inefficient preparation as described above.

Received: August 20, 2013
Revised: November 25, 2013
Accepted: December 2, 2013
Published: December 2, 2013

ACS Publications © 2013 American Chemical Society

In the current study, we suggest designing herbicide−micelle−clay formulations in which the clay is not an external ingredient but rather part of the target soil. The herbicide is solubilized in micelles, the herbicide−micelle formulation is directly applied to the soil, and herbicide leaching through the soil is suppressed due to its sorption, via micelle adsorption, to the soil. The herbicide and micelles are applied to the soil at the same time, in comparison to the two step application in other reports (soil modification and then herbicide application) which is advantageous. Furthermore, an "in situ" mode increases the percent of active ingredient, and since there is no clay in the employed formulation, preparation and application in the field is simplified.

MATERIALS AND METHODS

Materials. Wyoming Na-montmorillonite (SWy-2) (cation exchange capacity, 0.76 mmol/g; surface area, 700 m^2/g) was obtained from the Source Clays Repository of the Clay Mineral Society (Columbia, MO). Octadecyltrimethylammonium bromide (ODTMA) and Triton X-100 were purchased from Sigma-Aldrich (Stenheim, Germany). Acetonitrile and water, high-performance liquid chromatography (HPLC) grade, were purchased from Merck (Darmsradt, Germany). Sulfentrazone N-[2,4-dichloro-5-[4-(difluoromethyl)-4,5-dihydro-3-methyl-5-oxo-1*H*-1,2,4-triazol-1-yl[phenyl]methane-sulfonamide technical (purity 91.3%) was received from FMC (Princeton, NJ). Boral is a commercial formulation of the ai sulfentrazon (75% ai, water dispersible granular) 480 g ai/L liquid), metolachlor 2-chloro-*N*-(6-ethyl-*o*-tolyl)-*N*-[(1*RS*)-2-methoxy-1-methylethyl] acetamide technical (purity 98.6%), and commercial metolachlor (Dual-Gold 915 g ai/L liquid), which were obtained from Agan Chemicals (Ashdod, Israel). Rehovot sandy soil[51] was collected from the faculty's experimental farm. An Alluvial soil was collected from fields located a few miles east of the faculty's experimental farm (Na'an). The soil samples were air-dried and sieved through a 2 mm screen. The soils characteristics are shown in Table 1.

Table 1. Soil Characterization

soil	sand %	silt %	clay %	pH	OM %	CEC [mequiv/100 g]
alluvial	43.3	14.9	41.8	7.6	1.05	48.5
sandy	95.5	3.3	1.2	7.5	0.2	6.0

Methods. *Preparation of Herbicide−Micelle Formulations and Micelle−Clay and Herbicide−Micelle−Clay composites for Zeta Potential Measurements.* Throughout the study, the preparation of ODTMA micelles included heating the solutions to exceed the Krafft temperature, T_K point (40 °C) and reach a clear solution. Sulfentrazone (0.75−4.2 mmol/L) was added to an ODTMA solution (2.8 mM) which was stirred for 24 h. Micelle−clay and herbicide−micelle−clay composites were prepared by adding 2 g/L montmorillonite to the micelle solution (2.8 mM ODTMA) in the presence or absence of the herbicide (2.1 mM sulfentrazone) in the solution and stirred for another 24 h.

Zeta Potential Measurements of Micelle and Herbicide−Micelle Solutions and Clay and Composite Suspensions. The samples were allowed to settle for approximately 1 h, and a few milliliters of the suspension (of the clay, micelle−clay, and herbicide−micelle−clay composites) or the solution (of micelle and herbicide−micelle solutions) from the top of the flask was measured. ξ was measured using a Zetasizer Nanosystem (Malvern Instruments, Southborough, MA), where the ξ was deduced from the mobility of the particles using the Smoluchowski equation.

Micelle Size Measurements. Micelles and mixed micelles solutions were prepared by addition of ODTMA (2.8 mM), Triton X-100 (1.5 mM), or both surfactants (2.8 mM ODTMA and 1.5 mM Triton X-100) (by weight) to a stirred Erlenmeyer flask with distilled water, overnight. Size measurements were made after sample filtration (0.2 μm) by Zetasizer Nanosystem (Malvern Instruments, Southborough, MA). The corresponding apparent hydrodynamic radii were calculated as

$$R_{app} = \frac{kT}{6\pi\eta D}$$

where k is the Boltzmann constant, T is the absolute temperature, D is the diffusion coefficient, and η is the solvent viscosity in poise. The micelle size is expressed as apparent diameter $2R_{app}$.

Adsorption−Desorption of Commercial Herbicides and Herbicides Solubilized in Micelles to Soils. Sulfentrazone (300, 600, or 900 mg/L) was solubilized in ODTMA (2.8 mM), Triton X-100 (1.5 mM), or both surfactants (2.8 mM ODTMA and 1.5 mM Triton X-100) and stirred overnight. An alluvial soil was added to the herbicide−micelle solutions, reaching 67 g/L. The tubes were kept under continuous agitation, reaching equilibrium (for 24 h). Supernatants were separated by centrifugation at 15 000*g* for 20 min, and the herbicide concentrations in supernatants were measured by HPLC (see below).

Adsorption isotherms (adding 0−12 mg sulfentrazone/g soil) on a sandy or an alluvial soil (67 g/L) of sulfentrazone (0−800 mg/L) as is or solubilized in an ODTMA solution (3.36 mM) were obtained. The experiment was conducted in Teflon centrifuge tubes which were kept under continuous agitation for 24 h. Supernatants were separated by centrifugation at 15 000*g* for 20 min, and herbicide concentrations in supernatants were measured by HPLC (see below). Herbicide desorption was measured after 24 h by resuspending the precipitate (reaching 67 g soil/L) with distilled water. Supernatants were separated after 24 h of agitation by centrifugation, and the concentration of the desorbed herbicide in the supernatant was measured by HPLC. Sample analyses were performed in triplicate.

Herbicides Release and Leaching through Thin Soil Layers. Herbicide−micelle formulations were prepared by adding 800 mg/L herbicide (sulfentrazone or metolachlor) to ODTMA solutions (3.36−12.9 mM for the sulfentrazone and 3.36 mM for the metolachlor) and stirred overnight.

The release and leaching of sulfentrazone and metolachlor from herbicide−micelle formulations and from the commercial formulations was measured by applying the formulations on a thin sandy or alluvial soil layer (200 g and approximately 2 cm) deposited on a filter paper (Whatman 1442-125) in a Buchner funnel (area of 7.85×10^{-3} m^2). A second filter paper was placed on top of the soil to ensure uniform water distribution and to minimize disruption of the soil surface. No herbicide adsorption was obtained on the filter paper. Sulfentrazone leaching was also studied from the alluvial soil after washing it (10 pore volumes) to remove the dissolved organic matter. The herbicide−micelle and commercial formulations (Boral for sulfentrazone and Dual-Gold for metolachlor) were applied as solutions at a rate of 10.2 mg ai per funnel, equivalent to 1300 g/ha. Water was applied as a control. Soil pore volume was measured. The funnels were irrigated 8−14 times with 50 mm of water (40 mL per funnel) at uniform intervals between irrigations. The leachates were collected after each irrigation, and herbicide concentrations were measured by HPLC. Each treatment was performed in triplicate.

Herbicide Analysis. Supernatants were filtered with acrodisc (polypropylene) filters (Pall Corp., MA) of 0.45 μm pore diameter. The herbicides were analyzed by HPLC (Agilent Technologies 1200 series) equipped with a diode array detector set at 254 and 225 nm for sulfentrazone and metolachlor, respectivly. The HPLC column was a LiChroCARTR 250-4 PurospherR STAR RP-18 (5 μm) (Merck), operating at flow rate of 0.8 mL min^{-1}. For sulfentrazone detection, the mobile phase was 50% acetonitrile and 50% water with trifluoroacetic acid, pH ∼ 3. For metolachlor detection, the mobile phase was 70% acetonitrile and 30% water.

RESULTS AND DISCUSSION

Sulfentrazone Solubilization in Micelles. Zeta potential (ξ) of montmorillonite, ODTMA micelles, and an ODTMA−clay composite and ξ of ODTMA micelles as a function of sulfentrazone solubilized were monitored (Table 2). The ξ

dx.doi.org/10.1021/jf403456m | J. Agric. Food Chem. 2014, 62, 50−57

Table 2. Zeta Potential of ODTMA Micelles (2.8 mM) and Micelles Solubilized with Sulfentrazone (2.1 mM), Montmorillonite (2 g/L), and Montmorillonite-ODTMA Composite with and without Sulfentrazone (2.1 mM)

sample	ζ potential (mV)
ODTMA	46 ± 5
ODTMA + SFZ	44 ± 3.6
clay	−39 ± 0.6
ODTMA + clay	51 ± 1.2
ODTMA + SFZ → clay	48 ± 4.5

measured for montmorillonite, ODTMA micelle, and ODTMA−clay composite are in agreement with previous studies.[52] ODTMA micelle adsorption on the clay was complete and exceeded the CEC of the clay, resulting in charge reversal of the clay (51 ± 1.2 mV).[52] Surprisingly the positive ξ of ODTMA−clay composite did not decrease (less positive) upon adsorption of anionic sulfentrazone (48 ± 4.5 mV) with a 0.75 sulfentrazone/ODTMA mol/mol ratio. Furthermore, the positive ξ of ODTMA micelles did not decrease upon solubilization of anionic sulfentrazone at herbicide/surfactant mol at a ratio of 0.25−1.5 mol/mol.

Previously, we studied sulfentrazone solubilization in ODTMA micelles at a ratio of 0.1−0.5 mol/mol and found that upon increasing sulfentrazone concentrations solubilization in the micelles decreased from 72 to 60%, respectively.[11] Sulfentrazone solubilization in ODTMA micelles was explained by two mechanisms: 1. The cationic ODTMA micelles enhance sulfentrazone dissociation resulting in anion formation which binds electrostatically to the cationic micelles.[28] 2. Sulfentrazone molecules can interact with the hydrophobic micelle core (solubilized into the micelle). On the basis of the suggested mechanisms, we concluded that an increase in sulfentrazone concentration in the micelles decreases the positive charge on the micelles, resulting in lower affinity of sulfentrazone to the micelle.

However, our current results demonstrate that ξ of ODTMA micelles does not decrease upon sulfentrazone solubilization. Both mechanisms suggested above may take place and do not contradict the current ξ findings, when considering sulfentrazone solubilization mainly in the micelle core (Figure 1B)

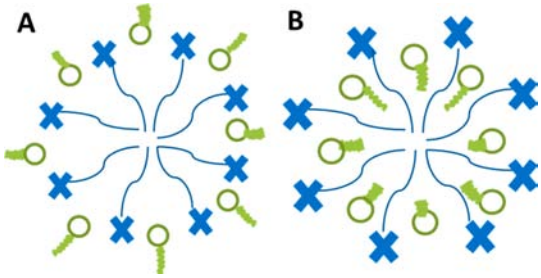

Figure 1. Suggested configurations of sulfentrazone solubilization in ODTMA micelles: (A) solubilization in the micelle shell and (B) solubilization in the micelle core.

and not at the surface (Figure 1A). Penetration into the core can explain (a) the decrease in solubilization upon increase in sulfentrazone concentration (solubilization limit and repulsion of excess positive changes in the micelles) and (b) the negligible changes in ξ of ODTMA micelles upon sulfentrazone solubilization. This implies that the suggested mechanisms[11] may be sequential with electorstatic attraction first and then sulfentrazone penetration into the micelles.

Adsorption−Desorption of Sulfentrazone Solubilized in Micelles to Soils. To maximize sulfentrazone adsorption to the soil via its solubilization in micelles which adsorb to the soil, two reactions, solubilization and micelle adsorption, need to be optimized. Herbicide solubilization may be increased by employing nonionic micelles with a lower CMC (than ODTMA) and which have high solubilization properties such as TX 100.[49,50,53−55] Many studies report the synergistic effect of mixed micelles.[56−61] Supporting these studies, the mixed micelles were found to have the largest micelle size (obtained from size measurements) which may enable higher solubilization due to larger core volume. The measured apparent micelle diameters of TX 100 micelles, ODTMA micelles, and the mixed micelles were 8.5, 7.5, and 9.5 ± 0.2 nm, respectively. Although sulfentrazone solubilization in TX100 micelles or in the mixed system may be higher than in ODTMA micelles, the latter's adsorption to the soil is predicted to be higher due to electrostatic attraction. To test the trade-off between solubilization and adsorption, sulfentrazone (300, 600, and 900 mg/L) adsorption to an alluvial soil was studied upon its solubilization in TX 100, ODTMA, and in mixed micelles of the two surfactants (Figure 2).

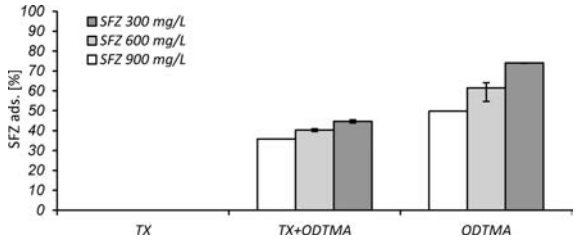

Figure 2. Adsorption of sulfentrazone (SFZ) (300, 600,900 mg/L) solubilized in micelles ODTMA (2.8 mM), TX 100 (1.5 mM), and mixed micelles of both surfactants to an alluvial soil (67 g/L).

Sulfentrazone adsorption to the soil upon its solubilization in TX 100 micelles was negligible, which demonstrates the poor adsorption of these micelles to the soil. Intermediate adsorption was obtained for the mixed micelles, and the highest adsorption was reached with the pure ODTMA micelles. These results indicate that although solubilization may be enhanced by the nonionic surfactant its adsorption to the soil is poor (lower than the adsorption of ODTMA micelles), causing lower sulfentrazone adsorption. Therefore, further adsorption and leaching studies of sulfentrazone were conducted with ODTMA micelles.

The adsorption of sulfentrazone (technical grade and Boral) and sulfentrazone (50−800 mg/L) solubilized in micelles (3.36 mM) to the sandy soil and to the heavy alluvial soil was studied (Figure 3). The adsorption of sulfentrazone, technical grade and Boral, to both soils, sandy or alluvial, was negligible. At the pH values of the soils 7.5 and 7.6, respectively, the herbicide is deprotonated, i.e., in its anionic form explaining the low adsorption to the soils and supporting reports on its high leaching.

The adsorption isotherms of sulfentrazone via its solubilization in ODTMA micelles have an L-shape and were in good agreement (R^2 > 0.986 or >0.972) with the Freundlich and Langmuir models, respectively (Table 3).

dx.doi.org/10.1021/jf403456m | J. Agric. Food Chem. 2014, 62, 50−57

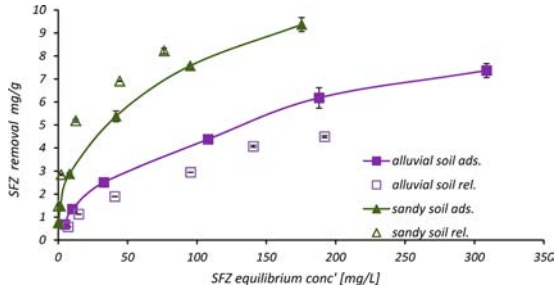

Figure 3. Adsorption/removal and desorption of Sulfentrazone (SFZ) (50–800 mg/L) solubilized in ODTMA micelles (3.36 mM) on/from soils (67 g/L).

Table 3. Adsorption Coefficients of Sulfentrazone Solubilized in ODTMA Micelles (3.36 mM) to Soils (67 g/L)

	Langmuir			Freundlich		
soil	X_m [mg/g]	K_L [L/mg]	R^2	K_f [L/mg]	n	R^2
sandy	9.8	0.057	0.972	1.11	0.42	0.994
alluvial	8.13	0.014	0.972	0.34	0.53	0.986

Higher adsorption of sulfentrazone (solubilized in ODTMA–micelles) to the alluvial soil was expected since the percent of clay in this soil is approximately 35 times higher than in the sandy soil and sulfentrazone adsorption to the soil is via the electrostatic adsorption of ODTMA micelles to the clay fraction. Surprisingly sulfentrazone affinity and loading to/on the sandy soil were higher than to the alluvial soil as indicated by the affinity coefficients which are 3–4 times higher for the sandy soil (for both models) and by X_m (Langmuir loading coefficient) which is higher for the sandy soil. Furthermore, the desorption from the sandy soil presents a normal hysteresis. However, the desorption from the alluvial soil exposes suspicious excessive desorption (inverse hysteresis).

The high adsorption of sulfentrazone on the sandier soil and the high desorption from the heavier soil can be explained by analyzing the molar ratio between the surfactant and the soil CEC. Mishael et al.[26] investigated sulfosulfuron adsorption to montmorillonite via its solubilization in ODTMA micelles. They found that the optimum ODTMA/CEC (mol/mol) ratio was ~1.5. Above this ratio not all the micelles adsorbed, resulting in herbicide solubilized in unadsorbed micelles, and below this ratio (i.e., high clay concentration) ODTMA adsorbed as monomers (which have a higher affinity to the clay than the micelles) causing decomposition of micelles and release of solubilized herbicide to the solution. The adsorption of sulfentrazone on the monomer–clay complexes is much lower than on the micelle–clay complexes as reported for sulfentrazone[28] and sulfometuron.[25]

The ODTMA/CEC mole ratio for the adsorption experiment with the sandy and with the alluvial soil were 1 and 0.12, respectively, which explains the higher adsorption to the sandy soil (ratio close to optimum ratio) and perhaps can explain precipitation of sulfentrazone in the experiment with the heavier soil due to the high clay concentration releasing sulfentrazone above its water solubility from the micelles. During the desorption experiment the unadsorbed sulfentrazone is released to the solution, resulting in excessive release. This implies that not all of the sulfentrazone (in the case of the alluvial soil) adsorbed but rather precipitated; therefore, the Y axis denoted sulfentrazone removal and not adsorption.

These results emphasize the importance of selecting an optimal surfactant/CEC ratio.

Sulfentrazone and Metolachlor Release and Leaching from Micelle Treated and Nontreated Soils. *Sulfentrazone Release and Leaching from Micelle Treated and Nontreated Soils.* We suggest that the cationic micelles solubilized with sulfentrazone adsorb to the soil which in turn inhibits both herbicide release from the micelles and leaching through the soil without compromising weed control.[11] To test the reduction in sulfentrazone leaching when applied to that solubilized in micelles, Boral, sulfentrazone (800 mg/L) solubilized in ODTMA micelles (3.36–13 mM), and water (control) were applied to a thin layer of the sandy or alluvial soil, and the soils were irrigated with 0–8 pore volumes; also, sulfentrazone concentrations in the leachates were measured (Figures 4). Sulfentrazone

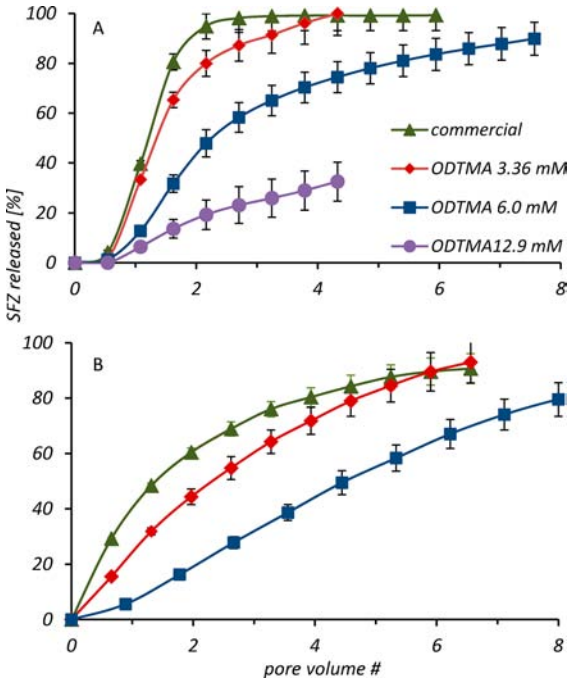

Figure 4. Sulfentrazone (SFZ) release and leaching applied as a commercial Boral or sulfentrazone–micelle formulations applied on thin layer of soil (A) alluvial or (B) sandy.

leaching from the commercial formulation was higher than from the herbicide–micelle ones, through both soils. For the alluvial soil, after 2.7 pore volumes irrigations (equivalent to 300 mm of rain), 98% of the sulfentrazone from the commercial formulation (Boral) leached through the soil layer, whereas 87, 58, and 23% leached from the 3.36, 6.0, and 12.9 mM ODTMA formulations, respectively. In the sandy soil, after 2.6 pore volume irrigations (equivalent to 200 mm of rain), 69% of the SFZ from the commercial formulation leached through the soil layer, whereas 54 and 27% leached from the 3.36 and 6.0 mM ODTMA formulations, respectively.

The decrease in sulfentrazone leaching upon the increase in surfactant concentration emphasizes the contribution of the adsorbed micelles to the inhibited leaching.

Effect of Soil on Sulfentrazone Release and Leaching from Micelle Treated and Nontreated Soils. In agreement with the adsorption/desorption results (Figure 3), sulfentrazone leaching (applied solubilized in micelles) through the alluvial soil

dx.doi.org/10.1021/jf403456m | J. Agric. Food Chem. 2014, 62, 50–57

was higher than through the sandy soil (Figure 4b). An irrigation of 2.6 pore volumes resulted in 87% and 48% leaching of sulfentrazone applied to the alluvial and sandy soils, respectively. The enhanced leaching from the alluvial soil can be explained by micelle decomposition caused by "excess" clay in the alluvial soil as described and calculated in the adsorption experiments. For the leaching experiments it is problematic to estimate the volume of soil the micelles can access, since the micelle solution is applied on top of the soil and not in a batch array. Therefore, the micelle/CEC mol/mol ratio was not calculated, but the enhanced leaching from the alluvial soil implies that the optimal ratio was exceeded.

The enhanced leaching of sulfentrazone from the commercial formulation through the alluvial soil, obviously, cannot be explained by a low micelle/CEC mol/mol ratio (Figure 4a). Four alternative explanations were raised and examined.

1. High adsorption of sulfentrazone to iron oxides, common in this sandy soil (Hamra), which could explain inhibited leaching. It is well documented that herbicides have high affinity to oxides.[62−64] However, sulfentrazone (technical and as Boral) adsorption experiments to iron oxides resulted in negligible adsorption, excluding this mechanism.
2. Transport of herbicides via their interaction with the dissolved organic matter (DOM) may also be considered. Indeed, the percent of DOM in the alluvial soil was higher than in the sandy soil. To test this hypothesis the DOM was washed from the alluvial soil and the leaching experiment was repeated with the washed soil; however, no significant differences were observed (Figure 5) indicating that in this case the DOM had a minor role in sulfentrazone transport (not surprising since both are negatively charged).

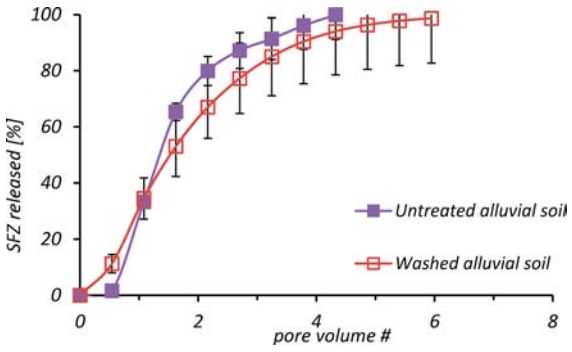

Figure 5. Sulfentrazone release and leaching from a sulfentrazone−micelle (3.36 mM ODTMA) formulation applied on a thin soil layer of an untreated alluvial soil and on a thin soil layer of alluvial soil in which the DOM was washed.

3. The well aggregated structure of the alluvial soil (in comparison to the sandy soil) may decrease the accessible soil adsorption sites, enhancing sulfentrazone leaching. If so, the leaching pattern, higher leaching through the alluvial soil, of other herbicides should be the same. As seen in Figure 6, metolachlor leaching through the two soils is not very different, and when plotted as a function of number of washes the leaching through both soils is nearly the same. In contrast, upon plotting the leaching of sulfentrazone as a function of number of washes the leaching from the alluvial soil remained higher (plot not shown). This suggests that the soil structure and that the kinetics are not the governing factors.
4. Finally, the repulsion of anionic sulfentrazone from the alluvial soil with a high clay concentration may explain the enhanced leaching through this soil. Metolachlor which is nonionic would not be as repelled from the heavy soil, and indeed its leaching through the sandy and heavy soils is not very different (Figure 6).

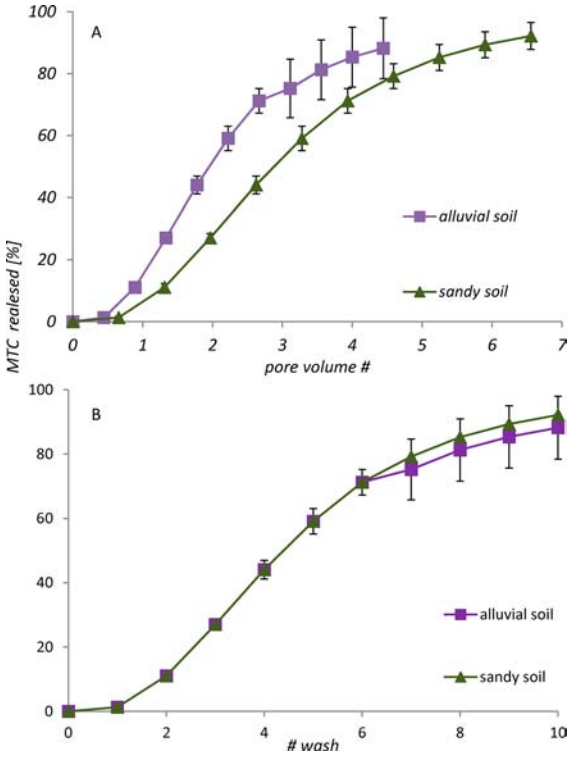

Figure 6. Metolachlor (S-dual gold) release and leaching from a thin layer of alluvial soil as a function of (A) irrigation pore volume and (B) number of irrigations.

Metolachlor Release and Leaching from Micelle Treated and Nontreated Soils. Leaching of metolachlor (solubilized in 3.36 mM ODTMA or as the commercial formulation, S-Dual Gold) through the alluvial soil was tested, in order to demonstrate that employing herbicides in micelles reduces their leaching is valid not just for sulfentrazone (Figure 7).

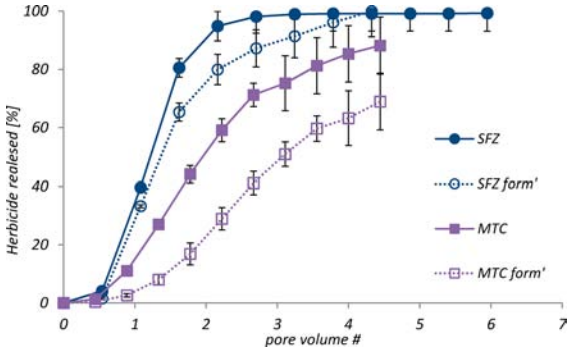

Figure 7. Herbicide release from commercial and herbicide−micelle (ODTMA 3.36 mM) formulations applied on thin layer of alluvial soil.

dx.doi.org/10.1021/jf403456m | J. Agric. Food Chem. 2014, 62, 50−57

Metolachlor leaching in both cases applied as the commercial or as a micelle formulation was restricted in comparison to sulfentrazone leaching. After irrigating 2.7 pore volumes, 98 and 87% of the sulfrentrazone leached from the commercial and from the micelle formulation, respectively, whereas metolachlor leaching after irrigating 2.7 pore volumes reached only 71 and 41% of the applied herbicide as the commercial or micelle formulation, respectively. As expected, leaching of anionic sulfentrazone was higher than the leaching of nonionic metolachlor.

Metolachlor leaching was inhibited when employed solubilized in micelles. Furthermore, metolacher leaching was inhibited to a higher degree (~50%) than that of sulfentrazone (~16%).

As discussed above due to a low surfactant/CEC mol/mol ratio in the alluvial soil micelle decomposition and monomer adsorption are expected. Nevertheless, metolachlor (unlike sulfentrazone) has high affinity to organo−clay complexes [34] which explains its high inhibition even under conditions of micelle decomposition.

Metolachlor leaching, when applied solubilized in micelles (3.36 mM ODTMA), was reduced by up to 2-fold, and sulfentrazone leaching, when applied solubilized in micelles (13 mM ODTMA), was reduced by up to 5-fold. These reduction rates are much higher than values previously reported for in situ slow release formulations.[39,65]

Gamiz et al. reported a reduction in fluometuron leaching of 1.25 upon adding 12.5% (surfactant (w)/soil (w)).[39] Rodriguez-Cruz et al. studied the retention of three pesticides in soil columns modified with ODTMA (w/w ratio of 2.5%). The leaching of linuron, atrazine, and metalaxyl through the soil treated with ODTMA was 3−4-fold less than from the nontreated soil.[65] In the current study, for sulfentrazone, not only were ODTMA doses much lower but herbicide reduction rates were higher. Sulfentrazone leaching was reduced by 5-fold upon adding only 0.3% ODTMA, and metolachlor leaching was reduced by 2-fold upon adding only 0.075% ODTMA.

The current study demonstrated four advantages when comparing the leaching retention to other reports on in situ soil modification: (1) Upon adding low loadings of ODTMA (0.075−0.3% w/w), herbicide leaching is significantly reduced. (2) ODTMA has been reported as toxic to microbial soil processes.[66] However, surfactant concentrations employed in this study are below the reported limit (1−10% w/w). (3) The herbicide is solubilized in the micelles as a formulation and both are applied to the soil at the same time, in comparison to the two step application in other reports (soil modification and then herbicide application). (4) An optimized surfactant/soil CEC mol/mol ratio is taken into account to maximize herbicide retention via micelle adsorption.

To conclude, herbicides were solubilized in micelles, and these formulations were applied to soils, for reduced herbicide leaching. This mode of application is more efficient than the common two step application, soil modification, and then herbicide application. Sulfentrazone (as Boral or technical) adsorption to a sandy or alluvial soil was negligible; however, its adsorption via its solubilization in ODTMA micelles was significant and in good agreement with the Freundlich and Langmuir models. An optimized surfactant/soil CEC mol/mol ratio was taken into account to maximize herbicide retention via micelle adsorption. Even upon adding low loadings of surfactant (0.075−0.3% w/w soil) herbicide leaching was significantly reduced.

AUTHOR INFORMATION

Corresponding Author

*(Y.G.M.) Tel.: 972-8-948-9171. Fax: 972-8-948-9856. E-mail: mishael@agri.huji.ac.il.

Present Address

[†]Samaria and the Jordan Rift regional R Center, Science park, Ariel, Israel.

Funding

This research was supported by internal funding for applied sciences of Hebrew University.

Notes

The authors declare no competing financial interest.

ABBREVIATIONS USED

SFZ, sulfentrazone; MTC, metolachlor; ODTMA, octadecyltrimethyl ammonium; TX, Triton X-100; ai, active ingredient; ads, adsorbed; rel, released

REFERENCES

(1) Carter, A. D. Herbicide movement in soils: principles, pathways and processes. *Weed Res.* **2000**, *40*, 113−122.

(2) Rice, P. J.; Anderson, T. A.; Coats, J. R. Degradation and persistence of metolachlor in soil: Effects of concentration, soil moisture, soil depth, and sterilization. *Environ. Toxicol. Chem.* **2002**, *21*, 2640−2648.

(3) Gevao, B.; Semple, K. T.; Jones, K. C. Bound pesticide residues in soils: a review. *Environ. Pollut.* **2000**, *108*, 3−14.

(4) Clerk, H. *Sulfentrzone; Establishment of Tolerances*; United States Environmental Protection Agency: 1997; pp 10703−10708.

(5) Miller, J. I. *Pesticide Fact Sheet, Registration of a New Chemical*; United States Environmental Protection Agency: 1997.

(6) Hela, D. G.; Lambropoulou, D. A.; Konstantinou, A. K.; Albanis, T. A. Environmental monitoring and ecological risk assessment for pesticide contamination and effects in Lake Pamvotis, northwestern Greece. *Environ. Toxicol. Chem.* **2005**, *24*, 1548−1556.

(7) Ahrens, H. W. *Herbicide Handbook*, 8th ed.; Weed Science Society of America: Champaign, IL, 2002.

(8) Ahrens, H. W. *Herbicide Handbook*, 7th ed.; Weed Science Society of America: Champaign, IL, 1994.

(9) Patakioutas, G.; Albanis, T. A. Adsorption-desorption studies of alachlor, metolachlor, EPTC, chlorothalonil and pirimiphos-methyl in contrasting soils. *Pest Manage. Sci.* **2002**, *58*, 352−362.

(10) Bakhtiary, S.; Shirvani, M.; Shariatmadari, H. Adsorption-desorption behavior of 2,4-D on NCP-modified bentonite and zeolite: Implications for slow-release herbicide formulations. *Chemosphere* **2013**, *90*, 699−705.

(11) Ziv, D.; Mishael, Y. G. Herbicide solubilization in micelle-clay composites as a basis for controlled release sulfentrazone and metolachlor formulations. *J. Agric. Food Chem.* **2008**, *56*, 9159−9165.

(12) Bojemueller, E.; Nennemann, A.; Lagaly, G. Enhanced pesticide adsorption by thermally modified bentonites. *Appl. Clay Sci.* **2001**, *18*, 277−284.

(13) Bruna, F.; Pavlovic, I.; Celis, R.; Barriga, C.; Cornejo, J.; Ulibarri, M. A. Organohydrotalcites as novel supports for the slow release of the herbicide terbuthylazine. *Appl. Clay Sci.* **2008**, *42*, 194−200.

(14) Cardoso, L. P.; Celis, R.; Cornejo, J.; Valim, J. B. Layered double hydroxides as supports for the slow release of acid herbicides. *J. Agric. Food Chem.* **2006**, *54*, 5968−5975.

(15) Carrizosa, M. J.; Calderon, M. J.; Hermosin, M. C.; Cornejo, J. Organosmectites as sorbent and carrier of the herbicide bentazone. *Sci. Total Environ.* **2000**, *247*, 285−293.

(16) Celis, R.; Hermosin, M. C.; Carrizosa, M. J.; Cornejo, J. Inorganic and organic clays as carriers for controlled release of the herbicide hexazinone. *J. Agric. Food Chem.* **2002**, *50*, 2324−2330.

(17) Cornejo, L.; Celis, R.; Dominguez, C.; Hermosin, M. C.; Cornejo, J. Use of modified montmorillonites to reduce herbicide

leaching in sports turf surfaces: Laboratory and field experiments. *Appl. Clay Sci.* **2008**, *42*, 284−291.
(18) El-Nahhal, Y.; Nir, S.; Polubesova, T.; Margulies, L.; Rubin, B. Lezaching, phytotoxicity, and weed control of new formulations of alachlor. *J. Agric. Food Chem.* **1998**, *46*, 3305−3313.
(19) El-Nahhal, Y.; Nir, S.; Serban, C.; Rabinovitz, O.; Rubin, B. Organo-clay formulation of acetochlor for reduced movement in soil. *J. Agric. Food Chem.* **2001**, *49*, 5364−5371.
(20) Huh, K. M.; Min, H. S.; Lee, S. C.; Lee, H. J.; Kim, S.; Park, K. A new hydrotropic block copolymer micelle system for aqueous solubilization of paclitaxel. *J. Controlled Release* **2008**, *126*, 122−129.
(21) Kenawy, E. R.; Sakran, M. A. Controlled release formulations of agrochemicals from calcium alginate. *Ind. Eng. Chem. Res.* **1996**, *35*, 3726−3729.
(22) Kumar, J.; Nisar, K.; Shakil, N. A.; Walia, S.; Parsad, R. Controlled release formulations of metribuzin: Release kinetics in water and soil. *J. Environ. Sci. Health, Part B* **2010**, *45*, 330−335.
(23) Li, J. F.; Li, Y. M.; Dong, H. P. Controlled release of herbicide acetochlor from clay/carboxylmethylcellulose gel formulations. *J. Agric. Food Chem.* **2008**, *56*, 1336−1342.
(24) Li, J. F.; Jiang, M.; Wu, H.; Li, Y. M. Addition of Modified Bentonites in Polymer Gel Formulation of 2,4-D for Its Controlled Release in Water and Soil. *J. Agric. Food Chem.* **2009**, *57*, 2868−2874.
(25) Mishael, Y. G.; Undabeytia, T.; Rytwo, G.; Papahadjopoulos-Sternberg, B.; Rubin, B.; Nir, S. Sulfometuron incorporation in cationic micelles adsorbed on montmorillonite. *J. Agric. Food Chem.* **2002**, *50*, 2856−2863.
(26) Mishael, Y. G.; Undabeytia, T.; Rabinovitz, O.; Rubin, B.; Nir, S. Sulfosulfuron incorporated in micelles adsorbed on montmorillonite for slow release formulations. *J. Agric. Food Chem.* **2003**, *51*, 2253−2259.
(27) Nennemann, A.; Mishael, Y.; Nir, S.; Rubin, B.; Polubesova, T.; Bergaya, F.; van Damme, H.; Lagaly, G. Clay-based formulations of metolachlor with reduced leaching. *Appl. Clay Sci.* **2001**, *18*, 265−275.
(28) Polubesova, T.; Nir, S.; Rabinovitz, O.; Borisover, M.; Rubin, B. Sulfentrazone adsorbed on micelle-montmorillonite complexes for slow release in soil. *J. Agric. Food Chem.* **2003**, *51*, 3410−3414.
(29) Radian, A.; Mishael, Y. G. Characterizing and designing polycation - Clay nanocomposites as a basis for imazapyr controlled release formulations. *Environ. Sci. Technol.* **2008**, *42*, 1511−1516.
(30) Sanchez-Verdejo, T.; Undabeytia, T.; Nir, S.; Maqueda, C.; Morillo, E. Environmentally friendly slow release formulations of alachlor based on clay-phosphatidylcholine. *Environ. Sci. Technol.* **2008**, *42*, 5779−5784.
(31) Undabeytia, T.; Nir, S.; Rubin, B. Organo-clay formulations of the hydrophobic herbicide norflurazon yield reduced leaching. *J. Agric. Food Chem.* **2000**, *48*, 4767−4773.
(32) Undabeytia, T.; Mishael, Y. G.; Nir, S.; Papahadjopoulos-sternberg, B.; Rubin, B.; Morillo, E.; Maqueda, C. A novel system for reducing leaching from formulations of anionic herbicides: Clay-liposomes. *Environ. Sci. Technol.* **2003**, *37*, 4475−4480.
(33) Undabeytia, T.; Recio, E.; Maqueda, C.; Sanchez-Verdejo, T.; Balek, V. Slow diuron release formulations based on clay-phosphatidylcholine complexes. *Appl. Clay Sci.* **2012**, *55*, 53−61.
(34) El-Nahhal, Y.; Nir, S.; Serban, C.; Rabinovitch, O.; Rubin, B. Montmorillonite-phenyltrimethyl ammonium yields environmentally improved formulations of hydrophobic herbicides. *J. Agric. Food Chem.* **2000**, *48*, 4791−4801.
(35) Mishael, Y. G.; Undabeytia, T.; Rabinovitz, O.; Rubin, B.; Nir, S. Slow-release formulations of sulfometuron incorporated in micelles adsorbed on montmorillonite. *J. Agric. Food Chem.* **2002**, *50*, 2864−2869.
(36) Undabeytia, T.; Nir, S.; Gomara, M. J. Clay-vesicle interactions: Fluorescence measurements and structural implications for slow release formulations of herbicides. *Langmuir* **2004**, *20*, 6605−6610.
(37) Singh, M.; Tan, S.; Sharma, S. D. Leaching and sorption of norflurazon in soils as affected by cationic surfactants. *Bull. Environ. Contam. Toxicol.* **2002**, *68*, 901−907.
(38) Rodriguez-Cruz, M. S.; Sanchez-Martin, M. J.; Andrades, M. S.; Sanchez-Camazano, M. Modification of clay barriers with a cationic surfactant to improve the retention of pesticides in soils. *J. Hazard. Mater.* **2007**, *139*, 363−372.
(39) Gamiz, B.; Celis, R.; Hermosin, M. C.; Cornejo, J. Soil Clay Modification with Spermine and Its Effect on the Behavior of the Herbicide Fluometuron. *Soil Sci. Soc. Am. J.* **2012**, *76*, 432−440.
(40) Boyd, S. A.; Mortland, M. M.; Chiou, C. T. Sorption characteristics of organic-compounds on hexadecyltrimethylammonium-smectite. *Soil Sci. Soc. Am. J.* **1988**, *52*, 652−657.
(41) Smith, L. W.; Bayer, D. E. Soil adsorption of diuron as influenced by surfactants. *Soil Sci.* **1967**, *103*, 328−&.
(42) Gaynor, J. D.; Volk, V. V. Surfactant effects on picloram adsorption by soils. *Weed Sci.* **1976**, *24*, 549−552.
(43) Elworthy, P. H.; Lipscomb, F. J. Solubilization of Griseofulvin by Nonionic Surfactants. *J. Pharm. Pharmacol.* **1968**, *20*, 817−824.
(44) Dunaway, C. S.; Christian, S. D.; Scamehorn, J. F. Overview and history of the study of solubilization. *Surf. Sci. Ser.* **1995**, *55*, 3−31.
(45) Rosen, M. J. *Surfactants and interfacial phenomena*, 3rd ed.; John Wiley & Sons, Inc.: Hoboken, NJ, 2004; p 444.
(46) Scamehorn, J. F.; Harwell, J. H. Surfactants in Emerging Technologies. In *Surfactant Science Series*, Rosen, M. J., Ed.; Marcel Dekker: New York, 1987; Vol. *26*, p 169.
(47) Zana, R. Aqueous surfactant-alcohol systems: a review. *Adv. Colloid Interface Sci.* **1995**, *57*, 1−64.
(48) Nagarajan, R.; Ruckenstein, E. Theory of Surfactant Self-Assembly - a Predictive Molecular Thermodynamic Approach. *Langmuir* **1991**, *7*, 2934−2969.
(49) Sanchez-Camazano, M.; Rodriguez-Cruz, S.; Sanchez-Martin, M. J. Evaluation of component characteristics of soil-surfactant-herbicide system that affect enhanced desorption of linuron and atrazine preadsorbed by soils. *Environ. Sci. Technol.* **2003**, *37*, 2758−2766.
(50) Wang, P.; Keller, A. A. Partitioning of hydrophobic organic compounds within soil-water-surfactant systems. *Water Res.* **2008**, *42*, 2093−2101.
(51) El-Nahhal, Y.; Nir, S.; Polubesova, T.; Margulies, L.; Rubin, B. Movement of metolachlor in soil: effect of new organo-clay formulations. *Pestic. Sci.* **1999**, *55*, 857−864.
(52) Zadaka, D.; Radian, A.; Mishael, Y. G. Applying zeta potential measurements to characterize the adsorption on montmorillonite of organic cations as monomers, micelles, or polymers. *J. Colloid Interface Sci.* **2010**, *352*, 171−177.
(53) West, C. C. Surfactant-enhanced solubilization of tetrachloroethylene and degradation products in pump and treat remediation. *ACS Symp. Ser.* **1992**, *491*, 149−158.
(54) Rodriguez-Cruz, M. S.; Sanchez-Martin, M. J.; Sanchez-Camazano, M. Enhanced desorption of herbicides sorbed on soils by addition of triton X-100. *J. Environ. Qual.* **2004**, *33*, 920−929.
(55) Xiarchos, I.; Doulia, D. Effect of nonionic surfactants on the solubilization of alachlor. *J. Hazard. Mater.* **2006**, *136*, 882−888.
(56) Khan, A.; Marques, E. F. Synergism and polymorphism in mixed surfactant systems. *Curr. Opin. Colloid Interface Sci.* **1999**, *4*, 402−410.
(57) Bergstrom, M.; Eriksson, J. C. A theoretical analysis of synergistic effects in mixed surfactant systems. *Langmuir* **2000**, *16*, 7173−7181.
(58) Zhu, L. Z.; Feng, S. L. Synergistic solubilization of polycyclic aromatic hydrocarbons by mixed anionic-nomonic surfactants. *Chemosphere* **2003**, *53*, 459−467.
(59) Mishael, Y. G.; Dubin, P. L. Toluene solubilization induces different modes of mixed micelle growth. *Langmuir* **2005**, *21*, 9803−9808.
(60) Zhou, W. J.; Zhu, L. Z. Solubilization of polycyclic aromatic hydrocarbons by anionic-nonionic mixed surfactant. *Colloids Surf., A* **2005**, *255*, 145−152.
(61) Yang, K.; Zhu, L. Z.; Xing, B. S. Enhanced soil washing of phenanthrene by mixed solutions of TX100 and SDBS. *Environ. Sci. Technol.* **2006**, *40*, 4274−4280.

(62) Kirkwood, R. C. Use and mode of action of adjuvants for herbicides - a review of some current work. *Pestic. Sci.* **1993**, *38*, 93−102.
(63) Leone, P.; Negre, M.; Gennari, M.; Boero, V.; Celis, R.; Cornejo, J. Adsorption of imidazolinone herbicides on smectite-humic acid and smectite-ferrihydrite associations. *J. Agric. Food Chem.* **2002**, *50*, 291−298.
(64) Rocha, W. S. D.; Regitano, J. B.; Alleoni, L. R. F.; Tornisielo, V. L. Sorption of imazaquin in soils with positive balance of charges. *Chemosphere* **2002**, *49*, 263−270.
(65) Rodriguez-Cruz, M. S.; Sanchez-Martin, M. J.; Andrades, M. S.; Sanchez-Camazano, M. Retention of pesticides in soil columns modified in situ and ex situ with a cationic surfactant. *Sci. Total Environ.* **2007**, *378*, 104−108.
(66) Sarkar, B.; Xi, Y. F.; Megharaj, M.; Krishnamurti, G. S. R.; Bowman, M.; Rose, H.; Naidu, R. Bioreactive Organoclay: A New Technology for Environmental Remediation. *Crit. Rev. Environ. Sci. Technol.* **2012**, *42*, 435−488.

JOURNAL OF AGRICULTURAL AND FOOD CHEMISTRY

Article

pubs.acs.org/JAFC

Peptidomic Profile of Milk of Holstein Cows at Peak Lactation

David C. Dallas,*[,†,‡] Andres Guerrero,[#] Evan A. Parker,[#] Luis A. Garay,[†] Aashish Bhandari,[†] Carlito B. Lebrilla,[‡,#] Daniela Barile,[†,‡] and J. Bruce German[†,‡]

[†]Department of Food Science and Technology, [‡]Foods for Health Institute, and [#]Department of Chemistry, University of California—Davis, One Shields Avenue, Davis, California 95616, United States

Supporting Information

ABSTRACT: Bovine milk is known to contain naturally occurring peptides, but relatively few of their sequences have been determined. Human milk contains hundreds of endogenous peptides, and the ensemble has been documented for antimicrobial actions. Naturally occurring peptides from bovine milk were sequenced and compared with human milk peptides. Bovine milk samples from six cows in second-stage peak lactation at 78−121 days postpartum revealed 159 peptides. Most peptides (73%) were found in all six cows sampled, demonstrating the similarity of the intramammary peptide degradation across these cows. One peptide sequence, ALPIIQKLEPQIA from bovine perilipin 2, was identical to another found in human milk. Most peptides derived from β-casein, α_{s1}-casein, and α_{s2}-casein. No peptides derived from abundant bovine milk proteins such as lactoferrin, β-lactoglobulin, and secretory immunoglobulin A. The enzymatic cleavage analysis revealed that milk proteins were degraded by plasmin, cathepsins B and D, and elastase in all samples.

KEYWORDS: *peptidomics, bovine milk, bioactive peptides, protease*

INTRODUCTION

The peptides that are naturally occurring in bovine milk have not been completely identified, nor have they all been investigated for biological activity. In this study, breakthroughs in the analytical chemistry of peptides have enabled us to perform a peptidomic profiling of the endogenous peptides in bovine milk.

Human milk contains hundreds of naturally occurring peptides released by plasmin and other milk proteases within the mammary gland.[1,2] Eighteen percent of the peptides in human milk had >50% homology with known functional peptides.[2] Most of these peptides matched known antimicrobial peptides. Assays demonstrated that an isolated ensemble of endogenous human milk peptides inhibited the growth of *Escherichia coli* and *Staphylococcus aureus*. As *S. aureus* and *E. coli* are common causative agents in human mastitis, these peptides may be a mechanism of maternal resistance to mastitis. This previous work in human milk demonstrated that naturally occurring milk peptides may influence the health of the mother and the infant.

The presence of active proteases—plasmin[3−5] (as well as tissue-type and urokinase-type plasminogen activators[6,7]) and possibly active cathepsin B and cathepsin D[8−10]—in non-mastitic bovine milk suggested that naturally occurring peptides would also be present in bovine milk. The appearance of low molecular weight bands in gel electrophoresis experiments has suggested that naturally occurring peptides exist in healthy bovine milk, typically referred to as the proteose peptone fraction.[11] The proteose peptone fraction has been separated into components and, for some, their sequences have been determined, typically with gel electrophoresis and amino acid sequencing.[12−14] That research showed this fraction to be composed of casein degradation products and some whey proteins.[15,16] A previous analysis of bovine milk peptides isolated by immobilized metal affinity chromatography and analyzed using matrix-assisted laser desorption/ionization tandem time-of-flight (MALDI-TOF/TOF) mass spectrometry identified 15 peptides but only 2 complete sequences, both from α_{s1}-casein.[17] Eleven naturally occurring phosphorylated peptides and one nonphosphorylated peptide from bovine milk β- and α_{s2}-casein were identified with MALDI-TOF/TOF and ultrahigh-pressure liquid chromatography electrospray ionization mass spectrometry.[18] In another paper, 21 peptide sequences were identified in healthy bovine milk by LC-MS/MS.[19]

This research analyzed naturally occurring peptides in bovine milk by a shotgun nanoliquid chromatography quadrupole time-of-flight tandem mass spectrometry approach. The cleavage sites were matched to cleavage patterns of known milk enzymes to determine which were likely responsible for protein cleavages in the mammary gland.

MATERIALS AND METHODS

Sample Collection. Bovine milk samples were collected from the University of California—Davis Dairy Barn in the winter from six Holstein cows. All six cows were deemed mastitis-free on the basis of the following criteria: (1) prior to milking, each teat was checked to ensure there was no abnormal milk (e.g., watery (serous) milk, flakes, or clots) or issues in the quarter (e.g., swelling, redness); (2) after milking, each pretank filter was checked to ensure no abnormal milk entered the tank; (3) milk weights were recorded, and any cows with low milk production were checked again for mastitis. None of the cows used in this study had abnormal milk, udder swelling, or low milk production. In addition, samples from the milk tank were cultured raw

Received: September 12, 2013
Revised: December 16, 2013
Accepted: December 17, 2013
Published: December 17, 2013

 © 2013 American Chemical Society

for total bacteria and coliform bacteria counts and then laboratory-pasteurized for thermophilic bacterial counts. All bacterial counts were normal. All cows sampled were lactating for the second time (second lactation period). Milk samples represented a range of days postpartum: 78−121 days. Animals were kept in free stall housing and fed a total mixed ration (a mixture of grain (barley and corn), alfalfa, cottonseed, almond hulls, oat hay, added minerals and salts, beet pulp, and canola meal) and had access to water ad libitum. Cows were milked twice daily, at 4 a.m. and 4 p.m. in a milking parlor managed according to American Association for Accreditation of Laboratory Animal Care guidelines. Samples employed in this study are all from 4 p.m. milkings. Cows were milked with automated milking machines (Metatron, GEA Farm Technologies) from all four quarters at once. The resulting stream of milk was split from delivery to the bulk tank throughout the pumping process to provide samples representative of each cow's individual milk for this study. Before the pumps were attached, all four teats were washed first with water and then with an antiseptic solution (Chlorhexidine Active Mastitis Prevention) with 0.5% chlorhexidine gluconate, a chemical antiseptic, as the active ingredient. The time from initiation of suction to end of milking was 5.5−6.5 min. The cows produced from 41 to 52 lbs of milk. After pumping, milk was immediately placed in a 100 °C water bath for 4 min to deactivate the milk proteases. Samples were then transferred to a −20 °C freezer.

Sample Preparation. Samples were removed from the freezer and allowed to thaw at room temperature. Then, they were vortexed for 3−4 min each. Peptides were extracted according the procedure of Dallas et al.[2] but adapted to a 96-well plate format for increased sample preparation speed, reproducibility, and throughput. Briefly, 50 μL of each milk sample was added to the 96-well plate with 150 μL of nanopure water followed by pipet mixing. The 96-well plates were centrifuged at 2800*g* for 30 min at 4 °C, and 160 μL of the infranate (skim milk) was removed from the upper lipid layer by multichannel pipet and added to a second 96-well plate. Proteins were precipitated with addition of 160 μL of 200 g/L trichloroacetic acid (TCA). A plate cap was added, and the samples were vortexed for 5 min. After centrifugation at 2800*g* for 30 min at 4 °C, the peptide supernatant was collected. The peptide supernatant was cleaned up on a C18 solid phase extraction column plate to remove salts, sugars, and TCA. Columns were prepared with 99.9% acetonitrile (ACN)/0.1% trifluoroacetic acid (TFA) (v/v), followed by 1% ACN and 0.1% TFA (v/v). The peptide samples were then added. Three column volumes (200 μL) of 1% ACN and 0.1% TFA (v/v) were added to remove sugars, salts, and TCA. Then, 3 column volumes of 80% ACN and 0.1% TFA (v/v) were used to elute peptides. Solvents were passed through the columns by centrifugation for 30 s at 2800*g* without heating. Peptides were dried in the plate by centrifugal evaporation. Peptides were resolubilized in 20 μL of nanopure water with 5 min of sonication and 30 min of plate vortexing. Samples were then centrifuged at 16000*g* for 30 min to pull down any remaining solids. Supernatants were transferred to sampling vials for Q-TOF analysis.

Mass Spectrometry. Peptides were analyzed by mass spectrometry according to the procedure of Dallas et al.[2] Samples were injected on the Agilent 6520 (Santa Clara, CA, USA) nano-LC-chip-Q-TOF MS/MS (Chip-Q-TOF) with an Agilent chip C18 column. Changes to the procedure in Dallas et al.[2] include using a drying gas flow rate of 3 L/min and a spectral acquisition rate of 1 spectra/s. The gradient elution solvents were (A) 3% ACN/0.1% FA (v/v) and (B) 90% ACN/0.1% FA (v/v). The gradient employed was ramped from 0 to 8% B from 0 to 5 min, from 8 to 26.5% B from 5 to 24 min, and from 26.5 to 100% B from 24 to 48 min, followed by 100% B for 2 min and 100% A for 10 min (to re-equilibrate the column). Ion polarity was set to positive. The peak collection thresholds were set at 200 ion counts or 0.01% relative intensity for MS spectra and 5 ion counts or 0.01% relative intensity for MS/MS. Automated precursor selection based on abundance was employed to select peaks for tandem fragmentation with an exclusion list consisting of all peptides identified in previous analyses in this study. The acquisition rate employed was 0.63 spectra/s for both MS and MS/MS modes. The isolation width for tandem analysis was 1.3 m/z. The collision energy was set by the formula (slope) × (m/z)/100 + offset, with slope = 3.6 and offset = −4.8. Five tandem spectra were collected after each MS spectrum, with active exclusion after 2 MS/MS for 2 min. Precursor ions were selected only if they had at least 1000 ion counts or 0.01% of the relative intensity of the spectra.

Spectral Analysis. Spectra were analyzed by database search according to the procedure of Dallas et al.[2] Briefly, data were exported from Agilent MassHunter in .mgf format and imported into the offline search engine X!Tandem.[20] X!Tandem searches were against a bovine milk library compiled from previous bovine milk proteome studies.[21−23] Peptides were accepted if e-values were ≤0.01, corresponding to a 99% confidence level. Masses were allowed 20 ppm error. No complete (required) modifications were included, but up to four potential modifications were allowed on each peptide. Potential modifications allowed were phosphorylation of serine, threonine, and tyrosine; oxidation of methionine and tryptophan; and deamidation of asparagine and glutamine. A nonspecific cleavage ([X]|[X]) (where 'X' is any amino acid) was used to search against the protein sequences. Because the instrument did not always select the monoisotopic ion for tandem fragmentation, isotope errors were allowed (allowing up to one C13). No model refinement was employed in X!Tandem.

Library Search. X!Tandem peptide results were used to construct a peptide library from all samples. Duplicates with the same sequence, protein, and modifications were removed. In addition, all peptides that were the same except for the position of the modification were reduced to a single entry for each. The library information consisted of neutral mass, retention time, and a peptide ID. Compounds were identified from MS-only runs of all six samples by the "Find by Molecular Feature" function in Agilent MassHunter Qualitative Analysis version 6. The target data type was small molecule (chromatographic). Retention time was restricted from 3.5 to 36 min (the range of library peptides). Only peaks with at least 1000 ion counts were selected. The selected charge carrier was "protons". The isotope model was "peptides", and the maximum assigned charge was 7. After compounds were extracted, they were matched to the peptide library by mass and retention time to identify peptides. The database match employed a mass error tolerance of 40 ppm and a retention time tolerance of 1 min. Each exact peptide mass in the library was converted to an m/z for all charge states from 1 to 7 for the search. All amino acid sequence ranges expressed throughout this paper will include the signal sequence.

Enzyme Analysis. A custom program written in Python was used to estimate the activity of selected enzymatic systems. This program works with the output from the peptide library from an individual trial. Each peptide is assigned a location within a protein on the basis of the unique sequence to determine the sequence context of the peptide. After assigning context, both termini of each peptide are compared to a selected set of proteolytic enzyme rules. As a measure of simplification, rules were assumed to only act on P1 and P1′. P1 is the amino acid directly before the cleavage site, and P1′ is the amino acid directly after the cleavage site, where the protein N-terminus is on the left and the C-terminus is on the right. Enzymatic cleavage rules were derived from a list published on ExPASy.[24] The enzyme specificity patterns used in the algorithm for evaluating cleavages are shown in Table 1. Peptides having termini that pass a comparison to an enzymatic rule have their mass spectral intensity (peak volume)

Table 1. Enzyme Cleavage Specificity Rules Used for Enzyme Analysis[a]

enzyme	P1	P1′
plasmin	R, K	any
cathepsin B	G, A, M, Q, T	F, G, I, V, L
cathepsin D	A, V, L, I, P, M, F, W	A, V, L, I, P, M, F
elastase	A, V, L, I, G, R	G, P, A, L, F

[a]Specificity rules were derived from PeptideCutter as described in ref 24.

dx.doi.org/10.1021/jf4040964 | J. Agric. Food Chem. 2014, 62, 58−65

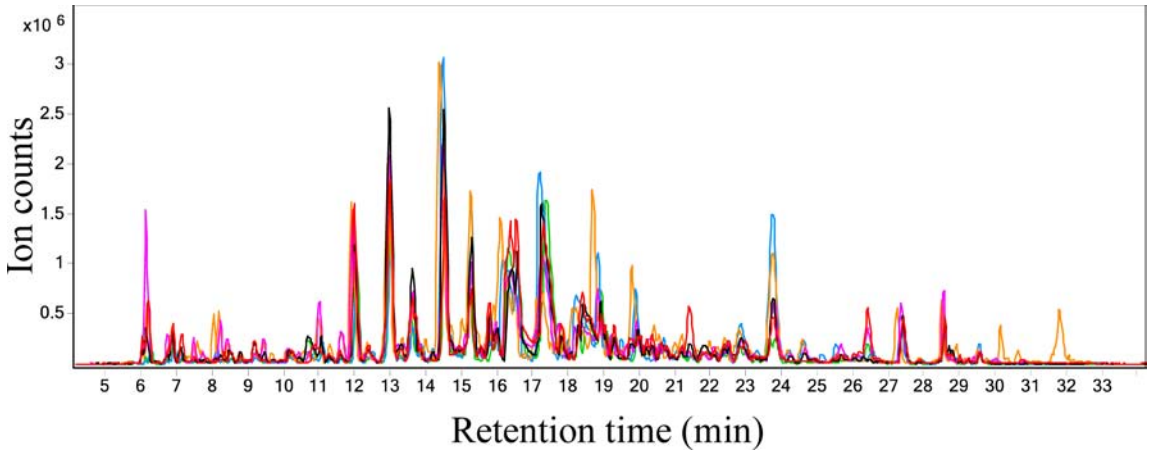

Figure 1. Base peak chromatograms of all six bovine milk samples overlapped.

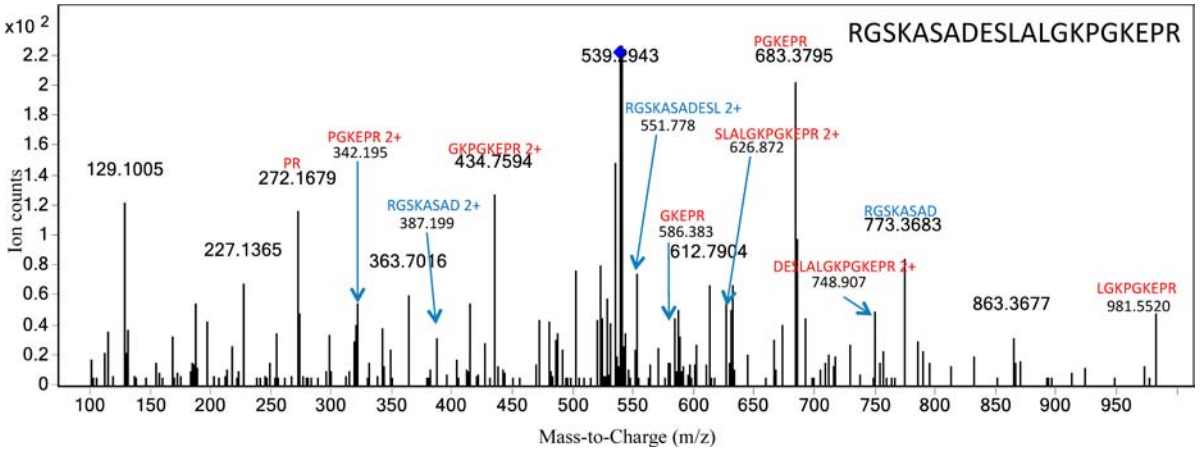

Figure 2. Tandem fragmentation of m/z ($z = 4$) 539.29 at one time point within its 8.3−8.8 min retention time with y-type ions in red, b-type ions in blue, and the precursor ion denoted by a blue diamond. The tandem fragmentation analysis confirms the presence of peptide RGSKASADESLALGKPGKEPR from fibroblast growth factor-binding protein 1.

added to the sum of the respective enzyme. In the case that a peptide matches multiple rules simultaneously, the full intensity of that peptide is added to both enzymatic sums; thus, the intensity value output represents potential activity rather than uniquely specific activity. Peptides failing all enzymatic comparisons have their intensity added to a list of remainders, the purpose of which is to assist in the identification of new enzymatic systems.

Homology Searches for Comparison of Bovine and Human Milk Peptides. Sequences identified in the bovine milk samples were searched for homology against endogenous peptides previously identified in human milk.[2] This search was performed with protein−protein BLAST. For each query, matches were retained only if peptides shared at least 50% identity (at least 50% of the amino acids were the same and in the same positions).

RESULTS AND DISCUSSION

The base peak chromatograms from all six samples (shown in Figure 1) have a substantial number of overlapping peaks. The large degree of overlap is interpreted to indicate that release of peptides in the mammary gland is thus similar across the six cows measured. The annotated tandem spectrum in Figure 2 demonstrates how peptide identifications were verified in an automated process in X!Tandem, in this case, confirmation of the presence of RGSKASADESLALGKPGKEPR from bovine fibroblast growth factor-binding protein 1 in all six samples from 8.3 to 8.8 min retention time.

The nano-LC Q-TOF and database searching methodologies developed for peptidomic analysis identified 159 endogenous peptides in the six bovine milk samples. All 159 peptide sequences are shown in Supplementary Table 1 in the Supporting Information. Previous research on endogenous bovine milk peptides revealed fewer peptides. One study employing MALDI-TOF/TOF identified two peptides sequences, both from α_{s1}-casein.[17] Another study employed MALDI-TOF and LC-MS to identify 11 phosphopeptides and 1 nonphosphorylated peptide.[18] Mansor et al. identified 21 peptide sequences from healthy bovine milk by LC-MS/MS.[19] The increased number of peptides identified in the present research is likely due to improved identification methods.

Six of the peptides found in Mansor et al. were identified in the present research (identified in Supplementary Table 1). Most of the other peptides in the work of Mansor et al. matched segments of the proteins identified here but were not identical sequence matches. The two bovine milk peptides found in Meltretter et al. were not found here, but overlapping peptides were identified in the present data.[17] Of the 12 peptides found in Baum et al.[18] 3 were identical to those found here (2 phosphorylated, 1 nonphosphorylated) (see Supplementary Table 1), 4 overlapped but were incomplete matches,

dx.doi.org/10.1021/jf4040964 | J. Agric. Food Chem. 2014, 62, 58−65

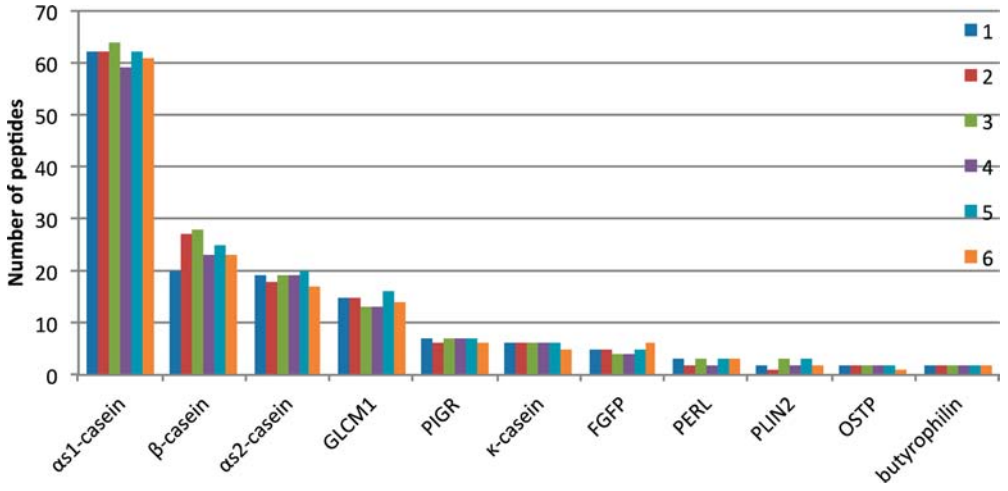

Figure 3. Number of peptides identified for each protein by each sample. GLCM1, glycosylation-dependent cell adhesion molecule 1; PIGR, polymeric immunoglobulin receptor; FGFP, fibroblast growth factor-binding protein 1; PLIN2, perilipin-2; PERL, lactoperoxidase; OSTP, osteopontin.

and 5 matched by sequence but had a lower degree of phosphorylation in the present paper.

The peptides identified ranged in charge states from 1 to 6. Peptide sequence length ranged from 8 to 45 amino acids. The average number of amino acids in a sequence was 16.7. Peptide mass ranged from 784.4 to 4416.2 Da. The average peptide mass was 1938.8 Da.

The majority of identified peptide sequences (73%) were present in all six samples. Sixteen percent were found in five of the six samples; thus, 89% of peptides identified were found in at least five of the samples. This data set was interpreted to indicate that the degradation processes within the mammary gland are relatively similar across these six healthy Holstein cows in second-stage peak lactation. Analysis of more cows would be necessary to extend this interpretation to healthy Holstein cows in general, as the cows examined had similar feed and climate.

The parent proteins for all peptides identified are present in healthy bovine milk as protein fragments and as intact proteins. Gel electrophoresis implied the presence of these intact milk proteins.[25] In the present research, 15 proteins gave rise to endogenous milk peptides, including α_{s1}-casein, α_{s2}-casein, β-casein, κ-casein, glycosylation-dependent cell adhesion molecule 1, polymeric immunoglobulin receptor, fibroblast growth-factor-binding protein 1, lactoperoxidase, perilipin-2, butyrophilin, and osteopontin. Previous research by Meltretter et al. identified only α_{s1}-casein-derived peptides.[17] The work of Baum et al. identified peptides only from α_{s2}-casein and β-casein.[18] Mansor et al. identified peptides from most of the proteins identified in the present research, but did not identify peptides from polymeric immunoglobulin receptor, perilipin-2, and butyrophilin.[19] The increased number of protein precursors identified in the present research compared to previous research is likely due to more exhaustive tandem fragmentation of peptide precursors and searching against the large in-house library of milk proteins with X!Tandem.

However, other high-abundance milk proteins including lactoferrin, β-lactoglobulin, and secretory IgA (sIgA) did not produce peptides. These proteins were also not present as peptides in human milk.[2] One peptide from β-lactoglobulin was found in healthy bovine milk in Mansor et al., but, like the present research, they detected no peptides from lactoferrin or sIgA.[19] Likewise, these peptides were not identified in milk in the previous works of Meltretter et al.[17] and Baum et al.[18]

This variation in which proteins are degraded in the mammary gland could be due to protein structural differences. Milk enzymes may more easily degrade the looser three-dimensional structure of the caseins[2] than the more rigid, compact, globular structures of lactoferrin, β-lactoglobulin, and sIgA.[2] The type and position of glycan post-translational modifications on lactoferrin and sIgA may also influence resistance to protein degradation.

Forty percent of all peptide sequences were derived from α_{s1}-casein. The number of peptides found for each protein is shown in Figure 3. In human milk, the majority of peptides identified in mothers studied were derived from β-casein,[2] whereas α_{s1}-casein peptides were present but less abundant. The number of peptides identified from each protein were similar across the six bovine milk samples (Figure 3). These data are interpreted to indicate that protein degradation in the cow mammary gland is well regulated and controlled across cows. However, evaluation of more milks is necessary to confirm this interpretation, as these cows were exposed to identical feeding and climate conditions. This similarity of peptides released across bovine milk samples was mirrored in the results showing that human milk peptide profiles are highly similar between mothers.[2]

Each sample had between 35 and 37 phosphorylated peptides. The total number of phosphorylated peptides for all six samples combined was 38 (24% of all peptides identified by count). The number of phosphopeptides identified here is higher than the 11 identified in Baum et al.[18] Research by Meltretter et al. and Mansor et al. did not identify any phosphopeptides.[17,19] The high number of phosphorylated peptides detected in the present research is not surprising as most of the phosphorylated peptides come from the four casein proteins, which are all known to be multiply phosphorylated.[18] Some of these phosphopeptides contained multiple phosphorylations: two had three phosphorylations, and four had two phosphorylations. This is less phosphorylation than found in the work of Baum et al.: they identified nine peptides with four phosphorylations.[18] The presence of phosphorylations on caseins is known to allow formation of organophosphate salts for minerals, especially calcium.[26] Peptides containing multiple phosphorylation sites may bind calcium and aid in calcium

dx.doi.org/10.1021/jf4040964 | J. Agric. Food Chem. 2014, 62, 58−65

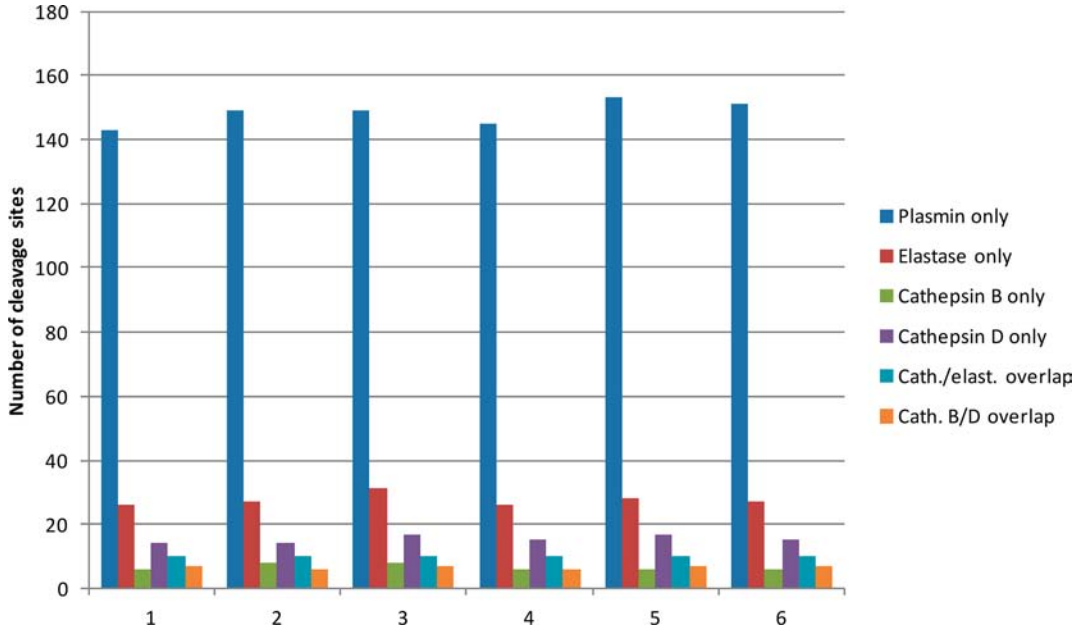

Figure 4. Cumulative intensities for all assigned cleavage sites for each bovine milk sample.

delivery.[27] Other modifications found include methionine oxidation, deamidation of glutamine, N-terminal acetylation, and pyroglutamination of glutamine. No glycosylated peptides were searched for with the methodology employed; therefore, no glycopeptides were identified.

Only one bovine milk peptide sequence matched exactly a known endogenous peptide in human milk: ALPIIQKLEPQIA from human and bovine perilipin 2 (amino acids 65−77 in both species, including the signal sequence). This peptide was not identified in milk peptide profiles in Mansor et al.,[19] Meltretter et al.,[17] and Baum et al.[18] No function has been ascribed to this peptide sequence. Although many bovine milk peptides derived from the same proteins as peptides found in human milk,[2] the amino acids within these sequences differed, presumably due to evolutionary changes.

All six cows released peptides from the same locations within each protein (α_{s1}-, α_{s2}-, β-, κ-casein, osteopontin, and glycosylation-dependent cell adhesion molecule 1), but with various levels. None of the protein fragments were derived from the protein signal sequence of any of the proteins.

Enzyme Cleavage. Plasmin (EC 3.4.21.7) was interpreted by computation to be a major agent of cleavage in the bovine mammary gland (see Figure 4). Plasmin is a serine protease that cleaves on the C-terminal side of arginine or lysine.[28] Cleavage after arginine or lysine accounts for the majority of released peptides by count. Plasmin and trypsin cannot be differentiated with these methods, because both cleave after arginine or lysine; however, no evidence for trypsin in bovine milk exists.[29] Plasmin is known to be present and active in bovine milk.[30] Plasmin is thought to enter milk from the blood,[30] and this interpretation is supported by the lack of mRNA for plasminogen in bovine mammary epithelial cells.[31] The remaining cleavage sites are interpreted to be created by elastase and cathepsins B and D (Figure 4) on the basis of their match to the cleavage specificity of the remainder of cleavages. More cleavages were attributed to cathepsin D than to cathepsin B for all milks. A separate column shows that many peptide cleavage sites could not be differentiated between cathepsins B and D. Likewise, several peptide cleavages were assigned to elastase in each milk sample, and a substantial number of cleavages could not be differentiated between the cathepsins and elastase. Cathepsin D (3.4.23.5), cathepsin B (EC 3.4.22.1), and elastase (EC 3.4.21.36) have been proven to exist in milk via either sequencing or antibody recognition.[32] Other cathepsins (i.e., cathepsins L (EC 3.4.22.15) and G (EC 3.4.21.20)) may also be present in milk, but their presence has not been confirmed.[32] Therefore, in this analysis, only plasmin, cathepsin B, cathepsin D, and elastase were assessed. Not all cleavage sites were matched to these enzymes: on average, 237.6 cleavage sites for each milk sample were assigned to plasmin, cathepsin B, cathepsin D, or elastase. However, on average, another 108.3 cleavage sites could not be assigned to these enzymes. This finding suggests that other enzymes not assessed here (nor proven to exist in bovine milk) are active in the bovine mammary gland. Further research to determine which enzymes are responsible is warranted.

***α_{s1}*-Casein.** Isracidin, a peptide derived from α_{s1}-casein (RPKHPIKHQGLPQEVLNENLLRF, 16−38) was identified in the bovine milks. Isracidin is known to be active against *S. aureus* and the yeast *Candida albicans*.[33] The signal sequence of α_{s1}-casein is amino acids 1−15, so in the terminology of this paper, the position would be 16−38 (which includes the signal sequence). This paper is the first to identify isracidin as a naturally occurring peptide in bovine milk. Previously, isracidin was identified after digestion with chymosin.[33]

α_{s1}-Casokinin-5 (FFVAP, 38−42) a known angiotensin converting enzyme inhibitory peptide,[34] is found within the sequences of three identified peptides (38−49 **FFVAP**FPEVFGK, 38−51 **FFVAP**FPEVFGKEK, 38−54 **FFVAP**FPEVFGKEKVNE). Whether the FFVAP sequence will exhibit identical actions within a longer sequence is unknown. A closely overlapping peptide with these, α_{s1}-casein (39−52), was previously found in Mansor et al.[19]

α-Casein exorphin (RYLGYLE, 105−111), a known opioid agonist peptide[35] from α_{s1}-casein, is found within three sequences found (95−115 HIQKEDVPSE**RYLGYLE**QLLR, 95−117 HIQKEDVPSE**RYLGYLE**QLLRLK, 95−119 HIQKEDVPSE**RYLGYLE**QLLRLKKY). It is not known whether

dx.doi.org/10.1021/jf4040964 | J. Agric. Food Chem. 2014, 62, 58−65

these longer sequences will retain the opioid inhibitory function. RYLGYLE has naloxone-inhibitable opioid-like properties.[36] RYLGYLE is a δ-selective opioid receptor ligand.[35] Opioid receptors are found in the digestive tract and the brain.

α_{s1}-Immunocasokinin-6, TTMPLW (208−214) from α_{s1}-casein, which has angiotensin-converting enzyme inhibitory[36] and immunomodulatory function,[37] is present within two sequences (187−214, 191−214). α_{s1}-Immunocasokinin-6 is known to decrease proliferation of lymphocytes,[38] decrease proliferation of human peripheral blood mononuclear cells,[39] increase antibody formation and macrophage phagocytosis,[40] and decrease *Klebsiella pneumoniae* infection in mice.[41,42]

Caseicin B (EVFGKEKVN, 45−53) from α_{s1}-casein inhibits the growth of *E. sakazakii* of α_{s1}-casein and is found within the sequence identified 40−54. Whether this longer sequence has antimicrobial function is unknown.

β-Casein. Peptide 16−39 from β-casein (RELEELNVPGEIVESLSSSEESIT) is a known caseinophosphopeptide that binds to calcium with its phosphorylation sites.[37] This binding of peptides to calcium hinders calcium phosphate precipitation in the milk, increasing the bioavailability of this mineral.[43] This peptide is present within the sequences of five peptide sequences found in this data set (16−40, 16−43, ranging from one to three phosphorylations).

Casoparan (41−45, INKKI)[44] is present within one larger sequence detected in β-casein: **INKKI**EKFQSEEQQQTEDELQDK (41−63). Casoparan activates macrophages to increase their phagocytic activity and peroxide release. Casoparan also acts as a bradykinin-potentiating peptide (i.e., increasing the duration or magnitude or bradykinin's vasodilatory effects).[44] Whether casoparan is functional within this larger sequence is unknown.

Casohypotensin (129−136, YPVEPFTE),[45] another bradykinin-potentiating peptide and a competitive inhibitor of angiotensin converting enzyme, is present within longer sequences in the identified β-casein protein fragment: HKEMPFPK**YPVEPFTE**SQSL (121−140). Whether casohypotensin is functional within this larger sequence is unknown.

β-Casokinin-7, an ACE inhibitor[46] from β-casein AVPYPQR 192−198, is present in several larger peptides in bovine milk but missing the initial alanine as 193−201 **VPYPQR**DMP and 193−204 **VPYPQR**DMPIQA. Whether the missing alanine is important to function as an ACE inhibitor is unknown. In addition, β-casein (193−209) in previous literature has been shown to have bitter taste perception.[47] β-Casein (193−204) found here may also have bitter taste.

Casecidin-15 YQEPVLGPVRGPFPI (208−222) from β-casein has been shown to be antimicrobial toward *E. coli*[48] and is present in the identified peptide sequences but lacking two amino acids: β-casein (210−222). A similar peptide, casecidin-17 YQEPVLGPVRGPFPIIV (208−224) that is also antimicrobial toward *E. coli*,[48] is also present but missing two amino acids: β-casein (210−224).

α_{s2}-Casein. A known antihypertensive peptide from α_{s2}-casein (TKVIP, 213-217) was present within an identified peptide sequence α_{s2}-casein (**TKVIP**YVRYL, 213−222). Whether this longer sequence will have antihypertensive function is unknown.

As endogenous milk peptides could be released by a variety of proteases, a nonspecific cleavage pattern was necessary for the X!Tandem searches. Searching X!Tandem with a nonspecific cleavage (rather than the typical tryptic cleavage employed for proteomic studies) against the full bovine proteome with modifications allowed resulted in a failed search because the search space was too large for the program. Therefore, to reduce the search space, a smaller list of proteins compiled from all proteins identified in proteomic studies of bovine milk was used. This restriction of the protein library used may have affected the results. Improvements in database searching speed would allow more thorough analysis of nonspecifically cleaved peptides.

Some endogenous milk peptides may be glycosylated. However, peptides with unknown glycosylation cannot be identified currently with X!Tandem. In addition, identification of glycopeptides with our approach is difficult as CID leads to mostly glycosidic cleavages rather than peptide chain cleavages.[49] This pattern allows identification of the glycan but not the peptide. The use of an alternate fragmentation strategy, such as electron transfer detection, which fragments both the glycan and peptide moieties,[49] could resolve this problem. In addition, glycopeptides ionize poorly in comparison with peptides,[49] thus making them difficult to detect without prior fractionation to increase their abundance. Identification of nonspecifically cleaved naturally occurring glycopeptides from a complex biological mixture remains a major challenge in glycobiology.[50]

The results of these healthy cow's milk are likely to differ from milks of cows with mastitis, an inflammation of the mammary gland. As somatic cell counts were not measured in these milks, we cannot rule out the possibility that some of these cows had subclinical mastitis, which could affect the results. Milks from cows with mastitis are known to have upregulated plasmin, cathepsin, and elastase[32,51,52] as well as urokinase-type plasminogen activator.[7] In addition, invading bacteria present in mastitis are also known to release exogenous enzymes into the milk, including elastase.[53] Previous work has shown that mastitic milks, compared to healthy milks, significantly differ in relative abundance of 33 identified peptide sequences.[19] All six of the peptides identified in this work that matched those identified in Mansor et al. were found in both healthy and mastitis cows but at different levels. As absolute quantification is employed for neither the work of Mansor et al. nor the present research, the abundances of peptides between these cows and the mastitic cows in the previous work are not comparable.

■ ASSOCIATED CONTENT

Ⓢ Supporting Information

List of all peptides identified including their sequence, modifications, and peak volume in each of the bovine milk samples. This material is available free of charge via the Internet at http://pubs.acs.org.

■ AUTHOR INFORMATION

Corresponding Author

*(D.C.D.) E-mail: dcdallas@ucdavis.edu. Phone: (530) 752-4137.

Funding

We gratefully acknowledge funding from the National Science Foundation Graduate Research Fellowship Program and the USDA National Institute for Food and Agriculture Postdoctoral Fellowship, the National Institutes of Health (R01 HD059127 and UL1 TR000002).

Notes

The authors declare no competing financial interest.

■ ACKNOWLEDGMENTS

We thank Cora J. Dillard for editing the manuscript.

■ ABBREVIATIONS USED

MALDI-TOF/TOF, matrix-assisted laser desorption/ionization tandem time-of-flight; ACN, acetonitrile; TFA, trifluoroacetic acid; FA, formic acid; Q-TOF, quadrupole time-of-flight; Da, Dalton; GlyCAM-1, glycosylation-dependent cell adhesion molecule 1

■ REFERENCES

(1) Ferranti, P.; Traisci, M. V.; Picariello, G.; Nasi, A.; Boschi, V.; Siervo, M.; Falconi, C.; Chianese, L.; Addeo, F. Casein proteolysis in human milk: tracing the pattern of casein breakdown and the formation of potential bioactive peptides. *J. Dairy Res.* **2004**, *71*, 74−87.

(2) Dallas, D. C.; Guerrero, A.; Khaldi, N.; Castillo, P. A.; Martin, W. F.; Smilowitz, J. T.; Bevins, C. L.; Barile, D.; German, J. B.; Lebrilla, C. B. Extensive in vivo human milk peptidomics reveals specific proteolysis yielding protective antimicrobial peptides. *J. Proteome Res.* **2013**, *12*, 2295−2304.

(3) Politis, I. Plasminogen activator system: Implications for mammary cell growth and involution. *J. Dairy Sci.* **1996**, *79*, 1097−1107.

(4) Andrews, A. T. Proteinases in normal bovine milk and their action on caseins. *J. Dairy Res.* **1983**, *50*, 45−55.

(5) Nielsen, S. S. Plasmin system and microbial proteases in milk: characteristics, roles, and relationship. *J. Agric. Food Chem.* **2002**, *50*, 6628−6634.

(6) Heegaard, C. W.; Rasmussen, L. K.; Andreasen, P. A. The plasminogen activation system in bovine milk: Differential localization of tissue-type plasminogen activator and urokinase in milk fractions is caused by binding to casein and urokinase receptor. *Biochim. Biophys. Acta−Mol. Cell. Res.* **1994**, *1222*, 45−55.

(7) Heegaard, C. W.; Christensen, T.; Rasmussen, M. D.; Benfeldt, C.; Jensen, N.; Sejrsen, K.; Petersen, T. E.; Andreasen, P. Plasminogen activators in bovine milk during mastitis, an inflammatory disease. *Fibrinolysis* **1994**, *8*, 22−30.

(8) Hinz, K.; Larsen, L. B.; Wellnitz, O.; Bruckmaier, R.; Kelly, A. Proteolytic and proteomic changes in milk at quarter level following infusion with *Escherichia coli* lipopolysaccharide. *J. Dairy Sci.* **2012**, *95*, 1655−1666.

(9) Larsen, L. B.; Boisen, A.; Petersen, T. E. Procathepsin D cannot autoactivate to cathepsin D at acid pH. *FEBS Lett.* **1993**, *319*, 54−58.

(10) Kaminogawa, S.; Yamauchi, K. Acid protease of bovine milk. *Agric. Biol. Chem.* **1972**, *36*, 2351−2356.

(11) Eigel, W. Identification of proteose-peptone component 5 as a plasmin-derived fragment of bovine β-casein. *Int. J. Biochem.* **1981**, *13*, 1081−1086.

(12) Paquet, D.; Alais, C.; Aubert, F. Review: the proteose-peptone fraction of milk. *Lait* **1989**, *69*, 1−21.

(13) Girardet, J. M.; Linden, G. PP3 component of bovine milk: a phosphorylated whey glycoprotein. *J. Dairy Res.* **1996**, *63*, 333−350.

(14) Andrews, A. T.; Alichanidis, E. Proteolysis of caseins and the proteose-peptone fraction of bovine milk. *J. Dairy Res.* **1983**, *50*, 275−290.

(15) Andrews, A. T. The formation and structure of some proteose-peptone components. *J. Dairy Res.* **1979**, *46*, 215−218.

(16) Sørensen, E. S.; Petersen, T. E. Phosphorylation, glycosylation and amino acid sequence of component PP3 from the proteose peptone fraction of bovine milk. *J. Dairy Res.* **1993**, *60*, 535−542.

(17) Meltretter, J.; Schmidt, A.; Humeny, A.; Becker, C.-M.; Pischetsrieder, M. Analysis of the peptide profile of milk and its changes during thermal treatment and storage. *J. Agric. Food Chem.* **2008**, *56*, 2899−2906.

(18) Baum, F.; Ebner, J.; Pischetsrieder, M. Identification of multiphosphorylated peptides in milk. *J. Agric. Food Chem.* **2013**, *61*, 9110−9117.

(19) Mansor, R.; Mullen, W.; Albalat, A.; Zerefos, P.; Mischak, H.; Barrett, D. C.; Biggs, A.; Eckersall, P. D. A peptidomic approach to biomarker discovery for bovine mastitis. *J Proteomics* **2013**, *85*, 89−98.

(20) Craig, R.; Beavis, R. C. TANDEM: matching proteins with tandem mass spectra. *Bioinformatics* **2004**, *20*, 1466−1467.

(21) Reinhardt, T. A.; Lippolis, J. D. Bovine milk fat globule membrane proteome. *J. Dairy Res.* **2006**, *73*, 406−416.

(22) Wilson, N. L.; Robinson, L. J.; Donnet, A.; Bovetto, L.; Packer, N. H.; Karlsson, N. G. Glycoproteomics of milk: differences in sugar epitopes on human and bovine milk fat globule membranes. *J. Proteome Res.* **2008**, *7*, 3687−3696.

(23) Reinhardt, T.; Lippolis, J. Developmental changes in the milk fat globule membrane proteome during the transition from colostrum to milk. *J. Dairy Sci.* **2008**, *91*, 2307−2318.

(24) Gasteiger, E.; Hoogland, C.; Gattiker, A.; Duvaud, S. E.; Wilkins, M.; Appel, R.; Bairoch, A. Protein identification and analysis tools on the ExPASy server. In *The Proteomics Protocols Handbook*; Walker, J. M., Ed.; Humana Press: Totowa, NJ, USA, 2005; pp 571−607.

(25) Ng-Kwai-Hang, K.; Kroeker, E. Rapid separation and quantification of major caseins and whey proteins of bovine milk by polyacrylamide gel electrophoresis. *J. Dairy Sci.* **1984**, *67*, 3052−3056.

(26) Lönnerdal, B. Nutritional and physiologic significance of human milk proteins. *Am. J. Clin. Nutr.* **2003**, *77*, 1537S.

(27) Sato, R.; Noguchi, T.; Naito, H. Casein phosphopeptide (CPP) enhances calcium absorption from the ligated segment of rat small intestine. *J. Nutr. Sci. Vitaminol. (Tokyo)* **1986**, *32*, 67−76.

(28) Le Bars, D.; Gripon, J.-C. Specificity of plasmin towards bovine α_{s2}-casein. *J. Dairy Res.* **1989**, *56*, 817−821.

(29) O'Mahony, J.; Fox, P.; Kelly, A. Indigenous enzymes of milk. In *Advanced Dairy Chemistry*; Springer: New York, 2013; pp 337−385.

(30) Eigel, W.; Hofmann, C.; Chibber, B.; Tomich, J.; Keenan, T.; Mertz, E. Plasmin-mediated proteolysis of casein in bovine milk. *Proc. Natl. Acad. Sci. U.S.A.* **1979**, *76*, 2244−2248.

(31) Wickramasinghe, S.; Rincon, G.; Islas-Trejo, A.; Medrano, J. F. Transcriptional profiling of bovine milk using RNA sequencing. *BMC Genomics* **2012**, *13*, 45−58.

(32) Kelly, A.; O'Flaherty, F.; Fox, P. Indigenous proteolytic enzymes in milk: a brief overview of the present state of knowledge. *Int. Dairy J.* **2006**, *16*, 563−572.

(33) Lahov, E.; Regelson, W. Antibacterial and immunostimulating casein-derived substances from milk: casecidin, isracidin peptides. *Food Chem. Toxicol.* **1996**, *34*, 131−145.

(34) Maruyama, S.; Mitachi, H.; Awaya, J.; Kurono, M.; Tomizuka, N.; Suzuki, H. Angiotensin I-converting enzyme-inhibitors derived from an enzymatic hydrolysate of casein. 5. Angiotensin I-converting enzyme inhibitory activity of the c-terminal hexapeptide of α_{s1}-casein. *Agric. Biol. Chem.* **1987**, *51*, 2557−2561.

(35) Loukas, S.; Varoucha, D.; Zioudrou, C.; Streaty, R. A.; Klee, W. A. Opioid activities and structures of α-casein-derived exorphins. *Biochemistry (Moscow)* **1983**, *22*, 4567−4573.

(36) Gill, H.; Doull, F.; Rutherfurd, K.; Cross, M. Immunoregulatory peptides in bovine milk. *Br. J. Nutr.* **2007**, *84*, 111−117.

(37) Gobbetti, M.; Stepaniak, L.; De Angelis, M.; Corsetti, A.; Di Cagno, R. Latent bioactive peptides in milk proteins: proteolytic activation and significance in dairy processing. *Crit. Rev. Food Sci. Nutr.* **2002**, *42*, 223−239.

(38) Otani, H.; Hata, I. Inhibition of proliferative responses of mouse spleen lymphocytes and rabbit Peyer's patch cells by bovine milk caseins and their digests. *J. Dairy Res.* **1995**, *62*, 339−339.

(39) Kayser, H.; Meisel, H. Stimulation of human peripheral blood lymphocytes by bioactive peptides derived from bovine milk proteins. *FEBS Lett.* **1996**, *383*, 18−20.

(40) Jolles, P.; Fiat, A.; Migliore-Samour, D.; Drouet, L.; Caen, J. Peptides from milk proteins implicated in antithrombosis and

immunomodulation. In *New Perspectives in Infant Nutrition, Symposium Antwerp*; Thieme Medical Publishers: New York, 1993; pp 160−172.
(41) Schlimme, E.; Meisel, H. Bioactive peptides derived from milk-proteins − structural, physiological and analytical aspects. *Nahrung−Food* **1995**, *39*, 1−20.
(42) Meisel, H. Biochemical properties of regulatory peptides derived from milk proteins. *Biopolymers* **1997**, *43*, 119−128.
(43) Meisel, H.; Frister, H. Chemical characterization of a caseinophosphopeptide isolated from in vivo digests of a casein diet. *Biol. Chem. Hoppe-Seyler* **1988**, *369*, 1275−1280.
(44) Lebrun, I.; Cavallaro, V.; Juliano, L.; Juliano, M. A. Effects of 'casoparan', a peptide isolated from casein hydrolysates with mastoparan-like properties. *Mediators Inflamm.* **2004**, *13*, 263−268.
(45) Perpetuo, E. A.; Juliano, L.; Lebrun, I. Biochemical and pharmacological aspects of two bradykinin-potentiating peptides obtained from tryptic hydrolysis of casein. *J. Protein Chem.* **2003**, *22*, 601−606.
(46) Maruyama, S.; Nakagomi, K.; Tomizuka, N.; Suzuki, H. Angiotensin I-converting enzyme inhibitor derived from an enzymatic hydrolysate of casein. II. Isolation and bradykinin-potentiating activity on the uterus and the ileum of rats. *Agric. Biol. Chem.* **1985**, *49*, 1405−1409.
(47) Singh, T. K.; Young, N. D.; Drake, M.; Cadwallader, K. R. Production and sensory characterization of a bitter peptide from *β*-casein. *J. Agric. Food Chem.* **2005**, *53*, 1185−1189.
(48) Birkemo, G.; O'Sullivan, O.; Ross, R.; Hill, C. Antimicrobial activity of two peptides casecidin 15 and 17, found naturally in bovine colostrum. *J. Appl. Microbiol.* **2009**, *106*, 233−240.
(49) Mechref, Y. Use of CID/ETD mass spectrometry to analyze glycopeptides. In *Current Protocols in Protein Science*; Wiley: New York, 2001.
(50) Dallas, D. C.; Martin, W. F.; Hua, S.; German, J. B. Automated glycopeptide analysis − review of current state and future directions. *Brief. Bioinform.* **2012**, *14*, 361−374.
(51) Saeman, A. I.; Verdi, R.; Galton, D.; Barbano, D. Effect of mastitis on proteolytic activity in bovine milk. *J. Dairy Sci.* **1988**, *71*, 505−512.
(52) Kirschke, H.; Barrett, A.; Glaumann, H.; Ballard, F. *Lysosomes: Their Role in Protein Breakdown*; Academic Press: London, UK, 1987; pp 193−283.
(53) Fleminger, G.; Heftsi, R.; Uzi, M.; Nissim, S.; Gabriel, L. Chemical and structural characterization of bacterially-derived casein peptides that impair milk clotting. *Int. Dairy J.* **2011**, *21*, 914−920.

JOURNAL OF AGRICULTURAL AND FOOD CHEMISTRY

Article

pubs.acs.org/JAFC

Impact of the Nonvolatile Wine Matrix Composition on the *In Vivo* Aroma Release from Wines

Carolina Muñoz-González, Pedro J. Martín-Álvarez, M. Victoria Moreno-Arribas, and M. Ángeles Pozo-Bayón*

Instituto de Investigación en Ciencias de la Alimentación (CIAL) (CSIC-UAM) C/Nicolás Cabrera 9, 28049 Madrid, Spain

ABSTRACT: The impact of the nonvolatile wine matrix composition on the retronasal aroma release of four volatile compounds added to different types of wines has been evaluated. For this purpose, a tailor-made retronasal aroma trapping device (RATD) was used to entrap the exhaled breath of six panelists previously trained in a specific consumption procedure. Five wines of different composition (white wine, sparkling white wine, young red wine, aged red wine, and a sweet wine) were evaluated. Prior to the evaluation, with the exception of the sweet wine, the wines were adjusted to the same ethanol content and aromatized with a mixture of four target volatile compounds. Aroma release data were submitted to multivariate statistical analysis in order to relate wine chemical composition and aroma release during wine drinking. Results showed interindividual differences and a clustering of panelists among lower and higher aroma releasers, which was in agreement to the differences in their breathing capacity. A significant influence of the matrix composition in the low aroma releasers group during wine consumption was observed. The consumption of red wines provoked a significantly higher aroma release than the consumption of white and sweet wines. From the chemical composition determined in the wine samples (pH, total acidity, total polyphenols, neutral polysaccharides, residual sugar, and nitrogenous compounds), the amount of total polyphenols was better correlated with the observed effect.

KEYWORDS: *wine, nonvolatile wine matrix, retronasal aroma, in vivo aroma release, wine drinking*

INTRODUCTION

The hedonic behavior behind wine consumption is greatly influenced by wine aroma, which is one of the most outstanding characteristics in explaining wine quality. Wine aroma is composed of hundreds of volatile compounds which depending on their concentration and chemical structure will have a higher or lower impact on the overall flavor profile of a wine.[1,2] The characterization of these compounds and the elucidation of their sensory relevance for wine aroma have been the focus of many interesting works,[3−5] and taking into account the magnitude of this task, it is likely these works will continue in the future.

However, we already know that only the characterization of the overall flavor composition of a food (for example: the headspace profile) does not directly correlate with the perceived sensations during consumption.[6] The process of aroma release during food consumption is a sequential process, which starts when the food is smelled (orthonasal aroma) and continues during the processing of the food in the mouth. Within the oral cavity, volatile compounds are released from the food and from here breathing flow carries them to the olfactory region where they are perceived. This is a dynamic and complex process known as retronasal aroma, in which not only the physicochemical characteristics of the compounds, but other physiological factors such as breathing flow, the presence of saliva, and tongue movements are also involved.[6,7] For liquid foods, such as wine, although the processing in the mouth could not be as critical, there are some factors such as the formation of a coating on the pharyngeal mucosa, the flow rates, temperature, etc., that should be considered as important aspects for modulating the aroma released available for the olfactory receptors during consumption.[7−10]

In spite of the facts that retronasal aroma is directly related to flavor perception and it is a key modulator for food consumption and food preferences, there are not many scientific works directed toward understanding aroma release during wine consumption. This type of study would need new analytical approaches based on monitoring aroma release during drinking.[1] One possible approach is the use of artificial devices to simulate the drinking process. Following this *in vitro* approach, Genovese and collaborators[11] studied the influence of saliva on wine aroma release. Although, undoubtedly, the use of artificial devices has considerable advantages (better control of the variables of the study, many experimental repetitions, no requirements of human subjects avoiding ethical considerations, etc.), they cannot mimic the real situation during wine consumption; therefore, they do not take into consideration all the physiological factors involved in aroma release (such as swallowing), making their correlation with sensory perception difficult. Other approaches to monitor aroma release during *in vivo* food consumption, such as the use of real time monitoring (breath by breath analysis) using mass spectrometric techniques such as atmospheric pressure ionization or proton transfer reaction mass spectrometric techniques (API-MS and PTR-MS, respectively),[12,13] or the use of aroma trapping devices of exhaled breath during consumption,[14−16] which are

Received: July 26, 2013
Revised: December 11, 2013
Accepted: December 11, 2013
Published: December 11, 2013

ACS Publications © 2013 American Chemical Society

often employed to study aroma release in many types of liquid and solid foods, have not been often applied in the wine field. Only Lasekan et al.,[17] applied an exhaled odor trapping device to investigate the aroma compounds released during the consumption of palm wine.

On the other hand, in recent years, the influence of the nonvolatile matrix composition has been highlighted as an outstanding factor influencing wine aroma release.[18−24] Using specific wine nonvolatile components[19,22−24] or the whole wine matrix composition[20,21] it has been possible to determine the interaction effect between wine compounds and specific wine volatiles. Even the effect of these interactions on the sensory characteristics of wines has been shown.[25,26] Most of these analytical studies have been carried out in static conditions, which, although very valuable, do not represent the retronasal aroma delivery of volatiles during a real wine consumption situation.

Therefore, the objective of this work was to determine the impact of the nonvolatile wine matrix composition on the *in vivo* aroma release during the consumption of different types of wines. To achieve the objective of this work, a tailor-made retronasal aroma trapping device (RATD) was used to trap the exhaled breath of six panelists previously trained in a specific consumption procedure. Five wines of different composition were aromatized with a mixture of volatile compounds at the same concentration and the aroma release data were submitted to multivariate statistical analysis in order to relate wine chemical composition and aroma release during wine drinking.

MATERIAL AND METHODS

Wine Samples. Five commercial Spanish wines representative of different winemaking technologies and with different matrix compositions were selected for this study: a young Verdejo white wine (**WH-W**), a young Tempranillo red wine (**YR-W**), a 4-year old (16 months in oak barrels) Tempranillo red wine (**AR-W**), a Cava white wine (Spanish sparkling wine manufactured by the traditional method) (**SP-W**), and a sweet biologically aged wine made from Pedro Ximénez grapes (**SW-W**).

In order to minimize the effect of ethanol on the volatility of aroma compounds, all the wines, except the sweet wine that was kept at its initial concentration (15% v/v) were adjusted to the same ethanol content (13.5% v/v). All the wines were spiked with four *food-grade* aroma compounds from Sigma-Aldrich (Steinheim, Germany) characterized by presenting different physicochemical properties (Table 1). To do that, four independently aroma stock solutions in ethanol absolute were prepared and from here, each aroma compound was added to the wines to obtain a final concentration of 50 mg/L. The initial concentration of these aroma compounds in the original wines was also previously determined in the five types of wines (Rodriguez-Bencomo et al., 2011[20]) showing that endogenous aroma represent a 5% of the aroma added to the wines, except for β-phenyl ethanol, which concentration corresponded to 15%. The considerably lower amount of these compounds in the original wines compared to the higher amount of the exogenously added aroma should not interfere on the solubility or volatility properties of the added aroma compounds as has been previously shown (Athes et al., 2004[27]).

Table 1. Main Physicochemical Characteristics of the Aroma Compounds Used in the Study of Aroma Release during the Consumption of Different Types of Wine Matrices

compound	chemical group	molecular weight (g/mol)	log P^a	boiling point (°C)	solubility[b] (mg/L)
isoamyl acetate	ester	130.2	2.3	134.9	1070.0
ethyl hexanoate	ester	144.1	2.8	167.0	308.7
linalool	terpene	152.2	3.4	204.1	683.7
β-phenylethanol	alcohol	122.2	1.6	224.9	21990.0

[a]Hydrophobic constant. [b]Solubility in water at 25 °C estimated using molecular modeling software EPI Suite (U.S. EPA 2000−2007).

Retronasal Aroma Trapping Device (RATD). A tailor-made retronasal trapping device (RATD) was employed for this study. This glass device allowed the trapping of exhaled breath after wine consumption into a Tenax trap thanks to a nosepiece coupled to a hollow tube in which the trap was fitted. A vacuum pump connected to a rotameter allowed a steady flow through the trap. Finally, a flowmeter allowed us to know the exact flow through the trap. In preliminary experiments, an optimization and validation of the effectiveness of this device for the purposes of this study was performed. The retention time, ion of quantification, the range of concentration assayed for each volatile compound and regression lines, together with the values of the residual standard deviation (s) and the determination coefficient (R^2), which are estimators of the adequacy of the regression models, are presented in Table 2. In addition, the inter- and intratraps variability is presented. Adequate relative standard deviation between analysis, very low values of s and satisfactory values for the regression coefficients were obtained for the assayed compounds: isoamyl acetate (R^2 = 0.964), ethyl hexanoate (R^2 = 0.991), linalool (R^2 = 0.985), and β-phenylethanol (R^2 = 0.978).

Retronasal Aroma Trapping Procedure during Wine Consumption. Six volunteers (2 males and 4 females) between 26 and 34 years old previously trained in the retronasal aroma trapping procedure participated in this study. They were instructed not to eat, drink, or smoke 2 h before the experiments. They had no known illnesses and had self-reported normal olfactory and gustatory functions. Before each experiment, the panelists had to clean their mouths and rinse with a bicarbonate solution. The monitoring of the oral cavity of the panelists for the four compounds of interest was performed before each analysis.

The drinking procedure consisted in mainly two steps. In the first one, 20 mL of wine contained in a syringe were provided to the panelist, who had to keep it in the mouth for 10 s with the lips closed. After this time, the panelist had to swallow and breath normally through the nose into the glass nosepiece for 20 more seconds. During the experiment, a relatively small amount of wine, typically consumed with a meal (100 mL) was provided. Two repetitions of the same wine were performed on the same day but on different sessions (leaving at least 2 h between replications). The same procedure was followed with the original control wines (without aroma added), so that we could find out the amount of aroma initially present in the wines that could be trapped with this device. These results were used to correct the aroma release data.

Analysis of Volatile Compounds. The aroma compounds from the expiration of breath by the nose and trapped onto the Tenax cartridges were desorbed with 6 mL of a hexane/diethyl ether solution (1:1). Thirty microliters of an internal standard (3-octanol) were added, and the sample was then concentrated using a nitrogen stream to a final volume of 200 μL and analyzed in the GC-MS. A volume of 8 μL of the concentrated breath extract was injected in a cool injection system unit (CIS), (Gerstel, Mülheim an der Ruhr, Germany) in the solvent vent mode. The injector temperature ranged from −80 to 270 °C.

The identification of volatile compounds was carried out with a Gas Chromatograph Agilent 6890N coupled to a quadrupole Mass Detector Agilent 5973. After injection on the CIS, volatile compounds were separated on a Supra-Wax polar capillary column (60 m × 0.25 mm i.d. × 0.50 μm film thickness) from Konik (Barcelona, Spain). Helium was used as the carrier gas at a flow rate of 1 mL/min. The oven temperature was initially held at 50 °C for 2 min, then increased at 8 °C/min to 240 °C and held for 15 min.

For the MS system (Agilent 5973N), the temperatures of the transfer line, quadrupole, and ion source were 270, 150, and 230 °C, respectively. Electron impact mass spectra were recorded at 70 eV ionization voltages, and the ionization current was 10 μA. The acquisitions were performed in Scan (from 35 to 350 amu) and SIM

Table 2. Chromatographic and Regression Parameters ($y = a + bx$) Determined for the Added Aroma Compounds in the Breathing Trapping Experiments

			linear regression[c]					repeatability[d]	
	RT[a]	ion Q[b]	linear range (mg/L)	a	b	s	R^2	intercartridge RSD (%)	intracartridge RSD (%)
isoamyl acetate	11.42	43	25−100	0.2209	0.0126	0.0930	96.4	13.3	6.8
ethyl hexanoate	13.32	88	0−100		0.0142	0.0982	99.1	23.0	14.9
linalool	18.53	71	0−100		0.0053	0.0487	98.5	11.6	11.8
β-phenylethanol	24.35	91	0−90		0.0002	0.0018	97.8	19.0	19.5

[a]RT = Retention time (minutes). [b]Ion Q = quantification ion. [c]Linear regression parameters = intercept (a), slope (b), residual standard deviation (s), and determination coefficient (R^2); [d]Repeatability is expressed as an average of 5 assays performed in the same conditions

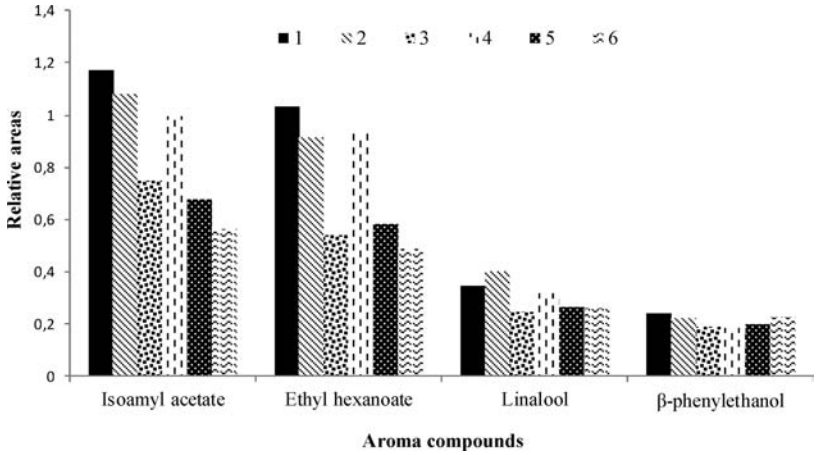

Figure 1. Average values of aroma release (relative peak areas) obtained for each panelist during wine consumption considering the five different wines (**WH-W**, **SP-W**, **YR-W**, **AR-W**, and **SW-W**) and two repetitions of the same wine. For better comparison, data for β-phenylethanol are multiplied by a factor of 10. Different background patterns mean different panelists.

modes. The identification of compounds was based on the comparison of retention times and mass spectra. The mass spectra were compared with those from NIST 2.0 database. Relative peak areas (RPAs) were obtained by calculating the relative peak area in relation to that of the internal standard. The use of RPAs data to express aroma release was sufficient for this type of analysis as the aim of the work was to compare the extent of aroma release between wine samples.

Wine Matrix Composition. Nitrogen compounds (total nitrogen, free amino acids, and peptides), neutral polysaccharides and residual sugars, total polyphenols, total acidity, and pH were determined in the five types of wines following the procedures previously described in Rodriguez-Bencomo et al., 2011.[20]

Statistical Analysis. The statistical methods used for data analysis were linear regressions to establish the regression parameters for each aroma compound released after wine drinking and the lack of fit test to judge the adequacy of the linear models: cluster analysis (the square Euclidean distance was taken as a measure of the proximity between two samples and Ward's method was used as linkage rule) to check the grouping of panelists depending on their aroma release performance; one-way ANOVA to test the influence of matrix composition on aroma release and to test compositional differences between wines; least significant difference (LSD) test for mean comparison; principal component analysis (PCA) to examine the relationship between compositional parameters and wine matrices; and correlation analysis to determine the existence of correlations between each of the compositional variables and the aroma release data of the four aroma compounds. The STATISTICA program for Windows Version 7.1 was used for data processing (StatSoft, Inc., 2005, www.statsoft.com).

RESULTS AND DISCUSSION

***In Vivo* Aroma Release from Wines.** Different published works have shown that wine matrix might play an important role on aroma release in static headspace conditions.[18−21,28,29] However, the relevance of this effect on a real wine consumption situation has not been evaluated so far. In this work, we have focused on the "in vivo" release (during wine consumption) of some target aroma compounds added to five wines with different matrix composition. We monitored, the so-called 'expiration breath', since it might be a good representation of the aroma compounds which interact with the olfactory system.[14] The type of aroma compounds (isoamyl acetate, ethyl hexanoate, linalool and β-phenylethanol) represented a wide range of physicochemical properties and the concentration was selected in order to make an easy-to-drink wine, preventing the possible tiredness and rejection of the wine by the panelists and avoiding analytical problems (sensitivity). To overcome the effect of ethanol, which has been shown, might significantly affect the partition coefficient of the aroma compounds,[19,30−33] all the wines, except the sweet wine were adjusted to the same ethanol concentration (13.5% v/v). The differences in ethanol content between the sweet wine (15% v/v) and the rest of the wines were of 1.5% (v/v), which is unlikely to exert a significant difference on the release of the aroma compounds. [33] Wines were consumed following a systematic procedure in order to minimize interindividual differences. Previous training sessions were performed with the panelists to familiarize them with the procedure. As it was described in Material and Methods, a tailor-made breathing trapping device, previously optimized and validated for this purpose was employed. Although this type of device did not allow us to monitor the retronasal aroma release in real time such as the breath by breath analysis using mass spectrometric techniques (PTR-MS; APCI-MS), other important advantages such as the unequivocally identification of the compounds of interest, the possibility of having a concentrated breath

extract,[14] and the facility to adapt it to any laboratory with a relatively low economical investment make it very interesting for the purposes of this type of study.

The average data (relative peak areas) corresponding to each of the aroma released by the six panelists, independent of the type of wine, is depicted in Figure 1. Previously, the same consumption procedure was employed to evaluate the five wines without spiked aromas, and only traces of the four aroma compounds were detected. However, all the release data were corrected taking into consideration these results. As can be observed in the figure, in spite that all the panelists followed a strict consumption procedure, for each single aroma compound, large differences in the released patterns between individuals were found. Interestingly, these differences seemed to be constant toward the same type of compound. For example, the interindividual release pattern of the two esters, isoamyl acetate and ethyl hexanoate, was quite similar; panelist #1 released the highest amount of these compounds, while panelist #6 always released the lowest. However, when considering a more chemically different compound, such as linalool, and β-phenylethanol, this pattern was different. For instance, linalool was more greatly released by panelists #1, #2, and #4, while the rest of subjects released almost the same amount. In addition, depending on the type of compound, differences between panelists were less pronounced, and for example, the release of β-phenylethanol was more or less the same for all of them. The existence of interindividual differences on aroma release patterns during food consumption have been extensively described, both in solid[34−36] and liquid food-matrices[6,8,9,37] and could be attributed to anatomical and physiological differences between panelists (respiratory flows, saliva composition, oral and pharyngeal mucosa, etc.).

To further investigate whether there was a trend in the aroma release pattern, a cluster analysis with the data corresponding to the aroma released by the 6 panelists during the consumption of the five different wines was performed. Figure 2 shows the dendrogram obtained from this analysis in which two groups of aroma releasers can be clearly observed. A first group formed by panelists #1, #2, and #4, and a second comprising of panelists #3, #5, and #6. Both groups could be called higher and lower releasers, respectively. A similar trend on flavor release was observed during the consumption of liquid emulsions,[37] and these differences between higher and lower releasers were also in agreement with previous works.[34,35] Although a higher number of individuals might be needed to confirm this trend, the preliminary results derived from this study indicated two behaviors on the aroma release during wine consumption.

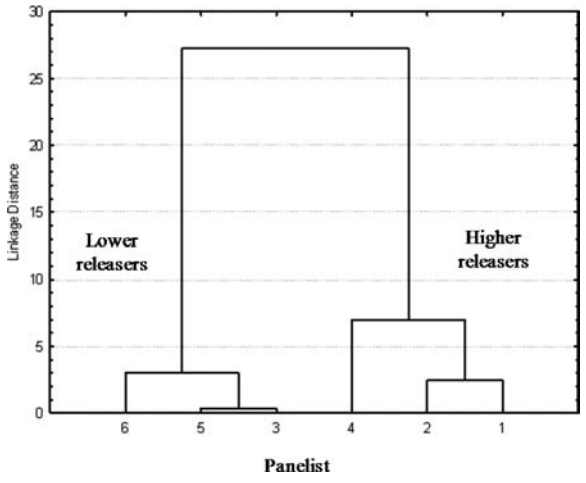

Figure 2. Dendrogram showing the grouping of panelists depending on their aroma release performance during the consumption of the five different types of wine.

Among the anatomical and physiological differences between panelists that might be responsible for the differences in the observed trends on aroma release, the variations in the flow rates between subjects might be an explanation. It has been suggested that a greater respiratory rate could contribute to bringing more volatiles to the upper airways, and consequently, more volatiles could be present in the expired air of the panelists.[36−38] However, in another study performed *in vivo* and *in vitro*, Well et al.[10] showed that an increase in flow rate resulted in a decrease in the aroma release.

To determine whether the breathing capacity might have an influence on the grouping of panelists in higher and lower releasers, two breathing related parameters corresponding to the vital capacity (VC) and forced vital capacity (FVC) were calculated. The vital capacity (VC) can be defined as the volume of air breathed out after the deepest inhalation,[39] while the forced vital capacity (FVC) is the determination of the vital capacity from a maximally forced expiratory effort.[40,41] In fact, FVC is the most basic maneuver in spirometry tests.[40,41] Both parameters were estimated considering different individual physiological variables such as age, sex, ethnic group, and height of the panelists. These data are shown in Table 3. As can be seen, the highest predicted FVC and VC values did indeed correspond to panelists from the first group (higher releasers), while the second group, the lower releasers, also showed the lowest FVC values. These results suggest that although other physiological variables might also affect the rate of aroma release during the consumption of wine, in the experimental conditions of this study, we have found a direct relationship between respiratory rate and aroma compounds in the expired air of the panelists, which might influence the sensory perception of wine aroma.

Table 3. Predicted Forced Vital Capacity (FVC) and Vital Capacity (VC) Values Calculated for the Panelists[a]

	FVC		VC	
panelist	predicted value (L)	SD	predicted value (L)	SD
1	4.75	0.43	4.47	0.13
2	5.63	0.86	5.75	0.12
3	4.12	0.43	3.90	0.13
4	5.72	0.86	5.65	0.12
5	4.52	0.43	4.28	0.13
6	4.00	0.43	3.81	0.13

[a]FVC and VC estimated using Dynamic Measurement Technologies software (www.dynamicmt.com) based on Hedenström et al., 1985−1986[40,41] and Langhammer et al., 2001,[39] respectively. SD: ± standard deviation.

Effect of Wine Matrix Composition on Aroma Release.

Considering the two types of behaviors between panelists regarding the aroma release during wine consumption (higher and lower releasers), release data (relative peak areas) obtained from both groups of panelists were separately treated and submitted to one-way ANOVA in order to know if the nonvolatile wine matrix composition could have a significant effect on aroma release during wine consumption. Surprisingly, we noticed that the effect of wine matrix was different

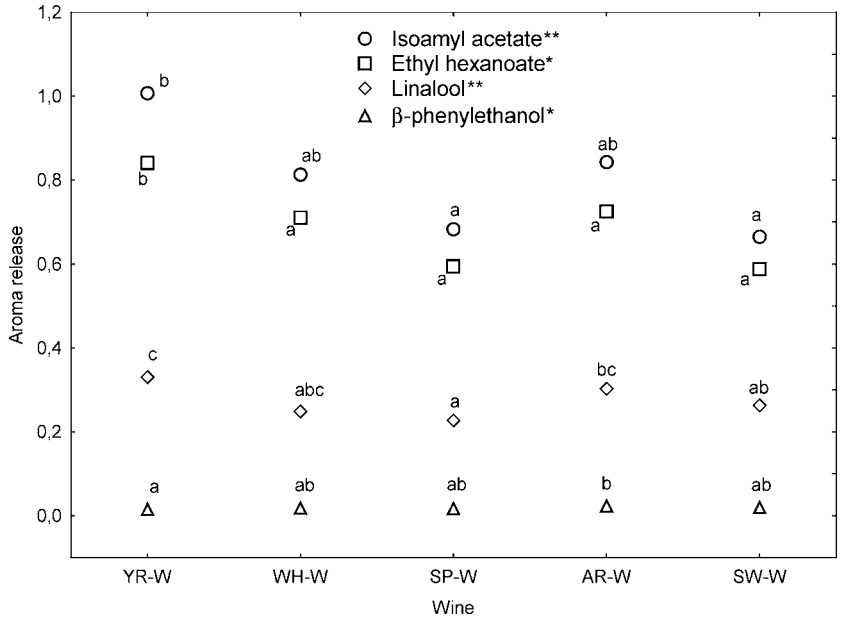

Figure 3. Results of the aroma release during the consumption of the five different types of wine for the lower releaser group. Significant differences on aroma release depending on matrix composition are indicated with * $0.05 < P < 0.1$ or ** $P < 0.05$. Different letters across the different wines denotes statistical differences after the application of LSD test.

Table 4. Mean ± Standard Deviation (SD) Values ($n = 3$) of the Chemical Composition of the Five Matrices: White Wine (WH-W), Sparkling Wine (SP-W), Young Red Wine (YR-W), Aged Red Wine (AR-W), Sweet Wine (SW-W)[a]

	WH-W		SP-W		YR-W		AR-W		SW-W	
	mean	SD	mean	SD	mean	SD	mean	SD	mean	SD
pH	2.99[a]	0.0	3.07[b]	0.0	3.93[d]	0.0	3.66[c]	0.0	4.12[e]	0.0
total acidity (mg tartaric acid/L)	5.60[e]	0.1	5.29[d]	0.1	4.06[b]	0.0	4.41[c]	0.1	3.68[a]	0.0
total polyphenols (mg gallic acid/L)	211.50[a]	0.6	173.23[a]	5.2	2009.67[d]	52.0	1859.67[c]	20.9	574.33[b]	41.1
neutral polysaccharides (g mannose/L)	1.82[a]	0.1	0.96[a]	0.1	2.66[a]	0.1	2.38[a]	0.1	171.07[b]	9.4
residual sugars (g/L)	1.59[a]	0.0	1.14[a]	0.0	3.82[b]	0.3	2.58[ab]	0.3	310.08[c]	2.7
total nitrogen (mg/L)	206.78[b]	3.8	129.36[a]	8.3	315.00[c]	51.1	358.68[c]	19.4	1010.80[d]	10.3
amino acids + peptides (mg N/L)	64.51[a]	0.7	104.38[b]	0.9	141.05[d]	3.2	113.07[c]	2.5	319.61[e]	2.4
amino acids (mg N/L)	36.39[a]	0.7	38.39[a]	0.4	69.59[c]	1.2	58.69[b]	3.2	67.20[c]	0.9
peptides (mg N/L)[b]	28.12[a]		65.99[c]		71.46[d]		54.39[b]		252.41[e]	

[a]Different letters across the different wines denotes statistical differences after the application of LSD test. [b]This data is indirectly determined as the difference between the analytical determination of amino acids plus peptides and free amino acids, therefore SD values are not included in the table.

depending on the group of panelists. For the higher releaser group, only the release of linalool was influenced by matrix composition ($0.05 < P < 0.1$). This result seemed to be related to some analytical constraints of the trapping device, such as the possible saturation of the Tenax trap during the experiment with higher releasers, which could have masked the wine matrix effect. However, considering the lower releaser group, all the compounds were significantly influenced by matrix composition; these results are shown in Figure 3 together with the results corresponding to the application of the LSD test with the five types of wine matrices. It is important to highlight that the differences on aroma release also depended on the type of aroma compound considered (e.g., we observed more differences on the release of linalool toward the different wines that on the release of β-phenylethanol); however, independently on the type of aroma compound considered, there was a clear trend, in which higher aroma release was always observed during the consumption of the two red wines (**YR-W** and **AR-W**) compared to the consumption of white wines (**WH-W** and **SP-W**) and the sweet wine (**SW-W**). As can be seen in Figure 3, the highest release of isoamyl acetate, ethyl hexanoate, and linalool was during the consumption of young red wine, while β-phenylethanol was more released during the consumption of aged red wine.

Therefore, in spite of the interindividual differences between panelists, the influence of wine matrix composition on the amount of aroma released during wine consumption was evidenced. This finding is in agreement with previous studies in the literature which have already demonstrated using static conditions, the existence of interaction between nonvolatile wine matrix components and aroma compounds, which might affect the release of aroma compounds into the headspace.[20,22−24,28] Moreover, the effect of wine matrix on aroma release has been shown in *in vitro*- dynamic conditions,[11] being this the first time that this effect is proven in an *in vivo*, real consumption situation.

In order to try to determine which component/s from the wine matrix were more involved on aroma release during wine consumption, the chemical characterization of the nonvolatile matrix composition of the five wines consumed by the panelists

was performed and it is shown in Table 4 together with the results of the LSD test. As can be seen, the five wines exhibited significant differences in their composition. As expected, the sweet wine (**SW-W**) was the most different, showing the highest pH (4.12), the lowest value of acidity (3.68 mg tartaric acid/L), and the highest content of neutral polysaccharides (171 g mannose/L) and residual sugars (310 g/L). In addition, this wine showed the highest levels of nitrogen compounds (total nitrogen, amino acids, and peptides). In spite of its *a priori*, higher matrix complexity, during the consumption of this wine, we did not observe a significant effect on aroma release, which was more similar to that experienced during the consumption of white wines (**WH-W** and **SW-W**). The lack of a clear interaction effect of this type of wine with typical wine aroma compounds is in agreement with previous results performed in static conditions.[20] It seems, at least, in static conditions, that the higher content of some small molecules in this wine, such as mono- and disaccharides or free amino acids[18,42] could be responsible for a "salting out" effect, which might compensate the retention effect exerted by other higher molecular weight compounds (such as polyphenols or proteins)[18,20] or by an increase in the solution hydrophobicity because of the presence of a large amount of hydrophobic sugars such as fructose.[33]

The consumption of the two white wines (**WH-W**, **SP-W**) provided in general, a lower aroma release. These wines exhibited the highest values of acidity (5.6−5.29 mg tartaric/L) and therefore lowest pH values (2.99−3.07), although these differences did not seem enough to explain the differences observed on aroma release compared with the aroma release during red wines consumption. In addition, white and sparkling wines showed the lowest values of the majority of nonvolatile compounds determined in the samples (polyphenols, polysaccharides, residual sugars, and nitrogen compounds). However, compared with red wines, the group of compounds that was dramatically different between the two types of samples was the content of total polyphenols. Red wines showed ten times more of these compounds (2010 and 1860 mg gallic acid/L for **YR-W** and **AR-W**, respectively) compared to white wines (211 and 173 mg gallic acid/L for **WH-W** and **SP-W**, respectively).

To better envisage the compositional differences between the five types of wines, a principal component analysis (PCA) was performed with the data from Table 4. Two principal components were obtained. The first one (PC1) was negatively related (|loadings| > 0.82) with all the compositional parameters (pH, neutral polysaccharides, residual sugars, nitrogen compounds) except total polyphenols and positively correlated with total acidity (0.92). The PC2 was positively correlated with the total polyphenol content (0.97). Figure 4 shows the representation of the wines on the plane defined by PC1 and PC2. Clearly, PC1 could distinguish between sweet wines, with high and negative values for this component from white and sparkling wines with high and positive values for PC1. Red wines appeared together between sweet and white wines. On the other hand, PC2 clearly separated red wines from the rest. This component was only defined by the polyphenol content, which clearly, as was previously commented, was much higher in these wines than in the rest.

Many works in the literature performed in static conditions have shown the existence of specific interactions between polyphenols and aroma compounds resulting in a reduction of the aroma released into the headspace.[22,28,33] For instance, it

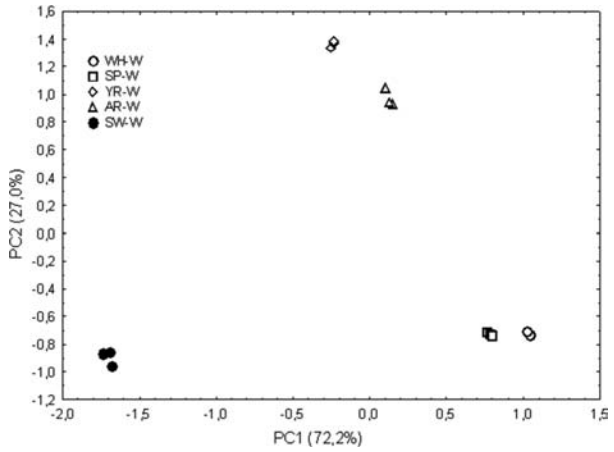

Figure 4. Representation of the wines on the plane defined by PC1 and PC2 obtained with the nonvolatile matrix composition data (Table 4).

has been shown that monomeric polyphenols, abundant in young red wines, can interact with terpenes in ethanolic solutions provoking a lower aroma release in *in vitro* conditions.[22] Other interactions that have been described involved the galloyl ring of some phenolic compounds and the aromatic ring of some aroma compound.[28,43] Moreover, the type and polymerization state, which is related with the polyphenol origin (from seed or skin), might be involved in different interaction with aroma molecules (Mitropoulou et al., 2011;[44] Lorrain et al., 2013[45]). Anyway, in dynamic real drinking conditions, as we have used in this study, aroma release seems to be enhanced by the presence of polyhenols. One possible explanation could be that after swallowing, these types of compounds could specifically interact with pharyngeal and/or esophageal mucosa contributing to the formation of a product coating on the throat and pharynx, which could increase the contact area between air and product, favoring aroma release.[8] In fact, some works in the literature have already suggested interactions between aroma compounds and oral/esophageal mucosa to explain a delay on aroma release, which to an extent might be dependent on product composition.[9,46] Another explanation, could be the formation of polyphenol−aroma complexes in the surface coating, acting as aroma reservoirs and resulting in a greater concentration of aroma molecules ready to be released by the expiration flows. In fact, in *in vitro* systems (static headspace), using reconstituted wine samples, Mitropoulou and co-workers[44] suggested the possible formation of a protein-polyphenol-carbohydrate complex able to encapsulate hydrophobic aroma molecules.

Although obtaining straightforward relationships between the aroma release behavior during wine drinking and the effect of wine matrix components is a difficult task not only because of the differences in compositional parameters but also because of the physicochemical characteristics of the aroma compounds and the physiological parameters affecting retronasal aroma release, a correlation analysis between compositional parameters (from Table 4) of all the wines of the study and the average values of aroma release considering the data from all the panelists was performed. Results showed that the matrix components, which better correlated with the aroma release where the total polyphenol content, which were positively correlated with the release of isoamyl acetate (r = 0.81), ethyl

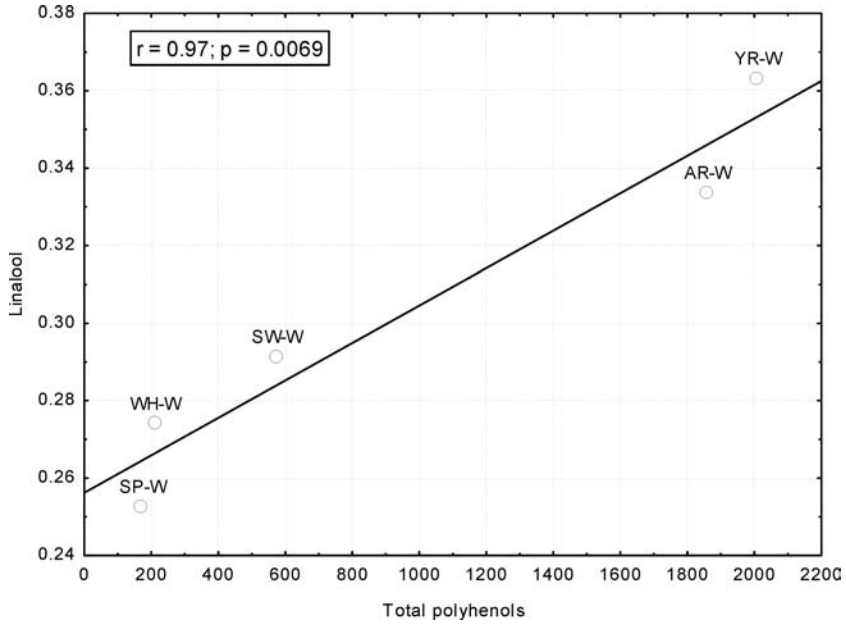

Figure 5. Correlation between the retronasal release of linalool during wine consumption and the polyphenol content in the five types of wines.

hexanoate (r = 0.80), and linalool (r = 0.97). Figure 5 shows this correlation, where it is possible to see how red wines showed the highest aroma release values, while the wines with the lowest polyphenol content showed the lowest aroma release for this compound. In spite of the greater aroma release that was observed by β-phenylethanol during the consumption of **AR-W**, the release of this compound did not correlate with the total polyphenol content or any other compositional parameter analyzed in the samples. This suggests that its release could be more affected by other chemicals of different nature or by specific interaction with different types of polyphenols more characteristic of aged wines (polymerized polyphenols), which will require further studies.

In conclusion, results of this work show that in spite of the interindividual differences due to certain physiological characteristics of the individuals (such as the breathing capacity), there is an influence of the wine matrix composition on the *in vivo* aroma release from wines and therefore in the amount of aroma available for the olfactory receptors. Among the different major wine matrix components, polyphenols, seem to enhance aroma release during wine drinking, which could be due to the involvement of these compounds on the formation of a wine coating after swallowing, which might increase the contact area between exhaled air and product and/or because of the formation of polyphenol−aroma complexes on the surface coating acting as a reservoir of aroma molecules ready to be released by the expiration flows. Ongoing work is directed to study the nature of these interactions and their meaning for the sensory characteristics of the wines.

AUTHOR INFORMATION

Corresponding Author

*Phone: +34 910 017 961. Fax: +34 910 017 905. E-mail: m.delpozo@csic.es.

Notes

The authors declare no competing financial interest.

ACKNOWLEDGMENTS

We sincerely thank the panelists for their participation in this study. This work was funded by the MINECO (AGL2012-04172-C02-01, and CONSOLIDER INGENIO 2010 (FUN-C-FOOD, CSD2007-063, Projects). C.M.G. thanks CSIC for her research contract cofunded by the European Social Fund.

REFERENCES

(1) Munoz-Gonzalez, C.; Rodriguez-Bencomo, J. J.; Moreno-Arribas, M. V.; Pozo-Bayon, M. A. Beyond the characterization of wine aroma compounds: Looking for analytical approaches in trying to understand aroma perception during wine consumption. *Anal. Bioanal. Chem.* **2011**, *401*, 1497−1512.

(2) Polaskova, P.; Herszage, J.; Ebeler, S. E. Wine flavor: Chemistry in a glass. *Chem. Soc. Rev.* **2008**, *37*, 2478−2489.

(3) Escudero, A.; Campo, E.; Farina, L.; Cacho, J.; Ferreira, V. Analytical characterization of the aroma of five premium red wines. Insights into the role of odor families and the concept of fruitiness of wines. *J. Agric. Food Chem.* **2007**, *55*, 4501−4510.

(4) Guth, H. Identification of character impact odorants of different white wine varieties. *J. Agric. Food Chem.* **1997**, *45*, 3022−3026.

(5) Kotseridis, Y.; Baumes, R. Identification of impact odorants in Bordeaux red grape juice, in the commercial yeast used for its fermentation, and in the produced wine. *J. Agric. Food Chem.* **2000**, *48*, 400−406.

(6) Buettner, A.; Beer, A.; Hannig, C.; Settles, M.; Schieberle, P. Physiological and analytical studies on flavor perception dynamics as induced by the eating and swallowing process. *Food. Qual. Prefer.* **2002**, *13*, 497−504.

(7) Linforth, R.; Taylor, A. J. Persistence of volatile compounds in the breath after their consumption in aqueous solutions. *J. Agric. Food Chem.* **2000**, *48*, 5419−5423.

(8) Buettner, A.; Beer, A.; Hannig, C.; Settles, M. Observation of the swallowing process by application of videofluoroscopy and real-time magnetic resonance imaging-consequences for retronasal aroma stimulation. *Chem. Senses* **2001**, *26*, 1211−1219.

(9) Deleris, I.; Saint-Eve, A.; Guo, Y.; Lieben, P.; Cypriani, M.-L.; Jacquet, N.; Brunerie, P.; Souchon, I. Impact of swallowing on the dynamics of aroma release and perception during the consumption of alcoholic beverages. *Chemical Senses* **2011**, *36*, 701−713.

(10) Weel, K. G. C.; Boelrijk, A. E. M.; Burger, J. J.; Verschueren, M.; Gruppen, H.; Voragen, A. G. J.; Smit, G. New device to simulate

swallowing and *in vivo* aroma release in the throat from liquid and semiliquid food systems. *J. Agric. Food Chem.* **2004**, *52*, 6564−6571.
(11) Genovese, A.; Piombino, P.; Gambuti, A.; Moio, L. Simulation of retronasal aroma of white and red wine in a model mouth system. Investigating the influence of saliva on volatile compound concentrations. *Food Chem.* **2009**, *114*, 100−107.
(12) Lindinger, W.; Hansel, A.; Jordan, A. Proton-transfer-reaction mass spectrometry (PTR-MS): On-line monitoring of volatile organic compounds at pptv levels. *Chem. Soc. Rev.* **1998**, *27*, 347−354.
(13) Taylor, A. J.; R. S., L, ., Techniques for measuring volatile release *in vivo* during consumption of food. In *Flavor Release*; ACS Symposium Series; D. D., R.; A. J., T., Eds.; American Chemical Society: Washington, DC, 2000; Vol. *763*, pp 8−21.
(14) Buettner, A.; Schieberle, P. Exhaled odorant measurement (EXOM)—A new approach to quantify the degree of in-mouth release of food aroma compounds. *Lebensm.-Wiss. Technol.-Food Sci. Technol.* **2000**, *33*, 553−559.
(15) Delahunty, C. M.; Piggott, J. R.; Conner, J. M.; Paterson, A. Comparison of dynamic flavour release from hard cheeses and analysis of headspace volatiles from the mouth with flavour perception during consumption. *J. Sci. Food Agric.* **1996**, *71*, 273−281.
(16) Linforth, R. S. T.; Savary, I.; Pattenden, B.; Taylor, A. J. Volatile compounds found in expired air during eating of fresh tomatoes and in the headspace above tomatoes. *J. Sci. Food Agric.* **1994**, *65*, 241−247.
(17) Lasekan, O.; Buettner, A.; Christlbauer, M. Investigation of the retronasal perception of palm wine (*Elaeis guineensis*) aroma by application of sensory analysis and exhaled odorant measurement (EOM). *Afr. J. Food, Agric., Nutr. Dev.* **2009**, *9*, 793−813.
(18) Pozo Bayón, M. A.; Reineccius, G., Interactions between wine matrix macro-components and aroma compounds. In *Wine Chemistry and Biochemistry*; Moreno-Arribas, M. V.; Polo, M. C., Eds.; Springer, New York, 2009; Vol. *II*, pp 417−435.
(19) Robinson, A. L.; Ebeler, S. E.; Heymann, H.; Boss, P. K.; Solomon, P. S.; Trengove, R. D. Interactions between wine volatile compounds and grape and wine matrix components influence aroma compound headspace partitioning. *J. Agric. Food Chem.* **2009**, *57*, 10313−10322.
(20) Rodriguez-Bencomo, J. J.; Munoz-Gonzalez, C.; Andujar-Ortiz, I.; Jose Martin-Alvarez, P.; Victoria Moreno-Arribas, M.; Angeles Pozo-Bayon, M. Assessment of the effect of the nonvolatile wine matrix on the volatility of typical wine aroma compounds by headspace solid phase microextraction/gas chromatography analysis. *J. Sci. Food Agric.* **2011**, *91*, 2484−2494.
(21) Saenz-Navajas, M. P.; Campo, E.; Cullere, L.; Fernandez-Zurbano, P.; Valentin, D.; Ferreira, V. Effects of the nonvolatile matrix on the aroma perception of wine. *J. Agric. Food Chem.* **2010**, *58*, 5574−5585.
(22) Dufour, C.; Bayonove, C. Interactions between wine polyphenols and aroma substances. An insight at the molecular level. *J. Agric. Food Chem.* **1999**, *47*, 678−684.
(23) Dufour, C.; Bayonove, C. L. Influence of wine structurally different polysaccharides on the volatility of aroma substances in a model system. *J. Agric. Food Chem.* **1999**, *47*, 671−677.
(24) Dufour, C.; Sauvaitre, I. Interactions between anthocyanins and aroma substances in a model system. Effect on the flavor of grape-derived beverages. *J. Agric. Food Chem.* **2000**, *48*, 1784−1788.
(25) Jones, P. R.; Gawel, R.; Francis, I. L.; Waters, E. J. The influence of interactions between major white wine components on the aroma, flavour, and texture of model white wine. *Food. Qual. Prefer.* **2008**, *19*, 596−607.
(26) Saenz-Navajas, M.-P.; Campo, E.; Fernandez-Zurbano, P.; Valentin, D.; Ferreira, V. An assessment of the effects of wine volatiles on the perception of taste and astringency in wine. *Food Chem.* **2010**, *121*, 1139−1149.
(27) Athes, V.; Lillo, M. P. Y.; Bernard, C.; Perez-Correa, R.; Souchon, I. Comparison of experimental methods for measuring infinite dilution volatilities of aroma compounds in water/ethanol mixtures. *J. Agric. Food Chem.* **2004**, *52*, 2021−2027.
(28) Aronson, J.; Ebeler, S. E. Effect of polyphenol compounds on the headspace volatility of flavors. *Am. J. Enol. Vitic.* **2004**, *55*, 13−21.
(29) Pineau, B.; Barbe, J.-C.; Van Leeuwen, C.; Dubourdieu, D. Which impact for β-damascenone on red wines aroma? *J. Agric. Food Chem.* **2007**, *55*, 4103−4108.
(30) Conner, J. M.; Birkmyre, L.; Paterson, A.; Piggott, J. R. Headspace concentrations of ethyl esters at different alcoholic strengths. *J. Sci. Food Agric.* **1998**, *77*, 121−126.
(31) Escalona, H.; Piggott, J. R.; Conner, J. M.; Paterson, A. Effect of ethanol strength on the volatility of higher alcohols and aldehydes. *Ital. J. Food Sci.* **1999**, *11*, 241−248.
(32) Rodriguez-Bencomo, J. J.; Conde, J. E.; Rodriguez-Delgado, M. A.; Garcia-Montelongo, F.; Perez-Trujillo, J. P. Determination of esters in dry and sweet white wines by headspace solid-phase microextraction and gas chromatography. *J. Chromatogr., A* **2002**, *963*, 213−223.
(33) Villamor, R. R.; Evans, M. A.; Mattinson, D. S.; Ross, C. F. Effects of ethanol, tannin, and fructose on the headspace concentration and potential sensory significance of odorants in a model wine. *Food Res. Int.* **2013**, *50*, 38−45.
(34) Blee, N.; Linforth, R.; Yang, N.; Brown, K.; Taylor, A. Variation in aroma release between panellists consuming different types of confectionary. *Flavour Fragrance J.* **2011**, *26*, 186−191.
(35) Gierczynski, I.; Laboure, H.; Guichard, E. *In vivo* aroma release of milk gels of different hardnesses: Inter-individual differences and their consequences on aroma perception. *J. Agric. Food Chem.* **2008**, *56*, 1697−1703.
(36) Pionnier, E.; Chabanet, C.; Mioche, L.; Le Quere, J. L.; Salles, C. 1. *In vivo* aroma release during eating of a model cheese: Relationships with oral parameters. *J. Agric. Food Chem.* **2004**, *52*, 557−564.
(37) Frank, D.; Appelqvist, I.; Piyasiri, U.; Wooster, T. J.; Delahunty, C. Proton transfer reaction mass spectrometry and time intensity perceptual measurement of flavor release from lipid emulsions using trained human subjects. *J. Agric. Food Chem.* **2011**, *59*, 4891−4903.
(38) Hanaoka, K.; Vallet, N.; Giampaoli, P.; Heyd, B.; MacLeod, P. Possible influence of breathing on detection frequency and intensity rating in gas chromatography-olfactometry. *Food Chem.* **2001**, *72*, 97−103.
(39) Langhammer, A.; Johnsen, R.; Gulsvik, A.; Holmen, T. L.; Bjermer, L. Forced spirometry reference values for Norwegian adults: The Bronchial Obstruction in North Trøndelag study. *Eur. Respir. J.* **2001**, *18*, 1−10.
(40) Hedenström, H.; Malmberg, P.; F., H. V. Reference values for lung function tests in men: Regression equations with smoking variables. *Upsala J. Med. Sci.* **1986**, *91*, 299−310.
(41) Hedenström, H.; Malmberg, P.; K., A. Reference values for lung function tests in females. *Bull. Eur. Physiopathol. Respir.* **1985**, *21*, 551−557.
(42) Delarue, J.; Giampaoli, P., Carbohydrate-flavour interactions. In *Flavour in Food*; Voilley, A.; Etievant, P. X., Eds.; Boca Raton: Woohead, 2006; pp 208−224.
(43) Jung, D. M.; de Ropp, J. S.; Ebeler, S. E. Study of interactions between food phenolics and aromatic flavors using one- and two-dimensional H-1 NMR spectroscopy. *J. Agric. Food Chem.* **2000**, *48*, 407−412.
(44) Mitropoulou, A.; Hatzidimitriou, E.; Paraskevopoulou, A. Aroma release of a model wine solution as influenced by the presence of non-volatile components. Effect of commercial tannin extracts, polysaccharides, and artificial saliva. *Food Res. Int.* **2011**, *44*, 1561−1570.
(45) Lorrain, B.; Tempere, S.; Iturmendi, N.; Moine, V.; de Revel, G.; Teissedre, P. L. Influence of phenolic compounds on the sensorial perception and volatility of red wine esters in model solution: An insight at the molecular level. *Food Chem.* **2013**, *140*, 76−82.
(46) Buettner, A. Investigation of potent odorants and afterodor development in two chardonnay wines using the buccal odor screening system (BOSS). *J. Agric. Food Chem.* **2004**, *52*, 2339−2346.

JOURNAL OF AGRICULTURAL AND FOOD CHEMISTRY

Article

pubs.acs.org/JAFC

Quantitation of Acrylamide in Foods by High-Resolution Mass Spectrometry

Antonio Dario Troise,[†,§] Alberto Fiore,[§] and Vincenzo Fogliano*[,†]

[†]Food Quality Design Group, Wageningen University, Wageningen, The Netherlands

[§]Department of Agricultural and Food Science University of Naples "Federico II", Naples, Italy

ABSTRACT: Acrylamide detection still represents one of the hottest topics in food chemistry. Solid phase cleanup coupled to liquid chromatography separation and tandem mass spectrometry detection along with GC-MS detection are nowadays the gold standard procedure for acrylamide quantitation thanks to high reproducibility, good recovery, and low relative standard deviation. High-resolution mass spectrometry (HRMS) is particularly suitable for the detection of low molecular weight amides, and it can provide some analytical advantages over other MS techniques. In this paper a liquid chromatography (LC) method for acrylamide determination using HRMS detection was developed and compared to LC coupled to tandem mass spectrometry. The procedure applied a simplified extraction, no cleanup steps, and a 4 min chromatography. It proved to be solid and robust with an acrylamide mass accuracy of 0.7 ppm, a limit of detection of 2.65 ppb, and a limit of quantitation of 5 ppb. The method was tested on four acrylamide-containing foods: cookies, French fries, ground coffee, and brewed coffee. Results were perfectly in line with those obtained by LC-MS/MS.

KEYWORDS: *acrylamide, Orbitrap, high-resolution mass spectrometry, Maillard reaction*

INTRODUCTION

Acrylamide has been a hot topic in food science, and in particular in Maillard chemistry,[1,2] since the first report highlighted its presence at high concentration in French fries, cereals, and coffee.[3] On the one hand, with regard to acrylamide toxicological and exposure outcomes,[4−6] a huge variety of papers dealt with the chemical and analytical insights of acrylamide determination. The chemical aspects of acrylamide formation have been studied more intensively in several pivotal papers: the determination of precursors,[7−9] the detection of a key intermediate,[10] the mechanism in heated food[11] and the kinetic modeling of formation.[12] On the other hand, in the past decade several methods for quantitative determination have been reviewed.[13,14] Generally, acrylamide analysis can be characterized by three steps: sample preparation including extraction, spiking with labeled internal standard with or without derivatization,[15] cleanup, chromatographic separation, and detection. With regard to the first step several techniques have been developed providing satisfactory results: pressurized liquid extraction (PLE) cation-exchange cartridges, hydrophilic−lipophilic balanced cartridges, and C-18 cartridges.[16−19] The chromatographic separations should take into consideration several drawbacks; among them the acrylamide high polarity as well as the poor retention, matrix effect, and solvent interferences,[20−22] that can be ruled out through derivatization procedures with mercaptobenzoic acid or through the use of the "bromination" method.[23−25] For the detection step the analytical techniques of choice were tandem mass spectrometry (MS/MS) acquisition performed by selected reaction monitoring (SRM) or multiple reaction monitoring (MRM), choosing the characteristic transitions m/z 72→55, 72→54, and 72→27,[26−28] Fourier transform infrared (FT-IR)[8] analysis, or time-of-flight mass spectrometry (TOF/MS),[29] or by fluorescence method.[30] To obviate the matrix effect and the poor retention of acrylamide and in addition to the above-mentioned analytical methods, many official institutions standardized and published their full validated methods for the determination of acrylamide, most of which focused on LC-MS/MS analysis and isotope dilution with ^{13}C or ^{2}H (Swiss Federal Office of Public Health; U.S. Food and Drug Administration).[28]

In this paper the performances of ultrahigh-pressure liquid chromatography coupled to Orbitrap high-resolution mass spectrometry (U-HPLC-HRMS) have been evaluated and accurately compared to the HPLC tandem mass spectrometry method (LC-MS/MS) to build a fast and sensitive procedure that can avoid the cleanup step as well as obtain a high mass accuracy.

MATERIALS AND METHODS

Chemicals. Methanol and water for U-HPLC-HRMS and LC-MS/MS determination were obtained from Merck (Darmstadt, Germany). Formic acid (98%), acrylamide, [2,3,3-d_3]-acrylamide, and Orbitrap calibration solution standards were purchased from Sigma (St. Louis, MO, USA). All of the samples were filtered through a 25 mm diameter and 0.22 μm pore size nylon filter using a 2.5 mL syringe (BD, Franklin Lakes, NJ, USA) equipped with a PTFE adapter (Phenomenex, Torrance, CA, USA). Carrez reagent potassium salt and Carrez reagent zinc salt were purchased from Carlo Erba (Milano, Italy).

High-Resolution Mass Spectrometry (HRMS). Acrylamide separation was performed on a U-HPLC Accela system 1250 (Thermo Fisher Scientific, San Jose, CA, USA) consisting of a degasser, a quaternary pump, a thermostated autosampler, and a column oven. Mobile phase A was 0.1% formic acid, and mobile phase B was 0.1%

Received: July 1, 2013
Revised: December 10, 2013
Accepted: December 15, 2013
Published: December 15, 2013

ACS Publications © 2013 American Chemical Society

formic acid in methanol. Four chromatographic columns were tested: Synergi Hydro (150 × 2.0 mm, 4.0 μm) Kinetex PFP (50 × 2.0 mm, 2.6 μm), Luna HILIC (150 × 2.0 mm, 3.0 μm), and Kinetex C18 (100 × 3.0 mm, 2.6 μm), all from Phenomenex. In all cases the binary gradient (min)/(% B) (0/5), (2/5), (4/80), (5/80), (6/5), (7/5) was used, and the flow rate was 0.2 mL/min, except for the C18 column, with which the flow rate was 0.3 mL/min, and HILIC column, for which the mobile phases consisted of (A) 0.1% formic acid in acetonitrile and (B) 0.1% formic acid in water. Volumes of 10 μL were injected using the thermostated autosampler at 18 °C. The separation temperature was set at 30 °C, and the autosampler needle was rinsed with 500 μL of a mixture of methanol/water 50:50 before each injection.

To set up the optimal condition, a water solution of acrylamide (concentration = 250 μg/mL) at a flow rate of 5 μL/min was pumped using a 500 μL syringe pump directly into the LC stream entering in the HRMS (6.25 μg/mL final concentration, according to the chromatographic flow rate that was 0.195 mL/min). The U-HPLC was coupled to an Exactive Orbitrap MS (Thermo Fisher Scientific) equipped with a heated electrospray interface operating in the positive mode and scanning the ions in the m/z range of 50−400. The resolving power was set to 50000 full width at half-maximum (fwhm, m/z 200), resulting in a scan time of 1 s. The automatic gain control was used to fill the C-trap and gain accuracy in mass measurements (ultimate mass accuracy mode, 5×10^5 ions); maximum injection time was 50 ms. The interface parameters were as follows: spray voltage, 4.5 kV; capillary voltage, 42.5 V; skimmer voltage, 14 V; capillary temperature, 300 °C; heater temperature, 250 °C; sheath gas flow, 40 (arbitrary units); and auxiliary gas flow, 6 (arbitrary units).

Before the acrylamide determination was run, the instrument was externally calibrated by infusion with a calibration solution that consisted of caffeine, Met-Arg-Phe-Ala (MRFA), Ultramark 1621, and acetic acid in a mixture of acetonitrile/methanol/water (2:1:1, v/v/v). Several reference masses (lock masses) were tested for the mass analyzer recalibration: methanol ($[M_2 + H]^+$, exact mass = 65.05971); methanol/water ($[A_2B_2 + H]^+$, exact mass = 101.08084); sodium adduct of methanol/water ($[A_2B_2 + Na]^+$, exact mass = 123.06278); [2,3,3-d_3]-acrylamide ($[M + H]^+$, exact mass = 75.06322); and diisooctyl phthalate ($[M + H]^+$, exact mass = 391.28429).[31] To optimize the HRMS conditions and the mass accuracy, 200 μL of the above-mentioned calibration solution was spiked with 10 μg of [2,3,3-d_3]-acrylamide and the scanning window was set in the m/z range of 70−1400 for the initial calibration procedure.

Preparation of Standard Solutions. A stock solution of acrylamide was prepared by dissolving 10 mg of standard in 1 mL of water. This solution was diluted and stored at −20 °C until use. A calibration curve was built in the range of 5−500 ng/mL according to the limit of detection (LoD) and the limit of quantitation (LoQ). Three replicates of the 0.5 ng/mL solutions were injected into the U-HPLC/HRMS system to verify the lowest concentration for which the signal-to-noise ratio was >3. Concentrations of <1 ng/mL resulted in no signal. The LoQ was 5 ng/mL for the standard solution, and the r^2 value was always >0.99 in the above-mentioned range. Reproducibility of the method was evaluated through the intraday and interday assay. The slope among the three subsequent calibration curves showed a % RSD of <7%. The same calibration points used for the above-mentioned curve were spiked with 1.25 μg of [2,3,3-d_3]-acrylamide to evaluate the potential differences in the presence or absence of the internal labeled standard.

Sample Preparation. *Cookies.* Model cookies (height = 3 mm, diameter = 30 mm) were prepared according to AACC Method 10-54 (AACC, 2000) as previously described.[32] Cookies were baked at 200 °C for 13 min in a forced-air circulation oven (Memmert, Schwabach, Germany).

French Fries. Ten pieces (5 cm × 0.7 cm × 0.7 cm, total amount = 50 g) were fried in 1 L of olive oil for 5 and 7 min. At the end of the cooking process the French fries were freeze-dried and stored until the acrylamide extraction.

Brewed Coffee and Ground Coffee. Ground coffee was purchased in a local market; an aliquot was directly analyzed without further preparation; instead, 15 g was brewed with 100 mL of water (100 °C for 15 min) under continuous stirring. Solid particles were removed through a paper filter, and 50 mL was stored at −20 °C until the analysis.

Acrylamide Extraction. French fries and cookies were ground in a knife mill Grindomix 200 (Retsch, Haan, Germany), and 100 mg were weighed in a volumetric flask; along with 4.8 mL of deionized water, 100 μL of Carrez reagent potassium salt and 100 μL of Carrez reagent zinc salt were added to each sample. The same protocol was followed for ground coffee. For coffee liquid samples 500 μL was diluted in 1 mL of deionized water. Each replicate of the different samples was prepared in two different ways: one was spiked with 125 μg of [2,3,3-d_3]-acrylamide, whereas the other was without the internal standard. All samples were vortexed for 10 min at 800 rpm at room temperature, and after centrifugation (2500 g, 4 °C, 10 min), 1 mL of the aqueous layer was accurately filtered and collected into a glass vial.

Tandem Mass Spectrometry (MS/MS). To validate the HRMS method, all of the above-mentioned samples were analyzed through LC-MS/MS according to the method of Gökmen et al.[16] Two grams of the freeze-dried French fries, cookies, or coffee powder were weighed; 8.9 mL of deionized water was added in a 15 mL centrifuge tube along with 500 μL of Carrez reagent potassium salt, 500 μL of Carrez reagent zinc salt, and 100 μL of internal standard [2,3,3-d_3]-acrylamide (final concentration = 90 ng/mL). For brewed coffee 1 mL was mixed along with 8.9 mL of water, 500 μL of both Carrez reagents, and 100 μL of internal standard. The tubes were shaken vigorously for 1 min, and the resulting mixture was centrifuged at 2500 g for 10 min at 4 °C. Then supernatant were collected in a 20 mL volumetric flask, and two further extractions were performed using 5 mL of deionized water, except for brewed coffee that was filtered and injected. Finally, the pellets were discarded, and the supernatants were filtered through a 0.45 μm nylon filter. One milliliter of supernatants was collected and passed through an Oasis HLB cartridge (Waters, Milford, MA, USA) previously activated with 1 mL of methanol and 1 mL of deionized water; 20 μL of the final solution were injected onto the LC column for quantitation by MS/MS. Identification and quantitative determination of acrylamide and [2,3,3-d_3]-acrylamide were carried out using an API 2000 triple-quadrupole mass spectrometer (Applied Biosystems, Carlsbad, CA, USA) coupled to an ion spray interface, equipped with an HPLC binary micropump series 200 (Perkin-Elmer, Waltham, MA, USA). Chromatographic separation of acrylamide and [2,3,3-d_3]-acrylamide was achieved through an Inertsil column, 250 × 4.6 mm, 5 μm (GLSciences, Torrance, CA, USA); the mobile phases were (A) 0.1% formic acid and (B) 0.1% formic acid in methanol, and the gradient elution (min)/(% B) (0/0), (3/0), (8/93), (12/0), (15/0) was applied at a flow rate of 0.8 mL/min, whereof 0.2 mL were split into the ion source. Quantitation was carried out in multiple reaction monitoring (MRM) mode at m/z ratios of 72 and 75 for acrylamide and [2,3,3-d_3]-acrylamide, respectively. Specific molecular fragments corresponding to m/z 55 and 44 for acrylamide and m/z 58 and 44 for [2,3,3-d_3]-acrylamide were also monitored. The daughter ions were obtained through fragmentation with the following conditions: the source temperature was set at 350 °C, nitrogen was used as nebulizer gas at a flow rate of 12 L/h, and the needle and cone voltages were set at 3.0 kV and 100 V, respectively. Under the above-mentioned chromatographic conditions the acrylamide and its corresponding deuterated standard eluted at 7.4 min. For LC-MS/MS analysis acrylamide was quantified using a linear calibration curve built in the range of 50−500 ng/mL, the LoD and LoQ were 10 and 20 ng/mL for acrylamide and [2,3,3-d_3]-acrylamide, respectively, and the coefficient of determination, r^2, was >0.99.

Statistical Analysis. All of the analyses were performed in triplicate for both HRMS and MS/MS; the results were reported as nanograms per gram of samples for cookies, French fries, and ground coffee or as nanograms per milliliter for brewed coffee or acrylamide solution. For HRMS, data were recorded using Xcalibur software version 2.1 (Thermo Fisher Scientific). For MS/MS data, Analyst version 1.4.2 (Applied Biosystems) was used.

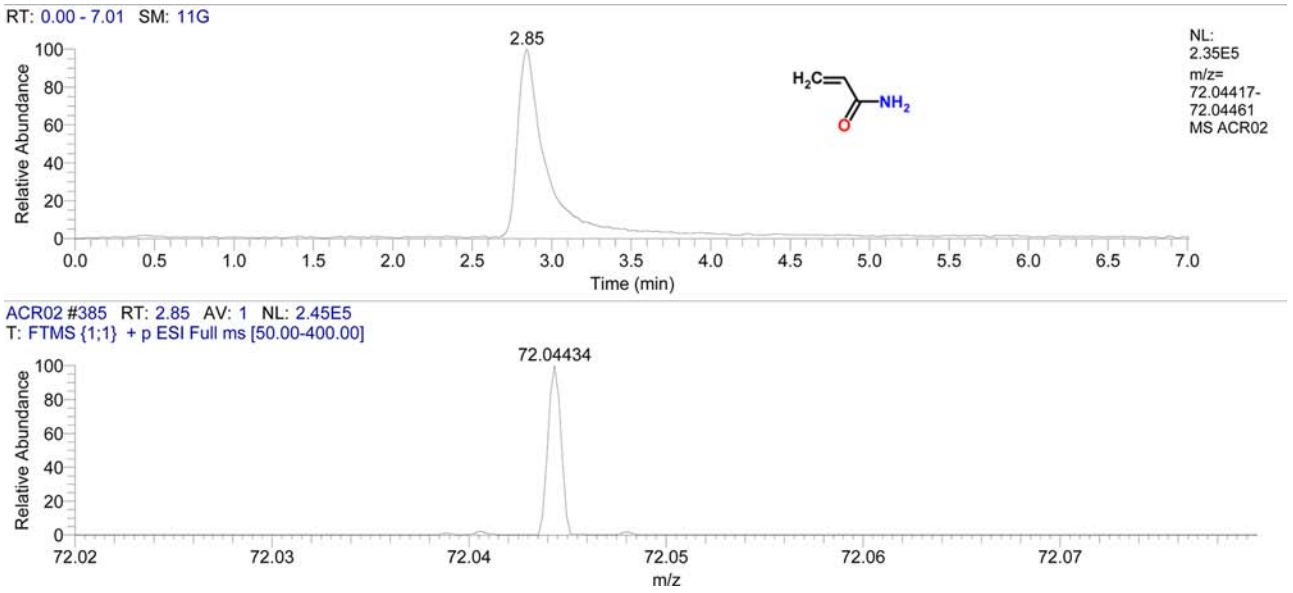

Figure 1. Typical extracted ion chromatogram and mass spectrum of acrylamide standard dissolved in water. Δ ppm = −0.7. Acrylamide theoretical mass = 72.04439.

RESULTS AND DISCUSSION

Method Development. Despite recent developments in acrylamide analysis, improvements in high-throughput quantitative procedures for its determination are still requested. The key point of this paper was to evaluate the potentialities of HRMS in the detection of this small amide in a complex mixture riding out the problems associated with the solid phase extraction and, possibly, to the use of internal standard.[13,14]

The first step of the work dealt with the optimization of chromatographic separation of acrylamide in combination with HRMS detection. It is well-known that acrylamide is a very polar molecule with poor retention ($k' < 2.0$) in conventional liquid chromatography reversed phase sorbents.[16,33] Four columns with different selectivities were tested by evaluating chromatographic performances, including retention time and reproducibility. Among the tested columns, including HILIC phase, pentafluorophenyl phase, and a core shell C18 phase, a polar end-capped stationary phase was selected to get a good reproducibility and avoid the interferences of the solvent, matrix, and unretained compounds that eluted along with the solvent front. A typical chromatogram of acrylamide standard is presented in Figure 1. Along with the polar end-capped column, the use of a core shell C18 phase can ensure a significant reproducibility for several subsequent injections even if the k' was always 1. From the chromatographic separation point of view, relevant results were obtained with HILIC phase, even if the use of acetonitrile interfered with the ionization of acrylamide.

Although the retention time was rather short (2.85 min), it ensured separation from the first eluting impurities; the peak shape was maintained, and the deviation of retention time was <0.1 min among assays of calibration standards, real samples, and recovery samples.

The following step of the experimental work was the HRMS optimization downstream the U-HPLC separation. Specifically, the use of auxiliary gas coupled to a capillary voltage higher than 4.0 kV caused the fragmentation of acrylamide in source. As a consequence it was decided to use an auxiliary gas flow rate of 6 AU to avoid undesired fragmentation of the molecules and the formation of the typical fragment (72→55).[26−28,34] The lens voltage was optimized by setting the mass on 72.0 by manual tuning. This procedure was repeated in two different conditions: direct infusion of the acrylamide standard solution in the ion source and its infusion in the liquid chromatography flow to evaluate the interferences of the solvents. The heater temperature and the capillary temperature were optimized to ensure the best solvent nebulization. Under the stated conditions in Materials and Methods, the Orbitrap MS analyzer showed the best compromise between selectivity and quantitative performance.

Method Performance. The method performance was tested against quality parameters such as specificity, carry-over, linearity of the calibration, coefficient of correlation (r^2), limit of quantitation, limit of detection, precision, accuracy, and recovery. The first point was checking for the absence of any contaminants with an exact mass similar to the one of acrylamide by injecting several times pure water. Subsequently, a calibration curve was built after determination of the LoD and LoQ. The LoD was calculated according to the method of Armbruster et al.[35] After 20 replicates, the limit of blank was 0.5 ppb, the limit of detection was 2.65 ppb, and the limit of quantitation was 5 ppb. Two different series of calibration curves were prepared: one spiked with the deuterated internal standard; another one without internal standard. For both series the linearity was achieved in the range of 5−500 ng/mL and the r^2 was always >0.99. Each point was injected three times each day and for three consecutive days. After each replicate, a blank sample (pure water) was injected in order to verify the absence of carry-over effect. The precision of the two methods was verified in the linearity range through the evaluation of the slope of three different calibration curves; the results, reported as %RSD, were <8% for both calibration curves; the accuracy of the method, calculated through the ratio observed amount/specified amount × 100, was always >90%. The recovery test was performed using two different concentrations of [2,3,3-d_3]-acrylamide (100 and 253 ng/mL final concentration, $n = 6$ for each matrix) to verify the matrix effect and the ion suppression. First, the ionization performance

dx.doi.org/10.1021/jf404205b | J. Agric. Food Chem. 2014, 62, 74−79

of [2,3,3-d_3]-acrylamide was evaluated through the injection of the pure standard dissolved in water, and then the recovery was calculated as the ratio between the area of the internal standard and the area of spiked samples. The results ranged from 90 to 99% and are shown in Table 2. In Figure 2 the recovery of

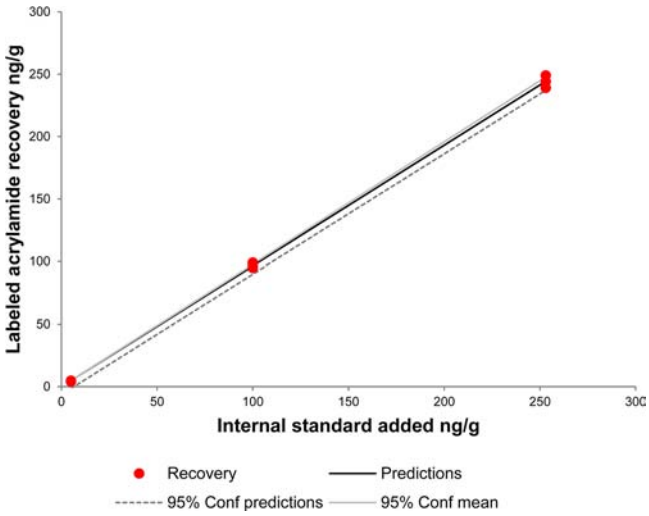

Figure 2. Recovery of internal standard spiked in French fries. The dotted lines represent the 95% confidence intervals calculated on the predictions and on the mean (n = 3).

internal standard spiked in French fries is presented. The setup of the condition for mass accuracy optimization was one of the prominent points of the paper. In a first set of fine-tuning trials several lock masses were used to recalibrate the instrument and reduce the mass error,[31] and the mass to charge ratio of some contaminants or interference ions was evaluated (Table 1), such as methanol ($[M_2 + H]^+$, exact mass = 65.05971); methanol/water ($[A_2B_2 + H]^+$, exact mass = 101.08084); and sodium adduct of methanol/water ($[A_2B_2 + Na]^+$, exact mass = 123.06278). Then, 1 μL of [2,3,3-d_3]-acrylamide solution ($[M + H]^+$, exact mass = 75.06322) was directly infused in the liquid chromatography flow with a final concentration of 3 μg/mL. The former trials gave unsatisfying results with a mass accuracy around 5 ppm, whereas the latter, which used deuterated acrylamide straight in the calibration solution, reduced the mass accuracy to −0.7 ppm. The calibration mixture was spiked with 10 μg of [2,3,3-d_3]-acrylamide to set the instrument for the optimal detection of small molecules with m/z <80. The presence of [2,3,3-d_3]-acrylamide in the calibration solution determined the reduction in the discrepancies between the observed mass ($[M + H]^+$, exact mass = 72.04434) and the theoretical mass of acrylamide ($[M + H]^+$, exact mass = 72.04439).

Measurement of Acrylamide Content in Foods. As described above, three of the most commonly consumed acrylamide-containing foods, French fries, coffee, and cookies, were selected to test the performance of the developed method. The determination of acrylamide in these food matrices showed different requirements in terms of extraction and cleanup before chromatographic separation.[14] Up to now acrylamide was detected through solid phase extraction along with liquid chromatography and tandem mass spectrometry detection,[28,34,36−38] by LC-MS after derivatization with 2-mercaptobenzoic acid,[15] by direct gas chromatography coupled to mass spectrometry,[39] and by pyrolysis GC-MS.[40] The extraction procedure used in this paper was exactly the same for cookies, French fries, and ground coffee, whereas for brewed coffee only a dilution in water was performed. The recovery test and the LoD were evaluated in the different matrix, with satisfactory results as presented in Table 2, where the LoD and LoQ in the

Table 2. LC-HRMS Performances for Acrylamide Detection in Three Different Foods[a]

	RT (min)	LOD (ppb)	LOQ (ppb)	recovery (%)	% RSD	% RSD*[a]	linearity
French fries	2.85	2.65	5	97	8	9	
brewed coffee	2.83	3	5	90	7	9	
ground coffee	2.85	3	5	90	7	5	
cookies	2.85	2.65	5	92	6	5	
standard	2.83	2.65	5		<7	<5	>0.99

[a]%RSD* indicates the set of samples performed with labeled internal standard.

tested foods and in standard solutions were almost similar. In Table 3 acrylamide concentrations obtained on the various foods with and without the use of internal standard are reported, and they were compared not only with those present in the literature but also with the results obtained by LC-MS/MS on the same samples. For French fries the value ranged from 270 ± 12.1 ng/g (254 ± 4.6 ng/g for internal standard analysis) to 424 ± 10.3 ng/g (490 ± 10.0 ng/g for internal standard analysis) according to the processing time (5 and 7 min, respectively).[41] These values were very similar to the ones obtained through LC-MS/MS as reported in Table 3.[27,42,43] For cookie samples two different typologies of cookies prepared de novo according to two recipes, already used in a previous paper from our group, were used for acrylamide determination.[32] The value varied from 276 ± 3.5 ng/g (cookies with 0.65% sodium chloride) to 317 ± 9.2 ng/g (cookies without 0.65% sodium chloride). The use of the internal standard resulted in similar values: 262 ± 4.0 and 340 ± 5.6 ng/g for cookies with and without sodium chloride, respectively. These data clearly showed the substantial agreement between the U-HPLC/HRMS method and the SPE LC-MS/MS method (Table 3).

Table 1. Contaminant or Interference Ions Used as Locking Mass To Recalibrate the Instruments during the Run[31]

monoisotopic ion mass	ion type	formula for M	compound ID	origin
65.05971	$[M_2 + H]^+$	CH_3OH	methanol	solvent
101.08084	$[A_2B_2 + H]^+$	$[MeOH]_n[H_2O]_m$	methanol/water	ESI solvents
123.06278	$[A_2B_2 + Na]^+$	$[MeOH]_n[H_2O]_m$	methanol/water	ESI solvents
391.28429	$[M + H^+]$	$C_{24}H_{38}O_4$	diisooctyl phtalate	plasticizer
75.06322	$[M + H^+]$	$C_3H_2D_3NO$	[2,3,3-d_3]-acrylamide	external infusion

dx.doi.org/10.1021/jf404205b | J. Agric. Food Chem. 2014, 62, 74−79

Table 3. Acrylamide Concentration in the Tested Foods, through LC-HRMS (with and without Labeled Internal Standard), through LC-MS/MS and Literature Data

food	no labeled standard	labeled standard	LC-MS/MS	literature data	ref
cookies (different formulations)	276 ± 3.5 ng/g	262 ± 4.0 ng/g	286 ± 15.3 ng/g	278−313 ng/g	32
	317 ± 9.2 ng/g	340 ± 5.6 ng/g	325 ± 9.3 ng/g	451−510	15
French fries (different frying times)	270 ± 12.1 ng/g	254 ± 4.6 ng/g	280 ± 18.8 ng/g	253−2688	42
	424 ± 10.3 ng/g	490 ± 10.0 ng/g	409 ± 11.1 ng/g	150−1200	43
				50−1800	27
brewed coffee	12 ± 0.1 ng/mL	15 ± 0.2 ng/mL	13 ± 0.2 ng/mL	6−16 ng/mL	46
				5−12	44
				14−21	45, 49
ground coffee	140 ± 3.6 ng/g	159 ± 8.1 ng/g	145 ± 3.2 ng/g	45−374 ng/g	46
				267; %RSD = 0.5	47

The method performances were tested also in brewed coffee sample and in ground coffee. In this case the acrylamide contents were 12.1 ± 0.1 ng/mL and 140 ± 3.6 ng/g for brewed coffee and ground coffee, respectively, and the previous results were fully confirmed,[44−47] even if with the use of [2,3,3-d_3]-acrylamide small differences were present: 15 ± 0.2 ng/mL and 159 ± 8.1 ng/g for brewed coffee and ground coffee, respectively. The key points for brewed coffee were the LoD and the recovery that were 3 ppb and 90%, respectively. Acrylamide detection in coffee is characterized by several drawbacks due to the matrix effect and the roasting of coffee beans.[44] For this reason for LC-MS/MS the use of internal standard is a key point that can be easily overcome thanks to the HRMS. This is presented in Table 3, where the analysis performed through HRMS or MS/MS showed similar results.

The results obtained with the developed methods were in any case in line with those present in the literature.[48,49] From the analytical point of view the use of [2,3,3-d_3]-acrylamide increased the robustness of the method, in particular, the variability due to the ion suppression or to the matrix effect was eliminated for each analysis. Interestingly, without the use of labeled internal standard the results were still satisfying, and the differences between the two methods were <14% in solid foods, thus suggesting that in the cases not requiring high precision the use of the HRMS method could theoretically allow also avoidance of the use of external standard.

A huge variety of papers have been published on quantitation procedures for acrylamide in foods. The method here developed using U-HPLC Orbitrap HRMS proved to be very effective as it negated the matrix effect and time consumption due to solid phase extraction. Moreover, the use of a modified calibration solution allowed the optimal set of the instrument and it improved enormously the mass accuracy for acrylamide detection. Also, the use of internal standard could be theoretically avoided with a negligible loss in method accuracy. From the analytical standpoint the performances were satisfactory: the relative standard deviation was <7%, the recovery in the three different matrix was always >90%, and the limit of detection was comparable to the ones of tandem mass spectrometry.

AUTHOR INFORMATION

Corresponding Author

*(V.F.) E-mail: vincenzo.fogliano@wur.nl. Phone: +31 317 485171.

Funding

This work was carried out within the framework of the PROMETHEUS project (PROcess contaminants: Mitigation and Elimination Techniques for High food quality and their Evaluation Using Sensors and Simulation) funded by the European Commission.

Notes

The authors declare no competing financial interest.

REFERENCES

(1) Friedman, M. Food browning and its prevention: an overview. *J. Agric. Food Chem.* **1996**, *44*, 631−653.

(2) Ledl, F.; Schleicher, E. New aspects of the Maillard reaction in foods and in the human-body. *Angew. Chem., Int. Ed.* **1990**, *29*, 565−594.

(3) Tareke, E.; Rydberg, P.; Karlsson, P.; Eriksson, S.; Tornqvist, M. Analysis of acrylamide, a carcinogen formed in heated foodstuffs. *J. Agric. Food Chem.* **2002**, *50*, 4998−5006.

(4) Dybing, E.; Farmer, P. B.; Andersen, M.; Fennell, T. R.; Lalljle, S. P. D.; Muller, D. J. G.; Olin, S.; Peterson, B. J.; Schlatter, J.; Scholz, G.; Scimeca, J. A.; Slimani, N.; Tornqvist, M.; Tuijtelaars, S.; Verger, P. Human exposure and internal dose assessments of acrylamide in food. *Food Chem. Toxicol.* **2005**, *43*, 365−410.

(5) Arribas-Lorenzo, G.; Morales, F. J. Dietary exposure to acrylamide from potato crisps to the Spanish population. *Food Addit. Contam. A* **2009**, *26*, 289−297.

(6) Konings, E. J. M.; Hogervorst, J. G. F.; van Rooij, L.; Schouten, L. J.; Sizoo, E. A.; van Egmond, H. P.; Goldbohm, R. A.; van den Brandt, P. A. Validation of a database on acrylamide for use in epidemiological studies. *Eur. J. Clin. Nutr.* **2010**, *64*, 534−540.

(7) Mottram, D. S.; Wedzicha, B. L.; Dodson, A. T. Acrylamide is formed in the Maillard reaction. *Nature* **2002**, *419*, 448−449.

(8) Yaylayan, V. A.; Wnorowski, A.; Locas, C. P. Why asparagine needs carbohydrates to generate acrylamide. *J. Agric. Food Chem.* **2003**, *51*, 1753−1757.

(9) Stadler, R. H.; Blank, I.; Varga, N.; Robert, F.; Hau, J.; Guy, P. A.; Robert, M. C.; Riediker, S. Acrylamide from Maillard reaction products. *Nature* **2002**, *419*, 449−450.

(10) Granvogl, M.; Jezussek, M.; Koehler, P.; Schieberle, P. Quantitation of 3-aminopropionamide in potatoes − a minor but potent precursor in acrylamide formation. *J. Agric. Food Chem.* **2004**, *52*, 4751−4757.

(11) Stadler, R. H.; Robert, F.; Riediker, S.; Varga, N.; Davidek, T.; Devaud, S.; Goldmann, T.; Hau, J.; Blank, I. In-depth mechanistic study on the formation of acrylamide and other vinylogous compounds by the Maillard reaction. *J. Agric. Food Chem.* **2004**, *52*, 5550−5558.

(12) Knol, J. J.; Van Loon, W. A. M.; Linssen, J. P. H.; Ruck, A. L.; Van Boekel, M. A. J. S.; Voragen, A. G. J. Toward a kinetic model for acrylamide formation in a glucose-asparagine reaction system. *J. Agric. Food Chem.* **2005**, *53*, 6133−6139.
(13) Wenzl, T.; de la Calle, M. B.; Anklam, E. Analytical methods for the determination of acrylamide in food products: a review. *Food Addit. Contam.* **2003**, *20*, 885−902.
(14) Zhang, Y.; Zhang, G. Y.; Zhang, Y. Occurrence and analytical methods of acrylamide in heat-treated foods − review and recent developments. *J. Chromatogr., A* **2005**, *1075*, 1−21.
(15) Jezussek, M.; Schieberle, P. A new LC/MS-method for the quantitation of acrylamide based on a stable isotope dilution assay and derivatization with 2-mercaptobenzoic acid. Comparison with two GC/MS methods. *J. Agric. Food Chem.* **2003**, *51*, 7866−7871.
(16) Gokmen, V.; Senyuva, H. Z.; Acar, J.; Sarioglu, K. Determination of acrylamide in potato chips and crisps by high-performance liquid chromatography. *J. Chromatogr., A* **2005**, *1088*, 193−199.
(17) Delatour, T.; Perisset, A.; Goldmann, T.; Riediker, S.; Stadler, R. H. Improved sample preparation to determine acrylamide in difficult matrixes such as chocolate powder, cocoa, and coffee by liquid chromatography tandem mass spectroscopy. *J. Agric. Food Chem.* **2004**, *52*, 4625−4631.
(18) Olsson, K.; Svensson, R.; Roslund, C. A. Tuber components affecting acrylamide formation and colour in fried potato: variation by variety, year, storage temperature and storage time. *J. Sci. Food Agric.* **2004**, *84*, 447−458.
(19) Yusa, V.; Quintas, G.; Pardo, O.; Marti, P.; Pastor, A. Determination of acrylamide in foods by pressurized fluid extraction and liquid chromatography-tandem mass spectrometry used for a survey of Spanish cereal-based foods. *Food Addit. Contam.* **2006**, *23*, 237−244.
(20) Ono, H.; Chuda, Y.; Ohnishi-Kameyama, M.; Yada, H.; Ishizaka, M.; Kobayashi, H.; Yoshida, M. Analysis of acrylamide by LC-MS/MS and GC-MS in processed Japanese foods. *Food Addit. Contam.* **2003**, *20*, 215−220.
(21) Cavalli, S.; Maurer, R.; Hofler, F. Fast determination of acrylamide in food samples using accelerated solvent extraction followed by ion chromatography with UV or MS detection. *LC GC Eur.* **2003**, 9−11.
(22) Rydberg, P.; Eriksson, S.; Tareke, E.; Karlsson, P.; Ehrenberg, L.; Tornqvist, M. Investigations of factors that influence the acrylamide content of heated foodstuffs. *J. Agric. Food Chem.* **2003**, *51*, 7012−7018.
(23) Ahn, J. S.; Castle, L.; Clarke, D. B.; Lloyd, A. S.; Philo, M. R.; Speck, D. R. Verification of the findings of acrylamide in heated foods. *Food Addit. Contam.* **2002**, *19*, 1116−1124.
(24) Hashimoto, A. Improved method for the determination of acrylamide monomer in water by means of gas−liquid chromatography with an electron-capture detector. *Analyst* **1976**, *101*, 932−938.
(25) Tareke, E.; Rydberg, P.; Karlsson, P.; Eriksson, S.; Tornqvist, M. Acrylamide: a cooking carcinogen? *Chem. Res. Toxicol.* **2000**, *13*, 517−522.
(26) Riediker, S.; Stadler, R. H. Analysis of acrylamide in food by isotope-dilution liquid chromatography coupled with electrospray ionization tandem mass spectrometry. *J. Chromatogr., A* **2003**, *1020*, 121−130.
(27) Becalski, A.; Lau, B. P. Y.; Lewis, D.; Seaman, S. W.; Sun, W. F. Determination of acrylamide in various food matrices − evaluation of LC and GC mass spectrometric methods. *Adv. Exp. Med. Biol.* **2005**, *561*, 271−284.
(28) Roach, J. A. G.; Andrzejewski, D.; Gay, M. L.; Nortrup, D.; Musser, S. M. Rugged LC-MS/MS survey analysis for acrylamide in foods. *J. Agric. Food Chem.* **2003**, *51*, 7547−7554.
(29) Hamdan, M.; Bordini, E.; Galvani, M.; Righetti, P. G. Protein alkylation by acrylamide, its N-substituted derivatives and cross-linkers and its relevance to proteomics: a matrix assisted laser desorption/ionization-time of flight-mass spectrometry study. *Electrophoresis* **2001**, *22*, 1633−1644.
(30) Schieberle, P.; Kohler, P.; Granvogl, M. New aspects on the formation and analysis of acrylamide. *Adv. Exp. Med. Biol.* **2005**, *561*, 205−222.
(31) Keller, B. O.; Suj, J.; Young, A. B.; Whittal, R. M. Interferences and contaminants encountered in modern mass spectrometry. *Anal. Chim. Acta* **2008**, *627*, 71−81.
(32) Fiore, A.; Troise, A. D.; Mogol, B. A.; Roullier, V.; Gourdon, A.; Jian, S. E.; Hamzalioglu, B. A.; Gokmen, V.; Fogliano, V. Controlling the Maillard reaction by reactant encapsulation: sodium chloride in cookies. *J. Agric. Food Chem.* **2012**, *60*, 10808−10814.
(33) Gokmen, V.; Senyuva, H. Z. Study of colour and acrylamide formation in coffee, wheat flour and potato chips during heating. *Food Chem.* **2006**, *99*, 238−243.
(34) Rosen, J.; Hellenas, K. E. Analysis of acrylamide in cooked foods by liquid chromatography tandem mass spectrometry. *Analyst* **2002**, *127*, 880−882.
(35) Armbruster, D. A.; Tillman, M. D.; Hubbs, L. M. Limit of detection (Lod) limit of quantitation (Loq) − comparison of the empirical and the statistical, methods exemplified with Gc-Ms assays of abused drugs. *Clin. Chem.* **1994**, *40*, 1233−1238.
(36) Napolitano, A.; Morales, F.; Sacchi, R.; Fogliano, V. Relationship between virgin olive oil phenolic compounds and acrylamide formation in fried crisps. *J. Agric. Food Chem.* **2008**, *56*, 2034−2040.
(37) Gokmen, V.; Senyuva, H. Z. A simplified approach for the kinetic characterization of acrylamide formation in fructose-asparagine model system. *Food Addit. Contam.* **2006**, *23*, 348−354.
(38) Pedreschi, F.; Moyano, P.; Kaack, K.; Granby, K. Color changes and acrylamide formation in fried potato slices. *Food Res. Int.* **2005**, *38*, 1−9.
(39) Biedermann, M.; Grob, K. In GC-MS, acrylamide from heated foods may be coeluted with 3-hydroxy propionitrile. *Eur. Food Res. Technol.* **2008**, *227*, 945−948.
(40) Yaylayan, V. A. Analysis of complex reaction mixtures: applications of Py-GG-MS and the microwave-assisted process. *Am. Lab.* **1999**, *31*, 30−31.
(41) Pedreschi, F.; Kaack, K.; Granby, K. Acrylamide generation in pre-treated potato chips. *Agro Food Ind. Hi-Tech* **2008**, *19*, 4−6.
(42) Capuano, E.; Fogliano, V. Acrylamide and 5-hydroxymethylfurfural (HMF): a review on metabolism, toxicity, occurrence in food and mitigation strategies. *LWT−Food Sci. Technol.* **2011**, *44*, 793−810.
(43) Parker, J. K.; Balagiannis, D. P.; Higley, J.; Smith, G.; Wedzicha, B. L.; Mottram, D. S. Kinetic model for the formation of acrylamide during the finish-frying of commercial French fries. *J. Agric. Food Chem.* **2012**, *60*, 9321−9331.
(44) Granby, K.; Fagt, S. Analysis of acrylamide in coffee and dietary exposure to acrylamide from coffee. *Anal. Chim. Acta* **2004**, *520*, 177−182.
(45) Perez, H. L.; Osterman-Golkar, S. A sensitive gas chromatographic-tandem mass spectrometric method for detection of alkylating agents in water: application to acrylamide in drinking water, coffee and snuff. *Analyst* **2003**, *128*, 1033−1036.
(46) Andrzejewski, D.; Roach, J. A. G.; Gay, M. L.; Musser, S. M. Analysis of coffee for the presence of acrylamide by LC-MS/MS. *J. Agric. Food Chem.* **2004**, *52*, 1996−2002.
(47) Granvogl, M.; Schieberle, P. Quantification of 3-aminopropionamide in cocoa, coffee and cereal products. *Eur. Food Res. Technol.* **2007**, *225*, 857−863.
(48) Guenther, H.; Anklam, E.; Wenzl, T.; Stadler, R. H. Acrylamide in coffee: review of progress in analysis, formation and level reduction. *Food Addit. Contam.* **2007**, *24*, 60−70.
(49) Lantz, I.; Ternite, R.; Wilkens, J.; Hoenicke, K.; Guenther, H.; van der Stegen, G. H. D. Studies on acrylamide levels in roasting, storage and brewing of coffee. *Mol. Nutr. Food Res.* **2006**, *50*, 1039−1046.

JOURNAL OF AGRICULTURAL AND FOOD CHEMISTRY

Article

pubs.acs.org/JAFC

Interlaboratory Comparison of a General Method To Screen Foods for Pesticides Using QuEChERs Extraction with High Performance Liquid Chromatography and High Resolution Mass Spectrometry

Brian D. Eitzer,*[,†] Walter Hammack,[‡] and Michael Filigenzi[§]

[†]Department of Analytical Chemistry, The Connecticut Agricultural Experiment Station, 123 Huntington Street, New Haven, Connecticut 06511, United States

[‡]Florida Department of Agriculture, 3125 Conner Blvd, Tallahassee, Florida 32399-1650, United States

[§]California Animal Health and Food Safety Laboratory, University of California at Davis, West Health Sciences Drive, Davis, California 95616, United States

Supporting Information

ABSTRACT: An interlaboratory comparison of a multipesticide residue analytical method is reported. The goal of the comparison was to evaluate the potential for liquid chromatography/high resolution mass spectrometry along with a specific automated screening procedure to allow the determination of the presence or absence of a set of targeted compounds without additional manual review. The method utilized an off the shelf QuEChERs based extraction followed by analysis with an orbitrap mass spectrometer with the data evaluated by ToxID. The method was tested at three laboratories, with three produce matrices (spinach, carrots, and oranges), and three levels of spiked pesticides with all analyses in triplicate. A series of 247 compounds were tested, and it was found that the three laboratories produced consistent data; however, manual review was still necessary. The data was shown to have no false negatives for 211 compounds in the three produce matrixes at 200 ppb. Of these 211 compounds, 189 had no false negatives at 50 ppb, and 129 had no false negatives at 10 ppb. The HRMS method was shown to be robust with similar data being achieved by all three laboratories and detectable concentrations only slightly above the range shown for triple quadrupole MS/MS.

KEYWORDS: *QuEChERs, pesticide residue, interlaboratory comparison, high resolution mass spectrometry*

INTRODUCTION

It has become evident that there are a multitude of potential contaminants in foods. The vast numbers of compounds include hundreds of different pesticides, mycotoxins, industrial compounds, and their byproducts. Insuring food safety therefore increasingly requires the use of methodologies that can monitor for hundreds of chemicals at the same time. These multiresidue methods combine a single extraction technique with analytical instrumentation capable of determining numerous compounds. Screening methods that can relatively quickly examine hundreds of compounds at relevant concentrations (i.e., below tolerance levels) have their place along with more rigorous quantitative methods. It has been noted that for screening to be effective for hundreds of compounds automated library based procedures will need to be implemented.[1]

Extraction protocols for multiresidue methods have been investigated by many researchers, with much of the recent efforts focused on modifications to the QuEChERS procedure as originally described by Anastassiades et al.[2] Versions with various buffers have been compared by Lehotay et al.[3] and a modified QuEChERS version was compared with aqueous acetonitrile extraction and pure acetonitrile extraction by Lacina.[4] Both groups report that the various different versions of QuEChERS perform reasonably well for most pesticides with the differences between the various procedures most pronounced for a couple of pH dependent pesticides.

The extracts produced in these multiresidue techniques have been commonly used along with liquid chromatography tandem mass spectrometry. These combined techniques lead to reports of the determination of pesticide residues in produce, wine, mango, watermelon, tea, and many other foods.[5−10] These quantitative methods require that the mass spectrometric procedures be targeted for a specific set of pesticides prior to analysis, so that the scan functions can be optimized for the selected reaction monitoring of each individual pesticide. One drawback of this optimization can be a limitation on the number of pesticides monitored at similar retention times due to the duty cycle of the instrument (the number of different scan functions that can be cycled through while still getting sufficient points across each chromatographic peak) Untargeted compounds will not be determined.

More recently the use of high resolution mass spectrometry (HRMS) rather than tandem mass spectrometry has been explored. Various instrumental configurations have been used: an orbitrap for the analysis of 350 pesticides in honey;[11] pesticide residues in fruits and vegetables with an orbitrap[12,13] and a quadrupole orbitrap;[14] organic contaminants in foods using a quadrupole time-of-flight MS;[15] a report of pesticide residues in ginseng and spinach using several different HRMS

Received: August 16, 2013
Accepted: December 9, 2013
Published: December 9, 2013

 © 2013 American Chemical Society

configurations.[16] One focus has been on how much mass resolution is necessary. Recent efforts have postulated that complex matrices require resolution greater than 50000 ($m/\Delta m$),[1] and in a comparison of HRMS to tandem MS, it was shown that above 50000 resolution, the selectivity of HRMS is greater than standard tandem MS.[17] In a later report, Kaufmann et al. stated that while "sensitivity was slightly inferior ... HRMS has advantages that will most likely never be met by MS/MS".[18] Among the advantages is the nontargeted nature of full-scan data acquisition. Signals for virtually all ions within the selected mass range are acquired as opposed to only those targeted for acquisition as occurs with multiple reaction monitoring in MS/MS. This makes it possible to analyze data retrospectively for analytes that were not considered at the time of acquisition. Potential drawbacks of the orbitrap based methods are some ion suppression issues that can occur in the c-cell of these instruments[12,19] and the need for robust automated methods to handle the abundance of data produced.[1,13]

Many of these recent efforts utilizing both time-of-flight and orbitrap platforms have been reviewed with the conclusion that these systems are "attractive for residue analysis in food".[20] It is, however, important to show that these methods are robust and rugged with results that agree across different users. This robustness can be best shown by comparing results on the same samples from different laboratories. We report here on such an interlaboratory comparison using an orbitrap HRMS to screen for pesticide residues in three diverse food matrices: spinach, a leafy green; oranges, watery fruit; and carrots, a root crop. The goal of the project was not the development of a full quantitative method but rather an examination of the utility of HRMS along with an automated data processing program to relatively quickly screen produce for the presence of pesticide residues. Our intent was not to investigate the method but to evaluate current procedure. We therefore chose to only utilize the 100000 resolution achievable by the orbitrap. As mentioned previously there are many versions of the QuEChERs extraction protocol, all of which do reasonably well for most compounds. We therefore chose to mimic a recently published validation of a QuEChERS LC-tandem mass spectrometric procedure[10] using the same matrices and extraction protocols. These choices would allow us to examine the utility of the HRMS screening procedure without going through optimization of the extraction or analysis protocols. To further examine the utility of the procedure, we chose to use a commercially available set of 247 pesticides, none of which were preselected to be amenable to the chosen QuEChERS procedure and LC-MS. Although this set of pesticides was not the same as the procedure that we were mimicking there was a sufficient overlap that we could compare our HRMS results with their tandem MS results. All samples were prepared at a single laboratory, frozen, and shipped to the other two laboratories. At each laboratory, the samples were spiked with the set of standards, extracted using the modified version QuEChERs, and analyzed by LC/HRMS on an orbitrap mass spectrometer.

MATERIALS AND METHODS

Reagents. The three laboratories in this study may have had different suppliers for some of the reagents so these are listed by specification. Water was supplied as 18.2 MΩ water from a Millipore Milli-Q source or purchased as HPLC grade. Acetonitrile was HPLC grade. When used for the mobile phases, the water and acetonitrile were either fortified at 0.1% with ACS reagent grade formic acid or purchased as prefortified HPLC grade reagents.

Materials. Prefilled QuEChERs extraction tubes containing 4 g of $MgSO_4$ and 1 g of NaCl (part no. ECMSS50CT, UCT, Bristol, PA) and prefilled QuEChERs extraction tubes containing 50 mg of PSA and 150 mg of $MgSO_4$ (part no. CUMPS2CT, UCT).

Standards. A mixed pesticide standard set was obtained from Accustandard (part no. S-21974-set, New Haven, CT). This set consists of 13 1 mL ampules each containing 16−22 pesticides at 100 μg/mL, for a total of 247 compounds. The stock standard was prepared by combining 400 μL from each of the ampules in a single 10 mL volumetric flask, and the final volume was brought to 10 mL with acetonitrile for a final concentration of 4 μg/mL. A diluted stock solution was prepared by bringing 2.5 mL of the stock solution to 10 mL with acetonitrile for a final concentration of 1 μg/mL. A 5 ppm solution of triphenylphosphate and d-6 malathion in acetonitrile was prepared as an internal standard.

Sample Preparation. Three different matrices were prepared. One pound or more of carrots, oranges, and spinach were chopped in a Hobart food chopper without peeling. The mixture was then thoroughly blended in a Robot Coupe, model R2 equipped with a 3 quart stainless steel bowl. The sample homogenate was frozen in 18 ounce Nasco whirl-pak bags with each bag containing about 250−300 g each. Bags of each matrix were shipped overnight to the other two laboratories for all subsequent work. At each laboratory, 12 10 g samples of each homogenized commodity were placed into 50 mL centrifuge tubes. Three tubes were left as unspiked matrix samples, three were spiked with 100 μL of the diluted stock standard (10 ppb in produce), three with 500 μL of the diluted stock standard (50 ppb in produce), three with 500 μL of the stock standard (200 ppb in produce). All were spiked with 100 μL of the internal standard solution. A reagent blank consisting of 10 mL water was also prepared. Acetonitrile was added to each of the tubes so that the total volume of acetonitrile added (spikes plus acetonitrile) was 10 mL. A ceramic stone was added to each tube, and the sample was vigorously shaken for 1 min. A UCT salt packet containing 4 g of $MgSO_4$ and 1 g of NaCl was then added, and again the samples were shaken for 1 min. The sample was centrifuged for 5 min at ≥3000 rpm. A 1 mL aliquot was transferred to a tube containing 50 mg of PSA and 150 mg of $MgSO_4$. The sample was shaken for 1 min. The sample was centrifuged for 5 min at ≥3000 rpm. A 0.5 mL aliquot was diluted with 0.5 mL of the aqueous mobile phase (water with 0.1% formic acid), and the sample was filtered into a microvial for LC-HRMS analysis.

Instrumental Analysis. Samples were analyzed using an Agilent (Santa Clara, CA) 1200 series rapid resolution liquid chromatograph interfaced to a Thermo Fisher Scientific (West Palm Beach, FL) Exactive orbitrap mass spectrometer. The LC was operated using a Thermo Fisher Scientific Hypersil Gold aQ C-18, 100 mm × 2.1 mm, 1.9 μm column held at 40 °C. The mobile phase flow rate was 0.25 mL/min, going from 99% water with 0.1% formic acid to 95% acetonitrile with 0.1% formic acid from 1 to 10 min followed by a 5 min hold at 95%, with a 5 min re-equilibration step for a total run time of 21.5 min. Three microliters of extract was injected. HRMS data was acquired in the positive electrospray mode using a metal needle at 3.5 kV, a source capillary temperature of 300 °C and mass resolution of 100000 (as specified in the tune page), the balanced mass accuracy setting, and an injection time of 20 ms. Data was acquired over the mass range of m/z = 75−1500. Prior to analysis, the mass spectrometer was tuned by infusion of azoxystrobin into the system. The tube lens, skimmer, and other parameters were adjusted so that the relative abundance of m/z 372 compared with m/z 404 was less than 10%. This tuning step was performed in order to ensure that any fragmentation of analytes through the tube lens and skimmer was minimized. A single tune file from each laboratory was used for the entire set of analyses though a mass calibration was performed prior to the analysis of each sample matrix.

It should be noted that the final extract concentration was 0.5 g sample/mL extract. At the 10 ppb concentration using a 3 μL injection, this would result in a total of 15 pg on column. While these low levels may help reduce ion suppression, they also can be a challenge to detect.

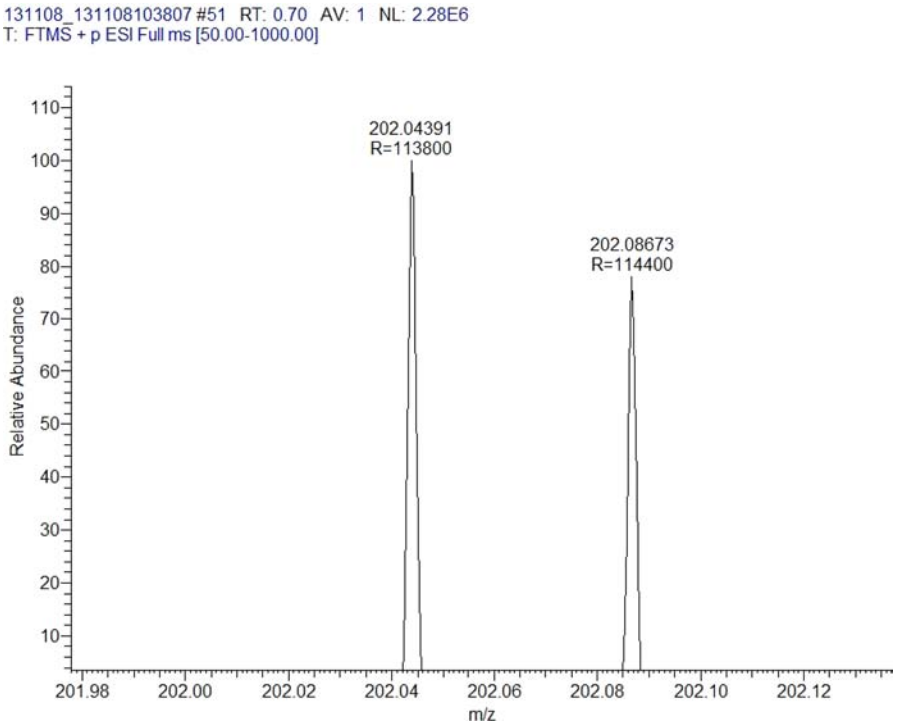

Figure 1. Mass profile for an infusion of thiobendazole and carbaryl on the orbitrap mass spectrometer at a resolving power of 100000. The theoretical m/z of the $(M + H)^+$ ions are 202.04334 and 202.08626, respectively.

Data Analysis. The raw pesticide data from the instrument was analyzed using the ToxID software package (Thermo Scientific). This program required an input file listing the molecular formula for each pesticide of interest, along with its expected retention time. During the setup of the method, the stock solution of 247 standards was injected on the instrument to determine retention times. Five compounds had distinctively split peaks and were entered into the input file twice (with separate retention times), while six compounds were not detected in the positive electrospray mode, thus in total there were 246 entries in the input file used for these tests. During operation of the software, the raw exact mass data for each entry was compared with the theoretically expected data (as computed from the entries molecular formula) for each of the individual pesticides in the input file. User parameters were set for detection at an elution time of ±0.25 min with a mass accuracy of ±5 ppm. The response threshold was set by each laboratory and had a slight variability depending on instrument but was in the range of 1000- 5000 counts. The ToxID data output for samples, spiked samples, and method blanks were reviewed to determine if analytes were found correctly and identified in amounts significantly greater (3x) than that observed in the method blanks.

Safety. Pesticides are considered hazardous materials. In accordance, all laboratory procedures were conducted with good chemical handling practices, and waste was disposed of as per the laboratory's hazardous waste plan.

RESULTS AND DISCUSSION

Specificity. Individual pesticide residues were identified in samples through two fundamental characteristics of the pesticide. The first was that the retention time for the pesticide must have been within 0.25 min of the time observed for an authentic standard of that pesticide. The second and more important characteristic was that the exact m/z of the pesticide must have been within 5 ppm of the calculated theoretical value.

As an example of the specificity that is provided by an exact mass instrument consider the case of the two pesticides, carbaryl and thiabendazole. Although carbaryl ($C_{12}H_{11}NO_2$) and thiabendazole ($C_{10}H_7N_3S$) have the same nominal mass of 201, the theoretical exact m/z's of their $(M + H)^+$ ion are 202.08626 and 202.04334, respectively. While these ions would be indistinguishable on unit resolution mass spectrometers, they are easily differentiated under high resolution conditions with a required resolution ($m/\Delta m$) of only 4700. This is clearly demonstrated in Figure 1, which shows the infusion (no chromatography) of these two compounds into the orbitrap system used in the current work. The protonated molecular ions of the two compounds are quite distinct. The work herein described was performed at a mass resolution of 100000. Isomeric compounds, having identical formulas, cannot be distinguished by differences in the exact mass of the molecular ion. However, these compounds can often still be distinguished by differences in relative retention time through the chromatographic system. Alternatively they can be differentiated by collisional fragments generated in the HCD cell of the instrument. These experiments could be conducted on the described instrumentation, but that is the subject of future work.

Interlaboratory Comparison. Data was reviewed for each individual pesticide at each level in each matrix. The number of detections (out of three samples) for each combination (matrix−pesticide−level) was recorded. All data from the three laboratories is included in the Supporting Information. The number of detections for the same combination was then compared across the three laboratories and is shown in Table 1. As can be seen in the table, the three different laboratories were very consistent in their ability to detect the pesticides. At the lowest level over 70% of the time either all three laboratories found a pesticide the same number of times in a particular matrix or did not see it at all in that matrix. By the highest concentration level the consistency in the data was almost at 90%. Clearly the entire method showed good consistency across the three laboratories.

dx.doi.org/10.1021/jf405128y | J. Agric. Food Chem. 2014, 62, 80−87

Reagent Blanks. With each set of samples, a reagent blank (using clean water and all other reagents including the internal standards) was analyzed. These samples were processed using the same ToxID protocol as used for all samples. A total of 43 of the compounds on the entry list were reported as a positive hit in at least one reagent blank sample by the ToxID software. Upon further inspection almost all of these "detections" appeared to be the result of software integrating noise. This points out the need for user accessible data integration parameters (other than intensity threshold) in the ToxID software. In addition, this also indicates that there needs to be a manual review of data.

Table 1. Comparison of the Percentage of Times That the Different Laboratories Agree on the Detection (Or Nondetection) At the Specified Concentration Level

concn level	% 0 of 3 agree	% 2 of 3 agree	% 3 of 3 agree
10	5.65	22.6	71.8
50	2.0	14.6	83.3
200	1.6	9.5	88.8

Table 2. The Number of Pesticides with the Specified Number of False Positive Hits in Each Matrix[a]

matrix	1 hit	2 hits	3 hits	4 hits	5 hits	6 hits	7 hits	8 hits	9 hits
oranges	13	6	11	3	1	4	0	1	1
carrots	5	2	10	3	0	0	0	0	1
spinach	11	6	13	3	1	2	0	0	1

[a]Each unspiked matrix was analyzed three times by each laboratory so the maximum number of hits is nine.

Unspiked Matrix. The analyzed samples were purchased at the supermarket with no *a prioi* knowledge of pesticide use. Therefore, the unspiked matrix samples were examined for the presence of any of the pesticides in the spiked mixture. Each laboratory extracted a set of three samples of each matrix without any spikes other than the internal standards. Three incurred residues were identified in the oranges (imazalil, pyriproxifen, and thiadendazole); two residues in the spinach (imidacloprid and spinosad), and none in the carrots. For these residues, in all cases there were good distinct peaks that appeared to be real in all nine samples analyzed of the unspiked matrix. There were a number of additional compounds tentatively identified by ToxID in the unspiked matrix that on closer inspection did not look like real peaks. These pesticides would be considered as false positves and are summarized in Table 2. There are two ways to consider the false positive rate: either (number of pesticides seen at least

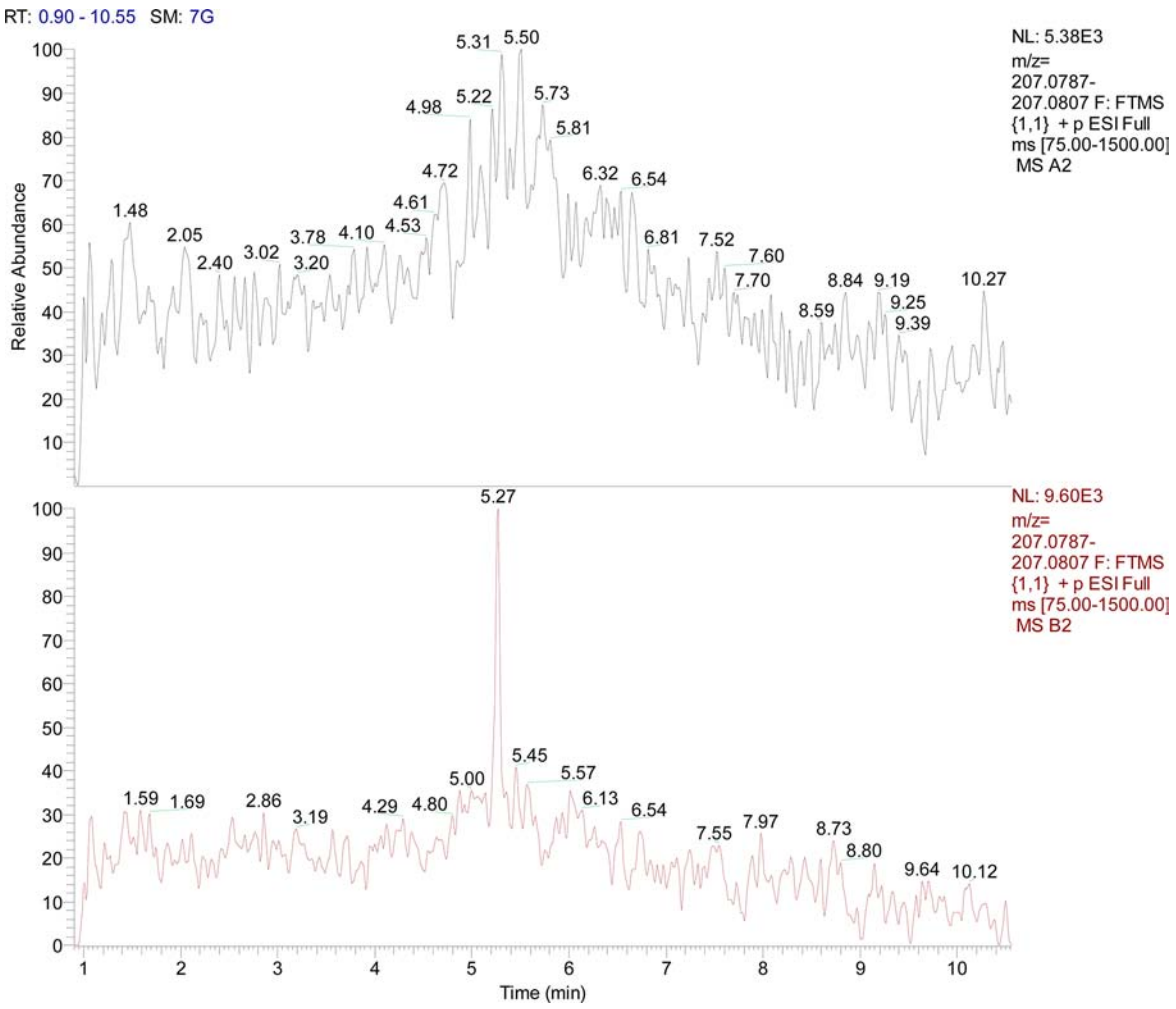

Figure 2. Selected ion chromatogram (5 ppm window) around $(M + H)^+$ ion for aldicarb sulfoxide spiked into oranges at 10 ppb (top) and 50 ppb (bottom). ToxID identifies a peak in both samples; however, the compound was not considered to be identified in the upper sample upon review.

dx.doi.org/10.1021/jf405128y | J. Agric. Food Chem. 2014, 62, 80−87

once)/(the total number of pesticides, 247) or (the total number of hits)/(total possible hits, 2223). Thus, the false positive rates for the three matrixes are as follow: oranges 16% and 5.2%, carrots 9% and 2.7%, spinach 15% and 4.5%. Although these rates are low, they again point to the need for additional data review beyond the library program.

False Negatives. A false negative occurs if a residue that should be reported was missed. To give a true assessment of the false negative rates, the data needed to be adjusted for positive detections based on the integration of noise. To do this, any pesticide that had a ToxID reported detection in either an unspiked matrix or reagent blank was carefully examined in the lowest spiked samples. In a few cases, the ToxID program integrated a noise peak at the 10 ppb level and then identified the compound as having been found. An example of this noise integration is shown in Figure 2 (top); however, in all of these cases, when the compound was examined at the 50 ppb level, the peak was present at sufficient signal-to-noise ratio to be correctly identified, Figure 2 (bottom). In these cases, the detections for the 10 ppb sample were manually changed to nondetects prior to the analysis of false negatives.

The false negative rate for each pesticide at each concentration level is defined by eq 1, where F is the false negative rate, N is the number of missed detections at a given concentration, and D is the number of possible detections at a given concentration. For most pesticides, D is 27, but for those pesticides for which there was an incurred residue, the data was adjusted to only use the matrixes without that incurred residue (D = 18 in those cases).

$$F = 100 \times N/D \quad (1)$$

The false negative rate for each pesticide at each concentration is included in the Supporting Information. The data is summarized in Table 3 showing the number of pesticides within a specified false negative percentage range. The method was tested with a mixed pesticide standard containing 247 different pesticides along with two internal standards. Seven compounds did not respond on the LC/MS system while five others gave split peaks creating a total of 246 distinct ToxID entries to examine for false negatives. At the 10 ppb spiking level, just over half (129) of the pesticides were seen in all spiked samples, with this number increasing to about 75% (189) at 50 ppb, and 85% (211) at 200 ppb. This table also shows that there were only a couple of truly problematic compounds that had false negative rates of over 50% at the higher concentration level. Several of these compounds also had poor (though) detectable response in the standards so likely lacked sensitivity to be detected at lower concentrations in matrix. It is also possible that a couple of these pesticides may have had problems with the chosen extraction procedure, though this was not evaluated. It should be noted that this version of QuEChERS has an overall dilution of the sample by a factor of 2. Some of the other versions of QuEChERs result in

Table 3. Number of Pesticides with the Specified False Negative Rate Using the ToxID Software at Each Concentration

concn	0%	0−25%	25−50%	50−75%	75−100%
10	129	34	30	16	37
50	189	18	16	14	9
200	211	9	13	11	2

Table 4. Comparison of the Minimum Concentration with Zero False Negatives with the Tandem MS MDL as Listed by Sack et al.[10] for the Same Compound[a]

compound	minimum concentration with zero false negatives	tandem MS MDL (ppb)
acephate	50	4
acetamiprid	50	5
acibenzolar S-methyl	50	8
alanycarb	*b*	8
aldicarb	50	6
aldicarb sulfoxide	50	4
aminocarb	10	4
azoxystrobin	10	4
benalaxyl	10	5
bendiocarb	50	4
benfuracarb	50	3
benzoximate	10	6
bifenazate	200	5
bitertanol	10	6
boscalid	50	6
bromuconazole-cis	50	7
bromuconazole-trans	50	7
bupirimate	10	7
buprofezin	10	5
butafenacil	50	5
butocarboxim	50	9
butoxycarboxim	*b*	6
carbaryl	50	5
carbendazim	10	5
carbetamide	10	4
carbofuran	10	4
carbofuran-3OH	50	5
chlorantraniliprole	200	5
chlorfluazuron	50	6
chloroxuron	10	7
clethodim	50	5
clofentezine	200	5
clothianidin	200	7
cyazofamid	50	8
cycluron	10	5
cyflufenamid	10	5
cymoxanil	*b*	5
cyproconazole	10	7
cyprodinil	10	6
cyromazine	*b*	4
desmedipham	50	5
diclobutrazol	10	7
dicrotophos	10	4
diethofencarb	10	5
difenoconazole	10	4
diflubenzuron	*b*	5
dimethoate	10	4
dimethomorph	50	6
dimoxystrobin	10	5
dinotefuran	50	5
dioxacarb	*b*	6
diuron	50	6
doramectin	200	13

dx.doi.org/10.1021/jf405128y | J. Agric. Food Chem. 2014, 62, 80−87

Table 4. continued

compound	minimum concentration with zero false negatives	tandem MS MDL (ppb)
emamectin benzoate B1a	10	6
emamectin benzoate B1b	200	6
ethiofencarb	10	4
ethiprole	50	7
ethirimol	10	3
etoxazole	10	4
fenamidone	10	6
fenazaquin	10	5
fenbuconazole	10	6
fenhexamid	50	6
fenobucarb	10	4
fenoxycarb	10	4
fenpyroximate	10	4
fenuron	10	5
flonicamid	50	6
flubendiamide	50	9
flufenoxuron	200	5
fluometuron	10	5
fluoxastrobin	10	5
flusilazole	10	5
flutolanil	10	6
flutriafol	10	6
forchlorfenuron	10	6
formetanate	10	5
fuberidazole	10	4
furathiocarb	10	5
halofenozide	50	5
hexaflumuron	*b*	9
hexythiazox	50	4
hydramethylnon	50	5
imazalil	10	5
imidacloprid	50	6
indoxacarb	50	8
ipconazole	10	7
iprovalicarb	10	4
isoprocarb	10	3
isoproturon	10	5
isoxaflutole	*b*	30
ivermectin	200	10
kresoxim-methyl	50	6
linuron	50	6
malathion	50	7
mandipropamid	10	6
mepanipyrim	10	6
metaflumizone	*b*	7
metalaxyl	10	5
metconazole	10	6
methamidophos	200	4
methiocarb	50	5
methomyl	50	5
methoxyfenozide	10	6
metobromuron	50	4
mevinphos	50	6
mexacarbate	10	6
monocrotophos	10	4

Table 4. continued

compound	minimum concentration with zero false negatives	tandem MS MDL (ppb)
monolinuron	10	4
moxidectin	200	8
myclobutanil	10	7
neburon	10	5
nitenpyram	50	5
novaluron	*b*	7
nuarimol	10	7
omethoate (dimethoate oxon)	10	4
oxadixyl	50	6
oxamyl	50	4
paclobutrazol	10	8
phenmedipham	50	5
picoxystrobin	10	6
piperonyl butoxide	10	5
pirimicarb	10	5
prochloraz	10	4
promecarb	10	5
propamocarb	10	4
propargite	*b*	4
propiconazole	10	6
propoxur	10	3
pyracarbolid	10	4
pyraclostrobin	10	4
pyridaben	10	5
pyrimethanil	10	6
pyriproxyfen	10	5
rotenone	10	6
siduron	10	9
spinetoram	10	4
spirodiclofen	50	17
spiromefisen	50	7
spirotetramat	50	6
spiroxamine	200	7
sulfentrazone	*b*	10
tebuconazole	10	7
tebufenozide	10	6
tebuthiuron	10	4
teflubenzuron	*b*	9
temephos	*b*	6
thiabendazole	10	5
thiacloprid	50	5
thiamethoxam	50	6
thidiazuron	10	7
thiophanate-methyl	200	5
triadimefon	10	6
triadimenol	10	9
tricyclazole	10	3
trifloxystrobin	10	4
triflumizole	10	5
triflumuron	200	6
triticonazole	10	7
vamidothion	10	5
zoxamide	50	7

[a]Average of two transitions used. [b]Never reached, there was always at least one false negative.

dx.doi.org/10.1021/jf405128y | J. Agric. Food Chem. 2014, 62, 80−87

Table 5. List of Compounds Tested for Which a Tolerance Has Been Established for One of the Matrixes Studied along with the Minimum Concentration with Zero False Negatives[a]

compound	minimum zero false negative concn (ppb)	carrots tolerance (ppb)	spinach tolerance (ppb)	oranges tolerance (ppb)
acetamiprid	50		3000	500
acibenzolar S-methyl	50		1000	
aldicarb	50			300
aldicarb sulfone	50			300
aldicarb sulfoxide	50			300
azoxystrobin	10	500		10 000
boscalid	50	1000	1000	1600
buprofezin	10		35 000	2500
carbaryl	50	2000	22 000	10 000
carfentrazone-ethyl	*b*		100	100
chlorantraniliprole	200		13 000	1400
clethodim	50	1000	2000	
clothianidin	200	800	3000	
cyazofamid	50	90	9000	
cyprodinil	10	750	30 000	8000
desmedipham	50		6000	
diazinon	10	750	700	
difenoconazole	10			600
dimethoate	10			2000
dinotefuran	50		5000	
diuron	50			50
emamectin benzoate B1a	10		100	
emamectin benzoate B1b	200		100	
EPTC (eptam)	10	100		
ethofumesate	*b*	7000		
fenamidone	10	150		
fenazaquin	10			500
fenbuconazole	10			1000
fenhexamid	50		30 000	
fenpyroximate	10			600
flonicamid	50	600	9000	
flubendiamide	50		11 000	
flufenoxuron	200			300
hexythiazox	50			350
imazalil[2]	10			10 000
imidacloprid[3]	50	400	3500	700
indoxacarb	50		14 000	
linuron	50	1000		
malathion	50	8000	8000	8000
mandipropamid	10		20 000	
metalaxyl	10	500	10 000	10 000
methidation	*b*			4000
methomyl	50	200	200-	2000
methoxyfenozide	10	100	30 000	10 000
metribuzin	10	300		
mevinphos	50		1000	
myclobutanil	10	30	30	
norflurazon	50			200
oxamyl	50	100		3000
phenmedipham	50		4000	
piperonyl butoxide	10			8000
prometryn	10	450		
propiconazole	10	250	5000	
pymetrozine	200		600	
pyraclostrobin	10	400	29 000	2000
pyridaben	10			500
pyrimethanil	10			10 000
pyriproxyfen	10	150	3000	300
spinetoram	10	100	8000	300
spinosad[5]	10	100	8000	300
spirodiclofen	50			500
spiromefisen	50		12 000	
spirotetramat	50		9000	600
tebufenozide	10		10 000	800
thiabendazole	10			10 000
thiamethoxam	50	50	4000	400
trifloxystrobin	10	100		600
triflumizole	10		3500	

[a]Tolerance values from Pesticide Chemical News Guide, Arlington VA;[21] also available from Code of Federal Regulations Title 40, 24, Part 180.[22]
[b]Never reached, there was always at least one false negative.

concentration of the extract by a factor of 2−5. It is possible that using one of these other versions would further reduce the false negative rate and improve the overall sensitivity of the method at the possible cost of increasing false positives.

It is useful to compare the overall performance of this HRMS method with that of the triple quadrupole MS/MS reported by Sack et al. for these same three matrixes using the same extraction scheme but with multiple reaction monitoring tandem mass spectrometry as the detection method.[10] This comparison is shown in Table 4. It should be noted that the Sack et al. data were reported using operating conditions that were optimized for each individual pesticide, whereas the current data was collected using a single scan function on the mass spectrometer. Furthermore, the Sack data are actual reported MDLs, while the current data only report on the minimum concentration in this screening project that had no false negatives; for many compounds, the detection limit is likely lower because there were many pesticides with strong signals at the lowest tested level. Nevertheless, the current data show a robust response with the minimum detection limits; over 50% of these 161 pesticides had a zero false positives at a concentration on the same order of magnitude as the reported MDL (i.e., minimum concentration of 10 vs an MDL of 5). There were clearly some pesticides that worked much better on the tandem MS system; further investigation is needed to see what is causing this to occur. Furthermore, the current methodology can easily be expanded to include many other pesticides (and other toxic organic contaminants). All that is necessary is the knowledge of the chemical formula of the compound; it can then be easily added to the screen (provided it extracts and is detectable by the LC/HRMS system). In fact, because the instrumental conditions do not change, items can be added to the list retroactively. This is one item that the triple quadrupole system could not do because it needs to have screened for a specific (and preset) transition.

It is also useful to examine the validated level in terms of what detection level is actually needed. This can be done by comparing the validated level to the tolerance for a particular pesticide in a given matrix as determined by the EPA and listed in the Code of Federal Regulations.[21] Table 5 compares the

minimum validated levels with the tolerances for those compounds for which a tolerance has been established. Examination of this table shows that in almost all cases the minimum validated level is below (and in most cases, well below) the United States tolerance and for many compounds meets the 10 ppb default detection limit of Europe. Thus, use of the reported screening method would succeed in observing the pesticides at the levels where they would need to be found. This being a screening method, follow-up would be required to determine whether they are below tolerance when found. Overall, there clearly is utility in the HRMS screening procedures, though improvements still need to be made in the software for dealing with these large multiresidue screens.

■ ASSOCIATED CONTENT

Ⓢ Supporting Information

All data from the three laboratories and the false negative rate for each pesticide at each concentration. This material is available free of charge via the Internet at http://pubs.acs.org.

■ AUTHOR INFORMATION

Corresponding Author

*E-mail: Brian.eitzer@ct.gov.

Funding

This work was supported by the Food and Drug Administration through the Food Emergency Response Networks Chemistry Cooperative Agreement Program.

Notes

The authors declare no competing financial interest.

■ ACKNOWLEDGMENTS

We thank the personnel of the FDA's Forensic Chemistry Center for suggestions during the study.

■ REFERENCES

(1) Kellmann, M.; Muenster, H.; Zomer, P.; Mol, H. Full Scan MS in Comprehesive Qualitative and Quantitative Residue Analysis in Food and Feed Matrices: How Much Resolving Power is Required? *J. Am. Soc. Mass Spectrom.* **2009**, *20*, 1464−1476.

(2) Anastassiades, M.; Lehotay, S. J.; Stajnbaher, D.; Schenck, F. J. Fast easy multiresidue method employing acetonitrile extraction partitioning and 'dispersive solid phase extraction' for determination of pesticide residues in produce. *J. AOAC Int.* **2003**, *86*, 412−431.

(3) Lehotay, S. J.; Son, K. A.; Kwon, H.; Koesukwiwat, U.; Fu, W.; Mastovska, K.; Hoh, E.; Leepipatpiboon, N. Comparison of QuEChERS Sample Preparation Methods for the Analysis of Pesticide Residues in Fruits and Vegetables. *J. Chromatogr. A* **2010**, *1217*, 2458−2560.

(4) Lacina, O.; Zachariasova, M.; Urbanova, J.; Vaclavikova, M.; Cajka, T.; Hajslova, J. Critical Assessment of Extraction Methods for the Simultaneous Determination of Pesticide Residues and Mycotoxins in Fruits, Cereals, Spices, and Oil Seeds Employing Ultra-High Performance Liquid Chromatography-Tandem Mass Spectrometry. *J. Chromatogr. A* **2012**, *1262*, 8−18.

(5) Ortelli, D.; Edder, P.; Corvi, C. Multiresidue analysis of 74 pesticides in fruits and vegetables by liquid chromatography-electrospray-tandem mass spectrometry. *Anal. Chim. Acta* **2004**, *520*, 33−45.

(6) Zhang, K.; Wong, J. W.; Hayward, D. G.; Sheladia, P.; Krynitsky, A. J.; Schenk, F. J.; Webster, M. G.; Ammann, J. A.; Ebeler, S. E. Multiresidue pesticide analysis of wines by dispersive solid-phase extraction and ultrahigh-performance liquid chromatography-tandem mass spectrometry. *J. Agric. Food Chem.* **2009**, *57*, 4019−29.

(7) Banerjee, K.; Oulkar, D. P.; Patil, S. B.; Jadhav, J.; Dasgupta, S.; Patil, S. B.; Bal, S.; Adsule, P. G. Multiresidue determination and uncertainty analysis of 87 pesticides in mango by liquid chromatography-tandem mass spectrometry. *J. Agric. Food Chem.* **2009**, *57*, 4068−78.

(8) Park, S.; Lee, S. J.; Kim, H. G.; Jeong, W. Y.; Shim, J. H.; Abd El-Aty, A. M.; Jeong, S. W.; Lee, W. S.; Kim, S. T.; Shin, S. C. Residue analysis of multi-class pesticides in watermelon by LC-MS/MS. *J. Sep Sci.* **2010**, *33*, 493−501.

(9) Huang, Z.; Zhang, Y.; Wang, L.; Ding, L.; Wang, M.; Yan, H.; Li, Y.; Zhu, S. Simultaneous determination of 103 pesticide residues in tea samples by LC-MS/MS. *J. Sep Sci.* **2009**, *32*, 1294−1301.

(10) Sack, C.; Smoker, M.; Chamkasem, N.; Thompson, R.; Satterfield, G.; Masse, C.; Mercer, G.; Neuhaus, B.; Cassias, I.; Chang, E.; Lin, Y.; MacMahon, S.; Wong, J.; Zhang, K.; Smith, R. E. Collaborative Validation of the QuEChERS Procedure for the Determination of Pesticides in Food by LC-MS/MS. *J. Agric. Food Chem.* **2011**, *59*, 6383−6411.

(11) Gomez-Perez, M. L.; Plaza-Bolanos, P.; Romero-Gonzalez, R.; Martinez-Vidal, J. L.; Garrido-Frenich, A. Comprehensive Qualitative and Quantitative Determination of Pesticides and Veterinary Drugs in Honey Using Liquid Chromatography-Orbitrap High Resolution Mass Spectrometry. *J. Chromatogr. A* **2012**, *1248*, 130−138.

(12) Adler, L.; Steinborn, A.; Bergelt, B. Suitability of an Orbitrap Mass Spectrometer for the Screening of Pesticide Residues in Extracts of Fruits and Vegetables. *J. AOAC Int.* **2011**, *94* (6), 1661−1673.

(13) Mol, H. G. J.; Zomer, P.; de Koning, M. Qualitative Aspects and Validation of a Screening Method for Pesticides in Vegetables and Fruits Based on Liquid Chromatography Coupled to Full Scan High Resolution (Orbitrap) Mass Spectrometry. *Anal. Bioanal. Chem.* **2012**, *403*, 2891−2908.

(14) Wang, J.; Chow, W.; Leung, D.; Chang, J. Application of Ultrahigh-Performance Liquid chromatography and Electrospray Ionization Quadrupole Orbitrap High-Resolution Mass Spectrometry for Determination of 166 Pesticides in Fruits and Vegetables. *J. Agric. Food Chem.* **2012**, *60*, 12088−12104.

(15) Diaz, R.; Ibanez, M.; Sancho, J. V.; Hernandez, F. Target and Non-Target Screening Stratagies for Organic Contaminants, Residues, and Illicit Substances in Food, Environmental and Human Biological Samples by UHPLC-QTOF-MS. *Anal. Methods* **2012**, *4*, 196−209.

(16) Hayward, D. G.; Wong, J. W.; Zhang, K.; Chang, J.; Shi, F.; Banerjee, K.; Yang, P. Multiresidue Pesticide analysis in Ginseng and Spinach by Nontargeted and Targeted Screening Procedures. *J. AOAC Int.* **2011**, *94* (6), 1741−1751.

(17) Kaufmann, A.; Butcher, P.; Maden, K.; Walker, S.; Widmer, M. Comprehensive comparison of liquid chromatography selectivity as provided by two types of liquid chromatography detectors (high resolution mass spectrometry and tandem mass spectrometry): "Where is the crossover point? *Anal. Chim. Acta* **2010**, *673*, 60−72.

(18) Kaufmann, A.; Dvorak, V.; Cruzer, C.; Butcher, P.; Maden, K.; Walker, S.; Widmer, M.; Schurmann, A. Study of high-resolution mass spectrometry as a replacement for tandem mass spectrometry in the field of quantitative pesticide analysis. *J. AOAC Int.* **2012**, 528−548.

(19) Kaufmann, A.; Widmer, M.; Maden, K. Post-Interface Signal Suppression, a Phenomenon Observed in a Single Stage Orbitrap Mass Spectrometer Coupled to an Electrospray Interfaced Liquid Chromatograph. *Rapid Commun. Mass Spectrom.* **2010**, *24*, 2162−2170.

(20) Gomez-Ramos, M. M.; Ferrer, C.; Malato, O.; Aguera, A.; Fernandez-Alba, A. R. Liquid chromatography-high-resolution-mass-spectrometry for pesticide residue analysis in fruit and vegetables: Screening and quantitative studies. *J. Chromatogr. A* **2013**, *1287*, 24−37.

(21) Code of Federal Regulations Title 40, 24, Part 180.

(22) Pesticide Chemical News Guide, Arlington VA.

JOURNAL OF AGRICULTURAL AND FOOD CHEMISTRY

Article

pubs.acs.org/JAFC

Effect of Cyclolinopeptides on the Oxidative Stability of Flaxseed Oil

Oyunchimeg Sharav,[†] Youn Young Shim,*[,‡] Denis P. Okinyo-Owiti,[‡] Ramaswami Sammynaiken,[§] and Martin J. T. Reaney*[,†,‡,⊥]

[†]Department of Food and Bioproduct Sciences, and [‡]Department of Plant Sciences, University of Saskatchewan, 51 Campus Drive, Saskatoon, Saskatchewan S7N 5A8, Canada

[§]Saskatchewan Structural Sciences Centre, University of Saskatchewan, 110 Science Place, Saskatoon, Saskatchewan S7N 5C9, Canada

[⊥]Department of Food Science and Engineering, Jinan University, 601 Huangpu Avenue West, Guangzhou, 510632, China

ABSTRACT: Polar compounds present in flaxseed oil increase its oxidative stability. Flaxseed oil becomes less stable to oxidation when filtered with silica. This observation may be linked to antioxidant compounds present in flaxseed oil. Flaxseed oil was passed over a silica adsorbent column to remove polar compounds. The polar compounds were then eluted from the silica absorbant using a series of increasingly polar solvents. The polar fractions from flaxseed oil were then added back to silica-treated flaxseed oil to determine the impact of fractions containing polar compounds on oxidative stability (induction time) at 100 °C. A polar fraction containing mainly cyclolinopeptide A (CLA, **1**), but also containing β/γ- and δ-tocopherol increased the induction time of silica-treated flaxseed oil from 2.36 ± 0.28 to 3.20 ± 0.41 h. When oxidative stability was determined immediately after addition of the polar fractions other flaxseed fractions and solvent controls did not affect oil stability. However, when the oxidative stability index (OSI) test was delayed for three days and oil samples were held at room temperature after the addition of the polar fractions to the flaxseed oil, it was observed that the control oil treated with silica had become highly sensitive to oxidation. A polar fraction containing a mixture of CLs (**1**, **5**, **7**, **9**, **11**), improved the oxidative stability of peptide-free oil with respect to the control when the OSI measurement was made three days after adding the fraction. In addition, effects of **1** on the oxidative stability of peptide-free oil containing divalent metal cations was investigated.

KEYWORDS: *Linum usitatissimum L., cyclolinopeptide, flaxseed, antioxidant, oxidative stability*

INTRODUCTION

Flaxseed (*Linum usitatissimum* L.) is an oilseed adapted to cool northern climates. Whole flaxseed contains 41% fat, 28% dietary fiber, and 21% protein having an amino acid profile comparable to that of soybean meal.[1] Flaxseed is one of the richest dietary sources of α-linolenic acid (ALA), having high levels of polyunsaturated fatty acids (73%).[2] Food and Agriculture Organization statistics show that global flaxseed production has been stable at ∼2 000 000 tonnes between 2008 and 2012 with the majority of the crop being produced in North America, Asia, and Europe.[3] Flaxseed oil is used predominantly as drying oil but it is increasingly being used as a source of dietary omega-3 fatty acids.[4]

Whereas the high content of unsaturated fatty acid present in flaxseed is important to its purported health benefits, its chemical structure makes it vulnerable to oxidation. Oxidation of flaxseed oil during improper processing and storage reduces its nutritional value and causes the development of undesirable flavors.[5,6] Despite its distinctive unstable oil content, flaxseed produces antioxidants that protect the meal in storage.[7−9] Flaxseed contains several known bioactive compounds, including lignans, phenolic acids, anthocyanin pigments, flavonols, flavones, and phytic acid, all of which may contribute to the seed's antioxidant capacity.[10] The concentration of these antioxidants in flaxseed oil depends on the extraction procedure and the treatment of the oil. Moreover, refining may also reduce minor compounds that have an effect on oil shelf life. The unrefined oil may have higher nutritional value and longer shelf life than refined flaxseed oil.[11] On the other hand, cold-pressing procedures do not involve heat or chemical treatments and the oil is extracted under mild conditions.[12] Siger et al.[11] reported several antioxidant compounds in cold-pressed flaxseed oil, including flavonoids (12.7−25.6 mg/100 g), phenolic acids (76.8−307.3 mg/100 g), α-tocopherols (0.55−9.11 mg/100 g), γ-tocopherols (10.56−15.00 mg/100 g), and plastochromanol-8 (3.37−5.53 mg/100 g). However, tocopherols are considered the main antioxidants in flaxseed oil. Some authors report weak[13] or no relationship between flaxseed oil oxidative stability and the content of tocopherols or phenol compounds in the oil.[14] Therefore, it is possible that other minor oil soluble compounds play a role in slowing the oxidation of flaxseed oil.

Cyclolinopeptides (CLs) are hydrophobic compounds present in flaxseed oil with polarity comparable to known natural antioxidants (Table 1 and Figure 1), but the antioxidant activity of these compounds has not been studied. The oxidative stability of CLs in vegetable oil was reported by Brühl et al.[6] while the stability of CLs in partially defatted flaxseed products was reported by Aladedunye et al.[7] The first discovered CL, CLA (**1**), was characterized in 1959.[15] Its unique structure induced researchers to investigate its

Received: August 25, 2013
Revised: December 8, 2013
Accepted: December 9, 2013
Published: December 9, 2013

ACS Publications © 2013 American Chemical Society

Table 1. Amino Acid Sequences and Chemical Formulas of CLs

CL (code)	name[a]	amino acid sequence (NαC-)[b]	molecular formula	protonated ion mass (m/z)[c]
CLA (**1**)	CLA[15]	Ile-Leu-Val-Pro-Pro-Phe-Phe-Leu-Ile	$C_{57}H_{85}N_9O_9$	1040.65
1-Met-CLB (**2**)	CLB[47]	Met-Leu-Ile-Pro-Pro-Phe-Phe-Val-Ile	$C_{56}H_{83}N_9O_9S$	1058.61
1-MetO-CLB (**3**)	CLC[47]	MetO-Leu-Ile-Pro-Pro-Phe-Phe-Val-Ile	$C_{56}H_{83}N_9O_{10}S$	1074.56
1-Met-CLD (**4**)	CLD′[48]	Met-Leu-Leu-Pro-Phe-Phe-Trp-Ile	$C_{57}H_{83}N_9O_8S$	1048.60
1-MetO-CLD (**5**)	CLD[47]	MetO-Leu-Leu-Pro-Phe-Phe-Trp-Ile	$C_{57}H_{77}N_9O_8S$	1064.54
1-Met-CLE (**6**)	CLE′[48]	Met-Leu-Val-Phe-Pro-Leu-Phe-Ile	$C_{51}H_{76}N_8O_8S$	961.59
1-MetO-CLE (**7**)	CLE[47]	MetO-Leu-Val-Phe-Pro-Leu-Phe-Ile	$C_{51}H_{76}N_8O_9S$	977.52
1-Met-CLF (**8**)	CLF′[48]	Met-Leu-Met-Pro-Phe-Phe-Trp-Val	$C_{55}H_{73}N_9O_8S_2$	1052.51
1-MetO,3-MetO-CLF (**9**)	CLF[49]	MetO-Leu-MetO-Pro-Phe-Phe-Trp-Val	$C_{55}H_{73}N_9O_{10}S_2$	1084.47
1-Met-CLG (**10**)	CLG′[48]	Met-Leu-Met-Pro-Phe-Phe-Trp-Ile	$C_{56}H_{75}N_9O_8S_2$	1066.56
1-MetO,3-MetO-CLG (**11**)	CLG[49]	MetO-Leu-MetO-Pro-Phe-Phe-Trp-Ile	$C_{56}H_{75}N_9O_{10}S_2$	1098.50
1-MetO,3-Met-CLG (**12**)	CLH[49]	MetO-Leu-Met-Pro-Phe-Phe-Trp-Ile	$C_{56}H_{75}N_9O_9S_2$	1082.38
1-Met,3-MetO-CLF (**13**)	CLI[49]	Met-Leu-MetO-Pro-Phe-Phe-Trp-Val	$C_{55}H_{73}N_9O_9S_2$	1068.35

[a]Peptides are named according to references where they are first described. [b]The first and third positions of amino acid sequences are highlighted in Figure 1. Abbreviations are Met for methionine and MetO for methionine *S*-oxide. [c]From reference and ESI-MS data obtained as described in supplemental file by Gui et al.[27]

bioactivity. Recent studies show that peptides possess a wide range of biological activities and can act as anticancer[16] and antimicrobial[17] agents. Peptides have also demonstrated immunomodulatory and antioxidant activities. Moreover, some peptides produced in living cells act as antioxidants. Well-known examples of such antioxidants include hormones (melatonin,[18] angiotensin, oxytocin, and enkephalin[19]) and skeletal muscle peptides carnosine and anserine.[20] The antioxidative mechanism of peptides is not well understood. Some authors suggest that peptides that contain aromatic residues (tyrosine, histidine, tryptophan, and phenylalanine) are able to stabilize reactive oxygen species (ROS) through electron transfer.[21] Peptides are also well-known metal chelators and this property may contribute to antioxidant properties. The antioxidant activity of peptides produced by protein digestion is often greater than that of the intact proteins and the amino acid order and structure affect antioxidant activity.[22]

In accelerated oxidation tests of lipids, the oxidation rate is normally low until natural antioxidants are consumed and then the rate of oxidation increases. The time required for the increase in oxidation rate is called the induction time. The active oxygen method (AOM) accelerates lipid oxidation by applying both elevated temperatures and oxygen to an oil. The oxidative stability index (OSI) is an accelerated oxidation assay that determines production of volatile organic compounds produced during oil oxidation. The main criticism of this assay is that the oxidation mechanism at high temperatures is not necessarily similar to the mechanism encountered under normal storage conditions. Nevertheless, it is reported that the shelf life of the sample at ambient conditions can be predicted based on OSI at elevated temperature.[23,24] In general, lipid oxidation is the result of many complex chemical processes and interactions. The reaction between unsaturated fatty acid groups in lipids and ROS created in different ways is important to the stability of lipids containing unsaturated fats.[25]

The presence of CLs in flaxseed oil has led us to hypothesize that these compounds may contribute to the stability of crude flaxseed oil. The purpose of this study is to isolate polar fractions present in flaxseed oil, including CLs, to determine if these fractions increased the oxidative stability of flaxseed oil that has been treated to remove polar compounds. The effect of CL-containing fractions obtained from crude flaxseed oil were tested for their effects on the oxidative stability of peptide-free flaxseed oil. Subsequently the effects of enriched CLs on the oxidative stability of flaxseed oil in the presence of metal cations were determined. Analysis of the compounds present in fractions that contribute to oxidative stability may reveal compounds contributing to the antioxidant mechanism in flaxseed oil. There are no previous reports of the antioxidant activity of CLs in flaxseed oils.

MATERIALS AND METHODS

General. Cold-pressed crude flaxseed oil was donated by Biorginal Food and Science, Inc. (Saskatoon, SK, Canada), and stored at 4 °C. Canola oil was purchased from a retail supplier (Saskatoon, SK, Canada). Silica gel 60 (particle size 0.040−0.063 mm, 230−400 mesh) was purchased from EMD Chemicals Inc. (Gibbstown, NJ, USA). High-pressure liquid chromatography (HPLC) and column chromatography solvents were HPLC grade and purchased from Fisher Scientific (Pittsburgh, PA, USA) unless otherwise noted. A Milli-Q system (Millipore, Bedford, MA, USA) was used to prepare deionized water for all mobile phases. Metal stearates (Zn^{2+}, Ni^{2+}, and Co^{2+}) were obtained from Sigma-Aldrich Canada Ltd. (Oakville, ON, Canada). CL **1** was prepared by reverse phase chromatography of a silica gel solid phase extraction of flaxseed oil according to Reaney et al.[26] and Gui et al.[27] At the time of this study highly enriched CL **1** was available in relatively large quantities while other peptides were not available in quantities sufficient to conduct similar studies.

Silica Gel Flash Column Chromatography. A cotton ball was placed in the bottom of the glass column (2.5-cm i.d.) which was then packed with silica gel (80 cm^3). A sand layer (1-cm; 50−70 mesh) was placed on top.[27] Flaxseed oil (400 mL) was introduced into the column at a ratio of 5:1 (v/v, oil to silica gel) and was allowed to elute through the column under gravity to yield peptide-free oil.[27] The column was eluted with 400 mL of 100% hexane (A), 250 mL of 20% (v/v) ethyl acetate (EtOAc) in hexane (B), 250 mL of 50% (v/v) EtOAc in hexane (C), 250 mL of 100% EtOAc, and (D) finally 250 mL of 10% (v/v) methanol (MeOH) in dichloromethane (DCM, E) (Figure 2). Each of the fractions B−E (~230 mL each) were collected in volumetric flasks and diluted to a final volume of 250 mL. Samples of each fraction (B−E; 20 mL each) were taken and concentrated under vacuum pressure at 40 °C using a Buchi Rotavapor R-200 evaporator (9000 Pa, Brinkman Instruments, Inc., Westbury, NY, USA) and the resulting residue was subjected to HPLC and HPLC-MS analysis.

HPLC Analysis. HPLC analysis was conducted using an Agilent 1200 series HPLC systems (Agilent Technologies Canada Inc., Mississauga, ON, Canada) equipped with a quaternary pump, an autosampler, and a variable-wavelength diode array detector (DAD,

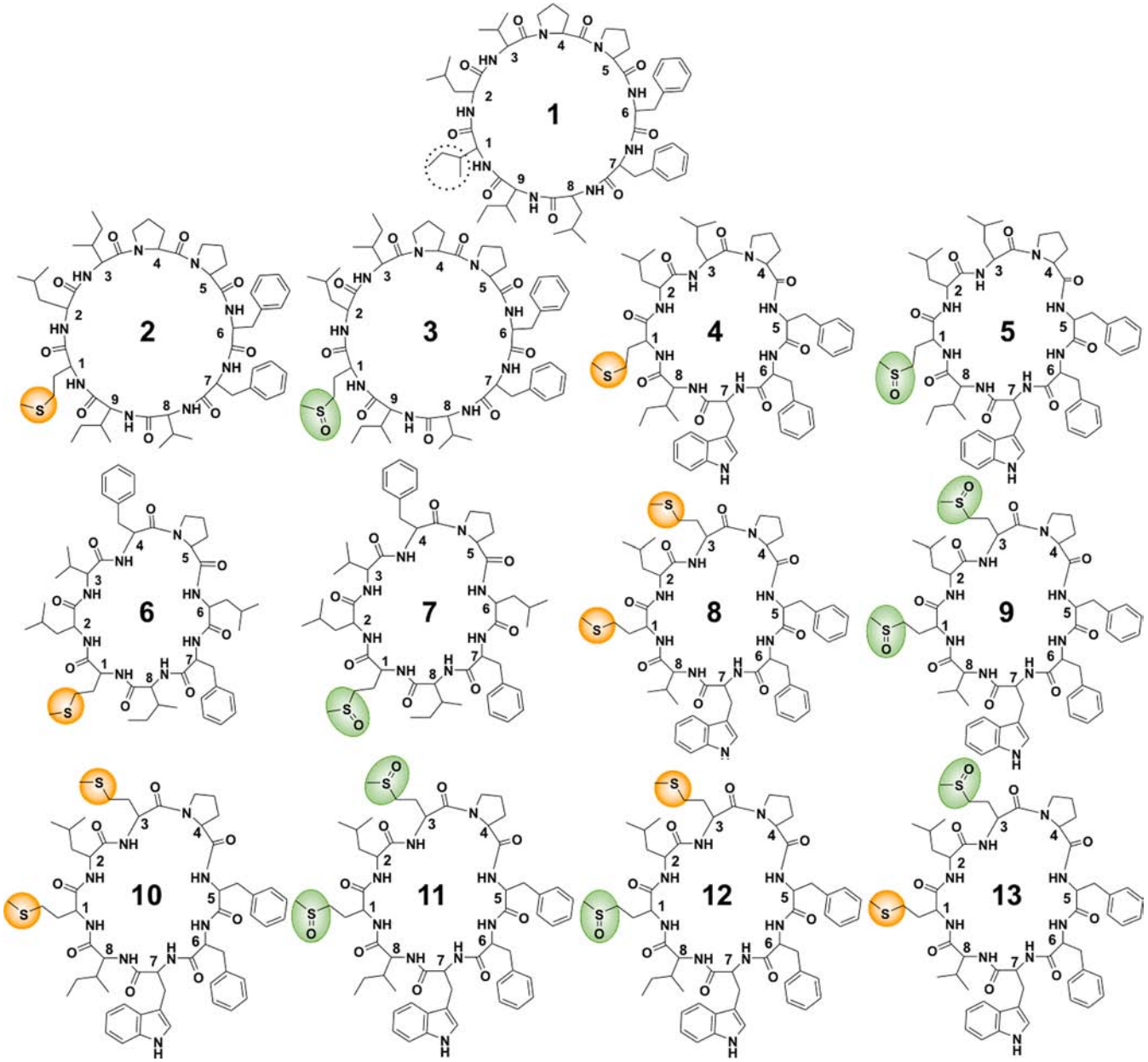

Figure 1. Structures of CLs. Met and MetO in the first and third positions of amino acid sequences are highlighted in CLs.

190−300 nm). The samples were separated on a ZORBAX Eclipse XDB-C18 column (150 × 4.6 mm i.d., 5 μm, Agilent Technologies Canada Inc.) with an in-line filter. The mobile phase consisted of a linear gradient of water−acetonitrile and a flow rate of 2 mL/min.[27] The injections of silica extracts onto the HPLC column were conducted to show if compounds were present and were not meant to be quantitative. Chromatograms of peptide extracts had peaks that exceeded an absorbance of 2.5 AU. With this strong absorbance quantative analysis of peptides was not possible.

Mass Spectrometry. Tocopherols in fraction D were separated using a Chromolith FastGradient RP-18e column (50 × 2.0 mm i.d., 3 μm, Merck KGaA, Darmstadt, Germany). An Agilent HPLC (1200 series) equipped with a quaternary pump, an autosampler, DAD (190−300 nm), and a degasser directly connected to a Bruker micrOTOF-Q II Mass Spectrometer (Hybrid Quadrupole-TOF MS/MS; Bruker, Bremen, Germany) with Apollo II ESI ion source (operated with Nebulizer gas at 4.0 bar and dry gas temperature held at 200 °C) was used in HPLC MS analysis. The mobile phase consisted of a linear gradient of 0.1% (v/v) formic acid in water and 0.1% (v/v) formic in acetonitrile (60:40 for 2 min, to 10:90 in 8 min, to 60:40 in 0.5 min, to equilibration for 5.5 min) and a flow rate of 0.40 mL/min.

OSI Analysis. *Effect of Polar Fractions on Oxidation of Silica-Treated Flaxseed Oil.* Eluate from each fraction (B−E; 30 mL) was added to 30 mL of silica-treated flaxseed oil, and the mixture was concentrated under vacuum at 40 °C using a Buchi Rotavapor R-200 evaporator (9000 Pa) to remove organic solvent. Control samples were prepared by adding the same solvent used to elute the column to silica-treated flaxseed oil and concentrating under vacuum pressure as described above. Crude and silica-treated flaxseed oil samples were kept under vacuum pressure in a desiccator for 24 h prior to OSI analysis (as described below).

Effect of the Concentration of Polar Fraction on the OSI of Silica-Treated Flaxseed Oil. Fractions D and E (200 mL) were collected from a silica gel flash column and concentrated as described above. The concentrate was added to 30 mL of silica-treated flaxseed oil and stored in a desiccator that was sealed and connected with a vacuum system for 24 h. The OSI of these samples was determined as described below.

dx.doi.org/10.1021/jf4037744 | J. Agric. Food Chem. 2014, 62, 88−96

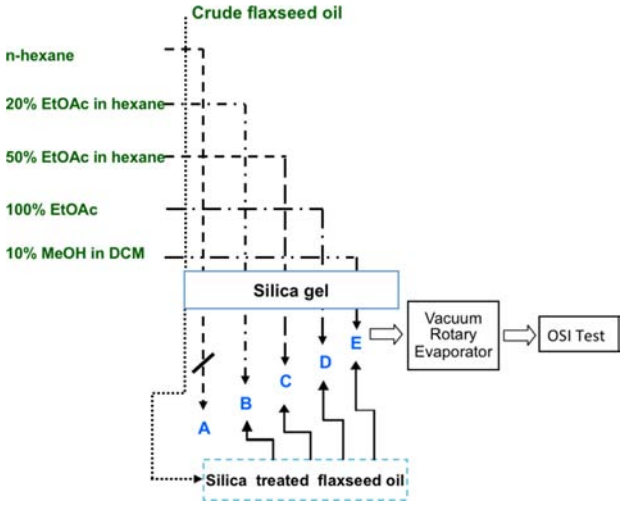

Figure 2. Flowchart for isolation of CL-containing fractions and sample preparation for OSI.

Effect of CL **1** *and Divalent Metal Cations on the OSI of Flaxseed Oil.* Stock solutions of metal stearates (Ni^{2+} and Zn^{2+}; 1.25 mM) and **1** (2.5 mM) were prepared in silica-treated flaxseed oil. The stock solutions were then added to silica-treated flaxseed oil to achieve the desired final concentrations of metal stearate (0.125 mM) and **1** (0.25 mM). The OSI of these samples was determined as described below. In a separate study, stock solutions of zinc stearate (1.0 mM) and **1** (1.0 mM) were prepared in canola oil. Subsequently, **1** (1 mL, 2 mL, 3 mL) and zinc stearate (4 mL) stock solutions were added to 23 mL of silica-treated flaxseed oil. The mixture volume was increased to 30 mL by the addition of canola oil. The final concentration of **1** was 0.03–0.09 mM and that of Zn^{2+} was 0.12 mM. The OSI of these samples was determined as described below. In a third study, stock solutions of **1** (0.625 mM) and cobalt stearate (0.625 mM) were prepared in canola oil. The canola oil along with metal-stearate-treated canola oil were added to 25 mL of silica-treated flaxseed oil until the volume of the oil was 32 mL. The addition of treated canola oil produced mixed oils with final concentrations of 0.04 or 0.12 mM **1** and/or 0.02 mM cobalt stearate. The OSI of these samples was determined as described below.

Measurement of OSI. OSI was measured with an OSI instrument (Omnion, ADM, Rockville, MD, USA) using AOCS official method Cd 12b-92.[28] Samples (5.0 ± 0.05 g) were taken in a glass test tube and then placed in the preheated (100 °C) OSI instrument. Air was bubbled through each sample (130 mL/min flow rate) during heating. Technical replicate samples (n = 4) were analyzed in each experiment. Crude oil and silica-treated flaxseed oil were taken as reference samples. OSI values were calculated using the Omnion OSI v 8.18 software, which detects the end point mathematically by determining the maximum of the second derivative of conductivity plotted against time.

Statistical Analysis. All analyses were performed using SPSS 13.0 software (SPSS Inc., Chicago, IL, USA) and data are presented as mean ± standard deviation (SD) (n = 4). Differences between mean values were evaluated using one-way analysis of variance (ANOVA) followed by a posthoc least significant difference (LSD) test, or an unpaired Student's t test. Statistical significance was accepted at $p < 0.05$.

RESULTS AND DISCUSSION

CL Isolation and Identification. UV absorbance indicated the presence of carotenoids in the oil. In the present study, CLs (**2**, **3**, **5**, and **7**) containing polar fractions from silica were prepared by flash column chromatography of cold-pressed flaxseed oil, and the solvent was removed from the fractions by concentrating under vacuum. The yields of the extracts obtained by silica gel flash chromatography are presented in units of g/100 mL of flaxseed oil (Table 2). Silica-treated flaxseed oil, with a clear yellow color, was obtained by passing fresh crude flaxseed oil through a silica gel column. Using an approach analogous to that applied in this study, Abuzaytoun and Shahidi[29] analyzed fractions obtained by passing cold-pressed hempseed and flaxseed oil through a column packed with two adsorbents (activated silicic acid and activated charcoal) and eluting the compounds with a series of organic solvents. They observed that after absorption on silica and carbon, the oil was essentially free of tocopherols and lacked light absorbance at 550–710 nm, which would indicate a loss of chlorophyll molecules as well. CLs were identified by their standard HPLC retention times as described by Gui et al.[27] The crude flaxseed oil was rich in **1**–**13** (Table 3 and Figure 3). HPLC analyses of fractions B–E revealed the presence of CLs in fractions D and E. Fraction D contained CLs (**1**–**8**, **10**, **12**), whereas fraction E contained a mixture of CLs (**1**–**13**) (Figure 4C and D). Peptides containing methionine (Met) group (**2**, **4**, **6**, **8**, and **10**) were decreased, and CLs (**9** and **11**) were not apparent in the HPLC chromatograms of polar compounds isolated from flaxseed oil. Oxidation of the Met group of CLs into methionine *S*-oxide (MetO) is observed regularly with the exposure of flaxseed oil to oxygen during oil extraction.[30] Most of the peptides were observed in fractions D and E. In addition, mass spectrometric analysis of fraction D indicated the presence of γ-tocopherol (Figure 5), β- and δ-tocopherols (data not shown).

Table 2. Yield of Flaxseed Oil Extracts in Different Solvents

fraction	yield g/100 mL[a]	details of content
B[b]	24.96 ± 0.12a	ND[c]
C[b]	2.29 ± 0.28b	ND[c]
D	1.11 ± 0.98b	CLs (**1**–**8**, **10**, **12**) and tocopherols (β-, γ-, and δ-)
E	1.09 ± 0.34b	CLs (**1**–**13**)

[a]Values are mean ± standard deviation (SD) (n = 4). Means followed by the same letter are not significantly different at $p < 0.05$. [b]Oil was a major component of these fractions. [c]ND: not detected.

Oxidative Stability Test. To determine the presence of antioxidant substances, the OSI values were determined at 100 °C on crude pressed flaxseed oil, silica-treated flaxseed oil, and silica-treated flaxseed oil with polar fractions (B–E) added (Table 4). Adding solvents to silica-treated flaxseed oil and subsequently evaporating them was conducted to act as a control. The OSIs of solvent-treated control oils, ranging from 2.03 to 2.65 h, were not significantly different from that of silica-treated flaxseed oil (Table 4). An effect of the addition and removal of solvents was observed with solvent D treated oils having lower stability (Table 4). This was not explored further. Crude flaxseed oil had higher oxidative stability than silica-treated flaxseed oil, indicating that some of the chemical constituents that were removed by silica gel play a significant role in reducing the rate of flaxseed oil oxidation. OSI times of crude and silica-treated flaxseed oils varied from 3.00 to 4.30 h and 1.15 to 2.75 h, respectively (Table 4). Abuzaytoun and Shahidi[26] observed that passing flaxseed oil over a silicic acid/charcoal column reduced markers of oxidation, thiobarbituric acid-reactive substances and conjugated dienes of cold-pressed flaxseed oil from 6.01 to 4.54 μM/g and from 1.65 to 1.09 μM/g, respectively. However, the oils were more susceptible to

dx.doi.org/10.1021/jf4037744 | J. Agric. Food Chem. 2014, 62, 88–96

Table 3. HPLC Profile of Crude Flaxseed Oil and its Fractions

		crude flaxseed oil		fraction D		fraction E	
CL	retention time (min)[a]	retention time (min)[b]	area (mAU × s)[c]	retention time (min)[b]	area (mAU × s)[c]	retention time (min)[b]	area (mAU × s)[c]
1	24.05	24.24[d]	2434[d]	24.20[d]	30743[d]	24.17[d]	55747[d]
2	21.55	21.59	654	21.73	24744	21.77	15135
3	13.61	13.74	5147	13.77	5718	13.78	39923
4	ND[e]	25.92	896	26.08	17842	26.01	2063
5	17.22	17.80	3950	17.90	2458	17.93	25429
6	ND[e]	24.24[d]	2434[d]	24.20[d]	30743[d]	24.17[d]	55747[d]
7	15.72	15.70	9679	15.72	5884	15.77	74445
8	ND[e]	23.22	204	23.33	5980	23.39	1022
9	ND[e]	12.35	736	ND[e]	ND[e]	12.36	4550
10	ND[e]	25.20	629	25.28	17650	25.32	1822
11	12.83	12.83	2467	ND[e]	ND[e]	12.85	16993
12	ND[e]	18.42	5696	18.53	3282	18.56	41303
13	ND[e]	16.58	1786	16.66	1027	16.68	11886

[a]Retention time assigned by Gui et al.[27] [b]Mean of retention time for 4 runs. [c]Mean of peak area for 4 runs. [d]Coeluted. [e]ND: not detected.

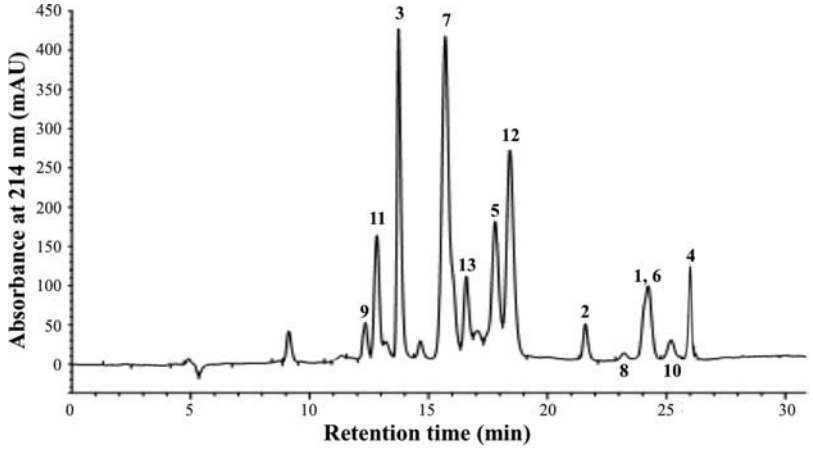

Figure 3. HPLC profile of fresh crude flaxseed oil.

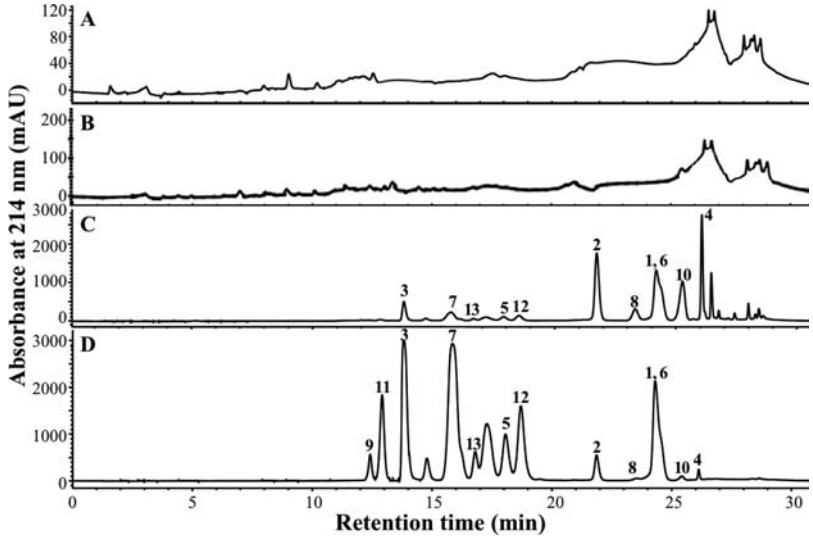

Figure 4. HPLC profile of polar fractions obtained by silica absorption of flaxseed oil: (A) fraction B; (B) fraction C; (C) fraction D; (D) fraction E.

oxidation with continued storage. Several natural antioxidant compounds have been determined in flaxseed oil and the quantity of these compounds depends on cultivar, growing conditions, and processing method. According to the study of Choo et al.,[12] cold-pressed flaxseed oil purchased in New Zealand, including locally produced and imported oil, contained 76.8−307.3 mg/100 g phenolic acid, 12.7−25.6 mg/100 g flavonoids, 3.4−5.5 mg/100 g plastochromanol-8, and 11.1−24.5 mg/100 g tocopherols. In addition, cold-pressed flaxseed oil may contain up to 150 mg/100 g CLs.[27] Therefore,

dx.doi.org/10.1021/jf4037744 | J. Agric. Food Chem. 2014, 62, 88−96

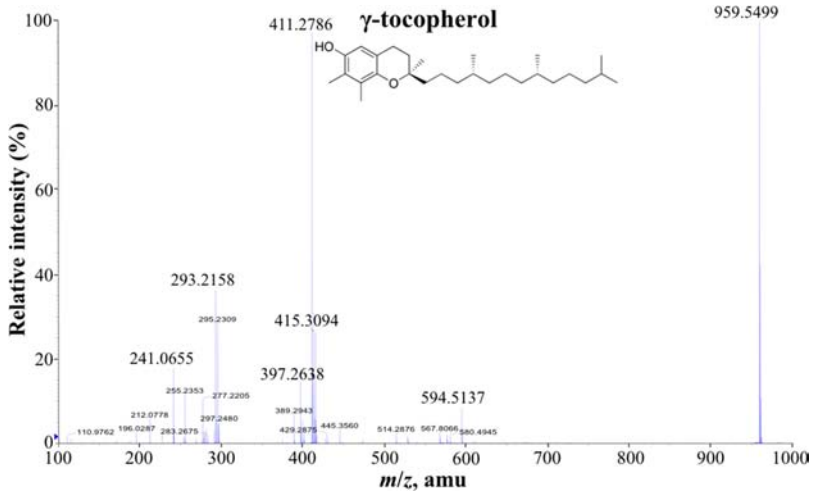

Figure 5. Mass spectrum of fraction D containing tocopherols.

Table 4. Oxidative Stability[a] of CLs-Containing Fractions and Flaxseed Oils

	OSI (h) 0 month	OSI (h) 10 months		
fraction	1st day	1st day	3rd day	reference (solvent)
B	2.78 ± 0.57c	ND[b]	ND[b]	2.65 ± 0.41a
C	2.41 ± 0.50c	ND[b]	ND[b]	2.54 ± 0.26a
D	3.20 ± 0.41b	3.56 ± 0.68a	2.86 ± 0.21b	2.03 ± 0.03a
E	2.77 ± 0.48c	3.02 ± 0.45ab	2.35 ± 0.27b	2.34 ± 0.30a
crude flaxseed oil	4.30 ± 0.56a	3.00 ± 0.10ab	3.07 ± 0.47a	ND[b]
silica-treated flaxseed oil	2.36 ± 0.28c	2.75 ± 0.20b	1.15 ± 0.07c	ND[b]

[a]Values are mean ± SD (n = 4). Means in the same vertical column followed by the same letter are not significantly different at $p < 0.05$. [b]ND: not detected.

reduced oxidative stability observed with silica treatment may be related to the removal of any or all of these polar compounds. The presence of other minor compounds and synergistic interaction among substances should be considered.[12,29] Addition of fraction D to silica-treated flaxseed oil increased its stability to oxidation when compared to silica-treated flaxseed oil and solvent treated control oil (Figure 6, Table 4). However, oils treated with fractions B, C, or E were not significantly different from solvent-treated oil controls (Table 4). Fraction D contained **1** and trace amounts of γ-, β-, and δ-tocopherols. These compounds could potentially contribute to the observed increase in oxidative stability.

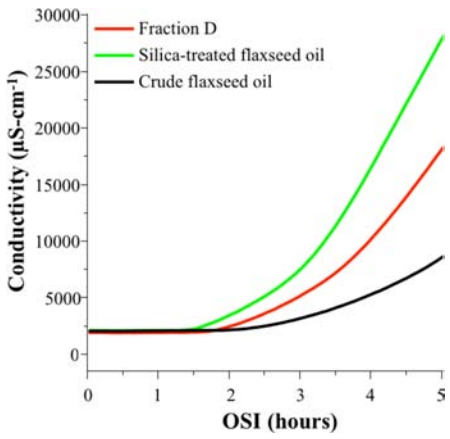

Figure 6. OSI of flaxseed oil and CLs-containing fractions.

Fractions B and C did not affect oxidative stability of silica-treated flaxseed oil when compared with appropriate controls. Fraction E contained more polar CLs than Fraction D (Table 4). The effect of silica treatment on other compounds such as phenolics and flavonoids with known antioxidant properties[31,32] was not investigated, but these compounds were not evident in extracts and may remain bound to the silica column.

Reports of the presence of phenolic compounds in flaxseed[11,12,33] are based on the use of colorimetric methods that employ low specificity reagents. For instance, the Folin–Ciocalteu reagent was used to determine the flavonoid content of cold-pressed flaxseed oil,[12] but this reagent may also react with a broad range of reducing substances including nitrogen-containing compounds such as indole derivatives.[34] D/L-tryptophan produces a strong absorbance at 745 nm when reacted with Folin–Ciocalteu reagent.[34] As indicated in Figure 4, fraction E contains **5**, **9**, and **11**. Each of these peptides contains tryptophan and MetO residues. It is possible that these substances reduce the Folin–Ciocalteu reagent, giving a false indication of the presence of phenolic compounds in flaxseed oil.

Many studies have revealed that polar fractions obtained from various vegetable oils contain phenolic compounds that contribute to antioxidant activity. For instance, Zhang et al.[35] contacted parsley essential oil with silica gel and conducted a stepwise solvent elution of the silica with EtOAc, EtOAc/MeOH (1:1, v/v), and MeOH. This study revealed that the antioxidant activity of the fractions increased with the polarity of the solvent used to elute that fraction from the silica. Phenolic compounds are also reported in fractions exhibiting

dx.doi.org/10.1021/jf4037744 | J. Agric. Food Chem. 2014, 62, 88–96

the strongest antioxidant activity. In comparison to fraction D and the solvent control, fraction E has little or no effect on flaxseed oil oxidation in spite of its higher polarity (Table 3). It is possible that fraction E does not contains phenolic compounds. Elevated induction time may be linked to specific CLs abundant in fraction D but are absent or less abundant in fraction E, or synergic activity of the peptides with tocopherols detected in fraction D. The dose−response and time-dependent activity of fractions D and E were studied after 10 months storage at 4 °C in a refrigerator (Table 4 and Figure 7). The

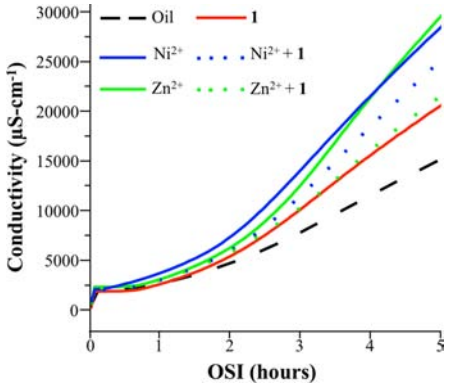

Figure 7. OSI of flaxseed oil and CL **1** + M^{2+}.

induction time of crude flaxseed oil decreased from 4.30 to 3.07 h during the 10-month storage period. Guseva et al.[36] observed that the peroxide value of cold-pressed flaxseed oil increased from 1.8 to 2.9 after six months storage at 10 °C, while Yildirim[34] reported that over 126 days storage at 4 °C, the peroxide value increased from 3.01 to 6.73. In addition, the fatty acid and antioxidant contents in crude flaxseed oil changed significantly over the first seven months of storage, after which no further changes were observed.[37] In this study the OSI times were measured over three days (Table 4) after removal from storage at 4 °C and maintaing the sample at room temperature. The oxidative stability of silica-treated flaxseed oil decreased significantly, by over 50%, after the temperature was increased, while oil subjected to other treatments was more stable. Silica-treated flaxseed oil with added fractions D and E decreased in induction period by 20% after three days removal from storage. Therefore, both fractions D and E have antioxidant properties that may be effective for long storage periods at low temperatures. It is important to note that the largest impact of fractions D and E was observed only after long storage followed by removal from storage for three days.

Influence of CL 1 on Metal Cation Induced Oxidation of Flaxseed Oil. Crude cold-pressed vegetable oil contains small amounts of metals. The quantity of trace metals varies depending on genetics, environmental conditions during plant growth, and processing methods used for oil extraction.[38,39] These metals potentially act as lipid oxidation catalysts. In this study, transition metal ions (Zn^{2+}, Co^{2+}, and Ni^{2+}) were added to flaxseed oil to determine their effects on the rate of oil oxidation. Also, if **1** binds to metals in flaxseed oil it may affect the rate of oil oxidation. Metal binding with **1** has been reported. Balasubramanian et al.[40] reported that **1** binds weakly to Ca^{2+} ions in MeOH. Moreover, Chatterji et al.[41] detected **1**:Tb^{3+} complexes stabilized by the f orbital of the lanthanide. Although binding of both ions with **1** was stabilized by Phe residues, the interaction with Ca^{2+} did not involve charge.

Silica gel adsorption readily removes divalent metal ions with high efficiency from different substrates.[42−44] Hence, silica-treated flaxseed oil is likely greatly reduced in, or free from. divalent metal ions. We observed that transition metal ions Zn^{2+} and Ni^{2+} accelerated the oxidation rate of silica-treated flaxseed oil (Table 5). Induction times of silica-treated flaxseed oil in the presence of these metals at 0.25 mM concentration were reduced by over 0.8 h when compared with controls without added metal. Whereas **1** had no effect on the oxidation of oil when added alone, **1** slowed oxidation induction by Ni^{2+} and Zn^{2+} by 17 and 37%, respectively (Table 5). The is the first study describing the impact of a CL on the rate of oil oxidation in the presence of a transition metal (Zn^{2+}, Ni^{2+}, and Co^{2+}). The observed results may be attributed to **1** binding with metal soaps, making them unavailable for oil oxidation. In addition, zinc ion is abundant in flaxseed (4 mg/100 g) and this study revealed that **1** could potentially interact with zinc. Additional experiments were focused on the dose-dependent interaction of zinc with **1**.

The effects of **1** and zinc ion on oxidation of silica-treated flaxseed oil at mole ratios of 1:4, 1:2, and 1:1.3 of **1** to Zn^{2+} were explored (Table 6). Canola oil was used as a more stable oil to dissolve metal stearates and **1** as dissolving these compounds in flaxseed oil led to unacceptably rapid oxidation (not shown). The addition of canola oil increased overall oil stability (from 2.35 h up to 3.5−8 h) and, hence, OSI times are not comparable to those in other studies. This agrees with other studies where blends of flaxseed oil with sesame, milk thistle,[36] and olive oil[37] have superior oxidative stability when compared to unblended flaxseed oil. This phenomenon occurs with other oils. For example, Isbell et al.[45] reported that adding just 5% of crude meadowfoam oil to triolein enhanced its stability by 35%.

The addition of canola oil modified the impact of zinc on oil OSI. Zinc soaps did not lower the OSI of blends of canola and flaxseed oil. It is possible that antioxidant compounds are present in canola oil that inhibit zinc oxidation pathways. Canola oil is rich in tocopherols; commercial canola oil contains up to 700 mg/kg tocopherols. Moreover, during refining processes, especially after bleaching and deodorizing, metal cations would have been almost cleared from the commercial oil used in this study.[46]

CL **1** improved the oxidative stability of canola/flax blends when added alone to the oil. However, the presence of zinc reduced the antioxidant effect of **1** (Table 6). At 0.12 mM concentration, **1** enhanced the induction time by 11.4 and 6.7% when canola oil was present at 26.0 and 16.6%, respectively. An interaction of **1** with zinc on oxidative stability was also observed in this study. As shown in Table 6, the OSI times of a

Table 5. OSI[a] of Flaxseed Oil with 1, Zn^{2+}, and Ni^{2+} Stearates

silica-treated flaxseed oil	**1** (0.125 mM)	Zn^{2+} (0.25 mM)	**1** + Zn^{2+} (1:2)	Ni^{2+} (0.25 mM)	**1** + Ni^{2+} (1:2)
2.36 ± 0.20a	2.21 ± 0.40a	1.50 ± 0.20b	2.05 ± 0.25ab	1.45 ± 0.15b	1.71 ± 0.13ab

[a]Values are mean ± SD (n = 4). Means in a horizontal row followed by the same letter are not significantly different at $p < 0.05$.

dx.doi.org/10.1021/jf4037744 | J. Agric. Food Chem. 2014, 62, 88−96

Table 6. OSI[a] of Flaxseed/Canola Oil Blends with 1 and Zn^{2+} Stearates

			1: Zn^{2+}		
flaxseed/canola oil blends	1 (0.12 mM)	Zn^{2+} (0.12 mM)	1:4	1:2	1:1.3
3.50 ± 0.33[b]c	3.90 ± 0.30a	3.50 ± 0.31c	3.58 ± 0.17c	3.65 ± 0.28bc	3.75 ± 0.13b
8.07 ± 0.33[c]c	8.61 ± 0.41a	8.25 ± 0.38b	8.08 ± 0.02c	8.20 ± 0.10b	8.77 ± 0.23a

[a]Values are mean ± SD (n = 4). Means in the same horizontal row followed by the same letter are not significantly different at $p < 0.05$. [b]Content of canola oil is 26.0% by volume of blend. [c]Content of canola oil is 16.6% by volume of blend.

Table 7. OSI[a] of Flaxseed/Canola Oil Blends with 1 and Co^{2+} Stearates

			1: Co^{2+}	1: Co^{2+}
flaxseed/canola oil blends	1 (0.08 mM)	Co^{2+} (0.02 mM)	2:1	6:1
3.41 ± 0.13[b]a	3.55 ± 0.16a	3.05 ± 0.15c	3.10 ± 0.14b	3.11 ± 0.15b

[a]Values are mean ± SD (n = 4). Means in a horizontal row followed by the same letter are not significantly different at $p < 0.05$. [b]Content of canola oil is 28.5% for volume canola oil.

the canola/flax blend with **1** is similar to that of the blend with highest ratio of **1** to Zn^{2+} studied (1:1.3). Addition of smaller amounts of **1** did not counteract the effect of Zn^{2+} on OSI. It is possible that CLA almost completely binds Zn^{2+} at this ratio. In contrast, oil with **1** and Zn^{2+} added at a molar ratio of 1:4 oxidizes at the same rate as oil in the presence of metal soaps with no **1** added. This likely indicates that the presence of excess amounts of metal ion exceeds the metal binding capacity of **1**. In addition, the effect of Co^{2+} ions on the oxidation of silica-treated flaxseed oil was studied. However, **1** had no effect on the rate of oil the oxidation in the presence of cobalt as there was no influence of **1** on OSI in the presence of cobalt stearate. Because cobalt has a strong redox potential it may be able to initiate oxidation. It cannot be determined if binding to **1** has occurred (Table 7).

In conclusion, crude flaxseed oil has higher oxidative stability than silica-treated flaxseed oil, indicating that some of the chemical constituents removed upon treatment with silica gel play a significant role in protecting flaxseed oil from oxidation. Fractions containing **1** and tocopherols (fraction D), and a mixture of CLs (**1**−**13**) (fraction E), improved the oxidative stability of peptide-free oil, suggesting the significant role played by these compounds in protecting oil from oxidation. CLs have their own role in the strong antioxidant system of flaxseed oil. They may behave as antioxidants or pro-oxidants depending on concentration and environment. Dose- and time-dependent antioxidant properties of these peptides were observed. CL **1** is able to interact with metals selectively. Further studies are required to determine if **1** inhibits oil oxidation processes by binding metals or other mechanisms. Although, the OSI test was able to illuminate an approximate picture of oxidation in the presence of CLs, possible trace compounds in the studied fractions prevented the conclusive demonstration of the direct role of CLs as antioxidants. Further research should be conducted with simplified model systems to definitively show the interaction of pure CLs with antioxidants and radicles.

AUTHOR INFORMATION

Corresponding Authors

*Tel: +1 306 9665050; fax: +1 306 9665015; e-mail: younyoung.shim@usask.ca.

*Tel: +1 306 9665027; fax: +1 306 9665015; e-mail: martin.reaney@usask.ca.

Funding

This research was funded by the Saskatchewan Ministry of Agriculture's Agriculture Development Fund (20080205) and Genome Canada support of Total Utilization of Flax GENomics (TUFGEN).

Notes

The authors declare no competing financial interest.

ACKNOWLEDGMENTS

We thank Dr. P. G. Arnison (Prairie Plant Systems Inc.) for helpful comments.

ABBREVIATIONS USED

HPLC, high-performance liquid chromatography; MeOH, methanol; EtOAc, ethyl acetate; AOM, active oxygen method; OSI, oxidative stability index; ROS, reactive oxygen species; Met, methionine; MetO, methionine *S*-oxide

REFERENCES

(1) DeClercq, D. R. Flaxseed quality in Canada; http://www.grainscanada.gc.ca/flax-lin/trend-tendance/qfc-qlc-eng.htm, August 25, 2013.

(2) Tolkachev, O. N.; Zhuchenko, A. A. Biological active substane of flax: Medicinal and nutritional properties (a review). *Pharm. Chem. J.* **2000**, *34* (7), 360−367.

(3) Food and Agricultural Organization of the United Nations. Rome, Italy. http://faostat3.fao.org/faostat-gateway/go/to/download/Q/QC/E, November 10, 2013.

(4) Ward, O. P.; Singh, A. Omega-3/6 fatty acids: Alternative sources of production. *Proc. Biochem.* **2005**, *40*, 3627−3652.

(5) Brühl, L.; Matthäus, B.; Fehling, E.; Wiege, B.; Lehmann, B.; Luftmann, H.; Bergander, K.; Quiroga, K.; Scheipers, A.; Frank, O.; Hofmann, T. Identification of bitter off-taste compounds in the stored cold pressed linseed oil. *J. Agric. Food Chem.* **2007**, *55*, 7864−7868.

(6) Brühl, L.; Matthäus, B.; Scheipers, A.; Hofmann, T. Bitter off-taste in stored cold-pressed linseed oil obtained from different varieties. *Eur. J. Lipid Sci. Technol.* **2008**, *110*, 625−631.

(7) Aladedunye, F.; Sosinska, E.; Przybylski, R. Flaxseed cyclolinopeptides: Analysis and storage stability. *J. Am. Oil Chem. Soc.* **2013**, *90*, 419−428.

(8) Przybylski, R.; Daun, J. K. Additional data on the storage stability of milled flaxseed. *J. Am. Oil Chem. Soc.* **2001**, *78*, 105−106.

(9) Malcolmson, L. J.; Przybylski, R.; Daun, J. K. Storage stability of milled flaxseed. *J. Am. Oil Chem. Soc.* **2000**, *77*, 235−238.

(10) Westcott, N. D.; Muir, A. D. Chemical studies on the constituents of *Linum* spp. In *Flax - The Genus Linum*; Muir, A. D., Westcott, N. D., Eds; Routledge: New York, 2003; pp 55−73.

(11) Siger, A.; Nogala-Kalucka, M.; Lampart-Szczapa, E. The content and antioxidant activity of phenolic compounds in cold-pressed plant oils. *J. Food Lipids* **2008**, *15* (2), 137−149.
(12) Choo, W. S.; Birch, J.; Dufour, J. P. Physicochemical and quality characteristics of cold-pressed flaxseed oils. *J. Food Compos. Anal.* **2007**, *20* (3−4), 202−211.
(13) Oomah, B. D.; Kenaschuk, E. O.; Mazza, G. Tocopherols in flaxseed. *J. Agric. Food Chem.* **1997**, *45* (6), 2076−2080.
(14) Bozan, B.; Temelli, F. Chemical composition and oxidative stability of flax, safflower and poppy seed and seed oils. *Bioresour. Technol.* **2008**, *99* (14), 6354−6359.
(15) Kaufmann, H. P.; Tobschirbel, A. Über ein oligopeptid aus leinsamen. *Chem. Ber.* **1959**, *92*, 2805−2809.
(16) Waldschläger, J.; Bergemann, C.; Ruth, W.; Effmert, U.; Jeschke, U.; Richter, D. U.; Kragl, U.; Piechulla, B.; Briese, V. Flaxseed extracts with phytoestrogenic effects on a hormone receptor-positive tumour cell line. *Anticancer Res.* **2005**, *25*, 1817−1822.
(17) Barbary, O. M.; El-sohaimy, S. A.; El-saadani, M. A.; Zeitoun, A. M. Antioxidant, antimicrobial and anti-HCV activities of lignan extracted from flaxseed. *Res. J. Agric. Biol. Sci.* **2010**, *6* (3), 247−256.
(18) Zang, L. Y.; Cosma, G.; Gardner, H.; Vallyathan, V. Scavenging of reactive oxygen species by melotonin. *Biochim. Biophys. Acta* **1998**, *1425* (3), 469−477.
(19) Moosmann, B.; Behl, C. Secretory peptides hormons are biochemical antioxidants: Structure-activity relationship. *Mol. Pharmacol.* **2002**, *61* (2), 260−268.
(20) Chan, K. M.; Decker, E. A. Endogenous skeletal muscle antioxidants. *Crit. Rev. Food Sci. Nutr.* **1994**, *34* (4), 403−426.
(21) Jung, W. K.; Rajapakse, N.; Kim, S. K. Antioxidative activity of a low molecular weight peptide derived from the sauce of fermented blue mussel *Myilus edulis*. *Eur. Food Res. Technol.* **2005**, *220* (5), 535−539.
(22) Chen, H. M.; Muramoto, K.; Yamauchi, F. Structural analysis of antioxidative peptides from soybean β-Conglycinin. *J. Agric. Food Chem.* **1995**, *43*, 574−578.
(23) Farhoosh, R. The effect of operational parameters of the Rancimat method on the determination of the oxidative stability measures and shelf-life prediction of soybean oil. *J. Am. Chem. Soc.* **2007**, *84*, 205−209.
(24) Koleva, I. I. *New methods for the screening of antioxidants in three Siberitis species*. Ph.D. Thesis, Wageningen University, Wageningen, The Netherlands, 2007.
(25) Min, D. B.; Boff, J. M. Chemistry and reaction of singlet oxygen in foods. *Comp. Rev. Food Sci. Food Saf.* **2002**, *1* (2), 58−72.
(26) Reaney, M. J. T.; Jia, Y.; Shen, J.; Schock, C.; Tyler, N.; Elder, J.; Singh, S. Recovery of hydrophobic peptides from oils. U.S. Patent 8,383,172, 2013.
(27) Gui, B.; Shim, Y. Y.; Datla, R. S. S.; Covello, P. S.; Stone, S. L.; Reaney, M. J. T. Identification and quantification of cyclolinopeptides in five flaxseed cultivars. *J. Agric. Food Chem.* **2012**, *60*, 8571−8579.
(28) AOCS. The oxidative stability index. In *Official Methods and Recommended Practices of the American Oil Chemists' Society*, 5th ed.; Firestone, D., Ed.; AOCS Press: Champaign, IL, 1999; method Cd 12b-92.
(29) Abuzaytoun, R.; Shahidi, F. Oxidative stability of flax and hemp oils. *J. Am. Oil Chem. Soc.* **2006**, *83* (10), 855−861.
(30) Gui, B. *Cyclolinopeptides in flaxseed & flaxseed products*. M.Sc. Thesis, University of Saskatchewan, Saskatoon, SK, Canada, 2011.
(31) Panagiotopoulou, P. M.; Tsimidou, M. Solid phase extraction: Applications to the chromatographic analysis of vegetable oils and fats. *Grasas Aceites* **2002**, *53* (1), 84−95.
(32) Bukhari, S. B.; Bhanger, M. I.; Memon, S. Antioxidative activity of extracts from fenugreek seeds (*Trigonella foenum-graecum*). *Pak. J. Anal. Environ. Chem.* **2008**, *9* (2), 78−83.
(33) Oomah, B. D.; Mazza, G.; Kenaschuk, E. O. Flavonoid content of flaxseed. Influence of cultivar and environment. *Euphytica* **1996**, *90* (2), 163−137.
(34) Ikawa, M.; Schaper, T. D.; Dollard, C. A.; Sasner, J. J. Utilization of Folin-Ciocalteu phenol reagent for the detection of certain nitrogen compounds. *J. Agric. Food Chem.* **2003**, *51* (7), 1811−1815.
(35) Zhang, H.; Chen, F.; Wang, X.; Yao, H. Y. Evaluation of antioxidant activity of parsley (*Petroselinum crispum*) essential oil and identification of its antioxidant constituents. *Food Res. Int.* **2006**, *39* (8), 833−839.
(36) Guseva, D. A.; Prozorovskaya, N. N.; Shironin, A. V.; Evteeva, N. M.; Rusina, I. F.; Kasaikina, O. T. Antioxidant activity of vegetable oils with different omega-6/omega-3 fatty acids ratio. *Biomed. Chem.* **2010**, *4* (4), 366−371.
(37) Yildirim, G. *Effect of storage time on olive oil quality*. M.Sc. Thesis, The Graduate School of Engineering and Sciences of İzmir Institute of Technology, Izmir, Turkey, 2009.
(38) Pehlivan, E.; Arslan, G.; Gode, F.; Altun, T.; Ozcan, M. M. Determination of some inorganic metals in edible vegetable oils by inductively coupled plasma atomic emission spectroscopy (ICP-AES). *Grasas Aceites* **2008**, *59* (3), 239−244.
(39) Anwar, F.; Kazi, T. G.; Saleem, R.; Bhanger, M. I. Rapid determination of some trace metals in several oils and fats. *Grasas Aceites* **2004**, *55*, 160−168.
(40) Balasubramanian, D.; Chopra, P.; Ardeshir, F. Cyclolinopeptide - An antamanide analog. *FEBS Lett.* **1976**, *65* (1), 69−72.
(41) Chatterji, D.; Sankaram, M. B.; Balasubramanian, D. Conformational and ion-binding properties of cyclolinopeptide A isolated from linseed. *J. Biosci.* **1987**, *11* (1−4), 473−484.
(42) Goswami, A.; Singh, A. K. Silica gel functionalized with resacetophenone: Synthesis of a new chelating matrix and its application as metal ion collector for their flame atomic absorption spectrometric determination. *Anal. Chim. Acta* **2002**, *454* (2), 229−240.
(43) Baytak, S.; Turker, A. R.; Cevrimli, B. S. Application of silica gel 60 loaded with *Aspergillus niger* as a solid phase extractor for the separation/preconcentration of chromium (III), copper (II), zinc (II), and cadmium (II). *J. Sep. Sci.* **2005**, *28* (18), 2482−2488.
(44) Prado, A. G. S.; Miranda, B. S.; Zara, L. F. Adsorption and thermochemical data of divalent cations onto silica gel surface modified with humic acid at solid/liquid interface. *J. Hazard. Mater.* **2005**, *120* (1−3), 243−247.
(45) Isbell, T. A.; Abbott, T. P.; Carlson, K. D. Oxidative stability index of vegetable oils in binary mixtures with meadowfoam oil. *Ind. Crops Prod.* **1999**, *9* (2), 115−123.
(46) Przybylski, R.; Mag, T.; Eskin, N. A. M.; McDonald, B. E. Canola oil. In *Bailey's Industrial Oil and Fat Products: Chemistry, Properties and Health Effects*; Shahidi, F., Ed; Wiley-Interscience: Hoboken, NJ, 2005; pp 61−122.
(47) Morita, H.; Shishido, A.; Matsumoto, T.; Itokawa, H.; Takeya, K. Cyclolinopeptides B−E, new cyclic peptides from *Linum usitatissimum*. *Tetrahedron* **1999**, *55*, 967−976.
(48) Stefanowicz, P. Detection and sequencing of new cyclic peptides from linseed by electrospray ionization mass spectrometry. *Acta Biochim. Pol.* **2001**, *48* (4), 1125−1129.
(49) Matsumoto, T.; Shishido, A.; Morita, H.; Itokawa, H.; Takeya, K. Cyclolinopeptides F−I, cyclic peptides from linseed. *Phytochemistry* **2001**, *57*, 251−260.

JOURNAL OF AGRICULTURAL AND FOOD CHEMISTRY

Article

pubs.acs.org/JAFC

Evaluation of Liquid Chromatographic Behavior of Lumazinic Derivatives, from α-Dicarbonyl Compounds, in Different C18 Columns: Application to Wine Samples Using a Fused-Core Column and Fluorescence Detection

María del Carmen Hurtado-Sánchez, Anunciación Espinosa-Mansilla, María Isabel Rodríguez-Cáceres, and Isabel Durán-Merás*

Department of Analytical Chemistry, University of Extremadura, 06006 Badajoz, Spain

ABSTRACT: Several C18 columns, packed with totally porous particles of different sizes and shell thicknesses, have been compared for simultaneous determination of α-dicarbonyl compounds, previous derivatization to lumazinic derivatives. Chromatographic conditions for the separation have been optimized for each column, and chromatographic parameters have been calculated and exhaustively compared. A core−shell C18 column provided the best results, and a HPLC method with fluorimetric detection has been proposed. The developed method has been validated in terms of linearity, precision, and sensitivity. Detection and quantification limits obtained were comprised between 0.02 and 0.30 and 0.07 and 1.0 ng mL^{-1}, respectively, while RSD values obtained were lower than 6% and 5% in intraday and interday repeatability studies, respectively. The method has been applied to analysis of the α-dicarbonyl compounds in different types of wines. The higher levels of the total α-dicarbonyl compounds were found in sweet wines and the lower levels in white wines.

KEYWORDS: *α-dicarbonyl compounds, lumazinic derivatives, C18 columns, fluorescence detection, wine samples*

1. INTRODUCTION

α-Dicarbonyl compounds are reactive intermediates formed in physiological systems by lipid peroxidation of polyunsaturated fatty acids[1,2] and biological systems through the Maillard reaction by degradation of sugars.[3,4] In processed foods, these compounds are formed from carbohydrates during thermal processing in the course of the Maillard reaction, and they are also important compounds present in food products obtained by fermentation processes, such as wine. In this matrix, α-dicarbonyl compounds are formed as a consequence of the malolactic fermentation, a process that can occur after or simultaneously with alcoholic fermentation. During malolactic fermentation decarboxylation of L-malic acid takes place, and in consequence, acidity levels are reduced and several compounds related with the aroma and flavors are formed.[5,6] Among the identified formed compounds, dicarbonyl compounds with a short chain such as diacetyl (DIA), glyoxal (Gly), methylglioxal (MGly), 2,3-pentanedione (2,3-Pen), and phenylglyoxal (PhGly) are included.[5−7] These compounds are present in all types of wines, with levels higher in red wines,[8] and these concentrations are increased during age.[9] They play an important role in wines because they have a great influence on flavor and sensory characteristics. Specifically, DIA and 2,3-Pen are the most important compounds in the aroma of wines, and DIA is responsible for the buttery flavor of certain wines.[10] In addition, α-dicarbonyl compounds present reactivity with other components, which contribute to the loss of nutritional quality and increment production of toxic compounds in the wine.[11]

Glucosones, such as glucosone (GS) and 3-deoxyglucosone (3-DG), are α-dicarbonyl compounds with a C-6 backbone, which can be also formed from hexoses through monosaccharide autoxidation.[12] To date, to our knowledge, no data about the quantities of these compounds in wines have been reported.

A number of methods have been developed for determination of α-dicarbonyl compounds in several matrices such as biological samples and processed and fermented foods, and the prelabeled HPLC method is the most common. The more frequent derivatization reaction is formation of quinoxaline derivatives, and different diaminobenzenes have been proposed as derivatizing reagents: 2,4-dinitrophenylhydrazine,[13] 1,2-diaminobenzene,[14] and 1,2-diamino-4,5-dimethoxybenzene.[15,16] Other reagents used have been 6-hydroxy-1,2,3-triaminopirimidine,[17,18] 2,3-diaminonaphthalene,[19] or 5,6-diamino-2,4-hydroxypyrimidine.[20]

For analysis of these compounds in wine samples, methods such as gas chromatography with a mass-selective detector (GC-MS)[21] or a thermoionic detector (GC-NPD)[22] have been proposed as alternative techniques. However, the methodology more frequently used is based on formation of quinoxaline derivatives and analysis by RP-LC with photometric detection.[22−24] All HPLC methods employ C18 columns with particles of 5 μm for chromatographic separation of the corresponding derivatives.[25]

In this point, development of packed columns with smaller particle diameter to work in reverse phase could improve analysis in terms of separation efficiency and also in terms of reduction of the analysis time, which is an important factor to

Received: September 17, 2013
Revised: December 4, 2013
Accepted: December 11, 2013
Published: December 11, 2013

ACS Publications © 2013 American Chemical Society

take into account. In this way, columns packed with core−shell and totally porous sub-2 μm particles have been most frequently employed in qualitative and quantitative analysis.[26] The efficiency of a packed column is described by the Deemter's plate height model,[27] which explains the variation of this parameter with the linear velocity. The key concept of porous shell (or fused-core) particles is to increase both efficiency and separation velocity by reducing the mass transfer (C term in the van Deemter curve).[28] This is possible because it has a silica core that allows keeping their diameter large enough to avoid pressure limitations at high linear velocities. This type of column is constituted by a solid silica core of 1.7 μm in size with a porous outer layer 0.5 μm thick and a total particle size of 2.7 μm. On the other hand, packing of columns with porous sub-2 μm particles consist of derivatized, high-purity porous-silica microspheres having reproducible bonded monolayers. The rigidity and extremely narrow particle-size distribution of totally porous particles allow high-resolution and fastest analysis since operation at high flow rates is possible. However, this column has the disadvantage that usually an ultra-high-pressure liquid chromatography (UPLC) system is required to achieve the best results, while a fused core column allows fast separation on a conventional LC system, without significant loss in efficiency or resolution.[29] In the past decade, comparative studies about the separation of compounds in columns with different particle size, such as pharmaceutical compounds[30] or aflatoxins,[29] among others, have been realized by several authors, and in all cases, they concluded that columns with small particle size achieve major separation efficiency and improve the analytical method developed. On the other hand, core−shell columns have been compared with sub-2 μm porous particles columns in pharmaceutical compound analysis,[31] and a higher capacity of the core−shell columns to accomplish better separation efficiency under the same operation conditions was demonstrated.

The present paper is focused in two ways: first, to investigate the chromatographic behavior, in different packed columns, of the lumazinic derivatives formed from α-dicarbonyl compounds, in order to explore the advantages of columns with core−shell and minor particle size in analysis of these compounds; second, apply the obtained results in development of a simple, rapid, and competitive method to determine these compounds in different types of wines.

2. MATERIALS AND METHODS

2.1. Chemicals, Standards, and Samples. DIA, 2,3-Pen, and PhGly, all of 97% purity, and aqueous solutions of Gly and MGly, 40% purity, were purchased from Sigma-Aldrich (Madrid, Spain). GS (98%) and 3-DG (95%) were obtained from Santa Cruz Biotechnology (California, USA). Stock standard solutions of 3-DG (100 μg mL^{-1}), GS (400 μg mL^{-1}), and PhGly (135 μg mL^{-1}) were prepared by dissolving in ultrapure water adequate amounts of the powder presentation of each compound. Stock solutions of DIA (600 μg mL^{-1}), 2,3-Pen (150 μg mL^{-1}), Gly (50 μg mL^{-1}), and MGly (70 μg mL^{-1}) were prepared by weighting and dilution of the adequate aliquots in ultrapure water. Stock analyte solutions were prepared separately and stored at 4 °C. Working standard mixture solutions were daily prepared by suitable dilution of stock analyte solutions with ultrapure water. 5,6-Diamino-2,4-hydroxypyrimidine sulfate (DDP) (95%) was purchased from Sigma-Aldrich, and a 8.6 mM stock solution was daily prepared by dissolving adequate amounts in ultrapure water containing 200 mM β-mercaptoethanol (β-ME), also provided from Sigma-Aldrich. Ammonia/ammonium chloride buffer was prepared by dissolving ammonium chloride from Panreac (Barcelona, Spain) in ultrapure water and fixing the pH at 10.0 with ammonia (Panreac). Phosphoric acid (85%) was provided by Scharlau (Barcelona, Spain), acetic acid (95.5%) by Romil Chemical LTD (Cambridge, England), and formic acid (98%) by Fluka (Seelze, Germany). Different solutions of pH between 2.9 and 4.0 were prepared by dilution of an adequate volume of concentrated acid in ultrapure water. Methanol (MeOH), HPLC grade, was purchased from Panreac. Ultrapure water was obtained from a Milli-Q water system (Millipore S.A.S., Molsheim, France). Wines analyzed were acquired from local markets and kept at 4 °C, avoiding exposure to direct light. Specifically, red wines (Monasterio de Tentudía, Ribera del Duero, and Merlot), white wines (Rioja Comportillo, Viña Canchal, and Manzanilla), red sweet wines (Vin Santo and Port Tawny), and white sweet wines (Málaga Dulce and Oremus Takaji) were purchased. Most of them are from Spain, with the exception of red sweet wines (from Italy and Portugal) and Oremus Tokaji wine (from Hungary).

2.2. Instrumentation and Software. Chromatographic studies were performed on an Agilent model 1100 LC instrument (Agilent Technologies, Palo Alto, CA, USA), equipped with an online degasser, quaternary pump, manual six-way injection valve, UV−vis diode-array detector, rapid scan fluorescence spectrophotometer detector, and the Chemstation software package to control the instrument, data acquisition, and data analysis. Chromatographic studies and analytical separation were carried out in columns purchased from Agilent. The column temperature was controlled by a coil with recirculating water, in which the temperature was selected through a thermostatic bath. The injection volume was set at 20 μL for the Zorbax-Eclipse XDB C18 column and at 10 μL for columns with minor particle size. The flow rate was 1 mL min^{-1} for Eclipse columns and 0.5 mL min^{-1} for the Poroshell column. Detection was performed with a fluorimetric detector at 450 nm, exciting at 270, 330, and 350 nm.

A Crison MicropH 501 m (Barcelona, Spain), equipped with a combined glass/saturated calomel electrode, was used for pH measurements.

Calibration curves and analytical figures of merit were performed by means of the ACOC program,[32] in MATLAB code.

2.3. General Procedure: Calibration Curves. To build the calibration curves, aliquots of each α-dicarbonyl compound in variable concentration were placed in 25 mL volumetric flasks, and 0.125 mL of ammonia/ammonium chloride buffer (0.5 M, pH = 10) and 1.5 mL of 8.6 mM DDP solution containing 200 mM β-ME were added. After 30 min at 60 °C, solutions were cooled in ice water and diluted with 0.4 mM phosphoric acid solution (pH 3.2) up to the mark. Resulting solutions were filtered through a 0.22 μm nylon filter, and aliquots of 10 μL were injected in the chromatographic system. Separation was performed with a Poroshell 120 column, employing a solution of 0.4 mM phosphoric acid solution (pH 3.2)/MeOH (95:5, v/v) (eluent A) and MeOH (eluent B) as mobile phase, with the following gradient mode: 0−5 min, 0% B; 5−13 min, 30% B; 13−13.5 min, 40% B. These conditions were maintained until 25 min, and finally, the eluent B content was decreased to the initial conditions (0% B) and the column was re-equilibrated for 5 min. The eluate was fluorimetrically monitored at 450 nm (exciting at 270, 330, and 350 nm), and peak areas were used as analytical signal. Three replicas of each standard were used. Temperature was fixed at 25 °C, and a flow rate of 0.5 mL min^{-1} was employed.

2.4. Analysis of α-Dicarbonyl Compounds in Wine Samples. Analysis of the α-dicarbonyl compounds in red, white, and sweet wines was carried out by the standard addition method. For each wine sample, adequate volumes were added in a 25 mL volumetric flask. Increasing volumes of a standard mixture of the dicarbonyl compounds were added, and the general procedure was followed for the derivatization step. Separation of derivatives was carried out in a Poroshell 120 column thermostated at 25 °C. A mobile phase composed of 0.4 mM phosphoric acid solution (pH 3.2)/MeOH (95:5, v/v) (eluent A) and MeOH (eluent B) was employed by following the same gradient mode described in section below. Fluorescence excitation/emission wavelengths of 330/450 nm were employed.

3. RESULTS AND DISCUSSION

The first aim of this work is to realize a comparative study of the chromatographic behavior of the lumazinic derivatives from α-dicarbonyl compounds using three different C18 columns. In any case, the focus was to obtain baseline separation of all compounds in the shortest time and with the lowest solvent consumption as possible in order to achieve a simple, a fast, and an environmental friendly method, susceptible of being applied to analysis of these compounds in wine samples.

3.1. Formation of Lumazinic Derivatives. The most extensively applied methods in wine analysis for control of α-dicarbonyl compounds levels are based on reaction with 2,3-diaminobenzene to form quinoxaline derivatives that can be determined by HPLC with UV detection at 313 nm,[22] fluorimetric detection exciting at 350 nm,[33] or GC with a MS or NPD detector.[34] These derivatization reactions need high temperatures and reaction times close to 3 h. In this paper, DDP is proposed as derivatizing reagent in order to simplify the derivatization reaction. Optimization of the conditions for formation of the lumazínic derivatives for Gly and MGly was described in previous work.[20] In this work, use of DDP as derivatizing reagent was expanded to the seven α-dicarbonyl compounds that can be present in wine samples. The scheme of the derivatization reaction is shown in Figure 1.

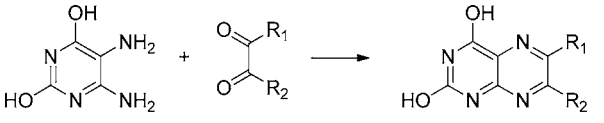

Gly: $R_1 = R_2 = H$

MGly: $R_1 = H$, $R_2 = CH_3$

DIA: $R_1 = R_2 = CH_3$

2,3-Pen: $R_1 = CH_3$, $R_2 = CH_2CH_3$

PhGly: $R_1 = H$, $R_2 = Ph$

3-DG: $R_1 = H$, $R_2 = -CH_2-(CHOH)_2-CH_2OH$

GS: $R_1 = H$, $R_2 = -(CHOH)_3-CH_2OH$

Figure 1. Derivatization reaction of α-dicarbonyl compounds with 5,6-diamino-2,4-dihydropyrimidine (DDP) to yield the corresponding lumazinic derivatives.

The physicochemical variables that influence the yield and reaction rate, such as pH, temperature, reaction time, and DDP excess, were studied chromatographically by monitoring the derivatization reaction. In accordance with previous studies, the yield of the reaction of α-dicarbonyl compounds with DDP was optimal at pH 10, and this value was fixed in all solutions with 0.125 mL of ammonia/ammonium chloride buffer (0.5 M). Temperature and reaction time are two very important parameters that influence in the DDP−dicarbonyl compound reaction rates. For this reason, a series of standard mixture solutions containing 1.0 μg mL^{-1} GS, 400.0 ng mL^{-1} 3-DG, 100.0 ng mL^{-1} Gly, 100.0 ng mL^{-1} MGly, 100.0 ng mL^{-1} DIA, 120.0 ng mL^{-1} 2,3-Pen, 500.0 ng mL^{-1} PhGly, and DDP solution (7.5×10^{-2} mM) (concentrations enough so that all obtained derivatives provide a good signal, easily measurable, and whose variations are detectable, when the conditions of the reaction are changed) were placed in 25 mL volumetric flasks at pH 10 and incubated at 45, 60, and 80 °C during several heating times in the range 2−60 min. After completing the reaction times, the flasks were cooled in ice water and made to volume with 0.4 mM phosphoric acid (pH 3.2), and aliquots of 10 μL of these solutions were injected in the chromatographic system. For all α-dicarbonyl compounds, except for DIA and PhGly, the peak area of the derivatives increased with temperature and is maintained constant between 60 and 80 °C. The peak area of DIA and PhGly derivatives increased up to 60 °C, and for higher temperatures, the signal decreases. Finally, we selected 60 °C as the optimum heating temperature. With respect to the heating time, the peak area of the seven lumazinic derivatives increased up to 15 min. However, the reaction rate for formation of GS and 3-DG lumazinic derivatives is more dependent on the heating time, and after 60 min, these reactions had not been completed. With the object of not extending the total time of the derivatization reactions, a compromise value of 30 min was selected as optimum.

In the optimized conditions of temperature and reaction time, the DDP/total aldehyde ratio was studied in a range between 10:1 and 70:1. For all compounds a 10:1 ratio was enough to obtain the maxima signal; however, for GS and DIA a 30:1 ratio was necessary, and this relation was chosen as optimum.

Studies carried out showed that in the derivatization conditions DDP is degraded into several products, with the object of minimizing the appearance of degradation products that can interfere in analysis of some of the lumazinic derivatives, and in accordance with previous research[14,18] β-ME is added to the DDP solution. The influence of this reagent in the stabilization of DDP has been studied by preparing DDP solutions (0.8 mM) in the presence of different concentrations of β-ME (200, 400, and 600 mM). Aliquots of each solution were placed in a 25 mL volumetric flask, heated at 60 °C for 30 min at pH 10, diluted with 0.4 mM phosphoric acid (pH = 3.2) until the mark, and injected into the chromatographic system. It can be observed that degradation of DDP was avoided in the same extension, independent of the concentration of β-ME employed. Therefore, a solution of DDP was prepared in the presence in 200 mM of this compound. Figure 2A shows the chromatograms of a DDP solution in the presence and in the absence of 200 mM β-ME, and it can be observed that, in the presence of β-ME, degradation of the reagent is practically avoided and signal decreases.

In Figure 2B, a representative chromatogram from lumazinic derivatives obtained in physicochemical-optimized conditions is shown. As can be seen, all α-dicarbonyl compounds become a single lumazinic derivative, except 2,3-Pen and PhGly, which form two derivatives. For unequivocal identification of the derivatives, a comparison of the retention time of Gly derivative with a reference standard of lumazine was done. A standard solution containing 50 ng mL^{-1} of lumazine was injected in the chromatographic system, in the conditions previously described. As expected, retention time and excitation spectra of both peaks are coincident, and this allows confirmation of formation of the lumazinic derivatives.

dx.doi.org/10.1021/jf404180t | J. Agric. Food Chem. 2014, 62, 97−106

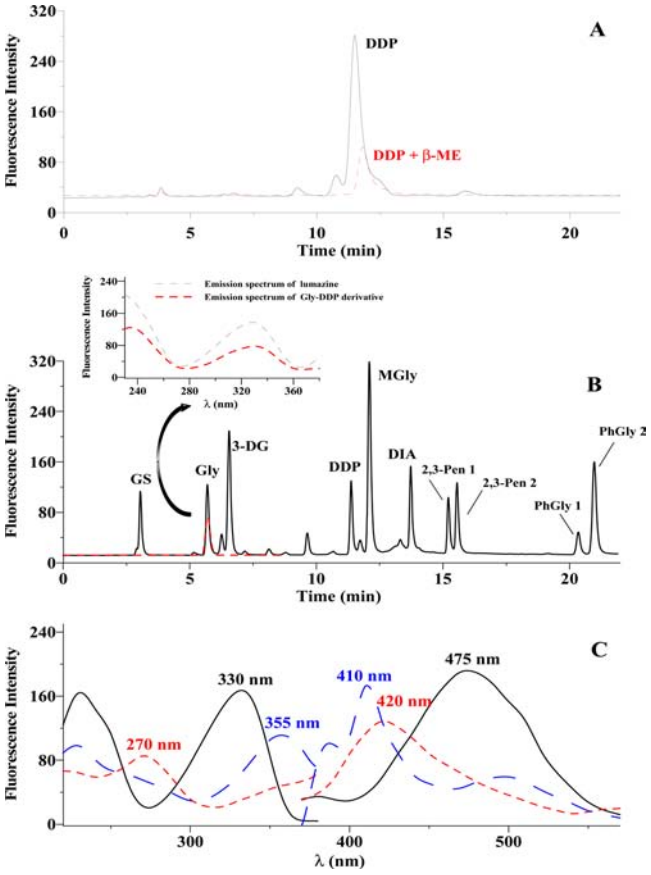

Figure 2. (A) Influence of the presence of β-ME in the degradation process of DDP in the derivatization reaction conditions. Chromatograms correspond to a DDP solution (7.5×10^{-2} mM) in the absence of β-ME (continuous line) and in the presence of 200 mM of β-ME (dashed line). $\lambda_{exc}/\lambda_{em}$ = 330/450 nm. (B) HPLC/FLD chromatograms from a stock standard solution of the α-dicarbonyl compounds in the presence of DDP solution (7.5×10^{-2} mM) at pH 10, derivatized in optimized conditions (heating for 30 min at 60 °C) (continuous line), and of a standard solution of lumazine, 50 ng mL^{-1} (dashed line). $\lambda_{exc}/\lambda_{em}$ = 330/450 nm. [GS] = 1.0 μg mL^{-1}, [3-DG] = 400.0 ng mL^{-1}, [Gly] = 100.0 ng mL^{-1}, [MGly] = 100.0 ng mL^{-1}, [DIA] = 100.0 ng mL^{-1}, [2,3-Pen] = 120.0 ng mL^{-1}, and [PhGly] = 500.0 ng mL^{-1}. (C) Excitation and emission spectra of lumazinic derivatives GS, 3-DG, Gly, MGly, DIA, and 2,3-Pen (—), PhGly 1 (---), and PhGly 2 (———).

Spectral characteristics of all derivatives were studied in order to achieve higher sensitivity in their analysis, and excitation and emission spectra were obtained for each peak (Figure 2C). All of them, except the PhGly derivatives, presented excitation and emission wavelengths characteristics of the lumazines at 330 and 475 nm, respectively. Also, the two derivatives of 2,3-Pen have identical spectral characteristics, with excitation and emission wavelengths at 330 and 475 nm, respectively, and both are formed in similar extension, as can be seen in the chromatogram shown in Figure 2B, where the peak areas of the two derivatives are similar. In the case of the PhGly derivatives, its spectral characteristics are different. Thus, the lumazinic derivative with minor elution time (PhGly 1) presents excitation and emission wavelengths at 270 and 420 nm, respectively, while the other derivative (PhGly 2) shows excitation at 355 nm and emission at 410 nm. On the other hand, in this case formation of one of the derivatives (PhGly 2) is more favorable that the other, probably due to steric impediments.

As a consequence of the different excitation and emission wavelengths of the lumazinic derivatives, a fluorescence detector was programed in multiexcitation mode and each chromatogram was recorded simultaneously exciting at 270, 330, and 350 nm. A wavelength of 450 nm was selected as the emission wavelength as a compromise in order to analyze all compounds in only one run.

3.2. Optimization of Separation and Comparison of Columns Efficiency. With the aim of selecting the more appropriate column for separation of the seven α-dicarbonyl-DDP derivatives, we realized a systematic comparison of three columns assayed. This study was performed in order to develop a simple, reliable, and robust method for efficient separation and quantification of these compounds. In this study, reversed-phase C18 columns with different dimensions and different size and surface particles were tested. The columns used were Zorbax-Eclipse XDB C18 (5.6 μm), Poroshell 120 (2.7 μm), and Zorbax-Eclipse XDB-C18 RRHT (1.8 μm). The most important parameters that influence chromatographic separation, such as mobile phase composition, flow rate, and column temperature, were assayed with each column.

The composition of the mobile phase has a large influence in complete resolution of the derivatives. Due to the analytes differing widely in polarity, isocratic elution is unviable and it was necessary to use a binary gradient. The two solvents employed in the gradient elution were mixtures of acid:MeOH, as solvent A, and MeOH 100% as solvent B. The presence of acid in the mobile phase is essential to complete resolution of the lumazinic derivatives, so the influence of the nature of the acid used in solvent A and the pH of the mobile phase was studied. Acetic, phosphoric, and formic acids were assayed, and the pH was varied between 2.9 and 4.0 for each acid. The behavior of the α-dicarbonyl−DDP derivatives was identical with the three columns assayed, independent of the acid used. In general, the retention times of DIA, 2,3-Pen, and PhGly lumazine derivatives are not affected, and the retention times of the less retained derivatives decreased as the pH increased. Finally, 0.4 mM phosphoric acid (pH 3.2) was selected as the aqueous component of solvent A for the three columns.

Below, the composition of solvent A was optimized for each column by modifying the phosphoric acid (0.4 mM)/MeOH ratio between 99/1 and 99/5, v/v. Also, different gradients with methanol as solvent B were assayed to achieve baseline separation of all derivatives in a time as short as possible. Optimized conditions for each column are summarized in Table 1.

Also, the influence of the temperature in the separation has been studied with the three columns. In general, the capacity factors decreased with increasing temperature for all compounds. It is noticeable that this effect is greater for the less retained compounds and when the mobile phase is 100% aqueous, as can be seen in Figure 3. In gradient mode, as the percentage of methanol increased and the mobile phase viscosity was varying, the effect of temperature in the capacity factors decrease, and the variation in the last four analytes eluted is lower.

Representative chromatograms obtained in the optimized conditions with the three columns assayed, XDB-C18, Poroshell, and XDB-C18 RRHT, are shown in Figure 4. As can be seen, use of a conventional monomeric C18 column results in a lack of complete separation between the peak of the

dx.doi.org/10.1021/jf404180t | J. Agric. Food Chem. 2014, 62, 97−106

Table 1. Column Characteristics and Optimum Chromatographic Parameters for Each Column

column	mobile phase	gradient mode	other parameters
Agilent Zorbax Eclipse XDB-C18 (150 mm × 4.6 mm, 5.6 μm)	40 mM H_3PO_4/MeOH (98/2, v/v) (eluent A) MeOH (eluent B)	0–8 min, 0% B; 8–13 min, 20% B; 13–14 min, 35% B; 35% B until 25 min flow rate: 1 mL min^{-1}	T_{column}: 30 °C $V_{injection}$: 20 μL t_0: 1.4 min P_0: 145 bar
Agilent Poroshell 120 EC-C18 (150 mm × 3 mm, 2.7 μm)	40 mM H_3PO_4/MeOH (95/5, v/v) (eluent A) MeOH (eluent B)	0–5 min, 0% B; 5–13 min, 30% B; 13–13.5 min, 40% B; 40% B until 25 min flow rate: 0.5 mL min^{-1}	T_{column}: 25 °C $V_{injection}$: 10 μL t_0: 1.8 min P_0: 245 bar
Agilent Zorbax Eclipse XDB-C18 RRHT (50 mm × 4.6 mm, 1.8 μm)	40 mM H_3PO_4/MeOH (98/2, v/v) (eluent A) MeOH (eluent B)	0–5 min, 0% B; 5–13 min, 35% B; 35% B until 18 min flow rate: 1 mL min^{-1}	T_{column}: 20 °C $V_{injection}$: 10 μL t_0: 0.5 min P_0: 180 bar

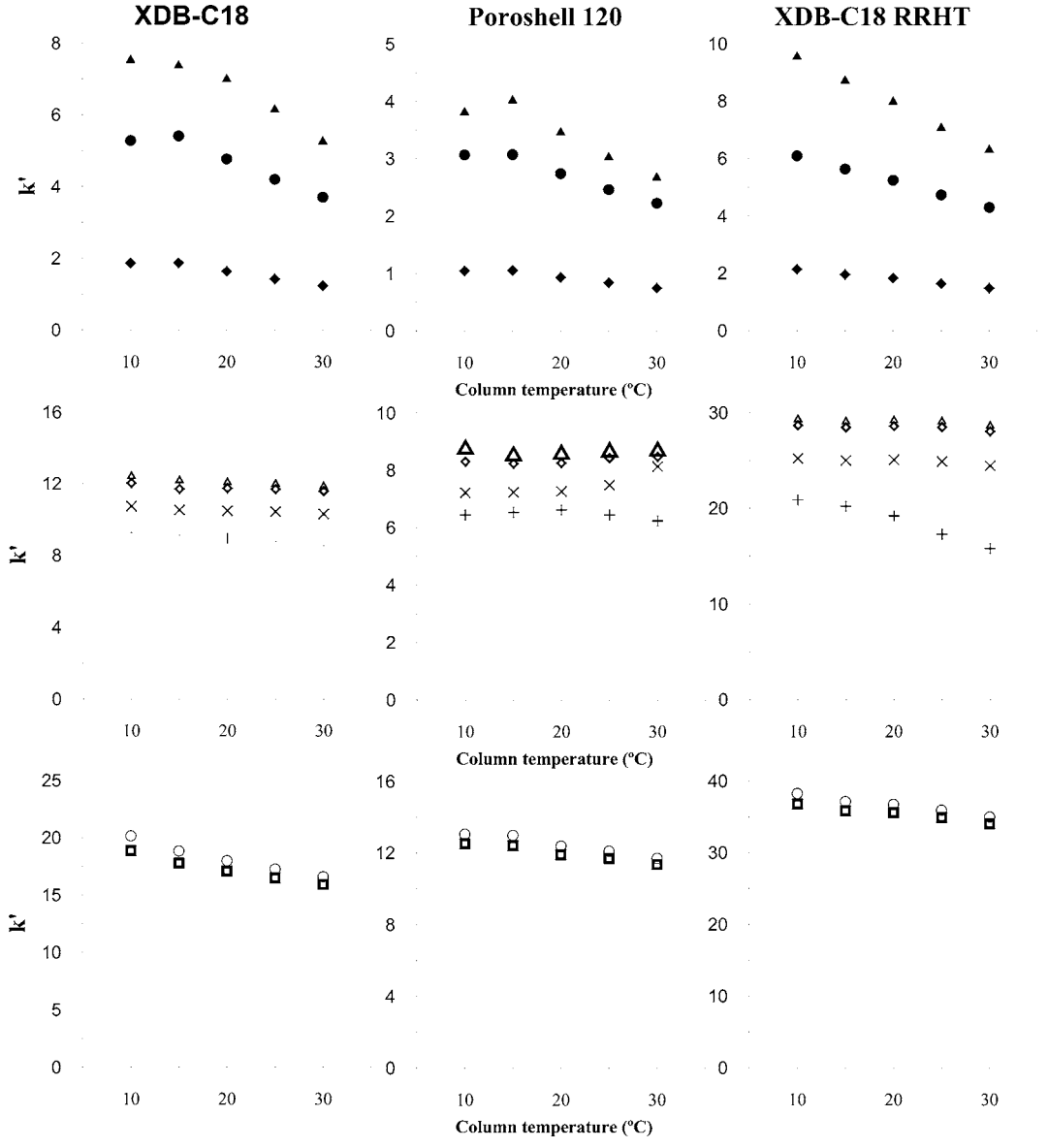

Figure 3. Variation of capacity factor (k') with column temperature for the three columns studied: (◆) GS, (●) Gly, (▲) 3-DG, (+) MGly, (×) DIA, (◇) 2,3-Pen (1), (△) 2,3-Pen (2), (□) PhGly (1), and (○) PhGly (2).

dx.doi.org/10.1021/jf404180t | J. Agric. Food Chem. 2014, 62, 97–106

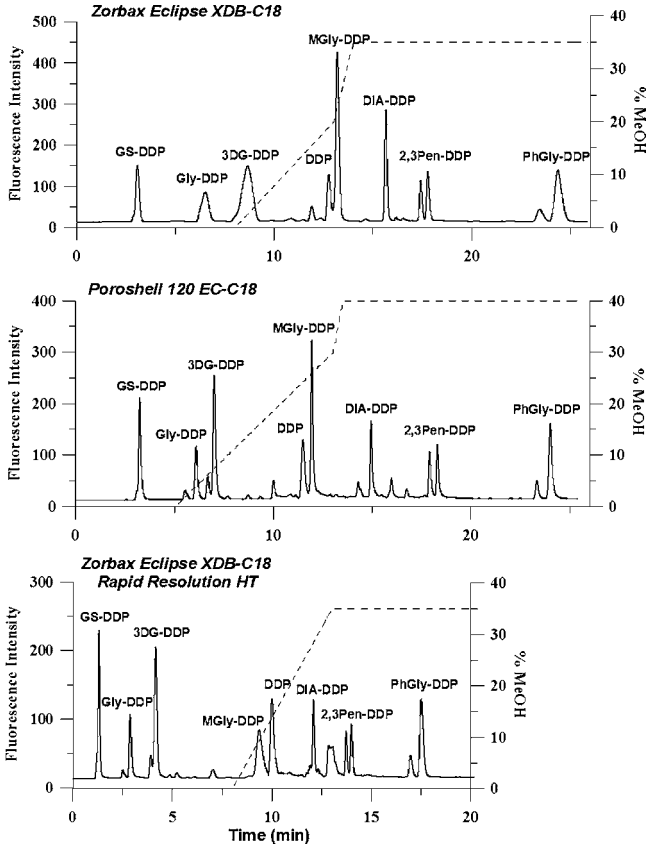

Figure 4. Optimum separation of lumazinic derivatives in the three columns assayed. Dashed lines indicated the gradient program employed. $\lambda_{exc}/\lambda_{em}$ = 330/450 nm.

MGly−DDP derivative and the peak of the DDP reagent. In addition, more polar analytes presented peak tailing, and in general, peak shape was wider than in the other columns. On the other hand, lower analysis time is obtained with the XDB-C18 RRHT column. It is important to remark that elution order of MGly derivative and DDP is inverted in this column. The Poroshell column achieves complete separation of the compounds in 25 min with narrow and symmetric peaks.

Once elution conditions were established, chromatographic parameters (column resolution (R), capacity factor (k'), and theoretical plate number (N)) were calculated to obtain information about the efficiency of each column in the chromatographic separation of the lumazinic derivatives. These parameters have been calculated following eqs 1−3, and the obtained values are summarized in Table 2.

$$R = \frac{1.17(t_{R_2} - t_{R_1})}{(w_{1/2})_1 + (w_{1/2})_2} \quad (1)$$

$$k' = \frac{t_R - t_0}{t_0} \quad (2)$$

$$N = 5.54x(t_R/w_{1/2})^2 \quad (3)$$

t_R is the retention time, t_0 is the dead time, and $w_{1/2}$ is the width of the peak at half height.

Retention time is the most important parameter to know the length of analysis. For all compounds, using the optimized elution conditions, retention times were shorter with the XDB-C1 8 RRHT column than with conventional C18 and Poroshell columns, getting a total scan time of 18 min, against the 25 min for the other two columns. Thus, the column length reduction decreases analysis time, as expected. Retention times of the lumazinic derivatives in the three columns assayed can be seen in Table 2.

Peak resolution describes the degree of separation between two compounds. Usually an R value of 1 is accepted to consider that a separation is satisfactory, but R must be equal to or higher than 1.5 to achieve a baseline resolution. As can be seen in Table 2, better resolution for all compounds is achieved when the separation was carried out with a Poroshell column. It is important to highlight that R has been calculated with respect to the previous peak eluted; thus, in the case of columns XDB-C18 and Poroshell, MGly resolution is referred to its separation from the DDP. However, as the order of elution between DDP and MGly derivative changes in XDB-C18 RRHT, the resolution of MGly is calculated with regard to the 3-DG derivative, with a resolution value of DDP-MGly of 1.4 ± 0.1. In relation to k' values, in the case of the Poroshell column, they are comprised between 0.84 and 12.7, which are near the ideal values (1 and 10),[35] while for XDB-C18 RRHT, k' values are too high (approximately 35 for the last derivative). This is in agreement with the fact that superficially porous particles typically have about one-half to three-quarters the surface area of totally porous particles, resulting in a smaller capacity factor value for columns of core−shell particles in size comprised between 2.5 and 2.7 μm.[36] On the other hand, N values, calculated based on the width of peak at half height, were greater for the Poroshell column in all cases, which indicates more efficient chromatographic separation.

Other aspects like solvent consumption were taken into account. In this way, although the analysis time for the XDB-C18 RRHT column is lower, solvent consumption is higher than with Poroshell (12.5 against 18 mL per run) due to the flow rate employed with this column being one-half.

In order to evaluate the precision of analysis with the three columns, repeatability was assessed by injection of 10 standard solutions, in the optimized conditions, for each column. The RSD from the signal of the peak area was between 1.6% and 7.4% for XDB-C18, 2.4% and 6.3% for XDB-C18 RRHT, and 2.4% and 6.1% for Poroshell. Therefore, significant differences were not found.

In summary, although the XDB-C18 RRHT column has the fastest elution time, resolution was enhanced with the core−shell column. Also, the solvent reduction achieved with this column is a good advantage with the aim of developing a method of analysis less polluting as possible; thus, the Poroshell 120 column was chosen for the following experiments.

3.3. Method Validation: Analytical Parameters. For validation of the method, a calibration curve of each compound was established employing the peak area as analytical signal and using the optimized conditions for the selected Poroshell column (Table 1). The linearity of the method was assessed by preparing calibration standards with concentrations ranging from 10.0 to 600 ng mL^{-1} of GS, from 4.0 to 120.0 ng mL^{-1} of Gly and 3-DG, from 4.0 to 40.0 ng mL^{-1} of MGly and DIA, from 4.0 to 150.0 ng mL^{-1} of PhGly, and from 4.0 to 60.0 ng mL^{-1} of 2,3-Pen. The pH 10 of the derivatization reaction was maintained with ammonia/ammonium chloride buffer, and the concentration of DDP was 0.86 mM, as previously explained in section 2.3. Standard solutions containing all α-dicarbonyl compounds were prepared in triplicate for each concentration level, and the analytical figures of merit were calculated

dx.doi.org/10.1021/jf404180t | J. Agric. Food Chem. 2014, 62, 97−106

Table 2. Chromatographic Parameters Calculated for Each α-Dicarbonyl Compound in the Three Columns Assayed

column	α-dicarbonyl compound	$t_R \pm SD^a$ (min)	$R \pm SD^a$	$k' \pm SD^a$	$N \pm SD^a$
Zorbax Eclipse XDB-C18	GS	2.89 ± 0.05	6.59 ± 0.06	1.06 ± 0.03	1480 ± 77
	Gly	5.90 ± 0.10	7.41 ± 0.18	3.24 ± 0.09	1984 ± 148
	3-DG	7.80 ± 0.20	3.03 ± 0.04	4.57 ± 0.16	2052 ± 145
	MGly	12.79 ± 0.07	1.17 ± 0.07	8.12 ± 0.03	27 283 ± 1593
	DIA	15.34 ± 0.03	8.57 ± 0.10	9.93 ± 0.02	47 071 ± 2150
	2,3-Pen (1)	17.20 ± 0.02	7.07 ± 0.06	11.27 ± 0.02	81 245 ± 1595
	2,3-Pen (2)	17.55 ± 0.02	1.34 ± 0.01	11.51 ± 0.02	72 407 ± 1703
	PhGly (1)	22.70 ± 0.06	12.67 ± 0.22	15.18 ± 0.04	27 549 ± 1303
	PhGly (2)	23.51 ± 0.07	1.40 ± 0.02	15.76 ± 0.04	24 488 ± 754
Poroshell 120 EC-C18	GS	3.30 ± 0.02	9.79 ± 0.08	0.84 ± 0.01	4348 ± 117
	Gly	6.25 ± 0.05	13.04 ± 0.11	2.49 ± 0.01	10 018 ± 177
	3-DG	7.31 ± 0.06	4.06 ± 0.03	3.07 ± 0.01	12 178 ± 149
	MGly	12.05 ± 0.04	1.58 ± 0.03	5.72 ± 0.04	34 227 ± 632
	DIA	15.04 ± 0.05	11.68 ± 0.11	7.39 ± 0.05	57 992 ± 688
	2,3-Pen (1)	18.03 ± 0.04	12.06 ± 0.12	9.05 ± 0.06	88 847 ± 2298
	2,3-Pen (2)	18.45 ± 0.04	1.68 ± 0.02	9.29 ± 0.06	82 818 ± 2207
	PhGly (1)	23.70 ± 0.10	17.63 ± 0.45	12.28 ± 0.10	74 283 ± 5729
	PhGly (2)	24.60 ± 0.10	2.08 ± 0.09	12.70 ± 0.11	76 963 ± 9321
Zorbax Eclipse XDB-C18 RRHT	GS	1.30 ± 0.02	6.34 ± 0.17	1.65 ± 0.05	931 ± 52
	Gly	2.88 ± 0.03	7.96 ± 0.16	4.87 ± 0.13	2605 ± 122
	3-DG	4.13 ± 0.04	5.10 ± 0.14	7.42 ± 0.21	4023 ± 188
	MGly	9.37 ± 0.09	12.13 ± 0.23	18.10 ± 0.44	3927 ± 186
	DIA	12.08 ± 0.03	8.54 ± 0.16	23.63 ± 0.55	69 012 ± 7705
	2,3-Pen (1)	13.73 ± 0.03	8.81 ± 0.20	27.00 ± 0.63	86 418 ± 4532
	2,3-Pen (2)	14.00 ± 0.03	1.45 ± 0.03	27.55 ± 0.64	80 582 ± 7418
	PhGly (1)	16.95 ± 0.06	10.83 ± 0.44	33.54 ± 0.75	39 543 ± 3950
	PhGly (2)	17.20 ± 0.10	1.57 ± 0.06	34.63 ± 0.77	43 576 ± 3225

[a]SD: standard deviation.

Table 3. Calibration Data and Validation Parameters

α-dicarbonyl compound	linear range (ng mL^{-1})	intercept ± SD[a]	slope ± SD[a] (ng mL^{-1})	R^2	LOD[b] (ng mL^{-1})	LOQ[c] (ng mL^{-1})	precision[d] intraday (n = 10)	precision[d] interday (n = 6)
GS	10–600	(−29) ± 17	2.10 ± 0.02	0.9989	0.31	1.03	2.9	5.0
Gly	4–120	464 ± 33	11.80 ± 0.20	0.9975	0.05	0.18	4.5	4.9
3-DG	4–125	70 ± 34	7.74 ± 0.08	0.9986	0.08	0.28	3.6	4.3
MGly	4–40	26 ± 26	32.50 ± 0.40	0.9978	0.02	0.07	4.5	2.1
DIA	4–30	188 ± 22	24.00 ± 0.50	0.9963	0.03	0.10	6.0	2.3
2,3-Pen (1)	4–150	(−72) ± 32	7.80 ± 0.10	0.9974	0.09	0.30	3.9	3.4
2,3-Pen (2)		(−12) ± 18	8.75 ± 0.06	0.9994	0.08	0.27	2.3	3.2
PhGly (1)	4–60	(−16) ± 13	8.00 ± 0.10	0.9978	0.16	0.52	4.7	5.0
PhGly (2)		32 ± 15	14.30 ± 0.10	0.9991	0.07	0.25	5.7	3.3

[a]SD: standard deviation. [b]Limit of detection. [c]Limit of quantification. [d]Expressed as relative standard deviation (% RSD). Standard solution employed containing 300.0 ng mL^{-1} GS, 60.0 ng mL^{-1} Gly, 3-DG, 20.0 ng mL^{-1} MGly, DIA, 75.0 ng mL^{-1} 2,3-Pen, and 30.0 ng mL^{-1} PhGly.

employing the peak areas as analytical signal. The analytical figures of merit obtained for each α-dicarbonyl compound are shown in Table 3. Evaluation of the precision of the optimized method was done by analyzing standard solutions of the α-dicarbonyl compounds in the same day (intraday precision, n = 10) and in consecutive days (interday precision, n = 6). Intraday and interday repeatability values, expressed as relative standard deviation (RSD), are lower than 6.0% and 5.0%, respectively, so they may be considered as a guarantee of the goodness of the proposed method, and use of an internal standard is not required. The limits of detection (LOD) and quantification (LOQ) were calculated as concentrations corresponding to 3 and 10 times the standard deviation of the signal from baseline from chromatograms obtained in intraday precision study. Low values are obtained that are indicative of the high sensitivity of the developed method. Results obtained are summarized in Table 3.

3.4. Quantitative Measurement of α-Dicarbonyl Compounds in Wines. After evaluation and selection of the optimum column for separation of seven α-dicarbonyl compounds, the proposed method was applied to analysis of different red, white, and sweets wines. To carry out quantification of the α-dicarbonyl compounds in wine samples, the influence of the matrix effect over chromatographic

dx.doi.org/10.1021/jf404180t | J. Agric. Food Chem. 2014, 62, 97−106

Table 4. Concentrations of the Six α-Dicarbonyl Compounds Detected in Commercial Wine Samples

type of wine	[GS][a]	[Gly][a]	[3-DG][a]	[MGly][a]	[DIA][a]	[2,3-Pen][a]	total α-DC[a]
red wines[b]							
Monasterio Tentudía, 2008 (Extremadura, Spain)	4.50 ± 0.20	1.85 ± 0.08	13.50 ± 0.30	1.58 ± 0.05	3.10 ± 0.60	3.00 ± 0.04	27.53 ± 0.71
Ribera Duero, 2010 (Spain)	0.50 ± 0.20	1.35 ± 0.03	7.70 ± 0.40	0.68 ± 0.01	8.80 ± 0.20	1.45 ± 0.02	20.48 ± 0.49
Merlot, 2009 (Extremadura, Spain)	1.70 ± 0.20	7.10 ± 0.20	10.40 ± 0.50	0.42 ± 0.02	1.22 ± 0.05	5.60 ± 0.03	26.46 ± 0.58
white wines[c]							
Rioja Comportillo, 2011 (D.O. Rioja, Spain)	0.70 ± 0.10	1.53 ± 0.08	4.90 ± 0.20	0.73 ± 0.03	0.29 ± 0.01	2.22 ± 0.03	10.37 ± 0.24
Viña Canchal, 2011 (Extremadura, Spain)	0.40 ± 0.10	1.12 ± 0.05	7.90 ± 0.30	0.21 ± 0.01	0.63 ± 0.02	1.17 ± 0.03	11.43 ± 0.32
Manzanilla, dry wine (D.O. SanLúcar de Barrameda, Spain)	5.20 ± 0.20	1.10 ± 0.10	6.10 ± 0.20	0.28 ± 0.01	0.64 ± 0.02	0.90 ± 0.04	14.22 ± 0.30
red sweet wines[d]							
Vin Santo (Toscana, Italy)	138 ± 11	4.50 ± 0.30	133 ± 5	1.68 ± 0.08	1.02 ± 0.06	2.30 ± 0.10	280 ± 12
Port Tawny (Porto, Portugal)	89 ± 13	8.90 ± 0.40	39 ± 4	0.95 ± 0.05	1.50 ± 0.09	1.90 ± 0.10	141 ± 14
white sweet wines[d]							
Málaga Dulce (Málaga, Spain)	261 ± 7	8.40 ± 0.20	126 ± 5	0.90 ± 0.05	2.80 ± 0.10	2.61 ± 0.08	402 ± 9
Oremus Tokaji, 2008 (Hungary)	37 ± 1	5.50 ± 0.20	75 ± 2	3.21 ± 0.06	0.60 ± 0.07	4.60 ± 0.10	126 ± 2

[a]Concentration expressed as μg mL^{-1} ± SD (standard deviation) [b]Aliquot of wine samples: 500 μL for Gly, MGly, DIA and 2,3-Pen, and 120 μL for 3-DG and DIA wine/water (1/50, v/v) for GS and 3-DG. [c]Aliquot of wine samples: 1500 μL wine/water (1/50, v/v) for GS and 3-DG. [d]Aliquot of wine samples: 120 μL for Gly, MGly, DIA and 2,3-Pen, and 50 μL of a solution wine/water (1/50, v/v) for GS and 3-DG.

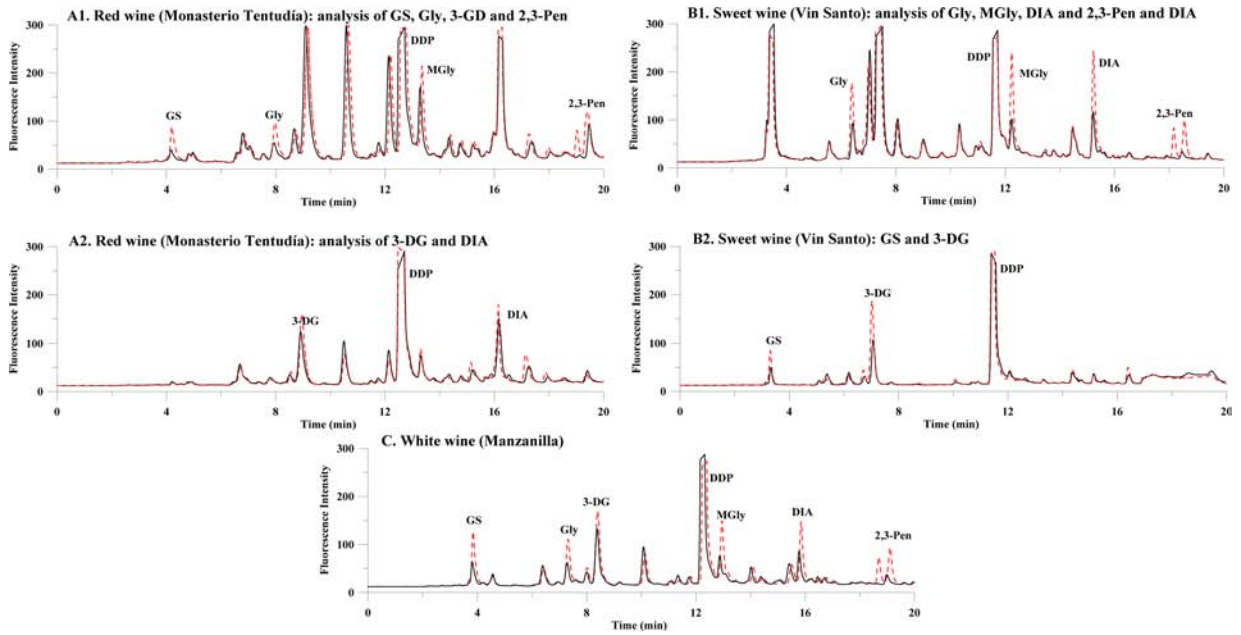

Figure 5. Chromatograms obtained from each type of wine analyzed (continuous line) and from wine samples spiked with 125.0 ng mL^{-1} GS, 60.0 ng mL^{-1} 3-DG, 40.0 ng mL^{-1} Gly, 6.0 ng mL^{-1} MGly, 6.0 ng mL^{-1} DIA, and 40.0 ng mL^{-1} 2,3-Pen (dashed line). (A1) Analysis of GS, Gly, MGly, and 2,3-Pen in red wine (Monasterio Tentudía, 0.50 mL of sample). (A2) Analysis of 3-DG and DIA in red wine (Monasterio Tentudía, 0.12 mL of sample. (B1) Analysis of Gly, MGly, DIA, and 2,3-Pen in sweet wine (Vin Santo, 0.12 mL of sample). (B2) Analysis of GS and 3-DG in sweet wine (Vin Santo, 0.50 mL of a solution wine/water (1/50 v/v)). (C) Analysis of six α-dicarbonyl compounds in white wine (Manzanilla, 1.50 mL of sample). $\lambda_{exc}/\lambda_{em}$ = 330/450 nm.

separation was first evaluated. For this standard addition calibration curves, from each of the α-dicarbonyl compounds in wine samples, were established, and calibration slopes were compared with the corresponding slopes of the external standard calibration plots of each analyte at the 95% confidence level. In all cases, considerable differences were obtained, and these results suggest that there is a matrix effect. As a consequence, calibration curves were constructed using the standard addition method for each of the wines analyzed and used to quantify each analyte in duplicate.

It is important to bear in mind that levels of α-dicarbonyl compounds vary with the type of wine, and for this reason, adequate sample dilutions were optimized for each type of wine analyzed. The volume chosen for each wine is shown in Table 4. The low volumes of samples needed for analysis, in comparison with other published methods, highlight the sensitivity of the proposed method.

Ten wines were analyzed following the methodology described in section 2.4: 3 red wines, 3 white wines, 2 sweet red wines, and 2 sweet white wines. Figure 5 shows an example of chromatograms obtained from each type of wine analyzed, and the results obtained for each α-dicarbonyl are shown in Table 4. Contrary to the literature,[22] PhGly was not detected in any of the different wines analyzed in this study. Also, in all

dx.doi.org/10.1021/jf404180t | J. Agric. Food Chem. 2014, 62, 97−106

samples, only one lumazinic derivative from 2,3-Pen was observed.

To date, the dicarbonyl compound more relevant in wines is DIA, since it has a pronounced butter odor and its presence in wines at high concentrations is undesirable.[8] Depending on the type of wine, the contents of DIA[37,38] ranged from 0.2 to 12 mg L^{-1}. As it can be seen in Table 4, in the samples analyzed in this paper the content of DIA varies between 0.29 and 8.8 mg L^{-1}. It can be observed that in red wines the content is higher than in white wines, in accordance with previous research, and no significant differences were found between not sweet and sweet wines, with the exception of Ribera Duero wine.

With respect to the other α-dicarbonyl compounds with a short chain, concentrations found for Gly and MGly were similar to those previously reported.[33] Values ranged from 1.1 to 1.85 mg L^{-1} for Gly and 0.28 to 1.68 mg L^{-1} for MGly, with the exception of Merlot wine, whose concentration of Gly found was 7.1 mg L^{-1}. Thus, the levels found in Merlot wine are close to the levels found for sweet wines, in which the quantities of Gly and MGly found were higher (between 4.5 and 8.9 mg L^{-1} and 0.9 and 3.2 mg L^{-1} for Gly and MGly, respectively). In all cases the relation Gly/MGly is greater than unity. With respect to the levels of 2,3-Pen, these are similar in all wines analyzed ranging between 0.9 and 5.60 mg L^{-1}, and no appreciable differences were found between sweet and not sweet wines.

On the other hand and with respect to the α-dicarbonyl sugars, 3-DG and GS have been detected in all wines analyzed. In red and white wines, the content of GS varies between 0.4 and 5.2 mg L^{-1} and the 3-DG content between 4.9 and 13.5 mg L^{-1}. In sweet wines, the concentration of both glucosones increases considerably, independent of whether they are red or white, and their concentrations vary between 37 and 261 mg L^{-1}.

Due to the high concentration of glucosones obtained in sweet wines, it was important to check if formation of the α-dicarbonyl compounds from sugars was not favored by the high temperature of the derivatization reaction conditions. Therefore, in sweet wines, the derivatization reaction was performed at room temperature for 2 h and 30 min and aliquots of these samples were analyzed. A comparison of the chromatograms, obtained at room temperature and higher temperature, does not show significant differences. This fact allows us to conclude that the elevated concentrations of glucosones found in sweet wines are related to its high levels of sugars.

Finally, if analyzing the total α-dicarbonyl concentration, it can be observed that no significant variations were found in each type of red or white wine analyzed. However, if we made a comparison between red and white wines, we can confirm that the total α-dicarbonyl concentration is significantly higher in red wines. On the other hand, in sweet wines, a great difference has been found between the wines analyzed, and values of total α-dicarbonyl concentration amounting to 402 mg L^{-1} have been found. In addition, Tokaji wine, which it is a sweet white wine produced with botrytized grapes, contains higher levels of MGly. In spite of this, the total α-dicarbonyl concentration found is lower compared to the other sweet wines analyzed.

In conclusion, all types of columns tested were able to separate the lumazinic derivatives with sufficient resolution and peak symmetry in the optimum chromatographic conditions, although they differed in analysis time and separation efficiency of the derivatives analyzed. The conventional C18 column had the lowest resolution and peaks wider than columns with minor particle size. By comparing the chromatographic behavior of lumazinic derivatives in small particle size columns, it can be observed that although the XDB-C18 RRHT column provides the lowest retention times the best separation efficiency and lowest solvent consumption is achieved with the Poroshell column. For this reason, the comparison study carried out showed that the Poroshell column was most appropriate for analysis of α-dicarbonyl compounds and previous derivatization to lumazines, and this column was selected for their analysis in wine samples. Derivatization reaction time, temperature, and sample volume employed in analysis have considerably decreased with respect to the previous published method. On the other hand, a very sensitive and reproducible method to analyze these compounds in different commercial wine samples has been developed, and no pretreatment of sample is required. The sensitivity of the method is presented as a useful alternative to other methods, even with MS detection, whose instrumentation is more costly and complicated and not available in many laboratories. A comparison between red and white wines shows that the total α-dicarbonyl concentration is significantly higher in red ones. In sweet wines, total amounts up to 400 mg mL^{-1} have been found.

AUTHOR INFORMATION

Corresponding Author

*Tel.: +34924289375. Fax: +34924274244. E-mail: iduran@unex.es.

Funding

The authors gratefully acknowledge funding from the Junta de Extremadura (Project GR10033 of Research Group FQM003) and the Ministerio de Economía y Competitividad of Spain (Project CTQ2011-25388), both cofinanced by the European FEDER Funds. M.C.H.S. is grateful to the Consejería de Economía, Comercio e Innovación of Junta de Extremadura for a fellowship (DOE 04/01/2011).

Notes

The authors declare no competing financial interest.

ABBREVIATIONS USED

GS, D-glucosone; 3-DG, 3-deoxyglucosone; Gly, glyoxal; MGly, methylglyoxal; DIA, diacetyl; 2,3-Pen, 2,3-pentanedione; PhGly, phenylglyoxal; DDP, 5,6-diamino-2,4-hydroxypyrimidine; β-ME, β-mercaptoethanol

REFERENCES

(1) Thornalley, P. J. Advanced glycation and development of diabetic complications: Unifying the involvement of glucose, methylglyoxal and oxidative stress. *Endocrinol. Metab.* **1996**, *3*, 149−166.

(2) Uchida, K.; Kanematsu, M.; Sakai, K.; Matsuda, T.; Hattori, N.; Suzuki, D.; Miyata, T.; Noguchi, N.; Niki, E.; Osawa, T. Protein-bound acrolein: Potential markers for oxidative stress. *Proc. Natl. Acad. Sci.* **1998**, *95*, 4882−4887.

(3) Van Boekel, M. A. J. S. Formation of flavour compounds in the Maillard reaction. *Biotechnol. Adv.* **2006**, *24*, 230−233.

(4) Chen, X. M.; Kitts, D. D. Identification and quantification of á-dicarbonyl compounds produced in different sugar-amino acid Maillard reaction model systems. *Food Res. Int.* **2011**, *4*, 2775−2782.

(5) Flamini, R.; De Luca, G.; Di Stefano, R. Changes in carbonyl compounds in Chardonnay and Cavernet Sauvignon wines as a consequence of a malolactic fermentation. *Vitis* **2002**, *41*, 107−112.

(6) Flamini, R.; Dalla Vedova, A. Glyoxal/Glycolaldehyde: A redox system involved in malolactic fermentation of wine. *J. Agric. Food Chem.* **2003**, *51*, 2300−2303.

(7) De Revel, G.; Bertrand, A. A method for the detection of carbonyl compounds in wine: glyoxal and methylglyoxal. *J. Sci. Food Agric.* **1993**, *61*, 267−272.
(8) Bartowsky, E. J.; Henschke, P. A. The buttery attribute of wine -diacetyl- desirability spoilage and beyond. *Int. J. Food Microbiol.* **2004**, *96*, 235−252.
(9) Oliveira, C. M.; Silva-Ferreira, A. C.; De Freitas, V.; Silva, A. M. S. Oxidation mechanisms ocurring in wines. *Food Res. Int.* **2011**, *44*, 1115−1126.
(10) Davis, C. R.; Wibowo, D.; Eschenbruch, R.; Lee, T. H.; Fleet, G. H. Practical implications of malolactic fermentation: A review. *Am. J. Enol. Viticult.* **1985**, *36*, 290−301.
(11) Ramos, R. M.; Grosso Pacheco, J.; Moreira Gonçalves, L.; Valente, I. M.; Rodrigues, J. A.; Araújo Barros, A. Determination of free and total diacetyl in wine by HPLC−UV using gas-diffusion microextraction and pre-column derivatization. *Food Control* **2012**, *24*, 220−224.
(12) Thornalley, P. J. Monosaccharide autoxidation in health and disease. *Environ. Health Perspect.* **1985**, *64*, 297−307.
(13) Deng, Y.; Yu, P. H. Simultaneous determination of formaldehyde and methylglyoxal in urine: involvement of semicarbazide-sensitive amine oxidase-mediated deamination in diabetic complications. *J. Chromatogr. Sci.* **1999**, *37*, 317−322.
(14) Cordeiro, C.; Ponces-Freire, A. Methylglyoxal assay in cells as 2-methylquinoxaline using 1,2-diaminobenzene as derivatizing reagent. *Anal. Biochem.* **1996**, *234*, 221−224.
(15) McLellan, A. C.; Phillips, S.; Thornalley, P. J. The assay of methylglyoxal in biological systems by derivatization with 1,2-diamino-4,5-dimethoxybenzene. *Anal. Biochem.* **1992**, *206*, 17−23.
(16) Akira, K.; Matsumoto, Y.; Hashimoto, T. Determination of urinary glyoxal and methylglyoxal by high-performance liquid chromatography. *Clin. Chem. Lab. Med.* **2004**, *42*, 147−153.
(17) Espinosa-Mansilla, A.; Durán-Merás, I.; Salinas, F. High-performance liquid chromatographic-fluorometric determination of glyoxal, methylglyoxal, and diacetyl in urine by prederivatization to pteridinic rings. *Anal. Biochem.* **1998**, *255*, 263−273.
(18) Hurtado-Sánchez, M. C.; Espinosa-Mansilla, A.; Rodríguez-Cáceres, M. I.; Martín-Tornero, E.; Durán-Merás, I. Development of a method for the determination of advanced glycation end products precursors by liquid chromatography and its application in human urine samples. *J. Sep. Sci.* **2012**, *35*, 2575−2584.
(19) Yamada, H.; Miyata, S.; Igaki, N.; Yatabe, H.; Miyauchi, Y.; Ohara, T.; Sakai, M.; Shoda, H.; Oimomi, M.; Kasuga, M. Increase in 3-deoxyglucosone levels in diabetic rat plasma. Specific in vivo determination of intermediate in advanced Maillard reaction. *J. Biol. Chem.* **1994**, *269*, 20275−20280.
(20) Espinosa-Mansilla, A.; Durán-Merás, I.; Cañada-Cañada, F.; Prado-Márquez, M. P. High-performance liquid chromatographic determination of glyoxal and methylglyoxal in urine by prederivatization to lumazinic rings using in serial fast scan fluorimetric and diode array detectors. *Anal. Biochem.* **2007**, *371*, 82−91.
(21) Hayasaka, Y.; Bartowsky, E. J. Analysis of diacetyl in wine using solid-phase microextraction combined with gas chromatography-mass spectrometry. *J. Agric. Food Chem.* **1999**, *47*, 612−617.
(22) De Revel, G.; Pripis Nicolau, L.; Barbe, J. C.; Bertrand, A. The detection of alpha-dicarbonyl compounds in wine by formation of quinoxaline derivatives. *J. Sci. Food Agric.* **2000**, *80*, 102−108.
(23) Barros, A.; Rodrigues, J. A.; Almeida, P. J.; Oliva-Teles, T. Determination of glyoxal, methylglyoxal, and diacetyl in selected beer and wine, by HPLC with UV spectrophotometric detection, after derivatization with o-phenylenediamine. *J. Liq. Chromatogr. Relat. Technol.* **1999**, *22*, 2061−2069.
(24) Ramos, R. M.; Pacheco, J. G.; Gonçalves, L. M.; Valente, I. M.; Rodrigues, J. A.; Barros, A. Determination of free and total diacetyl in wine by HPLC-UV using gas-diffusion microextraction and pre-column derivation. *Food Control* **2012**, *24*, 220−224.
(25) Shibamoto, T. Analytical methods for trace levels of reactive carbonyl compounds formed in lipid peroxidation systems. *J. Pharm. Biomed.* **2006**, *41*, 12−25.
(26) Fekete, S.; Oláh, E.; Fekete, J. Fast liquid chromatography: the domination of core-shell and very fine particles. *J. Chromatogr. A* **2012**, *1228*, 57−71.
(27) Neue, U. D. *HPLC Columns: Theory, Technology, and Practice*; Wiley-VCH: New York, 1997.
(28) McCalley, D. V. Instrumental considerations for the effective operation of short, highly efficient fused-core columns. Investigation of performance at high flow rates and elevated temperatures. *J. Chromatogr. A* **2010**, *1217*, 4561−4567.
(29) Abrahim, A.; Al-Sayah, M.; Skrdla, P.; Bereznitski, Y.; Chen, Y.; Wu, N. Practical comparison of 2.7 ìm fused-core silica particles and porous sub-2 ìm particles for fast separations in pharmaceutical process development. *J. Pharm. Biomed.* **2010**, *51*, 131−137.
(30) Nováková, L.; Solich, P. A comparison of performance of various analytical columns in pharmaceutical analysis: conventional C18 and high throughput C18 zorbax columns. *J. Chromatogr. A* **2005**, *1088*, 24−31.
(31) Medina, A.; Magan, N. Comparison of three different C18 HPLC columns with different particle sizes for the optimization of aflatoxins analysis. *J. Chromatogr. B* **2012**, *889−890*, 138−143.
(32) Espinosa-Mansilla, A.; Muñoz de la Peña, A.; González-Gómez, D. Using univariate linear regression calibration software in the MATLAB Environment, application to chemistry laboratory practices. *Chem. Educ.* **2005**, *10*, 337−345.
(33) Da Silva-Ferreira, A. C.; Reis, S.; Rodrigues, C.; Oliveira, C.; Guedes de Pinho, P. Simultaneous determination of ketoacids and dicarbonyl compounds, key Maillard intermediates on the generation of aged wine aroma. *J. Food Sci.* **2007**, *72*, S314−S318.
(34) Compendium of international analysis of methods: a-dicarbonyl compounds by GC after derivatization Method for the determination of a-dicarbonyl compounds of wine by GC after derivatization by 1,2-diaminobenzene (OIV-Oeno 386B-2010) Method OIV-MA-AS315−21 , 2010.
(35) Murphy, I. B.; Stutte, C. A. Analysis for substituted benzoic and cinnamic acids using high-pressure liquid chromatography. *Anal. Biochem.* **1978**, *86*, 220−228.
(36) DeStefano, J. J.; Schuster, S. A.; Lawhorn, J. M.; Kirkland, J. J. Performance characteristics of new superficially porous particles. *J. Chromatogr. A* **2012**, *1258*, 76−83.
(37) Guillou, J.; Bertrand, A.; De Revel, G.; Barbe, J. C. Occurrence of hydroxypropanedial in certain musts and wines. *J. Agric. Food Chem.* **1997**, *45*, 3382−3386.
(38) Peynaud, E. *Le Gout du Vin*; Dunod: Paris, 1980; pp 44−45.

JOURNAL OF AGRICULTURAL AND FOOD CHEMISTRY

Article

pubs.acs.org/JAFC

Comprehensive Multiphase NMR Spectroscopy of Intact ^{13}C-Labeled Seeds

Leayen Lam,[†,‡] Ronald Soong,[†,‡] Andre Sutrisno,[†,‡] Ries de Visser,[§] Myrna J. Simpson,[†,‡] Heather L. Wheeler,[#,⊥] Malcolm Campbell,[#,⊥] Werner E. Maas,[⊗] Michael Fey,[⊗] Antonie Gorissen,[§] Howard Hutchins,[⊗] Brian Andrew,[⊗] Jochem Struppe,[⊗] Sridevi Krishnamurthy,[⊗] Rajeev Kumar,[○] Martine Monette,[○] Henry J. Stronks,[○] Alan Hume,[○] and André J. Simpson*[,†,‡]

[†]Department of Physical and Environment Sciences, University of Toronto Scarborough, 1265 Military Trail, Toronto, Ontario, Canada M1C 1A4

[‡]Department of Chemistry, University of Toronto, 80 St. George Street, Toronto, Ontario, Canada M5S 3H6

[§]IsoLife BV, Droevendaalsesteeg 1, 6708 PB Wageningen, The Netherlands

[#]Department of Biological Sciences, University of Toronto Scarborough, 1265 Military Trail, Toronto, Ontario, Canada M1C 1A4

[⊥]Department of Cell Systems and Biology, University of Toronto, 33 Willcocks Street, Toronto, Ontario, Canada M5S 3B2

[⊗]Bruker BioSpin Corp., 15 Fortune Drive, Billerica, Massachusetts 01821-3991, United States

[○]Bruker BioSpin Canada, 555 Steeles Avenue East, Milton, Ontario, Canada L9T 1Y6

Supporting Information

ABSTRACT: Seeds are complex entities composed of liquids, gels, and solids. NMR spectroscopy is a powerful tool for studying molecular structure but has evolved into two fields, solution and solid state. Comprehensive multiphase (CMP) NMR spectroscopy is capable of liquid-, gel-, and solid-state experiments for studying intact samples where *all organic components* are studied and differentiated in situ. Herein, intact ^{13}C-labeled seeds were studied by a variety of 1D/2D ^{1}H/^{13}C experiments. In the mobile phase, an assortment of metabolites in a single ^{13}C-labeled wheat seed were identified; the gel phase was dominated by triacylglycerides; the semisolid phase was composed largely of carbohydrate biopolymers, and the solid phase was greatly influenced by starchy endosperm signals. Subsequently, the seeds were compared and relative similarities and differences between seed types discussed. This study represents the first application of CMP-NMR to food chemistry and demonstrates its general utility and feasibility for studying intact heterogeneous samples.

KEYWORDS: *multiphase, broccoli, corn, wheat, seeds, NMR spectroscopy, intact sample, in situ analysis, triacylglyceride (TAG)*

INTRODUCTION

Seeds are integral to world nutrition as they not only serve as a direct source of food rich with essential vitamins, fiber, sterols, and antioxidants but carry the potential to be cultivated into fruit- and vegetable-bearing plants.[1−4] Plant sterols have been shown to reduce low-density lipoprotein cholesterol absorption, whereby the structurally analogous sterols compete with cholesterol absorption sites in the intestine.[5] Similarly, high antioxidant intake has demonstrated protective effects against chronic diseases such as cancer, cardiovascular disease, osteoporosis, and diabetes by mitigating the damaging effects related to oxidative stress.[1,2,4] β-Carotene, a precursor to vitamin A, and other antioxidants such as vitamin C are not produced natively by the human body and must be obtained from extrinsic dietary sources, for which fruits and vegetables are naturally abundant.[6,7]

Historically, NMR spectroscopy has evolved into two separate fields, namely, solution-state and solid-state NMR. Seed components can be extracted for solution-state NMR, but this process is destructive and selective toward only a subset of chemicals present. Solid-state NMR can be used to study intact seeds, but in the case of soluble/gel components, the lack of pulse field gradients and a spectrometer lock restrict the type of experiments and information that can be extracted directly. Recently, NMR spectroscopy has been applied in seed analysis for the study of oil and protein composition, but often requires extensive and time-consuming sample preparation.[8,9] One study used wheat seeds that were initially milled into a flour, dissolved in a buffer solution, and centrifuged, and the supernatant was collected prior to NMR analysis.[10] Such methods of sample preparation can be detrimental as they potentially perturb the structure and native chemical and physical interactions that influence analyte kinetics across phase boundaries, which are important for analysis.

The first ^{1}H measurements of intact seeds, in which the oil content was determined for a variety of seeds, were likely performed in 1963.[11] This was followed by the first high-resolution ^{13}C measurements conducted in 1974, whereby the oil composition was measured for a single soybean.[12] Previous

Received: October 12, 2013
Revised: December 18, 2013
Accepted: December 19, 2013
Published: December 19, 2013

ACS Publications © 2013 American Chemical Society

analysis of intact seeds has been performed by high-resolution magic angle spinning (HR-MAS) of canola seeds to determine seed oil composition;[13] cross-polarization (CP)-MAS and HR-MAS to characterize *Arabidopsis*, pea, and lettuce seeds;[14] metabolite profiling to assess conifer seed quality,[15] as well as measuring the moisture content of garden cress seeds.[16] In all cases, although intact seeds were used, only select phases (liquid, gel, or solid) were studied in a given experiment.

Traditional solution-state NMR probes use low-power electronics, a lock channel, and pulsed field gradients and provide excellent line shape but only for dissolved samples. HR-MAS probes were introduced in 1996 and employ magic angle spinning, a magic angle gradient, and susceptibility-matched stators.[17] HR-MAS probes permit the study of swellable and liquid components. However, HR-MAS probes are designed using low-power circuitry; as such, they cannot generate the RF field required for high-power decoupling or cross-polarization, elements essential to the majority of solid-state NMR experiments. Solid-state probes, on the other hand, are designed to generate high RF fields, but as solid-state NMR spectroscopy has been predominantly reserved for the study of true solids, they lack a lock and gradients, which are required for the efficient study of liquid and gel components. Comprehensive multiphase (CMP) NMR, introduced in 2012, incorporates all of the aforementioned aspects, including magic angle spinning, a magic angle gradient, a lock, full susceptibility matching, and solid-state circuitry to permit high power handling. Therefore, it is built to study unaltered samples where *all organic components* can be observed and differentiated in situ, resulting in a universal approach.[18]

The use of separate probes to achieve the same goal is only an option for the most simple, structural studies, where the sample does not change. Even in this case, it is important to stress that in large part, due to independent development of liquid- and solid-state NMR, very few laboratories in the world would have separate liquid, HR-MAS, and solids probes, and even if they did, scheduling all to be available at the same time would be extremely challenging. More importantly, any study involving kinetics transfer between phases (e.g., growth, contaminant sequestration) or changes of one phase into another (for example, soil swelling/drying, feeding phenylalanine to follow lignin formation) will require a CMP probe as such studies are impossible to perform using separate probes. This is discussed in more detail later in this study.

CMP-NMR has been, thus far, used to determine the fate and binding of contaminants in soil.[18,19] Here, we introduce CMP-NMR to applications in food and agriculture. This study focuses on structural information that can be obtained from ^{1}H and ^{13}C CMP-NMR characterization of intact broccoli, corn, and wheat seeds. Wheat and corn were selected as they represent major global crops, whereas broccoli seeds were included as an example of a legume. The different seed types will be compared to each other for relative differences and similarities as well as further considerations of CMP probes (including quantification; need for labeling and future potential) will be discussed toward the end of this study.

Seeds are used here as an example that serves to demonstrate the general applicability of CMP-NMR for the analysis of all organic components in all phases in whole, unaltered samples. CMP-NMR is likely to find widespread application in the agricultural and food sciences due to versatility and ability to provide unsurpassed molecular detail on intact samples. CMP-NMR has potential to understand intact structure, processes that are involved in phase changes (drying, swelling), and molecular interactions (for example, between a herbicide and plant tissue) and, thus, has considerable potential for the analysis of food, soil, sediments, plants, and seeds.

MATERIALS AND METHODS

^{13}C Labeling of the seeds. Uniformly ^{13}C-enriched seeds of broccoli, corn, and wheat (*Brassica oleracea* var. *botrytis* 'Broccoli', *Zea mays*, and *Triticum aestivum*, respectively) were produced in specially designed, airtight, high-irradiance growth chambers[20] (IsoLife, Wageningen, The Netherlands). Plants were grown from ^{13}C-labeled seeds in a closed atmosphere containing 97 atom % $^{13}CO_2$ (from pressurized cylinders; Isotec, Inc., Miamisburg, OH, USA) from the seedling stage until full maturity. Internal wind speed ensured efficient pollination of the corn and wheat. Pollination of broccoli flowers was ensured by combining compatible parent plants and introducing bluebottle flies into the chambers. Mineral nutrients were supplied as Hoagland-type solutions with micronutrients and iron.[21,22] Climate conditions were as follows: irradiance (PPFD), 600 μmol m^{-2} s^{-1} (HPI) during a 16 h day; day/night temperatures, 24/16 °C; relative humidity, 75/85%.

Sample Preparation. Uniformly ^{13}C-labeled (>97% total carbon content) and nonlabeled (<1.2% total carbon content) seeds of broccoli, corn, and wheat (*B. oleracea* var. *botrytis* 'Broccoli', *Z. mays*, and *T. aestivum*, respectively) were used. The whole and intact seeds were placed directly into a 4 mm zirconium rotor and filled with D_2O (Andover, MA, USA) as a lock solvent. The seeds, which contained 6.7 and 6.6, 6.8 and 7.2, and 8.6 and 7.5% water for labeled and nonlabeled wheat, labeled and nonlabeled corn, labeled and nonlabeled broccoli, respectively, were not swollen beforehand. Because the goal of the study was to study seed structure and not the process of germination, 99.8% D_2O was deliberately used because seeds are found to either not germinate or germinate but do not continue to grow afterward when imbibed with D_2O.[23,24] No significant differences were noted over each 24 h acquisition period; all spectra data sets were consistent with each other. In addition, during longer experiments CP-MAS, direct carbon, and 2D NMR the spectra (collected over many hours) will represent the average state of the seeds during that time period and hence give a representative overview of the overall structural state. Seeds remained intact and were not damaged during the spinning process. In the case of corn, which was cut in half to fit into the rotor, the D_2O solvent may have been more likely to leach components from the seed into the aqueous solvent. The goal of this study was only to look at overall structural state; future studies that employ H_2O as the solvent (with an external D_2O lock) and kinetic experiments with high temporal resolution could be used to understand the molecular processes behind germination.

The rotor was sealed using a top insert made from Kel-F, a Kel-F sealing screw, and a Kel-F cap. For wheat, only one seed was used. For broccoli, 2 seeds were used for proton studies and 10 seeds for anything that required carbon to increase sensitivity. Finally, for corn, the seed had to be cut into half due to its size before being placed in the rotor. The nonlabeled equivalents were prepared identically.

1D NMR Spectroscopy. All NMR measurements were performed on a 500 MHz Bruker Avance III spectrometer at a spinning speed of 6666 Hz using a prototype CMP MAS 4 mm $^{1}H-^{13}C-^{19}F-^{2}H$ probe fitted with an actively shielded Z gradient (Bruker BioSpin) at 298 K. All experiments were locked on D_2O, and the lock was maintained for all experiments including the solid-state experiments. Decoupling was used in all 1D and 2D experiments to remove $^{1}H-^{13}C$ coupling from the labeled sample. For low-power experiments *garp* was used for proton observe and *waltz16* for carbon observe. For high-power decoupling *spinal-64* was used for carbon observe.

All ^{1}H NMR spectra were recorded using presaturation for water suppression except for when presaturation utilizing relaxation gradients and echoes (PURGE) was employed.[25] The 90° pulse was calibrated for each sample in the study. A spectral width of 20 ppm was used, 2K scans and 8K time domain points were acquired. T_1 times were measured using the standard inversion recovery approach and the

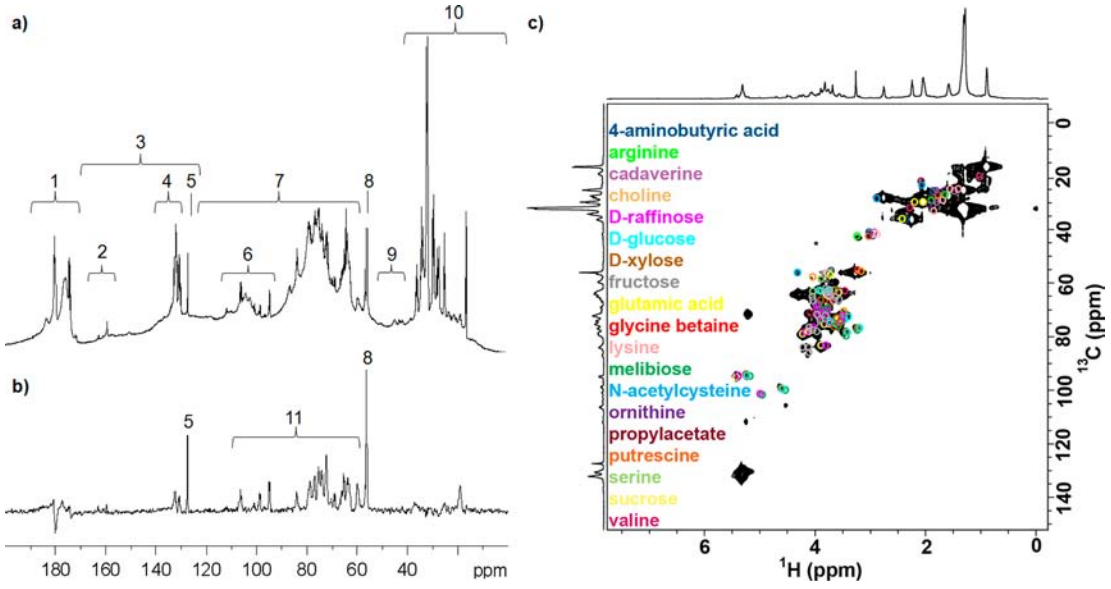

Figure 1. ^{13}C NMR spectra of a single ^{13}C-labeled wheat seed. (a) 1D carbon profile. Peaks: 1, carbonyls; 2, guanidine group carbon of arginine; 3, aromatic; 4, double bonds; 5, ethylene; 6, anomeric carbons; 7, overlapping carbohydrate and amino acids; 8, methanol; 9, amino acids; 10, aliphatic. (b) Spectrum showing the components with unrestricted diffusion (soluble) (by inverse diffusion edited, IDE). Peak: 11, small sugars. (c) Heteronuclear single-quantum coherence (HSQC) spectrum showing color-coded soluble/mobile species as determined by AMIX Bruker Bioreference spectra database. See Supporting Information Figure S2 for an expansion.

recycle delay set at 5 times the measured T_1 value. Spectra were processed using a zero-filling factor of 2 and an exponential function corresponding to a line broadening of 2 Hz.

One-dimensional ^{13}C NMR spectra were recorded with a spectral width of 400 ppm using inverse gate decoupling. Scans ranged from 2K to 12K and 16K time domain points. ^{13}C RAMPed-amplitude cross-polarization magic angle spinning (^{13}C RAMP CP-MAS)[26] was acquired with 2K scans, a 1 ms contact time, and a 2 s carbon recycle delay. T_1 times were measured using the standard inversion recovery approach and the recycle delay set at 5 times the measured T_1 value. Spectra were processed using a zero-filling factor of 2 and an exponential function corresponding to a line broadening of 5 Hz (conventional carbon) and 40 Hz (CP-MAS).

Spectral Editing. Diffusion-edited proton and carbon spectra were produced using a bipolar pulse pair longitudinal encode−decode (BPLED) sequence[27] with inverse gated decoupling. Scans were collected using encoding/decoding gradients of 1.8 ms at 50 gauss/cm and a diffusion time of 180 ms. Inverse diffusion edited (IDE) and recovering relaxation losses arising from diffusion editing (RADE) were created via difference from the appropriate controls as previously described.[18] Using CPMG (T_2 filtered) experiments to obtain the liquid phase components, the T_2 delay was rotor synchronized and set at 600 μs and the pulse train was repeated 100 times, yielding a total pulse train length of 120 ms.[18] To remove solid components, two CPMG echoes of 7.5 μs were inserted prior to cross-polarization. During this short period, signals from extremely broad ^{1}H signals (i.e., true crystalline solids) relax (or are not efficiently refocused), whereas signals from more mobile solids remain along the XY plane for subsequent cross-polarization. The approach has been discussed in detail by Courtier-Murias et al.[18] For spectral editing, the spectra were scaled until the dominant component being subtracted was nulled, leaving a difference spectrum containing positive peaks.[18]

2D NMR Spectroscopy. ^{1}H total correlation spectroscopy (TOCSY) spectra were acquired in the phase-sensitive mode, using a mixing sequence with rotor synchronized constant adiabatic WURST-2 pulses within an X_M16 mixing scheme.[28] Scans (128) were collected for each of the 196 increments in the F1 dimension. Data points (2048) were collected in F2 at a mixing time of 120 ms. Both dimensions were processed using sine-squared functions with a $\pi/2$ phase shift and a zero-filling factor of 2. Nuclear Overhauser effect spectroscopy (NOESY) spectra were acquired in phase-sensitive mode, using time proportional phase incrementation. Scans (128) and data points (2048) were collected for each of the 196 increments in the F1 dimension at a mixing time of 300 ms. Both dimensions were processed using sine-squared functions with a $\pi/2$ phase shift and a zero-filling factor of 2. The correlation spectroscopy (COSY) spectra were acquired in non-phase-sensitive mode, using gradients for selection. Scans (128) and data points (2048) were collected for each of the 196 increments in F1. Both dimensions were processed using unshifted sine-squared function, a zero-filling factor of 2, and a magnitude mode for projection.

^{1}H−^{13}C heteronuclear single-quantum coherence (HSQC) spectra were collected in phase-sensitive mode using echo/antiecho-TPPI gradient selection. Scans (128) were collected for each of the 196 increments in the F1 dimension. Data points (2048) were collected in F2 and a 1J ^{1}H−^{13}C of 145 Hz. Both dimensions were processed using sine-squared functions with a $\pi/2$ phase shift and a zero-filling factor of 2. Dipolar assisted rotational resonance (DARR) spectroscopy was acquired using 256 scans for each of 96 increments in F1 and a mixing time of 200 ms. F2 was processed using an exponential function corresponding to 35 Hz line broadening and F1 using a sine-squared function with a $\pi/2$ phase shift. Both dimensions were zero-filled by a factor of 2.

NMR Spectroscopy of Nonlabeled Samples. For nonlabeled samples, only basic 1D ^{13}C spectra and CP-MAS were acquired. Experiments such as diffusion-edited carbon and DARR are very insensitive and time prohibitive on a nonlabeled sample.

Compound Identification. Spectra were calibrated against a range of known compounds in the Bruker Biofluid Reference Compound Database (v 2.0.3). Pattern matching of both 1D and 2D spectra was performed using analysis of mixtures (AMIX, version 3.9.3, Bruker BioSpin) against the Bruker Biofluid Reference Compound Database (v 2.0.0−2.0.3) using a procedure previously developed for complex mixtures.[29] Compounds with a >80% confidence match (from automated searches) were further selected for detailed manual inspection. Only compounds that showed near perfect matches in all spectral regions were retained as assignments. The chemical shifts of the identified compounds were compared with database values (r^2 = 0.99, σ = 0.01). For quantification, spectra were also normalized to total intensity over the 200−0 ppm region in the carbon spectra. The multi-integration tool in AMIX (version 3.9.3, Bruker BioSpin) was used to compare the relative quantity of carbonyl

dx.doi.org/10.1021/jf4045638 | J. Agric. Food Chem. 2014, 62, 107−115

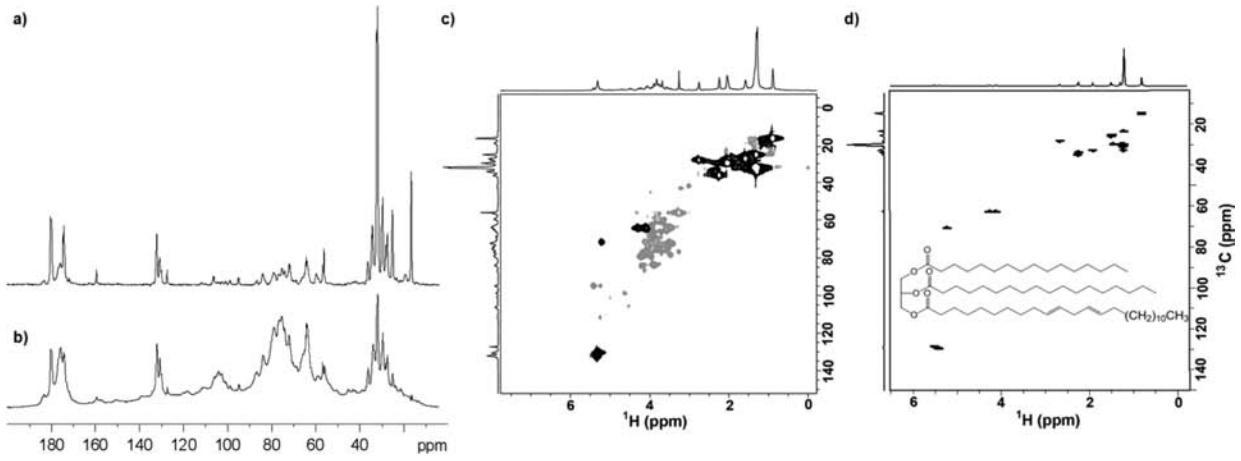

Figure 2. ^{13}C NMR spectra of a single ^{13}C-labeled wheat seed: (a) components with restricted diffusion (by diffusion editing, DE); (b) semisolids (by recovering relaxation losses arising from diffusion editing, RADE); (c) HSQC with triacylglyceride signals in black and all other signals gray; (d) ACD/Laboratories HSQC simulation of generic triacylglycerides structure (overlaid).

protein (defined as 190−170 ppm), carbohydrates (defined as 110−50 ppm), lipids/fatty acids (defined as 183−164, 135−121, and 44−3 ppm), and aliphatic proteins (defined as 60−40 ppm).

RESULTS AND DISCUSSION

Comprehensive Multiphase NMR Spectroscopy. In this study a number of spectral editing approaches have been used. These have been discussed in detail by Courtier-Murias et al.[18] Briefly, starting from the most liquid-like through the most solid-like, these experiments can be described as follows. (1) IDE is a difference-based approach that selects molecules that have unrestricted tumbling (i.e., truly dissolved molecules). Here, these components will be referred to as "components with unrestricted diffusion". (2) DE selects molecules with restricted diffusion and will include swollen biopolymers, mobile gels, and smaller molecules that are trapped or sorbed. In this study these components will be referred to as "components with restricted diffusion". There is no clear-cut diffusivity that separates all dissolved molecules from all those with restricted diffusion. Instead, the experiments should be considered as a continuum with the "fast diffusing molecules contained in IDE" and generally "the restricted molecules" being in DE. The strength of the diffusion editing has been developed on standard samples to give the best distinction between truly dissolved molecules from entrapped molecules and gels.[18] (3) RADE is an experiment that compensates for signals that otherwise may be lost through relaxation during diffusion editing. RADE selects semisolid components that may include gels and possibly some very dynamic solids. In this study these components will be referred to as "semisolids". (4) T_2 filtered CP-MAS selects the more mobile "true solids" that may include very rigid gels and solids that exhibit some dynamics. In this study these components will be referred to as "dynamic solids". It is important to note that although no components are missed, some components may be observed twice by ^{1}H RADE and ^{13}C T_2 CP-MAS.[18] (5) Finally, inverse T_2 filtered CP-MAS is a difference approach that selects just the truly rigid solids that show little to no dynamics. In this study these components will be referred to as "rigid solids".

Detailed Analysis of Wheat Seed. *Components with Unrestricted Diffusion (Soluble Components).* A conventional 1D carbon profile of the single ^{13}C-labeled (97 atom %) wheat seed was acquired with low-power *waltz-16* decoupling (Figure 1a). In this experiment carbons from true solid components are strongly attenuated as the lower power decoupling is insufficient to decouple broad proton resonances that are characteristic in solids. As such, the spectrum contained signals from components with and without restricted diffusion and semisolids, but signals from true solids are largely suppressed (Figure 1a). Due to the complex nature of the seeds, the conventional ^{13}C spectrum showed considerable overlap, which was reduced by spectral editing to obtain the IDE spectrum (Figure 1b). IDE shows only molecules that demonstrate unrestricted diffusion in solution. It requires the subtraction of the diffusion-edited spectrum (contains molecules with restricted diffusion) from a reference spectrum (without diffusion weighting, i.e., defocusing/refocusing gradients set to zero power) but otherwise acquired under identical conditions. The IDE spectrum (Figure 1b) emphasized a range of small molecules, but identification from the IDE spectrum alone is challenging. Two-dimensional HSQC correlations provided additional spectral dispersion as well as one-bond ^{1}H−^{13}C connectivity information. Database matching against the AMIX Bruker Bioreference spectral database of the HSQC data along with ^{1}H−^{1}H COSY, ^{1}H−^{1}H TOCSY, and ^{1}H−^{1}H NOESY (see Supporting Information Figure S1 for example COSY and TOCSY data) confirmed a wide range of metabolites present (Figure 1c; see Supporting Information Figure S2 for an expansion of Figure 1c and brief description of each metabolite identified).

After identification from the 2D spectrum, metabolite assignments were transferred to the 1D carbon spectrum (Figure 1a). Major regions can be summarized as follows: carbonyls from proteins and lipids (approximately 190−170 ppm); guanidine group of arginine (159 ppm); conjugated double bonds (135−130 ppm) from triacylglycerides (TAG, see next section); ethylene (sharp signal at 128.1 ppm); anomeric carbons of carbohydrates (90−110 ppm); various overlapping carbohydrate and amino acid signals (90−50 ppm); methanol (56.40 ppm) and amino acids and various metabolites (42−46 ppm including 4-aminobutyric acid, arginine, cadaverine, lysine, ornithine, putrescine) and aliphatics (50−5 ppm, mainly TAG, see next section).

As discussed above, the IDE spectrum (Figure 1b) highlighted the molecules that are most liquid-like or dynamic within the seed. To our knowledge, this is the first report of

dx.doi.org/10.1021/jf4045638 | J. Agric. Food Chem. 2014, 62, 107−115

ethylene, a gas within the seed,[30] detected by NMR spectroscopy. Strong signals from methanol and a range of small sugars dominated, indicating that these are present in a dissolved or dynamic state. Conversely, the aliphatic signals hardly contribute at all to the IDE spectrum and suggest many of these are in a more restricted environment. This will be discussed in the next section.

Components with Restricted Diffusion and Semisolid Components via Diffusion-Based Editing. Diffusion editing encodes the spatial position of a signal at the start of the experiment and decodes it at the end. If the molecule physically changes position during the experiment, it is not refocused and is attenuated. The result is a spectrum that contains signals from molecules that show very slow/no diffusion, such as macromolecules, swollen polymers, and small molecules trapped in an environment that prevents free diffusion.

Figure 2a shows the ^{13}C DE spectrum of the wheat seed. Small signals from carbohydrate were present, indicating that some carbohydrates were present in a restricted diffusion-like state. These could be swollen carbohydrate polymers (for example, starch) or smaller entities sorbed to other larger components. The dominant signals in the DE spectrum arose from triacylglycerides (TAG). The HSQC of the single ^{13}C-labeled wheat seed (Figure 2c) matches extremely well with the ACD/Laboratories HSQC simulation of the generic TAG structure overlaid (Figure 2d). Whereas generic TAG structures clearly dominate the lipid profile, individual TAG molecules could not be distinguished. Detailed assignments are present in Table 1 and are consistent with COSY, TOCSY, NOESY, and

Table 1. Proton (^1H) and Carbon (^{13}C) Chemical Shift Assignment of Fatty Acid and Lipidic Components of a Single ^{13}C-Labeled (97 Atom %) Wheat Seed

component	^1H (ppm)	^{13}C (ppm)
$\mathbf{CH_3}-(CH_2)_n-$	0.90	16.60
$CH_3-(\mathbf{CH_2})_n-$	1.31	25.30
$-(\mathbf{CH_2})_n-CH_2-CH_2$	1.31	32.20
$-(\mathbf{CH_2})_n-CH_2-CH_2$	1.31	34.20
$-(\mathbf{CH_2})-CH_2-CO-O-$	1.59	27.60
$-\mathbf{CH_2}-CH=CH-$	2.05	29.80
$-CH_2-\mathbf{CH_2}-CO-O-$	2.25	36.40
$-CH=CH-\mathbf{CH_2}-CH=CH-$	2.76	28.20
$-\mathbf{CH_2}O-$	4.08−4.28	64.40
$-\mathbf{CH}O-$	5.21	71.50
$-CH_2-\mathbf{CH}=\mathbf{CH}-$	5.32	130.90−132.20

the previous work by Sacco and co-workers.[31] Complete TAG oxidation yields twice the amount of energy that could be generated from protein or carbohydrates.[32] Thus, TAGs are considered highly compact energy reserves and are therefore an efficient way to maximize energy storage within the confines of a seed.[32] Most triglycerides exist as a "solid fat" somewhat analogous to butter; as such, it is logical that TAG within the seeds display restricted diffusion-like properties rather than true liquid or solid properties.

Diffusion editing is a useful experiment to emphasize components with restricted movement. However, the experiment uses a relatively long diffusion delay, which could potentially lead to the loss of signal from very large or semisolid components that exhibit fast relaxation. This rapidly relaxing signal can be fully recovered using an experiment termed RADE, the technicalities of which are discussed by Courtier-Murias and co-workers.[18] In simple terms, RADE accounts for signals from semisolids that otherwise could be missed by diffusion-based spectral editing alone. Figure 2b shows the RADE spectrum for the ^{13}C-labeled wheat seed. The spectrum contains signals from the components that relax extremely quickly and have a semisolid character. As with the spectrum of components with restricted diffusion, there is a strong signature from TAG suggesting that some of the TAG have a semisolid-like character as expected. Other lipid signals may arise from membrane structures within the seed. In addition to the aliphatic species, the RADE spectrum also contains significant carbohydrate signal, indicating strong contribution from carbohydrate polymers. These could arise from the starchy endosperm of wheat seeds[33] as well as cell walls and possibly more flexible components of the seed coat itself. These carbohydrate signals are strongly emphasized by CP-MAS (Figure 3a), which emphasizes the true solid in the seed coat.[34]

Solid Components. The above experiments focused on the unrestricted diffusion (soluble), restricted diffusion, and semisolid components of ^{13}C-labeled seeds. As CMP-NMR probes can handle the high-power RF requirements required for modern solid-state experiments, the solid components of the seeds can also be studied. CP-MAS is an excellent filter for the ^{13}C detection of true solid components.[18] During CP, magnetization is passed from proton on carbon via a strong dipole network. As such, CP is not efficient for dynamic systems (for example, solutions, mobile gels). However, in the true solids static H−C dipoles provide a useful framework for CP and the process is highly efficient. The result is that CP provides a strong bias toward the components in the sample with the most solid-like character. The solid-state NMR spectral profile is shown in Figure 3a and is dominated by starch, cellulose, and hemicellulose signals. Assignments for all peaks have previously been reported[14,35] and are labeled in Figure 3a. Absolute quantification is challenging because of overlap of signals, and additional in-depth research is required to understand how the editing procedure affects quantification. It is unclear how the different editing steps influence absolute quantification; however, it is possible to do relative quantification between the species (see next section) to estimate crude changes or differences. T_2 relaxation editing can be used to further edit the solid components with dynamics from the true solid domains. The proton T_2 filter is utilized prior to CP so that protons in the most solid environment with short T_2 will preferentially relax. This leaves only the resonances from the unrestricted diffusion or semimobile materials (Figure 3c). The most rigid signals with short T_2 can be recovered with spectral subtraction of the T_2-filtered CP-MAS spectrum (dynamic solids) from the regular CP-MAS spectrum (everything), leaving a spectrum containing the most rigid resonances (Figure 3b). For example, the peak for amorphous CH_2 does appear in T_2-filtered CP-MAS (labeled "9" in Figure 3c), demonstrating these chains exhibit motion and likely exist as restricted diffusion/semisolid state. Conversely, the signal labeled "5" (Figure 3b) arose from crystalline cellulose. Specifically, this signal represents the C4 position in crystalline cellulose and is the only signal that can be clearly resolved due to overlap. Crystalline cellulose behaves like a true solid; as such it is strongly emphasized along with the most rigid components (Figure 3b).

Other carbohydrate signals, mainly starch, are prominent in all spectra and come from the starchy endosperm of wheat seeds[33] and from the seed coat.[34] Next to TAG, starch and

dx.doi.org/10.1021/jf4045638 | J. Agric. Food Chem. 2014, 62, 107−115

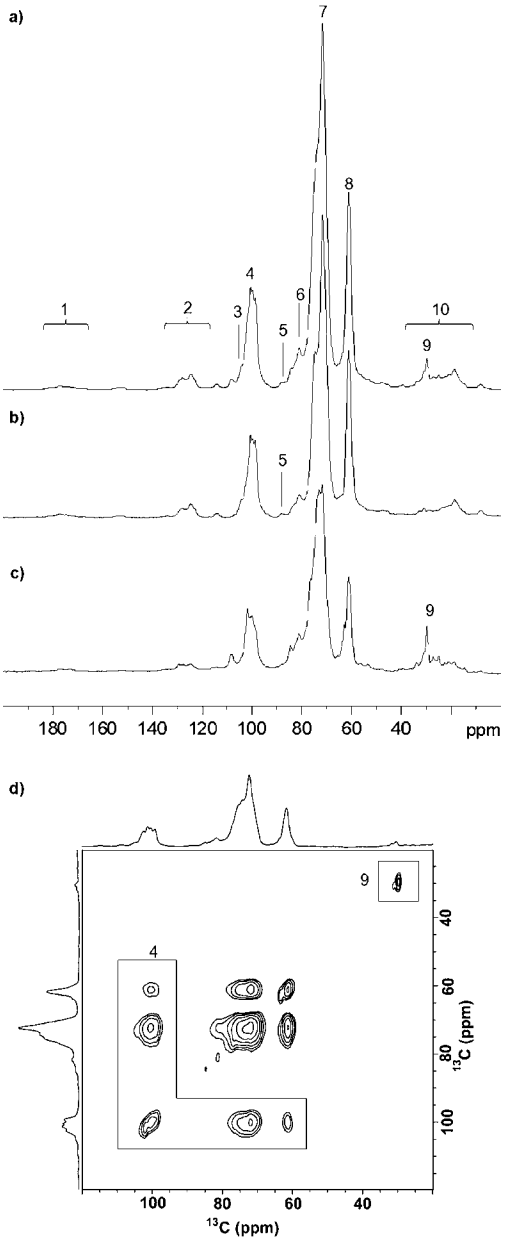

Figure 3. ^{13}C NMR spectra of a single ^{13}C-labeled wheat seed. (a) True solids (by cross-polarization magic angle spinning, CP-MAS). Peaks: 1, carbonyls in lignins, hemicelluloses, and proteins; 2, double bonds (lignins); 3, C1 of cellulose and hemicelluloses; 4, C1 of starch (anomeric carbon); 5, C4 of crystalline cellulose; 6, C4 of amorphous cellulose, hemicelluloses, and/or starch; 7, C2, C3, C5 in celluloses, hemicelluloses, and starch and C6 starch branch points; 8, C6 in celluloses, hemicelluloses, and starch; 9, amorphous CH_2; 10, aliphatic. (b) Spectral editing to emphasize rigid solids. (c) T_2-filtered CP-MAS to emphasize dynamic solids. (d) Dipolar assisted rotational resonance (DARR) to highlight connectivities between carbons for the truly solid components.

storage protein are the main storage reserves of cereal seeds. Higher plants produce starches, which are a critical nutritional source for humans.[36] DARR is able to identify ^{13}C−^{13}C correlations through space (Figure 3d) and is a very useful experiment to confirm and help assign structure. DARR confirms that the signals at 62−73, 62−100, and 73−100 ppm are correlated in the same structure, consistent with that of carbohydrates in general. DARR also confirms that the TAG at 30 ppm and carbonyl at 130 ppm (not shown) each are not correlated to carbohydrate signals.

Comparing Wheat, Broccoli, and Corn Seeds. For unrestricted diffusion (soluble) components (IDE), corn has the most signals in the free carbohydrate area (about 10% more than wheat and 55% more than broccoli, based on integration), with the majority of signals arising from glucose and fructose, which is consistent with the literature (Figure 4c).[37,38] It is important to note that in the case of corn, the seed was cut in half, and it is possible that some of this additional signal intensity from soluble molecules could arise from D_2O leaching components from the exposed interior of the seed. The IDE (unrestricted diffusion (soluble) components, Figure 4b) and DE (restricted diffusion components, Figure 4e) for broccoli looked quite similar, and both were dominated by lipids in large part because of the lower carbohydrate levels compared to the other two species. Broccoli had the highest lipid content (about 10% more than wheat and corn based on integration), and these findings are consistent with trends found in the literature.[39,40] The actual location of these small molecules within the seeds is unclear; previous MRI-based studies have indicated that water has some mobility within the endosperm,[41,42] and it is possible that some of these relatively free molecules are associated with this water. The RADE spectrum (semisolids) of corn and wheat (Figure 4i) emphasized a considerable contribution of carbohydrates.[40] Conversely, broccoli shows very few carbohydrates in the semisolid phase. Note that in wheat, broccoli, and corn the CH_3 signal of lipids (marked with an askterisk (∗) in Figure 4a−f) appeared in the IDE and DE but disappeared in the RADE spectrum. This likely resulted from the local motion of the CH_3 terminal groups that leads to longer relaxation times compared with other parts of the lipid/TAG molecules.

The CP-MAS of broccoli (Figure 4k) was very different from that of wheat (Figure 4j) mainly because it had stronger signals from proteins (about 2.5 times more intense based on integration) and from long chain fatty acyl groups than the wheat spectrum. This is consistent with the literature that lists protein in broccoli seeds to be ∼21 g/100 g[39] and in wheat to be ∼10 g/100 g.[40] The 60−0 ppm region mainly arises from aliphatic amino acids with the strong signals from long-chain aliphatics $(CH_2)_n$ superimposed at ∼30 ppm. α-Carbons from protein resonate in a band from ∼60 to 40 ppm centered at ∼50−55 ppm, and aromatic amino acids add to the aromatic region and are most prominent from 110 to 120 ppm. The carbonyl signals at 190−160 ppm arise from proteins, lignins, lipids, and hemicelluloses. The carbonyls are likely much more intense in the broccoli compared to the wheat (roughly 5.5 times more based on integration) in large part due to the additional protein and oil content.[39,40] The presence of a relatively strong $(CH_2)_n$ superimposed at ∼30 ppm in the broccoli is interesting. This suggests that in the broccoli, at least some of the aliphatic components are more solid-like than in the other seeds. As the characteristic double bonds from TAG are also present (∼125 ppm), it is most likely that the truly solid aliphatic component is a portion of TAG stored in the more solid form when compared to the other seeds. However, it is also possible that some of this additional CH_2 intensity also arises from lipoprotein, free fatty acids, or lipids other than TAG, which are known to be present in seeds.[15,43,44]

Other Considerations. CMP-NMR provides a unique insight into both chemical and physical attributes of molecular structure inside unaltered natural samples. Seeds here were

dx.doi.org/10.1021/jf4045638 | J. Agric. Food Chem. 2014, 62, 107−115

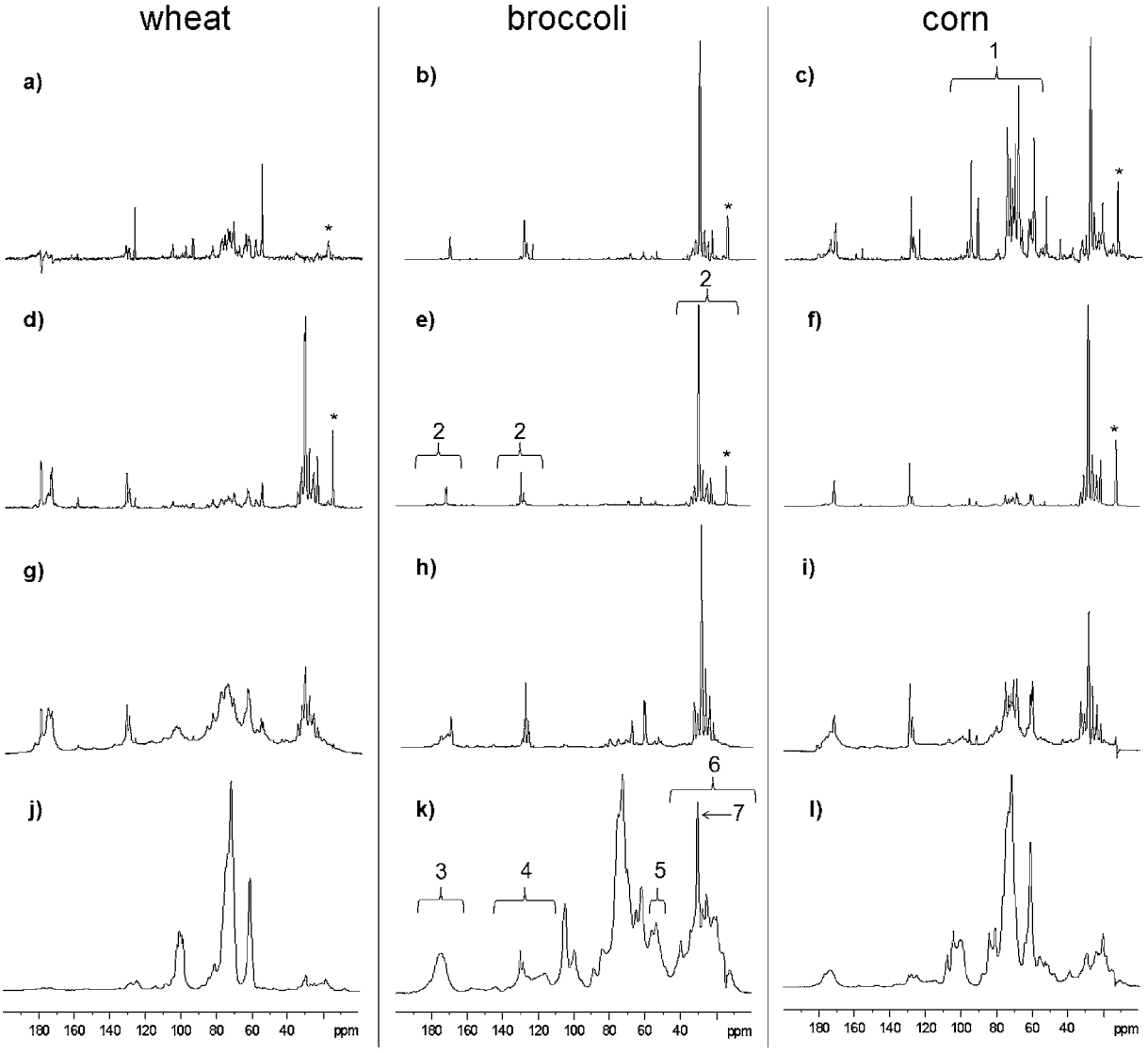

Figure 4. ^{13}C NMR spectra comparing ^{13}C labeled wheat, broccoli, and corn seeds: (a−c) unrestricted diffusion (soluble) components (by inverse diffusion edited, IDE); (d−f) restricted diffusion (by diffusion edited, DE); (g−i) semisolids (by recovering relaxation losses arising from diffusion editing, RADE); (j−l) true solids (by cross-polarization magic angle spinning, CP-MAS). The $-CH_3$ of TAG is marked with an *; 1, dominated by fructose in corn; 2, triacylglycerides; 3, carbonyls (result of increased protein content); 4, aromatic (result of increased protein content); 5, α carbon of amino acids; 6, dominated by aliphatic amino acids; 7, aliphatic $-(CH_2)-$ (dominated by TAG).

used to exemplify the approach to natural samples in general. Isotopic labeling is beneficial but not essential for CMP-NMR. Generally, labeling is necessary when less sensitive multidimensional spectra (for example, DARR in this study) are being obtained to abbreviate spectrometer time with enhanced signal-to-noise ratio. Natural abundance of ^{13}C can be used to acquire NMR spectra but will increase sampling time considerably. The ^{13}C-labeled CP of wheat was performed over a period of 1 h and 43 min for 2K scans (signal-to-noise = 690), whereas the unlabeled equivalent containing ^{13}C at the natural abundance took 16 h and 23 min for 20K scans (signal-to-noise = 69). Comparison of the ^{13}C-labeled spectra to natural abundance spectra are provided in the Supporting Information (Figures S3−S5). In the future, the use of 7 mm rotor diameters will allow ∼4−5 times the sample volume to be introduced, which should substantially increase signal from unlabeled samples and should make similar studies on unlabeled material more feasible. The main drawback of CMP-NMR probes in comparison to a dedicated HR-MAS or solid probe is loss of sensitivity. As discussed by Courtier Murias et al.,[18] the four-channel prototype probe used here suffers from a loss of ∼40% when compared to a two-channel solid probe. This loss mainly arises due to single circuit being quadrupley tuned in the four-channel design. If identical probes could be compared (note, no two-channel CMP-NMR probes have been built to date), it is predicted that the loss in sensitivity would be ∼10−15% (mainly associated with the addition of the gradient coil). Due to the sensitivity losses CMP-NMR probes should be restricted to studies of native sample where the study of the components in their native phase is critical. In such cases the potential for CMP-NMR to provide otherwise inaccessible molecular-level information in situ is considerable. In studies following developmental changes it may be important to study the development of the solid, gel, and liquid components over time. Here it may be important to interleave solid, gel, and liquid NMR experiments and measure not just the phases independently but kinetic transfer between the phases. Such

dx.doi.org/10.1021/jf4045638 | J. Agric. Food Chem. 2014, 62, 107−115

studies would be impossible using two or three separate NMR probes as it takes several hours to change and properly calibrate an NMR probe. Similarly, studies that follow the conversion of a molecule from liquid, to gel, to solid phases (for example, feeding phenylalanine to follow lignin growth or the binding and sequestration of a contaminant) also require the kinetic transfer between phases to be monitored and may find CMP-NMR probes useful in the future. These examples indicate a future potential of CMP-NMR in seed/plant/food research. Finally, as the CMP-NMR probes combine all aspects of solution, HR-MAS, and solids, they provide the potential to develop novel NMR experiments (for example, solids using gradients) to better select and study structure and interaction in situ.

Finally, it is important to note that quantification in complex systems such as seeds is complicated by spectral overlap. Spectral editing can extract molecules in the liquid, gel, semisolid, or solid state, and theoretically if the carbons were detected in exactly the same manner it would be possible to quantify the distribution between the different phases. However, in this study, this has been complicated by the fact CP-MAS was used for solid components, which enhances certain signals more than others, making this comparison inaccurate. Commonly, for quantification in solids, direct polarization magic angle spinning (DP-MAS)[45] would be used. With regard to CMP-NMR, the cross-polarization element was required to select the rigid bonds (i.e., spectral editing to select the solid components), further complicating the issue. It may possible to quantify in the future, but this would require advanced techniques such as spin counting.[46]

Although the focus of this study has been to demonstrate the general applicability of CMP-NMR to the chemical structures of seeds, nonlabeled broccoli seeds were collected after spinning to test if they would germinate. They successfully germinated after being transferred to a Petri dish with a filter paper moist with water. This indicates that the seeds were still alive during spinning, and the potential for monitoring them while germinating the seed exists. CMP-NMR holds potential to provide an unprecedented window into the germination process itself. This avenue opens potential for research in fields such as physiology (germination, vernalization processes), agriculture (seed viability), and food safety (pathogen test, purity). Specifically, applications are possible in selecting viable seeds (current methods are mutagenic, destructive, or time-consuming) or for seed selection breeding programs, which all require detailed yet nondestructive molecular analysis.[47]

■ ASSOCIATED CONTENT

Supporting Information

Example COSY and TOCSY spectra with TAG assignments labeled; expansion of Figure 1c (HSQC of a single ^{13}C labeled wheat seed) with brief description of the metabolites identified and figures comparing ^{13}C-labeled spectra to natural abundance spectra of a single wheat seed. This material is available free of charge via the Internet at http://pubs.acs.org.

■ AUTHOR INFORMATION

Corresponding Author

*(A.J.S.) E-mail: andre.simpson@utoronto.ca. Phone: +1 (416) 287-7547. Fax: +1 (416) 287-7279.

Funding

We thank the Natural Sciences and Engineering Research Council of Canada NSERC, Strategic and Discovery Grants Programs, the Canada Foundation for Innovation (CFI), the Ontario Ministry of Research and Innovation (MRI), and the Krembil Foundation for providing funding. A.J.S. thanks the Government of Ontario for an Early Researcher Award. We acknowledge the Dutch Innovation Program Food and Nutrition Delta for financial support (Project FND09002).

Notes

The authors declare no competing financial interest.

■ ACKNOWLEDGMENTS

We thank E. Koning and R. J. P. Baan (Koppert Cress BV) for kindly providing nonlabeled seeds of *Brassica oleracea* L. from which the ^{13}C-labeled plants and seeds were produced. L.L. thanks A. J. Veloso for constructive criticism and editing of the manuscript.

■ REFERENCES

(1) Byers, T.; Nestle, M.; McTiernan, A.; Doyle, C.; Currie-Williams, A.; Gansler, T.; Thun, M. American Cancer Society guidelines on nutrition and physical activity for cancer prevention: reducing the risk of cancer with healthy food choices and physical activity. *Ca—Cancer J. Clin.* **2002**, *52*, 92—119.

(2) Yang, J.; Liu, R. H.; Halim, L. Antioxidant and antiproliferative activities of common edible nut seeds. *LWT—Food Sci. Technol.* **2009**, *42*, 1—8.

(3) Elleuch, M.; Bedigian, D.; Roiseux, O.; Besbes, S.; Blecker, C.; Attia, H. Dietary fibre and fibre-rich by-products of food processing: characterisation, technological functionality and commercial applications: a review. *Food Chem.* **2011**, *124*, 411—421.

(4) Poutanen, K. Past and future of cereal grains as food for health. *Trends Food Sci. Technol.* **2012**, *25*, 58—62.

(5) Ostlund, R., Jr. Phytosterols, cholesterol absorption and healthy diets. *Lipids* **2007**, *42*, 41—45.

(6) Montel-Hagen, A.; Kinet, S.; Manel, N.; Mongellaz, C.; Prohaska, R.; Battini, J.-L.; Delaunay, J.; Sitbon, M.; Taylor, N. Erythrocyte Glut1 triggers dehydroascorbic acid uptake in mammals unable to synthesize vitamin C. *Cell* **2008**, *132*, 1039—1048.

(7) Lobo, G. P.; Amengual, J.; Palczewski, G.; Babino, D.; von Lintig, J. Mammalian carotenoid-oxygenases: key players for carotenoid function and homeostasis. *Biochim. Biophys. Acta, Mol. Cell Biol. Lipids* **2012**, *1821*, 78—87.

(8) Kouame, S.-D. B.; Perez, J.; Eser, S.; Benesi, A. ^{1}H-NMR monitoring of the transesterification process of Jatropha oil. *Fuel Process. Technol.* **2012**, *97*, 60—64.

(9) Jiao, Z.; Si, X.-x.; Zhang, Z.-m.; Li, G.-k.; Cai, Z.-w. Compositional study of different soybean (*Glycine max* L.) varieties by ^{1}H NMR spectroscopy, chromatographic and spectrometric techniques. *Food Chem.* **2012**, *135*, 285—291.

(10) Lamanna, R.; Cattivelli, L.; Miglietta, M. L.; Troccoli, A. Geographical origin of durum wheat studied by ^{1}H NMR profiling. *Magn. Reson. Chem.* **2011**, *49*, 1—5.

(11) Conway, T. F.; Earle, F. R. Nuclear magnetic resonance for determining oil content of seeds. *J. Am. Oil Chem. Soc.* **1963**, *40*, 265—268.

(12) Schaefer, J.; Stejskal, E. O. Carbon-13 nuclear magnetic resonance measurement of oil composition in single viable soybeans. *J. Am. Oil Chem. Soc.* **1974**, *51*, 210—213.

(13) Hutton, W. C.; Garbow, J. R.; Hayes, T. R. Nondestructive NMR determination of oil composition in transformed Canola seeds. *Lipids* **1999**, *34*, 1339—1346.

(14) Bardet, M.; Foray, M. F.; Bourguignon, J.; Krajewski, P. Investigation of seeds with high-resolution solid-state ^{13}C NMR. *Magn. Reson. Chem.* **2001**, *39*, 733—738.

(15) Terskikh, V. V.; Feurtado, J. A.; Borchardt, S.; Giblin, M.; Abrams, S. R.; Kermode, A. R. In vivo ^{13}C NMR metabolite profiling: potential for understanding and assessing conifer seed quality. *J. Exp. Bot.* **2005**, *56*, 2253−2265.
(16) Rachocki, A.; Latanowicz, L.; Tritt-Goc, J. Dynamic processes and chemical composition of *Lepidium sativum* seeds determined by means of field-cycling NMR relaxometry and NMR spectroscopy. *Anal. Bioanal. Chem.* **2012**, *404*, 3155−3164.
(17) Maas, W. E.; Laukien, F. H.; Cory, D. G. Gradient, high resolution, magic angle sample spinning NMR. *J. Am. Chem. Soc.* **1996**, *118*, 13085−13086.
(18) Courtier-Murias, D.; Farooq, H.; Masoom, H.; Botana, A.; Soong, R.; Longstaffe, J. G.; Simpson, M. J.; Maas, W. E.; Fey, M.; Andrew, B.; Struppe, J.; Hutchins, H.; Krishnamurthy, S.; Kumar, R.; Monette, M.; Stronks, H. J.; Hume, A.; Simpson, A. J. Comprehensive multiphase NMR spectroscopy: basic experimental approaches to differentiate phases in heterogeneous samples. *J. Magn. Reson.* **2012**, *217*, 61−76.
(19) Longstaffe, J. G.; Courtier-Murias, D.; Soong, R.; Simpson, M. J.; Maas, W. E.; Fey, M.; Hutchins, H.; Krishnamurthy, S.; Struppe, J.; Alaee, M.; Kumar, R.; Monette, M.; Stronks, H. J.; Simpson, A. J. In-situ molecular-level elucidation of organofluorine binding sites in a whole peat soil. *Environ. Sci. Technol.* **2012**, *46*, 10508−10513.
(20) Gorissen, A.; Kraut, N. U.; De Visser, R.; De Vries, M.; Roelofsen, H.; Vonk, R. J. No de novo sulforaphane biosynthesis in broccoli seedlings. *Food Chem.* **2011**, *127*, 192−196.
(21) Smakman, G.; Rinie, H. Energy metabolism of *Plantago lanceolata*, as affected by change in root temperature. *Physiol. Plant.* **1982**, *56*, 33−37.
(22) De Visser, R.; Vianden, H.; Schnyder, H. Kinetics and relative significance of remobilized and current C and N incorporation in leaf and root growth zones of *Lolium perenne* after defoliation: assessment by ^{13}C and ^{15}N steady-state labelling. *Plant, Cell Environ.* **1997**, *20*, 37−46.
(23) Blake, M. I.; Crane, F. A.; Uphaus, R. A.; Katz, J. J. Effect of heavy water on the germination of a number of species of seeds. *Planta* **1967**, *78*, 35−38.
(24) Siegel, S. M.; Halpern, L. A.; Giumarro, C. Germination and seedling growth of winter rye in deuterium oxide [47]. *Nature* **1964**, *201*, 1244−1245.
(25) Simpson, A. J.; Brown, S. A. Purge NMR: effective and easy solvent suppression. *J. Magn. Reson.* **2005**, *175*, 340−346.
(26) Metz, G.; Wu, X. L.; Smith, S. O. Ramped-amplitude cross polarization in magic-angle-spinning NMR. *J. Magn. Reson., Ser. A* **1994**, *110*, 219−227.
(27) Wu, D. H.; Chen, A. D.; Johnson, C. S. An improved diffusion-ordered spectroscopy experiment incorporating bipolar-gradient pulses. *J. Magn. Reson., Ser. A* **1995**, *115*, 260−264.
(28) Peti, W.; Griesinger, C.; Bermel, W. Adiabatic TOCSY for C,C and H,H J-transfer. *J. Biomol. NMR.* **2000**, *18*, 199−205.
(29) Woods, G. C.; Simpson, M. J.; Koerner, P. J.; Napoli, A.; Simpson, A. J. HILIC-NMR: toward the identification of individual molecular components in dissolved organic matter. *Environ. Sci. Technol.* **2011**, *45*, 3880−3886.
(30) Matilla, A. J.; Matilla-Vázquez, M. A. Involvement of ethylene in seed physiology. *Plant Sci.* **2008**, *175*, 87−97.
(31) Sacco, A.; Neri Bolsi, I.; Massini, R.; Spraul, M.; Humpfer, E.; Ghelli, S. Preliminary investigation on the characterization of durum wheat flours coming from some areas of south Italy by means of ^{1}H high-resolution magic angle spinning nuclear magnetic resonance. *J. Agric. Food Chem.* **1998**, *46*, 4242−4249.
(32) Theodoulou, F. L.; Eastmond, P. J. Seed storage oil catabolism: a story of give and take. *Curr. Opin. Plant Biol.* **2012**, *15*, 322−328.
(33) Calucci, L.; Galleschi, L.; Geppi, M.; Mollica, G. Structure and dynamics of flour by solid state NMR: effects of hydration and wheat aging. *Biomacromolecules* **2004**, *5*, 1536−1544.
(34) Oliveira, C. M. R. d.; Iacomini, M.; alquini, Y.; Gorin, P. A. J. Microscopic and NMR analysis of the external coat from seeds of *Magonia pubescens*. *New Phytol.* **2001**, *152*, 501−509.
(35) Jiang, J.; Shao, Y.; Li, A.; Zhang, Y.; Wei, C.; Wang, Y. FT-IR and NMR study of seed coat dissected from different colored progenies of *Brassica napus*−*Sinapis alba* hybrids. *J. Sci. Food Agric.* **2012**, 1898−1902.
(36) Tetlow, I. J. Starch biosynthesis in developing seeds. *Seed Sci. Res.* **2011**, *21*, 5−32.
(37) Whistler, R. L.; Kramer, H. H.; Smith, R. D. Effect of certain genetic factors on the sugars produced in corn kernels at different stages of development. *Arch. Biochem. Biophys.* **1957**, *66*, 374−380.
(38) García-Pérez, A.; Harrison, M.; Grant, B.; Chivers, C. Microbial analysis and chemical composition of maize (*Zea mays*, L.) growing on a recirculating vertical flow constructed wetland treating sewage on-site. *Biosyst. Eng.* **2013**, *114*, 351−356.
(39) Gu, Y.; Guo, Q.; Zhang, L.; Chen, Z.; Han, Y.; Gu, Z. Physiological and biochemical metabolism of germinating broccoli seeds and sprouts. *J. Agric. Food. Chem.* **2011**, *60*, 209−213.
(40) U.S. Department of Agriculture, Agricultural Research Service. USDA National Nutrient Database for Standard Reference; http://www.ars.usda.gov/nutrientdata (accessed June 1, 2013).
(41) Callaghan, P. T.; Jolley, K. W.; Lelievre, J. Diffusion of water in the endosperm tissue of wheat grains as studied by pulsed field gradient nuclear magnetic resonance. *Biophys. J.* **1979**, *28*, 133−141.
(42) Ishida, N.; Ogawa, H.; Kano, H. Diffusion of cell-associated water in ripening barley seeds. *Magn. Reson. Imaging* **1995**, *13*, 745−751.
(43) Austin, J. R.; Frost, E.; Vidi, P.-A.; Kessler, F.; Staehelin, L. A. Plastoglobules are lipoprotein subcompartments of the chloroplast that are permanently coupled to thylakoid membranes and contain biosynthetic enzymes. *Plant Cell.* **2006**, *18*, 1693−1703.
(44) Bréhélin, C.; Kessler, F.; van Wijk, K. J. Plastoglobules: versatile lipoprotein particles in plastids. *Trends Plant Sci.* **2007**, *12*, 260−266.
(45) Keeler, C.; Maciel, G. E. Quantitation in the solid-state ^{13}C NMR analysis of soil and organic soil fractions. *Anal. Chem.* **2003**, *75*, 2421−2432.
(46) Smernik, R. J.; Oades, J. M. The use of spin counting for determining quantitation in solid state ^{13}C NMR spectra of natural organic matter 1. Model systems and the effects of paramagnetic impurities. *Geoderma* **2000**, *96*, 101−129.
(47) Terry, J.; Probert, R. J.; Linington, S. H. Processing and maintenance of the Millennium Seed Bank collections. In *Seed Conservation: Turning Science into Practice*; Smith, R. D., Dickie, J., Linington, S., Pritchard, H., Probert, R., Eds.; Royal Botanic Gardens: Kew, UK, 2003; Chapter 17, pp 307−325.

JOURNAL OF AGRICULTURAL AND FOOD CHEMISTRY

Article

pubs.acs.org/JAFC

Coffee Modulates Transcription Factor Nrf2 and Highly Increases the Activity of Antioxidant Enzymes in Rats

Silvio J. V. Vicente,*[,†] Emília Y. Ishimoto,[‡] and Elizabeth A. F. S. Torres[‡]

[†]Department of Ecotoxicology, Santa Cecília University, Santos, SP, Brazil

[‡]Department of Nutrition, School of Public Health, University of São Paulo, São Paulo, SP, Brazil

ABSTRACT: This study investigated the effect of a 28 day administration of coffee brew on the activity of antioxidant enzymes in rats. After this period of 2.0 mL/day dosages of this beverage, the activities of hepatic superoxide dismutase, catalase, and glutathione peroxidase increased 74.8, 59.4, and 135.2%, respectively, whereas the cytosolic level of Nrf2 increased 131.3%. At the same time, the total antioxidant capacity of the hepatic tissue increased 25.1%, improving the defensive status against oxidative stress. At the end of the experiment, the levels of biomarkers alanine transaminase and aspartate transaminase remained equal to the control group, and no changes were observed in the hepatic histoarchiteture of the animals, suggesting that the liver tissue was not impaired by the exposure to coffee. The changes in enzyme activities and antioxidant capacity were statistically significant ($p < 0.05$), indicating that coffee could be considered an important alternative against oxidative stress and its correlated degenerative diseases.

KEYWORDS: *coffee, hepatic antioxidant enzymes, Nrf2, ORAC, rats*

INTRODUCTION

Chemoprevention has been accepted as one of the most successful strategy to fight cancers. In the past decades, studies have been developed to investigate natural and synthesized substances capable of restraining carcinogenic processes.[1] Some coffee bioactive substances such as phenolic compounds (including chlorogenic acids and phenolic acids released by the hydrolysis of chlorogenic acids), caffeine and other xanthines, Maillard reaction products, and the diterpenes cafestol and kahweol have been evaluated, and most results have suggested that the ingestion of these substances is inversely related to the incidence of liver and colon cancers.[2−7] The degree of roasting also affects coffee antioxidant capacity as it promotes the formation of Maillard reaction products and the partial conversion of trigonelline to *N*-methylpyridinium, both with defensive capacities.[5,7]

In general, a tumor is initiated by a permanent modification of DNA by the action of electrophilic or oxidant species. Once procarcinogens are introduced in organisms, they usually require an enzymatic activation to be converted into highly reactive intermediates that can attack important molecules such as DNA, RNA, and proteins. These enzymatic processes are frequently promoted by phase I enzymes. In opposition, phase II enzymes have the ability to neutralize dangerous species, generating less reactive and more soluble substances that can be eliminated from the organisms.[1,3,6,8,9] Antioxidant enzymes such as superoxide dismutase (SOD), catalase (CAT), and glutathione peroxidase (GPx) also play important defensive roles, reducing the levels of dangerous species such as O_2^- (superoxide anion radical), H_2O_2 (hydrogen peroxide), and O_2^{2-} (peroxide anion). This fact decreases the downstream formation of other reactive oxygen species (ROS), neutralizing or reducing their deleterious actions.[2,10] Therefore, considerable efforts have been made to identify substances that can modulate the transcription and increase the activity of these protective enzymes.

Different studies have produced strong evidence that the key point for the transcription of phase II and antioxidant enzymes is the protein nuclear factor-E2-related (Nrf2) factor. Under normal (reducing) condition, Nrf2 remains anchored to its inhibitor cytoplasmic complex Keap1−Nrf2 (Kelch-like ECH-associated protein-1) for its polyubiquitination and subsequent 26S proteasome-mediated degradation. However, under oxidative stress or exposure to inducers, Nrf2 is disrupted from this complex, allowing its translocation to the nucleus of the cells, where it binds to the antioxidant response element (ARE) or electrophile response element (EpRE) present in the promoter region of the mentioned enzymes, increasing their transcription.[3,6,8,9] Keap1 presents a dimeric structure formed through its BTB/POZ (broad-complex, tramtrak, bric-à-brac/pox virus-zinc finger) domains, sequestering one molecule of Nrf2 when thiol groups of the cysteine residues C273 and C288 are reduced (−SH). Oxidative stress and inducers act on these two cysteine residues to form intermolecular disulfides (−S−S−) that cause a conformational change of Keap1, releasing Nrf2 to migrate to the nucleus.[5,9] A post-translational phosphorylation also facilitates Nrf2 to dissociate from Keap1-Nrf2, and this change would be promoted by kinases such as protein kinase C (PKC), phosphatidyl inositol 3-kinase (PI3K), and mitogen-activated protein kinase (MAPK). Advances have accumulated in recent years, but some details still need to be elucidated on the pathway that activates this mechanism.[8,9]

Received: April 25, 2013
Revised: December 9, 2013
Accepted: December 13, 2013
Published: December 13, 2013

ACS Publications © 2013 American Chemical Society

Two studies published experimental evidence that the administration of phenolic acids (gentisic, gallic, ferulic, and *p*-coumaric acids) to rats increased the hepatic and cardiac activities of SOD, CAT, and GPx.[11,12] Simultaneously, these tissues showed higher levels of cytosolic Nrf2 and higher expressions of the mRNA for these enzymes. In both cases, a dose equal to 100 mg/kg of body weight (mg/kg BW) per day of each phenolic acid dissolved in propylene glycol/saline was administered to the animals over 14 days.

Aiming to evaluate the above-mentioned beneficial effect using a natural beverage, we decided to use coffee brew as it contains high levels of phenolic acids found as a family of chlorogenic acids.[13−15] Additionally, high levels of caffeine are also found in coffee brew (from 0.9 to 1.3% w/w dry basis in *Coffea arabica*; from 1.2 to 2.4% w/w dry basis in *Coffea robusta*),[16] and this xanthine has been reported as another bioactive substance capable of modulating antioxidant enzymes.[2,3,6] Another important fact for choosing coffee is that it is one of the most popular nonalcoholic beverages in the world,[2,5,6,17] and the eventual results of this study would have wide application.

In a previous publication,[18] we discussed the effect of a single and small dose of coffee brew (from 0.5 to 2.0 mL) on the activity of hepatic SOD, CAT, and GPx in rats, obtaining increases of 19.1, 22.1, and 25.1%, respectively, in relation to the control group. It was shown that doses containing from 2.0 to 8.0 mg/kg BW phenolic acids promoted measurable beneficial effects. As cited in the present study, besides phenolic acids, other bioactive compounds present in coffee certainly collaborated to achieve this positive answer.[2−6]

Motivated by these encouraging results, we decided to evaluate the effect of a repetitive administration of small doses of coffee brew to rats, (1) measuring the effect of this exposure in the activity of hepatic enzymes SOD, CAT, and GPx and in the cytosolic concentration of Nrf2; (2) evaluating the changes in the antioxidative status of the liver tissue; and (3) identifying any damage to the liver through the quantification of the hepatic biomarkers alanine transaminase (ALT) and aspartate transaminase (AST) together with histological observations.

MATERIALS AND METHODS

Chemicals. Caffeic, ferulic, and *p*-coumaric acids, 5-caffeoylquinic acid (5-CQA), 5-feruloylquinic acid (5-FQA), 2,2′-azobis(2-amidinopropane) dihydrochloride (AAPH), 6-hydroxy-2,5,7,8-tetramethylchroman-2-carboxylic acid (Trolox), tris(hydroxymethyl)-aminomethane hydrochloride (Tris-HCl) buffer, and fluorescein were acquired from Sigma-Aldrich (USA). The commercial kits Ransod and Ransel for SOD and GPx determinations were acquired from Randox Laboratories (UK). Hydrogen peroxide (30%), formic acid, and methanol were acquired from Merck KgaA (Germany). The kits for the determination of AST and ALT were acquired from LabTest Ltd.a. (Brazil). The Western blotting reagents were acquired from Amersham Biosciences (USA).

Coffee Description and Preparation. Medium roast (degree 3) Brazilian coffee (*C. arabica* var. Bourbon blended with 15−30% of *Coffea canephora* var. Robusta) produced in Minas Gerais state (Brazil), packed under vacuum in 500 g aluminized bags with an external cardboard box, was acquired from local stores. Packs were kept under vacuum, at 4 °C (refrigerator) and in the dark to preserve coffee characteristics during the tests. All tests were done using fresh coffee brews prepared with 80 g of coffee powder per liter of mineral water at 90 °C and filtered through paper filter as recommended by the Brazilian Association of Coffee Industry (ABIC).[17]

Animal Characteristics and Treatment. Male rats (*Ratus novergicus* var. Wistar) with 200 ± 10 g of BW were provided by the Animal Facility of the Medical School, University of São Paulo (FM-USP). A total of 12 animals were housed in individual plastic cages for 4 days (adaptation period), with free access to food (purified diet AIN-76) and water. The temperature was kept at 22 ± 2 °C, and the animals were exposed to 12 h light/dark cycles. On day 5, they were randomly distributed in two groups ($n = 6$) and given 2.0 mL of water (group 1) or 2.0 mL of coffee brew (group 2) per day by gavage. After 28 days, the animals were deprived of food for 12 h, anesthetized, and sacrificed by exsanguination (cardiac puncture). The liver tissue was washed with sterile ice-cold 0.9% NaCl solution and immediately frozen in liquid nitrogen. The procedures involving the animals were conducted at the Institute of Tropical Medicine (IMT-USP) in compliance with Brazilian laws and approved by the Committee of Ethics in Research of the IMT-USP under number CEP-IMT-10/07.

Liver Homogenate Preparation. The liver homogenates were prepared as described by Vicente et al.[18] Basically, 1.0 g of washed liver tissues was homogenized with 3 mL of phosphate buffer (0.1 M, pH 7.0) and centrifuged at 1000*g* (20 min at 4 °C); the supernatant was collected and centrifuged at 11200*g* (20 min at 4 °C), and then the supernatant was collected, diluted 1:10 (v/v) with phosphate buffer, and centrifuged at 76900*g* (60 min at 4 °C). The final supernatant was collected and stored at −80 °C in the dark until the end of the analytical determinations (within 48 h of sacrifice). The preparation of the homogenate was done within 2 h of sacrifice.

Instrumentation. The activities of antioxidant enzymes and the biomarkers AST and ALT were determined using a spectrophotometer model 1650 (Shimadzu, Japan). The antioxidant capacity was measured by oxygen radical absorbance capacity (ORAC) using a fluorimeter model FL-55 (Perkin-Elmer, UK). Both instruments were equipped with a 10 mm temperature-controlled cell. Free phenolic acids and caffeine were quantified by high-performance liquid chromatography (HPLC) using an equipment supplied by TSP (USA) and a C18 Microsorb MV column (Varian Inc., USA) with 250 × 4.6 mm (5 μm of particle size). The major chlorogenic acids were quantified by HPLC-DAD-MS using a chromatograph model 1200 SL (Agilent Technologies, USA) equipped with a diode array detector (DAD), a mass spectrophotometer detector (MS), and a Zorbax SB-C18 column (Agilent Technologies, USA) of 50 × 2.1 mm (1.8 μm particle size). The electrophoresis for the Western blotting analysis was developed using a Minive kit (Amersham Biosciences, USA), and the chemiluminescence was measured using an ECL-Plus ImageQuant CAS 4000 (GE Healthcare, USA).

Bioactive Compounds in Coffee Brew. Some of the bioactive substances (caffeic, ferulic, and *p*-coumaric acids) capable of modulating the transcription of antioxidant enzymes are present in coffee as a family of esters called chlorogenic acids formed through different combinations of these hydroxycinnamic acids with quinic acid. Taking into account that both chlorogenic acids and free phenolic acids have been reported as active substances, we decided to measure these two forms. The major chlorogenic acids present in coffee brew were quantified by HPLC-DAD-MS according to the method of Corrêa.[19] This analysis was done by injecting 20 μL of coffee brew, starting with an isocratic elution of 85% of phase A (deionized water with 0.1% of formic acid) and 15% of phase B (methanol) at 0.32 mL/min until 2 min. Between 2 and 6 min, a gradient from 15 to 30% of phase B was developed, ending with second gradient from 30 to 35% of phase B between 6 and 12 min. Operation conditions for MS were ionization voltage, 3000 V; N_2 flow, 12.0 L/min at 30 psig; and temperature, 350 °C. A previous standardization of this method was done (recovery, limit of detection, and limit of quantification),[19] the quantification was performed at 324 nm using external standard curves (five points, triplicate measurements), and the results were expressed in micrograms per milliliter. Because coffee brew does not present free phenolic acids, before the analysis of these substances a previous hydrolysis was done according to the method of Nardini et al.,[20] using 2 N NaOH containing 10 mM EDTA and 1% ascorbic acid to prevent phenolic acid decomposition. Next, these substances were quantified by HPLC as suggested by Kowalski and Wolski,[21] injecting 20 μL of hydrolyzed coffee brew. Water/methanol/acetic acid (75:24:1 v/v) was used as mobile phase at 0.8 mL/min, and the determinations were

done at 323 nm for caffeic and ferulic acids and at 309 nm for *p*-coumaric acid. A previous standardization of this method was done (recovery, limit of detection, and limit of quantification),[15] the quantification was performed using external standard curves (five points, triplicate measurements), and the results were expressed in micrograms per milliliter.

Caffeine is another substance capable of modulating the transcription of antioxidant enzymes, and it was quantified by HPLC as suggested by Vitorino et al.,[22] with small adaptations. Briefly, coffee brew was filtered (0.5 μm), and 20 μL was injected in the HPLC using water/methanol/acetic acid (80:19:1 v/v) as mobile phase at 1.0 mL/min. The wavelength 272 nm was selected for the detection of caffeine. A previous standardization of this method was done, the quantification was performed using external standard curves (five points, triplicate measurements), and the results were expressed in micrograms per milliliter.

Antioxidant Enzyme Activity and ORAC. The activity of SOD was measured by visible spectroscopy (505 nm) according to the method of Woolliams et al.,[23] with small modifications for the use of the kit Ransod.[15] The liver homogenate was diluted 1:20 v/v with phosphate buffer (75 mM, pH 7.4) for this assay. The activity of CAT was determined by ultraviolet spectroscopy (230 nm) using the method described by Aebi.[24] The liver homogenate was diluted 1:5 v/v with phosphate buffer to determine this enzyme. The activity of GPx was also determined by ultraviolet spectroscopy (340 nm) according to the method of Paglia and Valentine,[25] with small modifications for the use of the kit Ransel.[15] The liver homogenate was not diluted for this determination. These enzymatic activities were expressed in units per milligram of protein, micromoles per minute per milligram of protein, and units per milligram of protein, respectively. The quantifications of the proteins for the calculations of the antioxidant enzymes were done in accordance with Bradford[26] using bovine serum albumin (BSA) as standard.

The ORAC assay was developed by fluorescence spectroscopy (excitation, 493 nm; emission, 515 nm) according to the methods of Ou et al.[27] and Prior et al.[28] with small modifications.[15] The liver homogenate was diluted 1:40 v/v with phosphate buffer, and 300 μL of this dilution was used in each test. The results were expressed as micromoles of Trolox equivalent per liter (μmol TE/L).

Hepatic Biomarkers, Histopathological Analysis, and Western Blotting of Nrf2. The hepatic biomarkers AST and ALT were determined as described by Reitman and Frankel,[29] with small modifications for the use of the kits for these enzymes.[15] Both enzymes were determined by visible spectroscopy (505 nm) using a calibration curve (five points, triplicate measurements, from 0 to 200 IU/L).

For the histopathological analysis, a small section of the liver tissue was collected after the sacrifice, washed with sterile ice-cold 0.9% NaCl solution, fixed with 10% formaldehyde (48 h), embedded in liquid paraffin, and sliced (5 μm thick), the paraffin was removed by heat, and the tissue was stained with hematoxylin and eosin dyes (H&E) to be observed under the microscope.[30]

The determination of Nrf2 was done as described by Yeh and Yen[11] with small modifications, using the dye-binding assay proposed by Bradford[26] for the quantification of proteins (BSA as the standard). Briefly, 10 μL of the cytosolic fraction was separated by 10% SDS–polyacrylamide gel electrophoresis (20 V, 300 mA). After the electrophoresis, the proteins were electrotransferred from the gel to a PVDF membrane (25 V, 400 mA) using 25 mM Tris-HCl buffer with 20% of methanol; the membrane was washed with Tris-HCl buffer containing 0.05% (v/v) Tween-20, and free binding sites were blocked for 2 h with defatted dried milk (7% w/v). Next, the membrane was incubated overnight at 4 °C with rabbit polyclonal antibody against Nrf2, washed three times with Tris-HCl buffer, incubated with IgG secondary antibody coupled with horseradish peroxidase for 1 h at room temperature, and washed with Tris-HCl buffer; chemiluminescence was measured. The quantifications were adjusted for the corresponding β-actin level (loading control protein).

Statistical Calculations. Statistical calculations (Kolmogorov–Smirnov and Student's *t* test) were done using the SPSS 16.0 for Windows software package, with a significance level of $p < 0.05$. All tests were done in triplicate, and the results are presented as means ± standard deviations.

RESULTS AND DISCUSSION

Bioactive Compounds in Coffee Brew. As the main purpose of this study was to evaluate the effect of the administration of coffee brew on the activity of antioxidant enzymes, it was important to quantify the levels of the bioactive

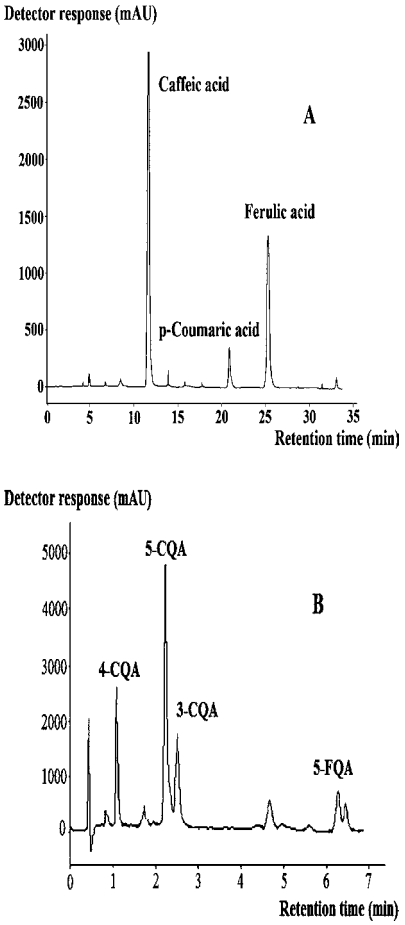

Figure 1. Typical chromatograms obtained during the quantification of free phenolic acids (A) and chlorogenic acids (B) in coffee brew.

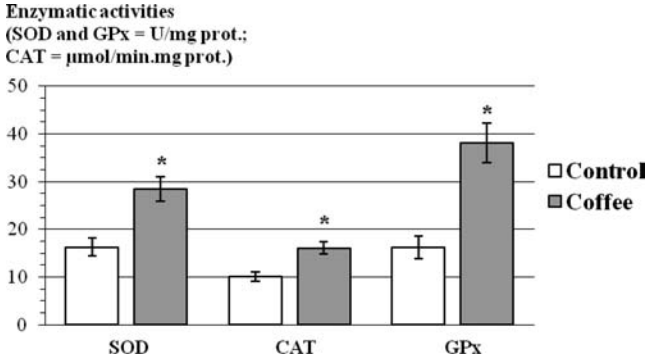

Figure 2. SOD (U/mg of protein), CAT (μmol/min/mg of protein), and GPx (U/mg of protein) average activities in the liver tissue of rats ($n = 6$) showing the differences between groups 1 (control) and 2 (coffee). (∗ indicates statistically significant difference from the control group at $p < 0.05$.)

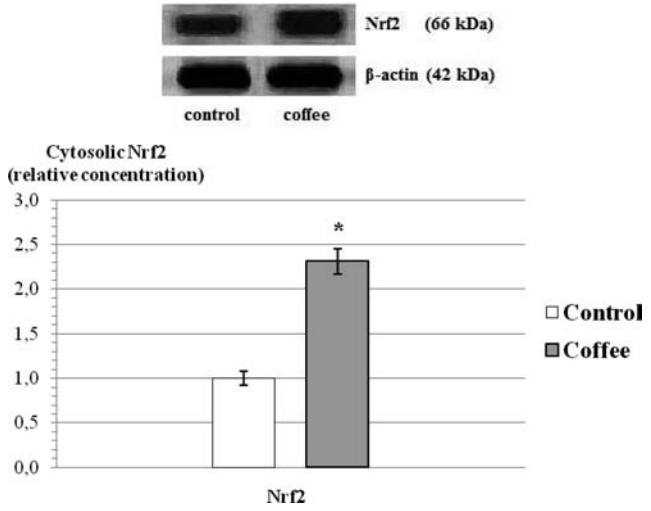

Figure 3. Cytosolic levels of Nrf2 (relative concentrations) in the liver tissue of groups 1 and 2 (n = 6): (top) original blotting; (bottom) average results of the densitometric analysis. (∗ indicates statistically significant difference from the control group at $p < 0.05$.)

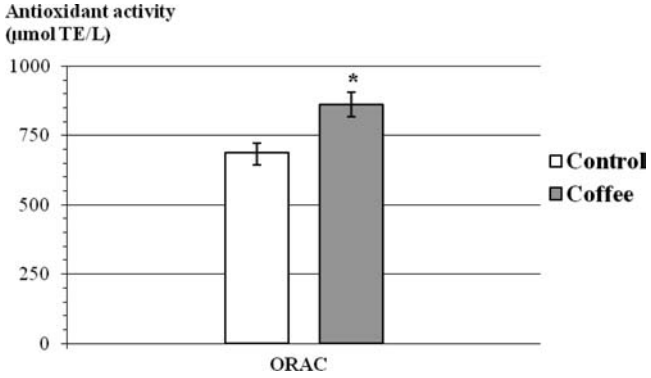

Figure 4. Total antioxidant capacity measured by ORAC (μmol TE/L) in the liver tissue of groups 1 and 2 (n = 6). (∗ indicates statistically significant difference from the control group at $p < 0.05$.)

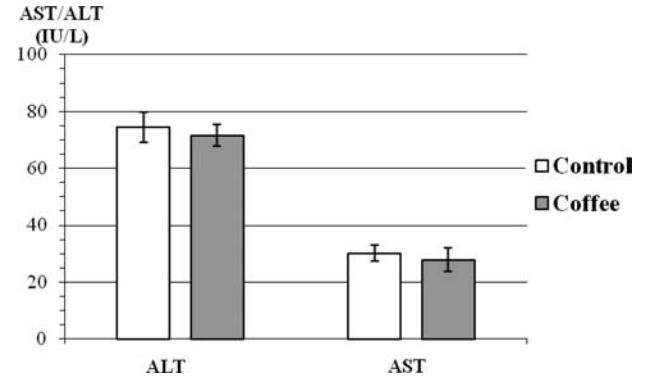

Figure 5. AST and ALT average levels in the liver tissue of groups 1 and 2 (n = 6). (No statistically differences from the control group were observed at $p < 0.05$.)

substances in this beverage. After the hydrolysis of coffee brew followed by chromatographic tests, a total of 793.3 μg of free phenolic acids/mL of coffee was found (685.1 ± 30.8 μg/mL of caffeic acid, 97.9 ± 8.0 μg/mL of ferulic acid, 10.3 ± 1.3 μg/mL of p-coumaric acid), confirming that this beverage is a rich source of these substances originally present as different chlorogenic acids (Figure 1A). The total concentration of phenolic acids was shown to be 28.7−39.7% lower than the results issued in other publications,[13,14] and these differences could be related to the use of automatic brewing machines in the mentioned studies (longer contact between coffee powder and water). Another possible reason could be the origin of coffee samples. As shown by Farah and Donangelo,[31] the variety Bourbon widely cultivated in Brazil showed the second lowest result for chlorogenic acids among 19 coffees from different origins, probably due to the mild Brazilian climate given that phenolic acids are secondary metabolites produced as a defensive response against stressful environmental conditions.

There is a lot of controversial data regarding whether chlorogenic acids or free phenolic acids are actually absorbed. Some studies affirm that chlorogenic acids are absorbed in the intestine being found intact in plasma and urine.[32,33] However, most publications mention an extensive hydrolysis of chlorogenic acids promoted by esterases in the colon to yield quinic acid and free hydroxycinnamic acids that are rapidly transformed to different derivatives such as glucuronide and sulfate conjugates.[13,34−36] For this reason, the major chlorogenic acids present in coffee brew were quantified (Figure 1B), resulting in 1155.2 μg/mL (1002.3 ± 87.0 μg/mL of 3-, 4-, and 5-CQA, 152.9 ± 10.3 μg/mL of 5-feruloylquinic acid). The results obtained in the present study were similar to the ones issued by Boettler et al.[5] (1040 μg/mL of 5-CQA) and Corrêa[19] (864.0 μg/mL of 3-, 4-, and 5-CQA isomers, 128.1 μg/mL of FQA isomers), all converted to 80 g/L of Brazilian *Arabica* coffee powder. In view of these results, a single dose of 2 mL/day of coffee brew given to rats with 200 g of BW represented approximately 8 mg of phenolic acids/kg of BW per day (or approximately 12 mg of chlorogenic acids/kg of BW per day), which fits the purpose of this study to administer small doses of the active substances.

Caffeine is another bioactive compound present in coffee. The level of this substance was also determined in coffee brew, and an average concentration equal to 728.1 ± 20.5 μg/mL was found. This value was 39.7% lower than the result issued by Natella et al.,[37] and the possible reasons were already discussed (the use of automatic brewing machine and the nature of coffee). This result indicated that 2 mL/day of coffee brew to rats represented approximately 7 mg of caffeine/kg of BW per day, which fits the intention to administer small doses of the bioactive substances.

Antioxidant Enzymes, Nrf2, and Antioxidant Capacity. The activities of antioxidant enzymes in group 1 (control) showed average results equal to 16.3 ± 1.9 U/mg of protein for SOD, 10.1 ± 1.0 μmol/min/mg of protein for CAT, and 16.2 ± 2.4 U/mg of protein for GPx, well-suited to the figures obtained in other studies with similar animal models.[1,11,12,38,39] At the same time, group 2 (coffee) average results were 28.5 U/mg of protein for SOD, 16.1 μmol/min/mg of protein for CAT, and 38.1 U/mg of protein for GPx, showing increases of 74.8, 59.4, and 135.2%, respectively, in relation to the control group (Figure 2). The results of groups 1 and 2 were compared (independent samples), and the differences were statistically significant according to the Student t test ($p < 0.001$ for all enzymes). This finding showed that even a small quantity of a natural beverage containing phenolic acids (released by the hydrolysis of chlorogenic acids in the organism), caffeine, and other unquantified bioactive substances was capable of producing notable changes in the activity of hepatic SOD, CAT, and GPx. As filtered coffee was used, the

dx.doi.org/10.1021/jf401777m | J. Agric. Food Chem. 2014, 62, 116−122

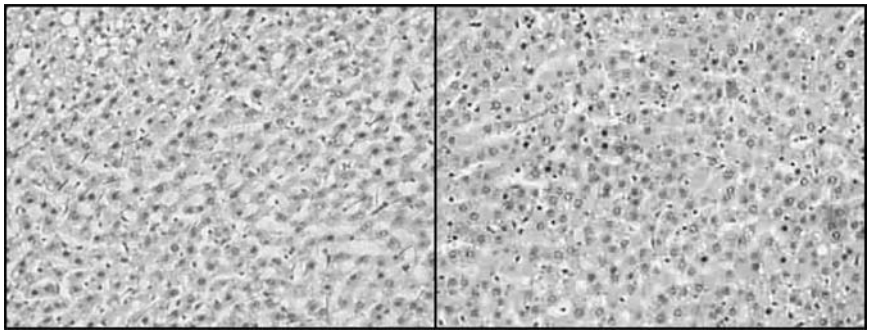

Figure 6. Liver tissues (group 1, left; group 2, right) showing normal architectures and no apparent damage.

contribution of the diterpenes cafestol and kahweol was negligible as they were absorbed by the paper filter.[3]

In a preceding publication, we showed that a single dose of 2.0 mL of coffee brew increased the activities of SOD, CAT, and GPx, but this effect was transitory and the activities started to return to basal levels a couple of hours after the administration.[18] In the present study, even after 12 h of fasting, the enzymatic activities remained much higher than the levels obtained after a single dose. This indicated that a daily ingestion of a small dose of coffee brew produced an accumulative effect that increased and maintained the activities of antioxidant enzymes far above the basal levels.

Another remarkable issue was the concomitant increase in the activities of SOD, CAT, and GPx, also observed in the previous publication using a single dose of coffee.[18] As these enzymes work in a sequential process[10,15] (SOD converts O_2^- to O_2^{2-} or H_2O_2 that is converted to H_2O by CAT or GPx), the simultaneous increases indicate an interesting solution found by evolution to avoid excessive concentration of any dangerous intermediate during hepatic detoxification. Increased levels of SOD could efficiently reduce O_2^- naturally produced in the mitochondrial domain to form O_2^{2-} (or H_2O_2) and subsequently water by the action of CAT and GPx, protecting the cells against the attack of these and other downstream ROS.

Because Nrf2 acts in DNA promoter regions as a direct factor for the transcription of the antioxidant enzymes as well as itself,[3,7−9] it was important to verify if coffee could also affect the concentration and the expression of this protein. The cytosolic level of Nrf2 was measured in groups 1 and 2, showing an increase equal to 131.3% (relative concentrations) in group 2 in relation to group 1 (Figure 3). Increased levels of cytosolic Nrf2 certainly promote the translocation of this protein to the nucleus, activating the transcription of ARE-responsive genes.[3,7−9] These results were compared and indicated a statistically significant difference according to the Student t test ($p < 0.001$). As Nrf2 plays an important role in the transcription of antioxidant enzymes, its increased level certainly collaborated to raise the expression of SOD, CAT, and GPx, resulting in higher activities for these enzymes.

Using the same samples, the total antioxidant capacity of the liver tissue was measured by ORAC. The control group showed an average result equal to 689 ± 34 μmol TE/L, which rose to 862 ± 44 μmol TE/L in group 2 (Figure 4), resulting in a statistically significant difference according to the Student t test ($p < 0.001$). As the ORAC assay measures the total antioxidant capacity of the samples, part of the observed effect must be assigned to the increased activities of the antioxidant enzymes and part to the phenolic compounds present in coffee as they are potent antioxidant molecules through the formation of resonance-stabilized phenoxy radicals.[39] Once more, the accumulative effect already mentioned was observed as a single dose of coffee brew promoted only a small and not statistically significant increase of ORAC ($p = 0.403$).[18]

On the basis of these results it was possible to conclude that a small and repetitive dose of coffee brew was sufficient to modulate the protein Nrf2, increasing the activity of antioxidant enzymes and improving the defensive status against oxidative stress. By comparison of the two studies involving a single dose and repetitive doses of coffee, it was possible to verify an accumulative effect that can be considered a beneficial consequence for coffee drinkers.

Evolution of Body Weight and Changes in Liver Tissue. Next, it was important to verify the occurrence of any damage to the health of the animals. The evolution of body weight is a parameter that could indicate eventual toxicity of coffee. At the beginning of the study, group 1 (control) showed an average weight equal to 203.86 ± 7.00 g, whereas group 2 (coffee) showed an average weight equal to 201.80 ± 6.83 g. These results were compared, and no statistically significant difference was obtained ($p = 0.617$). After the 28 day period, group 1 showed an average value equal to 349.10 ± 10.97 g, whereas group 2 showed 356.66 ± 19.55 g, indicating no statistically significant difference between them ($p = 0.428$). This result suggests that coffee did not present systemic toxicity and did not affect the appetite of the animals or the growing curve.[15]

The levels of the hepatic biomarkers AST and ALT were determined for group 1, showing average results equal to 74.5 ± 5.3 IU/L for AST and 30.2 ± 2.9 IU/L for ALT, compatible with the figures reported in other publications.[1,30,39] Group 2 was evaluated using the same methodology, showing average values equal to 71.5 ± 3.8 IU/L for AST and 27.9 ± 4.0 IU/L for ALT (Figure 5), not statistically different from group 1 according to the Student t test ($p = 0.290$ for AST; $p = 0.284$ for ALT). This finding was an excellent indication that no injury was caused to the liver by a continued exposure to coffee.

To strengthen the previous conclusion, a histopathological analysis of the liver tissue was done. After the preparation of the samples, it was observed that the hepatic histoarchitecture of both groups showed no alterations, presenting normal structures without inflammatory infiltration or necrosis when observed under the microscope (Figure 6). In addition, no fat accumulation in the liver was observed after sacrifice, and the health indicators for both groups (increase of weight, appearance of eyes and skin, physical activity, and response to external stimulus) were identical.

It was possible to conclude that the administration of 2 mL of coffee brew per day to rats greatly increased the cytosolic

levels of Nrf2 and the activity of antioxidant enzymes, improving the defensive status against oxidative stress with no apparent damage to the liver tissue. As a comparison, a human of 70 kg BW would have to consume three to four medium-size cups per day of coffee brew, which means approximately 550 mg of phenolic acids and 500 mg of caffeine.

AUTHOR INFORMATION

Corresponding Author

*(S.J.V.V.) Mailing address: R. Oswaldo Cruz 266, Santos/SP, Brazil 11045-907. E-mail: laq@unisanta.br. Phone: +55 13 3202.7100. Fax: +55 13 3234.5297.

Funding

This work was financially supported by the State of São Paulo Research Foundation, FAPESP, and the National Council for Scientific and Technological Development, CNPq.

Notes

The authors declare no competing financial interest.

ABBREVIATIONS USED

SOD, superoxide dismutase; CAT, catalase; GPx, glutathione peroxidase; Nrf2, nuclear factor E2-related factor; Keap1, Kelch-like ECH-associated protein-1; Tris-HCl buffer, tris-(hydroxymethyl)aminomethane hydrochloride; ORAC, oxygen radical absorbance capacity; TE, Trolox equivalent; O_2^{-}, superoxide radical; O_2^{2-}, peroxide anion; BW, body weight; AST, aspartate transaminase; ALT, alanine transaminase; ROS, reactive oxygen species; ARE, antioxidant response element; HPLC, high-performance liquid chromatography; CQA, caffeoylquinic acid; FQA, feruloylquinic acid

REFERENCES

(1) Kim, H. J.; Yu, M. H.; Lee, I. S. Inhibitory effects of methanol extract of plum (*Prunus salicina* L., cv 'Soldam') fruits against benzo(α)pyrene-induced toxicity in mice. *Food Chem. Toxicol.* **2008**, *46*, 3407−3413.

(2) Bichler, J.; Cavin, C.; Simic, T.; Chakraborty, A.; Ferk, F.; Hoelzl, C.; et al. Coffee consumption protects human lymphocytes against oxidative and 3-amino-1-methyl-5*H*-pyrido[4,3-*b*]indole acetate (Trp-P-2) induced DNA-damage: results of an experimental study with human volunteers. *Food Chem. Toxicol.* **2007**, *45*, 1428−1436.

(3) Tao, K. S.; Wang, W.; Wang, L.; Cao, D. Y.; Li, Y. Q.; Wu, S. X.; Dou, K. F. The multifaceted mechanisms for coffee's anti-tumorigenic effect on liver. *Med. Hypotheses* **2008**, *71*, 730−736.

(4) Higgins, L. G.; Cavin, C.; Itoh, K.; Yamamoto, M.; Hayes, J. D. Induction of cancer chemopreventive enzymes by coffee is mediated by transcription factor Nrf2. Evidence that the coffee-specific diterpenes cafestol and kahweol confer protection against acrolein. *Toxicol. Appl. Pharmacol.* **2008**, *226*, 328−337.

(5) Boettler, U.; Sommerfeld, K.; Volz, N.; Pahlke, G.; Teller, N.; Somoza, V.; Lang, R.; Hofmann, T.; Marko, D. Coffee constituents as modulators of Nrf2 nuclear translocation and ARE (EpRE)-dependent gene expression. *J. Nutr. Biochem.* **2011**, *22*, 426−440.

(6) Muriel, P.; Arauz, J. Coffee and liver diseases. *Fitoterapia* **2010**, *81*, 297−305.

(7) Volz, N.; Boettler, U.; Winkler, S.; Teller, N.; Schwarz, C.; Bakuradze, T.; Eisenbrand, G.; Haupt, L.; Griffiths, L. R.; Stiebitz, H.; Bytof, G.; Lantz, I.; Lang, R.; Hofmann, T.; Somoza, V.; Marko, D. Effect of coffee combining green coffee bean constituents with typical roasting products on the Nrf2/ARE pathway in vitro and in vivo. *J. Agric. Food Chem.* **2012**, *60*, 9631−9641.

(8) Kwak, M. K.; Wakabayashi, N.; Kensler, T. W. Chemoprevention through the Keap1-Nrf2 signaling pathway by phase 2 enzyme inducers. *Mutat. Res.* **2004**, *555*, 133−148.

(9) Giudice, A.; Montella, M. Activation of the Nrf2-ARE signaling pathway: a promising strategy in cancer prevention. *BioEssays* **2006**, *28*, 169−181.

(10) Valko, M.; Leibfritz, D.; Moncol, J.; Cronin, M. T. D.; Mzur, M.; Telser, J. Free radicals and antioxidants in normal physiological functions and human disease. *Int. J. Biochem. Cell Biol.* **2007**, *39*, 44−84.

(11) Yeh, C. T.; Yen, G. C. Induction of hepatic antioxidant enzymes by phenolic acids in rats is accompanied by increased levels of multidrug resistance-associated protein 3 mRNA expression. *J. Nutr.* **2006**, *136*, 11−15.

(12) Yeh, C. T.; Ching, L. C.; Yen, G. C. Inducing gene expression of cardiac antioxidant enzymes bydietary phenolic acids in rats. *J. Nutr. Biochem.* **2009**, *20*, 163−171.

(13) Nardini, M.; Cirillo, E.; Natella, F.; Scaccini, C. Absorption of phenolic acids in humans after coffee consumption. *J. Agric. Food Chem.* **2002**, *50*, 5735−5741.

(14) Mattila, P.; Hellström, J.; Törrönen, R. Phenolic acids in berries, fruits and beverages. *J. Agric. Food Chem.* **2006**, *54*, 7193−7199.

(15) Vicente, S. J. V. Antioxidant characterization of coffee (*Coffea arabica*, L) and effects of its oral administration to rats. Thesis, University of São Paulo, São Paulo, Brazil, 2009; available at www.teses.usp.br.

(16) Toci, A.; Farah, A.; Trugo, L. C. Efeito do processo de descafeinação com diclorometano sobre a composição química dos cafés *Arabica* e *Robusta* antes e após a torrefação. *Quim. Nova* **2006**, *29*, 965−971.

(17) Associação Brasileira da Indústria do Café (ABIC); http://www.abic.com.br/scafe_dicas.hmtl (accessed Jan 2013).

(18) Vicente, S. J. V.; Ishimoto, E. Y.; Cruz, R. J.; Pereira, C. D. S.; Torres, E. A. F. S. Increase of the activity of phase II antioxidant enzymes in rats after a single dose of coffee. *J. Agric. Food Chem.* **2011**, *59*, 10887−10892.

(19) Corrêa, T. A. F. Comparison of the antioxidant capacity of coffee roasts and their effects on cardiovascular risks factors in healthy subjects. Thesis, University of São Paulo, São Paulo, Brazil, 2012; available at www.teses.usp.br.

(20) Nardini, M.; Cirillo, E.; Natella, F.; Mencarelli, D.; Comisso, A.; Scaccini, C. Detection of bond phenolic acids: prevention by ascorbic acid and ethylenediaminetetraacetic acid of degradation of phenolic acids during alkaline hydrolysis. *Food Chem.* **2002**, *79*, 119−124.

(21) Kowalski, R.; Wolski, T. Evaluation of phenolic acid content in *Silphium perfoliatum* L. leaves, inflorescences and rhizomes. *Electr. J. Polish Agric. Univ.* **2003**, *6*, 9−17.

(22) Vitorino, M. D.; França, A. S.; Oliveira, L. S.; Borges, M. L. A. Metodologia de obtenção de extrato de café visando a dosagem de compostos não voláteis. *Rev. Bras. Armaz.* **2001**, *26*, 17−24.

(23) Woolliams, J. A.; Wiener, G.; Anderson, P. H.; McMurray, C. H. Variation in the activities of glutathione peroxidase and superoxide dismutase and in the concentration of copper in the blood of various breed crosses of sheep. *Res. Vet. Sci.* **1983**, *34*, 253−256.

(24) Aebi, H. Catalase *in vitro*. In *Methods in Enzymology*; Packer, L., Ed.; Academic Press: Orlando, FL, USA, 1984; Vol. 105, pp 121−126.

(25) Paglia, D. E.; Valentine, W. N. Studies on the quantitative and qualitative characterization of erythrocyte glutathione peroxidase. *J. Lab. Clin. Med.* **1967**, *70*, 158−169.

(26) Bradford, M. M. A rapid and sensitive method for the quantification of microgram quantities of protein utilizing the principle of protein-dye binding. *Anal. Biochem.* **1976**, *72*, 248−254.

(27) Ou, B.; Hampsch-Woodill, M.; Prior, R. L. Development and validation of an improved oxygen radical absorbance capacity assay using fluorescein as the fluorescent probe. *J. Agric. Food Chem.* **2001**, *49*, 4619−4626.

(28) Prior, R. L.; Hoang, H.; Gu, L.; Wu, X.; Bacchiocca, M.; Howard, L.; et al. Assays for hydrophilic and lipophilic antioxidant capacity (oxygen radical absorbance capacity ($ORAC_{FL}$)) of plasma and other biological and food samples. *J. Agric. Food Chem.* **2003**, *51*, 3273−3279.

(29) Reitman, S.; Frankel, S. A colorimetric method for the determination of serum glutamic oxalacetic and glutamic pyruvic transaminases. *Am. J. Clin. Pathol.* **1957**, *28*, 56−63.
(30) Pari, L.; Prasath, A. Efficacy of caffeic acid in preventing nickel induced oxidative damage in liver of rats. *Chem. Biol. Interact.* **2008**, *173*, 77−83.
(31) Farah, A.; Donangelo, C. M. Phenolic compounds in coffee. *Braz. J. Plant Physiol.* **2006**, *18*, 26−36.
(32) Lafay, S.; Gil-Izquierdo, A.; Manach, C.; Morand, C.; Besson, C.; Scalbert, A. Chlorogenic acid is absorbed in its intact form in the stomach of rats. *J. Nutr.* **2006**, *136*, 1192−1197.
(33) Monteiro, M.; Farah, A.; Perrone, D.; Trugo, L. C.; Donangelo, C. Chlorogenic acid compounds from coffee are differentially absorbed and metabolized in humans. *J. Nutr.* **2007**, *137*, 2196−2201.
(34) Lafay, S.; Morand, C.; Manach, C.; Besson, C.; Scalbert, A. Absorption and metabolism of caffeic acid and chlorogenic acid in the small intestine of rats. *Br. J. Nutr.* **2006**, *96*, 39−46.
(35) Suri, R.; Crozier, A. Free phenolic acids in human urine after drinking coffee rich in chlorogenic acids. *J. Trop. Agric. Food Sci.* **2012**, *40*, 221−232.
(36) Redeuil, K.; Smarrito-Menozzi, C.; Guy, P.; Rezzi, S.; Dionisi, F.; Williamson, G.; Nagy, K.; Renouf, M. Identification of novel circulating coffee metabolites in human plasma by liquid chromatography−mass spectrometry. *J. Chromatogr., A* **2011**, *1218*, 4678−4688.
(37) Natella, F.; Nardini, M.; Gianetti, I.; Dattilo, C.; Scaccini, C. Coffee dirnking influences plasma antioxidant capacity in humans. *J. Agric. Food Chem.* **2002**, *50*, 6211−6216.
(38) Kakarla, P.; Vadluri, G.; Kesireddy, S. R. Response of hepatic antioxidant system to exercise training in aging female rat. *J. Exp. Zool.* **2005**, *303*, 203−208.
(39) Shanmugarajan, T. S.; Krishnakumar, E.; Somasundaram, I.; Sivaraman, D.; Arunsundar, M.; Balaji, R.; Sivakumar, S. M. Salutary effect of ferulic acid against D-galactosamine challenged liver damage. *J. Biol. Sci.* **2008**, *8*, 1271−1279.

JOURNAL OF AGRICULTURAL AND FOOD CHEMISTRY

Article

pubs.acs.org/JAFC

Structural Analysis of Proanthocyanidins Isolated from Fruit Stone of Chinese Hawthorn with Potent Antityrosinase and Antioxidant Activity

Wei-Ming Chai,[†] Chih-Min Chen,[†] Yu-Sen Gao,[†] Hui-Ling Feng,[†] Yu-Mei Ding,[†] Yan Shi,[†] Han-Tao Zhou,[‡] and Qing-Xi Chen*[,†]

[†]State Key Laboratory of Cellular Stress Biology, School of Life Sciences, Xiamen University, Xiamen 361005, China

[‡]Key Laboratory of the Ministry of Education for Coastal and Wetland Ecosystems, College of the Environment and Ecology, Xiamen University, Xiamen 361005, China

ABSTRACT: Proanthocyanidins were isolated from fruit stone of Chinese hawthorn (*Crataegus pinnatifida* Bge. var. *major* N.E.Br.). Their structures were analyzed and elucidated by methods of matrix-assisted laser desorption/ionization time-of-flight mass spectrometry (MALDI-TOF MS) and high performance liquid chromatography electrospray ionization mass spectrometry (HPLC-ESI-MS). The results demonstrated that these compounds are complicated mixtures of homo- and heteropolymers consisting of procyanidin/procyanidin gallate and prodelphinidin. They possessed structural heterogeneity in monomer units, polymer length, and interflavan linkage (A-type and B-type). Their antityrosinase and antioxidant activity were then investigated. The results revealed that they can inhibit tyrosinase activities, including the monophenolase activity and the diphenolase activity. In addition, proanthocyanidins possessed potent antioxidant activity. Our studies revealed that proanthocyanidins isolated from fruit stone of Chinese hawthorn may be applied in food, agriculture, pharmaceutical, and cosmetic industries.

KEYWORDS: *hawthorn proanthocyanidins, structural analysis, MALDI-TOF MS, HPLC-ESI-MS, antityrosinase activity, antioxidant activity*

INTRODUCTION

Proanthocyanidins are polyphenol compounds. They are most commonly found in the plants and have aroused considerable interest and received more and more attention in recent years due to their bioactive functions. These compounds are composed of flavan-3-ol monomer units (Figure 1), which are joined together through C4−C8 or C4−C6 bonds to B-type oligomers and high polymers.[1] When C2 and C7 are linked by an additional ether linkage, these compounds are A-type proanthocyanidins (Figure 1).[2] The structural variability of monomer units, interflavan linkage, and distribution of polymerization degree contribute to the diversity of proanthocyanidins.[2,3] The qualitative and quantitative analysis of these compounds remains very challenging because of their structural diversity and complexity.

In our previous report, proanthocyanidins isolated from stem bark, fruit, and leaf of *Delonix regia* were found with potent tyrosinase inhibitory activity.[4] Tyrosinase (EC 1.14.18.1) is a kind of oxidase that contains copper and possesses two successive catalytic activities: the monophenolase activity (hydroxylation of monophenols to *o*-diphenols) and diphenolase activity (the oxidation of *o*-diphenols to *o*-quinones).[5] It causes melanization in animals and browning in plants.[6,7] In addition, tyrosinase is important in normal developmental processes in insects.[8] This indicates that tyrosinase inhibitors are potential insect control agents as well as whitening agents, food additives, and medicine. Plants are rich in bioactive compounds that have few side effects; thus researchers have shown increasing interest in employing them as a source of tyrosinase inhibitors.[9]

Hawthorn is one of the most popular medicinal and food materials in the world. Its fruits, leaves, bark, and flowers contain significant amounts of phenolic compounds, which exhibit potent antioxidant activity.[10−12] Most of these compounds belonged to proanthocyanidins.[13,14] In addition, Svedström et al. found that oligomeric proanthocyanidins in different tissue of hawthorn range from 2-mers to 6-mers.[15] However, detailed structure information and antityrosinase and antioxidant activity of purified proanthocyanidins extracted from Chinese hawthorn fruit stone have not been reported. Our study primarily aims to provide thorough structural analysis of proanthocyanidins from fruit stone of Chinese hawthorn using reflectron pattern MALDI-TOF MS, linear pattern MALDI-TOF MS, reversed-phase HPLC-ESI/MS, and normal-phase HPLC-ESI/MS analysis. These techniques are initially applied on Chinese hawthorn fruit stone proanthocyanidins to clarify the elementary units, distribution of DP, and type of linkage. The antityrosinase and antioxidant activity information on these compounds are also provided in this study.

MATERIALS AND METHODS

Chemicals. HPLC standards (catechin and epicatechin), Sephadex LH-20, trifluoroacetic acid, benzyl mercaptan, Amberlite IRP-64 cation-exchange resin, CsCl, and 2,5-dihydroxybenzoic acid were

Received: July 23, 2013
Revised: December 7, 2013
Accepted: December 8, 2013
Published: December 8, 2013

ACS Publications © 2013 American Chemical Society

dx.doi.org/10.1021/jf405385j | J. Agric. Food Chem. 2014, 62, 123−129

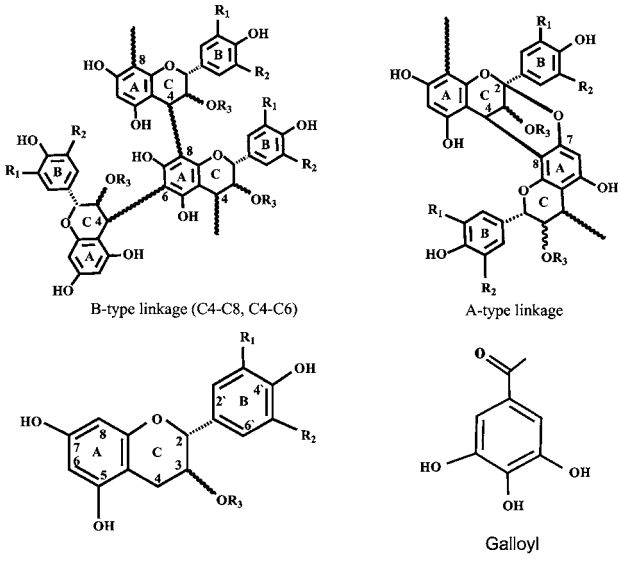

R1	R2	R3	flavan-3-ol	proanthocyanidins
OH	H	H	(Epi)catechin	Procyanidin
OH	OH	H	(Epi)gallocatechin	Prodelphindin
OH	H	galloyl	(Epi)catechin gallate	Procyanidin gallate

Figure 1. Chemical structure of flavan-3-ol monomer units and proanthocyanidins.

obtained from Sigma-Aldrich (St. Louis, Missouri, USA). Mushroom tyrosinase, L-tyrosine, 3,4-dihydroxyphenylalanine, dimethyl sulfoxide, DPPH, ABTS, TPTZ, AAPH, and ascorbic acid, were also obtained from Sigma-Aldrich. The solvents with standard analytical purity were acquired from Sinopharm (Shanghai, China). Acros Organics (New Jersey, USA) is the company that provided the fluorescein and trolox.

Plant Material and Sample Preparation. Hawthorn fruits at commercial maturation were picked on the campus of Jiangxi Normal University (Nanchang, Jiangxi Province, China) in July. Fruit stones were isolated manually and immediately freeze-dried and then were ground to fine powders. The powders were placed at −80 °C before next analysis.

Extraction and Purification of Hawthorn Fruit Stone Proanthocyanidins. The powders (10.0 g) were ultrasonically extracted three times (each 200 mL) with acetone−water (7:3, v/v) solution containing 0.1% ascorbic acid at 25 °C. The acetone was eliminated in a rotary evaporator at 38 °C. Chlorophyll and lipophilic compounds remained in aqueous fraction were eliminated by extracting them with petroleum ether three times (each 150 mL). The remaining aqueous fraction was purified by using chromatography on Sephadex LH-20 column (Pharmacia Biotech, Uppsala, Sweden). Methanol (50% dissolved in water) and 70% acetone (dissolved in water) were used to elute successionally. The latter was freeze-dried to get dry proanthocyanidin powders after the acetone was removed by rotary evaporation. These powders were stored in the refrigerator (−20 °C) prior to structure and activity analysis.

MALDI-TOF MS Analysis of Hawthorn Fruit Stone Proanthocyanidins. Bruker Reflex III instrument (Bruker-Franzen, Bremen, Germany) was used for MALDI-TOF MS analysis. Samples (proanthocyanidins powders) were irradiated at 337 nm with a nitrogen laser. Angiotensin I (M + H 1296.7, monoisotopic) and angiotensin II (M + H 1046.5, monoisotopic) were employed to calibrate mass spectra. Parameters for positive pattern spectra in the reflectron pattern were as follows: accelerating voltage, 20 kV; reflectron voltage, 23.0 kV; delayed extraction voltage, 16.32 kV; lens voltage, 9.45 kV. Parameters for positive pattern spectra in the linear pattern were as follows: accelerating voltage, 20.0 kV; delayed extraction voltage, 16.25 kV; lens voltage, 10.0 kV. DHB was used as the matrix, and Cs^+ was selected as the cationization reagent. Amberlite IRP-64 cation-exchange resin was dissolved in deionized water, which was used to remove ions in the sample and matrix solution. The mixture volumetric ratio of the sample solutions and the matrix solution was 1:3. The final mixed solution (1 μL) was then dripped to the steel target.[16]

Reversed-Phase HPLC-ESI-MS Analysis Followed Thiolysis Reaction. With an Agilent 1200 system (Agilent, Palo Alto, CA, USA) coupled to a QTRAP 3200 (Applied Biosystems, Foster, USA), reversed-phase HPLC-ESI-MS analysis was conducted. The column employed in the analysis was a 250 mm × 4.6 mm i.d., 5 μm, Li-Chrospher 100 RP-18, with a 4 mm × 4 mm i.d. guard column of the same material (Elite, Dalian, China). The linear gradient elution process was performed as follows (two solvents were used as mobile phase, 0.5% trifluoroacetic acid and acetonitrile): 0−45 min, 12−80% acetonitrile; 45−50 min, 80−12% acetonitrile. The flow rate was kept at 1 mL/min, and the chromatogram was detected at 280 nm. In addition, instrument parameters for MS analysis in the negative ion pattern were set as follows: ion spray voltage, 4.5 kV; declustering potential, 50 V; entrance potential, 10 V; curtain gas, 20 psi; source temperature, 400 °C.

Normal-Phase HPLC-ESI-MS Analysis. Analysis was performed on a 250 mm × 4.6 mm i.d., 5 μm Silica Luna (Phenomenex, Darmstadt, Germany). The column temperature was controlled at 35 °C. The HPLC and MS system were the same as reversed-phase HPLC-ESI-MS analysis. Two solvents were used: A = water/acetic acid/methanol/dichloromethane (1:1:7:41, v/v/v/v) and B = water/acetic acid/methanol/dichloromethane (1:1:5:43, v/v/v/v). The linear gradient elution program was as follows: 0−20 min, 0−13.5% B; 20−50 min, 13.5−29.2% B; 50−55 min, 29.2−100% B; 55−60 min, 100% B.[17] Conditions for MS analysis were the same as the reversed-phase HPLC-ESI-MS analysis described previously.

Assay of the Enzyme Activity. Enzyme reaction was performed in compliance with the program of our previous study.[18] L-Tyrosine (2.17 mg/mL) was used as substrate for monophenolase activity assay and 3,4-dihydroxyphenylalanine (1 mg/mL) was used as substrate for diphenolase activity assay. The substrate and tyrosinase were mixed well in the absence or presence of the sample (3 mL reaction system) with different concentrations. The final concentrations of tyrosinase were 33.33 μg/mL for monophenolase activity assay and 6.67 μg/mL for diphenolase activity assay. Their enzyme activities were recorded on a Beckman UD-800 spectrophotometer (Beckman coulter, Pasadena, California, USA) at 475 nm. Lag time (the time for the reaction system reaching steady-state rate) and steady-state rate (a constant rate) were employed to measure the effect of proanthocyanidins on the enzyme activity of monophenolase. The effect of proanthocyanidins on the diphenolase reaction was expressed as percentage.

Fluorescence Analysis. Varian Cary Eclipse fluorescence spectrophotometer was used to record the fluorescence spectra. The reaction system (3 mL) contained 300 μL of mushroom tyrosinase solution, 300 μL of sample solution with different concentrations, and 2.4 mL of sodium phosphate buffer (50 mM, pH 6.8). Excitation wavelength was 290 nm. All the tests were peformed at room temperature.

Determination of Cu^{2+} Chelating Activity. The reaction system (3 mL) contained 100 μL of sample (2 mg/mL) solution, 100 μL of copper sulfate solution with different concentrations (25, 50, 100 μM), and 2.8 mL of sodium phosphate buffer (50 mM, pH 6.8). The mixture was shaken well and kept at 25 °C for 10 min prior to UV−vis analysis.

DPPH Radical Scavenging Activity Assay. DPPH analysis was performed in accordance with the report of Brand-Williams et al.[19] The reaction system was comprised of 0.1 mL of sample solution (dissolved in methanol) and 3 mL of DPPH solution (25 mg/L in methanol). The results were detected at 517 nm after the reaction mixture was shaken well and kept at 25 °C for 30 min. The scavenging effect was determined on the basis of the following equation:

$$\text{DPPH\% inhibition} = [(A_1 - A_2)/A_1] \times 100$$

dx.doi.org/10.1021/jf405385j | J. Agric. Food Chem. 2014, 62, 123−129

where A_1 is the absorbance in the absence of the sample and A_2 represents the absorbance in the presence of the sample. The IC_{50} value (μg/mL) is the sample concentration that caused 50% scavenging.

ABTS Radical Scavenging Activity Assay. ABTS radical scavenging activity was conducted according to the method of Re et al.[20] ABTS solution (7 mM) and potassium persulfate solution (2.45 mM) were mixed and stored in the dark for 16 h to obtain the $ABTS^+$ solution. It was diluted with 80% ethanol to get the $ABTS^+$ working solution. The working solution was detected at 734 nm with an absorbance of 0.700 ± 0.050. Tested sample (0.1 mL) was then mixed with 3.9 mL of $ABTS^+$ working solution. The absorbance was detected on a Beckman UD-800 spectrophotometer (Beckman coulter, Pasadena, California, USA) after incubation for 6 min. The result was expressed as IC_{50} value.

Ferric Reducing Antioxidant Power (FRAP) Assay. The FRAP assay was carried out in compliance with the method described by Benzie and Strain.[21] TPTZ solution (10 mM), ferric chloride solution (20 mM), and sodium acetate buffer (300 mM, pH 3.6) were mixed in a ratio of 1:1:10 to get the FRAP working solution. Sample (0.1 mL) was then added into 3 mL of freshly made working solution. The wavelength for the detection was 593 nm. Reaction mixture was kept at room temperature for 10 min before the detection. FRAP values were expressed as millimoles of ascorbic acid equivalents (AAE) per gram of purified proanthocyanidins.

Oxygen Radical Absorbance Capacity (ORAC) Assay. The ORAC method was performed on the basis of Ou et al.[22] The reaction system (300 μL) included 100 μL (0.33 μM) of fluorescein, 50 μL of extract or Trolox, and 150 μL of AAPH (60 mM). They were shaken well and recorded on a POLARstar Omega (BMG Labtech, Offenburg, Germany) with a 96-well microplate. The detection was performed after that the mixture was kept in 37 °C for 20 min. ORAC value was calculated as micromoles of trolox equivalents per gram of proanthocyanidins (dry weight).

Statistical Analysis. All the enzyme assays were repeated three times. The curves present in the picture were made according to the average value. The data for the antioxidant assay were obtained from three independent determinations, and they were analyzed by one-way analysis of variance. It indicated the significant differences when $p < 0.05$. The software used for the statistical analyses is SPSS 13.0.

RESULTS AND DISCUSSION

MALDI-TOF MS Analysis. Reflectron MALDI-TOF MS spectra of proanthocyanidins extracted from fruit stone of Chinese hawthorn are displayed in Figure 2A,B. Results indicated that hawthorn fruit stone proanthocyanidins exhibit mass spectra with a primary set of peaks with differences of 288 Da. It can be concluded that 288 Da is a mass difference of one catechin/epicatechin. A subset mass 14 Da higher was also found in the spectra (Figure 2A) except the detected mass series mentioned above. They were produced by gallocatechin/epigallocatechin. Additionally, the A-type interflavan linkages of 2 Da less than B-type were also detected in the main set of peaks (Figure 2B). These findings suggested that proanthocyanidins extracted from fruit stone of Chinese hawthorn are composed of procyanidin and prodelphindin. B-type procyanidin dominates. These compounds possess structural heterogeneity in monomer units and interflavan linkage (A-type and B-type). Besides the series of peaks described above, 152 Da mass distances following the main set of peaks were also observed (Figure 2A), which are in line with the addition of one galloyl group at the heterocyclic C-ring.[23] Also, 132 Da mass distances following the main set of peaks were produced by synchronous attachment of two Cs^+ and absence of a proton $[M + 2Cs^+ - H]^+$.[24] Additionally, these compounds had polymer chain length varying from 2-mers to 12-mers, with most intensity in 4-mers.

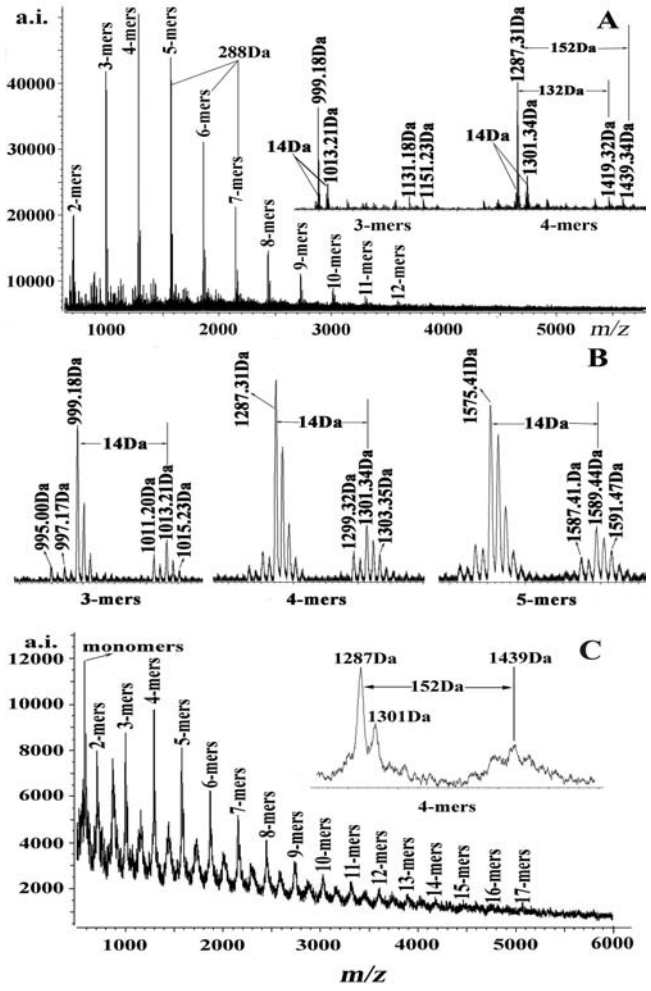

Figure 2. MALDI-TOF mass spectra of Chinese hawthorn fruit stone proanthocyanidins. The *y* axis represents absolute intensity (ai), that is the number of ions of each species that reach the detector.

To detect polymeric proanthocyanidins higher than those shown above, it is necessary to operate the linear pattern MALDI-TOF MS analysis. Figure 2C reveals a series of peaks separated by 288 Da, which are in keeping with the mass difference of one catechin/epicatechin. These compouds had polymer chain length ranging from monomer to 17-mers. In comparison with spectrum obtained from reflectron pattern (Figure 2A), linear pattern (Figure 2C) had weak resolution, but gave detection of mass information in line with higher DP. Linear MALDI-TOF MS analysis revealed the detection of litchi seed proanthocyanidins up to 27-mers.[16] In addition, in our study, proanthocyanidins showed galloyl ester units up to 6-mers in the reflectron pattern, while up to 17-mers in the linear pattern.

Reversed-Phase HPLC-ESI-MS Analyses. Chromatogram of thiolytic degraded proanthocyanidins from fruit stone of Chinese hawthorn is shown in Figure 3A. Results indicated that terminal units are mainly epicatechin (peak 2) and the extension units are primarily epicatechin benzylthioethers (peak 8). In addition, catechin (peak 1) and its benzylthioether (peak 7), catechin gallate (peak 3), and epigallocatechin benzylthioether (peak 5) were detected in Chinese hawthorn fruit stone proanthocyanidins by the thiolysis-HPLC method. Because A-type linkage is stable in the process of thiolytic degradation, the A-type terminal unit would be present in the

dx.doi.org/10.1021/jf405385j | J. Agric. Food Chem. 2014, 62, 123−129

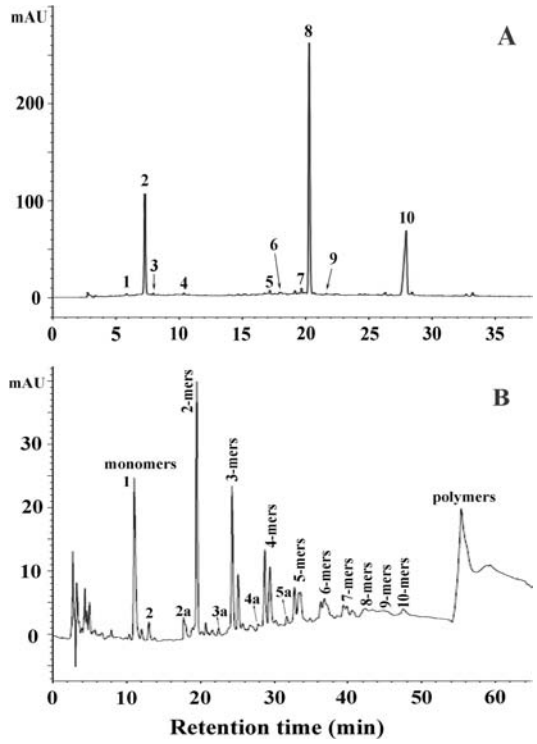

Figure 3. (A) Reversed-phase HPLC-ESI-MS chromatogram of Chinese hawthorn fruit stone proanthocyanidins after thiolytic degradation. Peaks are as follows: 1, catechin (289 Da, $[M - H]^-$); 2, epicatechin (289 Da, $[M - H]^-$); 3, epicatechin gallate (441 Da, $[M - H]^-$); 4, A-type dimer (575 Da, $[M - H]^-$); 5, epigallocatechin benzylthioether (427 Da, $[M - H]^-$); 6, A-type trimer benzylthioether (985 Da, $[M - H]^-$); 7, catechin benzylthioether (411 Da, $[M - H]^-$); 8, epicatechin benzylthioether (411 Da, $[M - H]^-$); 9, A-type dimer benzylthioether (697 Da, $[M - H]^-$); and 10, benzyl mercaptan. (B) Normal-phase HPLC-ESI-MS chromatogram of Chinese hawthorn fruit stone proanthocyanidins. Peaks are as follows: 1, epicatechin (289 Da $[M - H]^-$); 2, catechin (289 Da $[M - H]^-$); 2a, A-type dimer (575 Da $[M - H]^-$); 3a, A-type trimer (863 Da, $[M - H]^-$); 4a, A-type tetramer (1151 Da, $[M - H]^-$) and 5a, A-type pentamer (1439 Da, $[M - H]^-$), respectively.

form of A-type oligomers, while the A-type linkage between the extension units produced an A-type oligomer benzylthioether.[25] Peak 4 was authenticated as A-type dimer. Peaks 6 and 9 were A-type trimer benzylthioether and A-type dimer benzylthioether, respectively. In conclusion, the chromatogram after thiolysis indicated that proanthocyanidins are mainly constituted by the epicatechin unit. In addition, A-type linkage and B-type linkage are both involved in the formation of polymers, with B-type linkage dominating. These results were consistent with the results that achieved by MALDI-TOF MS analysis.

Normal-Phase HPLC-ESI-MS Analyses. Normal-phase HPLC profile of proanthocyanidins from fruit stone of Chinese hawthorn is illustrated in Figure 3B. The result indicated that DP of proanthocyanidins range from monomers to the 10-mers. In the chromatogram, peaks 1 and 2 are epicatechin (289 Da, $[M - H]^-$) and catechin (289 Da, $[M - H]^-$), respectively. Peaks 2a (575 Da $[M - H]^-$), 3a (863 Da, $[M - H]^-$), 4a (1151 Da, $[M - H]^-$), and 5a (1439 Da, $[M - H]^-$) are peaks of 2-mers, 3-mers, 4-mers, and 5-mers with A-type linkage, respectively. HPLC performance implied the precise separation of proanthocyanidins from monomers to 7-mers and the presence of isomers. However, the polymers higher than 10-mers could not be separated and showed a single broad peak at the end of the chromatograms (55.7 min). Our results were similar to the results of Gu et al.[26] and a good supplement of the reversed phase HPLC-ESI-MS analysis.

Effect of Chinese Hawthorn Fruit Stone Proanthocyanidins on the Monophenolase Reaction of Mushroom Tyrosinase. Kinetic courses of L-tyrosine oxidation by mushroom tyrosinase were tested in the presence of different concentrations of hawthorn proanthocyanidins. When L-tyrosine was used as substrate, the monophenolase activity of tyrosinase was assayed in the absence of inhibitor, and it was found that there was a remarkable lag time. The system reached steady-state rate after the lag period (lag time).[27] The steady-state rate of monophenolase activity can be negatively affected by addition of proanthocyanidins from fruit stone of Chinese hawthorn. The steady-state rate decreased in a dose-dependent way following the increase of the inhibitor concentration. When the final concentration of the proanthocyanidins in the system is 166.67 μg/mL, the steady-state rate decreased from 100% to 37.5%. The IC_{50} value was estimated as 37 $\pm$ 0.5 μg/mL for monophenolase activity. However, the corresponding lag time decreased from 94.8 s of the initial state to 47.6 s in the presence of 166.67 μg/mL proanthocyanidins.

In our previous study, the samples lengthened the lag time of the enzyme reaction or had no influence on it.[28] In the present study, however, proanthocyanidins isolated from fruit stone of Chinese hawthorn accelerated the reaction process (decreased the lag time) of the enzyme. To explain this phenomenon, 3,4-dihydroxyphenylalanine, catechin, and epicatechin in different concentrations were added into the enzyme−tyrosine reaction systems (3 mL), and the result showed that all the three compounds can obviously decrease the lag time at a low concentrations. The initial lag time decreased from 277.0 to 140.5, 14.4, and 9.6 s in the presence of 10 μM 3,4-dihydroxyphenylalanine, catechin, and epicatechin, respectively. The results showed that *o*-diphenol could affect the lag period of the monophenolase activity. The presence of *o*-diphenol in the monophenolase reaction system shortens the lag time, because the lag time is the time required to reach the steady *o*-diphenol concentration.[29] These findings further indicated that catechin and epicatechin existing in the extract of fruit stone of Chinese hawthorn are responsible for the particular phenomenon, and the effects of catechin/epicatechin are obviously better than that of 3,4-dihydroxyphenylalanine, which is commonly the substrate of the diphenolase reaction, to shorten the lag period. In summary, proanthocyanidins inhibit monophenolase activity of tyrosinase by reducing its steady-state rate.

Effect of Chinese Hawthorn Fruit Stone Proanthocyanidins on the Diphenolase Reaction of Mushroom Tyrosinase. The substrate for the assay of the diphenolase reaction was 3,4-dihydroxyphenylalanine. The relative activity increased before reaching a maximum (124.6% at 40 μg/mL) and decreased after that as concentration of the samples increased (Figure 4A). When the concentration reached 400 μg/mL, the relative activity decreased to 83.3%.

Gowda et al.[30] found that diphenol can activate diphenolase activity of polyphenol oxidase obtained from field bean (*Dolichos lablab*). Proanthocyanidins isolated from fruit stone of Chinese hawthorn increased diphenolase reaction absorption of tyrosinase in low concentration. To explain the phenomenon, 3,4-dihydroxyphenylalanine was replaced by catechin/epicatechin in 3 mL reaction system. The results indicated that both catechin and epicatechin can be better catalyzed by

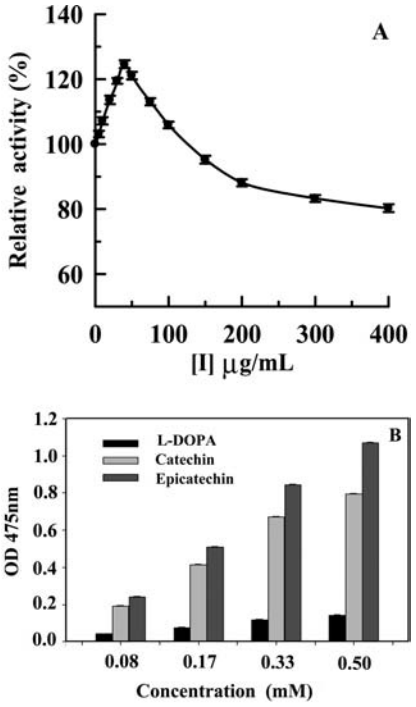

Figure 4. (A) Effects of Chinese hawthorn fruit stone proanthocyanidins on the diphenolase activity of mushroom tyrosinase. [I] represent concentrations of inhibitor. (B) Comparison of diphenolase activity of mushroom tyrosinase after adding 3,4-dihydroxyphenylalanine, catechin, and epicatechin as substrate.

tyrosinase than 3,4-dihydroxyphenylalanine and they are more effective substrates of tyrosinase (Figure 4B). This can be explained because catechin and epicatechin are substrate (3,4-dihydroxyphenylalanine) analogues. The increase of relative activity between 0 and 127 μg/mL is mainly because of the high absorption of products produced from catechin/epicatechin (exist in proanthocyanidins of hawthorn fruit stone) and tyrosinase at 475 nm. However, absorptions were not obvious when hawthorn fruit stone proanthocyanidins were mixed with tyrosinase in the absence of 3,4-dihydroxyphenylalanine. It can be speculated that oligomeric proanthocyanidins, such as dimer and trimer, may combine with tyrosinase and produce absorption at 475 nm. These findings suggested that hawthorn proanthocyanidins may inhibit (not activate) the reaction of 3,4-dihydroxyphenylalanine and tyrosinase by competing for the enzyme.

Fluorescence Emission Spectra of Mushroom Tyrosinase Solution in the Presence of Chinese Hawthorn Fruit Stone Proanthocyanidins with Different Concentrations. Combining capacities with proanthocyanidins of tyrosinase and its conformational alteration were evaluated by measuring the inherent fluorescence intensity of the enzyme in the absence/presence of proanthocyanidins. The fluorescence emission spectrum is recorded from a range of 300−500 nm with excitation wavelength set at 290 nm. As shown in Figure 5, the tyrosinase produces a strong fluorescence emission (337 nm, curve 0), while proanthocyanidins have a peak at 319 nm (curve A). The concentrations of samples for the curves 1−4 are 30, 60, 150, and 300 μg/mL, respectively. The result showed that fluorescence emission intensity reduced markedly with an increasing concentration of proanthocyanidins. The fluorescence intensity decreased from 64.7 to 13.5 (by 79.4%),

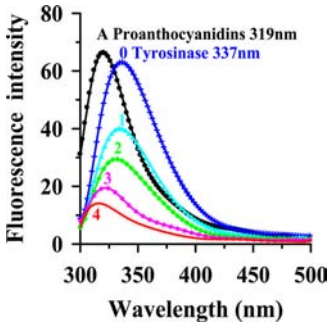

Figure 5. Fluorescence emission spectra of mushroom tyrosinase solution in the presence of Chinese hawthorn fruit stone proanthocyanidins with different concentrations. The concentrations of samples for the curves 0−4 are 0, 30, 60, 150, and 300 μg/mL, respectively. The curve A is fluorescence emission spectra of proanthocyanidins at the concentration of 300 μg/mL.

when the concentration of proanthocyanidins increased from 0 to 0.30 mg/mL. In addition, an obvious blue shift is also present in the spectra. The results indicated that when the proanthocyanidins bind to the enzyme molecule, it can induce the enzyme conformation to change and the enzyme activity to decrease.

Cu^+ Chelating Activity of Proanthocyanidins from Fruit Stone of Chinese Hawthorn. The copper-chelating properties of the proanthocyanidins from fruit stone of Chinese hawthorn were investigated. The increase of Cu(II) concentration to proanthocyanidins solution caused increased absorbance at 280 nm, which shows proanthocyanidins' binding to Cu(II). There is no absorbance difference at 280 nm when Na_2SO_4 is added to the proanthocyanidins solution. The inhibitory effect of proanthocyanidins on the tyrosinase may due to the combining capacity between their −OH group and copper ions in the catalytic center of mushroom tyrosinase. Because the −OH groups of proanthocyanidins present anionic form at pH 6.8, they may interact electrostatically with copper ions.

Determination of Antioxidant Property. Antioxidant activity of proanthocyanidins isolated from fruit stone of Chinese hawthorn was evaluated by DPPH, ABTS, FRAP, and ORAC assays. Figure 6A,B show DPPH and ABTS radical scavenging activities of proanthocyanidins from fruit stone of Chinese hawthorn and ascorbic acid at different concentrations. The results demonstrated that these compounds could eliminate DPPH and ABTS radicals in a dose-dependent manner. The quality of antioxidants was determined by IC_{50} values (antioxidant concentration that reduces the DPPH/ABTS radical by 50%). A much lower value of IC_{50} indicated better antioxidant activity. The proanthocyanidins had potent DPPH (IC_{50} 170.04 ± 5.17 μg/mL) and ABTS (IC_{50} 122.90 ± 1.25 μg/mL) free radical scavenging activity. One thing special is that proanthocyanidins possessed effective ABTS radical scavenging activity that was significantly better than ascorbic acid (140.52 ± 3.40 μg/mL) ($p < 0.05$). Noteworthy, the proanthocyanidins from fruit stone of Chinese hawthorn bleached the DPPH and ABTS radical immediately, which suggests that these compounds could be classified as dynamic antioxidants. Next, FRAP assay was used to measure the antioxidant activity of proanthocyanidins, and the same dose-dependent activity was found (Figure 6C). The FRAP value was calculated to be 5.83 ± 0.04 mmol AAE/g.

dx.doi.org/10.1021/jf405385j | J. Agric. Food Chem. 2014, 62, 123−129

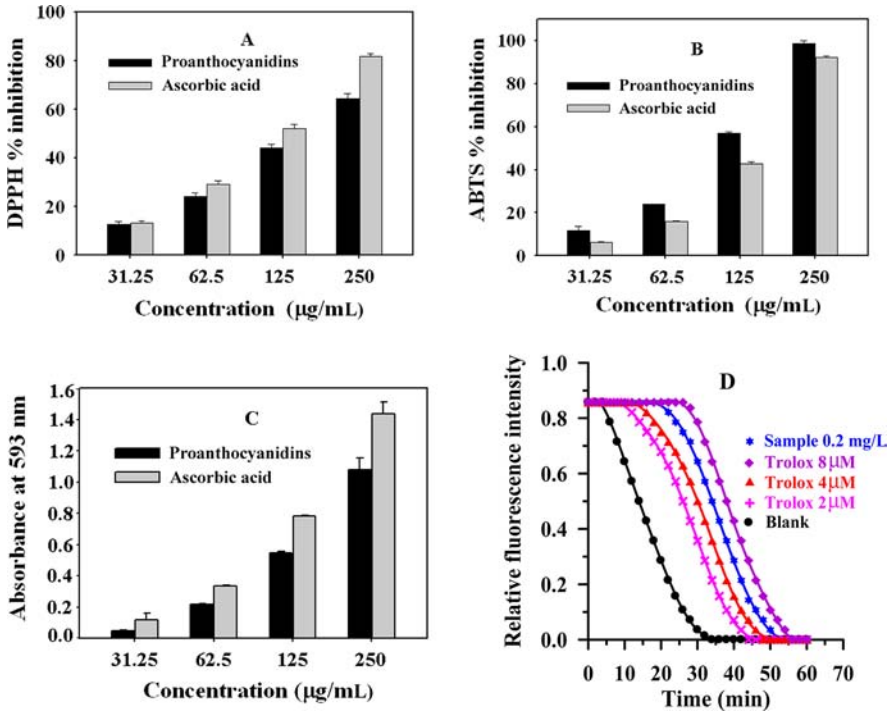

Figure 6. Evaluation of antioxidant activities of Chinese hawthorn fruit stone proanthocyanidins by using (A) DPPH, (B) ABTS, (C) FRAP, and (D) ORAC methods.

Furthermore, ORAC assay was performed. In the presence of antioxidative compounds, fluorescence decay was inhibited, and fluorescence intensity could be measured at 525 nm with excitation wavelength at 485 nm. The scavenging effect of proanthocyanidins against peroxyl radicals is illustrated in Figure 6D. This effect can be calculated from net integrated area under the kinetic curve and compared with that of Trolox. Our results demonstrated that proanthocyanidins scavenge peroxyl radicals effectively; the ORAC value was 29204.40 ± 870.12 μmol Trolox/g proanthocyanidins, measured at the proanthocyanidins concentration of 0.2 mg/L.

The antioxidant activity of proanthocyanidins can be affected by their chemical structure including monomer units, DP, and type of linkage.[31] Hagerman et al.[32] has conducted insightful research on the mechanism of procyanidin as potential antioxidants, the results of which showed that high molecular weight and hydroxyl group play important roles in free radical scavenging. Therefore, it can be speculated that the procyanidin with high DP in hawthorn fruit stone proanthocyanidins is the reason for the potent activity. Antioxidants have broad application prospects, and researchers have done a great deal of work to search for feasible and effective antioxidants. In this study, our results revealed that proanthocyanidins from fruit stone of Chinese hawthorn may be a good resource for further development as an antioxidant.

AUTHOR INFORMATION

Corresponding Author

*Tel: 86-592-2185487. Fax: 86-592-2185487. E-mail: chenqx@xmu.edu.cn.

Funding

This study was supported by the Natural Science Foundation of China (Grant Nos. 31071611 and 31070522) and the Science and Technology Foundation of Fujian Province (Grant No. 2010N5013).

Notes

The authors declare no competing financial interest.

ABBREVIATIONS USED

MALDI-TOF MS, matrix-assisted laser desorption/ionization time-of-flight mass spectrometry; HPLC-ESI-MS, high performance liquid chromatography electrospray ionization mass spectrometry; FRAP, ferric reduced antioxidant power; ORAC, oxygen radical absorbing capacity; ABTS, 2,2-azinobis(3-ethylbenzothiazoline-6-sulfonic acid) diammonium salt; DPPH, 2,2′-diphenyl-1-picrylhydrazyl; TPTZ, 2,4,6-tripyridyl-*S*-triazine; AAPH, 2,20-azobis (2-methylpropionamidine) dihydrochloride

REFERENCES

(1) Bravo, L. Polyphenols: Chemistry, dietary sources, metabolism, and nutritional significance. *Nutr. Rev.* **1998**, *56*, 317−333.

(2) Hümmer, W.; Schreier, P. Analysis of proanthocyanidins. *Mol. Nutr. Food Res.* **2008**, *52*, 1381−1398.

(3) Dixon, R. A.; Xie, D. Y.; Sharma, S. B. Proanthocyanidins-a final frontier in flavonoid research? *New Phytol.* **2005**, *165*, 9−28.

(4) Chai, W. M.; Shi, Y.; Feng, H. L.; Qiu, L.; Zhou, H. C.; Deng, Z. W.; Yan, C. L.; Chen, Q. X. NMR, HPLC-ESI-MS, and MALDI-TOF MS analysis of condensed tannins from *Delonix regia* (Bojer ex Hook.) Raf. and their bioactivities. *J. Agric. Food Chem.* **2012**, *60*, 5013−5022.

(5) Espin, J.; Garcia-Ruiz, P.; Tudela, J.; Garcia-Canovas, F. Study of stereospecificity in mushroom tyrosinase. *Biochem. J.* **1998**, *331*, 547−551.

(6) Korner, A.; Pawelek, J. Mammalian tyrosinase catalyzes three reactions in the biosynthesis of melanin. *Science* **1982**, *217*, 1163−1165.

(7) Friedman, M. Food browning and its prevention: An overview. *J. Agric. Food Chem.* **1996**, *44*, 631−653.

(8) Chase, M. R.; Raina, K.; Bruno, J.; Sugumaran, M. Purification, characterization and molecular cloning of prophenoloxidases from *Sarcophaga bullata*. *Insect Biochem. Mol. Biol.* **2000**, *30*, 953−967.

(9) Maisuthisakul, P.; Gordon, M. H. Antioxidant and tyrosinase inhibitory activity of mango seed kernel by product. *Food Chem.* **2009**, *117*, 332−341.
(10) Kirakosyan, A.; Seymour, E.; Kaufman, P. B.; Warber, S.; Bolling, S.; Chang, S. C. Antioxidant capacity of polyphenolic extracts from leaves of *Crataegus laevigata* and *Crataegus monogyna* (hawthorn) subjected to drought and cold stress. *J. Agric. Food Chem.* **2003**, *51*, 3973−3976.
(11) Barros, L.; Carvalho, A. M.; Ferreira, I. C. Comparing the composition and bioactivity of *Crataegus monogyna* flowers and fruits used in folk medicine. *Phytochem. Anal.* **2011**, *22*, 181−188.
(12) Sokół-Łętowska, A.; Oszmiański, J.; Wojdyło, A. Antioxidant activity of the phenolic compounds of hawthorn, pine and skullcap. *Food Chem.* **2007**, *103*, 853−859.
(13) Liu, P.; Kallio, H.; Yang, B. Phenolic compounds in hawthorn (*Crataegus grayana*) fruits and leaves and changes during fruit ripening. *J. Agric. Food Chem.* **2011**, *59*, 11141−11149.
(14) Liu, P.; Kallio, H.; Lü, D.; Zhou, C.; Yang, B. Quantitative analysis of phenolic compounds in Chinese hawthorn (*Crataegus* spp.) fruits by high performance liquid chromatography-electrospray ionisation mass spectrometry. *Food Chem.* **2011**, *127*, 1370−1377.
(15) Svedström, U.; Vuorela, H.; Kostiainen, R.; Huovinen, K.; Laakso, I.; Hiltunen, R. High-performance liquid chromatographic determination of oligomeric procyanidins from dimers up to the hexamer in hawthorn. *J. Chromatogr. A* **2002**, *968*, 53−60.
(16) Zhou, H. C.; Lin, Y. M.; Chai, W. M.; Wei, S. D.; Liao, M. M. Characterization of condensed tannins from litchi seed by reflectron modes and linear modes of MALDI-TOF MS. *Acta Chim. Sin.* **2011**, *69*, 2981−2986.
(17) Hellström, J.; Sinkkonen, J.; Karonen, M.; Mattila, P. Isolation and structure elucidation of procyanidin oligomers from saskatoon berries (*Amelanchier alnifolia*). *J. Agric. Food Chem.* **2007**, *55*, 157−164.
(18) Li, Z. C.; Chen, L. H.; Yu, X. J.; Hu, Y. H.; Song, K. K.; Zhou, X. W.; Chen, Q. X. Inhibition kinetics of chlorobenzaldehyde thiosemicarbazones on mushroom tyrosinase. *J. Agric. Food Chem.* **2010**, *58*, 12537−12540.
(19) Brand-Williams, W.; Cuvelier, M.; Berset, C. Use of a free radical method to evaluate antioxidant activity. *LWT—Food Sci. Technol.* **1995**, *28*, 25−30.
(20) Re, R.; Pellegrini, N.; Proteggente, A.; Pannala, A.; Yang, M.; Rice-Evans, C. Antioxidant activity applying an improved ABTS radical cation decolorization assay. *Free Radical Biol. Med.* **1999**, *26*, 1231−1237.
(21) Benzie, I. F.; Strain, J. The ferric reducing ability of plasma (FRAP) as a measure of "antioxidant power": the FRAP assay. *Anal. Biochem.* **1996**, *239*, 70−76.
(22) Ou, B.; Hampsch-Woodill, M.; Prior, R. L. Development and validation of an improved oxygen radical absorbance capacity assay using fluorescein as the fluorescent probe. *J. Agric. Food Chem.* **2001**, *49*, 4619−4626.
(23) Reed, J. D.; Krueger, C. G.; Vestling, M. M. MALDI-TOF mass spectrometry of oligomeric food polyphenols. *Phytochemistry* **2005**, *66*, 2248−2263.
(24) Xiang, P.; Lin, Y.; Lin, P.; Xiang, C.; Yang, Z.; Lu, Z. Effect of cationization reagents on the matrix-assisted laser desorption/ionization time-of-flight mass spectrum of Chinese gallotannins. *J. Appl. Polym. Sci.* **2007**, *105*, 859−864.
(25) Gu, L.; Kelm, M. A.; Hammerstone, J. F.; Beecher, G.; Holden, J.; Haytowitz, D.; Prior, R. L. Screening of foods containing proanthocyanidins and their structural characterization using LC-MS/MS and thiolytic degradation. *J. Agric. Food Chem.* **2003**, *51*, 7513−7521.
(26) Gu, L.; Kelm, M.; Hammerstone, J. F.; Beecher, G.; Cunningham, D.; Vannozzi, S.; Prior, R. L. Fractionation of polymeric procyanidins from lowbush blueberry and quantification of procyanidins in selected foods with an optimized normal-phase HPLC-MS fluorescent detection method. *J. Agric. Food Chem.* **2002**, *50*, 4852−4860.
(27) Espín, J. C.; Varón, R.; Fenoll, L. G.; Gilabert, M.; García-Ruíz, P. A.; Tudela, J.; García-Cánovas, F. Kinetic characterization of the substrate specificity and mechanism of mushroom tyrosinase. *Eur. J. Biochem.* **2000**, *267*, 1270−1279.
(28) Chen, L. H.; Hu, Y. H.; Song, W.; Song, K. K.; Liu, X.; Jia, Y. L.; Zhuang, J. X.; Chen, Q. X. Synthesis and antityrosinase mechanism of benzaldehyde thiosemicarbazones: novel tyrosinase inhibitors. *J. Agric. Food Chem.* **2012**, *60*, 1542−1547.
(29) Chazarra, S.; García-Carmona, F.; Cabanes, J. Characterization of monophenolase activity of polyphenol oxidase from iceberg lettuce. *J. Agric. Food Chem.* **1999**, *47*, 1422−1426.
(30) Gowda, L. R.; Paul, B. Diphenol activation of the monophenolase and diphenolase activities of field bean (*Dolichos lablab*) polyphenol oxidase. *J. Agric. Food Chem.* **2002**, *50*, 1608−1614.
(31) Schofield, P.; Mbugua, D.; Pell, A. Analysis of condensed tannins: A review. *Anim. Feed Sci. Technol.* **2001**, *91*, 21−40.
(32) Hagerman, A. E.; Riedl, K. M.; Jones, G. A.; Sovik, K. N.; Ritchard, N. T.; Hartzfeld, P. W.; Riechel, T. L. High molecular weight plant polyphenolics (tannins) as biological antioxidants. *J. Agric. Food Chem.* **1998**, *46*, 1887−1892.

JOURNAL OF AGRICULTURAL AND FOOD CHEMISTRY

Article

pubs.acs.org/JAFC

Revisiting the Prospects of Plastein: Thermal and Simulated Gastric Stability in Relation to the Antioxidative Capacity of Casein Plastein

Chibuike C. Udenigwe,* Sihong Wu, Kiesha Drummond, and Min Gong

Health and Bioproducts Research Laboratory, Department of Environmental Sciences, Faculty of Agriculture, Dalhousie University, Truro, Nova Scotia B2N 5E3, Canada

ABSTRACT: Plastein, a product of protease-induced peptide aggregation, is thought to possess unique physical properties and bioactivity, although its formation, stability, and functional mechanisms remain unclear. This study demonstrates that plastein is formed from bovine casein peptides with Alcalase by hydrophobic and electrostatic interactions and less likely by covalent bonding. The peptide aggregation enhanced the Fe(III) reducing potential and decreased the Fe(II) chelating activity ($p < 0.05$) of casein peptides, but there was no difference in inhibition of Fe-induced linoleic acid peroxidation after plastein reaction. The casein plastein product retained its antioxidative activities after being heated at 100 °C. However, simulated gastric protease treatment with pepsin and pancreatic enzymes resulted in enhanced reducing potential and metal chelation of the casein plastein and reduction of the inhibitory effect on lipid peroxidation. It appears that the plasteins were disintegrated and further hydrolyzed by gastric proteases on the basis of the antioxidative capacity and RP-HPLC profile being similar to those of the casein hydrolysates. Therefore, plastein reaction may not confer metabolic stability or enhance the antioxidative capacity of casein peptides for prospective functional food applications.

KEYWORDS: *plastein, peptide aggregation, antioxidant, bioactive peptide, stability, gastric protease*

INTRODUCTION

Plastein is a product of physical aggregation of peptides catalyzed by proteases at high substrate concentrations. First reported in 1902 by Danilevski and Okuneff, and originally thought to be resynthesized proteins,[1] plasteins are held together mostly by hydrophobic interaction of aggregating peptides.[2] However, the molecular events catalyzed by the protease during plastein formation remain unclear. Currently, plasteins are yet to be applied in the food system, and decades of research explored utilization of its gel-like physical properties in food.[3] Moreover, plastein has prospects for use in delivering desirable amino acids and enhancing the nutritional composition, quality, and health applications of proteins.[4] Furthermore, plastein has been explored for masking the bitterness of protein hydrolysates since hydrophobic amino acid residues that contribute to bitterness are buried within the plastein,[3] possibly limiting their interactions with taste receptors. Recently, a number of studies reported that plastein formation enhances the bioactivity of peptides, particularly their antioxidative and angiotensin-converting enzyme inhibitory activities.[5−7] Consequently, plastein can be explored as a multifunctional peptide-based ingredient for developing functional foods with desirable sensory, physicochemical, and bioactive properties. However, the mechanisms and structural requirements of plastein for enhanced bioactivity are presently not known, although this can be related to the surface property and availability of active functional groups in the peptide aggregates. Moreover, there is a dearth of information on the stability of plastein, which can be susceptible to thermal degradation during food processing and gastric proteolysis during ingestion, potentially leading to loss of structure and bioactivity. The objective of this study was to evaluate the antioxidative property of casein plastein on the basis of the reducing potential, metal chelation, and inhibition of Fe-induced lipid peroxidation with respect to their structural and functional stability against thermal and gastric protease treatments.

MATERIALS AND METHODS

Casein Hydrolysis and Plastein Formation. Casein was prepared by isoelectric precipitation by adjusting commercial skim bovine milk to pH 4.6 using 0.5 M HCl followed by centrifugation at 10000*g* for 15 min and freeze-drying the resulting precipitate. Thereafter, an aqueous suspension of the casein powder (5%, w/v) was heated at 90 °C for 10 min and cooled to 55 °C, followed by addition of protease from *Bacillus licheniformis* ([Alcalase] ≥ 2.4 U/g) at 0.01 g/g of casein to initiate hydrolysis. After 5 h of reaction maintained at 55 °C and pH 8.5 (adjusted by adding 0.5 M NaOH), the mixture was heated at 90 °C for 15 min to inactivate the enzyme, and the resulting product was freeze-dried. The degree of casein hydrolysis (DH) was determined by the *O*-phthaldialdehyde (OPA) method[8] and the average peptide chain length calculated as previously reported.[9] To produce casein plastein, a 40% aqueous suspension of the freeze-dried casein hydrolysates was mixed with 0.01 g of Alcalase/g of hydrolysates at 43 °C for 6 h at pH 6.5. Sample aliquots were withdrawn from the reaction every 1 h to monitor plastein formation and antioxidative activities. After termination of the plastein reaction by heating, the resulting products were freeze-dried and stored at −20 °C for further analysis.

Free Amino Nitrogen Determination. Free amino nitrogen present in the casein hydrolysates and plasteins was analyzed using OPA reagent containing sodium dodecyl sulfate (SDS) and dithiothreitol.[8] The OPA reagent (3 mL) was mixed with a 0.4 mL sample (1 mg/mL), and the absorbance of the solution was measured at 340 nm after 2 min. Serine (0.1 mg/mL) was used as the standard,

Received: August 1, 2013
Revised: December 5, 2013
Accepted: December 11, 2013
Published: December 11, 2013

ACS Publications © 2013 American Chemical Society

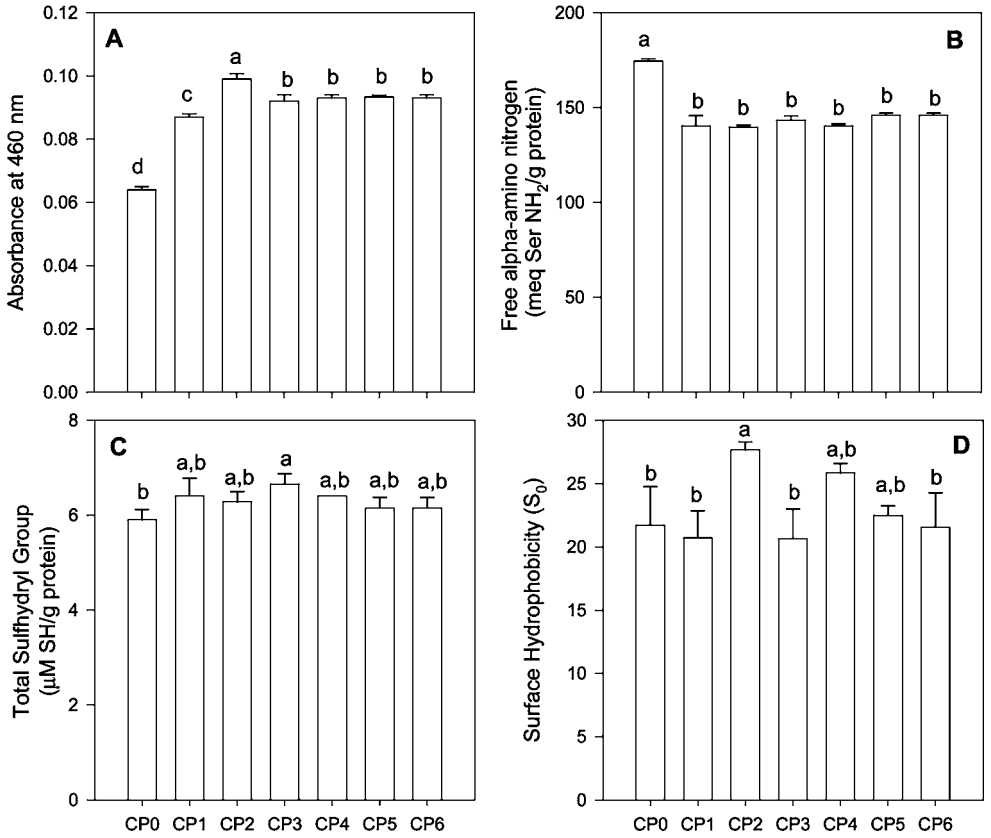

Figure 1. (A) Turbidity in deionized water, (B) free amino nitrogen concentration, (C) total sulfhydryl group concentration , and (D) surface hydrophobicity of casein hydrolysates (CP0) and plasteins after 1−6 h of reaction (CP1−CP6). Bars with different letters within each graph represent statistically significant means with $p < 0.05$.

and the free amino nitrogen was calculated as milliequiv of serine NH_2/g of protein as previously reported.[8]

Surface Hydrophobicity (S_o). The surface hydrophobicity of the casein hydrolysates and plastein reaction products was determined by the fluorescence method using a hydrophobic probe, 8-anilino-1-naphthalenesulfonic acid, as previously reported.[10] The samples were assayed at concentrations of 0.0009−0.015% with excitation and emission wavelengths of 390 and 470 nm, respectively. The surface hydrophobicity was determined as the slope of the fluorescence vs concentration (%) plot.

Turbidity Measurement. The solution turbidity was measured as reported[9] with modifications. The casein hydrolysates and plasteins were dissolved in deionized water at 3 mg/mL and allowed to stand for 15 min at room temperature followed by vortex mixing. The absorbance of the solution was then measured at 460 nm. The same process was repeated with the samples dissolved in 0.2 M SDS or 2 M NaCl instead of distilled water as previously reported[9] to evaluate the respective roles of hydrophobic and electrostatic interactions during plastein formation.

Sulfhydryl Group Analysis. The total sulfhydryl group concentration of the hydrolysates and plasteins was measured as reported[11] with modifications. Samples (0.5 mL, 10 mg/mL) were mixed with 2 mL of 0.1 M Tris−glycine buffer containing 10 M urea (pH 8.0) and incubated at 40 °C for 30 min. Then 62.5 μL of 5,5′-dithiobis(2-nitrobenzoic acid) (4 mg/mL 0.1 M Tris−glycine buffer, pH 8) was added to the mixture, the resulting mixture was incubated at room temperature for 10 min, and the absorbance was measured at 412 nm. The total sulfhydryl group concentration (μM SH/g of protein) was calculated as $73.53A_{412nm}(D/C)$, where D = the dilution factor and C = the sample concentration.[11]

Antioxidative Assays. Three assays were used to evaluate the antioxidant property of the plasteins. First, the Fe(III) to Fe(II) reducing potential of casein hydrolysates and plasteins was assayed using the potassium ferricyanide method.[12] The samples and glutathione (positive control) were analyzed at 1 mg/mL final concentration, and the reducing potential was expressed as the absorbance at 700 nm. Thereafter, the Fe(II) chelating assay was conducted as previously reported[12] with modifications. Briefly, the 3 mL assay mixture contained 1 mL of peptide solution or EDTA (positive control) at a final concentration of 0.05 mg/mL, 0.05 mL of $FeCl_2$ (2 mM), and 1.85 mL of deionized water. A 0.1 mL solution of 5 mM ferrozine was then added followed by mixing; an equal volume of deionized water was used in the blank assay. The absorbance was then measured at 562 nm and the Fe(II) chelating effect (%) calculated. Last, the assay for inhibition of Fe(II)-induced lipid peroxidation was also conducted as previously reported[13] with modifications. A 70 μL solution of the samples or glutathione (final concentration 0.05 mg/mL) was mixed with 3.2 mL of 0.1 M sodium phosphate buffer containing 1% (v/v) Triton X-100 (pH 7), 50 mM linolenic acid (0.72 mL), and 20 mM $FeCl_2$ (10 μL). The mixture was incubated at 80 °C for 1 h, and a 0.1 mL aliquot was mixed with 75% ethanol (4.5 mL), 30% ammonium thiocyanate (0.1 mL), 1 M HCl (0.2 mL), and 20 mM $FeCl_2$ (0.1 mL in 1 M HCl). The absorbance of the solution was then measured at 500 nm followed by calculation of the inhibition (%) of Fe(II)-induced linoleic acid peroxidation.

Thermal and Gastric Stability. For thermal stability, aqueous solutions of casein hydrolysates and plastein were heated in a water bath (97−100 °C) for 10 min and cooled to room temperature followed by vortex mixing and measurement of the turbidity and antioxidative properties as described earlier. For gastric stability, the casein hydrolysates and plastein samples (50 mg) were mixed with pepsin solution (1 mg/mL in 0.1 M HCl−KCl buffer, pH 2.0) and incubated at 37 °C for 2 h followed by the addition of 1 mL of NaOH to neutralize the solution and inactivate pepsin.[14] Thereafter, 1 mL of pancreatin suspension (3 mg/mL in 0.1 M sodium phosphate buffer, pH 8.0) was added to the mixture, and the resulting mixture was

incubated at 37 °C for 14 h followed by enzyme inactivation at 90 °C for 15 min. The resulting samples were analyzed for free amino group, ferric reducing potential, metal chelation, and inhibition of Fe(II)-induced linoleic acid peroxidation.

Reversed-Phase (RP) HPLC Analysis. Solutions (20 μL) of 5 mg/mL casein hydrolysates and plastein (dissolved in solvent A, 0.05% trifluoracetic acid (TFA) in water) before and after gastric protease treatment were injected into a Waters 515 HPLC system fitted with a Phenomenex C18 column (250 × 4.6 mm, 5 μm). The samples were eluted at a 1 mL/min flow rate using a linear gradient of 0−66% solvent B (0.05% TFA in acetonitrile) for 45 min and then 66−100% for 5 min and equilibration with 100% solvent A for 10 min. The samples and solvents were filtered through 0.2 μm membrane filters prior to analysis, and peptide elution was monitored at 214 nm with a Waters 2487 dual λ absorbance detector fitted to the HPLC equipment.

Statistical Analysis. All data were collected in triplicate and are expressed as the mean ± standard deviation. The statistical significance of difference between treatments was analyzed by one-way analysis of variance and the Holm−Sidak multiple comparison test using SigmaPlot for Windows, version 11.0 (Systat Software, San Jose, CA).

RESULTS AND DISCUSSION

Plasteins are believed to be products of entropy-driven physical aggregation of mostly low molecular size peptides induced by proteases at substrate concentrations often higher than 30% (w/v).[2,3,15−18] Although proteolytic activity is not required, native enzymes are preferred in inducing peptide aggregation during plastein formation.[2] In the present study, Alcalase was used for casein hydrolysis to produce small-chain peptides due to its broad specificity. Extensive proteolysis with the microbial enzyme for 5 h resulted in a 20.4 ± 0.12% degree of casein hydrolysis and a calculated average peptide chain length of 4.9 ± 0.03. The turbidity of the casein peptide solutions was measured at a low concentration (0.3%, w/v) to monitor peptide aggregation induced by the protease during plastein reaction.[9,16] In this study, casein peptide aggregation occurred as observed from the increase in the absorbance value at 460 nm (turbidity) by 45% from 0 to 6 h (CP0−CP6), with the highest increase of 54% observed at 2 h of reaction (CP2) (Figure 1A). These results agree with similar studies that reported an increase in solution turbidity during peptide aggregation.[9,16] Moreover, the plastein reaction resulted in a decrease in free amino nitrogen of the casein peptide solution by 16% after the 6 h reaction, with CP2 showing the lowest value (Figure 1B). A decrease in free amino nitrogen of protein hydrolysates has been reported to occur during plastein formation.[5−7] A possible explanation of the observed changes in free amino nitrogen during peptide aggregation is the enzyme-induced covalent modification of free amino groups, leading to amide bond formation and peptide condensation. However, there is evidence that plastein formation is reversible and that no detectable peptide bonds are formed in casein plasteins.[2,17] An earlier study indicated that blocking the amino and carboxyl groups of peptides reduced the plastein yield,[2] which supports the possible involvement of free amino groups in peptide aggregation during plastein reaction, although the mechanism remains unclear. It is important to note that peptide aggregation did not occur in the absence of the protease. Another possible contributor to peptide aggregation is covalent disulfide bond formation. However, it appears that disulfide linkages are not involved in casein peptide aggregation in this study since the limited sulfhydryl group concentration in the casein hydrolysates did not decrease during plastein reaction (Figure 1C).

Several studies have demonstrated that hydrophobic interaction plays a major role in peptide aggregation.[2,15−17] This was confirmed during casein plastein reaction as the turbidity of the plastein solutions decreased in the presence of a surfactant, SDS (data not shown), which can disrupt hydrophobic interactions in peptide aggregates.[2,16,17] This decrease was highest at 2 h of reaction (CP2), corresponding to the highest turbidity value (Figure 1A) and surface hydrophobicity, S_o (Figure 1D). The peptides' surface hydrophobicity can impact their physiological biomolecular interactions and influence bioactivity especially if hydrophobic interaction with target molecules (e.g., lipids) is required. Apart from CP2, S_o did not change with peptide aggregation during casein plastein formation (Figure 1D). Moreover, considering the phosphates and other charged amino acid species in casein, electrostatic interactions may have also played minor roles in plastein formation as demonstrated by the decreased turbidity of the plastein in a high-ionic-strength NaCl solution (data not shown), which disrupted electrostatic interactions in the casein plastein, similar to previous observations during peptide aggregation.[15−17] On the basis of these data, it is plausible that most of the casein plasteins are held together by noncovalent bonds, especially for the casein plastein product at 2 h (CP2) under our experimental conditions.

Plastein reaction has recently been reported to enhance the bioactivity of peptides including antioxidative properties,[5−7] although there is a dearth of clearly defined mechanisms and structural requirements of the aggregates for the enhanced bioactivity. Results from the present study demonstrate that there is no substantial increase in the physiologically relevant antioxidative properties of casein peptides to justify the additional plastein reaction step. However, there were statistically significant ($p < 0.05$) increases in the ferric reducing potential of the casein plasteins, especially at 2 h (CP2), which enhanced bioactivity by 19% (Figure 2A). In contrast, plastein reaction resulted in a reduced metal (FeII) chelating activity of the casein peptides with up to 42% loss of activity observed in CP3 (Figure 2B). Since the chemical compositions of the casein hydrolysates and plasteins are similar, it appears that molecular rearrangement during aggregation induced the negative effect on bioactivity. Plausibly, the metal chelating residues and phosphates in casein peptides may have participated in stabilizing the plasteins by hydrophobic and electrostatic interactions, respectively, making them unavailable to chelate Fe(II) during the assay. In addition, peptide aggregation during plastein formation did not seem to impact the inhibitory effects of the casein peptides on Fe(II)-induced linoleic acid peroxidation (Figure 2C). It was also observed that the reducing potential of the casein peptides is not related to their total sulfhydryl groups, which is a key electron-donating functionality in peptides. Therefore, the enhanced reducing potential of the plasteins may be due to other antioxidative functionalities of amino acid residues that became proximal and perhaps collectively more reactive within the peptide aggregates. Moreover, the observed inhibitory activities against Fe(II)-induced linoleic acid peroxidation are not exclusively due to their metal chelating effects since there was no correlation between the two antioxidative properties, and a strong metal chelating agent (EDTA) did not inhibit the Fe(II)-catalyzed oxidative process during the assay. Overall, the casein hydrolysates and plasteins competed favorably with equal amounts of the positive controls (EDTA chelated 100% Fe(II) and glutathione inhibited 13% lipid peroxidation) except

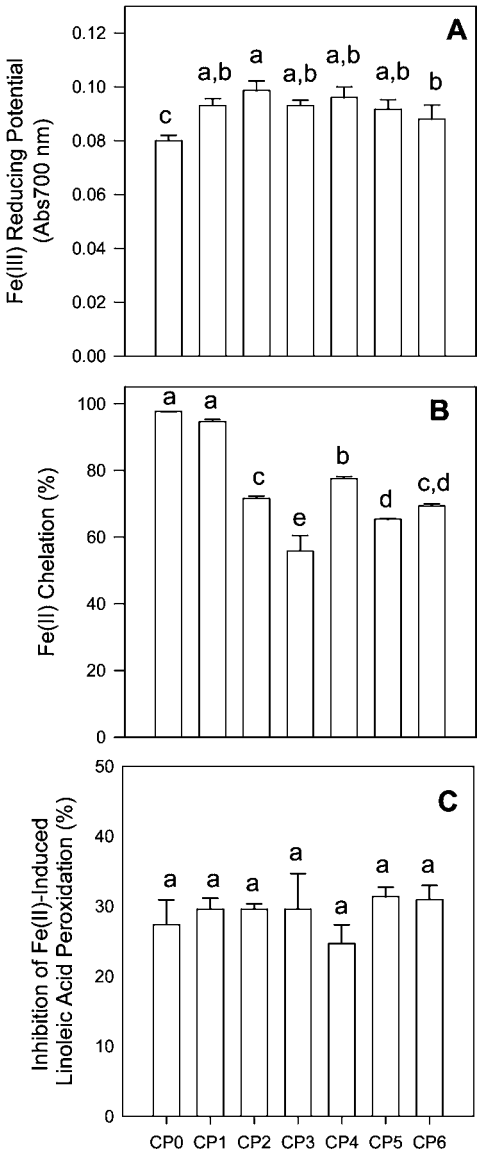

Figure 2. Antioxidative properties of casein hydrolysates (CP0) and plasteins after 1−6 h of reaction (CP1−CP6): (A) Fe(III) reducing potential, (B) Fe(II) chelating activity, and (C) inhibition of Fe(II)-induced linoleic acid peroxidation. Bars with different letters within each graph represent statistically significant means with $p < 0.05$.

in the case of the high reducing potential of glutathione (A_{700nm} = 1.91) due to its substantially higher molar amount of reducing sulfhydryl functionality in the assay compared to that of the casein products.

For decades, an important driver of the need to explore plasteins in food applications has included the modified physicochemical functionality of the peptide aggregates that can purportedly confer unique properties such as molecular stability. However, the mechanism of protease-induced plastein formation remains unclear, and the peptide aggregates have yet to find a major place in food product development. Our study has demonstrated that the intramolecular interactions holding the casein peptides together in the plastein appear stable to heat treatment at 100 °C for 10 min on the basis of the solution turbidity (data not shown). Moreover, the antioxidative properties of the hydrolysates and plasteins were conserved after heat treatment, except that the plastein lost about 8% of its ability to inhibit Fe(II)-induced lipid peroxidation (Table 1). There was also a slight but statistically significant ($p < 0.05$) increase in the ferric reducing potential and metal chelating activity of plastein, indicating possible changes in the noncovalent molecular interactions that exposed functional amino acid residues after heating. That notwithstanding, the same trend was observed for the antioxidative activities of the treated and untreated samples, indicating that the plastein did not have a substantial advantage over the unmodified casein hydrolysates in these model assay systems, which casts doubts on the purported enhanced value and prospective use of casein plasteins in functional food applications.

In contrast, gastric treatment resulted in altered antioxidative activities of the hydrolysates and plastein. The gastric enzymes induced a 4-fold increase in the ferric reducing potential of both samples and enhanced the metal chelating effect of the plastein to a value similar to that of the hydrolysates (Table 1). However, there was loss of over 24% of their inhibitory effects on lipid peroxidation after gastric modification. It appears that the casein hydrolysates and plasteins are similar after gastric treatment on the basis of their similar antioxidative activities (Table 1). Moreover, the HPLC profiles of the casein peptides before and after plastein reaction also appeared similar (Figure 3), indicating limited covalent bond formation induced by the microbial protease during aggregation. This suggests that noncovalent interactions played major roles in casein plastein formation in this study, as earlier suggested using other proteases.[2] Furthermore, simulated gastric protease treatment resulted in further hydrolysis, especially for highly hydrophobic peptides, yielding similar HPLC profiles for the casein hydrolysates and plastein (Figure 3). These data indicate that the aggregated peptides in the plasteins formed by hydrophobic and ionic interactions (and possibly covalent bonds) are not resistant to further gastric proteolysis, similar to peptides in the original casein hydrolysates. A previous study suggested that plastein reaction can confer stability on peptides against further

Table 1. Residual Antioxidative Properties of Casein Hydrolysates (CP0) and Plastein (CP2) after Thermal and Gastric Protease Treatments[a]

	Fe(III) reducing potential[b]	Fe(II) chelation (%)	inhibition of Fe(II)-induced lipid peroxidation (%)
		Thermal Treatment (100 °C for 10 min)	
CP0	0.098 ± 0.005 d (1.22)[c]	97.93 ± 3.42 a (1.00)	28.06 ± 2.79 a (1.02)
CP2	0.119 ± 0.002 c (1.20)	82.73 ± 4.23 b (1.15)	27.27 ± 4.36 a (0.92)
		Gastric Protease (Pepsin and Pancreatin) Treatment	
CP0	0.346 ± 0.012 a (4.33)	100 ± 0.00 a (1.02)	21.02 ± 1.10 b (0.76)
CP2	0.320 ± 0.005 b (3.99)	100 ± 0.00 a (1.39)	21.02 ± 1.10 b (0.71)

[a]Data with different letters within a column are statistically significant ($p < 0.05$). [b]Absorbance values of assay mixtures at 700 nm. [c]Fold change in activity in parentheses.

dx.doi.org/10.1021/jf403405r | J. Agric. Food Chem. 2014, 62, 130−135

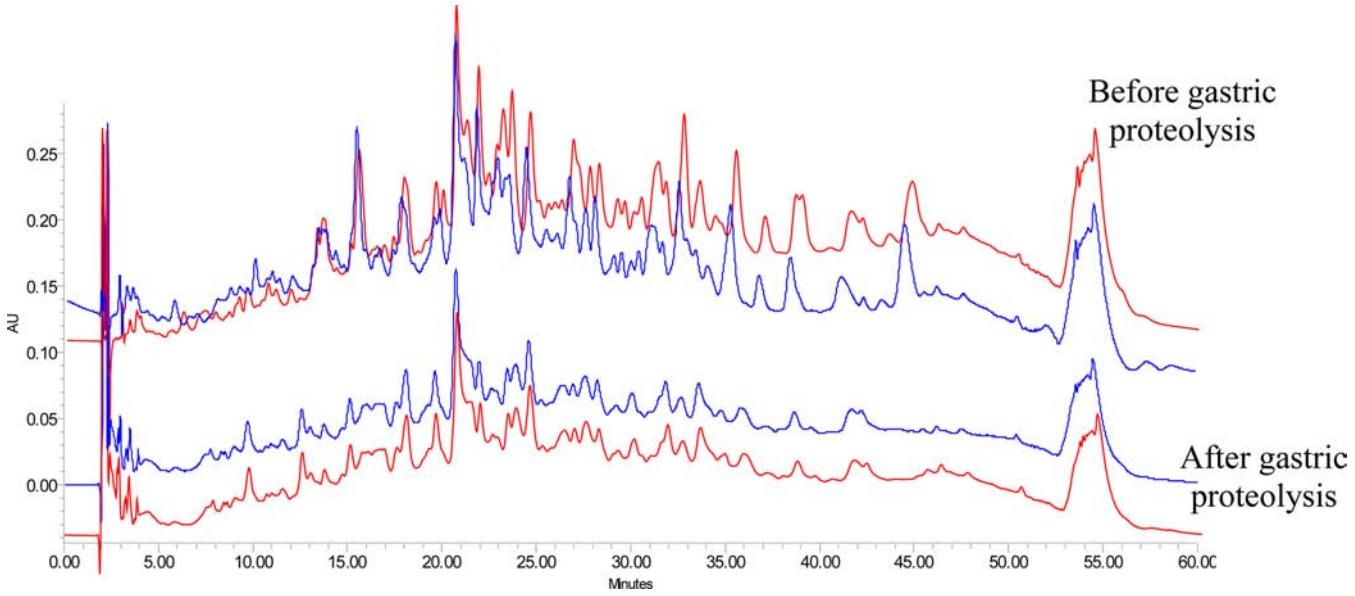

Figure 3. Reversed-phase HPLC profiles of casein hydrolysates (blue) and plastein (red) before and after gastric protease treatment.

proteolysis after short-term (up to 30 min) exposure to proteases, including gastric trypsin and pepsin.[7] However, plastein stability may not be guaranteed since the authors' conclusion was based on short-term exposure to proteases and retention of bioactivity and did not consider the peptide aggregate structure or fingerprints, although the authors observed an increase in free amino group postprotease treatment,[7] suggesting susceptibility of the plastein to proteolysis. Gastric metabolic instability of peptides has been a major concern in translating food peptide research due to potential loss of structure and function. However, the present study demonstrated that the overall antioxidative potential of the casein plastein was enhanced as a result of gastric proteolysis, possibly due to further release of cryptic antioxidative peptides. Despite the enhanced bioactivity, the lack of clear distinction in the molecular profile and antioxidative activities of the casein hydrolysates and plastein postmodification by gastric proteases indicates that plastein reaction did not enhance gastric metabolic stability and overall prospects of the casein peptide aggregates.

In conclusion, this study has demonstrated that plastein reaction catalyzed by microbial proteases resulted in the formation of peptide aggregates that are held together mostly by hydrophobic and electrostatic interactions and less likely by covalent bonding. Although plastein reaction enhanced the reducing potential and decreased the metal chelating ability, the overall activity of the casein plastein did not differ substantially from that of the hydrolysates, especially in their effects in inhibiting linoleic acid peroxidation. Despite the thermal stability and retention of antioxidative activities after heating, the structure and bioactivity of casein plastein were modified substantially after simulated gastric treatment. These findings suggest that the aggregates in the plastein product may not improve the metabolic stability of casein peptides in functional food applications.

AUTHOR INFORMATION

Corresponding Author

*E-mail: cudenigwe@dal.ca. Phone: (902) 893-6625. Fax: (902) 893-1404.

Funding

The research program of CCU is supported by the Natural Sciences and Engineering Research Council of Canada (NSERC) through a Discovery Grant.

Notes

The authors declare no competing financial interest.

REFERENCES

(1) Beard, H. H. The nutritive value of plastein. *J. Biol. Chem.* **1927**, *71*, 477−480.

(2) Andrews, A. T.; Alichanidis, E. The plastein reaction revisited: Evidence for a purely aggregation reaction mechanism. *Food Chem.* **1990**, *35*, 243−261.

(3) Eriksen, S.; Fagerson, I. S. The plastein reaction and its applications: A review. *J. Food Sci.* **1976**, *41*, 490−493.

(4) Yamashita, M.; Arai, S.; Fujimaki, M. Plastein reaction for food protein improvement. *J. Agric. Food Chem.* **1976**, *24*, 1100−1104.

(5) Zhao, X. H.; Li, Y. Y. An approach to improve ACE-inhibitory activity of casein hydrolysates with plastein reaction catalyzed by Alcalase. *Eur. Food Res. Technol.* **2009**, *229*, 795−805.

(6) Zhao, X. H.; Wu, D.; Li, T. J. Preparation and radical scavenging activity of papain-catalyzed casein plastein. *Dairy Sci. Technol.* **2010**, *90*, 521−535.

(7) Sun, H.; Zhao, X. H. Angiotensin I converting enzyme inhibition and enzymatic resistance in vitro of casein treated by plastein reaction and fractionated with ethanol/water or methanol/water. *Int. Dairy J.* **2012**, *24*, 27−32.

(8) Nielsen, P. M.; Petersen, D.; Dambmann, C. Improved method for determining food protein degree of hydrolysis. *J. Food Sci.* **2001**, *66*, 642−646.

(9) Doucet, D.; Gauthier, S. F.; Otter, D. E.; Foegeding, E. A. Enzyme-induced gelation of extensively hydrolysed whey proteins by Alcalase: Comparison with the plastein reaction and characterization of interactions. *J. Agric. Food Chem.* **2003**, *51*, 6036−6042.

(10) Horax, R.; Hettiarachchy, N. S.; Chen, P.; Jalaluddin, M. Preparation and characterization of protein isolate from cowpea (*Vigna unguiculata* L. Walp). *J. Food Sci.* **2004**, *69*, 114−118.

(11) Mine, Y. Effect of dry heat and mild alkaline treatment on functional properties of egg white proteins. *J. Agric. Food Chem.* **1997**, *45*, 2924−2928.

(12) Pownall, T. L.; Udenigwe, C. C.; Aluko, R. E. Amino acid composition and antioxidant properties of pea seed (*Pisum sativum* L.)

enzymatic protein hydrolysate fractions. *J. Agric. Food Chem.* **2010**, *58*, 4712−4718.
(13) Chen, H. M.; Muramoto, K.; Yamauchi, F. Structural analysis of antioxidative peptides from soybean β-conglycinin. *J. Agric. Food Chem.* **1995**, *43*, 574−578.
(14) Wu, J.; Aluko, R. E.; Muir, A. D. Purification of angiotensin I-converting enzyme-inhibitory peptides from the enzymatic hydrolysate of defatted canola meal. *Food Chem.* **2008**, *111*, 942−950.
(15) Van Hofsten, B.; Lalasidis, G. Protease-catalyzed formation of plastein products and some of their properties. *J. Agric. Food Chem.* **1976**, *24*, 460−465.
(16) Groleau, P. E.; Morin, P.; Gauthier, S. F.; Pouliot, Y. Effect of physicochemical conditions on peptide−peptide interactions in a tryptic hydrolysate of β-lactoglobulin and identification of aggregating peptides. *J. Agric. Food Chem.* **2003**, *51*, 4370−4375.
(17) Sukan, G.; Andrews, A. T. Application of the plastein reaction to caseins and to skim-milk powder: II. Chemical and physical properties of the plasteins and the mechanism of plastein formation. *J. Dairy Res.* **1982**, *49*, 279−293.
(18) Sukan, G.; Andrews, A. T. Application of the plastein reaction to caseins and to skim-milk powder: I. Protein hydrolysis and plastein formation. *J. Dairy Res.* **1982**, *49*, 265−278.

JOURNAL OF AGRICULTURAL AND FOOD CHEMISTRY

Article

pubs.acs.org/JAFC

Maize Genotype and Food Matrix Affect the Provitamin A Carotenoid Bioefficacy from Staple and Carrot-Fortified Feeds in Mongolian Gerbils (*Meriones unguiculatus*)

Samantha Schmaelzle, Bryan Gannon, Serra Crawford, Sara A. Arscott,[‡] Shellen Goltz, Natalia Palacios-Rojas,[#] Kevin V. Pixley,[#] Philipp W. Simon, and Sherry A. Tanumihardjo*

Interdepartmental Graduate Program in Nutritional Sciences, University of Wisconsin—Madison, Madison, Wisconsin 53706, United States

Supporting Information

ABSTRACT: Biofortification to increase provitamin A carotenoids is an agronomic approach to alleviate vitamin A deficiency. Two studies compared biofortified foods using in vitro and in vivo methods. Study 1 screened maize genotypes (n = 44) using in vitro analysis, which demonstrated decreasing micellarization with increasing provitamin A. Thereafter, seven 50% biofortified maize feeds that hypothesized a one-to-one equivalency between β-cryptoxanthin and β-carotene were fed to Mongolian gerbils. Total liver retinol differed among the maize groups (P = 0.0043). Study 2 assessed provitamin A bioefficacy from 0.5% high-carotene carrots added to 60% staple-food feeds, followed by in vitro screening. Liver retinol was highest in the potato and banana groups, maize group retinol did not differ from baseline, and all treatments differed from control (P < 0.0001). In conclusion, β-cryptoxanthin and β-carotene have similar bioefficacy; meal matrix effects influence provitamin A absorption from carrot; and in vitro micellarization does not predict bioefficacy.

KEYWORDS: *α-retinol, biofortification, carrots, nixtamalization*

INTRODUCTION

Biofortification of staple crops to improve provitamin A carotenoid concentrations is a promising agronomic approach to increase vitamin A (VA) intake in populations. One such crop is maize, which makes up 55−70% of energy intake in countries such as Mexico and Zambia.[1,2] The provitamin A carotenoids, β-carotene (βC), β-cryptoxanthin (βCX), and α-carotene (αC), are present in typical yellow maize in low concentrations[3] and in higher concentrations in biofortified varieties.[4,5] The bioefficacy to make retinol from provitamin A carotenoids in maize was demonstrated by maintaining liver retinol stores of VA-depleted Mongolian gerbils (*Meriones unguiculatus*).[4,6] Furthermore, favorable bioconversion factors, which were more efficient than the Institute of Medicine (IOM) values of 12 μg of βC equivalents to 1 μg of retinol,[7] were measured from single test meals made with biofortified maize in U.S. women[8] and Zimbabwean men.[9]

Several studies have evaluated the effects of the relative carotenoid ratio, food matrices, meal components, and food processing on bioavailability, which is defined as provitamin A carotenoid that is absorbed and available for physiological function. For example, βCX and βC from biofortified maize are equally efficacious at maintaining baseline retinol stores in gerbils.[10] Cooking carotenoid-containing foods increases bioefficacy,[11] and dietary fat in meals increases carotenoid absorption.[12−14] However, carotenoid bioavailability from combined meals prepared with staple crops (biofortified or not) and vegetables, such as carrots and green leaves,[5] has not been determined.

In vitro carotenoid bioaccessibility screening methods (i.e., measuring provitamin A carotenoid released from the food matrix) involve digestion assays and may predict carotenoid bioavailability in vivo.[15−18] The micellarization efficiency (i.e., the fraction of carotenoid transferred from digesta to aqueous fraction) of maize carotenes was higher for porridge than extruded puffs and bread,[17] indicating that wet-cooking enhances bioaccessibility. In vitro digestions have been coupled with Caco-2 cell uptake as a model to screen the relative absorption of carotenoids from micelles with direct proportionality to the amount of provitamin A in cassava.[16] In vitro digestions were used to determine carotenoid bioavailability from vegetables;[19,20] however, it has not been coupled with animal studies to assess the same foods.

Two studies coupled in vitro and in vivo components. Study 1 screened 44 maize genotypes (*Zea mays* sp.) with different βCX to βC ratios. Thereafter, 50% maize feeds, assuming 1:1 rather than the theoretical 2:1 retinol activity equivalency between βCX and βC, were fed to Mongolian gerbils to assess in vivo bioaccessibility and bioconversion to VA, that is, bioefficacy. The hypothesis was that bioaccessibility of provitamin A carotenoids is correlated to concentration when measured by in vitro methods and that βCX will be as bioefficacious as βC in maize at the molar level in vivo. Study 2 assessed the bioefficacy of αC and βC from a small amount of biofortified, high-βC carrots (*Daucus carota* L.) when added to 60% staple-food feeds of gerbils and compared this with in vitro carotenoid bioaccessibility. In prior studies, high-βC carrots

Received: August 12, 2013
Revised: December 10, 2013
Accepted: December 16, 2013
Published: December 16, 2013

ACS Publications © 2013 American Chemical Society

Table 1. Provitamin A Carotenoid Concentrations, Fiber and Resistant Starch Contents of Feeds, Feed Intake, and Theoretical Retinol Intake for Mongolian Gerbils (Studies 1 and 2)[a,b]

Study 1								
component	β-cryptoxanthin (nmol/g feed)	β-carotene (nmol/g feed)	hypothetical retinol (nmol/g feed)	neutral detergent fiber (%)	resistant starch (%)	feed intake/cage (g/day)	daily hypothetical intake/cage[c] (nmol/day)	daily theoretical intake/cage[d] (nmol/day)
P value	<0.0001	<0.0001	0.53	0.048	<0.0001	<0.0001	<0.0001	<0.0001
VA−	ND	ND	ND			NM		
G1	0.005 ± 0.001^{C}	4.45 ± 0.60^{A}	4.46 ± 0.60	10.6 ± 0.07^{A}	5.13 ± 0.14^{D}	10.6 ± 1.8^{D}	47.2 ± 8.1^{D}	94.3 ± 16.1^{C}
G2	4.08 ± 0.62^{A}	0.92 ± 0.19^{B}	5.00 ± 0.79	9.46 ± 0.45^{C}	5.73 ± 0.14^{BC}	11.5 ± 2.1^{B}	57.3 ± 10.7^{B}	67.8 ± 12.6^{F}
G3	0.006 ± 0.000^{C}	4.41 ± 0.35^{A}	4.41 ± 0.35	10.6 ± 0.33^{AB}	5.98 ± 0.08^{AB}	11.3 ± 2.2^{BC}	49.9 ± 9.7^{C}	99.8 ± 19.4^{B}
G4	4.25 ± 0.55^{A}	1.13 ± 0.20^{B}	5.39 ± 0.75	9.85 ± 0.58^{ABC}	5.87 ± 0.06^{AB}	10.9 ± 1.9^{CD}	58.5 ± 10.4^{AB}	71.0 ± 12.8^{EF}
G5	3.50 ± 0.35^{B}	1.52 ± 0.16^{B}	5.02 ± 0.49	9.08 ± 0.69^{C}	5.42 ± 0.01^{CD}	12.0 ± 1.9^{A}	60.2 ± 9.6^{A}	78.4 ± 12.5^{D}
G6	4.26 ± 0.49^{A}	1.04 ± 0.23^{B}	5.30 ± 0.67	9.55 ± 0.90^{BC}	5.97 ± 0.02^{AB}	11.5 ± 1.9^{AB}	60.9 ± 9.9^{A}	72.9 ± 11.8^{E}
G7	0.030 ± 0.046^{C}	4.99 ± 0.84^{A}	5.02 ± 0.86	10.1 ± 0.71^{ABC}	6.08 ± 0.02^{A}	11.3 ± 2.7^{BC}	56.5 ± 13.6^{B}	113 ± 27.0^{A}
VA+						NM	49.9	

Study 2							
component	α-carotene	β-carotene	theoretical retinol	neutral detergent fiber	resistant starch	feed intake	daily theoretical intake/cage
P value	<0.0001	<0.0001	<0.0001	<0.0001	<0.0001	0.024	<0.0001
VA−	ND	ND	ND	NM	0.31 ± 0.01^{D}	10.8 ± 0.20^{AB}	ND
60% rice	4.23 ± 0.40^{B}	11.8 ± 0.46^{B}	29.5 ± 2.92^{B}	2.65 ± 0.53^{D}	4.54 ± 0.21^{A}	9.89 ± 0.66^{C}	291 ± 19.5^{B}
60% potato	4.05 ± 0.52^{B}	12.1 ± 1.49^{B}	28.3 ± 3.75^{B}	4.63 ± 0.98^{C}	1.20 ± 0.01^{C}	10.4 ± 0.63^{BC}	294 ± 17.8^{B}
60% banana	6.42 ± 0.94^{A}	16.8 ± 2.19^{A}	40.0 ± 4.89^{A}	4.62 ± 0.76^{C}	4.76 ± 0.78^{A}	11.3 ± 0.80^{A}	452 ± 32.2^{A}
60% white maize	4.15 ± 0.63^{B}	12.3 ± 1.62^{B}	28.7 ± 4.40^{B}	6.29 ± 0.90^{B}	2.35 ± 0.96^{B}	10.4 ± 0.67^{BC}	297 ± 19.3^{B}
carrot only	4.17 ± 0.68^{B}	12.2 ± 1.81^{B}	28.6 ± 4.89^{B}	9.96 ± 0.51^{A}	0.32 ± 0.02^{D}	10.5 ± 0.41^{BC}	300 ± 11.9^{B}

[a]Values are means ± SD, $n \geq 3$ replicates (diet analysis), and $n = 5$ (feed intake and daily theoretical retinol intake). Means in a column without a common capital letter differ. Feed intake and theoretical retinol are per cage ($n = 2$/cage, $n = 10$/treatment group). ND, not detected; NM, not measured; VA+, positive control; VA−, negative control. [b]The limit for detection for carotenoids is <0.001 nmol and that for resistant starch is 0.08%. Assay includes all resistant starch. [c]Daily hypothetical retinol intake assumes 1 mol of β-carotene = 1 mol of β-cryptoxanthin = 1 mol of retinol. [d]Daily theoretical retinol intake assumes 100% bioefficacy (i.e., 1 mol of β-carotene provides 2 mol of retinol and 1 mol of α-carotene or β-cryptoxanthin provides 1 mol of retinol). This calculation (theoretical retinol × feed intake) accounts for losses in provitamin A concentrations over time.

provided an abundant amount of retinol to gerbils.[21] In study 2, the hypothesis was that small amounts of high-βC carrots will be an effective complementary food to maintain liver retinol reserves in gerbils despite potential effects of the combined food matrix.

MATERIALS AND METHODS

Maize and Carrots. Maize genotypes, including lines and synthetics, from the International Maize and Wheat Improvement Center (CIMMYT)/HarvestPlus maize provitamin A biofortification project were grown in Mexico at Agua Fria, Puebla (20°32′ N, 97°28′ W; 110 m above sea level). Ears were harvested and dried, and grain was stored at −20 °C before shipment to the University of Wisconsin (UW)—Madison. Genotypes were selected on the basis of carotenoid profile and contrasting βCX/βC. Carrots from the USDA carrot breeding and genetics program were grown by the University of California Desert Research and Extension Station in sandy, loam soil in October and harvested in March the following year. Carrots were refrigerated at 2 °C until shipped overnight from California to Wisconsin. Upon arrival, they were immediately returned to 2 °C and utilized for feed preparation after freeze-drying. Genotypes used (i.e., HCM and B2327) were selected for high βC concentrations.

In Vitro Digestion, Isolation of Micellarized Fraction, and Analyses. For study 1, maize genotypes ($n = 44$) were prescreened using HPLC (Supplemental Table 1 in the Supporting Information) and in vitro methods.[16,17] From these data, four genotypes were selected along with three others for gerbil study 1. Three genotypes had high βC and four had high βCX concentrations (Table 1). Biofortified maize and feeds from study 2 were weighed (~3 g) in triplicate and subjected to in vitro digestion as described by Thakkar et al.[16] and modified by Kean et al.[17] The method involves an oral phase using α-amylase, a gastric phase with porcine pepsin and pH adjustment with HCl, and an intestinal phase using porcine pancreatin, lipase, and bile extracts to mimic what happens in vivo. After the intestinal phase, the digesta is composed of the fluid and food products. Digesta were transferred to polycarbonate tubes for high-speed centrifugation (10000*g* for 1 h). Aqueous fractions (5−10 mL) were collected and syringe filtered into 15 mL centrifuge tubes, covered with nitrogen, and stored at −80 °C until analysis.[21−23] Digesta and aqueous fractions (3 mL) were placed in glass tubes with internal standard (β-apo-8′-carotenal, 50 μL) and ethanol with 0.1% butylated hydroxytoluene (500 μL). The carotenoids were extracted three times with hexanes (1 mL), pooled, dried under nitrogen, and reconstituted in 100 μL of 50:50 methanol/dichloroethane, and 50 μL was injected into a photodiode array HPLC.

Gerbil Study Designs. For studies 1 and 2, male 34−40-day-old Mongolian gerbils (Charles River Laboratories, Kingston, NY, USA) were group housed (2−3/cage) during VA depletion and treatment (2/cage). During depletion, gerbils were weighed daily for 2 weeks and, thereafter, three times per week. Room temperature and humidity were held constant with a 12 h light/dark cycle. Animal handling procedures were approved by the College of Agriculture and Life Sciences Animal Care and Use Committee at UW—Madison.

For study 1, gerbils ($n = 97$) were fed 50% white maize feed as a wash-out for 5 weeks. A baseline kill ($n = 7$) was performed via exsanguination while the gerbils were under isoflurane anesthesia. Remaining gerbils were divided into nine treatment groups ($n = 10$/group) and fed 50% white (VA− and VA+ groups) or seven orange maize feeds (G1−G7) prepared as published.[6] The feeds were developed by hypothesizing that 1 molecule of βC = 1 molecule of βCX = 1 molecule of retinol from the feed or supplement (Table 1). This contrasts with the theoretical relationship of 0.5 molecule of βC = 1 of molecule βCX = 1 molecule of retinol. Oral supplements,

administered using a positive displacement pipet, consisted of retinyl acetate (VA+ group) or oil only, which was given to groups G1−G7 and the VA− control. The VA+ dose was matched to the nanomoles of βC + βCX consumed from the orange maize on the prior day, and oil doses were matched by volume. Gerbils were fed for 4 weeks and then killed for tissue collection.

For study 2, gerbils (n = 66) were randomly separated into six treatment groups and acclimated to their study treatment by increasing staple amounts by 15% each week during depletion (4 weeks). Feeds ultimately contained 60% white staple food [i.e., potato (PT), rice (RC), banana (BN), or maize (MZ)] + carrot or VA-free feed with (CA) and without (VA−) carrot (Table 2). After depletion, one gerbil from each group (n = 6) was killed to determine initial serum and liver retinol concentrations. During treatment (4 weeks), 0.5% freeze-dried high-βC carrot was added to the staple feeds and the CA group. After treatment, the gerbils were killed, and blood and livers were collected. Blood was centrifuged for 15 min at 2200g in serum separator Vacutainer tubes (Becton Dickinson, Franklin Lakes, NJ, USA). Livers and serum were stored at −80 °C.

Table 2. Composition of Experimental Feeds for Study 2 Designed in Consultation with a Nutritionist at the Feed Supplier (Harlan-Teklad, Madison, WI, USA) That Were Fed to Mongolian Gerbils To Determine Vitamin A Efficacy of High β-Carotene Carrot Mixed with a Variety of Staple Foods

	g/kg feed				
ingredient	60% potato	60% rice	60% banana[a]	60% white maize	vitamin A-free[b]
component	600	600	600	600	
casein	146	149	172	140	200
L-cystine	2.57	2.57	2.57	2.57	3
sucrose	145	143	75.1	170	360.5
maltodextrin	0	0	21.7	0	120
corn starch	0	0	29.4	0	150
cottonseed oil[c]	55.6	53.7	48.5	36.5	60
cellulose	0	0	0	0	60
mineral mix, AIN-93M-MX	34.6	34.6	34.6	34.6	35
magnesium oxide	1.73	1.73	1.73	1.73	1.75
calcium phosphate, dibasic	1.98	1.98	1.98	1.98	2
vitamin mix[d], w/o choline, A, D, E[2]	4.94	4.94	4.94	4.94	5
vitamin E, DL-α-tocopheryl acetate	0.239	0.239	0.239	0.239	0.242
vitamin D3, cholecalciferol	0.004	0.004	0.004	0.004	0.044
choline bitartrate	0.004	0.004	0.004	0.004	2.5
fiber	146	149	172	140	200

[a]All banana was chopped, freeze-dried, and ground. [b]Vitamin A-free feed was used for both the VA− diet and the 0.5% carrot diet. [c]Fat content was equalized in the feeds as well as nitrogen and energy. [d]Vitamin mix provided the following, mg/kg purified diet: biotin, 0.4; calcium; pantothenate, 66.1; folic acid, 2; inositol, 110.1; menadione, 49.6; niacin, 99.1; p-aminobenzoic acid, 110.1; pyridoxine-HCl, 22; riboflavin, 22; thiamin-HCl, 22; vitamin B12 (0.1% in mannitol), 29.7; ascorbic acid (97.5%), 1016.6.

Feed Preparation for Study 2. Green bananas were purchased from a local grocery store, peeled and sliced, lyophilized for ∼6 days, ground into flour, and kept frozen (−20 °C) until mixed into feeds. Nixtamalized (processed) white maize meal that contained no carotenoids (masa), precooked dehydrated potato flakes (Roundy's), and precooked instant rice (Roundy's) were purchased from a grocery store. Nixtamalization is a common processing method whereby the maize grains are soaked in limewater prior to grinding to improve consistency, increase calcium, reduce phytic acid, and enhance niacin bioavailability from the maize.[24] Potato flakes and rice were ground into fine powders using a Vitamix blender. Basal mixes were formulated for each food item with assistance from a feed nutritionist (Harlan-Teklad, Madison, WI, USA) to provide VA- and carotenoid-free, isoenergetic, and isonitrogenous feeds, which were mixed weekly with 0.5% carrot and stored at −20 °C (Table 2).

Carotenoid, Retinoid, Resistant Starch, and Fiber Analyses. Maize (0.6 g), feeds (0.6 g), and carrots (0.01 g) were analyzed each week in triplicate for carotenoid concentrations using a modified procedure after grinding with a mortar and pestle.[23] Serum preparation followed published methods.[22] Originally, the livers were analyzed for retinyl esters and carotenoids without saponification;[4] however, after initial data analyses, liver retinol was reanalyzed using a saponification procedure to better assess total retinol in study 1 and total α-retinol concentrations in study 2 derived from carrot αC.[22] For liver carotenoids, an unsaponified 5 mL aliquot of the 25 mL liver extract was dried and resuspended in 100 μL of 50:50 methanol/dichloroethane, and 50 μL was injected into an HPLC system as published.[23] Resistant starch and fiber were analyzed using previously published methods.[25,26]

Statistical Analysis and Calculation of Bioconversion Factors. Values are reported as means ± SD. Data were analyzed using the General Linear Model procedure in the Statistical Analysis System (SAS Institute, version 9.2). Outcomes of interest (i.e., gerbil weights, retinol, α-retinol, and carotenoid concentrations) were evaluated using one-way ANOVA, and differences among treatment groups were determined using least significant difference tests. One- and two-tailed t tests were used when appropriate. For calculation of bioconversion factors, the mean total liver retinol of the negative control group was subtracted from each treatment group prior to calculation. In study 1, bioconversion factors were calculated in reference to the retinyl acetate dosed group.[6] In study 2, bioconversion factors were calculated by taking into account the amount of retinol utilized during the treatment period by the negative control group and the amount of provitamin A carotenoids ingested.[27] α < 0.05 was considered significant.

RESULTS

Study 1. *In Vitro Digestion of Maize Genotypes.* Typically, when the βCX to βC ratio was <0.045, micellarized βCX was ≤6%. However, above this parameter, βCX was highly micellarized at all concentrations (Figure 1A). Incorporating all data points resulted in a positive relationship of βCX concentration and micellarization (P = 0.017). After removal of the βCX/βC < 0.045 maize genotypes (n = 6), the slope was not different from zero (P = 0.58). βC micellarization efficiency and total carotenoid micellarized had significant negative relationships with the amount in the maize (Figure 1, panels B and C, respectively, P < 0.0001). At lower βC concentrations, that is, < 5.5 μg/g maize, micellarization was 35.2 ± 12.6%; at concentrations >8.1 μg/g, it was 17.2 ± 6.6% (Figure 1B, P < 0.0001). The total amount of βCX + βC micellarized was stable across genotypes (Figure 1D, r = 0.12, P = 0.45).

Weights and Feed Intakes. Final gerbil body weights (73.0 ± 5.43 g) and liver weights (2.49 ± 0.46 g) were not different among groups. Feed intake differed among groups and therefore affected daily hypothetical and theoretical retinol intake (Table 1). Fiber differed by 1.5% (P = 0.048) and resistant starch by 1% (P < 0.0001) of total dietary content among the feeds (Table 1).

Tissue Concentrations. Serum retinol concentrations did not differ among groups (1.87 ± 0.90 μmol/L, data not shown). Total liver retinol and retinol concentrations differed among groups (Figure 2, P ≤ 0.0043). All biofortified maize groups showed no difference in liver retinol concentration from

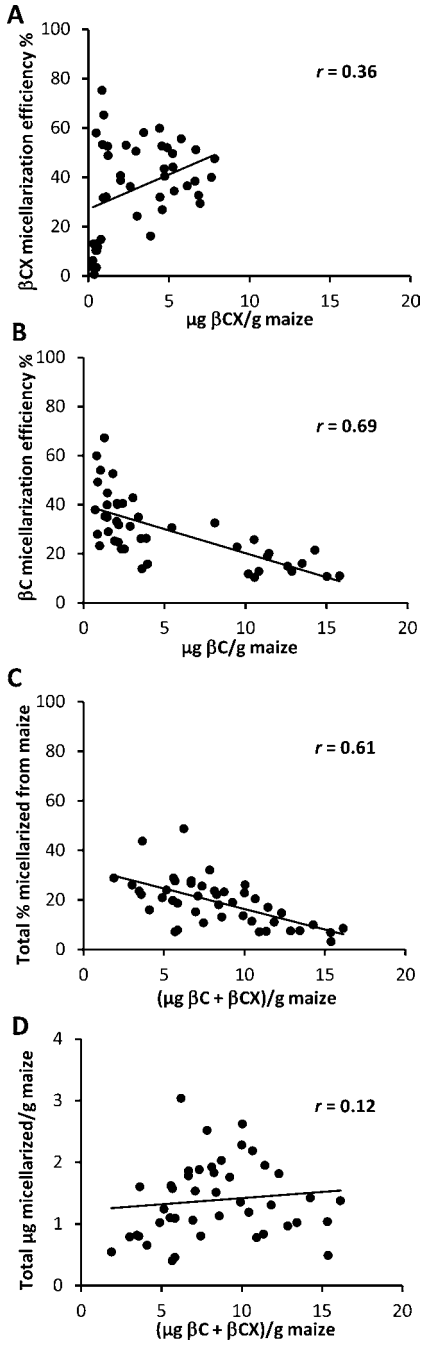

Figure 1. Micellarization efficiencies (concentration in aqueous micellar fraction/concentration in internal digesta × 100%) of provitamin A carotenoids from biofortified maize genotypes in relationship to the amount of the carotenoid, either β-cryptoxanthin (βCX, panel A) or β-carotene (βC, panel B); total percent micellarized [(μg βC + βCX in aqueous micellar fraction)/(μg βC + βCX in maize)] in relationship to (μg βC + βCX) in maize (panel C); total (βC + βCX) micellarized per gram maize in relationship to (μg βC + βCX) in maize (panel D). It is worth noting that the amount of total provitamin A carotenoid micellarized was the same across combined concentrations. Values are means ± SD.

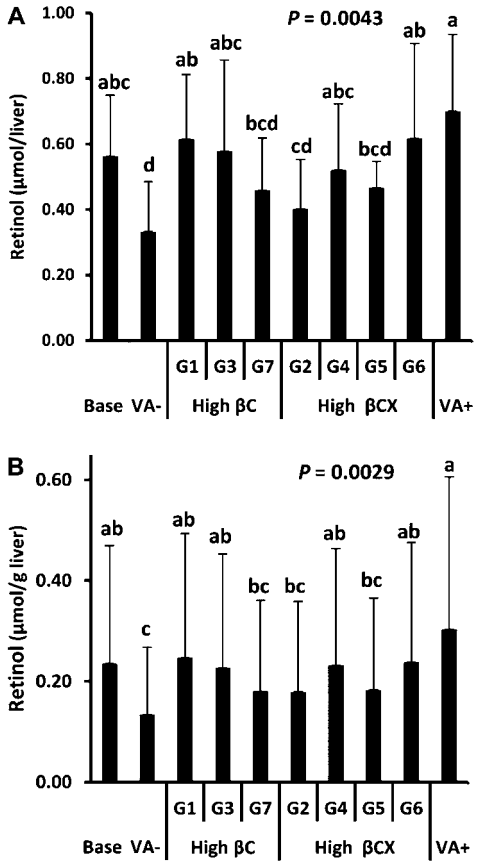

Figure 2. Total liver retinol (A) and retinol concentrations (B) from saponified livers in Mongolian gerbils at baseline after 5 weeks of being fed a vitamin A-free feed (base, n = 7) or fed vitamin A-free (VA−), 50% high β-carotene maize (G1, G3, G7), high β-cryptoxanthin maize (G2, G4, G5, G6), or vitamin A-free feed with daily retinyl acetate doses (VA+) in study 1 (n = 10/group). All other treatment groups received a plain oil dose matched to the VA+ group for 4 weeks. Values are means ± SD.

each other (Figure 2B), and all maize groups maintained baseline concentrations. When corrected for total retinol/liver by multiplying by liver weight, treatment groups differed, but remained similar to baseline. Two of three high-βC maize genotypes achieved liver retinol similar to VA+, whereas the other was not different from VA− (Figure 2A). Two of four high-βCX maize genotypes achieved total liver retinol similar to VA+, whereas the other two were not different from VA− (Figure 2A). When the theoretical retinol intakes (Table 1) are compared between the high-βC and -βCX groups, intakes differed (P = 0.010), but this difference was not reflected in the increase in liver retinol, which supports the hypothesis that βCX is as bioefficacious as βC on a molar level. The bioconversion factors calculated in reference to the VA in oil dose ranged from 1.2 to 6.1 μmol of provitamin A carotenoid to 1 μmol of retinol and did not differ between the high -βC and -βCX maize genotypes (Table 3).

Liver provitamin A carotenoid concentrations reflected those in the feeds and therefore differed (P < 0.0001). Total liver βCX was the same among the four high-βCX groups (0.754 ± 0.285 nmol/liver) and low in the high-βC groups (0.125 ± 0.203 nmol/liver). Although there were slight differences in βC concentrations in the high-βC groups, total liver βC did not differ among high-βC groups (3.21 ± 1.16 nmol/liver) or among the high-βCX groups (1.54 ± 0.53 nmol/liver). Combined βC and βCX concentrations per gram of liver [(nmol βC + nmol βCX)/g liver] did not differ among treatment groups, but total liver carotenoid amounts were different (P = 0.031), with more carotenoids generally found in

dx.doi.org/10.1021/jf403548w | J. Agric. Food Chem. 2014, 62, 136−143

Table 3. Bioconversion Factors in Mongolian Gerbils Fed High-β-Carotene or High-β-Cryptoxanthin Maize or 0.5% Freeze-Dried Carrots with Different Staple Food Matrices

	μmol provitamin A/ μmol retinol	μg provitamin A/ μg retinol	IOM reference[a]	% IOM value
Study 1				
high β-carotene				
G1	1.2	2.3	12.0	19
G3	1.5	2.8	12.0	23
G7	3.3	6.3	12.1	52
high β-cryptoxanthin				
G2	6.1	11.8	21.8	54
G4	2.3	4.4	21.5	20
G5	3.3	6.4	20.4	31
G6	1.6	3.0	21.6	14
Study 2				
carrot alone	3.2	6.0	15.1	40
rice matrix	3.0	5.7	15.2	38
potato matrix	2.7	5.1	15.0	34
banana matrix	4.4	8.2	15.3	54
maize matrix	4.6	8.5	15.0	57

[a]The Institute of Medicine (IOM) values[7] were calculated by determining the proportion of β-cryptoxanthin and α-carotene in the diet compared with the β-carotene and multiplying by the IOM values of 12:1 for β-carotene and 24:1 for β-cryptoxanthin and α-carotene.

the high-βC groups than in the high-βCX groups, which supports preferential bioconversion of βCX. Furthermore, the βCX/βC ratio in the feed and liver did not differ in the groups fed high-βC maize, but was much lower in the liver than in the feed in those fed high-βCX maize ($P = 0.0065$).

Study 2. *Carotenoid, Fiber, and Resistant Starch Concentrations and Micellarization.* The concentrations of αC and βC were higher in the BN feed than in other feeds ($P < 0.0001$) due to naturally occurring carotenoids in banana.[11] The theoretical retinol, based on 100% bioefficacy of all feeds (Table 1), exceeded gerbil requirements, which allowed for ample liver storage. Fiber content was lowest in RC feed and highest in the VA-free feeds ($P < 0.0001$). Resistant starch concentration was highest in the BN and RC feeds and lowest in controls ($P < 0.0001$). Micellarization efficiency did not differ or predict findings in vivo (Table 4; $r = 0.02$), where MZ resulted in lower liver retinol concentrations than PT, RC, BN, and CA (Figure 3).

Weights and Intakes. Final gerbil weights were higher in the BN and MZ (74.1 ± 6.2 g) groups than in CA, VA−, and RC groups (68.4 ± 3.0 g, $P = 0.0036$). Liver weights were highest in the PT group (2.61 ± 0.59 g) and lowest in the CA, RC, and BN groups (2.20 ± 0.27 g). Percent liver weight was higher in PT, MZ, and VA− groups (3.46 ± 0.53%) than in the BN group (2.91 ± 0.23%, $P = 0.020$). Feed ($P = 0.024$) and theoretical retinol intakes ($P < 0.0001$) were highest in the BN group and lowest in the RC group (Table 1).

Tissue Concentrations. Serum retinol concentrations did not differ (1.34 ± 0.19 μmol/L, data not shown). Total liver retinol was highest in the PT and BN groups and lowest in VA− (Figure 3A, $P < 0.0001$). Liver retinol concentrations did not differ among the PT, RC, BN, and CA groups, but the MZ group was lower and did not differ from baseline or VA− groups (Figure 3B, $P < 0.0001$). Total liver α-retinol differed (Figure 4A, $P < 0.0001$) and was highest in the BN group, which reflected the higher αC concentration. The MZ group had lower α-retinol than the BN and PT groups, but did not differ from the RC and CA groups. Liver α-retinol concentrations differed (Figure 4B, $P < 0.0001$) and were highest in the BN group followed by PT, RC, and CA groups, which did not differ, and MZ, which was lowest. Bioconversion factors were adjusted for differences in provitamin A carotenoid intakes and ranged from 2.7 μmol of carrot provitamin A from the PT matrix to 4.6 μmol from the MZ matrix, producing 1 μmol of retinol (36 ± 15% of IOM values; Table 3).

Table 4. Micellarization Efficiencies (Aqueous Divided by Digesta Fraction × 100) of α- and β-Carotene from 0.5% Freeze-Dried Carrot Powder Mixed with Staple Foods in Feeds Fed to Mongolian Gerbils in Study 2[a]

component	micelle fraction α-carotene (%)	micelle fraction β-carotene (%)	micelle fraction theoretical retinol (%)
60% potato	6.5 ± 5.0	5.7 ± 3.0	18 ± 5.3
60% rice	12 ± 7.4	13 ± 5.4	37 ± 11
60% banana	26 ± 20	14 ± 14	54 ± 23
60% maize	10. ± 0.2	12 ± 1.0	33 ± 11
carrot only	11 ± 5.0	9.0 ± 5.2	29 ± 8.3

[a]Values are means ± SD, $n = 3$/staple food. Methods were those of Thakkar et al.[16] as modified by Kean et al.[17] No differences in micellarized carotenoids were observed among the feeds ($P > 0.05$).

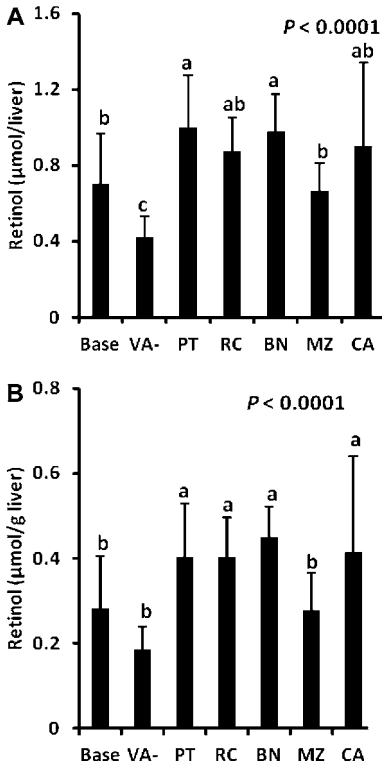

Figure 3. Total liver retinol (A) and retinol concentrations (B) from saponified livers in Mongolian gerbils at baseline after 4 weeks of being fed a vitamin A-free feed (base, $n = 6$) or fed 60% potato (PT), rice (RC), banana (BN), or maize (MZ) with 0.5% high β-carotene carrot or vitamin A-free feed with (CA) or without (VA−) 0.5% high β-carotene carrot for 4 weeks in study 2 ($n = 10$/group). Values are means ± SD.

dx.doi.org/10.1021/jf403548w | J. Agric. Food Chem. 2014, 62, 136−143

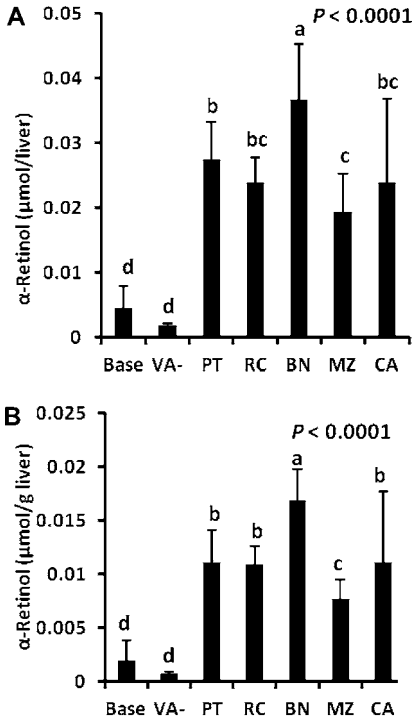

Figure 4. Total liver α-retinol (A) and liver α-retinol concentrations (B) from saponified livers in Mongolian gerbils at baseline after 4 weeks of being fed a vitamin A-free feed (base, n = 6) or fed 60% potato (PT), rice (RC), banana (BN), or maize (MZ) with 0.5% high β-carotene carrot or vitamin A-free feed with (CA) or without (VA−) 0.5% high β-carotene carrot for 4 weeks in study 2 (n = 10/group). Values are means ± SD.

The PT, RC, and BN (8.11 ± 3.27 nmol αC/liver) groups had more αC than the MZ and CA (4.01 ± 2.04 nmol αC/liver) groups (P = 0.0009). Similarly, βC was higher in the PT, RC, and BN (12.8 ± 5.77 nmol βC/liver) groups than in the MZ and CA (6.47 ± 3.41 nmol βC/liver) groups (P = 0.0025). Liver provitamin A carotenoid concentrations did not reflect those in the feeds. The ratio of αC to βC in the feeds (0.35 ± 0.02) was approximately half that in the liver (0.63 ± 0.04) (P < 0.0001), which may reflect preferential cleavage of βC. The ratio in the in vitro micellarized fraction was 0.49 ± 0.16, which is midway between these two ratios.

DISCUSSION

Biofortification of staple and horticultural crops with provitamin A carotenoids is a promising technique to diminish VA deficiency.[28,29] In study 1, percent total carotenoid and βC micellarized were negatively correlated with the total amount of provitamin A carotenoid, but the absolute amount micellarized remained relatively stable and was not related to genotype. βCX was not well-micellarized when concentrations were <0.5 μg/g and βC concentrations were >8 μg/g. Considering the physiochemical properties of micelles, several reasons explain these findings, which were consistent in this study and largely based on maize genotypes with a similar pedigree (entries 17, 19−22, and 27 in Supplemental Table 1 in the Supporting Information). In vitro, βCX likely did not meet a critical concentration needed for micelle incorporation in the genotypes that had a low βCX/βC.[30] Carotenoid interactions are well-documented;[31,32] therefore, the polarity difference between βC and βCX may not have allowed the βCX into the overwhelmingly nonpolar micellar microenvironment formed from the high βC content in these genotypes. Furthermore, the lipid profile differentially affects incorporation of xanthophyll and hydrocarbon carotenoids into micelles.[33] Future studies on maize lines that are close to commercialization should include characterization of the endogenous oil. Study 2 demonstrated good micellarization of αC and βC (6−26%) compared with other studies (0.2−16.7%),[18,31] but perhaps higher variability. This is due to the small amount of carrot added to the feed, which acts more like a fortificant and not an endogenous component, which may lead to higher variability among replicates.

In study 1, gerbil feeds were equalized for total carotenoid content by assuming that 1 mol of βC or βCX would supply 1 mol of retinol; βCX was as good as βC on a molar basis for maintaining VA status, confirming previous studies.[6,10] If 2 βCX/1 βC applied, the high-βC maize should have resulted in 2 times the amount of retinol over the high-βCX maize because of the hypothetical study design. Although the gerbils maintained balance, based on no difference from baseline regardless of feed, differences in liver reserves existed among genotypes. This important finding, not explained by fiber or resistant starch, demonstrates that other factors, such as endogenous interactive nutrients, must be investigated especially among commercial biofortified lines that are being developed and released.[28,34] A recent study in Zambian children showed a genotype effect with biofortified maize intake due to different cooking properties.[35] Furthermore, the current study was able to quantify βCX in the livers of gerbils fed biofortified maize. Although βCX was quantifiable in a study that fed fruits,[36] prior studies with maize did not find quantifiable βCX. Thus, the amounts in the maize likely exceeded gerbil requirements because βCX was absorbed intact and stored.

A review of human studies concluded that the apparent bioavailability of βCX is much higher than that of βC from Western foods.[37] Researchers need to consider resources available and the question being asked when selecting an experimental model. No animal model can replace human studies, but Mongolian gerbils are better predictors of provitamin A bioefficacy than rats or mice.[38] For example, the range of bioconversion factors among the maize genotypes in study 1 was 2.3−11.8 μg of provitamin A carotenoids to 1 μg of retinol, which is similar to the range from single test meals of biofortified maize in young U.S. women (3.9−13.3 μg of βC equivalents to 1 μg of retinol)[8] and Zimbabwean men (1.5−5.3 μg of βC equivalents to 1 μg of retinol).[9]

In study 2, α-retinol, retinol, αC, and βC were quantified. A negative matrix effect occurred on the uptake and storage of αC and βC from carrot and bioconversion to α-retinol and retinol when gerbils consumed 60% nixtamalized MZ feed, which was not found in the in vitro analysis. On the other hand, PT exhibited the least matrix effects. On the basis of the gerbil studies, in vitro digestion, which evaluates carotenoid release from the food matrix and micellarization, did not predict bioefficacy, which is regulated by in vivo processes, such as cellular uptake, bioconversion, and chylomicron packaging and secretion.

In agreement with a prior study in gerbils that were fed high-carotene carrot,[21] as αC increased, αC liver reserves increased; however, in that study, α-retinol was not quantified. Nonetheless, in a subsequent study, αC was as effective as βC in maintaining liver retinol reserves when fed at double the

amount, and quantification of α-retinol implied central cleavage of αC.[22] Bioconversion factors in that study revealed 2 αC to 1 βC, but factors were less efficient than IOM values for supplements.[7,22] In the current study, a small amount of carrot was fed so that the regulatory systems would not be overwhelmed by carotenoids. In the prior carrot study, the group that was fed high-carotene carrots had only 14% more retinol in the liver than the group fed typical orange carrots but had 120% more βC.[21] Although postabsorptive bioconversion occurs,[39] the major site for meeting daily retinol needs is bioconversion at the gut level. The relative amount of carotenoid fed affects bioconversion.[34] In humans and gerbils, extra dietary carotenoid that is not converted to retinol is absorbed and stored, but not currently considered when determining bioavailability. The βC absorbed from biofortified carrot and stored in the liver was 2650% higher in the prior study at 3.3%[21] than the current study at 0.5% of the feed. Carrot intake, in contrast to VA supplements, affects antioxidant capacity of tissues and may support optimal health.[40,41]

The food matrix effect on the uptake of carotenoids from MZ feed was not due to fiber because the CA feed had more fiber. Soluble fiber had no effect on βC efficacy when gerbils were fed orange sweet potato.[14] White maize, as in masa meal, is soaked in limewater (i.e., nixtamalized) to increase some nutrients' bioavailability, and other nutrients are sometimes added, which may have affected the bioavailability of the carrot carotenoids. If nixtamalization, which is widely practiced, does have a negative effect on carotenoid utilization, it needs to be further investigated in biofortifed maize products. The processed maize in this study had a negative impact on the bioconversion factor, which is a similar finding to commercially processed banana.[36] The BN group utilized endogenous carotenoids despite the presence of resistant starch, which is congruent with previous studies[11] and supported by the higher liver α-retinol. All of the mixed feeds maintained or enhanced total liver reserves by the addition of a small amount of carrot as a source of provitamin A carotenoids. As a global measure of bioavailability, the nanomoles/liver of (retinol + α-retinol + βC + αC) was summed after correction for the negative control group and differed among the treatments ($P = 0.05$). PT had the most desirable matrix, endogenous BN carotenoids are bioavailable, and nixtamalized MZ had the least desirable outcome for provitamin A bioefficacy from mixed food.

Determining the many factors that affect carotenoid absorption and utilization from biofortified and mixed foods is important for biofortification and nutrition education efforts to alleviate VA deficiency. Although biofortification of staple crops with provitamin A carotenoids is efficacious, adding a little carrot (and perhaps other high provitamin A fruits and vegetables) to the diet had a greater impact on VA status of the gerbils, which highlights the importance of multipronged approaches to eradicate VA deficiency.

■ ASSOCIATED CONTENT

Supporting Information

Supplemental Table 1. This material is available free of charge via the Internet at http://pubs.acs.org.

■ AUTHOR INFORMATION

Corresponding Author

*(S.A.T.) Mailing address: 1415 Linden Drive, UW—Madison, Madison, WI 53706, USA. Phone: (608) 265-0792. E-mail: sherry@nutrisci.wisc.edu. Reprints will not be available.

Present Addresses

‡(S.A.A.) Standard Process, Palmyra, WI, USA.

#(N.P.-R.) International Maize and Wheat Improvement Center (CIMMYT), Texcoco, Mexico.

Author Contributions

S.S. and S.C. conducted gerbil studies. S.S., B.G., and S.A.A. conducted in vitro analyses. S.S., B.G., and S.A.T. analyzed data. S.G. analyzed samples. N.P.-R. and K.V.P. selected and provided biofortified maize. P.W.S. provided high-βC carrots. S.A.T., N.P.-R., and K.V.P. designed research. S.S., B.G., and S.A.T. wrote the manuscript. All authors have read and approved the final version of the paper.

Funding

This work was supported by USDA Hatch WIS01528 (S.A.T.), an endowment to S.A.T. entitled "Friday Chair for Vegetable Processing Research", NIH Grant T32-DK007665 (B.G.), California Fresh Carrot Advisory Board (P.W.S.), and HarvestPlus Agreement 5204 (K.V.P.). HarvestPlus (www.harvestplus.org) is a global alliance of agriculture and nutrition research institutions working to increase the micronutrient density of staple food crops through biofortification. The views expressed do not necessarily reflect those of HarvestPlus.

Notes

The authors declare no competing financial interest.

■ ACKNOWLEDGMENTS

We thank Peter Crump for statistical assistance and Mario Ferruzzi's laboratory at Purdue University for the hands-on training of SAA in the in vitro analysis procedures.

■ ABBREVIATIONS USED

αC, α-carotene; BN, banana group; βC, β-carotene; βCX, β-cryptoxanthin; CA, carrot group; IOM, Institute of Medicine; MZ, maize group; PT, potato group; RC, rice group; UW, University of Wisconsin; VA, vitamin A

■ REFERENCES

(1) FAO. Agricultural commodities: profiles and relevant WTO negotiating issues, 2003; 5−25; http://www.fao.org/docrep/006/Y4343E/y4343e02.htm (accessed Oct 31, 2012).

(2) Nuss, E. T.; Tanumihardjo, S. A. Maize: a paramount staple crop in the context of global nutrition. *Compr. Rev. Food Sci. Food Saf.* **2010**, *9*, 417−436.

(3) Ortiz-Monasterio, J. I.; Palacios-Rojas, N.; Meng, E.; Pixley, K.; Trethowan, R.; Peña, R. J. Enhancing the mineral and vitamin content of wheat and maize through plant breeding. *J. Cereal Sci.* **2007**, *46*, 293−307.

(4) Howe, J. A.; Tanumihardjo, S. A. Carotenoid-biofortified maize maintains adequate vitamin A status in Mongolian gerbils. *J. Nutr.* **2006**, *136*, 2562−2567.

(5) Nuss, E. T.; Arscott, S. A.; Bresnahan, K.; Pixley, K. V.; Rocheford, T.; Hotz, C.; Siamusantu, W.; Chileshe, J.; Tanumihardjo, S. A. Comparative intake of white- versus orange-colored maize by Zambian children in the context of promotion of biofortified maize. *Food Nutr. Bull.* **2012**, *33*, 63−71.

(6) Davis, C.; Jing, H.; Howe, J. A.; Rocheford, T.; Tanumihardjo, S. A. β-Cryptoxanthin from supplements or carotenoid-enhanced maize maintains liver vitamin A in Mongolian gerbils (*Meriones unguiculatus*)

better than or equal to β-carotene supplements. *Br. J. Nutr.* **2008**, *100*, 786−793.
(7) Institute of Medicine. Food and Nutrition Board. *Dietary Reference Intakes for Vitamin A, Vitamin K, Arsenic, Boron, Chromium, Copper, Iodine, Iron, Manganese, Molybdenum, Nickel, Silicon, Vanadium, and Zinc*; National Academy Press: Washington, DC, 2001; pp 65−126.
(8) Li, S.; Nugroho, A.; Rocheford, T.; White, W. S. Vitamin A equivalence of the β-carotene in β-carotene-biofortified maize porridge consumed by women. *Am. J. Clin. Nutr.* **2010**, *92*, 1105−1112.
(9) Muzhingi, T.; Gadaga, T. H.; Siwela, A. H.; Grusak, M. A.; Russell, R. M.; Tang, G. Yellow maize with high β-carotene is an effective source of vitamin A in healthy Zimbabwean men. *Am. J. Clin. Nutr.* **2011**, *94*, 510−519.
(10) Davis, C. R.; Howe, J. A.; Rocheford, T. R.; Tanumihardjo, S. A. The xanthophyll composition of biofortified maize (*Zea mays* Sp.) does not influence the bioefficacy of provitamin A carotenoids in Mongolian gerbils (*Meriones unguiculatus*). *J. Agric. Food Chem.* **2008**, *56*, 6745−6750.
(11) Bresnahan, K. A.; Arscott, S. A.; Khanna, H.; Arinaitwe, G.; Dale, J.; Tushemereirwe, W.; Mondloch, S.; Tanumihardjo, J. P.; De Moura, F. F.; Tanumihardjo, S. A. Cooking enhances but the degree of ripeness does not affect provitamin A carotenoid bioavailability from bananas in Mongolian gerbils. *J. Nutr.* **2012**, *142*, 2097−2104.
(12) Brown, M. J.; Ferruzzi, M. G.; Nguyen, M. L.; Cooper, D. A.; Eldridge, A. L.; Schwartz, S. J.; White, W. S. Carotenoid bioavailability is higher from salads ingested with full-fat than with fat-reduced salad dressings as measured with electrochemical detection. *Am. J. Clin. Nutr.* **2004**, *80*, 396−403.
(13) Goltz, S. R.; Campbell, W. W.; Chitchumroonchokchai, C.; Failla, M. L.; Ferruzzi, M. G. Meal triacylglycerol profile modulates postprandial absorption of carotenoids in humans. *Mol. Nutr. Food Res.* **2012**, *56*, 866−877.
(14) Mills, J. P.; Tumuhimbise, G.; Jamil, K. M.; Thakkar, S.; Failla, M. L.; Tanumihardjo, S. A. Sweet potato β-carotene bioefficacy is enhanced by dietary fat and not reduced by soluble fiber intake in Mongolian gerbils. *J. Nutr.* **2009**, *139*, 44−50.
(15) Reboul, E.; Richelle, M.; Perrot, E.; Desmoulins-Malezet, C.; Pirisi, V.; Borel, P. Bioaccessibility of carotenoids and vitamin E from their main dietary sources. *J. Agric. Food Chem.* **2006**, *54*, 8749−8755.
(16) Thakkar, S. K.; Maziya-Dixon, B.; Dixon, A. G.; Failla, M. L. β-Carotene micellarization during in vitro digestion and uptake by Caco-2 cells is directly proportional to β-carotene content in different genotypes of cassava. *J. Nutr.* **2007**, *137*, 2229−2233.
(17) Kean, E. G.; Hamaker, B. R.; Ferruzzi, M. G. Carotenoid bioaccessibility from whole grain and degermed maize meal products. *J. Agric. Food Chem.* **2008**, *56*, 9918−9926.
(18) Thakkar, S. K.; Failla, M. L. Bioaccessibility of pro-vitamin A carotenoids is minimally affected by non pro-vitamin A xanthophylls in maize (*Zea mays* sp.). *J. Agric. Food Chem.* **2008**, *56*, 11441−11446.
(19) Chitchumroonchokchai, C.; Schwartz, S. J.; Failla, M. L. Assessment of lutein bioavailability from meals and a supplement using simulated digestion and Caco-2 human intestinal cells. *J. Nutr.* **2004**, *134*, 2280−2286.
(20) Granado-Lorencio, F.; Olmedilla-Alonso, B.; Herrero-Barbudo, C.; Pérez-Sacristan, B.; Blanco-Navarro, I.; Blazquez-García, S. Comparative in vitro bioaccessibility of carotenoids from relevant contributors to carotenoid intake. *J. Agric. Food Chem.* **2007**, *55*, 6387−6394.
(21) Dosti, M. P.; Mills, J. P.; Simon, P. W.; Tanumihardjo, S. A. Bioavailability of β-carotene (βC) from purple carrots is the same as typical orange carrots while high-βC carrots increase βC stores in Mongolian gerbils (*Meriones unguiculatus*). *Br. J. Nutr.* **2006**, *96*, 258−267.
(22) Tanumihardjo, S. A; Howe, J. A. Twice the amount of α-carotene isolated from carrots is as effective as β-carotene in maintaining the vitamin A status of Mongolian gerbils. *J. Nutr.* **2005**, *135*, 2622−2626.
(23) Howe, J. A.; Tanumihardjo, S. A. Evaluation of analytical methods for carotenoid extraction from biofortified maize (*Zea mays* sp.). *J. Agric. Food Chem.* **2006**, *54*, 7992−7997.
(24) Bressani, R.; Rooney, L. W.; Saldivar, S. O. S. *Fortification of Corn Masa Flour with Iron and/or Other Nutrients − a Literature and Industry Experience Review*; U.S. Agency for International Development: Washington, DC, 1997.
(25) Champ, M. Determination of resistant starch in foods and food products: interlaboratory study. *Eur. J. Clin. Nutr.* **1992**, *46*, S51−S62.
(26) Mertens, D. R. Gravimetric determination of amylase-treated neutral detergent fiber in feeds with refluxing in beakers or crucibles: collaborative study. *J. AOAC Int.* **2002**, *85*, 1217−1240.
(27) Mills, J. P.; Simon, P. W.; Tanumihardjo, S. A. β-Carotene from red carrot maintains vitamin A status, but lycopene bioavailability is lower relative to tomato paste in Mongolian gerbils. *J. Nutr.* **2007**, *137*, 1395−1400.
(28) Pixley, K.; Palacios-Rojas, N.; Babu, R.; Mutale, R.; Surles, R.; Simpungwe, E. Biofortification of maize with provitamin A carotenoids. In *Carotenoids and Human Health*; Tanumihardjo, S. A., Ed.; Springer Science and Business Media: New York, 2013; pp 271−292.
(29) Simon, P. W.; Bowman, M. J.; Tanumihardjo, S. A. Horticultural crops as a source of carotenoids. In *Carotenoids and Human Health*; Tanumihardjo, S. A., Ed.; Springer Science and Business Media: New York, 2013; pp 293−301.
(30) Moulik, S. P. Micelles: self-organized surfactant assemblies. *Curr. Sci.* **1996**, *71*, 368−376.
(31) Tyssandier, V.; Lyan, B.; Borel, P. Main factors governing the transfer of carotenoids from emulsion lipid droplets to micelles. *Biochim. Biophys. Acta* **2001**, *1533*, 285−292.
(32) Kostic, D.; White, W. S.; Olson, J. A. Intestinal absorption, serum clearance, and interactions between lutein and β-carotene when administered to human adults in separate or combined oral doses. *Am. J. Clin. Nutr.* **1995**, *62*, 604−610.
(33) Fernandez-Garcia, E.; Minguez-Mosquera, M. I.; Perez-Galvez, A. Changes in composition of the lipid matrix produce a differential incorporation of carotenoids in micelles. Interaction effect of cholesterol and oil. *Innovative Food Sci. Emerging Technol.* **2007**, *8*, 379−384.
(34) Tanumihardjo, S. A.; Palacios, N.; Pixley, K. V. Provitamin A carotenoid bioavailability: what really matters? *Int. J. Vitam. Nutr. Res.* **2010**, *80*, 336−350.
(35) Schmaelzle, S.; Kaliwile, C.; Arscott, S. A.; Gannon, B.; Masi, C.; Tanumihardjo, S. A. Nutrient and non-traditional food intakes by Zambian children in a controlled feeding trial. *Food Nutr. Bull.* **2014**, in press.
(36) Arscott, S. A.; Howe, J. A.; Davis, C. R.; Tanumihardjo, S. A. Carotenoid profiles in provitamin A-containing fruits and vegetables affect the bioefficacy in Mongolian gerbils. *Exp. Biol. Med.* **2010**, *235*, 839−848.
(37) Burri, B. J.; Chang, J. S. T.; Neidlinger, T. R. β-Cryptoxanthin- and α-carotene-rich foods have greater apparent bioavailability than β-carotene-rich foods in Western diets. *Br. J. Nutr.* **2011**, *105*, 212−219.
(38) Tanumihardjo, S. A. Mammalian models for understanding mechanisms of retinol and retinoid actions. In *WHO Technical Consultation on Vitamin A in Newborn Health: Mechanistic Studies*; World Health Organization: Geneva, Switzerland, 2012; pp 93−108.
(39) Tang, G.; Qin, J.; Dolnikowski, G. G.; Russell, R. M. Short-term (intestinal) and long-term (postintestinal) conversion of β-carotene to retinol in adults as assessed by a stable-isotope reference method. *Am. J. Clin. Nutr.* **2003**, *78*, 259−266.
(40) Mills, J. P.; Simon, P. W.; Tanumihardjo, S. A. Biofortified carrot intake enhances liver antioxidant capacity and vitamin A status in Mongolian gerbils. *J. Nutr.* **2008**, *138*, 1692−1698.
(41) Sun, T.; Simon, P. W.; Tanumihardjo, S. A. Antioxidant phytochemicals and antioxidant capacity of biofortified carrots (*Daucus carota* L.) of various colors. *J. Agric. Food Chem.* **2009**, *57*, 4142−4147.

JOURNAL OF AGRICULTURAL AND FOOD CHEMISTRY

Article

pubs.acs.org/JAFC

Radical-Scavenging Compounds from Olive Tree (*Olea europaea* L.) Wood

Mercedes Pérez-Bonilla,[†] Sofía Salido,[†] Teris A. van Beek,[‡] and Joaquín Altarejos*[,†]

[†]Departamento de Química Inorgánica y Orgánica, Facultad de Ciencias Experimentales, Universidad de Jaén, Campus de Excelencia Internacional Agroalimentario, ceiA3, 23071 Jaén, Spain

[‡]Laboratory of Organic Chemistry, Natural Products Chemistry Group, Wageningen University, Dreijenplein 8, Wageningen, Huet Brothers 6703, The Netherlands

ABSTRACT: The purpose of this study was to complete knowledge on the chemical composition and radical-scavenging activity of olive tree wood. Two new monoterpene glycosides, (−)-oleuropeic acid 6′-*O*-α-D-glucopyranosyl ester (**6a**) and (−)-perillic acid 1′-*O*-β-D-primeverosyl ester (**8**), together with the known compounds (−)-oleuropeic acid (**1**), (−)-olivil (**2**), the aldehydic form of oleuropein aglycone (**3**), (+)-1-hydroxypinoresinol 1-*O*-β-D-glucopyranoside (**4**), (−)-oleuropeic acid 1′-*O*-β-D-glucopyranosyl ester (**5**), (−)-oleuropeic acid 6′-*O*-β-D-glucopyranosyl ester (**6b**), and (−)-olivil 4-*O*-β-D-glucopyranoside (**7**) were isolated from an ethyl acetate extract. The radical scavengers found (**2**−**4** and **7**) were detected and isolated with the help of the online HPLC-DAD-DPPH/ABTS technique. Compounds **2**−**4** and **7** displayed a higher antioxidative effect against the free radical DPPH than the reference BHT and lower than hydroxytyrosol, whereas compounds **1**, **5**, **6a**, **6b**, and **8** showed no activity.

KEYWORDS: *olive tree wood, Olea europaea, agricultural byproducts, online HPLC-DAD-radical-scavenging technique, (−)-oleuropeic acid, (−)-olivil, aldehydic form of oleuropein aglycone, (+)-1-hydroxypinoresinol 1-O-β-D-glucopyranoside, (−)-oleuropeic acid 1′-O-β-D-glucopyranosyl ester, (−)-oleuropeic acid 6′-O-α-D-glucopyranosyl ester, (−)-oleuropeic acid 6′-O-β-D-glucopyranosyl ester, (−)-olivil 4-O-β-D-glucopyranoside, (−)-perillic acid 1′-O-β-D-primeverosyl ester*

INTRODUCTION

Reactive oxygen species (ROS) are widely believed to cause or aggravate several human pathologies such as neurodegenerative diseases, cancer, stroke, and many other ailments.[1] ROS are also the main factor responsible for complete spoilage of lipid-containing foods.[2] For both reasons antioxidants are of great importance nowadays in medicine and in the food industry. In the latter field, some concerns have been expressed about the safety of certain synthetic (artificial) antioxidants commonly used to preserve food, such as *tert*-butylhydroquinone (TBHQ) and *tert*-butyl-4-hydroxyanisole (BHA),[3] which has driven much attention to natural antioxidants and the search of new plant sources containing them. Thus, much work has been done to find interesting sources of potentially safe natural antioxidants in any material of vegetable origin, such as medicinal plants,[4] foods, and drinks,[5] etc., or even in agroindustrial waste materials.[6]

The olive tree (*Olea europaea* L., Oleaceae) is one the most important fruit trees in the Mediterranean countries. The chemical composition of the tree and that of olive oil has been intensively studied for years.[7−9] Among the phytochemicals reported in olive tree, the phenolic compounds constitute an interesting group whose presence has been investigated in practically all parts of the plant: fruits,[10] leaves,[11] stems,[12] bark,[13] wood,[14] stones,[15] and roots.[16] Due to the high interest of phenolic compounds for the food and pharmacy industries great efforts are also being directed toward their recovery from any byproducts and residues generated in olive oil industrial production.[17]

Olive tree wood constitutes a very important agricultural byproduct since large amounts of biomass from pruning are generated every year in all olive oil producing countries. Just in Spain more than 7 million tonnes per year are produced of this biomass, which consists mainly of wood together with leaves and small stems. Olive tree wood is an untapped resource since nowadays it is basically used for house heating in rural areas. For that reason, alternative uses for olive tree wood are being investigated such as a raw material for production of activated carbon,[18] lignin,[19] cellulose pulp,[20] and bioethanol[21] or as a fuel source.[22] However, no information is available on the antioxidant activity of the extracts obtained from this part of the olive tree, with the exception of our previous work.[14,23−25] With the help of HPLC online assay for antioxidants,[26] we detected and isolated the active components of ethyl acetate and ethanol extracts of olive tree wood:[14,24,25] oleuropein, ligustroside, hydroxytyrosol, (+)-cycloolivil, oleuropein-3″-methyl ether, (7″*R*)-7″-ethoxyoleuropein, (7″*S*)-7″-ethoxyoleuropein, (7″*S*)-7″-hydroxyoleuropein, ligustroside 3′-*O*-β-D-glucoside, oleuropein 3′-*O*-β-D-glucoside, jaspolyanoside, jaspolyoside, and isojaspolyoside A (Figure 1). In addition, during the purification work of antioxidants, other compounds which exhibited weak antioxidant activity, such as tyrosol (Figure 1), were also isolated.[24] Two of these compounds, oleuropein and (+)-cycloolivil, were included in a study to determine their

Received: September 20, 2013
Revised: December 7, 2013
Accepted: December 11, 2013
Published: December 11, 2013

ACS Publications © 2013 American Chemical Society

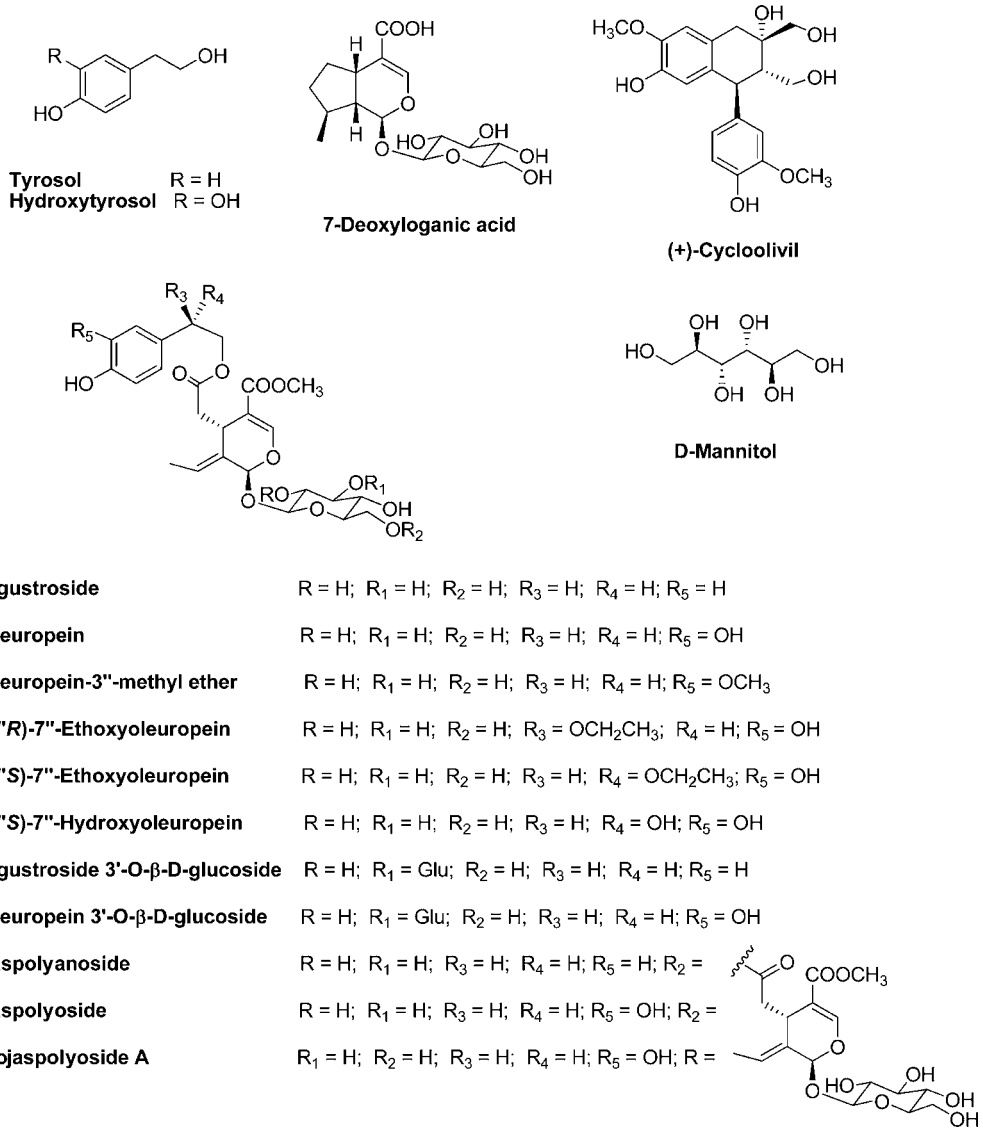

Figure 1. Compounds previously isolated from olive tree wood.[14,24,25,28]

antiplatelet aggregation properties.[27] More recently, a procedure to obtain D-mannitol and elenolic acid from olive tree wood, along with extracts enriched in antioxidants hydroxytyrosol and oleuropein, have been patented by us.[28] Similarly, further work has been reported by others on the composition and applications of fractions obtained from olive tree wood[29−32] and also from the whole byproduct obtained during pruning work on olive grooves.[33−37]

All the work developed on radical scavengers from olive tree wood extracts shows that this agricultural byproduct could become a very interesting source of natural antioxidants, as commercial olive leaf extracts already are,[38] i.e., further research is needed. Thus, in this work, an additional activity-guided isolation of antioxidants from olive tree wood and evaluation of their antioxidant activities are reported. To perform the study, the online HPLC-DAD-DPPH/ABTS technique has been used, since it has demonstrated to be a very useful tool for rapid identification of antioxidants in plant extracts, foods, and beverages.[39,40] This work complements previous studies from our laboratory to give an overall picture of the chemical constituents present in olive tree wood, a renewable source of natural antioxidants rather unknown until a few years ago.

MATERIALS AND METHODS

General Experimental Procedures. Optical rotations ($[\alpha]_D$) were recorded in methanol on a Perkin-Elmer 241 automatic polarimeter (Perkin-Elmer Instruments, Norwalk, CT, USA) in a 10 cm 2 mL cell. UV spectra were obtained in methanol on a Perkin-Elmer Lambda 19 UV/vis/NIR spectrophotometer (Perkin-Elmer Instruments, Norwalk, CT, USA). IR spectra were measured, in liquid films (neat) between KBr plates, on a Perkin-Elmer model 1760X FTIR spectrometer (Perkin-Elmer Instruments, Norwalk, CT, USA). ^{1}H (400 MHz), ^{13}C (100 MHz), and 2D NMR (500 MHz) spectra were taken on Bruker DPX 400 and Bruker AMX 500 spectrometers (Bruker Daltonik GmbH, Rheinstetten, Germany) using CD_3OD as solvent and tetramethylsilane (TMS) as internal reference. When necessary, due to small amounts of samples, NMR spectra were recorded using SHIGEMI tubes (Campro Scientific, The Netherlands) and a Zirconia zircon oxide rotor (Wilmad Labglass, USA). Mass spectra were recorded on two different mass spectrometers: (a) a Hewlett-Packard model HP 5989B mass spectrometer (Agilent Technologies, Santa Clara, CA, USA) using the electron impact ionization method (70 eV), ion source temperature of the MS unit = 250 °C, scan range from m/z 35 to m/z 400 and (b) a Finnigan MAT LCQ ion trap mass spectrometer (Waters Integrity System, Milford, MA, USA) with ESI interface used in both modes, with a capillary temperature of 200 °C and spray voltage of −4.5 kV. High-resolution

dx.doi.org/10.1021/jf403998t | J. Agric. Food Chem. 2014, 62, 144−151

Table 1. ^{1}H and ^{13}C NMR Spectroscopy Data (400 MHz, CD_3OD) and HMBC (500 MHz, CD_3OD) Correlations of Compounds 6a and 6b

	(−)-oleuropeic acid 6′-*O*-α-D-glucopyranosyl ester (**6a**)			(−)-oleuropeic acid 6′-*O*-β-D-glucopyranosyl ester (**6b**)		
position	δ_H mult. (*J*, Hz)	δ_C, mult.	HMBC	δ_H mult. (*J*, Hz)	δ_C, mult.	HMBC
1		131.2, qC			131.2, qC	
2	6.97−7.00, m	141.4, CH	3, 4, 6, 7	6.97−7.00, m	141.4, CH	3, 4, 6, 7
3ax	1.92−2.03, m	28.5, CH_2	1, 2, 4, 6, 8, CH_3-8	1.92−2.03, m	28.5, CH_2	1, 2, 4, 6, 8, CH_3-8
3eq	2.26−2.33, m		1, 2, 4, 5	2.26−2.33, m		1, 2, 4, 5
4	1.45−1.53, m	45.5, CH	3, 5, 6, 8, CH_3-8, CH_3′-8,	1.45−1.53, m	45.5, CH	3, 5, 6, 8, CH_3-8, CH_3′-8,
5ax	1.13−1.21, m	24.5, CH_2	1, 3, 4, 6, 8	1.13−1.21, m	24.5, CH_2	1, 3, 4, 6, 8
5eq	1.92−2.03, m		1, 2, 3, 4, 8, CH_3-8	1.92−2.03, m		1, 2, 3, 4, 8, CH_3-8
6ax	2.04−2.14, m	26.3, CH_2	1, 3	2.04−2.14, m	26.3, CH_2	1, 3
6eq	2.43−2.50, m		1, 2, 4, 5, 7	2.43−2.50, m		1, 2, 4, 5, 7
7		168.9, qC			168.9, qC	
8		72.8, qC			72.8, qC	
CH_3-8	1.13, s	26.4, CH_3	3, 4, 5, 8, CH_3′-8	1.13, s	26.4, CH_3	3, 4, 5, 8, CH_3′-8
CH_3′-8	1.13, s	27.0, CH_3	3, 4, 5, 8, CH_3-8	1.13, s	27.0, CH_3	3, 4, 5, 8, CH_3-8
1′	5.03, d (3.7)	94.0, CH	3′, 5′	4.44, d (7.8)	98.2, CH	2′, 3′, 5′
2′	3.27−3.35, m	73.8, CH	3′, 5′, 6′	3.27−3.35, m	77.9, CH	4′
3′	3.63, t (9.3)	74.8, CH	1′, 2′, 4′	3.09, t (8.5)	76.2, CH	1′, 2′
4′	3.27−3.35, m	72.0, CH	5′, 6′	3.27−3.35, m	71.7, CH	2′, 3′, 5′, 6′
5′	3.94, ddd (1.9, 5.1, 9.3)	70.8, CH	3′, 4′	3.44−3.49, m	75.4, CH	3′, 4′
6′a	4.34, dd (1.9, 11.3)	64.8, CH_2	7, 4′, 5′	4.40, dd (1.7, 12.1)	64.8, CH_2	7, 4′, 5′
6′b	4.21, dd (5.1, 11.3)		7, 4′, 5′	4.19, dd (5.8, 12.1)		7, 5′

mass spectra (HRESIMS) were recorded on a Waters Micromass AutoSpec NT spectrometer (Waters Integrity System, Milford, MA, USA). Silica gel 60 (Merck), particle size 40−63 μm, was used for column chromatography. Silica gel 60 F_{254} precoated aluminum sheets (0.25 mm, Merck) were employed for thin-layer chromatography (TLC). High-performance liquid chromatography (HPLC) analyses were performed by an analytical RP-HPLC (Spherisorb ODS-2 column, 250 mm × 3 mm i.d., 5 μm, Waters Chromatography Division, Milford, MA, USA) on a Waters 600E instrument (Waters Chromatography Division, Milford, MA, USA) equipped with a diode array detector, scan range = 190−800 nm (Waters CapLC 2996 Photodiode Array Detector, Waters Chromatography Division, Milford, MA, USA), and operating at 30 °C. Samples of the extracts were prepared in MeOH at a concentration of 10 mg/mL, and the injection volume was 10 μL. The best separation was obtained with H_2O:CH_3COOH, 99.8:0.2 v/v (solvent A), and CH_3OH:CH_3COOH, 99.8:0.2, v/v (solvent B), at a flow rate of 0.7 mL/min: linear gradient from 20% to 70% B for 55 min and another 10 min to return to the initial conditions. Preparative HPLC separations were performed with a Alltima C18 column (250 mm × 22 mm i.d., 5 μm, Alltech Associates Inc., Deerfield, IL, USA) on a Shimadzu preparative HPLC instrument (Shimadzu, Kyoto, Japan) equipped with a diode array detector, scan range = 190−600 nm (SPD-M10Ap Photodiode Array Detector, Shimadzu, Kyoto, Japan), and a sample collector FRC-10A (Shimadzu, Kyoto, Japan), operating at 30 °C and a flow rate of 12 mL min^{-1}.

Chemicals. Solvents used for extraction and chromatographic separation (dichloromethane, ethyl acetate, ethanol, and chloroform) were glass distilled prior to use. Methanol used for radical-scavenging activity assays was of HPLC grade. Deuterated methanol was used to prepare solutions of purified compounds for NMR analysis. The following reagents were used for radical-scavenging assays: 2,2-diphenyl-1-picrylhydrazyl radical ($DPPH^{\bullet}$) (95%, Sigma-Aldrich Chemie, Steinheim, Germany), 2,2′-azino-bis(3-ethylbenzothiazoline-6-sulfonic acid) diammonium salt (ABTS) (95%, Fluka Chemie, Buchs, Switzerland), potassium persulfate (99%, Sigma-Aldrich Chemie, Steinheim, Germany), NaCl (99%, Panreac, Barcelona, Spain), KH_2PO_4 (99.5%, Riedel de Haën, Seeize, Germany), Na_2HPO_4 (99.5%, Riedel de Haën, Seeize, Germany), KCl (99%, Panreac, Barcelona, Spain), hydroxytyrosol (Extrasynthese, Genay, France), and 2,6-di-*tert*-butyl-hydroxytoluene (BHT) (99%, Sigma-Aldrich Chemie, Steinheim, Germany).

Plant Material. The wood sample of *O. europaea* L. (Picual variety) used in this study was collected from the pruning of a tree growing near the town of Fuensanta (province of Jaén, Spain) in April 2003 and consisted of a single piece of 25 cm diameter and 70 cm length. The sample was stored for 3 months in a dry and dark place at room temperature with passive ventilation prior to extraction. Just before starting the extraction process, the wood piece was scraped in a local sawmill (wood shavings length 3−5 cm, thickness 0.1−0.3 mm).

Extraction and Prefractionation of Olive Wood Extract. Nine individual but identical batches of 250 g of wood chips (9 × 250 g) were extracted successively by maceration during 24 h at room temperature with dichloromethane (9 × 3.5 L) and then for 2 h at reflux with ethyl acetate (9 × 3.5 L). Solvents were evaporated under reduced pressure to give the corresponding dichloromethane (9.2 g) and ethyl acetate (31.2 g) extracts. An aliquot of the ethyl acetate extract (23.4 g) was chromatographed by open column chromatography on silica gel 60 (230 g, 40−63 μm) using $CHCl_3$:EtOH mixtures of increasing polarity. Fractions of 350 mL were collected, monitored by TLC, pooled, and evaporated to give 11 major fractions: C_1 (0.38 g), C_2 (2.75 g), C_3 (3.35 g), C_4 (3.17 g), C_5 (4.98 g), C_6 (4.00 g), C_7 (1.09 g), C_8 (1.17 g), C_9 (0.60 g), C_{10} (1.27 g), and C_{11} (0.20 g).

Activity-Guided Chromatographic Isolation of Antioxidants. Fractions C_1−C_{11} were assessed for their ability to scavenge the DPPH radical by the offline spectrophotometric DPPH assay (calculated as radical-scavenging percentage, RSP) according to the procedure described below. Among all these fractions, the most active ones were C_3, C_5, C_4, and C_6, with RSP values of 91.8%, 90.4%, 76.9%, and 55.6%, respectively. These active fractions were further monitored by online HPLC-DAD-DPPH/ABTS assays to detect the active components present in each fraction according to the procedure described below. Thus, analysis of fraction C_5 revealed that the active constituent was the previously isolated antioxidant oleuropein (Figure 1),[14] and analyses of fractions C_3, C_4, and C_6 showed the presence of some further minor active constituents not reported yet. Accordingly, fraction C_3 (3.3 g) was subjected to silica gel 60 (235 g, 40−63 μm) column chromatography using $CHCl_3$:EtOH mixtures of increasing polarity. Fractions of 50 mL were collected and combined on the basis of TLC into 16 fractions (C_3-I−C_3-XVI). These latter fractions were again monitored by the online assays, which allowed focusing attention

on fractions C_3-VII and C_3-X. Thus, an aliquot of fraction C_3-VII (101 mg) was further chromatographed by preparative RP-HPLC. Separation was carried out with H_2O:CH_3COOH, 99.8:0.2 v/v (solvent A), and CH_3OH:CH_3COOH, 99.8:0.2 v/v (solvent B): isocratic conditions of 25% B for 10 min and then a linear gradient from 25% to 30% B in 10 min yielded pure compound **1**: (−)-oleuropeic acid (10 mg). An aliquot of fraction C_3-X (104 mg) was further chromatographed by preparative RP-HPLC. Separation was carried out with isocratic conditions of 30% B for 25 min yielding pure compound **2**: (−)-olivil (17.3 mg). Fraction C_4 (3.0 g) was subjected to silica gel 60 (177 g, 63−200 μm) column chromatography using $CHCl_3$:EtOH mixtures of increasing polarity. Fractions of 50 mL were collected and combined on the basis of TLC into 20 fractions (C_4-I−C_4-XX). These latter fractions were again monitored by online assays. This allowed focusing attention on fraction C_4-III (10.4 mg), which was identified as pure compound **3**: the aldehydic form of oleuropein aglycone. Fraction C_6 (4.0 g) was fractionated by column chromatography over silica gel 60 (180 g, 40−63 μm) and eluted with $CHCl_3$:EtOH mixtures of increasing polarity. Fractions of 50 mL were collected and combined on the basis of TLC into 13 fractions (C_6-I−C_6-XIII). These latter fractions were again monitored by online assays. This allowed focusing attention on fractions C_6-VIII, C_6-X, and C_6-XII. An aliquot of fraction C_6-VIII (237 mg) was further chromatographed by preparative RP-HPLC. Separation was carried out with a linear gradient from 25% to 40% B in 40 min yielding pure compound **4**: (+)-1-hydroxypinoresinol 1-*O*-β-D-glucopyranoside (5.1 mg). An aliquot of fraction C_6-X (207.2 mg) was further separated by preparative RP-HPLC. Separation was carried out with H_2O:CH_3OH:CH_3COOH, 79.8:20:0.2 v/v (solvent C), and CH_3OH:CH_3COOH, 99.8:0.2 v/v (solvent B); isocratic conditions of 15% B for 5 min and then a linear gradient from 15% to 100% B in 30 min to yield pure compound **5**: (−)-oleuropeic acid 1′-*O*-β-D-glucopyranosyl ester (4.5 mg). Similarly, another aliquot of fraction C_6-X (31.4 mg) was further separated by preparative RP-HPLC with isocratic conditions of 10% B for 60 min to yield a mixture of compounds **6a** ((−)-oleuropeic acid 6′-*O*-α-D-glucopyranosyl ester) and **6b** ((−)-oleuropeic acid 6′-*O*-β-D-glucopyranosyl ester) (8.3 mg). Fraction C_6-XII (1.1 g) was chromatographed on silica gel 60 (172 g, 40−63 μm), eluting with a 90:10 EtOAc:EtOH mixture. Fractions of 30 mL were collected and combined on the basis of TLC into 13 fractions (C_6-XIIa−C_6-XIIm). These latter fractions were again monitored by online assays. This allowed focusing attention on fraction C_6-XIIj. Thus, an aliquot of fraction C_6-XIIj (214.1 mg) was further separated by preparative RP-HPLC with isocratic conditions of 15% B for 10 min and then a linear gradient from 15% to 100% B in 20 min to yield pure compound **7**: (−)-olivil 4-*O*-β-D-glucopyranoside (7.5 mg). Finally, another aliquot of fraction C_6-XIIj (91.8 mg) was further separated by preparative RP-HPLC with a linear gradient from 20% to 70% B in 55 min to yield pure compound **8**: (−)-perillic acid 1′-*O*-β-D-primeverosyl ester (3.5 mg).

Structural Elucidation of New Natural Products. *(−)-Oleuropeic Acid 6′-O-α/β-D-Glucopyranosyl Esters (**6a** and **6b**).* Yellowish syrup; UV (MeOH) λ_{max} (log ε) 218.8 (3.8) nm; IR (neat) ν_{max} 3384, 2925, 1701, 1649, 1384, 1258, 1058 cm^{-1}; ESIMS *m*/*z* 369.2 ($[M + Na]^+$), 345.2 ($[M - H]^-$); HRESIMS *m*/*z* 347.1701 $[M + H]^+$ (calcd for $C_{16}H_{27}O_8$, 347.3856), 391.1594 $[M + HCOO]^-$ (calcd for $C_{17}H_{27}O_{10}$, 391.3954); ^1H and ^{13}C NMR, see Table 1.

*(−)-Perillic Acid 1′-O-β-D-Primeverosyl Ester (**8**).* Yellowish syrup; $[\alpha]_D^{25}$ −41° (*c* 0.10, MeOH); UV (MeOH) λ_{max} (log ε) 222 (3.6), 302.8 (2.9) nm; IR (neat) ν_{max} 3356, 1702, 1654, 1070 cm^{-1}; ESIMS *m*/*z* 483.2 ($[M + Na]^+$), 942.7 $[2M + Na]^+$, 459.1 $[M - H]^-$, 919.0 $[2M - H]^-$; HRESIMS *m*/*z* 483.1831 $[M + Na]^+$ (calcd for $C_{21}H_{32}O_{11}Na$, 483.4683), 505.1927 $[M + HCOO]^-$ (calcd for $C_{22}H_{33}O_{13}$, 505.4962); ^1H and ^{13}C NMR, see Table 2.

Offline Spectrophotometric DPPH Assay. Radical-scavenging activity of chromatographic fractions, purified compounds, and reference compounds was determined spectrophotometrically with the stable DPPH radical.[41] Methanolic solutions (2.4 mL) of DPPH• (~7×10^{-5} M) with an absorbance at 515 nm of 0.80 ± 0.03 AU were mixed with methanolic solutions (1.2 mL) of samples at different concentrations by dissolving the dry samples in methanol. The experiment was carried out in triplicate. Samples were shaken and kept in the dark for 15 min at room temperature, and then the decrease of absorbance was measured at 515 nm.

Radical-scavenging activity of chromatographic fractions, using a concentration of 50 μg/mL, is expressed as radical-scavenging percentage (RSP) and was calculated by the following formula[41]

$$\mathrm{RSP} = \left[\frac{A_B - A_A}{A_B}\right] \times 100$$

where A_B is the absorbance of the blank (t = 0 min) and A_A is the absorbance of tested sample solution (t = 15 min).

Radical-scavenging activity of purified and reference compounds, using different concentrations (4−100 μg/mL), is expressed in terms of the antioxidant concentration (μM) required to decrease the initial DPPH• concentration by 50% (efficient concentration, EC_{50}). The percentage of DPPH• remaining, calculated by the following equation[42]

$$\%\mathrm{DPPH}_{rem} = \frac{[\mathrm{DPPH}]}{[\mathrm{DPPH}]_0} \times 100$$

where [DPPH] is the concentration of DPPH• at the time measured (t = 15 min) and $[DPPH]_0$ is the initial concentration of DPPH• (t = 0 min), was plotted against the sample concentration (μg/mL), a linear or logarithmic regression curve being established in order to calculate the EC_{50}.

Online HPLC-DAD-DPPH/ABTS Assays. Online HPLC radical-scavenging assays of the fractions from the olive tree wood ethyl acetate extract were performed to detect active compounds in complex mixtures.[39] The setup for online assessment of radical-scavenging

Table 2. ^1H and ^{13}C NMR Spectroscopy Data (400 MHz, CD_3OD) and HMBC (500 MHz, CD_3OD) Correlations of Compound 8

	(−)-perillic acid 1′-*O*-β-D-primeverosyl ester (**8**)		
position	δ_H mult. (*J* in Hz)	δ_C, mult.	HMBC
1		130.51, qC	
2	7.14, bs	142.50, CH	6, 7
3eq	2.34−2.49, m	32.27, CH_2	2
3ax	2.16−2.27, m		
4	2.34−2.49, m	41.36, CH	
5eq	1.85−1.97, m	28.18, CH_2	
5ax	1.44−1.56, m		3, 4
6eq	2.34−2.49, m	25.41, CH_2	
6ax	2.16−2.27, m		
7		167.26, qC	
8		150.02, qC	
9a	4.76, s	109.79, CH_2	4, 10
9b	4.73, s		4, 10
10	1.75, s	20.87, CH_3	4, 8, 9
1′	5.49, d (7.5)	95.74, CH	7
2′	3.35−3.50, m	73.92, CH	1′, 4′
3′	3.50−3.56, m	77.75,[a] CH	2′
4′	3.35−3.50, m	70.96,[b] CH	
5′	3.35−3.50, m	77.88,[a] CH	
6′a	4.08, bd (11.2)	69.42, CH_2	3′, 4′, 1″
6′b	3.70, dd (4.8, 11.2)		
1″	4.27, d (7.5)	105.14, CH	6′, 5″
2″	3.12−3.21, m	74.87, CH	1″, 4″
3″	3.35−3.50, m	77.70,[a] CH	5″
4″	3.35−3.50, m	71.16,[b] CH	
5″a	3.83, dd (5.8, 11.3)	66.91, CH_2	1″, 3″, 4″
5″b	3.12−3.21, m		1″

[a]Interchangeable signals. [b]Interchangeable signals.

dx.doi.org/10.1021/jf403998t | J. Agric. Food Chem. 2014, 62, 144−151

activity consisted of an eluent pump, a photodiode array detector, and a Agilent 1100 Series controller, equipped with a C18 Waters Spherisorb S5 ODS2 (250 × 3 mm, 5 μm) analytical column. Methanolic solutions of fractions were prepared by dilution in methanol at a concentration of 10 mg/mL, and the injection volume was 10 μL. Separation was performed by a linear gradient from 20% to 70% B in 55 min, isocratic hold at 100% B for 5 min, linear gradient from 100% to 20% B in 10 min, and 10 min isocratic hold at 20% B for re-equilibration of the column. After HPLC separation and UV detection, the flow was mixed with a methanolic DPPH$^{\bullet}$ solution or an ABTS$^{\bullet+}$ solution in PBS.[43] Radical solutions were delivered using a Gilson model 302 pump at 0.5 mL/min for both DPPH$^{\bullet}$ and ABTS$^{\bullet+}$ solutions. The reaction between separated compounds and radicals took place in a 3.5 m × 0.25 mm i.d. PEEK reaction coil. The decrease in absorbance was measured at 515 nm for DPPH$^{\bullet}$ and at 414 nm for ABTS$^{\bullet+}$ in an Applied Biosystems UV/vis 759A spectrophotometer equipped with a tungsten lamp.

RESULTS AND DISCUSSION

Isolation of Compounds from the Olive Wood Extract. Olive wood chips were sequentially extracted with dichloromethane and ethyl acetate at room temperature and under reflux conditions, respectively. Dichloromethane extraction (0.4% yield) allowed removing the nonpolar components, which showed low antioxidant activity.[25] The resulting ethyl acetate extract (1.4% yield) was prefractionated by open column chromatography on silica gel, yielding 11 major fractions (C_1−C_{11}). These fractions were assessed for their ability to scavenge the DPPH radical by offline spectrophotometric measurements. This approach was chosen because it is generally known that lipid oxidation is initiated by a free radical attack and due to their simplicity and worldwide acceptance for comparative purposes. Among all these fractions, in terms of DPPH radical-scavenging percentages (RSP), the most active fractions were, in this order, C_3 (14.3% yield), C_5 (21.3% yield), C_4 (13.5% yield), and C_6 (17.1% yield). These active fractions were further monitored by online HPLC-DAD-DPPH/ABTS assays to detect the active components present in each fraction.[14] After a combination of conventional silica gel column chromatography and preparative RP-HPLC the following antioxidants were finally isolated: (−)-olivil (**2**), the aldehydic form of oleuropein aglycone (**3**), (+)-1-hydroxypinoresinol 1-*O*-*β*-D-glucopyranoside (**4**), and (−)-olivil 4-*O*-*β*-D-glucopyranoside (**7**) (Figure 2). In addition, during the purification work of antioxidants, several nonactive compounds, such as (−)-oleuropeic acid (**1**), (−)-oleuropeic acid 1′-*O*-*β*-D-glucopyranosyl ester (**5**), (−)-oleuropeic acid 6′-*O*-*α*-D-glucopyranosyl ester (**6a**), (−)-oleuropeic acid 6′-*O*-*β*-D-glucopyranosyl ester (**6b**), and (−)-perillic acid 1′-*O*-*β*-D-primeverosyl ester (**8**) (Figure 2), were also isolated.

Structure Elucidation of the Isolated Compounds. Compounds **1**−**8** were characterized and identified by UV, IR, MS, HRMS, ^{1}H NMR, ^{13}C NMR, 2D NMR, and specific optical rotation measurements. Spectral and physical data of compounds **1**−**5**, **6b**, and **7** are in agreement with earlier published data: (−)-oleuropeic acid (**1**),[44] (−)-olivil (**2**),[45] the aldehydic form of oleuropein aglycone (**3**),[46] (+)-1-hydroxypinoresinol 1-*O*-*β*-D-glucopyranoside (**4**),[13] (−)-oleuropeic acid 1′-*O*-*β*-D-glucopyranosyl ester (**5**),[44] (−)-oleuropeic acid 6′-*O*-*β*-D-glucopyranosyl ester (**6b**),[44] and (−)-olivil 4-*O*-*β*-D-glucopyranoside (**7**) (Figure 2).[47] Compounds **2**−**4** and **7** have been reported before from other parts of the olive tree. Compounds **1**, **5**, and **6b** have been previously found in the leaves of *Cunila spicata* L.[44] esterified with acylated glucose,

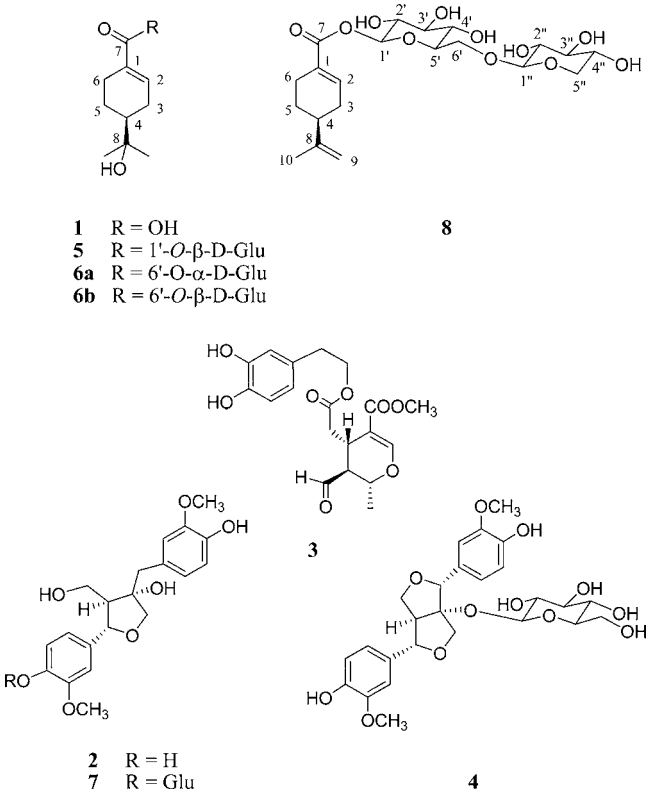

Figure 2. Compounds isolated in this work from an olive tree wood EtOAc extract.

while the methyl ester of compound **1** has been also isolated from *Eucalyptus cypellocarpa* leaves.[48]

Compounds **6a** and **6b** were assigned a molecular formula of $C_{16}H_{26}O_8$ by HRESIMS. They are anomeric glucosides, and their ^{1}H NMR spectrum showed, apart from signals corresponding to two monoterpene aglycone units, similar to that of compound **1**, a set of signals assignable to two glucose moieties; one anomeric proton is centered at 4.44 ppm (1H, d, 7.8 Hz), consistent with the configuration for a *β*-D-glucopyranosyl group, while the other is centered at 5.03 ppm (1H, d, 3.7 Hz), consistent with the configuration for an *α*-D-glucopyranosyl group (Table 1). In the HMBC spectrum, cross peaks between the proton signals H-6′a and H-6′b and the carbon C-7 indicate the linkage of the monoterpene residues and the glucose units. Further cross peaks between the proton signal at *δ* 5.03 (H-1′), from the *α* anomer, and the carbons at *δ* 74.8 (C-3′) and 70.8 (C-5′) and between the proton signal at *δ* 4.44 (H-1′), from the *β* anomer, and the carbons at *δ* 77.9 (C-2′), 76.2 (C-3′), and 75.4 (C-5′) allowed us to assign ^{13}C peaks for each anomer. Accordingly, the structure of compound **6a** was determined to be (−)-oleuropeic acid 6′-*O*-*α*-D-glucopyranosyl ester, while **6b** was determined to be (−)-oleuropeic acid 6′-*O*-*β*-D-glucopyranosyl ester (Figure 2). Integration of anomeric protons in the ^{1}H NMR spectrum indicated an equilibrium mixture of anomers, **6a** and **6b**, with a ratio of 1:1.

Compound **8** was assigned a molecular formula of $C_{21}H_{32}O_{11}$ by HRESIMS. The ^{1}H NMR spectrum (Table 2) showed signals of an isopropenyl moiety [*δ* 1.75 (3H, s), 4.73 (1H, s), and 4.76 (1H, s)], an olefinic proton [*δ* 7.14 (1H, br s)], three methylene groups [*δ* 1.44−2.49 (6H, m)], and a methyne group [*δ* 2.34−2.49 (1H, m)], corresponding to a mono-

dx.doi.org/10.1021/jf403998t | J. Agric. Food Chem. 2014, 62, 144−151

terpene aglycone unit. Additionally, a set of signals assignable to two sugar moieties was observed; one anomeric proton is centered at 4.27 ppm (1H, d, 7.5 Hz), while the other is centered at 5.49 ppm (1H, d, 7.5 Hz), indicating the β configuration for both sugar units. The ^{13}C NMR spectrum showed the presence of an isopropenyl group (a methyl [δ 20.87 (C-10)], a terminal methylene [δ 109.79 (C-9)], and a quaternary carbon [δ 150.02 (C-8)]), three methylene groups [δ 25.41 (C-6), 28.18 (C-5), and 32.27 (C-3)], a methyne carbon [δ 41.36 (C-4)], two olefinic carbons [δ 130.51 (C-1) and 142.50 (C-2)], and a quaternary carbon of an α,β-unsaturated ester [167.26 (C-7)]. The ^{13}C NMR spectrum also showed 11 signals in the sugar region, two of them being anomeric carbons [δ 95.74 (C-1′) and 105.14 (C-1″)]. The two sugars were identified as glucose and xylose. In the HMBC spectrum, cross peaks between the proton signals at δ 5.49 (H-1′) and the carbon at δ 167.26 (C-7) indicate the linkage between the monoterpene residue and the glucose unit. Similarly, cross peaks between the proton signal at δ 4.27 (H-1″) and the carbon at δ 69.42 (C-6′) and between the protons at δ 4.08 (H-6′a) and δ 3.70 (H-6′b) with the carbon at δ 105.14 (C-1″) showed the linkage between the xylose and the glucose units. A glucose and xylose moiety linked via C-6′ → C-1″ is known as the disaccharide primeverose. This linkage explained the upfield shifts observed for the glucose carbons C-1′, C-2′, and C-5′ and the downfield shifts for carbon C-6′. Accordingly, the structure of compound **8** was determined to be (−)-perillic acid 1′-*O*-β-D-primeverosyl ester, which is a new natural product (Figure 2).

Radical-Scavenging Activity of the Isolated Antioxidants. The antioxidant activity of the isolated compounds from olive tree wood was determined with the DPPH radical-scavenging assay and expressed in terms of the antioxidant concentration (μM) required to reduce the initial DPPH$^{\bullet}$ concentration after 15 min by 50% (efficient concentration, EC_{50}). In Table 3, EC_{50} values for the active compounds **2**−**4** and **7** and the reference compounds BHT and hydroxytyrosol are presented as the average of three replicates. The activities of compounds **2**−**4** and **7** were higher than that of reference BHT (505 μM) and lower than that of hydroxytyrosol (39 μM), which was the most active component identified in olive tree wood together to oleuropein (32 μM).[27] Hydroxytyrosol is more active than tyrosol (826 μM),[24] which could be related to the stabilization by delocalization of the *o*-diphenolic moiety present in hydroxytyrosol, since *o*-quinone formation is favored. Thus, the aldehydic form of oleuropein aglycone (**3**) exhibited marked activity; its efficient concentration (45 μM) was just somewhat lower than that of oleuropein (32 μM) and higher than those observed for other secoiridoids, such as jaspolyoside (55 μM), oleuropein 3′-*O*-β-D-glucoside (66 μM), isojaspolyoside A (108 μM), 7″*S*-hydroxyoleuropein (113 μM), oleuropein-3″-methyl ether (170 μM), ligustroside (233 μM), ligustroside 3′-*O*-β-D-glucoside (290 μM), and jaspolyanoside (847 μM), and iridoids, such as 7-deoxyloganic acid (742 μM).[14,27] The lignans (−)-olivil (**2**), (+)-1-hydroxypinoresinol 1-*O*-β-D-glucopyranoside (**4**), and (−)-olivil 4-*O*-β-D-glucopyranoside (**7**) showed EC_{50} values of 176, 164, and 134 μM, respectively. These activities are lower than that observed for lignan (+)-cycloolivil (90 μM).[27] Monoterpenoids **1**, **5**, **6a**, **6b**, and **8** did not show any antioxidant activity.

Table 3. DPPH Radical-Scavenging Activity of the Isolated Active Compounds from Olive Wood Ethyl Acetate Extract, Expressed as Efficient Concentration (EC_{50})

compounds	EC_{50} (μM)[a]
hydroxytyrosol	39
aldehydic form of oleuropein aglycone (**3**)	45
(−)-olivil 4-*O*-β-D-glucopyranoside (**7**)	134
(+)-1-hydroxypinoresinol 1-*O*-β-D-glucopyranoside (**4**)	164
(−)-olivil (**2**)	176
BHT[b]	505

[a] EC_{50} values are means of three replicates, and the RSD is less than 1%. [b] 2,6-Di-*tert*-butyl-4-methylphenol.

In summay, this work completes previous studies on the composition of an ethyl acetate extract from olive tree wood,[14,24,25] as well as their antioxidant activity. On the basis of their chemical structures, the 25 compounds isolated from olive tree wood can be classified into various phytochemical subclasses including simple phenols [hydroxytyrosol, tyrosol], monoterpenoids [(−)-oleuropeic acid (**1**), (−)-oleuropeic acid 1′-*O*-β-D-glucopyranosyl ester (**5**), (−)-oleuropeic acid 6′-*O*-α-D-glucopyranosyl ester (**6a**), (−)-oleuropeic acid 6′-*O*-β-D-glucopyranosyl ester (**6b**), and (−)-perillic acid 1′-*O*-β-D-primeverosyl ester (**8**)], lignans [(+)-cycloolivil, (−)-olivil (**2**), (+)-1-hydroxypinoresinol 1-*O*-β-D-glucopyranoside (**4**), and (−)-olivil 4-*O*-β-D-glucopyranoside (**7**)], iridoids [7-deoxyloganic acid], secoiridoids [ligustroside, oleuropein, the aldehydic form of oleuropein aglycone (**3**), oleuropein-3″-methyl ether, (7″*R*)-7″-ethoxyoleuropein, (7″*S*)-7″-ethoxyoleuropein, (7″*S*)-7″-hydroxyoleuropein, ligustroside 3′-*O*-β-D-glucoside, oleuropein 3′-*O*-β-D-glucoside, jaspolyanoside, jaspolyoside, and isojaspolyoside A], and a sugar alcohol [D-mannitol]. The results obtained here complete the current knowledge of olive tree wood composition and confirm that this agricultural byproduct contains diverse phytochemicals, among which secoiridoids predominate, which in turn could offer interesting potential applications in the food, cosmetic, and pharmaceutical industries.

AUTHOR INFORMATION

Corresponding Author

*Tel.: +34 953 212743. Fax: +34 953 211876. E-mail: jaltare@ujaen.es.

Funding

This study was supported by the Spanish Ministerio de Educación y Ciencia (R+D Project CTQ2005-07005/PPQ; partial financial support from the FEDER funds of the European Union). M.P.-B. was the recipient of a predoctoral fellowship granted by the Andalusian Government Junta de Andalucía. Part of the work was supported by the Centro de Instrumentación Científico-Técnica of the University of Jaén.

Notes

The authors declare no competing financial interest.

ACKNOWLEDGMENTS

We thank Dr. P. de Waard for his technical assistance in recording NMR spectra.

REFERENCES

(1) Firuzi, O.; Miri, R.; Tavakkoli, M.; Saso, L. Antioxidant therapy: current status and future prospects. *Curr. Med. Chem.* **2011**, *18*, 3871−3888.

(2) Finley, J. W.; Kong, A.-N.; Hintze, K. J.; Jeffery, E. H.; Ji, L. L.; Lei, X. G. Antioxidants in foods: state of the science important to the food industry. *J. Agric. Food Chem.* **2011**, *59*, 6837−6846.
(3) Gharavi, N.; Haggarty, S.; El-kadi, A. O. S. Chemoprotective and carcinogenic effects of *tert*-butylhydroquinone and its metabolites. *Curr. Drug Metab.* **2007**, *8*, 1−7.
(4) Sati, S. C.; Sati, N.; Rawat, U.; Sati, O. P. Medicinal plants as a source of antioxidants. *Res. J. Phytochem.* **2010**, *4*, 213−224.
(5) Vuong, Q. V.; Stathopoulos, C. E.; Nguyen, M. H.; Golding, J. B.; Roach, P. D. Isolation of green tea catechins and their utilization in the food industry. *Food Rev. Int.* **2011**, *27*, 227−247.
(6) Balasundram, N.; Sundram, K.; Samman, S. Phenolic compounds in plants and agri-industrial by-products: antioxidant activity, occurrence, and potential uses. *Food Chem.* **2006**, *99*, 191−203.
(7) Bianco, A.; Ramunno, A. The chemistry of *Olea europaea*. In *Studies in Natural Products Chemistry*; Atta-ur-Rahman, Ed.; Elsevier B.V.: Amsterdam, The Netherlands, 2006; Vol. 33, pp 859−903.
(8) Boskou, D. Phenolic compounds in olives and olive oil. In *Olive oil*; Boskou, D., Ed.; CRC Press: Boca Raton, FL, 2009; pp 11−44.
(9) Ghanbari, R.; Anwar, F.; Alkharfy, K. M.; Gilani, A.-H.; Saari, N. Valuable nutrients and functional bioactives in different parts of olive (*Olea europaea* L.) - a review. *Int. J. Mol. Sci.* **2012**, *13*, 3291−3340.
(10) Bianco, A.; Uccella, N. Biophenolic components of olives. *Food Res. Int.* **2000**, *33*, 475−485.
(11) Erbay, Z.; Icier, F. The importance and potential uses of olive leaves. *Food Rev. Int.* **2010**, *26*, 319−334.
(12) Japón-Luján, R.; Luque de Castro, M. D. Small branches of olive tree: a source of biophenols complementary to olive leaves. *J. Agric. Food Chem.* **2007**, *55*, 4584−4588.
(13) Tsukamoto, H.; Hisada, S.; Nishibe, S. Lignans from bark of the *Olea* plants. II. *Chem Pharm. Bull.* **1985**, *33*, 1232−1241.
(14) Pérez-Bonilla, M.; Salido, S.; van Beek, T. A.; de Waard, P.; Linares-Palomino, P. J.; Sánchez, A.; Altarejos, J. Isolation of antioxidative secoiridois from olive wood (*Olea europaea* L.) guided by on-line HPLC−DAD−radical scavenging detection. *Food Chem.* **2011**, *124*, 36−41.
(15) Spizzirri, U. G.; Restuccia, D.; Parisi, O. I.; Cirillo, G.; Curcio, M.; Iemma, F.; Puoci, F.; Picci, N.; Chiricosta, S. Olive stones as a source of antioxidants for food industry. *J. Food Nutr. Res.* **2011**, *50*, 57−67.
(16) Ortega-García, F.; Peragón, J. HPLC analysis of oleuropein, hydroxytyrosol, and tyrosol in stems and roots of *Olea europaea* L. cv. Picual during ripening. *J. Agric. Food Chem.* **2010**, *90*, 2295−2300.
(17) Sabatini, N. Recent patents in olive oil industry: new technologies for the recovery of phenols compounds from olive oil, olive oil industrial by-products and waste waters. *Recent Pat. Food, Nutr. Agric.* **2010**, *2*, 154−159.
(18) Ould-Idriss, A.; Stitou, M.; Cuerda-Correa, E. M.; Fernández-González, C.; Macías-García, A.; Alexandre-Franco, M. F.; Gómez-Serrano, V. Preparation of activated carbons from olive-tree wood revisited. I. Chemical activation with H_3PO_4. *Fuel Process. Technol.* **2010**, *92*, 261−265.
(19) Toledano, A.; Serrano, L.; Labidi, J. Enhancement of lignin production from olive tree pruning integrated in a green biorefinery. *Ind. Eng. Chem. Res.* **2011**, *50*, 6573−6579.
(20) Moral, A.; Hernández, M. D.; de la Torre, M. J.; Torrecilla, J. S. Pulp and paper obtained from olive tree trimmings. *Adv. Environ. Res.* **2012**, *20*, 237−244.
(21) Ruiz, E.; Cara, C.; Ballesteros, M.; Manzanares, P.; Ballesteros, I.; Castro, E. Ethanol production from pretreated olive tree wood and sunflower stalks by an SSF process. *Appl. Biochem. Biotechnol.* **2006**, *130*, 631−643.
(22) Jung, C. G. Pyrolysis and gasification of industrial waste towards substitution fuels valorization. *High Temp. Mater. Processes* **2008**, *27*, 299−304.
(23) Altarejos, J.; Salido, S.; Pérez-Bonilla, M.; Linares-Palomino, P. J.; van Beek, T. A.; Nogueras, M.; Sánchez, A. Preliminary assay on the radical scavenging activity of olive wood extracts. *Fitoterapia* **2005**, *76*, 348−351.
(24) Pérez-Bonilla, M.; Salido, S.; van Beek, T. A.; Linares-Palomino, P. J.; Altarejos, J.; Nogueras, M.; Sánchez, A. Isolation and identification of radical scavengers in olive tree (*Olea europaea*) wood. *J. Chromatogr. A* **2006**, *1112*, 311−318.
(25) Pérez-Bonilla, M.; Salido, S.; Sánchez, A.; van Beek, T. A.; Altarejos, J. Effect of extraction conditions on the antioxidant activity of olive wood extracts. *Int. J. Food Sci.* **2013**, *1* (719593), 1−13.
(26) Koleva, I. I.; Niederländer, H. A. G.; van Beek, T. A. An on-line HPLC method for detection of radical scavenging compounds in complex mixtures. *Anal. Chem.* **2000**, *72*, 2323−2328.
(27) Zbidi, H.; Salido, S.; Altarejos, J.; Pérez-Bonilla, M.; Bartegi, A.; Rosado, J. A.; Salido, G. M. Olive tree wood phenolic compounds with human platelet antiaggregant properties. *Blood Cells Mol. Dis.* **2009**, *42*, 279−285.
(28) Salido, S.; Pérez-Bonilla, M.; Linares-Palomino, P. J.; Nogueras, M.; Sánchez, A.; Altarejos, J. Procedimiento de extracción de madera de olivo y extractos enriquecidos en productos de interés alimentario. Span. Patent ES 2386860, 2012.
(29) Castro, E.; Conde, E.; Moure, A.; Falque, E.; Cara, C.; Ruiz, E.; Domínguez, H. Antioxidant activity of liquors from steam explosion of *Olea europea* wood. *Wood Sci. Technol.* **2008**, *42*, 579−592.
(30) Requejo, A.; Peleteiro, S.; Rodríguez, A.; Garrote, G.; Parajó, J. C. Second-generation bioethanol from residual woody biomass. *Energy Fuels* **2011**, *25*, 4803−4810.
(31) El-Sheikh, A. H.; Alzawahreh, A. M.; Sweileh, J. A. Preparation of an efficient sorbent by washing then pyrolysis of olive wood for simultaneous solid phase extraction of chloro-phenols and nitro-phenols from water. *Talanta* **2011**, *85*, 1034−1042.
(32) Hemmasi, A. H. Manufacturing paper sheets from olive wood by soda, sulphite and kraft pulping. *World Appl. Sci. J.* **2012**, *18*, 510−513.
(33) Conde, E.; Cara, C.; Moure, A.; Ruiz, E.; Castro, E.; Domínguez, H. Antioxidant activity of the phenolic compounds released by hydrothermal treatments of olive tree pruning. *Food Chem.* **2009**, *114*, 806−812.
(34) López, F. J.; Pinzi, S.; Ruiz, J. J.; López, A.; Dorado, M. P. Economic viability of the use of olive tree pruning as fuel for heating systems in public institutions in South Spain. *Fuel* **2010**, *89*, 1386−1391.
(35) Manzanares, P.; Negro, M. J.; Oliva, J. M.; Sáez, F.; Ballesteros, I.; Ballesteros, M.; Cara, C.; Castro, E.; Ruiz, E. Different process configurations for bioethanol production from pretreated olive pruning biomass. *J. Chem. Technol. Biotechnol.* **2011**, *86*, 881−887.
(36) Requejo, A.; Rodríguez, A.; Colodette, J. L.; Gomide, J. L.; Jiménez, L. TCF bleaching sequence in kraft pulping of olive tree pruning residues. *Bioresour. Technol.* **2012**, *117*, 117−123.
(37) Mateo, S.; Puentes, J. G.; Sánchez, S.; Moya, A. J. Oligosaccharides and monomeric carbohydrates production from olive tree pruning biomass. *Carbohydr. Polym.* **2013**, *93*, 416−423.
(38) De la Fuente, P.; Chamorro, P.; Moreno, M.; Poza, M. A. Antioxidant properties of Olixxol (hydroxytyrosol) from olive leaves (*Olea europaea* L.). *Innov. Food Technol.* **2005**, *26*, 76−79.
(39) van Beek, T. A.; Tetala, K. K. R.; Koleva, I. I.; Dapkevicius, A.; Exarchou, V.; Jeurissen, S. M. F.; Claassen, F. W.; van der Klift, E. J. C. Recent developments in the rapid analysis of plants and tracking their bioactive constituents. *Phytochem. Rev.* **2009**, *8*, 387−399.
(40) Shi, S. Y.; Zhou, H. H.; Zhang, Y. P.; Jiang, X. Y.; Chen, X. Q.; Huang, K. L. Coupling HPLC to on-line, post-column (bio)chemical assays for high-resolution screening of bioactive compounds from complex mixtures. *Trends Anal. Chem.* **2009**, *28*, 865−877.
(41) von Gadow, A.; Joubert, E.; Hansmann, C. F. Comparison of the antioxidant activity of aspalathin with that of other plant phenols of rooibos tea (*Aspalathus linearis*), α-tocopherol, BHT, and BHA. *J. Agric. Food Chem.* **1997**, *45*, 632−638.
(42) Huang, D.; Ou, B.; Prior, R. L. The chemistry behind antioxidant capacity assays. *J. Agric. Food Chem.* **2005**, *53*, 1841−1856.
(43) Exarchou, V.; Fiamegos, Y. C.; van Beek, T. A.; Nanos, C.; Vervoort, J. Hyphenated chromatographic techniques for the rapid screening and identification of antioxidants in methanolic extracts of pharmaceutically used plants. *J. Chromatogr. A* **2006**, *1112*, 293−302.

(44) Manns, D.; Hartmann, R. Monoterpene glucosides from *Cunila spicata*. *Planta Med.* **1994**, *60*, 467−469.
(45) Tsukamoto, H.; Hisada, S.; Nishibe, S. Lignans from bark of the *Olea* plants. I. *Chem Pharm. Bull.* **1984**, *32*, 2730−2735.
(46) Christophoridou, S.; Dais, P.; Tseng, L.-H.; Spraul, M. Separation and identification of phenolic compounds in olive oil by coupling high-performance liquid chromatography with postcolumn solid-phase extraction to nuclear magnetic resonance spectroscopy (LC-SPE-NMR). *J. Agric. Food Chem.* **2005**, *53*, 4667−4679.
(47) Abe, F.; Yamauchi, T.; Wan, A. S. C. *Cerbera*. VI. Lignans related to olivil from genus *Cerbera*. *Chem. Pharm. Bull.* **1988**, *36*, 795−799.
(48) Ito, H.; Koreishi, M.; Tokuda, H.; Nishino, H.; Yoshida, T. Cypellocarpins A−C, phenol glycosides esterified with oleuropeic acid, from *Eucalyptus cypellocarpa*. *J. Nat. Prod.* **2000**, *63*, 1253−1257.

JOURNAL OF AGRICULTURAL AND FOOD CHEMISTRY

Article

pubs.acs.org/JAFC

Identification of IgE-Binding Peptides in Hen Egg Ovalbumin Digested in Vitro with Human and Simulated Gastroduodenal Fluids

Sara Benedé, Iván López-Expósito, Rosina López-Fandiño, and Elena Molina*

Instituto de Investigación en Ciencias de la Alimentación (CIAL), CSIC-UAM, Nicolás Cabrera 9, 28049 Madrid, Spain

Supporting Information

ABSTRACT: The digestibility of the major egg allergen ovalbumin (OVA, Gal d 2) with human and simulated digestive fluids was assessed. Degradation of OVA was faster when treated with human fluids, particularly following duodenal digestion, leading to gastrointestinal digests with lower IgE binding. Gastric digestion with both systems yielded 52 identical cleavage sites and a similar peptide pattern with 47 peptides in common. Subsequent duodenal digestion showed that the human fluid released fewer and shorter peptides. Several high-frequency IgE-binding epitopes were detected among the fragments of molecular mass lower than 3 kDa identified in the digests: OVA (141−154) and OVA (164−176) in the gastrointestinal digests produced with human fluids; and OVA (125−134), OVA (159−172), OVA (141−154), OVA (188−198), OVA (326−336), and OVA (370−385) in the gastrointestinal digests produced with simulated fluids. The high binding frequency of the fragment OVA (370−385), which reacted with 80% of the sera from allergic patients used, was noteworthy.

KEYWORDS: *egg allergy, ovalbumin, in vitro digestion, human digestive fluids, IgE, epitope*

INTRODUCTION

Egg allergy is one of the most frequent food allergies in children below the age of three, with common symptoms frequently involving the skin as well as the gut and, in more severe cases, anaphylaxis.[1] A meta-analysis of double-blind placebo-controlled food challenges confirmed a prevalence of >1.7%,[2] with most children not outgrowing their egg allergy by school age but, instead, showing a long progression to egg allergy resolution.[3]

Ovalbumin (OVA, Gal d 2), the most abundant protein in egg white (up to 54% w/w of the protein content), is considered one of the dominant allergens.[4] It is a phosphoglycoprotein with a molecular mass of 45 kDa, the sequence of which (with 385 amino acids) includes six cysteines, with a single disulfide bond between Cys_{73} and Cys_{120}, a glycosylation site at Asn_{292}, and two phosphorylation sites at Ser_{68} and Ser_{344}. As many other allergenic proteins, OVA partially resists hydrolysis with pepsin and pancreatic enzymes, an aspect that could contribute to its ability to sensitize or elicit allergic reactions.[5]

So far, studies investigating the gastrointestinal stability of OVA have been performed in vitro by the use of enzymes of bovine or porcine origin as part of different digestion models, ranging from simple one-step hydrolyses[6,7] to advanced physiologically relevant systems in which subsequent gastric and duodenal digestions are conducted under conditions that mimic the in vivo processes in infants and adults.[8,9] These latter studies have highlighted the effects that the enzyme to substrate ratio, pH, and concentration of physiological surfactants, such as phospatidylcholine and bile salts, exert on the gastrointestinal stability of OVA and their influence in the resulting immunoreactivity of the digests. However, these relevant parameters regarding digestion, such as enzyme activity, volume of digestive juices secreted, pH, or surfactant level, vary widely among individuals and also with the type and amount of food ingested and the time of the day, making in vivo conditions very difficult to simulate.[10] In addition, human gastrointestinal juices contain complex mixtures of enzymes, which could present either broader or different specificities or vary in their functional parameters with respect to purified commercial enzymes from animal sources.[11] In the present work, the digestibility of OVA using human gastric and duodenal juices was assessed, the peptides released were characterized, and the IgE-binding properties of the most relevant digestion products were evaluated. Digestions were also conducted with simulated fluids for comparative purposes. This allowed the identification of relevant IgE-binding epitopes that resisted digestion in both systems and could contribute to the allergenic potential of the protein.

MATERIALS AND METHODS

Human Digestive Fluids. Human gastric and duodenal fluids were collected by gastroscopy of four different patients without any gastrointestinal pathology at the Hospital Universitario La Paz (Madrid, Spain) after 8 h of fasting. Gastric and duodenal fluids were separately pooled and frozen at −20 °C before use. Pepsin activity of the pooled gastric fluid (pH 2.13) was 728.9 U/mL. Trypsin and chymotrypsin activities of the duodenal fluid (pH 7.8) were 167.2 and 2.8 U/mL, respectively, with a bile salt concentration of 0.7 mM.[12]

Human Sera. Individual serum samples from 22 children with proven allergy to egg white proteins were kindly donated by the Hospital Infanta Sofía (San Sebastián de los Reyes, Madrid, Spain). The diagnosis of IgE-mediated egg allergy was made on the basis of objective symptoms of an acute reaction after egg ingestion, together with evidence of specific IgE antibodies against egg (Table S1 in the

Received: September 20, 2013
Revised: December 12, 2013
Accepted: December 18, 2013
Published: December 18, 2013

ACS Publications © 2013 American Chemical Society

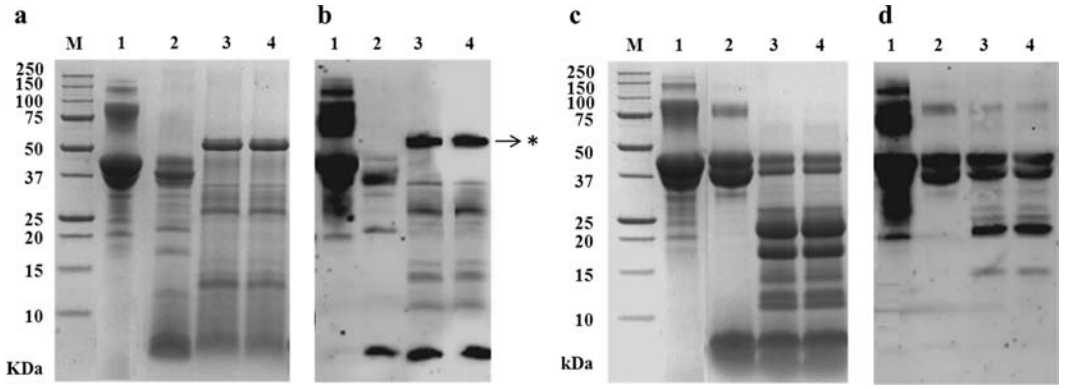

Figure 1. SDS-PAGE patterns (a, c) and Western blotting (b, d) of OVA after in vitro gastric and gastroduodenal digestions with human (a, b) and simulated (c, d) fluids. Electrophoresis was performed using Bis-Tris 12% acrylamide gel with reducing agents. Lanes: M, molecular mass marker (Precision Plus Protein standards (Bio Rad), ranging in molecular mass from 10 to 250 kDa; 1, OVA; 2, 60 min gastric digest; 3, gastroduodenal digest (60 min of gastric followed by 30 min of duodenal digestion); 4, gastroduodenal digest (60 min of gastric followed by 60 min of duodenal digestion). ∗, IgE-binding fragment originally present in the human duodenal fluid.

Supporting Information). Serum samples from two nonallergic donors were also used.

In Vitro Digestions. In vitro gastric and duodenal digestions with simulated fluids, based upon the procedure described by Moreno et al.,[13] were performed as described in Benedé et al.,[12] using albumin (EC232-692-7) from chicken egg white grade V (Sigma-Aldrich, St. Louis, MO, USA). Gastric digestions were conducted at pH 2.0 for 60 min at 37 °C, with 182 U/mg OVA of porcine pepsin. Duodenal digestions were conducted on the 60 min gastric digests, readjusted to pH 6.5, and stopped after either 30 or 60 min at 37 °C with Bowman−Birk trypsin−chymotrypsin inhibitor. The final composition of the simulated duodenal mixture was 3.9 mg/mL OVA, 3.3 mg/mL phosphatidylcholine, 7.4 mM bile salts (BS; sodium glycodeoxycholate and sodium taurocholate), 7.6 mM $CaCl_2$, and 20.3 mM Bis-Tris, with pancreatic porcine lipase (24.7 U/mg OVA), pancreatic porcine colipase (1:895 mg/mg OVA), pancreatic bovine trypsin (34.5 U/mg OVA), and pancreatic bovine α-chymotrypsin (0.44 U/mg OVA), all from Sigma-Aldrich.

In vitro protein digestion with human fluids, mimicking gastric and duodenal phases, followed the method of Benedé et al.[12] OVA was mixed with the pool of human gastric fluids at pH 2.1 at a pepsin to OVA ratio of 182 U/mg. After 1 h of incubation at 37 °C, the pH was adjusted to pH 6.5 with 1 M $NaHCO_3$, and the pool of human duodenal fluids was added, so that the enzyme to substrate ratio was 34.5 U/mg trypsin and 0.49 U/mg chymotrypsin. The reaction was stopped after 30 and 60 min with Bowman−Birk trypsin−chymotrypsin inhibitor.

SDS-PAGE Analyses. OVA and its hydrolysates were diluted to 1 mg/mL in sample buffer containing 2% (w/v) SDS and 5% (v/v) β-mercaptoethanol and heated at 95 °C for 4 min. Samples were analyzed on Precast Criterion XT 12% Bis-Tris gels, and electrophoretic separations were carried out at 150 V using XT-MES as running buffer (Bio-Rad, Richmond, CA, USA) in the Criterion cell (Bio-Rad). Gels were stained with Bio-Safe Coomassie G-250 (Bio-Rad).

Western Blotting. After SDS-PAGE separation, the gels (loaded with 50 μL of a 1 mg/mL sample solution) were soaked in transfer buffer (48 mM Tris, 39 mM glycine, 20% methanol, pH 9.2) for 20 min and subjected to semidry transfer in a Trans-Blot SD (Bio-Rad) for 30 min at 18 V. Transfer effectiveness to the membrane was assessed by staining with Ponceau reagent. Western blotting was conducted as explained in Benedé et al.,[12] using pooled sera from six children with egg allergy (patients 7−12, Table S1 in the Supporting Information), diluted 1/50 in Tris buffer saline (50 mM Tris, 150 mM NaCl, pH 7.6, TBS), containing Tween 20 (0.05% v/v) (TBTS) and BSA 0.1% (w/v).

Human IgE Binding by Inhibition ELISA. Human IgE binding of OVA and its digests was assessed by inhibition ELISA as previously reported Jiménez-Saiz et al.,[14] using individual sera from patients 1−6 (Table S1 in the Supporting Information).

Peptide Sequencing by RP-HPLC-MS/MS. RP-HPLC-MS/MS analyses of the digested samples were performed as described in Benedé et al. on an Agilent 1100 HPLC System (Agilent Technologies, Waldbron, Germany) with an RP318 C18 column (250 × 4.6 mm, Bio-Rad). The HPLC system was connected online to an Esquire 3000 quadrupole ion trap (Bruker Daltonik, Bremen, Germany) equipped with an electrospray ionization source. Mass spectra were recorded over the range of m/z 100−3000 for MS spectra. Tandem MS was applied by using a signal threshold of 10000, a window width of 4.0 m/z, and a voltage ramp from 0.3 to 2 V. Using Data Analysis (version 4.0, Bruker), the m/z spectral data were processed and transformed to spectra representing mass values. BioTools (version 3.1, Bruker) was used to process the MS(n) spectra and perform peptide sequencing.

Dot-Blot. Twenty-seven peptides representative of those identified in the in vitro gastroduodenal digests were commercially synthesized (JPT peptide Technologies, Berlin, Germany). Among the peptides selected, those with 8 and 9 amino acids were extended to 10 amino acids with the preceding and following amino acids of the protein chain. Peptides, at a concentration of 1 mM, were diluted 1/3 in TBS. Then, 1 μL of each peptide was spotted onto the membrane and allowed to dry.

The nitrocelullose membranes were conditioned in transfer buffer for 20 min, and 1 μL from each peptide was spotted onto the membrane and allowed to dry. Then, the nitrocellulose membranes were blocked with TBST containing 1% w/v BSA for 60 min and washed with TBST. Immunolabeling with 10 individual serum samples (patients 13−22, Table S1 in the Supporting Information) was conducted as described for the Western blotting experiments.

Ethical Concerns. All human samples in this study have been obtained with written consent of the subjects. The researchers involved in the process handled and used such material sensitively and responsibly. All procedures received ethical approval by CSIC.

RESULTS

In Vitro Digestion of Ovalbumin with Human and Simulated Fluids. Figure 1 shows the SDS-PAGE patterns (Figure 1a,c) and Western blots (Figure 1b,d) of OVA, after being subjected to two-step digestion protocols, mimicking the stomach and duodenal stages, by using human and simulated fluids. In general terms, after 60 min of incubation with human gastric fluid a remarkable amount of OVA remained undigested, whereas the intact protein virtually disappeared following the subsequent duodenal phase (Figure 1a). Gastric and, particularly, duodenal hydrolyses were much faster with

human fluids as compared with simulated fluids, with the appearance of more degradation products after the gastric phase, of ~40, 22, 18, 13, and 5 kDa, and fewer degradation products, within the range from ~25 to 5 kDa, after the duodenal phase (Figure 1a,c). As a result, there was less IgE binding from intact OVA and its 40 kDa fragment following gastroduodenal digestion with human fluids. Remarkably, a strong IgE-binding band of ~21 kDa, which formed during duodenal digestion with simulated fluid, was absent from the corresponding digests produced with human fluid, which, in turn, yielded lower molecular mass immunoreactive degradation products (Figure 1b,d). It should be mentioned that no differences in the degradation patterns were detected when 30 and 60 min of duodenal digestion were compared with either system.

In consonance with these results, inhibition ELISA (Figure 2) showed that the gastric and gastroduodenal digests produced

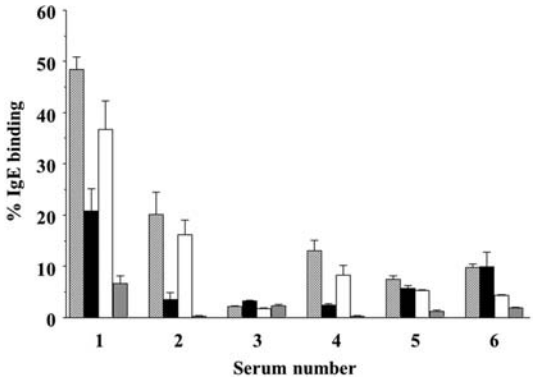

Figure 2. IgE binding of OVA, expressed as percentage of the EC_{50} of the intact protein, as estimated by inhibition ELISA with sera from six allergic patients (patients 1–6, Table S1 in the Supporting Information), after in vitro gastric digestion with simulated (gray dotted bars) and human (black bars) fluids and gastroduodenal digestion with simulated (white bars) and human (gray bars) fluids.

with human fluids exhibited the lowest IgE binding to three individual sera from egg-allergic patients (patients 1, 2, 4, and 5, Table S1 in the Supporting Information). With another two sera (patients 3 and 6, Table S1 in the Supporting Information), IgE reactivities toward the gastric digests produced by both systems were very similar, although the lowest IgE binding always corresponded to the human gastroduodenal digests. No IgE binding to sera from non-allergic donors was detected.

Identification of IgE-Binding Epitopes. Figure 3 shows the sequences of the peptides identified by RP-HPLC/MS-MS in the gastric (60 min) and gastroduodenal (30 min) digests of OVA. No peptides covering the first 50 amino acids of the protein sequence were found in either model. Following gastric digestion with human and simulated fluids, 84 and 118 peptides were identified, respectively, with 47 peptides in common. There were 52 identical pepsin cleavage sites in both systems, including Leu (83, 105, 114, 124, 183, 216, 232, 242, 252, 255, 282, 312, 321, and 365), Glu (70, 108, 143, 202, 248, 266, 274, 336, 340, and 357), Phe (59, 99, 134, 198, 217, and 261), Ala (141, 171, 177, 187, 195, 332, and 345), Met (210, 211, 222, 239, and 241), and Gln (89, 140, 203, and 325). Eighty-one of the 118 sequences identified after gastric hydrolysis with simulated fluid resisted subsequent duodenal hydrolysis, appearing as end products of digestion. Most of the remaining peptides found in the duodenal digests produced with simulated fluid could be products of hydrolysis of the low molecular mass peptides previously released by pepsin action, except for the C-terminal sequence HIATNAVLFFGRCVS, resulting from the trypsin cleavage at Lys369. In addition, in this digestion system, breakdown at the trypsin cleavage sites Lys (55, 92, 226, 228, 277, 279, 286, and 322) and Arg (50, 84, 104, 142, 158, and 276) was detected. Only 47 peptides were identified after gastrointestinal digestion with human fluids. In this case, there were several fragments that could not arise from the peptides previously identified after gastric digestion and, thus, they could derive from the hydrolysis of either intact OVA or the big proteolysis fragments that resisted pepsin hydrolysis. Only six peptides were coincident with those produced with simulated duodenal fluid and, in general terms, the human fluid gave rise to less numerous and shorter peptides. Hydrolysis by trypsin at Lys290 and Arg (50, 158, 284, and 359) was detected (Figure 3 and Table S2 in the Supporting Information).

Twenty-seven peptides, ranging from 10 to 16 amino acids, representative of those found in the gastroduodenal digests with simulated and human fluids were chemically synthesized, and their IgE binding to 10 individual sera from egg-allergic patients was assessed by dot-blot. As shown in Figure 3, all peptides were recognized by, at least, one serum, except for two fragments, OVA (299–308) and (351–360), which did not react with any of the patient's sera employed in the study. A high IgE binding corresponded to the region comprised between positions 125 and 176, because 40–60% of the patients reacted to the synthetic peptides OVA (125–134), OVA (135–144), OVA (141–154), OVA (159–172), and OVA (164–176). The fragments OVA (188–198) and OVA (326–336) were recognized by sera from 60 and 50% of the patients, respectively. The highest IgE binding corresponded to the C-terminal fragment OVA (370–385), which reacted with 80% of the sera.

DISCUSSION

Proteolyses of OVA with human and simulated digestive fluids were compared. The results obtained with simulated gastric fluid agree with previously published information showing that OVA is quite stable to porcine pepsin at an E:S ratio of 182 U/mg and pH 2.0.[9] A digestion pattern with two main degradation products, of 40.1 and 4.1 kDa, has been described,[7,15,16] the first one probably corresponding to the fragment Ala23–Pro385.[9] Moreover, Dupont et al.,[8] using a gastric model under similar conditions (E:S 182 U/mg, pH 2.5) reported, in addition to smaller peptides of ~5400 and 4600 Da, the appearance of digestion products of ~21700 and 17800 Da, which are analogous to those found in the gastric digests produced with human fluid in the present study (Figure 1a). In any case, and although there was intact protein remaining after the gastric phase in both systems, degradation of OVA was faster when digested with human than with simulated fluid (Figure 1a,c), an aspect that was already observed with β-CN.[12] This suggests a more efficient performance of pepsin of human origin despite specificity being similar, as judged by the existence of 52 identical cleavage sites and a similar peptide pattern with 47 peptides in common (Figure 3 and Table S2 in the Supporting Information). It is noteworthy that the in vitro digestion with human gastric juice released peptides with antihypertensive activity that either act as inhibitors of angiotensin-I-converting enzyme or exert a vasodilator action, such as FRADHPFL, YAEERYPIL, YRGGLEPINF, ESSINF, or YQIGL, which were

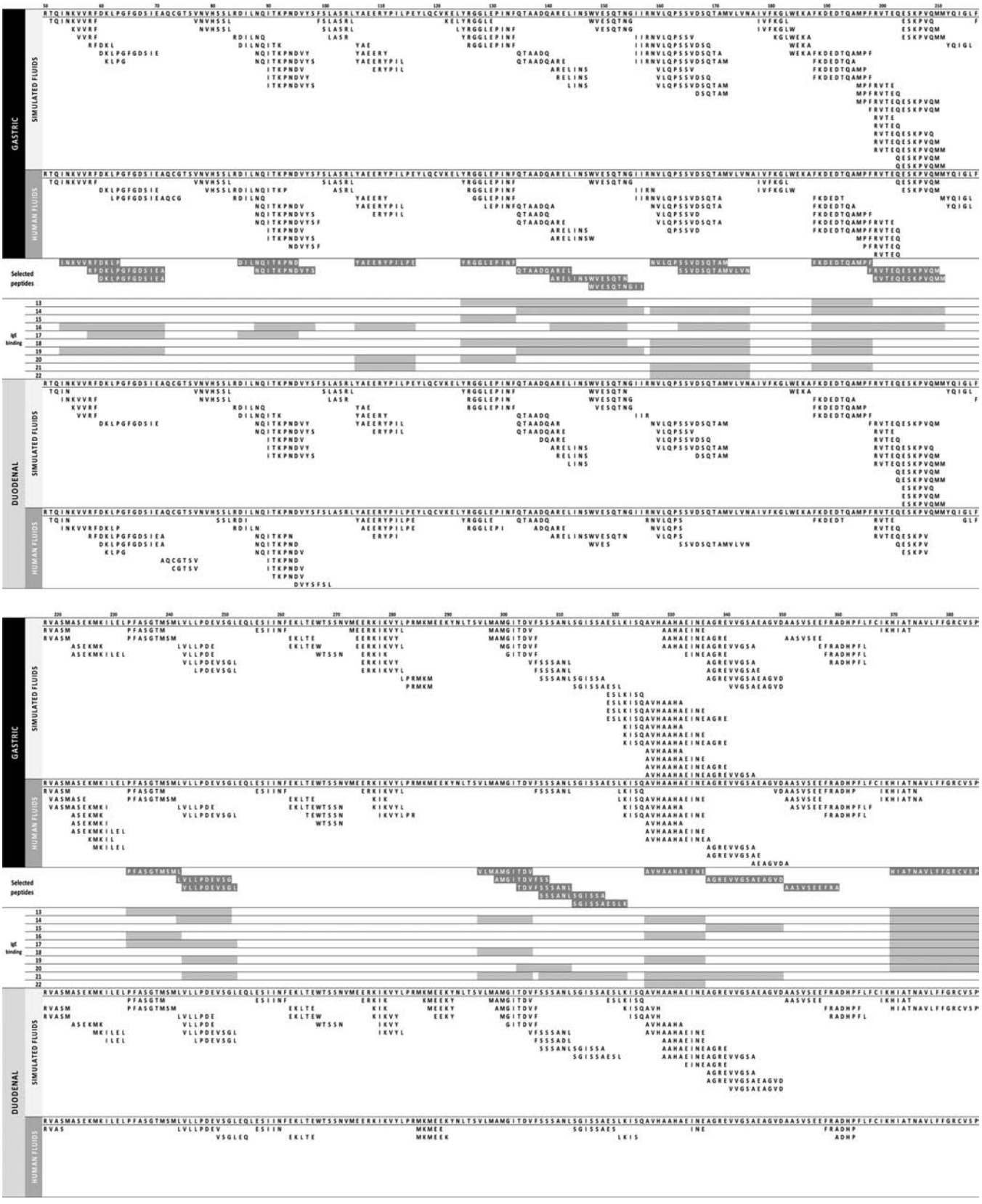

Figure 3. Peptide sequences, identified by RP-HPLC-MS/MS, in the gastric (60 min) and subsequent duodenal digests of OVA (60 min of gastric followed by 30 min of duodenal digestion), and IgE binding, estimated by dot-blot with 10 sera of egg-allergic patients (patients 13−22, Table S1 in the Supporting Information), of 27 synthetic peptides selected within the peptides identified in the simulated digestions.

dx.doi.org/10.1021/jf404226w | J. Agric. Food Chem. 2014, 62, 152−158

previously produced from OVA by hydrolysis with porcine pepsin for 3 h and also appeared in the hydrolysates produced with simulated fluid.[17,18]

Following in vitro duodenal hydrolysis with trypsin (E:S 40 U/mg) and chymotrypsin (E:S 0.5 U/mg), the appearance of digestion products of ~20700, 17000, 12500, 10400, and 6500 Da has been described,[8] which could coincide with those formed during duodenal digestion with the simulated fluid in our study (Figure 1c). These degradation products were absent from the gastroduodenal digests produced with human duodenal fluid (Figure 1a), as this caused a much more extensive proteolysis of the gastric digests than the simulated fluid. A difference between both duodenal digestion systems laid in the concentration of BS, which was much lower in the pool of human fluids, probably due to the prolonged fasting that preceded their extraction. It has been found that BS, at the concentration present in the simulated duodenal fluid, which is typical of a fed state, considerably increase the proteolysis of OVA by pancreatic enzymes.[9] However, despite the lower concentration of bile acids in the human duodenal fluid, it promoted very effectively the proteolysis of intact OVA and of the peptides generated from it by pepsin hydrolysis. This could be attributed to differences in the specificity between human trypsin and α-chymotrypsin and their bovine counterparts, as well as to the presence of peptidases in the human pancreatic extracts.[19] In fact, it has been reported that intact OVA and its 40 kDa fragment partially resist hydrolysis by porcine trypsin and chymotrypsin, but they are more readily degraded by an enzyme preparation from the pig pancreas gland that, in addition to both proteases, contains amino and carboxypeptidases.[9] Furthermore, comparison of the peptide patterns produced by both systems showed that in vitro gastroduodenal digestion with human fluids released fewer and shorter peptides, revealing a most extensive liberation of free amino acids from the short fragments previously formed during the gastric phase (Figure 3 and Table S2 in the Supporting Information).

In accordance with the least extensive proteolytic degradation and although there were, as expected, differences in donor's specificity,[20] inhibition ELISA with individual sera from allergic patients revealed a comparatively higher IgE reactivity to the gastroduodenal digests produced with simulated fluids (Figure 2). This is probably because of the presence, in addition to intact OVA and its 40 kDa fragment, of a strong IgE-binding band of ~21 kDa and of other minor immunoreactive degradation products (Figure 1d). This pattern is similar to that previously observed after in vitro digestion of egg white with simulated gastroduodenal fluids that allowed the identification of several IgE-binding fragments with molecular masses in the range of 35−20 kDa, as well as others of 15 and 11 kDa, which derived from the hydrolysis of OVA.[21] The corresponding digests produced with human fluids showed fainter and lower molecular mass IgE-binding degradation products and the virtual absence of intact protein and its high molecular mass fragment (Figure 1b).

In addition, several IgE-binding epitopes were detected among the peptide fragments of molecular mass <3 kDa identified in the digests by RP-HPLC-MS/MS (Figure 3). Considering the binding frequency to human sera of the 27 synthetic peptides that mimicked the products of the gastrointestinal digestion, 4 main areas of the protein were recognized by >40% of the sera from egg-allergic patients: 125−176, 188−198, 326−336, and 370−385.

Within the first one, 125−176, at least five distinct epitopes were found, including OVA (125−134) and OVA (159−172), as well as OVA (141−154) and OVA (164−176), which were present in the gastrointestinal digests produced with simulated and human fluids, respectively. The peptides OVA (188−198) and OVA (326−336), found in the gastrointestinal digests produced with simulated fluids that bound, respectively, 60 and 50% of the sera from allergic patients, are related to previously defined allergenic epitopes. OVA (188−198) partially coincides with one of the five dominant human IgE-binding epitopes described by Mine and Rupa,[20] (38−49, 95−102, 191−200, 243−248, and 251−260), whereas OVA (326−336) is comprised within the fragment 323−339, considered an immunodominant B and T cell epitope.[22] The discovery of this latter epitope gave rise to a transgenic mouse carrying the MHC class II restricted rearranged T cell receptor transgene, Tg(DO11.10)10Dlo, specific for OVA (323−339), broadly used in in vitro studies of T cell differentiation and in vivo studies of tolerance and immune responses.[23] Finally, the C-terminal fragment, OVA (370−385), showed the highest binding frequency, reacting with 80% of the sera. Human IgE binding has been demonstrated to broader areas of the C-terminal region of OVA, such as 301−385[24] and 347−385.[25] On the other hand, the existence of, at least, two epitopes within the shorter fragment OVA (367−385) was implied from a positive basophil stimulation in one allergic patient.[25] Interestingly, the peptide OVA (375−384) was recognized by IgE from orally sensitized BALB/c mice but not from mice submitted to intraperitoneal or subcutaneous immunization,[26] which suggests that, even if it is protected within the native structure (Figure 4), it can be specifically exposed as a result of

Figure 4. Representation of the IgE-binding epitope OVA (370−385) in the 3D structure of the protein obtained from the RCSB Protein Data Bank (PDB ID 1OVA) with the UCSF Chimera package.

digestion. This immunoreactive fragment was present in the gastrointestinal digests produced with simulated fluids, but it could not be found in the gastrointestinal digests produced with human fluids.

In agreement with a previous study comparing the in vitro digestibility of bovine β-casein with human and simulated digestive fluids[12] and despite human fluids leading to a much faster proteolytic degradation, a high degree of similarity within the peptide patterns arising from gastric digestion was detected, which was not so evident following duodenal digestion, likely

because of the presence of active exopeptidases in the human duodenal extract. The accumulation of large degradation fragments and low molecular mass peptides with IgE-binding properties could contribute to the stronger residual IgE-binding capacity of the gastroduodenal digests produced with simulated fluids as compared with those produced with human fluids, although the gastrointestinal digests produced with human fluids also contained IgE-binding epitopes that could play a role in the allergenic potential of OVA. Among the epitopes released, OVA (370−385) seemed to be of special importance, as it was able to bind IgE of 80% of the sera employed in the study. More research is needed to elucidate the biological activity of this fragment.

■ ASSOCIATED CONTENT

Supporting Information

Tables S1 and S2. This material is available free of charge via the Internet at http://pubs.acs.org.

■ AUTHOR INFORMATION

Corresponding Author

*(E.M.) Phone: +34 91 001 7938. Fax: +34 91 001 7905. E-mail: e.molina@csic.es.

Funding

This work was funded by the project AGL2011-24740. S.B, I.L.-E., and E.M. are participants of COST-Infogest FA 1005. S.B. and I.L.-E. acknowledge the financial support of CSIC through JAE Pre and JAE Doc grants.

Notes

The authors declare no competing financial interest.

■ ACKNOWLEDGMENTS

We thank Dr. F. Gea from Hospital Universitario La Paz (Madrid, Spain) and Dr. M. Reche and Dr. T. Valbuena from Hospital Infanta Sofía (San Sebastián de los Reyes, Madrid, Spain) for providing, respectively, human samples of gastrointestinal fluids and sera.

■ ABBREVIATIONS USED

OVA, ovalbumin; BS, bile salts; BSA, bovine serum albumin

■ REFERENCES

(1) Benhamou, A. H.; Caubet, J. C.; Eigenmann, P. A.; Nowak-Wegrzyn, A.; Marcos, C. P.; Reche, M.; Urisu, A. State of the art and new horizons in the diagnosis and management of egg allergy. *Allergy* **2010**, *65*, 283−289.

(2) Rona, R. J.; Keil, T.; Summers, C.; Gislason, D.; Zuidmeer, L.; Sodergren, E.; Sigurdardottir, S. T.; Lindner, T.; Goldhahn, K.; Dahlstrom, J.; McBride, D.; Madsen, C. The prevalence of food allergy: a meta-analysis. *J. Allergy Clin. Immunol.* **2007**, *120*, 638−646.

(3) Savage, J. H.; Matsui, E. C.; Skripak, J. M.; Wood, R. A. The natural history of egg allergy. *J. Allergy Clin. Immunol.* **2007**, *120*, 1413−1417.

(4) Mine, Y.; Yang, M. Recent advances in the understanding of egg allergens: basic, industrial, and clinical perspectives. *J. Agric. Food Chem.* **2008**, *56*, 4874−4900.

(5) Ruiter, B.; Shreffler, W. G. Innate immunostimulatory properties of allergens and their relevance to food allergy. *Semin. Immunopatol.* **2012**, *34*, 617−632.

(6) Fu, T. J.; Abbott, U. R.; Hatzos, C. Digestibility of food allergens and nonallergenic proteins in simulated gastric fluid and simulated intestinal fluid − a comparative study. *J. Agric. Food Chem.* **2002**, *50*, 7154−7160.

(7) Takagi, K.; Teshima, R.; Okunuki, H.; Sawada, J.-I. Comparative study of *in vitro* digestibility of food proteins and effect of preheating on the digestion. *J. Biol. Pharm. Bull.* **2003**, *26*, 969−973.

(8) Dupont, D.; Mandalari, G.; Molle, D.; Jardin, J.; Léonil, J.; Faulks, R. M.; Wickham, M. S. J.; Mills, E. N. C.; Mackie, A. R. Comparative resistance of food proteins to adult and infant *in vitro* digestion models. *Mol. Nutr. Food Res.* **2010**, *54*, 767−780.

(9) Martos, G.; Contreras, P.; Molina, E.; López-Fandiño, R. Egg white ovalbumin digestion mimicking physiological conditions. *J. Agric. Food Chem.* **2010**, *58*, 5640−5648.

(10) Hur, S. J.; Lim, B. O.; Decker, E. A.; McClements, D. J. *In vitro* human digestion models for food applications. *Food Chem.* **2011**, *125*, 1−12.

(11) Furlund, C. B.; Ulleberg, E. K.; Devold, T. G.; Flengsrud, R.; Jacobsen, M.; Sekse, C.; Holm, H.; Vegarud, G. E. Identification of lactoferrin peptides generated by digestion with human gastrointestinal enzymes. *J. Dairy Sci.* **2012**, *96*, 75−88.

(12) Benedé, S.; López-Expósito, I.; Giménez, G.; Grishina, G.; Bardina, L.; Sampson, H. A.; Molina, E.; López-Fandiño, R. *In vitro* digestibility of bovine β-casein with simulated and human oral and gastrointestinal fluids. Identification and IgE-reactivity of the resultant peptides. *Food Chem.* **2014**, *143*, 514−521.

(13) Moreno, F. J.; Mellon, F. A.; Wickham, M. S. J.; Bottrill, A. R.; Mills, E. N. C. Stability of the major allergen Brazil nut 2S albumin (Ber e1) to physiologically relevant in vitro gastrointestinal digestion. *FEBS J.* **2005**, *272*, 341−352.

(14) Jiménez-Saiz, R.; López-Exposito, I.; Molina, E.; López-Fandiño, R. IgE-binding and in vitro gastrointestinal digestibility of egg allergens in the presence of polysaccharides. *Food Hydrocolloids* **2013**, *30*, 597−605.

(15) Bannon, G. A.; Bartels, M.; Dearman, R. J.; Esdaile, D. J.; Fu, T. J.; Glatt, C. M.; Hadfield, N.; Hatzos, C.; Hefle, S. L.; Heylings, J. R.; Goodman, R. E.; Henry, B.; Herouet, C.; Holsapple, M.; Ladics, G. S.; Landry, T. D.; MacIntosh, S. C.; Rice, E. A.; Privalle, L. S.; Steiner, H. Y.; Teshima, R.; van Ree, R.; Woolhiser, M.; Zawodny, J. A multi-laboratory evaluation of a common in vitro pepsin digestion assay protocol used in assessing the safety of novel proteins. *Regul. Toxicol. Pharmacol.* **2004**, *39*, 87−98.

(16) Dearman, R. J.; Caddick, H.; Stone, S.; Kenna, J. G.; Basketter, D. A.; Kimber, I. Immunogenic properties of rapidly digested food proteins following gavage exposure to mice: a comparison of ovalbumin with a potato acid phosphatase preparation. *Food Chem. Toxicol.* **2002**, *40*, 625−633.

(17) Miguel, M.; Recio, I.; Gómez-Ruiz, J. A.; Ramos, M.; López-Fandiño, R. Angiotensin I-converting enzyme inhibitory activity of peptides derived from egg white proteins by enzymatic hydrolysis. *J. Food Prot.* **2004**, *67*, 1914−1920.

(18) García-Redondo, A. B.; Roque, F. R.; Miguel, M.; López-Fandiño, R.; Salaices, M. Vascular effects of egg white-derived peptides in resistance arteries form rats. Structure-activity relatioships. *J. Sci. Food Agric.* **2010**, *90*, 1988−1993.

(19) Lyons, P. J.; Fricker, L. D. Carboxypeptidase O is a glycosylphosphatidylinositol-anchored intestinal peptidase with acidic amino acid specificity. *J. Biol. Chem.* **2011**, *286*, 39023−39032.

(20) Mine, Y.; Rupa, P. Fine mapping and structural analysis of immunodominant IgE allergenic epitopes in chicken ovalbumin. *Protein Eng.* **2003**, *16*, 747−752.

(21) Martos, G.; López-Fandiño, R.; Molina, E. Immunoreactivity of hen egg allergens: influence on *in vitro* gastrointestinal digestion of the presence of other egg white proteins and of egg yolk. *Food Chem.* **2013**, *136*, 775−781.

(22) Elsayed, S.; Apold, J.; Holen, E.; Vik, H.; Florvaag, E.; Dybendal, T. The structural requirements of epitopes with IgE binding capacity demonstrated by three major allergens from fish, egg and tree pollen. *Scand. J. Clin. Lab. Invest.* **1991**, *204* (Suppl.), 17−31.

(23) Sato, T.; Sasahara, T.; Nakamura, Y.; Osaki, T.; Hasegawa, T.; Tadakuma, T.; Arata, Y.; Kumagai, Y.; Katsuki, M.; Habu, S. Naive T-cells can mediate delayed-type hypersensitivity response in T-cell receptor transgenic mice. *Eur. J. Immunol.* **1994**, *24*, 1512−1516.

(24) Kahlert, H.; Petersen, A.; Becker, W. M.; Schlaak, M. Epitope analysis of the allergen ovalbumin (Gal d II) with monoclonal antibodies and patients' IgE. *Mol. Immunol.* **1992**, *29*, 1191−1201.
(25) Honma, K.; Kohno, Y.; Saito, K.; Shimojo, N.; Horiuchi, T.; Hayashi, H.; Suzuki, N.; Hosoya, T.; Tsunoo, H.; Niimi, H. Allergenic epitopes of ovalbumin (OVA) in patients with hen's egg allergy: inhibition of basophil histamine release by haptenic ovalbumin peptide. *Clin. Exp. Immunol.* **1996**, *103*, 446−453.
(26) Mine, Y.; Yang, M. Epitope characterization of ovalbumin in BALB/c mice using different entry routes. *Biochim. Biophys. Acta−Proteins Proteomics* **2007**, *1774*, 200−212.

JOURNAL OF AGRICULTURAL AND FOOD CHEMISTRY

Article

pubs.acs.org/JAFC

Production and *in Vitro* Fermentation of Soluble, Non-digestible, Feruloylated Oligo- and Polysaccharides from Maize and Wheat Brans

Junyi Yang, María X. Maldonado-Gómez, Robert W. Hutkins, and Devin J. Rose*

Department of Food Science and Technology, University of Nebraska—Lincoln, Lincoln, Nebraska 68583-0919, United States

Supporting Information

ABSTRACT: High-pressure hydrothermal treatment of cereal bran results in fragmentation of the cell wall, releasing soluble, non-digestible, feruloylated oligo- and polysaccharides (FOPS), which may be beneficial to gut health. The objectives of this study were to (1) determine treatment temperatures for production of FOPS from maize bran and wheat bran and (2) determine the fermentation properties of partially purified FOPS from maize bran and wheat bran. FOPS were produced by heating bran and water (10%, w/v) in a high-pressure stirred reactor until the slurry reached 160−200 °C (in 10 °C increments). Final temperatures of 190 °C for maize bran and 200 °C for wheat bran resulted in the highest release of FOPS (49 and 50% of starting non-starch polysaccharide, respectively). Partial purification with ion exchange and dialysis resulted in a final product containing 63 and 57% total carbohydrate and 49 and 30% FOPS, respectively (other carbohydrate was starch). Following *in vitro* digestion (to remove starch), *in vitro* fermentation revealed that wheat FOPS were more bifidogenic than maize FOPS. However, maize FOPS led to continual production of short-chain fatty acid (SCFA), resulting in the highest SCFA and butyrate production at the end of the fermentation. In addition, maize FOPS showed significantly higher antioxidant activity than wheat FOPS. This study identified a process to produce FOPS from maize bran and wheat bran and showed that, considering the overall beneficial effects, FOPS from maize bran may exhibit enhanced benefits on gut health compared to those of wheat bran.

KEYWORDS: *maize, short-chain fatty acids, butyrate, prebiotic, Bifidobacterium*

INTRODUCTION

The basic structure of arabinoxylan, the predominant non-starch polysaccharide in grains, is a (1,4)-linked β-D-xylopyranosyl backbone substituted at C(O)-2 and/or C(O)-3 with α-L-arabinofuranosyl moieties, some of which are themselves substituted with ferulic acid that can be involved in oxidative cross-linkages with other arabinoxylan chains and other cell-wall components.[1] Beyond these basic structures, arabinoxylan can also contain oligosaccharide side chains comprised of pentose or hexose sugars or uronic acids. Dependent upon botanical source and location within the kernel, arabinoxylan can differ in distributions and types of side chains, molecular weight, ferulate content, and degree of cross-linking.[1,2] Because of its complex nature, arabinoxylan is sometimes referred to as glucuronoarabinoxylan or heteroxylan.[3−5] For simplicity, arabinoxylan will be used in this paper to refer to this complex class of polysaccharides.

Two sources of divergent arabinoxylan structures are those from maize and wheat. Enzymatic or dilute acid degradation accompanied by partial methylation analysis of alkali-solubilized arabinoxylan from maize bran and wheat bran has revealed greater branch density and complexity in maize arabinoxylan compared to that of wheat.[4,6,7]

In its native form, arabinoxylan is mostly insoluble and cross-linked, making it a poorly fermentable substrate for gut bacteria.[8−10] However, partial hydrolysis of arabinoxylan from wheat bran with xylanase releases arabinoxylan oligosaccharides (AXOS), which are highly fermentable in the gut and stimulate the growth of bifidobacteria and other beneficial bacteria.[11] AXOS have also been shown to reduce blood serum triglyceride and cholesterol levels, facilitate diabetic weight loss, and enhance antioxidant capacity in liver.[11]

Arabinoxylan may also be released from its insoluble matrix by autohydrolysis,[12,13] but the structure of the carbohydrates released are different from those released by enzyme. For instance, autohydrolysis breaks down the arabinoxylan into many size pieces ranging from monosaccharides on up to polysaccharides with a degree of polymerization (DP) of 750 or more,[12,13] while enzymatic treatment releases mostly shorter chain oligosaccharides.[14] Additionally, autohydrolysis can release arabinoxylan structures that are resistant to enzymatic hydrolysis, as evidenced by increased yields with autohydrolysis (ca. 50% from maize bran and wheat bran)[12,13] compared to enzymatic release (ca. 30% in wheat bran[10,14] and <3% in maize bran[15]).

Although the fermentation properties of AXOS have been reported extensively,[11] utilization of the soluble, non-digestible, feruloylated oligo- and polysaccharides (FOPS) released by autohydrolytic processing have only been studied in a few instances, and in these cases, the hydrolytic product was further treated with xylanase.[16−18] Because maize bran and wheat bran contain vastly different arabinoxylan structures[4,6,7] and the parent arabinoxylans from these two sources have been shown

Received: September 25, 2013
Revised: December 5, 2013
Accepted: December 11, 2013
Published: December 11, 2013

ACS Publications © 2013 American Chemical Society

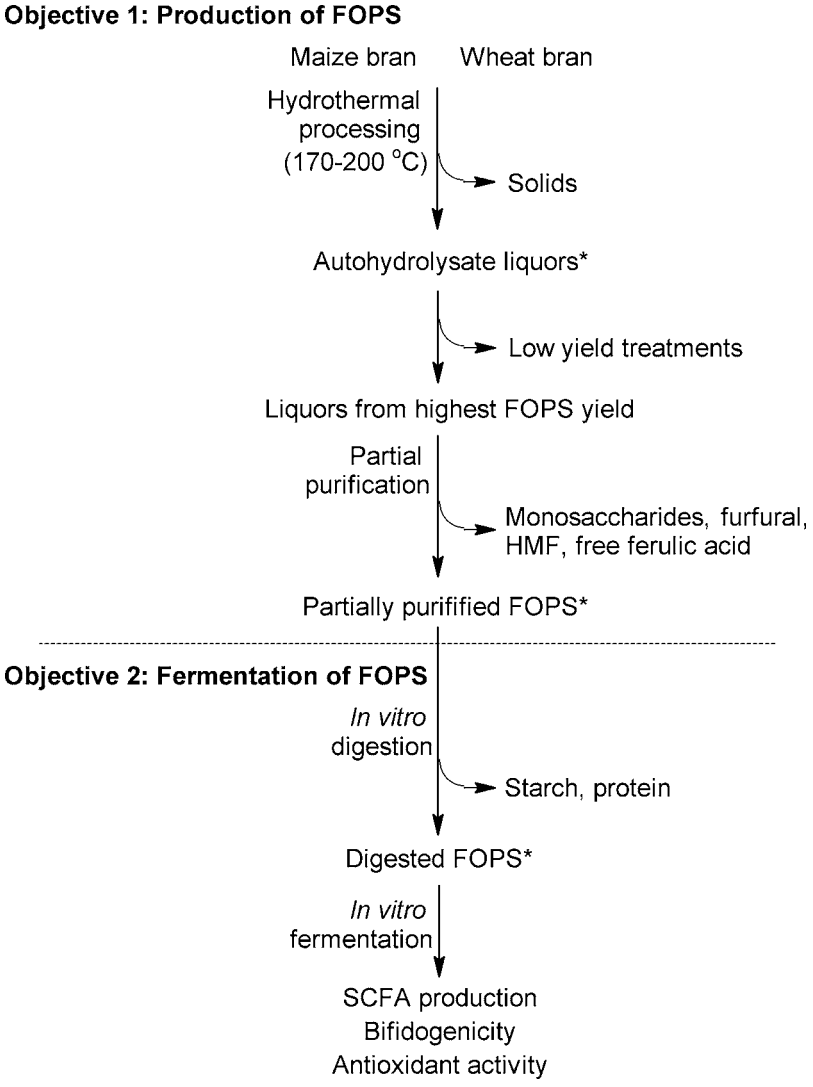

Figure 1. Flowchart of the protocol, which consisted of two objectives: (1) production of FOPS and (2) fermentation of FOPS. (∗) Compositional analysis was performed at these stages, including: total FOPS, monosaccharides, furfural, HMF, free ferulic acid, total starch, protein, antioxidant activity, and molecular weight distribution.

to be used very differently by gut bacteria,[8] the objectives of this study were to (1) determine treatment temperatures for production of FOPS from maize bran and wheat bran and (2) determine the fermentation properties of partially purified FOPS from these substrates.

MATERIALS AND METHODS

Safety. The high-pressure processing followed the safety portions of the instrument manual (4848, Parr Instrument Co., Moline, IL). The chemicals used in this study required no special safety considerations.

Production of FOPS. Maize bran was obtained from Bunge Milling (Crete, NE), and wheat bran was obtained from Horizon Mills (Newton, KS) and milled with a cyclone sample mill (UDY, Boulder, CA) equipped with a 1 mm screen. A total of 150 g of milled bran and 1350 mL of water were combined in a 2 L high-pressure reactor (model 4848, Parr, Moline, IL). The slurry was heated to 170, 180, 190, or 200 °C at full power (ca. 4 °C/min) under constant stirring at a speed of 400 rpm. The slurry was then cooled to 80 °C using an internal serpentine cold water cooling coil (ca. 15 min). Following the treatment, the slurries were centrifuged at 10000*g* for 10 min and the supernatant was retained. The supernatant was referred to as the autohydrolysate liquor (Figure 1). Each treatment was performed in duplicate.

Total carbohydrate, total starch, free monosaccharides, free and esterified ferulic acid, furfural, hydroxymethylfurfural (HMF), total starch, and protein were determined in all autohydrolysate liquors (see Compositional Analyses). FOPS were calculated according to the following equation:

$$\text{FOPS}\ (\%) = W_{ara} + W_{xyl} + W_{man} + W_{gal} + W_{glc} + W_{fa}$$

where W_{ara} is total arabinan (%), W_{xyl} is total xylan (%), W_{man} is total mannan (%), W_{gal} is total galactan (%), W_{glc} is total non-starch glucan (%), determined as the difference between the total glucan content after acid hydrolysis and the starch content, and W_{fa} is total esterified ferulate. Autohydrolysate liquors corresponding to treatment temperatures that resulted in the highest release of FOPS were also analyzed for molecular weight distribution and antioxidant activity (see Compositional Analyses).

The autohydrolysate liquors from treatment temperatures corresponding to the highest release of FOPS were pooled and dialyzed (molecular weight cut-off of 500, Spectrum Laboratories, Rancho Dominguez, CA). The retentate was mixed with ion-exchange resin (AG501-X8, Bio-Rad, Hercules, CA) at a rate of 1 g/20 mL and stirred gently overnight. After ion-exchange resin was filtered, the sample was treated under partial vacuum at 80 °C to concentrate the solids and

dx.doi.org/10.1021/jf404305y | J. Agric. Food Chem. 2014, 62, 159−166

remove volatile compounds. The material, referred to as partially purified FOPS, was then freeze-dried and assayed for total carbohydrate, free monosaccharides, free ferulic acid and esterified ferulate, furfural, HMF, starch, protein, antioxidant activity, and molecular weight distribution (see Compositional Analyses).

Fermentation of FOPS. To prepare for fermentation, *in vitro* digestion of partially purified FOPS was performed according to Yang et al.[19] The digested content was dialyzed (molecular weight cut-off of 500). Dialyzed material was freeze-dried and analyzed for total carbohydrate, free monosaccharides, free ferulic acid and esterified ferulate, starch, furfural, HMF, protein, antioxidant activity, and molecular weight distribution (see Compositional Analyses). This material was referred to as digested FOPS.

In vitro fermentation of digested FOPS was performed according to Hartzell et al.,[20] except that the sample size was 70 mg of carbohydrate instead of 100 mg. Fructooligosaccharides (FOS, Beneo, Morris Plains, NJ) were included as a positive control, and tubes containing no substrate were used as blanks. Samples (1 mL each) were taken at predetermined time points and stored at −80 °C. At times 0, 12, and 24 h, samples were assayed for short-chain fatty acid (SCFA), *Bifidobacterium*, and antioxidant activity (see Fermentation Analysis and Compositional Analyses). At other time points, samples were only assayed for SCFA.

Compositional Analyses. Total carbohydrate and free monosaccharides were determined according to Rose et al.[13] Briefly, 1 mL of liquid sample or 30 mg of solid sample were analyzed in tandem for carbohydrate content with or without chemical hydrolysis.[21] With hydrolysis constituted total carbohydrate, and without hydrolysis gave free monosaccharides. Oligo- and polymeric carbohydrates were determined as the differences between total carbohydrate and free monosaccharides.

Free ferulic acid and esterified ferulate were measured using methods described by Yuan et al.[22] and Carole et al.[23] For bran samples, 10 mg of sample was weighed into a tube. If the sample was a liquid (such as autohydrolysate liquors), 0.2 mL of sample was used. If sample was a freeze-dried powder, it was dissolved in water at 3% (w/v) and 0.2 mL of sample was used. Two tubes were prepared for analysis per replicate. To one of the tubes, which represented the total ferulic acid content, 0.2 mL of 0.4 M sodium hydroxide was added. The tube was shaken for 2 h at room temperature, and then 0.3 mL of 0.4 M phosphoric acid was added, followed by 0.2 mL of water. Free ferulic acid was assayed in the other tube in the same manner, except that sodium hydroxide was replaced by water. Each tube was then extracted with 1 mL of ethyl acetate 3 times. The pooled ethyl acetate extracts were evaporated using a partial vacuum, and the extract was dissolved in 2 mL of 50% aqueous methanol. Samples were filtered through a 0.45 μm membrane, and 15 μL was injected into high-performance liquid chromatography (HPLC, 1260, Agilent, Santa Clara, CA) equipped with a C18 column (C-18-4E, Skowa Denko K.K., Tokyo, Japan) and ultraviolet (UV) detector at 320 nm. Elution was performed using the gradient described by Carole et al.[23] Quantification was by means of external calibration with a ferulic acid standard (MP Biomedicals, Solon, OH). Esterified ferulate content was calculated by the difference between the total ferulic acid and the free ferulic acid.

Samples were analyzed for furfural and HMF by means of external calibration with authentic standards (Sigma-Aldrich, St. Louis, MO) following Gomis et al.,[24] except that the mobile phase was 96:4 (v/v) water/acetonitrile rather than 92:8. If the sample was a liquid, it was analyzed directly or after appropriate dilution (in samples containing high furfural or HMF concentration). If the sample was a freeze-dried powder, it was dissolved at 3% (w/v) for analysis.

Total starch was measured in solid samples using a kit (K-TSTA, Megazyme, Bray, Ireland). In liquid samples, the total starch content was measured following the method from Rose et al.[12]

The protein content of solid samples was obtained by a FP528 nitrogen/protein determinator (LECO Corporation, St. Joseph, MI) after using a conversion factor of 6.25 for percent nitrogen to percent protein.[25] In liquid samples, the protein content was measured using the Bradford method with bovine serum albumin (Pierco, Rockford, IL) used to create a standard curve.[26]

To determine the molecular weight distribution, 10 mg of freeze-dried powder was dissolved in 2 mL of water. Samples were filtered through a 0.45 μm membrane, and 100 μL was injected into HPLC (Agilent) equipped with Shodex SB-G, SB-804 HQ, and SB-802 HQ (Skowa Denko K.K., Tokyo, Japan) columns connected in series followed by a refractive index detector (Agilent). The mobile phase was 0.02% sodium azide at 0.5 mL/min. Molecular weight calibration was accomplished by means of external pullulan (P-82, Shodex) and glucooligosaccharide (4-7265, Sigma-Aldrich, St. Louis, MO) standards.

Antioxidant activity was determined using the 1,1-diphenyl-2-picrylhydrazyl (DPPH) and 2,2-azino-bis-3-ethylbenzthiazoline-6-sulfonic acid (ATBS) methods. The DPPH assay was performed by reacting 0.2 mL of appropriately diluted sample with 1 mL of DPPH as described by Sensoy et al.,[27] except that, after incubating for 30 min, the tubes were centrifuged for 10 min at 3000*g* to remove the cloudiness. The ATBS assay was conducted according to Re et al.[28] Antioxidant activity was expressed relative to the antioxidant activity of 6-hydroxy-2,5,7,8-tetramethylchroman-2-carboxylic acid (Trolox, Sigma-Adrich, St. Louis, MO).

Fermentation Analysis. Samples taken during fermentation were thawed and centrifuged (10000*g* for 5 min). The supernatant was used for analysis of SCFA after Hartzell et al.[20] and for antioxidant activity (see Compositional Analyses). The pellet was used for analysis of *Bifidobacterium* by quantitative real-time polymerase chain reaction (PCR) as described.[20]

Data Analysis. For autohydrolytic processing, two replications at each temperature were performed. Each replicate was analyzed twice. Differences in chemical compositions were analyzed using analysis of variation (ANOVA) in combination with Fisher's protected least significant difference. The replicates from autohydrolysis were pooled for the *in vitro* fermentation stage. Differences in SCFA production between treatments were analyzed with three replicates using ANOVA with repeated measures followed by Fisher's protected least significant difference using SAS (version 9.2, SAS Institute, Cary, NC). Differences among substrate treatment on the population of *Bifidobacterium* and antioxidant activity were computed using ANOVA in combination with Fisher's protected least significant difference.

RESULTS AND DISCUSSION

Production of FOPS. Maize bran and wheat bran contained high concentrations of total dietary fiber (Table 1), most of which was water-insoluble.[29] Higher ferulic acid content was

Table 1. Selected Composition of Maize Bran and Wheat Bran (% Dry Basis)[a]

component	maize bran	wheat bran
starch	10.6 ± 0.2	14.4 ± 0.3
total dietary fiber	64.6 ± 1.4	47.2 ± 1.4
arabinan	12.5 ± 0.5	9.8 ± 0.2
xylan	24.7 ± 1.6	13.9 ± 1.0
mannan	0.772 ± 0.060	0.691 ± 0.000
galactan	2.82 ± 0.03	0.440 ± 0.020
glucan	16.2 ± 1.7	12.1 ± 1.9
uronic acid	3.23 ± 0.04	0.988 ± 0.031
Klason lignin	4.38 ± 0.11	9.25 ± 0.11
ferulic acid	2.51 ± 0.05	0.150 ± 0.011
protein	5.33 ± 0.01	17.1 ± 0.0
other (by difference)	17.0	21.2

[a]Mean values ± standard deviation (SD) (n = 2). Total dietary fiber is expressed as the sum of neutral sugars, uronic acids, and Klason lignin. Glucan refers to non-starch glucan.

dx.doi.org/10.1021/jf404305y | J. Agric. Food Chem. 2014, 62, 159−166

observed in maize bran compared to wheat bran. Maize has the highest ferulic acid content among major cereal brans, which exhibits high antioxidant activity and displays potential health benefits.[29]

The composition of the autohydrolysate liquors differed depending upon the treatment temperature (Figure 2A). The

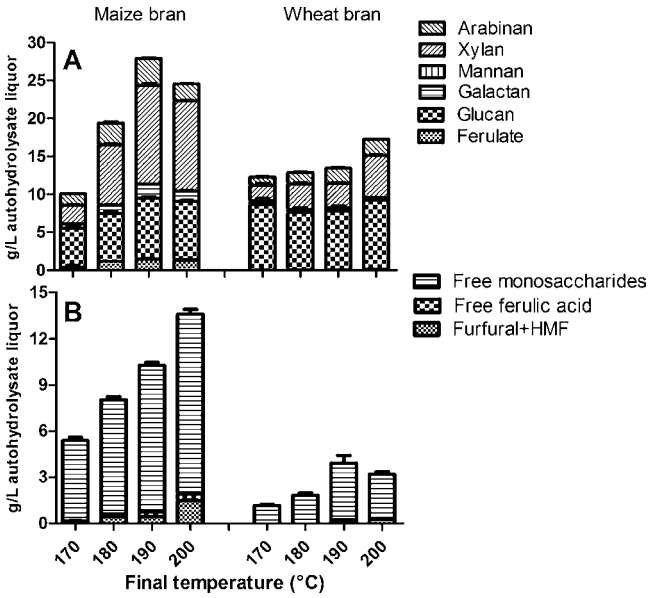

Figure 2. Composition of autohydrolysate liquor upon hydrothermal treatment to selected temperatures: (A) FOPS and (B) non-FOPS material released by autohydrolysis treatment. HMF = hydroxymethylfurfural. Error bars show standard deviation (n = 2). Some error bars were too small to plot.

release of FOPS was increased in autohydrolysate liquor from maize bran as the temperature increased from 170 to 190 °C and then showed a marked decrease from 190 to 200 °C. The highest yield represented 49% of the starting non-starch polysaccharide content and 44% of the initial ferulic acid content. With wheat bran, an increased final temperature resulted in a steady increase in the concentration of FOPS in the autohydrolysate liquor, ultimately releasing 50% of the initial non-starch polysaccharide content and 82% of the ferulic acid content at a final treatment temperature of 200 °C. These yields agree well with the percentage of cell-wall polysaccharides released by hydrothermal treatment of other agricultural byproducts[30] and were substantially higher than the AXOS released by enzymatic hydrolysis.[14] Thus, 190 and 200 °C were selected as the desirable temperatures to release FOPS from maize bran and wheat bran, respectively.

The autohydrolysate liquors also contained high concentrations of non-FOPS material (Figure 2B). The release of arabinose and xylose was largely affected by the treatment temperature, with more arabinose being released (mainly side chain) than xylose (mainly backbone), suggesting that arabinoxylan was partially debranched during autohydrolysis (data not shown). Furfural and HMF increased as the treatment temperature increased. These compounds are one of the thermal degradation compounds of pentoses and hexoses, respectively.[31] Starch and protein were also present in autohydrolysate liquors (10.9−15.3 and 0.180−2.01 g/L, respectively), but the concentration did not vary as a function of the treatment temperature.

Dialysis, ion-exchange, and vacuum concentration were used to partially remove non-FOPS material from autohydrolysate liquors. The partially purified material from maize bran contained a higher percentage of FOPS compared to wheat bran (49 versus 30%, respectively; see Table S1 of the Supporting Information). Nearly 4-fold higher antioxidant activity was observed on partially purified maize FOPS compared to wheat when using ATBS radical; when using DPPH radical, maize FOPS showed 2-fold higher antioxidant activity compared to wheat (see Table S1 of the Supporting Information).

The purification process removed furfural, HMF, and free ferulic acid (i.e., these compounds were not detectable in the partially purified samples; see Table S1 of the Supporting Information). More than 90% of the free monosaccharaides present in autohydrolysate liquors from both maize bran and wheat bran was removed with the partial purification process (see Table S1 of the Supporting Information).

Because the purification process only concentrated oligo- and polysaccharides and removed non-carbohydrate material, there was still substantial starch contamination in the partially purified FOPS preparations (15.5 and 27.1% in maize bran and wheat bran freeze-dried material, respectively; see Table S1 of the Supporting Information). Pretreatments are often employed to remove starch prior to producing FOPS-like materials.[12,13] However, this step was not performed to simplify the production process because it was anticipated that the digestion phase would remove any contaminating starch prior to determining fermentation characteristics.

Partially purified FOPS showed a broad molecular weight distribution, resulting from the fragmentation of arabinoxylan caused by high-pressure hydrothermal treatment. The majority of polymers ranged from 0.24×10^5 to 1.9×10^5 g/mol (data not shown). The presence of high-molecular-weight polymers could have been due to the release of polysaccharides or from the release of oligosaccharides that were covalently linked through diferuloyl groups.

Fermentation of FOPS. Because the partially purified FOPS contained appreciable starch (see Table S1 of the Supporting Information), prior to *in vitro* fermentation, *in vitro* digestion was performed. *In vitro* digestion removed nearly all of the starch and, consequently, increased the percentage of FOPS in the freeze-dried material compared to the partially purified FOPS (see Table S1 of the Supporting Information). The digestion process also resulted in concentrating the ferulate content and, subsequently, increasing the antioxidant activity (see Table S1 of the Supporting Information). Protein decreased after digestion, but a small percentage persisted (2.37 and 3.27% in maize bran and wheat bran samples, respectively). Some of this protein could have been denatured enzymes from the digestion process as well as enzyme-resistant protein from the starting material. The difficulty in completely removing protein from cereal grain materials has been noted previously.[32]

In vitro digestion removed some of the shortest polymers in wheat FOPS (data not shown), suggesting that starch may have been fragmented into small dextrins. However, the digested FOPS contained a similar broad molecular weight distribution compared to before *in vitro* digestion.

In vitro fermentation was performed to determine how FOPS from maize bran and wheat bran were metabolized by fecal bacteria. Wheat FOPS resulted in lower SCFA production at 4 h compared to FOS (included as a positive control), and there

Table 2. SCFA Production (μmol/100 mg of Initial Carbohydrate) during *in Vitro* Fermentation of Blank, FOS, and FOPS from Maize and Wheat Brans[a]

	fermentation time (h)			
metabolite/sample	4	8	12	24
		Acetate		
blank	213 ± 18 c	198 ± 21 b	203 ± 31 b	300 ± 23 c
maize FOPS	370 ± 26 b	541 ± 52[b] a	530 ± 40 a	886 ± 173[b] a
wheat FOPS	433 ± 20 b	472 ± 75 a	485 ± 45 a	454 ± 29 b
FOS	560 ± 30 a	517 ± 74 a	495 ± 98 a	563 ± 30 b
		Propionate		
blank	45.5 ± 5.2 d	61.6 ± 6.0 c	62.8 ± 7.1 c	85.2 ± 8.7[b] b
maize FOPS	71.7 ± 6.7 c	106 ± 11[b] ab	111 ± 11 b	179 ± 34[b] a
wheat FOPS	95.4 ± 3.8 b	90.8 ± 10.9 b	100 ± 9 b	91 ± 6 b
FOS	137 ± 10 a	121 ± 14 a	155 ± 19[b] a	164 ± 9 a
		Butyrate		
blank	58 ± 6 d	57.0 ± 3.2 c	52.7 ± 15.4 c	77.3 ± 3.4[b] c
maize FOPS	104 ± 7 c	146 ± 8[b] b	181 ± 13[b] b	244 ± 6[b] a
wheat FOPS	150 ± 5 b	182 ± 15[b] a	209 ± 9[b] a	206 ± 10 b
FOS	181 ± 19 a	183 ± 16[b] a	207 ± 17[b] a	216 ± 6 b
		Total SCFA		
blank	316 ± 26 c	317 ± 28 b	318 ± 52 b	462 ± 31 d
maize FOPS	546 ± 26 b	795 ± 74[b] a	822 ± 43 a	1040 ± 218[b] a
wheat FOPS	679 ± 32 b	745 ± 100 a	794 ± 58 a	751 ± 30 c
FOS	878 ± 46 a	821 ± 82 a	715 ± 131 a	943 ± 131[b] b

[a]Values are reported as mean ± SD of three replicates. Units are μmol/100 mg of initial carbohydrate. Means followed by different letters within each column and SCFA type are significantly different. [b]Significantly different from the previous time point ($p < 0.05$).

was no significant change in SCFA production after 4 h (Table 2). Maize FOPS also showed low SCFA production relative to FOS at 4 h but brought about continual production of SCFA thereafter, resulting in the highest SCFA production at the end of the fermentation.

The steadily fermentation profile of maize FOPS suggests that fermentation may persist into the distal part of the colon, where protein fermentation otherwise predominates, resulting in the production of toxic compounds, such as ammonia, phenol, indoles, thiols, amines, and sulfides.[34] A greater increase in SCFA production in distal colon may result in protective effects by lowering the pH and inhibiting the fermentation of protein.[33]

The difference in chemical structure between maize and wheat arabinoxylan may be responsible for their different fermentation profiles. As mentioned, maize arabinoxylan contains higher branch density and complexity, coupled with higher levels of esterified ferulic acid compared to wheat arabinoxylan.[4,6,7] Notably, extended fermentation properties for alkali-extracted maize arabinoxylan[8] as well as its hydrolysate[34] have been shown previously. Thus, slow fermentation appears to be an inherent property of maize arabinoxylan, independent of the DP or method of release from the cell-wall matrix.

Individual SCFA production also differed among substrates. After 24 h of fermentation, microbial butyrate production on maize FOPS was significantly higher than that on other substrates (Table 2). Butyrate has been shown to inhibit inflammatory responses by inhibiting activation of nuclear factor κB.[35] Thus, the high butyrate production of maize FOPS may exert potential health benefits compared to the other substrates.[33,35,36] Significantly higher propionate was also observed on maize FOPS compared to wheat FOPS. Propionate may reduce serum lipid as well as the risk of cardiovascular diseases.[37] Propionate has also been shown to have the potential to prevent obesity-related inflammation and associated diseases.[38]

Because the target of many prebiotic studies is to increase *Bifidobacterium*,[33,39] and because AXOS produced by enzyme treatment have been shown to be particularly bifidogenic,[40−42] the shift in *Bifidobacterium* upon FOPS treatment was investigated. Both maize and wheat FOPS showed a significant increase in *Bifidobacterium* compared to the blank and baseline after 12 and 24 h of fermentation, although the increase was not as great as FOS (except for wheat FOPS after 12 h of fermentation; Figure 3). Wheat FOPS exhibited higher bifidogenicity than maize at the end of the fermentation.

These results are contrary to previous reports demonstrating that AXOS can be a more potent bifidogenic substrates than FOS.[40,41] This is likely because FOPS (released by autohydrolysis) contained more complex, higher DP structures compared to AXOS (released by enzyme).[14] The higher branch density and complexity of maize arabinoxylan compared to wheat may account for the lower bifidogenicity of maize FOPS, whereas other bacteria may have greater capacity to use these substrates. For instance, the SCFA data suggest that maize FOPS supported butyrate producers (Table 2). The main butyrate producers in the gut include *Eubacterium rectale*/*Roseburia* spp. and *Faecalibacterium prausnitzii*, which have shown beneficial effects on the gut.[43] Other members of the gut microbiota also contribute to the SCFA pool.

Although the gut is an anaerobic environment, the gut epithelia release reactive oxygen species into the lumen of the gut in response to environmental stresses and, in some cases, even commensal bacteria.[44] Numerous diseases, such as inflammatory bowel diseases and colon cancer, are associated with an imbalance in the gut cellular redox system.[45] When the antioxidant activity in the medium was measured, the potential ability of FOPS to prevent oxidative damage in the gut was investigated.

dx.doi.org/10.1021/jf404305y | J. Agric. Food Chem. 2014, 62, 159−166

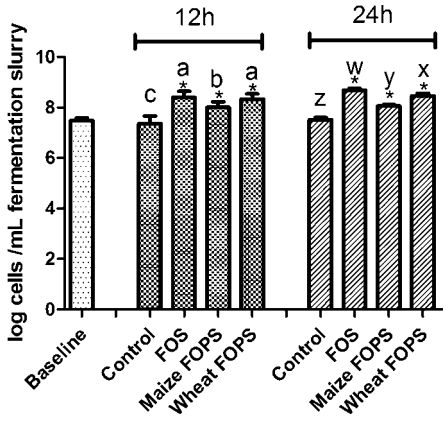

Figure 3. Enumeration of *Bifidobacterium* during *in vitro* fermentation. The baseline represents *Bifidobacterium* in the fecal inoculum before fermentation (0 h). The control represents a sample after fermentation with no added carbohydrate substrate. FOPS = feruloylated oligo- and polysaccharides. FOS = fructooligosaccharides. Bars marked with different letters are significantly different within each time point. (∗) Significantly different from the baseline ($p < 0.05$). $n = 2$ (baseline) or 3 (fermentation samples). Error bars show standard deviation.

As expected, because of the high ferulate content, at 0 h, the highest antioxidant activity was observed on maize FOPS (Figure 4). During fermentation, antioxidant activities changed depending upon the substrate and radical used for the antioxidant assay. On ATBS, the blank and FOS showed decreasing antioxidant activity as fermentation time progressed. The decrease was delayed when wheat FOPS was used, and maize FOPS showed an increase at 12 h before a decrease was experienced. In contrast to ATBS, radical scavenging ability against DPPH increased in all samples, including the blank and FOS, from 0 to 12 h of fermentation, followed by a significant decrease in all samples, except maize FOPS at 24 h.

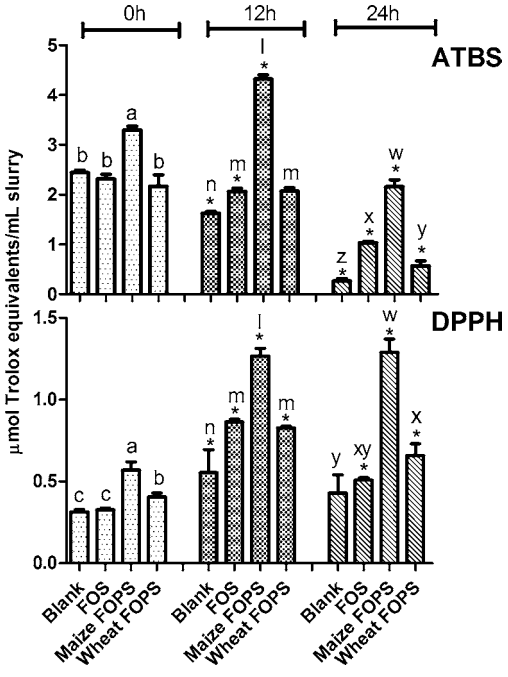

Figure 4. Antioxidant activity of fermentation medium before and after 12 and 24 h *in vitro* fermentation. The blank represents a sample after fermentation with no added carbohydrate substrate. FOPS = feruloylated oligo- and polysaccharides. FOS = fructooligosaccharides. Bars marked with different letters are significantly different within each time point. (∗) Significantly different from the corresponding substrates at the previous time point ($p < 0.05$). $n = 3$. Error bars show standard deviation.

The human microbiota can express several enzymes that are capable of releasing and metabolizing ferulic acid,[46,47] the major antioxidant in FOPS. This has a dramatic effect on biological activity.[46−50] First, gut bacteria probably hydrolyze the ester linkage and release free ferulic acid.[51] This would likely increase the antioxidant activity because free ferulic acid possesses higher antioxidant activity than esterified ferulate.[52] Upon release of the ferulic acid, modification of function groups by microbial enzymes could further affect the antioxidant activity. Metabolism of ferulic acid first involves hydrogenation of the propen-2-oic acid side chain and demethylation of the ring ether[46] to form 3,4-dihydroxyphenylpropionic acid.[46] This compound has been shown to possess higher antioxidant activity than ferulic acid in edible oil systems;[53] however, this compound is only transient and, subsequently, dehydroxylated to 3-hydroxyphenylpropionic acid and, finally, phenylpropionic acid.[46] These conversions likely decrease antioxidant activity.

Other factors not directly related to the bioconversion of ferulic acid may also contribute to changes in antioxidant activity. For instance, higher antioxidant activity has been observed for free ferulic acid in the presence of AXOS compared to without AXOS.[52] As mentioned, ferulic acid is initially de-esterified by the gut microbiota, and this could be analogous to free ferulic acid in the presence of AXOS. As fermentation progresses, however, AXOS are removed from the system by microbial metabolism. Microbial metabolism of AXOS also leads to production of SCFA, which lower the pH and could affect antioxidant activity.[54]

This study identified a high-pressure hydrothermal treatment of cereal bran that resulted in fragmentation of the cell wall. Final temperatures of 190 °C for maize bran and 200 °C for wheat bran resulted in the highest release of FOPS (49 and 50% of initial non-starch polysaccharide, respectively) and esterified ferulic acid (44 and 82% of initial ferulic acid, respectively). Maize FOPS displayed a desirable protracted fermentation profile with higher butyrate production compared to wheat FOPS and FOS. Both maize and wheat FOPS exhibited bifidogenic activity, although weaker than FOS. Maize FOPS exhibited high antioxidant capacity during fermentation that could have beneficial properties *in vivo*. Because FOPS can possibly combine beneficial fermentation properties and antioxidant activities, it may have potential to become a functional food ingredient to promote gut health.

■ ASSOCIATED CONTENT

Ⓢ Supporting Information

Composition of freeze-dried partially purified FOPS and digested FOPS from maize bran and wheat bran (Table S1). This material is available free of charge via the Internet at http://pubs.acs.org.

■ AUTHOR INFORMATION

Corresponding Author

*Telephone: +1-402-472-2802. E-mail: drose3@.unl.edu.

Funding

This work was supported by a grant from the Nebraska Research Initiative Fund.

Notes

The authors declare no competing financial interest.

■ ABBREVIATIONS USED

AXOS, arabinoxylan oligosaccharides; DP, degree of polymerization; FOPS, soluble, non-digestible, feruloylated oligo- and polysaccharides; HMF, hydroxymethylfurfural; FOS, fructooligosaccharides; SCFA, short-chain fatty acid; DPPH, 1,1-diphenyl-2-picrylhydrazyl; ATBS, 2,2-azino-bis-3-ethylbenzthiazoline-6-sulfonic acid; Trolox, 6-hydroxy-2,5,7,8-tetramethylchroman-2-carboxylic acid

■ REFERENCES

(1) Izydorczyk, M. S.; Biliaderis, C. G. Cereal arabinoxylans: Advances in structure and physicochemical properties. *Carbohydr. Polym.* **1995**, *28*, 33−48.

(2) Saulnier, L.; Thibault, J. F. Ferulic acid and diferulic acids as components of sugar-beet pectins and maize bran heteroxylans. *J. Sci. Food Agric.* **1999**, *79*, 396−402.

(3) Chanliaud, E.; Saulnier, L.; Thibault, J. F. Alkaline extraction and characterisation of heteroxylans from maize bran. *J. Cereal Sci.* **1995**, *21*, 195−203.

(4) Schooneveld-Bergmans, M.; Beldman, G.; Voragen, A. Structural features of (glucurono) arabinoxylans extracted from wheat bran by barium hydroxide. *J. Cereal Sci.* **1999**, *29*, 63−75.

(5) Ebringerová, A.; Hromádková, Z.; Heinze, T. Hemicellulose. In *Polysaccharides I: Advances in Polymer Science*; Heinze, T., Ed.; Springer: Berlin, Germany, 2005; Vol. *186*, pp 1−67.

(6) Chanliaud, E.; Saulnier, L.; Thibault, J. F. Alkaline extraction and characterisation of heteroxylans from maize bran. *J. Cereal Sci.* **1995**, *21*, 195−203.

(7) Saulnier, L.; Vigouroux, J.; Thibault, J. F. Isolation and partial characterization of feruloylated oligosaccharides from maize bran. *Carbohydr. Res.* **1995**, *272*, 241−253.

(8) Rose, D. J.; Patterson, J. A.; Hamaker, B. R. Structural differences among alkali-soluble arabinoxylans from maize (*Zea mays*), rice (*Oryza sativa*), and wheat (*Triticum aestivum*) brans influence human fecal fermentation profiles. *J. Agric. Food Chem.* **2009**, *58*, 493−499.

(9) Karppinen, S.; Liukkonen, K.; Aura, A. M.; Forssell, P.; Poutanen, K. *In vitro* fermentation of polysaccharides of rye, wheat and oat brans and inulin by human faecal bacteria. *J. Sci. Food Agric.* **2000**, *80*, 1469−1476.

(10) Dintzis, F.; Legg, L.; Deatherage, W.; Baker, F.; Inglett, G.; Jacob, R.; Reck, S.; Munoz, J.; Klevay, L.; Sandstead, H. Human gastrointestinal action on wheat, maize, and soy hull bran: Preliminary findings. *Cereal Chem.* **1979**, *56*, 123−127.

(11) Broekaert, W. F.; Courtin, C. M.; Verbeke, K.; Van de Wiele, T.; Verstraete, W.; Delcour, J. A. Prebiotic and other health-related effects of cereal-derived arabinoxylans, arabinoxylan-oligosaccharides, and xylooligosaccharides. *Crit. Rev. Food Sci. Nutr.* **2011**, *51*, 178−194.

(12) Rose, D. J.; Inglett, G. E. Two-stage hydrothermal processing of wheat (*Triticum aestivum*) bran for the production of feruloylated arabinoxylooligosaccharides. *J. Agric. Food Chem.* **2010**, *58*, 6427−6432.

(13) Rose, D. J.; Inglett, G. E. Production of feruloylated arabinoxylooligosaccharides from maize (*Zea mays*) bran by microwave-assisted autohydrolysis. *Food Chem.* **2010**, *119*, 1613−1618.

(14) Swennen, K.; Courtin, C. M.; Lindemans, G. C.; Delcour, J. A. Large-scale production and characterisation of wheat bran arabinoxylooligosaccharides. *J. Sci. Food Agric.* **2006**, *86*, 1722−1731.

(15) Rose, D. J.; Inglett, G. E. A method for the determination of soluble arabinoxylan released from insoluble substrates by xylanases. *Food Anal. Methods* **2011**, *4*, 66−72.

(16) Gullón, P.; González-Muñoz, M. J.; Parajó, J. C. Manufacture and prebiotic potential of oligosaccharides derived from industrial solid wastes. *Bioresour. Technol.* **2011**, *102*, 6112−6119.

(17) Gullón, P.; González-Muñoz, M. J.; van Gool, M. P.; Schols, H. A.; Hirsch, J.; Ebringerová, A.; Parajó, J. C. Production, refining, structural characterization and fermentability of rice husk xylooligosaccharides. *J. Agric. Food Chem.* **2010**, *58*, 3632−3641.

(18) Gullón, P.; Moura, P.; Esteves, M. P.; Girio, F. M.; Domínguez, H.; Parajó, J. C. Assessment on the fermentability of xylooligosaccharides from rice husks by probiotic bacteria. *J. Agric. Food Chem.* **2008**, *56*, 7482−7487.

(19) Yang, J.; Rose, D. J. Impact of dietary fiber fermentation from cereal grains on metabolite production by the fecal microbiota from normal weight and obese individuals. *J. Med. Food* **2013**, *16*, 862−867.

(20) Hartzell, A. L.; Maldonado-Gómez, M. X.; Hutkins, R. W.; Rose, D. J. Synthesis and *in vitro* digestion and fermentation of acylated inulin. *Bioact. Carbohydr. Diet. Fibre* **2013**, *1*, 81−88.

(21) American Association of Cereal Chemists (AACC). *Approved Methods of the American Association of Cereal Chemists*, 10th ed.; AACC: St. Paul, MN, 2000.

(22) Yuan, X.; Wang, J.; Yao, H. Production of feruloyl oligosaccharides from wheat bran insoluble dietary fibre by xylanases from *Bacillus subtilis*. *Food Chem.* **2006**, *95*, 484−492.

(23) Antoine, C.; Peyron, S.; Lullien-Pellerin, V.; Abecassis, J.; Rouau, X. Wheat bran tissue fractionation using biochemical markers. *J. Cereal Sci.* **2004**, *39*, 387−393.

(24) Gomis, D. B.; Alvarez, M. G.; Naredo, L. S.; Alonso, J. M. High-performance liquid chromatographic determination of furfural and hydroxymethylfurfural in apple juices and concentrates. *Chromatographia* **1991**, *32*, 45−48.

(25) AOAC International. *Official Methods of Analysis of AOAC International*; AOAC International: Arlington, VA, 1995.

(26) Bradford, M. M. A rapid and sensitive method for the quantitation of microgram quantities of protein utilizing the principle of protein−dye binding. *Anal. Biochem.* **1976**, *72*, 248−254.

(27) Şensoy, Í.; Rosen, R. T.; Ho, C.-T.; Karwe, M. V. Effect of processing on buckwheat phenolics and antioxidant activity. *Food Chem.* **2006**, *99*, 388−393.

(28) Tsai, J. C.; Huang, G. J.; Chiu, T. H.; Huang, S. S.; Huang, S. C.; Huang, T.-H.; Lai, S.-C.; Lee, C.-Y. Antioxidant activities of phenolic components from various plants of *Desmodium* species. *Afric. J. Pharm. Pharmacol.* **2011**, *5*, 468−476.

(29) Vitaglione, P.; Napolitano, A.; Fogliano, V. Cereal dietary fibre: A natural functional ingredient to deliver phenolic compounds into the gut. *Trends Food Sci. Technol.* **2008**, *19*, 451−463.

(30) Parajó, J.; Garrote, G.; Cruz, J.; Dominguez, H. Production of xylooligosaccharides by autohydrolysis of lignocellulosic materials. *Trends Food Sci. Technol.* **2004**, *15*, 115−120.

(31) Chheda, J. N.; Román-Leshkov, Y.; Dumesic, J. A. Production of 5-hydroxymethylfurfural and furfural by dehydration of biomass-derived mono- and polysaccharides. *Green Chem.* **2007**, *9*, 342−350.

(32) Lebet, V.; Arrigoni, E.; Amadò, R. Measurement of fermentation products and substrate disappearance during incubation of dietary fibre sources with human faecal flora. *LWT—Food Sci. Technol.* **1998**, *31*, 473−479.

(33) Macfarlane, S.; Macfarlane, G.; Cummings, J. Review article: Prebiotics in the gastrointestinal tract. *Aliment. Pharmacol. Ther.* **2006**, *24*, 701−714.

(34) Hamaker, B. R.; Rose, D. J.; Keshavarzian, A.; Rumpagaporn, P.; Campanella, O. H. Slowly fermentable soluble dietary fiber. U.S. Patent Application US20100303953 A1, 2010.

(35) Segain, J.; De La Blétiere, D. R.; Bourreille, A.; Leray, V.; Gervois, N.; Rosales, C.; Ferrier, L.; Bonnet, C.; Blottiere, H.; Galmiche, J. Butyrate inhibits inflammatory responses through NFκB inhibition: Implications for Crohn's disease. *Gut* **2000**, *47*, 397−403.

(36) Wächtershäuser, A.; Stein, J. Rationale for the luminal provision of butyrate in intestinal diseases. *Eur. J. Nutr.* **2000**, *39*, 164−171.

(37) Hosseini, E.; Grootaert, C.; Verstraete, W.; Van de Wiele, T. Propionate as a health-promoting microbial metabolite in the human gut. *Nutr. Rev.* **2011**, *69*, 245−258.

(38) Al-Lahham, S.; Roelofsen, H.; Rezaee, F.; Weening, D.; Hoek, A.; Vonk, R.; Venema, K. Propionic acid affects immune status and metabolism in adipose tissue from overweight subjects. *Eur. J. Clin. Invest.* **2012**, *42*, 357−364.

(39) Roberfroid, M.; Gibson, G. R.; Hoyles, L.; McCartney, A. L.; Rastall, R.; Rowland, I.; Wolvers, D.; Watztl, B.; Szajewska, H.; Stahl, B. Prebiotic effects: Metabolic and health benefits. *Br. J. Nutr.* **2010**, *104*, S1−S63.
(40) Hsu, C. K.; Liao, J. W.; Chung, Y. C.; Hsieh, C. P.; Chan, Y. C. Xylooligosaccharides and fructooligosaccharides affect the intestinal microbiota and precancerous colonic lesion development in rats. *J. Nutr.* **2004**, *134*, 1523−1528.
(41) Gobinath, D.; Madhu, A. N.; Prashant, G.; Srinivasan, K.; Prapulla, S. G. Beneficial effect of xylo-oligosaccharides and fructo-oligosaccharides in streptozotocin-induced diabetic rats. *Br. J. Nutr.* **2010**, *104*, 40−47.
(42) Van Craeyveld, V.; Swennen, K.; Dornez, E.; Van de Wiele, T.; Marzorati, M.; Verstraete, W.; Delaedt, Y.; Onagbesan, O.; Decuypere, E.; Buyse, J. Structurally different wheat-derived arabinoxylooligosaccharides have different prebiotic and fermentation properties in rats. *J. Nutr.* **2008**, *138*, 2348−2355.
(43) Louis, P.; Flint, H. J. Diversity, metabolism and microbial ecology of butyrate-producing bacteria from the human large intestine. *FEMS Microbiol. Lett.* **2009**, *294*, 1−8.
(44) Jones, R. M.; Mercante, J. W.; Neish, A. S. Reactive oxygen production induced by the gut microbiota: Pharmacotherapeutic implications. *Curr. Med. Chem.* **2012**, *19*, 1519−1529.
(45) Aw, T. Y. Molecular and cellular responses to oxidative stress and changes in oxidation−reduction imbalance in the intestine. *Am. J. Clin. Nutr.* **1999**, *70*, 557−565.
(46) Anson, N. M.; Selinheimo, E.; Havenaar, R.; Aura, A. M.; Mattila, I.; Lehtinen, P.; Bast, A.; Poutanen, K.; Haenen, G. R. Bioprocessing of wheat bran improves in vitro bioaccessibility and colonic metabolism of phenolic compounds. *J. Agric. Food Chem.* **2009**, *57*, 6148−6155.
(47) Rechner, A. R.; Kuhnle, G.; Bremner, P.; Hubbard, G. P.; Moore, K. P.; Rice-Evans, C. A. The metabolic fate of dietary polyphenols in humans. *Free Radical Biol. Med.* **2002**, *33*, 220−235.
(48) Russell, W. R.; Scobbie, L.; Chesson, A.; Richardson, A. J.; Stewart, C. S.; Duncan, S. H.; Drew, J. E.; Duthie, G. G. Anti-inflammatory implications of the microbial transformation of dietary phenolic compounds. *Nutr. Cancer* **2008**, *60*, 636−642.
(49) Manso, I.; Torres, B.; Andreu, J. M.; Menéndez, M.; Rivas, G.; Alfonso, C.; Díaz, E.; García, J. L.; Galán, B. 3-Hydroxyphenylpropionate and phenylpropionate are synergistic activators of the MhpR transcriptional regulator from *Escherichia coli*. *J. Biol. Chem.* **2009**, *284*, 21218−21228.
(50) Monagas, M.; Khan, N.; Andrés-Lacueva, C.; Urpi-Sarda, M.; Vázquez-Agell, M.; Lamuela-Raventos, R. M.; Estruch, R. Dihydroxylated phenolic acids derived from microbial metabolism reduce lipopolysaccharide-stimulated cytokine secretion by human peripheral blood mononuclear cells. *Br. J. Nutr.* **2009**, *102*, 201−206.
(51) Andreasen, M. F.; Kroon, P. A.; Williamson, G.; Garcia-Conesa, M.-T. Esterase activity able to hydrolyze dietary antioxidant hydroxycinnamates is distributed along the intestine of mammals. *J. Agric. Food Chem.* **2001**, *49*, 5679−5684.
(52) Snelders, J.; Dornez, E.; Delcour, J. A.; Courtin, C. M. Ferulic acid content and appearance determine the antioxidant capacity of arabinoxylanoligosaccharides. *J. Agric. Food Chem.* **2013**, *61*, 10173−10182.
(53) Dziedzic, S. Z.; Hudson, B. J. Phenolic acids and related compounds as antioxidants for edible oils. *Food Chem.* **1984**, *14*, 45−51.
(54) Ruenroengklin, N.; Zhong, J.; Duan, X.; Yang, B.; Li, J.; Jiang, Y. Effects of various temperatures and pH values on the extraction yield of phenolics from litchi fruit pericarp tissue and the antioxidant activity of the extracted anthocyanins. *Int. J. Mol. Sci.* **2008**, *9*, 1333−1341.

JOURNAL OF AGRICULTURAL AND FOOD CHEMISTRY

Article

pubs.acs.org/JAFC

Inhibition of the β-Catenin/Tcf Signaling by Caffeoylquinic Acids in Sweet Potato Leaf through down Regulation of the Tcf-4 Transcription

Junsei Taira,* Masatsugu Uehara, Eito Tsuchida, and Wakana Ohmine

Department of Bioresource Technology, Okinawa National College of Technology, 905 Henoko, Nago City, Okinawa, 905-2192 Japan

ABSTRACT: Sweet potato leaves contain the highest levels of functional polyphenols. In this study the effects of the sweet potato leaf extract and its contents, such as mono (3, 4, and 5)-caffeoylquinic acid (CQA), di-CQA (4,5-diCQA, 3,5-diCQA, and 3,4-diCQA) and caffeic acid (CA), were evaluated on the β-catenin/Tcf-4 signaling in human colorectal cancer HCT116 cells. The extract and the CQA derivatives inhibited the β-catenin/Tcf-4 signaling, and the inhibition of the di-CQA (with two caffeoyl groups) was higher than that of the mono-CQA (one-caffeoyl group) and CA, suggesting that the caffeoyl structure in the presence of a catechol group plays a significant role in interfering with the β-catenin/Tcf-4 signaling. In addition, the CQA derivatives had no effect on the β-catenin protein expression, but all test compounds inhibited the expression of the Tcf-4 transcription, and the inhibition of the di-CQA derivatives was stronger than those of the mono-CQA derivatives as well as the β-catenin/Tcf-4 transcriptional activity. These compounds can modulate the downstream Wnt signaling pathway, suggesting that sweet potato leaves can be a protective food for colorectal cancer.

KEYWORDS: *caffeoylquinic acid, HCT 116 cells, colorectal cancer, β-catenin/Tcf signaling, sweet potato*

INTRODUCTION

Recent studies have demonstrated that sweet potato (*Ipomoea batatas* L.) leaves contain the highest levels of polyphenols compared to other commercial vegetables.[1,2] The leaves were found to be an inhibitor of the growth of colon and stomach cancer cells, leukemia, and viruses[3,4] and to reduce the effects of diabetes in humans.[5] The sweet potato leaves contain phenolic compounds, such as caffeoylquinic acid (CQA) derivatives, a family of esters formed from certain cinnamic acids and quinic acid, including the mono-CQA (chlorogenic acid derivatives) and di-CQA, such as 3,5-diCQA, 3,4-diCQA, and 4,5-diCQA.[6−8] The CQA derivatives are the main sweet potato polyphenols and they have an anti-LDL oxidation activity, DPPH-radical scavenging action, and antimutagen and antitumor activities.[8−11] Colorectal cancer is a human malignance as well as stomach and lung cancer which are causes of human death. The incidence tends to increase due to changing Japanese dietary habits. Recent studies have indicated that in most of the colorectal cancers associated with the aberrant Wnt signaling pathway, the expression of β-catenin plays critical roles in cell proliferation and differentiation. The glycogen synthase kinase (GSK)-3β/Axin complex normally promotes the proteolytic degradation of the β-catenin intracellular signaling molecule. When the β-catenin destruction complex is inhibited, a pool of cytoplasmic β-catenin stabilizes and is able to enter the nucleus and interact with the T-cell factor/lymphoid enhancer-binding factor (Tcf/Lef) family transcription factors to promote a specific gene expression and the signaling is an early progression event in colorectal cancer.[12] In previous studies over the past decade, several naturally occurring dietary compounds, such as flavonoids, curcumin, and the tea polyphenol epigallocatechin-3-gallate (EGCG), have been shown to target intermediates in the Wnt/β-catenin signaling pathway.[13,14] These active compounds have shown antioxidant activity; thus, caffeoylquinic acids will be expected to have a similar activity. This study was designed to confirm whether caffeoylquinic acid derivatives can modulate β-catenin/Tcf-4 signaling.

MATERIALS AND METHODS

Materials. Caffeic acid (CA) and 3-caffeoylquinic acid were obtained from the Wako Pure Chemical Co. (Osaka, Japan). FuGENE 6 as a transfection reagent and the Lucyferase Assay System containing the luciferase substrate and lysis buffer to assess the reporter assay were obtained from the Promega Corporation (CA). Polyclonal anti-β-catenin (mouse monoclonal antibody, BD Biosciences, CA) and Tcf-4 monoclonal antibody (mouse monoclonal antibody, Exalpha Biologicals, Inc., MA) were used to detect the protein expression.

Isolation of CQA Derivatives. The CQA derivatives were isolated from the methanol (MeOH) extract of the sweet potato leaf as previously reported.[8,9] Briefly, the MeOH extract was partitioned between dichloromethane and H_2O (50/50 v/v) and the H_2O fraction was continuously partitioned with n-BuOH. The H_2O fraction was freeze-dried, then separated by HPLC (Agilent 1200, Agilent Technologies, CA) with an ODS-column (COAMOSIL Packed column 5C18-MS-II, 10 I.D. × 250 mm, Nacalai Tesque, Tokyo, Japan), and monitored at 326 nm at the flow rate of 2.0 mL/min at 40 °C. The mobile phase consisting of a formic acid aqueous solution (0.5%) and acetonitrile was carried out by a linear gradient to 2, 45, and 100% for 15, 50, and 60 min, respectively. Each peak of the mono (4 and 5)-CQA and di-CQA, such as 4,5- diCQA, 3,5-diCQA, and 3,4-diCQA, was collected by a fraction collector (Analyte FC, Agilent Technologies). These compounds were used in the β-catenin/Tcf-4

Received: October 1, 2013
Revised: December 2, 2013
Accepted: December 5, 2013
Published: December 5, 2013

ACS Publications © 2013 American Chemical Society

reporter assay and as the standard substances for determining the quantity of the content in the sweet potato leaf extract.

Sample Preparation. The sweet potato leaf powder (1 g) was extracted with distilled water (50 mL) at 85 °C for 45 min. The extract was filtered and then freeze-dried (Tokyo Rikakiki Co. Ltd., Tokyo, Japan). The sample (430.1 mg) dissolved in MQ-water (1 mL) was filtered using a disk filter (0.45 μm, Millipore, MA) and used for the assay and analysis of the contents in the sweet potato leaf.

LC/MS Analysis. The content of each component in the extract of the sweet potato leaves was determined by an LC/MS analysis. The LC/MS (Agilent1200, Agilent Technologies) was carried out using a photodiode array detector and monitored in the operating wavelength range from 210 to 700 nm at the flow rate of 0.80 mL/min on a reversed-phase chromatographic column, YMC-Pack Pro C18 (100 × 4.6 mm I.D., 5 μm particle size, YMC Co., Ltd., Kyoto, Japan) at 40 °C. The mass spectra were measured under the following conditions: ESI negative ion mode; desolvation temperature, 350 °C; desolvation pressure, 35 psi; and desolvation gas flow, 12.01 mL/min (6120 Quadrupole LC/MS spectrometer, Agilent Technologies).

Cell Culture. HCT116 human colon cancer cells (American Type Culture Collection) were cultured in DMEM (Gibco-BRL, Life Technologies, CA) medium (including 10% FBS, 100 U/ml penicillin and 100 μg/mL streptomycin) at 37 °C in a 5% CO_2 atmosphere.

Cell Viability. The cell viability due to treatment with a test sample was examined by an MTT assay as previously reported.[15] Briefly, the cells were seeded at a density of 5.0×10^5 cells/mL and cultured for 24 h with or without the test sample. After the culture, MTT (0.05%) was added to each well and incubated for 3 h, and then the suspension was carefully removed. Extraction with DMSO (50 μL) was measured at 540 nm with the reference at 655 nm using a microplate reader (BIO-RAD model 550, BIO-RAD, CA).

Reporter Assay. The HCT116 cells with or without the test sample were cultured on a 12-well microplate (5×10^5 cells/well) for 24 h the day before being transiently cotransfected in triplicate with Tcf-4 and the β-catenin plasmid using the FuGENE 6 transfection reagent. After 24 h, the cells were washed twice in phosphate-buffered saline (PBS) and lysed in 100 μL of lysis buffer. The lucyferase activity of the lysate cells (50 μL) was assayed with a luciferase substrate, then the chemiluminescence (CL) was measured by a microplate reader (GLOMAX MULTI Detection system, Promega). The protein concentration was determined using a BCA protein assay kit (Thermo Fisher Scientific, Inc., IL).

Western Blot. After stimulation, the cells were washed with PBS and then treated with the lysis buffer. The cellular lysates were centrifuged at 13800*g* for 5 min. The total cellular extracts were separated on SDS-polyacrylamide gels (4−12% SDS-polyacrylamide, Invitrogen, CA) and transferred to a nitrocellulose membrane (iBlot Gel Transfer Mini, Invitrogen) using an iBlot Gel Transfer Device (Invitrogen). The membrane treatment and detection of the protein expression were carried out by manual procedures using an immunodetection system (Invitrogen) while incubated with the polyclonal anti-β-catenin or Tcf-4 overnight at 4 °C.

Statistical Analysis. Data were expressed as mean ± SD. Analysis of data was carried out using one-way analyses of variance (ANOVA) and Tukeỳs method for multiple comparison. Significance $P < 0.05$ was considered statistically significant.

RESULTS AND DISCUSSION

Figure 1 shows the LC−MS chromatogram of the CQA derivatives obtained from the hot-water extract of the sweet potato leaves. It indicated mono-CQA, 5-CQA (24.70 min, 353.0 m/z), 3-CQA (27.19 min, 353.0 m/z), 4-CQA (27.55, 353.0 m/z), CA (27.71 min, 179.1 m/z), and di-CQA, such as 4,5-diCQA (33.62 min, 515.1 m/z), 3,5-diCQA (33.94 min, 515.1 m/z), and 3,4-diCQA (34.89 min, 515.1 m/z). These chemical structures of the CQA derivatives in the sweet potato leaf extract were depicted in Figure 2. Figure 3 shows that the content in the extract and the di-CQA was higher than those of

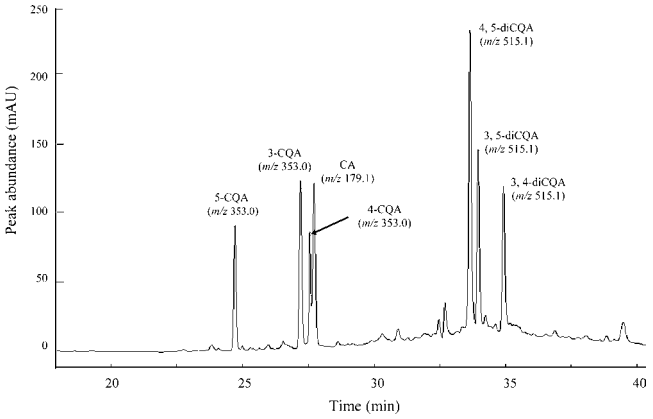

Figure 1. LC/MS chromatogram obtained from the hot-water extract of the sweet potato leaves. The LC/MS was carried out by the analytical condition as shown in the text. Each peak indicated the mono (3, 4, and 5)-caffeoylquinic acid (CQA, m/z = 353.0), di-CQA (4,5-diCQA, 3,5-diCQA, and 3,4-diCQA, m/z = 515.1), and caffeic acid (CA, m/z = 179.1).

the other mono-CQA derivatives and CA, particularly, the 4,5-diCQA had the highest content. Similar results were obtained from the ethanol extract of the sweet potato leaves.[8,9] The CQA derivatives are the antitumor main sweet potato polyphenols and they have DPPH-radical scavenging action, antimutagen, and activities.[10,11] A recent study revealed that the CQA derivatives have an anti-LDL oxidation activity suggesting that they may prevent the development of atherosclerosis caused by the oxidative modification of LDL.[8,9] In previous studies over the past decade, several naturally occurring dietary polyphenols, such as quercetin, EGCG, and curcumin, have been shown to modulate genes in the Wnt/β-catenin signaling pathway.[16−18] Based on the sweet potato leaf extract and the main polyphenol contents, the CQA derivatives were expected to modulate the Wnt/β-catenin signaling pathway; thus, the reporter assay of the test sample was carried out on the β-catenin/Tcf-4 signaling pathway in the human colorectal cancer HCT116 cells. Figure 4 shows the result of the reporter assay by the combination of β-catenin and Tcf-4 plasmid DNAs with or without the test sample. As shown in Figure 4, the chemiluminescence (CL) reporter activity of β-catenin and Tcf-4 transfected in cells increased when compared to Tcf-4 alone. When cells transfected with the β-catenin and Tcf-4 genes were treated with the sweet potato leaf extract, the induction of the CL reporter activity, suppressed in a dose dependent manner (0.22, 1.10, and 2.20 mg/mL). Each compound from the extract also inhibited the CL reporter activity, and the activity of the di-CQA derivatives was higher than those of mono-CQA. The concentration range of these compounds used in the reporter assay did not show any cytotoxicity, indicating that the reduction of the CL reporter activity is due to the interference of the β-catenin/Tcf-4 signaling (Table 1). The antioxidant activity of the phenolic compound is due to the function of the OH group in the molecule, specifically, the presence of a catechol group contributes to the effective radical scavenging activity.[15,19] The CQA derivatives having a catechol group in the caffeoyl structure have an effective antioxidant activity, such as the DPPH-radical scavenging action and the anti LDL-oxidation activity.[7−9] The antioxidant activity of the CQA derivatives was related to the number of caffeoyl groups in the structure, for example, the antioxidant activity is decreasing as follows: tri-CQA, which has three caffeoyl groups, di-CQA

dx.doi.org/10.1021/jf404411r | J. Agric. Food Chem. 2014, 62, 167−172

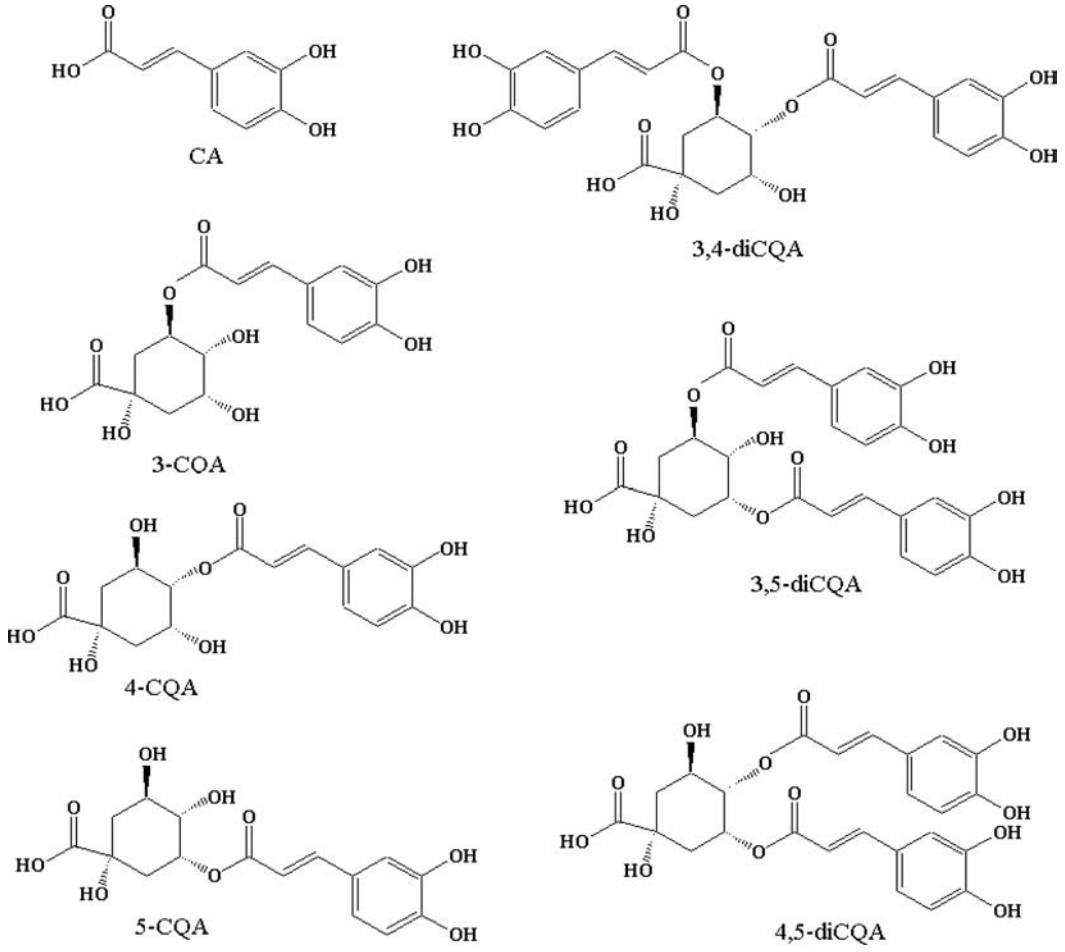

Figure 2. Chemical structures of caffeoylquinic acid (CQA) derivatives including caffeic acid (CA) from sweet potato leaves. The sweet potato leaves were extracted with methanol. The CQA derivatives, except for CA and 3-CQA, were separated from the extract by the procedures shown in the text.

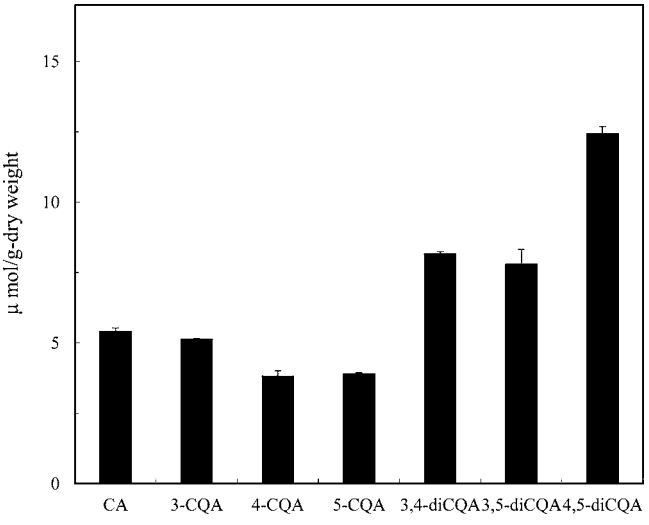

Figure 3. Composition of the CQA derivatives in the sweet potato leaf. The content of each component in the hot-water extract of the sweet potato leaf was determined by an LC/MS analysis using the procedures shown in the text. The content of each compound is expressed as mean ± SD of three experiments.

(with 2 caffeoyl groups) derivatives, and mono-CQA (with one caffeoyl group). The CL reporter activity of the CQA derivatives including CA having a catechol structure similar to that of the antioxidant activity. Quercetin, the major representative of the flavonol subclass of flavonoids, has been shown to be a potent inhibitor of the β-catenin/Tcf signaling in SW480 human colon adenocarcinoma cells. Quercetin also has a catechol function in the A-ring of the molecule.[16] Caffeic acid phenethyl esters, a phenolic component of propolis, having a catechol structure in the molecule inhibited the colorectal cancer cell growth in a dose and time-dependent manner by decreasing the β-catenin.[20,21] Therefore, the caffeoyl structure in the presence of a catechol group of the CQA derivatives may play a functional role in interfering the Wnt/β-catenin signaling pathway.

The cytoplasmic β-catenin levels are normally low through continuous proteasome-mediated degradation by an APC/GSK-3β/Axin complex. When cells receive the Wnt signal, the degradation of β-catenin is inhibited and the levels of β-catenin increase in the cytoplasm and nucleus. Nuclear β-catenin interacts with the transcription factors, such as the Tcf/Lef, and lead to tumor formation and progression.[12] The inhibition of the GSK-3β kinase activity might lead to the onset of the β-catenin/Tcf/Lef-mediated gene transcription, representing a potentially mitogenic stimulus. The molecules, such as GSK-3β, β-catenin, and the transcription factor, and Tcf are the key factors in the Wnt pathway involved in the regulation of the β-catenin homeostasis. In previous studies, it was reported that the naturally occurring dietary compounds inhibited the β-catenin/Tcf-4 transcriptional signaling in the cancer cells. A

dx.doi.org/10.1021/jf404411r | J. Agric. Food Chem. 2014, 62, 167−172

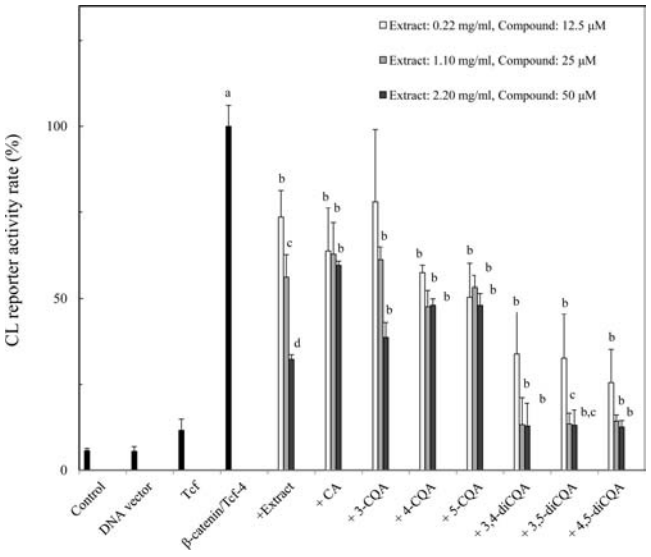

Figure 4. Inhibition of the chemiluminescence reporter activity on β-catenin/Tcf-4 signaling in the HCT116 colorectal cancer cells. The chemiluminescence (CL) of the β-catenin/Tcf-4 signaling in the HCT116 colorectal cancer cells with or without the test sample was measured by the CL reporter assay and indicated as the CL reporter activity rate (%) for the control and β-catenin/Tcf-4 plasmid transfected cells. Data were expressed as mean ± SD of three experiments and groups with different letters are significantly different ($p < 0.05$).

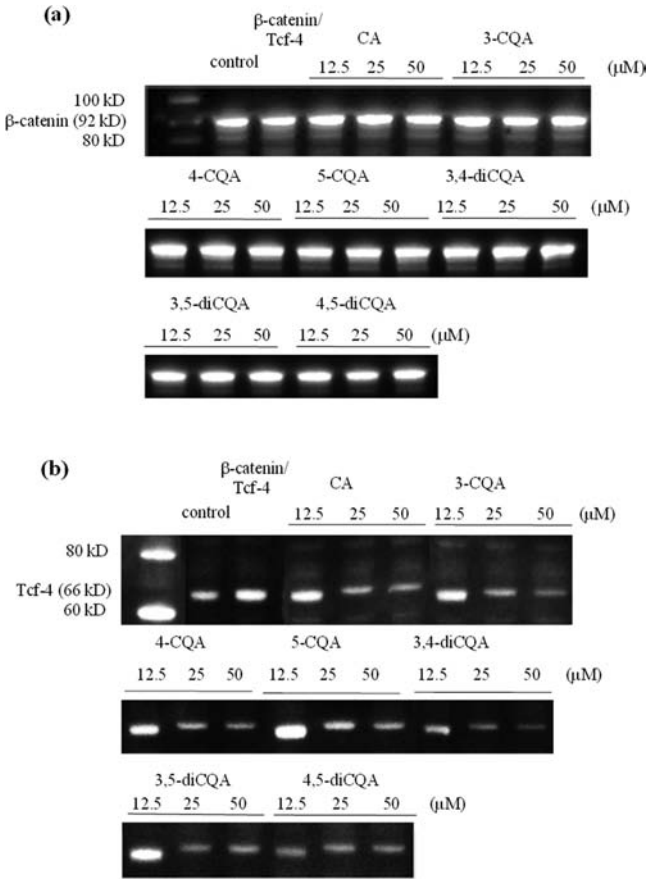

Figure 5. Suppression of the CQA derivatives for the β-catenin and Tcf-4 protein expression in HCT116 colorectal cancer cells. Western blot analysis of protein expression for the β-catenin/Tcf-4 plasmid transfected cells with or without the test sample (12.5, 25, and 50 μM). (a) Effect of the CQA derivatives on β-catenin protein expression and (b) inhibition of the Tcf-4 protein expression. A representative example of two experiments is shown.

polyphenol-rich apple juice extract was found to effectively inhibit the kinase activity of GSK-3β.[22] Curcumin derivative treatment of a variety of colon cancer cell lines reduced in a dose dependent manner the β-catenin transcriptional activity by increasing the degradation of the cytoplasmic β-catenin.[17] EGCG treatment in HEK293 cells inhibited the β-catenin transcriptional activity,[18] and resveratrol also significantly decreased the level of β-catenin in the nucleus of colon cancer cells.[23] In this study, the target molecule by the CQA derivatives in the β-catenin/Tcf-4 signaling was examined in cells transfected with the β-catenin/Tcf-4 plasmid DNAs with or without test compounds (Figure 5). The expression of β-catenin in cells transfected with the β-catenin/Tcf-4 plasmid DNAs was at a level similar to that of the vector alone. As shown in Figure 5a, the CQA derivatives treatment in cells had no effect on the reduction of the β-catenin protein suggesting that the inhibition of the β-catenin/Tcf-4 transcriptional activity is due to the downregulation of the signaling pathway. In the same experiment, the Tcf-4 protein expression in cells transfected with the β-catenin/Tcf-4 plasmid DNAs was greater than that of the vector alone (control). When all of the test compounds were treated at 25 μM in the cells, the production of the Tcf-4 protein was completely suppressed (Figure 5b).

Table 1. Cytotoxicity of Sweet Potato Leaf Extract and the CQA Derivatives in HCT 116 Colorectal Cancer Cells

	cells survival rate (%)[b]						
		extract (mg/mL)			CQA derivatives (μM)		
group	control[a]	0.22	1.10	2.20	12.5	25	50
	100 ± 9.28						
extract		97.64 ± 3.38	98.16 ± 5.16	95.15 ± 4.81			
CA					96.06 ± 4.24	87.54 ± 1.97	85.75 ± 6.47
3-CQA					101.28 ± 10.63	86.85 ± 3.37	91.82 ± 3.37
4-CQA					99.29 ± 7.33	97.07 ± 6.59	94.53 ± 7.22
5-CQA					97.54 ± 7.23	105.27 ± 5.88	97.17 ± 2.51
3,4-diCQA					91.78 ± 6.80	93.55 ± 5.12	91.31 ± 1.18
3,5-diCQA					96.13 ± 2.98	92.72 ± 2.47	90.21 ± 1.45
4,5-diCQA					94.48 ± 8.75	95.70 ± 7.77	93.34 ± 3.20

[a]β-catenin/Tcf-4 plasmid transfected cells without test sample. [b]Cells survival rate (%) for control was determined by MTT assay. Data are expressed as mean ± SD of four experiments.

dx.doi.org/10.1021/jf404411r | J. Agric. Food Chem. 2014, 62, 167−172

The result clearly indicated that the CQA derivatives targeted the transcription factor Tcf-4 on the Wnt/β-catenin signaling pathway. In previous papers, it was reported that the naturally occurring dietary compounds inhibited the β-catenin/Tcf-4 transcriptional signaling due to modulating the Wnt signaling gene expression. Quercetin inhibits the β-catenin/Tcf-4 signaling in SW480 human colon adenocarcinoma cells by decreasing the levels of β-catenin and Tcf-4 in the nucleus, resulting in a decreased downstream Wnt signaling gene expression of *c-myc*.[16] Curcumin treatment inhibits the mRNA expression of the Wnt target genes *c-myc*, *c-fos*, and *c-jun* in a variety of cancer cells.[24] EGCG reduced the expression of the β-catenin/Tcf-4 signaling target genes *c-jun* and *cyclin D1*.[25,26] Resveratrol decreased the localization of β-catenin in the nucleus due to the expression of *lgs* and *pygol*, the activator of β-catenin in all cell lines.[23] The caffeic acid phenethyl ester significantly suppressed the β-catenin, *c-myc*, and *cyclin D1* protein expression in SW480 cells.[21] The CQA derivatives may have also affected the Wnt target genes, such as the cell cycle prompting genes *c-myc* and *cyclin D1*. In addition, the CQA derivatives may have a potential modulation of the Wnt/β-catenin signaling pathway in various cancer cells. These subjects will be the focus of future research.

In conclusion, this study demonstrated that the edible sweet potato leaf extract and its contents, such as mono (3, 4, and 5)-caffeoylquinic acid (CQA), di-CQA (4,5-diCQA, 3,5-diCQA, and 3,4-diCQA), and caffeic acid (CA), inhibit the β-catenin/Tcf-4 transcriptional activity in HCT116 cells. Particularly, the di-CQA derivatives (with 2 caffeoyl groups) were greater than that of the mono-CQA derivatives (one caffeoyl group) and CA, suggesting that the caffeoyl structure in the presence of a catechol group plays a significant role in the reduction of the β-catenin transcriptional activity. In addition, the compounds targeted the molecular transcription factor Tcf-4 for the inhibition of the β-catenin/Tcf-4 transcriptional activity. Sweet potato leaf containing the β-catenin signaling inhibitor, CQA derivatives, may be a protective diet for colorectal cancer.

AUTHOR INFORMATION

Corresponding Author

*E-mail: taira@okinawa-ct.ac.jp.

Notes

The authors declare no competing financial interest.

ACKNOWLEDGMENTS

We thank Dr. A. Nagafuchi (Kumamoto University, Japan) for providing a constitutively active form of mouse β-catenin (caβ-catenin) cDNA. We thank Dr. T. Shimotono (University of Kyoto, Japan) for providing TCF-BP-Luc plasmid.

REFERENCES

(1) Islam, M. S.; Yoshimoto, M.; Yahara, S.; Okuno, S.; Ishiguyro, K.; Yamakawa, O. Identification and characterization of foliar polyphenolic composition in sweetpotato (*Ipomoae batatas* L.) genotypes. *J. Agric. Food Chem.* **2002**, *50*, 3718−3722.

(2) Taira, J.; Ohmi, N.; Uechi, K. Characteristics of folic acid and polyphenol in Okinawan sweet potato (*Ipomoea batatas* L.) foliage. *Nippon Shokuhin Kagaku Kogaku Kaishi* **2007**, *54*, 215−221.

(3) Kurata, R.; Adachi, M.; Yamakawa, O.; Yoshimoto, M. Growth suppression of human cancer cells by polyphenolics from sweetpotato (*Ipomoea batatas* L.) leaves. *J. Agric. Food Chem.* **2007**, *55*, 185−190.

(4) Mahmood, N.; Moore, P. S.; DeTommasi, N.; DeSmone, F.; Colman, S.; Hay, A. J.; Pizza, C. Inhibition of HIV infection by caffeoylquinic acid derivatives. *Antivial Chem. Chemother.* **1993**, *4*, 235−240.

(5) Ludivik, B.; Hanefeld, M.; Pacini, M. Improved metabolic control by *Ipomoea batatas* (Caiapo) is associated with increased adiponectin and decreased fibrinogen levels in type 2 diabetic subjects. *Diab. Obes. Metabol.* **2008**, *10*, 586−592.

(6) Cliffold, M. N.; Johnson, K. L.; Knight, S.; Kuhnert, N. Hierarchical scheme for LC-MS identification of chlorogenic acids. *J. Agric. Food Chem.* **2003**, *51*, 2900−2911.

(7) Ishiguro, K.; Yahara, S.; Yoshimoto, M. Changes in polyphenols contents and radical-scavenging activity of sweetpotato (*Ipomoea batatas* L.) during storage at optimal and low temperature. *J. Agric. Food Chem.* **2007**, *55*, 10773−10778.

(8) Taira, J.; Ohmine, W. Characteristics of Caffeic acid derivatives in Okinawan sweet potato (*Ipomoea batatas* L.) leaves and the anti-LDL oxidation activity. *Nippon Shokuhin Kagaku Kogaku Kaishi* **2011**, *58*, 16−20.

(9) Taira, J.; Taira, K.; Ohmine, W.; Nagata, J. Mineral determination and anti-LDL oxidation activity of sweet potato (*Ipomoea batatas* L.) leaves. *J. Food Comp. Anal.* **2013**, *29*, 117−125.

(10) Oki, T.; Masuda, M.; Furuya, S.; Nishiba, Y.; Terahara, N.; Suda, I. Involvement of anthocyanins and other phenolic compounds in radical-scavenging activity of purple-fleshed sweet potato cultivars. *J. Food Sci.* **2002**, *67*, 1752−1756.

(11) Yoshimoto, M.; Yahara, S.; Okuno, S.; Islam, M. S.; Ishiguro, K.; Yamakawa, O. Antimutagenecity of mono-, di-, and tricaffeoylquinic acid derivatives isolated from sweetpotato (*Impomoae batatas* L.) leaf. *Biosci. Biotechnol. Biochem.* **2002**, *66*, 2336−2341.

(12) Bienz, M.; Clevers, H. Linking Colorectal Cancer to Wnt Signaling Review. *Cell* **2000**, *103*, 311−320.

(13) Tarapore, R. S.; Siddique, I. A.; Mukhter, H. A.; Mukhtar, H. Modulating of Wnt/β-catenin signaling pathway by bioactive food components. *Carcinogenesis* **2011**, *0*, 1−9.

(14) Teiten, M.-H.; Gaascht, F.; Dicato, M.; Diederich, M. Targeting the Wingless signaling pathway with natural compounds as chemo-preventive or chemotherapeutic agents. *Curr. Pharmaceut. Biotechnol.* **2012**, *13*, 245−254.

(15) Taira, J.; Nanbu, H.; Ueda, K. Nitric oxide-scavenging compounds in *Agrimonia pilosa* Ledeb on LPS-induced RAW264.7 macrophages. *Food Chem.* **2009**, *115*, 1221.

(16) Park, C. H.; Chang, J.-Y.; Hahm, E. R.; Park, S.; Kim, H.-K.; Yang, C. H. Quercetin, a potent inhibitor against β-catenin/Tcf signaling in SW480 colon cancer cells. *Biochem. Biophys. Res. Commun.* **2005**, *328*, 227−254.

(17) Ryu, M.-J.; Cho, M.; Song, J.-Y.; Yun, Y.-S.; Choi, II-W.; Kim, D.-E.; Park, B.-S.; Oh, S. Natural derivatives of curcumin attenuate the Wnt/β-catenin pathway through down regulation of the transcriptional coactivator p300. *Biochem. Biophys. Res. Commun.* **2008**, *377*, 1304−1308.

(18) Dashwood, W.-M.; Orner, G. A.; Dashwood, R. H. Inhibition of β-catenin/Tcf activity by white tea, green tea, and epigallocatechin-3-gallate (EGCG): minor contribution of H_2O_2 at physiologically relevant EGCG concentrations. *Biochem. Biophys. Res. Commun.* **2002**, *296*, 584−588.

(19) Haenen, G. R. M. M.; Paqary, J. B. G.; Korthouwer, R. E. M.; Bast, A. Peroxynitrite scavenging by flavonoids. *Biochem. Biophys. Res. Commun.* **1997**, *236*, 591−593.

(20) Wang, D.; Xiang, D.-B.; He, Y.-J.; Li, Z.-P.; Wu, X.-H.; Mou, J.-H.; Xiao, H.-L.; Zhang, Q.-H. Effect of caffeic acid phenythyl ester on proliferation and apoptosis of colorectal cancer cells *in vitro*. *World J. Gastroenterol.* **2005**, *11*, 4008−4012.

(21) He, Y.-J.; Liu, B.-H.; Xiang, D.-B.; Qiao, Z-Yi.; Fu, T.; He, Yu-H. Inhibitory effect of caffeic acid phenythyl ester on the growth of SW480 colorectal tumor cells involves β-catenin associated signaling pathway down-regulation. *World J. Gastroenterol.* **2006**, *31*, 4981−4985.

(22) Kern, M.; Pahlkb, G.; Ngiewjh, Y.; Marko, D. Modulation of key elements of the Wnt pathway by apple polyphenols. *J. Agric. Food Chem.* **2006**, *54*, 7011−7046.

(23) Hope, C.; Kestutis, P.; Marina, P.; Moyer, M. P.; Johal, K. S.; Woo, J.; Santoso, C.; Hanson, J. A.; Holcombe, R. F. Low concentration of resveratrol inhibit Wnt signal throughout in colon-derived cells: Implications for colon cancer prevention. *Mol. Nutr. Food Res.* **2008**, *52* (Suppl 1), 852−861.

(24) Lin, J.-K. Molecular targets of curcumin. *Adv. Exp. Med. Biol.* **2007**, *595*, 227−243.

(25) Issa, A. Y.; Volate, S. R.; Muga1, S. J.; Nitcheva, D.; Smith, T.; Wargovich1, M. J. Green tea selectively targets initial stages of intestinal carcinogenesis in the AOM-Apc^{Min} mouse model. *Carcinogenesis* **2007**, *28*, 1978−1984.

(26) Ju, J.; Hong, J.; Zhou, J.; Pan, Z.; Bose, M.; Liao, J.; Yang, G-yu.; Liu, Y. Y.; Hou, Z.; Lin, Y.; Ma, J.; Shih, W. J.; Carothers, M.; Yang, C. S. Inhibition of intestinal tumorigenesis in $Apc^{min/+Mice}$ by (-)-epigallocatechin-3-gallate, the major catechin in green tea. *Cancer Res.* **2005**, *65*, 10623−10631.

JOURNAL OF AGRICULTURAL AND FOOD CHEMISTRY

Article

pubs.acs.org/JAFC

Antihypertensive Mechanism of Lactoferrin-Derived Peptides: Angiotensin Receptor Blocking Effect

Ricardo Fernández-Musoles,[†] María Castelló-Ruiz,[‡,§,#] Cristina Arce,[⊥] Paloma Manzanares,[†] M. Dolores Ivorra,[⊥] and Juan B. Salom*[,‡,§,#]

[†]Departamento de Biotecnología de Alimentos, Instituto de Agroquímica y Tecnología de Alimentos, Consejo Superior de Investigaciones Científicas, Avenida Agustín Escardino 7, 46980 Paterna, Valencia, Spain

[‡]Centro de Investigación, Hospital Universitario 'La Fe', Avenida Campanar 21, 46009 Valencia, Spain

[§]Departamento de Fisiología, Facultad de Medicina y Odontología, Universidad de Valencia, Avenida Blasco Ibáñez 17, 46010 Valencia, Spain

[#]Unidad Mixta de Investigación Cerebrovascular, IIS-Fundación Investigación Hospital La Fe−Universidad de Valencia, Valencia, Spain

[⊥]Departamento de Farmacología, Facultad de Farmacia, Universidad de Valencia, Avenida Vicent Andrés Estellés s/n, 46100 Burjassot, Valencia, Spain

ABSTRACT: Looking for antihypertensive mechanisms beyond ACE inhibition, we assessed whether lactoferrin (LF)-derived peptides can act as receptor blockers to inhibit vasoconstriction induced by angiotensin II or endothelin-1. The lactoferricin B (LfcinB)-derived peptide $LfcinB_{20-25}$ (RRWQWR), the low molecular weight LF hydrolysate (LFH < 3 kDa), and two peptides identified in LFH < 3 kDa (LIWKL and RPYL) were tested in ex vivo assays of vasoactive responses. The peptide RPYL was tested in radioligand receptor binding assays. Both LFH < 3 kDa and individual peptides inhibited angiotensin II-induced vasoconstriction. RPYL showed the highest ex vivo inhibitory effect and also inhibited binding of [^{125}I]-(Sar^1,Ile^8)-angiotensin II to AT_1 receptors. By contrast, neither LFH < 3 kDa nor RPYL inhibited endothelin-1 and depolarization-induced vasoconstrictions. In conclusion, LF-derived peptides selectively inhibit angiotensin II-induced vasoconstriction by blocking angiotensin AT_1 receptors. Therefore, inhibition of angiotensin II-induced vasocontriction is suggested as a mechanism contributing along with ACE inhibition to the antihypertensive effect of some LF-derived peptides.

KEYWORDS: *bovine lactoferrin hydrolysate, lactoferrin-derived peptides, antihypertensive mechanism, renin−angiotensin system, angiotensin-converting enzyme inhibition, angiotensin receptor blocker*

INTRODUCTION

Hypertension is probably the most important modifiable risk factor for cardiovascular disease, and its management includes not only pharmacological treatment but also lifestyle changes including physical activity and dietary habits.[1] The increasing perception about the relationship between food and health is fostering the development of functional foods providing health benefits beyond basic nutrition.[2] Some food proteins contain embedded peptides that once released behave as bioactive peptides with different health-promoting properties including blood pressure lowering effects.[3]

The renin angiotensin system (RAS) is one of the main targets for the treatment of hypertension. Its inhibition at three possible levels, angiotensin-converting enzyme (ACE), upstream renin activity, or downstream angiotensin receptors, is the pharmacological basis for commonly used antihypertensive drugs.[4] ACE inhibition is also the most aimed target for antihypertensive food-derived peptides developed as an alternative to drugs.[5] Although different animal and plant proteins have been used, milk is the main source of antihypertensive ACE-inhibitory peptides reported to date.[6]

In contrast to casein, there was much less information about the potential of milk whey proteins as sources of antihypertensive peptides when some years ago we focused on whey protein lactoferrin (LF)[7] and its well-known functional domain lactoferricin B (LfcinB).[8] First, we have shown that a set of peptides derived from LfcinB had inhibitory effects on in vitro ACE activity and ex vivo angiotensin I-induced ACE-dependent vasoconstriction[9] and were orally effective antihypertensive peptides in spontaneously hypertensive rats (SHRs).[10] With regard to the parent protein, we have reported the inhibitory effects of a LF pepsin hydrolysate (LFH) on ACE activity and ACE-dependent vasoconstriction.[11] Then, we have recently described that the ultrafiltered hydrolysate (LFH < 3 kDa) showed increased inhibitory effect on ACE activity and orally antihypertensive effect in SHRs after both acute[12] and chronic[13] administration. Finally, we have isolated and identified novel non-LfcinB-derived peptides with ACE-inhibitory and antihypertensive properties, which could contribute to the antihypertensive effects of LFH < 3 kDa.[12]

The search for in vitro ACE inhibition is the most common strategy in the selection of potential antihypertensive peptides derived from food proteins. However, it is difficult to establish a

Received: October 15, 2013
Revised: December 18, 2013
Accepted: December 19, 2013
Published: December 19, 2013

ACS Publications © 2013 American Chemical Society

direct relationship between ACE-inhibitory effect in vitro and antihypertensive effect in vivo. On one hand, the in vitro ACE-inhibitory potency of food-derived peptides is around 1000 times lower than that of ACE-inhibitory drugs such as captopril, but there are no substantial differences when their antihypertensive effects are compared.[14] On the other hand, there is no correlation between in vitro and in vivo effects when different individual peptides or protein hydrolysates are compared. To explain these apparent discrepancies, one should take into account both bioavailability issues and mechanisms of action other than ACE inhibition when bioactive peptides are assayed in vivo.[15] Alternative antihypertensive mechanisms reported for food-derived bioactive peptides include short-term vasoactive mechanisms as well as long-term antioxidant and anti-inflammatory mechanisms.[16]

Looking for antihypertensive mechanisms beyond ACE inhibition in milk protein derived bioactive peptides, we have shown that some LfcinB-derived peptides were dual vasopeptidase inhibitors. In addition to ACE, they inhibit endothelin-converting enzyme (ECE), a key enzyme of the endothelin system also involved in vascular tone and blood pressure regulation.[17] We have also reported that orally effective antihypertensive LF hydrolysates may act as dual vasopeptidase (ACE/ECE) or as single ECE inhibitors with different antivasoconstrictor effects depending on the protease used to release bioactive peptides.[18] In the present study, we aimed to assess whether LF-derived peptides, in addition to inhibiting the converting enzymes of the angiotensin and endothelin systems, can act as receptor blockers to inhibit vasoconstriction induced by angiotensin II or endothelin-1. For this purpose, we included in the study the LfcinB-derived peptide $LfcinB_{20-25}$ (RRWQWR), the low molecular weight LF pepsin hydrolysate LFH < 3 kDa, and two peptides identified in LFH < 3 kDa (LIWKL and RPYL), all of them with proven antihypertensive effects in SHRs.

MATERIALS AND METHODS

Materials. Bovine lactoferrin (LF) was provided by FrieslandCampina Domo (Zwolle, The Netherlands). Porcine pepsin, porcine kidney ACE, human endothelin-1 (ET-1), captopril, valsartan, and protease inhibitor cocktail were purchased from Sigma-Aldrich Química (Tres Cantos, Madrid, Spain). Angiotensin II was supplied by Calbiochem Co. (La Jolla, CA, USA), and fluorescent ACE substrate *o*-aminobenzoylglycyl-*p*-nitrophenylalanylproline was from Bachem Feinchemikalien (Bubendorf, Switzerland). [^{125}I]-(Sar^1,Ile^8)-angiotensin II and angiotensin AT_1 receptor (human) membrane preparation were from PerkinElmer, Inc. (Waltham, MA, USA), where membranes were prepared from transfected Chinese hamster ovary cells (cell line CHO-K1).

Peptides ($LfcinB_{20-25}$, LIWKL, and RPYL) were ordered at >95% purity from GenScript Corp. (Piscataway, NJ, USA) where they were synthesized by solid phase methods using *N*-(9-fluorenyl)-methoxycarbonyl (Fmoc) chemistry. $LfcinB_{20-25}$ was acetylated at the N-terminus and amidated at the C-terminus, because such a modified peptide was used in our previous studies showing its vasoactive[9] and antihypertensive[10] effects. Actual peptide purities of supplied batches were 99.8% for $LfcinB_{20-25}$, 97.7% for LIWKL, and 99.5% for RPYL. Stock solutions of each peptide were prepared at 5 mM concentration in Milli-Q water (Millipore Corp., Bedford, MA, USA) and stored at −20 °C. $LfcinB_{20-25}$ (RRWQWR) and LIWKL concentrations were determined on the basis of the extinction coefficient of W residues by measuring the absorbance at 280 nm (ε_{280} = 5600 M^{-1} cm^{-1} for W residue), whereas RPYL concentration was based on the dry weight of the peptide.

A low molecular weight fraction of an LF hydrolysate obtained by enzymatic treatment with pepsin (LFH < 3 kDa) was prepared as described previously,[11,12] and the resulting permeate was freeze-dried and kept at room temperature until use. LFH < 3 kDa was subjected to determination of protein content by the bicinchoninic acid method (BCA; Sigma-Aldrich Química) using BSA as standard and to in vitro assay of ACE-inhibitory potency (IC_{50}) using the method described by Sentandreu and Toldrá[19] as previously reported.[12]

Animal Welfare. Rabbits were housed in temperature-controlled rooms (23 °C) with 12 h light/dark cycles and consumed tap water and standard diet ad libitum. Euthanasia was carried out in accordance with the Spanish legislation on "Protection of Animals used for Experimental and other Scientific Purposes". The study was approved by the Ethics Committee for Animal Welfare of the Hospital 'La Fe' to be carried out in its accredited animal research facility (ES462500001001).

Isolation of Rabbit Carotid Arteries and Preparation of Membrane Microsomal Fraction. Thirty male New Zealand White rabbits (Technology Transferring Center, Polytechnic University of Valencia, Valencia, Spain), weighing 2.5−3 kg, were killed by injection of 25 mg/kg sodium thiopental and 1.5 mL of 10 mM KCl solution through the ear vein. A midline throat incision provided access to both common carotid arteries, which were dissected free and cut into four 4 mm long segments, each one for the ex vivo functional assays in organ bath. On the other hand, the membrane microsomal fraction from carotid arteries was obtained for radioligand binding assays according to the method of Faber et al.[20] with some modifications. Briefly, frozen tissue was pulverized in liquid N_2 and homogenized (500 μL for 100 mg of tissue) in 4 °C buffer (25 mM Tris-HCl, 1 mM EDTA, 2 mM $MgCl_2$, and 100 mM KCl, pH 7.4) plus protease inhibitor cocktail (1% v/v) with an Ultra-Turrax T8 homogenizer (IKA-Werke, Staufen, Germany) at maximal speed (5 × 10 s). All procedures specified below were carried out at 4 °C. The homogenate was subjected to three strokes at 4 W in a Microson XL ultrasonic cell disruptor (Misonix, Farmingdale, NY), treated with 0.6 M KCl for 20 min to remove major contractile proteins, and centrifuged at 1000*g* for 10 min; the supernatant was centrifuged at 10000*g* for 10 min, and again the supernatant ultracentrifuged at 110000*g* for 1 h. The final pellet was resuspended in storage buffer (50 mM Tris-HCl, 0.5 mM EDTA, 10 mM $MgCl_2$, 10% sucrose, pH 7.4, protease inhibitor cocktail) and kept at −80 °C until used. The concentration of the membrane protein was determined by using the bicinchoninic acid method.

Ex Vivo Functional Assays of Vasoactive Responses. The arterial segments were mounted in an organ bath containing Ringer−Locke solution (120 mM NaCl, 5.4 mM KCl, 2.2 mM $CaCl_2$, 1.0 mM $MgCl_2$, 25 mM $NaHCO_3$, and 5.6 mM glucose) for computer-assisted isometric tension recording, as described previously.[9] The contractile capacity of every arterial segment was checked by exposure to 50 mM KCl Ringer−Locke solution (NaCl replaced with an equimolar amount of KCl). Carotid arteries contracting less than 1 g were discarded.

To assess effects on angiotensin receptor-mediated vasoconstriction, every arterial segment was challenged with angiotensin II (1 μM). After washing out, each arterial segment was subjected to one of the following protocols: (i) control, a second challenge to angiotensin II to check for response reproducibility, or (ii) treated, preincubation (20 min) with LFH < 3 kDa (100 μg/mL), one of the LF-derived peptides (20 μM), the ACE-inhibitor drug captopril (0.1 μM), or the angiotensin II AT_1 receptor blocker drug valsartan (10 nM) and a second challenge to angiotensin II to check for their effect on angiotensin II-induced contraction. Concentration-dependent effects were assessed for the LF-derived peptide RPYL (20−200 μM) and valsartan (10−100 nM).

To assess effects on endothelin receptor-mediated vasoconstriction, every arterial segment was challenged with KCl (50 mM). After washing out, each arterial segment was subjected to one of the following protocols: (i) a challenge with endothelin-1 (10 nM) to obtain the control contractile response, or (ii) treated, preincubation (20 min) with LFH < 3 kDa (100 μg/mL), the LF-derived peptide RPYL (20 μM), or the angiotensin II AT_1 receptor blocker drug valsartan (0.1 μM), and a challenge with endothelin-1 to check for their effect on endothelin-1-induced contraction.

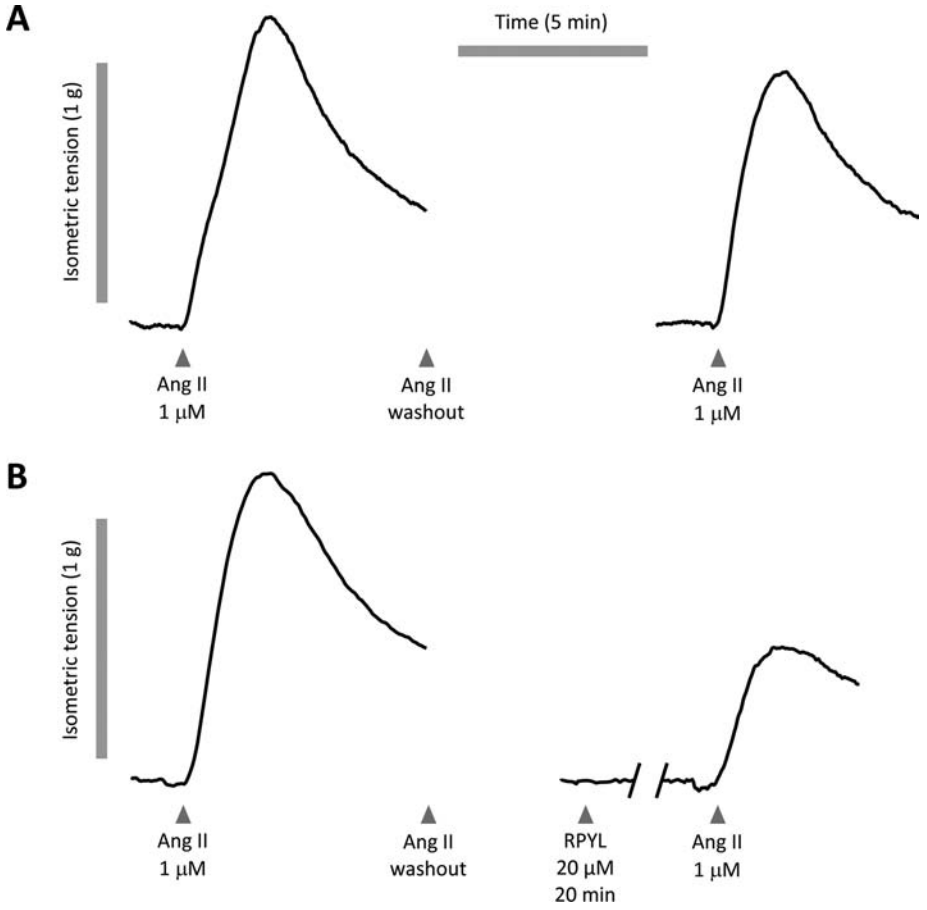

Figure 1. Typical vasoconstrictor effects of angiotensin II (Ang II) in carotid artery segments isolated from New Zealand White rabbits: (A) successive vasoconstrictions to Ang II in control conditions; (B) effect of the LF-derived peptide RPYL on Ang II-induced vasoconstriction.

Finally, some arterial segments were subjected to two successive challenges to 50 mM KCl with or without LFH < 3 kDa (100 μg/mL), the LF-derived peptide RPYL (20 μM), or valsartan (0.1 μM) between to check for nonspecific effects of the treatments on arterial contractile capacity.

Radioligand Receptor Binding Assays. Competition binding assays were carried out with both a membrane preparation containing human angiotensin AT_1 receptor and a membrane microsomal fraction from rabbit carotid artery. The human receptor membrane preparation (0.6 μg protein) was incubated at 27 °C for 60 min in a total volume of 200 μL of assay buffer (50 mM Tris-HCl, 5 mM $MgCl_2$, pH 7.4) with [^{125}I]-(Sar^1,Ile^8)-angiotensin II (0.03 nM) and various concentrations of unlabeled competitors. Experiments were terminated by rapid vacuum filtration through Whatman GF/C fiberglass filters (GE Healthcare Europe GmbH, Barcelona, Spain) presoaked in 0.5% BSA using a Brandel cell harvester (M24R, Valley Research Iberica, Madrid, Spain). The filters were then washed five times with 1 mL of ice-cold 50 mM Tris-HCl buffer (pH 7.4), and the filter-bound radioactivity was measured in a gamma counter (2480 WIZARD, PerkinElmer, Waltham, MA, USA). Nonspecific binding was determined in the presence of 1 μM unlabeled valsartan. Specific binding is defined as total binding minus nonspecific binding. For the rabbit carotid artery membrane preparation, 40 μg of protein and [^{125}I]-(Sar^1,Ile^8)-angiotensin II (0.06 nM) were used instead. A full competition binding assay curve (1 pM−1 μM) was carried out for valsartan, and selected concentrations of RPYL were assayed according to the vasoactive responses in the ex vivo functional assays.

Statistical Analyses. Values are expressed as the mean ± SEM. Unpaired Student's t test was used to assess differences between two groups. Analysis of variance (ANOVA) followed by Student−Newman−Keuls test or Dunnett's test was used for multiple comparisons among more than two groups. P values <0.05 were considered significant. The calculation of IC_{50} values was performed by nonlinear regression analysis. GraphPad Prism software (GraphPad Software Inc., La Jolla, CA, USA) was used.

RESULTS

Lactoferrin-Derived Peptides Inhibit Angiotensin II-Induced Vasoconstriction. Challenge of rabbit carotid arterial segments with a depolarizing solution (50 mM KCl) induced phasic contraction followed by active tone maintained until KCl wash-out. Average active tone amounted to 3424 ± 106 mg in all viable arterial segments included in the study (n = 200).

Angiotensin II (1 μM) induced phasic, transient contractions that were almost completely reproducible in two consecutive challenges to the same arterial segment (Figure 1A). Average contractile response to the second challenge was 82 ± 2% of the first response (n = 30). The inhibitory effects of the different treatments on angiotensin II-induced vasoconstriction were assessed as shown for RPYL in the representative recording of Figure 1B. $LfcinB_{20-25}$ (20 μM), LFH < 3 kDa (100 μg/mL), LIWKL (20 μM), and RPYL (20 μM) produced significant inhibition of angiotensin II-induced vasoconstriction when compared to control vasoconstriction (Figure 2A). The degree of inhibition ranged from 21% response reduction over the control conditions for the weakest $LfcinB_{20-25}$ to 44% response reduction for the strongest RPYL. Figure 2A also shows the lack of effect of the ACE inhibitor captopril (0.1 μM) on angiotensin II-induced vasoconstriction and the significant inhibitory effect of the angiotensin II AT_1 receptor blocker

dx.doi.org/10.1021/jf404616f | J. Agric. Food Chem. 2014, 62, 173−181

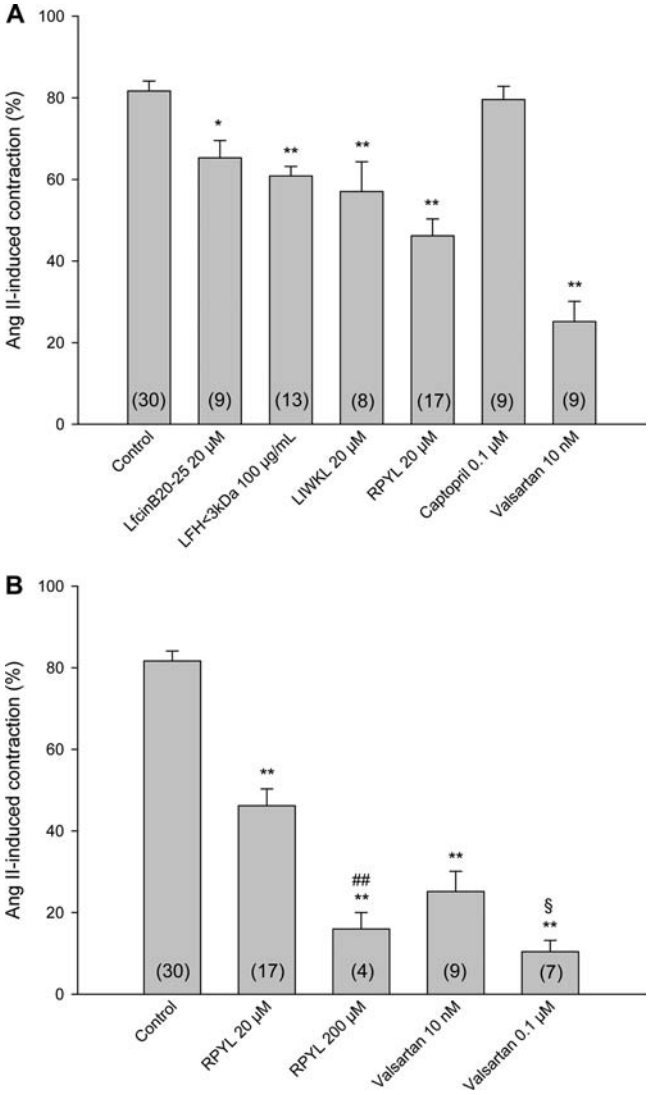

Figure 2. Inhibitory effects of lactoferrin-derived peptides on angiotensin II (Ang II)-induced vasoconstriction in carotid artery segments isolated from New Zealand White rabbits. (A) $LfcinB_{20-25}$, LFH < 3 kDa, the LF-derived peptides LIWKL and RPYL, the ACE-inhibitor captopril, and the Ang II AT_1 receptor blocker valsartan were applied before the second addition of Ang II (1 μM). (B) Concentration-dependent inhibitory effects of RPYL and valsartan on Ang II-induced vasoconstriction. Vasoconstrictor responses are expressed as a percentage of previous Ang II-induced contraction. Data are the mean ± SEM from (n) arterial segments. ∗, $P < 0.05$, and ∗∗, $P < 0.01$, compared with Ang II alone (control), respectively. ##, $P < 0.01$, compared with RPYL (20 μM), and §, $P < 0.05$, compared with valsartan (10 nM).

valsartan (10 nM). Finally, concentration-dependent inhibitory effects on the contractile response to angiotensin II are shown for RPYL (20−200 μM) as well as for valsartan (10−100 nM) (Figure 2B).

Lactoferrin-Derived Peptide RPYL Inhibits Binding of [^{125}I]-(Sar^1,Ile^8)-Angiotensin II to AT_1 Receptors. The competitive angiotensin II AT_1 receptor blocker valsartan (1 pM−1 μM) induced concentration-dependent inhibition of [^{125}I]-(Sar^1,Ile^8)-angiotensin II (0.03 nM) specific binding to human angiotensin AT_1 receptors (Figure 3A) with a calculated IC_{50} value of 0.79 ± 0.15 nM (n = 6). The peptide RPYL (3−300 μM) also induced significant concentration-dependent inhibition of [^{125}I]-(Sar^1,Ile^8)-angiotensin II specific binding to human angiotensin AT_1 receptors (Figure 3B), amounting to 62% binding inhibition at the highest RPYL concentration assayed (300 μM). On the other hand, RPYL (100 μM) also significantly reduced to 38.2 ± 5.0% (n = 3, $P < 0.01$) specific binding of [^{125}I]-(Sar^1,Ile^8)-angiotensin II (0.06 nM) to rabbit carotid artery angiotensin AT_1 receptors.

Lactoferrin-Derived Peptides Do Not Inhibit Endothelin-1 and Depolarization-Induced Vasoconstrictions. Endothelin-1 (10 nM) induced slow contraction (Figure 4A) with maximum effect amounting to 108 ± 5% relative to previous response to KCl, reached at 67 ± 6 min, with a mean slope of 61 ± 7 mg/min (n = 16). The effects of the different treatments on endothelin-1-induced vasoconstriction were assessed as shown for LFH < 3 kDa in the representative recording of Figure 4B. LFH < 3 kDa (100 μg/mL), the peptide RPYL (20 μM), or valsartan (0.1 μM) did not induce significant modification of the contractile response to endothelin-1 (Table 1).

Finally, the effects of some treatments inhibiting angiotensin II-induced vasoconstriction were assayed also against KCl-induced vasoconstriction. In control conditions, the second vasoconstriction to KCl-induced depolarization was 116 ± 2% of the first response in the same arterial segment (n = 19), and the responses to KCl were not significantly different after incubation with LFH < 3 kDa (100 μg/mL), RPYL (20 μM), or valsartan (0.1 μM) (Table 1).

DISCUSSION

We have found that some lactoferrin (LF)-derived antihypertensive peptides inhibit angiotensin II-induced vasoconstriction due to their blocking effect on angiotensin AT_1 receptors. This effect is selective for angiotensin AT_1 receptors as endothelin-1-induced, ET_A receptor-mediated vasoconstriction is not inhibited, and no unspecific effects on depolarization-induced vasoconstriction are shown.

We have previously reported that the low molecular weight LF hydroysate included in this study (LFH < 3 kDa) shows antihypertensive effects in SHRs. Single-dose LFH < 3 kDa induces acute blood pressure reduction in SHRs,[12] and long-term intake attenuates progression of hypertension.[13] LFH < 3 kDa inhibits both in vitro ACE activity[12] and ACE-dependent angiotensin I-induced vasoconstriction.[18] The ACE inhibitory effect of LFH < 3 kDa has been confirmed as an in vivo mechanism for the antihypertensive effect.[13] The present results point to inhibition of angiotensin II-induced vasoconstriction as a potential mechanism also contributing along with ACE inhibition to the antihypertensive effect of the hydrolysate. We have also previously shown that individual peptides embedded in different regions of the LF sequence, either derived from the lactoferricin B domain (LfcinB) or identified in LFH < 3 kDa, are ACE inhibitors and have antihypertensive effects when acutely administered to SHRs.[9,10,12] The present study shows that $LfcinB_{20-25}$ also has a slight inhibitory effect on angiotensin II-induced vasoconstriction. On the other hand, the inhibitory effects of individual peptides such as LIWKL and, to a higher extent, RPYL on angiotensin II-induced vasoconstriction would contribute at least in part to the inhibitory effect of the whole hydrolysate LFH < 3 kDa.

The mechanism involved in the inhibitory effects of LF-derived peptides on angiotensin II-induced vasoconstriction has been further investigated using the most effective peptide

dx.doi.org/10.1021/jf404616f | J. Agric. Food Chem. 2014, 62, 173−181

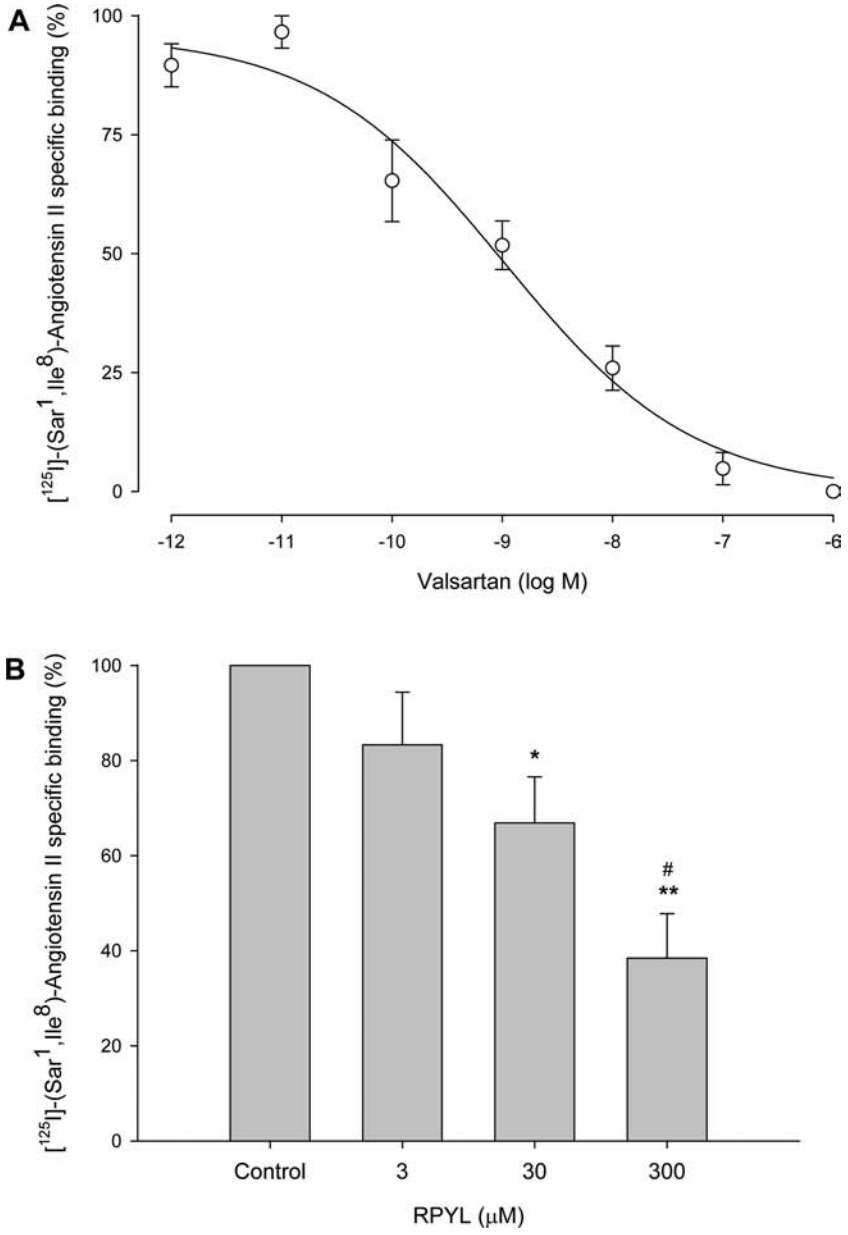

Figure 3. Inhibition of [^{125}I]-(Sar^1,Ile^8)-angiotensin II specific binding to a membrane preparation from CHO-K1 cells expressing the human angiotensin AT$_1$ receptor. Nonspecific binding was 29.3 ± 2.9%, mean ± SEM, from nine independent experiments (each performed in duplicate or triplicate). (A) Sigmoidal curve for concentration-dependent inhibitory effects of the angiotensin II AT$_1$ receptor blocker valsartan. Data are the mean ± SEM from six independent experiments (each performed in duplicate or triplicate). (B) Concentration-dependent inhibitory effects of the LF-derived peptide RPYL. Data are the mean ± SEM from at least three independent experiments (each performed in duplicate or triplicate). ∗, $P < 0.05$, and ∗∗, $P < 0.01$, compared with [^{125}I]-(Sar^1,Ile^8)-angiotensin II alone (control), respectively. #, $P < 0.05$, compared with RPYL (30 μM).

RPYL. Our results show that the inhibitory effect of RPYL on angiotensin II-induced vasoconstriction was concentration-dependent. Moreover, RPYL displaced the binding of [^{125}I]-(Sar^1,Ile^8)-angiotensin II to human angiotensin AT$_1$ receptors also in a concentration-dependent manner. These human recombinant receptors, expressed in transfected Chinese hamster ovary cells, are commonly used for AT$_1$ receptor binding assays both in whole cells[21] and in membrane preparations.[22] Finally, the inhibitory effect of RPYL on [^{125}I]-(Sar^1,Ile^8)-angiotensin II specific binding was confirmed in membranes from rabbit carotid artery, the native tissue used in vasoconstriction experiments. All of these results support an angiotensin AT$_1$ receptor-blocking mechanism for the inhibitory effect of RPYL on angiotensin II-induced vasoconstriction.

Angiotensin receptor blocker (ARB) drugs are a series of chemically related imidazole derivatives used in the clinical setting for hypertension treatment because of their ability to bind to angiotensin AT$_1$ receptors, thereby inhibiting vasoconstriction and other cellular actions of angiotensin II.[23,24] Valsartan, a member of this drug family,[25] has been used in our study as a positive control in both vasoconstriction and binding experiments. At the concentrations used, RPYL was much less potent than valsartan in both experimental settings.

The inhibitory effects of food-derived antihypertensive peptides on angiotensin II-induced vasoconstriction have not been extensively studied, and when studied, no inhibition has been found. Others have reported the lack of effect of the milk-derived tripeptide IPP[26] and the sardine muscle-derived

dx.doi.org/10.1021/jf404616f | J. Agric. Food Chem. 2014, 62, 173−181

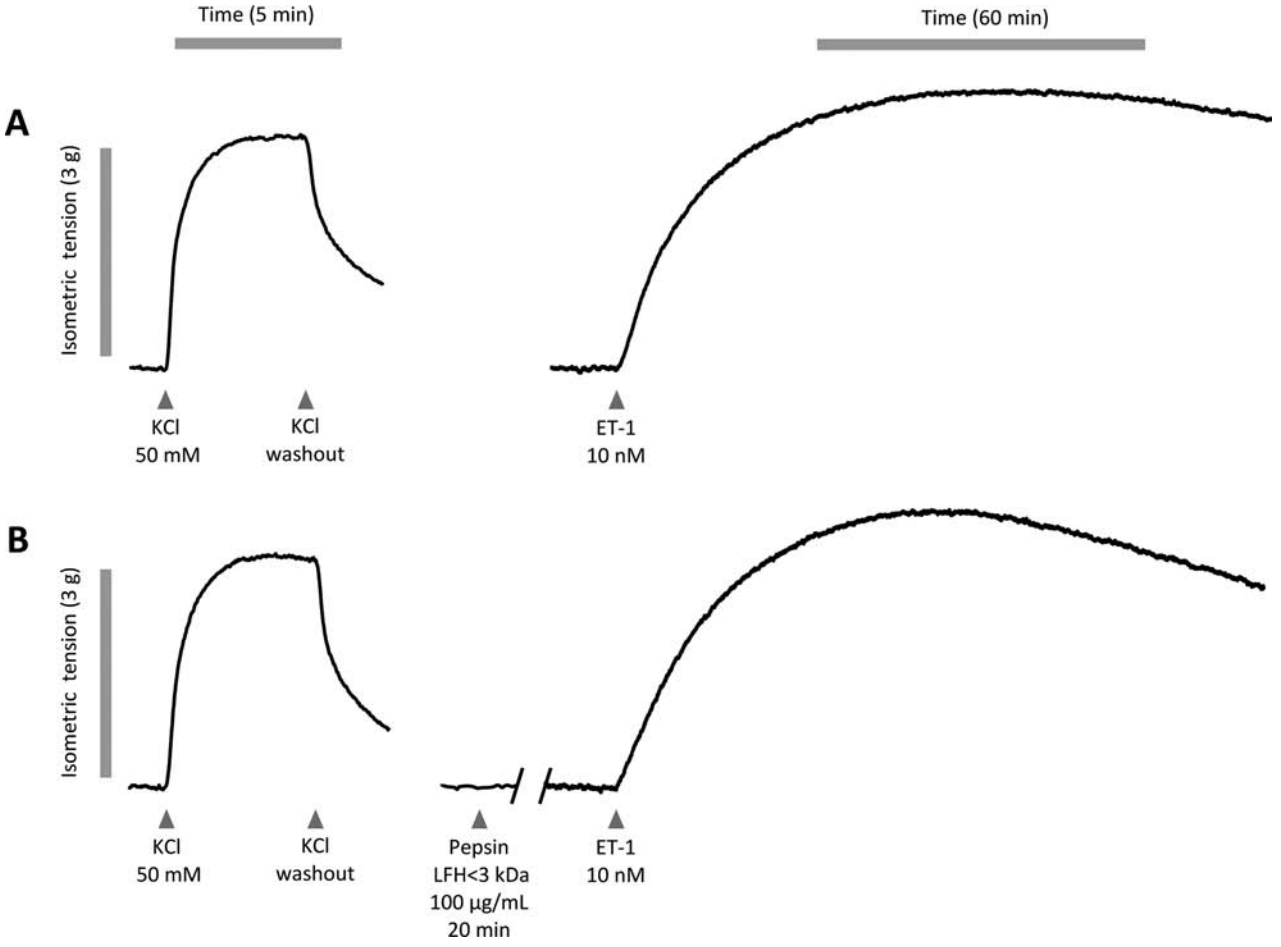

Figure 4. Typical vasoconstrictor effects of endothelin-1 (ET-1) in carotid artery segments isolated from New Zealand White rabbits: (A) vasoconstriction to high-KCl and to ET-1 in control conditions; (B) effect of LFH < 3 kDa on ET-1-induced vasoconstriction.

Table 1. Vasoconstrictor Responses of Carotid Artery Segments Isolated from New Zealand White Rabbits to Endothelin-1 and KCl-Induced Depolarization, in Control Conditions and after Treatment with LFH < 3 kDa, the LF-Derived Peptide RPYL, the Angiotensin II AT_1 Receptor Blocker Valsartan, and the Selective ET_A Endothelin Receptor Antagonist BQ-123[a]

	endothelin-1 (10 nM)	KCl (50 mM)
control	124 ± 2 (3)	117 ± 2 (8)
LFH < 3 kDa (100 µg/mL)	113 ± 6 (9)	113 ± 2 (8)
control	106 ± 11 (7)	109 ± 2 (7)
RPYL (20 µM)	93 ± 5 (8)	109 ± 3 (7)
control	103 ± 3 (6)	124 ± 8 (4)
valsartan (0.1 µM)	109 ± 3 (16)	128 ± 5 (12)
control	123 ± 7 (12)	nd
BQ-123 (1 µM)[b]	49 ± 3 (8)[c]	

[a]Vasoconstrictor responses are expressed as a percentage of previous KCl-induced contraction. Data are the mean ± SEM from (*n*) arterial segments (nd, not determined). [b]Taken from Fernández-Musoles et al.[17] [c]Significantly different from control, $P < 0.01$. Unpaired Student's *t* test.

dipeptide VY[27] on angiotensin II-induced vasoconstriction. In a previous study with rationally designed heptapeptides, we found that the ACE inhibitor antihypertensive heptapeptide PACEI50 (RKWHFLW) did not modify angiotensin II-induced vasoconstriction.[28] With regard to LF-derived peptides, the crude LF pepsin hydrolysate before ultrafiltration (LFH) did not inhibit angiotensin II-induced vasoconstriction, did not modify blood pressure in SHRs and showed much less inhibitory potency on ACE than LFH < 3 kDa,[11,12] thus indicating that the antihypertensive effects of the LF hydrolysate are due to the bioactive properties of its low molecular weight peptides such as LIWKL and RPYL.

To the best of our knowledge, the present study for the first time shows the ability of antihypertensive bioactive peptides to inhibit angiotensin II-induced vasoconstriction by an angiotensin AT_1 receptor blocking mechanism. With regard to nonpeptide substances, inhibition of angiotensin II-induced vasoconstriction has been reported to underlie the antihypertensive effects of compounds such as nitro-oleic acid, a NO-derived fatty acid,[29] and especially plant extracts used in folk medicine.[30−34] Moreover, proanthocyanidins and alkaloids from some plant extracts are angiotensin AT_1 receptor binding compounds.[21,35,36] On the other hand, inhibitory effects on renin activity, the rate-limiting enzyme upstream of the RAS,[37] have been reported for hemp seed protein hydrolysates,[38] flaxseed protein hydrolysate fractions,[39] and peptides from pea protein hydrolysates,[40] as well as for peptides from a protein hydrolysate of the macroalga *Palmaria palmate*.[41] In most of these cases, inhibitory effects were observed on both renin and

dx.doi.org/10.1021/jf404616f | J. Agric. Food Chem. 2014, 62, 173−181

ACE activities.[38−40] Therefore, bioactive peptides with antihypertensive potential can be multifunctional peptides inhibiting more than one of the RAS steps: generation of angiotensin I from angiotensinogen by renin, generation of vasoactive angiotensin II from angiotensin I by ACE, or activation of the AT_1 receptor by angiotensin II.[37]

The endothelin system, similar to the RAS, is another peptidic system with an increasingly recognized role in blood pressure regulation and hypertension pathophysiology.[42] Of particular relevance in the cardiovascular system, endothelin-1 has powerful vasoconstrictor and pressor properties. The gene product preproendothelin-1 is cleaved by a furin-like endopeptidase to form a biologically inactive intermediate termed big endothelin-1. Next, big ET-1 is cleaved by an endothelin-converting enzyme (ECE) to form endothelin-1, which binds to vascular ET_A receptors to induce vasoconstriction.[43] Both AT_1 and ET_A receptors belong to class 1 of G protein-coupled receptors,[44] and dual-action AT_1 and ET_A receptor antagonists reduce blood pressure in experimental hypertension.[45] Moreover, angiotensin AT_1 receptor binding alkaloids from the root of *Bocconia frutescens* also show weaker binding to endothelin ET_A receptors.[35] Our results show that neither LFH < 3 kDa nor RPYL, the peptide with the highest inhibitory effect on angiotensin II-induced vasoconstriction, modified the vasoconstriction induced by endothelin-1, thus supporting the selective effects of LF-derived peptides on the AT_1 receptor. In a previous study, we reported that LfcinB-derived peptides hinder endothelin-1 generation by inhibiting ECE activity but do not act on downstream ET_A receptors or intracellular signal transduction mechanisms leading to vasoconstriction.[17]

Some considerations have to be made regarding the availability of LF-derived peptides both in the present experiments and in in vivo circumstances. Peptidases are present in the wall of blood vessels, both in the endothelial layer and in the smooth muscle.[46] In addition to ACE[9] and ECE[17] activities previously shown in the isolated rabbit carotid artery used in our ex vivo assays, some other vascular peptidases hydrolyze endogenous vasoactive peptides, thus interfering with their biological effects.[47,48] A possible hydrolytic effect of vascular peptidases on LF-derived peptides during their incubation with the carotid arteries cannot be dismissed. Furthermore, depending on the acid−base nature of their amino acid residues, peptide−peptide ionic interactions can occur to form quite stable noncovalent complexes.[49] In our study, interaction between LF-derived peptides and angiotensin II to form peptide complexes unable to bind to AT_1 receptors has not been assessed. The influence of such a mechanism on the availability of LF-derived peptides and their inhibitory effects on angiotensin II-induced contraction cannot be discarded. Finally, bioavailability of peptides after oral administration is needed to guarantee bioactivity.[14] The few bioavailability studies performed in vivo show the detection of VPP and IPP in plasma in picomolar to nanomolar concentrations[50] with elimination half-lives of about 2 min.[51] The low bioavailability found for most natural peptides raises questions as to whether those peptides lower blood pressure only via an ACE-inhibiting mechanism in blood vessels. Although plasma levels of the peptides were not measured in our studies reporting the antihypertensive effects of orally administered $LfcinB_{20-25}$,[10] LIWKL, and RPYL,[12] we showed RPYL to be particularly resistant to simulated gastrointestinal digestion.[12] Moreover, RPYL and the other LF-derived peptides add their inhibitory effects on angiotensin II effects to ACE inhibition.

In conclusion, LF-derived peptides released from different regions of the protein inhibit angiotensin II-induced vasoconstriction by blocking angiotensin AT_1 receptors. The lack of effects on endothelin-1-induced and ET_A receptor-mediated vasoconstriction as well as on depolarization-induced vasoconstriction points to a selective effect of the peptides. Therefore, inhibition of angiotensin II-induced vasocontriction is suggested as a potential mechanism also contributing along with ACE inhibition to the antihypertensive effect of some LF-derived peptides.

AUTHOR INFORMATION

Corresponding Author

*(J.B.S.) Phone: +34 96 386 2797. Fax: +34 96 197 3018. E-mail: salom_jba@gva.es.

Funding

This work was supported by Grants AGL2010-21009 from Ministerio de Educación y Ciencia − FEDER, Consolider Ingenio 2010, Fun-C-Food, CSD2007-00063, and network RETICS INVICTUS − RD12/0014/0004 from Instituto de Salud Carlos III. R. Fernández-Musoles is the recipient of a fellowship from Ministerio de Educación y Ciencia (BES-2008-004472).

Notes

The authors declare no competing financial interest.

ACKNOWLEDGMENTS

We thank Javier López-Díez and Sonia Ruiz-Piquer for technical assistance.

ABBREVIATIONS USED

ACE, angiotensin-converting enzyme; AT_1, angiotensin receptor 1; ECE, endothelin-converting enzyme; ET-1, endothelin-1; ET_A, endothelin receptor A; IC_{50}, half-maximal effective concentration; LF, lactoferrin; LfcinB, lactoferricin B; LFH, lactoferrin hydrolysate; RAS, renin angiotensin system; SHR, spontaneously hypertensive rat

REFERENCES

(1) Ruilope, L. M. Current challenges in the clinical management of hypertension. *Nat. Rev. Cardiol.* **2011**, *9*, 267−275.

(2) Roberfroid, M. B. Global view on functional foods: European perspectives. *Br. J. Nutr.* **2002**, *88* (Suppl.8), S133−S138.

(3) Hartmann, R.; Meisel, H. Food-derived peptides with biological activity: from research to food applications. *Curr. Opin. Biotechnol.* **2007**, *18*, 163−169.

(4) Fragasso, G.; Maranta, F.; Montanaro, C.; Salerno, A.; Torlasco, C.; Margonato, A. Pathophysiologic therapeutic targets in hypertension: a cardiological point of view. *Expert Opin. Ther. Targets* **2012**, *16*, 179−193.

(5) Hong, F.; Ming, L.; Yi, S.; Zhanxia, L.; Yongquan, W.; Chi, L. The antihypertensive effect of peptides: a novel alternative to drugs? *Peptides* **2008**, *29*, 1062−1071.

(6) Hernández-Ledesma, B.; del Mar Contreras, M.; Recio, I. Antihypertensive peptides: production, bioavailability and incorporation into foods. *Adv. Colloid Interface Sci.* **2011**, *165*, 23−35.

(7) González-Chávez, S. A.; Arévalo-Gallegos, S.; Rascón-Cruz, Q. Lactoferrin: structure, function and applications. *Int. J. Antimicrob. Agents* **2009**, *33*, 301.e1−301.e8.

(8) Wakabayashi, H.; Takase, M.; Tomita, M. Lactoferricin derived from milk protein lactoferrin. *Curr. Pharm. Des.* **2003**, *9*, 1277−1287.

(9) Centeno, J. M.; Burguete, M. C.; Castelló-Ruiz, M.; Enrique, M.; Vallés, S.; Salom, J. B.; Torregrosa, G.; Marcos, J. F.; Alborch, E.; Manzanares, P. Lactoferricin-related peptides with inhibitory effects on ACE-dependent vasoconstriction. *J. Agric. Food Chem.* **2006**, *54*, 5323−5329.
(10) Ruiz-Giménez, P.; Ibáñez, A.; Salom, J. B.; Marcos, J. F.; López-Díez, J. J.; Vallés, S.; Torregrosa, G.; Alborch, E.; Manzanares, P. Antihypertensive properties of lactoferricin B-derived peptides. *J. Agric. Food Chem.* **2010**, *58*, 6721−6727.
(11) Ruiz-Giménez, P.; Burguete, M. C.; Castello-Ruiz, M.; Marcos, J. F.; Salom, J. B.; Vallés, S.; Torregrosa, G.; Alborch, E.; Manzanares, P. Bovine lactoferrin pepsin hydrolysate exerts inhibitory effect on angiotensin I-converting enzyme-dependent vasoconstriction. *Int. Dairy J.* **2007**, *17*, 1212−1215.
(12) Ruiz-Giménez, P.; Salom, J. B.; Marcos, J. F.; Valles, S.; Martínez-Maqueda, D.; Recio, I.; Torregrosa, G.; Alborch, E.; Manzanares, P. Antihypertensive effect of a bovine lactoferrin pepsin hydrolysate: identification of novel active peptides. *Food Chem.* **2012**, *131*, 266−273.
(13) Fernández-Musoles, R.; Manzanares, P.; Burguete, M. C.; Alborch, E.; Salom, J. B. *In vivo* angiotensin I-converting enzyme inhibition by long-term intake of antihypertensive lactoferrin hydrolysate in spontaneously hypertensive rats. *Food Res. Int.* **2013**, *54*, 627−632.
(14) Vermeirssen, V.; Van Camp, J.; Verstraete, W. Bioavailability of angiotensin I converting enzyme inhibitory peptides. *Br. J. Nutr.* **2004**, *92*, 357−366.
(15) Martínez-Maqueda, D.; Miralles, B.; Recio, I.; Hernández-Ledesma, B. Antihypertensive peptides from food proteins: a review. *Food Funct.* **2012**, *3*, 350−361.
(16) Marques, C.; Amorim, M. M.; Pereira, J. O.; Pintado, M. E.; Moura, D.; Calhau, C.; Pinheiro, H. Bioactive peptides: are there more antihypertensive mechanisms beyond ACE inhibition? *Curr. Pharm. Des.* **2012**, *18*, 4706−4713.
(17) Fernández-Musoles, R.; López-Díez, J. J.; Torregrosa, G.; Vallés, S.; Alborch, E.; Manzanares, P.; Salom, J. B. Lactoferricin B-derived peptides with inhibitory effects on ECE-dependent vasoconstriction. *Peptides* **2010**, *31*, 1926−1933.
(18) Fernández-Musoles, R.; Salom, J. B.; Martínez-Maqueda, D.; López-Díez, J. J.; Recio, I.; Manzanares, P. Antihypertensive effects of lactoferrin hydrolysates: inhibition of angiotensin- and endothelin-converting enzymes. *Food Chem.* **2013**, *139*, 994−1000.
(19) Sentandreu, M. A.; Toldrá, F. A rapid, simple and sensitive fluorescence method for the assay of angiotensin-I converting enzyme. *Food Chem.* **2006**, *97*, 546−554.
(20) Faber, J. E.; Yang, N.; Xin, X. Expression of alpha-adrenoceptor subtypes by smooth muscle cells and adventitial fibroblasts in rat aorta and in cell culture. *J. Pharmacol. Exp. Ther.* **2001**, *298*, 441−452.
(21) Caballero-George, C.; Vanderheyden, P. M.; De Bruyne, T.; Shahat, A. A.; Van den Heuvel, H.; Solis, P. N.; Gupta, M. P.; Claeys, M.; Pieters, L.; Vauquelin, G.; Vlietinck, A. J. *In vitro* inhibition of [^{3}H]-angiotensin II binding on the human AT_1 receptor by proanthocyanidins from *Guazuma ulmifolia* bark. *Planta Med.* **2002**, *68*, 1066−1071.
(22) Zhang, J.; Wang, J. L.; Zhou, Z. M.; Li, Z. H.; Xue, W. Z.; Xu, D.; Hao, L. P.; Han, X. F.; Fei, F.; Liu, T.; Liang, A. H. Design, synthesis and biological activity of 6-substituted carbamoyl benzimidazoles as new nonpeptidic angiotensin II AT_1 receptor antagonists. *Bioorg. Med. Chem.* **2012**, *20*, 4208−4216.
(23) Taylor, A. A.; Siragy, H.; Nesbitt, S. Angiotensin receptor blockers: pharmacology, efficacy, and safety. *J. Clin. Hypertens. (Greenwich)* **2011**, *13*, 677−686.
(24) Sica, D. A. Angiotensin receptor blockers: new considerations in their mechanism of action. *J. Clin. Hypertens. (Greenwich)* **2006**, *8*, 381−385.
(25) Criscione, L.; de Gasparo, M.; Bühlmayer, P.; Whitebread, S.; Ramjoué, H. P.; Wood, J. Pharmacological profile of valsartan: a potent, orally active, nonpeptide antagonist of the angiotensin II AT_1-receptor subtype. *Br. J. Pharmacol.* **1993**, *110*, 761−771.
(26) Sipola, M.; Finckenberg, P.; Santisteban, J.; Korpela, R.; Vapaatalo, H.; Nurminen, M. L. Long-term intake of milk peptides attenuates development of hypertension in spontaneously hypertensive rats. *J. Physiol. Pharmacol.* **2001**, *52*, 745−754.
(27) Vercruysse, L.; Morel, N.; Van Camp, J.; Szust, J.; Smagghe, G. Antihypertensive mechanism of the dipeptide Val-Tyr in rat aorta. *Peptides* **2008**, *29*, 261−267.
(28) Ruiz-Giménez, P.; Marcos, J. F.; Torregrosa, G.; Lahoz, A.; Fernández-Musoles, R.; Valles, S.; Alborch, E.; Manzanares, P.; Salom, J. B. Novel antihypertensive hexa- and heptapeptides with ACE-inhibiting properties: from the *in vitro* ACE assay to the spontaneously hypertensive rat. *Peptides* **2011**, *32*, 1431−1438.
(29) Zhang, J.; Villacorta, L.; Chang, L.; Fan, Z.; Hamblin, M.; Zhu, T.; Chen, C. S.; Cole, M. P.; Schopfer, F. J.; Deng, C. X.; Garcia-Barrio, M. T.; Feng, Y. H.; Freeman, B. A.; Chen, Y. E. Nitro-oleic acid inhibits angiotensin II-induced hypertension. *Circ. Res.* **2010**, *107*, 540−548.
(30) Poh, T. F.; Ng, H. K.; Hoe, S. Z.; Lam, S. K. *Gynura procumbens* causes vasodilation by inhibiting angiotensin II and enhancing bradykinin actions. *J. Cardiovasc. Pharmacol.* **2013**, *61*, 378−384.
(31) Xue, B.; Li, J.; Chai, Q.; Liu, Z.; Chen, L. Effect of total flavonoid fraction of *Astragalus complanatus* R. Brown on angiotensin II-induced portal-vein contraction in hypertensive rats. *Phytomedicine* **2008**, *15*, 759−762.
(32) Lau, Y. S.; Kwan, C. Y.; Ku, T. C.; Hsieh, W. T.; Wang, H. D.; Nishibe, S.; Dharmani, M.; Mustafa, M. R. *Apocynum venetum* leaf extract, an antihypertensive herb, inhibits rat aortic contraction induced by angiotensin II: a nitric oxide and superoxide connection. *J. Ethnopharmacol.* **2012**, *143*, 565−571.
(33) Kono, R.; Okuno, Y.; Nakamura, M.; Inada, K.; Tokuda, A.; Yamashita, M.; Hidaka, R.; Utsunomiya, H. Peach (*Prunus persica*) extract inhibits angiotensin II-induced signal transduction in vascular smooth muscle cells. *Food Chem.* **2013**, *139*, 371−376.
(34) Guerrero, E. I.; Morán-Pinzón, J. A.; Ortíz, L. G.; Olmedo, D.; del Olmo, E.; López-Pérez, J. L.; San Feliciano, A.; Gupta, M. P. Vasoactive effects of different fractions from two Panamanians plants used in Amerindian traditional medicine. *J. Ethnopharmacol.* **2010**, *131*, 497−501.
(35) Caballero-George, C.; Vanderheyden, P. M.; Apers, S.; Van den Heuvel, H.; Solis, P. N.; Gupta, M. P.; Claeys, M.; Pieters, L.; Vauquelin, G.; Vlietinck, A. J. Inhibitory activity on binding of specific ligands to the human angiotensin II AT_1 and endothelin 1 ET_A receptors: bioactive benzo[c]phenanthridine alkaloids from the root of *Bocconia frutescens*. *Planta Med.* **2002**, *68*, 770−775.
(36) Caballero-George, C.; Vanderheyden, P. M.; Solis, P. N.; Gupta, M. P.; Pieters, L.; Vauquelin, G.; Vlietinck, A. *In vitro* effect of sanguinarine alkaloid on binding of [^{3}H]candesartan to the human angiotensin AT_1 receptor. *Eur. J. Pharmacol.* **2003**, *458*, 257−262.
(37) Herichova, I.; Szantoova, K. Renin-angiotensin system: upgrade of recent knowledge and perspectives. *Endocr. Regul.* **2013**, *47*, 39−52.
(38) Girgih, A. T.; Udenigwe, C. C.; Abayomi, H. L.; Adebiyi, P.; Aluko, R. E. Kinetics of enzyme inhibition and antihypertensive effects of hemp seed (*Cannabis sativa* L.) protein hydrolysates. *J. Am. Oil Chem. Soc.* **2011**, *88*, 1767−1774.
(39) Udenigwe, C. C.; Lin, Y. S.; Houc, W. C.; Aluko, R. E. Kinetics of the inhibition of renin and angiotensin I-converting enzyme by flaxseed protein hydrolysate fractions. *J. Funct. Foods* **2009**, *1*, 199−207.
(40) Li, H.; Aluko, R. E. Identification and inhibitory properties of multifunctional peptides from pea protein hydrolysate. *J. Agric. Food Chem.* **2010**, *58*, 11471−11476.
(41) Fitzgerald, C.; Mora-Soler, L.; Gallagher, E.; O'Connor, P.; Prieto, J.; Soler-Vila, A.; Hayes, M. Isolation and characterization of bioactive pro-peptides with *in vitro* renin inhibitory activities from the macroalga *Palmaria palmata*. *J. Agric. Food Chem.* **2012**, *60*, 7421−7427.
(42) Schiffrin, E. L. Vascular endothelin in hypertension. *Vasc. Pharmacol.* **2005**, *43*, 19−29.

(43) Kedzierski, R. M.; Yanagisawa, M. Endothelin system: the double-edged sword in health and disease. *Annu. Rev. Pharmacol. Toxicol.* **2001**, *41*, 851−876.
(44) Foord, S. M.; Bonner, T. I.; Neubig, R. R.; Rosser, E. M.; Pin, J. P.; Davenport, A. P.; Spedding, M.; Harmar, A. J. International Union of Pharmacology. XLVI. G protein-coupled receptor list. *Pharmacol. Rev.* **2005**, *57*, 279−288.
(45) Kowala, M. C.; Murugesan, N.; Tellew, J.; Carlson, K.; Monshizadegan, H.; Ryan, C.; Gu, Z.; Kane, B.; Fadnis, L.; Baska, R. A.; Beyer, S.; Arthur, S.; Dickinson, K.; Zhang, D.; Perrone, M.; Ferrer, P.; Giancarli, M.; Baumann, J.; Bird, E.; Panchal, B.; Yang, Y.; Trippodo, N.; Barrish, J.; Macor, J. E. Novel dual action AT_1 and ET_A receptor antagonists reduce blood pressure in experimental hypertension. *J. Pharmacol. Exp. Ther.* **2004**, *309*, 275−284.
(46) Palmieri, F. E.; Bausback, H. H.; Ward, P. E. Metabolism of vasoactive peptides by vascular endothelium and smooth muscle aminopeptidase M. *Biochem. Pharmacol.* **1989**, *38*, 173−180.
(47) Ryan, J. W. Peptidase enzymes of the pulmonary vascular surface. *Am. J. Physiol.* **1989**, *257*, L53−L60.
(48) Rouissi, N.; Nantel, F.; Drapeau, G.; Rhaleb, N. E.; Dion, S.; Regoli, D. Inhibitors of peptidases: how they influence the biological activities of substance P, neurokinins, kinins and angiotensins in isolated vessels. *Pharmacology* **1990**, *40*, 185−195.
(49) Woods, A. S.; Huestis, M. A. A study of peptide-peptide interaction by matrix-assisted laser desorption/ionization. *J. Am. Soc. Mass Spectrom.* **2001**, *12*, 88−96.
(50) Foltz, M.; Meynen, E. E.; Bianco, V.; Van Platerink, C.; Koning, T. M.; Kloek, J. Angiotensin converting enzyme inhibitory peptides from a lactotripeptide-enriched milk beverage are absorbed intact into the circulation. *J. Nutr.* **2007**, *137*, 953−958.
(51) Van der Pijl, P. C.; Kies, A. K.; Ten Have, G. A.; Duchateau, G. S.; Deutz, N. E. Pharmacokinetics of proline-rich tripeptides in the pig. *Peptides* **2008**, *29*, 2196−2202.

JOURNAL OF AGRICULTURAL AND FOOD CHEMISTRY

Article

pubs.acs.org/JAFC

Chlorogenic Acid and Coffee Prevent Hypoxia-Induced Retinal Degeneration

Holim Jang,[†,‡] Hong Ryul Ahn,[‡] Hyoung Jo,[‡] Kyung-A Kim,[‡] Eun Ha Lee,[‡] Ki Won Lee,[§] Sang Hoon Jung,*[,‡,¶] and Chang Y. Lee*[,†,¶]

[†]Department of Food Science, Cornell University, Ithaca, New York 14850, United States

[‡]Functional Food Center, Korea Institute of Science and Technology (KIST), Daejeon-dong, Gangneung 210-340, Republic of Korea

[§]Department of Agricultural Biotechnology, Seoul National University, Seoul 151-742, Republic of Korea

ABSTRACT: This study explored whether chlorogenic acid (CGA) and coffee have protective effects against retinal degeneration. Under hypoxic conditions, the viability of transformed retinal ganglion (RGC-5) cells was significantly reduced by treatment with the nitric oxide (NO) donor *S*-nitroso-*N*-acetylpenicillamine (SNAP). However, pretreatment with CGA attenuated cell death in a concentration-dependent manner. In addition, CGA prevented the up-regulation of apoptotic proteins such as Bad and cleaved caspase-3. Similar beneficial effects of both CGA and coffee extracts were observed in mice that had undergone an optic nerve crush (ONC) procedure. CGA and coffee extract reduced cell death by preventing the down-regulation of Thy-1. Our *in vitro* and *in vivo* studies demonstrated that coffee and its major component, CGA, significantly reduce apoptosis of retinal cells induced by hypoxia and NO, and that coffee consumption may help in preventing retinal degeneration.

KEYWORDS: *coffee, chlorogenic acid, neuroprotection, retinal degeneration, hypoxia, RGC-5, glaucoma*

INTRODUCTION

The retina, a thin layer of tissue on the inside back wall of the eye, contains millions of light-sensitive cells and other nerve cells that receive and organize visual information. Collectively, these cells send visual information to the brain through the optic nerve. The retina is one of the most metabolically active tissues in the body, consuming oxygen more rapidly than any other tissues, including the brain. Therefore, it is susceptible to a variety of diseases caused by oxidative stress, including age-related macular degeneration, diabetic retinopathy, and glaucoma—all of which can lead to partial or complete blindness.[1]

One mechanism of retinal degeneration is hypoxia, a reduction in retinal oxygen supply caused by pathologies such as central retinal artery occlusion, ischemic central retinal vein thrombosis, complications of diabetic eye disease, and some types of glaucoma that cause vascular eye diseases.[2,3] Retinal hypoxia can negatively impact both tissue function and cell viability, and is a potential risk factor for sight-threatening disorders.[4]

Unsurprisingly, there has been great interest in identifying neuroprotective compounds that inhibit hypoxia. Particularly promising in this capacity are natural products and phytochemicals that act as antioxidants and can be taken regularly without causing significant side effects.[5−7]

One important group of neuroprotectants comprises derivatives of chlorogenic acid (CGA). Collectively, these phenolic phytochemicals are known to have hepatoprotective, antibacterial, anti-inflammatory, DNA protective, and anti-cancer activities, among others.[8−13] Several studies have also suggested that the antioxidant properties of CGA make it a powerful neuroprotectant.[14−16]

CGA derivatives are found in a variety of edible plants, including tea, fruits, and vegetables. However, the major source of CGA intake in humans is coffee.[17] CGA is 4−12% of raw coffee, while a 200 mL cup of prepared coffee contains 200 mg of total CGA.[18,19] It has also been reported that part of CGA from foods enters into the blood circulation with relatively high absorption rate (33%) in the small intestine of humans.[20] There are also many reports for the bioavailability and pharmacokinetic profile of CGA after coffee consumption.[21−23] Previous studies by Farah et al. showed that major CGA compounds from green coffee are highly absorbed and metabolized in humans by a different manner throughout the whole gastrointestinal tract.[22]

Coffee consumption appears to decrease the risk of developing chronic diseases such as Parkinson's, prostate cancer, and diabetes.[24−27] It also reduces the extent of cognitive declines associated with aging.[28−30] The latter pattern, in particular, supports the idea that the neuroprotective effects of CGA derivatives stem from their antioxidant activities.

Despite these generally positive results, the effects of coffee consumption on ocular health are not yet clear. In particular, clinical studies on the relationship between coffee consumption and risk of glaucoma have yielded conflicting results.[31,32] Thus, we designed the current study to investigate whether coffee and, in particular, its main polyphenol, CGA has protective effects against the degeneration of retinal ganglion cells (RGC-5), both *in vitro* and *in vivo*.

Received: October 16, 2013
Revised: November 26, 2013
Accepted: December 2, 2013
Published: December 2, 2013

ACS Publications © 2013 American Chemical Society

MATERIALS AND METHODS

Chemicals. Hoechst 33342 and propidium iodide (PI) were purchased from Molecular Probes (Eugene, OR, USA). Fluorogold was purchased from Invitrogen (Carlsbad, CA, USA). Anticleaved caspase-3, anti-Bad, and anti-Thy-1 were purchased from Cell Signaling Technology (Danvers, MA, USA). Anti-β-actin and secondary antibodies were purchased from Santa Cruz Biotechnology (Santa Cruz, CA, USA).

The VECTASHIELD Mounting Medium was purchased from Vector Laboratories (Burlingame, CA, USA). Zoletil and Rumpun were used as anesthesia and purchased from Virbac Laboratories (Fort Worth, TX, USA) and Bayer (Newbury, UK), respectively.

Chlorogenic acid (C3878) and all other chemicals and reagents were purchased from Sigma-Aldrich (St. Louis, MO, USA).

Animals. All animal studies were carried out in a pathogen-free barrier zone at the KIST Gangneung Institute and were done in accordance with the procedure outlined in the Association for Research in Vision and Ophthalmology (ARVO) Statement for the Use of Animals in Ophthalmic and Vision Research. Procedures used in this study were approved by the Animal Care and Use Committee of KIST.

Male ICR mice weighing between 30 and 35 g (5 weeks of age) were used in the present study and were acclimated for at least one week, were caged in groups of five or less, and were fed with a diet of animal chow and water *ad lib.* They were housed at 23 ± 0.5 °C and 10% humidity with a 12 h light-dark cycle.

Preparation of the Crude Extract from Coffee Powder. The coffee sample was obtained from a local supermarket (Colombian roast and ground coffee, Tesco, U.K.). Ground coffee (30.0 g) was refluxed with 70% EtOH (600 mL) three times each for 3 h, and the combined solution was filtered and evaporated under vacuum to give a 70% EtOH extract (9.76 g).

HPLC Analysis. Coffee extract (CE) was analyzed by HPLC to quantify CGA using an Agilent 1200 series system, equipped with a G1379B vacuum degasser, a G1312A binary pump, a G1329A autosampler, a G1316A column oven, and a G1315B DAD detector (Agilent, Palo Alto, CA, USA). The separation was carried out on a Shiseido MGII C-18 column (250 mm × 4.6 mm i.d., 5 μm particle size). The mobile phase consisted of 0.1% TFA in water and acetonitrile (93:7) with a flow rate of 1.0 mL/min during 45 min. The UV detector was set at 330 nm with full spectral scanning from 200 to 400 nm, and the sample injection volume was 10 μL.

A standard solution of CGA (31.25−1000 μg/mL) was prepared in methanol, and 10 μL of each was injected into the HPLC column via the autoinjector. The linearity was evaluated by linear regression analysis, which was calculated by the least-squares regression method. The limit of detection (LOD) and the lower limit of quantification (LOQ) were defined as the minimum concentration at the signal-to-noise ratio (S/N), equal to 3.3 and 10, respectively. The precision, accuracy, and recovery were evaluated by analyzing three different concentrations on the same day and on three different days. All the experiments were carried out in triplicate.

Culture of RGC-5 Cells. RGC-5 cells that are proven to be of mice origin are highly relevant to the study of glaucomatous neurodegeneration and have been previously shown to express ganglion cell markers and ganglion cell-like behavior in culture.[33,34]

To mimic physiological hypoxic stress, RGC-5 cultures were transferred into a closed hypoxic chamber (Billups-Rothenberg Inc., Del Mar, CA, USA) in which the gas levels (1% O_2, 5.13% CO_2, and 93.87% N_2) and temperature (37 °C) were automatically controlled, and they were incubated for 24 h. Under hypoxic conditions, cells were cotreated with *S*-nitroso-*N*-acetylpenicillamine (SNAP), a nitric oxide (NO) donor, with low glucose (5.5 mM) Dulbecco's modified Eagles's medium (DMEM; Gibco, Carlsbad, CA), which mimics physiological normal blood sugar levels *in vivo*. Culture of RGC-5 cells in 96-well plates was analyzed 24 h later for cell viability, and the cells in a 60 mm^2 dish were analyzed 24 h later for Western blot analysis.

Cell Viability. To measure the relative number of living cells, an EZ cytox cell viability assay kit (Daeil Labservice, Seoul, Korea) for a WST-1 assay was used.

The number of living cells in each well was determined by measuring the optical density (OD) at 460 nm with a microplate reader (BioTek Instruments, Winooski, VT, USA). This quantity was expressed relative to the control value.

Microscopic Analysis of Cell Viability by Hoechst 33342 and PI Double Staining. The Hoechst 33342 and PI double staining method was used to determine whether cell death occurred as a result of apoptosis or necrosis.[35] The cells were stained with 8 μM Hoechst 33342 and 1.5 μM PI for 30 min at 37 °C. After being washed twice with serum free media, the cells were imaged using a fluorescence microscope (Olympus, Tokyo, Japan).

Protein Extraction and Western Blot Analysis. The cells were scraped using a cell scraper and centrifuged at 14,000*g* for 10 min. The cell pellets were resuspended in cell lysis buffer [1 M Tris pH 7.4, 2 M NaCl, 1 M EDTA, 10% NP40, 1 × protease inhibitors, 1 mM PMSF] and then incubated on ice for 10 min. The extracted cells were centrifuged at 14,000*g* for 30 min at 4 °C. The supernatant was sonicated, and the total protein concentration was determined using a Bio-Rad Protein Assay kit (Bio-Rad Laboratories, Hercules, CA, USA).

Western blot analysis was performed with the primary antibodies, including anticleaved caspase-3, anti-Bad, anti-Thy-1 (1:1000, Cell Signaling Technology, Beverly, MA, USA), and β-actin (1:3000, Santa Cruz Biotechnology, CA, USA). Secondary antibodies were purchased from Santa Cruz Biotechnology Co. Ltd. (1:3000, Santa Cruz Biotechnology, CA, USA). Immunoreactive bands were detected using enhanced chemiluminescence reagents (Amersham Bioscience, GE Healthcare, U.K.) and were measured via densitometry using a LAS-4000 image reader and Multi Gauge 3.1 software (Fuji Photo Film, Japan).

Histological Analysis. For Hematoxilin and Eosin staining, the enucleated eyes were fixed in 10% formalin for 24 h, embedded in paraffin, and sectioned through an equatorial plane at 4 μm thickness using a HM340E microtome (Walldof, Germany). Four sections (n = 4) were used for analysis.

Hematoxylin solution was added to the retina section (0.1% hematoxylin, 10% ammonium) for 8 min. The sections were then washed three times with distilled water. Bluing reagent (0.2% lithium carbonate solution) was added to the section for 1 min. The sections were quickly rinsed in 95% alcohol, and 1% Eosin Y solution was added to the sections for 1 min. Eosin Y was washed off with 95% alcohol three times, and the sections were cover-slipped with a mounting medium and observed under a light microscope (Olympus, Tokyo, Japan).[36]

For TUNEL staining, the sections were submitted to enzymatic digested with 20 μg/mL of proteinase K for 15 min and then washed with PBS and incubated with 3% hydrogen peroxide in PBS for 5 min at room temperature and twice rinsed in PBS. They were then immersed, incubated with a stock solution of terminal deoxynucleotidyl transferase (TdT) reaction enzyme in a humidified chamber at 37 °C for 1 h, and then washed three times in PBS for 1 min. The sections were subsequently incubated with antidigoxygenin peroxidase conjugate and peroxidase substrate. Histological analysis was performed with a light microscope (Olympus, Tokyo, Japan), allowing us to look for signs of apoptosis (brown staining).

Optic Nerve Crush. Five-week-old ICR mice with a body weight of 30−35 g were used in the study.

Animals were anaesthetized by intraperitoneal injection with a mixture of Zoletil (1.6 μg/g, Verbac Laboratories 06515, France) and Rompun (0.05 μL/g, Bayer), and retinal damage was induced using optic nerve crush (ONC).[37] The optic nerve of the left eye in all treatment groups was exposed by opening the meninges of the optic nerve with the sharp tips of a forceps, followed by blunt dissection. Then the exposed optic nerve was partially crushed 2 mm behind the globe for 10 s with a cross-action calibrated forceps. In each case, a "sham" operation was performed in the same way on the partner eye, but without closing the forceps, to check for any falsifying influence of surgery on the treatment effects. In all cases the retinal blood supply

remained grossly intact, as judged on the basis of a direct ophthalmoscopic inspection. After ONC in mice, CGA or CE was dissolved in PBS, and administered orally at a dose of 10 mg/kg and 30 mg/kg for 2 weeks once a day.

All eyeballs were enucleated immediately after mice were sacrificed, and then fixed for retrograde labeling of retinal ganglion cells (RGCs).

RGC Labeling and Retinal Flat Mount Preparation. Mice were anesthetized by intraperitoneal or intramuscular administration of a mixture of Zoletil (1.6 μg/g, Verbac Laboratories 06515, France) and Rompun (0.05 μL/g, Bayer) 9 days after CGA or CE treatment. The skin over the cranium was incised, and the scalp was exposed. Holes approximately 2 mm in diameter were drilled in the skull 4 mm posterior to the bregma, 1 mm lateral to the midline, with a dentist's drill on both sides of the midline raphe. These positions correspond to the superior colliculi as determined from a stereotactic mouse brain atlas.

The superior colliculi were exposed by gentle aspiration of the overlying occipital cortex. A piece of Gelfoam soaked in a 5% solution of the neurotracer dye Fluorogold (Invitrogen, NY, USA) was directly applied to each superior colliculus. Skull openings were then sealed with a petrolatum-based antibiotic ointment. The overlying skin was sutured and antibiotic ointment applied externally.

Five days after the application of Fluorogold (enough time to allow retrograde uptake of the dye and labeling of the RGC somata), mice were sacrificed by transcardial perfusion with 4% buffered paraformaldehyde (Sigma-Aldrich, St. Louis, MO, USA) while under the same anesthesia as that used for RGC labeling. Eyes were immediately enucleated, and the retinas were detached at the ora serrata and cut with a trephine around the optic nerve head. Four radial relaxing incisions were made and the retinas prepared as flattened whole mounts on silane-coated microscope slides.[38]

Statistical Analysis. The data are expressed as a mean percentage of the control value plus standard error of the mean (SEM). Statistical comparisons were made using a one-way ANOVA followed by a Dunnett's test. Statistical analyses were conducted using GraphPad Prism (version 4.0) (GraphPad, San Diego, CA, USA). Significance was defined as $p < 0.05$.

RESULTS AND DISCUSSION

Cell Viability Following Treatment with SNAP and/or Hypoxia. Under normoxic conditions, we observed no changes in cell viability when RGC-5 cells were treated with SNAP (data not shown). Likewise, the two lowest concentrations of SNAP did not have any noticeable effects on the viability of RGC-5 cells exposed to hypoxic conditions (Figure 1). However, both the 50 and 100 μM treatments resulted in highly significant reductions in viability ($p < 0.001$). The 100 μM treatment had a particularly noticeable effect, causing a 41% reduction of viability. Thus, this is the concentration that was used in the *in vitro* experiments (Figure 1).

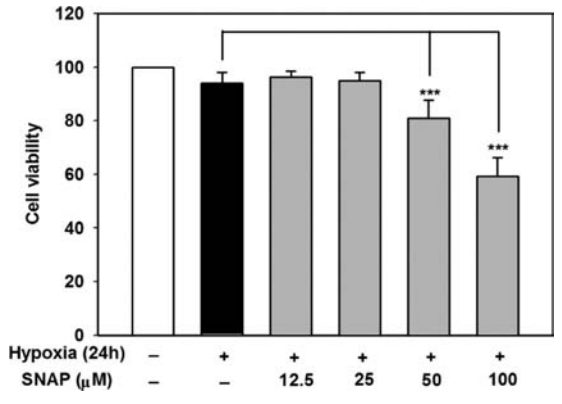

Figure 1. Effects of *S*-nitroso-*N*-acetylpenicillamine (SNAP) on the viability of retinal ganglion (RGC-5) cells cultured under hypoxic conditions for 24 h. Values are presented as means ($n = 6$ independent experiments per treatment); error bars indicate SEM. Triple asterisks (***) indicate $p < 0.001$.

The negative effects of SNAP observed here are similar to those previously reported by Sato et al. (2010).[39] They found that treatment with SNAP under hypoxic conditions resulted from activation of caspase and the formation of superoxide anions and peroxynitrite.[39]

Cell Viability Following Treatment with SNAP and CGA. CGA significantly blunted the negative effect of SNAP on RGC-5 cells (Figure 2). This effect was dose-dependent, with cell viability increased by 72.6%, 92.7%, and 101.6% in response to 25, 50, and 100 μM CGA pretreatments, respectively (all $p <$ 0.001 in comparison with the control; Figure 2A).

The antioxidant *N*-acetylcysteine (NAC) and the NO scavenger 2,4-carboxyphenyl-4,4,5,5-tetramethylimidazoline-1-oxyl-3-oxide (CPTIO) were used as positive controls. Both

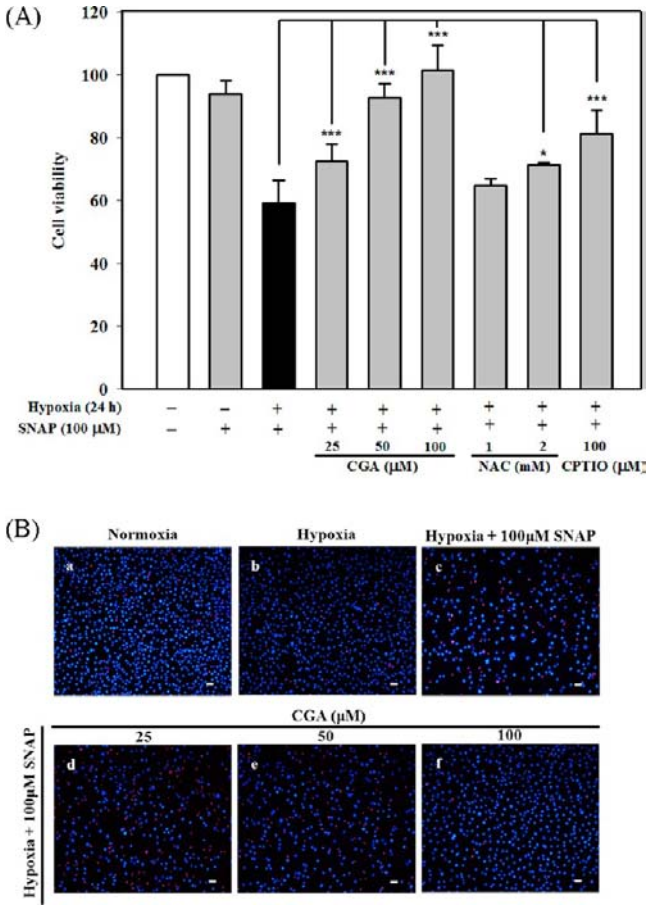

Figure 2. Effects of the chlorogenic acid (CGA) treatment on retinal ganglion (RGC-5) cells exposed to *S*-nitroso-*N*-acetyl-penicillamine (SNAP) under hypoxic conditions. (A) Results of the WST-1 assay. Values are presented as means ($n = 6$ independent experiments per treatment); error bars indicate SEM. Single asterisks (*) indicate $p <$ 0.05; triple asterisks (***) indicate $p < 0.001$. (B) Representative fluorescence microscopy of PI (red) and Hoechst 33342 (blue) staining. (a) Control RGC-5 cells under normoxic conditions. (b) RGC-5 cells under hypoxic conditions. (c) RGC-5 cells treated with 100 μM SNAP under hypoxic conditions. (d–f) RGC-5 cells pretreated with CGA (25, 50, and 100 μM concentrations, respectively) prior to being exposed to 100 μM SNAP under hypoxic conditions. Scale bar =50 μm.

dx.doi.org/10.1021/jf404285v | J. Agric. Food Chem. 2014, 62, 182–191

treatments also significantly reduced the negative impacts of SNAP observed in the untreated controls ($p < 0.05$ for the 2 mM NAC treatment, and $p < 0.001$ for the 100 μM CPTIO treatment; Figure 2A). Previous work has shown that the benefits of CPTIO stem from its suppression of both caspase activation and NO production.[39] CGA has been considered an antioxidant agent; moreover, CGA is a potent inhibitor of NO production by the inhibition of the expression of inflammatory proteins such as COX-2 and iNOS, without cytotoxic effects.[40,41]

The similar viabilities observed in cells treated with CPTIO and CGA treatments suggest that CGA may protect cells by scavenging NO that might otherwise lead to neurodegeneration of RGC-5 cells under hypoxic conditions.

Fluorescence microscopy of Hoechst 33342- and PI-stained cells revealed similar patterns to those produced by the WST-1 assay (Figure 2B). More apoptotic/necrotic cells were observed in cultures treated with SNAP than in control cultures. However, lower levels of cell death were observed in cultures that had been pretreated with CGA; this was particularly noticeable in response to the 100 μM CGA treatment.

Our Western blot analysis showed up-regulation of Bad and cleaved caspase-3 in cells that had been exposed to SNAP under hypoxic conditions, in relation to β-actin of the control (Figure 3). However, this response was noticeably suppressed in cells given a 100 μM CGA pretreatment. A similar pattern was observed in cells treated with CPTIO as a positive control.

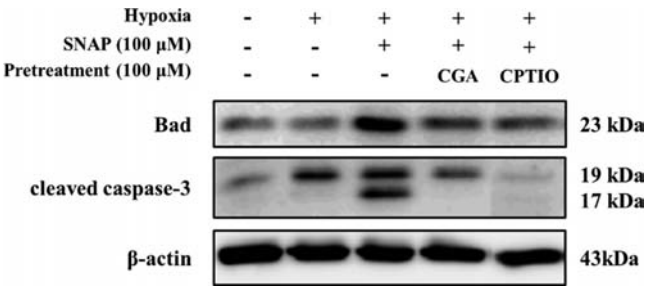

Figure 3. Western blot of apoptotic proteins in RGC-5 cells subjected to 100 μM SNAP for 24 h under hypoxic conditions. The nitric oxide (NO) scavenger 2,4-carboxyphenyl-4,4,5,5-tetramethylimidazoline-1-oxyl-3-oxide (CPTIO) was used as a positive control. Pretreatment with CGA appeared to have antiapoptotic effects on hypoxia and NO-induced down-regulation of both Bad and cleaved caspase-3.

Bad (BCL-2 antagonist of cell death), a pro-apoptotic protein in the BH3 domain-only group,[42] is the key regulator of apoptosis and is, itself, regulated primarily by phosphorylation.[43,44] Bad can be cleaved into a shortened form by caspases, which are cysteine proteases that play an important role in apoptosis.[45−47] When this cleavage occurs, Bad can be a more potent inducer of apoptosis.[46,47] Apoptosis is also facilitated by the activity of caspase-3, which is known to promote neuronal apoptosis.[48,49]

Effects of CGA on Optic Nerve Crush-Induced Retinal Damage in Mouse. ONC is a well-known experimental model for chronic glaucoma. During the procedure, the surgically exposed optic nerve is clamped for several seconds, resulting in both primary RGC death due to the optic nerve injury and secondary death of surrounding, uninjured RGCs.[50]

Results from our histological hematoxylin and eosin staining assay can be seen in Figure 4A. Relative to tissues that underwent no ONC (Figure 4A, a), those that were crushed but received no chemical treatment exhibited a clear thinning of the inner plexiform layer (IPL) (Figure 4A, b). However, this thinning appears to have been inhibited in tissues treated with CGA (Figure 4A, c and d).

In addition to investigating these morphological patterns, we also used TUNEL staining to explore whether CGA could also reduce ganglion cell apoptosis associated with ONC (Figure 4B). Control tissues (Figure 4B, a) had fewer TUNEL-positive cells than those subjected to ONC (Figure 4B, b). As with the hematoxylin and eosin assay, however, we found that the negative effects of ONC were mitigated by treatment with CGA; in this case, there were notably fewer TUNEL-positive cells in the ganglion cell layer (GCL) of tissues treated with CGA (Figure 4B, c and d).

RGC survival was much lower in tissues that had undergone optic nerve crush (ONC) than in controls (Figure 4C, a−d). In tissues that had been treated with CGA, however, RGC survival was markedly higher (Figure 4C, e−h). This was particularly true in tissues that had been dosed with 30 mg/kg of CGA (Figure 4C, g and h). Further, both CGA treatments appeared to prevent the dramatic decrease (52.7%) in Thy-1 protein that occurred in tissues that had undergone ONC (Figure 4D). Thy-1 is a surface glycoprotein expressed uniquely in RGCs; it serves as an early marker of RGC loss in models of retinal damage.[51]

Indeed, 30 mg/kg CGA was similar or more effective for the neuroprotective effects on retinal degeneration than the same concentration of epigallocatechin gallate (EGCG) used as positive control; thus, the patterns reported here strongly suggest that CGA is a powerful neuroprotectant that can prevent retinal cell death.

Previously reported mechanisms for the degeneration by ONC include blockade of axonal transport resulting in inadequate supply of neurotrophic factors, disturbances of intracellular calcium homeostasis, activation of cell death genes, and local excitotoxicity due to uncontrolled activation of NMDA receptors.[52,53] ONC induces apoptotic cascades during which cytochrome *c* is released and both caspases-9 and -3 are subsequently activated.[54,55]

Injury of the optic nerve also causes an inflammatory response involving the release of cytotoxic compounds such as free radicals, NO, and glutamate.[56]

Administration of SNAP under hypoxic conditions has been associated with NO release, causing RGC-5 cell death by decreasing mitochondrial membrane potential, increasing the formation of superoxides, and activating caspases.[39] Thus, our current data suggest that the beneficial effects of CGA on retinal cells, both *in vitro* and *in vivo*, are partly due to its NO scavenging activity.

HPLC Chromatograms of CE and Standardization of CGA in CE. HPLC chromatograms of CE showed a CGA peak retention time at 28.5 min (Figure 5). We observed no interference from other materials in the extract, indicating that the specificity of the method was reliable. The limits of detection (LOD) and limits of quantification (LOQ) for CGA were 7.67 μg/mL and 23.26 μg/mL, respectively (Table 1). Precision is the measure of how close the data values are to each other for a number of measurements under the same analytical conditions and expressed as the % relative standard deviation (%RSD) of each analyte concentration. Our analyses were associated with very low levels of relative standard deviation (RSD: intraday, >2.57%; interday, >2.60%), indicating that our CGA measurements were highly precise (Table 2).

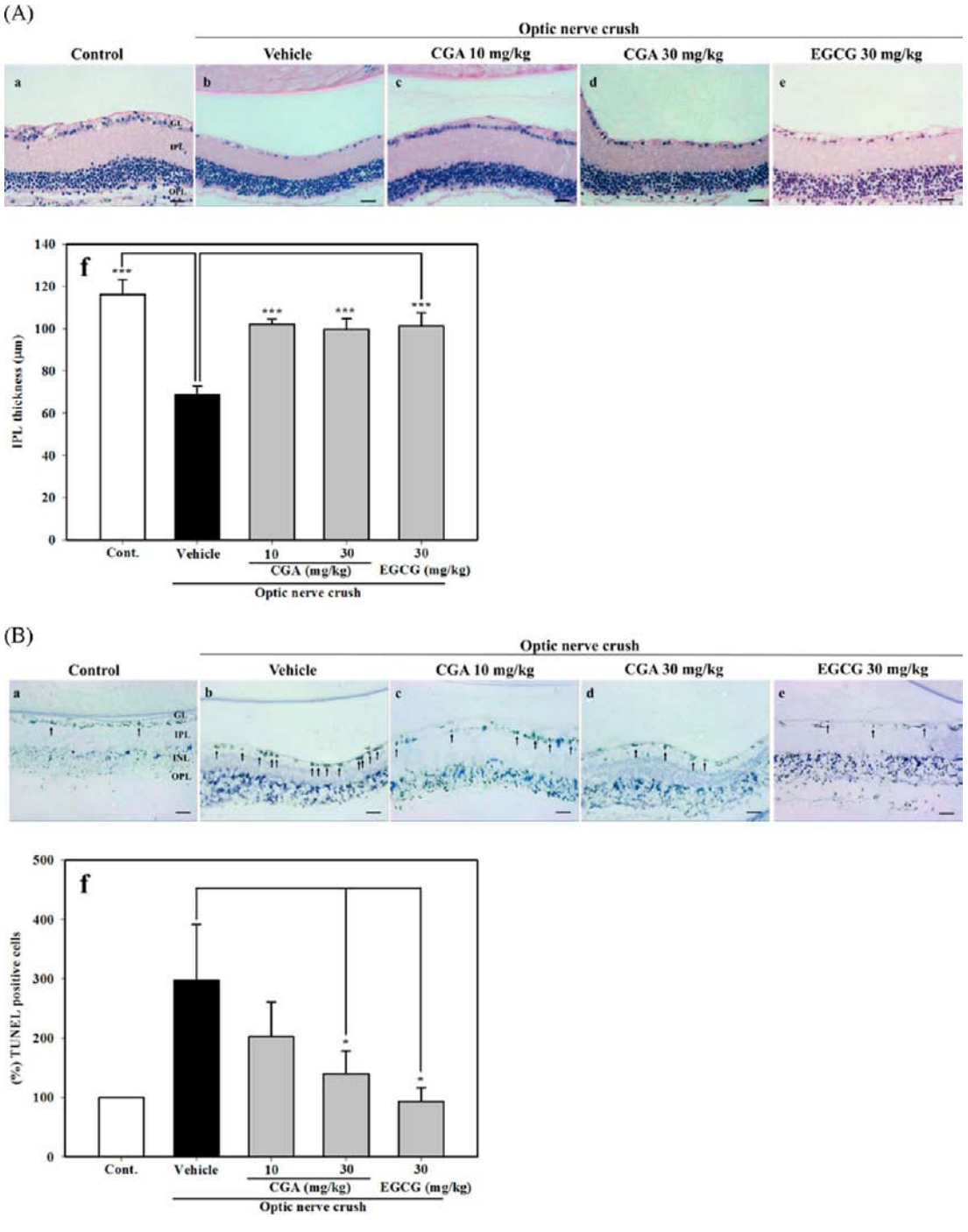

Figure 4. continued

dx.doi.org/10.1021/jf404285v | *J. Agric. Food Chem.* 2014, 62, 182−191

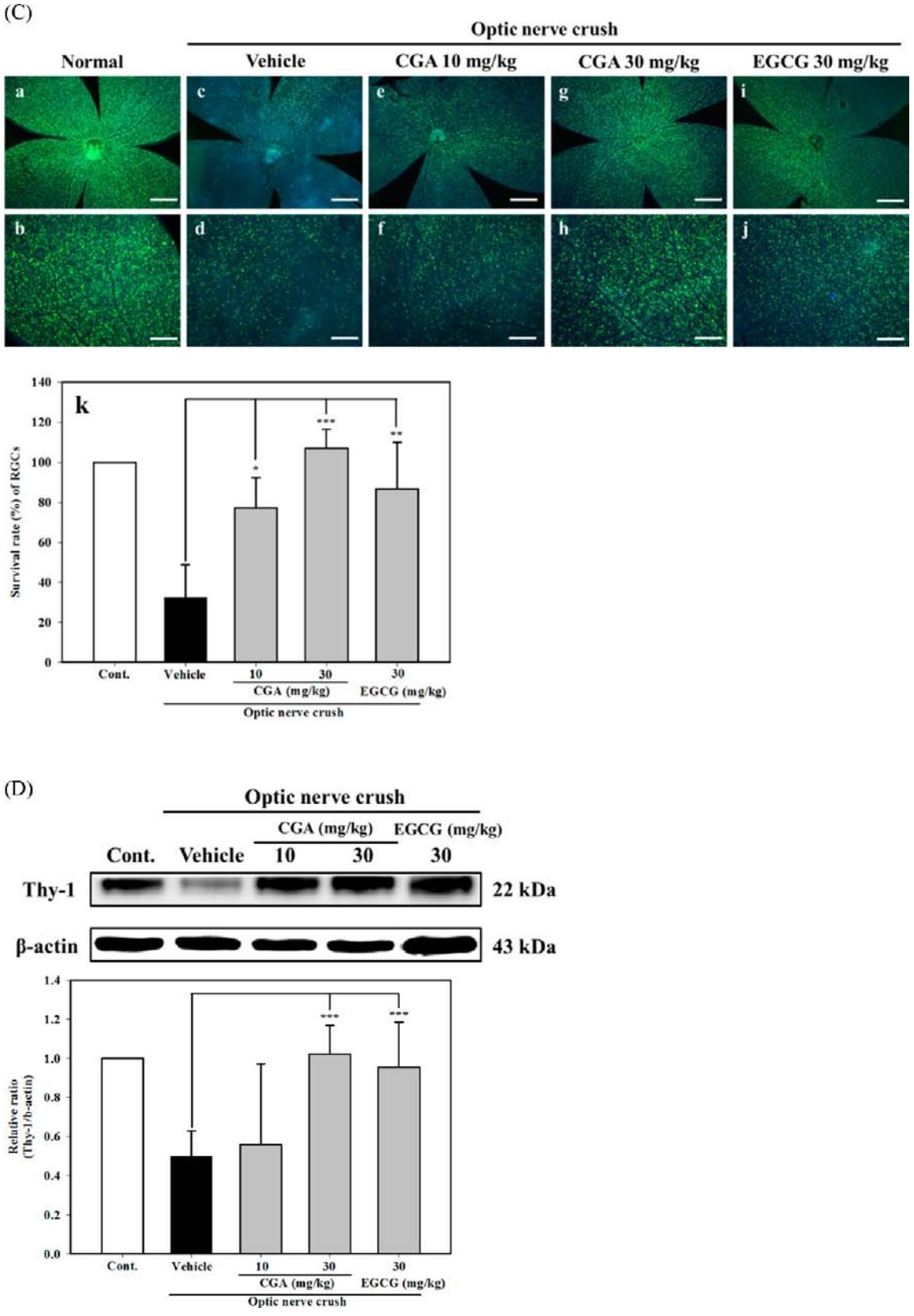

Figure 4. Optic nerve crush (ONC) experiments on the impacts of a CGA treatment on retinal tissues of mice. (A) Representative photomicrographs of tissues stained with hematoxylin and eosin. Tissues from (a) a control, (b) a mouse that underwent ONC only, (c) a mouse that underwent ONC and was treated with 10 mg/kg of CGA, (d) a mouse that underwent ONC and was treated with 30 mg/kg, and (e) a mouse that underwent ONC and was treated with 30 mg/kg of epigallocatechin gallate (EGCG). The thickness of IPL (f). Results are mean values, with error bar indicating mean SEM. Triple asterisks (***) indicate $p < 0.001$. (B) Representative photomicrographs of TUNEL-stained cells. Arrows indicate TUNEL-positive cells (brown stain). Scale bar = 50 μm. The quantification of TUNEL positive cells (f). Results are mean values with error bar indicating mean SEM. Single asterisk (*) indicates $p < 0.05$. (C) Representative micrographs showing Fluorogold-labeled retinal ganglion cells

dx.doi.org/10.1021/jf404285v | J. Agric. Food Chem. 2014, 62, 182−191

Figure 4. continued

(RGCs) harvested from mice 14 days after optic nerve crush (ONC). Retina from (a) an untreated control mouse, (c) a mouse that underwent ONC only, (e) a mouse that underwent ONC and was treated with 10 mg/kg of CGA, (g) a mouse that underwent ONC and was treated with 30 mg/kg of CGA, and (i) a mouse that underwent ONC and was treated with 30 mg/kg EGCG. Images in the lower row are 100× magnifications of the images above them; scale bars in the upper row represent 500 μm, while scale bars in the lower row represent 100 μm. (k) Quantitative analysis of the survival (%) rate of RGCs 14 days after ONC. Experimental values are expressed as mean SEM. Single asterisks (*) indicate $p < 0.05$; double asterisks (**) indicate $p < 0.01$; triple asterisks (***) indicate $p < 0.001$. (D) Results of Western blot analysis investigating Thy-1 expression in RGCs 14 days after the ONC procedure. Densitometric analysis of Thy-1 levels; data are shown as mean SEM. Single asterisks (*) indicate $p < 0.05$.

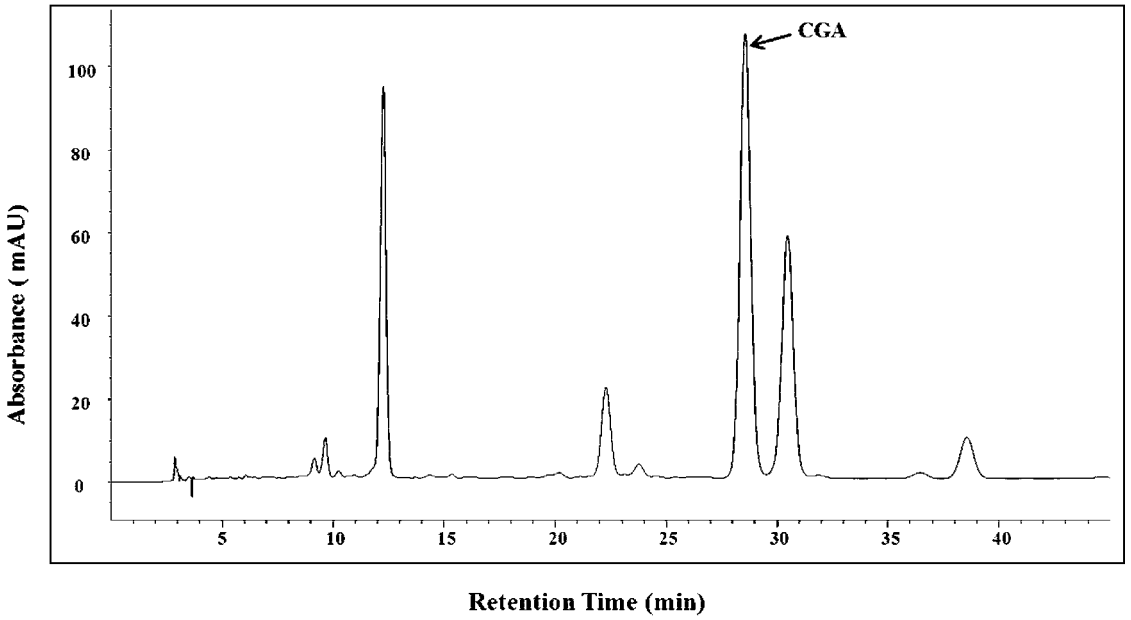

Figure 5. High-performance liquid chromatography analysis of coffee extract (prepared in 70% EtOH); ultraviolet detection was performed at 330 nm. The arrow indicates the peak corresponding to CGA.

Table 1. Calibration Curve, Correlation Coefficients, Limits of Detection (LOD), and Limits of Quantification (LOQ) of CGA

standard sample	range (μg/mL)	slope	intercept	R^2	LOD[a] (μg/mL)	LOQ[a] (μg/mL)
CGA	31.25−1000	24.226	167.56	1.0	7.67	23.26

[a]$n = 3$ replicates.

Table 2. Intra- and Interday Precision and Accuracy for the Determination of CGA

		intraday ($n = 3$)			interday ($n = 3$)		
stand sample	conc (μg/mL)	found conc (μg/mL) ± SD	recovery (%)	%RSD[a]	found conc (μg/mL) ± SD	recovery (%)	%RSD[a]
CGA	61.25	64.42 ± 0.94	103.07	1.46	61.60 ± 1.60	98.56	2.60
	125	126.88 ± 3.06	101.50	2.41	125.28 ± 0.45	100.22	0.36
	250	253.45 ± 6.51	101.38	2.57	246.47 ± 0.40	98.59	0.16

[a]RSD refers to the relative standard deviation.

The accuracy by mean recovery (%) for CGA ranged from 98.56 to 103.07% (Table 2), thus it can be accurately determined by this method from any small changes in the standard sample concentration.[57]

Effects of CE on Optic Nerve Crush-Induced Retinal Damage in Mouse. In addition to investigating the effects of pure CGA on retinal degeneration, we also explored whether CE, a major source of CGA, has similar benefits. As we observed in the CGA activity, lower levels of RGC death were found in control tissues (Figure 6A, a and b) than in those that were crushed but not treated with exogenous compounds (Figure 6A, c and d). In tissues treated with 50 mg/kg of CE, however, cell death was markedly reduced (Figure 6A, i and j). The protective effects of CE occur in a dose-dependent manner (Figure 6A, e−j). Likewise, while the 50 mg/kg CE treatment was associated with a preservation of Thy-1 expression, the 10- and 30 mg/kg CE treatments were less effective than the group of 50 mg/kg CE treatments (Figure 6B).

Based on the HPLC chromatogram of CE, we found 14.7 mg/g of CGA in CE. Although the amount of CGA in CE is less than the reported amount, the group of CE treatment shows similar protective effects with the CGA treatments (Figures 4C and 6A).[19]

Since significant amounts of CGA are metabolized in the human intestine and some phenolic metabolites of coffee are known to possess high antioxidant activity,[58] we expect that the

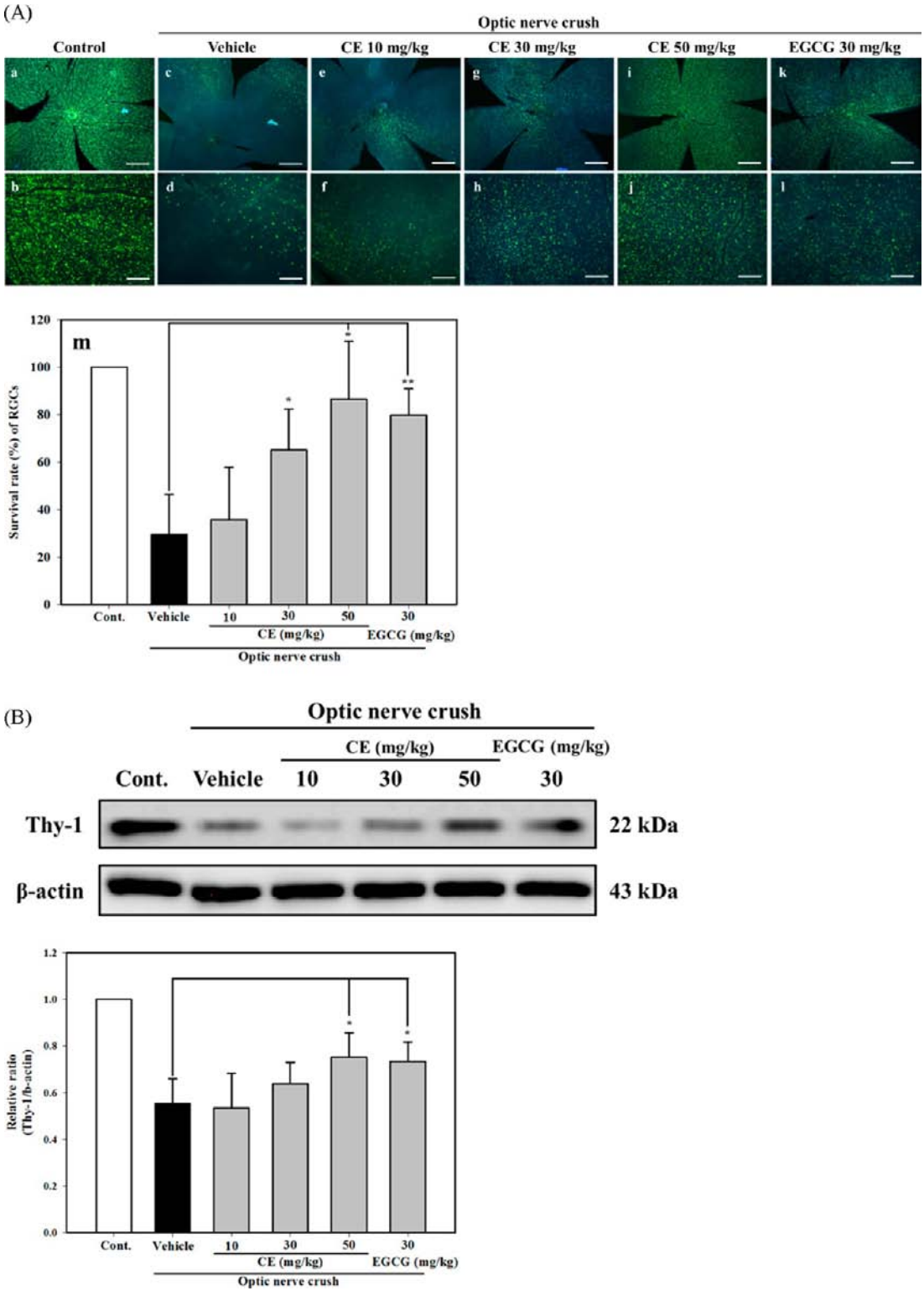

Figure 6. Optic nerve crush (ONC) experiments on the impacts of CE treatment on retinal tissues of mice. (A) Representative micrographs of Fluorogold-labeled tissues from (a) a control, (c) a mouse that underwent ONC, (e) a mouse that underwent ONC and was treated with 10 mg/kg of CE, (g) a mouse that underwent ONC and was treated with 30 mg/kg of CE, (i) a mouse that underwent ONC and was treated with 50 mg/kg of CE, and (k) a mouse that underwent ONC and was treated with 30 mg/kg EGCG. Images in the lower row are 100 × magnifications of the images in the row above them; scale bars in the upper row represent 500 μm, while scale bars in the lower row represent 100 μm. (m) Quantitative analyses of the survival (%) rate of RGCs 14 days after ONC. Experimental values are expressed as mean SEM. Single asterisks (*) indicate $p < 0.05$; double asterisks (**) indicate $p < 0.01$. (B) Results of Western blot analysis investigating Thy-1 expression in RGCs 14 days after the ONC procedure. Densitometric analysis of Thy-1 levels; data are shown as mean SEM. Single asterisks (*) indicate $p < 0.05$.

dx.doi.org/10.1021/jf404285v | J. Agric. Food Chem. 2014, 62, 182−191

additional bioactivities are originated from those metabolites. Therefore, the research on the protective effects of CGA and coffee metabolites on retina is being conducted.

In conclusion, this study shows that CGA and coffee extract are responsible for reduction of the RGC apoptosis induced by hypoxia and NO. Therefore, coffee consumption may provide additional health benefits by preventing retinal degeneration.

AUTHOR INFORMATION

Corresponding Authors

*E-mail: shjung507@gmail.com. Phone: +82-33-650-3653. Fax: +82-33-650-3679.

*E-mail: cyl1@cornell.edu. Phone: +1-607-255-0114. Fax: +1-607-254-4868.

Author Contributions

¶S.H.J. and C.Y.L. equally contributed to this article.

Funding

This work was financially supported by an intramural grant (2Z03943, 2Z03850) from the Korea Institute of Science and Technology (KIST), Republic of Korea.

Notes

The authors declare no competing financial interest.

ACKNOWLEDGMENTS

The RGC-5 cells were a generous gift from Alcon Research, Ltd.

ABBREVIATIONS

SNAP, *S*-nitroso-*N*-acethyl-DL-penicillamine; ONC, optic nerve crush; CGA, chlorogenic acid; CE, coffee extract; LOD, limit of detection; LOQ, limit of quantification; RGC, retinal ganglion cell; IOP, intraocular pressure; DCFH-DA, dichlorofluorescin diacetate; PI, propidium iodide; ARVO, Association for Research in Vision and Ophthalmology; HPLC, high-performance liquid chromatography; CPTIO, 2,4-carboxyphenyl-4,4,5,5-tetramethylimidazoline-1-oxyl-3-oxide; IPL, inner plexiform layer; GCL, ganglion cell layer; DMEM, Dulbecco's modified Eagle's medium; FBS, fetal bovine serum; NMDA, *N*-methyl-D-aspartate; NAC, *N*-acetyl-L-cysteine; NO, nitric oxide; DMSO, dimethyl sulfoxide; ROS, reactive oxygen species; PMSF, phenylmethylsulfonyl fluoride; PVDF, polyvinylidene difluoride; TdT, terminal deoxynucleotidyl transferase; TUNEL, terminal deoxynucleotidyl transferase dUTP nick end labeling; SEM, standard error of the mean; COX-2, cyclooxygenase-2; iNOS, inducible nitric oxide synthase

REFERENCES

(1) Ames, A. Energy requirements of CNS cells as related to their function and to their vulnerability to ischemia - a commentary based on studies on retina. *Can. J. Physiol. Pharmacol.* **1992**, *70*, S158−S164.

(2) Levin, L. A. Retinal ganglion cells and neuroprotection for glaucoma. *Surv. Ophthalmol.* **2003**, *48* (Suppl 1), S21−24.

(3) Sennlaub, F.; Courtois, Y.; Goureau, O. Inducible nitric oxide synthase mediates retinal apoptosis in ischemic proliferative retinopathy. *J. Neurosci.* **2002**, *22*, 3987−3993.

(4) Kaur, C.; Foulds, W. S.; Ling, E. A. Hypoxia-ischemia and retinal ganglion cell damage. *Clin. Ophthalmol.* **2008**, *2*, 879−889.

(5) Mozaffarieh, M.; Grieshaber, M. C.; Orgul, S.; Flammer, J. The potential value of natural antioxidative treatment in glaucoma. *Surv. Ophthalmol.* **2008**, *53*, 479−505.

(6) Losso, J. N.; Bawadi, H. A. Hypoxia inducible factor pathways as targets for functional foods. *J. Agric. Food Chem.* **2005**, *53*, 3751−3768.

(7) Lu, K. T.; Chiou, R. Y. Y.; Chen, L. G.; Chen, M. H.; Tseng, W. T.; Hsieh, H. T.; Yang, Y. L. Neuroprotective effects of resveratrol on cerebral ischemia-induced neuron loss mediated by free radical scavenging and cerebral blood flow elevation. *J. Agric. Food Chem.* **2006**, *54*, 3126−3131.

(8) Henry-Vitrac, C.; Ibarra, A.; Roller, M.; Merillon, J. M.; Vitrac, X. Contribution of chlorogenic acids to the inhibition of human hepatic glucose-6-phosphatase activity in vitro by Svetol, a standardized decaffeinated green coffee extract. *J. Agric. Food Chem.* **2010**, *58*, 4141−4144.

(9) Lou, Z.; Wang, H.; Zhu, S.; Ma, C.; Wang, Z. Antibacterial activity and mechanism of action of chlorogenic acid. *J. Food Sci.* **2011**, *76*, M398−403.

(10) Belkaid, A.; Currie, J. C.; Desgagnes, J.; Annabi, B. The chemopreventive properties of chlorogenic acid reveal a potential new role for the microsomal glucose-6-phosphate translocase in brain tumor progression. *Cancer Cell Int.* **2006**, *6*, 7.

(11) dos Santos, M. D.; Almeida, M. C.; Lopes, N. P.; de Souza, G. E. Evaluation of the anti-inflammatory, analgesic and antipyretic activities of the natural polyphenol chlorogenic acid. *Biol. Pharm. Bull.* **2006**, *29*, 2236−2240.

(12) Bouayed, J.; Rammal, H.; Dicko, A.; Younos, C.; Soulimani, R. Chlorogenic acid, a polyphenol from *Prunus domestica* (Mirabelle), with coupled anxiolytic and antioxidant effects. *J. Neurol. Sci.* **2007**, *262*, 77−84.

(13) Xu, J.-G.; Hu, Q.-P.; Liu, Y. Antioxidant and DNA-protective activities of chlorogenic acid isomers. *J. Agric. Food Chem.* **2012**, *60*, 11625−11630.

(14) Sato, Y.; Itagaki, S.; Kurokawa, T.; Ogura, J.; Kobayashi, M.; Hirano, T.; Sugawara, M.; Iseki, K. In vitro and in vivo antioxidant properties of chlorogenic acid and caffeic acid. *Int. J. Pharm.* **2011**, *403*, 136−138.

(15) Lee, K.; Lee, J. S.; Jang, H. J.; Kim, S. M.; Chang, M. S.; Park, S. H.; Kim, K. S.; Bae, J.; Park, J. W.; Lee, B.; Choi, H. Y.; Jeong, C. H.; Bu, Y. Chlorogenic acid ameliorates brain damage and edema by inhibiting matrix metalloproteinase-2 and 9 in a rat model of focal cerebral ischemia. *Eur. J. Pharmacol.* **2012**, *689*, 89−95.

(16) Kim, J.; Lee, S.; Shim, J.; Kim, H. W.; Kim, J.; Jang, Y. J.; Yang, H.; Park, J.; Choi, S. H.; Yoon, J. H.; Lee, K. W.; Lee, H. J. Caffeinated coffee, decaffeinated coffee, and the phenolic phytochemical chlorogenic acid up-regulate NQO1 expression and prevent H_2O_2-induced apoptosis in primary cortical neurons. *Neurochem. Int.* **2012**, *60*, 466−474.

(17) Clifford, M. N. Chlorogenic acids and other cinnamates - nature, occurrence, dietary burden, absorption and metabolism. *J. Sci. Food Agric.* **2000**, *80*, 1033−1043.

(18) Matei, M. F.; Jaiswal, R.; Kuhnert, N. Investigating the chemical changes of chlorogenic acids during coffee brewing: conjugate addition of water to the olefinic moiety of chlorogenic acids and their quinides. *J. Agric. Food Chem.* **2012**, *60*, 12105−12115.

(19) Farah, A.; de Paulis, T.; Moreira, D. P.; Trugo, L. C.; Martin, P. R. Chlorogenic acids and lactones in regular and water-decaffeinated arabica coffees. *J. Agric. Food Chem.* **2006**, *54*, 374−381.

(20) Olthof, M. R.; Hollman, P. C.; Katan, M. B. Chlorogenic acid and caffeic acid are absorbed in humans. *J. Nutr.* **2001**, *131*, 66−71.

(21) Monteiro, M.; Farah, A.; Perrone, D.; Trugo, L. C.; Donangelo, C. Chlorogenic acid compounds from coffee are differentially absorbed and metabolized in humans. *J. Nutr.* **2007**, *137*, 2196−2201.

(22) Farah, A.; Monteiro, M.; Donangelo, C. M.; Lafay, S. Chlorogenic acids from green coffee extract are highly bioavailable in humans. *J. Nutr.* **2008**, *138*, 2309−2315.

(23) Erk, T.; Williamson, G.; Renouf, M.; Marmet, C.; Steiling, H.; Dionisi, F.; Barron, D.; Melcher, R.; Richling, E. Dose-dependent absorption of chlorogenic acids in the small intestine assessed by coffee consumption in ileostomists. *Mol. Nutr. Food Res.* **2012**, *56*, 1488−1500.

(24) Ross, G. W.; Abbott, R. D.; Petrovitch, H.; Morens, D. M.; Grandinetti, A.; Tung, K. H.; Tanner, C. M.; Masaki, K. H.; Blanchette, P. L.; Curb, J. D.; Popper, J. S.; White, L. R. Association

of coffee and caffeine intake with the risk of Parkinson disease. *JAMA* **2000**, *283*, 2674−2679.
(25) van Dam, R. M.; Hu, F. B. Coffee consumption and risk of type 2 diabetes - a systematic review. *JAMA* **2005**, *294*, 97−104.
(26) Wilson, K. M.; Kasperzyk, J. L.; Rider, J. R.; Kenfield, S.; van Dam, R. M.; Stampfer, M. J.; Giovannucci, E.; Mucci, L. A. Coffee consumption and prostate cancer risk and progression in the Health Professionals Follow-up Study. *J. Natl. Cancer Inst.* **2011**, *103*, 876−884.
(27) Higdon, J. V.; Frei, B. Coffee and health: a review of recent human research. *Crit. Rev. Food Sci. Nutr.* **2006**, *46*, 101−123.
(28) van Gelder, B. M.; Buijsse, B.; Tijhuis, M.; Kalmijn, S.; Giampaoli, S.; Nissinen, A.; Kromhout, D. Coffee consumption is inversely associated with cognitive decline in elderly European men: the FINE Study. *Eur. J. Clin. Nutr.* **2007**, *61*, 226−232.
(29) Shukitt-Hale, B.; Miller, M.; Chu, Y.-F.; Lyle, B.; Joseph, J. Coffee, but not caffeine, has positive effects on cognition and psychomotor behavior in aging. *Age (Dordrecht, Neth.)* **2013**, 1−10.
(30) Chu, Y.-F.; Brown, P. H.; Lyle, B. J.; Chen, Y.; Black, R. M.; Williams, C. E.; Lin, Y.-C.; Hsu, C. W.; Cheng, I. H. Roasted coffees high in lipophilic antioxidants and chlorogenic acid lactones are more neuroprotective than green coffees. *J. Agric. Food Chem.* **2009**, *57*, 9801−9808.
(31) Pasquale, L. R.; Wiggs, J. L.; Willett, W. C.; Kang, J. H. The relationship between caffeine and coffee consumption and exfoliation glaucoma or glaucoma suspect: a prospective study in two cohorts. *Invest. Ophthalmol. Vis. Sci.* **2012**, *53*, 6427−6433.
(32) Jiwani, A. Z.; Rhee, D. J.; Brauner, S. C.; Gardiner, M. F.; Chen, T. C.; Shen, L. Q.; Chen, S. H.; Grosskreutz, C. L.; Chang, K. K.; Kloek, C. E.; Greenstein, S. H.; Borboli-Gerogiannis, S.; Pasquale, D. L.; Chaudhry, S.; Loomis, S.; Wiggs, J. L.; Pasquale, L. R.; Turalba, A. V. Effects of caffeinated coffee consumption on intraocular pressure, ocular perfusion pressure, and ocular pulse amplitude: a randomized controlled trial. *Eye (London)* **2012**, *26*, 1122−1130.
(33) Krishnamoorthy, R. R.; Agarwal, P.; Prasanna, G.; Vopat, K.; Lambert, W.; Sheedlo, H. J.; Pang, I. H.; Shade, D.; Wordinger, R. J.; Yorio, T.; Clark, A. F.; Agarwal, N. Characterization of a transformed rat retinal ganglion cell line. *Brain Res. Mol. Brain Res.* **2001**, *86*, 1−12.
(34) Van Bergen, N. J.; Wood, J. P. M.; Chidlow, G.; Trounce, I. A.; Casson, R. J.; Ju, W. K.; Weinreb, R. N.; Crowston, J. G. Recharacterization of the RGC-5 retinal ganglion cell line. *Invest. Ophthalmol. Vis. Sci.* **2009**, *50*, 4267−4272.
(35) Jung, S. H.; Kim, B. J.; Lee, E. H.; Osborne, N. N. Isoquercitrin is the most effective antioxidant in the plant *Thuja orientalis* and able to counteract oxidative-induced damage to a transformed cell line (RGC-5 cells). *Neurochem. Int.* **2010**, *57*, 713−721.
(36) Matsunaga, N.; Imai, S.; Inokuchi, Y.; Shimazawa, M.; Yokota, S.; Araki, Y.; Hara, H. Bilberry and its main constituents have neuroprotective effects against retinal neuronal damage in vitro and in vivo. *Mol. Nutr. Food Res.* **2009**, *53*, 869−877.
(37) Li, Y.; Schlamp, C. L.; Nickells, R. W. Experimental induction of retinal ganglion cell death in adult mice. *Invest. Ophthalmol. Vis. Sci.* **1999**, *40*, 1004−1008.
(38) Danias, J.; Lee, K. C.; Zamora, M. F.; Chen, B.; Shen, F.; Filippopoulos, T.; Su, Y. L.; Goldblum, D.; Podos, S. M.; Mittag, T. Quantitative analysis of retinal ganglion cell (RGC) loss in aging DBA/2NNia glaucomatous mice: Comparison with RGC loss in aging C57/BL6 mice. *Invest. Ophthalmol. Vis. Sci.* **2003**, *44*, 5151−5162.
(39) Sato, T.; Oku, H.; Tsuruma, K.; Katsumura, K.; Shimazawa, M.; Hara, H.; Sugiyama, T.; Ikeda, T. Effect of hypoxia on susceptibility of RGC-5 cells to nitric oxide. *Invest. Ophthalmol. Vis. Sci.* **2010**, *51*, 2575−86.
(40) Hwang, S. J.; Kim, Y. W.; Park, Y.; Lee, H. J.; Kim, K. W. Anti-inflammatory effects of chlorogenic acid in lipopolysaccharide-stimulated RAW 264.7 cells. *Inflamm. Res.* **2013**, 1−10.
(41) Mullen, W.; Nemzer, B.; Stalmach, A.; Ali, S.; Combet, E. Polyphenolic and hydroxycinnamate contents of whole coffee fruits from china, India, and Mexico. *J. Agric. Food Chem.* **2013**, *61*, 5298−5309.
(42) Huang, D. C.; Strasser, A. BH3-Only proteins-essential initiators of apoptotic cell death. *Cell* **2000**, *103*, 839−842.
(43) Franke, T. F.; Cantley, L. C. Apoptosis. A Bad kinase makes good. *Nature* **1997**, *390*, 116−117.
(44) Gross, A.; McDonnell, J. M.; Korsmeyer, S. J. BCL-2 family members and the mitochondria in apoptosis. *Genes Dev.* **1999**, *13*, 1899−1911.
(45) Cohen, G. M. Caspases: the executioners of apoptosis. *Biochem. J.* **1997**, *326* (Pt 1), 1−16.
(46) Fujita, N.; Nagahashi, A.; Nagashima, K.; Rokudai, S.; Tsuruo, T. Acceleration of apoptotic cell death after the cleavage of Bcl-XL protein by caspase-3-like proteases. *Oncogene* **1998**, *17*, 1295−1304.
(47) Condorelli, F.; Salomoni, P.; Cotteret, S.; Cesi, V.; Srinivasula, S. M.; Alnemri, E. S.; Calabretta, B. Caspase cleavage enhances the apoptosis-inducing effects of BAD. *Mol. Cell. Biol.* **2001**, *21*, 3025−3036.
(48) Keane, R. W.; Srinivasan, A.; Foster, L. M.; Testa, M. P.; Ord, T.; Nonner, D.; Wang, H. G.; Reed, J. C.; Bredesen, D. E.; Kayalar, C. Activation of CPP32 during apoptosis of neurons and astrocytes. *J. Neurosci. Res.* **1997**, *48*, 168−180.
(49) Kuida, K.; Zheng, T. S.; Na, S.; Kuan, C.; Yang, D.; Karasuyama, H.; Rakic, P.; Flavell, R. A. Decreased apoptosis in the brain and premature lethality in CPP32-deficient mice. *Nature* **1996**, *384*, 368−372.
(50) Levkovitch-Verbin, H.; Quigley, H. A.; Kerrigan-Baumrind, L. A.; D'Anna, S. A.; Kerrigan, D.; Pease, M. E. Optic nerve transection in monkeys may result in secondary degeneration of retinal ganglion cells. *Invest. Ophthalmol. Vis. Sci.* **2001**, *42*, 975−982.
(51) Huang, W.; Fileta, J.; Guo, Y.; Grosskreutz, C. L. Down-regulation of Thy1 in retinal ganglion cells in experimental glaucoma. *Curr. Eye Res.* **2006**, *31*, 265−271.
(52) Kreutz, M. R.; Seidenbecher, C. I.; Sabel, B. A. Molecular plasticity of retinal ganglion cells after partial optic nerve injury. *Restor. Neurol. Neurosci.* **1999**, *14*, 127−134.
(53) Schuettauf, F.; Rejdak, R.; Thaler, S.; Bolz, S.; Lehaci, C.; Mankowska, A.; Zarnowski, T.; Junemann, A.; Zagorski, Z.; Zrenner, E.; Grieb, P. Citicoline and lithium rescue retinal ganglion cells following partial optic nerve crush in the rat. *Exp. Eye Res.* **2006**, *83*, 1128−1134.
(54) Kermer, P.; Klocker, N.; Labes, M.; Thomsen, S.; Srinivasan, A.; Bahr, M. Activation of caspase-3 in axotomized rat retinal ganglion cells in vivo. *FEBS Lett.* **1999**, *453*, 361−364.
(55) Kermer, P.; Ankerhold, R.; Klocker, N.; Krajewski, S.; Reed, J. C.; Bahr, M. Caspase-9: involvement in secondary death of axotomized rat retinal ganglion cells in vivo. *Brain Res. Mol. Brain Res.* **2000**, *85*, 144−150.
(56) Magharious, M.; D'Onofrio, P. M.; Hollander, A.; Zhu, P.; Chen, J.; Koeberle, P. D. Quantitative iTRAQ analysis of retinal ganglion cell degeneration after optic nerve crush. *J. Proteome Res.* **2011**, *10*, 3344−3362.
(57) Lim, S. S.; Lee, M. Y.; Ahn, H. R.; Choi, S. J.; Lee, J. Y.; Jung, S. H. Preparative isolation and purification of antioxidative diarylheptanoid derivatives from *Alnus japonica* by high-speed counter-current chromatography. *J. Sep. Sci.* **2011**, *34*, 3344−3352.
(58) Gomez-Ruiz, J. A.; Leake, D. S.; Ames, J. M. In vitro antioxidant activity of coffee compounds and their metabolites. *J. Agric. Food Chem.* **2007**, *55*, 6962−6969.

JOURNAL OF AGRICULTURAL AND FOOD CHEMISTRY

Article

pubs.acs.org/JAFC

Variations in the Efficacy of Resistant Maltodextrin on Body Fat Reduction in Rats Fed Different High-Fat Models

Hui-Fang Chu,[†,∥] Min-Hsiung Pan,[§] Chi-Tang Ho,[‡] Yu-Han Tseng,[†] William Wei-Li Wang,[†] and Chi-Fai Chau*[,†,⊥]

[†]Department of Food Science and Biotechnology, National Chung Hsing University, Taichung 40227, Taiwan

[‡]Department of Food Science, Rutgers University, New Brunswick, New Jersey 08901, United States

[§]Institute of Food Science and Technology, National Taiwan University, Taipei, 10617, Taiwan

[∥]Standard Chem. Pharm. Co., Ltd., 154 Kaiyuan Road, Sinying City, Tainan County 73055, Taiwan

[⊥]Agricultural Biotechnology Center, National Chung Hsing University, 250 Kuo-Kuang Road, Taichung 40227, Taiwan

ABSTRACT: Many studies have utilized a variety of methods to induce obesity in rodents, but they often received inconsistent results. The present study intended to use resistant maltodextrin (RMD) as a means to investigate the variations in its efficacy on body fat accumulation under the influence of four high-fat (HF) models of 23% or 40% total fat, comprising soybean oil, lard, and/or condensed milk. Results indicated that integrating condensed milk into the diets could help increase diet intake, boost energy intake, increase weight gain, and enhance fat formation. Supplementation of RMD (2.07 g/kg) notably reduced total body fat levels in three HF models, with the exception of a condensed-milk-added 40%-fat diet that may have misrepresented the functions of RMD. The uses of the 23% HF diets, with and without milk, and the milk-free 40% HF diet were therefore recommended as suitable models for antiobesity evaluations of RMD, or other fiber-rich products.

KEYWORDS: *Resistant maltodextrin, body fat, high-fat diet*

INTRODUCTION

Obesity is a medical condition that facilitates the development of metabolic disorders including diabetes, hypertension, and cardiovascular disease.[1] In recent decades, many studies, including human trials and animal tests, have been widely performed to investigate the relationship between dietary lipid absorption and body fat accumulation, in hopes of finding ways to reduce lipid absorption and body weight.[2−4]

To study the mechanisms involved in body fat reduction, obese rodent models are commonly used. A variety of methods have been developed to induce obesity in rodents. For example, obesity could be induced by feeding them fat-enriched, high-sugar, or high-calorie diets. Among these diet choices, a high-fat (HF) diet was commonly used to induce obesity in rodents. A wide range of fat contents, ranging from 10% to 63% (w/w), have been used in different studies, with fat contents around 23% and 40% being the two most frequently used models.[5] Dietary lipid types also varied between animal-derived fats (e.g., lard or beef tallow) and plant oils (e.g., corn or safflower oil) in previous studies. In some studies, a portion of condensed milk or fructose was also added into the HF diets to help induce obesity.[6,7] However, different combinations of fat contents and fat types have been found to induce diversified increases in body fat, ranging from 38% to 169%.[8,9]

In the past few decades, the potential inhibitory effects of many food ingredients on lipid absorption and its accumulation in body have been investigated, but the results have not always been consistent.[8−12] For instance, though green tea (at 1−3 mg/kg per day) has commonly been reported to have body-fat-reducing effects, contradicting results were observed between rats fed a 15%-fat HF diet and those fed a 30%-fat HF diet.[12,13] It was therefore speculated from these studies that different HF feeding models could lead to different outcomes to the assessments of the same ingredient.

New ingredients possessing potential for body fat-reducing effect have been reported in recent years. Resistant maltodextrin (RMD), as one of the candidates, is a type of colorless and tasteless water-soluble fiber, composed of short-chain glucose polymers that are resistant to digestion in the human digestive system. Studies have reported that RMD could delay absorption of carbohydrates, reduce dietary lipid absorption and serum triglyceride level, and suppress elevation of postprandial blood glucose.[14−17] Its high stability against temperature variations and acidic conditions has driven RMD to become a popular water-soluble fiber component in many nutritional supplements.

The present study intends to use RMD as a means to demonstrate and compare the various possible influences of different HF diet compositions on body fat accumulation in rats. In particular, the variations in the efficacy of RMD in different HF dietary models will be accurately evaluated and discussed. Relationships between different HF diets and food intake, body weight, visceral fat, or total body fat will also be addressed.

Received: October 25, 2013
Revised: December 7, 2013
Accepted: December 8, 2013
Published: December 9, 2013

ACS Publications © 2013 American Chemical Society

dx.doi.org/10.1021/jf404809v | *J. Agric. Food Chem.* 2014, 62, 192−197

Table 1. Compositions of the Normal Chow Diet and the Experimental High-Fat Diets

	23% fat high fat diet[a]			23% fat high fat diet (with condensed milk)[a]			40% fat high fat diet[a]			40% fat high fat diet (with condensed milk)[a]			normal chow diet[b]
ingredient (g/100 g diet)	23-C	23-1xF	23-2xF	23M-C	23M-1xF	23M-2xF	40-C	40-1xF	40-2xF	40M-C	40M-1xF	40M-2xF	(ND)
chow	81	81	81	52	52	52	63	63	63	29	29	29	100
oil	4	4	4	5	5	5	10	10	10	12	12	12	
lard	15	15	15	13	13	13	27	27	27	24	24	24	
condensed milk[c]				30	30	30				30	30	30	
casein										5	5	5	
supplementation of RMD (g/kg bw)[d]		1.03	2.07		1.03	2.07		1.03	2.07		1.03	2.07	
carbohydrate	39	39	39	42	42	42	31	31	31	30	30	30	49
fat	23	23	23	23	23	23	40	40	40	40	40	40	5
protein	19	19	19	14	14	14	14	14	14	14	14	14	23

[a]High-fat basal diet groups (23-C, 23M-C, 40-C, and 40M-C) were used as controls for their corresponding RMD-supplemented groups including low doses (23-1xF, 23M-1xF, 40-1xF, and 40M-1xF, respectively) and high doses (23-2xF, 23M-2xF, 40-2xF, and 40M-2xF, respectively). [b]Chow (PMI Nutrition International, St. Louis, MO) contained crude protein (23.0 g/100 g), crude lipid (4.5 g/100 g), and carbohydrate (72.5 g/100 g). [c]Condensed milk contained crude protein (7.3 g/100 g), crude lipid (8.2 g/100 g), and carbohydrate (84.5 g/100 g). [d]The energies of 23-C, 23M-C, 40-C, and 40M-C diets were 443.2, 432.4, 544.7, and 517.1 kcal/100 g, respectively, while that of ND diet was 336 kcal/100 g.

Table 2. Effects of Different High Fat Diets on Food Intake, Energy Intake, Fat Intake, Body Weight Gain, and Feed Efficiency in Rats[a]

	23% fat high fat diet			23% fat high fat diet (with condensed milk)			40% fat high fat diet			40% fat high fat diet (with condensed milk)			normal chow diet
	23-C	23-1xF	23-2xF	23M-C	23M-1xF	23M-2xF	40-C	40-1xF	40-2xF	40M-C	40M-1xF	40M-2xF	(ND)
food intake[b] (g)	1272m	1258	1268	1428n	1427	1401	1042o	1040	1030	1339p	1232	1253	1509n
energy intake (kcal)	5632m	5575	5619	6168n	6164	6051	5677m	5667	5615	6925o	6372	6478	5071p
fat intake[b] (g)	292m	289	292	328n	328	322	417o	416	412	536p	493	501	76q
body weight gain[b] (g)	277mn	267	259	299n	296	277	260m	260	253	299n	278	280	196o
feed efficiency[b]	21.7m	21.1	20.4	20.9m	20.9	19.8	25.0n	25.0	24.5	22.4n	22.5	22.3	13.0o

[a]Values with different letters (m−q) among the five diets (23-C, 23M-C, 40-C, 40M-C, and ND) are significantly different (Duncan, $p < 0.05$). [b]Data are expressed as mean ($n = 8$).

MATERIALS AND METHODS

Experimental Diets and Design. One hundred and four male Sprague−Dawley rats (6 weeks old) weighing 137 ± 5 g were purchased from the National Laboratory Animal Center (Taipei, Taiwan). The animals were individually housed in stainless steel screen-bottomed cages and placed in a room maintained at 22 ± 2 °C with a 12-h light/dark cycle. After a two-week acclimation period, the rats were divided into eight weight classes of thirteen animals each. The rats in each weight class were randomly assigned to one of the thirteen diet groups, including one normal chow diet (ND), and twelve HF diet experimental groups.

The compositions of the ND diet and twelve high-fat experimental diets are shown in Table 1. All HF diets contained either 23% or 40% (w/w) total fat contents. The HF diet groups included soybean oil and lard, with or without condensed milk. Specifically, the twelve high-fat diets were designed for 4 distinct HF-diet arrangements (namely, 23, 23M, 40, and 40M), each with its own experimental control (-C) group, low-dose treatment (-1xF) group, and high-dose treatment (-2xF) group. In more detail, the twelve HF-diet groups comprised three groups (23-C, 23-1xF, and 23-2xF) receiving 23%-fat diets without condensed milk, three groups (23M-C, 23M-1xF, and 23M-2xF) receiving 23%-fat diets with condensed milk, three groups (40-C, 40-1xF, and 40-2xF) receiving 40%-fat diets without condensed milk, and three groups (40M-C, 40M-1xF, and 40M-2xF) receiving 40%-fat diets with condensed milk. Animals in all -1xF groups received a single dose of RMD (1.03 g/kg body weight) each day, and each animal in the -2xF groups was given a double dose of RMD (2.07 g/kg body weight) every day. The doses of RMD (at 1.03 and 2.07 g/kg) are approximately equivalent to 10 and 20 g/day, respectively, for a 60-kg human. These dose equivalents are in accordance with body surface area calculation as recommended by the U.S. FDA.[18] The actual amounts of RMD supplement for the rats were constantly recalculated every three days to adjust for changes in body weights throughout the test period.

Animals were allowed free access to food and water during the experimental period. Food intake and body weights were recorded daily. At the end of the experimental period, animals were anesthetized by carbon dioxide after fasting for 12 h. After blood samples were drawn from the orbital sinus, the anesthetized rats were sacrificed by exsanguination. The visceral fat pads were immediately excised, blot dried, and weighed. The coats were shaved and the remaining carcasses were then weighed and stored at −20 °C until analysis. The institutional guidelines for the care and use of laboratory animals were carefully followed. This study protocol was approved by the Institutional Animal Care and Use Committee of National Chung Hsing University.

Feed Efficiency. Feed efficiency was determined after 8 weeks on the experiment diets for each rat using the following formula:

$$\text{Feed efficiency} = \text{body weight gained (g)} / \text{food intake (g)} \times 100$$

Measurement of Total Visceral Fat. Total visceral fat was defined as the sum of the mesenteric, epididymal, and perirenal fat depots.[19] All fat along the mesentery starting at the lesser curvature of the stomach and ending at the sigmoid colon was considered mesenteric fat. At sacrifice, the mesenteric, epididymal, and perirenal fat depots were dissected from the rats and weighed before freezing.

$$\text{Visceral fat\%} = \text{total visceral fat (g)} / \text{final body weight (g)} \times 100$$

Measurement of Crude Carcass Fat. For the present study, the carcass was defined as the entire shaved rat torso minus the visceral fat

dx.doi.org/10.1021/jf404809v | J. Agric. Food Chem. 2014, 62, 192−197

Figure 1. Effects of different diet models on visceral fat mass in control groups. (A) Epididymal fat of normal diet (ND) group; (B) peri-renal fat of normal diet (ND) group; (C) epididymal fat of nonmilk 23%-fat control (23-C) group; (D) peri-renal fat of nonmilk 23%-fat control (23-C) group; (E) epididymal fat of milk-containing 23%-fat control (23M-C) group; (F) peri-renal fat of milk-containing 23%-fat control (23M-C) group; (G) epididymal fat of nonmilk 40%-fat control (40-C) group; (H) peri-renal fat of nonmilk 40%-fat control (40-C) group; (I) epididymal fat of milk-containing 40%-fat control (40M-C) group; (J) peri-renal fat of milk-containing 40%-fat control (40M-C) group.

pads removed during sacrifice. Following the method of Janis et al. with slight modifications, rat carcasses were dried at 80 °C for 4 h, followed by drying at 105 °C for another 24 h.[20] Dried carcasses were weighed and ground individually without deboning. Furthermore, fat extractions were performed on all shaved coats and the carcasses. Following the AOAC method with slight modifications, carcass fats were extracted from the dried carcass powder by ether (1:20, w/v), and total crude carcass fats were quantified gravimetrically after evaporating the solvents in the lipid extracts.[21]

$$\text{Carcass fat\%} = \text{crude carcass fat (g)} / \text{final body weight (g)} \times 100$$

Determination of Body Fat Percentage. Total body fat was defined as the sum of total visceral fat and crude carcass fat. Body fat percentage of each rat was therefore calculated using the following formula:

$$\text{Body fat (\%)} = (\text{visceral fat (g)} + \text{crude carcass fat (g)}) / \text{final body weight(g)} \times 100$$

Statistical Analysis. All experiments were performed on groups of eight animals. Data are presented as means ± standard deviation. Numerical data were analyzed with SPSS 19.0 statistics software (Chicago, IL, USA). The significance level was set to $p < 0.05$ (Duncan).

RESULTS

The food intakes, energy intakes, fat intakes, body weight gains, and feed efficiencies of the animals fed the different diets are shown in Table 2. After the acclimation period, there were no differences in the initial body weights (249−280 g) among the thirteen dietary groups. Throughout eight weeks of observation, all animals remained healthy and active. All animals on the four HF control diets (i.e., 23-C, 23M-C, 40-C, and 40M-C) consumed lesser amounts of feed (−5 to −31%) cumulatively than the ND group (1509 g). Feed consumptions for the 40%-fat groups (40-C and 40M-C) were lower than those of the 23%-fat groups (23-C and 23M-C, respectively). Owing to the higher energy density in the 40%-fat diets (Table 1), the actual fat and energy intakes in the 40%-fat groups were significantly higher, demonstrating that the actual energy intake could be a collective consequence of the consumption level and energy density. Furthermore, it was also noted that the incorporation of condensed milk into the HF diets might help increase food intakes. Total energy intakes (6051−6925 kcal) for all six condensed milk-feeding groups were higher than those (5575−5677 kcal) of the other milk-free HF groups.

In terms of the body weight changes during the experimental period, all four HF control groups gained significantly ($p < 0.05$) more weight (133−153%) than the ND group due to higher fat intake in these HF groups. Similarly, the feed efficiencies of the four HF control diets (20.9−25.0) were significantly ($p < 0.05$) higher than that of ND diet (13.0) (Table 2). The results revealed that fat intake and feed efficiency were positively correlated. It seemed that the fat component was a major factor affecting the feed efficiency while both condensed milk and RMD supplementation only led to some slight but consistent decreases in feed efficiencies.

The apparent differences in visceral fat sizes are visually presented in Figure 1. The organs were removed before the measurement of fat mass. The ND control group was shown to have the lowest fat mass in the epididymal and peri-renal area (Figure 1A and B), while all four HF diet control groups had greater fat mass than ND, with the milk-containing 40%-fat diet (40M-C) control group showing the greatest fat mass in the same visceral area (Figure 1I and J). More specifically, Table 3 shows that the visceral accumulations of fat in four HF control groups were all markedly ($p < 0.05$) higher (1.6- to 2.4-fold)

Table 3. Effects of the Administration of RMD on Visceral Fat Percentage[a]

	high-fat controls[b]	RMD treatment groups[c]	
treatment	(without RMD)	low dose (1.03 g/kg bw)	high dose (2.07 g/kg bw)
23% fat	9.9 ± 1.0nx	9.5 ± 0.7xy	8.6 ± 1.0y
23% fat (with condensed milk)	13.5 ± 1.3ox	12.4 ± 1.0x	10.5 ± 0.7y
40% fat	13.0 ± 1.2ox	12.6 ± 1.5x	10.9 ± 1.5y
40% fat (with condensed milk)	15.5 ± 1.7px	15.5 ± 0.9x	15.3 ± 1.0x

[a]Data are expressed as mean ± standard derivation ($n = 8$). [b]The visceral fat percentage of the ND group (6.4 ± 1.4%) was significantly ($p < 0.05$) lower than that of all high-fat controls. Values with different letters (n−p) in the high-fat control column are significantly different (Duncan, $p < 0.05$). [c]Values in the same row with different letters (x−y) are significantly different (Duncan, $p < 0.05$).

than that of the ND group (6.4%). The visceral fats of 40%-fat HF controls (40-C and 40M-C) were significantly ($p < 0.05$) higher than those of the 23%-fat controls (23-C and 23M-C, respectively). The incorporation of condensed milk in both the 23%- and 40%-fat diets led to significant ($p < 0.05$) increases in visceral fat (1.36- and 1.19-fold, respectively) against their corresponding milk-free diets. Furthermore, our results revealed that the administration of RMD at a high dose (2.07 g/kg) could result in significant ($p < 0.05$) reductions in the levels of visceral fat (−13% to −22% against the controls) among different HF models excluding the 40M model.

Moreover, the effects of RMD administration on crude carcass fat (nonvisceral fat) accumulation are demonstrated in Table 4. Similar to the findings in the visceral fat, the carcass fat accumulations in all four HF control groups were significantly ($p < 0.05$) higher (1.67- to 2.0-fold) than that of the ND group (3.3%). Among the four HF controls, the 40%-fat diet with condensed milk was again the most effective model in accumulating fat (6.6%). In the other three models (i.e., 23-C, 23M-C, and 40-C), different amounts of fat consumption (292−417 g) and total energy intakes (5635−6359 kcal) (Table 2) merely led to comparable levels of carcass fat accumulation (5.5% to 5.8%). Nonetheless, administration of RMD at 2.07 g/kg was again able to significantly reduce ($p < 0.05$) the carcass fat (−16% to 28% against the controls) in different HF models, except the 40M model. It was interesting to note that RMD was similarly more effective in reducing the carcass fat in diets without condensed milk. These results reaffirmed that the ability of RMD in reducing fat accumulation was basically affected by dietary compositions such as fat content and condensed milk.

Lastly, the present study also compared total body fat in the animals as a sum of total visceral fat and crude carcass fat. As shown in Figure 2, the total body fat accumulations in all four HF control groups were significantly ($p < 0.05$) higher (1.3- to 2.3-fold) than that of the ND group (9.7%), with a visceral-to-carcass fat ratio of approximately 2:1. Higher levels of body fat ($p < 0.05$) were observed for groups with higher dietary fat consumption as well as with condensed milk. Specifically, the effectiveness of the four HF controls in inducing the accumulations of total body fat was ranked as follows: 40M-C (22.1%) > 23M-C (19.0%) ≥ 40-C (18.8%) > 23-C (15.7%), demonstrating that HF diets with condensed milk could produce greater amounts of body fat than HF diets alone, regardless of fat content. In contrast, the ability of RMD in reducing body fat accumulation declined in the reverse order,

Table 4. Effects of the Administration of RMD on Crude Carcass Fat Percentage[a]

treatment	high fat controls[b] (without RMD)	RMD groups[c] low dose (1.03 g/kg bw)	RMD groups[c] high dose (2.07 g/kg bw)
23% fat	5.8 ± 0.4nx	5.5 ± 0.6x	4.2 ± 0.5y
23% fat (with condensed milk)	5.5 ± 0.5nx	5.2 ± 0.5x	4.6 ± 0.5y
40% fat	5.8 ± 0.5nx	5.6 ± 0.5x	4.7 ± 0.4y
40% fat (with condensed milk)	6.6 ± 0.9ox	6.3 ± 0.3x	6.5 ± 0.8x

[a]Data are expressed as mean ± standard derivation ($n = 8$). [b]The carcass fat percentage of the ND group (3.3 ± 0.8%) was significantly ($p < 0.05$) lower than that of all high-fat controls. Values with different letters (n−o) in the high-fat control column are significantly different (Duncan, $p < 0.05$). [c]Values in the same row with different letters (x−y) are significantly different (Duncan, $p < 0.05$).

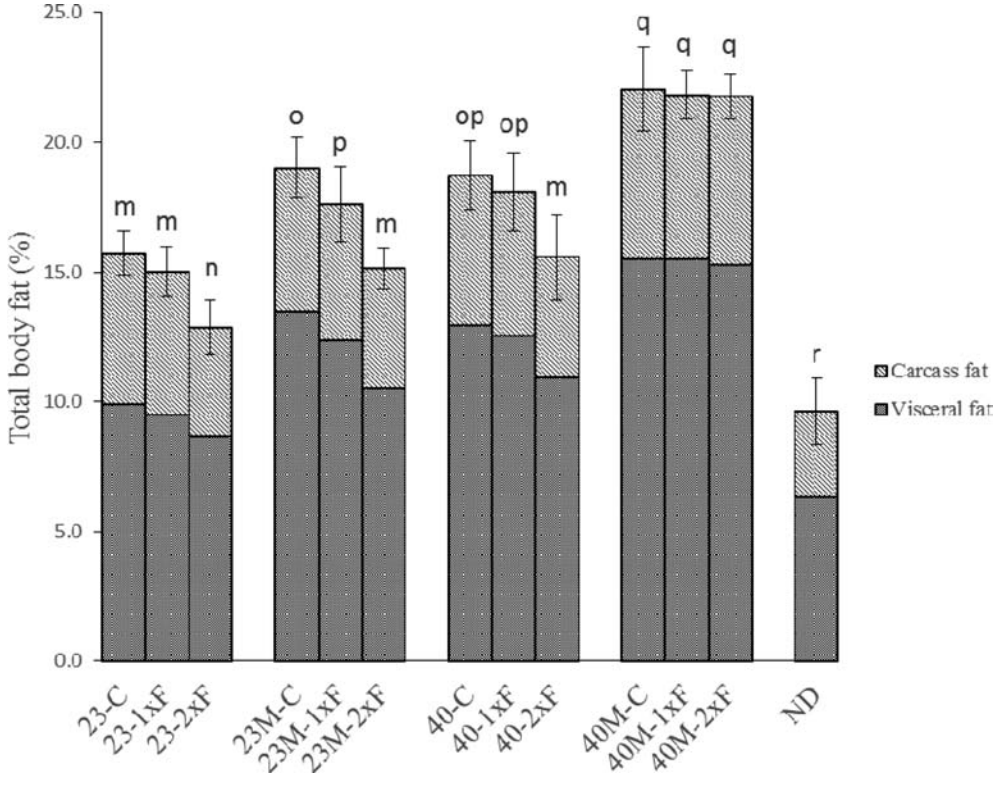

Figure 2. Effects of different diet groups on total body fat percentage. Bars with different letters (m−r) are significantly different (Duncan, $p < 0.05$).

dx.doi.org/10.1021/jf404809v | J. Agric. Food Chem. 2014, 62, 192−197

with the 40M diets showing the least body fat reduction after the RMD supplementation.

DISCUSSION

From many in vivo studies on the abilities of various ingredients to affect accumulation of body fat, a multitude of high-fat diets with fat levels between 10 and 63% have been used. Total fat contents of 23% and 40% were chosen for this study based on the prevalence of common fat levels used in previous studies.[5] Condensed milk has also been incorporated into two of the experimental models as an extra palatable component, since such a supplementation was practiced in some high-fat studies, for the purposes of boosting dietary intake and levels of obesity.[5,22] In addition, after comparing the nutrient profiles of the experimental diets to the estimated nutrient requirements, casein was incorporated into the 40 M diet to compensate for the protein content for the maintenance of the rats.

After feeding the rats for eight weeks, the findings in our study agreed with the observations that both the dietary fat level and uses of condensed milk played important roles in total body fat accumulation.[6,14] The consumption of condensed milk was actually found to be associated with higher body fat levels (Table 3), though the 23%-fat (with condensed milk) and 40%-fat groups were found to have similar amounts of visceral fat. Such a connection between palatable dietary component and visceral fat formation has previously been reported in some other studies.[22,23] Therefore, it was inferred that the addition of condensed milk (84.5% carbohydrate) would induce obesity more effectively in rats through improving feed and energy intake, and the combination of condensed milk and high levels of dietary fat might have a concrete effect on boosting the visceral fat accumulation of a 23%-fat diet to a level comparable to that of a milk-free 40%-fat diet.

Kishimoto et al. has suggested that resistant maltodextrin could potentially suppress lipid absorption and promote lipid excretion by inhibiting the decomposition of micelles and the release of fatty acids from micelles in the lipid absorption process.[15] Similarly, our results demonstrated that long-term consumption of RMD at 2.07 g/kg under various high-fat models (excluding the 40% fat diet with condensed milk) could be promising in reducing the body fat effectively ($p < 0.05$) (Figure 2). The works from other authors have also proclaimed the efficacy of resistant maltodextrin on body fat accumulation. In 2004, Okuma and Kishimoto asserted that persistent RMD consumption could significantly decrease body fat ratio and body fat area in obese objects.[17] Later in 2007, Gordon has reported that providing 30 g of RMD to overweight hyperlipidemia patients in addition to their daily regular diet could significantly reduce body fat ratio and the area of visceral and subcutaneous fats, though total weight did not significantly decline, in three months.[24] More recently, Hashizume et al. also recorded that providing metabolic syndrome patients with 27 g of RMD for 12 weeks in addition to their normal diet could significantly decrease waist circumference and visceral fat area.[25] The consistency of these studies reinforced our observations on the efficacy of RMD on body fat reduction.

Nonetheless, our results also suggested that the promotional effects of condensed milk plus high fat (i.e., 40 M groups) might have been too effective in inducing body fat accumulation, which then resulted in the diminishment of the fat-reduction capability of the high dose RMD supplement. In other words, the functions of RMD might be underestimated and misrepresented in a 40%-fat diet model when used with condensed milk. Thus, it should be noted that the 40M diet model might be a nutrient-wise extreme diet, with micronutrient contents close to the minimum limit of daily requirement, for inducing obesity, and thus it should not be considered as an appropriate model for the above-mentioned evaluation of RMD at the present dosages.

In sum, it was concluded from our results that the composition of HF models could affect the consistency of the evaluations of a sample's efficacy for comparison purposes. Both 23%-fat models (with and without condensed milk) and the 40%-fat diet without condensed milk can be considered as suitable experimental models for body fat reduction assessment trials of RMD or other fiber-rich products. However, since the recommended daily total fat intake for adults (ages 19 and older) is between 20 and 35% of dietary calories according to the USDA,[26] having 40% fat in an experimental diet (equivalent to about 67% of dietary calories) is in fact considered extremely high for attempting to mimic the actual dietary patterns of the general population. Thus, when shorter periods of obesity-induction or greater levels of body fat formation were desired, the inclusion of condensed milk in HF diets (around 23% dietary fat) could be considered over milk-free HF diets.

AUTHOR INFORMATION

Corresponding Author

*Phone: (886)-4-22852420. Fax: (886)-4-22876211. E-mail: chaucf@nchu.edu.tw. Mail: Department of Food Science and Biotechnology, National Chung Hsing University, 250 Kuokuang Road, Taichung 40227, Taiwan.

Notes

The authors declare no competing financial interest.

ACKNOWLEDGMENTS

We appreciate Sina Vakili for his technical support. This work is supported in part by the Ministry of Education, Taiwan, ROC, under the ATU plan.

ABBREVIATIONS USED

HF, high fat; RMD, resistant maltodextrin; ND, normal chow diet

REFERENCES

(1) Marta, G.; Arantxa, R. Dietary phytochemicals and their potential effects on obesity: A review. *Pharmacol. Res.* **2011**, *64*, 438−455.

(2) Lina, B.; Gemma, V.; Teresa, P. Nutraceuticals and Atherosclerosis: Human trials. *Cardiovasc. Ther.* **2010**, *28*, 202−215.

(3) Shinji, I.; Mayumi, T.; Nobuyo, T.; Kayo, M.; Hiroshige, I.; Osamu, E. High-Fat Diet-Induced Hyperglycemia and Obesity in Mice: Differential Effects of Dietary Oils. *Metabolism* **1996**, *45*, 1539−1546.

(4) Nobuyo, T.; Shinji, I.; Mayumi, T.; Kayo, M.; Hiroyuki, W.; Naohiro, G.; Osamu, E. High-Monounsaturated Fat Diet-Induced Obesity and Diabetes in C57BL/6J Mice. *Metabolism* **1998**, *47*, 724−730.

(5) Hariri, N.; Thibault, L. High-fat diet-induced obesity in animal models. *Nutr. Res. Rev.* **2010**, *23*, 270−299.

(6) Mohan, P. F.; Ihnen, J. S.; Levin, B. E.; Cleary, M. P. Effects of dehydroepiandrosterone treatment in rats with diet-induced obesity. *J. Nutr.* **1990**, *120*, 1103−1114.

(7) Haring, S. J.; Harris, R. B. The relation between dietary fructose, dietary fat and leptin responsiveness in rats. *Physiol. Behav.* **2011**, *104*, 914−922.

(8) Kobayashi-Hattori, K.; Mogi, A.; Matsumoto, Y.; Takita, T. Effect of caffeine on the body fat and lipid metabolism of rats fed on a high-fat diet. *Biosci. Biotechnol. Biochem.* **2005**, *69*, 2219−2223.
(9) Santas, J.; Espadaler, J.; Mancebo, R.; Rafecas, M. Selective *in vivo* effect of chitosan on fatty acid, neutral sterol and bile acid excretion: A longitudinal study. *Food Chem.* **2012**, *134*, 940−947.
(10) Song, W. Y.; Chun, S. S.; Ku, K. H.; Choi, J. H. Effect of red pepper seeds powder on lipid composition in rats fed high-fat high-cholesterol Diets. *J. Food Sci. Nutr.* **2010**, *15*, 184−188.
(11) Han, L. K.; Kimura, Y.; Okuda, H. Reduction in fat storage during chitin-chitosan treatment in mice fed a high-fat diet. *Int. J. Obes. Relat. Metab. Disord.* **1999**, *23*, 174−179.
(12) Choo, J. J. Green tea reduces body fat accretion caused by high-fat diet in rats through beta-adrenoceptor activation of thermogenesis in brown adipose tissue. *J. Nutr. Biochem.* **2003**, *14*, 671−676.
(13) Chen, N.; Bezzina, R.; Hinch, E.; Lewandowski, P. A.; Cameron-Smith, D.; Mathai, M. L.; Jois, M.; Sinclair, A. J.; Begg, D. P.; Wark, J. D.; Weisinger, H. S.; Weisinger, R. S. Green tea, black tea, and epigallocatechin modify body composition, improve glucose tolerance, and differentially alter metabolic gene expression in rats fed a high-fat diet. *Nutr. Res. (N.Y.)* **2009**, *29*, 784−793.
(14) Kishimoto, Y.; Oga, H.; Tagami, H.; Okuma, K.; Gordon, D. T. Suppressive effect of resistant maltodextrin on postprandial blood triacylglycerol elevation. *Eur. J. Nutr.* **2007**, *46*, 133−138.
(15) Kishimoto, Y.; Yoshikawa, Y.; Miyazato, S.; Oga, H.; Yamada, T.; Tagami, H.; Hashizume, C.; Yamamoto, K. Effects of resistant maltodextrin on digestion and absorption of lipids. *J. Health Sci.* **2009**, *55*, 838−844.
(16) Sharma, A.; Singh, N. K.; Sharma, M.; Singh, R.; Katiyar, C. Determination of fortified resistant maltodextrin in juices by high performance liquid chromatography. *Int. J. Chem. Anal. Sci.* **2013**, *4*, 39−43.
(17) Okuma, K.; Kishimoto, Y. Effect of resistant maltodextrin on metabolism of glucose and lipids. In *Dietary Fiber: Bioactive Carbohydrates for Food and Feed*; Van Der Kamp, J. W., Asp, N.-G., Jones, J. M., Schaafsma, G., Eds.; Wageningen Academic Publishers: Wageningen, The Netherlands, 2004; pp 219−230.
(18) U.S. FDA. Guidance for Industry: Estimating the Maximum Safe Starting Dose in Initial Clinical Trials for Therapeutics in Adult Healthy Volunteers, 2005. http://www.fda.gov/downloads/Drugs/Guidances/UCM078932.pdf.
(19) Kishino, E.; Ito, T.; Fujita, K.; Kiuchi, Y. A mixture of the Salacia reticulate (*Kotala himbutu*) aqueous extract and cyclodextrin reduces the accumulation of visceral fat mass in mice and rats with high-fat diet-induced obesity. *J. Nutr.* **2006**, *136*, 433−439.
(20) Fisler, J. S.; Warden, C. H.; Pace, M. J.; Lusis, A. J. BSB: A new mouse model of multigenic obesity. *Obes. Res.* **1993**, *1*, 271−280.
(21) Folch, J.; Lees, M.; Sloane Stanley, G. H. A simple method for the isolation and purification of total lipids from animal tissues. *J. Biol. Chem.* **1957**, *226*, 497−509.
(22) Levin, B. E.; Dunn-Meynell, A. A. Defense of body weight depends on dietary composition and palatability in rats with diet-induced obesity. *Am. J. Physiol. Regul. Integr. Comp. Physiol.* **2002**, *282*, R46−R54.
(23) Surwit, R. S.; Feinglos, M. N.; Rodin, J.; Sutherland, A.; Petro, A. E.; Opara, E. C.; Kuhn, C. M.; Rebuffé-Scrive, M. Differential effects of fat and sucrose on the development of obesity and diabetes in C57BL/6J and A/J mice. *Metabolism* **1995**, *44*, 645−651.
(24) Gordon, D. T. The effect of resistant maltodextrin on blood glucose, insulin and triacylglyceride levels, and fat accumulation after meal feeding in humans. In *Dietary Fibre Components and Functions*; Salovaara, H., Gates, F, Tenkanen, M., Eds.; Wageningen: Wageningen Academic Pub: Wageningen, The Netherlands, 2007; pp 305−322.
(25) Hashizume, C.; Kishimoto, Y.; Kanahori, S.; Yamamoto, T.; Okuma, K.; Yamamoto, K. Improvement effect of resistant maltodextrin in humans with metabolic syndrome by continuous administration. *J. Nutr. Sci. Vitaminol.* **2012**, *58*, 423−430.
(26) U.S. Department of Agriculture (USDA). http://www.health.gov/dietaryguidelines/dga2005/recommendations.htm (accessed Oct 19, 2013).

JOURNAL OF AGRICULTURAL AND FOOD CHEMISTRY

Article

pubs.acs.org/JAFC

Pyrosequencing as a Tool for Rapid Fish Species Identification and Commercial Fraud Detection

Cristian De Battisti,*[,†] Sabrina Marciano,[†] Cristian Magnabosco,[‡,⊥] Sara Busato,[†] Giuseppe Arcangeli,[‡] and Giovanni Cattoli[†]

[†]Research & Innovation Department, Istituto Zooprofilattico Sperimentale delle Venezie, Viale dell'Università 10, 35020 Legnaro, Padova, Italy

[‡]Istituto Zooprofilattico Sperimentale delle Venezie, Via L. da Vinci, 39, 45011 Adria, Rovigo, Italy

Supporting Information

ABSTRACT: The increased consumption of fish products, as well as the occurrence of exotic fish species in the Mediterranean Sea and in the fish market, has increased the risk of commercial fraud. Furthermore, the great amount of processed seafood products has greatly limited the application of classic identification systems. DNA-based identification allows a clear and unambiguous detection of polymorphisms between species, permitting differentiation and identification of both commercial fraud and introduction of species with potential toxic effects on humans. In this study, a novel DNA-based approach for differentiation of fish species based on pyrosequencing technology has been developed. Raw and processed fish products were tested, and up to 25 species of fish belonging to *Clupeiformes* and *Pleuronectiformes* groups were uniquely and rapidly identified. The proper identification based on short and unique genetic sequence signatures demonstrates that this approach is promising and cost-effective for large-scale surveys.

KEYWORDS: *Clupeiformes, Pleuronectiformes, commercial fraud, fish species identification, pyrosequencing*

INTRODUCTION

The consumption of fish products in Europe has increased in recent decades mainly because of the growing awareness of the importance of a healthy diet and the consequent demand for new sources of healthy food.[1] This factor, in combination with the globalization of the fish markets, has contributed to the introduction of novel fish species in the European fish markets and to an increased risk of commercial and/or sanitary fraud. In this regard, a commercial fraud consists of the illegal substitution of one species with another.[2] These economic corruptions can greatly affect the seafood commerce. Considering an estimated conservative worldwide substitution rate of 10%, the economic losses for worldwide fisheries is about US$ 24 billion/year.[3] For instance, in the case of red snapper (*Lutjanus campechanus*) fraudulent substitutions can account for three-quarters of the fish sold,[4] whereas for fish products sold as Alaska pollock (*Theragra chalcogramma*) more than 80% of the analyzed samples were prepared with species different from the one indicated on the label.[5] In the Mediterranean sea, high levels of market mislabeling were reported in different countries, to quote but a few, hake in Spain and Greece[6] and cod in Italy.[7] Besides the economic impact, these substitutions could also introduce species with potential toxic effects on humans.[8] All these issues combined with the increase in seafood consumption may well explain why it is mandatory to assign a unique market name to a given fish species in order to be unambiguously identified.[1,8] The European Union (EU) regulation 104/2000 imposes that commercial name, method of production (Directive 2200/13/EC), and capture area (EU Commission Regulation No 2065/2001) must be clearly indicated on the product label prior to its submission to the commercial circuit.[9] Despite these regulations, the process of labeling can still have some drawbacks.[10]

Identification of fish species is traditionally based on external morphological features (i.e., body shape, pattern of colors, position of fins, and number); otoliths count and shape analysis are also occasionally used. However, these identification systems are not considered useful or reliable for processed products subject to filleting, beheading, and/or skinning due to the obvious lack of morphological distinct features.[11] In more recent times, methods based on the separation and characterization of specific proteins using electrophoretic techniques, such as isoelectric focusing (IEF),[12] have been officially recognized and adopted to identify and assign species to fish products characterized by poor morphological integrity.[13] Some processing procedures often remove or damage key species signatures, as might be the case for proteins denatured by cooking,[13,14] making identification of species by morphological or protein-based taxonomic means extremely difficult if not impossible. The percentage of processed seafood related to the total seafood consumed in Europe can be relevant, for instance, up to 80% in the German market according to Horstkotte and Rehbein,[15] or to about 50% in Italy (ISMEA, 2007, http://www.ismea.it/flex/cm/pages/ServeBLOB.php/L/IT/IDPagina/2756). Taking these data into account, traditional

Received: August 9, 2013
Revised: November 19, 2013
Accepted: December 11, 2013
Published: December 18, 2013

ACS Publications © 2013 American Chemical Society

dx.doi.org/10.1021/jf403545m | J. Agric. Food Chem. 2014, 62, 198−205

Table 1. Samples Analyzed in This Study[a]

family	genera species (number of samples)	phase 1	phase 2
Engraulidae	*Engraulis encrasicolus* (11)	not unambiguously identified	*E. encrasicolus* 77.8−100
	Engraulis japonicus (0)	no samples available	
	Coilia spp (3)	*Coilia spp* 88.8−92.9	
Clupeidae	*Sardinops sagax* (1)	*Sardinops sagax* 96.5	
	Sprattus sprattus (2)	*Sprattus sprattus* 95.6−100	
	Sardinella aurita (4)	*Sardinella aurita* 100	
	Sardinella fimbriata (1)	*Sardinella fimbriata* 93.4	
	Sardina pilchardus (15)	Sardina pilchardus 66.8−93	
	Clupea harengus (12)	*Clupea harengus* 95.2−100	
	Sardinella jussieu (1)	*Sardinella jussieu/gibbosa/fimbriata* 93.4	
	Alosa spp (7)	*Alosa spp* 100	
Pleuronectidae	*Pleuronectes platessa* (20)	not unambiguously identified	*Pleuronectes platessa* 86.1−100
	Limanda limanda (2)	not unambiguously identified	*Limanda limanda* 93.1−93.6
	Atheresthes stomias (1)	*Atheresthes stomias* 100	
	Reinhardtius hippoglossoides (2)	*Reinhardtius hippoglossoides* 95.5−100	
	Paralichthys patagonicus (1)	*Paralichthys patagonicus* 100	
	Lepidopsetta polyxystra (5)	not unambiguously identified	*Lepidopsetta polyxystra* 93.6−100
	Platichthys flesus (3)	not unambiguously identified	*Platichthys flesus* 79.4−87.2
	Eopsetta jordani (1)	*Eopsetta jordani 100*	
Soleidae	*Solea solea* (6)	*Solea solea 96.8−100*	
	Solea senegalensis (1)	*Solea senegalensis* 100	
	Solea lascaris (3)	*Solea lascaris* 83.1−86.6	
	Synaptura lusitanica (8)	*Synaptura lusitanica* 94.2−100	
	Microchirus azevia (2)	*Microchirus azevia 100*	
Psettodidae	*Psettodes belcheri* (1)	*Psettodes belcheri* 78.6	
Bothidae	*Arnoglossus spp* (3)	*Arnoglossus laterna* 100	

[a]Column 2, species genera analyzed and number of samples tested. Column 3, identifications of phase 1. Column 4, identifications of phase 2. The identification score for the different species is also reported.

morphological and protein-based methods are not sufficient for correct species identification.[8]

The advancement of genomic technologies in recent years has made the DNA-based identification system a new and powerful option to accurately identify the fish species of high commercial value or of those frequently involved in commercial fraud. Generally speaking, this system is based on the presence of species-specific polymorphisms naturally occurring in the genomes.[16] The DNA-based methods present several advantages, such as high sensitivity, high specificity, large scale throughput, and the possibility to apply different types of analyses on the same specimen (e.g., PCR, sequencing, cloning, phylogenetic analysis, etc.). A variety of DNA-based identification approaches have been developed, as reported by refs 13 and 17, mainly based on PCR reaction: PCR-RFLP,[18−20] PCR-SSCP,[21] real time PCR,[22] PCR-RAPD,[23] and PCR-AFLP.[24] Besides the DNA-based approaches, DNA barcoding is the most widely adopted method for species identification.[25,26] Over the past decade, Sanger sequencing technology has become largely available, and at present it is considered one of the best methodologies to overcome the limitations of the morphology-based approach.[8,27−30] Microarray and next generation sequencing (NGS) technology has been also considered but not implemented to date for fish species identification.[11]

A novel and powerful DNA-based technology with a potential for species identification is pyrosequencing.[17,31] Using this technique, short stretches of nucleotides (approximately 30−40 nucleotides in length) downstream from a sequencing primer can be sequenced with high efficiency and accuracy.[32,33]

In this study, we evaluated the application of an alternative and modular technique to the Sanger sequencing (DNA barcoding) based on PCR followed by pyrosequencing for the rapid identification of two groups of fish commonly present in fish markets and frequently involved in commercial fraud. The first group includes species belonging to the genus *Clupeidae* as well as other species potentially used as fraudulent substitutes of *Clupeids*. The second group includes species belonging to the genus *Pleuronectidae* as well as other flat fish, such as *Solea solea*, *Hipoglossus hipoglossus*, etc.

It is interesting to note that products derived from these species are often commercialized as fillets in various forms, for example, fresh, frozen, marinated, salted, or breaded, all of which are unsuitable for morphological means of identification and sometimes even for protein-based species identification. Although pyrosequencing was previously applied for the identification of genetic lineages of *Salmo trutta* species,[34] to date, this is the first application of pyrosequencing-based analysis that aims at the identification of commercial fraud involving fish species.

MATERIALS AND METHODS

Sample Collection and DNA Extraction. One-hundred and sixteen (57 *Clupeiformes* and 59 *Pleuronectiformes*) specimens consisting of whole fishes and processed seafoods were collected from the fish market in Chioggia (Venice, Italy) and from local shops. Scientific and common names of fish species (11 *Clupeiformes* and 15 *Pleuronectiformes*) were assigned following identification by species-specific morphological traits following classification criteria and Sanger sequence DNA analysis; species names are listed in Table 1. DNA was extracted from 25 to 50 mg of fish muscles or processed seafood with the High Pure PCR Template Preparation kit (Roche Diagnostics,

Mannheim, Germany) according to the manufacturer's instructions. Specimens represented the most common product types present on the market in the commerce, such as fresh (skinned, filleted, eviscerated, etc.) or processed products (dried, salted, marinated, smoked, etc.). In detail, the samples analyzed were frozen fillet (59 samples), smoked (7 samples), cooked/precooked (12 samples), whole fresh fish (5 samples), marinated (6 samples), fermented (2 samples), salted in oil (14 samples), and frozen in breadcrumbs fillets (11 samples).

Preliminary Identification. *Morphological Analysis.* The specimens represented by the whole fish (n = 5) included in this study were at first identified by morphological analysis. Whole fish, with intact skin and fins, were identified using the dichotomous keys approach proposed by the FAO and available on the Web site http://www.fao.org/fishery/species/search/en, which refers to specific monographs (ref 35 for the Mediterranean Sea).

Sanger Sequence-Based Identification. All the specimens were identified by using cytochrome c oxidase I (COI) sequence. Briefly, the samples were amplified by using the PCR reaction previously described.[36] Sanger sequencing method was applied on the obtained PCR products. The sequences were generated using the Big Dye Terminator v3.1 cycle sequencing kit (Applied Biosystem, Foster City, CA). The products of the sequencing reactions were cleaned-up using PERFORMA DTR Ultra 96-Well kit (Edge BioSystems, Gaithersburg, MD) and sequenced by using ABI PRISM 3130xl Genetic Analyzer (Applied Biosystem, Foster City, CA). COI sequences obtained were compared to the COI sequences deposited in the GenBank database.

PCR Design and PCR Amplification for Pyrosequencing. Sequences of conserved regions of mitochondrial DNA (mtDNA) from different species present in the public database GenBank were aligned using the software MEGA 5.[37] On the basis of the analysis of the alignment, a set of PCR primers targeting 16S rRNA conserved region (16SForbio 5′-biotin-ACGAGAAGACCCTDTGGAG-3′, 16SRev 5′-TGTTATCCCTAGGGTAACTTG-3′) and a sequencing primer (16Sseq 5′-GTCGCCCCAACCGAAGA-3′) for pyrosequencing were designed. This set of primer was developed to amplify all the commercial species of interest in this study. On the basis of the *in silico* analysis, not all the originated pyrosequences showed the polymorphisms needed to be correctly and uniquely differentiated as in the case of *Cluipeidae*, that is, *Engraulis encrasicolus* and *Engraulis japonicus.* As for *Pleuronectidae*, *Hippoglossoides elassodon*, *Reinhardtius hippoglossoides*, *Limanda limanda*, *Limanda aspera*, *Pleuronectes quadrituberculatus*, *Pleuronectes platessa*, *Platichtys flesus*, and *Lepidopsetta bilineata* were not uniquely identified. Then, two other set of primers targeting different genomic sequences were designed. The first set of primers (Engra JEF 5′-biot- GCAGCCTTCCTTACCTTAAACA-3′ and Engra JER 5′-GTAGGAGGTTTGTGGCGAGAG-3′ for amplification, Engra JES 5′-AGTCACTTGGGTAAGAATC-3′ for sequencing), targeting the NADH dehydrogenase subunit II gene (ND2), allows discrimination of *Engraulis japonicus* from *Engraulis encrasicolus* on the basis of the pyrosequences obtained. The second set (PleuFbio 5′-ATCGCAAACGATGCTTTAG-3′ and PleuRseq1 5′-GGAARAGAAAGTGGAAKGC-3′ for amplification, PleuRseq2 5′-GGAAGAGRAAGTGGAATGC-3′ for sequencing), targeting a portion of the *cytb* gene of the *Pleuronectiformes*, discriminates species of *Hippoglossoides elassodon*, *Reinhardtius hippoglossoides*, *Limanda limanda*, *Limanda aspera*, *Pleuronectes quadrituberculatus*, *Pleuronectes platessa*, *Platichtys flesus*, and *Lepidopsetta bilineata*.

For each set, one of the amplification primer had to be biotinylated according to the pyrosequencing chemistry to allow the purification and selection of the specific fragment in the subsequent procedures.

Amplification of DNA was performed by using a PCR in a 50 μL reaction volume with 5 μL of DNA, 1.5 U AmpliTaq Gold (Roche Diagnostics, Mannheim, Germany), 2 mM $MgCl_2$, 1 mMdNTPs, and 0.5 μM of each specific primer (Eurofins MWG-Operon, Ebersberg, Germany). PCR was performed with the following thermal conditions: 10 min at 95 °C, 40 cycles consisting in 30 s at 95 °C, 30 s at 58 °C, 55 °C, 52 °C respectively for ND2, 16S and cyt B amplification, 30 s at 72 °C, with a final extension of 5 min at 72 °C. The amplified products, 289 bp for 16S, 520bp for cyt B and 291bp for ND2, were analyzed on a 2% agarose gel (Sigma-Aldrich, St. Louis, MO) in TAE buffer with 0.1 μL/mL GelRed (Biotium, Hayward, CA) and visualized under UV illumination.

Pyrosequencing Reaction and Sequence Library. The biotinylated PCR products were purified and prepared for the pyrosequencing reaction according to the manufacturer's instructions (Biotage, Uppsala, Sweden). Briefly, 20 μL of the biotinylated PCR product was immobilized onto 4 μLof Streptavidine-Sepharose (GE Healthcare, Uppsala, Sweden) beads in 40 μL of binding buffer with 20 μL of DEPC water at room temperature for 30 min. Single-stranded DNA was prepared with the PyroMark Vacuum Prep Workstation (Biotage, Uppsala, Sweden). The single-stranded, biotinylated DNA products were hybridized to sequencing primer (final concentrations of 0.5 μM) in a 96-well plate . The reaction was performed in 40 μL of annealing buffer in a sample plate heated at 80 °C for 4 min and then cooled to room temperature for 10 min before being placed into the pyrosequencing instrument. Pyrosequencing was performed using PyroGold reagents according to manufacturer's recommendations. The sequences originated by the analysis were automatically compared with a sequences library containing all the reference sequences of the species of interest in this study. The sequences library was generated, and the analysis was performed using the IdentiFire software (Biotage, Uppsala, Sweden).

For some of the fish species included in this project, sequences of the target genes were not available in the public databases. Those sequences were generated using the classical sequencing protocol (Sanger), added to the library (IdentiFire software), and deposited in a public database (see following section).

This software will assign a score value to each tested sequence, indicating the quality and the affordability of the result. This score is not only based on the sequence homology, but also on the position of any possible mismatch, the quality of the pyrogram, and the intensity of the peaks. Thus, the same number of mismatches may give different scores according to the positions of the polymorphisms along the pyrosequence. Mismatches closer to the 5′-end of the pyrosequences can affect the score value, which can be decreased more than a mismatch close to the 3′-end.

RESULTS

Preliminary Identification. The samples analyzed in this study originated from species belonging to *Clupeiformes* (n = 57) and *Pleuronectiformes* (n = 59) (Table 1).

Sequences obtained by the Sanger method were used as the gold standard for pyrosequences identification. For some of the species analyzed in the present study, the sequence of 16S gene was not available in the public databases, and therefore the newly Sanger-generated 16S sequences were submitted to Genbank [accession numbers: KC461225 (*Alosa falla nilotica*), KC461223, KC461224 (*Alosa fallax lacustris*), and KC461222 (*Sardinella fimbriata*)]. Similarly, *cytb* PCR products from samples of *Lepidopsetta polyxystra* (identified by COI gene Sanger sequence DNA analysis) were submitted to GenBank (Acc numbers: KF007183, KF007184, KF007185).

Pyrosequencing Identification: Experimental Design and Proposed Workflow. In order to correctly and unambiguously identify all the 25 fish species targeted in this study, the entire procedure was divided into two phases (herein, phase 1 and phase 2). Phase 1 was based on the use of one PCR reaction targeting the 16S rRNA gene, followed by the pyrosequencing analysis to identify and differentiate 20 out of the 25 targeted species. For those sequences not uniquely identified in phase 1, two other PCR amplifications followed by pyrosequencing were performed (phase 2), specifically targeting the group of *Clupeiformes* (two species) and the *Pleuronectiformes* (four species). The proposed workflow is schematically illustrated in Figure 1.

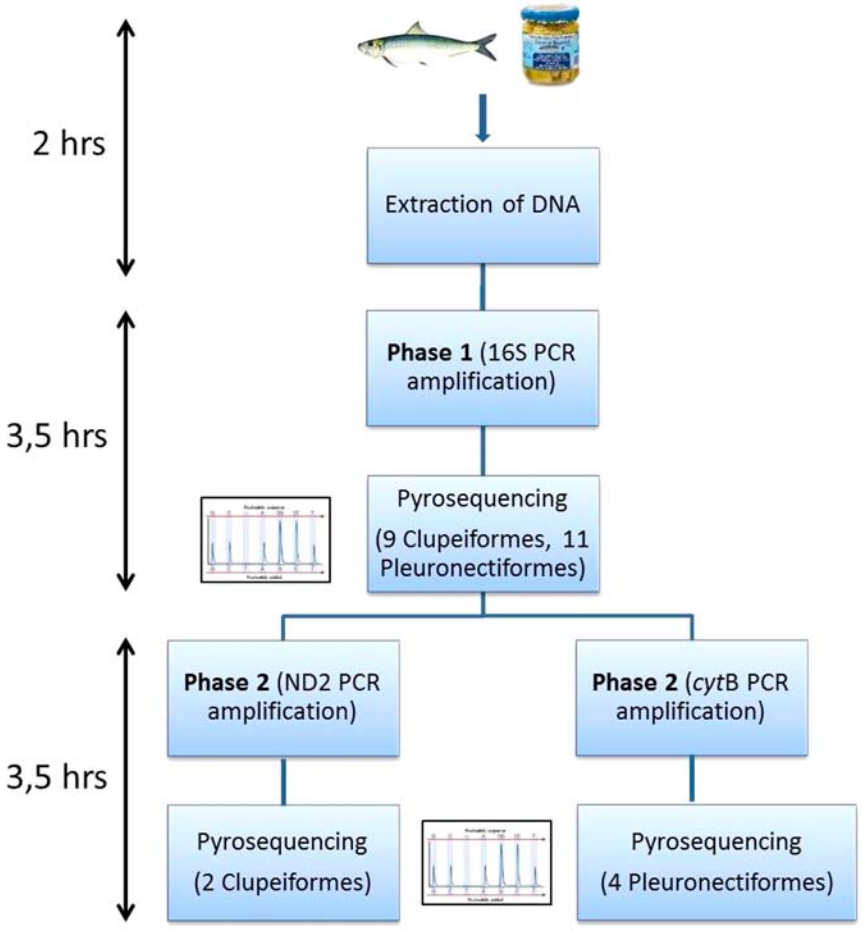

Figure 1. Schematic representation of pyrosequencing workflow. The number of fish species identified throughout the two phases is indicated as well as the analysis turn-around time. Overall, 20 fish species can be identified with this procedure in 3.5 h. The identification of the 25 species targeted in this study is achieved in a maximum time frame of 7 h. It can be reduced if phase 1 and 2 are performed simultaneously.

Phase 1 – Targeting the 16S rRNA Gene. The DNA isolated from all the fresh and processed samples collected in this study was amplified using the PCR targeting the 16S rRNA gene.

The pyrosequencing reaction was able to produce the short sequences, and the subsequent comparison of the query sequences was carried out with the reference sequences in the library database (based on the Identifire software). The results demonstrated that for 20/25 species the 16S rRNA sequences identified correctly and uniquely with a score range in the Identify software between 66.8 and 100 (*Coilia spp, Sardinops sagax, Sprattus sprattus, Sardinella aurita, Sardinella fimbriata, Sardina pilchardus, Clupea harengus, Sardinella jusseu, Alosa spp., Atheresthes stomias, Reinhardtius hippoglossoides, Paralitchthys patagonicus, Eopsetta jordani, Solea solea, Solea senegalensis, Solea lascaris, Synaptura lusitanica, Microchirus azevia, Psettodes belcheri, Arnoglossus spp.*) (Table 1). Some samples were ambiguously identified because of the similarity of their sequences with more than one reference sequences included in the database, as was the case for two samples identified in the *Clupeiformes* group as *Engraulis encrasicolus* and *Engraulis japonicus.* As illustrated in Figure S-1 (Supporting Information), the same score with three different reference sequences, *Engraulis australis*, *Engraulis encrasicolus*, and *Engraulis japonicus* was obtained. Similarly, a unique and precise identification of *Limanda limanda*, *Pleuronectes platessa*, *Platichthys flesus*, and *Lepidopsetta polyxystra* in the *Pleuronctiformes* group was not possible in phase 1 (Figure S-2, Supporting Information).

Phase 2 – Targeting NADH and cyt b Gene. The samples assigned to *Clupeiformes* group but ambiguously identified in phase 1 were tested with a PCR assay targeting the NADH dehydrogenase subunit II gene (ND2). The subsequent pyrosequencing procedure enabled the discrimination between genetic sequences belonging to *Engraulis encrasicolus* and *Engraulis japonicus* and the correct identification of these species with scores ranging from 77.8 to 100 (Figure 2).

The samples assigned to the *Pleuronectiformes* group but ambiguously identified in phase 1 were tested with a distinct PCR targeting the cytochrome *b* (*cyt* b) gene. The sequences obtained allowed the correct and unambiguous identification of four of the previously misclassified species (*Limanda limanda, Pleuronectes platessa, Platichtys flesus, Lepidopsetta polyxystra*), with scores ranging from 79.4 (in the case of *Platichtys flesus*) to 100 (in the case of *Pleuronectes platessa*) (Figure S-3, Supporting Information).

DISCUSSION

The identification of a species substitution using morphological detection or other classical systems (IEF) can fail when processed fish products are considered, since the diagnostic

dx.doi.org/10.1021/jf403545m | *J. Agric. Food Chem.* 2014, 62, 198−205

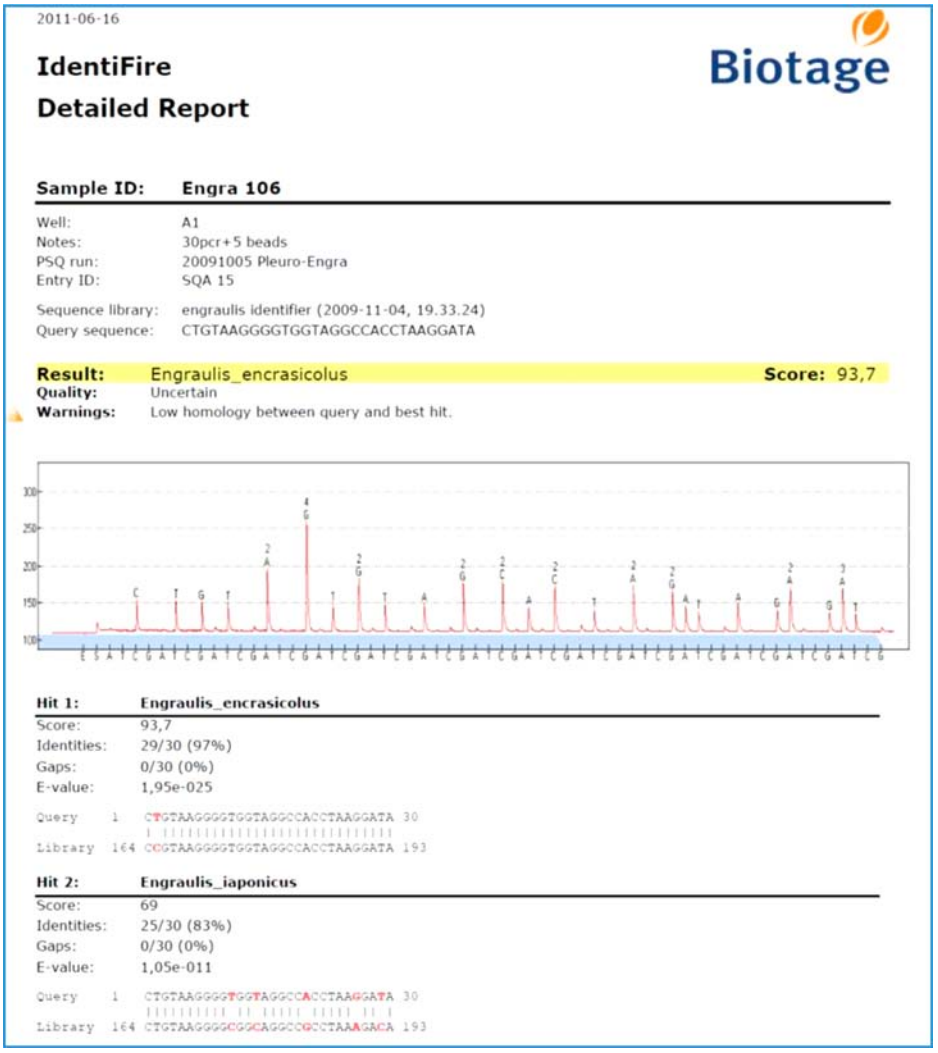

Figure 2. Example of IdentiFire results of the phase 2 discriminating *Engraulis encrasicolus* from *Engraulis japonicus*. The different score assigned indicates a level of polymorphism that enables correct identification.

target can be damaged. In those cases, traditional methods do not always provide satisfactory results.[8]

The selection of the proper DNA target is a crucial point in the DNA-based fish species identification methods. The DNA target should be present in large amounts to ensure it will always be detectable and show a sufficient number of polymorphisms between the species to be unequivocally assigned to a given species.[13] Several genes or genomic sequences satisfy these criteria, but the mtDNA has been widely used because of its particular features: it is present in several copies into the cell (up to 1000 times more than in the nuclear DNA), and it shows more polymorphisms than nuclear DNA because of its faster evolution.[13] Besides this, mtDNA is more stable because of its circular structure that may constitute a crucial advantage in the case of processed seafood, where thermal treatment could reduce the integrity of DNA originating fragments from less than 100 bp up to about 500 bp.[2] Among the mtDNA, some genes have been widely used for fish species identification, especially cytochrome oxidase c subunit 1 (COI), cytochrome *b* (*cytb*), and 16S rRNA.[1,2,11,13,38−44] The 650 base pairs sequence of COI is the main barcode for animal species identification and can discriminate all the commercially available fish species.[45,46] The pyrosequencing technique provides the sequence of a conserved region containing a short stretch of nucleotides (30−40) with a number of polymorphisms sufficient enough to enable differentiation of the species under investigation.

The testing protocol developed in this study is based on three different PCR reactions followed by pyrosequencing analysis and provides a rapid, sensitive, specific, and robust system to identify fish species based on the nucleotide sequence of a specific locus.[34]

The simple workflow schematically illustrated in Figure 1 allowed for an efficient and accurate identification of 25 species (11 *Clupeiformes* and 15 *Pleuronectiformes*), and the analysis detected some of the most important commercial frauds related to these groups of fish that could have a great impact on the market.[47]

The precise and unambiguous discrimination of *Engraulis encrasicolus* (commercially, a high-value species) is relevant in the framework of the official control of commercial fish frauds.[48] *E. encrasicolus* can also be substituted by *Sprattus sprattus*,[49] and this fraud can be clearly identified by the pyrosequencing protocol as well. The lack of available samples belonging to *E.* japonicus in this study did not allow for testing of this species in the laboratory; nevertheless, the *in silico* analysis confirmed the clear DNA discrimination between *E.*

japonicus and *E. encrasicolus* on the basis of the *cyt* b available sequences from public databases.

In *Pleuronectiformes*, *Pleuronectes platessa* and *Solea solea* are the two species that are most widely substituted by various low-value species such as members of the genus *Limanda* and *Lepidopsetta*. The results presented showed that *P. platessa* and *S. solea* can be unambiguously differentiated. It is clear that the identification of species by using sequence data is strongly affected by the availability of reference sequences in public databases.

A major point of interest is that the method developed in this study has proven to be highly efficient on processed fish products as well. As a matter of fact, the DNA from all these samples was amplified and correctly assigned to a given species, indicating that the method developed is not affected by the various processing methods.

As for other barcoding techniques, such as mini-barcoding,[50] one of the advantages of the pyrosequencing protocol is that the relatively small size of the amplified PCR products, less than 520 bp, coupled with the high efficiency and accuracy of this sequencing method for short sequence fragments allows detection of high quality genetic sequences, even in samples where DNA may be partially damaged or degraded by the processing, providing a robust identification system.[2]

It was possible to identify the specimens at the species level in most of the analyzed samples; however, in some cases the identification limited to the Genus level (e.g., *Arnoglossus sp*, *Coilia sp*, and *Alosa sp*) was still considered sufficient for commercial purposes. In those cases, all the members of the genus presented comparable commercial values and/or the same commercial denomination. The analysis in phase 1 can be considered as a primary screening test to identify most of the species of interest being capable to identify 20 species in 3.5 h (Figure 1). Phase 2 analysis acts as a fine-tuned identification step, but both can be performed simultaneously to reduce the turn-around time, if necessary (Figure 1). To make the entire process as fast as possible (i.e., about 3.5 h), all three PCR reactions (phase 1 and 2) can be performed at the same time, and the resulting PCR products can then be analyzed in a single run on the pyrosequencing platform. Furthermore, depending on the species to be investigated (and the correspondent fraud), only one specific PCR could be performed. Indeed, in most cases of mislabeling fraud, only one of the PCR presented was sufficient to identify the species involved. According to this, the system presented can be considered as a modular system, and either phase can be used independently. This reduces the total analysis time to that of a single PCR step.

The classical sequencing system (Sanger method) is a very useful tool to identify fish species, but it still is rather expensive and time-consuming; therefore, its use is not recommended for routine analyses to date.[51] On the basis of the commercial value of the reagents and platform, the cost per sample of PyroMark ID pyrosequencing analysis ranges from 5 to 6 euro (from 480 to 576 euro/96 plate). On the other hand, the cost per sample of the Sanger sequencing system is of about 11 or 12 euro (1056 to 1152 euro/96 plate). Interestingly, the pyrosequencing pipeline is more time-efficient and cheaper than Sanger sequencing. Indeed, pyrosequencing requires only few protocol steps, and the sequence detection is performed in real-time. The additional mandatory steps to be performed in the Sanger protocol, consisting of big-dye terminator sequencing reaction, postreaction purification, and final electrophoresis, prolong the total time of the analysis and increase costs.[50] Conversely, the total cost of the pyrosequencing analysis has decreased since it does not need terminator enzymes and time-consuming purification steps.[52−54]

The newest upgrade to PyroMark platform makes the read-length up to 140 nucleotides (instead of the current 30−40) longer (www.qiagen.com). This improvement could extend the application field of the pyrosequencing technique to a wider target range. In addition, the cost of the new upgraded platform is still lower than the Sanger sequencing platform commercially available making pyrosequencing even cheaper and more powerful.

In conclusion, the analysis of the 30-bp fragment following the sequencing primer enabled the discrimination of 25 fish species in 3.5−7 h, indicating that the fish species identification system based on pyrosequencing analysis is a powerful tool to discriminate the most important cases of commercial fraud regarding *Clupeiformes* and *Pleuronectiformes* groups.

■ ASSOCIATED CONTENT

Supporting Information

IdentiFire analysis figures. Figure S-1: IdentiFire results of phase 1 on species belonging of the Clupeiformes group. The maximum score was assigned to more than one reference sequence, indicating that for some samples the phase 1 was not sufficient for the correct and unambiguous identification. Figure S-2: Example of IdentiFire results of phase 1 on species belonging to the Pleuronectiformes group. The maximum score was assigned to more than one reference sequence, indicating that for some samples the phase 1 was not sufficient for a correct and unambiguous identification. Figure S-3: IdentiFire results of the phase 2 discriminating *Pleuronectes platessa* from its major substitutions. The different score assigned indicates a level of polymorphism which enables correct identification. This material is available free of charge via the Internet at http://pubs.acs.org.

■ AUTHOR INFORMATION

Corresponding Author

*Tel. +390498084381; fax +390498084360; e-mail cdebattisti@izsvenezie.it.

Present Address

⊥(C.M.) Sacco Srl, Via Manzoni 29/A, 22071 Cadorago (Co), Italy.

Funding

This work was supported by the RC VE 3-09 (Italian Ministry of Health) and partially by the Italian Ministry of Agriculture (INRAN, no. E12900E1).

Notes

The authors declare no competing financial interest.

■ ACKNOWLEDGMENTS

We are grateful to Francesca Ellero and Samantha Kasloff (Research & Innovation Department, IZSVe, Italy) for revising the manuscript.

■ REFERENCES

(1) Comi, G.; Iacumin, L.; Rantsiou, K.; Cantoni, C.; Cocolin, L. Molecular methods for the differentiation of species used in production of cod-fish can detect commercial frauds. *Food Control* **2005**, *16*, 37−42.

(2) Rasmussen, R. S.; Morrissey, M. T. DNA-Based Methods for the Identification of Commercial Fish and Seafood Species. *Compr. Rev. Food Sci. Food Saf.* **2008**, *7*, 280−295.
(3) Hanner, R.; Becker, S.; Ivanova, N. V.; Steinke, D. FISH-BOL and seafood identification: Geographically dispersed case studies reveal systemic market substitution across Canada. *Mitochondrial DNA* **2011**, *22*, 106−122.
(4) Marko, P. B.; Lee, S. C.; Rice, A. M.; Gramling, J. M.; Fitzhenry, T. M.; McAlister, J. S.; Harper, G. R.; Moran, A. L. Fisheries: mislabelling of a depleted reef fish. *Nature* **2004**, *430*, 309−310.
(5) Pepe, T.; Trotta, M.; Di Marco, I.; Anastasio, A.; Bautista, J. M.; Cortesi, M. L. Fish species identification in surimi-based products. *J. Agric. Food Chem.* **2007**, *55*, 3681−3685.
(6) Garcia-Vazquez, E.; Perez, J.; Martinez, J. L.; Pardinas, A. F.; Lopez, B.; Karaiskou, N.; Casa, M. F.; Machado-Schiaffino, G.; Triantafyllidis, A. High level of mislabeling in Spanish and Greek hake markets suggests the fraudulent introduction of African species. *J. Agric. Food Chem.* **2011**, *59*, 475−480.
(7) Di Pinto, A.; Di Pinto, P.; Terio, V.; Bozzo, G.; Bonerba, E.; Ceci, E.; Tantillo, G. DNA barcoding for detecting market substitution in salted cod fillets and battered cod chunks. *Food Chem.* **2013**, *141*, 1757−1762.
(8) Yancy, H. F.; Zemlak, T. S.; Mason, J. A.; Washington, J. D.; Tenge, B. J.; Nguyen, N. L.; Barnett, J. D.; Savary, W. E.; Hill, W. E.; Moore, M. M.; Fry, F. S.; Randolph, S. C.; Rogers, P. L.; Hebert, P. D. Potential use of DNA barcodes in regulatory science: applications of the Regulatory Fish Encyclopedia. *J. Food Prot.* **2008**, *71*, 210−217.
(9) Civera, T. Species identification and safety of fish products. *Vet. Res. Commun.* **2003**, *27* (Suppl 1), 481−489.
(10) Sanchez, A.; Quinteiro, J.; Rey-Mendez, M.; Perez-Martin, R. I.; Sotelo, C. G. Identification of European Hake species (*Merluccius merluccius*) using real-time PCR. *J. Agric. Food Chem.* **2009**, *57*, 3397−3403.
(11) Kochzius, M.; Seidel, C.; Antoniou, A.; Botla, S. K.; Campo, D.; Cariani, A.; Vazquez, E. G.; Hauschild, J.; Hervet, C.; Hjorleifsdottir, S.; Hreggvidsson, G.; Kappel, K.; Landi, M.; Magoulas, A.; Marteinsson, V.; Nolte, M.; Planes, S.; Tinti, F.; Turan, C.; Venugopal, M. N.; Weber, H.; Blohm, D. Identifying Fishes through DNA Barcodes and Microarrays. *PLoS One* **2010**, *5*, e12620.
(12) Rehbein, H. Electrophoretic techniques for species identification of fishery products. *Z. Lebensmittel-Untersuchung Forschung A* **1990**, *191*, 1−10.
(13) Teletchea, F. Molecular identification methods of fish species: reassessment and possible applications. *Rev. Fish Biol. Fisheries* **2009**, *19*, 265−293.
(14) Calo-Mata, P.; Sotelo, C. G.; Pérez-Martín, R. I.; Rehbein, H.; Hold, G. L.; Russell, V. J.; Pryde, S.; Quinteiro, J.; Rey-Méndez, M.; Rosa, C.; Santos, A. T. Identification of gadoid fish species using DNA-based techniques. *Eur. Food Res. Technol.* **2003**, *217*, 259−264.
(15) Horstkotte, B.; Rehbein, H. Fish Species Identification by Means of Restriction Fragment Length Polymorphism and High-Performance Liquid Chromatography. *J. Food Sci.* **2003**, *68*, 2658−2666.
(16) Liu, Z. J.; Cordes, J. F. DNA marker technologies and their applications in aquaculture genetics. *Aquaculture* **2004**, *238*, 1−37.
(17) Hellberg, R. S.; Morrissey, M. T. Advances in DNA-based techniques for the detection of seafood species substitution on the commercial market. *J. Lab. Autom.* **2011**, *16*, 308−321.
(18) Perez, J.; Garcia-Vazquez, E. Genetic identification of nine hake species for detection of commercial fraud. *J. Food Prot.* **2004**, *67*, 2792−2796.
(19) Perez, M.; Presa, P. Validation of a tRNA-Glu-cytochrome b key for the molecular identification of 12 hake species (Merluccius spp.) and Atlantic Cod (*Gadus morhua*) using PCR-RFLPs, FINS, and BLAST. *J. Agric. Food Chem.* **2008**, *56*, 10865−10871.
(20) Aranishi, F.; Okimoto, T.; Izumi, S. Identification of gadoid species (Pisces, Gadidae) by PCR-RFLP analysis. *J. Appl. Genet.* **2005**, *46*, 69−73.
(21) Weder, J.; Rehbein, H.; Kaiser, K. On the specificity of tuna-directed primers in PCR-SSCP analysis of fish and meat. *Eur. Food Res. Technol.* **2001**, *213*, 139−144.
(22) Casper, R. M.; Jarman, S. N.; Deagle, B. E.; Gales, N. J.; Hindell, M. A. Detecting prey from DNA in predator scats: A comparison with morphological analysis, using Arctocephalus seals fed a known diet. *J. Exp. Mar. Biol. Ecol.* **2007**, *347*, 144−154.
(23) Lakra, W. S.; Goswami, M.; Gopalakrishnan, A. Molecular identification and phylogenetic relationships of seven Indian Sciaenids (Pisces: Perciformes, Sciaenidae) based on 16S rRNA and cytochrome c oxidase subunit I mitochondrial genes. *Mol. Biol. Rep.* **2009**, *36*, 831−839.
(24) Maldini, M.; Nonnis Marzano, F.; Fortes, G. G.; Papa, R.; Gandolfi, G. Fish and seafood traceability based on AFLP markers: Elaboration of a species database. *Aquaculture* **2006**, *261*, 487−494.
(25) Wong, E.H.-.; Hanner, R. H. DNA barcoding detects market substitution in North American seafood. *Food Res. Int.* **2008**, *41*, 828−837.
(26) Keskin, E.; Atar, H. H. Genetic structuring of European anchovy (*Engraulis encrasicolus*) populations through mitochondrial DNA sequences. *Mitochondrial DNA* **2012**, *23*, 62−69.
(27) Allander, T.; Emerson, S. U.; Engle, R. E.; Purcell, R. H.; Bukh, J. A virus discovery method incorporating DNase treatment and its application to the identification of two bovine parvovirus species. *Proc. Natl. Acad. Sci. U. S. A.* **2001**, *98*, 11609−11614.
(28) Pace, N. R. A molecular view of microbial diversity and the biosphere. *Science* **1997**, *276*, 734−740.
(29) Hamels, S.; Gala, J. L.; Dufour, S.; Vannuffel, P.; Zammatteo, N.; Remacle, J. Consensus PCR and microarray for diagnosis of the genus Staphylococcus, species, and methicillin resistance. *BioTechniques* **2001**, *31*, 1364−6, 1368, 1370−2.
(30) Nanney, D. L. Genes and phenes in Tetrahymena. *Bioscience* **1982**, *32*, 783−788.
(31) Balitzki-Korte, B.; Anslinger, K.; Bartsch, C.; Rolf, B. Species identification by means of pyrosequencing the mitochondrial 12S rRNA gene. *Int. J. Legal Med.* **2005**, *119*, 291−294.
(32) Ronaghi, M. Pyrosequencing sheds light on DNA sequencing. *Genome Res.* **2001**, *11*, 3−11.
(33) Woolfe, M.; Primrose, S. Food forensics: using DNA technology to combat misdescription and fraud. *Trends Biotechnol.* **2004**, *22*, 222−226.
(34) Keller, I.; Taverna, A.; Seehausen, O. A pyrosequencing assay for the rapid discrimination of mitochondrial lineages in the Salmo trutta species complex. *Mol. Ecol. Resour.* **2011**, *11*, 196−199.
(35) Fischer W.; Bauchot, M. L.; Schneider, M. *Fiches FAO d'identification des espèces pour les besoins de la pêche. Méditerranée et mer Noire. Zone de Pêche 37 (rev. 1)*; Commission des Communautés Européennes and FAO: Rome, 1987; Vol. *II*, pp 891−1421.
(36) Baldwin, C. C.; Weight, L. A.; Smith, D. G.; Mounts, J. H. Reconciling Genetic Lineages with Species in Western Atlantic Coryphopterus (Teleostei: Gobiidae). *Smithsonian contributions to the marine science* **2009**, 111−138.
(37) Tamura, K.; Dudley, J.; Nei, M.; Kumar, S. MEGA4: Molecular Evolutionary Genetics Analysis (MEGA) software version 4.0. *Mol. Biol. Evol.* **2007**, *24*, 1596−1599.
(38) Kartavtsev, Y. P.; Sharina, S. N.; Goto, T.; Chichvarkhin, A. Y.; Balanov, A. A.; Vinnikov, K. A.; Ivankov, V. N.; Hanzawa, N. Cytochrome oxidase 1 gene sequence analysis in six flatfish species (Teleostei, Pleuronectidae) of Far East Russia with inferences in phylogeny and taxonomy. *Mitochondrial DNA* **2008**, *19*, 479−489.
(39) Aquino, L. M.; Tango, J. M.; Canoy, R. J.; Fontanilla, I. K.; Basiao, Z. U.; Ong, P. S.; Quilang, J. P. DNA barcoding of fishes of Laguna de Bay, Philippines. *Mitochondrial DNA* **2011**, *22*, 143−153.
(40) Ribeiro, A. O.; Caires, R. A.; Mariguela, T. C.; Pereira, L. H.; Hanner, R.; Oliveira, C. DNA barcodes identify marine fishes of Sao Paulo State, Brazil. *Mol. Ecol. Resour.* **2012**, *12*, 1012−1020.
(41) Kochzius, M. Trends in Fishery Genetics. In *The Future of Fisheries Science in North America, 1*; Beamish, R. J., Rothschild, B. J.,

Eds.; Springer Netherlands: AK Houten, Netherlands, 2009; Vol. *31*, pp 453−493.
(42) Espineira, M.; Gonzalez-Lavin, N.; Vieites, J. M.; Santaclara, F. J. Authentication of anglerfish species (Lophius spp) by means of polymerase chain reaction-restriction fragment length polymorphism (PCR-RFLP) and forensically informative nucleotide sequencing (FINS) methodologies. *J. Agric. Food Chem.* **2008**, *56*, 10594−10599.
(43) Espineira, M.; Gonzalez-Lavin, N.; Vieites, J. M.; Santaclara, F. J. Development of a method for the genetic identification of flatfish species on the basis of mitochondrial DNA sequences. *J. Agric. Food Chem.* **2008**, *56*, 8954−8961.
(44) Rasmussen, R. S.; Morrissey, M. T.; Hebert, P. D. DNA barcoding of commercially important salmon and trout species (Oncorhynchus and Salmo) from North America. *J. Agric. Food Chem.* **2009**, *57*, 8379−8385.
(45) Hebert, P. D.; Ratnasingham, S.; deWaard, J. R. Barcoding animal life: cytochrome c oxidase subunit 1 divergences among closely related species. *Proc. Biol. Sci.* **2003**, *270* (Suppl 1), S96−9.
(46) Hebert, P. D.; Cywinska, A.; Ball, S. L.; deWaard, J. R. Biological identifications through DNA barcodes. *Proc. Biol. Sci.* **2003**, *270*, 313−321.
(47) Lahsen, A. *World Inventory of Fisheries. Trade Implications of Fish Species Identification. Issues Fact Sheets*; Food and Agriculture Organization of the United Nations, Fisheries and Aquaculture Department: Rome, Italy, 2005; http://www.fao.org/fishery/topic/14807/en.
(48) Santaclara, F.; Cabado, A.; Vieites, J. Development of a method for genetic identification of four species of anchovies: *E. encrasicolus*, *E. anchoita*, *E. ringensand*, *E. japonicus*. *Eur. Food Res. Technol.* **2006**, *223*, 609−614.
(49) Sebastio, P.; Zanelli, P.; Neri, T. M. Identification of anchovy (*Engraulis encrasicholus* L.) and gilt sardine (*Sardinella aurita*) by polymerase chain reaction, sequence of their mitochondrial cytochrome b gene, and restriction analysis of polymerase chain reaction products in semipreserves. *J. Agric. Food Chem.* **2001**, *49*, 1194−1199.
(50) Shokralla, S.; Zhou, X.; Janzen, D. H.; Hallwachs, W.; Landry, J. F.; Jacobus, L. M.; Hajibabaei, M. Pyrosequencing for mini-barcoding of fresh and old museum specimens. *PLoS One* **2011**, *6*, e21252.
(51) Durand, J. D.; Diatta, M. A.; Diop, K.; Trape, S. Multiplex 16S rRNA haplotype-specific PCR, a rapid and convenient method for fish species identification: an application to West African Clupeiform larvae. *Mol. Ecol. Resour.* **2010**, *10*, 568−572.
(52) Pizzuto, M. S.; De Battisti, C.; Marciano, S.; Capua, I.; Cattoli, G. Pyrosequencing analysis for a rapid classification of fowl adenovirus species. *Avian Pathol.* **2010**, *39*, 391−398.
(53) Dudley, D. M.; Chin, E. N.; Bimber, B. N.; Sanabani, S. S.; Tarosso, L. F.; Costa, P. R.; Sauer, M. M.; Kallas, E. G.; O'Connor, D. H. Low-Cost Ultra-Wide Genotyping Using Roche/454 Pyrosequencing for Surveillance of HIV Drug Resistance. *PLoS One* **2012**, *7*, e36494.
(54) Timbs, A. T.; Rugless, M. J.; Gallienne, A. E.; Haywood, A. M.; Henderson, S. J.; Old, J. M. Prenatal diagnosis of hemoglobinopathies by pyrosequencing: a more sensitive and rapid approach to fetal genotyping. *Hemoglobin* **2012**, *36*, 144−150.

JOURNAL OF AGRICULTURAL AND FOOD CHEMISTRY

Article

pubs.acs.org/JAFC

Ara h 6 Complements Ara h 2 as an Important Marker for IgE Reactivity to Peanut

Audrey E. Koid,[†] Martin D. Chapman,[†] Robert G. Hamilton,[‡] Ronald van Ree,[§] Serge A. Versteeg,[§] Stephen C. Dreskin,[∥] Stef J. Koppelman,[⊥,¶] and Sabina Wünschmann*,[†]

[†]INDOOR Biotechnologies, Incorporated, 1216 Harris Street, Charlottesville, Virginia 22903, United States

[‡]Johns Hopkins University School of Medicine, 600 North Wolfe Street, 6-113, Baltimore, Maryland 21287, United States

[§]Academic Medical Center, Meibergdreef 9, 1105 AZ Amsterdam-Zuidoost, Netherlands

[∥]School of Medicine, University of Colorado Denver, 1250 14th Street, Denver, Colorado 80202, United States

[⊥]HAL Allergy, J.H. Oortweg 15, 2333 CH Leiden, Netherlands

ABSTRACT: The similarities of two major peanut allergens, Ara h 2 and Ara h 6, in molecular size, amino acid sequence, and structure have made it difficult to obtain natural Ara h 6 free of Ara h 2. The objectives of this study were to purify natural Ara h 6 that is essentially free of Ara h 2 and to compare its IgE reactivity and potency in histamine release assays to Ara h 2. Sodium dodecyl sulfate−polyacrylamide gel electrophoresis of the highly purified allergen (<0.01% Ara h 2) revealed a single 14.5 kD band, and the identity of Ara h 6 was confirmed by liquid chromatography−tandem mass spectrometry. Ara h 6 showed a higher seroprevalence in chimeric IgE enzyme-linked immunosorbent assay (n = 54) but a weaker biological activity in basophil histamine release assays than Ara h 2. Purified Ara h 6 will be useful for diagnostic IgE antibody assays as well as molecular and cellular studies to investigate the immunological mechanisms of peanut allergy.

KEYWORDS: *peanut, allergen, IgE reactivity, histamine release*

INTRODUCTION

Peanut allergy is an important food allergy in the United States that affects 1.4% of children and 0.6% of adults.[1,2] In the United Kingdom, approximately 1.8% of children have an allergy to peanut.[3,4] While most children outgrow food allergies to milk, egg, or wheat, allergy to peanut is more persistent and often continues into adulthood.[5] Minute amounts of peanut, as little as 0.4 g, are enough to elicit milder allergic symptoms that include rashes, angioedema, and gastrointestinal symptoms.[5,6] However, peanut is also one of the main triggers of severe anaphylactic reactions that can be fatal.[7]

Currently, 12 peanut allergens have been documented by the World Health Organization (WHO)/International Union of Immunological Societies (IUIS) Allergen Nomenclature committee.[8] Ara h 1 and Ara h 2 have been well-studied and are recognized as major allergens. Ara h 2 has a higher predictive value for diagnosis of clinical peanut allergy than Ara h 1, Ara h 3, Ara h 8, and Ara h 9.[9] Ara h 2 is also more potent than Ara h 1 or Ara h 3 in histamine release assays and skin prick tests.[10−12]

Another peanut allergen, Ara h 6, has recently emerged as an important allergen, which, together with Ara h 2, has been associated with clinical peanut allergy.[13] Ara h 6 has approximately the same seroprevalence as Ara h 2 and thus is considered a major peanut allergen.[13,14] Ara h 6 and Ara h 2 are of similar molecular size; Ara h 2 is 17−19 kDa, and Ara h 6 is 14.5 kDa. Both allergens are 2S albumins that are heat-stable, immunogenic, and resistant to digestion in the gut.[15−17] The nucleotide (and amino acid) sequences of Ara h 2.0101 and Ara h 6.0101 are 50% identical and 58% similar (EMBOSS Needle alignment). The structure of the protease-resistant core of Ara h 6 has previously been determined by nuclear magnetic resonance (NMR), and the folds of this allergenic core were found to be virtually identical to those of Ara h 2.[15] The three-dimensional folds determine the IgE epitopes, which are lost upon unfolding.[18] More recently, the structure of Ara h 2 was determined by X-ray crystallography, and molecular modeling studies predict that half of the residues on the surfaces of both proteins are conserved.[19] These factors contribute to the difficulty in obtaining purified natural Ara h 6 (nAra h 6) that is free of Ara h 2. Ara h 7, the third peanut allergen of the 2S albumin family, also shows sequence homology to Ara h 2 and Ara h 6.[20] However, attempts to identify natural Ara h 7 protein in peanut extracts have failed. Recently, Schmidt et al. found low abundance of natural Ara h 7.0201 and Ara h 7.0202 in peanut extracts after enrichment of the low-molecular-mass peanut proteins.[21]

Highly purified allergens are important for allergen standardization.[22,23] There is extensive variability in allergen composition and potency between different commercially available peanut extracts, including those used for skin prick testing that could lead to misdiagnosis.[24,25] "Component-resolved" or molecular diagnostics is based on measuring IgE antibodies to multiple individual allergens rather than to heterogeneous extracts. The use of molecular diagnostics tends to lower false-positive IgE antibody results caused by the interaction with profilins and cross-reactive carbohydrate

Received: May 23, 2013
Revised: December 9, 2013
Accepted: December 11, 2013
Published: December 11, 2013

 © 2013 American Chemical Society

determinants that are present in diverse plant-based food.[26−29] Some birch pollen-allergic patients were found to be cross-sensitized to peanut through cross-reactivity between Bet v 1 and Ara h 8, which are homologous proteins that belong to the PR-10 family.[30] Moreover, pea-allergic patients, who later developed peanut allergy, recognized only Ara h 1 but not Ara h 2 or Ara h 3.[31] Vicilin homologues in pea and peanut (Ara h 1) are the molecular basis for this cross-reactivity. Most peanut-allergic patients that react to Ara h 2 also have IgE against Ara h 6; however, a recent case study reported that Ara h 6 caused severe reactions to peanut in the absence of sensitization to Ara h 2.[32] Thus, it is important to have pure, single-component peanut allergens for accurate diagnosis of peanut allergy.

Our objective in this study was to obtain purified nAra h 6 that is essentially free of Ara h 2 and compare its IgE reactivity and potency in histamine release assays to Ara h 2.

MATERIALS AND METHODS

Purified Natural Ara h 6. Peanut flour was extracted into phosphate-buffered saline (PBS) at pH 7.4 containing 1 M sodium chloride for 2 h at 60 °C. The mixture was centrifuged at 13500*g* for 25 min, and the supernatant was sterile-filtered. Ammonium sulfate precipitation was used to remove contaminating Ara h 1. The 70−100% pellet containing Ara h 6 and Ara h 2 was redissolved in PBS and passed over a 1C4 monoclonal antibody column to remove the contaminating Ara h 2. Size-exclusion chromatography (HiPrep 16/60 Sephacryl S-100 HR, GE Life Sciences, Uppsala, Sweden) was used as a final polishing step. The identity of purified nAra h 6 was confirmed by liquid chromatography−tandem mass spectrometry (LC−MS/MS), and its purity was analyzed by sodium dodecyl sulfate−polyacrylamide gel electrophoresis (SDS−PAGE) and silver staining. The concentration of the purified protein was determined by the Advanced Protein Assay (Cytoskeleton, Denver, CO), and the Ara h 2 content was measured using a two-site antibody enzyme-linked immunosorbent assay (ELISA) with monoclonal antibody 1C4 as the capture antibody and rabbit-polyclonal antibody anti-Ara h 2 for detection.[33] Ara h 6 was measured by ELISA using capture monoclonal antibody 3B8 and detection antibody 3E12. Another nAra h 6 preparation available from TNO Quality of Life, Zeist, Netherlands (T-Ara h 6) was tested for comparison.

Sera. Sera for the immunoblotting, chimeric IgE ELISA, and cross-inhibition ELISA were obtained from Bioreclamation, Inc. (East Meadow, NY) (n = 24), which operates in full compliance with the Food and Drug Administration guidelines, the Department of Allergy and Clinical Immunology at Johns Hopkins University (n = 25), and kindly provided by Dr. Peter Heymann, University of Virginia (n = 8). Sera for the Basophil Histamine Release Assay were provided by the Department of Allergy, Asthma, and Clinical Immunology at the University of Colorado (n = 20). All donors signed informed consent and, for minors, assent. Sera were collected with approval from the respective institutions' human investigation committees.

Immunoblotting. IgE reactivity of purified nAra h 6 was compared to natural Ara h 2 (nAra h 2), peanut extract, and T-Ara h 6 by immunoblot using pooled sera from six peanut-allergic patients (≥100 kU/L by chimeric IgE ELISA, PWH6, BR13, BR21, BR22, BR23, and BR24). Proteins loaded at 0.5 mg/mL and separated by SDS−PAGE under non-reducing conditions (20% homogenous, GE Lifesciences, Uppsala, Sweden) were transferred to a polyvinylidene difluoride (PVDF) membrane (Bio-Rad Laboratories, Hercules, CA) by electroblotting. The membrane was blocked with 5% non-fat dry milk in 25 mM Tris, 150 mM NaCl at pH 7.4, and 0.05% Tween-20 for 16 h at 4 °C and then incubated with the pooled sera at a 1:2 dilution in blocking buffer for 2 h at room temperature. Bound IgE was detected with peroxidase-labeled goat anti-human IgE (Kirkegaard and Perry Laboratories, Inc., Gaithersburg, MD) followed by ECL Western Blotting Analysis System (GE Lifesciences, Uppsala, Sweden), which produced a detectable chemiluminescent signal.

Chimeric IgE ELISA. IgE antibody binding to nAra h 6 was compared to IgE binding to T-Ara h 6 and nAra h 2 by a modified chimeric IgE ELISA as described previously.[34−36] Briefly, microtiter plates coated to saturation with one allergen at 0.5 μg/well were incubated with sera from peanut-allergic patients (ImmunoCAP values ranged from 0.45 to >100 kUA/L, with an average of 15.2 ± 21.4 kUA/L; n = 54). Bound IgE antibody was detected using biotinylated goat anti-human IgE (Kierkegaard and Perry, Gaithersburg, MD), followed by streptavidin peroxidase. The intensity of the color developed by 2,2′-azino-bis(3-ethylbenzothiazoline-6-sulfonic acid) (ABTS) was measured at 405 nm. A chimeric anti-Der p 2 antibody, 2B12-IgE, was used to establish a standard curve from 0.4 to 115 U/mL IgE to quantify the bound specific IgE as previously reported.[36] Ara h 6- and Ara h 2-specific IgE for each serum sample were extrapolated from the linear portion of the 2B12−IgE curve. Levels of specific IgE antibody reactive with nAra h 6 and nAra h 2 or T-Ara h 6 were plotted and modeled using linear regression. Pearson correlations were used to analyze the relationship between specific IgE to nAra h 6 and nAra h 2 or T-Ara h 6 in sera of peanut-allergic patients.

Cross-inhibition ELISA. The chimeric IgE ELISA was modified for cross-inhibition assays. Microtiter plates were saturated with nAra h 6 or nAra h 2 at 0.5 μg/well for 16 h at 4 °C.[34] A serum pool of the same sera used in the immunoblot was incubated with increasing concentrations of the inhibitor (either nAra h 6 or nAra h 2) for 1 h prior to performing the assays. The protein concentration of the inhibiting allergen was increased in 10-fold increments from 10 to 10 000 ng/mL. The pooled sera with or without the inhibitor were added to their respective wells and incubated at room temperature for 1 h. Bound IgE was detected as described for the chimeric IgE ELISA. The percent inhibition was calculated on the basis of the optical density at 405 nm. A 0% inhibition was assumed for the wells that had no inhibitor.

Basophil Histamine Release Assay. The stripped basophil histamine release assay was performed as previously described.[37] Briefly, basophil cells were stripped of membrane-bound IgE and sensitized with each serum from peanut-allergic patients (Ara h 6-specific IgE values ranged from 5 to 480 kUA/L, with an average of 87.8 ± 125 kUA/L; n = 20). The cells were then stimulated with increasing concentrations of allergen, and histamine release was measured by fluorometric analysis. Histamine release was expressed as a percentage of the total amount of histamine in the cells determined after lysis of the cells with perchloric acid (100% release). EC_{50} was the allergen concentration required to stimulate 50% of the maximum release. Histamine release dose response curves for nAra h 6 and nAra h 2 were generated for concentrations between 0.001 and 1000 ng/mL.

RESULTS

Protein Characterization. Purified nAra h 6 (lane 4) and T-Ara h 6 (lane 5) migrated as single bands on silver-stained SDS−PAGE at the predicted molecular weight of 14.5 kDa (Figure 1A). The Ara h 6 content was 1.05 mg/mL, while the

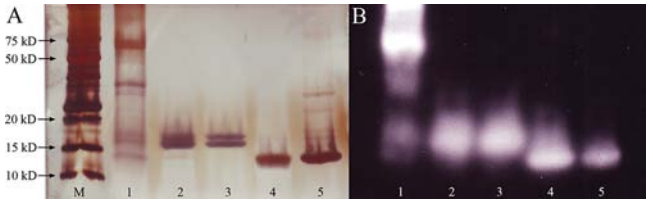

Figure 1. Silver stain and immunoblot of nAra h 2, nAra h 6, and peanut extract using pooled sera from six peanut-allergic patients. (A) Silver-stained gel. (B) Proteins transferred onto a PVDF membrane were probed with sera, and bound IgE was detected with a peroxidase-labeled goat anti-human IgE. Lane M, marker; lane 1, peanut extract; lanes 2 and 3, nAra h 2; lane 4, nAra h 6; and lane 5, T-Ara h 6.

dx.doi.org/10.1021/jf4022509 | J. Agric. Food Chem. 2014, 62, 206−213

concentration of Ara h 2 was less than 0.1 μg/mL (0.01%) as measured by two-site antibody ELISA. The results of LC−MS/MS confirmed the identity of the purified allergen as Ara h 6.0101 with 74.5% sequence coverage (Figure 2).

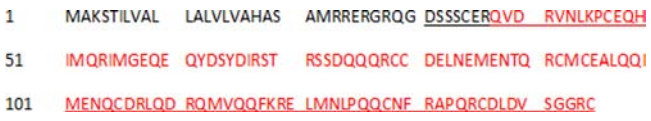

Figure 2. Sequence coverage of purified nAra h 6 with Ara h 6.0101. Underlined red letters indicate identical amino acids between the purified allergen and the published sequence.

IgE Binding Analysis. Immunoblotting demonstrated strong IgE reactivity to nAra h 2 (lanes 2 and 3), nAra h 6 (lanes 4 and 5), and peanut extract (lane 1; Figure 1B). The major allergens, Ara h 1 (63 kDa), Ara h 2 (18−20 kDa), and Ara h 6 can be seen as major bands in the peanut extract. Ara h 2 was not detected in the purified nAra h 6 preparation.

More sera showed IgE binding to nAra h 6 than to nAra h 2 (45 versus 39) using a chimeric IgE ELISA; however, the levels of Ara h 2-specific IgE were on average 13% higher than the levels of Ara h 6-specific IgE. A total of 25 of these patients had higher levels of specific IgE to one allergen but not to the other (Table 1). For example, patient BR1 had 4-fold higher Ara h 2-specific IgE than Ara h 6-specific IgE, while patient BH25 had 5-fold higher Ara h 6-specific IgE than Ara h 2-specific IgE (Table 1). There was a strong quantitative correlation between the levels of specific IgE to nAra h 6 and specific IgE to nAra h 2 ($r = 0.91$; $n = 54$; $p < 0.001$; Figure 3A). The levels of Ara h 6-specific IgE binding to purified nAra h 6 correlated well with the same Ara h 6-specific IgE binding to T-Ara h 6 ($r = 0.98$; $n = 39$; $p < 0.001$; Figure 3B). On average, the IgE binding to the purified nAra h 6 material was 46% higher than that observed interacting with T-Ara h 6.

Results obtained in the cross-inhibition assay indicate that nAra h 2 inhibited IgE allergen binding more effectively than nAra h 6. At 70 ng/mL, Ara h 2 inhibited 50% of IgE−Ara h 2 and IgE−Ara h 6 interactions (Figure 4). However, 600 and 5000 ng/mL of Ara h 6 were required to inhibit 50% IgE binding to Ara h 6 and Ara h 2, respectively.

Biological Activity. Natural Ara h 6 showed less biological activity than nAra h 2 in the basophil histamine release assay (Figure 5). At a concentration of 0.1 μg/mL, Ara h 2 stimulated 50% of the maximum histamine release, while 1 μg/mL of Ara h 6 was required to achieve 50% of maximum histamine release. In general, histamine release was 10% lower for nAra h 6 than nAra h 2 at the same allergen concentration. The dose−response curve of histamine release by nAra h 6 was shifted to the right of the dose response curve for nAra h 2 (Figure 5). On average, histamine release began to plateau at 0.001 μg/mL Ara h 2 and continued an upward trend even to a concentration of 1 μg/mL Ara h 6.

DISCUSSION

Peanut allergy is on the rise, as evidenced by a 1% increase in just over an 11 year period (1997−2008) in the U.S.[2] Traces of peanut can be found in many processed foods, and this poses a danger to peanut-allergic patients because miniscule amounts can trigger an allergic reaction.[6] Previous studies have demonstrated significant variability in the protein content and allergenicity of commercially available peanut extracts.[38] There is a critical need for ultrapure allergens to clarify research results and improve the accuracy of diagnostic tests in an attempt to better understand the mechanisms associated with the induction of allergic diseases. Analysis of single components

Table 1. Ara h 2- and Ara h 6-Specific IgE Concentrations of Sera of Peanut-Allergic Patients That Were Positive to at Least One of the Two Allergens as Measured by Chimeric ELISA[a]

INDOOR ID	Ara h 2 (kUA/L)	nAra h 6 (kUA/L)	INDOOR ID	Ara h 2 (kUA/L)	nAra h 6 (kUA/L)
BH1	8.96	10.9	**BH25**	58.3	326
BH2	223	109	**BR1**	270	61.7
BH3	9.59	7.02	**BR2**	38.4	89.2
BH4	3.61	8.7	**BR4**	<0.4	0.7
BH5	8.43	20	**BR5**	20.2	4.17
BH6	345	383	BR6	3.67	3.51
BH7	499	814	**BR8**	0.89	4.89
BH8	1.03	10.8	**BR11**	<0.4	0.6
BH9	40.1	7.9	BR12	0.4	<0.4
BH10	0.56	0.89	BR13	568	520
BH11	<0.4	0.7	**BR14**	0	0.8
BH12	58.3	79.5	BR16	2.63	3.07
BH13	108	187	**BR17**	58.4	6.71
BH14	1.89	3.62	**BR18**	96.8	36.1
BH15	0.93	0.92	BR21	208	145
BH16	<0.4	1.71	BR22	140	151
BH17	13.6	10.1	BR23	299	164
BH18	1.05	13.3	**BR24**	269	93.1
BH19	7.32	17.4	PWH1	<0.4	0.57
BH21	0.35	0.6	**PWH3**	0.8	5.31
BH22	1.47	1.23	**PWH4**	0.33	0.66
BH23	14.2	28.9	**PWH5**	<0.4	0.71
BH24	4.83	2.06	PWH6	1657	1113

[a]Sera with a ratio of Ara h 2-specific IgE/Ara h 6-specific IgE of >2 or <0.5 are highlighted in bold font.

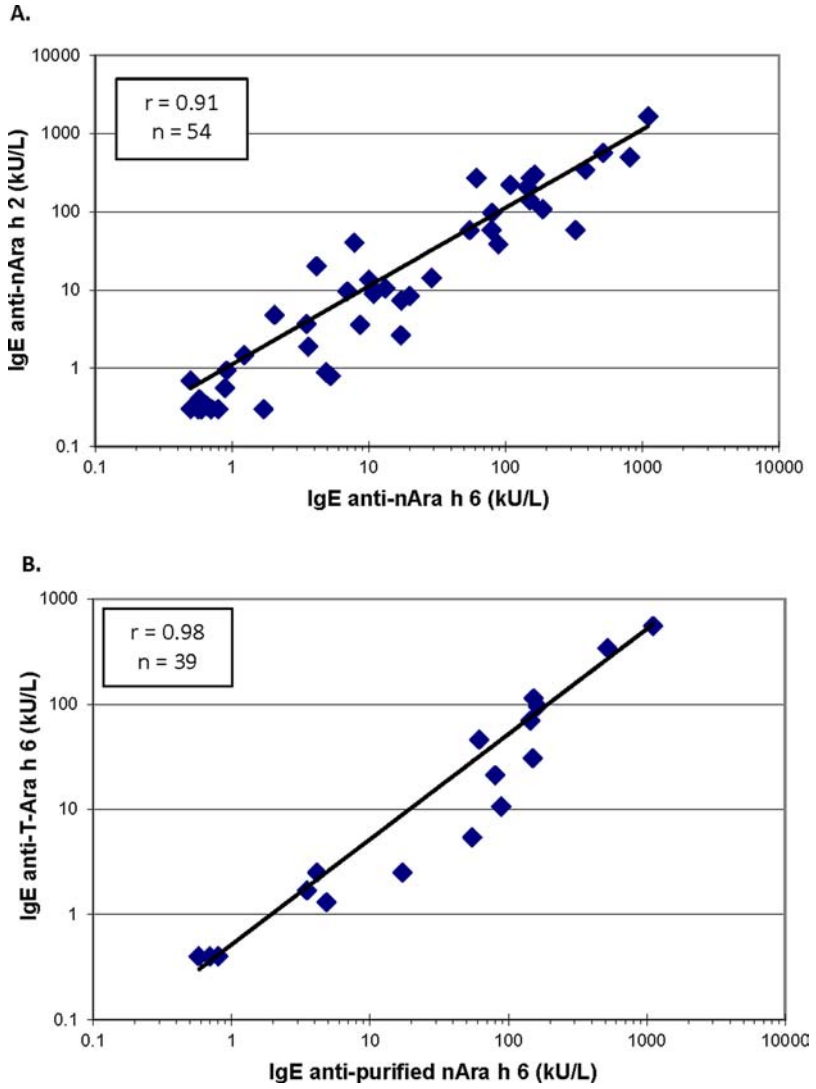

Figure 3. Correlation between (A) IgE binding to purified nAra h 6 and purified nAra h 2 and (B) purified nAra h 6 and T-Ara h 6. Allergen coated onto microtiter plates was incubated with sera from peanut-allergic patients, and bound IgE was detected by biotin-labeled goat anti-human IgE, followed by streptavidin peroxidase. The intensity of the color development of ABTS was measured at 405 nm.

allows for more effective dissection of cross-reactivity among structurally similar allergens and aids in identifying the cross-reactive allergen from the allergen that initially elicited the sensitization. For food allergy studies in particular, molecular diagnostics more effectively reveal patterns of sensitization and cross-reactivity among allergenic homologues across food groups.[39]

Ara h 2 has been extensively studied and established as a major allergen, while Ara h 6 has only recently gained interest in peanut allergy research. Ara h 2 and Ara h 6 belong to the 2S albumin family that are characterized by having a stable core formed by four disulfide bridges, which makes these proteins resistant to high-temperature processing and proteolytic digestion.[16,40] The stability of these proteins and their resistance to digestive enzymes in the gut has been identified as major factors contributing to their allergenicity.[15,41] The sequence and structural similarity between Ara h 6 and Ara h 2 has made it difficult to produce nAra h 6 free of nAra h 2.[19] Recombinant Ara h 6 has been produced, but conformational differences between the natural and recombinant forms have yielded recombinant Ara h 6 with low IgE reactivity.[20] More recently, a recombinant Ara h 6 produced in *Pichia pastoris* has shown improved biological potency similar to that of nAra h 6.[42]

Highly purified nAra h 6 has analytically been shown to be free of Ara h 2. Similar to natural Ara h 2, natural Ara h 7 also shares sequence similarity with Ara h 6 and thus may co-purify with Ara h 6. However, natural Ara h 7 has a very low abundance in peanut extracts, which greatly minimizes the risk of contamination.[21]

Purified natural Ara h 6 displayed its own unique immunological activity patterns. While a strong correlation was shown between the relative levels of Ara h 2-specific IgE and Ara h 6-specific IgE, sera from 25 individuals reacted more strongly to one allergen than the other, as reported in previous studies.[16,32,43] Interestingly, only 8 of the 25 tested sera had higher Ara h 2-specific IgE, even though Ara h 2 is the predominantly recognized allergen by peanut-allergic patients.[13]

In our cross-inhibition analyses, Ara h 2 inhibited Ara h 6-specific IgE binding more effectively than Ara h 6 inhibited Ara h 2-specific IgE binding as reported previously.[16] The inhibitory

dx.doi.org/10.1021/jf4022509 | J. Agric. Food Chem. 2014, 62, 206−213

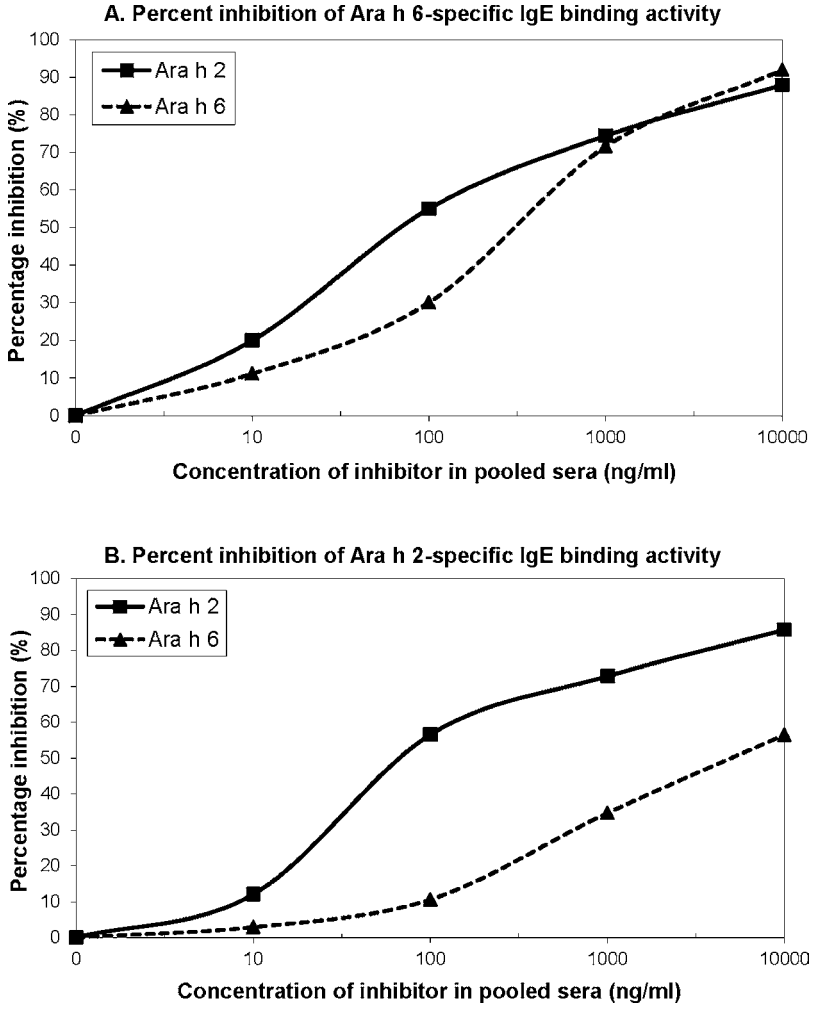

Figure 4. Specific IgE cross-inhibition assay with increasing inhibitor allergen concentrations of Ara h 2 and Ara h 6. (A) Percent inhibition of Ara h 6-specific IgE binding activity. (B) Percent inhibition of Ara h 2-specific IgE binding activity.

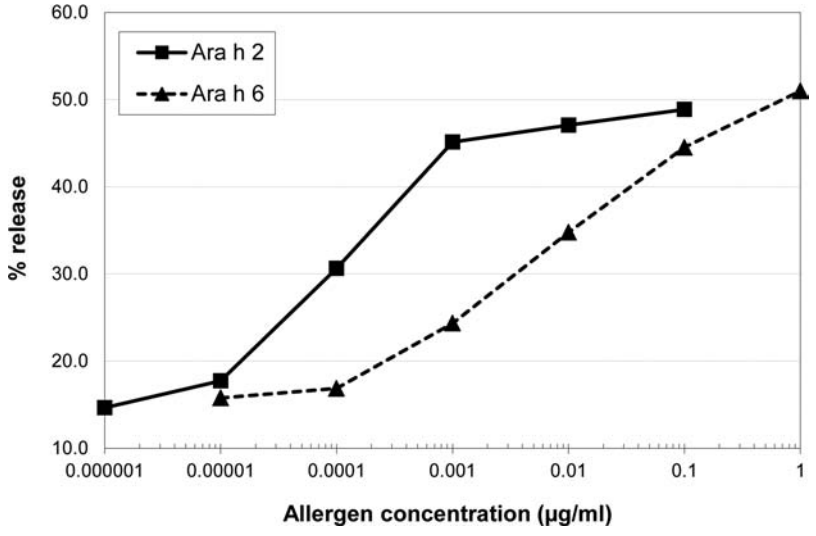

Figure 5. Average basophil histamine release by nAra h 2 and nAra h 6 (n = 20) using increasing concentrations of allergen.

effect of Ara h 2 may be due to its unique IgE-binding epitopes that are not present in Ara h 6, while Ara h 6 contains IgE-binding epitopes that are also present on Ara h 2.[44] However, we did not achieve complete inhibition of Ara h 6−IgE binding by Ara h 2 even at 10 μg/mL, which suggests that Ara h 6 could have unique IgE-binding epitope(s). This is supportive of the report by Lehmann et al., who performed an enzyme allergosorbent test and found that maximal inhibition by

dx.doi.org/10.1021/jf4022509 | J. Agric. Food Chem. 2014, 62, 206−213

recombinant Ara h 2 and recombinant Ara h 6 was only 70 and 60%, respectively.[15,45]

Ara h 2 consistently induced higher levels of histamine release than Ara h 6 in basophil studies. In general, a 10-fold lower concentration of Ara h 2 than Ara h 6 was required to induce the same amount of histamine release. Similarly, Ara h 2 was recently found to be more potent than Ara h 6 using the RBL SX-38 cells assay, although the magnitude of the difference was less than we report here with the stripped basophil assay.[46] Ara h 2 also elicited a higher magnitude of mediator release at lower concentrations than Ara h 6.[15] However, as the allergen concentration increased, Ara h 6 induced the release of higher percentages of β-hexosaminidase than Ara h 2.[47]

While most published data suggest that Ara h 2 is more potent than Ara h 6, there are exceptions. Ara h 6 had a higher seroprevalence (83.3%) than Ara h 2 (72.2%) in our study that involved testing 54 sera from peanut-allergic patients. In another study, Ara h 6 was shown to produce a stronger Th2 response than Ara h 2 in peripheral blood mononuclear cells of peanut-allergic children.[48] The depletion of Ara h 2 or Ara h 6 alone from crude peanut extract did not cause a significant reduction in the maximal net level of mediator release from SBX-38 cells, but the removal of both allergens decreased effector activity by approximately 20%.[49] Previously, Ara h 2 and Ara h 6 together were shown to be responsible for over 60% of the effector activity.[50] Furthermore, *in vivo* studies using murine models showed that desensitization with the Ara h 2/Ara h 6 mixture and crude peanut extract produced comparable results.[51,52]

Peanut allergy associated with sensitization to storage proteins (Ara h 1, Ara h 2, Ara h 3, Ara h 6, and Ara h 7) presents the most serious form of peanut allergy.[53] While Ara h 1 and Ara h 3 are the most abundant storage proteins in peanut (11−31 and 38−76% of protein content in peanut extracts, respectively), patients with peanut allergy recognize predominantly Ara h 2 and Ara h 6.[13,14,54] Molecular diagnostics have shown that the combined results of IgE reactivity to the two storage proteins Ara h 2 and Ara h 6 yielded the highest diagnostic sensitivity and specificity for detecting clinically evident peanut allergy.[13] By themselves, Ara h 2 and Ara h 6 had high diagnostic sensitivity and specificity compared to Ara h 1 and Ara h 3, but together, the two 2S albumin proteins were able to predict peanut allergy with 98% sensitivity and 85% specificity at a predictive threshold of 0.1 kU/L. The addition of specific IgE tests for other storage proteins, such as Ara h 6, or Ara h1, and Ara h 3, will increase specificity and sensitivity of molecular diagnosis, because not all patients with clinical peanut allergy show sensitization to Ara h 2.[32,53,55] Thus, purified nAra h 6 should be considered an important diagnostic reagent for both *in vitro* and *in vivo* assays that, together with nAra h 2 will improve diagnostic, immunologic, and biologic assays used in the investigation of peanut allergy, T-cell studies, and mouse models of asthma.

AUTHOR INFORMATION

Corresponding Author

*Telephone: +1-434-984-2304. Fax: +1-434-984-2709. E-mail: sabina@inbio.com.

Present Address

[¶]DBV Technologies, Green Square, Bâtiment, D 80/84 rue des Meuniers, 92220 Bagneux, France.

Funding

Stephen C. Dreskin and Stef Koppelman received funding from HAL Allergy for part of the research carried out in this work. This work was also partially supported by Grant RO1-AI052164 to Stephen C. Dreskin from the National Institute of Allergy and Infectious Diseases (National Institutes of Health) 89130-898.

Notes

The authors declare the following competing financial interest(s): Audrey E. Koid, Martin D. Chapman, and Sabina Wünschmann are employees of INDOOR Biotechnologies, Inc. that manufactures peanut allergens.

ACKNOWLEDGMENTS

The authors are grateful to Dr. Peter Heymann for the peanut allergic patients' sera. The authors also thank Dr. Govardus A. H. de Jong for providing the T-Ara h 6.

ABBREVIATIONS USED

nAra h 6, natural Ara h 6; nAra h 2, natural Ara h 2; T-Ara h 6, TNO-produced Ara h 6 used as a reference; SDS−PAGE, sodium dodecyl sulfate−polyacrylamide gel electrophoresis; LC−MS/MS, liquid chromatography−tandem mass spectrometry; ELISA, enzyme-linked immunosorbent assay; WHO, World Health Organization; PR-10, pathogenesis-related class 10 protein; PVDF, polyvinylidene difluoride; ABTS, 2,2′-azinobis(3-ethylbenzothiazoline-6-sulfonic acid)

REFERENCES

(1) Gupta, R. S.; Springston, E. E.; Warrier, M. R.; Smith, B.; Kumar, R.; Pongracic, J.; Holl, J. L. The prevalence, severity, and distribution of childhood food allergy in the United States. *Pediatrics* **2011**, *128* (1), e9−e17.

(2) Sicherer, S. H.; Munoz-Furlong, A.; Godbold, J. H.; Sampson, H. A. US prevalence of self-reported peanut, tree nut, and sesame allergy: 11-year follow-up. *J. Allergy Clin. Immunol.* **2010**, *125* (6), 1322−1326.

(3) Hourihane, J. O.; Aiken, R.; Briggs, R.; Gudgeon, L. A.; Grimshaw, K. E.; DunnGalvin, A.; Roberts, S. R. The impact of government advice to pregnant mothers regarding peanut avoidance on the prevalence of peanut allergy in United Kingdom children at school entry. *J. Allergy Clin. Immunol.* **2007**, *119* (5), 1197−1202.

(4) Du, T. G.; Katz, Y.; Sasieni, P.; Mesher, D.; Maleki, S. J.; Fisher, H. R.; Fox, A. T.; Turcanu, V.; Amir, T.; Zadik-Mnuhin, G.; Cohen, A.; Livne, I.; Lack, G. Early consumption of peanuts in infancy is associated with a low prevalence of peanut allergy. *J. Allergy Clin. Immunol.* **2008**, *122* (5), 984−991.

(5) Finkelman, F. D. Peanut allergy and anaphylaxis. *Curr. Opin. Immunol.* **2010**, *22* (6), 783−788.

(6) Perry, T. T.; Matsui, E. C.; Conover-Walker, M. K.; Wood, R. A. Risk of oral food challenges. *J. Allergy Clin. Immunol.* **2004**, *114* (5), 1164−1168.

(7) Bock, S. A.; Munoz-Furlong, A.; Sampson, H. A. Further fatalities caused by anaphylactic reactions to food, 2001−2006. *J. Allergy Clin. Immunol.* **2007**, *119* (4), 1016−1018.

(8) Chapman, M. D.; Pomes, A.; Breiteneder, H.; Ferreira, F. Nomenclature and structural biology of allergens. *J. Allergy Clin. Immunol.* **2007**, *119* (2), 414−420.

(9) Nicolaou, N.; Murray, C.; Belgrave, D.; Poorafshar, M.; Simpson, A.; Custovic, A. Quantification of specific IgE to whole peanut extract and peanut components in prediction of peanut allergy. *J. Allergy Clin. Immunol.* **2011**, *127* (3), 684−685.

(10) Astier, C.; Morisset, M.; Roitel, O.; Codreanu, F.; Jacquenet, S.; Franck, P.; Ogier, V.; Petit, N.; Proust, B.; Moneret-Vautrin, D. A.; Burks, A. W.; Bihain, B.; Sampson, H. A.; Kanny, G. Predictive value of skin prick tests using recombinant allergens for diagnosis of peanut allergy. *J. Allergy Clin. Immunol.* **2006**, *118* (1), 250−256.

(11) Koppelman, S. J.; Wensing, M.; Ertmann, M.; Knulst, A. C.; Knol, E. F. Relevance of Ara h 1, Ara h 2 and Ara h 3 in peanut-allergic patients, as determined by immunoglobulin E Western blotting, basophil-histamine release and intracutaneous testing: Ara h 2 is the most important peanut allergen. *Clin. Exp. Allergy* **2004**, *34* (4), 583−590.

(12) Palmer, G. W.; Dibbern, D. A., Jr.; Burks, A. W.; Bannon, G. A.; Bock, S. A.; Porterfield, H. S.; McDermott, R. A.; Dreskin, S. C. Comparative potency of Ara h 1 and Ara h 2 in immunochemical and functional assays of allergenicity. *Clin. Immunol.* **2005**, *115* (3), 302−312.

(13) Codreanu, F.; Collignon, O.; Roitel, O.; Thouvenot, B.; Sauvage, C.; Vilain, A. C.; Cousin, M. O.; Decoster, A.; Renaudin, J. M.; Astier, C.; Monnez, J. M.; Vallois, P.; Morisset, M.; Moneret-Vautrin, D. A.; Brulliard, M.; Ogier, V.; Castelain, M. C.; Kanny, G.; Bihain, B. E.; Jacquenet, S. A novel immunoassay using recombinant allergens simplifies peanut allergy diagnosis. *Int. Arch. Allergy Immunol.* **2011**, *154* (3), 216−226.

(14) Flinterman, A. E.; van Hoffen, E.; den Hartog Jager, C. F.; Koppelman, S.; Pasmans, S. G.; Hoekstra, M. O.; Bruijnzeel-Koomen, C. A.; Knulst, A. C.; Knol, E. F. Children with peanut allergy recognize predominantly Ara h2 and Ara h6, which remains stable over time. *Clin. Exp. Allergy* **2007**, *37* (8), 1221−1228.

(15) Lehmann, K.; Schweimer, K.; Reese, G.; Randow, S.; Suhr, M.; Becker, W. M.; Vieths, S.; Rosch, P. Structure and stability of 2S albumin-type peanut allergens: Implications for the severity of peanut allergic reactions. *Biochem. J.* **2006**, *395* (3), 463−472.

(16) Suhr, M.; Wicklein, D.; Lepp, U.; Becker, W. M. Isolation and characterization of natural Ara h 6: Evidence for a further peanut allergen with putative clinical relevance based on resistance to pepsin digestion and heat. *Mol. Nutr. Food Res.* **2004**, *48* (5), 390−399.

(17) Starkl, P.; Krishnamurthy, D.; Szalai, K.; Felix, F.; Lukschal, A.; Oberthuer, D.; Sampson, H. A.; Swoboda, I.; Betzel, C.; Untersmayr, E.; Jensen-Jarolim, E. Heating affects structure, enterocyte adsorption and signalling, as well as immunogenicity of the peanut allergen Ara h 2. *Open Allergy J.* **2011**, *4*, 24−34.

(18) Starkl, P.; Felix, F.; Krishnamurthy, D.; Stremnitzer, C.; Roth-Walter, F.; Prickett, S. R.; Voskamp, A. L.; Willensdorfer, A.; Szalai, K.; Weichselbaumer, M.; O'Hehir, R. E.; Jensen-Jarolim, E. An unfolded variant of the major peanut allergen Ara h 2 with decreased anaphylactic potential. *Clin. Exp. Allergy* **2012**, *42* (12), 1801−1812.

(19) Mueller, G. A.; Gosavi, R. A.; Pomes, A.; Wunschmann, S.; Moon, A. F.; London, R. E.; Pedersen, L. C. Ara h 2: Crystal structure and IgE binding distinguish two subpopulations of peanut allergic patients by epitope diversity. *Allergy* **2011**, *66* (7), 878−885.

(20) Kleber-Janke, T.; Crameri, R.; Appenzeller, U.; Schlaak, M.; Becker, W. M. Selective cloning of peanut allergens, including profilin and 2S albumins, by phage display technology. *Int. Arch. Allergy Immunol.* **1999**, *119* (4), 265−274.

(21) Schmidt, H.; Krause, S.; Gelhaus, C.; Petersen, A.; Janssen, O.; Becker, W. M. Detection and structural characterization of natural Ara h 7, the third peanut allergen of the 2S albumin family. *J. Proteome. Res.* **2010**, *9* (7), 3701−3709.

(22) van Ree, R.; Chapman, M. D.; Ferreira, F.; Vieths, S.; Bryan, D.; Cromwell, O.; Villalba, M.; Durham, S. R.; Becker, W. M.; Aalbers, M.; Andre, C.; Barber, D.; Cistero, B. A.; Custovic, A.; Didierlaurent, A.; Dolman, C.; Dorpema, J. W.; Di, F. G.; Eberhardt, F.; Fernandez, C. E.; Fernandez, R. M.; Fiebig, H.; Focke, M.; Fotisch, K.; Gadermaier, G.; Das, R. G.; Gonzalez, M. E.; Himly, M.; Kinaciyan, T.; Knulst, A. C.; Kroon, A. M.; Lepp, U.; Marco, F. M.; Mari, A.; Moingeon, P.; Monsalve, R.; Neubauer, A.; Notten, S.; Ooievaar-de Heer, P.; Pauli, G.; Pini, C.; Purohit, A.; Quiralte, J.; Rak, S.; Raulf-Heimsoth, M.; San Miguel Moncin, M. M.; Simpson, B.; Tsay, A.; Vailes, L.; Wallner, M.; Weber, B. The CREATE project: Development of certified reference materials for allergenic products and validation of methods for their quantification. *Allergy* **2008**, *63* (3), 310−326.

(23) Chapman, M. D.; Ferreira, F.; Villalba, M.; Cromwell, O.; Bryan, D.; Becker, W. M.; Fernandez-Rivas, M.; Durham, S.; Vieths, S.; van Ree, R. The European Union CREATE project: A model for international standardization of allergy diagnostics and vaccines. *J. Allergy Clin. Immunol.* **2008**, *122* (5), 882−889.

(24) Hefle, S. L.; Helm, R. M.; Burks, A. W.; Bush, R. K. Comparison of commercial peanut skin test extracts. *J. Allergy Clin. Immunol.* **1995**, *95* (4), 837−842.

(25) Akkerdaas, J. H.; Wensing, M.; Knulst, A. C.; Krebitz, M.; Breiteneder, H.; de, V. S.; Penninks, A. H.; Aalberse, R. C.; Hefle, S. L.; van Ree, R. How accurate and safe is the diagnosis of hazelnut allergy by means of commercial skin prick test reagents? *Int. Arch. Allergy Immunol.* **2003**, *132* (2), 132−140.

(26) Mari, A.; Ooievaar-de Heer, P.; Scala, E.; Giani, M.; Pirrotta, L.; Zuidmeer, L.; Bethell, D.; van Ree, R. Evaluation by double-blind placebo-controlled oral challenge of the clinical relevance of IgE antibodies against plant glycans. *Allergy* **2008**, *63* (7), 891−896.

(27) Valenta, R.; Duchene, M.; Ebner, C.; Valent, P.; Sillaber, C.; Deviller, P.; Ferreira, F.; Tejkl, M.; Edelmann, H.; Kraft, D. Profilins constitute a novel family of functional plant pan-allergens. *J. Exp. Med.* **1992**, *175* (2), 377−385.

(28) van Ree, R. Carbohydrate epitopes and their relevance for the diagnosis and treatment of allergic diseases. *Int. Arch. Allergy Immunol.* **2002**, *129* (3), 189−197.

(29) Santos, A.; van Ree, R. Profilins: mimickers of allergy or relevant allergens? *Int. Arch. Allergy Immunol.* **2011**, *155* (3), 191−204.

(30) Mittag, D.; Akkerdaas, J.; Ballmer-Weber, B. K.; Vogel, L.; Wensing, M.; Becker, W. M.; Koppelman, S. J.; Knulst, A. C.; Helbling, A.; Hefle, S. L.; van Ree, R.; Vieths, S. Ara h 8, a Bet v 1-homologous allergen from peanut, is a major allergen in patients with combined birch pollen and peanut allergy. *J. Allergy Clin. Immunol.* **2004**, *114* (6), 1410−1417.

(31) Wensing, M.; Knulst, A. C.; Piersma, S.; O'Kane, F.; Knol, E. F.; Koppelman, S. J. Patients with anaphylaxis to pea can have peanut allergy caused by cross-reactive IgE to vicilin (Ara h 1). *J. Allergy Clin. Immunol.* **2003**, *111* (2), 420−424.

(32) Asarnoj, A.; Glaumann, S.; Elfstrom, L.; Lilja, G.; Lidholm, J.; Nilsson, C.; Wickman, M. Anaphylaxis to peanut in a patient predominantly sensitized to Ara h 6. *Int. Arch. Allergy Immunol.* **2012**, *159* (2), 209−212.

(33) Chapman, M. D.; Tsay, A.; Vailes, L. D. Home allergen monitoring and control—Improving clinical practice and patient benefits. *Allergy* **2001**, *56* (7), 604−610.

(34) Trombone, A. P.; Tobias, K. R.; Ferriani, V. P.; Schuurman, J.; Aalberse, R. C.; Smith, A. M.; Chapman, M. D.; Arruda, L. K. Use of a chimeric ELISA to investigate immunoglobulin E antibody responses to Der p 1 and Der p 2 in mite-allergic patients with asthma, wheezing and/or rhinitis. *Clin. Exp. Allergy* **2002**, *32* (9), 1323−1328.

(35) Schuurman, J.; Perdok, G. J.; Aalberse, R. C. Mouse/human chimeric antibodies directed to two nonoverlapping epitopes of the house dust mite allergen, Der p 2. *Int. Arch. Allergy Immunol.* **1997**, *113* (1−3), 262−263.

(36) Schuurman, J.; Perdok, G. J.; Lourens, T. E.; Parren, P. W.; Chapman, M. D.; Aalberse, R. C. Production of a mouse/human chimeric IgE monoclonal antibody to the house dust mite allergen Der p 2 and its use for the absolute quantification of allergen-specific IgE. *J. Allergy Clin. Immunol.* **1997**, *99* (4), 545−550.

(37) Kleine, B. I.; de Heer, P. G.; van der Zee, J. S.; Aalberse, R. C. The stripped basophil histamine release bioassay as a tool for the detection of allergen-specific IgE in serum. *Int. Arch. Allergy Immunol.* **2001**, *126* (4), 277−285.

(38) Hourihane, J. O. Peanut allergy. *Pediatr. Clin. North Am* **2011**, *58* (2), 445−458.

(39) Steckelbroeck, S.; Ballmer-Weber, B. K.; Vieths, S. Potential, pitfalls, and prospects of food allergy diagnostics with recombinant allergens or synthetic sequential epitopes. *J. Allergy Clin. Immunol.* **2008**, *121* (6), 1323−1330.

(40) Koppelman, S. J.; Hefle, S. L.; Taylor, S. L.; de Jong, G. A. Digestion of peanut allergens Ara h 1, Ara h 2, Ara h 3, and Ara h 6: A comparative in vitro study and partial characterization of digestion-resistant peptides. *Mol. Nutr. Food Res.* **2010**, *54* (12), 1711−1721.

(41) Moreno, F. J.; Clemente, A. 2S albumin storage proteins: What makes them food allergens? *Open Biochem. J.* **2008**, *2*, 16−28.
(42) Zhuang, Y.; Durrani, S.; Hodges, B. D.; Dreskin, S. C.; Chen, X. Expression of recombinant Ara h 6 in *Pichia pastoris* but not in *Escherichia coli* preserves allergic effector function and allows assessment of specific mutations. *Mol. Nutr. Food Res.* **2012**, *56* (6), 986−995.
(43) Bernard, H.; Mondoulet, L.; Drumare, M. F.; Paty, E.; Scheinmann, P.; Thai, R.; Wal, J. M. Identification of a new natural Ara h 6 isoform and of its proteolytic product as major allergens in peanut. *J. Agric. Food Chem.* **2007**, *55* (23), 9663−9669.
(44) Koppelman, S. J.; de Jong, G. A.; Laaper-Ertmann, M.; Peeters, K. A.; Knulst, A. C.; Hefle, S. L.; Knol, E. F. Purification and immunoglobulin E-binding properties of peanut allergen Ara h 6: Evidence for cross-reactivity with Ara h 2. *Clin. Exp. Allergy* **2005**, *35* (4), 490−497.
(45) Bernard, H.; Drumare, M. F.; Guillon, B.; Paty, E.; Scheinmann, P.; Wal, J. M. Immunochemical characterisation of structure and allergenicity of peanut 2S albumins using different formats of immunoassays. *Anal. Bioanal. Chem.* **2009**, *395* (1), 139−146.
(46) Chen, X.; Wang, Q.; El-Mezayen, R.; Zhuang, Y.; Dreskin, S. C. Ara h 2 and Ara h 6 have similar allergenic activity and are substantially redundant. *Int. Arch. Allergy Immunol.* **2012**, *160* (3), 251−258.
(47) Blanc, F.; Adel-Patient, K.; Drumare, M. F.; Paty, E.; Wal, J. M.; Bernard, H. Capacity of purified peanut allergens to induce degranulation in a functional in vitro assay: Ara h 2 and Ara h 6 are the most efficient elicitors. *Clin. Exp. Allergy* **2009**, *39* (8), 1277−1285.
(48) Flinterman, A. E.; Pasmans, S. G.; den Hartog Jager, C. F.; Hoekstra, M. O.; Bruijnzeel-Koomen, C. A.; Knol, E. F.; van Hoffen, E. T cell responses to major peanut allergens in children with and without peanut allergy. *Clin. Exp. Allergy* **2010**, *40* (4), 590−597.
(49) Chen, X.; Zhuang, Y.; Wang, Q.; Moutsoglou, D.; Ruiz, G.; Yen, S. E.; Dreskin, S. C. Analysis of the effector activity of Ara h 2 and Ara h 6 by selective depletion from a crude peanut extract. *J. Immunol. Methods* **2011**, *372* (1−2), 65−70.
(50) Porterfield, H. S.; Murray, K. S.; Schlichting, D. G.; Chen, X.; Hansen, K. C.; Duncan, M. W.; Dreskin, S. C. Effector activity of peanut allergens: A critical role for Ara h 2, Ara h 6, and their variants. *Clin. Exp. Allergy* **2009**, *39* (7), 1099−1108.
(51) Kulis, M.; Chen, X.; Lew, J.; Wang, Q.; Patel, O. P.; Zhuang, Y.; Murray, K. S.; Duncan, M. W.; Porterfield, H. S.; Burks, W.; Dreskin, S. C. The 2S albumin allergens of *Arachis hypogaea*, Ara h 2 and Ara h 6, are the major elicitors of anaphylaxis and can effectively desensitize peanut-allergic mice. *Clin. Exp. Allergy* **2012**, *42* (2), 326−336.
(52) Zhuang, Y.; Dreskin, S. C. Redefining the major peanut allergens. *Immunol. Res.* **2013**, *55* (1−3), 125−134.
(53) Vereda, A.; van, H. M.; Ahlstedt, S.; Ibanez, M. D.; Cuesta-Herranz, J.; van, O. J.; Wickman, M.; Sampson, H. A. Peanut allergy: Clinical and immunologic differences among patients from 3 different geographic regions. *J. Allergy Clin. Immunol.* **2011**, *127* (3), 603−607.
(54) Koppelman, S.; Apostolovic, D.; Warmenhoven, H.; Verbart, D.; Taylor, S.; Isleib, T.; Maleki, S. The content of allergens Ara h1, Ara h2, Ara h3, and Ara h6 in different peanut cultivars commonly consumed in Europe and the USA. *Allergy* **2012**, *67* (Supplement 96), 548.
(55) Pedrosa, M.; Boyano-Martinez, T.; Garcia-Ara, M. C.; Caballero, S. Q. Peanut seed storage proteins are responsible for clinical reactivity in Spanish peanut-allergic children. *Pediatr. Allergy Immunol.* **2012**, 654−659.

JOURNAL OF AGRICULTURAL AND FOOD CHEMISTRY

Article

pubs.acs.org/JAFC

Potato and Mushroom Polyphenol Oxidase Activities Are Differently Modulated by Natural Plant Extracts

Tomas F. M. Kuijpers,[†] Teunie van Herk,[‡] Jean-Paul Vincken,[†] Renske H. Janssen,[†] Deborah L. Narh,[‡] Willem J. H. van Berkel,[‡] and Harry Gruppen*,[†]

[†]Laboratory of Food Chemistry, Wageningen University, P.O. Box 17, 6700 AA Wageningen, The Netherlands

[‡]Laboratory of Biochemistry, Wageningen University, Wageningen, The Netherlands

Supporting Information

ABSTRACT: Enzymatic browning is a major quality issue in fruit and vegetable processing and can be counteracted by different natural inhibitors. Often, model systems containing a single polyphenol oxidase (PPO) are used to screen for new inhibitors. To investigate the impact of the source of PPO on the outcome of such screening, this study compared the effect of 60 plant extracts on the activity of PPO from mushroom (*Agaricus bisporus*, AbPPO) and PPO from potato (*Solanum tuberosum*, StPPO). Some plant extracts had different effects on the two PPOs: an extract that inhibited one PPO could be an activator for the other. As an example of this, the mate (*Ilex paraguariensis*) extract was investigated in more detail. In the presence of mate extract, oxygen consumption by AbPPO was found to be reduced >5-fold compared to a control reaction, whereas that of StPPO was increased >9-fold. RP-UHPLC-MS analysis showed that the mate extract contained a mixture of phenolic compounds and saponins. Upon incubation of mate extract with StPPO, phenolic compounds disappeared completely and saponins remained. Flash chromatography was used to separate saponins and phenolic compounds. It was found that the phenolic fraction was mainly responsible for inhibition of AbPPO and activation of StPPO. Activation of StPPO was probably caused by activation of latent StPPO by chlorogenic acid quinones.

KEYWORDS: *enzymatic browning, tyrosinase, LC-MS, plant extracts, Ilex paraguariensis*

INTRODUCTION

Polyphenol oxidases (PPOs) catalyze enzymatic browning by oxidizing phenolic compounds to their respective *o*-quinones, which subsequently undergo nonenzymatic reactions with each other and other compounds present, resulting in the formation of dark-colored pigments, also referred to as melanins.[1] This phenomenon is a major quality problem in fruit and vegetable processing (e.g., apple, potato, mushroom), but it is also associated with discoloration of shrimps[2] and formation of hyperpigmentation in human skin.[3]

To control enzymatic browning, much research is dedicated to finding natural inhibitors of enzymatic browning.[4−7] In such research, it is important to distinguish between (i) actual PPO inhibitors that prevent the formation of *o*-quinones, (ii) compounds that reduce the *o*-quinones to their *o*-diphenolic precursors (e.g., ascorbic acid[8]), and (iii) compounds that form colorless addition products with *o*-quinones (e.g., cysteine[9]).

Inhibition studies have been conducted on PPOs from a range of sources. Because of its commercial availability, mushroom tyrosinase is often used in model browning systems, both for browning of food products and for skin pigmentation.[10] Little is known on whether results of inhibition studies with one PPO can be extrapolated to another PPO, as most such studies were conducted with a single PPO. To address this issue, we compared the effect of a selection of plant extracts on two different PPOs in the same model system of enzymatic browning. A commercially available mushroom (*Agaricus bisporus*) tyrosinase (AbPPO) and a PPO isolated from potato tubers (*Solanum tuberosum*) (StPPO) were used.

MATERIALS AND METHODS

Materials. Potato (*S. tuberosum* cv. Celino) tubers were obtained from Gemüse Meyer (Twistringen, Germany). Mushroom (*A. bisporus*) tyrosinase, L-3,4-dihydroxyphenylalanine (L-DOPA), chlorogenic acid, and theobromine were obtained from Sigma-Aldrich (St. Louis, MO, USA). Ultrahigh-performance liquid chromatography−mass spectrometry (UHPLC-MS) grade acetonitrile (ACN) was obtained from Biosolve BV (Valkenswaard, The Netherlands), and caffeine was from Boom (Meppel, The Netherlands). Water was prepared using a Milli-Q water purification system (Millipore, Billerica, MA, USA).

Plant Extracts. Commercial, food grade plant extracts (Table 1) were obtained from Frutarom (Wädenswil, Switzerland). The solvents used in the production of the extracts are specified in Table S1 in the Supporting Information.

Purification of Mushroom Tyrosinase. The mushroom tyrosinase was purified by a single gel filtration step.[11] A HiLoad 26/60 Superdex 200 column connected to an Akta Explorer system (GE Healthcare, Uppsala, Sweden) was used. Fifty milligrams of the commercial enzyme (dissolved in 50 mM HEPES buffer, pH 6.8) was loaded and eluted with 50 mM HEPES buffer, pH 6.8, at 4 mL/min. Fractions (5 mL) were collected, and activity was assayed by a spectrophotometric assay: 50 μL of each fraction was combined with 100 μL of 0.8 mM tyrosine in a 96-well plate, and absorbance at 520 nm was monitored in time. Active fractions were pooled and stored at −20 °C until use. Tyrosinase activity was expressed in units (U), according to the suppliers definition (1 U increases the A_{280} by 0.001/

Received: June 27, 2013
Revised: December 17, 2013
Accepted: December 17, 2013
Published: December 17, 2013

ACS Publications © 2013 American Chemical Society

Table 1. Effect of Plant Extracts on the Rate of Dopachrome Formation by AbPPO and StPPO

	extract	plant species	relative activity[a] (%)	
			AbPPO	StPPO
1	green mate leaf	*Ilex paraguariensis*	27 ± 1.0	354 ± 41.5
2	oats herb	*Avena sativa*	73 ± 1.8	88 ± 10.6
3	olive leaf	*Olea europaea*	85 ± 3.2	224 ± 2.3
4	echninacea dry pressed juice	*Echinaceae purpurea*	104 ± 3.7	105 ± 6.7
5	echninacea purpurea root	*Echinaceae purpurea*	91 ± 2.2	102 ± 7.3
6	pumpkin seed	*Curcubita pepo*	85 ± 1.6	101 ± 3.7
7	green tea leaf	*Camillia sinensis*	22 ± 1.1	61 ± 1.9
8	nettle leaf	*Urtica dioica, Urtica urens*	84 ± 2.7	106 ± 3.8
9	balm herb	*Melissa officinalis*	30 ± 2.9	216 ± 9.9
10	sage leaf	*Salvia officinalis*	31 ± 2.6	181 ± 4.1
11	rhubarb	*Rheum rhabarbarum*	50 ± 1.1	85 ± 3.4
12	red vine leaf	*Vitis vinifera*	63 ± 7.2	89 ± 0.8
13	peppermint leaf	*Mentha piperita*	44 ± 3.3	124 ± 13.8
14	dandelion herb and root	*Taraxum officinale*	79 ± 8.6	100 ± 8.4
15	thyme herb	*Thymus vulgaris*	37 ± 1.8	156 ± 0.2
16	pink rockrose herb	*Cistus incanus*	37 ± 2.1	70 ± 1.5
17	passion flower herb	*Passiflora incarnata*	67 ± 3.5	95 ± 4.3
18	damiana leaf	*Turnera diffusa*	75 ± 3.3	93 ± 10.7
19	goldenrod herb	*Solidago* sp.	43 ± 0.2	189 ± 11.2
20	artichoke leaf	*Cynara scolymus*	63 ± 2.2	102 ± 25.4
21	java tea	*Orthosiphon stamineus*	34 ± 0.2	107 ± 0.13
22	eyebright herb	*Euphrasia* sp.	42 ± 2.7	146 ± 3.9
23	ivy leaf	*Hedera helix*	53 ± 3.8	123 ± 1.4
24	marshmallow root	*Althea officinalis*	99 ± 2.7	96 ± 1.4
25	bearberry leaf	*Arctostaphylos uva-ursi*	36 ± 6.6	61 ± 0.9
26	schisandra fruit	*Schisandra chinensis*	88 ± 5.7	92 ± 2.2
27	licorice root	*Glycyrrhiza glabra*	4 ± 1.8	15 ± 1.1
28	chasteberry	*Vitex agnus-castus*	51 ± 12.8	115 ± 0.4
29	juniper fruit	*Juniperus* sp.	84 ± 3.2	96 ± 1.3
30	rosemary leaf	*Rosmarinus officinalis*	29 ± 3.4	160 ± 0.0
31	devil's claw root	*Harpagophytum procumbens* and/or *H. zeyheri*	41 ± 1.5	117 ± 1.6
32	pelargonium root	*Pelargonium sidoides*	25 ± 1.0	44 ± 9.6
33	chamomile flower	*Chamomilla recutita*	33 ± 0.2	102 ± 1.9
34	caraway seed	*Carum carvu*	56 ± 1.0	97 ± 2.4
35	puslane herb	*Potulaca oleracea*	62 ± 3.3	86 ± 8.7
36	rosehip	*Rosa canina*	98 ± 0.5	84 ± 13.0
37	SoyLife 40	*Glycine max*	48 ± 0.5	103 ± 17.0
38	LinumLife EXTRA	*Linum usitatissimum*	82 ± 2.9	103 ± 9.4
39	brocoraphanin 10% glucoraphanin	*Brassica oleracea* var. *italica*	118 ± 11.5	80 ± 12.7
40	biocurcumin	*Curcuma longa*	–[b]	–[b]
41	Pomactiv AGE	*Malus* sp.	44 ± 2.7	90 ± 5.8
42	SuperBerry 6000	blend of seven berries	37 ± 8.0	78 ± 3.7
43	acai	*Euterpe oleracea*	94 ± 5.5	82 ± 10.2
44	black currant 25% anthocyanins	*Ribes nigrum*	11 ± 10.3	90 ± 18.1
45	Origanox WS-LB	*Origanum vulgare* and/or *Melissa officinalis*	31 ± 2.4	213 ± 3.0
46	Origanox WS	*Origanum vulgare*	44 ± 2.1	125 ± 3.0
47	Cranberry High PAC 25:1	*Vaccinum macrocarpon*	176 ± 4.5	90 ± 1.6
48	OPC Grape Seed ActiVin	*Vitis vinifera*	18 ± 0.4	67 ± 0.7
49	neohesperidine dihydrochalcone (NHDC)	extracted from citrus and chemically modified	19 ± 0.8	73 ± 2.3
50	neohesperidine	extracted from citrus	40 ± 4.9	97 ± 4.0
51	hesperidine	extracted from citrus	45 ± 5.1	99 ± 1.3
52	black garlic	*Allium sativum*	109 ± 3.0	95 ± 0.6
53	horseradish	*Armoracia rusticana*	110 ± 1.2	86 ± 12.9
54	hibiscus	*Hibiscus* sp.	114 ± 12.3	54 ± 15.0
55	baobab	*Adansonia digitata*	107 ± 0.1	94 ± 1.5
56	coriander	*Coriandrum sativum*	79 ± 4.5	105 ± 2.4
57	cinnamon	*Cinnamomum* sp.	69 ± 5.6	91 ± 4.3
58	cinnamon 2	*Cinnamomum* sp.	104 ± 40.4	95 ± 4.0
59	Pomactiv HFV	*Malus* sp.	48 ± 1.8	107 ± 13.7

dx.doi.org/10.1021/jf4043375 | J. Agric. Food Chem. 2014, 62, 214−221

Table 1. continued

	extract	plant species	relative activity[a] (%) AbPPO	StPPO
60	Pomactiv Shape	*Malus* sp.	40 ± 2.4	183 ± 4.6

[a]The rate of dopachrome formation relative to the appropriate control (L-DOPA with AbPPO or StPPO and the solvent used to dissolve the plant extract). [b]Biocurcumin was not included in the spectrophotometric assay due to interfering color of the extract.

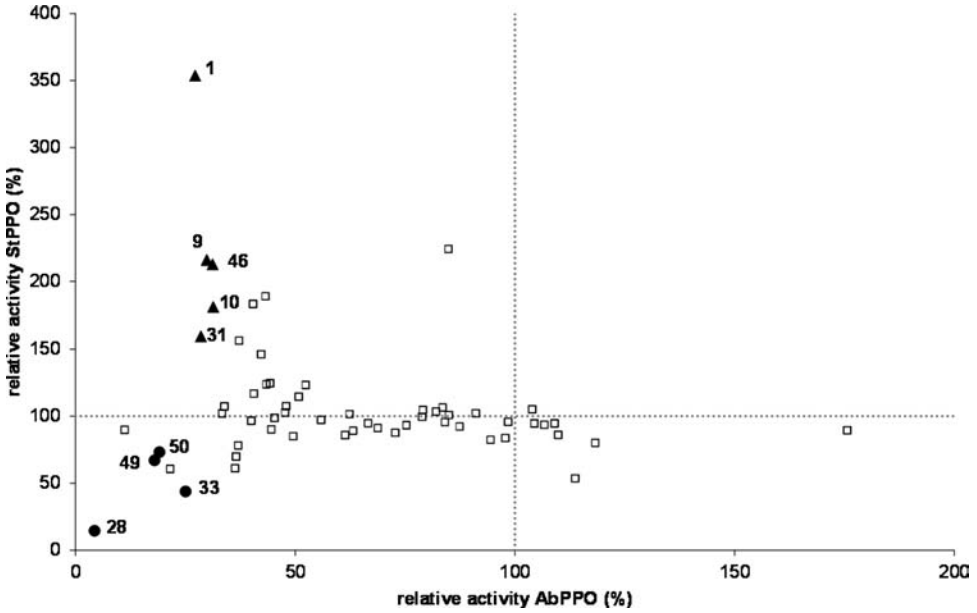

Figure 1. Comparison of the influence of different plant extracts on the conversion of L-DOPA to dopachrome by AbPPO and StPPO. Solid circles indicate extracts that were relatively good inhibitors for both reactions, solid triangles indicate extracts that showed a large difference in inhibition, and open squares indicate all other plant extracts. Numbers refer to Table 1.

min with L-tyrosine as substrate, at pH 6.5 and 25 °C). Purified mushroom tyrosinase is further referred to as AbPPO.

Purification of Potato PPO. One kilogram of potatoes was cooled to 4 °C, washed, and homogenized in 1 L of ice-cold 50 mM HEPES buffer, pH 6.9, containing 1% ascorbic acid and two tablets of protease inhibitor (Complete - EDTA free, Roche Diagnostics GmbH) using a commercial blender. The homogenate was filtered through four layers of cheesecloth, and the filtrate was centrifuged at 13600*g* at 4 °C for 1 h (crude extract, CE). Ammonium sulfate was added to 40% saturation, and the resulting solution was stirred overnight at 4 °C. The precipitate was collected by centrifugation at 13600*g* at 4 °C for 1.5 h and dissolved in a minimal amount of 50 mM HEPES buffer, pH 6.9, containing 1% ascorbic acid. The obtained protein solution was three times dialyzed against 2 L of 50 mM HEPES buffer, pH 6.9, containing 0.1% ascorbic acid and two tablets of the protease inhibitor, after which it was centrifuged at 13600*g* at 4 °C for 30 min.

All subsequent chromatographic steps were performed using an Akta Explorer system (GE Healthcare) at room temperature. The dialyzed protein solution (268 mL) was applied onto a Fast Flow Q-sepharose column (2.6 × 10 cm), pre-equilibrated with 50 mM HEPES buffer, pH 6.9. After a washing with 400 mL of starting buffer, bound protein was eluted using an 800 mL linear gradient of 0−1 M NaCl in the same buffer. The flow rate was 4 mL/min, and 15 mL fractions were collected. Fractions showing maximal PPO activity were pooled and concentrated using a 10 kDa Amicon membrane filter (Millipore) under air pressure.

The concentrated enzyme solution (5 mL) was applied onto a Superdex S-200 column (2.6 × 100 cm) and eluted with 50 mM HEPES buffer, pH 6.9, at a flow rate of 1.5 mL/min. Fractions (5 mL) showing maximal PPO activity were concentrated as described above.

This purification procedure gave an activity yield of 10.6% and resulted in an 11-fold purified enzyme preparation with a specific activity of 5.9 U/mg (Supporting Information Table S2).

Fractionation of Mate Extract. Mate extract was fractionated using a 12 g Reveleris C18 column on a Reveleris flash chromatography system (Grace, Deerfield, IL, USA) operated at 30 mL/min. Twenty milliliters of a 30 g/L solution of mate extract in MQ was applied onto the column. Water acidified with 0.1% (v/v) acetic acid, eluent A, and ACN acidified with 0.1% (v/v) acetic acid, eluent B, were used as eluents. The following elution profile was used: 0−2 min, isocratic on 0% (v/v) B; 2−3 min, linear gradient from 0 to 30% (v/v) B; 3−8 min, isocratic at 30% (v/v) B; 8−13 min, linear gradient from 30 to 100% (v/v) B; 13−15 min, isocratic at 100% (v/v) B. Fractions of 10 mL were collected and pooled on the basis of RP-UHPLC-MS analysis.

Screening of Plant Extracts. Inhibitory activity of plant extracts was assayed using a spectrophotometric assay. Plant extracts (5 g/L) dissolved in either water or dimethyl sulfoxide were diluted (0.16 g/L) into 0.2 mM L-DOPA and 6.5 U/mL AbPPO or 0.4 mM L-DOPA and 0.19 U/mL StPPO in 50 mM HEPES buffer, pH 6.9, in a total volume of 155 μL in a 96-well plate. The absorbance at 520 nm was measured every 20 s for 20 min at 25 °C. The initial rate of color formation (100−240 s) was compared to the appropriate water or dimethyl sulfoxide controls and expressed as relative activity. To ensure that potential competitive inhibition could be observed, substrate concentrations were chosen below the K_m of the two PPOs for L-DOPA.

Oxygen Consumption Measurements. Oxygen consumption of AbPPO or StPPO with selected extracts was measured using an Oxytherm System (Hansatech, Kings Lynn, UK). Incubations with plant extracts or fractionated mate extracts (0.16 g/L) were done with 0.4 mM L-DOPA and 0.19 U/mL StPPO or 0.2 mM L-DOPA and 65 U/mL AbPPO in a total volume of 1 mL of 50 mM HEPES buffer, pH 6.9, at 25 °C. Data acquisition and analysis were performed using Oxygraph Plus software (Hansatech).

RP-UHPLC Analysis. Samples were analyzed on an Accela UHPLC system (Thermo Scientific, San Jose, CA, USA) equipped with a pump, autosampler, and PDA detector. Samples (1 μL) were injected onto a Hypersil Gold column (2.1 × 150 mm, particle size 1.9 μm; Thermo Scientific). Water acidified with 0.1% (v/v) acetic acid, eluent A, and ACN acidified with 0.1% (v/v) acetic acid, eluent B, were used as eluents. The flow rate was 400 μL/min, and the column oven temperature was controlled at 30 °C. The PDA detector was set to measure the range 200−600 nm. The following elution profile was used: 0−1 min, isocratic on 5% (v/v) B; 1−21 min, linear gradient from 5 to 75% (v/v) B; 21−21.1 min, linear gradient from 75 to 100% (v/v) B; 21.1−24 min, isocratic on 100% (v/v) B; 24−24.1 min, linear gradient from 100 to 5% (v/v) B; 24.1−27 min, isocratic on 5% (v/v) B.

Electrospray Ionization Mass Spectrometry (ESI-MS). Mass spectrometric data were obtained by analyzing samples on an LTQ-Velos (Thermo Scientific) equipped with a heated ESI probe coupled to the RP-UHPLC system. Nitrogen was used as sheath gas and auxiliary gas. Data were collected over the m/z range 150−1500. Data-dependent MS^n analysis was performed with a normalized collision energy of 35%. The MS^n fragmentation was performed on the most intense product ion in the MS^{n-1} spectrum. Most settings were optimized via automatic tuning using Tune Plus (Xcalibur 2.1, Thermo Scientific). The system was tuned with a mate extract in negative ionization (NI) mode. The source heater temperature was 45 °C, the transfer tube temperature was 350 °C, and the source voltage was 3.5 kV. Data acquisition and analysis were done with Xcalibur 2.1 (Thermo Scientific).

RESULTS

Screening of Plant Extracts for PPO Inhibitory Activity. The effect of 60 different plant extracts on dopachrome formation by AbPPO and StPPO was compared by expressing the rate of dopachrome formation as activity relative to the appropriate control (L-DOPA with AbPPO or StPPO and the solvent used to dissolve the plant extract) (Table 1). To facilitate this comparison, the relative activities were plotted against each other (Figure 1). From this plot it can be observed that, in general, the StPPO-mediated color formation seemed to be less inhibited than color formation caused by AbPPO. Interestingly, some extracts seemed to inhibit AbPPO, whereas they stimulated StPPO. It should be taken into account that the observed effect on color formation is not necessarily caused by influencing the enzymatic activity. An alternative explanation for an observed inhibition of color formation could be the presence of reducing compounds in the plant extracts, which can either reduce the enzymatically formed *o*-quinone back to the corresponding *o*-diphenol (e.g., ascorbic acid[12]) or combine with the *o*-quinone in an addition product (e.g., cysteine[9] or sulfite[13]). An explanation for enhanced color formation could be the presence of substrates for enzymatic browning in the plant extract itself. To investigate whether enzymatic activity was truly affected, five extracts that showed a large difference in effect on AbPPO and StPPO and four extracts that appeared to be relatively good inhibitors for both the AbPPO and StPPO-mediated color formation were selected for oxygen consumption measurements.

Oxygen Consumption Measurements Discriminate between Inhibition of Color Formation and Enzyme Activity. The four extracts indicated with a circle in Figure 1 (licorice root, pelargonium root, OPC grape seed ActiVin, and NHDC) were used in oxygen consumption measurements to determine whether the observed inhibitory effect on dopachrome formation for both enzymes was caused by inhibition of PPO activity. Biocurcumin was also used in this assay, as the color of this extract was found to interfere with the spectrophotometric assay. The trend of color formation with StPPO being less inhibited than that with AbPPO (Figure 1) was confirmed by oxygen consumption of the two enzymes (Figure 2). Remarkably, the relative oxygen consumption of

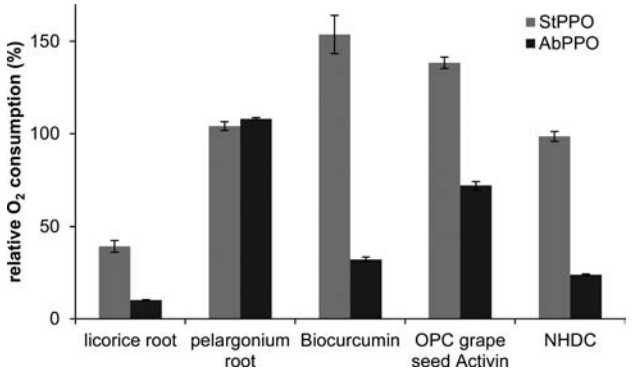

Figure 2. Relative oxygen consumption rates of StPPO and AbPPO with combinations of plant extracts and L-DOPA. Bars represent averages of duplicate determinations; error bars indicate standard deviation.

StPPO in the presence of biocurcumin, grape seed, pelargonium root, and NHDC was 100% or more, whereas the relative color formation with StPPO and these extracts was below 100%. Possibly, the extract contained substrates for StPPO, the oxidation of which did not result in products with an absorption at 520 nm, the wavelength used for the screening assay. If these substrates are preferentially used by StPPO, no color development at 520 nm would be observed, while oxygen consumption occurs. It is unlikely that this effect could be attributed to the presence of reducing compounds in the extracts, as no differences between StPPO and AbPPO would then be expected.

The influence on oxygen consumption of StPPO and AbPPO of five extracts that showed a large difference in their effect on StPPO- and AbPPO-mediated color formation (mate, balm herb, sage leaf, rosemary, and oregano, indicated with triangles in Figure 1) was investigated. Because compounds present in the extracts could potentially be substrates for either of the PPOs, in this way possibly enhancing enzyme activity, incubations of PPO with only plant extract were compared to incubations of PPO, plant extracts, and L-DOPA (Figure 3). The oxygen consumption of StPPO with all of the plant extracts alone was higher than that of the control reaction (StPPO with L-DOPA) used for standardization, indicating that these plant extracts contained either substrates that had a higher affinity for StPPO than L-DOPA or substrates in a considerably higher concentration than the L-DOPA used (0.4 mM). Assuming a molecular weight of 150−300 g/mol for possible substrates in the plant extracts and assuming that these extracts consisted only of substrate, it can be calculated that the maximum theoretical substrate concentration is approximately 0.5−1 mM, with the concentration of plant extracts used in the assay. Balm herb, sage, rosemary, and oregano are all members of the Lamiaceae plant family, which are known to contain a variety of phenolics, including phenolic acids, flavonoids, and phenolic terpenes.[14,15] LC-MS analysis of the extracts used confirmed the presence of a range of compounds, with the most abundant compounds being rosmarinic acid and derivatives of rosmarinic acid (data not shown). The fact that the extracts

dx.doi.org/10.1021/jf4043375 | J. Agric. Food Chem. 2014, 62, 214−221

Figure 3. Relative oxygen consumption rates of StPPO and AbPPO in the presence of plant extracts alone or combinations of plant extracts and L-DOPA. Oxygen consumption was expressed relative to the control reaction of either StPPO or AbPPO with L-DOPA. Bars represent averages of duplicate determinations; error bars indicate standard deviation.

consisted of multiple components indicated that substrates present in the extracts had higher affinities for StPPO than L-DOPA. The relative activity of AbPPO on the plant extracts alone was lower than the activity on combinations of plant extract and L-DOPA, and activity of both reactions was lower than that of the control reaction (AbPPO with L-DOPA). This indicated that the selected plant extracts effectively reduced the rate of AbPPO-mediated color formation by inhibiting the enzyme. The observation that AbPPO showed some activity on the plant extracts alone indicated that besides inhibitors for AbPPO, the extracts also contained substrates for AbPPO. Furthermore, comparing the activity of StPPO and AbPPO on the plant extracts alone, it can be concluded that the substrates present in the extracts are probably better substrates for StPPO than for AbPPO.

Comparing the effect of the plant extracts in combination with L-DOPA on StPPO to the activity of StPPO on the plant extracts alone, the effect of the mate extract stands out. Whereas the activity of StPPO on the mate extract alone was approximately double that of StPPO on L-DOPA, the activity of StPPO on a combination of L-DOPA and mate extract was >9 times that of StPPO on L-DOPA alone. It seems unlikely that this effect can be attributed only to the presence of substrates in the mate extract. As an example of the contrasting effects a plant extract can have on the activity of different PPOs, the effect of mate extract on StPPO and AbPPO was further investigated.

Mate Extract Accelerates Oxygen Consumption of StPPO, whereas It Inhibits That of AbPPO. The effect of sequential addition of mate extract and L-DOPA to StPPO was compared to a control incubation of StPPO with L-DOPA alone and an incubation of StPPO with L-DOPA and mate extract added simultaneously (Figure 4A). The initial activity of StPPO on mate extract is comparable to that on the combination of mate extract and L-DOPA, both of which are higher than the activity on L-DOPA alone. The activity of StPPO on mate extract alone started to decrease shortly after the beginning of the reaction and eventually leveled off, indicating that the substrates present in mate extract were all converted. When L-DOPA was added after complete conversion of the substrates present in the mate extract, enhanced StPPO activity was still observed. This is an indication that the enhanced oxygen consumption of StPPO with combinations of L-DOPA and mate extract not only is due to supplementation of L-DOPA with additional substrates present in the extract but rather points toward activation of StPPO.

The activity of AbPPO on mate extract was much lower than that of StPPO, and the L-DOPA oxidation rate of AbPPO was lower in the presence of mate extract than without mate extract (Figure 4B). AbPPO was also inhibited upon sequential addition of mate extract and L-DOPA.

These results seemed to indicate that the mate extract used contained one or more activators for StPPO and one or more inhibitors for AbPPO. It is not known whether the same compounds are responsible for the activation of StPPO and the inhibition of AbPPO or whether activators for StPPO are present alongside inhibitors for AbPPO.

Characterization of Mate Extract. To identify the compound(s) responsible for activation of StPPO and inhibition of AbPPO, the composition of the mate extract was characterized on the basis of RP-UHPLC-MS analysis (Figure 5A). Peaks were annotated on the basis of comparison of MS/MS fragmentation with published data (Table 2).[16−18] Two distinct groups of compounds were found, hydroxycinnamic acid conjugates and saponins. Furthermore, quercetin-3-*O*-rutinoside, a glycosylated flavonol, caffeine, and theobromine were found. The hydroxycinnamic acid conjugates were, besides a small amount of feruloylquinic acid, all chlorogenic acid-like compounds, that is, different caffeoyl- and dicaffeoylquinic acid isomers. Chlorogenic acid is a well-known substrate

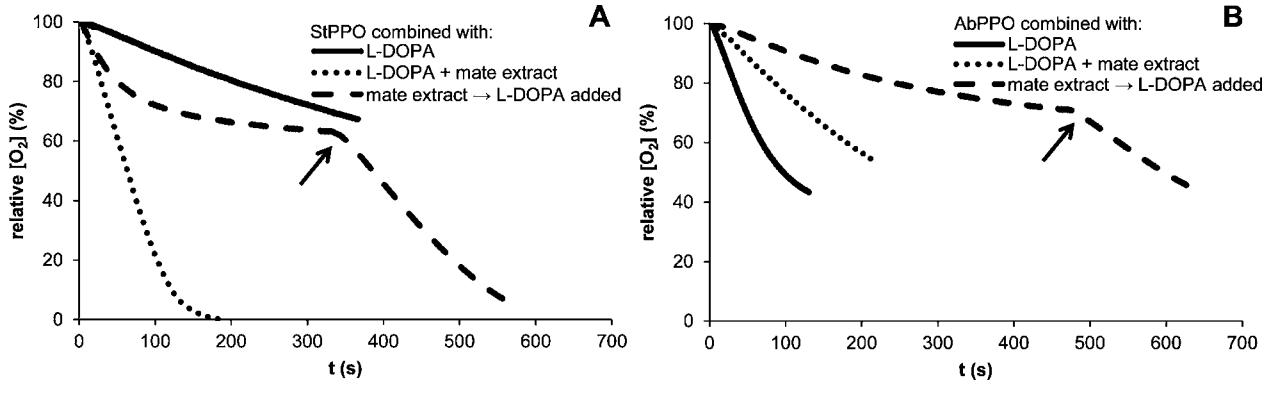

Figure 4. Oxygen consumption in time of incubations of StPPO (A) and AbPPO (B) with L-DOPA and mate extract. Arrows indicate the time point at which L-DOPA was added.

dx.doi.org/10.1021/jf4043375 | J. Agric. Food Chem. 2014, 62, 214−221

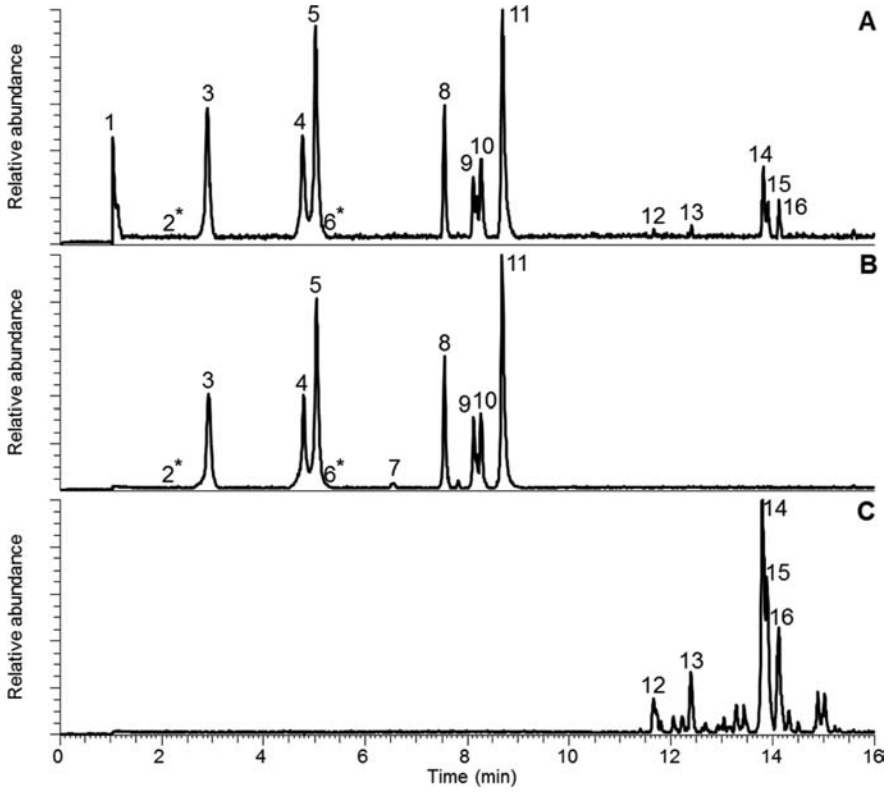

Figure 5. RP-UHPLC-MS traces of mate extract (A), polar mate fraction (B), and apolar mate fraction (C). Peak numbers refer to annotation in Table 2. ∗ indicates the retention time of theobromine and caffeine, which were observed only in the UV trace, not in negative ionization mode MS.

Table 2. RP-UHPLC-MS Characterization of Mate Extract[a]

peak	retention time	$[M-H]^-$	MS^2 fragments (relative abundance)	tentative identification
1	1.04	191	191 (100), 111 (42), 127 (30), 85 (30), 93 (17), 87 (7), 109 (6), 155 (4), 71 (3), 153 (3)	quinic acid
2	2.15			theobromine
3	2.90	353	191 (100), 179 (39), 353 (8), 135 (3), 173 (1)	3-*O*-caffeoylquinic acid
4	4.76	353	191 (100), 179 (1)	5-*O*-caffeoylquinic acid
5	5.02	353	173 (100), 179 (72), 191 (28), 353 (9), 135 (4), 155 (1)	4-*O*-caffeoylquinic acid
6	5.18			caffeine
7	6.57	367	191 (100), 173 (73), 193 (15), 285 (7), 307 (3), 367 (2), 203 (2), 325 (1), 155 (1)	feruloylquinic acid
8	7.56	609	301 (100), 300 (48), 609 (9), 343 (8), 271 (8), 255 (5), 179 (2), 273 (1)	quercetin-3-rutinoside
9	8.12	515	353 (100), 335 (11), 173 (1), 515 (8), 179 (8), 191 (6), 203 (3), 255 (2), 299 (2)	dicaffeoylquinic acid
10	8.28	515	353 (100), 191 (3), 179 (1)	dicaffeoylquinic acid
11	8.70	515	353 (100), 203 (6), 173 (5), 299 (5), 255 (4), 179 (3), 335 (2), 317 (2), 191 (1)	dicaffeoylquinic acid
12	11.67	1073	911 (100), 749 (76), 893 (12), 603 (10), 983 (9), 927 (6), 765 (5), 901 (5), 1043 (5)	matesaponin 3
13	12.42	1219	895 (100), 733 (13), 937 (2)	matesaponin 4
14	13.82	1057	895 (100), 733 (14), 937 (8), 587 (5)	matesaponin 2
15	13.91	1057	895 (100), 733 (64), 893 (8), 587 (7)	matesaponin 2 isomer
16	14.13	911	749 (100), 791 (19)	matesaponin 1

[a]Peaks were annotated on the basis of MS^2 fragmentation.

for PPO,[19,20] so the presence of these compounds explains the observed activity of StPPO and AbPPO when incubated with mate extract as substrate. Chlorogenic acids are the most abundant phenolic compounds in potato,[21] which might explain the much higher activity of StPPO than AbPPO on the mate extract, considering that chlorogenic acid is likely to be the natural substrate for StPPO. To investigate whether indeed the different chlorogenic acid isomers were used as substrate by PPO, RP-UHPLC-MS analysis of incubations of mate extract with StPPO and AbPPO was done. The MS traces of these samples revealed that the different chlorogenic acids and quercetin-3-*O*-rutinoside were converted, whereas the saponins remained (data not shown). No reaction products of the oxidation of the different substrates were found, whereas the mate extract after incubation with PPO visibly turned brown. This might be explained by the formation of a wide variety of reaction products from the *o*-quinones resulting from PPO oxidation, which individually fall below the detection limit of the RP-UHPLC analysis.

Polar Compounds in Mate Extract Are Responsible for Activation of StPPO. The fact that the saponins remained after PPO activity led to the hypothesis that they might be responsible for the observed activation of StPPO and inhibition of AbPPO. Saponins extracted from *Paris polyphylla* have been

dx.doi.org/10.1021/jf4043375 | J. Agric. Food Chem. 2014, 62, 214−221

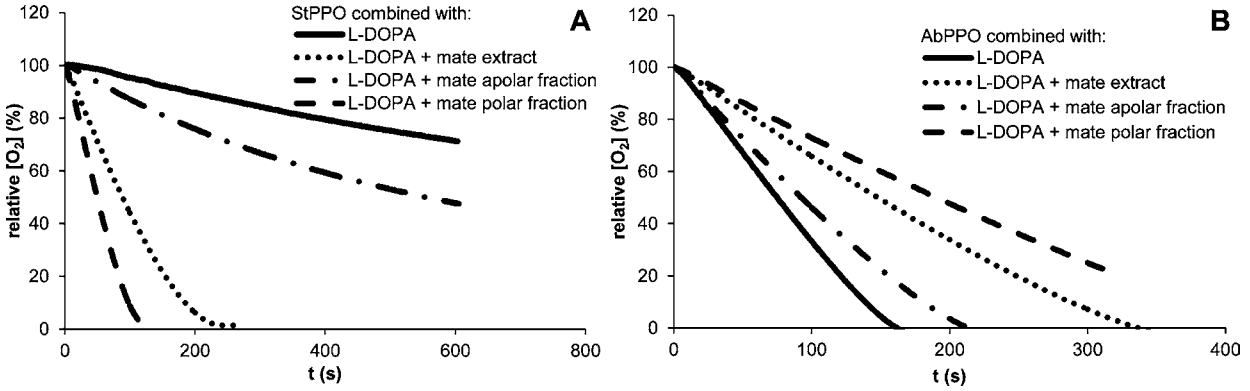

Figure 6. Oxygen consumption in time of incubations of StPPO (A) and AbPPO (B) with L-DOPA (blank) and L-DOPA combined with mate extract, the polar mate fraction, and the apolar mate fraction.

found to inhibit AbPPO.[22] To investigate this, reversed-phase flash chromatography was used to fractionate the mate extract to investigate the effect of the saponins separately from the chlorogenic acid-like compounds. Fractions from flash chromatography were pooled such that a fraction containing mainly chlorogenic acid-like compounds (polar fraction, Figure 5B) and a fraction containing mainly saponins (apolar fraction, Figure 5C) were obtained.

Oxygen consumption measurements with L-DOPA and StPPO in the presence of the apolar or polar mate fraction (Figure 6A) showed that the polar mate fraction seemed to be mainly responsible for activation of StPPO: whereas StPPO was slightly more active in the presence of the apolar mate fraction than with only L-DOPA, activity in the presence of the polar mate fraction was much higher than the blank incubation.

Besides chlorogenic acid-like compounds, caffeine and theobromine were also present in the polar fraction. Whereas the chlorogenic acid-like compounds were converted after incubation with PPO, caffeine and theobromine remained. Experiments with pure caffeine and theobromine showed that they were not responsible for activation of StPPO or inhibition of AbPPO (data not shown). Apparently, the substrates present in the mate extract activated StPPO, also after they had reacted (Figure 4A). To investigate whether the activation of StPPO was indeed due to the chlorogenic acid-like substrates present in the mate extract, StPPO was incubated with pure chlorogenic acid. When oxygen consumption had leveled off, L-DOPA was added. The results obtained were similar to those obtained with mate: oxygen consumption with sequential chlorogenic acid and L-DOPA addition was accelerated compared to a control of StPPO with only L-DOPA (data not shown).

Because of the inhibition of AbPPO by mate, fractionation of the extract indicated that the polar fraction was mainly responsible for inhibition (Figure 6B). In the presence of the apolar mate fraction, oxygen consumption of AbPPO with L-DOPA was comparable to that in the blank reaction, whereas in the presence of the polar fraction the oxygen consumption was decreased compared to that with the blank.

■ DISCUSSION

Our results of screening 60 plant extracts for StPPO and AbPPO inhibitory activity demonstrated that the effect that an extract can have on PPO-catalyzed browning is dependent on the source of PPO. Some extracts showed inhibitory activity toward both PPOs, whereas other extracts inhibited only one PPO or even inhibited one and activated the other PPO. As an example, a mate extract was investigated in more detail, and it was found to be an activator for StPPO and an inhibitor for AbPPO.

Inhibition of PPOs by Plant Extracts. Of 60 plant extracts screened for inhibitory effects on StPPO and AbPPO, 4 were further investigated by measuring their influence on oxygen consumption. Only the extract of licorice root was found to inhibit the activity of both StPPO and AbPPO (Figure 2), indicating that the observed inhibitory effect on color formation of the other extracts was most likely caused by reducing compounds in the extracts. These compounds only prevent formation of color, but do not inhibit enzyme activity.

The inhibitory effect of licorice root on AbPPO has been described before, and several inhibitory (iso)flavonoids and chalcones have been identified.[23−25] Licorice extracts were found to inhibit both mushroom tyrosinase in vitro and melanin formation in cultured human melanocytes.[24] In addition to this, our results demonstrated that licorice also inhibited StPPO. This might indicate that the inhibitors present in licorice are inhibitors with a wide application range.

Activation of StPPO by Mate Extract. When StPPO was incubated with mate extract, oxygen consumption and conversion of substrates present in the extract was observed. Incubation of StPPO with mate extract had an activating effect on L-DOPA oxidation by the enzyme (Figure 4A). Fractionation of the mate extract demonstrated that chlorogenic acid-like compounds were responsible for this activation, which was confirmed by experiments with pure chlorogenic acid. An explanation for the increased StPPO activity observed might be activation of StPPO, which was extracted in a latent state, by *o*-quinones resulting from chlorogenic acid oxidation. Similarly, activation of latent PPO from red clover (*Trifolium pretense*) by *o*-quinones resulting from oxidation of endogenous substrates has been demonstrated.[26] It was proposed that a conformational change of clover PPO occurred through interaction of *o*-quinones with the protein. Conformational changes have been implicated before in the activation of latent plant PPOs. Treatment with surfactants such as SDS, addition of fatty acids, and pH-induced conformational change have been reported to activate plant PPOs, by making the active site more accessible.[27−30] Possibly, interaction of chlorogenic acid quinones with StPPO induced a conformational change, in this way making its active site more accessible.

In conclusion, our results showed that care should be taken when results of inhibitor studies obtained with one specific PPO are generalized to broader food or cosmetic applications.

dx.doi.org/10.1021/jf4043375 | J. Agric. Food Chem. 2014, 62, 214−221

Although screening with a commercially available PPO might be a convenient way to find potential inhibitors, experiments with the target PPO should be done before an inhibitor can be applied in a specific product. Moreover, when a different PPO is used for inhibitor screening than for the final application, potentially useful inhibitors might be overlooked.

■ ASSOCIATED CONTENT

Supporting Information

Solvents used in the production of plant extracts and purification table of potato polyphenol oxidase. This material is available free of charge via the Internet at http://pubs.acs.org.

■ AUTHOR INFORMATION

Corresponding Author

*(H.G.) Phone: +31-317-483211. Fax: +31-317-484893. E-mail: harry.gruppen@wur.nl.

Funding

This study has been carried out with financial support from the Commission of the European Communities within the Seventh Framework Programme for research and technological development (FP7), Grant Agreement 226930, title "Replacement of sulphur dioxide (SO_2) in food keeping the SAme qualitY and shelf-life of the products", acronym SO2SAY.

Notes

The authors declare no competing financial interest.

■ REFERENCES

(1) Friedman, M. Food browning and its prevention: an overview. *J. Agric. Food Chem.* **1996**, *44*, 631−653.

(2) Nirmal, N. P.; Benjakul, S. Effect of ferulic acid on inhibition of polyphenoloxidase and quality changes of Pacific white shrimp (*Litopenaeus vannamei*) during iced storage. *Food Chem.* **2009**, *116*, 323−331.

(3) Smit, N.; Vicanova, J.; Pavel, S. The hunt for natural skin whitening agents. *Int. J. Mol. Sci.* **2009**, *10*, 5326−5349.

(4) Chang, T.-S. An updated review of tyrosinase inhibitors. *Int. J. Mol. Sci.* **2009**, *10*, 2440−2475.

(5) Loizzo, M. R.; Tundis, R.; Menichini, F. Natural and synthetic tyrosinase inhibitors as antibrowning agents: an update. *Compr. Rev. Food Sci. Food Saf.* **2012**, *11*, 378−398.

(6) Kim, Y. J.; Uyama, H. Tyrosinase inhibitors from natural and synthetic sources: structure, inhibition mechanism and perspective for the future. *Cell. Mol. Life Sci.* **2005**, *62*, 1707−1723.

(7) Parvez, S.; Kang, M.; Chung, H.-S.; Bae, H. Naturally occurring tyrosinase inhibitors: mechanism and applications in skin health, cosmetics and agriculture industries. *Phytother. Res.* **2007**, *21*, 805−816.

(8) Ros, J. R.; Rodriguez-Lopez, J. N.; Garcia-Canovas, F. Effect of L-ascorbic acid on the monophenolase activity of tyrosinase. *Biochem. J.* **1993**, *295*, 309−312.

(9) Richard, F. C.; Goupy, P. M.; Nicolas, J. J.; Lacombe, J. M.; Pavia, A. A. Cysteine as an inhibitor of enzymic browning. 1. Isolation and characterization of addition compounds formed during oxidation of phenolics by apple polyphenol oxidase. *J. Agric. Food Chem.* **1991**, *39*, 841−847.

(10) Adhikari, A.; Devkota, H. P.; Takano, A.; Masuda, K.; Nakane, T.; Basnet, P.; Skalko-Basnet, N. Screening of Nepalese crude drugs traditionally used to treat hyperpigmentation: *in vitro* tyrosinase inhibition. *Int. J. Cosmetic Sci.* **2008**, *30*, 353−360.

(11) Schurink, M.; van Berkel, W. J. H.; Wichers, H. J.; Boeriu, C. G. Novel peptides with tyrosinase inhibitory activity. *Peptides* **2007**, *28*, 485−495.

(12) Iyengar, R.; McEvily, A. J. Anti-browning agents: alternatives to the use of sulfites in foods. *Trends Food Sci. Technol.* **1992**, *3*, 60−64.

(13) Kuijpers, T. F. M.; Narváez-Cuenca, C.-E.; Vincken, J.-P.; Verloop, A. J. W.; van Berkel, W. J. H.; Gruppen, H. Inhibition of enzymatic browning of chlorogenic acid by sulfur-containing compounds. *J. Agric. Food. Chem.* **2012**, *60*, 3507−3514.

(14) Hossain, M. B.; Rai, D. K.; Brunton, N. P.; Martin-Diana, A. B.; Barry-Ryan, A. C. Characterization of phenolic composition in lamiaceae spices by LC-ESI-MS/MS. *J. Agric. Food Chem.* **2010**, *58*, 10576−10581.

(15) Koukoulitsa, C.; Karioti, A.; Bergonzi, M. C.; Pescitelli, G.; Di Bari, L.; Skaltsa, H. Polar constituents from the aerial parts of *Origanum vulgare* L. ssp. *hirtum* growing wild in Greece. *J. Agric. Food Chem.* **2006**, *54*, 5388−5392.

(16) Bravo, L.; Goya, L.; Lecumberri, E. LC/MS characterization of phenolic constituents of mate (*Ilex paraguariensis*, St. Hil.) and its antioxidant activity compared to commonly consumed beverages. *Food Res. Int.* **2007**, *40*, 393−405.

(17) Puangpraphant, S.; Berhow, M. A.; de Mejia, E. G. Mate (*Ilex paraguariensis* St. Hilaire) saponins induce caspase-3-dependent apoptosis in human colon cancer cells *in vitro*. *Food Chem.* **2011**, *125*, 1171−1178.

(18) Martinet, A.; Ndjoko, K.; Terreaux, C.; Marston, A.; Hostettmann, K.; Schutz, Y. NMR and LC-MS^n characterisation of two minor saponins from *Ilex paraguariensis*. *Phytochem. Anal.* **2001**, *12*, 48−52.

(19) Kermasha, S.; Goetghebeur, M.; Monfette, A.; Metche, M.; Bovel, B. Studies on inhibition of mushroom polyphenol oxidase using chlorogenic acid as substrate. *J. Agric. Food Chem.* **1993**, *41*, 526−531.

(20) Oszmianski, J.; Lee, C. Y. Enzymic oxidative reaction of catechin and chlorogenic acid in a model system. *J. Agric. Food Chem.* **1990**, *38*, 1202−1204.

(21) Narváez-Cuenca, C.-E.; Vincken, J.-P.; Gruppen, H. Identification and quantification of (dihydro) hydroxycinnamic acids and their conjugates in potato by UHPLC−DAD−ESI-MS^n. *Food Chem.* **2012**, *130*, 730−738.

(22) Devkota, K. P.; Khan, M. T. H.; Ranjit, R.; Meli Lannang, A.; Samreen; Iqbal Choudhary, M. Tyrosinase inhibitory and antileishmanial constituents from the rhizomes of *Paris polyphylla*. *Nat. Prod. Res.* **2007**, *21*, 321−327.

(23) Fu, B.; Li, H.; Wang, X.; Lee, F. S. C.; Cui, S. Isolation and identification of flavonoids in licorice and a study of their Inhibitory effects on tyrosinase. *J. Agric. Food Chem.* **2005**, *53*, 7408−7414.

(24) Nerya, O.; Vaya, J.; Musa, R.; Izrael, S.; Ben-Arie, R.; Tamir, S. Glabrene and isoliquiritigenin as tyrosinase inhibitors from licorice roots. *J. Agric. Food Chem.* **2003**, *51*, 1201−1207.

(25) Yokota, T.; Nishio, H.; Kubota, Y.; Mizoguchi, M. The inhibitory effect of glabridin from licorice extracts on melanogenesis and inflammation. *Pigment Cell Res.* **1998**, *11*, 355−361.

(26) Winters, A. L.; Minchin, F. R.; Michaelson-Yeates, T. P. T.; Lee, M. R. F.; Morris, P. Latent and active polyphenol oxidase (PPO) in red clover (*Trifolium pratense*) and use of a low PPO mutant to study the role of PPO in proteolysis reduction. *J. Agric. Food Chem.* **2008**, *56*, 2817−2824.

(27) Kanade, S. R.; Paul, B.; Rao, A. G. A.; Gowda, L. R. The conformational state of polyphenol oxidase from field bean (*Dolichos lablab*) upon SDS and acid-pH activation. *Biochem. J.* **2006**, *395*, 551−562.

(28) Mayer, A. M. Polyphenol oxidases in plants and fungi: going places? A review. *Phytochemistry* **2006**, *67*, 2318−2331.

(29) Pérez-Gilabert, M.; Morte, A.; García-Carmona, F. Histochemical and biochemical evidences of the reversibility of tyrosinase activation by SDS. *Plant Sci.* **2004**, *166*, 365−370.

(30) Golbeck, J. H.; Cammarata, K. V. Spinach thylakoid polyphenol oxidase: isolation, activation, and properties of the native chloroplast enzyme. *Plant Physiol.* **1981**, *67*, 977−984.

JOURNAL OF AGRICULTURAL AND FOOD CHEMISTRY

Article

pubs.acs.org/JAFC

Crystal Structure of Korean Pine (*Pinus koraiensis*) 7S Seed Storage Protein with Copper Ligands

Tengchuan Jin,*[,†,⊥] Yang Wang,[†] Yu-Wei Chen,[†,#] Tong-Jen Fu,[‡] Mahendra H. Kothary,[§] Tara H. McHugh,[∥] and Yuzhu Zhang*[,∥]

[†]Department of Biology, Illinois Institute of Technology, 3101 South Dearborn Street, Chicago, Illinois 60616, United States

[‡]Center for Food Safety and Applied Nutrition, U.S. Food and Drug Administration, 6502 South Archer Road, Bedford Park, Illinois 60501, United States

[§]Center for Food Safety and Applied Nutrition, U.S. Food and Drug Administration, 8301 Muirkirk Road, Laurel, Maryland 20708, United States

[∥]Agricultural Research Service, Western Regional Research Center, U.S. Department of Agriculture, 800 Buchanan Street, Albany, California 94710, United States

Supporting Information

ABSTRACT: The prevalence of food allergy has increased in recent years, and Korean pine vicilin is a potential food allergen. We have previously reported the crystallization of Korean pine vicilin purified from raw pine nut. Here we report the isolation of vicilin mRNA and the crystal structure of Korean pine vicilin at 2.40 Å resolution. The overall structure of pine nut vicilin is similar to the structures of other 7S seed storage proteins and consists of an N-terminal domain and a C-terminal domain. Each assumes a cupin fold, and they are symmetrically related about a pseudodyad axis. Three vicilin molecules form a doughnut-shaped trimer through head-to-tail association. Structure characterization of Korean pine nut vicilin unexpectedly showed that, in its native trimeric state, the vicilin has three copper ligands. Sequence alignments suggested that the copper-coordinating residues were conserved in winter squash, sesame, tomato, and several tree nuts, while they were not conserved in a number of legumes, including peanut and soybean. Additional studies are needed to assess whether the copper-coordinating property of vicilins has a biological function in the relevant plants. The nutritional value of this copper-coordinating protein in tree nuts and other edible seeds may be worth further investigations.

KEYWORDS: *7S vicilin, pine nut, allergen, X-ray crystallography, copper protein*

1. INTRODUCTION

Food allergies have become a major global health concern.[1,2] Most food allergies are triggered by immunoglobulin E (IgE) recognition of food allergens.[3] To date, there is no cure for food allergies, although immunotherapy using a very small amount of food, recombinant allergens, and engineered hypoallergenic proteins is considered promising.[4−7] Peanut and tree nuts account for the majority of fatal and near-fatal food allergy cases in the United States.[8,9] Cross-reactivity exhibited by peanut allergic patients to other tree nuts, legumes, and oil seeds[10,11] poses an additional risk to these patients.

Pines (family Pinaceae, genus *Pinus*) are widely distributed around the world and are among the most important forest trees. One single species, the loblolly pine (*Pinus taeda* L.), provides ∼16% of the world's annual timber supply.[12] Pine woods are also widely used in the pulp and paper industries. The edible seeds of pine trees (pine nuts) have been consumed in Asia and Europe since prehistoric times, and in some regions, people may have survived winters by consuming only pine nuts.[13] About 30 species of pine produce seeds that are large enough for harvesting.[14] Korean pine nuts are extensively harvested in northeastern China. More than 80% of the pine nuts sold in the United States are imported, primarily from China.[15] Pine nuts are considered a delicacy in many of the world's cultures,[14] and they are frequently used in the preparation of bakery products, vegetable dishes, and other foods.[16,17] Pine nuts are also of high nutritional value. Proteins make up as much as 31.6% of the total dry weight of the edible portion of pine nuts.[17,18] Pine nuts contain a considerable number of vitamins (e.g., vitamins A, B1, and B2), potassium, magnesium, copper, and other minerals as well as dietary fiber.[17,19]

Unfortunately, pine nuts, similar to peanuts and other tree nuts, are reported to cause allergic reactions in certain patients,[20,21] although no pine proteins have been officially recognized as allergens by the World Health Organization and International Union of Immunological Societies (WHO/IUIS) Allergen Nomenclature Subcommittee. The 7S vicilin type seed storage proteins belong to the cupin protein superfamily, which also includes the 11S legumins. Both the 7S and 11S proteins in peanut, hazelnut, cashew nut, pistachios, and walnuts are known to be allergens.[22,23] The crystal structures of a few of these allergens have been reported, including Ara h 3[24] and Ara h 1[25,26] from peanut and Pru du 6[27] from almond. Structural studies on a related protein from *Amaranthus hypochondriacus*

Received: September 6, 2013
Revised: November 27, 2013
Accepted: December 11, 2013
Published: December 11, 2013

ACS Publications © 2013 American Chemical Society

dx.doi.org/10.1021/jf4039887 | J. Agric. Food Chem. 2014, 62, 222−228

were also attempted.[28] To understand the allergenicity of the cupin family of proteins, additional information about the structural properties of the 7S and 11S proteins is needed. In this paper, we describe the cloning of Korean pine vicilin and X-ray crystallographic study of the structure of this potential allergen.

2. MATERIALS AND METHODS

2.1. Plasmid Construction. *2.1.1. Total RNA Extraction.* The 7S vicilin of Korean pine was first purified from pine nut and identified by aligning its N-terminal peptides with the available sequence of vicilin from loblolly pine.[29] To determine the mRNA sequence of Korean pine vicilin, fresh tissues of female flowers and young cones of Korean pine were collected at the Chicago Botanic Garden (Chicago, IL). Total RNA from young Korean pine cones was extracted using the QIAGEN (Valencia, CA) RNeasy Plus Mini Kit according to the manufacturer's protocol with minor modifications. Briefly, 100 mg of fresh tissues/seeds of young cone were ground in liquid nitrogen and collected in a microcentrifuge tube. As soon as the liquid nitrogen evaporated, 450 μL of buffer RLT was added, and the sample was mixed by inversion. RLT and RW1 and RPE mentioned below are proprietary buffers provided by the kit, and their compositions are not described. After centrifugation, the supernatant was transferred to a gDNA Eliminator Mini Spin column and subjected to centrifugation. The flow-through was mixed with 1/2 volume of ethanol and loaded onto an RNeasy Mini Spin column. The column was washed with 700 μL of RW1 buffer and 500 μL of RPE buffer, and the total RNA was eluted with 50 μL of RNase-free water. Two microliter (80 units) of RNaseOUT recombinant ribonuclease inhibitor (Invitrogen, Carlsbad, CA) was added to the sample immediately after elution. Fresh total RNA was used as a template for reverse transcription (RT).

2.1.2. RT and PCR. An Omniscript Reverse Transcription Kit (QIAGEN, Valencia, CA) was used to synthesize cDNAs from the total RNA of various pine tissues. The RT reaction was carried out using a 20-nucleotide poly-dT primer at a 6 μM concentration and 2 μL of the fresh total RNA as the template in a 20 μL RT mixture. The RT reaction was allowed to proceed for 1 h at 37 °C, and the reverse transcriptase was inactivated by incubation at 95 °C for 5 min. The RT product was either used immediately as a template in PCR or stored at −80 °C for further use.

Previously, we reported the purification and biochemical and biophysical characterization of the Korean pine vicilin.[29] N-terminal peptide sequencing of the purified protein indicated that it was similar but not identical to that of loblolly pine.[29] To isolate the mRNA sequence of Korean pine vicilin, PCR primers (atggcttttgtttctttacttacc-attcttc, forward; cgtggagaaactctagt, reverse) were designed on the basis of the loblolly pine vicilin mRNA sequence, and PCR was carried out using Phusion DNA polymerase (New England BioLabs, Ipswich, MA). By blunt end ligation using quick ligase, the PCR product was inserted into a pBluescript SKII vector digested with *Eco*RV to generate pBlue−vicilin. Two colonies were sent to a commercial vender for sequencing, and the resulting mRNA sequence was deposited in GenBank (access ID KF530834).

2.2. Identification of Metal Ligands. A Varian AA 55B atomic absorption spectrophotometer (Agilent Technologies, Santa Clara, CA) was used to determine and quantify possible metal ligands in Korean pine vicilin. An air/acetylene (oxidant/fuel) mixture was used as the flame source. Standard solutions of Cu, Ni, Zn, Mg, Mn, Ca, Fe, and Al ions were prepared fresh for each measurement according to the spectrophotometer manufacturer's instructions and were used for the calibration of the instrument. A vicilin sample of 0.161 mM monomer concentration in Milli-Q H_2O was used for metal content determination.

2.3. Structure Refinement. Korean pine vicilin was purified from raw pine nut and crystallized by the vapor-diffusion method as described previously.[30] X-ray diffraction data were collected at the SER-CAT 22ID beamline at the Advanced Photon Source (APS), Argonne National Laboratory. Data processing with HKL2000[31] and a structure solution by PHASER[32,33] molecular-replacement calculations have been previously reported.[30]

Structure refinement was carried out with REFMAC5[34] implemented in CCP4i[35] and with PHENIX[36] alternated with model building and model improvement using Coot.[37]

The final structure was refined with all data to a 2.40 Å resolution, and the final model was checked by PROCHECK[38] and MolProbity validation.[39] The quality of the structure model was also checked with a shake-and-omit protocol by first introducing random errors up to 0.3 Å to the coordinates of the final refined structure using the program PDSET distributed with CCP4.[35] For each region to be checked, the concerned region of the shaken structure was manually omitted and 20 cycles of restrained refinements were carried out using REFMAC5.[34] This was followed by inspecting the $F_o - F_c$ map together with the final refined structure.

The structure of pine nut vicilin has been submitted to the Protein Data Bank with the accession code 4LEJ. Molecular graphics were prepared using the programs RASMOL,[40] MOLSCRIPT,[41] Raster3D,[42] and Pymol (http://pymol.org/).

3. RESULTS

3.1. Isolation of Korean Pine Vicilin cDNA. To allow characterization of the physicochemical, structural, and immunological properties of Korean pine vicilin, the availability of purified protein is needed. Toward this end, we sought to isolate the vicilin gene and deduce its peptide sequence. The coding sequence of Korean pine vicilin was cloned, sequenced, and deposited in GenBank (KF530834). The coding sequence of vicilin as well as its encoded peptide sequence is shown in the Supporting Information (Figure S1). The signal peptide was determined by comparing the predicted pro-protein with the result of N-terminal sequencing of the native protein purified from mature seeds.[29] The isolation of the coding sequence of pine nut vicilin and production of the recombinant protein can be used in future studies to investigate pine nut allergy and the allergenicity of this protein.

3.2. Structure of Pine Nut Vicilin. The translated peptide sequence from the newly cloned Korean pine vicilin was used for structure refinement. The refined structure gave R/R_{free} values of 0.1924/0.2414 for all data to 2.40 Å (Figure 1 and Table 1). The RMSDs from ideal empirical values[43] were 0.004 Å for the bond lengths and 0.80° for the bond angles, with no main-chain bond length deviating more than 0.05 Å or main-chain bond angle deviating more than 10° from the "ideal" small-molecule values. On the Ramachandran plot calculated with MolProbity validation,[39] all residues were in allowed

Figure 1. Structure of pine vicilin. A vicilin molecule in one asymmetric unit is shown in a ribbon diagram with a rainbow coloring scheme (N-terminal, blue; C-terminal, red). A copper ligand of the protein is shown as a bronze sphere, and the side chains of copper-binding residues are shown as sticks with the CPK coloring scheme.

dx.doi.org/10.1021/jf4039887 | J. Agric. Food Chem. 2014, 62, 222−228

Table 1. X-ray Crystallographic Statistics and Refinement

Data Collection	
space group	$I2_13$
unit cell (a, b, c) (Å)	148.78, 148.78, 148.78
wavelength (Å)	1.0
resolution (last shell) (Å)	50.00−2.40 (2.48−2.40)
no. of reflns (total/unique)	153081/21278
completeness (last shell) (%)	98.9 (100.00)
Wilson B-factor	58.65
redundancy (last shell)	7.2 (7.3)
$I/\sigma(I)$ (last shell)	10.46 (4.51)
R_{merge} (last shell)[a]	0.105 (0.660)
R_{pim} (last shell)[b]	0.044 (0.263)
Refinement	
total no. of atoms	2874
no. of protein atoms	2832
no. of ligand atoms	12
no. of solvent atoms	30
av B-factor (Å^2)	71.95
RMSD(bond lengths) (Å)	0.004
RMSD(bond angles) (deg)	0.80
R_{work}[c]	0.1924
R_{free}[d]	0.2414
Ramachandran plot favored/disallowed (%)	96.3/0.0

[a] $R_{merge} = \sum_h\sum_i|I_i(h) - \langle I(h)\rangle|/\sum_h\sum_i I_i(h)$, where $I_i(h)$ and $\langle I(h)\rangle$ are the ith and mean measurements of the intensity of reflection h. [b] $R_{pim} = \sum_h[(1/n - 1)^{1/2}]\sum_i|I_i(h) - \langle I(h)\rangle|/\sum_h\sum_i I_i(h)$, where $I_i(h)$ and $\langle I(h)\rangle$ are the ith and mean measurements of the intensity of reflection h and n is the redundancy of reflection h and was calculated with unmerged intensities using PHENIX merging statistic utilities. [c] $R_{work} = \sum_h||F_o(h)| - |F_c(h)||/\sum_h|F_o(h)|$, where $F_o(h)$ and $F_c(h)$ are the observed and calculated structure factors, respectively. No I/σ cutoff was applied. [d] R_{free} was calculated from 5% of the total data set randomly selected that was not used in the refinement.

regions, and 96.3% of all residues were in favored regions (Table 1). In the final refined structure, there was one vicilin molecule in the crystallographic asymmetric unit with 355 protein residues located in the electron density map. Eight residues at the N-terminal and nine residues at the C-terminal of the mature protein could not be located in the electron density map and were not included in the refined structure. Two flexible loop regions (residues N241−A261 and G342−H355) were also not located in the structure. In addition, the final structure included 30 water molecules, 1 glycerol molecule, 1 phosphate ion, and 1 metal ligand. Flame atomic absorption spectrometry was used to determine the identity of the metal ligand of vicilin. The results indicated that there was one copper ion in each vicilin molecule. No Ni, Zn, Mg, Mn, Ca, Fe, or Al ions could be detected in the sample (data not shown).

The overall structure of pine nut vicilin consists of an N-terminal domain and a C-terminal domain. Each assumes a cupin fold, and the two domains are symmetrically related about a pseudodyad axis. Three vicilin molecules form a doughnut-shaped trimer through head-to-tail association (Figure 2). The structures of several 7S seed storage proteins from other plants have been reported, including adzuki bean (PDB 2EAA), mung bean (PDB 2CV6), soybean (PDB 1UIK and 1IPK), kidney bean (PDB 2PHL), jack bean (PDB 2CAU), and peanut (PDB 3S7I and 3SMH). All these previously reported structures, however, were from legumes, and they did not contain any metal ligands.

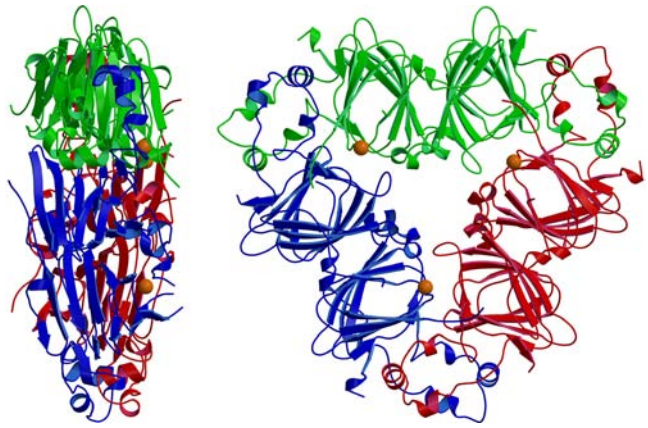

Figure 2. Trimeric structure of pine vicilin. The trimeric vicilins are shown in a ribbon diagram with the monomers colored in cyan, green, and magenta. The trimer is shown in two orthogonal views and with the copper atoms in all three monomers shown in space-fill and colored in bronze.

On the basis of patient serum recognition and LC/MS/MS sequencing of peptides resulting from protease digestion of a 50 kDa protein, *Pinus pinea* (stone pine) vicilin was suggested to be a pine nut allergen.[44] The three peptides identified in that study (ASSEAGEIR, QFLAGK, and FGVPSGHTFY) can be separately aligned with Korean pine vicilin isolated in this study with 100% identity, except for the second peptide, which would align with a sequence of EFLAGK, with one amino acid residue not identical (data not shown). A total of 23 linear IgE epitopes in peanut allergen Ara h 1 were identified, and the smallest IgE-binding sequence was determined to contain six amino acids.[45] When pine vicilin isolated in this study was aligned with Ara h 1 (data not shown), the longest stretch of exact matches contained six residues but did not reside in any of the known linear epitopes of Ara h 1. The second longest match only contained less than 6 amino acids. To date, the allergenicity of food proteins is still poorly understood, and the reliability of using sequence comparison alone to predict protein allergenicity may be questionable. Structural properties may provide clues that contribute to the understanding of the allergenicity of these proteins. Unfortunately, very little information is available regarding conformational IgE epitopes of known allergens. The availability of three-dimensional structures of additional food allergens may help the understanding and mitigation of the allergenicity of food proteins in the future when more information about conformational epitopes is obtained.

3.3. Copper Center in Pine Nut Vicilin. The copper center of pine nut vicilin consists of a cysteine (C338), a tyrosine (Y67), and two histidines (H340 and H379). The sulfur of C338, the ND1 of H340, and the NE2 of H379 form a trigonal planar structure with the copper ion in the center, but slightly away from the plane. The hydroxyl group of Y67 provides the fourth, axial ligand with a longer coordinating distance (Figure 3).

On the basis of the structural and spectroscopic properties of copper proteins, their Cu centers are classified into different types (types I, II, III, Cu_A, Cu_B, and Cu_Z).[46] Modification of the Cu center by protein engineering has also generated a so-called type I and half copper site.[47] Type I copper proteins are also called blue copper proteins because of their strong absorbance at about 600 nm, and they function in electron transfer.[48] This type of Cu center is typically coordinated by two His residues

dx.doi.org/10.1021/jf4039887 | J. Agric. Food Chem. 2014, 62, 222−228

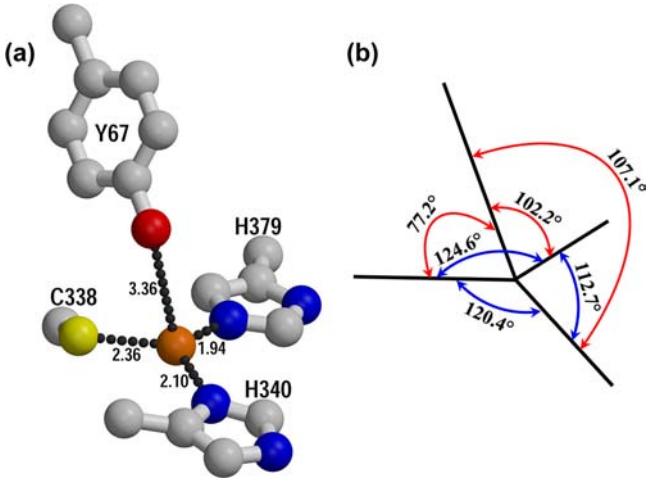

Figure 3. Type II copper center in pine nut vicilin. (a) Ball-and-stick representation of copper coordination in vicilin. The distances (Å) are shown next to the dotted lines between the copper ion and its coordinating residues. Atom colors are gray, red, blue, yellow, and bronze for C, O, N, S, and Cu, respectively. (b) Coordination geometry parameters about the copper. The lines between the copper ion and its coordinating atoms are shown in the same orientation as in (a). The angles formed by two distances connecting the Cu and two of its coordination atoms are shown in degrees.

and a Cys residue in a trigonal planar arrangement with an additional axial Met coordinated, distorting the geometry toward tetrahedral. Type II Cu centers lack the strong, distinctive absorbance at 600 nm and have no evident color. The amino acid coordination and geometries of type II Cu centers are diverse.[49] A typical type II Cu center is coordinated with four His residues in a square pyramidal geometry and is generally considered not to have a Cys ligand.[50] The Cu center in pine nut vicilin has features of both type I and type II Cu sites. Its ligands include the side chain sulfur of a Cys residue, but it was colorless and the absorbance spectra of the protein were featureless in the visible region (data not shown). Unlike in type I proteins where both the His residues bind to the Cu ion through ND1,[51] H379 in Korean pine vicilin interacts with the Cu ion through its NE2. In addition, the distance between the sulfur of C338 and the Cu ion (2.36 Å) is longer than its counterpart in a typical type I copper protein.[52] Thus, it does not fit a type I copper protein, and for now, we will group it in the more divergent type II category.

3.4. Possible Copper Binding in Other Vicilin Orthologues. Free copper ions in the cell can be toxic even at low concentrations, so the ability of certain proteins to bind copper might provide a mechanism to detoxify the cell. It is unclear whether the existence of a copper ligand of the 7S protein is unique to Korean pine. It is also unclear whether this copper center of the vicilin protein has an important biological

(a)

```
Korean pine          60 EEEREENPYVFHSDRFRIRASSEAGEIRAL
Loblolly pine        60 EEEREENPYVFHSDRFRMRASSEAGEIRAL
White spruce         46 EE-REENPYVFHSDSFRTRASSEAGEIRAL
Black walnut         63 EQQRH-NPYYFHSQSIRSRHESEEGEVKYL
English walnut      175 EQQRH-NPYYFHSQSIRSRHESEEGEVKYL
Pecan               364 EQQRH-NPYYFHSQGLRSRHESGEGEVKYL
Pistachio           123 EED--ENPYVFEDEHFTTRVKTEQGKVVVL
Cashew              147 EED--ENPYVFEDEDFTTKVKTEQGKVVLL
Hazelnut             56 EQE--ENPYVFQDEHFESRVKTEEGRVQVL
Winter squash       384 QEQ-SNNPYYFQEQRFQSRYRSDEGHWRVL
Sesame              187 EQGRGRIPYVFEDQHFITGFRTQHGRMRVL
Tomato              140 QQEKSNNPYLFESQRFRSRFRASHGDFRIL

Korean pine         318 NTKATSIAIVMEGEGRIEMACPHLGQEHGW
Loblolly pine       319 NTKATSIAIVTQGEGRIEMACPHLGQQHGW
White spruce        304 NSKSTSIGIVTNGEGRIEMACPHLG-QHGW
Black walnut        324 NSKATVVVYVVEGTGRYEMACPH-VSSQSF
English walnut      436 NSKATVVVYVVEGTGRYEMACPH-VSSQSY
Pecan               624 NSKATVVVYVVEGTGRFEMACPHDVSSQSY
Pistachio           379 NSRATKIAIVVSGEGRLEIACPHLSSSKNS
Cashew              403 NSRATKIAIVVSGEGCVEIACPHLSSSKSS
Hazelnut            313 NSRATKISVVVEGEGFFEMACPHLSSSSGS
Winter squash       643 NSRATWVVFVSEGAGSFEMACPHIQSSQWQ
Sesame              445 NSKATKIALVVDGEGYFEMACPHMSRSRGS
Tomato              397 NTKSTKLVMVIEGNARFEMACPHLGRQSQS

Korean pine         367 LRTGTVYVVPAGHPITEIASTNGRLEILWF
Loblolly pine       368 LRTGTVYVVPAGHPITEIACTEGHLEILWF
Shite spruce        352 LRTGSVYIVPAGHPITEIASTNSRLQILWF
Black walnut        376 LARGDIFVIPAGHPIAITASQNENLRLLGF
English walnut      488 LARGDIFVIPAGHPIAITASQNENLRLLGF
Pecan               678 LARGDIFVIPAGHPIAITASQNENLRLVGF
Pistachio           424 IRTDSVFVVPAGHPFVTVASGNQNLEILCF
Cashew              443 IRKDTVFIVPAGHPFATVASGNENLEIVCF
Hazelnut            350 LRRGVVFVAPAGHPVAVIASQNNNLQVLCF
Winter squash       704 LSEGGVLVIPAGHPIAIMASPNENLRLVGF
Sesame              492 LTRGTVVIIPAGHPFVAVASSNQNLQVLCF
Tomato              458 LNVGDVLVIPAGHPITFVATGNSNLRIVGF
```

(b)

```
Korean pine          60 EEEREENPYVFHS-DRFRIRASSEAGEIRALPNFG
adzuki bean          13 DSRGENNPFYFSSDRRFHTLFTNQYGHLRILHRFD
mung bean             9 VSRGKNNPFYFNSDRWFHTLFRNQFGHLRVLQRFD
soybean               1 RRHKNKNPFHFNS-KRFQTLFKNQYGHVRVLQRFN
kidney bean           3 VREDENNPFYFRSSNSFQTLFENQNGRIRLLQRFN
kidney bean           6 EEESQDNPFYFNSDNSWNTLFKNQYGHIRVLQRFD
jack bean            41 ESRAQNNPYLFRS-NKFLTLFKNQHGSLRLLQRFN
peanut              167 EETSRNNPFYFPS-RRFSTRYGNQNGRIRVLQRFD
thale cress          73 EEESTNHPYHFRK-RSFSDWFQSKEGFVRVLPKFT

Korean pine         318 NTKATSIAIVMEGEGRIEMACPHLGQEHGWS
adzuki bean         283 NSKAIVIMVINEGEAKIELVGLSDQQ-QQKQ
2CV6_A              279 NSKAIVILVINEGKANIELVGQREQQKQQEE
1UIK_A              269 NSKAIVVLVINEGEANIELVGIKEQQQRQQQ
1IPK_A              267 NSKAIVILVINEGDANIELVGIKEQQQKQKQ
2PHL_A              257 YSKAIVILVVNEGEAHVELVG-------PKG
2CAU_A              299 NSRATVILVANEGRAEVELVGLEQQ---QQQ
3S7E_A              449 NSKAMVIVVVNKGTGNLELVAVRKEQQQRGR
NP_566714           329 NSKTTFVTFVENGCARFEMATPYKFQRGQQQ

Korean pine         367 LRTGTVYVVPAGHPITEIASTNGRLEILWF
adzuki bean         326 LSEDDVFVIPAAYPVAINATS--NLNFFAF
2CV6_A              323 LSEDDVFIIPATYPVAINATS--NLNFFAF
1UIK_A              313 LSEQDIFVIPAGYPVVVNATS--DLNFFAF
1IPK_A              311 LSEDDVFVIPAAYPFVVNATS--NLNFLAF
2PHL_A              294 LSKDDVFVIPAAYPVAIKATS--NVNFTGF
2CAU_A              340 LSEGDIIVIPSSFPVALKAAS--DLNMVGI
3S7E_A              504 LKEGDVFIMPAAHPVAINASS--ELHLLGF
NP_566714           381 VCKGEVFIVPAGHPFTILSQDQ-DFIAVGF
```

Figure 4. Multiple sequence alignments of vicilins from different species. The sequence of Korean pine vicilin isolated in this study was aligned with those of other species identified by a BLAST search of the nonredundant protein sequence (NR) database at NCBI (see the text). The copper-coordinating residues in pine nut vicilin, and the corresponding conserved residues in other vicilins, are shown in red. Only the alignments around the copper-coordinating residues are shown. (a) Vicilins with conserved copper-coordinating residues and a possible copper center. (b) Vicilins without the copper-coordinating residues conserved. These include the 7S proteins for which the crystal structures were reported previously (and for whose structures were solved the PDB access codes were also used to label the sequences).

dx.doi.org/10.1021/jf4039887 | J. Agric. Food Chem. 2014, 62, 222−228

function. To assess whether the copper-binding property is shared by vicilins from other species, ClustalW was used to align available vicilin sequences from different species. The copper-coordinating residues in pine nut are conserved in the 7S seed storage proteins of *Picea glauca* (white spruce, NR accession number CAA44873), *Juglans nigra* (black walnut, AAM54366), *Juglans regia* (English walnut, AAF18269), *Carya illinoinensis* (pecan, ABV49593), *Pistacia vera* (pistachio, ABO36677), *Anacardium occidentale* (cashew, AAM73730), *Corylus avellana* (hazelnut, AAL86739), *Cucurbita maxima* (winter squash, BAA34056), *Sesamum indicum* (sesame, AAK15089), and *Solanum lycopersicum* (tomato, CAP69670). On the other hand, the copper-coordinating residues are not universally conserved in the 7S storage proteins in a number of legumes. These include the 7S proteins in *Vigna angulariz* (adzuki bean, 2EAA_A), *Vigna radiata* var. *radiata* (mung bean, 2CV6_A), *Glycine max* (soybean, 1UIK_A (conglycinin α) and 1IPK_A (conglycinin β)), *Phaseolus vulgaris* (kidney bean, 2PHL_A), *Canavalia ensiformis* (jack bean, 2CAU_A), and *Arachis hypogaea* (peanut, P43238). These residues are also not conserved in the extensively studied model plant *Arabidopsis thaliana* (thale cress, NP_566714). Regardless of whether the copper-coordinating residues are presented or not, many of these vicilins have been identified as food allergens, including Ara h 1 in peanut, Gly m 5 in soybean, Vig r 2 in mung bean, Ses I 3 in sesame, Cor a 11 in hazelnut, Ana o 1 in cashew, Pis v 3 in pistachio, Jug r 2 in English walnut, and Jug n 2 in black walnut. Thus, the presence of a copper center is unlikely to be related to the allergenicity of the 7S proteins.

Multiple sequence alignments of pine nut vicilin and its orthologues with and without the conserved copper coordination residues are shown in parts a and b, respectively, of Figure 4. The alignment of the full sequences of these 7S proteins is shown in the Supporting Information (Figure S2). Copper-coordinating residues are conserved in a large number of seed plants, including conifers and a subset of flowering plants, suggesting that copper is a ligand of vicilin in these species. Copper is an essential trace element in nearly all organisms.[53] As a seed storage protein, besides preserving nitrogen, carbon, and sulfur for the development of young plants, no other biological function for vicilin is known. The identification of pine nut vicilin as a copper protein indicates that it may have a function in copper reservation.

The biological roles of copper include transportation of dioxygen and iron, electron transfer, oxidation of organic substrates and metal ions, and reduction of nitrite, nitrous oxide, an dioxygen.[54] The diverse category of proteins with a type II Cu center also includes peptidylglycine α-hydroxylating monooxygenase whose function requires two copper centers[55] and galactose oxidase whose activity involves a covalently modified tyrosine.[56] To our knowledge, the 7S seed storage protein has not been reported to contain a copper center. The copper center of pine vicilin does not readily reveal a possible biological function. As the copper ion binds to residues from both the N- and C-terminal domains of the protein, it may contribute to the stability of the protein. Future investigations are needed to unveil whether the presence of a copper ligand is required by an unknown catalytic activity of vicilin in pine and other plants. Further studies on whether copper centers exist in the vicilins from other species may result in valuable information and provide insights into the molecular evolution of this seed storage protein and reveal the nutritional value of this type of abundant copper-binding protein in seeds.

■ ASSOCIATED CONTENT

Supporting Information

Figures showing the coding sequence of Korean pine vicilin and its translated peptide sequence and sequence alignment of 7S proteins. This material is available free of charge via the Internet at http://pubs.acs.org.

■ AUTHOR INFORMATION

Corresponding Authors

*Phone: 301-594 2114. E-mail: tengchuan@gmail.com.

*Phone: 510-559-5981. Fax: 510-559-5818. E-mail: yuzhu.zhang@ars.usda.gov.

Present Addresses

[⊥]T.J.: Structural Immunobiology Unit, Laboratory of Immunology, National Institute of Allergy and Infectious Diseases, National Institutes of Health, Bethesda, MD 20892, United States.

[#]Y.-W.C.: MERIAL Ltd., Duluth, GA 30601, United States.

Funding

Use of the APS was supported by the U.S. Department of Energy, Office of Science, Office of Basic Energy Sciences, under Contract W-31-109-Eng-38. This work was partially supported by a fund from the Illinois Institute of Technology and by Cooperative Agreement 5U01FD003801 between the U.S. Food and Drug Administration and Institute for Food Safety and Health, Illinois Institute of Technology.

Notes

The authors declare no competing financial interest. Mention of trade names or commercial products in this publication is solely for the purpose of providing specific information and does not imply recommendation or endorsement by the U.S. Department of Agriculture.

■ ACKNOWLEDGMENTS

X-ray diffraction data were collected at the Southeast Regional Collaborative Access Team (SER-CAT) 22-ID beamline at the Advanced Photon Source (APS), Argonne National Laboratory.

■ REFERENCES

(1) Jackson, K. D.; Howie, L. D.; Akinbani, L. J. Trends in allergic conditions among children: United States, 1997−2011; NCHS Data Brief No. 121, May 2013. http://www.cdc.gov/nchs/data/databriefs/db121.pdf (accessed Sept 5, 2013).

(2) Wang, J.; Sampson, H. A. Food anaphylaxis. *Clin. Exp. Allergy* **2007**, *37*, 651−60.

(3) Asero, R.; Ballmer-Weber, B. K.; Beyer, K.; Conti, A.; Dubakiene, R.; Fernandez-Rivas, M.; Hoffmann-Sommergruber, K.; Lidholm, J.; Mustakov, T.; Oude Elberink, J. N.; Pumphrey, R. S.; Stahl Skov, P.; van Ree, R.; Vlieg-Boerstra, B. J.; Hiller, R.; Hourihane, J. O.; Kowalski, M.; Papadopoulos, N. G.; Wal, J. M.; Mills, E. N.; Vieths, S. IgE-mediated food allergy diagnosis: Current status and new perspectives. *Mol. Nutr. Food Res.* **2007**, *51*, 135−47.

(4) Sampson, H. A. Update on food allergy. *J. Allergy Clin. Immunol.* **2004**, *113*, 805−19, quiz p 820.

(5) Pons, L.; Palmer, K.; Burks, W. Towards immunotherapy for peanut allergy. *Curr. Opin. Allergy Clin. Immunol* **2005**, *5*, 558−62.

(6) de Leon, M. P.; Rolland, J. M.; O'Hehir R, E. The peanut allergy epidemic: Alergen molecular characterisation and prospects for specific therapy. *Expert Rev.Mol.Med.* **2007**, *9*, 1−18.

(7) Li, X. M.; Srivastava, K.; Grishin, A.; Huang, C. K.; Schofield, B.; Burks, W.; Sampson, H. A. Persistent protective effect of heat-killed *Escherichia coli* producing "engineered," recombinant peanut proteins in a murine model of peanut allergy. *J. Allergy Clin. Immunol.* **2003**, *112*, 159−67.

(8) Sampson, H. A.; Mendelson, L.; Rosen, J. P. Fatal and near-fatal anaphylactic reactions to food in children and adolescents. *N. Engl. J. Med.* **1992**, *327*, 380−4.
(9) Yunginger, J. W.; Sweeney, K. G.; Sturner, W. Q.; Giannandrea, L. A.; Teigland, J. D.; Bray, M.; Benson, P. A.; York, J. A.; Biedrzycki, L.; Squillace, D. L.; Helm, R. M. Fatal food-induced anaphylaxis. *JAMA, J. Am. Med. Assoc.* **1988**, *260*, 1450−2.
(10) Beardslee, T. A.; Zeece, M. G.; Sarath, G.; Markwell, J. P. Soybean glycinin G1 acidic chain shares IgE epitopes with peanut allergen Ara h 3. *Int. Arch. Allergy Immunol.* **2000**, *123*, 299−307.
(11) de Leon, M. P.; Drew, A. C.; Glaspole, I. N.; Suphioglu, C.; O'Hehir, R. E.; Rolland, J. M. IgE cross-reactivity between the major peanut allergen Ara h 2 and tree nut allergens. *Mol. Immunol.* **2007**, *44*, 463−71.
(12) Liang, C.; Wang, G.; Liu, L.; Ji, G.; Fang, L.; Liu, Y.; Carter, K.; Webb, J. S.; Dean, J. F. ConiferEST: an integrated bioinformatics system for data reprocessing and mining of conifer expressed sequence tags (ESTs). *BMC Genomics* **2007**, *8*, 134.
(13) Cordenunsi, B. R.; De Menezes Wenzel, E.; Genovese, M. I.; Colli, C.; De Souza Goncalves, A.; Lajolo, F. M. Chemical composition and glycemic index of Brazilian pine (*Araucaria angustifolia*) seeds. *J. Agric. Food Chem.* **2004**, *52*, 3412−6.
(14) FAO. Pine nuts. *Non-Wood Forest Products from Conifers*; Publications Division, Food and Agriculture Organization (FAO) of the United Nations: Rome, Italy, 1998.
(15) Geisler, M.; Huntrods, D. Pine nuts profile. http://www.agmrc.org/commodities__products/nuts/pine-nuts-profile/ (ccessed Sept 5, 2013).
(16) Özgüven, F.; Vursavuş, K. Some physical, mechanical and aerodynamic properties of pine (*Pinus pinea*) nuts. *J. Food Eng.* **2005**, *68*, 191−196.
(17) Nergiz, C.; Dönmez, I. Chemical composition and nutritive value of *Pinus pinea* L. seeds. *Food Chem.* **2004**, *86*, 365−368.
(18) Venkatachalam, M.; Sathe, S. K. Chemical composition of selected edible nut seeds. *J. Agric. Food Chem.* **2006**, *54*, 4705−14.
(19) USDA National Nutrient Database for Standard Reference. http://www.nal.usda.gov/fnic/foodcomp/search/ (accessed Sept 5, 2013).
(20) Añó, M. A.; Maselli, J. P.; Sanz Mf, M. L.; Fernandez-Benitez, M. Allergy to pine nut. *Allergol. Immunopathol.* **2002**, *30*, 104−8.
(21) Garcia-Menaya, J. M.; Gonzalo-Garijo, M. A.; Moneo, I.; Fernandez, B.; Garcia-Gonzalez, F.; Moreno, F. A 17-kDa allergen detected in pine nuts. *Allergy* **2000**, *55*, 291−3.
(22) Roux, K. H.; Teuber, S. S.; Sathe, S. K. Tree nut allergens. *Int. Arch. Allergy Immunol.* **2003**, *131*, 234−44.
(23) Allergen nomenclature. http://www.allergen.org/Allergen.aspx (accessed Sept 5, 2013).
(24) Jin, T.; Guo, F.; Chen, Y.-w.; Howard, A.; Zhang, Y.-Z. Crystal structure of Ara h 3, a major allergen in peanut. *Mol. Immunol.* **2009**, *46*, 1796−804.
(25) Cabanos, C.; Urabe, H.; Tandang-Silvas, M. R.; Utsumi, S.; Mikami, B.; Maruyama, N. Crystal structure of the major peanut allergen Ara h 1. *Mol. Immunol.* **2011**, *49*, 115−23.
(26) Chruszcz, M.; Maleki, S. J.; Majorek, K. A.; Demas, M.; Bublin, M.; Solberg, R.; Hurlburt, B. K.; Ruan, S.; Mattisohn, C. P.; Breiteneder, H.; Minor, W. Structural and immunologic characterization of Ara h 1, a major peanut allergen. *J. Biol. Chem.* **2011**, *286*, 39318−27.
(27) Jin, T.; Albillos, S. M.; Guo, F.; Howard, A.; Fu, T. J.; Kothary, M. H.; Zhang, Y. Z. Crystal structure of prunin-1, a major component of the almond (*Prunus dulcis*) allergen amandin. *J. Agric. Food Chem.* **2009**, *57*, 8643−51.
(28) Vasco-Mendez, N. L.; Soriano-Garcia, M.; Moreno, A.; Castellanos-Molina, R.; Paredes-Lopez, O. Purification, crystallization, and preliminary X-ray characterization of a 36 kDa amaranth globulin. *J. Agric. Food Chem.* **1999**, *47*, 862−6.
(29) Jin, T.; Albillos, S. M.; Chen, Y. W.; Kothary, M. H.; Fu, T. J.; Zhang, Y. Z. Purification and characterization of the 7S vicilin from Korean pine (*Pinus koraiensis*). *J. Agric. Food Chem.* **2008**, *56*, 8159−8165.
(30) Jin, T.; Fu, T.-J.; Kothary, M. H.; Howard, A.; Zhang, Y.-Z. Crystallization and initial crystallographic characterization of a vicilin-type seed storage protein from *Pinus koraiensis*. *Acta Crystallogr.* **2007**, *F63*, 1041−3.
(31) Otwinowski, Z.; Minor, W. Processing of X-ray diffraction data collected in oscillation mode. *Methods Enzymol.* **1997**, *276*, 307−326.
(32) McCoy, A. J.; Grosse-Kunstleve, R. W.; Storoni, L. C.; Read, R. J. Likelihood-enhanced fast translation functions. *Acta Crystallogr.* **2005**, *D61*, 458−464.
(33) Storoni, L. C.; McCoy, A. J.; Read, R. J. Likelihood-enhanced fast rotation functions. *Acta Crystallogr.* **2004**, *D60*, 432−438.
(34) Vagin, A. A.; Steiner, R. A.; Lebedev, A. A.; Potterton, L.; McNicholas, S.; Long, F.; Murshudov, G. N. REFMAC5 dictionary: Organization of prior chemical knowledge and guidelines for its use. *Acta Crystallogr.* **2004**, *D60*, 2184−95.
(35) Potterton, E.; Briggs, P.; Turkenburg, M.; Dodson, E. A graphical user interface to the CCP4 program suite. *Acta Crystallogr.* **2003**, *D59*, 1131−1137.
(36) Adams, P. D.; Afonine, P. V.; Bunkoczi, G.; Chen, V. B.; Davis, I. W.; Echols, N.; Headd, J. J.; Hung, L. W.; Kapral, G. J.; Grosse-Kunstleve, R. W.; McCoy, A. J.; Moriarty, N. W.; Oeffner, R.; Read, R. J.; Richardson, D. C.; Richardson, J. S.; Terwilliger, T. C.; Zwart, P. H. PHENIX: A comprehensive Python-based system for macromolecular structure solution. *Acta Crystallogr.* **2010**, *D66*, 213−21.
(37) Emsley, P.; Cowtan, K. Coot: Model-building tools for molecular graphics. *Acta Crystallogr.* **2004**, *D60*, 2126−32.
(38) Laskowski, R. A.; MacArthur, M. W.; Moss, D. S.; Thornton, J. M. PROCHECK: A program to check the stereochemical quality of protein structures. *J. Appl. Crystallogr.* **1993**, *26*, 283−291.
(39) Lovell, S. C.; Davis, I. W.; Arendall, W. B., 3rd; de Bakker, P. I.; Word, J. M.; Prisant, M. G.; Richardson, J. S.; Richardson, D. C. Structure validation by Cα geometry: ϕ,ψ and Cβ deviation. *Proteins* **2003**, *50*, 437−50.
(40) Sayle, R. A.; Milner-White, E. J. RASMOL: Biomolecular graphics for all. *Trends Biochem. Sci.* **1995**, *20*, 374.
(41) Kraulis, P. J. MOLSCRIPT: A program to produce both detailed and schematic plots of protein structures. *J. Appl. Crystallogr.* **1991**, *24*, 946−950.
(42) Merritt, E. A.; Murphy, M. E. Raster3D version 2.0. A program for photorealistic molecular graphics. *Acta Crystallogr.* **1994**, *D50*, 869−73.
(43) Engh, R. A.; Huber, R. Accurate bond and angle parameters for X-ray protein structure refinement. *Acta Crystallogr.* **1991**, *A47*, 392−400.
(44) Cabanillas, B.; Cheng, H.; Grimm, C. C.; Hurlburt, B. K.; Rodriguez, J.; Crespo, J. F.; Maleki, S. J. Pine nut allergy: Clinical features and major allergens characterization. *Mol. Nutr. Food Res.* **2012**, *56*, 1884−93.
(45) Burks, A. W.; Shin, D.; Cockrell, G.; Stanley, J. S.; Helm, R. M.; Bannon, G. A. Mapping and mutational analysis of the IgE-binding epitopes on Ara h 1, a legume vicilin protein and a major allergen in peanut hypersensitivity. *Eur. J. Biochem.* **1997**, *245*, 334−9.
(46) Belle, C.; Rammal, W.; Pierre, J. L. Sulfur ligation in copper enzymes and models. *J. Inorg. Biochem.* **2005**, *99*, 1929−36.
(47) Canters, G. W.; Gilardi, G. Engineering type 1 copper sites in proteins. *FEBS Lett.* **1993**, *325*, 39−48.
(48) Rubino, J. T.; Franz, K. J. Coordination chemistry of copper proteins: How nature handles a toxic cargo for essential function. *J. Inorg. Biochem.* **2012**, *107*, 129−43.
(49) MacPherson, I. S.; Murphy, M. E. Type-2 copper-containing enzymes. *Cell. Mol. Life Sci.* **2007**, *64*, 2887−99.
(50) McGuirl, M. A.; Dooley, D. M. Copper proteins with type 2 sites. *Encyclopedia of Inorganic Chemistry*; John Wiley & Sons, Ltd.: Hoboken, NJ, 2006.
(51) Katz, A. K.; Shimoni-Livny, L.; Navon, O.; Navon, N.; Bock, C. W.; Glusker, J. P. Copper-binding motifs: Structural and theoretical aspects. *Helv. Chim. Acta* **2003**, *86*, 1320−1338.

(52) Guss, J. M.; Bartunik, H. D.; Freeman, H. C. Accuracy and precision in protein structure analysis: Restrained least-squares refinement of the structure of poplar plastocyanin at 1.33 Å resolution. *Acta Crystallogr.* **1992**, *B48*, 790−811.
(53) Nakamura, K.; Go, N. Function and molecular evolution of multicopper blue proteins. *Cell. Mol. Life Sci.* **2005**, *62*, 2050−66.
(54) Frausto da Silva, J. J. R.; Williams, R. J. P. *The Biological Chemistry of the Elements: The Inorganic Chemistry of Life*, 2nd ed.; Oxford University Press: New York, 2001.
(55) Siebert, X.; Eipper, B. A.; Mains, R. E.; Prigge, S. T.; Blackburn, N. J.; Amzel, L. M. The catalytic copper of peptidylglycine α-hydroxylating monooxygenase also plays a critical structural role. *Biophys. J.* **2005**, *89*, 3312−9.
(56) Rokhsana, D.; Dooley, D. M.; Szilagyi, R. K. Systematic development of computational models for the catalytic site in galactose oxidase: Impact of outer-sphere residues on the geometric and electronic structures. *J. Biol. Inorg. Chem.* **2008**, *13*, 371−83.

JOURNAL OF AGRICULTURAL AND FOOD CHEMISTRY

Article

pubs.acs.org/JAFC

Polysaccharide from Seeds of *Plantago asiatica* L. Affects Lipid Metabolism and Colon Microbiota of Mouse

Jie-Lun Hu,[†,§] Shao-Ping Nie,*[,†] Qi-Meng Wu,[†] Chang Li,[†] Zhi-Hong Fu,[†] Joshua Gong,[†,§] Steve W. Cui,[†,§] and Ming-Yong Xie[†]

[†]State Key Laboratory of Food Science and Technology, Nanchang University, Nanchang 330047, China

[§]Guelph Food Research Center, Agriculture and Agri-Food Canada, 93 Stone Road West, Guelph, Ontario N1G 5C9, Canada

Supporting Information

ABSTRACT: Polysaccharide from the seeds of *Plantago asiatica* L. was given via oral administration to mice (0.4 g/kg body weight, 30 days) to observe its effects on mouse nutrient metabolism and colon microbiota. It was found the polysaccharide intake could lower the apparent absorption of lipid. Total triglyceride, cholesterol, and atherogenic index in blood serum with total lipid and cholesterol levels in liver of polysaccharide group mice were all significantly lower than those of the control group ($p < 0.05$). Furthermore, the effect of the polysaccharide intake on mouse colon bacterial communities was investigated. Mice from the polysaccharide group showed a higher colon bacterial diversity than the control group. *Bacteroides* sp., *Eubacterium* sp., butyrate-producing bacteria *Butyrivibrio* sp., and probiotics *Bifidobacterium bifidum*, *Lactobacillus fermentum*, and *Lactobacillus reuteri* in mouse colon were all increased after polysaccharide intake. These indicated that the intake of polysaccharide from *P. asiatica* L. could be beneficial for lipid metabolism and colon microbiota.

KEYWORDS: *Plantago asiatica L., polysaccharide, lipid metabolism, colon microbiota*

INTRODUCTION

In recent years, the influence of polysaccharides on major nutrient (carbohydrate, protein, and lipid) metabolism has been of particular interest because major nutrient metabolism is related to many chronic diseases.[1,2] In addition, the effects of polysaccharide on colon microbiota were also paid much attention because of its benefits for the colon health, which is of more and more concern nowadays.[3] The gut microbiota in colon contact with its host takes part in a great number of metabolic processes.[4] The supply of fermentable carbohydrate is an important factor limiting the growth of bacteria in colon and, as in other environments, bacteria that can transform the available substrates most rapidly will occur in the greatest numbers.[5]

Polysaccharides can be extracted from many kinds of herbal or plant materials. Some *Plantago* plants, such as *Plantago afra* L., *Plantago psyllium* L., *Plantago ovata* Forsk. (isabgul), *Plantago indica* L., and *Plantago major* L., are often used in traditional medicine throughout the world because the soluble fibers in their seeds are able to improve some intestinal functions.[6] Our research group has recently isolated a pure and homogeneous polysaccharide from the seeds of *Plantago asiatica* L. with a molecular mass of 1894 kDa.[7] The polysaccharide was found to be a highly branched heteroxylan, which consisted of a β-1,4-linked Xyl*p* backbone with side chains attached to *O*-2 or *O*-3. The side chains consisted of β-T-linked Xyl*p*, α-T-linked Ara*f*, α-T-linked GlcA*p*, β-Xyl*p*-(1→3)-α-Ara*f*, and α-Ara*f*-(1→3)-β-Xyl*p*, etc.[8] In addition, our recent studies have also shown that this polysaccharide may induce maturation of murine dendrite cells, have antioxidant activity in vitro, promote mouse defecation, increase short-chain fatty acid (SCFA) production in mouse colon and in vitro fermentation, and have some effects on intestinal function in vitro.[9−14] However, the influence of the polysaccharide from *P. asiatica* L. on nutrient metabolism and colon microbiota in mouse has not been studied.

In this study, the effect of the polysaccharide from *P. asiatica* L. on mouse nutrient metabolism was evaluated by determining the apparent absorption of major nutrients, blood serum ingredients, and liver lipid contents. Additionally, the effect of the polysaccharide on mouse colonic bacterial communities was investigated. Amplicons of the V3 variable regions of bacterial 16S rDNA were analyzed by denaturing gradient gel electrophoresis (DGGE), cloning, and sequencing. Furthermore, the relationship between lipid metabolism difference and bacterial community change of mouse after polysaccharide intake was also discussed.

MATERIALS AND METHODS

Materials and Animals. The seeds of *P. asiatica* L. were purchased from Ji'an, Jiangxi, China, and dried in the sun before use. All reagents used were of analytical grade and purchased from Shanghai Chemicals and Reagents Co. (Shanghai, China).

Kunming mice, weighing 20.0 ± 2.0 g [grade II, certificate SCXK (gan) 2006-0001], were purchased from Jiangxi College of Traditional Chinese Medicine, Jiangxi Province, China. All animals used in this study were cared for in accordance with the *Guidelines for the Care and Use of Laboratory Animals* published by the U.S. National Institutes of Health (NIH Publication 85-23, 1996), and all procedures were

Received: September 12, 2013
Revised: December 4, 2013
Accepted: December 16, 2013
Published: December 16, 2013

ACS Publications © 2013 American Chemical Society

approved by the Animal Care Review Committee (Animal application approval 0064257), Nanchang University, China.

Polysaccharide Preparation. Polysaccharide from *P. asiatica* L. seeds was prepared using our published method.[7] Briefly, the seeds of *P. asiatica* L. (50 g) were defatted with 1 L of ethanol at room temperature for 24 h under stirring and then extracted with 500 mL of doubly distilled water at 100 °C for 2 h. The residue was re-extracted. The combined aqueous extract (a highly viscous gel) was centrifuged (4800*g*, 10 min) and prefiltered through a cotton cloth bag. After that, the filtrate was concentrated by a rotary evaporator under reduced pressure at 55 °C to yield *P. asiatica* L. water extract. The filtrate was mixed with 1.5 g/L papain and heated in water at 60 °C for 2 h. The resulting aqueous solution was extensively dialyzed against doubly distilled water for 72 h and precipitated by adding 4 volumes of anhydrous ethanol at 4 °C for 12 h. After centrifugation, the precipitate was washed with anhydrous ethanol, dissolved in water, and lyophilized to yield the polysaccharide.

Animal Experiment Design. Male 6-week-old Kunming mice (20.0 ± 2.0 g) were individually housed in stainless steel cages in a room with controlled temperature (25 ± 0.5 °C), relative humidity (50 ± 5%), and a 12 h/12 h light/dark cycle. All mice were fed the same amount of basal diet (Table 1), which was prepared according to the published formula,[15] and water was provided ad libitum. All mice were randomly divided into two groups: (1, Polysaccharide group) Mice were orally administered polysaccharide at the dose of 0.4 g/kg body weight of mice. The dose for the polysaccharide administration was selected according to our previous research.[11,12] (2, Control group) Mice were given distilled water of the same volume as the mean volume of the polysaccharide groups. Each group had 12 mice, and mice were housed individually. All of the mice were given oral administration of polysaccharide or water at about 9:00 a.m. every day for 30 days. In addition, we determined the body weight of each mouse every day before gavage and changed the volume of the polysaccharide to ensure that the mice were given polysaccharide at the dose of 0.4 g/kg body weight by gavage every day. Throughout the experiment, the animals' general health status and body mass were observed twice daily.

Table 1. Composition of the Basal Diet for Mice

component	g/kg dry weight (DW) basis
corn starch	454
soybean meal	240
sucrose	100
corn oil	60
cellulose	50
gelatinized starch	10
vitamin mixture[a]	10
mineral mixture[b]	76

[a]Containing, in g/kg (DW basis): 0.25 (250000 IU) vitamin A; 0.002 (65000 IU) vitamin D_3; 2 (2000 IU) vitamin E; 0.41 menadinoe; 0.07 folic acid; 1.25 niacin; 0.5 calcium pantothenate; 0.2 riboflavin; 0.25 thiamin; 0.5 pyridoxine; 0.003 cyanocobalamine; 0.025 biotin; 70.0 cholin chloride. [b]Containing, in g/kg (DW basis): 69.6 $CaCO_3$; 313.1 $C_{12}H_{10}Ca_3{\cdot}4H_2O$; 114.6 $CaHPO_4{\cdot}2H_2O$; 222.2 $K_2HPO_4{\cdot}3H_2O$; 126.7 KCl; 78.3 NaCl; 38.9 $MgCO_3$; 35.8 $MgCO_3$; 0.204 $MnSO_4{\cdot}H_2O$; 0.042 KI; 0.515NaF; 0.091 $AlNH_4(SO_4)_2{\cdot}12H_2O$.

At the end of the designated experiment period, feces of the mice were collected individually and used to measure the apparent absorption of major nutrients (carbohydrate, protein, and fat). Blood was drawn from the eyes of the mice, and the serum was isolated by brief centrifugation of the whole blood. After that, the mice were sacrificed, and the liver and colon (with contents) were obtained. Then the colons were aseptically removed immediately and placed on an ice-cold plate and longitudinally opened, and the colon contents were collected. The feces, liver, and colon content were then kept at −20 °C for further analysis.

Measurement of the Apparent Absorption of Major Nutrients (Carbohydrate, Protein, and Lipid). The feeds and freeze-dried feces were crushed and measured for their carbohydrate, crude protein, and crude lipid.[16] The carbohydrate content was determined colorimetrically: To an aliquot of the feed (200 mg) or feces (200 mg) was added 10 mL of a 0.2 M acetate buffer (pH 4.8) and 5 mL of a 0.12% glucoamylase solution (Biochemical Co., Shanghai, China). After the addition of distilled water to give 50 mL of the solution, a few drops of toluene were added, and the mixture was incubated at 37 °C for 24 h. After hydrolysis, the mixture was filtered, and an aliquot of the solution was used for determining the reducing sugar according to the method of Somoyi-Nelson, 0.9 being adopted as the conversion factor to carbohydrate. The crude protein content was determined by titration: An aliquot of the feed (200 mg) or feces (200 mg) was weighed and degraded by H_2SO_4. The nitrogen content was determined using the Kjeldahl method with a Kjeltec TM 8400 instrument (Foss, Denmark), 6.25 being adopted as the conversion factor to protein. The crude lipid content was determined gravimetrically according to the Soxhlet method, using an aliquot of the feed (200 mg) or feces (200 mg). The apparent absorption of major nutrients (carbohydrate, protein, and lipid) was calculated by using the following equation:

$$\text{apparent nutrient absorption (\%)} = [(\text{intake} - \text{excretion})/\text{intake}] \times 100 \quad (1)$$

Measurement of Blood Serum Ingredients and Liver Lipid Contents. Total serum protein, albumin, albumin/globulin ratio, glucose, urea nitrogen, creatinine, triglyceride, total cholesterol, high-density lipoprotein (HDL)-cholesterol, low-density lipoprotein (LDL)-cholesterol, atherogenic index, glutamic oxalacetic transaminase activity (GOT), and glutamic pyruvic transaminase activity (GPT) were determined by using an Automatic Biochemical Analyzer (AU2700, Olympus, Hamburg, Germany). Freeze-dried livers were ground, and the lipids were extracted with chloroform/methanol (2:1, v/v).[17] The total lipid content was quantified gravimetrically, and the total cholesterol and triglycerides were determined by using the Automatic Biochemical Analyzer, whereas phospholipid contents were determined colorimetrically with a determiner assay kit (Jinghao Medix Co., Beijing, China).

Colon Content DNA Extraction and PCR Amplification. To describe bacterial diversity in the mouse colon tract, total DNA was isolated from colon content samples and used as a template for PCR amplification. Amplicons of the V3 regions of bacterial 16S rDNA were analyzed using the DGGE analysis method. Sample DNA extraction (200 mg of frozen colon content for every mouse) was performed by using a QIAamp DNA Stool Mini Kit (QIAGEN, Inc., Shanghai, China), according to the manufacturer's instruction. For DGGE analysis, PCR amplifications with V3 region primers against the 16S rDNA were performed in a 25 μL (total volume) mixture containing 1.2 μL of forward primer with a GC-clamp [primer F338-GC, sequence (5′−3′), CGCCCGCCGCGCGCGGCGGGCGGG-GCGGGGGCACGGGGGGACTCCTACGGGAGGCAGCAG] and 1.2 μL pf reverse primer [primer R518, sequence (5′−3′), ATTACC-GCGGCTGCTGG], 0.5μL of deoxynucleoside triphosphate at a concentration of 10 mM, 2.5 μL of PCR reaction buffer, 0.2 μL of DNA polymerase (5 U/μL), 1.0 μL of DMSO (4%, v/v), 1 μL of DNA template with an appropriate amount, and 17.4 μL of sterile water.[18] PCR amplification was performed with a Biosci PCR system as follows: an initial denaturation of 94 °C for 4 min, followed by 30 cycles of 94 °C for 0.5 min, 56 °C for 0.5 min, and 72 °C for 1 min, and a final elongation at 72 °C for 10 min. Aliquots of 5 μL were analyzed by electrophoresis on an agarose gel (1%) to check the size and amounts of the amplicons.

DGGE Profiling. DGGE was performed with the Bio-Rad DCodeTM system (Bio-Rad Ltd., Hercules, CA, USA). PCR products were loaded onto 1 mm thick 8% (w/v) polyacrylamide (acrylamide/bisacrylamide = 37.5:1) gels containing a 35−65% linear denaturing gradient. TAE buffer (1×, 40 mM Tris-acetate, 1 mM Na-EDTA, pH 8.0) was used as the electrophoresis buffer. The electrophoresis was

initiated by prerunning for 5 min at a voltage of 220 V and subsequently run at a fixed voltage of 85 V for 16 h at 60 °C. The gel was stained with $AgNO_3$ and developed after completion of electrophoresis. The obtained DGGE patterns were subsequently normalized and analyzed with Bio-Rad Quantity One 4.4.0 software. During the processing, the different lanes were defined, background was subtracted, differences in the intensity of the lanes were compensated during normalization, and the correlation matrix was calculated. Clustering was done with Pearson correlation and the unweighted pair group mean average (UPGMA) method.

Identification of DGGE DNA Bands. The bands of interest were excised from the gel using a sterile blade and incubated overnight at 4 °C in Tris−EDTA buffer (pH 8.0) for future sequencing. PCR amplifications of the DNA fragments from the excised gel were carried out according to the same protocols described above with the corresponding primers [forward primer F338, sequence (5′−3′), ACTCCTACGGGAGGCAGCAG; reverse primer R518, sequence (5−3′), ATTACCGCGGCTGCTGG] and 1 μL aliquot of the gel elution.[18] PCR products were excised from a 1.0% agarose gel and purified with a DNA Gel Extraction Kit (Tiangen, China). Isolation of DNA bands from the DGGE gel, cloning of excised bands, and sequence analysis were performed as described by Gong et al.[19] The sequences were submitted to GenBank and the RDP database to determine their most related bacterium. The DNA sequences are available in the GenBank database with accession numbers.

Statistical Analysis. All of the experiments were done in triplicate. Statistical analysis was carried out using SPSS (version 16.0, Chicago, IL, USA). The results were expressed as the mean ± standard deviation and compared using the Tukey test at a 5% confidence level. DGGE banding patterns in each group were digitalized by Quantity One software (Bio-Rad). The intensity and relative position of each DGGE band were determined manually with background subtraction. The intensity of each band was expressed as percentage of the integrated intensity of the entire lane. The matrix of intensity and relative position was analyzed by principal component analysis (PCA) using SPSS software.

RESULTS AND DISCUSSION

General Health Status of Mice. Throughout the experiment period, no noticeable behavioral or activity changes were observed in the mice, and no treatment-related illness or death occurred. The growth of mice appeared normal throughout the experiment period, and no mouse experienced diarrhea or constipation. There was no observable difference in the animals' body mass and hair luster between the polysaccharide-treated group and control group.

Effect of Polysaccharide on Absorption of Major Nutrient of Mice. The apparent absorption of major nutrients (carbohydrate, protein, and lipid) is summarized in Table 2. Although the values for nutrient absorption were all nearly quantitative, there was a significant difference ($p < 0.05$) between the control group (94.8 ± 0.2%) and polysaccharide group (87.4 ± 0.3%) for lipid apparent absorption. This observation suggested that the polysaccharide from *P. asiatica* L. may have had some influence on lowering the absorption of lipid, which was consistent with our previous finding that the polysaccharide from *P. asiatica* L. could inhibit some pancreatic lipase activity and reduce cholesterol available for absorption.[13] The polysaccharide from *P. asiatica* L., which was found to promote mouse defection in our previous study, might also have some effect on promoting cholesterol and lipid excretion.[11] In addition, the polysaccharide was found to increase the propionic acid production in mouse colon, which might influence the lipid metabolism.[12] Furthermore, the polysaccharide from *P. asiatica* L. was found to bind bile acid in vitro,[13] which may also affect the excretion and metabolism of cholesterol and lipid. Other studies showed that some other polysaccharides could enhance the excretion of lipids in feces,[20] which was similar to our results.

Table 2. Effect of Polysaccharide from *P. asiatica* L. on Apparent Absorption of Carbohydrate, Protein, and Lipid in Mice[a]

	apparent absorption (%)	
	control group	polysaccharide group
carbohydrate	99.9 ± 0.0 a	99.6 ± 0.3 a
lipid	94.8 ± 0.2 a	87.4 ± 0.3 b
protein	99.9 ± 0.1 a	99.9 ± 0.1 a

[a]Each value is the mean ± standard deviation ($n = 12$); means in the same row not sharing a common letter are significantly different ($p < 0.05$).

Effect of Polysaccharide on the Characteristics of Blood Serum and Liver Lipid Levels. The characteristics of the blood serum and the liver lipid levels in mice of the polysaccharide group or control group are given in Tables 3 and 4, respectively. There was in general no marked difference in serum chemistry, apart from total triglyceride, total cholesterol, and atherogenic index (Table 3). Total triglyceride, total cholesterol, and atherogenic index in blood serum tended to be lower in the group of mice given oral administration of polysaccharide, with the difference between the control group

Table 3. Effect of Polysaccharide from *P. asiatica* L. on Characteristic Blood Serum Chemistry of Mice[a]

	control group	polysaccharide group
glucose (mmol/L)	6.72 ± 0.51 a	6.56 ± 0.39 a
total protein (g/L)	55.3 ± 1.1 a	54.0 ± 1.1 a
albumin (g/L)	31.3 ± 0.9 a	31.6 ± 0.5 a
albumin/globulin	1.3 ± 0.1 a	1.4 ± 0.1 a
urea nitrogen (mmol/L)	9.5 ± 0.6 a	9.4 ± 0.5 a
creatinine (μmol/L)	33 ± 2 a	35 ± 3 a
triglyceride (mmol/L)	1.90 ± 0.11 a	1.25 ± 0.12 b
total cholesterol (mmol/L)	3.27 ± 0.26 a	2.65 ± 0.28 b
HDL-cholesterol (mmol/L)	2.62 ± 0.11 a	2.34 ± 0.14 a
LDL-cholesterol (mmol/L)	0.58 ± 0.14 a	0.32 ± 0.09 a
atherogenic index[b]	0.22 ± 0.01 a	0.17 ± 0.01 b
GOT (U/L)[c]	193 ± 21 a	192 ± 29 a
GPT (U/L)[d]	132 ± 19 a	134 ± 21 a

[a]Each value is the mean ± standard deviation ($n = 12$); means in the same row not sharing a common letter are significantly different ($p < 0.05$). [b]Atherogenic index = (LDL-cholesterol)/(HDL-cholesterol). [c]GOT, glutamic oxalacetic transaminase activity. [d]GPT, glutamic pyruvic transaminase activity.

Table 4. Effect of Polysaccharide from *P. asiatica* L. on Liver Lipid Levels in Mice[a]

	control group	polysaccharide group
cholesterol (μmol/g of liver)	6.4 ± 0.4 a	5.5 ± 0.2 b
triglyceride (μmol/g of liver)	33.5 ± 1.2 a	32.9 ± 0.9 a
phospholipid (μmol/g of liver)	35.4 ± 2.2 a	35.9 ± 1.8 a
total lipid (mg/g liver)	49.6 ± 2.2 a	44.6 ± 2.2 b

[a]Each value is the mean ± standard deviation ($n = 12$); means in the same row not sharing a common letter are significantly different ($p < 0.05$).

dx.doi.org/10.1021/jf4040942 | J. Agric. Food Chem. 2014, 62, 229−234

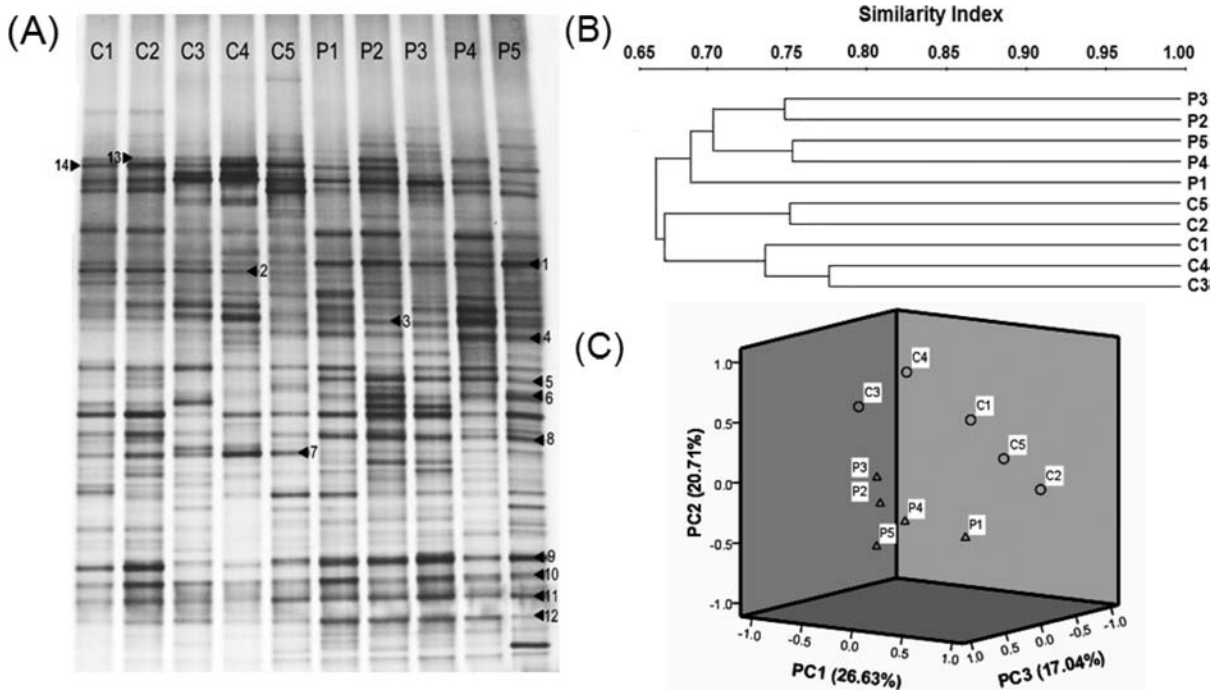

Figure 1. Microbiota analysis for the colon content in mice from polysaccharide group and control group: (A) denaturing gradient gel electrophoresis (DGGE) of V3 regions of bacterial 16S rDNA amplifications; (B) UPGMA cluster analysis of DGGE bacterial profiles; (C) PCA scores plot of DGGE bacterial profiles. PC1, PC2, and PC3 represent principal factors and their probability (%) of influence on the bacterial profiles. C1−C5, colon content samples individually from five mice randomly chosen from the control group after 30 days of administration; P1−P5, colon content samples individually from five mice randomly chosen from the polysaccharide group after 30 days of administration.

Table 5. Diversity Indices Calculated from the DGGE Banding Profiles Generated from the V3 Region of Bacterial 16S rDNA

treatment	richness (S)	H'^{a}	$H'_{max}{}^{b}$	evenness (E)
control group	24.60 ± 3.05 a[c]	3.02 ± 0.13 a	3.10 ± 0.12 a	0.97 ± 0.01 a
polysaccharide group	30.80 ± 3.96 b	3.34 ± 0.14 b	3.42 ± 0.13 b	0.98 ± 0.01 a

[a] H', Shannon−Wiener index. [b] H'_{max}, maximum Shannon−Wiener index. [c] Values are mean of three determinations ± standard deviation. Different letters indicate significant difference ($p < 0.05$) from each other in the same column.

and the polysaccharide group being significant ($p < 0.05$). Studies have shown that an elevation of serum lipids, especially cholesterol, is one of the most important risk factors leading to coronary heart disease.[21] Thus, the cholesterol-lowering effect of the polysaccharide from *P. asiatica* L. was beneficial for health.

A difference in liver lipid levels was apparent for cholesterol and total lipid (Table 4). The liver cholesterol and total lipid level in mice given oral administration of polysaccharide were both significantly lower ($p < 0.05$) than that of the control group. Thus, the polysaccharide from *P. asiatica* L. appears to play a role in lowering the liver cholesterol level. Some other studies also indicated that polysaccharides present in some food materials could reduce the cholesterol in serum and lipid in liver,[22] which was similar to our results.

In contrast to liver cholesterol level, the liver triglyceride level in mice was not significantly decreased after polysaccharide administration for 30 days (Table 4, $p > 0.05$). We have observed that the polysaccharide intake could significantly lower the serum triglyceride level of mice (Table 3, $p < 0.05$). The influence of the polysaccharide on serum triglyceride level may be faster than its effect on liver triglyceride level because the triglyceride was accumulated in liver and the reducing effect by polysaccharide intake may need more time. However, for cholesterol, the polysaccharide could significantly reduce both the serum and liver cholesterol levels (Tables 3 and 4, $p < 0.05$). Although cholesterol was also accumulated in the liver, the liver cholesterol level was significantly reduced by the polysaccharide intake. This may be because except for the polysaccharide itself, the organic acids, particularly propionate, that are produced by colonic fermentation could also influence the liver cholesterol metabolism.[23] The polysaccharide from *P. asiatica* L. was found to increase the propionic acid production of mouse colon in our previous study.[12] Thus, the effect of the polysaccharide on lowering the liver cholesterol level may be stronger than its effect on lowering the liver triglyceride level.

Effect of Polysaccharide on Mice Colon Microbiota. Diversity indices for the DGGE bacterial profiles (Figure 1A) generated from the 16S rDNA V3 region are shown in Table 5. The richness of the DGGE banding profiles for the polysaccharide group (30.80 ± 3.96) was significantly higher than for the control group (24.60 ± 3.05, $p < 0.05$) after 30 days of administration. In addition, a significant increase was also observed in the Shannon−Wiener index and maximum Shannon−Wiener index for the polysaccharide group relative to the control group ($p < 0.05$). There was no significant difference for the evenness between the polysaccharide group and control group ($p > 0.05$).

The effect of polysaccharide on the bacterial communities after 30 days of oral administration was investigated by PCR-

dx.doi.org/10.1021/jf4040942 | J. Agric. Food Chem. 2014, 62, 229−234

DGGE bacterial profiling and identification of putative bacterial species through sequence analysis of recovered DGGE DNA bands. To compare the predominant bacterial communities between different treatments, PCR amplification of the V3 region of the 16S rRNA gene was carried out with corresponding primers. DGGE banding patterns of the V3 region of colon content of each group are shown in Figure 1A. The influence of polysaccharide intake on bacterial community structure was investigated. DGGE image analysis showed that the bacterial community structure from the colon content samples of the polysaccharide group was similar (Figure 1A) and also grouped together in the UPGMA cluster analysis (Figure 1B). In addition, it could also be seen that the bacterial community structure of colon content from polysaccharide group mice was low in similarity with the control group, which means the influence of polysaccharide intake appeared to be a major factor affecting the community. Furthermore, the PCA scores plot (Figure 1C) was also used to compare the differences between banding patterns of different treatments. In the PCA scores plot, "sit together" demonstrates similarity between samples. As shown in Figure 1C, the banding pattern of the control group was different from that of the polysaccharide group. Because banding patterns were related to the bacterial communities, the above results suggest that the predominant bacterial communities in the colon content of polysaccharide group mice were different from those of the control group mice.

Several numerically dominant bacterial species in the colon content for the polysaccharide group corresponding to the presence of some intense DGGE DNA bands, which were different from the control group, were observed (Figure 1A). To further clarify the differences, bands that showed different percentages of density among groups were sequenced for determining their putative identity of bacteria. The putative identity of bacteria is presented in Table 6, which may suggest their possible role in the utilization of the polysaccharide. As shown in Figure 1A and Table 6, 14 interesting excised bands were identified.

Although bands 1, 3−6, and 8−12 have the same migration in different lanes, higher peak density of bands can be observed in the polysaccharide-treated group than in the control group (Figure 1A). Sequencing results showed that their most related bacteria (bands 9−12) were *Bacteroides* sp. *Bacteroidetes* can degrade polysaccharides and metabolic intermediates. They were also able to produce SCFAs such as acetate, lactate, propionate, and others.[24] Band 1 was closest to butyrate-producing bacteria and affiliated with the family of *Butyrivibrio*. A few species-related bands, 5, 6, and 8, had a closer relationship with probiotics *Bifidobacterium bifidum*, *Lactobacillus fermentum*, and *Lactobacillus reuteri*, respectively. These putative butyrate-producing bacteria or probiotics were observed to increase after polysaccharide intake in this study, similar to these bacteria reported to utilize fibers previously.[25] Bands 3 and 4 were sequenced and identified as belonging to *Eubacterium* sp., which were reported to be very active fermentation bacteria for fiber.[26]

Bands 2, 7, 13, and 14 were sequenced as well (Figure 1A), which had higher peak density in the control group than in the polysaccharide-treated groups. The sequencing results showed that their most related bacteria were *Clostridiales* sp. and *Helicobacter* sp., which are the common commensal bacteria in the colon and not good for health in a large amount.[18] These sequencing results indicated that polysaccharide treatment could decrease *Clostridiales* sp. and *Helicobacter* sp. in the mouse colon microbiota.

On the basis of the banding patterns (Figure 1A) and sequencing results (Table 6), it can be inferred that orally administered polysaccharide could substantially affect the mouse colon microbiota. In addition, some other papers have indicated that the predominant increased species in colon microbiota belong to the genera *Bacteroides*, *Eubacterium*, and *Bifidobacterium* after the supply of fermentable carbohydrates. Many other bacteria also occur in high numbers, including *Lactobacilli* and various anaerobic Gram-positive cocci.[27] Their results were similar to ours.

It was reported that there were some relationships between lipid metabolism difference and bacterial community change. The intestinal microbiota develops an important biochemical activity within the host body by providing additional metabolic functions. Specific components of the commensal microbiota also regulate serum lipids and cholesterol by taking part in metabolism.[28] Some intestinal bacteria could influence lipid metabolism. *Butyrivibrio proteoclasticus*, a butyrate-producing ruminal bacterium, could have some effects on cholesterol and lipid utilization.[29] Lactic acid bacteria and *Bifidobacteria* could remove cholesterol or carry out cholesterol assimilation. For example, *Lactobacillus fermentum* was reported to reduce serum lipids and cholesterol in subjects.[30] Low lipid level was associated with higher *Bifidobacterium* numbers in cecal content in mice.[31] Furthermore, *Eubacterium rectale*, *Bacteroides thetaiotaomicrometer*, and *Bacteroides vulgatus* were also found to be cholesterol-reducing bacteria.[32] Thus, the *Bacteroides* sp., *Eubacterium* sp., *Butyrivibrio proteoclasticus*, *Bifidobacterium bifidum*, *Lactobacillus fermentum*, and *Lactobacillus reuteri*, which were found increased in mouse colon after the intake of polysaccharide *P. asiatica* L., may have some effect on the mouse lipid metabolism in this study.

In addition, some probiotics-related metabolites might also exert beneficial effects on cholesterol and lipid metabolism. Propionic acid was reported to affect the liver cholesterol metabolism.[23] The polysaccharide from *P. asiatica* L. was found to increase the propionic acid production in mice colon in a previous study,[12] which might influence the lipid metabolism. Bile acid was found to be closely related to cholesterol and lipid metabolism; thus, the polysaccharide from *P. asiatica* L., which

Table 6. Band Identification for Searching the Bacterial Identity in Denaturing Gradient Gel Electrophoresis (DGGE) Using Bacterial V3 Primers

strain	closest relative	similarity (%)	GenBank no.
1	*Butyrivibrio proteoclasticus*	96	U37378.1
2	*Clostridiales* sp.	97	AB781636.1
3	*Eubacterium rectale*	100	AB626630.1
4	*Eubacterium* sp.	98	AY169428.1
5	*Bifidobacterium bifidum*	95	GU936674.1
6	*Lactobacillus fermentum*	98	JQ669802.1
7	*Helicobacter pylori*	96	JX455160.1
8	*Lactobacillus reuteri*	100	HQ615667.1
9	*Bacteroides salanitronis*	100	AB253731.1
10	*Ruminococcus torques*	99	NR_036777.1
11	*Bacteroides thetaiotaomicrometer*	99	NR_074277.1
12	*Bacteroides vulgatus*	95	HQ012024.1
13	*Clostridium clariflavum*	98	NR_041235.1
14	*Clostridium caenicola*	99	NR_041311.1

dx.doi.org/10.1021/jf4040942 | J. Agric. Food Chem. 2014, 62, 229−234

was found to bind bile acid in vitro,[13] might also affect cholesterol and lipid metabolism.

Our results showed the effect of polysaccharide from *P. asiatica* L. on mouse lipid metabolism and colon microbiota for the first time. The intake of polysaccharide from *P. asiatica* L. could lower the apparent absorption of lipid and decrease the serum and liver lipid level in mice. Mice from the polysaccharide group showed a higher colon bacterial diversity than the control group. *Bacteroides* sp., *Eubacterium* sp., butyrate-producing bacteria *Butyrivibrio* sp., and probiotics *Bifidobacterium bifidum*, *Lactobacillus fermentum*, and *Lactobacillus reuteri* in mouse colon were all increased after mice were given oral administration of the polysaccharide. These suggested that the intake of polysaccharide from *P. asiatica* L. may be beneficial for lipid metabolism and colon microbiota. The changed colon bacteria may play a role in utilization of the polysaccharide and mouse lipid metabolism, which was also affected by polysaccharide intake.

■ ASSOCIATED CONTENT

Supporting Information

Structure of the polysaccharide from the seeds of *P. asiatica* L. This material is available free of charge via the Internet at http://pubs.acs.org.

■ AUTHOR INFORMATION

Corresponding Author

*(S.-P.N.) Phone/fax: +86-791-88304452. E-mail: spnie@ncu.edu.cn.

Funding

This study is financially supported by the Key Program of the National Natural Science Foundation of China (31130041), the National Key Technology R&D Program of China (2012BAD33B06), the National Natural Science Foundation of China (20802032 and 21062012), the Program for New Century Excellent Talents in University (NCET-12-0749), and Research Projects of the State Key Laboratory of Food Science and Technology (SKLF-ZZA-201301 and SKLF-KF-201202), which are gratefully acknowledged.

Notes

The authors declare no competing financial interest.

■ ABBREVIATIONS USED

HDL, high-density lipoprotein; LDL, low-density lipoprotein; DGGE, denaturing gradient gel electrophoresis; PCA, principal component analysis; UPGMA, unweighted pair group mean average; SCFA, short-chain fatty acid

■ REFERENCES

(1) Neyrinck, A. M.; Possemiers, S.; Verstraete, W.; De Backer, F.; Cani, P. D.; Delzenne, N. M. *J. Nutr. Biochem.* **2012**, *23*, 51−59.
(2) Gropper, S. S.; Smith, J. L. In *Advanced Nutrition and Human Metabolism*, 1st ed.; Wadsworth Publishing: New York, 2012.
(3) Xu, X.; Xu, P.; Ma, C.; Tang, J.; Zhang, X. *Biotechnol. Adv.* **2012**, *31*, 318−337.
(4) Topping, D. L.; Clifton, P. M. *Physiol. Rev.* **2001**, *81*, 1031−1064.
(5) Cummings, J. H.; Macfarlane, G. T. *J. Appl. Microbiol.* **1991**, *70*, 443−459.
(6) Mahady, G. B.; Fong, H. S.; Farnsworth, N. R. In *WHO Monographs on Selected Medicinal Plants*, 1st ed.; World Health Organisation: Geneva, Switzerland, 1999.
(7) Yin, J. Y.; Nie, S. P.; Zhou, C.; Wan, Y.; Xie, M. Y. *J. Sci. Food Agric.* **2010**, *90*, 210−217.
(8) Yin, J.; Lin, H.; Li, J.; Wang, Y.; Cui, S. W.; Nie, S.; Xie, M. *Carbohydr. Polym.* **2012**, *87*, 2416−2424.
(9) Huang, D. H.; Xie, M. Y.; Yin, J. Y.; Nie, S. P.; Tang, Y. F.; Zhou, C. *J. Ethnopharmacol.* **2009**, *124*, 493−498.
(10) Tang, Y.; Huang, D.; Yin, J.; Zhou, C.; Xie, X.; Xie, M. *Food Sci.* **2007**, *28*, 517−520.
(11) Wu, G.; Tian, Y.; Xie, M.; Li, C. *Food Sci.* **2007**, *28*, 514−516.
(12) Hu, J. L.; Nie, S. P.; Min, F. F.; Xie, M. Y. *J. Agric. Food Chem.* **2012**, *60*, 11525−11532.
(13) Hu, J. L.; Nie, S. P.; Li, C.; Xie, M. Y. *Int. J. Biol. Macromol.* **2013**, *54*, 264−269.
(14) Hu, J. L.; Nie, S. P.; Li, C.; Fu, Z. H.; Xie, M. Y. *J. Agric. Food Chem.* **2013**, *61*, 6092−6101.
(15) Adachi, T.; Ono, Y.; Koh, K. B.; Takashima, K.; Tainaka, H.; Matsuno, Y.; Nakagawa, S.; Todaka, E.; Sakurai, K.; Fukata, H. *Food Chem. Toxicol.* **2004**, *42*, 445−452.
(16) Takahashi, T.; Maeda, H. *Biosci., Biotechnol., Biochem.* **1999**, *63*, 1340−1345.
(17) Folch, J.; Lees, M.; Sloane-Stanley, G. *J. Biol. Chem.* **1957**, *226*, 497−509.
(18) Muyzer, G.; De Waal, E. C.; Uitterlinden, A. G. *Appl. Environ. Microbiol.* **1993**, *59*, 695−700.
(19) Gong, J.; Yu, H.; Liu, T.; Gill, J.; Chambers, J.; Wheatcroft, R.; Sabour, P. *J. Appl. Microbiol.* **2008**, *104*, 1372−1382.
(20) Dall'Agnol, R.; Lino von Poser, G. *J. Ethnopharmacol.* **2000**, *71*, 337−341.
(21) Kannel, W. B.; Castelli, W. P.; Gordon, T. *Ann. Intern. Med.* **1979**, *90*, 969−975.
(22) Gallaher, C. M.; Munion, J.; Hesslink, J. R.; Wise, J.; Gallaher, D. D. *J. Nutr.* **2000**, *130*, 2753−2759.
(23) Nishimura, N.; Nishikawa, H.; Kiriyama, S. *J. Nutr.* **1993**, *123*, 1260−1269.
(24) Duncan, S.; Louis, P.; Flint, H. *Lett. Appl. Microbiol.* **2007**, *44*, 343−350.
(25) Crittenden, R.; Karppinen, S. *J. Sci. Food Agric.* **2002**, *82*, 781−789.
(26) Varel, V. H.; Yen, J. T. *J. Anim. Sci.* **1997**, *75*, 2715−2722.
(27) Finegold, S. M.; Attebery, H. R.; Sutter, V. L. *Am. J. Clin. Nutr.* **1974**, *27*, 1456−1469.
(28) Gill, S. R.; Pop, M.; DeBoy, R. T.; Eckburg, P. B.; Turnbaugh, P. J.; Samuel, B. S.; Gordon, J. I.; Relman, D. A.; Fraser-Liggett, C. M.; Nelson, K. E. *Science* **2006**, *312*, 1355−1359.
(29) Moon, C. D.; Pacheco, D. M. *Int. J. Syst. Evol. Microbiol.* **2008**, *58*, 2041−2045.
(30) Simons, L. A.; Amansec, S. G. *Nutr. Metab. Cardiovasc.* **2006**, *16*, 531−535.
(31) Cani, P. D.; Amar, J.; Iglesias, M. A.; Poggi, M.; Knauf, C.; Bastelica, D.; Neyrinck, A. M.; Fava, F.; Tuohy, K. M.; Chabo, C. *Diabetes* **2007**, *56*, 1761−1772.
(32) Sadzikowski, M.; Sperry, J.; Wilkins, T. *Appl. Environ. Microbiol.* **1977**, *34*, 355−362.

JOURNAL OF AGRICULTURAL AND FOOD CHEMISTRY

Article

pubs.acs.org/JAFC

Identification and Characterization of Dimeric Oxidation Products of *p*-Cymene-2,3-diol Isolated from *Thymus vulgaris* L.

Guido Rainis and Waldemar Ternes*

Department of Analytical Chemistry, Institute of Food Toxicology and Analytical Chemistry, University of Veterinary Medicine Hannover, Foundation, Bischofsholer Damm 15, D-30173 Hannover, Germany

ABSTRACT: The aim of this study was to investigate the oxidation products of *p*-cymene-2,3-diol, a major antioxidative constituent of thyme (*Thymus vulgaris* L.). Although a dimeric form of *p*-cymene-2,3-diol and some derivative substances exhibiting valuable food technological and health-promoting properties have been reported in earlier publications, no obvious correlation has been shown between these substances. A modified HPLC-ESI-MS method made it possible to prove that two dimers, 3,4,3′,4′-tetrahydroxy-5,5′-diisopropyl-2,2′-dimethylbiphenyl (**1**) and the newly identified 3′,4′-dihydroxy-5,5′-diisopropyl-2,2′-dimethylbiphenyl-3,4-dione (**2**), are oxidation products of *p*-cymene-2,3-diol. **2** was characterized by the fragmentation pattern determined by multiple mass spectrometry, ^{1}H NMR, ^{13}C NMR, H−H COSY, HSQC, and HMBC. Both biphenyls were also quantitated in freeze-dried thyme as well as in a food matrix spiked with thyme extract. Model experiments using raw and cooked minced pork meat as matrix and sodium nitrite as oxidizing and reduction agent with and without ascorbic acid as protective reagent showed the correlation between food processing and dimer generation.

KEYWORDS: *p-cymene-2,3-diol, Thymus vulgaris L., oxidation products, HPLC, LC-ESI-MS, hydrodistillation*

INTRODUCTION

Members of the botanical family of Lamiaceae (or Labiateae) have been intensively investigated as well-known sources of antioxidant and antimicrobial components, and the best-studied[1−6] genera include *Origanum*, *Rosmarinus*, *Salvia*, and *Thymus*. The most often cultivated and commercially most widespread species of that genus is *Thymus vulgaris* L. (garden or common thyme).[7] Native to the Iberian peninsula, it is traditionally used as a flavoring herb for many dishes in Mediterranean cuisine as well as for medicinal purposes.[7] The main functional constituents of *T. vulgaris* L. are the odorous monoterpene phenols thymol and carvacrol, which have been widely discussed in the literature in regard to their antioxidant,[1,8−11] antimicrobial,[2,10] and anti-inflammatory[10] effects. However, *Thymus citriodorus* L. (lemon thyme), another commonly available species, is reported to contain no carvacrol[12,13] and only small amounts of thymol.[13] Despite the beneficial health effects of thymol and carvacrol, their use as ingredients in food is limited by their strong odorous activity. Whereas thymol and carvacrol have been known for more than 100 years, another important component, *p*-cymene-2,3-diol, was not detected until much later,[14] probably due to the fact that thyme (*T. vulgaris* L.) has mainly been analyzed by means of gas chromatography, as the putative substances of interest, that is, thymol and carvacrol (and, e.g., compounds of essential oils), are volatile. In contrast, the semivolatile *p*-cymene-2,3-diol is hard to determine by gas chromatography; it is much easier to detect with liquid chromatographic methods such as HPLC-DAD.[14,15] *p*-Cymene-2,3-diol is sometimes included[16,17] and sometimes not[18,19] in the literature on the nonvolatile substances of *T. vulgaris* L. Furthermore, only marginal information is available about the formation, chemical behavior due to food processing, and possible oxidation products of *p*-cymene-2,3-diol. In comparison with thymol and carvacrol, *p*-cymene-2,3-diol possesses one additional hydroxyl group on the aromatic ring system and exhibits similar functional properties.[14,15] Thymoquinone has been suggested as a possible oxidation product of thymol and carvacrol.[16,20,21] Furthermore, Nakatani and Miura isolated from the leaves of thyme five biphenyl compounds[22,23] proven to have deodorizing,[22−24] antioxidative,[5,17,24,25] and human platelet aggregation-inhibiting activities.[26] The biphenyls occur in the same fraction as flavonoids and other nonvolatile natural compounds described and analyzed in several newer publications,[16,17,19,27−31] but only two of these[16,17] mention at least one of the biphenyls mentioned above, 3,4,3′,4′-tetrahydroxy-5,5′-diisopropyl-2,2′-dimethylbiphenyl (**1**),[22] along with other nonvolatile compounds. One further biphenyl described by Nakatani and Miura is assumed to be a dimer of thymoquinone, that is, the quinoid form of **1**, 3,3′-diisopropyl-6,6′-dimethylbiphenyl-1,2,1′,2′-tetraone (**3**).[23] Each of the other three postulated compounds contains one thymol molecule dimerized with one of the following substances: *p*-cymene-2,3-diol (named 3,4,4′-trihydroxy-5,5′-diisopropyl-2,3-dimethylbiphenyl),[22] hydroxy thymoquinone (named 4,4′-dihydroxy-5,5′-diisopropyl-2,2′-dimethylbiphenyl-3,6-dione),[23] or thymoquinone (named 4′-hydroxy-5,5′-diisopropyl-2,2′-dimethylbiphenyl-3,4-dione).[23] For better comparability, we have maintained the nomenclature of these substances, which was established by Nakatani and Miura.[22] To date, nothing is known about the formation and content of the biphenyls in commercial thyme in consideration of the fact that it exhibits the various exploitable characteristics mentioned above. There is no clear and coherent information

Received: September 18, 2013
Revised: November 17, 2013
Accepted: November 23, 2013
Published: November 23, 2013

ACS Publications © 2013 American Chemical Society

about the correlation of monomeric and dimeric substances or their formation pathway under experimental or even native conditions. **1** has recently been described as a major antioxidative component of a supercritical CO_2 extract of *T. vulgaris* L. and as a dimer of *p*-cymene-2,3-diol.[16,17] To investigate the potential chemical pathway between *p*-cymene-2,3-diol and its postulated dimeric oxidation products in the nonvolatile part of *T. vulgaris* L., we planned to add supercritical CO_2 extracts of thyme to a minced pork meat matrix to determine the oxidation stability of *p*-cymene-2,3-diol and its dimeric oxidation products. Considering previous results,[16,17] we intended to develop an HPLC-ESI-MS method for chromatographic analysis of *p*-cymene-2,3-diol along with the biphenyls that should also be applicable to minced meat and other food matrices. In consideration of the potentially high amounts of *p*-cymene-2,3-diol and dimeric substances in freeze-dried thyme (and thyme byproducts), the intended results of the present study should facilitate the industrial exploitation of the functional substances of thyme and make it possible to utilize their advantageous properties in specific applications in the future.

MATERIALS AND METHODS

Sample Material. Seedlings of known varieties of common and lemon thyme, *T. vulgaris* L. (variety 'Faustini') and *T. citriodorus* L. (variety 'Silver Queen') were obtained from a local market and grown in a kitchen garden for 3 months in 2012. The leaves were harvested and freeze-dried in June. The *T. vulgaris* L. and *T. citriodorus* L. leaves contained 26.7 and 23.8% dry matter, respectively. Minced, conventionally packaged pork meat was obtained from a local market. A commercial supercritical CO_2 extract of nonspecified *T. vulgaris* L. varieties was obtained from Raps (Kulmbach, Germany).

Chemicals. Water (18 MΩ × cm) was obtained from a water purification system (Millipore, San Jose, CA, USA). Silica gel was obtained from Riedel-de-Haën (Seelze, Germany). The reference standard of *p*-cymene-2,3-diol and diethyl ether were obtained from Sigma-Aldrich (Steinheim, Germany). *p*-Coumaric acid, ascorbic acid, hydrogen peroxide (30%), sodium chloride, and sodium nitrite were obtained from Carl Roth (Karlsruhe, Germany). Three nitrite curing salt formulations were prepared by mixing sodium chloride with 1.0, 3.0, and 6.0% (w/w) sodium nitrite. **1** and **2** (3′,4′-dihydroxy-5,5′-diisopropyl-2,2′-dimethylbiphenyl-3,4-dione) were isolated from a supercritical CO_2 extract of thyme by means of preparative HPLC as described below. Samples and standards were diluted in methanol (LC-MS grade, Sigma-Aldrich); the ascorbic acid and nitrite curing salt were dissolved in purified water. Acetonitrile (LC-MS grade, Sigma-Aldrich) and purified water (Millipore) were used for chromatographic purposes.

Steam Distillation. Freeze-dried leaves of thyme were ground to a fine powder in an A 11 basic analytical mill (IKA, Staufen, Germany). To remove the volatile substances, approximately 1 g of the powder was steam-treated in a laboratory glass apparatus according to the method of Antonacopoulos[32] until approximately 100 mL of aqueous distillate had been collected. The aqueous distillate containing the volatile substances was discarded. The steam distillation residue was dried at room temperature.

Extraction and Purification. Freeze-dried thyme and the residue from steam distillation were extracted three times with methanol/water (70:30, v/v) for 30 min at room temperature on a magnetic stirrer. The extracts were transferred through a folded filter into a round-bottom flask; the combined extracts concentrated using a rotary evaporator at 50 °C under vacuum and then collected with methanol. The extract was further purified by solid-phase extraction (SPE) applying Chromabond C-18 "Hydra" cartridges (500 mg, Macheray-Nagel, Düren, Germany) conditioned with water. The extract was mixed with water before loading into the cartridge, which had been rinsed with water. The substances were eluted with 5 mL of methanol into a 5 mL volumetric flask, and the flask was filled to volume with methanol. To compare experimental conditions with previously published preparation methods,[22,23] purification by silica gel chromatography was conducted using a glass column half-filled with silica gel and diethyl ether as eluent. Eluted solutions were evaporated to dryness on a rotary evaporator and collected with methanol. All solutions obtained were diluted with methanol for analytical use.

Oxidation Assays. A storage assay was performed on six 1000 mg/L preparations of *p*-cymene-2,3-diol solutions, which were stored at room temperature and constantly stirred in a sealed round-bottom glass flask. Samples were obtained from each assay immediately and after 1, 2, and 6 days of storage. All solutions were purified with Chromabond C-18 Hydra cartridges (500 mg, Macheray-Nagel) as described above and analyzed by HPLC-MS as described below.

Experiments under food-relevant conditions were carried out on a mixture of minced pork meat with a 1.0% (w/w) supercritical CO_2 extract of thyme (containing *p*-cymene-2,3-diol, **1**, and **2**) and 1.0% (w/w) nitrite curing salt mixtures containing either 1.0, 3.0, or 6.0% sodium nitrite (all percentages w/w: 100, 300, and 600 mg/kg of the entire matrix) and with or without 1.0% (w/w) ascorbic acid in a conventional mixer. The mixtures were heated in a closed plastic vessel at 80 °C in a water bath for 30 min. The cooked minced meat was homogenized again, extracted three times with methanol/water (70:30, v/v) with an Ultra-Turrax (IKA, Staufen, Germany), filtered through a folded filter, purified by means of SPE as described above, and analyzed by HPLC-MS as described below.

3 as reference substance was produced by spiking 1 part hydrogen peroxide (30% solution in water) to 9 parts of a highly concentrated standard solution of *p*-cymene-2,3-diol (5000 mg/L), stirring in a clear round-bottom flask for several days at room temperature (no direct sunlight), and subsequent isolation of the resulting **3** by preparative HPLC (as described below).

Preparative HPLC-UV. Preparative chromatography was carried out on a Knauer Smartline 1000 pump connected to a Smartline Manager 5000 and a Knauer 8700 variable-wavelength detector, controlled by EuroChrom 3.05 software (Knauer, Berlin, Germany) on a Knauer IF 2 interface box. A 250 mm Nucleodur C 18 Isis column with an inner diameter (i.d.) of 4.8 mm and a particle size of 5 μm (Macheray Nagel) was used for chromatographic separation. Solvent A was purified water with 0.1% (v/v) acetic acid; solvent B was acetonitrile mixed with 0.1% (v/v) acetic acid. Isocratic separation was achieved with 50% A and 50% B with a flow rate of 1.0 mL/min for 15 min, followed by a washing step with 95% B for 5 min and recalibration to starting conditions for 5 min. Detection was carried out by the Knauer 8700 variable-wavelength detector at 273 nm. The injection volume for the preparative separation of **1**, **2** (both from methanol solution of supercritical CO_2 thyme extract), and the produced **3** (as described above) was 200 μL. Substances were repeatedly collected, purified by means of SPE, and, after removal of the eluent under vacuum, the greasy, dark brown residue (95% purity, estimated by means of NMR and MS data) was weighed out and determined by HPLC-MS.

Analytical HPLC-UV. HPLC-UV was carried out at 273 nm on the same HPLC system as described above. Water with 0.1% acetic acid (solvent A) and acetonitrile mixed with 0.1% acetic acid (solvent B) were used at a flow rate of 1.0 mL/min. The gradient started with 70% A for 2 min, followed by a linear decrease to 50% A within 10 min, then to 10% A within 3 min, back to 70% within 5 min, and then recalibration to starting conditions for 10 min. The injection volume of each sample was 20 μL.

Analytical HPLC-MS. Chromatographic separation was carried out on a Waters 616 gradient pump and a Waters 171 plus autosampler (Waters, Eschborn, Germany) controlled by a Waters 600 controller unit. The interior temperature of the autosampler was set to 10 °C. A Nucleodur C 18 Isis column (150 mm × 2.1 mm i.d.) with a particle size of 5 μm (Macheray-Nagel) was used for chromatographic separation at 20 °C. The temperature was kept stable by means of a column oven (LabSource, Manchester, UK). Water with 0.1% (v/v) acetic acid (solvent A) and acetonitrile with 0.1% (v/v) (solvent B) were used at a flow rate of 0.2 mL/min. The gradient started with 80%

Table 1. Statistical Parameters of the HPLC-ESI-MS Method Validation

analyte	eq calcd from quadratic (polynomial) regression[a]	R^{2a}	MSD (mg/L)[b]	MVC (%)[b]	LOD (mg/L)[c]	LOC (mg/L)[c]	LOQ (mg/L)[c]
p-cymene-2,3-diol	$y = 0.085 + 0.5137x - 0.003x^2$	0.9952	1.426	10.60	0.178	0.356	0.536
1	$y = -0.049 + 0.7648x - 0.006x^2$	0.9964	0.571	4.29	0.099	0.197	0.307
2	$y = -0.047 + 0.7560x - 0.005x^2$	0.9952	0.572	4.30	0.099	0.197	0.307

[a]Calibration data confirmed with XCalibur 1.3 software in the range of 0.5−50 mg/L, calculated from quadratic polynomial regression as calibration function of the second degree. [b]Calculated by means of calibration data and Valoo 2.5 software.[32] [c]DIN 32645:2008-11.[31]

A for 10 min, followed by a linear decrease to 70% A within 5 min, then to 50% A in 5 min, which was held for 10 min, followed by an increase to 90% B within 5 min, and held for 5 min (washing step); recalibration to starting conditions was then allowed for 15 min. The injection volume of each sample was 5.0 μL.

The HPLC system was connected with a Finnigan LCQ Classic mass spectrometer (Thermo Scientific, Bonn, Germany) with an electrospray ionization (ESI) source operating in negative ion mode. Mass spectra were recorded in total ion chromatogram (TIC, *m/z* 150−1000) mode during the chromatographic separation and in selected ion monitoring (SIM) mode for quantitation purposes. The instrument was tuned by optimization of *m/z* 327 while a standard solution of 1.0 mg/L **2** was infused directly into the ESI source by a syringe pump with a flow rate of 3.0 μL/min. Tuning parameters were as follows: capillary temperature, 250 °C; sheath gas flow, 60 arbitrary units; and auxiliary gas flow 10, arbitrary units. Automatically set parameters after tuning were as follows: source voltage, 4.5 kV; capillary voltage, 32 V; tube lens offset, 55 V; multipole 1 offset, −3.0 V; multipole 2 offset, −4.5 V; interpole lens voltage, −24 V; trap DC offset voltage, 10 V. Chromatographic and mass spectrometric data were acquired with XCalibur 1.3 software (Thermo Scientific). To obtain structural information, collision-induced fragmentation spectra were recorded using TunePlus 1.3 (Thermo Scientific) software. Preparatively isolated substances were infused by a syringe pump with a flow rate of 3.0 μL/min. Collision energy values were adjusted to between 35 and 41 arbitrary units.

HPLC-ESI-MS Calibration, Method Validation, and Statistical Analysis. Stock solutions of 1000 mg/L were prepared on the basis of the commercially available standard of *p*-cymene-2,3-diol and isolated **2**. The internal standard was *p*-coumaric acid. The concentration of the internal standard in each calibration standard and sample was 5.0 mg/L. Calibration was conducted using XCalibur 1.3 software. The analytical parameters as configured in the software were as follows: Genesis peak detection algorithm with minimum peak height of 3.0 arbitrary units, 5-point-smooth, minimum signal-to-noise ratio (S/N ratio) of 0.5 arbitrary unit, and valley detection with a 20 s expected width. The calibration curve was created with standard amounts of 0.5, 1.0, 2.5, 5.0, 10, 25, and 50 mg/L *p*-cymene-2,3-diol and **2**. To cover a wide range of concentration, quadratic (polynomial) regression and a calibration function of the second order were applied. **1** was quantitated as **2** equivalents (using the calibration standards of **2**). Statistical differences were determined by a paired (two-tailed) Student's *t* test. All statistical tests were conducted at a significance level of $\alpha = 0.05$ ($p < 0.05$). The sensitivity of the HPLC-ESI-MS instrument was evaluated by determining the limits of detection (LOD), quantitation (LOQ), and capability (LOC) by means of the calibration function method according to DIN 32645:2008-11[33] (Table 1). The calibration curves were tested for outliers (Grubbs test). All statistical parameters were calculated using Valoo 2.5 software.[34] Formation/decomposition rates (FDRs) in the matrices were determined by spiking freeze-dried thyme and minced pork meat (raw and cooked) with a *p*-cymene-2,3-diol standard solution containing *p*-cymene-2,3-diol, **1**, and **2**. No interferences were detected due to unwanted coelutions. FDRs were expressed in percentage of untreated standard contents (minus analyte amounts in plain matrix) and of contents after extraction to determine content changes during extraction and processing.

Nuclear Magnetic Resonance Spectroscopy (NMR). ^{1}H NMR (400 MHz), ^{13}C NMR (100 MHz), correlation spectroscopy (H−H COSY), heteronuclear single-quantum coherence (HSQC), and heteronuclear multiple-bond correlation (HMBC) spectra were obtained in deuterated chloroform (**1**, **2**) or deuterated methanol (**3**) with a Bruker DPX 400 MHz NMR spectrometer. The chemical shift of protons and carbons is expressed here as δ values with tetramethylsilane (TMS; δ = 0) as the internal standard.

RESULTS AND DISCUSSION

Identification of 1 and 2 by Means of HPLC-MS and NMR Spectroscopy. As depicted in Figure 1A,B, chromatographic analysis of *p*-cymene-2,3-diol (MW = 166 g/mol, no. II) standard in methanolic solutions by HPLC-ESI-MS in negative ion mode and in TIC mode revealed two additional distinct peaks after storage. These peaks potentially represent the *p*-cymene-2,3-diol oxidation products **1** and **2**, as peaks III and IV have molecular weights consistent with those calculated for **1** (330 g/mol) and **2** (328 g/mol). Considering that *p*-cymene-2,3-diol is very sensitive to oxidation in air, oxidation of *p*-cymene-2,3-diol may already take place in the unharvested

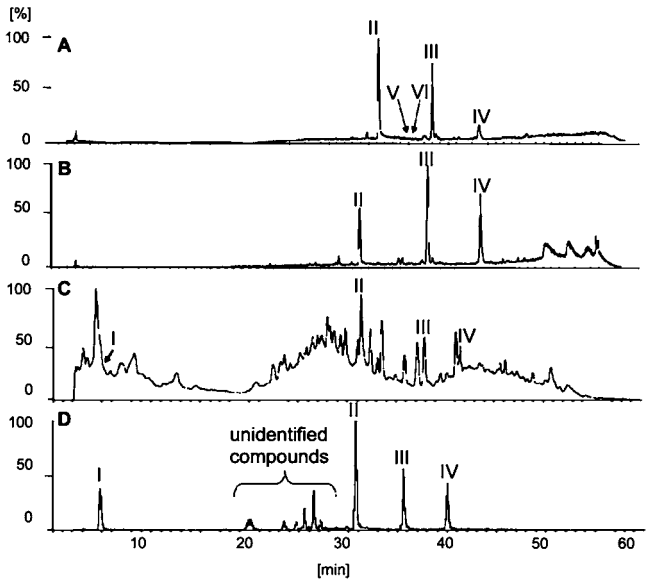

Figure 1. Chromatographic separations in negative ion mode of *p*-coumaric acid (*m/z* 163) (I), *p*-cymene-2,3-diol (*m/z* 165) (II), 3,4,3′,4′-tetrahydroxy-5,5′-diisopropyl-2,2′-dimethylbiphenyl (**1**, *m/z* 329) (III), and 3′,4′-dihydroxy-5,5′-diisopropyl-2,2′-dimethylbiphenyl-3,4-dione (**2**, *m/z* 327) (IV). V and VI are approximate retention times for carvacrol (V) and thymol (VI) (neither detectable by means of ESI-MS). (A) Freshly prepared solution of *p*-cymene-2,3-diol commercially available standard (100 mg/L in methanol) in total ion chromatogram (TIC) mode (*m/z* 150−1000); (B) standard solution after 4 days of storage in a glass envelope at room temperature in TIC mode (*m/z* 150−1000); (C) extraction solution of freshly harvested freeze-dried *Thymus vulgaris* L. in TIC mode (*m/z* 150−1000); (D) extraction solution of freshly harvested freeze-dried *T. vulgaris* L. in selected ion monitoring (SIM) mode (*m/z* 163, 165, 327, 329).

dx.doi.org/10.1021/jf404193y | J. Agric. Food Chem. 2014, 62, 235−243

thyme plant. The two potential dimeric oxidation products of *p*-cymene-2,3-diol were already present in the freshly prepared *p*-cymene-2,3-diol solution (Figure 1A), but after storage, the signal intensities of those increased, whereas that of *p*-cymene-2,3-diol decreased (Figure 1B). As the dimers have nonvolatile characteristics, they are suitable for examination by HPLC-ESI-MS detection, a technique that is mainly applied for analysis of nonvolatile secondary plant material such as flavonoids and phenolic acids. Because thymol and carvacrol, the major constituents of thyme, are volatile, they cannot be detected by that method and have to be analyzed by means of other detection techniques such as UV−vis or gas chromatography. The expected retention times of thymol and carvacrol as determined by analytical HPLC-UV are shown in Figure 1A (arrows V and VI).

The preparatively isolated substances with m/z 329 ($[M - H^-]$) **1** and m/z 327 ($[M - H^-]$) **2** were identified by means of ESI-MS detection by the characteristic fragmentation pattern (Figures 2 and 3). Due to the negative ion mode setting, the

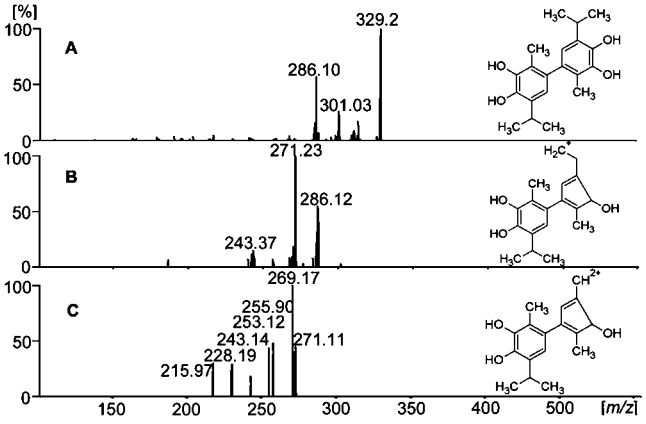

Figure 2. ESI product ion spectrum in negative ion mode ($[M - H]^-$) of **1** m/z 329 (A) and selected daughter ions m/z 286 (B) and m/z 271 (C).

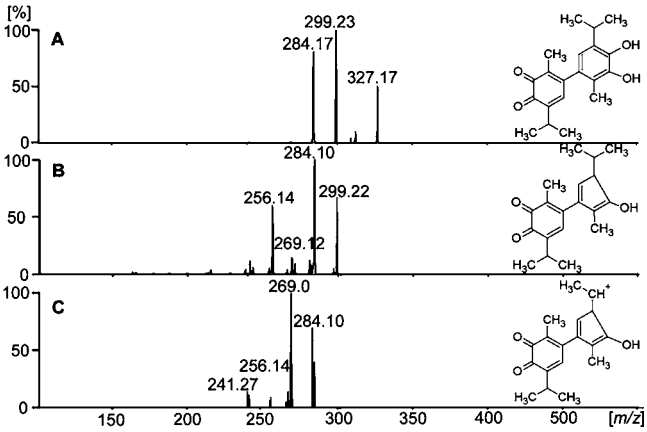

Figure 3. ESI product ion spectrum in negative ion mode ($[M - H]^-$) of m/z 327 (**2**) (A) and selected daughter ions m/z 299 (B) and m/z 284 (C).

base peaks are displayed as $[M - H]^-$. Therefore, the correct molecular weights of the substances are 330 g/mol, which is consistent with the molecular formula of **1**, and 328 g/mol, consistent with that of **2**. Figure 2 shows the fragmentation pattern of **1**: The first fragmentation step resulted in m/z 301 by phenol-characteristic loss of [CO] as reported in the literature on general mass spectrometry,[35] followed by splitting off [CH_3], on the one hand, and loss of [CO], on the other, so that m/z 286 is formed. The ion with m/z 286 can be observed even at the first fragmentation step (Figure 2B), as m/z 301 is very unstable and fragments immediately to m/z 286. In the further fragmentation step (Figure 2B), m/z 286 lost one [CH_3], so that m/z 271 was formed, followed by m/z 256 due to the loss of [CH_3] and by m/z 228 and further loss of [CO] (Figure 2C).

Table 2 shows ^{1}H NMR (400 MHz) and ^{13}C NMR (100 MHz) data as well as results from HMBC of **2** (MW = 328 g/mol), which have not yet been reported in the literature. The ^{1}H NMR spectrum showed the presence of two aromatic protons (singlets at 6.62 and 6.57 ppm), two hydroxyl groups (broad singlets at 5.34 and 5.43 ppm), two isopropyl groups (septets at 3.00 and 3.20 ppm and doublets at 1.13 and 1.29 ppm), and two methyl groups (singlets at 1.78 and 2.15 ppm). Assignment of directly coupling protons was confirmed by H−H COSY. The ^{13}C NMR spectrum exhibited 20 signals, and allocations were confirmed by means of HSQC and HMBC experiments. The HSQC experiment indicated that the ^{13}C NMR signal at 116.63 ppm correlates with the ^{1}H NMR signal at 6.57 ppm and the ^{13}C NMR signal at 138.39 ppm with the ^{1}H NMR signal 6.62 ppm. By means of the HMBC experiment, which shows C−H correlations over multiple bondings, it could also be shown that the ^{1}H NMR signal at 6.62 ppm correlates with the ^{13}C NMR signal at 180.23 ppm assigned to be one of the carbonyl carbons (position 3 or 4). This fact confirms that the ^{1}H NMR signal at 6.62 ppm and the ^{13}C NMR signal at 138.06 ppm correspond to position 6, just as the ^{13}C NMR

Table 2. ^{1}H NMR and ^{13}C NMR Spectroscopic Characteristics and HMBC of 3′,4′-Dihydroxy-5,5′-diisopropyl-2,2′-dimethylbiphenyl-3,4-dione (2)

position[a]	^{1}H NMR shift[b] (ppm) (multiplicity)	^{13}C NMR shift (ppm)	HMBC (H to C correlations)
1		148.99	
2		133.73	
3		181.60	
4		180.23	
5		145.55	
6	6.62 (s)	138.39	2, 4, 8, 1′
7	1.78 (s)	12.93	1, 2, 3
8	3.00 (sept)	27.07	4, 5, 6, 9, 10
9	1.13 (d)	21.48	5, 10
10′	1.13 (d)	21.64	5, 9
1′		130.74	
2′		118.51	
3′		141.22	
4′		142.32	
5′		132.59	
6′	6.57 (s)	116.63	2′, 4′, 8′, 1
7′	2.15 (s)	12.95	1′, 2′, 3′
8′	3.20 (sept)	27.32	4′, 5′, 6′, 9′, 10′
9′	1.29 (d)	22.55	5′, 10′
10′	1.29 (d)	22.60	5′, 9′
OH-3′	5.43 (bs)		
OH-4′	5.34 (bs)		

[a]Numbering of atoms is shown in Figure 4. [b]δ values (ppm) in $CDCl_3$. s = singlet; sept = septet; d = doublet; bs = broad singlet.

dx.doi.org/10.1021/jf404193y | J. Agric. Food Chem. 2014, 62, 235−243

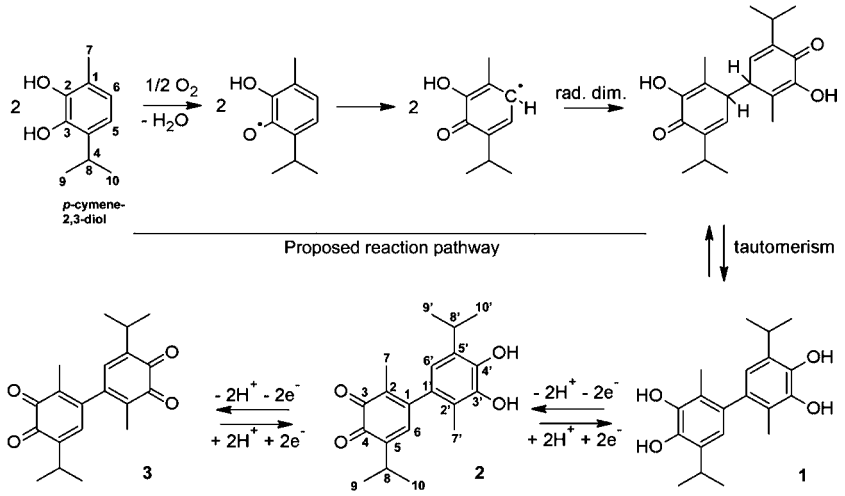

Figure 4. Proposed reaction pathway (upper part) leading to the formation of *p*-cymene-2,3-diol dimeric oxidation products **1**, **2**, and **3** identified by comparing retention times, MS, ^{1}H NMR, and ^{13}C NMR spectra. rad. dim. = radical dimerization.

signal at 180.23 ppm refers to position 4. On the other hand, the ^{1}H NMR signals at 3.20 ppm (isopropyl CH) and 6.57 ppm (aromatic CH) correspond to the ^{13}C NMR signal at 141.22 ppm, which in turn must suggest that this signal refers to position 4′. Thus, all ^{13}C NMR signals could be allocated distinctively. These data therefore prove that the isolated compound with the molecular mass of 328 g/mol has to be 1′,2′-dihydroxy-3,3′-disopropyl-6,6′-dimethylbiphenyl-1,2-dione **2** as depicted in Figures 3 and 4. Although Nakatani and Miura isolated and characterized a dimer with the same molecular weight (328 g/mol), they determined a different structure by NMR experiments,[23] but this was not confirmed in our studies. We were able to identify naturally occurring substances such as flavonoids and phenolic acids, but found no dimeric oxidation products other than **1** and **2**, in methanolic extracts either from steam-treated thyme (Figure 1D) or from the eluent of silica gel chromatography (data not shown). The ^{1}H NMR and ^{13}C NMR data for **1** and **3** correspond with those reported earlier.[22,23] We isolated **1** and **2** from thyme extract by extraction techniques and preparative HPLC as described above. Here, **2** was characterized for the first time as a further oxidation product. On the other hand, we found only traces of **3** in thyme extract (retention time of approximately 50 min), so we isolated it from a standard solution of *p*-cymene-2,3-diol, where it occurred as an oxidation product. **3** was obtained through oxidation of *p*-cymene-2,3-diol and subsequent preparative HPLC. The results are listed below.

*3,4,3′,4′-Tetrahydroxy-5,5′-diisopropyl-2,2′-dimethylbiphenyl (**1**):* ^{1}H NMR (400 MHz, chloroform-*d*) δ 1.27 (d, 12, J = 7 Hz, CH$\underline{CH_3}$), 1.96 (s, 4 H), 3.15−3.26 (sept, 2, J = 7 Hz, $\underline{CH}CH_3$), 5.39 (bs, 4, OH), 6.59 (s, 2, CH); ^{13}C NMR (100 MHz, chloroform-*d*) δ 12.70 (C-7, C-7′), 22.66 (C-9, C-9′), 22.77 (C-10, C-10′), 27.19 (C-8, C-8′), 119.30 (C-6, C-6′), 119.98 (C-2, C-2′), 131.52 (C-5, C-5′), 134.08 (C-1, C-1′), 139.85 (C-3, C-3′), 141.38 (C-4, C-4′).

*3,3′-Diisopropyl-6,6′-dimethylbiphenyl-1,2,1′,2′-tetraone (**3**):* ^{1}H NMR (400 MHz, methanol-d_4) δ 1.17 (d, 12, J = 7 Hz, CH$\underline{CH_3}$), 1.89 (s, 10, CH_3), 2.91−3.02 (sept, 2, J = 7 Hz, $\underline{CH}CH_3$), 6.69 (s, 2, CH); ^{13}C NMR (100 MHz, methanol-d_4) δ 11.53 (C-7, C-7′), 20.35 (C-9, C-9′, C-10, C-10′), 27.44 (C-8, C-8′), 133.49 (C-1, C-1′) 134.04 (C-6, C-6′) 144.41 (C-2, C-2′), 147.63 (C-5, C-5′), 179.20 (C-4, C-4′), 180.09 (C-3, C-3′).

Assumed Reaction Pathway of *p*-Cymene-2,3-diol, 1, 2, and 3 under Oxidative Conditions. The proposed reaction pathway of *p*-cymene-2,3-diol leading to the formation of the oxidation products **1**, **2**, and **3** shown in Figure 4 was created on the basis of the reaction products identified and general reference literature.[36] It follows a common reaction pathway of phenols. The reaction starts with oxygen-catalyzed radical formation of two *p*-cymene-2,3-diol molecules and loss of two protons (one from each molecule) and then proceeds with electron migration from a hydroxyl group to the unsubstituted *para* carbon atom, forming a quinoid radical transitional state.[36] The resulting radicals form a quinoid dimer, which immediately reacts to its hydrolyzed form, accompanied by intramolecular migration of two protons. That reaction step can be explained as a tautomerism, which is promoted by *para*-substituents on both aromatic parts of the dimer. The resulting product with a molecular weight of 330 g/mol (**1**) has been described in the literature[22,23] (as mentioned above) and can be specified as the dimeric form of *p*-cymene-2,3-diol. By means of further oxidation of one part of the dimeric compound and formation of a stable quinoid structure containing two ortho keto groups, the newly identified **2** is formed with a molecular weight of 328 g/mol followed by the quinoid dimer **3** with a molecular weight of 326 g/mol. We observed that the kinetics of the phenolic dimerization reaction and further oxidation of one aromatic part were very slow at room temperature and without further addition of oxidizing agents. However, HPLC-MS showed that the presence of oxidation reagents such as sodium nitrite in acid medium sped the reactions. These processes can even be observed macroscopically, as a freshly prepared solution of *p*-cymene-2,3-diol changes from clear and colorless to dark brown during a few days of storage at room temperature. This process took place within a few minutes upon heating and addition of oxidizing agents.

Previously, five substances had been reported that were assumed to be dimeric oxidation products of *p*-cymene-2,3-diol and thymol,[22,23] but only two of them (**1** and **3**) could be definitely identified in the present work. One dimer, **2**, was newly identified, as described above. Furthermore, **3** could be identified only on the basis of a highly concentrated standard

dx.doi.org/10.1021/jf404193y | J. Agric. Food Chem. 2014, 62, 235−243

Table 3. Formation/Decomposition Rates (FDRs) of *p*-Cymene-2,3-diol, 1, and 2 Determined in the Matrices Freeze-Dried Thyme, Raw Minced Meat, and Cooked Minced Meat and in Elution Solution[a] after Extraction and Purification

matrix		*p*-cymene-2,3-diol	1	2
thyme extract[b]	content in extract of spiked standard[e] (mg/L)	99.74 ± 4.82	20.17 ± 1.16	10.25 ± 0.67
	content in extract of plain matrix (mg/L)	17.85 ± 1.85	32.36 ± 2.50	5.89 ± 2.91
	expected content in extract of spiked matrix (mg/L)	117.6	52.53	16.14
	content in extract of spiked matrix (mg/L)	114.8 ± 4.21	45.23 ± 1.04	23.13 ± 2.74
	FDR (%)[f]	98.01	82.94	143.3
raw minced meat[c]	content in extract of spiked standard[e] (mg/L)	92.56 ± 4.06	23.71 ± 1.35	6.16 ± 0.58
	content in extract of plain matrix (mg/L)	<LOD	<LOD	<LOD
	content in extract of spiked matrix (mg/L)	78.39 ± 3.40	15,37 ± 1.12	9.87 ± 2.87
	FDR (%)[f]	84.69	64.82	160.4
cooked minced meat[c,d]	content in extract of spiked standard[e] (mg/L)	92.56 ± 4.06	23.71 ± 1.35	6.16 ± 0.58
	content in extract of plain matrix (mg/L)	<LOD	<LOD	<LOD
	content in extract of spiked matrix (mg/L)	70.41 ± 5.73	16.70 ± 0.76	7.01 ± 0.52
	FDR (%)[f]	76.07	70.46	113.9

[a]Five milliliter elution volume (in methanol) after purification by SPE. [b]Each data point represents the mean of three determinations (n = 3). [c]Each data point represents the mean of four determinations (n = 4). [d]Minced meat was cooked at 80 °C without standard addition and used as plain matrix after cooking. [e]Contents of analytes determined from diluted (5 mL) and nonpurified standard solution. [f]Formation/decomposition rate (FDR) = [content in extract of spiked matrix/(content in utilized standard solution + content in extract of plain matrix)] × 100, expressed in percentage of contents of standard solution plus contents in plain matrix and contents in extracts of spiked matrices to examine content changes during processing.

solution of *p*-cymene-2,3-diol and not in methanolic thyme extract. We detected traces of appropriate masses of the other compounds described here (3,4,4′-trihydroxy-5,5′-diisopropyl-2,3-dimethylbiphenyl, 4,4′-dihydroxy-5,5′-diisopropyl-2,2′-dimethylbiphenyl-3,6-dione, 4′-hydroxy-5,5′-diisopropyl-2,2′-dimethylbiphenyl-3,4-dione)[22,23] by means of LC-ESI-MS in standard solutions of *p*-cymene-2,3-diol, but we could not identify them in methanolic extracts of freeze-dried thyme. One reason for this may be that the present method of extraction and isolation of the biphenyls differs distinctively from the conditions described in the literature.[22,23] For example, Nakatani and Miura used a preparation technique involving steam distillation and silica gel column chromatography in which multiple further oxidation reactions can take place, which may have resulted in the artificial production of some of the previously characterized structures during isolation that do not naturally occur in large amounts. To test this assumption, we conducted silica gel chromatography with a standard of *p*-cymene-2,3-diol and a freshly prepared extract of freeze-dried thyme for comparison, but our HPLC-ESI-MS method showed that the eluates contained only artifacts of the expected appropriate masses (data not shown). In particular, the three biphenyls deriving from thymol described by Nakatani and Miura[22,23] may be formed under conditions created by the method applied by these authors, which presumably promoted more oxidation purification. The biphenyls characterized in this work (**1** and **2**) are major constituents of thyme extracts; however, the other previously described substance, **3**, as well as the three biphenyls deriving from thymol described by Nakatani and Miura[22,23] were not definitely identified in a thyme extract by means of the current standard HPLC-MS method. As mentioned above, the literature provides no coherent information on this subject: whereas one of the biphenyls described by Nakatani and Miura[22,23] has been reported as being extracted from thyme,[22,23] in a later report it is described as a synthetic compound,[5] so that its natural occurrence in thyme must be considered questionable. Additionally, the possibility of oxygen-coupled dehydrodimers was also considered, but there was no indication of these substances in the chromatographic and mass spectrometric data.

Analytical Method. The method described under Analytical HPLC-MS was developed considering previously reported methods,[16,17] especially for the oxidation products of thyme, but it may be used in further studies for effective analysis of the whole nonvolatile phase of thyme and other natural materials. Validation data including instrumental detection and quantitation limits are given in Table 1. The limits of detection (LOD) and quantitation (LOQ) of **1** and **2** are the same, 0.099 and 0.307 mg/L, whereas those of *p*-cymene-2,3-diol are clearly higher (0.178 and 0.536 mg/L). Table 3 shows the formation/decomposition rates (FDRs) in three matrices: freeze-dried thyme, raw minced meat, and cooked minced meat. Minced meat was used to examine oxidation reactions in a food matrix that is within the scope of subsequent industrial application of the functional oxidation products. The postulated reaction pathway from *p*-cymene-2,3-diol to **1** and **2** can be understood in light of their FDRs. Whereas the amounts of *p*-cymene-2,3-diol decreased, those of **1** first increased and then decreased, and those of **2** increased distinctly in all defined matrices. These facts support the reaction pathway postulated above, as **2** is assumed to be a secondary product of *p*-cymene-2,3-diol and **1**, and oxidation reactions take place intensely during storage. Thus, the FDRs determined for extraction techniques have to be interpreted not only as decreases in amounts due to extraction and purification but also as being due to unavoidable oxidation processes. Therefore, the FDRs specified in Table 3 have to be regarded as an indication for the conversion of *p*-cymene-2,3-diol, **1**, and **2**, and not only as process-related losses of substance. Not surprisingly, the losses of *p*-cymene-2,3-diol and **1** caused by the more complex extraction of raw and cooked minced meat matrix are considerably higher than for freeze-dried thyme, as the oxidation reactions indicated also take place. Therefore,

both losses and conversions have to be regarded as part of a systematic, coherent process.

Amounts of 1 and 2 in *T. vulgaris* L. and *T. citriodorus* L. and Their Hydrodistillation Residues. *p*-Cymene-2,3-diol, **1**, and **2** were found in extracts of freshly harvested, freeze-dried samples of *T. vulgaris* L. (Figure 1C,D) and *T. citriodorus* L. **1** and **2** were determined for the first time in thyme species. As shown in Figure 5, both thyme species contain larger amounts of **1** than of *p*-cymene-2,3-diol and **2**, whereas *T. vulgaris* L. has distinctly higher amounts of all three analytes than *T. citriodorus* L. Thus, **1** and **2** can be assumed to occur in the unharvested plant, where oxidation reactions possibly take place immediately after metabolic production of *p*-cymene-2,3-diol (Figure 5A).

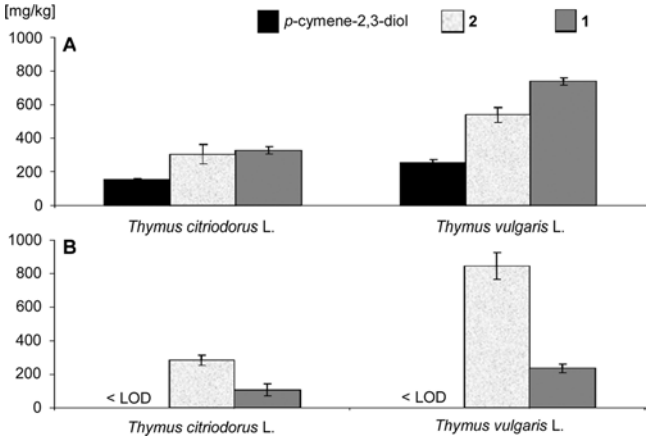

Figure 5. Amounts of *p*-cymene-2,3-diol, **2**, and **1** in freshly harvested, freeze-dried thyme species (A) and of **2** and **1** in hydrodistillation residue of thyme species (B). Each data point represents the mean of three determinations (n = 3) in dry matter.

After immediate hydrodistillation of the samples, the concentration of analytes in the remaining residues (results in dry matter) differed greatly (Figure 5B) from that of freshly harvested, freeze-dried thyme species. The concentration of the semivolatile *p*-cymene-2,3-diol was below the LOD when it was transferred (together with other volatile and semivolatile compounds) into the aqueous distillate, where it could have been identified (data not shown). However, before being transferred, some *p*-cymene-2,3-diol may have been oxidized, resulting in **1**, and total **1** may have been oxidized, resulting in **2**. As **1** and **2** are nonvolatiles, they were therefore predominately found in the residue. Notably, the ratio of **1** and **2** changed after hydrodistillation, after which **2** was the dominant dimer in the residue. This is not surprising, as **2** is suspected of being the oxidation product of **1**; furthermore, hydrodistillation conditions (heat treatment) accelerated the oxidation reactions described above. From these results it can be deduced that the functional biphenyls can be partly formed and enriched by means of a simple hydrodistillation treatment.

Kinetics of *p*-Cymene-2,3-diol in Methanol Solution and Meat Matrix. As proved in preliminary experiments with commercial standards of *p*-cymene-2,3-diol, thymol, and carvacrol, formation of **1** and **2** could be determined only in solutions containing *p*-cymene-2,3-diol and not from those prepared only from thymol or carvacrol, proving that the dimeric oxidation products identified were not formed from the major constituents thymol and carvacrol as reported earlier.[6,22,37] This may be explained by the fact that the half-wave potentials of thymol (+790 mV)[14] and carvacrol (+840 mV)[14] are higher than that of *p*-cymene-2,3-diol (+640 mV),[14] whereas *p*-cymene-2,3-diol is more sensitive to oxidation than thymol and carvacrol. In consideration of the circumstances of the sophisticated sample preparation including steam distillation and silica gel chromatography conducted earlier,[22,23] and the differences in half-wave potentials, the biphenyls including thymol monomers may be formed simply under intensive oxidative conditions. However, our easier and faster purification procedure described above suggests the possibility of milder conditions and less time for possible reactions.

In freshly prepared standard solutions, *p*-cymene-2,3-diol was always accompanied by **1** and **2** (Figure 1A,B). Figure 6 shows a storage experiment with a freshly prepared solution of *p*-cymene-2,3-diol. Storage for 1 day at room temperature under stirring led to significant ($p < 0.05$) degradation of *p*-cymene-2,3-diol and (to a lesser extent) **1**, whereas the **2** concentration increased significantly ($p < 0.05$). During the next 5 days, only marginal changes were observed in concentrations of *p*-cymene-2,3-diol, **1**, and **2**. During storage, the concentration of total analytes (sum of *p*-cymene-2,3-diol, **1**, and **2** contents) decreased successively from 1154 mg/L on the first day to 930 mg/L on the sixth. Therefore, it cannot be excluded that further, unidentified oxidation products were generated in addition to those postulated in the present work.

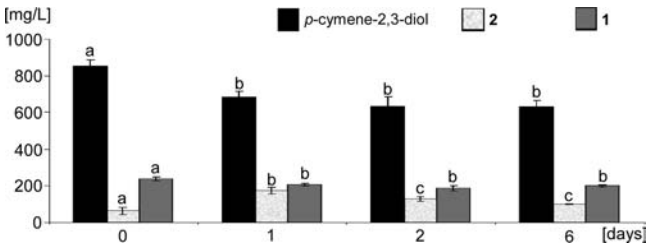

Figure 6. Amounts of *p*-cymene-2,3-diol, **2**, and **1** in freshly prepared solution of commercially available *p*-cymene-2,3-diol after 1, 2, and 6 days of storage. Each data point represents the mean of four determinations (n = 4). Values with the same letter within one data series are not significantly ($p > 0.05$) different between days of storage. Values with the letter "a" are starting values. Values with the letter "b" are significantly distinguished from those with the letters "a" and "c", and values with the letter "c" are significantly distinguished from values with the letters "a" and "b".

In another experiment, supercritical CO_2 thyme extract was added to minced pork meat as a representative food matrix to which the dimers could be supplemented. Figure 7 shows the amounts of *p*-cymene-2,3-diol as well as **1** and **2** after heat treatment: I (raw minced meat) and II (cooked minced meat) are control conditions including raw and cooked matrix with 1.0% (w/w) thyme extract; III, IV, and V contained 1.0% (w/w) nitrite curing agent with 1.0% (III), 3.0% (IV), and 6.0% (V) sodium nitrite (all w/w) as an additional reagent; whereas VI, VII, and VIII contained the same amount of nitrite curing salt (1.0%, w/w) with the same amounts of nitrite (1.0% (VI), 3.0% (VII), and 6.0% (VIII)) and with the addition of 1.0% (w/w) ascorbic acid. The resulting sodium nitrite concentrations in minced meat (100, 300, and 600 mg/kg) were chosen in consideration of the usual additions of sodium nitrite in food processing in accordance with the German food additive law (Zusatzstoff-Zulassungsverordnung, ZZulV), which specifies a maximum of 150 mg/kg sodium nitrite for meat products. To

dx.doi.org/10.1021/jf404193y | J. Agric. Food Chem. 2014, 62, 235−243

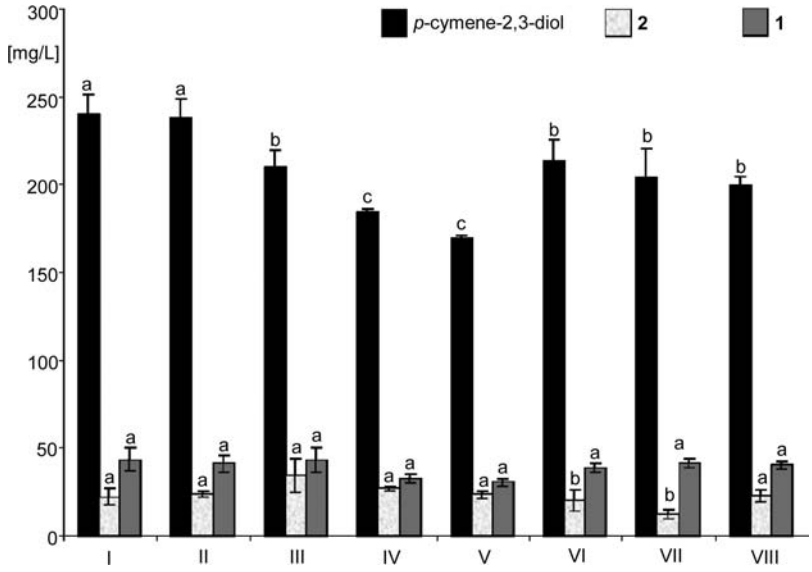

Figure 7. Amounts of *p*-cymene-2,3-diol, **2**, and **1** in minced meat under the following conditions: I, raw with 1% thyme extract; II, cooked with 1% thyme extract; III, cooked with 1% thyme extract and 0.01% sodium nitrite; IV, cooked with 1% thyme extract and 0.03% sodium nitrite; V, cooked with 1% thyme extract and 0.06% sodium nitrite; VI, cooked with 1% thyme extract, 0.01% sodium nitrite, and 1% ascorbic acid; VII, cooked with 1% thyme extract, 0.03% sodium nitrite, and 1% ascorbic acid; VIII, cooked with 1% thyme extract, 0.06% sodium nitrite, and 1% ascorbic acid. All percentages are related to weight of minced meat. Each data point represents the determination of mean of four determinations ($n = 4$). Values with the same letter within one data series are not significantly ($p > 0.05$) different between assays I and VIII. Values with the letter "a" are starting values. Values with the letter "b" are significantly distinguished from those with the letters "a" and "c", and values with the letter "c" are significantly distinguished from those with the letters "a" and "b".

test the efficiency of sodium nitrite as an oxidizing agent, concentrations (300 and 600 mg/kg) were also used that are considerably higher than allowed by law. As shown in Figure 7, cooked minced meat containing thyme extract but without further addition of sodium nitrite (II) showed a significantly ($p < 0.05$) higher amount of *p*-cymene-2,3-diol than samples with 1.0% (III), 3.0% (IV), or 6.0% (V) sodium nitrite (all w/w) after cooking. As described in the previous sections, at room temperature, *p*-cymene-2,3-diol initially reacts slowly to **1** and then to **2** as second step (and finally to **3**). It could be shown that these reactions can be accelerated by heat treatment and oxidizing agents. Assays with further addition of ascorbic acid (VI, VII, and VIII), a well-known antioxidant food preservative, showed that the decrease in *p*-cymene-2,3-diol was significantly ($p < 0.05$) lower than without ascorbic acid (IV and V) due to enhanced degradation of the responsible oxidizing agent, NO_2^-.

As stated above, no other oxidation products of *p*-cymene-2,3-diol were identified in the present work, but a further reaction of **2** and **3** caused by oxidation reagents can be considered possible and must be investigated in future experiments.

In summary, a method for the quantitative HPLC-MS analysis of *p*-cymene-2,3-diol along with its oxidation products has been established that is applicable for meat and other food matrices. This study revealed high contents of **1** and the newly identified **2** in methanol extracts of *T. vulgaris* L., its hydrodistillation residue, and supercritical CO_2 thyme extracts. Large amounts of industrially produced residues from the production of essential oils, that is, industrial waste (by-products), that are usually discarded by producers can now be viewed as potential sources for **1** and above all **2**, if species such as *T. vulgaris* L. are used. In addition, **1** and **2** are characterized by relatively low odorous activity compared with thymol, carvacrol, and other volatile antioxidants and antimicrobials, which constitutes a clear advantage over other sources. For efficient exploitation of the functional substances of thyme and utilization of these advantageous properties, further investigations should be conducted on the possible applicability of these species as a food additive.

AUTHOR INFORMATION

Corresponding Author

*(W.T.) Phone: +49-511-8567544. Fax: +49-511-8567674. E-mail: waldemar.ternes@tiho-hannover.de.

Funding

We gratefully acknowledge the Fritz-Ahrberg-Stiftung (Hannover, Germany) for their support.

Notes

The authors declare no competing financial interest.

ABBREVIATIONS USED

HPLC, high-performance liquid chromatography; DAD, diode array detector; SPE, solid-phase extraction; NMR, nuclear magnetic resonance spectrometry; COSY, correlation spectroscopy; HSQC, heteronuclear single quantum coherence; HMBC, heteronuclear multiple bond correlation; ESI, electrospray ionization; MS, mass spectrometry; TIC, total ion chromatogram; SIM, selected ion monitoring; MW, molecular weight; FDR, formation/decomposition rate; UV, ultraviolet spectrometry; MSD, method standard deviation; MVC, method variation coefficient; IDL, instrument detection limit; LOQ, limit of quantitation; LOC, limit of capability

REFERENCES

(1) Brewer, M. S. Natural antioxidants: sources, compounds, mechanisms of action, and potential applications. *Compr. Rev. Food Sci. Food Saf.* **2011**, *10* (4), 221−247.

(2) Lang, G. R.; Buchbauer, G. A review on recent research results (2008−2010) on essential oils as antimicrobials and antifungals. A review. *Flavour Fragrance J.* **2012**, *27* (1), 13−39.
(3) Madsen, H. L.; Bertelsen, G.; Skibsted, L. H. Antioxidative activity of spices and spice extracts. In *Spices: Flavor Chemistry and Antioxidant Properties*; American Chemical Society: Washington, DC, 1997; Vol. 660, pp 176−187.
(4) Miguel, M. G. Antioxidant activity of medicinal and aromatic plants. A review. *Flavour Fragrance J.* **2011**, *25* (5), 291−312.
(5) Nakatani, N. Chemistry of antioxidants from Labiateae herbs. In *Food Phytochemicals for Cancer Prevention II: Teas, Spices, and Herbs*; American Chemical Society: Washington, DC, 1994; Vol. 547, pp 144−153.
(6) Yanishlieva, N. V.; Marinova, E.; Pokorny, J. Natural antioxidants from herbs and spices. *Eur. J. Lipid Sci. Technol.* **2006**, *108* (9), 776−793.
(7) Peter, K. V., Ed. *Handbook of Herbs and Spices*; Woodhead Publishing/CRC Press: Cambridge, UK, 2004; Vol. 2, p 297.
(8) Aeschbach, R.; Loliger, J.; Scott, B. C.; Murcia, A.; Butler, J.; Halliwell, B.; Aruoma, O. I. Antioxidant actions of thymol, carvacrol, 6-gingerol, zingerone and hydroxytyrosol. *Food Chem. Toxicol.* **1994**, *32* (1), 31−36.
(9) Yanishlieva, N. V.; Marinova, E. M.; Gordon, M. H.; Raneva, V. G. Antioxidant activity and mechanism of action of thymol and carvacrol in two lipid systems. *Food Chem.* **1999**, *64* (1), 59−66.
(10) Tsai, M. L.; Lin, C. C.; Lin, W. C.; Yang, C. H. Antimicrobial, antioxidant, and anti-Inflammatory activities of essential oils from five selected herbs. *Biosci., Biotechnol., Biochem.* **2011**, *75* (10), 1977−1983.
(11) Chizzola, R.; Michitsch, H.; Franz, C. Antioxidative properties of *Thymus vulgaris* leaves: comparison of different extracts and essential oil chemotypes. *J. Agric. Food Chem.* **2008**, *56* (16), 6897−6904.
(12) Sacchetti, G.; Maietti, S.; Muzzoli, M.; Scaglianti, M.; Manfredini, S.; Radice, M.; Bruni, R. Comparative evaluation of 11 essential oils of different origin as functional antioxidants, antiradicals and antimicrobials in foods. *Food Chem.* **2005**, *91* (4), 621−632.
(13) Stahl-Biskup, E.; Holthuijzen, J. Essential oil and glycosidically bound volatiles of lemon-scented thyme, *Thymus* × *citriodorus*. *Flavour Fragrance J.* **1995**, *10* (3), 225−229.
(14) Ternes, W.; Gronemeyer, M.; Schwarz, K. Determination of *p*-cymene-2,3-diol, thymol, and carvacrol in different foodstuffs. *Z. Lebensm.-Unters.-Forsch.* **1995**, *201* (6), 544−547.
(15) Schwarz, K.; Ernst, H.; Ternes, W. Evaluation of antioxidative constituents from thyme. *J. Sci. Food Agric.* **1996**, *70* (2), 217−223.
(16) Babovic, N.; Djilas, S.; Jadranin, M.; Vajs, V.; Ivanovic, J.; Petrovic, S.; Zizovic, I. Supercritical carbon dioxide extraction of antioxidant fractions from selected Lamiaceae herbs and their antioxidant capacity. *Innovative Food Sci. Emerging Technol.* **2010**, *11* (1), 98−107.
(17) Dapkevicius, A.; van Beek, T. A.; Lelyveld, G. P.; van Veldhuizen, A.; de Groot, A.; Linssen, J. P. H.; Venskutonis, R. Isolation and structure elucidation of radical scavengers from *Thymus vulgaris* leaves. *J. Nat. Prod.* **2002**, *65* (6), 892−896.
(18) Fecka, I.; Turek, S. Determination of polyphenolic compounds in commercial herbal drugs and spices from Lamiaceae: thyme, wild thyme and sweet marjoram by chromatographic techniques. *Food Chem.* **2008**, *108* (3), 1039−1053.
(19) Hossain, M. B.; Rai, D. K.; Brunton, N. P.; Martin-Diana, A. B.; Barry-Ryan, C. Characterization of phenolic composition in Lamiaceae spices by LC-ESI-MS/MS. *J. Agric. Food Chem.* **2010**, *58* (19), 10576−10581.
(20) Jukic, M.; Milos, M. Catalytic oxidation and antioxidant properties of thyme essential oils (*Thymus vulgarae* L.). *Croatica Chem. Acta* **2005**, *78* (1), 105−110.
(21) Martins, R. R. L.; Neves, M.; Silvestre, A. J. D.; Silva, A. M. S.; Cavaleiro, J. A. S. Oxidation of aromatic monoterpenes with hydrogen peroxide catalysed by Mn(III) porphyrin complexes. *J. Mol. Catal. A: Chem.* **1999**, *137* (1−3), 41−47.
(22) Miura, K.; Inagaki, T.; Nakatani, N. Structure of new deodorant biphenyl compounds from thyme (*Thymus vulgaris* L.). *Chem. Pharm. Bull.* **1989**, *37* (7), 1816−1819.
(23) Nakatani, N.; Miura, K.; Inagaki, T. Structure of new deodorant biphenyl compounds from thyme (*Thymus vulgaris* L.) and their activity against methyl mercaptan. *Agric. Biol. Chem.* **1989**, *53* (5), 1375−1381.
(24) Miura, K.; Nakatani, N. Antioxidative activity of biphenyl compounds from thyme (*Thymus vulgaris* L.). *Chem. Express* **1989**, *4* (4), 237−240.
(25) Haraguchi, H.; Saito, T.; Ishikawa, H.; Date, H.; Kataoka, S.; Tamura, Y.; Mizutani, K. Antiperoxidative components in *Thymus vulgaris*. *Planta Med.* **1996**, *62* (3), 217−221.
(26) Okazaki, K.; Kawazoe, K.; Takaishi, Y. Human platelet aggregation inhibitors from thyme (*Thymus vulgaris* L.). *Phytother. Res.* **2002**, *16* (4), 398−399.
(27) Nagy, T. O.; Solar, S.; Sontag, G.; Koenig, J. Identification of phenolic components in dried spices and influence of irradiation. *Food Chem.* **2011**, *128* (2), 530−534.
(28) Guillen, M. D.; Manzanos, M. J. Study of the composition of the different parts of a Spanish *Thymus vulgaris* L. plant. *Food Chem.* **1998**, *63* (3), 373−383.
(29) Justesen, U. Negative atmospheric pressure chemical ionisation low-energy collision activation mass spectrometry for the characterisation of flavonoids in extracts of fresh herbs. *J. Chromatogr., A* **2000**, *902* (2), 369−379.
(30) Horwath, A. B.; Grayer, R. J.; Keith-Lucas, D. M.; Simmonds, M. S. J. Chemical characterisation of wild populations of *Thymus* from different climatic regions in southeast Spain. *Biochem. Syst. Ecol.* **2008**, *36* (2), 117−133.
(31) Miron, T. L.; Plaza, M.; Bahrim, G.; Ibanez, E.; Herrero, M. Chemical composition of bioactive pressurized extracts of Romanian aromatic plants. *J. Chromatogr., A* **2011**, *1218* (30), 4918−4927.
(32) Antonacopoulos, N. Verbesserte Apparatur zur quantitativen Destillation wasserdampfflüchtiger Stoffe. *Z. Lebensm.-Unters.-Forsch. A* **1960**, *113* (2), 113−116.
(33) Deutsches Institut fuer Normung. *DIN 32645: Chemical Analysis - Decision Limit, Detection Limit, and Determination Limit under Repeatability Conditions - Terms, Methods, Evaluation*; Beuth Verlag: Berlin, Germany, 2008.
(34) Nieto-Ernst, S. *Valoo, 2.5*; Analytik Software: Leer, 2009.
(35) MacLafferty, F. W.; Turecek, F. *Interpretation von Massenspektren*; Spektrum-Akademischer Verlag: Heidelberg, Germany, 1995.
(36) Sykes, P. *Reaktionsmechanismen der Organischen Chemie*, 9th ed.; Wiley-VCH: Weinheim, Germany, 1988; p 531.
(37) Nakatani, N. Phenolic antioxidants from herbs and spices. *Biofactors* **2000**, *13* (1−4), 141−146.

JOURNAL OF AGRICULTURAL AND FOOD CHEMISTRY

Article

pubs.acs.org/JAFC

Effect of pH on the Complexation of Kaempferol-4′-glucoside with Three β-Cyclodextrin Derivatives: Isothermal Titration Calorimetry and Spectroscopy Study

Yan Zheng,[†] Li-Na Dong,[‡] Min Liu,*[,†] Aiju Chen,[†] Shangcai Feng,[§] Bingquan Wang,[∥] and Dezhi Sun*[,†]

[†]School of Chemistry and Chemical Engineering, Liaocheng University, Liaocheng, 252059 China

[‡]Shandong Experimental High School, Jinan, Shandong, 250001 China

[§]School of Chemistry and Chemical Engineering, Linyi University, Linyi, 276000 China

[∥]School of Pharmacrutical, Liaocheng University, Liaocheng, 252059 China

ABSTRACT: The utilization of kaempferol and its glycosides in food and pharmaceutical industries could be improved by the formation of inclusion complexes with cyclodextrins at different pH. This study explores the complexation of kaempferol-4′-glucoside with sulfobutyl ether-β-cyclodextrin (SBE-β-CD), hydroxypropyl-β-cyclodextrin (HP-β-CD), and methylated-β-cyclodextrin (M-β-CD) in phosphate buffer solutions of different pH using isothermal titration calorimetry, UV−vis absorption and proton nuclear magnetic resonance spectroscopy at 298.2 K. Experimental results showed that kaempferol-4′-glucoside binds with the three β- cyclodextrins in the same 1:1 stoichiometry. The rank order of stability constants is SBE-β-CD > HP-β-CD > M-β-CD at the same pH level and pH 6.0 > pH 7.4 > pH 9.0 for the same cyclodextrin. The binding of kaempferol-4′-glucoside with the three β-cyclodextrin derivatives is synergistically driven by enthalpy and entropy at pH 6.0 and enthalpy-driven at pH 7.4 and 9.0. The possible inclusion mode was that in the cavity of β-CD is included the planar benzopyranic-4-one part of the kaempferol-4′-glucoside.

KEYWORDS: *kaempferol-4′-glucoside, β-cyclodextrin, complexation, isothermal titration calorimetry, NMR, UV−vis*

INTRODUCTION

Consumption of fruits and vegetables has been consistently associated with a reduced risk of human cancers.[1] Flavonoids are polyphenolic phytochemicals that are ubiquitous in vegetables and fruits. They are components in the human diet and constitute a large group of secondary plant metabolities.[2,3] The average intake of all flavonoids is 23 mg/day.[4] The antioxidant and anti-inflammatory capacities of these natural products are well documented,[5] and many display a cancer fighting potential.[6] As a typical kind of flavonoid, kaempferol (3,4′,5,7-tetrahydroxyflavone) is widely distributed in onion leaves, carrot, and black tea with the contents of 832, 140, and 118 mg/kg of dry weight, respectively.[7] Several biological activities have been attributed to kaempferol, including antioxidant,[8] antiatherogenic activities[9] and anti-inflammatory properties.[10] Significantly, kaempferol inhibits cancer cell growth and angiogenesis and induces cancer cell apoptosis.[11] Kaempferol-4′-glucoside (KG, Figure 1) is a glucosylated form of kaempferol with β-D-glucopyranoside substitution on the 4′ position of the B-ring. Kaempferol and its glycosides are characterized by the presence of hydroxyl groups that can be ionized depending on the working conditions. It was found that the biochemical activity of flavonoids is correlated to the position of these groups and their corresponding p*K*a values.[12] In addition, the type and degree of glycosylation may be important in determining the ability of these compounds to cross the intestinal wall.[13]

In recent years, the food, cosmetic, pharmaceutical, and chemical industries have become increasingly interested in kaempferol and its glycosides due to their health-promoting effects.[14] However, their poor water solubility and sensitivity to external agents such as air, light, and oxidative enzymes severely restrict their bioavailability, formulation, and manipulation in the elaboration of functional foods. However, these limitations can be overcome by the formation of inclusion complexes with cyclodextrins (CDs). β-Cyclodextrin (β-CD) is a cyclic oligosaccharide consisting of seven glucose units connected by α-(1,4) glycoside bonds. This molecular structure confers to β-CD the shape of a truncated cone, with the outer side formed by the secondary hydroxyl groups and the narrow side by the primary hydroxyl groups. This conformation makes β-CD have hydrophobic internal cavity and hydrophilic external surface and form inclusion complexes with various guest molecules

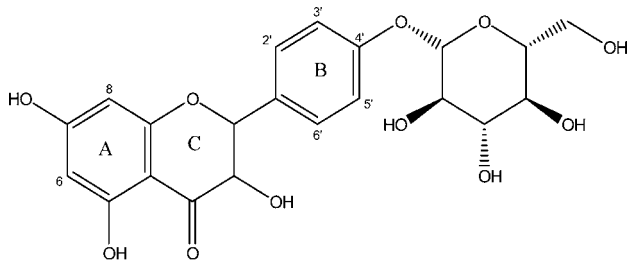

Figure 1. Molecular structure of kaempferol-4′-glucoside.

Received: September 26, 2013
Revised: December 6, 2013
Accepted: December 6, 2013
Published: December 6, 2013

ACS Publications © 2013 American Chemical Society

through noncovalent interactions.[15−18] The complexation has many applications in food, cosmetics, and pharmaceutical industries due to the improvement of the solubility, stability, and bioactivity of guest molecules. However, β-CD is unsuitable for parenteral administration due to its low aqueous solubility. A universal solution to this problem is the use of CD derivatives.[19] β-CD derivatives of pharmaceutical interest include hydroxypropyl-β-CD (HP-β-CD), methylated-β-CD (M-β-CD), sulfobutyl ether β-CD (SBE-β-CD), and the so-called branched CDs such as maltosyl-β-CD (G_2-β-CD).

Several papers have been published on the complexation of kaempferol by CDs.[20−25] However, to the best of our knowledge, there is no report about the inclusion complexation between KG and different β-cyclodextrin derivatives. Among various measuring techniques, isothermal titration calorimetry (ITC) is an extremely powerful and highly sensitive technique for the characterization of the interaction mechanisms of CDs with drugs.[26] It has been used with great success in the study of weak interactions from thermodynamic and kinetics points of view. In this work, the complexations of KG with three different cyclodextrins (SBE-β-CD, HP-β-CD, and M-β-CD) in aqueous solutions of different pH were studied using complementary techniques of ITC, UV−vis absorption spectroscopy, and ^{1}H nuclear magnetic resonance spectroscopy (^{1}H NMR). The resulting thermodynamic parameters may promote the application of KG in the food and pharmaceutical industries.

MATERIALS AND METHODS

Materials. Kaempferol-4′-glucoside (KG, purity >98%) was purchased from Shanghai Forever Biotech Ltd., Co. (Shanghai, China). HP-β-CD (average molecular weight =1460), SBE-β-CD (total degree of substitution = 6.8), and M-β-CD (average molecular weight = 1310) were obtained from Aldrich (St. Louis, MO, USA), Shandong Binzhou Zhiyuan Bio-Technology Co., Ltd. (Binzhou, China), and J&K Chemical (Beijing, China), respectively. Dimethyl sulfoxide-d_6 (DMSO), containing 0.03% (v/v) tetra methyl silane (TMS), was from Aldrich (St. Louis, MO, USA). All other reagents were of analytical grade. Deionized and double-distilled water were used throughout the study. All solutions of different pH values (pH 6.0, 7.4 and 9.0) were prepared with 0.05 M phosphate buffer solution (PBS) as solvent. The final concentrations of KG and three β-CD derivatives were adjusted for individual analytical instruments, as detailed below.

Isothermal Titration Calorimetry (ITC). ITC experiments were carried out with a nanowatt scale isothermal titration microcalorimeter supported by Thermal Activity Monitor-2277 (Thermometric, Sweden). The instrument was periodically calibrated either electrically using an internal electric heater or chemically by measuring the dilution enthalpy of a concentrated sucrose solution.[27] The titrant was CD (SBE-β-CD, HP-β-CD, or M-β-CD) at the concentration of 4.0×10^{-3} M in PBS, and all solutions were degassed before each titration. The sample cell and reference cell of the calorimeter were initially loaded with 0.50 mL of KG solution and 0.75 mL of PBS, respectively. The concentration of KG in PBS was 1.0×10^{-3} M. The programmable titration was controlled by Digitam 4.1 software, and the titrant was injected into the stirred sample cell in 30 portions of 15 μL using a 500 μL Hamilton syringe. The interval between two injections was sufficiently long for the signal to return to the baseline. To correct the thermal effect due to mixing and dilution, a control experiment was performed by injecting the β-CD solution into PBS and PBS into the KG solution, respectively. All experiments were performed at a fixed temperature of (298.2 ± 0.1) K and repeated 3-fold.

UV−vis Absorption Spectroscopy. A stock solution of KG (2.0×10^{-5} M) was prepared in PBS and was dissolved by vortexing. An accurately weighed quantity of β-CD (SBE-β-CD, HP-β-CD, or M-β-CD) was dissolved into each specific volume of KG solution to obtain a series of solutions for each kind of the CDs and the largest concentration of the host is 6.0×10^{-3} M. All solution samples were then equilibrated in an electro-heating standing-temperature cultivator maintained at 25 °C for 60 min. Spectra for each of the solution transferred into a quartz cuvette (1 cm × 1 cm × 4 cm) was recorded using a HP 8453 UV−vis spectrophotometer (Hewlett-Packard Company, USA). The temperature was controlled by an externally coupled bath at 25 °C. All experiments were performed in triplicate.

^{1}H Nuclear Magnetic Resonance (NMR) Spectroscopy. ^{1}H NMR spectra were performed on a Varian Mercury Plus 400 MHz nuclear magnetic resonance spectrometer (USA). KG and CDs were dissolved in D_2O in presence of 40% (v/v) deuterated dimethlsulfoxide-d_6 (DMSO) due to the poor solubility of KG in D_2O. TMS was employed as an internal standard.

RESULTS AND DISCUSSION

Calorimetric Characterization of Complexation at Different pH Conditions. ITC is one of the most sensitive methods available for the determination of the stoichiometry (n), equilibrium constant (K_a) and enthalpy change (ΔH°), for host−guest association, based on direct determination of the heat released or taken up during the interaction.

Complex formation between a CD (derivative) and KG can easily reach the equilibrium

$$m\mathrm{CD} + n\mathrm{KG} \rightleftharpoons \mathrm{CD}_m\cdot\mathrm{KG}_n \quad (1)$$

in which m and n = 1, 2, 3. Therefore, there are five possible inclusion models. The experimental association constant K_c can be expressed by equilibrium concentrations

$$K_c = \frac{[\mathrm{CD}_m\cdot\mathrm{KG}_n]}{[\mathrm{CD}]^m[\mathrm{KG}]^n} \quad (2)$$

The total concentration of CDs and KG can be obtained according to the following formulas

$$[\mathrm{CD}]_0 = [\mathrm{CD}] + mK_a[\mathrm{CD}]^m[\mathrm{KG}]^n \quad (3)$$

$$[\mathrm{KG}]_0 = [\mathrm{KG}] + nK_a[\mathrm{CD}]^m[\mathrm{KG}]^n \quad (4)$$

ΔH° and K_a can be obtained by the multinonlinear regression equation analysis with the Ligand Binding program available within the Digitam 4.1 software. By comparing the fitness between the simulation curve and the experiment point, the most reasonable result can be obtained as final result. A representative titration curve is given in Figure 2A. The excellent fit between experimental and calculated points is observed for 1:1 complex formation between the three substituted CDs and KG, as illustrated in Figure 2B. Furthermore, the standard association Gibbs free energy (ΔG°) and the standard association entropy (ΔS°) can be obtained from ΔH° and K_a according to the following thermodynamic formulas:

$$\Delta G^0 = -RT \ln K_a \quad (5)$$

where $K_a = K_c(c^0)^{m+n-1}$, c^0 = 1 mol dm^{-3}

$$\Delta S^0 = (\Delta H^0 - \Delta G^0)/T \quad (6)$$

The calculated association constants as well as the changes in Gibbs free energy, enthalpy, and entropy for the inclusion complexations of SBE-β-CD, HP-β-CD, and M-β-CD with KG are listed in Table 1.

As shown, the K_a values of KG with the three investigated β-CDs evidently decrease with the increase of pH of buffer solution from pH 6.0 to pH 9.0. This result indicates that acidity of buffer aqueous media has strong impact on the

dx.doi.org/10.1021/jf404320w | J. Agric. Food Chem. 2014, 62, 244−250

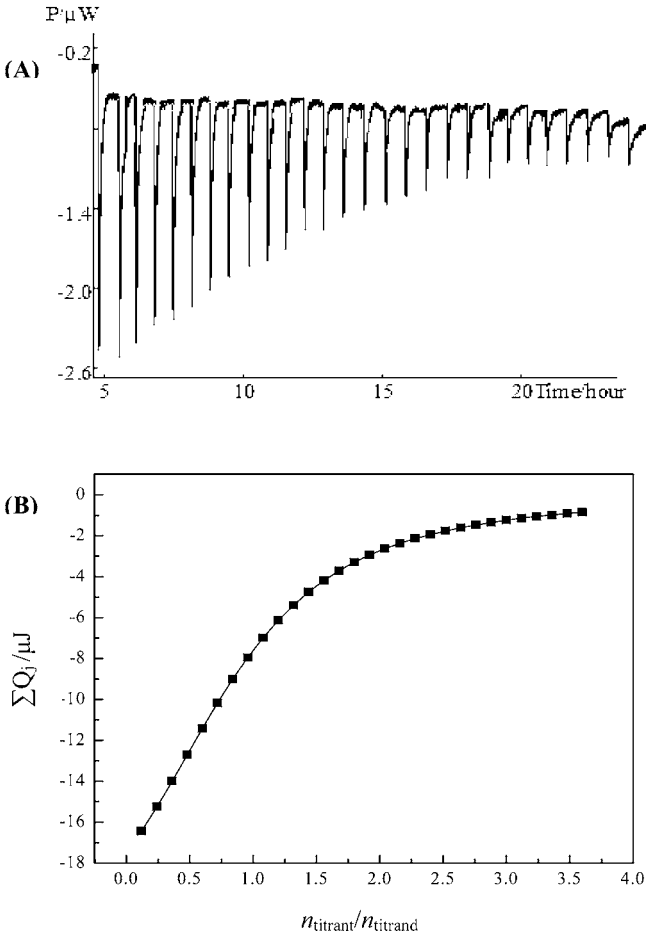

Figure 2. (A) Variation of heat-flow/electrical power P as a function of time t at pH 7.4, titrant: 4.0×10^{-3} M SBE-β-CD; titrand: 1.0×10^{-3} M kaempferol-4′-glucoside. (B) Experimental thermal effect for binding process versus the concentration ratio of titrant to titrand, where data points are derived from experiments and the line is the result of calculations at pH 7.4.

Table 1. Stability Constants and Thermodynamic Parameters of Kaempferol-4′-glucoside Inclusion Complexation with SBE-β-CD, HP-β-CD, and M-β-CD Obtained from Isothermal Titration Calorimetry Data

	SBE-β-CD	HP-β-CD	M-β-CD
	pH 6.0		
K_a/(L mol^{-1})	6381 ± 105	5773 ± 20	5425 ± 33
ΔH^0/(kJ mol^{-1})	−8.64 ± 0.03	−7.90 ± 0.01	−6.53 ± 0.01
$T\Delta S^0$/(J mol^{-1} K^{-1})	13.08 ± 0.07	13.56 ± 0.02	14.75 ± 0.02
ΔG^0/(kJ mol^{-1})	−21.72 ± 0.04	−21.47 ± 0.01	−21.31 ± 0.02
	pH 7.4		
K_a/(L mol^{-1})	2610 ± 10	1793 ± 9	1487 ± 4
ΔH^0/(kJ mol^{-1})	−23.53 ± 0.02	−18.70 ± 0.02	−17.91 ± 0.02
$T\Delta S^0$/(J mol^{-1} K^{-1})	−4.03 ± 0.03	−0.13 ± 0.01	0.19 ± 0.01
ΔG^0/(kJ mol^{-1})	−19.49 ± 0.01	−18.57 ± 0.01	−18.11 ± 0.01
	pH 9.0		
K_a/(L mol^{-1})	2107 ± 5	1360 ± 2	1200 ± 1
ΔH^0/(kJ mol^{-1})	−45.46 ± 0.04	−43.14 ± 0.03	−40.97 ± 0.02
$T\Delta S^0$/(J mol^{-1} K^{-1})	−26.49 ± 0.04	−25.07 ± 0.03	−23.39 ± 0.02
ΔG^0/(kJ mol^{-1})	−18.97 ± 0.01	−17.89 ± 0.01	−17.57 ± 0.01

complexation process. Hydroxyl groups of KG molecules are sequentially dissociated into anions with the elevation of pH values. Ionized KG exhibits much weaker binding with CD derivatives due to their enhanced hydrophilic character. Similar results have been observed in many other CD/guest complexation studies.[28] So the controlled release of KG could be achieved by the complexation with β-CD at different pH values. It was also noted that the stability of KG inclusion complexes is in the order SBE-β-CD > HP-β-CD > M-β-CD at the same pH. These differences are due to the variety of substituent group of the three CDs.[29] The hydrophility of the substituent group on the outer surface of SBE-β-CD, HP-β-CD, and M-β-CD decreases successively. The most probable binding mode of native and modified CDs with various guests involves the insertion of the hydrophobic part of the guest molecule into the CD cavity, while the hydrophilic, often charged, group remains outside the rim of the cavity.[30] The main driving forces for complex formation include hydrophobic interactions, electrostatic interactions (ion−ion interaction, ion−dipole interaction, and dipole−dipole interaction), van der Waals force interactions, hydrogen binding and the release of "high energy water" molecules from the cavities of CD to bulk water. Therefore, the binding process is the cooperative effects of the above driving forces. In many cases, hydrophobic interactions are the principal intermolecular weak forces responsible for the formation of stable supramolecular complexes. However, in some cases, where neutral or charged guest molecules and charged CDs mutually interact, strong complexations have been observed.[31,32] In such cases, the improvement in complexation has been associated with additional interaction sites provided by the CD charge. The mode of interaction is presumed to be hydrophobic interaction with the cavity interior along with additional electrostatic interactions between the guest and host molecules. Therefore, electrostatic interactions, including ion-dipole interactions,[33] maybe contribute to the formation of inclusion complexes. The stronger electrostatic interactions between the anions of the outer surface of SBE-β-CD and the hydroxyl groups of KG lead to a stronger complexation. In contrast, the hydrophobic−hydrophilic interactions between the methyl group of the outer surface of M-β-CD and the hydroxyl groups of KG are unfavorable to the complexation process.

The study of ΔH^0 and ΔS^0 obtained from ITC data leads to the determination of the driving force of the interaction. The main factors contributing to the formation of the complexation include release of cavity-bound water, partial destruction of hydration shells and noncovalent interactions (van der Waals, hydrophobic and electrostatic interactions as well as H-bonding).[34] Thermodynamic parameters of complex formation are the result of the competitive equilibrium among the above effects.

The three complexation reactions have negative ΔH^0, indicating that the association is exothermic in the order SBE-β-CD > HP-β-CD > M-β-CD at the same pH levels. The most negative ΔH^0 value for KG/SBE-β-CD complex may be attributed to the strong electrostatic interaction, which is consistent with the conclusion obtained from values of stability constant K_a, since the hydrophobic molecular cavity of the CDs is the same.[33] In addition, for the same CD, the heat released from the complexation increases with increasing pH. This could also be caused by the stronger electrostatic interaction at higher pH values.

The entropy effect is due to the total result of the host−guest combination which includes two opposite effects.[35] The negative contribution to entropy is due to the association of two molecules and the restriction of rotational and translational degrees of freedom, in particular those of the guest molecule. The positive contribution is due to the release of the highly ordered solvent molecules surrounding the host and guest molecules. The strong electrostatic interaction leads to the loss of degree of freedom. Therefore, the entropy change is in the order SBE-β-CD < HP-β-CD < M-β-CD at the same pH level and pH 6.0 > pH 7.4 > pH 9.0 for the same CD.

The differences in the proportion by which the binding entropy and enthalpy contribute to the Gibbs energy reflect the differences in the interaction established between the various CDs and KG molecules. It can be concluded from the above discussion that the binding of KG with the three β-CD derivatives is synergistically driven by enthalpy and entropy ($\Delta H^0 < 0$ and $T\Delta S^0 > 0$) at pH 6.0 and enthalpy-driven ($|\Delta H^0| > |T\Delta S^0|$) at pH 7.4 and 9.0.

UV−vis Absorption Spectroscopy. Figure 3 shows the absorption spectra of KG (2.0×10^{-5} M) in PBS of different pH values in the presence and absence of the three β-CD derivatives at 298.2 K. The higher wavelength band at about 265 nm is related to the $\pi \rightarrow \pi^*$ transition absorbance in the A-ring.[36] As can be seen from Figure 3, the addition of CDs results in a corresponding decrease in the absorbance intensity of KG. Similar reduction in absorption profile was observed upon the inclusion of resveratrol within HP-β-CD,[37] rosmarinic acid within natural and derivative cyclodextrins,[38] puerarin within glucosyl-β-cyclodextrin,[17] and *trans*-ferulic acid within HP-β-CD.[39] According to the symmetry forbidden rule, the $\pi \rightarrow \pi^*$ transition in KG may be less intense in the case of being included inside the cavity of the three β-CD derivatives than of being exposed in the polar solution.[40] SBE-β-CD shows a more pronounced absorbance decrease, probably due to a greater propensity to form inclusion complexes with KG. UV−vis spectra of KG (2.0×10^{-5} M) in the presence of various concentrations of SBE-β-CD at pH 7.4 is illustrated in Figure 4A. As shown, the absorbance intensity of KG gradually decreases with the stepwise addition of SBE-β-CD. The change in the absorption peak strength is characteristic of the interaction of KG with CDs.

Assuming a 1:1 stoichiometry of complex formation between the KG molecule and each of the three investigated β-CDs, the stability constant (K_a) can be obtained from the analysis of the sequential changes of absorption (ΔA) at various CD concentrations by using the modified Benesi−Hildebrand equation[41]

$$\frac{1}{\Delta A} = \frac{1}{K_a \Delta\varepsilon [\mathrm{KG}]_0 [\mathrm{CD}]_0} + \frac{1}{\Delta\varepsilon [\mathrm{KG}]_0} \quad (7)$$

where $[\mathrm{CD}]_0$ and $[\mathrm{KG}]_0$ refer to the total concentration of CD and KG, respectively, $\Delta\varepsilon$ is the change in molar extinction coefficient between the free and associated host, and ΔA denotes the change in absorbance of KG upon stepwise addition of CD. An exemplary double reciprocal Benesi−Hildebrand plot, i.e. plot of $1/\Delta A$ (at 268 nm) versus $1/[\text{SBE-}\beta\text{-CD}]_0$, was constructed and is shown in Figure 4B. The good linearity indicates that the presumed 1:1 stoichiometry of the complex is reasonable. Stability constants of complexation between KG and SBE-β-CD, HP-β-CD, and M-β-CD obtained by the spectroscopic analysis are listed in Table 2. The results show that the general rank order and order of magnitude of stability constants are consistent with those obtained from ITC data. Therefore, the rank order of stability constants is SBE-β-CD > HP-β-CD > M-β-CD.

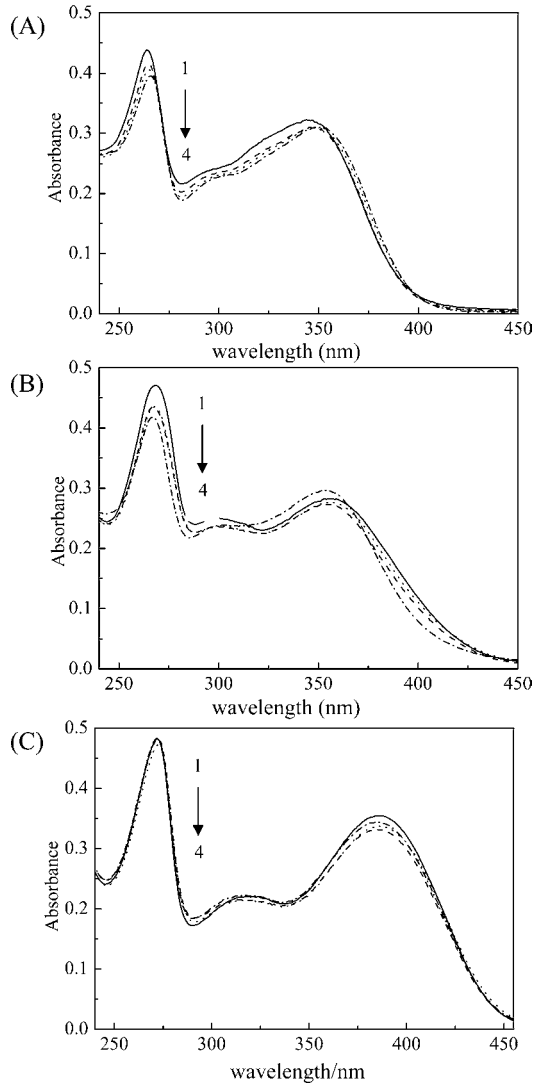

Figure 3. UV−vis spectra of KG (2.0×10^{-5} M) in the absence and presence of different β-CDs (1.0×10^{-3} M) in PBS of different pH values at 298.2 K: (A) pH 6.0, (B) 7.4, and (C) 9.0. Curves 1−4 correspond to KG (——), KG + M-β-CD (− − −), KG + HP-β-CD (· · ·), and KG + SBE-β-CD (− · − ·), respectively.

Characterization of Complexes by NMR. The formation of complexes was also studied by proton nuclear magnetic resonance spectroscopy (^{1}H NMR), where the relative orientation of the guest in the hydrophobic cavity of the host was obtained.[42,43]

The chemical shifts of protons in β-CD derivatives were not reliable for the NMR characterization due to the purity problem, caused by the degree and position of substitution.[44] Thus, only those of the protons in the guest were considered in this presentation. The spectra of ^{1}H NMR of KG in the absence and presence of CDs are presented in Figure 5. The detailed change of the chemical shifts ($\Delta\delta$) calculated for the protons in KG by using eq 8 were shown in Figure 6.

$$\Delta\delta = \delta_{(\text{complexation})} - \delta_{(\text{guest})} \quad (8)$$

dx.doi.org/10.1021/jf404320w | J. Agric. Food Chem. 2014, 62, 244−250

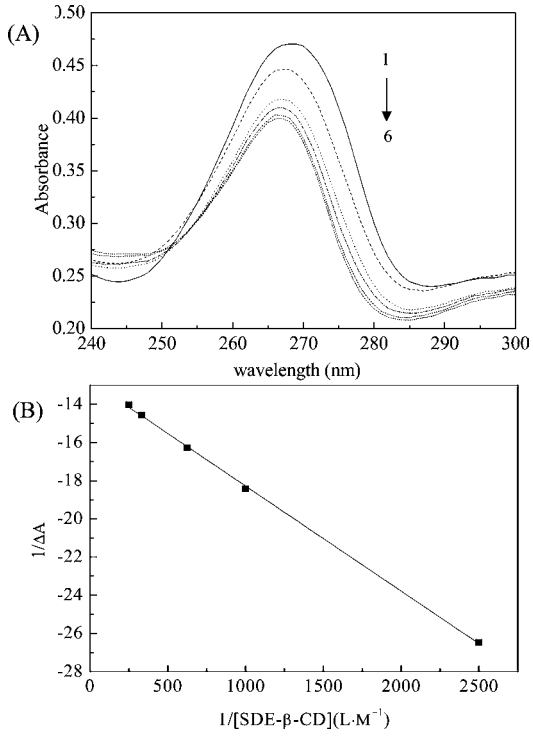

Figure 4. (A) UV−vis spectra of KG in the presence of SBE-β-CD of various concentrations at 298.2 K and pH 7.4. The concentration of KG was 2.0×10^{-5} M, and the concentrations of SBE-β-CD were 0, 0.4, 1.0, 1.6, 3.0, and 4.0×10^{-3} M corresponding to curves 1−6. (B) Double reciprocal plot of the data at 268 nm according to eq 7.

Table 2. Stability Constants of Complexation between Kaempferol-4′-glucoside and SBE-β-CD, HP-β-CD, and M-β-CD Derived from Double Reciprocal Benesi−Hildebrand Plot

	K/(L mol^{-1})		
	SBE-βCD	HP-βCD	M-βCD
pH 6.0	6154 ± 321	5300 ± 158	4722 ± 120
pH 7.4	2322 ± 16	1452 ± 9	1272 ± 10
pH 9.0	2081 ± 72	1304 ± 6	1176 ± 8

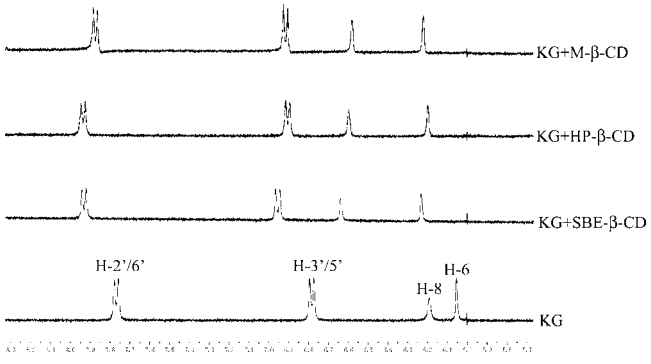

Figure 5. Chemical shifts of aromatic protons of KG in the absence and presence of different β-CDs in D_2O/DMSO (V:V = 6:4) solution.

where $\delta_{(complexation)}$ and $\delta_{(guest)}$ are the ^{1}H chemical shift of associated and free guest, respectively. The final results of $\Delta\delta$ were the average of triplicate values.

Although added DMSO may reduce the binding strength of the KG-β-CD complex, the general trend was revealed by the change of chemical shift.[44] As shown in Figure 6, the presence of CDs caused a downfield shift for all of the protons, which was probably due to their relatively strong interaction with β-CDs. In addition, Figure 6 indicates that the chemical shift change of H8 is the largest. It can therefore be inferred that the most possible binding mode is that the planar benzopyranic-4-one part of KG is included in the cavity of β-CD, as shown in Figure 7. The protrusion of A-ring is hindered due to the steric effect of 5-hydroxyl and 7-hydroxyl of A-ring and the intramolecular hydrogen bonding between 5-hydroxy of A-ring and 4-carbonyl group oxygen of C-ring.

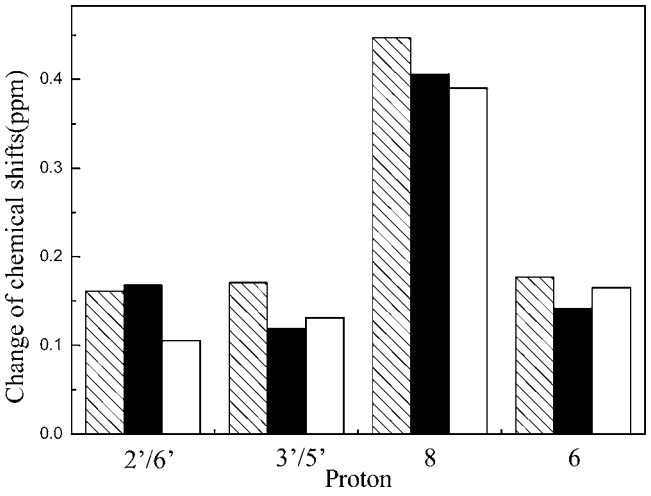

Figure 6. Chemical shifts change of aromatic protons of KG in presence and absence of βCDs in D_2O/DMSO (V: V = 6:4) solution. Cross-hatched bar, SBE-β-CD; black bar, HP-β-CD; white bar, M-β-CD.

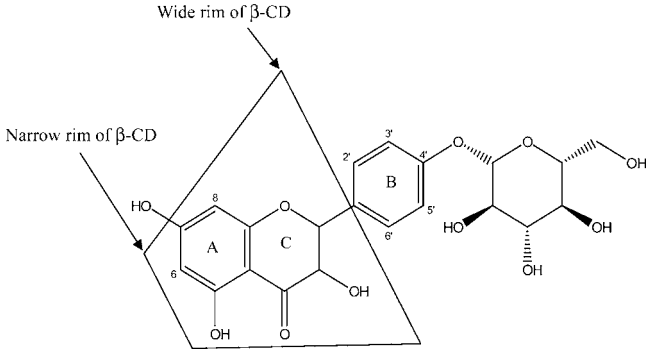

Figure 7. Possible inclusion mode of KG/SBE-β-CD, KG/HP-β-CD, and KG/M-β-CD inclusion complexes.

This binding model has been verified by Yang et al. for the interaction of rutin with β-CD.[45] Rutin (quercetin-3-rhamnosylglucoside) is a natural flavone derivative whose molecular structure is similar to that of KG molecule. It is also found in Figure 6 that the chemical shift change of SBE-β-CD is most prominent among the three β-CD derivatives, indicating that stronger interaction between KG and SBE-β-CD. The results are in good agreement with those of ITC and UV−vis absorption spectra analyses.

AUTHOR INFORMATION

Corresponding Authors

*E-mail: panpanliumin@163.com.

*E-mail: sundezhisdz@163.com. Tel: +86-635-8230612. Fax: +86-635-8239880.

Funding

We thank the Natural Science Foundation of China for Funding (Nos. 21103079 and 21373106). This work was also supported by Tai-Shan Scholar Research Fund of Shandong Province.

Notes

The authors declare no competing financial interest.

■ ABBREVIATIONS USED

KG, kaempferol-4′-glucoside; β-CD, β-cyclodextrin; SBE-β-CD, sulfobutyl ether-β-cyclodextrin; HP-β-CD, hydroxypropyl-β-cyclodextrin; M-β-CD, methylated-β-cyclodextrin; DMSO, dimethyl sulfoxide-d_6; PBS, phosphate buffer solution; TMS, tetra methyl silane

■ REFERENCES

(1) Neuhouser, M. L. Dietary flavonoids and cancer risk: Evidence from human population studies. *Nutrit. Cancer* **2004**, *50*, 1−7.
(2) Herrmann, K. Flavonols and flavones in food plants: a review. *J. Food Technol.* **1976**, *11*, 433−448.
(3) Wojdyło, A.; Oszmianski, J.; Czemerys, R. Antioxidant activity and phenolic compounds in 32 selected herbs. *Food Chem.* **2007**, *105*, 940−949.
(4) Park, Y. K.; Lee, C. Y. Identification of isorhamnetin 4′-glucoside in onions. *J. Agric. Food Chem.* **1996**, *44*, 34−36.
(5) Jovanovic, S. V.; Steenken, S.; Tosic, M.; Marjanovic, B.; Simic, M. G. Flavonoids as antioxidants. *J. Am. Chem. Soc.* **1994**, *116*, 4846−4851.
(6) Papadopoulou, A.; Green, R. J.; Frazier, R. A. Interaction of flavonoids with bovine serum albumin: A fluorescence quenching study. *J. Agric. Food Chem.* **2005**, *53*, 158−163.
(7) Miean, K. H.; Mohamed, S. Flavonoid (myricetin, quercetin, kaempferol, luteolin, and apigenin) content of edible tropical plants. *J. Agric. Food Chem.* **2001**, *49*, 3106−3112.
(8) Park, J. S.; Rho, H. S.; Kim, D. H.; Chang, I. S. Enzymatic preparation of kaempferol from green tea seed and its antioxidant activity. *J. Agric. Food Chem.* **2006**, *54*, 2951−2956.
(9) Tu, Y. Ch.; Lian, T. W.; Yen, J. H.; Chen, Z. T.; Wu, M. J. Antiatherogenic effects of kaempferol and rhamnocitrin. *J. Agric. Food Chem.* **2007**, *55*, 9969−9976.
(10) Chen, G. F.; Ma, X.; Meng, F. B.; Li, G. X. The electron transfer reactivity of kaempferol and its interaction with amino acid residues. *Bioelectrochemistry* **2008**, *72*, 169−173.
(11) Chen, A. Y.; Chen, Y. Ch. A review of the dietary flavonoid, kaempferol on human health and cancer chemoprevention. *Food Chem.* **2013**, *138*, 2099−2107.
(12) Iulia, M.; Sorana, I.; Mihaela, H. Kaempferol−human serum albumin interaction: characterization of the induced chirality upon binding by experimental circular dichroism and TDDFT calculations. *Spectrochim. Acta Part A* **2012**, *96*, 709−715.
(13) Gee, J. M.; DuPont, M. S.; Rhodes, M. J. C.; Johnson, I. T. Quercetin glucosides interact with the intestinal glucose transport pathway. *Free Radic. Biol. Med.* **1998**, *25*, 19−25.
(14) Zhu, X. Y.; Lin, H. M.; Chen, X.; Xie, J.; Wang, P. Mechanochemical-assisted extraction and antioxidant activities of kaempferol glycosides from *Camellia oleifera* Abel. meal. *J. Agric. Food Chem.* **2011**, *59*, 3986−3993.
(15) Zhang, Q. F.; Nie, H. Ch.; Shangguang, X. Ch.; Yin, Zh. P.; Zheng, G. D.; Chen, J. G. Aqueous solubility and stability enhancement of astilbin through complexation with cyclodextrins. *J. Agric. Food Chem.* **2013**, *61*, 151−156.
(16) Koontz, J. L.; Marcy, J. E. Formation of natamycin: cyclodextrin inclusion complexes and their characterization. *J. Agric. Food Chem.* **2003**, *51*, 7106−7110.
(17) Liu, B. G.; Zhao, J.; Liu, Y. H.; Zhu, X. A.; Zeng, J. Physiochemical properties of the inclusion complex of puerarin and glucosyl-β-cyclodextrin. *J. Agric. Food Chem.* **2012**, *60*, 12501−12507.
(18) Lucas-Abellán, C.; Fortea, I.; López-Nicolás, J. M.; Núnez-Delicado, E. Cyclodextrins as resveratrol carrier system. *Food Chem.* **2007**, *104*, 39−44.
(19) Kurkov, S. V.; Loftsson, T. Cyclodextrins. *Int. J. Pharm.* **2012**, *453*, 167−180.
(20) Mercader−Ros, M. T.; Lucas−Abellán, C.; Gabaldón, J. A.; Fortea, M. I.; Martínez-Cachá, A.; Núnez-Delicado, E. Kaempferol complexation in cyclodextrins at basic pH. *J. Agric. Food Chem.* **2010**, *58*, 4675−4680.
(21) Bergonzi, M. C.; Bilia, A. R.; Bari, L. Di.; Mazzi, G.; Vincieri, F. Studies on interaction between some flavonols and cyclodextrins. *Bioorg. Med. Chem. Lett.* **2007**, *17*, 5744−5748.
(22) Lucas-Abellán, C.; Fortea, I.; Gabaldón, J. A.; Núnez-Delicado, E. Encapsulation of quercetin and myricetin in cyclodextrins at acidic pH. *J. Agric. Food Chem.* **2008**, *56*, 255−259.
(23) Mercader-Ros, M. T.; Lucas-Abellán, C.; Fortea, M. I.; Gabaldón, J. A.; Núnez-Delicado, E. Effect of HP-β-cyclodextrins complexation on the antioxidant activity of flavonols. *Food Chem.* **2010**, *118*, 769−773.
(24) Jullian, C.; Brossard, V.; Gonzalez, I.; Alfaro, M.; Olea-Azar, C. Cyclodextrins−kaempferol inclusion complexes: Spectroscopic and reactivity studies. *J. Solution Chem.* **2011**, *40*, 727−739.
(25) Kim, H.; Choi, J.; Jung, S. Inclusion complexes of modified cyclodextrins with some flavonols. *J. Incl. Phenom. Macrocycl. Chem.* **2009**, *64*, 43−47.
(26) Bouchemal, K.; Mazzaferro, S. How to conduct and interpret ITC experiments accurately for cyclodextrin−guest interactions. *Drug Discovery Today.* **2012**, *17*, 623−629.
(27) Liu, M.; Zhu, L.-Y.; Qu, X.-K.; Sun, D.−Zh.; Li, L.-W.; Lin, R.-S. Studies on the binding of paeonol and two of its isomers to human serum albumin by using microcalorimetry and circular dichroism. *J. Chem. Thermodyn.* **2007**, *39*, 1565−1570.
(28) Veiga, F.; Teixeira-Dias, J. J. C.; Kedzierewicz, F.; Sousa, A.; Maincent, P. Inclusion complexation of tolbutamide with β-cyclodextrin and hydroxypropyl-β-cyclodextrin. *Int. J. Pharm.* **1996**, *129*, 63−71.
(29) Jullian, C.; Moyano, L.; Yañez, C.; Olea-Azar, C. Complexation of quercetin with three kinds of cyclodextrins: An antioxidant study. *Spectrochim. Acta Part A* **2007**, *67*, 230−234.
(30) Rekharsky, M. V.; Inoue, Y. Complexation and chiral recognition thermodynamics of 6-Amino-6-deoxy-β-cyclodextrin with anionic, cationic, and neutral chiral guests: Counterbalance between van der Waals and coulombic interactions. *J. Am. Chem. Soc.* **2002**, *124*, 813−826.
(31) Zia, V.; Rajewski, R. A.; Stella, V. J. Effect of cyclodextrin charge on complexation of neutral and charged substrates: Comparison of $(SBE)_{7M}$-β-CD to HP-β-CD. *Pharm. Res.* **2001**, *18*, 667−673.
(32) Zia, V.; Rajewski, R. A.; Stella, V. J. Thermodynamics of binding of neutral molecules to sulfobutyl ether β-cyclodextrins (SBE-β-CDs): The effect of total degree of substitution. *Pharm. Res.* **2000**, *17*, 936−941.
(33) Mohanty, J.; Bhasikuttan, A. C.; Nau, W. M.; Pal, H. Host-Guest complexation of neutral red with nacrocyclic host molecules: Contrasting pK_a shifts and binding affinities for cucurbit[7]uril and β-cyclodextrin. *J. Phys. Chem. B* **2006**, *110*, 5132−5138.
(34) Terekhova, I. V. Comparative thermodynamic study on complex formation of native and hydroxypropylated cyclodextrins with benzoic acid. *Thermochim. Acta* **2011**, *526*, 118−121.
(35) Smith, V. J.; Rougier, N. M.; Rossi, R. H.; Caira, M. R.; Buján, E. I.; Fernández, M. A.; Bourne, S. A. Investigation of the inclusion of the herbicide metobromuron in native cyclodextrins by powder X-ray diffraction and isothermal titration calorimetry. *Carbohydr. Res.* **2009**, *344*, 2388−2393.
(36) Sandipan, C.; Soumalee, B.; Ansuman, L.; Soumen, B. Inclusion of chrysin in β-cyclodextrin nanocavity and its effect on antioxidant

potential of chrysin: A spectroscopic and molecular modeling approach. *J. Mol. Struct.* **2010**, *977*, 180−188.
(37) Lu, Zh.; Cheng, B.; Hu, Y. L.; Zhang, Y. H.; Zou, G. L. Complexation of resveratrol with cyclodextrins: Solubility and antioxidant activity. *Food Chem.* **2009**, *113*, 17−20.
(38) Çelik, S. E.; Özyürek, M.; Tufan, A. N.; Güçlü, K.; Apak, R. Spectroscopic study and antioxidant properties of the inclusion complexes of rosmarinic acid with natural and derivative cyclodextrins. *Spectrochim. Acta Part A* **2011**, *78*, 1615−1624.
(39) Wang, J.; Cao, Y. P.; Sun, B. G.; Wang, Ch. T. Characterisation of inclusion complex of trans-ferulic acid and hydroxypropyl-β-cyclodextrin. *Food Chem.* **2011**, *124*, 1069−1075.
(40) Ibrahim, M. S.; Shehatta1, I. S.; Al-Nayeli, A. A. Voltammetric studies of the interaction of lumazine with cyclodextrins and DNA. *J. Pharm. Biomed. Anal.* **2002**, *28*, 217−225.
(41) Fan, Y. X.; Li, J. F.; Dong, Ch. Preparation and study on the inclusion complexes of two tanshinone compounds with β-cyclodextrin. *Spectrochim. Acta Part A* **2005**, *61*, 135−140.
(42) Sun, D. Zh.; Li, L.; Qiu, X. M.; Liu, F.; Yin, B. L. Isothermal titration calorimetry and ^{1}H NMR studies on host−guest interaction of paeonol and two of its isomers with β-cyclodextrin. *Int. J. Pharm.* **2006**, *316*, 7−13.
(43) Yang, L. J.; Chen, W.; Ma, Sh. X.; Gao, Y. T.; Huang, R.; Yan, Sh. J.; Lin, J. Host−guest system of taxifolin and native cyclodextrin or its derivative: Preparation, characterization, inclusion mode, and solubilization. *Carbohyd. Polym.* **2011**, *85*, 629−637.
(44) Zheng, Y.; Haworth, I. S.; Zuo, Z.; Chow, M. S. S.; Chow, A. H. L. Physicochemical and structural characterization of quercetin-β-cyclodextrin complexes. *J. Pharm. Sci.* **2005**, *94*, 1079−1089.
(45) Yang, G. J.; Xu, J. J.; Chen, H. Y.; Leng, Z. Z. Studies on the interaction between rutin and DNA in the absence and presence of β-cyclodextrin by electrochemical and spectroscopic methods. *Chin. J. Chem.* **2004**, *22*, 1325−1329.

JOURNAL OF AGRICULTURAL AND FOOD CHEMISTRY

Article

pubs.acs.org/JAFC

Effect of Addition of Olive Leaves before Fruits Extraction Process to Some Monovarietal Tunisian Extra-Virgin Olive Oils Using Chemometric Analysis

Ammar Sonda,[†] Zribi Akram,[†] Gargouri Boutheina,[†] Flamini Guido,[§] and Bouaziz Mohamed*[,†,‡]

[†]Laboratoire d'Electrochimie et Environnement, Ecole Nationale d'Ingénieurs de Sfax BP ⟨1173⟩ 3038, Université de Sfax, Sfax, Tunisia

[‡]Institut Supérieur de Biotechnologie de Sfax, Université de Sfax, BP ⟨1175⟩ 3038, Sfax, Tunisia

[§]Dipartimento di Farmacia, via Bonanno 33, 56126 Pisa, Italy

ABSTRACT: The analysis of the effect of cultivar and olive leaves addition before the extraction on the different analytical values revealed significant differences ($p < 0.05$) in some parameters, mainly in peroxide value, phenols and tocopherol contents, and oxidative stability. Aroma profiles were also influenced by the different varieties and the addition of different amounts (0% and 3%) of olive leaves. Twenty-three compounds were characterized, representing 86.1−99.2% of the total volatiles. Chétoui cultivar has the highest amount of (*E*)-2-hexenal, followed by Chemlali cultivar, whereas (*E*)-2-hexen-1-ol was the major constituent of Zalmati and crossbreeding Chemlali by Zalmati cultivars. Sensory analysis showed that Chemlali and Chétoui Zarzis possessed a high fruity, bitter, and pungent taste, whereas the Zalmati and crossbreeding Chemlali by Zalmati had a 'green' taste among its attributes. Indeed, the taste panel found an improvement of the oil quality when an amount of olive leaves (3%) added to the olives fruits.

KEYWORDS: *olive leaves, extra-virgin olive oil, volatile compounds, Tunisian cultivars, sensory characteristics, principal component analysis*

INTRODUCTION

Extra-virgin olive oil is a valuable vegetable oil that is produced without any preliminary refining process. It plays a very important role in the agronomy and economy, providing both employment and export revenue. Olive trees in Tunisia cover an area of 1.7 million ha and account for more than 4% of the olive oil produced in the world. Indeed, with an annual production of 170.000 tons, Tunisia is the fourth largest producer and exporter of olive oil in the world.[1] More than 50 different olive oil cultivars exist in Tunisia such as Chemlali, Chétoui, Meski, Chemchali, Oueslati, and Zalmati. However, two important varieties dominate most of the arable land: Chétoui and Chemlali.[2]

In fact, Chemlali is the main cultivated variety, covering 60% of the olive-growing surface, spread from the northeast of the country to the extreme south.[3] In addition, despite its ordinary organoleptic and taste characteristics, olive oil composition is different according to the geographical origin.[4] In contrast, the Chétoui variety can be found mostly in the north of the country. The oil of the latter's cultivar is characterized by high amounts of total phenols and tocopherols.[5] Almost all research studies on Tunisian virgin olive oil have focused on the characterization and improvement of these two varieties.[6] However, the work on other cultivars could be very interesting as it aims at planting new cultivars with a high yield of oil, good quality, and good stability. The minor components and the unsaponifiables are the delicate and the interesting fractions of the lipid matter,[7] rising to about 2% of the total oil weight. They include many chemical compounds such as aliphatic and triterpenic alcohols, sterols, hydrocarbons, volatile compounds, and antioxidants. In fact, olive oil has a special flavor that is generated from a number of volatile molecules present at extremely low concentrations.[8] These molecules mainly include aldehydes, alcohols, ketones, and esters.[9] The main volatile compounds usually found in high sensory quality virgin olive oil are produced from polyunsaturated fatty acids through the cascade of reactions collectively called the lipoxygenase (LOX) pathway.[10−12] Many positive attributes and sensory defects in olive oil can be associated with volatile compounds. The absence of sensory defects is necessary for the olive oil to be classified as EVOO.[13] Cultivar type influences the formation of volatile compounds in oil and is an important factor for determining the final olive oil quality.

Olive leaves are one of the farming byproducts of the olive groove and are considered as a cheap raw material that can be used as a useful source of highly added value products,[14] particularly phenolic compounds[15] exhibiting a strong protective effect against oils oxidation.[16,17] On the other hand, the addition of olive leaves during the oil extraction process could cause mechanical problems associated with the flow of olive paste. Moreover, the presence of leaves before olive fruits extraction may further enhance the flavor and did not distort the aroma of such oils. Di Giovacchino et al.[18] suggested that the analyses of the volatile components of the oil, in fact, show no newly formed substances or considerable

Received: September 30, 2013
Revised: December 8, 2013
Accepted: December 12, 2013
Published: December 12, 2013

ACS Publications © 2013 American Chemical Society

changes in the majority of volatile components. An exception is a noticeable increase in the trans-2-hexenal, hexanal content, and some alcohols, such as cis-3-hexenol, trans-2-hexenol, and 1-hexanol.This increase could be explained by release of chloroplasts from crushing olive leaves.[18]

In this context, we intend to study if the addition of olive leaves before the extraction process of olive oil introduces a favorable effect on the chemical composition and quality of olive oils of two widespread olive cultivars (Chemlali and Chétoui) of Zalmati cultivar and for the first time a new cultivar obtained by crossbreeding Chemlali by Zalmati. Different lots with over mature olives and with increasing quantities of olive leaves (0% to 3%) of the four samples were processed. The extracted olive oils were characterized for several quality parameters, oxidative stability (through Rancimat method), fatty acids composition, tocopherols, volatile compounds, and sensory analyses.

MATERIALS AND METHODS

Olive Origin. Monovarietal virgin olive oil samples were obtained from four Tunisian olive varieties: Chemlali, Chétoui, Zalmati, and crossbreeding Chemlali by Zalmati, which were harvested in Zarzis, (south of Tunisian) during two crop seasons (2011/2012 and 2012/2013). In order to eliminate the influence of maturation state on olive oil quality, the ripening degree was the same for the four studied olive samples (maturation indices were 6.07, 6.14, 6.88, and 6.86 for Chemlali, Chétoui, Zalmati, and crossbreeding Chemlali by Zalmati cv., respectively). The olive samples were collected from the olive trees in triplicate from orchards in the same neighborhood carried out with the same cultural practices. The olive ripening index (RI) was determined according to the method developed in ref 19, on the basis of the evaluation of the olive skin and pulp colors. RI values range from 0 (100% intense green skin) to 7 (100% purple flesh and black skin).

Chemicals. Methanol, hexane, acetone, acetic acid, and cyclohexane HPLC-grade solvents were purchased from Riedel-deHaen (Switzerland). The solvents were of appropriate purity. Double distilled water was used in the HPLC mobile phase. Folin−Ciocalteu reagent was obtained from Fluka (Switzerland).

Oil Extraction. After harvesting, samples of Chemlali, Chétoui, Zalmati, and crossbreeding Chemlali by Zalmati olives were transported the same day to the laboratory to be transformed into oil within 24 h. For each olive sample, fruits were processed and olive oil was obtained using a two-phase centrifugation: about 1.5−2 kg of olives from each sample were crushed with a hammer crusher, and the paste mixed at a temperature of about 27 °C for 30 min, centrifuged in a decanter (3500 rpm for 3 min) without the addition of warm water and then transferred into dark glass bottles, and stored at 4 °C until analysis.

Analytical Methods. *Quality Indices Determinations.* The determination of acidity (given as % of oleic acid), peroxide value (PV) (meqO_2/kg of oil) were carried out following the analytical methods described by the International Olive Council.[20]

Fatty Acid Methyl Ester Analysis. The fatty acid composition of the oils was determined by gas chromatography (GC) as fatty acid methyl esters (FAMEs). FAMEs were prepared by saponification/methylation with sodium methylate according to the EEC Reg 2568/91.[21] A chromatographic analysis was performed in a SHIMADZU set 17 A Series II gas chromatography using a capillary column (stabilwax, Restek, length 50 m, internal diameter 0.32 mm, and film thickness 0.25 μm). The column temperature was isothermal at 180 °C, and the injector and detector temperatures were 230 and 250 °C, respectively. Fatty acids have been identified by comparing retention times with standard compounds, palmitic (16:0), hypogeic (16:1(n − 9)) + palmitoleic (16:1(n − 7)), heptadecanoic (C17:0), heptadecenoic (C17:1n-8), stearic (18:0), (Z)-vaccenic (18:1(n − 7)) + oleic (18:1(n − 9)), linoleic (18:2), linolenic (18:3), arachidic (20:0), and gondoïc (C20:1(n − 9)) behenic (22:0) and lignoceric (24:0) acids they have been expressed as percentages of fatty acid methyl esters.

Tocopherol Determination. HPLC analysis for α-tocopherol was performed with an Agilent (1100) Series HPLC (Hewlett-Packard, Waldbronn, Germany) apparatus. Detection was performed at 290 nm for α-tocopherol. The column was C-18, 4.6 × 250 mm, particle size 5 μm, shim-pack, VP-ODS, Shimadzu, Kyoto, Japan. The elution solvents used were A (2% acetic acid in water), B (methanol), C (acetonitrile), and D (isopropanol). The samples were eluted according to the following gradient: 95% A/5% B in 2 min; 60% A/10% B/30% C in 8 min; 25% B/75% C in 22 min, and this percentage was maintained for 10 min; 40% C/60% D in 10 min; and this percentage was maintained for 15 min; 25% B/75% C in 2 min, and finally, 95% A/5% B in 3 min. Flow rate was 1 mL/min and run time was 70 min. The run was performed at 32 °C. The sample injection volume was 20 μL. The identification of α-tocopherol was achieved by comparing its retention time values with a standard.[22] The α-tocopherol content was determined by diluting approximately 1100 mg of olive oil in 1 mL of n-hexane and analyzing the sample solution by HPLC. Besides, the concentrations of α-tocopherol were calculated by integrating peak areas of the samples and the calibration curve of the α-tocopherol standard. Then, acceptable linearity was achieved in the range 300−1100 mg kg^{-1} (y = 1.30x, R^2 = 0.899).

Analysis of Phenolic Compound. *Extraction of Phenolic Fraction from Olive Oil.* The phenols containing extracts were obtained following the procedure of Mraicha et al.,[23] with some modification. Briefly, the oil sample (4 g) was added to 2 mL of n-hexane and 4 mL of a methanol/water (60:40, v/v) solution in a 20 mL centrifuge tube. After vigorous mixing, they were centrifuged for 3 min. The hydroalcoholic phase was collected, and the hexane phase was re-extracted twice with 4 mL of methanol/water (60:40, v/v) solution each time. Finally, the hydroalcoholic fractions were combined, washed with 4 mL of n-hexane to remove the residual oil, then concentrated and dried by evaporative centrifuge in vacuum at 35 °C.

Determination of Total Phenols. The determination of the total phenolic compounds was performed by means of the Folin−Ciocalteau reagent using the method that was described by Bouaziz et al.[3] The total phenols content was expressed as milligrams of gallic acid (GA) equivalents per kilogram of oil (y = 0.011x, R^2 = 0.990).

Volatile Compound Analyses. *Extraction.* Solid-phase microextraction was used as a technique for headspace sampling of virgin olive oils. Supelco SPME devices coated with polydimethylsiloxane (PDMS, 100 μm) were used to sample the headspace of 2 mL of olive oil inserted into a 5-mL glass septum vial and allowed to equilibrate for 30 min at 22 ± 1 °C. After the equilibration time, the fiber was exposed to the headspace for 50 min. Extraction temperature and times were optimized in previous studies.[24]

Identification. GC analyses were performed using a HP-5890 series II instrument equipped with a DB-5 capillary column (30 m × 0.25 mm i.d., 0.25 μm film thickness), working with the following temperature program: 60 °C for 10 min, ramp of 5 °C min 1 to 220 °C; injector and detector temperatures, 250 °C; carrier gas, helium (1 mL min^{-1}); detector FID; splitless injection. The components were identified by the comparison of their retention times with those of pure authentic standards and by means of their linear retention indices (LRI) relative to the series of n-hydrocarbons. GC−EIMS analyses were performed using a Varian CP 3800 gas-chromatograph equipped with a DB-5 capillary column (30 m × 0.25 mm i.d., 0.25 μm film thicknesses) and a Varian Saturn 2000 ion trap mass detector. Analytical conditions were as follows: injector and transfer line temperature at 250 and 240 °C, respectively; oven temperature was programmed from 60 to 240 °C at 3 °C min^{-1}; carrier gas, helium at 1 mL min^{-1}; splitless injection. The identification of the constituents was based on the comparison of the retention times with those of authentic samples, comparing their LRI relative to the series of n-hydrocarbons, and on computer matching against commercial (NIST 98 and ADAMS) and homemade library mass spectra built from pure substances and components of known oils and MS literature data.[25] Moreover, the molecular weights of all the

identification substances were confirmed by GC-CI-MS, using MeOH as CI ionizing gas.[26]

Determination of Oxidative Stability by Rancimat Method. The oil samples (5.0 g) were heated in a Rancimat equipment at 120 °C (Metrohm Ltd., Herisau, Switzerland), with a continuous air flow of 20 L/h passing through the samples. The conductivity cells were filled with 60 mL of deionized water. The time needed (hours) for the appearance of a sudden water conductivity rise, caused by the adsorption of volatiles derived from oil oxidation, was registered as the induction time.

Sensory Assessment. Sensory evaluation was carried out by a panel composed by eight judges who were fully trained in the evaluation of virgin olive oil (VOO) according to the official methods of the International Olive Oil Council (IOOC).[20]

Statistical Analysis. The results were expressed as mean ± standard deviation (SD) of three measurements for the analytical determination. Significant differences between the values of all parameters were determined at $p < 0.05$ according to the one way ANOVA: Student−Newman−Keuls test, using SPSS Statistics 17.0 for Windows (SPSS Inc., 2008).

Nonstandardized principal component analysis (PCA) was applied to show the effect of addition of olive leaves (3%) on the quality of different varieties of olive oils from Zarzis region according to all the parameters investigated, using the Varimax rotation with Kaiser Normalization. The PCA type was Pearson (n), the biplot type was correlation biplot and the coefficient was automatic. PCA plots were performed using XLSTAT software for Windows (v.2013.2.03, Addinsoft, NY, U.S.A.).

RESULTS AND DISCUSSION

Quality Indices. Table 1 shows the physicochemical quality parameters of olive oils from the studied cultivars with different olive leaves amounts (0% and 3%) added before the extraction process.

The free fatty acid content is an important quality factor and has been extensively used as a traditional criterion for classifying olive oil in various commercial grades.[27] The free fatty acids of oils produced from the four olive varieties extracted with different percentages of olive leaves (Table 1) did not exceed the upper limits of 0.8% established by the COI norm, and they all corresponded to the extra-virgin olive oil class.[28] The addition of olive leaves (3%) to all studied samples before the extraction of olive oil did not significantly ($p > 0.05$) change the free acidity in these samples except for the Zalmati and crossbreeding Chemlali by Zalmati samples ($p < 0.05$). Compared to the results obtained by Malheiro et al.[29] and Di-Giovacchino et al.[8] for the other cultivar, our free acidity values are lower. Malheiro et al.[29] have reported that the addition of olive leaves may also increase the presence of lipolytic enzymes which consequently entails an increase in the free acidity, explaining the observed increments in this parameter.

The peroxide values (PV) evaluate the hydroperoxide content and offer a measure of lipid oxidation.[30] In the studied oils, the PV ranged between 9.00 and 16.63 meq O_2 kg^{-1}, resulting in values lower than the maximum indicated by the EEC Regulations.[31] The highest PV was observed in the oil from crossbreeding Chemlali by Zalmati oil (13.15 and 16.63 meq O_2 kg^{-1}, respectively for 0% and 3% of added leaves). While, the lowest ones were detected in the Chemlali olive oils, it tends to 9.00 without the addition of olive leaves and 11.50 meq O_2 kg^{-1} with the addition of 3% of olive leaves. Concerning the Chétoui and Zalmati varieties, they showed intermediate PV, comprised between 12.75 to 15.45 and 11.00 to 13.50 meq O_2/kg in the olive oils with added leaves at 0% and 3%, respectively. As observed, the varietal selection of

Table 1. Quality Parameters of the Four Olive Oil Varieties Extracted with and without Addition of Olive Leaves (3%)[a]

	Chemlali		Chétoui		Zalmati		crossbreeding Chemlali by Zalmati	
	0%	3%	0%	3%	0%	3%	0%	3%
free fatty acid (% oleic)	0.20 ± 0.01*a	0.21 ± 0.01*a	0.18 ± 0.00*b	0.18 ± 0.00*b	0.16 ± 0.00*c	0.20 ± 0.01**a	0.29 ± 0.00*d	0.35 ± 0.01**c
peroxide value (meq O_2/kg)	9.00 ± 0.27*a	11.50 ± 0.18**a	12.75 ± 0.41*b	15.45 ± 0.38**b	11.00 ± 0.19*c	13.50 ± 0.60**c	13.15 ± 0.29*b	16.63 ± 0.52**d
oxidative stability (h)	6.21 ± 0.15*a	5.53 ± 0.19**a	8.85 ± 0.39*b	8.18 ± 0.14**b	5.10 ± 0.11*c	4.62 ± 0.16**c	4.80 ± 0.21*d	4.12 ± 0.09**d
total phenols (ppm)	101.07 ± 2.53*a	122.14 ± 3.01**a	253.67 ± 4.80*b	264.29 ± 3.96**b	343.61 ± 4.93*c	355.00 ± 5.21**c	275.71 ± 3.17*d	289.81 ± 2.77**d
total tocopherols (ppm)	254.49 ± 3.18*a	234.53 ± 3.60**a	274.14 ± 2.05*b	254.74 ± 2.67**b	126.40 ± 1.64*c	109.71 ± 1.23**c	135.44 ± 1.08*d	128.74 ± 1.56**d

[a]Each value represents the mean of three determinations ($n = 3$) and three independent experiments. Different symbols (*,**) within the same line indicate significant differences ($p < 0.05$) between 0 and 3% percents of olive leaves for each variety. Different lower-case letters (a,b,c,d) within the same line indicate significant differences ($p < 0.05$) for the same percentage of olive leaves between the different varieties.

dx.doi.org/10.1021/jf404395x | J. Agric. Food Chem. 2014, 62, 251−263

Table 2. Fatty Acids Composition (%) of Chétoui, Chemlali, Zalmati, and Chemlali Crossbreeding by Zalmati Olive Oils from Zarzis Region Extracted with Different Percentages of Olive Leaves[a]

	Chemlali		Chétoui		Zalmati		crossbreeding Chemlali by Zalmati	
fatty acids (%)	0%	3%	0%	3%	0%	3%	0%	3%
C14:0	0.01 ± 0.00*a	0.01 ± 0.00*a	0.02 ± 0.00*b	0.22 ± 0.00**b	0.01 ± 0.00*a	0.01 ± 0.00*a	0.01 ± 0.00*a	0.01 ± 0.00*a
C16:0	16.37 ± 0.24*a	16.09 ± 0.20*a	11.00 ± 0.09*b	10.90 ± 0.17*b	18.00 ± 0.16*c	17.80 ± 0.20*c	18.34 ± 0.14*d	18.13 ± 0.17*d
C16:1($n-7$) + C16:1($n-9$)	2.17 ± 0.04*a	2.12 ± 0.02*a	0.56 ± 0.01*b	0.44 ± 0.00**b	2.24 ± 0.02*c	2.20 ± 0.05*c	2.66 ± 0.02*d	2.49 ± 0.03**d
C17:0	0.04 ± 0.00*a	0.04 ± 0.00*a	0.05 ± 0.00*b	0.04 ± 0.00**a	0.03 ± 0.00*c	0.04 ± 0.00**a	0.04 ± 0.00*a	0.03 ± 0.00**b
C17:1($n-8$)	0.06 ± 0.00*a	0.06 ± 0.00*a	0.04 ± 0.00*b	0.04 ± 0.00*b	0.07 ± 0.00*c	0.07 ± 0.00*c	0.07 ± 0.00*c	0.06 ± 0.00**a
C18:0	3.51 ± 0.05*a	3.46 ± 0.04*a	3.03 ± 0.01*b	3.00 ± 0.05*b	2.44 ± 0.02*c	2.47 ± 0.02*c	2.32 ± 0.01*d	2.38 ± 0.01**d
C18:1($n-7$) + C18:1($n-9$)	67.84 ± 1.02*a	67.88 ± 0.79*a	64.77 ± 0.61*b	64.50 ± 1.13*b	58.75 ± 0.52*c	58.98 ± 0.67*c	55.73 ± 0.44*d	56.41 ± 0.53*d
C18:2($n-6$)($n-9$)	8.76 ± 0.13*a	9.07 ± 0.11**a	18.76 ± 0.09*b	19.11 ± 0.29*b	17.26 ± 0.15*c	17.23 ± 0.20*c	19.47 ± 0.16*d	19.22 ± 0.18*b
C18:3($n-3$)($n-6$)($n-9$)	0.97 ± 0.01*a	0.53 ± 0.01**a	0.69 ± 0.01*b	0.70 ± 0.01*b	0.51 ± 0.00*c	0.49 ± 0.00**c	0.62 ± 0.00*d	0.56 ± 0.00**d
C20:0	0.15 ± 0.00 *a	0.43 ± 0.00**a	0.45 ± 0.00*b	0.44 ± 0.00**b	0.38 ± 0.00*c	0.40 ± 0.00**c	0.39 ± 0.00*d	0.40 ± 0.00**c
C20:1($n-9$)	0.09 ± 0.00*a	0.15 ± 0.00**a	0.45 ± 0.00*b	0.45 ± 0.00*b	0.17 ± 0.00*c	0.15 ± 0.00**a	0.18 ± 0.00*d	0.15 ± 0.00**a
C22:0	0.03 ± 0.00*a	0.10 ± 0.00**a	0.12 ± 0.00*b	0.11 ± 0.00**b	0.09 ± 0.00*c	0.10 ± 0.00**a	0.11 ± 0.00*d	0.10 ± 0.00**a
C24:0		0.06 ± 0.00a	0.06 ± 0.00*a	0.05 ± 0.00**b	0.05 ± 0.00*b	0.06 ± 0.00**a	0.06 ± 0.00*a	0.06 ± 0.00*a
C18:1/C18:2	7.74	7.48	3.45	3.37	3.40	3.42	2.86	2.93
ΣSFA	20.11 ± 0.29*a	20.19 ± 0.24*a	14.73 ± 0.10*b	14.76 ± 0.22*b	21.00 ± 0.18*c	20.88 ± 0.22*c	21.27 ± 0.15*c	21.11 ± 0.18*c
ΣMUFA	70.16 ± 1.06*a	70.21 ± 0.81*a	65.82 ± 0.62*b	65.43 ± 1.13*b	61.23 ± 0.54*c	61.40 ± 0.72*c	58.64 ± 0.46*d	59.11 ± 0.56*d
ΣPUFA	9.73 ± 0.14*a	9.60 ± 0.12*a	19.45 ± 0.10*b	19.81 ± 0.30*b	17.77 ± 0.15*c	17.72 ± 0.20*c	20.09 ± 0.16*d	19.78 ± 0.18**b
ΣUFA	79.89 ± 1.20*a	79.81 ± 0.93*a	85.27 ± 0.72*b	85.24 ± 1.43*b	79.00 ± 0.69*a	79.12 ± 0.92*a	78.73 ± 0.62*a	78.89 ± 0.74*a
ΣMUFA/ΣPUFA	7.21	7.31	3.38	3.30	3.44	3.46	2.91	2.98

[a]SFA: saturated fatty acids. MUFA: monounsaturated fatty acids. PUFA: polyunsaturated fatty acids. UFA: unsaturated fatty acids. Each value represents the mean of three determinations ($n = 3$) and three independent experiments. Different symbols (*, **) within the same line indicate significant differences ($p < 0.05$) between 0 and 3% percents of olive leaves for each variety. Different lower-case letters (a, b) within the same line indicate significant differences ($p < 0.05$) for the same percentage of olive leaves between the different varieties.

dx.doi.org/10.1021/jf404395x | J. Agric. Food Chem. 2014, 62, 251−263

olives and addition of olive leaves before the extraction of olive oils induce significant ($p < 0.05$) increases in all the peroxide values. These results are in agreement with those obtained by Di Giovacchino et al.[8] and Malheiro et al.[29]

Fatty Acid Profile. As shown in Table 2, many fatty acids were detected in the extra-virgin olive oils of the studied varieties extracted with different percentages of olive leaves. As expected, the most abundant one in all the samples was oleic acid (C18:1), followed by palmitic (C16:0) and linoleic acids (C18:2), while palmitoleic, stearic, linolenic, and arachidic acids were present in small amounts, independently of the percentage of olive leaves added. The four EVOO showed a fatty acid composition (Table 2) in compliance with the established limits[31] and variety-depending ranges. Oleic acid, the major monounsaturated fatty acid, also showed a wide variability depending on the varieties. Chemlali Zarzis had the highest percentage of oleic acid which did not follow any tendency with the increasing quantity of olive leaves added ($p > 0.05$), varying from 67.84% to 67.88% (samples with 0% and 3% of leaves, respectively). While Zalmati Zarzis and crossbreeding Chemlali by Zalmati Zarzis showed the lowest values in the oleic acid varying from 58.75% to 58.98% and 55.73% to 56.41% for samples with 0% and 3% of added leaves, respectively. Chétoui Zarzis had a good value of C18:1, which remained almost the same for 0% and 3% of added leaves before the extraction process of olive oil (64.77% to 64.50%, respectively). Palmitic acid (C16:0) is the major saturated fatty acid in olive oil; its content was not influenced by the amount of the added leaves ($p > 0.05$), but it was instead strongly affected by the cultivar ($p < 0.05$). The highest percentage was observed in crossbreeding Chemlali by Zalmati oils (18.34 to 18.13 for samples with 0% and 3% of added leaves, respectively), whereas the lowest values were present in Chétoui oil (11.00% and 10.90% for samples with 0% and 3% of added leaves, respectively). Concerning linoleic acid, crossbreeding Chemlali by Zalmati oil samples had the highest mean values (19.47% and 19.22% for samples with 0% and 3% of added leaves, respectively) whereas the lowest one was found in Chemlali Zarzis (from 8.76 to 9.07% in the olive oils without addition of olive leaves to 3% of added leaves). The Chétoui and Zalmati varieties presented intermediate percentages, comprised between 18.76 and 19.11% and between 17.26 and 17.23% in samples with 0% and 3% of added leaves, respectively. The percentages of the other fatty acids, including palmitoleic (C16:1), stearic (C18:0), linolenic (C18:3) and arachidic (C20:0) acids, vary from one olive oil to another, but the amounts were quite small. The levels of these fatty acids in the various tested oils were close to those required by the IOOC (2011).[31] The percentages of saturated, monounsaturated and polyunsaturated fatty acids and the oleic acid/linoleic acid ratio (O/L) in the studied olive oils were also evaluated. It was observed that crossbreeding Chemlali by Zalmati oil was the richest in total saturated fatty acids (SFA) (21.27% and 21.11% from oil samples with 0% to 3% of added leaves, respectively) essentially due to its high content in palmitic acid, which represents the major acid of the SFA fraction.

With respect to the total monounsaturated fatty acids (MUFA), Chemlali Zarzis olive oil contained the highest percentage (70.21%) because of its high content in oleic acid. Crossbreeding Chemlali by Zalmati olive oil was the richest in total polyunsaturated fatty acids (20.09%) because of its high contents in linoleic acid, representing the major fatty acid component of that fraction. The oleic acid/linoleic acid ratio varied between 2.86 and 7.74% according to the varieties. This ratio can be useful to characterize olive cultivars and have a relationship with stability.[32] We can then claim that fatty acid composition may be an important factor to identify the monovarietal olive oils. Notably, the percentages of the fatty acids did not follow any tendency with the increasing quantity of the added olive leaves.[29]

Total Phenols. Olive oil usually contains considerable amounts of phenolic compounds. The four varieties showed different amounts of total phenols (Table 1). The highest content of these components was detected in Zalmati olive oil, with 343.61 to 355.00 ppm with 0% and 3% of added leaves, respectively, while the lowest amount was recorded for Chemlali olive oil (101.07 and 122.14 for 0% and 3% of added leaves, respectively). The effect of the cultivar on these compounds is obvious. These results are in agreement with those obtained by Issaoui et al.[33] Moreover, the data in Table 1 show that the total phenols contents (ppm) of oils oils increase slightly but significantly ($p < 0.05$) when the different percentages of leaves were added to olives. This is due to the fact that the concentration of the phenolic compounds (glycosides) of leaves is similar to that in olive flesh. Moreover, the phenolic substances are present in leaves as glycosides, soluble in water but not in oil.[8]

Total Tocopherols Content. Tocopherols constitute the lipophilic antioxidant fraction and are well-known for their effective inhibition of lipid oxidation in all vegetable oils. The tocopherols content in these four Tunisian olive oil samples (Table 1) extracted with olive leaves can be considered as medium−high (comprised between 109.71 and 254.74 ppm). Chemlali and Chétoui olive oils showed the highest values of tocopherol (254.49 to 234.53 ppm and 274.14 to 254.74 ppm for 0% and 3% of added leaves, respectively), whereas Zalmati and crossbreeding Chemlali by Zalmati oils contained the lowest levels of these compounds (126.40 to 109.71 ppm and 135.44 to 128.74 ppm for 0% and 3% of added leaves, respectively). Notably, the tocopherol level is highly variety-dependent. These results are in agreement with those previously reported, which showed that tocopherols contents vary between cultivars.[34] Indeed, the contents of tocopherols presented a slight difference but also significant ($p < 0.05$) between the olive oils without addition of leaves and those up to 3% of the added leaves. In addition, these observations are in agreement with the research studies of Malheiro et al.[29]

Oil Stability. The oxidative stability of EVOO measured by Rancimat test (at 120 °C) showed that the induction time varied according to the cultivar. The highest level was attributed to the cultivar Chétoui Zarzis (from 8.85 to 8.18 h samples with 0% and 3% of added leaves, respectively). The different induction times of all the samples are probably due to the combination of fatty acid composition, and in particular to the relatively low content of polyunsaturated fatty acids, expressed by the O/L ratio. Furthermore, the effect of various pro/antioxidants present in the oils should not be neglected.[35,36] Chemlali Zarzis olive oils presented intermediate values, varying between 6.21 and 5.53 h with 0% and 3% of added leaves. Zalmati and crossbreeding Chemlali by Zalmati oil seem to have a lower stability value that does not exceed 5.10 h for both oils extracted with different percentages of olive leaves. Indeed, the results showed that the addition of leaves also did slightly but significantly ($p < 0.05$) affect the induction time. Furthermore, our results are in agreement with those obtained by Di-Giovacchino et al.[8] On the contrary, Malheiro et al.[29]

Table 3. Composition of the Volatile Fraction (%) Obtained from the Four Olive Oil Varieties from Zarzis (Tunisia) Extracted with Different Percentages of Olive Leaves

		Chemlali		Chétoui		Zalmati		crossbreeding Chemlali by Zalmati	
volatile compd	LRI[a]	0%	3%	0%	3%	0%	3%	0%	3%
				Aldehydes					
hexanal	804	2.60	3.60	3.40	4.70	2.10	4.60		
(*E*)-2-hexenal	856	9.60	12.60	27.90	32.60		5.20		
(*Z*)-2-octenal	1046					1.80	1.10	2.30	1.90
nonanal	1104		0.80	0.30		1.80	1.20	2.50	1.60
(*E*)-2-nonenal	1164							2.80	1.90
				Alcohols					
1-pentanol	762					8.30		9.50	7.80
(*E*)-2-hexen-1-ol	864	18.00	20.50	16.50	18.50	30.00	58.00	35.20	45.40
(*E*)-2-octen-1-ol	1072		0					1.2	
phenyl ethyl alcohol	1111	1.30	8.90			3.20	2.30	5.90	2.70
(*E*)-2-nonen-1-ol	1171							0.8	1.0
1-nonanol	1173								0.80
2-decanol	1206	38.40	31.20	19.70	16.30	22.60	17.80	15.10	19.70
				Esters					
(*Z*)-3-hexenyl acetate	1008	6.40	6.70	6.30	9.60				
1-hexyl acetate	1010	12.50	11.40	6.20	8.50				
methyl salicylate	1192					2.80			1.10
				Alkanes					
n-dodecane	1200	1.70	0.60	0.80		2.50		8.50	1.70
n-tetradecane	1400	0.40						0.90	
				Terpene Hydrocarbons					
				Monoterpene Hydrocarbons					
limonene	1032						0.50	1.80	
(*E*)-*β*-ocimene	1052		0.40	0.90	1.00	7.30	5.10	4.30	5.60
				Sesquiterpene Hydrocarbons					
α-copaene	1377			1.10	1.20				
(*Z*)-*β*-farnesene	1444			0.50	0.50				
valencene	1493		0.30	0.80	0.70			1.20	0.50
(*E*,*E*)-*α*-farnesene	1508	3.00	2.20	4.60	5.30	3.70	2.10	0.80	3.00
				Totals					
total aldehydes		12.20	170	31.60	37.30	5.70	12.10	7.60	5.40
total alcohols		57.70	60.60	36.20	34.80	64.10	78.10	67.70	77.40
total esters		18.90	18.10	12.50	18.10	2.80	0	0	1.10
total C6 compd		49.10	51.80	60.30	73.90	32.10	67.80	35.20	45.40
total C5 compd						8.30		9.50	7.80
identified compd		93.90	99.20	890	98.90	86.10	97.90	92.80	94.70
nonidentified compd		6.10	0.80	11	1.10	13.90	2.10	7.20	5.30

[a]LRI, linear retention index.

have reported that the induction times are clearly associated with changes induced in the composition of olive oils due to leaves addition, namely by the extraction of antioxidative components into the olive oils.

Aroma Profiles. The characteristic and the unique flavor of extra-virgin olive oil, in particular, its green and fruity attributes depends on many volatile compounds.[13,6,37] The concentration and odors threshold of volatile compounds, whether major or minor, are crucial to extra-virgin olive oil quality. Table 3 displays the compounds identified in the volatile fractions of the oils obtained from the four varieties of *Olea europaea L.* (Chemlali, Chétoui, Zalmati, and crossbreeding Chemlali by Zalmati) extracted with different percentages of olive leaves using SPME-GC/MS. It proves that the virgin olive oil headspace consists of a complex mixture of 23 compounds, representing 86.1−99.2% of the total volatile compounds. Moreover, 17 unknown minor volatile compounds detected in olive oils samples were presented in Table 4. These results indicate that olive oil volatile compounds accumulate differently, according to the cultivar kind and the increase of the percentage of olive leaves. The present results are in agreement with other studies, such as Ouni et al.[38] Commonly, each volatile compound is characterized by an odor threshold. So, even if different fruits have similar qualitative compositions, the aroma could considerably vary when the relative proportions in olive leaves are different. The detected compounds can be divided into four chief chemical groups: aldehydes, alcohols, esters, and terpene hydrocarbons (monoand sesquiterpenes). Their main aromatic notes can be classified as green, fruity, bitter, pungent, and fatty.[39] In detail, within the main chemical groups, we have identified seven alcohols (34.8−78.1% of total volatile fraction), five aldehydes (5.4−37.3%), three esters (0−18.9%), two monoterpenes (0−7.3%), and four sesquiterpenes (2−7.7%). On the contrary, a ketone fraction was not identified

dx.doi.org/10.1021/jf404395x | J. Agric. Food Chem. 2014, 62, 251−263

Table 4. LRI and the Main Mass Fragments of the Biggest Unidentified Peaks

	LRI[a]	mass fragments, *m/z* (%)
Chemlali 0%	1033	39 (100), 93 (91), 79 (86), 67 (64), 91 (63), 95 (55)
	1043	87 (100), 55 (54), 39 (48), 84 (47), 41 (46), 86 (40
	1106	41 (100), 39 (71), 57 (54), 56 (47), 43 (46), 67 (44)
	1264	44 (100), 41 (84), 67 (75), 40 (45), 56 (45), 42 (41)
Chemlali 3%	1043	87 (100), 55 (54), 39 (48), 84 (47), 41 (46), 86 (40)
Chétoui 0%	1043	87 (100), 55 (54), 39 (48), 84 (47), 41 (46), 86 (40)
	1048	41 (100), 87 (92), 55 (65), 91 (54), 105 (38), 142 (35)
	1002	41 (100), 39 (86), 69 (58), 67 (54), 40 (52), 68 (25)
	1069	40 (100), 39 (48), 41 (29), 44 (26), 43 (17), 55 (13)
	1106	41 (100), 39 (71), 57 (54), 56 (47), 43 (46), 67 (44)
	1398	40 (100), 39 (49), 41 (45), 44 (27), 57 (23), 43 (21)
Chétoui 3%	1118	69 (100), 41 (98), 39 (75), 79 (32), 91 (25), 77 (18)
	1438	40 (100), 39 (41), 41 (37), 44 (30), 69 (17), 94 (12)
Zalmati 0%	1033	39 (100), 93 (91), 79 (86), 67 (64), 91 (63), 95 (55)
	1060	40 (100), 39 (85), 41 (63), 43 (34), 44 (26), 55 (24)
	1065	91 (100), 39 (98), 95 (57),55 (63), 38 (45), 105 (37)
	1327	73 (100), 40 (63), 39 (41), 41 (31), 45 (22), 147 (20)
Zalmati 3%	860	39 (100), 67 (69), 41 (66), 69 (52), 55 (49), 42 (23)
	1002	41 (100), 39 (86), 69 (58), 67 (54), 40 (52), 68 (25)
crossbreeding Chemlali by Zalmati 0%	806	41 (100), 43 (85), 39 (78), 56 (53), 57 (49), 58 (20)
	860	39 (100), 67 (69), 41 (66), 69 (52), 55 (49), 42 (23)
	1097	57 (100), 39 (69), 41 (67), 43 (63), 71 (53), 44 (32)
	1158	39 (100), 55 (91), 41 (78), 67 (63), 68 (33), 69 (31)
crossbreeding Chemlali by Zalmati 3%	806	41 (100), 43 (85), 39 (78), 56 (53), 57 (49), 58 (20)
	1158	39 (100), 55 (91), 41 (78), 67 (63), 68 (33), 69 (31)

[a]LRI, linear retention index.

in all the studied oils, indicating an extremely low content or activity of alcohol acetyl transferase.[40]

Aldehydes and alcohols were the main chemical classes detected in the analyzed oils (Table 3). Indeed, alcohols in olive oil are connected to positive sensory characteristics: olive fruity, other fruits, green, and aromatic. However, since they have higher threshold values, they also have a lower sensory significance than aldehydes.[41] Besides, alcohols were the most abundant volatile compounds in these studied oils, ranging between a minimum of 57.70% and 60.60% in 0 and 3% of the added leaves samples for oils produced from Chemlali Zarzis to a maximum of 64.10% to 78.10% for 0 and 3% of leaves for oil produced from Zalmati Zarzis cultivars, with the exception of Chétoui olive oil processed with 0% and 3% leaves, which showed the highest percentages of aldehydes (31.60% and 37.30% of the total aroma, respectively). The difference between cultivars became much stronger when considering the highest levels of esters observed in Chétoui and Chemlali olive oil (18.90% to 18.10% and 12.50% to 18.10% for 0% to 3% of leaves, respectively). These results therefore indicate that the level of ester was strongly affected by the leaves added to the olives.

The major components of the volatile fraction of extra-virgin oils were the C6 compounds, which derive from the cascade of enzymatic reactions starting with the formation by lipoxygenase action (LOX pathway occurring during the crushing of olive fruit and the malaxation of paste), of 13-hydroperoxides from linoleic and linolenic acids.[11,12,39] The different accumulations of metabolites from the lipoxygenase cascade were highly dependent on the levels of enzymes involved, the extraction conditions, the variety, the storage time, and the degree of ripening of olives.[6] Their quantitative composition basically changed according to the cultivar. However, some modifications of the concentration of C6 compounds from the LOX pathways should be attributed to the addition of olive leaves before the extraction of olive oil. The chemical compositions of all Tunisian olive oil headspaces showed that C6 aldehydes (hexanal and (*E*)-2-hexenal) were the most abundant compounds. Chétoui cultivars had the highest amount of (*E*)-2-hexenal (27.90% and 32.60% for 0% to 3% of added leaves, respectively) followed by Chemlali Zarzis (9.60% and 12.60% for 0% to 3% of leaves added, respectively), while Zalmati Zarzis registered the lowest amounts of this compound, (0% and 5.20% from 0% to 3% of added leaves, respectively). Interestingly, this compound was not detected at all in crossbreeding Chemlali by Zalmati Zarzis. Therefore, we can affirm that the analysis of aroma matrix showed similarities between Zalmati and crossbreeding Chemlali by Zalmati Zarzis. These results agree with previous findings suggesting that monovarietal VOO could be distinguished by their (*E*)-2-hexenal content. Moreover, the amount of hexanal that confer apple and green fruity attributes[38] was lower and varied between 0% for crossbreeding Chemlali by Zalmati and 4.70% in Chétoui olives oil samples with 3% of added leaves. According to Brkic Bubola et al.[42] a low hexanal/(*E*)-2-hexenal ratio indicates better quality and lower oxidation degree of the oil. Zalmati and crossbreeding Chemlali by Zalmati oils had no influence on these two aldehydes nor on its ratio, and it can be concluded that oxidative changes in the oils did not occur with 0% and 3% of the added leaves. In Chemlali and Chétoui oils, the hexanal/(*E*)-2-hexenal ratio was very low due to the low hexanal content and the high levels of (*E*)-2-hexenal. Indeed, Di-Giovacchino et al.[42] stated that the taste panel found a quality improvement in oil when the percentage of leaves added to olives was increased, even though there was a slight decrease in the evaluation of the oil obtained from olives containing 5% leaves. This result can be explained by the increase in the content of hexanal, an unpleasant to the taste aldehyde. Therefore, when evaluating olive oil quality, the importance to

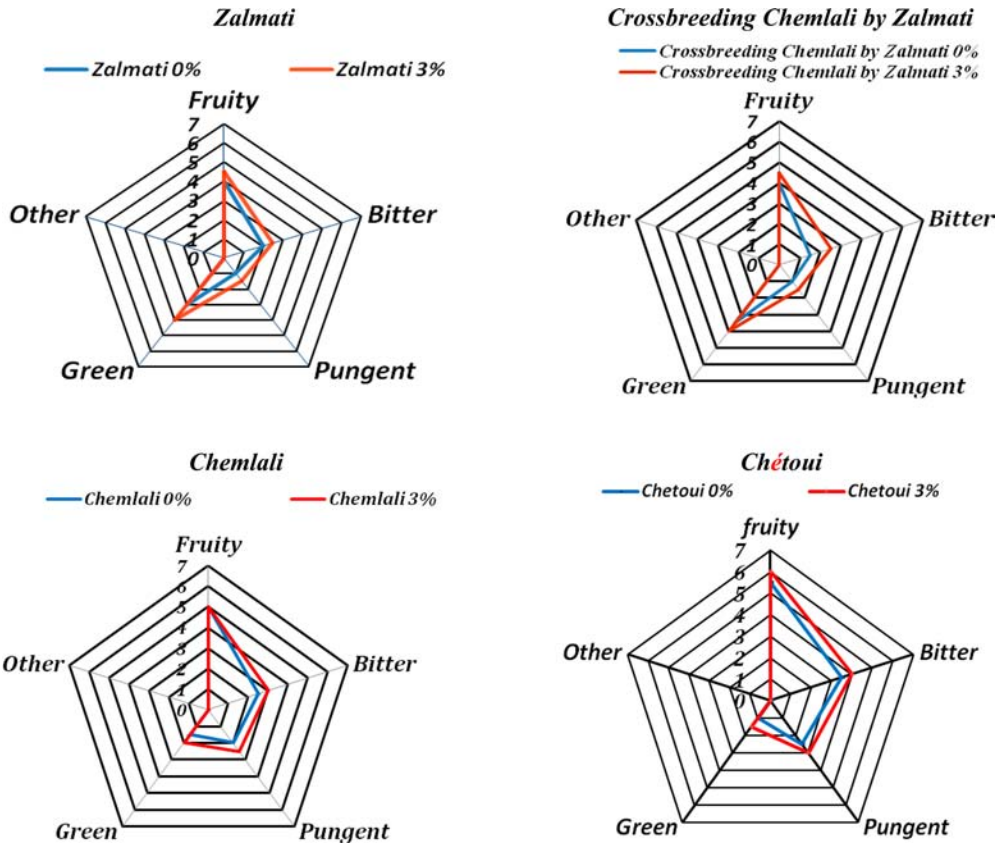

Figure 1. Sensory spider plot of extra-virgin olive oils for the Tunisian olive cultivars: Chemlali, Chétoui, Zalmati, and crossbreeding Chemlali by Zalmati from Zarzis region extracted with different percentages (0 and 3%) of olive leaves.

study the ratio between hexanal and (*E*)-2-hexenal content was confirmed.

In the volatile alcohols component of the oil, no newly formed substances or considerable changes in the majority of volatile components was proven. An exception is a noticeable increase in some C6 alcohols, such as (*E*)-2-hexenol. The role of this compound in the flavor of olive oil is not clear. In fact, in the literature, only very few papers[25] have reported the presence of this compound, which could play a very important role in the fragrance of this valuable food. The highest percentage of this volatile fraction was detected in Zalmati and crossbreeding Chemlali by Zalmati oils. Such an increase could be explained by the method of olive leaves crushing (30.0% to 58.0% and 35.20% to 45.40% in 0% and 3% of added leaves added, respectively). The same observation is true in the case of Chemlali Zarzis. It has been shown that the enzymatic conversion of 13-L-hydroperoxides from linoleic and linolenic acids to the corresponding alcohols occurs primarily in the lamellae of chloroplasts.[18] Thus, we can estimate that the overall amounts of C6 aldehydes were clearly higher than the sum of C6 alcohols in Chétoui samples, as reported for virgin olive oil analyzed by others variety. Nevertheless, in Chemlali, Zalmati and crossbreeding Chemlali by Zalmati oils, the sums of C6 alcohols was generally higher than those of C6-aldehydes. However, Baccouri et al.[6] have shown that, in Chétoui oils, the sum of C6-alcohols was generally higher than that of C6-aldehydes. These results may be explained by the differential activity of the alcohol dehydrogenase (ADH) enzyme, which reduces the C6-aldehydic compounds to the corresponding alcohols due, among genetic factors, also to the region of growing of the plants.[43] Indeed, the Chétoui cultivar studied in this research work grows in the south of the country, while the samples studied by Baccouri et al.[6] have been harvested in the north.

1-Hexyl acetate and (*Z*)-3-hexenyl acetate, which contribute to the elicitation of pleasant fruity perceptions, are present in the aroma of all the studied olive oil samples, but they are minor components when compared with aldehydes or alcohols. These esters are synthesized by alcohol acetyl transferase (AAT) within the LOX pathway. Moreover, the absence of esters in the varieties Zalmati and crossbreeding Chemlali by Zalmati also point out the absence of alcohol acetyl transferase (AAT) activity in the olive oils compared with Chemlali and Chétoui varieties (6.40% to 6.70% and 6.30% to 9.60% with 0 and 3% leaves).

Several terpene hydrocarbons (mono- and sesquiterpenes) were detected in all the analyzed samples. Most of them were minor compounds of the volatile fraction not derived from fatty acid transformations. However, even if they occur in EVOO below their olfactory threshold they may provide useful quality markers. It is important to note that the main sesquiterpene (*E*,*E*)-α-farnesene a tetraun-saturated acyclic sesquiterpene, detected in all the oils was more abundant in Chétoui olive oil (4.60% to 5.30% for 0% and 3% of the added leaves, respectively) than in crossbreeding Chemlali by Zalmati olive oils (0.80% and 3% for 0% to 3% of added leaves, respectively). Zalmati and Chemlali olive oil had similar percentage to crossbreeding Chemlali by Zalmati olive oils with 3% of added leaves. α-Copaene is a monounsaturated sesquiterpene that has already been detected in Tunisian oils, mainly in those obtained from olives of the Oueslati variety.[44] The addition of 0−3% olives leaves seemed to slightly influence the contents of α-

dx.doi.org/10.1021/jf404395x | J. Agric. Food Chem. 2014, 62, 251−263

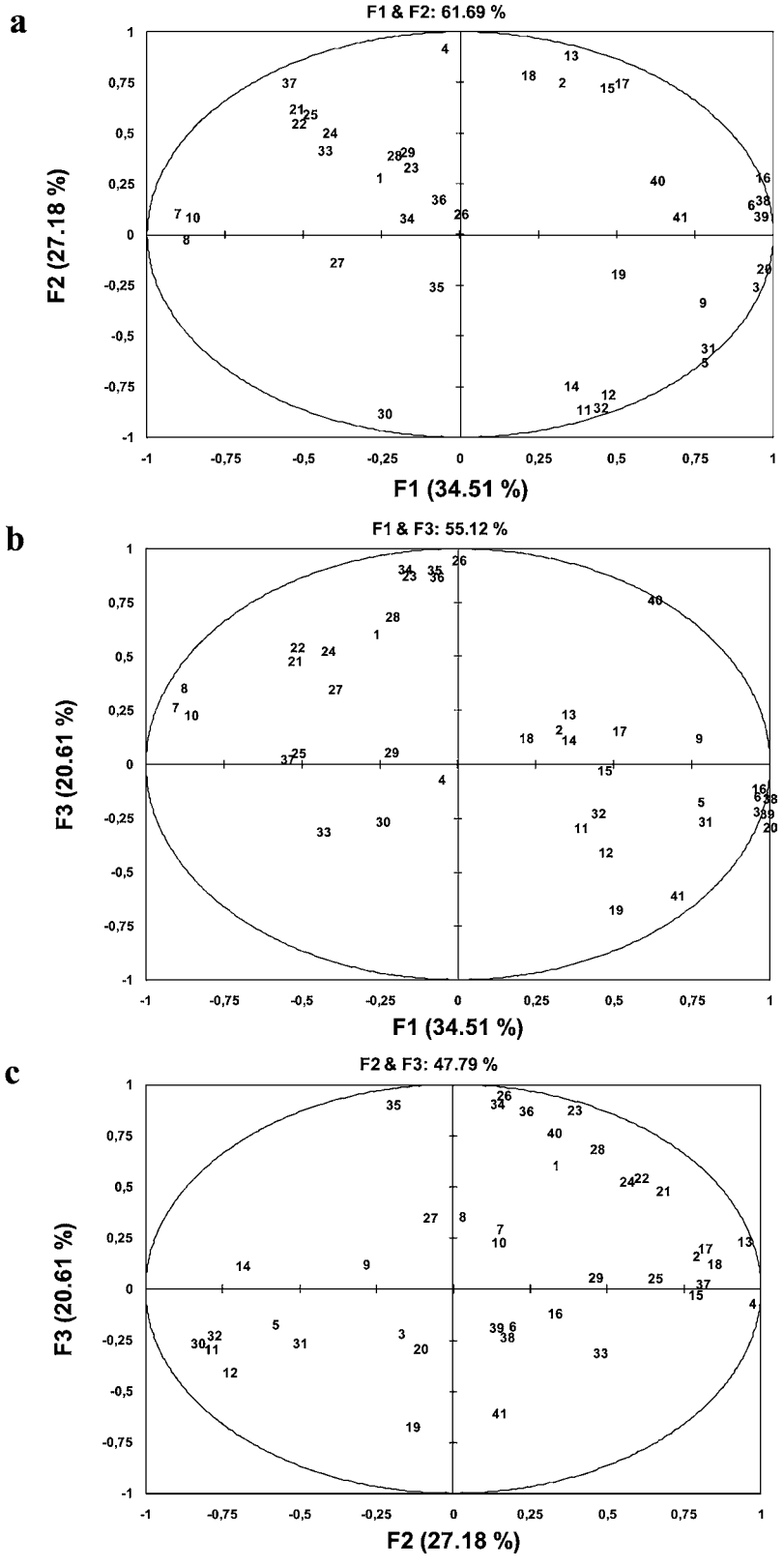

Figure 2. (a, b, and c) Principal component analysis applied to all samples considering 41 variables: Plot of component weights. 1, free fatty acids; 2, peroxide value; 3, oxidative stability; 4, total phenols; 5, total tocopherols; 6, C14:0; 7, C16:0; 8, C16:1($n-7$) +,C16:1($n-9$); 9, C17:0; 10, C17:1($n-8$); 11, C18:0; 12, C18:1($n-7$) + C18:1($n-9$); 13, C18:2($n-6$)($n-9$); 14, C18:3($n-3$)($n-6$)($n-9$); 15, C20:0; 16, C20:1($n-9$); 17, C22:0; 18, C24:0; 19, Hexanal; 20, (*E*)-2-hexenal; 21, (*Z*)-2-octenal; 22, nonanal; 23, (*E*)-2-nonenal; 24, 1-pentanol; 25, (*E*)-2-hexen-1-ol; 26, (*E*)-2-octen-1-ol; 27, phenyl ethyl alcohol; 28, (*E*)-2-nonen-1-ol; 29, 1-nonanol; 30, 2-decanol; 31, (*Z*)-3-hexenyl acetate; 32, 1-hexyl acetate; 33, methyl salicylate; 34, *n*-dodecane; 35, *n*-tetradecane; 36, limonene; 37, (*E*)-β-ocimene; 38, α-copaene; 39, (*Z*)-β-farnesene; 40, valencene; 41, (*E*,*E*)-α-farnesene.

dx.doi.org/10.1021/jf404395x | *J. Agric. Food Chem.* 2014, 62, 251−263

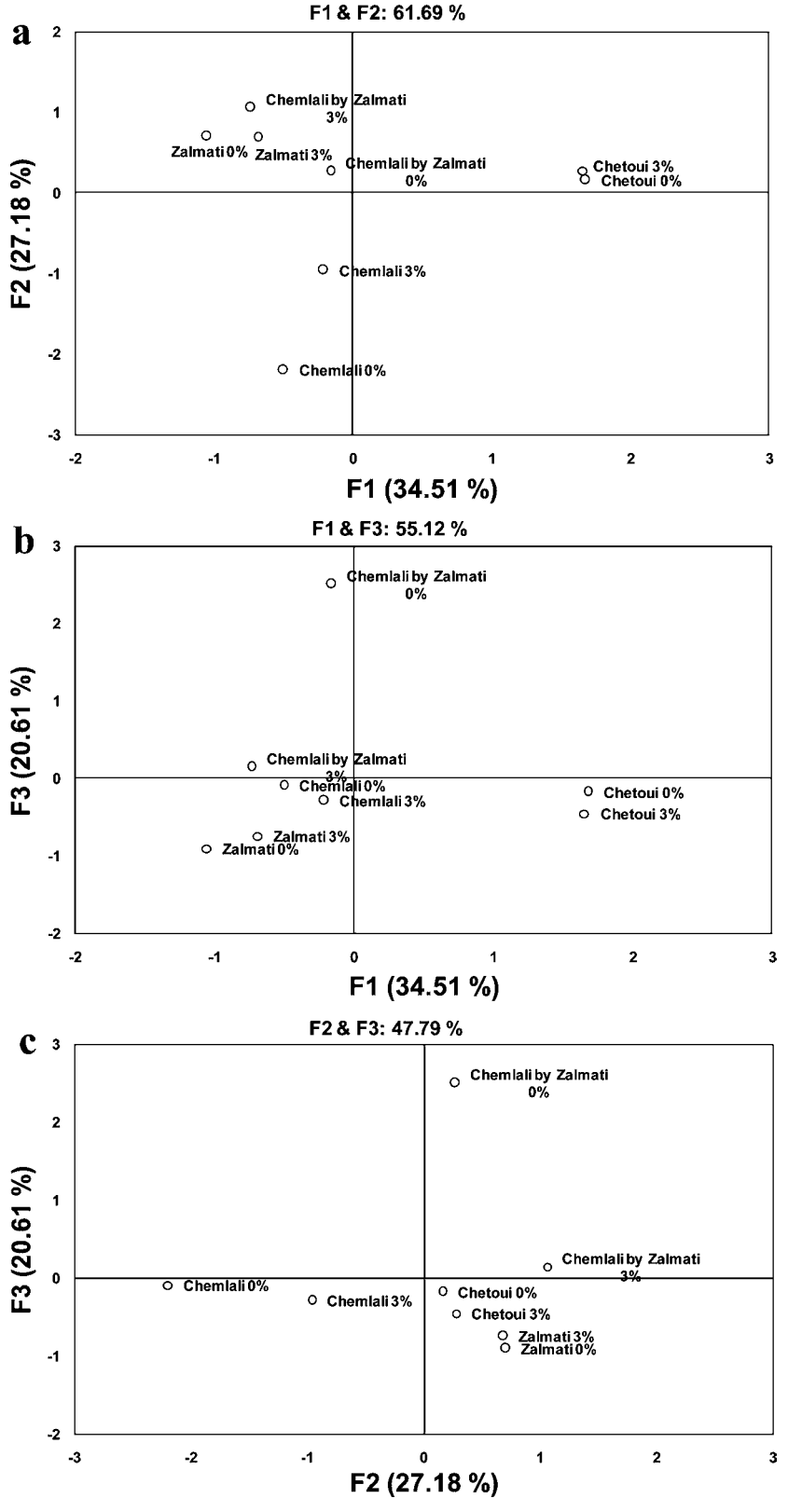

Figure 3. (a, b, and c) Principal components analysis based on all the analyses performed for the four olive oil varieties extracted with and without addition of olive leaves (3%).

copaene as also reported by Vichi et al.[45] Furthermore, this chemical was not detected in Chemlali, Zalmati, and cross-breeding Chemlali by Zalmati. It was only detected in low percentages in Chétoui olives oil (Table 3). These results are in agreement with those of Cecchi et al.,[46] which showed that terpene hydrocarbons show a large variability that depend on the olives variety.

dx.doi.org/10.1021/jf404395x | J. Agric. Food Chem. 2014, 62, 251−263

Sensory Analysis. Chemlali, Chétoui, Zalmati, and crossbreeding Chemlali by Zalmati cv, growing in Zarzis location, gave extra-virgin olive oils that are endowed with four positive descriptors: fruity, green, bitter, and pungent (Figure 1). The eight olive oils samples with and without the addition of olive leaves also showed the absence of any defects and had the typical fruity flavor preferred by consumers. Chemlali and Chétoui olive oils from Zarzis location were bitter and pungent, but very fruity. This result can be explained by the increase in the content of C6-compounds, especially the aldehydes, as reported by Angerosa.[13] This class of compounds is usually characterized by intense sensory descriptions associated with fruity and bitter sensory notes.[47] On the contrary, Zalmati and crossbreeding Chemlali by Zalmati oils from Zarzis were less bitter and pungent and acquired well-balanced fruity and green tastes probably due to the presence of C6-alcohols such as (*E*)-2-hexen-1-ol.[41]

On the other hand, in contrast to what is postulated by Angerosa,[13] incorporating leaves in concentrations of about 0−3% prior crushing, enhances the flavor of the oils from overripe fruits and improves their quality. The aroma is not distorted and tasters perceive higher intensities of green fruity, pungent and bitter taste. In fact, the analysis of the volatile compounds did not show any newly formed substances but a noticeable increase in C6 aldehydes (hexanal and (*E*)-2-hexenal) and C6-alcohols ((*E*)-2-hexen-1-ol), which are in good agreement with the results of the organoleptic evaluation.

Chemometric Analysis. PCA was used in exploratory analysis to characterize the effect of addition of olive leaves (3%) on the components of the extra-virgin olive oils from different varieties of Zarzis region, before the extraction process. PCA was applied to the data set of all performed analyses of EVOOs using the Varimax rotation with Kaiser Normalization, and three factors were selected justifying 82.30% of total variance (F1, 34.51%; F2, 27.18%; and F3, 20.61%) (Figures 2 and 3). Regarding these factors, the different varieties (enriched and unenriched oils with 3% of olive leaves) could be discriminated on the PCA diagrams (Figure 3a, b, and c). According to Figures 2(a, b) and 3(a, b), Chétoui and crossbreeding Chemlali by Zalmati varieties were related to the axe F1 which was dominated after the Varimax rotation by the following variables: oxidative stability, total tocopherols, C14:0, C16:0, C16:1($n-7$) + C16:1($n-9$), C17:0, C17:1($n-8$), C20:1($n-9$), (*E*)-2-hexenal, (*Z*)-3-hexenyl acetate, α-copaene, (*Z*)-β-farnesene, and (*E*,*E*)-α-farnesene.

According to Figures 2(a, c) and 3(a, c), Chemlali variety was related to the F2 axe which was dominated after the Varimax rotation by the following variables: peroxide value, total phenols, C18:0, C18:1($n-7$) + C18:1($n-9$), C18:2($n-6$)($n-9$), C18:3($n-3$)($n-6$)($n-9$), C20:0, C22:0, C24:0, 2-decanol, 1-hexyl acetate, and (*E*)-β-ocimene. Indeed, F2 clearly showed the effect of the enrichment of Chemlali oil with 3% of olive leaves, which is consistent with the results of mean comparison (Student−Newman−Keuls test).

Finally, Zalmati variety was related to the axe F3 according to Figures 2(b, c) and 3(b, c), which was dominated after the Varimax rotation by the following variables: free fatty acids, hexanal, (*E*)-2-nonenal, (*E*)-2-octen-1-ol, (*E*)-2-nonen-1-ol, *n*-dodecane, *n*-tetradecane, limonene and valencene.

In conclusion, our results confirm that olive oil quality is cultivar dependent. Hence, fatty acid compositions are useful for distinguishing the monovarietal olive oils belonging to particular cultivars, in which Chemlali and Chétoui oils showed the best fatty acid composition compared to that of Zalmati and crossbreeding Chemlali by Zalmati (lowest palmitic acid and the highest oleic acid). Concerning the leaves addition prior the fruits extraction process, it induces significant increases ($p < 0.05$) mainly in peroxide value and phenols and tocopherols contents, as well as oxidative stability. In addition, the application of SPME to the analysis of extra-virgin olive oil headspace allowed the detection of significant differences in the proportions of volatile constituents from oils of different varieties and the addition of olive leaves prior the fruits extraction processes. Evidently, the addition of 3% of olive leaves promoted the increase in C6 compounds specially the hexanal, (*E*)-2-hexanal and (*E*)-2-hexan-1-ol. Finally, the results obtained provide information on the performance of the studied Tunisian cultivars. The studied olive oils showed chemical profiles corresponding to extra-virgin olive oil category (high quality) and good sensory attributes highly appreciated by the consumers.

AUTHOR INFORMATION

Corresponding Author

*Tel: +216 98 667 581. Fax: +216 74 674 364. E-mail: mohamed.bouaziz@fsg.rnu.tn.

Funding

The authors thank the Ministère de l'Enseignement Supérieur et de la Recherche Scientifique, Tunisia, for the support of this research work.

Notes

The authors declare no competing financial interest.

ACKNOWLEDGMENTS

The authors thank Hazem Jaber and Ikram Trabelsi for their precious help with sensorial evaluation, HPLC, and GC analysis. They are also grateful to Leila Mahfoudhi, an English teacher at the Sfax Faculty of Science, for having proofread the paper.

ABBREVIATIONS USED

AAT, alcohol acetyl transferase enzyme; ADH, alcohol dehydrogenase enzyme; CI, chemical ionization; EVOO, extra-virgin olive oil; FAMEs, fatty acid methyl esters; GA, gallic acid; GC, gas chromatography; GC-CI-MS, gas chromatography with chemical ionization mass spectrometry; HPLC, high-performance liquid chromatography; IOOC, International Olive Oil Council; LOX, lipoxygenase enzyme; LRI, linear retention indices; MeOH, methanol; MS, mass spectrometry; MUFA, mono-unsaturated fatty acids; O/L, oleic acid/linoleic acid ratio; PCA, principal compounds analysis; PDMS, polydimethylsiloxane; PV, peroxide value; RI, ripening index; SD, standard deviation; SFA, saturated fatty acids; SPME, solid-phase microextraction

REFERENCES

(1) Issaoui, M.; Flamini, G.; Brahmi, F.; Dabbou, S.; Ben Hassine, K.; Taamali, A.; Chehab, H.; Ellouz, M.; Zarrouk, M.; Hammami, M. Effect of the growing area conditions on differentiation between Chemlali and Chétoui olive oils. *Food Chem.* **2010**, *119*, 220−225.

(2) Bouaziz, M.; Chamkha, M.; Sayadi, S. Comparative study on phenolic content and antioxidant activity during maturation of the olive cultivar Chemlali from Tunisia. *J. Agric. Food. Chem.* **2004**, *52*, 5476−5481.

(3) Bouaziz, M.; Feki, I.; Ayadi, M.; Jemai, H.; Sayadi, S. Stability of refined olive oil and olive pomace oil added by phenolic compounds from olive leaves. *Eur. J. Lipid Sci. Technol.* **2010**, *112*, 21−24.
(4) Gargouri, B.; Ammar, S.; Zribi, A.; Ben Mansour, A.; Bouaziz, M. Effect of growing region on quality characteristics and phenolic compounds of chemlali extra-virgin olive oils. *Acta. Physiol Plant.* **2013**, *35*, 2801−2812.
(5) Ben Temime, S.; Baccouri, B.; Taamalli, W.; Abaza, L.; Daoud, D.; Zarrouk, M. Location effects on Chetoui virgin olive oil stability. *J. Food Biochem.* **2006**, *30*, 659−670.
(6) Baccouri, O.; Bendinib, A.; Cerretanib, L.; Guerfel, M.; Baccouri, B.; Lercker, G.; Zarrouk, M.; Daoud-Ben Miled, D. Comparative study on volatile compounds from Tunisian and Sicilian monovarietal virgin olive oils. *Food Chem.* **2008**, *111*, 322−328.
(7) Cunha, S. C.; Amaral, J. S.; Fernandes, J. O.; Oliveira, M. B. P. P. Quantification of tocopherols and tocotrienols in Portuguese olive oils using HPLC with three different detection systems. *J. Agric. Food. Chem.* **2006**, *54*, 3351−3356.
(8) Di Giovacchino, L.; Sestili, S.; Di Vincenzo, D. Influence of olive processing on virgin olive oil quality. *Eur. J. Lipid Sci. Technol.* **2002**, *104*, 587−601.
(9) Kalua, C. M.; Allen, M. S.; Bedgood, D. R.; Bishop, A. G.; Prenzler, P. D.; Robards, K. Olive oil volatile compounds, flavour development and quality: A critical review. *Food Chem.* **2007**, *100*, 273−286.
(10) Manai, H.; Mahjoub-Haddada, F.; Oueslati, I.; Daoud, D.; Zarrouk, M. Characterization of monovarietal virgin olive oils from six crossing varieties. *Sci. Hortic.* **2008**, *115*, 252−260.
(11) Flamini, G. Headspace analyses in valuable and functional foods: Application of SPME in the quality control and characterization of olive oils. *Curr. Anal. Chem.* **2007**, *3*, 149−159.
(12) Brahmi, F.; Dabbou, S.; Flamini, G.; Edziri, H.; Mastouri, M.; Hammami, M. Fatty acid composition and biological activities of volatiles from fruits of two Tunisian olive cultivars. *Int. J. Food Sci. Technol.* **2011**, *46*, 1316−1322.
(13) Angerosa, F. Influence of volatile compounds on virgin olive oil quality evaluated by analytical approaches and sensor panels. *Eur. J. Lipid Sci. Technol.* **2002**, *104*, 639−660.
(14) Korukluoglu, M.; Sahan, Y.; Yigit, A.; Ozer, E. T.; Gücer, S. Antibacterial activity and chemical constitutions of *Olea Europaea* L. leaf extracts. *J. Food Proc. Preserv.* **2010**, *34*, 383−396.
(15) Bouaziz, M.; Sayadi, S. Isolation and evaluation of antioxidants from leaves of a Tunisian cultivar olive tree. *Eur. J. Lipid Sci. Technol.* **2005**, *107*, 497−504.
(16) Bouaziz, M.; Feki, I.; Jemai, H.; Ayadi, M.; Sayadi, S. Effect of storage on refined and husk olive oils composition; stabilization by addition of natural antioxidants from Chemlali olive leaves. *Food Chem.* **2008**, *108*, 253−262.
(17) Paiva-Martins, F.; Correia, R.; Felix, S.; Ferreira, P.; Gordon, M. H. Effects of enrichment of refined olive oil with phenolic compounds from olive leaves. *J. Agric. Food Chem.* **2007**, *55*, 4139−4143.
(18) Di-Giovacchino, L.; Angerosa, F.; Di Giacinto, L. Effect of mixing leaves with olives on organoleptic quality of oil obtained by centrifugation. *J. Am. Oil Chem. Soc.* **1996**, *73*, 371−374.
(19) Boskou, D. *Olive Oil: Chemistry and Technology*; AOCS Press: Champaign, IL, 1996; pp 85−127.
(20) International Olive Council (2010). http://www.internationaloliveoil.org(accessed July 8, 2011).
(21) European Union Commission. Regulation EEC 2568/91 on the characteristics of olive and olive pomace oils and their analytical methods. *Off. J. Eur. Communities* **1991**, *L248*, 0001−0082.
(22) Zhishen, J.; Mengcheng, T.; Jianming, W. The determination of flavonoid contents in mulberry and their scavenging effects on superoxide radicals. *Food Chem.* **1999**, *64*, 555−559.
(23) Mraicha, F.; Ksantini, M.; Zouch, O.; Ayadi, M.; Sayadi, S.; Bouaziz, M. Effect of olive fruit fly infestation on the quality of olive oil from *Chemlali cultivar* during ripening. *Food. Chem Toxicol.* **2010**, *48*, 3235−3241.
(24) Campeol, E.; Flamini, G.; Chericoni, S.; Catalano, S.; Cremonini, R. Volatile compounds from three cultivars of *Olea europea* from Italy. *J. Agric. Food. Chem.* **2001**, *49*, 5409−5411.
(25) Adams, R. P. Identification of Essential Oil Components by Gas Chromatography/Mass Spectroscopy; Allured: Carol Stream, IL, 1995.
(26) Flamini, G.; Cioni, P. L.; Morelli, I. Volatiles from leaves, fruits, and virgin oil from *Olea europaea* C v. *Olivastra seggianese* from Italy. *J. Agric. Food. Chem.* **2003**, *51*, 1382−1386.
(27) Salvador, M. D.; Arand, A. F.; Gomez-Alonso, S.; Fregapane, G. Quality characteristics of Cornicabra virgin olive oil. *Res. Adv. Oil Chem.* **2000**, *1*, 31−39.
(28) International Olive Council, COI/T, 15/NC No. 3 Rev 6. Principe de Ergara, 154, 28002: Madrid, Spain, 2011.
(29) Malheiro, R.; Casal, S.; Teixeira, H.; Bento, A.; Pereira, J. A. Effect of olive leaves addition during the extraction process of overmature fruits on olive oil quality. *Food Bioprocess Technol.* **2013**, *6*, 509−521.
(30) Haddada, F. M.; Krichène, D.; Manai, H.; Oueslati, I.; Daoud, D.; Zarrouk, M. Analytical evaluation of six monovarietal virgin olive oils from Northern Tunisia. *Eur. J. Lipid Sci. Technol.* **2008**, *110*, 905−913.
(31) European Union Commission Regulation EEC No 1169/2011 on the characteristics of olive and olive pomace oils and their analytical methods. *Off. J. Eur. Communities* **2011**, *3*, 18−63.
(32) Allalout, A.; Krichéne, D.; Methenni, K.; Taamalli, A.; Oueslati, I.; Daoud, D.; Zarrouk, M. Characterization of virgin olive oil from super intensive Spanish and Greek varieties grown in northern Tunisia. *Sci. Hortic.* **2009**, *120*, 77−83.
(33) Issaoui, M.; Dabbou, S.; Echbili, A.; Rjiba, I.; Gazzah, N.; Trigui, A.; Hammami, M. Biochemical characterisation of some Tunisian virgin olive oils obtained from different cultivars growing in Sfax National Collection. *J. Food, Agri. Environ.* **2007**, *5*, 17−21.
(34) Oueslati, I.; Anniva, C.; Daoud, D.; Tsimidou, M. Z.; Zarrouk, M. Virgin olive oil (VOO) production in Tunisia: The commercial potential of the major olive varieties from the arid Tataouine zone. *Food Chem.* **2009**, *112*, 733−741.
(35) Chtourou, M.; Gargouri, B.; Jaber, H.; Abdelhedi, R.; Bouaziz, M. Comparative study of olive oil quality from Chemlali Sfax versus Arbequina cultivated in Tunisia. *Eur. J. Lipid Sci. Technol.* **2013**, *115*, 631−640.
(36) Dabbou, S.; Selvaggini, R.; Urbani, S.; Taticchi, A.; Servili, M.; Hammami, M. Comparison of the chemical composition and the organoleptic profile of virgin olive oil from two wild and two cultivated Tunisian Olea europaea. *Chem. Biodiv.* **2011**, *8*, 189−202.
(37) Ouni, Y.; Flamini, G.; Guerfel, M.; Ben Youssef, N.; Daoud-Ben Miled, D.; Zarrouk, M. The compositional quality and volatile compounds of samples from the blend of monovarietal olive oils cultivated in Tunisia. *Int. J. Food Sci. Technol.* **2011a**, *46*, 678−686.
(38) Ouni, Y.; Flamini, G.; Issaoui, M.; Ben Youssef, N.; Pier Luigi, C.; Hammami, M.; Daoud, D.; Zarrouk, M. Volatile compounds and compositional quality of virgin olive oil from Oueslati variety: Influence of geographical origin. *Food Chem.* **2011b**, *124*, 1770−1776.
(39) Dabbou, S.; Issaoui, M.; Esposto, S.; Sifi, S.; Taticchi, A.; Servili, M.; Montedoro, G. F.; Hammemi, M. Cultivar and growing area effects on minor compounds of olive oil from autochthonous and European introduced cultivars in Tunisia. *J. Sci. Food Agric.* **2009**, *89*, 1314−1325.
(40) Cavalli, J. F.; Fernandez, X.; Lizzani-Cuvelier, L.; Loiseau, A. M. haracterization of volatile compounds of French and Spanish virgin olive oils by HS-SPME: Identification of quality-freshness markers. *Food Chem.* **2004**, *88*, 151−157.
(41) Luna, G.; Morales, M. T.; Aparicio, R. Characterisation of 39 varietal virgin olive oils by their volatile compositions. *Food Chem.* **2006**, *98*, 243−252.
(42) Brkic Bubola, K.; Koprivnjak, O.; Sladonja, B. Influence of filtration on volatile compounds and sensory profile of virgin olive oils. *Food Chem.* **2012**, *132*, 98−103.
(43) Reboredo-Rodríguez, P.; González-Barreiro, C.; Cancho-Grande, B.; Simal-Gándara, J. Dynamic headspace/GC−MS to control

the aroma fingerprint of extra-virgin olive oil from the same and different olive varieties. *Food Control* **2012**, *25*, 684−695.
(44) Ouni, Y.; Guerfel, M.; Abdelly, C.; Salma Nayet, M.; Zarrouk, M.; Flamini, G. Changes in volatile compounds and oil quality with alaxation time of Tunisian cultivars of *Olea europea*. *Int. J. Food Sci Technol.* **2013**, *48*, 74−81.
(45) Vichi, S.; Pizzale, L.; Conte, L. S.; Buxaderas, S.; López-Tamames, E. Solid phase microextraction in the analysis of virgin olive oil volatiles fraction: Characterization of virgin olive oils from two distinct geographical areas of northern Italy. *J. Agric. Food Chem.* **2003**, *51*, 6572−6577.
(46) Cecchi, T.; Alfei, B. Volatile profiles of Italian monovarietal extra virgin olive oils via HS-SPME-GC-MS: Newly identified compounds, flavors molecular markers, and terpenic profile. *Food Chem.* **2013**, *141*, 2025−2035.
(47) Reboredo-Rodríguez, P.; González-Barreiro, C.; Cancho-Grande, B.; Simal-Gándara, J. Concentrations of aroma compounds and odor activity values of odorant series in different olive cultivars and their oils. *J. Agric. Food Chem.* **2013**, *61*, 5252−5259.

JOURNAL OF AGRICULTURAL AND FOOD CHEMISTRY

Article

pubs.acs.org/JAFC

Characterization and Thermal Isomerization of (*all-E*)-Lycopene

Munenori Takehara,*[,†] Masatoshi Nishimura,[†] Takahiro Kuwa,[†] Yoshinori Inoue,[†] Chitoshi Kitamura,[†] Tsutomu Kumagai,[†] and Masaki Honda[‡]

[†]Department of Materials Science, The University of Shiga Prefecture, Hassaka, Hikone 522-8533, Japan

[‡]Research Institute, Kagome Company, Limited, Nishitomiyama, Nasushiobara 329-2762, Japan

ABSTRACT: A large amount of (*all-E*)-lycopene was successfully purified from tomato paste using an improved method that included a procedure to wash crystalline powder with acetone. The total yield of the pure (*all-E*) form was at least 30%. The melting point of (*all-E*)-lycopene was determined to be 176.35 °C by differential scanning calorimetry (DSC) measurements. Bathochromic shifts were observed in the absorption maxima of all solvents tested (at most a 36 nm shift for λ_2 in carbon disulfide, as was observed in hexane) and were accompanied by absorbance decreases, namely, a hypochromic effect, showing a higher correlation between the position and the intensity of the main absorption bands. This bathochromic shift was dependent upon the polarizability of the solvent rather than its polarity. The structure of (*all-E*)-lycopene in $CDCl_3$ and C_6D_6 was identified on the basis of one- and two-dimensional nuclear magnetic resonance (NMR) spectra, including ^1H and ^{13}C NMR, homonuclear correlation spectroscopy ($^1H-^1H$ COSY), heteronuclear multiple-quantum coherence (HMQC), and heteronuclear multiple-bond connectivity (HMBC). The rate constants of the decrease in (*all-E*)-lycopene with hexane and benzene were calculated to be 3.19×10^{-5} and 3.55×10^{-5} s^{-1}, respectively. The equilibrium constants between (*all-E*) and (13*Z*) isomers were estimated to be 0.29 in hexane and 0.31 in benzene, respectively, from the point at which the amount of (13*Z*)-lycopene reached its maximum.

KEYWORDS: *lycopene, purification, tomatoes, spectrum analysis, thermal isomerization, density functional theory*

INTRODUCTION

Lycopene is a well-known carotenoid found abundantly in vegetables and fruits with a red color, such as tomatoes, red carrots,[1] watermelons, and gac (*Momordica cochinchinensis*),[2] as well as in microorganisms, such as *Dunaliella salina*,[3] *Chlorella* spp.,[4,5] and *Blakeslea trispora*.[6,7] Lycopene, like other carotenoids, is responsible for the characteristic bright color of these organisms and plays a protective role against oxidative stress.[8−10] The natural benefits of lycopene have been applied not only to food and dietary supplements as edible colorants and antioxidants but also to medical approaches to cancer and arteriosclerosis prevention,[11−13] taking advantage of its physiological properties and biocompatibility. These useful functions of lycopene, the molecular formula of which is $C_{40}H_{56}$, have been attributed to its chemical structure containing many unsaturated bonds, in which 11 double bonds are conjugated (Figure 1), and more effectively allow for the absorption of relatively long-wavelength light and quench singlet oxygen. Therefore, many researchers have studied this useful pigment and published excellent reports from the middle of the 20th century.[14−19] However, these studies were performed with lycopenes prepared from different origins and with different purification degrees, which may lead to a misunderstanding because of different values for basic physicochemical properties.

Although most of the lycopenes are known to be present in the (*all-E*) configuration in tomatoes and other vegetables, 71 kinds of (*Z*) isomers are theoretically possible.[20] However, bioavailability of the (*Z*) isomers of lycopene by lymph-cannulated ferrets[21] and a human intestinal cell model[22] was shown to be significantly greater than that of the (*all-E*) isomer. Therefore, an efficient method to improve the isomerization of (*all-E*) to the (*Z*) configuration is desired, with isomerization kinetics only being investigated in unpurified mixtures.[23,24]

Under these circumstances, we performed an extraction of (*all-E*)-lycopene with higher purity from a tomato paste and determined its physical and chemical properties, including some spectrophotometric measurements. The isomerization of lycopene by a heating apparatus was also investigated by chromatography. The results of our study give new criteria for the identification of lycopene and contribute to the fundamental chemistry of this carotenoid in the food science and technology field.

MATERIALS AND METHODS

Reagents. All reagents and solvents used were analytical-grade, except for methanol, which was high-performance liquid chromatography (HPLC)-grade (Sigma-Aldrich, St. Louis, MO), and were used without any further purification.

Extraction and Purification of (*all-E*)-Lycopene. All procedures were performed at room temperature, unless otherwise indicated. A total of 500 mL of dichloromethane was added to 50 g of tomato paste (Kagome Co., Ltd., Tokyo, Japan; lycopene content, 8−12 g/kg) in an Erlenmeyer flask, and the mixture was stirred for 60 min in darkness. The organic layer was separated with a separatory funnel, and repetitive extraction was performed on the resulting suspension by the same volume of dichloromethane. The solvent was evaporated on a rotary evaporator under a vacuum (170 mmHg) at 25 °C for 30 min. The crude extract (345 mg) containing lycopene was dissolved in 15

Received: October 6, 2013
Revised: December 17, 2013
Accepted: December 19, 2013
Published: December 19, 2013

ACS Publications © 2013 American Chemical Society

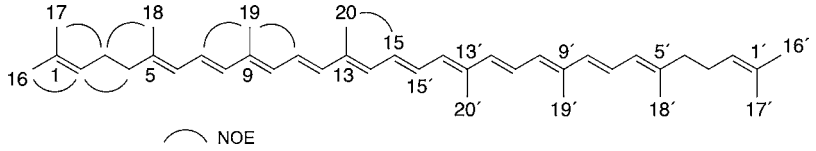

Figure 1. Chemical structure of (*all-E*)-lycopene. The nuclear Overhauser effect (NOE) correlations observed in the two-dimensional NMR measurements are shown as curved lines in one half side of the symmetrical structure of the lycopene.

Table 1. Absorption Maxima and Molar Extinction Coefficients of (*all-E*)-Lycopene from Tomato[a]

solvent	λ_1		λ_2		λ_3		λ_{max} calcd[b]
methanol	444.0	*c*	469.5	*c*	501.5	*c*	486.5
hexane	444.0	(118)	471.0	(182)	502.5	(168)	470.5
hexane/chloroform (98:2)[d]	443	(123)	470	(187)	502	(172)	*c*
MTBE[e]	445.5	(120)	472.0	(180)	503.5	(164)	*c*
ethanol	446.0	*c*	472.5	*c*	504.0	*c*	473.0
acetonitrile	446.0	*c*	472.5	*c*	504.0	*c*	*c*
acetone	447.0	(118)	474.0	(178)	505.5	(162)	*c*
ethyl acetate	447.5	(118)	474.0	(179)	506.0	(162)	*c*
cyclohexane	448.5	(116)	476.0	(177)	508.5	(159)	478.0
tetrahydrofuran	452.0	(114)	479.0	(173)	512.0	(153)	*c*
dichloromethane	455.0	(113)	482.5	(170)	515.5	(150)	*c*
chloroform	456.5	(110)	484.5	(164)	518.0	(143)	483.5
toluene	456.5	(110)	485.0	(165)	519.5	(144)	*c*
benzene	457.5	(110)	485.5	(164)	520.0	(144)	487.5
anisole	460.5	(104)	489.0	(157)	524.5	(137)	*c*
dimethyl phthalate	461.5	*c*	489.5	*c*	525.0	*c*	*c*
pyridine	462.5	(104)	490.5	(155)	526.0	(137)	490.0
benzonitrile	463.5	(101)	491.5	(150)	527.0	(132)	*c*
N,*N*-dimethylaniline	464.0	(102)	492.5	(148)	529.0	(130)	*c*
carbon disulfide	478.0	(89)	507.0	(133)	544.5	(123)	505.5

[a] λ_{1-3} in nm; values in parentheses, $\varepsilon \times 10^{-3}$. [b] Calculated according to the literature.[32−34] [c] Not determined. [d] Synthetic (*all-E*)-lycopene.[38] [e] Methyl *tert*-butyl ether, containing 0.1% dichloromethane.

mL of benzene at 60 °C within 10 min and recrystallized at 4 °C for 4 h under shading. The resulting crystals were collected by suction filtration on a Kiriyama funnel (number 5B filter paper), rinsed with 100 mL of acetone, and dried *in vacuo*: 188 mg of fine red crystalline powder, with a melting point (mp) of 176.35 °C [differential scanning calorimetry (DSC)]; HPLC, ≥99.3%; ultraviolet/visible (UV/vis), Table 1; infrared (IR) (KBr), Table 2; nuclear magnetic resonance (NMR), Table 3; high-resolution mass spectrometry−fast atom bombardment (HRMS−FAB) (*m*/*z*) [M + H] $^+$ calcd for $C_{40}H_{57}$, 537.4460; found, 537.4418.

Thermal Isomerization of Lycopene. Purified (*all-E*)-lycopene dissolved in 100 mL of organic solvent (hexane, 9.76 μM; benzene, 198 μM) was transferred into a three-neck flask equipped with a mechanical stirrer, a reflux condenser, and a gas inlet tube. The isomerization of lycopene was conducted at 50 °C with an oil bath in darkness under an argon stream. The reaction mixtures were sampled at intervals, and the contents of the lycopene isomers were analyzed by reversed-phase HPLC. The recoveries of the total lycopene isomers with hexane and benzene during the sampling periods were estimated to be 87.5 and 61.9%, respectively, by the HPLC method.

Table 2. IR Absorption Bands of (*all-E*)-Lycopene Extracted and Purified from Tomato Paste and Their Calculated Values

	frequency (cm^{-1})	
origin	found	calcd
C−H stretch, alkene	3038, 3020 m	3072−3055, 3033−3007 m
C−H stretch, methylene/methyl	2968, 2912, 2854 s	2981−2962, 2926−2894, 2894 m to s
C═C stretch	1627, 1552 w	1636, 1558 m
C−H deformation, methylene/methyl	1441 m	1460−1444 m
C−H deformation, methyl	1391, 1364 m	1399−1375, 1364−1350 m
C−H out-of-plane, (*E*) disubstituted double bond	960 s	976−946 s

UV−Vis, Fourier Transform Infrared (FTIR), Mass, and NMR Spectroscopic Analyses. UV−vis spectra of the purified lycopene were measured in organic solvents over a scanning range of 200−600 nm, and the λ maxima of the compounds were determined. Spectra were recorded with a Hitachi U-2910 spectrophotometer (Tokyo, Japan).

IR spectra were obtained by JASCO FT/IR 4100 (Tokyo) using the KBr disc in the range of 4000−400 cm^{-1}.

The HRMS of (*all-E*)-lycopene was recorded in the positive-ion mode by FAB+ on a JEOL JMS-700T instrument (Tokyo), using 3-nitrobenzyl alcohol as the matrix.

NMR spectra of (*all-E*)-lycopene were recorded using a JEOL JMN-LA400 FT 400 NMR spectrometer at 400 MHz (^{1}H) and 100 MHz (^{13}C). Chemical shifts were recorded as the δ value (ppm) using tetramethylsilane (TMS) as an internal standard. Spectra were observed on $CDCl_3$ and benzene-d_6 (C_6D_6).

DSC. The melting point of purified (*all-E*)-lycopene was determined by DSC using a DSC-60A system (Shimadzu, Kyoto, Japan). DSC measurements were performed with aluminum sample pans and empty reference pans. Both the sample and reference were scanned at a heating rate of 5 K/min from 303 to 473 K under a nitrogen atmosphere with a flow rate of 50 mL/min. The mass of the sample was 7 mg. All measurements were performed in triplicate.

dx.doi.org/10.1021/jf404497k | J. Agric. Food Chem. 2014, 62, 264−269

Table 3. Refinement of ^{1}H and ^{13}C NMR Assignments of (*all-E*)-Lycopene from Tomato[a]

proton	*d* in ppm (multiplicity, coupling constant in Hz)		carbon	*d* in ppm	
	in $CDCl_3$ [synthetic lycopene][38]	in C_6D_6		in $CDCl_3$ [synthetic]	in C_6D_6
			C(1), C(1′)	131.72 [131.64]	131.58
H−C(2), H−C(2′)	5.11 (m) [5.11]	5.23 (m)	C(2), C(2′)	123.96 [124.12]	124.50
2H−C(3), 2H−C(3′)	2.11 (m) [ca. 2.11]	2.18 (m)	C(3), C(3′)	26.70 [26.83]	27.10
2H−C(4), 2H−C(4′)	2.11 (m) [ca. 2.11]	2.18 (m)	C(4), C(4′)	40.23 [40.30]	40.62
			C(5), C(5′)	139.47 [139.30]	138.95
H−C(6), H−C(6′)	5.95 (d, *J* = 11.0) [5.95]	6.16 (d, *J* = 11.0)	C(6), C(6′)	125.74 [125.94]	126.77
H−C(7), H−C(7′)	6.49 (dd, *J* = 11.0, 15.0) [6.49]	6.67 (dd, *J* = 11.0, 15.1)	C(7), C(7′)	124.79 [124.87]	125.31
H−C(8), H−C(8′)	6.25 (d, *J* = 15.0) [6.25]	6.44 (d, *J* = 15.1)	C(8), C(8′)	135.40 [135.54]	136.17
			C(9), C(9′)	136.15 [136.15]	136.37
H−C(10), H−C(10′)	6.18 (d, *J* = 11.4) [6.18]	6.36 (d, *J* = 11.6)	C(10), C(10′)	131.55 [131.64]	132.39
H−C(11), H−C(11′)	6.64 (dd, *J* = 11.4, 14.9) [6.64]	6.77 (dd, *J* = 11.6, 15.0)	C(11), C(11′)	125.15 [125.21]	125.66
H−C(12), H−C(12′)	6.35 (d, *J* = 14.9) [6.35]	6.49 (d, *J* = 15.0)	C(12), C(12′)	137.35 [137.46]	138.00
			C(13), C(13′)	136.56 [136.54]	136.83
H−C(14), H−C(14′)	6.24 (m) [6.25]	6.34 (AA′ of AA′BB′ system)	C(14), C(14′)	132.64 [132.71]	133.39
H−C(15), H−C(15′)	6.62 (m) [6.62]	6.70 (BB′ of AA′BB′ system)	C(15), C(15′)	130.07 [130.17]	130.70
3H−C(16), 3H−C(16′)	1.687 (s) [1.688]	1.674 (s)	C(16), C(16′)	25.68 [25.66]	25.84
3H−C(17), 3H−C(17′)	1.614 (s) [1.612]	1.568 (s)	C(17), C(17′)	17.70 [17.70]	17.73
3H−C(18), 3H−C(18′)	1.818 (s) [1.818]	1.749 (s)	C(18), C(18′)	16.99 [16.97]	16.90
3H−C(19), 3H−C(19′)	1.968 (s) [1.968]	1.925 (s)	C(19), C(19′)	12.90 [12.90]	12.98
3H−C(20), 3H−C(20′)	1.968 (s) [1.968]	1.876 (s)	C(20), C(20′)	12.79 [12.81]	12.86

[a] ^{1}H and ^{13}C NMR were recorded at 400 and 100 MHz, respectively. s, singlet; d, doublet; dd, doublet of doublets; and m, multiplet.

HPLC Analysis. Reversed-phase HPLC analysis with a photodiode array detector (SPD-M10AVP, Shimadzu, Kyoto, Japan) was performed under the following conditions: column, YMC Carotenoid (250 × 4.6 mm inner diameter, 5 μm particles, YMC, Kyoto, Japan); solvent A, methanol/methyl *tert*-butyl ether (MTBE)/ H_2O (75:15:10, v/v/v); solvent B, methanol/MTBE/H_2O (7:90:3, v/v/v); gradient, started with 100% eluent A and ended with 100% eluent B over a period of 35 min; flow rate, 3.0 mL/min; and column temperature, 22 °C. A typical chromatogram of the lycopene isomers was obtained with a retention time and absorption maxima at (13*Z*)-lycopene [24.6 min; 440.0, 465.0, and 496.5 nm; and (*Z*) peak[25] at 361 nm with a relative intensity of 59.2% D_B/D_{II}], (9*Z*)-lycopene [27.6 min; 441.0, 467.0, and 497.5 nm; and (*Z*) peak at 361 nm with 13.7% D_B/D_{II}], (*all-E*)-lycopene (31.9 min; 445.0, 472.5, and 503.5 nm); and (5*Z*)-lycopene (32.6 min; 445.0, 472.0, and 503.5 nm). The quantification of all lycopenes was performed by peak area integration at 470 nm, showing a reliable approximation for the analysis of isomers.[26,27]

Computational Analysis. *Ab initio* and density functional theory (DFT) calculations on the infrared spectrum of (*all-E*)-lycopene were performed with Gaussian 03 software using the B3LYP functional and 6-31G(*d*) basis set.

RESULTS AND DISCUSSION

Physical Properties of (*all-E*)-Lycopene. In this study, a large amount of (*all-E*)-lycopene was successfully purified from tomato samples without laborious chromatographic procedures.[28,29] This improved method included a procedure to wash crystalline powder with acetone, in which the solubility of (*all-E*)-lycopene was low (ca. 0.75 mg/mL).[30] The total yield of the pure (*all-E*) form (purity ≥ 99.3% by HPLC) was at least 30% when the lycopene content of the tomato paste was considered. The DSC curve for the purified lycopene showed two possible melting points of 170.66 and 176.35 °C. The lower value may be attributed to the (*Z*)-lycopenes, which arose from the (*all-E*) form because of the heating process. The content of the (*all-E*) form was reduced to 61.6% by reversed-phase HPLC for

dx.doi.org/10.1021/jf404497k | J. Agric. Food Chem. 2014, 62, 264−269

lycopene samples after the DSC measurement. The melting point of (*all-E*)-lycopene was then determined to be 176.35 °C, which was consistent with the value obtained by Manchand et al.[18]

Lycopene has an electron spectrum characterized by 11 conjugated double bonds, which geometrically impose a linear and highly planar structure. In hexane, (*all-E*)-lycopene showed strong absorption maxima at 502.5, 471.0, and 444.0 nm with molar extinction coefficients estimated as 168×10^3, 182×10^3, and 118×10^3 (Table 1), corresponding to vibrational transition energies of 0−0, 0−1, and 0−2, respectively. The peak at approximately 360 nm, the so-called (*Z*) peak,[25,31] was not observed in this sample.

Furthermore, absorption maxima and molar extinction coefficients with (*all-E*)-lycopene were measured in various organic solvents to investigate the solvent effect on the electronic spectrum of the molecule (Table 1). All values for the maxima (λ_2) of the fine structure in this study were also consistent with the calculated values according to an empirical rule.[32−34] The values (λ_1, λ_2, and λ_3) listed in this table were plotted as a function of wavelength in Figure 2A. From these

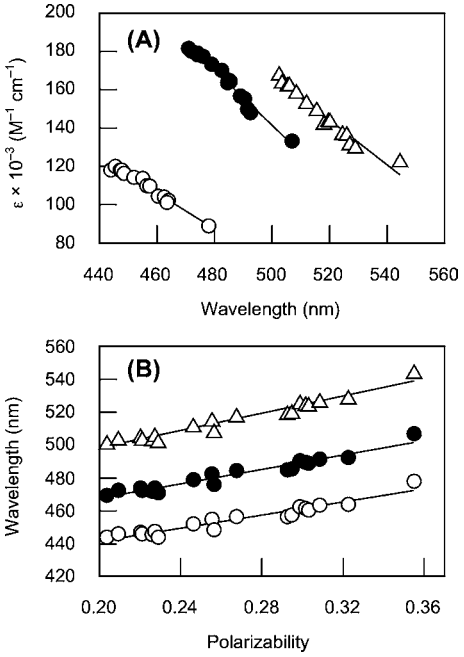

Figure 2. Relationships (A) between the absorption maxima and molar extinction coefficients of (*all-E*)-lycopene in various solvents and (B) between the polarizabilities of the solvents and the absorption maxima. The values of (○) λ_1, (●) λ_2, and (△) λ_3 are from Table 1. Polarizability of the solvent is calculated as follows: $(n^2 - 1)/(n^2 + 2)$, where *n* is the refractive index of the solvent.[39]

results, bathochromic shifts in the absorption maxima were observed in all solvents tested (at most a 36 nm shift for λ_2 in carbon disulfide, as was observed in hexane) and were accompanied by absorbance decreases, namely, a hypochromic effect, showing a higher correlation between the position and the intensity of the main absorption bands. Although many studies suggested that the bathochromic shift had been independently reported previously,[35,36] the highly purified (*all-E*)-lycopene had first enabled a discussion of the solvent effect on this carotenoid. This bathochromic shift depends upon the polarizability of the solvent because of high correlation between them (Figure 2B)[37] rather than its polarity (data not shown). This is the first report showing the solvent effect on the electron spectra of (*all-E*)-lycopene, because this was difficult to evaluate before as a result of samples having different purification grades with different origins. This finding contributes to the fundamental chemistry of carotenoids and will be a new criterion for the identification and evaluation of lycopene in agriculture, food, and medical fields.

The IR spectrum of (*all-E*)-lycopene was measured, and characteristic absorptions were shown in Table 2, along with those calculated by the Gaussian program. Observed and calculated values from C−H and C═C stretches and C−H out-of-plane attributed to the alkene as well as other origins were consistent with each other. This computational estimation with high fidelity may depend upon the restriction of the molecular motion of lycopene caused by the 11 conjugated double bonds. Therefore, these observations will facilitate an evaluation of the relative free energy of (*Z*) isomer lycopenes, which may be contained in foods or originate from heat-induced isomerization.

NMR Assignment of (*all-E*)-Lycopene. The structure of (*all-E*)-lycopene has been identified on the basis of one- and two-dimensional NMR spectra, including ^{1}H and ^{13}C NMR, homonuclear correlation spectroscopy (^{1}H−^{1}H COSY), heteronuclear multiple-quantum coherence (HMQC), and heteronuclear multiple-bond connectivity (HMBC). Chemical shifts for proton and carbon signals of the (*all-E*)-lycopene in this work were good accordance with those of the synthetic (*all-E*)-lycopene[38] (Table 3). Spectral data on (*all-E*)-lycopene in $CDCl_3$ were also independently reported by different literature;[40−42] however, some values reported were not consistent among the previous studies, e.g., for the coupling constants of protons H−C(11), H−C(11′) and the chemical-shift value of carbon atoms C(14), C(14′). In our study with thoroughly purified lycopene, the coupling constant values between H−C(11), H−C(11′) and H−C(10), H−C(10′) and between H−C(11), H−C(11′) and H−C(12), H−C(12′) were measured as 11.4 and 14.9 Hz, respectively. The chemical shift for C(14), C(14′) could be assigned to the signal observed at 132.64 ppm by the HMQC experiment, and refinement of the NMR signal assignment of (*all-E*)-lycopene was then achieved in $CDCl_3$.

Measurements were subsequently performed in another solvent, C_6D_6, in expectation of NMR signal charts distinct from those obtained in $CDCl_3$ because of differences in their physical properties, such as polarity, resonance, and viscosity. Proton and ^{13}C signals in C_6D_6 were preliminarily assigned by the results obtained in $CDCl_3$ and ascertained by ^{1}H homonuclear decoupling and the nuclear Overhauser effect difference (NOE-dif) experiments in addition to the above two-dimensional measurements. As shown in Table 3, chemical shifts in methyl protons between H−C(19), H−C(19′) and H−C(20), H−C(20′) were discriminated in C_6D_6 at 1.925 and 1.876 ppm, respectively (Table 3), whereas these signals appeared as a singlet at 1.968 ppm in $CDCl_3$ (this study and refs 40 and 41). Furthermore, the coupling system between H−C(14), H−C(14′) and H−C(15), H−C(15′) could be analyzed in C_6D_6, whereas their corresponding signals in $CDCl_3$ overlapped with H−C(8), H−C(8′) and H−C(11), H−C(11′), respectively, and were assigned to a multiplet. The observed spin signal occurred in the AA′BB′-type system, to which similar coupling was assigned in some carotenoids, such as prolycopene and (9*Z*,9′*Z*)-7,8,7′,8′-tetrahydrolycopene,[38,43]

dx.doi.org/10.1021/jf404497k | J. Agric. Food Chem. 2014, 62, 264−269

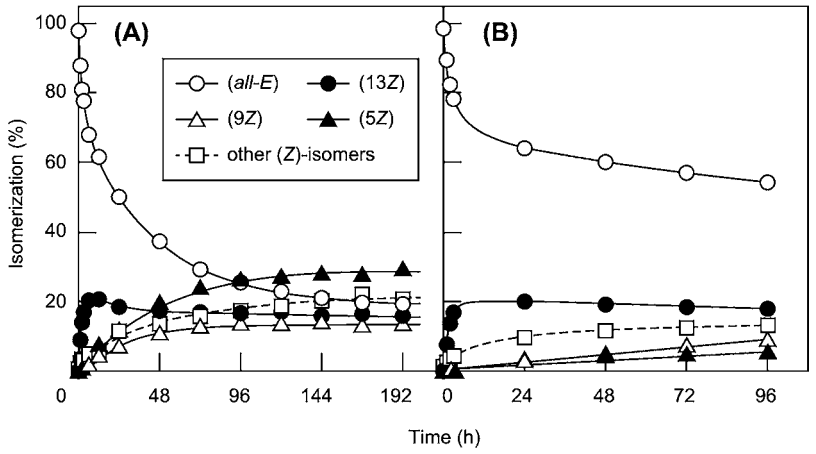

Figure 3. Isomerization of (*all-E*)-lycopene to (*Z*) isomers in (A) hexane and (B) benzene at 50 °C. Changes in the content percentage of (○) (*all-E*)-, (●) (13*Z*)-, (△) (9*Z*)-, and (▲) (5*Z*)-lycopene, as well as the other (*Z*) isomers (□), are presented with regard to the total amount of lycopenes resulting at each point of sampling.

and the full assignment of ^{1}H and ^{13}C signals was then given in Table 3. The unambiguous determination attained in this study will also help to analyze the (*Z*) isomers occurring in natural sources and those generated from the isomerization of (*all-E*)-lycopene by a heating process.

Thermal Isomerization of (*all-E*)-Lycopene. The isomerization of (*all-E*)-lycopene to (*Z*) isomers was investigated in hexane and benzene at 50 °C. The contents of (*all-E*)-lycopene rapidly decreased within a few hours in both solvents at this temperature and reached less than 20% for hexane and 55% for benzene during the test periods (Figure 3). Corresponding to the decrease in (*all-E*)-lycopene, (13*Z*)-lycopene emerged as the first (*Z*) isomer observed, and the content of the isomer gradually decreased after reaching its maximum of ca. 20% at 10 h. These decreases reflect the regeneration of (*all-E*)-lycopene and subsequent isomerization to other (*Z*) forms. The generation rates for (9*Z*) and (5*Z*) isomers were different in both solvents, and this may have led to the selective enrichment of a desirable isomer by taking advantage of the solvent effect.

The rate constants for the isomerization of lycopenes were then investigated on approximation to the one-order reaction.[44,45] The rate constants of the decrease in (*all-E*)-lycopene with hexane and benzene were calculated as 3.19×10^{-5} and 3.55×10^{-5} s^{-1}, respectively. It is necessary to evaluate the main kinetic parameters of lycopene isomerization in such a complex system that several equilibrium states can coexist. At the very early stage of these reactions, the reaction rate for the formation of (13*Z*)-lycopene overcome that of other isomers, which indicated that the reduction rate of (*all-E*)-lycopene could be approximate to the production rate of (13*Z*) isomer. The values obtained with lycopene were shown to be greater than those of the corresponding (13*Z*)-*β*-carotene and its derivative at 64 °C, apart from (15*Z*)-lycopene, which could not be observed in our or other studies.[44] According to the above approximation, the equilibrium constants between (*all-E*) and (13*Z*) isomers were estimated to be 0.29 in hexane and 0.31 in benzene, respectively, from the point at which the amount of (13*Z*)-lycopene reached its maximum.

Fundamental data for (*all-E*)-lycopene were obtained in the present study using an extremely purified extract from tomato paste, which provided a new insight into the spectroscopic and geometrical properties of lycopene. Moreover, the obtained thermal information of (*E*–*Z*) isomerization will contribute not only to the efficient production of (*Z*)-lycopenes that may give many benefits to human wellness but also to the identification of chemical and physical properties of the (*Z*) isomers.

AUTHOR INFORMATION

Corresponding Author

*Telephone: +81-749-28-8373. Fax: +81-749-28-8515. E-mail: takehara@mat.usp.ac.jp.

Notes

The authors declare no competing financial interest.

ACKNOWLEDGMENTS

We thank Toshio Morita, technical staff of the Department of Applied Chemistry and Biotechnology, University of Fukui, Fukui, Fukui Prefecture, Japan, for HRMS measurements.

REFERENCES

(1) Horvitz, M. A.; Simon, P. W.; Tanumihardjo, S. A. Lycopene and *β*-carotene are bioavailable from lycopene 'red' carrots in humans. *Eur. J. Clin. Nutr.* **2004**, *58*, 803–811.

(2) Aoki, H.; Kieu, N. T.; Kuze, N.; Tomisaka, K.; Van Chuyen, N. Carotenoid pigments in GAC fruit (*Momordica cochinchinensis* SPRENG). *Biosci., Biotechnol., Biochem.* **2002**, *66*, 2479–2482.

(3) Orset, S. C.; Young, A. J. Exposure to low irradiances favors the synthesis of 9-*cis* *β*,*β*-carotene in *Dunaliella salina* (Teod.). *Plant Physiol.* **2000**, *122*, 609–618.

(4) Ishikawa, E.; Abe, H. Lycopene accumulation and cyclic carotenoid deficiency in heterotrophic *Chlorella* treated with nicotine. *J. Ind. Microbiol. Biotechnol.* **2004**, *31*, 585–589.

(5) Renju, G. L.; Muraleedhara Kurup, G.; Saritha Kumari, C. H. Anti-inflammatory activity of lycopene isolated from *Chlorella marina* on type II collagen induced arthritis in Sprague Dawley rats. *Immunopharmacol. Immunotoxicol.* **2013**, *35*, 282–291.

(6) Estrella, A.; López-Ortiz, J. F.; Cabri, W.; Rodríguez-Otero, C.; Fraile, N.; Erbes, A. J.; Espartero, J. L.; Carmona-Cuenca, I.; Chaves, E.; Muñoz-Ruiz, A. Natural lycopene from *Blakeslea trispora*: *all-trans* lycopene themochemical and structural properties. *Thermochim. Acta* **2004**, *417*, 157–161.

(7) López-Nieto, M. J.; Costa, J.; Peiro, E.; Méndez, E.; Rodríguez-Sáiz, M.; de la Fuente, J. L.; Cabri, W.; Barredo, J. L. Biotechnological lycopene production by mated fermentation of *Blakeslea trispora*. *Appl. Microbiol. Biotechnol.* **2004**, *66*, 153–159.

(8) Di Mascio, P.; Kaiser, S.; Sies, H. Lycopene as the most efficient biological carotenoid singlet oxygen quencher. *Arch. Biochem. Biophys.* **1989**, *274*, 532–538.

(9) Stahl, W.; Sies, H. Antioxidant activity of carotenoids. *Mol. Aspects Med.* **2003**, *24*, 345−351.
(10) Cantrell, A.; McGarvey, D. J.; Truscott, T. G.; Rancan, F.; Böhm, F. Singlet oxygen quenching by dietary carotenoids in a model membrane environment. *Arch. Biochem. Biophys.* **2003**, *412*, 47−54.
(11) Dahan, K.; Fennal, M.; Kumar, N. B. Lycopene in the prevention of prostate cancer. *J. Soc. Integr. Oncol.* **2008**, *6*, 29−36.
(12) Gann, P. H.; Ma, J.; Giovannucci, E.; Willett, W.; Sacks, F. M.; Hennekens, C. H.; Stampfer, M. J. Lower prostate cancer risk in men with elevated plasma lycopene levels: Results of a prospective analysis. *Cancer Res.* **1999**, *59*, 1225−1230.
(13) Palozza, P.; Parrone, N.; Simone, R. E.; Catalano, A. Lycopene in atherosclerosis prevention: an integrated scheme of the potential mechanisms of action from cell culture studies. *Arch. Biochem. Biophys.* **2010**, *504*, 26−33.
(14) Zechmeister, L.; LeRosen, A. L.; Schroeder, W. A.; Polgár, A.; Pauling, L. Spectral characteristics and configuration of some stereoisomeric carotenoids including prolycopene and pro-γ-carotene. *J. Am. Chem. Soc.* **1943**, *65*, 1940−1951.
(15) Davis, W. B. Preparation of lycopene from tomato paste for use as a spectrophotometric standard. *Anal. Chem.* **1949**, *21*, 1226−1228.
(16) Karrer, P.; Jucker, E. *Carotenoids*; Elsevier: Amsterdam, Netherlands, 1950.
(17) Surmatis, J. D.; Ofner, A. Total synthesis of spirilloxanthin, dehydrolycopene, and 1,1′-dihydroxy-1,2,1′,2′-tetrahydrolycopene. *J. Org. Chem.* **1963**, *28*, 2735−2739.
(18) Manchand, P. S.; Rüegg, R.; Schwieter, U.; Siddons, P. T.; Weedon, B. C. L. Carotenoids and related compounds. Part XI. Syntheses of δ-carotene and ε-carotene. *J. Chem. Soc.* **1965**, 2019−2026.
(19) Davis, B. H. Carotenoid. In *Chemistry and Biochemistry of Plant Pigments*; Goodwin, T. W., Ed.; Academic Press: London, U.K., 1976; pp 38−165.
(20) Zechmeister, L.; LeRosen, A. L.; Went, F. W.; Pauling, L. Prolycopene, a naturally occuring stereoisomer of lycopene. *Proc. Natl. Acad. Sci. U. S. A.* **1941**, *27*, 468−474.
(21) Boileau, A. C.; Merchen, N. R.; Wasson, K.; Atkinson, C. A.; Erdman, J. W., Jr. *cis*-Lycopene is more bioavailable than *trans*-lycopene in vitro and in vivo in lymph-cannulated ferrets. *J. Nutr.* **1999**, *129*, 1176−1181.
(22) Failla, M. L.; Chitchumroonchokchai, C.; Ishida, B. K. In vitro micellarization and intestinal cell uptake of *cis* isomers of lycopene exceed those of *all-trans* lycopene. *J. Nutr.* **2008**, *138*, 482−486.
(23) Moraru, C.; Lee, T. C. Kinetic studies of lycopene isomerization in a tributyrin model system at gastric pH. *J. Agric. Food Chem.* **2005**, *53*, 8997−9004.
(24) Colle, I. J.; Lemmens, L.; Tolesa, G. N.; Van Buggenhout, S.; De Vleeschouwer, K.; Van Loey, A. M.; Hendrickx, M. E. Lycopene degradation and isomerization kinetics during thermal processing of an olive oil/tomato emulsion. *J. Agric. Food Chem.* **2010**, *58*, 12784−12789.
(25) Britton, G. UV/visible spectroscopy. In *Carotenoids*; Britton, G., Liaaen-Jensen, S., Pfander, H., Eds.; Birkhäuser Verlag: Basel, Switzerland, 1995; Vol. *1B*: Spectroscopy, pp 13−62.
(26) Schierle, J.; Bretzel, W.; Bühler, I.; Faccin, N.; Hess, D.; Steiner, K.; Schüep, W. Content and isomeric ratio of lycopene in food and human blood plasma. *Food Chem.* **1997**, *59*, 459−465.
(27) Ishida, B. K.; Ma, J.; Chan, B. A simple, rapid method for HPLC analysis of lycopene isomers. *Phytochem. Anal.* **2001**, *12*, 194−198.
(28) Zhang, J.-P.; Chen, C.-H.; Koyama, Y. Vibrational relaxation and redistribution in the $2Ag^-$ state of *all-trans*-lycopene as revealed by picosecond time-resolved absorption spectroscopy. *J. Phys. Chem. B* **1998**, *102*, 1632−1640.
(29) Choksi, P. M.; Joshi, V. Y. A review on lycopene—Extraction, purification, stability and applications. *Int. J. Food Prop.* **2007**, *10*, 289−298.
(30) Craft, N. E.; Soares, J. H., Jr. Relative solubility, stability, and absorptivity of lutein and β-carotene in organic solvents. *J. Agric. Food Chem.* **1992**, *40*, 431−434.
(31) Zechmeister, L.; Polgár, A. *cis*−*trans* Isomerization and spectral characteristics of carotenoids and some related compounds. *J. Am. Chem. Soc.* **1943**, *65*, 1522−1528.
(32) Hirayama, K. Relation between chemical structure and visible and ultra-violet spectra. I−II. II. Polyenes and alkylated polyenes. *Nippon Kagaku Zassi* **1954**, *75*, 29−35.
(33) Hirayama, K. Relation between chemical structure and visible and ultra-violet spectra. III. Solvents effects on absorption of polyenes. *Nippon Kagaku Zassi* **1954**, *75*, 667−674.
(34) Hirayama, K. Relation between chemical structure and visible and ultra-violet spectra. IV. Effects of substituents and special structures. *Nippon Kagaku Zassi* **1954**, *75*, 674−678.
(35) Naviglio, D.; Pizzolongo, F.; Ferrara, L.; Naviglio, B.; Aragòn, A.; Santini, A. Extraction of pure lycopene from industrial tomato waste in water using the extractor Naviglio. *Afr. J. Food Sci.* **2008**, *2*, 37−44.
(36) Hertzberg, S.; Liaaren-Jensen, S. Bacterial carotenoids: The carotenoids of *Mycobacterium phlei* strain Vera. 2. The structure on the phlei-xanthophylls—two novel tertiary glycoside. *Acta Chem. Scand.* **1967**, *21*, 15−41.
(37) Mimuro, M.; Nagashima, U.; Nagaoka, S.; Nishimura, Y.; Takaichi, S.; Katoh, T.; Yamazaki, I. Quantitative analysis of the solvent effect on the relaxation processes of carotenoids showing dual emissive characteristics. *Chem. Phys. Lett.* **1992**, *191*, 219−224.
(38) Hengartner, U.; Bernhard, K.; Meyer, K.; Englert, G.; Glinz, E. Synthesis, isolation, and NMR-spectroscopic characterization of fourteen (*Z*)-isomers of lycopene and of some acetylenic didehydro- and tetradehydrolycopenes. *Helv. Chim. Acta* **1992**, *75*, 1848−1865.
(39) Budavari, S.; O'Neil, M. J.; Smith, A.; Heckelman, P. E. *The Merck Index*, 13th ed.; Merck: Rahway, NJ, 2001.
(40) Tiziani, S.; Schwartz, S. J.; Vodovotz, Y. Profiling of carotenoids in tomato juice by one- and two-dimensional NMR. *J. Agric. Food Chem.* **2006**, *54*, 6094−6100.
(41) Fröhlich, K.; Conrad, J.; Schmid, A.; Breithaupt, D. E.; Böhm, V. Isolation and structural elucidation of different geometrical isomers of lycopene. *Int. J. Vitam. Nutr. Res.* **2007**, *77*, 369−375.
(42) Kishimoto, S.; Maoka, T.; Sumitomo, K.; Ohmiya, A. Analysis of carotenoid composition in petals of calendula (*Calendula officinalis* L.). *Biosci., Biotechnol., Biochem.* **2005**, *69*, 2122−2128.
(43) Englert, G. NMR spectroscopy. In *Carotenoids*; Britton, G., Liaaen-Jensen, S., Pfander, H., Eds.; Birkhäuser Verlag: Basel, Switzerland, 1995; Vol. *1B*: Spectroscopy, pp 147−260.
(44) Doering, W. v. E.; Sotiriou-Leventis, C.; Roth, W. R. Thermal interconversions among 15-*cis*-, 13-*cis*-, and *all-trans*-β-carotene: Kinetics, Arrhenius parameters, thermochemistry, and potential relevance to anticarcinogenicity of *all-trans*-β-carotene. *J. Am. Chem. Soc.* **1995**, *117*, 2747−2757.
(45) Yuan, J.-P.; Chen, F. Isomerization of *trans*-astaxanthin to *cis*-isomers in organic solvents. *J. Agric. Food Chem.* **1999**, *47*, 3656−3660.

JOURNAL OF AGRICULTURAL AND FOOD CHEMISTRY

Article

pubs.acs.org/JAFC

Characterization and Phylogenetic Analysis of Allergenic Tryp_alpha_amyl Protein Family in Plants

Jing Wang,[†,‡] Litao Yang,[†] Xiaoxiang Zhao,[†,‡] Jing Li,*[,‡] and Dabing Zhang*[,†]

[†]National Center for Molecular Characterization of Genetically Modified Organisms, State Key Laboratory of Hybrid Rice, School of Life Science and Biotechnology, Shanghai Jiao Tong University, 800 Dongchuan Road, Shanghai 200240, People's Republic of China

[‡]Department of Bioinformatics and Biostatistics, School of Life Sciences and Biotechnology, Shanghai Jiao Tong University, Shanghai 200240, People's Republic of China

Supporting Information

ABSTRACT: Most known allergenic proteins in rice (*Oryza sativa*) seed belong to the Tryp_alpha_amyl family (PF00234), but the sequence characterization and the evolution of the allergenic Tryp_alpha_amyl family members in plants have not been fully investigated. In this study, two specific motifs were found besides the common alpha-amylase inhibitors (AAI) domain from the allergenic Tryp_alpha_amyl family members in rice seeds (trRSAs). To understand the evolution and functional importance of the Tryp_alpha_amy1 family and the specific motifs for the allergenic one, a BLAST search identified 75 homologous proteins of trRSAs (trHAs) from 22 plant species including main crops such as rice, maize (*Zea mays*), wheat (*Triticum aestivum*), and sorghum (*Sorghum bicolor*) from all available sequences in the public databases. Statistical analysis showed that the allergenicity of trHAs is closely associated with these two motifs with high number of cysteine residues (p value = 0.00026), and the trHAs with and without the two motifs were clustered into separate clades, respectively. Furthermore, significant difference was observed on the secondary and tertiary structures of allergenic and nonallergenic trHAs. In addition, expression analysis showed that trHA-encoding genes of purple false brome (*Brachypodium distachyon*), barrel medic (*Medicago truncatula*), rice, and sorghum are dominantly expressed in seeds. This work provides insight into the understanding of the properties of allergens in the Tryp_alpha_amyl family and is helpful for allergy therapy.

KEYWORDS: *rice seed allergen, allergenic protein, Tryp_alpha_amyl family, evolution of trHAs, allergen-specific characteristics*

INTRODUCTION

Allergy is a major health problem frequently caused by allergens, which are recognized by the immune system and induce type-I hypersensitivity reaction in atopic individuals.[1] Common allergens in our daily lives are mainly proteins from plants including crops.[2] It has been reported that several proteins in wheat (*Triticum aestivum*), rice (*Oryza sativa*), soybean (*Glycine max*), peanut (*Arachis hypogaea*), and maize (*Zea mays*) can cause allergic responses in susceptible individuals.[3−6] Most of the plant food allergens that have been identified are proteins belonging to a few protein families and superfamilies, among which the Tryp_alpha_amyl family (pfam: PF00234) is the most widespread group, accounting for 16.88% of plant food allergens.[7]

The Tryp_alpha_amyl family includes plant lipid transfer proteins (LTP), seed storage proteins, and trypsin-alpha amylase inhibitors, and they share the alpha-amylase inhibitors (AAI) domain with a similar structure.[8−11] Pru p 3 (*Prunus persica*) and Cor a 8 (*Corylus chinensis*) were shown to be allergenic plant LTPs.[12,13] The structure of 7−9 kDa monomeric LTPs contains a hydrophobic tunnel formed by four disulfide bonds.[14,15] Some of the seed storage proteins such as Ber e 1 (*Bertholletia excelsa*) and Ses i 2 (*Sesamum indicum*) were shown to trigger allergy in hypersensitive patients.[16,17] Typical 2S albumin, a major group of storage proteins of the Tryp_alpha_amyl family, contains four disulfide bonds that link two polypeptide chains, forming a heterodimeric protein complex.[18] Trypsin-alpha amylase inhibitors such as Hor v 15 and Sec c 1 from barley (*Hordeum vulgare*) and rye (*Secale cereal*) also have been reported as allergenic multimers that contain four disulfide bonds.[19−22] Furthermore, studies showed that the Tryp_alpha_amyl family allergenic proteins are rich in cysteine and form three-dimensional structures with α-helices.[7,23,24]

In rice seeds, eight proteins, Os07g11320.1, Os07g11330.1, Os07g11360.1, Os07g11380.1, Os07g11380.2, Os07g11410.1, Os07g11510.1, and Os08g09250.1, have been reported as allergens because of their IgE-binding activity.[4,25−29] Particularly, seven of these seed allergens belong to the Tryp_alpha_amyl protein family, indicating that the Tryp_alpha_amyl protein family might play an important role in the allergenicity of plant foods. However, the genome-wide characterization and evolutionary analysis of the allergenic Tryp_alpha_amyl family members in plants have not been fully investigated.

In this study, we characterized the sequence features of trRSAs, rice seed allergens belonging to the Tryp_alpha_amyl family, and in silico identified the homologous proteins of trRSAs (trHAs) in all organisms with available genome sequence. In addition, the structures related to allergenicity of these trHAs were analyzed, and their evolutionary relationship

Received: January 21, 2013
Revised: October 28, 2013
Accepted: December 12, 2013
Published: December 12, 2013

ACS Publications © 2013 American Chemical Society

Table 1. Known *trRSA* Genes Localized on Chromosome 7

model	function	PfamAcc	PfamName	*E* value
LOC_Os07g11320.1	RAL1: seed allergenic protein RA5/RA14/RA17 precursor, expressed	PF00234	Tryp_alpha_amyl	2.90×10^{-5}
LOC_Os07g11330.1	RAL1: seed allergenic protein RA5/RA14/RA17 precursor, expressed	PF00234	Tryp_alpha_amyl	4.70×10^{-12}
LOC_Os07g11360.1	RAL1: seed allergenic protein RA5/RA14/RA17 precursor, expressed	PF00234	Tryp_alpha_amyl	2.30×10^{-12}
LOC_Os07g11380.1	RAL1: seed allergenic protein RA5/RA14/RA17 precursor, expressed	PF00234	Tryp_alpha_amyl	1.10×10^{-13}
LOC_Os07g11380.2	RAL1: seed allergenic protein RA5/RA14/RA17 precursor, expressed	PF00234	Tryp_alpha_amyl	4.80×10^{-7}
LOC_Os07g11410.1	RAL1: seed allergenic protein RA5/RA14/RA17 precursor, expressed	PF00234	Tryp_alpha_amyl	6.80×10^{-13}
LOC_Os07g11510.1	RAL1: seed allergenic protein RA5/RA14/RA17 precursor, expressed	PF00234	Tryp_alpha_amyl	5.40×10^{-14}

was also performed. Finally, the expression profiles were also discussed.

MATERIALS AND METHODS

Motif Identification and Annotation. The MEME tool (version 4.8.1) was used to elucidate conserved motifs among all rice proteins of the Tryp_alpha_amyl family.[30] To check whether trHAs contain the trRSAs-specific motifs, the FIMO tool (version 4.8.1) was used with a *p* value threshold of 0.001.[31] The sequence logo of motifs was retrieved from the output of MEME results and confirmed by WebLogo3.[32]

Homology Search and Tree Building. To search a comprehensive and nonredundant set of trHA homologues, the BLAST program was performed.[33] First, trRSAs' sequences were used for BLASTP in the nr (nonredundant protein sequences) database (organism: rice) of NCBI (National Center for Biotechnology Information) and MSU-RGAP (Rice Genome Annotation Project, release 7) protein sequences. Each obtained sequence was then used as the query sequence to perform TBLASTN in the following databases: NCBI nucleotide collection (nt), TAIR (The *Arabidopsis* Information Resource), Phytozome genome (version 8.0), and genomic databases in JGI (Joint Genome Institute). The algorithm parameters were set to be default. The redundant sequences within species with >95% identity were removed from our data set. The remaining sequences with *E* values below 1×10^{-4} were combined in our data set. To confirm the sequences we obtained, the amino acid sequences were searched using Pfam,[34] and the ones that were not included in the Tryp_alpha_amyl family (PF00234) were excluded from further analyses.

ClustalX2 was used for multiple sequence alignments with the default parameters, and Muscle was used to recheck the result.[35,36] The alignment was then adjusted manually by GeneDoc software.[37] A neighbor-joining (NJ) tree was constructed with the aligned trHAs protein sequences using MEGA (version 5) with the following parameters: poisson correction, pairwise deletion, and bootstrap (1000 replicates; random seed).[38] The views of the tree were constructed by interactive Tree Of Life (iTOL).[39]

Allergen Prediction Approaches. The allergen in trHAs was predicted using the criterion defined by FAO/WHO (Food and Agriculture Organization of the United Nations/World Health Organization) Codex alimentarius and SVM-AAC (Support Vector Machine–Amino Acid Composition).[40,41] The FAO/WHO criterion of exact match of a stretch of 8 or more amino acids was used in this study, because the evaluation showed that this level could ensure high sensitivity and specificity.[42] To study whether the allergenicity of trHAs is related to specific motifs significantly, one statistical method, Fisher's exact test, was performed by R.[43]

Expression Pattern Analysis. The expression data of rice trHAs were collected from RiceGE (Rice Functional Genomics Database) of SIGnAL (Salk Institute Genomic Analysis Laboratory, http://signal.salk.edu/) and SeedGeneDB (http://ibi.cqupt.edu.cn/sgdb/index.php), which integrated the raw array data from GEO (Gene Expression Omnibus). The corresponding data of trHAs of purple false brome (*Brachypodium distachyon*), barrel medic (*Medicago truncatula*), and sorghum (*Sorghum bicolor*) were collected from GEO (GSE10055, GSE10151, GSE36689, GSE30249, and GSE33391).

Statistical Analysis and 3D Structure Modeling. The instability index, GRAVY (grand average of hydropathicity), and amino acid composition of all trHAs were analyzed by ProtParam,[44] and the 3D structure of trHAs was modeled by SWISS-MODEL.[45] To understand the role of disulfide bonds in allergenic trHAs, Fisher's exact test was performed on trHAs in the number of sulfur atoms. For amino acid composition, a permutation test was used to analyze the statistical significance of the amounts of cysteine in allergenic trHAs, with random sampling 10000 times.[46] The Wilcoxon test was used on the differential analysis of secondary structure and cysteine enrichment analysis.[47] All of the *p* values of multiple tests in this study were corrected using the Benjamini–Hochberg procedure.[48]

RESULTS AND DISCUSSION

Sequence Characterization of Rice trRSAs. Previously seven proteins including Os07g11320.1, Os07g11330.1, Os07g11360.1, Os07g11380.1, Os07g11380.2, Os07g11410.1, and Os07g11510.1 from rice were identified as allergenic proteins within the Tryp_alpha_amyl family (trRSAs).[4,25] These *trRSA* genes are all localized on chromosome 7 (Table 1) and expressed dominantly in seeds, particularly in mature seeds, from the available microarray data (http://signal.salk.edu/cgi-bin/RiceGE) (Supplemental Figure 1). To study the sequence differences and conservation between trRSAs and other rice proteins in Tryp_alpha_amly family, we obtained a total of 114 rice proteins belonging to the Tryp_alpha_amyl family from RGAP (Rice Genome Annotation Project, http://

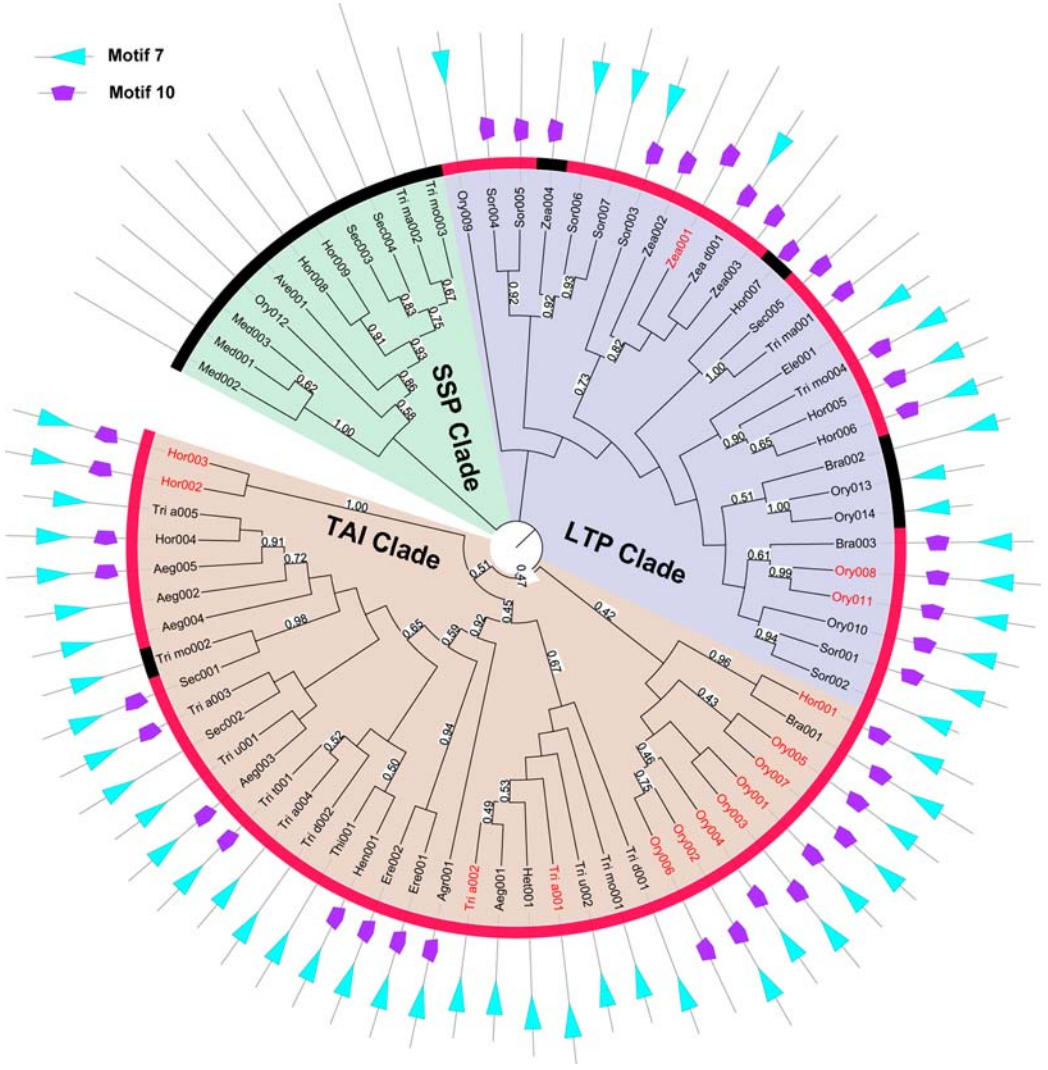

Figure 1. Phylogenetic tree of trHAs. 75 trHAs (see Supplemental Table 2) are grouped into three clades shaded in different colors. Bootstrap values are indicated in the branches of different clades. The color strip represents the putative allergenicity of each trHA: red identifies the trHAs predicted as allergen; black identifies the trHAs predicted as nonallergens. The outer domain architecture represents the existence of motif 7 and motif 10 and the relative length of each trHA.

rice.plantbiology.msu.edu/index.shtml) (Supplemental Table 1).

To characterize the sequence of these rice proteins of the Tryp_alpha_amyl family and explore the relationship among them, we searched the dominant motifs in these 114 proteins using MEME (with the parameters of $6 \leq$ width ≤ 50 and maximum number of motifs = 15)[49] and performed phylogenetic analysis using MEGA.[38] For conciseness of the display, we renamed all of the proteins in abbreviations containing the family domain name and the sequential number (Supplemental Table 1). As shown in Supplemental Figure 2, the seven known allergenic trRSAs were grouped into a specific subclade highlighted with red branches, and motif 7 having a length of 41 amino acids and motif 10 with 29 amino acids were found to be enriched among these trRSAs (Supplemental Figure 2). Thus, we proposed that the two specific motifs might be critical for the allergenicity of these proteins, and further analyses were performed to verify this point.

Phylogenetic Analysis of trHAs in Plants. To understand more trHAs from other organisms, we used the seven known rice trRSAs as BLASTP queries against all species with available genome sequences. We observed 75 putative trHAs encoded by 74 genes from 22 plant species, in which there were 21 grass species and barrel medic. This result suggests that trHAs might originate after the divergence of grass species; alternatively, the ancestors of trHAs may be lost in many other species during evolution. Similarly, all trHAs were renamed in abbreviations using the species name and the sequential number (Supplemental Table 2). To analyze the evolutionary relationship of the *trHA* genes, a NJ phylogenetic tree was generated through the multiple sequence alignments of the trHAs sequences using 1000 replicates (Figure 1).

As illustrated in Figure 1, these 75 trHAs were grouped into three clades: the seed storage protein (SSP) clade, the lipid transfer protein (LTP) clade, and the trypsin-alpha amylase inhibitor (TAI) clade named on the functional annotation. The SSP clade contained 11 members from 7 species: 3 from barrel medic, 1 from rice, 1 from wild oat (*Avena fatua*), 2 from barley, 2 from rye, 1 from *Triticum macha*, and 1 from einkorn wheat (*Triticum monococcum*) (Supplemental Table 3). Among them, Ory012 (LOC_Os05g41970.1) was identified as a 2S albumin seed storage protein, and the other 10 trHAs have

dx.doi.org/10.1021/jf402463w | J. Agric. Food Chem. 2014, 62, 270−278

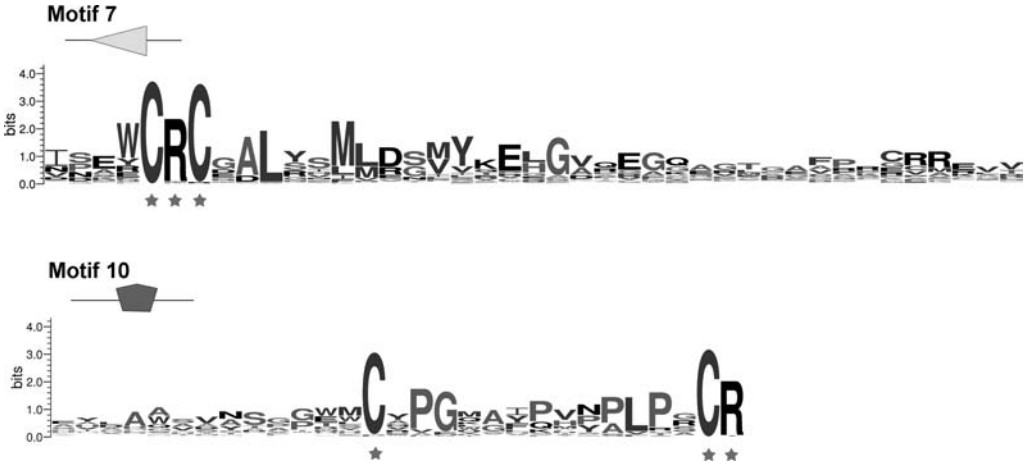

Figure 2. Analysis of conserved amino acid residues of motifs 7 and 10 in trHAs. Motifs are represented by position-specific probability matrices that specify the probability of each possible letter appearing at each possible position in an occurrence of the motif. The total height of the stack is the information content of that position in the motif in bits. The height of the individual letters in a stack is the probability of the letter at that position multiplied by the total information content of the stack. The bigger characters indicate the higher conserved residues by the alignment of motif sequences in trHAs. Highly conservative sites are marked with a star (★).

been reported as homologues of Ory012.[50] The LTP clade consisted of 27 trHAs from 10 species including rice, sorghum, purple false brome, barley, *Triticum macha*, einkorn wheat, finger millet (*Eleusine coracana*), rye, *Zea diploperennis*, and maize (Supplemental Table 3). An allergen from maize (Zea m 14, Zea001) in the LTP clade has been described as a LTP,[51,52] and six LTPs from rice named Ory008−Ory011, Ory013, and Ory014 are in this clade.[53] The third clade contained 37 trHAs from 15 species including rice, wheat, barley, goatgrass (*Aegilops*), einkorn wheat, rye, red wild einkorn (*Triticum urartu*), *Triticum timopheevii* subsp. *Armeniacum*, emmer wheat (*Triticum dicoccoides*), *Thinopyrum bessarabicum*, *Henrardia persica*, *Eremopyrum bonaepartis*, *Agropyron desertorum*, *Heteranthelium piliferum*, and purple false brome (Supplemental Table 3). Likewise, we called the third clade the trypsin-alpha amylase inhibitor clade because it had 7 rice trHAs and 11 wheat trHAs defined as trypsin-alpha amylase inhibitor (Figure 1).[19,26]

Figure 1 shows that all members of barrel medic were grouped into one subclade in the SSP clade and that all members of another subclade in the SSP clade were from Triticeae except one from rice. All trHAs in the LTP and TAI clades were from only monocot grasses (Figure 1). In addition, trHAs of Andropogoneae (sorghum, *Zea diploperennis*, and maize) were observed only in the LTP clade.

To analyze the evolution of the two motifs, motif 7 and motif 10, and their association with allergenicity in plants, we investigated their distribution in all trHAs shown in Figure 1. Interestingly, the trHAs with none of motif 7 and 10 were grouped into one clade (SSP clade, including a subclade of barrel medic members), whereas the trHAs containing motif 7 and/or motif 10 were clustered into the LTP and TAI clades (Figure 1).

Allergenic Analysis of trHAs in Plants. Among the 75 trHAs, 13 members including 7 rice trRSAs, 3 barley trHAs, 2 wheat trHAs, and 1 maize trHA have been reported as allergens (Supplemental Table 3).[3,26,51,54−56] To understand the allergenicity of all trHAs, we scanned each by allergen prediction approaches. One way is recommended by the FAO/WHO criteria by matching eight or more continuous amino acids with known allergens.[42] Another prediction method is SVM-AAC for measuring the false-positive rate (FDR).[41] We considered the candidates to be allergenic trHAs when they were identified as allergens by both of the two approaches. As shown in Figure 1, 58 trHAs were predicted as allergens (color strip, colored in red) and 17 trHAs were nonallergens (color strip, colored in black). All 13 reported allergenic trHAs were included in the putative allergens by prediction (Figure 1, red leaves).

From Figure 1, we observed that the trHAs in the SSP clade were all predicted as nonallergens, whereas most of the trHAs in the LTP and TAI clades were predicted as allergens (color strip). Specifically, all candidates containing neither motif 7 nor motif 10 were identified as nonallergens and 90.63% (58/64) of the members with motif 7 and/or motif 10 as putative allergens. To further investigate whether these two motifs are associated with trHAs' allergenicity, we compared the prediction results of trHAs with none of the two motifs to other trHAs, and the results showed the significant correlation between allergenicity and the existence of one or both motif 7 and motif 10 (Fisher's exact test, p value = 0.00026), suggesting that motifs 7 and 10 are involved in allergenicity.

Structure Analysis in Plant trHAs. *Enrichment of Cysteine Residues.* To further characterize the sequence features of motifs 7 and 10, we did alignment analysis of the trHAs containing motifs 7 and 10, respectively, and three consensus sites for motif 7 (5-C, 6-R, 7-C) and three for motif 10 (14-C, 28-C, 29-R) were observed (Figure 2, Supplemental Figure 3). Given that cysteines are the main conserved amino acids in these two motifs of trHAs, we analyzed the amino acid preferences of trHAs by comparing the amino acid compositions of trHAs with Swiss-Prot proteins to understand the importance of these cysteine residues. Here, the definition of amino acid composition is the percentage of each amino acid in a protein. As shown in Figure 3A, the amount of cysteine was significantly enriched in trHAs (permutation test, p value < 0.0001). As disulfide bonds are a typical feature for allergens in the Tryp_alpha_amyl family,[14,18] we further analyzed the distribution of sulfur atoms among trHAs and observed that the putative allergenic trHAs had more sulfur atoms than those of nonallergenic ones (Wilcoxon test, p value = 1.768×10^{-9}) (Figure 3B).

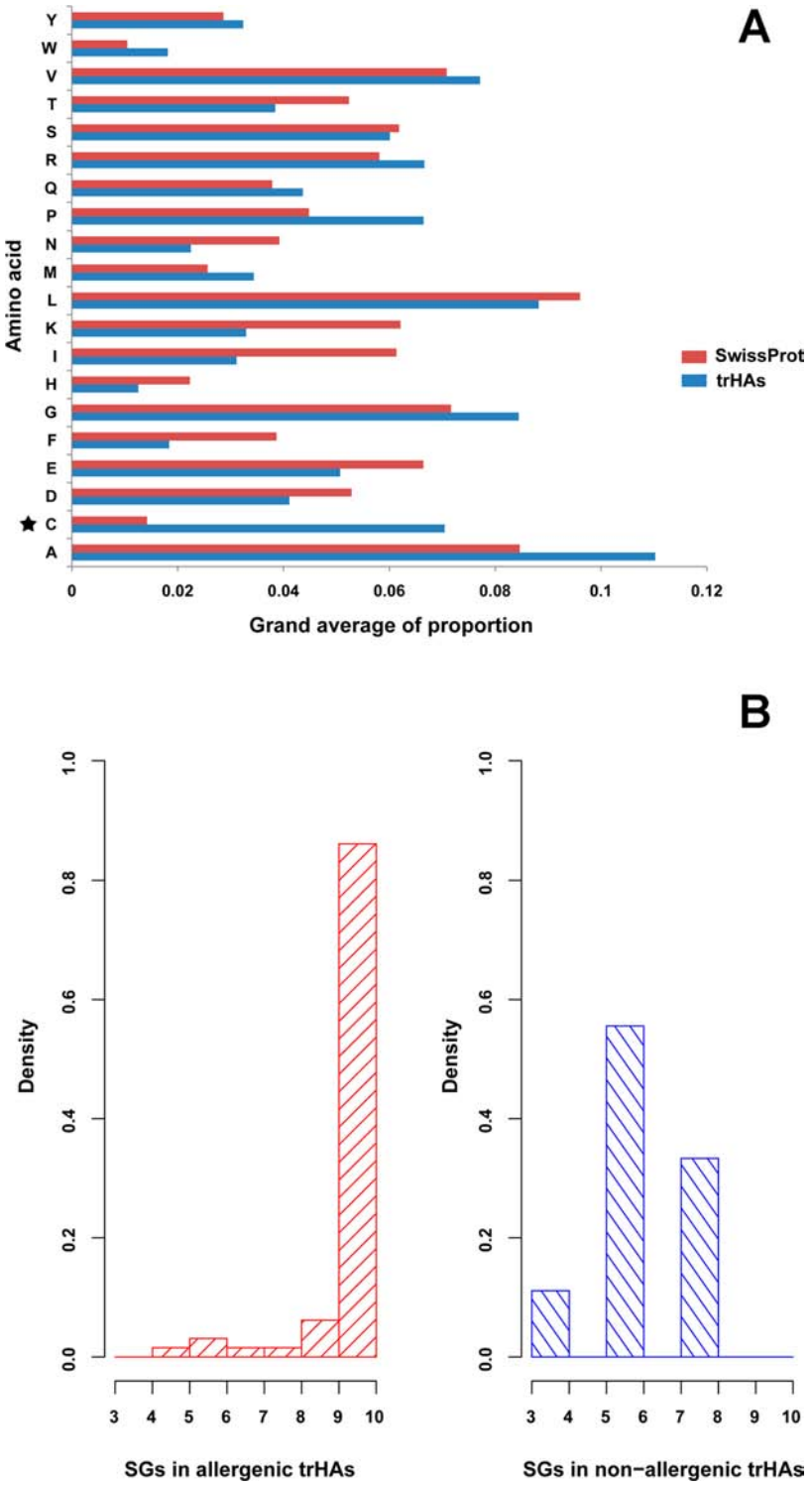

Figure 3. Comparison of amino acid composition of trHAs with the proteins in Swiss-Prot database. (A) The horizontal axis is the proportion of each amino acid in protein sequence, and the letters beside the vertical axis represent the 20 amino acids. Statistical results show significance on the amount of cysteine in trHAs (permutation test, p value < 0.0001), which is marked by a star (★). (B) Comparison of the number of sulfur atoms (labeled SG) of allergenic trHAs and nonallergenic trHAs (Wilcoxon test, p value = 1.768×10^{-9}).

Secondary Structure. We also analyzed the secondary structure of trHAs, which is associated with the protein's stability and function.[12,57] Generally, the secondary structure assignments of protein by DSSP are grouped into eight types including H (α helix), B (residue in isolated beta-bridge), E (extended strand, participates in beta ladder), G (3-helix, 3/10 helix), I (5 helix, pi helix), T (hydrogen bonded turn), S (bend), and blank (loop or irregular).[58] Our analysis data showed that the average percentage of H content in both putative allergenic and nonallergenic trHAs was the highest, which accounted for 40.75 and 48.43%, respectively, followed by the blank, T, and S, whereas the average percentages of B, E and G were much lower, and no I was observed in any trHAs (Figure 4). We made statistical analysis about the difference of

dx.doi.org/10.1021/jf402463w | J. Agric. Food Chem. 2014, 62, 270−278

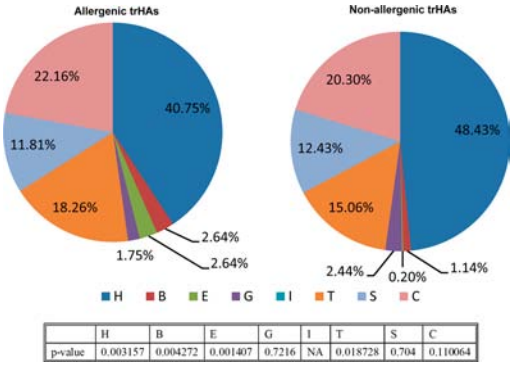

	H	B	E	G	I	T	S	C
p-value	0.003157	0.004272	0.001407	0.7216	NA	0.018728	0.704	0.110064

Figure 4. Preference of the secondary structure in trHAs. The types of secondary structure are from DSSP including H (α helix), B (residue in isolated beta-bridge), E (extended strand, participates in beta ladder), G (3-helix, 3/10 helix), I (5 helix, pi helix), T (hydrogen-bonded turn), S (bend), and blank (loop or irregular, represented as C here). The bottom table in this figure gives the p values of Wilcoxon tests showing the degree of variance of each secondary structure type between putative allergenic and nonallergenic trHAs.

each secondary structure of putative allergenic and non-allergenic trHAs. The results showed a significant difference in the compositions of H, B, E, and T between the two groups (Figure 4, Wilcoxon test). Specifically, nonallergenic trHAs contained more H-type secondary structure than those of allergenic ones with a p value of 0.0032. On the contrary, the contents of B, E, and T in the allergens are higher than in the nonallergens, and the corresponding p values are 0.0043, 0.0014, and 0.019, respectively (Figure 4).

3D Structure and Allergenicity. Three-dimensional (3D) structure is closely related to a protein's function.[59] To find the correlation of the characteristics of 3D structure with allergenicity of plant trHAs, we analyzed the 3D structure for all trHAs.[60] Analysis of the 3D structures of four representative trHAs randomly selected from four distinct groups, three allergenic trHAs groups containing both motifs 7 and 10, motif 7 only, motif 10 only, and one group of nonallergenic trHAs without any motif 7 or motif 10, revealed that allergenic trHAs were different from nonallergenic trHAs in 3D structure (Figure 5). The allergenic trHAs seemed more likely to have four alpha-helix and at least four disulfide bonds than nonallergenic trHAs (Fisher's exact test, p value = 1.259×10^{-5}) (Figure 5). Supportively, the trHAs with and without motif 7/10 were separated into different clusters by root mean square deviation (RMSD) analysis (Supplemental Figure 4A). Furthermore, analysis of the physicochemical properties also showed a distinct difference between the trHAs with and without specific motifs in grand average of hydropathicity (GRAVY). Specially, the GRAVY of most trHAs containing neither of the two motifs was below −0.2, whereas the figure for trHAs containing any/both of the specific motifs was > −0.2 (Supplemental Figure 4B), suggesting that the two specific motifs may increase the ability of hydropathicity.

Expression Patterns of trHAs of Purple False Brome, Barrel Medic, Rice, and Sorghum. To further understand the biological role of trHAs, we analyzed their expression patterns using the available information of purple false brome,

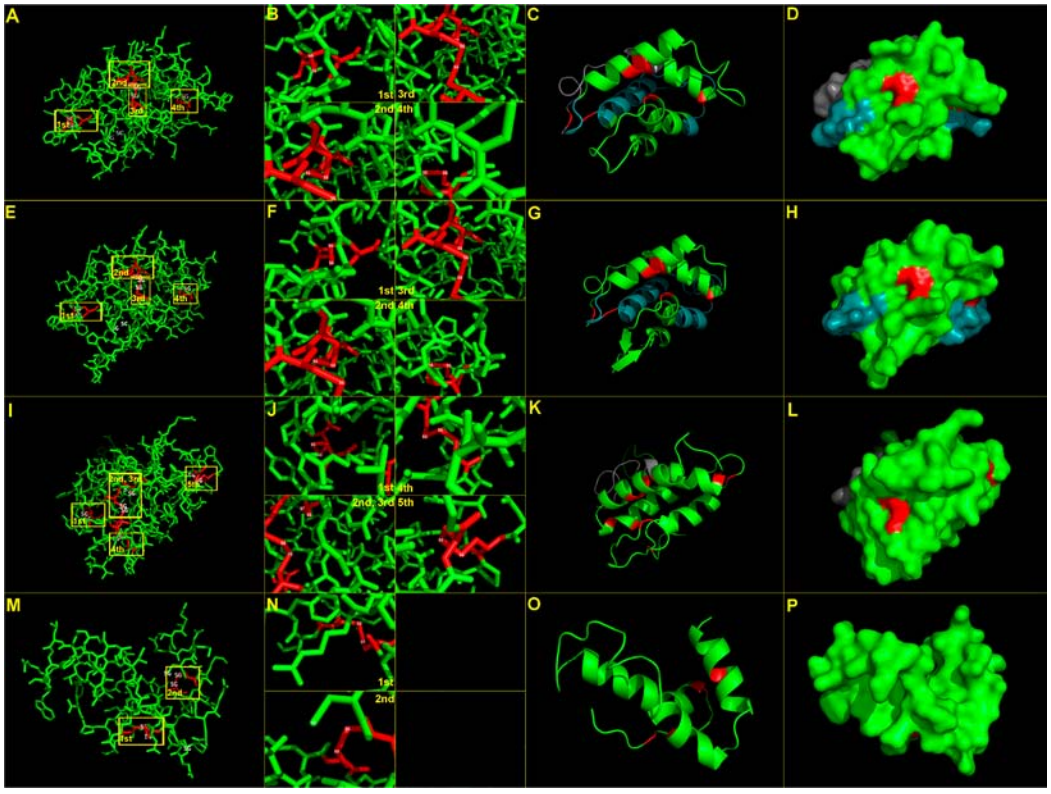

Figure 5. 3D structure of four representative trHAs. (A–D) Ory 002, allergenic trHA contains both motif 7 and motif 10; (E–H) Aeg 001, allergenic trHA contains motif 7 only; (I–L) Zea 003, allergenic trHA contains motif 10 only; (M–P) Tri_ma002, nonallergenic trHA without motif 7 and motif 10. (A, E, I, M) Stick models: cysteines providing sulfur atoms of disulfide bonds are colored in red; (B, F, J, N) stick models of disulfide bonds; (C, G, K, O) cartoon models, motif 7 is colored in cyan and motif 10 is colored in gray; (D, H, L, P) surface models.

dx.doi.org/10.1021/jf402463w | J. Agric. Food Chem. 2014, 62, 270–278

barrel medic, rice, and sorghum. Expression data of rice *trHA* genes from SIGnAL, and *trHA* genes of purple false brome, barrel medic, and sorghum from GEO (Figure 6) showed that

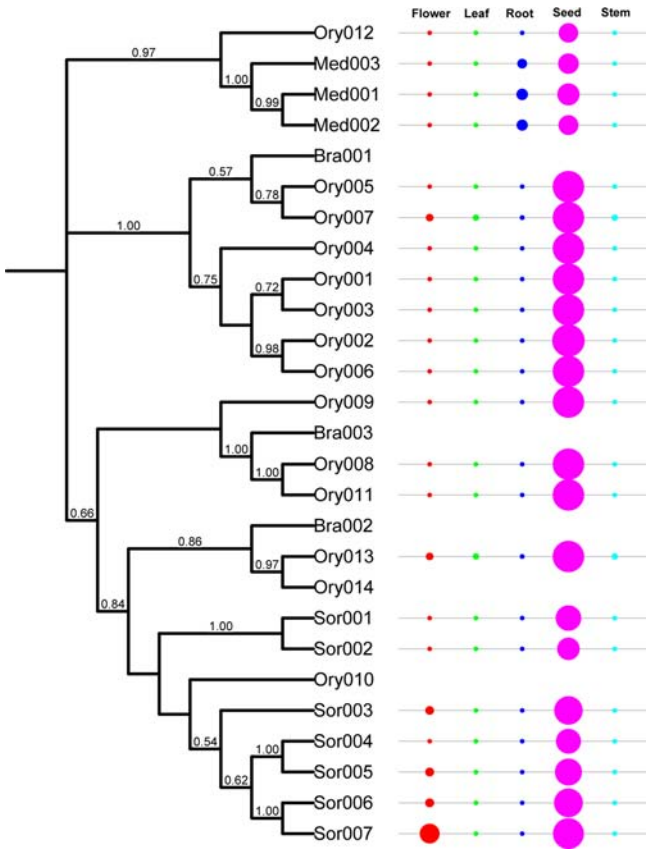

Figure 6. Expression patterns of trHAs in four species: expression pattern represented by solid circles in five tissues, that is, flower, leaf, root, seed, and stem. The area of the circle indicates the expression level, and higher expression level is indicated by a larger area.

trHA genes were preferentially expressed in seeds, suggesting that the trHAs have conserved transcriptional regulation in grass seeds. Supportively, previous papers showed the expression of rice trRSAs in maturing seeds.[4,25−29] Interestingly, trHAs of barrel medic had a higher expression in root than the other three species, suggesting that trHAs may be involved in root development processes in barrel medic (Figures 1 and 6).

■ ASSOCIATED CONTENT

Supporting Information

Additional figures and tables. This material is available free of charge via the Internet at http://pubs.acs.org.

■ AUTHOR INFORMATION

Corresponding Authors

*(J.L.) E-mail: jing.li@sjtu.edu.cn.

*(D.Z.) E-mail: zhangdb@sjtu.edu.cn.

Funding

This work was supported by funds from the National Basic Research Program of China (973 Program) (2012CB720804), the National Transgenic Plant Special Fund (2011BAK10B03, 2013ZX080125002, and 2013ZX08011-006), the Program for "Chen Xing" Young Scholars, Shanghai Jiao Tong University, and the Pujiang Talent program (12PJ1406600).

Notes

The authors declare no competing financial interest.

■ ACKNOWLEDGMENTS

We thank Dr. Hong Sun from Shanghai Center for Bioinformation Technology for her great help in the phylogenetic analysis and also Dr. Haifeng Chen and Wei Ye for the valuable suggestion in 3D structure modeling.

■ REFERENCES

(1) Goldsby, R. A.; Kindt, T. J.; Osborne, B. A.; Kuby, J. *Immunology*, 5th ed.; Freeman: New York, 2003; p 9.

(2) Midoro-Horiuti, T.; Brooks, E. G.; Goldblum, R. M. Pathogenesis-related proteins of plants as allergens. *Ann. Allergy Asthma Immunol.* **2001**, *87* (4), 261−271.

(3) Armentia, A.; Sanchez-Monge, R.; Gomez, L.; Barber, D.; Salcedo, G. In vivo allergenic activities of eleven purified members of a major allergen family from wheat and barley flour. *Clin. Exp. Allergy* **1993**, *23* (5), 410−415.

(4) Izumi, H.; Adachi, T.; Fujii, N.; Matsuda, T.; Nakamura, R.; Tanaka, K.; Urisu, A.; Kurosawa, Y. Nucleotide sequence of a cDNA clone encoding a major allergenic protein in rice seeds. Homology of the deduced amino acid sequence with members of alpha-amylase/trypsin inhibitor family. *FEBS Lett.* **1992**, *302* (3), 213−216.

(5) Gu, X.; Beardslee, T.; Zeece, M.; Sarath, G.; Markwell, J. Identification of IgE-binding proteins in soy lecithin. *Int. Arch. Allergy Immunol.* **2001**, *126* (3), 218−225.

(6) Petersen, A.; Dresselhaus, T.; Grobe, K.; Becker, W. M. Proteome analysis of maize pollen for allergy-relevant components. *Proteomics* **2006**, *6* (23), 6317−6325.

(7) Breiteneder, H.; Radauer, C. A classification of plant food allergens. *J. Allergy Clin. Immunol.* **2004**, *113* (5), 821−830 (quiz 831).

(8) Lin, K. F.; Liu, Y. N.; Hsu, S. T.; Samuel, D.; Cheng, C. S.; Bonvin, A. M.; Lyu, P. C. Characterization and structural analyses of nonspecific lipid transfer protein 1 from mung bean. *Biochemistry* **2005**, *44* (15), 5703−5712.

(9) Pantoja-Uceda, D.; Bruix, M.; Gimenez-Gallego, G.; Rico, M.; Santoro, J. Solution structure of RicC3, a 2S albumin storage protein from *Ricinus communis*. *Biochemistry* **2003**, *42* (47), 13839−13847.

(10) Oda, Y.; Matsunaga, T.; Fukuyama, K.; Miyazaki, T.; Morimoto, T. Tertiary and quaternary structures of 0.19 alpha-amylase inhibitor from wheat kernel determined by X-ray analysis at 2.06 A resolution. *Biochemistry* **1997**, *36* (44), 13503−13511.

(11) Gourinath, S.; Alam, N.; Srinivasan, A.; Betzel, C.; Singh, T. P. Structure of the bifunctional inhibitor of trypsin and alpha-amylase from ragi seeds at 2.2 A resolution. *Acta Crystallogr. D: Biol. Crystallogr.* **2000**, *56* (Part 3), 287−293.

(12) Schocker, F.; Luttkopf, D.; Scheurer, S.; Petersen, A.; Cistero-Bahima, A.; Enrique, E.; San Miguel-Moncin, M.; Akkerdaas, J.; van Ree, R.; Vieths, S.; Becker, W. M. Recombinant lipid transfer protein Cor a 8 from hazelnut: a new tool for in vitro diagnosis of potentially severe hazelnut allergy. *J. Allergy Clin. Immunol.* **2004**, *113* (1), 141−147.

(13) Diaz-Perales, A.; Sanz, M. L.; Garcia-Casado, G.; Sanchez-Monge, R.; Garcia-Selles, F. J.; Lombardero, M.; Polo, F.; Gamboa, P. M.; Barber, D.; Salcedo, G. Recombinant Pru p 3 and natural Pru p 3, a major peach allergen, show equivalent immunologic reactivity: a new tool for the diagnosis of fruit allergy. *J. Allergy Clin. Immunol.* **2003**, *111* (3), 628−633.

(14) Shin, D. H.; Lee, J. Y.; Hwang, K. Y.; Kim, K. K.; Suh, S. W. High-resolution crystal structure of the non-specific lipid-transfer protein from maize seedlings. *Structure* **1995**, *3* (2), 189−199.

(15) Han, G. W.; Lee, J. Y.; Song, H. K.; Chang, C.; Min, K.; Moon, J.; Shin, D. H.; Kopka, M. L.; Sawaya, M. R.; Yuan, H. S.; Kim, T. D.; Choe, J.; Lim, D.; Moon, H. J.; Suh, S. W. Structural basis of non-

specific lipid binding in maize lipid-transfer protein complexes revealed by high-resolution X-ray crystallography. *J. Mol. Biol.* **2001**, *308* (2), 263−278.
(16) Beyer, K.; Bardina, L.; Grishina, G.; Sampson, H. A. Identification of sesame seed allergens by 2-dimensional proteomics and Edman sequencing: seed storage proteins as common food allergens. *J. Allergy Clin. Immunol.* **2002**, *110* (1), 154−159.
(17) Pastorello, E. A.; Farioli, L.; Pravettoni, V.; Ispano, M.; Conti, A.; Ansaloni, R.; Rotondo, F.; Incorvaia, C.; Bengtsson, A.; Rivolta, F.; Trambaioli, C.; Previdi, M.; Ortolani, C. Sensitization to the major allergen of Brazil nut is correlated with the clinical expression of allergy. *J. Allergy Clin. Immunol.* **1998**, *102* (6 Part 1), 1021−1027.
(18) Shewry, P. R.; Napier, J. A.; Tatham, A. S. Seed storage proteins: structures and biosynthesis. *Plant Cell* **1995**, *7* (7), 945−956.
(19) Mena, M.; Sanchez-Monge, R.; Gomez, L.; Salcedo, G.; Carbonero, P. A major barley allergen associated with baker's asthma disease is a glycosylated monomeric inhibitor of insect alpha-amylase: cDNA cloning and chromosomal location of the gene. *Plant Mol. Biol.* **1992**, *20* (3), 451−458.
(20) Nakase, M.; Usui, Y.; Alvarez-Nakase, A. M.; Adachi, T.; Urisu, A.; Nakamura, R.; Aoki, N.; Kitajima, K.; Matsuda, T. Cereal allergens: rice-seed allergens with structural similarity to wheat and barley allergens. *Allergy* **1998**, *53* (46 Suppl.), 55−57.
(21) Gomez, L.; Martin, E.; Hernandez, D.; Sanchez-Monge, R.; Barber, D.; del Pozo, V.; de Andres, B.; Armentia, A.; Lahoz, C.; Salcedo, G.; et al. Members of the alpha-amylase inhibitors family from wheat endosperm are major allergens associated with baker's asthma. *FEBS Lett.* **1990**, *261* (1), 85−88.
(22) Feng, G. H.; Richardson, M.; Chen, M. S.; Kramer, K. J.; Morgan, T. D.; Reeck, G. R. alpha-Amylase inhibitors from wheat: amino acid sequences and patterns of inhibition of insect and human alpha-amylases. *Insect Biochem. Mol. Biol.* **1996**, *26* (5), 419−426.
(23) Breiteneder, H.; Mills, E. N. Molecular properties of food allergens. *J. Allergy Clin. Immunol.* **2005**, *115* (1), 14−23 (quiz 24).
(24) Dominguez, J.; Cuevas, M.; Urena, V.; Munoz, T.; Moneo, I. Purification and characterization of an allergen of mustard seed. *Ann. Allergy* **1990**, *64* (4), 352−357.
(25) Adachi, T.; Izumi, H.; Yamada, T.; Tanaka, K.; Takeuchi, S.; Nakamura, R.; Matsuda, T. Gene structure and expression of rice seed allergenic proteins belonging to the alpha-amylase/trypsin inhibitor family. *Plant Mol. Biol.* **1993**, *21* (2), 239−248.
(26) Alvarez, A. M.; Adachi, T.; Nakase, M.; Aoki, N.; Nakamura, R.; Matsuda, T. Classification of rice allergenic protein cDNAs belonging to the alpha-amylase/trypsin inhibitor gene family. *Biochim. Biophys. Acta* **1995**, *1251* (2), 201−204.
(27) Matsuda, T.; Nakase, M.; Adachi, T.; Nakamura, R.; Tada, Y.; Shimada, H.; Takahashi, M.; Fujimura, T. In *Allergenic Proteins in Rice: Strategies for Reduction and Evaluation*; Food Allergies and Intolerances: Symposium; Wiley: Weinheim, Germany, 1996; pp 161−169.
(28) Matsuda, T.; Sugiyama, M.; Nakamura, R.; Torii, S. Purification and properties of an allergenic protien in rice grain. *Agric. Biol. Chem.* **1988**, *52* (1), 465−470.
(29) Urisu, A.; Yamada, K.; Masuda, S.; Komada, H.; Wada, E.; Kondo, Y.; Horiba, F.; Tsuruta, M.; Yasaki, T.; Yamada, M.; et al. 16-kilodalton rice protein is one of the major allergens in rice grain extract and responsible for cross-allergenicity between cereal grains in the Poaceae family. *Int. Arch. Allergy Appl. Immunol.* **1991**, *96* (3), 244−252.
(30) Bailey, T. L.; Elkan, C. Fitting a mixture model by expectation maximization to discover motifs in biopolymers. *Proc. Int. Conf. Intell. Syst. Mol. Biol.* **1994**, *2*, 28−36.
(31) Grant, C. E.; Bailey, T. L.; Noble, W. S. FIMO: scanning for occurrences of a given motif. *Bioinformatics* **2011**, *27* (7), 1017−1018.
(32) Crooks, G. E.; Hon, G.; Chandonia, J. M.; Brenner, S. E. WebLogo: a sequence logo generator. *Genome Res.* **2004**, *14* (6), 1188−1190.
(33) Altschul, S. F.; Gish, W.; Miller, W.; Myers, E. W.; Lipman, D. J. Basic local alignment search tool. *J. Mol. Biol.* **1990**, *215* (3), 403−410.
(34) Punta, M.; Coggill, P. C.; Eberhardt, R. Y.; Mistry, J.; Tate, J.; Boursnell, C.; Pang, N.; Forslund, K.; Ceric, G.; Clements, J.; Heger, A.; Holm, L.; Sonnhammer, E. L.; Eddy, S. R.; Bateman, A.; Finn, R. D. The Pfam protein families database. *Nucleic Acids Res.* **2012**, *40* (database issue), D290−D301.
(35) Thompson, J. D.; Gibson, T. J.; Plewniak, F.; Jeanmougin, F.; Higgins, D. G. The CLUSTAL_X windows interface: flexible strategies for multiple sequence alignment aided by quality analysis tools. *Nucleic Acids Res.* **1997**, *25* (24), 4876−82.
(36) Edgar, R. C. MUSCLE: multiple sequence alignment with high accuracy and high throughput. *Nucleic Acids Res.* **2004**, *32* (5), 1792−1797.
(37) Nicholas, K. B.; Nicholas, H. B. J.; Deerfield, D. W. I. GeneDoc: analysis and visualization of genetic variation. *EMBNEW* **1997**, *4*, 14.
(38) Tamura, K.; Peterson, D.; Peterson, N.; Stecher, G.; Nei, M.; Kumar, S. MEGA5: molecular evolutionary genetics analysis using maximum likelihood, evolutionary distance, and maximum parsimony methods. *Mol. Biol. Evol.* **2011**, *28* (10), 2731−2739.
(39) Letunic, I.; Bork, P. Interactive Tree Of Life (iTOL): an online tool for phylogenetic tree display and annotation. *Bioinformatics* **2007**, *23* (1), 127−128.
(40) FAO/WHO. *Evaluation of Allergenicity of Genetically Modified Foods*; Rome, Italy, 2003.
(41) Saha, S.; Raghava, G. P. AlgPred: prediction of allergenic proteins and mapping of IgE epitopes. *Nucleic Acids Res.* **2006**, *34* (Web Server issue), W202−W209.
(42) Stadler, M. B.; Stadler, B. M. Allergenicity prediction by protein sequence. *FASEB J.* **2003**, *17* (9), 1141−1143.
(43) Fisher, R. A. *Statistical Methods for Research Workers*; Oliver & Boyd: Edinburgh, Scotland, 1954.
(44) Gasteiger, E.; Hoogland, C.; Gattiker, A.; Duvaud, S.; Wilkins, M. R.; Appel, R. D.; Bairoch, A. Protein identification and analysis tools on the ExPASy server. In *The Proteomics Protocols Handbook*; Walker, J. M., Ed.; Humana Press: Totowa, NJ, USA, 2005.
(45) Arnold, K.; Bordoli, L.; Kopp, J.; Schwede, T. The SWISS-MODEL workspace: a web-based environment for protein structure homology modelling. *Bioinformatics* **2006**, *22* (2), 195−201.
(46) Nichols, T. E.; Holmes, A. P. Nonparametric permutation tests for functional neuroimaging: a primer with examples. *Hum. Brain Mapp* **2002**, *15* (1), 1−25.
(47) Wilcoxon, F. Individual comparisons of grouped data by ranking methods. *J. Econ. Entomol.* **1946**, *39*, 269.
(48) Benjamini, Y.; Hochberg, Y. Controlling the false discovery rate: a practical and powerful approach to multiple testing. *J. R. Stat. Soc. Ser. B (Methodol.)* **1995**, 289−300.
(49) Bailey, T. L.; Boden, M.; Buske, F. A.; Frith, M.; Grant, C. E.; Clementi, L.; Ren, J.; Li, W. W.; Noble, W. S. MEME SUITE: tools for motif discovery and searching. *Nucleic Acids Res.* **2009**, *37* (WebServer issue), W202−W208.
(50) Shorrosh, B. S.; Wen, L.; Zen, K. C.; Huang, J. K.; Pan, J. S.; Hermodson, M. A.; Tanaka, K.; Muthukrishnan, S.; Reeck, G. R. A novel cereal storage protein: molecular genetics of the 19 kDa globulin of rice. *Plant Mol. Biol.* **1992**, *18* (1), 151−154.
(51) Pastorello, E. A.; Farioli, L.; Pravettoni, V.; Ispano, M.; Scibola, E.; Trambaioli, C.; Giuffrida, M. G.; Ansaloni, R.; Godovac-Zimmermann, J.; Conti, A.; Fortunato, D.; Ortolani, C. The maize major allergen, which is responsible for food-induced allergic reactions, is a lipid transfer protein. *J. Allergy Clin. Immunol.* **2000**, *106* (4), 744−751.
(52) Pastorello, E. A.; Pompei, C.; Pravettoni, V.; Farioli, L.; Calamari, A. M.; Scibilia, J.; Robino, A. M.; Conti, A.; Iametti, S.; Fortunato, D.; Bonomi, S.; Ortolani, C. Lipid-transfer protein is the major maize allergen maintaining IgE-binding activity after cooking at 100 degrees C, as demonstrated in anaphylactic patients and patients with positive double-blind, placebo-controlled food challenge results. *J. Allergy Clin. Immunol.* **2003**, *112* (4), 775−783.
(53) Lin, H.; Ouyang, S.; Egan, A.; Nobuta, K.; Haas, B. J.; Zhu, W.; Gu, X.; Silva, J. C.; Meyers, B. C.; Buell, C. R. Characterization of paralogous protein families in rice. *BMC Plant Biol.* **2008**, *8*, 18.

(54) Barber, D.; Sanchez-Monge, R.; Gomez, L.; Carpizo, J.; Armentia, A.; Lopez-Otin, C.; Juan, F.; Salcedo, G. A barley flour inhibitor of insect alpha-amylase is a major allergen associated with baker's asthma disease. *FEBS Lett.* **1989**, *248* (1−2), 119−122.
(55) Satoh, R.; Nakamura, R.; Komatsu, A.; Oshima, M.; Teshima, R. Proteomic analysis of known and candidate rice allergens between non-transgenic and transgenic plants. *Regul. Toxicol. Pharmacol.* **2011**, *59* (3), 437−444.
(56) Sander, I.; Rozynek, P.; Rihs, H. P.; van Kampen, V.; Chew, F. T.; Lee, W. S.; Kotschy-Lang, N.; Merget, R.; Bruning, T.; Raulf-Heimsoth, M. Multiple wheat flour allergens and cross-reactive carbohydrate determinants bind IgE in baker's asthma. *Allergy* **2011**, *66* (9), 1208−1215.
(57) Richard, C.; Leduc, V.; Battais, F. Plant lipid transfer proteins (LTPS): biochemical aspect in panallergen − structural and functional features, and allergenicity. *Eur. Ann. Allergy Clin. Immunol.* **2007**, *39* (3), 76−84.
(58) Kabsch, W.; Sander, C. Dictionary of protein secondary structure: pattern recognition of hydrogen-bonded and geometrical features. *Biopolymers* **1983**, *22* (12), 2577−2637.
(59) Orengo, C. A.; Michie, A. D.; Jones, S.; Jones, D. T.; Swindells, M. B.; Thornton, J. M. CATH − a hierarchic classification of protein domain structures. *Structure* **1997**, *5* (8), 1093−1108.
(60) Bordoli, L.; Kiefer, F.; Arnold, K.; Benkert, P.; Battey, J.; Schwede, T. Protein structure homology modeling using SWISS-MODEL workspace. *Nat. Protoc.* **2009**, *4* (1), 1−13.

JOURNAL OF AGRICULTURAL AND FOOD CHEMISTRY

Article

pubs.acs.org/JAFC

Inhibitory Effect of Liposomal Solutions of Grape Seed Extract on the Formation of Heterocyclic Aromatic Amines

Daniela Natale,[†] Monika Gibis,*[,‡] Maria Teresa Rodriguez-Estrada,[†] and Jochen Weiss[‡]

[†]Department of Agricultural and Food Sciences, Alma Mater Studiorum-Università di Bologna, Viale Fanin 40, 40127 Bologna, Italy

[‡]Department of Food Physics and Meat Science, Institute of Food Science and Biotechnology, University of Hohenheim, Garbenstrasse 21/25, 70599 Stuttgart, Germany

Supporting Information

ABSTRACT: The effectiveness of grape seed extract (GSE) encapsulated in liposomes to inhibit the formation of heterocyclic aromatic amines (HAA) during frying of beef patties was assessed. All liposomal systems were prepared by high pressure homogenization at 22 500 psi. A total of six samples (rapeseed oil (control), GSE at 0.1% and 0.2%, and GSE-containing liposomes with 1%, 2%, and 5% soy lecithin) were investigated. MeIQx (2-amino-3,8-dimethylimidazo[4,5-*f*]quinoxaline), PhIP (2-amino-1-methyl-6-phenylimidazo[4,5*b*]pyridine), Norharman, and Harman were found after the marinade application and frying. PhIP concentrations decreased upon marination with GSE (0.1%) and GSE-containing liposomes (1% and 5%) ($p < 0.05$). MeIQx contents decreased in all samples compared to the oil control ($p < 0.01$) while no effect on β-carboline formation was observed. Results are in contrast to previous studies that had shown that liposomal encapsulation may enhance effectiveness of polyphenols to inhibit radical reactions. A mechanistic model was proposed to explain the observed differences.

KEYWORDS: *liposomes, grape seed extract, heterocyclic aromatic amines, phenolic compounds, beef patties*

INTRODUCTION

Diet plays a vital role in maintaining human health, and many studies have been carried out that demonstrate a cause and effect relationship between diet and disease, especially if harmful substances are present in food. Heterocyclic aromatic amines (HAA) are such compounds, as they have been shown to exhibit carcinogenic and mutagenic activities. They are formed in meat and fish when cooked at high temperatures (≥150 °C).[1,2] HAA are classified into two groups based on the temperatures that are prevalent during their formation. HAA formed at temperatures between 100 °C and 300 °C are known as "thermic HAA", IQ type, or aminoimidazoazaarenes (AIA) while HAA produced at higher temperatures (>300 °C) are known as "pyrolytic HAA" or non-IQ type.[3] Their concentration has been found to depend on meat type, cooking parameters (duration, temperature, equipment, and methods), pH, water activity, creatine concentration, amount, and type of carbohydrates, as well as free amino acid content.[4] Several studies have demonstrated the progressive decrease of HAA in the presence of compounds with antioxidant activity, such as vitamin E, fruit extracts, plant extracts, carotenoids, spices, beer, wine, and polyphenols.[5−8]

A wide variety of polyphenols exist in nature, with compounds exhibiting significant antioxidant activities thereby inhibiting radical reactions. Moreover, they have been found to display beneficial physiological functions, such as, for example, anticarcinogenic activity.[9] These potent antioxidants, however, can lose their efficacy when subjected to high temperatures or exposed to oxygen or light-sources. To improve their stability and also control release, researchers have worked on a rational design of encapsulation systems that are compatible with the application matrix and enable protection from degradation.[10,11] Such encapsulation approaches have shown to not only improve chemical stability but also to alleviate unpleasant taste or flavor and improve the compounds' in vivo and in vitro bioavailabilities.[12] Different studies have demonstrated that the activity of polyphenols in particular may be maintained and/or enhanced by encapsulation.[13]

Microencapsulation can be performed by different techniques, such as spray drying, spray chilling, fluidized bed coating, extrusion coating, coacervation, inclusion complexation, centrifugal extrusion, rotational suspension separation, and liposome entrapment.[14] The latter method involves the use of lipid bilayer vesicles that enclose aqueous compartments, allowing in principal the conveyance of a wide variety of molecules having different polarities. Recent studies have shown that liposomes are particularly well suited to carry bioactive compounds of an amphiphilic nature.[15] Liposomal encapsulation, therefore, is a powerful technological tool that can be helpful in producing high-quality foods. The controlled delivery of bioactive compounds can lead to an enhanced absorption of such molecules and to food systems that are more stable having extended shelf-lives.[16−18]

The polyphenols in grape seed extract (GSE) consist mainly of flavonoids, including gallic acid, monomeric flavan-3-ols catechin, epicatechin, gallocatechin, epigallocatechin, and epicatechin 3-*O*-gallate, and procyanidin dimers and trimers and the more highly polymerized procyanidin.[19] Such compounds, when encapsulated in liposomes, have shown to be predominately localized in the bilayer membrane, and only a small part of the substances are found in the inner

Received: April 16, 2013
Revised: December 8, 2013
Accepted: December 9, 2013
Published: December 9, 2013

ACS Publications © 2013 American Chemical Society

dx.doi.org/10.1021/jf4035332 | *J. Agric. Food Chem.* 2014, 62, 279−287

Table 1. Experimental Design Used for This Study (each treatment, $n = 6$)[a]

	systems	treatments
controls	(1) no liposomes (0% of soy lecithin)	(a) patties marinated with rapeseed oil (b) patties marinated with pure GSE (0.1%) (c) patties marinated with pure GSE (0.2%)
liposomes	(1) liposome with 1% of soy lecithin	(a) control without GSE (b) marinated with 0.1% of GSE (c) marinated with 0.2% of GSE
	(2) liposome with 2% of soy lecithin	(a) control without GSE (b) marinated with 0.1% of GSE (c) marinated with 0.2% of GSE
	(3) liposome with 5% of soy lecithin	(a) control without GSE (b) marinated with 0.1% of GSE (c) marinated with 0.2% of GSE

[a]Seventy-two deep-frozen beef patties marinated with 10 g of each solution.

compartment of the liposomes.[20] In model systems these capsules have proven to be highly effective in inhibiting radical reactions.[21] However, only a few studies have been conducted that have investigated their functionalities in complex foods such as, for example, meats and meat products.

The aim of this work was to evaluate the efficiency of the encapsulation of polyphenols from GSE in liposomes and to assess their functionality with respect to HAA formation in fried beef patties after marination. We hypothesized that liposomal-entrapped GSE may have a higher inhibitory effect on the formation of HAA, as liposomes provide large surfaces which can readily interact with the meat compounds that generate HAA. Moreover, liposomes could facilitate a burst release upon heating, which might be beneficial to inhibit the initial stages of the propagating reaction.

MATERIALS AND METHODS

Materials. Soy lecithin (Lipoid S75) was provided by Lipoid (Ludwigshafen, Germany). The contents of phosphatidylcholine, phosphatidylethanolamine, and lysophosphatidylcholine were 69.3%, 9.8%, and 2.1%, respectively, according to the company's specifications. The concentration of the antioxidant DL-α-tocopherol was 0.18%, and the fresh lecithin standard had a maximal peroxide value specification of 3 mequiv O_2/kg (1.5 mmol O_2/kg). The grape seed extract (GSE; *Vitis vinifera L.*) had a procyanidins content of ≥30% (calculated as cyanidin chloride) and a total content of polyphenols of ≥40% (calculated as anhydrous gallic acid) according to the manufacturer's specification; GSE was provided by the Martin Bauer Group Plantextrakt GmbH & Co.KG. (Vestenbergsgreuth, Germany). SephadexG50, Triton X100, gallic acid, sodium acetate, acetic acid, hydrochloric acid, ammonium hydroxide solution, sodium hydroxide, and Folin−Ciocalteu reagent were purchased from Sigma-Aldrich (St. Louis, MO). Ethyl acetate, toluene, methanol, acetonitrile (HPLC grade), triethylamine, and orthophosphoric acid (20%) were supplied by Merck (Darmstadt, Germany). A silica column, propylsulfonic acid (PRS) (500 mg), and C18 (500 mg and 100 mg) solid-phase extraction (SPE) cartridges were purchased from Varian (Palo Alto, CA). The HAA standards IQ, IQx, MeIQ, MeIQx, 4,8-DiMeIQx, 7,8-DiMeIQx, PhIP, Trp-P-1, Trp-P-2, Glu-P-1, Glu-P-2, AαC, and MeAαC were obtained from Toronto Research Chemicals (Toronto, Ontario, Canada). Norharman and harman were supplied by Sigma-Aldrich (St. Louis, MO). The standards were used to prepare a mixed stock standard solution with final concentration of 19.7, 22.8, 21.3, 13.6, 12.9, 12.5, 9.6, 6.5, 5.9, 7.4, 9.4, 5.3, 5.0, 4.9, and 4.1 ng in 100 μL of methanol, respectively (concentrations of HAA in order as described above). All stock solutions were corrected by means of the extinction coefficient.[22] Caffeine was used as an internal standard at a concentration of 2.5 μg/mL in ultrapure water and methanol (1:1, v/v).

Preparation of Liposomes. Liposomes were prepared with different percentages of soy lecithin (1%, 2%, and 5%). Soy lecithin was dispersed in an acetate buffer system (0.25 mol/L, pH 3.8) containing GSE at 0.1% and 0.2%. The GSE-containing buffer system was prepared in ultrapure water and filtered with a folded cellulose filter (Whatman-VWR, Darmstadt, Germany). The GSE solution had been characterized in an earlier study by LC/MS/MS,[23] by a method suggested by Maier et al.[19] The main components of the filtered extract were procyanidin B1 (19.3 mg/g), (+)-catechin (19.1 mg/g), (−)-epicatechin (10.3 mg/g), procyanidin B2 (5.3 mg/g), gallic acid (2.6 mg/g), and (−)-epicatechin gallate (2.1 mg/g). Galloylated dimeric procyanidin and dimeric procyanidins were also found by HPLC-ESI-MS/MS.[19] The mixture was predispersed using a magnetic stirrer overnight and was passed five times through a high-pressure homogenizer consisting of a diamond chamber at 22 500 psi (M110-EH-30, Microfluidics International Cooperation, Newton, MA) to form finely dispersed liposomes incorporating GSE.

Zeta Potential and Average Particle Diameter Measurements of Liposomes. Liposomal charge and z-average particle diameter were determined by dynamic light-scattering (Zetasizer Nano ZS, model ZEN3600, Malvern Instruments, Malvern, UK) at 25 °C. The samples were diluted approximately nine times with the acetate buffer (0.25 mol/L, pH 3.8) and transferred into cuvettes for size determination (DTS1060, Malvern Instruments). The instrument measures the size of particles by determining their Brownian motion at a backscattering angle of 173°. The charge of particles is determined by applying an oscillating electric field and measuring the electrophoretic mobility of particles via light scattering. The z-average particle size and zeta potential were determined immediately after liposome preparation and throughout the four weeks of storage. For each sample, the measurement was repeated twice at 25 °C.

Determination of Total Phenolic Compounds by Folin−Ciocalteu Assay. Two GSE solutions (0.1% and 0.2%) were prepared by dissolving the dried GSE in acetate buffer (pH 3.8 ± 0.2; 0.25 M), stirring for 30 min, and filtering with folded filters. The amount of phenolic compounds was determined in the extract and in the liposomes after encapsulation and after gel filtration according to the Folin−Ciocalteu assay.[24] Liposomes were deliberately destabilized by adding 3 mL of 15 wt % Triton X100 to the samples for the determination of polyphenols in bilayers. The spectrophotometric measurements were carried out at 720 nm, after a 60-min reaction. The results were expressed as milligrams of gallic acid per gram of extract. The encapsulation efficiency of liposomes containing extract was calculated by the amount of total polyphenols of liposomes containing GSE after gel filtration and treatment with the surfactant Triton X-100 divided by the concentration of total polyphenols treated with Triton X-100.

Preparation of Samples and Pan-Frying Trials. Deep-frozen beef patties were obtained from Salomon Hitburger (Grossostheim, Germany). A total of 72 deep-frozen beef patties (62.5 g, 112 × 105 mm, thickness 10 mm) were marinated with 10 g of marinade solution ($n = 6$ for each experimental treatment). As controls, a treatment marinated with rapeseed oil and two treatments marinated with 0.1% and 0.2% unencapsulated (free) GSE were used. Liposomal treatments consisted of solutions containing 1%, 2%, and 5% of soy lecithin and two different GSE concentrations (0.1% and 0.2%) (Table 1). The

dx.doi.org/10.1021/jf4035332 | J. Agric. Food Chem. 2014, 62, 279−287

marination time was 3 h at 8 °C. The marinated beef patties were fried on a double contact grill (Nevada, Neumarker, Hemer, Germany) and heated at 220 °C for 2 min 40 s, as previously described by Gibis et.[6] The core temperature was monitored using a data logger (Therm 3280-8M, Ahlborn, Holzkirchen, Germany). Meat samples were stored under vacuum conditions in the freezer (−18 °C) until analysis. All measurements were repeated at least three times using two replicates. Means and standard deviations were calculated from these measurements with Excel (Microsoft, Redmond, VA).

Determination of HAA. Concentrations of 15 polar and nonpolar HAA were determined using a modified HPLC method[25] based on the method described by Gross and Grueter.[26] Briefly, crushed patties were homogenized with 1 M sodium hydroxide solution. Two homogenates were spiked with 100 μL of the standard mixture. Diatomaceous earth was added and mixed to each of the four equivalent homogenates. HAA were extracted from the patties by multiple solid-phase extractions. HAA were eluted with an ethyl acetate solution containing 5% toluene (100 mL) and adsorbed onto a coupled preconditioned cation exchanger PRS cartridge which had been preconditioned with a mixture of ethyl acetate and 5% toluene. After the PRS cartridge had been dried and washed with 0.01 M HCl solution, the nonpolar HAA were eluted with 15 mL of a mixture of 0.01 M HCl:methanol (2:3, v/v). The nonpolar fraction was purified, first by being adsorbed onto a C18 cartridge (500 mg). After a cleaning step with ultrapure water and drying, the nonpolar HAA were eluted with a 1.2 mL of methanol:ammonia (25%) mixture (90:10, v/v) into a vial. After drying, the eluate was redissolved in 100 μL of caffeine solution (internal standard). The polar HAA were eluted from the PRS cartridges with 20 mL of 0.5 M ammonia acetate solution (pH 8.5) and adsorbed onto a coupled C18 cartridge that had been conditioned with methanol for cleanup. After washing with ultrapure water (2 mL) and drying, the polar HAA were eluted with a 0.8 mL of methanol:ammonia (25%) mixture (90:10, v/v), dried under nitrogen, and redissolved in 100 μL of caffeine solution (internal standard). A Gynkotek HPLC-system (Gynkotek, Germering, Germany) with a M480 pump, a Gina 50 autosampler, a degasser (DG 1310 S) connected to a fluorescence detector (RF 1002), and a diode array detector (UVD 320) were used for the analytical determination of HAA. The system was equipped with a Gynkosoft chromatography data software (version 5.50). HAA were analyzed using a TSK-gel ODS-80TM 250−4.6 mm, 5 μm analytical column (Tosoh Bioscience, Stuttgart, Germany) and a Supelguard LC-18-DB guard column (Supelco, Bellefonte, PA). The injection volume was 60 μL. The mobile phase contained 10 mM triethylamine adjusted with phosphoric acid to pH 3.2 as eluent A, 10 mM triethylamine adjusted to pH 3.6 as eluent B, and acetonitrile as eluent C. HAA were separated with the following gradient program: 82−75% A, 10% B, and 8−15% C from 0 to 10 min; 0% A, 85−75% B, and 15−25% C from 10 to 20 min; 0% A, 75−55% B, and 25−45% C from 20 to 29 min; 0−82% A, 55−10% B, and 45−8% C from 29 to 33 min; 82−15% A, 10% B, and 8−75% C from 33 to 35 min. The flow rate was 1 mL/min. The mobile phase with 75% C was run for 4 min to recover the HPLC column. The HPLC system was then reset to its original starting conditions and equilibrated for 10 min. UV-detection was carried out at 258 nm, and a 3D-field was used for spectral plots at 200−360 nm. The fluorescence detector (ex/em) was adjusted to 360/450 nm at 0 min, 300/440 nm at 14 min, 265/410 nm at 22 min, 305/390 nm at 24 min, 265/410 nm at 25.5 min, and 335/410 nm at 28 min. The peaks of HAA, norharman, and harman were identified by comparing their retention times and UV-spectra with those of the corresponding standards. Quantification was performed with an external calibration (norharman, harman) or standard addition using a single point in duplicate (MeIQx, PhIP) (two samples and two standard mixture spiked samples). The limit of detection (LOD) was 0.017−0.03 ng/g for UV and 0.002−0.015 ng/g for fluorescence detection.[27]

Statistical Method. All data for the concentrations of HAA, the diameter of liposomes, and the ratio of shell volume to total liposome volume were subjected to the Shapiro−Wilk test to assess whether the data was normally distributed. If the data were normally distributed, the values would be analyzed using an analysis of variance with the procedure GLM and the Tukey test ($\alpha = 0.05$ and/or $\alpha = 0.01$) of SAS program version 9.3 (SAS Institute Inc., Cary, NC). If the data was not normally distributed, a nonparametric test (Kruskal−Wallis test, $\alpha = 0.05$) would be used to determine differences. The coefficients of determination (R^2) were calculated (SAS program) for the particle diameter of liposomes, as well as for the ratio of GSE to lecithin concentration.

RESULTS AND DISCUSSION

Determination of Liposomal Stability. The diameter of each liposomal preparation, with and without extract, was measured immediately after production and during storage for four consecutive weeks. Figure 1A−C shows that the diameters of the liposomes without extract were significantly smaller than those of liposomes with GSE. The 5% lecithin liposomes had the smallest z-average particle diameter when compared to the 1% and 2% trials. The differences in z-average diameter between the control (without extract) and liposomes with

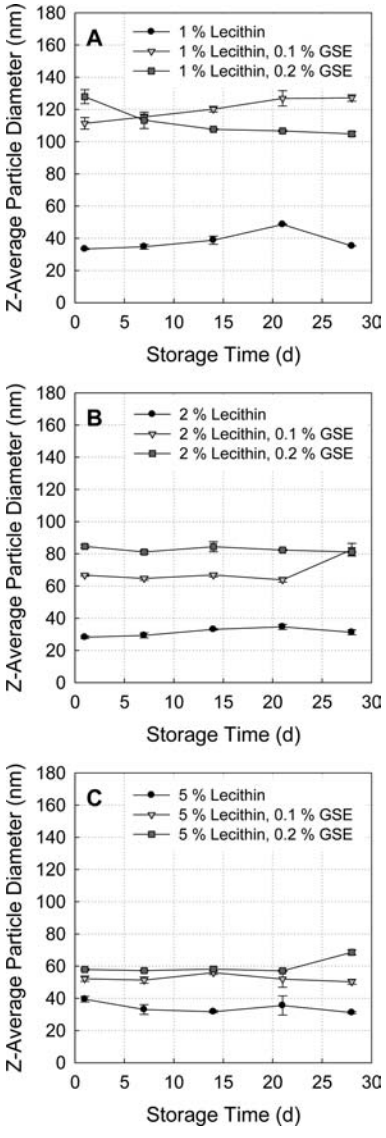

Figure 1. Evaluation of z-average particle diameter of liposomal solutions with different lecithin (1−5%) and GSE (0−0.2%) concentrations, during storage (0−28 days) ($n = 8$). (A) 1% lecithin, (B) 2% lecithin, (C) 5% lecithin.

dx.doi.org/10.1021/jf4035332 | J. Agric. Food Chem. 2014, 62, 279−287

extract suggest that the polyphenolic compounds had been incorporated into the liposomal bilayer, because liposomes with extract were larger than liposomes without it (3-, 2.5-, and 1.6-fold for the 1%, 2%, and 5% trials with 0.2% GSE, respectively). Particle diameters remained virtually unchanged during the four weeks of storage, an indication of the good stability of the liposomal preparations (Figure 1A–C).

The ratio of GSE content to lecithin had a linear, positive correlation (R^2 = 0.97, p < 0.001) to the particle diameter (Figure 2). The largest particle diameter had a ratio of 20%

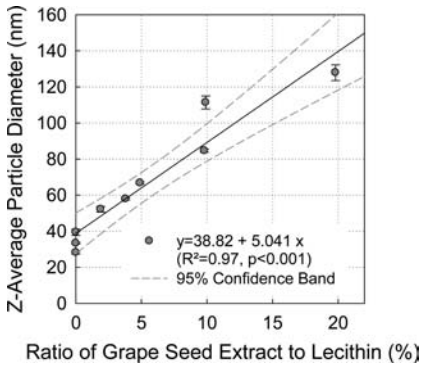

Figure 2. z-Average particle diameter as a function of the ratio of content of GSE to lecithin concentration (0–20%) (n = 8).

GSE in the liposomal lecithin at 1% liposomes containing 0.2% GSE. The correlation shown in Figure 2 confirms that higher ratios of GSE led to liposomes having higher z-average particle diameters. It was not possible to encapsulate more than 20% of GSE because at higher concentrations, large GSE–lecithin aggregates were formed that rapidly developed a sediment layer at the bottom of the sample container. Such sediment-containing solutions could not be processed with the microfluidizer, i.e., the aggregates blocked the homogenization valve. In Figure 3, the zeta potential of liposomes containing GSE concentrations ranging from 0% to 0.2% is depicted as a function of storage time. The zeta potential decreased on average about −14 mV for 0.1% GSE and −9 mV for 0.2% GSE. Similar results had been reported in an earlier study, where liposomes containing GSE had a more negative surface charge with respect to the controls.[21] The zeta potential slightly decreased in all liposomal systems during storage (Figure 3).

Determination of Total Phenolic Compounds by Folin–Ciocalteu Assay. The analysis of the polyphenolic content using the Folin–Ciocalteu assay confirmed that most of the polyphenolic compounds had been incorporated in liposomes (Figure 4). The mean encapsulation efficiency for all liposomal systems containing GSE was 94% ± 14.9%. For example, the amount of unbound polyphenols was particularly low in liposomes containing 5% lecithin, suggesting that the ratio of GSE to lecithin affected the amount being encapsulated (Table 2). The fact that higher ratios of GSE to lecithin resulted in higher amounts of phenols being present in liposomes is in agreement with results from a prior study.[21] To gain more insight into the distribution of polyphenols between the liposomal membrane and the interior, the volume of the inner compartment of liposomes and thus the concentration of GSE there can be calculated by considering the ratio of shell to total volume of liposomes V_{shell}/V_{total} (eq 2) (Table 2).

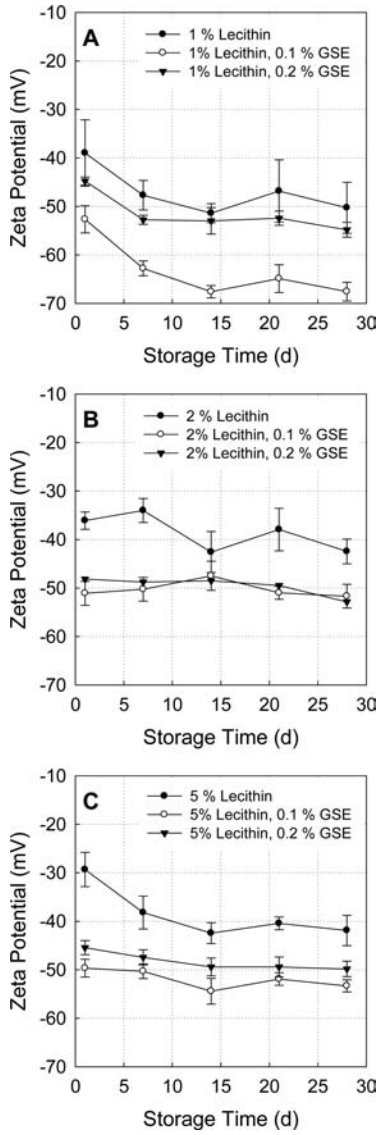

Figure 3. Zeta potential of the liposomes containing GSE as a function of storage time (0–28 days) (n = 8). (A) liposomes 2% containing 0–0.2% GSE, (B) liposomes 5% containing 0–0.2% GSE.

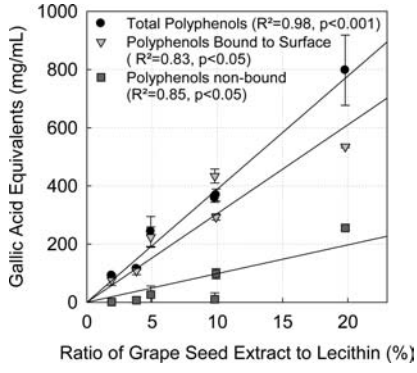

Figure 4. Concentration of phenolic compounds (calculated as gallic acid equivalents) in liposomal solution, as a function of the ratio of GSE to lecithin content (0–20%) (n = 4).

$$\frac{V_{shell}}{V_{total}} = \frac{\frac{4}{3}\pi {r_2}^3 - \frac{4}{3}\pi(r_2 - \Delta r)^3}{\frac{4}{3}\pi {r_2}^3} \quad (1)$$

dx.doi.org/10.1021/jf4035332 | J. Agric. Food Chem. 2014, 62, 279–287

Table 2. Theoretical Calculations of the Ratio of Shell to Total Volume of Liposomes (V_{shell}/V_{total})[a]

concentration of GSE (% w/v)	concentration of lecithin (% w/w)					
	1%		2%		5%	
	particle radius (nm)[b–d]	V_{shell}/V_{total} (% v/v)[b–d]	particle radius (nm)[b–d]	V_{shell}/V_{total} (% v/v)[b–d]	particle radius (nm)[b–d]	V_{shell}/V_{total} (% v/v)[b–d]
0	16.5 ± 0.23^{Aa}	56.1 ± 0.6^{Aa}	14.1 ± 0.42^{Ba}	63.2 ± 1.3^{Ba}	19.7 ± 0.42^{Ca}	49.3 ± 1.6^{Ca}
0.1	55.7 ± 1.80^{Ab}	20.0 ± 0.1^{Ab}	33.4 ± 0.2^{Bb}	31.8 ± 0.2^{Bb}	26.1 ± 0.33^{Cb}	39.3 ± 0.2^{Cb}
0.2	64.0 ± 2.18^{Ac}	17.6. ± 0.1^{Ac}	42.3 ± 0.1^{Bc}	25.8 ± 0.1^{Bc}	29.0 ± 0.31^{Cc}	36.0 ± 0.3^{Cc}

[a]Calculations were carried out with eq 2, considering Δr_{shell} = 4 nm and the measured radius of each liposome. [b]Data are reported as mean ± SD. [c]Means with different letters are significantly different ($p < 0.05$). [d]Lower case for 0–0.2% GSE, upper case for 1–5% lecithin.

Table 3. Concentrations of HAA in Fried Beef Patties after Marination with GSE, Rapeseed Oil, and Liposomes (1, 2, and 5% w/w lecithin) Containing GSE (0.1% and 0.2%) ($n = 6$, $p < 0.01$)

samples	HAA in fried beef patties[a]			
	MeIQx (ng/g) mean ± SD	PhIP (ng/g) mean ± SD	norharman (ng/g) mean ± SD	harman (ng/g) mean ± SD
control I (rapeseed oil)	1.9 ± 0.06^{a}	1.0 ± 0.21^{bcd}	9.2 ± 0.64^{cd}	3.8 ± 0.26^{cd}
control II 0.1% GSE	1.2 ± 0.07^{b}	0.5 ± 0.12^{cd}	8.9 ± 0.6^{d}	3.3 ± 0.11^{d}
control III 0.2% GSE	1.3 ± 0.27^{b}	0.8 ± 0.21^{bcd}	11.3 ± 0.27^{ab}	4.0 ± 0.2^{bcd}
lip. 1% lec.	1.2 ± 0.09^{b}	1.2 ± 0.04^{bc}	9.4 ± 0.05^{cd}	4.6 ± 0.02^{bc}
lip. 1% lec., 0.1% GSE	1.0 ± 0.13^{b}	0.5 ± 0.15^{cd}	9.2 ± 0.64^{cd}	4.7 ± 0.24^{bc}
lip. 1% lec., 0.2% GSE	1.1 ± 0.10^{b}	0.9 ± 0.11^{bcd}	9.0 ± 0.45^{cd}	4.6 ± 0.78^{bc}
lip. 2% lec.	1.0 ± 0.05^{b}	0.7 ± 0.24^{bc}	10.4 ± 0.26^{cd}	4.4 ± 0.12^{bc}
lip. 2% lec., 0.1% GSE	0.9 ± 0.18^{b}	1.1 ± 0.17^{bc}	10.5 ± 1.03^{abc}	4.8 ± 0.56^{ab}
lip. 2% lec., 0.2% GSE	1.3 ± 0.01^{b}	1.2 ± 0.10^{abc}	11.9 ± 0.93^{a}	5.7 ± 0.36^{a}
lip.5% lec.	1.4 ± 0.14^{b}	1.9 ± 0.69^{a}	9.9 ± 0.02^{bcd}	4.4 ± 0.01^{bc}
lip. 5% lec., 0.1% GSE	1.2 ± 0.17^{b}	0.3 ± 0.03^{d}	4.1 ± 0.01^{e}	2.0 ± 0.01^{e}
lip. 5% lec. 0.2% GSE	1.4 ± 0.39^{b}	1.4 ± 0.16^{ab}	11.0 ± 0.01^{ab}	4.7 ± 0.01^{bc}

[a]lip. = liposomes, lec. = lecithin, and GSE = grape seed extract. Means with different letters are significantly different.

$$\frac{V_{shell}}{V_{total}} = 1 - \frac{(r_2 - \Delta r)^3}{r_2^3} \quad (2)$$

with r_2 being the mean radius after microfluidization. A shell thickness of 44.5 Å ± 0.3 Å for unilamellar 1,2-dimyristoyl-phosphatidylcholine vesicles of approximately 4 nm (Δr) has been reported for small unilamillar vesicular liposomes containing a single bilayer.[28,29] The ratio of the core volume to the total volume thus increased from 37% to 82% in liposomes containing extract (Table 2). Consequently, at higher loading capacities of GSE where lipsomes have larger particle diameters, GSE is increasingly located in the interior of liposomes rather than in the membrane, simply due to spatial constraints (Figure 2).

Effect on the Formation of HAA in Fried Beef Patties. The effectiveness of application of liposomal-encapsulated GSE on beef patties on weight loss and formation of HAA was assessed. The weight loss of patties during frying was determined as the weight difference of the beef patties before and after frying. The internal temperature was continually monitored by using a data logger, and it was around 72 °C at the end of the frying process. The mean weight loss of the patties was between 29.3% and 34.9% for the different batches, with an overall standard deviation of 2.7%. The results of the weight loss measurements showed that all patties were subjected to similar frying conditions.

In the polar fraction of HAA method, the two most important polar HAA (MeIQx and PhIP) were identified. The HPLC-chromatograms are shown in Figure S1 in Supporting Information. The concentrations of PhIP were quantified using the higher sensitively fluorescence detection. β-Carbolines norharman and harman were found in the nonpolar fraction (data not shown). The average recoveries for HAA were 61% for MeIQx, 47% for PhIP, and 55% for norharman and harman, which confirms the high efficiency of the method used for such substances. These recoveries are similar to those reported in other studies.[27]

Table 3 shows the content of HAA in fried beef patties. The most predominant HAA found in the beef samples for the polar fractions was MeIQx. Generally, the content of polyphenols had an inhibiting effect on the formation of MeIQx during frying of beef. In comparison to control samples (marinated with rapeseed oil), a significant decrease of MeIQx ($p < 0.01$) was observed with respect to all other samples. However, no significant differences were found between different experimental treatments marinated with liposomes and liposomal-encapsulated GSE (Table 3). In contrast, significant differences were detected in the MeIQx concentration in the control trial, in particular between the samples marinated with rapeseed oil and those marinated with pure GSE. The concentration of extract (0.1% and 0.2%) did not have an impact on the formation of MeIQx. However, significant differences were detected between the control treatment (marinated with rapeseed oil), and the encapsulation trials (1%, 2%, and 5% of soy lecithin) regardless of the soy lecithin percentage. The MeIOx concentration was approximately 1.6-fold higher in the sample marinated with rapeseed oil than in samples marinated with liposomal-encapsulated GSE solution.

Various studies have demonstrated the positive effect exerted by molecules with antioxidant activity on the inhibition of HAA formation, with a particular focus on the inhibition of formation of MeIQx.[30,31] The marination of meats with barbeque sauces,

dx.doi.org/10.1021/jf4035332 | J. Agric. Food Chem. 2014, 62, 279–287

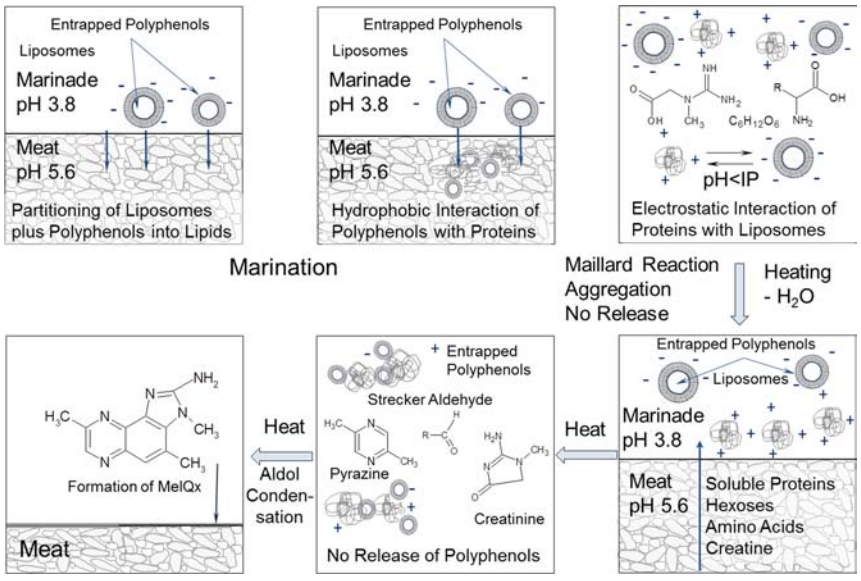

Figure 5. Schematic overview of HAA formation (e.g., MeIQx) and the proposed mechanism with possible interactions between the marinade consisting of liposome-entrapped GSE and the meat matrix.

mixtures of spices, red wine, beer, or plant extracts before frying mostly led to a reduction in the HAA content.[5−7,25,32−34] Similarly in the present study, an inhibitory effect on formation of HAA was found when compounds with antioxidant activities were used to marinate the beef patties. However, liposomal encapsulation of GSE did not lead to a significant improvement in the inhibition of the HAA formation compared to the use of free GSE. Complex interplays take place that depend on oil/lipid type and concentration. For example, authors reported an increasing effect of oxidized oil on the formation of HAA after different storage times.[35,36]

These somewhat disappointing results with respect to MeIQx may be due to the formation mechanism of polar amines, which are generated by the reaction of hexose and amino acids via Maillard and Strecker degradation reactions, whereby the free radical intermediate form of pyridines and pyrazines will react with creatine.[37,38] The apparent positive impact on the diminution of polar MeIQx may not be solely due to the action of the polyphenols but may be attributed to an antioxidant effect exerted by soy lecithin, which contained 0.18% DL-α-tocopherols, according to its specification. Therefore, approximately 4−8 mg of polyphenolic compounds and 0.2−0.9 mg of α-tocopherols were calculated per patty marinated with GSE-entrapped liposomes.

With PhIP, a different behavior was observed compared to that of the other polar HAA. No differences at a level of significance of $p = 0.01$ were found between the control and samples treated with GSE, regardless of the polyphenol concentration. In other words, an antioxidant effect from the polyphenolic compounds was not evident. A significant decrease of PhIP was detected in the trials with liposomes prepared with 5% of soy lecithin that contained 0.1% GSE ($p < 0.05$). Nevertheless, no systematic correlation between the concentration of PhIP and the GSE content in liposomes could be established.

A significant increase of norharman compared to the rapeseed oil control was observed after marination with 0.2% pure extract, and 2% and 5% liposomes containing 0.2% GSE. The β-carboline norharman levels varied between 8.9 and 11.9 ng/g, except for the 5% liposomes containing 0.1% GSE (Table 3). Harman concentration ranged from 3.3 to 5.7 ng/g. The β-carboline harman generally increased with GSE content with results being significantly different for samples marinated with 2% liposomes containing GSE. These results are similar to those reported in an earlier study, where β-carbolines increased with the addition of GSE.[23] The concentration of norharman and harman are comparable to those reported by Totsuka et al.[39] One can conclude from these results that the use of GSE is somewhat detrimental to the formation of β-carbolines norharman and harman and that the application form (encapsulated or free) does not affect the β-carboline levels. This may be related to the formation mechanism of norharman and harman, which does not involve a free radical action and, for this reason, cannot be inhibited by the addition of antioxidants such as polyphenols.[37] In the formation pathway of these compounds, tryptophan has been identified as their precursor, whereas glucose enhances norharman formation. In aqueous model systems containing creatine, glucose, and various single amino acids, norharman and harman were formed in mixtures containing isoleucine, arginine, phenylalanine, and tryptophan, and this mixture combined with tyrosine generated norharman upon heating at 180 °C for 10 min. [40] When iron (Fe^{2+}) and copper (Cu^{2+}) were added to a model system, norharman was generated even at temperatures as low as 40 °C.[40]

Mechanistic Insights. The fact that entrapped GSE polyphenols in liposomes had no additional inhibitory effect on the formation of MeIQx and PhIP is somewhat surprising, considering that liposomal-encapsulated polyphenols have previously been found to improve inhibition of, for example, lipid oxidation in model systems.[21] Moreover, in another study, the use of a different encapsulation system, a water-in-oil marinade with GSE being encapsulated in water droplets suspended in an oil phase, was found to significantly reduce formation of the mutagenic compounds MeIQx and PhIP compared to water-in-oil marinade without extract.[23] There, the water-in-oil marinade contained 0.2−0.8% GSE (pH 5.6) and had been applied before frying of beef patties. In consequence, the content of MeIQx and PhIP decreased by approximately 57% and 90%, respectively.[23]

dx.doi.org/10.1021/jf4035332 | J. Agric. Food Chem. 2014, 62, 279−287

The observed differences between the results in this study and the results of the above cited former studies may be due to a variety of physical mechanisms that are influenced by the structure and physical properties of the encapsulation system used and its interaction with the application matrix (Figure 5):

(i) Diffusion and partitioning behavior: Liposomes containing GSE had a very small particle size and a hydrophilic surface and thus were water-soluble. Thus similar to free GSE, once applied on the surface of the meat matrix, they are able to rapidly diffuse into the interior of the meat matrix. Once in the interior, they are effectively unable to inhibit the formation reaction of HAA that occurs mostly at the surface where high temperatures are prevalent. This is notably different from the above-described water-in-oil system, which is hydrophobic and has much larger particle sizes. There, water droplets containing GSE are enclosed by an oil matrix and are thus mostly present at the surface of the meat product. The heating may lead to an evaporation of the internal water droplets, which in turn leads to a release of the polyphenols able to inhibit the reaction.

(ii) Interaction behavior: The encapsulation of GSE in liposomes may have also not prevented the polyphenols from interacting with dissolved proteins in the meat matrix. During grinding, some of the proteins are solubilized, leading to a characteristic binding of meat and fat particles in ground beef patties. Studies have shown that the interaction of both phosphatidylcholine liposomes and polyphenols with dissolved proteins generally leads to the formation of protein−polyphenol[41] and liposomes−protein complexes,[42] respectively, rendering polyphenols unable to effectively inhibit radical reactions. These interactions may be driven by hydrophobic as well as electrostatic interactions, the latter being due to the fact that both the liposomes and the free GSE were negatively charged (Figure 3) while the surface charge of meat proteins at the pH of the buffered marinade of 3.8 was below the isoelectric point and therefore positively charged. The former may be due to the fact that most proteins possess significant surface hydrophobicities, and because GSE was bound mostly to the surface or was part of the liposomal membrane, an interaction may readily occur. This would again be noticeably different from the functionality of a water-in-oil emulsion, in which the polyphenols are protected from interaction with proteins by the oil phase that surrounds the internal water droplets containing the GSE.

Finally, the formation of PhIP differs from the formation of MeIQx. On the basis of literature studies, while glucose does not seem to be a necessary precursor when using dry heating in a model system, it may however enhance or inhibit the formation of PhIP.[43] In a model system with only phenylalanine and creatinine as precursors, the Strecker aldehyde phenylacetaldehyde is initially formed. In a second step an aldol condensation of the aldehyde with creatinine and subsequent dehydration takes place. The products of the addition as well as the condensation product were identified in the model system and in heated meat.[44]

Our working hypothesis that a liposomal encapsulation may inhibit HAA formation due to the increased surface of the liposomes was therefore not supported by the data obtained. In fact, the system proved to be ineffective with results being analogous to those of trials with free GSE. However, the study led to new mechanistic insights that should help to more effectively and rationally design encapsulation systems for antioxidants. A functional encapsulation system for polyphenols must not only be able to contain high contents of the active ingredient such as for example the polyphenol, but it must be designed such that is ensures that high concentrations of an active compound are present at the required site of release. If the reaction takes place at the surface of a product, then the generation of small particles that are compatible with the properties of the food matrix may not be ideal. Rather, larger particles with a certain "incompatibility", preventing a migration into the matrix, should be manufactured. In contrast, if the reaction takes place in the interior of the matrix, small carriers that are compatible with the matrix may be well suited to influence the reaction. This study therefore should be helpful to food manufacturers to better understand chemical or physical interactions in complex food matrixes (such as meat), by means of encapsulated active compounds as well as the encapsulating material.

■ ASSOCIATED CONTENT

Ⓢ Supporting Information

Figure S1: HPLC UV (258 nm) and fluorescence chromatograms of polar HAA in fried beef patties marinated with 5% liposomes. This material is available free of charge via the Internet at http://pubs.acs.org.

■ AUTHOR INFORMATION

Corresponding Author

*Tel: +49 711 459 22293. Fax: +49 711 459 24446. E-mail: gibis@uni-hohenheim.de.

Funding

This project was supported financially by funds from the University of Hohenheim Experiment Station.

Notes

The authors declare no competing financial interest.

■ ACKNOWLEDGMENTS

The authors thank Lipoid GmbH and the Plantextrakt−Martin Bauer Group for donation of sample materials.

■ ABBREVIATIONS USED

GSE, grape seed extract; Lip, liposomes; Lec, lecithin; SD, standard deviation; HAA, heterocyclic aromatic amines; IQ, 2-amino-3-methylimidazo[4,5-*f*]quinoline (CAS no.: 76180-96-6); IQx, 2-amino-3-methylimidazo[4,5-*f*]quinoxaline (CAS no.: 108354-47-8); MeIQ, 2-amino-3,4-dimethylimidazo[4,5-*f*]-quinoline (CAS no.: 77094-11-2); MeIQx, 2-amino-3,8-dimethylimidazo[4,5-*f*]quinoxaline (CAS no.: 77500-04-0); 4,8-DiMeIQx, 2-amino-3,4,8-trimethylimidazo[4,5-*f*]-quinoxaline (CAS no.: 95896-78-9); 7,8-DiMeIQx, 2-amino-3,7,8-trimethylimidazo[4,5-*f*]quinoxaline (CAS no.: 92180-79-5); PhIP, 2-amino-1-methyl-6-phenylimidazo[4,5-*b*]pyridine (CAS no.: 105650-23-5); Trp-P-1, 3-amino-1,4-dimethyl-5*H*-pyrido[4,3-*b*]indole (CAS no.: 62450-06-0), monoacetate (CAS no.: 68808-54-8); Trp-P-2, 3-amino-1-methyl-5*H*-pyrido-[4,3-*b*]indole (CAS no.: 62450-07-1); Glu-P-1, 2-amino-6-methyldipyrido[1,2-a:3′,2′-*d*]imidazole (CAS no.: 67730-11-4); Glu-P-2, 2-aminodipyrido[1,2-*a*:3′,2′-*d*]imidazole (CAS no.: 67730-10-3); AαC, 2-amino-9*H*-pyrido[2,3-*b*]indole (CAS no.: 26148-68-5); MeAαC, 2-amino-3-methyl-9*H*-pyrido[2,3-*b*]indole (CAS no.: 68006-83-7); harman, 1-methyl-9*H*-pyrido-[3,4-*b*]indole (CAS no.: 486-84-0); norharman, 9*H*-pyrido[3,4-*b*]indole (CAS no.: 244-63-3)

REFERENCES

(1) Arvidsson, P.; Van Boekel, M. A. J. S.; Skog, K.; Jägerstad, M. Kinetics of formation of polar heterocyclic amines in a meat model system. *J. Food Sci.* **1997**, *62*, 911−916.

(2) Jägerstad, M.; Skog, K.; Arvidsson, P.; Solyakov, A. Chemistry, formation and occurrence of genotoxic heterocyclic amines identified in model systems and cooked foods. *Z. Lebensm.-Unters. Forsch.* **1998**, *207*, 419−427.

(3) Alaejos, M. S.; Afonso, A. M. Factors that affect the content of heterocyclic aromatic amines in foods. *Compr. Rev. Food Sci. Food Saf.* **2011**, *10*, 52−108.

(4) Oz, F.; Kaya, M. Heterocyclic aromatic amines in meat. *J. Food Process. Preserv.* **2011**, *35*, 739−753.

(5) Viegas, O.; Amaro, L. F.; Ferreira, I. M. P. L. V. O.; Pinho, O. Inhibitory effect of antioxidant-rich marinades on the formation of heterocyclic aromatic amines in pan-fried beef. *J. Agric. Food Chem.* **2012**, *60*, 6235−6240.

(6) Gibis, M.; Weiss, J. Inhibitory effect of marinades with hibiscus extract on formation of heterocyclic aromatic amines and sensory quality of fried beef patties. *Meat Sci.* **2010**, *85*, 735−742.

(7) Smith, J. S.; Ameri, F.; Gadgil, P. Effect of marinades on the formation of heterocyclic amines in grilled beef steaks. *J. Food Sci.* **2008**, *73*, T100−T105.

(8) Murkovic, M.; Steinberger, D.; Pfannhauser, W. Antioxidant spices reduce the formation of heterocyclic amines in fried meat. *Z. Lebensm.-Unters. Forsch.* **1998**, *207*, 477−480.

(9) Bendini, A.; Cerretani, L.; Carrasco-Pancorbo, A.; Gómez-Caravaca, A. M.; Segura-Carretero, A.; Fernández-Gutiérrez, A.; Lercker, G. Phenolic molecules in virgin olive oils: A survey of their sensory properties, health effects, antioxidant activity and analytical methods. An overview of the last decade. *Molecules* **2007**, *12*, 1679−1719.

(10) Mozafari, M. R.; Flanagan, J.; Matia-Merino, L.; Awati, A.; Omri, A.; Suntres, Z. E.; Singh, H. Recent trends in the lipid-based nanoencapsulation of antioxidants and their role in foods. *J. Sci. Food Agric.* **2006**, *86*, 2038−2045.

(11) McClements, D. J. Design of nano-laminated coatings to control bioavailability of lipophilic food components. *J. Food Sci.* **2010**, *75*, R30−R42.

(12) Fang, J.-Y.; Hung, C.-F.; Hwang, T.-L.; Huang, Y.-L. Physicochemical characteristics and in vivo deposition of liposome-encapsulated tea catechins by topical and intratumor administrations. *J. Drug Targeting* **2005**, *13*, 19−27.

(13) Jones, O. G.; McClements, D. J. Functional biopolymer particles: Design, fabrication, and applications. *Compr. Rev. Food Sci. Food Saf.* **2010**, *9*, 374−397.

(14) Gibbs, B. F.; Kermasha, S.; Alli, I.; Mulligan, C. N. Encapsulation in the food industry: A review. *Int. J. Food Sci. Nutr.* **1999**, *50*, 213−224.

(15) Mozafari, R. M.; Johnson, C.; Hatziantoniou, S.; Demetzos, C. Nanoliposomes and their applications in food nanotechnology. *J. Liposome Res.* **2008**, *18*, 309−327.

(16) McClements, D. J.; Decker, E. A.; Park, Y.; Weiss, J. Structural design principles for delivery of bioactive components in nutraceuticals and functional foods. *Crit. Rev. Food Sci. Nutr.* **2009**, *49*, 577−606.

(17) McClements, D. J.; Li, Y. Structured emulsion-based delivery systems: Controlling the digestion and release of lipophilic food components. *Adv. Colloid Interface Sci.* **2010**, *159*, 213−228.

(18) Taylor, T. M.; Davidson, P. M.; Bruce, B. D.; Weiss, J. Liposomal nanocapsules in food science and agriculture. *Crit. Rev. Food Sci. Nutr.* **2005**, *45*, 587−605.

(19) Maier, T.; Schieber, A.; Kammerer, D. R.; Carle, R. Residues of grape (Vitis vinifera L.) seed oil production as a valuable source of phenolic antioxidants. *Food Chem.* **2008**, *112*, 551−559.

(20) Nakayama, T.; Kajiya, K.; Kumazawa, S. Interaction of plant polyphenols with liposomes. *Adv. Planar Lipid Bilayers Liposomes* **2006**, *4*, 107−133.

(21) Gibis, M.; Vogt, E.; Weiss, J. Encapsulation of polyphenolic grape seed extract in polymer-coated liposomes. *Food Funct.* **2012**, *3*, 246−254.

(22) Hatch, F. T.; Felton, J. S.; Stuermer, D. H.; Bjeldanes, L. F. Identification of mutagens from the cooking of food. *Chem. Mutagens* **1984**, *9*, 111−164.

(23) Gibis, M.; Weiss, J. Antioxidant capacity and inhibitory effect of grape seed and rosemary extract in marinades on the formation of heterocyclic amines in fried beef patties. *Food Chem.* **2012**, *134*, 766−774.

(24) Singleton, V. L.; Orthofer, R.; Lamuela-Raventos, R. M. Analysis of total phenols and other oxidation substrates and antioxidants by means of Folin-Ciocalteu reagent. *Methods Enzymol.* **1999**, *299*, 152−178.

(25) Gibis, M. Effect of oil marinades with garlic, onion, and lemon juice on the formation of heterocyclic aromatic amines in fried beef patties. *J. Agric. Food Chem.* **2007**, *55*, 10240−10247.

(26) Gross, G. A.; Grueter, A.; Heyland, S. Optimization of the sensitivity of high-performance liquid chromatography in the detection of the heterocyclic aromatic amine mutagens. *Food Chem. Toxicol.* **1992**, *30*, 491−498.

(27) Gibis, M. Optimized HPLC method for analysis of polar and nonpolar heterocyclic amines in cooked meat products. *J. AOAC Int.* **2009**, *92*, 715−724.

(28) Laye, C.; McClements, D. J.; Weiss, J. Formation of biopolymer-coated liposomes by electrostatic deposition of chitosan. *J. Food Sci.* **2008**, *73*, N7−15.

(29) Kucerka, N.; Kiselev, M. A.; Balgavy, P. Determination of bilayer thickness and lipid surface area in unilamellar dimyristoylphosphatidylcholine vesicles from small-angle neutron scattering curves: A comparison of evaluation methods. *Eur. Biophys. J.* **2004**, *33*, 328−334.

(30) Salmon, C. P.; Knize, M. G.; Felton, J. S. Effects of marinating on heterocyclic amine carcinogen formation in grilled chicken. *Food Chem. Toxicol.* **1997**, *35*, 433−441.

(31) Shin, H. S.; Lee, S. Influence of honey containing marinades on heterocyclic aromatic amine formation and overall mutagenicity in fried pork chops. *Food Sci. Biotechnol.* **2004**, *13*, 651−656.

(32) Tikkanen, L. M.; Latva-Kala, K. J.; Heinio, R. L. Effect of commercial marinades on the mutagenic activity, sensory quality and amount of heterocyclic amines in chicken grilled under different conditions. *Food Chem. Toxicol.* **1996**, *34*, 725−730.

(33) Busquets, R.; Puignou, L.; Galceran, M. T.; Skog, K. Effect of red wine marinades on the formation of heterocyclic amines in fried chicken breast. *J. Agric. Food Chem.* **2006**, *54*, 8376−8384.

(34) Puangsombat, K.; Jirapakkul, W.; Smith, J. S. Inhibitory activity of Asian spices on heterocyclic amines formation in cooked beef patties. *J. Food Sci.* **2011**, *76*, T174−T180.

(35) Johansson, M. A. E.; Fredholm, L.; Bjerne, I.; Jägerstad, M. Influence of frying fat on the formation of heterocyclic amines in fried beefburgers and pan residues. *Food Chem. Toxicol.* **1995**, *33*, 993−1004.

(36) Persson, E.; Graziani, G.; Ferracane, R.; Fogliano, V.; Skog, K. Influence of antioxidants in virgin olive oil on the formation of heterocyclic amines in fried beefburgers. *Food Chem. Toxicol.* **2003**, *41*, 1587−1597.

(37) Tsen, S. Y.; Ameri, F.; Smith, J. S. Effects of rosemary extracts on the reduction of heterocyclic amines in beef patties. *J. Food Sci.* **2006**, *71*, C469−C473.

(38) Milić, B. i. L.; Djilas, S. M.; Čanadanović-Brunet, J. M. Synthesis of some heterocyclic aminoimidazoazarenes. *Food Chem.* **1993**, *46*, 273−276.

(39) Totsuka, Y.; Ushiyama, H.; Ishihara, J.; Sinha, R.; Goto, S.; Sugimura, T.; Wakabayashi, K. Quantification of the co-mutagenic β-carbolines, norharman and harman, in cigarette smoke condensates and cooked foods. *Cancer Lett.* **1999**, *143*, 139−143.

(40) Pfau, W.; Skog, K. Exposure to β-carbolines norharman and harman. *J. Chromatogr. B: Anal. Technol. Biomed. Life Sci.* **2004**, *802*, 115−126.

(41) Hagerman, A. E.; Butler, L. G. The specificity of proanthocyanidin-protein interactions. *J. Biol. Chem.* **1981**, *256*, 4494−7.
(42) Dimitrova, M. N.; Tsekov, R.; Matsumura, H.; Furusawa, K. Size dependence of protein-induced flocculation of phosphatidylcholine liposomes. *J. Colloid Interface Sci.* **2000**, *226*, 44−50.
(43) Skog, K. I.; Johansson, M. A.; Jägerstad, M. I. Carcinogenic heterocyclic amines in model systems and cooked foods: A review on formation, occurrence and intake. *Food Chem. Toxicol.* **1998**, *36*, 879−896.
(44) Murkovic, M. Formation of heterocyclic aromatic amines in model systems. *J. Chromatogr. B: Anal. Technol. Biomed. Life Sci.* **2004**, *802*, 3−10.

JOURNAL OF AGRICULTURAL AND FOOD CHEMISTRY

Article

pubs.acs.org/JAFC

Metabolism, Distribution, and Excretion of Deoxynivalenol with Combined Techniques of Radiotracing, High-Performance Liquid Chromatography Ion Trap Time-of-Flight Mass Spectrometry, and Online Radiometric Detection

Dan Wan, Lingli Huang, Yuanhu Pan, Qinghua Wu, Dongmei Chen, Yanfei Tao, Xu Wang, Zhenli Liu, Juan Li, Liye Wang, and Zonghui Yuan*

National Reference Laboratory of Veterinary Drug Residues (HZAU) and Ministry of Agriculture (MOA) Key Laboratory for the Detection of Veterinary Drug Residues in Foods, Huazhong Agricultural University, Wuhan, Hubei 430070, People's Republic of China

ABSTRACT: Dispositions of deoxynivalenol (DON) in rats and chickens were investigated, using a radiotracer method coupled with a novel γ-accurate radioisotope counting (γ-ARC) radio-high-performance liquid chromatography ion trap time-of-flight tandem mass spectrometry (radio-HPLC-IT-TOF-MS/MS) system. 3β-^{3}H-DON was chemically synthesized and orally administrated to both sexes of rats and chickens as single or multiple doses. The results showed that DON was widely distributed and quickly eliminated in all tissues. The highest concentration was found in the gastrointestinal tract at 6 h post-administration. Substantially lower levels were detected in the kidney, liver, heart, lung, spleen, and brain. Three new metabolites were identified tentatively as 10-deoxynivalenol-sulfonate, 10-deepoxy-deoxynivalenol (DOM-1)-sulfonate, and deoxynivalenol-3α-sulfate. Deoxynivalenol-3α-sulfate was a major metabolite in chickens, while the major forms in rats were DOM-1 and DON. Additionally, a higher excretion rate in urine was observed in female rats than in male rats. The differences in metabolite profiles and excretion rates, which suggested diverse ways to detoxify, may relate to the different tolerances in different genders or species.

KEYWORDS: *metabolism, disposition, deoxynivalenol, tritium labeled*

INTRODUCTION

Deoxynivalenol [DON (Figure 1)], one of the primary trichothecene toxins produced by *Fusarium culmorum* and *Fusarium graminearum* species, is a widespread contaminant in grains, such as wheat, barley, oat, and maize. The presence of DON in grains is considered as an important limit for economic benefits in the livestock industry. It reduces feed intake, body weight, and reproductive capacities of food-producing animals while increases disease incidence and, thus, leads to significant economic losses.[1] Upon consumption of DON-contaminated grains or food products, it is known to trigger a wide range of disorders in humans and animals, including vomiting, diarrhea, and gastroenteritis, by targeting ribosome and endoplasmic reticulum (ER), ultimately leading to inhibition of protein synthesis.[2,3] Because of these mycotoxicosis, the Joint FAO/WHO Expert Committee on Food Additives (JECFA) has recently set the limit of group provisional maximum tolerable daily intake (PMTDI) of DON for 1 μg kg^{-1} of body weight (bw) day^{-1}.[4]

Previous studies revealed that DON was widely distributed and rapidly excreted in rats and chickens. Following a single oral administration of 10 mg/kg of bw of [^{14}C] DON to rats, DON was detectable in the gastrointestinal tract, liver, testes, prostate, seminal vesicles, and heart, with negligible radioactivity retained in the above tissues in 96 h. Excretion in the urine and feces accounts for 25 and 64%, respectively, of the administered dose.[5] In chickens, after a single dose of 2.2 mg of [^{14}C] DON per bird, radioactivity was detectable in all tissues, including the gastrointestinal tract, liver, spleen, heart, kidney, fat, and brain in 3 h, and 78.6 ± 21% was excreted within 24 h.[6] DON can be extensively metabolized mainly into deepoxy-deoxynivalenol [DOM-1 (Figure 1)] and DON conjugates.[7] Using unlabeled DON, DOM-1 was identified in rat feces by gas chromatography−mass spectrometry (GC−MS) and shown later to be a major form in rat excreta.[5,8] After *in vitro* incubation with the contents of large intestines or intestinal microbes of chickens, DON was completely converted into DOM-1.[9,10] Glucuronide conjugations appear to be important phase II metabolites in rats, swine, sheep, cows, and humans, including DOM-1-glucuronide and three DON-glucuronide conjugates.[7,11,12] One of the major glucuronide conjugations, DON-3α-glucuronide, could be a biomarker for monitoring DON exposure in human urine.[13] Additionally, minor DON sulfate conjugation was also found, which involved 2% of the recovered dose in sheep urine, following intravenous administration.[14]

Although research on metabolism, distribution, and excretion of DON in rodent and poultry has been partially performed, information on *in vivo* metabolism of DON in poultry is still limited. The gender differences in metabolism, distribution, and excretion were not investigated in rats or any other species. In

Received: June 19, 2013
Revised: December 14, 2013
Accepted: December 16, 2013
Published: December 16, 2013

ACS Publications © 2013 American Chemical Society

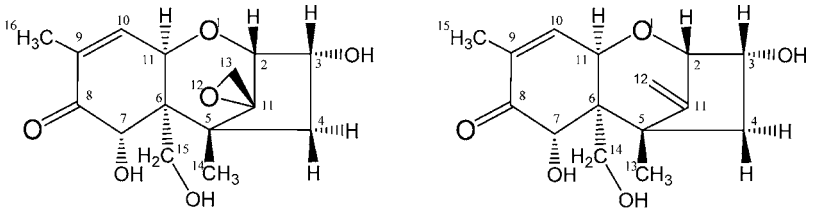

Figure 1. Structures of DON and DOM-1.

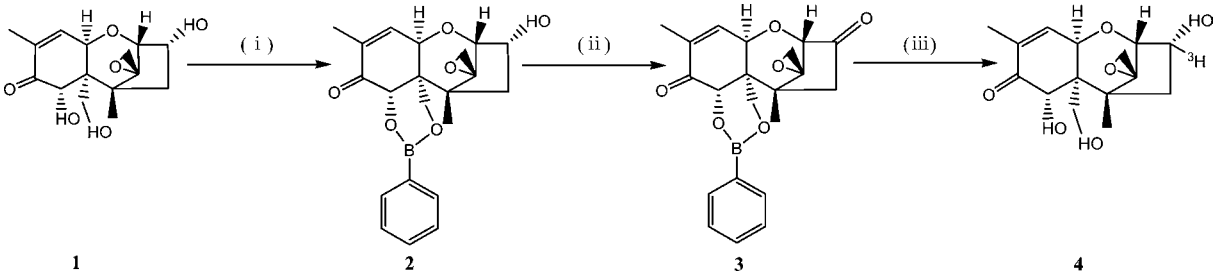

Figure 2. Synthesis of [3β-^{3}H] DON: (i) 1.1 equiv phenylboronic acid, acetone, reflux, 10 h, (ii) Swern oxidation, CH_2Cl_2, −80 °C, 15 min, and (iii) 1/4 equiv NaB^3H_4, isopropanol, room temperature, 30 min.

this study, a comparison study on metabolism, distribution, and excretion of DON in both sexes of rats and chickens was investigated by a radiotracer method, coupled with a novel γ-accurate radioisotope counting (γ-ARC) radio-high-performance liquid chromatography mass spectrometry (radio-HPLC-MS) system. The γ-ARC radio detector was specifically designed for enhanced sensitivity of radioactivity and online radioisotope detection. The full understanding of the dispositions of DON in both sexes of rodents and poultry would provide basis data of DON for future food safety evaluation and toxicological research.

MATERIALS AND METHODS

Chemicals. DON for the animal experiment was produced according to the method by Altpeter and Posselt.[15] DON and DOM-1 for structure confirmation were commercially purchased from Sigma-Aldrich Co. (St. Louis, MO). NaB^3H_4 (500 mCi/mmol) was from American Radiolabeled Chemicals, Inc. (St. Louis, MO). Phenylboronic acid (>98%) and oxayl chloride (>98%) were provided by Aladdin, Inc. (Shanghai, China). Other organic solvents were of analytical grade and from Sinopharm Chemical Reagent Co., Ltd. (Shanghai, China).

Tritium-Labeled DON. Tritium-labeled DON (3β-^{3}H-DON) was prepared using a modified method, as illustrated in Figure 2.[16] Briefly, the mixture of DON (**1**) and phenylboronic acid in dry acetone was refluxed for 4 h to give the 7,15-dihydroxyl-protected product (**2**), followed by Swern oxidation to afford a 3-keto-DON-7,15-phenylboronic acid ester (**3**). After reduction with NaB^3H_4 in isopropanol, 3β-^{3}H-DON (**4**) was obtained in moderate yields. Further purification of DON was conducted using model 2695 HPLC with a 2996 detector (Waters, Milford, MA). The separation procedure was performed on a 150 × 21.5 mm inner diameter, 10 μm, Venusil XBP-18 column (Agela Techonologies, Inc., Tianjin, China), eluting with MeOH/water (1:4, v/v) at a flow rate of 5 mL/min at 30 °C. Fractions containing pure ^{3}H-DON were pooled and concentrated under nitrogen, then subjected to a freeze-drying procedure, and finally dissolved in absolute EtOH to afford 110 mCi of 3β-^{3}H-DON (22% yield) with a radiochemical purity of 99%.

Subjects. Wistar rats (8 weeks, 200 ± 10 g) were supplied by the Hubei Provincial Center for Disease Control and Prevention (Wuhan, China). Avian broilers (4 weeks, 1.5 ± 0.3 kg) were from Charoen Pokphand Group (Hubei, China). After routine immunization, both species were placed in all-stainless-steel metabolism cages and fasted overnight with free access to DON-free feed and water. A constant environmental temperature of 25 ± 2 °C was maintained with a relative humidity of 55 ± 5% and 12 h light/dark cycle. All experimental procedures were conducted in accordance with the guidelines of the Committee on the Care and Use of Laboratory Animals of China (permit number SYXK 2007-0044).

Instrumentation. The γ-ARC radio-HPLC-MS system consisted of an online isotope detector system (γ-ARC 2.0, AIM Research Co., Hockessin, DE), an ion trap time-of-flight mass spectrometry (IT-TOF-MS) instrument and high-performance liquid chromatography (HPLC). The online isotope detector (γ-ARC) is fitted with a 750 μL flow cell and a splitter (600-PO10-06). The IT-TOF-MS instrument is equipped with an orthogonal spray electrospray ionization (ESI) source (Shimadzu Corp., Kyoto, Japan), while the HPLC system (Shimadzu Corp., Kyoto, Japan) contains a solvent delivery pump (LC-20AD), an autosampler (SIL-20AC), a DGU-20A3 degasser, a photodiode array detector (PDA, SPD-M20A), a communication base module (CBM-20A), and a column oven (CTO-20AC). This γ-ARC detector uses dynamic flow counting technologies to accurately detect and quantitate radioisotopes and is controlled by LC Solutions software (Shimadzu Corp., Kyoto, Japan). A liquid scintillation counter, Tri-Carb 2900TR, includes a quench standards set, which contains the same amount of nuclide with varying amounts of quenching agent (PerkinElmer, Waltham, MA).

Dosing and Sample Collection. *Excretion and Metabolism of [^{3}H] DON.* Animals were divided into three dose groups (0.5 and 2.5 mg/kg of bw dose rat group and 2.5 mg/kg of bw dose chicken group), with males (n = 3) and females (n = 3) in each group. On the basis of the dose levels, a single dose of [^{3}H] DON (1.1 mCi/mg) was administered orally. The excreta were collected 6, 12, and every 24 h thereafter (24, 48, 72, 96 h, etc.) after administration until radioactivity was no longer detectable in urine or feces. Each feces sample was homogenized in an equal amount of MeOH/water (50:50, v/v), while each urine sample was divided into two parts and stored at −20 °C prior to total radioactivity determination and metabolite profiling.

Distribution and Depletion of [^{3}H] DON. Three groups of animals, including two rat groups and one chicken group (each group with 15 males and 15 females), were given [^{3}H] DON for 5 days. In accordance with the excretion and metabolism tests, rats were dosed 0.5 and 2.5 mg kg^{-1} of bw day^{-1}, respectively, and chickens received 2.5 mg kg^{-1} of bw day^{-1}. According to the above excretion rate of

dx.doi.org/10.1021/jf4047946 | J. Agric. Food Chem. 2014, 62, 288−296

DON in these animals, rats were sacrificed at 6, 24, 48, 72, and 96 h after dosing, while chickens were sacrificed at 6, 12, 24, 48, and 72 h. The following samples were obtained from both rats and chicken: gastrointestinal tract, plasma, bile, brain, heart, liver, kidney, lung, spleen, pancreas, urinary bladder, ovary/testis, adipose, muscle, and skin. Above tissues were thoroughly rinsed with phosphate-buffered saline (PBS) to avoid external blood contamination and stored at −20 °C prior to analysis.

Determination of Total Radioactivity and Radioactivity Profiles. Radioactivity was determined on Tri-Carb 2900TR, with samples mixed with 10 mL Ultima Gold scintillation cocktail (PerkinElmer, Waltham, MA) and counted for 5 min unless 2σ of 0.4% was reached. An external standard quench curve was used to correct for differences in counting efficiency and calculate disintegrations per minute (dpm), where dpm = counts per minute (cpm)/efficiency. Urine (200 μL), plasma (200 μL), and bile (10 μL) were directly mixed with Ultima Gold scintillation cocktail and counted on Tri-Carb 2900TR. Air-dried feces (190−210 mg) were powdered and burned in oxygen in an autosampler oxidizer (PerkinElmer, Waltham, MA) to generate ^3H_2O by combustion before analysis. Individual tissues (190−210 mg) were dissolved in a 2 mL tissue Solvable solubilizer (PerkinElmer, Waltham, MA) in unquenched standard vials for 12 h. A total of 0.2 mL of 30% H_2O_2 was added dropwise with swirling to bleach. After standing for 10 min at ambient temperature, samples were warmed to 37 °C for 15 min to decompose peroxides and, thus, minimize chemiluminescence. Quantification of radioactivity in HPLC elutes was performed on the γ-ARC detector, using a dynamic flow mode at a flow of 1.0 mL/min. A linear relationship exists between cpm (X), obtained from the γ-ARC detector, and dpm (Y) from Tri-Carb 2900TR: $Y = 4.37X + 175.93$ ($r = 0.997$).

Metabolite Profiling. The Strata-X column (Phenomenex, Torrance, CA) was conditioned with 2 mL of MeOH followed by 2 mL of H_2O. A total of 0.4 mL of urine sample was diluted with 1.5 mL of 2% phosphoric acid in 10 mM ammonium acetate, mixed, and applied to the preconditioned Strata-X column. After washing with 2 mL of 0.1% phosphoric acid, followed by 2 mL of 5% aqueous ammonia in MeOH, the eluate was concentrated under nitrogen at 50 °C, followed by reconstitution with 0.1 mL of mobile phase (10% MeOH, containing 5 mM ammonium acetate). A total of 2 g of the homogenized feces was extracted twice with an equal volume of MeOH and centrifuged at 8000 rpm at 25 °C for 10 min. The combined extracts were concentrated under nitrogen at 50 °C, followed by reconstitution with a mobile phase up to 0.1 mL. Recovery was determined by detection of radioactivity in an equal amount of samples before and after above procedures on Tri-Carb 2900TR. The chromatographic separation was performed on a 150 × 2.1 mm inner diameter, 5 μm, Thermo Hypersil Gold (Thermo Fisher Scientific, Inc., Waltham, MA) using a linear gradient at a flow rate of 0.2 mL/min at 40 °C. The mobile phases were 5 mmol/L ammonium acetate (A) and MeOH (B). The gradient was programmed as follows: 0−30 min, 1−20% B; 30−50 min, 20% B; 50−52 min, 20−95% B; 52−53 min, 95−1% B; and 53−60 min, 1% B. A total of 20 μL of sample was injected each time. The eluate from the chromatographic separation was divided into two portions. The portion for metabolic quantification was applied to a γ-ARC 2.0, and the rest was analyzed and identified by ion trap time-of-flight tandem mass spectrometry (IT-TOF-MS/MS). To obtain the abundant signal for the product ion scan, mass spectrometric analysis was carried out on a full-scan mass spectrometer, operated in both positive and negative modes with a mass range of m/z 150−650. The MS/MS spectra were produced by collision-induced dissociation (CID) of the selected precursor ions using argon as the collision gas with a relative energy of 50%. Prior to data acquisition, external mass calibration was carried out using a direct infusion of reference standards from 50 to 2000 Da, including 0.25 mL/L trifluoroacetic acid and 0.1 g/L sodium hydroxide. Mass errors (5 mDa) were allowed after calibration.

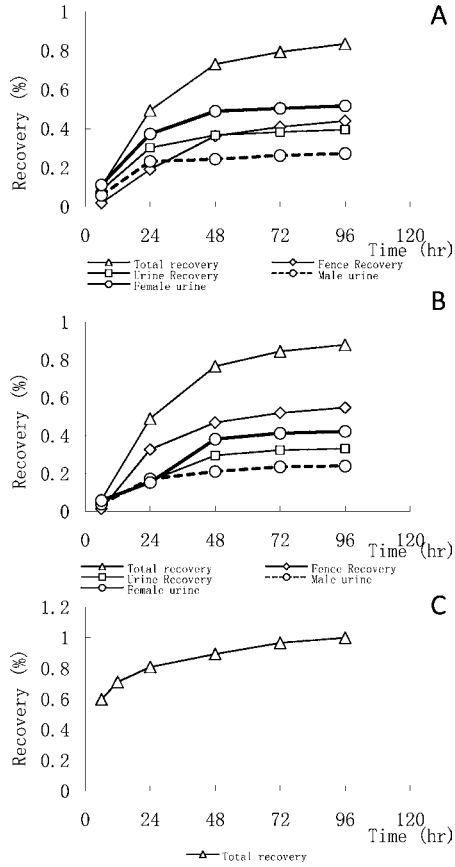

Figure 3. Mean cumulative excretion of total radioactivity in rat and chicken excreta: (A) 0.5 mg/kg of bw rat group, (B) 2.5 mg/kg of bw rat group, and (C) 2.5 mg/kg of bw chicken group.

RESULTS AND DISCUSSION

Synthesis of the Tritium-Labeled DON. Tritium-labeled DON was partially synthesized from DON via a three-step route. Protection of 7,15-dihydroxyl groups with phenylboronic acid and oxidation of the secondary hydroxyl of compound **2** to the 3-ketone derivative (**3**) were preceded smoothly in good yields as reported earlier.[17,18] Afterward, tritiated sodium borohydride was used for reduction of the 3-keto group, and tritium was introduced to DON with high specific radioactivity. A previous study on the synthesis of [^{3}H] T-2 toxin revealed a mixture of 3α- and 3β-hydroxyl epimeric products in a ratio of 4:1.[16] In this study, the absence of a 4β-hydroxyl group in 3-keto DON has resulted in a unique 3α-hydroxyl product when reduced with $NaBH_4$; no β epimer was found. The stereoselectivity and regioselectivity of this reduction of compound **3** with $NaBH_4$ have been described previously.[19] Thus, the desired compound 3β-^{3}H-DON was obtained. To ascertain the "exchange risk" of radioactive samples quantitatively, total radioactivity in plasma and urine was measured on Tri-Carb 2900TR before and after freeze-drying. Because no tritiated water was formed, the "exchange risk" could be ignored[20] (data not shown).

Excretion of the Radioactivity. DON was rapidly eliminated in rats and chickens. In rats, 73.08 ± 11.92% (n = 6; 0.5 mg/kg of bw) and 76.63 ± 8.91% (n = 6; 2.5 mg/kg of bw) of the radioactive dose were recovered from urine and feces in 48 h. By 96 h, they were accumulated to 87.99 ± 10.30% (n = 3; 0.5 mg/kg of bw) and 83.44 ± 7.88% (n = 3; 2.5 mg/kg of bw), respectively. In chickens, 80.90 ± 6.24% (n =

dx.doi.org/10.1021/jf4047946 | J. Agric. Food Chem. 2014, 62, 288−296

Table 1. Tissue Distribution and Depletion Rates of Radioactivity in Wistar Rats Following a Multi-dose of [^{3}H] DON at 2.5 mg kg^{-1} of bw Day^{-1} for 5 Days

	concentration (μg/kg)					elimination kinetics[a]	
tissues	6 h	24 h	48 h	72 h	96 h	K_e ($\times 10^{-2}$)	$t_{1/2}$ (h)
plasma	160.4 ± 22.1	80.8 ± 7.5	30.2 ± 6.6	4.5 ± 3.7	ND[b]	5.33	13.0
muscle	132.0 ± 29.3	81.6 ± 9.0	23.4 ± 9.0	17.8 ± 4.9	7.4 ± 6.3	3.18	21.8
abdominal fat	50.1 ± 7.0	25.8 ± 1.3	8.9 ± 2.7	5.3 ± 1.3	3.3 ± 1.7	2.06	33.7
stomach	1795.9 ± 43.6	753.0 ± 19.2	33.9 ± 15.1	23.5 ± 5.6	6.3 ± 3.7	6.48	10.7
large intestine	5226.2 ± 38.8	1970.8 ± 28.7	53.0 ± 6.3	22.3 ± 2.9	3.7 ± 0.9	8.35	8.3
small intestine	1473.7 ± 38.3	642.8 ± 17.5	43.2 ± 15.9	15.6 ± 2.7	3.7 ± 2.2	5.13	13.5
liver	776.6 ± 34.0	365.4 ± 20.3	50.8 ± 10.0	20.8 ± 1.8	5.6 ± 2.0	5.59	12.4
kidney	418.7 ± 40.3	220.9 ± 20.0	52.0 ± 8.6	30.5 ± 8.9	11.2 ± 1.8	3.98	17.4
heart	211.3 ± 36.8	134.3 ± 16.0	50.8 ± 9.9	24.2 ± 4.8	8.8 ± 1.3	3.69	18.8
lung	254.0 ± 46.0	157.5 ± 19.0	65.0 ± 14.2	36.5 ± 9.8	20.0 ± 3.1	2.46	28.2
skin	194.0 ± 23.4	123.1 ± 12.3	49.9 ± 2.1	27.2 ± 5.2	5.0 ± 3.7	3.89	17.8
spleen	235.4 ± 55.4	161.7 ± 25.4	66.5 ± 19.4	38.3 ± 6.5	15.9 ± 4.1	3.00	23.1
brain	100.0 ± 43.9	73.5 ± 13.6	43.7 ± 19.5	27.9 ± 19.5	11.3 ± 7.8	2.35	29.5
testes	218.4 ± 56.9	118.7 ± 12.5	40.7 ± 12.3	23.0 ± 8.4	8.9 ± 4.8	3.52	19.7
ovary	171.1 ± 23.5	115.5 ± 22.3	53.1 ± 9.6	34.9 ± 7.9	15.4 ± 6.7	2.63	26.3
adrenals	172.9 ± 22.2	94.1 ± 9.9	36.1 ± 7.4	ND	ND	3.7	18.5

[a]The terminal slope (β) for determining the elimination constant (K_e) and half-life ($t_{1/2}$) of tissues was calculated by linear regression analysis using points by WinNonlin Enterprise, version 5.2.1. [b]ND = not detectable.

Table 2. Tissue Distribution and Depletion Rates of Radioactivity in Wistar Rats Following a Multi-dose of [^{3}H] DON at 0.5 mg kg^{-1} of bw Day^{-1} for 5 Days

	concentration (μg/kg)					elimination kinetics[a]	
tissues	6 h	24 h	48 h	72 h	96 h	K_e ($\times 10^{-2}$)	$t_{1/2}$ (h)
plasma	41.8 ± 2.4	ND[b]	ND	ND	ND	—[c]	—
muscle	31.0 ± 8.4	ND	ND	ND	ND	—	—
abdominal fat	11.5 ± 4.6	ND	ND	ND	ND	—	—
stomach	775.1 ± 7.8	123.9 ± 9.2	ND	ND	ND	—	—
large intestine	760.8 ± 38.8	123.3 ± 28.7	26.7 ± 6.3	8.7 ± 2.8	3.7 ± 0.9	4.13	16.8
small intestine	834.4 ± 30.3	87.8 ± 17.5	10.6 ± 8.9	4.3 ± 2.7	ND	7.97	8.7
liver	249.5 ± 30.2	35.1 ± 20.3	50.8 ± 10.0	ND	ND	4.50	15.4
kidney	154.9 ± 35.6	22.7 ± 21.1	11.3 ± 8.6	6.8 ± 6.0	ND	2.52	27.5
heart	211.4 ± 13.8	163.4 ± 24.5	97.5 ± 18.7	18.9 ± 5.0	ND	4.50	15.4
lung	107.4 ± 35.4	38.6 ± 18.9	19.3 ± 14.2	4.8 ± 2.2	ND	4.53	15.3
skin	47.3 ± 8.9	6.4 ± 5.8	ND	ND	ND	—	—
spleen	95.4 ± 55.4	47.4 ± 25.4	31.3 ± 19.4	15.0 ± 6.5	ND	2.68	25.9
brain	26.8 ± 6.1	14.7 ± 12.6	ND	ND	ND	—	—
testes	80.3 ± 10.9	17.7 ± 4.5	9.4 ± 5.5	4.8 ± 3.4	ND	2.72	25.5
ovary	52.7 ± 13.6	19 ± 6.8	11.9 ± 5.6	8.2 ± 3.8	2.7 ± 1.5	2.95	23.5
adrenals	39.34 ± 6.56	ND	ND	ND	ND	—	—

[a]The terminal slope (β) for determining the elimination constant (K_e) and half-life ($t_{1/2}$) of tissues was calculated by linear regression analysis using points by WinNonlin Enterprise, version 5.2.1. [b]ND = not detectable. [c]— = not determined.

3; 2.5 mg/kg of bw) of the radioactive dose was recovered in 24 h and accumulated to 94.52 ± 3.59% (n = 6) in 72 h from excreta (Figure 3). The urine radioactivity excretion rate was 39.51 ± 13.41% (n = 6) of the radioactive dose in the 0.5 mg/kg of bw group and reduced to 33.12 ± 10.31% (n = 6) in the 2.5 mg/kg of bw group. Significant differences in the dose- and sex-dependent excretions were found in rats. For female rats, urine radioactivity excretion rates were 57.13 ± 1.18% (0.5 mg/kg of bw; n = 3) and 42.26 ± 3.07% (2.5 mg/kg of bw; n = 3), while for males, they were 27.29 ± 0.67 and 23.97 ± 2.26%, respectively. This difference in the urine excretion rate may relate to the previous report that the female rats were less sensitive than male rats in response to DON.[21]

Distribution and Depletion of Total Radioactivity in Tissues. After DON was administered to rats and chickens for 5 days, the animal body weight, urine volume, feces weight, and general appearance of the animals were not affected, except for a slight reduction in food intake in rats at the high dosage. The concentrations of the DON-related substance in the tissues at each time point was shown in Tables 1−3. The terminal slope (β) for determining the elimination constant (K_e) and half-life ($t_{1/2}$) of tissues was calculated by linear regression analysis using points by WinNonlin Enterprise, version 5.2.1. DON was widely distributed in 6 h and quickly depleted in all tissues from rats and chickens. In rats, the highest concentration of radioactivity was detected at 6 h post-administration in the gastrointestinal tract at 5226.2 and 834.4 μg/kg, which declined to 50.3 and 10.6 μg/kg in 48 h, for the 2.5 and 0.5 mg/kg of bw groups, respectively; substantially lower levels were detected in the kidney, liver, heart, lung, spleen, and brain. In the 0.5 mg/

dx.doi.org/10.1021/jf4047946 | J. Agric. Food Chem. 2014, 62, 288−296

Table 3. Tissue Distribution and Depletion Rates of Radioactivity in Chickens Following a Multi-dose of [^{3}H] DON at 2.5 mg kg^{-1} of bw Day^{-1} for 5 Days

	concentration (μg/kg)					elimination kinetics[a]	
tissues	6 h	12 h	24 h	48 h	72 h	K_e ($\times 10^{-2}$)	$t_{1/2}$ (h)
bile	822.5 ± 261.1	111.2 ± 27.2	89.8 ± 45.5	4.0 ± 1.3	ND[b]	11.36	6.1
plasma	209.6 ± 63.3	94.4 ± 7.7	35.9 ± 13.1	5.5 ± 4.7	ND	7.88	8.8
muscle	295.9 ± 14.9	132.9 ± 32.3	91.4 ± 23.4	56.1 ± 9.4	ND	2.34	29.6
abdominal fat	492.2 ± 14.4	146.3 ± 30.1	86.3 ± 21.9	56.8 ± 19.3	ND	2.50	27.7
gizzard	1009.6 ± 39.6	316.2 ± 21.7	164.7 ± 52.2	44.7 ± 19.1	24.7 ± 13.4	4.33	16
large intestine	1776.2 ± 53.8	187.3 ± 23.0	294.0 ± 19.1	70.0 ± 11.9	50.0 ± 37.4	3.69	18.8
small intestine	1666.3 ± 208.1	200.9 ± 12.8	96.3 ± 27.2	39.3 ± 10.3	19.3 ± 15.0	3.35	20.7
crop	1928.7 ± 24.4	569.5 ± 88.1	225.1 ± 44.6	69.0 ± 5.0	28.9 ± 1.1	4.28	16.2
bursal	1726.7 ± 88.1	300.0 ± 13.8	112.5 ± 10.1	47.2 ± 19.5	ND	4.91	14.1
liver	531.9 ± 14.0	165.3 ± 36.5	90.2 ± 12.2	54.1 ± 5.3	ND	2.96	23.4
kidney	1025.5 ± 24.4	262.3 ± 65.0	104.1 ± 22.6	55.7 ± 8.0	ND	4.08	17
heart	565.1 ± 33.2	131.0 ± 46.7	81.3 ± 14.0	50.5 ± 8.7	ND	2.56	27.1
lung	649.2 ± 32.3	154.5 ± 57.6	79.8 ± 19.7	54.3 ± 10.6	ND	2.72	25.5
skin	148.9 ± 79.9	138.6 ± 57.8	72.7 ± 36.6	13.2 ± 4.1	ND	6.60	10.5
spleen	408.9 ± 107.0	146.4 ± 54.8	79.0 ± 8.6	53.9 ± 12.4	ND	2.61	26.6
pancreas	230.8 ± 22.3	123.2 ± 35.1	42.2 ± 32.6	21.5 ± 4.9	ND	5.46	12.7
brain	133.6 ± 32.1	99.8 ± 23.7	78.8 ± 13.7	42.8 ± 6.1	ND	3.24	21.4
testes	2353.3 ± 1134.9	296.1 ± 41.2	130.1 ± 51.6	72.1 ± 10.7	ND	3.71	18.7
ovary	1015.0 ± 452.5	303.0 ± 32.5	131.8 ± 32.0	56.8 ± 9.5	ND	4.50	15.4

[a]The terminal slope (β) for determining the elimination constant (K_e) and half-life ($t_{1/2}$) of tissues was calculated by linear regression analysis using points by WinNonlin Enterprise, version 5.2.1. [b]ND = not detectable

Table 4. Measured Masses, Predicted Masses, Mass Errors, and Major Fragment Ions of Identified DON Metabolites

compounds	retention time (min)	measured mass (Da)	predicted mass (Da)	error (mDa)	error (ppm)	elemental composition	major fragment ions	identification
MD1	5.6	377.1005	377.0912	9.3	24.6	$[M - H]^-$ $C_{15}H_{21}O_9S^-$	347, 295, 265, 247, 217, and 138	10-deoxynivalenol-sulfonate
MD2	7.5	471.149	471.1508	1.8	3.8	$[M - H]^-$ $C_{21}H_{27}O_{12}^-$	411, 307, 265, 247, 229, and 217	DON-3α-glucuronide
MD3	9.2	361.0991	361.0963	2.8	6.6	$[M - H]^-$ $C_{15}H_{21}O_8S^-$	331, 261, 249, 231, and 215	10-DOM-1-sulfonate
MD4	12.3	375.0714	375.0755	4.1	10.9	$[M - H]^-$ $C_{15}H_{19}O_9S^-$	345, 327, 265, 247, 229, and 217	deoxynivalenol-3α-sulfate
MD5	18.8	355.135	355.1398	4.8	13.5	$[M + CH_3COO]^-$ $C_{16}H_{23}O_8^-$	295, 265, 247, and 138	DON
MD6	27.5	339.1426	339.1449	2.3	6.8	$[M + CH_3COO]^-$ $C_{16}H_{23}O_7^-$	279, 261, 249, 231, and 215	DOM-1

kg of bw group in rats, the radioactivity in the plasma, muscle, fat, and adrenals was not detectable at 24 h, while at 96 h after administration, the radioactivity was not detectable in most tissues, except the large intestine and ovary. Nevertheless, in the 2.5 mg/kg of bw group in rats, at 96 h after administration, the radioactivity can be detected at very low levels (<20 μg/kg) in most of the tissues, except the plasma and adrenals. In chickens, the radioactivity was eliminated even faster. The highest concentration was also found at 6 h post-administration in the gastrointestinal tract at 1928.7 μg/kg, and it declined to 225 μg/kg in 24 h. At 72 h after administration, radioactivity was detectable in the gastrointestinal tract only and the concentrations were less than 50 μg/kg. Initially, higher specific radioactivity in the gastrointestinal tract appeared to undergo fast, with $t_{1/2}$ ranging from 8.3 to 20.7 h. Estimated clearance rates for radioactivity varied slightly among the various tissues examined, with the elimination half-life values occurring between 6 and 34 h. The gastrointestinal tract, the first barrier against food contaminants, is highly sensitive to mycotoxins, especially DON. Moreover, the results of the distribution showed that DON could be detected in the brain, which suggested that DON or its metabolites may deliver across the blood−brain barrier in rats and chickens.

Structural Determination of Identified Ions. *DON (MD5) and DOM-1 (MD6).* As shown in Table 4, MD5 (t_R = 18.8 min) gave a deprotonated ion $[M + CH_3COO - H]^-$ and its molecular formula was deduced as $C_{15}H_{20}O_6$. A product ion scanning spectrum provided its characteristic fragment ions at m/z 295 $[M - H]^-$, 265 $[M - H - 30]^-$, 247 $[M - H - 48]^-$, and 217 $[M - H - 78]^-$, suggesting that it was the parent product (DON). The molecular form of metabolite MD6 (t_R = 27.5 min) was calculated as $C_{15}H_{20}O_5$ by IT-TOF-MS ($[M + CH_3COO - H]^-$). The difference of the 16 Da mass between m/z 339 and 355 indicated the neutral loss of oxygen based on DON. Its major product ions were m/z 279 $[M - H]^-$, 261 $[M - H - 18]^-$, 249 $[M - H - 30]^-$, and 231 $[M - H - 48]^-$, suggesting that it was DOM-1, a de-epoxy product of DON. The structures of those two compounds were confirmed by comparison of their retention times and MS/MS spectra on liquid chromatography−mass spectrometry (LC−MS) to the standards.

dx.doi.org/10.1021/jf4047946 | J. Agric. Food Chem. 2014, 62, 288−296

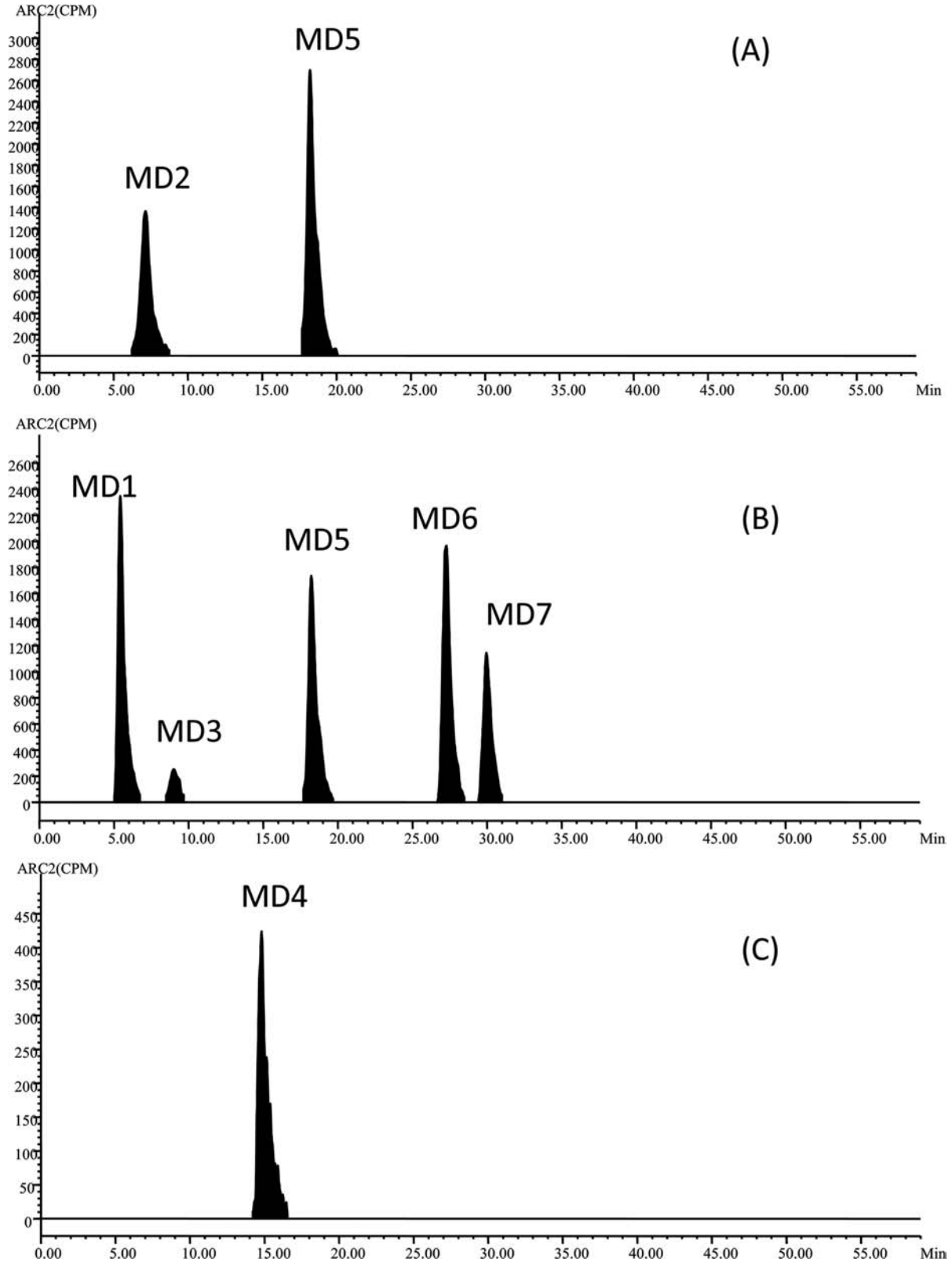

Figure 4. Representative radio-HPLC chromatograms of excreta from [^{3}H]-DON-treated animals: (A) 0−6 h urine from [^{3}H]-DON-treated rats, (B) 6−24 h feces extracts from [^{3}H]-DON-treated rats, and (C) 0−48 h excreta from [^{3}H]-DON-treated chickens.

MD2 and MD4 (3α-Hydroxy Conjugates). Metabolites MD2 and MD4 were expected for phase II metabolites, because the skeleton was identical with DON according to the MS/MS fragments (Figure 5A). MD2 (t_R = 7.5 min) gave a $[M - H]^-$ molecule. The product ion spectrum of MD2 displayed a fragment ion at m/z 411, 265, 247, 217, and 175. The mass loss of 206 Da (176 + 30 Da) and the fragment ion m/z 175 indicated that it is a DON-3α-glucuronide conjugate. MD4 (t_R = 12.3 min) showed a $[M - H]^-$ molecule with a series of product ions at m/z 345, 327, 265, 247, 229, and 217.

dx.doi.org/10.1021/jf4047946 | J. Agric. Food Chem. 2014, 62, 288−296

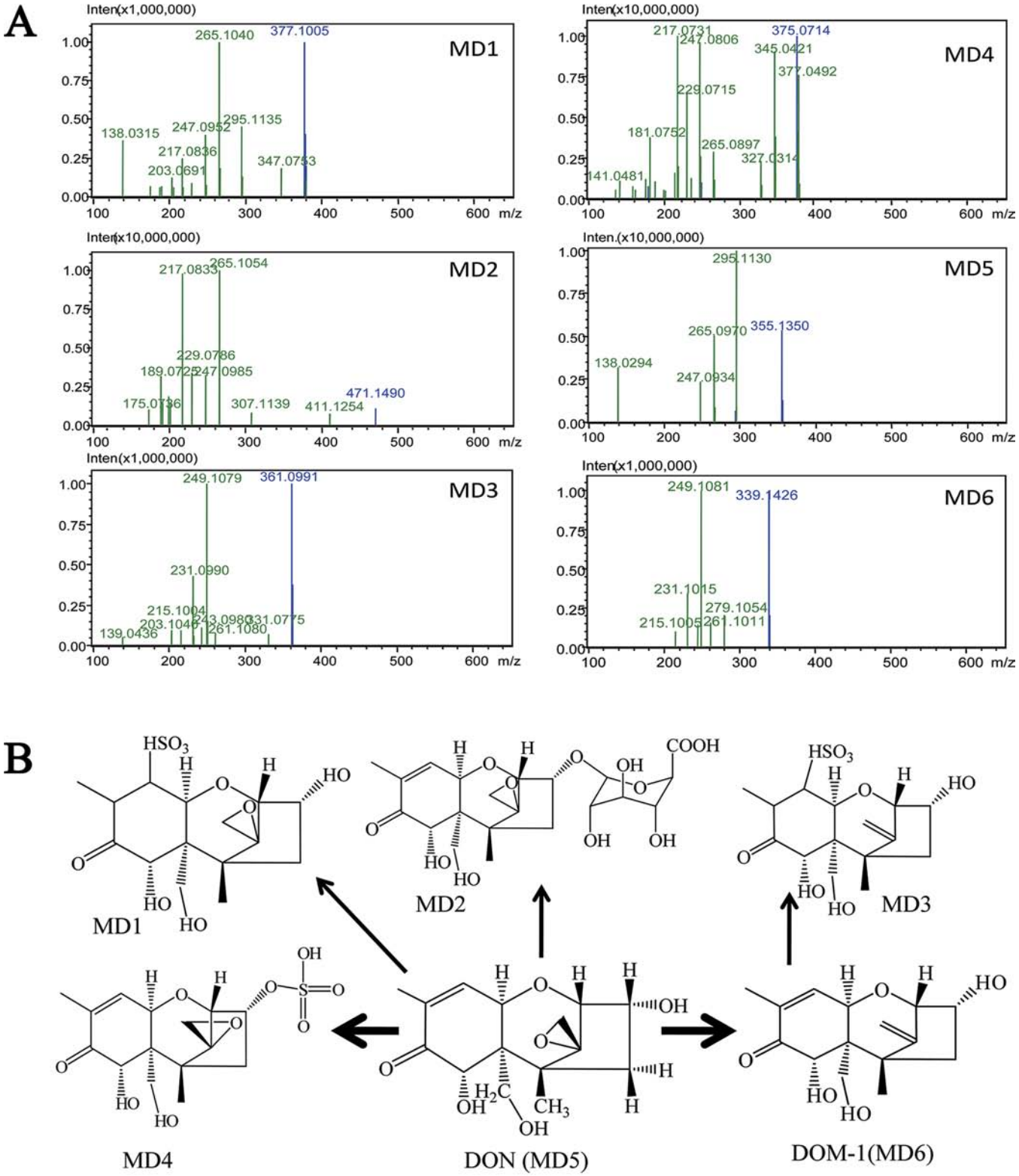

Figure 5. MS and MS^2 of the metabolites of DON and the potential metabolism pathway in the excreta of rats and chickens. (A) MS and MS^2 of the identified metabolites. (B) Structure of the identified metabolites and the potential metabolism pathway.

Subsequent neutral loss of 80 Da from fragment ions m/z 345 and 327 yielded fragment ions at m/z 265 and 247, respectively, which is a specific signature for sulfate conjugates. The product ion at m/z 345 because of the loss of 30 Da ($-CH_2O$) indicated that the sulfate is conjugated at the 3α-hydroxy position. For deoxynivalenol-sulfate, first reported in sheep urine,[14] the details of structural elucidation are missing. Here, the fragmentation patterns (m/z 345, 327, 265, 247, and 217) in MS/MS confirmed that the sulfate was conjugated with a 3α-hydroxyl group.

dx.doi.org/10.1021/jf4047946 | J. Agric. Food Chem. 2014, 62, 288−296

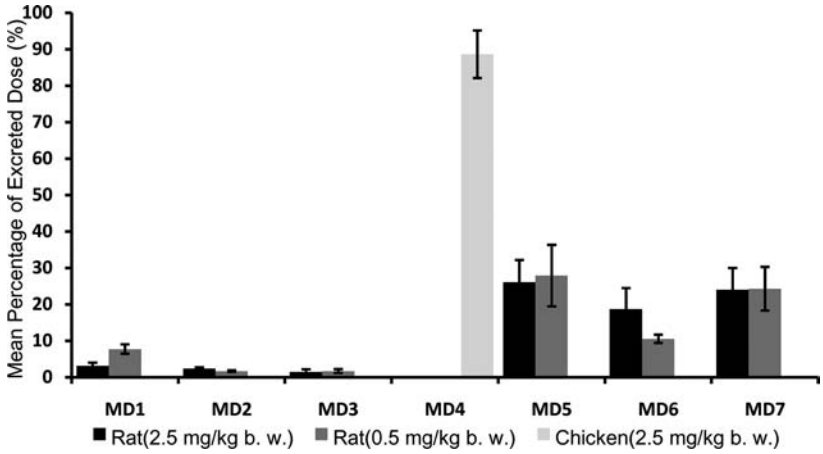

Figure 6. Total excretion of metabolites from rats and chickens (n = 6) 0−96 h after single-dose administration [means ± standard deviation (SD)].

MD1 and MD3 (Sulfonate Acid Conjugates). Two new metabolites, MD1 (t_R = 5.6 min) and MD3 (t_R = 9.2 min), were found in radiometric HPLC (Figure 4B). MD1 gave a $[M - H]^-$ molecule in IT-TOF-MS, and its molecular formulas was deduced as $C_{15}H_{22}O_9S$ (Table 4). Its mass fragments (m/z 295 $[M - H - 82]^-$, 265 $[M - H - 82 - 30]^-$, 247 $[M - H - 82 - 48]^-$, 217 $[M - H - 82 - 78]^-$, and 138 $[M - H - 82 - 157]^-$) were identical to those of DON. The mass neutral loss of 82 Da was deduced as H_2SO_3 (calculated 81.9725) by IT-TOF-MS (Figure 5A). The keto group or the 9,10 double bond of DON could potentially undergo an addition with H_2SO_3, which suggested that MD1 was generated from a rare sulfonation metabolic pathway. Further comparison of MS fragmentation patterns and retention time of MD1 with 10-deoxynivalenol-sulfonate, a reference substance that was synthesized on the basis of the protocol by Beyer et al.,[22] confirmed that it was 10-deoxynivalenol-sulfonate. Similarly, MD3 (m/z 361, 331, 279, 249, 261, and 231) was proposed to be 10-DOM-1-sulfonate.

Profiles of Excreted Metabolites. The radioactivity in excreta was completely recovered, as the recovery efficiencies were 98.7 ± 2.4% in rat urine, 96.1 ± 3.6% in rat feces, 99.6 ± 4.1% in chicken excreta. Seven peaks were observed in HPLC radiochromatograms (Figure 4), and six of them were identified as deoxynivalenol-sulfonate, DON-3α-glucuronide, DOM-1-sulfonate, deoxynivalenol-3α-sulfate, DON, and DOM-1. An unexpected metabolite (MD7), which was found in rat urine and feces, was not identified because of its weak ion response in this high-performance liquid chromatography ion trap time-of-flight tandem mass spectrometry (HPLC-IT-TOF-MS/MS) system. In rats, deoxynivalenol-sulfonate, DON-3α-glucuronide, DOM-1-sulfonate, DOM-1, and DON were detected in both dose groups and both genders. DON existed in all samples, while DOM-1 was detected in urine and feces after 24 h post-administration, DON-3α-glucuronide was found only in urine during 0−6 h after dosing, and deoxynivalenol-sulfonate and DOM-1-sulfonate were found only in feces after 24 h post-administration. In chickens, the toxin residue mainly existed in the form of deoxynivalenol-3α-sulfate and DON but DOM-1, deoxynivalenol-sulfonate, DOM-1-sulfonate, and DON-glucuronide were not detectable. In total, the new metabolites, deoxynivalenol-sulfonate and DOM-1-sulfonate, comprised 10% or less of the total radioactivity, while DON-3α-glucuronide involved 2% of the radioactivity. The major compounds, DON, DOM-1, and MD7, accounted for 27.89 ± 8.44, 10.55 ± 1.14, and 24.28 ± 5.99% of the original dose in the 2.5 mg/kg of bw rat group and 26.08 ± 6.09, 18.73 ± 5.74, and 24.02 ± 5.96% in the 0.5 mg/kg of bw rat group, respectively (Figure 6). The new metabolite deoxynivalenol-3α-sulfate, a major metabolite in chickens, accounted for about 88.63 ± 6.53% of the dose. This O-sulfate conjugation was considered to be a detoxification or deactivation pathway.[23] The specific capability of chicken to biotransform DON to deoxynivalenol-sulfate effectively seems to be a rational reason why poultry is less sensitive than rodents to the toxin DON.[24]

A rare sulfonation metabolic pathway, which led to new [M + 82] metabolites of DON and DOM-1 in rats, was found for the first time. Earlier studies have reported that a few chemicals can be converted into [M + 82] metabolites in rats, such as (*R*)-(+)-menthofuran, gambogic acid, and xanthohumol.[25−27] These compounds, including DON, containing an α,β-unsaturated carbonyl group, might result in this biotransformaition *in vivo*. To date, these metabolites were not identified in chicken and swine. It seems that it is a specific metabolic pathway for rats. Although the enzymes involved in this metabolic pathway were not clear, several hypotheses were proposed. One possible mechanism involves an addition of glutathione (GSH) to the unsaturated ketoaldehyde, followed by further metabolism to give the sulfonic acid conjugates.[25] Thus, it can be hypothesized that, if *in vivo* reversibility of the GSH adduct of DON could occur, it could represent a mechanism for DON delivering and regenerating to the toxicological target. The addition of GSH to the double bond of DON was found in wheat, for which nuclear magnetic resonance (NMR) evidence was provided, most likely a 1,4 addition of α,β-unsaturated ketones.[28] In that case, the proposed structures of the sulfonates, the GSH conjugate-processing products, were 10-deoxynivalenol-sulfonate and 10-DOM-1-sulfonate. Alternatively, it might also result from microbial metabolism. However, the action of gut flora was not to catalyze the sulfonation directly but to transform inorganic sulfate to sulfite. The sulfur-containing chemical substance reacted with DON from bile excretion by a well-known Michael addition reaction. In any case, it is a detoxification or deactivation pathway, because the increased polarity of deoxynivalenol-sulfonate is associated with fast excretion of the molecule.[17]

In summary, the metabolism, distribution, and excretion of DON in rats and chicken were investigated in the present study. DON and its metabolites were quickly distributed to the entire body and eliminated from all tissues. Gender and species

dx.doi.org/10.1021/jf4047946 | J. Agric. Food Chem. 2014, 62, 288−296

appear to play a role in the excretion rate and metabolic pathway. In addition, to some known metabolites, sulfate-conjugated DON and sulfones were identified as important detoxification routes in chickens and rats. This quick elimination and extensive detoxification of DON in chicken strongly suggested that DON residues from poultry meat would probably be non-toxic to humans, as long as these poultry were exposed to feeds contaminated with a low level of DON 24 h before sacrifice. Metabolites in other species need to be established *in vivo*, as indicated by different metabolism profiles in chickens and rats from this study.

AUTHOR INFORMATION

Corresponding Author

*Telephone: 0086-27-8728-7186. Fax: 0086-27-8767-2232. E-mail: yuan5802@mail.hzau.edu.cn.

Funding

This work was financially supported by the National Basic Research Program of China (2009CB118800).

Notes

The authors declare no competing financial interest.

ABBREVIATIONS USED

DON, deoxynivalenol; ARC, accurate radioisotope counting; bw, body weight; ER, endoplasmic reticulum; JECFA, Joint FAO/WHO Expert Committee on Food Additives; PMTDI, provisional maximum tolerable daily intake; DOM-1, deepoxy-deoxynivalenol; dpm, disintegrations per minute; cpm, counts per minute; CID, collision-induced dissociation; ESI, electrospray ionization

REFERENCES

(1) Binder, E. M.; Tan, L. M.; Chin, L. J.; Handl, J.; Richard, J. Worldwide occurrence of mycotoxins in commodities, feeds and feed ingredients. *Anim. Feed Sci. Technol.* **2007**, *137*, 265−282.

(2) Pestka, J. J. Deoxynivalenol: Toxicity, mechanisms and animal health risks. *Anim. Feed Sci. Technol.* **2007**, *137*, 283−298.

(3) Pestka, J. J. Mechanisms of deoxynivalenol-induced gene expression and apoptosis. *Food Addit. Contam., Part A* **2008**, *25*, 1128−1140.

(4) Joint FAO/WHO Expert Committee on Food Additives (JECFA). *Summary Report of the Seventy-Second Meeting of the Joint FAO/WHO Expert Committee on Food Additives (JECFA)*; JECFA: Rome, Italy, 2010; http://www.who.int/foodsafety/chem/summary72_rev.pdf (accessed June 1, 2010).

(5) Lake, B. G.; Phillips, J. C.; Walters, D. G.; Bayley, D. L.; Cook, M. W.; Thomas, L. V. Studies on the metabolism of deoxynivalenol in the rat. *Food Chem. Toxicol.* **1987**, *25*, 589−592.

(6) Prelusky, D. B.; Hamilton, R. M.; Trenholm, H. L. Transmission of residues to eggs following long-term administration of ^{14}C-labelled deoxynivalenol to laying hens. *Poult. Sci.* **1989**, *68*, 744−748.

(7) Wu, Q.; Dohnal, V.; Huang, L.; Kuca, K.; Yuan, Z. Metabolic pathways of trichothecenes. *Drug Metab. Rev.* **2010**, *42*, 250−267.

(8) Yoshizawa, T.; Takeda, H.; Ohi, T. Structure of a novel metabolite from deoxynivalenol, a trichothecene mycotoxin, in animals. *Agric. Biol. Chem.* **1983**, *47*, 2133−2135.

(9) He, P.; Young, L. G.; Forsberg, C. Microbial transformation of deoxynivalenol (vomitoxin). *Appl. Environ. Microb.* **1992**, *58*, 3857−3863.

(10) Young, J. C.; Zhou, T.; Yu, H.; Gong, J. Degradation of trichothecene mycotoxins by chicken intestinal microbes. *Food Chem. Toxicol.* **2007**, *45*, 136−143.

(11) Lattanzio, V. M. T.; Solfrizzo, M.; Girolamo, A. D.; Chulze, S. N.; Torres, A. M.; Visconti, A. LC−MS/MS characterization of the urinary excretion profile of the mycotoxin deoxynivalenol in human and rat. *J. Chromatogr. B: Anal. Technol. Biomed. Life Sci.* **2011**, *879*, 707−715.

(12) Warth, B.; Sulyok, M.; Berthiller, F.; Schuhmacher, R.; Krska, R. New insights into the human metabolism of the *Fusarium* mycotoxins deoxynivalenol and zearalenone. *Toxicol. Lett.* **2013**, *220*, 88−94.

(13) Warth, B.; Sulyok, M.; Berthiller, F.; Schuhmacher, R.; Fruhmann, P.; Hametner, C.; Gerhard, A.; Johannes, F.; Krska, R. Direct quantification of deoxynivalenol glucuronide in human urine as biomarker of exposure to the *Fusarium* mycotoxin deoxynivalenol. *Anal. Bioanal. Chem.* **2011**, *401*, 195−200.

(14) Preluskya, D. B.; Veiraa, D. M.; Trenholma, H. L.; Fostera, B. C. Metabolic fate and elimination in milk, urine and bile of deoxynivalenol following administration to lactating sheep. *J. Environ. Sci. Health, Part B* **1987**, *22*, 125−148.

(15) Altpeter, F.; Posselt, U. K. Production of high quantities of 3-acetyldeoxynivalenol and deoxynivalenol. *Appl. Microbiol. Biotechnol.* **1994**, *41*, 384−387.

(16) Wallace, E. M.; Pathre, S. V.; Mirocha, C. J.; Robison, T. S.; Fenton, S. W. Synthesis of radiolabeled T-2 toxin. *J. Agric. Food Chem.* **1977**, *25*, 836−838.

(17) Savard, M.; Blackwell, B. A.; Greenhalgh, R. An ^{1}H nuclear magnetic resonance study of derivatives of 3-hydroxy-12,13-epoxy-trichothec-9-enes. *Can. J. Chem.* **1987**, *65*, 2254−2262.

(18) Bretz, M.; Beyer, M.; Cramer, B.; Humpf, H. Stable isotope dilution analysis of the *Fusarium* mycotoxins deoxynivalenol and 3-acetyldeoxynivalenol. *Mol. Nutr. Food Res.* **2006**, *50*, 251−260.

(19) Grove, J. F. Regioselective reactions with derivatives of the trichothecene mycotoxins, nivalenol and vomitoxin. *J. Nat. Prod.* **1994**, *57*, 1491−1497.

(20) Shaffer, C. L.; Gunduz, M.; Thornburgh, B. A.; Fate, G. D. Using a tritiated compound to elucidate its preclinical metabolic and excretory pathways *in vivo*: Exploring tritium exchange risk. *Drug Metab. Dispos.* **2006**, *34*, 1615−1623.

(21) Rotter, B. A.; Prelusky, D. B.; Pestka, J. J. Toxicology of deoxynivalenol (vomitoxin). *J. Toxicol. Environ. Health, Part A* **1996**, *48*, 1−34.

(22) Beyer, M.; Dänicke, S.; Rohweder, D.; Humpf, H. Determination of deoxynivalenol-sulfonate (DONS) in cereals by hydrophilic interaction chromatography coupled to tandem mass spectrometry. *Mycol. Res.* **2010**, *26*, 109−117.

(23) Yi, L.; Dratter, J.; Wang, C.; Tunge, J. A; Desaire, H. Identification of sulfation sites of metabolites and prediction of the compounds' biological effects. *Anal. Bioanal. Chem.* **2006**, *386*, 666−674.

(24) Pestka, J. J.; Smolinski, A. T. Deoxynivalenol: Toxicology and potential effects on humans. *J. Toxicol. Environ. Health, Part B* **2005**, *8*, 39−69.

(25) Chen, L. J.; Lebetkin, E. H.; Burka, L. T. Metabolism of (*R*)-(+)-menrhofuran in fischer-344 rats: Identification of sulfonic acid metabolites. *Drug Metab. Dispos.* **2003**, *31*, 1208−1213.

(26) Jirásko, R.; Holčapek, M.; Vrublová, E.; Ulrichová, J.; Šimánek, V. Identification of new phase II metabolites of xanthohumol in rat *in vivo* biotransformation of hop extracts using high-performance liquid chromatography electrospray ionization tandem mass spectrometry. *J. Chromotogr., A* **2010**, 4100−4108.

(27) Yang, J.; Ding, L.; Hu, L.; Qian, W.; Jin, S.; Sun, X.; Wang, Z.; Xiao, W. Metabolism of gambogic acid in rats: A rare intestinal metabolic pathway responsible for its final disposition. *Drug Metab. Dispos.* **2011**, *39*, 617−626.

(28) Kluger, B.; Bueschl, C.; Lemmens, M.; Berthiller, F.; Häubl, G.; Jaunecker, G.; Adam, G.; Krska, R.; Schuhmacher, R. Stable isotopic labeling-assisted untargeted metabolic profiling reveals novel conjugates of the mycotoxin deoxynivalenol in wheat. *Anal. Bioanal. Chem.* **2013**, *405*, 1−6.

JOURNAL OF AGRICULTURAL AND FOOD CHEMISTRY

Article

pubs.acs.org/JAFC

Synthesis, Characterization, and Antimicrobial Activity of Kojic Acid Grafted Chitosan Oligosaccharide

Xiaoli Liu, Wenshui Xia,* Qixing Jiang, Yanshun Xu, and Peipei Yu

State Key Laboratory of Food Science and Technology, School of Food Science and Technology, Jiangnan University, Lihu Road 1800, Wuxi, 214122 Jiangsu, People's Republic of China

Supporting Information

ABSTRACT: A novel water-soluble chitosan oligosaccharide (COS) derivative, chitosan oligosaccharide/kojic acid grafts assigned as COS/KA, was prepared by using the selective partial alkylation of *N*-benzylidene COS and chlorokojic acid in the presence of dimethyl sulfoxide (DMSO) and pyridine (Py). The derivative was characterized by UV−vis spectroscopy, FTIR, ^{1}H NMR, TGA, SEM, and XRD techniques, which showed that the alkylation reaction took place at the C-6 and C-3 positions of COS. The results showed that the degree of substitution (DS) for COS/KA was from 0.38 to 1.21, and the product exhibited an excellent solubility in organic solvents and distilled water. The antibacterial results indicated that the antibacterial activity of COS/KA was strengthened relative to COS with the increase of DS for *Staphylococcus aureus*, *Escherichia coli*, *Aspergillus niger* and *Saccharomyces cerevisiae*. These findings provide important supports for developing new antibacterial agents and expand the scope of application of COS in the food industry.

KEYWORDS: *chitosan oligosaccharide, kojic acid, antimicrobial activity*

INTRODUCTION

Many researchers have focused on chitosan as a source of potential bioactive material during the past few decades. However, it has several drawbacks for its utilization in biological applications, including poor solubility and absorption under physiological conditions.[1] Unlike chitosan, chitosan oligosaccharide (COS), the hydrolyzed product of chitosan, is a mixture of oligomers of β-1,4-linked D-glucosamine residues that have better biocompatibility and solubility due to their shorter chain lengths and free amino groups in D-glucosamine units.[2] Many of the biological activities reported for COS, such as antifungal,[3,4] antibacterial,[5] and antitumor,[6] are dependent on their physicochemical properties, which allow COS to be considered as a potential novel functional food ingredient, particularly in the preparation of low-calorie foods.[7] Recently, it has been shown that COS and its derivatives exert antimicrobial effects against different groups of microorganisms such as bacteria, fungi, and yeast.[7] Therefore, it has also been used as an antibacterial agent and additive to improve the shelf life of food products.[8] There are three types of reactive functional groups present in COS (an amino group as well as both primary and secondary alcoholic OH groups at the C-2, C-3, and C-6 positions, respectively), which can be readily subjected to chemical derivatization, allowing its antibacterial activity to be increased.[9] However, the antibacterial activity of COS is low, and chemical modification may lead to enhancement of its antibacterial activity.

Kojic acid (KA), 2-hydroxymethyl-5-hydroxy-4*H*-pyran-4-one, which is an organic acid, is a metabolic compound produced by several species of economically valuable fungi, such as *Aspergillus*, *Acetobacter*, and *Penicillium*.[10] At present, kojic acid and its derivatives have drawn attention because they have been shown to possess various bioactivities such as antimicrobial and antiviral,[11] anti-inflammatory,[12] antitumor,[13] antidiabetic,[14] and skin-whitening activities.[15] Recently, methods for the synthesis of various kojic acid derivatives, such as kojic acid esters kojic acid laureate and kojic acid dipalmitate, have been reported in many studies.[16,17] Moreover, kojic acid provides a promising skeleton for development of new more potent derivatives such as chlorokojic acid (2-chloromethyl-5-hydroxy-4*H*-pyran-4-one), which is a good ligand for the nucleophilic and electrophilic substitution reaction depending on the reagent type and can inhibit *Aeromonas aerogenes*, *Micrococcus pyogenes* var. *aureus*, *Salmonella typhosa*, *Penicillium digitalum*, *Russula nigricans*, and *Saccharomyces cerevisiae* growth.[10] Marwaha and co-workers reported that organomercury(II) complexes of kojic acid and maltol demonstrated greater antibacterial activity than kojic acid.[18] Nevertheless, at present, there is little information available regarding the synthesis of COS/KA graft complexes and their antibacterial activity.

Both COS and kojic acid are good natural food preservatives for improving food quality and safety. Herein we report the preparation of a derivative of COS, *N*-benzylidene COS, by alkylation with chlorokojic acid. The chemical structure and physical properties of products were characterized by UV−vis spectroscopy, FTIR, ^{1}H NMR, TGA, SEM, and XRD techniques. Besides, the solubility and the antibacterial activity against *Staphylococcus aureus*, *Escherichia coli*, *Aspergillus niger*, and *Saccharomyces cerevisiae* were also studied. These two chemical groups are expected to supplement each other for their antibacterial activity in the preparation of new effective and environmentally friendly biocides.

Received: September 13, 2013
Revised: November 18, 2013
Accepted: December 12, 2013
Published: December 23, 2013

ACS Publications © 2013 American Chemical Society

dx.doi.org/10.1021/jf404026f | *J. Agric. Food Chem.* 2014, 62, 297−303

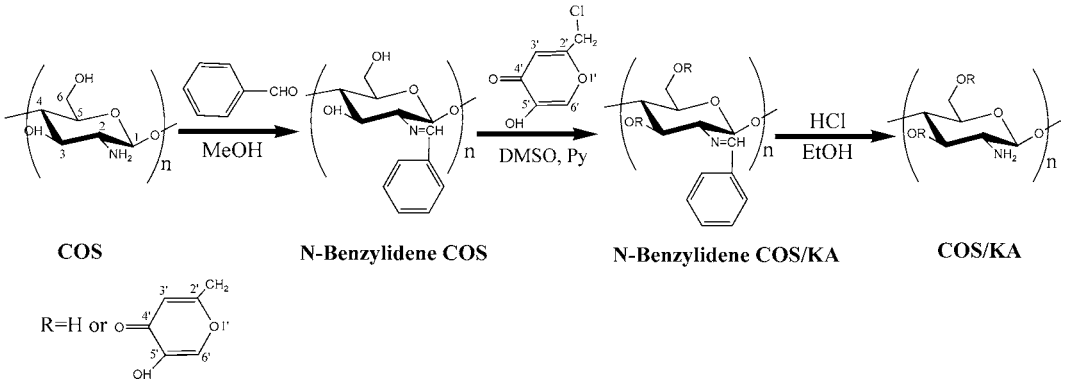

Figure 1. Reaction scheme for the synthesis of COS/KA.

MATERIALS AND METHODS

Materials. Chitosan oligosaccharide (MW = 1 kDa), with a degree of deacetylation of 90%, was made from crab shell and obtained from Zhejiang Jinke Biochemical Co. Ltd. (Zhejiang, China). Kojic acid (2-hydroxymethyl-5-hydroxy-4*H*-pyran-4-one) was purchased from Wuhan Weisheng Biochemical Co. Ltd. (Hubei, China). Chlorokojic acid (2-chloromethyl-5-hydroxy-4*H*-pyran-4-one) was prepared by the reaction of kojic acid with thionyl chloride in chloroform according to the method of Uher and Hudecová.[19] Chlorination of the 2-hydroxymethyl moiety of kojic acid using thionyl chloride at room temperature produced chlorokojic acid, with the ring alcoholic OH being unaffected. Dimethyl sulfoxide (DMSO), deuterium oxide (D_2O), pyridine, and benzaldehyde were purchased from Sigma-Aldrich (St. Louis, MO, USA). *Staphylococcus aureus*, *Escherichia coli*, *Aspergillus niger*, and *Saccharomyces cerevisiae* used for the antibacterial assay were provided by the School of Food Science and Technology of Jiangnan University. All of the reagents used were of a highly pure grade and were used without further purification, and deionized water was used for all reagent solutions.

Synthesis of Chitosan Oligosaccharides/Kojic Acid (COS/KA). Three chitosan oligosaccharide/kojic acid grafts designated COS/KA1−3 were prepared by the reaction of *N*-benzylidene COS with chlorokojic acid in DMSO and pyridine (Py) (Figure 1). Reaction conditions are summarized in Supplemental Table 1 of the Supporting Information. COS (ca. 6 g) was dissolved in 70 mL of 1% acetic acid and diluted with 120 mL of methanol. Then 6 mL of benzaldehyde was slowly added into the COS solution over 30 min to obtain *N*-benzylidene COS, and the reaction was conducted at 60 °C for 12 h to protect amino groups of COS as Schiff base. After the reaction was completed, the reaction mixture was filtered using a sintered glass filter, and the residue was washed three times sequentially with ethanol and water to remove unreacted benzaldehyde and finally freeze-dried for 24 h. Chlorokojic acid (2.16−1.07 mol) was dissolved in DMSO. By stirring, *N*-benzylidene COS (1 mol) was added to this solution, and then Py was added dropwise at room temperature. Both *N*-benzylidene COS and chlorokojic acid dissolved completely in DMSO, so the reaction was homogeneous in this case. The reaction mixtures were stirred at different temperatures for 6 h and cooled to room temperature. Then an excess of acetone was poured into the DMSO solution, and the product was precipitated. The solid was recovered by filtration, washed repeatedly with acetone, Soxhlet-extracted with ethanol for 24 h, and finally oven-dried at 40 °C for 16 h to obtain *N*-benzylidene COS/KA. Then, the *N*-benzylidene COS/KA was suspended in 1000 mL of 0.25 mol/L hydrochloric acid solution at room temperature for 12 h, followed by filtration and three washings with ethanol and water, respectively, and oven-dried at 60 °C for 12 h to obtain the product.

UV−Vis Spectroscopy. UV−vis absorption spectra of 0.2% (w/v) solutions were obtained using a UV1000 spectrophotometer (Techcomp Ltd., China) in the spectral region of 190−600 nm and with a beam width of 2 nm.

FTIR Spectroscopy. Fourier transform infrared (FTIR) spectrum was recorded on a Nicolet NexuS470 instrument (Nicolet Instrument, Thermo Co., Madison, WI, USA). Samples were prepared as KBr pellet and scanned against a blank KBr pellet background at wavenumber range 4000−400 cm^{-1} with resolution of 4.0 cm^{-1}.

^{1}H NMR Spectroscopy. ^{1}H NMR spectra were obtained on a Bruker AV400 MHz (Bruker, Rneinstetten, Germany). Samples were dissolved in D_2O with tetramethylsilane (TMS) as internal standard.

Thermogravimetric Analysis (TGA). The TGA for the samples was performed on a Mettler Toledo TGA/SDTA851 thermogravimeter (Zurich, Switzerland) at the heating rate of 10 °C/min under N_2 atmosphere in the temperature range of 25−500 °C. STARe software (version 9.01) was used to analyze the thermal stability of the samples.

X-ray Diffraction (XRD). Crystallinity measurements were made using a Bruker D8 Advance diffractometer with an area detector operating at a voltage of 40 kV and a current of 50 mA at Cu Kα radiation of k = 0.154 nm. The scanning rate was 2°/min, and the scanning scope was set from 5° to 80° at room temperature.

Scanning Electron Microscopy (SEM). The morphological characteristics of COS and KA1−3 were checked using SEM (Hitachi S-4800, Hitachi Co., Japan). The samples were attached to SEM stubs using two-sided adhesive tape and spray-coated with gold powder (<10 nm) to improve the conductivity of the surface.

Solubility Test. The solutions of COS, KA, and COS/KA 1−3 were evaluated at a concentration of 5 mg/mL in different solvents including distilled water, anhydrous ethanol, acetone, diethyl ether, ethyl acetate, and glacial acetic acid at room temperature (25 °C).

Antimicrobial Activity. The antibacterial activities of the COS, KA, and COS/KA1−3 were tested using a modified colony counting method on bacteria selected for their resistance to common antimicrobial agents. A representative microbe colony was picked off with a wire loop, placed in nutrient broth, and then incubated at 37 °C overnight. By dilution with sterile normal saline (0.9%) solution, the cultures of *Staphylococcus aureus* and *Escherichia coli* containing 10^7 CFU/mL were prepared and used for the antibacterial test. The bacterial suspension (0.1 mL) was inoculated under aseptic condition into 10 mL of liquid peptone medium containing COS, KA, and COS/KA1−3. Each sample contained test materials at a concentration of 1.0, 1.25, 1.5, 2.0, 2.5, 3.0, 4.0, 5.0, 6.0, or 8.0 mg/mL, whereas a blank without test materials was prepared for comparison. All of the samples were incubated at 37 °C under constant agitation. During incubation, 0.1 mL of each suspension was taken to determine the bacteria count by serial dilution with triplicate plating on agar plates. Then the plates were taken out of the incubator, and the inhibitory activity was calculated.

The inhibitory activity (I) was calculated using eq 1 and expressed as percentage:

$$I\ (\%) = N_1 - N_2/N_1 \times 100 \quad (1)$$

N_1 is the initial cell number (CFU/mL), and N_2 is the cell number after treatment (CFU/mL).

In the determination of the inhibition rate of COS, KA, and COS/KA1−3 on the growth of *Aspergillus niger* and *Saccharomyces cerevisiae* by the same method, the differences were that all of the samples were incubated at 28 °C under constant agitation. The cultures were filtered, the pellet was washed with distilled water and dried at 80 °C to constant weight, and then measured the dry cell weight and the inhibitory activity were calculated.

The inhibitory activity (I) was calculated using eq 2 and expressed as percentage:

$$I(\%) = W_1 - W_2/W_1 \times 100 \quad (2)$$

W_1 is the dry cell weight of *Aspergillus niger* and *Saccharomyces cerevisiae* in the control culture medium, and W_2 is the dry cell weight of *Aspergillus niger* and *Saccharomyces cerevisiae* in the COS, KA, and COS/KA1−3 culture medium, respectively.

The 50% inhibitory concentrations (IC_{50}) against microorganisms were determined for COS, KA, and COS/KA1−3. Fitting of the data was performed by linear regression using the concentration versus percent inhibition. The calculated IC_{50} was submitted to analysis of variance, and the means were compared by the Tukey test ($p \leq 0.05$) using SPSS 20.0.

RESULTS AND DISCUSSION

UV−Vis Spectroscopy Analysis of COS/KA. In the UV−vis spectra of COS, KA, and COS/KA1−3 (Supporting Information, Supplemental Figure 1), broad absorption bands between 200 and 300 nm were observed for all five samples. On the basis of the data reported in the published literature, the broad absorption band of COS might be ascribed to the C═O group.[20] In the UV spectrum of KA, obvious absorption peaks appeared at 219 and 273 nm, ,whereas the UV−vis absorption spectra of COS/KA1−3 obtained at different reaction conditions were quite similar to each other. Two absorption bands of COS/KA1−3 at 207 and 271 nm indicated the presence of a 5-hydroxypyranone group. These bands were assigned to intraligand n→π^* and $\pi\rightarrow\pi^*$ transitions of the chromophoric C═O group,[18,21] indicating that KA had been substituted onto the COS.

FTIR Spectroscopy Analysis of COS/KA. FTIR spectroscopy of COS and COS/KA1−3 is shown in Figure2. From the FTIR spectrum of COS, a characteristic peak at 3422.36 cm^{-1} appeared, and this can be attributed to the −NH and −OH group stretching vibration, as well as inter- and extramolecular hydrogen bonding of COS molecules. The weak band at 2923.83 cm^{-1} was attributed to the −CH− stretch of COS. The characteristic peaks at 1628.76, 1519.37, and 1322.79 cm^{-1} were assigned to the carbonyl stretching $\nu_{C=O}$ (amide I), amine bending δ_{N-H} (amide II), and amide three absorption band of COS, respectively. The absorption band at 1155.97 cm^{-1} was the asymmetric stretching of the C−O−C bridge. In addition, the adsorption band at 1071.52 and 1034.16 cm^{-1} corresponded to the involved skeletal vibration of the C−O stretching and the band at 890.44 cm^{-1} had been assigned to the β (1→4) glycoside linkage. The FTIR spectra of the COS/KA1−3 samples were quite similar to each other. The intense band at 1216.72 cm^{-1} and the shoulder at 911.09 cm^{-1} were broadened and shifted from the corresponding features of chlorokojic acid that could be due to covalent bonding of the kojic acid residues onto the COS.[18] Compared with the NH_2 characteristic absorption band of COS and the absorption band of COS/KA1−3, the characteristic peak at 1519.37 cm^{-1} for the NH_2 group is present in both COS and COS/KA1−3, but the absorption peaks at 1030 and 1074 cm^{-1}, which were attributed to ν_{C-O} of C6−OH and C3−OH of COS, respectively, were substantially weakened. These results indicate that the alkylation reaction mainly occurred not on the amine group but on the alcoholic OH groups of COS.

^{1}HNMR Spectroscopy Analysis of COS/KA. The ^{1}HNMR spectra of COS and COS/KA1 in D_2O solvent are shown in Figure 3. In Figure 3A, the peak at 1.98 ppm existed because of the presence of $-CH_3$ of the N-alkylated glucosamine residue. A singlet at 2.98 ppm was assigned to H_2 of glucosamine and N-acetylated GlcN, and multiplets from 3.24 to 3.94 ppm corresponded to H_3, H_4, H_5, and H_6 of the methine protons of glucosamine and N-acetylated glucosamine.

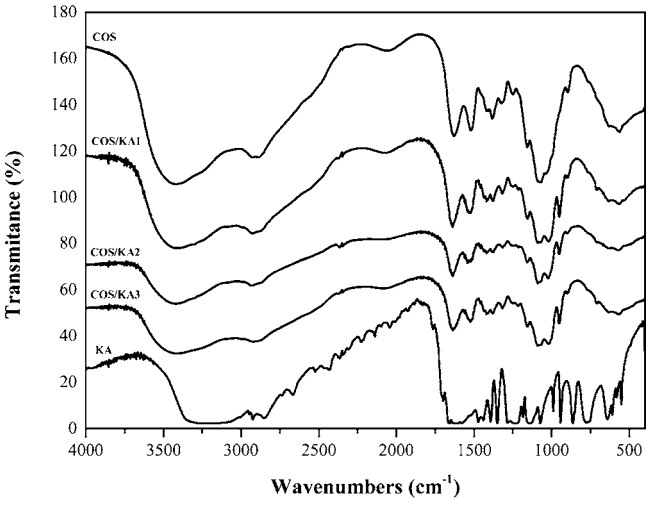

Figure 2. FTIR spectra of COS, KA, and COA/KA1−3.

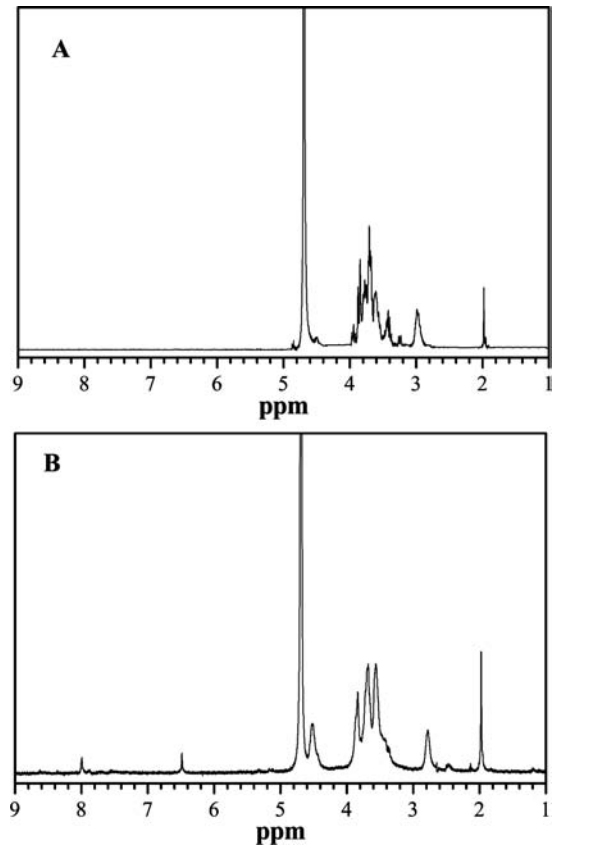

Figure 3. ^{1}H NMR spectrum of COS (A) and COS/KA1 (B).

dx.doi.org/10.1021/jf404026f | J. Agric. Food Chem. 2014, 62, 297−303

The peak at 4.5 ppm was attributed to H_1 of glucosamine, N-acetylated glucosamine. The solvent proton resonates at 4.7 ppm.[22,23] For the ^{1}H NMR spectrum of COS/KA1, the signals of COS protons at 1.98 and 2.98 and from 3.24 to 3.94 ppm did not change significantly their chemical shifts. In Figure 3B, signals of the newly formed three resonance signals appeared at 4.19 (CH_2), 6.59 (H-3′), and 8.07 (H-6′) ppm. These new peaks were assigned to the protons of kojic acid residues bound to the polysaccharide.[10,11] In free kojic acid, the signals due to CH_2, H-3′, and H-6′ have been reported in 4.52, 6.45, and 7.92 ppm regions, respectively.[18] Therefore, compared with kojic acid the signals of aromatic proton H-3′ and H-6′ in COS/KA1 were upfield shifted by 0.14 and 0.15 ppm, respectively, whereas the CH_2 signal was downfield shifted by 0.33 ppm. Hence, the observed shifts confirm that the kojic acid moiety is bound to COS via the CH_2 group.

COS contains two hydroxyl groups in every monosaccharide residue and potentially is able to undergo many reactions of alcohols. One of the most common reactions of alcohols is etherification, which takes place between OH groups of alcohols or between an OH group of an alcohol and a halogen group of an alkyl halide.[24] Aromatic protons of the 4-pyrone ring are much less sensitive to the chlorine substitution than the methylene protons. Hence, the KA moiety is covalently bound to GlcN of COS via the CH_2 group.

TGA of COS/KA. TGA and the first derivative of weight loss (DTG) have been widely used to evaluate the thermal properties of materials and to show the mechanism by which a material loses weight as a result of controlled heating.[25] Figure 4 shows the TGA and DTG curves of COS and COS/KA1−3. Despite some differences in terms of the presence of bound water and residual mass, similar profiles in the curves of mass loss were observed. Both COS and COS/KA1−3 involved two steps of weight loss. In the case of COS, the first stage of weight loss of about 10% between 30 and 100 °C was observed corresponding to the water content. The weight loss of about 47% in the second step was attributed to a complex process including degradation of saccharide rings and disintegration of macromolecule chains in the sample. It had a rapid decomposition between 150 and 320 °C, reaching its peak temperature at 214 °C. As for COS/KA1−3, the first stage, with weight loss of about 6% before 100 °C, was ascribed to the volatile low molecular products and water. The second event, approximately from 160 to 350 °C, refers to a complex process including dehydration of the saccharide rings, depolymerization, and decomposition of the alkylated units of the polymer with weight loss of about 50%.[26] COS/KA1, COS/KA2, and COS/KA3 had similar curves, which showed a maximum degradation temperature (T_{max}) at about 198 °C. This indicates that they have similar thermal stabilities. The T_{max} values of COS and COS/KA1−3 were about 214 and 198 °C, respectively. It was suggested that the thermal stability of COS/KA1−3 decreased compared with COS, which might be attributed to the disruption of crystalline structure. For COS a slight change in crystalline structure could cause significant alteration in thermal stability.[27]

XRD Analysis of COS/KA. The XRD patterns of COS and COS/KA1 are presented in Figure 5. The COS exhibited two peaks at around $2\theta = 11°$ and $2\theta = 21°$, respectively, characteristic of crystallinity of COS, as has been shown previously.[27,28] In contrast, the peak at $2\theta = 11°$ completely disappeared in COS/KA1, and the peak at $2\theta = 21°$ was wider and weaker, indicating that COS/KA1 was considerably more amorphous than COS.

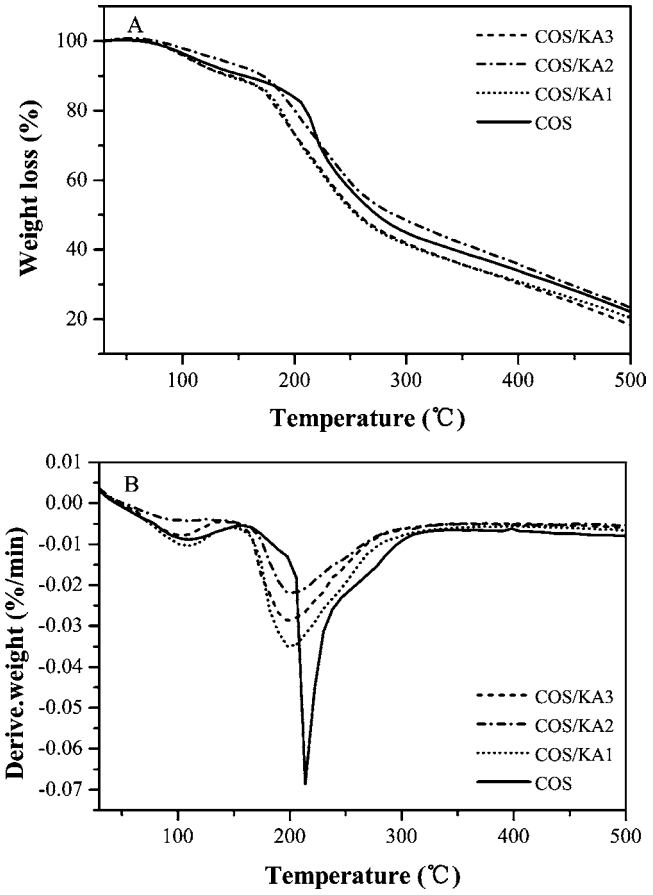

Figure 4. Thermogravimetric curves of COS (solid) and the modified COS: COS/KA1 (short dot), COS/KA2 (short dash dot), COS/KA3 (short dash).

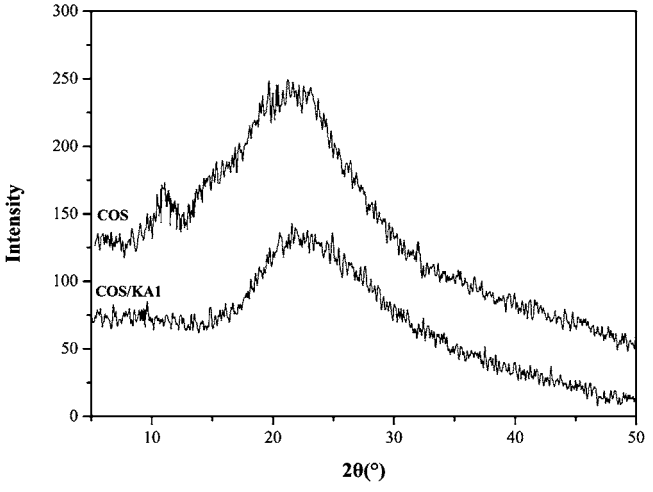

Figure 5. XRD patterns of COS and COS/KA1.

SEM Analysis of COS/KA. Surface morphological studies of COS and COS/KA1 have been investigated using SEM (Supporting Information, Supplemental Figure 2). Because the SEM images of COS/KA1−3 were quite similar, only the image of COS/KA1 is presented here for comparison with COS. The SEM image of COS shows a smooth surface and a more or less spherical shape, because there is stronger

dx.doi.org/10.1021/jf404026f | J. Agric. Food Chem. 2014, 62, 297−303

interaction between the COS molecules, whereas the particles of COS/KA1 were observed to be in the form of irregular flakes and the surfaces of COS/KA1 had many indentations. This could be attributed to effects of drying rate. High drying rates, associated with small particles, usually led to rapid wall solidification, and thus dent smoothing cannot occur.[29] This indicated that the alkylate reaction changed the fiber's microstructure and surface morphology.

Solubility Test of COS/KA. The solubilities of COS, KA, and COS/KA1−3 were investigated in various solvents (Supporting Information, Supplemental Table 1). The results showed that COS did not dissolve in the acetone and diethyl ether, but did dissolve in the other four solvents (distilled water, anhydrous ethanol, ethyl acetate, and glacial acetic acid). KA has better solubility compared with COS. However, COS/KA1−3 could be dissolved in all of the solvents except acetone. In these solvents, COS/KA1−3 showed improved solubility as compared with COS. This can be explained by the contribution of decreased crystallinity confirmed by XRD and TGA.

COS/KA1−3 with different DS values were synthesized by adjusting the molar ratio of chlorokojic acid to COS and the reaction temperature. The DS of derivatives increased when the molar ratio of chlorokojic acid to COS was increased and decreased when the reaction temperature was increased. This might be due to the introduction of a 5-hydroxypyranone group, which disturbed the formation of the ordered structure of COS and hindered the formation of inter- and intramolecular hydrogen bonds. Hence, it was helpful to dissolve.[18]

Antimicrobial Activity Assessment. The antimicrobial effect of chitosans has been reported to be dependent on MW[2,30] and degree of deacetylation,[31] which suggested that chitosans and highly deacetylated COS were more effective at inhibiting the growth of *Staphylococcus aureus*, *Escherichia coli*, *Aspergillus niger*, and *Saccharomyces cerevisiae* than COS with low deacetylation. The COS used in this study was highly deacetylated (90%). The antibacterial activities of COS, KA, and COS/KA1−3 against *Staphylococcus aureus*, *Escherichia coli*, *Saccharomyces cerevisiae*, and *Aspergillus niger* are shown in Table 1. At tested conditions, COS/KA1−3 could inhibit the growth of all four tested microorganisms, whereas COS and KA could not inhibit *Aspergillus niger*. The result indicated no noticeable antimicrobial activity when COS and KA were tested against *Aspergillus niger* at concentrations up to 8.0 mg/mL. However, COS/KA1−3 markedly inhibited growth of *Aspergillus niger* with IC_{50} values ranging from 2.15 and 2.46 mg/mL. *Aspergillus niger* belongs to the fungus category, whereas the fungal cell wall contains chitosan. Therefore, *Aspergillus niger* has a certain resistance to the antifungal performance of chitosan.[32] However, COS/KA1−3 showed an excellent antifungal activity and expanded the antimicrobial spectrum.

Table 1. Antimicrobial Activity of COS, KA, and COS/KA1-3 against *Staphylococcus aureus*, *Escherichia coli*, *Aspergillus niger*, and *Saccharomyces cerevisiae*

	IC_{50} (mg/mL)				
	COS	KA	COS/KA1	COS/KA2	COS/KA3
Staphylococcus aureus	6.30	6.63	1.04	1.15	1.24
Escherichia coli	7.39	6.04	1.23	1.38	1.58
Saccharomyces cerevisiae	7.37	7.58	1.56	1.63	1.75
Aspergillus niger			2.15	2.37	2.46

It can be observed that the antimicrobial activities of COS/KA1−3 were enhanced with increasing of DS. COS/KA1 (DS = 1.21) displayed the highest antibacterial activity followed by COS/KA2 (DS = 1.13) and COS/KA3 (DS = 0.38) against the four microorganisms with IC_{50} values from 1.04 to 2.15 mg/mL, from 1.15 to 2.37 mg/mL, and from 1.24 to 2.46 mg/mL, respectively. However, COS and KA possessed a weaker antimicrobial activity (IC_{50} from 6.30 to 7.58 mg/mL) compared to COS/KA1−3. The IC_{50} values of COS/KA against antimicrobial activities were 3−7 times lower than those of KA and COS. Hence, the introduction of a 5-hydroxypyranone group to the COS chain greatly enhanced the antimicrobial activity of the COS/KA.

There were also some differences in the inhibition activity against *Staphylococcus aureus* and *Escherichia coli* for COS, KA, and COS/KA1−3. Both COS and COS/KA1−3 showed higher activity against *Staphylococcus aureus* (IC_{50} = 6.30, 1.04−1.24 mg/mL) than against *Escherichia coli* (IC_{50} = 7.39, 1.23−1.58 mg/mL). On the contrary, KA showed higher activity against *Escherichia coli* (IC_{50} = 6.04 mg/mL) than against *Staphylococcus aureus* (IC_{50} = 6.63 mg/mL). This result accorded with the previous studies[33,34] and may be attributed to their different cell walls. The cell wall of Gram-positive bacteria (*Staphylococcus aureus*) is fully composed of peptide polyglycogen. The peptidoglycan layer is composed of networks with plenty of pores, which allow COS and COS/KA molecules to come into the cell without difficulty and allow more rapid absorption of COS and COS/KA into the cell. However, the cell wall of Gram-negative bacteria (*Escherichia coli*) is made up of a thin membrane of peptide polyglycogen and an outer membrane constituted of lipopolysaccharide, lipoprotein, and phospholipids. Because of the complicated bilayer cell structure, the outer membrane is a potential barrier against COS and COS/KA molecules. Therefore, the samples have different effects on the two kinds of bacteria.

As discussed above, the probable antimicrobial mechanisms of COS/KA are suggested as being, on one hand, the positive charge of the amino group at the C-2 in the glucosamine monomer of COS/KA allows interactions with negatively charged microbial cell membranes that lead to the leakage of intracellular constituents. On the other hand, the 5-hydroxypyranone group was introduced along the molecular chain, which can form complexes with various metal ions. The hydroxyl group at the carbon 5 position acting as a weak acid is capable of forming salts with a few metals such as sodium, zinc, copper, calcium, nickel, and cadmium, which is important in cell membranes. The catechol groups readily interact with phospholipids of the cell membrane subsequently disrupting the microbial membrane and may also denature proteins. Hence, we can deduce that COS/KA showed a synergistic effect against four microorganisms. More work is needed to confirm this hypothesis.

In this study, the COS/KA derivatives with different DS values from 0.38 to1.21 were successfully prepared by alkylation reaction of chitosan oligosaccharide and chlorokojic acid in the presence of DMSO and Py. The product was characterized by UV, FTIR, and ^{1}H NMR, and XRD confirmed that the amino groups of COS reacted with chlorokojic acid to form the alkylate chitosan. TGA showed that the thermal stability of COS/KA was lower than that of COS. COS/KA exhibited an excellent solubility in organic solvents and distilled water. The

antimicrobial activity of COS was significantly enhanced by the kojic acid derivative of COS, and it increased with DS for *Staphylococcus aureus*, *Escherichia coli*, *Aspergillus niger*, and *Saccharomyces cerevisiae*. Thus, COS/KA may have potential as an antimicrobial agent in food applications. However, more biological studies are needed to understand their mechanisms of action, to improve their activity by other modifications of those molecules, and to determine their safety for food applications.

■ ASSOCIATED CONTENT

Supporting Information

UV−vis absorption spectra of COS, KA, and COS/KA1−3, SEM image of COS and COS/KA1, and reaction conditions for *N*-benzylidene COS with chlorokojic acid, DS, yield and solubility for the derivatives. This material is available free of charge via the Internet at http://pubs.acs.org.

■ AUTHOR INFORMATION

Corresponding Author

*(W.X.) Phone: +86 510 85919121. Fax: +86 510 85919121. E-mail: xiaws@jiangnan.edu.cn.

Funding

This research was financially supported by the Twelfth Five Year National Science and Technology Plan of rural field research mission contract (2011BAD23B00), and the Fund Project for Transformation of Scientific and Technological Achievements of Jiangsu Province (BA2009082).

Notes

The authors declare no competing financial interest.

■ ACKNOWLEDGMENTS

We thank the staff at our laboratory for the assistance they have provided in this study.

■ REFERENCES

(1) Rinaudo, M. Chitin and chitosan: properties and applications. *Prog. Polym. Sci.* **2006**, *31*, 603−632.

(2) Jeon, Y. J.; Kim, S. K. Production of chitooligosaccharides using an ultrafiltration membrane reactor and their antibacterial activity. *Carbohydr. Polym.* **2000**, *41*, 133−141.

(3) Xia, W.; Liu, P.; Zhang, J.; Chen, J. Biological activities of chitosan and chitooligosaccharides. *Food Hydrocolloids* **2011**, *25*, 170−179.

(4) Xu, J.; Zhao, X.; Han, X.; Du, Y. Antifungal activity of oligochitosan against *Phytophthora capsici* and other plant pathogenic fungi in vitro. *Pestic. Biochem. Physiol.* **2007**, *87*, 220−228.

(5) Kendra, D. F.; Hadwiger, L. A. Characterization of the smallest chitosan oligomer that is maximally antifungal to *Fusarium solani* and elicits pisatin formation in *Pisum sativum*. *Exp. Mycol.* **1984**, *8*, 276−281.

(6) Qin, C.; Zhou, B.; Zeng, L.; Zhang, Z.; Liu, Y.; Du, Y.; Xiao, L. The physicochemical properties and antitumor activity of cellulase-treated chitosan. *Food Chem.* **2004**, *84*, 107−115.

(7) Jeon, Y. J.; Kamil, J. Y.; Shahidi, F. Chitosan as an edible invisible film for quality preservation of herring and Atlantic cod. *J. Agric. Food Chem.* **2002**, *50*, 5167−5178.

(8) Kim, S.-K.; Rajapakse, N. Enzymatic production and biological activities of chitosan oligosaccharides (COS): a review. *Carbohydr. Polym.* **2005**, *62*, 357−368.

(9) Can, Z.; Ya, D.; Yu, L.; Qi, P. Polymeric micelle systems of hydroxycamptothecin based on amphiphilic *N*-alkyl-*N*-trimethyl chitosan derivatives. *Colloids Surf. B: Biointerfaces* **2007**, *50*, 192−199.

(10) Aytemir, M. D.; Ozcelik, B. Synthesis and biological activities of new Mannich bases of chlorokojic acid derivatives. *Med. Chem. Res.* **2011**, *20*, 443−452.

(11) Aytemir, M. D.; Ozcelik, B. A study of cytotoxicity of novel chlorokojic acid derivatives with their antimicrobial and antiviral activities. *Eur. J. Med. Chem.* **2010**, *45*, 4089−4095.

(12) Blumenthal, C. Z. Production of toxic metabolites in *Aspergillus niger*, *Aspergillus oryzae*, and *Trichoderma reesei*: justification of mycotoxin testing in food grade enzyme preparations derived from the three fungi. *Regul. Toxicol. Pharmacol.* **2004**, *39*, 214−228.

(13) Higa, Y.; Kawabe, M.; Nabae, K.; Toda, Y.; Kitamoto, S.; Hara, T.; Tanaka, N.; Kariya, K.; Takahashi, M. Kojic acid-absence of tumor-initiating activity in rat liver, and of carcinogenic and photo-genotoxic potential in mouse skin. *J. Toxicol. Sci.* **2007**, *32*, 143−159.

(14) Xiong, X.; Pirrung, M. C. Modular synthesis of candidate indole-based insulin mimics by Claisen rearrangement. *Org. Lett.* **2008**, *10*, 1151−1154.

(15) Burdock, G. A.; Soni, M. G.; Carabin, I. G. Evaluation of health aspects of kojic acid in food. *Regul. Toxicol. Pharmacol.* **2001**, *33*, 80−101.

(16) Khamaruddin, N. H.; Basri, M.; Lian, G.; Salleh, A. B.; Abdul-Rahman, R.; Ariff, A.; Mohamad, R.; Awang, R. Enzymatic synthesis and characterization of palm-based kojic acid ester. *J. Oil Palm Res.* **2008**, *20*, 461−469.

(17) Lee, Y. S.; Park, J. H.; Kim, M. H.; Seo, S. H.; Kim, H. J. Synthesis of tyrosinase inhibitory kojic acid derivative. *Arch. Pharm.* **2006**, *339*, 111−114.

(18) Marwaha, S. S.; Kaur, J.; Sodhi, G. S. Organomercury(II) complexes of kojic acid and maltol: synthesis, characterization, and biological studies. *J. Inorg. Biochem.* **1994**, *54*, 67−74.

(19) Uher, M.; Hudecová, D.; Brtko, J.; Dobias, J.; Kováč, J.; ŠturdíkE. Antifungal preparation. CS Patent 259592, 1989.

(20) Cai, Q.; Gu, Z.; Chen, Y.; Han, W.; Fu, T.; Song, H.; Li, F. Degradation of chitosan by an electrochemical process. *Carbohydr. Polym.* **2010**, *79*, 783−785.

(21) Sima, J.; Chochulová, B.; Veverka, M.; Makánová, J.; Hajselova, M.; Bradiaková, A. Efficiency of the photoreduction of iron (III) complexes with kojic acid derivatives. *Pol. J. Chem.* **1993**, *67*, 1369−1374.

(22) Fernandez-Megia, E.; Novoa-Carballal, R.; Quiñoá, E.; Riguera, R. Optimal routine conditions for the determination of the degree of acetylation of chitosan by ^{1}H-NMR. *Carbohydr. Polym.* **2005**, *61*, 155−161.

(23) Lavertu, M.; Xia, Z.; Serreqi, A.; Berrada, M.; Rodrigues, A.; Wang, D.; Buschmann, M.; Gupta, A. A validated ^{1}H NMR method for the determination of the degree of deacetylation of chitosan. *J. Pharm. Biomed. Anal.* **2003**, *32*, 1149−1158.

(24) Natalija, G.; Ricardas, M. Synthesis and study of water-soluble chitosan-*O*-poly(ethylene glycol) graft copolymers. *Eur. Polym. J.* **2004**, *40*, 685−691.

(25) Hong, J. H.; Choi, Y. H. Physico-chemical properties of protein-bound polysaccharide from *Agaricus blazei* Murill prepared by ultrafiltration and spray drying process. *Int. J. Food Sci. Technol.* **2007**, *42*, 1−8.

(26) Peniche, C.; Zaldivar, D.; Bulay, A.; Román, J. S. Study of the thermal degradation of poly(furfuryl methacrylate) by thermogravimetry. *Polym. Degrad. Stab.* **1993**, *40*, 287−295.

(27) Qin, C.; Du, Y.; Xiao, L.; Li, Z.; Gao, X. Enzymic preparation of water-soluble chitosan and their antitumor activity. *Int. J. Biol. Macromol.* **2002**, *31*, 111−117.

(28) Rhim, J. W.; Hong, S. I.; Park, H. M.; Ng, P. K. Preparation and characterization of chitosan-based nanocomposite films with antimicrobial activity. *J. Agric. Food Chem.* **2006**, *54*, 5814−5822.

(29) Rosenberg, M.; Kopelman, I. J.; Talmon, Y. A scanning electron microscopy study of microencapsulation. *J. Food Sci.* **1985**, *50*, 139−144.

(30) No, H. K.; Young Park, N.; Ho Lee, S.; Meyers, S. P. Antibacterial activity of chitosans and chitosan oligomers with different molecular weights. *Int. J. Food Microbiol.* **2002**, *74*, 65−72.

(31) Chung, Y. C.; Su, Y. P.; Chen, C. C.; Jia, G. W.; Huey, W. Relationship between antibacterial activity of chitosan and surface characteristics of cell wall. *Acta Pharmacol. Sinica* **2004**, *25*, 932−936.
(32) Wang, J.; Wang, H. Preparation of soluble *p*-aminobenzoyl chitosan ester by Schiff's base and antibacterial activity of the derivatives. *Int. J. Biol. Macromol.* **2011**, *48*, 523−529.
(33) Xing, K.; Chen, X. G.; Kong, M.; Liu, C. S.; Cha, D. S.; Park, H. J. Effect of oleoyl-chitosan nanoparticles as a novel antibacterial dispersion system on viability, membrane permeability and cell morphology of *Escherichia coli* and *Staphylococcus aureus*. *Carbohydr. Polym.* **2009**, *76*, 17−22.
(34) Mutlu, D. A.; Berrin, Ö. Original article, A study of cytotoxicity of novel chlorokojic acid derivatives with their antimicrobial and antiviral activities. *Eur. J. Med. Chem.* **2010**, *45*, 4089−4095.

JOURNAL OF AGRICULTURAL AND FOOD CHEMISTRY

Article

pubs.acs.org/JAFC

Screening for the Presence of Patulin in Molded Fresh Produce and Evaluation of Its Stability in the Production of Tomato Products

Evelien Van de Perre, Liesbeth Jacxsens, Wendy Van Der Hauwaert, Ine Haesaert, and Bruno De Meulenaer*

NutriFOODchem Unit, Department of Food Safety and Food Quality, Faculty of Bioscience Engineering, Ghent University, Coupure Links 653, 9000 Ghent, Belgium

ABSTRACT: A screening for the presence of patulin in molded fresh produce was conducted. Patulin was present in 11% of the sweet bell peppers and in 8% of the soft red fruits, but not in onions. Patulin was also found in tomatoes, but could not be detected in derived tomato products. When the production process of tomato concentrates was simulated, none of the evaluated hypotheses could however explain a complete degradation of patulin. It was thus concluded that the tomato varieties used for further processing are probably less susceptible to infestation by patulin-producing molds compared to tomatoes used for the fresh market. This was confirmed by screening for patulin throughout the production process of tomato concentrate, gazpacho, and salmorejo in three different countries; all 191 samples were negative for patulin. Therefore, it can be concluded that no health risk can be associated with derived tomato products considering this particular mycotoxin.

KEYWORDS: *patulin, tomato products, UPLC, stability of mycotoxins*

INTRODUCTION

Patulin is a well-known mycotoxin in several fruits, especially in apple and apple-derived products such as apple juice, cider, or apple puree.[1−5] It is also found in other fruits or fruit-derived products such as blueberry, cranberry, raspberry syrup, and grape juice.[6−8] When contaminated fruits are used as raw material for the manufacture of derived products, the final product is likely to be contaminated as well, because patulin is not readily degraded during the processing of fruits.[9] Different treatments during the production process can have an influence on the final patulin concentration in the product. In apple juices it is shown that an average loss of patulin of 39% is obtained for conventional clarification.[10] A study on the effect of heat treatments showed that as the heating and evaporation time increased, the concentration of patulin in apple juice samples decreased.[11]

Patulin is produced by more than 60 fungal species, of which *Penicillium expansum* is the most important.[4] Growth of the fungi on fruits occurs mainly if the surface tissue of the fruit is damaged and is thus mostly a postharvest problem.[12,13] In contrast to its original description as an antibiotic, patulin can cause symptoms of acute and chronic toxicity and has teratogenic properties.[14] After absorption in the gastrointestinal tract, patulin degrades quickly before reaching other tissues.[15] The International Agency for Research on Cancer (IARC) concluded that there is inadequate evidence that patulin is carcinogenic in animals.[16] The "no observable effect level" (NOEL) was set at 43 μg/kg bw/ay and a provisional maximum tolerable daily intake (PMTDI) of 0.4 μg/kg bw was established.[17] The maximum permitted level of patulin in apples and derived products in Europe is 50 μg/kg, and that in baby food is 10 μg/kg. [18] Thus, the presence of patulin in fruits and derived products is a potential and relevant food-related health risk, especially for vulnerable consumers.[5,19] The structural formula of patulin is given in Figure 1.

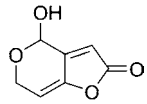

Figure 1. Structural formula of patulin.

The first objective of this study was to evaluate the presence of patulin in molded vegetable and fruit matrices other than previously reported (i.e., tomatoes, onions, sweet bell peppers, soft red fruits (small berries such as strawberries, blueberries, blackberries, red currants, and raspberries) and derived tomato products). After the observation that patulin was found in fresh molded tomatoes, but was absent in derived tomato products, hypotheses linked to the potential degradation of patulin during tomato processing were evaluated, under both laboratory and industrial conditions.

MATERIALS AND METHODS

Reagents and Chemicals for Patulin Analysis. Ethyl acetate (pa), ultrapure water, and acetic acid (99−100%) (pa) were purchased from ChemLab, Zedelgem, Belgium. Perchloric acid 70% and acetonitrile were bought from Fisher Scientific, Aalst, Belgium, and patulin was obtained from Sigma, Diegem, Belgium. A stock standard solution of patulin was prepared by dissolving 5 mg of patulin in 25 mL of ethyl acetate. The working standards were further prepared by making dilutions in water at pH 4. Standards were kept at −28 °C. Ascorbic acid, malic acid, and citric acid were bought from ChemLab. L-Glutamate (sodium salt) was bought from Fluka, Diegem, Belgium, and aspartate (sodium salt) was purchased from Merck, Overijse, Belgium.

Received: September 18, 2013
Revised: December 4, 2013
Accepted: December 10, 2013
Published: December 10, 2013

ACS Publications © 2013 American Chemical Society

dx.doi.org/10.1021/jf404192n | J. Agric. Food Chem. 2014, 62, 304−309

Analyses for Patulin and Screening of Molded Products and Derived Tomato Products. *Molded Tomatoes, Bell Peppers, and Onions.* To evaluate the method for screening of patulin, the protocol described by Sanzani et al.[20] was adapted. Potato dextrose agar (PDA) Petri plates (Oxoid, Drongen, Belgium) were inoculated with *P. expansum* MUM 00.01 and incubated for 10 days at 25 °C. Three different types of samples were taken to evaluate which contained the highest patulin concentration: only fungi/mycelium (1 cm^2), only agar (1 cm^2), and combination of fungi and agar (1 cm^3). This procedure was conducted in triplicate. Results showed that when fungi were taken together with some agar (up to 1 cm^3), the highest peak of patulin was obtained. Therefore, it was decided to take a piece of fungus combined with a piece of the molded matrix for the screening. Because the objective was to evaluate the possible presence of patulin producing molds, this qualitative method proved to be sufficient.

A 1 cm^2 piece of fungus together with 1 cm depth of product was put into a Falcon tube together with 3 mL of acidified water (pH adjusted to 4 with pure acetic acid). This was centrifuged for 10 min at 9000*g*, filtered through a 0.45 μm syringe filter, and analyzed by HPLC-UV (Thermo, Aalst, Belgium). The results were expressed as present/absent and are qualitative. This method allowed an easy screening to determine the presence of patulin-producing molds on the molded products (i.e., tomatoes, sweet bell peppers, and onions).

Molded Soft Red Fruits and Derived Tomato Products. Patulin was extracted from frozen soft red fruits and derived tomato products by adding 2 mL of ethyl acetate to 1 g of homogenized sample. After vortexing, it was mixed using a rotary shaker for 1 h. The mixture was centrifuged during 10 min at 9000*g*. A volume of 750 μL of extract was transferred into Eppendorf tubes, dried under a gentle stream of nitrogen, and reconstituted in 750 μL of water pH 4. After vortexing and sonication, the reconstituted extract was filtered through a 0.45 μm syringe filter and analyzed by UPLC (Dionex, Aalst, Belgium). This method is quantitative, and the results are expressed as micrograms patulin per kilogram product.

Instrumental Parameters. The HPLC was a Varian Vista 5500 (Thermo). It was equipped with a Rheodyne model 7125 six-way injector with a 20 μL loop. The column used was a 250 mm × 4.6 mm i.d., 5 μm, Inertsil 5 ODS-2 stainless steel (Varian, Diegem, Belgium) column. As a mobile phase acetonitrile/0.0175% perchloric acid in water (7/93, v/v) was used at 1 mL/min. After 13 min, a change was made to 90% acetonitrile to elute interfering compounds from the extract. After 15 min, there was again a shift to acetonitrile/0.0175% perchloric acid in water (7:93, v/v). The column and guard column were maintained at 36 °C during the HPLC analysis. Detection was carried at 276 nm, and run time was 38 min.

UPLC separation was achieved on an Ultimate 3000 RS system (Dionex), consisting of a vacuum degasser, quaternary pump, cooled autosampler, and column oven (30 °C) and equipped with a 150 × 2.1 mm i.d., 2.2 μm, Acclaim RSLC 120 C18 column (Dionex). As a mobile phase acetonitrile/perchloric acid in water (0.0175%) (7/93, v/v) was used at 0.5 mL/min. After 5 min, a change was made to 90% acetonitrile to elute polluting compounds from the extract. After 6.6 min, there was again a shift to acetonitrile/0.0175% perchloric acid in water (7:93, v/v). The column was maintained at 30 °C during the UPLC analysis. Detection was carried out at 276 nm by a diode array detector, and run time was 10 min.

Validation of the Quantitative Method for Determining Patulin in Molded Soft Red Fruits and Derived Tomato Products. The analytical method was validated by spiking fresh soft red fruit (strawberry, red currant, blackberry, and blueberry) that had been homogenized to a juice and tomato concentrates with patulin (0.1, 0.5, 1, and 1.5 μg/mL). This procedure was done in duplicate. After spiking with patulin, the samples were mixed for 1 h using a rotary shaker to allow equilibration with the matrix. The total recovery (TR) was calculated as described by Sulyok et al.:[21]

$$\mathrm{TR}\ (\%) = 100 \times \text{slope } b/\text{slope } a$$

a is the slope of spiked pure solvents, and b is the slope of the calibration curve from blank extracts spiked before extraction. The LOD and LOQ were determined using the equations

$$\mathrm{LOD} = 3s_{\mathrm{bl}}/S$$

where s_{bl} is the standard error of the intercept and S the slope of the respective calibration curve) and

$$\mathrm{LOQ} = 3\mathrm{LOD}$$

Evaluation of the Stability of Patulin in the Production Process of Tomato-Derived Products. *Binding of Patulin with Compounds Present in the Tomato Matrix.* Fresh tomatoes were visually checked for the absence of molds and then mixed to prepare a tomato juice using a blender. The tomato juice was spiked with three patulin concentrations (0.5, 1.0, and 1.5 μg/mL) and left between 0 and 5 days at 4 °C before the extraction procedure was begun. This was done in duplicate.

Influence of Ascorbic Acid (Vitamin C) and Free Amino Acids on the Stability of Patulin. Different tomato simulants were made to investigate the influence of vitamin C on patulin. Tomato juice was first analyzed for the presence of free amino acids[22] and vitamin C.[23] On the basis of these results, the formulation of the tomato simulants was made to evaluate the effect of vitamin C and amino acids on the stability of patulin during the heating process of the production of tomato concentrate. The simulant was made by adding citric acid and malic acid (respectively 9 and 4% on dry matter (DM) (5% DM in tomato)) and vitamin C (0.14 g/5 g DM) to water. The same was done without the addition of vitamin C but with the addition of amino acids glutamate (0.07 g/5 g DM) and aspartate (0.02 g/5 g DM). These amino acids proved to be the two dominant amino acids representing, respectively, 63 and 21% of the total free amino acids present in tomatoes. To simulate the production process of tomato concentrate, the simulants were thickened from 5 to 12% DM using a rotary evaporator (100 °C) (Heidolph, Schwabach, Germany). Each experiment was done in duplicate and analyzed for patulin using the previously presented extraction procedure.

Influence of the Heating Process on the Stability of Patulin. Tomatoes, visually checked for the absence of molds, were inoculated with *P. expansum* MUM 00.01 and incubated at 25 °C for 2 weeks. After homogenization, the sample was preheated in a warm water bath at 95 °C for 30 min and then put on a rotary evaporator at 77 °C for 20 min, thus simulating the cold break procedure. This was done in quintuplicate. Samples were taken before preheating, after preheating, after 10 min of evaporation, and at the end (20 min of evaporation). Samples were analyzed for patulin using the previously presented extraction procedure.

Sampling in Industrial Production Process of Derived Tomato Products. Samples were taken from the field stage through the end product at different companies producing tomato concentrate (in Spain, Portugal, and Poland), salmorejo (Spain), and gazpacho (Spain). The type and number of samples that were analyzed for patulin were molded tomatoes in the field (preharvest) (n = 49), molded tomatoes entering the factory (postharvest) (n = 36), skin and seeds (removed from process) (n = 17), intermediate products (n = 61), and end products (i.e., concentrates, gazpacho, and salmorejo) (n = 28).

Data Evaluation. Prevalence data of patulin for each type of fresh produce and each country were expressed, and the standard deviation of a sample proportion was calculated with eq 1

$$s_p = \sqrt{\frac{p(1-p)}{n}} \tag{1}$$

with p the proportion of positive samples and n the number of samples tested.[24] Statistics were performed with Excel (2007).

RESULTS AND DISCUSSION

Development and Validation of the Quantitative Method for Analyzing Patulin in Molded Soft Red Fruits and Derived Tomato Products. Because the molded soft red fruits were liquid after defrosting, the described qualitative method could not be used to screen for the presence of patulin and thus for patulin-producing molds in these samples.

dx.doi.org/10.1021/jf404192n | J. Agric. Food Chem. 2014, 62, 304−309

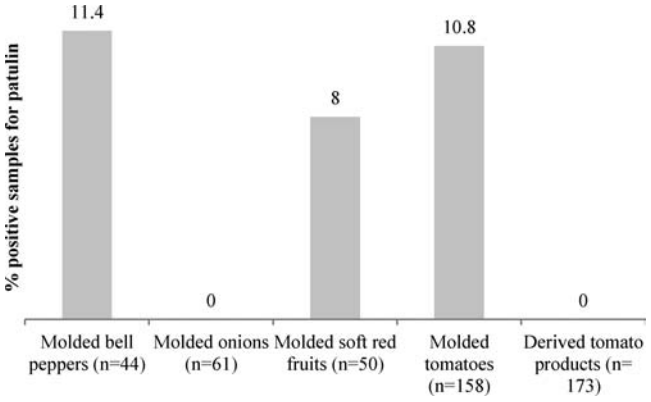

Figure 2. Percentage of positive samples for patulin for molded bell peppers (n = 44), molded onions (n = 61), molded soft red fruits (n = 50), molded tomatoes (n = 158), and derived tomato products (n = 173).

Table 1. Results of Binding of Patulin on Tomato Matrix as a Function of Days Expressed as Recovery of Spiked Tomato Juice (n = 2)

spiked concen on day 0 (μg/mL of patulin)	recovery[a] ± SD (%)		
	day 0	day 1	day 5
0.5	108.4 ± 11.4a	82.2 ± 8.5b	80.9 ± 5.8b
1	95.1 ± 0.2a	73.7 ± 0.4b	79.4 ± 1.1b
1.5	85.9 ± 1.5a	67.6 ± 3.4b	7.9 ± 1.8b

[a]Different letters indicate significant difference within the same concentration..

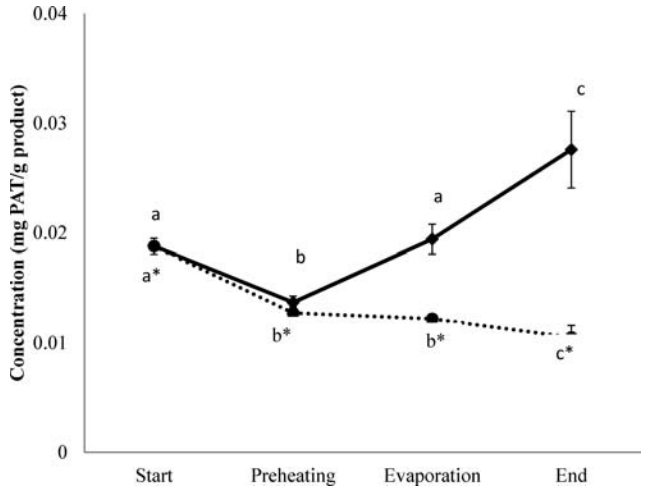

Figure 3. Evolution of patulin concentration in tomatoes throughout the production process of concentrated tomatoes: (solid line) patulin concentration on total product (mg patulin/g tomato product) (mean ± SD, n = 5; a, b, and c are significantly different); (dotted line) patulin concentration on dry matter content; (a*, b*, and c* are significantly different. Start, juice molded tomatoes; preheating = 95 °C, 30 min, evaporation = 77 °C, 10 min, and end = final product tomato concentrate (77 °C, 10 min).

Therefore, a more complex method was used to detect patulin. All derived tomato products were also screened with this method.

Patulin standards were analyzed at different levels (0.1, 0.5, 1, and 1.5 μg/mL). The linearity was assessed by plotting the peak area versus the patulin concentration, resulting in a good linearity with R^2 > 0.99. The RSD values obtained at different levels were 3.9% for 1.5 μg/mL and 4.7% for 0.1 μg/mL (n = 10; two repetitions over 5 days). The recovery of patulin in the different matrices was 96.5 ± 11.0% for tomato concentrate, 77.5 ± 7.4% for blueberry, 76.1 ± 12% for red currant, 76.4 ± 8.6% for strawberry, and 71.1 ± 6.8% for blackberry. A good recovery above 70% was achieved for all matrices. The recovery for tomato concentrate was higher than the recoveries for soft red fruit. A LOD of 13 μg/kg and a LOQ of 39 μg/kg were obtained. These are below the maximum permitted level of 50 μg patulin/kg in apples and derived products in Europe.[18]

Screening for Patulin in Molded Products. In total, 44 molded sweet bell peppers, 61 molded onions, 50 molded soft red fruits, and 158 molded tomatoes were screened for the presence of patulin. The results of the screening are shown in Figure 2. In molded onions no patulin was found. Patulin was present in 16.7% of the molded sweet bell peppers from Belgium (n = 30, Sp = standard deviation of a sample proportion = 6.8%) and in none of the molded sweet bell peppers from India (n = 14). Currently, in the literature there is no information on patulin occurrence in sweet bell peppers available. It is reported that after inoculation with *P. expansum*, patulin was found in sweet bell peppers, but not in onions.[23] Up to 8% of the molded soft red fruits were contaminated with patulin (n = 50, Sp = 3.8%). Frank[23] also mentioned the occurrence of patulin on strawberries after inoculation with patulin-producing molds. Additionally, patulin was present in 11% of molded tomatoes (n = 158, Sp = 2.5%). Fourteen percent of the tomatoes from the Belgian market were positive for patulin (n = 107, Sp = 3.4%), and patulin was present in 7.4% of the molded tomatoes from the Spanish market (n = 27, Sp = 5%). So far, no information on the presence of patulin in molded tomatoes is available in the literature. Because of the high number of tomatoes contaminated with patulin, it was decided to screen further for the presence of patulin in derived tomato products, because they form a higher risk for exposure to patulin for consumers than the molded tomatoes, which are not likely to be consumed as such.

Screening for Patulin in Derived Tomato Products. In total, 173 derived tomato samples (purees, concentrates, juices, dried tomatoes, soups) were screened for patulin (from Belgium (n = 114), Spain (n = 13), South Africa (n = 13), Brazil (n = 7), Egypt (n = 16), Cyprus (n = 7), and Finland (n = 5)) by applying the qualitative screening method. Although 11% of the molded fresh tomato samples were positive for patulin, none of the derived tomato samples tested positive (173 samples < LOD). At the moment there is no reported knowledge on the presence of patulin in processed tomato products. A study in Brazil analyzed 48 samples of tomato pulp after processing, and no patulin was found in any of the samples.[24] The Ministry of Agriculture, Fisheries and Food (MAFF) of the United Kingdom analyzed 26 samples of tomato products, and none of the samples were contaminated with patulin.[25] In view of the fact that patulin was found in 11% of the molded fresh tomatoes, and none was found in the derived tomato products, different hypotheses on the behavior and stability of patulin throughout the production process of tomato products were evaluated.

Evaluation of the Stability of Patulin in Tomato Product Production Processes. *Binding of Patulin with Compounds Present in the Tomato Matrix.* In a first experiment the possibility of patulin binding with compounds from the tomato matrix was evaluated. Previously, it was shown

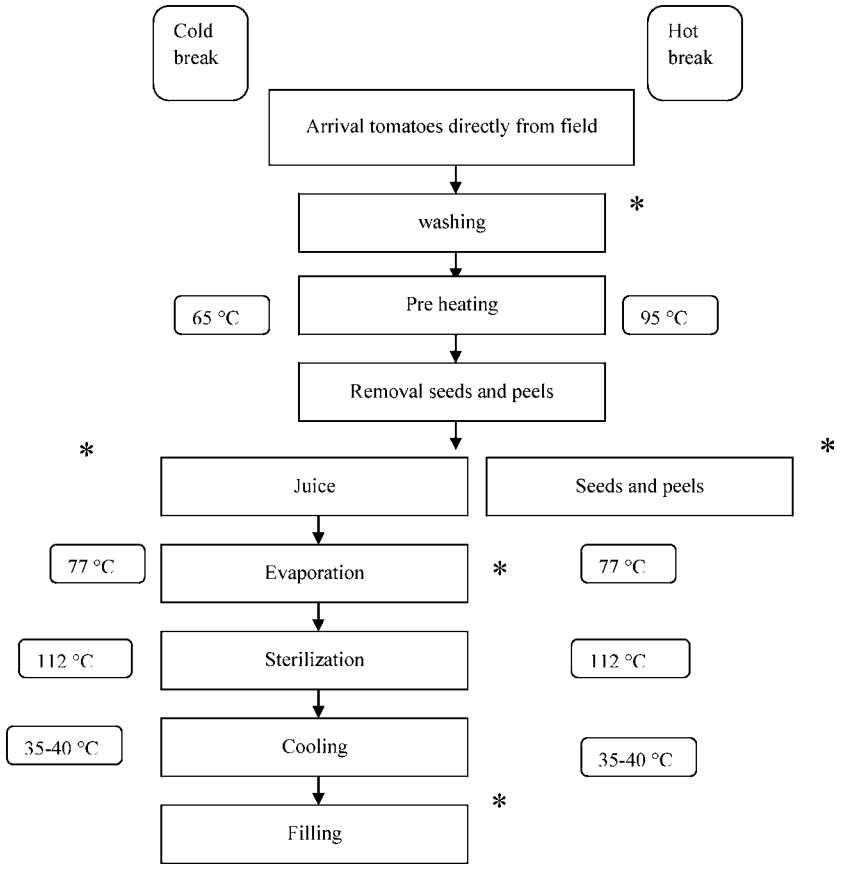

Figure 4. Flowchart of derived tomato product production process and indication of sampling in various steps (sampling is indicated by ∗).

that the clarification process reduced significantly the concentration of patulin in apple juice.[26] Moreover, a study on patulin in apple juices showed that patulin was able to bind with the solid particles of cloudy apple juice, probably due to binding with proteins.[27] It has been reported before that patulin is able to bind with thiol groups from small molecules such as amino acids.[13] Therefore, a spiking experiment with patulin was performed on laboratory-made tomato juice. The tomato juice was spiked with three patulin concentrations and left during 0−5 days at 4 °C before the extraction procedure was begun. As can be seen in Table 1, a reduction of patulin of 18−26% was observed after 1 day. After 5 days, no further significant reduction was observed. These results reveal that patulin is binding only partially to compounds in the tomato matrix, probably with proteins or free amino acids, and remains available for detection.

Influence of Ascorbic Acid and Free Amino Acids on the Stability of Patulin during the Heating Process of the Production of Tomato Concentrate. In a second experiment the influence of specific tomato matrix compounds on the stability of patulin during the production process of tomato concentrate was investigated. Therefore, different tomato simulants were made and spiked with three concentrations of patulin. The simulants were subsequently heated using a rotary evaporator (20 min, 95 °C), mimicking the tomato concentration process. The results showed that the heating process did not induce the binding of patulin with the amino acids evaluated (recovery of 88.3 ± 15%). On the other hand, the average recovery of patulin in the simulant to which vitamin C was added (59.9 ± 9.2%) was significantly lower than the average recovery of patulin in the simulant with only amino acids ($p = 0.027 < 0.05$). This confirms previous findings that ascorbic acid reduces the concentration of patulin.[28−32] In one study the addition of ascorbic acid reduced the presence of patulin by 30% after 34 days at acidic conditions in an aqueous juice-like model system.[30]

Overall Influence of the Production Process on the Stability of Patulin in Tomatoes. In a third experiment, the impact of the whole production process of tomato concentrates on the stability of patulin in a tomato matrix was evaluated on a laboratory scale. Figure 3 shows the evolution of the patulin concentration as a function of the different steps in the production of tomato concentrate. The full line shows that the patulin concentration decreased 27% after preheating (30 min at 95 °C), whereas after 20 min in the rotary evaporator, the concentration of patulin was increased by 47% compared to the original concentration. However, this increase was due to the concentration process of the tomato juice. To investigate the effect of the heating treatments on patulin alone, the evaporation of water was thus taken into account. By doing so, a decrease of the patulin content by 44% is observed in the final product, mainly due to a decrease after the preheating (30 min at 95 °C). Overall, however, the observed absence of patulin in the derived tomato products cannot be explained by the impact of the production process on patulin. In the literature it is shown that patulin is relatively heat stable, confirming our results.[10,28] Therefore, a screening for patulin in products taken during the industrial production process of tomato concentrates, gazpacho, and salmorejo was performed in various production countries.

Screening of Patulin during the Production Process of Tomato Concentrate, Gazpacho, and Salmorejo. Samples

dx.doi.org/10.1021/jf404192n | J. Agric. Food Chem. 2014, 62, 304−309

were taken from the field until the end product in the production process of tomato concentrates in different companies in producing regions in Spain, Portugal, and Poland, gazpacho (Spain), and salmorejo (Spain). Figure 4 gives a flowchart of the production process and shows the steps in the production process where samples were collected. None of the samples tested positive for patulin. The products tested were molded tomatoes in the field (preharvest) (n = 49), molded tomatoes entering the factory (postharvest) (n = 36), skin and seeds (removed from the process) (n = 17), intermediate products (n = 61), and end products (i.e., concentrates, gazpacho, and salmorejo) (n = 28). Agronomics at the different fields in Spain and Portugal, where the tomatoes for further production are cultivated, confirmed the observation that the tomatoes in the field are not infected by *P. expansum*, hence supporting the findings about the absence of patulin in the derived tomato products. However, to confirm and in particular explain this observation, extra studies have to be performed, for example, with a genetic approach. It is currently not clear why tomatoes for the fresh market are clearly more susceptible for infestation with patulin-producing molds, whereas tomatoes that are further processed are not. It is striking though that the dry matter content of the different tomatoes is significantly different: 0.5−0.6% dry matter for the tomatoes of the fresh market versus 3−4% dry matter for the tomatoes that are used for further processing. Interestingly, Konstantinou et al.[33] observed that the susceptibility to *P. expansum* was negatively correlated to the fruit firmness. In addition, *P. expansum* is a postharvest problem, whereas the tomatoes used for further processing are stored for no longer than 48 h after harvesting before further processing. However, it cannot be excluded that other factors are involved in the observed differences in the vulnerability to mold infestation.

Fresh tomatoes, soft red fruits, and sweet bell peppers in the fresh market are likely to be contaminated with patulin upon mold infestation. Remarkably, no patulin was found in processed tomato products, although it was shown that patulin is not likely to be completely degraded during processing. It could be concluded that the tomato varieties used for further processing are not vulnerable to infestation by patulin-producing molds and thus that patulin is not a relevant safety risk in processed tomato products although it is in molded fresh tomatoes.

AUTHOR INFORMATION

Corresponding Author

*(B.D.M.) Phone: +32-(0)9 264 61 66. Fax: +32 9 264 62 15. E-mail: Bruno.DeMeulenaer@UGent.be.

Funding

We are grateful to the European Community's Seventh Framework Programme (FP7) under Grant Agreement 244994 (Project VEG-i-TRADE) for financial support.

Notes

The authors declare no competing financial interest.

ACKNOWLEDGMENTS

We thank the Council for Scientific and Industrial Research in Pretoria, South Africa (CSIR); the Royal International Inspection Laboratory in Suez, Egypt (RILL); the Tamil Nadu Agricultural University in Coimbatore, India (TNAU); the Universidade Federal do Rio Grande do Sul in Porto Alegro, Brazil (UFRGS); and the Consejo Superior de Investigaciones Cientificad in Madrid, Spain (CSIC), for the different samples.

ABBREVIATIONS USED

IARCInternational Agency for Research on Cancer; NOELno observable effect level; PMTDIprovisional maximum tolerable daily intake

REFERENCES

(1) Baert, K.; De Meulenaer, B.; Kamala, A.; Kasase, C.; Devlieghere, F. Occurrence of patulin in organic, conventional, and handcrafted apple juices marketed in Belgium. *J. Food Prot.* **2006**, *69*, 1371−1378.

(2) Beretta, B.; Gaiaschi, A.; Galli, C. L.; Restani, P. Patulin in apple-based foods: occurrence and safety evaluation. *Food Addit. Contam. A* **2000**, *17*, 399−406.

(3) de Sylos, C. M.; Rodriguez-Amaya, D. B. Incidence of patulin in fruits and fruit juices marketed in Campinas, Brazil. *Food Addit. Contam. A* **1999**, *16*, 71−74.

(4) Lai, C. L.; Fuh, Y. M.; Shih, D. Y. C. Detection of mycotoxin patulin in apple juice. *J. Food Drug Anal.* **2000**, *8*, 85.

(5) Tangni, E. K.; Theys, R.; Mignolet, E.; Maudoux, M.; Michelet, J. Y.; Larondelle, Y. Patulin in domestic and imported apple-based drinks in Belgium: occurrence and exposure assessment. *Food Addit. Contam. A* **2003**, *20*, 482−489.

(6) Weidenbörner, M. *Encyclopedia of Food Mycotoxins*; Springer: New York, 2001.

(7) Rychlik, M.; Schieberle, P. Quantification of the mycotoxin patulin by a stable isotope dilution assay. *J. Agric. Food Chem.* **1999**, *47*, 3749−3755.

(8) Asam, S.; Liu, Y.; Konitzer, K.; Rychlik, M. Development of a stable isotope dilution assay for tenuazonic acid. *J. Agric. Food Chem.* **2011**, *59*, 2980−2987.

(9) Boonzaaijer, G.; Bobeldijk, I.; van Osenbruggen, W. A. Analysis of patulin in dutch food, an evaluation of a SPE based method. *Food Control* **2005**, *16*, 587−591.

(10) Acar, J.; Gökmen, V.; Taydas, E. E. The effects of processing technology on the patulin content of juice during commercial apple juice concentrate production. *Z. Lebensm. Unters. Forsch.* **1998**, *207*, 328−331.

(11) Kadakal, C.; Nas, S. Effect of heat treatment and evaporation on patulin and some other properties of apple juice. *J. Sci. Food Agric.* **2003**, *83*, 987−990.

(12) Battilani, P.; Barbano, C.; Logrieco, A. Risk assessment and safety evaluation of mycotoxins in fruits. In *Mycotoxins in Fruits and Vegetables*; Barkai-Golan, R., Paster, N., Eds.; Elsevier: Amsterdam, The Netherlands, 2008; pp 1−26.

(13) Baert, K.; Devlieghere, F.; Amiri, A.; De Meulenaer, B. Evaluation of strategies for reducing patulin contamination of apple juice using a farm to fork risk assessment model. *Int. J. Food Microbiol.* **2012**, *154*, 119−129.

(14) Speijers, G. Patulin. In *Mycotoxins in Food: Detection and Control*; Magan, N., Olsen, M., Eds.; Woodhead Publishing: New York, 2004.

(15) Rychlik, M. Rapid degradation of the mycotoxin patulin in man quantified by stable isotope dilution assays. *Food Addit. Contam. A* **2003**, *20*, 829−837.

(16) IARC International Agency for Research on Cancer. Last update 1998; http://monographs.iarc.fr/ENG/Monographs/vol40/volume40.pdf (accessed Nov 15, 2013).

(17) JECFA evaluation of certain food additives and contaminants. *WHO Technical Report Series 859*; Geneva, Switzerland, 1995.

(18) EC Commission Regulation (EC) of 19 December 2006, setting maximum levels for certain contaminants in foodstuffs. *Off. J. European Union* **2006**, *L364*, 5−24.

(19) Baert, K.; De Meulenaer, B.; Verdonck, F.; Huybrechts, I.; De Henauw, S.; Vanrolleghem, P. A.; Debevere, J.; Devlieghere, F. Variability and uncertainty assessment of patulin exposure for

preschool children in Flanders. *Food Chem. Toxicol.* **2007**, *45*, 1745−1751.
(20) Sanzani, S.; Schena, L.; Nigro, F.; De Girolamo, A.; Ippolito, A. Effect of quercetin and umbelliferone on the transcript level of *Penicillium expansum* genes involved in patulin biosynthesis. *Eur. J. Plant Pathol.* **2009**, *125*, 223−233.
(21) Sulyok, M.; Berthiller, F.; Krska, R.; Schuhmacher, R. Development and validation of a liquid chromatography/tandem mass spectrometric method for the determination of 39 mycotoxins in wheat and maize. *Rapid Commun. Mass Spectrom.* **2006**, *20*, 2649−2659.
(22) Mestdagh, F.; Kerkaert, B.; Cucu, T.; De Meulenaer, B. Interaction between whey proteins and lipids during light-induced oxidation. *Food Chem.* **2011**, *126*, 1190−1197.
(23) Van Bree, I.; Baetens, J. M.; Samapundo, S.; Devlieghere, F.; Laleman, R.; Vandekinderen, I.; Noseda, B.; Xhaferi, R.; De Baets, B.; De Meulenaer, B. Modelling the degradation kinetics of vitamin C in fruit juice in relation to the initial headspace oxygen concentration. *Food Chem.* **2012**, *134*, 207−214.
(24) Uyttendaele, M.; Busschaert, P.; Valero, A.; Geeraerd, A. H.; Vermeulen, A.; Jacxsens, L.; Goh, K. K.; De Loy, A.; Van Impe, J. F.; Devlieghere, F. Prevalence and challenge tests of *Listeria monocytogenes* in Belgian produced and retailed mayonnaise-based deli-salads, cooked meat products and smoked fish between 2005 and 2007. *Int. J. Food Microbiol.* **2009**, *133*, 94−104.
(25) Frank, H. K. Occurrence of patulin in fruit and vegetables. *Ann. Nutr. Aliment.* **1977**, *31*, 459−465.
(26) Kawashima, L. M.; Soares, L. M. V.; de Massaguer, P. R. The development of an analytical method for two mycotoxins, patulin and verruculogen, and survey of their presence in commercial tomato pulp. *Braz. J. Microbiol.* **2002**, *33*, 269−273.
(27) MAFF MAFF UK − Survey of fruit juices and tomato products for patulin, 1995, *63*.
(28) Bissessur, J.; Permaul, K.; Odhav, B. Reduction of patulin during apple juice clarification. *J. Food Prot.* **2001**, *64*, 1216−1219.
(29) Baert, K.; De Meulenaer, B.; Kasase, C.; Huyghebaert, A.; Ooghe, W.; Devlieghere, F. Free and bound patulin in cloudy apple juice. *Food Chem.* **2007**, *100*, 1278−1282.
(30) Brackett, R. E.; Marth, E. H. Ascorbic acid and ascorbate cause disappearance of patulin from buffer solutions and apple juice. *J. Food Prot.* **1979**, *42*, 864−866.
(31) Aytac, S. A.; Acar, J. The effect of L-ascorbic acid and sulfur dioxide on the stability of patulin in apple juice and buffer solutions. *Ernaehrung/Nutrition* **1994**, *18*, 15−17.
(32) Drusch, S.; Kopka, S.; Kaeding, J. Stability of patulin in a juice-like aqueous model system in the presence of ascorbic acid. *Food Chem.* **2007**, *100*, 192−197.
(33) Konstantinou, S.; Karaoglanidis, G. S.; Bardas, G. A.; Minas, I. S.; Doukas, E.; Markoglou, A. N. Postharvest fruit rots of apple in Greece: pathogen incidence and relationships between fruit quality parameters, cultivar susceptibility, and patulin production. *Plant Dis.* **2011**, *95*, 666−672.

JOURNAL OF AGRICULTURAL AND FOOD CHEMISTRY

Article

pubs.acs.org/JAFC

Processing Treatments for Mitigating Acrylamide Formation in Sweetpotato French Fries

Van-Den Truong,*[,†] Yvette T. Pascua,[†] Rong Reynolds,[†] Roger L. Thompson,[†] T. Koray Palazoğlu,[§] Burce Atac Mogol,[#] and Vural Gökmen[#]

[†]USDA-ARS, SAA Food Science Research Unit, North Carolina State University, Raleigh, North Carolina 27695, United States

[§]Department of Food Engineering, University of Mersin, 33343 Ciftlikkoy, Mersin, Turkey

[#]Department of Food Engineering, Hacettepe University, 06532 Beytepe, Ankara, Turkey

ABSTRACT: Acrylamide formation in sweetpotato French fries (SPFF) is likely a potential health concern as there is an increasing demand for good-quality fries from carotene-rich sweetpotatoes (SP). This is the first report on acrylamide formation in SPFF as affected by processing methods. Acrylamide levels in SPFF from untreated SP strips fried at 165 °C for 2, 3, and 5 min were 124.9, 255.5, and 452.0 ng/g fresh weight, which were reduced by about 7 times to 16.3, 36.9, and 58.3 ng/g, respectively, when the strips were subjected to processing that included water blanching and soaking in 0.5% sodium acid pyrophosphate before frying. An additional step of strip soaking in 0.4% calcium chloride solution before par-frying increased the calcium content from 0.2 to 0.8 mg/g and decreased the acrylamide levels to 6.3, 17.6, and 35.4 ng/g, respectively. SPFF with acrylamide level of <100 ng/g or several times lower than that of white potato French fries can be obtained by integrating processing treatments commonly used in the food industry.

KEYWORDS: *sweet potatoes, Ipomoea batatas, sugars, asparagine, acrylamide French fries*

INTRODUCTION

Consumer demands for French fries processed from orange-fleshed sweetpotatoes (SP) as a carotene-rich food have increased in recent years.[1] In response to the increasing market demand, many food companies have thus ventured into commercial production of sweetpotato French fries (SPFF). For commercial success, the product should be of consistent quality regardless of root storage duration. Our previous studies demonstrated that consistent quality SPFF can be produced year round from SP roots stored under appropriate conditions. SPFF have relatively low fat content, 10% fresh weight (fw), and high carotene content, 10 mg/100 g fw.[2] However, aside from quality, acrylamide formation in SPFF can be a potential health concern.

Acrylamide is potentially carcinogenic in humans, and its formation is found to be associated with the Maillard reaction in thermally processed foods. Free amino acids, especially asparagine and reducing sugars, are the most important precursors for the acrylamide formation that occurs during the heat processing of foods.[3] Various studies on acrylamide intake indicated that French fries and potato chips (referred to as potato crisps in the United Kingdom and some other places), bread and bakery products, coffee, and breakfast cereals are the main sources of dietary acrylamide exposure.[4,5] French fries containing less than a proposed value of 100 μg/kg are recommended for reducing the dietary acrylamide intake.[6]

Numerous studies have been conducted to determine factors affecting its formation and to develop possible mitigation strategies to limit acrylamide levels in various foods, especially fried potato products.[7−11] The mitigation strategies include lowering reducing sugars and free asparagine in the raw materials through potato cultivar selection, application of appropriate agronomical practices, control of storage conditions (>8 °C), and tuber reconditioning for reduction of reducing sugars before processing.[12−14] Processing strategies recommended for reducing acrylamide formation in potato French fries include having the appropriate shape and size of potato cuts, that is, surface to volume ratio,[15] blanching temperature and time,[16] and soaking in water containing various additives or processing aids including calcium and sodium acid pyrophosphate (SAPP).[10] The effects of frying time, temperature, and oil type on acrylamide formation in fried potato products have been studied in detail.[8,10] Gökmen and others[17] reported a linear relationship between frying time and acrylamide content in potato French fries and an exponential increase with increased frying temperature between 150 and 190 °C. A frying model was developed for a close estimate of acrylamide content in potato French fries as a function of reducing sugar level, strip thickness, frying time, and temperature.[18]

For SPFF, several studies have been reported on the effects of SP cultivars, postharvest handling, processing treatments, and frying conditions on product quality.[2,19−23] However, limited information is available on acrylamide content in SP fries and other SP processed products. Therefore, research in this area would be beneficial to SP processors in delivering good-quality SPFF with low acrylamide levels to the consumers. We report, hereto, the effect of processing treatment and frying time on acrylamide formation in SPFF. To our knowledge, this is the first study on acrylamide

Received: September 24, 2013
Revised: December 11, 2013
Accepted: December 15, 2013
Published: December 15, 2013

ACS Publications © 2013 American Chemical Society

formation in SPFF as affected by common practices of French fry processing.

MATERIALS AND METHODS

Chemicals. Food grade chemicals, namely, SAPP and anhydrous calcium chloride ($CaCl_2$), were purchased from Spectrum Chemical MFG Corp. (Gardena, CA, USA) and Tetra Chemicals (Woodlands, TX, USA), respectively. High-pressure liquid chromatography (HPLC) grade methanol (99.9%) was purchased from Sigma-Aldrich (St. Louis, MO, USA). Water used for HPLC analysis was purified with a deionized water system (Pure Water Solutions, Hillsborough, NC, USA). Cellobiose and asparagine standards were obtained from Sigma-Aldrich (St. Louis, MO, USA). Acrylamide (>99%) was purchased from Sigma-Aldrich (Diesenhofen, Germany). Potassium hexacyanoferrate, zinc sulfate, and formic acid (98%) were obtained from Merck (Darmstadt, Germany). Carrez I solution was prepared by dissolving 15 g of potassium hexacyanoferrate in 100 mL of water, and Carrez II solution was prepared by dissolving 30 g of zinc sulfate in 100 mL of water. The Oasis MCX solid phase extraction (SPE) cartridges (30 mg, 1 mL) were obtained from Waters Corp. (Berkshire, UK). All other chemicals were of analytical grade (Fisher Scientific, Suwannee, GA, USA).

Sweetpotato Cultivar and French Fry Processing. Orange-fleshed SP (cv. Covington) was grown at the experimental fields of the Sweetpotato Breeding Program (Clinton, NC, USA), North Carolina State University. The harvested roots were cured at 30 °C and 85−90% relative humidity for 7 days and stored at 13−16 °C and 80−90% relative humidity for 4 months prior to sampling for the experiments.

Sweetpotatoes were washed, peeled, and cut into 0.9 × 0.9 cm strips using a manual French fry cutter (model 29, Vollrath, Bloomfield, IN, USA). Strips were trimmed by hand to a uniform length of 9 cm and divided into three batches, one for each processing treatment. For treatment 1 (Trt 1), strips were not subjected to any soaking or blanching treatments. Strips were cut and fried as commonly practiced for home preparation of French fries. A par-frying step was included in Trt 1 for parallel comparison with the other treatments in this study. For treatment 2 (Trt 2), samples were blanched in tap water at 95 ± 2 °C for 3 min using a steam-jacketed kettle. Immediately after blanching, the strips were drained and soaked in 0.5% SAPP at 62 ± 1 °C for 10 min followed by soaking in tap water at 21 ± 1 °C for 10 min. The strips were then drained, placed on a stainless steel rack, and partially air-dried at 65 ± 5 °C for 10 min to obtain up to 10−15% weight loss using a 1600 W food dehydrator (model D-14, The Sausage Maker Inc., Buffalo, NY, USA). For treatment 3 (Trt 3), the materials were processed as described in Trt 2 with an additional step of soaking the blanched SAPP-treated strips in 0.4% $CaCl_2$ at 62 ± 1 °C for 10 min before air-drying. All strips (120 g) were par-fried at 165 °C for 1 min in 22 L of canola oil in an electric fryer (1ER50 Series, Vuncan-Hart Co., Louisville, KY, USA) and drained on absorbent paper towels. This frying temperature is 10 °C lower than the maximum frying temperature recommended by the European Food Safety Authority for white potato French fries.[24] Due to the high reducing sugar content in SP, frying temperatures above 170 °C as commonly applied in potato French fries[8,11] would produce SPFF with an undesirable brown color. Par-fried strips were cooled to room temperature, covered, and frozen at −20 °C. Final frying was also done in canola oil at 165 °C for 2, 3, and 5 min.

Sample Preparation for Chemical Analyses. Samples were collected at each processing step and stored at −20 °C for analyses of dry matter, asparagine, calcium, and sugar contents. For calcium and acrylamide determination, the collected samples were dried for 24 h in a convection oven at 50 ± 1 °C and pulverized using a Mr. Coffee precision coffee grinder (Sunbeam, Boca Raton, FL, USA). Raw SP strips were freeze-dried for several days using a VirTis Genesis 25XL freeze-dryer (Gadiner, NY, USA), operated at −35 to −40 °C, and pulverized as other samples. The dry matter content of all samples was determined by using the oven method at 100 °C for 24 h.

Quantitation of Sugars. Duplicate specimens (5 g) from each frozen sample were ground in 15 mL of boiling 80% ethanol with a Tekmar tissuemizer (type SDT-1810; Tekmar Co., Cincinnati, OH, USA) and centrifuged at 5000 rpm for 10 min. Each sample was extracted two more times with 15 mL of 80% ethanol, and the combined supernatants were brought to 50 mL and filtered with a 0.25 μm syringe filter. Sugars were analyzed using a Shimadzu HPLC system equipped with a SIL-20AC HT autosampler, DGU-20a_3 degasser, LC 20AD pump, CTO-20A column oven, and CBM-20A controller hooked to an Antec Leyden model Decade II electrochemical detector in the pulsed mode using a gold electrode and LabSoultions/LC Solution Acquisition software (Shimadzu Corp., Kyoto, Japan). Sugar separation (glucose, fructose, sucrose, and maltose) was achieved by a 250 × 4 mm CarboPac-PA1 column attached to a 50 × 4 mm CarboPac guard column (Thermo Scientific, Waltham, MA, USA). The eluent was 0.15 N NaOH at a flow rate of 1 mL/min and temperature of 30 °C. An internal standard of cellobiose was used for peak area quantitation of the separated sugars.[25] All standard curves had a goodness of fit coefficient of at least 0.99 with the intercept being set to zero.

Quantitation of Asparagine. Free asparagine was analyzed by HPLC using the method described by Palazoğlu and Gökmen[26] with minor modifications. Duplicate specimens (5 g) from each frozen sample were ground in 25 mL of cold deionized water using a Tekmar tissuemizer (type SDT-1810) for 2 min. An additional 20 mL of cold water was used to rinse the dispersion probe, and the extraction was continued for 5 min with occasional shaking. The suspension was then centrifuged at 5000 rpm and 10 °C for 10 min, and the extract was adjusted to a final volume of 50 mL with cold water. Asparagine was converted to its 9-fluorenylmethylchloroformate (FMOC) by mixing 0.8 mL of the extract with 0.1 mL of 50 mM borate buffer, pH 10, and 0.1 mL of derivatizing agent (2 mg/mL FMOC-Cl reagent in acetonitrile) for 2 min. Hexane was added to remove the excess FMOC-Cl reagent after derivatization. This step was repeated three times to ensure the removal of the unused fluorescent reagent. Aliquots were taken for injection into a Thermo Finnigan HPLC system equipped with a fluorescent detector FL3000 set at 265/340 nm and ChromQuest data acquisition software (Thermo Electron Corp., San Jose, CA, USA). A Zorbax Eclipse Plus C8 column (150 × 4.6 mm, 5 μm) was used, and the fluorescent compound was eluted at a flow rate of 1 mL/min and 25 °C by mixtures of 50 mM sodium acetate buffer (A) and acetonitrile (B) with the following gradient: from 100 to 75% A from 0 to 10 min, from 75 to 55% A from 10 to 17 min, from 55 to 0% A from 17 to 25 min, then to 100% A in 5 min, and equilibrated for 37 min. Asparagine was calculated on the basis of an external standard with a range from 0.05 to 0.2 mM.

Quantitation of Calcium. Samples of SP strips and SPFF were oven-dried at 100 °C for 24 h and ground into powders. Calcium analysis was conducted at the Analytical Spectroscopy Service Laboratory, North Carolina State University, Raleigh, NC, USA. Duplicate specimens (1 g) from each sample were subjected to acid digestion into liquid and diluted further before analysis for calcium concentration using an inductively coupled plasma atomic emission spectromery (Perkin-Elmer Optima 2000DV, Boston, MA, USA).

Quantitation of Acrylamide Formation. All par-fried and finish-fried SP samples were dried at 50 °C for 24 h and ground into fine powder for acrylamide analysis as previously described.[26,27] Sample (1 g) was extracted with 20 mL of 10 mM formic acid in three stages (10, 5, and 5 mL). The coextracted colloids were precipitated with Carrez I and Carrez II reagents. Fat was separated by means of cold centrifugation (0 °C) at 5000 rpm for 10 min. The extract was cleaned up using a cation-exchanger SPE cartridge to remove positive charged coextractives, which may interfere during the mass spectrometric detection of acrylamide. The clear extract was eluted through a preconditioned Oasis MCX cartridge at a rate of 1 drop/s. After the first seven to eight drops had been discarded, the remaining drops were collected and filtered through a 0.45 μm nylon filter prior to analysis.

The samples were analyzed by using a Waters Acquity UPLC system coupled to a TQ detector operated in ESI(+) mode. Chromatographic separations were performed on an Acquity UPLC HSS T3 column using 10 mM formic acid with 0.5% methanol as

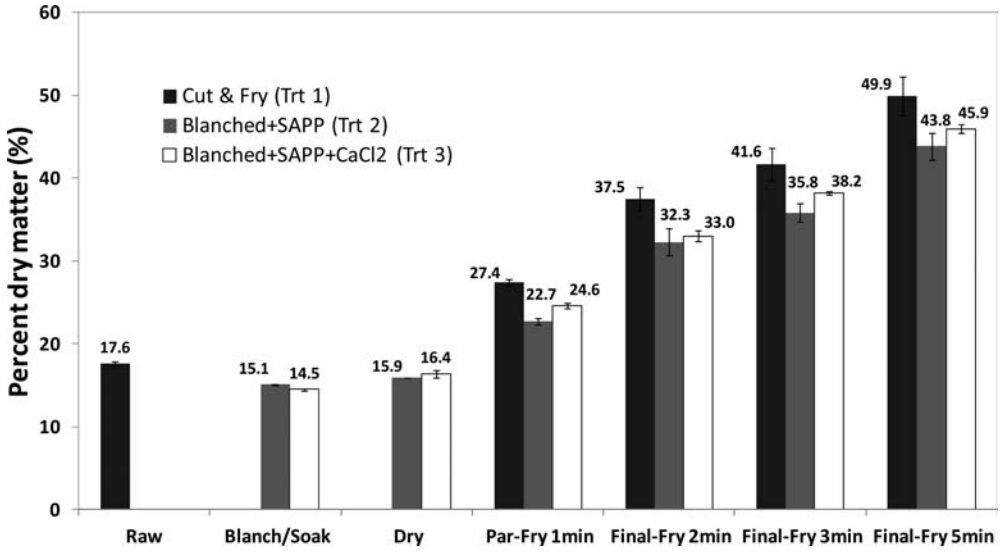

Figure 1. Dry matter content of SP strips at different processing stages.

Figure 2. Typical samples of SP French fry processing: (a) blanched SP strips; (b) par-fried, 165 °C; (c) final frying, 165 °C, 3 min.

mobile phase at the flow rate of 0.3 mL/min. The column was equilibrated at 40 °C, and a Waters Acquity FTN autosampler was held at 10 °C during the analysis. The electrospray source had the following settings: capillary voltage, 0.75 kV; cone voltage, 21 V; extractor voltage, 4 V; source temperature, 120 °C; desolvation temperature, 450 °C; desolvation gas (nitrogen) flow, 900 L/h. Acrylamide was identified by MRM of two channels. Collision gas (argon) had the flow of 0.25 mL/min. The precursor ion $[M + H]^+$ 72 was fragmented, and product ions 55 (collision energy = 9 V) and 44 (collision energy = 12 V) were monitored. The dwell time was 0.2 s for all MRM transitions. Concentration of acrylamide was calculated by means of an external calibration curve built in a range between 1 and 20 ng/mL (1, 2, 5, 10, and 20 ng/mL).

Statistical Analysis. The experiment was conducted with two replicates in a completely randomized design with a covariate. Two samples per replicate were taken for analysis. The General Linear Model procedure in the Statistical Analysis System (SAS, v. 9.2, SAS Institute Inc., Cary, NC, USA) was used to compute the statistical interferences. Group differences were evaluated using t tests with $p < 0.05$ considered to be a statistically significant difference. Means were compared with Duncan's multiple-range test with $\alpha = 0.05$.

RESULTS AND DISCUSSION

Dry Matter, Sugar, and Free Asparagine Contents. The dry matter content of the orange-fleshed SP such as the Covington cultivar used in this study is about 20% after harvest.[28] Respiration and metabolism during storage decreased the dry matter content of raw SP used in this study to 17.6%. Soluble solid leaching out during blanching further decreased the dry matter content to 14.5−15.1% in Trts 2 and 3 (Figure 1). Partial drying of SP strips before par-frying resulted in increases of dry matter content by 5.6−13.6%, which were in accordance with previous studies.[22] The final-fried samples that were fried for 2, 3, and 5 min at 165 °C had dry matter contents of 32.3−49.9% (Figure 1). With the results on dry matter content in Figure 1, all of the fresh weight (fw) data can be converted into dry weight (dw) basis for comparison with information from other studies. For commercial potato French fries, white potato tubers with dry matter content of 20−24% are preferred,[29] and after final-frying, a good-quality product should have residual moisture in the range of 38−45 or 55−62% dry matter.[11,15] After blanching and soaking, potato strips are usually subjected to partial drying to remove surface water, increasing dry matter content, shortening frying time, and consequently reducing acrylamide formation.[17] The SP French fries from all three treatments in this study had lower dry matter contents than commercial potato French fries and a softer creamy texture in the interior. The typical appearances of blanched, par-fried, and final French fry samples of the orange-fleshed SP are shown in Figure 2.

As the name implies, raw SP have a much higher sugar content than white potatoes. The sugar levels of the SP samples from different stages of the three SPFF processing schemes are shown in Figure 3. Raw strips had high concentrations of glucose, 10.22 ± 0.22 mg/g fw (1.0%); fructose, 8.09 ± 0.04 mg/g (0.8%); and sucrose, 41.91 ± 0.63 mg/g (4.2%). The total reducing sugar (sum of glucose and fructose) content was 18.31 mg/g fw (1.8%). This was 9- and 3.6-fold higher than the maximum levels of 0.2 and 0.5% reducing sugar content in white potato cultivars, which was set for limiting the browning color and acrylamide formation in the industrial processing of potato chips and French fries, respectively.[25,29]

Blanching and soaking in water or $CaCl_2$ solution decreased glucose, fructose, and sucrose contents to 0.9, 0.6, and 3.5%,

dx.doi.org/10.1021/jf404290v | J. Agric. Food Chem. 2014, 62, 310−316

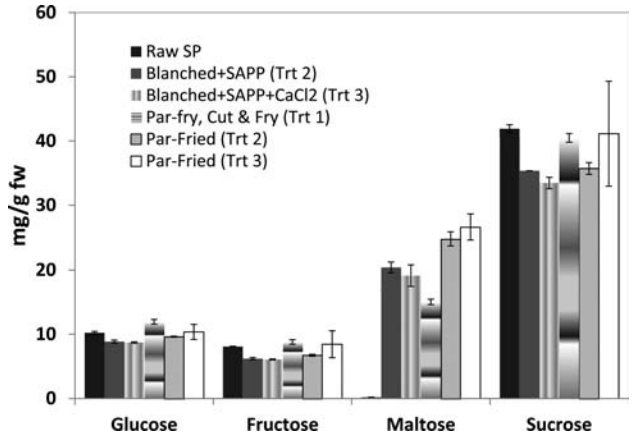

Figure 3. Effects of processing treatments and par-frying on sugar profiles of SP samples.

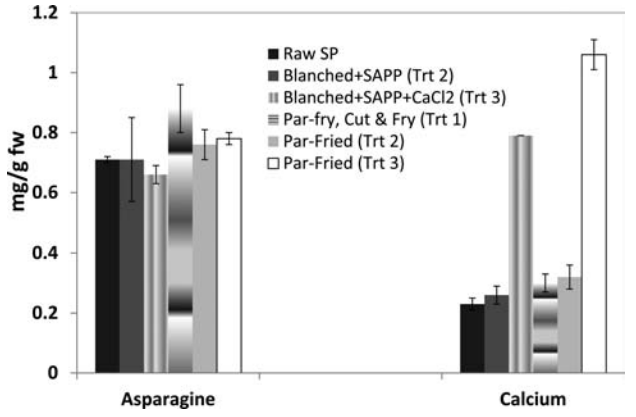

Figure 4. Asparagine and calcium contents in the raw, blanched, and par-fried SP samples.

respectively, accounting for about a 17% reduction of sugar levels in the raw SP strips. This amount of sugar leaching was much lower than the 85% decrease of reducing sugars due to water blanching of potato strips reported by Mestdagh and others.[16] Raw SP strips had negligible maltose content (0.19 ± 0.01 mg/g), which was significantly increased in the blanched and par-fried samples of all three treatments (Figure 3). The starch−maltose conversion during heating is due to hydrolysis of gelatinized starch by endogenous amylases in SP roots.[30,31] The par-fried SP samples of the cut and fry process (Trt 1) had a maltose content of 15.05 ± 0.42 mg/g (Figure 3). This maltose level was lower than the levels of the blanching and soaking treatments, which were 24.86 ± 1.11 mg/g for Trt 2 and 26.66 ± 1.98 mg/g for Trt 3. The differences can be attributed to direct application of the raw SP strips in Trt 1 to the high frying temperature and shorter time (165 °C, 1 min), which were less suitable for amylase hydrolysis of gelatinized starch into maltose as compared to blanching conditions (95 °C, 3 min). The sugar levels, except maltose, were not significantly changed by par-frying ($p > 0.05$). In the final-fried samples, the contents of total reducing sugars (sum of glucose, fructose, maltose) were 50.21−59.93 mg/g (5.02−5.99%) and sucrose levels were 52.34−70.55 mg/g (5.2−7.0%) (Table 1); these compounds provide the natural sweetness and unique flavor of SPFF as compared to white potato French fries.[23]

The asparagine content among the SP samples was found to be from 0.66 to 0.88 mg/g fw (Figure 4), which was at the low end of a range of 0.5−4.2 mg/g fw reported for eight SP varieties harvested in different years in Japan.[32] Lim and others[33] recently reported an asparagine content of 1.97 mg/g dw, equivalent to 0.68 mg/g fw of a purple-fleshed SP cultivar. The concentrations of asparagine in SP are thus much lower than the levels of 1.5−17.7 mg/g fw reported for various white potato cultivars.[13,34,35] Asparagine is the most abundant free amino acid in white potato tubers, accounting for approximately 30% of the total amino acid pool.[13] On a molar basis, asparagine concentration was about 3.7 and 5.6 times higher than that of glucose and fructose, respectively. Therefore, in white potatoes, asparagine has not been considered as a limiting factor in the Maillard reactions and acrylamide formation is mainly governed by reducing sugars during frying of potato products.[11,36] On the contrary, the amount of total reducing sugars in SP was 25 times more than that of asparagine, suggesting that asparagine is likely a limiting factor in acrylamide formation during frying of SP strips. Okuno and others[37] reported a high correlation ($R^2 = 0.803$) between free asparagine content in 15 SP varieties and acrylamide levels of 5 mm thick root slices fried in soybean oil for 4 min at 197 °C. However, there was no significant correlation between acrylamide formation with either glucose or fructose concentration in the fried crisps. In cereals such as wheat, in which the

Table 1. Sugar, Asparagine, and Calcium Content in Sweetpotato Samples As Affected by Final-Frying Time[a]

sample/treatment	frying time at 165 °C (min)	glucose (mg/g fw)	fructose (mg/g fw)	maltose (mg/g fw)	sucrose (mg/g fw)	asparagine (mg/g fw)	calcium (mg/g fw)
1. cut and fry	2	14.16 ± 1.26 ab	13.64 ± 1.58 abc	14.76 ± 1.38 f	64.40 ± 2.13 ab	0.77 ± 0.03 ab	0.35 ± 0.02 cd
(Trt 1)	3	14.71 ± 0.92 ab	11.85 ± 1.73 bcd	25.02 ± 6.89 cde	65.12 ± 5.27 ab	0.69 ± 0.06 bcd	0.39 ± 0.04 cd
	5	14.82 ± 0.68 ab	14.53 ± 1.26 ab	25.84 ± 9.97 bcde	70.55 ± 4.82 a	0.54 ± 0.10 cde	0.42 ± 0.00 cd
2. blanched + SAPP	2	11.39 ± 1.34 c	9.98 ± 1.57 de	29.30 ± 1.96 abcd	52.34 ± 5.36 d	0.67 ± 0.03 bcd	0.40 ± 0.11 c
(Trt 2)	3	13.87 ± 1.47 ab	10.83 ± 1.68 cde	25.51 ± 7.78 cde	62.89 ± 5.63 bc	0.65 ± 0.05 bcd	0.45 ± 0.09 f
	5	14.92 ± 1.97 a	15.37 ± 3.04 a	26.14 ± 9.35 bcde	64.87 ± 3.45 ab	0.53 ± 0.00 cde	0.46 ± 0.13 c
3. blanched +	2	12.73 ± 0.92 b	11.73 ± 0.81 bcd	34.00 ± 4.98 ab	58.42 ± 3.99 cd	0.65 ± 0.04 bcd	1.31 ± 0.07 b
SAPP + $CaCl_2$	3	13.56 ± 0.13 ab	11.23 ± 1.07 cde	35.14 ± 0.25 a	61.02 ± 0.31 bc	0.55 ± 0.06 cde	1.48 ± 0.08 ab
(Trt 3)	5	14.16 ± 0.21 ab	13.36 ± 0.46 abc	30.05 ± 2.34 abc	63.51 ± 0.94 bc	0.42 ± 0.08 e	1.62 ± 0.10 a

[a]Values within columns having the same letter are not significantly different ($p > 0.05$).

dx.doi.org/10.1021/jf404290v | J. Agric. Food Chem. 2014, 62, 310−316

sugar concentrations are relatively higher as compared with free amino acids, the asparagine level can be a limiting factor in acrylamide formation. Selection of wheat cultivars and growing conditions for low asparagine content is among the recommended practices in mitigating acrylamide formation in heated wheat products.[38]

Processing Treatments and Acrylamide Formation. The cut and fry process without par-frying is one of the common methods for home preparations of French fries. In this study, a par-frying step was inserted in Trt 1 for comparison with the processing effects in Trts 2 and 3. The acrylamide concentration in the par-fried SP strips of the cut-fry process was 10.7 ng/g, which linearly increased to 125−452 ng/g on a fresh weight basis (Figure 5) and 324−874 ng/g on a dry

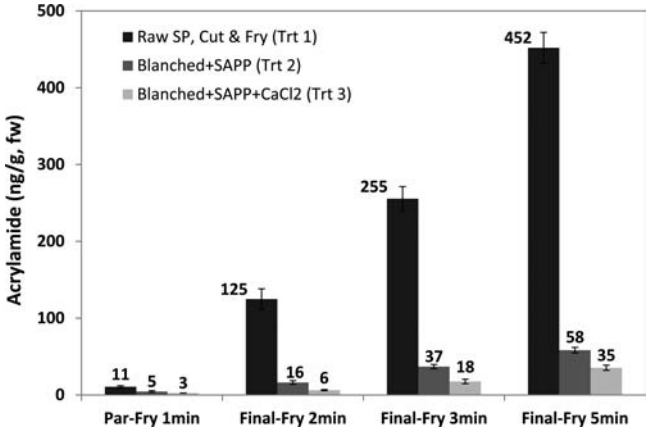

Figure 5. Acrylamide levels in sweetpotato French fries (ng/g fresh weight).

weight basis during final frying at 165 °C for 2, 3, and 5 min. The linear relationship between acrylamide formation and frying time was in accordance with the previous studies on white potato French fries.[18] The acrylamide levels obtained for the nonblanched SPFF samples (Trt 1) (Figure 5) were within the 50−1823 ng/g range of acrylamide content in white potato French fries from various commercial varieties and breeding lines.[34] Acrylamide levels up to 2970 ng/g were reported for home preparation of white potato French fries from potato varieties with wide variations in reducing sugars, 0.015−0.788% fw.[35] Mestdagh and others[16] found an acrylamide level of 833 ng/g from unblanched strips of a potato variety having low reducing sugars (0.061%) fried at 180 °C for 5 min. Commercial white potato French fries in Canada had acrylamide levels that fluctuated from 60 to 1800 ng/g.[34] Acrylamide data gathered from food monitoring in 2007−2010 by the European Food Safety Authority indicated a range of 277−356 μg/kg in white potato French fries.[39,40]

Unlike white potato French fries, information on acrylamide levels in fried SP products is very limited. Acrylamide levels up to 3000 ng/g were formed in 0.5 cm thick root slices of different SP varieties fried at 197 °C for 4 min.[37] The type of vegetable oil and the number of batches fried consecutively in the same oil affect acrylamide formation. The levels of acrylamide varied from 296 to 2019 ng/g in fried chips of a SP cultivar, which were deep-fried in different vegetable oils for 10 consecutive frying sessions, 2 min each at 180 °C.[32] On the basis of the regression of the browning index and the acrylamide content among the fried and roasted food items from different roots and tubers in Africa, the fried SP had the highest estimated acrylamide formation of 1043 ng/g.[41] Sweetpotato fries with acrylamide content of 136.3−366.1 ng/g were among the acrylamide survey of traditional snacks in Thailand.[42]

The results presented in Figure 5 demonstrate the beneficial effect of blanching and soaking SP strips in 0.5% SAPP (pH 4.4) to reduce acrylamide formation in SPFF. Blanching and soaking SP strips in SAPP as described in Trt 2 significantly ($p < 0.05$) reduced the acrylamide content to levels of 16, 37, and 58 ng/g in the final SPFF fried for 2, 3, and 5 min, respectively. The reductions were equivalent to 85−87% on fw (Figure 5) and 83−85% on dw (based on the dry matter content in Figure 1), as compared to the SPFF samples of the cut and fry process (Trt 1). Leaching out of the acrylamide precursors, reducing sugars and asparagines (Figures 3 and 4) contributed to the acrylamide reduction in the SPFF samples. It has been demonstrated that acrylamide formation mainly occurred at the surface of the white potato French fries.[6] Therefore, any processing treatments that result in decreasing the levels of reducing sugars and asparagine on the strip surface would be effective strategies in mitigating acrylamide formation. Further studies need to be conducted to determine the blanching and soaking effects on chemical components at the outer layers of SP strips and acrylamide formation in SPFF. Blanching is commonly practiced in the industrial processing of white potato French fries to inactivate oxidases associated with enzymatic browning and to develop a layer of gelatinized starch, which reduces oil absorption and improves the texture of the fried products. Acrylamide content in potato French fries was reduced from 833 ng/g in the unblanched treatment to 365 ng/g or 56% reduction and to 254 ng/g or 70% reduction by blanching white potato strips in tap water and industrially used blanching water before frying, respectively.[16]

Soaking the potato cuts in acidic solutions, for example, SAPP, citric acids, and other organic acids to reduce darkening has also been reported as a effective way to reduce acrylamide formation in white potato French fries.[10] The SAPP treatment has also been applied in processing of various SP products including purees, chips, and French fries.[23,31] Measurements of pH on the surface of SP strips was performed using a flat electrode of a pH meter (Accumet electrode 13-620-299, Fisher Scientific Accumet AR50). The results showed that the water-blanched SP strips had a pH of 6.2, which was decreased to 5.2 after soaking in 0.5% SAPP for 10 min at 65 °C. Jung and others[43] reported that soaking the potato cuts in citric acid and other organic acid has a mitigating effect by protonating asparagine amino groups at low pH and preventing the formation of Schiff bases, intermediates in the Maillard reaction and acrylamide formation.

Soaking the blanched SAPP-treated strips in 0.4% $CaCl_2$ solution (Trt 3) further decreased the acrylamide levels to 6, 18, and 35 ng/g in the final SPFF fried for 2, 3, and 5 min, respectively (Figure 5). These reductions were equivalent to 40−62% on fresh weight and 42−62% on dry weight as compared to the SPFF samples with no $CaCl_2$ (Trt 2). Therefore, the combined effects of water blanching and soaking SP strips in SAPP and $CaCl_2$ resulted in 92−95% reduction of acrylamide formation in the final frying of SPFF. Soaking the blanched SP strips in 0.4% $CaCl_2$ resulted in a 3.4-fold increase in calcium content (Figure 4). Calcium content in the potato strips after soaking was not always measured in previous studies on acrylamide formation in potato French fries.[9,10] Gökmen and Senyuva[9] reported that dipping potato strips in 0.1 M

$CaCl_2$ solution inhibited the acrylamide formation by up to 95% during frying. In the same mechanism, Kalita and Javanty[44] reported that soaking the potato strips in 0.001, 0.01, and 0.1 M vanadyl sulfate solutions before frying can reduce acrylamide formation by 30.3, 53.3, and 89.3%, respectively. It was postulated that cations such as Na^+, Ca^{2+}, and VO^{+2} could interact with asparagine and prevent the Schiff base reaction involved in acrylamide formation.

In summary, blanching the SP strips and using processing aids and additives, such as SAPP and $CaCl_2$, were effective in reducing acrylamide formation in SP French fries. These processing treatments, especially blanching and SAPP soaking, have been widely used in SP processing and unlikely affected SPFF sensory quality. Overall acceptability scores of SPFF prepared with these treatments were rated >6.0 on a nine-point hedonic scale as reported in previous studies.[2,23] Unlike white potatoes, SP contain low asparagine and high reducing sugar levels, and therefore asparagine is likely a limiting factor in acrylamide formation in SP fried products. Acrylamide formation in SPFF linearly increased with frying time. SPFF with acrylamide levels of <100 ng/g or several times lower than those of regular white potato French fries can be obtained by integrating processing treatments commonly used in the food industry.

AUTHOR INFORMATION

Corresponding Author

*(V.D.T.) E-mail: den.truong@ars.usda.gov. Phone: (919) 513-7781. Fax: (919) 513-0180.

Notes

Mention of a trademark or proprietary product does not constitute a guarantee or warranty of the product by the U.S. Department of Agriculture or North Carolina Agricultural Research Service nor does it imply approval to the exclusion of other products that may be suitable.

The authors declare no competing financial interest.

REFERENCES

(1) ConAgra Foods. Sweetpotato fries: opportunity overview. Presented at the U.S. Sweetpotato Council Annual Meeting, Biloxi, MS, Jan 24−26, 2010.

(2) Truong, V. D.; Pascua, Y. T.; Reynolds, R.; Thompson, R. L.; Dean, L. O.; Boyette, M. D.; Schultheis, J. R.; Yencho, G. C.; Kimber, J. *Chemical changes in sweetpotatoes during long-term storage as related to French fry processing quality*. Abstract and Poster Presentation 238-18, IFT Annual Meeting, New Orleans, LA, June 11−14, 2011.

(3) Mottram, D. S.; Wedzicha, B. L.; Dodson, A. T. Acrylamide is formed in the Maillard reaction. *Nature* **2002**, *419*, 448−449.

(4) JECFA. Safety evaluation of certain contaminants in food. Acrylamide. 72nd meeting of the Joint FAO/WHO Expert Committee on Food Additives (JECFA); FAO JECFA Monograph 8; 2011; pp 1−151 (*WHO Food Additive Series 63*; http://whqlibdoc.who.int/publications/2011/9789241660631_eng.pdf).

(5) Lineback, D. R.; Coughlin, J. R.; Stadler, R. H. Acrylamide in foods: a review of the science and future considerations. *Annu. Rev. Food Sci. Technol.* **2012**, *3*, 15−35.

(6) Grob, K.; Biedermann, M.; Biedermann-Brem, S.; Noti, A.; Imhof, D.; Amrein, T.; Pfefferle, A.; Bazzocco, D. French fries with less than 100 μg/kg acrylamide. A collaboration between cooks and analysts. *Eur. Food Res. Technol.* **2003**, *217*, 185−194.

(7) Tareke, E.; Rydberg, P.; Karlsson, P.; Erickson, S.; Törnqvist, M. Analysis of acrylamide, a carcinogen formed in heated foodstuffs. *J. Agric. Food Chem.* **2002**, *50*, 4998−5006.

(8) Friedman, M.; Levin, C. E. Review of methods for reduction of dietary content and toxicity of acrylamide. *J. Agric. Food Chem.* **2008**, *56*, 6113−6140.

(9) Gökmen, V.; Senyuva, H. Z. Acrylamide formation is prevented by divalent cations during the Maillard reaction. *Food Chem.* **2007**, *103*, 196−203.

(10) Medeiros Vinci, R.; Mestdagh, F.; Meulenaer, B. D. Acrylamide formation in fried potato products − present and future, a critical review on mitigation strategies. *Food Chem.* **2012**, *133*, 1138−1154.

(11) Palazoğlu, T. K.; Gökmen, V. Reduction of acrylamide level in French fries by employing a temperature program during frying. *J. Agric. Food Chem.* **2008**, *56*, 6162−6166.

(12) De Wilde, T.; De Meulenaer, B.; Mestdagh, F.; Govaert, Y.; Ooghe, W.; Fraselle, S.; Demeulemeester, K.; Van Peteghem, C.; Calus, A.; Degroodt, J.-M.; Verhea, R. Selection criteria for potato tubers to minimize acrylamide formation during frying. *J. Agric. Food Chem.* **2006**, *54*, 2199−2205.

(13) Halford, N. G.; Muttucumaru, N.; Powers, S. J.; Gillatt, P. N.; Hartley, L.; Elmore, J. S.; Mottram, D. S. Concentrations of free amino acids and sugars in nine potato varieties: effects of storage and relationship with acrylamide formation. *J. Agric. Food Chem.* **2012**, *60*, 12049−12055.

(14) Marchettini, N.; Focardi, S.; Guarnieri, M.; Guerranti, C.; Perra, G. Determination of acrylamide in local and commercial cultivar of potatoes from biological farm. *Food Chem.* **2013**, *136*, 1426−1428.

(15) Matthäus, B.; Haase, N. U.; Vosmann, K. Factors affecting the concentration of acrylamide during deep-fat frying of potatoes. *Eur. J. Lipid Sci. Technol.* **2004**, *106*, 793−801.

(16) Mestdagh, F.; De Wilde, T.; Fraselle, S.; Govaert, Y.; Ooghe, W.; Degroodt, J. M. Optimization of the blanching process to reduce acrylamide in fried potatoes. *LWT − Food Sci. Technol.* **2008**, *41*, 1648−1654.

(17) Gökmen, V.; Palazoglu, T. K.; Senyuva, H. Z. Relation between the acrylamide formation and time-temperature history of surface and core regions of French fries. *J. Food Eng.* **2006**, *77*, 972−976.

(18) Palazoğlu, T. K.; Gökmen, V. Development and experimental validation of a frying model to estimate acrylamide levels in French fries. *J. Food Sci.* **2008**, *73*, E109−E114.

(19) Ali, N.; Falade, K. O.; Akingbala, J. O. Effect of cultivar on quality attributes of sweet potato fries and crisps. *Food Nutr. Sci.* **2012**, *3*, 224−232.

(20) Farinu, A.; Baik, O.-D. Heat transfer coefficients during deep fat frying of sweetpotato: effects of product size and oil temperature. *Food Res. Int.* **2007**, *40*, 989−994.

(21) Odenigbo, A.; Rahimi, J.; Ngadi, M.; Wees, D.; Mustafa, A.; Seguin, P. Quality changes in different cultivars of sweet potato during deep-fat frying. *J. Food Process. Technol.* **2012**, *3*, 2−5.

(22) Walter, W. M., Jr.; Hoover, M. W. Preparation, evaluation and analysis of a French fry-type product from sweet potatoes. *J. Food Sci.* **1986**, *51*, 967−970.

(23) Walter, W. M., Jr.; Collins, W. W.; Truong, V. D.; Fine, T. I. Physical, compositional and sensory properties of French fry-type products from five sweetpotato selections. *J. Agric. Food Chem.* **1997**, *45*, 383−388.

(24) Food Drink Europe. Acrylamide Toolbox 2011; http://www.fooddrinkeurope.eu/uploads/publications_documents/Toolboxfinal260911.pdf (accessed Dec 9, 2013).

(25) Pattee, H. E.; Isleib, T. G.; Giesbrecht, F. G.; McFeeters, R. F. Investigations into genotypic variations of peanut carbohydrates. *J. Agric. Food Chem.* **2000**, *48*, 750−756.

(26) Palazoğlu, T. K.; Savran, D.; Gökmen, V. Effect of cooking method (baking compared with frying) on acrylamide level of potato chips. *J. Food Sci.* **2010**, *75*, E25−E29.

(27) Şenyuva, H. Z.; Gökmen, V. Interference-free determination of acrylamide in potato and cereal-based foods by a laboratory validated liquid chromatography−mass spectrometry method. *Food Chem.* **2006**, *97*, 539−545.

(28) Yencho, G.; Pecota, K. V.; Schultheis, J. R.; Pesic-Vanesbroeck, Z.; Holmes, G. J.; Little, B. E.; Thornton, A. C.; Truong, V. D. Covington sweetpotato. *HortScience* **2008**, *43*, 1911−1914.
(29) Alverez Torres, M. D.; Canet Parreño, W. Thermal processing and quality optimization. In *Advances in Potato Chemistry and Technology*; Singh, J., Kaur, L., Eds.; Elsevier: New York, 2009; pp 163−219.
(30) Ridley, S. C.; Lim, M.; Heenan, S.; Bremer, P. Evaluation of sweet potato cultivars and heating methods for control of maltose production, viscosity and sensory quality. *J. Food Qual.* **2005**, *28*, 191−204.
(31) Truong, V. D.; Avula, R. Y. Sweet potato purees and powders for functional food ingredients. In *Sweet Potato: Post Harvest Aspects in Food, Feed and Industry*; Ray, R. C., Tomlins, K. I., Eds.; Nova Science Publishers: New York, 2010; pp 117−161.
(32) Takahata, Y.; Noda, T.; Nagata, T. Varietal differences in chemical composition of the sweetpotato storage root. *Acta Hortic.* **1993**, *343*, 77−80.
(33) Lim, P. K.; Jinap, S.; Sanny, M.; Tan, C. P.; Khatib, A. The influence of deep frying using various vegetable oils on acrylamide formation in sweetpotato (*Ipomoea batatas* L. Lam) chips. *J. Food Sci.* **2013**, DOI: 10.1111/1750-3841.12250.
(34) Becalski, A.; Lau, B. P.; Lewis, D.; Seaman, S. W.; Hayward, S.; Sahagian, M.; Ramesh, M.; Leclerc, Y. Acrylamide in French fries: influence of free amino acids and sugars. *J. Agric. Food Chem.* **2004**, *52*, 3801−3806.
(35) Brunton, N. P.; Gormley, R.; Butler, F.; Cummins, E.; Danaher, M.; Minihan, M.; O'Keeffe, M. A survey of acrylamide precursors in Irish ware potatoes and acrylamide levels in French fries. *LWT − Food Sci. Technol.* **2007**, *40*, 1601−1609.
(36) Amrein, T. M.; Bachmann, S.; Noti, A.; Biedermann, M.; Barbosa, M. F.; Biedermann-Brem, S.; Grob, K.; Keiser, A.; Realini, P.; Escher, F.; Amadó, R. Potential of acrylamide formation, sugars, and free asparagine in potatoes: a comparison of cultivars and farming systems. *J. Agric. Food Chem.* **2003**, *51*, 5556−5560.
(37) Okuno, S.; Ishiguro, K.; Yoshimoto, M.; Ono, H.; Chuda, Y.; Yada, H.; Yoshida, M.; Kai, Y. Relationship between acrylamide formed during heating and components of sweetpotato roots. *Sweetpotato Res. Front.* **2007**, *21* (3), 3.
(38) Curtis, T. Y.; Muttucumaru, N.; Shewry, P. R.; Parry, M. J.; Powers, S. J.; Elmore, J. S.; Mottram, D. S.; Hook, S.; Halford, N. G. Effects of genotype and environment on free amino acid levels in wheat grain: implications for acrylamide formation during processing. *J. Agric. Food Chem.* **2009**, *57*, 1013−1021.
(39) European Food Safety Authority (EFSA).. Update on acrylamide levels in food from monitoring years 2007 to 2010. *EFSA J.* **2012**, *10*, 2938−2976.
(40) Pedreschi, F.; Mariotti, M. S.; Granby, K. Current issues in dietary acrylamide: formation, mitigation and risk assessment. *J. Sci. Food Agric.* **2013**, *94*, 9−20.
(41) Quayson, E. T.; Ayernor, G. S. Non-enzymatic browning and estimated acrylamide in roots, tubers and plantain products. *Food Chem.* **2007**, *105*, 1525−1529.
(42) Komthong, P.; Suriyaphan, O.; Charoenpanich, J. Determination of acrylamide in Thai-conventional snacks from Nong Mon market, Chonburi using GC-MS technique. *Food Addit. Contam.: Part B* **2012**, *5* (1), 20−28.
(43) Jung, M. Y.; Choi, D. S.; Ju, J. W. A novel technique for limitation of acrylamide formation in fried and baked corn chips and in French fries. *J. Food Sci.* **2003**, *68*, 1287−1290.
(44) Kalita, D.; Jayanty, S. S. Reduction of acrylamide formation by vanadium salt in potato French fries and chips. *Food Chem.* **2013**, *138*, 644−649.

JOURNAL OF AGRICULTURAL AND FOOD CHEMISTRY

Article

pubs.acs.org/JAFC

Minor Groove Binding of the Food Colorant Carmoisine to DNA: Spectroscopic and Calorimetric Characterization Studies

Anirban Basu and Gopinatha Suresh Kumar*

Biophysical Chemistry Laboratory, Chemistry Division, CSIR–Indian Institute of Chemical Biology, Kolkata 700 032, India

ABSTRACT: The interaction of the food additive carmoisine with herring testes DNA was studied by multifaceted biophysical techniques. Carmoisine exhibited hypochromic effects in absorbance, whereas in fluorescence the intensity enhanced upon complexation with DNA. Energy transfer from the DNA base pairs to carmoisine molecules occurred upon complexation. A groove binding model of interaction was envisaged for carmoisine–DNA complexation from 4′,6-diamidino-2-phenylindole (DAPI) and Hoechst displacement studies. The binding of carmoisine stabilized the DNA structure against thermal denaturation. The binding induced moderate conformational perturbations in the B-form structure of DNA. The binding affinity (10^4 M^{-1}) values, calculated from absorbance and fluorescence data, and calorimetry titrations were in close agreement with each other. The binding was characterized to be exothermic and favored by small negative enthalpic and large positive entropic contributions. Salt-dependent calorimetric studies revealed that the binding reaction was dominated by nonpolyelectrolytic forces. The negative heat capacity value suggested the role of hydrophobic effect in the interaction.

KEYWORDS: *carmoisine, DNA binding, groove binder, thermodynamics*

INTRODUCTION

Food colorants, either natural or synthetic, are widely used to enhance the aesthetic appeal of food. Azo dyes constitute one such class of synthetic organic colorants, which are extensively used in the food, textile, paper, cosmetics, agrochemical, and pharmaceutical industries.[1] Carmoisine (Figure 1) is a synthetic

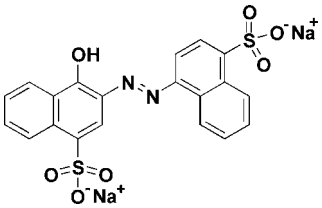

Figure 1. Molecular structure of carmoisine.

azo food dye. It is also known as Azorubine, Food Red 3, Azorubin S, Brillant carmoisine O, Acid Red 14, and C.I. 14720. It usually exists as a disodium salt and is obtained as a red to maroon powder. It has been employed for heat treatment of food after fermentation. It has E number E122 and is found in a number of food items such as blancmange, marzipan, Swiss roll, jams, preserves, yogurts, jellies, breadcrumbs, and cheesecake mixes. Carmoisine is also used as a colorant in oraldene mouthwash.[2] Owing to the presence of an azo group, carmoisine can be reduced in organisms to an aromatic amine, which is highly sensitizing.[2] Sulfanylic acid is the main metabolite of carmoisine that has been reported to date.[3] Carmoisine exercised histopathological effects on the hepatic and renal tissues of rats, which were indicated by vacuolation, swelling, necrosis, and pyknosis of their cells.[4] Histopathological studies revealed that carmoisine induced brown pigment deposition in the portal tracts and Van Küpffer cells of the liver and kidney.[5] The response was dependent not only on dose, age, gender, nutritional status, and genetic factors but also on long-term exposure to low doses.[2,6] It was recently reported that carmoisine can affect adversely and alter biochemical markers in vital organs even at low doses.[2] Significant increase in ALT, AST, ALP, urea, creatinine, total protein, and albumin in the serum of rats dosed with carmoisine have been observed. These changes were found to be more pronounced at higher doses.[2] Amin et al. reported that carmoisine induced changes in the hepatic and renal parameters, and induced oxidative stress by formation of free radicals at higher doses.[2] In the light of the above health hazards, much more safety assessment of carmoisine is essential and the use of this synthetic azo food dye should be thoroughly checked by laws, regulations, and acceptable daily intake (ADI) values.[7]

Deoxyribonucleic acid (DNA) is the key genetic substance that encodes the genetic instructions used in the development and functioning of all known living organisms. It is the carrier of hereditary information and promotes the biological synthesis of proteins and enzymes through replication and transcription.[7,8] DNA is most often the prime cellular target for natural and synthetic organic materials. In anticancer therapy specific interaction of organic molecules with genomic DNA may be exploited in preventing retrieval of further information, thereby leading to the arrest of cell division. Noninvasive therapeutic action of organic molecules may also involve photosensitization leading to energy transfer from a photoexcited molecule to molecular oxygen, generating a singlet state that may directly or indirectly damage the cellular DNA.[9] Hazardous organic materials, such as dyes, heavy metals, and pesticides, that enter into the biological system by inhalation, ingestion, or absorption through the skin can interact with

Received: November 5, 2013
Revised: December 16, 2013
Accepted: December 16, 2013
Published: December 16, 2013

ACS Publications © 2013 American Chemical Society

DNA directly or indirectly in vivo, which may alter the DNA morphology and bring about DNA damage, thereby adversely affecting its function and genetic expression.[7,10] A few studies on the interaction of synthetic azo dyes with DNA have been undertaken.[11,12] The results suggested a groove binding model for these azo dyes and proposed that these colorants had a toxic potential to DNA in vitro.[11,12] Hence, studies on the interaction of carmoisine with DNA are of great significance as they could provide useful insights into the toxicological aspects of the dye. A preliminary spectroscopic investigation on carmoisine–DNA binding has been reported,[11] but detailed aspects on the mode, mechanism, affinity, and energetics of its DNA binding are still obscure. Therefore, in this study we present the outcome of our detailed investigation on the binding of carmoisine to DNA from multifaceted biophysical studies.

MATERIALS AND METHODS

Materials. Herring testes DNA (HT DNA, Type XIV, 41 mol % GC), carmoisine (disodium 4-hydroxy-3-[(4-sulfo-1-naphthalenyl)-azo]-1-naphthalenesulfonate, ~98% purity), bisbenzimide (Hoechst 33258, ≥98% purity), and 4′,6-diamidino-2-phenylindole (DAPI, ≥98% purity) were purchased from Sigma-Aldrich Corp. (St. Louis, MO, USA). DNA was purified by phenol extraction and ethanol precipitation. DNA samples were sonicated to uniform size of about 280 ± 50 base pairs in a Labsonic sonicator (B. Brown, Germany) and were dialyzed under sterile conditions at 5 °C into the experimental buffer. The DNA exhibited characteristic ultraviolet absorption spectrum with an A_{260}/A_{280} ratio between 1.88 and 1.92 and an A_{260}/A_{230} ratio between 2.12 and 2.22. Concentration of the DNA was determined spectrophotometrically using a molar extinction coefficient value of 13200 M^{-1} cm^{-1} expressed in terms of base pairs. The nativeness of the DNA sample was confirmed from optical melting studies in which a sharp cooperative melting profile with about 40% hyperchromicity was observed. Carmoisine was highly soluble in aqueous buffer and hence its solution was freshly prepared and kept protected in the dark to prevent any light-induced photochemical changes. All of the buffer salts and other reagents were of analytical grade. All experiments were performed in filtered 10 mM citrate–phosphate (CP) buffer, pH 7.0, containing 5 mM Na_2HPO_4 prepared in deionized and triple-distilled water. The pH of the buffer solution was adjusted with citric acid.

Absorbance and Fluorescence Spectral Titrations. The absorption spectral titrations were performed at 20 ± 0.5 °C on a Jasco V660 unit (Jasco International Co. Ltd., Hachioji, Japan) equipped with a thermoelectrically controlled cell holder and temperature controller in matched quartz cuvettes of 1 cm path length, following generally the methods standardized in our laboratory and reported earlier.[13,14] Steady state fluorescence measurements were performed on a Shimadzu RF-5301PC fluorometer in fluorescence-free quartz cuvettes of 1 cm path length as described previously.[13,15] The excitation wavelength for carmoisine was 324 nm. All of the measurements were carried out under conditions of stirring and keeping excitation and emission band passes of 10 nm. The sample temperature of the fluorometer was maintained at 20 ± 1.0 °C using an Eylea Uni Cool U55 water bath (Tokyo Rikakikai Co. Ltd., Tokyo, Japan).

Estimation of the Binding Parameters. The spectral titration data were analyzed by employing the Benesi–Hildebrand plot.[16] The apparent equilibrium constant (K_{BH}) was measured using the relationship

$$\frac{1}{\Delta A} = \frac{1}{\Delta A_{max}} + \frac{1}{K_{BH}(\Delta A_{max})} \times \frac{1}{[M]} \quad (1)$$

where ΔA is the change in absorbance or fluorescence intensity at a given wavelength and [M] is the concentration of DNA. By plotting the reciprocal of the difference in absorbance or fluorescence intensity against the reciprocal of DNA concentration, the Benesi–Hildebrand association constant (K_{BH}) for the carmoisine–DNA association was calculated from the ratio of the intercept to the slope.[16]

Quantum Efficiency Measurements. The quantum efficiency (Q) of DNA binding to carmoisine is defined as the energy transferred from the DNA to carmoisine upon association and is determined from the ratio of the quantum efficiency of carmoisine bound to DNA (q_b) to the quantum efficiency of free carmoisine (q_f). It is calculated using the equation[17]

$$Q = \frac{q_b}{q_f} = \frac{I_b \varepsilon_f}{I_f \varepsilon_b} \quad (2)$$

where ε_f and ε_b represent the molar extinction coefficients of the free and DNA-bound carmoisine and I_b and I_f are the fluorescence intensities of complexed and free ligands, respectively. The quantum efficiency was determined according to a procedure reported earlier.[18]

Measurement of Energy Transfer. Energy transfer from DNA base pairs to the bound carmoisine was measured from the excitation spectra of the complexes in the wavelength range of 220–310 nm.[19−21] Excitation spectra were recorded at the emission maximum of carmoisine. The ratio $Q = q_b/q_f$, where q_b and q_f are the quantum efficiencies of bound and free carmoisine, respectively, was calculated for each wavelength using eq 2. A plot of the ratio Q_i/Q_{310} against wavelength was constructed. The wavelength of 310 nm was selected as the normalization wavelength owing to the negligible absorbance of DNA here.

Determination of the Binding Stoichiometry: Job Plot Analysis. The continuous variation method of Job was employed to determine the binding stoichiometry from fluorescence spectroscopy.[22,23] The fluorescence signal was recorded for solutions having the concentrations of both DNA and carmoisine varied while the sum of their concentrations was kept constant. The difference in fluorescence intensity (ΔF) in the absence and presence of DNA was plotted as a function of the input mol fraction of carmoisine. In the resulting plot the break point corresponded to the mole fraction of bound carmoisine in the complex. The stoichiometry was obtained in terms of DNA–carmoisine $[(1 - \chi_{carmoisine})/\chi_{carmoisine}]$, where $\chi_{carmoisine}$ denotes the mole fraction of carmoisine. The results reported are averages of three experiments.

Minor Groove Displacement Assay. Two well-known minor groove binders, DAPI and Hoechst 33258, were used to perform the minor groove displacement assays as reported earlier.[24−26] In a typical experiment, the changes in the emission spectra of DAPI and Hoechst complexed with the DNA were monitored upon addition of increasing concentrations of carmoisine at room temperature.

Hydrodynamic Studies. Viscometry studies were performed using a Cannon–Manning semimicrodilution viscometer type 75 (Cannon Instruments Co., State College, PA, USA) submerged vertically in a constant-temperature water bath (Cannon Instruments Co.) maintained at 20 ± 0.5 °C; 750 μL of the DNA solution was placed in the viscometer, and aliquots of concentrated carmoisine solution were added directly into the viscometer to obtain increasing D/P [carmoisine/DNA molar ratio] values. The two solutions were mixed thoroughly by gently bubbling dry nitrogen gas through the viscometer. Flow times of DNA alone and DNA complexed with different ratios of carmoisine were measured in triplicate with an accuracy of ±0.01 s using a Casio model HS-30W electronic stop watch (Casio Computer Co. Ltd., Japan), and the relative specific viscosity (η'_{sp}/η_{sp}) was determined using the equation

$$\eta'_{sp}/\eta_{sp} = \{(t_{complex} - t_0)/t_0\}/\{(t_{control} - t_0)/t_0\} \quad (3)$$

as reported.[14] In eq 3 η'_{sp} and η_{sp} are the specific viscosity of DNA in the presence and absence of carmoisne, $t_{control}$ and $t_{complex}$ are the average efflux times of DNA alone and carmoisine–DNA complex, and t_0 is average efflux time for the buffer.

Circular Dichroism (CD) Studies. CD spectra were recorded on a PC-controlled Jasco J815 unit (Jasco International Co. Ltd.) equipped with a temperature controller and thermal programmer model PFD 425L/15 in rectangular quartz cuvettes of 1 cm path length at 20 ± 0.5 °C as reported earlier.[27] Each spectrum was averaged from five

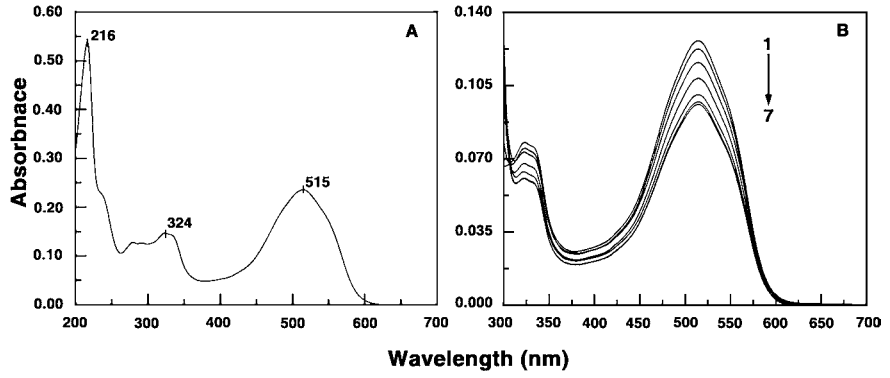

Figure 2. (A) Absorption spectrum of carmoisine. (B) Absorption spectral titration of carmoisine (curve 1) with increasing concentration of DNA (curves 2−7).

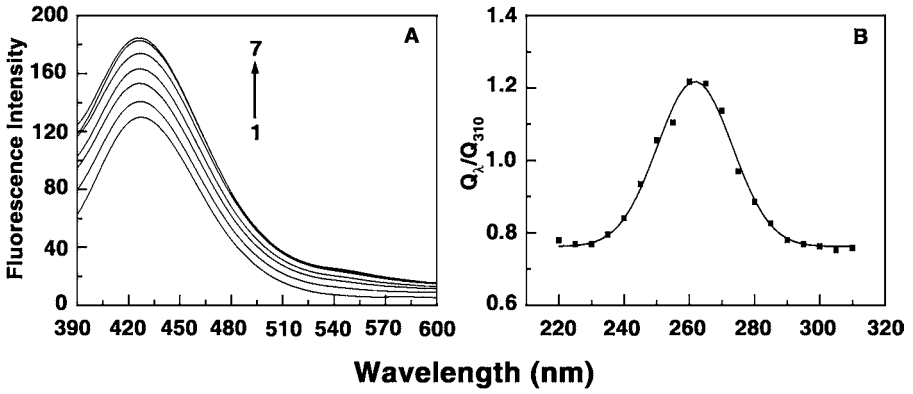

Figure 3. (A) Fluorescence spectral titration of carmoisine (curve 1) with increasing concentration of DNA (curves 2−7). (B) Variation of the relative fluorescence quantum yield of carmoisine in the presence of DNA as a function of excitation wavelength.

successive scans at a scan rate of 100 nm/min using a bandwidth of 1 nm at a sensitivity of 100 millidegree and was baseline corrected and smoothed within permissible limits using the built-in Jasco software. The molar ellipticity values $[\theta]$ are expressed in terms of DNA base pairs.

Optical Melting and Differential Scanning Calorimetry Studies. Thermal melting profiles of carmoisine−DNA complexes were measured on a Shimadzu Pharmaspec 1700 spectrophotometer equipped with a Peltier-controlled TMSPC-8 model accessory (Shimadzu Corp.). In a typical melting experiment, DNA samples were mixed with carmoisine and diluted into the degassed buffer in the micro-optical eight-chambered cuvette of 1 cm path length. The temperature of the microcell accessory was raised at a heating rate of 0.5 °C, monitoring the absorbance change at 260 nm. The midpoint of the transition profiles obtained from the maxima of the first-derivative plots gave the melting temperature (T_m).

Excess heat capacities as a function of temperature were measured on a Microcal VP-differential scanning calorimeter (DSC) (MicroCal, Inc., Northampton, MA, USA) as described previously.[28] In a series of DSC scans, both the calorimeter cells were loaded at first with the buffer, equilibrated at 35 °C for 15 min, and scanned from 35 to 95 °C at a rate of 50 °C/h. The buffer scans were repeated until a reproducible baseline was obtained (noise specification <0.5 μcal/°C and repeatability specification <1.3 μcal/°C). Once a steady baseline was achieved, on cooling, the sample cell was rinsed with the experimental buffer, loaded with the DNA sample followed by the DNA−carmoisine complex, and scanned in the same range. Each experiment was repeated twice with separate fillings. The DSC thermograms of excess heat capacity versus temperature were analyzed with Origin 7.0 software. The area under the experimental heat capacity (C_p°) curves was used to calculate the calorimetric transition enthalpy (ΔH_{cal}) by employing the equation

$$\Delta H_{cal} = \int C_p^\circ \, dT \tag{4}$$

where T is the absolute scale temperature in kelvins. This calorimetrically determined enthalpy being model-independent is unrelated to the nature of the transition. The temperature at which excess heat capacity reaches a maximum defines the transition temperature (T_m). The model-dependent van't Hoff enthalpy (ΔH_v) was obtained by shape analysis of the calorimetric data, and the cooperativity factor was obtained from the ratio of ΔH_{cal} and ΔH_v. Temperature calibration of the DSC unit was performed using the built-in calibration heaters of the unit.

Isothermal Titration Calorimetry (ITC). ITC experiments were performed on a MicroCal VP-ITC microcalorimeter (MicroCal, Inc.). Instrument control, data acquisition, and analysis were carried out using the dedicated Origin 7.0 software provided with the unit as described previously.[14,18] In a typical ITC experiment, aliquots of 10 μL of degassed DNA solution were injected from a rotating syringe (stirring speed = 290 rpm) into the isothermal sample chamber containing carmoisine solution (1.4235 mL). This protocol enabled us to keep a low concentration of carmoisine in the calorimeter cell, thereby preventing the possibility of aggregation of the dye. The reference cell was filled with degassed deionized water. Corresponding control experiments to determine the heat of dilution of the injectant were performed. The area under each heat burst curve was determined by integration using Origin 7.0 software. The heat associated with each DNA−buffer mixing was subtracted from the corresponding heat of carmoisine−DNA reaction to obtain the heat of carmoisine−DNA binding. The heat of dilution for injecting the buffer alone into the carmoisine solution was found to be negligible. The resulting corrected injection heats were plotted as a function of the molar ratio. The experimental data were fitted using a nonlinear least-squares minimization algorithm to one site binding to obtain the binding affinity (K), binding stoichiometry (N), and standard molar enthalpy

dx.doi.org/10.1021/jf404960n | J. Agric. Food Chem. 2014, 62, 317−326

of binding ($\Delta H°$). The standard molar binding Gibbs energy ($\Delta G°$) was calculated from standard relationship

$$\Delta G° = -RT \ln K \quad (5)$$

where R signifies the universal gas constant (1.9872041 cal K^{-1} mol^{-1}) and the entropic contribution ($T\Delta S°$) was obtained from the relationship

$$T\Delta S° = \Delta H° - \Delta G° \quad (6)$$

RESULTS AND DISCUSSION

Absorbance and Fluorescence Spectral Studies. Carmoisine has a characteristic absorption spectrum in the 200−700 nm region with three well-defined intense peaks with maxima around 216, 324, and 515 nm, respectively (Figure 2A). The interaction of carmoisine with DNA was monitored in the 300−700 nm region, where the absorbance of DNA is negligible. The absorption spectra of carmoisine exhibited 24% hypochromicity at 515 nm upon addition of increasing concentrations of DNA, revealing strong intermolecular association (Figure 2B). Such spectral changes have often been attributed to a strong interaction between the π electron cloud of the interacting ligand and the DNA base pairs.[11,29,30]

Carmoisine exhibited an emission maximum at 427 nm upon excitation at 324 nm. The interaction was studied by titrating a constant concentration of carmoisine with increasing concentrations of DNA. In the presence of increasing concentrations of DNA, enhancement of the fluorescence intensity of carmoisine was observed without any noticeable shift in the emission maximum (Figure 3A). This enhancement of the fluorescence intensity upon binding to DNA suggested an effective interaction of the bound carmoisine molecules with the DNA base pairs. This also indicated the location of the bound carmoisine molecules to be in a hydrophobic environment.

Evaluation of Binding Affinity Values. The spectral data obtained from absorbance and fluorescence titration studies were used to construct Benesi−Hildebrand plots to determine the apparent equilibrium constant (K_{BH}) for carmoisine−DNA complexation. The ratio of the intercept to slope afforded the apparent equilibrium constant as described earlier as per eq 1. From spectrophotometry, the magnitude of the apparent equilibrium constant was deduced to be 2.88×10^4 M^{-1}. Similarly, from spectrofluorometry the value of K_{BH} was estimated to be 2.41×10^4 M^{-1}. It can be seen that these two values, obtained from spectrophotometry and spectrofluorometry, were in very close agreement with each other.

Measurement of Quantum Efficiency and Energy Transfer. The quantum efficiency (Q) of a DNA binding ligand gives a measure of the energy transferred from the DNA to the bound ligand upon complexation and is calculated from the ratio of the quantum efficiency of the ligand bound to the nucleic acid (q_b) to the quantum efficiency of the free ligand (q_f). Determination of quantum efficiency (Q) further testifies to the strong binding of carmoisine to DNA. A plot of ΔAbs versus the inverse of the DNA concentration gave an exponential plot (not shown) from which a quantum efficiency value of 1.883 was determined for the complexation of carmoisine with DNA, which indicates enhancement of the energy of the bound carmoisine. $Q > 1$ is indicative of enhancement of fluorescence intensity and greater retention of fluorescence energy by the bound carmoisine molecules due to shielding within the binding site from quenching by the solvent.[17,18]

Energy transfer from the DNA base pairs to carmoisine upon complexation can serve as an evidence for strong intermolecular association. In Figure 3B the variation of Q_λ/Q_{310} with wavelength for the complexation of carmoisine with DNA is presented. An enhancement in the quantum yield is observed in the 230−290 nm region with maximum around 262 nm, which is the characteristic DNA absorbing region. The increase in quantum yield suggested that the DNA−carmoisine complexation resulted in significant energy transfer from the DNA base pairs to the carmoisine molecules.

Determination of the Binding Stoichiometry by Job Plot. The stoichiometry of the complexation was determined independently by continuous variation analysis (Job plot) in fluorescence.[22,23] At constant temperature, the fluorescence intensity was monitored for solutions in which the concentrations of both DNA and carmoisine were varied while the sum of their concentrations was kept constant. The plot of the difference in fluorescence intensity (ΔF) at 427 nm versus the mole fractions of carmoisine revealed a single binding mode for carmoisine−DNA complexation. The intersection of least-squares fitted lines at $\chi_{carmoisine} = 0.192$ corresponds to a stoichiometry value (number of DNA base pairs bound per carmoisine molecule) of 4.21 base pairs for the carmoisine−DNA complexation.

Minor Groove Displacement Assay. DAPI is a well-known minor groove binder having a fluorescence intensity that is enhanced upon complexation with DNA.[24,25] In the presence of another minor groove binding ligand, there would be competition between the new probe and DAPI for binding to the DNA, thereby leading to a decrease in the fluorescence intensity of the DAPI−DNA complex. Such competitive binding assay enables the location of the binding site of the new ligand. A pronounced decrease (~76%) in the fluorescence intensity of the DAPI−DNA complex was observed upon the addition of carmoisine (Figure 4A). This quenching in the

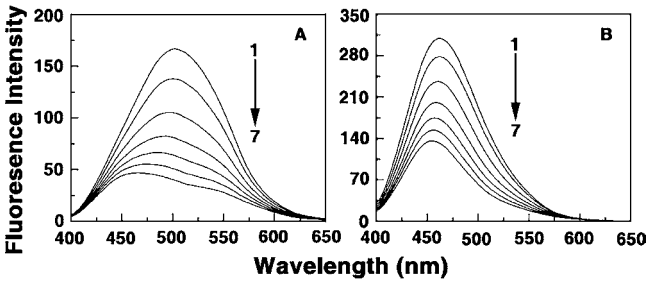

Figure 4. Changes in the fluorescence emission spectra of (A) DAPI−DNA and (B) Hoechst−DNA complexes (curve 1) upon addition of increasing concentration of carmoisine (curves 2−7). The excitation and emission band passes were fixed at 3 nm.

fluorescence intensity suggested that carmoisine has the ability to displace DAPI from the minor grooves of the DNA. Therefore, carmoisine is most likely to be a minor groove binder of DNA.

Hoechst 33258, 2-(4-hydroxyphenyl)-5-[5-(4-methylpiperazine-1-yl)benzimidazo-2-yl]bezimidazole, a synthetic *N*-methylpiperazine derivative, is another classical DNA minor groove binder with specificity for A-T-rich sequences.[26,31−36] The fluorescence intensity of Hoechst 33258 enhances significantly on binding to DNA.[37] The displacement of DNA-bound Hoechst molecules by a new ligand competing for the same sites on the DNA may be reflected as a decrease in the

dx.doi.org/10.1021/jf404960n | J. Agric. Food Chem. 2014, 62, 317−326

fluorescence intensity of the Hoechst−DNA complex upon addition of the competing ligand. The fluorescence spectral changes of Hoechst−DNA complex upon addition of increasing concentration of carmoisine are shown in Figure 4B. The decrease (∼57%) in the fluorescence intensity of DNA-bound Hoechst 33258 in the presence of carmoisine confirms that carmoisine is also an A-T-specific minor groove binder.

Hydrodynamic Studies. In another assay we checked the intercalation ability of carmoisine. The viscosity of a rod-like DNA enhances upon intercalation of ligands to accommodate the stacked molecules between the base pairs. This leads to an increase in the helix contour length of the DNA.[38] Very minor alterations in relative viscosity occur for ligands binding to the grooves of DNA. To prove the mode of binding, the viscosity of DNA in the presence and absence of carmoisine was measured in terms of flow time, which was obtained as an average of four readings. The viscosity of the DNA solution was estimated in the presence of increasing concentrations of carmoisine, and the change in the relative viscosities with increasing D/P values was calculated. The relative viscosities of the DNA solution, determined employing eq 3 (vide supra), showed only marginal alterations in the presence of carmoisine. Such minor changes in relative viscosity rule out intercalation and may be correlated to a groove binding model.[11,26]

Circular Dichroism Studies. The DNA in its B conformation exhibits a positive band at around 278 nm (due to base stacking) and a negative band at around 245 nm (due to polynucleotide helicity).[39] Intercalative binding results in an increase in the molar ellipticity of the positive bands due to the stacking interaction of the intercalator between the base pairs of DNA.[40] However, the groove binders generally do not cause significant unwinding of the DNA base pairs.[41] Figure 5 depicts

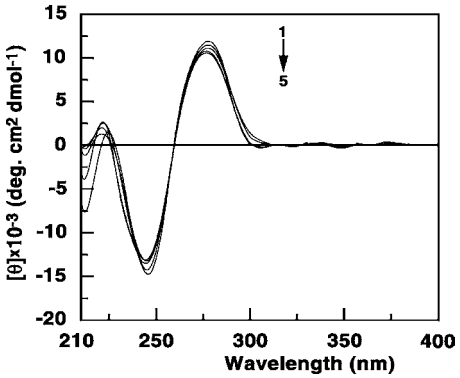

Figure 5. Circular dichroism spectra of DNA (curve 1) treated with increasing concentrations of carmoisine (curves 2−5).

the CD spectra of DNA in the absence and in the presence of increasing concentrations of carmoisine in the 210−450 nm region. A moderate decrease in the positive band upon addition of carmoisine was observed with no change in the band shape or induction of new bands. Besides, minor perturbations in the negative CD band at 245 nm were also evident. Thus, no significant conformational change or unwinding of the DNA base pairs or formation of any altered form of DNA were observed upon the addition of carmoisine, indicating that it most likely binds in the minor groove.[26] The decrease in the positive CD band of DNA in the presence of carmoisine may be attributed to a transition from the extended double-helix form to a more compact Ψ-structure form.[42] Small molecules having achiral chromophores do not exhibit any CD spectra, but on binding to the chiral DNA double helix, the ligand can acquire an induced CD signal. The sign and magnitude of the induced CD spectra are governed by the binding mode, DNA sequence, depth of intercalation, and orientation of the transition dipoles of the ligand.[43] However, carmoisine did not exhibit any induced CD spectra upon complexation with DNA in the studied wavelength region.

Optical Melting and Differential Scanning Calorimetry Results. The ability of carmoisine to enhance the stability of the double-stranded DNA against strand separation was studied by optical melting and by DSC experiments. Under the experimental conditions, native DNA melted cooperatively at 65.0 °C without any hysteresis. The binding of carmoisine enhanced the thermal stability of DNA against strand separation. Under saturating conditions, the melting temperature of DNA increased to around 71.5 °C. A ΔT_m value of about 6.5 °C was obtained for carmoisine−DNA complexation. The optical melting profiles of native DNA and DNA complexed with carmoisine are presented in Figure 6A. This enhancement in the melting temperature further substantiates the binding of carmoisine to double-stranded DNA.

DSC studies also showed identical stabilization of the double-stranded DNA by carmoisine against strand separation (Figure 6B). ΔH_{cal} is the sum total of endothermic contributions, such as the disruption of hydrogen bonds[44] and exothermic contributions such as the breakup of hydrophobic interactions.[45] It is model independent and is not governed by the nature of the transition. This also holds true for the van't Hoff enthalpy (ΔH_v).[46] The ratio $\Delta H_v/\Delta H_{cal} > 1$ gives a measure of the average number of DNA base pairs that melt as a single thermodynamic entity,and tends to suggest a significantly populated intermediate state.[47] The data obtained from the helix melting experiments were used to evaluate the binding constant (K_{obs}) of the DNA association at 20 °C using the equation derived by Crothers[48] as described in detail earlier:[9,14,49]

$$1/T_m^{\circ} - 1/T_m = (R/n\Delta H_{wc}) \ln(1 + K_{T_m}\alpha) \quad (7)$$

T_m° is the optical melting temperature of the DNA in the absence of carmoisine, T_m is the melting temperature in the presence of saturating amounts of carmoisine, ΔH_{wc} is the enthalpy of DNA melting, R is the universal gas constant (1.9872041 cal K^{-1} mol^{-1}), K_{T_m} is the drug binding constant at the T_m, α is the free drug activity, which may be estimated by half of the total drug concentration, and n is the site size of the drug binding. The calculated apparent binding constant at the melting temperature can be extrapolated to a reference temperature (say 293.15 K) using the standard relationship

$$\partial[\ln(K_{obs})]/\partial(1/T) = -(\Delta H_b/R) \quad (8)$$

where K_{obs} is the drug binding constant at the reference temperature T (in kelvin) and ΔH_b is the standard molar binding enthalpy, which was directly determined from the ITC experiment. The data obtained from the helix melting experiments are collated in Table 1. The magnitude of the binding constant (K_{obs}) for carmoisine−DNA complexation from the helix melting experiments was deduced to be 2.91×10^4 M^{-1}. This value is of the same order and in close agreement with that obtained from the spectroscopic studies.

dx.doi.org/10.1021/jf404960n | J. Agric. Food Chem. 2014, 62, 317−326

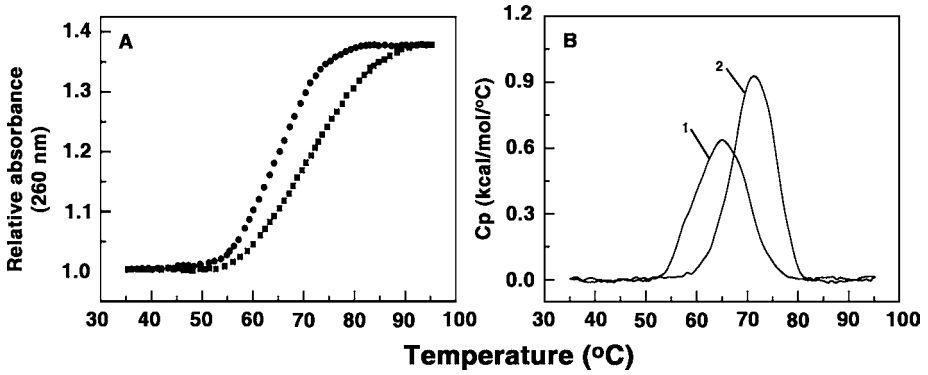

Figure 6. (A) Optical melting profile of DNA (■) and carmoisine–DNA complex (●). (B) DSC thermograms of DNA (curve 1) and carmoisine–DNA complex (curve 2).

Table 1. Optical Melting Data and Binding Constants from Melting Data at Saturating Concentrations of Carmoisine with DNA[a]

	T_m (°C) (optical melting)	T_m (°C) (DSC)	ΔT_m (°C)	ΔH_{cal} (kcal/mol)	ΔH_v (kcal/mol)	$K_{T_m} \times 10^{-4}$ (M^{-1})	$K_{obs} \times 10^{-4}$ (M^{-1})
DNA	65.0	64.7		8.95	64.09		
DNA + carmoisine	71.5	71.4	6.50	10.07	90.30	2.74	2.91

[a]Melting stabilization of DNA in the presence of saturating amounts of carmoisine. ΔH_{cal} is the calorimetric enthalpy, ΔH_v is the van't Hoff enthalpy, K_{T_m} is the binding constant at the melting temperature, and K_{obs} is the carmoisine binding constant at 20 °C determined using equations described in the text. ΔH_{cal} and ΔH_v were obtained from the DSC data.

Elucidating the Thermodynamics of the Interaction. Thermodynamic analysis of the complexation of a ligand to a biomacromolecule provides valuable insights into the molecular forces governing the complexation. Here we present a detailed calorimetric studies on the interaction of carmoisine and DNA. Figure 7A presents the representative primary data from the isothermal calorimetric titration of DNA into a solution of carmoisine at 293.15 K. It can be seen from the plot of power versus time that the binding reaction was characterized by exothermic heats. The integrated heat data after correction of heat of dilution showed only one monophasic binding; hence, it was fitted to a single-site model. This was also based on the results of the Job plot analysis, which revealed a single binding mode for carmoisine–DNA complexation. The binding affinity value obtained from ITC was $(2.62 \pm 0.06) \times 10^4$ M^{-1} and is in very close agreement with the value calculated from spectroscopic studies. The binding of carmoisine to DNA was driven by a positive standard molar entropic contribution of 5.695 kcal/mol and a negative standard molar enthalpic contribution of −0.235 kcal/mol. Thus, the binding reaction was dominated by large positive entropy changes and relatively small negative enthalpy changes. This strong positive entropy term is suggestive of the disruption and release of DNA-bound water molecules, and the negative enthalpy term originates from noncovalent interactions such as stacking.[50,51] The standard molar Gibbs energy for carmoisine–DNA complexation was estimated to be −5.93 ± 0.06 kcal/mol. The overall binding affinity and the binding site size values obtained from ITC analysis (Table 2) are in excellent agreement with the affinity values and the stoichiometry values derived from spectroscopy studies. These values are also comparable to those evaluated from the thermal melting data.

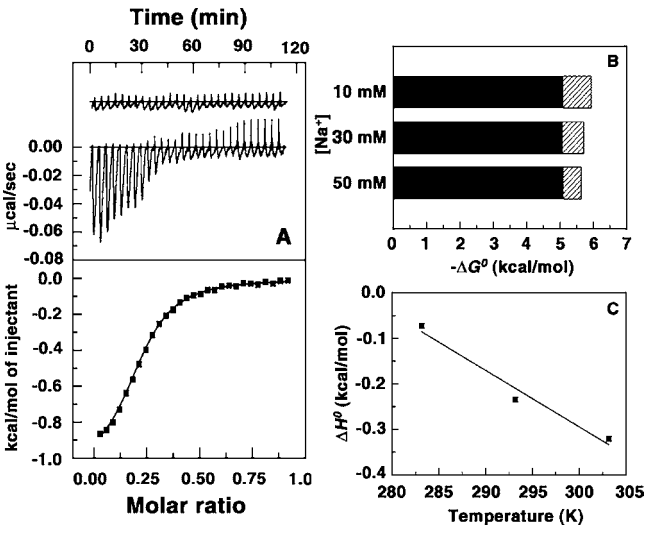

Figure 7. (A) ITC profiles for the complexation of carmoisine with DNA. The top panel represents the raw data for sequential injection of DNA into carmoisine solution, and the bottom panel shows the integrated heat data after correction of heat of dilution against molar ratio of DNA/carmoisine. The data points (■) were fitted to a one-site model, and the solid line represents the best fit data. Experiments were performed at 293.15 K. (B) Partitioned polyelectrolytic ($\Delta G°_{pe}$) (shaded) and nonpolyelectrolytic ($\Delta G°_t$) (black) contributions to the binding Gibbs energy at different [Na^+]. (C) Plot of variation of $\Delta H°$ (■) with temperature for carmoisine–DNA complexation.

Influence of Ionic Strength of the Medium on Binding and Parsing of the Standard Molar Gibbs Energy Change. The analysis of carmoisine–DNA complexation in the salt concentration range 10–50 mM Na^+ in conjunction with van't Hoff analysis revealed the contributions from polyelectrolytic and nonpolyelectrolytic forces. A relationship between the binding constant (K) and Na^+ ion concentration has been given by Record and co-workers[52]

$$\partial \log(K)/\partial \log([Na^+]) = -z\varphi \quad (9)$$

dx.doi.org/10.1021/jf404960n | J. Agric. Food Chem. 2014, 62, 317–326

Table 2. Thermodynamic Parameters for the Association of Carmoisine with DNA from ITC at Different Salt Concentrations[a]

	$[Na^+]$ (mM)	$K \times 10^{-4}$ (M^{-1})	n	ΔH° (kcal/mol)	$T\Delta S^\circ$ (kcal/mol)	ΔG° (kcal/mol)	ΔG°_t (cal/(mol K))	ΔG°_{pe} (kcal/mol)
carmoisine	10	2.62 ± 0.06	4.55 ± 0.02	−0.235 ± 0.009	5.695	−5.93 ± 0.06	−5.08	−0.85
	30	1.80 ± 0.05	3.66 ± 0.01	−0.214 ± 0.007	5.496	−5.71 ± 0.03	−5.07	−0.64
	50	1.59 ± 0.04	4.92 ± 0.01	−0.211 ± 0.006	5.429	−5.64 ± 0.02	−5.09	−0.55

[a]All of the data in this table are derived from ITC experiments conducted at different $[Na^+]$, pH 7.0, and are the average of four determinations. K and ΔH° values were determined from ITC profiles fitting to Origin 7.0 software as described in the text. The values of ΔG° and $T\Delta S^\circ$ were determined using the equations $\Delta G^\circ = -RT \ln K$ and $T\Delta S^\circ = \Delta H^\circ - \Delta G^\circ$. ΔG°_t and ΔG°_{pe} are the Gibbs energy contributions from the nonpolyelectrolytic and polyelectrolytic forces, respectively. All of the ITC profiles were fitted to a model of single binding. Uncertainties correspond to regression standard errors.

Table 3. Thermodynamic Parameters for the Association of the Carmoisine with DNA from ITC at Different Temperatures[a]

temperature (T) (K)	$K \times 10^{-4}$ (M^{-1})	n	ΔH° (kcal/mol)	$T\Delta S^\circ$ (kcal/mol)	ΔG° (kcal/mol)	ΔC_p^0 (cal/(mol K))	ΔG°_{hyd} (kcal/mol)
283.15	3.27 ± 0.06	5.41 ± 0.03	−0.073 ± 0.004	5.777	−5.85 ± 0.06		
293.15	2.62 ± 0.06	4.55 ± 0.02	−0.235 ± 0.009	5.695	−5.93 ± 0.06	−12.4	−0.99
303.15	1.32 ± 0.03	4.56 ± 0.02	−0.321 ± 0.009	5.399	−5.72 ± 0.04		

[a]All of the data in this table are derived from the ITC experiments and are the average of four determinations. T denotes the temperatures studied. K, the binding affinity and ΔH°, the enthalpy change, were determined from ITC profiles fitting to Origin 7.0 software as described in the text. The values of ΔG°, Gibbs energy change, and $T\Delta S^\circ$, the entropy contribution, were determined using the equations $\Delta G^\circ = -RT \ln K$ and $T\Delta S^\circ = \Delta H^\circ - \Delta G^\circ$. ΔG°_{hyd} is the Gibbs energy contribution from the hydrophobic transfer of binding of the analogs and ΔC_p^0 denotes the heat capacity changes. All of the ITC profiles were fit to a model of single binding sites. Uncertainties correspond to regression standard errors.

where z is the apparent charge of the bound ligand and φ is the fraction of sodium ions bound per DNA phosphate group. With increasing $[Na^+]$ from 10 to 50 mM, the binding affinity reduced from $(2.62 \pm 0.06) \times 10^4$ to $(1.59 \pm 0.04) \times 10^4$ M^{-1}. However, the binding stoichiometry varied only marginally. The slope of the plot of log K versus log $[Na^+]$ yielded a value of −0.315. With increasing salt conditions, the negative enthalpy and positive entropy values decreased in magnitude. The binding Gibbs energies of the complexation reduced by about 0.29 kcal mol^{-1} (in absolute values) with changing salt concentration from 10 to 50 mM (Table 2). There are contributions from various physical factors to the total binding Gibbs energy for a ligand−DNA reaction, and a better understanding of the energetics of the complexation can be achieved from detailed partitioning of the binding Gibbs energy. From the dependence of K on $[Na^+]$, the observed binding Gibbs energy can be partitioned between the polyelectrolytic (ΔG°_{pe}) and nonpolyelectrolytic (ΔG°_t) components. The uncharged molecules can also have polyelectrolytic contribution owing to separation of phosphates that reduces the extent of counterion condensation that releases cations.[53−55] The contribution to the binding Gibbs energy from the electrostatic forces (polyelectrolytic) is given by the standard relationship[56,57]

$$\Delta G^\circ_{pe} = -z\varphi RT \ln([Na^+]) \quad (10)$$

where $z\varphi$ is the slope of the van't Hoff plot. At 10, 30, and 50 mM $[Na^+]$, the value of ΔG°_{pe} has been calculated to be −0.85, −0.64, and −0.55 kcal mol^{-1}, respectively, which accounts for about 14, 11, and 10% of the total binding Gibbs energy. The ΔG°_{pe} contains contribution from an enthalpic term, originating from the coulombic interaction of the solute molecules with the counterions present in solution, and an entropic term, arising from the disruption of the ion atmosphere upon complexation of carmoisine. A graphical representation of the partitioning of the binding Gibbs energy between polyelectrolytic (ΔG°_{pe}) and nonpolyelectrolytic (ΔG°_t) components is depicted in Figure 7B. It can be seen that the ΔG°_{pe} contribution decreased with increasing $[Na^+]$, whereas ΔG°_t had large magnitude in all cases and remained almost invariant with change in salt concentration (Table 2). The ΔG°_t term originates from noncovalent molecular interactions such as H-bonding, hydrophobic contacts, van der Waals forces, and $\pi-\pi$ stacking between the aromatic rings of carmoisine and the DNA base pairs.

Temperature-Dependent Isothermal Titration Calorimetry: Determination of Heat Capacity Changes. To obtain insight about the nature of forces driving the interaction, ITC experiments were performed in the temperature range of 283.15−303.15 K. The constant-pressure heat capacity change (ΔC_p^0) was determined by employing the standard relationship

$$\Delta C_p^0 = \partial \Delta H^\circ / \partial T \quad (11)$$

Heat capacity change data can lend valuable information about the type and magnitude of forces governing the complexation phenomenon. The thermodynamic quantities deduced from ITC experiments conducted at three temperatures, namely, 283.15, 293.15, and 303.15 K, are depicted in Table 3. The binding constant of the reaction decreased from $(3.27 \pm 0.06) \times 10^4$ to $(2.62 \pm 0.06) \times 10^4$ M^{-1} when the temperature was raised from 283.15 to 293.15 K. An additional rise in temperature from 293.15 to 303.15 K further reduced the K value to $(1.32 \pm 0.03) \times 10^4$ M^{-1}. Furthermore, there were remarkable changes in the enthalpy and entropy contributions; while the ΔH° values increased, the $T\Delta S^\circ$ values decreased (Table 3). Variation of the ΔH° with temperature can provide information on the heat capacity changes (ΔC_p^0). The observed enthalpy change (ΔH°) varied linearly within the experimental temperature range, suggesting that there is no measurable shift in the preexisting equilibrium between the conformational states of DNA. The variation of ΔH° with temperature afforded a ΔC_p^0 value of −12.40 cal K^{-1} mol^{-1} (Figure 7C). The finite value of ΔC_p^0 indicated temperature dependence of the enthalpy change. Furthermore, change in solvent-accessible surface area has also been revealed to be a significant component of ΔC_p^0.[58−60] Besides, the change in the structured water like the water of hydrophobic hydration as well as the transfer of nonpolar groups into the DNA grooves may also

dx.doi.org/10.1021/jf404960n | J. Agric. Food Chem. 2014, 62, 317−326

result in the release of water, which can contribute a negative term to the ΔC_p^0. The negative ΔC_p^0 value observed here for carmoisine−DNA complexation indicated that the binding is specific and accompanied by burial of nonpolar surface area.[51,58,59] Furthermore, this suggested the involvement of a significant hydrophobic component in the complexation process. ΔG°_{hyd}; the Gibbs energy contribution for the hydrophobic transfer step was calculated from the relationship $\Delta G^\circ_{hyd} = (80 \pm 10) \times \Delta C_p^0$, given by Record et al.[61] The value of ΔG°_{hyd} for carmoisine−DNA complexation was found to be −0.99 kcal mol^{-1}.

This study delineates the structural and thermodynamic aspects of the binding of the food colorant carmoisine to DNA through multifaceted spectroscopic and calorimetric studies. The thermodynamics of the binding reaction correlated well with the structural aspects, thereby enabling a complete and unambiguous understanding of the interaction profile. Carmoisine exhibited hypochromic shift absorbance, and its fluorescence intensity enhanced upon complexation with DNA. The magnitude of the association constant calculated from the Benesi−Hildebrand analysis of the absorption and fluorescence data was of the order 10^4 M^{-1}. Helix melting studies revealed that carmoisine enhanced the thermal stability of DNA by about 6.5 °C. Job plot analysis revealed a single binding mode for carmoisine−DNA complexation. The quantum efficiency value provided evidence for energy transfer from the DNA base pairs to carmoisine. CD studies showed that carmoisine induced moderate conformational perturbations in the secondary structure of DNA. DAPI and Hoechst displacement assay revealed a groove binding model for carmoisine−-DNA complexation. The energetics of the interaction showed that the binding was predominantly entropy driven with a smaller but favorable enthalpy term, which enhanced significantly with temperature. The strong positive entropic terms suggested the disruption and release of DNA-bound water molecules by carmoisine. Salt-dependent ITC studies showed that the contribution from the nonelectrostatic forces to the binding Gibbs energy was clearly dominant and accounted for about 85−90% of the total binding Gibbs energy. The negative heat capacity change observed here can be attributed to the involvement of dominant hydrophobic forces in the complexation process, corroborating the low polyelectrolytic contribution to the binding Gibbs energy. This study presents for the first time a complete structural and thermodynamic profile of the minor groove interaction of carmoisine with double-stranded DNA that further advances our knowledge of the interaction of small molecules with DNA that may be useful for assessing the toxicological effects of this important food additive.

AUTHOR INFORMATION

Corresponding Author

*(G.S.K.) Mailing address: Biophysical Chemistry Laboratory, CSIR−Indian Institute of Chemical Biology, 4 Raja S. C. Mullick Road, Jadavpur, Kolkata 700 032, India. Phone: +91 33 2499 5723/2472 4049. Fax: +91 33 2472 3967. E-mail: gskumar@csiriicb.in, gsk.iicb@gmail.com.

Funding

This work was supported by grants from the CSIR network project ORIGIN (CSC0123). A.B. is a NET qualified Senior Research Fellow of the University Grants Commission (UGC), Government of India.

Notes

The authors declare no competing financial interest.

ACKNOWLEDGMENTS

We thank all of the colleagues of the Biophysical Chemistry Laboratory for their help and cooperation at every stage of this work. We greatly appreciate the critical and judicious comments of the anonymous reviewers that enabled considerable improvement in the presentation of the manuscript.

REFERENCES

(1) Snehalathaa, M.; Ravikumar, C.; Hubert Joe, I.; Sekar, N.; Jayakumar, V. S. Spectroscopic analysis and DFT calculations of a food additive carmoisine. *Spectrochim. Acta A* **2009**, *72*, 654−662.

(2) Amin, K. A.; Abdel Hameid, H., II; Abd Elsttar, A. H. Effect of food azo dyes tartrazine and carmoisine on biochemical parameters related to renal, hepatic function and oxidative stress biomarkers in young male rats. *Food Chem. Toxicol.* **2010**, *48*, 2994−2999.

(3) Chung, K. T.; Stevens, J. R.; Cerniglia, C. E. The reduction of dyes by the intestinal microflora. *Crit. Rev. Microbiol.* **1992**, *18*, 175−190.

(4) Mekkawy, H. A.; Ali, M. O.; El-Zawahry, A. M. Toxic effect of synthetic and natural food dyes on renal and hepatic functions in rats. *Toxicol. Lett.* **1998**, *95*, 155.

(5) Aboel-Zahab, H.; El-Khyat, Z.; Sidhom, G.; Awadallah, R.; Abdel-al, W.; Mahdy, K. Physiological effects of some food coloring additives on rats. *Boll. Chim. Farm.* **1997**, *136*, 615−627.

(6) Sasaki, Y. F.; Kawaguchi, S.; Kamaya, A.; Ohshita, M.; Kabasawa, K.; Iwama, K.; Taniguchi, K.; Tsuda, S. The comet assay with 8 mouse organs: results with 39 currently used food additives. *Mutat. Res.* **2002**, *519*, 103−119.

(7) Ma, Y.; Zhang, G.; Pan, J. Spectroscopic studies of DNA interactions with food colorant indigo carmine with the use of ethidium bromide as a fluorescence probe. *J. Agric. Food Chem.* **2012**, *60*, 10867−10875.

(8) Ni, Y. N.; Wei, M.; Kokot, S. Electrochemical and spectroscopic study on the interaction between isoprenaline and DNA using multivariate curve resolution-alternating least squares. *Int. J. Biol. Macromol.* **2011**, *49*, 622−628.

(9) Paul, P.; Hossain, M.; Yadav, R. C.; Suresh Kumar, G. Biophysical studies on the base specificity and energetics of the DNA interaction of photoactive dye thionine: spectroscopic and calorimetric approach. *Biophys. Chem.* **2010**, *148*, 93−103.

(10) Arakawa, H.; Ahmad, R.; Naoui, M.; Tajmir-Riahi, H. A. A comparative study of calf thymus DNA binding to Cr(III) and Cr(VI) ions. *J. Biol. Chem.* **2000**, *275*, 10150−10153.

(11) Arvin, M.; Dehghan, G.; Hosseinpourfeizi, M. A.; Moosavi-Movahedi, A. A. Spectroscopic and electrochemical studies on the interaction of carmoisine food additive with native calf thymus DNA. *Spectrosc. Lett.* **2013**, *46*, 250−256.

(12) Kashanian, S.; Zeidali, S. H. DNA binding studies of tartrazine food additive. *DNA Cell Biol.* **2011**, *30*, 499−505.

(13) Bhadra, K.; Maiti, M.; Suresh Kumar, G. Molecular recognition of DNA by small molecules: AT base pair specific intercalative binding of cytotoxic plant alkaloid palmatine. *Biochim. Biophys. Acta* **2007**, *1770*, 1071−1080.

(14) Islam, M. M.; Roy Chowdhury, S.; Suresh Kumar, G. Spectroscopic and calorimetric studies on the binding of alkaloids berberine, palmatine and coralyne to double stranded RNA polynucleotides. *J. Phys. Chem. B* **2009**, *113*, 1210−1224.

(15) Sinha, R.; Islam, M. M.; Bhadra, K.; Suresh Kumar, G.; Banerjee, A.; Maiti, M. The binding of DNA intercalating and non-intercalating compounds to A-form and protonated form of poly(rC)·poly(rG): spectroscopic and viscometric study. *Bioorg. Med. Chem.* **2006**, *14*, 800−814.

(16) Benesi, H. A.; Hildebrand, J. H. A spectrophotometric investigation of the interaction of iodine with aromatic hydrocarbons. *J. Am. Chem. Soc.* **1949**, *71*, 2703−2707.

(17) Garbett, N. C.; Hammond, N. B.; Graves, D. E. Influence of the amino substituents in the interaction of ethidium bromide with DNA. *Biophys. J.* **2004**, *87*, 3974−3981.
(18) Basu, A.; Jaisankar, P.; Suresh Kumar, G. Binding of the 9-*O*-*N*-aryl/arylalkyl amino carbonyl methyl substituted berberine analogs to $tRNA^{phe}$. *PLoS One* **2013**, *8*, e58279.
(19) Sari, M. A.; Battioni, J. P.; Dupre, D.; Mansuy, D.; Le Pecq, J. B. Interaction of cationic porphyrins with DNA: importance of the number and position of the charges and minimum structural requirements for intercalation. *Biochemistry* **1990**, *29*, 4205−4215.
(20) Reinhardt, C. G.; Roques, B. P.; Le Pecq, J. B. Binding of bifunctional ethidium intercalators to transfer RNA. *Biochem. Biophys. Res. Commun.* **1982**, *104*, 1376−1385.
(21) Scaria, P. V.; Shafer, R. H. Binding of ethidium bromide to a DNA triple helix. *J. Biol. Chem.* **1991**, *266*, 5417−5423.
(22) Job, P. Formation and stability of inorganic complexes in solution. *Ann. Chim.* **1928**, *9*, 113−203.
(23) Islam, M. M.; Sinha, R.; Suresh Kumar, G. RNA binding small molecules: studies on t-RNA binding by cytotoxic plant alkaloids berberine, palmatine and the comparison to ethidium. *Biophys. Chem.* **2007**, *125*, 508−520.
(24) Zaitsev, E. N.; Kowalczykowski, S .C. Binding of double stranded DNA by *Escherichia coli* RecA protein monitored by a fluorescent dye displacement assay. *Nucleic Acids Res.* **1998**, *26*, 650−654.
(25) Kunwar, A.; Simon, E.; Singh, U.; Chittela, R. K.; Sharma, D.; Sandur, S. K.; Priyadarsini, I. K. Interaction of a curcumin analogue dimethoxycurcumin with DNA. *Chem. Biol. Drug Des.* **2011**, *77*, 281−287.
(26) Sahoo, B. K.; Ghosh, K. S.; Bera, R.; Dasgupta, S. Studies on the interaction of diacetylcurcumin with calf thymus DNA. *Chem. Phys.* **2008**, *351*, 163−169.
(27) Islam, M. M.; Basu, A.; Hossain, M.; Sureshkumar, G.; Hotha, S.; Suresh Kumar, G. Enhanced DNA binding of 9-ω-amino alkyl ether analogs from the plant alkaloid berberine. *DNA Cell Biol.* **2011**, *30*, 123−133.
(28) Giri, P.; Suresh Kumar, G. Self-structure induction in single stranded poly(A) by small molecules: studies on DNA intercalators, partial intercalators and groove binding molecules. *Arch. Biochem. Biophys.* **2008**, *474*, 183−192.
(29) Basu, A.; Suresh Kumar, G. Synthesis of novel 9-*O*-*N*-aryl/arylalkyl amino carbonyl methyl substituted berberine analogs and evaluation of DNA binding aspects. *Bioorg. Med. Chem.* **2012**, *20*, 2498−2505.
(30) Basu, A.; Suresh Kumar, G. Biophysical studies on curcumin−deoxyribonucleic acid interactions: spectroscopic and calorimetric approach. *Int. J. Biol. Macromol.* **2013**, *62*, 257−264.
(31) Muller, W.; Gautier, F. Interactions of heteroaromatic compounds with nucleic acids. A-T-specific non-intercalating DNA ligands. *Eur. J. Biochem.* **1975**, *54*, 385−394.
(32) Latt, S. A.; Wohlleb, J. C. Optical studies of the interaction of 33258 Hoechst with DNA, chromatin, and metaphase chromosomes. *Choromosoma* **1975**, *52*, 297−316.
(33) Murray, V.; Martin, R. F. Sequence specificity of ^{125}I-labelled Hoechst 33258 in intact human cells. *J. Mol. Biol.* **1988**, *201*, 437−442.
(34) Murray, V.; Martin, R. F. Sequence specificity of ^{125}I-labelled Hoechst 33258 damage in six closely related DNA sequences. *J. Mol. Biol.* **1988**, *203*, 63−73.
(35) Haq, I.; Ladbury, J. E.; Chowhdry, B. Z.; Jenkins, T. C.; Chaires, J. B. Specific binding of Hoechst 33258 to the d-(CGCAAATTTGCG)2 duplex: calorimetric and spectroscopic studies. *J. Mol. Biol.* **1997**, *271*, 244−257.
(36) Harshman, K. D.; Dervan, P. B. Molecular recognition of B-DNA by Hoechst 33258. *Nucleic Acids Res.* **1985**, *13*, 4825−4835.
(37) Weisblum, B.; Haenssler, E. Fluorometric properties of the bibenzimidazole derivative Hoechst 33258, a fluorescent probe specific for AT concentration in chromosomal DNA. *Choromosoma* **1974**, *46*, 255−260.
(38) Lerman, L. S. Structural considerations in the interaction of DNA and acridines. *J. Mol. Biol.* **1961**, *3*, 18−30.
(39) Rajendran, A.; Nair, B. U. Unprecedented dual binding behaviour of acridine group of dye: a combined experimental and theoretical investigation for the development of anticancer chemotherapeutic agents. *Biochim. Biophys. Acta* **2006**, *1760*, 1794−1801.
(40) Uma, V.; Kanthimathi, M.; Weyhermuller, T.; Nair, B. U. Oxidative DNA cleavage mediated by a new copper(II) terpyridine complex: crystal structure and DNA binding studies. *J. Inorg. Biochem.* **2005**, *99*, 2299−2307.
(41) Silverman, R. B. *The Organic Chemistry of Drug Design and Drug Action*, 2nd ed.; Elsevier: New York, 2004.
(42) Jordan, C. F.; Lerman, L. S.; Venable, J. H. Structure and circular dichroism of DNA in concentrated polymer solutions. *Nat. New Biol.* **1972**, *236*, 67−70.
(43) Armitage, B. A. Cyanine dye−DNA interactions: intercalation, groove binding and aggregation. *Top. Curr. Chem.* **2005**, *253*, 55−76.
(44) Privalov, P. L.; Khechinashvili, N. N. J. A thermodynamic approach to the problem of stabilization of globular protein structure: a calorimetric study. *J. Mol. Biol.* **1974**, *86*, 665−684.
(45) Arntfield, S. D.; Murray, E. D. The influence of processing parameters on food protein functionality. I. Differential scanning calorimetry as an indicator of protein denaturation. *Can. Inst. Food Sci. Technol. J.* **1981**, *14*, 289−294.
(46) Bruylants, G.; Wouters, J.; Michaux, C. Differential scanning calorimetry in life science: thermodynamics, stability, molecular recognition and application in drug design. *Curr. Med. Chem.* **2005**, *12*, 2011−2020.
(47) Hofr, C.; Brabec, V. Thermal stability and energetics of 15-mer DNA duplex interstrand crosslinked by trans-diamminedichloroplatinum(II). *Biopolymers* **2005**, *77*, 222−229.
(48) Crothers, D. M. Statistical thermodynamics of nucleic acid melting transitions with coupled binding equilibria. *Biopolymers* **1971**, *10*, 2147−2160.
(49) Das, A.; Suresh Kumar, G. Probing the binding of two sugar bearing anticancer agents aristololactam−β-D-glucoside and daunomycin to double stranded RNA polynucleotides: a combined spectroscopic and calorimetric study. *Mol. BioSyst.* **2012**, *8*, 1958−1969.
(50) Haq, I. Thermodynamics of drug−DNA interactions. *Arch. Biochem. Biophys.* **2002**, *403*, 1−15.
(51) Ren, J.; Jenkins, T. C.; Chaires, J. B. Energetics of DNA intercalation reactions. *Biochemistry* **2000**, *39*, 8439−8447.
(52) Record, M. T., Jr.; Anderson, C. F.; Lohman, T. M. Thermodynamic analysis of ion effects on the binding and conformational equilibria of proteins and nucleic acids: the role of ion association or release, screening, and ion effects on water activity. *Q. Rev. Biophys.* **1978**, *11*, 103−178.
(53) Wilson, W. D.; Lopp, I. G. Analysis of cooperativity and ion effects in the interaction of quinacrine with DNA. *Biopolymers* **1979**, *18*, 3025−3041.
(54) Friedman, R. A. G.; Manning, G. S. Polyelectrolyte effects on site-binding equilibria with application to the intercalation of drugs into DNA. *Bipolymers* **1984**, *23*, 2671−2714.
(55) Das, A.; Suresh Kumar, G. Drug−DNA binding thermodynamics: a comparative study of aristololactam-β-D-glucoside and daunomycin. *J. Chem. Thermodyn.* **2012**, *54*, 421−428.
(56) Record, M. T., Jr.; Spolar, R. S. In *The Biology of Nonspecific DNA−Protein Interactions*; Revzin, A., Ed.; CRC Press: Boca Raton, FL, USA, 1990; pp 33.
(57) Record, M. T., Jr.; Ha, J. H.; Fisher, M. A. Analysis of equilibrium and kinetic measurements to determine thermodynamic origins of stability and specificity and mechanism of formation of site-specific complexes between proteins and helical DNA. *Methods Enzymol.* **1991**, *208*, 291−343.
(58) Buchmueller, K. L.; Bailey, S. L.; Matthews, D. A.; Taherbhai, Z. T.; Register, J. K.; Davis, Z. S.; Bruce, C. D.; O'Hare, C.; Hartley, J. A.; Lee, M. Physical and structural basis for the strong interactions of the -ImPycentral pairing motif in the polyamide f-ImPyIm. *Biochemistry* **2006**, *45*, 13551−13565.

(59) Guthrie, K. M.; Parenty, A. D. C.; Smith, L. V.; Cronin, L.; Cooper, A. Microcalorimetry of interaction of dihydro-imidazo-phenanthridinium (DIP)-based compounds with duplex DNA. *Biophys. Chem.* **2007**, *126*, 117−123.
(60) Nguyen, B.; Stanek, J.; Wilson, W. D. Binding-linked protonation of a DNA minor-groove agent. *Biophys. J.* **2006**, *90*, 1319−1328.
(61) Ha, J. H.; Record, M. T., Jr. Role of the hydrophobic effect in stability of site-specific protein−DNA complexes. *J. Mol. Biol.* **1989**, *209*, 801−816.

JOURNAL OF AGRICULTURAL AND FOOD CHEMISTRY

Addition/Correction

pubs.acs.org/JAFC

Correction to Comparative Metabolomics in *Glycine max* and *Glycine soja* under Salt Stress To Reveal the Phenotypes of Their Offspring

Yonghai Lu, Honming Lam, Erxu Pi, Qinglei Zhan, Sauna Tsai, Chunmei Wang, Yiuwa Kwan, and Saiming Ngai*

J. Agric. Food Chem. **2013**, *61* (36), 8711−8721. DOI: 10.1021/jf402043m

The funding statement should read as follows:

AUTHOR INFORMATION

Funding

The work is supported by the Hong Kong RGC Collaborative Research Fund, CUHK03/CRF/11G.

Published: December 20, 2013

ACS Publications © 2013 American Chemical Society

JOURNAL OF AGRICULTURAL AND FOOD CHEMISTRY

Article

pubs.acs.org/JAFC

Synthesis and Evaluation of Heterocyclic Analogues of Bromoxynil

Matthew A. Cutulle,*[,†,¶] Gregory R. Armel,[†] James T. Brosnan,[†] Michael D. Best,[‡] Dean A. Kopsell,[†] Barry D. Bruce,[#] Heidi E. Bostic,[§] and Donovan S. Layton[⊥]

[†]Department of Plant Sciences, University of Tennessee, Knoxville, Tennessee 37996, United States

[‡]Department of Chemistry, University of Tennessee, Knoxville, Tennessee 37996, United States

[#]Department of Biochemistry Cell Biology and Molecular Biology, University of Tennessee, Knoxville, Tennessee 37996, United States

[§]Department of Chemistry, Wofford College, Spartanburg, South Carolina 29303, United States

[⊥]Department of Chemical and Biomolecular Engineering, University of Tennessee, Knoxville, Tennessee 37996, United States

ABSTRACT: One attractive strategy to discover more active and/or crop-selective herbicides is to make structural changes to currently registered compounds. This strategy is especially appealing for those compounds with limited herbicide resistance and whose chemistry is accompanied with transgenic tools to enable herbicide tolerance in crop plants. Bromoxynil is a photosystem II (PSII) inhibitor registered for control of broadleaf weeds in several agronomic and specialty crops. Recently at the University of Tennessee—Knoxville several analogues of bromoxynil were synthesized including a previously synthesized pyridine (2,6-dibromo-5-hydroxypyridine-2-carbonitrile sodium salt), a novel pyrimidine (4,6-dibromo-5-hydroxypyrimidine-2-carbonitrile sodium salt), and a novel pyridine *N*-oxide (2,6-dibromo-1-oxidopyridin-1-ium-4-carbonitrile). These new analogues of bromoxynil were also evaluated for their herbicidal activity on soybean (*Glycine max*), cotton (*Gossypium hirsutum*), redroot pigweed (*Amaranthus retroflexus*), velvetleaf (*Abutilon theophrasti*), large crabgrass (*Digitaria sanguinalis*), and pitted morningglory (*Ipomoea lacunose*) when applied at 0.28 kg ha^{-1}. A second study was conducted on a glyphosate-resistant weed (*Amaranthus palmeri*) with the compounds being applied at 0.56 kg ha^{-1}. Although all compounds were believed to inhibit PSII by binding in the quinone binding pocket of D1, the pyridine and pyridine-*N*-oxide analogues were clearly more potent than bromoxynil on *Amaranthus retroflexus*. However, application of the pyrimidine herbicide resulted in the least injury to all species tested. These variations in efficacy were investigated using molecular docking simulations, which indicate that the pyridine analogue may form a stronger hydrogen bond in the pocket of the D1 protein than the original bromoxynil. A pyridine analogue was able to control the glyphosate-resistant *Amaranthus palmeri* with >80% efficacy. The pyridine analogues of bromoxynil showed potential to have a different weed control spectrum compared to bromoxynil. A pyridine analogue of bromoxynil synthesized in this research controlled several weed species greater than bromoxynil itself, potentially due to enhanced binding within the PSII binding pocket. Future research should compare this analogue to bromoxynil using optimized formulations at higher application rates.

KEYWORDS: *bromoxynil, herbicide resistance, glyphosate resistance, Palmer amaranth*

INTRODUCTION

No new herbicidal mode of action has been incorporated into weed management strategies in over 20 years.[1] Prior to 1991 a new mode of action was introduced to the market approximately every three years. The dearth of novel herbicidal modes of action has led to selection pressure for herbicide-resistant weed biotypes in many different cropping systems. Currently, over 400 weedy biotypes exist that are resistant to at least one herbicide active ingredient.[2] To that end, optimization of molecules with the potential to either provide new modes of action or target established sites where resistance is not problematic is important for the future of weed management.[3,4]

A known target site with the potential to be exploited further is the plastoquinone binding site (Q_B) of the photosystem II (PSII) reaction center. PSII consists of multiple protein subunits and acts as a water:quinol oxidoreductase in all oxygenic organisms including cyanobacteria, algae, and plants. Upon illumination, the reaction center primary donor P680 becomes excited to a singlet state, where it then rapidly undergoes charge separation. P680 chlorophyll donates an electron to a proximal pheophytin (Ph) molecule, which leads to the formation of a $P680^{\bullet+}Ph^{\bullet-}$ radical pair. The occurrence of the radical pair is brief, as an electron is transferred from the Ph anion to the nonmobile plastoquinone electron acceptor Q_A to form the $P680^{\bullet+}Q_A{}^{\bullet-}$ radical.[6,7] Subsequently, an electron is transferred to Q_B via several intermediates. $P680^+$ is then rereduced by extracting an electron from Tyr_{161} of the D1 protein, which leads to the formation of a $TyrZ^{\bullet}(H^+)Q_A{}^{\bullet}$ radical pair.[8,9] This cation is then stabilized by the Mn_4Ca cluster in the oxygen-evolving complex, which upon further illumination extracts four electrons from two H_2O molecules to evolve O_2. On the other side of the membrane the electron is transferred from Q_A to Q_B via the nonheme Fe. After accepting

Received: August 1, 2013
Revised: December 16, 2013
Accepted: December 19, 2013
Published: December 19, 2013

ACS Publications © 2013 American Chemical Society

dx.doi.org/10.1021/jf404209d | *J. Agric. Food Chem.* 2014, 62, 329−336

two electrons Q_B is converted to plastoquinol and released from the D1 binding pocket.[5]

Generally, PSII-inhibiting herbicides bind at the exchangeable Q_B site of the D1 protein in the PSII reaction center.[10−14] Binding of these herbicides displaces plastoquinone at the Q_B site; thus, the less mobile Q_A is unable to be oxidized. This leads to a charge recombination pathway resulting in the formation of triple chlorophyll and singlet oxygen species, which causes lipid peroxidation and general oxidative stress.[5,15] However, PSII inhibitors can interact with different portions of this binding pocket of the D1 protein. On the basis of simulation modeling and D1 mutant studies, phenolic herbicides such as bromoxynil and ioxynil form hydrogen bonds with His_{215} in the D1 protein, whereas it is believed that triazines and ureas do not form a hydrogen bond at this residue; rather they form a hydrogen bond at Ser_{264} of the D1 protein.[16,17]

Currently, there are approximately 70 weedy biotypes that are resistant to triazine herbicides, and many of the biotypes contain a Ser to Gly_{264} mutation.[2,18] Comparatively, only one weedy biotype is resistant to phenolic herbicides, and the mechanism of resistance is metabolism based.[2] Also, weedy biotypes containing the Gly_{264} mutation are hypersensitive to phenolic herbicides.[19,20] Resistance to phenolic herbicides is less likely to occur for two reasons: (1) bromoxynil and ioxynil typically have limited residual soil activity when compared to triazine herbicides; thus, there is less selection pressure on the seed bank for resistant biotypes[21,22]; and (2) $Hist_{215}$ and three other histidine residues form hydrogen bonds with the nonheme iron. This amino acid residue is more conserved than Ser_{264}; thus, resistance is less likely to occur due to target site mutations.

Physiologically, the interaction of His_{215} with phenolic herbicides could be exploited further with analogues of different electronegative properties because of the proximity of phenolic herbicides to Q_A.[16] Essentially, a molecular bridge forms between Q_A, His_{214} of the D2 protein, the nonheme iron, His_{215} of the D1 protein, and Q_B. The CO group on bromoxynil, which is deprotonated at physiological pH, forms a stronger hydrogen bond with the NH imidazole group on His_{215} than plastoquinone.[16] The tighter bond coupled with slightly different electron density characteristics of the herbicide likely affects the conformation of the Q_A−His_{214}−iron−His_{215}−Q_B system. Specifically, the hydrogen bond strength of the Q_A CO group and the imidazole NH group off His_{214} is likely altered.[23] Subsequently, the redox potential of Q_A is reduced, which leads to a charge recombination that favors $P680^+pPheo^-$, ultimately leading to a triplet chlorophyll state. Evaluation of analogues of phenolic herbicides is warranted given how important the Q_A−His_{214}−iron−His_{215}−Q_B molecular bridge is in PSII. In particular, heterocyclic[24] analogues (cyclic structures containing atoms other than carbon) of the phenolic herbicides would be interesting candidates for evaluation because of the potential impact that a ring structure with different electronegative properties would have on the π electron system of the molecular bridge, Q_B binding site, and redox potential of Q_A.

Bromoxynil is an ideal phenolic PSII inhibitor for structural modification because of its current significance to the marketplace, limited environmental impact due to rapid degradation in the soil, and effectiveness when applied postemergence (POST) for control of many problematic broadleaf weeds including pitted morningglory.[25,26] Bromoxynil is labeled for use in alfalfa (*Medicago sativa*), cereals, corn (*Zea mays*), flax (*Linum usitatissimum*), mint (*Mentha spicata*), garlic (*Allium sativum*), and onions (*Allium cepa*).[22] Commercially, bromoxynil is formulated as an ester to help penetrate the hydrophobic cuticle of weeds. Subsequently, the herbicide is then hydrolyzed by plant enzymes to a free acid molecule.[27] Typically, bromoxynil absorption is greater in shoots than in roots because bromoxynil is conjugated in the soil and does not translocate as easily to leaves.[28,29]

An understanding of bromoxynil's impact on plant physiology, availability of the target crystal structure of the D1 protein, and bromoxynil's importance to weed management make bromoxynil an interesting compound for optimization. Research was conducted to evaluate novel heterocyclic analogues of bromoxynil synthesized on site for crop tolerance and weed control. Further analysis was performed by simulating the interaction of bromoxynil analogues in the binding pocket.

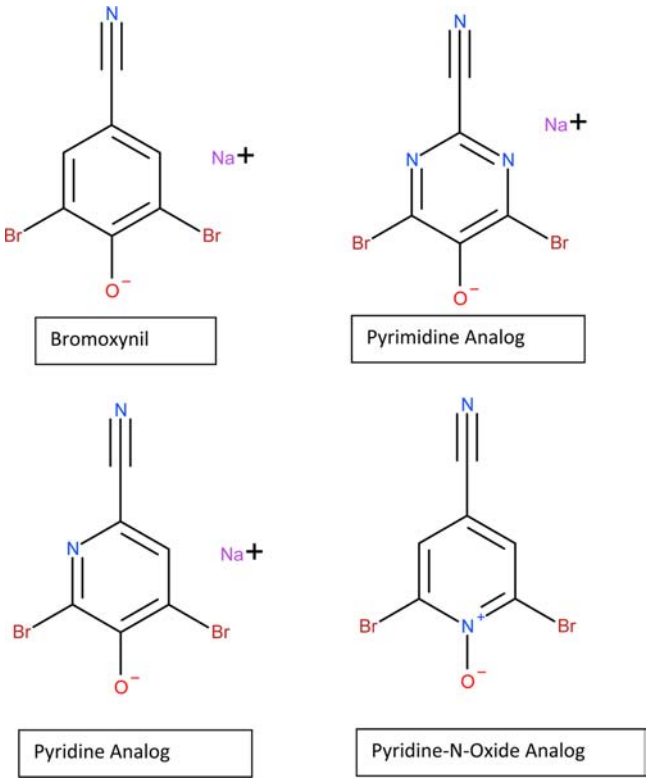

Figure 1. Chemical structures of bromoxynil and the heterocyclic analogues synthesized and tested at the University of Tennessee (Knoxville, TN, USA) during 2012 and 2013.

MATERIALS AND METHODS

Compound Synthesis (Figure 1). A 3,5-dibromo-4-hydroxybenzonitrile bromoxynil salt (bromoxynil, Figure 2) compound was synthesized following procedures from Gulbenk and Ruetman.[30] A total of 300 mg of 4-hydroxybenzonitrile, 1500 mg of sodium bromate, and 2050 mg of sodium bromide was dissolved in 15 mL of deionized water in a 250 mL round-bottom flask with a magnetic stir bar. Subsequently, the flask was capped with a rubber stopper and vented with a nitrogen balloon while 6 mL of concentrated hydrochloric acid (HCl) was slowly added to the reaction with a syringe over a period of 10 min. The flask was kept over a magnetic stir plate for 24 h at 20 °C. Finally, the solution was subjected to vacuum rotary evaporation

dx.doi.org/10.1021/jf404209d | J. Agric. Food Chem. 2014, 62, 329−336

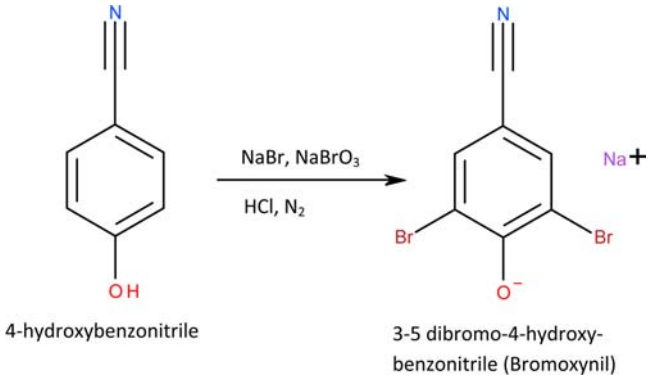

Figure 2. Synthesis of 3,5-dibromo-4-hydroxybenzonitrile (bromoxynil) evaluated in greenhouse trials at the University of Tennessee (Knoxville, TN, USA) during 2012 and 2013.

(Buchi R-114. Nine Buchi Labortechnik AG, Flawil, Switzerland). Structural conformation was determined by direct analysis in real time (DART) HR mass spectrometry MS (m/z): 276.91 (found). A 2,4-dibromo-6-cyano-5-pyridin-3-olate sodium salt (pyridine) was also brominated using the same technique using 5-hydroxypyridine-2-carbonitrile starting material (pyridine; Figure 3). Structural

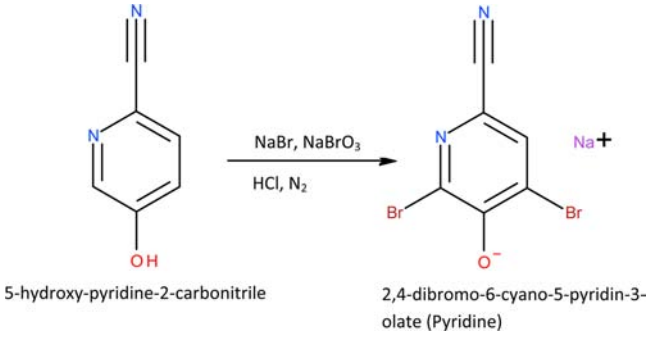

Figure 3. Synthesis of 2,4-dibromo-6-cyano-5-pyridin-3-olate (pyridine) evaluated in greenhouse trials at the University of Tennessee (Knoxville, TN, USA) during 2012 and 2013.

conformation was determined by DART HR mass spectrometry MS (m/z): 277.9 (found). However, because 5-hydroxypyridine-2-carbonitrile is more electrophilic than 4-hydroxybenzonitrile, fewer equivalencies of sodium bromate (753 mg) and sodium bromide (1028 mg) were required to make pyridine.

The first time step of the synthesis of 4,6-dibromo-2-cyanopyrimidin-5-olate sodium salt (pyrimidine; Figure 4) required 300 mg of 5-benzyloxypyrimidine-2-carbonitrile (Waterstone Techology, St. Carmel, IN, USA), which was dissolved in 20 mL of acetic acid and mixed with 30 mg of a 10% carbon palladium catalyst (Strem Chemicals, Newburyport, MA, USA) in a 250 mL round-bottom flask with a magnetic stir bar. Subsequently, the flask was capped and vented with hydrogen gas and reacted over a magnetic stir plate for 36 h at 20 °C. After 36 h, the solution was poured onto a Celite filter aid (Fisher Scientific, Fair Lawn, NJ, USA) covered Büchner funnel connected to an aspirator. The liquid phase was subjected to vacuum rotary evaporation and then dried under a high vacuum for 24 h. The structure of 5-hydroxypyrimidine-2-carbonitrile was confirmed by DART HR mass spectrometry (m/z): 121.1 (found). Next, 600 mg of sodium bromate and 900 mg of sodium bromide were dissolved in 15 mL of deionized water with 250 mg of 5-hydroxypyrimidine-2-carbonitrile in a 250 mL round-bottom flask with magnetic stir bar. Subsequently, the flask was capped with a rubber stopper and vented with a nitrogen balloon while 6 mL of HCl was slowly added to the reaction with a syringe over 10 min. The flask was kept over a magnetic stir plate for 24 h at 20 °C. The solution was then subjected to vacuum rotary evaporation. The structure of 4,6-dibromo-2-cyanopyrimidin-5-olate sodium was confirmed by DART HR mass spectrometry MS (m/z): 278.89 (found).

Synthesis of 2,6-dibromo-1-oxidopyridin-1-ium-4-carbonitrile (pyridine-*N*-oxide; Figure 5) required a different bromination technique. Bromination of pyridine at the 2- and 6-positions within the ring structure of pyridine is difficult and requires drastic conditions that typically involve high pressure and vapor phase reactions at temperatures >500 °C.[24] However, displacement of chlorine with bromine at the 2,6-positions on pyridine had previously been performed under less drastic conditions.[31] To avoid vapor phase reactions, 213 mg of 2,6-dichloro-4-pyridinecarbonitrile was dissolved in 10 mL of acetic acid in a capped 250 mL three-neck round-bottom flask with a magnetic stir bar vented with a nitrogen balloon. The flask was attached to a condenser and an addition funnel in a hot oil bath at 103 °C over a magnetic stir plate. A total volume of 2 mL of hydrobromic acid was added to the solution through the addition funnel over a period of 5 min. After 9 h, 2.9 mL of phosphorus

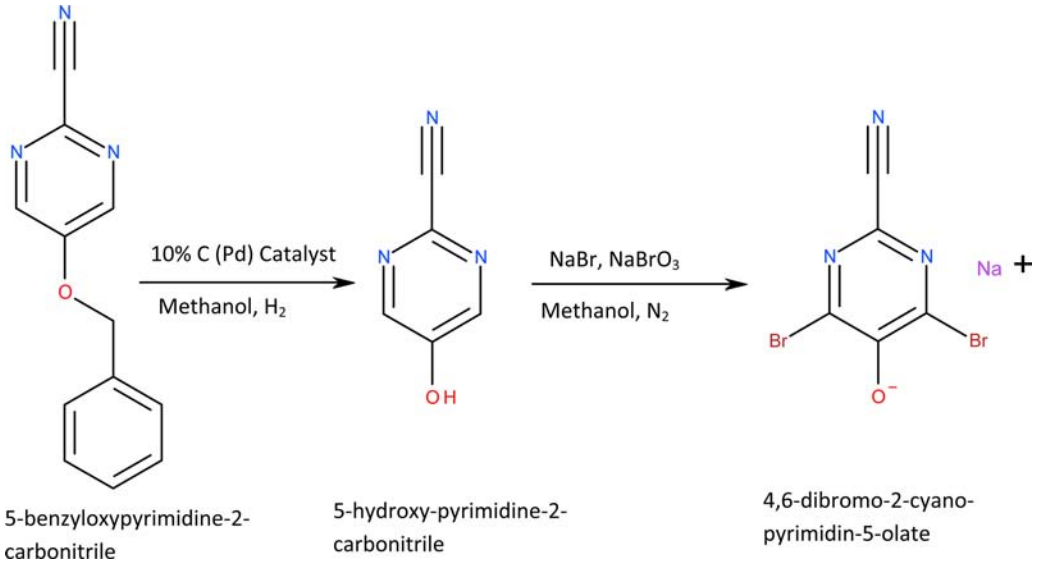

Figure 4. Synthesis of 4,6-dibromo-5-hydroxypyrimidine-2-carbonitrile (pyrimidine) evaluated in greenhouse trials at the University of Tennessee (Knoxville, TN, USA) during 2012 and 2013.

dx.doi.org/10.1021/jf404209d | *J. Agric. Food Chem.* 2014, 62, 329−336

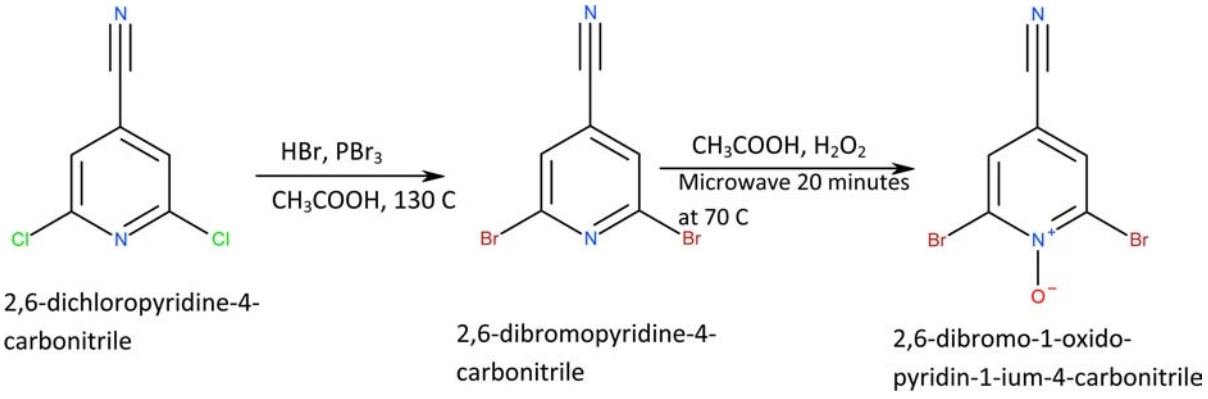

Figure 5. Synthesis of 2,6-dibromo-1-oxidopyridin-1-ium-4-carbonitrile (pyridine-*N*-oxide) evaluated in greenhouse trials at the University of Tennessee (Knoxville, TN, USA) during 2012 and 2013.

tribromide was added to the reaction with a syringe over 45 min and the reaction continued for an additional 16 h at 130 °C. The product of this reaction was a red solution that was cooled in an ice bath and diluted with 20 mL of dichloromethane and 40 mL of deionized water. The phases were mixed in a separation funnel, and the organic layer was extracted and subjected to vacuum rotary evaporation. The structure of the product, 2,6-dibromopyridine-4-carbonitrile, was confirmed through DART HR mass spectrometry MS (m/z): 272.5 (found). A total of 200 mg of 2,6-dibromopyridine-4-carbonitrile was then dissolved in 3 mL of glacial acetic acid and 1.5 mL of 30% hydrogen peroxide. The reaction mixture was exposed to 70 W of microwave irradiation for 20 min at normal absorption using a Biotage Initiator robot (Biotage, Kungsgatan, Sweden) following a protocol by Khrustalev et al.[32] Next, 15 mL of deionized water was added to the final solution and later removed using vacuum rotary evaporation. The product, 2,6-dibromo-1-oxidopyridin-1-ium-4-carbonitrile (pyridine-*N*-oxide), was confirmed using DART HR mass spectrometry MS (m/z): 277.6 (found).

All mass spectrometry analyses were conducted at the Mass Spectrometry Center located in the Department of Chemistry at the University of Tennessee. The DART analyses were performed using a JEOL AccuTOF-D time-of-flight (TOF) mass spectrometer with a DART ionization source from JEOL USA, Inc. (Peabody, MA, USA). Mass spectrometry solutions were prepared with methanol.

Weed and Crop Response Greenhouse Study. To evaluate the crop tolerance and weed control efficacy of synthesized bromoxynil analogues (bromoxynil, pyridine, pyrimidine, and pyridine-9*N*-oxide), an array of crops and weeds were propagated at the University of Tennessee Plant Science Greenhouse (Knoxville, TN, USA; 35.946471 latitude, 83.938558 longitude) including soybean, cotton, redroot pigweed, velvetleaf, large crabgrass, and pitted morningglory. All plants were grown in plastic 10.2 × 10.2 cm circular pots (Dillen Products/Myers Industries, Inc., Middlefield, OH, USA) containing peat-based growing media (ProMix BX Mycorrhizae, Premier Tech Horticulture, Quakertown, PA, USA) and treated 10 days after seeding. The experiment was conducted from Octboer 6 until 30, 2012, and repeated from November 14 until December 8, 2012. During both experimental runs the average air temperature in the climate-controlled greenhouse was 23 °C, whereas the lowest/highest air temperatures recorded were 20/30 °C. Mean daytime light levels during this period were 280 μmol m^{-2} s^{-1}. Irrigation was supplied through an overhead mist system and was withheld for 24 h after experimental herbicide application to ensure adequate time for foliar absorption of the experimental herbicides.

The compounds were applied POST at a rate of 0.28 kg ha^{-1}. This rate was chosen because it is the lowest labeled rate of bromoxynil recommended for weed control.[22] Additionally, the quantities of the analogues for use in studies were limited given that the yields of the aforementioned synthesis processes ranged from 20 to 35%. All compounds were dissolved in a mixture of acetone (3 mL) and deionized water (32 mL) and agitated using a (CL-18) sonicator (Fisher Scientific International Inc., Hampton, NH, USA) prior to application. Subsequently, the solutions were mixed with 0.1% nonionic surfactant. The solutions were then applied to the plants using an enclosed spray chamber (Generation III track sprayer; DeVries 10 Manufacturing, Hollandale, MN, USA) in deionized water carrier at 215 L ha^{-1} with an 8004 EVS nozzle (Teejet, Wheaton, IL, USA).

Visual percent plant injury ratings were recorded 7 days after treatment (DAT), whereas dry aboveground biomass was recorded 14 days after treatment. Aboveground biomass was harvested from every plant and oven-dried (Thelco 130D laboratory oven, Precision Scientific) at 65 °C for 3 days and weighed. Chlorophyll fluorescence (F_V/F_M) was recorded 10 DAT from soybean using a pulse-modulated fluorometer (OS1-FL, Opti-Sciences, Inc., Hudson, NH, USA).

Glyphosate Resistant Palmer Amaranth (*Amaranthus palmeri*) Greenhouse Study. A second study was conducted to evaluate bromoxynil, pyridine, pyrimidine, and pyridine-*N*-oxide for control of glyphosate-resistant Palmer amaranth (gift from Dr. Chad Brommer, BASF Research Triangle Park, NC, USA) from February 20 to March 13, 2013. Potting medium and irrigation conditions in the greenhouse were the same as previously described for the weed and crop response greenhouse study. The application rate in this study was increased to 0.56 kg ha^{-1} considering that these compounds imparted minimal injury to Palmer amaranth when applied at 0.28 kg ha^{-1} in prior experiments.

Statistical Analysis. All experiments were conducted in a completely randomized design (CRD) with three replications. All data were subjected to analysis of variance (ANOVA), and means were separated using Fisher's protected LSD at α = 0.05 in SAS (SAS Institute v. 9.2, Cary, NC, USA). Percent visual injury ratings were arscine transformed prior to analysis. Interpretations were not different from nontransformed data. Thus, nontransformed percent visual ratings are presented for clarity.

Docking Calculations. A crystal structure of the D1 and D2 proteins was extracted from the PSII complex of *Thermosynechococcus elongatus* at 2.9 Å resolution (Protein Data Bank entry 3BZ1)[33] and incorporated into the Molecular Operating Environment (MOE, 2012.10; Chemical Computing Group Inc., Montreal, QC, Canada) program. Structural optimization was performed on the Q_B binding site to include the nonheme iron, the four surrounding histidine ligands (D1-Hist$_{215}$, D1-His$_{272}$, D2-His$_{214}$, and D2-His$_{268}$), and the D1 residues of the QB binding site that consisted of Met$_{214}$, Leu$_{218}$, Val$_{219}$, Tyr$_{246}$, Ile$_{248}$, Ala $_{251}$, His$_{252}$, Phe$_{255}$, Ser$_{264}$, Phe$_{265}$, and Leu $_{271}$). The bromoxynil compounds were constructed in MOE; subsequently, Amber forcefield was used to optimize molecular mechanics.[34] Geometry optimization and energy minimization were applied to the system containing bromoxynil and the 3BZI protein. Bromoxynil was then inserted proximal to the binding pocket, and docking simulations were performed. Heterocyclic analogues were substituted for bromoxynil, and docking simulations were repeated with the analogues. To simulate physiological pH conditions, the CO group

Table 1. Crop and Weed Species Injury 7 Days following Applications of Bromoxynil and the Heterocyclic Analogues of Bromoxynil at 0.28 kg ai ha^{-1}[a]

	injury[b,c] (%)					
treatment	soybean	cotton	pitted morningglory	redroot pigweed	velvetleaf	large crabgrass
bromoxynil	35 a	36 b	45 b	12 b	21 a	6 a
pyridine	41 a	16 c	45 b	30 a	11 a	9 a
pyrimidine	16 b	25 c	22 c	18 b	18 a	5 a
pyridine-*N*-oxide	45 a	38 b	55 a	33 a	25 a	13 a

[a]Means were combined from two runs of a greenhouse experiment conducted in Knoxville, TN, USA, in 2012. [b]Injury was evaluated visually on a 0 (no injury) to 100% (complete kill) scale relative to a nontreated check. [c]Means within the same column followed by the same letter are not significantly different according to Fisher's protected least significant difference test at the 0.05 level.

Table 2. Crop and Weed Species Aboveground Biomass 14 Days following Applications of Bromoxynil and the Heterocyclic Analogues of Bromoxynil at 0.28 kg ai ha^{-1}[a]

	aboveground biomass[b,c] (g per pot)					
treatment	soybean	cotton	pitted morningglory	redroot pigweed	velvetleaf	large crabgrass
bromoxynil	1.20 a	0.30 bc	0.95 b	0.24 ab	0.60 a	0.36 b
pyridine	0.92 b	0.21 c	0.79 bc	0.18 b	0.45 bc	0.26 b
pyrimidine	1.18 a	0.4 b	0.90 b	0.23 ab	0.46 bc	0.30 b
pyridine-*N*-oxide	0.84 b	0.19 c	0.35 e	0.10 c	0.48 bc	0.25 b
nontreated	1.33 a	0.68 a	1.30 a	0.25 a	0.62 a	0.50 a

[a]Means were combined from two runs of a greenhouse experiment conducted in Knoxville, TN, USA, in 2012. [b]Means within a column followed by the same letter are not significantly different according to Fisher's protected least significant difference test at the 0.05 level. [c]Above ground biomass was harvested from every plant and oven-dried at 65 °C for 3 days and weighed.

from all compounds was deprotonated. The simulation distance between herbicide and target amino acids in the binding pocket was transcribed in Symx Draw (version 4.0, Accelrys Inc., San Diego, CA, USA) to enhance visual clarity.

RESULTS AND DISCUSSION

Weed and Crop Response. No treatment-by-experimental run interactions were detected in percent injury or aboveground biomass data; therefore, data from both runs were combined.

Application of bromoxynil resulted in >35% injury to soybean, cotton, and pitted morningglory (Table 1). However, when bromoxynil was applied to velvetleaf, redroot pigweed, or large crabgrass, injury measured <25% (Table 1).

Different trends were observed with applications of heterocyclic bromoxynil analogues. Applications of the pyridines (pyridine and pyridine-*N*-oxide) generally injured all plant species more than pyrimidine. Injury ratings were similar when pyridine and pyridine-*N*-oxide were compared; however, applications of pyridine-*N*-oxide resulted in more injury to pitted morningglory and cotton than pyridine (Table 1). This response was especially pronounced following treatment to cotton, where application of pyridine-*N*-oxide resulted in 38% injury whereas application of pyridine resulted in only 16% injury. Interestingly, pyridine and pyridine-*N*-oxide were also more injurious to redroot pigweed when compared to bromoxynil. None of the herbicides injured large crabgrass >13%.

Generally, aboveground biomass data supported visual assessments of plant injury (Table 2). However, pyridine reduced velvetleaf aboveground biomass more than bromoxynil, which caused greater visual injury than pyridine. Technical grade material was applied in our research, and volatility in the spray chamber may have limited the effectiveness of the compound. Commercially formulated herbicides often have emulsifiers, detergents, wetting agents, and other surfactants that improve herbicide efficacy.[35]

Pyridine reduced photosynthetic efficiency more than any other treatment (Table 3.). Analysis of F_V/F_M data did not always correlate with visual ratings. For example, pyridine reduced PSII efficiency significantly more than pyridine-*N*-oxide; however, pyridine-*N*-oxide generally induced more phytotoxicity than pyridine (Tables 2 and 3). Pyrimidine did not reduce F_V/F_M significantly more than the nontreated check.

Table 3. Impact of Compounds Applied to Soybeans at 0.28 kg ai ha^{-1} on F_V/F_M Values Taken 10 Days after Treatment

treatment	F_V/F_M[a]
bromoxynil	0.456 b
pyridine	0.222 c
pyrimidine	0.671 a
pyridine-*N*-oxide	0.456 b
nontreated	0.804 a

[a]Means within a column followed by the same letter are not significantly different according to Fisher's protected least significant difference test at the 0.05 level.

The most interesting trend observed in the weed and crop response study was the ability of the pyridine analogues (pyridine and pyridine-*N*-oxide) to inflict greater phytotoxicity on redroot pigweed than bromoxynil. Although the redroot pigweed injury observed in this study would not be considered acceptable, the potential impact on weed management that the pyridine herbicides would have when applied as a formulated product at higher rates is intriguing.

Glyphosate-Resistant Palmer Amaranth Study. Applications of bromoxynil and pyridine all injured glyphosate-resistant Palmer amaranth >80% (Table 4). Although it cannot be determined statistically, it appeared that doubling the application rate to 0.56 kg ha^{-1} in this study greatly improved

Table 4. Glyphosate-Resistant Palmer Amaranth (*Amaranthus palmeri*) Injury and Aboveground Biomass following Applications of Bromoxynil and the Heterocyclic Analogues of Bromoxynil at 0.56 kg ai ha^{-1} in a Greenhouse Experiment Conducted in Knoxville, TN, USA, in 2013[a]

treatment	injury[b,c] (%)	aboveground biomass[c,d]
bromoxynil	87 a	0.18 cd
pyridine	83 a	0.08 d
pyrimidine	25 b	0.41 b
pyridine-*N*-oxide	25 b	0.30 bc
nontreated		0.80 a

[a]Injury and aboveground biomass data were collected 7 and 14 days after treatment, respectively. [b]Injury was evaluated visually on a 0 (no injury) to 100% (complete kill) scale relative to the nontreated check. [c]Means within a column followed by the same letter are not significantly different according to Fisher's protected least significant difference test at the 0.05 level. [d]Aboveground biomass was harvested from every plant and oven-dried at 65 C for 3 days and weighed.

the efficacy of bromoxynil and pyridine against pigweed species. Application of pyrimidine and pyridine-*N*-oxide injured glyphosate-resistant Palmer amaranth ~25%. This response was surprising considering the level of redroot pigweed injury observed with pyridine-*N*-oxide in the weed and crop tolerance study (Table 1). Whereas pyridine-*N*-oxide reduced glyphosate-resistant Palmer amaranth aboveground biomass more than pyrimidine, reductions in aboveground biomass were less than with bromoxynil and pyridine (Table 4). Glyphosate-resistant Palmer amaranth biotypes typically exhibit increased transcription of EPSP-synthase.[36] Therefore, increased expression of cytochrome-P450s, glutathione-*S*-transferases, and altered ABC-transporters in Palmer amaranth are likely not responsible for the decreased effectiveness of pyridine-*N*-oxide in this study.

Docking Simulations. Bromoxynil docking in our research was similar to work done by Takahashi et al.[16] Interestingly, the distance of the hydrogen bond between the CO group from the pyridine and the D1 His_{215} was closer than was observed with bromoxynil (Figure 6). This may explain why pyridine performed better than bromoxynil in the weed and crop response study. However, pyridine is supposedly less injurious to broadleaf crops as described by Gullbenk and Ruetman.[30] The decreased susceptibility of broadleaf crops to pyridine may be due to metabolism. The pyrimidine analogue was inverted in the binding pocket relative to the other compounds tested, and the CN group formed a hydrogen bond with His_{215} during the simulation. Hydrogen bonding with a CN group is typically weaker when compared to a CO group; additionally, the bond distance was greater in the pyrimidine simulation than in the pyridine simulation. This could explain why pyridine resulted in more injury than pyrimidine during our greenhouse trials. Pyrimidine did not form a strong hydrogen bond with His_{215}. Different parameters likely need to be applied to the environment to account for the unique properties of a pyridine-*N*-oxide bromoxynil analogue. An alternative simulation performed with pyridine-*N*-oxide showed that the oxyanion interacted with the hydrogen backbone of His_{215} as opposed to the imidazole ring. Additionally, a hydrogen bond formed between the ring of pyridine-*N*-oxide and the sulfur atom on Met_{214}. The presence of a cation at the QB binding site may influence the π electron system of the Q_A–His_{214}–Iron–His_{215}–Q_B bridge, which is interesting information that could be used to design future compounds.

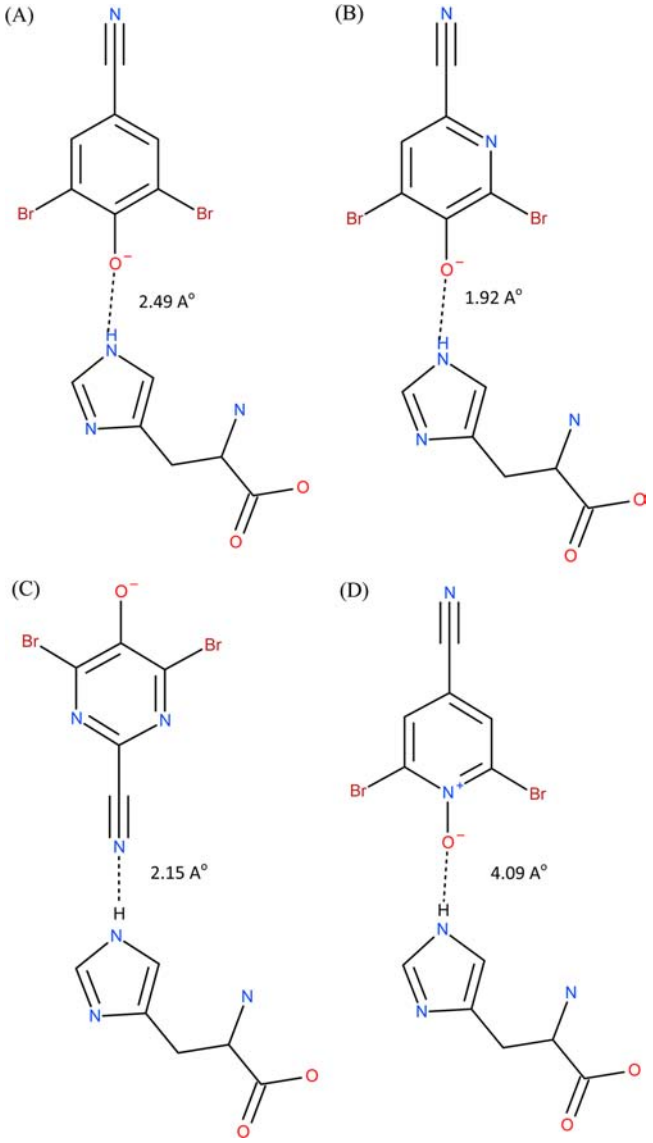

Figure 6. Docking simulations of bromoxynil and heterocyclic analogues (A) bromoxynil, (B) pyridine, (C) pyrimidine, and (D) pyridine-*N*-oxide. The hydrogen bond distance between the ligand and $histidine_{215}$ is in angstroms (A°).

Structure–Activity Relationship. The primary metabolite of bromoxynil in nonsusceptible plants and microbial soil systems results from the hydrolysis of the nitrile group to a carboxylic acid or amide.[37,38] Additionally, replacement of the bromines with hydroxyl groups results in a less herbicidal metabolite.[8,37] This hydroxylation reaction involves the formation of a hydroxide anion, which then initiates an S_N2 reaction by attacking the meta-positioned carbons on bromoxynil. An electron pair is then donated to bromine, which leaves the ring and forms a Br^- ion. Pyridine and pyrimidine analogues are less electron dense compared to bromoxynil and would be more susceptible to hydroxylation and other nucleophilic attacks. If hydroxylation of bromine is the metabolic mechanism that results in decreased efficacy of bromoxynil, then pyrimidine would be the most readily metabolized analogue tested because it is the most electrophilic. This theory is supported by the results of the greenhouse trials as well as what was observed in the docking calculations. Pyrimidine did not bind as strongly to His_{215} in the binding

dx.doi.org/10.1021/jf404209d | J. Agric. Food Chem. 2014, 62, 329–336

pocket as bromoxynil or pyridine and is likely easier to metabolize, thus reducing weed and crop injury. Pyridine formed a stronger hydrogen bond with His_{215} in the binding pocket compared to bromoxynil; however, it is likely metabolized more easily than bromoxynil, and thus did not significantly injure all plants more than bromoxynil. As mentioned earlier, the pyridine-*N*-oxide analogue is similar to bromoxynil with regard to electrophilicity and therefore may not be as easily hydroxylated as the pyridine and pyrimidine analogues. Interestingly, application of pyridine-*N*-oxide resulted in greater redroot pigweed control than bromoxynil with less damage to cotton and soybean. Alternatively, the structure of pyridine-*N*-oxide may be altered by metabolism in both crop and weed species, resulting in greater herbicidal activity. This scenario could be possible because the docking simulations indicated that pyridine-*N*-oxide hydrogen bond distance with His_{215} was not optimal.

Evaluating the stability of pyridine-*N*-oxide, synthesizing ester analogues of pyridine and pyrimidine, and optimizing formulations for all of these compounds would be important for further characterizing the potential of these heterocyclic bromoxynil analogues as new herbicides. The ability of the nonformulated pyridine herbicides to inflict significant damage to multiple weed species necessitates evaluating these compounds within multiple formulations. Additionally, evaluating the safety of the heterocyclic compounds on *bxn* crops would be of interest. The *bxn* trait consists of a nitrilase gene that detoxifies bromoxynil by converting the nitrile group into a carboxylic acid.[39] Cotton containing this trait may be safely sprayed with bromoxynil. The effectiveness of pyridine on glyphosate-resistant Palmer amaranth and the potential safety of the compounds in *bxn* plants may provide a new tool for farmers to manage cropping systems where glyphosate-resistant weeds are problematic.

AUTHOR INFORMATION

Present Address

[¶](M.A.C.) Syngenta Crop Protection, Vero Beach, Florida 32967.

Notes

The authors declare no competing financial interest.

REFERENCES

(1) Duke, S. O. Why have no new herbicide modes of action appeared in recent years? *Pest Manag. Sci.* **2011**, *68*, 505−512.

(2) Heap I. M., The international survey of herbicide-resistant weeds; available at http://www.weedscience.org/in.asp (accessed May 9, 2013).

(3) Witschel, M.; Rohl, F.; Niggeweg, R.; Newton, T. In search of new herbicidal inhibitors of the non-mevalonate pathway. *Pest Manag. Sci.* **2013**, *69*, 559−563.

(4) Grossman, K.; Christiansen, N.; Looser, R.; Tresch, S.; Hutzler, J.; Pollmannc, S.; Ehrhardt, T. Physionomics and metabolomics − two key approaches in herbicidal mode of action discovery. *Pest Manag. Sci.* **2012**, *68*, 494−504.

(5) Rutherford, A. W.; Krieger-Liszkay, A. Herbicide-induced oxidative stress in photosystem II. *Trends Biochem. Sci.* **2001**, *26*, 648−653.

(6) Diner, B. A.; Schlodder, E.; Nixon, P. J.; Coleman, W. J.; Rappaport, F.; Lavergne, J.; Vermaas, W. F. J.; Chisholm, D. A. Site-directed mutations at D1-His_{198} and D2-His_{197} of photosystem II in *Synechocystis* PCC 6803: sites of primary charge separation and cation and triplet stabilization. *Biochemistry* **2001**, *40*, 9265−9281.

(7) Diner, B. A.; Babcock, G. T. Structure, dynamics, and energy conversion efficiency in photosystem II. In *Oxygenic Photosynthesis: The Light Reactions*; Ort, D., Yocum, C. F., Eds.; Kluwer Academic Publishers: Dordrecht, The Netherlands, 1996; pp 213−247.

(8) Debus, R. J. Amino acid residues that modulate the properties of tyrosine YZ and the manganese cluster in the water oxidizing complex of photosystem II. *Biochim. Biophys. Acta* **2001**, *1503*, 164−176.

(9) Diner, B. A. Amino acid residues involved in the coordination and assembly of the manganese cluster of photosystem II. Proton-coupled electron transport of the redox-active tyrosines and its relationship to water oxidation. *Biochim. Biophys. Acta* **2001**, *1503*, 147−163.

(10) Oettmeier, W. Herbicide resistance and supersensitivity in photosystem II. *Cell. Mol. Life Sci.* **1999**, *55*, 1255−1277.

(11) Trebst, A. Inhibitors in the functional dissection of the photosynthetic electron transport system. *Photosynth. Res.* **2007**, *92*, 217−224.

(12) Trebst, A. The molecular basis of plant resistance to photosystem II herbicides. In *Molecular Genetics and Evolution of Pesticide Resistance*; Brown, T. M., Ed.; ACS Symposium Series 645; American Chemical Society: Washington, DC, 1996; pp 44−51.

(13) Trebst, A. The three-dimensional structure of the herbicide binding niche on the reaction center polypeptides of photosystem II. *Z. Naturforsch.* **1987**, *C42*, 742−750.

(14) Wraight, C. A. Oxidation−reduction physical chemistry of the acceptor quinone complex in bacterial photosynthetic reaction centers: evidence for a new model of herbicide activity. *Isr. J. Chem.* **1981**, *21*, 349−354.

(15) Ido, K.; Gross, C. M.; Guerrero, F.; Sedoud, A.; Lai, T.; Ifuku, K.; Rutherford, A. W.; Krieger-Liszkay, A. High and low potential forms of the QA quinone electron acceptor in photosystem-II of *Thermosynechococcus elongatus* and spinach. *J. Photochem. Photobiol. B: Biol.* **2011**, *104*, 154−157.

(16) Takahashi, R.; Hasegawa, K.; Takano, A.; Noguchi, T. Structures and binding sites of phenolic herbicides in the Q_B pocket of photosystem II. *Biochemistry* **2010**, *49*, 5445−5454.

(17) Devine, M. D.; Shukla, A. Altered target sites as a mechanism of herbicide resistance. *Crop Prot.* **2000**, *19*, 881−889.

(18) Gronwald, J. W. Resistance to photosystem II inhibiting herbicides. In *Herbicide Resistance in Plants: Biology and Biochemistry*; Powles, S. B., Holtum, J. A. M., Eds.; CRC Press: Boca Raton, FL, USA, 1994; pp *27*−60.

(19) Van Oorschot, J. L.; Van Leeuwen, P. H. Inhibition of photosynthesis in intact plants of biotypes resistant or susceptible to atrazine and cross-resistant to other herbicides. *Weed Res.* **1988**, *28*, 223−230.

(20) Gressel, .J Why get resistance? It can be prevented or delayed. In *Herbicide Resistance in Weeds and Crops*; Caseley, J. C., Cussans, G. W., Atkin, R. K., Eds.; Butterworth-Heinemann: Oxford, UK, 1991; pp 1−26.

(21) Carpenter, K.; Cottrell, H. J.; De Silva, W. H.; Heywood, B. J.; Leeds, W. G.; Rivett, K. F.; Soundy, M. L. Chemical and biological properties of two new herbicides − ioxynil and bromoxynil. *Weed Res.* **1964**, *4*, 175−195.

(22) Senseman, S. A., Ed. *Herbicide Handbook*, 9th ed.; Weed Science Society of America: Lawrence, KS, USA, xxxx; p 22.

(23) Takano, A.; Takahashi, R.; Suzuki, H.; Noguchi, T. Herbicide effect on the hydrogen-bonding interaction of the primary quinone electron acceptor QA in photosystem II as studied by Fourier transform infrared spectroscopy. *Photosynth. Res.* **2008**, *98*, 159−167.

(24) Katritzky, A. R.; Ramsden, C. A.; Joule, J. A.; Zhdankin, V. V. *Handbook of Heterocyclic Chemistry*, 3rd ed.; Oxford, UK, 2010.

(25) Patterson, M. G.; Norris, B. E. Transgenic cotton allows over-the top weed control. In *Highlights of Agricultural Research*; Alabama Agricultural Experiment Station, Auburn University: Auburn, AL, USA, 1993; Vol. 40, p 13.

(26) Smith, M. C.; Jordan, D. L.; Frans, R. E.; McClelland, M. R. Influence of application rate and timing on efficacy of bromoxynil. *Proc. Beltwide Cotton Conf.* **1993**, *17*, 1519.

(27) Eberlein, C. V.; Guttieri, M. J.; Steffen-Campbell, J. Bromoxynil resistance in transgenic potato clones expressing the *bxn* gene. *Weed Sci.* **1998**, *46*, 150−157.
(28) Gentsch, B. J.; Weber, J. B. Absorption and translocation of bromoxynil following application to roots, stems, and leaves of two *Ipomoea* spp. *Abstr. Weed Sci. Soc. Am.* **1986**, *26*, 19.
(29) Boydston, R. A.; Al-Khatib, K. Efficacy, site of uptake, and retention of bromoxynil in common lambsquarters with conventional and sprinkler application. *Weed Sci.* **1993**, *41*, 166−171.
(30) Gulbenk, A. H.; Ruetman, S. H. (Dow Chemical Co.) U.S. Patent 3,956,338, 1975.
(31) McKendry, L. H. Synthesis of a substituted cyclopropanecurboxylate. *J. Labelled Compd. Radiopharm.* **1984**, *21*, 401−408.
(32) Khrustalev, D. P.; Khamzina, G. T.; Fazylov, S. D.; Muldakhmetov, Z. M. Microwave activation in the synthesis of nitrogen heterocycles, *N*-oxides of pyridine series. *Russ. J. Gen. Chem.* **2008**, *78*, 1577−1578.
(33) Guskov, A.; Kern, J.; Gabdulkhakov, A.; Broser, M.; Zouni, A.; Saenger, W. Cyanobacterial photosystem II at 2.9-Å resolution and the role of quinones, lipids, channels and chloride. *Nat. Struct. Mol. Biol.* **2009**, *16*, 334−342.
(34) Hornak, V.; Abel, R.; Okur, A.; Strockbine, B.; Roitberg, A.; Simmerling, C. Comparison of multiple Amber force fields and development of improved protein backbone parameters. *Proteins* **2006**, *65*, 712−725.
(35) Behrens, R. W. The physical and chemical properties of surfactants and their effects on formulated herbicides. *Weeds* **1964**, *12*, 255−258.
(36) Gaines, T. A.; Shaner, D. L.; Ward, S. M.; Leach, J. E.; Preston, C.; Westra, P. Mechanism of resistance of evolved glyphosate-resistant Palmer amaranth (*Amaranthus palmeri*). *J. Agric. Food Chem.* **2011**, *59*, 5886−5889.
(37) Buckland, J. F.; Collins, R. F.; Pullin, E. M. Metabolism of bromoxynil octanoate in growing wheat. *Pest Manag. Sci.* **1973**, *4*, 149−162.
(38) Graß, B.; Mayer, H.; Nolte, J.; Preuß, G.; Zullei-Seibert, N. Studies on the metabolism of hydroxybenzonitrile herbicides: I. Mass spectrometric identification. *Pest Manag. Sci.* **2000**, *56*, 49−59.
(39) Stalker, D. M.; McBride, K. E.; Malyj, L. D. Herbicide-resistance in transgenic plants expressing a bacterial detoxification gene. *Science* **1988**, *242*, 419−423.

JOURNAL OF AGRICULTURAL AND FOOD CHEMISTRY

Article

pubs.acs.org/JAFC

Identification of Volatile Markers in Potato Brown Rot and Ring Rot by Combined GC-MS and PTR-MS Techniques: Study on in Vitro and in Vivo Samples

Sonia Blasioli,*[,†] Enrico Biondi,[†] Devasena Samudrala,[§] Francesco Spinelli,[†] Antonio Cellini,[†] Assunta Bertaccini,[†] Simona M. Cristescu,[§] and Ilaria Braschi[†]

[†]Department of Agricultural Sciences, University of Bologna, Viale G. Fanin 44, 40127 Bologna, Italy

[§]Molecular and Laser Physics, IMM, Radboud University, Heyendaalseweg 135, 6525 AJ Nijmegen, The Netherlands

Supporting Information

ABSTRACT: *Ralstonia solanacearum* (Rs) and *Clavibacter michiganensis* subsp. *sepedonicus* (Cms) are the bacterial causal agents of potato brown and ring rot, respectively, and are included in the A2 list of quarantine pathogens in Europe. Identification by GC-MS analysis of volatile organic compounds from Rs or Cms cultured on different nutrient media was performed. GC-MS and PTR-MS analysis were carried out also on unwounded potato tubers infected with the same pathogens. Infected tubers were produced by experimental inoculations of the plants. In in vitro experiments, Rs or Cms emitted volatile compounds, part of which were specific disease markers of potato (2-propanol and 3-methylbutanoic acid), mainly originating from bacterial metabolism (i.e., amino acid degradation, carbohydrate and fatty acid oxidation). In potato tubers, pathogen metabolism modified the volatile compound pattern emitted from healthy samples. Both bacteria seem to accelerate metabolic processes ongoing in potatoes and, in the case of Rs, disease markers (1-hepten-3-ol, 3,6-dimethyl-3-octanone, 3-ethyl-3-methylpentane, 1-chloroctane, and benzothiazole) were identified.

KEYWORDS: *Ralstonia solanacearum, Clavibacter michiganensis subsp. sepedonicus, volatile compounds*

INTRODUCTION

Brown rot and ring rot caused by bacteria *Ralstonia solanacearum* race 3 biovar 2 (Rs) and *Clavibacter michiganensis* subsp. *sepedonicus* (Cms), respectively, are among the most severe potato diseases worldwide. Rs occurs mostly in Solanaceous plants (e.g., *Capsicum* spp., eggplant, potato, and tomato) and many weeds and wild plants,[1] and it is spread wordwide.[2,3] Cms has a host range restricted to potato, tomato, eggplant, and some Solanaceous weeds; it occurs in northern America, northeastern Europe, and Asia. Both bacteria are included in the A2 list of quarantine pathogens in Europe and are subject to EU directives (2006/63/EC and 2006/56/EC for Rs and Cms, respectively). Tuber internal symptoms of potato brown rot (see symptoms shown in Table 1) are discoloration and decay localized at vascular ring and a bacterial slime oozing from the area until the complete destruction of tubers.[4] When tubers, infected with potato ring rot, are cut and squeezed, a cheesy cream comes out from the vascular ring; as the infection develops, destruction of vascular tissue occurs and cracks appear on the tuber surface.[5] The absence of internal symptoms does not exclude the absence of the pathogens (latent infections).

It is well-known that both microorganisms and plants emit volatile compounds, some of which may have odors that are characteristic of the species. As reported in Turner and Magan,[6] the microbial species, as well as the type of culture media and growth time, may influence the amount and pattern of volatile compounds that are produced. In case these compounds are formed in the presence of pathogens, they can be used as markers for their presence. No studies about the volatile molecules emitted from bacterial cultures of Rs and Cms are reported in the literature.

Potato flavor has been extensively studied due to its importance in nutrition: volatile compounds predominantly include aldehydes, alcohols, ketones, acids, esters, hydrocarbons, amines, furans, and sulfur compounds. The pattern and the number of volatile components obtained from potatoes can be quite different, depending on whether potatoes are raw or cooked and the cooking method used to prepare them.[7] All studies reported in the literature on raw potato flavor are conducted on sliced or peeled tubers to favor smell diffusion.

Fungi, prokaryotes (bacteria and mollicutes), parasitic plants, viruses and viroids, nematodes, and protozoa can modify the volatile pattern emitted from diseased species.[8] Potatoes inoculated with *Pectobacterium carotovorum* ssp. *carotovorum* and *P. carotovorum* ssp. *atrosepticum*,[9,10] *Phytophthora infestans*, *Pythium ultimum*, and *Botrytis cinerea*,[11,12] and *Fusarium sambucinum*[13] produce volatile molecules that can be considered markers of infection. Potatoes used for these studies have been wounded before the experimental inoculation. Stinson et al.[14] found that potatoes infected with Rs and Cms emit molecules associated with disease: 3-methyl-2-pentanone has been indentified as a marker of ring rot, and the variation of peak intensity of short-chain alcohols and ketones is indicative of brown rot disease. In this study, potatoes were at the final stage of

Received: August 2, 2013
Revised: December 7, 2013
Accepted: December 8, 2013
Published: December 8, 2013

ACS Publications © 2013 American Chemical Society

Table 1. Phytopathometric Classes of Symptomatic Diseased Potato Tubers; Severity Classes Are Laddered on the Basis of Vascular Ring Symptoms

Symptom level	Class	Sample specimen	
		Rs	*Cms*
asymptomatic	0		
very low	1		
low	2		
low/medium, medium, medium/high	3		
high	4		
very high	5		

infection when the whole tuber rots away; at this stage, other secondary microorganisms such as *Fusarium* sp. and *Erwinia* spp. or other saprophytic microrganisms can contribute to the degradation of the tuber tissues[15,16] and can affect the visual symptom analysis, making difficult the discrimination of brown and ring rot from other tuber rots.

The present work describes part of the results of the Q-Detect project performed in the EU's seventh Framework Program (FP7); its aim was to develop reliable detection methods for quarantine pests and pathogens to be used by National Plant Protection Organizations (NPPO) and Inspection Services also through the detection of volatile organic compounds emitted from diseased species.

The work was focused on detection of brown rot and ring rot of potato, by the identification of volatile markers or specific fingerprints of the diseases using gas chromatography and proton transfer reaction coupled with mass spectrometry (GC-MS and PTR-MS) analysis. For the first time, volatile compounds emitted from (i) bacterial cultures of Rs and Cms (in vitro assays) and (ii) unwounded potatoes (in vivo assays) without external disease symptoms and with a low disease severity (to avoid cross-contaminations due to the presence of other secondary microorganisms) were investigated.

MATERIALS AND METHODS

Chemicals. Reference compounds were injected, when available, to confirm identification of volatile compounds detected. Methanol, acetaldehyde, 2-propanone, 2-propanol, 2-butanone, propanoic acid, 3-methylbutanal, 2-methylpropanoic acid, toluene, dimethyl disulfide, 3-methylbutanoic acid, benzaldehyde, methyl 2-methylbutanoate, benzothiazole, and 1-hepten-3-ol were purchased as pure or analytical standards from Sigma-Aldrich Co. LLC (USA). Reference volatile concentration for GC-MS analysis was 100 μM.

Bacterial Strains. The virulent strains IPV-BO 5836 of Rs and IPV-BO 7695 of Cms were routinely grown on tetrazolium (TZ)[17] and yeast dextrose calcium carbonate (YDC)[18] media at 27.0 ± 0.1 °C for 72−96 h, respectively. The IPV-BO 5836 (Mazzucchi and Traversa, unpublished data) and IPV-BO 7695 (Mazzucchi and Mucini, unpublished data) strains were isolated from potato tubers.

In Vitro Assays. *Rs and Cms in Solid Media.* Preliminary studies were carried out to identify volatile compounds produced by the metabolism of Rs and Cms cultured on specific substrates chosen as a model for their growth. The Rs and Cms strains were streaked on agar media such as TZ, "*levure*" peptone glucose (LPG),[19] potato dextrose (PDA; Difco, Becton, Dickinson and Co., USA), and PD prepared using peeled potato tubers,[20] referred to hereafter as natural PD (NPD). The plates were incubated at 27.0 ± 0.1 °C for appropriate time durations, based on the growth rate on each specific solid medium: 5 days for Rs on TZ-agar (TZA; Cms was not cultured on TZA); 2 days on LPG-agar (LPGA), 11 days on PDA, and 12 days on NPD-agar (NPDA) for both Rs and Cms. Agar media without pathogens have been used as a negative control. All experiments were carried out in duplicate.

Rs and Cms in Liquid Media. To follow the development of volatile compounds as a function of bacterial growth, time course studies were performed on broth cultures of the pathogens. RS or Cms bacterial strains were inoculated in TZ (only Rs), LPG, PD, and NPD broths to obtain an initial suspension (time point = 0 h) of ca. 10^6 CFU mL^{-1} for each pathogen; sterile deionized water (SDW) was added as a negative control. The inoculated broths were incubated in a rotary incubator at 27.0 ± 0.1 °C at 80 rpm. At days 2 and 7, 1 mL of suspension was collected, and 10-fold dilutions of the suspension were plated (10 μL drops) on LPGA and incubated at 27.0 ± 0.1 °C. Each suspension concentration was determined by counting the number of Rs and Cms colonies grown after 3 and 5 days of incubation, respectively, when by a naked eye each single colony was visible. Experiments were carried out in duplicate.

In Vivo Assays. Infected potatoes were obtained by experimental inoculations with both bacterial pathogens in potato plants; cultivars 'Spunta' and 'Kennebec' were chosen as sensitive hosts and inoculated with Rs and Cms, respectively.

Rs and Cms Experimental Inoculations. For Rs, ca. 100 potato plants were grown in the field following standard agronomical procedures; within the end of blooming time (after 2 months from the tuber seeding), 30 μL of water suspension containing the pathogen (ca. 10^9 CFU mL^{-1}) was experimentally injected into a wound made at the stem (one-third to two-thirds of the total stems). Cms was inoculated in two distinct phenological phases (seed and third−fourth-leaf stage) to increase the disease incidence and the spectrum of variability of the disease severity in the daughter tubers. Half of the total plants were experimentally inoculated at the seed stage (around 50 potato tubers) by injection of 180 μL of pathogen water suspension (ca. 10^9 CFU mL^{-1}) in a well, made at the heal end. The inoculated tubers were then placed in a dark chamber at 95% humidity for 48 h and then left for an additional 24 h at 23 ± 1 °C to dry the tubers. The next day the inoculated tubers were seeded in the field. The remaining plants (about fifty) were experimentally inoculated at the stem in the third−fourth-leaf stage (two-thirds of the total stems) following the procedure used for Rs inoculation. SDW was employed as a negative control.

At approximately 4 months after the inoculation, the tubers from experimental fields were harvested and stored in a dark climatic chamber at 4 ± 1 °C. Negative controls and tubers inoculated with the pathogens were harvested and stored separately to avoid cross-contaminations. At storing temperature, Rs just survives,[3,4,21] whereas Cms decreases its activity.[5,22] Before volatile compound analysis, to promote the reactivation and, indeed, the bacterial growth of both pathogens, the tubers were left at room temperature from 1 to 10 days.

Volatile Compounds Headspace Sampling for GC-MS Analysis. Volatile compounds analysis on in vitro samples were performed on slices of medium with the grown Rs and Cms strains, which were placed in glass tubes sealed with Teflon caps (Figure 1a). A slice of medium without the pathogen was used as a negative control. Unwounded tubers (healthy or Rs/Cms experimentally inoculated) without external visible symptoms of diseases, were placed in 500 mL jars, and the jars were filled to volume and sealed with Teflon caps (Figure 1b). Due to the low intensity of measured signals, analysis was carried out on pooled tubers. Eight pooled Rs-diseased samples with 4 healthy samples as control, and 10 pooled Cms-diseased samples with 5 control samples were analyzed.

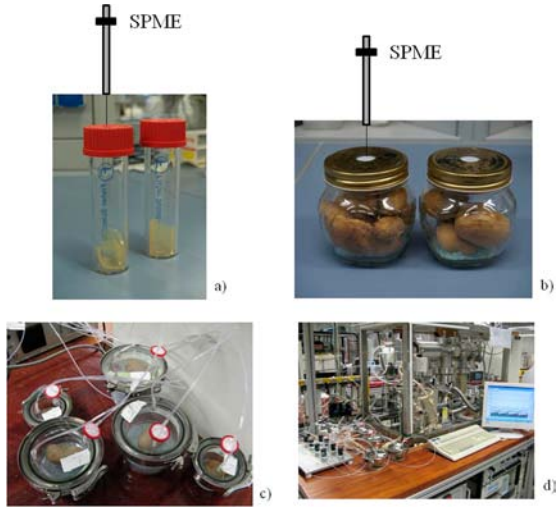

Figure 1. In vitro and in vivo sample preparation for GC-MS analysis: (a) slices of Rs or Cms cultured agar medium in glass tubes and (b) unwounded potato tubers infected with Rs or Cms in jars. Both container types were sealed with a Teflon cap. CAR/PDMS (Supelco) SPME fibers were used for headspace sampling. In vivo sample preparation for PTR-MS analysis is reported in (c), where single potato tubers were placed in glass cuvettes and flushed with 2 L h^{-1} air for headspace analysis. Panel d shows a view of the PTR-MS instrument measuring low molecular weight volatile compounds from tubers placed in glass cuvettes.

Detection of volatile compounds emitted from in vivo or in vitro samples was performed by sampling the headspace with solid phase microextraction (SPME) fibers. Supelco 75 μm carboxen/polydimethylsiloxane fibers were used to monitor gases emitted from Rs or Cms cultures and infected potatoes. SPME fibers were exposed for 24 h to headspace of in vitro solid media and in vivo samples and for 30 min to headspace of broth samples.

After GC-MS analysis, tubers have been examined by visual analysis of symptoms on the vascular ring and by bacterial strain reisolation and identification.

GC-MS Analyses. Volatile compounds adsorbed by SPME fibers from in vitro and in vivo samples were thermally desorbed in the GC injector (kept at 250 °C) of a Finnigan Mat ion trap gas chromatograph GC-MS (Thermo Fisher Scientific, USA) and analyzed for the masses. Transfer line and source temperatures were kept at 250 and 200 °C, respectively. Mass spectra were recorded with a 1 s scan time in the m/z range from 20 to 350 using electronic ionization (ionization energy, 70 eV) as a source. The carrier gas was helium (pressure, 35 kPa). Chromatographic separation was performed on a fused-silica bonded-phase capillary column Supelco SPB-5 poly (5% diphenyl/95% dimethylsiloxane) 30 × 0.32 mm; 0.25 mm film thickness (Sigma-Aldrich Co. LLC, USA). Volatile compounds were separated by applying the following GC oven temperature program: 40 °C for 3 min, raised at 3 °C min^{-1} to 130 °C, raised at 10 °C min^{-1} to 260 °C, and held at 260 °C for 10 min. The identification of volatile compounds was achieved by comparing their mass spectra with the mass database stored in the National Institute of Standards and Technology U.S. Government library (NIST, 1998).

Quantitative analysis of detected volatiles emitted by in vitro samples was done by integration of peak area, whereas, for in vivo samples, by area normalization to sample weight. Data were statistically processed using the semimaximal dispersion (maximal error) or the standard deviation.

Volatile Compound Headspace Sampling for PTR-MS Analysis. Potato tubers experimentally inoculated with Rs (18 samples) and Cms (23 samples) and controls (mocked or healthy, 18 tubers as Rs and 23 tubers as Cms control) were shipped from Bologna (Italy) and stored in the refrigerator at Radboud University, Nijmegen (The Netherlands). A few hours before the PTR-MS measurements, they were kept in the laboratory at 20 °C. A single unwounded potato was placed in a leaktight glass cuvette and flushed with 2 L h^{-1} hydrocarbon-free air (Figure 1c). An automatic valve system was used to connect up to five cuvettes to the PTR-MS (Figure 1d) in alternate sequences of 30 min.[23] After the volatile compound analyses, the samples were returned to the Bologna laboratory for establishment of the symptomatic and asymptomatic features by expert visual inspection.

PTR-MS Analysis. PTR-MS analysis was carried out with a custom-built mass spectrometer at the Trace Gas Research Group at the Radboud University, Nijmegen (The Netherlands). A detailed description of the instrument has been given elsewhere.[24,25] Trace quantities of volatile compounds are sampled directly, and those having proton affinity (PA) greater than that of water (PA = 691 kJ mol^{-1}) undergo ion−molecule reactions by receiving a proton from the hydronium cation, H_3O^+. The protonated compounds are mass filtered with a quadrupole mass spectrometer and quantified by a secondary electron multiplier as mass to charge ratio, m/z. The calibration was performed with different concentrations ranging from 0.035 to 1 ppmv (parts per million volume) obtained from a reference mixture of 1 ± 0.05 ppmv (of methanol (m/z 33), acetaldehyde (m/z 45), 2-propanone (m/z 59), isoprene (m/z 69), benzene (m/z 79), toluene (m/z 93), m-xylene (m/z 107), and α-pinene (m/z 137) in nitrogen dilution gas (Linde, Dieren, The Netherlands).

Symptom Analysis. After GC-MS and PTR-MS analyses, each tuber was cut in half, and the disease symptoms on the vascular ring were visually analyzed and photographed: to better evaluate the disease severity, a phytopathometric class ladder was built (Table 1).

Bacterial Pathogen Reisolation and Identification. *Sample Processing.* After the symptom visual analysis, from each tuber, at the

dx.doi.org/10.1021/jf403436t | J. Agric. Food Chem. 2014, 62, 337−347

Table 2. Volatile Compounds Emitted from Rs and Cms Cultured on Different Agar Media at Different Times from Inoculation (5 Days for Rs Grown on TZA; 2 Days for Rs and Cms on LPGA; 11 Days on PDA; and 12 Days on NPDA) and from Potato Tubers from Plants That Were Experimentally Inoculated with the Pathogens[a]

medium					
TZA	LPGA	PDA	NPDA	potato	volatile compd identification[b]
			Rs Bacterium		
dimethyl disulfide	**2-propanone**				MS, RS
	dimethyl disulfide				MS, RS
		2-butanone			MS, RS
		3-methylbutanoic acid		3-methylbutanoic acid	MS, RS
		2-furancarboxaldehyde			MS (tentatively identified)
		propanoic acid			MS, RS
	methyl 2-methylbutanoate	**methyl 2-methylbutanoate**			MS, RS
		unknown (*m*/*z* 84)			
	dimethyl trisulfide				MS (tentatively identified)
		styrene			MS (tentatively identified)
				1-hepten-3-ol	MS, RS
				3,6-dimethyl-3-octanone	MS (tentatively identified)
				3-ethyl-3-methylpentane	MS (tentatively identified)
				1-chloroctane	MS (tentatively identified)
				benzothiazole	MS, RS
				2,2,3,4-tetramethylpentane	MS (tentatively identified)
				2,3,4-trimethylhexane/4-methyloctane	MS (tentatively identified)
				4-methyl-2-propyl-1-pentanol	MS (tentatively identified)
not available	**3-methylbutanal**				MS, RS
	dimethyl trisulfide				MS (tentatively identified)
			Cms Bacterium		
		2-propanol	**2-propanol**	2-propanol	MS, RS
		2-methylpropanoic acid	**2-methylpropanoic acid**		MS, RS
		unknown (*m*/*z* 86)			
		3-methylbutanoic acid	**(3-methylbutanoic acid)**		MS, RS
			2-hydroxy-3-pentanone		MS (tentatively identified)
		benzaldehyde			MS, RS
				3-methyl-3-buten-2-one	MS (tentatively identified)
				toluene	MS, RS

[a]Specific markers of Rs and Cms are highlighted in bold. Methods used to confirm volatile compound detected are also reported. [b]MS, identification by comparison with NIST mass spectrum; RS, identification by injection of reference standards.

heal end, a core was crushed in 2 mL of SDW and left to settle. After 15 min, 1.5 mL of extract was collected to carry out microbiological and molecular assays.

Reisolation and Identification of the Pathogen. Each core extract was centrifuged for 20 min at 10000*g* at 4 ± 1 °C; the pellet was resuspended in 1 mL of SDW, and 50 μL of resuspension was inoculated on SMSA agar(for Rs, as specified in the EU Directives) and YDC or NCP-88 (for Cms, EU Directives) agar and incubated at 27 ± 1 °C from 3 to 7 days to isolate Rs and Cms pathogens. The Rs-like and Cms-like colonies were purified on appropriate media and identified with pathogenicity test (EU Directives).

Molecular Assays. The remaining 950 μL resuspended pellet was used for DNA extraction using a DNeasy Plant Mini Kit (Qiagen, Germany). The DNA was then stored at −20 °C for PCR assays. The protocols of Seal et al.[26] and Pastrik et al.[27] were followed for PCR assays to identify Rs and Cms, respectively (EU Directives). The PCR method of Pastrik et al.[27] was slightly modified, and the use of the endogenous control primers was avoided to increase the sensitivity of the assay.

RESULTS AND DISCUSSION

GC-MS Analysis. *In Vitro Assays.* Volatile compounds emitted from bacterial cultures of Rs or Cms grown on different media (TZA, LPGA, PDA, and NPDA) were detected by SPME-GC-MS analysis (Table 2). These media were chosen to study the metabolism of Rs or Cms in matrices less complex than that represented by potato tuber. PDA and NPDA were chosen to

simulate a simplified potato substrate. Depending on media characteristics, volatile compound analysis was done when the single colonies have shown their typical morphology on agar media: after 5 days for Rs grown on TZA, and after 2, 11, and 12 days for Rs or Cms grown on LPGA, PDA, and NPDA, respectively (EU Directives). Because no data about the incubation time on PDA and NPDA (these media are basically used as standard in mycology but not in bacteriology) are reported in EU Directives, the required time to evaluate the morphology of a typical colony was deduced by visual analysis of Rs or Cms cultured plates.

The microorganism activity in cultured media was related to the increase of volatile compound concentration in comparison with that of uncultured media. Indeed, although samples were prepared in sterile conditions and hermetically sealed, the occurrence of volatile compounds released by the substrate incubated at 27 °C could not be avoided.

In Table 2, only volatile compounds emitted in amounts significantly different from the control or detected in cultured agar media are reported. Volatile compounds emitted from the metabolic activity of the two pathogens were broadly similar, and only minor differences were observed.

Dimethyl disulfide (DMDS) was the main volatile compound metabolized by Rs on TZA. Cms was not cultured on this medium that is typical for Rs, and it is also not recommended because of its slow growth rate.

A mixture of polysulfides (DMDS and dimethyl trisulfide) was produced by Rs on LPGA along with 2-propanone and methyl 2-methylbutanoate. 2-Propanone, DMDS, and methyl 2-methylbutanoate were markers for Rs on LPGA, whereas dimethyl trisulfide was a degradation product detected in uncultured LPGA, the concentration of which increased in the presence of pathogen. Considering the slow growth of Cms with respect to Rs, only a few molecules were identified as markers of pathogen presence: 3-methylbutanal was a compound characteristic of the Cms metabolism on LPGA, and an increase of dimethyl trisulfide concentration was revealed in comparison with the control.

Volatile compound pattern of Rs metabolism on PDA was more complex than that observed on the other agar media as highlighted from the number of volatile compounds detected (Table 2 and Figure S1 in the Supporting Information). Among these, 3-methylbutanoic acid, propanoic acid, methyl 2-methylbutanoate, and an unknown compound with m/z 84 were detected only in Rs cultured on PDA. Moreover, the metabolic activity of Rs pathogen on PDA was related to the increase of 2-butanone, 2-furancarboxaldehyde, and styrene concentrations. 2-Propanol and 3-methylbutanoic acid were markers of Cms metabolism cultured on PDA. The pathogen favored also the increase of 2-methylpropanoic acid, an unknown compound with m/z 86, and benzaldehyde concentrations.

No disease markers and no variations of volatile compound concentration were detected in Rs cultured on NPDA. On the contrary, similar to what was observed on PDA, the metabolism of Cms on NPDA was related to the variation of 2-propanol, 2-methylpropanoic acid, and 2-hydroxy-3-pentanone concentrations (Figure S2 in the Supporting Information). 3-Methylbutanoic acid was also detected but with a concentration too low to be taken into consideration as a disease marker on NPDA.

All volatile compounds detected seemingly come from degradation reactions of amino acids.[28−33] The short-chain alcohols, acids, aldehydes, and ketones detected are known as degradation products of carbohydrates.[7] As far as methyl 2-methylbutanoate is concerned, it can be produced by oxidation of very long chain unsaturated fatty acids.[34]

Time Course Study on in Vitro Samples. The distribution of volatile compounds emitted from bacteria kept for 2 and 7 days at 27 ± 1 °C in liquid suspensions was analyzed in relation with time. Time course studies were carried out in a time range arbitrarily chosen but adequate to allow the growth of the two bacterial pathogens. In general, the presence of water coupled with shaking increases the bacterial growth speed with respect to that in agar media. In our experimental conditions, the pathogen growth was maximal at day 2 in all bacterium−broth systems with the exception of Rs suspended in NPD broth, in which even after 7 days, the bacterium kept growing (data not shown). For Cms in both LPG and NPD broths, the death phase was observed at day 7. No bacterial growth was observed in PD broth for both Rs and Cms within 7 days as confirmed by SPME-GC-MS analysis, which did not reveal differences between inoculated samples and controls (data not shown). As shown in Table 3, Rs growth rate in different broths calculated at 2 days increased in the order TZ ≥ LPG ≫ NPD, whereas for Cms inoculated in LPG and NPD broths the growth rates were comparable. Rs growth rate in LPG broth doubled that of Cms in the same liquid medium; in NPD broth, on the contrary, the Rs growth rate was significantly lower than that of Cms (3 and 20 generation number × 10^{-5} min^{-1} for Rs and Cms, respectively).

Table 3. Number of Cells Generated and Growth Rate Calculated at Day 2 for Rs or Cms in Different Liquid Media

	substrate					
	generation no.			growth rate (generation no.× 10^{-5} min^{-1})		
bacterial pathogen	TZ	LPG	NPD	TZ	LPG	NPD
Rs	14	13	0.8	49	45	3
Cms		6	6		20	20

As was already observed for Rs cultured in TZA, dimethyl disulfide was the marker of Rs metabolism in TZ broth: after 7 days, its concentration increased 5 times compared with that at day 2 (data reported in the Supporting Information, Figure S3). In Figure 2, volatile compounds emitted during the Rs and Cms bacterial growth in LPG broth are reported. The pattern of detected volatile compounds was different for Rs and Cms because the growth rates of the two bacteria in LPG broth were different (the growth rate of Rs doubled that of Cms, Table 3). The increase of toluene concentration after 2 days from inoculation of Rs in LPG broth along with the emission of DMDS confirmed the bacterial growth. Similar to what it was observed for methyl 2-methylbutanoate, also toluene can be considered a product of long-chain unsaturated fatty acid oxidation.[34]

As expected, for Cms at day 0, control and inoculated broths produced similar volatile compound patterns. After 2 days and more markedly at day 7, concentrations of 2-methylpropanal and 3-methylbutanal (both derived from amino acid Strecker degradation) considerably decreased in the inoculated samples in contrast with what has been observed in LPGA medium. After 7 days, the Cms growth curve achieved the death phase and the decrease of volatile compounds concentrations could be due reasonably to the reduction of living cell number that metabolized the substrate. At this stage, volatile compound distribution differences were observed between inoculated and control samples: the concentration of dimethyl disulfide and an

dx.doi.org/10.1021/jf403436t | J. Agric. Food Chem. 2014, 62, 337−347

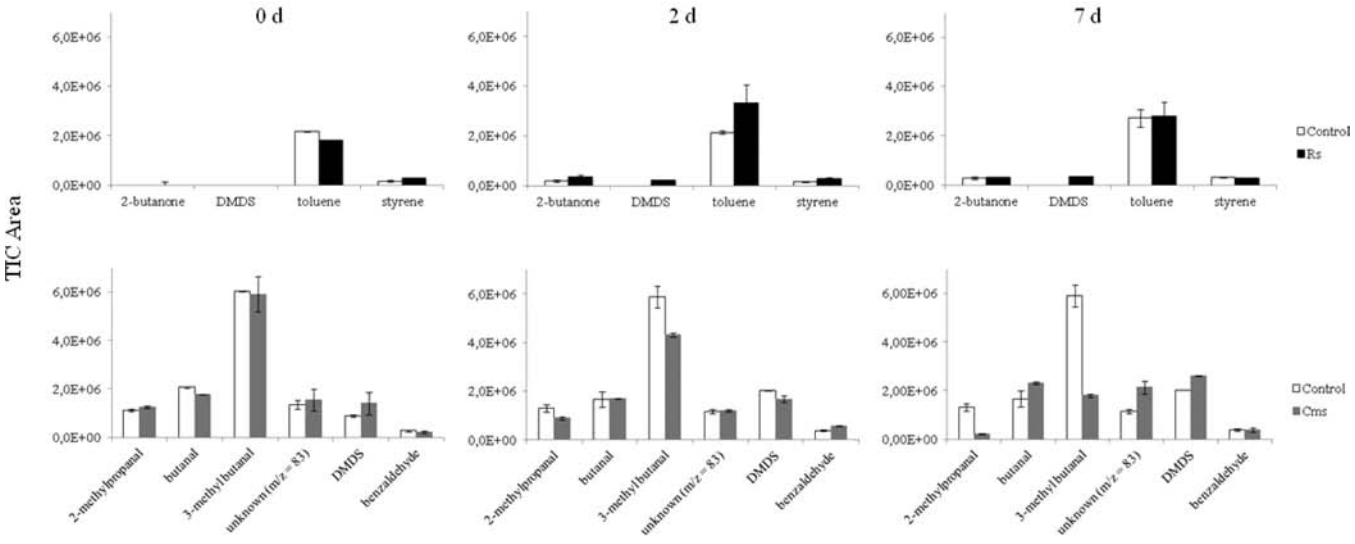

Figure 2. Volatile compounds emission from Rs or Cms cultured in LPG broth after 0, 2, and 7 days of growth. Volatile compounds emitted from uncultured LPG broth samples are reported as a control (mean of two replicates; semimaximal dispersions in vertical bars). TIC, total ion current; DMDS, dimethyl disulfide.

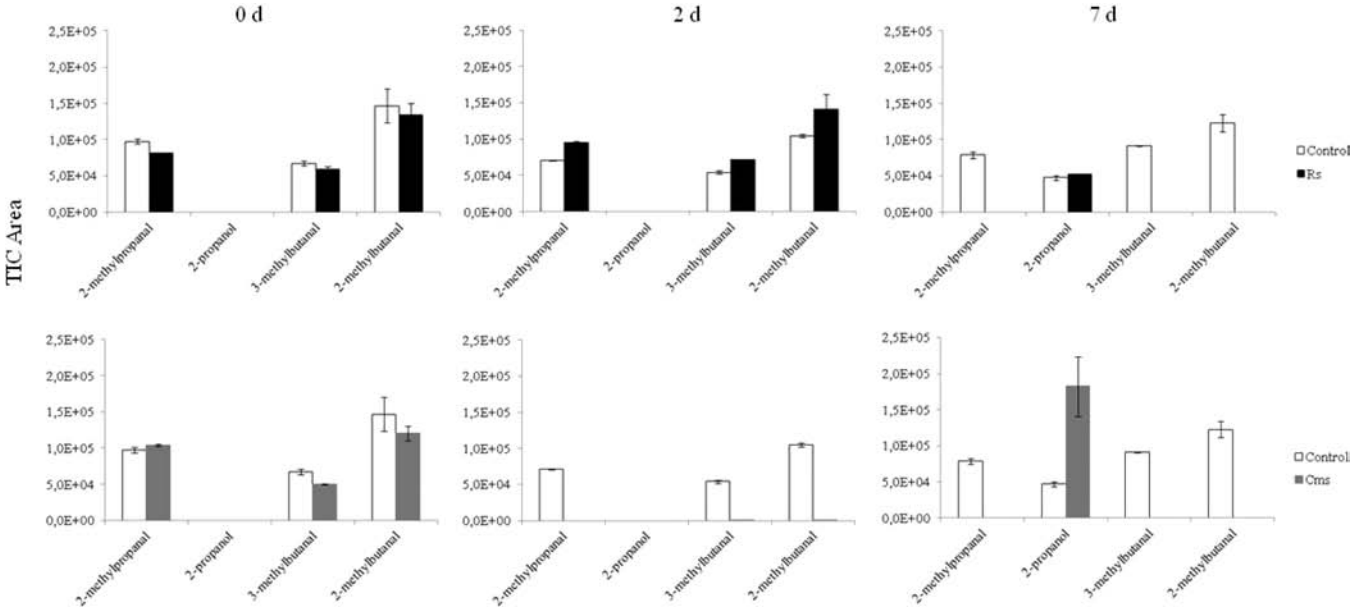

Figure 3. Volatile compound emission from Rs or Cms cultured on NPD broth after 0, 2, and 7 days of growth. Volatile compounds emitted from uncultured NPD broth samples are reported as a control (mean of two replicates; semimaximal dispersions in vertical bars). TIC, total ion current.

unknown molecule (m/z 83) in the Cms−LPG broth system increased compared to the control.

The volatile compound pattern detected in the headspace of Rs or Cms inoculated in NPD broths was very similar (Figure 3) but different from the patterns observed on NPDA media. A mixture of methyl-aldehydes containing three or four carbon atoms were detected in both inoculated and control samples, whereas a mixture of methyl-carboxylic acids containing three or four carbon atoms were identified in Cms cultured on NPDA (no disease markers and no variation of volatile compound concentration were detected in Rs cultured on the same medium). Slight differences (i.e., an increase of 2-methylpropanal, 3-methylbutanal, and 2-methylbutanal concentrations) were observed after 2 days in Rs−NPD broth system compared with control sample. After 7 days, the metabolism of Rs in NPD broth changed: the mixture of aldehydes disappeared, and 2-propanol was the only volatile compound to be detected. For the Cms−NPD system, after 2 days, negligible volatile compound amounts were detected and, after 7 days, 2-propanol was the only identified volatile. The concentration of 2-propanol in the presence of Cms in NPD broth was about 3 times higher than that measured in Rs−NPD sample due to the higher growth rate of Cms (20 and 3×10^{-5} generation number min^{-1} for Cms and Rs, respectively).

The different pattern of volatile compounds detected depends on pathogen growth rate as well as chemical composition of the substrate. The large amount of dimethyl disulfide released by Rs−TZ solid and liquid media samples might derive from casamino acids present in TZ composition (BD Biosciences, USA), which contains cystine (derived from cysteine oxidation). LPG contains Bacto Peptone (BD Biosciences, USA), an enzymatic digest of animal proteins that can contain traces of

dx.doi.org/10.1021/jf403436t | J. Agric. Food Chem. 2014, 62, 337−347

Table 4. Detected Pathogen Markers, Their Average Total Ion Current (TIC) Abundance Normalized to the Sample Weight (SD in Parentheses), and Their Frequency of Appearance Related to 4 Control and 8 Diseased Rs Samples and to 5 Control and 10 Diseased Cms Samples, Respectively

	control		Rs-infected sample		Cms-infected sample		
volatile	av TIC abundance ($g^{-1} \times 10^4$)	appearance frequency	av TIC abundance ($g^{-1} \times 10^4$)	appearance frequency	av TIC abundance ($g^{-1} \times 10^4$)	appearance frequency	volatile compd identification[a]
3-methylbutanoic acid	0.73 (0.15)	2	1.08 (0.47)	4			MS, RS
2,2,3,4-tetramethylpentane	1.33 (0.21)	3	2.29 (1.16)	5			MS (tentatively identified)
2,3,4-trimethylhexane/4-methyloctane	0.94 (0.13)	3	1.38 (0.43)	5			MS (tentatively identified)
4-methyl-2-propyl-1-pentanol	1.13 (0.19)	3	1.96 (0.35)	5			MS (tentatively identified)
2-propanol	1.12 (0.00)	1			2.31 (0.06)	3	MS, RS
3-methyl-3-buten-2-one	1.66 (1.19)	2			1.56 (0.59)	5	MS (tentatively identified)
toluene	2.60 (0.00)	1			3.01 (0.34)	2	MS, RS

[a]MS, identification by comparison with NIST mass spectrum; RS, identification by injection of reference standards.

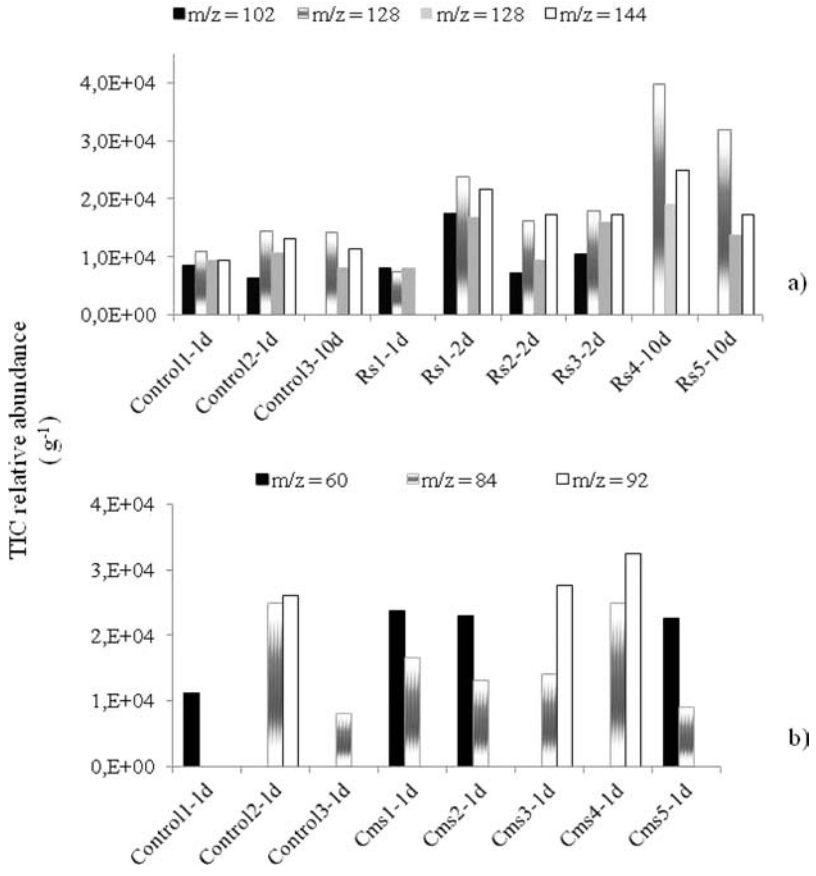

Figure 4. Total ion current (TIC) relative abundance (peak area normalized to sample weight) of (a) 3-methylbutanoic acid (m/z 102), 2,2,3,4-tetramethylpentane (m/z 128), 2,3,4-trimethylhexane/4-methyloctane (m/z 128), and 4-methyl-2-propyl-1-pentanol (m/z 144) detected in Rs infected potato samples and (b) 2-propanol (m/z 60), 3-methyl-3-buten-2-one (m/z 84), and toluene (m/z 92) in Cms samples. (Abundances lower than 10^3 are not reported.)

fatty acids, the oxidation of which produces toluene. Both PD and NPD contain potato derivatives such as starch, sugar, protein, minerals, and glycoalkaloids. Solanine and chaconine glycoalkaloids are usually found concentrated in potato peel, and thus they can be present in commercial PD, but they can be insignificant in NPD, extracted from peeled potatoes. As has been already reported for fungi,[35] these toxic compounds could have an inhibitory effect on bacteria, which explains the slow Rs and Cms growth in PD broth. The yeast extract contained in LPG and the carbohydrates naturally present in potato (i.e., PD and NPD media) might explain the formation of carbohydrate degradation products. On the basis of these considerations, it was possible to explain the occurrence of volatile compounds produced by the degradation of amino acids and fatty acids (detected in the first two days) and of carbohydrates (detected at day 7): note that the final degradation products as CO_2 and H_2O were not detected because they are not retained and separated from the GC column used.

dx.doi.org/10.1021/jf403436t | J. Agric. Food Chem. 2014, 62, 337−347

In Vivo Assays. Infected tubers produced under field conditions by Rs or Cms experimental inoculations were analyzed by SPME-GC-MS to identify markers of brown and ring rot diseases and compared with those identified in in vitro assays.

Harvested tubers showed a high percentage of disease incidence but not all were symptomatic: 78 and 91% of tubers were found infected by Rs and Cms, respectively, 49 and 46% of which showed the typical tuber symptoms of brown and ring rot. Among the symptomatic tubers, the severity of diseases was variable, and the evaluation of the disease severity of the tuber vascular ring (Table 1) assigned the lowest value to healthy potatoes and to the class of infected but asymptomatic tubers (latently infected) and was rated 0 (zero). The remaining classes were rated between 1 and 5 according to five levels of disease severity (from "very low" to "very high" level) as shown by the pictures reported in Table 1. At the highest level of the phytopathometric scale (corresponding to class 5), symptoms of the tubers were ascribed to Rs or Cms as well as to other secondary microorganisms as *Fusarium* sp. and *Erwinia* spp. that contributed to the degradation of potato tissues.[15,16,36] All samples analyzed were composed for the most part by tubers belonging to class 1 or 2. Moreover, all Rs-infected and 50% of Cms-infected samples contained at least one tuber with medium or high symptom level (class 3 or 4).

Chromatograms and corresponding mass spectra were collected (Figure S4) for infected and control samples kept at room temperature for different times.

Some significant differences, which increase with the reactivation time, could be observed in the GC-MS chromatograms of Rs-infected potato samples with respect to controls (see the Supporting Information, Figure S5 (left), and Table 2): 1-hepten-3-ol (m/z 114), 3,6-dimethyl-3-octanone (m/z 156), 3-ethyl-3-methylpentane (m/z 142), 1-chloroctane (m/z 148), and benzothiazole (m/z 135) were identified as markers of brown rot disease (their presence in diseased samples was confirmed for about 50% analyzed samples). In addition, the presence of symptoms of brown rot disease seemed to be related to the increase of relative intensities of the peaks assigned to 3-methylbutanoic acid (m/z 102), 2,2,3,4-tetramethylpentane (m/z 128), 2,3,4-trimethylhexane/4-methyloctane (m/z 128), or 4-methyl-2-propyl-1-pentanol (m/z 144) (Table 2). The collected chromatograms showed variations of the relative intensity of peaks in the entire acquisition range (peaks with m/z 158 and 186 attributable to 2-propyl-1-heptanol and 2-ethyl-1-decanol, respectively, showed the most evident variations but the frequency of appearance was <25%).

The average abundance and appearance frequency of 3-methylbutanoic acid, 2,2,3,4-tetramethylpentane, 2,3,4-trimethylhexane/4-methyloctane, and 4-methyl-2-propyl-1-pentanol are reported in Table 4: these volatile compounds were detected both in control and Rs-diseased samples with a frequency percentage of about 75 and 63%, respectively, even if their average abundance was slightly lower in the control samples than in diseased ones. Their relative abundances (peak area normalized to sample weight) are reported in Figure 4a. Samples named Control3-10d, Rs4-10d, and Rs5-10d were kept at 25 °C for 10 days before GC-MS analyses. Generally, volatile compound emission normalized to sample weight was higher from the diseased samples than controls and seemed to depend on the reactivation time duration, as clearly shown in volatile compounds composition emitted from Rs4-10d and Rs5-10d samples. For these samples, an increase of 2,2,3,4-tetramethylpentane and the corresponding disappearance of 3-methylbutanoic acid were observed. Disease severity analysis revealed that the samples contained tubers with medium to high symptom level (class ≥3).

No specific markers of ring rot have been identified after GC-MS analysis of Cms-diseased samples kept for 1 day at room temperature, but an increase of the relative intensity of two peaks, which were identified as 2-propanol (m/z 60) and 3-methyl-3-buten-2-one (m/z 84), in diseased samples was observed (see Supporting Information, Figure S5 (right), and Table 2). Further analyses performed on Cms suspected diseased samples showed significant intensity variations of the peak assigned to toluene (m/z 92). Different from what has been observed in Rs samples, volatile compound production of Cms-diseased samples did not seem related to the time of bacterial reactivation (data not shown) as a confirmation of the different biology of the two pathogens.[3,5,21,22]

The average abundance and appearance frequency of volatile compounds detected are reported in Table 4. The appearance frequency was low (30, 50, and 20% of total analyzed samples for 2-propanol, 3-methyl-3-buten-2-one, and toluene, respectively), but the differences between the average abundances of control and diseased samples were significant. The trend was confirmed by the relative abundances of the volatile compounds normalized to each sample weight (Figure 4b): 2-propanol and toluene allowed discrimination between healthy and Cms-diseased samples.

The 2-propanol and 3-methylbutanoic acid were already identified as markers of Cms metabolism in cultured agar media PDA and NPDA; 3-methylbutanoic acid was also a marker of Rs metabolism in PDA. The similarity between potato tubers and PDA in terms of chemical composition can explain the detection of the same volatile compounds. However, potato is a matrix more complex than PDA, especially for the presence of unwounded peel, which creates a barrier between the tuber internal part and the environment. Peel reduces the potato smell diffusion and, at the same time, adsorbs on its surface odors from the environment such as soil or fungi smell, making very complex the detection of possible diseases markers due to the presence of these interfering volatile compounds. To minimize this effect, potato tubers used in our study have been gently brushed to remove residues of soil and possible spores of saprophytic fungi. Moreover, the absence of external disease symptoms and low disease severity in assayed tubers were responsible for the limited production of volatile compounds characteristic of brown and ring rot diseases. An attempt to identify brown and ring rot markers by GC-MS analysis has been made by Stinson et al.[14] Unfortunately, these results are not comparable with those reported in the present paper because they used potatoes with clear disease symptoms (comparable with our class 5 symptom level, Table 1), whereas in our study potato tubers belonging to the lower classes were used. Moreover, a comparison between the two analytical approaches is not allowed as Stinson et al.[14] did not report details of GC-MS analysis. Similarly, in a recent review[7] on volatile compounds emitted from raw potatoes, tubers have been analyzed after peeling and for this reason the results cannot fit with our findings.

Volatile compounds detected in our bacterial cultures are organic compounds usually produced in the main metabolic processes. On the contrary, in potato samples, with the exception of 2-propanol and 3-methylbutanoic acid, volatile compounds from the metabolism of Rs or Cms were mostly identified as branched-chain alkanes and alcohols with a C atom number >5.

No data are available in the literature to explain the formation of these products. Likely, they might be carbohydrate degradation intermediates, more complex than volatiles with three or four carbon atoms detected in bacterial cultures. As far as the detection of other volatile compounds is concerned, benzothiazole is a degradation product of S-containing amino acid and toluene, as previously reported, along with detected ketones are products of fatty acid degradation. 2-Propanol, toluene, and benzothiazole were also detected in the headspace of tubers infected with *Phytophthora infestans* and *Fusarium solani* var. *coeruleum*.[37] In our case infected tubers were chosen to avoid contamination due to other saprophytic organisms such as *Fusarium* spp. and *Pectobacterium* spp: moreover, the presence of *Phytophthora infestans* in tubers used for this study was excluded.

PTR-MS in Vivo Analysis. PTR-MS is a useful tool for real-time monitoring of low molecular mass volatile compound emissions, such as ethanol, methanol, propanol, and 2-propanone. Most of these volatile compounds are not in the range of the compounds measured with GC-MS.

High levels of several m/z were measured in diseased samples of Rs and Cms as compared to the controls; their abundance is given in Table 5.

Identification of the measured m/z is not straightforward, as PTR-MS cannot distinguish between product ions with the same mass. However, previous experimental determinations in similar conditions as used here (e.g., E/N = 120 V cm^2, where E is the electric field strength expressed as V cm^{-1} and N is the density of the neutral molecules expressed as molecule number cm^{-3} in the reaction chamber); reaction chamber pressure (2 mbar) together with the isotopic ratio analysis[38] allows assignment of several compounds such as methanol (m/z 33), acetaldehyde (m/z 45), ethanol (m/z 47), 2-propanone (m/z 59), dimethyl sulfide (DMS, m/z 63), and dimethyl disulfide (DMDS, m/z 95). Possible candidates or their major fragment for the ions measured are indicated in Table 5. Two of them, with m/z 43 and 93, were specific to Cms-diseased tubers and were attributed to 2-propanol and toluene, respectively, as confirmed by GC-MS analysis in this study. For some of the remaining compounds the most probable candidates were indicated on the basis of the literature.

Most of the volatile compounds were common for tubers infected with Rs as well as for those infected with Cms. 2-Butanone and sulfur-containing compounds (DMS and DMDS) were identified only in Rs-diseased tubers (DMDS was also the marker of Rs presence in TZ and LPG solid and liquid media). Ethanol and toluene were mainly produced by the Cms-diseased samples with symptomatic characteristics of class 3 or higher (identified after the measurements). These volatile compounds could be considered specific markers for Rs and Cms infection, respectively.

The PTR-MS analysis provided a profile of low molecular mass volatile compounds complementary to the GC-MS analysis. However, 2-butanone, dimethyl disulfide, ethanol, ethyl acetate, acetaldehyde, and 2-propanone were also found in the headspace of potatoes inoculated with *Pectobacterium carotovorum* ssp. *carotovorum* and *atrosepticum*.[9,39] Hexanal and traces of toluene and acetic acid were reported from tubers inoculated with *Phytophthora infestans* and *Fusarium solani* var. *coeruleum*.[37]

In conclusion, GC-MS and PTR-MS techniques allowed recognition of potato tubers infected by Rs or Cms through the identification of specific disease markers: 1-hepten-3-ol, 3,6-dimethyl-3-octanone, 3-ethyl-3-methylpentane, 1-chloroctane, and benzothiazole were markers of potato brown rot, whereas 2-propanol and toluene were markers of potato ring rot. The techniques provided also a promising alternative to the molecular assays.

Within the framework of the development of innovative and rapid techniques for the detection of quarantine pathogens to be used by National Plant Protection Organizations and Inspection Services in the European Union, these findings represent the first step toward the realization of plant pathogen noninvasive diagnostic methods alternative to the standard methods reported in EU Directives, which require costly and time-consuming microbiological, serological, and molecular assays.

Further studies will be addressed to the volatile compound detection by electronic nose due to the importance of accelerating potato disease analysis.

Table 5. Possible Volatile Compounds Detected in the Headspace of Rs- and Cms-Diseased Potatoes by PTR-MS Analysis, Percentage of Diseased Tubers That Emitted the Specific Volatile Compounds, and Related Literature

		diseased tubers (% abundance)			
m/z	possible compd/ major fragment	Rs	Cms	intercomparison GC-MS studies	volatile compd identification[a]
33	methanol	83	65	Waterer and Pritchard[10]	IA, RS
43	2-propanol	55	55	Waterer and Pritchard[40] Stinson et al.[14]	MS (tentatively identified)
45	acetaldehyde	89	95		IA, RS
47	ethanol		35		IA (tentatively identified)
59	2-propanone	67	65	Stinson et al.[14]	IA, RS
61	acetic acid	5	26		MS (tentatively identified)
	ethyl acetate				
63	dimethyl sulfide	55			IA (tentatively identified)
73	2-butanone	55	13	Stinson et al.[14]	MS (tentatively identified)
83	cyclohexene	66	65		MS (tentatively identified)
	hexanal				
85	3-methyl-3-buten-2-one	55	61	this study	MS (tentatively identified)
87	3-methyl-2-buten-1-ol	28	48		MS (tentatively identified)
	2,3-butanedione				
	2-pentanone			Stinson et al.[14]	
93	toluene		18	this study	MS, RS
95	dimethyl disulfide	54			IA (tentatively identified)

[a]IA, identification by isotopic ratio analysis;[41] MS, identification by comparison with NIST mass spectrum; RS, identification by injection of reference standards.

dx.doi.org/10.1021/jf403436t | J. Agric. Food Chem. 2014, 62, 337−347

■ ASSOCIATED CONTENT

Supporting Information

Additional figures. This material is available free of charge via the Internet at http://pubs.acs.org.

■ AUTHOR INFORMATION

Corresponding Author

*(S.B.) Phone: +39 051 2096207. Fax: +39 051 2096203. E-mail: sonia.blasioli@unibo.it.

Funding

This work was financed as Q-Detect project, which was a part of the EU's 7th Framework Program (FP7-KBBE-2009-3).

Notes

The authors declare no competing financial interest.

■ ACKNOWLEDGMENTS

We gratefully thank C. E. Gessa and U. Mazzucchi for their precious work and suggestions, which helped us in setting up the experiments. We acknowledge A. Galeone for her contribution to molecular assays. We also thank A. Nastri and S. Vecchi for the excellent management of the fields used for the tuber production, S. Grandi for the GC-MS maintenance, and S. Brigati and P. Bertolini for the use of the refrigerated cells. We are grateful to the Phytosanitary Service of Emilia Romagna Region for providing special permissions to export infected tubers to project partners.

■ REFERENCES

(1) Pradhanang, P. M.; Elphinstone, J. G.; Fox, R. T. V. Identification of crop and weed hosts of *Ralstonia solanacearum* biovar 2 in the hills of Nepal. *Plant Pathol.* **2000**, *49*, 403−413.

(2) Elphinstone, J. G. The current bacterial wilt situation: a global overview. In *Bacterial Wilt: The Disease and the Ralstonia solanacearum Species Complex*; Allen, C., Prior, P., Hayward, A. C., Eds.; APS: St. Paul, MN, USA, 2005; pp 9−28.

(3) Milling, A.; Meng, F.; Denny, T. P.; Allen, C. Interactions with hosts at cool temperatures, not cold tolerance, explain the unique epidemiology of *Ralstonia solanacearum* race 3 biovar 2. *Phytopathology* **2009**, *99*, 1127−1134.

(4) Álvarez B.; Biosca E. G.; López, M. M. On the life of *Ralstonia solanacearum*, a destructive bacterial plant pathogen. In *Current Research, Technology and Education Topics in Applied Microbiology and Microbial Biotechnology*; Méndez-Vilas, A.; Ed.; Formatex Research Center: Badajoz, Spain, 2010; pp 267−279.

(5) van der Wolf, J. M.; Elphinstone, J. G.; Stead, D. E.; Metzler, M.; Müller, P.; Hukkanen A.; Karjalainen, R. Epidemiology of *Clavibacter michiganensis* subsp. *sepedonicus* in relation to control of bacterial ring rot. In *Plant Research International B.V. Report 95*; Wageningen, The Netherlands, 2005; pp 1−38.

(6) Turner, A. P. F.; Magan, N. Electronic noses and disease diagnostics. *Nat. Rev. Microbiol.* **2004**, *2*, 161−166.

(7) Dresow, J. F.; Böhm, H. The influence of volatile compounds of the flavour of raw, boiled and baked potatoes: impact of agricultural measures on the volatile components. *Landbauforschung − vTI Agric. For. Res.* **2009**, *4* (59), 309−338.

(8) Jansen, R. M. C.; Wildt, J.; Kappers, I. F.; Bouwmeester, H. J.; Hofstee, J. W.; van Henten, E. J. Detection of diseased plants by analysis of volatile organic compound emission. *Annu. Rev. Phytopathol.* **2011**, *49*, 23.1−23.18.

(9) Varns, J. L.; Glynn, M. T. Detection of disease in stored potatoes by volatile monitoring. *Am. Potato J.* **1979**, *56*, 185−197.

(10) Waterer, D. R.; Pritchard, M. K. Production of volatile metabolites in potatoes infected by *Erwinia carotovora* var. *carotovora* and *E. carotovora* var. *atroseptica*. *Can. J. Plant Pathol.* **1985**, *7*, 47−51.

(11) Lui, L.; Vikram, A.; Hamzehzarghani, H.; Kushalappa, A. C. Discrimination of three fungal diseases of potato tubers based on volatile metabolic profiles developed using GC/MS. *Potato Res.* **2005**, *48*, 85−96.

(12) Laothawornkitkul, J.; Jansen, R. M. C.; Smid, H. M.; Bouwmeester, H. J.; Muller, J.; vanBruggen, A. H. Volatile organic compounds as a diagnostic marker of late blight infected potato plants: apilot study. *Crop Prot.* **2010**, *29*, 872−878.

(13) Kushalappa, A. C.; Lui, L. H.; Chen, C. R.; Lee, B. Volatile fingerprinting (SPME-GC-FID) to detect and discriminate diseases of potato tubers. *Plant Dis.* **2002**, *86* (2), 131−137.

(14) Stinson, J. A.; Persaud, K. C.; Bryning, G. Generic system for the detection of statutory potato pathogens. *Sens. Actuators, B* **2006**, *116*, 100−106.

(15) Rich, A. E. *Potato Diseases*; Academic Press: New York, 1983; pp 20−25.

(16) Rowe, R. C.; Miller, S. A.; Riedel, R. M. Bacterial ring rot of potatoes (online). 1995; http://ohioline.osu.edu/hyg-fact/3000/3103.html (accessed July 10, 2013).

(17) Kelman, A. The relationship of pathogenicity in *Pseudomonas solanacearum* to colony appearance on a tetrazolium medium. *Phytopathology* **1954**, *44*, 693−695.

(18) Wilson, E. E.; Zeitoun, F. M.; Fredrickson, D. L. Bacterial phloem canker, a new disease of Persian walnut trees. *Phytopathology* **1967**, *57*, 618−621.

(19) Ridé, M.; Ridé, S.; Novoa, D. Connaissances actuelles sur la necrose bacterienne de la vigne [*Xanthomonas ampelina*; evolution, symptomes, cycle biologique, lutte, fongicides]. *Bull. Tech. Pyrenees Orientales* **1983**, *106*, 10−45.

(20) U.S. Food and Drug Administration. http://www.fda.gov/Food/FoodScienceResearch/ LaboratoryMethods/ucm063519.htm (accessed July 24, 2013).

(21) Scherf, J. M.; Milling, A.; Allen, C. Moderate temperature fluctuations rapidly reduce the viability of *Ralstonia solanacearum* race 3, biovar 2, in infected geranium, tomato, and potato plants. *Appl. Environ. Microbiol.* **2010**, *76* (21), 7061−7067.

(22) Eddins, A. H. Some characteristics of bacterial ring rot of potatoes. *Am. Potato J.* **1939**, *16*, 309−322.

(23) van Dam, N. M.; Samudrala, D.; Harren, F. J. M.; Cristescu, S. M. Real-time analysis of sulfur-containing volatiles in *Brassica* plants infested with root-feeding *Delia radicum* larvae using proton-transfer reaction mass spectrometry. *AoB Plants* **2012**, *2012*10.1093/aobpla/pls021.

(24) Steeghs, M.; Bais, H. P.; de Gouw, J.; Goldan, P.; Kuster, W.; Northway, M.; Fall, R.; Vivanco, J. M. Proton-transfer-reaction mass spectrometry as a new tool for real time analysis of root-secreted volatile organic compounds in *Arabidopsis*. *Plant Physiol.* **2004**, *135*, 47−58.

(25) Boamfa, E. I.; Steeghs, M. M. L.; Cristescu, S. M.; Harren, F. J. M. Trace gas detection from fermentation processes in apples; an intercomparison study between proton-transfer-reaction mass spectrometry and laser photoacoustics E.I. *Int. J. Mass Spectrom.* **2004**, *239*, 193−201.

(26) Seal, S. E.; Jackson, L. A.; Young, J. P. W.; Daniels, M. J. Differentiation of *Pseudomonas solanacearum, P. syzygii, P. picketti* and the blood disease bacterium by partial 16S rRNA sequencing: construction of oligonucleotide primers for sensitive detection by polymerase chain reaction. *J. Gen. Microbiol.* **1993**, *139*, 1587−1594.

(27) Pastrik, K.-H. Detection of *Clavibacter michiganensis* subsp. *sepedonicus* in potato tubers by multiplex PCR with coamplification of host DNA. *Eur. J. Plant Pathol.* **2000**, *106*, 155−165.

(28) Van Ruth, S. M.; Roozen, J. P.; Cozijnsen, J. L. Volatile compounds of rehydrated French beans, bell peppers and leeks. Part 1. Flavour release in the mouth and in three mouth model systems. *Food Chem.* **1995**, *53*, 15−22.

(29) Cremer, D. R.; Eichner, K. Formation of volatile compounds during heating of spice paprika (*Capsicum annuum*) powder. *J. Agric. Food Chem.* **2000**, *48*, 2454−2460.

(30) Dickinson, J. R.; Lanterman, M. M.; Danner, D. J.; Pearsoni, B. M.; Sanz, P.; Harrison, S. J.; Hewlins, M. J. E. A ^{13}C nuclear magnetic

resonance investigation of the metabolism of leucine to isoamyl alcohol in *Saccharomyces cerevisiae*. *J. Biol. Chem.* **1997**, *272* (43), 26871−26878.
(31) Boatright, J.; Negre, F.; Chen, X.; Kish, C. M.; Wood, B.; Peel, G.; Orlova, I.; Gang, D.; Rhodes, D.; Dudareva, N. Understanding in vivo benzenoid metabolism in petunia petal tissue. *Plant Physiol.* **2004**, *135*, 1993−2011.
(32) Blasioli, S.; Biondi, E.; Braschi, I.; Mazzucchi, U.; Bazzi, C.; Gessa, C. E. Electronic nose as an innovative tool for the diagnosis of grapevine crown gall. *Anal. Chim. Acta* **2010**, *672*, 20−24.
(33) Shu, C. K.; Ho, C. T. Effect of pH on the volatile formation from the reaction between cysteine and 2,5-dimethyl-4-hydroxy-3(2*H*)-furanone. *J. Agric. Food Chem.* **1988**, *36*, 801−803.
(34) Rios, J. J.; Fernández-García, E.; Mínguez-Mosquera, M. I.; Pérez-Gálvez, A. Description of volatile compounds generated by the degradation of carotenoids in paprika, tomato and marigold oleoresins. *Food Chem.* **2008**, *106*, 1145−1153.
(35) Sindsen, S. L.; Goth, R. W.; O'Brien, M. J. Effect of potato alkaloids on the growth of *Alternaria solani* and their possible role as resistance factors in potatoes. *Phytopathology* **1972**, *63*, 303−307.
(36) Atlantic Committee on Potatoes. http://www.gnb.ca/0029/00290033-e.asp (accessed June 24, 2013).
(37) De Lacy Costello, B. P. J.; Evans, P.; Ewen, R. J.; Gunson, H. E.; Jones, P. R. H.; Ratcliffe, N. M.; Spencer-Phillips, P. T. N. Gas chromatography-mass spectrometry analyses of volatile organic compounds from potato tubers inoculated with *Phytophthora infestans* or *Fusarium coeruleum*. *Plant Pathol.* **2001**, *50*, 489−496.
(38) Danner, H.; Samudrala, D.; Cristescu, S. M.; Van Dam, N. M. Tracing hidden herbivores: time-resolved non-invasive analysis of belowground volatiles by proton-transfer-reaction mass spectrometry (PTR-MS). *J. Chem. Ecol.* **2012**, *38*, 785−794.
(39) Lui, L. H.; Vikram, A.; Abu-Nada, Y.; Kushalappa, A. C.; Raghavan, G. S. V.; Al-Mughrabi, K. Volatile metabolic profiling for discrimination of potato tubers inoculated with dry and soft rot pathogens. *Am. J. Potato Res.* **2005**, *82*, 1−8.
(40) Waterer, D. R.; Pritchard, M. K. Monitoring of volatiles: a technique for detection of soft rot (*Erwinia carotovora*) in potato tubers. *Am. Potato. J. Res.* **1984**, *61*, 345−353.
(41) Hansel, A.; Jordan, A.; Holzinger, R.; Prazeller, P.; Vogel, W.; Lindinger, W. Proton transfer reaction mass spectrometry: on-line trace gas analysis at the ppb level. *Int. J. Mass Spectrom. Ion Processes* **1995**, *149/150*, 609−619.

JOURNAL OF AGRICULTURAL AND FOOD CHEMISTRY

Article

pubs.acs.org/JAFC

Comparison of Simulated Pesticide Concentrations in Surface Drinking Water with Monitoring Data: Explanations for Observed Differences and Proposals for a New Regulatory Modeling Approach

Michael F. Winchell[†,*] and Nathan J. Snyder[‡]

[†]Stone Environmental, Inc., 535 Stone Cutters Way, Montpelier, Vermont 05602, United States

[‡]Waterborne Environmental, Inc., 897-B Harrison Street S.E., Leesburg, Virginia 20175, United States

ABSTRACT: A primary component to human health risk assessments required by the U.S. Environmental Protection Agency in the registration of pesticides is an estimation of concentrations in surface drinking water predicted by environmental models. The assumptions used in the current regulatory modeling approach are designed to be "conservative", resulting in higher predicted pesticide concentrations than would actually occur in the environment. This paper compiles previously reported modeling and monitoring comparisons and shows that current regulatory modeling methods result in predictions that universally exceed observed concentrations from the upper end of their distributions. In 50% of the modeling/monitoring comparisons, model predictions were more than 229 times greater than the observations, while, in 25% of the comparisons, model predictions were more than 4500 times greater than the observations. The causes for these overpredictions are identified, followed by suggestions for alternative modeling approaches that would result in predictions of pesticide concentrations closer to those observed.

KEYWORDS: *pesticide, modeling, monitoring, surface water, water supply*

INTRODUCTION

Regulation of agricultural pesticides use in the Unites States is required to be protective of both human health and the environment. The U.S. Environmental Protection Agency (EPA) assesses the risk of a particular pesticide use to human health from all nonoccupational sources by determining an estimated drinking water concentration (EDWC) of the pesticide, generally using simulation models, and combining this with other possible routes of exposure (food and residential sources) for comparison against human health effects metrics (the pesticide toxicity). Occupational exposure is assessed under a separate paradigm. The aggregate exposure is compared with effects data so that the risk manager may make an informed decision based on the risk characterization. The EDWC is often the determining factor in a risk assessment, and the accurate estimations of exposure are worthy of evaluation and improvements as technology and available data improve. EDWCs are calculated for both groundwater and surface water, with the higher of the two values representing the exposure level in the risk assessment. While challenges exist in the determination of groundwater and surface water EDWCs, this paper will focus on surface water. Surface water EDWCs can be determined from direct monitoring of raw and finished water in surface water supplies (for already registered products), modeling the pesticide fate and transport in surface drinking water using established regulatory tools or refined tools, or a combination of the two approaches. While extensive monitoring of pesticide residues in drinking water systems has occurred in the US over the past few decades, the need to calculate EDWCs for certain types of water systems and pesticides lacking more extensive monitoring records (especially limited and new use products) will continue. For this reason, modeling of pesticide EDWCs is the most common approach taken when conducting risk assessments; however, the usefulness of existing monitoring programs should not be ignored in their ability to validate the regulatory process and modeling predictions made by the EPA.

Current Regulatory Modeling Approach. In pesticide registration review, the U.S. EPA follows a tiered risk assessment process that applies more conservative aquatic exposure modeling methods for estimating pesticide EDWCs at the lower tiers and only applies more complex, refined modeling approaches for those pesticides that have not passed the risk assessment at the lower tiers. The Tier 1 modeling approach (designed to be most conservative) uses EPA's FIRST model,[1] and because most pesticides fail this initial tier, a Tier 2 assessment is often required. In a Tier 2 assessment, the EPA requires that a standard modeling approach utilizing the Pesticide Root Zone Model (PRZM) field scale hydrologic model[2] and the Exposure Analysis Modeling System (EXAMS) receiving water model[3] be followed when estimating pesticide EDWCs for the purpose of product registration. Refinements including Percent Crop Area (PCA) adjustments to the assumption of 100% cropping are within the Tier 2 guidance, but other refinements are limited. Registrants have at times submitted more complex modeling approaches that incorporate site specific environmental conditions (e.g., soil and weather), probabilistic methods (e.g., Monte Carlo simulation), specialized models, spatial analysis of model input parameters, and monitoring data as a Tier 3 and Tier 4 assessment to further refine exposure predictions.[4] US EPA acceptance of Tier 3 and

Received: August 25, 2013
Revised: December 12, 2013
Accepted: December 13, 2013
Published: December 13, 2013

ACS Publications © 2013 American Chemical Society

Tier 4 has been limited, so in practice, exposure modeling beyond the screening level assessment provided in Tier 2 is rarely conducted, making the Tier 2 modeling results the most relevant for comparison with monitoring data.

The modeling results reported on in this study were generated using the Tier 2 modeling approaches that were prescribed by the EPA at the time the studies were conducted. The Tier 2 approach simulates daily concentrations of a pesticide in an "Index Reservoir" over a 30-year period. The Index Reservoir was characterized by the US EPA as being "designed to mimic drinking water reservoirs in the central Midwest known to be highly vulnerable to contamination from pesticides used in agriculture".[5] This Index Reservoir and its associated watershed is based on the Shipman Reservoir in Illinois. The Shipman Reservoir covers approximately 5.3 ha, has a mean depth of 2.7 m, and has a watershed that drains approximately 172.8 ha. These geometric characteristics result in a drainage area to normal capacity ratio (DA/NC) of 12, which is higher than approximately 90% of drinking water reservoirs.[5] Because higher DA/NC ratios lead to higher pesticide exposure vulnerability, the geometric characteristics of the Index Reservoir place it on the high end (90th percentile) of vulnerability.

The use of Shipman Reservoir to represent the Index Reservoir scenario for estimating EDWCs was designed to be conservative; therefore, the predicted pesticide concentrations are expected to be higher than would be found in most drinking water reservoirs.[6] Another important input assumption when applying the Index Reservoir scenario to calculate EDWCs is the percent cropped area (PCA) adjustment factor. A PCA adjustment factor is necessary because, for watersheds greater than a few hectares in size, the percentage of the watershed being cropped will be less than 100%. The PCA is a critical input assumption to the Index Reservoir modeling approach because it dictates the fraction of the reservoir watershed that will be treated with the pesticide under evaluation. The US EPA has recently developed updated guidance on how PCA adjustment factors should be determined for major crop and crop groups for both national and regional assessments.[7] This guidance provides recommendations of national and regional PCA values for major crops, for combinations of major crops, and for all agriculture, as well as a prescribed methodology for choosing the appropriate PCA value for a given pesticide use pattern scenario. While this recent guidance supersedes the approaches to PCA calculation that were effective at the time when several of the modeling studies in this report were conducted, the differences in PCA values between current and past guidance are small relative to the magnitude of the modeled versus monitoring data concentrations. Furthermore, the recommended PCA values in the most recent guidance are generally higher than the previously guidance, making the current model predictions more conservative than past analogous predictions. The national maximum PCAs for the major crops that were recommended for use during the period between 2000 and 2012[8] and the current post-2012 guidance are shown in Table 1.

The only legal constraints on pesticide use are the conditions for use placed on a product label. These conditions (for agricultural products, the application rates and timing on specific crops) are what EPA uses as a basis for modeling exposure, focusing on what could occur as opposed to what actually occurs or is likely to occur. Following the EPA modeling approach, the PCA and subsequently the fraction of the watershed treated with pesticide are constant for all pesticides that are labeled for use on a particular crop, regardless of the relative market share of individual products or the prevalence of actual use. Additionally, it is assumed that application of the pesticide is made over the entire cropped area in the watershed on the same day. The assumption that the entire cropped area is treated on the same day is likely to be more accurate for very small watersheds and low acreage crops consisting of a few fields under the management of few farmers, but it quickly becomes less realistic as the watershed size increases or for high acreage crops (due to farmer equipment constraints or pest and weed management strategies). Misrepresentation of actual product use spatially and temporally can have a significant impact on EDWCs. In order for models to successfully predict pesticide concentrations that can realistically be expected to occur under high vulnerability conditions, the product use assumptions must reflect reality. A comparison of modeling results with monitoring data will give an indication of model performance but also how well assumptions used for input values reflect actual conditions.

Table 1. Comparison of National Percent Cropped Area (PCA) Adjustment Factors for Major Crops from US EPA Guidance during 2000−2012 and Updated Guidance for 2012−Present

crop	max percent cropped area (2000−2012)	max percent cropped area (2012−current)
corn	0.46	0.61
soybeans	0.41	0.57
wheat	0.56	0.38
cotton	0.2	0.33
all agricultural land	0.87	0.91

Comparing Modeling to Monitoring Data. Making comparisons of water quality modeling results and monitoring data is a common activity used in model calibration and validation. Often times, these comparisons are not straightforward due to monitoring frequency and sampling methods relative to the modeling data.

One common comparison approach is to perform time series analysis where monitoring data and modeling results are evaluated over specific time periods (typically daily) where the two co-occur. A time series analysis can also occur based on longer duration time steps (monthly or annually) where both the monitoring and modeling data are aggregated over the duration being assessed. Obtaining an accurate assessment of model performance from time series analysis can be challenging in pesticide simulation modeling due to the uncertainties in pesticide application timing and subsequent transport to receiving waters. These uncertainties make the quantification of differences between model and monitoring data difficult, because the time series goodness of fit statistics are very sensitive to small timing errors in the model. The difficulty in applying time series comparison methods is even more difficult in situations where the number of monitoring samples is small compared to the number of model predictions. In situations where pesticide application timing is very well understood and monitoring data is more abundant, a time series analysis can be a meaningful approach for assessing the performance of pesticide concentration simulations. Another approach for comparing modeling and monitoring data is to perform statistical comparisons of the probability distributions of the two data sets. This type of approach places less emphasis on

assessing the model's ability to match temporal signals in the monitoring data and, instead, looks to assess the model's ability to predict concentration magnitude and frequency. This approach is particularly appropriate for pesticides where the specific temporal use patterns are often highly uncertain and where the monitoring data may not be able to capture the details of day to day temporal variability.

When making comparisons between modeling and monitoring data, the uncertainties inherent in both need to be considered. Uncertainties in modeling arise from the identification of model parameters, measured model inputs, and the underlying conceptual model and model structure. Uncertainties in model parameters have long been recognized in pesticide exposure modeling, and parameter space sampling techniques, such as Monte Carlo Analysis, Latin Hypercube Sampling, and Deterministic Equivalent Modeling Method (DEMM), have been used to address them.[9−12] Unfortunately, techniques such as Monte Carlo analysis often do not include errors and uncertainties in model inputs, such as weather and pesticide application timing, which can often be as or more important as many model parameters included in a probabilistic approach. Often times, model uncertainty is reduced by the refinement of model parameters accomplished through calibration with monitoring data.

Uncertainty in monitoring data used to calibrate and validate hydrologic and water quality models is also well acknowledged, and can lead to poor identification of model parameters. Efforts to quantify this uncertainty and development of tools to aid in the comparison of monitoring data with model data have been developed[13,14] and may be used to improve model calibration. Techniques for quantification of uncertainties associated with a conceptual model and model structure are not commonly applied to water quality models with a static form used in pesticide exposure modeling; however, the existence of these uncertainties should be acknowledged.

One of the greatest sources of uncertainty associated with monitoring data is the potential bias in the monitoring data resulting from low sampling frequency. Arguments can be made that infrequent sampling at regular intervals in a monitoring program can sometimes miss the peaks in concentration which are important in the determination of EDWCs for use in risk assessments. While this argument cannot be disputed, the question of the sampling frequency required to enable accurate prediction of the "true" distribution in concentration levels remains a topic of interest and continued investigation. Crawford[15] evaluated the sampling frequency required to accurately predict various exceedance probabilities of annual maximum concentrations. Crawford found that required sampling frequency was dependent upon watershed size and the exceedance probability being detected. For example, the median annual concentration in water bodies draining lager watersheds (e.g., 16,400 km^2) can be estimated sufficiently by sampling 7 times per year. For the 95th percentile annual concentrations (5% exceedance probability) on smaller watersheds (90−250 km^2), a sampling frequency of 10 times per month during the runoff season following pesticide applications was required. In addition, Mosquin et al.[16] presented an approach for estimating higher percentile (lower exceedance probability) pesticide concentrations in surface drinking water from monitoring data sets of various frequencies. In addition, they provided estimates of the number of samples required to derive confidence bounds for the upper percentiles of concentration distributions. For example, an effective sample size of 59−69 can provide the estimates for the 95th percentile concentrations with sufficient statistical confidence (e.g., 95%), and increasing the sample size to 212 reduces the relative standard error to 30% or below. Other recent work has sought to quantify the potential bias in the estimates of higher percentile pesticide concentrations based on nondaily monitoring data.[17,18] These studies have suggested that bias factors (defined as the 95th percentile of the ratios of a true concentration end point derived from daily monitoring data to the corresponding estimate from nondaily sampling) increase as monitoring frequency decreases and as the desired averaging interval decreases in duration (i.e., the bias factor increases if estimating maximum versus 14-day average). Chen et al.[18] found an average bias factor of 2.4 when using 7-day sampling interval data to estimate an annual peak value, and Hetrick[17] found bias factors averaging 1.79 for estimating peaks from 4-day sampling data or 8.35 when using 28-day sampling data. The development of bias factors for estimating higher percentile pesticide concentrations from monitoring data of various sampling frequencies provides an important basis for the comparisons between modeling results and monitoring data obtained from nondaily sampling studies. While the development of methods for using monitoring data in statistical estimation of higher percentile pesticide concentrations will continue, modeling tools will always be required when assessing EDWCs for newly registered crop protection products.

The question of if and by how much pesticide EDWCs derived from the standard regulatory modeling approach overestimate actual pesticide concentrations in drinking water has long been one of considerable interest. Several authors have published comparisons of modeling and monitoring data within the past ten years.[19−24] These studies (and others) have determined that the regulatory modeling based EDWCs consistently overpredict the concentrations of pesticides found in surface drinking water monitoring data sets. As was stated, the US EPA's modeling approach is understandably designed to be conservative; however, the magnitude of the gap between modeled and observed pesticide concentrations in surface drinking water should be fully understood so that the modeling results can be applied more appropriately in the context of better understood certainty/uncertainty of the modeled estimates. This paper brings together a collection of previously published comparisons between monitoring data and regulatory modeling-based EDWCs, with the objective of evaluating how accurately the regulatory modeling approach being used by the U.S. EPA reflects what has been observed in monitoring studies. In combining data from multiple past studies, the analysis contained in this paper is based on the most comprehensive set of data on the subject to date. A secondary objective of this paper is to identify the possible factors leading to the overprediction of EDWCs following the current modeling approach and to propose alternative assumptions and methods that produce results closer to observed values of pesticide concentrations in surface drinking water.

MATERIALS AND METHODS

This comparison of modeling and monitoring data of pesticide concentrations focused on modeled EDWCs derived from standard US EPA Tier 2 regulatory modeling and monitoring data covering a wide range of water body types (flowing and nonflowing) and sizes. A preliminary literature review on the subjects of pesticide modeling and monitoring identified 179 documents from peer reviewed journal

articles, technical reports, conference proceedings and presentations, and Web sites. This initial bibliography was then screened to identify the studies that contained explicit comparisons between Tier 2 PRZM/EXAMS modeling results and monitoring data. This screening resulted in seven studies from which the data for evaluation were compiled. All the monitoring and modeling results reported in each of the seven studies selected were designed to select either the maximum or a higher percentile monitoring data concentration for comparison with the modeled values (which were generally the 1 in 10 year annual maximum values used in regulatory risk assessments). The discussion that follows and footnotes to the individual data tables will provide the information concerning each of the data sources and describe the methodology for the modeling/monitoring data comparisons made in this report.

Data Sources. The data sets, and descriptions of the source studies they came from, are provided in this section. First was the paper by Jones.[19] This study reported on four pesticides that were part of targeted monitoring studies that sought to identify community drinking water systems (CWS) that were in locations most vulnerable to potential exposure to each individual pesticide. The study included between 5 and 28 CWS for each pesticide, with between 233 and 2120 samples of raw water and between 30 and 306 samples of finished water (total samples per pesticide ranging from 263 to 2426). The sampling associated with these studies lasted between 2 and 3 years and included weekly or biweekly sampling frequency during and after the application season. The study compared both daily maximum concentrations and annual average concentrations. A summary of the data compiled from this study is provided in Table 2. In Table 2, the highest modeled concentrations represent the highest daily maximum value based on 30-year simulations of all multiple crop scenarios simulated for the pesticide shown. The highest monitoring concentration represents the highest of finished water over the duration of the study (2 to 3 years).

Table 2. Summary of Modeling and Monitoring Data from Jones[17]

pesticide	highest modeled conc[e] (μg/L)	max monitoring conc (μg/L)	EDWC duration	tot samples[f]
aldicarb[a]	17	0.68	acute (daily max)	2426
bromoxynil[b]	11	0.38	acute (daily max)	543
carbaryl[c]	745	0.16	acute (daily max)	2369
ethoprophos[d]	127	0.012	acute (daily max)	263
aldicarb[a]	5.8	0.07	chronic (annual avg)	2426
bromoxynil[b]	0.2	0.01	chronic (annual avg)	543
carbaryl[c]	31	0.005	chronic (annual avg)	2369
ethoprophos[d]	13	<0.003	chronic (annual avg)	263

[a]Includes 28 sites monitored for 3 years with weekly sampling during application season. [b]Includes 16 sites monitored for 2 years with biweekly sampling during application season. [c]Includes 20 sites monitored for 3 years with weekly sampling during application season. [d]Includes 5 sites monitored for 3 years with weekly sampling during application season. [e]Modeling conducted by EPA and represents 90th percentile annual maximum; for bromoxynil, value represents the average of annual maxima. [f]Raw water plus finished water samples.

The second source of data by Jackson et al.[20] examined 25 different pesticides, making predictions of EDWCs following the standard EPA PRZM/EXAMS regulatory modeling approach and comparing those results with monitoring data collected in the study of water supply reservoirs conducted by the US Geological Survey (USGS) and the US EPA.[25] The USGS study monitored 12 reservoirs over a period of one to two years (1999−2000) extending geographically across 12 different states, from California to New York . The reservoirs selected focused on small reservoirs with high pesticide use, and were thus highly vulnerable to elevated pesticide concentrations. A sampling strategy was designed to be able to estimate higher percentile (90th, 95th, and 99th percentile) with high confidence. The strategy was derived from an evaluation of a 2-year record of daily pesticide concentrations from Perry Lake reservoir in Kansas, and PRZM/EXAMS simulations. Three different sampling schemes were developed (11, 26, and 37 times per year), each of which focused samples during the pesticide application season. One of the 12 reservoirs received the highest sampling frequency (37 times per year), four reservoirs received the middle frequency (26 times per year), and seven received the lower frequency sampling, resulting in 537 to 551 samples per pesticide. In addition to data from the 2-year reservoir monitoring study, Jackson et al.[20] also presented monitoring data from the USGS National Water Quality Assessment (NAWQA) program as an additional data set for comparison. The NAWQA data set analysis included a longer record of water quality sampling (1992−2004) and a larger total number of samples for each pesticide, ranging from 105 to 23,726. The NAWQA sampling locations are not specifically targeted as sites having a high vulnerability to pesticide exposure, but rather represent a cross section of agricultural, developed, and mixed land use watersheds spread geographically across the United States. Sampling for NAWQA is generally conducted on a biweekly basis. One of the primary objectives of the NAQWA program is to monitor trends in surface water quality. A summary of the PRZM/EXAMS modeling and the monitoring results from the USGS reservoir monitoring and the NAWQA database analysis is provided in Table 3. The highest modeling concentration reported is the highest 90th percentile annual maximum concentration (from the 30-year PRZM/EXAMS simulations) simulated from one or more crop scenarios. The 90th percentile annual maximum concentrations are calculated by first determining the maximum concentration in each simulation year and then ranking those annual maximum concentrations and calculating the 90th percentile of those values. The data presented for the reservoir monitoring program represents the maximum concentration detected, while the data from the NAWQA program is the 95th percentile of the collection of samples. Although these two monitoring data sets are not equivalent, the additional NAWQA data provide a valuable comparison with both the modeled concentrations and the reservoir data.

A conference presentation by Hertl et al.[21] also compared modeling results following the EPA PRZM/EXAMS regulatory modeling approach with monitoring data from the USGS reservoir monitoring program.[19] This study evaluated several pesticides in addition to the Jackson et al.[20] study and also looked at both acute (short-term) and chronic (long-term) concentrations. The acute concentrations were represented by the maximum individual sample values, and the chronic concentrations were calculated as the 95th percentile of the time weighted annual average. In addition, the monitoring data evaluated in the Hertl et al.[21] study represented only the raw water samples, whereas the Jackson et al. paper included finished water as well, with a total number of samples per pesticide ranging from 312 to 323. For the vast majority of the pesticides analyzed, the raw water samples had higher concentrations than the finished water samples (highlighting another area of conservatism in the regulatory approach). These data are summarized in Table 4.

The most recent report reviewed that compared monitoring data to regulatory model simulation results was prepared by the US EPA.[7] The purpose of this report was to present an updated methodology for selecting appropriate PCA adjustment factors based on analysis of the most recent land use and cropping data sets. In addition to presenting the updated methodology, the report also showed monitoring data comparisons of the regulatory modeling simulations using the new PCA adjustment factors. In addition, the report included monitoring data from multiple sources (some were the same as those used in the earlier studies described) compiled over the past 20 years. These monitoring data sets included the following: USGS monitoring data from community water systems presented in *Concentration Data for*

dx.doi.org/10.1021/jf4036996 | J. Agric. Food Chem. 2014, 62, 348−359

Table 3. Summary of Modeling and Monitoring Data from Jackson et al.[16]

pesticide	highest modeled conc[a] (μg/L)	USGS reservoir program, max monitoring conc (μg/L)[b,c]	tot samples[f]	USGS NAWQA program, 95th percentile monitoring conc (μg/L)[e]	no. of NAWQA samples
2,4-D	145	0.634	537	0.362	7,129
2,4-DB	140	0.054	537	<0.24	5,938
acifluorfen	13.4	0.062	537	<0.035	6,014
aldicarb	98.7	0.082[d]	537	<0.55	5,980
atrazine(H)	438	11.6	551	1.4	23,726
benomyl	9.34	0.215	537	0.024	1,182
bentazon	32.5	0.344	537	0.1	6,488
bromoxynil	88.3	0.057	537	<0.035	5,877
clopyralid	15.8	0.17	537	<0.23	5,976
dicamba	32.5	0.192	537	<0.035	6,043
flumetsulam	2.25	0.088	537	<0.11	1,084
imazaquin	3.09	0.351	537	0.058	1,214
imazethapyr	3.06	0.133	537	0.028	1,128
linuron	35	0.035	537	<0.08	259
MCPA	81	0.121	537	<0.07	6,218
metalaxyl	101	0.351	538	0.04	656
methomyl	16.3	0.077[d]	537	<0.017	105
nicosulfuron	1.92	0.139	537	<0.013	1,089
norflurazon	215	0.414	537	<0.042	6,101
oryzalin	161	0.127	537	<0.31	6,056
picloram(H)	5.27	1.441	537	<0.05	5,763
propiconazole	125	0.064	537	<0.021	1,112
sulfometuron-methyl	1.87	0.16	537	0.025	1,165
tebuthiuron	1350	0.077	537	0.049	14,133
terbacil	125	0.1	537	<0.034	10,223

[a]Modeled values represent 90th percentile of annual maxima. [b]Data presented in Jackson et al. (2005) was graphical. Specific values reported were extracted directly from Bloomquist et al. (2001). [c]Includes 12 sites monitored for 1 to 2 years with 11 to 37 samples per year, focused during application season (up to every 3 days for 1 month). [d]No detections occurred in sampling. Value represents detection limit. [e]Values preceded by "<" were below the level of quantification for the analytical method. [f]Raw water plus finished water samples.

Anthropogenic Organic Compounds in Ground Water, Surface Water, and Finished Water of Selected Community Water Systems in the United States, 2002–05 (http://pubs.usgs.gov/ds/2007/268/); USGS NAWQA surface water data (http://infotrek.er.usgs.gov/nawqa_queries/); the USDA's Pesticide Data Program (PDP); the California Department of Pesticide Regulation's Surface Water database (http://www.cdpr.ca.gov/docs/emon/surfwtr/surfdata.htm); and data obtained from crop-specific monitoring studies submitted to EPA. The comparisons in Echeverria et al.[7] represent the most current implementation of EPA's regulatory modeling approach as well as the most comprehensive compilation of monitoring data comparison. These data comparisons from the EPA report are summarized in Table 5. The highest modeling concentration shown represents the 1 in 10 year peak, or 90th percentile annual maximum concentration (see footnote earlier in this section). The total number of samples per pesticide was not provided in the EPA report; however, given that NAWQA was one of the sources, the number of samples likely well exceeded 1000 for many of the pesticides.

The four studies presented thus far accounted for the majority of the modeling results monitoring data comparisons. Three other studies provided additional comparisons of regulatory modeling results with monitoring data. The first study focused on the fungicide vinclozolin and its use on golf courses.[22] In this study, 10 CWS watersheds with high numbers of golf courses were monitored for over a two year period for vinclozolin. The second study assessed the herbicide oxadiazon, which is also used on turf.[23] In this study, three community water systems were monitored for a period of three years. The third study was an analysis of fungicide iprodione use on turf and included its degradate product, 3,5-DCA.[24] This study compared monitoring data of finished water collected over three years from three different CWS with regulatory modeling predictions. The modeling and monitoring data from these three studies, including the total number of monitoring samples (ranging from 480 to 639), are presented in Table 6.

Data Compilation and Analysis. The modeling/monitoring data comparison from the seven studies presented in Tables 2–6 were combined for an assessment of the modeled data overprediction in surface water EDWCs. For the Jackson et al.[20] study, only the monitoring data from the USGS reservoir study was included for the combined comparison. This was done because, for all pesticides, the monitoring data from the USGS reservoir monitoring found greater concentrations than the 95th percentile data from the NAWQA analysis. There were a total of 85 modeling/monitoring data points for evaluation. These 85 data points included 68 acute and 17 chronic EDWC concentrations spread over 52 different pesticides (52 acute and 15 chronic). The overprediction in the modeled concentration was calculated as the ratio of modeled concentration to monitored concentration. The results of this analysis follow.

RESULTS AND DISCUSSION

Analysis of Modeling and Monitoring Data Comparisons. All monitoring and modeling data comparisons from the seven studies compiled are shown in Figure 1a. The 85 data points are sorted from highest modeled concentration to lowest modeled concentration. Figure 1b shows only the 25 data points with the lowest modeled concentrations. The modeled concentrations ranged from a high value of 1350 μg/L (for tebuthiuron acute concentration) to a low value of 0.2 μg/L (for bromoxynil chronic concentration). The median modeled concentration was 32.5 μg/L (for bentazon, acute concentration), which had an associated monitoring concentration 2 orders of magnitude lower at 0.344 μg/L. In total, 96.5% of the

Table 4. Summary of Modeling and Monitoring Data from Hertl et al.[20]

pesticide	highest modeled conc[a] (μg/L)	max monitoring conc[b,c,d] (μg/L)	EDWC duration	tot samples[e]
acifluorfen	14.03	0.062	acute (daily max)	312
aldicarb	17.4	0.082	acute (daily max)	312
atrazine	205.1	11.6	acute (daily max)	323
azinphos-methyl	87.8	0.144	acute (daily max)	323
carbaryl	274	0.063	acute (daily max)	323
disulfoton	26.8	0.021	acute (daily max)	323
fenamiphos	651	0.016	acute (daily max)	317
metolachlor	134.6	3.32	acute (daily max)	323
triallate	7.76	0.002	acute (daily max)	323
tribuphos	14	0.016	acute (daily max)	317
acifluorfen	2.97	0.062	chronic (annual avg)	312
aldicarb	5.8	0.082	chronic (annual avg)	312
atrazine	194.2	2.016	chronic (annual avg)	323
azinphos-methyl	7.2	0.018	chronic (annual avg)	323
carbaryl	79	0.063	chronic (annual avg)	323
disulfoton	1.1	0.017	chronic (annual avg)	323
fenamiphos	329	0.016	chronic (annual avg)	317
metolachlor	77.9	0.417	chronic (annual avg)	323
triallate	0.88	0.001	chronic (annual avg)	323
tribuphos	2	0.016	chronic (annual avg)	317

[a]Modeling conducted by EPA and Represents 90th percentile annual maximum. [b]For nondetections, where the 95th percentile could not be determined (chronic), the detection limit was used. [c]Includes 12 sites monitored for 1 to 2 years with 11 to 37 samples per year, focused during application season (up to every 3 days for 1 month). [d]Acute represents the maximum detected, and chronic represents the 95th percentile of the time-weighted average. [e]Raw water samples.

Table 5. Summary of Modeling and Monitoring Data from Echeverria et al.[5]

pesticide	highest modeled conc[b] (μg/L)	max monit conc[b] (μg/L)	EDWC duration
acetochlor	50.1	4.77	acute (daily max)
acifluoren	49.5	0.011	acute (daily max)
atrazine	130.3	85	acute (daily max)
bentazon	11.7	0.12	acute (daily max)
bromacil	62.7	0.0927	acute (daily max)
bromoxynil	2	0.0046	acute (daily max)
carbofuran	25.2	0.0141	acute (daily max)
chlorthalonil	328.5	0.71	acute (daily max)
chlorthalonil	75.9	0.71	acute (daily max)
cycloate	44.4	0.6	acute (daily max)
cypermethrin	1.9	0.246	acute (daily max)
dcpa	416.7	0.0049	acute (daily max)
diazinon	135.8	0.0855	acute (daily max)
dicrotovos	16.6	6.83	acute (daily max)
fipronil	0.5	0.0375	acute (daily max)
fluometuron	29.7	0.0065	acute (daily max)
imazaquin	11	0.16	acute (daily max)
iprodione	163.2	0.018	acute (daily max)
linuron	17.7	5.28	acute (daily max)
mcpa	15.3	0.47	acute (daily max)
oryzalin	61.1	0.065	acute (daily max)
phosmet	2.6	0.074	acute (daily max)
picloram	8.6	0.17	acute (daily max)
triallate	3.3	0.65	acute (daily max)
triclopyr	516.6	0.45	acute (daily max)

[A]Modeled values represent 90th percentile of annual maxima. [b]Value represents maxima from multiple sources over many sites and many years. Refer to source report for details. [c]Total number of samples was not reported in source.

Table 6. Summary of Modeling and Monitoring Data from Jackson et al.,[21] Nandihalli et al.,[18] and Jones[22]

pesticide[a]	highest modeled conc[d] (μg/L)	max monit conc (μg/L)	EDWC duration	tot samples[e]
3,5-DCA[b]	153	<0.032	acute (daily max)	587
iprodione[b]	361	0.6	acute (daily max)	587
oxadiazon[b]	52	0.175	acute (daily max)	639
vinclozolin[c]	84.3	0.025	acute (daily max)	480
3,5-DCA[b]	36	<0.025	chronic (annual avg)	587
iprodione[b]	1.6	0.037	chronic (annual avg)	587
oxadiazon[b]	18.6	0.025	chronic (annual avg)	639

[a]Vinclozolin data from Jackson et al. (2010); oxadiazon data from Nandihalli et al. (2010); iprodione and 3,5-DCA data from Jones (2012). [b]Includes 3 sites monitored for 3 years with weekly/biweekly sampling. [c]Includes 10 sites monitored for 3 years with biweekly sampling for first 6 months, then monthly. [d]Modeled values represent 90th percentile of annual maxima. [e]Raw water plus finished water samples.

modeled concentrations were greater than 1 μg/L, while the monitoring data values were greater than 1 μg/L only 10.6% of the time. In all 85 comparisons, the monitoring data were lower than the modeling data.

The magnitude of the overprediction by the modeling results was quantified by calculating the ratio of the modeling concentration to the monitoring concentration. These ratios are plotted from low to high in Figure 2 using percentiles calculated from the Weibull plotting position. In addition, the 85 data points were split into acute and chronic comparisons. Based on the population of all 85 data points, the range in overprediction is from 1.5 to 85,041, with the median overprediction greater than 2 orders of magnitude (229×). More than 90% of the comparisons had a model overprediction of greater than 1 order of magnitude (10×). For one-third of all comparisons, the overprediction by the modeling results was greater than 1000×. When comparing the distribution of model overprediction for acute versus chronic EDWCs, the distributions are very similar between from the 30th through 90th percentiles. Below the 30th percentile, the chronic EDWC overpredictions are somewhat higher than the acute overpredictions. The smallest overprediction in the chronic EDWCs

dx.doi.org/10.1021/jf4036996 | J. Agric. Food Chem. 2014, 62, 348−359

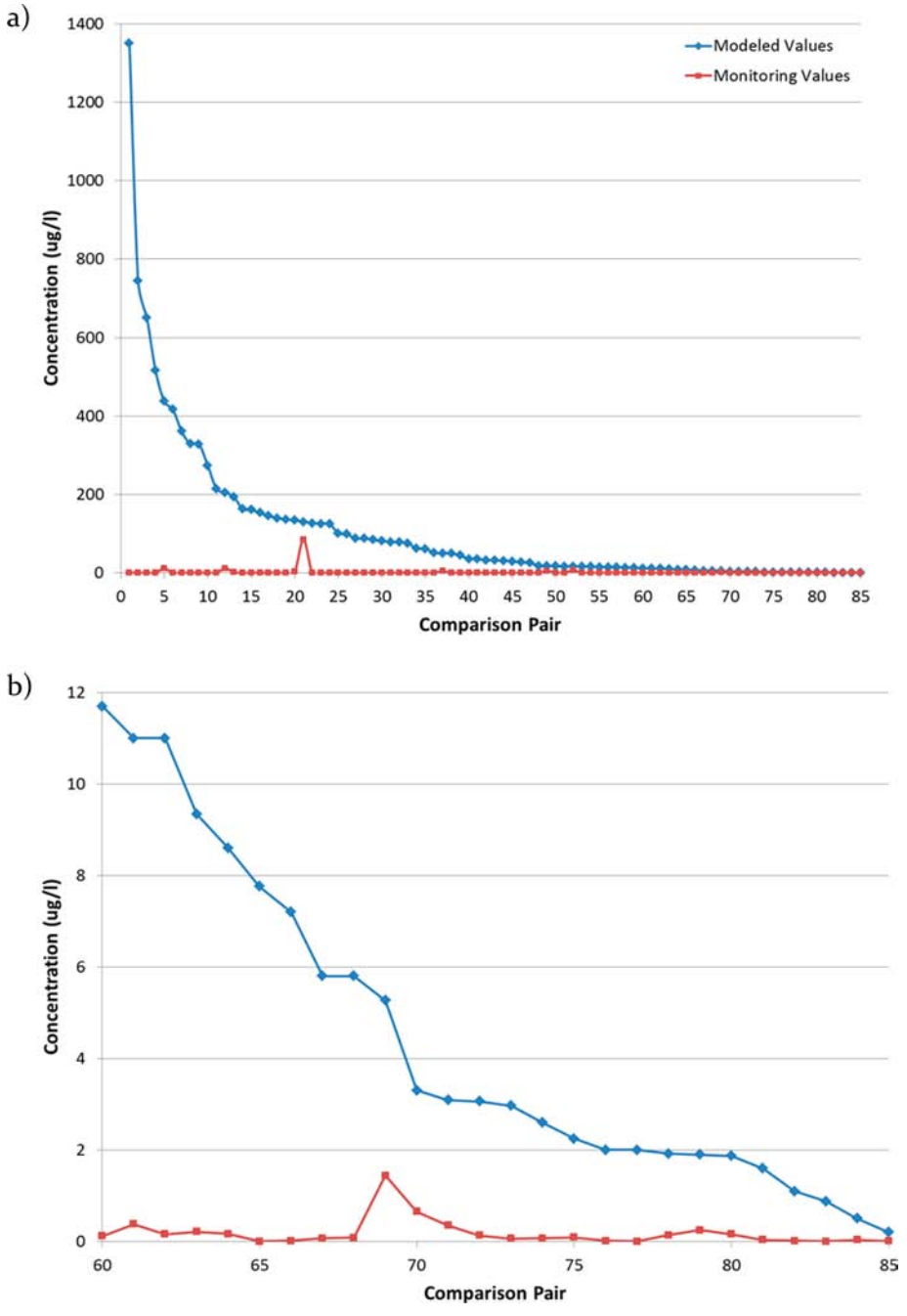

Figure 1. (a) Comparison of modeled and monitoring data concentrations for all pesticides, all data points. (b) Comparison of modeled and monitoring data concentrations for all pesticides, low concentration data points.

was 20× while the smallest acute overprediction was 1.16×. This suggests that, even as the regulatory modeling approach results in peak concentrations that are too high, the persistence of elevated concentrations that it predicts can lead to more significant overprediction of longer duration concentrations. This persistence of high concentrations may be in part due to the underestimation of inflows and outflows associated with the index reservoir assumptions.

The overprediction ratios by pesticide for the acute EDWC comparisons are shown in Figure 3. The average (arithmetic mean) was calculated for those pesticides (e.g., atrazine) where multiple comparisons of modeling and monitoring data were available. In the figure, (I) indicates an insecticide, (H) indicates a herbicide, (F) indicates a fungicide, (F,D) indicates a fungicide degradate, and (N) represents a nematocide. Based on the data in Figure 3, there are a few trends to note. First, three of the pesticides in the top ten highest overprediction ratios were fungicides or associated degradates, while no fungicides occurred among the lowest ten ratios. In addition, two of the pesticides in the top ten lowest overprediction ratios (acetochlor and atrazine) are among the top 5 highest use pesticides in the US in 2007.[26] Of the ten pesticides with the highest overprediction ratios shown in Figure 3, none of them were among the 25 pesticides with the highest use in the US in 2007. While the data available concerning actual pesticides use associated with each modeling/monitoring data comparison are limited at best, the comparison trend demonstrates a

dx.doi.org/10.1021/jf4036996 | J. Agric. Food Chem. 2014, 62, 348−359

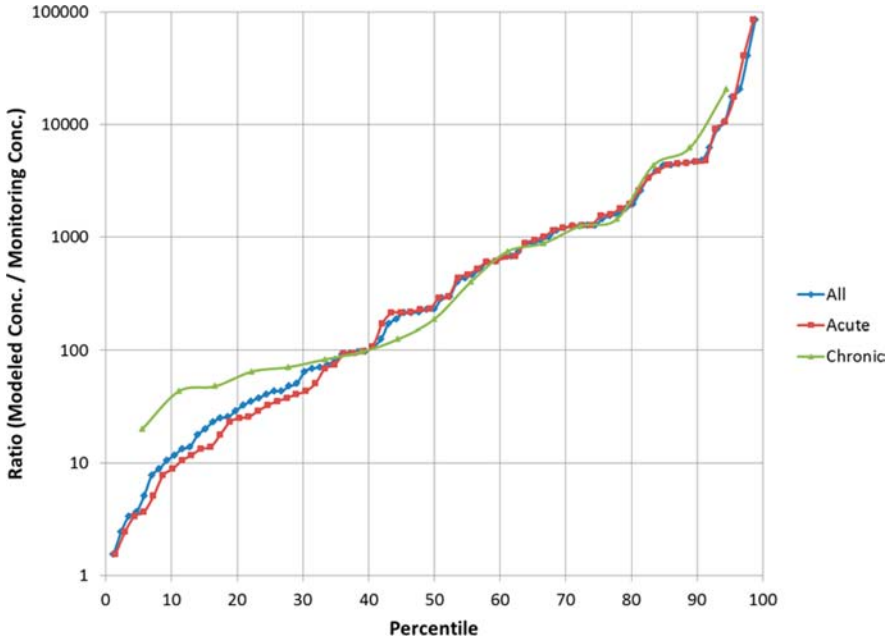

Figure 2. Overprediction ratios of EDWCs for acute, chronic, and all predictions pooled together.

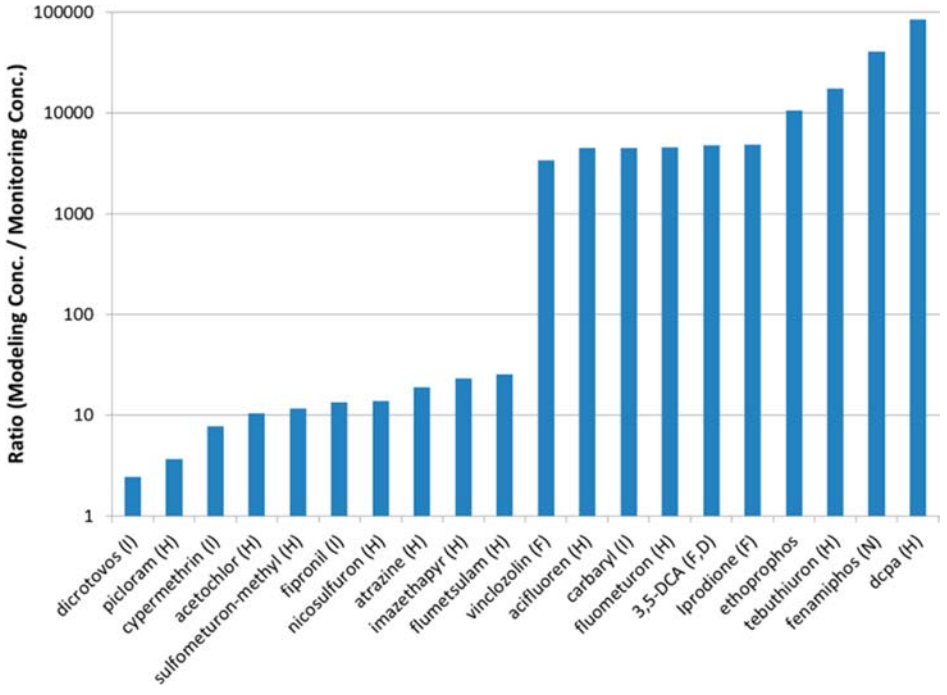

Figure 3. Top 10 and bottom 10 acute overprediction ratios of EDWCs by pesticide.

correlation between lower use pesticides and higher overprediction ratios.

Factors Affecting Model Comparisons with Monitoring Data. It must be acknowledged that the comparisons between the modeled EDWCs and monitoring data are not, and cannot be, absolutely equivalent comparisons, as the regulatory modeling was not conducted on a site-specific basis under monitoring watershed conditions (e.g., specific weather or soil characteristics). They were run under the generic Index Reservoir standard setting. One aspect of the monitoring data sets that is different than the modeling data is the sampling interval. The modeling data EDWCs are based on daily predictions, whereas the monitoring data sets are based on different prescribed sampling intervals. As has been discussed, the data sets cited in this paper all had annual sampling frequency in the range of once every 3-days to biweekly samples during the high runoff season. Although these nondaily sampling frequencies might have missed the true maximum concentration in a particular year, the annual mean (chronic end point) and/or the 90th percentiles (acute) concentrations over the many sites and years (up to 20 years) should provide sufficient statistical power for estimating these end points based on Crawford[15] and Mosquin et al.[16] Recall that Crawford[15] found that seven samples per year was sufficient to estimate median annual concentrations for larger watersheds, and 95th percentile annual maximum concentrations could be con-

dx.doi.org/10.1021/jf4036996 | J. Agric. Food Chem. 2014, 62, 348−359

fidently estimated with ten samples per month (every three days) during the runoff season. The sampling frequency in the monitoring studies contained in this report all exceeded the frequency required for estimates of annual mean concentrations (chronic), and several met or approached the frequency required to estimate the 95th percentile annual concentration (a level requiring more frequent sampling than the standard 90th percentile annual acute concentration). In addition, research concerning the bias factors between the true peak concentrations and peak concentrations[17,18] inferred from a nondaily sampling scheme indicated a weekly based sampling scheme could likely underestimate peak concentrations by a factor of 2.4 on average, whereas a 28-day sampling scheme could underestimate peak concentrations by a factor of 8.35 on average. The monitoring programs evaluated in the comparisons contained in this study included targeted monitoring (designed to sample high vulnerability sites), with weekly or sometimes more frequent sampling (sampling information is provided as footnotes associated with each data table and earlier in the text). A monitoring bias factor of around 3x is very small compared to the median model overprediction of 280x reported in the studies evaluated here.

A second aspect of the modeling data that differs from the monitoring data is the length of the model simulation compared to the monitoring sampling period. Model simulations for Tier 2 regulatory modeling are run for 30 years in order to account for climate variability. Although some of the monitoring data sets included in this study included longer periods of record (>10 years), such as some sources included in Echeverria et al.,[7] many were based on durations of two to three years.[19−24] If these monitoring studies were each considering only a single site, one might conclude that the shorter duration of the monitoring data would be expected to show potentially lower peak pesticide concentrations compared to a model simulation representative of a 30-year weather time series (with greater extremes). In the case of the studies presented in this report, this conclusion would not be valid, because all of the studies evaluated multiple sites throughout the monitoring period, effectively multiplying the number of sample years by the number of sites. For example, in the Jones study,[19] individual pesticide monitoring ranged from five sites for three years (15 effective site-years) to 28 sites for three years (56 effective site-years). The USGS targeted reservoir monitoring program,[25] which was used in model comparisons in several studies,[20,21] intensively monitored 12 sites for two years (24 effective site-years). By including multiple sites monitoring for the same pesticide, the potential for a low bias in the monitoring data due to having less climate variability than a 30-year modeling period is likely to be low. This can also be supported by the statistical work of Crawford[15] and Mosquin et al.,[16] who have shown that nondaily sampling data sets over many sites and years (up to 20 years in our cited data) should provide sufficient statistical power for estimating the annual mean (chronic end point) and/or the 90th (acute) concentrations. Recall that Mosquin et al.[16] found that an effective sample size of 212 is sufficient to estimate the 95th percentile concentrations with a relative error of 30% or less for a target population of monitoring. As can be seen in reviewing Tables 2−6, the total number of samples per pesticide used to compare with model results ranged from a minimum of 263 samples for ethoprophos (Table 2) to 23,736 samples in the case of the NAWQA atrazine data (Table 3), with most pesticides having greater than 500 samples. These findings suggest that the sample sizes in the monitoring data sets evaluated in this study are large enough to allow meaningful estimation of both chronic (annual mean) and acute (90th percentile) concentrations.

Framework for More Accurate Modeling of Drinking Water Exposures. This study included comparisons of modeling results generated by using standard EPA regulatory practices with monitoring data dating back to 2002,[21] continuing up through a comprehensive assessment compiled by the US EPA using that latest parametrization methodology.[7] Each of these studies concludes that, to varying degrees, the regulatory modeling approach overpredicts drinking water EDWCs. While overprediction by the modeling approach is consistent with the regulatory objective of protecting human health, the degree of overprediction identified in this study (median of nearly 280×) suggests that for most pesticides the current modeling approach may have unrealistically predicted a higher potential health risk than actually exists. Evaluation of the current modeling approach is thus warranted, including a critical review of the inputs and assumptions in the current approach that are responsible for the significant overprediction of EDWCs.

Many of the assumptions leading to the large overpredictions have been identified by the authors of previous publications on the subject. Hertl et al.[21] mention several factors leading to the overprediction, foremost among them being the overrepresentation of pesticide use in the Index Reservoir watershed. Even though a PCA adjustment factor is applied to lower the effective fraction of the Index Reservoir watershed receiving pesticide application, this PCA is based on a conservative estimate of crop extent and does not take into consideration information on actual pesticide use. The assumption that 100% of a given crop is applied across the whole watershed with the same pesticide under consideration at the maximum labeled rate (as is the assumption in regulatory modeling) is never true in reality, and for many pesticides with small market share, it is a gross overestimate of actual use. Hertl et al.[21] goes on to mention issues associated with the appropriateness of the PRZM/EXAMS model scale compared to the scale it is being used to simulate. PRZM is a single field model which is being used to simulate the hydrochemical behavior of a heterogeneous watershed. The PRZM model cannot account for watershed scale attenuation and the effects of interaction between adjacent landscape units (such as vegetated and/or riparian buffers) which have been shown to significantly reduce off-field transport of pesticides.[27] Furthermore, the issue of scale is a key factor in the assumptions of pesticide spray drift contributions to EDWCs in the index reservoir modeling scenario, which assumes that all treated fields are adjacent to water bodies contributing to the reservoir and that those water bodies are always downwind of the field treated with pesticide; an assumption that is physically an impossibility. Other factors contributing to the regulatory modeling overprediction include the compounding of conservative assumptions such as the following: selection of only a single representative but runoff vulnerable soil and the interpretation of product labels assuming the maximum rates at the minimum intervals to all fields within a watershed on the same day. The chemical specific environmental fate parameters chosen as inputs to the models are selected with each parameter individually representing the upper 90th of sample values for that parameter's data set. Collectively, however, combining these parameter values creates a vulnerability scenario much higher

than the 90th. Other authors[19,20] have identified similar factors contributing to regulatory model overprediction, with Jackson et al.[20] proposing a correction factor based on the total pesticide applied in the model simulation.

The authors of this paper support the suggestions by previous authors on the subject regarding the causes for overprediction in the regulatory modeling approach that are most responsible for model overprediction. There are several other factors that deserve mentioning and reinforcement. First, as stated in the Introduction, the Index Reservoir scenario is based on CWS with a very low drainage area to normal capacity ratio (DA/NC), and according to the EPA,[5] 90% of surface drinking water reservoirs will have higher DA/NC ratios. This issue of CWS watershed characteristics becomes even more relevant in the context of drinking water supplies located along flowing water bodies, where the characteristics of pesticide concentrations are very different than static water supply reservoirs. The use of a high vulnerability static water body to represent pesticide exposure potential in a broad range of both static and flowing water bodies does not capture the variability in these types of drinking water supplies. Second, while the overrepresentation of pesticide use has already been discussed, another related problem is the implicit assumption that all fields in a watershed receive the pesticide application at the same time. This assumption is inappropriate for even the smallest sized watersheds that can support an adequate drinking water supply (such as the 172.8 ha Shipman Reservoir) and has greater invalidity as the size of the CWS watershed increases and the variability of agronomic practices of multiple farms contributes to a broad range in pesticide application dates. Accounting for the variability in application timing when modeling pesticide fate and transport at the watershed scale has been shown to have a significant effect on predicted concentrations in flowing water bodies.[28,29] We have discussed the many factors that are contributing to the unrealistically high estimates of drinking water concentrations of pesticides using the current regulatory modeling approach. Refined approaches to applying the current Tier 2 models, as well as methods for applying alternative models, already exist and have shown promise in their ability to accurately predict pesticide residues in surface water.

These alternative modeling approaches include both newly developed tools as well as models with a longer history. The US EPA is currently working on developing updated modeling tools, such as the Surface Water Calculator (Young, 2013)[30] and the Spatial Aquatic Model,[31] that may be able to address some of the shortcomings of the current modeling approach. The Surface Water Calculator (SWC) is expected to include a replacement to the EXAMS receiving water model called the Variable Volume Water Model (VVWM) which will allow for simulation of dynamic water volumes and a wider range in hydrologic conditions. The Spatial Aquatic Model (SAM) is being designed to simulate both static and flowing water bodies draining a watershed with heterogeneous land use and soils. In addition to US EPA efforts to improve the accepted regulatory modeling tools, several other models reported in the scientific literature have been shown to perform well at the prediction of pesticides in complex watersheds that are typical of surface drinking water systems. The United States Geological Survey Watershed Regressions for Pesticides (WARP) model[32] was designed to predict annual atrazine concentration percentiles in flowing water bodies across the US. The WARP model was shown by both Jones[19] and Jackson et al.[22] to predict pesticide concentrations closer to monitoring data than the standard Index Reservoir modeling method. The WARP model was originally developed based on a statistical analysis of atrazine monitoring data and has since been adopted for use with other pesticides through incorporation of a surface water mobility index.[33] The strength of the WARP model is that it was built on robust monitoring data sets; however, because it is not physically based, it is unable to provide important functions such as the simulation of alternative Best Management Practices. This model also has limited testing on pesticides for target crops with a smaller geographic extent than corn.

Promising opportunities for developing a modeling approach that addresses the shortcomings in the current regulatory modeling method reside in the application of exiting watershed scale models that have a proven ability to accurately represent the hydrochemical processes that are necessary for pesticide fate and transport prediction. These tools could easily work into the current regulatory process as a higher tier refinement and could be utilized to simulate either additional representative scenarios or individual drinking water−watersheds of specific concern. One of the most widely used watershed scale models is the Soil and Water Assessment Tool (SWAT) developed and maintained by the United States Department of Agriculture.[34] SWAT is a watershed-scale, continuous, physically based, semidistributed model that has been used in a broad range of hydrologic and water quality applications.[35] One of SWAT's strengths is its ability to simulate the water quality impact of alternative management practices, including tillage practices, buffers and grassed waterways, and pesticide application practices. The use of the SWAT model in the simulation of pesticide transport at the watershed scale has been reported in the literature since at least 2005, and SWAT was recently selected from a pool of 36 models as one of the most appropriate for watershed-scale simulation of pesticides.[36] Pesticide transport modeling with SWAT has included assessments of pesticides in both static and flowing water bodies. Winchell et al.[28] and Peranginangin et al.[37] developed and evaluated a SWAT modeling methodology which focused on identifying a parametrization approach that takes advantage of intelligent use of data in place of extensive site-specific calibration for use in aquatic pesticide concentration predictions in complex watersheds. Another watershed-scale modeling approach based on the PRZM model is the PRZM-Hybrid modeling method described by Snyder et al.[38] and in reports by Miller and colleagues.[29,39] The PRZM-Hybrid approach utilizes spatially explicit high-resolution NEXRAD radar rainfall data, additional meteorology data, field-scale soil properties from the US national SSURGO database, and spatially explicit land use data as input data to model daily watershed runoff concentrations. Both the SWAT and PRZM-Hybrid models are designed for simulation of complex, spatially heterogeneous watersheds and could be readily adapted to serve the purposes of modeling EDWCs for the purposes of human exposure risk assessments. In order for either of these models to generate accurate pesticide concentration predictions when compared to monitoring data, a good understanding of pesticide use information needs to be incorporated. If used in a regulatory context, the models have the ability to represent more complex and realistic hydrology, soil, weather, and application technologies than is possible with the models currently used by EPA. USEPA scientists and pesticide registrants have evaluated the use of watershed modeling

approaches in the past,[40] and because many of the tools have matured, a similar effort should be explored again.

Regardless of the model platform, achieving more realistic model predictions of EDWCs will require incorporating accurate assumptions on pesticide use intensity (i.e., pounds of pesticide per acre of watershed) into the regulatory modeling framework. The current assumption that any pesticide evaluated is applied to 100% of the maximum possible extent defined by its label is overly conservative for even the most widely used pesticides. This implausible assumption is the driving factor leading to the common occurrence of 3 to 5 orders of magnitude model overpredictions of EDWCs that were shown in Figure 2. Strong evidence to support the incorporation of realistic pesticide use assumptions in watershed scale modeling is found in recent studies where WARP (which explicitly accounts for pesticide use intensity) was shown to much more closely match monitoring data than the current regulatory modeling approach.[19,22] Information and techniques similar to those used by the USGS in their recently released national pesticide use maps[41] could serve as the foundation for more realistic use estimates but may require additional scale adjustments to be representative of small watersheds.

The data compiled in this paper represents the most complete collection to date of pesticide modeling and monitoring data. The accuracy of the concentration predictions made by the current regulatory modeling approach was shown to be poor, with significant overprediction common. Some of the primary reasons for this overprediction were discussed, including the regulatory modeling assumptions of pesticide use, a lack of application timing variability, reservoir and watershed geometry, and missing spatial heterogeneity of the watershed. In order for many of these shortcomings to be addressed, a watershed scale modeling approach will need to be adopted and databases of more accurate pesticide use information will need to be compiled. Several existing watershed modeling approaches were proposed, each of which has already shown promise in predicting pesticide concentrations in watersheds of similar size and complexity to typical CWS watersheds. A suggested next step is to take a closer look at several of the watershed scale models introduced in this discussion and determine which ones best fit the needs of regulatory modeling and result in more accurate predictions of EDWCs.

AUTHOR INFORMATION

Corresponding Author

*Phone: 802-229-1882. Fax: 802-229-5417. E-mail: mwinchell@stone-env.com.

Notes

The authors declare no competing financial interest.

REFERENCES

(1) USEPA. 2007, About Water Models—Water Exposure Models Used by the Office of Pesticide Programs, Available at http://www.epa.gov/oppefed1/models/water/models4.htm (Accessed November 20, 2013).

(2) Suarez, L. A. *PRZM-3, A Model for Predicting Pesticide and Nitrogen Fate in Crop Root and Unsaturated Zones: Users Manual for Release 3.12.3*; EPA/600/R-05/111 (NTIS PB2006-101105); National Exposure Research Laboratory, U.S. Environmental Protection Agency: Washington, DC, 2005; p 426.

(3) Burns, L. *Selected water supply reservoirs and finished drinking water 1999−2000: Summary of results from a pilot monitoring program*; United States Environmental Protection Agency: Sacramento, CA, 2004; Publication 01-456.

(4) ECOFRAM. ECOFRAM Aquatic Report, Ecological Committee on FIFRA Risk Assessment Methods (ECOFRAM). US Environmental Protection Agency: Washington, DC, 1999.

(5) Jones, R. D.; Abel, S.; Effland, W.; Matzner, R.; Parker, R. An Index Reservoir for Use in Assessing Drinking Water Exposure. Chapter IV in Proposed Methods for Basin Scale Estimation of Pesticide Concentrations in Flowing Water and Reservoirs for Tolerance Reassessment. Presentation given at the FIFRA Science Advisory Panel; Washington, DC, 1998.

(6) Jones, R. D.; Costello, K.; Hetrick, J. A.; Parker, R. D.; Thurman, N.; Peck, C. *Development and Use of the Index Reservoir in Drinking Water Exposure Assessments*; Office of Pesticide Programs, Environmental Protection Agency: Washington, DC, 2010.

(7) Echeverria, M.; Jones, R. D.; Peck, C.; Ruhman, M.; Shelby, A.; Thawley, S.; Thurman, N. *Development and Use of Percent Cropped Area and Percent Turf Area Adjustment Factors in Drinking Water Exposure Assessments: 2012 Update*; Office of Pesticide Programs, US Environmental Protection Agency: Washington, DC, 2012.

(8) OPP. 2010. *Development and Use of Percent Cropped Area Adjustment Factors in Drinking Water Exposure Assessments. Environmental Fate and Effects Division. September 9, 2010.*

(9) Dubus, I. G.; Brown, C. D.; Beulke, S. Sources of uncertainty in pesticide fate modeling. In *Pesticide Behavior in Soils and Water: BCPC Symposium Proceedings No. 78*; British Crop Protection Council: Farnham, UK, 2001; pp 239−244.

(10) Havens, P. L.; Carbone, J. P.; Warren-Hicks, W.; Fouch, M. A. Development of a Monte Carlo sampling shell for the pesticide root zone model and its application by the Federal Insecticide, Fungicide, and Rodenticide Act Environmental Modeling Validation Task Force. *Environ. Toxicol. Chem.* **2002**, *21*, 1566−1569.

(11) Carbone, J. P.; Havens, P. L.; Warren-Hicks, W. Validation of pesticide root zone model 3.12: Employing uncertainty analysis. *Environ. Toxicol. Chem.* **2002**, *21*, 1578−1590.

(12) Cryer, S. A.; Applequist, G. E. Direct treatment of uncertainty. Part II—Applications in pesticide runoff, leaching and spray drift exposure modeling. *Environ. Eng. Sci.* **2003**, *20*, 169−181.

(13) Harmel, R. D.; Smith, P. K. Consideration of Measurement Uncertainty in the Evaluation of Goodness-of-fit in Hydrologic and Water Quality Modeling. *J. Hydrol.* **2007**, *337*, 326−336.

(14) Harmel, R. D.; Smith, D. R.; King, K. W.; Slade, R. M. Estimating storm discharge and water quality data uncertainty: A software tool for monitoring and modeling applications. *Environ. Model. Software* **2009**, *24*, 832−842.

(15) Crawford, C. G. Sampling strategies for estimating acute and chronic exposures of pesticides in streams. *J. Am. Water Resour. Assoc.* **2004**, *40*, 485.

(16) Mosquin, P.; Whitmore, R. W.; Chen, W. Estimation of Upper Centile Concentrations Using Historical Atrazine Monitoring Data from Community Water Systems. *J. Environ. Qual.* **2012**, *41*, 834.

(17) Hetrick, J. A. Development and Use of Bias Factors. Presentation given at the CLA and Rise Spring Conference, Crystal City, CA, 2013.

(18) Chen, W.; Mosquin, P.; Truman, C. C. Sampling Bias Factors: Compensation for "Missing the Peak. Presentation given at the CLA and Rise Spring Conference. Crystal City, CA, 2013.

(19) Jones, R. L. Comparison of regulatory estimates of drinking water concentrations with monitoring data. *J. Agric. Food Chem.* **2005**, *53*, 8835−9.

(20) Jackson, S.; Hendley, P.; Jones, R.; Poletika, N.; Russell, M. Comparison of regulatory method estimated drinking water exposure concentrations with monitoring results from surface drinking water supplies. *J. Agric. Food Chem.* **2005**, *53*, 8840−8847.

(21) Hertl, P.; Gustafson, D. I.; Jackson, S. H.; Jones, R. L.; Russell, M. H.; Schocken, M. J. A Comparison of US EPA's Tier 1 and 2 Index Reservoir Model Estimates to Drinking Water Reservoir Monitoring Results in Selected US Systems in 1999/2000. Poster 5c.05 presented

at the 10th International Congress Pesticide Chemistry, Basel, August 2002. In *Book of Abstracts*; Basel, Switzerland, 2002; Vol. 2, p 125.
(22) Jackson, S. H.; Jones, J. J.; Hanzas, J. Comparison of Regulatory Method Estimated Drinking Water Exposure Concentrations with Monitoring Results from Surface Water Drinking Supplies. In *Pesticide Exposure Assessment and Predictive Modeling Tools*; ACS Symposium Series; American Chemical Society: Washington, DC, 2010; Vol. *1028*, pp 71−95.
(23) Nandihalli, U. B.; Jones, R. L.; Allen, R.; Ramanarayanan, T. S.; Sabbagh, G. J. Surface Drinking Water Assessment and Monitoring for Oxadiazon Herbicide on Golf Courses. In *Turf Grass: Pesticide Exposure Assessment and Predictive Modeling Tools*; ACS Symposium Series; 2010; pp 57−69.
(24) Jones, R. D. Measuring and Estimating Concentrations of Pesticides in Drinking Water: A Historical Perspective. Presentation given at the EPA Exposure Modeling Public Meeting; Washington, DC, 2012.
(25) Blomquist, J. D.; Denis, J. M.; Cowles, J. L.; Hetrick, J. A.; Jones, R. D.; Birchfield, N. B. *Pesticides in selected water-supply reservoirs and finished drinking water, 1999−2000: Summary of results from a pilot monitoring program*; Publication 01-456; U.S. Dept. of the Interior, U.S. Geological Survey: Baltimore, MD, 2001; p 65.
(26) Grube, A.; Donaldon, D.; Kiely, T.; Wu, L. *Pesticides Industry Sales and Usage: 2006 and 2007 Market Estimates*; Biological and Economic Analysis Division, Office of Pesticide Programs, Office of Chemical Safety and Pollution Prevention, U.S. Environmental Protection Agency: Washington, DC, 2011.
(27) United States Department of Agriculture (USDA). *Conservation Buffers to Reduce Pesticide Losses*; USDA Natural Resources Conservation Service: Washington, DC, 2000; p 21.
(28) Winchell, M.; Peranginangin, N.; Srinivasan, R. A Comparison of SWAT Pesticide Simulations Based on Different Input Resolutions Using a Minimal Calibration Approach. Presentation at the International SWAT Conference, Toledo, Spain, 2011.
(29) Miller, P. S.; Northcott, W. J.; Andrus, J. M.; Harbourt, C. M.; Hendley, P. *PRZM-Hybrid Modeling System Utilizing an Agronomic Approach to Define Watershed Scale Chemical Applications*; Syngenta Task No. TK0023394; Syngenta: Wilmington, DE, 2012.
(30) Young, D. F. Surface Water Calculator. Presentation given at the EPA Exposure Modeling Public Meeting; Washington, DC, 2013.
(31) Thurman, N. Spatial Aquatic Model (SAM) Pilot Project. Presentation given at the EPA Exposure Modeling Public Meeting; Washington, DC, 2013.
(32) Larson, S. J.; Crawford, C. G.; Gilliom, R. J., Development and application of Watershed Regressions for Pesticides (WARP) for estimating atrazine concentration distributions in streams; *U.S. Geological Survey Water-Resources Investigations Report 03-4047*; 2004; p 68.
(33) Chen, W.; Hertl, P.; Chen, S.; Tierney, D. P. A pesticide surface water mobility index and its relationship with concentrations in agricultural drainage watersheds. *Environ. Toxicol. Chem.* **2002**, *21*, 298−308.
(34) Arnold, J. G.; Srinivasan, R.; Muttiah, R. S.; Williams, J. R. Large-area hydrologic modeling and assessment. Part I. Model development. *J. Am. Water Resour. Assoc.* **1998**, *34*, 73−89.
(35) Gassman, P. W.; Reyes, M. R.; Green, C. H.; Arnold, J. G. The Soil and Water Assessment Tool: Historical development, applications, and future research directions. *Trans. ASABE* **2007**, *50*, 1211−1240.
(36) Quilbe, R.; Rousseau, P.; Lafrance, P.; Leclerc, J.; Amrani, M. Selecting a Pesticide Fate Model at the Watershed Scale Using a Multi-criteria Analysis. *Water Qual. Res. J. Canada* **2006**, *41*, 283−295.
(37) Peranginangin, N.; Winchell, M.; Folle, S. Evaluation of a Simplified SWAT Model Approach for Prediction of Insecticide Concentrations in a Small Watershed in Northwestern Oregon. Presentation given at the 244th ACS National Meeting & Exposition; American Chemical Society: Philadelphia, PA, 2012.
(38) Snyder, N. J.; Harbourt, C. M.; Miller, P. S.; Trask, J. R.; Hendley, P.; Johnston, E. A. *Analysis of Chemograph Behavior Between Grab Samples - Measurement and Hybrid PRZM Approaches*; Syngenta Task No. T001508-03; Syngenta: Wilmington, DE, 2007.
(39) Miller, P. S.; Northcott, W. J.; Andrus, J. M.; Zwilling, L. F.; Cheplick, J. M.; Harbourt, C. M.; Hendley, P. *Development of the PRZM-Hybrid Watershed Exposure Modeling System Methodology Report*; Syngenta Task No. TK0023394; Syngenta: Wilmington, DE, 2011.
(40) Parker, R.; Arnold, J. G.; Barrett, M.; Burns, L.; Carrubba, L.; Neitsch, S. L.; Snyder, N. J.; Srinivasan, R. Evaluation of Three Watershed-Scale Pesticide Environmental Transport and Fate Models. *J. Am. Water Resour. Assoc.* **2007**, *43*, 1424−1443.
(41) Stone, W. W. *Estimated annual agricultural pesticide use for counties of the conterminous United States, 1992−2009*; U.S. Geological Survey Data Series 752; Pamphlet; United States Geological Survey: Washington, DC, 2013; p 1.

JOURNAL OF AGRICULTURAL AND FOOD CHEMISTRY

Article

pubs.acs.org/JAFC

Enantioselective Determination of Triazole Fungicide Epoxiconazole Bioaccumulation in Tubifex Based on HPLC-MS/MS

Chunxiao Liu,[†] Bo Wang,[†] Peng Xu,[§] Tiantian Liu,[†] Shanshan Di,[†] and Jinling Diao*[,†]

[†]Department of Applied Chemistry, China Agricultural University, Yuanmingyuan West Road 2, Beijing 100193, China

[§]Research Center for Eco-Environmental Sciences, Chinese Academy of Sciences, Shuangqing Road 18, Beijing 100085, China

ABSTRACT: In this study, the enantioselective bioaccumulation of epoxiconazole enantiomers in tubifex (Oligochaeta, Tubificida) was investigated in two uptake pathways. A sensitive and rapid chiral method was developed for the determination of epoxiconazole enantiomers in tubifex and soil based on high-performance liquid chromatography coupled with triple-quadrupole mass spectrometry (HPLC-MS/MS). In the spiked-water or spiked-soil treatments, enantioselective bioaccumulation of epoxiconazole in tubifex was obersved. For spiked-water treatment, (−)-epoxiconazole accumulated in tubifex to a greater extent than (+)-epoxiconazole, leading to enrichments with a composition (−) > (+). However, for spiked-soil treatment, the enantioselectivity in tubifex was reversed with a preferential accumulation of (+)-epoxiconazole. Calculated accumulation factors (AFs) indicated that epoxiconazole in spiked-water treatment had higher bioaccumulation potential than that in spiked-soil treatment. The results from the spiked-soil treatment also revealed that the dissipation of epoxiconazole in soil was enantioselective, and tubifex has positive effects on epoxiconazole diffusion from soil to overlying water.

KEYWORDS: *epoxiconazole, tubifex, enantioselectivity, bioaccumulation*

INTRODUCTION

Epoxiconazole is a broad-spectrum triazole fungicide and extensively used worldwide to control diseases caused by fungi, such as Ascomycetes, Basidiomycetes, and Deuteromycetes, in cereals, sugar beet, peanuts, oilseed rape, apple, and ornamentals.[1] It is also used to regulate plant growth by acting as an inhibitor of C-14 demethylase in sterol biosynthesis. Epoxiconazole also plays an important role in the formation of ergosterol, a component of fungal cell membrane.[2] This fungicide, which is widely used on wheat, sugar beet, triticale, barley, and oat,[3] persists in soil and aquatic sediment.[4,5] Hence, epoxiconazole in sediment may lead to serious noxious effects on benthic organisms that use sediment as food resources and living environments. After prolonged repeated applications, epoxiconazole could enter into fresh-water circulations. Therefore, the influence of epoxiconazole on the aquatic ecosystem should be investigated.

Epoxiconazole, *cis*-1-{[3-(2-chlorophenyl)-2-(4-fluorophenyl)oxiranyl]ethyl}-1*H*-1,2,4-triazole, was first produced by BASF Corp. in 1993.[6] It consists of two chiral centers in its molecular structure and therefore presents two diastereoisomers with four stereoisomers. However, present commercial epoxiconazole pesticide contains only a pair of enantiomers with 2*R*,3*S*- and 2*S*, 3*R*-configurations.[7] The chemical structures and molecular weights (MWs) of four epoxiconazole stereoisomers are shown in Figure 1. Thus, epoxiconazole is a member of the chiral pesticide family. Organic pesticides play a crucial role in agricultural protection, and among these pesticides, >25% are chiral compounds with at least two mirror-image enantiomers.[8] However, most of the currently used chiral pesticides are produced and released into the environment as racemates. Theoretically, enantiomers have identical physical and chemical properties, as well as abiotic degradation rates,[9] whereas their individual toxicities, biological activities, and microbial degradation rates have been shown to differ.[9−13] Thus, the mechanism, exposure, and effect of each enantiomer should be evaluated when the risk of chiral pesticides to human and wildlife populations is assessed.[13] This necessity has led to extensive research on the enantioselectivity of chiral compounds. Several studies have

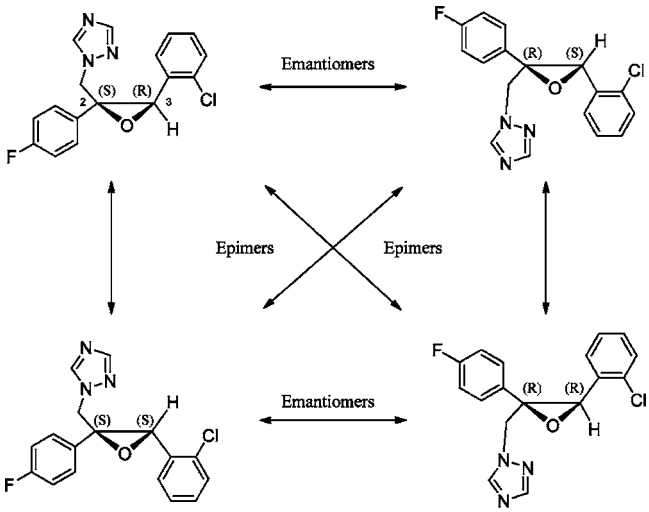

Figure 1. Structures of epoxiconazole stereoisomers. The present commercial product refers to the *cis*-stereoisomers with 2*S*,3*R* and 2*R*,3*S* configurations.

Received: September 9, 2013
Revised: December 13, 2013
Accepted: December 23, 2013
Published: December 23, 2013

ACS Publications © 2013 American Chemical Society

shown that enantiomers of epoxiconazole behave differently during biodegradation in the environment.[14] Liang et al.[6] reported that the dissipation of epoxiconazole enantiomers in grape is enantioselective with relative enrichment of (+)-epoxiconazole, and an enantioselective dissipation also occurred in soil with preferential degradation of the (−)-form under field condition. However, other aspects such as enantioselective bioaccumulation of epoxiconazole in tubifex have not been investigated.

Tubifex is a cosmopolitan freshwater oligochaete (Tubificidea). It forms an important link in aquatic food chains.[15,16] Given their endobenthic lifestyle, this oligochaete is in intimate contact with the solid phase and the pore water of the sediment.[16] In addition, this worm ingests the substrates and utilizes adhering micro-organisms and detrital material.[17,18] Tubifex is widely cultured as a fish food.[19] Therefore, it is prone to transfer sediment-associated contaminants to higher trophic levels. Thus, tubifex plays an important role in the aquatic ecosystem and has been designated as a representative freshwater benthic infauna for aquatic system bioassays. Several studies have chosen tubifex to study bioaccumulation and sediment toxicity.[20−23] However, data on enantioselective bioaccumulation of epoxiconazole enantiomers in *Tubifex tubifex* have not been reported.

The differences in the bioaccumulation behavior of the two enantiomers of epoxiconazole in tubifex were investigated in the present study. Effective methods for the extraction, purification, and detection by high-performance liquid chromatography coupled with triple-quadrupole mass spectrometry (HPLC-MS/MS) have been developed to study epoxiconazole enantiomers in tubifex tissue under laboratory conditions. We compared the effect of two different contamination sources, spiked water and spiked soil, on the bioaccumulation of epoxiconazole. The results showed that bioaccumulations of epoxiconazole were both enantioselective in the two contamination treatments. Additionally, we evaluated the effects of tubifex on the diffusion and dissipation of epoxiconazole.

MATERIALS AND METHODS

Chemicals and Reagents. Reference standards of *rac*-epoxiconazole (98.4%) were purchased from Shanghai Pesticide Research Institute (Shanghai, China). Acetone, formic acid, methanol, *n*-hexane, and ethyl acetate were of analytical grade and purchased from Beijing Chemical Reagent Co. Ltd. (Beijing, China). Acetonitrile was of HPLC grade and purchased from J. T. Baker (Phillipsburg, NJ, USA). The Florisil solid phase extraction (SPE) cartridges (500 mg/6 mL) were obtained from Agela Technologies (Tianjin, China) and conditioned with 5 mL of acetone/*n*-hexane (1:3, v/v) ether before use.

Worms and Soil Collection. *T. tubifex* was obtained from Beijing Xiyuan Flower Market (Beijing, China). The worms were maintained in 2 L plastic tanks containing uncontaminated soil and deionized water at 21 ± 1 °C under 12 h light/12 h darkness. The water was continuously aerated, 75% of which was replaced weekly. The worms were fed TetraMin Flakes (Tetra Werke, Melle, Germany) weekly. For the experiments, adult *T. tubifex* (aged 5−7 weeks) were used. Prior to the introduction of worms into the treatments, tubifex worms were allowed to live in the uncontaminated environment for 1 week to acclimate.

The experimental substrate was terrestrial soil collected from Baiwang Forest National Park northwest of Beijing, China. No detectable epoxiconazole was found at detectable levels in this soil. After the superficial layer of 1−2 cm was removed, the soil was collected to a depth of 10 cm, sieved through a 500 μm mesh, air-dried at room temperature, and stored in the dark until use within a few days. Physicochemical properties of the soil were as follows: organic carbon (OC), 4.28 ± 1.05%; moisture content (MC), 1.37%; clay, 4.31 ± 0.02%; sand, 58.42 ± 0.25%; silt, 37.19 ± 0.22%; and pH, 8.2 ± 0.2.

Soil Handling and Spiking. To disperse the test substance epoxiconazole homogeneously within the 100 g dry weight of soil, we performed a stepwise dilution spike procedure.[24] First, racemic epoxiconazole was dissolved in acetone to make a stock solution at a concentration of 1000 mg/L. Then, 0.1 mL of acetone solution was added dropwise into the dry soil (100 g) while the mixture was continuously mixed manually for approximately 5 min with a stainless steel laboratory spoon, yielding a nominal epoxiconazole concentration of 1 mg/kg_{dwt}. The spiked soil was left in a fume cupboard for >12 h. After complete evaporation of the solvent, the contaminated soil (100 g dry weight) was transferred to a 500 mL beaker and rehydrated with 100 mL of deionized water. The height of the bottom substrate was 2−3 cm, and the overlying water was 2−3 cm. The test vessels were incubated for a 24 h equilibration period. Prior to tubifex addition, four 50 mL samples of wet soil were weighed, dried at room temperature until the weight became stable, and then reweighed to estimate the moisture content.

Bioassay Procedure. To examine the influence of different uptake pathways of epoxiconazole on the total bioaccumulation in tubifex, two types of uptake kinetics were examined resulting from the spiked-water and spiked-soil treatments. The first scenario was designated {+Tub +water}, in which epoxiconazole was accumulated from spiked water. For each individual experiment, acclimated tubifex (10 g) were placed into beakers (21 beakers, 7 sampling points, and triplicates for one sampling point), and the spiking solutions were prepared by adding epoxiconazole dissolved in acetone to deionized water to obtain a final concentration of 1 mg/L. After an exposure period (0.5, 1, 3, 5, 7, 10, and 14 days), the living worms were removed from the beaker, gently passed through a 500 μm sieve to a clean pan, and then washed three times with deionized water. Finally, the peripheral water of the worm samples was dried using absorbent paper, and samples were weighed before storage at −20 °C, and the worm sample for extraction was 5 g. In the present study, only the uptake from the aqueous phase was studied for 14 days of exposure, and this treatment was performed in semistatic conditions with daily water renewal.

The second scenario, which consisted of tubifex, water, and spiked soil, was designated {+Tub+soil}, in which epoxiconazole was accumulated from overlying water, pore water, and ingestion of soil particles. Acclimated tubifex (10 g) were added to the test beaker containing unspiked water and spiked soil (21 beakers, 7 sampling points, and triplicates for one sampling point). For the {+Tub+soil} treatment, test organisms, overlying water, and soil were also sampled after an exposure period (1, 3, 5, 7, 10, 14, and 20 days). At each sample point, overlying water was gently poured and initially sampled. Then, the beakers were placed on ice for 2 h, during which the tubifex worms climbed to the soil surface and intertwined slowly together. At this moment, worm aggregation was sampled with forceps and rinsed in deionized water. Water on the surface of the worms was carefully dried by absorbent paper. Soil samples, overlying water, and tubifex sampled from each beaker were weighed and frozen at −20 °C.

To compare with the second scenario, a separate experiment (negative control), which was designated {−Tub+soil}, that used only water and spiked soil, was performed (21 beakers, 7 sampling points, and triplicates for one sampling point). The sampling times were also 1, 3, 5, 7, 10, 14, and 20 days. At these sampling points, overlying water and aliquots of 3.15 g of soil (based on dry weight) were removed from each beaker and transferred into 50 mL plastic centrifuge tube for extraction and analysis.

For the {+Tub+soil} and {−Tub+soil} treatments, the test beakers were weighed daily, and the loss of water resulting from evaporation was compensated for by adding deionized water. All beakers were cultured in a dark environmental chamber, and temperature was controlled to 20 ± 2 °C. The treatment beakers were arranged in a randomized block design.

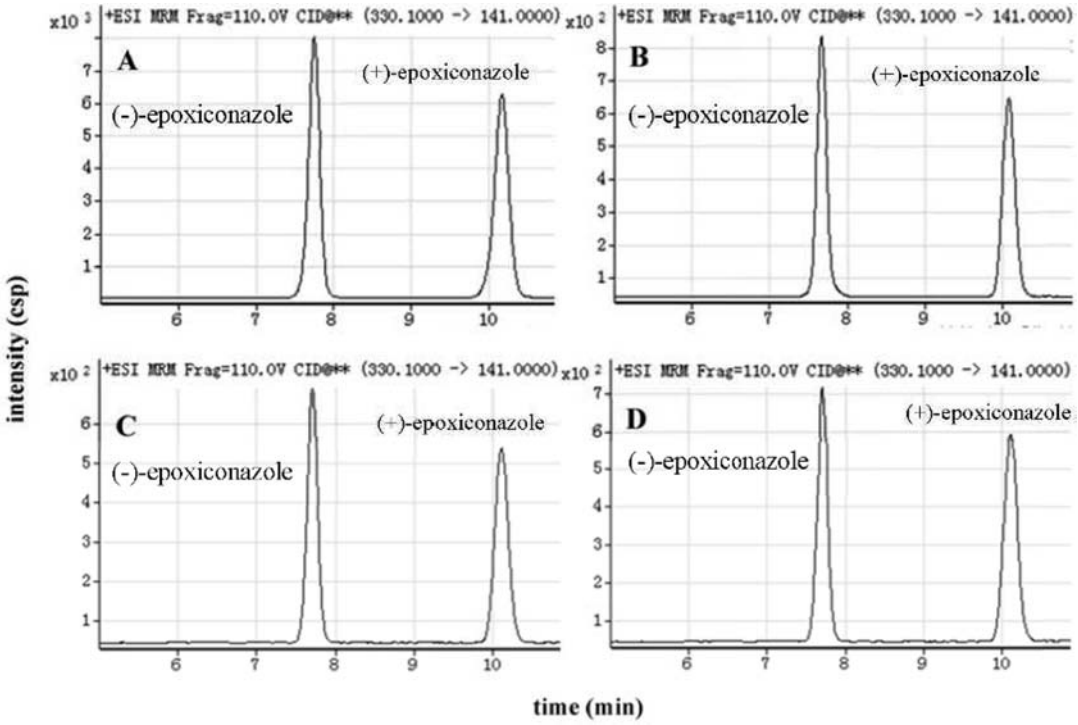

Figure 2. Chromatograms of (A) standard solution at 1 mg/L, (B) overlying water spiked at 0.1 mg/L, (C) soil spiked at 0.1 mg/L, and (D) tubifex spiked at 0.1 mg/L.

Sample Extraction. The water and overlying water samples (5 mL) were extracted by 10 mL of acetone/ethyl acetate (1:3, v/v) in glass separatory funnels after removal of the solid matter by vacuum filtration. This extraction was repeated twice using fresh solvent. The combined solvent phase was filtered through 5 g of anhydrous sodium sulfate for dehydration, transferred to a pear-shaped flask, and then evaporated to dryness at 35 °C by a vacuum rotary vaporator. The dry extract was redissolved to 1 mL with methanol for analysis on HPLC-MS/MS.

The wet soil samples were extracted by acetone/ethyl (1:3, v/v) acetate, and interfering substances were cleaned up by Florisil SPE (500 mg) on a cartridge (6 mL). Briefly, soil samples (5 g wet weight per sample), 20 mL of acetone/ethyl (1:3, v/v) acetate, and 2 g of anhydrous sodium sulfate were added to a 50 mL polypropylene centrifuge tube. The tube was capped, vortex-mixed for 3 min, and centrifuged at 3500 rpm for 5 min. The extract was filtered through 5 g of anhydrous sodium sulfate for dehydration and transferred to a pear-shaped flask. The remaining part was re-extracted following the same extraction step. Then, the combined extract was concentrated to dryness on a vacuum rotary evaporator at 35 °C. The SPE cartridge was preconditioned by elution with 5 mL of acetone followed by 5 mL of *n*-hexane and equilibrated with 10 mL of acetone/*n*-hexane (1:4, v/v). The sample of dry extract was recovered in 3 mL of 20% acetone in *n*-hexane, and then the solution was passed through the SPE cartridge. The cartridge was eluted with an additional 7 mL of acetone/*n*-hexane (1:4, v/v). The eluates were combined with the loading eluates. The combined 10 mL of eluates was collected in a glass tube, evaporated to dryness under a stream of nitrogen, and diluted to 1 mL with methanol after passage through a filter membrane (pore size = 0.45 μm).

The tubifex samples were thawed for about 15 min at room temperature. Then, 20 mL of acetone/ethyl (1:3, v/v) acetate was added to a 50 mL polypropylene centrifuge tube containing 5 g of worms. The mixture was homogenized with an Ultra-Turrax T18 homogenizer for 30 s, vortex-mixed for 5 min, and then separated by centrifugation at 3500 rpm for 5 min. The upper organic phase was passed through a funnel with about 5 g of anhydrous sodium sulfate to a pear-shaped flask. The extraction was repeated two more times. The combined extracts were evaporated to dryness at 35 °C and reconstituted in 5 mL of acetonitrile. Then 5 mL of *n*-hexane was added for liquid−liquid partition to extract most of the lipid, and this procedure was repeated three times. The upper layer of *n*-hexane was discarded, and the acetonitrile layer was evaporated to dryness by a vacuum rotary evaporator. The purification process was similar to that of the soil samples described above.

Chemical Analysis. A chiral liquid chromatograph coupled with a tandem mass spectrometer was used to determine the concentrations of epoxiconazole enantiomers in the samples. The liquid chromatograph was an Agilent 1200 HPLC system equipped with a G1322A degasser, a G1311A quatpump, a G1316B column compartment, a G1329A autosampler, and a 100 μL sample loop. Stereoselective separation was performed on a new highly efficient chiral column [Phenomenex LuxCellulose-1 column, 250 × 4.6 mm (i.d.)] packed with a chiral stationary phase of cellulose tris(3,5-dimethylphenylcarbamate). The mobile phase consisted of a mixture of acetonitrile/water/formic acid (5:95:0.1, v/v/v) at flow rate of 0.5 mL/min. Chromatographic separation was conducted at a temperature of 30 °C. The injection volume was maintained at 5 μL. According to a previous paper,[25] the enantiomeric elution order of epoxiconazole on the Lux Cellulose-1 column was (−)-isomer first and (+)-isomer second with acetonitrile/water as mobile phase at an optical rotation detection wavelength of 426 nm.

An Agilent 6460 triple-quadrupole mass spectrometer equipped with an electrospray ionization source was used for MS/MS analysis (Agilent, USA). The analyses were performed in the positive mode with a 3500 V capillary voltage, 110 V fragmentor, and a 350 °C dry gas temperature. An 11 L/h dry gas flow was used. The nebulizer gas was 99.95% nitrogen with a pressure of 40 psi, and the collision gas was 99.999% nitrogen. The transitions of precursor ion (m/z 330.1) to production (m/z 121 and 141) of epoxiconazole were detected with multiple reaction monitoring (MRM) in positive ion (ESI+) mode. The collision energies for m/z 121 and 141 were 10 and 14 V, respectively, ,and the ion m/z 141 was used for quantification. Masshunter (Agilent, USA) software was used to collect and analyze the data obtained.

The linear regression equations and the correlation coefficients of each stereoisomer were obtained from the peak area ratio plotted

dx.doi.org/10.1021/jf403996g | J. Agric. Food Chem. 2014, 62, 360−367

Table 1. Summary Recoveries for Epoxiconazole Stereoisomers in Overlying Water, Soil and Tubifex

		overlying water		soil		tubifex	
compound	spiked level (mg/kg)	av recovery (%, n = 3)	RSD	av recovery (%, n = 3)	RSD	av recovery (%, n = 3)	RSD
(−)-epoxiconazole	0.05	89.2	4.8	83.6	4.2	84.6	8.3
	0.5	86.0	5.6	80.3	4.9	83.1	4.2
	2.5	88.3	8.2	78.2	6.8	88.5	6.4
(+)-epoxiconazole	0.05	92.4	5.2	81.4	7.8	90.2	5.9
	0.5	89.3	7.6	85.7	6.9	85.8	7.8
	2.5	95.2	9.3	88.2	5.4	88.7	9.6

against its respective concentration (0.01−10 mg/L). Calibration curves were generated by plotting peak area versus the concentration of each enantiomer. The relative standard deviation (RSD) was calculated at the standard range. The standard curves for (−)- and (+)-enationmers showed excellent linearity in the range of 0.01−10 mg/L of each enatiomer (n = 3). For (−)-epoxiconazole, $y = 114043x + 23890$, $R^2 = 0.9973$; for (+)-epoxiconazole, $y = 129131x + 24593$, $R^2 = 0.9963$. The precisions of peak areas at the six concentration levels were also good with RSDs of 0.4−0.8% for (−)-epoxiconazole and 0.1−0.8% for (+)-epoxiconazole.

A series of blank samples fortified *rac*-epoxiconazole at 0.1, 1, and 5 mg/kg were determined immediately after fortification into the overlying water, soil, and tubifex tissue. In this work, the LC-MS/MS method was successfully developed to analyze epoxiconazole stereoisomers in water, soil, and tubifex samples. As shown in Figure 2, two stereoisomers were baseline separated. There were no interference peaks eluted at the same retention times as those of the stereoisomers. Table 1 shows the fortified results of epoxiconazole stereoisomers in water, soil, and tubifex samples. Thus, recovery rates and their standard error were acceptable. The LOQs and LODs for both stereoisomers in overlying water were found to be 0.005 and 0.001 mg/kg, and those in soil and tubifex tissue were both 0.03 and 0.006 mg/kg.

Data Analysis. The enantiomer fraction (EF) was used to measure the enantioselectivity behavior of epoxiconazole in our experiment. The EF values ranged from 0 to 1, with EF = 0.5 representing the racemic mixture. EF was expressed as

$$\mathrm{EF} = \text{peak area of } (-)/[(-) + (+)]$$

where (−) is the first eluted chromatograph peak of (−)-epoxiconazole and (+) is the second eluted peak of (+)-epoxiconazole.

Data presented correspond to mean ± standard deviation of three independent experiments (n = 3). Statistical analysis for the enantioselectivity of epoxiconazole enantiomers was performed using SPSS 18.0. A one-sample t test was used to compare the means of the EF values in tubifex and sediment samples with EF = 0.5. The concentrations and accumulation factors (AFs) of the two enantiomers of epoxiconazole were analyzed using one-way ANOVA, and a pairwise multiple-comparison procedure (S−N−K test) was used to compare results at $P < 0.05$.

RESULTS AND DISCUSSION

Enantioselective Bioaccumulation in Spiked-Water Treatment. For the spiked-water treatment ({+Tub+water}), in which water was the only supply of living environment and the worm can accumulate contamination via a single skin exposure, concentrations of the two enantiomers of epoxiconazole in tubifex tissue were detected. The typical LC-MS/MS chromatograms in tubifex obtained from this treatment at different times are shown in Figure 3A,B. Figure 4 shows the bioaccumulation concentrations of each enantiomer of epoxiconazole in tubifex samples under this treatment. On the seventh day, the concentrations of the two enantiomers reached the highest levels. Then, a significant decrease in concentrations was observed between 7 and 10 days of exposure, which could be the metabolism and excretion of epoxiconazole caused by the self-detoxification of tubifex. At the end of exposure, the concentrations tended toward a steady state. Additionally, Figure 4 also shows a clearly greater bioaccumulation of (−)-epoxiconazole than of (+)-epoxiconazole. The EF values in tubifex tissue were calculated and are shown in Figure 5. A one-sample t test was performed to compare the means of the EF values in tubifex with EF = 0.5, and the result showed that the EF values significantly deviated from 0.5 ($P < 0.005$). Therefore, the bioaccumulation of epoxiconazole in tubifex tissue under this treatment was enantioselective.

In this study, AF was used to express the bioaccumulation of epoxiconazole enantiomers in tubifex tissue. AF is a function of the relative sorptive capacities of the organism versus the surrounding environment. It is often used to compare the body burden of an organism with the degree of contamination in the water. The following definition is used here:

$$\mathrm{AF} = C_{\mathrm{worm}}/C_{\mathrm{water}}$$

C_{worm} and C_{water} are concentrations of epoxiconazole enantiomers in tubifex and water, respectively. The AF value at each sampling point was plotted against time. The AF values of (−)-enantiomer were larger than those of (+)-enantiomer, indicating that the (−)-enantiomer was preferentially accumulated over the (+)-enantiomer in tubifex tissue, and a significant difference was observed between the two enantiomers (Figure 4). Thus, the bioaccumulation of epoxiconazole in tubifex tissue exposure was enantioselective.

Enantioselective Dissipation of Epoxiconazole in Soil. In general, the residues of both enantiomers of epoxiconazole decreased with prolonged time in the {+Tub+soil} and {−Tub +soil} treatments (Figure 6). For worm-free treatment, the dissipation kinetics of (−)-epoxiconazole and (+)-epoxiconazole in soil followed first-order kinetics with $R^2 = 0.96$ and 0.98, respectively. The first-order kinetic equations were $C(t) = 0.4615e^{-0.063t}$ and $C(t) = 0.4781e^{-0.051t}$, respectively, where $C(t)$ was the concentration at time t (days). The corresponding half-life was calculated as $t_{1/2} = \ln 2/k = 0.693/k$, where k is the dissipation rate constant. The (−)-epoxiconazole and (+)-epoxiconazole had half-lives of 11.0 and 13.6 days in soil, respectively, resulting in relative enrichment of the (+)-form in soil (Figure 3C,D). For the worm-present treatment, the dissipation kinetics of (−)-epoxiconazole and (+)-epoxiconazole in soil also followed first-order kinetics with $R^2 = 0.92$ and 0.93, respectively, and the first-order kinetic equations were $C(t) = 0.3854e^{-0.105t}$ and $C(t) = 0.4217e^{-0.079t}$, respectively. The half-lives of (−)- and (+)-epoxiconazole were 6.6 and 9.2 days in soil, respectively, resulting in preferential dissipation of the (−)-form in soil (Figure 3E,F). Therefore, enantioseletive

dx.doi.org/10.1021/jf403996g | J. Agric. Food Chem. 2014, 62, 360−367

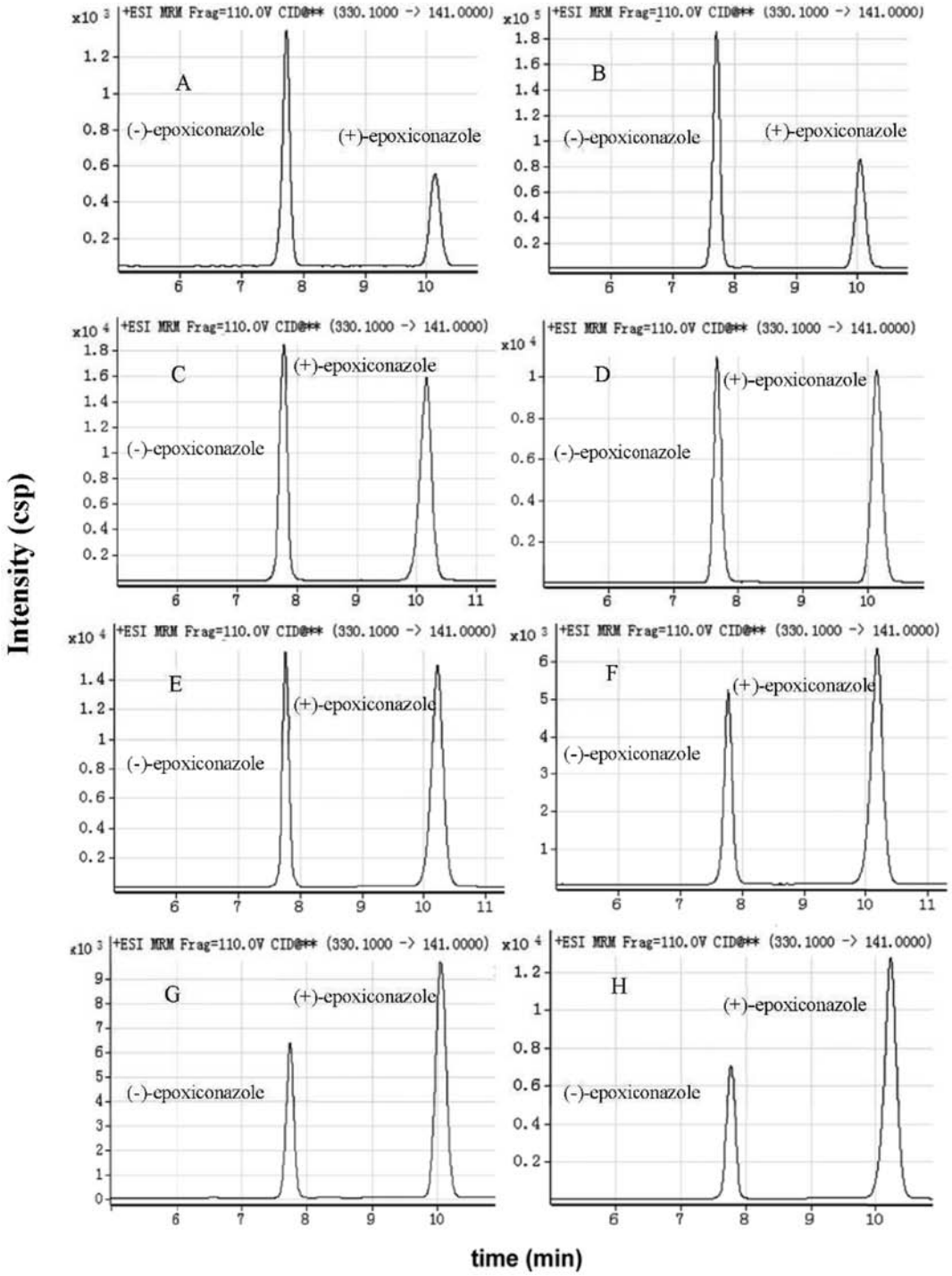

Figure 3. Typical chromatograms of extracts from water in {+Tub+water} treatment after 0.5 days (A) and 7 days (B), extracts from soil in {−Tub +soil} treatment after 1 day (C) and 14 days (D), extracts from soil in {+Tub+soil} treatment after 1 day (E) and 14 days (F), and extracts from tubifex in {+Tub+soil} treatment after 1 day (G) and 14 days (H).

behaviors were detected in the dissipation of the epoxiconazole in soil. During the whole 20-day exposure, the concentrations of the two enantiomers of epoxiconazole in soil under worm-present conditions were lower than those under worm-free conditions. Hence, epoxiconazole had lower persistence in soil with the existence of tubifex. In other words, tubifex could play an important role in remediation of contaminated soil.

Enantioselective Bioaccumulation in Spiked-Soil Treatment. For the {+Tub+soil} treatment, in which soil was the initial contamination source and tubifex can accumulate epoxiconazole via skin and ingestion exposure routes, concentrations of epoxiconazole enantiomers in tubifex tissue, overlying water, and spiked soil were evaluated. Figure 7 shows the bioaccumulation curves of the two enantiomers of epoxiconazole in tubifex tissue. Both concentrations of the two enantiomers of epoxiconazole in tubifex tissue persistently increased from days 1 to 5. After a 5 day decline, concentrations increased again and reached steady state as the duration of exposure increased. A significant difference between the two enantiomers was observed during the whole uptake period. The

dx.doi.org/10.1021/jf403996g | J. Agric. Food Chem. 2014, 62, 360−367

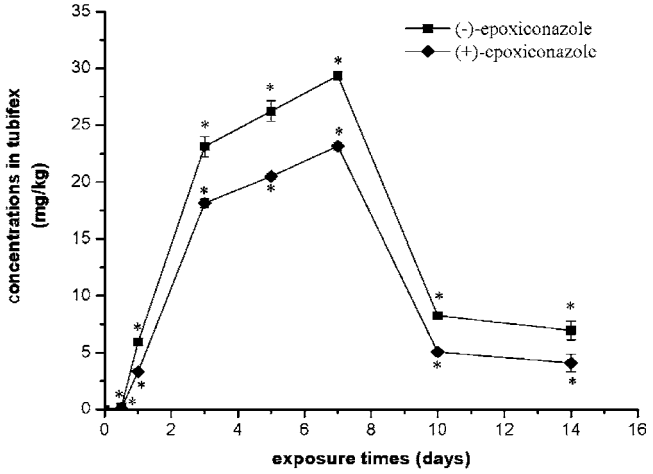

Figure 4. Accumulation curves for epoxiconazole in tubifex tissue in spiked-water treatment (bars are standard error). ∗ indicates significant difference between the two enantiomers at the same time point ($P < 0.05$, S−N−K test).

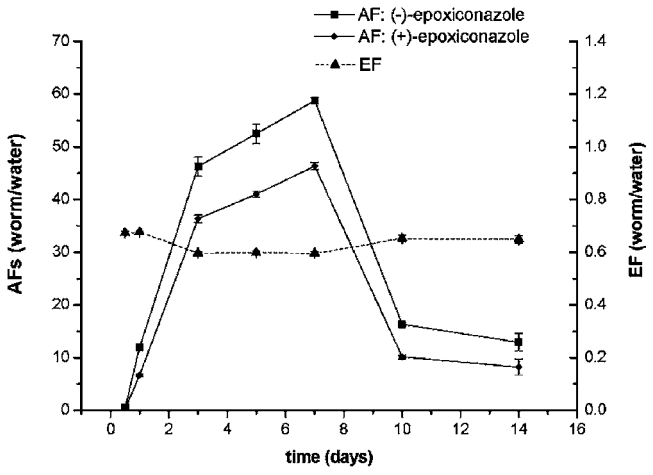

Figure 5. Calculated AF and EF values for epoxiconazole enantiomers in spiked-water treatment (bars are standard error). ∗ indicates significant difference between the two enantiomers at the same time point ($P < 0.05$, S−N−K test).

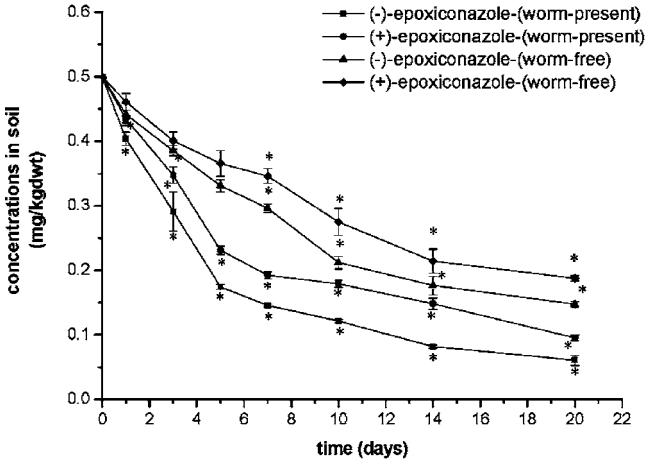

Figure 6. Dissipation curves of epoxiconazole in spiked soil (bars are standard error). ∗ indicates significant difference between the two enantiomers at the same time point ($P < 0.05$, S−N−K test).

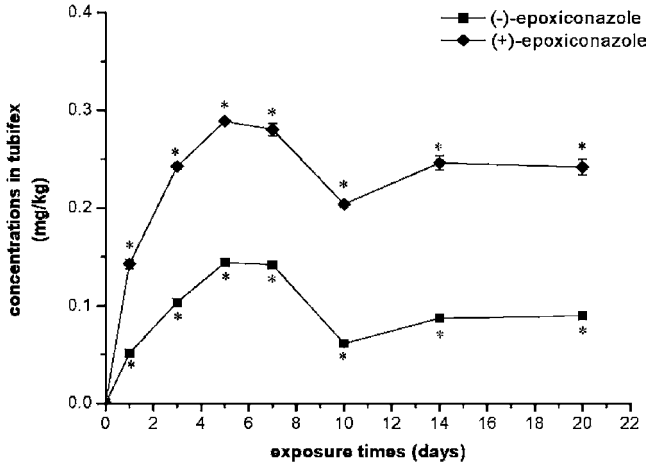

Figure 7. Accumulation curves for epoxiconazole enantiomers in tubifex tissue for spiked-soil treatment (bars are standard error). ∗ indicates significant difference between the two enantiomers at the same time point ($P < 0.05$, S−N−K test).

concentrations of (+)-enantiomer in tubifex tissues were higher than those of (−)-enantiomer, resulting in relative enrichment of the (+)-epoxiconazole (Figure 3G,H). The EF values of epoxiconazole changed with time as shown in Figure 8. A one-

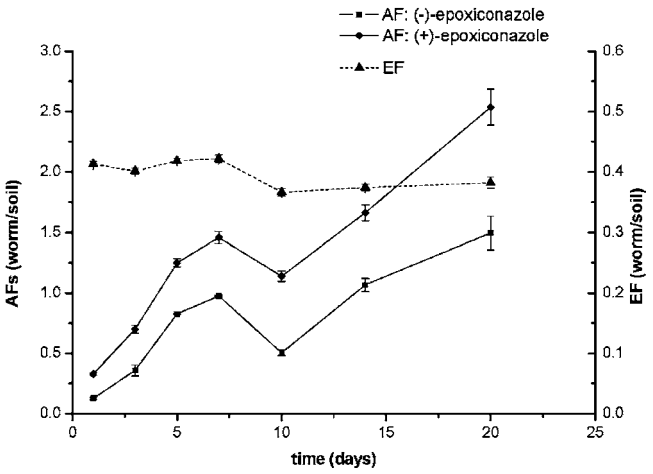

Figure 8. Calculated AF and EF values for epoxiconazole enantiomers in spiked-soil treatment (bars are standard error). ∗ indicates significant difference between the two enantiomers at the same time point ($P < 0.05$, S−N−K test).

sample *t* test between the EF values of epoxiconazole in tubifex and EF = 0.5 yielded a *P* value of 0.001. These results showed that enantioselective bioaccumulation of epoxiconazole in tubifex occurred. For this treatment ({+Tub+soil}), the AF was defined as

$$AF = C_{worm}/C_{soil}$$

where concentrations of epoxiconazole enantiomers in tubifex and soil were expressed as C_{worm} and C_{soil}, respectively. The AF values versus the duration of exposure are plotted in Figure 8. On the basis of the S−N−K test, a significant difference between the AF values of the two enantiomers was observed, and the (+)-enantiomer was preferentially accumulated over the (−)-enantiomer in tubifex tissue. According to Figures 5 and 8, we found that the direction of the enantioselectivity

dx.doi.org/10.1021/jf403996g | J. Agric. Food Chem. 2014, 62, 360−367

varied with incubation conditions. Epoxiconazole was found to be enriched in the (−)-enantiomer in spiked-water treatment. However, enantioselectivity reversal in spiked-soil treatment was observed, resulting in concentrations enriched in (+)-enantiomer. Furthermore, the AF values in spiked-soil treatment were lower than those in spiked-water treatment during the whole exposure period. These interesting phenomena may have resulted from the different uptake pathways of the two treatments. For the spiked-water treatment, the accumulation activities of tubifex are absorbed merely through the epidermis. For spiked-soil treatment, bioaccumulation of epoxiconazole in tubifex may have occurred through ingestion of the soil particles and exposure in overlying water or pore water. Hence, the relative bioaccumulation capacities and bioaccumulation enantioselectivity of epoxiconazole in tubifex are related to the different chiral environments that play a role in the uptake of epoxiconazole.

Influence of Bioturbation. Bioturbation is caused by the activity of animal species living at the surface and/or within the sediment superficial layers.[26,27] Previous studies have investigated the effects of freshwater infaunal invertebrates on sediment transport and solute composition.[27−32] Bioturbation was found to induce a significant release of some xenobiotics from the sediment to the overlying waters. In this study, the concentrations of epoxiconazole enantiomers in overlying water for {+Tub+soil} and {−Tub+soil} treatments were detected. Data from Figure 9 illustrate that the concentrations of

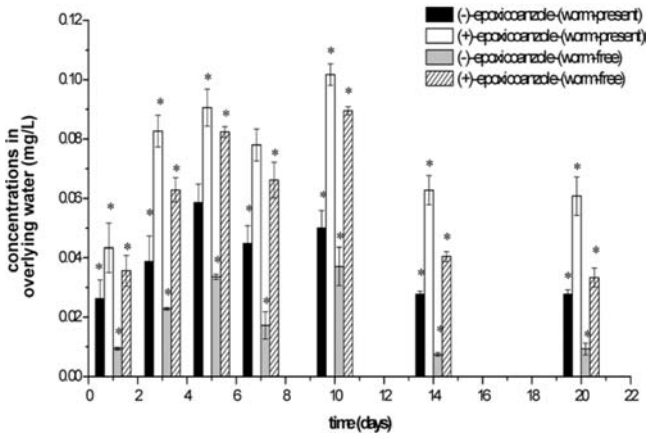

Figure 9. Concentrations of epoxiconazole in the overlying water (bars are standard error). ∗ indicates significant difference between the two enantiomers at the same time point ($P < 0.05$, S−N−K test).

(+)-epoxiconazole in overlying water samples in the two treatments were higher than those of (−)-epoxiconazole. Furthermore, the results also indicated that the concentrations of the two enantiomers in worm-present experiments were higher than those in worm-free experiments. This phenomenon could have been explained by the traversal of epoxiconazole to the spiked soil into the overlying water by simple diffusion processes in the worm-free treatment. However, for the worm-present treatment, epoxiconazole could pass through the spiked soil into the overlying water by two processes, diffusion and bioturbation. Thus, bioturbation has a positive effect on epoxiconazole diffusion from soil to overlying water.

AUTHOR INFORMATION

Corresponding Author

*(J.D.) Phone: +86 13811992249. Fax: +8610-62733547. E-mail: lingyinzi1201@gmail.com.

Funding

This work was funded by the National Natural Science Foundation of China (Contracts 41201499 and 21177154) and the Special Fund for Agro-scientific Research in the Public Interest (No. 201203022).

Notes

The authors declare no competing financial interest.

REFERENCES

(1) Bertelsen, J.; Neergaard, E.; Smedegaard-Petersen, V. Fungicidal effects of azoxystrobin and epoxiconazole on phyllosphere fungi, senescence and yield of winter wheat. *Plant Pathol.* **2001**, *50*, 190−205.

(2) Barber, J.; Parkin, C.; Chowdhury, A. Effect of application method on the control of powdery mildew (*Bulmeriagraminis*) on spring barley. *Crop Prot.* **2003**, *22*, 949−957.

(3) Tomlin, C., Ed. *The Pesticide Manual: A World Compendium*; British Crop Protecton Council/BCPC: Surrey, UK, 2003; pp 305−306.

(4) Lin, H.; Wong, S.; Li, G. Dissipation of epoxiconazole in the paddy field under subtropical conditions of Taiwan. *J. Environ. Sci. Health B* **2001**, *36*, 409−420.

(5) Passeport, E.; Benoit, P.; Bergheaud, V.; Coquet, Y.; Tournebize, J. Epoxiconazole degradation from artificial wetland and forest buffer substrates under flooded conditions. *Chem. Eng. J.* **2011**, *173*, 760−765.

(6) Liang, H.; Qiu, J.; Li, L.; Li, W.; Zhou, Z.; Liu, F.; Qiu, L. Stereoselective dissipation of epoxiconazole in grape (*Vitis vinifera* cv. Kyoho). *Chemosphere* **2012**, *87*, 982−987.

(7) Tomlin, C., Ed. *The Pesticide Manual, A World Compendium*, XIIth ed.; British Crop Protection Council: Surrey, UK, 2000.

(8) Williams, A. Opportunities for chiral agrochemicals. *Pestic. Sci.* **1996**, *46*, 3−9.

(9) Garrison, A.; Schmitt, P.; Martens, D.; Kettrup, A. Enantiomeric selectivity in the environmental degradation of dichlorprop as determined by high-performance capillary electrophoresis. *Environ. Sci. Technol.* **1996**, *30*, 2449−2455.

(10) Overmyer, J.; Rouse, D.; Avants, J.; Garrison, A.; DeLorenzo, M.; Chung, K.; Key, P.; Wilson, W.; Black, M. Toxicity of fipronil and its enantiomers to marine and freshwater non-targets. *J. Environ. Sci. Health B* **2007**, *42*, 471−480.

(11) Kodama, S.; Yamamoto, A.; Saitoh, Y.; Matsunaga, A.; Okamura, K.; Kizu, R.; Hayakawa, K. Enantioseparation of vinclozolin by γ-cyclodextrin-modified micellar electrokinetic chromatography. *J. Agric. Food Chem.* **2002**, *50*, 1312−1317.

(12) Liu, W.; Gan, J.; Schlenk, D.; Jury, W. Enantioselectivity in environmental safety of current chiral insecticides. *Proc. Natl. Acad. Sci. U.S.A.* **2005**, *102*, 701−706.

(13) Garrison, A. Probing the enantioselectivity of chiral pesticides. *Environ. Sci. Technol.* **2006**, *40*, 16−23.

(14) Bromilow, R.; Evans, A.; Nicholls, P. Factors affecting degradation ratesof five triazole fungicides in two soil types: 1. Laboratory incubations. *Pestic. Sci.* **1999**, *55*, 1129−1134.

(15) Fargasova, A. Toxicity of metals on *Daphnia magna* and *Tubifex tubifex*. *Ecotoxicol. Environ. Saf.* **1994**, *27*, 210−213.

(16) Egeler, P.; Meller, M.; Roembke, J.; Spoerlein, P.; Streit, B.; Nagel, R. *Tubifex tubifex*as a link in food chain transfer of hexachlorobenzene from contaminated sediment to fish. *Hydrobiologia* **2001**, *463*, 171−184.

(17) Kosiorek, D. Development cycle of *Tubifex tubifex* Müll. In experimental culture. *Pol. Arch. Hydrobiol.* **1974**, *21*, 411−422.

(18) Patrick, F.; Loutit, M. Passage of metals in effluents through bacteria to higher organisms. *Water Res.* **1976**, *10*, 333−335.

(19) Oplinger, R.; Bartley, M.; Wagner, E. Culture of *Tubifex tubifex*: effect of feed type, ration, temperature, and density on juvenile recruitment, production, and adult survival. *N. Am. J. Aquacult.* **2011**, *73*, 68−75.
(20) Paris-Palacios, S.; Mosleh, Y.; Almohamad, M.; Delahaut, L.; Conrad, A.; Arnoult, F.; Biagianti-Risbourg, S. Toxic effects and bioaccumulation of the herbicide isoproturonin *Tubifex tubifex* (Oligocheate, Tubificidae): a study of significance of autotomy and its utility as a biomarker. *Aquat. Toxicol.* **2010**, *98*, 8−14.
(21) Redeker, E.; Blust, R. Accumulation and toxicity of cadmium in the aquatic oligochaete *Tubifex tubifex*: a kinetic modeling approach. *Environ. Sci. Technol.* **2004**, *38*, 537−543.
(22) Stanley, J.; Coleman, J.; Wess, C.; Steevens, J. Sediment toxicity and bioaccumulation of nano and micro-sized aluminum oxide. *Environ. Toxicol. Chem.* **2010**, *29*, 422−429.
(23) Ciutat, A.; Gerino, M.; Mesmer-Dudons, N.; Anschutz, P.; Boudou, A. Cadmium bioaccumulation in Tubificidae from the overlying water source and effects on bioturbation. *Ecotoxicol. Environ. Saf.* **2005**, *60*, 237−246.
(24) Xu, P.; Liu, D.; Diao, J.; Lu, D.; Zhou, Z. Enantioselective acute toxicity and bioaccumulation of benalaxyl in earthworm (*Eiseniafedtia*). *J. Agric. Food Chem.* **2009**, *57*, 8545−8549.
(25) Qiu, J.; Dai, S.; Zheng, C.; Yang, S.; Chai, T.; Bie, M. Enantiomeric separation of triazole fungicides with 3-μm and 5-μm particle chiral columns by reverse-phase high-performance liquid chromatography. *Chirality* **2011**, *23*, 479−486.
(26) Rhoads, D. Organism-sediment relations on the muddy sea floor. *Oceanogr. Mar.* **1974**, *12*, 263−300.
(27) Ciutat, A.; Anschutz, P.; Gerino, M.; Boudou, A. Effects of bioturbation on cadmium transfer and distribution into freshwater sediment. *Environ. Toxicol. Chem.* **2005**, *24*, 1048−1058.
(28) Robbins, J.; McCall, P.; Fisher, J.; Krezoski, J. Effect of deposit feeders on migration of ^{137}Cs in lake sediments. *Earth Planet. Sci. Lett.* **1979**, *42*, 277−287.
(29) Matisoff, G. Effects of bioturbation on solute and particle transport in sediments. *Metal Contaminated Aquatic Sediments* **1995**, 201−272.
(30) Rasmusse, A.; Banta, G.; Andersen, O. Cadmium dynamics in estuarine sediments: Effects of salinity and lugworm bioturbation. *Environ. Toxicol. Chem.* **2000**, *19*, 380−386.
(31) Liu, T.; Xu, P.; Lu, Y.; Zhou, G.; Diao, J.; Zhou, Z. Enantioselective bioaccumulation of soil-associated fipronil enantiomers in *Tubifex tubifex*. *J. Hazard. Mater.* **2012**, *219*−*220*, 50−56.
(32) Di, S.; Liu, T.; Diao, J.; Zhou, Z. Enantioselective bioaccumulation and degradation of sediment-associated metalaxyl enantiomers in *Tubifex tubifex*. *J. Agric. Food Chem.* **2013**, *61*, 4997−5002.

JOURNAL OF AGRICULTURAL AND FOOD CHEMISTRY

Article

pubs.acs.org/JAFC

Holadysenterine, a Natural Herbicidal Constituent from *Drechslera australiensis* for Management of *Rumex dentatus*

Muhammad Akbar,[†] Arshad Javaid,*[,†] Ejaz Ahmed,[‡] Tariq Javed,[§] and Jacob Clary[∥]

[†]Institute of Agricultural Sciences, University of the Punjab, Lahore 54590, Pakistan

[‡]Institute of Chemistry, University of the Punjab, P.O. Box 54590, Lahore, Pakistan

[§]Centre of Excellence in Molecular Biology, University of the Punjab, P.O. Box 54590, Lahore, Pakistan

[∥]Department of Chemistry and Biochemistry, University of California, 1156 High Street, Santa Cruz , California 95064, United States

ABSTRACT: *Rumex dentatus* L. is a problematic weed of wheat. Bioassay-directed isolation of culture filtrates of a plant pathogenic fungus *Drechslera australiensis* gave holadysenterine as the main herbicidal constituent against this weed of wheat. Leaf disc bioassay showed that herbicidal activity of holadysenterine was comparable to that of synthetic herbicide 2,4-D. This is the first report of this herbicidal compound from the genus *Drechslera*.

KEYWORDS: *Drechslera australiensis, leaf disc bioassay, natural herbicides, Rumex dentatus, weed of wheat*

INTRODUCTION

Rumex dentatus L. (family Polygonaceae) is a broad-leaf densely populated weed of wheat (*Triticum aestivum* L.) fields.[1,2] It is an extremely competitive annual herb that causes remarkable reduction in the yield of wheat.[3,4] Besides, the weed is also known for its allelopathic activity.[5] Anjum and Bajwa[3] reported 83% reduction in grain yield of wheat due to *R. dentatus* infestation. To control this weed, use of chemical herbicides is on the increase to boost up crop productivity.[6,7] However, we are now facing new challenges regarding weed control, especially emergence of resistance in weeds to herbicides[8] and concerns about herbicide effects in food, soil, groundwater, and atmosphere.[9,10] Because of these ill effects of herbicides coupled with increasing demand for organic farming in the world, isolation of new herbicides from natural sources is gaining importance.[11,12] Use of natural herbicidal constituents from microbes is one of the alternative strategies to manage the weeds.[13,14]

There have been many successful attempts to control weeds by metabolites of fungi of genus *Drechslera*.[15−17] Some bioactive compounds have been isolated from some species of this genus and proposed as potent natural herbicides.[18−20] Kastanias and Chrysayi-Tokousbalides[21] isolated macrodiolide (8*R*,16*R*)-(−)-pyrenophorin (8,16-dimethyl-1,9-dioxa-cyclohexadeca-3,11-diene-2,5,10,13-tetraone) from cultures of *Drechslera avenae* (Eidam) Shoem. The isolated compound inhibited seed germination of wild oats (*Avena fatua* L.). Another herbicidal compound drazepinone was identified from culture filtrates of *Drechslera siccans* (Drechsler) Shoemaker.[15] Evidente et al.[17] isolated a number of herbicidal metabolites from culture filtrate of *D. gigantea* Heald & Wolf including ophiobolin A that proved to be a potent herbicide against several grass and dicotyledonous weeds including *Avena ludoviciana* Dur., *Phalaris canariensis* L., *Chenopodium album* L., and *Sonchus oleraceus* L. Ophiobolin A proved to be the most potent phytotoxin as compared to the other related compounds. Preliminary investigations on culture filtrates of some species of *Drechslera* from Pakistan, namely *D. australiensis*, *D. hawaiiensis*, *D. biseptata*, and *D. holmii*, revealed their herbicidal activity against some problematic weeds of wheat and *Parthenium hysterophorus*.[22−24] However, detailed studies regarding isolation of herbicidal compounds from Pakistani *Drechslera* species are lacking. Therefore, the present study was carried out to identify the herbicidal constituents present in culture filtrates of *D. australiensis*.

MATERIALS AND METHODS

Preparation of Culture Filtrates of the Test Fungus. Culture of *D. australiensis* was procured from Fungal Culture Bank of Pakistan, Institute of Agricultural Sciences, University of the Punjab, Lahore, Pakistan. M-1-D growth medium was prepared by following the procedure described by Evidente et al.[17] First, 100 mL of medium was poured in 500 mL conical flasks and autoclaved. These flasks were then inoculated with actively growing culture discs of *D. australiensis* and incubated at 25 ± 2 °C in an incubator. After 28 days of incubation, cultures were filtered through muslin cloth, centrifuged, and finally filtered through Whatman filter paper no. 1. to get crude fungal culture filtrates free of fungal mycelia and spores.

Organic Solvent Extraction. A total of 4 L of crude fungal culture filtrate of *D. australiensis* was collected and evaporated (45 °C) to yield 1.5 L of concentrated filtrate. Four organic solvents, viz. *n*-hexane, chloroform, ethyl acetate, and *n*-butanol, were successively used for extraction. These organic solvents were used in order of their increasing polarity. The organic solvent phases were collected and evaporated under vacuum in a rotary evaporator to yield crude organic fractions.[25]

Bioassays with Crude Organic Fractions. Bioassays with crude organic fractions were carried out following procedure described by Sarpeleh et al.[26] with some modifications. Seeds of *R. dentatus* were sown in plastic pots under natural environmental conditions. Young leaves from 30-day-old plants were detached, and discs of 1 cm diameter were cut with the help of a cork borer. These leaf discs were

Received: September 17, 2013
Revised: December 12, 2013
Accepted: December 23, 2013
Published: December 23, 2013

ACS Publications © 2013 American Chemical Society

Table 1. Herbicidal Effect of Crude Organic Fractions of Culture Filtrate of *D. australiensis* on Leaf Discs of *R. dentatus*

	DMSO effect			effect of crude organic fractions							
				n-hexane		chloroform		ethyl acetate		*n*-butanol	
DMSO conc (μL mL^{-1})	color[a]	necrotic spot[b]	organic fraction conc (mg mL^{-1})	color[a]	necrotic spot[b]	color[a]	necrotic spot[b]	color[a]	necrotic spot[b]	color[a]	necrotic spot[b]
0	0	4	0	0	4	0	4	0	4	0	4
1.560	0	4	0.0625	0–1	4	1–2	4	0	4	0	4
3.125	1	4	0.1250	1	4	2	4	1	4	0	4
6.250	0–1	4	0.2500	1	4	2–3	4	1	4	1	4
12.500	0–1	4	0.5000	1–2	4	3	4	1–2	4	1	4
25.000	0–1	4	1.0000	2	4	3	5	2	4	1–2	4
50.000	0–1	4	2.0000	2	4	3	7	2	5	2	4
100.000	0–1	4	4.0000	2	4	3	10	3	7	2	4

[a]Color scale: 0 = no change; 1 = light discoloration; 2 = moderate discoloration; 3 = severe discoloration. [b]Necrotic spot scale: 4 = no necrotic spot; 5 = necrotic spot ≤ 1 mm; 6 = necrotic spot ≤ 2 > 1 mm; 7 = necrotic spot ≤ 3 > 2 mm; 8 = necrotic spot ≤ 4 > 3 mm; 9 = necrotic spot ≤ 5 > 4 mm; 10 = necrotic spot ≤ 6 > 5 mm.

placed on glass slides and punctured with the help of a fine needle. Glass slides were placed in a Petri plate on a filter paper wetted with 2 mL of sterilized distilled water.

Then 4 mg of each of the four crude fractions were dissolved in 100 μL of dimethylsulfoxide (DMSO). Final volume of each fraction was raised to 1.0 mL with distilled water to prepare a stock solution of 4 mg mL^{-1} concentration. The stock solution was serially double diluted by adding distilled water to prepare lower concentrations of 2, 1, ..., 0.0625 mg mL^{-1}. Droplets of 15 μL of each of the seven concentrations were applied on the punctured leaf discs surfaces. Ten leaf discs of the test weed species were used for each concentration. For blank control treatments, 100 μL of DMSO were dissolved in distilled water to prepare a 1.0 mL mixture and subsequent lower concentrations were made by double diluting it with distilled water. Petri plates were incubated at 25 °C under continuous fluorescent light in a growth room. Symptoms regarding appearance of necrotic spot and discoloration of leaf discs were observed after 72 h. Color scale 0–3 and necrotic spot scale 4–10 were used for comparisons following Mahoney et al.[27] with some modifications.

Color Scale

0 = no change
1 = light discoloration
2 = moderate discoloration
3 = severe discoloration

Necrotic Spot Scale

4 = no necrotic spot
5 = necrotic spot ≤ 1 mm
6 = necrotic spot ≤ 2 > 1 mm
7 = necrotic spot ≤ 3 > 2 mm
8 = necrotic spot ≤ 4 > 3 mm
9 = necrotic spot ≤ 5 > 4 mm
10 = necrotic spot ≤ 6 > 5 mm

Isolation of Compounds through Chromatographic Techniques. Crude chloroform fraction of culture filtrate of *D. australiensis* were selected for thin layer chromatography (TLC) analysis followed by separation of compounds through preparative thin layer chromatography (PTLC) and reversed phase high performance liquid chromatography.

A thin strip of aluminum foil backed TLC was used as chromatogram. First, 5 mg of crude chloroform fraction was taken in an Eppendorf tube and was dissolved in 1 mL of methanol. Then 10 mL of solvent (chloroform, ethyl acetate, and *n*-hexane) in a 10:6:84 ratio was used to elute the mixture of compounds spotted on chromatogram strip. Spots were located under UV transilluminator, both at short and long wavelengths as well as visualized by spraying ceric sulfate solution accompanied by heating with heat gun. Retention factor (R_f) value for each spot was calculated using the formula:

$$R_f = \frac{\text{distance traveled by component}}{\text{distance traveled by the solvent}}$$

Six fractions, namely **A** (R_f 0.096), **B** (R_f 0.130), **C** (R_f 0.170), **D** (R_f 0.269), **E** (R_f 0.480), and **F** (R_f 0.576), were isolated from chloroform fraction.

TLC fractions were further purified by preparative thin layer chromatography (PTLC). For preparative thin layer chromatography, precoated silica gel GF-254 preparative plates (20 cm × 20 cm, 0.5 mm thick, E-Merck) were used. Solvent system was same as in TLC. When developed with the solvent, the compounds separated in horizontal bands. These bands were scraped from the plates and eluted with methanol. Soluble compounds were carefully collected separately in another vial through filtration and were evaporated at 40 °C to dryness and weighed.

Compounds separated through PTLC were further subjected to reversed phase high performance liquid chromatography. For elution, acetonitrile (HPLC grade) with 0.1% formic acid was added and deionized water with 0.1% formic acid was used as solvent system. Gradient elution was employed with initial ratio of acetonitrile and deionized water as 10:90 with an increasing ratio of acetonitrile to water as 100:0. Fractions containing purified compounds were collected in glass vials, and solvent was evaporated under continuous currents of clean air at room temperature.

Bioassays with Purified Chromatographic Fractions. Bioassays with purified chromatographic fractions were generally carried out using the same method as was adopted in case of crude organic fractions. Stock solutions of 2 mg mL^{-1} of the various purified isolated constituents were prepared by dissolving 2 mg of the compound in 50 μL of DMSO and raised the volume to 1.0 mL by adding distilled water. Lower concentrations of 1, 0.5, ..., 0.03125 mg mL^{-1} were prepared by serially double diluting the stock solutions. In total, seven concentrations were made with distilled water viz. 2, 1, 0.5, 0.25, 0.125, 0.0625, and 0.03125 mg mL^{-1}. A set of blank control treatments with different concentrations of DMSO corresponding to DMSO concentration in various treatments of pure compounds was also included. Different concentrations of a known herbicidal compound 2,4-D (2,4- dichlorophenoxyacetic acid) were also included as positive control to compare with efficacy of the isolated compounds. Symptoms regarding appearance of necrotic spots and discoloration of leaf discs were observed after 72 h.

Spectroscopic Analyses. Structural elucidation by 1D and 2D NMR techniques of only the most active compounds was carried out. Less bioactive compounds were not subjected to mass spectroscopy because their bioactivity was far too low as compared to synthetic herbicide in use.

Proton nuclear magnetic resonance (^{1}H NMR) spectra were recorded in CD_3OD using TMS as internal standard at 600 MHz on Bruker AM-500 nuclear magnetic resonance spectrometers. The ^{13}C

dx.doi.org/10.1021/jf403860b | J. Agric. Food Chem. 2014, 62, 368–372

Table 2. Herbicidal Activity of Purified Chromatographic Fractions from Chloroform Fraction of Culture Filtrates of *D. australiensis* on Leaf Discs of *R. dentatus*

						effect of purified chromatographic fractions											
	DMSO effect			effect of 2,4-D		A		B		C		D		E		F	
DMSO conc (μL mL^{-1})	color[a]	NS[b]	2,4-D conc (mg mL^{-1})	color[a]	NS[b]	color[a]	NS[b]	color[a]	NS[b]	color[a]	NS[b]	color[a]	NS[b]	color[a]	NS[b]	color[a]	NS[b]
0	0	4	0	0	4	0	4	0	4	0	4	0	4	0	4	0	4
0.780	0	4	0.0312	0–1	4	0	4	0	4	0	4	0	4	0	4	0	4
1.560	0	4	0.0625	0–1	4	0–1	4	0–1	4	0–1	4	0–1	4	0–1	4	0–1	4
3.125	0	4	0.1250	1	4	0–1	4	0–1	4	1	4	1	4	0–1	4	0–1	4
6.250	0	4	0.2500	1	6	1	4	0–1	4	1	4	1	4	0–1	4	0–1	4
12.500	0–1	4	0.5000	1	7	1	6	1	4	2	4	1	4	1	4	1	6
25.000	0–1	4	1.0000	1	10	1–2	7	1	4	2	7	2	4	1	4	2	7
50.000	0–1	4	2.0000	1	10	2	9	1	4	3	8	2	7	1	4	3	9

[a]Color scale: 0 = no change; 1 = light discoloration; 2 = moderate discoloration; 3 = severe discoloration. [b]NS = necrotic spot. Necrotic spot scale: 4 = no necrotic spot; 5 = necrotic spot ≤ 1 mm; 6 = necrotic spot ≤ 2 > 1 mm; 7 = necrotic spot ≤ 3 > 2 mm; 8 = necrotic spot ≤ 4 > 3 mm; 9 = necrotic spot ≤ 5 > 4 mm; 10 = necrotic spot ≤ 6 > 5 mm.

NMR spectra were recorded in CD_3OD at 125 MHz on the same instrument.

EIMS spectra were recorded on a Finnigan MAT 311 with MASSPEC data system.

RESULTS AND DISCUSSION

Bioassays with Crude Organic Fractions. Positive reaction showing necrotic spots was recorded on punctured *R. dentatus* leaf discs surfaces. The chloroform fraction produced the most prominent necrotic spots followed by the ethyl acetate fraction. A 1.0 mg mL^{-1} concentration of crude chloroform fraction produced necrotic spot, while ethyl acetate fraction produced necrotic spots at a minimum concentration of 2.0 mg mL^{-1}. *n*-Hexane and *n*-butanol fractions did not produce any necrotic spot. Severe discoloration was also observed in the case of bioassays that performed well. In the case of the chloroform fraction, severe discoloration was observed due to 0.25 mg mL^{-1} and higher concentrations. In the case of the ethyl acetate fraction, severe discoloration was observed only at the highest concentration of 4.0 mg mL^{-1}. In the case of *n*-hexane and *n*-butanol fractions, discoloration was not much pronounced. Leaf sections treated with DMSO as a positive control exhibited only light discoloration (Table 1).

Bioassays with Purified Chromatographic Fractions. In these bioassays, out of six purified chromatographic fractions from crude chloroform fraction of culture filtrate of *D. australiensis*, four, viz. **A**, **C**, **D**, and **F**, were found effective in producing necrotic spot on leaf discs of *R. dentatus*. Among these, **A** and **F** were found to be the most herbicidal and produced necrotic spots on leaf discs surfaces at a minimum concentration of 0.5 mg mL^{-1}. Fraction **C** was found active at a minimum concentration of 1.0 mg mL^{-1}, while fraction **D** was found active at the highest concentration of 2.0 mg mL^{-1}. Chromatographic fractions **B** and **E** did not produce any necrotic spots. In the case of bioassays performed with reference compound 2,4-D, maximum bioactivity was observed at minimum concentration of 0.25 mg mL^{-1}. Discoloration of leaf discs was also observed to a variable extent in all the treatments. Fraction **C** and **F** induced severe discoloration at a concentration of 2.0 mg mL^{-1}. In contrast, only light discoloration was observed in case of 2,4-D, even at the highest concentration of 2.0 mg mL^{-1} (Table 2).

Spectroscopic Data of the Isolated Compound. Chromatographic fraction **F** exhibited the highest herbicidal activity, therefore, spectroscopic analysis of only this compound was carried out. Chromatographic fraction **F** was identified as compound **1** (Figure 1).

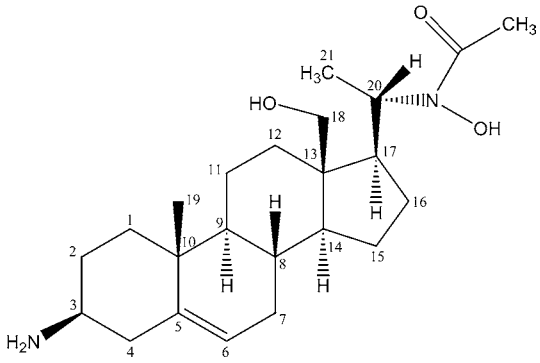

Figure 1. Chemical structure of holadysenterine.

Compound 1. Holadysenterine. Colorless amorphous powder; $[\alpha]_D^{28}$ −14.6° (*c* = 1.0, MeOH); mp 219.5–220.5 °C. EIMS *m*/*z*: $[M]^+$ 390 (2.0), 317 (4.5), 354 (3.5), 307 (60), 289 (22), 278 (65), 154 (25), 136 (54), 115 (48), 107 (50), 85 (100). HREIMS *m*/*z*: $[M]^+$ 390.3030 (calcd for $C_{23}H_{38}N_2O_3$ 390.3083). ^{1}H NMR (CD_3OD, 600 MHz) δ_H: 1.19 (1H, m, H-1), 1.33 (1H, m, H-1), 1.35 (1H, m, H-2), 1.44 (1H, m, H-2), 2.99 (1H, brm, H-3), 5.44 (brs 1H, m, H-6), 1.84 (2H, m, H-12), 1.33 (1H, m, H-17), 4.01 (1H, d, *J* = 10.9, H-18), 3.70 (1H, d, *J* = 10.9), 1.29 (s, 3H, H-19), 3.45 (1H, m, H-20), 1.38 (1H, d, *J* = 7.1 H-21), 2.01 (s, 3H, CO-Me).

Compound **1** (holadysenterine) was isolated as amorphous solid from the chloroform extraction. Molecular formula was obtained by HREIMS, showing a peak at *m*/*z* 390.3030 for $C_{23}H_{38}N_2O_3$ showing six degrees of unsaturation in the compound. Four unsaturations were accounted for by a tetracyclic pregnane type skeleton, and two were due to the endocyclic double bond and was due to the carboxyl function. The UV spectrum was inconclusive. Inspection of ^{1}H NMR spectrum of compound **1** showed olefinic proton at δ 5.44 (1H, br singlet). The spectra showed two doublets at δ 3.70 (1H, d, *J* = 10.9 Hz) assignable to the hydroxyl methylene protons. At δ 2.99 and 3.45, two broad multiplets were observed and were assigned to the H-3α and 20β, respectively. Two methyl singlets were observed at δ 1.29 and δ 2.0, while at δ 1.38 a

dx.doi.org/10.1021/jf403860b | J. Agric. Food Chem. 2014, 62, 368–372

characteristic methyl doublet was observed having J = 7.1 Hz. The downfield shift of methyl group at δ 2.0 indicated the presence of acetamide functionality in the molecule. A solvent exchangeable proton singlet due to *N*-hydroxy was observed at δ 4.98,[28] indicated its attachment at amine side chain functionality. EIMS spectrum gave peaks at m/z 317 [M + H − CH_3CONOH]+ (−C−N bond cleavage), 289 [M + H − $C_4H_8NO_2$]+ (C17−C20 bond cleavage) and 278 [M + H − $C_5H_8NO_2$]+ (C13−C17 and C16−C17 bond cleavage). This proves the attachment of a hydroxyl methyl group at the amine center. On the basis of this evidence and comparison with the literature data, compound **1** was assigned as (20*S*)-20 acetylhydroxylamine,3β-amino,13β-hydroxymethylenepregn-5-ene and named previously as holadysenterine.[29] Because of a lack of amount, ^{13}C spectrum was unpredictable, however, some 2D NMR spectra (HMBC, ^{1}H−^{1}H COSY) were showing some signals of ^{13}C and from which final structure of compound **1** was concluded.

In earlier studies, some herbicidal constituents have been isolated from other species of *Drechslera*. The culture of *Drechslera siccans* (Drechsler) Shoemaker is also reported to yield a phytotoxin named as 6,8-dihydroxy-3-(2′-hydroxypropyl) isocoumarin (de-*o*-methyldiaporthin). Phytotoxicity of this compound has been estimated in terms of necrotic spot area when tested on *Avena sativa*, *Echinochloa crus-galli*, and *Amaranthus spinosus*.[30] Capio et al.[20] isolated two phytotoxic compounds, namely cytochalasin B and dihydrocytochalasins, from extracts of dried mycelia and liquid culture filtrates of *Drechslera wirreganensis* Wallwork, Lichon & Sivan and *D. campanulata* (Lév.) B. Sutton. Similarly, another metabolite namely drazepinone with broad spectrum herbicidal activity has been isolated from *Drechslera siccans*.[15] The present study concludes that herbicidal activity of culture filtrates of *D. australiensis* is mostly due to holadysenterine.

AUTHOR INFORMATION

Corresponding Author

*Phone: +92 42 99231846. Fax: +92 42 99231187. E-mail: arshadjpk@yahoo.com.

Funding

The Higher Education Commission of Pakistan provided funding to accomplish part of this work at the University of California, USA.

Notes

The authors declare no competing financial interest.

REFERENCES

(1) Siddiqui, I.; Bajwa, R. Variation in weed composition in wheat fields of Lahore and Gujranwala divisions. *Pak. J. Biol. Sci.* **2001**, *4*, 492−504.

(2) Qureshi, R.; Waheed, A.; Arshad, M. Weed communities of wheat crop in district Toba Tek Singh, Pakistan. *Pak. J. Bot.* **2009**, *41*, 239−245.

(3) Anjum, T.; Bajwa, R. Competition losses caused by *Rumex dentatus* L. and *Chenopodium album* L. in wheat (*Triticum aestivum* L.). *Philipp. Agric. Sci.* **2010**, *93*, 365−368.

(4) Siddiqui, I.; Bajwa, R.; Zil-e-Huma; Javaid, A. Effect of six problematic weeds on growth and yield of wheat. *Pak. J. Bot.* **2010**, *42*, 2461−2471.

(5) Hussain, F.; Mobeen, B. S.; Yoo, S. Allelopathic suppression of wheat and mustard by *Rumex dentatus* ssp. *lotzschianus*. *J. Plant Biol.* **1997**, *40*, 120−124.

(6) Ashiq, M.; Muhammad, N.; Ahmed, N. Comparative efficacy of different herbicides against broad leaf weeds in wheat. *Pak. J. Weed Sci. Res.* **2007**, *13*, 149−156.

(7) Hulting, A. G.; Dauer, J. T.; Hinds-Cook, B.; Curtis, D.; Koepke-Hill, R. M.; Mallory-Smith, C. Management of Italian Ryegrass (*Lolium perenne* ssp. *multiflorum*) in Western Oregon with Preemergence Applications of Pyroxasulfone in Winter Wheat. *Weed Technol.* **2012**, *26*, 230−235.

(8) Llewellyn, R. S.; D'Emden, F. H.; Owen, M. J. Herbicide resistance in rigid ryegrass (*Lolium rigidum*) has not led to higher weed densities in western Australian cropping fields. *Weed Sci.* **2009**, *57*, 61−65.

(9) Marín, A.; Oliva, J.; Garcia, C.; Navarro, S.; Barba, A. Dissipation rates of cyprodinil and fludioxonil in lettuce and table grape in the field and under cold storage conditions. *J. Agric. Food Chem.* **2003**, *51*, 4708−4711.

(10) Rial-Otero, R.; Arias-Estévez, M.; López-Periago, E.; Cancho-Grande, B.; Simal- Gándar, J. Variation in concentrations of the fungicides tebuconazole and dichlofluanid following successive applications to greenhouse-grown lettuces. *J. Agric. Food Chem.* **2005**, *53*, 4471−4475.

(11) Naylor, R. E. *Weed Management Handbook*; Blackwell Publishing, Oxford, 2002.

(12) Jamil, M.; Cheema, Z. A.; Mushtaq, M. N.; Farooq, M.; Cheema, M. A. Alternative control of wild oat and canary grass in wheat fields by allelopathic plant water extracts. *Agron. Sustainable Dev.* **2009**, *29*, 475−482.

(13) Javaid, A. Herbicidal potential of allelopathic plants and fungi against *Parthenium hysterophorus*—a review. *Allelopathy J.* **2010**, *25*, 331−344.

(14) Zhang, L.; Kang, Z.; Xu, J.; Xu, W.; Zhang, J.l. Isolation and structural indentification of herbicidal toxin fractions produced by *Pythium aphanidermatum*. *Agric. Sci. China* **2010**, *9*, 995−1000.

(15) Evidente, A.; Andolfi, A.; Vurro, M.; Fracchiolla, M.; Zonno, M. C.; Motta, A. Drazepinone, a trisubstituted tetrahydronaphthofuroazepinone with herbicidal activity produced by *Drechslera siccans*. *Phytochemistry* **2005**, *66*, 715−721.

(16) Evidente, A.; Andolfi, A.; Cimmino, A.; Vurro, M.; Fracchiolla, M.; Charudattan, R.; Motta, A. Ophiobolin E and 8-epi-ophiobolin J produced by *Drechslera gigantea*, a potential mycoherbicide of weedy grasses. *Phytochemistry* **2006**, *67*, 2281−2287.

(17) Evidente, A.; Andolfi, A.; Cimmino, A.; Vurro, M.; Fracchiolla, M.; Charudattan, R. Herbicidal potential of ophiobolins produced by *Drechslera gigantea*. *J. Agric. Food Chem.* **2006**, *54*, 1779−1783.

(18) Kastanias, M. A.; Chrysayi-Tokousbalides, M. Herbicidal potential of pyrenophorol isolated from a *Drechslera avenae* pathotype. *Pest Manage. Sci.* **2000**, *56*, 227−232.

(19) Zhang, W.; Watson, A. K. Isolation and partial characterization of phytotoxins produced by *Exserohilum monoceras*, a potential bioherbicide for control of *Echinochloa* species. Proceedings of the X International Symposium on Biological Control of Weeds, Bozeman, Montana, July 4−14, 1999; Montana State University: Bozeman, Montana, 1999. Spencer, N.R. (ed.). 2000, pp 125−130.

(20) Capio, E. R.; Tate, M. E.; Wallwork, H. Phytotoxic metabolites from *Drechslera wirreganensis* and *D. campanulata*. *Austral. Plant Pathol.* **2004**, *33*, 23−28.

(21) Kastanias, M. A.; Chrysayi-Tokousbalides, M. Bioactivity of the fungal metabolite (8*R*,16*R*)-(−)-pyrenophorin on graminaceous plants. *J. Agric. Food Chem.* **2005**, *53*, 5943−5947.

(22) Javaid, A.; Adrees, H. Parthenium management by cultural filtrates of phytopathogenic fungi. *Nat. Prod. Res.* **2009**, *23*, 1541−1551.

(23) Akbar, M.; Javaid, A. Management of some problematic weeds of wheat by metabolites of *Drechslera* sp. prepared in malt extract medium. *Pak. J. Weed Sci. Res.* **2010**, *16*, 145−151.

(24) Javaid, A.; Javaid, A.; Akbar, M. Herbicidal potential of *Drechslera* spp. culture filtrates against *Parthenium hysterophorus* L. *Chil. J. Agric. Res.* **2011**, *71*, 634−637.

(25) Javaid, A.; Ali, S. Herbicidal activity of culture filtrates of *Trichoderma* spp. against two problematic weeds of wheat. *Nat. Prod. Res.* **2011**, *25*, 730−740.
(26) Sarpeleh, A.; Tate, M. E.; Wallwork, H.; Catcheside, D.; Able, A. J. Characterisation of low molecular weight phytotoxins isolated from *Pyrenophora teres*. *Physiol. Mol. Plant Pathol.* **2009**, *73*, 154−162.
(27) Mahoney, N.; Lardner, R.; Molyneux, R. J.; Scottb, B.; Leverett, E. S.; Smith, R.; Schoch, T. K. Phenolic and heterocyclic metabolite profiles of the grapevine pathogen *Eutypa lata*. *Phytochemistry* **2003**, *64*, 475−484.
(28) Bhutani, K. K.; Vaid, R. M.; Ali, M.; Kapoor, R.; Soodan, S. R.; Kumar, D. Steroidal alkaloids from *Holarrhena antidysenterica*. *Phytochemistry* **1990**, *29*, 969−972.
(29) Kumar, N.; Singh, B.; Bhandari, P.; Gupta, A. P.; Kaul, V. K. Steroidal alkaloids from *Holarrhena antidysenterica* (L.) WALL. *Chem. Pharm. Bull.* **2007**, *55*, 912−914.
(30) Hallock, Y. F.; Clardy, J.; kenfield, D. S.; Strobel, G. De-*O*-methyldiaporthin, a phytotoxin from *Drechslera siccans*. *Phytochemistry* **1988**, *27*, 3123−3125.

JOURNAL OF AGRICULTURAL AND FOOD CHEMISTRY

Article

pubs.acs.org/JAFC

Interactions of Aluminum with Biochars and Oxidized Biochars: Implications for the Biochar Aging Process

Linbo Qian and Baoliang Chen*

Department of Environmental Science and Zhejiang Provincial Key Laboratory of Organic Pollution Process and Control, Zhejiang University, Hangzhou, Zhejiang 310058, China

Supporting Information

ABSTRACT: Interactions of aluminum with primary and oxidized biochars were compared to understand the changes in the adsorption properties of aged biochars. The structural characteristics of rice straw-derived biochars, before and after oxidation by HNO_3/H_2SO_4, were analyzed by element composition, FTIR, and XPS. The adsorption of Al to primary biochars was dominated by binding to inorganic components (such as silicon particles) and surface complexation of oxygen-containing functional groups via esterification reactions. Oxidization (aging) introduced carboxylic functional groups on biochar surfaces, which served as additional binding sites for Al^{3+}. At pH 2.5−3.5, the Al^{3+} binding was significantly greater on oxidized biochars than primary biochars. After loading with Al, the −COOH groups anchored to biochar surfaces were transformed into COO^- groups, and the negative surface charge diminished, which indicated that Al^{3+} coordinated with COO^-. Biochar is suggested as a potential adsorbent for removing Al from acidic soils.

KEYWORDS: *oxidized biochar, carboxyl functional groups, aluminum, aging process, soil remediation*

INTRODUCTION

Biochar is a carbon-rich material produced during the pyrolysis of biomass, and its biogeochemical cycles have received much attention in recent years.[1,2] Following the amendment of contaminated soils or sediments with biochar, physical and biochemical processes (aging) can affect the biochar properties. Yao et al. reported that mineral elements (such as K, S, Ca, and P) were released from biochar during weathering.[3] The formation of carbonyl and carboxylic functional groups on the surface of aged biochar was also observed.[3] This trend was confirmed by long-term studies of the dynamics of black carbon in which the O/C ratios and carboxyl groups of aged biochar increased by over 133 and 192% after the first 10 and 30 years, respectively.[4] Mao et al. used quantitative ^{13}C NMR to show that Terra Preta soils (with char >800 years) consisted predominantly of char residues with about six fused aromatic rings with COO^- substituents.[5] Obviously, oxidation is an important process controlling the quality of biochars and black carbon in the environment.[4]

Typically, minerals (such as P and Si) and oxygen-containing groups in biochars control the mobility and bioavailability of toxic metals in soil amended with biochars.[6−10] Cao et al. reported that the precipitation of phosphorus-containing minerals dominated Pb adsorption.[7] Uchimiya et al. showed that carboxyl functional groups of biochar controlled heavy metal retention in soil, and biochar oxidized by HNO_3/H_2SO_4 (to simulate aging) can enhance this process.[6,11] Qian et al. demonstrated that biochar amendments effectively reduced aluminum (Al) phytotoxicity due to biochar's liming effect and adsorption properties, and the complexation of Al with organic hydroxyl and carboxyl groups and the surface adsorption and coprecipitation of Al with silicate particles both contributed to Al adsorption on biochars.[8,9] However, more studies of the interaction of Al with aged biochar are needed to understand the long-term effects of biochar on the remediation of soils that contain Al.

Aluminum is a major limitation on plant productivity in acidic soils in up to 30% of the world's total land area,[12] and this issue is receiving more attention because of increasing soil acidification trends.[13,14] Biochars can display variable physicochemical properties and, therefore, their interaction with aluminum can vary over the long term. To improve our knowledge of the long-term behavior of biochar in acidic soil, we simulated the oxidative aging of biochars with HNO_3/H_2SO_4 to gain insights into the mechanisms of interactions between biochar and aluminum. A series of biochars were produced from rice straw at different temperatures (350, 500, and 700 °C), and the corresponding oxidized samples were prepared. The structures of biochars before and after oxidation were analyzed by Fourier transform infrared spectra (FTIR) and X-ray photoelectron spectroscopy (XPS). The effect of pH on aluminum adsorption was investigated. To investigate binding mechanisms, the surface and structural changes of Al-loaded biochars were further characterized by FTIR and zeta potential.

MATERIALS AND METHODS

Biochar Preparation and Oxidation. Rice straw (RS) was chosen as a precursor for biochar. Rice straw was collected from the farm at the Zijingang campus of Zhejiang University, Hangzhou, China. Samples were air-dried for 2 days and subsequently oven-dried overnight at 70−80 °C, ground, and then passed through a 0.154 mm sieve to produce raw biomass material. Temperature is presumably a

Received: October 15, 2013
Revised: December 21, 2013
Accepted: December 23, 2013
Published: December 23, 2013

ACS Publications © 2013 American Chemical Society

Table 1. Elemental Composition, Atomic Ratio, Ash Content, and Soluble Si Content of Rice Straw (RS)-Derived Biochars before and after Oxidation Using HNO_3/H_2SO_4[a]

sample[b]	C/%	H/%	O/%	N/%	H/C[c]	O/C[d]	ash/%	soluble Si/%
RS350	47.03 ± 0.11	2.85 ± 0.04	13.4 ± 0.58	1.39 ± 0.02	0.73	0.21	35.33 ± 0.00	1.240 ± 0.044
RS350-NS0	56.69 ± 0.13	3.41 ± 0.04	14.21 ± 0.51	1.89 ± 0.28	0.72	0.19	23.80 ± 0.00	0.076 ± 0.005
RS350-NS20	41.33 ± 0.16	2.35 ± 0.03	20.79 ± 1.41	3.57 ± 0.04	0.68	0.38	31.96 ± 0.01	0.021 ± 0.000
RS350-NS40	37.36 ± 0.35	2.05 ± 0.00	22.8 ± 0.16	3.76 ± 0.23	0.66	0.46	34.03 ± 0.00	0.023 ± 0.003
RS350-NS60	37.48 ± 0.07	2.10 ± 0.00	18.94 ± 0.01	3.52 ± 0.00	0.67	0.38	37.96 ± 0.00	0.019 ± 0.002
RS500	47.31 ± 0.13	1.46 ± 0.01	7.70 ± 0.69	1.50 ± 0.01	0.37	0.12	42.03 ± 0.01	3.657 ± 0.016
RS500-NS0	58.12 ± 0.15	1.80 ± 0.01	6.37 ± 0.01	1.90 ± 0.01	0.37	0.08	34.81 ± 0.00	0.547 ± 0.012
RS500-NS60	44.09 ± 0.05	1.42 ± 0.01	16.85 ± 0.80	2.91 ± 0.06	0.39	0.29	34.73 ± 0.01	0.006 ± 0001
RS700	47.76 ± 0.27	0.61 ± 0.00	6.42 ± 0.68	1.03 ± 0.18	0.15	0.10	44.18 ± 0.00	4.647 ± 0.043
RS700-NS0	57.12 ± 0.79	1.80 ± 0.04	5.97 ± 0.02	1.89 ± 0.05	0.38	0.08	33.22 ± 0.00	0.892 ± 0.015
RS700-NS60	46.67 ± 0.06	0.91 ± 0.00	12.96 ± 0.30	1.33 ± 0.01	0.23	0.21	38.13 ± 0.00	0.020 ± 0.001

[a]Values are given as the mean ± SD, which are from duplicated experiments. [b]The numbers following "RS" in the sample names refer to the pyrolysis temperatures. NS, concentrated HNO_3/H_2SO_4 = 1/3, the following numbers referring to the percent of NS. [c]H/C, atomic ratio of hydrogen to carbon. [d]O/C, atomic ratio of oxygen to carbon.

key parameter affecting the structure of organic and inorganic components, and thus temperature was the controlled variable in this study. On the basis of multiple lots within a specific temperature, biochars were produced by pyrolyzing rice straw at 350, 500, and 700 °C under nitrogen using a modified method.[15,16] Briefly, the powdered rice straw (100 g) was packed tightly in a ceramic pot, covered with a fitted lid, and then pyrolyzed at different temperatures in a furnace (1100-40, Shanghai HAOYUE Instrument and Equipment Co. Ltd., China) under nitrogen atmosphere for 6 h to prevent calcination of the biomass in the presence of oxygen. The heating rate was controlled at 5 °C/min for slow pyrolysis to produce more solid residue (biochar). The charred solids were passed through a 0.154 mm sieve to produce the final biochar samples. Rice straw biochars were referred to as RS350, RS500, and RS700; these numbers refer to the pyrolysis temperatures.

A mixture of concentrated HNO_3 and H_2SO_4 was selected to oxidize these rice straw biochars and simulate the aging process in acidic environments (acid rain), because NO_3^- and SO_4^{2-} were the main anions in acid rain in China[17] and these acids were shown previously to significantly increase the carboxyl content of biochars.[6,18] Biochars were oxidized with an HNO_3/H_2SO_4 mixture (1:3 (v/v)) using a modified method.[6,18] Each biochar sample (5 g) was immersed in 400 mL of a different HNO_3/H_2SO_4 solution, 20, 40, or 60% (e.g., concentrated HNO_3 and H_2SO_4 were mixed at a ratio of 1/3 and then diluted to 20, 40%, or 60%). The other samples without acid oxidation were treated with deionized water instead. The reaction was highly exothermic, so the solution was maintained at 70 °C for 6 h. To remove residual acid, oxidized biochars were first drained through a 325 mesh sieve and then washed repeatedly with 1 L of deionized water for 1 h until the pH stabilized (Supporting Information Figure S1). Samples that were not treated with HNO_3/H_2SO_4 (NS0) were rinsed until the pH reached 7. The oxidized biochar samples are denoted RS350-NS0 (without the HNO_3/H_2SO_4 mixture), RS350-NS20 (oxidized with a 20% solution of the HNO_3/H_2SO_4 mixture), RS350-NS40, and RS350-NS60. After treatment, the RS500 and RS700 samples are denoted RS500-NS0 and RS500-NS60 and RS700-NS0 and RS700-NS60, respectively. The preparation of each biochar and treated biochar was replicated.

Sample Characterization. Elemental (C, H, N) analysis was conducted using an EA112 CHN elemental analyzer (Thermo Finnigan). The Na, K, Ca, and Mg contents in these biochars were extracted by digestion in HNO_3 for 24 h at 150 °C.[19] Elemental concentrations in the extraction solution were determined by inductively coupled plasma atomic emission spectroscopy (ICP-AES). The biochars were also examined using FTIR and XPS analysis. Biochar samples in KBr wafers (0.5%) were prepared for FTIR measurements. The FTIR spectra were recorded in the 4000−400 cm^{-1} region by a Nicolet FTIR spectrophotometer (model 7600, Thermo Scientific, USA) with a resolution of 1.0 cm^{-1}. For XPS analysis, RS350 and RS350-NS60 were tested. The chemical bonding state at the biochar surface was obtained by using an XPS (VG ESCALAB MARK II) with Mg Kα (1253.6 eV) radiation emitted from a double anode at 50 W.

Batch Adsorption Experiment. The adsorption experiment (run in duplicate) was conducted in 8 mL vials by mixing 4 mg of biochar with 8 mL of 0.5 mmol/L $CaCl_2$ (to simulate the soil interstitial water) as a background solution containing 500 μmol/L Al at an initial pH ranging from 2.0 to 4.5. The adsorption experiments including the blank and calibration control were performed in duplicate. The mixtures were agitated on a reciprocating shaker at 120 rpm for 24 h. A preliminary experiment showed that Al sorption reached equilibrium after 12 h. After 24 h, the solid and liquid phases were separated by centrifugation at 3000 rpm for 15 min, and the solution was filtered through a 0.22 μm Millipore filter. The filtrate was acidified immediately with 0.2% (v/v) HNO_3 for Al analysis. The total Al concentration in the supernatant fluid was determined using a Perkin-Elmer Analyst 700 (PE700, USA) atomic adsorption spectrometer equipped with an HGA-800 graphite furnace. The residual solid was vacuum-dried for FTIR analysis.

Zeta Potential Analysis. Surface charge properties of biochars were measured with the zeta potential. Biochar (0.25 g/L) was suspended in deionized water or 100 μmol/L Al solutions and adjusted to pH 1.0−9.0, and the zeta potential was measured with a Zetasizer (Malvern ZEN3690). The pH of the biochar suspensions was adjusted using 1 mol/L HCl or 1 mol/L NaOH. On the basis of the measured total aqueous Al concentration and the final pH value, the concentrations of various Al species, including Al^{3+}, $AlOH^{2+}$, $Al(OH)_2^+$, and $Al(OH)_3^0$, were calculated using the Visual MINTEQ model.[20]

RESULTS AND DISCUSSION

Structural Characterization of Biochars. The chemical properties of the rice straw-derived biochars processed over a range of temperatures and their oxidized derivatives are shown in Table 1. Elemental analysis showed the progressive decrease of the H/C and O/C ratios with increasing pyrolysis temperature, which was attributed mainly to the thermal conversion of organic matter to carbonized organic matter and indicative of the formation of structures containing condensed carbons such as aromatic rings.[16,21−23] After samples were washed with water, the O/C ratio decreased due to the release of soluble minerals. When samples were oxidized with HNO_3/H_2SO_4, the O/C ratio increased to 0.38, 0.29, and 0.21 for RS350-NS60, RS500-NS60, and RS700-NS60, respectively, indicating that oxygen-containing groups were introduced on biochar surfaces. An increase in the O/C ratios was also

dx.doi.org/10.1021/jf404624h | J. Agric. Food Chem. 2014, 62, 373−380

observed when soot and biochars were oxidized using HNO_3/H_2SO_4.[6,24] Meanwhile, the increase of the O/C ratio during the aging of biochars was also confirmed.[25] The nitrogen content in oxidized samples increased with the increasing concentration of HNO_3/H_2SO_4. The nitrogen content of RS350-NS60 was nearly 3-fold greater than that in RS350. This observation is attributed to the treatment with nitric acid.[26]

The FTIR spectra of these rice straw-derived biochars and their oxidized samples are presented in Figure 1. At higher

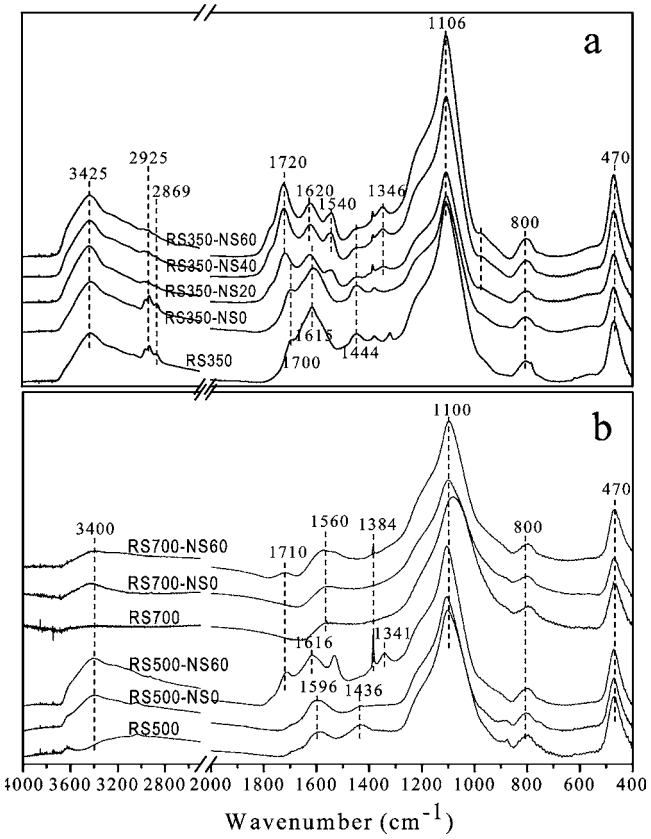

Figure 1. FTIR spectra of the rice straw-derived biochars before and after oxidation using HNO_3/H_2SO_4 (RS350 (a), RS500 and RS700 (b)). The numbers in the sample names represent the pyrolysis temperatures. NS, concentrated HNO_3/H_2SO_4 = 1/3; the following numbers refer to the percent of NS.

pyrolytic temperatures, the intense bands for aliphatic CH_2 groups (2925, 2869, and 1444 cm^{-1}) disappeared abruptly, and the intensity of the band at 1620 cm^{-1} (for aromatic C═C and C═O bonds) diminished for RS500 and RS700, which was attributed to a decrease in the nonpolar groups and the surface functional groups.[16,27] With oxidation by HNO_3/H_2SO_4, there is a large increase in the intensity of the band at 1720 cm^{-1} (the C═O stretching vibration), indicating the increase of carboxyl acid groups of RS350.[6,16,28] An increase in the level of oxygen-containing functionalities strongly suggests that substantial amounts of solid organic oxidation products are formed during the oxidation process (Table 1) and retained on the biochar surfaces. Additionally, the peaks at 1540 and 1346 cm^{-1} are assigned to asymmetric NO_2 and symmetric NO_2 vibration, respectively.[26] The nitric acid mixed with concentrated sulfuric acid formed nitronium ions, which then reacted via electrophilic substitution of the hydrogen ions in the carbon matrix.[24,29] Some studies of activated carbon oxidized by HNO_3 also revealed the presence of nitrate and nitro surface groups.[26,29,30] The oxidized samples of RS500 and RS700 enhanced peaks in these regions to a much lesser extent than RS350. Further analysis of the C and O bonding states was performed by XPS for both RS350 and RS350-NS60 to identify the change in C and O bonding states on biochar surfaces after oxidation by HNO_3/H_2SO_4 (Figure S-2 in the Supporting Information and Figure 2). Figure S-2 showed that the O 1s peak was

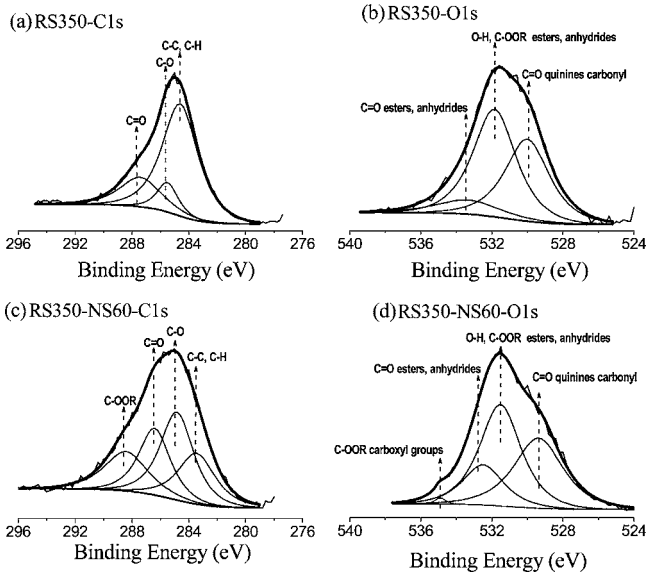

Figure 2. XPS C 1s (a and c) and O 1s (b and d) region scans and peak fitting for rice straw-derived biochars before (RS350, a and b) and after (RS350-NS60, c and d) oxidation using HNO_3/H_2SO_4. The numbers in the sample names represent the pyrolysis temperatures. NS, concentrated HNO_3/H_2SO_4 = 1/3, the following numbers refer to the percent of NS.

strengthened after oxidization. From Figure 2, a new peak appeared at the binding energy of 288.4 eV after HNO_3/H_2SO_4 treatment, which can be attributed to the carboxylic groups, esters, and lactones (−COOR). The new peak appearing at the binding energy of the O 1s spectra (534.9 eV) confirmed that carboxylic groups formed.[31] A previous study about mineral ash-rich biochar geochemical weathering in a modified Soxhlet reactor has also shown a considerable increase in carbonyl and carboxylic functional groups.[3]

The ash content and alkaline elements (Na, K, Mg, and Ca) in biochars increased with temperature (350−700 °C) (Table S-1). When treated with water, the ash content and alkaline elements decreased significantly. Because the alkaline elements were lost during water washing, the pH decreased to neutral (Supporting Information Figure S-1). In samples oxidized by HNO_3/H_2SO_4, the alkaline elements (K, Mg, and Ca) also showed a decreasing trend because these elements were released during oxidation. The release of alkaline elements is a typical process for biochars during geochemical weathering. Previous studies demonstrated that the alkaline elements were released from biochar during weathering or aging.[3] The release of such elements (Ca and Mg) supplies nutrients to plants, but this result also indicated that the liming effect of biochar may be a short-term effect. Unlike alkaline elements, the silicon content in biochar remained high (Figure 1). The bands at 1100−1000, 880−780, and 470 cm^{-1} were characteristic of Si−O−Si asymmetric stretching, symmetric stretching, and bending,

dx.doi.org/10.1021/jf404624h | J. Agric. Food Chem. 2014, 62, 373−380

respectively. All biochars and oxidized samples exhibited a relatively strong Si−O−Si stretching band, which corresponded to results for biochars with high silicon contents.[9] As the concentrations of HNO_3/H_2SO_4 increased, the intensity of the Si−O−Si stretching band became much stronger, indicating that the oxidation process concentrated Si-containing minerals. The XPS data confirmed this observation. After oxidation by HNO_3/H_2SO_4, the intensities of Si 2p and Si 2s were strengthened (Supporting Information Figure S-2). Remarkably, the soluble Si was decreased after water treatment and acid oxidation (Table 1). Notably, Si is common in grasses such as rice but uncommon in biochar from non-Poaceae plants.

Effect of pH on Aluminum Adsorption. The pH-dependent adsorption of Al from aqueous solution on biochar samples is shown in Figure 3. When the initial pH was below

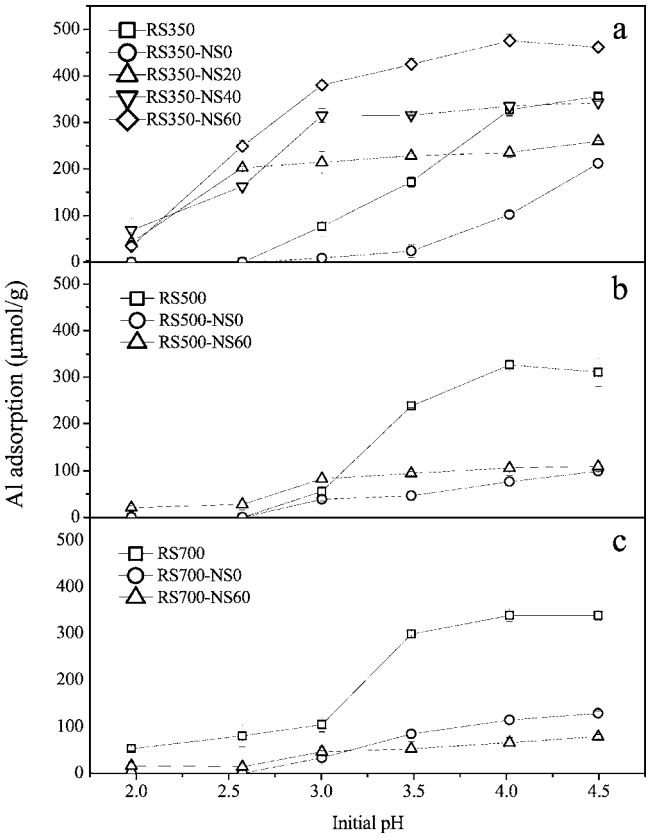

Figure 3. Effect of pH on Al adsorption by rice straw-derived biochars before and after oxidation using HNO_3/H_2SO_4 (RS350 (a), RS500 (b), and RS700 (c)). The numbers in the sample names represent the pyrolysis temperatures. NS, concentrated HNO_3/H_2SO_4 = 1/3, the following numbers refer to the percent of NS. Values are given as the mean ± SD, which are from duplicated experiments.

3.0, little Al adsorption by RS350 and RS350-NS0 was observed. The RS500, RS500-NS0, RS700, and RS700-NS0 samples displayed the same trend. The competition of H^+ led to little electrostatic bonding of Al to biochars. The Al adsorption by oxidized samples occurred at an initial pH of 2.5 and reached 203, 163, and 249 μmol/g for RS350-NS20, RS350-NS40, and RS350-NS60, respectively. This result is attributed primarily to the lower pK_a of oxidized samples. The lower pK_a of oxidized samples was mainly attributed to the nitro groups added to biochar surface (Figure 1 and Figure S-2) and the multicarbxylic groups.[32,33] Nitro groups can form an extended conjugated π-system with the benzene ring and exhibit strong enhancement of the acidity.[33] Additionally, oxidation may also increase the ionic strength of the linear charge density and, thus, lower the pK_a of the oxidized samples. For RS500 and RS700, as the pyrolytic temperature increased, the organic matter carbonized and formed condensed carbons; it is difficult to oxidize, and few carboxylic groups formed on RS500 and RS700 surfaces (Table 1 and Figure 1). Therefore, little Al adsorption by RS500-NS60 and RS700-NS60 occurred below pH 3.0. When the initial pH was increased to 3.5, enhanced adsorption of Al was observed for RS350 (172 μmol/g), RS500 (238 μmol/g), and RS700 (298 μmol/g). These observations may be attributed to the liming effect of primary biochar, and the final pH of RS350, RS500, and RS700 reached 4.14, 4.35, and 4.43, respectively (Figure 4). At these pH values,

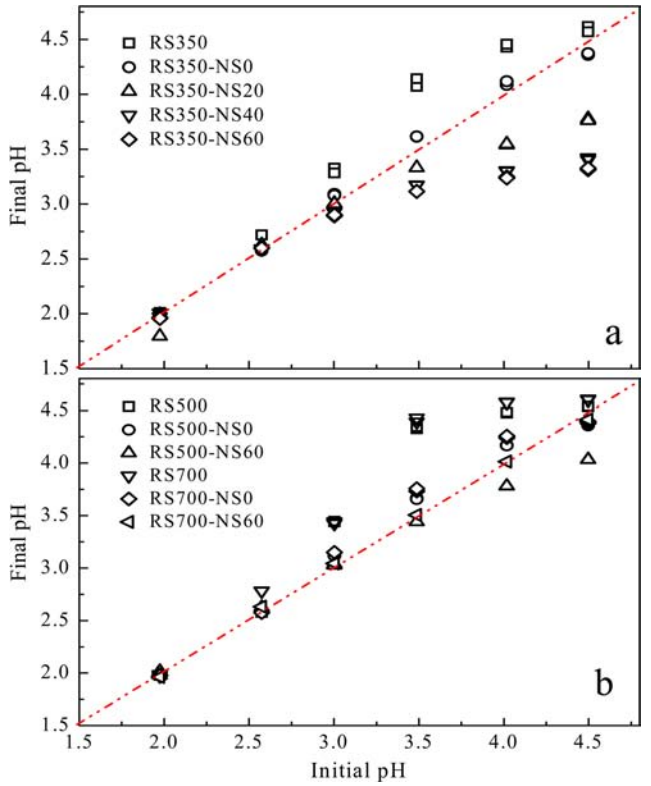

Figure 4. pH changes with Al adsorption by rice straw-derived biochars before and after oxidation using HNO_3/H_2SO_4 (RS350 (a), RS500 and RS700 (b)). The numbers in the sample names represent the pyrolysis temperatures. NS, concentrated HNO_3/H_2SO_4 = 1/3, the following numbers refer to the percent of NS.

some carboxylic groups started to dissociate. Below this pH value, it is possible that the Al hydrolysis reacted with dissociated carboxylic groups and silicon particle.[9,34]

Remarkably, the adsorption of Al by washed biochars (RS350-NS0, RS500-NS0, and RS700-NS0) was significantly lower than that by the corresponding primary biochars. As carboxyl groups formed on oxidized samples (RS350-NS20, RS350-NS40, and RS350-NS60), the adsorption of Al maintained a high level at pH 3.5. When the initial pH value increased to 4.0 and 4.5, Al adsorption by the oxidized samples reached a plateau at pH 4.0, which suggests that available binding sites are saturated by Al. In a comparison, Al adsorption by the primary samples (RS350, RS500, and RS700) increased progressively. This phenomenon may be

dx.doi.org/10.1021/jf404624h | J. Agric. Food Chem. 2014, 62, 373−380

related to the pH-dependent Al adsorption mechanism. At the final pH 4.0−4.5 for adsorption by primary samples, additional Al adsorption sites such as silica surfaces were introduced.[9]

FTIR Spectra of the Biochars before and after Loading with Al. The FTIR spectra of aluminum-loaded RS350 and RS350-NS60 at different pH values are shown in Figure 5. The

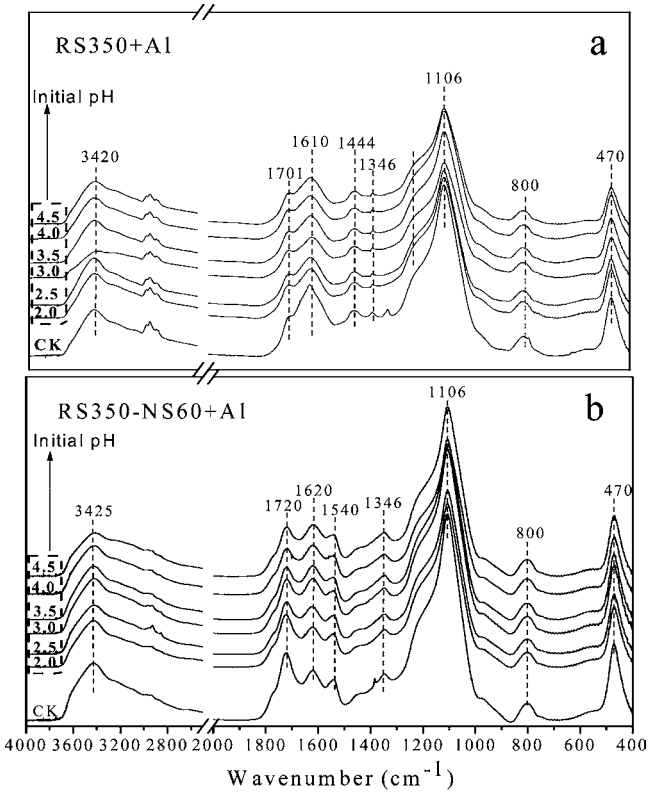

Figure 5. FTIR spectra of Al-loaded rice straw-derived biochars before (RS350) and after oxidation using HNO_3/H_2SO_4 (RS350-NS60 (b)). CK represents the absence of Al reaction, and the numbers from 2.0 to 4.5 represent the initial pH of Al adsorption by biochar. The numbers in the sample names represent the pyrolysis temperatures. NS60, concentrated HNO_3/H_2SO_4 = 1/3, the following numbers refer to the percent of NS.

peaks at 1609 and 1444 cm^{-1} were assigned to asymmetric and symmetric COO^- stretching, respectively.[35] On the basis of Figure 5, as the initial pH increased, the peak at 1609 cm^{-1} shifted toward higher wavenumbers and the adsorbed aluminum increased. The difference in the calculated wavenumbers between the asymmetric and symmetric COO^- stretching regions increased as the initial pH increased, that is, 169, 169, 169, 170, 172, and 172 cm^{-1} for pH 2.0, 2.5, 3.0, 3.5, 4.0, and 4.5, respectively. The increase in the wavenumber difference between the asymmetric and symmetric COO^- stretching peaks suggested that the adsorption of Al was associated with carboxyl groups.[9,35] Surface complexation, the dominant adsorption mechanism between the carboxylate groups and Al, is attributed mainly to the esterification reactions of carboxylate groups and Al hydrolysis.[34] Furthermore, the band at 1100 cm^{-1} shifted or became broader, and the band at 1160−1200 cm^{-1} became narrower, which indicated that Al reacted with silicon.[9,36]

Increasing numbers of carboxyl functional groups and additional nitro groups were observed after oxidation by HNO_3/H_2SO_4 (Figure 1a), and the FTIR spectra of the aluminum-loaded samples showed more obvious variations (Figure 5b). The bands at 1720 and 1620 cm^{-1} were characteristic of C═O stretching vibrations of ester bonds and C═C or C═O stretching in aromatic rings, respectively.[16] The intensities of the bands at 1720 and 1620 cm^{-1} were reversed when associated with Al. Without added Al, the intensity of the band at 1720 cm^{-1} was stronger than that of the band at 1620 cm^{-1}. After Al was added, the band at 1620 cm^{-1} became more intense, whereas the band at 1720 cm^{-1} became less intense. This was evidence of the conversion of COOH groups to COO^- groups in the biochar.[37] Meanwhile, the changes in the bands at 1720 and 1620 cm^{-1} coincided with the Al adsorption by samples (Figure 3a). This result indicated that carboxyl groups were the adsorption sites of Al. In a previous investigation of the adsorption of Al onto biomaterials derived from the cell walls of *Datura inoxia*, ^{27}Al NMR spectroscopy revealed that carboxylate groups were responsible for Al^{3+} adsorption at pH 3.5.[38]

Zeta Potential of Biochar Particles with and without Al Loading. The results for zeta potential measurements of primary biochars and oxidized samples (with and without added Al) are illustrated in Figure 6 and Figure S-3 in the Supporting Information. Because biochars are amphoteric in nature due to the various functional groups on their surfaces, it is always important to evaluate their isoelectric point (IEP), which is the pH at which the zeta potential is zero. These results show a marked difference in the pH_{IEP} of the primary biochars and the oxidized samples. The pH_{IEP} values for primary biochars were approximately 3.0, 4.0, and 4.0 for RS350, RS500, and RS700, respectively. The organic components ($-COO^-$ and $-OH$) and the mineral fractions both potentially contribute to the biochar surface charge. Without oxidation, the concentrations of oxygen-containing functional groups (e.g., $-COO^-$ and $-OH$) decreased and eventually disappeared as the pyrolysis temperature increased (Figure 1). Crystalline minerals formed (e.g., calcite and albite), and thus RS500 and RS700 had less negative surface charges. In contrast, the pH_{IEP} decreased to approximately 1.0 for oxidized biochars. This sequence indicated that after treatment with HNO_3/H_2SO_4, the biochar surface fixed a larger number of oxygen complexes. The low pH_{IEP} values for oxidized samples are due to the presence of weakly acidic carboxylic functional groups and nitro groups.[29,32,33]

The negatively charged surfaces of the tested samples dramatically changed after they interacted with Al. However, these changes were sample dependent, which indicated that different mechanisms were involved. For RS350 and RS350-NS0, the pH−zeta potential curves before and after Al loading had the same trends when the pH values were below 3.0 (Figure 6a,b). In contrast, the negative surface charge of oxidized samples partially diminished after Al loading at pH 2.0−3.0 (Figure 6c−e). As the dominant Al species at pH 2−3 was Al^{3+}, the free energy of dehydration of Al^{3+} was too large for adsorption to occur on silica-like minerals.[39] The diminished negative surface charge was attributed mainly to the electrostatic attraction of Al^{3+} to biochars. Before oxidation, when the pH value was below 3, none of the primary biochars (except RS700) reacted with Al^{3+}, whereas after oxidation by HNO_3/H_2SO_4, adsorption occurred. This phenomenon demonstrated that Al may concentrate on biochar surfaces following aging processes even in strongly acidic environments.

Mechanisms of Aluminum Adsorption. For primary biochars, Al adsorption was dominated by binding to inorganic

dx.doi.org/10.1021/jf404624h | J. Agric. Food Chem. 2014, 62, 373−380

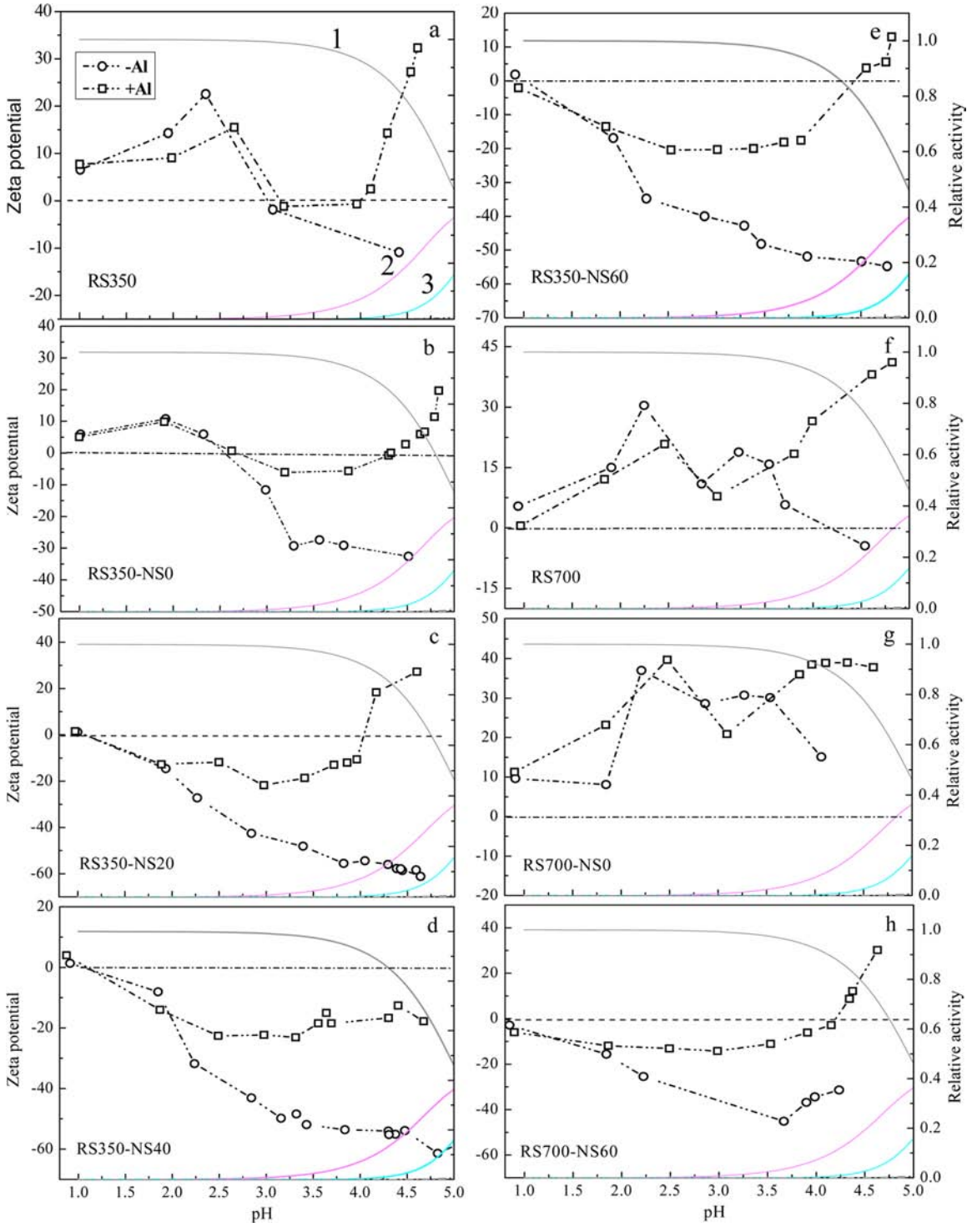

Figure 6. Zeta potential data of rice straw-derived biochars before and after oxidation using HNO_3/H_2SO_4 (RS350 (a–e), RS700 (f–h)): before (−Al) and after (+Al) reaction with aqueous Al. The numbers in the sample names represent the pyrolysis temperatures. NS, concentrated HNO_3/H_2SO_4 = 1/3, the following numbers refer to the percent of NS. The shaded lines in the figure represent the Al speciation distributions at different solution pH values: 1, Al^{3+}; 2, $Al(OH)^{2+}$; 3, $Al(OH)_2^{+}$.

matter (alkaline elements and silicon particles) and surface complexation to functional groups containing organic oxygen by esterification reactions. Qian and Chen found that the organic components and silicate particles within the biochars served as dual adsorptive sites for Al.[9] After aging with water, as the inorganic matter was leached by water, the Al adsorption sharply decreased. For the oxidized samples, the most likely mechanism for aluminum adsorption was the creation of oxygenated adsorption sites by HNO_3/H_2SO_4 oxidation, which was attributed mainly to the electrostatic interaction of Al^{3+} with the negative surfaces of oxidized biochars. This finding was consistent with the adsorption of Pb by mesoporous carbon foams oxidized by HNO_3.[40] It is important to reveal the interaction between the biochar aging process and Al, not only

dx.doi.org/10.1021/jf404624h | J. Agric. Food Chem. 2014, 62, 373–380

because the adsorption capacity increased following the aging process but also to respond to the trend of increasing soil acidity due to acid rain.[13] Furthermore, the existence of ancient, char-rich Terra Preta in the Amazon and similar char-rich soils elsewhere in the world provides important examples of the long-term carbon sequestration potential of anthropogenic amendment with charred organic matter. This long-term carbon stability serves as a durable structure for silica attachment, thus resisting geochemical weathering. Binding organic ligands with Al is likely to increase soil organic carbon storage.[41] Thus, the binding of biochar with Al may increase the stability of biochar. Carbonyl and carboxylic functional groups were formed on biochar surfaces by HNO_3/H_2SO_4 oxidation (simulation of aging processes). The carboxylic functional groups controlled Al adsorption at low pH values of 2.0−3.5 through electrostatic attractions. When pH values were above 3.5, Al adsorption primarily involved complexation with organic hydroxyl and carboxyl functional groups of biochars. Additional coprecipitation and surface adsorption on silica particle surfaces were confirmed by zeta potential measurements. The results indicated that Al concentrated on biochar surface during geochemical weathering. However, the effects of biochar aging should be addressed fully by considering additional processes such as the coating of biochar surfaces by minerals, organic matter, and silt components of soil. Our future studies on biochar biogeochemical samples as well as field trials will provide additional information for implementing large-scale biochar soil amendment.

■ ASSOCIATED CONTENT

Ⓢ Supporting Information

Alkaline elements of rice straw-derived biochars before and after oxidation using HNO_3/H_2SO_4 are presented in Table S-1. The final pH changes of rice straw-derived biochars and oxidized samples are presented in Figure S-1. The XPS spectra RS350 and RS350-NS60 are given in Figure S-2, and zeta potential data for RS500 before and after oxidation by HNO_3/H_2SO_4 are shown in Figure S-3. This material is available free of charge via the Internet at http://pubs.acs.org.

■ AUTHOR INFORMATION

Corresponding Author

*(B.C.) E-mail: blchen@zju.edu.cn. Phone: (0086) 571-8898-2587. Fax: (0086) 571-8898-2587.

Funding

This project is supported by the National Natural Science Foundation of China (41071210, 20890111), The National High-Tech Research and Development Program of China (Grant 2012AA06A203), and the Doctoral Fund of Ministry of Education of China (J20091588).

Notes

The authors declare no competing financial interest.

■ REFERENCES

(1) Lehmann, J. A handful of carbon. *Nature* **2007**, *447*, 143−144.

(2) Hale, S. E.; Hanley, K.; Lehmann, J.; Zimmerman, A. R.; Cornelissen, G. Effects of chemical, biological, and physical aging as well as soil addition on the sorption of pyrene to activated carbon and biochar. *Environ. Sci. Technol.* **2011**, *45*, 10445−10453.

(3) Yao, F. X.; Arbestain, M. C.; Virgel, S.; Blanco, F.; Arostegui, J.; Macia-Agullo, J. A.; Macias, F. Simulated geochemical weathering of a mineral ash-rich biochar in a modified soxhlet reactor. *Chemosphere* **2010**, *80*, 724−732.

(4) Nguyen, B. T.; Lehmann, J.; Kinyangi, J.; Smernik, R.; Riha, S. J.; Engelhard, M. H. Long-term black carbon dynamics in cultivated soil. *Biogeochemistry* **2008**, *89*, 295−308.

(5) Mao, J. D.; Johnson, R. L.; Lehmann, J.; Olk, D. C.; Neves, E. G.; Thompson, M. L.; Schmidt-Rohr, K. Abundant and stable char residues in soils: implications for soil fertility and carbon sequestration. *Environ. Sci. Technol.* **2012**, *46*, 9571−9576.

(6) Uchimiya, M.; Bannon, D. I.; Wartelle, L. H. Retention of heavy metals by carboxyl functional groups of biochars in small arms range soil. *J. Agric. Food Chem.* **2012**, *60*, 1798−1809.

(7) Cao, X.; Ma, L.; Gao, B.; Harris, W. Dairy-manure derived biochar effectively sorbs lead and atrazine. *Environ. Sci. Technol.* **2009**, *43*, 3285−3291.

(8) Qian, L.; Chen, B.; Hu, D. Effective alleviation of aluminum phytotoxicity by manure-derived biochar. *Environ. Sci. Technol.* **2013**, *47*, 2737−2745.

(9) Qian, L.; Chen, B. The dual role of biochars as adsorbents for aluminum: the effects of oxygen-containing organic components and the scattering of silicate particles. *Environ. Sci. Technol.* **2013**, *47*, 8759−8768.

(10) Beesley, L.; Moreno-Jimenez, E.; Gomez-Eyles, J. L.; Harris, E.; Robinson, B.; Sizmur, T. A review of biochars' potential role in the remediation, revegetation and restoration of contaminated soils. *Environ. Pollut.* **2011**, *159*, 3269−3282.

(11) Uchimiya, M.; Chang, S.; Klasson, K. T. Screening biochars for heavy metal retention in soil: Role of oxygen functional groups. *J. Hazard. Mater.* **2011**, *190*, 432−441.

(12) Vonuexkull, H. R.; Mutert, E. Global extent, development and economic-impact of acid soils. *Plant Soil* **1995**, *171*, 1−15.

(13) Guo, J.; Liu, X.; Zhang, Y.; Shen, J.; Han, W.; Zhang, W.; Christie, P.; Goulding, K. W. T.; Vitousek, P.; Zhang, F. Significant acidification in major chinese croplands. *Science* **2010**, *327*, 1008−1010.

(14) Cronan, C. S.; Schofield, C. L. Aluminum leaching response to acid precipitation − effects on high-elevation watersheds in the northeast. *Science* **1979**, *204*, 304−306.

(15) Zhou, Z.; Shi, D.; Qiu, Y.; Sheng, G. Sorptive domains of pine chars as probed by benzene and nitrobenzene. *Environ. Pollut.* **2010**, *158*, 201−206.

(16) Chen, B.; Zhou, D.; Zhu, L. Transitional adsorption and partition of nonpolar and polar aromatic contaminants by biochars of pine needles with different pyrolytic temperatures. *Environ. Sci. Technol.* **2008**, *42*, 5137−5143.

(17) Cao, Y.; Wang, S.; Zhang, G.; Luo, J.; Lu, S. Chemical characteristics of wet precipitation at an urban site of Guangzhou, South China. *Atmos. Res.* **2009**, *94*, 462−469.

(18) Cho, H. H.; Wepasnick, K.; Smith, B. A.; Bangash, F. K.; Fairbrother, D. H.; Ball, W. P. Sorption of aqueous Zn(II) and Cd(II) by multiwall carbon nanotubes: the relative roles of oxygen-containing functional groups and graphenic carbon. *Langmuir* **2010**, *26*, 967−981.

(19) Silber, A.; Levkovitch, I.; Graber, E. R. pH-dependent mineral release and surface properties of cornstraw biochar: agronomic implications. *Environ. Sci. Technol.* **2010**, *44*, 9318−9323.

(20) Kinraide, T. B. Identity of the rhizotoxic aluminum species. *Plant Soil* **1991**, *134*, 167−178.

(21) Keiluweit, M.; Nico, P. S.; Johnson, M. G.; Kleber, M. Dynamic molecular structure of plant biomass-derived black carbon (biochar). *Environ. Sci. Technol.* **2010**, *44*, 1247−1253.

(22) Wang, Z. Y.; Zheng, H.; Luo, Y.; Deng, X.; Herbert, S.; Xing, B. S. Characterization and influence of biochars on nitrous oxide emission from agricultural soil. *Environ. Pollut.* **2013**, *174*, 289−296.

(23) Xu, Y.; Chen, B. Investigation of thermodynamic parameters in the pyrolysis conversion of biomass and manure to biochars using thermogravimetric analysis. *Bioresour. Technol.* **2013**, *146*, 485−493.

(24) Chen, B.; Huang, W. H. Effects of compositional heterogeneity and nanoporosity of raw and treated biomass-generated soot on adsorption and absorption of organic contaminants. *Environ. Pollut.* **2011**, *159*, 550−556.

(25) Lin, Y.; Munroe, P.; Joseph, S.; Kimber, S.; Van Zwieten, L. Nanoscale organo-mineral reactions of biochars in ferrosol: an investigation using microscopy. *Plant Soil* **2012**, *357*, 369−380.
(26) Seredych, M.; Hulicova-Jurcakova, D.; Lu, G. Q.; Bandosz, T. J. Surface functional groups of carbons and the effects of their chemical character, density and accessibility to ions on electrochemical performance. *Carbon* **2008**, *46*, 1475−1488.
(27) Chen, Z.; Chen, B.; Chiou, C. T. Fast and slow rates of naphthalene sorption to biochars produced at different temperatures. *Environ. Sci. Technol.* **2012**, *46*, 11104−11111.
(28) Sun, K.; Gao, B.; Zhang, Z. Y.; Zhang, G. X.; Zhao, Y.; Xing, B. S. Sorption of atrazine and phenanthrene by organic matter fractions in soil and sediment. *Environ. Pollut.* **2010**, *158*, 3520−3526.
(29) Chingombe, P.; Saha, B.; Wakeman, R. J. Surface modification and characterisation of a coal-based activated carbon. *Carbon* **2005**, *43*, 3132−3143.
(30) Saha, B.; Tai, M. H.; Streat, M. Study of activated carbon after oxidation and subsequent treatment characterization. *Process Saf. Environ.* **2001**, *79*, 211−217.
(31) Zhou, J. H.; Sui, Z. J.; Zhu, J.; Li, P.; De, C.; Dai, Y. C.; Yuan, W. K. Characterization of surface oxygen complexes on carbon nanofibers by TPD, XPS and FT-IR. *Carbon* **2007**, *45*, 785−796.
(32) Evanko, C. R.; Dzombak, D. A. Influence of structural features on sorption of nom-analogue organic acids to goethite. *Environ. Sci. Technol.* **1998**, *32*, 2846−2855.
(33) Dong, H. T.; Du, H. B.; Wickramasinghe, S. R.; Qian, X. H. The effects of chemical substitution and polymerization on the p*K*(a) values of sulfonic ccids. *J. Phys. Chem. B* **2009**, *113* (43), 14094−14101.
(34) Wehr, J. B.; Blamey, F. P.; Hanna, J. V.; Kopittke, P. M.; Kerven, G. L.; Menzies, N. W. Hydrolysis and speciation of Al bound to pectin and plant cell wall material and its reaction with the dye chrome azurols. *J. Agric. Food Chem.* **2010**, *58*, 5553−5560.
(35) Mimmo, T.; Marzadori, C.; Montecchio, D.; Gessa, C. Characterisation of Ca- and Al-pectate gels by thermal analysis and FT-IR spectroscopy. *Carbohydr. Res.* **2005**, *340*, 2510−2519.
(36) Murthy, M. K.; Kirby, E. M. Infrared study of compounds and solid solutions in the system lithia-alumina-silica. *J. Am. Ceram. Soc.* **1962**, *45*, 324−329.
(37) Lu, X. Q.; Chen, Z. L.; Yang, X. H. Spectroscopic study of aluminium speciation in removing humic substances by Al coagulation. *Water Res.* **1999**, *33*, 3271−3280.
(38) Xia, H. Y.; Rayson, G. D. Investigation of aluminum binding to a datura innoxia material using ^{27}Al NMR. *Environ. Sci. Technol.* **1998**, *32*, 2688−2692.
(39) Johnson, S. B.; Dixon, D. R.; Scales, P. J. The electrokinetic and shear yield stress properties of kaolinite in the presence of aluminium ions. *Colloid Surf. A* **1999**, *146*, 281−291.
(40) El-Hendawy, A.-N. A. Influence of HNO_3 oxidation on the structure and adsorptive properties of corncob-based activated carbon. *Carbon* **2003**, *41*, 713−722.
(41) Yu, G. H.; Wu, M. J.; Wei, G. R.; Luo, Y. H.; Ran, W.; Wang, B. R.; Zhang, J. C.; Shen, Q. R. Binding of organic ligands with Al(III) in dissolved organic matter from soil: implications for soil organic carbon storage. *Environ. Sci. Technol.* **2012**, *46*, 6102−6109.

JOURNAL OF AGRICULTURAL AND FOOD CHEMISTRY

Article

pubs.acs.org/JAFC

Design, Synthesis, Crystal Structures, and Insecticidal Activities of Eight-Membered Azabridge Neonicotinoid Analogues

Renbo Xu, Rui Xia, Ming Luo, Xiaoyong Xu,* Jiagao Cheng, Xusheng Shao, and Zhong Li*

Shanghai Key Laboratory of Chemical Biology, School of Pharmacy, East China University of Science and Technology, Shanghai 200237, China

Supporting Information

ABSTRACT: Three series of novel azabridge neonicotinoid analogues were designed and synthesized, which were constructed by starting material **A**, glutaraldehyde, and primary amine hydrochlorides (aliphatic amines, phenylhydrazines, and anilines). Most of the eight-membered azabridge compounds presented higher insecticidal activities than oxabridged compound **B** against cowpea aphid (*Aphis craccivora*) and brown planthopper (*Nilaparvata lugens*). Compared with imidacloprid, some azabridged compounds exhibited excellent insecticidal activity against brown planthopper. The crystal structures and bioassay indicated that changing bridge atoms from O to N could lead to entirely different conformations, which might be the important influential factor of the bioactivities.

KEYWORDS: *oxabridge, azabridge, neonicotinoids, insecticide*

INTRODUCTION

Based on the natural alkaloid nicotine, imidacloprid, discovered by Kagabu et al.,[1] was the forerunner of neonicotinoid insecticides. Moreover, following the organophosphates, carbamates, and pyrethroids, neonicotinoids were regarded as fourth-generation insecticides in modern crop protection.[2] Experimental research indicated that the neonicotinoids act selectively as agonist of the insect nicotinic acetylcholine receptors (nAChRs), one of the most important insect targets in mediating rapid excitatory neurotransmission in the central nervous system (CNS) of piercing−sucking insects.[3−7]

The neonicotinoid compounds have the characteristics of high efficiency, low mammalian toxicity, no cross-resistance, and unique mode of action (MoA), which had showed great development in agriculture and animal health markets in the past 20 years.[8] Recently, Dow AgroSciences launched a neonicotinoid insecticide, Sulfoxaflor[9] (Figure 1), which is a new member of the neonicotinoids.[10]

In our previous work,[11] by introducing succinaldehyde and glutaraldehyde, two unexpected oxabridged compounds, **B** and cycloxaprid (Figure 2), were synthesized. Interestingly, according to the crystallographic diffraction analysis and biological tests, the two oxabridged compounds exhibited large differences in overall conformation and insecticidal activities (Figure 2), which implied that the molecular structure could significantly influence the bioactivities. Therefore, an effort to modify the structure was carried out, in which the oxabridge was converted to an azabridge, by replacing O with N, to increase the insecticidal activities of bridged compounds.

Owing to the difficulties of obtaining succinaldehyde, in this paper, the synthesis and insecticidal activities of three series of eight-membered azabridged neonicotinoids are first reported; these compounds were constructed by starting material **A**,

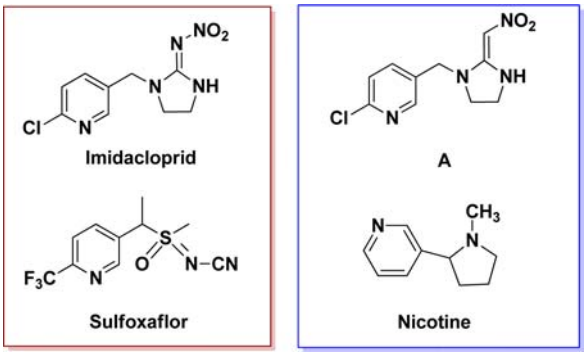

Figure 1. Nicotine and neonicotinoids.

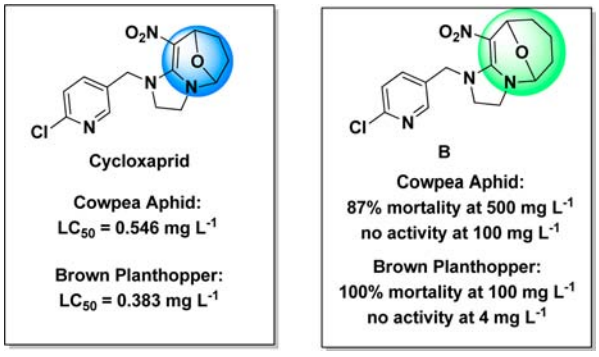

Figure 2. Comparison of biological activities between compound **B** and cycloxaprid.

Received: October 16, 2013
Revised: December 12, 2013
Accepted: December 23, 2013
Published: December 23, 2013

ACS Publications © 2013 American Chemical Society

glutaraldehyde, and three kinds of primary amine hydrochlorides (Scheme 1).

Scheme 1. Reaction Route To Synthesize Three Series of Compounds

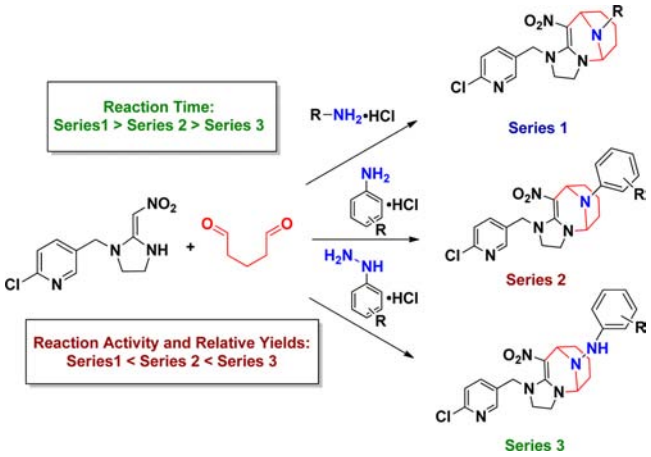

MATERIALS AND METHODS

Instruments and Chemicals. All melting points were obtained with a Büchi Melting Point B540 and are uncorrected. Nuclear magnetic resonance spectra were recorded on a Bruker AM-400 spectrometer with $CDCl_3$ or DMSO-d_6 as the solvent (^{1}H at 400 MHz and ^{13}C at 100 MHz) and TMS as the internal standard. Chemical shifts are reported in parts per million (δ). Coupling constants (J) are reported in hertz (Hz). High-resolution electron mass spectra (ESI-TOF) were performed on a Micromass LC-TOF spectrometer. Analytical thin-layer chromatography (TLC) was carried out on precoated plates (silica gel 60 F_{254}), and spots were visualized with ultraviolet (UV) light. All other solvents and reagents were obtained from commercial sources without further purification.

General Procedure for the Preparation of Aliphatic Amine Hydrochlorides. The corresponding aliphatic amine (20 mmol) was dissolved in diethyl ether (20 mL). With cooling and vigorous stirring, HCl gas was introduced into the mixture to yield an off-white precipitate. This was collected by filtration, washed with plenty of Et_2O, and used immediately.

General Procedure for the Preparation of Substituted Aniline Hydrochlorides. The corresponding aniline (20 mmol) in ethyl acetate (20 mL) was cooled to 0 °C. A solution of concentrated HCl was dropwise added and adjusted the pH value of the reaction mixture to 1−2. After the addition was completed, precipitate was filtered and washed with less concentrated HCl and ethyl acetate. After drying under vacuum, the obtained corresponding aniline hydrochloride could be used without further purification.

General Procedure for the Preparation of Substituted Phenylhydrazine Hydrochlorides. A suspension of the corresponding aniline (20 mmol) in concentrated HCl (40 mL) was cooled to −10 °C. A solution of $NaNO_2$ (20.2 mmol) in water (2 mL) was dropwise added, keeping the reaction temperature below 0 °C. After 30 min of stirring, a solution of $SnCl_2{\cdot}2H_2O$ (40.4 mmol) in concentrated HCl (15 mL) was slowly added. Amounts of precipitate were immediately formed. After the addition was completed, the mixture was stirred overnight and filtered. The precipitate was washed with less concentrated HCl and dichloromethane. After drying under vacuum, the obtained corresponding phenylhydrazine hydrochloride could be used without further purification.

General Procedure for the Preparation of Three Series. A mixture of starting material **A** (2 mmol), corresponding primary amine hydrochloride (2.5 mmol), and 50% mol NaH_2PO_4 (1 mmol) in acetonitrile (20 mL) was stirred at 0 °C. After 5 min of stirring, 25% glutaraldehyde aqueous solution (1 mL) was added slowly. Then the reaction mixture was stirred at 0 °C to room temperature and monitored by TLC. After completion, the pH value of the reaction mixture was adjusted to 7−8 by saturated aqueous $NaHCO_3$, and the solvent was removed under reduced pressure. The resulting mixture was extracted with dichloromethane (3 × 50 mL), and the organic layer was washed with brine, dried over anhydrous sodium sulfate, filtered, and concentrated. The residue was purified by silica gel column chromatography to afford the corresponding product.

Series 1: Compounds 1a−1d. *1-((6-Chloropyridin-3-yl)methyl)-11-methyl-10-nitro-1,2,3,5,6,7,8,9-octahydro-5,9-epiminoimidazo-[1,2-a]azocine (**1a**):* yield, 51.5%; mp, 165.6−166.2 °C; ^{1}H NMR (400 MHz, DMSO-d_6) δ 8.37 (d, J = 1.6 Hz, 1H), 7.84 (dd, J = 8.0, 2.0 Hz, 1H), 7.52 (d, J = 8.0 Hz, 1H), 4.88 (d, J = 15.2 Hz, 1H), 4.74 (d, J = 15.2 Hz, 1H), 4.20 (s, 1H), 3.96 (s, 1H), 3.77−3.49 (m, 4H), 2.11 (s, 3H), 1.84−1.68 (m, 2H), 1.66−1.51 (m, 2H), 1.48−1.35 (m, 1H), 1.17−0.98 (m, 1H); ^{13}C NMR (100 MHz, DMSO-d_6) δ 156.66, 149.78, 149.74, 139.91, 133.33, 124.48, 104.10, 72.83, 56.33, 51.63, 49.76, 49.06, 47.15, 29.41, 28.20, 15.45; HRMS (ES+) calcd for $C_{16}H_{20}{}^{35}ClN_5O_2Na$ $(M + Na)^+$ 372.1203; found, 372.1185; calcd for $C_{16}H_{20}{}^{37}ClN_5O_2Na$ $(M + Na)^+$ 374.1174; found, 374.1168.

*1-((6-Chloropyridin-3-yl)methyl)-11-ethyl-10-nitro-1,2,3,5,6,7,8,9-octahydro-5,9-epiminoimidazo[1,2-a]azocine (**1b**):* yield, 20%; mp, 130.4−131.1 °C; ^{1}H NMR (400 MHz, DMSO-d_6) δ 8.36 (d, J = 2.4 Hz, 1H), 7.83 (dd, J = 8.4, 2.4 Hz, 1H), 7.52 (d, J = 8.4 Hz, 1H), 4.86 (d, J = 15.6 Hz, 1H), 4.75 (d, J = 15.6 Hz, 1H), 4.32 (s, 1H), 4.10 (s, 1H), 3.76−3.50 (m, 4H), 2.37−2.20 (m, 1H), 2.19−2.06 (m, 1H), 1.84−1.72 (m, 2H), 1.66−1.50 (m, 2H), 1.50−1.40 (m, 1H), 1.20−1.04 (m, 1H), 0.95 (t, J = 7.2 Hz, 3H); ^{13}C NMR (100 MHz, DMSO-d_6) δ 157.34, 149.78, 149.73, 139.90, 133.01, 124.45, 104.84, 71.35, 53.86, 51.58, 49.82, 49.06, 47.17, 29.48, 28.41, 16.13, 13.18; HRMS (ES+) calcd for $C_{17}H_{23}{}^{35}ClN_5O_2$ $(M + H)^+$ 364.1540; found, 364.1535; calcd for $C_{17}H_{23}{}^{37}ClN_5O_2$ $(M + H)^+$ 366.1511; found, 366.1517.

*1-((6-Chloropyridin-3-yl)methyl)-11-isopropyl-10-nitro-1,2,3,5,6,7,8,9-octahydro-5,9-epiminoimidazo[1,2-a]azocine (**1c**):* yield, 3%; mp, 149.8−150.5 °C; ^{1}H NMR (400 MHz, DMSO-d_6) δ 8.36 (d, J = 1.6 Hz, 1H), 7.82 (dd, J = 8.4, 2.4 Hz, 1H), 7.51 (d, J = 8.0 Hz, 1H), 4.84 (d, J = 15.2 Hz, 1H), 4.78 (d, J = 15.2 Hz, 1H), 4.53 (s, 1H), 4.35 (s, 1H), 3.80−3.53 (m, 4H), 2.37−2.27 (m, 1H), 1.86−1.68 (m, 2H), 1.62−1.40 (m, 3H), 1.20−1.05 (m, 1H), 0.98 (d, J = 6.0 Hz, 3H), 0.89 (d, J = 6.4 Hz, 3H); ^{13}C NMR (100 MHz, DMSO-d_6) δ 157.87, 149.76, 149.74, 139.87, 133.02, 124.45, 105.39, 68.44, 51.72, 51.47, 49.98, 49.41, 46.79, 29.61, 29.01, 21.57, 21.42, 16.27; HRMS (ES+) calcd for $C_{18}H_{25}{}^{35}ClN_5O_2$ $(M + H)^+$ 378.1697; found, 378.1699; calcd for $C_{18}H_{25}{}^{37}ClN_5O_2$ $(M + H)^+$ 380.1667; found, 380.1674.

*1-((6-Chloropyridin-3-yl)methyl)-10-nitro-11-propyl-1,2,3,5,6,7,8,9-octahydro-5,9-epiminoimidazo[1,2-a]azocine (**1d**):* yield, 5%; mp, 152.3−153.2 °C; ^{1}H NMR (400 MHz, $CDCl_3$) δ 8.37 (d, J = 1.6 Hz, 1H), 7.86 (dd, J = 8.4, 2.4 Hz, 1H), 7.35 (d, J = 8.4 Hz, 1H), 5.00 (d, J = 15.2 Hz, 1H), 4.81 (d, J = 15.2 Hz, 1H), 4.39 (s, 1H), 4.17 (s, 1H), 3.80−3.45 (m, 4H), 2.38−2.01 (m, 3H), 1.85−1.75 (m, 2H), 1.69−1.61 (m, 2H), 1.55−1.41 (m, 2H), 1.38−1.17 (m, 1H), 0.90 (t, J = 6.8 Hz, 3H); ^{13}C NMR (100 MHz, $CDCl_3$) δ 157.20, 151.29, 149.12, 139.56, 131.24, 124.58, 105.82, 72.97, 55.32, 54.38, 52.18, 49.23, 46.93, 29.73, 28.05, 20.90, 16.03, 11.71; HRMS (ES+) calcd for $C_{18}H_{24}{}^{35}ClN_5O_2Na$ $(M + Na)^+$ 400.1520; found, 400.1511; calcd for $C_{18}H_{24}{}^{37}ClN_5O_2Na$ $(M + Na)^+$ 402.1487; found, 402.1493.

Series 2: Compounds 2a−2n. *1-((6-Chloropyridin-3-yl)methyl)-10-nitro-11-phenyl-1,2,3,5,6,7,8,9-octahydro-5,9-epiminoimidazo-[1,2-a]azocine (**2a**):* yield, 16.5%; mp, 186.8−187.6 °C; ^{1}H NMR (400 MHz, DMSO-d_6) δ 8.26 (d, J = 1.6 Hz, 1H), 7.59 (dd, J = 8.4, 2.4 Hz, 1H), 7.36 (d, J = 8.4 Hz, 1H), 7.27−7.18 (m, 2H), 6.96−6.85 (m, 3H), 5.37 (s, 1H), 5.01 (s, 1H), 4.77 (d, J = 15.6 Hz, 1H), 4.72 (d, J = 15.6 Hz, 1H), 3.78−3.48 (m, 4H), 2.06−1.95 (m, 1H), 1.95−1.84 (m, 1H), 1.84−1.71 (m, 2H), 1.65−1.51 (m, 1H), 1.33−1.22 (m, 1H); ^{13}C NMR (100 MHz, DMSO-d_6) δ 157.59, 149.70, 149.67, 148.74, 139.50, 132.65, 129.68, 124.42, 121.27, 117.49, 105.51, 68.88, 52.77, 51.25, 49.71, 46.77, 28.94, 28.53, 15.95; HRMS (EI+) calcd for

dx.doi.org/10.1021/jf4046683 | J. Agric. Food Chem. 2014, 62, 381−390

$C_{21}H_{22}{}^{35}ClN_5O_2$ $(M)^+$ 411.1462; found, 411.1458; calcd for $C_{21}H_{22}{}^{37}ClN_5O_2$ $(M)^+$ 413.1433; found, 413.1433.

*1-((6-Chloropyridin-3-yl)methyl)-10-nitro-11-(p-tolyl)-1,2,3,5,6,7,8,9-octahydro-5,9-epiminoimidazo[1,2-a]azocine (**2b**):* yield, 34.2%; mp, 200.8−201.7 °C; ^{1}H NMR (400 MHz, DMSO-d_6) δ 8.25 (d, J = 2.0 Hz, 1H), 7.59 (dd, J = 8.4, 2.4 Hz, 1H), 7.37 (d, J = 8.0 Hz, 1H), 7.02 (d, J = 8.4 Hz, 2H), 6.79 (d, J = 8.8 Hz, 2H), 5.31 (s, 1H), 4.94 (s, 1H), 4.79 (d, J = 15.2 Hz, 1H), 4.70 (d, J = 15.2 Hz, 1H), 3.75−3.50 (m, 5H), 2.23 (s, 3H), 2.04−1.94 (m, 1H), 1.94−1.85 (m, 1H), 1.85−1.70 (m, 2H), 1.65−1.53 (m, 1H), 1.33−1.17 (m, 1H); ^{13}C NMR (100 MHz, DMSO-d_6) δ 157.50, 149.69, 149.67, 146.41, 139.54, 132.65, 130.11, 130.07, 124.41, 117.51, 105.61, 69.18, 52.90, 51.15, 49.73, 46.86, 29.03, 28.41, 20.56, 16.00; HRMS (ES+) calcd for $C_{22}H_{24}{}^{35}ClN_5O_2Na$ $(M + Na)^+$ 448.1516; found, 448.1510; calcd for $C_{22}H_{24}{}^{37}ClN_5O_2Na$ $(M + Na)^+$ 450.1487; found, 450.1487.

*1-((6-Chloropyridin-3-yl)methyl)-10-nitro-11-(o-tolyl)-1,2,3,5,6,7,8,9-octahydro-5,9-epiminoimidazo[1,2-a]azocine (**2c**):* yield, 41.7%; mp, 164.4−165.2 °C; ^{1}H NMR (400 MHz, DMSO-d_6) δ 8.35 (d, J = 2.0 Hz, 1H), 7.79 (dd, J = 8.0, 2.0 Hz, 1H), 7.50 (d, J = 8.0 Hz, 1H), 7.17 (d, J = 6.8 Hz, 1H), 7.11−7.01 (m, 1H), 7.02−6.93 (m, 1H), 6.71 (d, J = 8.0 Hz, 1H), 4.86 (d, J = 15.2 Hz, 1H), 4.80 (d, J = 15.2 Hz, 1H), 4.72 (s, 1H), 4.47 (s, 1H), 3.85−3.72 (m, 2H), 3.72−3.58 (m, 2H), 2.28 (s, 3H), 2.00−1.91 (m, 1H), 1.91−1.77 (m, 3H), 1.69−1.53 (m, 1H), 1.36−1.19 (m, 2H); ^{13}C NMR (100 MHz, DMSO-d_6) δ 157.60, 149.81, 148.63, 139.90, 132.80, 132.10, 131.66, 127.13, 124.53, 123.94, 119.73, 105.51, 70.36, 55.39, 51.36, 49.92, 46.20, 29.08, 28.86, 18.50, 16.03; HRMS (ES+) calcd for $C_{22}H_{24}{}^{35}ClN_5O_2Na$ $(M + Na)^+$ 448.1516; found, 448.1514; calcd for $C_{22}H_{24}{}^{37}ClN_5O_2Na$ $(M + Na)^+$ 450.1487; found, 450.1500.

*1-((6-Chloropyridin-3-yl)methyl)-10-nitro-11-(m-tolyl)-1,2,3,5,6,7,8,9-octahydro-5,9-epiminoimidazo[1,2-a]azocine (**2d**):* yield, 39.0%; mp, 150.4−151.2 °C; ^{1}H NMR (400 MHz, DMSO-d_6) δ 8.27 (d, J = 2.4 Hz, 1H), 7.59 (dd, J = 8.0, 2.4 Hz, 1H), 7.36 (d, J = 8.0 Hz, 1H), 7.11 (t, J = 8.0 Hz, 1H), 6.77 (s, 1H), 6.72 (d, J = 7.2 Hz, 1H), 6.69−6.63 (m, 1H), 5.35 (s, 1H), 5.00 (s, 1H), 4.78 (d, J = 15.6 Hz, 1H), 4.72 (d, J = 15.6 Hz, 1H), 3.75−3.65 (m, 2H), 3.62−3.57 (m, 2H), 2.24 (s, 3H), 1.94−1.86 (m, 1H), 1.84−1.71 (m, 2H), 1.63−1.55 (m, 1H), 1.33−1.20 (m, 2H); ^{13}C NMR (100 MHz, DMSO-d_6) δ 157.65, 149.69, 149.67, 148.76, 139.50, 138.84, 132.66, 129.50, 124.39, 122.11, 118.36, 114.36, 105.59, 68.84, 52.84, 51.25, 49.67, 46.77, 28.95, 28.50, 21.87, 15.99; HRMS (ES+) calcd for $C_{22}H_{24}{}^{35}ClN_5O_2Na$ $(M + Na)^+$ 448.1516; found, 448.1504; calcd for $C_{22}H_{24}{}^{37}ClN_5O_2Na$ $(M + Na)^+$ 450.1487; found, 450.1494.

*11-(4-Bromophenyl)-1-((6-chloropyridin-3-yl)methyl)-10-nitro-1,2,3,5,6,7,8,9-octahydro-5,9-epiminoimidazo[1,2-a]azocine (**2e**):* yield, 29.2%; mp, 192.0−192.9 °C; ^{1}H NMR (400 MHz, $CDCl_3$) δ 8.25 (d, J = 2.0 Hz, 1H), 7.54 (dd, J = 8.0, 2.0 Hz, 1H), 7.37 (d, J = 8.8 Hz, 2H), 7.23 (d, J = 8.0 Hz, 1H), 6.80 (d, J = 8.8 Hz, 2H), 5.15 (s, 1H), 5.07 (s, 1H), 4.87 (d, J = 15.6 Hz, 1H), 4.74 (d, J = 15.6 Hz, 1H), 3.74−3.60 (m, 2H), 3.52−3.38 (m, 2H), 2.33−2.24 (m, 1H), 2.04 − 1.96 (m, 2H), 1.94−1.81 (m, 1H), 1.78−1.70 (m, 1H), 1.56−1.40 (m, 1H); ^{13}C NMR (100 MHz, $CDCl_3$) δ 157.32, 151.32, 149.07, 147.34, 138.83, 132.42, 130.85, 124.57, 119.23, 114.15, 106.04, 71.09, 52.52, 51.96, 49.04, 46.94, 29.86, 27.54, 16.07; HRMS (ES+) calcd for $C_{21}H_{21}{}^{35}Cl^{79}BrN_5O_2Na$ $(M + Na)^+$ 512.0465; found, 512.0456; calcd for $C_{21}H_{21}{}^{37}Cl^{81}BrN_5O_2Na$ $(M + Na)^+$ 516.0415; found, 516.0428.

*1-((6-Chloropyridin-3-yl)methyl)-10-nitro-11-(2-nitrophenyl)-1,2,3,5,6,7,8,9-octahydro-5,9-epiminoimidazo[1,2-a]azocine (**2f**):* yield, 7.2%; mp, 193.1−193.6 °C; ^{1}H NMR (400 MHz, DMSO-d_6) δ 8.33 (d, J = 2.0 Hz, 1H), 7.92−7.85 (m, 1H), 7.76 (dd, J = 8.0, 2.4 Hz, 1H), 7.57 (t, J = 7.2 Hz, 1H), 7.48 (d, J = 8.4 Hz, 1H), 7.26 (t, J = 7.6 Hz, 1H), 7.04 (d, J = 8.0 Hz, 1H), 4.87 (s, 1H), 4.84−4.75 (m, 2H), 4.58 (s, 1H), 3.83−3.62 (m, 4H), 2.03−1.93 (m, 1H), 1.80−1.74 (m, 2H), 1.66−1.54 (m, 1H), 1.32−1.18 (m, 2H); ^{13}C NMR (100 MHz, DMSO-d_6) δ 157.30, 149.82, 149.74, 144.09, 142.72, 139.80, 134.56, 132.66, 126.09, 124.49, 124.28, 122.25, 104.63, 70.21, 56.22, 51.46, 50.01, 46.10, 28.81, 28.65, 15.52; HRMS (ES+) calcd for $C_{21}H_{21}{}^{35}ClN_6O_4Na$ $(M + Na)^+$ 479.1211; found, 479.1219; calcd for $C_{21}H_{21}{}^{37}ClN_6O_4Na$ $(M + Na)^+$ 481.1181; found, 481.1175.

*1-((6-Chloropyridin-3-yl)methyl)-11-(2-fluorophenyl)-10-nitro-1,2,3,5,6,7,8,9-octahydro-5,9-epiminoimidazo[1,2-a]azocine (**2g**):* yield, 22.4%; mp, 148.7−149.3 °C; ^{1}H NMR (400 MHz, $CDCl_3$) δ 8.29 (d, J = 2.0 Hz, 1H), 7.74 (dd, J = 8.0, 2.4 Hz, 1H), 7.29 (d, J = 8.0 Hz, 1H), 7.09−6.99 (m, 3H), 6.87−6.80 (m, 1H), 5.01−4.91 (m, 3H), 4.77 (d, J = 15.2 Hz, 1H), 3.74−3.56 (m, 2H), 3.55−3.39 (m, 2H), 2.32−2.22 (m, 1H), 2.15−2.04 (m, 1H), 2.00−1.86 (m, 2H), 1.80−1.67 (m, 1H), 1.58−1.43 (m, 1H); ^{13}C NMR (100 MHz, $CDCl_3$) δ 157.31, 155.14 (d, J = 243.4 Hz, 1C), 151.30, 149.09, 139.18, 130.95, 124.87 (d, J = 3.6 Hz, 1C), 124.58, 123.61 (d, J = 7.9 Hz, 1C), 119.70, 116.46 (d, J = 20.6 Hz, 1C), 106.27, 71.54 (d, J = 7.9 Hz, 1C), 53.16, 52.07, 49.21, 46.68, 29.62, 27.82, 16.20; HRMS (ES+) calcd for $C_{21}H_{21}{}^{35}ClFN_5O_2Na$ $(M + Na)^+$ 452.1266; found, 452.1250; calcd for $C_{21}H_{21}{}^{37}ClFN_5O_2Na$ $(M + Na)^+$ 454.1236; found, 454.1235.

*11-(2-Chlorophenyl)-1-((6-chloropyridin-3-yl)methyl)-10-nitro-1,2,3,5,6,7,8,9-octahydro-5,9-epiminoimidazo[1,2-a]azocine (**2h**):* yield, 22.9%; mp, 199.8−200.6 °C; ^{1}H NMR (400 MHz, DMSO-d_6) δ 8.35 (d, J = 2.0 Hz, 1H), 7.78 (dd, J = 8.4, 2.4 Hz, 1H), 7.50 (d, J = 8.4 Hz, 1H), 7.45 (dd, J = 8.0, 1.6 Hz, 1H), 7.27−7.20 (m, 1H), 7.13−7.06 (m, 1H), 6.91−6.84 (m, 1H), 4.89 (s, 1H), 4.85 (d, J = 15.6 Hz, 1H), 4.79 (d, J = 15.6 Hz, 1H), 4.75 (s, 1H), 3.86−3.74 (m, 2H), 3.74−3.64 (m, 2H), 2.04−1.86 (m, 2H), 1.87−1.74 (m, 2H), 1.67−1.56 (m, 1H), 1.34−1.19 (m, 1H); ^{13}C NMR (100 MHz, DMSO-d_6) δ 157.40, 149.81, 149.78, 146.31, 139.87, 132.74, 131.02, 128.68, 128.14, 125.20, 124.53, 121.72, 105.00, 69.94, 54.82, 51.40, 50.00, 46.13, 28.81, 28.67, 15.75; HRMS (ES+) calcd for $C_{21}H_{21}{}^{35}Cl_2N_5O_2Na$ $(M + Na)^+$ 468.0970; found, 468.0982; calcd for $C_{21}H_{21}{}^{37}Cl_2N_5O_2Na$ $(M + Na)^+$ 472.0911; found, 472.0932.

*11-(2-Bromophenyl)-1-((6-chloropyridin-3-yl)methyl)-10-nitro-1,2,3,5,6,7,8,9-octahydro-5,9-epiminoimidazo[1,2-a]azocine (**2i**):* yield, 12.7%; mp, 193.0−193.7 °C; ^{1}H NMR (400 MHz, DMSO-d_6) δ 8.35 (d, J = 2.0 Hz, 1H), 7.79 (dd, J = 8.0, 2.4 Hz, 1H), 7.66−7.58 (m, 1H), 7.50 (d, J = 8.4 Hz, 1H), 7.34−7.23 (m, 1H), 7.08−6.98 (m, 1H), 6.95−6.85 (m, 1H), 4.86 (s, 1H), 4.84 (d, J = 15.6 Hz, 1H), 4.79 (d, J = 15.6 Hz, 1H), 4.74 (s, 1H), 3.85−3.74 (m, 2H), 3.75−3.64 (m, 2H), 2.05−1.89 (m, 2H), 1.89−1.75 (m, 2H), 1.69−1.55 (m, 1H), 1.35−1.18 (m, 1H); ^{13}C NMR (100 MHz, DMSO-d_6) δ 157.43, 149.82, 149.79, 147.65, 139.88, 134.22, 132.76, 129.28, 125.81, 124.53, 122.20, 119.39, 104.90, 70.22, 55.21, 51.40, 50.00, 46.10, 28.81, 28.64, 15.70; HRMS (ES+) calcd for $C_{21}H_{21}{}^{35}Cl^{79}BrN_5O_2Na$ $(M + Na)^+$ 512.0465; found, 512.0463; calcd for $C_{21}H_{21}{}^{37}Cl^{81}BrN_5O_2Na$ $(M + Na)^+$ 516.0415; found, 516.0424.

*1-((6-Chloropyridin-3-yl)methyl)-10-nitro-11-(3-nitrophenyl)-1,2,3,5,6,7,8,9-octahydro-5,9-epiminoimidazo[1,2-a]azocine (**2j**):* yield, 4.4%; mp, 215.3-216.3 °C; ^{1}H NMR (400 MHz, DMSO-d_6) δ 8.21 (d, J = 2.0 Hz, 1H), 7.78−7.70 (m, 2H), 7.61 (dd, J = 8.0, 2.4 Hz, 1H), 7.52 (t, J = 8.0 Hz, 1H), 7.41−7.32 (m, 2H), 5.57 (s, 1H), 5.14 (s, 1H), 4.80 (d, J = 15.6 Hz, 1H), 4.71 (d, J = 15.6 Hz, 1H), 3.84−3.55 (m, 4H), 2.09−1.98 (m, 1H), 1.99−1.88 (m, 1H), 1.88−1.75 (m, 2H), 1.68−1.56 (m, 1H), 1.37−1.21 (m, 1H); ^{13}C NMR (100 MHz, DMSO-d_6) δ 157.40, 149.76, 149.72, 149.55, 149.29, 139.55, 132.47, 131.04, 124.34, 123.76, 115.84, 111.73, 104.93, 68.40, 52.80, 51.24, 49.98, 46.71, 28.73, 28.35, 15.68; HRMS (ES+) calcd for $C_{21}H_{21}{}^{35}ClN_6O_4Na$ $(M + Na)^+$ 479.1211; found, 479.1206; calcd for $C_{21}H_{21}{}^{37}ClN_6O_4Na$ $(M + Na)^+$ 481.1181; found, 481.1188.

*1-((6-Chloropyridin-3-yl)methyl)-10-nitro-11-(4-nitrophenyl)-1,2,3,5,6,7,8,9-octahydro-5,9-epiminoimidazo[1,2-a]azocine (**2k**):* yield, 5.2%; mp, 209.9−210.7 °C; ^{1}H NMR (400 MHz, DMSO-d_6) δ 8.22 (d, J = 2.4 Hz, 1H), 8.11 (d, J = 9.6 Hz, 2H), 7.63 (dd, J = 8.0, 2.4 Hz, 1H), 7.35 (d, J = 8.4 Hz, 1H), 7.11 (d, J = 9.2 Hz, 2H), 5.67 (s, 1H), 5.27 (s, 1H), 4.80 (d, J = 15.6 Hz, 1H), 4.71 (d, J = 15.6 Hz, 1H), 3.82−3.60 (m, 4H), 2.09−1.99 (m, 1H), 2.00−1.89 (m, 1H), 1.86−1.72 (m, 2H), 1.67−1.57 (m, 1H), 1.40−1.21 (m, 1H); ^{13}C NMR (100 MHz, DMSO-d_6) δ 157.34, 153.88, 149.71, 149.54, 140.32, 139.57, 132.45, 125.99, 124.35, 116.44, 105.27, 67.56, 52.31, 51.27, 50.18, 46.82, 28.63, 28.07, 15.67; HRMS (ES+) calcd for $C_{21}H_{21}{}^{35}ClN_6O_4Na$ $(M + Na)^+$ 479.1211; found, 479.1196; calcd for $C_{21}H_{21}{}^{37}ClN_6O_4Na$ $(M + Na)^+$ 481.1181; found, 481.1175.

11-(4-Bromo-2,6-dimethylphenyl)-1-((6-chloropyridin-3-yl)methyl)-10-nitro-1,2,3,5,6,7,8,9-octahydro-5,9-epiminoimidazo[1,2-

dx.doi.org/10.1021/jf4046683 | J. Agric. Food Chem. 2014, 62, 381−390

*a]azocine (**2l**):* yield, 32.8%; mp, 174.4−175.1 °C; ^{1}H NMR (400 MHz, DMSO-d_6) δ 8.40 (d, J = 2.4 Hz, 1H), 7.85 (dd, J = 8.0, 2.4 Hz, 1H), 7.54 (d, J = 8.4 Hz, 1H), 7.27 (s, 1H), 7.19 (s, 1H), 4.92 (d, J = 15.2 Hz, 1H), 4.79−4.64 (m, 2H), 4.32 (s, 1H), 3.82−3.59 (m, 4H), 2.31 (s, 3H), 2.15 (s, 3H), 2.10−1.96 (m, 1H), 1.96−1.85 (m, 1H), 1.86−1.72 (m, 1H), 1.72−1.53 (m, 2H), 1.46−1.27 (m, 1H); ^{13}C NMR (100 MHz, DMSO-d_6) δ 158.59, 149.80, 149.73, 146.75, 139.91, 136.21, 132.87, 131.76, 124.51, 117.09, 108.21, 69.60, 55.15, 51.45, 49.57, 46.24, 29.11, 28.66, 20.77, 19.70, 16.15; HRMS (ES+) calcd for $C_{23}H_{26}{}^{35}Cl^{79}BrN_5O_2$ (M + H)$^+$ 518.0958; found, 518.0958; calcd for $C_{23}H_{26}{}^{37}Cl^{81}BrN_5O_2$ (M + H)$^+$ 522.0908; found, 522.0917.

*11-(4-Chlorophenyl)-1-((6-chloropyridin-3-yl)methyl)-10-nitro-1,2,3,5,6,7,8,9-octahydro-5,9-epiminoimidazo[1,2-a]azocine (**2m**):* yield, 32.3%; mp, 186.4−187.3 °C; ^{1}H NMR (400 MHz, DMSO-d_6) δ 8.26 (d, J = 1.6 Hz, 1H), 7.60 (dd, J = 8.0, 2.4 Hz, 1H), 7.37 (d, J = 8.4 Hz, 1H), 7.26 (d, J = 8.4 Hz, 2H), 6.93 (d, J = 8.4 Hz, 2H), 5.37 (s, 1H), 4.99 (s, 1H), 4.79 (d, J = 15.2 Hz, 1H), 4.72 (d, J = 15.2 Hz, 1H), 3.77−3.52 (m, 4H), 2.05−1.96 (m, 1H), 1.96−1.85 (m, 1H), 1.85−1.70 (m, 2H), 1.65−1.52 (m, 1H), 1.35−1.18 (m, 1H); ^{13}C NMR (100 MHz, DMSO-d_6) δ 157.42, 149.74, 149.67, 147.66, 139.50, 132.59, 129.42, 125.03, 124.38, 119.22, 105.25, 68.82, 52.82, 51.22, 49.84, 46.80, 28.89, 28.34, 15.81; HRMS (ES+) calcd for $C_{21}H_{22}{}^{35}Cl_2N_5O_2$ (M + H)$^+$ 446.1151; found, 446.1150; calcd for $C_{21}H_{22}{}^{37}Cl_2N_5O_2$ (M + H)$^+$ 450.1092; found, 450.1094.

*1-((6-Chloropyridin-3-yl)methyl)-11-(2,5-dimethoxyphenyl)-10-nitro-1,2,3,5,6,7,8,9-octahydro-5,9-epiminoimidazo[1,2-a]azocine (**2n**):* yield, 17.2%; mp, 71.2−72.1 °C; ^{1}H NMR (400 MHz, DMSO-d_6) δ 8.34 (d, J = 1.6 Hz, 1H), 7.74 (dd, J = 8.4, 2.4 Hz, 1H), 7.44 (d, J = 8.4 Hz, 1H), 6.88 (d, J = 7.2 Hz, 1H), 6.55 (d, J = 8.8 Hz, 1H), 6.21 (s, 1H), 5.02 (s, 1H), 4.87−4.72 (m, 3H), 3.76 (s, 3H), 3.73−3.67 (m, 2H), 3.65 (s, 3H), 3.64−3.54 (m, 2H), 2.00−1.90 (m, 1H), 1.89−1.75 (m, 3H), 1.63−1.54 (m, 1H), 1.34−1.19 (m, 1H); ^{13}C NMR (100 MHz, DMSO-d_6) δ 157.61, 153.99, 149.74, 149.69, 146.31, 139.66, 139.22, 132.78, 124.45, 113.67, 106.53, 106.48, 105.44, 69.47, 56.73, 55.50, 53.59, 51.43, 49.58, 46.39, 28.82, 28.69, 15.95; HRMS (ES+) calcd for $C_{23}H_{27}{}^{35}ClN_5O_4$ (M + H)$^+$ 472.1753; found, 472.1746; calcd for $C_{23}H_{27}{}^{37}ClN_5O_4$ (M + H)$^+$ 474.1722; found, 474.1726.

Series 3: Compounds 3a−3u. *1-((6-Chloropyridin-3-yl)methyl)-10-nitro-N-phenyl-1,2,3,5,6,7,8,9-octahydro-5,9-epiminoimidazo-[1,2-a]azocin-11-amine (**3a**):* yield, 42%; mp, 181.6−182.2 °C; ^{1}H NMR (400 MHz, DMSO-d_6) δ 8.46 (d, J = 1.6 Hz, 1H), 7.93 (dd, J = 8.0, 2.0 Hz, 1H), 7.54 (d, J = 8.0 Hz, 1H), 7.14 (t, J = 7.6 Hz, 2H), 6.90 (d, J = 8.0 Hz, 2H), 6.67 (m, 1H), 5.06 (d, J = 15.6 Hz, 1H), 4.64 (d, J = 15.6 Hz, 1H), 4.39 (s, 1H), 4.21 (s, 1H), 3.78−3.52 (m, 4H), 2.01−1.73 (m, 4H), 1.51−1.42 (m, 1H), 1.30−0.98 (m, 1H); ^{13}C NMR (100 MHz, DMSO-d_6) δ 157.47, 150.98, 149.75, 149.62, 147.98, 139.93, 133.31, 129.29, 124.41, 113.50, 104.07, 73.58, 57.25, 52.51, 50.02, 46.57, 29.76, 29.08, 15.16; HRMS (ES+) calcd for $C_{21}H_{24}{}^{35}ClN_6O_2$ (M + H)$^+$ 427.1649; found, 427.1647; calcd for $C_{21}H_{24}{}^{37}ClN_6O_2$ (M + H)$^+$ 429.1620; found, 429.1633.

*1-((6-Chloropyridin-3-yl)methyl)-10-nitro-N-(p-tolyl)-1,2,3,5,6,7,8,9-octahydro-5,9-epiminoimidazo[1,2-a]azocin-11-amine (**3b**):* yield, 45.5%; mp, 179.0−179.6 °C; ^{1}H NMR (400 MHz, DMSO-d_6) δ 8.45 (d, J = 1.6 Hz, 1H), 7.92 (dd, J = 8.0, 2.0 Hz, 1H), 7.54 (d, J = 8.0 Hz, 1H), 6.96 (d, J = 7.8 Hz, 2H), 6.81 (d, J = 8.0 Hz, 2H), 5.05 (d, J = 15.6 Hz, 1H), 4.63 (d, J = 15.6 Hz, 1H), 4.38 (s, 1H), 4.20 (s, 1H), 3.76−3.51 (m, 4H), 2.18 (s, 3H), 1.95−1.70 (m, 4H), 1.55−1.39 (m, 1H), 1.28−1.00 (m, 1H); ^{13}C NMR (100 MHz, DMSO-d_6) δ 157.39, 149.76, 149.62, 145.64, 139.93, 133.32, 129.72, 127.43, 124.40, 113.87, 103.99, 73.56, 57.13, 52.47, 50.01, 46.59, 29.89, 29.22, 20.63, 15.12; HRMS (ES+) calcd for $C_{22}H_{26}{}^{35}ClN_6O_2$ (M + H)$^+$ 441.1806; found, 441.1801; calcd for $C_{22}H_{26}{}^{37}ClN_6O_2$ (M + H)$^+$ 443.1776; found, 443.1770.

*1-((6-Chloropyridin-3-yl)methyl)-N-(4-fluorophenyl)-10-nitro-1,2,3,5,6,7,8,9-octahydro-5,9-epiminoimidazo[1,2-a]azocin-11-amine (**3c**):* yield, 43%; mp, 191.6−192.4 °C; ^{1}H NMR (400 MHz, DMSO-d_6) δ 8.46 (d, J = 1.6 Hz, 1H), 7.93 (dd, J = 8.4, 2.4 Hz, 1H), 7.55 (d, J = 8.0 Hz, 1H), 6.99 (t, J = 8.8 Hz, 2H), 6.94−6.86 (m, 2H), 5.06 (d, J = 15.6 Hz, 1H), 4.64 (d, J = 15.6 Hz, 1H), 4.39 (s, 1H), 4.21 (s, 2H), 3.71−3.55 (m, 4H), 1.98−1.71 (m, 4H), 1.52−1.38 (m, 1H), 1.27−0.99 (m, 1H); ^{13}C NMR (100 MHz, DMSO-d_6) δ 156.18 (d, J = 258.2 Hz, 1C), 154.89, 149.77, 149.61, 144.66, 139.95, 133.31, 129.64, 124.41, 115.68 (d, J = 22.0 Hz, 1C), 114.53 (d, J = 7.4 Hz, 1C), 104.01, 73.52, 57.24, 52.52, 49.98, 46.58, 29.76, 29.14, 15.14; HRMS (ES+) calcd for $C_{21}H_{22}{}^{35}ClFN_6O_2Na$ (M + Na)$^+$ 467.1374; found, 467.1371; calcd for $C_{21}H_{22}{}^{37}ClFN_6O_2Na$ (M + Na)$^+$ 469.1345; found, 469.1367.

*1-((6-Chloropyridin-3-yl)methyl)-N-(2-methoxyphenyl)-10-nitro-1,2,3,5,6,7,8,9-octahydro-5,9-epiminoimidazo[1,2-a]azocin-11-amine (**3d**):* yield, 28.8%; mp, 169.6−170.5 °C; ^{1}H NMR (400 MHz, DMSO-d_6) δ 8.42 (d, J = 1.6 Hz, 1H), 7.87 (dd, J = 8.4, 2.4 Hz, 1H), 7.55 (d, J = 8.0 Hz, 1H), 7.14 (d, J = 7.6 Hz, 1H), 6.91−6.84 (m, 2H), 6.79−6.73 (m, 1H), 4.93 (d, J = 15.6 Hz, 1H), 4.83 (d, J = 15.6 Hz, 1H), 4.46 (s, 1H), 4.19 (s, 1H), 3.87−3.78 (m, 2H), 3.76 (s, 3H), 3.72−3.53 (m, 2H), 2.21−1.71 (m, 4H), 1.53−1.39 (m, 1H), 1.13−0.96 (m, 1H); ^{13}C NMR (100 MHz, DMSO-d_6) δ 157.31, 149.80, 149.72, 147.01, 139.88, 136.29, 132.83, 124.54, 121.52, 119.70, 113.99, 111.05, 102.96, 73.78, 57.32, 56.05, 51.62, 49.80, 46.52, 29.40, 29.25, 14.90; HRMS (ES+) calcd for $C_{22}H_{25}{}^{35}ClN_6O_3Na$ (M + Na)$^+$ 479.1574; found, 479.1574; calcd for $C_{22}H_{25}{}^{37}ClN_6O_3Na$ (M + Na)$^+$ 481.1545; found, 481.1544.

*N-(2-Chlorophenyl)-1-((6-chloropyridin-3-yl)methyl)-10-nitro-1,2,3,5,6,7,8,9-octahydro-5,9-epiminoimidazo[1,2-a]azocin-11-amine (**3e**):* yield, 66.5%; mp, 165.9−166.6 °C; ^{1}H NMR (400 MHz, DMSO-d_6) δ 8.42 (d, J = 1.6 Hz, 1H), 7.88 (dd, J = 8.0, 2.0 Hz, 1H), 7.54 (d, J = 8.0 Hz, 1H), 7.33−7.23 (m, 3H), 6.84−6.78 (m, 1H), 4.94 (d, J = 15.6 Hz, 1H), 4.84 (d, J = 15.6 Hz, 1H), 4.50 (s, 1H), 4.22 (s, 1H), 3.86−3.74 (m, 2H), 3.73−3.55 (m, 2H), 2.04−1.76 (m, 4H), 1.54−1.41 (m, 1H), 1.15−0.99 (m, 1H); ^{13}C NMR (100 MHz, DMSO-d_6) δ 156.66, 149.84, 149.80, 143.09, 139.92, 132.83, 129.63, 128.62, 124.59, 120.76, 118.39, 115.89, 102.75, 73.63, 57.73, 51.60, 49.95, 46.53, 29.39, 29.29, 14.80; HRMS (ES+) calcd for $C_{21}H_{22}{}^{35}Cl_2N_6O_2Na$ (M + Na)$^+$ 483.1079; found, 483.1064; calcd for $C_{21}H_{22}{}^{37}Cl_2N_6O_2Na$ (M + Na)$^+$ 487.1020; found, 487.1024.

*N-(4-Bromophenyl)-1-((6-chloropyridin-3-yl)methyl)-10-nitro-1,2,3,5,6,7,8,9-octahydro-5,9-epiminoimidazo[1,2-a]azocin-11-amine (**3f**):* yield,75.0%; mp, 195.0−195.8 °C; ^{1}H NMR (400 MHz, DMSO-d_6) δ 8.46 (d, J = 1.6 Hz, 1H), 7.93 (dd, J = 8.0, 2.0 Hz, 1H), 7.54 (d, J = 8.0 Hz, 1H), 7.29 (d, J = 8.0 Hz, 2H), 6.88 (d, J = 8.0 Hz, 2H), 5.06 (d, J = 15.6 Hz, 1H), 4.64 (d, J = 15.6 Hz, 1H), 4.39 (s, 1H), 4.20 (s, 1H), 3.77−3.56 (m, 4H), 1.97−1.73 (m, 4H), 1.53−1.40 (m, 1H), 1.31−1.00 (m, 1H); ^{13}C NMR (100 MHz, DMSO-d_6) δ 157.46, 149.77, 149.65, 147.53, 139.95, 133.30, 131.86, 124.40, 115.28, 109.20, 103.99, 73.46, 57.35, 52.55, 50.00, 46.54, 29.74, 29.14, 15.11; HRMS (ES+) calcd for $C_{21}H_{22}{}^{35}Cl^{79}BrN_6O_2Na$ (M + Na)$^+$ 527.0574; found, 527.0577; calcd for $C_{21}H_{22}{}^{37}Cl^{81}BrN_6O_2Na$ (M + Na)$^+$ 531.0524; found, 531.0526.

*N-(4-Chlorophenyl)-1-((6-chloropyridin-3-yl)methyl)-10-nitro-1,2,3,5,6,7,8,9-octahydro-5,9-epiminoimidazo[1,2-a]azocin-11-amine (**3g**):* yield, 66.5%; mp, 199.7−200.6 °C; ^{1}H NMR (400 MHz, DMSO-d_6) δ 8.46 (d, J = 1.6 Hz, 1H), 7.93 (dd, J = 8.0, 2.0 Hz, 1H), 7.54 (d, J = 8.0 Hz, 1H), 7.29 (d, J = 8.0 Hz, 2H), 6.88 (d, J = 8.0 Hz, 2H), 5.06 (d, J = 15.6 Hz, 1H), 4.64 (d, J = 15.6 Hz, 1H), 4.39 (s, 1H), 4.20 (s, 1H), 3.77−3.56 (m, 4H), 1.97−1.73 (m, 4H), 1.53−1.40 (m, 1H), 1.31−1.00 (m, 1H); ^{13}C NMR (100 MHz, DMSO-d_6) δ 157.48, 149.77, 149.62, 147.15, 139.95, 133.30, 129.02, 124.40, 121.69, 114.74, 104.00, 73.46, 57.34, 52.55, 49.99, 46.56, 29.73, 29.12, 15.09; HRMS (ES+) calcd for $C_{21}H_{22}{}^{35}Cl_2N_6O_2Na$ (M + Na)$^+$ 483.1079; found, 483.1076; calcd for $C_{21}H_{22}{}^{37}Cl_2N_6O_2Na$ (M + Na)$^+$ 487.1020; found, 487.1040.

*1-((6-Chloropyridin-3-yl)methyl)-10-nitro-N-(4-nitrophenyl)-1,2,3,5,6,7,8,9-octahydro-5,9-epiminoimidazo[1,2-a]azocin-11-amine (**3h**):* yield, 65%; mp, 186.5−187.2 °C; ^{1}H NMR (400 MHz, DMSO-d_6) δ 8.47 (d, J = 1.6 Hz, 1H), 8.07 (d, J = 8.8 Hz, 2H), 7.93 (dd, J = 8.0, 2.0 Hz, 1H), 7.55 (d, J = 8.0 Hz, 1H), 6.99 (d, J = 8.8 Hz, 2H), 5.06 (d, J = 15.6 Hz, 1H), 4.66 (d, J = 15.6 Hz, 1H), 4.47 (s, 1H), 4.22 (s, 1H), 3.77−3.59 (m, 4H), 1.99−1.79 (m, 4H), 1.53−1.42 (m, 1H), 1.21−1.01 (m, 1H); ^{13}C NMR (100 MHz, DMSO-d_6) δ 157.46, 153.83, 149.79, 149.64, 139.95, 137.77, 133.22, 126.56, 124.41, 111.30, 103.67, 73.07, 57.71, 52.57, 50.02, 46.40, 29.51, 29.18, 14.87; HRMS (ES+) calcd for $C_{21}H_{22}{}^{35}ClN_7O_4Na$ (M + Na)$^+$ 494.1319; found,

dx.doi.org/10.1021/jf4046683 | J. Agric. Food Chem. 2014, 62, 381−390

494.1318; calcd for $C_{21}H_{22}{}^{37}ClN_7O_4Na$ $(M + Na)^+$ 496.1290; found, 496.1280.

*1-((6-Chloropyridin-3-yl)methyl)-N-(2-ethyl-6-methylphenyl)-10-nitro-1,2,3,5,6,7,8,9-octahydro-5,9-epiminoimidazo[1,2-a]azocin-11-amine (**3i**):* yield, 22.5%; mp, 100.0−100.6 °C; ^{1}H NMR (400 MHz, DMSO-d_6) δ 8.45 (d, J = 1.6 Hz, 1H), 7.92 (dd, J = 8.4, 2.4 Hz, 1H), 7.55 (d, J = 8.0 Hz, 1H), 7.00 (d, J = 7.2 Hz, 1H), 6.95 (d, J = 7.2 Hz, 1H), 6.90−6.83 (m, 1H), 5.03 (d, J = 15.6 Hz, 1H), 4.73 (d, J = 15.6 Hz, 1H), 4.60 (s, 1H), 4.12 (s, 1H), 3.81−3.65 (m, 4H), 2.57 (q, J = 7.2 Hz, 2H), 2.16 (s, 3H), 1.97−1.88 (m, 1H), 1.79−1.59 (m, 3H), 1.58−1.46 (m, 1H), 1.45−1.34 (m, 1H), 1.17 (t, J = 7.2 Hz, 3H); ^{13}C NMR (100 MHz, DMSO-d_6) δ 157.10, 149.86, 149.72, 142.39, 139.89, 136.35, 133.11, 129.84, 128.77, 127.27, 124.52, 123.33, 103.05, 74.08, 57.03, 52.07, 50.11, 46.54, 29.64, 29.05, 24.29, 18.46, 15.41, 15.20; HRMS (ES+) calcd for $C_{24}H_{29}{}^{35}ClN_6O_2Na$ $(M + Na)^+$ 491.1938; found, 491.1938; calcd for $C_{24}H_{29}{}^{37}ClN_6O_2Na$ $(M + Na)^+$ 493.1909; found, 493.1901.

*1-((6-Chloropyridin-3-yl)methyl)-10-nitro-N-(m-tolyl)-1,2,3,5,6,7,8,9-octahydro-5,9-epiminoimidazo[1,2-a]azocin-11-amine (**3j**):* yield, 76.3%; mp, 175.9−176.6 °C; ^{1}H NMR (400 MHz, DMSO-d_6) δ 8.46 (d, J = 1.6 Hz, 1H), 7.94 (dd, J = 8.0, 2.0 Hz, 1H), 7.55 (d, J = 8.0 Hz, 1H), 7.02 (t, J = 7.2 Hz, 1H), 6.78−6.66 (m, 2H), 6.50 (d, J = 6.8 Hz, 1H), 5.06 (d, J = 15.2 Hz, 1H), 4.64 (d, J = 15.2 Hz, 1H), 4.38 (s, 1H), 4.20 (s, 1H), 3.82−3.54 (m, 4H), 2.22 (s, 3H), 1.96−1.72 (m, 4H), 1.52−1.40 (m, 1H), 1.25−1.01 (m, 1H); ^{13}C NMR (100 MHz, DMSO-d_6) δ 157.46, 149.77, 149.60, 148.01, 139.96, 138.31, 133.35, 129.17, 124.41, 119.55, 113.99, 110.76, 104.05, 73.60, 57.24, 52.56, 50.07, 46.63, 29.80, 28.97, 21.83, 15.19; HRMS (ES+) calcd for $C_{22}H_{25}{}^{35}ClN_6O_2Na$ $(M + Na)^+$ 463.1625; found, 463.1627; calcd for $C_{22}H_{25}{}^{37}ClN_6O_2Na$ $(M + Na)^+$ 465.1620; found, 465.1609.

*1-((6-Chloropyridin-3-yl)methyl)-N-(2,6-diethylphenyl)-10-nitro-1,2,3,5,6,7,8,9-octahydro-5,9-epiminoimidazo[1,2-a]azocin-11-amine (**3k**):* yield, 12.2%; mp, 169.6−170.1 °C; ^{1}H NMR (400 MHz, DMSO-d_6) δ 8.45 (d, J = 1.6 Hz, 1H), 7.92 (dd, J = 8.0, 2.0 Hz, 1H), 7.56 (d, J = 8.0 Hz, 1H), 7.02−6.89 (m, 3H), 5.04 (d, J = 14.8 Hz, 1H), 4.72 (d, J = 14.8 Hz, 1H), 4.61 (s, 1H), 4.14 (s, 1H), 3.83−3.64 (m, 4H), 2.01−1.85 (m, 1H), 1.81−1.59 (m, 3H), 1.58−1.45 (m, 1H), 1.45−1.33 (m, 1H), 1.30−0.95 (m, 10H); ^{13}C NMR (100 MHz, DMSO-d_6) δ 157.03, 149.87, 149.72, 141.64, 139.90, 136.07, 133.06, 126.94, 124.52, 123.60, 102.99, 74.01, 56.93, 52.03, 50.08, 46.60, 29.69, 28.98, 24.26, 15.43, 15.20; HRMS (ES+) calcd for $C_{25}H_{31}{}^{35}ClN_6O_2Na$ $(M + Na)^+$ 505.2095; found, 505.2093; calcd for $C_{25}H_{31}{}^{37}ClN_6O_2Na$ $(M + Na)^+$ 507.2065; found, 507.2059.

*1-((6-Chloropyridin-3-yl)methyl)-10-nitro-N-(o-tolyl)-1,2,3,5,6,7,8,9-octahydro-5,9-epiminoimidazo[1,2-a]azocin-11-amine (**3l**):* yield, 41.9%; mp, 180.0−180.4 °C; ^{1}H NMR (400 MHz, DMSO-d_6) δ 8.44 (d, J = 1.6 Hz, 1H), 7.90 (dd, J = 8.0, 2.0 Hz, 1H), 7.55 (d, J = 8.4 Hz, 1H), 7.12−7.08 (m, 2H), 7.03 (d, J = 7.2 Hz, 1H), 6.81−6.69 (m, 1H), 4.98 (d, J = 14.8 Hz, 1H), 4.77 (d, J = 14.8 Hz, 1H), 4.47 (s, 1H), 4.23 (s, 1H), 3.84−3.72 (m, 2H), 3.72−3.58 (m, 2H), 2.04 (s, 3H), 1.94−1.86 (m, 1H), 1.85−1.70 (m, 3H), 1.50−1.40 (m, 1H), 1.15−1.00 (m, 1H); ^{13}C NMR (100 MHz, DMSO-d_6) δ 157.03, 149.79, 149.76, 145.09, 139.96, 133.04, 130.76, 127.06, 124.53, 124.01, 120.18, 114.97, 103.24, 73.64, 57.31, 51.83, 49.92, 46.65, 29.54, 29.15, 17.69, 15.08; HRMS (ES+) calcd for $C_{22}H_{25}{}^{35}ClN_6O_2Na$ $(M + Na)^+$ 463.1625; found, 463.1610; calcd for $C_{22}H_{25}{}^{37}ClN_6O_2Na$ $(M + Na)^+$ 465.1596; found, 465.1597.

*1-((6-Chloropyridin-3-yl)methyl)-10-nitro-N-(2-nitrophenyl)-1,2,3,5,6,7,8,9-octahydro-5,9-epiminoimidazo[1,2-a]azocin-11-amine (**3m**):* yield, 11.8%; mp, 139.6−140.2 °C; ^{1}H NMR (400 MHz, DMSO-d_6) δ 8.70 (s, 1H), 8.44 (d, J = 1.6 Hz, 1H), 8.07 (d, J = 8.4 Hz, 1H), 7.91 (dd, J = 8.0, 2.0 Hz, 1H), 7.71−7.60 (m, 1H), 7.55 (d, J = 8.0 Hz, 1H), 6.92−6.83 (m, 1H), 5.00 (d, J = 15.6 Hz, 1H), 4.74 (d, J = 15.6 Hz, 1H), 4.59 (s, 1H), 4.31 (s, 1H), 3.87−3.54 (m, 4H), 2.07−1.77 (m, 4H), 1.56−1.42 (m, 1H), 1.20−1.00 (m, 1H); ^{13}C NMR (100 MHz, DMSO-d_6) δ 156.76, 149.80, 149.75, 144.34, 139.85, 137.31, 132.74, 131.67, 126.33, 124.56, 118.23, 116.34, 102.72, 73.50, 58.35, 51.94, 49.88, 46.61, 29.26, 28.98, 14.66; HRMS (ES+) calcd for $C_{21}H_{22}{}^{35}ClN_7O_4Na$ $(M + Na)^+$ 494.1319; found, 494.1311; calcd for $C_{21}H_{22}{}^{37}ClN_7O_4Na$ $(M + Na)^+$ 496.1290; found, 496.1287.

*1-((6-Chloropyridin-3-yl)methyl)-10-nitro-N-(3-nitrophenyl)-1,2,3,5,6,7,8,9-octahydro-5,9-epiminoimidazo[1,2-a]azocin-11-amine (**3n**):* yield, 49.3%; mp, 190.7−191.4 °C; ^{1}H NMR (400 MHz, DMSO-d_6) δ 8.47 (d, J = 1.6 Hz, 1H), 7.95 (dd, J = 8.0, 2.0 Hz, 1H), 7.71 (s, 1H), 7.56 (d, J = 7.6 Hz, 1H), 7.49 (d, J = 6.0 Hz, 1H), 7.47−7.38 (m, 1H), 7.34 (d, J = 6.8 Hz, 1H), 5.07 (d, J = 15.2 Hz, 1H), 4.66 (d, J = 15.2 Hz, 1H), 4.45 (s, 1H), 4.24 (s, 1H), 3.78−3.58 (m, 4H), 1.99−1.80 (m, 4H), 1.56−1.41 (m, 1H), 1.31−1.03 (m, 1H); ^{13}C NMR (100 MHz, DMSO-d_6) δ 157.48, 149.78, 149.64, 149.48, 149.16, 139.96, 133.27, 130.63, 124.42, 119.17, 112.57, 106.69, 103.89, 73.37, 57.53, 52.61, 50.01, 46.54, 29.72, 29.22, 14.98; HRMS (ES+) calcd for $C_{21}H_{22}{}^{35}ClN_7O_4Na$ $(M + Na)^+$ 494.1319; found, 494.1320; calcd for $C_{21}H_{22}{}^{37}ClN_7O_4Na$ $(M + Na)^+$ 496.1290; found, 496.1311.

*1-((6-Chloropyridin-3-yl)methyl)-N-(2,4-dinitrophenyl)-10-nitro-1,2,3,5,6,7,8,9-octahydro-5,9-epiminoimidazo[1,2-a]azocin-11-amine (**3o**):* yield, 37.1%; mp, 206.4−207.4 °C; ^{1}H NMR (400 MHz, DMSO-d_6) δ 9.20 (s, 1H), 8.83 (s, 1H), 8.46 (d, J = 1.6 Hz, 1H), 8.39 (d, J = 8.8 Hz, 1H), 7.91 (dd, J = 8.0, 2.0 Hz, 1H), 7.76 (d, J = 8.8 Hz, 1H), 7.55 (d, J = 8.0 Hz, 1H), 5.01 (d, J = 15.2 Hz, 1H), 4.77 (d, J = 15.2 Hz, 1H), 4.63 (s, 1H), 4.39 (s, 1H), 3.87−3.57 (m, 4H), 2.07−1.82 (m, 4H), 1.59−1.45 (m, 1H), 1.24−1.05 (m, 1H); ^{13}C NMR (100 MHz, DMSO-d_6) δ 156.54, 149.85, 149.80, 147.63, 139.83, 137.16, 132.71, 130.80, 130.19, 124.55, 123.49, 116.80, 102.37, 73.10, 58.37, 52.01, 49.95, 46.45, 29.20, 28.91, 14.56; HRMS (ES+) calcd for $C_{21}H_{21}{}^{35}ClN_8O_6Na$ $(M + Na)^+$ 539.1163; found, 539.1165; calcd for $C_{21}H_{21}{}^{37}ClN_8O_6Na$ $(M + Na)^+$ 541.1141; found, 541.1150.

*4-((1-((6-Chloropyridin-3-yl)methyl)-10-nitro-1,2,3,5,6,7,8,9-octahydro-5,9-epiminoimidazo[1,2-a]azocin-11-yl)amino)benzonitrile (**3p**):* yield, 40.8%; mp, 218.9−219.7 °C; ^{1}H NMR (400 MHz, DMSO-d_6) δ 8.47 (d, J = 1.6 Hz, 1H), 8.03 (s, 1H), 7.93 (dd, J = 8.0, 2.0 Hz, 1H), 7.55 (d, J = 8.0 Hz, 2H), 6.96 (d, J = 8.0 Hz, 2H), 5.06 (d, J = 15.6 Hz, 1H), 4.64 (d, J = 15.6 Hz, 1H), 4.42 (s, 1H), 4.20 (s, 1H), 3.77−3.54 (m, 4H), 2.00−1.73 (m, 4H), 1.53−1.39 (m, 1H), 1.19−1.01 (m, 1H); ^{13}C NMR (100 MHz, DMSO-d_6) δ 157.43, 151.73, 149.80, 149.66, 139.93, 133.96, 133.20, 124.41, 120.74, 112.50, 103.72, 98.55, 73.22, 57.59, 52.48, 49.96, 46.39, 29.49, 29.28, 14.89; HRMS (ES+) calcd for $C_{22}H_{22}{}^{35}ClN_7O_2Na$ $(M + Na)^+$ 474.1421; found, 474.1426; calcd for $C_{22}H_{22}{}^{37}ClN_7O_2Na$ $(M + Na)^+$ 476.1392; found, 476.1401.

*N-(4-Bromo-2,6-dimethylphenyl)-1-((6-chloropyridin-3-yl)methyl)-10-nitro-1,2,3,5,6,7,8,9-octahydro-5,9-epiminoimidazo[1,2-a]azocin-11-amine (**3q**):* yield, 32.8%; mp, 173.7−174.5 °C; ^{1}H NMR (400 MHz, DMSO-d_6) δ 8.45 (d, J = 1.6 Hz, 1H), 7.92 (dd, J = 8.4, 2.4 Hz, 1H), 7.55 (d, J = 8.4 Hz, 1H), 7.17 (s, 2H), 5.01 (d, J = 15.6 Hz, 1H), 4.72 (d, J = 15.6 Hz, 1H), 4.58 (s, 1H), 4.08 (s, 1H), 3.80−3.62 (m, 4H), 2.17 (s, 6H), 1.97−1.85 (m, 1H), 1.76−1.60 (m, 2H), 1.60−1.45 (m, 1H), 1.46−1.34 (m, 1H), 1.13−1.07 (m, 1H); ^{13}C NMR (100 MHz, DMSO-d_6) δ 157.16, 149.71, 149.70, 142.62, 139.89, 133.14, 132.88, 131.17, 124.48, 114.81, 102.94, 73.97, 65.39, 57.22, 52.16, 50.11, 46.47, 29.53, 29.13, 15.64, 15.15; HRMS (ES+) calcd for $C_{23}H_{27}{}^{35}Cl^{79}BrN_6O_2$ $(M + H)^+$ 533.1067; found, 533.1070; calcd for $C_{23}H_{27}{}^{37}Cl^{81}BrN_6O_2$ $(M + H)^+$ 537.1017; found, 537.1039.

*1-((6-Chloropyridin-3-yl)methyl)-10-nitro-N-(4-(trifluoromethyl)-phenyl)-1,2,3,5,6,7,8,9-octahydro-5,9-epiminoimidazo[1,2-a]-azocin-11-amine (**3r**):* yield, 32.1%; mp, 212.2−212.9 °C; ^{1}H NMR (400 MHz, DMSO-d_6) δ 8.47 (d, J = 1.6 Hz, 1H), 7.94 (dd, J = 8.0, 2.0 Hz, 1H), 7.71 (s, 1H), 7.55 (d, J = 8.4 Hz, 1H), 7.47 (d, J = 8.4 Hz, 2H), 7.02 (d, J = 8.4 Hz, 2H), 5.07 (d, J = 15.6 Hz, 1H), 4.64 (d, J = 15.6 Hz, 1H), 4.43 (s, 1H), 4.22 (s, 1H), 3.77−3.58 (m, 4H), 1.98−1.89 (m, 1H), 1.88−1.75 (m, 3H), 1.52−1.42 (m, 1H), 1.20−1.03 (m, 1H); ^{13}C NMR (100 MHz, DMSO-d_6) δ 157.45, 151.29, 149.77, 149.64, 139.91, 133.24, 126.71 (d, J = 3.7 Hz, 1C), 125.85 (d, J = 213.6 Hz, 1C), 124.51 (d, J = 56.6 Hz, 1C), 124.38, 118.03 (q, J = 31.8 Hz, 1C), 112.34, 103.83, 73.34, 57.51, 52.52, 49.96, 46.45, 29.60, 29.24, 14.97; HRMS (ES+) calcd for $C_{22}H_{22}{}^{35}ClF_3N_6O_2Na$ $(M + Na)^+$ 517.1353; found, 517.1337; calcd for $C_{22}H_{22}{}^{37}ClF_3N_6O_2Na$ $(M + Na)^+$ 519.1313; found, 519.1307.

*1-((6-Chloropyridin-3-yl)methyl)-N-(3-methoxyphenyl)-10-nitro-1,2,3,5,6,7,8,9-octahydro-5,9-epiminoimidazo[1,2-a]azocin-11-amine (**3s**):* yield, 9%; mp, 113.1−114.1 °C; ^{1}H NMR (400 MHz, DMSO-d_6) δ 8.47 (d, J = 1.6 Hz, 1H), 7.94 (dd, J = 8.0, 2.0 Hz, 1H),

dx.doi.org/10.1021/jf4046683 | J. Agric. Food Chem. 2014, 62, 381−390

7.55 (d, J = 8.0 Hz, 1H), 7.10−6.99 (m, 1H), 6.88 (s, 1H), 6.48 (s, 1H), 6.27 (d, J = 8.0 Hz, 1H), 5.07 (d, J = 15.6 Hz, 1H), 4.63 (d, J = 15.6 Hz, 1H), 4.39 (s, 1H), 4.22 (s, 1H), 3.70 (s, 3H), 3.69−3.55 (m, 4H), 1.97−1.88 (m, 1H), 1.88−1.70 (m, 3H), 1.53−1.40 (m, 1H), 1.13−1.06 (m, 1H); ^{13}C NMR (100 MHz, DMSO-d_6) δ 160.70, 157.45, 149.77, 149.63, 149.54, 139.93, 133.32, 130.12, 124.40, 106.04, 104.20, 104.00, 99.03, 73.55, 57.33, 55.17, 52.52, 49.99, 46.55, 29.75, 29.15, 15.14; HRMS (ES+) calcd for $C_{22}H_{25}{}^{35}ClN_6O_3Na$ $(M + Na)^+$ 479.1573; found, 479.1569; calcd for $C_{22}H_{25}{}^{37}ClN_6O_3Na$ $(M + Na)^+$ 481.1545; found, 481.1538.

*1-((6-Chloropyridin-3-yl)methyl)-N-(2,6-difluorophenyl)-10-nitro-1,2,3,5,6,7,8,9-octahydro-5,9-epiminoimidazo[1,2-a]azocin-11-amine (**3t**):* yield, 15.6%; mp, 159.9−160.5 °C; ^{1}H NMR (400 MHz, DMSO-d_6) δ 8.45 (d, J = 1.6 Hz, 1H), 7.92 (dd, J = 8.0, 2.0 Hz, 1H), 7.53 (d, J = 8.0 Hz, 1H), 7.11− 6.98 (m, 3H), 5.02 (d, J = 15.6 Hz, 1H), 4.70 (d, J = 15.6 Hz, 1H), 4.55 (s, 1H), 4.34 (s, 1H), 3.82−3.60 (m, 4H), 1.94−1.85 (m, 1H), 1.85−1.75 (m, 1H), 1.72−1.54 (m, 2H), 1.44−1.33 (m, 1H), 1.15−1.00 (m, 1H); ^{13}C NMR (100 MHz, DMSO-d_6) δ 157.07, δ 155.65 (dd, J = 244.9, 5.9 Hz, 1C), 139.79, 133.20, 124.60 (d, J = 14.1 Hz, 1C), 124.53, 124.41, 123.58 (t, J = 9.5 Hz, 1C), 112.26 (dd, J = 17.0, 6.8 Hz, 1C), 103.19, 74.24, 58.26, 52.32, 50.11, 46.76, 29.85, 29.10, 14.98; HRMS (ES+) calcd for $C_{21}H_{21}{}^{35}ClF_2N_6O_2Na$ $(M + Na)^+$ 485.1289; found, 485.1275; calcd for $C_{21}H_{21}{}^{37}ClF_2N_6O_2Na$ $(M + Na)^+$ 487.1251; found, 487.1245.

*N-(2-Bromophenyl)-1-((6-chloropyridin-3-yl)methyl)-10-nitro-1,2,3,5,6,7,8,9-octahydro-5,9-epiminoimidazo[1,2-a]azocin-11-amine (**3u**):* yield, 35.8%; mp, 182.4−183.3 °C; ^{1}H NMR (400 MHz, DMSO-d_6) δ 8.43 (d, J = 1.6 Hz, 1H), 7.88 (dd, J = 8.0, 2.0 Hz, 1H), 7.55 (d, J = 8.4 Hz, 1H), 7.45 (d, J = 8.0 Hz, 1H), 7.34−7.22 (m, 2H), 6.76 (t, J = 6.8 Hz, 1H), 4.95 (d, J = 15.6 Hz, 1H), 4.83 (d, J = 15.6 Hz, 1H), 4.51 (s, 1H), 4.22 (s, 1H), 3.86−3.76 (m, 2H), 3.74−3.64 (m, 2H), 2.01−1.90 (m, 1H), 1.88−1.75 (m, 3H), 1.51−1.42 (m, 1H), 1.14−0.98 (m, 1H); ^{13}C NMR (100 MHz, DMSO-d_6) δ 156.66, 149.85, 149.80, 143.89, 139.95, 132.78, 132.71, 129.24, 124.61, 121.52, 116.25, 108.75, 102.62, 73.70, 57.78, 51.64, 49.95, 46.62, 29.38, 29.23, 14.78; HRMS (ES+) calcd for $C_{21}H_{22}{}^{35}Cl^{79}BrN_6O_2Na$ $(M + Na)^+$ 527.0574; found, 527.0568; calcd for $C_{21}H_{22}{}^{37}Cl^{81}BrN_6O_2Na$ $(M + Na)^+$ 531.0524; found, 531.0517.

X-ray Diffraction Analysis. Compound **2a** was recrystallized by slow evaporation from a mixture of acetone, dichloromethane, and cyclohexane to afford a suitable single crystal. Green blocks of **2a** (0.23 mm × 0.18 mm × 0.13 mm) were mounted on a quartz fiber. Cell dimensions and intensities were measured at 293 K on a Bruker SMART CCD area detector diffractometer with graphite monochromated Mo Kα radiation (λ = 0.71073 Å); θ_{max} = 25.99°; 11673 measured reflections; 3763 independent reflections (R_{int} = 0.0277). Data were corrected for Lorentz and polarization effects and for absorption (t_{min} = 0.4568 and t_{max} = 1.0000). The structure was solved by direct methods using SHELXS-97;[12] all other calculations were performed with a Bruker SAINT System and Bruker SMART programs.[13] Full-matrix least-squares refinement based on F^2 using the weight of $1/[\sigma^2 (F_o^2) + (0.0613P)^2 + 0.0371P]$ gave final values of R = 0.0331, ωR = 0.0844, and GOF (F) = 1.035 for 263 variables and 3763 contributing reflections. Maximum shift/error = 0.000(3) and max/min residual electron density = 0.178/−0.156 e Å^{-3}. Hydrogen atoms were observed and refined with a fixed value of their isotropic displacement parameter.

Compound **3o** was recrystallized by slow evaporation from a mixture of acetone, dichloromethane, and cyclohexane to afford a suitable single crystal. Yellow blocks of **3o** (0.36 mm × 0.30 mm × 0.20 mm) were mounted on a quartz fiber. Cell dimensions and intensities were measured at 293 K on a Bruker SMART CCD area detector diffractometer with graphite monochromated Mo Kα radiation (λ = 0.71073 Å); θ_{max} = 32.64°; 24369 measured reflections; 7970 independent reflections (R_{int} = 0.0222). Data were corrected for Lorentz and polarization effects and for absorption (t_{min} = 0.9203 and t_{max} = 0.9546). The structure was solved by direct methods using SHELXS-97; all other calculations were performed with a Bruker SAINT System and Bruker SMART programs. Full-matrix least-squares refinement based on F^2 using the weight of $1/[\sigma^2 (F_o^2) + (0.0613P)^2 + 0.0371P]$ gave final values of R = 0.0378, ωR = 0.1077, and GOF (F) = 1.033 for 325 variables and 7970 contributing reflections. Maximum shift/error = 0.000(3) and max/min residual electron density = 0.521/−0.639 e Å^{-3}. Hydrogen atoms were observed and refined with a fixed value of their isotropic displacement parameter.

Biological Assay. All bioassays were performed on representative test organisms reared in the laboratory. The bioassay was repeated at 25 ± 1 °C according to statistical requirements. All compounds were dissolved in *N*,*N*-dimethylformamide (AP, Shanghai Chemical Reagent Co., Ltd., Shanghai, China) and diluted with distilled water containing Triton X-100 (0.1 mg L^{-1}) to obtain series concentrations of 500, 100, and 4 mg L^{-1} and others for bioassays. For comparative purposes, imidacloprid, cycloxaprid and oxabridged compound **B** were tested under the same conditions.

Insecticidal Test. The insecticidal activities of the synthetic compounds against cowpea aphid (*Aphis craccivora*) and brown planthopper (*Nilaparvata lugens*) were tested according to our previously reported procedure.[11,14]

RESULTS AND DISCUSSION

Synthesis. Generally, the eight-membered nitrogen-containing rings (azocines) were constructed by intra- or intermolecular reactions.[15,16] Among these, Robinson−Schöpf reaction was regarded as a classical and efficient intermolecular methodology to synthesize azabridged bicyclic systems, which involved 1,3-dicarbonyl compounds, methylamine hydrochloride, and dialdehydes via double-Mannich condensation.[17] Thus, by comparing the 1,3-dicarbonyl derivatives and cyclic β-nitroenamines (starting material **A**), it was discovered that these two structures have very similar nucleophilic centers (Figure 3), which indicated the possibility of synthesizing eight-membered azabridge neonicotinoid analogues by reacting with various primary amine hydrochlorides and glutaraldehyde (Scheme 2).

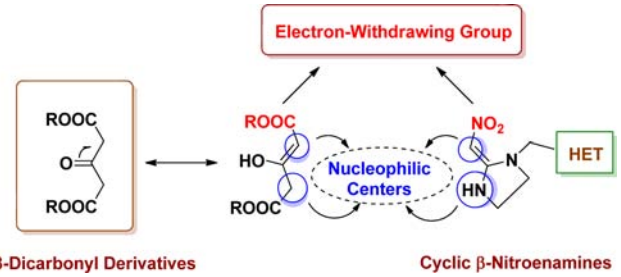

Figure 3. Structural comparison of the 1,3-dicarbonyl derivatives and cyclic β-nitroenamines.

When compound **1a** was synthesized, oxabridged compound **B** and a lot of unreacted starting material **A** were observed, which resulted in low yield (Table 1, entry 1). To optimize this reaction, several buffer salts and Lewis acids, such as $MgCl_2$, $NiCl_2$, $BF_3{\cdot}Et_2O$, $ZnCl_2$, $CoCl_2$, NH_4OAc, NaH_2PO_4, and Na_2HPO_4, were investigated (Table 1, entries 2−9). According to the screening of catalysts, NaH_2PO_4 presented higher yield. Furthermore, through adjusting the amounts of NaH_2PO_4, it was observed that 50 mol % was more appropriate to the reaction (Table 1, entry 10). Then, the influence of reaction temperature was studied. The results showed that increasing the reaction temperature led to decreasing yields. However, when the temperature was below 0 °C, the yield of **1a** was no longer improved (Table 1, entries 10 and 12−14). The effect of the solvent in the reaction was also investigated; various solvents such as acetonitrile, tetrahydrofuran (THF), H_2O,

dx.doi.org/10.1021/jf4046683 | J. Agric. Food Chem. 2014, 62, 381−390

Scheme 2. Retrosynthetic Strategy for Eight-Membered Azabridge Neonicotinoids

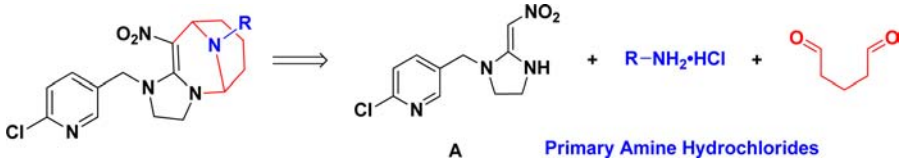

Table 1. Optimization of Compound 1a[a]

entry	solvent	catalyst	catalyst amount (mol %)	temperature[b] (°C)	yield[c] (%)
1	acetonitrile	none		25	19
2	acetonitrile	$MgCl_2$	10	25	20
3	acetonitrile	$NiCl_2$	10	25	20
4	acetonitrile	$BF_3{\cdot}Et_2O$	10	25	18
5	acetonitrile	$ZnCl_2$	10	25	16
6	acetonitrile	$CoCl_2$	10	25	18
7	acetonitrile	NH_4OAc	10	25	16
8	acetonitrile	Na_2HPO_4	10	25	NR[d]
9	acetonitrile	NaH_2PO_4	10	25	30
10	acetonitrile	NaH_2PO_4	50	25	47
11	acetonitrile	NaH_2PO_4	100	25	45
12	acetonitrile	NaH_2PO_4	50	40	11
13	acetonitrile	NaH_2PO_4	50	0	60
14	acetonitrile	NaH_2PO_4	50	−5	51
15	MeOH	NaH_2PO_4	50	0	10
16	acetone	NaH_2PO_4	50	0	16
17	dioxane	NaH_2PO_4	50	0	18
18	THF	NaH_2PO_4	50	0	24
19	CH_2Cl_2	NaH_2PO_4	50	0	14
20	H_2O	NaH_2PO_4	50	0	tr[e]
21	EtOH	NaH_2PO_4	50	0	4.7
22	1,2-dichloroethane	NaH_2PO_4	50	0	2.2

[a]All reactions were performed with glutaraldehyde (1.2 equiv mol), methylamine hydrochloride (1.2 equiv mol), and starting material **A** (1 equiv mol). [b]All reaction time were 12 h. [c]Yields were determined by HPLC. [d]No reaction. [e]Trace.

acetone, EtOH, CH_2Cl_2, 1,2-dichloroethane, and dioxane were employed. According to the yields of HPLC, acetonitrile was more suitable to carry out the reaction (Table 1, entries 13 and 15−22).

On the basis of the optimizations above, various aliphatic amine hydrochlorides were introduced to obtain series **1** (compounds **1a**−**1d**). With the extension of the alkyl chains, it was found the R_f values of the corresponding compounds were very close to those of the unreacted starting material **A** or oxabridged compound **B**, which resulted in the difficulties of isolation. For studying the effects of substituents on the bridged nitrogen atom, other primary amine hydrochlorides such as aniline hydrochlorides (series **2**) and phenylhydrazine hydrochlorides (series **3**) were employed. Consequently, another two series of azabridged analogues were synthesized. Compared to series **1**, the compounds of series **2** and **3** could be obtained with higher yields and the reaction could finish in shorter reaction time because of the different reaction activities among the three primary amine hydrochlorides (Scheme 1). However, the oxabridged compound **B** was still observed in the mixtures, which led to the low yields.

Crystal Structure Analysis. Azabridged compounds **2a** and **3o** were recrystallized by slow evaporation from mixed solvent of dichloromethane and acetone (v/v = 1:1), and their single-crystal structures were determined by X-ray crystallography as illustrated in Figures 4 and 5.

In these two crystal structures, the pharmacophore nitro groups lay approximately in the same plane with the imidazole ring. Under the delocalization role of the lone pair electron on the amine and the electron-withdrawing effect of the nitro group, a coplanar olefin-amine extended π electron network was formed in these two compounds. It resulted in the corresponding bond lengths of C—N (Table 2, entries 3 and 4) being shorter than the typical C—N single bond (1.47 Å) but close to the length of C═N (1.33 Å).[18,19] The bond lengths of C═C in **2a** and **3o** were 1.408 and 1.401 Å, respecitvely, which were longer than the normal C═C (1.34 Å), and the C—NO_2 was shorter than the typical C—NO_2 (1.49 Å) (Table 2, entry 1). Whereas the pyridine ring and the bridged oxygen atom of oxabridged compound **B** were directed in same orientation,[11] the pyridine and benzene rings of **2a** pointed in opposite directions. For **3o**, the directions of the nitrogen atom in the pyridine plane and the bridged nitrogen atom were contrary. Obviously, from the crystal structures, it was exhibited that the changing of bridge atoms or the substituents of the bridged nitrogen atom could lead to entirely different conformations, which might be important influential factors of the bioactivities.

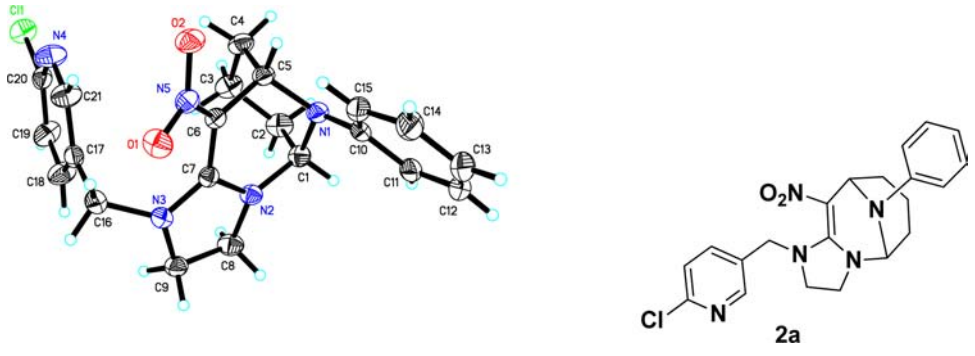

Figure 4. Crystal structure of compound **2a**.

dx.doi.org/10.1021/jf4046683 | J. Agric. Food Chem. 2014, 62, 381−390

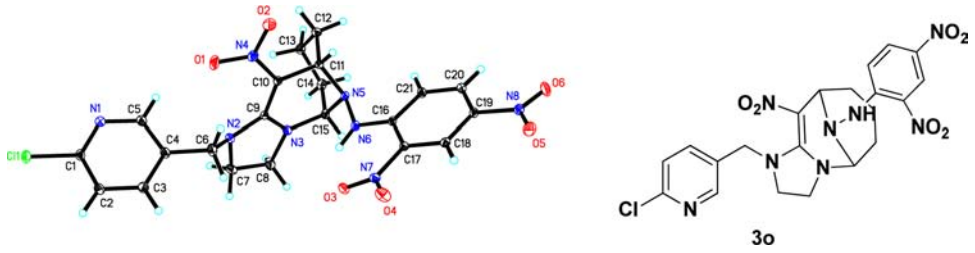

Figure 5. Crystal structure of compound **3o**.

Table 2. Compared Bond Lengths of Compounds 2a and 3o

	bond lengths (Å)			
entry	**2a**		**3o**	
1	N(5)−C(6)	1.361	N(4)−C(10)	1.380
2	C(6)−C(7)	1.408	C(9)−C(10)	1.401
3	N(2)−C(7)	1.347	N(2)−C(9)	1.373
4	N(3)−C(7)	1.344	N(3)−C(9)	1.350

Insecticidal Activities. The insecticidal activities of series **1** are shown in Table 3. At the concentration of 100 mg L^{-1}, the mortality of all tested compounds reached 100% against cowpea aphid (*A. craccivora*) and brown planthopper (*N. lugens*). Compared with imidacloprid, compounds **1b** and **1c** exhibited excellent insecticidal activity against brown planthopper (Table 6).

Table 3. Insecticidal Activities of Series 1

		mortality (%)			
		Aphis craccivora		*Nilaparvata lugens*	
compd	R	100 mg L^{-1}	4 mg L^{-1}	100 mg L^{-1}	4 mg L^{-1}
1a	Me	100	20	100	10
1b	Et	100	0	100	100
1c	i-Pr	100	0	100	90
1d	n-Pr	100	50	100	20
B		0	0	100	0
cycloxaprid		100	100	100	100
imidacloprid		100	100	100	100

The insecticidal activities of series **2** are listed in Table 4. Most of the azabridged compounds showed 100% mortality at 500 mg L^{-1}, which were higher than the oxabridged compound **B** against cowpea aphid. Compared to the unsubstituted compound **2a**, introducing electron-withdrawing groups, electron-donating groups, or halogen atoms did not contribute to great improvement of the bioactivities of the corresponding compounds. Moreover, when a bromine atom was introduced into the phenyl ring, related compounds **2e**, **2i**, and **2l** showed lower insecticidal activity than oxabridged compound **B** against cowpea aphid, which indicated that a bromine atom on position 2 or 4 of the phenyl ring would decrease the insecticidal activity. Meanwhile, compounds **2c**, **2g**, **2h**, and **2n** with electron-donating groups or halogen atoms (except Br) on position 2 of the phenyl group showed relatively high mortality at 4 mg L^{-1} against cowpea aphid, which confirmed that position 2 was the key substitution site for structural derivation to obtain high-activity molecules.

The bioactivities of series **3** are shown in Table 5. At the concentration of 100 mg L^{-1}, the mortality of most tested compounds reached 100% against cowpea aphid and brown planthopper, which was much higher than that of oxabridged compound **B**. Introducing halogen atoms into position 2 (**3e**, **3t**, and **3u**) and position 4 (**3c**, **3f**, and **3g**) of the phenyl ring could increase the activity against brown planthopper. Furthermore, the compounds with electron-donating groups

Table 4. Insecticidal Activities of Series 2

		mortality (%)			
		Aphis craccivora		*Nilaparvata lugens*	
compd	R	500 mg L^{-1}	4 mg L^{-1}	500 mg L^{-1}	4 mg L^{-1}
2a	H	100	20	100	0
2b	4-Me	100	5	100	50
2c	2-Me	100	30	100	0
2d	3-Me	100	10	100	0
2e	4-Br	0	0	0	0
2f	2-NO_2	100	5	100	0
2g	2-F	100	20	100	0
2h	2-Cl	100	30	100	0
2i	2-Br	34	5	100	0
2j	3- NO_2	80	15	100	0
2k	4-NO_2	100	0	100	0
2l	2,6-$(Me)_2$-4-Br	40	0	100	0
2m	4-Cl	14	0	100	0
2n	2,5-$(OMe)_2$	100	20	100	20
B		87	0	100	0
cycloxaprid		100	100	100	100
imidacloprid		100	100	100	100

dx.doi.org/10.1021/jf4046683 | J. Agric. Food Chem. 2014, 62, 381−390

Table 5. Insecticidal Activities of Series 3

		mortality (%)			
		Aphis craccivora		*Nilaparvata lugens*	
compd	R	100 mg L^{-1})	4 mg L^{-1})	100 mg L^{-1})	4 mg L^{-1})
3a	H	100	45	100	0
3b	4-Me	40	0	100	0
3c	4-F	100	40	100	80
3d	2-OMe	100	5	100	50
3e	2-Cl	100	4	100	60
3f	4-Br	100	40	100	60
3g	4-Cl	100	30	100	90
3h	4-NO_2	100	15	100	50
3i	2-Me-6-Et	100	45	100	50
3j	3-Me	100	30	100	80
3k	2,6-$(Et)_2$	100	15	100	0
3l	2-Me	100	20	100	0
3m	2-NO_2	100	5	100	0
3n	3- NO_2	100	20	85	0
3o	2,4- $(NO_2)_2$	60	20	50	0
3p	4-CN	100	20	100	0
3q	2,6-$(Me)_2$-4-Br	100	20	100	100
3r	4-CF_3	100	45	100	100
3s	3-OCH_3	100	30	100	90
3t	2,6-$(F)_2$	100	30	100	100
3u	2-Br	100	30	100	50
B		0	0	100	0
cycloxaprid		100	100	100	100
imidacloprid		100	100	100	100

on position 3 (**3j** and **3s**) also had higher insecticidal activity against brown planthopper compared with unsubstituted compound **3a**.

In conclusion, three series of eight-membered azabridged neonicotinoid analogues were designed and synthesized. All of the target compounds were obtained in optimized reaction conditions. The azabridged compounds constructed by aliphatic amine and phenylhydrazine hydrochlorides exhibited excellent insecticidal activities against cowpea aphid and brown planthopper among three series. On the basis of the LC_{50} values (Table 6), compounds **1b**, **1c**, **3c**, **3g**, **3j**, and **3r** showed higher bioactivity than imidacloprid against brown planthopper (Table 6). Most of the azabridged compounds presented higher bioactivities than eight-membered oxabridged compound **B** against cowpea aphid and brown planthopper, which indicated that the modification on the bridge atom was an effective strategy to discover new candidates as pesticides. However, the insecticidal activities against cowpea aphid and brown planthopper were lower than that of seven-membered oxabridged compound cycloxaprid. Therefore, the obtaining of seven-membered azabridges and study of their biological behavior are underway.

Table 6. LC_{50} Values of Some Azabridged Compounds against Brown Planthoppper

compd	$Y=a+bx$	LC_{50} (mg L^{-1})	95% limits
1b	$Y = 5.419 + 1.445x$	0.584	0.427−0.784
1c	$Y = 5.195 + 1.486x$	0.739	0.533−0.983
3c	$Y = 4.981 + 1.439x$	1.032	0.794−1.338
3e	$Y = 4.875 + 1.049x$	1.315	0.967−1.817
3f	$Y = 4.896 + 1.082x$	1.248	0.895−1.786
3g	$Y = 5.130 + 1.302x$	0.794	0.599−1.038
3j	$Y = 5.211 + 1.118x$	0.647	0.453−0.882
3q	$Y = -0.739 + 1.867x$	2.489	1.672−4.554
3r	$Y = 0.526 + 1.705x$	0.491	0.403−0.593
3s	$Y = -0.771 + 1.768x$	2.730	2.204−3.581
3t	$Y = -0.624 + 1.850x$	2.175	1.797−2.732
cycloxaprid	$Y = 5.743 + 1.786x$	0.383	0.197−0.593
imidacloprid	$Y = 4.908 + 2.477x$	1.089	0.973−1.218

■ ASSOCIATED CONTENT

Supporting Information

Crystallographic information files (CIFs) of compounds **2a** and **3o**. This material is available free of charge via the Internet at http://pubs.acs.org.

■ AUTHOR INFORMATION

Corresponding Authors

*(Z.L.) Phone: +86-21-64253540. Fax: +86-21-64252603. E-mail: lizhong@ecust.edu.cn.

*(X.X.) E-mail: xyxu@ecust.edu.cn

Funding

This work was financially supported by the National Basic Research Program of China (973 Program, 2010CB126100), the National High Technology Research and Development Program of China (863 Program, 2011AA10A207), and the National Natural Science Foundation of China (21272071). This work was also partly supported by the National Key Technology R&D Program of China (2011BAE06B01) and the Fundamental Research Funds for the Central Universities.

Notes

The authors declare no competing financial interest.

REFERENCES

(1) Zapol'skii, V. A; Fischer, R.; Namyslo, J. C.; Kaufmann, D. E. Chemistry of polyhalogenated nitrobutadienes, 8: nitropolychlorobutadienes – precursors for insecticidal neonicotinoids. *Bioorg. Med. Chem.* **2009**, *17*, 4206–4215.

(2) Tomizawa, M.; Casida, J. E. Neonicotinoid insecticides: highlights of a symposium on strategic molecular designs. *J. Agric. Food Chem.* **2011**, *59*, 2883–2886.

(3) Jepson, J. E. C.; Brown, L. A.; Sattelle, D. B. The actions of the neonicotinoid imidacloprid on cholinergic neurons of *Drosophila melanogaster*. *Invert. Neurosci.* **2006**, *6*, 33–40.

(4) Kagabu, S.; Ishihara, R.; Hieda, Y.; Nishimura, K.; Naruse, Y. Insecticidal and neuroblocking potencies of variants of the imidazolidine moiety of imidacloprid-related neonicotinoids and the relationship to partition coefficient and charge density on the pharmacophore. *J. Agric. Food Chem.* **2007**, *55*, 812–818.

(5) Tomizawa, M.; Casida, J. E. Molecular recognition of neonicotinoid insecticides: the determinants of life or death. *Acc. Chem. Res.* **2009**, *42*, 260–269.

(6) Tomizawa, M.; Casida, J. E. Unique neonicotinoid binding conformations conferring selective receptor interactions. *J. Agric. Food Chem.* **2011**, *59*, 2825–2828.

(7) Kagabu, S. Discovery of imidacloprid and further developments from strategic molecular designs. *J. Agric. Food Chem.* **2010**, *59*, 2887–2896.

(8) Jeschke, P.; Nauen, R.; Schindler, M.; Elbert, A. Overview of the status and global strategy for neonicotinoids. *J. Agric. Food Chem.* **2011**, *59*, 2897–2908.

(9) Zhu, Y. M.; Lose, M. R.; Watson, G. B.; Sparks, T. C.; Rogers, R. B.; Huang, J. X.; Gerwick, B. C.; Babcock, J. M.; Kelley, D.; Hegde, V. B.; Nugent, B. M.; Renga, J. M.; Denholm, I.; Gorman, K.; DeBoer, G. J.; Hasler, J.; Meade, T.; Thomas, J. D. Discovery and characterization of sulfoxaflor, a novel insecticide targeting sap-feeding pests. *J. Agric. Food Chem.* **2011**, *59*, 2950–2957.

(10) Qian, W. J.; Shi, X. L. Sulfoxaflor: a novel pesticide developed by Dow AgroSciences. *Pestic. Market News* **2010**, *23*, 35–35.

(11) Shao, X. S.; Fu, H.; Xu, X. Y.; Xu, X. L.; Liu, Z. W.; Li, Z.; Qian, X. H. Divalent and oxabridged neonicotinoids constructed by dialdehydes and nitromethylene analogues of imidacloprid: design, synthesis, crystal structure, and insecticidal activities. *J. Agric. Food Chem.* **2010**, *58*, 2696–2702.

(12) Sheldrick, G. M. *SHELXTL* (version 5.0); University of Göttingen: Göttingen, Germany, 2001.

(13) Bruker. *SMART* (version 5.628), *SAINT* (version 6.45), and *SADABS*; Brucker AXS: Madison, WI. USA, 2001.

(14) Tian, Z. Z.; Shao, X. S.; Li, Z.; Qian, X. H.; Huang, Q. C. Synthesis, insecticidal activity, and QSAR of novel nitromethylene neonicotinoids with tetrahydropyridine fixed cis configuration and exo-ring ether modification. *J. Agric. Food Chem.* **2007**, *55*, 2288–2292.

(15) Ohno, H.; Tanaka, T. Palladium(0)-catalyzed synthesis of medium-sized heterocycles by using bromoallenes as an allyl dication equivalent. *J. Am. Chem. Soc.* **2004**, *126*, 8744–8754.

(16) Majumdar, K. C.; Chattopadhyay, B. Synthesis of highly substituted dibenzoazocine derivatives by the aza-Claisen rearrangement and intramolecular Heck reaction via 8-exo-trig mode of cyclization. *Tetrahedron Lett.* **2009**, *50*, 3178–3181.

(17) Simon, S.; Constantieux, T.; Rodriguez, J. Utilisation of 1,3-dicarbonyl derivatives in multicomponent reactions. *Eur. J. Org. Chem.* **2004**, 4957–4980.

(18) Sasada, Y. Molecular and crystal structure. In *Chemistry Handbook*, 3rd ed.; Springer: Berlin, Germany, 1984.

(19) Kagabu, S.; Matsuno, H. Chloronicotinyl insecticides. 8. Crystal and molecular structures of imidacloprid and analogous compounds. *J. Agric. Food Chem.* **1997**, *45*, 276–281.

JOURNAL OF AGRICULTURAL AND FOOD CHEMISTRY

Article

pubs.acs.org/JAFC

Characterization of the Key Aroma Compounds in Turkish Olive Oils from Different Geographic Origins by Application of Aroma Extract Dilution Analysis (AEDA)

Songul Kesen,[†] Hasim Kelebek,[§] and Serkan Selli*[,#]

[†]Department of Food Technology, Naci Topcuoglu Vocational High School, Gaziantep University, 27600 Gaziantep, Turkey

[§]Department of Food Engineering, Faculty of Engineering and Natural Sciences, Adana Science and Technology University, 01110 Adana, Turkey

[#]Department of Food Engineering, Faculty of Agriculture, Cukurova University, 01330 Adana, Turkey

ABSTRACT: The aroma and aroma-active compounds of olive oils obtained from Nizip Yaglik (NY) and Kilis Yaglik (KY) cultivars and the effect of the geographical area (southern Anatolian and Aegean regions) on these compounds were analyzed by gas chromatography−mass spectrometry−olfactometry (GC-MS-O). For this purpose, two oil samples were obtained from their native geographical area including NY from Nizip province and KY from Kilis province (southern Anatolian region of Turkey). Another two oils of the same cultivar, NY-Bornova (NY-B) and KY-Bornova (KY-B), were obtained from the Olive Oil Research Center-Bornova, Izmir province (Aegean region of Turkey) to compare geographical effect on aroma and aroma-active compounds. Simultaneous distillation and extraction (SDE) with dichloromethane was used for extraction of volatile components. SDE gave a highly representative aromatic extract of the studied olive oil based on the sensory analysis. Totals of 61, 48, 59, and 48 aroma compounds were identified and quantified in olive oils obtained from NY, NY-B, KY, and KY-B cultivars, respectively. The results of principal component analysis (PCA) showed that the aroma profile of native region oils was discriminately different from those of Bornova region oils. Aldehydes and alcohols were qualitatively and quantitatively the most dominant volatiles in the oil samples. Aroma extract dilution analysis (AEDA) was used for the determination of aroma-active compounds of olive oils. The number of aroma-active compounds in native region oils was higher than in Bornova region oils. Within the compounds, aldehydes and alcohols were the largest aroma-active compounds in all olive oils.

KEYWORDS: *olive oil, olfactometry, aroma, aroma-active compounds, geographical effect*

INTRODUCTION

Olive oil is obtained from the olive (*Olea europaea*), a traditional tree crop of the Mediterranean area. It is almost unique among oils as it can be consumed in crude form without refining, possessing increased stability as well as nutritional and healthy features with respect to other vegetable oils.[1] According to olive oil production data released in 2012, Spain (992,000 tonnes), Italy (570,000 tonnes), Greece (351,800 tonnes), Turkey (206,300 tonnes), Syria (200,000 tonnes), and Tunisia (192,600 tonnes) are the leading production countries.[2]

Aroma compounds stimulate much more qualities and therefore are mainly responsible for the characteristic flavor of foods.[3] Olive oil aroma consists of a complex mixture of volatile compounds, which includes mainly aldehydes, alcohol, ketones, and esters. Enzymatic reactions and autoxidation play crucial roles in the occurrence of aroma substances. The formation of these compounds starts at the moment of cell disruption during crushing of olives and continues during the extraction process. Synthesis of the aroma compounds of virgin olive oil (VOO) occurs through the lipoxygenase (LOX) pathway comprising mainly the actuation of LOX and hydroperoxide-lyase enzymes. The volatile compounds found in virgin olive oil are mainly C-6 and C-5 compounds biogenerated from polyunsaturated fatty acids through the lipoxygenase pathway. These compounds are mainly responsible for the characteristic aroma of olive oil, which is of prime importance in the food industry, because it plays a significant role in consumer choice.[4−6]

More than 180 different aroma compounds have been found in olive oils.[6] However, it is well-accepted that only a small fraction on the large number of volatile compounds occurring in food actually contribute to the overall aroma. The technology of gas chromatography−olfactometry (GC-O) made it possible to divide identified volatiles into odor-active and non-odor-active compounds with regard to their existing concentration in the studied sample.[7,8] Limited numbers of researchers have analyzed the aroma-active compounds of olive oils: Guth and Grosch[9] determined potent odorants of different virgin olive oils using aroma extract dilution analysis (AEDA). They indicated that (*Z*)-3 hexenol, (*E*)-2-hexenal, and (*Z*)-3-hexenal were mainly responsible for the green odor notes of four different olive oils. Reiners and Grosch[10] studied the aroma-active compounds of virgin olive oils from Italy, Spain, and Morocco by AEDA and GC-O of headspace samples. Morales and Aparicio[7] investigated the best extraction conditions (temperature and time of malaxing) on the basis of odor-active compounds that are responsible for the unique

Received: October 8, 2013
Revised: December 24, 2013
Accepted: December 27, 2013
Published: December 27, 2013

ACS Publications © 2013 American Chemical Society

attributes of virgin olive oil. Collin et al.[11] determined the aroma-active compounds in extracts obtained by simultaneous extraction/distillation (SDE) of Moroccan black and green olives. In this study, odor-active compounds were identified by using the AEDA method and GC-O.

Cultivar is one of the most important factors that significantly influences volatile compound composition and sensorial characteristics of virgin olive oil. The same olive cultivar grown in different locations produces oils with different volatile profiles.[6] In addition to cultivar, the degree of fruit ripening, environment, growing season, traditional growing habits of various cultivars, extraction methods, processing techniques, and storage conditions affect the aroma profiles of olive oils.[12,13] It is well-known that VOO obtained from different cultivars, under identical growth conditions, harvested at roughly equal ripeness degree, and processed in the same manner, is characterized by more or less different composition and concentration of minor components.[8,14]

Up to now, there is no information on the identification of the main odorants in Turkish olive oils. NY and KY are economically important cultivars to olive production of the southern Anatolian region and used mainly for producing oil. Therefore, the aim of the present study was to investigate aroma and aroma-active compounds in two of the most important monovarietal olive oils (cvs. Nizip Yaglik (NY) and Kilis Yaglik (KY)) produced in two geographical areas of Turkey. Before the GC-MS-O analysis, the aromatic extract obtained from SDE was analyzed by sensory evaluation to assess its representativeness.

MATERIALS AND METHODS

Chemicals. The water used in the study was purified by a Millipore-Q system (Millipore Corp., Saint-Quentin, France). The reference aroma compounds were obtained from the following sources: Hexanal, (*E*)-2-pentenal, (*E*)-2-hexenal, (*Z*)-3-hexenal, nonanal, nonanol, (*E*)-2-heptenal, (*E*)-2-octenal, and (*E*)-2-decenal were obtained from Fluka (Buchs, Switzerland). 2-Methyl-1-propanol, 1-penten-3-ol, pentanol, 3-penten-2-ol, hexanol, (*E*)-3-hexenol, (*Z*)-3-hexenol, (*E*)-2-hexenol, 2-hexanol, heptanol, 2-ethyl-1-hexanol, (*Z*)-2-pentenol, phenol, hexyl acetate, (*Z*)-3-hexenyl acetate, ethyl salicylate, methyl palmitate, ethyl palmitate, limonene, linalool, (*Z*)-4-heptenal, 1-octen-3-ol, (*E*)-2-nonenal, benzaldehyde, (*E*,*E*)-2,4-heptadienal, (*E*,*E*)-2,4-decadienal, δ-octalactone, γ-nonalactone, γ-decalactone, δ-decalactone, δ-dodecalactone, and γ-dodecalactone were purchased from Sigma-Aldrich (Steinheim, Germany). Octanal, octanol, (*E*)-2-octenol, heptanal, benzyl alcohol, 2-phenylethanol, 6-methyl-5-hepten-2-one, β-pinene, α-copaene, α-farnesene, farnesol, acetic acid, octanoic acid, nonanoic acid, decanoic acid, hexanoic acid, dodecanoic acid, and guaiacol came from Merck (Darmstadt, Germany). Pentane, dichloromethane, 4-nonanol, sodium chloride, and sodium sulfate were also obtained from Merck (Darmstadt, Germany). Dichloromethane was freshly distilled prior to use. All chemicals used as standards and solvents were of GC grade having purity up to 99.0%.

Olives. Olive varieties (NY, KY, NY-B, and KY-B) averaging 50−70 kg were used in this study. Two olive samples were obtained from their native geographical area including NY from Nizip province and KY from Kilis province (southern Anatolian region of Turkey). To investigate geographical effect, the same olive cultivars were bought from the Olive Research Center located in Bornova-Izmir province (NY-B and KY-B; Aegean region of Turkey). Sound olives were harvested at the optimum maturity stage in 2011 seasons. The maturity indices were calculated according to the International Olive Oil Council method.[15]

Extraction of the Olive Oils. First, leaves were removed and then the healthy olives washed with water. Then, the cold-press with dual-phase centrifuge (Olio Mio Mini, Italy) was used for olive oil extraction. Cold-press has been a widely used method for many years to produce high-quality olive oils.[16] Olives in the mill after grinding for 30 min underwent malaxation (kneading). Then fractions were divided into decanters. These fractions were oil and wastewater plus oil cake. Fresh olive oils were put into glass bottles and were kept in a dark and cool place until analysis.

Standard Chemical Analysis. Moisture, oil content, percentage of free fatty acidity, and peroxide values of the samples were calculated following the methods described in the regulation of the European Economic Commission.[17] The color of the olive oil was measured in a colorimeter using a HunterLab Color QuestXE (Reston, VA, USA). Results for L^*, a^*, and b^* color system profile were recorded using CIE. Measurements were made at room temperature. Olive oils were placed in a sample cell (6 cm diameter), 2 cm deep, and the data were read.

Extraction of the Volatile Compounds. The volatile compounds of olive oils were extracted by SDE in a Likens-Nickerson apparatus (Neubert-Glas, Geschwenda, Germany). This method has already shown its reliability for the extraction of volatile components of olive oils.[18,19] For the extraction, 40 mL of olive oil, 100 mL of pure water, 25 mL of 30% NaCl, and 40 μg of 4-nonanol as the internal standard were put into a 500 mL distillation flask on one hand, and on the other 40 mL of dichloromethane solvent was pipetted into another (a 100 mL distillation flask). Both flasks were placed in a heater, and then extraction was performed for approximately 3 h. The temperatures of the sample mixture and the dichloromethane flasks were maintained by a water bath at 70 and 50 °C, respectively. After the dehydration by anhydrous sodium sulfate, the resulting organic extract was condensed to 5 mL in a Kuderna Danish concentrator (Sigma-Aldrich, St. Louis, MO, USA) and then to 200 μL under a gentle stream of pure nitrogen.[18] Olive oils were extracted in triplicate, and three independent extracts were obtained for each sample. The extracts were subsequently kept at −20 °C in a 2 mL glass vial before the analysis.

Representativeness Test of the Extract. *Sample Preparation and Presentation.* The panel was composed of seven assessors (two females and five males between 25 and 46 years old) from the Department of Food Engineering, University of Cukurova. The assessors were previously trained in odor recognition and sensory evaluation techniques and had experience in gas chromatography−olfactometry. In the present study, we used a cardboard smelling strip (reference 7140 BPSI, Granger-Veyron, Lyas, France) for checking the representativeness of the aromatic extract obtained by SDE. Smelling strips have already given good results for the representativeness test of orange juice[20] and Dwarf Cavendish banana extracts.[21] Two solvents (dichloromethane and pentane plus dichloromethane) were evaluated for the representativeness using SDE. First, 5 mL of olive oil was placed in a 25 mL brown coded flask as a reference for representativeness tests. Olive oil aromatic extracts obtained from two solvents were adsorbed onto a cardboard smelling strip. After 1 min (the time necessary for solvent evaporation), the extremities of the strips were cut off, and then they were placed in dark coded flasks (25 mL) and presented to the panel after 15 min. Dichloromethane and pentane/dichloromethane (2:1) are very volatile solvents. After evaporation, no panelists detected the odor of the solvents. Samples were assessed at room temperature (20 °C) and in neutral conditions.

Similarity and Intensity Tests. Similarity and intensity tests were performed to demonstrate the closeness between the odor of extracts and the olive oil. These test procedures were well documented in our previous studies.[20] Results were analyzed with an analysis of variance with Statgraphics Plus software (Manugistic, Inc., Rockville, MD, USA).

GC-FID, GC-MS, and GC-MS-O Analyses of Aroma Compounds. The GC system consisted of an Agilent 6890 chromatograph equipped with a flame ionization detector (FID) (Wilmington, DE, USA), an Agilent 5973-network-mass selective detector (MSD), and a Gerstel ODP-2 (Linthicum, MD, USA) sniffing port using deactivated capillary column (30 cm × 0.3 mm) heated at 240 °C and supplied with humidified air at 40 °C. This system allowed us to simultaneously obtain a FID signal for the quantification, an MS signal for the

dx.doi.org/10.1021/jf4045167 | J. Agric. Food Chem. 2014, 62, 391−401

Table 1. Olive Fruits and Olive Oils General Properties[a]

olive/olive oil property	NY	NY-B	KY	KY-B
maturity index	4.1 ± 0.00a	3.9 ± 0.00b	4.2 ± 0.00a	3.9 ± 0.00b
oil content (%)	26.30 ± 0.12b	21.80 ± 0.10d	30.50 ± 0.17a	24.50 ± 0.14c
moisture content (%)	50.33 ± 0.62a	47.46 ± 0.75b	47.04 ± 1.07b	43.62 ± 0.42c
free fatty acidity (oleic acid %)	0.68 ± 0.08a	0.77 ± 0.18a	0.67 ± 0.14a	0.69 ± 0.08a
peroxide value (mequiv oxygen/kg oil)	6.40 ± 0.16c	8.02 ± 0.13a	7.40 ± 0.18b	8.30 ± 0.16a
L^*	60.64 ± 0.06c	64.86 ± 0.04b	51.70 ± 0.05d	68.60 ± 0.03a
a^*	−1.87 ± 0.03c	2.37 ± 0.02a	−2.11 ± 0.02d	1.17 ± 0.01b
b^*	73.05 ± 1.69b	102.21 ± 0.13a	74.38 ± 0.10b	101.13 ± 0.10a

[a]Results are mean of three replications ± standard deviation. Values with different letters in same row are significant statistically ($p < 0.05$).

identification, and the odor characteristics of each compound detected by sniffing port. GC effluent was split 1:1:1 among the FID, MSD, and sniffing mode via a Dean's switch. Aroma compounds were separated on the DB-WAX (30 m length × 0.25 mm i.d. × 0.5 μm thickness; J&W Scientific, Folsom, CA, USA) column. A total of 3 μL of extract was injected each time in pulsed splitless (40 psi; 0.5 min) mode. The injector and FID detectors were set at 270 and 280 °C, respectively. The flow rate of carrier gas (helium) was 1.5 mL/min. The oven temperature of the DB-WAX column was first increased from 50 to 200 °C at a rate of 5 °C/min and then to 260 °C at 8 °C/min with a final hold at 260 °C for 5 min. The same oven temperature programs were used for the MSD. The mass detector was operated in scan mode, with an electronic impact ionization energy of 70 eV. The GC-MS interface and ionization source temperatures were set at 250 and 180 °C, respectively. Identification and quantification were performed in full scan mode with a mass/charge range of 30−300 amu at 2.0 scan/s scan rate. The compounds were identified by comparing their retention index and Wiley 6 and NIST 98 mass spectral data libraries installed in the GC-MS and the instrument's internal library created from previous laboratory studies. Some of the identifications were confirmed by the injection of the chemical standards into the GC-MS system. Retention indices of the compounds were calculated by using the retention data of the linear alkane series. After identification, the concentrations of aroma compounds were calculated according to the internal standard.[20]

Aroma Extract Dilution Analysis. The original aroma extracts were analyzed by GC-MS-O using three experienced sniffers. For AEDA, the concentrated aromatic extract (200 μL) of olive oils was stepwise diluted 1:1 using dichloromethane as the solvent to obtain dilutions of 1:1, 1:2, 1:4, 1:8, 1:16, and up to 1:1024 of the original extracts.[22] Sniffing of dilutions was continued until no odor could be detected by GC-MS-O. Each odor was thus assigned a flavor dilution factor (FD factor) representing the last dilution in which the odor was still detectable. As the FD factor of aroma compounds increases, also the degree of flavor activity increases.[23,24] This method has been used in different foods such as green olives[25] and orange juices.[26]

Sensory Analysis of Olive Oils. Sensory analysis of olive oil samples was made by a group of 10 trained panelists according to the published methods of the International Olive Oil Council determining the terms of organoleptic assessment.[27] Olive oil samples (15 mL) were placed in tasting glasses coded with different four-digit numbers. The temperatures of samples were kept at 28 ± 2 °C. A profile sheet was used by tasters. Each panelist smelled and then tasted the oil in the tasting glass and detected the intensity of the positive (fruity, bitter, pungent) and negative attributes (fusty/muddy, musty/humid, winey-vinegar, metallic, and rancid) on a 10 cm scale.

Statistical Analyses. The findings of this study were subjected to analysis of variance using the SPSS 17 software package, and Duncan's multiple-comparison test was used to find significant differences.[28] On the other hand, principal component analysis (PCA) was carried out using XLStat-Pro7.5 (2007) for Windows (Addinsoft, New York, NY, USA).

RESULTS AND DISCUSSION

Chemical Composition of Olive Oils. General properties of the assayed samples are shown in Table 1. As can be seen in Table 1, maturity indices were found between 3.9 and 4.2. This is an important factor in determining the harvest time of olives and must be between 2.5 and 4.5 for processed olive oil.[29] Oil and moisture contents of olives were found between 21.80 and 30.50% and between 43.62 and 50.33%, respectively. Oil contents of olive samples grown in the native region were higher than in olives grown in the Bornova geographical area. In addition, a similar situation was observed in the moisture content of the samples. This finding agrees with previous studies[30,31] reporting that a significant difference of olive oil composition exists among the different growing regions.

The percentage of free fatty acidity, peroxide values, and color values are usually used for quality characteristics and depend on the quality of the olives and on possible enzymatic alteration of olive fruits.[32] The percentage of free fatty acidity values of all olive oils were not significantly different ($p < 0.05$) and under the limit of 0.8% established for extra virgin olive oil. Peroxide values also were below the limit of 20 mequiv oxygen/kg oil, which is accepted as the limit for extra quality of VOO (Table 1). Peroxide values of native area oils were lower than in oils obtained from the Bornova area. In a previous study, acidity and peroxide values of olive oils obtained from 12 olive samples grown on islands of Italy and France were measured within the ranges of 0.20−1.34% and 3.28−16.15 mequiv oxygen/kg of oil, respectively.[33] Color properties of olive oils influence consumer acceptance. Color values varied depending on the cultivar and growing region. The L^*, a^*, and b^* values of olive oils obtained from olives grown in the Bornova area were higher than those of olives grown in native areas.

Representativeness of the Extract. *Intensity and Similarity Evaluation.* The intensity scores of the aromatic extract obtained from dichloromethane and pentane/dichloromethane solvents on smelling strips were found to be 63.5 and 64.2 mm on a 100 mm unstructured scale, respectively. The intensity scores of both extracts were close to each other. The differences of intensity scores for the two tests were not found as statistically significant. With regard to similarity evaluation, this score of dichloromethane extract (75.7 mm on a 100 mm unstructured scale) was found to be better than that of pentane/dichloromethane (50.2 mm on a 100 mm unstructured scale). The similarity scores of two solvents were found to be significantly different ($p < 0.05$). The similarity score of the dichloromethane extract was found to be acceptable and quite high and also scored relatively more closely to the reference sample. On the basis of these results, we selected the dichloromethane solvent for extracting olive oil aroma

dx.doi.org/10.1021/jf4045167 | J. Agric. Food Chem. 2014, 62, 391−401

Table 2. Volatile Compounds of Olive Oil Samples

			concentration[a] (μg/kg)				
no.	LRI[b]	aroma compound	NY	NY-B	KY	KY-B	identification[c]
1	1074	hexanal	3163.3a	1485.7d	2124.9b	1966.6c	LRI, MS, std
2	1077	(*E*)-hexyl-2-butenoate	46.7b	42.1b	192.0a	0.0	LRI, MS tent.
3	1104	2-methyl-1-propanol	243.2a	59.0b	223.0a	68.8b	LRI, MS, std
4	1108	*β*-pinene	0.0	0.0	140.7a	73.4b	LRI, MS, std
5	1121	(*E*)-2-pentenal	70.2b	37.8c	108.2a	75.1b	LRI, MS, std
6	1135	(*Z*)-3-hexenal	372.2a	244.0c	143.6d	317.5b	LRI, MS, std
7	1140	2-ethyl-(*E*)-2-butenal	391.2a	0.0	141.4b	0.0	LRI, MS tent.
8	1157	1-penten-3-ol	708.8a	188.1b	140.8c	108.6d	LRI, MS, std
9	1177	3-penten-2-ol	655.5b	487.2d	803.6a	544.1c	LRI, MS, std
10	1180	heptanal	0.0	48.3c	241.0a	170.9b	LRI, MS, std
11	1182	3-methyl-2-butenal	307.7a	0.0	133.0b	0.0	LRI, MS, std
12	1186	limonene	707.7a	179.6c	582.7b	93.0d	LRI, MS, std
13	1190	(*E*)-2-hexenal	9772.9a	5754.0c	9247.0b	4995.2d	LRI, MS, std
14	1197	3-hdroxy-3-methyl-2-butanone	63.3b	86.8a	0.0	83.8a	LRI, MS, tent
15	1248	pentanol	0.0	127.0b	199.8a	0.0	LRI, MS, std
16	1254	2-ethenyl-2-butenal	0.0	663.1a	406.6b	0.0	LRI, MS tent.
17	1285	hexyl acetate	0.0	211.6a	0.0	142.2b	LRI, MS, std
18	1292	octanal	135.6c	128.0c	360.8a	204.2b	LRI, MS, std
19	1295	4-heptanol	22.9b	0.0	53.6a	0.0	LRI, MS, std
20	1307	2-hexanol	923.5a	231.0c	439.3b	431.8b	LRI, MS, std
21	1309	ethyl chloroacetate	0.0	52.2a	0.0	45.9b	LRI, MS tent.
22	1311	(*E*)-2-heptenal	0.0	0.0	96.4b	319.2a	LRI, MS, std
23	1312	(*Z*)-3-hexenyl acetate	0.0	846.3a	0.0	160.1b	LRI, MS, std
24	1313	(*Z*)-4-heptenal	269.5a	0.0	42.2b	0.0	LRI, MS, std
25	1325	3-methyl-2-butenol	115.6b	0.0	0.0	145.2a	LRI, MS tent.
26	1328	(*Z*)-2-pentenol	997.9a	267.7c	564.8b	0.0	LRI, MS, std
27	1332	6-methyl-5-hepten-2-one	87.3a	35.1c	88.5a	68.5b	LRI, MS, std
28	1350	hexanol	1971.6a	849.6c	1877.4a	1346.6b	LRI, MS, std
29	1373	(*E*)-3-hexenol	521.6a	0.0	0.0	0.0	LRI, MS, std
30	1378	(*Z*)-3-hexenol	681.7c	779.5c	1426.1a	1066.2b	LRI, MS, std
31	1384	nonanal	163.8b	244.5a	237.4a	224.6a	LRI, MS, std
32	1386	3-octanol	47.9b	0.0	103.2a	0.0	LRI, MS tent.
33	1388	(*E*)-2-hexenol	2658.1a	1158.6c	2410.3b	657.7d	LRI, MS, std
34	1413	acetic acid	20.7b	0.0	50.7a	23.6b	LRI, MS, std
35	1434	(*E*)-2-octenal	211.7a	0.0	150.4b	104.4c	LRI, MS, std
36	1485	(*E*,*E*)-2,4-heptadienal	97.5c	73.0c	302.3a	222.8b	LRI, MS, std
37	1492	1-octen-3-ol	59.8b	0.0	70.2a	0.0	LRI, MS, std
38	1498	heptanol	44.0c	60.0b	151.9a	25.1d	LRI, MS, std
39	1505	*α*-copaene	663.6a	0.0	0.0	451.1b	LRI, MS, std
40	1508	2-ethyl-1-hexanol	70.9b	81.1b	475.0a	0.0	LRI, MS, std
41	1527	benzaldehyde	49.0c	55.6c	159.6b	215.3a	LRI, MS, std
42	1530	(*E*)-2-nonenol	0.0	77.2a	22.0b	80.8a	LRI, MS, std
43	1536	(*E*)-2-nonenal	118.3a	0.0	94.9b	0.0	LRI, MS, std
44	1537	linalool	103.7a	0.0	99.4a	54.4b	LRI, MS, std
45	1554	octanol	91.6b	50.3c	233.8a	18.4d	LRI, MS, std
46	1590	(*E*)-2-octenol	25.2a	0.0	15.8b	0.0	LRI, MS, std
47	1616	(*E*)-2-decenal	223.7b	202.2c	737.8a	163.4d	LRI, MS, std
48	1665	nonanol	55.8b	33.9c	74.5a	0.0	LRI, MS, std
49	1666	(*E*)-*β*-farnesene	32.5a	0.0	0.0	0.0	LRI, MS tent.
50	1685	*α*-terpinolene	0.0	87.6a	18.5c	37.9b	LRI, MS tent.
51	1692	*α*-muurolene	0.0	101.9b	301.7a	75.0c	LRI, MS tent.
52	1711	3-dodecenal	0.0	69.0b	282.0a	0.0	LRI, MS tent.
53	1719	(*E*,*E*)-*α*-farnesene	985.1a	0.0	20.1b	0.0	LRI, MS tent.
54	1745	*α*-farnesene	0.0	142.9c	2104.7a	514.5b	LRI, MS, std
55	1763	(*E*,*E*)-2,4-decadienal	331.4b	152.1d	365.4a	203.2c	LRI, MS, std
56	1792	ethyl salicylate	0.0	15.1a	0.0	22.5a	LRI, MS, std
57	1840	hexanoic acid	62.7b	27.8d	93.8a	48.9c	LRI, MS, std
58	1849	guaiacol	110.4a	71.2b	0.0	0.0	LRI, MS, std
59	1861	benzyl alcohol	91.5a	78.0b	0.0	0.0	LRI, MS, std

dx.doi.org/10.1021/jf4045167 | J. Agric. Food Chem. 2014, 62, 391−401

Table 2. continued

			concentration[a] (μg/kg)				
no.	LRI[b]	aroma compound	NY	NY-B	KY	KY-B	identification[c]
60	1870	2-phenylethanol	546.9a	208.9c	48.5d	258.0b	LRI, MS, std
61	1881	δ-octalactone	90.6a	0.0	42.8b	0.0	LRI, MS, std
62	1995	phenol	20.8b	0.0	0.0	43.3a	LRI, MS, std
63	2042	γ-nonalactone	127.4a	62.5c	0.0	87.1b	LRI, MS, std
64	2049	farnesol	289.2a	119.9c	0.0	143.7b	LRI, MS, std
65	2091	octanoic acid	52.8b	42.5b	77.3a	95.7a	LRI, MS, std
66	2103	γ-decalactone	240.9a	0.0	49.6b	54.5b	LRI, MS, std
67	2157	nonanoic acid	212.2b	137.9c	328.6a	199.0b	LRI, MS, std
68	2192	3-ethylphenol	74.3b	0.0	45.2	229.2a	LRI, MS tent.
69	2216	δ-decalactone	150.0a	0.0	82.6b	0.0	LRI, MS, std
70	2220	δ-dodecalactone	85.6a	0.0	0.0	0.0	LRI, MS, std
71	2233	methyl palmitate	93.9b	0.0	421.2a	0.0	LRI, MS, std
72	2270	ethyl palmitate	96.3b	0.0	168.9a	0.0	LRI, MS, std
73	2293	decanoic acid	95.3c	74.8d	185.6a	120.6b	LRI, MS, std
74	2384	γ-dodecalactone	255.2a	0.0	33.7b	0.0	LRI, MS, std
75	2391	dodecanoic acid	110.2a	52.9b	0.0	0.0	LRI, MS, std
		general total	31090a	16285b	29837a	16802b	

[a]Results are the means of three repetitions as μg/kg. Values with different letters in the same row are significant statistically ($p < 0.05$) [b]Linear retention index calculated on DB-WAX capillary column. [c]Methods of identification: LRI (linear retention index); MS tent., (tentatively identified by MS); std (chemical standard). When only MS or LRI is available for the identification of a compounds, it must be considered as an attempt of identification. Standard deviation of all aroma compounds was below 10%.

compounds. As previously stated, it is of great importance to assess the representativeness of the aromatic extracts in a matrix with characteristics similar to those of the original product.[34] When we compared other studies, the similarity score of the banana extracts was found to be 66.7 mm,[21] and that of rainbow trout (*Oncorhynchus mykiss*) was found to be 51.1 mm.[34] Briefly, the similarity and intensity results indicated that the representative aromatic extracts were achieved with the SDE method to determine the aroma-active compounds of olive oils. Similarly, the SDE technique has shown to be a reliable method for the determination of Moroccan black olive odor active compounds by Collin et al.[11] and hazelnut oils odorants by Pfnuer et al.[35]

Volatile Composition of Olive Oils. The volatile compounds identified in olive oils and linear retention index values on the DB-WAX column for these compounds are presented in Table 2. Mean values (μg/kg) of the GC analyses of triplicate extractions are reported. As can be seen in Table 2, a wide variety of volatile compounds was found in the VOO samples. Differences were observed in terms of the number of volatile compounds depending on growing regions. Totals of 61, 48, 59, and 48 compounds, including aldehydes, alcohols, ketones, esters, terpenes, lactones, carboxylic acids, and phenols, were identified and quantified in NY, NY-B, KY, and KY-B olive oils, respectively. The highest amount of volatiles was found in NY oil (31090 μg/kg), followed by KY (29837 μg/kg), KY-B (16802 μg/kg), and NY-B (16285 μg/kg). When the geographical effect was compared, the major difference observed was that the total amount of volatile compounds in the native region oils was approximately 2 times higher than that found in the Bornova region oils (Table 2). To evaluate the possibility of differentiating the oil samples taking into account the aromatic profile, we applied a multivariate statistical analysis using the total concentration of volatile in each of the eight chemical groups from Table 2. The variables were selected for the PCA, and the explained variance was 90.81% (factor 1, 54.32%; factor 2, 36.50%). Figure 1A represents the projection of the variables with regard to the single factor (PC1 or PC2) on the factor plane (PC1 × PC2). The application of the PCA algorithm showed two distinct groups (Figure 1B). The first group represents the results of NY and KY oils. The second one was characterized by KY-B and NY-B. The first group was positively associated with PC1 (lactones, alcohols, aldehydes, terpenes, and carboxylic acids), whereas the second group was negatively associated with PC1 (ketones and esters). It seems that each sample results in a different quarter of the PCA space: for example, KY-B has a higher quantity of ketones, NY-B is richer in esters, NY is characterized by a higher amount of lactones, and finally KY is characterized by terpenes and carboxylic acids. As previously stated, growing areas affected the aroma profiles of olive oils by different researchers. Issaoui et al.[36] studied the aroma profiles of virgin olive oils from the Tunisian Chemlali and Chétoui cultivars, grown in two different locations. They found significant differences of aroma profiles between the oils from both cultivars when grown in the different locations. In the results of their study, they stated that aroma profiles were influenced by the pedoclimatic conditions. Our data were also in accordance with the results obtained by Tura et al.[37] The authors investigated the geographical origin and cultivar effects on the typical volatile profile of extra virgin olive oils. They noted that the growing area and cultivars significantly affected the aroma profiling of oils. Most of the volatile compounds identified in the present study have already been identified in Italian, Spanish, and Greek olive oils.[16,18,31]

Aldehydes and alcohols quantitatively and qualitatively represent the main group of the volatile fraction in all olive oils compared to other volatile compounds. The main aldehyde compounds in oil samples were (*E*)-2-hexenal and hexanal (Table 2). The total concentration of these compounds in cv. NY (15678 μg/kg) was greater than those of the KY (15375 μg/kg), KY-B (9182.5 μg/kg), and NY-B (9157.4 μg/kg) oils.

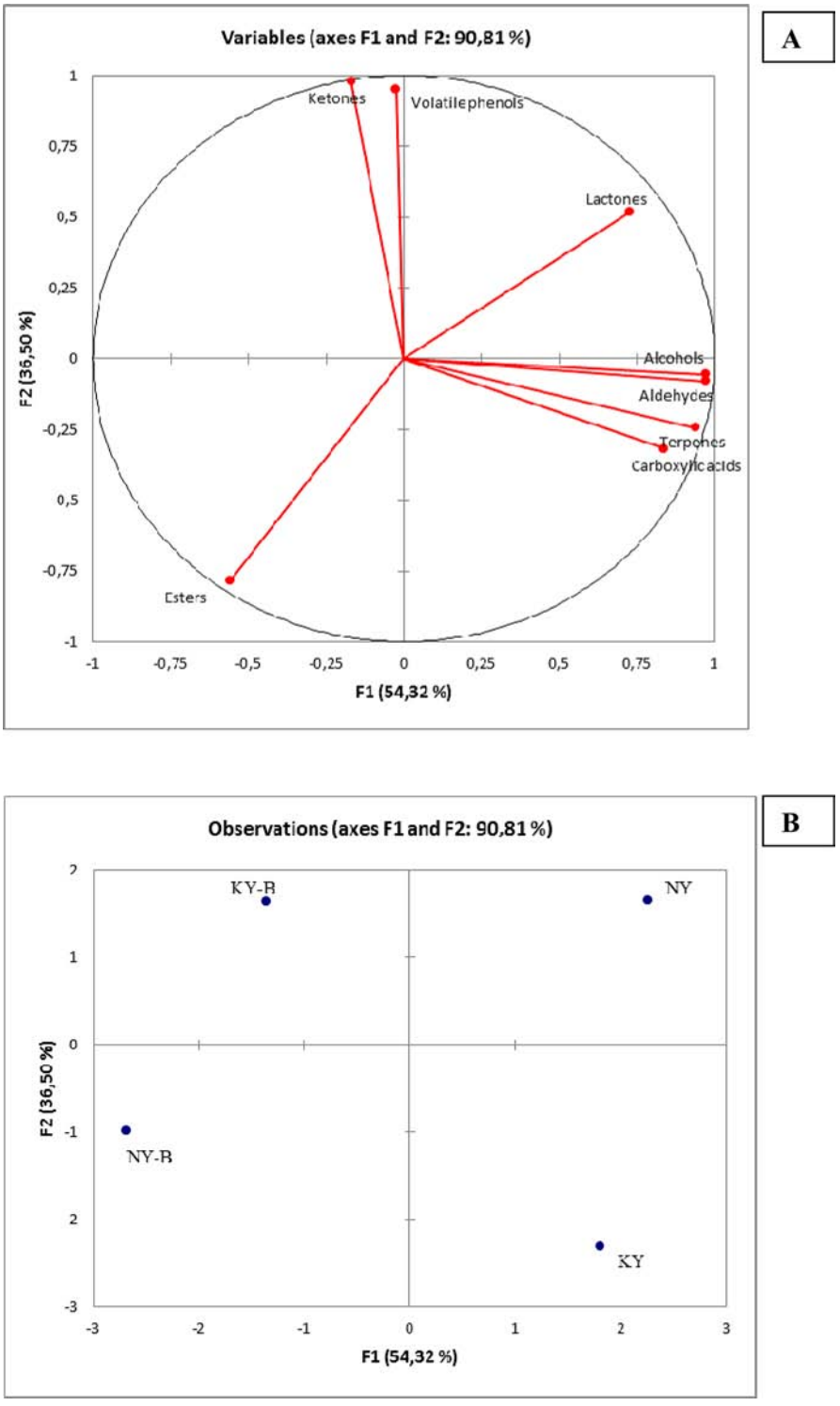

Figure 1. (A) Projection of the variables on the factor plane (PC1 × PC2) considering the aroma compounds quantified. (B) Score plot for the two principal components showing the two geographical origins studied.

Significant difference between the two growing areas was found for aldehydes, which were found in higher concentrations of the native region oils than the Bornova region oils. Kiralan et al.[38] also pointed out a significant difference in the composition of volatile components between the oils from the same cultivar and from different geographic regions. (*E*)-2-Hexenal and hexanal were present at the highest concentration in all oils, which accounted for between 13.82 and 21.42% and between 54.39 and 62.83% of total aldehyde compounds, respectively. The amounts of (*E*)-2-hexenal and hexanal in the native region oils reached higher levels than the Bornova region oils. Similarly, Aparicio et al.[39] reported that the major aroma compounds identified in most virgin olive oils from European countries are (*E*)-2-hexenal, hexanal, hexanol, and 3-methyl-butan-1-ol. (*E*)-2-Hexenal is produced by the enzymatic breakdown of the 13-hydroperoxide of linolenic acid in leaf homogenates, whereas hexanal is formed by the action of the enzyme aldehyde-lyase.[4,5] These aldehydes are widespread, as

dx.doi.org/10.1021/jf4045167 | *J. Agric. Food Chem.* 2014, 62, 391−401

Table 3. Aroma-Active Compounds of Olive Oil Samples (FD ≥ 8)

				FD factor[a]			
no.	LRI[b]	aroma compound	odor description[c]	NY	NY-B	KY	KY-B
1	1074	hexanal	cut grass	128	64	64	64
2	1108	β-pinene	green plant, floral			32	16
3	1121	(E)-2-pentenal	green plant, grassy	8		16	8
4	1135	(Z)-3-hexenal	vegetables, grassy, herbal	128	64	64	128
5	1171	2-ethyl-(E)-2-butenal	grassy, floral	256			
6	1176	1-penten-3-ol	grassy, green plant	1024	128	128	64
7	1178	3-penten-2-ol	green, grassy	64	16	128	16
8	1180	heptanal	green plant, oily			128	64
9	1182	3-methyl-2-butenal	floral, sweet	16			
10	1186	limonene	light floral	128		64	
11	1190	(E)-2-hexenal	cut grass, green	512	256	512	256
12	1243	unknown	citrus				16
13	1254	2-ethenyl-2-butenal	fruity, green		512	512	
14	1269	unknown	pickled olive			16	16
15	1285	hexyl acetate	fruity		32		16
16	1292	octanal	citrus, lemon	16		256	64
17	1300	(Z)-3-hexenyl acetate	fruity, green		128		32
18	1326	(Z)-2-pentenol	fatty	128		64	
19	1350	hexanol	floral, grass	128	32	64	64
20	1378	(Z)-3-hexenol	cut grass, herbal	128	128	256	256
21	1403	unknown	floral		16		
22	1408	(E)-2-octenal	green plant, fatty	16			
23	1412	(E)-2-hexenol	grassy, green, fruity	64	32	64	16
24	1485	(E,E)-2,4-heptadienal	fatty			32	16
25	1498	heptanol	margarine, fatty			16	
26	1521	α-copaene	sweet, fruity	64			32
27	1544	unknown	sweet, floral	32	16		
28	1547	linalool	lilac, lavender	128		128	32
29	1554	octanol	floral, grassy			16	
30	1563	unknown	sweet, fruity		16		16
31	1592	α-terpinolene	floral, light		16		
32	1616	(E)-2-decenal	soapy, fatty			16	
33	1665	nonanol	citrus	8		8	
34	1708	(E)-2-nonenol	fruity, waxy		32		32
35	1711	3-dodecenal	fatty			16	
36	1719	(E,E)-α-farnesene	floral, herb	32			
37	1745	α-farnesene	floral, green plant			64	16
38	1755	unknown	cocoa powder, chocolate				16
39	1763	(E,E)-2,4-decadienal	fatty, solvent	8	8	8	8
40	1824	guaiacol	olive paste, soapy	32	16		
41	1874	unknown	green plant		128		32
42	1922	2-phenylethanol	floral, rose	128	32		32
43	1980	unknown	floral	8		8	
44	2103	γ-decalactone	fruity	32		8	8
45	2216	δ-decalactone	fruity	64		8	
46	2233	methyl palmitate	fruity	8		128	
47	2270	ethyl palmitate	fruity	32		256	
48	2384	γ-dodecalactone	fruity	512			

[a]FD factor is the highest dilution of the extract at which an odorant is determined by aroma extract dilution analysis. [b]Linear retention index calculated on DB-WAX capillary column. [c]Odor description as perceived by panelists during olfactometry.

they have already been found in many other olive oils, such as Spanish cvs. Arbequina, Cornicabra, Morisca, Picolimon, Picudo, and Picual[40] and Tunisian cvs. Jemri Ben Gerdane, Chemlali Zarzis, and Zalmati.[41] Vichi et al.[42] studied the effect of different growing regions on the aroma profile of same cultivars. The authors noted that there were significant differences in the mean values of hexanal of the oils in relation to different regions. Among the aldehydes, the ratio hexanal/nonanal was found to be an appropriate way to detect the beginning of oxidation and its evolution,[19] and Morales et al.[43] proposed that, when the ratio of hexanal to nonanal was below 2, the oil should be considered as rancid. The ratios of these two aldehydes in NY, NY-B, KY, and KY-B olive oils were found to be 19.3, 6.1, 9.0, and 8.8, respectively.

Alcohols are produced by the action of ADH enzyme. It is widespread in the plant kingdom and is responsible for the

dx.doi.org/10.1021/jf4045167 | J. Agric. Food Chem. 2014, 62, 391−401

formation of volatile alcohols that contribute to the aroma of olive oils. The native region olive oils contained more alcohols than the Bornova region olive oils. The total amount of alcohols in the native region oils was approximately 2 times higher than the that of the Bornova region oils. The highest amount of alcohols was observed in NY oil (10534 μg/kg), probably related to higher activity of the alcohol dehydrogenase (ADH) enzyme, followed by KY (9333.6 μg/kg), KY-B (4751.4 μg/kg), and NY-B (4737.2 μg/kg) oils. Within the alcohols, C-6 alcohols such as hexanol, (*E*)-2-hexenol, and (*Z*)-3-hexenol were observed as high amounts in oil samples. When compared to other studies, a similar pattern of the three mentioned C-6 alcohols was identified in virgin olive oils from Spain,[40] Italy,[42] and Tunisia.[44] (*E*)-2-Hexenol predominated in NY (2658.1 μg/kg) and KY (2410.3 μg/kg) oil samples. Similarly, hexanol was observed in highest amount in the native region (NY = 1971.6 μg/kg and KY = 1877.4 μg/kg) oil samples. In previous studies, higher amounts of C-6 alcohols were determined in Tunisian and Italian olive oils, and the amount of hexanol and (*E*)-2-hexenol ranged between 50 and 2970 μg/kg and between 410 and 6920 μg/kg, respectively.[44]

GC-MS-O Results. The results of olfactometric analysis are given in Table 3. Application of the AEDA on the olive oil extracts revealed 29, 20, 30, and 27 aroma-active compounds in the NY, NY-B, KY, and KY-B oils, respectively. The differences in the number of aroma-active compounds of the oils are mainly caused by concentration differences of these compounds. As can be seen in Table 3, the native region oils contained more aroma-active compounds than the Bornova region oils. The FD factors of the compounds were detected to fall within the range of ≥8−1024 (Table 3). The compound having the highest FD factor (1024) was 1-penten-3-ol for NY oil, 2-ethenyl-2-butenal (FD = 512) for NY-B oil, (*E*)-2-hexenal and 2-ethenyl-2-butenal (FD = 512) for KY oil, and (*E*)-2-hexenal and (*Z*)-3-hexenol for KY-B oil.

Aldehydes were the largest class of aroma-active components of the olive oil extracts. Odor threshold values of these compounds are generally lower than those of volatile compounds; thus, they have important potential effect of the overall aroma of olive oils. A total of 14 aldehydes were identified in olive oils as key compounds (Table 3). Aldehydes are generally characterized by intense sensory description by panelists and are associated with green, cut grass, green plant, citrusy, fatty, and sweet notes. The total numbers of aroma-active aldehydes were 9, 5, 11, and 8 in NY, NY-B, KY, and KY-B oils, respectively. Among these compounds, hexanal, (*Z*)-3-hexenal, (*E*)-2-hexenal, and (*E*,*E*)-2,4-decadienal were common to all varieties. These aldehydes are widespread, as they have already been found in many other olive oils.[9,10] Within the aroma-active aldehydes, (*E*)-2-hexenal (FD = 512) for NY and KY oils and 2-ethenyl-2-butenal (FD = 512) for NY-B and KY oils were the most powerful aroma-active compounds to contribute to the aroma profile of oils. The first has a cut grass note, and the latter has a fruity, green note. The FD factor of (*E*)-2-hexenal was 256 for NY-B and KY-B. Solinas et al.[45] suggest that monovarietal virgin olive oils could be distinguished by the (*E*)-2-hexenal compound. This aldehyde is a well-known powerful odorant that contributes to the characteristic aromas of olive oils.[9] The other most important aldehydes, which have FD factors of 256, were 2-ethyl-(*E*)-2-butenal (grassy, floral) and octanal (citrus, lemon) for NY and KY, respectively. In a previous study, Dierkes et al.[46] stated that hexanal (green), (*E*)-2-hexenal (green, apple-like), nonanal (citrus-like), (*E*)-2-nonenal (paper-like, fatty), and (*E*,*E*)-2,4-decadienal (fatty, solvent) were potent aldehyde compounds in olive oils. Similarly, hexanal (fresh cut grass), (*E*)-2-hexenal (green), and heptanal (fatty, soapy) have been detected as aroma-active aldehyde compounds in Portuguese extra virgin olive oils from Galega Vulgar and Cobrançosa cultivars by Peres et al.[47]

Alcohols were the second largest class of odor-active compounds in the oil samples. A total of 11 aroma-active alcohol compounds were found in the samples. These were 1-penten-3-ol (grassy, green plant), 3-penten-2-ol (green, grassy), (*Z*)-2-pentenol (fatty), hexanol (floral, grassy), (*Z*)-3-hexenol (cut grass, herbal), (*E*)-2-hexenol (grassy, green plant, fruity), heptanol (margarine, fatty), octanol (floral, grassy), nonanol (citrus), (*E*)-2-nonenol (fruity, waxy), and 2-phenylethanol (rose). Within these, 1-penten-3-ol, 3-penten-2-ol, hexanol, (*Z*)-3-hexenol, and (*E*)-2-hexenol were common aroma-active alcohol compounds in all oil samples. The FD factors of these compounds varied depending on cultivar. Alcohols have less sensorily significant than aldehydes due to their higher odor threshold values. The most powerful aroma-active alcohol compound was 1-penten-3-ol to contribute to the aroma profile of the olive oils. The FD factor of these compounds was 1024 for NY. This compound was generated from polyunsaturated fatty acids (PUFA) by the influence of an enzyme such as lipoxygenase or hydroperoxidase.[48] (*Z*)-3-Hexenol (FD = 256 for KY and KY-B) was the second most important aroma-active alcohol compound in the oils. Most of the potent alcohols found in our samples have already been identified in olive oils by Luna et al.[8] and Dierkes et al.[46] and in green olives by Iraqi et al.[25] Among the alcohols, 2-phenylethanol was detected in NY, NY-B, and KY-B oils with FD factors of 128, 32, and 32, respectively, and described as a floral-rose odor. As stated previously, 2-phenylethanol has been cited as a major aroma-active compound in Moroccan black olives by Collin et al.[11] and in olive oils by Dierkes et al.,[46] providing a floral-fruity and sweet-winey odor, respectively.

β-Pinene (green plant, floral), limonene (light floral), *α*-copaene (sweet, fruity), linalool (lilac, lavender), *α*-terpinolene (floral, light), (*E*,*E*)-*α*-farnesene (floral, herb), and *α*-farnesene (floral, green plant) were detected as aroma-active terpene compounds in the olive oil extracts. The samples NY, KY, and KY-B contained four aroma-active terpene compounds, but NY-B only one. On the basis of GC-O, the most potent aroma-active terpenes were limonene and linalool, which have 128 FD factors. *β*-Pinene and *α*-farnesene were detected only in KY and KY-B oils. In addition, limonene was not sensed in oil obtained from the Bornova region. Among the terpenes, limonene, linalool, and *α*-farnesene were identified as being the key odorants in Moroccan green olives.[25]

Hexyl acetate (fruity, green), (*Z*)-3-hexenyl acetate (fruity, green), methyl palmitate (fruity), and ethyl palmitate (fruity) were detected in oil aromatic extracts as aroma-active compounds. Esters are the main volatile compounds found in most fruits and are responsible for the fruity notes.[20] Increasing the alcohol acetyl transferases (AAT) activity can enhance the production of volatile esters in olive oils.[42] Within the esters, ethyl palmitate had the highest FD factor (256) value detected by GC-O in KY oil.

Lactones contribute to the characteristic fruity odors of the olive oil samples. *γ*-Decalactone (fruity), *δ*-decalactone (fruity), and *γ*-dodecalactone (fruity) were identified as aroma-active lactone compounds. As summarized in Table 3, oil produced

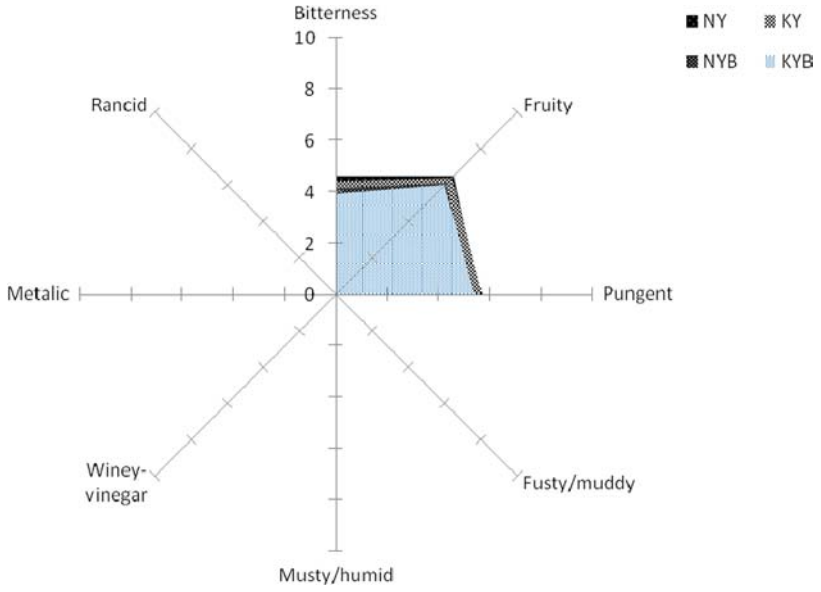

Figure 2. Sensory properties of olive oils.

from NY olives had a higher number and FD factors than the others. On the basis of the FD factor values, the most powerful aroma-active lactone compound was γ-dodecalactone in NY oil, qualified as having a fruity odor. The FD factor of this compound was 512. All of the potent lactones found in our samples have already been identified in black olives by Collin et al.[11]

The other aroma-active compound identified in the olive oils was guaiacol (olive paste, soapy). This compound was detected only in NY and NY-B oils. The FD factors of this volatile phenol were 32 and 16, respectively. This compound was also determined in Italian, Spanish, and Moroccan olive oils as the aroma-active compound. The highest FD value (128) of this compound was determined in Moroccan olive oils.[10]

A total of eight unknown compounds may contribute to the overall aroma of the olive oil samples. Among the unknowns, **14** (LRI = 1269) was found to be the pickled olive odor in KY and KY-B oils. Unknown **27** (LRI = 1544), with a sweet, floral note, was detected in only NY and NY-B oils. Unknowns **30** and **41** were found in oils obtained from the Bornova region, whereas unknown **43** was found in oils obtained from the native region.

Sensory Analysis of Olive Oils. The results of the positive and negative sensory attributes of the olive oils are given in Figure 2. Olive oils are classified as extra virgin olive oils if the median of defects is equal to zero and the median of fruity is more than zero.[27] The studied oils showed no defects in the sensory analysis, so they were considered extra virgin olive oils. The highest fruity median was found in NY oil (6.50). This value was quoted at 6.40, 6.10, and 6.0 for KY, NY-B, and KY-B oils, respectively. The bitterness values of olive oils were detected between 3.90 and 4.60. According to median value of positive attributes (fruity, bitterness, and pungent), oils from the native region had the higher values than those from the Bornova region. The highest value (5.70) of pungent property was detected in olive oil obtained from cv. KY. According to Regulation EEC/640/2008,[49] the term "medium" may be used when the median of the positive attribute concerned is between 3 and 6. In our research olive oil samples were characterized as medium for all criteria (fruity, bitter, and pungent). In a previous study, sensory properties of olive oils were evaluated by using the medians of defects and positive attributes.[50]

In conclusion, this first study revealed key aroma compounds of olive oils obtained from NY and KY cultivars and the effect of growing regions on these compounds. The results suggest that besides cultivars, growing area influences volatile formation in olive oil. The native region oils were distinguished from the Bornova region samples by their number and quantity of volatile compounds. Totals of 61, 48, 59, and 48 aroma compounds were identified and quantified in olive oils obtained from NY, NY-B, KY, and KY-B cultivars, respectively. Aldehydes were found as, qualitatively and quantitatively, the majority of aroma-active compounds in the oil samples. On the basis of sensory analysis, the olive oils studied in the present work were defined as extra virgin olive oils, and the highest fruity median was found in NY oil followed by KY, NY-B, and KY-B oils, respectively.

AUTHOR INFORMATION

Corresponding Author

*(S.S.) E-mail: sselli@cu.edu.tr. Phone: + (90)-322-3386173. Fax: + (90) 322 338 66 14.

Funding

We thank the Scientific and Technical Research Council of Turkey (TUBITAK, Project 110O602) and Cukurova University Research Fund (ZF-2010-D24) for financial support.

Notes

The authors declare no competing financial interest.

ACKNOWLEDGMENTS

We thank all of the members of our sensory panel, who devoted much of their precious time to the sensory assessment of olive oil extracts.

REFERENCES

(1) De la Torre, F.; Bautista, R.; Canovas, F. M.; Claros, G. Isolation of DNA from olive oil and oil sediments: application in oil fingerprinting. *J. Food Agric. Environ.* **2004**, *2*, 84−89.

(2) FAO. Agricultural Statistical Database, 2013 (http://www.faostat.fao.org).

(3) Grosch, W. *Handbook of Food Analysis: Physical Characterization and Nutrient Analysis − Aroma Compounds*; Nollet, L. M. L., Ed.; CRC Press: Boca Raton, FL, USA, 2004; p 717.
(4) Kiritsakis, A. K. Flavor components of olive oil − a review. *J. Am. Oil Chem. Soc.* **1998**, *75*, 673−681.
(5) Ridolfi, M.; Terenziani, S.; Patumi, M.; Fontanazza, G. Characterization of the lipoxygenases in some olive cultivars and determination of their role in volatile compounds formation. *J. Agric. Food Chem.* **2002**, *50*, 835−839.
(6) Kalua, C. M.; Allen, M. S.; Bedgood, D. R.; Bishop, A. G.; Prenzler, P. D.; Robards, K. Olive oil volatile compounds, flavor development and quality: a critical review. *Food Chem.* **2007**, *100*, 273−286.
(7) Morales, M. T.; Aparicio, R. Effect of extraction conditions on sensory quality of virgin olive oil. *J. Agric. Food Chem.* **1999**, *76*, 295−300.
(8) Luna, G.; Morales, M. T.; Aparicio, R. Characterisation of 39 varietal virgin olive oils by their volatile compositions. *Food Chem.* **2006**, *98*, 243−252.
(9) Guth, G.; Grosch, W. A comparative-study of the potent odorants of different virgin olive oils. *Fat Sci. Technol.* **1991**, *93*, 335−339.
(10) Reiners, J.; Grosch, W. Odorants of virgin olive oils with different flavor profiles. *J. Agric. Food Chem.* **1998**, *46*, 2754−2763.
(11) Collin, S.; Nizet, S.; Muls, S.; Iraqi, R.; Bouseta, A. Characterization of odor-active compounds in extracts obtained by simultaneous extraction/distillation from Moroccan black olives. *J. Agric. Food Chem.* **2008**, *56*, 3273−3278.
(12) Gomez-Rico, A.; Salvador, M. D.; La Greca, M.; Fregapane, G. Phenolic and volatile compounds of extra virgin olive oil (*Olea europaea* L. cv. Cornicabra) with regards to fruit ripening and irrigation management. *J. Agric. Food Chem.* **2006**, *54*, 7130−7136.
(13) Rodriguez, P. R.; Barreiro, C. G.; Grande, B. C.; Gandara, J. S. Dynamic headspace/GC-MS to control the aroma fingerprint of extra-virgin olive oil from the same and different olive varieties. *Food Control.* **2012**, *25*, 684−695.
(14) Koprivnjak, O.; Majetic, V.; Bubola, K. B.; Kosic, U. Variability of phenolic and volatile compounds in virgin olive oil from Leccino and Istarska Bjelica cultivars in relation to their fruit mixtures. *Food Technol. Biotechnol.* **2012**, *50*, 216−221.
(15) IOOC, International Olive Council. Guide for the Determination of the Characteristics of Oil-Olives, COI/OH/Doc. No 1, Nov 2011 (http://www.internationaloliveoil.org).
(16) Ranalli, A.; Contento, S.; Schiavone, C.; Simone, N. Malaxing temperature affects volatile and phenol composition as well as other analytical features of virgin olive oil. *Eur. J. Lipid Sci. Technol.* **2001**, *103*, 228−238.
(17) EEC, European Economic Commission. Regulation EEC/1429/92 Amending Regulation EEC2568/91 on the characteristics of olive oil and olive residue oil and on the relevant methods of analysis. *Off. J. Eur. Communities* **1992**, *150*, 17.
(18) Vichi, S.; Guadayol, J. M.; Caixach, J.; Tamames, E. L.; Buxaderas, S. Comparative study of different extraction techniques for the analysis of virgin olive oil aroma. *Food Chem.* **2007**, *105*, 1171−1178.
(19) Kesen, S.; Kelebek, H.; Selli, S. Characterization of the volatile, phenolic and antioxidant properties of monovarietal olive oil obtained from cv. Halhali. *J. Am. Oil Chem. Soc.* **2013**, *90*, 1685−1696.
(20) Selli, S.; Kelebek, H. Aromatic profile and odor-activity value of blood orange juices obtained from Moro and Sanguinello (*Citrus sinensis* L. Osbeck). *Ind. Crop Prod.* **2011**, *33*, 727−733.
(21) Selli, S.; Gubbuk, H.; Kafkas, E.; Gunes, E. Comparison of aroma compounds in Dwarf Cavendish banana (*Musa* spp. AAA) grown from open-field and protected cultivation area. *Sci. Hortic.* **2012**, *141*, 76−82.
(22) Schieberle, P.; Grosch, W. Evaluation of the flavor of wheat and rye crust by aroma extract dilution analysis. *Z. Lebensm. Unters. Forsch.* **1987**, *185*, 111−113.
(23) Fickert, B.; Schieberle, P. Identification of the key odorants in barly malt (caramalt) using GC/MS tecniques and odor dilution analyses. *Nahrung* **1998**, *42*, 371−375.
(24) Tairu, A. O.; Hofmann, T.; Schieberle, P. Studies on tke key odorants formed by roasting of wild mango seeds (*Irvingia gabonensis*). *J. Agric. Food Chem.* **2000**, *48*, 2391−2394.
(25) Iraqi, R.; Vermeulen, C.; Benzekri, A.; Bouseta, A.; Collin, S. Screening for key odorants in Moroccan green olives by gas chromatography-olfactometry/aroma extract dilution analysis. *J. Agric. Food Chem.* **2005**, *53*, 1179−1184.
(26) Averbeck, M.; Schieberle, P. Characterization of the key aroma compounds in a freshly reconstituted orange juice from concentrate. *Eur. J. Lipid Sci. Technol.* **2009**, *229*, 611−622.
(27) IOOC, International Olive Council. Sensory Analysis of Olive Oil Method for the Organoleptic Assessment of Virgin Olive Oil, COI/T.20/Doc. No 15/Rev. 4, 2011 (http://www.internationaloliveoil.org).
(28) Benincasa, C.; De Nino, A.; Lombardo, N.; Perri, E.; Giovanni, S.; Tagarelli, A. Assay of aroma active components of virgin olive oils from southern Italian regions by SPME-GC/ion trap mass spectrometry. *J. Agric. Food Chem.* **2003**, *51*, 733−741.
(29) Ferguson, L.; Sibbett, G. S. *Olive Production Manual*, 2nd ed.; 180s; University of California, Agriculture & Natural Resources Publishing: Los Angeles, CA, USA, 2004.
(30) Ogutcu, M.; Yilmaz, E. Comparison of the virgin olive oils produced in different regions of Turkey. *J. Sensory Stud.* **2009**, *24*, 332−353.
(31) Longobardi, F.; Ventrella, A.; Casiello, G.; Sacco, D.; Tasioula-Margari, M.; Kiritsakis, A. K. Characterization of the geographical origin of western Greek virgin olive oils based on instrumental and multivariate statistical analysis. *Food Chem.* **2012**, *133*, 169−175.
(32) Di Giovacchino, L.; Solinas, M.; Miccoli, M. Effect of extraction systems on the quality of virgin olive oil. *J. Am. Oil Chem. Soc.* **1994**, *71*, 1189−1194.
(33) Cerretani, L.; Bendini, A.; Del Caro, A.; Piga, A.; Vacca, V.; Caboni, M. F.; Toschi, T. G. Preliminary characterisation of virgin olive oils obtained from different cultivars in Sardinia. *Eur. Food Res. Technol.* **2006**, *222*, 354−361.
(34) Selli, S.; Rannou, C.; Prost, C.; Robin, J.; Serot, T. Characterization of aroma-active compounds in rainbow trout (*Oncorhynchus mykiss*) eliciting an off-odor. *J. Agric. Food Chem.* **2006**, *54*, 9496−9502.
(35) Pfnuer, P.; Matsui, T.; Grosch, W.; Guth, H.; Hofmann, T.; Schieberle, P. Development of a stable isotope dilution assay for the quantification of 5-methyl-(*E*)-2-hepten-4-one: application to hazelnut oils and hazelnuts. *J. Agric. Food Chem.* **1999**, *47*, 2044−2047.
(36) Issaoui, M.; Flamini, G.; Brahmi, F.; Dabbou, S.; Hassine, K. B.; Taamali, A.; Chehab, H.; Ellouz, M.; Zarrouk, M.; Hammami, M. Effect of the growing area conditions on differentiation between Chemlali and Chétoui olive oils. *Food Chem.* **2010**, *119*, 220−225.
(37) Tura, D.; Failla, O.; Bassi, D.; Attilio, C.; Serraiocco, A. Regional and cultivar comparison of Italian single cultivar olive oils according to flavor profiling. *Eur. J. Lipid Sci. Technol.* **2013**, *115*, 196−210.
(38) Kiralan, M.; Ozkan, G.; Koyluoglu, F.; Ugurlu, H. A.; Bayrak, A.; Kiritsakis, A. Effect of cultivation area and climatic conditions on volatiles of virgin olive oil. *Eur. J. Lipid Sci. Technol.* **2012**, *114*, 552−557.
(39) Aparicio, R.; Morales, M. T.; Alonso, V. Authentication of European extra-virgin olive oils by their chemical compounds, sensory attributes and consumers' attitudes. *J. Agric. Food Chem.* **1997**, *45*, 1076−1083.
(40) Gomez-Rico, A.; Fregapane, G.; Salvador, M. D. Effect of cultivar and ripening on minor components in Spanish olive fruits and their corresponding virgin olive oils. *Food Res. Int.* **2008**, *41*, 433−440.
(41) Zarrouk, W.; Haddada, F. M.; Baccouri, B.; Oueslati, I.; Taamalli, X. F.; Lizzani-Cuvelier, L.; Daoud, D.; Zarrouk, M. Characterization of virgin olive oil from southern Tunisia. *Eur. J. Lipid Sci. Technol.* **2008**, *110*, 81−88.

(42) Vichi, S.; Pizzale, L.; Conte, L.; Buxaderas, S.; Tamames, E. L. Solid phase microextraction in the analysis of virgin olive oil volatile fraction: characterization of virgin olive oils from two distinct geographical areas of northern Italy. *J. Agric. Food Chem.* **2003**, *51*, 6572−6577.
(43) Morales, M. T.; Rios, J. J.; Aparicio, R. Changes in the volatile composition of virgin olive oil during oxidation: flavors and off-flavors. *J. Agric. Food Chem.* **1997**, *45*, 2666−2673.
(44) Baccouri, O.; Bendini, A.; Cerretani, L.; Guerfel, M.; Baccouri, B.; Lercker, G.; Zarrouk, M.; Ben Miled, D. D. Comparative study on volatile compounds from Tunisian and Sicilian monovarietal virgin olive oils. *Food Chem.* **2008**, *111*, 322−328.
(45) Solinas, M. F.; Angerosa, F.; Marsili, V. Research of some flavor components of virgin olive oil in relation to olive varieties. *Riv. Ital. Sostanze Grasse* **1988**, *65*, 361−368.
(46) Dierkes, G.; Bongartz, A.; Guth, H.; Hayen, H. Quality evaluation of olive oil by statistical analysis of multicomponent stable isotope dilution assay data of aroma active compounds. *J. Agric. Food Chem.* **2012**, *60*, 394−401.
(47) Peres, F.; Jelen, H. H.; Majcher, M. M.; Arraias, M.; Martins, L. L.; Ferreira-Dias, S. Characterization of aroma compounds in Portuguese extra virgin olive oils from Galega Vulgar and Cobrançosa cultivars using GC-O and GC X GC −ToFMS. *Food Res. Int.* **2013**, *54*, 1979−1986.
(48) Ganeko, N.; Shoda, M.; Hirohara, I.; Bhadra, A.; Ishida, T.; Matsuda, H.; Takamura, H.; Matoba, T. Analysis of volatile flavor compounds of sardine (*Sardinops melanostica*) by solid phase microextraction. *J. Food Sci.* **2008**, *73*, 83−88.
(49) EEC, Commission Regulation (EC) No. 640. *Off. J. Eur. Union* **2008**, *178*, 11−16.
(50) Escuderos, M. E.; Uceda, M.; Sanchez, S.; Jimenez, A. Instrumental technique evolution for olive oil sensory analysis. *Eur. J. Lipid Sci. Technol.* **2007**, *109*, 536−546.

JOURNAL OF AGRICULTURAL AND FOOD CHEMISTRY

Article

pubs.acs.org/JAFC

Rapid Method for Glutathione Quantitation Using High-Performance Liquid Chromatography with Coulometric Electrochemical Detection

Banu Bayram,[†] Gerald Rimbach,*[,†] Jan Frank,[§] and Tuba Esatbeyoglu[†]

[†]Institute of Human Nutrition and Food Science, Christian-Albrechts-University, Hermann Rodewald Strasse 6, 24098 Kiel, Germany

[§]Institute of Biological Chemistry and Nutrition, Division Biofunctionality and Safety of Food, University of Hohenheim, Garbenstrasse 28, 70599 Stuttgart, Germany

ABSTRACT: A rapid, sensitive, and direct method (without derivatization) was developed for the detection of reduced glutathione (GSH) in cultured hepatocytes (HepG2 cells) using high-performance liquid chromatography with electrochemical detection (HPLC-ECD). The method was validated according to the guidelines of the U.S. Food and Drug Administration in terms of linearity, lower limit of quantitation (LOQ), lower limit of detection (LOD), precision, accuracy, recovery, and stabilities of GSH standards and quality control samples. The total analysis time was 5 min, and the retention time of GSH was 1.78 min. Separation was carried out isocratically using 50 mM sodium phosphate (pH 3.0) as a mobile phase with a fused-core column. The detector response was linear between 0.01 and 80 μmol/L, and the regression coefficient (R^2) was >0.99. The LOD for GSH was 15 fmol, and the intra- and interday recoveries ranged between 100.7 and 104.6%. This method also enabled the rapid detection (in 4 min) of other compounds involved in GSH metabolism such as uric acid, ascorbic acid, and glutathione disulfite. The optimized and validated HPLC-ECD method was successfully applied for the determination of GSH levels in HepG2 cells treated with buthionine sulfoximine (BSO), an inhibitor, and α-lipoic acid (α-LA), an inducer of GSH synthesis. As expected, the amount of GSH concentration-dependently decreased with BSO and increased with α-LA treatments in HepG2 cells. This method could also be useful for the quantitation of GSH, uric acid, ascorbic acid, and glutathione disulfide in other biological matrices such as tissue homogenates and blood.

KEYWORDS: *glutathione, electrochemical detection, hepatocytes, method validation, buthionine sulfoximine*

INTRODUCTION

Glutathione (γ-L-glutamyl-L-cysteinglycine, GSH) is a tripeptide nonprotein thiol antioxidant molecule composed of cysteine, glutamic acid, and glycine. The thiol group of the cysteine residue is the biologically active site of GSH.[1,2] GSH has a number of important roles in human metabolism including scavenging of free radicals, detoxifying xenobiotics, maintaining cell homeostasis, protecting against oxidative stress, controlling gene expression, detoxifying heavy metals, and in-signal transduction.[2−6] GSH is also involved in regenerating antioxidants involved in the antioxidant network system, such as vitamin E and ascorbic acid.[2] GSH is present in all organs with particularly high levels in the liver.[1] Severe oxidative stress leads to oxidation of GSH and the formation of glutathione disulfide (GSSG).[7]

The identification and quantitation of GSH are of great interest due to its critical protective functions in the body. Furthermore, it may be a useful biomarker for oxidative stress, a common occurrence in many disease states. Various chemiluminescence,[8] spectrofluorometric,[9] and spectrophotometric[7] methods are available for the determination of GSH in biological samples. In addition, chromatographic methods with improved specificity and sensitivity have been developed using high-performance liquid chromatography (HPLC) coupled to ultraviolet,[10] fluorescence,[11] and coulometric electrochemical detections[12] as well as mass spectroscopy[13] and capillary electrophoresis.[14,15] Most of these methods require either precolumn or postcolumn derivatization of GSH with fluorogenic (monobromobimane, *o*-phthalaldehyde), and chromophoric (*N*-ethylmaleimide or iodoacetic acid) agents or reduction with reducing agents (tributylphosphine, tris(2-carboxyethyl)phosphine),[16] which is time-consuming.

Among the chromatographic techniques, coulometric electrochemical detection facilitates the resolution and accurate identification of trace amounts of electroactive compounds, including redox-reactive compounds such as thiols and disulfides.[17] Thus, HPLC coupled to electrochemical detection (HPLC-ECD) is a valuable tool for analyzing GSH with high specificity and sensitivity without the need of prior derivatization.[12,18] In addition, run time is an important aspect of any chromatographic method. The currently available methods for GSH analysis are often longer than 3 min.[12,19,20]

In this study, we aimed to develop a rapid and sensitive HPLC-ECD method for the analysis of GSH in HepG2 cells and to validate it according to FDA guidelines for bioanalytical method validation.[21] The measurement of GSH levels is crucial for determining the influence of treatments on the GSH−GSSG redox system. We therefore tested the application of this method by measuring changes in GSH levels in HepG2 cells treated with buthionine sulfoximine (BSO), an inhibitor, and α-lipoic acid (α-LA), an inducer of GSH synthesis.

Received: September 13, 2013
Revised: December 10, 2013
Accepted: December 15, 2013
Published: December 15, 2013

ACS Publications © 2013 American Chemical Society

dx.doi.org/10.1021/jf403857h | *J. Agric. Food Chem.* 2014, 62, 402−408

MATERIALS AND METHODS

Chemicals. Standards of glutathione, ascorbic acid, α-lipoic acid, and sodium dihydrogen phosphate monohydrate were purchased from Sigma-Aldrich (Steinheim, Germany). Glutathione disulfide, dimethyl sulfoxide (DMSO), and metaphosphoric acid were from Carl Roth (Karlsruhe, Germany), and orthophosphoric acid was from Merck (Darmstadt, Germany). Uric acid and buthionine sulfoximine were from Fluka (Buchs, Switzerland). Reference standards of analyzed compounds had purities >98%. Water was of Milli-Q grade, purified by a Milli-Q UV purification system (Millipore, Bedford, MA, USA).

Preparation of Standard Solutions. A stock solution of GSH standard was prepared in 1% metaphosphoric acid at a concentration of 10 mM, and working standards were prepared daily from this stock solution by dilution in 1% metaphosphoric acid. It is recommended to prepare the standards daily as an effect of temperature and storage time was observed for GSH in our stability studies.

Cell Culture Conditions. HepG2 cells were obtained from Applied Cell Culture (IAZ, München, Germany). Dulbecco's modified Eagle's medium (DMEM), fetal calf serum (FCS), and penicillin/streptomycin were purchased from PAA (Coelbe, Germany). HepG2 cells were cultured in DMEM containing 10% FCS and 1% penicillin/streptomycin in a temperature- and humidity-controlled incubator (95% air, 5% CO_2) at 37 °C. Cells were grown in T75 flasks (Sarstedt, Nümbrecht, Germany) at a density of 8×10^6 cells in DMEM and subcultured twice a week when at 80% confluence. Confluent cells were harvested by trypsination.

Extraction of GSH from HepG2 Cells. Confluent cells were seeded at a density of 1.2×10^6 cells per well in 12-well plates (Corning Inc., NY, USA) and cultivated for 24 h. Cells were washed with cold PBS and then incubated with 500 μL of trypsin/EDTA per well for 10 min. Cells were suspended in 1 mL of DMEM and pelleted by centrifugation at 2000*g* for 5 min at 4 °C. Cell pellets were suspended in 300 μL of PBS and frozen at −80 °C. The cell suspension was then thawed and mixed with 600 μL of PBS. An equal volume of 1% metaphosphoric acid (900 μL) was added before homogenization with a Qiagen TissueLyser (Hilden, Germany) for 2 min. The cell suspension was then centrifuged at 13000*g* for 10 min at 4 °C, and the supernatants were transferred into HPLC vials for GSH analysis. GSH content was expressed as micromoles per liter.

Cytotoxicity Test for BSO and α-LA. The cytotoxicity of BSO and α-LA was determined using the neutral red (NR) assay.[22] Viable cells incorporate NR in lysosomes, which can then be photometrically measured at 540 nm. Cell viability was expressed as a percentage of solvent-only exposed control cells. HepG2 cells were incubated with BSO (prepared in distilled water) or with α-LA (prepared in DMSO and the final concentration of DMSO was <0.1%) at concentrations of 1−1000 μmol/L to establish the highest nontoxic concentration. In concentration−response experiments, HepG2 cells were exposed to increasing concentrations of BSO and α-LA ranging from 1 to 250 μmol/L for 24 h. For each treatment, three independent experiments were performed in duplicate ($n = 6$).

HPLC Analysis of GSH. HPLC analyses were carried out on a Jasco system (Jasco GmbH Deutschland, Gross-Umstadt, Germany) consisting of a pump (PU-2085) and autosampler (XLC-3059AS), whereas detection was carried out on a four-channel ESA 5600A CoulArray detector with an integrated column oven (ESA Inc., Chelmsford, MA, USA). For analyte detection, increasing potentials of 250, 400, 600, and 800 mV were applied. Separation of phenolics was achieved on a Kinetex C18 column (100 × 4.6 mm, 2.6 μm; Phenomenex, Aschaffenburg, Germany) using isocratic elution with 50 mM NaH_2PO_4. The pH of the aqueous eluent was adjusted to 3.0 with orthophosphoric acid, and the eluent was vacuum-filtered through a 0.2 μm hydrophilic polypropylene membrane filter (Pall Corp., MI, USA). The column temperature was maintained at 30 °C, the flow rate was set at 1.0 mL/min, and the injection volume was 10 μL. GSH was quantified against an external standard using the sum of peak heights.

Method Validation. The analytical method for the determination of GSH was validated according to the requirements of FDA guidelines for bioanalytical method validation in terms of linearity, limit of quantitation (LOQ), limit of detection (LOD), accuracy, precision, recovery, stock solution stability, short-term stability, freeze−thaw stability, and benchtop stability. All of the analyses were performed three times.

Linearity, Lower LOD, and Lower LOQ. The linear range of detection was determined using serial dilutions of the stock solution. Calibration curves were obtained by plotting the sum of the peak heights of GSH versus its concentration for eight different concentrations. Standard solutions corresponding to each point in the calibration curve were injected in triplicate and regression parameters calculated. The LOQ was defined as the lowest concentration that could be determined with a deviation from the actual concentration and a coefficient of variation of precision of <20%, respectively. The LOD was the lowest concentration of the analyte of interest that could be reliably discerned from the baseline (signal-to-noise ratio ≈ 3).

Precision and Accuracy. The precision and accuracy of the method were ascertained by measuring five replicates of control samples with known amounts of GSH (low, medium, and high concentrations) on three consecutive days. After thawing, 600 μL of 1% metaphosphoric acid or GSH (2, 10, or 40 μmol/L prepared in 1% metaphosphoric acid) was added to cell suspensions and treated according to the protocol outlined under Extraction of GSH from HepG2 Cells. These concentrations were determined according to the amount of GSH in HepG2 cells found in the literature. Also, lower limit of detection and upper limit of detection values of the method were taken into account. The calculated concentration of GSH extracted from the spiked cell suspensions was compared with the known concentration within the same day (intraday) and from day-to-day (interday). The precision is given as the intra- and interday coefficients of variation (% CV). The accuracy was expressed as the absolute percentage error and calculated as follows: accuracy (%) = [(mean of measured concentration − known added concentration)/known added concentration] × 100.

Recovery. The recovery of GSH was calculated by analyzing the peak heights of five replicate spiked cell suspensions (spiked cell sample − cell sample) for each GSH concentration (low, medium, and high) and comparing them with calibration standards of the same concentration. The recovery (in percent) was calculated as follows: recovery (%) = [(peak height of spiked cell sample − peak height of cell sample)/peak height of standard] × 100.

Stock Solution Stability. The stability of three concentrations (low, medium, and high) of stock solution was determined at room temperature and 4, −20, and −80 °C for 24 h. The sum of peak heights of GSH prestorage was compared to those poststorage, and the results were expressed as percent degradation.

Short- and Long-Term Stability. Five aliquots of spiked cell suspensions were prepared at two concentrations (low and high). The aliquots were initially analyzed, and the remaining samples were stored at room temperature and 4, −20, and −80 °C for 24 h to assess short-term stability and at −20 and −80 °C for 4 months to assess long-term stability. The initial values were compared with those obtained after storage and the results expressed as percent degradation.

Freeze−Thaw Stability. Three aliquots of spiked cell suspensions were prepared at two concentrations (low and high). The aliquots were initially analyzed, and remaining samples were frozen at −80 °C for 24 h, thawed at room temperature, and then frozen again for 12−24 h at −80 °C. The freeze−thaw cycle was repeated two additional times and the stability determined by comparing initial values to those obtained after repeated freeze−thaws. Results were expressed as percent degradation.

Benchtop Stability. Three aliquots of spiked cell suspensions were prepared at two concentrations (low and high), and the effect of length of time in the autosampler on sample stability was determined by injecting samples at 6 h intervals (6, 12, and 18 h). The samples were injected from the same HPLC vial, and the screw-caps were replaced after each injection to minimize solvent loss. The results were expressed as percent degradation.

Statistical Analysis. Statistical analysis was performed using SPSS version 16.0 (SPSS Inc., Chicago, IL, USA). Data were analyzed for

dx.doi.org/10.1021/jf403857h | J. Agric. Food Chem. 2014, 62, 402−408

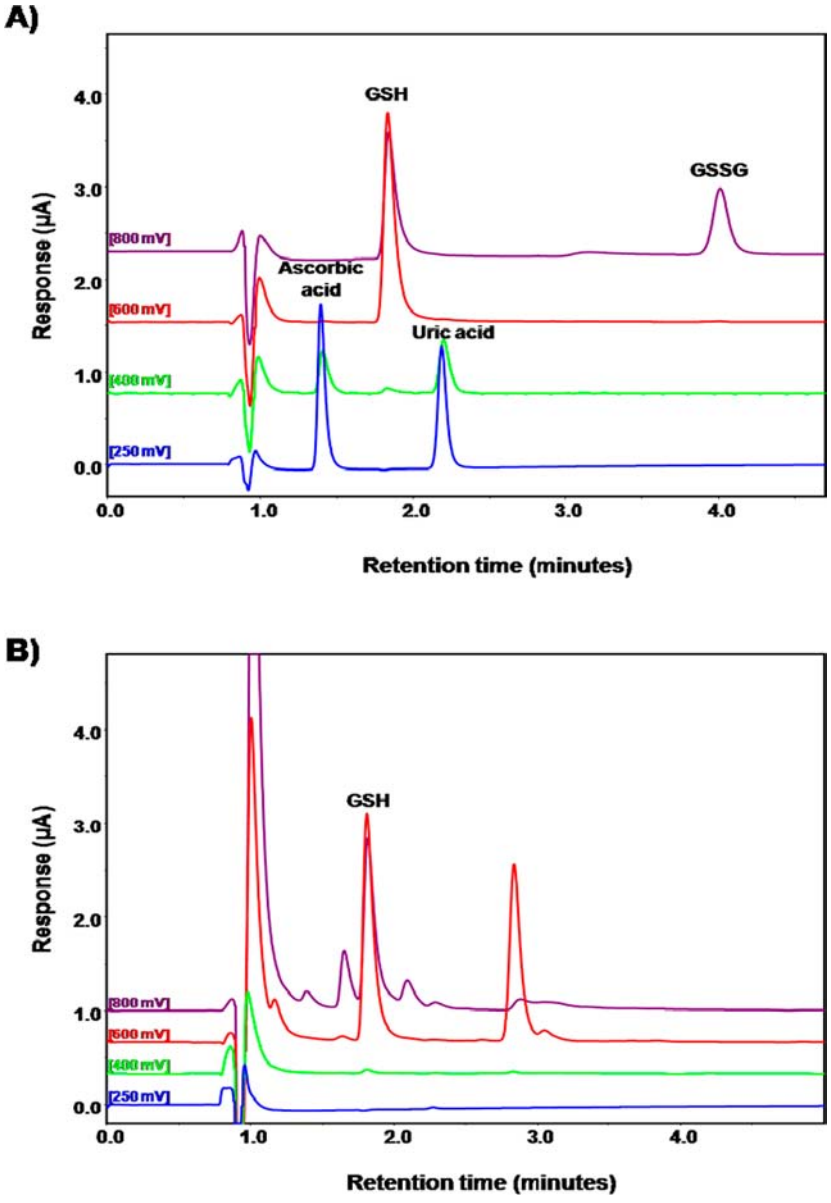

Figure 1. (A) Representative chromatogram of ascorbic acid, GSH, uric acid, and GSSG standards. The injection volume was 10 μL, and the concentrations of ascorbic acid, GSH, uric acid, and GSSG in the standard mixture were 5 μM. (B) GSH extracted from HepG2 cells resolved by isocratic elution on a Kinetex C18 fused-core column and detected by four-channel coulometric electrochemical detection. The retention times of the analytes (in minutes) are given in parentheses: 1, ascorbic acid (1.39); 2, GSH (1.78); 3, uric acid (2.19); 4, GSSG (4.00).

normality of distribution (Kolmogorow−Smirnov and Shapiro−Wik tests) and equality of variance (Levene test). For the comparison of group means, one-way ANOVA was performed with the Dunnet post hoc test. Results are expressed as mean values with standard deviation (SD). Differences were considered significant when the P value was $\leq$0.05.

RESULTS AND DISCUSSION

We developed and validated a method for the direct measurement of GSH in HepG2 cells without the requirement of prior derivatization. Cell extracts were acidified with metaphosphoric acid to facilitate protein precipitation and minimize oxidation of GSH. This newly developed and validated method enables the detection of GSH with a retention time of only 1.78 min (Figure 1) and a total run time of 5 min. Currently, we know of no other method for GSH analysis that has a shorter total run time. In addition, the method we describe herein also enables the detection of ascorbic acid, uric acid, and GSSG to be achieved within 4 min (Figure 1). However, validation according to FDA guidelines for bioanalytical method validation was applied only to GSH. The developed method is important because it can be used to efficiently detect and measure GSH as well as three other key molecules involved in GSH metabolism and its biological activity, namely, ascorbic acid, uric acid, and GSSG. GSH can regenerate the exogenous antioxidant ascorbic acid from its radical form, which results in the conversion of GSH to its oxidized form GSSG. However, one particular challenge in the analysis of GSSG with electrochemical detectors is that it requires the application of high voltages (>800 mV), which can cause detrimental effects to the detection system over time. Therefore, an amperometric boron-doped diamond electrode rather than a coulometric graphite electrode would be preferable if GSSG is analyzed with this method.[23] Uric acid

dx.doi.org/10.1021/jf403857h | J. Agric. Food Chem. 2014, 62, 402−408

Table 1. Comparison of the Lower Limits of Detection (Given as Total Amount Injected; LOD), Retention Times, Detection Methods, Sample Matrices, and Derivatization Procedures of the Present Method with Other Sensitive Methods for the Quantitation of GSH in Biological Samples Published in the Literature[a]

LOD	RT (min)	detector	sample	derivatization	ref
50 fmol	3.7	HPLC-FL	red blood cells and cultured fibroblasts	derivatization with OPA	11
2 fmol	12.3	HPLC-ECD	HL-60 cells	none	12
0.2 pmol	5.1	LC-MS/MS	mouse liver	none	13
10 fmol	4.4	LC-CE	red blood cells	derivatization with NEM	14
0.33 pmol	5.23	HPLC-ECD	DU145 and A549 cells	none	18
na (LOQ = 0.5 pmol)	7.74	HPLC-FL	U373-MG human astrocytoma cell	derivatization with ABD-F	20
4 pmol	3.7	LC-MS/MS	whole blood	derivatization with NEM	28
15 fmol	1.8	HPLC-ECD	HepG2 cells	none	this study

[a]Abbreviations: ABD-F, 4-fluoro-7-aminosulfonylbenzofurazan; CE, capillary electrophoresis; ECD, electrochemical detection; FL, fluorescence; IAA, iodoacetic acid; LC, liquid chromatography; MS, mass spectrometry; NEM, *N*-ethylmaleimide; OPA, *o*-phthalaldehyde.

is a powerful antioxidant and has recently been reported to increase cysteine uptake and GSH synthesis in the brain[24] and liver.[25]

Linearity, Lower LOD, and Lower LOQ. The linearity of the detector response for GSH was evaluated by triplicate injection of standard solutions corresponding to each point on the standard curve on three different days. The detector response was linear between 0.01 and 80 μmol/L with a regression coefficient (R^2) >0.99. The LOQ and LOD of GSH were 50 and 15 fmol (given as total amount injected), respectively, which are lower than reported in the literature for most other studies (Table 1).

Precision, Accuracy, and Recovery. Precision, accuracy, and recovery were determined by adding low, medium, and high concentrations of the GSH standard to HepG2 cell suspensions (n = 5). Intra- and interday repeatability studies were carried out by analyzing five cell suspensions on three consecutive days. Intraday precision values were 3.75, 1.67, and 0.71%, and interday precision results were 5.27, 6.89, and 9.86% for low, medium, and high GSH concentrations, respectively (Table 2). These precision and accuracy values are within the limits prescribed by the FDA (≤20% for concentrations near the LOQ and ≤15% for other concentration levels). The intraday and interday recovery values of GSH in cell suspensions ranged from 100.7 to 104.6% (Table 2).

Table 2. Intra- and Interday Precision, Accuracy, and Recovery of GSH Added to Cell Suspensions of HepG2 Cells at Low, Medium, or High Concentrations and Determined in Five Replicate Analyses (n = 5)

concn (μmol/L)	calcd concn (μmol/L)	recovery (%)	accuracy (%)	precision (CV%)
		Intraday		
2	2.01	100.7	−0.71	3.75
10	10.36	103.7	−3.68	1.67
40	41.35	103.5	−3.45	0.71
		Interday		
2	2.09	104.6	−4.59	5.27
10	10.40	104.2	−4.23	6.89
40	41.76	104.6	−4.59	9.86

Stability. The stability of analytes prior to injection is an important issue that is often neglected during method development. Therefore, in the present study, we determined both the stability of GSH stock solutions and GSH-spiked cell extracts. Aliquots of GSH stock solutions (low, medium, and high concentrations) were stored at room temperature and 4, −20, or −80 °C for 24 h. The concentrations after storage were compared with the prestorage values (Table 3). The low-concentration GSH stock solution showed the highest level of degradation (−7.60%) when stored at −20 °C for 24 h. No significant differences in 24 h stability were observed between temperatures. During long-term storage for 4 months, GSH was less stable when stored at −20 °C compared to −80 °C, with the highest level of degradation being observed for the low GSH (Table 3). These results indicate that, to optimize stability, long-term storage of GSH stock solutions and standards should be at −80 °C.

Table 3. Stock Solution Stability of GSH Standards at Low, Medium, or High Concentration after Storage at Room Temperature or 4, −20, or −80 °C for 24 h (Short-Term Stability) and at −20 or −80 °C for 4 Months (Long-Term Stability)

	degradation (%)					
	short-term stability				long-term stability	
concn (μmol/L)	room temp	4 °C	−20 °C	−80 °C	−20 °C	−80 °C
0.4	4.85	−5.48	−7.60	−5.54	27.29	1.93
4	2.23	0.08	0.66	−2.24	17.01	10.97
40	0.25	−2.40	−3.30	2.81	13.06	11.04

To assess short-term stability in cell extracts, HepG2 cells were spiked with GSH at two concentrations (low and high) and analyzed after storage at room temperature or 4, −20, or −80 °C for 24 h. The highest degradation was observed in samples with high concentrations of GSH at −20 °C (−3.68%). There were no clear differences in the stability of GSH between samples stored at room temperature or 4, −20, or −80 °C for 24 h (Table 4). To assess long-term stability, the GSH-spiked HepG2 cells were also stored at −20 or −80 °C for 4 months. Significant degradation was seen in the sample spiked with the high concentration of GSH at −20 °C (12.53%). As with the GSH stock solutions, −80 °C is preferable for long-term storage of cell extracts to protect GSH from degradation (0.13 and 1.16% for high and low concentrations, respectively).

The effect of repeated freezing and thawing on the stability of GSH-spiked cell extracts was also assessed. GSH degraded by 2.01% and by −1.87% at low and high concentrations, respectively, indicating that GSH withstands freeze−thawing in cell extracts (Table 4).

The stability of HepG2 cell extracts during the time in the autosampler was also investigated. The autosampler temper-

dx.doi.org/10.1021/jf403857h | J. Agric. Food Chem. 2014, 62, 402−408

Table 4. Short-Term (24 h), Long-Term (4 Months), Freeze−Thaw, and Postpreparative Stabilities (Expressed as Percent Degradation) of GSH-Spiked HepG2 Cell Extracts at Low and High Concentrations

	degradation (%)									
	short-term stability				long-term stability		freeze−thaw stability	postpreparative stability		
concn (μmol/L)	room temp	4 °C	−20 °C	−80 °C	−20 °C	−80 °C		6 h	12 h	18 h
2	0.97	−0.32	−2.16	−2.91	9.83	1.16	2.01	0.6	0.5	0.8
40	1.50	−0.57	−3.68	−1.66	12.53	0.13	−1.87	−2.6	−3.7	−3.9

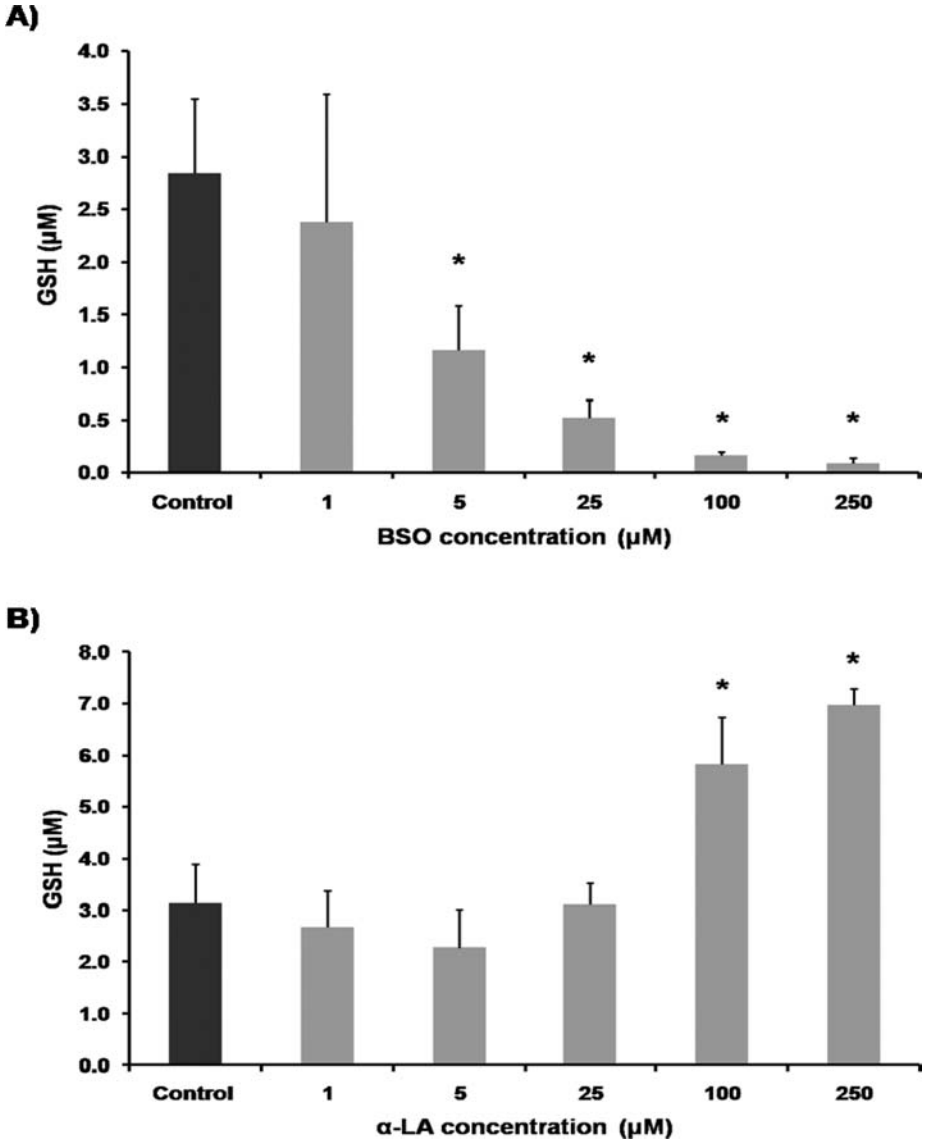

Figure 2. (A) Concentrations of GSH (μmol/L) in HepG2 cells treated with buthionine sulfoximine (BSO) or (B) α-lipoic acid (α-LA) at concentrations ranging between 1 and 250 μmol/L. Values are expressed as arithmetic means ± SD from three individual experiments performed in duplicate (n = 6). Comparison of mean values to control was performed by one-way ANOVA with the Dunnett post hoc test, and significant differences are indicated by asterisks: ∗, $P < 0.001$.

ature was maintained at 4 °C. Cell extracts containing high and low GSH concentrations were found to be stable for 18 h in the autosampler (Table 4). The highest degradation was observed after 18 h (−3.9%) in the high GSH-spiked samples.

Application of the Method for the Quantitation of GSH in HepG2 Cells Treated with BSO and α-LA. The measurement of GSH is useful in assessing the effectiveness of treatments that may affect synthesis of GSH. The developed and validated method was used to analyze the content of GSH in BSO- and α-LA-treated HepG2 cells. The sensitivity of the analytical method is an important issue when GSH is altered in cells by depleting agents, oxidative stress, or physical agents. BSO acts as an inhibitor of GSH synthesis and has been shown to be effective at lowering GSH levels in a number of cell types both in vitro and in vivo.[26,27] According to the results of the neutral red test, no toxic effect of either BSO or α-LA on HepG2 cells was detected at concentrations between 1 and 1000 μmol/L. HepG2 cells were concentration-dependently

dx.doi.org/10.1021/jf403857h | J. Agric. Food Chem. 2014, 62, 402−408

treated with 1−250 μmol/L of BSO, and significant GSH depletion was achieved even at a low concentration (5 μmol/L) (Figure 2A, $P < 0.001$). Conversely, treatment with the GSH inducer α-LA, when used at concentrations of 100 and 250 μmol/L, significantly increased cellular GSH (Figure 2B, $P < 0.001$).

In conclusion, we developed and validated a simple, fast, direct, sensitive, and specific HPLC-ECD method for the determination of GSH in HepG2 cells. This chromatographic method has a number of advantages, including a quick sample preparation, as it requires no derivatization step, a very good sensitivity with markedly lower LOD than for most other methods reported in the literature, and a very short retention time of GSH of only 1.78 min, which results in the fastest analysis time among the published HPLC methods for GSH. This method furthermore allows the elution of GSH as well as three other compounds involved in GSH metabolism (ascorbic acid, uric acid, and GSSG) in 4 min, resulting in a total analysis time of under 5 min. The method may thus be useful for the analysis of these compounds, too. The developed method was successfully applied to analyze GSH in HepG2 cells treated with BSO and α-LA. It needs to be established whether our method can also be applied for the analysis of GSH in other biological samples such as blood and tissues.

AUTHOR INFORMATION

Corresponding Author

*(G.R.) E-mail: rimbach@foodsci.uni-kiel.de. Phone: +49 431 880 2583. Fax: +49 431 880 2628.

Notes

The authors declare no competing financial interest.

REFERENCES

(1) Pastore, A.; Federici, G.; Bertin, E.; Piemonte, F. Analysis of glutathione: implication in redox and detoxification. *Clin. Chim. Acta* **2003**, *333*, 19−39.

(2) Valko, M.; Leibfritz, D.; Moncol, J.; Cronin, M.; Mazur, M.; Telser, J. Free radicals and antioxidants in normal physiological functions and human disease. *Int. J. Biochem. Cell B* **2007**, *39*, 44−84.

(3) Bald, E.; Chwatko, G.; Głowacki, R.; Kusmierek, K. Analysis of plasma thiols by high-performance liquid chromatography with ultraviolet detection. *J. Chromatogr., A* **2004**, *1032*, 109−115.

(4) Potesil, D.; Petrlova, J.; Adam, V.; Vacek, J.; Klejdus, B.; Zehnalek, J.; Trnkova, L.; Havel, L.; Kizek, R. Simultaneous femtomole determination of cysteine, reduced and oxidized glutathione, and phytochelatin in maize (*Zea mays* L.) kernels using high-performance liquid chromatography with electrochemical detection. *J. Chromatogr., A* **2005**, *1084*, 134−144.

(5) Petrlova, J.; Mikelova, R.; Stejskal, K.; Kleckerova, A.; Zitka, O.; Petrek, J.; Havel, L.; Zehnalek, J.; Adam, V.; Trnkova, L. Simultaneous determination of eight biologically active thiol compounds using gradient elution-liquid chromatography with Coul-Array detection. *J. Sep. Sci.* **2006**, *29*, 1166−1173.

(6) Livingstone, C.; Davis, J. Targeting therapeutics against glutathione depletion in diabetes and its complications. *Br. J. Diabetes Vasc. Dis.* **2007**, *7*, 258−265.

(7) Rossi, R.; Milzani, A.; Dalle-Donne, I.; Giustarini, D.; Lusini, L.; Colombo, R.; Di Simplicio, P. Blood glutathione disulfide: In vivo factor or in vitro artifact? *Clin. Chem.* **2002**, *48*, 742−753.

(8) Wang, S.; Ma, H.; Li, J.; Chen, X.; Bao, Z.; Sun, S. Direct determination of reduced glutathione in biological fluids by Ce(IV)-quinine chemiluminescence. *Talanta* **2006**, *70*, 518−521.

(9) Pullela, P. K.; Chiku, T.; Carvan, M. J.; Sem, D. S. Fluorescence-based detection of thiols in vitro and in vivo using dithiol probes. *Anal. Biochem.* **2006**, *352*, 265−273.

(10) Giustarini, D.; Dalle-Donne, I.; Colombo, R.; Milzani, A.; Rossi, R. An improved HPLC measurement for GSH and GSSG in human blood. *Free Radical Biol. Med.* **2003**, *35*, 1365−1372.

(11) Cereser, C.; Guichard, J.; Drai, J.; Bannier, E.; Garcia, I.; Boget, S.; Parvaz, P.; Revol, A. Quantification of reduced and total glutathione at the femtomole level by high-performance liquid chromatography with fluorescence detection: application to red blood cells and cultured fibroblasts. *J. Chromatogr., B* **2001**, *752*, 123−132.

(12) Hiraku, Y.; Murata, M.; Kawanishi, S. Determination of intracellular glutathione and thiols by high performance liquid chromatography with a gold electrode at the femtomole level: comparison with a spectroscopic assay. *Biochim. Biophys. Acta* **2002**, *1570*, 47−52.

(13) Norris, R. L.; Eaglesham, G. K.; Shaw, G. R.; Smith, M. J.; Chiswell, R. K.; Seawright, A. A.; Moore, M. R. A sensitive and specific assay for glutathione with potential application to glutathione disulfide, using high-performance liquid chromatography−tandem mass spectrometry. *J. Chromatogr., B* **2001**, *762*, 17−23.

(14) Piccoli, G.; Fiorani, M.; Biagiarelli, B.; Palma, F.; Potenza, L.; Amicucci, A.; Stocchi, V. Simultaneous high-performance capillary electrophoretic determination of reduced and oxidized glutathione in red blood cells in the femtomole range. *J. Chromatogr., A* **1994**, *676*, 239−246.

(15) Yao, X.; Wang, Y.; Chen, G. Simultaneous determination of aminothiols, ascorbic acid and uric acid in biological samples by capillary electrophoresis with electrochemical detection. *Biomed. Chromatogr.* **2007**, *21*, 520−256.

(16) Monostori, P.; Wittmann, G.; Karg, E.; Túri, S. Determination of glutathione and glutathione disulfide in biological samples: an in-depth review. *J. Chromatogr., B* **2009**, *877*, 3331−3346.

(17) Iwasaki, Y.; Saito, Y.; Nakano, Y.; Mochizuki, K.; Sakata, O.; Ito, R.; Saito, K.; Nakazawa, H. Chromatographic and mass spectrometric analysis of glutathione in biological samples. *J. Chromatogr., B* **2009**, *877*, 3309−3317.

(18) Spadaro, A.; Bousquet, E.; Santagati, N. A.; Vittorio, F.; Ronsisvalle, G. Simple analysis of glutathione in human colon carcinoma cells and epidermoid human larynx carcinoma cells by HPLC with electrochemical detection. *Chromatographia* **2005**, *62*, 11−15.

(19) Khan, A.; Khan, M. I.; Iqbal, Z.; Shah, Y.; Ahmad, L.; Nazir, S.; Watson, D. G.; Khan, J. A.; Nasir, F.; Khan, A. A new HPLC method for the simultaneous determination of ascorbic acid and aminothiols in human plasma and erythrocytes using electrochemical detection. *Talanta* **2011**, *84*, 789−801.

(20) Steele, M. L.; Ooi, L.; Münch, G. Development of a high-performance liquid chromatography method for the simultaneous quantification of glutathione and related thiols. *Anal. Biochem.* **2012**, *429*, 45−52.

(21) U.S. FDA. Guidance for Industry: Bioanalytical Method Validation; U.S. Departmentof Health and Human Services, FDA, Center for Drug Evaluation and Research, Rockville, MD, 2001; www.fda.gov/downloads/drugs/guidancecomplianceregulatoryinformation/guidances/ucm070107.pdf.

(22) Valacchi, G.; Rimbach, G.; Saliou, C.; Weber, S. U.; Packer, L. Effect of benzoyl peroxide on antioxidant status, NF-κB activity and interleukin-1α gene expression in human keratinocytes. *Toxicology* **2001**, *165*, 225−234.

(23) Park, H. J.; Mah, E.; Bruno, R. S. Validation of high-performance liquid chromatography-boron-doped diamond detection for assessing hepatic glutathione redox status. *Anal. Biochem.* **2010**, *407*, 151−159.

(24) Aoyama, K.; Matsumura, N.; Watabe, M.; Wang, F.; Kikuchi-Utsumi, K.; Nakaki, T. Caffeine and uric acid mediate glutathione synthesis for neuroprotection. *Neuroscience* **2011**, *181*, 206−215.

(25) Allameh, A.; Maleklou, N.; Zargar, M.; Sanati, M. H. The influence of uric acid treatments on liver glutathione system prevents oxidative damages in experimental autoimmune encephalomyelitis mice. *Neurosci. Lett.* **2008**, *439*, 111−115.

(26) Beddowes, E. J.; Faux, S. P.; Chipman, J. K. Chloroform, carbon tetrachloride and glutathione depletion induce secondary genotoxicity in liver cells via oxidative stress. *Toxicology* **2003**, *187*, 101−115.
(27) Will, O.; Mahler, H. C.; Arrigo, A. P.; Epe, B. Influence of glutathione levels and heat-shock on the steady-state levels of oxidative DNA base modifications in mammalian cells. *Carcinogenesis* **1999**, *20*, 333−337.
(28) Moore, T.; Le, A.; Niemi, A. K.; Kwan, T.; Cusmano-Ozog, K.; Enns, G. M.; Cowan, T. M. A new LC−MS/MS method for the clinical determination of reducedand oxidized glutathione from whole blood. *J. Chromatogr., B* **2013**, *929*, 51−55.

JOURNAL OF AGRICULTURAL AND FOOD CHEMISTRY

Article

pubs.acs.org/JAFC

Quantification of Individual Phenolic Compounds' Contribution to Antioxidant Capacity in Apple: A Novel Analytical Tool Based on Liquid Chromatography with Diode Array, Electrochemical, and Charged Aerosol Detection

Merichel Plaza,*[,†] James Kariuki,[§] and Charlotta Turner[†]

[†]Department of Chemistry, Centre for Analysis and Synthesis, Lund University, P.O. Box 124, SE-221 00 Lund, Sweden

[§]Department of Science, Augustana Campus, University of Alberta, 4901-46 Avenue, Camrose, Alberta, Canada T4V 2R3

Supporting Information

ABSTRACT: Phenolics, particularly from apples, hold great interest because of their antioxidant properties. In the present study, the total antioxidant capacity of different apple extracts obtained by pressurized hot water extraction (PHWE) was determined by cyclic voltammetry (CV), which was compared with the conventional antioxidant assays. To measure the antioxidant capacity of individual antioxidants present in apple extracts, a novel method was developed based on high-performance liquid chromatography (HPLC) with photodiode array (DAD), electrochemical (ECD), and charged aerosol (CAD) detection. HPLC-DAD-ECD-CAD enabled rapid, qualitative, and quantitative determination of antioxidants in the apple extracts. The main advantage of using CAD was that this detector enabled quantification of a large number of phenolics using only a few standards. The results showed that phenolic acids and flavonols were mainly responsible for the total antioxidant capacity of apple extracts. In addition, protocatechuic acid, chlorogenic acid, hyperoside, an unidentified phenolic acid, and a quercetin derivative presented the highest antioxidant capacities.

KEYWORDS: *antioxidant capacity, charged aerosol detector, cyclic voltammetry, electrochemical detector, hyphenation, phenolic compounds*

INTRODUCTION

Flavonoids represent a highly diverse class of secondary plant metabolites with about 9000 structures.[1] Flavonoids are polyphenolic compounds derived from 2-phenylchromone, commonly found in many plants, vegetables, and flowers.[2] They have received considerable attention in the literature, specifically due to their biological and physiological importance. They are also known to have benefits to human health, including antioxidant activity,[3] metal chelation,[4] and anti-proliferative, anticarcinogenic, antibacterial, anti-inflammatory, antiallergenic, and antiviral effects.[5−7]

In this context, the apple is an interesting vegetable plant species due to its natural high content of polyphenols (500−2700 mg/kg) and its widespread popularity all over the world.[8] Thus, there is considerable research interest toward the production of polyphenols and their enriched extracts, for use as food supplements or active ingredients by the cosmetics and pharmaceutical industries. Due to this ongoing interest, in this work, various apple extracts were investigated as sources of natural antioxidants.

Pressurized hot water extraction (PHWE) has been successfully used at an analytical level for the quantitative recovery of target analytes.[9−13] For instance, in a previous study, PHWE was used to extract antioxidants from apple byproducts.[14] This study showed the optimum conditions to extract antioxidants while minimizing the formation of undesirable compounds, such as Maillard and caramelization reaction products, during the extraction. The extraction conditions used in the present work to extract phenolic compounds from different types of apples were based on that previous, study although slightly modified.

There is an increased interest in assessing the total antioxidant capacity of complex samples, that is, the total number of moles of a given free radical that is scavenged by the sample. The *antioxidant capacity* should be distinguished from the *antioxidant activity*, of which the latter corresponds to the rate constant of a reaction between a specific antioxidant and a specific oxidant.[15] Several methods to measure antioxidant properties have been proposed and were recently reviewed.[16,17] Among these, trolox equivalent antioxidant capacity (TEAC), scavenging of stable radical 2,2-diphenyl-1-picrylhydrazyl (DPPH), oxygen radical absorbance capacity (ORAC), total radical-trapping antioxidant parameter (TRAP), ferric reducing antioxidant power (FRAP), and cupric ions (Cu^{2+}) reducing power (Cuprac) were employed in foods.[16] These methods are related to the capacity of a sample to compete for and scavenge a specific reactive oxygen species (ROS).

Even though these methods provide useful information, they are not sufficient for the evaluation of the overall antioxidant profile of biological fluids, tissue homogenate, or plant extract. Besides, these procedures present some drawbacks because

Received: September 23, 2013
Revised: December 14, 2013
Accepted: December 18, 2013
Published: December 18, 2013

ACS Publications © 2013 American Chemical Society

they require the use of specific reagents and they are tedious and time-consuming. Furthermore, the DPPH$^{\bullet}$ and ABTS$^{\bullet+}$ radicals are not representative of biomolecules found in any biological system. In this context, cyclic voltammetry (CV) methodology allows a rapid production of the electrochemical profile of samples and is especially suitable for screening studies. It is based on the analysis of the anodic current (AC) waveform, which is a function of the reactive potential of a given compound in the sample or a mixture of compounds. The CV tracing indicates the ability of a compound to donate electrons at the potential of the anodic wave. A CV also provides information describing the integrated antioxidant capacity without the specific determination of the contribution of each individual component. Therefore, in the past couple of years, CV has been suggested as an instrumental methodology for the evaluation of the total antioxidant capacity of foods.[18−21] Therefore, we have used CV methodology to evaluate the antioxidant capacity of apple extracts and then compared it with the traditional methods such as DPPH and TEAC.

The main purpose of the current study was, however, to assess the contribution of individual components of apple extracts to the overall antioxidant capacity of the extracts. Recently, online HPLC methods for analyzing radical-scavenging activity have been developed.[22−24] Such methods require a stable model free radical system, such as DPPH$^{\bullet}$ and ABTS$^{\bullet+}$, with radical-scavenging activity assessed in comparison to the water-soluble synthetic vitamin E derivative 6-hydroxy-2,5,7,8-tetramethylchroma-2-carboxylic acid (trolox). Online assessment of antioxidant activity allows complex mixtures to be separated by HPLC and the antioxidant contribution of individual components to be evaluated. Instead, likewise to CV, electrochemical properties of the individual compounds can be used for quantifying their antioxidant capacity. In our previous work, we have developed a separation system useful for characterizing antioxidants in complex samples, which was based on the hyphenation of high-performance liquid chromatography with diode array, electrochemical, and mass spectrometry detection (HPLC-DAD-ECD-MS/MS).[25,26] However, a large drawback is that none of these detectors can give any information about the quantity of the analyzed compounds without their respective standards. Because chemical standards are rarely available for most flavonoids found in plants and herbs, and the available flavonoid standards are generally very expensive, the quantification of these compounds is a true challenge.

Recently, a novel detector has been suggested to overcome this drawback; the charged aerosol detector (CAD), which is based on a technique that adds charges to each particle containing analytes eluting from HPLC column. The size of the charge is not dependent on chemical properties of the analytes, which makes the CAD relatively generic, thereby requiring only a limited number of chemical standards to quantify a large number of analytes in complex samples.

The aim of this work was to develop a method to measure the total antioxidant capacity of apple extracts obtained by PHWE from different apple varieties and, additionally, to evaluate the contribution of individual compounds to the total antioxidant capacity of the extracts, as well as to quantify the compounds present. Hence, this paper presents for the first time the use of a hyphenated system, HPLC-DAD-ECD-CAD, to directly screen and characterize antioxidants in apples. This system shows great potential in all applications involving the analysis of antioxidants in complex samples.

MATERIALS AND METHODS

Chemicals and Reagents. All of the chemicals were of analytical grade. 2,2′-Azinobis(3-ethylbenzothiazoline-6-sulfonic acid) (ABTS) was purchased from Fluka (Buchs, Switzerland). Trolox, ammonium formate, potassium persulfate, chlorogenic acid, caffeic acid, protocatechuic acid, homovanillic acid, rutin, and phloridzin were supplied by Sigma-Aldrich (Steinheim, Germany). Formic acid was from Merck (Darmstadt, Germany). Methanol, LC-MS grade, was provided by Scharlau (Barcelona, Spain). The flavonoid standards were purchased from Extrasynthese (Lyon, France). Deagglomerated alumina (α-Al_2O_3) suspensions with grain size = 0.1 μm was provided by Struers (Ballerup, Denmark). The ultrapure water used was obtained from a Milli-Q (Millipore, Billerica, MA, USA) instrument.

Samples. The apple samples (Fuji, Golden Delicious, Granny Smith, Jonagold, Royal Gala, organic Golden Delicious, and organic Royal Gala, one of each) were obtained from a local market in Lund, Sweden. The apple samples were cut in small cubes (3 mm) composed of skin and flesh.

PHWE. Extractions were performed on a Dionex ASE 200 system (Thermo Fisher, Germering, Germany). At the beginning of the day, the water was sonicated for 40 min. Extractions were performed at 112 °C for 10 min on the basis of an experimental method used in a previous study.[14] Prior to each experiment, heating of an extraction cell was carried out for 6 min. Likewise, all extractions were performed in 11 mL extraction cells, containing 5 g of fresh sample. Samples were prepared in duplicate.

The dry weight of apple was calculated by subtracting water content from the total weight. The fresh apple was led to dryness in an oven at 125 °C for 24 h.[27] This process was carried out in triplicate. The water contents in the apples, Fuji, Golden Delicious, Granny Smith, Jonagold, Royal Gala, organic Golden Delicious, and organic Royal Gala, were 84.5 ± 0.3, 85.1 ± 0.2, 85.3 ± 0.1, 86.1 ± 0.1, 83.4 ± 0.2, 88.1 ± 0.1, and 84.5 ± 0.4%, respectively.

The extraction procedure was as follows: (i) the extraction cell was loaded into the oven; (ii) the cell was filled with solvent up to a pressure of 1500 psi; (iii) heating time was applied; (iv) a static extraction with all system valves closed was performed; (v) the cell was rinsed (with 60% cell volume using extraction solvent); (vi) solvent was purged from the cell with nitrogen gas; and (vii) depressurization took place. Between extractions, a rinse of the complete system was made to prevent any extract carry-over. The extracts obtained were protected from light, freeze-dried, and stored at −20 °C until analysis. To prepare the sample solutions, the freeze-dried extracts were redisolved in water at a concentration of 20 mg/mL.

Evaluation of Antioxidant Capacity. *TEAC Assay.* The TEAC assay described by Re et al.[28] with some modifications was used to measure the antioxidant capacity of the extracts. The ABTS radical cation (ABTS$^{\bullet+}$) was produced by reacting 7 mM ABTS with 2.45 mM potassium persulfate and allowing the mixture to stand in the dark at room temperature for 12−16 h before use. The aqueous ABTS$^{\bullet+}$ solution was diluted with 5 mM phosphate buffer (pH 7.4) to an absorbance of 0.70 (±0.02) at 734 nm. Ten microliters of sample solution (four different concentrations) was added to 1 mL of diluted ABTS$^{\bullet+}$ radical solution. After 50 min at 30 °C, 300 μL of the mixture was transferred into a well of the microplate, and the absorbance was measured at 734 nm in a microplate spectrophotometer reader (Multiskan GO, Thermo Fisher). Trolox was used as a reference standard, and results were expressed as TEAC values (mmol trolox/g extract). These values were obtained from at least four different concentrations of each extract tested in the assay giving a linear response between 20 and 80% of the initial absorbance. All analyses were done in triplicate for each extract.

DPPH Radical-Scavenging Assay. The antioxidant capacity of all the obtained extracts was measured using the DPPH radical-scavenging assay based on the protocol by Brand-Williams et al.[29] Briefly, a solution was prepared by dissolving 23.5 mg of DPPH in 100

mL of methanol. This stock solution was further diluted 1:10 with methanol. Both solutions were stored at 4 °C until use. Four different concentrations of extracts were tested. Twenty-five microliters of these solutions was added to 975 μL of DPPH diluted solution to complete the final reaction medium (1 mL). After 4 h at room temperature, 300 μL of the mixture was transferred into a well of the microplate, and the absorbance was measured at 516 nm in a microplate spectrophotometer reader (Multiskan GO, Thermo Fisher). A DPPH−methanol solution was used as a reference sample. The DPPH concentration remaining in the reaction medium was calculated from a calibration curve. The percentage of remaining DPPH against the extract concentration was then plotted to obtain the amount of antioxidant necessary to decrease the initial DPPH concentration by 50%, or EC_{50}. Therefore, the lower the EC_{50}, the higher the antioxidant capacity. To enhance the clarity of the results, the antioxidant capacity was determined as the inverse value of the efficient concentration EC_{50} (μg/mL), representing a comparable term for the effectiveness of antioxidant and radical-scavenging capacity ($1/EC_{50}$). The larger the antioxidant capacity, the more efficient the antioxidant. Measurements were done in triplicate for each extract.

Cyclic Voltammetry. Cyclic voltammetric experiments were performed in 50:50 (methanol/water, v/v) extracts mixed with sodium formate buffer (pH 3.0) at a 1:1 (v/v) ratio and 0.5 M $NaNO_3$ following the method of Zettersten et al.[26] The sodium formate buffer consisted of 200 mM NaHCOO/HCOOH in water. The sodium formate buffer and $NaNO_3$ served as supporting electrolytes for the voltammetric measurement.

Cyclic voltammetry measurements were performed in a sealed-bottom three-electrode cell in which the electrode area was defined by an elastomeric O-ring (area ∼ 0.5 cm^2) using a glassy carbon electrode. A platinum auxiliary electrode and a silver/silver chloride reference electrode were used. The glassy carbon electrode was slightly polished on a polishing cloth with Al_2O_3 before each voltammetric experiment. All voltammograms were obtained at a scan rate of 20 mV/s. The homemade three-electrode cell used had angled openings allowing the reference and the working electrodes to be placed as close as possible to each other. The cell was connected to a battery-powered potentiostat (PalmSens, Palm Instruments BV, Houten, The Netherlands). The potentiostat was controlled by an HP iPAQ Pocket PC (HP 2200 series, Hewlett-Packard Co.) using PalmScan software (vs 1.4.2, Palm Instruments BV). All apple extract solutions (concentration = 10 mg/mL) were purged for 5 min with nitrogen gas prior to use. Measurements were done in triplicate.

For the purpose of testing, the total anodic peak wave area (S) of the voltammogram was calculated.[30] This method is based on the correlation between the total anodic peak wave area of cyclic voltammograms and the antioxidant capacity of the sample and reference substance. For the reference, an 80% methanol solution of trolox within the concentration range of 0.05−2.50 mM was used, and the results were expressed as micromoles of Trolox per gram of dry extract.

HPLC with Hyphenated Diode Array, Electrochemical, and Charged Aerosol Detection. *Instrumentation.* The HPLC-DAD-ECD-CAD setup is described schematically in Figure 1. It consisted of an UltiMate-3000 HPLC system from Dionex (Thermo Fisher) with an online degasser, a quarternary solvent pump, and an autosampler with cooler, column oven, and photodiode array detector (DAD) with scanning capabilities, all controlled by Chromeleon 6.80 (Thermo Fisher) software. The detection wavelengths used were 200, 280, 350, 370, and 520 nm.

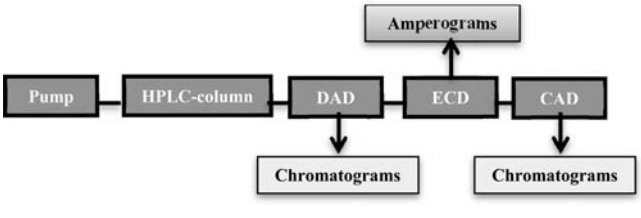

Figure 1. Employed online HPLC-DAD-ECD-CAD system.

An ECD instrument was attached just after the DAD. The online amperometric detection setup included a thin layer flow cell (Bioanalytical System Inc., West Lafayette, IN, USA) with a series dual glassy carbon disk electrodes (3 mm diameter) working electrode imbedded in a PEEK block (Bioanalytical System Inc.). A spacer gasket with a thickness of 16 μm (Bioanalytical System Inc.) was placed between the PEEK block comprising the working electrode and the stainless steel block serving as counter electrode. This resulted in a total cell volume of 1.0−1.2 μL. The reference electrode was fixed in a compartment in the stainless steel block. The ECD redox potential measured at +0.6 V vs Ag/AgCl was found to yield antioxidant capacity results comparable with those of the DPPH and ABTS assays. A battery-powered potentiostat (Palmsens, Palm Instrument BV) was connected to the flow cell and was controlled by an HP iPAQ Pocket PC (HP 2200 series, Hewlett-Packard Co.). PalmTime software (vs 2.3.0.0, Palmsens) was used to collect data.

A Corona CAD instrument from ESA Biosciences Inc. (part of Thermo Fisher) was placed in series after the ECD detector. Data processing was carried out with Chromeleon 6.8 software (Thermo Fisher). Nitrogen gas flow rate was regulated automatically and monitored by the CAD device regulated at 35 psi. Response range was set to 20 pA full scale. Medium filter was applied.

Chromatographic Separation. A porous-shell fused core Ascentis Express C18 (150 mm × 2.1 mm, 2.7 μm) from Supelco (Bellefonte, PA, USA) was used as an analytical column for LC separation. The mobile phases consisted of (A) ammonium formate buffer (pH 3.0), 60 mM (NH_4HCOO/HCOOH) in water; and (B) methanol with 0.2% of formic acid in a gradient elution analysis programmed as follows: 0 min, 5% (B); 0−5 min, 5% (B); 5−35 min, 40% (B); 35−40 min, 40% (B), with 10 min of post-time at a flow rate of 300 μL/min. The mobile phases were purged with nitrogen to remove oxygen. The column temperature was set at 50 °C, the injection volume was 2 μL, and the vial tray was held at 4 °C.

Statistical Analysis. The KaleidaGraph 4.03 (Synergy Software, Reading, PA, USA) program was employed for statistical analysis of the data with the level of significance set at 95%. Student's t test was used to assess significant differences between antioxidant assays.

RESULTS AND DISCUSSION

As mentioned in the Introduction, the aim of this work was mainly to develop a method that can be used to characterize and quantify antioxidants in complex samples. Hence, the focus was not to identify the different types of antioxidants found in apples.

Antioxidant Capacity of Apple Extracts Produced by PHWE. PHWE is an environmentally friendly technique that presents important advantages over traditional solvent extraction techniques, mainly achieving safe, green, and rapid extractions. Increasing the temperature decreases the dielectric constant of water, resulting in the possibility of tuning its solvent properties, as has been shown for aromatic plants.[11] In this work, PHWE was used to obtain a variety of extracts from seven different apples: Fuji, Golden Delicious, Granny Smith, Jonagold, Royal Gala, organic Golden Delicious, and organic Royal Gala. The extraction yield (percent dry weight) obtained from apple PHWE extraction was around 63% (Table 1), being maximum in Jonagold (67%) and minimum in organic Golden Delicious (60%).

In this study, we conducted a critical evaluation of a cyclic voltammetry method for the determination and rapid screening of antioxidant capacity of different apple type extracts compared with ABTS and DPPH assays. The representative cyclic voltammograms of the apple extracts (10 mg/mL concentration) were recorded from 0 to 700 mV at a scan rate of 20 mV/s (Figure 2). The obtained voltammograms

Table 1. Extraction Yield and DPPH, ABTS, and Cyclic Voltammetry Antioxidant Capacity Values Obtained for the Different Varieties of Apple Extracts after PHWE at 112 °C and 10 min[a]

	extraction yield		ABTS		DPPH		CV	
apple variety	% (dry wt)	RSD (%)	TEAC (mmol/g dry extract)	RSD (%)	$1/EC_{50}$ (μg/mL)	RSD (%)	mmol trolox/g dry extract	RSD (%)
Golden Delicious	60	1.7	0.12	4.0	3.4	1.7	7.9	3.0
Royal Gala	64	4.9	0.082	7.8	2.7	2.2	7.4	1.1
Fuji	64	5.5	0.050	8.0	1.5	2.0	5.1	6.1
Granny Smith	62	1.7	0.13	1.9	3.5	1.0	7.4	4.7
Jonagold	67	4.8	0.18	3.3	4.9	2.2	12	4.3
organic Golden Delicious	59	8.0	0.16	6.0	4.2	4.9	9.3	7.1
organic Royal Gala	63	2.4	0.10	4.0	2.9	2.3	6.7	8.7

[a]All measurements were done in triplicate for each extraction. The data are presented as the average of six measurements from two extracts (mean and relative standard deviation (RSD)).

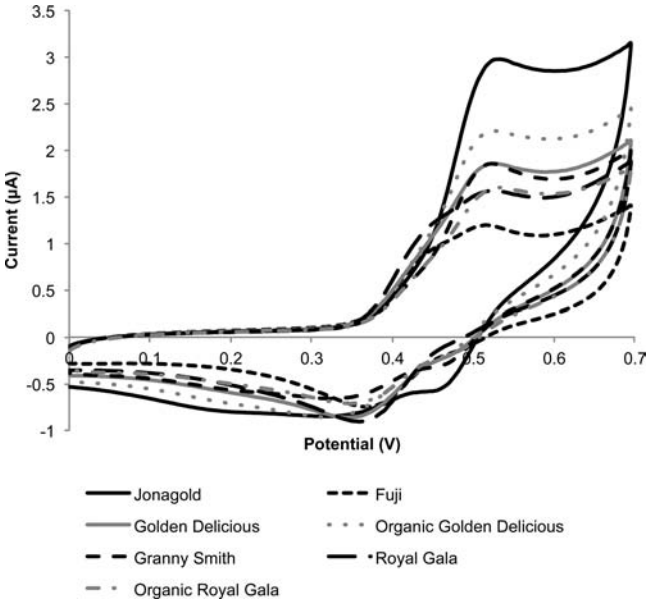

Figure 2. Cyclic voltammograms of PHWE extracts from different apple varieties. Operative conditions: concentration of each extract, 10 mg/mL; scan rate, 20 mV/s.

show that the different apple extracts exhibit well-defined oxidation and reduction votammetric peaks. The area of each voltammetric peak is related to the concentration of antioxidants.[31,32] A broad anodic peak between 0.4 and 0.6 V was observed. The peak is due to the response of several antioxidants with different oxidation potentials, which are mainly flavonoids and phenolic acids.[14] The results show that the samples contain multiple reducing agents in the respective extracts. Therefore, the area under the anodic current waveform (AUC) was taken to reflect the total antioxidant capacity of the samples compared to a set of trolox solutions, as suggested by Chevion et al.,[31] Martínez et al.,[32] and Zielinska et al.[30] This provides a marked advantage in some cases, particularly when the AUC wave represents more than a single component. Higher AUC area indicates a higher antioxidant capacity of the investigated extract.

Furthermore, the use of three different methods to measure the antioxidant capacity of different apple extracts allowed us to gain insight into their reaction mechanism. The results obtained are summarized in Table 1. All extracts were able to act against $ABTS^{\bullet+}$ and DPPH radicals and were susceptible to oxidation. Extracts from different apple varieties show significant differences in their antioxidant capacity, although the extraction yields are similar.

To correlate the CV data for different apple varieties with the ABTS and DPPH, the results in Figure 3 have been normalized so that the values range from 0 to 1, 1 being the maximum value of total antioxidant capacity in each method. The results from CV strongly correlate with those determined using well-known spectrophotometric methodologies such as DPPH and ABTS assays. There was no statistically significant difference between the different assays ($p > 0.05$). From the above results it follows that a good correlation exists between antioxidant capacity (obtained from the oxidation peak areas in CV) and antiradical power, indicating that the voltammetric method can be used for the determination of antioxidant capacity, in the same way as the DPPH and ABTS assays. At least this is true for water-soluble antioxidants in apples.

This means that the values of the oxidation potentials can be interpreted in the same way as the antiradical power values obtained from DPPH and ABTS, and the quality of the information obtained is the same in all cases. This result is in agreement with other studies, in which CV was shown to be an efficient instrumental tool for evaluating the antioxidant capacity of plant, food, and biological samples.[21,30,33,34] An advantage of the electrochemical measurement compared to the DPPH and ABTS methods is that it is fast. The CV measurement is carried out in <10 min; that is, it is less tedious. Moreover, there is no necessity to use expensive reagents that include free radicals, thus lowering the cost. In addition, the use of a small amount of organic solvent reduces the amount of organic waste produced.

Optimization of an Online HPLC-DAD-ECD-CAD Method. The separation of all phenolic compounds in the fruit extract using HPLC is a crucial and challenging task. Considerable effort was required to develop the HPLC conditions used in this paper. Apples are rich in flavonoids with similar skeleton structures. Because acidic conditions are known to create uncharged hydroxyl groups, the pH of the analytes should be kept below the pK_a of the flavonoids, thus achieving better separation for flavonoid derivatives by reducing the tailing of the peaks. This was achieved by adding acid into the mobile phase used in this work.[35,36] It was also necessary to use a mobile phase that could also serve as a supporting electrolyte in the EC cell. To meet these conditions, an ammonium formate buffer (pH 3) was used as the mobile phase and contained 60 mM $NH_4HCOO/HCOOH$ in water.[26] In the course of optimizing the conditions of separation, the system conditions including gradient program (gradient time, gradient shape, and initial composition of the mobile phase),

dx.doi.org/10.1021/jf404263k | J. Agric. Food Chem. 2014, 62, 409−418

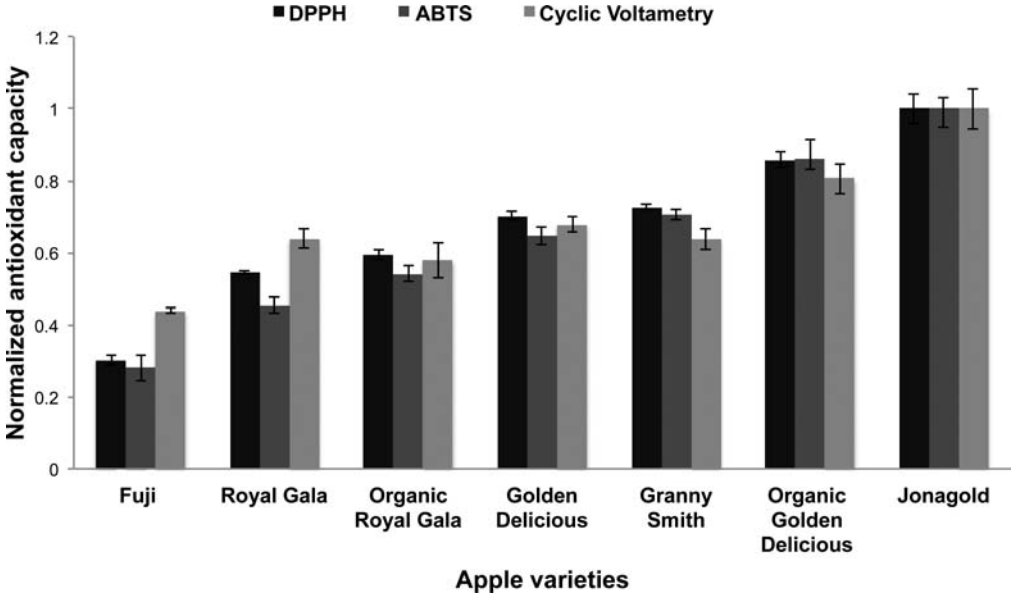

Figure 3. Normalized antioxidant capacity of DPPH, ABTS, and cyclic voltammetry values obtained for the different varieties of apple extracts after PHWE at 112 °C and 10 min. All measurements were done in triplicate for each extraction. The data are presented as the average of six measurements from two extracts.

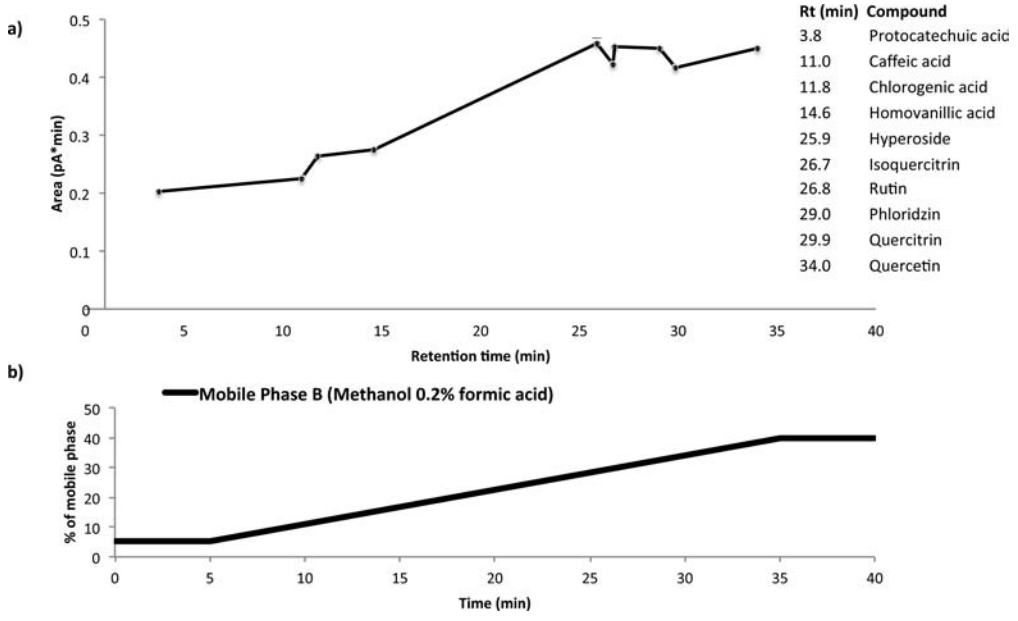

Figure 4. Charged aerosol detection response for a selection of phenolic compounds injected at the same concentration (0.1 mg/mL) (a) and a HPLC gradient of mobile phases employed for the analysis of these compounds (b). All measurements were done in triplicate.

column temperature (25−50 °C), flow rate (0.2−0.4 mL/min), injection volume (1−5 μL), and detection wavelength (200, 280, 350, 370, and 520 nm) were investigated. The final results showed that the best resolution and shortest analysis time were achieved when a gradient elution was composed of solvent (A) ammonium formate buffer (pH 3.0)−60 mM (NH_4HCOO/HCOOH) in water and solvent (B) methanol with 0.2% formic acid programmed as follows: 0 min, 5% B; 0−5 min, 5% B; 5−35 min, 40% B; 35−40 min, 40% B; and a 10 min post-time at final composition. The selected flow rate was 300 μL/min, the column temperature was 50 °C, and the injection volume was 2 μL. The vial tray was held at 4 °C.

The analytes were detected by a DAD, which was set to record chromatograms between 200 and 600 nm, with selected wavelengths of 280 nm (for identification of the phenolic acids and chalcones) and 350 nm (for flavonols and chlorogenic acid). The DAD allowed a preliminary characterization of the compounds based on their retention time and UV−vis spectra by comparison with standards, when available, or with data appearing in the literature.[37,38]

The DAD was coupled online to an ECD to estimate the antioxidant capacity of each compound and its contribution to the total antioxidant capacity of the apple extracts. The oxidation potential for the phenolic compounds from apples was determined on the basis of the cyclic voltammograms. The oxidation peak for the phenolic compounds from apples occurred at a potential of about 0.55 V. This peak is due to the oxidation of hydroxyl groups on the extracted phenolic

dx.doi.org/10.1021/jf404263k | J. Agric. Food Chem. 2014, 62, 409−418

Table 2. Calibration Curves Using Various Standards of Phenolic Compounds in HPLC-CAD and the Error Obtained When Calibration Curves of Chlorogenic Acid (for Phenolic Acids) and Hyperoside (for Flavonols and Chalcones) Were Used Instead of Their Respective Standards To Carry Out the Quantification of These Standards[a]

RT (min)	compound	regression coefficient	R^2	LOD[b] (μg/mL)	LOQ[c] (μg/mL)	error (%)
3.76	protocatechuic acid	$2.097x + 0.003$	0.992	4.6	16.7	11.7
10.98	caffeic acid	$2.295x + 0.001$	0.998	4.4	14.4	7.3
11.80	chlorogenic acid	$2.655x - 0.006$	0.997	5.8	18.8	
14.61	homovanillic acid	$2.729x + 0.006$	0.998	7.5	30.4	1.4
25.87	hyperoside	$4.662x + 0.004$	0.998	1.5	5.4	
26.67	isoquercitrin	$4.184x - 0.0001$	0.999	1.6	5.9	5.4
26.81	rutin	$4.501x + 0.005$	0.999	1.5	5.2	1.7
29.04	phloridzin	$4.494x - 0.002$	0.999	1.3	5.4	1.8
29.88	quercitrin	$4.116x + 0.001$	0.999	1.8	6.2	6.2
34.04	quercetin	$4.594x - 0.002$	0.997	1.6	7.8	0.7

[a]All measurements were done in triplicate. [b]LOD, limit of detection. [c]LOQ, limit of quantification.

compounds and, unfortunately, cannot be used to identify individual antioxidants.[31] More in-depth information about oxidation of phenolic compounds is given by Yakovleva et al.[39] In conclusion, for the ECD experiments, we used a fixed potential of 0.60 V to ensure all of the phenolic compounds were oxidized.

To carry out the quantification of the phenolic compounds, the HPLC-DAD-ECD system was hyphenated online to a corona CAD detector. CAD is now established as a universal detector for HPLC applications, which has been shown to produce direct quantification of compounds relative to a known standard.[40,41] CAD involves first nebulizing the HPLC column eluent with nitrogen and then drying in a drift tube to produce analyte particles. A secondary flow of nitrogen becomes positively charged as it passes through a corona generated by high voltage. This charged nitrogen is then mixed with the stream of analyte particles where the charge migrates to the analyte.[42] Charged analyte particles proceed to a collector region, where a highly sensitive electrometer produces a signal that is proportional to the weight of sample present, independent of chemical structure.[43] This results in an equal response for equal mass amounts.[44]

To measure the detector response of the CAD, different phenolic compounds (flavonols, chalcones, and phenolic acids), which have been previously described in apples,[14,37] were injected in triplicate at the same concentration of 0.1 mg/mL (see Figure 4a). As can be seen in Figure 4a, the response obtained was different, dividing the compounds into two groups. The phenolic acids, protocatechuic, caffeic, chlorogenic, and homovanillic acids, which had shorter retention times, had similar response areas around 0.20−0.27 pA·min. On the other hand, the flavonols and chalcone, hyperoside, isoquercitrin, rutin, quercitrin, quercetin, and phloridzin, which had longer retention times, had similar response areas around 0.42−0.46 pA·min. The differences observed may have been due to mobile phase composition. As can be seen in Figure 4, it is evident that the response factors increased with increasing concentration of methanol in the mobile phase. As has been reported before, a weakness of all detectors employing a nebulization process is that the response is dependent on the composition of the mobile phase and increases with the organic solvent content.[45] A solution to this is to use a second gradient pump that applies a reverse gradient. We are currently carrying out experiments to test this hypothesis.

The data concerning the validation of the quantification of phenolic compounds method by HPLC-CAD are summarized in Table 2. The linearity of the detector response was determined by the square correlation coefficients of the calibration curves generated by three repeated injections of standard solutions at nine concentration levels (Table 2). Quercetin-3-*O*-galactoside (hyperoside), quercetin-3-*O*-glucoside (isoquercitrin), quercetin-3-*O*-rutinoside (rutin), phloretin-2′-*O*-glucoside (phloridzin), quercetin-3-*O*-rhamnoside (quercitrin), and quercetin were injected in concentrations from 1 to 100 μg/mL each; chlorogenic acid, protocatechuic acid, and caffeic acid were injected in concentrations from 2 to 200 μg/mL each; and homovanillic acid was injected in concentrations from 3 to 200 μg/mL.

The calibration curves were obtained by plotting peak area as a function of concentration (in micrograms per milliliter). Although it is known that Corona CAD response is nonlinear at a range of 4 orders of magnitude, its signal is nearly linear in the smaller ranges.[46] Responses obtained in the examined ranges were expressed by a linear equation, $y = ax \pm b$, with good r^2 determination coefficient values (Table 2). Estimations of the limit of detection (LOD) and limit of quantification (LOQ) of the phenolic compounds were determined on the basis of the signal-to noise ratio (S/N) of 3 and 10, respectively (Table 2). The analytical methodology revealed good linearity (Table 2). The regression coefficients using the CAD were very similar for the phenolic acids and for the flavonols and chalcones. In this sense, the calibration curve of one phenolic acid and one flavonol could be used to quantify other phenolic compounds present in the apple extracts. The calibration curves of chlorogenic acid and hyperoside were selected to quantify all of the phenolic compounds, because they are normally found in high concentration in the different apple extracts.[14] The error obtained by using the two selected standards (chlorogenic acid and hyperoside) instead of the corresponding standard for each sample was calculated at concentrations of LOQ. The data are given in Table 2. The maximum error obtained was <12%, and the average error was 5%. Our results suggest that CAD shows great promise as an appropriate universal detector for quantifying phenolics from apple extracts using only the calibration curves of one phenolic acid and one flavonoid. A disadvantage of CAD is its relatively low sensitivity compared to DAD. For instance, the obtained values for LOD and LOQ were 5.8 and 18.8 μg/mL for chlorogenic acid and 1.5 and 5.4 μg/mL for hyperoside, respectively (see Table 2), which are around 5−18 times higher than those described in the literature for these compounds and other flavonoids analyzed with a similar method but with DAD.[47−49]

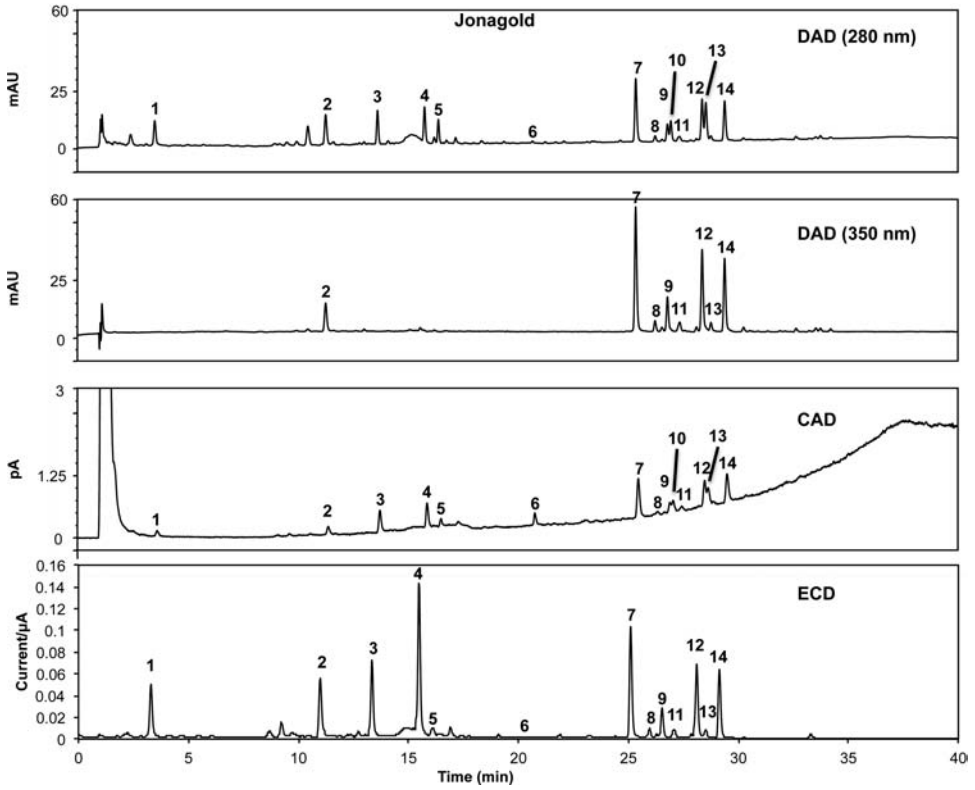

Figure 5. Chromatograms and amperogram corresponding to the HPLC-DAD-ECD-CAD analysis of Jonagold apple extract at 280 nm (a) and 350 nm (b), CAD chromatogram (c), and amperogram (d). Analytical conditions are given under Material and Methods. For peak identification, see Table 3.

Quantification and Tentative Identification of Phenolic Compounds in Apples. The developed online HPLC-DAD-ECD-CAD method was tested with the different apple extracts. Selected chromatograms and amperogram obtained from the Jonagold sample are shown in Figure 5. The data clearly demonstrate that several phenolic acids and polyphenols could be separated in an analysis time of around 40 min. As shown in Figure 5, the peak profile of the HPLC-ECD amperogram corresponded well with the chromatographic peaks in the DAD and CAD profiles. The careful analysis of the separated compounds, using the information provided by the DAD detector together with the information found in the literature[37,38] and from commercial standards (when available), allowed the tentative identification of 14 antioxidant compounds in the different apple extracts, which belong to the phenolic family (Table 3).

As discussed above, the quantification of phenolic compounds was carried out with a CAD detector using the calibration curve of chlorogenic acid for phenolic acids and hyperoside for flavonols and chalcones. This detector allowed the quantification of all of the separated phenolic compounds without their respective standards. All of the results for the quantification of phenolic compounds in apple varieties are shown in Table 1 of the Supporting Information.

Determination of Individual Phenolic Compound Contributions to the Total Antioxidant Capacity in Apples. The use of cyclic voltammetry for the determination of the antioxidant capacity has been reported. The intensity of the anodic peak current or the area under the anodic peak can be used as an indicator of the antioxidant capacity.[31] As a result, in this work, the ECD was used to study the oxidation of phenolic compounds to indicate the antioxidant capacity of each compound. To carry out the determination of the contribution of individual phenolic compounds to the total antioxidant capacity of the apple extracts, the concentration of each compound as determined by CAD and the peak areas obtained by ECD for each compound were correlated in scatter plots (Figure 6 and Table 3). The complete set of data is given in Table 1 of the Supporting Information.

Table 3. Linear Coefficient (R^2) and Slope of the Regression Line for a Side-by-Side Comparison between CAD Response (Concentration (Milligrams per Gram Dry Extract)) and ECD Response (Area (nA·s)) for Each Phenolic Compound Found in Seven Different Varieties of Apple Extracts Injected at a Concentration of 20 mg/mL[a]

peak	RT (min)	compound	R^2	slope ± 95% CI
1	3.6	protocatechuic acid	0.993	1269 ± 21
2	11.5	chlorogenic acid	0.907	948 ± 30
3	13.8	phenolic 1	0.782	646 ± 31
4	15.9	phenolic 2	0.938	1320 ± 57
5	16.5	phenolic 3	0.880	248 ± 20
6	20.9	phenolic 4	0.799	29 ± 3
7	25.5	hyperoside	0.980	1014 ± 15
8	26.4	isoquercitrin	0.944	873 ± 29
9	26.9	quercetin derivative 1	0.820	107 ± 6
10	27.1	phloretin glycoside		
11	27.5	quercetin derivative 2	0.907	362 ± 10
12	28.6	quercetin derivative 3	0.983	1145 ± 11
13	28.9	phloridzin	0.961	265 ± 14
14	29.6	quercitrin	0.972	754 ± 14

[a]The data are presented as the average of four measurements from two extracts. CI, confidence interval.

dx.doi.org/10.1021/jf404263k | J. Agric. Food Chem. 2014, 62, 409−418

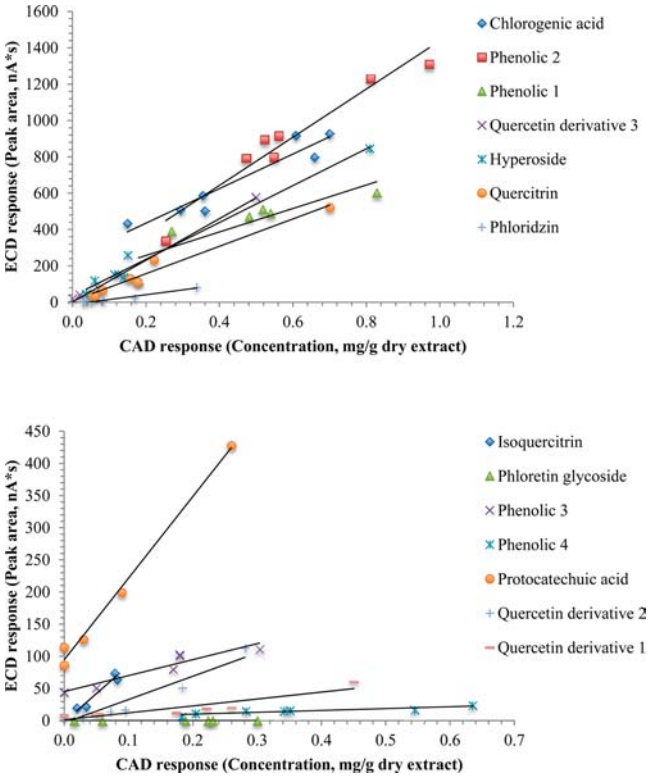

Figure 6. Scatterplots of ECD response (area (nA·s)) versus CAD response (concentration (mg/g dry extract)) for each phenolic compound found in seven different varieties of apple extracts injected at a concentration of 20 mg/mL. The data are presented as an average of four measurements from two extracts.

As shown in Table 3, the response between both detectors was fairly linear, with the R^2 of 14 compounds being ≥0.782. Using the slope, it was possible to calculate the antioxidant capacity and the contribution of each phenolic compound to the total antioxidant capacity of the apple extracts. The higher the slope, the higher the antioxidant capacity. The results revealed that phenolic 2 (not identified), protocatechuic acid, quercetin derivative 3 (not identified), hyperoside, and chlorogenic acid with slopes of 1320, 1269, 1145, 1013, and 948, respectively, were the phenolic compounds with higher antioxidant capacity. On the contrary, the phenolic compounds with lower antioxidant capacity were phenolic 4 (not identified), quercetin derivative 1 (not identified), phenolic 3 (not identified), and phloridzin, with slopes of 29, 107, 248, and 265, respectively. Phloretin glycoside was not possible to detect with ECD due to the low concentration present in the apple extracts. For this reason, it was not possible to calculate the R^2 and the slope for phloretin glycoside. This result suggests that this chalcone is not a significant contributor to the total antioxidant capacity of apple extracts. On the other hand, protocatechuic acid was present in concentrations lower than the detection limit of the CAD detector in several of the apple extracts, but showed high antioxidant capacity as observed with the ECD. In conclusion, phenolic 2, chlorogenic acid, phenolic 1, and hyperoside were found in high concentrations and also exhibited higher antioxidant capacity. Therefore, these compounds can be expected to contribute the most to the total antioxidant capacity of apple extracts (see Figure 6).

Figure 7 shows the sum of all peak areas obtained for each apple from the ECD voltammograms. The area represents the

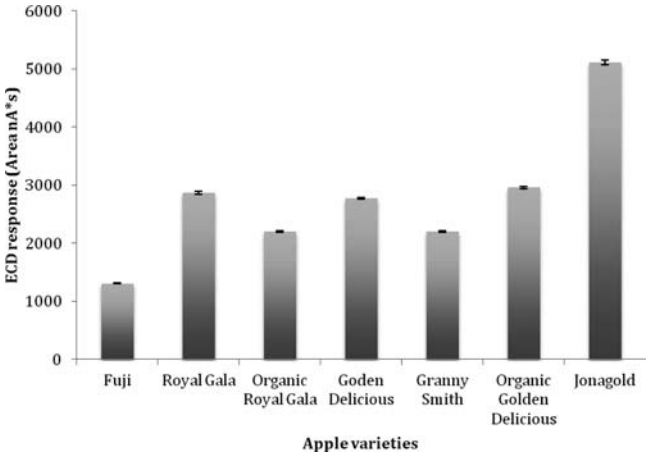

Figure 7. Total areas of phenolic compound peaks obtained by ECD for the different varieties of apple extracts. The data are presented as an average of four measurements from two extracts.

total antioxidant capacity of phenolic compounds found in the apple extracts. As can be seen in Figure 7, the highest antioxidant capacity was observed in Jonagold apple followed by organic Golden Delicious, Royal Gala, Golden Delicious, organic Royal Gala, Granny Smith, and Fuji. These results were similar to the data observed in Figure 3, which indicated that the total antioxidant capacity of apple extracts may be contributed mainly by phenolic compounds. However, in complex samples, synergism and antagonism reactions between different compounds may occur, and these reactions affect the total antioxidant capacity.[50−52]

In conclusion, a cyclic voltammetry assay was demonstrated to be an effective method for measuring the antioxidant capacity of apple extracts. It was comparable with conventional ABTS and DPPH antioxidant assays. Furthermore, for the first time, a HPLC-DAD-ECD-CAD method was developed for the determination and quantification of phenolic compounds in apple extracts. The main advantage of the developed hyphenated method is its selectivity, because it not only separates and detects polyphenols but also determines the compounds' potential functionality in terms of antioxidant capacity by utilizing ECD in combination with CAD responses.

Clearly, the advantage of online antioxidant measurement lies in its ability to distinguish the antioxidant capacity of compounds that can hardly be separated by fractionation. The relative importance of these compounds for antioxidant capacity is measured directly, without time-consuming techniques. Furthermore, an independent measurement of the quantity of antioxidant compounds is performed by CAD. This latter detector proved to enable quantification for different classes of compounds, relative to each other. This is particularly useful when no standards are available, as is usually the case for many flavonoids.

■ ASSOCIATED CONTENT

Supporting Information

Additional table. This material is available free of charge via the Internet at http://pubs.acs.org.

■ AUTHOR INFORMATION

Corresponding Author

*(M.P.) E-mail: Merichel.Plaza@chem.lu.se, merichelpla@gmail.com. Phone: +46 76 585 5167. Fax: +46 46 222 8209.

Funding

The presented work has been supported by the Antidiabetic Food Centre, a VINNOVA VINN Excellence Centre at Lund University, Sweden, and the Swedish Research Council Formas (229-2009-1527) (SuReTech).

Notes

The authors declare no competing financial interest.

■ ACKNOWLEDGMENTS

We thank Victor Abrahamsson, Center for Analysis and Synthesis (Lund University), for helpful suggestions regarding the presentation of the results. J.K. acknowledges the provision of sabbatical leave from the University of Alberta.

■ ABBREVIATIONS USED

ABTS, 2,2′-azinobis(3-ethylbenzothiazoline-6-sulfonic acid); AC, anodic current; AUC, area under the anodic current waveform; CAD, charged aerosol detector; Cuprac, cupric ions (Cu^{2+}) reducing power; CV, cyclic voltammetry; DAD, diode array detector; DPPH, scavenging of stable radical 2,2-diphenyl-1-picrylhydrazyl; ECD, electrochemical detector; FRAP, ferric reducing antioxidant power; HPLC, high-performance liquid chromatography; LOD, limit of detection; LOQ, limit of quantification; MS, mass spectrometry; ORAC, oxygen radical absorbance capacity; PHWE, pressurized hot water extraction; *S*, total anodic peak wave area; ROS, reactive oxygen species; TEAC, trolox equivalent antioxidant capacity; TRAP, total radical-trapping antioxidant parameter; trolox, 6-hydroxy-2,5,7,8-tetramethylchroma-2-carboxylic acid

■ REFERENCES

(1) Martens, S.; Mithofer, A. Flavones and flavone synthases. *Phytochemistry* **2005**, *66*, 2399−2407.
(2) Harborne, J. B.; Williams, C. A. Advances in flavonoid research since 1992. *Phytochemistry* **2000**, *55*, 481−504.
(3) Pietta, P. G. Flavonoids as antioxidants. *J. Nat. Prod.* **2000**, *63*, 1035−1042.
(4) Mira, L.; Fernandez, M. T.; Santos, M.; Rocha, R.; Florencio, M. H.; Jennings, K. R. Interactions of flavonoids with iron and copper ions: a mechanism for their antioxidant activity. *Free Radical Res.* **2002**, *36*, 1199−1208.
(5) Formagio, A. S. N.; Kassuya, C. A. L.; Neto, F. F.; Volobuff, C. R. F.; Iriguchi, E. K. K.; Vieira, M. D. C.; Foglio, M. A. The flavonoid content and antiproliferative, hypoglycaemic, anti-inflammatory and free radical scavenging activities of *Annona dioica* St. Hill. *BMC Complement. Altern. Med.* **2013**, *13*.
(6) Khan, N.; Mukhtar, H. Tea polyphenols for health promotion. *Life Sci.* **2007**, *81*, 519−533.
(7) Quiñones, M.; Miguel, M.; Aleixandre, A. Beneficial effects of polyphenols on cardiovascular disease. *Pharmacol. Res.* **2013**, *68*, 125−131.
(8) Wojdyło, A.; Oszmiański, J.; Laskowski, P. Polyphenolic compounds and antioxidant activity of new and old apple varieties. *J. Agric. Food Chem.* **2008**, *56*, 6520−6530.
(9) Stavikova, L.; Polovka, M.; Hohnová, B.; Karásek, P.; Roth, M. Antioxidant activity of grape skin aqueous extracts from pressurized hot water extraction combined with electron paramagnetic resonance spectroscopy. *Talanta* **2011**, *85*, 2233−2240.
(10) Arapitsas, P.; Turner, C. Pressurized solvent extraction and monolithic column-HPLC/DAD analysis of anthocyanins in red cabbage. *Talanta* **2008**, *74*, 1218−1223.
(11) Herrero, M.; Plaza, M.; Cifuentes, A.; Ibáñez, E. Green processes for the extraction of bioactives from Rosemary: Chemical and functional characterization via ultra-performance liquid chromatography-tandem mass spectrometry and in-vitro assays. *J. Chromatogr., A* **2010**, *1217*, 2512−2520.
(12) Cheigh, C. I.; Chung, E. Y.; Chung, M. S. Enhanced extraction of flavanones hesperidin and narirutin from *Citrus unshiu* peel using subcritical water. *J. Food Eng.* **2012**, *110*, 472−477.
(13) Gil-Ramírez, A.; Mendiola, J. A.; Arranz, E.; Ruíz-Rodríguez, A.; Reglero, G.; Ibáñez, E.; Marín, F. R. Highly isoxanthohumol enriched hop extract obtained by pressurized hot water extraction (PHWE). Chemical and functional characterization. *Innovative Food Sci. Emerging Technol.* **2012**, *16*, 54−60.
(14) Plaza, M.; Abrahamsson, V.; Turner, C. Extraction and neoformation of antioxidant compounds by pressurized hot water extraction from apple byproducts. *J. Agric. Food Chem.* **2013**, *61*, 5500−5510.
(15) MacDonald-Wicks, L. K.; Wood, L. G.; Garg, M. L. Methodology for the determination of biological antioxidant capacity in vitro: a review. *J. Sci. Food Agric.* **2006**, *86*, 2046−2056.
(16) Gülçin, I. Antioxidant activity of food constituents: an overview. *Arch. Toxicol.* **2012**, *86*, 345−391.
(17) Sánchez-Moreno, C. Review: Methods used to evaluate the free radical scavenging activity in foods and biological systems. *Food Sci. Technol. Int.* **2002**, *8*, 121−137.
(18) Lugonja, N. M.; Stanković, D. M.; Spasić, S. D.; Roglić, G. M.; Manojlović, D. D.; Vrvić, M. M. Comparative electrochemical determination of total antioxidant activity in infant formula with breast milk. *Food Anal. Methods* **2013**, 1−8.
(19) Gulaboski, R.; Mirčeski, V.; Mitrev, S. Development of a rapid and simple voltammetric method to determine total antioxidative capacity of edible oils. *Food Chem.* **2013**, *138*, 116−121.
(20) Pekal, A.; Drozdz, P.; Pyrzynska, K. Comparison of the antioxidant properties of commonly consumed commercial teas. *Int. J. Food Prop.* **2012**, *15*, 1101−1109.
(21) Arteaga, J. F.; Ruiz-Montoya, M.; Palma, A.; Alonso-Garrido, G.; Pintado, S.; Rodríguez-Mellad, J. M. Comparison of the simple cyclic voltammetry (CV) and DPPH assays for the determination of antioxidant capacity of active principles. *Molecules* **2012**, *17*, 5126−5138.
(22) Stewart, A. J.; Mullen, W.; Crozier, A. On-line high-performance liquid chromatography analysis of the antioxidant activity of phenolic compounds in green and black tea. *Mol. Nutr. Food Res.* **2005**, *49*, 52−60.
(23) Zhang, Y.; Li, Q.; Xing, H.; Lu, X.; Zhao, L.; Qu, K.; Bi, K. Evaluation of antioxidant activity of ten compounds in different tea samples by means of an on-line HPLC-DPPH assay. *Food Res. Int.* **2013**, *53*, 847−856.
(24) Gioti, E. M.; Fiamegos, Y. C.; Skalkos, D. C.; Stalikas, C. D. Antioxidant activity and bioactive components of the aerial parts of *Hypericum perforatum* L. from Epirus, Greece. *Food Chem.* **2009**, *117*, 398−404.
(25) Co, M.; Zettersten, C.; Nyholm, L.; Sjöberg, P. J. R.; Turner, C. Degradation effects in the extraction of antioxidants from birch bark using water at elevated temperature and pressure. *Anal. Chim. Acta* **2012**, *716*, 40−48.
(26) Zettersten, C.; Co, M.; Wende, S.; Turner, C.; Nyholm, L.; Sjöberg, P. J. R. Identification and characterization of polyphenolic antioxidants using on-line liquid chromatography, electrochemistry, and electrospray ionization tandem mass spectrometry. *Anal. Chem.* **2009**, *81*, 8968−8977.
(27) Wang, W. C.; Sastry, S. K. Effects of thermal and electrothermal pretreatments on hot air drying rate of vegetable tissue. *J. Food Process. Eng.* **2000**, *23*, 299−319.
(28) Re, R.; Pellegrini, N.; Proteggente, A.; Pannala, A.; Yang, M.; Rice-Evans, C. Antioxidant activity applying an improved ABTS radical cation decolorization assay. *Free Radical Biol. Med.* **1999**, *26*, 1231−1237.
(29) Brand-Williams, W.; Cuvelier, M. E.; Berset, C. Use of a free radical method to evaluate antioxidant activity. *LWT−Food Sci. Technol.* **1995**, *28*, 25−30.

(30) Zielinska, D.; Szawara-Nowak, D.; Ornatowska, A.; Wiczkowski, W. Use of cyclic voltammetry, photochemiluminescence, and spectrophotometric methods for the measurement of the antioxidant capacity of buckwheat sprouts. *J. Agric. Food Chem.* **2007**, *55*, 9891−9898.
(31) Chevion, S.; Roberts, M. A.; Chevion, M. The use of cyclic voltammetry for the evaluation of antioxidant capacity. *Free Radical Biol. Med.* **2000**, *28*, 860−870.
(32) Martinez, S.; Valek, L.; Rešetić, J.; Ružić, D. F. Cyclic voltammetry study of plasma antioxidant capacity − comparison with the DPPH and TAS spectrophotometric methods. *J. Electroanal. Chem.* **2006**, *588*, 68−73.
(33) Psotova, J.; Zahalkova, J.; Hrbac, J.; Simanek, V.; Bartek, J. Determination of total antioxidant capacity in plasma by cyclic voltammetry. Two case reports. *Biomed. Papers Med. Fac. Univ. Palacky, Olomouc, Czechoslovakia* **2001**, *145*, 81−83.
(34) Zielinska, D.; Wiczkowski, W.; Piskula, M. K. Determination of the relative contribution of quercetin and its glucosides to the antioxidant capacity of onion by cyclic voltammetry and spectrophotometric methods. *J. Agric. Food Chem.* **2008**, *56*, 3524−3531.
(35) Inbaraj, B. S.; Lu, H.; Kao, T. H.; Chen, B. H. Simultaneous determination of phenolic acids and flavonoids in *Lycium barbarum* Linnaeus by HPLC−DAD−ESI-MS. *J. Pharm. Biomed. Anal.* **2010**, *51*, 549−556.
(36) Wang, S.-P.; Huang, K.-J. Determination of flavonoids by high-performance liquid chromatography and capillary electrophoresis. *J. Chromatogr., A* **2004**, *1032*, 273−279.
(37) Alonso-Salces, R. M.; Korta, E.; Barranco, A.; Berrueta, L. A.; Gallo, B.; Vicente, F. Pressurized liquid extraction for the determination of polyphenols in apple. *J. Chromatogr., A* **2001**, *933*, 37−43.
(38) Lu, Y.; Foo, L. Y. Identification and quantification of major polyphenols in apple pomace. *Food Chem.* **1997**, *59*, 187−194.
(39) Yakovleva, K. E.; Kurzeev, S. A.; Stepanova, E. V.; Fedorova, T. V.; Kuznetsov, B. A.; Koroleva, O. V. Characterization of plant phenolic compounds by cyclic voltammetry. *Appl. Biochem. Microbiol.* **2007**, *43*, 661−668.
(40) Hutchinson, J. P.; Li, J.; Farrell, W.; Groeber, E.; Szucs, R.; Dicinoski, G.; Haddad, P. R. Universal response model for a corona charged aerosol detector. *J. Chromatogr., A* **2010**, *1217*, 7418−7427.
(41) Granica, S.; Krupa, K.; Klebowska, A.; Kiss, A. K. Development and validation of HPLC-DAD-CAD-MS (3) method for qualitative and quantitative standardization of polyphenols in *Agrimoniae eupatoriae* herba (Ph. Eur.). *J. Pharm. Biomed. Anal.* **2013**, *86*, 112−122.
(42) Novakova, L.; Lopez, S. A.; Solichova, D.; Satinsky, D.; Kulichova, B.; Horna, A.; Solich, P. Comparison of UV and charged aerosol detection approach in pharmaceutical analysis of statins. *Talanta* **2009**, *78*, 834−839.
(43) Gamache, P. H.; Ryan, S. M.; Freeto, S. M.; Asa, D. J.; Woodcock, M. J.; Laws, K.; Cole, R. O. HPLC analysis of non-volatile analytes using charged aerosol detection. *LCGC Eur.* **2005**, *18*, 345−354.
(44) Sinclair, I.; Gallagher, R. Charged aerosol detection: factors for consideration in its use as a generic quantitative detector. *Chromatogr. Today* **2008**, *1*, 42−46.
(45) Gorecki, T.; Lynen, F.; Szucs, R.; Sandra, P. Universal response in liquid chromatography using charged aerosol detection. *Anal. Chem.* **2006**, *78*, 3186−3192.
(46) Vervoort, N.; Daemen, D.; Torok, G. Performance evaluation of evaporative light scattering detection and charged aerosol detection in reversed phase liquid chromatography. *J. Chromatogr., A* **2008**, *1189*, 92−100.
(47) Cheng, S.; Qiu, F.; Huang, J.; He, J. Simulataneous determination of vitexin-2″-*O*-glucoside, vitexin-2″-*O*-rhamnoside, rutin, and hyperoside in the extract of hawthorn (*Crataegus pinnatifida* Bge.) leaves by RP-HPLC with ultraviolet photodiode array detection. *J. Sep. Sci.* **2007**, *30*, 717−721.
(48) Nugroho, A.; Lim, S. C.; Byeon, J. S.; Choi, J. S.; Park, H. J. Simultaneous quantification and validation of caffeoylquinic acids and flavonoids in *Hemistepta lyrata* and peroxynitrite-scavenging activity. *J. Pharm. Biomed. Anal.* **2013**, *76*, 139−144.
(49) Nugroho, A.; Lim, S. C.; Lee, C. M.; Choi, J. S.; Park, H. J. Simultaneous quantitative determination and validation of quercetin glycosides with peroxynitrite-scavenging effects from *Saussurea grandifolia*. *J. Pharm. Biomed. Anal.* **2012**, *61*, 247−251.
(50) Reber, J. D.; Eggett, D. L.; Parker, T. L. Antioxidant capacity interactions and a chemical/structural model of phenolic compounds found in strawberries. *Int. J. Food Sci. Nutr.* **2011**, *62*, 445−452.
(51) Kirakosyan, A.; Mitchell Seymour, E.; Noon, K. R.; Urcuyo Llanes, D. E.; Kaufman, P. B.; Warber, S. L.; Bolling, S. F. Interactions of antioxidants isolated from tart cherry (*Prunus cerasus*) fruits. *Food Chem.* **2010**, *122*, 78−83.
(52) Wang, S.; Meckling, K. A.; Marcone, M. F.; Kakuda, Y.; Tsao, R. Synergistic, additive, and antagonistic effects of food mixtures on total antioxidant capacities. *J. Agric. Food Chem.* **2011**, *59*, 960−968.

JOURNAL OF AGRICULTURAL AND FOOD CHEMISTRY

Article

pubs.acs.org/JAFC

Identification, Characterization, and Quantification of an Anti-pyridoxine Factor from Flaxseed Using Ultrahigh-Performance Liquid Chromatography–Mass Spectrometry

Shyamchand Mayengbam,[†] Haifeng Yang,[†,‡] Veronique Barthet,[§] Michel Aliani,[†] and James D. House*[,†,‡,#]

[†]Department of Human Nutritional Sciences, [‡]Richardson Centre for Functional Foods and Nutraceuticals, and [#]Department of Animal Science, University of Manitoba, Winnipeg, Manitoba R3T 2N2, Canada

[§]Canadian International Grain Commission, Winnipeg,Manitoba R3C 3G8, Canada

Supporting Information

ABSTRACT: In the present study, the anti-pyridoxine compounds linatine (1-[(*n*-γ-L-glutamyl)amino]-D-proline) and 1-amino-D-proline (1ADP) were quantified following extraction from defatted flaxseed using aqueous isopropanol as a solvent, with extraction variables including time, temperature, and the solid/solvent ratio. Both linatine and 1ADP were identified, characterized, and quantified via UPLC/ESI-MS using authentic standards. To optimize the extraction conditions for these anti-pyridoxine compounds, a response surface methodology was applied using a second-order polynomial to describe the experimental data. The predicted model for the optimal extraction was significant ($P < 0.05$) with a R^2 of 0.82. A varietal analysis showed that the amount of anti-pyridoxine present in flaxseed ranged from 177 to 437 μg 1ADPE/g of whole seed. The current study establishes the content of specific anti-pyridoxine factors in flaxseed and positions the data for use in subsequent risk assessment modeling.

KEYWORDS: *anti-pyridoxine, linatine, 1-amino-D-proline, flaxseed*

INTRODUCTION

The seeds of the flax plant (*Linum usitatissimum* L.) contain several nutritionally relevant compounds. Flaxseeds contain 35–45% oil by weight, of which 52% is α-linolenic acid (ALA), an omega-3 fatty acid.[1] Dietary ALA supplementation lowers the production of inflammatory biomolecules such as interleukin-6 (IL-6) and C-reactive protein (CRP).[2,3] Flaxseed consumption suppressed the development of atherosclerosis by reducing plasma total cholesterol (TC), low-density lipoprotein (LDL), and triglycerides (TGs) in a rat model.[4] For humans, the dietary reference intake (DRI) process led to the establishment of adequate intakes of ALA in the amounts of 1.1 and 1.6 g/day for women and men, respectively.[5] Given its enriched status, flaxseed has been positioned as a good source of ALA for the human diet. Additionally, flaxseed also represents a good source of cyclolinopeptides,[6,7] fiber, and contains significant levels of lignans, especially isolariciresinol, pinoresinol, and secoisolariciresinol diglucoside (SDG).[8−10] The latter phytoestrogenic compounds possess putative antitumorigenic,[10,11] antioxidant,[12] and hypotensive properties.[13] Given the increased interest in the potential health-promoting aspects of whole flaxseed, its utilization in the commercial food supply has expanded. Whereas the positive attributes of flax consumption have been the focus of attention in recent years, it is important to recognize the potential antinutritive factors present in whole seeds.

Flaxseed contains several antinutritive compounds, including phytic acid,[14] cyanogenic glycosides,[5,15,16] and the dipeptide linatine.[17] Linatine (1-[(*n*-γ-L-glutamyl)amino]-D-proline), is a polar compound first identified by Kratzer[18] to possess anti-pyridoxine activity. Chicks fed a diet containing linseed meal established signs of vitamin B_6 deficiency.[19] Subsequent studies confirmed the structure of the compound as $C_{10}H_{17}N_3O_5$ with an observed molecular weight of 259.26. It is a dipeptide formed by 1-amino-D-proline (1ADP) bound to a glutamic acid by a peptide bond through the γ-carbonyl of the glutamic acid[17] (Figure 1). The potent anti-pyridoxine component of linatine is

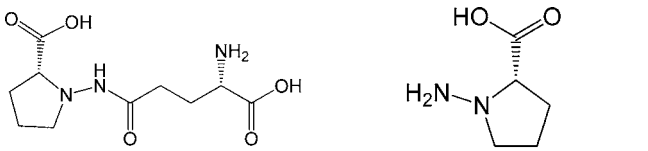

Linatine 1-amino D-proline

Figure 1. Structures of anti-pyridoxines from flaxseed.

purported to be 1ADP, which has a molecular weight of 130.15. The latter compound acts as an asymmetrically substituted secondary hydrazine that is thus responsible for the in vivo hydrazone toxicity of the active pyridoxyl-5-phosphate (PLP), ultimately leading to the vitamin B_6 deficiency symptoms.[19] Numerous PLP-dependent enzymes, including glutamic amino-transferase, tryptophanase, tyrosine decarboxylase, and glutamic

Received: October 24, 2013
Revised: December 17, 2013
Accepted: December 19, 2013
Published: December 19, 2013

ACS Publications © 2013 American Chemical Society

decarboxylase, demonstrated marked activity inhibition when treated, in vitro, with 1ADP.[20] Additionally, the intraperitoneal injection of 1ADP greatly disturbed methionine metabolism, resulting in the accumulation of L-cystathionine and its derivatives.[21] Given the recognized potential for the presence of an anti-pyridoxine factor in the food supply, the establishment of an analytical technique for the measurement of linatine and 1ADP in flaxseed is required prior to any risk assessment analysis.

Previous research has relied upon the use of first-generation chromatography (paper, thin layer) techniques coupled with ninhydrin-based, spectrophotometric analysis for linatine and 1ADP analysis.[17,22−24] The present study was designed to develop an ultrahigh-performance liquid chromatography−mass spectrometry (UPLC-MS) technique for the measurement of linatine and 1ADP. Additionally, the objectives included the optimization of extraction conditions using response surface methodology (RSM) with four factors (solvent concentration, time, and temperature, and the liquid/solid ratio), each tested at three distinct levels. The final objective of this study was the determination of the content of the anti-pyridoxine components in selected varieties of commercial flaxseed.

MATERIALS AND METHODS

Materials. Flaxseed samples [a harvest composite sample made of flaxseed samples (150) harvested within one year in western Canada and nine different varieties] were provided by the Canadian International Grain Commission, Winnipeg, Canada. Isotopically labeled D-proline (2,5,5-d_3) was obtained from C/D/N Isotopes (QC, Canada), whereas 1-amino D-proline was purchased from Santa Cruz Biotech (Dallas, TX, USA). All solvents (analytical and HPLC grades) were purchased from Sigma-Aldrich (Oakville, ON, Canada). A bulk of composite flaxseed was defatted through the use of a Soxhlet apparatus, using hexane as solvent. After drying, it was reground using a commercial seed/bean grinder, passed through 50 mesh sieves to obtain a fine powder (particle size = 300 μm), and used for optimization experiments.

Ultrasound-Assisted Extraction of Anti-pyridoxine Factors from Flaxseed. Ultrasound-assisted extraction was performed in a VWR 250 HT ultrasonic cleaning bath (VWR International, AB, Canada). The flaxseed samples (500 mg) were accurately weighed in a 50 mL centrifuge tube, the required amount of extracting solvent was added, and the contents were homogenized at 13500 rpm for 1 min using an Ultra-Turrax T25 homogenizer (IKA-Labortechnik, Wilmington, NC, USA). The mixture was transferred into a 100 mL volumetric flask and sonicated for the designated times and at designated temperatures. Temperatures were controlled through the use of a circulating thermostatic water bath. The resultant flaxseed extracts were centrifuged at 5000*g* for 20 min at 4 °C and the supernatants collected. The extracts were concentrated using a rotary evaporator set to 35 °C. The concentrated extracts were diluted to a constant volume (10 mL) followed by centrifugation at 12000*g* for 20 min and filtered through a 0.2 μm filter before injection onto the UPLC-MS system. All extracted samples were freshly analyzed.

UPLC-MS Conditions. An Acquity UPLC system coupled with a Quattro Micro Atmospheric pressure ionization (API) tandem mass spectrometer (Waters Corp., Milford, MA, USA) was used for the analysis. Deionized water (18.2 MΩ) as solvent A and acetonitrile as solvent B, both containing 0.1% formic acid, were used as mobile phases, and the column was a Hypersil Gold C18 column, 150 × 3.0 mm, 3 μm (Thermo Scientific Inc., Waltham, MA, USA). The gradient elution was programmed at 0, 2, 3, 3.4, 3.5, and 8 min with 0, 20, 50, 50, 0, and 0% of solvent B, respectively, at a flow rate of 0.16 mL/min. The column was maintained at 35 °C, whereas the autosampler was maintained at a temperature of 4 °C. The tandem mass spectrometer was operated in positive electrospray ionization (ESI+) mode, with the conditions tuned on the basis of 1ADP. The main parameters of MS were as follows: capillary voltage, 3 kV; cone voltage, 20 V; source temperature, 120 °C; desolvation temperature, 500 °C; desolvation gas (N_2) flow, 600 L/h; and cone gas flow, 50 L/h. Multiple reaction monitoring (MRM) mode was set to monitor the mass transition of precursor ion to the product ion. The mass transition was monitored at 118.9 → 72.9 for d_3-D-proline (internal standard), at 131.0 → 85 for 1ADP, and at 259.9 → 85 for linatine. Data acquisition and processing were done using MassLynx V4.1 (Waters Corp.).

Purity Analysis and Validation of the Presence of Linatine in Flaxseed Extracts. The flaxseed extract was concentrated in a rotary evaporator to form a crude linatine extract. It was fractionated using a Varian 920LC high-performance liquid chromatography (HPLC) system, equipped with a UV- detector and fraction collection capabilities (Varian Inc., Palo Alto, CA, USA). Fractions of each 15 s were collected using a reverse phase Luna C18 $_{(2)}$ column (250 × 4.6 mm, 5 μm (Phenomenex, Torrance, CA, USA)) and solvent conditions as described above. The identification of linatine in the fraction was confirmed on the basis of the theoretical mass spectrum, using UPLC-MS. The final linatine fraction collected was lyophilized to obtain a white amorphous solid. The amorphous solid was dissolved in deionized water and scanned at 200−400 nm to identify λ_{max} using a DU 8000 spectrophotometer (Beckman Coulter Inc., Brea, CA, USA). The purity of the linatine in the solution was determined by normalizing the peak areas detected by the UV detector of the HPLC at λ_{max} using the same column and method mentioned above.

The amorphous linatine fraction at a concentration of 50 μg/mL was analyzed by an Agilent 6538 Q-TOF mass spectrometer coupled with a dual ESI source (Agilent Technologies, Santa Clara, CA, USA) in positive mode using a Poroshell C18 column (2.1 × 50 mm, 2.7 μm (Agilent Technologies, Santa Clara, CA, USA)) with a flow rate of 0.6 mL/min using the same solvent and the gradient system mentioned above for UPLC-MS method. For the mass spectrometry and MS/MS analyses, data were acquired for the fragment range of m/z 50−1200. ESI capillary voltage was set at fast switch polarity mode ESI± with 4000 V (±) ion mode with a fragmentor voltage of 60 V. A drying gas (N_2) at a temperature of 300 °C was supplied at a flow rate of 11 L/min. The reference masses used were 121.050873, 922.00978, and119.03632 (Agilent Technologies, Mississauga, ON, Canada). Find by auto and targeted MS/MS algorithms options within the Agilent MassHunter Qualitative Analysis B.05.00 were used to verify the presence of linatine in the sample using the Metlin database and library.

Furthermore, to confirm the presence of linatine in the amorphous solid, 1 mg of the sample was hydrolyzed in 1 M HCl for 2 h at 100 °C. The hydrolyzed solution was passed through a H^+-form resin column (Bio-Rad, Hercules, CA, USA). It was then washed with deionized water and the sample was eluted with 3 M NH_4OH solution. The eluate was dried under N_2 at 35 °C and reconstituted with deionized water to 5 mL. Verification was done by comparing the retention time and daughter ion mass spectrum as described above for the UPLC-MS/MS method.

Preparation of Calibration Curve and Quantification of Anti-pyridoxines. A calibration curve was prepared according to FDA guidelines.[25] Fifty milliliters of the sample extract was incubated at 70 °C in a water bath for 48 h until all of the 1ADP and linatine had been degraded. A calibration curve was prepared by spiking the resulting extract with known concentrations of the analyte, either 1ADP or linatine, into the same sample matrix. The concentrations of standards were chosen on the basis of the concentration range of the sample. A blank sample matrix was also run concurrently with the calibration curve. The concentrations of anti-pyridoxine factors in the samples were determined on the basis of the peak area response of 1ADP and linatine with respect to the internal standard (d_3-D-proline) at a concentration of 200 ng/mL. The total anti-pyridoxine content was expressed as 1-amino D-proline equivalents (1ADPE) using eq 1 given below. The limit of detection (LOD) and the lower limit of quantification (LLOQ) were also determined.

$$\text{total anti-pyridoxine (1ADPE } \mu\text{g/g)} = \frac{1}{2}(\text{linatine}) + \text{1ADP} \quad (1)$$

Experimental Design of Extraction Procedures. An isopropanol−water mixture was used as the extraction solvent.[17] Four factors, isopropanol concentration (A, % v/v), time (B, min), temperature (C,

°C) and liquid/solid ratio (D, mL/g), were selected as the primary influential parameters for extraction yield. The anti-pyridoxine compounds (1ADP and linatine) from flaxseed were first extracted on the basis of a single-factor experiment to determine the three levels of each factor. During the entire extraction process, the chosen temperature of the sonication bath was kept steady (within ±1.5 °C).

After examination of the test results obtained from single-factor extraction, a design based on a central composite model with three levels and four variables was used to find the best extraction parameter combination to optimize the recovery of anti-pyridoxines from flaxseed. The variables were generated according to the equation[26]

$$x_i = (X_i - X_0)/\Delta X \quad (2)$$

where x_i was the value of the independent variable X_i, X_0 was the value of X_i at the center point, and ΔX was the step change value.

Table 1 shows the four independent variables with their respective levels. The central composite design matrix and experimental extraction values are listed in Table 2. Of the three responses (1ADP, linatine, and total 1ADPE), extraction of total 1ADPE was considered as the response for the regression analysis. The model was fitted on the second-order polynomial function as[27]

$$Y = b_0 + \sum_{i=1}^{4} A_i X_i + \sum_{i=1}^{4} A_{ii} X_i^2 + \sum_{i=1}^{3} \sum_{j=i+1}^{4} A_{ij} X_i X_j \quad (3)$$

where Y is the predicted variable function and A_i, A_{ii}, and A_{ij} are the regression coefficients of linear, quadratic, and interaction terms of the independent variables X_i and X_j.

The experimental design and calculation of the predicted data were carried out using Design Expert 8.0.7.1 software to estimate the best response. The predicted model was verified by conducting three additional experiments. The final response was also compared with the samples extracted with either ethanol or methanol.

Varietal Analysis and Stability of Anti-pyridoxine on Storage. Nine flaxseed varieties, grown in different locations, were defatted with SER 148 solvent extractor (VELP Scientifica, Via Stazione, MB, Italy) using hexane as solvent according to the AOAC official method guidelines[28] to avoid the interference of oil during extraction procedures. Anti-pyridoxine contents of those samples were determined using the optimized extraction parameters. To check the storage stability of anti-pyridoxines, 1ADP and linatine in solution or in the sample extract were incubated at 3 and 37 °C for 48 h. Every 6 h, the samples were injected in UPLC-MS and the changes in peak area ratio were noted.

Statistical Analysis. The design of the experiment for the optimization of extraction using RSM was performed using Design Expert 8.0.7.1 software (Trial Version, State-Ease Inc., Minneapolis, MN, USA). Statistical analysis was performed using SigmaPlot 11.0 (Systat Software Inc., San Jose, CA, USA). All data were analyzed using one-way ANOVA with Bonferroni's multiple comparison, and $p < 0.05$ was set for all analyses to reflect statistically significant differences.

Table 1. Factors and Levels of Response Surface Methodology

	levels		
independent variable	−1	0	1
isopropanol concentration (A, %)	30	40	50
extraction time (B, min)	20	30	40
extraction temperature (C, °C)	25	35	45
liquid/solid ratio (D, mL/g)	30	40	50

Table 2. Central Composite Design Matrix and Experimental Extraction Values of Anti-pyridoxines

std	run	A	B	C	D	1ADP (μg/g)	linatine (μg/g)	total 1ADPE[a] (μg/g)
9	1	30	20	25	50	47.5	995.5	545.2
24	2	40	30	35	50	5.8	620.3	315.9
23	3	40	30	35	30	43.1	784.6	435.4
8	4	50	40	45	30	17.8	828.6	432.1
28	5	40	30	35	40	33.7	854.1	460.7
4	6	50	40	25	30	16.7	641.9	337.7
14	7	50	20	45	50	10.8	948.3	485.0
1	8	30	20	25	30	51.0	637.0	369.4
18	9	50	30	35	40	22.6	839.7	442.4
21	10	40	30	25	40	29.2	902.7	480.6
16	11	50	40	45	50	19.7	945.8	492.7
20	12	40	40	35	40	37.4	898.1	486.5
6	13	50	20	45	30	12.5	801.8	413.4
30	14	40	30	35	40	39.3	850.5	464.5
12	15	50	40	25	50	23.5	858.9	452.9
13	16	30	20	45	50	29.3	843.7	451.2
10	17	50	20	25	50	23.7	728.8	388.1
19	18	40	20	35	40	31.6	897.7	480.5
29	19	40	30	35	40	31.0	861.9	462.0
22	20	40	30	45	40	14.5	713.4	371.3
26	21	40	30	35	40	37.7	943.5	509.4
11	22	30	40	25	50	18.7	907.9	472.7
7	23	30	40	45	30	33.8	659.8	363.7
25	24	40	30	35	40	40.6	874.8	478.0
5	25	30	20	45	30	31.4	532.6	297.7
2	26	50	20	25	30	21.2	766.5	404.4
3	27	30	40	25	30	17.4	449.9	242.4
27	28	40	30	35	40	41.5	894.7	488.8
15	29	30	40	45	50	34.3	835.0	451.8
17	30	30	30	35	40	29.2	797.5	427.9

[a]Total 1ADPE = 1/2(linatine) + 1ADP.

RESULTS AND DISCUSSION

Identification and Characterization of Anti-pyridoxines in Flaxseed. The anti-pyridoxines were detected using an ESI+ mode in MRM mass chromatograms. These compounds were identified by comparing the retention times and daughter ion mass spectra of the authentic standards. 1ADP was eluted at 5.48 min, whereas linatine was eluted at 7.33 min (Figure 2). There was an increase in the peak area of 1ADP when the sample was spiked with synthetic standard. This confirmed the presence of free 1 ADP in flaxseed (Figure S1, Supporting Information). It was verified by comparing the mass spectra of the authentic standard parent ion at m/z 131 and base ion at m/z 85 (Figure 3).

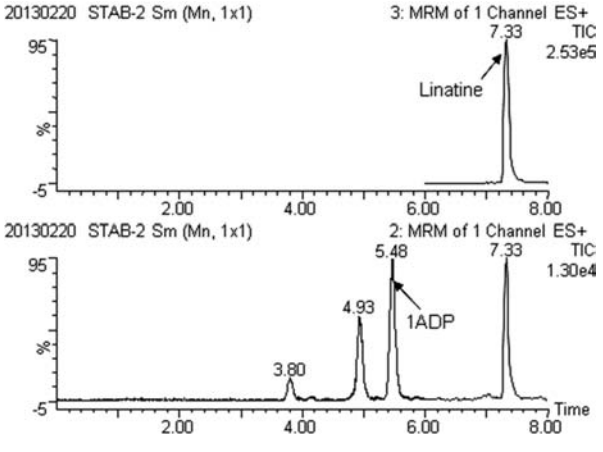

Figure 2. Chromatograms of linatine and 1-amino-D-proline (1ADP) from a flaxseed extract.

dx.doi.org/10.1021/jf404786v | J. Agric. Food Chem. 2014, 62, 419−426

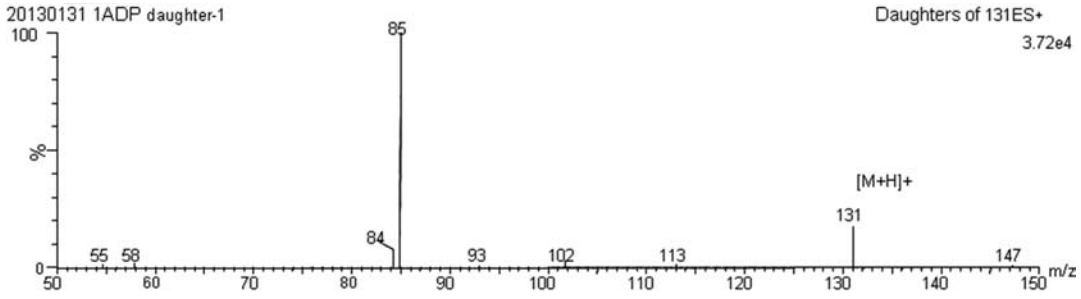

Figure 3. UPLC-mass spectrum of 1ADP: parent ion at m/z 131, $[M + H]^+$, and base ion m/z 85.

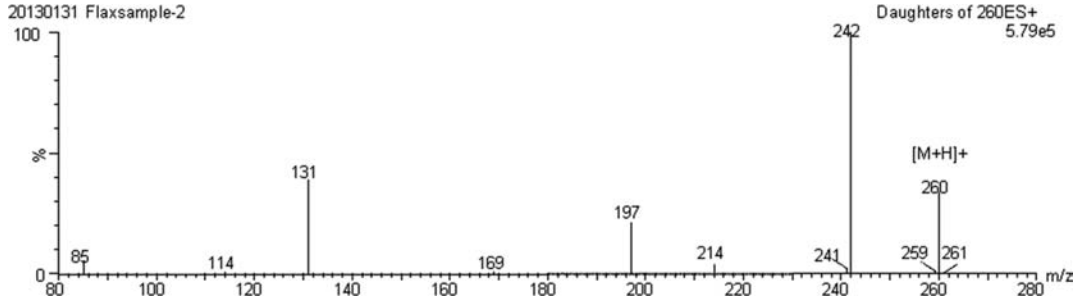

Figure 4. UPLC-mass spectrum of linatine in flaxseed extract: parent ion at m/z 260, $[M + H]^+$.

This was the first report indicating the presence of free 1ADP in flaxseed. Earlier, it was suggested that free 1ADP was not detected in the freshly prepared flaxseed extract when quantified using either the pyridoxal phosphate assay or an amino acid analyzer.[17] The latter results may be due to the lack of sensitivity of the methods and the instruments used at the time. In the current study, the limit of detection (S/N = 5) and lower limit of quantification (S/N = 10) for 1ADP were 10 and 15 ng/mL, respectively, showing the higher sensitivity of the new method.

Linatine was identified and characterized on the basis of its supposed mass spectral profile. We could not obtain a synthetic linatine standard as it was not commercially available. The mass spectrum of the chromatogram, obtained by scanning the flaxseed extract at m/z 260 $[M + H]^+$, was analyzed to validate the authenticity of linatine (Figure 4). Besides the parent ion, there were two major base peaks at m/z 242 $[M + H - 18]^+$ and m/z 131 $[M + H - 129]^+$. The first base peak was formed by losing a H_2O molecule (−18u), whereas the second base peak was formed by losing the glutamyl group (−129 u) as $[M + H - C_5H_7NO_3]^+$ to give the 1ADP spectrum. Apart from those two major base peaks, the minor peak obtained with m/z 197 $[M + H - 63]^+$ was due to the loss of a H_2O (−18 u) plus a COOH group (−63 u) as $[M + H - H_2O - COOH]^+$. The occurrence of common peaks at m/z 131 and 85 in both 1ADP and sample extract provided additional evidence supporting the presence of linatine in flaxseed.

Purity Analysis and Validation of the Presence of Linatine. The λ_{max} of a linatine solution prepared by dissolving the amorphous solid, obtained after the fractionation of crude flaxseed extract, into deionized water was found at 268 nm. The purity of linatine in the solution calculated after normalizing the peak area of three consecutive HPLC injections detected at $\lambda_{268\ nm}$ was 78%. The mass spectrum from Q-TOF (Figure S2, Supporting Information) showed a similar fragmentation of linatine as mentioned above in the case of UPLC-MS with a m/z value of 260.1217, $[M + H]^+$. Targeted MS/MS molecular feature analysis had provided a compatibility score of 99.15 of linatine compared to the database available in online Mass-Hunter software. This indicated a very high chance of the presence of linatine in the sample. Moreover, linatine was hydrolyzed into 1ADP, which was not found in the unhydrolyzed sample (Figure S3, Supporting Information). The appearance of the 1ADP peak in the chromatogram of the hydrolyzed sample also confirmed the presence of linatine in the amorphous solid fractionated from the crude extract. This amorphous solid was used as an authentic linatine standard for quantification.

Extraction Parameters. Ultrasound-assisted extraction of bioactive compounds from plant sources have been documented to be affected by extraction solvent, time, temperature, and ratio of liquid/solid.[22−24] The effects of the specific test parameters (isopropanol concentration, sonication time, temperature, and liquid/solid ratio) on the anti-pyridoxines extraction are displayed in Figure 5.

An isopropanol concentration of 30% resulted in the highest amount of 1ADP and linatine extraction. These results indicated that the efficiency of extraction was higher when the proportion of organic solvent was the lowest. Opportunities to use solvent concentrations lower than 30% were hampered by the increased extraction of water-soluble flax-derived gums and mucilages,[29−31] which created challenges during sample preparation (gelation). Therefore, the range for optimum isopropanol concentration was considered to be 30−50%. A similar trend was also observed in liquid/solid ratio, as the extraction efficiency was highest when the ratio was 50:1, indicating that higher water contents enhanced the extraction efficiency. The range for the liquid/solid ratio for extraction was selected as 30−50:1 (v/w). Similarly, ranges of sonication time and temperature were selected as 20−40 min and 25−45 °C, respectively. The above selected parameters were used for the RSM design.

Optimization of Extraction Conditions. On the basis of the values obtained from the single-factor experiments, the levels of independent variables chosen for the central composite design, that is, isopropanol concentration (A, % v/v), sonication time (B, min), sonication temperature (C, °C), and liquid/solid

dx.doi.org/10.1021/jf404786v | J. Agric. Food Chem. 2014, 62, 419−426

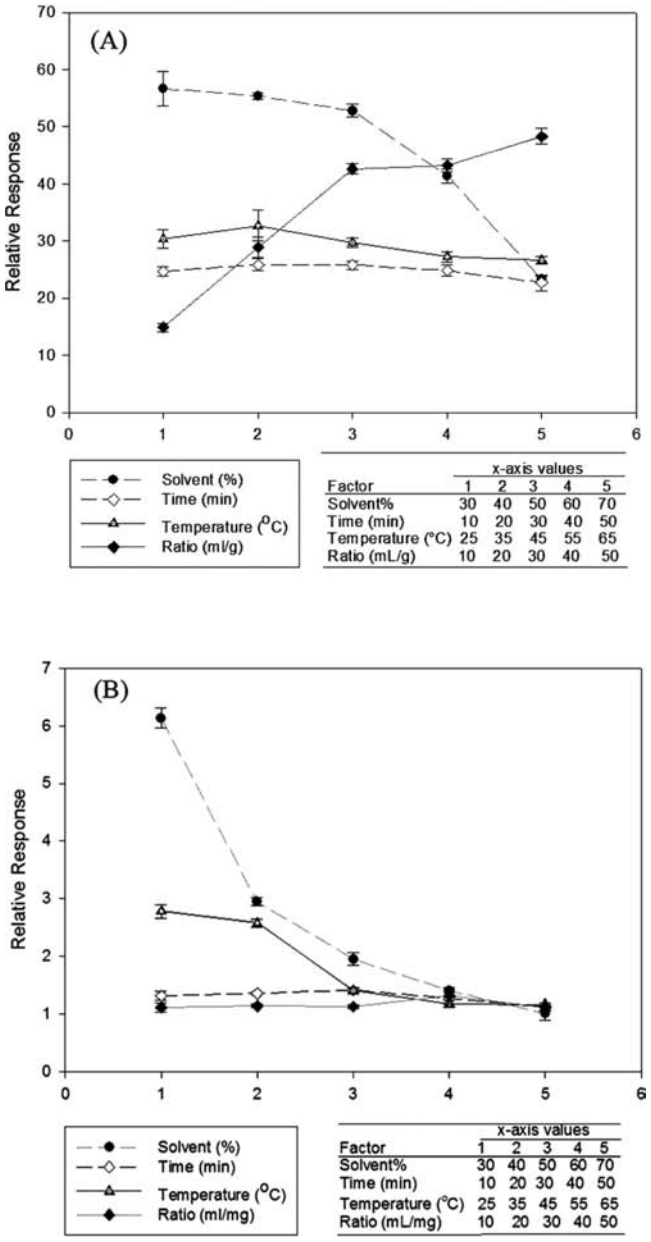

Figure 5. Effect of single-factor test on linatine (A) and 1ADP (B) extraction from flaxseed. Values on *x*-axis represent the five levels of each factor.

ratio (D, mL/g), were selected as design variables in the RSM (Table 1). Of the three anti-pyridoxine responses, that is, 1ADP, linatine, and total 1ADPE (Table 2), extraction of total 1ADPE was employed as the response value with four factors and three levels for the optimization using RSM design. Analysis of variance (ANOVA) for response surface of quadratic model analyses was chosen to test the significance and adequacy of the design. The value of "prob > F" of the model was significant with $p = 0.0082$, and the lack of fit was not significant ($p = 0.052$). This suggested that the model terms were precise and applicable (Table 3). The coefficient of determination (R^2) of the model was 0.82, and the regression equation after replacing experimental points was

Table 3. Analysis of Variance for the Fitted Quadratic Polynomial Model on Total 1ADPE

source	SS	DF	MS	F value	prob > F	
model	68404.14	14	4886.01	4.04	0.0082	significant
residual	15717.47	13	1209.04			
lack of fit	13879.53	8	1734.94	4.72	0.0521	not significant
pure error	1837.94	5	367.59			
cor total	84121.61	27				

$$Y = -307.92 + 26.54A - 11.28B + 17.48C + 0.63D + 0.02AB + 0.27AC - 0.18AD + 0.1BC - 0.01BD - 0.003CD - 0.36A^2 + 0.12B^2 - 0.45C^2 + 0.15D^2 \quad (4)$$

Each 3D plot (Figure 6) represents the number of combinations of the two test variables. After carrying out optimization of all the parameters on the basis of the mathematical model, the points of prediction for maximum extraction of total anti-pyridoxine were as follows: isopropanol concentration, 35.97% (v/v); time, 24.89 min; temperature, 31.54 °C; liquid/solid ratio, 44.68:1 (mL/g). At these points the predicted values for linatine, 1ADP, and total anti-pyridoxine (as 1ADPE) were 916.5, 41.3, and 499.5 μg/g, respectively.

Verification of the Predicted Model. To validate the adequacy of the model equation, a verification experiment was carried out under the optimal condions. Extraction conditions were adjusted to the following: isopropanol concentration, 36%; sonication time, 25 min; temperature, 32 °C; and liquid/solid ratio, 45:1 (mL/g). The results showed that the anti-pyridoxine content values were linatine, 1030 ± 21.7 μg/g; 1ADP, 42 ± 1.0 μg/g; and total 1ADPE, 557.9 ± 10.8 μg/g (of defatted flaxseed, $n = 3$). These results provide evidence that the experimental values were not only consistent with the predicted values but also better than any single-factor experiment. Therefore, the extraction conditions obtained by response surface methodology were considered optimized and repeatable.

The efficiency of anti-pyridoxine extraction using different solvents at optimized conditions were also evaluated (Table 4). Isopropanol has significantly ($p < 0.001$) higher capacity to extract both linatine and 1ADP compared to ethanol and methanol. Ethanol was able to extract more 1ADP than methanol; however, linatine extraction efficiencies were not significantly different for either of the solvents.

Varietal Analysis and Stability of Anti-pyridoxines on Storage. The oil removed from the nine varieties of flaxseed ranged from 32 to 43%. The amount of anti-pyridoxine compounds present in the nine varieties was significantly different (Table 5). The total amount of anti-pyridoxine content (1ADPE) in the tested varieties ranged from 177 to 437 μg/g for whole seed. Of the nine varieties, Normandy had the highest amount of anti-pyridoxine (437 ± 10.8 μg/g), whereas Taurus had the lowest (177.3 ± 5 μg/g). These results may provide evidence of genotypic variation in the 1ADPE content of flaxseed, but this remains to be rigorously tested.

The stability of 1ADP and linatine during storage is shown in Figure S4 (Supporting Information). Standard 1ADP solution was stable for 48 h at 3 °C but, it was readily degraded in 3 h at 37 °C. The amount of 1ADP content in sample increased during storage at both temperatures up to 12 h of incubation. The slight degradation of linatine likely results in the release of 1ADP in the

dx.doi.org/10.1021/jf404786v | J. Agric. Food Chem. 2014, 62, 419−426

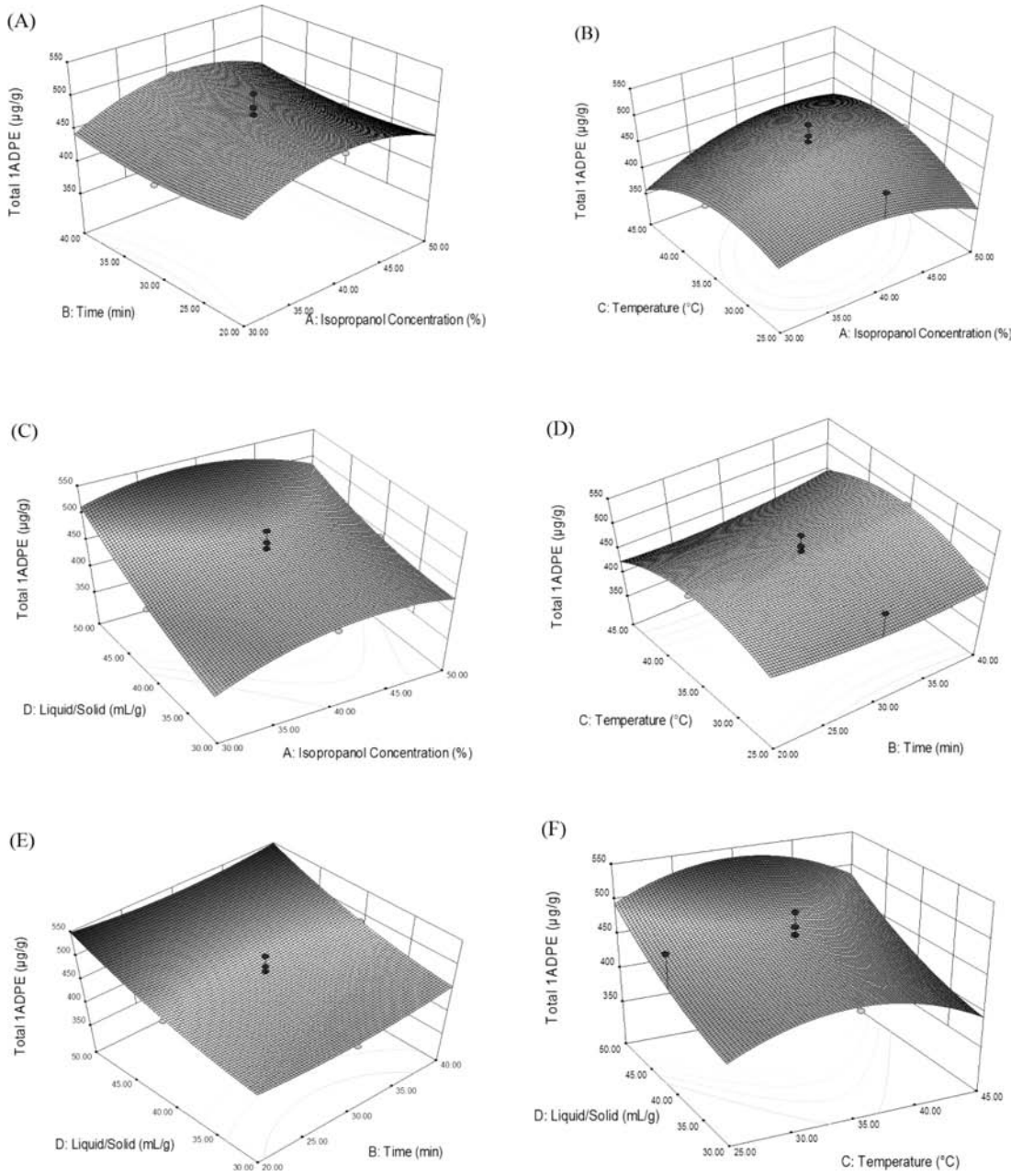

Figure 6. 3D plot showing the correlative effects of different parameters on total anti-pyridoxine extraction.

Table 4. Comparison of 1ADP and Linatine Extraction from Flaxseed Using Different Solvents

	concentration (μg/g)[a] of defatted flaxseed	
solvent type	1ADP	linatine
ethanol	32 ± 0.7b	919.3 ± 15.4b
methanol	15.2 ± 0.9c	850.9 ± 26.4b
isopropanol	42 ± 1.0a	1030 ± 21.7a

[a]Data represent means ± SE, n = 3. Values with different letters are significantly different ($p < 0.05$).

sample solution. Linatine in the sample also degraded at both temperatures; however, the rate of degradation was faster at 37 °C as compared to 3 °C.

In conclusion, this study establishes a new method for assessing the anti-pyridoxine content of flaxseed in advance of risk assessment modeling for specific populations. Our method provided a better extraction of 1ADP and linatine from flaxseed by optimizing the extraction parameters using a RSM design. The UPLC-MS/MS method, which has higher specificity and sensitivity for those analytes, revealed that the amount of anti-pyridoxine content in flaxseed was up to 437 μg/g of whole seed, much higher than previously reported by Klosterman et al.[17] Furthermore, we have documented the presence of free 1ADP in flaxseed, which has never been reported before. Although varietal differences in 1ADP equivalents were apparent, further work is required to ascertain the impact of genotype by environment effects on the anti-pyridoxine content of flaxseed. Future work will assess the oral toxicity of anti-pyridoxines, especially 1ADP and linatine, as it will be important to assess the risk factors associated with the consumption of flaxseed and its related products.

dx.doi.org/10.1021/jf404786v | J. Agric. Food Chem. 2014, 62, 419−426

Table 5. Varietal and Environmental Effects on the Content of Anti-pyridoxine Compounds in Flaxseed

			anti-pyridoxine content in defatted flaxseed[a] (μg/g)				anti-pyridoxine content in whole flaxseed[a] (μg/g)		
SL	variety	place grown	linatine	1ADP	total 1ADPE	fat removed (%)	linatine	1ADP	total 1ADPE
1	Taurus	MB, Canada	530.9 ± 15.8	11.6 ± 0.7	277.0 ± 7.8e	36.0	339.8 ± 10.1	7.4 ± 0.5	177.3 ± 5.0f
2	CDC-Sorrel	MB, Canada	919.7 ± 12.1	3.5 ± 0.2	463.4 ± 6.1d	39.8	554.6 ± 7.3	2.1 ± 0.1	279.4 ± 3.6e
3	CDC-Bethune	MB, Canada	794.0 ± 29.2	56.1 ± 3.2	453.1 ± 13.0d	32.8	533.5 ± 19.6	37.7 ± 2.2	304.5 ± 8.7de
4	CDC-Arras	SK, Canada	1138.6 ± 13.0	6.5 ± 0.4	575.7 ± 6.6c	40.9	672.9 ± 7.7	3.8 ± 0.2	340.3 ± 3.9c
5	Lightening	MB, Canada	1038.0 ± 17.0	32.6 ± 1.9	551.6 ± 7.0c	43.5	586.5 ± 9.6	18.4 ± 1.1	311.7 ± 3.9de
6	Normandy	MB, Canada	1331.9 ± 33.9	47.8 ± 2.2	713.7 ± 17.6a	38.8	816.4 ± 20.8	29.3 ± 1.4	437.5 ± 10.8a
7	Hanley	MB, Canada	1083.7 ± 13.6	24.8 ± 1.6	566.6 ± 7.7c	34.6	708.7 ± 8.9	16.2 ± 1.0	370.6 ± 5.1b
8	Vimy	SK, Canada	1255.0 ± 35.8	6.7 ± 0.2	634.2 ± 18.1b	38.1	776.8 ± 22.1	4.1 ± 0.1	392.6 ± 11.2b
9	Jantarop	Poland	868.6 ± 17.4	20.0 ± 0.9	454.3 ± 8.3d	32.5	586.3 ± 11.7	13.5 ± 0.6	306.7 ± 5.6de

[a]Data represent means ± SE, $n = 3$. Values with different letters are significantly different ($p < 0.05$).

■ ASSOCIATED CONTENT

Supporting Information

Figures representing chromatograms of samples before and after spiking with 1ADP (S1), a Q-TOF mass spectrum of linatine (S2), a chromatogram of a purified fraction of linatine before and after hydrolysis (S3), and data on the stability of 1ADP and linatine (S4). This material is available free of charge via the Internet at http://pubs.acs.org.

■ AUTHOR INFORMATION

Corresponding Author

*(J.D.H.) E-mail: james.house@ad.umanitoba.ca. Phone: +1 (204) 474-6837. Fax: +1 (204) 474-7593.

Funding

Funding for this research was provided through the Discovery Grants Program of the Natural Sciences and Engineering Research Council of Canada (NSERC). S.M. was the recipient of a scholarship through the NSERC CREATE-funded training program "FAST".

Notes

The authors declare no competing financial interest.

■ REFERENCES

(1) Singh, K. K.; Mridula, D.; Rehal, J.; Barnwal, P. Flaxseed: a potential source of food, feed and fiber. *Crit. Rev. Food Sci. Nutr.* **2011**, *51*, 210−222.

(2) Bemelmans, W. J. E.; Lefrandt, J. D.; Feskens, E. J. M.; van Haelst, P. L.; Broer, J.; Meyboom-de Jong, B.; May, J. F.; Cohen Tervaert, J. W.; Smit, A. J. Increased α-linolenic acid intake lowers C-reactive protein, but has no effect on markers of atherosclerosis. *Eur. J. Clin. Nutr.* **2004**, *58*, 1083−1089.

(3) Rallidis, L. S.; Paschos, G.; Liakos, G. K.; Velissaridou, A. H.; Anastasiadis, G.; Zampelas, A. Dietary α-linolenic acid decreases C-reactive protein, serum amyloid A and interleukin-6 in dyslipidaemic patients. *Atherosclerosis* **2003**, *167*, 237−242.

(4) Ratnayake, W. M. N.; Behrens, W. A.; Fischer, P. W. F.; L'Abbé, M. R.; Mongeau, R.; Beare-Rogers, J. L. Chemical and nutritional studies of flaxseed (variety Linott) in rats. *J. Nutr. Biochem.* **1992**, 3, 232−240.

(5) Institute of Medicine Dietary Reference Intakes for Energy, Carbohydrate, Fiber, Fat, Fatty Acids, Cholesterol, Protein, and Amino Acids, 2005; http://www.iom.edu/Activities/Nutrition/SummaryDRIs/ (accessed July 24, 2013).

(6) Gui, B.; Shim, Y. Y.; Datla, R. S. S.; Covello, P. S.; Stone, S. L.; Reaney, M. J. T. Identification and quantification of cyclolinopeptides in five flaxseed cultivars. *J. Agric. Food Chem.* **2012**, *60*, 8571−8579.

(7) Gui, B.; Shim, Y. Y.; Reaney, M. J. T. Distribution of cyclolinopeptides in flaxseed fractions and products. *J. Agric. Food Chem.* **2012**, *60*, 8580−8589.

(8) Meagher, L. P.; Beecher, G. R.; Flanagan, V. P.; Li, B. W. Isolation and characterization of the lignans, isolariciresinol and pinoresinol, in flaxseed meal. *J. Agric. Food Chem.* **1999**, *47*, 3173−3180.

(9) Sicilia, T.; Niemeyer, H. B.; Honig, D. M.; Metzler, M. Identification and stereochemical characterization of lignans in flaxseed and pumpkin seeds. *J. Agric. Food Chem.* **2003**, *51*, 1181−1188.

(10) Prasad, K. Flaxseed and cardiovascular health. *J. Cardiovasc. Pharmacol.* **2009**, *54*, 369−377.

(11) Thompson, L. U.; Seidl, M. M.; Rickard, S. E.; Orcheson, L. J.; Fong, H. H. S. Antitumorigenic effect of a mammalian lignan precursor from flaxseed. *Nutr. Cancer* **1996**, *26*, 159−165.

(12) Kitts, D. D.; Yuan, Y. V.; Wijewickreme, A. N.; Thompson, L. U. Antioxidant activity of the flaxseed lignan secoisolariciresinol diglycoside and its mammalian lignan metabolites enterodiol and enterolactone. *Mol. Cell. Biochem.* **1999**, *202*, 91−100.

(13) Prasad, K. Antihypertensive activity of secoisolariciresinol diglucoside (SDG) isolated from flaxseed: role of guanylate cyclase. *Int. J. Angiol.* **2004**, *13*, 7−14.

(14) Oomah, B. D.; Kenaschuk, E. O.; Mazza, G. Phytic acid content of flaxseed as influenced by cultivar, growing season, and location. *J. Agric. Food Chem.* **1996**, *44*, 2663−2666.

(15) Barthet, V. J.; Bacala, R. Development of optimized extraction methodology for cyanogenic glycosides from flaxseed (*Linum usitatissimum*). *J. AOAC Int.* **2010**, *93*, 478−484.

(16) Kobaisy, M.; Oomah, B. D.; Mazza, G. Determination of cyanogenic glycosides in flaxseed by barbituric acid-pyridine, pyridine-pyrazolone, and high-performance liquid chromatography methods. *J. Agric. Food Chem.* **1996**, *44*, 3178−3181.

(17) Klosterman, H. J.; Lamoureux, G. L.; Parsons, J. L. Isolation, characterization, and synthesis of linatine. A vitamin B6 antagonist from flaxseed (*Linum usitatissimum*). *Biochemistry (N.Y.)* **1967**, *6*, 170−177.

(18) Kratzer, F. H. The treatment of linseed meal to improve its feeding value of chicks. *Poult. Sci.* **1946**, *25*, 541−542.

(19) Kratzer, F. H.; Williams, D. E.; Marshall, B.; Davis, P. N. Some properties of the chick growth inhibitor in linseed oil meal. *J. Nutr.* **1954**, *52*, 555−563.

(20) Klosterman, J. H. Vitamin B6 antagonists of natural origin. *J. Agric. Food Chem.* **1974**, *22*−*1*, 13−16.

(21) Kimoto, M.; Ogawa, T.; Sasaoka, K. Effect of 1-aminoproline on methionine metabolism in rats. *Arch. Biochem. Biophys.* **1981**, *206*, 336−341.

(22) Evenstad, E. T.; Lamoureux, G. L.; Klosterman, H. J. Pilot scale extraction of the anti-pyridone factor in linseed meal. *Proc. N.D. Acad. Sci.* **1965**, *XIX*, 110−114.

(23) Klosterman, H. J.; Olsgaard, R. B.; Lockhart, W. C.; Magill, J. W. Extraction of anti-pyridoxine factor inflax cotyledons. *Proc. N.D. Acad. Sci.* **1960**, *XIV*, 87−94.

(24) Yang, L.; Jiang, J.; Li, W.; Chen, J.; Wang, D.; Zhu, L. Optimum extraction process of polyphenols from the bark of *Phyllanthus emblica* L. based on the response surface methodology. *J. Sep. Sci.* **2009**, *32*, 1437−1444.

(25) Food and Drug Administration Guidance for Industry: Biological Method Validation, 2001; pp 1−22; http://www.fda.gov/drugs/GuidanceComplianceRugulatoryInformation/Guidances/default.htm (accessed December 4, 2013).
(26) XuJie, H.; Wei, C. Optimization of extraction process of crude polysaccharides from wild edible BaChu mushroom by response surface methodology. *Carbohydr. Polym.* **2008**, *72*, 67−74.
(27) Lu, C.; Li, Y.; Fu, G.; Yang, L.; Jiang, J.; Zhu, L.; Lin, F.; Chen, J.; Lin, Q. Extraction optimization of daphnoretin from root bark of *Wikstroemia indica* (L.) C.A. and its anti-tumour activity tests. *Food Chem.* **2011**, *124*, 1500−1506.
(28) AOAC official method: crude fat in feeds, cereal grains, and forages, 2006.
(29) Zhang, W.; Xu, S.; Wang, Z.; Yang, R.; Lu, R. Demucilaging and dehulling flaxseed with a wet process. *LWT−Food Sci. Technol.* **2009**, *42*, 1193−1198.
(30) Oomah, B. D.; Mazza, G. Fractionation of flaxseed with a batch dehuller. *Ind. Crop Prod.* **1998**, *9*, 19−27.
(31) Madhusudhan, B.; Wiesenborn, D.; Schwarz, J.; Tostenson, K.; Gillespie, J. A dry mechanical method for concentrating the lignan secoisolariciresinol diglucoside in flaxseed. *LWT−Food Sci. Technol.* **2000**, *33*, 268−275.

JOURNAL OF AGRICULTURAL AND FOOD CHEMISTRY

Article

pubs.acs.org/JAFC

Characterization of Antidiabetic and Antihypertensive Properties of Canary Seed (*Phalaris canariensis* L.) Peptides

Patricia A. Estrada-Salas,[†] Gabriela M. Montero-Morán,[†] Pedro P. Martínez-Cuevas,[§] Carmen González,[§] and Ana P. Barba de la Rosa*[,†]

[†]IPICyT, Instituto Potosino de Investigación Científica y Tecnológica A.C., Camino a la Presa San José No. 2055, Lomas 4ª sección, 78216 San Luis Potosí, S.L.P., Mexico

[§]Facultad de Ciencias Químicas, Universidad Autónoma de San Luis Potosí, San Luis Potosí, S.L.P., Mexico

Supporting Information

ABSTRACT: Canary grass is used as traditional food for diabetes and hypertension treatment. The aim of this work is to characterize the biological activity of encrypted peptides released after gastrointestinal digestion of canary seed proteins. Canary peptides showed 43.5% inhibition of dipeptidyl peptidase IV (DPPIV) and 73.5% inhibition of angiotensin-converting enzyme (ACE) activity. An isolated perfused rat heart system was used to evaluate the canary seed vasoactive effect. Nitric oxide (NO), a major vasodilator agent, was evaluated in the venous effluent from isolated perfused rat heart. Canary seed peptides (1 μg/mL) were able to induce the production of NO (12.24 μM) in amounts similar to those induced by captopril (CPT) and bradykinin (BK). These results show that encrypted peptides in canary seed have inhibitory activity against DPPIV and ACE, enzymes that are targets for diabetes and hypertension treatments.

KEYWORDS: *angiotensin-converting enzyme, canary seed, dipeptidyl peptidase IV, encrypted peptides, nitric oxide*

INTRODUCTION

The canary seed (*Phalaris canariensis* L.) belongs to the Graminea family with production practices and life cycle similar to those of other winter cereal crops such as wheat and oats.[1,2] The grain is cultivated in many areas of the temperate climates and, currently, its production is concentrated in the southwestern provinces of Canada and, on a smaller scale, in Argentina, Thailand, and Australia.[3−5] Its main use is as food for birds, alone or mixed with other grains such as millet, sunflower seeds, and flaxseeds.[3,4]

Due to its good nutritional value, interest in canary seed has increased as an alternative nongluten cereal.[1,2] Compared to common cereals, canary seed contains high levels of protein (21%), although more deficient in both lysine and threonine than wheat proteins. Canary seed is very rich in cysteine, tryptophan, and phenylalanine.[6] The groats contain 61% starch, which are composed by small polygonal granules with diameters of 1.5−3.5 μm with lower amylose contents than wheat and high pasting temperatures forming rigid and highly stable gels when cooked or frozen.[7] Canary seed groats are rich in crude fat (8.7%), which is mainly composed of linoleic (55%), oleic (29%), palmitic (11%), and linolenic acids (2.5%).[8] The sterol and triterpene alcohol esters of caffeic acid are the major effective antioxidant components in the crude oil of a canary seed.[9] The major carotenoid compounds identified in canary seed are lutein, zeaxanthin, and β-carotene.[10]

Traditionally, canary seeds are also used as a "folk medicine" for diabetes and hypertension treatments; however, there is no scientific information about the possible bioactives responsible for such effects. Type 2 diabetes mellitus is a metabolic disorder characterized by a hyperglycemic chronic state due to several fundamental defects such as insulin resistance in muscles and liver and an impaired insulin secretion by pancreatic β-cells.[11] The incretin-based therapy is actually used as diabetic treatment. Incretins are responsible for >50% of postprandial insulin secretion, especially the hormone glucagon-like peptide 1 (GLP-1).[12] However, the half-life of incretins is very short due to the cleavage and inactivation of these proteins by dipeptidyl peptidase IV (DPPIV).[13] Hence, DPPIV inhibitors are the actual therapies that have shown promising results as antidiabetic agents.[14] Hypertension is about twice as common in a diabetic as in nondiabetics and has become the most common public health problem worldwide.[15] Hypertension treatments are based on inhibition of the angiotensin converting enzyme (ACE). ACE is a peptidylpeptidase hydrolase that plays an important physiological role in the regulation of blood pressure. ACE catalyzes the conversion of the inactive decapaptide angiotensin I into a powerful vasoconstrictor octapeptide, angiotensin II.[16] ACE also catalyzes the inactivation of the vasodilator bradykinin (BK) that regulates different biological processes including vascular endothelial nitric oxide (NO) release mediated by the activation of eNOS. NO exert its effects on the vascular smooth muscles, promoting vascular relaxation.[17]

Peptides with inhibitory activity of DPPIV and ACE have been found in several food proteins,[18,19] but there are no reports about the presence of these peptides encrypted in canary seed proteins that could be responsible for its claimed health benefits. Thus, the aim of this work was to test the

Received: July 8, 2013
Revised: December 16, 2013
Accepted: December 26, 2013
Published: December 26, 2013

ACS Publications © 2013 American Chemical Society

hydrolysis conditions to release the canary seed peptides and to evaluate the inhibitory activity of these peptides against DPPIV and ACE. In addition, the antihypertensive function of canary seed peptides was tested on isolated perfused rat heart system.

MATERIALS AND METHODS

Biological Material. Canary seed (Birdseed "Marabu") and commercial canary seed flour ("more Lait"), used as folk medicine, were purchased in local markets. Seeds were ground in a mill (Krup Coffe, Medford, MA, USA) and passed through 80 mesh. Defatted flours were obtained according to a reported protocol.[20] Canary seeds were placed in water (1:5 w/v, flour/water) overnight at room temperature. The soaking water was removed, the seeds were dried and milled, and the resultant flour was named canary seed milk.

Seed Storage Protein Fractionation. Proteins from (a) canary seed flours, (b) commercial flour "more Lait", and (c) canary seed milk were fractionated on the basis of their solubility.[20,21] The albumin fraction was solubilized with distilled water, and the suspension of flour/water (1:10 w/v) was under agitation for 1 h and centrifuged at 20000*g* for 30 min. The resulting pellet was resuspended in 0.1 M NaCl, 0.01 M KH_2PO_4, and 1 mM EDTA, pH 7.5, agitated and centrifuged as above, and the soluble protein was named 7S globulins. The pellet was resuspended in 0.8 M NaCl solution, 0.01 M KH_2PO_4, and 1 mM EDTA, pH 7.5, to obtain the 11S globulin fraction. Prolamins were extracted from the resulting pellet with 70% ethanol, and the final pellet was extracted with 0.1 M NaOH to obtain the glutelins fraction. Total proteins were extracted from canary seed flours (1 g) with 10 mL of buffer containing 7.5 M urea, 63 mM CHAPS, 2.2 M thiourea, 22 mM Tris-HCl, 17.3 mM trizma base, and 0.25% (v/v) Triton X-100, pH 3.1; the suspension was mixed with vortex and centrifuged for 10 min at 20000*g*, and the supernatant was named total protein. All extractions were performed in triplicate.

Tryptic Digestion of Canary Seed Proteins. Total protein extracts were used for protein digestion using trypsin from porcine pancreas (Sigma-Aldrich, St. Louis, MO, USA) at a ratio of enzyme/substrate 1:5 (w/w). Hydrolysis was carried out in a 100 mM Tris buffer, pH 8, at 37 °C for 6 h. The reaction was stopped by freezing, and the enzyme was removed by ultrafiltration using 10 kDa MWCO filters (Millipore, Billerica, MA, USA).

Simulation of Gastrointestinal Digestion Method. The protein hydrolysis of canary seed samples was also performed using the simulated gastrointestinal method.[19] Flour (1 g) was resuspended in 20 mL of 0.03 M NaCl, pH 2, heated in a water bath at 80 °C for 5 min, and allowed to cool to room temperature. Porcine pepsin (Sigma-Aldrich) previously dissolved in 0.03 M NaCl, pH 2.0, was added in a 1:40 ratio (w/w enzyme to substrate). The samples were digested at a constant pH for 3 h at 37 °C under constant agitation. Next, the pH was adjusted to 7.5, and a mixture of trypsin/pancreatin from porcine pancreas (Sigma-Aldrich) was added at a ratio of 1:1 w/w; enzymes were previously dissolved in 0.1 N $NaHCO_3$ at a ratio of 1:5000 (w/w enzyme/substrate). Samples were incubated at a constant pH for 3 h. Digestion was stopped by heating the samples at 75 °C for 20 min; the samples were allowed to cool and centrifuged at 20000*g* for 30 min. To remove the enzymes, the digests were ultrafiltered using 10 kDa MWCO membranes (Millipore).

Protein Quantification. Canary seed protein fractions were quantified using the kit Pierce BCA Protein Assay (Thermo Scientific, Rockford, IL, USA). The concentration of peptides released by the tryptic and gastrointestinal digestion methods was determined using the Lowry-based DC Protein Assay (Bio-Rad, Hercules, CA, USA). Bovine serum albumin was used as a standard.

Electrophoresis. Sodium dodecyl sulfate–polyacrylamide gel electrophoresis (SDS-PAGE) was carried out according to the method of Laemmli.[22] Protein samples (5 μg) were dissolved in 0.1 M Tris-HCl, pH 6.8, and 2% SDS. Electrophoresis was conducted at a constant current of 20 mA per gel for 2–3 h. After electrophoresis, the gel was stained with Phast Gel Blue R-350 (GE Healthcare Bio-Science AB, Uppsala, Sweden) in a final concentration of 0.02%. Destaining was accomplished by washing the gel with a solution of 30% methanol, 10% acetic acid, and water. Gels were digitalized in a Gel-Doc XR (Bio-Rad).

Assay for Inhibitory Activity of Dipeptidyl Peptidase IV. The assay for in vitro activity of DPPIV was carried out as reported previously.[19] The chromogenic substrate Gly-Pro-pNA (500 μM) and 100 ng/mL dipeptidyl peptidase IV isolated from a porcine kidney (Sigma) were used. Different concentrations (0, 200, 400, 600, 800, 1000, 1200, and 1400 μg/mL) of canary seed peptides were tested. The reaction was carried out for 1 h at 37 °C, and the absorbance of *p*-nitroaniline (pNA) released was read at 415 nm in a microplate reader (Bio-Rad). Diprotin A (Ile-Pro-Ile) was used as positive control of inhibition. All assays were performed in triplicate.

Assay for Inhibitory Activity of Angiotensin Converting Enzyme. The ACE inhibition assay was conducted following the protocol described previously.[18] The reaction was performed at 37 °C for 30 min in 100 μL of 0.1 M potassium phosphate buffer, pH 8.3, containing 0.3 M NaCl, 5 mM hippuryl-histidyl-leucine, 2 mU of ACE, and 25 μL of canary seed peptides at different concentrations (0, 83, 166, 249, 332, 415, 498, and 581 μg/mL). The reaction was stopped with the addition of 100 μL of 1 M HCl. The hippuric acid that formed was extracted with 1 mL of ethyl acetate, evaporated, and dissolved in 1 mL of distilled water; the hippuric acid absorbance was measured at 228 nm. The activity of each sample was tested in triplicate. Captopril (CPT) was used as a positive control. The IC_{50} value was defined as the peptide concentration (μg/mL) needed to inhibit 50% ACE activity, calculated by the ACE inhibition (%) versus log peptide concentration (μg/mL) linear regression.

Bioassay of Isolated Perfused Rat Heart (Langendorff Perfusion System). To evaluate the effect of vasoactive canary seed peptides, the Langendorff method was used.[23−25] Briefly stated, male Wistar rats (300−350 g) were euthanized with 50 mg/kg sodium pentobarbital intraperitoneally and 500 IU of heparin following the Animal Care Protocols (UASLP, Mexico). The rats' heart were removed and cannulated via the ascending aorta in a retrograde perfusion system (IsoHearth-SR Harvard Apparatus, Holliston, MS, USA) and were maintained at a constant flow rate of 10 mL/min. The perfusion medium was Krebs–Henseleit solution, pH 7.4,[21] equilibrated with 95% O_2 and 5% CO_2 at 37 °C. Increasing concentrations (0.01, 0.1, and 1 μg/mL) of canary seed peptides were administered intracoronary. BK at 10 μM and CPT at 50 μM were used as controls of vasodilation. Angiotensin I (ANG I) and/or angiotensin II (ANG II) at 1 μM were used as controls of vasoconstriction.

Quantification of Nitric Oxide in the Venous Effluent of Isolated Perfused Rat Heart. The concentration of NO, as nitrite and nitrate, was determined by using the Griess method.[18] Venous effluents from isolated hearts (100 μL) were collected and incubated at 37 °C for 30 min in the presence of 80 μL of vanadium chloride (VCl_3) followed by the addition of 20 μL of Griess reagent (1% sulfanilamide, 0.1% of naphthylethylenediamine in 2.5% phosphoric acid). Absorbance was read at 540 nm, and sodium nitrate ($NaNO_3$) was used as a standard.

Statistical Analysis. All experiments were carried out in triplicates, and results are reported as the mean values ± standard deviation. Statistical analyses were performed using GradphPad Prism 5 software (GraphPad Software Inc., La Jolla, CA, USA). One-way ANOVA and Tukey's test ($P < 0.05$) were performed to detect statistical differences.

RESULTS AND DISCUSSION

Extraction and Quantification of Canary Seed Storage Proteins. As shown in Figure 1, no differences were observed in protein fractions among canary seed flour (white bars), commercial flour "more Lait" (gray bars), and canary seed milk (black bars). The main fraction of canary seed storage proteins was prolamins with values ranging from 31 to 36% and glutelins (35−39%). Albumins fraction represented around 16%, and globulins were found in low concentrations (6%). The protein fraction values were similar to those in previous studies;[7] however, the electrophoretic profile has not been reported, and

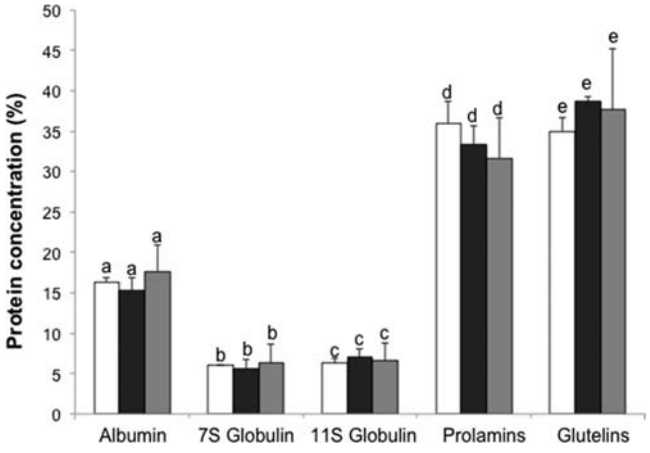

Figure 1. Distribution of canary seed storage proteins fractions expressed in percentage: canary seed flour (white bars); flour obtained from soaked seeds in water (black bars); commercial flour "more Lait" (gray bars). In each case the bar is the average of three replicates and standard deviation is indicated. The same letters mean no significant differences at $P < 0.05$ in the same fraction.

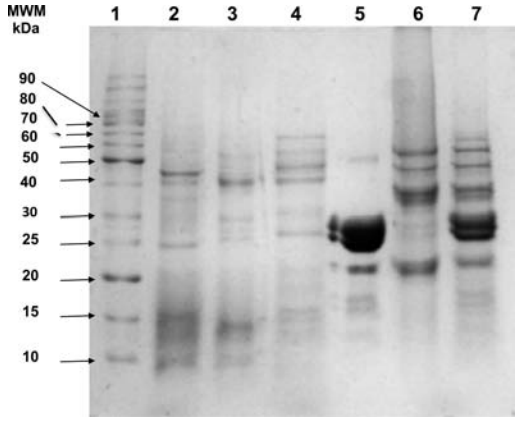

Figure 2. Electrophoretic profile of canary seed storage proteins. Canary seed storage proteins from commercial flour "more Lait" were extracted according to their solubility in different solvents. Lanes: 1, molecular weight marker (MW); 2, albumins; 3, 7S globulins; 4, 11S globulins; 5, prolamins; 6, glutelins; 7, total seeds proteins.

then we proceeded to characterize the protein profile of the canary seed storage protein fractions.

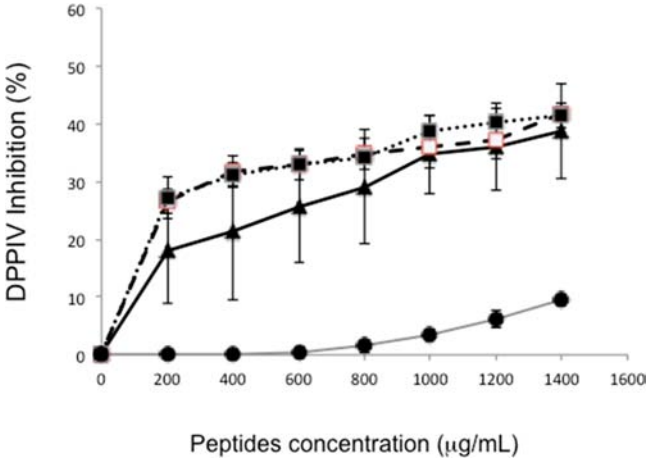

Figure 4. Inhibitory function of canary seed peptides against DPPIV activity. Canary seed proteins were digested by gastrointestinal digestion method, and fragments smaller than 10 kDa, obtained by ultrafiltration, were tested. The percentage of DPPIV inhibition was measured in the presence of increasing concentrations of canary seed peptides from canary seed flour (solid triangles), canary seed milk (open squares), and commercial canary seed flour "more Lait" (solid squares). Negative control used was nondigested canary seed proteins (solid circles). Error bars ± SD ($N = 3$).

Electrophoretic Profile of Canary Seed Storage Proteins. The electrophoretic profile under denaturing conditions of canary seed fractions obtained from commercial flour "more Lait" is shown in Figure 2. This pattern was similar to canary seed flour and canary seed milk (Supporting Information Figure 1S). Canary seed albumins pattern showed bands of molecular masses of 9.8, 12.8, 15.8, 19.3 23.4, 25.9, 39.2, and 43.4 kDa similar to the components of oat albumin (14−17, 20−27, and 36−47 kDa).[23] The 7S globulins profile was similar to that of albumin with the addition of another band of 37.8 kDa; 11S globulins showed bands at 62.8, 57.1, 46.5, 39.2, 25.8, 15.3, and 12.8 40 kDa. Prolamins patterns in canary seed showed a broad band containing at least two bands of 26.6 and 24.9 kDa. Prolamins patterns were similar to those of the oat (17−34 kDa), barley (15−20 kDa), and the zeins or prolamins from corn (23−24 and 26.5−27 kDa).[26,27] Glutelins main bands were located at 53.3, 41.5, 34.7, and 31.9 kDa, which are within a range similar to that of barley glutelins (35 and 42−46 kDa).[28] These results suggest that the electrophoretic profile of the canary seed storage proteins is

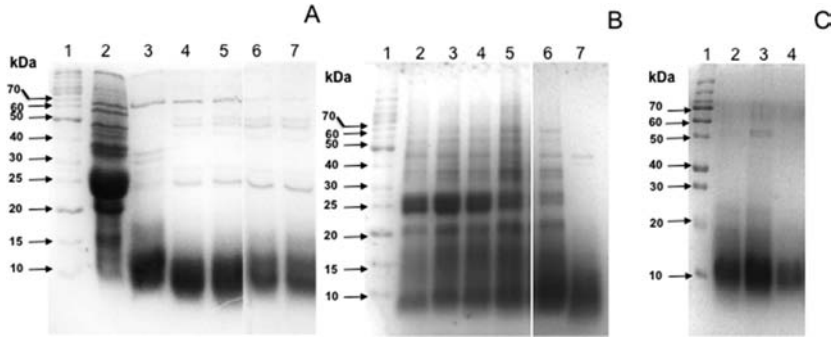

Figure 3. Digestion profile of total soluble proteins extracted from canary seed commercial flour "more Lait": (A) tryptic digestion; (B) gastrointestinal digestion. Lanes: 1, molecular weight marker; 2, nondigested canary seed proteins; 3−7, digestions at 0.1, 0.5, 1, 5, and 6 h, respectively. (C) Lanes: 1, molecular weight marker; 2−4, 10 kDa ultrafiltrates obtained from commercial flour "more Lait", canary seed flour, canary seed milk, respectively.

dx.doi.org/10.1021/jf404539y | J. Agric. Food Chem. 2014, 62, 427−433

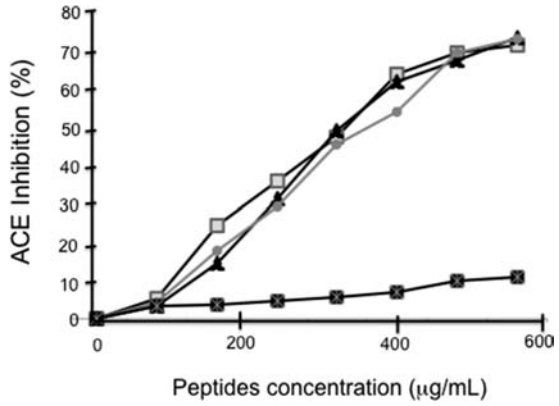

Figure 5. Inhibitory function of canary seed peptides against ACE activity. Canary seed proteins were digested by gastrointestinal digestion method, and fragments smaller than 10 kDa, obtained by ultrafiltration, were tested. The percentage of ACE inhibition was measured in the presence of increasing concentrations of canary seed peptides from canary seed flour (light-dotted dark squares), canary seed milk (solid triangles), and commercial canary seed flour "more Lait (gray circles). Nondigested canary seed proteins were used as negative control (gray-crossed black squares).

characteristic of the subfamily Pooideae cereals such as barley and oats and cereal family Poaceae (grass) such as corn.

Digestion of Canary Seed Proteins. The tryptic and gastrointestinal digestion (Figure 3) hydrolysis patterns of canary seed flour "more Lait" were similar to those of canary seed flour and canary seed milk patterns (Supporting Information Figure 2S). It was observed that at 6 h of gastrointestinal digestion, the bands of high molecular mass disappeared with the concomitant increasing of a smear below 10 kDa (Figure 3A). At this time, with tryptic digestion, bands of high molecular mass are still undigested (Figure 3B). Large protein fragments were removed by ultrafiltration using membranes of 10 kDa MWCO (Figure 3C), and eluted peptides were used for enzyme inhibition assays.

Characterization of Canary Seed Peptides Inhibitory Function against DPPIV Activity. Canary seed peptides obtained by gastrointestinal digestion showed an inhibition of DPPIV activity in a dose-dependent manner, where the highest inhibition of 43.4% was obtained at the higher peptide concentration (1.4 mg/mL). This behavior was similar among the three samples of canary seed under study (Figure 4). Nondigested canary seed proteins showed very low inhibition (9.3%). The tryptic digests (Supporting Information Figure 3S) had a lower percentage of inhibition (23%), and from this observation followed experiments that were evaluated using peptides obtained from gastrointestinal digestion. Diprotin A (Ile-Pro-Ile), the inhibition control for DPPIV, had an IC_{50} of 2 μg/mL

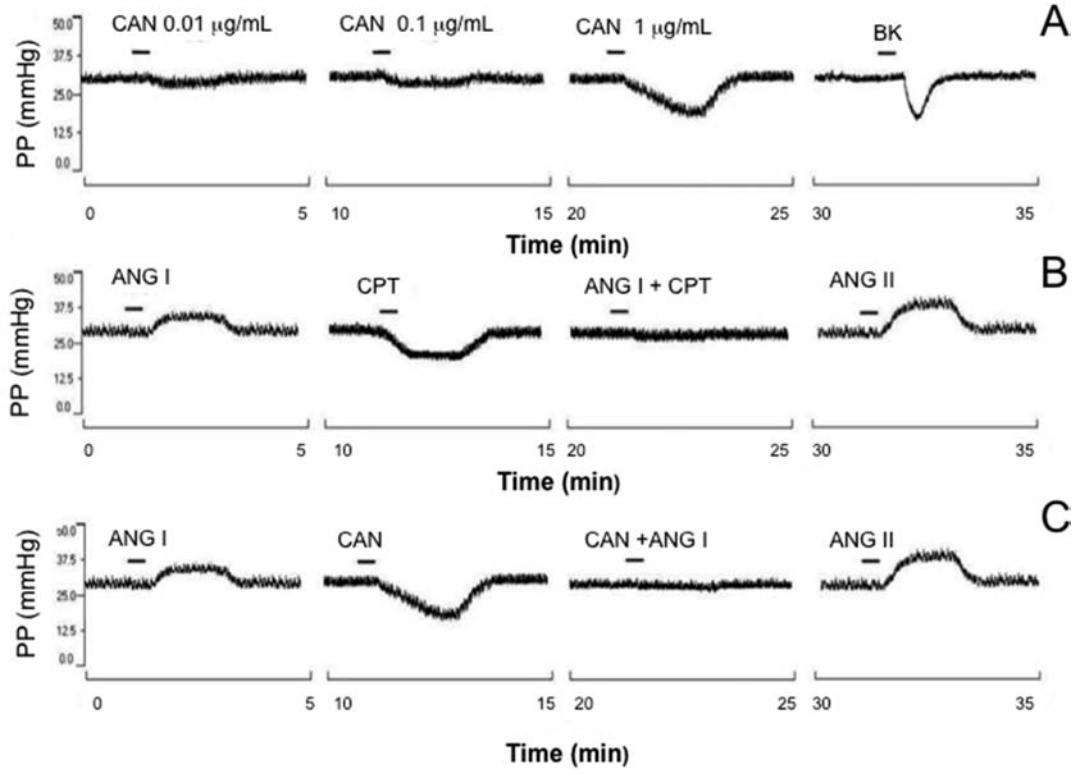

Figure 6. Representative trace recordings of the vasodilator effect induced by canary seed peptides in Langendorff system. Perfusion pressure (PP) was taken as an index of vascular tone (vasodilation/vasoconstriction) recorded from isolated perfused rat heart. PP representative trace recordings were in response to (A) increasing and independent administrations of canary seed peptides obtained by gastrointestinal digestion (CAN, 0.01, 0.1, and 1 μg/mL). Bradykinin (BK, 10 μM) was infused as control of vasodilation. (B) Vascular tone controls: Angiotensin I (ANG I; 1 μM), the precursor of the formation of ANG II. ANG II (1 μM) was administered as control of vasoconstriction, and captopril (CPT, 50 μM), an ACE inhibitor, was administered as control of vasodilation. The administration of ANG I in the presence of CPT blocked the vasoconstriction induced by ANG I. (C) ANG (1 μM) was administered as control of vasoconstriction, and the vasodilation action of CAN (1 mg/mL) was measured. ANG I in the presence of CAN blocked the vasoconstriction induced by ANG I. ANG II was infused as control of vasoconstriction. Canary seed peptides and controls were administered in all cases after washout periods. All experiments were carried out in triplicates.

dx.doi.org/10.1021/jf404539y | J. Agric. Food Chem. 2014, 62, 427−433

(Supporting Information Figure 4SA), this value being similar to values reported in the literature.[29,30]

Characterization of Canary Seed Peptide Inhibitory Function against ACE Activity. The antihypertensive action of canary seed peptides was evaluated as the capacity to inhibit ACE activity. Increasing concentrations of the gastrointestinal digestion derived peptides (0−581 μg/mL) were evaluated. The highest inhibition value was 73.5% (Figure 5), a value similar to that reported for the bovine whey peptides.[31] The IC_{50} of canary seed peptides was 332 μg/mL, similar to the IC_{50} value of the peptides of chickpea,[32] pea,[32] soybean,[33] wheat gliadin,[34] and sardine muscle.[35] All canary seed presentations had the same inhibition pattern. Nondigested samples reached only 10.7% inhibition at its highest concentration. Captopril, used as a positive control of ACE inhibition, showed an IC_{50} value of 4.074 μg/mL (Supporting Information Figure 4SB), similar to that reported in the literature.[37]

Assessment of the Vascular Tone Induced by Canary Seed Peptides in Isolated Perfused Rat Heart. In the Langendorff system, the perfusion pressure (PP) was taken as an index of vascular tone (vasodilation/vasoconstriction).[17] Three different concentrations (0.01, 0.1, and 1 μg/mL) of canary seed peptides were tested. The vasodilator effect was observed in a dose-dependent manner, where the lowest pressure was observed at 1 μg/mL, similar to the vasodilation induced by BK (10 μM) (Figure 6A). It has been reported that ANG I causes vasoconstriction in biological systems in perfusion[36−39] and is blocked by ACE inhibitors;[37,40−42] then ANG I and ANG II (1 μM) were tested as vasoconstriction controls, and CPT (50 μM) was used as vasodilation control and blocker of ACE (Figure 6B). In Figure 6C canary seed peptides (1 μg/mL) were used instead of CPT. It was observed that both CPT (Figure 6B) and canary seed peptides (Figure 6C) counteract the vasoconstrictor effect induced by ANG I. Vasodilation by canary seed peptides (1 μg/mL) was 82.7% compared to the 100% vasodilation induced with CPT and BK (Figure 7A). Figure 7B shows the percentage of vasoconstriction of ANG I (72%) and ANG II (100%), and it was observed that both CPT and canary seed peptides completely block the ANG I-induced vasoconstriction, suggesting the endogenous activity of ACE in the coronary vessels of the isolated and perfused rat hearts. Thereby, it was proposed that canary seed peptides are potential candidates as inhibitors of ACE activity (Figure 7B).

Nitric Oxide in the Venous Effluent Isolated Perfused Rat Heart. To determine whether the vasodilator effect of the canary seed peptides was also associated with NO production, NO was determined in venous effluent from the isolated perfused rat heart. The highest amount of NO produced by canary seed peptides at 1 μg/mL was 12.24 μM, whereas CPT induced the production of 20.27 μM and BK 19.24 μM (Figure 8). These data suggest an important function of canary seed peptides in the regulation of vascular tone through NO production. The NO produced in the inner layer of the blood vessel diffuses at the cardiac cell, blocking the release of calcium needed for muscle contraction, and therefore promotes a state of relaxation.[18,43] ACE inhibitors induce vasodilation due the formation of a BK−NO-dependent pathway.[18] Then, canary seed peptides are ACE type inhibitors stimulating NO production by this route.

In conclusion, the protein profile of canary seed protein fractions is more similar to those of cereals such as oats and maize and is farther from wheat electrophoretic patterns. Canary seed proteins contain encrypted peptides with

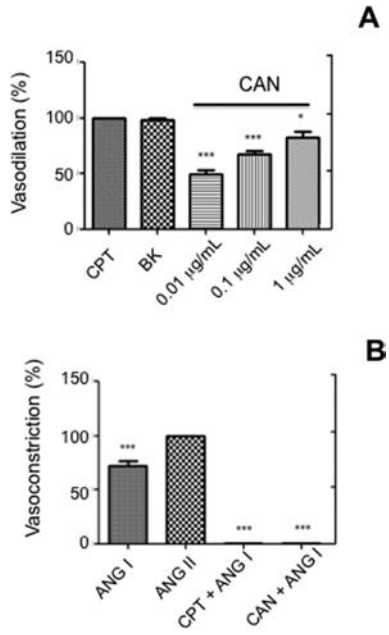

Figure 7. Vasodilation/vasoconstriction exerted by canary seed peptides (CAN) obtained by gastrointestinal digestion. (A) Vasodilation induced by different CAN concentrations (0.01, 0.1, 1 μg/mL). Vasodilation controls: captopril (CPT, 50 μM) and bradykinin (BK, 10 μM). (B) Vasoconstriction effect of CPT in the presence of angiotensin I (ANG I) or CAN in the presence of ANG I. Vasoconstriction controls (1 μM ANG I or ANG II). Values are expressed as the mean of three independent experiments. Asterisks indicate statistical differences at $P < 0.05$.

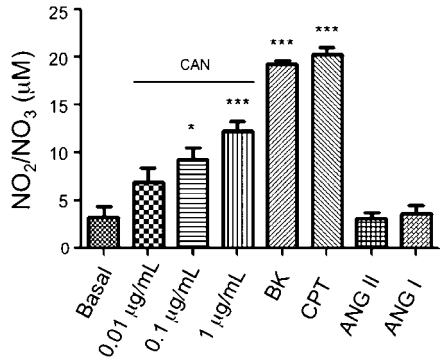

Figure 8. Induction of nitric oxide (NO) production by different concentrations of canary seed peptides (CAN; 0.01, 0.1, 1 μg/mL) obtained by gastrointestinal digestion. The NO (NO_2/NO_3) was measured in the venous effluent of the heart of rat isolated perfused. Results are representative of three independent experiments. Values are expressed as the mean ± standard error (SE). Asterisks indicate statistical differences at $P < 0.05$ versus basal.

inhibitory activity against DPPIV and ACE. The inhibition of DPPIV is the basis of modern antidiabetic therapy, whereas inhibition of ACE is the drug therapy against hypertension. In addition we have demonstrated that canary seed peptides are able to induce the production of NO, a potent vasodilator, at levels similar to those produced by CPT and BK.

■ ASSOCIATED CONTENT

Ⓢ Supporting Information

Supplementary Figures 1S−4S. This material is available free of charge via the Internet at http://pubs.acs.org.

dx.doi.org/10.1021/jf404539y | J. Agric. Food Chem. 2014, 62, 427−433

AUTHOR INFORMATION

Corresponding Author

*(A.P.B.R.) E-mail: apbarba@ipicyt.edu.mx. Phone: +52 444 8342000. Fax: +52 444 8342010.

Funding

PA Estrada-Salas thanks CONACyT for Fellowship 4234.

Notes

The authors declare no competing financial interest.

ACKNOWLEDGMENTS

We thank Alberto Barrera-Pacheco for his technical assistance and Jonathan Simon for review of the English grammar.

REFERENCES

(1) Boye, J. I.; Achouri, A.; Raymond, N.; Cleroux, C.; Weber, D.; Koerner, T. B.; Hucl, P.; Patterson, C. A. Analysis of glabrous canary seeds by ELISA, mass spectrometry, and western blotting for the absence of cross-reactivity with major plant food allergens. *J. Agric. Food Chem.* **2013**, *61*, 6102−6112.

(2) Robinson, R. G. Chemical composition and potential uses of annual canary grass. *Agron. J.* **1979**, *70*, 797−800.

(3) Cogliatti, M. Canary seed. *Crop. Sci. Agropecu.* **2012**, *1*, 75−88.

(4) Matus-Cadiz, M.; Hucl, P. Outcrossing in annual canarygrass. *Can. J. Plant Sci.* **2006**, *46*, 243−246.

(5) Putnam, D. H.; Miller, P. R.; Hucl, P. Potential for production and utilization of annual canarygrass. *Cereal Foods World* **1996**, *41*, 75−83.

(6) Abdel-Aal, E.-S. M.; Hucl, P. J.; Sosulski, F. W. Structural and compositional characteristics of canary seed (*Phalaris canariensis* L.). *J. Agric. Food Chem.* **1997**, *45*, 3049−3055.

(7) Abdel-Aal, E.-S. M.; Hucl, P.; Sosulski, F. W. Characteristics of canaryseed (*Phalaris canariensis* L.) starch. *Starch/Staerke* **1997**, *49*, 475−480.

(8) Malik, M. Y.; Williams, W. D. Composition of the seed oil of *Phalaris canariensis*. *J. Sci. Food Agric.* **1966**, *17*, 174−175.

(9) Takagi, T.; Iida, T. Antioxidant for fats and oils from canary seed: sterol and triterpene alcohol esters of caffeic acid. *J. Am. Oil Chem. Soc.* **1980**, *57*, 326−330.

(10) Li, W.; Beta, T. An evaluation of carotenoid levels and composition of glabrous canaryseed. *Food Chem.* **2012**, *133*, 782−786.

(11) Campbell, R. K. Fate of the beta-cell in the pathophysiology of type 2 diabetes. *J. Am. Pharm. Assoc.* **2009**, *49*, S10−S15.

(12) Holst, J. J.; Knop, F. K.; Vilsboll, T.; Krarup, T.; Madsbad, S. Loss of incretin effect is a specific, important, and early characteristic of type 2 diabetes. *Diabetes Care* **2011**, *34*, S251−S257.

(13) Stephan, M.; Radicke, A.; Leutloff, S.; Shimiedl, A.; Pabst, R.; von Hörsten, S.; Dettmer, S.; Lotz, J.; Nave, H. Dipeptidyl peptidase IV (DPPIV)-deficiency attenuates diet-induced obesity in rats: possible implications for the hypothalamic neuropeptidergic system. *Behav. Brain Res.* **2011**, *216*, 712−718.

(14) Keating, G. M. Vildagliptin. A review of its use in type 2 diabetes mellitus. *Drugs* **2010**, *70*, 2089−2112.

(15) Gokce, N. L-Arginine and hypertension. *J. Nutr.* **2004**, *134*, 2807S−2811S.

(16) Fleming, L. Signaling by the angiotensin-converting enzyme. *Circ. Res.* **2007**, *98*, 887−896.

(17) González, C.; Corbacho, A. M.; Eiserich, J. P.; García, C.; López-Barrera, F.; Morales-Tlalpan, V.; Barajas-Espinosa, A.; Díaz-Muñoz, M.; Rubio, R.; Lin, S. H.; Martinez de la Escalera, G.; Clapp, C. 16K-prolactin inhibits activation of endothelial nitric oxide synthase, intracellular calcium mobilization, and endothelium-dependent vaso-relaxation. *Endocrinology* **2004**, *145*, 5714−5722.

(18) Barba de la Rosa, A. P.; Barba, A.; Martínez, P.; Hernández, B.; León, F.; De León, A.; González, C. Tryptic amaranth glutelin digests induce endothelial nitric oxide production through inhibition of ACE: antihypertensive role of amaranth peptides. *Nitric Oxide* **2010**, *23*, 106−111.

(19) Velarde-Salcedo, A. J.; Barrera-Pacheco, A.; Lara-González, S.; Montero-Morán, G. M.; Díaz-Gois, A.; González de Mejía, E.; Barba de la Rosa, A. P. In vitro inhibition of dipeptidyl peptidase IV by peptides derived from the hydrolysis of amaranth (*Amaranthus hypochondriacus* L.) proteins. *Food Chem.* **2013**, *136*, 758−764.

(20) Barba de la Rosa, A. P.; Gueguen, J.; Paredes, O.; Virobent, G. Fractionation procedures, electrophoretic characterization, and amino acid composition of amaranth seed proteins. *J. Agric. Food Chem.* **1992**, *40*, 931−936.

(21) Osborne, T. Solubility of vegetable proteins. In *The Vegetable Proteins*, 2nd ed.; Longmans: London, UK, 1909; Vol. 1, pp 30−33.

(22) Laemmli, U. K. Cleavage of structural proteins during the assembly of the head of bacteriophage T4. *Nature* **1970**, *227*, 680−685.

(23) Gonzalez, C.; Rubio, R.; Zenteno, T. Coronary flow-induced inotropism is modulated by binding of dextrans to the endothelial luminal surface. *Am. J. Physiol. Heart Circ. Physiol.* **2003**, *284*, 1348−1357.

(24) Riascos, B.; Baltaxe, E.; Pascual, G. La preparación de Langendorff: corazón de mamífero aislado perfundido. *Univ. Med.* **2004**, *45*, 111−117.

(25) Rubio, R.; Ceballos, G. Role of the endothelial glycocalyx in dromotropic, inotropic, and arrythmogenic effects of coronary flow. *Am. J. Physiol. Heart Circ. Physiol.* **2000**, *278*, 106−116.

(26) Klose, C.; Arendt, E. Proteins in oats; their synthesis and changes during germination: a review. *Crit. Rev. Food Sci. Nutr.* **2012**, *52*, 629−639.

(27) Shewry, P.; Halford, N. Cereal seed storage proteins: structures, properties and role in grain utilization. *J. Exp. Bot.* **2002**, *53*, 947−958.

(28) Shewry, P. R.; Tatham, A. S. The prolamin storage proteins of cereal seeds: structure and evolution. *Biochem. J.* **1990**, *267*, 1−12.

(29) Rituparna, C.; Singh, B.; Prakrith, N.; Nimisha, V.; Lalthanzama, V.; Mohamed, H.; Kavitha, T. Dipeptidyl peptidase-IV inhibitory activity of *Berberis aristata*. *J. Nat. Prod.* **2011**, *4*, 158−163.

(30) Sudhanshu, B.; Neeraj, S.; Amit, K.; Sudhir, J.; Supriya, K.; Ashok, G.; Ashis, G.; Om, P. Dipeptidyl peptidase IV inhibitory activity of seed extract of *Castanospermum australe* and molecular docking of their alkaloids. *Topclass J. Herb. Med.* **2012**, *1*, 029−035.

(31) Pihlanto, A.; Rokka, T.; Korhonen, H. Angiotensin I converting enzyme inhibitory peptides derived from bovine milk proteins. *Int. Dairy J.* **1998**, *8*, 325−331.

(32) Barbana, C.; Boye, I. Angiotensin I-converting enzyme inhibitory activity of chickpea and pea protein hydrolysates. *Food Res. Int.* **2010**, *43*, 1642−1649.

(33) Tsai, S.; Lin, Y.; Pan, S.; Chen, J. Antihypertensive peptides and γ-aminobutyric acid from Prozyme 6 facilitated lactic acid bacteria fermentation of soymilk. *Process Biochem.* **2006**, *41*, 1282−1288.

(34) Motoi, H.; Kodama, T. Isolation and characterization of angiotensin I-converting enzyme inhibitory peptides from wheat gliadin hydrolysate. *Nahrung/Food* **2003**, *47*, 354−358.

(35) Vercruysse, L.; Camp, J. V.; Smagghe, G. ACE inhibitory peptides derived from enzymatic hydrolysates of animal muscle protein: a review. *J. Agric. Food Chem.* **2005**, *53*, 8106−8115.

(36) Vermeirssen, V.; Camp, J. V.; Verstraete, W. Bioavailability of angiotensin I converting enzyme inhibitory peptides. *Br. J. Nutr.* **2004**, *92*, 357−366.

(37) Hayes, M.; Stanton, C.; Slattery, H.; Sullivan, O.; Hill, C.; Fitzgerald, G.; Ross, R. Casein fermentate of *Lactobacillus animalis* DPC6134 Contains a range of novel propeptide angiotensin-converting enzyme inhibitors. *Appl. Environ. Microbiol.* **2007**, *73*, 4658−4667.

(38) Nishimura, H.; Buikema, H.; Baltau, O.; Ganten, D.; Urata, H. Functional evidence for alternative ANG II-forming pathways in hamster cardiovascular system. *Am. J. Physiol. Heart Circ. Physiol.* **1998**, *275*, 1307−1312.

(39) Van Kats, J. P.; Danser, A. H.; Van Meegen, J. R.; Sassen, L. M.; Verdouw, P. D.; Schalekamp, M. A. Angiotensin production by the heart a quantitative study in pigs with the use of radiolabeled angiotensin infusions. *Circulation* **1998**, *98*, 73−81.

(40) Wei, C. C.; Meng, C.; Palmer, R.; Hageman, G.; Durand, J.; Bradley, E.; Farrell, D.; Hankes, G.; Oparil, S.; Dell'Italia, L. Evidence for angiotensin converting enzyme and chymase-mediated angiotensin II formation in the interstitial fluid space of the dog heart in vivo. *Circulation* **1999**, *99*, 2583−2589.
(41) Coviello, A.; Soria, M. O.; Proto, M.; Peral de Bruno, M.; Berman, D. M.; Khosla, M. C.; Bumpus, F. M. Effects of angiotensin I of the American bullfrog *Rana catesbeiana* on amphibian tissue. *Comp. Biochem. Physiol.* **1993**, *104*, 113−116.
(42) Mauer, K.; Exaire, J.; Escalante, B. Importance of angiotensin converting enzyme in coronary circulation. *Arch. Cardiol. Mex.* **2001**, *71*, 278−285.
(43) Oliveira de Oliveira, U.; Reischak de Oliveira, Á.; Kucharski, L.; Fabres, U.; Irigoyen, M.; D'Agord, B. Efectos de la angiotensina-I e isquemia en la recuperación funcional en corazones aislados. *Arq. Bras. Cardiol.* **2011**, *97*, 390−396.

JOURNAL OF AGRICULTURAL AND FOOD CHEMISTRY

Article

pubs.acs.org/JAFC

Beneficial Effect of Betulinic Acid on Hyperglycemia via Suppression of Hepatic Glucose Production

Soo Jung Kim, Hai Yan Quan, Kyong Ju Jeong, Do Yeon Kim, Go woon Kim, Hee Kyung Jo, and Sung Hyun Chung*

Department of Pharmacology and Clinical Pharmacy, College of Pharmacy, Kyung Hee University, 1 Hoegi-dong, Dongdaemun-gu, Seoul 130-701, Korea

Supporting Information

ABSTRACT: The inhibitory effect of betulinic acid (BA) on hepatic glucose production was examined in HepG2 cells and high fat diet (HFD)-fed ICR mice. BA significantly inhibited the hepatic glucose production (HGP) and gene expression levels of PGC-1α, PEPCK, and G6Pase. BA activated AMPK and suppressed the expression level of phosphorylated CREB. These effects were all abolished in the presence of compound C (an AMPK inhibitor). Moreover, inhibition of AMPK by overexpression of dominant negative AMPK prevented BA from suppression of HGP, indicating that the inhibitory effect of BA on HGP is AMPK-dependent. In addition, BA markedly phosphorylated CAMKK, and phosphorylation of AMPK and ACC, and suppression of HGP were all reversed in the presence of STO-609 (a CAMKK inhibitor), suggesting that CAMKK is an upstream kinase for AMPK. In an animal study, HFD-fed ICR mice were orally administered with 5 or 10 mg of BA per kg (B5 and B10) for three weeks. Plasma glucose, triglyceride, and the insulin resistance index of the B10 group were decreased by 34%, 59%, and 38%, respectively. In a pyruvate tolerance test, pyruvate-induced glucose excursion was decreased by 27% when mice were pretreated with 10 mg/kg of BA. In summary, BA effectively ameliorates hyperglycemia through inhibition of hepatic gluconeogenesis via modulating the CAMKK-AMPK-CREB signaling pathway.

KEYWORDS: *AMPK, betulinic acid, CREB, hepatic glucose production, type 2 diabetes*

INTRODUCTION

Type 2 diabetes mellitus (T2DM), characterized by insulin resistance and β-cell dysfunction, is one of the leading causes of death and disability. Despite the great advances that have been made in the understanding and management of this complex, multifactorial disease, T2DM has become a worldwide epidemic in the 21st century.[1] Because of the variable and progressive pathophysiological changes associated with T2DM, pharmacological compounds acting on multiple targets are needed at different stages of the disease to complement the benefits of lifestyle changes, which can be effective but difficult to maintain.[2] Antidiabetic agents, however, have some limitations, including no sustainability of efficacy because of continued β-cell dysfunction and having side effects such as hypoglycemia, weight gain, gastrointestinal disturbances, peripheral edema, and potential cardiovascular effects.[3,4] Therefore, new therapeutic agents need to be developed that will sustain glycemic control, reverse or halt the decline in β-cell function, assist with weight loss, improve insulin action, avoid hypoglycemia, and have a favorable effect on cardiovascular disease. There is an increasing demand for the use of natural products with antidiabetic activity. In this context, phytochemicals derived from natural sources, including foods, are of worth to examine their beneficial effects on chronic diseases such as T2DM.

As part of the search for biologically active antidiabetic agents, more than 200 phytochemicals were evaluated, and betulinic acid (BA) was found to be one of the active ingredients that ameliorate hyperglycemia. BA is a pentacyclic triterpene isolated from the bark of *Albizia Julibrissin*. BA has been reported to show a wide spectrum of biological and pharmacological activities, such as anti-inflammation,[5,6] anticancer,[7−9] antimalaria,[10] anti-AIDS,[11] antifatty liver,[12] antidiabetes,[13,14] and antidepression[15] effects. However, whether BA exerts a suppressive effect on hepatic glucose production is unknown yet. In this study, we investigated whether BA inhibits hepatic gluconeogenesis in human hepatoma HepG2 cells and in high fat diet (HFD)-fed ICR mice, and underlying mechanisms. These studies reveal that suppression of the hepatic glucose production by BA as an AMP-activated protein kinase (AMPK) activator is of key therapeutic importance for T2DM.

MATERIALS AND METHODS

Chemicals. BA was kindly provided by Prof. N. I. Baek (Institute of Life Sciences and Resources, Kyung Hee University) and dissolved in DMSO. Antibodies against AMPK, phospho-AMPK, acetyl-CoA carboxylase (ACC), phospho-ACC, cAMP response element-binding protein (CREB), phospho-CREB, CREB-regulated transcription coactivator 2 (CRTC2), and IgG were from Cell Signaling Technology (Beverly, MA, USA), and actin was from Santa Cruz Biotechnology (Santa Cruz, CA, USA). Ca^{2+}-calmodulin dependent protein kinase kinase (CAMKK) and phospho-Ser/Thr antibodies were from BD Biosciences (San Jose, CA, USA). Reverse transcriptase, Taq polymerase, and cell proliferation assay kits were supplied by Promega (Madison, WI, USA), and SYBR premix Ex Taq was from Takara Bio Inc. (Dalian, China). Compound C (AMPK inhibitor)[16] and STO-609 (CAMKK inhibitor)[17] were from Calbiochem (Darmstadt, Germany). Protein

Received: July 13, 2013
Revised: December 14, 2013
Accepted: December 19, 2013
Published: December 19, 2013

ACS Publications © 2013 American Chemical Society

extraction, easy-BLUE total-RNA extraction, and enhanced chemiluminescence (ECL) reagent were from Invitron Biotechnology Inc. (Beverly, MA, USA). Jet-PEI Hepatocyte DNA transfection reagent was from Polyplus transfection Inc. (San Marcos, CA, USA), and the glucose production assay kit was from Roche Applied Sciences (Indianapolis, IN, USA). Regular diet (RD) and HFD (Table 1) were purchased from Research Diets, Inc. (New Brunswick, NJ, USA). The other reagents and chemicals were of the highest grade commercially available.

Table 1. Compositions of the Experimental Diets

	RD 10% (kcal)		HFD 45% (kcal)	
	g %	kcal %	g %	kcal %
protein	19.2	20	24	20
carbohydrate	67.3	70	41	35
fat	4.3	10	24	45
total		100		100
kcal/g	3.85		4.73	
ingredient	**gm**	**kcal**	**gm**	**kcal**
casein, 80 mesh	200	800	200	800
L-cystine	3	12	3	12
corn starch	315	1260	72.8	291
maltodextrin 10	350	140	100	400
sucrose	50	1400	172.8	691
cellulose, BW 200	25	0	50	0
soybean oil	20	225	25	225
lard	10	180	177.5	1598
mineral mix S10026	13	0	10	0
dicalcium phosphate	5.5	0	13	0
calcium carbonate	16.5	0	5.5	0
potassium citrate	10	0	16.5	0
vitamin mix V10001	2	40	10	40
choline bitartrate		0	2	0
FD&C yellow dye #5 (RD) red dye #40 (HFD)	0.05	0	0.05	0
total	**1055.05**	**4057**	**858.15**	**4057**

Cell Culture and Viability Assay. The human hepatoma cell line HepG2 was purchased from the American Type Culture Collection (Rockville, MD, USA). HepG2 cells were grown in high glucose DMEM (Gibco BL, Grand Island, NY, USA), supplemented with 10% fetal bovine serum (FBS) and antibiotics (100 unit/mL penicillin and 100 μg/mL streptomycin). Cells were maintained at subconfluent conditions in a humidified incubator at 37 °C with ambient oxygen and 5% CO_2. The cytotoxicity of BA was determined by a Cell Titer 96 AQueous One solution Cell Proliferation Assay kit. In brief, cells were seeded at 3×10^4 cells/well in a 96-well plate and treated with BA as indicated for 24 h. After one day of treatment, 20 μL of 3-(4,5-dimethylthiazol-2-yl)-5-(3-carboxymethoxyphenyl)-2-(4-sulfophenyl)-2H-tetrazolium (MTS) solution was added and incubated at 37 °C for 30 min, and the absorbance was recorded at 490 nm using an ELISA plate reader (Thermo LabSystem, Helsinki, Finland).

Stable Transfection. Expression plasmids for the Myc-tagged AMPKα1 wild type (WT) and dominant negative (DN) form, in which Asp157 was replaced with Ala, were generously provided by Prof. Ha (Department of Biochemistry, School of Medicine of Kyung Hee University). The HepG2 cells were seeded in 6-well plates and grown to 60% confluences, and the pdDNA3-AMPK α1-WT or -DN vectors were transfected into HepG2 cells using a jet-PEI transfection reagent. Briefly, each 1 μg of DNA vector was diluted to a volume of 100 μL with FBS-free and antibiotic-free DMEM, and then incubated with 10 μL of transfection reagent at room temperature for 15 min. Antibiotic-free DMEM containing 10% FBS was then added to a final volume of 1.5 mL before addition to the cells in a 6-well plate. Cells were incubated with the recombinant complexes for 48 h and then replaced with the selective medium containing 5 mg/mL G418. The stably expressed clones were screened through limiting dilution and Western blot analysis.

Glucose Production Assay. Cells were cultured in a 12-well plate at the density 3×10^5 cells/well, attached for 12 h, and then maintained in serum-free DMEM with or without BA for 3 h. Cells were washed twice with phosphate buffered saline (PBS) to remove glucose and incubated for 3 h in glucose production assay medium (glucose- and phenol red-free DMEM supplemented with 2 mM sodium pyruvate and 20 mM sodium lactate). Glucose in the media was quantified using an Amplex Red Glucose/Glucose Oxidase Assay Kit (Invitrogen, CA, USA) and normalized to the cellular protein concentration measured with a Bio-Rad protein assay kit (Hercules, CA, USA). The total glucose production is derived from glycogenolysis and gluconeogenesis in the liver. The glucose production from glycogenolysis was measured in the absence of gluconeogenic substrates. Thereafter, the glucose production via gluconeogenesis can be measured by the difference between the total glucose production and the glucose derived from glycogenolysis.

Animal Study. Five-week-old ICR mice were purchased from Orient Bio Inc. (Seongnam, Korea). The animal experiment protocol was reviewed and approved by the Institutional Animal Ethics Committee of Kyung Hee University (permission number: KHP-2010-12-9). Mice were housed in environmentally controlled conditions with a 12 h light/12 h dark cycle, and given free access to food and water under constant room temperature (22 ± 2 °C) and humidity (50 ± 5%). After 1 week acclimation, a pyruvate tolerance test (PTT) was performed using fasted 6-week-old ICR mice to examine the effect of a single administration of BA on hepatic glucose production. Ten mg/kg of BA (dissolved in 0.5% CMC) was orally administered to the ICR mice, and after 2 h, mice were intraperitoneally injected with 2 g/kg of pyruvate and blood glucose was obtained from the tail vein every 30 min until the 3 h period. Glucose levels were measured using an Accu-chek Advantage glucometer (Roche Diagnostics, Indianapolis, IN, USA). Next, to evaluate the effect of chronic administration of BA on blood glucose and lipid levels, mice were randomly divided into four groups (n = 8 for each group): regular diet fed group (RD), high fat diet fed group (HFD); HFD plus BA at 5 mg/kg body weight (BA5); and HFD plus BA at 10 mg/kg (BA10). Mice were orally administered with BA once a day for 3 weeks. Upon completion of treatment, mice were anesthetized by diethyl ether inhalation after overnight fasting. Blood was collected by cardiac puncture, and liver was dissected and snap-frozen in liquid nitrogen for further experiments.

Blood Chemistry Analysis. The plasma concentrations of glucose and triglyceride were determined using commercial kits (Stanbio Laboratory, Boerne, TX, USA) and an automatic analyzer (SMART-TLAB, Mannheim, Germany). The plasma insulin concentration was determined using a Bio-Plex Pro Mouse Diabetes Assay Kit (Bio-Rad, Hercules, CA, USA).

Immunoprecipitation and Western Blot Analysis. To detect proteins in whole cell lysates, cells were washed with ice-cold PBS and lysed using a protein extraction kit. Insoluble protein was removed by centrifugation at 13,000 rpm for 20 min. The protein concentration of the cell lysates was measured using a Bio-Rad protein assay kit. To determine protein expression in livers, the livers were removed and homogenized for 30 s, and then the protein concentration was measured as described above. For immunoprecipitation, 300 μg of cell lysate was cleared with 20 μL of protein G-sepharose beads (Santa Cruz, CA, USA) and 1 μg of antibody (anti-CAMKK or anti-CRTC2) was used. After the addition of 20 μL of G-Sepharose beads, incubation was continued for an additional 2 h at 4 °C. The beads were then collected by centrifugation and washed three times with PBS, the supernatant was removed, 30 μL of 2× loading buffer was added, and samples were run on a 8% SDS-polyacrylamide electrophoresis gel (SDA-PAGE). For Western blot assays, equal amounts of protein (40 μg/lane) were resolved by 8% SDS-PAGE and transferred to polyvinylidene difluoride membranes (Millipore, Bedford, MA, USA). Levels of protein and actin were detected with a 1:1000 dilution of each antibody in a nonfat dry milk solution (Tris-buffered saline with 5% nonfat dry milk and 0.1% Tween 20), followed by incubation with a horseradish peroxidase-

dx.doi.org/10.1021/jf4030739 | J. Agric. Food Chem. 2014, 62, 434−442

Table 2. RT-PCR and Real Time-PCR Primer Sequence and Annealing Temperature

gene (RT-PCR/real time-PCR)	forward primer	reverse primer	annealing temp (°C)
hPGC-1α	TGAGTGAATCCACTGTTTGT	TGGTAACAATATTTGTCAGG	58
hPEPCK	GGTTCCCAGGGTGCATGAAA	CACGTAGGGTGAATCCGTCAG	64
hG6Pase	GGGTGTAGACCTCCTGTGGA	GAGCCACTTGCTGAGTTTCC	65
hGAPDH	ACCACAGTCCATGCCATCAC	TCCACCACCCTGTTGCTGTA	55
mPGC-1α	AGAGCAAGTATGACTCTCTGG	GTCCTCACATGTGTACATATG	61
mPEPCK	TGCTGATCCTGGGCATAACTA	TGGGTACTCCTTCTGGAGATT	61
	TGACAGACTCGCCCTATGTG	TGCAGGCACTTGATGAACTC	60
mG6Pase	AAGACTCCCAGGACTGGTTCATCC	TAGCAGGTAGAATCCAAGCGC	65
	TGGAACCAGATGGGAAAGAG	AGGAAGGATGGAGGAAGGAA	60
mActin	GGACTCCTATGGTGGGTGACGAGG	GGGAGAGCATAGCCCTCGTAGAT	58
	TGACAGGATGCAGAAGGAGA	CGCTCAGGAGGAGCAATG	60

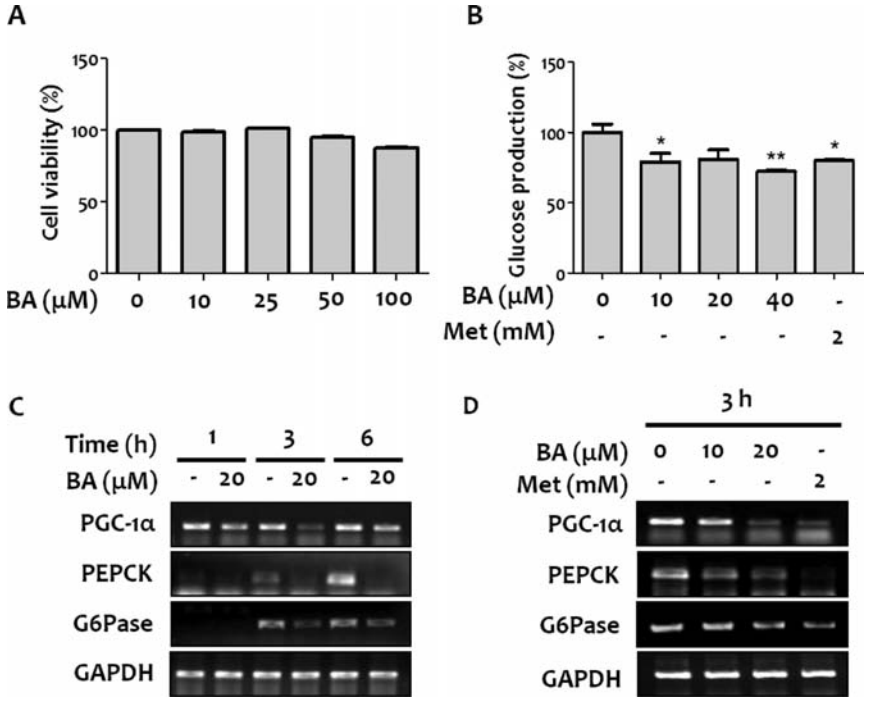

Figure 1. Effects of BA on glucose production and mRNA expression of gluconeogenic proteins in HepG2 cells. (A) HepG2 cells were treated with different concentrations (10, 25, 50, and 100 μM) of BA for 24 h, and cell viability was determined by MTS assay. (B) Cells were cultured in a 12-well plate, attached for 12 h, and then maintained in serum-free DMEM with or without BA at indicated concentrations for 3 h. Cells were washed twice with PBS to remove glucose and incubated for 3 h in glucose production assay medium (glucose and phenol red-free DMEM supplemented with 2 mM sodium pyruvate and 20 mM sodium lactate). The glucose concentration was determined using a glucose assay kit and normalized to cellular protein concentration. (C) Cells were treated with 20 μM BA for up to 6 h or (D) cells were treated with 10 or 20 μM BA for 3 h, and mRNA expression levels of PGC-1α, PEPCK, and G6Pase were analyzed by RT-PCR. Data are represented as the mean ± SE: *$p < 0.05$, **$p < 0.01$ compared to control cells.

conjugated secondary antibody (diluted 1:2000) for 2 h at room temperature. Protein bands were detected using an ECL Western blot detection kit.

RT- and Real Time-PCR. To determine the levels of gene expression of phosphoenolpyruvate carboxykinase (PEPCK), glucose-6-phosphatase (G6Pase), and peroxisome proliferation-activated receptor γ coactivator-1α (PGC-1α), total RNA was isolated from cultured HepG2 cells and liver tissue using an easy-BLUE total-RNA extraction kit according to the manufacturer's protocol. Five micrograms of extracted RNA was used to synthesize single-strand cDNA with oligo (15) dT primers and reverse transcriptase in a reaction volume of 50 μL. PCR reactions were performed in a total volume of 20 μL comprising 2 μL of cDNA product, 0.2 mM of each dNTP, 20 pmol of each primer, and 0.8 unit of Taq polymerase. PCR was performed at 95 °C for 30 s, followed by an annealing procedure for 30 s, and incubated at 72 °C for 1 min. The final extension was done at 72 °C for 10 min. The RT-PCR products were electrophoresed in 1% agarose gels under 100 V and were stained with 0.5 g/mL ethidium bromide. Levels of the house-keeping genes GAPDH and actin were used to correct for differences in RNA isolation, RNA degradation, and the efficiency of the reverse transcription reaction. To determine gene expression levels of PEPCK and G6Pase in a more accurate way, quantitative PCR was performed using 1 μg of cDNA in a 20 μL reaction volume with the LightCycler real-time PCR System (Roche Applied Science, Indianapolis, IN, USA). A relative gene expression quantification method was used to calculate the fold change of mRNA expression according to the comparative threshold cycle method using house-keeping gene as an endogenous control. The primers and annealing temperatures for both procedures are shown in Table 2.

Statistical Analysis. The results were shown as the mean ± standard error mean (SEM) of triplicate experiments. Comparisons between groups were made using ANOVA, and the significance was determined by Tukey's Test. Differences of $p < 0.05$ were considered to be statistically significant.

dx.doi.org/10.1021/jf4030739 | J. Agric. Food Chem. 2014, 62, 434−442

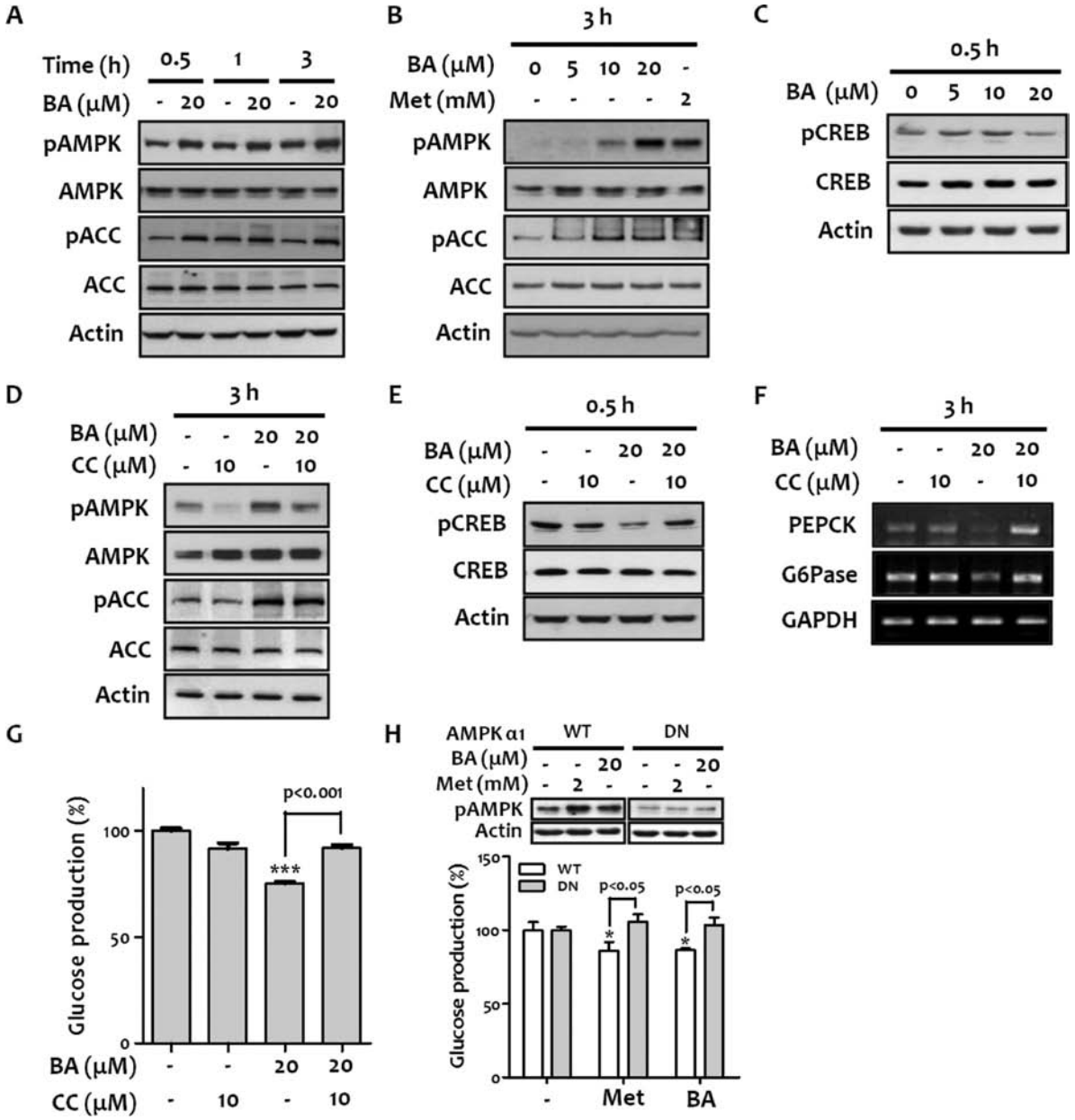

Figure 2. Effects of compound C (a chemical AMPK inhibitor) and AMPKα1-DN on BA-induced suppression of glucose production and the AMPK signaling pathway in Hep2 cells. (A) Cells were treated with 20 μM BA for up to 3 h or (B) cells were treated with 5−20 μM BA for 3 h, and phosphorylated forms of AMPK and ACC were determined by Western blot. (C) Cells were treated with 5−20 μM BA for 30 min, and the phosphorylated form of CREB was determined by Western blot. (D, E) Cells were pretreated with 10 μM compound C for 2 h and incubated with 20 μM BA for 3 h or 30 min, and phosphorylated forms of AMPK, ACC, and CREB were determined by Western blot. (F). Cells were pretreated with 10 μM compound C for 2 h and incubated with 20 μM BA for 3 h, and mRNA expression levels of PEPCK and G6pase were analyzed by RT-PCR. (G) Cells were pretreated with 10 μM compound C and incubated with 20 μM BA for 3 h in serum-free DMEM containing gluconeogenic substrates, and glucose production was determined. (H) HepG2 cells transfected with AMPKα1-WT or -DN were treated with 20 μM BA or 2 mM metformin for 3 h, and the protein expression level of phosphorylated AMPK was analyzed by Western blot. Under the same conditions, glucose production was also determined. Data are represented as the mean ± SE: *p < 0.05, ***p < 0.001 compared to control cells.

RESULTS

BA Inhibits Hepatic Glucose Production via Suppression of mRNA Expression of Gluconeogenic Proteins. First, we investigated the effect of BA on the viability of HepG2 cells using the MTS assay. The growth profile observed over one day of culture in the presence of BA at up to 50 μM was similar to that of the control (Figure 1A), but concentrations of BA greater than 50 μM resulted in cytotoxicity in HepG2 cells. Therefore, less than 50 μM BA was used in the following study. To examine the inhibitory effect of BA on hepatic glucose production, liver cells were treated with the indicated concentrations of BA for 6 h. The glucose contents were decreased in a concentration-dependent manner (Figure 1B). To elucidate the underlying mechanism of BA, the mRNA expression levels of PGC-1α, PEPCK, and G6Pase were examined using RT-PCR (Figure 1C and D). Gene expression levels of these proteins in 20 μM BA-treated cells were comparable to those in 2 mM metformin-treated cells (Figure 1D). Treatment with BA suppressed the gene expression of gluconeogenic proteins in HepG2 cells, and

dx.doi.org/10.1021/jf4030739 | J. Agric. Food Chem. 2014, 62, 434−442

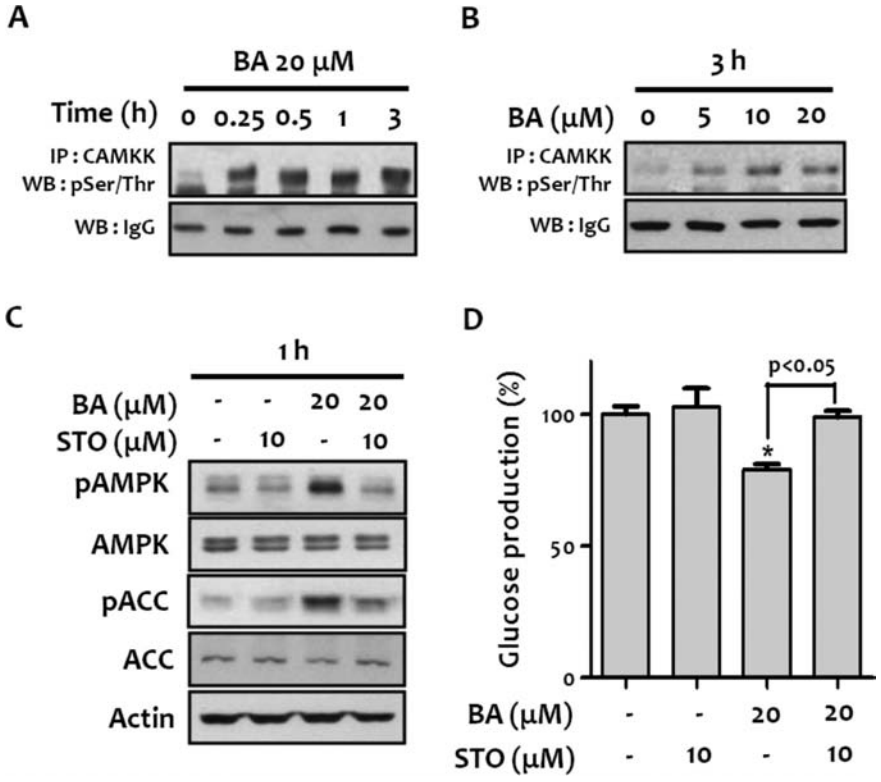

Figure 3. Effect of STO-609, a specific inhibitor of CAMKK, on BA-induced AMPK phosphorylation in HepG2 cells. (A) Cells were treated with 20 μM BA for up to 3 h or (B) cells were treated with BA at indicated concentrations for 3 h, and cell lysates were immunoprecipitated with an antibody against CAMKK, and then phospho-Ser/Thr was analyzed by Western blot. (C) Cells were pretreated with 10 μM STO-609 for 2 h and incubated with 20 μM BA for 3 h, and the protein expression levels of AMPK and ACC were analyzed by Western blot. (D) Cells were pretreated with 10 μM STO-609 for 2 h and incubated with 20 μM BA for 2 h in serum-free DMEM containing gluconeogenic substrates, and glucose production was determined. Data are represented as the mean ± SE: *$p < 0.05$ compared to control cells.

these results were parallel to the reduction of hepatic glucose production, as shown in Figure 1B.

BA Inhibits Hepatic Glucose Production via Activation of the AMPK Signaling Pathway. We examined whether BA stimulates the phosphorylation of AMPK in HepG2 cells because activated AMPK is known to generate ATP by increasing fatty acid oxidation and reducing ATP hydrolysis through decreased lipogenesis and gluconeogenesis.[18] When HepG2 cells were treated with BA, BA markedly phosphorylated AMPK and ACC, an immediate substrate of AMPK, in a concentration-dependent manner (Figure 2B). Next, downstream of the AMPK signaling pathway, including CREB, was examined, because phosphorylated CREB acts as a scaffold for coregulators such as CBP, p300, and CRTC2 that activate gluconeogenesis genes.[19] The expression of the phosphorylated form of CREB was significantly suppressed in 20 μM BA-treated cells (Figure 2C). To confirm whether the glucose-suppressive effect of BA was associated with AMPK, a chemical inhibitor of AMPK (compound C) and the dominant negative (DN) AMPK expression vector were employed. HepG2 cells were pretreated with 10 μM compound C for 2 h and then incubated with 20 μM BA for up to 3 h. The increases in AMPK and ACC phosphorylation, the decrease in the phosphorylation of CREB, the decreases in PEPCK and G6Pase gene expression, and the decrease in hepatic glucose production in 20 μM BA-treated cells were all completely reversed in the presence of compound C (Figure 2D−G). Next, HepG2 cells were transfected with either AMPKα1-WT or -DN and the phosphorylated form of AMPK was determined. As shown in Figure 2H, BA and metformin could not induce phosphorylation of AMPK in AMPKα1-DN transfected cells when compared to those in AMPKα1-WT transfected cells. Moreover, AMPKα1-DN transfected HepG2 cells could not suppress hepatic glucose production (Figure 2G) when these cells were treated with BA or metformin, indicating that the AMPK signaling pathway is positively associated with a suppressive effect of BA on hepatic glucose production.

CAMKK Is an Upstream Kinase that Acts on AMPK. Next, to identify the upstream kinase that acts on AMPK, liver kinase B1 (LKB1) and CAMKK were examined in BA-treated HepG2 cells. As shown in Figure 3A and B, CAMKK was significantly phosphorylated in time- and concentration-dependent manners when the cells were treated with BA, but not LKB1 (data not shown). To confirm whether CAMKK acts as a kinase for AMPK, the protein expression levels of phosphorylated AMPK and ACC were measured in the presence of a specific CAMKK inhibitor (STO-609). BA-induced AMPK and ACC phosphorylation and suppression of hepatic glucose production were markedly reversed when the cells were pretreated with 10 μM STO-609 (Figure 3C and D).

BA Improves Pyruvate Tolerance and Insulin Resistance. Having *in vitro* experimental results, we tested whether BA has a beneficial effect on hyperglycemia through suppression of hepatic glucose production. To directly assess the effect of BA on hepatic glucose production, mice were challenged with the gluconeogenic precursor pyruvate in which 10 mg/kg of BA was orally administered to ICR mice prior to intraperitoneal injection of pyruvate. Single administration of BA improved pyruvate tolerance, as represented by significant reduction in AUC of 27%

dx.doi.org/10.1021/jf4030739 | J. Agric. Food Chem. 2014, 62, 434−442

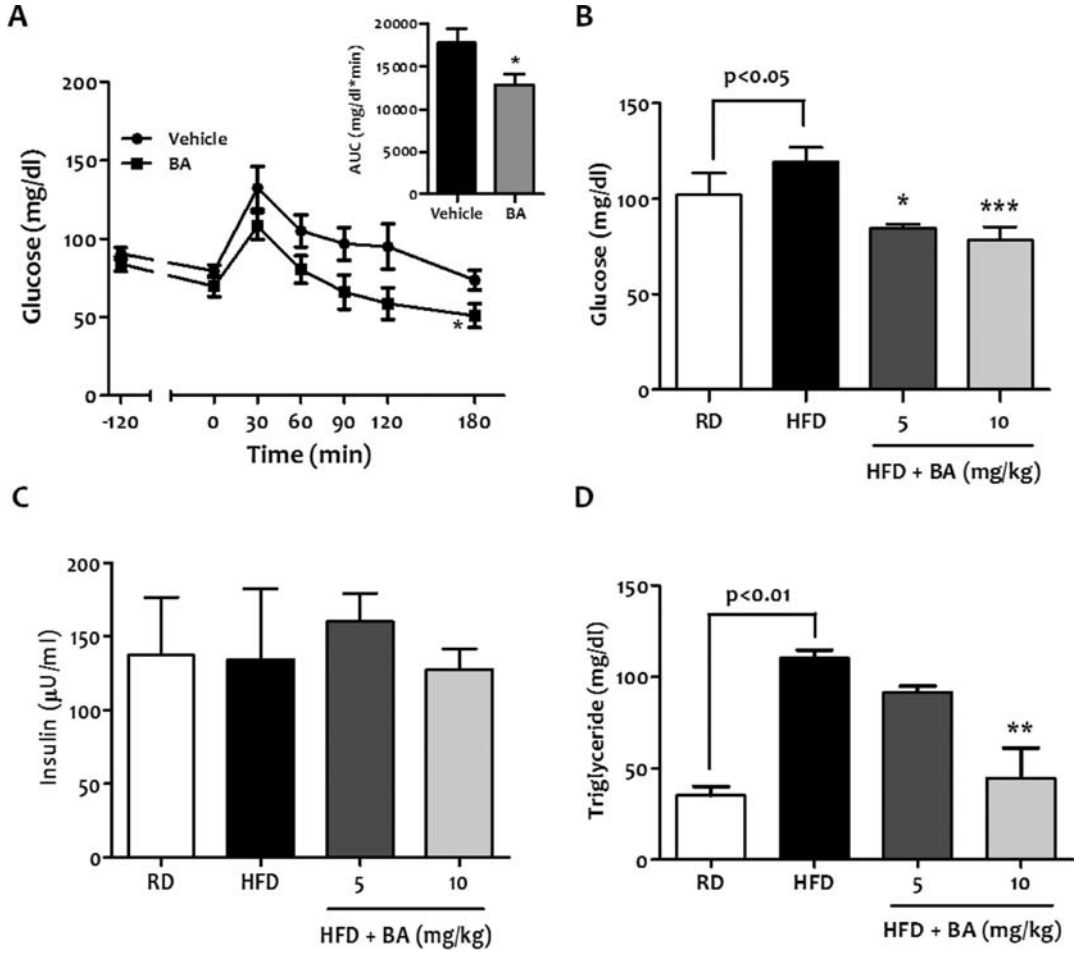

Figure 4. Effects of BA on pyruvate tolerance and the plasma levels of glucose, insulin, and triglyceride in ICR mice. (A) 10 mg/kg of BA was orally administered to the ICR mice, and after 2 h, mice were intraperitoneally injected with 2 g/kg of pyruvate and blood glucose was obtained from the tail vein every 30 min until the 3 h period. (B) Mice were fed either a regular diet (RD) or high fat diet (HFD) for 3 weeks with 5 or 10 mg/kg of BA. At the end of the treatment, plasma levels of fasting glucose (B), insulin (C), and triglyceride (D) were determined as described in the Materials and Methods. Data are represented as the mean ± SE: $*p < 0.05$; $**p < 0.01$; $***p < 0.001$ compared to the HFD group.

compared to that in vehicle-treated mice (Figure 4A). To affirm the results from *in vitro* and pyruvate tolerance test, ICR mice were treated with either 5 or 10 mg/kg of BA for a 3 week period. Plasma glucose, insulin, and triglyceride levels were determined in the blood at the end of the treatment. The results showed that BA5- and BA10-treated groups decreased the plasma glucose level by 29% and 34% (Figure 4B) and decreased plasma triglyceride levels by 17% and 59% (Figure 4D), respectively, when compared to those in the HFD-fed control group. However, no significant changes were observed in plasma insulin level after BA treatment (Figure 4C). In order to evaluate the improving effect of BA on insulin resistance, which was induced by HFD feeding to ICR mice, homeostasis model assessment (HOMA)-insulin resistance (IR) was used to calculate an index of insulin resistance as insulin (μU/mL) × glucose (mM)/22.5.[20] HOMA-IR of the HFD control group was increased to 40 from 35 of the RD control group, and this value was decreased to 34 and 25 in the BA5- and BA10-treated groups, respectively. When 5 and 10 mg/kg of BA were administered to HFD-fed mice for a 3-week period, HOMA-IR values for these groups were decreased by 15% and 38%, respectively, compared to that in the HFD-fed control group.

BA Suppresses Hepatic Glucose Production via Modulation of a CAMKK-AMPK-CREB Signaling Pathway in the HFD-Fed ICR Mice. Six-week-old ICR mice were fed a HFD with BA for 3 weeks, after which they were sacrificed and their liver tissues removed. Liver protein and mRNA were extracted to examine levels of CAMKK, AMPK, CREB, the CRTC2·CREB complex, PGC-1α, PEPCK, and G6Pase. The protein expression levels of activated CAMKK, AMPK, and ACC were increased, but the protein expression levels of pCREB and the CRTC2·CREB complex were decreased in a dose-dependent manner in the liver tissues of BA-treated mice when compared to those in HFD-fed control mice (Figure 5A), mimicking the effects observed *in vitro*. To determine the functional consequences of AMPK activation, the mRNA expression levels of key target proteins were assessed by RT- and real time-PCR (Figure 5B). The mRNA expression levels of gluconeogenic proteins were markedly enhanced in the HFD control group compared to mice fed a RD, whereas BA treatment significantly reduced the mRNA expression of all of these proteins in a dose-dependent manner.

DISCUSSION

Hepatic glucose production (HGP) is a key physiological process that becomes altered in diabetic patients[21] and represents the main target of the antihyperglycemic agents such as metformin.[22] Metformin reduces cellular respiration in hepatocytes by

dx.doi.org/10.1021/jf4030739 | J. Agric. Food Chem. 2014, 62, 434−442

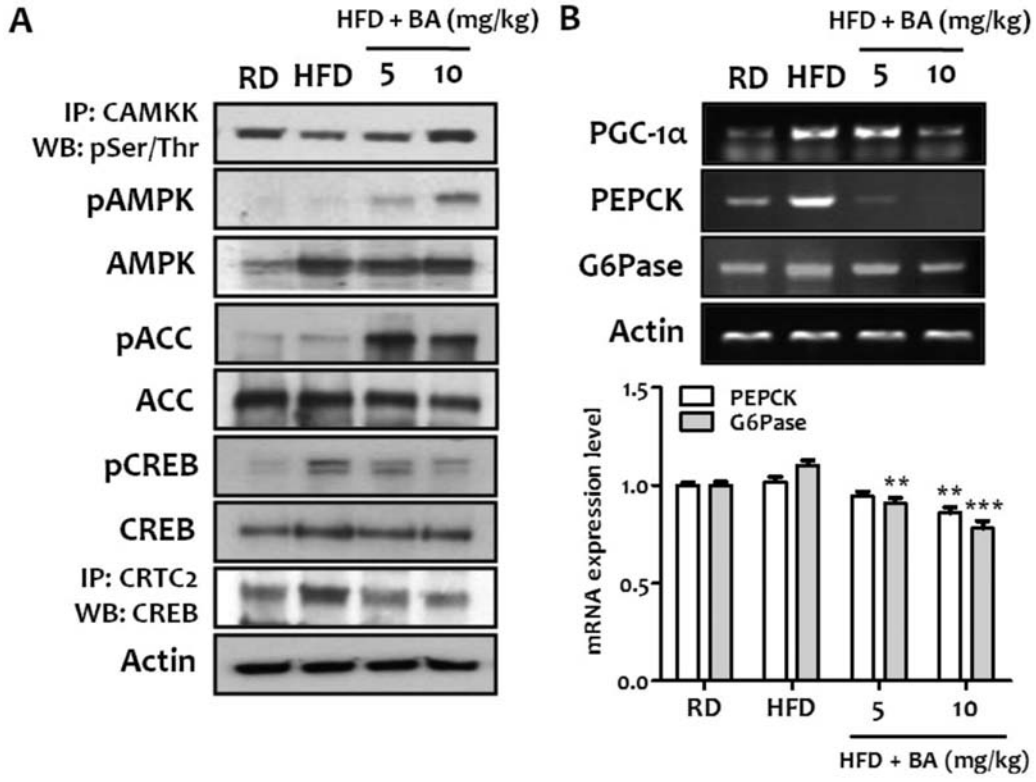

Figure 5. Effects of BA on protein and mRNA expression levels in the liver of HFD-fed ICR mice. (A) Protein expression levels of AMPK, ACC and CREB were analyzed by Western blot. The CAMKK and CRTC2●CREB complex were determined using immunoprecipitation followed by Western blot. (B) Gene expression levels of PGC-1α, PEPCK and G6Pase were estimated by RT-PCR and real time-PCR.

inhibiting the mitochondrial respiratory chain complex[23] and might thus blunt gluconeogenesis by reducing intracellular ATP. Although metformin is likely to be the main therapy due to its efficacy and tolerability, its use in diabetic patients is limited because of side effects such as lactic acidosis. There is a need for safer hypoglycemic agents that act on HGP. Dietary intake from plant food and their ingredients could be a more effective strategy for the management of T2DM because they act on multiple target sites and are relatively low cost. Recently, aloe vera phytosterols and decaffeinated green coffee extract (Svetol) were reported to show antidiabetic activity, primarily due to suppression of HGP.[24,25]

In this study, human hepatoma HepG2 cells and ICR mice fed HFD were used to examine the antihyperglycemic activity of BA and its underlying mechanisms, because the antidiabetic activity of BA has not been thoroughly studied yet. Based upon *in vitro* and pyruvate tolerance tests, we assumed that the antihyperglycemic activity of BA is mainly ascribed to suppression of hepatic glucose production. Therefore, we attempted to elucidate the underlying mechanisms that regulate the production of glucose by the liver, focusing on modulation of the AMPK signaling pathway by BA treatment.

In the cell studies using HepG2, hepatic glucose production and mRNA expression levels of PGC-1α and rate-limiting enzymes for gluconeogenesis (PEPCK and G6Pase) were all suppressed compared to those in vehicle-treated cells when the cells were treated with BA at indicated time and concentrations (Figure 1). Next, we examined whether BA activates the AMPK signaling pathway, because AMPK has been implicated in the control of hepatic glucose and lipid homeostasis by many additional effects, both on genes and on the short-term regulation of specific enzymes.[26] In vitro and in vivo studies showed that BA administration caused enhanced phosphorylation of AMPK and ACC (Figures 2A, 2B, and 5A) but inhibited phosphorylation of CREB, a scaffold for coregulators such as CBP, p300, and CRTC2 (Figures 2C and 5A). However, the protein expression of pAMPK, pACC, and pCREB, the mRNA expression of PEPCK and G6Pase, and HGP were all completely reversed when the cells were exposed to 10 μM compound C (an AMPK inhibitor) before treatment with BA (Figure 2D−G). In addition, HepG2 cells transfected with negative dominant AMPKα1 could not induce phosphorylation of AMPK and suppress glucose production when the cells were treated with BA or metformin compared to those in wild type AMPKα1 (Figure 2H), indicating that AMPK is strongly associated with the suppressive effect of BA on HGP.

Recently, as a molecular mechanism underlying AMPK-mediated PEPCK gene suppression, the phosphorylation of CRTC2, a coactivator of CREB protein, by AMPK was reported.[27] Phosphorylation of CRTC2 at Ser171 by AMPK confers binding of the protein 14-3-3 and sequestration of CRTC2 out of the nucleus, resulting in the inhibition of gluconeogenic gene expression.[28] In response to fasting, CRTC2 controls the gluconeogenic program in the liver via its nuclear translocation and association with the CREB, driving the expression of the PGC1α coactivator. Expression of the coactivator PGC-1α in turn drives the transcription of key gluconeogenic enzymes such as PEPCK and G6Pase. With this notion, HFD-fed mice seem to stimulate HGP through the induction of CREB phosphorylation, CRTC2·CREB interaction, and the expression of gluconeogenic enzymes. When ICR mice were treated with BA for 3 weeks, CREB phosphorylation, the CRTC2·CREB complex, and mRNA expression levels of PGC-1α, PEPCK, and G6Pase were all suppressed in a dose-

dx.doi.org/10.1021/jf4030739 | J. Agric. Food Chem. 2014, 62, 434−442

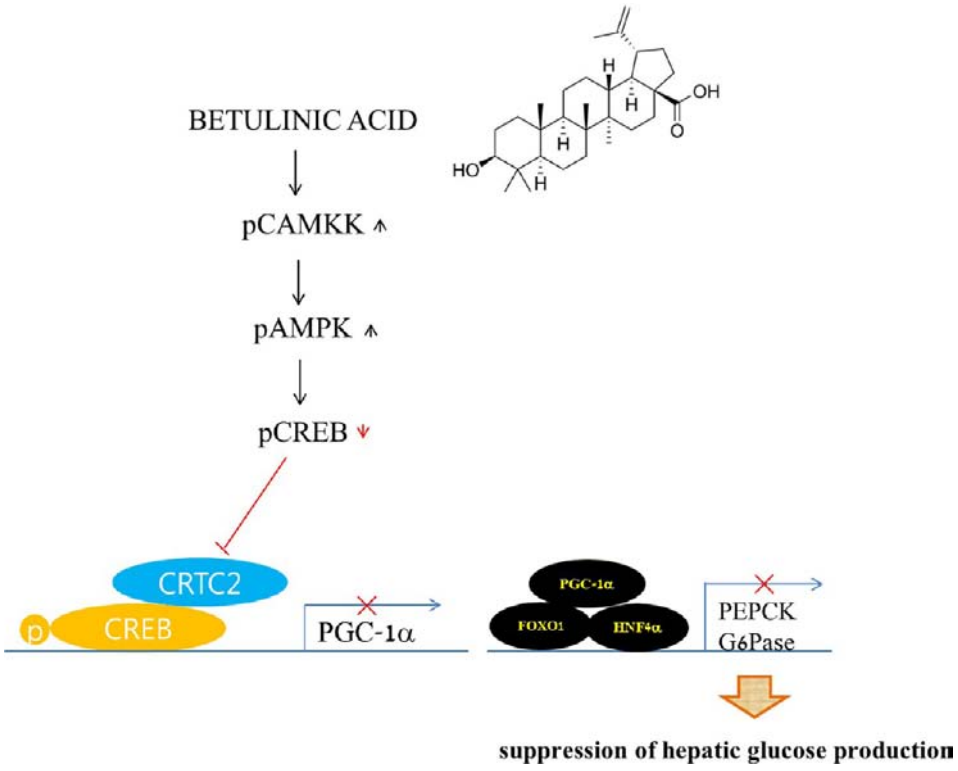

Figure 6. Schematic diagram illustrating the proposed mechanism by which betulinic acid inhibits hepatic gluconeogenesis. Inhibition of hepatic gluconeogenesis by betulinic acid may result from the activation of the CAMKK-AMPK-CREB signaling pathway.

dependent manner (Figure 5A and B), indicating that the inhibitory effect of BA on HGP is mediated through the AMPK-CREB-PGC-1α signaling pathway. Finally, to identify the upstream kinase that acts on AMPK, LKB1 and CAMKK were examined in BA-treated HepG2 cells, and BA activates AMPK by increasing its phosphorylation by CAMKK in HepG2 cells (Figure 3A and B) and liver tissues of ICR mice fed a HFD (Figure 5A). The fact that CAMKK acts as an upstream kinase for AMPK was verified by pretreatment with the STO-609, a specific inhibitor of CAMKK (Figure 3C and D). At this time, we do not know exactly how BA activates AMPK in HepG2 cells and liver tissue of HFD-fed ICR mice, although a calcium-dependent pathway involving phosphorylation of AMPK by CAMKK is evidently provided in this study. As alternative or additional explanations, mechanisms involving either inhibition of mitochondrial ATP synthesis or an SIRT1-dependent pathway via increase in NAD^+ levels should be tested to elucidate further how BA activates AMPK in hepatocytes.

ACC is an important rate-controlling enzyme for the synthesis of malonyl-CoA, which is a critical precursor for biosynthesis of fatty acids and a potent inhibitor of mitochondrial fatty acid oxidation. Phosphorylation of ACC by AMPK lead to a fall in malonyl-CoA content and a subsequent decrease in triglyceride synthesis concomitant with an increase in β-oxidation.[29] This was evidenced by the decrease in plasma triglyceride levels after BA treatment in HFD-fed ICR mice (Figure 4D). In addition, insulin resistance was also significantly reduced in BA-treated mice compared to that in HFD control mice even though there are no significant differences in plasma insulin levels among groups (HOMA-IR was decreased by 15% and 38% in BA5 and BA10 groups, respectively). Significant reduction of triglyceride levels in the plasma and the liver tissue may partly contribute to improvement of insulin resistance. Based upon *in vitro* and *in vivo* studies, an action mechanism of antihyperglycemic activity of BA might be due to the suppression of HGP, and this plausible mechanism was verified by a pyruvate tolerance test in which BA administration significantly reduced the AUC by 27% compared to that in vehicle-treated mice (Figure 4A).

In conclusion, BA has beneficial effects on hyperglycemia and insulin resistance by modulating the CAMKK-AMPK-CREB signaling pathway (Figure 6), and BA itself or BA-containing medicinal plants could represent a promising therapeutic agent to prevent type 2 diabetes.

■ ASSOCIATED CONTENT

Supporting Information

Tables of compositions of the experimental diets and RT-PCR and real time-PCR primer sequences and annealing temperatures. This material is available free of charge via the Internet at http://pubs.acs.org.

■ AUTHOR INFORMATION

Corresponding Author

*Phone: +82 2 961 0373. Fax: +82 2 957 0384. E-mail: suchung@khu.ac.kr.

Funding

This work was supported by a grant from the Kyung Hee University in 2011 (KHU-20111709).

Notes

The authors declare no competing financial interest.

■ ACKNOWLEDGMENTS

The authors thank Prof. Ha for providing expression vectors for AMPKα1-WT and -DN.

ABBREVIATIONS USED

ACC, acetyl CoA carboxylase; AMPK, AMP-activated protein kinase; CAMKK, Ca+2-calmodulin dependent protein kinase kinase; CBP, CREB-binding protein; CMC, carboxymethyl cellulose; CREB, cAMP-response element-binding protein; CRTC2, CREB-regulated transcription coactivator 2; FBS, fetal bovine serum; G6Pase, glucose-6-phosphatase; HFD, high fat diet; HGP, hepatic glucose production; LKB1, liver kinase B1; MTS, 3-(4,5-dimethylthiazol-2-yl)-5-(3-carboxymethoxyphenyl)-2-(4-sulfophenyl)-2H-tetrazolium; PEPCK, phosphoenolpyruvate carboxykinase; PGC-1α, peroxisome proliferation-activated receptor γ coactivator-1α; T2DM, type 2 diabetes mellitus

REFERENCES

(1) Stumvoll, M.; Goldstein, B. J.; van Haeften, T. W. Type 2 diabetes: principles of pathogenesis and therapy. *Lancet* **2005**, *365*, 1333−1346.

(2) Diabetes Prevention Program Research Group. Reduction in the incidence of type 2 diabetes with lifestyle intervention or metformin. *N. Engl. J. Med.* **2002**, *346*, 393-403.

(3) Kahn, S. E.; Haffner, S. M.; Heise, M. A.; Herman, W. H.; Holman, R. R.; Jones, N. P.; Kravitz, B. G.; Lachin, J. M.; O'Neill, M. C.; Zinman, B.; Viberti, G. Glycemic durability of rosiglitazone, metformin, or glyburide monotherapy. *N. Engl. J. Med.* **2006**, *355*, 2427−2443.

(4) Black, C.; Donnelly, P.; McIntyre, L.; Royle, P. L.; Shepherd, J. P.; Thomas, S. Meglitinide analogues for type 2 diabetes mellitus. *Cochrane Database Syst. Rev.* **2007**, *2*, CD004654.

(5) Nader, M. A.; Baraka, H. N. Effect of betulinic acid on neutrophil recruitment and inflammatory mediator expression in lipopolysaccharide-induced lung inflammation in rats. *Eur. J. Pharm. Sci.* **2012**, *46*, 106−113.

(6) Viji, V.; Helen, A.; Luxmi, V. R. Betulinic acid inhibits endotoxin-stimulated phosphorylation cascade and pro-inflammatory prostaglandin E(2) production in human peripheral blood mononuclear cells. *Br. J. Pharmacol.* **2011**, *162*, 1291−1303.

(7) Majeed, R.; Sangwan, P. L.; Chinthakindi, P. K.; Khan, I.; Dangroo, N. A.; Thota, N.; Hamid, A.; Sharma, P. R.; Saxena, A. K.; Koul, S. Synthesis of 3-O-propargylated betulinic acid and its 1,2,3-triazoles as potential apoptotic agents. *Eur. J. Med. Chem.* **2013**, *63*, 782−792.

(8) Reiner, T.; Parrondo, R.; de Las Pozas, A.; Palenzuela, D.; Perez-Stable, C. Betulinic acid selectively increases protein degradation and enhances prostate cancer-specific apoptosis: possible role for inhibition of deubiquitinase activity. *PLoS One* **2013**, *8*, e56234.

(9) Sun, Y. F.; Song, C. K.; Viernstein, H.; Unger, F.; Liang, Z. S. Apoptosis of human breast cancer cells induced by microencapsulated betulinic acid from sour jujube fruits through the mitochondria transduction pathway. *Food Chem.* **2013**, *138*, 1998−2007.

(10) Innocente, A. M.; Silva, G. N.; Cruz, L. N.; Moraes, M. S.; Nakabashi, M.; Sonnet, P.; Gosmann, G.; Garcia, C. R.; Gnoatto, S. C. Synthesis and antiplasmodial activity of betulinic acid and ursolic acid analogues. *Molecules* **2012**, *17*, 12003−12014.

(11) Theo, A.; Masebe, T.; Suzuki, Y.; Kikuchi, H.; Wada, S.; Obi, C. L.; Bessong, P. O.; Usuzawa, M.; Oshima, Y.; Hattori, T. Peltophorum africanum, a traditional South African medicinal plant, contains an anti HIV-1 constituent, betulinic acid. *Tohoku J. Exp. Med.* **2009**, *217*, 93−99.

(12) Quan, H. Y.; Kim, D. Y.; Kim, S. J.; Jo, H. K.; Kim, G. W.; Chung, S. H. Betulinic acid alleviates non-alcoholic fatty liver by inhibiting SREBP1 activity via the AMPK-mTOR-SREBP signaling pathway. *Biochem. Pharmacol.* **2013**, *85*, 1330−1340.

(13) Genet, C.; Strehle, A.; Schmidt, C.; Boudjelal, G.; Lobstein, A.; Schoonjans, K.; Souchet, M.; Auwerx, J.; Saladin, R.; Wagner, A. Structure-activity relationship study of betulinic acid, a novel and selective TGR5 agonist, and its synthetic derivatives: potential impact in diabetes. *J. Med. Chem.* **2010**, *53*, 178−190.

(14) Alqahtani, A.; Hamid, K.; Kam, A.; Wong, K. H.; Abdelhak, Z.; Razmovski-Naumovski, V.; Chan, K.; Li, K. M.; Groundwater, P. W.; Li, G. Q. The pentacyclic triterpenoids in herbal medicines and their pharmacological activities in diabetes and diabetic complications. *Curr. Med. Chem.* **2013**, *20*, 908−931.

(15) Machado, D. G.; Cunha, M. P.; Neis, V. B.; Balen, G. O.; Colla, A.; Bettio, L. E.; Oliveira, A.; Pazini, F. L.; Dalmarco, J. B.; Simionatto, E. L.; Pizzolatti, M. G.; Rodrigues, A. L. Antidepressant-like effects of fractions, essential oil, carnosol and betulinic acid isolated from Rosmarinus officinalis L. *Food Chem.* **2013**, *136*, 999−1005.

(16) Zhou, G.; Myers, R.; Li, Y.; Chen, Y.; Shen, X.; Fenyk-Melody, J.; Wu, M.; Ventre, J.; Doebber, T.; Fujii, N.; Musi, N.; Hirshman, M. F.; Goodyear, L. J.; Moller, D. E. Role of AMP-activated protein kinase in mechanism of metformin action. *J. Clin. Invest.* **2001**, *108*, 1167−1174.

(17) Tokumitsu, H.; Inuzuka, H.; Ishikawa, Y.; Ikeda, M.; Saji, I.; Kobayashi, R. STO-609, a specific inhibitor of the Ca(2+)/calmodulin-dependent protein kinase kinase. *J. Biol. Chem.* **2002**, *277*, 15813−15818.

(18) Zhang, B. B.; Zhou, G.; Li, C. AMPK: an emerging drug target for diabetes and the metabolic syndrome. *Cell Metab.* **2009**, *9*, 407−416.

(19) Koo, S. H.; Flechner, L.; Qi, L.; Zhang, X.; Screaton, R. A.; Jeffries, S.; Hedrick, S.; Xu, W.; Boussouar, F.; Brindle, P.; Takemori, H.; Montminy, M. The CREB coactivator TORC2 is a key regulator of fasting glucose metabolism. *Nature* **2005**, *437*, 1109−1111.

(20) Matthews, D. R.; Hosker, J. P.; Rudenski, A. S.; Naylor, B. A.; Treacher, D. F.; Turner, R. C. Homeostasis model assessment: insulin resistance and beta-cell function from fasting plasma glucose and insulin concentrations in man. *Diabetologia* **1985**, *28*, 412−419.

(21) Bogardus, C.; Lillioja, S.; Howard, B. V.; Reaven, G.; Mott, D. Relationships between insulin secretion, insulin action, and fasting plasma glucose concentration in nondiabetic and noninsulin-dependent diabetic subjects. *J. Clin. Invest.* **1984**, *74*, 1238−1246.

(22) Stumvoll, M.; Nurjhan, N.; Perriello, G.; Dailey, G.; Gerich, J. E. Metabolic effects of metformin in non-insulin-dependent diabetes mellitus. *N. Engl. J. Med.* **1995**, *333*, 550−554.

(23) El-Mir, M. Y.; Nogueira, V.; Fontaine, E.; Avéret, N.; Rigoulet, M.; Leverve, X. Dimethylbiguanide inhibits cell respiration via an indirect effect targeted on the respiratory chain complex I. *J. Biol. Chem.* **2000**, *175*, 223−228.

(24) Misawa, E.; Tanaka, M.; Nomaguchi, K.; Nabeshima, K.; Yamada, M.; Toida, T.; Iwatsuki, K. Oral ingestion of Aloe vera phytosterols alters hepatic gene expression profiles and ameliorates obesity-associated metabolic disorders in Zucker diabetic fatty rats. *J. Agric. Food Chem.* **2012**, *60*, 2799−2806.

(25) Henry-Vitrac, C.; Ibarra, A.; Roller, M.; Mérillon, J. M.; Vitrac, X. Contribution of chlorogenic acids to the inhibition of human hepatic glucose-6-phosphatase activity in vitro by svetol, a standardized decaffeinated green coffee extract. *J. Agric. Food Chem.* **2010**, *58*, 4141−4144.

(26) Viollet, B.; Foretz, M.; Guigas, B.; Horman, S.; Dentin, R.; Bertrand, L.; Hue, L.; Andreelli, F. Activation of AMP-activated protein kinase in the liver: a new strategy for the management of metabolic hepatic disorders. *J. Physiol.* **2006**, *574*, 41−53.

(27) Lin, H. V.; Accili, D. Hormonal regulation of hepatic glucose production in health and disease. *Cell Metab.* **2011**, *14*, 9−19.

(28) Yuan, H. D.; Kim, D. Y.; Quan, H. Y.; Kim, S. J.; Jung, M. S.; Chung, S. H. Ginsenoside Rg2 induces orphan nuclear receptor SHP gene expression and inactivates GSK3β via AMP-activated protein kinase to inhibit hepatic glucose production in HepG2 cells. *Chem. Biol. Interact.* **2012**, *195*, 35−42.

(29) Velasco, G.; Geelen, M. J.; Guzmán, M. Control of hepatic fatty acid oxidation by 5′-AMP-activated protein kinase involves a malonyl-CoA-dependent and a malonyl-CoA-independent mechanism. *Arch. Biochem. Biophys.* **1997**, *337*, 169−175.

JOURNAL OF AGRICULTURAL AND FOOD CHEMISTRY

Article

pubs.acs.org/JAFC

Absorption, Metabolism, and Effects at Transcriptome Level of a Standardized French Oak Wood Extract, Robuvit, in Healthy Volunteers: Pilot Study

Fausta Natella,[†,§] Guido Leoni,[†,§] Mariateresa Maldini,[†] Lucia Natarelli,[†] Raffaella Comitato,[†] Frank Schonlau,[‡] Fabio Virgili,[†] and Raffaella Canali*[,†]

[†]Consiglio per la Ricerca e Sperimentazione in Agricoltura, Food and Nutrition Research Centre, via Ardeatina 546, 00178 Roma, Italy

[‡]Horphag Research (U.K.) Ltd. 28 Old Brompton Road, Suite 393, South Kensington, London SW7 3SS, United Kingdom

ABSTRACT: The consumption of wine and spirits, traditionally aged in oak barrels, exposes humans to roburin ingestion. These molecules belong to a class of ellagitannins (ETs), and their only known source is oak wood. Very little is currently known about roburin bioavailability and biological activity. We reported for the first time human absorption of roburins from a French oak wood (*Quercus robur*) water extract (Robuvit) by measuring the increase of total phenols (from 0.63 ± 0.06 to 1.26 ± 0.18 μg GAE equiv/mL plasma) and the appearance of roburin metabolites (three different glucoronidate urolithins and ellagic acid), in plasma, after 5 days of supplementation. Robuvit supplementation induced also the increase of plasma antioxidant capacity from 1.8 ± 0.05 to 1.9 ± 0.01 nmol Trolox equiv/mL plasma. Moreover, utilizing a combined ex vivo cell culture approach, we assessed the effect of *Q. robur* metabolites (present in human serum after supplementation) on gene expression modulation, utilizing an Affymetrix array matrix, in endothelial, neuronal, and keratinocyte cell lines. The functional analysis reveals that Robuvit metabolites affect ribosome, cell cycle, and spliceosome pathways

KEYWORDS: *ellagitannins, roburins, Quercus robur, human study, gene array*

INTRODUCTION

In the past decades, epidemiological surveys pointed out the association between a significantly lower risk for cardiovascular, metabolic, and cancer diseases, cognitive decline, and neurodegeneration and the consumption of diets rich in plant polyphenols.[1,2] The beneficial role of polyphenols was initially attributed to a "nonspecific" antioxidant capacity. After a first enthusiasm, it became apparent that health contributions of polyphenols were not (only) associated with cellular protection from oxidation but are due to a more complex mechanism involving the induction of cellular response to potentially harmful stimuli finally resulting in a number of specific adaptive and defensive responses. Despite a consensus about this "hormetic" (*para*-hormetic) activity,[3] comprehensive knowledge about the absorption, metabolism, and specific biological activities of the different classes of polyphenols is still scarce.

Tannins are a specific family of polyphenols having a relatively large molecular structure. Tannins are considered to be "secondary" compounds of plant physiology, not functioning in "primary" metabolism such as biosynthesis or energy conversions, although they serve biological purposes such as protecting plants from herbivores and microbial infections. Tannins are divided into two groups on the basis of their structural characteristics: hydrolyzable and condensed tannins. In the hydrolyzable tannins, a carbohydrate is partially or totally esterified with phenolic groups such as gallic acid (gallotannins, GTs) or ellagic acid (ellagitannins, ETs). These compounds are present in significant amounts in many berries, nuts, pomegranates, muscadine grapes, and edible dark-colored fruits.[4,5]

The French oak water extract Robuvit is a registered proprietary water extract obtained from fresh *Quercus robur* wood, standardized to provide a specific profile of tannins and in particular a mixture of ≥20% roburins (A−E) including grandinin. The main ETs in *Q. robur* are two diastereoisomers, vescalagin and castalagin, which were originally isolated and described by Mayer et al.[6] Sugar derivatives of vescalagin with aldopentoses xylose and lyxose are defined as roburin E and grandinin, respectively (Figure 1).[7] Roburins A−D are dimers, with roburin D consisting of vescalagin and castalagin and roburin A of two vescalagin subunits. Roburins B and C resemble the structure of roburin A with additional xylose (roburin C) or lyxose (roburin B) bound to one vescalagin unit (Figure 2). Further to the roburins, Robuvit contains monomeric vescalagin and castalagin, as well as ellagic acid (EA) and gallic acid (GA). Oak wood is currently the only known source of roburins, and according to this specificity, the major source of roburins in human diets results from the consumption of wine and spirits (cognac and whiskey) traditionally matured, aged, and stored in oak barrels. In fact, oak wood constituents contribute to the improvement of the aroma, taste, and color and to the building up of the sensation of "mouth-fullness". As a result of this technological practice, humans have been exposed to roburins for centuries. In wines and spirits, roburins (including grandinin and the monomers

Received: August 7, 2013
Revised: December 16, 2013
Accepted: December 19, 2013
Published: December 19, 2013

ACS Publications © 2013 American Chemical Society

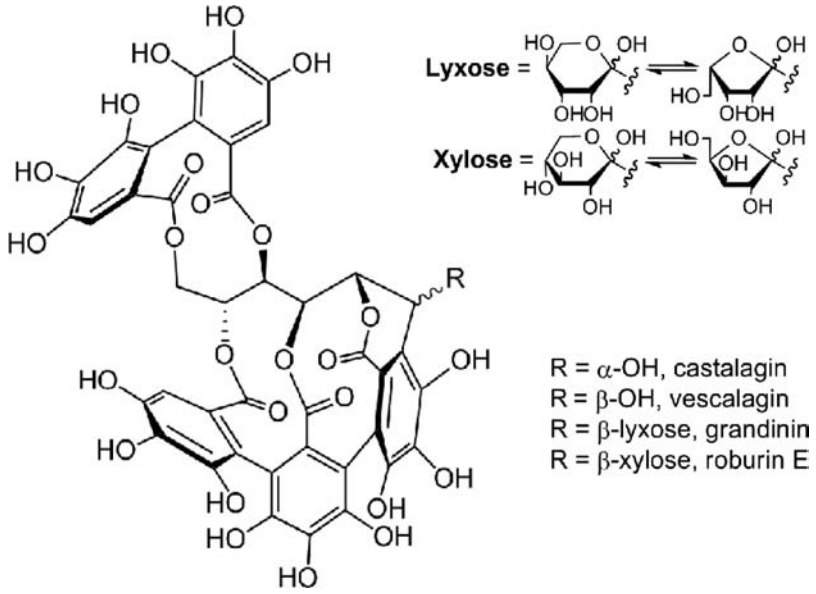

Figure 1. Chemical structures of the monomers, castalgin, vescalgin, and their sugar derivatives roburin E and grandinin.

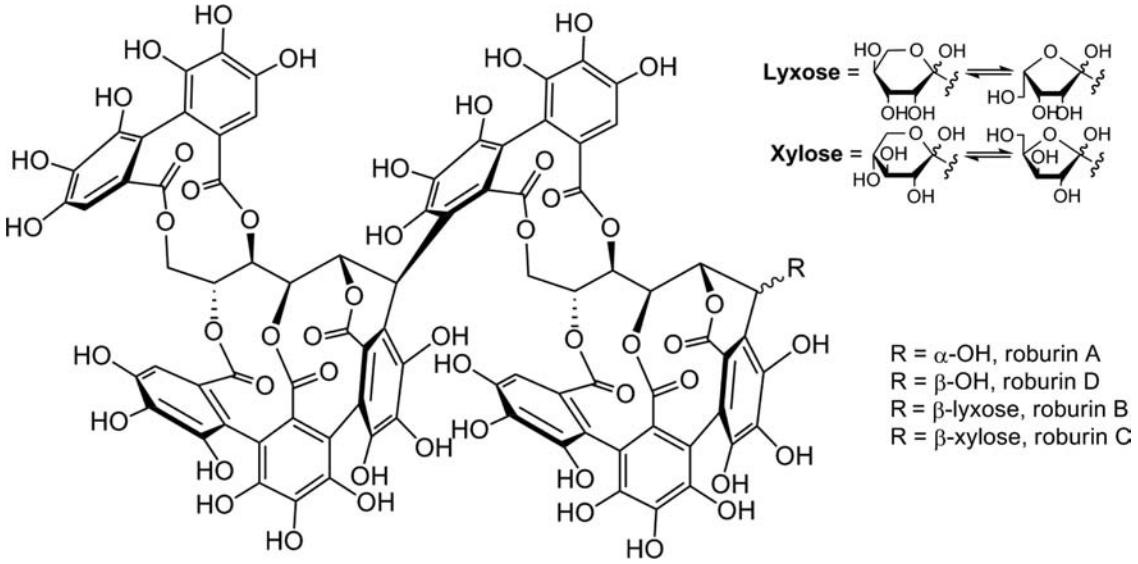

Figure 2. Chemical structure of roburins A–D.

castalagin and vescalagin) have been found to range between 1.2 mg/L (bourbon whiskey) and 9.4 mg/L (red wines).[8] A number of indications suggest that, similarly to other polyphenols, ETs and their metabolites may exert beneficial effects on human health.[9] Despite the traditional consumption of roburins with wine and spirits, very little is currently known about their bioavailability in humans. In general, ET from berries, pomegranate, walnuts, pecans, and pistachios are known to require the involvement of the colonic microflora to be metabolized into dibenzopyranone species (urolithins).[10] The consumption of oak-aged red wine was found to result in only trace amounts of urolithin-B aglycone and glucuronide in urine.[11] Furthermore, several kinds of grapes have been found to contain EA, and therefore excreted urolithins may not necessarily be attributed to oak constituents extracted following wine aging in barrels. The aim of our study is to investigate the absorption and metabolism of Robuvit extract in healthy volunteers and to evaluate the effect of Robuvit consumption on gene expression in cultured endothelial, neuronal, and keratinocyte cells to obtain a solid background for further studies addressing the understanding of possible beneficial effects of this family of molecules on human health.

MATERIALS AND METHODS

Chemicals. MeOH, HOCOOH, gallic acid, ellagic acid, Trolox, fluorescein, perchloric acid, and 2,2-azobis(2-amidinopropane) dihydrochloride (AAPH) were purchased from Sigma-Aldrich (Milano, Italy); randomly methylated *β*-cyclodextrin (RMCD) was purchased from Cyclolab (Budapest, Hungary).

In Vivo Study. *Experimental Design.* Three healthy, nonsmoker, volunteers participated in this study, which was approved by the CRA-NUT ethical committee. The investigation conforms to the principles outlined in the Declaration of Helsinki and its amendments. None of subjects was taking any medication or vitamin supplementation for the 2 weeks before the beginning of the experiment. The day before the experiment subjects abstained from drinking coffee, tea, wine, and beer, and they ate no chocolate, fruits, and vegetables. The first day of the in vivo experimental protocol, blood was withdrawn in fasting

dx.doi.org/10.1021/jf403493a | J. Agric. Food Chem. 2014, 62, 443–453

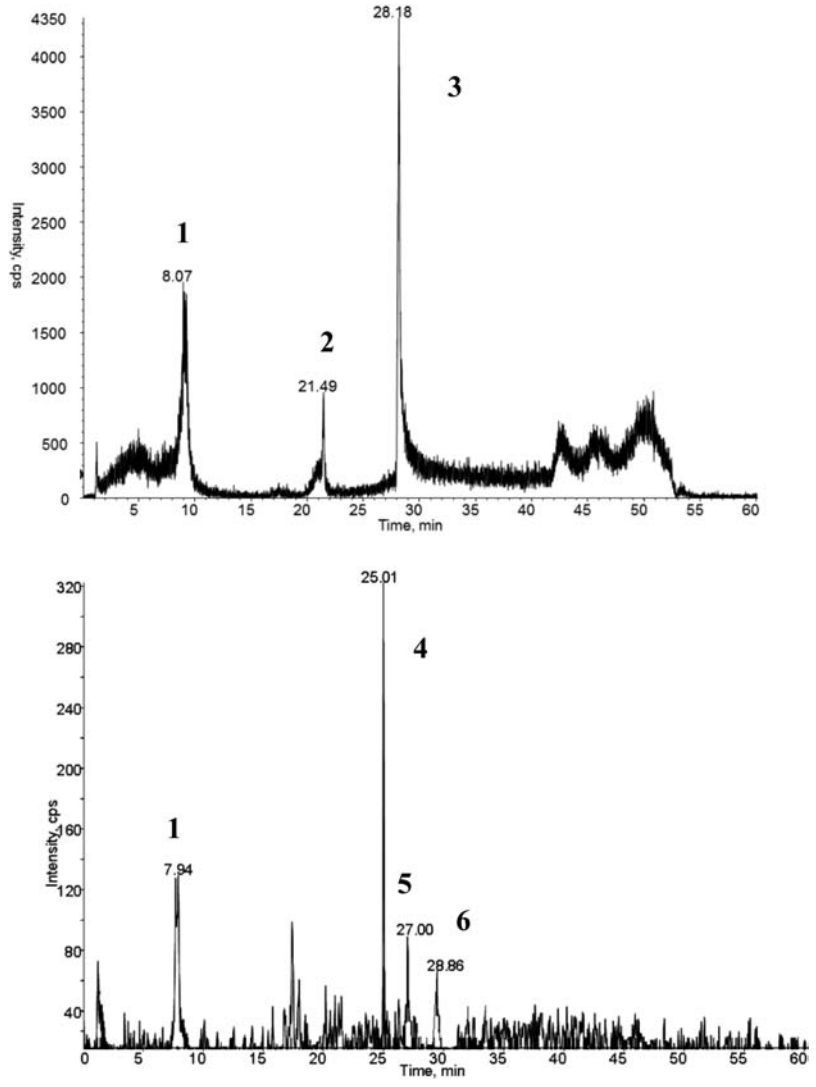

Figure 3. LC-MS total ion current (TIC) chromatograms of standards (top) and a representative plasma sample (bottom). Peaks: 1, gallic acid; 2, methyl gallate; 3, ellagic acid; 4, urolithin C diglucuronide; 5, urolithin A glucuronide; 6, urolithin B glucuronide.

condition and serum isolated and stored at −80 °C until its utilization. Volunteers were then supplemented with one capsule of Robuvit (containing 100 mg of *Q. robur* extract) three times a day for 5 days. During the 5 days of the supplementation, the subjects were encouraged to reduce as much as possible the consumption of polyphenol-rich foods. The last day of the supplementation, subjects were administered 300 mg of Robuvit in fasting condition, about 1 h before blood withdrawal, and serum was collected and isolated again as described above.

Q. robur Capsule Analyses. Robuvit capsule was extracted with 50 mL of MeOH/H_2O 80:20 (v/v) in a shaking bath overnight in reduced light and temperature conditions. Subsequently, the extract was centrifuged for 10 min at 2000*g* and 4 °C. The supernatant was filtered through a 0.20 mm PVDF filter (Whatman, USA) and diluted 1:1 with methanol before the analyses.

Plasma Sample Preparation. Plasma samples were acidified immediately to pH 3 with 1 N HCl immediately after blood withdrawal and stored at −80 °C. Once thawed, samples were mixed with acetonitrile 1:4 (v/v) to precipitate plasma proteins and then centrifuged for 10 min at 25000 rpm and 4 °C. The supernatant was recovered, dried under nitrogen (N_2), and reconstituted with 0.5 mL of H_2O acidified with 0.1% HCOOH. Extraction of metabolites was performed using solid-phase extraction (SPE) OASIS HLB 1 cm^3 (30 mg) extraction cartridges (Waters, Milford, MA, USA). The SPE procedure consisted of the following steps: activation of SPE cartridges with 1 mL of MeOH acidified with 0.1% HCOOH, conditioning with 1 mL of H_2O acidified with 0.1% HCOOH, loading of the sample, washing with H_2O acidified with 0.1% HCOOH (2 mL) and with water/methanol (95:5) (2 mL), and finally elution of metabolites with MeOH acidified with 0.1% HCOOH (2 mL). The eluted fraction was evaporated under nitrogen, and the residue was reconstituted with mobile phase to 0.3 mL and filtered through a 0.2 mm PVDF filter (Whatman) into a vial insert for LC-MS/MS analyses. We determined only the principal compounds that were extracted in MeOH/H_2O. However, several ETs are insoluble and should be measured after hydrolysis (by detection of the produced EA). Moreover, our MS has a maximum limit of m/z 1500; therefore, ETs that have higher molecular weights (such as roburin dimers) cannot be measured.

ESI-MS, ESI-MS/MS, LC-ESI-MS, and LC-ESI- MS/MS Analyses. Quantitative online HPLC-ESI-MS/MS analysis of the capsule extract and plasma sample were performed using a Perkin-Elmer series 200 HPLC system interfaced to an Applied Biosystems (Foster City, CA, USA) API 3200 instrument equipped with a Turbo ionspray source. A gradient elution was performed by using a mobile phase A represented by water acidified with formic acid (0.1%) and a mobile phase B represented by acetonitrile acidified with formic acid (0.1%). The gradient started from 0% of eluent B, remained at 0% of B for 10 min, then rose from 0 to 60% B in 40 min and subsequently to 100% B in 25 min. The flow (0.300 mL min^{-1}) generated by chromatographic separation was directly injected into the electrospray ion source. The

dx.doi.org/10.1021/jf403493a | *J. Agric. Food Chem.* 2014, 62, 443−453

chromatographic separation was carried out using a Restek Ultra C18 column (100 × 2.1 mm, 3 μm).

The API 3200 ES source was tuned by infusing standard solutions of EA, GA, and methylgallate (1 mg/mL in methanol) into the source at a flow rate of 0.01 mL/min. The mass spectrometer was operated in the negative ion mode under the following conditions: declustering potential, −75 eV; entrance potential, −6.2 eV; collision energy, −45 eV; and collision cell exit potential, −23.3 eV for EA; declustering potential, −40 eV; entrance potential, −4.2 eV; collision energy, −20 eV; and collision cell exit potential, −18.4 eV for GA; declustering potential, −40 eV; entrance potential, −4.2 eV; collision energy, −35 eV; and collision cell exit potential, −19 eV for methyl gallate. MS and MS-MS daughter spectra were measured from m/z 150 to 500 for plasma sample and from m/z 150 to 1500 for *Q. robur* capsule. The spectrometer was used in the MS/MS mode with multiple reaction monitoring (MRM) of fragmentation reactions selected for each compound. Volume injection for capsule extract was 0.01 mL and that for plasma samples, 0.03 mL. Because of the absence of commercially available standards for metabolites, the same MS/MS conditions of EA were used for other compounds. For calibration curves, stock solutions of EA (1 mg 5 mL^{-1}) and GA standards were prepared by dissolving each compound in MeOH. Eight different solutions, containing, respectively, 0.1, 0.5, 1, 5, 10, 25, 50, and 100 mg mL^{-1} of each compound (external standards), were prepared in MeOH and used for method development. A volume of 0.01 mL was injected in the chromatographic system. The calibration curves for each standard were made by linear regression by a graph reporting the area ratio of external standard against the known concentration of external standard. The result represents the average of curves performed by three injection of each concentration. All quantitative data were elaborated with the aid of Analyst software (Applied Biosystems). ETs and ET metabolites were identified according to their ion mass spectra, retention times, and MS-MS fragments.[12] For quantification purposes data were collected in MRM tracking the transition of parent and product ions specific for each compound. Because of the absence of commercially available standards for metabolites, quantification was calculated on the basis of EA calibration curve. In Figure 3 the HPLC-TIC-MS chromatograms of standards and a representative post-supplementation plasma sample are shown.

Plasmatic Total Phenols. Folin−Ciocalteu colorimetry was used to measure the total phenolic amount in plasma isolated from the three subjects before and after *Q. robur* supplementation. To remove plasmatic protein interference, 0.5 M perchloric acid (1:1) was used, whereas the hydrolysis of the conjugated forms of polyphenols was performed according to Serafini.[13] Results are expressed as micrograms of GA equivalent (GAE) per milliliter of plasma. This assay was also carried out on *Q. robur* capsule after extraction with 80% MeOH.

Antioxidant Capacity Analysis. The total antioxidant capacity has been evaluated using the oxygen radical absorbance capacity (ORAC) assay. Plasma was treated according to the method of Prior[14] to obtain the hydrophilic and lipophilic components of the plasma and to remove the interference of protein fraction. Briefly, 100 μL of plasma was mixed with 200 μL of ethanol and 100 μL of water. Then 400 μL of hexane was added twice. The hexane layers were removed, combined, and dried under nitrogen. For the lipophilic antioxidant assay, the dried hexane extract was dissolved in 250 μL of acetone and then diluted with a 7% randomly methylated β-cyclodextrin (RMCD) solution as a solubility enhancer. For the hydrophilic antioxidant assay, the residual aqueous plasma sample was treated with 400 μL of 0.5 M perchloric acid to precipitate proteins and then dissolved in phosphate buffer. ORAC assay was performed in a microplate fluorescence reader (TECAN) according to the method of Huang et al.[15] Briefly, ORAC is a method that utilizes the peroxyl radical generator 2,2-azobis(2-amidinopropane) dihydrochloride (AAPH) and fluorescein as an oxidizable substrate. AAPH induces oxidative damage to the substrate, which is inhibited by the presence of reductants. The inhibition measured is related to the antioxidant capacity of the reductants under analysis. Results are expressed as nanomoles of Trolox equivalent per milliliter of plasma.

Ex Vivo Study. Serum isolated before and after the supplementation of Robuvit from the three healthy subjects was used to enrich the medium of different cell cultures, that is, a permanent human endothelial cell, obtained by cell fusion of HUVEC, primary human endothelial cells, and immortalized human alveolar epithelial cells (EA.hy 926), human keratinocytes (HaCaT), and human neuroblastoma cells (SH-SY5Y). Cells were cultured in the absence of bovine serum in culture media supplemented with 10% (v/v) of the isolated human serum for 3 h.

RNA Extraction and Gene Array. At the end of the incubation, RNA was isolated using an RNAeasy Plus Mini kit (Qiagen). The concentration, purity, and integrity were analyzed using the Agilent 2100 bioanalyzer, before gene expression analysis was performed. Two micrograms of each isolated RNA samples was sent to the FIRC Institute of Molecular Oncology Foundation (IFOM), Milano, Italy, to be processed and hybridized on Gene 1.0 ST array chips according to the Affymetrix protocol. These arrays allow the assessment of the expression level of 28869 genes represented by approximately 26 probes spread across the full length of the gene, providing a more complete and accurate picture of gene expression than the classical 3′ -based expression array designs. Cell intensity files for each Gene 1.0 ST chip processed were generated utilizing Command Console software. Microarray statistical analysis was performed utilizing the OneChannelGUI R package.[16] Raw signal intensities were normalized utilizing the gene-chip robust multiarray average (GCRMA) method employing the empirical Bayes approach for background correction followed by quantile normalization. Differentially expressed genes were identified using the "limma package", applying linear models and moderated t statistics that implement empirical Bayes regularization of standard errors. Differences in expression values were expressed by means of $\log_2$ fold change (FC). A minimum difference threshold of FC ± 0.5 with a p value ≤0.05 was selected as gene differentially expressed in cells incubated with serum isolated after the supplementation with respect to cells incubated with serum isolated before the supplementation. To highlight small variations on a quantitative scale, we decided to decrease the threshold of FC. The lists of significantly differentially expressed genes in association with the administration of Robuvit-enriched serum were analyzed by using DAVID[17] and FIDEA[18] Web servers to identify statistically over-represented biological processes annotated in gene ontology (GO). Enriched GO biological processes (level 5) and Kegg pathways were identified according to p value threshold <0.05.

Both tools produced overlapping lists of enriched terms, and over-represented biological processes highlighted by DAVID were further clustered utilizing the functional annotation clustering utility included in the Web server. Most representative terms were selected and are listed under Results.

Statistical Analysis. Data obtained by total phenol analysis and antioxidant capacity analysis were analyzed using a paired, two-tailed, Student's t test. The threshold for significance was set at $p < 0.05$.

RESULTS

Phenolic Composition of *Q. robur* Capsules. Each Robuvit capsule contains a total phenol amount equivalent to 59.91 ± 14.67 mg of GA equivalents (GAE). On the basis of these data, each volunteer ingested approximately 179 mg of total phenols per day, expressed as GAE, for 5 days. The content of the principal soluble ETs in Robuvit capsule is presented in Table 1. The capsule contains EA and GA and peculiar ETs, such as vescalagin, castalagin, castalin or vescalin, and grandinin or roburin E. The soluble ETs were about 1.8 mg/capsule.

Plasmatic Total Phenols and ET Metabolites. Five days of Robuvit supplementation are associated with doubling of total plasmatic phenolic concentration up to 1.26 μg GAE/mL (Table 2). Table 3 shows the identification and relative quantification of six ET metabolites obtained by HPLC-MS^2 analysis of plasma isolated after supplementation. EA, GA, and

Table 1. Analysis of Soluble ETs in Robuvit and Milligrams of Polyphenols Consumed Each Day by the Volunteers

	μg/capsule	mg/day (three capsules per day)
gallic acid	643 ± 152	1.9 ± 0.4
ellagic acid	491 ± 52	1.5 ± 0.1
castalin/vescalin[a]	306 ± 69	0.9 ± 0.2
grandinin/roburin E[a]	120 ± 20	0.4 ± 0.1
HHDP-galloyl-glucose[a]	87 ± 5	0.3 ± 0.1
castalagin[a]	84 ± 1	0.2 ± 0.1
vescalagin[a]	76 ± 4	0.2 ± 0.1
HHDP-glucose[a]	traces	

[a]Data are expressed as μg ellagic acid equivalent (EAE)/tablet.

Table 2. Increase of Plasmatic Total Phenols Measured after Supplementation

	μg GAE equiv/mL plasma
before supplementation	0.63 ± 0.06
after supplementation	1.26 ± 0.18[a]

[a]Significantly different, $p < 0.005$.

four EA-derived metabolites, conjugated with glucuronic acid, namely, urolithin B-glucuronide, urolithin A-glucuronide, urolithin C-diglucuronide, and EA methyl ether glucuronide, were detected. The total concentration of metabolites in plasma was in the order of 0.2 μM. With the exception of EA, none of these metabolites was present in plasma collected before Robuvit supplementation. No sulfate derivatives were detected in our analysis. The interindividual variability observed among the volunteers was quite high.

Antioxidant Capacity Analysis. To assess if the administration of Robuvit resulted in an increase of plasmatic antioxidant capacity, we performed a classical "antioxidant capacity test", according to the ORAC assay. Five days of Robuvit supplementation was associated with a significant increase of the ORAC value related to the hydrophilic plasmatic component, but not to the lipohilic fraction (Table 4). When the assay was directly performed on a Robuvit capsule, an ORAC value equal to 648 nmol Trolox eq/mg *Q. robur* was obtained.

Microarray Results. As mentioned under Materials and Methods, human serum isolated before and after 5 days of Robuvit supplementation was used to enrich the culture medium of cells at a concentration of 10% v/v.

Microarray results show that, in this experimental condition, the presence of Robuvit metabolites induces a differential expression of a limited number of genes. In HaCaT (stabilized human keratinocites), only one gene (PRPF8, a component of the spliceosome that removes introns from a transcribed pre-RNA) was modulated with a FC ≥ 1, and 13 genes were modulated with a FC between ±1 and ±0.5 (Table 5).

Table 4. Plasmatic Antioxidant Capacity Analysis (ORAC) Partitioned in Hydrophilic and Lipophilic Components[a]

	nmol Trolox equiv/mL plasma	
	hydrophilic component	lipophilic component
before supplementation	1.8 ± 0.05	1.2 ± 0.07
after supplementation	1.9 ± 0.01[b]	1.2 ± 0.06

[a]Data are expressed as nmol Trolox equiv/mL plasma and measured before and after supplementation. [b]Significantly different $p < 0.05$.

In EA.hy.926 (permanent human endothelial cells), the genes RPL30 and RPL24 (60S ribosomal proteins) have been found to be up-regulated with a FC > 1 and 12 genes up-regulated with a FC between 0.5 and 1. Eight genes were down-regulated with a FC between −0.5 and −1 (Table 6).

In SHSY5Y cells (human bone marrow neuroblastoma), two genes (SMNDC1, a component of the spliceosome that removes introns from a transcribed pre-RNA, and FAU, involved in translation) were down-regulated with a FC ≤ 1 and 12 genes were up-regulated with a FC number between 0.5 and 1. Conversely, 23 genes have been found to be down-regulated with a FC between −0.5 and −1 (Table 7). Despite these cell-specific differences, the genes modulated by Robuvit supplementation are mainly involved in translation, cell cycle, RNA splicing, and ribosome biogenesis in all cell types, according to the statistical pathway enrichment analysis.

On the basis of the evidence of a non-negligible interindividual difference of *Q. robur* metabolite profile we considered that the effect of Robivit supplementation on gene expression modulation could be flattened out. We therefore assessed the effect of sera isolated from each subject (1,2 or 3) separately on the different cell lines. Table 8 shows the total number of genes modulated within a FC≤ ≥1. However, because most of the genes regulated are pseudogenes, not mapped in any GO term, the pathway analysis is only able to capture a percentage ranging from 30 to 50% of the total number of the modulated genes measured (shown in the second column). Moreover, the table shows the list of the genes, up- and down-regulated by each serum, that were used by the software to enrich the GO pathways and the resulting over-represented pathway in the three cell lines: ribosome, aminoacyl tRNA biosynthesis, and spliceosome. These results show that, independently of the individual profile metabolites resulting by Robuvit supplementation, the over-represented pathways associated with the three sera are similar in the three cell lines considered in the study.

Table 3. Analysis of the Metabolites Contained in Plasma Isolated before and after Supplementation from Each Subject

	before supplementation				after supplementation			
	subject				subject			
	1	2	3	mean	1	2	3	mean
gallic acid	0	0	0	0 ± 0	0	2.9	6.5	3 ± 3
ellagic acid	13.5	4.5	0	6 ± 7	14.5	14.5	9.5	13 ± 11
urolithin A glucuronide[a]	0	0	0	0 ± 0	8.1	11.8	12.2	11 ± 2
urolithin B glucuronide[a]	0	0	0	0 ± 0	96.1	7.1	7.9	37 ± 51
urolithin C diglucuronide[a]	0	0	0	0 ± 0	0	24.1	46.9	24 ± 23
EA methyl ether glucuronide	0	0	0	0 ± 0	5.6	0	0	2 ± 3

[a]Data are expressed as ng of ellagic acid equivalent (EAE)/mL plasma.

dx.doi.org/10.1021/jf403493a | J. Agric. Food Chem. 2014, 62, 443−453

Table 5. Gene Expression Regulation by the Metabolites of *Q. robur* in HaCaT[a]

official gene symbol	gene name	FC	*p* value	representative pathways
USP22	ubiquitin specific peptidase 22	0.51	0.007	cell cycle
EIF4G2	eukaryotic translation initiation factor 4 γ 2	−0.55	0.003	cell cycle
NPM1	nucleophosmin	−0.77	0.004	ribosome biogenesis; cell cycle
RPS7	40S ribosomal protein S7	0.71	0.002	ribosome biogenesis; RNA processing
C1D	C1D nuclear receptor corepressor	−0.60	0.034	ribosome biogenesis; RNA processing
PRPF8	pre-mRNA processing factor 8 homologue	1.00	0.018	RNA processing
TARDBP	TAR DNA-binding protein 43	−0.77	0.027	RNA processing; cell cycle
TP53TG3	TP53TG3	0.58	0.002	
LYZL2	lysozyme 2	0.53	0.007	
CD69	CD69	0.51	0.032	
EIF3D	eukaryotic translation initiation factor 3 subunit D	−0.51	0.012	
CAMTA2	calmodulin binding transcription activator 2	−0.56	0.022	
SNX3	sorting nexin-3	−0.76	0.041	
FMN1	formin 1	−0.83	0.023	

[a]FC threshold is $\leq \geq 0.5$; *p* value ≤ 0.05.

Table 6. Gene Expression Regulation by the Metabolites of *Q. robur* in EA.hy.926[a]

official gene symbol	gene name	FC	*p* value	representative pathways
NPM1	nucleophosmin	0.82	0.042	cell cycle
RPL24	60S ribosomal protein L24	1.08	0.011	cell cycle; M phase mitotic cycle
SEPT2	septin 2	0.52	0.028	cell cycle; M phase mitotic cycle
SMC4	structural maintenance of chromosomes protein 4	0.50	0.007	cell cycle; M phase mitotic cycle
RPL30	60S ribosomal protein L30	1.28	0.001	
ELMO1	engulfment and cell motility protein 1	0.95	0.047	
MT-ND2	NADH-ubiquinone oxidoreductase chain 2	0.75	0.037	
HNRNPC	heterogeneous nuclear ribonucleoproteins C1/C2	0.59	0.045	
NONO	non-POU domain-containing octamer-binding protein	0.58	0.045	
EIF4E3	eukaryotic translation initiation factor 4E member 3	0.57	0.005	
ADAM21	ADAM metallopeptidase domain 21	0.54	0.034	
B3GNT5	βGal β-1,3-*N*-acetylglucosaminyltransferase 5	0.53	0.004	
EPCAM	epithelial cell adhesion molecule	−0.83	0.013	
IK	IK cytokine	−0.51	0.008	
CYP1A1	cytochrome P450, family 1	−0.53	0.006	
MYST2	histone acetyltransferase	−0.72	0.011	
CD69	CD69	−0.73	0.004	
C8orf73		−0.73	0.002	
C22orf28		0.73	0.021	
AC007688.1		−0.61	0.002	
LOC642947		−0.51	0.002	
HOMER2		0.55	0.007	

[a]FC threshold is $\leq \geq 0.5$; *p* value ≤ 0.05.

DISCUSSION

This study represents the first investigation on standardized French oak wood extract, Robuvit, absorption/metabolism and on the effect of Robuvit metabolites on gene expression modulation, by utilizing a combined ex vivo cell culture approach.[19] To the best of our knowledge we have reported for the first time absorption of ETs from *Q. robur* in humans; in fact, to date, metabolites resulting from human consumption of oak wood constituents remained unknown.

The HPLC-MS^2 analysis of Robuvit capsule shows that it is mainly composed of GA and EA and of several ETs such as castalagin, vescalagin, and roburin E. Our data show that the consumption of about 180 mg of total phenols per day (three capsules a day of Robuvit) resulted in a significant increase of GA and EA in plasma. GA is generally rapidly absorbed and has a good bioavailability,[20,21] whereas ETs are hydrolyzed in vivo to EA, which is further metabolized by gut microbiota mostly to produce the derivative urolithins. Similarly to isoflavone metabolism, where there is a quite clear-cut separation between equol and nonequol producers,[22] it has been proposed that humans can be divided into high and low urolithin producers due to their microbiota, supporting the large variability in the metabolism of ETs.[23,24] The appearance of *three* glucuronated urolithin (urolithin B-glucuronide, urolithin A-glucuronide, urolithin C-diglucuronide) moieties in plasma isolated after the supplementation, absent at baseline, suggests that oak wood ETs are bioavailable. Although glucuronidated urolithin A was present in all three subjects, only one subject showed high urolithin B (about 0.1 μg/mL) but not detectable urolithin C levels. ET bioavailability has been already studied addressing the consumption of different foods and beverages.[11] EA and urolithin glucoronides were detected in human plasma at 6 h from pomegranate juice (PJ) administration (providing 318 mg of punicalagins and 12 mg of free EA)[9,25] or pomegranate

Table 7. Gene Expression Regulation by the Metabolites of *Q. robur* in SHSY-5Y[a]

official gene symbol	gene name	FC	*p* value	representative pathways
EIF4G2	eukaryotic translation initiation factor 4 γ 2	0.91	0.000	translation
RBMY1D	RNA binding motif protein	0.56	0.000	RNA splicing
HNRNPK	heterogeneous nuclear ribonucleoprotein K	−0.52	0.005	RNA splicing
SNRNP200	small nuclear ribonucleoprotein 200 kDa	−0.69	0.029	RNA splicing
HNRNPM	heterogeneous nuclear ribonucleoprotein M	−0.91	0.001	RNA splicing
SMNDC1	survival motor neuron domain containing 1	−1.10	0.003	RNA splicing
EIF3D	eukaryotic translation initiation factor 3 subunit D	0.69	0.014	translation
RPL17	ribosomal protein L17	−0.58	0.001	translation; ribosome
RPL4	60S ribosomal protein L4	0.58	0.029	translation; ribosome
RPS13	40S ribosomal protein S13	0.56	0.013	translation; ribosome
FAU	Finkel−Biskis−Reilly murine sarcoma virus	−1.00	0.002	translation; ribosome
PSMB2	proteasome subunit, β type, 2	0.85	0.002	
EFCAB4B	calcium release-activated calcium channel regulator 2A	0.75	0.002	
ACAA1	acetyl-eoenzyme A acyltransferase 1	0.66	0.003	
OR5L1	olfactory receptor 5L1	0.62	0.031	
STARD7	StAR-related lipid transfer (START) domain containing 7	0.55	0.005	
TSPAN33	tetraspanin 33	0.53	0.017	
FLJ25758		0.50	0.025	
BBS9	Bardet−Biedl syndrome 9	−0.53	0.039	
FOLH1	folate hydrolase	−0.54	0.036	
FOXK2	forkhead box	−0.56	0.034	
CR769776.1	ankyrin repeat domain 20 family	−0.59	0.008	
LIAS	lipoic acid synthetase	−0.60	0.010	
AC068775.1		−0.61	0.025	
ZNF846	zinc finger protein 846	−0.62	0.015	
ANKRD20A4	ankyrin repeat domain 20 family	−0.63	0.003	
ZNF117	zinc finger protein 117	−0.65	0.013	
ARF1	ADP-ribosylation factor 1	−0.66	0.047	
ARF3	ADP-ribosylation factor 3	−0.67	0.023	
CITED1	Cbp/p300-interacting transactivator	−0.69	0.008	
XCL1	chemokine (C motif)	−0.69	0.013	
SLC2A14	solute carrier family 2 (facilitated glucose transporter)	−0.76	0.004	
CBX3	chromobox homologue 3	−0.80	0.027	
HSD3B1	hydroxy-δ-5-steroid dehydrogenase, 3 β- and steroid δ-isomerase 1	−0.85	0.039	
C19orf50		−0.87	0.042	
USP22	ubiquitin specific peptidase 22	−0.92	0.000	
SART3	squamous cell carcinoma antigen recognized by T cells 3	−1.01	0.027	

[a]FC threshold is $\leq \geq 0.5$; *p* value ≤ 0.05.

extract (providing 330 mg of punicalagin and 21 mg of EA).[26] Glucuronides were the only urolithin metabolites found in plasma of subjects supplemented for 5 weeks with PJ consumption.[27] Urolithin glucuronides and EA derivatives were detected after 3 days of walnut consumption.[28] Stoner and co-workers found EA in human plasma at 2 h after the administration of 45 g of freeze-dried black rasberries (containing 13.5 mg of EA).[29] However, neither EA nor any of ET metabolites have been found in detectable quantities in human plasma over a 24 h period after 300 g of rasberry consumption.[12] According to the authors, this negative result is not a real proof of absence as it could be due to the high detection limit of the method used in the study. In agreement with our data, no sulfate metabolites have been found in humans after ET-rich food supplementation.[10]

EA structure presents two *o*-dihydroxy groups, and it may therefore be transformed by the activity of catechol-*O*-methyltransferase (COMT) (in the liver) in mono- and/or dimethyl ether of EA. These metabolites can be further metabolized by enzymatic glucuronic acid derivatization. In fact, dimethylellagic acid glucuronide has been found in the urine[9] and plasma[28] of subjects supplemented with PJ and in the plasma of rats supplemented with 6% punicalagin.[30] In the present study, we detected a low amount of methylellagic glucuronide in plasma isolated after the supplementation in only one of three subjects. Also in agreement with our study, a high interindividual variability of metabolic profile has been already frequently reported.[9,24,27,28]

Moreover, as expected, the total plasma polyphenol amount increased significantly by on average 100% in all volunteers. The consumption of the aqueous oak wood extract Robuvit led, also, to a statistically significant increase of hydrophilic blood oxygen radical absorbance capacity (ORAC) in healthy volunteers, even if the small change observed may not have a biological relevance.

The methodologies utilized to assess plasma polyphenol concentration and plasma antioxidant capacity are known to be non specific. In fact, it has been reported that the Folin assay provides polyphenol estimation consistently 2−4 times greater than that obtained by HPLC methods,[31] because it measures the reducing capacity of phenolic components by detecting nonspecific hydroxyl groups. GA and EA contain three and four

Table 8. Gene Expression Regulation Associated with Each Serum Isolated from the Healthy Subjects (Sera 1, 2, and 3) in HaCaT, EA.hy.926, and SHSY-5Y Cell Lines[a]

serum	total genes modulated	up-regulated	down-regulated	over-represented pathway
		HaCaT		
1	36	APOBE3CA, USP22, ZNF259	CANX, EIF3F, FNTA, HNRNPM, ILF2, NPM1, RPL11, SART3, SEPT2, TCEB2, TARDBP, ZNF737,	
2	29	CANX, NARS, PRPF8, RPS7, SART3	ANAPC5, EIF3D, FNTA, HRNPC, IK, ZNF259, ZNF737	spliceosome
3	52	IL10RA, LYZL2, NPM1, PRPF8, RPL11, RPL17, SEPT2, ZNF259	ARF3, C22orf28,CBX3, EIF3D, HNRNPC, IL18R1, IK, KARS, NONO, SMNCD1, SNX3, SNX32	spliceosome, ribosome
		EA.hy.926		
1	47	ANAPC5, ARF3, CASZ1, C1D, EIF3F, FNTA, MT-ND2, NPM1, RHOA,RPL11, RPL30, SMNDC1, SART3, SEPT2, SNX32, TARDBP	DEPDC5, EPCAM, HNRNPC, RPL34, TCEB2	ribosome
2	48	CANX, ELMO1, IL10RA, KARS, NARS, RPL11, RPL17, RPL24, RPL30, RPL34, SART1, SART3	CD69, CYP1A1,EPCAM, PDE5A, HSD3B1, IK, ILF2, ILF2, RASA4	ribosome, aminoacyl-tRNA biosynthesis, steroid hormone biosynthesis
3	50	AREG, ANAPC5, CANX, CBX3, EIF4E3, IK, MT-CYB, NARS, NONO, RPL34, RPL24, RPL30, SEPT2, SERPIND2,SMNDC1, TAF1D, ZNF28	ARF3, EIF3F, HNRNPK, SART3, TCEB2	ribosome
		SHSY-5Y		
1	38	CDC26, EPCAM, JTB	ACTR3C, C1D, EIF3D, FAU, GUK1, HNRNPK, EFCAB4B, IK, IL10RA, KARS, NARS, NPM1, RPL24, SART1, TARDBP, TCEB2	aminoacyl-tRNA biosynthesis
2	101	ANAPC5, AREG, CANX, CBX3, EIF3F, FNTA, NPM1, RBMYD1D, SLC25A43, SMNDC1, TMED2, ZNF259, ZNF487P, ZNF492	ARF3, ATP6 V0B, C1D, c22orf28, CCL4, EIF3D, HNRNPK, HNRNPM, ILF2, NARS, NONO, RHOA, RPL4, RPS27A, SEPT2, SNX3, SRP14, USP22, XCL1	
3	95	ARF3, C1D, CBX3, EIF3F, GPC2, HSD3B1, KARS, MT-ND3, PTCH2, RABGGTB, RPNS1, SART1	C22orf28, CANX, HNRNPC, HNRNPM, IK, INF2, NPM1, PSMB2,PTH2R, RPL11, SART3, SLCO4C1 SMNDC1, TARDBP, TMED2	spliceosoma

[a]FC threshold is $\leq \geq 1$.

dx.doi.org/10.1021/jf403493a | J. Agric. Food Chem. 2014, 62, 443−453

hydroxyl groups, respectively, and they strongly contribute to Folin and possess high antioxidant properties. However, in our results the extent of the increase of plasmatic GA and EA, after the supplementation, is not sufficient to explain the observed increase of ORAC and Folin. It is known that urolithins exhibited a significant antioxidant action correlated with the number of hydroxyl groups,[32] whereas no antioxidant activity has been reported for the glucuronide derivative forms.[24,33] Therefore, we have to hypothesize that a synergic activity of all *Q. robur* metabolites occurs.

Dietary EA and its metabolites, either independently or synergistically, are good candidates to be among the most active molecules responsible for a wide spectrum of molecular effects. In vivo and in vitro studies have shown that EA and urolithins have antiproliferative effects in human bladder cancer cells and antitumoral properties in several lines of cultured human cancer cells,[34,35] in hamster buccal carcinoma[36] and anti-inflammatory properties in colon fibroblasts,[4] and in human primary endothelial cells.[37] EA and urolithin A have been demonstrated to down-regulate the expression of COX-2 and iNOS and other inflammatory markers and to modulate the expression of genes involved in cell cycle in colonic mucosa in a colitis rat model.[4] Moreover, CaCo2 cells exposed to concentrations of EA and urolithins achievable in the colon from the diet arrested cell growth at the S and G_2/M phases. Transcriptional profiling obtained by microarray and functional analysis revealed significant changes in the expression levels genes involved in MAPK signaling such as growth factor receptors (*FGFR2*, *EGFR*), oncogenes (*K-Ras*, *c-Myc*), and tumor suppressors (*DUSP6*, *Fos*) as well as the modulation of genes involved in cell cycle (*CCNB1*,*CCNB1IP1*).[38] Similarly, GA has been shown to inhibit carcinogenesis in animal models and in vitro cancerous cell lines. The inhibitory effect of GA on cancer cell growth has been reported to be mediated by the modulation of the expression of genes encoding for proteins involved in cell cycle, metastasis, angiogenesis, and apoptosis.[39,40] Upstream to gene expression, GA has been reported to inhibit activation of NF-κB and Akt signaling pathways along with the activity of COX and inflammatory cytokines.[41,42]

The present study provides an original background to the understanding of possible effects of *Q. robur* extract metabolites on the modulation of gene expression in endothelial, neuronal, and keratinocyte cell lines. Our methodological approach allows the assessment of the effects of *Q. robur* metabolites at concentrations physiologically achievable in vivo and in a profile prevailing in humans. The transcriptome of each cell line was identified utilizing an Affymetrix customized array that recognizes a total number of 28869 genes.

Subsequent, functional analysis revealed that culturing cells in serum obtained from subjects administered *Q. robur* extract results in a moderate although significant modulation of the expression of genes related to specific GO categories, namely, cell cycle, ribosome biogenesis, and RNA processing pathways in HaCaT (stabilized human keratinocytes) cells; cell cycle, M phase mitotic cycle in Ea.Hy.926 cells (a permanent human endothelial cells); translation, RNA splicing, and ribosome pathways in SHSY5Y cells (human bone marrow neuroblastoma). Obviously, changes of gene expression at the level of mRNA do not necessarily imply that corresponding changes occur at the level of protein. Nonetheless, an understanding of the effect of dietary bioactive molecules at the transcriptional level is important to the building up of a conceptual background to be exploited in future studies addressing the putative effect of these botanical extracts in human health and disease.

Specific interindividual differences in the metabolization of *Q. robur* extract components may have differently influenced the final outcome in terms of the single gene expression. However, surprisingly, the functional analysis reveals that the three sera, independently of the individual profile metabolites, modulate similar pathways, ribosome, aminoacyl tRNA biosynthesis, and spliceosome, suggesting that the ET metabolites display a uniform behavior, in a cell-type independent way. However, the small differences in FC of most of the genes do not let us assign to the modulated pathways either a positive or a negative health concern. Moreover, it is important to note that the rate of cell proliferation was not affected by serum containing *Q. robur* metabolites compared to control sera (data not shown).

In conclusion, we demonstrate that Robuvit, a proprietary patented extract from *Q. robur*, is (at least in part) bioavailable to humans and that despite the very low concentration of the metabolite in serum, its consumption is associated with a statistically significant increase of the antioxidant capacity and to specific changes of gene expression profile.

AUTHOR INFORMATION

Corresponding Author

*(R. Canali) Phone: +39 06 51494519. Fax: +39 06 51494550. E-mail: raffaella.canali@entecra.it.

Author Contributions

§F.N. and G.L. equally contributed.

Funding

This study was supported by Horphag Research, Geneva, Switzerland, and by Italian Ministry of Agriculture, Food and Forestry (MiPAAF) Grants "NUME" (DM 3688/7303/08).

Notes

The authors declare the following competing financial interest(s): F.S. worked at Horphag Research Ltd. The other authors declare no competing financial interest.

ACKNOWLEDGMENTS

We are grateful to Prof. Michael Jourdes (Université Bordeaux Segalen, Faculté d'Oenologie, Unité de recherche Oenologie, Villenave d'Ornon, France) for his help with the chemical structure drawing.

ABBREVIATIONS USED

ETs, ellagitannins; EA, ellagic acid; GA, gallic acid

REFERENCES

(1) Arts, I. C.; Hollman, P. C. Polyphenols and disease risk in epidemiologic studies. *Am. J. Clin. Nutr.* **2005**, *81*, 317S−325S.

(2) Queen, B. L.; Tollefsbol, T. O. Polyphenols and aging. *Curr. Aging Sci.* **2010**, *3*, 34−42.

(3) Forman, H. J.; Davies, K. J.; Ursini, F. How do nutritional antioxidants really work: nucleophilic tone and para-hormesis versus free radical scavenging in vivo. *Free Radical Biol. Med.* **2013**, DOI: 10.1016/j.freeradbiomed.2013.05.045.

(4) Larrosa, M.; Gonzalez-Sarrias, A.; Yanez-Gascon, M. J.; Selma, M. V.; Azorin-Ortuno, M.; Toti, S.; Tomas-Barberan, F.; Dolara, P.; Espin, J. C. Anti-inflammatory properties of a pomegranate extract and its metabolite urolithin-A in a colitis rat model and the effect of colon inflammation on phenolic metabolism. *J. Nutr. Biochem.* **2010**, *21*, 717−725.

(5) Wu, S. B.; Dastmalchi, K.; Long, C.; Kennelly, E. J. Metabolite profiling of jaboticaba (*Myrciaria cauliflora*) and other dark-colored fruit juices. *J. Agric. Food Chem.* **2012**, *60*, 7513−7525.
(6) Mayer, W.; Gabler, W.; Riester, A.; Korger, H. On tannins compounds from the wood of chestnut and oak wood−IIs. Isolation of castalagin, vescalagin, castalin and vescaline. *Liebigs Ann. Chem.* **1967**, *707*, 177−181.
(7) García-Estévez, I.; Escribano-Bailón, M. T.; Rivas-Gonzalo, J. C.; Alcalde-Eon, C. Development of a fractionation method for the detection and identification of oak ellagitannins in red wines. *Anal. Chim. Acta* **2010**, *660*, 171−176.
(8) Glabasnia, A.; Hofmann, T. Sensory-directed identification of taste-active ellagitannins in American (*Quercus alba* L.) and European oak wood (*Quercus robur* L.) and quantitative analysis in bourbon whiskey and oak-matured red wines. *J. Agric. Food Chem.* **2006**, *54*, 3380−3390.
(9) Seeram, N. P.; Henning, S. M.; Zhang, Y.; Suchard, M.; Li, Z.; Heber, D. Pomegranate juice ellagitannin metabolites are present in human plasma and some persist in urine for up to 48 h. *J. Nutr.* **2006**, *136*, 2481−2485.
(10) Espín, J. C.; González-Barrio, R.; Cerdá, B.; López-Bote, C.; Rey, A. I.; Tomás-Barberán, F. A. Iberian pig as a model to clarify obscure points in the bioavailability and metabolism of ellagitannins in humans. *J. Agric. Food Chem.* **2007**, *55*, 10476−10485.
(11) Cerda, B.; Tomas-Barberan, F. A.; Espin, J. C. Metabolism of antioxidant and chemopreventive ellagitannins from strawberries, raspberries, walnuts, and oak-aged wine in humans: identification of biomarkers and individual variability. *J. Agric. Food Chem.* **2005**, *53*, 227−235.
(12) Gonzalez-Barrio, R.; Borges, G.; Mullen, W.; Crozier, A. Bioavailability of anthocyanins and ellagitannins following consumption of raspberries by healthy humans and subjects with an ileostomy. *J. Agric. Food Chem.* **2010**, *58*, 3933−3939.
(13) Serafini, M.; Maiani, G.; Ferro-Luzzi, A. Alcohol-free red wine enhances plasma antioxidant capacity in humans. *J. Nutr.* **1998**, *128*, 1003−1007.
(14) Prior, R. L.; Hoang, H.; Gu, L.; Wu, X.; Bacchiocca, M.; Howard, L.; Hampsch-Woodill, M.; Huang, D.; Ou, B.; Jacob, R. Assays for hydrophilic and lipophilic antioxidant capacity (oxygen radical absorbance capacity (ORAC(FL))) of plasma and other biological and food samples. *J. Agric. Food Chem.* **2003**, *51*, 3273−3279.
(15) Huang, D.; Ou, B.; Hampsch-Woodill, M.; Flanagan, J. A.; Prior, R. L. High-throughput assay of oxygen radical absorbance capacity (ORAC) using a multichannel liquid handling system coupled with a microplate fluorescence reader in 96-well format. *J. Agric. Food Chem.* **2002**, *50*, 4437−4444.
(16) Sanges, R.; Cordero, F.; Calogero, R. A. oneChannelGUI: a graphical interface to Bioconductor tools, designed for life scientists who are not familiar with R language. *Bioinformatics* **2007**, *23*, 3406−3408.
(17) Huang da, W.; Sherman, B. T.; Tan, Q.; Kir, J.; Liu, D.; Bryant, D.; Guo, Y.; Stephens, R.; Baseler, M. W.; Lane, H. C.; Lempicki, R. A. DAVID Bioinformatics Resources: expanded annotation database and novel algorithms to better extract biology from large gene lists. *Nucleic Acids Res.* **2007**, *35*, W169−175.
(18) D'Andrea, D.; Grassi, L.; Mazzapioda, M.; Tramontano, A. FIDEA: a server for the functional interpretation of differential expression analysis. *Nucleic Acids Res.* **2013**, *41*, W84−88.
(19) Canali, R.; Ambra, R.; Stelitano, C.; Mattivi, F.; Scaccini, C.; Virgili, F. A novel model to study the biological effects of red wine at the molecular level. *Br. J. Nutr.* **2007**, *97*, 1053−1058.
(20) Shahrzad, S.; Aoyagi, K.; Winter, A.; Koyama, A.; Bitsch, I. Pharmacokinetics of gallic acid and its relative bioavailability from tea in healthy humans. *J. Nutr.* **2001**, *131*, 1207−1210.
(21) Manach, C.; Williamson, G.; Morand, C.; Scalbert, A.; Remesy, C. Bioavailability and bioefficacy of polyphenols in humans. I. Review of 97 bioavailability studies. *Am. J. Clin. Nutr.* **2005**, *81*, 230S−242S.
(22) Shor, D.; Sathyapalan, T.; Atkin, S. L.; Thatcher, N. J. Does equol production determine soy endocrine effects? *Eur. J. Nutr.* **2012**, *51*, 389−398.
(23) Cerda, B.; Periago, P.; Espin, J. C.; Tomas-Barberan, F. A. Identification of urolithin a as a metabolite produced by human colon microflora from ellagic acid and related compounds. *J. Agric. Food Chem.* **2005**, *53*, 5571−5576.
(24) Cerda, B.; Espin, J. C.; Parra, S.; Martinez, P.; Tomas-Barberan, F. A. The potent in vitro antioxidant ellagitannins from pomegranate juice are metabolised into bioavailable but poor antioxidant hydroxy-6*H*-dibenzopyran-6-one derivatives by the colonic microflora of healthy humans. *Eur. J. Nutr.* **2004**, *43*, 205−220.
(25) Seeram, N. P.; Lee, R.; Heber, D. Bioavailability of ellagic acid in human plasma after consumption of ellagitannins from pomegranate (*Punica granatum* L.) juice. *Clin. Chim. Acta* **2004**, *348*, 63−68.
(26) Mertens-Talcott, S. U.; Jilma-Stohlawetz, P.; Rios, J.; Hingorani, L.; Derendorf, H. Absorption, metabolism, and antioxidant effects of pomegranate (*Punica granatum* L.) polyphenols after ingestion of a standardized extract in healthy human volunteers. *J. Agric. Food Chem.* **2006**, *54*, 8956−8961.
(27) Cerda, B.; Soto, C.; Albaladejo, M. D.; Martinez, P.; Sanchez-Gascon, F.; Tomas-Barberan, F.; Espin, J. C. Pomegranate juice supplementation in chronic obstructive pulmonary disease: a 5-week randomized, double-blind, placebo-controlled trial. *Eur. J. Clin. Nutr.* **2006**, *60*, 245−253.
(28) Gonzalez-Sarrias, A.; Gimenez-Bastida, J. A.; Garcia-Conesa, M. T.; Gomez-Sanchez, M. B.; Garcia-Talavera, N. V.; Gil-Izquierdo, A.; Sanchez-Alvarez, C.; Fontana-Compiano, L. O.; Morga-Egea, J. P.; Pastor-Quirante, F. A.; Martinez-Diaz, F.; Tomas-Barberan, F. A.; Espin, J. C. Occurrence of urolithins, gut microbiota ellagic acid metabolites and proliferation markers expression response in the human prostate gland upon consumption of walnuts and pomegranate juice. *Mol. Nutr. Food Res.* **2010**, *54*, 311−322.
(29) Stoner, G. D.; Sardo, C.; Apseloff, G.; Mullet, D.; Wargo, W.; Pound, V.; Singh, A.; Sanders, J.; Aziz, R.; Casto, B.; Sun, X. Pharmacokinetics of anthocyanins and ellagic acid in healthy volunteers fed freeze-dried black raspberries daily for 7 days. *J. Clin. Pharmacol.* **2005**, *45*, 1153−1164.
(30) Cerda, B.; Llorach, R.; Ceron, J. J.; Espin, J. C.; Tomas-Barberan, F. A. Evaluation of the bioavailability and metabolism in the rat of punicalagin, an antioxidant polyphenol from pomegranate juice. *Eur. J. Nutr.* **2003**, *42*, 18−28.
(31) Robbins, R. J.; Kwik-Uribe, C.; Hammerstone, J. F.; Schmitz, H. H. Analysis of flavanols in foods: what methods are required to enable meaningful health recommendations? *J. Cardiovasc. Pharmacol.* **2006**, *47*, S110−S121.
(32) Bialonska, D.; Kasimsetty, S. G.; Khan, S. I.; Ferreira, D. Urolithins, intestinal microbial metabolites of pomegranate ellagitannins, exhibit potent antioxidant activity in a cell-based assay. *J. Agric. Food Chem.* **2009**, *57*, 10181−10186.
(33) Ito, H.; Iguchi, A.; Hatano, T. Identification of urinary and intestinal bacterial metabolites of ellagitannin geraniin in rats. *J. Agric. Food Chem.* **2008**, *56*, 393−400.
(34) Qiu, Z.; Zhou, B.; Jin, L.; Yu, H.; Liu, L.; Liu, Y.; Qin, C.; Xie, S.; Zhu, F. In vitro antioxidant and antiproliferative effects of ellagic acid and its colonic metabolite, urolithins, on human bladder cancer T24 cells. *Food Chem. Toxicol.* **2013**, *59*, 428−437.
(35) Losso, J. N.; Bansode, R. R.; Trappey, A., 2nd; Bawadi, H. A.; Truax, R. *In vitro* anti-proliferative activities of ellagic acid. *J. Nutr. Biochem.* **2004**, *15*, 672−678.
(36) Vidya Priyadarsini, R.; Kumar, N.; Khan, I.; Thiyagarajan, P.; Kondaiah, P.; Nagini, S. Gene expression signature of DMBA-induced hamster buccal pouch carcinomas: modulation by chlorophyllin and ellagic acid. *PLoS One* **2012**, *7*, e34628.
(37) Gimenez-Bastida, J. A.; Gonzalez-Sarrias, A.; Larrosa, M.; Tomas-Barberan, F.; Espin, J. C.; Garcia-Conesa, M. T. Ellagitannin metabolites, urolithin A glucuronide and its aglycone urolithin A, ameliorate TNF-alpha-induced inflammation and associated molecular

markers in human aortic endothelial cells. *Mol. Nutr. Food Res.* **2012**, *56*, 784−796.
(38) Gonzalez-Sarrias, A.; Azorin-Ortuno, M.; Yanez-Gascon, M. J.; Tomas-Barberan, F. A.; Garcia-Conesa, M. T.; Espin, J. C. Dissimilar *in vitro* and *in vivo* effects of ellagic acid and its microbiota-derived metabolites, urolithins, on the cytochrome P450 1A1. *J. Agric. Food Chem.* **2009**, *57*, 5623−5632.
(39) Ho, H. H.; Chang, C. S.; Ho, W. C.; Liao, S. Y.; Lin, W. L.; Wang, C. J. Gallic acid inhibits gastric cancer cells metastasis and invasive growth via increased expression of RhoB, downregulation of AKT/small GTPase signals and inhibition of NF-kappaB activity. *Toxicol. Appl. Pharmacol.* **2013**, *266*, 76−85.
(40) Yeh, R. D.; Chen, J. C.; Lai, T. Y.; Yang, J. S.; Yu, C. S.; Chiang, J. H.; Lu, C. C.; Yang, S. T.; Yu, C. C.; Chang, S. J.; Lin, H. Y.; Chung, J. G. Gallic acid induces G(0)/G(1) phase arrest and apoptosis in human leukemia HL-60 cells through inhibiting cyclin D and E, and activating mitochondria-dependent pathway. *Anticancer Res.* **2011**, *31*, 2821−2832.
(41) Verma, S.; Singh, A.; Mishra, A. Gallic acid: molecular rival of cancer. *Environ. Toxicol. Pharmacol.* **2013**, *35*, 473−485.
(42) Al-Halabi, R.; Bou Chedid, M.; Abou Merhi, R.; El-Hajj, H.; Zahr, H.; Schneider-Stock, R.; Bazarbachi, A.; Gali-Muhtasib, H. Gallotannin inhibits NFkB signaling and growth of human colon cancer xenografts. *Cancer Biol. Ther.* **2011**, *12*, 59−68.

JOURNAL OF AGRICULTURAL AND FOOD CHEMISTRY

Article

pubs.acs.org/JAFC

Acidolysis of *p*-Coumaric Acid with Omega-3 Oils and Antioxidant Activity of Phenolipid Products in in vitro and Biological Model Systems

Jiankang Wang[†] and Fereidoon Shahidi*[,†,‡]

[†]Departments of Biology and [‡]Biochemistry, Memorial University of Newfoundland, St. John's, Newfoundland and Labrador A1B 3 × 9, Canada

ABSTRACT: Lipase-catalyzed acidolysis of *p*-coumaric acid with seal blubber oil (SBO) and menhaden oil (MHO) was carried out, followed by identification of major phenolipids in the resultant acidolysis mixture using high-performance liquid chromatography/mass spectrometry. Separation of phenolipid components from the resultant acidolysis mixture was achieved using flash column chromatography. The antioxidant activities of the phenolipids were examined in in vitro assays and biological model systems. The major phenolipids identified from acidolysis mixtures with both SBO and MHO included eight phenolic monoacylglycerols and eight phenolic diacylglycerols. Phenolipids derived from SBO and MHO generally showed good antioxidant potential in the systems tested. The prepared phenolipids exhibited high scavenging capacity toward 1,1-diphenyl-2-picrylhydrazyl (DPPH) and peroxyl radicals and displayed reducing power, strong inhibitory effect on bleaching of *β*-carotene, human low-density lipoprotein (LDL) cholesterol oxidation, as well as radical-induced DNA cleavage, thus suggesting that phenolipids derived from omega-3 oils may be used as potential stable products for health promotion and disease risk reduction.

KEYWORDS: *lipase-catalyzed acidolysis, p-coumaric acid, seal blubber oil, menhaden oil, phenolipid, DPPH radical scavenging activity, oxygen radical absorbance capacity, reducing power, β-carotene−linoleate, human LDL cholesterol, DNA*

INTRODUCTION

The omega-3 oils from marine origin, especially those from fish such as menhaden and from marine mammals such as seal blubber, are commonly used as supplements due to their high content of omega-3 fatty acids, such as eicosapentaenoic acid (EPA), docosapentaenoic acid (DPA), and docosahexaenoic acid (DHA).[1] The beneficial effects of omega-3 fatty acids have been associated with their ability to lower triacylglycerol levels in the circulatory system and in the treatment and/or prevention of hypertension, arrhythmia, arthritis, and inflammatory, immune, as well as mental disorders.[2−4] For instance, DHA is believed to be essential for normal development of the central nervous system and visual acuity in humans.[5] However, the high degree of unsaturation of these oils decreases their oxidative stability. Synthetic antioxidants such as butylated hydroxytoluene (BHT), butylated hydroxyanisole (BHA), and *tert*-butylhydroquinone (TBHQ), as well as natural antioxidants such as mixed tocopherols are often added to edible oils and foods in order to enhance their stability.[6] However, synthetic antioxidants have fallen out of favor due to concerns about their safety when used in high doses in animals.[7−9] Furthermore, effectiveness of tocopherols as antioxidants can be compromised by the presence of metal ions, including those of iron and copper, which are commonly present in marine oils.[2,3] Therefore, studies on the potential use of other forms of naturally occurring antioxidants to stabilize edible oils have been pursued.

Investigations on the search for natural antioxidants such as phenolics in foods and food processing byproducts have been widely reported, and most of them have proven to reduce the extent of lipid oxidation as well as rendering health benefits by reducing oxidative stress and the risk of associated diseases. For instance, *p*-coumaric acid occurs in various food sources and beverages, including tomatoes, carrots, garlics, as well as wines and vinegars.[10] Its strong antioxidant and anticancer effects have been reported in a number of studies.[11,12]

Modifying the structure of triacylglycerols can be used as a strategy and an effective means to improve nutritional and health benefits of highly unsaturated oils. Acidolysis is a modification process, which incorporates desired fatty acids or other forms of organic acids, such as phenolic acids, into triacylglycerols using enzyme catalysts.[13] For example, acidolysis of phenolic acids and triacylglycerols has been successfully conducted and reported in several studies.[14,15] Synthesis of phenolipids using *p*-coumaric acid and triolein was successfully conducted in our laboratory (unpublished work). The purified lipid derivatives of *p*-coumaric acid, monooleyl and dioleyl *p*-coumarates, demonstrated great antioxidant activity in a number of model systems, which may be explained by changes of lipophilicity and the steric conformation of modified lipids. In this study, acidolysis of *p*-coumaric acid with seal blubber oil (SBO) and menhaden oil (MHO) was conducted, and the phenolipids produced were purified from the resultant mixture using column chromatography and identified by using high-performance liquid chromatography/mass spectrometry (HPLC-MS). Antioxidant activity of synthesized phenolipids was also tested in several in vitro

Received: September 18, 2013
Revised: November 27, 2013
Accepted: December 2, 2013
Published: December 2, 2013

ACS Publications © 2013 American Chemical Society

assays, including 1,1-diphenyl-2-picrylhydrazyl (DPPH) radical scavenging activity, oxygen radical absorbance capacity (ORAC), and reducing power evaluations. In addition, antioxidant activity of synthesized phenolipids was further examined in a β-carotene−linoleate model system. The efficacy of the phenolipids so obtained in reducing the extent of oxidation of human low-density lipoprotein (LDL) cholesterol and prevention of DNA scission was also examined in order to obtain a better understanding of their antioxidant capacity and their potential use in food and supplements for health promotion.

MATERIALS AND METHODS

Novozyme 435 and *p*-coumaric acid were obtained from Sigma−Aldrich Canada Ltd. (Oakville, ON, Canada). Trolox was purchased from Acros Organics (Fair Lawn, NJ, USA). Human LDL cholesterol and supercoiled plasmid pBR322 DNA were purchased from Sigma−Aldrich Canada Ltd. (Oakville, ON, Canada). SYBR safe gel stain was obtained from Invitrogen Corporation (Carlsbad, CA, USA). All solvents used were of HPLC grade and purchased from Fisher Scientific (Nepean, ON, Canada).

Methods. *Lipase-Catalyzed Acidolysis of p-Coumaric Acid with SBO and MHO.* Lipase-catalyzed acidolysis of *p*-coumaric acid with SBO and MHO was carried out according to the method employed in the synthesis of phenolipids using *p*-coumaric acid and triolein (unpublished study). A stock solution of *p*-coumaric acid (10 mM) was freshly prepared in 2-butanone, and stock solutions of the oils (53.36 mM; the average molecular weight of the oils was calculated from the weight of the oil sample used and the amount of base used for its saponification.) were prepared in hexane. A 30 mL amount of the *p*-coumaric acid stock solution and 90 mL of each oil stock solution were transferred to a 250 mL round-bottom flask followed by addition of 645 mg of immobilized Novozyme 435 (15%, w/w of substrates). The final reaction solutions contained 2.5 mM of *p*-coumaric acid and 40 mM (calculated based on the average molecular weight of SBO and MHO) of SBO or MHO. Flasks were flushed with a stream of nitrogen and sealed properly. The acidolysis reaction was performed in an orbital shaking water bath at 50 °C and 170 rpm. Reaction mixtures were removed from the water bath after 12 days. The reaction mixture (0.1 mL) was transferred to a 4 mL vial, and the solvent was removed under a stream of nitrogen. The sample was redissolved in 2 mL of methanol/acetonitrile (41:59, v/v) for HPLC-MS analysis.

HPLC-MS Analysis of Synthesized Products. Phenolipids derived from SBO and MHO in the final acidolysis mixture were identified using reversed-phase HPLC-MS according to Sabally et al.[14] with minor modifications. An Agilent 1100 HPLC unit (Agilent Technologies, Palo Alto, CA, USA) with a UV−diode array detector (UV-DAD) was used. Separation was achieved on a C-18 column (4.6 mm × 250 mm coupled with a guard column; Agilent) by gradient elution using a methanol/acetonitrile/isopropanol mobile phase at a flow of 0.8 mL/min; fractions were detected at both 215 and 300 nm. The mobile phase used initially was methanol/acetonitrile/isopropanol (41:59:0, v/v/v), which was maintained for 15 min, but then gradually changed to 16.5:23.5:60 (v/v/v) from 15 to 25 min, then allowed to reach 100% isopropanol from 25 to 35 min, and kept there for 10 min. The mobile phase was changed to its initial components, methanol/acetonitrile/isopropanol (41:59:0, v/v/v) in the next 5 min and was subsequently maintained for 10 min in order to recondition the column. LC flow was further analyzed online by a mass spectrometric detector (LC-MSD-Trap-SL, Agilent) with atmospheric pressure chemical ionization (APCI) at alternative mode for identification of each fraction. The operating conditions used were 121 V for the fragmentor voltage, a drying temperature of 350 °C, an APCI temperature of 400 °C, a nebulizer pressure of 60 psi, and a drying gas flow of 7 L/min.

Purification and Identification of Derivatives of p-Coumaric Acid. Separation of phenolipid components from the final acidolysis mixture was achieved using flash column chromatography in order to investigate the antioxidant activity of produced phenolipids in test systems. The mixture was eluted from a column (40 cm × 5 cm i.d.) packed with silica gel (Selecto Scientific, Suwannee, GA, USA) with a series of solvent mixtures consisting of 350 mL of hexane, 100 mL of hexane/ethyl acetate/formic acid (95:5:2, v/v/v), 400 mL of hexane/ethyl acetate/formic acid (85:15:2, v/v/v), 400 mL of hexane/ethyl acetate/formic acid (75:25:2, v/v/v), and 400 mL of hexane/ethyl acetate/formic acid (65:35:2, v/v/v), in the order stated. Fractions corresponding to each component were collected, and then, solvents were removed using a rotary evaporator.

Antioxidant Activity Tests. DPPH Radical Scavenging Activity. The effect of phenolipid mixtures obtained from SBO (PSBO) and phenolipid mixtures obtained from MHO (PMHO) on the scavenging of DPPH radicals was determined according to the method described by Madhujith and Shahidi[16] with slight modifications. *p*-Coumaric acid was used as a reference in this study. *p*-Coumaric acid, PSBO, and PMHO were dissolved in ethanol in order to attain a concentration of 2.5 mM, which was followed by the addition of 2 mL of ethanolic solution of DPPH (0.18 mM). Contents of each test solution were thoroughly mixed and injected to the sample cavity of a Bruker E-scan electron paramagnetic resonance (EPR) spectrometer (Bruker Biospin Co., Billercia, MA, USA), and the spectrum was recorded after 10 min. Ethanol was used as the control in place of the test compounds. Meanwhile, trolox solutions (12.5−200 mM) were prepared for constructing a standard curve. The operating parameters of the Bruker E-scan were set as follows: 5.02 × 102 receiver gain, 1.86 G modulation amplitude, 2.621 s sweep time, 8 scans, 100.00 G sweep width, 3495.53 G center field, 5.12 ms time constant, 9.795 GHz microwave frequency, and 86.00 kHz modulation frequency. DPPH radical scavenging capacities of test compounds were calculated using the equation shown below:

$$\text{DPPH radical scavenging capacity}(\%) = 100 \times (1 - \text{signal intensity}_{\text{sample}}/\text{signal intensity}_{\text{control}})$$

where the control contained no trolox or test compounds. The DPPH radical scavenging capacities of the test compounds were expressed as millimolar trolox equivalents (TE) per millimolar sample.

ORAC Assay. The determination of ORAC was carried out using a Fluostar optima plate reader (BMG Labtech, Durham, NC, USA) equipped with an incubator and two injector pumps as described by Madhujith and Shahidi.[17] Fluorescein and 2,2′-azobis(2-amino-propane) dihydrochloride (AAPH) were used as the probe and radical generator, respectively. Solutions of *p*-coumaric acid (5 mM), PSBO (5 mM), PMHO (5 mM), and trolox standards (6.25−100 μM) were prepared in 7% (w/v, in H_2O) randomly methylated β-cyclodextrin (RMCD). An aliquot of each solution (20 μL) was injected into a 96-well Costar black plate (Corning Incorporated, Corning, NY, USA), followed by the addition of 75 μL of AAPH (17.2 mg/mL) in phosphate-buffered saline (PBS) (75 mM, pH 7.0). The RMCD solution without antioxidant was used as a blank. Samples were incubated at 37 °C for 10 min prior to the autoinjection of 75 μL of AAPH (17.2 mg/mL in PBS) to each sample. The operating conditions were set as follows: 0.3 s position delay, 8 s orbital shaking before each cycle with 4 mm width, 210 s cycle time, and 48 cycles. Fluorescence was measured at excitation and emission wavelengths of 485 and 520 nm, respectively. A standard curve was constructed from the trolox standards, and the results were expressed as millimolar trolox per millimolar sample.

Determination of Reducing Power. Reducing power of *p*-coumaric acid, PSBO, and PMHO was measured according to Duh et al.[18] with minor modifications. A 1 mL amount of the test compounds (1 mM in 95% ethanol) was transferred to centrifuge tubes containing 2.5 mL of PBS (0.2 M, pH 6.6) and 2.5 mL of potassium ferricyanide solution. The mixture was incubated at 50 °C for 20 min, which was followed by addition of 2.5 mL of trichloroacetic acid (TCA) (10%, w/v), and then, the content was centrifuged at 3000*g* for 10 min. After incubation, a portion (2.5 mL) of the supernatant was transferred to

dx.doi.org/10.1021/jf404140v | J. Agric. Food Chem. 2014, 62, 454−461

the test tube containing 2.5 mL of distilled water and 0.5 mL of ferric chloride (0.1%). The contents were thoroughly mixed, and the absorbance was read at 234 nm using a Hewlett−Packard model 845LA diode array spectrophotometer (Agilent, Palo Alto, CA, USA). Increased absorbance of the reaction mixture indicated increased reducing power. A series of ascorbic acid solutions (1−6 mM in 95% ethanol) were prepared for use in order to construct a standard curve.

Antioxidant Activity in a β-Carotene−Linoleate Model System. Antioxidant activity of *p*-coumaric acid, PSBO, and PMHO was assessed using the β-carotene bleaching assay according to Amarowicz and Shahidi[19] with minor modifications. β-Carotene (10 mg) was dissolved in chloroform (10 mL), and an aliquot (1.0 mL) of this solution was transferred into a 150 mL round-bottom flask containing linoleic acid (20 mg) and Tween 40 (200 mg). A blank without β-carotene was also prepared (20 mg of linoleic acid and 200 mg of Tween 40). After removal of chloroform under a stream of nitrogen, 50 mL of aerated distilled water was added to each flask, and the contents were then thoroughly mixed using a magnetic stirrer. Test compounds (30 μL, 1 mM in ethanol) and the control, ethanol, were injected into the Costar 96-well white plates (Corning Incorporated, Corning, NY, USA). The β-carotene−linoleic acid emulsion and the blank emulsion were injected to the test vials by the built-in injector pump. The absorbance was read immediately after the addition of emulsion to samples at 450 nm by using a Fluostar optima (BMG LABTECH Inc., Durham, NC, USA) plate reader. The operating parameters of the Fluostar optima were set as follows: 24 cycle no., 420 s cycle time, 4 s shaking time, 5 mm orbital width, and 310 μL/s injection speed.

Antioxidant activity of test compounds in protecting β-carotene-linoleic acid against oxidation was calculated using the following equation.

$$\text{Inhibition}(\%) = 100 \times [1 - (A_{s0} - A_{st})/(A_{c0} - A_{ct})]$$

where $A_{s0} - A_{st}$ are corrected absorbance values for test samples measured at zero time and after incubation, respectively; while $A_{c0} - A_{ct}$ are corrected absorbance values for control at zero time and after incubation, respectively.

Inhibition Effect on Copper-Induced LDL Cholesterol Oxidation. The inhibitory activity of *p*-coumaric acid, PSBO, and PMHO against copper-induced LDL cholesterol oxidation was assessed according to Lebeau et al.[20] with minor modifications. Human LDL cholesterol solution was dialyzed in PBS (10 mM, 0.15 M NaCl, pH 7.4) at 4 °C under a nitrogen blanket for 12 h. Sample solutions were prepared by dissolving the test compounds in ethanol at 1.0 mM. Sample solutions (10 μL) were transferred into Eppendorf tubes, and the solvent was removed under a stream of nitrogen. To each tube, 100 μL of PBS was added, followed by vortexing for 1 min. An aliquot (0.8 mL of the dialyzed and diluted LDL cholesterol solution (0.125 mg/mL)) was added to each tube; the contents were mixed well and incubated at 37 °C for 15 min. The induced oxidation reaction was initiated by the addition of 100 μL of $CuSO_4$ solution (20 μM, previously incubated at 37 °C). A blank containing only the sample without LDL or $CuSO_4$ was prepared for each test compound. After incubation of the reaction mixture at 37 °C for 22 h, the conjugated dienes formed were measured spectrophotometrically at 234 nm using a Hewlett−Packard model 8452A diode array spectrophotometer. Antioxidant activities of test compounds were expressed as percentage inhibition of conjugated dienes formation, as calculated according to the following equation:

$$\text{Inhibition } (\%) = 100 \times (A_{\text{control}} - A_{\text{sample}})/(A_{\text{control}} - A_{\text{native LDL}})$$

where the control contained LDL cholesterol and $CuSO_4$ without antioxidants and native LDL cholesterol contained LDL cholesterol only. All absorbance values for samples were blank-corrected.

Inhibition Effect on Radical-Induced DNA Scission. Antioxidant activity of *p*-coumaric acid, PSBO, and PMHO against radical-induced DNA scission was determined as described by Zhong and Shahidi[21] with slight modifications. Oxidation and nicking of DNA strands was induced by hydroxyl and peroxyl radicals and monitored by gel electrophoresis, respectively. For hydroxyl radical induced DNA oxidation, 2 μL of ethanolic solution (15 μM) of test compounds was added into a 0.5 mL Eppendorf tube, and the solvent was then removed under a stream of nitrogen. To the tube, 2 μL of PBS (0.5 M, pH 7.4) was added followed by thorough vortexing for 1 min. The following reagents were subsequently added to the tube in the order stated: 2 μL of PBS (0.5 M, pH 7.4), 4 μL of supercoiled pBR322 DNA (20 μg/mL in PBS), 2 μL of H_2O_2 (0.5 mM), and 2 μL of Fe_2SO_4 (0.5 mM). The mixture was then incubated at 37 °C for 1 h. For peroxyl radical induced DNA oxidation, a higher concentration (50 μM) of samples was used, and H_2O_2 and Fe_2SO_4 were replaced with 4 μL of AAPH (9 mM). A blank (containing only DNA) and a control (containing DNA and one of the radicals) were also prepared for both assays.

Upon completion of the incubation, l μL of loading dye (0.25% bromophenol blue/0.25% xylene cyanol/50% glycerol) was added, and the whole mixture was centrifuged and loaded onto an agarose gel, which was prepared by dissolving 0.7% (w/v) agarose in Tris−acetic acid−ethylenediaminetetraacetic acid (EDTA) buffer (TAE, pH 8.5) and stained with SYBR safe gel stain (1:10 000, v/v). Gel electrophoresis was performed at 80 V for 80 min in TAE buffer using a horizontal submarine gel electrophoresis apparatus (Sigma−Aldrich Canada Ltd., Oakville, ON, Canada). The DNA bands were visualized under ultraviolet light. Images were photographed by a GelDoc apparatus equipped with a Sony digital camera and analyzed using AlphaEase stand-alone software (Alpha Innotech Co., San Leandro, CA, USA). The intensity of the bands (obtained from a densitometer) was used as an indicator of the concentration of the supercoiled and nicked DNA fractions. Antioxidant activity was calculated as percent retention of DNA according to the following equation:

$$\text{Retention } (\%) = 100 \times (\text{intensity of supercoiled DNA}_{\text{sample}}/\text{intensity of supercoiled DNA}_{\text{blank}})$$

RESULTS AND DISCUSSION

Identification of Phenolipids. The HLPC profiles of samples were monitored by a UV detector at both 215 and 300 nm. Each compound was identified by comparing its retention time with that of its corresponding standard and/or the characterization of the molecular ion so generated from mass spectrometry. The major phenolipid compounds derived from *p*-coumaric acid are listed in Table 1, which include eight phenolic monoacylglycerols and eight phenolic diacylglycerols. The mass spectra of the representative identified ions and their corresponding chemical structures are shown in Figure 1. Although esterification of the hydroxyl group of *p*-coumaric acid with the released fatty acid is possible, formation of such products was not evident.

DPPH Radical Scavenging Activity. The DPPH radical scavenging assay is frequently used for examining antioxidant activity because of the relatively short analysis time required.[22] Phenolic compounds may act as free radical scavengers by virtue of their hydrogen atom donating ability.[23] The strong DPPH radical scavenging capacity of *p*-coumaric acid has been reported by Fukumoto and Mazza.[24]

The results of the DPPH radical scavenging assay on test compounds are summarized in Figure 2. The signal intensity in the EPR spectra of the DPPH radical as affected by the test compounds decreased significantly, which revealed the scavenging capacity of *p*-coumaric acid and its lipid derivatives on DPPH radicals. All test compounds exhibited effective DPPH radical scavenging activity. When comparing the scavenging capacity of *p*-coumaric acid and its derivatives, *p*-coumaric acid demonstrated a significantly lower ($P < 0.05$) capacity as trolox equivalents than both PSBO and PMHO.

Table 1. Lipid Derivatives of *p*-Coumaric Acid Identified in Both Acidolysis Mixtures of *p*-Coumaric Acid with SBO and MHO

phenolipid	fragmentation pattern	*m/z*
Phenolic Monoacylglycerol		
monomyristyl *p*-coumarate[b]	$[M + H - H_2O]^+$	431.3
monocetyl *p*-coumarate[c]	$[M + H - H_2O]^+$	459.3
monopalmitoleyl *p*-coumarate[c]	$[M + H - H_2O]^+$	457.3
monostearyl *p*-coumarate[c]	$[M + H - H_2O]^+$	487.3
monooleyl *p*-coumarate[c]	$[M + H - H_2O]^+$	485.3
monolinoleyl *p*-coumarate[b]	$[M + H - H_2O]^+$	483.3
monoeicosenyl *p*-coumarate[c]	$[M + H - H_2O]^+$	513.3
monoeicosapentaenyl *p*-coumarate[c]	$[M]^+$	523.5
Phenolic Diacylglycerol		
dimyristyl *p*-coumarate[c]	$[M]^+$	661.5
myristyl myristeyl *p*-coumarate[b]	$[M + H - H_2O]^+$	639.5
myristeyl cetyl *p*-coumarate[a]	$[M + H - H_2O]^+$	667.5
myristyl cetyl *p*-coumarate[b]	$[M + H - H_2O]^+$	669.5
cetyl palmitoleyl *p*-coumarate[a]	$[M + H - H_2O]^+$	695.5
myristeyl elaidolinolenyl *p*-coumarate[b]	$[M + H - H_2O]^+$	689.5
myristeyl stearidonyl *p*-coumarate[a]	$[M + H - H_2O]^+$	687.5
myristeyl eicosapentaenyl *p*-coumarate[b]	$[M + H - H_2O]^+$	713.5

[a]Indicates phenolipid compounds derived only from SBO. [b]Indicates phenolipid compounds derived only from MHO. [c]Indicates phenolipid compounds derived from both SBO and MHO; $[M + H - H_2O]^+$ resulting from the loss of a molecule of H_2O and addition of a proton; and $[M]^+$ resulting from the loss of an electron.

Meanwhile, PMHO showed superior DPPH radical scavenging activity compared to PSBO. Lipophilicity of phenolic compounds plays an important role in their antioxidant activity in certain systems; higher lipophilicity of phenolic compounds may lead to greater antioxidant activity.[25] In this case, esterification of *p*-couamric acid improved its lipophilicity, and thus, its lipid derivatives showed higher DPPH radical scavenging capacity. Although the improved lipophilicity of PSBO and PMHO may extend their application in more lipophilic environments, further investigation is required to obtain a better understanding of their antioxidant efficacy in different model systems and test media.

ORAC. *p*-Coumaric acid and its derivatives PSBO and PMHO demonstrated strong activity in the DPPH radical scavenging assay. However, the results obtained from the DPPH assay may not well reflect the antioxidant capacity of these compounds in the real food and biological systems, where the lifetime of their radicals are much shorter than the stable and artificial DPPH radical.[26] Therefore, the radical scavenging efficacy of *p*-coumaric acid and its derivatives was further evaluated by an oxygen radical (peroxyl radical) absorbance capacity assay, which uses a biologically relevant radical source.[21]

Dávalos et al.[27] reported that the ORAC value of *p*-coumaric acid was 4.5 fold that of trolox, which was 2 times higher than that of BHA. The ORAC values of *p*-coumaric acid and its lipid derivatives are summarized in Figure 2. All test compounds exhibited strong peroxyl radical scavenging activity. Both PSBO and PMHO showed significantly higher ($P < 0.05$) ORAC values than *p*-coumaric acid, and the trend of the results was correlated with the result of the DPPH radical scavenging assay. The improved antioxidant activity of PSBO and PMHO may be caused by changes of chemical and physical characteristics of the lipid derivatives, such as lipophilicity, electron distribution, and steric effect. For instance, the improved lipophilicity may have a positive effect on radical scavenging activity as higher lipophilicity of phenolic compounds may lead to improved antioxidant activity.[25] However, the weak electron-donating ester group may compromise the hydrogen-donation activity of *p*-coumaric acid, which leads to lower antioxidant activity.[28] It appears that the weaker hydrogen atom donating ability caused by the ester group was overwhelmed by the effect of improved lipophilicity, and thus, a postitive effect of esterification on peroxyl radical scavenging capacity became evident.

Reducing Power. The ferric reducing antioxidant power assay is frequently employed to assess the efficiency of antioxidants for their electron transfer capacity. The reducing power of antioxidants and its measurement is based on the reduction of Fe^{3+} to Fe^{2+} by antioxidants in an acidic environment.[28,29]

p-Coumaric acid demonstrated strong reducing power in the study conducted by Medina et al.[30] In this work, the results summarized in Figure 3 show effective reducing power of *p*-coumaric acid and its derivatives. Compared to *p*-coumaric acid, PSBO did not show significant difference ($P > 0.05$), and PMHO showed significantly higher ($P < 0.05$) reducing power. This phenomenon may be caused by the decrease of the ionization potential of *p*-coumaric acid when it was esterified to bulky acylglycerol substituents[31] as decreased ionization potential facilitates the electron transfer in PMHO and PSBO. The results of the reducing power of PSBO and PMHO are correlated with those of both DPPH radical scavenging and ORAC assays as shown in Figure 2. However, the reducing power of PSBO is not significantly different from that of *p*-coumaric acid, which may partially be due to the decreased hydrophilicity of *p*-coumaric acid after esterification in the aqueous test system. In the reducing power assay, the capacity of an antioxidant is strongly solvent-dependent as the solvent facilitates the stability of charged ions.[28] The reducing power of derivatives might be compromised under the hydrophilic test environment; however, such an effect was overwhelmed by the effect of decreased ionization potential.

Antioxidant Activity in a β-Carotene−Linoleate Model System. High surface-to-volume ratio of oil-in-water emulsions normally occurs in food systems. Therefore, it is essential to investigate the effectiveness of antioxidants in oil-in-water emulsions to achieve a comprehensive assessment of their antioxidant activity prior to their application in food systems.[25]

Gadow et al.[32] studied the antioxidant activity of *p*-coumaric acid in the β-carotene−linoleic acid model system and reported its strong inhibitory effect on β-carotene bleaching. In this work, the results (Figure 4) indicated that PSBO inhibited the bleaching of β-carotene by 50.1% over the entire incubation period, followed by PMHO (12.2%) and *p*-coumaric acid (8.35%). On the basis of the "polar paradox" theory, nonpolar antioxidants exhibit higher efficacy than that of polar ones in emulsion systems, which implies that the derivatives with improved lipophilicity may exhibit a higher inhibitory effect on β-carotene bleaching than *p*-coumaric acid.[21] However, the efficacy of an antioxidant is also determined by its hydrogen-donation capacity. In this case, esterification of *p*-coumaric acid may have changed the surrounding molecular structure of its hydroxyl group on the aromatic ring as well as the bond dissociation enthalpy of the O−H bond. The steric hindrance to the hydroxyl group and the changed bond dissociation enthalpy of the O−H bond may decrease the hydrogen atom donation capacity and lead to compromised antioxidant activity

dx.doi.org/10.1021/jf404140v | J. Agric. Food Chem. 2014, 62, 454−461

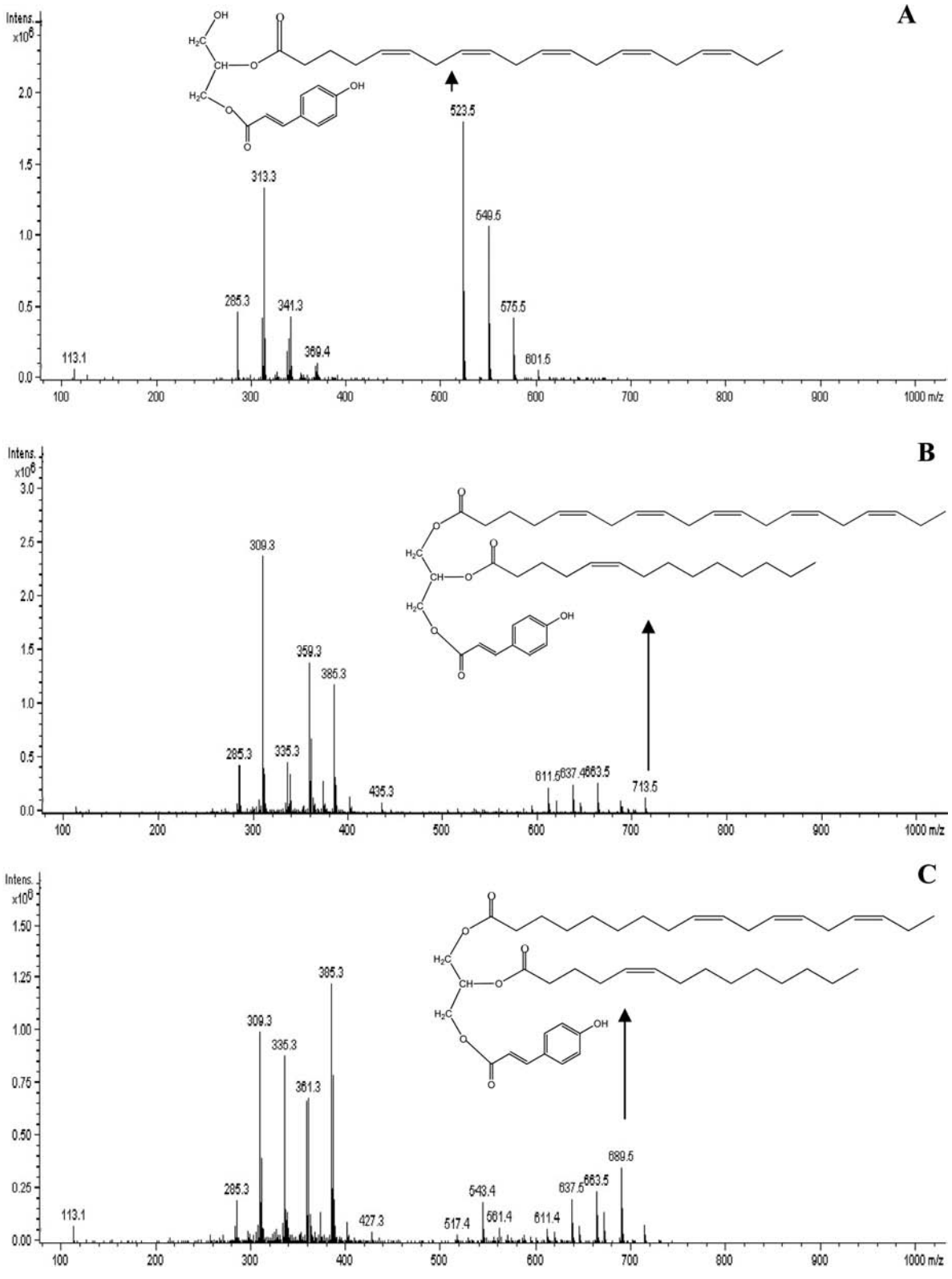

Figure 1. Chemical structures and mass spectrometric data of (A) monoeicosapentaenyl *p*-coumarate, (B) myristeyl eicosapentaenyl *p*-coumarate, and (C) myristeyl elaidolinolenyl *p*-coumarate.

of the test lipid derivatives. This may partially explain that the inhibitory activity of PMHO on β-carotene bleaching did not show any significant difference ($P > 0.05$) compared to that of *p*-coumaric acid.

Inhibitory Effect on Human LDL Cholesterol Oxidation. LDL cholesterol is one of the five major cholesterol carriers in the blood. It has been proven that the risk of atherosclerosis is positively associated with the increased plasma level of LDL.[33] The oxidized products of LDL have

dx.doi.org/10.1021/jf404140v | J. Agric. Food Chem. 2014, 62, 454−461

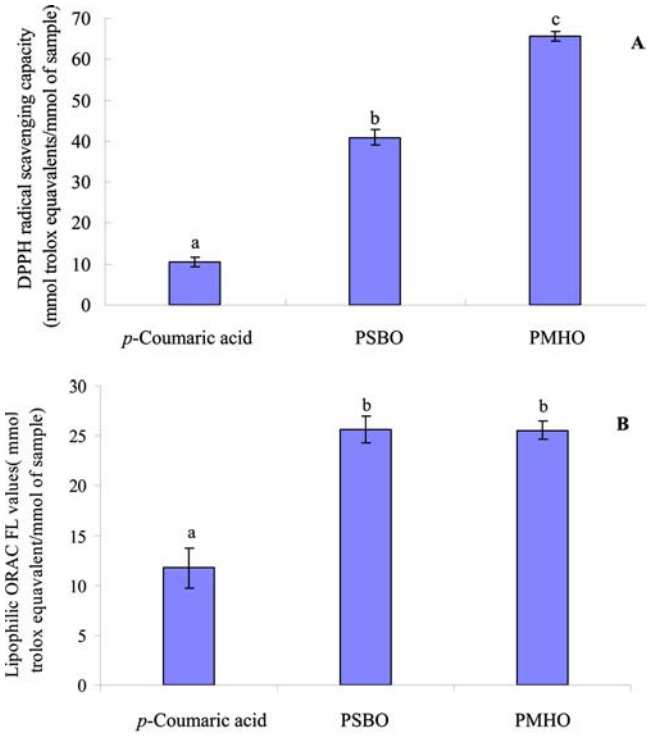

Figure 2. (A) DPPH radical scavenging capacity and (B) oxygen radical absorbance capacity of *p*-coumaric acid, PSBO (phenolipids mixture obtained from SBO), and PMHO (phenolipids mixture obtained from MHO) as trolox equivalents (TE); bars with different letters are significantly different ($P < 0.05$).

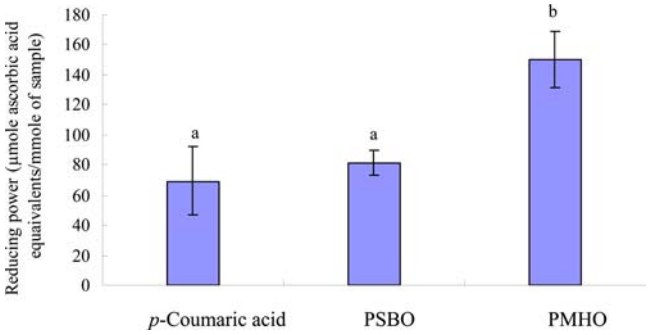

Figure 3. Reducing power of *p*-coumaric acid, PSBO (phenolipids mixture obtained from SBO), and PMHO (phenolipids mixture obtained from MHO) as ascorbic acid equivalents; bars with different letters are significantly different ($P < 0.05$).

been recognized as contributors to the formation of atherosclerotic plaques in arteries, hence providing incentive for preventing LDL oxidation.[34] Dietary antioxidants such as phenolic acids are believed to be effective inhibitors of LDL oxidation caused by free radical attack.[35−37]

In this work, the inhibitory effects of *p*-coumaric acid, PSBO, and PMHO on Cu^{2+}-induced LDL cholesterol oxidation were evaluated, and the results are summarized in Figure 5. LDL cholesterol was oxidized to different levels at the end of a 22 h incubation period, which depended on the type of antioxidant added to the samples. All test compounds showed high inhibitory capacity on LDL cholesterol oxidation. Inhibition percentage of LDL cholesterol upon addition of *p*-coumaric acid was 37.3%, which is much higher than the value reported by Andreasen et al.[35] due to the higher concentration of *p*-

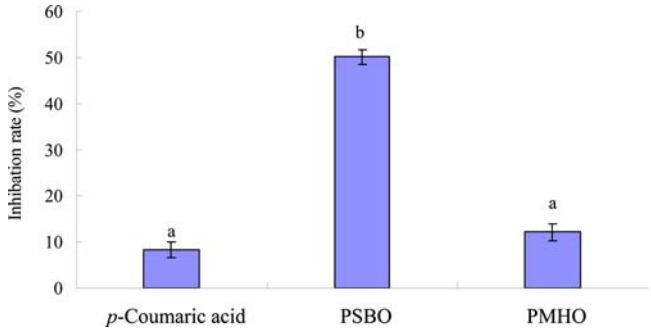

Figure 4. Inhibitory effects of *p*-coumaric acid, PSBO (phenolipids mixture obtained from SBO), and PMHO (phenolipids mixture obtained from MHO) against β-carotene bleaching; bars with different letters are significantly different ($P < 0.05$).

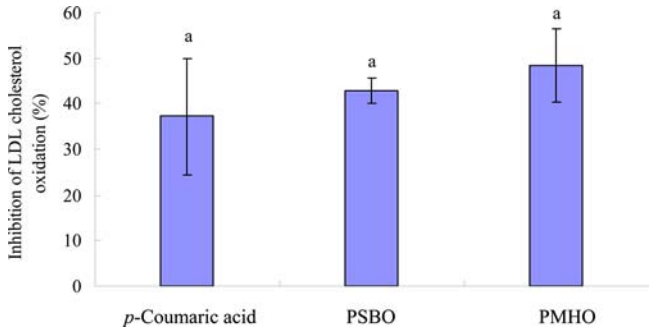

Figure 5. Inhibitory effect of *p*-coumaric acid, PSBO (phenolipids mixture obtained from SBO), and PMHO (phenolipids mixture obtained from MHO) on LDL cholesterol oxidation; bars with different letters are significantly different ($P < 0.05$).

coumaric acid employed in this work. Meanwhile, the inhibition percentages shown by derivatives of *p*-coumaric acid PSBO and PMHO were 42.8% and 48.4%, respectively, which are not significantly higher than that of *p*-coumaric acid ($P > 0.05$). The slightly improved inhibitory capacity of PSBO and PMHO against LDL cholesterol oxidation may be due to their improved lipophilicity as the higher lipophilicity allowed these lipid derivatives to have greater affinity to the major components on the surface of LDL cholesterol, that is, the phospholipids. Moreover, hydrophilic *p*-coumaric acid and a lipophilic fatty acid chain may lead to better amphiphilicity of the lipid derivatives, which further allowed them to exert their antioxidant activities within the LDL particles and/or on the surface of LDL cholesterol.[21] Thus, the potential use of PSBO and PMHO as antiatherosclerosis agents is supported by their high inhibitory activity on LDL cholesterol oxidation.

DNA Scission Assay. Oxidative stress in cells caused by reactive oxygen species such as hydroxyl and peroxyl radicals leads to DNA damage. Hydroxyl and peroxyl radicals react with DNA by possible addition to double bonds of DNA bases or abstraction of a hydrogen atom from the methyl group of thymine, among others.[38] Therefore, oxidative damage of DNA may occur at both the nucleotide bases and the phosphate backbone resulting in strand breakage and sister chromatid exchange, DNA−DNA and DNA−protein cross-linking, and base modification.[39] A background level of oxidative DNA damage is an inevitable consequence of cellular metabolism and can be repaired in normal tissues. However, the oxidative stress caused by excess free radicals may lead to severe DNA damage, which is implicated in mutagenesis, carcinogenesis, and

dx.doi.org/10.1021/jf404140v | J. Agric. Food Chem. 2014, 62, 454−461

cytostasis. Thus, the effect of various antioxidants such as phenolic acids on DNA oxidation inhibitory activity has been widely studied.[40,41]

In this study, the inhibitory activity of *p*-coumaric acid, PSBO, and PMHO on hydroxyl and peroxyl radical induced supercoiled DNA strand oxidation was evaluated, and the results are shown in Figures 6 and 7. The oxidative damage

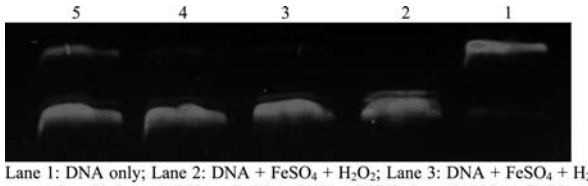

Lane 1: DNA only; Lane 2: DNA + $FeSO_4$ + H_2O_2; Lane 3: DNA + $FeSO_4$ + H_2O_2 + *p*-coumaric acid; Lane 4: DNA + $FeSO_4$ + H_2O_2 + PSBO; Lane 5: DNA + $FeSO_4$ + H_2O_2 + PMHO.

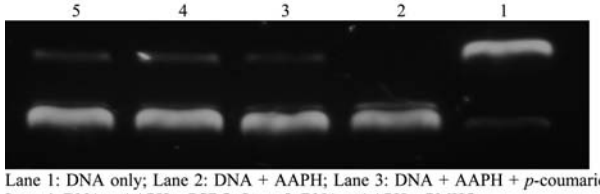

Lane 1: DNA only; Lane 2: DNA + AAPH; Lane 3: DNA + AAPH + *p*-coumaric acid; Lane 4: DNA + AAPH + PSBO; Lane 5: DNA + AAPH + PMHO.

Figure 6. Inhibitory effect of *p*-coumaric acid, PSBO (phenolipids mixture obtained from SBO), and PMHO (phenolipids mixture obtained from MHO) on radical-induced DNA scission (top: hydroxyl-induced DNA scission; bottom: peroxyl-induced DNA scission).

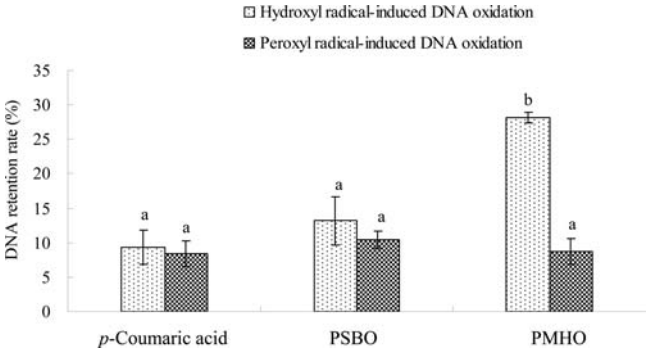

Figure 7. DNA retention rate (%) in radical-induced oxidative scission; bars within the same group with different letters are significantly different ($P < 0.05$); PSBO: phenolipids mixture obtained from SBO; PMHO: phenolipids mixture obtained from MHO.

caused by hydroxyl and peroxyl radicals led to supercoiled plasmid DNA strand nicking and formation of a nicked open circular form as a result of single strand cleavage. At higher concentrations, the free radicals can even cause double-bond breakage and convert the supercoiled plasmid DNA strand to a linear form of DNA. However, no linear form of DNA was observed due to the modest concentration of radicals employed in the test. The results from Figure 7 showed effective DNA retention in all test compounds in hydroxyl radical induced DNA tests due to their high radical scavenging capacity and for eliminating hydroxyl radicals generated from H_2O_2 through the Fenton reaction.[42] Of these, the lipid derivatives PSBO showed a slightly higher retention percentage than *p*-coumaric acid at an insignificant level ($P > 0.05$); meanwhile, PMHO exhibited a significantly ($P < 0.05$) higher retention percentage than *p*-coumaric acid. The trend of retention percentage of *p*-coumaric acid and its lipid derivatives in hydroxyl radical induced DNA nicking is positively correlated to that of the inhibitory effect of these compounds in the LDL cholesterol oxidation assay, which may result from the greater amphiphilic nature of these lipid derivatives.

The oxidation of supercoiled DNA was also successfully induced by peroxyl radical and resulted in the occurrence of nicked open circular DNA at the end of incubation, but no linear DNA was observed (Figure 6). All test compounds showed high retention of DNA. The derivatives, PSBO and PMHO, exhibited a slightly higher inhibitory capacity compared to *p*-coumaric acid although this was statistically insignificant ($P > 0.05$) (Figure 7). The different performance of test compounds on DNA retention between hydroxyl and peroxyl radical induced DNA oxidation may be due to the better stability of the peroxyl radical compared to the hydroxyl radical that helps it reach specific targets before being degraded or eliminated.

Derivatives of *p*-coumaric acid PSBO and PMHO showed variable levels of antioxidant capacity due to different antioxidant mechanisms involved in different testing systems employed. The improved lipophilicity and the decreased ionization potential of the lipid derivatives are the major factors that lead to the changes of antioxidant efficacy of *p*-coumaric acid. The good antioxidant activity of the phenolipids obtained from the acidolysis of *p*-coumaric acid with SBO and MHO, displayed in different assays employed, suggests that the phenolipids so produced may be used as potential ingredients in functional foods, supplements, or cosmetics for health promotion and disease risk reduction.

AUTHOR INFORMATION

Corresponding Author

*Phone: 1 (709) 864-8552; fax: 1 (709) 864-4000; e-mail: fshahidi@mun.ca.

Funding

F.S. thanks the Natural Sciences and Engineering Research Council (NSERC) of Canada for financial support in the form of a discovery grant.

Notes

The authors declare no competing financial interest.

REFERENCES

(1) Wanasundara, U. N.; Shahidi, F. Stabilization of seal blubber and menhaden oils with green tea catechins. *J. Am. Oil Chem. Soc.* **1996**, *73*, 1183−1190.

(2) Shahidi, F.; Miraliakbari, H. Omega-3 fatty acids in health and disease: Part 2−health effects of omega-3 fatty acids in autoimmune diseases, mental health, and gene expression. *J. Med. Food* **2005**, *8*, 133−148.

(3) Wanasundara, U. N.; Shahidi, F. Positional distribution of fatty acids in triacylglycerols of seal blubber oil. *J. Food Lipids* **1997**, *4*, 51−64.

(4) Reiffel, J. A.; McDonald, A. Antiarrhythmic effects of omega-3 fatty acids. *Am. J. Cardiol.* **2006**, *98*, 50−60.

(5) Kim, H. Y.; Edsall, L. The role of docosahexaenoic acid (22:6n-3) in neural signaling. *Lipids* **1999**, *34*, 249−250.

(6) Shahidi, F.; Ke, P. J.; Zhao, X.; Yang, Z.; Wanasundara, P. K. J. P. D Antioxidative activity of green and black tea in meat model systems. In *Proceedings of the 38th International Congress of Meat Science and Technology*, Clermont-Ferrand, France, 1992; pp 599−602.

(7) Lindenschmidt, R. C.; Tryka, A. F.; Goad., M. E.; Witschi, H. P. The effects of dietary butylatedhydroxytoluene on liver and colon tumor development in mice. *Toxicology* **1986**, *38*, 151−160.

(8) Bauer, A. K.; Dwyer-Nield, L. D.; Keil, K.; Koski, K.; Malkinson, A. M. Butylated hydroxytoluene (BHT) induction of pulmonary inflammation: A role in tumor promotion. *Exp. Lung Res.* **2001**, *27*, 197−216.
(9) Hirose, M.; Yada, H.; Hakoi, K.; Takahashi, S.; Ito, N. Modification of carcinogenesis by α-tocopherol, t-butylhydro-quinone, propyl gallate and butylated hydroxytoluene in a rat multi-organ carcinogenesis model. *Carcinogenesis* **2010**, *14*, 2359−2364.
(10) Ferguson, L. R.; Shuo-tun, Z.; Harris, P. J. Antioxidant and antigenotoxic effects of plant cell wall hydroxycinnamic acids in cultured HT-29. *Mol. Nutr. Food Res.* **2005**, *49*, 585−693.
(11) Kikugawa, K.; Hakamada, T.; Hasunuma, M.; Kurechi, T. Reaction of *p*-hydroxycinnamic acid derivatives with nitrite and its relevance to nitrosamine formation. *J. Agric. Food Chem.* **1983**, *1*, 780−785.
(12) Rosskopf, F.; Kraus, J.; Franz, G. Immunological and antitumor effects of coumarin and some derivatives. *Pharmazie* **1992**, *47*, 139−142.
(13) Senanayake, S. P. J. N.; Shahidi, F. Enzyme-catalyzed synthesis of structured lipids via acidolysis of seal (*Phoca groenlandica*) blubber oil with capric acid. *Food Res. Int.* **2002**, *35*, 745−752.
(14) Sabally, K.; Karboune, S.; St-Louis, R.; Kermasha, S. Lipase-catalyzed transesterification of dihydrocaffeic acid with flaxseed oil for the synthesis of phenolic lipids. *J. Biotechnol.* **2006**, *127*, 167−176.
(15) Safari, M.; Karboune, S.; St-Louis, R.; Kermasha, S. Enzymatic synthesis of structured phenolic lipids by incorporation selected phenolic acids into triolein. *Biocatal. Biotransform.* **2006**, *24*, 272−279.
(16) Madhujith, T.; Shahidi, F. Optimization of the extraction of antioxidative constituents of six barley cultivars and their antioxidant properties. *J. Agric. Food Chem.* **2006**, *54*, 8048−8057.
(17) Madhujith, T.; Shahidi, F. Antioxidative and antiproliferative properties of selected barley (*Hordeum vulgarae* L.) cultivars and their potential for inhibition of low density lipoprotein (LDL) cholesterol oxidation. *J. Agric. Food Chem.* **2007**, *55*, 5018−5024.
(18) Duh, P. D.; Yen, C. G.; Yen, W. J.; Chang, L. W. Antioxidant effects of water extracts from barley *Hordeum vulgare* L. prepared under different roasting temperatures. *J. Agric. Food Chem.* **2001**, *49*, 1455−1463.
(19) Amarowicz, R.; Shahidi, F. Antioxidant activity of green tea catechins in a β-carotene-linoleate model system. *J. Food Lipids* **1995**, *2*, 47−56.
(20) Lebeau, J.; Furman, C.; Bernier, J. L.; Duriez, P.; Teissier, E.; Cotelle, N. Antioxidant properties of di-tert-butylhydroxylated flavonoids. *Free Radical Biol. Med.* **2000**, *29*, 900−912.
(21) Zhong, Y.; Shahidi, F. Lipophilised epigallocatechin gallate (EGCG) derivatives and their antioxidant potential in food and biological systems. *Food Chem.* **2012**, *131*, 22−30.
(22) Chen, Y.; Wang, M.; Rosen, R. T.; Ho, C. T. 2,2-Diphenyl-1-picrylhydrazyl radical-scavenging active components from *Polygonum multiflorum Thunb*. *J. Agric. Food Chem.* **1999**, *47*, 2226−2228.
(23) Castelluccio, C.; Bolwell, G. P.; Gerrish, C.; Rice-Evans, C. Differential distribution of ferulic acid to the major plasma constituents in relation to its potential as an antioxidant. *Biochem. J.* **1996**, *316*, 691−694.
(24) Fukumoto, L. R.; Mazza, G. Assessing antioxidant and prooxidant activities of phenolic Compounds. *J. Agric. Food Chem.* **2000**, *48*, 3597−3604.
(25) Zhong, Y.; Shahidi, F. Lipophilized epigallocatechin gallate (EGCG) derivatives as novel antioxidants. *J. Agric. Food Chem.* **2011**, *59*, 6526−6533.
(26) Tan, Z.; Shahidi, F. Chemoenzymatic synthesis of phytosteryl ferulates and evaluation of their antioxidant activity. *J. Agric. Food Chem.* **2011**, *59*, 12375−12383.
(27) Dávalos, A.; Gómez-Cordovés, C.; Bartolomé, B. Extending applicability of the oxygen radical absorbance capacity (ORAC−fluorescein) assay. *J. Agric. Food Chem.* **2004**, *52*, 48−54.
(28) Wright, J. S.; Johnson, E. R.; DiLabio, G. A. Predicting the activity of phenolic antioxidants: Theoretical method, analysis of substituent effects, and application to major families of antioxidants. *J. Am. Chem. Soc.* **2001**, *123*, 1173−1183.
(29) Wojdylo, A.; Oszmiański, J.; Czemerys, R. Antioxidant activity and phenolic compounds in 32 selected herbs. *Food Chem.* **2007**, *105*, 940−949.
(30) Medina, I.; Gallardo, J. M.; González, M. J.; Lois, S.; Hedges, N. Effect of molecular structure of phenolic families as hydroxycinnamic acids and catechins on their antioxidant effectiveness in minced fish muscle. *J. Agric. Food Chem.* **2007**, *55*, 3889−3895.
(31) Sato, N.; Saito, G.; Inokuchi, H. Ionization potentials and polarization energies of tetraselenafulvalene (TSF) derivatives determined from ultraviolet photoelectron spectroscopy. *Chem. Phys.* **1983**, *76*, 79−88.
(32) Gadow, A.; Joubert, E.; Hansmann, C. F. Comparison of the antioxidant activity of aspalathin with that of other plant phenols of rooibos tea (*Aspalathus linearis*), α-tocopherol, BHT, and BHA. *J. Agric. Food Chem.* **1997**, *45*, 632−638.
(33) Ross, R. The pathogenesis of atherosclerosis: A perspective for the 1990s. *Nature* **1993**, *362*, 801−809.
(34) Esterbauer, H.; Gebicki, J.; Puhl, H.; Jürgens, G. The role of lipid peroxidation and antioxidants in oxidative modification of LDL. *Free Radical Biol. Med.* **1992**, *13*, 341−390.
(35) Andreasen, M. F.; Landbo, A.; Christensen, L. P.; Hansen, A.; Meyer, A. S. Antioxidant effects of phenolic rye (*Secale cereale* L.) extracts, monomeric hydroxycinnamates, and ferulic acid dehydrodimers on human low-density lipoproteins. *J. Agric. Food Chem.* **2001**, *49*, 4090−4096.
(36) Nardini, M.; D'Aquino, M.; Tomassi, G.; Gentili, V.; Felice, M. D.; Scaccini, C. Inhibition of human low-density lipoprotein oxidation by caffeic acid and other hydroxycinnamic acid derivatives. *Free Radical Biol. Med.* **1995**, *19*, 541−552.
(37) Slavin, J.; Jacobs, D.; Marquart, L. Whole-grain consumption and chronic disease: Protective mechanisms. *Nutr. Cancer* **1997**, *27*, 14−21.
(38) Cooke, M. S.; Evens, M. D.; Dizdaroglu, M.; Lune, J. Oxidative DNA damage: Mechanisms, mutation, and disease. *FASEB J.* **2003**, *17*, 1195−1214.
(39) Dizdaroglu, M. Chemistry and free radical damage to DNA and nucleoproteins. In *DNA and Free Radicals*; Halliwell, B., Aruoma, O. I., Eds.; Ellis Harwood: Chichester, U.K., 1993; pp 19−39.
(40) Lodovici, M.; Guglielmi, F.; Meoni, M.; Dolara, P. Effect of natural phenolic acids on DNA oxidation *in vitro*. *Food Chem. Toxicol.* **2001**, *39*, 1205−1210.
(41) Nabi, G.; Liu, Z.-q. Ferulic and couamric acids: Application to release oxidative stress of DNA and methyl linoleate. *J. Food Biochem.* **2012**, *36*, 38−45.
(42) Perron, N. R.; Hodges, J. N.; Jenkins, M.; Brumaghim, J. L. Predicting how polyphenol antioxidants prevent DNA damage by binding to iron. *Inorg. Chem.* **2008**, *47*, 6153−6161.

JOURNAL OF AGRICULTURAL AND FOOD CHEMISTRY

Article

pubs.acs.org/JAFC

Inhibitory Effects of 4-Hydroxyderricin and Xanthoangelol on Lipopolysaccharide-Induced Inflammatory Responses in RAW264 Macrophages

Michiko Yasuda,[†,⊥] Kyuichi Kawabata,*[,‡] Miki Miyashita,[‡] Mayu Okumura,[‡] Norio Yamamoto,[§] Masakazu Takahashi,[‡] Hitoshi Ashida,[∥] and Hajime Ohigashi[‡]

[†]Organization of Advanced Science and Technology, Kobe University, 1-1 Rokkodai-cho, Nada-ku, Kobe 657-8501, Japan

[‡]Department of Bioscience, Faculty of Biotechnology, Fukui Prefectural University, 4-1-1 Matsuoka Kenjojima, Eiheiji-cho, Yoshida-gun, Fukui 910-1195, Japan

[§]Food Science Research Center, House Wellness Foods Corporation, 3-20 Imoji, Itami, Hyogo 664-0011, Japan

[∥]Department of Agrobioscience, Graduate School of Agricultural Science, Kobe University, 1-1 Rokkodai-cho, Nada-ku, Kobe 657-8501, Japan

ABSTRACT: The Japanese herb, Ashitaba (*Angelica keiskei* Koidzumi), contains two prenylated chalcones, 4-hydroxyderricin and xanthoangelol, which are considered to be the major active compounds of Ashitaba. However, their effects on inflammatory responses are poorly understood. In the present study, we investigated the effects and underlying molecular mechanisms of 4-hydroxyderricin and xanthoangelol on lipopolysaccharide (LPS)-induced inflammatory responses in RAW264 mouse macrophages. LPS-mediated production of nitric oxide (NO) was markedly reduced by 4-hydroxyderricin (10 μM) and xanthoangelol (5 μM) compared with their parent compound, chalcone (25 μM). They also inhibited LPS-induced secretion of tumor necrosis factor-alpha (TNF-α) and expression of inducible NO synthase (iNOS) and cyclooxygenase-2 (COX-2). Although chalcone decreased the DNA-binding activity of both activator protein-1 (AP-1) and nuclear factor-kappa B (NF-κB), 4-hydroxyderricin and xanthoangelol suppressed only AP-1 and had no effect on NF-κB. On the other hand, all of the tested chalcones reduced the phosphorylation (at serine 536) level of the p65 subunit of NF-κB. 4-Hydroxyderricin and xanthoangelol may be promising for the prevention of inflammatory diseases.

KEYWORDS: *4-hydroxyderrin, xanthoangelol, Angelica keiskei Koidzumi (Ashitaba), anti-inflammation, NF-κB, AP-1*

INTRODUCTION

Chronic inflammation plays a critical role in the development of several diseases, including asthma, rheumatoid arthritis, atherosclerosis, inflammatory bowel diseases, and various human cancers.[1] Infection or injury stimulates inflammatory cells to produce proinflammatory mediators, such as NO, reactive oxygen species, prostaglandins, and cytokines.[2] AP-1 and NF-κB are well-known to be an important regulator of the expression of iNOS, COX-2, and TNF-α.[3−5]

Natural dietary sources, such as fruits, vegetables, herbs, and spices, have been reported to provide beneficial effects for human health,[1,2,4] thus drawing attention for their prevention against various diseases. Many types of compounds, including 1′-acetoxychavicol acetate (a phenylpropanoid derived from ginger),[6] nobiletin (a citrus polymethoxyflavonoid),[6] and xanthohumol (a prenylated chalcone contained in hop),[7] exhibit anti-inflammatory activity and decrease the transcriptional activity of AP-1 and NF-κB in inflammatory cells.

The Japanese herb, Ashitaba (*Angelica keiskei* Koidzumi, Apiaceae), is a perennial plant grown along the Pacific coast of Japan (Izu islands and the Izu, Bouso, and Miura peninsulas). Ashitaba is enriched with numerous active compounds such as coumarins, flavanones, and chalcones. Among these compounds, prenylated chalcones 4-hydroxyderricin and xanthoangelol (Figure 1) are more abundant and exhibit anti-bacterial,[8] anti-cancer,[9−11] and anti-diabetic actions.[12,13] However, the anti-inflammatory activity of 4-hydroxyderricin and xanthoangelol remains unclear. Although the *n*-hexane extract of Ashitaba has been found to suppress inflammatory responses in LPS-treated macrophages, active compounds were not identified.[14] Sugii et al. (2005)[15] have reported that xanthoangelol D, a xanthoangelol derivative, suppresses TNF-α-induced NF-κB activation in cultured porcine aortic endothelial cells. Also, Ohkura et al. (2011)[16] have found that xanthoangelol B and D reduced plasminogen activator

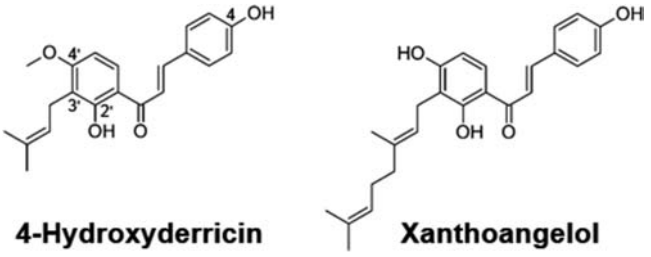

Figure 1. Chemical structure of 4-hydroxyderricin and xanthoangelol.

Received: September 19, 2013
Revised: November 22, 2013
Accepted: December 26, 2013
Published: December 26, 2013

ACS Publications © 2013 American Chemical Society

inhibitor-1 production in TNF-α-stimulated human umbilical vein endothelial cells. To our knowledge, there have been no reports evaluating an anti-inflammatory action of 4-hydroxyderricin and xanthoangelol. In the current study, we investigated the effects and underlying mechanisms of 4-hydroxyderricin, xanthoangelol, and their parent compound chalcone (1,3-diphenyl-prop-2-en-1-one framework)[17] on LPS-induced inflammatory responses in the murine macrophage RAW264 cell line.

MATERIALS AND METHODS

Chemicals. 4-Hydroxyderricin and xanthoangelol were purified as described previously.[13] Their purity (>90%) were confirmed by high-performance liquid chromatography. Nobiletin and 1′-acetoxychavicol acetate were kindly donated by Dr. Akira Murakami (Kyoto University, Japan). The anti-iNOS and COX-2 antibodies were purchased from Cayman Chemical Company (Ann Arbor, MI, USA). The anti-p65, phospho-p65 (Ser536), c-jun N-terminal kinase (JNK), phospho-JNK (Thr183/Tyr185), and lamin B1 antibodies were from Cell Signaling Technology (Beverly, MA, USA). Horseradish peroxidase-conjugated anti-rabbit IgG and anti-goat IgG antibodies were obtained from Calbiochem (San Diego, CA, USA) and Sigma (St. Louis, MO, USA), respectively. Anti-β-actin antibody was purchased from Santa Cruz Biotechnology. Can Get Signal immunoreaction enhancer solution was obtained from Toyobo (Osaka, Japan). All other chemicals were purchased from Wako Pure Chemicals (Osaka, Japan) unless specified otherwise.

Cell Culture. RAW264 mouse macrophages (RCB0535; RIKEN Bio Resource Center, Tsukuba, Japan) were grown in Dulbecco's Modified Eagle Medium (DMEM, Sigma) supplemented with 10% (v/v) heat-inactivated fetal bovine serum (FBS, Thermo Fisher Scientific, Waltham, MA, USA), penicillin (100 U/mL), and streptomycin (100 μg/mL). L929 mouse fibroblast cells (RCB1422, RIKEN Bio Resource Center) were cultured in Roswell Park Memorial Institute (RPMI) medium 1640 containing 10% heat-inactivated FBS, penicillin (100 U/mL), and streptomycin (100 μg/mL). Cells were grown at 37 °C under a humidified atmosphere of 95% air and 5% CO_2. RAW264 cells (2.5×10^5 cells/mL) and L929 cells (2.3×10^5 cells/mL) were seeded (in culture medium) on 96-well plates (for NO and TNF-α measurements), 48-well plates (for western immunoblotting), 12-well plates (for real-time reverse transcription-polymerase chain reaction (RT-PCR)), or 60 mm dishes (for electrophoretic mobility shift assay) in the culture medium. After 24 h incubation, cells were used for their respective assay. The final concentration of LPS was 100 ng/mL.

Determination of the Production of NO. NO production was determined via the Griess reaction,[18] which is based on the amount of nitrite, a stable end-product of NO. Briefly, RAW264 cells were treated with the tested compounds (4-hydroxyderricin (10 μM), xanthoangelol (5 μM), chalcone, (25 μM), nobiletin (50 μM), or 1′-acetoxychavicol acetate (6 μM)), which were dissolved in dimethyl sulfoxide (DMSO) in serum-free DMEM for 30 min and then exposed to LPS for a further 24 h. The supernatants (0.1 mL) were mixed with 0.1 mL of Griess reagent 1% (w/v) sulfanilamide and 0.1% (w/v) *N*-(1-naphthyl) ethylenediamine dihydrochloride in 2.5% (v/v) phosphoric acid) in 96-well plates. Absorbance was measured at 543 nm using the SPECTRAmax 190 (Molecular Devices, Sunnyvale, CA, USA). The half-maximal inhibitory concentration (IC_{50}) was defined as the concentration of each compound that inhibited NO production by 50%.

Measurement of Cell Viability. Cell viability was measured via crystal violet staining. RAW264 cells were fixed and stained with crystal violet solution (0.2% (w/v) in 2% (v/v) ethanol) for 10 min. The stained cells were then extracted with sodium dodecyl sulfate (SDS) solution (0.5% (w/v) in 50% (v/v) ethanol). The optical density was measured at 570 nm with a reference wavelength of 630 nm using the SPECTRAmax 190. The positive control (DMSO + LPS-treated cells) was taken as 100% cell viability.

Measurement of TNF-α Production. TNF-α was measured using the L929 fibroblast killing assay with some modifications.[19] Briefly, RAW264 macrophages were treated with DMSO, 4-hydroxyderricin (10 μM), xanthoangelol (5 μM), chalcone (25 μM), or nobiletin (50 μM) in the presence of LPS as described above. The culture supernatant was collected at 1, 3, 6, 12, and 24 h and diluted (500-fold) with RPMI1640 containing 10% FBS, which were used as the sample for the Killing assay. L929 cells were exposed to 2 μg/mL actinomycin D-containing medium and the sample for 20 h. Viability of L929 cells was measured by the crystal violet staining as described above. TNF-α levels in the supernatants were calculated from a standard curve that was constructed using the viability of L929 cells and the concentration of recombinant mouse TNF-α.

Real-Time RT-PCR. RAW264 macrophages were incubated for 30 min in serum-free DMEM containing DMSO or the tested compounds (4-hydroxyderricin (10 μM), xanthoangelol (5 μM), chalcone, (25 μM), nobiletin (50 μM), or 1′-acetoxychavicol acetate (6 μM)). After a further 4 h incubation with LPS, total RNA was isolated from the cells using TRIzol reagent (Invitrogen, Carlsbad, CA, USA), followed by cDNA synthesis from 20 ng of total RNA using PrimeScript RT reagent kit with gDNA Eraser (Takara, Shiga, Japan). Thermal cycling was performed on a Thermal Cycler Dice real-time system TP860 (Takara) using SYBR Premix Ex *Taq*II (Takara). The primers used were purchased from Takara (for primers: *β-actin* and *iNOS*) and Rikaken (Nagoya, Japan) (for primer: *COX-2*). Primer sequences were as follows: *β-actin* as a control (5′- CATCCGTAAAGACCTCTATGCCAAC-3′ and 5′-ATGGAGCCACCGATCCACA-3′), *iNOS* (5′-TAGGCAGAGATTGGAGGCCTTG-3′ and 5′-GGGTTGTTGCTGAACTTCCAGTC-3′), *COX-2* (5′-CCCCCACAGTCAAAGACACT-3′ and 5′-AGTTGCTCATCACCCCACTC-3′).

Western Immunoblot Analysis. RAW264 cells were incubated with DMEM containing DMSO or the tested compounds (4-hydroxyderricin (10 μM), xanthoangelol (5 μM), chalcone, (25 μM), nobiletin (50 μM), or 1′-acetoxychavicol acetate (6 μM)) for 30 min and then treated with LPS for a further 2 and 24 h. Whole cell lysates (for iNOS, COX-2, and β-actin, 24 h) and nuclear and cytoplasmic extracts (for p65, lamin B1, and JNK, 2 h) were made with RIPA buffer and the NE-PER nuclear and cytoplasmic extraction reagents kit (Pierce Biotechnology, Rockford, IL, USA), respectively. The cells were lysed with RIPA buffer (50 mM Tris, pH 8.0, 150 mM sodium chloride, 0.5% (w/v) sodium deoxycholate, 0.1% (w/v) SDS, and 1 mM 1,4-dithiothreitol) containing the protease inhibitor cocktail, Complete (Roche, Mannheim, Germany), and the phosphatase inhibitor cocktail, PhosSTOP (Roche). Cell lysates were centrifuged (15000*g* for 5 min at 4 °C), and the supernatant was used as the whole cell lysate. Nuclear and cytoplasmic extraction was performed according to the manufacturer's instruction. Protein concentrations were determined via the BioRad protein assay (BioRad Laboratories, Hercules, CA, USA) against the standard curve of γ-globulin. Equal amounts (10 μg) of protein were separated by 10% SDS polyacrylamide gel electrophoresis for 60 min at 120 V and transferred to polyvinylidene difluoride membranes (Millipore, Billerica, MA, USA) for 60 min at 100 V using the Mini Trans-Blot electrophoretic transfer cell (Bio-Rad Laboratories). After blocking with Blocking One or Blocking One-P (Nacalai Tesque, Kyoto, Japan), the membranes were treated with the primary antibodies diluted in Tris buffer (0.1 M Tris, pH 7.5, 0.15 M NaCl, 0.1% (v/v) Tween 20) containing 5% (v/v) Blocking One (for anti-iNOS (1:2000), anti-COX-2 (1:8000), or β-actin (1:500)) or Can Get Signal solution 1 (for total and phospho-p65 (both 1:4000), total and phospho-JNK (both 1:4000), or Lamin B1 (1:2000)) overnight at 4 °C. Corresponding horseradish peroxidase-conjugated secondary antibodies were diluted in Tris buffer (0.1 M Tris, pH 7.5, 0.15 M NaCl, 0.1% (v/v) Tween 20) containing 5% (v/v) Blocking One (for rabbit IgG (1:4000) or goat IgG, (1:2000)) or Can Get Signal solution 2 (for rabbit IgG (1:10000)) and added to the membranes for 1 h at room temperature. The blots were detected by enhanced chemiluminescence using ImmunoStar LD and developed by the LAS4000 mini (Fujifilm, Tokyo, Japan).

Electrophoretic Mobility Shift Assay. RAW264 macrophages were treated with DMSO or the tested compounds (4-hydroxyderricin (10 μM), xanthoangelol (5 μM), chalcone, (25 μM), nobiletin (50 μM), or 1′-acetoxychavicol acetate (6 μM)) in DMEM for 30 min followed by the exposure to LPS for a further 2 h. Nuclear extracts and protein concentration determination were performed as described above. Equal amounts (7 μg) of protein were subjected to the LightShift chemiluminescent EMSA kit (Thermo Fisher scientific, Waltham, MA, USA) according to the manufacturer's instructions. The 3′-biotin-labeled oligonucleotide sequences for *NF-κB* were 5′-AGTTGAGGGGACTTTCCCAGGC-3′ and 5′-GCCTGGGAAAGTCCCCTCAACT-3′ and for *AP-1* were 5′-CGCTTGATGACTCACCGGAA-3′ and 5′-TTCCGGCTGAGTCATCAAGCG-3′ (STAR Oligo; Rikaken, Nagoya, Japan).

Statistical Analysis. All data are expressed as the mean ± standard deviation from at least three independent experiments. Each treatment for the NO and TNF-α assays was performed in triplicate from at least three independent experiments. Comparisons between groups were analyzed by the Dunnett test. Statistical analysis was performed by SPSS 16.0J (SPSS Inc., Chicago, IL, USA). Significance was reached at values of $P < 0.05$.

RESULTS

4-Hydroxyderricin and Xanthoangelol Down-Regulated LPS-Mediated Production of NO in Mouse Macrophages. We first determined the effect of 4-hydroxyderricin and xanthoangelol on LPS-induced NO production (Figure 2A). NO production was induced in RAW264 macrophage cells exposed to LPS for 24 h (Figure 2A), and 6 μM 1′-acetoxychavicol acetate or 50 μM nobiletin, which are anti-

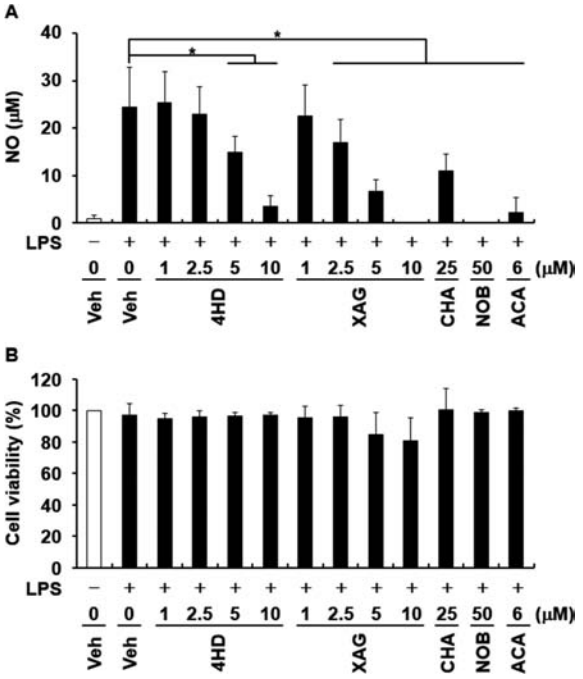

Figure 2. 4-Hydroxyderricin and xanthoangelol decrease NO production in LPS-treated RAW264 macrophages. RAW264 cells were incubated with 4-hydroxyderricin (4HD, 1−10 μM), xanthoangelol (XAG, 1−10 μM), chalcone (CHA, 25 μM), nobiletin (NOB, 50 μM), 1′-acetoxychavicol acetate (ACA, 6 μM), or DMSO (vehicle, Veh) for 30 min and then treated with or without LPS (100 ng/mL) for 24 h. The cell culture supernatant was collected and (A) NO production was determined. (B) Quantification of cells stained with crystal violet to estimate the cytotoxicity of the tested phytochemicals. *$p < 0.05$.

inflammatory dietary factors[6] and were used as the positive controls, significantly suppressed this response (Figure 2A). Furthermore, 4-hydroxyderricin (5 and 10 μM) and xanthoangelol (2.5−10 μM) significantly inhibited LPS-induced NO production in a concentration-dependent manner, with IC_{50} values of 5.0 ± 1.2 and 2.9 ± 0.4 μM, respectively. At 10 μM, 4-hydroxyderricin and xanthoangelol suppressed the production of NO by 90% and 100%, and both compounds had negligible effects on cell viability at this concentration (Figure 2B). Chalcone (25 μM) significantly reduced NO production. Treatment with each phytochemical alone did not affect the production of NO (data not shown).

4-Hydroxyderricin and Xanthoangelol Suppressed LPS-Induced Production of TNF-α in Mouse Macrophages. We next evaluated the effects of 4-hydroxyderricin and xanthoangelol on the production of TNF-α. LPS-stimulated RAW264 cells secreted TNF-α into the culture medium in a time-dependent manner (Figure 3). Xanthoange-

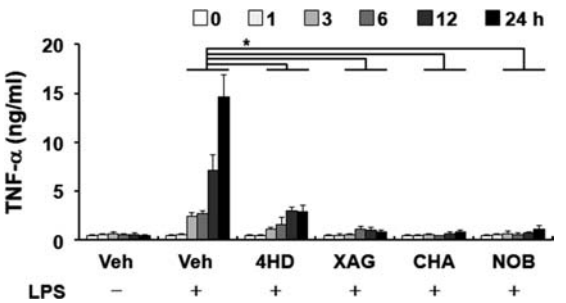

Figure 3. 4-Hydroxyderricin and xanthoangelol inhibit LPS-mediated secretion of TNF-α from RAW264 macrophages. RAW264 cells were treated with 4-hydroxyderricin (4HD, 10 μM), xanthoangelol (XAG, 5 μM), chalcone (CHA, 25 μM), nobiletin (NOB, 50 μM), or DMSO (vehicle, Veh) for 30 min and then stimulated with LPS. The TNF-α level in the culture supernatant at the various time-points was measured using L929 Killing assay as described in Materials and Methods. *$p < 0.05$.

lol, chalcone, and nobiletin strongly decreased the secretion of TNF-α from 3 to 24 h by 57−94% ($P < 0.05$), respectively, and 4-hydroxyderricin suppressed it by 40−80% ($P < 0.05$), respectively (Figure 3).

4-Hydroxyderricin and Xanthoangelol Inhibited LPS-Induced Expression of iNOS and COX-2. To assess whether the suppression of NO production by 4-hydroxyderricin or xanthoangelol is due to the reduction in the expression of iNOS, western immunoblots and RT-PCR were performed for iNOS. RAW264 cells treated with LPS for 24 h significantly induced the expression of iNOS protein and mRNA (parts A and B of Figure 4, respectively). All of the tested compounds down-regulated the expression of iNOS protein and mRNA (parts A and B of Figure 4, respectively). Similar responses were found with COX-2 (Figure 4A,B). These data indicate that the prenylated chalcones may attenuate LPS-induced NO production via the suppression of iNOS at the transcriptional level.

4-Hydroxyderricin and Xanthoangelol Reduced the DNA-Binding Activity of AP-1 and Inhibited the Phosphorylation of NF-κB but Not Its DNA-Binding Activity. We then investigated the effects of the prenylated chalcones on transcription factors, AP-1 and NF-κB. 4-Hydroxyderricin showed partial inhibition of AP-1 DNA-binding activity, while xanthoangelol and other compounds

dx.doi.org/10.1021/jf404175t | J. Agric. Food Chem. 2014, 62, 462−467

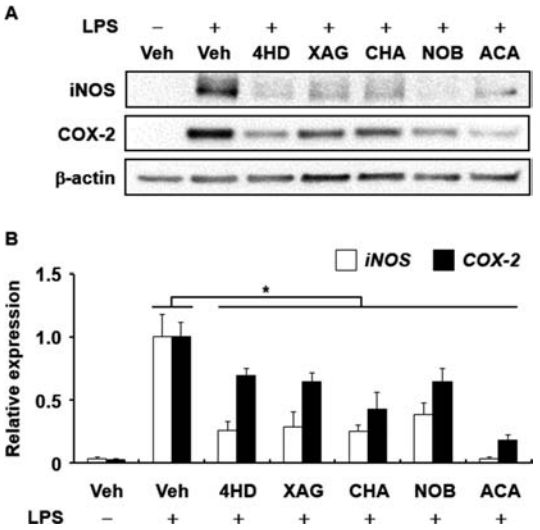

Figure 4. 4-Hydroxyderricin and xanthoangelol reduce the expression levels of iNOS and COX-2 in LPS-treated RAW264 macrophages. RAW264 cells were treated with 4-hydroxyderricin (4HD, 10 μM), xanthoangelol (XAG, 5 μM), chalcone (CHA, 25 μM), nobiletin (NOB, 50 μM), 1′-acetoxychavicol acetate (ACA, 6 μM), or DMSO (vehicle, Veh) for 30 min and then treated with LPS (100 ng/mL) for 24 h for (A) western immunoblots and for 4 h for (B) reverse-transcription-polymerase chain reaction. *β-Actin* and *gapdh* were used as the internal standard for (A) and (B), respectively. Results shown are representative of three independent experiments. *$p < 0.05$.

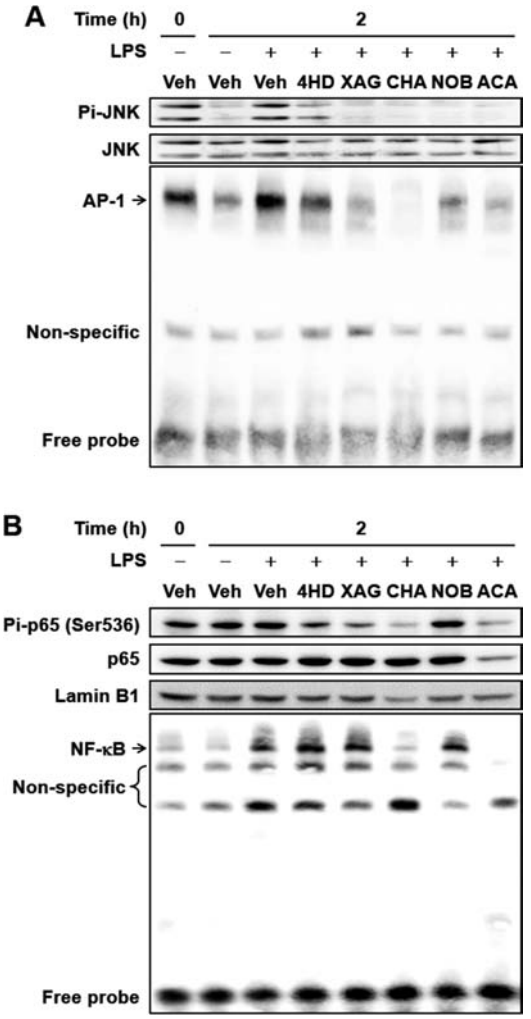

Figure 5. Effects of 4-hydroxyderricin and xanthoangelol on the activation of AP-1 and NF-κB. Nuclear and cytoplasmic extraction, western immunoblotting, and an electrophoretic mobility shift assay were performed on RAW264 cells treated with 4-hydroxyderricin (4HD, 10 μM), xanthoangelol (XAG, 5 μM), chalcone (CHA, 25 μM), nobiletin (NOB, 50 μM), 1′-acetoxychavicol acetate (ACA, 6 μM), or DMSO (vehicle, Veh) for 30 min and followed by LPS (100 ng/mL) for 2 h. The nuclear and cytoplasmic extracts prepared from cells immediately after the preincubation was set as 0 h. (A) JNK phosphorylation and AP-1 DNA-binding activity, (B) p65 phosphorylation and NF-κB-DNA binding activity. The NF-κB complex (indicated by the arrow) was confirmed by a supershift assay using the anti-p65 antibody (data not shown). Lamin B1 was used as the internal standard. Results shown are representative of three independent experiments.

completely abolished it (Figure 5A). A similar pattern of inhibition was observed in the phosphorylation level of JNK (Figure 5A). On the other hand, the prenylated chalcones did not affect the DNA-binding activity of NF-κB (Figure 5B). Interestingly, however, 4-hydroxyderricin and xanthoangelol decreased LPS-induced p65 phosphorylation at Ser536 (Figure 5B). In contrast, chalcone suppressed p65 phosphorylation and reduced its activity (Figure 5B). 1′-Acetoxychavicol acetate decreased the phosphorylation, nuclear translocation, and DNA-binding activity of p65 (Figure 5B). However, nobiletin had no effect on the phosphorylation and the activity of p65 (Figure 5B).

DISCUSSION

Proinflammatory mediators play important roles in chronic inflammation, which is associated with the development of obesity, cancer, cardiovascular diseases, and diabetes mellitus.[1,3,4] In the current study, we investigated the anti-inflammatory activities of 4-hydroxyderricin and xanthoangelol under in vitro conditions. Our findings reveal that these two compounds significantly decrease the production of NO and TNF-α in LPS-treated RAW264 mouse macrophages. Furthermore, the expression of iNOS and COX-2 genes are reduced. These findings are the first to report that 4-hydroxyderricin and xanthoangelol attenuate LPS-mediated inflammatory responses in macrophages. Their parent compound chalcone also display similar effects but at concentrations 5- to 10-fold higher than those of the prenylated chalcones. In addition, xanthoangelol, which has the geranyl group (two isoprene units), showed more strong activity (2-fold) than 4-hydroxyderricin, which has the dimethylallyl group (one isoprene unit). This may be because that the prenylation increases hydrophobicity and thus the uptake ratio into the cells. In other types of prenylated chalcones, both xanthohumol containing the dimethylally group at 3′ position and licochalcone A containing 2-methyl-3-buten-2-yl group at 4 position are known to have an anti-inflammatory activity,[7,20] suggesting the position of a prenyl group may be not important for exhibiting an anti-inflammatory activity. 1′-Acetoxychavicol acetate and nobiletin are widely accepted as the potent anti-inflammatory and cancer chemopreventive agents.[6,21−24] 4-Hydroxyderricin and xanthoangelol showed the anti-inflammatory activity at a concentration below that of nobiletin and lower toxicity to macrophages compared with 1′-acetoxychavicol acetate because toxic concentrations of the prenylated chalcones and 1′-acetoxychavicol acetate were above 25 and 10 μM, respectively (data not shown). Taken together, 4-

dx.doi.org/10.1021/jf404175t | J. Agric. Food Chem. 2014, 62, 462−467

hydroxyderricin and xanthoangelol with increased hydrophobicity by the prenyl group may effectively accumulate and work in the cells and hence be more potent than compounds with no prenyl group.

The expression of several proinflammatory mediators, including iNOS, COX-2, and TNF-α, are regulated by the transcription factors AP-1 and NF-κB.[5] Inflammatory stimuli, such as LPS, activate the pathways of mitogen-activated protein kinase (MAPK) and inhibitor of κB kinase (IKK), which then induce the nuclear translocation and increase the transcriptional activity of AP-1 and NF-κB, respectively. Nobiletin and 1′-acetoxychavicol acetate are known to exhibit anti-inflammatory activity via the inhibition of the activation of these transcription factors.[6] Like them, 4-hydroxyderricin, xanthoangelol, and chalcone reduced the DNA-binding activity of AP-1 and suppressed the activation of upstream kinase JNK. On the other hand, they reduced the phosphorylation of the p65 subunit of NF-κB, whereas only chalcone completely abolishes the DNA-binding activity of NF-κB. Moreover, all of the tested chalcones do not affect p65 nuclear translocation. In the present study, because the actions of the prenylated chalcones on NF-κB were distinct from those of chalcone, prenylation may have thus affected these mechanisms and bioavailability in macrophages. In the report by Murakami et al. (2005),[6] 1′-acetoxychavicol acetate inhibited gene transcription of COX-2 via reducing the activation of MAPKs, the translocation of p65, and the transcriptional activity of NF-κB, while nobiletin suppressed the COX-2 expression via reducing NF-κB transcriptional activity without affecting MAPK activation and p65 translocation. They showed nearly the same results in our study (though nobiletin suppressed the phosphorylation of JNK). The inhibition patterns of NF-κB by chalcone and the prenylated chalcones are similar to 1′-acetoxychavicol acetate and nobiletin, respectively. However, other prenylated chalcone xanthohumols have shown the chalcone-like action mechanism, namely the reduction of both p65 phosphorylation at Ser536 and NF-κB DNA-binding acivity.[7] Murakami et al. (2005)[6] supposed that nobiletin may disrupt binding of NF-κB with transcription coactivators such as p300. Buss et al. (2004)[25] have suggested that Ser536 phosphorylation disrupts the hydrogen bond between Ser536 and Asp533, thus leading to a lower and higher affinity of p65 for transcription corepressors and coactivators, respectively. IKKβ is considered to be an essential kinase in LPS-induced p65 phosphorylation at Ser536.[26] In addition, LPS-mediated and cAMP-independent activation of the catalytic subunit of protein kinase A increases the transcriptional activity of NF-κB through the phosphorylation of p65 at Ser276.[27] Licochalcone A suppressed the expression of inflammatory mediators including TNF-α without affecting nuclear translocation and DNA-binding activity of NF-κB.[20] This compound inhibited LPS-induced phosphorylation of p65 at Ser276, but not Ser536, resulting in reduced association with coactivator p300.[20] Furthermore, the acetylation of NF-κB affects the DNA-binding activity.[28,29] Therefore, 4-hydroxyderricin and xanthoangelol may regulate the interaction of NF-κB with transcriptional cofactors by inhibiting phosphorylation at Ser536 and at other sites (e.g., Ser276) and chalcone may suppress the NF-κB activation through the control of phosphorylation and acetylation statuses.

4-Hydroxyderricin and xanthoangelol have been found to suppress adipocyte differentiation by reducing the expression of adipocyte-specific transcription factors.[30] Furthermore, enhanced glucose uptake activity by the prenylated chalcones in muscle cells and adipocytes in vitro has been shown to occur via the activation of glucose transporter 4.[12,13] Anti-diabetic activities of 4-hydroxyderricin in KK-A^y mice was also reported.[12] Nakamura et al. (2012)[31] have demonstrated that 4-hydroxyderricin and xanthoangelol are distributed as both aglycone and conjugated forms to various tissues, such as liver, muscle, and fat, when mice are orally administered with Ashitaba extract. Generally, flavonoids are rapidly metabolized via glucuronidation, methoxylation, and/or sulfation and then circulate throughout the body. Interestingly, however, 4-hydroxyderricin and xanthoangelol are more abundant as aglycones than glucuronides in plasma and tissues.[31] 4-Hydroxyderricin and xanthoangelol predominantly accumulate in mesenteric fat tissue as aglycones,[31] possibly because of the hydrophobicity by the prenyloxy group. Chronic inflammation accompanying hypertrophy of mesenteric fat is known to cause insulin resistance, resulting in abnormal control of blood glucose by skeletal muscle tissue.[32] Taken together, 4-hydroxyderricin and xanthoangelol may be promising dietary factors for the prevention and improvement of metabolic syndromes.

Various components from Ashitaba inhibit inflammatory responses. For example, the coumarin derivative, selinidin, suppresses allergic inflammatory responses in mast cells.[33] Xanthoangelol B and D was shown to inhibit TNF-α-induced inflammatory responses in cultured endothelial cells.[15,16] Therefore, the Japanese herb, Ashitaba, which is rich in prenylated chalcones, may thus be a promising food source for the prevention of chronic inflammatory diseases

In conclusion, our study reveals that 4-hydroxyderricin and xanthoangelol are potent suppressors of inflammatory responses and may have distinct mechanisms of action than the parent compound, chalcone. We will address the investigation of the contribution of prenyl groups to their bioavailability and the elucidation of more details of their action mechanisms in the near future.

AUTHOR INFORMATION

Corresponding Author

*Phone: +81-776-61-6000. Fax: +81-776-61-6015. E-mail: kawaba-k@fpu.ac.jp.

Present Address

⊥For M.Y.: Graduate School of Nutritional and Environmental Sciences, Graduate School of Integrated Pharmaceutical and Nutritional Sciences, University of Shizuoka, 52-1 Yada, Suruga-ku, Shizuoka 422-8526, Japan.

Funding

This study was partially supported by a Grant-in-Aid for Scientific Research (C) (No. 20580139) and Special Coordination Funds for Promoting Science and Technology, Creation of Innovation Centers for Advanced Interdisciplinary Research Areas (Innovative Bioproduction Kobe) from the Ministry of Education, Culture, Sports, Science and Technology (MEXT) of Japan.

Notes

The authors declare no competing financial interest.

ACKNOWLEDGMENTS

We are grateful to Dr. Akira Murakami of Kyoto University for a kind donation of nobiletin and 1′-acetoxychavicol acetate.

REFERENCES

(1) Pan, M.; Lai, C.; Ho, C. Anti-inflammatory activity of natural dietary flavonoids. *Food. Funct.* **2010**, *1*, 15−31.

(2) Murakami, A.; Ohigashi, H. Targeting NOX, iNOS and COX-2 in inflammatory cells: chemoprevention using food phytochemicals. *Int. J. Cancer* **2007**, *121*, 2357−2363.

(3) Chung, H. Y.; Cesari, M.; Anton, S.; Marzetti, E.; Giovannini, S.; Seo, A. Y.; Carter, C.; Yu, B. P.; Leeuwenburgh, C. Molecular inflammation: underpinnings of aging and age-related diseases. *Ageing. Res. Rev.* **2009**, *8*, 18−30.

(4) Prasad, S.; Phromnoi, K.; Yadav, V. R.; Chaturvedi, M. M.; Aggarwal, B. B. Targeting inflammatory pathways by flavonoids for prevention and treatment of cancer. *Planta Med.* **2010**, *76*, 1044−1063.

(5) Guha, M.; Mackman, N. LPS induction of gene expression in human monocytes. *Cell. Signalling* **2001**, *13*, 85−94.

(6) Murakami, A.; Shigemori, T.; Ohigashi, H. Zingiberaceous and citrus constituents, 1′-acetoxychavicol acetate, zerumbone, auraptene, and nobiletin, suppress lipopolysaccharide-induced cyclooxygenase-2 expression in RAW264.7 murine macrophages through different modes of action. *J. Nutr.* **2005**, *135*, 2987S−2992S.

(7) Harikumar, K. B.; Kunnumakkara, A. B.; Ahn, K. S.; Anand, P.; Krishnan, S.; Guha, S.; Aggarwal, B. B. Modification of the cysteine residues in IkappaBalpha kinase and NF-kappaB (p65) by xanthohumol leads to suppression of NF-kappaB-regulated gene products and potentiation of apoptosis in leukemia cells. *Blood* **2009**, *113*, 2003−2013.

(8) Inamori, Y.; Baba, K.; Tsujibo, H.; Taniguchi, M.; Nakata, K.; Kozawa, M. Antibacterial activity of two chalcones, xanthoangelol and 4-hydroxyderricin, isolated from the root of *Angelica keiskei* KOIDZUMI. *Chem. Pharm. Bull. (Tokyo)* **1991**, *39*, 1604−1605.

(9) Kimura, Y.; Taniguchi, M.; Baba, K. Antitumor and antimetastatic activities of 4-hydroxyderricin isolated from *Angelica keiskei* roots. *Planta Med.* **2004**, *70*, 211−219.

(10) Kimura, Y.; Baba, K. Antitumor and antimetastatic activities of *Angelica keiskei* roots, part 1: isolation of an active substance, xanthoangelol. *Int. J. Cancer.* **2003**, *106*, 429−437.

(11) Okuyama, T.; Takata, M.; Takayasu, J.; Hasegawa, T.; Tokuda, H.; Nishino, A.; Nishino, H.; Iwashima, A. Anti-tumor-promotion by principles obtained from *Angelica keiskei*. *Planta. Med.* **1991**, *57*, 242−246.

(12) Enoki, T.; Ohnogi, H.; Nagamine, K.; Kudo, Y.; Sugiyama, K.; Tanabe, M.; Kobayashi, E.; Sagawa, H.; Kato, I. Antidiabetic activities of chalcones isolated from a Japanese herb, *Angelica keiskei*. *J. Agric. Food. Chem.* **2007**, *55*, 6013−6017.

(13) Kawabata, K.; Sawada, K.; Ikeda, K.; Fukuda, I.; Kawasaki, K.; Yamamoto, N.; Ashida, H. Prenylated chalcones 4-hydroxyderricin and xanthoangelol stimulate glucose uptake in skeletal muscle cells by inducing GLUT4 translocation. *Mol. Nutr. Food. Res.* **2011**, *55*, 467−475.

(14) Lee, H. J.; Choi, T. W.; Kim, H. J.; Nam, D.; Jung, S. H.; Lee, E. H.; Lee, H. J.; Shin, E. M.; Jang, H.; Ahn, K. S.; Shim, B. S.; Choi, S.; Kim, S.; Sethi, G.; Ahn, K. S. Anti-Inflammatory activity of *Angelica keiskei* through suppression of mitogen-activated protein kinases and nuclear factor-kappaB activation pathways. *J. Med. Food* **2010**, *13*, 691−699.

(15) Sugii, M.; Ohkita, M.; Taniguchi, M.; Baba, K.; Kawai, Y.; Tahara, C.; Takaoka, M.; Matsumura, Y. Xanthoangelol D isolated from the roots of *Angelica keiskei* inhibits endothelin-1 production through the suppression of nuclear factor-kappaB. *Biol. Pharm. Bull.* **2005**, *28*, 607−610.

(16) Ohkura, N.; Nakakuki, Y.; Taniguchi, M.; Kanai, S.; Nakayama, A.; Ohnishi, K.; Sakata, T.; Nohira, T.; Matsuda, J.; Baba, K.; Atsumi, G. Xanthoangelols isolated from *Angelica keiskei* inhibit inflammatory-induced plasminogen activator inhibitor 1 (PAI-1) production. *Biofactors* **2011**, *37*, 455−461.

(17) Baba, K.; Nakata, K.; Tahiguchi, M.; Kido, T.; Kozawa, M. Chalcones from *Angelica keiskei*. *Phytochemistry* **1990**, *29*, 3907−3910.

(18) Green, L. C.; Wagner, D. A.; Glogowski, J.; Skipper, P. L.; Wishnok, J. S.; Tannenbaum, S. R. Analysis of nitrate, nitrite, and [15N]nitrate in biological fluids. *Anal. Biochem.* **1982**, *126*, 131−138.

(19) Flick, D. A.; Gifford, G. E. Comparison of in vitro cell cytotoxic assays for tumor necrosis factor. *J. Immunol. Methods* **1984**, *68*, 167−175.

(20) Furusawa, J.; Funakoshi-Tago, M.; Tago, K.; Mashino, T.; Inoue, H.; Sonoda, Y.; Kasahara, T. Licochalcone A significantly suppresses LPS signaling pathway through the inhibition of NF-kappaB p65 phosphorylation at serine 276. *Cell. Signalling* **2009**, *21*, 778−785.

(21) Kohno, H.; Yoshitani, S.; Tsukio, Y.; Murakami, A.; Koshimizu, K.; Yano, M.; Tokuda, H.; Nishino, H.; Ohigashi, H.; Tanaka, T. Dietary administration of citrus nobiletin inhibits azoxymethane-induced colonic aberrant crypt foci in rats. *Life Sci.* **2001**, *69*, 901−913.

(22) Moffatt, J.; Hashimoto, M.; Kojima, A.; Kennedy, D. O.; Murakami, A.; Koshimizu, K.; Ohigashi, H.; Matsui-Yuasa, I. Apoptosis induced by 1′-acetoxychavicol acetate in Ehrlich ascites tumor cells is associated with modulation of polyamine metabolism and caspase-3 activation. *Carcinogenesis* **2000**, *21*, 2151−2157.

(23) Murakami, A.; Nakamura, Y.; Torikai, K.; Tanaka, T.; Koshiba, T.; Koshimizu, K.; Kuwahara, S.; Takahashi, Y.; Ogawa, K.; Yano, M.; Tokuda, H.; Nishino, H.; Mimaki, Y.; Sashida, Y.; Kitanaka, S.; Ohigashi, H. Inhibitory effect of citrus nobiletin on phorbol ester-induced skin inflammation, oxidative stress, and tumor promotion in mice. *Cancer. Res.* **2000**, *60*, 5059−5066.

(24) Kawabata, K.; Tanaka, T.; Yamamoto, T.; Ushida, J.; Hara, A.; Murakami, A.; Koshimizu, K.; Ohigashi, H.; Stoner, G. D.; Mori, H. Suppression of *N*-nitrosomethylbenzylamine-induced rat esophageal tumorigenesis by dietary feeding of 1′-acetoxychavicol acetate. *Jpn. J. Cancer Res.* **2000**, *91*, 148−155.

(25) Buss, H.; Dorrie, A.; Schmitz, M. L.; Hoffmann, E.; Resch, K.; Kracht, M. Constitutive and interleukin-1-inducible phosphorylation of p65 NF-kappaB at serine 536 is mediated by multiple protein kinases including IkappaB kinase (IKK)-alpha, IKKbeta, IKKepsilon, TRAF family member-associated (TANK)-binding kinase 1 (TBK1), and an unknown kinase and couples p65 to TATA-binding protein-associated factor II31-mediated interleukin-8 transcription. *J. Biol. Chem.* **2004**, *279*, 55633−55643.

(26) Yang, F.; Tang, E.; Guan, K.; Wang, C. IKK beta plays an essential role in the phosphorylation of RelA/p65 on serine 536 induced by lipopolysaccharide. *J. Immunol.* **2003**, *170*, 5630−5635.

(27) Zhong, H.; SuYang, H.; Erdjument-Bromage, H.; Tempst, P.; Ghosh, S. The transcriptional activity of NF-kappaB is regulated by the IkappaB-associated PKAc subunit through a cyclic AMP-independent mechanism. *Cell* **1997**, *89*, 413−424.

(28) Kiernan, R.; Bres, V.; Ng, R. M.; Coudart, M.; El Messaoudi, S.; Sardet, C.; Jin, D.; Emiliani, S.; Benkirane, M. Post-activation turn-off of NF-kappa B-dependent transcription is regulated by acetylation of p65. *J. Biol. Chem.* **2003**, *278*, 2758−2766.

(29) Chen, L.; Fischle, W.; Verdin, E.; Greene, W. C. Duration of nuclear NF-kappaB action regulated by reversible acetylation. *Science* **2001**, *293*, 1653−1657.

(30) Zhang, T.; Sawada, K.; Yamamoto, N.; Ashida, H. 4-Hydroxyderricin and xanthoangelol from Ashitaba (*Angelica keiskei*) suppress differentiation of preadiopocytes to adipocytes via AMPK and MAPK pathways. *Mol. Nutr. Food. Res.* **2013**, *57*, 1729−1740.

(31) Nakamura, T.; Tokushima, T.; Kawabata, K.; Yamamoto, N.; Miyamoto, M.; Ashida, H. Absorption and metabolism of 4-hydroxyderricin and xanthoangelol after oral administration of *Angelica keiskei* (Ashitaba) extract in mice. *Arch. Biochem. Biophys.* **2012**, *521*, 71−76.

(32) Lyon, C. J.; Law, R. E.; Hsueh, W. A. Minireview: adiposity, inflammation, and atherogenesis. *Endocrinology* **2003**, *144*, 2195−2200.

(33) Kishiro, S.; Nunomura, S.; Nagai, H.; Akihisa, T.; Ra, C. Selinidin suppresses IgE-mediated mast cell activation by inhibiting multiple steps of Fc epsilonRI signaling. *Biol. Pharm. Bull.* **2008**, *31*, 442−448.

JOURNAL OF AGRICULTURAL AND FOOD CHEMISTRY

Article

pubs.acs.org/JAFC

Soluble Phenolic Compounds in Fresh and Ensiled Orchard Grass (*Dactylis glomerata* L.), a Common Species in Permanent Pastures with Potential as a Biomass Feedstock

Barbara Hauck, Joe A. Gallagher, S. Michael Morris, David Leemans, and Ana L. Winters*

Institute of Biological, Environmental and Rural Sciences, Aberystwyth University, Gogerddan, Aberystwyth, Ceredigion SY23 3EE, United Kingdom

Supporting Information

ABSTRACT: High-value coproducts can greatly improve the feasibility of utilizing plant feedstocks for biorefining and biofuel production. Plant polyphenolics have potential application in the pharmaceutical and cosmetic industries. Orchard grass varieties have been noted for accumulation of polyphenolic compounds, and the current study determined the soluble phenol profile and content in the orchard grass variety 'Abertop'. Hydroxycinnamates and flavonoids were monitored during the transition from vegetative to flowering stage at maximum crop yield. Caffeic acid derivatives, related to bioactives in the Asian medicinal herb *Salvia miltiorrhiza*, and novel hydroxycinnamate−flavone conjugates were also identified in extracts. Harvest yields of hydroxycinnamates and flavonoids ranged from 2.6 to 4.0 kg/ha and from 2.1 to 5.1 kg/ha, respectively. Abundant compounds showed high levels of antioxidant activity comparable with that of trolox. Minimal changes in soluble phenol content and composition were observed after ensiling with the exception of increases in caffeic acid, a caffeic acid derivative, and a caffeic acid breakdown product, dihydroxystyrene.

KEYWORDS: *Dactylis glomerata, orchard grass, phenolic acid esters, flavonoid glycosides, caffeic acid derivatives*

INTRODUCTION

Orchard grass (*Dactylis glomerata*) is a relatively coarse, tussock-forming grass that is native to Europe, temperate Asia, and North Africa.[1] It has been introduced as a forage grass into most temperate countries in the world and is one of the most important sown species in Australia and New Zealand.[2] Plants are either diploid ($2n = 14$) or, more commonly, autotetraploid ($2n = 28$), and subspecies are morphologically distinguishable according to area of origin. For example, plants of the Eurasian (or Northern) group are typically large with broad leaves and winter-dormant, whereas plants from the Mediterranean region are relatively small, narrow-leaved, and summer-dormant. Although this species has a lower nutritional value compared to other forage species such as perennial ryegrass, it is more tolerant to heat and drought, resulting in higher production during summer dry periods.

Phenolic compounds are generally abundant in orchard grass compared with other temperate grass species. The presence of phenolic compounds in this species was first reported in 1926 by Landsborough-Thompson,[3] who described the isolation of a flavone glycoside and a free flavone from plant extracts. More recently, Parveen et al.[4] identified a number of hydroxcinnamate esters in a commercial variety of orchard grass (*D. glomerata*). There is a strong tendency for chemotaxonomically related plants to produce similar types of flavonoids,[5] and a number of studies have reported characteristic variation in the flavonoid profile of different populations of orchard grass.[6,7]

Although temperate grasses have a fundamental role in ruminant nutrition, recent studies have focused on their potential as feedstocks for biorefining.[8−10] Increased recovery of components with a marketable value can improve the feasibility of grasses as biorefining feedstocks. Valuable components can be recovered from the liquid fractions of ensiled grass biomass including lactic acid and amino acids,[11] whereas the residual presscake has potential as a combustible feedstock.[12] Alternatively, residual biomass may be used to produce bioethanol[9] or biogas.[13] Polyphenols have been identified as potential high value coproducts in a biorefinery, and processes have been developed for their recovery from olive mill wastewater.[14] These classes of compounds are of interest to the pharmaceutical, cosmetics, and nutraceutical sectors, and there is an increasing body of evidence demonstrating the health benefits of plant phenols.[15] Orchard grass is reported to be a traditional remedy for tumors, kidney, and bladder ailments.[16]

Here we report on the identification and quantitative analysis of flavonoids/phenolic compounds in a commercial variety of orchard grass, 'Abertop'. This variety has been developed to provide a high-yielding conservation cut and good ground cover. We monitor the phenol profile during the transition from vegetative stage to flowering stage, which corresponds with maximum yield. We also present data on changes in soluble phenol profile following a short period of ensiling.

MATERIALS AND METHODS

Chemicals. HPLC grade methanol was obtained from Fisher Scientific (Loughborough, UK), and commercial standards for phenolic acids and flavone aglycones were from Sigma-Aldrich (Gillingham, UK) and PhytoLab (Vestenbergsgreuth, Germany).

Received: September 11, 2013
Revised: December 16, 2013
Accepted: December 17, 2013
Published: December 17, 2013

ACS Publications © 2013 American Chemical Society

Plant Material. *D. glomerata* cv. Abertop was established in 1.2 m^2 plots (replicated × 4) at Aberystwyth University, Gogerddan, Aberystwyth (52°19′22″ N, 3°56′54″ W). Plots were harvested with a Haldrop plot harvester at regular intervals during May 2010. Plant yields were recorded during harvesting. Following harvesting, plant material was transported to the laboratory within a period of 1 h and stored at −20 °C for subsequent analysis.

Ensiling. Plant material was harvested from plots on May 8, 2010. Leaf material was chopped into 1 in. lengths and packed into three silage tubes (approximately 200 mL size) and capped with silo air traps. Tubes were incubated at 25 °C and opened after 2 weeks. Freshly sampled material was extracted for phenols, and remaining material was frozen at −20 °C for further chemical analysis. Samples were analyzed for dry matter content, pH, volatile fatty acids, and water-soluble carbohydrates.

Extraction and Analysis of Water-Soluble Carbohydrates and Organic Acids. Fresh and ensiled material was extracted by immersing 2.5 g in 10 mL of water. Samples were homogenized and centrifuged at 3000*g* for 15 min. The supernatant was recovered and the pellet discarded. Fifty microliters of extract was added to 950 μL of a buffer comprising 5 μM H_2SO_4, containing 5 μM crotonic acid as an internal standard. These samples were analyzed with a Jasco HPLC system (Jasco Ltd., Great Dunmow, Essex, UK), and the column used was a 150 mm × 7.8 mm Rezex ROA-Organic Acid (Phenomenex, Macclesfield, UK) with a mobile phase of 5 μM H_2SO_4 at 0.6 mL/min. Peaks were detected with a refractive index detector, identified using Jasco EZChrom Elite HPLC software (Jasco Ltd., Essex, UK), and quantitated by comparison with standard samples of fructan, sucrose, glucose, fructose, lactic acid, and acetic acid.

Phenol Extraction. Plant material was chopped and immersed in 70% methanol at 80 °C for 5 min to inactivate polyphenol oxidases (typically 1 g FW of sample was extracted for monitoring variation over a growing season, and a bulk sample of approximately 6 g was extracted for detailed profiling of phenolic compounds). The supernatant was decanted, and the pellet was extracted with methanol/water (8:2) and centrifuged for 20 min at 3000*g*. The fractions were then combined to give a total soluble phenol extract. Methanol was removed from the extracts by rotary evaporation, and extracts were then partially purified on a 500 mg Sep-Pak C_{18} 3 cc Vac RC cartridge (Waters Ltd., Elstree, UK). Cartridges were prepared with 4 mL of methanol (100%) followed by 4 mL of 5% acetic acid. Samples were then loaded, washed with 2.5 mL of water, and subsequently eluted with 4 mL of methanol (100%), dried down at 50 °C under nitrogen, and redissolved in 70% MeOH.

HPLC. Flavonoid and phenolic end products were analyzed by reverse-phase HPLC with online photodiode array detection with and without electrospray ionization−ion trap mass spectrometry.

HPLC analysis was carried out on a Waters system with a 996 photodiode array detector (PDA) and a 8 mm × 100 mm i.d., 4 μm, C_{18} Nova-Pak radial compression column (Waters), equilibrated with 100% solvent A (5% acetic acid) at a flow rate of 2 mL/min.

Compounds were eluted by linear gradient to 100% solvent B (100% methanol) over 50 min and monitored from 240 to 400 nm. Compounds were quantitated by comparison to calibration curves for appropriate standards.

HPLC−ion trap mass spetrometry (HPLC-MS^n) analysis was performed on a Thermo Finnigan LC-MS system (Thermo Electron Corp., Waltham, MA, USA) comprising a Finnigan Surveyor PDA Plus detector and a Finnigan LTQ linear ion trap with ESI source, and the column used was a 3.9 mm × 100 mm i.d., 4 μm, C_{18} Nova-Pak (Waters). The autosampler tray temperature was maintained at 5 °C and the column temperature at 30 °C. Sample injection volume was typically 10 μL, the detection wavelength was set to 240−400 nm, and the flow rate was 1 mL/min, with 100 μL/min going to the mass spectrometer. The mobile phase consisted of water/formic acid (A; 100:0.1, v/v) and MeOH/formic acid (B; 100:0.1, v/v). The column was equilibrated with 95% solvent A, and the percentage of B increased linearly to 60% over 65 min.

Ionization parameters were optimized by infusion of chlorogenic acid standard at a constant rate into the LC flow. Mass spectra were acquired in negative ionization mode with the following interface and MS parameters: nitrogen sheath gas, 30 arbitrary units; nitrogen auxiliary gas, 15 units; spray voltage, 4 kV; capillary temperature, 320 °C; capillary voltage, −1 V; and tube lens offset, −68 V. MS/MS fragmentation was carried out at a normalized collision energy of 35% and isolation width m/z 2.0.

Purification of Selected Compounds and Acid Hydrolysis. Abundant phenolic compounds were purified by reverse-phase chromatography with the Waters system described above. Fractions were concentrated by rotary evaporation, and a portion was retained for acid and alkali hydrolysis. Acid hydrolysis was performed by combining a volume of purified compound with an equal volume of 2 M HCl. The solution was heated to 90 °C for 1 h, and the pH was then adjusted to 4−5 with NaOH. Alkali hydrolysis was performed by combining a volume of purified compound with an equal volume of 2 M NaOH. The solution was incubated for 16 h under N_2, and the pH was then adjusted to 4−5 with HCl. Purified compounds and neutralized hydrolysates were partially purified on a 500 mg Sep-Pak C_{18} 3 cc Vac RC cartridge (Waters Ltd.) as described above, dried down at 50 °C under nitrogen, and redissolved in 70% MeOH.

Antioxidant Assays. Antioxidant activity was expressed as trolox equivalents (TE) by comparison of tested compounds to trolox calibration curves in the range of 5−50 μmol/L. The diphenylpicrylhydrazyl (DPPH) radical scavanging assay was carried out according to the method of Brand-Williams et al.[17] A 140 μM solution of DPPH was prepared in 50:50 methanol/water. This was combined with an equal volume of sample in a 1.5 mL cuvette, with 50:50 methanol/water as a control. Mixtures were left to stand for 30 min at room temperature, after which time absorbance at 517 nm was determined. A range of sample concentrations were tested to identify the range giving partial reduction of the DPPH in the reaction mixture.

A second radical-scavanging assay based on the positive radical ion, $ABTS^{\bullet+}$, was carried out according to the protocol of Re et al.[18] The radical form was prepared by adding potassium persulfate to a 7 mM stock solution of ABTS to give a final concentration of 2.45 mM and allowing the mixture to stand for 16 h at room temperature in the dark. At the time of assay, the $ABTS^{\bullet+}$ solution was diluted with water to give an absorbance of 0.700 (±0.2) at 743 nm. Sample volumes of 25 μL were added to 1475 μL of reagent in a 1.5 mL cuvette, and absorbance was measured after 6 min. A range of sample concentrations were tested to identify the range giving partial reduction of the $ABTS^{\bullet+}$ in the reaction mixture.

The ferric reducing capacity of samples was measured by the FRAP assay, which detects reduction of the ferric ion (Fe^{3+}) to the ferrous ion (Fe^{2+}).[19] The assay reagent was prepared by combining 10 mM TPTZ, 20 mM ferric chloride, and 300 mM sodium acetate buffer (pH 3.6) in the ratio of 1:1:10. Sample volumes of 25 μL were added to 1475 μL of reagent in a 1.5 mL cuvette, and absorbance was measured at 593 nm after 10 min.

RESULTS AND DISCUSSION

Phenol Profile. Figure 1 shows a typical profile of soluble phenols extracted from 'Abertop'. Analysis by LC ESI-MS with PDA detection revealed approximately 50 compounds that could be easily distinguished (Table 1). Several compounds were readily identified by comparison of retention times and fragmentation patterns with known standards. Others were tentatively identified by the similarity of UV absorbance characteristics and fragmentation patterns with known standards and compounds reported in the literature.[5,20,21] Representative structures are shown in Figure 2.

Compounds identified by LC-MS include hydroxycinnamoyl esters, flavone glycosides, salvianolic acids, and hydroxycinnamoyl flavone conjugates. Relatively abundant hydroxycinnamate esters, which have been previously reported by Parveen et al.[4] in orchard grass, were identified in extracts including 5-caffeoyl quinate (chlorogenic acid), 2-*O*-caffeoylisocitrate, and 2-*O*-caffeoylisocitrate 6-methyl ester (compounds **5**, **9**, and **18a** as shown in Table 1).

dx.doi.org/10.1021/jf4040749 | J. Agric. Food Chem. 2014, 62, 468−475

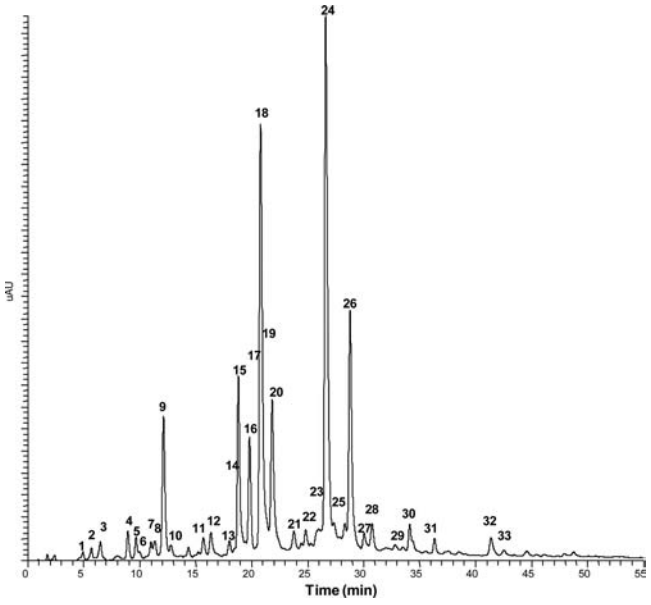

Figure 1. HPLC chromatogram showing separation of soluble phenolic compounds in extracts of orchard grass detected by photodiode array at 340 nm. Peak numbering corresponds with Table 1.

Hydroxycinnamate Esters. A number of hydroxycinnamate esters that have not previously been reported in orchard grass were detected in 'Abertop' extracts. Compound **7** with M_r 268 Da at t_R 11 min showed characteristics consistent with a caffeoyl/feruloyl ester with UV maxima at 303sh and 326 nm. MS^2 of m/z 267 in negative mode produced a base peak at m/z 161 $[\text{caffeic acid} - H_2O - H^+]^-$ and a secondary peak at m/z 105 $[\text{glyceric acid} - H^+]^-$. Further fragmentation of the m/z 105 ion produced a base peak at m/z 75 $[\text{glyceric acid} - \text{HCOH} - H^+]^-$ and corresponded with the fragmentation pattern observed for glyceric acid. This compound is identified as caffeoylglycerate. 2-Caffeoylglycerate has previously been identified in extracts of the medicinal plant, *Mercurialis perennis* L.[22]

A second hydroxycinnamoyl ester (M_R 352 Da), compound **22a**, was detected at t_R 24.8 min, showing maximal UV absorbance at 315 nm. This compound produced an MS^2 base peak at m/z 163 $[\text{coumaric acid} - H^+]^-$ and secondary ions at m/z 169 $[\text{methylisocitric acid} - 2 \times H_2O - H^+]^-$, 205 $[\text{methylisocitric acid} - H^+]^-$, and 119 $[\text{coumaric acid} - CO_2 - H^+]^-$. Further fragmentation of the 205 ion in MS^3 produced a base peak at m/z 173 $[\text{methylisocitric acid} - CH_3OH - H^+]^-$ and secondary ions at m/z 111 $[\text{methylisocitric acid} - CH_3OH - CO_2 - H_2O - H^+]^-$ and 155 $[\text{methylisocitric acid} - CH_3OH - H_2O - H^+]^-$. Caffeoylisocitrate methyl ester has been previously identified in orchard grass,[4] and this compounded yielded an ion at m/z 205 in MS^2 with an equivalent fragmentation pattern in MS^3 to the 205 ion reported here. On this basis this compound is identified as coumaroylisocitrate methyl ester.

Compound **8** with M_r 430 Da showed a fragmentation pattern related to that of compound **7** and was detected at t_R 11.4 min. This compound also showed a UV profile consistent with a caffeoyl/feruloyl ester with UV maxima at 300sh and 324 nm. It produced an MS^2 base peak in negative mode at m/z 267 corresponding to the neutral loss of 162 Da and secondary peaks at m/z 179 and 411 $[M - H_2O - H^+]^-$. The 179 ion was confirmed as $[\text{caffeic acid} - H^+]^-$ in MS^3. Further fragmentation of the 267 ion in MS^3 yielded a base peak at m/z 249 $[267 - H_2O - H^+]^-$ and secondary peaks at m/z 113, 175, 85, 87, and 205, and the 249 ion in MS^4 yielded a base peak at 113 and secondary peaks at 205, 157, 87, and 85. This indicates that the 157 ion yielded in MS^4 is released from the 175 ion yielded in MS^3. These fragments are consistent with neutral losses of CO_2 (−44 Da), dehydrophenoxy radical (−92 Da), dehydrophenoxy radical and CO_2 (−136 Da), and dehydrophenoxy radical, CO_2, and C_2H_2/C_2H_4 (−162/−164 Da). These fragments may be accounted for by whole or partial loss of a coumaroyl moiety, and the ion at m/z 87 is consistent with a dehydro-glycerate moiety. On this basis it is proposed that compound **8** is caffeoylglycerate conjugated with coumaric acid formed via an oxidative radical coupling reaction.

Caffeic Acid Derivatives. Antioxidant, antithrombotic, antitumor, and antiviral properties of the popular Asian medicinal herb, danshen (*Salvia miltiorrhiza*), have been attributed to constituent caffeic acid derivatives known as salvianolic and lithospermic acids.[23] A number of compounds with structural properties consistent with these caffeic acid derivatives were detected in orchard grass extracts. These included compounds **15**, **19a**, **19b**, **22b**, **23c**, **23d**, **25a**, and **25b** with M_r 360, 492, 538, 556, and 736 Da. ESI MS^n spectra of negative ions showed characteristic fragmentation patterns of lithospermic and salvianolic acids with products derived from neutral losses of 198, 180, 162, 110, and 44 Da corresponding to losses of 3,4-dihydroxyphenyl-lactic acid (danshensu), caffeic acid, caffeic acid dehydrate, catechol, and CO_2 moieties, respectively. They also yielded characteristic fragment ions of salvianolic acids at m/z 537, 493, 383, 339, 313, 295, 197, and 179.[24]

Compound **25b** with M_r 360 Da shows retention time, UV absorption profile (maxima at 276 and 331 nm), and fragmentation pattern consistent with those of rosmarinic acid (MS^2 fragments at m/z 161, 179, and 197). The remaining members of the group have been identified on the basis of their MS and UV spectra where detected.

Compound **23d** with M_r 492 Da at t_r 26.0 min shows characteristic features of caffeic acid derivatives. This compound showed a base peak in negative mode at m/z 339 and a secondary peak at m/z 447 corresponding to neutral losses of 152 and 44 Da. The fragmentation pattern suggests a molecular structure consistent with lithospermic acid less CHOOH. The loss of 152 Da is equivalent to the loss of 198 Da observed during fragmentation of lithospermic acid in negative mode resulting from a cleavage of the ester bond between the carboxyl oxygen and second oxygen atom, yielding a negative ion at m/z 339 as observed here. Other fragments in common with those yielded by lithospermic acid include negative ions at m/z 295 and 185. Other fragments observed include ions at 447 and 337, which may correspond with ions observed at m/z 493 and 383 in lithospermic MS spectra (447 + CHOOH and 337 + CHOOH, respectively).

Compounds **19b** and **25a** with M_r 556 and 736 Da at t_r 21.6 and 27.3 min, respectively, yielded fragment ions in negative MS at m/z 537 and 717, respectively, corresponding with lithospermic acid and lithospermic acid B. Similar compounds with equivalent masses have been reported in sage tea.[25] A 736 Da isomer gave rise to a base peak at m/z 537 (198 Da loss), which in MS^3 yielded fragment ions typical of lithospermic acid as reported by Zeng et al.[24]

Caffeic acid derivatives, including rosmarinic, lithospermic, and salvianolic acids, have potent radical-scavenging activity related to the number of catechol moieties contained in the

dx.doi.org/10.1021/jf4040749 | J. Agric. Food Chem. 2014, 62, 468−475

Table 1. Phenolic Compounds in Orchard Grass Leaf Extracts

peak/ ID	t_r	$[M-H]^-$ (m/z)	main fragments(m/z)	λ_{max}(nm)	tentative compound identification
1	4.9	353	**191**, 179 (45), 135 (8), 173 (3)	299sh, 323	3-caffeoylquinate
2	5.7	297	**135**, 179 (29), 279 (5), 229 (3)	301sh, 326	2-*O*-caffeoylthreonate
3	6.5	297	**135,** 179 (29), 279 (3), 229 (2), 117 (1)	299sh, 326	2-*O*-caffeoylthreonate
4a	8.9	179	**135**, 179 (76), 151 (1)	300sh,322	caffeic acid
4b		367	**193**, 134 (5), 173 (3), 191 (2)	300sh, 322	feruloyl quinate
5	9.7	353	**191**, 179 (5), 173 (1), 135 (0.5), 161 (1)	300sh, 321	5-caffeoylquinate
6	10.0	353	**173**, 179 (54), 191 (33), 135 (5)	301sh, 323	4-caffeoylquinate
7	11.0	267	**161**, 105 (64), 179 (33), 221 (6), 135(5)	303sh, 326	caffeoylglycerate
8	11.4	429	**267**, 411 (3), 179 (3)	300sh, 324	caffeoylglycerate *p*-coumaric conjugate
9	12.1	353	**173**, 191 (75), 111 (13), 155 (6), 179 (2)	304sh, 328	2-*O*-caffeoylisocitrate
10	12.8	163	**119**, 163 (8)	312	*p*-coumaric acid
11	15.7	337	**173**, 111 (13), 155 (5), 191 (3)	314	2-*O*-coumaroylisocitrate
12	16.4	609	**489**, 519 (26), 490 (12), 399 (9), 591 (8), 369 (7)	270, 342	luteolin-6-*C*-hexoside-8-*C*-hexoside
13a	18.0	593	**473**, 503 (32), 353 (27), 474 (22), 383 (14), 575 (11)	ND	apigenin-6-*C*-hexoside-8-*C*-hexoside
13b		367	**173**, 111 (13), 155 (7), 179 (7), 135 (3)	ND	2-*O*-caffeoylisocitrate methyl ester
14	18.4	609	**327**, 357 (65), 411 (25), 328 (11), 591 (10), 358 (8), 447 (7)	ND	iso-orientin-*O*-hexoside
15	18.8	537	**339**, 493 (5), 357 (1),	252, 285, 318sh, 344	lithospermic acid isomer
16	19.8	579	**489**, 459 (20), 519 (17), 561 (16), 399 (12), 369 (8), 471 (6)	270, 349	luteolin-6-*C*-pentoside-8-*C*-hexoside
17	20.5	447	**327**, 357 (46), 369 (6), 393 (4)	ND	orientin
18a	20.8	367	**179**, 205 (56), 169 (8), 135 (7), 173 (5), 187 (1), 111 (1)	302sh, 330	2-*O*-caffeoylisocitrate 6-methyl ester
18b		579	**429**, 459 (20), 357 (19), 309 (14), 561 (6), 447 (4)	ND	luteolin-*C*-hexosyl pentoside
19a	21.6	537	**493**, 295 (61), 357 (6), 383 (6), 313 (6), 337 (4)	ND	lithospermic acid isomer
19b		555	**537**, 511 (62), 269 (8), 493 (7), 313 (4)	ND	salvianolic acid K isomer
20a	21.8	447	**327**, 357 (49), 429 (15), 387 (3)	ND	iso-orientin
20b		563	**443**, 473 (60), 353 (20), 383 (15), 545 (14), 503 (7)	ND	apigenin-6-*C*-hexoside-8-*C*-pentoside
21a	23.8	563	**413,** 293 (20), 443 (3)		apigenin-*C*-hexosyl pentoside
21b		593	**473**, 503 (83), 383 (33), 413 (21), 474 (20), 504 (17), 575 (15), 533 (7)		chryseriol-6-*C*-hexoside-8-*C*-pentoside
22a	24.8	351	**163**, 169 (78), 205 (38), 119 (5)	315	2-*O*-coumaroylisocitrate methyl ester
22b		555	**511**, 537 (64), 357 (61), 269 (47), 285 (38), 313 (33), 449 (27), 241 (22), 339 (18), 197 (10)	ND	caffeic acid derivative
22c		431	**311**, 341 (28), 312 (10), 413 (7)	ND	isovitexin
22d		563	**443**, 473 (50), 444 (18), 353 (16), 545 (11), 474 (10), 383 (8), 455 (4)	ND	apigenin-6-*C*-hexoside-8-*C*-pentoside
23a	26.0	743	**607**, 581 (10), 487 (7), 625 (1), 553 (1)	ND	2-*O*-caffeoylthreonate orientin conjugate
23b	26.6	713	**607**, 581 (20), 607 (17), 487 (15), 581 (3), 517 (3), 553 (2), 625 (2)	ND	2-*O*-caffeoylglycerate orientin conjugate
23c		735	**493**, 537 (66), 717 (50), 313 (45), 691 (20), 475 (18), 555 (15), 431 (11), 519 (11), 295 (10), 339 (8)	ND	caffeic acid derivative
23d		491	**339**, 447 (33)	ND	caffeic acid derivative
24		799	**581**, 607 (2), 461 (1), 625 (1), 755 (1), 491 (1)	269, 349	2-*O*-caffeoylisocitrate orientin conjugate
25a	27.3	735	**537**, 717 (80), 493 (26), 339 (22), 475 (20), 449 (15), 519 (13), 465 (12), 313 (12), 673 (10), 357 (9), 295 (8)	ND	salvianolic acid isomer
25b	27.3	359	**161**, 179 (29), 197 (24), 223 (15), 133 (3), 135 (2)	ND	rosmarinic acid
26	28.8	813	**581**, 607 (10), 461 (2), 625 (2), 487 (1), 491 (1)	270, 349	2-*O*-caffeoylisocitrate methyl ester orientin conjugate
27	30.0	491	**329**, 330 (5), 371 (3), 314 (1)	260, 343	tricin-*O*-hexoside
28	30.8	813	**595**, 639 (19), 581 (8), 607 (1), 769 (1), 625 (1), 461 (1)	270, 345	2-*O*-caffeoylisocitrate methyl ester orientin conjugate
29	32.8	827	**595**, 639 (3)	271, 335	2-*O*-caffeoylisocitrate methyl ester luteolin-methyl-ether conjugate
30	34.1	577	**533**, 491 (1)	260, 345	tricin-*O*-hexosyl -malonate
31	34.4	687	**491**, 669 (49), 643 (33), 329 (30), 492 (13), 525 (12),	326	tricin conjugate
32	41.4	329	**314**, 329 (50), 299 (1)	267, 349	tricin
33	42.5	525	**329**, 477 (2), 195 (2), 314 (2), 507 (2), 165 (1)	270, 331	tricin conjugate

structure and are reported to have a range of protective and antimicrobial properties.[26,27]

Hydroxycinnamate Esters and Flavone Glycoside Conjugates. UV combined with MS analysis revealed a novel group of compounds in *D. glomerata* extracts with distinctive fragmentation patterns in negative mode MS. These compounds show neutral losses consistent with cleavage of ester-linked organic acids and, where detected, UV absorption maxima at 269−270 and 349 nm. UV profiles were typical of the profile produced by orientin (luteolin-8-*C*-glucoside) standard. Compound **24** with M_r 800 Da eluted at t_R 26.6 min and in negative mode produced a mass spectrum with a base peak at m/z 581 and further peaks at m/z 607 and 625. This corresponds to neutral losses of 218, 192, and 174 Da, respectively. Interestingly, full MS

dx.doi.org/10.1021/jf4040749 | J. Agric. Food Chem. 2014, 62, 468−475

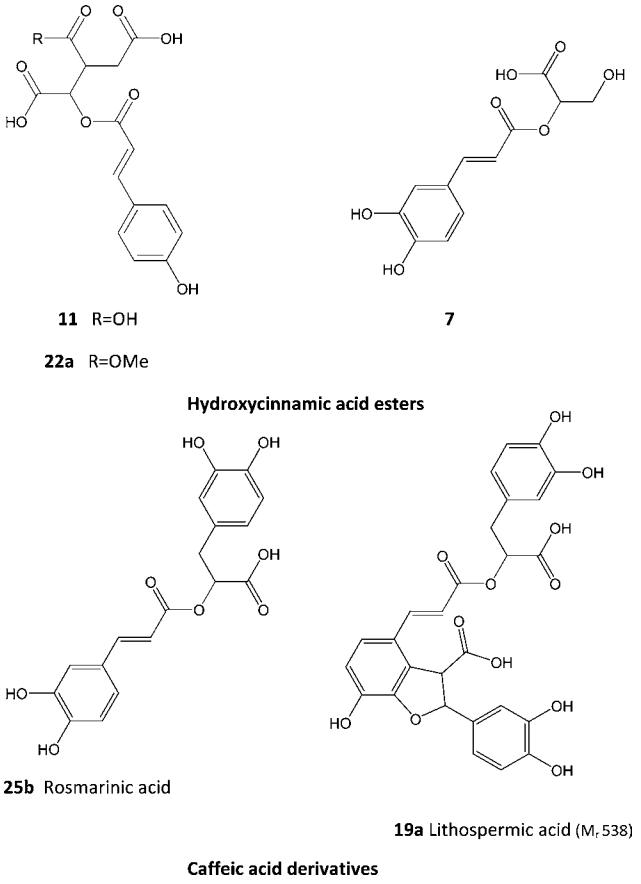

Figure 2. Structures of phenolic compounds in orchard grass.

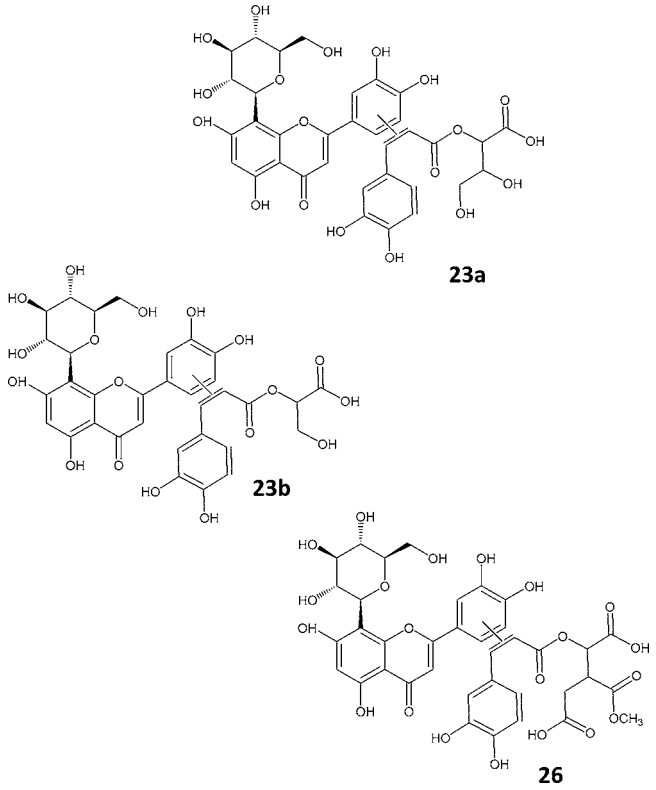

Figure 3. Caffeic acid ester−orientin conjugates detected in orchard grass extracts including caffeoylthreonate orientin conjugate (**23a**), caffeoylglycerate orientin conjugate (**23b**), and 2-*O*-caffeoylisocitrate methyl ester orientin conjugate (**26**).

Table 2. Variation in Composition and Yield of Orchard Grass during the Transition from Vegatative to Flowering Stage

	May 8	May 13	May 18	May 23	May 29
crude protein (g/kg DM)	166.6	161.3	129.1	126.9	106.9
WSC (g/kg DM)	152.7	114.3	165.4	150.9	130.6
NDF (g/kg DM)	430.9	480.0	465.1	469.1	522.4
ADF (g/kg DM)	206.0	236.2	230.8	234.7	264.0
DMD (g/kg DM)	759.6	722.4	744.8	720.2	692.1
yield (t/ha)	2.58	3.05	3.68	3.87	6.36

in positive mode revealed major ions at m/z 801 and 627 at t_R 26.6, whereas only one ion was observed in negative mode, suggesting a neutral fragment of 174 Da is readily lost in positive mode. Losses of 192 and 174 Da correspond to cleavage of an isocitrate or quinate moiety on either side of the ether linkage in an ester bond. The neutral loss of 218 Da could be accounted for by cleavage at the far side of the carbonyl group (174 + 44 Da). Further fragmentation of the 581 ion in MS^3 yielded ions at m/z 461 and 491, which correspond to neutral losses of 120 and 90 Da, typical of C-linked flavonoid hexosides.[28] Additional fragments at m/z 471 and 351 correspond to neutral losses of 110 and 230 Da. These may be accounted for by loss of a catechol moiety (110 Da) and a catechol moiety combined with a C-linked hexoside fragment (110 and 120 Da). Spectra in MS^4 of the ions at m/z 491 and 461 showed base peaks at m/z 381 and 351, respectively, corresponding to the loss of a catechol moiety. Compound **24** was purified by reverse phase chromatography and incubated with 1 M HCl with heat or with 1 M NaOH at room temperature to hydrolyze ester and O-glycosidic linkages. Major products of acid and alkali hydrolysis experiments included compounds with M_r 626, 582, and 472 Da. These compounds yielded identical fragment ions in MS^2 corresponding to fragment ions described above and may be accounted for by hydrolysis of ester linkages, acid-catalyzed decarboxylation, and release of pyrocatechol by decomposition. Minor products included compounds with M_r 192, 354, and 447 Da. These compounds showed fragmentation patterns identical to those of isocitric acid, 2-*O*-caffeoylisocitrate, and orientin.

On the basis of this evidence, this molecule is composed of 2-*O*-caffeoylisocitrate and orientin residues. The fragmentation patterns observed in MS^n experiments including the release of isocitrate and catechol moieties and CO_2 indicate that this compound is formed by a condensation reaction with bonds formed between C2 and C3 on the alkyl side chain of the caffeoyl moiety and the luteolin B-ring. Similar condensation products include naturally occurring oxyneolignans, americanin A[29] and eusiderin,[30] and the coumarinolignoid, daphneticin.[31] Other related compounds include a hydroxcinnamate−mandelonitrile conjugate, which has been reported in *Miscanthus* × *giganteus* stem extracts.[32] These compounds are postulated to be formed by oxidative coupling mechanisms, and conjugates identified in orchard grass extracts may be formed by similar pathways. Activity of plant oxidative enzymes during the extraction process could potentially catalyze formation of these products. To eliminate this possibility, we repeated the extraction procedure including 50 mM ascorbic acid in the extraction solvent. An identical profile of phenolic compounds was obtained by this method (data not presented), indicating that these conjugates were not formed during the extraction procedure.

dx.doi.org/10.1021/jf4040749 | J. Agric. Food Chem. 2014, 62, 468−475

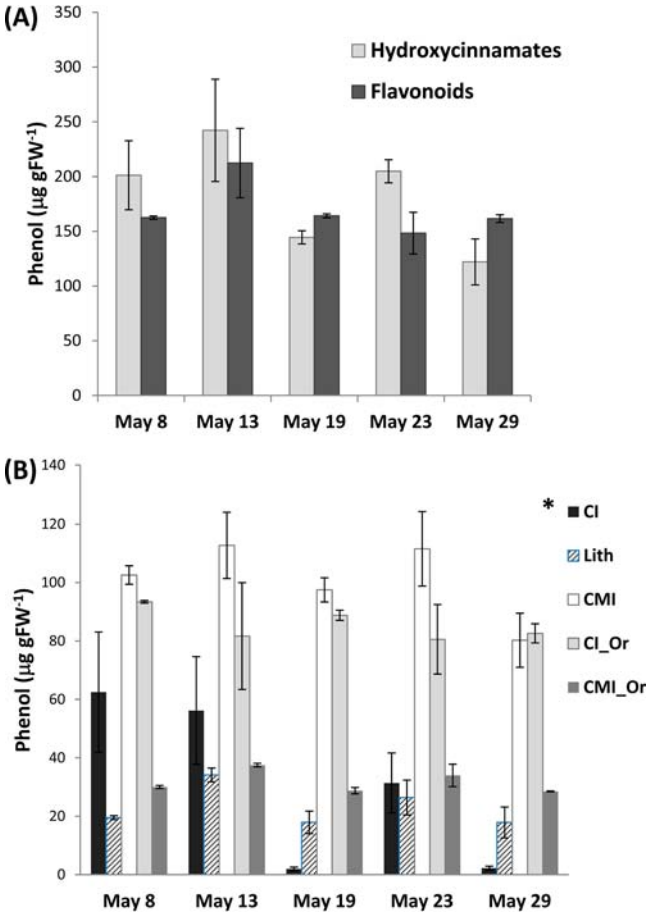

Figure 4. Variation in phenolic composition of orchard grass during the transition from vegetative to flowering stage: (A) changes in total flavonoids and hydroxycinnamates; (B) changes in abundant phenolic compounds. CI, 2-*O*-caffeoylisocitrate, **9**; Lith, lithospermic, **15**; CMI, 2-*O*-caffeoylisocitrate 6-methyl ester, **18a**; CI-Or, 2-*O*-caffeoylisocitrate orientin conjugate, **26**; CMI-Or, 2-*O*-caffeoylisocitrate methyl ester orientin conjugate, **28**.

Other compounds assigned to this group on the basis of fragmentation patterns include compounds **23a**, **23b**, **26**, **28**, and **29** with M_r 744, 714, 814, 814, and 828 Da. Common fragments detected in negative mode ESI MS^n spectra include ions at m/z 625, 607, 581, 491, 487, and 461 Da. Compounds with M_r 714, 744, and 814 Da have been tentatively identified as conjugates of orientin with caffeoylthreonate, caffeoylglycerate, and caffeoylisocitrate methyl ester, respectively (Figure 3), and a compound with M_r 828 Da has a fragmentation pattern consistent with a conjugate of hispidulin-*C*-glycoside with caffeoylisocitrate methyl ester.

Variation in Phenolic Profiles during Transition from Vegetative to Flowering Stage. Orchard grass production was monitored during transition from vegetative to flowering stage, which corresponds with maximum yield of biomass. Table 2 shows changes in composition in harvested material. Changes in composition reflect the alteration in morphology that occurs during flowering, that is, increasing proportion of stem tissue with a corresponding decrease in leaf tissue. Neutral detergent fiber (NDF) and acid detergent fiber (ADF) show an increasing trend, whereas the opposite pattern is observed with dry matter digestibility and crude protein, which generally decrease with plant maturity. Biomass yield showed a steady increase during this period. Figure 4A shows changes in total hydroxycinnamate and flavonoid content during flowering. Levels remained high throughout this period, with potential yields of hydroxycinnamates and flavonoids ranging from 2.6 to 4.0 kg/ha and from 2.1 to 5.1 kg/ha, respectively. Levels of the most abundant phenolic compounds are shown in Figure 4B. These included compounds 2-*O*-caffeoylisocitrate, **9**; 2-*O*-caffeoylisocitrate methyl ester, **18a**; lithospermic acid isomer, **19**; 2-*O*-caffeoylisocitrate orientin conjugate, **24**; and 2-*O*-caffeoylisocitrate methyl ester orientin conjugate, **26**. Some variation in content was observed with 2-*O*-caffeoylisocitrate concentrations decreasing over time. Analysis of the antioxidant activity of these compounds by a range of assays, including DPPH, ABTS, and FRAP, showed levels of activity comparable with that of trolox (Table 3) and indicate that the lithospermic isomer is the most potent antioxidant of the compounds tested.

Table 4. Composition of Fresh and Ensiled 'Abertop' Plant Material

	fresh	ensiled
DM (g/kg fw)	22.00	19.13
pH	6.40	5.95
WSC (g/kg dm)	167.41	147.59
lactic acid (g/kg dm)		23.86
acetic acid (g/kg dm)		14.31

Ensiling. Orchard grass was ensiled in laboratory silos for 14 days to investigate the effect of conservation on the phenol profile of the plant material. The composition of the silage is shown in Table 4. Limited fermentation occurred during this period with reduced production of fermentation acids, minimal depletion of WSC content, and little change in pH.

Analysis of phenolic compounds in ensiled orchard grass showed that many of these compounds persisted during the ensiling period (Figure 5). Whereas all compounds were not fully resolved in these extracts, differences in compound abundance were verified by total ion counts. There was evidence of hydrolysis of caffeoyl esters with accumulation of free caffeic acid, **4a**. There was also evidence of further catabolism of caffeic acid with accumulation of dihydroxystyrene (X, Figure 5). 2-*O*-Caffeoylisocitrate, **9**, showed a decrease, while an increase in the lithospermic acid isomer, **15**, was also evident. It is noteworthy

Table 3. Antioxidant Capacity of Abundant Phenolic Compounds in Orchard Grass

	TE (μM trolox/μM phenol)		
compound	DPPH	ABTS	FRAP
2-*O*-caffeoylisocitrate, **9**	0.531 ± 0.033	0.911 ± 0.054	1.500 ± 0.009
lithospermic acid, **15**	1.652 ± 0.011	3.565 ± 0.049	4.133 ± 0.003
2-*O*-caffeoylisocitrate 6-methyl ester, **18a**	0.388 ± 0.007	0.725 ± 0.024	1.325 ± 0.029
2-*O*-caffeoylisocitrate orientin conjugate, **26**	1.187 ± 0.008	0.581 ± 0.099	0.884 ± 0.041
2-*O*-caffeoylisocitrate methyl ester orientin conjugate, **28**	1.535 ± 0.016	0.831 ± 0.064	2.283 ± 0.054

dx.doi.org/10.1021/jf4040749 | J. Agric. Food Chem. 2014, 62, 468−475

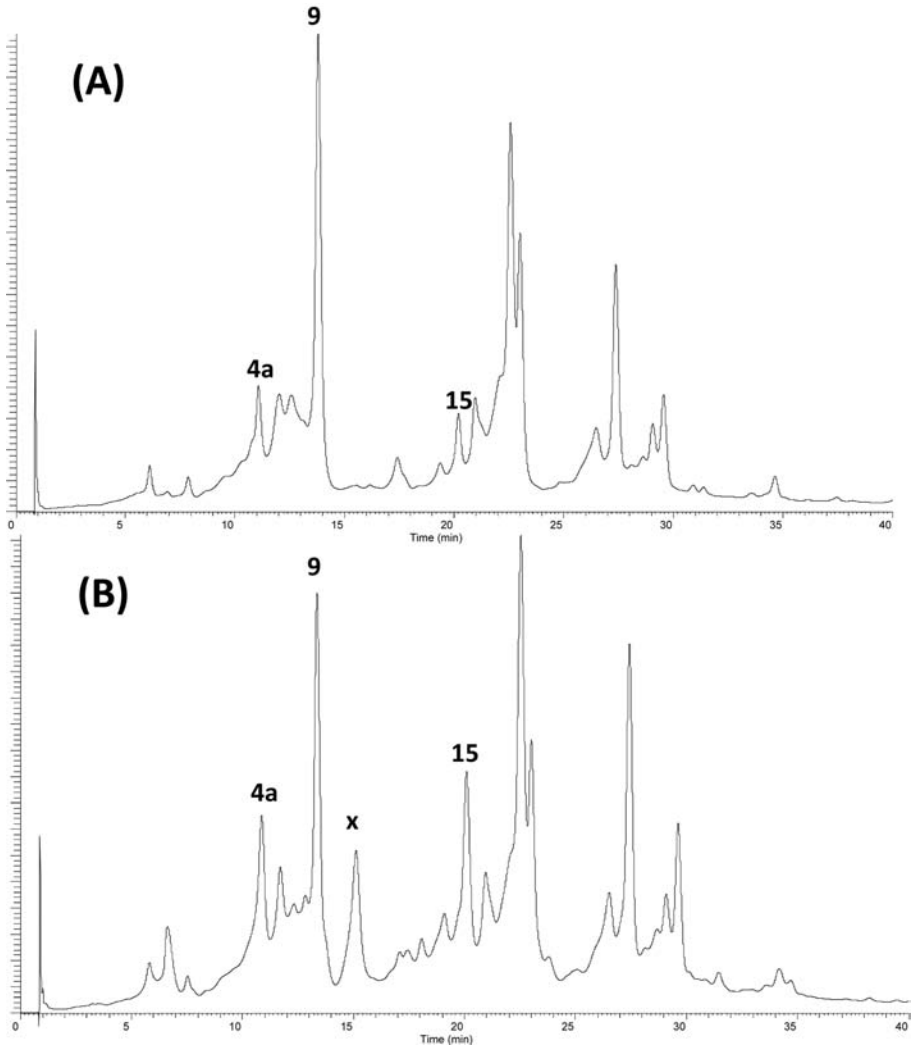

Figure 5. LC chromatogram showing separation of soluble phenolic compounds detected by photodiode array at 340 nm: (A) before ensiling; (B) after ensiling. Peaks that showed a change in content during ensiling are labeled according to numbering in Table 1. X denotes dihydroxystyrene peak.

that dramatic increases in levels of the compound salvianolic acid B, which is a bioactive component in the medicinal herb danshen (*Salvia miltiorrhiza*), were observed during postharvest drying of the herbal material.[33] This observation may be significant as this component is potentially of therapeutic value.

This study suggests that restricted silage fermentation may be advantageous from a biorefining perspective. Limited degradation of metabolites offers increased scope for recovery of high-value components, and a high WSC content provides a fermentable substrate in extracted juice for the production of ethanol or lactic acid.

In summary, there is currently much interest in developing biorefineries based on grass feedstocks, and ensilage is the preferred method for stabilizing harvested biomass for biorefining and biofuel production. Processes have been developed at pilot scale for the extraction of amino acids and lactic acid from silage juice.[10] Recovery of other potential high-value components such as soluble phenolic compounds with bioactive properties can improve the economic feasibility of these biorefineries. It is noteworthy that we have demonstrated in previous experiments that compounds identified in orchard grass can also be extracted with ethanol, a solvent compatible with the production of nutraceuticals. Moreover, biorefining can enable recovery of these compounds on a large scale as coproducts when profit margins would prohibit an operation based solely on these molecules.

■ ASSOCIATED CONTENT

Ⓢ Supporting Information

Proposed fragmentation route for compound **24**, which is representative of fragmentation patterns observed for other compounds in this group. This material is available free of charge via the Internet at http://pubs.acs.org.

■ AUTHOR INFORMATION

Corresponding Author

*(A.L.W.) Phone: +44 (0) 1970 823207. Fax: +44 (0) 1970 828357. E-mail: alg@aber.ac.uk.

Funding

This work was supported by funding from the Biotechnology and Biological Sciences Research Council (BBSRC) Institute Strategic Programme Grant (BB/J0042/1), the European Regional Development Fund through funding provided for the BEACON project by the Welsh European Funding Office, and the Technology Strategy Board through the Succinic Esters from Renewable Feedstocks (SERF) project.

Notes

The authors declare no competing financial interest.

REFERENCES

(1) Beddows, A. R. Biological flora of the British Isles. *Dactylis glomerata* L. *J. Ecol.* **1959**, *47*, 223−239.

(2) Lolicato, S.; Rumball, W. Past and present improvement of orchard grass (*Dactylis glomerata* L.) in Australia and New Zealand. *N. Z. J. Agric. Res.* **1994**, *37*, 379−390.

(3) Landsborough-Thompson, D. The pigments of butterflies' wings. II. Occurrence on the pigment of *Melanargia galatea* in *Dactylis glomerata*. *Biochem. J.* **1926**, *20*, 1026−1027.

(4) Parveen, I.; Winters, A.; Threadgill, M. D.; Hauck, B.; Morris, P. Extraction, structural characterisation and evaluation of orchard grass (*Dactylis glomerata*) as substrates for polyphenol oxidase. *Phytochemistry* **2008**, *69*, 2799−2806.

(5) Cuyckens, F.; Claeys, M. Mass spectrometry in the structural analysis of flavonoids. *J. Mass Spectrom.* **2004**, *39*, 1−15.

(6) Jay, M.; Plenet, D.; Ardouin, P.; Lumaret, R.; Jacquard, P. Flavonoid variation in seven tetraploid populations of *Dactylis glomerata* L. (Graminae). *Biochem. Syst. Ecol.* **1984**, *12*, 193−198.

(7) Jay, M.; Lumaret, R. Variation in the subtropical group of *Dactylis glomerata* L. 2. Evidence from phenolic compound pattern. *Biochem. Syst. Ecol.* **1995**, *23*, 523−531.

(8) Mandl, M. G. Status of biorefining in Europe. *Biofuels, Bioprod. Biorefin.* **2010**, *4*, 268−274.

(9) Sieker, T.; Neuner, A.; Dimitrova, D.; Tippkötter, N.; Muffler, K.; Bart, H. J.; Heinzle, E.; Ulber, R. Ethanol production from grass silage by simultaneous pretreatment, saccharification and fermentation: first steps in process development. *Eng. Life. Sci.* **2011**, *11*, 436−442.

(10) Ecker, J.; Schaffenberger, M.; Koschuh, W.; Mandl, M.; Böchzelt, H. G.; Schnitzer, H.; Harasek, M.; Steinmüller, H. Green biorefinery Upper Austria − pilot plan operation. *Sep. Purif. Technol.* **2012**, *96*, 237−247.

(11) Schaffenberger, M.; Ecker, J.; Koschuh, W.; Essl, R.; Mandl, M. G.; Boechzelt, H. G.; Steinmueller, H.; Schnitzer, H. Green biorefinery − production of amino acids from grass silage juice using an ion exchanger device at pilot scale. *Chem. Eng. Trans.* **2012**, *29*, 505−510.

(12) McEniry, J.; Finnan, J.; King, C.; Kiely, P. The effect of ensiling on the suitability for combustion of three common grassland species at sequential harvest dates. *Grass Forage Sci.* **2012**, *67*, 559−568.

(13) O'Keeffe, S. O.; Schulte, R. P. O.; Sanders, J. P. M.; Struik, P. C., II Economic assessment for first generation green biorefinery (GBR): scenarios for an Irish GBR blueprint. *Biomass Bioenergy* **2012**, *41*, 1−13.

(14) Bertin, L.; Ferri, F.; Scoma, A.; Marchetti, L.; Fava, F. Recovery of high added value natural polyphenols from actual olive mill wastewater through solid phase extraction. *Chem. Eng. J.* **2011**, *171*, 1287−1293.

(15) Boudet, A. Evolution and current status of research in phenolic compounds. *Phytochemistry* **2007**, *68*, 2722−2735.

(16) Duke, J. A.; Wain, K. K. *Medicinal Plants of the World*, computer index with more than 85000 entries, 1981; *3* vol.

(17) Brand-Williams, W.; Cuvelier, M. E.; Berset, C. Use of a free radical method to evaluate antioxidant activity. *LWT−Food Sci. Technol.* **1995**, *28*, 25−30.

(18) Re, R.; Pellegrini, N.; Pannala, A.; Yang, M.; Rice-Evans, C. Antioxidant activity applying an improved ABTS radical decolorization assay. *Free Radical Biol. Med.* **1999**, *26*, 1231−1237.

(19) Benzie, I. F. F.; Strain, J. J. The ferric reducing ability of plasma (FRAP) as a measure of "antioxidant power". The FRAP assay. *Anal. Biochem.* **1996**, *239*, 70−76.

(20) Ferreres, F.; Andrade, P.; Valentão, P.; Gil-Izquierdo, A. Further knowledge on barley (*Hordeum vulgare* L.) leaves *O*-glycosyl-*C*-glycosyl flavones by liquid chromatography-UV diode array detection-electrospray ionisation mass spectrometry. *J. Chromatogr., A* **2007**, *22*, 56−64.

(21) Vukics, V.; Guttman, A. Structural characterization of flavonoid glycosides by multi-stage mass spectrometry. *Mass Spectrom. Rev.* **2010**, *29*, 1−16.

(22) Lorenz, P.; Conrad, J.; Bertrams, J.; Berger, M.; Duckstein, S.; Meyer, U.; Stintzing, F. C. Investigations into the phenolic constituents of dog's mercury (*Mercurialis perennis* L.) by LC-MS/MS and GC-MS analyses. *Phytochem. Anal.* **2012**, *23*, 60−71.

(23) Chen, J.; Wang, F.; Lee, F. S-C.; Wang, X.; Xie, M. Separation and identification of water-soluble salvianolic acids from *Salvia miltiorrhiza* Bunge by high-speed counter-current chromatography and ESI-MS analysis. *Talanta* **2006**, *69*, 172−179.

(24) Zeng, G.; Xiao, H.; Liu, J.; Liang, X. Identification of phenolic constituents in Radix *Salvia miltiorrhizae* by liquid chromatography/electrospray ionization mass spectrometry. *Rapid Commun. Mass Spectrom.* **2006**, *20*, 499−506.

(25) Zimmermann, B. F.; Walch, S. G.; Tinzoh, L. N.; Stühlinger, W.; Lachenmeier, D. W. Rapid UHPLC determination of polyphenols in aqueous infusions of *Salvia officinale* L. (sage tea). *J. Chromatogr., B* **2011**, *879*, 2459−2464.

(26) Nuengchamnong, N.; Krittasilp, K.; Ingkaninan, K. Characterisation of phenolic antioxidants in aqueous extract of *Orthosiphon grandiflorus* tea by LC-ESI-MS/MS coupled to DPPH assay. *Food Chem.* **2011**, *127*, 1287−1293.

(27) Ho, J. H. C.; Hong, C.-Y. Salvianolic acids: small compounds with multiple mechanisms for cardiovascular protection. *J. Biomed. Sci.* **2011**, *18*, 30.

(28) Ferreres, F.; Silva, B. M.; Andrade, P. B.; Seabra, R. M.; Ferreira, M. A. Approach to the study of *C*-glycosyl flavones by ion trap HPLC-PAD-ESI/MS/MS: application to seeds of quince (*Cydonia oblonga*). *Phytochem. Anal.* **2003**, *14*, 352−359.

(29) Woo, W. S.; Kang, S. S.; Wagner, H.; Chari, V. M. The structure of Americanin, a neolignan from *Phytolacca americana*. *Tetrahedron Lett.* **1978**, *25*, 3239.

(30) Dias, M. C.; Fernandes, J. B.; Maia, J. G. S.; Gottlieb, O. R.; Gottlieb, H. E. Eusiderins and other neolignans from an *Aniba* species. *Phytochemistry* **1985**, *25*, 213−217.

(31) Zhuang, L.-G.; Seligmann, O.; Wagner, H. Daphneticin, a coumarinolignoid from *Daphne tangutica*. *Phytochemistry* **1983**, *22*, 617−619.

(32) Parveen, I.; Threadgill, M. D.; Hauck, B.; Donnison, I.; Winters, A. Isolation, identification and quantification of hydroxycinnamic acid conjugates, potential platform chemicals, in leaves and stems of *Miscanthus* × *giganteus* using LC-ESI-MS*n*. *Phytochemistry* **2011**, *72*, 2376−2384.

(33) Li, X. B.; Wang, W.; Zhou, G. J.; Li, Y.; Xie, X. M.; Zhou, T. S. Production of salvianolic acid B in roots of *Salvia miltiorrhiza* (Danshen) during the post-harvest drying process. *Molecules* **2012**, *17*, 2388−2407.

JOURNAL OF AGRICULTURAL AND FOOD CHEMISTRY

Article

pubs.acs.org/JAFC

Synthesis of the Insecticide Prothrin and Its Analogues from Biomass-Derived 5-(Chloromethyl)furfural

Fei Chang,[†] Saikat Dutta,[†] James J. Becnel,[‡] Alden S. Estep,[§] and Mark Mascal*[,†]

[†]Department of Chemistry, University of California Davis, 1 Shields Avenue, Davis, California 95616, United States

[‡]Center for Medical, Agricultural, and Veterinary Entomology (CMAVE), Agricultural Research Service (ARS), United States Department of Agriculture (USDA), 1600 Southwest 23rd Drive, Gainesville, Florida 32608, United States

[§]Navy Entomology Center of Excellence, Box 43, Naval Air Station, Jacksonville, Florida 32212, United States

Supporting Information

ABSTRACT: Prothrin, a synthetic pyrethroid insecticide, was synthesized from the biomass-derived platform chemical 5-(chloromethyl)furfural in six steps and overall 65% yield. Two structural analogues of prothrin were also prepared following the same synthetic approach. Preliminary testing of these furan-based pyrethroids against the yellow fever mosquito *Aedes aegypti* indicates promising insecticidal activities.

KEYWORDS: *biomass, furans, pyrethroids, synthesis, 5-(chloromethyl)furfural*

INTRODUCTION

Previously, we have described the synthesis of the natural herbicide δ-aminolevulinic acid (**2**)[1] and the anti-ulcer drug ranitidine (Zantac) (**3**)[2] from the renewable platform chemical 5-(chloromethyl)furfural (CMF) (**1**), which can be derived in a single step from either sugars, cellulose, or raw biomass in isolated yields between 80 and 90%.[3] In a continuing effort to expand the derivative markets of CMF (**1**), we now report a simple, six-step approach to the furan-based pyrethroid insecticide prothrin (**4**) alongside five-step routes to analogues **5** and **6**.

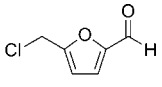

1

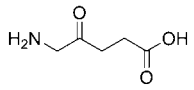

2

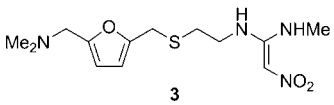

3

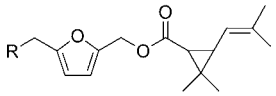

4 R=CCH
5 R=CN
6 R=OPh

The naturally occurring insecticide pyrethrum, isolated from flowers of *Chrysanthemum* sp., has been in commercial use for over 100 years.[4] Elucidation of the chemical structure of its active constituents [i.e., pyrethrins (**7**)] in 1924 ultimately led to the production of several synthetic pyrethroids.[5] As a result of extensive structure−activity studies, the insecticidal and toxicological properties of these compounds typically surpass those of the natural products. Prothrin (**4**) is a member of the synthetic furan-based pyrethroids,[6] which class also includes resmethrin (**8**), a high-volume commercial insecticide.[7]

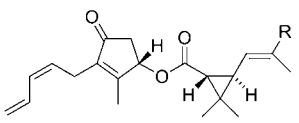

7a R= Me
7b R= CO_2Me

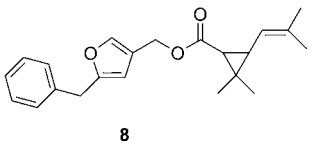

8

Pyrethroids are generally well-suited for agricultural and household uses because of their biodegradability and low mammalian toxicity, and demand for these products has increased in the past decade with the declining use of organophosphates. However, all United States Environmental Protection Agency (U.S. EPA)-registered pesticides are regularly submitted to a process by which they are systematically reviewed to establish that they can still perform their intended function without unreasonable adverse effects on human health or the environment, and this process applies constant pressure on the development of new generations of products that are even more selective in their mode of action.

The synthesis of prothrin (**4**) was first reported in 1969 and is always completed by esterification of 5-propargylfurfuryl alcohol (**10**) with chrysanthemic acid chloride.[6] Because chrysanthemic acid is commercially available as a synthetic version of the natural product,[8] the actual target of prothrin syntheses becomes compound **10**, and most approaches to this molecule have centered around either the reaction of a metalated derivative of furfuryl alcohol (**9**) with a propargyl electrophile[9] or a metalated acetylene with a 5-methyl-substituted furfuryl alcohol derivative incorporating a leaving group (**11**) (Scheme 1).[10,11] Looking to the structures of both compound **10** and CMF (**1**), it becomes apparent that a concise route connecting them should be achievable, and we

Received: October 14, 2013
Revised: December 18, 2013
Accepted: December 19, 2013
Published: December 19, 2013

ACS Publications © 2013 American Chemical Society

dx.doi.org/10.1021/jf4045843 | *J. Agric. Food Chem.* 2014, 62, 476−480

Scheme 1. Approaches to the Synthesis of 5-Propargylfurfuryl Alcohol (10)[a]

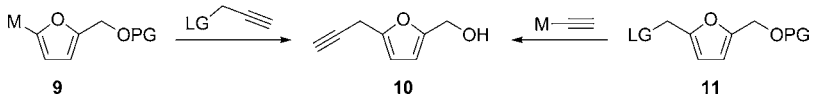

[a]LG, leaving group; PG, protecting group.

Scheme 2. [a]

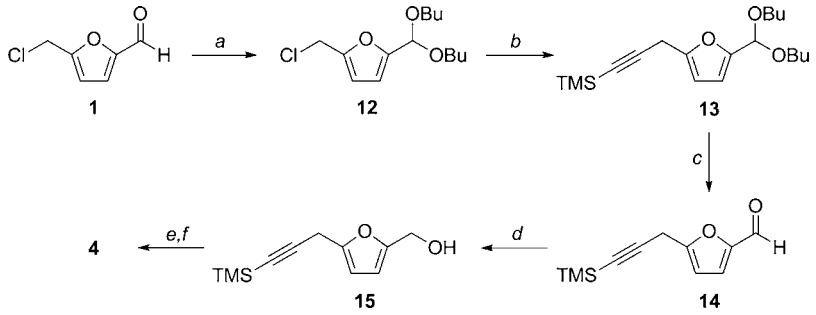

[a]Reagents: *a*, 1-butanol, concentrated HCl (catalyst), 98%; *b*, TMS−acetylene, CuI, K_2CO_3, CH_3CN, 55 °C, 88%; *c*, 1 M aqueous HCl, 97%; *d*, $NaBH_4$, MeOH, 0 °C, 98%; *e*, chrysanthemic acid chloride, benzene, reflux, 95%; and *f*, Bu_4NF, THF, −20 °C, 84%.

were naturally attracted to published methods that involved CMF (**1**) as a precursor to structure **11**[10] but considered the use of organometallics a serious drawback to any industrial application of this synthetic approach. We proposed that the installation of the propargyl group could instead be achieved by copper(I)-mediated coupling of the chloromethyl functionality to an acetylene derivative.[12] The synthesis is shown in Scheme 2.

Attempts to couple compound **1** and trimethylsilyl (TMS) acetylene in the presence of the aldehyde group were unsuccessful; thus, CMF (**1**) was protected as the dibutyl acetal (**12**). Coupling of the alkyne to compound **12** proceeded to give compound **13** in good yield, which was hydrolyzed to the furfural derivative (**14**). Reduction of compound **14** with sodium borohydride gave alcohol **15**. Compound **15** is essentially a protected form of compound **10**, but to complete the synthesis of prothrin (**4**), we esterified compound **15** with chrysanthemic acid chloride and, finally, desilylated with tetrabutylammonium fluoride. It was necessary to retain the TMS protecting group until the end of the synthesis, because any attempt to remove it at an earlier stage resulted in gradual isomerization of the triple bond to the allene.

The above-described route to prothrin (**4**) does not necessitate the synthesis of a 5-methylfurfuryl precursor to compound **10** but rather derives it directly from biomass. It also involves no organometallic reagents, requires no chromatographic separations until the final step, and proceeds in an overall 65% yield. The efficiency of this approach and the ready availability of CMF (**1**) presented an attractive opportunity to carry out analoging studies on the prothrin framework.

A highly apparent analogue to prothrin (**4**) is the cyanomethylfuran derivative (**5**), and this was targeted for synthesis along with the known resmethrin-like aryloxymethyl analogue (**6**).[13] Thus, in the approach to analogues **5** and **6**, the acetylene nucleophile is exchanged for cyanide and phenoxide, respectively. We had initially supposed that conversion of CMF (**1**) into acetal **12** would not be necessary in these cases, because compound **1** is known to be effectively substituted with nucleophiles, such as alcohols[3a] and azide anion.[1] However, attempts to directly substitute the chloromethyl group in compound **1** with either phenol or cyanide were unsuccessful. From substituted acetals **16** and **17**, the syntheses proceeded as for compound **4** but are one step shorter, because no deprotection is required at the end (Scheme 3). The overall yields of analogues **5** and **6** from CMF (**1**) were 51 and 70%, respectively.

Scheme 3. [a]

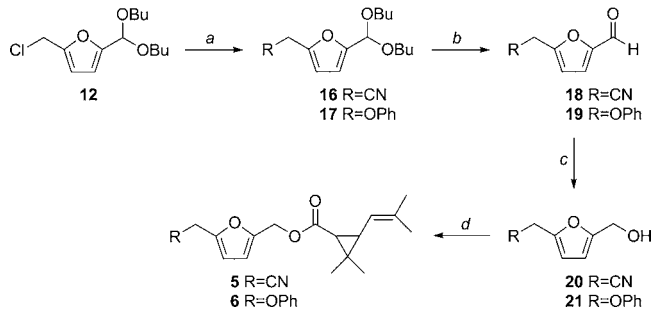

[a]Reagents: *a*, for compound **16**, NaCN, DMSO, 85 °C, 78%; for compound **17**, phenol, K_2CO_3, DMSO, 50 °C, 87%; *b*, 1 M aqueous HCl; *c*, $NaBH_4$, $MeOH/CH_2Cl_2$, 0 °C; and *d*, chrysanthemic acid chloride, benzene, reflux.

MATERIALS AND METHODS

2-(Chloromethyl)-5-(dibutoxymethyl)furan (12).[14] CMF (**1**) (2.00 g, 13.8 mmol) was dissolved in 1-butanol (40 mL), and concentrated HCl (0.1 mL) was added. The solvent was then removed using a rotary evaporator under high vacuum (0.1 mmHg) while cooling the evaporating flask in an ice−water bath. The product **12** was obtained as a yellow oil (3.721 g, 98%). ^{1}H NMR (300 MHz, $CDCl_3$) δ: 6.32 (s, 1H), 6.29 (s, 1H), 5.47 (s, 1H), 4.53 (s, 2H), 3.51 (m, 4H), 1.52 (m, 4H), 1.35 (m, 4H), 0.88 (t, 7.3 Hz, 6H). ^{13}C NMR (75 MHz, $CDCl_3$) δ: 153.1, 150.1, 110.4, 109.4, 96.5, 65.7, 37.7, 31.9, 19.5, 14.0. HRMS: $(M - OBu)^+$, $C_{10}H_{14}O_2Cl$ calculated, 201.0682; found, 201.0678.

2-(Dibutoxymethyl)-5-[3-(trimethylsilyl)prop-2-yn-1-yl]furan (13). Copper(I) iodide (0.269 g, 1.41 mmol), potassium carbonate (0.328 g, 2.37 mmol), and (trimethylsilyl)acetylene (0.21 mL, 0.15 g, 1.5 mmol) were added to a solution of compound **12** (0.328 g, 1.19

dx.doi.org/10.1021/jf4045843 | J. Agric. Food Chem. 2014, 62, 476−480

mmol) in anhydrous acetonitrile (10 mL) under argon. The suspension was heated to 55 °C and stirred overnight. Saturated aqueous $NaHCO_3$ (50 mL) was added and the layers were separated. The aqueous layer was extracted with dichloromethane, the organic layers were combined and dried over sodium sulfate, and the solvent was evaporated to give compound **13** as a yellow oil (0.353 g, 88%). ^{1}H NMR (300 MHz, $CDCl_3$) δ: 6.31 (d, 3.1 Hz, 1H), 6.17 (d, 3.1 Hz, 1H), 5.45 (s, 1H), 3.61 (s, 2H), 3.56−3.44 (m, 4H), 1.59−1.52 (m, 4H), 1.40−1.32 (m, 4H), 0.90 (t, 7.5 Hz, 6H), 0.16 (s, 9H). ^{13}C NMR (75 MHz, $CDCl_3$) δ: 151.0, 150.1, 109.0, 106.7, 101.0, 96.5, 86.5, 65.4, 31.8, 20.1, 19.4, 13.9, 0.0. HRMS: $(M - OBu)^+$, $C_{15}H_{23}O_2Si$ calculated, 263.1462; found, 263.1469.

5-[3-(Trimethylsilyl)prop-2-yn-1-yl]furfural (14). A mixture of compound **13** (0.210 g, 0.624 mmol) and 1 M HCl (10 mL) was stirred for 2 h and then extracted with dichloromethane. The combined organic layers were dried over sodium sulfate and the solvent was evaporated to give compound **14** as a yellow solid (0.125 g, 97%) with a melting point (mp) of 46 °C. ^{1}H NMR (300 MHz, $CDCl_3$) δ: 9.55 (s, 1H), 7.19 (d, 3.6 Hz, 1H), 6.49 (d, 3.6 Hz, 1H), 3.72 (s, 2H), 0.18 (s, 9H). ^{13}C NMR (75 MHz, $CDCl_3$) δ: 177.2, 157.5, 152.5, 123.1, 109.9, 98.9, 88.1, 20.5, −0.1. HRMS: $(M + H)^+$, $C_{11}H_{15}O_2Si$ calculated, 207.0835; found, 207.0833.

2-(Hydroxymethyl)-5-[3-(trimethylsilyl)prop-2-yn-1-yl]furan (15). Sodium borohydride (0.0720 g, 1.90 mmol) was added to a solution of compound **14** (0.391 g, 1.90 mmol) in methanol (10 mL) at 0 °C. The mixture was allowed to come to room temperature over 2 h with stirring. The solvent was evaporated and the residue was taken up in dichloromethane (25 mL), which was washed with saturated aqueous NH_4Cl solution. The aqueous layer was back-extracted with dichloromethane, the organic layers were combined and dried over sodium sulfate, and the solvent was evaporated to give compound **15** as a pale yellow oil (0.388 g, 98%). ^{1}H NMR (300 MHz, $CDCl_3$) δ: 6.21 (d, 3.0 Hz, 1H), 6.16 (d, 3.0 Hz, 1H), 4.56 (s, 2H), 3.62 (s, 2H), 1.73 (s, 1H), 0.17 (s, 9H). ^{13}C NMR (75 MHz, $CDCl_3$) δ: 153.4, 150.2, 108.8, 107.1, 101.1, 86.6, 57.3, 20.0, 0.0. HRMS: $(M + H)^+$, $C_{11}H_{17}O_2Si$ calculated, 209.0992; found, 209.0987.

Mixture of (±)-*cis*- and (±)-*trans*-{5-[3-(Trimethylsilyl)prop-2-yn-1-yl]furan-2-yl}methyl-2,2-dimethyl-3-(2-methylprop-1-en-1-yl)cyclopropane-1-carboxylate. Compound **15** (0.157 g, 0.754 mmol) was dissolved in dry benzene (25 mL) under argon. A mixture of (±)-*cis*- and (±)-*trans*-chrysanthemic acid chloride (0.156 g, 0.836 mmol) was added and the solution was heated at reflux for 5 h. The reaction was allowed to cool to room temperature and the solvent was evaporated. Excess chrysanthemic acid chloride was removed under high vacuum (0.1 mmHg) to give the product as a brown oil (0.257 g, 95%). ^{1}H NMR (300 MHz, $CDCl_3$) δ: 6.32 (m, 1H, H_d and $H_{d'}$), 6.19 (m, 1H, H_c and $H_{c'}$), 5.38 (d, 8.5 Hz, 0.4H, H_j), 5.09−4.90 (m, 2H, H_e and $H_{e'}$), 4.88 (d, 7.7 Hz, 0.6H, $H_{j'}$), 3.62 (s, 2H, H_b and $H_{b'}$), 2.06 (dd, 7.7 Hz, 5.5 Hz, 0.6H, $H_{i'}$), 1.88 (t, 8.5 Hz, 0.4H, H_i), 1.75−1.65 (m, 6H, H_k, $H_{k'}$, H_l, and $H_{l'}$), 1.41 (d, 5.5 Hz, 0.6 H, $H_{f'}$), 1.25−1.11 (m, 6H, H_g, $H_{g'}$, H_h, and $H_{h'}$), 0.18 (s, 9H). ^{13}C NMR (75 MHz, $CDCl_3$) δ: 172.2, 170.7, 151.1, 151.0, 149.2, 149.1, 135.6, 134.9, 121.2, 118.1, 111.6, 111.4, 107.4, 100.8, 86.7, 58.1, 57.7, 34.7, 33.1, 32.6, 31.1, 29.0, 28.9, 26.8, 26.0, 25.7, 22.2, 20.5, 20.1, 18.6, 18.4, 14.8, 0.1. HRMS: $(M + H)^+$, $C_{21}H_{31}O_3Si$ calculated, 359.2037; found, 359.1999.

Mixture of (±)-*cis*- and (±)-*trans*-Prothrin (4). A mixture of (±)-*cis*- and (±)-*trans*-{5-[3-(trimethylsilyl)prop-2-yn-1-yl]furan-2-yl}methyl-2,2-dimethyl-3-(2-methylprop-1-en-1-yl)cyclopropane-1-carboxylate (0.143 g, 0.399 mmol) was dissolved in tetrahydrofuran (THF) (10 mL) and the solution was cooled to −20 °C in a dry-ice/ethylene glycol bath. A solution of tetrabutylammonium fluoride in THF (1.0 M, 0.44 mL, 0.44 mmol) was added dropwise with stirring. After 15 min at −20 °C, saturated ammonium chloride (50 mL) was added and the aqueous layer was separated and extracted with ethyl acetate. The organic layers were combined and dried over sodium sulfate, and the solvent was evaporated. The residue was purified by flash column chromatography on silica gel (20:1 hexanes/ethyl acetate) to give compound **4** as a pale yellow oil (0.095 g, 84%). ^{1}H NMR (300 MHz, $CDCl_3$) δ: 6.30 (t, 3.0 Hz, 1H, H_d and $H_{d'}$), 6.18 (d, 3.0 Hz, 1H, H_c and $H_{c'}$), 5.35 (d, 8.4 Hz, 0.4H, H_j), 5.04−4.90 (m, 2H, H_e and $H_{e'}$), 4.85 (d, 7.9 Hz, 0.6H, $H_{j'}$), 3.56 (d, 2.4 Hz, 2H, H_b and $H_{b'}$), 2.13 (t, 2.4 Hz, 1H, H_a and $H_{a'}$), 2.05 (dd, 7.9 Hz, 5.4 Hz, 0.6H, $H_{i'}$), 1.87 (t, 8.4 Hz, 0.4H, H_i), 1.72−1.65 (m, 6H, H_k, $H_{k'}$, H_l, and $H_{l'}$), 1.40 (d, 5.4 Hz, 0.6H, $H_{f'}$), 1.24−1.09 (m, 6H, H_g, $H_{g'}$, H_h, and $H_{h'}$). ^{13}C NMR (75 MHz, $CDCl_3$) δ: 171.9, 170.5, 150.5, 150.4, 149.2, 149.1, 135.4, 134.6, 121.1, 118.1, 111.4, 111.3, 107.3, 78.6, 70.3, 57.9, 57.5, 34.5, 32.9, 32.4, 30.9, 28.8, 28.7, 26.6, 25.9, 25.5, 22.1, 20.3, 18.5, 18.4, 18.2, 14.7. HRMS: $(M + H)^+$, $C_{18}H_{23}O_3$ calculated, 287.1642; found, 287.1639.

2-(Cyanomethyl)-5-(dibutoxymethyl)furan (16). Sodium cyanide (0.174 g, 3.55 mmol) was added to a solution of compound **12** (0.811 g, 2.95 mmol) in dimethyl sulfoxide (DMSO) (6 mL) and the mixture was stirred at 90 °C under argon for 3 h. Saturated aqueous $NaHCO_3$ (50 mL) was added and the mixture was extracted with hexanes. The combined organic layers were washed with saturated aqueous $NaHCO_3$, dried over sodium sulfate, and decolorized with charcoal. The solvent was evaporated to give compound **16** as a light yellow oil (0.608 g, 78%). ^{1}H NMR (300 MHz, $CDCl_3$) δ: 6.34 (s, 1H), 6.28 (s, 1H), 5.44 (s, 2H), 3.60−3.42 (m, 4H), 1.65−1.47 (m, 4H), 1.45−1.27 (m, 4H), 0.90 (t, 7.5 Hz, 6H). ^{13}C NMR (75 MHz, $CDCl_3$) δ: 152.8, 143.1, 115.6, 109.4, 109.2, 96.5, 65.9, 31.9, 19.5, 17.8, 14.1. HRMS: $(M - OBu)^+$, $C_{11}H_{14}NO_2$ calculated, 192.1019; found, 192.1019.

5-(Cyanomethyl)furfural (18). A mixture of compound **16** (0.224 g, 0.844 mmol) and 1 M HCl (10 mL) was stirred for 2 h and then extracted with dichloromethane. The organic layers were combined and dried over sodium sulfate, and the solvent was evaporated to give compound **18** as a brown oil (0.109 g, 95%). ^{1}H NMR (300 MHz, $CDCl_3$) δ: 9.55 (s, 1H), 7.20 (d, 3.0 Hz, 1H), 6.56 (d, 3.0 Hz, 1H), 3.88 (s, 2H). ^{13}C NMR (75 MHz, $CDCl_3$) δ: 177.6, 153.2, 149.9, 122.7, 114.6, 111.7, 18.2. HRMS: $(M + H)^+$, $C_7H_6NO_2$ calculated, 136.0393; found, 136.0389.

2-(Cyanomethyl)-5-(hydroxymethyl)furan (20). Sodium borohydride (0.0560 g, 1.47 mmol) was added to a solution of compound **18** (0.155 g, 1.15 mmol) in methanol (10 mL) at 0 °C. The reaction was allowed to stir for 2 h at 0 °C. Saturated aqueous NH_4Cl (25 mL) was added and the mixture was extracted with dichloromethane. The organic layers were combined and dried over sodium sulfate, and the solvent was evaporated to give compound **20** as a brown liquid (0.142 g, 90%). ^{1}H NMR (300 MHz, $CDCl_3$) δ: 6.22 (d, 3.0 Hz, 1H), 6.20 (d, 3.0 Hz, 1H), 4.48 (s, 2H), 3.72 (s, 2H), 3.16 (br, 1H, OH). ^{13}C NMR (75 MHz, $CDCl_3$) δ: 154.9, 142.8, 115.7, 109.3, 108.9, 56.9, 17.5. HRMS: $(M - OH)^+$, C_7H_6NO calculated, 120.0444; found, 120.0435.

Mixture of (±)-*cis*- and (±)-*trans*-[5-(Cyanomethyl)furan-2-yl]methyl-2,2-dimethyl-3-(2-methylprop-1-en-1-yl)-cyclopropane-1-carboxylate (5). Compound **20** (0.152 g, 1.11 mmol) was dissolved in dry benzene (25 mL) under argon. A mixture of (±)-*cis*- and (±)-*trans*-chrysanthemic acid chloride (0.247 g, 1.32 mmol) was added and the solution was heated at reflux for 2 h. The reaction was allowed to cool to room temperature and the solvent was evaporated. The residue was taken up in dichloromethane (20 mL), which was then washed with brine. The aqueous layer was back-extracted with dichloromethane. The organic layers were combined and dried over sodium sulfate, and the solvent was evaporated. The crude product was purified by flash column chromatography on silica gel (10:1 hexanes/ethyl acetate) to give compound **5** as a light yellow oil (0.244 g, 77%). ^{1}H NMR (300 MHz, $CDCl_3$) δ: 6.28 (s, 1H, H_d and $H_{d'}$), 6.22 (s, 1H, H_c and $H_{c'}$), 5.28 (d, 8.3 Hz, 0.4H, H_j), 5.01−4.84 (m, 2H, H_e and $H_{e'}$), 4.80 (d, 7.0 Hz, $H_{j'}$), 3.70 (s, 2H, H_b and $H_{b'}$), 1.99 (t, 7.0 Hz, 0.6H, $H_{i'}$), 1.83 (t, 8.3 Hz, 0.4H, H_i), 1.68−1.56 (m, 6H, H_k, $H_{k'}$, H_l, and $H_{l'}$), 1.33 (d, 5.4 Hz, 0.6H, $H_{f'}$), 1.20−1.00 (m, 6H, H_g, $H_{g'}$, H_h, and $H_{h'}$). ^{13}C NMR (75 MHz, $CDCl_3$) δ: 172.0, 170.6, 150.9, 150.8, 144.0, 144.0, 135.7, 135.0, 121.1, 118.1, 115.6, 111.8, 111.7, 109.6, 57.8, 57.4, 34.6, 33.2, 32.7, 31.0, 29.1, 28.8, 26.9, 26.0, 25.7, 22.2, 20.5, 18.6, 18.5, 17.6, 14.9. HRMS: $(M + H)^+$, $C_{17}H_{22}NO_3$ calculated, 288.1600; found, 288.1612.

2-(Dibutoxymethyl)-5-(phenoxymethyl)furan (17). Phenol (0.232 g, 2.47 mmol) and potassium carbonate (0.360 g, 2.61

dx.doi.org/10.1021/jf4045843 | J. Agric. Food Chem. 2014, 62, 476−480

mmol) were added to a solution of compound **12** (0.564 g, 2.05 mmol) in DMSO (5 mL), and the mixture was stirred at 50 °C under argon for 5 h. Saturated aqueous $NaHCO_3$ (50 mL) was added and the mixture was extracted with hexanes. The organic layers were combined, washed with saturated aqueous $NaHCO_3$, and dried over sodium sulfate. The solvent was evaporated to give compound **17** as a pale yellow oil (0.592 g, 87%). ^{1}H NMR (300 MHz, $CDCl_3$) δ: 7.34−7.25 (m, 2H), 7.02−6.93 (m, 3H), 6.42 (d, 3.3 Hz, 1H), 6.40 (d, 3.3 Hz, 1H), 5.55 (s, 1H), 4.99 (s, 2H), 3.65−3.49 (m, 4H), 1.70−1.55 (m, 4H), 1.51−1.35 (m, 4H), 0.95 (t, 7.2 Hz, 6H). ^{13}C NMR (75 MHz, $CDCl_3$) δ: 158.3, 152.4, 150.2, 129.4, 121.2, 114.9, 110.3, 109.0, 96.5, 65.5, 62.4, 31.8, 19.4, 13.9. HRMS: $(M - OBu)^+$, $C_{16}H_{19}O_3$ calculated, 259.1329; found, 259.1331.

5-(Phenoxymethyl)furfural (19).[15] A mixture of compound **17** (0.322 g, 0.970 mmol) and 1 M HCl (10 mL) was stirred for 2 h and then extracted with dichloromethane (20 mL). The organic layers were combined and dried over sodium sulfate, and the solvent was evaporated to give compound **19** as a yellow solid (0.194 g, 99%), with a mp of 84 °C. ^{1}H NMR (300 MHz, $CDCl_3$) δ: 9.64 (s, 1H), 7.36−7.20 (m, 3H), 7.05−6.91 (m, 3H), 6.61 (d, 3.3 Hz, 1H), 5.10 (s, 2H). ^{13}C NMR (75 MHz, $CDCl_3$) δ: 178.0, 158.1, 157.0, 152.9, 129.9, 122.4, 122.0, 115.0, 111.9, 62.7. HRMS: $(M + H)^+$, $C_{12}H_{11}O_3$ calculated, 203.0703; found, 203.0706.

2-(Hydoxymethyl)-5-(phenoxymethyl)furan (21).[13] Sodium borohydride (0.269 g, 7.08 mmol) was added to a solution of compound **19** (1.196 g, 5.915 mmol) in a 1:1 mixture of methanol and dichloromethane (20 mL) at 0 °C. The reaction was allowed to come to room temperature over 2 h with stirring. The solvent was evaporated, and the residue was taken up in dichloromethane (20 mL) and washed with brine. The aqueous layer was back-extracted with dichloromethane. The organic layers were combined, dried over sodium sulfate, and evaporated to give compound **21** as a pale yellow liquid (1.156 g, 96%). ^{1}H NMR (300 MHz, $CDCl_3$) δ: 7.36−7.25 (m, 2H), 7.04−6.94 (m, 3H), 6.37 (d, 2.7 Hz, 1H), 6.26 (d, 2.7 Hz, 1H), 4.96 (s, 2H), 4.56 (s, 2H), 2.91 (s, 1H, OH). ^{13}C NMR (75 MHz, $CDCl_3$) δ: 158.5, 155.0, 150.3, 129.8, 121.6, 115.1, 111.1, 108.9, 62.6, 57.6. HRMS: $(M + H)^+$, $C_{12}H_{13}O_3$ calculated, 205.0859; found, 205.0861.

Mixture of (±)-*cis*- and (±)-*trans*-[5-(Phenoxymethyl)furan-2-yl]methyl-2,2-dimethyl-3-(2-methylprop-1-en-1-yl)-cyclopropane-1-carboxylate (6).[13] Compound **21** (0.331 g, 1.62 mmol) was dissolved in dry benzene (25 mL) under argon. A mixture of (±)-*cis*- and (±)-*trans*-chrysanthemic acid chloride (0.364 g, 1.95 mmol) was added and the solution was heated at reflux for 3 h. The reaction was allowed to cool to room temperature and the solvent was evaporated. The residue was taken up in dichloromethane (25 mL), which was then washed with brine. The aqueous layer was back-extracted with dichloromethane. The organic layers were combined and dried over sodium sulfate, and the solvent was evaporated. The crude product was purified by flash column chromatography on silica gel (15:1 hexanes/ethyl acetate) to give compound **6** as a colorless oil (0.484 g, 85%). ^{1}H NMR (300 MHz, $CDCl_3$) δ: 7.35−7.24 (m, 2H), 7.03−6.93 (m, 3H), 6.39 (s, 2H, H_c, $H_{c'}$, H_d, and $H_{d'}$), 5.37 (d, 8.3 Hz, 0.15H, H_j), 5.13−4.95 (m, 4H, H_b, $H_{b'}$, H_e, and $H_{e'}$), 4.88 (d, 7.5 Hz, 0.85H, $H_{j'}$), 2.08 (t, 7.5 Hz, 0.85H, $H_{i'}$), 1.90 (t, 8.3 Hz, 0.15H, H_i), 1.81−1.65 (m, 6H, H_k, $H_{k'}$, H_l, and $H_{l'}$), 1.43 (d, 5.1 Hz, 0.85H, H_f), 1.30−1.08 (m, 6H, H_g, $H_{g'}$, H_h, and $H_{h'}$). ^{13}C NMR (75 MHz, $CDCl_3$) δ: 172.3, 170.9, 158.5, 151.1, 151.1, 150.8, 150.6, 135.8, 135.1, 129.7, 121.5, 121.3, 118.3, 115.1, 111.6, 111.5, 111.1, 62.6, 58.2, 57.9, 34.8, 33.3, 32.8, 31.3, 29.2, 29.0, 27.0, 26.2, 25.8, 22.4, 20.6, 18.8, 18.6, 15.0. HRMS: $(M + H)^+$, $C_{22}H_{27}O_4$ calculated, 355.1909; found, 355.1925.

Entomological Studies. *Mosquitoes.* The Orlando strain of *Aedes aegypti* (established 1952) was reared in the insectary of the Mosquito and Fly Research Unit at the Center for Medical, Agricultural, and Veterinary Entomology (CMAVE), Agricultural Research Service (ARS), United States Department of Agriculture (USDA), according to the procedures described by Pridgeon et al.[16] Briefly, eggs were hatched in a flask with deionized water, left overnight, and transferred to a plastic tray containing distilled water. A powdered diet (2:1 pot belly pig chow/brewer's yeast) was added to each tray. Mosquitoes were reared in an environmental chamber at 28 °C, 80% relative humidity, and a photoperiod of 14 h/10 h (light/dark). Adults were held in a screened cage and provided 10% sucrose *ad libitum*. Female adults were used for all bioassays.

Adult Topical Bioassays. To determine the toxicity of each compound against female *A. aegypti*, samples were initially diluted to a 10% solution in DMSO. This solution was then serially diluted 1:10 in acetone and then topically applied to individual mosquitoes. Each addition of diluent and stock solution was weighed to allow for accurate concentration calculations and to account for pipetting variability because of the volatility of acetone. Prior to application, 5−7-day-old females were cold-anaesthetized and placed on a 4 °C chill table (BioQuip Products, Rancho Dominguez, CA). A 0.5 μL droplet of chemical solution was applied to the thorax using a 700 series gastight syringe and a PB 600 repeating dispenser (Hamilton, Reno, NV). Control treatments with 0.5 μL of acetone alone gave control mortality of less than 10%. After treatment, mosquitoes were kept in plastic cups and supplied with 10% sucrose solution for 24 h before mortality was recorded. Temperature and relative humidity were maintained at 26−27 °C and 80%, respectively. Cohorts of 20−30 mosquitoes were treated at each dose. Bioassays were replicated 3 times. Technical-grade permethrin (Chemservice, West Chester, PA), a combination of 46.1% *cis* and 53.2% *trans* isomers, was used as the positive control in all assays and diluted in the same manner as the test compounds. This system reliably results in a LD_{50} for permethrin of around 0.1 ng per mosquito.

RESULTS AND DISCUSSION

Preliminary entomological testing of pyrethroids **5** and **6** was conducted against prothrin (**4**) and the commercial insecticide permethrin as standards using the "Orlando" strain of the pesticide-susceptible mosquito *A. aegypti*, as described above. Mortality was recorded at 24 h post-application, and three replicates were performed. Averaged mortality counts are included in Table S1 of the Supporting Information, and the estimated LD_{50} values are given in Table 1. The activities of analogues **5** and **6** are thus within about a log of that of prothrin (**4**), which itself is more active than the natural pyrethrins.[17] Further testing will determine whether these derivatives show any useful selectivity in their action.

Table 1. Estimated LD_{50} Values (ng/Mosquito) of Analogues 5 and 6 with Prothrin (4) and Permethin Standards against *A. aegypti* "Orlando" Strain Mosquitos

toxicant	LD_{50}
permethrin	0.07
prothrin (**4**)	0.50
5	7.0
6	3.3

In conclusion, CMF (**1**), a biomass-derived platform chemical, is an attractive starting material for the high-yield synthesis of prothrin (**4**) and analogues **5** and **6**. This scalable synthetic approach could be generalized toward the renewable-sourced production of a variety of furan-based pyrethroids, which will enable further structure−activity studies and potential commercial development of this important family of insecticides.

ASSOCIATED CONTENT

Supporting Information

Details of entomological data and ^{1}H and ^{13}C NMR data for all compounds prepared in this work. This material is available free of charge via the Internet at http://pubs.acs.org.

dx.doi.org/10.1021/jf4045843 | J. Agric. Food Chem. 2014, 62, 476−480

AUTHOR INFORMATION

Corresponding Author

*E-mail: mjmascal@ucdavis.edu.

Notes

The authors declare no competing financial interest.

REFERENCES

(1) Mascal, M.; Dutta, S. *Green Chem.* **2011**, *13*, 40.
(2) Mascal, M.; Dutta, S. *Green Chem.* **2011**, *13*, 3101.
(3) (a) Mascal, M.; Nikitin, E. B. *Angew. Chem., Int. Ed.* **2008**, *47*, 7924. (b) Mascal, M.; Nikitin, E. B. *ChemSusChem* **2009**, *2*, 859.
(4) Metcalf, R. L. *Ullmann's Encyclopedia of Industrial Chemistry*; Wiley-VCH: Weinheim, Germany, 2000; Vol. *19*, pp 264−325, DOI: 10.1002/14356007.a14_263.
(5) Staudinger, H.; Ruzicka, L. *Helv. Chim. Acta* **1924**, *7*, 177.
(6) Katsuda, Y.; Chikamoto, T.; Ogami, H.; Hirobe, H.; Kunishige, T. *Agric. Biol. Chem.* **1969**, *33*, 1361.
(7) Approximately 50 000 pounds of resmethrin are used annually in the U.S., mostly for adult mosquito abatement: United States Environmental Protection Agency (U.S. EPA). *Reregistration Eligibility Decision for Resmethrin*; U.S. EPA: Washington, D.C., June 2006; EPA 738-R-06-003, www.epa.gov/oppsrrd1/REDs/resmethrin_red.pdf.
(8) Commerical chrysanthemic acid is a synthetic mixture of *cis* and *trans* isomers.
(9) (a) Inamasu, S.; Oe, T.; Tsuruta, M. *Jpn. Tokkyo Koho* 1970, JP 45025687. (b) Mukai, T.; Inamasu, S.; Tsuruta, M. *Jpn. Tokkyo Koho* 1970, JP 45034374. (c) Katsuda, S. *Jpn. Tokkyo Koho* 1971, JP 46023729. (d) Nishida, N.; Inoue, M.; Nakayama, K. *Jpn. Kokai Tokkyo Koho* 2002, JP 2002308864. Gu, S. *Faming Zhuanli Shenqing Gongkai Shuomingshu* 2004, CN 1546480.
(10) (a) Katsuda, S. *Jpn. Tokkyo Koho* 1972, JP 47003342. (b) Bohlmann, F.; Fanghaenel, L.; Kleine, K. M.; Kramer, H. D.; Moench, H.; Schuber, J. *Chem. Ber.* **1965**, *98*, 2596.
(11) Other approaches: (a) Katsuda, S. *Jpn. Tokkyo Koho* 1971, JP 46023728. (b) Katsuda, J. *Jpn. Tokkyo Koho* 1971, JP 46031221. (c) Matsuda, S. *Jpn. Tokkyo Koho* 1972, JP 47003343. (d) Mai, L.; Lin, X. *Huadong Shifan Daxue Xuebao, Ziran Kexueban* **1997**, 51.
(12) Davies, K. A.; Abel, R. C.; Wulff, J. E. *J. Org. Chem.* **2009**, *74*, 3997.
(13) French Patent FR 2043019, 1971.
(14) (a) Raja, S.; Xavier, N.; Arulraj, S. J. *Indian J. Chem., Sect. B: Org. Chem. Incl. Med. Chem.* **1989**, *28B*, 687. (b) Pevzner, L. M.; Ignat'ev, V. M.; Ionin, B. I. *Z. Obshch. Khim.* **1990**, *60*, 1061.
(15) (a) Middendorp, J. A. *Rec. Trav. Chim. Pays-Bas Belg.* **1919**, *38*, 1. (b) Jew, S. S.; Park, H. G.; Park, B. S.; Lim, D. Y. PCT International Application WO 2004037808, 2004. (c) Raboisson, P. J.-M. B.; McGowan, D. C.; Vandyck, K.; Vendeville, S. M. H.; Bonfanti, J.-F.; Van den Broeck, W. M. M.; Nyanguile, O.; Amssoms, K. I. E.; Hu, L.; Boutton, C. W. M.; Tahri, A.; Last, S. J.; Rombauts, K.; Rebstock, A.-S. H. M.; Fortin, J. M. C.; Muller, P. PCT International Application WO 2008099019, 2008.
(16) Pridgeon, J. W.; Pereira, R. M.; Becnel, J. J.; Allan, S. A.; Clark, G. G.; Linthicum, K. J. *J. Med. Entomol.* **2008**, *45*, 82.
(17) Nishizawa, Y. *Bull. W. H. O.* **1971**, *44*, 325.

JOURNAL OF AGRICULTURAL AND FOOD CHEMISTRY

Article

pubs.acs.org/JAFC

Accurate Determination of Genetic Identity for a Single Cacao Bean, Using Molecular Markers with a Nanofluidic System, Ensures Cocoa Authentication

Wanping Fang,[†,‡] Lyndel W. Meinhardt,[†] Sue Mischke,[†] Cláudia M. Bellato,[†] Lambert Motilal,[§] and Dapeng Zhang*[,†]

[†]Sustainable Perennial Crops Laboratory (SPCL), Beltsville Agricultural Research Center (BARC), Agricultural Research Service (ARS), United States Department of Agriculture (USDA), 10300 Baltimore Avenue, Building 001, Room 223, BARC-W, Beltsville, Maryland 20705, United States

[‡]College of Horticulture, Nanjing Agricultural University, Nanjing, Jiangsu 210095, People's Republic of China

[§]Cocoa Research Centre, The University of the West Indies, St. Augustine, Republic of Trinidad and Tobago, West Indies

ABSTRACT: Cacao (*Theobroma cacao* L.), the source of cocoa, is an economically important tropical crop. One problem with the premium cacao market is contamination with off-types adulterating raw premium material. Accurate determination of the genetic identity of single cacao beans is essential for ensuring cocoa authentication. Using nanofluidic single nucleotide polymorphism (SNP) genotyping with 48 SNP markers, we generated SNP fingerprints for small quantities of DNA extracted from the seed coat of single cacao beans. On the basis of the SNP profiles, we identified an assumed adulterant variety, which was unambiguously distinguished from the authentic beans by multilocus matching. Assignment tests based on both Bayesian clustering analysis and allele frequency clearly separated all 30 authentic samples from the non-authentic samples. Distance-based principle coordinate analysis further supported these results. The nanofluidic SNP protocol, together with forensic statistical tools, is sufficiently robust to establish authentication and to verify gourmet cacao varieties. This method shows significant potential for practical application.

KEYWORDS: *authentication, chocolate, conservation, fair trade, fluidigm, food forensics, food adulteration, gourmet food, germplasm, molecular markers, Theobroma cacao, traceability, tropical tree*

INTRODUCTION

Cacao (*Theobroma cacao* L.) is an important tropical crop because it is the source of cocoa butter and powder for the confectionery industry. This species comprises a large number of highly morphologically variable populations, which can all be crossed with one another.[1,2] The upper Amazon, including parts of Ecuador, Peru, Brazil, and Colombia, is generally believed to be the center of origin of cacao, because of the high morphological and genetic diversity observed in this region.[1,3,4] Cacao was domesticated by the Mayas and Aztecs,[5,6] and this crop was widely grown in Mexico and Central America in pre-Columbian times.[7,8]

Production and marketing of differentiated (or specialty) high-value cocoa provides socioeconomic opportunities for cacao growers, the chocolate industry, and especially for consumers. From the conservation perspective, the higher farm-gate revenues from this premium market can provide strong economic incentives for demand-driven, *in situ*/on-farm conservation of cacao genetic diversity. However, among premium cacao varieties, adulteration is common and can happen at different steps of the cocoa chain, from farm to port. Cacao varietal authentication, therefore, is of considerable interest to the various stakeholders in the chocolate value chain.

DNA-based authentication has been widely investigated in various crop species.[9−12] Examples of these methods include identifying different varieties of cereals,[13,14] fruits,[15] olives,[16,17] tea,[18] and coffee.[19] Thus far, microsatellite markers have been used in the majority of the published research.[12] Microsatellite markers have been commonly used in cacao breeding, germplasm management, and propagation of planting materials.[20,21] However, comparisons of microsatellite genotyping results from different laboratories have not been straightforward. Data generated from different genotyping platforms are often difficult to compare to one another because the same allele may be binned differently, which can lead to false conclusions. Moreover, an additional challenge for cocoa anthentication is that the DNA profile needs to be established for a single bean (seed) rather than leaves or other tissues. This is because, during fermentation, drying, or packaging, cacao beans from different varieties may be mixed into a lot being sold to traders. Adulteration may be intentional or unintentional at any of these steps.

A cacao bean is a botanical seed. The integument of the matured ovule develops into the seed coat, which thus shares the same diploid genotype with the mother tree. The seed coat is, therefore, ideal for tracing the genetic identity of the mother tree, which provides strong evidence for the authentication of a cacao variety. Nevertheless, there has thus far been no research on molecular authentication in cacao, partially because of the

Received: September 30, 2013
Revised: December 12, 2013
Accepted: December 19, 2013
Published: December 19, 2013

ACS Publications © 2013 American Chemical Society

Table 1. Cacao Varieties (and Clones) Used in the Experiment and Their Source of Origin

sample name	country of origin	tissue	provider
Fortunato No. 4	Peru	fermented dry bean	Marañón Chocolate, San Diego, CA
CCN 51	Ecuador	leaves	Cocoa Research Centre, Trinidad
ICS 1	Trinidad	leaves	Cocoa Research Centre, Trinidad
ICS 84	Trinidad	leaves	Cocoa Research Centre, Trinidad
ICS 98	Trinidad	leaves	Cocoa Research Centre, Trinidad
LCT EEN 241	Ecuador	leaves	Cocoa Research Centre, Trinidad
LCT EEN 302	Ecuador	leaves	Cocoa Research Centre, Trinidad
LCT EEN 83/S	Ecuador	leaves	Cocoa Research Centre, Trinidad
IMC 47	Peru	leaves	Cocoa Research Centre, Trinidad
IMC 60	Peru	leaves	Cocoa Research Centre, Trinidad
NA 32	Peru	leaves	Cocoa Research Centre, Trinidad
NA 702	Peru	leaves	Cocoa Research Centre, Trinidad
NA 111	Peru	leaves	Cocoa Research Centre, Trinidad
PA 150	Peru	leaves	Cocoa Research Centre, Trinidad
PA 300	Peru	leaves	Cocoa Research Centre, Trinidad
AMELONADO 22	Brazil	leaves	Cocoa Research Centre, Trinidad
CATONGO	Brazil	leaves	Cocoa Research Centre, Trinidad
CRIOLLO 13	Costa Rica	leaves	CATIE, Costa Rica
CRIOLLO 22	Trinidad	leaves	Cocoa Research Centre, Trinidad

difficulty in extracting sufficient DNA from beans that has acceptable quality for DNA fingerprinting.

Recent progress in the development of cacao genomics has led to the use of single nucleotide polymorphism (SNP) markers in cacao DNA fingerprinting. SNPs are the most abundant class of polymorphisms in plant genomes.[22] In comparison to simple sequence repeat (SSR) markers, accurate identification of SNPs can be performed without requiring DNA separation by size and can, therefore, be automated in an assay array format or on microchips. The diallelic nature of SNPs offers a much lower error rate in allele calling than with SSRs, and genotyping can be multiplexed and performed very quickly at lower costs. TaqMan-based SNP assays have been developed for cacao genotyping under field conditions.[23,24] SNP genotyping through the Sequenom genotyping platform has been applied to molecular identification of farmer varieties of cacao in Nicaragua and Honduras.[25] However, the application of SNP markers for cacao authentication has not been investigated. The objective of this work was to develop a SNP-based analysis enabling authentication of a fine-flavor cacao variety from northern Peru. The SNP-based DNA fingerprints were compared to other cacao varieties that were cultivated in the same region, including the most commonly used adulterant variety.

MATERIALS AND METHODS

Cacao Bean Samples. Dried cacao bean samples of the fine-flavor variety "Fortunato No. 4" were provided by Marañón Chocolate, San Diego, CA. These cacao beans, from a single source in northern Peru, are from an indigenous variety enjoying premium market price. On the basis of their relative cultivation area in Cajamarca province of Peru,[26] five other varieties were chosen for testing as the "adulterant varieties". These varieties included the most widely cultivated variety in Peru "CCN-51", which is considered an inferior variety in terms of flavor and quality. In addition, DNA samples of 18 international clones were included in this experiment as reference clones (Table 1). The genetic identities of these clones are known through an international initiative for DNA fingerprinting of the cacao germplasm.[27−29] The majority of the accessions were maintained in the international genebanks in Trinidad.

Extraction and Treatment of DNA from Cacao Seed Coat Samples. DNA was extracted from seed coats of single fermented and dried cacao beans with the DNeasy Plant Mini Kit Tissue Kit (Qiagen, Inc., Valencia, CA), which is based on the use of silica as an affinity matrix. The thin seed coat was carefully separated from the seed, and 30 mg of this dry tissue was placed in a 2 mL microcentrifuge tube with one $^1/_4$ in. ceramic sphere and 0.15 g of garnet matrix (Lysing Matrix A, MP Biomedicals, Solon, OH). The seed coat samples were disrupted by high-speed shaking in a TissueLyser II (Qiagen) at 30 Hz for 1 min, followed by an additional 1 min, with a 1 min rest between disruptions. Lysis solution (buffer AP1 containing 25 mg/mL polyvinylpolypyrrolidone), along with ribonuclease I or ribonucleate 3′-pyrimidinooligonucleotidohydrolase (RNase A), was added to the powdered seed coat, and the mixture was incubated at 65 °C, as specified in the kit instructions. The remainder of the extraction method followed the suggestions of the manufacturer. DNA was eluted from the silica column with two washes of 50 μL of buffer AE, which were pooled, resulting in 100 μL of DNA solution. Using a NanoDrop spectrophotometer (Thermo Scientific, Wilmington, DE), the DNA concentration was determined by absorbance at 260 nm. DNA purity was estimated by the 260/280 ratio and the 260/230 ratio.

Over a total of 51 extractions, the DNA concentration ranged from 3.4 to 21.7 ng/μL; 260/280 ratios were from 1.06 to 2.08; and 260/230 ratios were from 0.20 to 1.01. To mitigate possible problems of low concentration or quality in DNA samples during polymerase chain reaction (PCR), each DNA was first subjected to a multiplex specific target amplification (STA) procedure using primer pools provided by Fluidigm Corp. (South San Francisco, CA), Qiagen 2× Multiplex PCR Master Mix (PN 206143), and the protocol recommended in the Fluidigm SNP Genotyping User Guide.[30]

SNP Markers and Genotyping. The 48 cacao SNP markers were selected from 1560 candidate SNPs that were developed from cDNA sequences from a wide range of cacao tissues (Boccara, personal communication).[31−33] The selection of SNPs was based on the level of polymorphism and their distribution across the 10 chromosomes in cacao. The chosen 48 markers were used to design and manufacture primers for a SNPtype genotyping panel (Fluidigm Corp.). Genotyping was performed on the high-throughput Fluidigm EP1 system, using the Fluidigm SNPtype Genotyping Reagent Kit according to the instructions of the manufacturer and a nanofluidic 48.48 Dynamic Array integrated fluidic circuit (IFC, Fluidigm Corp.). This chip automatically assembles PCR reactions, enabling simultaneous testing of up to 48 samples with 48 SNP markers.

Fluorescent intensity was measured with the EP1 reader and plotted in two axes. Genotypic calls were made using the Fluidigm SNP Genotyping Analysis program.[30]

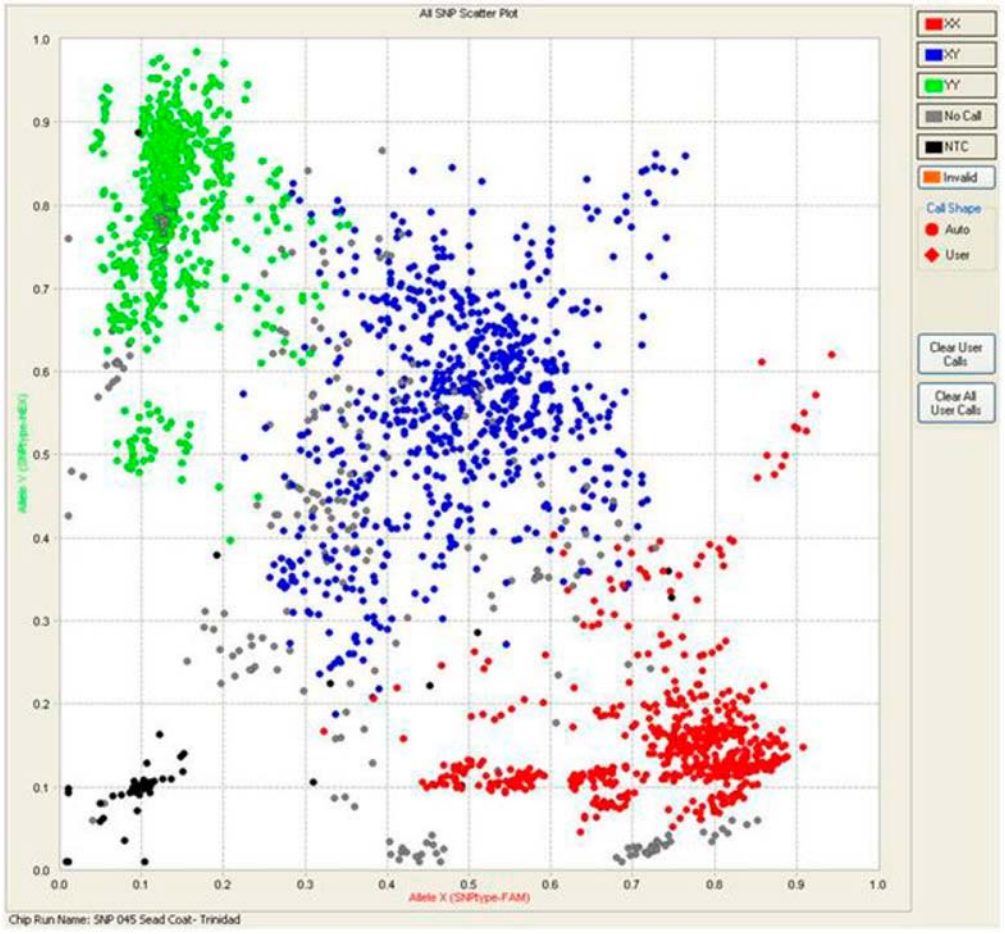

Figure 1. Cluster plots for the 48 SNP assays and 48 cacao DNA samples obtained from Fluidigm Dynamic Array IFCs.

Data Analysis. Key descriptive statistics for measuring the informativeness of these SNP markers were calculated, including minor allele frequency, observed heterozygosity, expected heterozygosity, Shannon's information index, and probability of identity.[34,35] The program GenAlEx 6.2[36,37] was used for computation.

Two approaches were taken to identify the adulterant varieties in the tested samples. Initially, SNP profiles of the authentic variety and the putative adulterant variety were compared at every locus using a pairwise multilocus matching procedure, as implemented in the computer program GenAlEx 6.2.[36,37] To assess the differentiation power of the SNP markers, we calculated the probability of identity (PID).[35] We computed the probability of identity among siblings (PID-sib), which was defined as the probability that two sibling individuals drawn at random from a population have the same multilocus genotype.[34]

The second approach employed assignment tests to check if all of the cacao beans claimed as "Fortunato No. 4" were truly from the "home population". An exclusion test,[38] as implemented in the program GeneClass,[39] was used to identify if there was a presence of the adulterant variety in the tested samples. Both Bayesian assignment test and classical frequency-based assignment were applied. In both cases, the resampling algorithm of Cornuet et al.[39] was used and the minimum number of simulated individuals was set at 10 000. The "type I error" was set at 0.01.

To understand and visualize the relationship among the authentic and adulterant varieties, we also computed the genetic distances for each possible pair of tested individuals. Principle coordinate analysis (PCoA), implemented in GenAlEx 6.2,[36,37] was used for computation.

RESULTS

Summary Information of SNP Fingerprints and Multilocus Matching. From the 48 SNPs tested, 46 primer pairs generated polymorphic fingerprints (Figures 1 and 2). Locus 226, 836 and locus 1038, 1114 had more than 20% no call, and they were therefore excluded from subsequent analyses. At the remaining 44 marker loci, two alleles were detected for each locus in the 45 DNA samples. The average polymorphism information content (PIC) was 0.60, ranging from 0.356 to 0.692. The mean observed heterozygosity was 0.284, ranging from 0.043 to 0.563, whereas the mean expected heterozygosity was 0.412, ranging from 0.203 to 0.499 (Table 2). Repeated tests, using three independently extracted DNAs from the same seed, showed that the genotyping result was highly consistent. The five repeatedly genotyped beans (each with three replications) always generated the same SNP profiles.

Individual genotype matching (pairwise comparisons) based on multilocus SNP profiles showed that there were no matched pairs, either within the 30 putative "Fortunato No. 4" samples or between the "Fortunato No. 4" samples and CCN 51, the targeted adulterant variety. The 30 "Fortunato No. 4" samples differed by at least three loci, showing that each bean came from a different mother tree. The "Fortunato No. 4" samples differed from CCN-51 by at least six loci, thus demonstrating no mixture of CCN-51 in the examined "Fortunato No. 4" samples. The probability that two unrelated accessions will have

dx.doi.org/10.1021/jf404402v | J. Agric. Food Chem. 2014, 62, 481−487

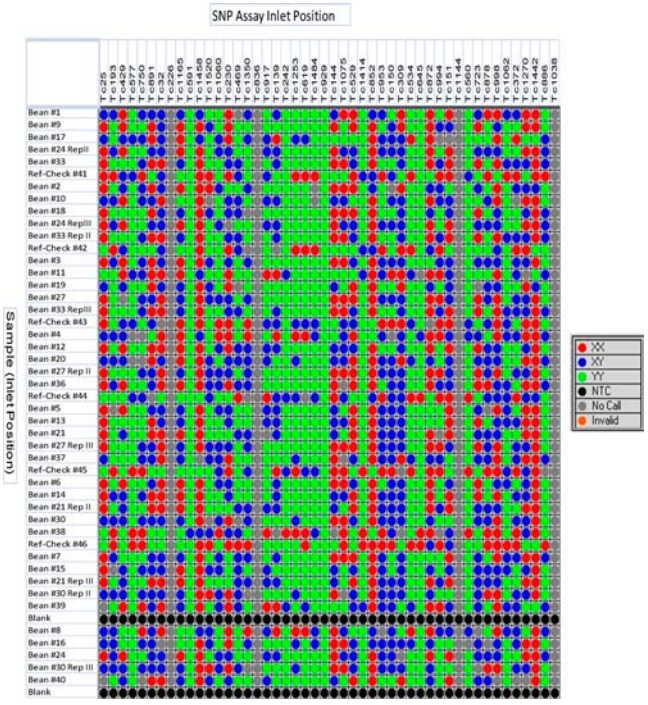

Figure 2. Call map view shows the overall calls for the Dynamic Array IFC, displaying 2304 data points at one time. The 48 accessions include 30 DNA samples extracted from fermented/dry beans from a single source provider in northern Peru, six reference clones, and two blank used as checks.

the same genotype at the 44 SNP loci is approximately 1 in 100 000 for the tested samples.

Assignment Test. The result of assignment by the exclusion−simulation method[39] showed that the 30 "Fortunato No. 4" samples should be assigned into one genetic cluster if the threshold probability of >0.50 was taken. Because CCN 51 and the other 17 international clones had an assignment probability ranging from <0.001 to 0.012, they were categorized as the putative adulterant variety (Table 3). When the algorithm was changed from Bayesian clustering analysis to frequency-based assignment, the overall result remain unchanged (Table 3).

PCoA. The genetic relationships among the tested varieties/clones were shown by PCoA (Figure 3). The plane of the first three main principle coordinate (PCO) axes accounted for 53.7, 14.2, and 11.2% of total variation, respectively. In the plane of coordinate 1 versus 2 (Figure 1), the 30 accessions of the authentic variety "Fortunato No. 4" formed a relatively homogeneous group, whereas the assumed adulterant variety "CCN-51" was clearly separated from the authentic group, indicating its "non-resident" status. All of the other reference accessions were well-differentiated from "Fortunato No. 4" as well. The result of distance-based multivariate analysis is fully compatible with the Bayesian method as well as the frequency-based assignment test.

DISCUSSION

Rapid segmentation in the chocolate market has resulted in a strong demand for sustainably and responsibly produced cocoa products. To meet this demand, scientific tools for verification of cacao genetic identity is essential to provide authentication in the value chain. A DNA fingerprint from a single fermented

Table 2. Characteristics of the 44 SNPs from the 48 Cacao Samples

locus	information index	observed heterozygosity	expected heterozygosity	inbreeding coefficient
25	0.662	0.208	0.469	0.556
32	0.682	0.479	0.489	0.021
139	0.675	0.313	0.482	0.352
144	0.621	0.417	0.430	0.030
150	0.626	0.468	0.435	−0.077
151	0.690	0.417	0.497	0.161
193	0.643	0.438	0.451	0.030
226	0.637	0.222	0.444	0.500
230	0.685	0.375	0.492	0.238
242	0.356	0.146	0.203	0.281
309	0.629	0.563	0.437	−0.286
372	0.678	0.391	0.485	0.193
429	0.675	0.271	0.482	0.439
469	0.654	0.426	0.462	0.078
529	0.688	0.396	0.495	0.200
534	0.498	0.271	0.317	0.147
560	0.451	0.125	0.278	0.550
577	0.382	0.043	0.223	0.809
591	0.415	0.125	0.249	0.498
619	0.525	0.104	0.342	0.695
645	0.538	0.083	0.353	0.764
723	0.691	0.396	0.498	0.205
750	0.692	0.391	0.499	0.216
836	0.533	0.150	0.349	0.570
852	0.584	0.167	0.395	0.578
872	0.669	0.348	0.476	0.270
878	0.692	0.422	0.499	0.154
886	0.512	0.292	0.330	0.116
891	0.688	0.438	0.495	0.115
917	0.653	0.326	0.460	0.291
929	0.495	0.063	0.269	0.768
953	0.688	0.438	0.495	0.115
994	0.667	0.273	0.474	0.425
998	0.600	0.447	0.409	−0.091
1038	0.677	0.091	0.483	0.812
1060	0.525	0.354	0.342	−0.036
1062	0.573	0.271	0.385	0.297
1075	0.605	0.239	0.415	0.423
1144	0.637	0.133	0.444	0.700
1165	0.690	0.333	0.497	0.329
1253	0.594	0.229	0.404	0.433
1270	0.600	0.277	0.409	0.324
1350	0.666	0.426	0.473	0.100
1414	0.643	0.063	0.451	0.861
1442	0.451	0.083	0.278	0.700
1458	0.498	0.146	0.317	0.541
1484	0.530	0.178	0.346	0.486
1520	0.574	0.391	0.386	−0.015
mean	0.601	0.284	0.412	0.331
SE	0.013	0.020	0.012	0.040

cacao bean is essential for cocoa authentication. Thus far, it is not possible to distinguish the genetic identity of cacao beans from their morphological characteristics. The only available method to assess the authentication of cacao bean is for an experienced sensory panel to taste the cocoa liquor. This practice is not practical when dealing with large number of samples because there is a limit to the number of samples a sensory panel can evaluate before losing its accuracy. Plus, the

dx.doi.org/10.1021/jf404402v | J. Agric. Food Chem. 2014, 62, 481−487

Table 3. Self-Assignment Test of 30 Cacao Beans of Resident Variety "Fortunato No. 4" and 18 Non-resident Clones Based on Their Multilocus SNP Profiles

	probability of self-assignment		
sample name	Bayesian method	allele frequency	Nei's standard distance
Fortunato No. 4-bean 1	0.986	0.995	0.986
Fortunato No. 4-bean 2	0.685	0.742	0.625
Fortunato No. 4-bean 3	0.990	1.000	0.996
Fortunato No. 4-bean 4	0.985	0.991	0.978
Fortunato No. 4-bean 5	0.900	0.932	0.855
Fortunato No. 4-bean 6	0.900	0.913	0.824
Fortunato No. 4-bean 7	0.955	0.969	0.934
Fortunato No. 4-bean 8	0.992	0.996	0.993
Fortunato No. 4-bean 9	0.716	0.773	0.592
Fortunato No. 4-bean 10	0.984	0.986	0.974
Fortunato No. 4-bean 11	0.982	0.985	0.962
Fortunato No. 4-bean 12	0.890	0.930	0.847
Fortunato No. 4-bean 13	0.952	0.966	0.939
Fortunato No. 4-bean 14	0.986	0.998	0.974
Fortunato No. 4-bean 15	0.972	0.984	0.984
Fortunato No. 4-bean 16	0.950	0.968	0.981
Fortunato No. 4-bean 17	0.998	1.000	0.994
Fortunato No. 4-bean 18	0.947	0.965	0.908
Fortunato No. 4-bean 19	0.885	0.914	0.790
Fortunato No. 4-bean 20	0.990	0.991	0.998
Fortunato No. 4-bean 21	0.951	0.970	0.932
Fortunato No. 4-bean 24	0.986	0.990	0.983
Fortunato No. 4-bean 27	0.995	0.991	0.980
Fortunato No. 4-bean 30	0.993	0.998	0.992
Fortunato No. 4-bean 33	0.961	0.991	0.954
Fortunato No. 4-bean 36	0.784	0.835	0.747
Fortunato No. 4-bean 37	0.975	0.986	0.990
Fortunato No. 4-bean 38	0.835	0.962	0.927
Fortunato No. 4-bean 39	0.941	0.991	0.985
Fortunato No. 4-bean 40	0.955	0.976	0.925
CCN 51	<0.001	<0.001	<0.000
ICS 1	<0.001	<0.001	0.048
ICS 84	<0.001	<0.001	<0.000
ICS 98	<0.001	<0.001	<0.000
LCT EEN 241	<0.001	<0.001	0.006
LCT EEN 302	0.004	<0.001	<0.013
LCT EEN 83S	0.076	<0.001	0.206
IMC 47	0.012	<0.001	0.078
IMC 60	<0.001	<0.001	<0.000
NA 32	<0.001	<0.001	<0.000
NA 702	<0.001	<0.001	<0.000
NA 111	0.030	0.058	0.076
PA 150	<0.001	<0.001	<0.000
PA 300	<0.001	<0.001	<0.000
AMELONADO 22	<0.001	<0.001	<0.000
CATONGO	<0.001	<0.001	<0.000
CRIOLLO 13	<0.001	<0.001	<0.000
CRIOLLO 22	<0.001	<0.001	<0.000

evaluation result of the sensory panel is difficult for statistical analysis. Moreover, it cannot be performed on a single bean basis. In the present study, we demonstrated a DNA fingerprinting method that uses a small set of SNP markers to verify the genetic identity of a single cacao bean. This method can handle a large amount of samples in a short period of time, and the result is highly robust and repeatable.

Our results showed that single bean genotyping using the nanofluidic array of SNP markers is particularly suitable for this purpose. The STA protocol, performed before genotyping, is a multiplex PCR reaction using primers for all loci of interest, but without targeting the specific alleles, thus proportionally increasing the copies of these loci.[40] This procedure has been demonstrated to significantly improve call rates for SNPs[41] and solved our problem of the low concentration of DNA obtained from a single seed coat. Cacao seed coat, similar to the cacao leaves, contains a high level of polyphenolic compounds and other PCR inhibitory compounds, and in addition, the seed coat is encrusted in a dried plant and microorganism residue that is a direct result of the fermentation and drying processes. The STA protocol efficiently dealt with problems of the DNA quality extracted from cacao.

Results from the repeatedly genotyped five beans (three independent DNA extractions were performed from the same seed coat of each bean) showed 100% concordance. SNP profiles of CCN 51 as well as of the 17 other reference clones fully matched their established genotypes, determined by previous independent methodology, suggesting that the nanofluidic system is a reliable platform for generating cacao DNA fingerprints with high accuracy.

The present study used CCN 51 as the targeted adulterant variety because this variety is the most widely cultivated bulk cocoa variety in Peru. According to the report from the Peruvian Ministry of Agriculture,[26] CCN 51 accounted for 50% of the production in the region where the authentic variety ("Fortunato No. 4") is grown. CCN 51 is also the number one bulk cocoa variety in Ecuador, where the fine flavor Nacional cacao is produced. Knowing the targeted adulterant variety (e.g., CCN 51 in Ecuador and Peru) made the identification straightforward. A conclusion can be reached by multilocus matching the SNP profiles without any ambiguity. Nevertheless, in this situation, the effectiveness of individual identification via SNP fingerprints depends upon the number of loci used for genotyping. An important statistical parameter for determining the number of loci required to identify all distinct individuals with a needed confidence level is the probability of identity (PID). Multilocus PID values can be obtained by multiplying together single-locus PID values, assuming independence of loci. A stringent PID value is needed for domesticated crop species, because they often share similar ancestors. Therefore, PID calculated for sibs would provide a highly conservative boundary for domesticated crop species. The present result shows that, using 44 SNP loci, the chance of sampling identical genotypes from a random mating population would be 1 out of 100 000. It thus predicts the high statistical power of using this set of SNPs for cacao genotype verification.

When the adulterant varieties are unknown, direct multilocus matching cannot be applied; therefore, the DNA fingerprints need to be used with an assignment test to single out unknown adulterant varieties, as well as to confirm the authentic variety. Among the different kinds of assignment tests, an exclusion test is the most suitable for cacao beans because it can be used even if only one variety (i.e., the authentic variety) has been sampled. In reality, this is the case for most of the authentication issues in the cocoa trade. For example, the fine-flavor varieties produced in Peru and Ecuador were often mixed with other high-yielding varieties of bulk cocoa, such as CCN 51. This situation is equivalent to a small number of "non-resident" individuals mixed into the resident population in typical population genetics. Using self-assignment test, such as the one

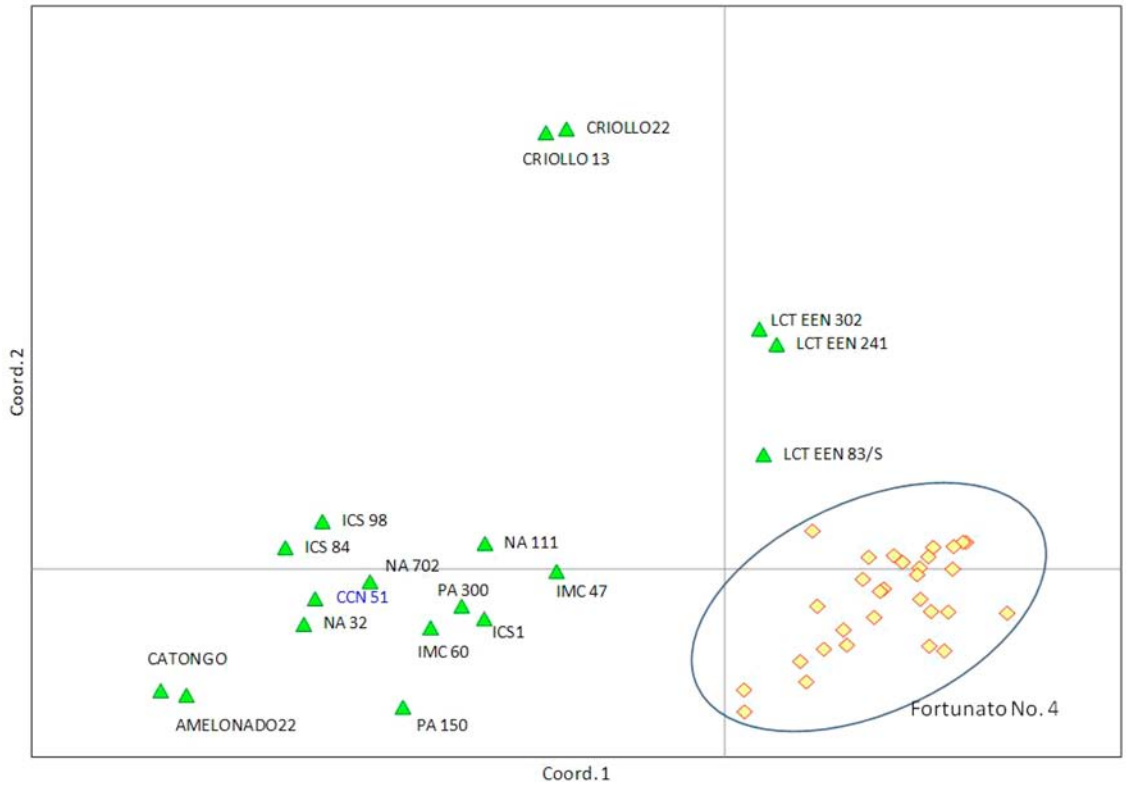

Figure 3. PCoA plot of 45 cacao accessions, including 30 DNA samples extracted from fermented/dry beans from a single source provider in northern Peru, 1 putative adulterant clone (CCN 51), and 17 international clones serving as reference samples. The plane of the first three main PCO axes accounted for 89.6% of total variation. First axis = 53.7% of the total information; second axis = 14.2% of the total information; and third axis = 11.2% of the total information.

implemented in GeneClass2,[39] one could calculate the observed allele frequencies in the resident group, simulate a distribution of random multilocus genotypes that are expected to occur in the resident group (on the basis of the observed allele frequencies), and exclude the resident group (the authentic variety) as the origin of the cacao bean if its multilocus genotype lies outside the distribution of the simulated genotypes. As demonstrated in the present study, the non-resident cacao genotypes, including some Forastero-type clones indigenous to Peru, all received low assignment probability (<0.0001−0.02 for the Bayesian method and <0.0001−0.037 for the allele frequency method). In contrast, all 30 samples in the resident group received high assignment probability (>0.50). The genetic relationship among the analyzed samples was further visualized by distance-based PCoA (Figure 3). The concordant results of the assignment test and distance-based PCoA suggest that the protocol for authentication testing is robust and accurate.

In conclusion, we conducted a pilot study on verification of authentication for cacao. We applied single bean genotyping using a nanofluidic array and SNP markers. This technology enabled us to generate high-quality SNP-profile-based DNA extracted from a single seed coat. Together with forensic statistical tools, the single-bean-based DNA fingerprints allowed for an unambiguous identification of the targeted adulterant variety. It also enabled the assignment test to authenticate and exclude adulterated samples. To our knowledge, this is the first authentication study in cacao using molecular makers. This approach is robust for authentication verification of gourmet cacao varieties and, thus, has significant potential for practical application.

AUTHOR INFORMATION

Corresponding Author

*Telephone: 1-301-504-7477. Fax: 1-301-504-1998. E-mail: dapeng.zhang@ars.usda.gov.

Funding

This work was funded by ARS, USDA, and by a financial gift from Lindt and Sprüngli chocolate company through the World Cocoa Foundation. References to a company and/or product by the USDA are only for the purposes of information and do not imply approval or recommendation of the product to the exclusion of others that may also be suitable.

Notes

The authors declare no competing financial interest.

ACKNOWLEDGMENTS

The authors give special thanks to Katica Ilic, Xiaohui Wang, Robert Jones, and Jun Wang in Fluidigm Corporation for designing the 48.48 SNP assay. The authors also acknowledge the Fine Chocolate Industry Association and Marañón Chocolate for supplying samples.

ABBREVIATIONS USED

SNP, single nucleotide polymorphism; SSR, simplet sequence repeat; RNase A, ribonuclease I or ribonucleate 3′-pyrimidino-oligonucleotidohydrolase; PCR, polymerase chain reaction; IFC, integrated fluidic circuit; PID, probability of identity; PID-sib, probability of identity among siblings; PCoA, principle coordinate analysis; PIC, polymorphism information content; PCO, principle coordinate; STA, specific target amplification

REFERENCES

(1) Cheesman, E. E. Notes on the nomenclature, classification and possible relationships of cocoa populations. *Trop. Agricult.* **1944**, *21*, 144−159.

(2) Bartley, B. G. D. *The Genetic Diversity of Cacao and Its Utilization*; CABI Publishing, Wallingford, U.K., 2005.

(3) Pound, F. J. A note on the cocoa population of South America. *Proceedings of the 1945 Cocoa Conference*, London, U.K., 1945; pp 131−133.

(4) Dias, L. A. S. Origin and distribution of *Theobroma cacao* L: A new scenario. In *Genetic Improvement of Cacao*; Dias, L. A. S., Ed.; EcoPort, Food and Agriculture Organization (FAO): Rome, Italy, 2001; (http://ecoport.org/ep?SearchType=earticleView&earticleId=197&page=2683) (accessed Sept 29, 2013).

(5) Gómez-Pompa, A.; Flores, J. S.; Fernandez, M. A. The sacred cacao groves of the Maya. *Lat. Am. Antiq.* **1990**, *1*, 247−257.

(6) Henderson, J. S.; Joyce, R. A.; Hall, G. R.; Hurst, W. J.; McGovern, P. E. Chemical and archaeological evidence for the earliest cacao beverages. *Proc. Natl. Acad. Sci. U. S. A.* **2007**, *104*, 18937−18940.

(7) Bergman, J. F. The distribution of cacao cultivation in pre-Columbian America. *Ann. Assoc. Am. Geogr.* **1969**, *59*, 85−96.

(8) Young, A. M. *The Chocolate Tree: A Natural History of Cacao*; University Press of Florida: Gainsville, FL, 2007; pp 92, 93, and 219.

(9) Woolfe, M.; Primrose, S. Food forensics: Using DNA technology to combat misdescription and fraud. *Trends Biotechnol.* **2004**, *22*, 222−226.

(10) Mafra, I.; Ferreira, I. M. P. V. O.; Oliveira, M. B. P. P. O. Food authentication by PCR-based methods. *Eur. Food Res. Technol.* **2008**, *227*, 649−665.

(11) Galimberti, A.; De Mattiaa, F.; Losaa, A.; Brunia, I.; Federicia, S.; Casiraghia, M.; Martellosb, S.; Labra, M. DNA barcoding as a new tool for food traceability. *Food Res. Int.* **2013**, *50*, 55−63.

(12) Martins-Lopes, P.; Gomes, S.; Pereira, L.; Guedes-Pinto, H. Molecular markers for food traceability. *Food Technol. Biotechnol.* **2013**, *51*, 198−207.

(13) Prins, T. W.; Dijk, J. P.; Hoef, A. M. A.; Voorhuijzen, M. M.; Broeders, S.; Trapmann, S.; Seyfarth, R.; Pardigol, A.; Schoen, C. D.; Aarts, H. J. M.; Kok, E. J. Towards a multiplex cereal traceability tool using padlock probe ligation on genomic DNA. *Food Chem.* **2010**, *118*, 966−973, DOI: 10.1016/j.foodchem.2008.10.085.

(14) Chuang, H.; Lur, H.; Hwu, K.; Chang, M. Authentication of domestic Taiwan rice varieties based on fingerprinting analysis of microsatellite DNA markers. *Bot. Stud.* **2011**, *52*, 393−405.

(15) Palmieri, L.; Bozza, E.; Giongo, L. Soft fruit traceability in food matrices using real-time PCR. *Nutrients* **2009**, *2*, 316−28.

(16) Montealegre, C.; Alegre, M. L. M.; García-Ruiz, V. Traceability markers to the botanical origin in olive oils. *J. Agric. Food Chem.* **2010**, *58*, 28−38.

(17) Agrimonti, C.; Vietina, M.; Pafundo, S.; Marmiroli, N. The use of food genomics to ensure the traceability of olive oil. *Trends Food Sci. Technol.* **2011**, *22*, 237−244.

(18) Stoeckle, M. Y.; Gamble, C. C.; Kirpekar, R.; Young, G.; Ahmed, S.; Little, D. P. Commercial teas highlight plant DNA barcode identification successes and obstacles. *Sci. Rep.* **2011**, *1*, 42.

(19) Tornincasa, P.; Furlan, M.; Pallavicini, A.; Graziosi, G. Coffee species and varietal identification. In *Tools for Identifying Biodiversity: Progress and Problems*; Nimis, P. L., Vignes Lebbe, R., Eds.; Oxford Press: Oxford, U.K., 2010; pp 307−313, ISBN: 978-88-8303-295-0.

(20) Guiltinan, M. J.; Verica, J.; Zhang, D.; Figueira, A. Genomics of *Theobroma cacao*, "the food of the Gods". In *Genomics of Tropical Crop Plant*; Moore, P. H., Ming, R., Eds.; Springer: New York, 2008; pp 145−170.

(21) Zhang, D.; Figueira, A.; Motilal, L.; Lachenaud, P.; Meinhardt, L. W. Theobroma. In *Wild Crop Relatives: Genomic and Breeding Resources, Plantation and Ornamental Crops*; Kole, C., Ed.; Springer-Verlag: Berlin, Germany, 2012; pp 277−296. DOI: 10.1007/978-3-642-21201-7_13.

(22) Buckler, E. S.; Thornsberry, J. Plant molecular diversity and applications to genomics. *Curr. Opin. Plant Biol.* **2002**, *5*, 107−111.

(23) Livingstone, D. S.; Freeman, B.; Motamayor, J. C.; Schnell, R. J.; Royaert, S.; Takrama, J.; Meerow, A. W.; Kuhn, D. N. Optimization of a SNP assay for genotyping *Theobroma cacao* under field conditions. *Mol. Breed.* **2012**, *30*, 33−52, DOI: 10.1007/s11032-011-9596-4.

(24) Takrama, J.; Dadzie, A. M.; Opoku, F. K.; Padi, F. K.; Adomako, B.; Asu-Ampomah, Y.; Livingstone, D. S.; Motamayor, J. C.; Schnell, R. J.; Kuhn, R. J. Applying SNP marker technology in the cacao breeding programme in Ghana. *Afr. Crop Sci. J.* **2012**, *20*, 67−75.

(25) Ji, K.; Zhang, D. P.; Motilal, L.; Boccara, M.; Lachenaud, P.; Meinhardt, L. W. Genetic diversity and parentage in farmer varieties of cacao (*Theobroma cacao* L.) from Honduras and Nicaragua as revealed by single nucleotide polymorphism (SNP) markers. *Genet. Resour. Crop Evol.* **2013**, *60*, 441−453.

(26) Ministerio de Agricultura. *Caracterización de las Zonas Productoras de Cacao en el Perú y Su Competitividad*; Ministerio de Agricultura: Lima, Peru, 2003; p 209.

(27) Zhang, D.; Mischke, S.; Goenaga, R.; Hemeida, A. A.; Saunders, J. A. Accuracy and reliability of high-throughput microsatellite genotyping for cacao clone identification. *Crop Sci.* **2006**, *46*, 2084−2092.

(28) Zhang, D.; Mischke, S.; Johnson, E. S.; Mora, A.; Phillips-Mora, W.; Meinhardt, L. W. Molecular characterization of an international cacao collection using microsatellite markers. *Tree Genet. Genomes* **2009**, *5*, 1−10.

(29) Motilal, L.; Zhang, D.; Umaharan, P.; Mischke, S.; Mooleedhar, V.; Meinhardt, L. W. The relic *Criollo cacao* in Belize—Genetic diversity and relationship with *Trinitario* and other cacao clones held in the International Cocoa Genebank, Trinidad. *Plant Genet. Resour.* **2010**, *8*, 106−110.

(30) Fluidigm. *Fluidigm SNP Genotyping User Guide, Revision H1*; Fluidigm Corporation: South San Francisco, CA, 2011; PN 68000098.

(31) Argout, X.; Fouet, O.; Wincker, P. Towards the understanding of the cocoa transcriptome: Production and analysis of an exhaustive dataset of ESTs of *Theobroma cacao* generated from various tissues and under various conditions. *BMC Genomics* **2008**, *9*, 512.

(32) Argout, X.; Salse, J.; Aury, J. M. The genome of *Theobroma cacao*. *Nat. Genet.* **2011**, *43*, 101−108, DOI: 10.1038/ng.736.

(33) Lanaud, C.; Fouet, O.; Gramacho, K.; Argout, X.; et al. A large EST resource for Theobroma cacao including cDNAs isolated from various organs and under various biotic and abiotic stresses. *Proceedings of the 15th International Cocoa Research Conference*; San Jose, Costa Rica, 2006; pp 185−191.

(34) Evett, I. W.; Weir, B. S. *Interpreting DNA Evidence: Statistical Genetics for Forensic Scientists*; Sinauer, Sunderland, MA, 1998.

(35) Waits, L. P.; Luikart, G.; Taberlet, P. Estimating the probability of identity among genotypes in natural populations: Cautions and guidelines. *Mol. Ecol.* **2001**, *10*, 249−256.

(36) Peakall, R.; Smouse, P. E. Genalex 6: Genetic analysis in Excel. Population genetic software for teaching and research. *Mol. Ecol. Notes* **2006**, *6*, 288−295.

(37) Peakall, R.; Smouse, P. E. GenAlEx 6.5: Genetic analysis in Excel. Population genetic software for teaching and research-an update. *Bioinformatics* **2012**, *28*, 2537−2539.

(38) Rannala, B.; Mountain, J. L. Detecting immigration by using multilocus genotypes. *Proc. Natl. Acad. Sci. U. S. A.* **1997**, *94*, 9197−9201.

(39) Cornuet, J. M.; Piry, S.; Luikart, G.; Estoup, A.; Solignac, M. New methods employing multilocus genotypes to select or exclude populations as origins of individuals. *Genetics* **1999**, *153*, 1989−2000.

(40) Qin, J.; Jones, R. C.; Ramakrishnan, R. Studying copy number variations using a nanofluidic platform. *Nucleic Acids Res.* **2008**, *36*, No. e1162008, DOI: 10.1093/nar/gkn518.

(41) Wang, J.; Lin, M.; Crenshaw, A.; Hutchinson, A.; Hicks, B.; Yeager, M.; Berndt, S.; Huang, W.-Y.; Hayes, R. B.; Chanock, S. J.; Jones, R. C.; Ramakrishnan, R. High-throughput single nucleotide polymorphism genotyping using nanofluidic dynamic arrays. *BMC Genomics* **2009**, *10*, 561 DOI: 10.1186/1471-2164-10-561.

JOURNAL OF AGRICULTURAL AND FOOD CHEMISTRY

Article

pubs.acs.org/JAFC

New Triterpenoid Saponins from *Ilex cornuta* and Their Protective Effects against H_2O_2-Induced Myocardial Cell Injury

Shanshan Li,[†] Jianping Zhao,[‡] Yanli Liu,[†] Zhong Chen,[†] Qiongming Xu,*[,†,‡] Ikhlas A. Khan,[†,‡] and Shilin Yang[†]

[†]College of Pharmaceutical Science, Soochow University, Suzhou 215123, China

[‡]National Center for Natural Products Research, and Department of Pharmacognosy, Research Institute of Pharmaceutical Sciences, School of Pharmacy, University of Mississippi, University, Mississippi 38677, United States

Supporting Information

ABSTRACT: Five new triterpenoid saponins, **1**−**5**, together with 10 known ones, **6**−**15** were isolated from the aerial parts of *Ilex cornuta*. The structures of compounds **1**−**5** were determined as 3*β*-*O*-*α*-L-arabinopyranosyl-19*α*,23-dihydroxy-20*α*-urs-12-en-28-oic acid 28-*O*-*β*-D-glucopyranosyl ester, **1**; 3*β*-*O*-*β*-D-glucopyranosyl-(1→2)-*α*-L-arabinopyranosyl-19-hydroxy-20*α*-urs-12-en-28-oic acid 28-*O*-*β*-D-glucopyranosyl ester, **2**; 19*α*,23-dihydroxyurs-12-en-28-oic acid 3*β*-*O*-*β*-D-glucuronopyranoside-6-*O*-methyl ester, **3**; 19*α*,23-dihydroxyurs-12-en-28-oic acid 3*β*-*O*-[*β*-D-glucuronopyranoside-6-*O*-methyl ester]-28-*O*-*β*-D-glucopyranosyl ester, **4**; and 3*β*-*O*-[*α*-L-arabinopyranosyl-(1→2)-*β*-D-glucuronic acid]-oleanolic acid 28-*O*-*β*-D-glucopyranosyl ester, **5**, on the basis of spectroscopic analyses (IR, ESI-MS, HR-ESI-MS, 1D and 2D NMR) and chemical reactions. Protective effects of compounds **1**−**15** were tested against H_2O_2-induced H9c2 cardiomyocyte injury, and the data showed that compounds **1**, **4**, **6**, and **13** had significant cell-protective effects. No significant DPPH radical scavenging activity was observed for compounds **1**−**15**.

KEYWORDS: *Ilex cornuta, Aquifoliaceae, triterpenoid saponins, structure identification, cardiomyocyte oxidative injury, DPPH radical scavenging activity*

INTRODUCTION

Ilex cornuta Lindl. et Paxt. (Aquifoliaceae family) is an evergreen shrub with dense foliage. Its leaves are the major source of "Ku-Ding-Cha", a popular herbal tea consumed in China and other countries.[1] The tea is widely used for its health benefits, such as relief of sore throat and weight loss.[2] According to the Traditional Chinese Medicine theory, the leaves of *I. cornuta*, which are bitter and cool-natured, can invigorate the liver and kidney and can expel "wind" and "heat". It has been used to cure weakness of waist, knees, arthrodynia, head-wind, acute conjunctivitis, toothache, and urticaria.[3] The results from modern pharmacology research showed that the plant had many therapeutic effects, such as increase of coronary blood flow[4] and anticancer[5] and antibacterial properties.[6] Previous phytochemical investigation on the *Ilex* genus led to the isolation of triterpenes, triterpenoid saponins,[7] flavones, flavonoid glycosides,[8] polyphenols,[9] and fatty acids.[10]

Cardiovascular disease is one of the major causes of deaths worldwide. Oxidative stress is considered as a causative factor in the pathogenesis of cardiomyocyte ischemic injury. Activation of oxidative stress leads to a variety of intracellular signaling events that ultimately cause dysfunction of the endothelium, proliferation of vascular smooth muscle cells, expression of pro-inflammatory genes, and reconstruction of the extracellular matrix.[11] Growing evidence has suggested that the intake of foods rich in antioxidants can result in a lower risk of cardiovascular disease.[12] In our effort to develop the extract of *I. cornuta* as a herbal dietary supplement for the prevention of coronary artery disease, a phytochemical investigation of its aerial parts was undertaken, which led to the isolation of 5 new triterpenoid saponins, **1**−**5** (Figure 1), along with 10 known ones. In this paper, we report the isolation and structural elucidation of the new compounds, as well as the protective effects of the isolates against cardiomyocyte injury induced by H_2O_2. In addition, their radical scavenging activity was evaluated by DPPH assay.

MATERIALS AND METHODS

General. The specific optical rotation values were determined with a Perkin-Elmer model 241 polarimeter (Perkin-Elmer Inc., Waltham, MA, USA). IR spectra were determined on a Perkin-Elmer 983 G spectrometer. ^{1}H and ^{13}C NMR and 2D NMR spectra were recorded on a Varian Inova 500 spectrometer (Varian Inc., Palo Alto, CA, USA) in C_5D_5N using tetramethylsilane (TMS) as the internal standard. HR-ESI-MS spectra were determined on a Micromass Q-TOF2 spectrometer (Micromass Corp., London, UK).

Chromatography. HPLC analysis and purification were performed with an Agilent Zorbax SB-C18 semipreparative HPLC column (250 × 9.4 mm i.d., 5 *μ*m, Agilent Corp., Palo Alto, CA, USA) on a Shimadzu HPLC system composed of an LC-20AT pump with an SPD-20A detector (Shimadzu Corp., Kyoto, Japan), and the wavelength for detection was 203 nm. Medium-pressure liquid chromatography (MPLC) purification was performed on a Büchi flash chromatography system composed of a C-650 pump and a flash column (460 × 26 mm i.d., Büchi Corp., Flawil, Switzerland). Silica gel (60−100 mesh) used for column chromatography and precoated silica gel for TLC plates were purchased from Qingdao Marine Chemical

Received: October 16, 2013
Revised: December 27, 2013
Accepted: December 29, 2013
Published: December 29, 2013

ACS Publications © 2013 American Chemical Society

dx.doi.org/10.1021/jf4046667 | J. Agric. Food Chem. 2014, 62, 488−496

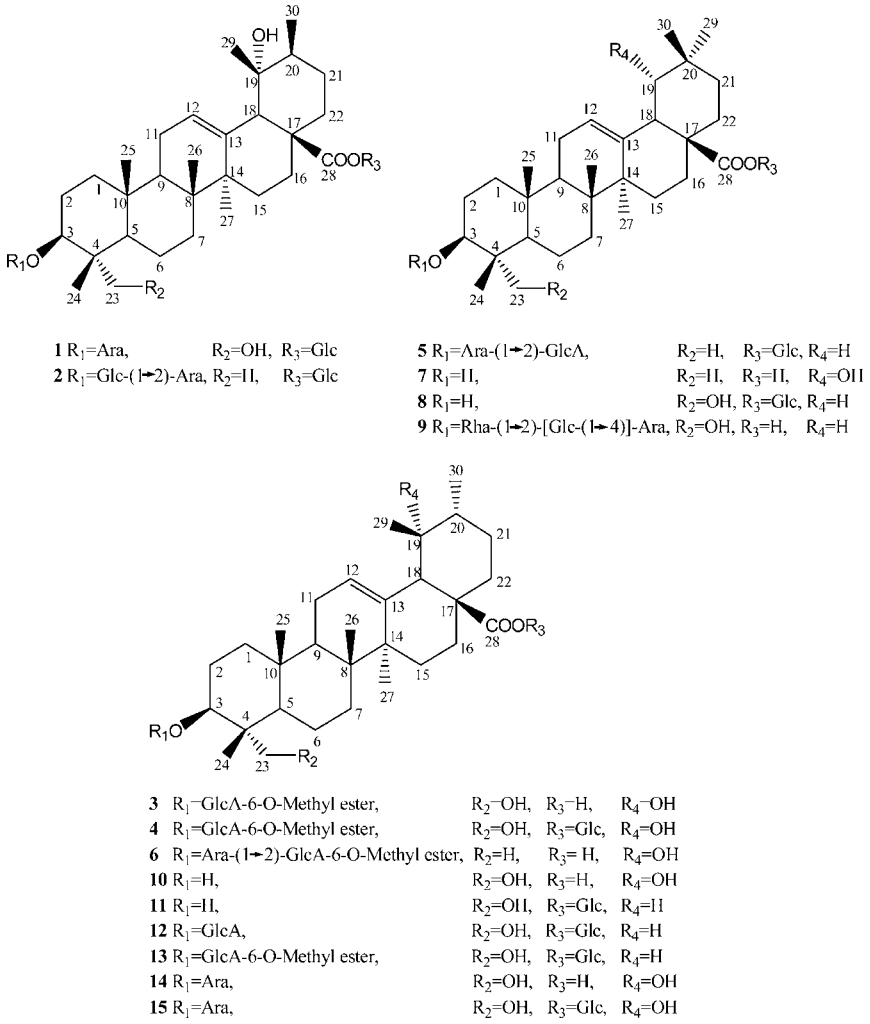

Figure 1. Structures of compounds **1**−**15**.

Factory (Qingdao, China). A 10% sulfuric acid alcohol solution was used for TLC colorization. Sephadex LH-20 for column chromatography was purchased from GE Corp. (Piscataway, NJ, USA). D101 macroporous resin for column chromatography was purchased from Xi'an Sunresin New Materials Co. Ltd. (Xi'an, China). GC analyses were conducted on a GC-14C (Shimadzu Corp.) instrument with a flame ionization detector (FID), and the analytical conditions were as follows: DB-5 column (i.d. = 0.25 μm, length = 30 m, Suzhou Huitong Chromatography Technology Co., Ltd., Suzhou, China); column temperature at 210 °C; injector temperature at 270 °C; detector temperature at 300 °C.

Materials. The aerial parts of *I. cornuta* were collected from Liuan City of Anhui province, in April 2011, and were authenticated by Professor Xiao-ran Li. A voucher specimen (04-21-01-11) was deposited in the herbarium of the College of Pharmaceutical Science, Soochow University.

Extraction and Isolation. The dried plant material (10 kg) was crushed into powder and extracted twice with 50% EtOH at 80 °C under reflux. The solvent was subsequently removed under reduced pressure to yield a residue (325 g), which was then dissolved in 30 L of distilled water and passed through D101 macroporous resin column (200 × 30 cm i.d.), eluted with a gradient of aqueous EtOH (EtOH/H_2O 0, 30, 60, 90%). The 90% EtOH eluate (30 g) was further vacuum chromatographed on a silica gel (60−100 mesh) column (30 × 18 cm i.d.), eluted with a gradient of $CHCl_3$/MeOH (90:10, 80:20, 70:30, 60:40, 50:50, 40:60, 30:70, 0:100, each 6.0 L). The $CHCl_3$/MeOH (90:10) eluate (1.5 g) was then separated by MPLC over an ODS column, eluted with MeOH/H_2O (60:40, 70:30, 80:20, 90:10, 100:0, each 500 mL) to afford five fractions. Fraction 2 (125 mg) was separated by semipreparative HPLC to yield compounds **7** (25 mg, t_R 35.27 min), **8** (8 mg, t_R 38.28 min), and **9** (33 mg, t_R 41.32 min). The $CHCl_3$/MeOH (80:20) eluate (4.9 g) yielded five fractions after separation by MPLC. Fraction 3 (90 mg) was further separated by using semipreparative HPLC to yield compounds **1** (9 mg, t_R 60.27 min) and **10** (19 mg, t_R 63.19 min). From fraction 4 (1500−2000 mL, 180 mg) compounds **3** (40 mg, t_R 70.15 min) and **4** (8 mg, t_R 73.23 min) were obtained after it was subjected to the semipreparative HPLC separation. In a similar way, the $CHCl_3$/MeOH (70:30) eluate (6.7 g) from the vacuum chromatography was first separated into six fractions by MPLC over the ODS column, and then these fractions were further separated by using semipreparative HPLC to yield compounds **6** (20 mg), **12** (55 mg), **13** (10 mg), **14** (9 mg), and **15** (14 mg). Moreover, compounds **2** (10 mg), **5** (17 mg), and **11** (36 mg) were obtained from the $CHCl_3$/MeOH (60:40) eluate (4.8 g) after MPLC and semipreparative HPLC separations as described above.

3β-O-α-L-Arabinopyranosyl-19α,23-dihydroxy-20α-urs-12-en-28-oic acid 28-O-β-D-glucopyranosyl ester (1): white amorphous powder; $[\alpha]_D^{25}$ −9.5 (*c* 0.12, MeOH); IR (KBr) ν_{max} 3385 (OH), 2943, 1745 (C═O), 1692, 1641, 1460, 1050 (C—O—C), 876 cm^{-1}; ^1H NMR (C_5D_5N, 500 MHz) and ^{13}C NMR (C_5D_5N, 125 MHz) spectroscopic data, see Tables 1 and 2; HR-ESI-MS (positive ion mode) *m*/*z* 805.4303 ($[M + Na]^+$; calcd for $C_{41}H_{66}O_{14}Na$, 805.4350).

3β-O-β-D-Glucopyranosyl-(1→2)-α-L-arabinopyranosyl-19-hydroxy-20α-urs-12-en-28-oic acid 28-O-β-D-glucopyranosyl ester (2): white amorphous powder; $[\alpha]_D^{25}$ −15.4 (*c* 0.15, MeOH); IR (KBr) ν_{max}

dx.doi.org/10.1021/jf4046667 | J. Agric. Food Chem. 2014, 62, 488−496

Table 1. NMR Spectroscopic Data for Aglycone Moieties of Compounds 1−5 (in C_5D_5N)

	1		2		3		4		5	
no.	δ_C	δ_H	δ_C	δ_H	δ_C	δ_H	δ_C	δ_H	δ_C	δ_H
1	38.9	1.16m, 1.69m	38.9	0.96m, 1.60m	38.8	1.01m, 1.56m	38.9	1.00m, 1.58m	38.8	0.90m, 1.44m
2	26.3	2.12m, 2.34m	26.6	1.92m, 2.16m	26.2	2.04m, 2.26m	26.2	2.06m, 2.28m	26.8	1.94m, 2.32m
3	82.0	4.34m	89.0	3.27dd (5.0, 15.0[a])	82.3	4.36m	82.4	4.36m	89.2	3.37dd (4.0, 11.5)
4	43.6		39.6		43.6		43.6		39.7	
5	47.7	1.78m	56.0	0.83d (15.0)	47.6	1.76m	47.6	1.76m	55.9	0.80d (11.5)
6	18.5	1.46m, 1.75m	18.8	1.40m, 1.53m	18.4	1.45m, 1.79m	18.4	1.43m, 1.76m	18.6	1.39m, 1.56m
7	33.2	1.50m, 1.80m	33.6	1.55m, 1.65m	33.3	1.42m, 1.80m	33.3	1.49m, 1.81m	33.3	1.39m, 1.52m
8	40.6		40.6		40.5		40.7		40.0	
9	48.0	2.01m	47.9	1.85m	47.9	1.97m	47.9	1.98m	48.1	1.68m
10	37.1		37.1		36.9		37.0		37.0	
11	24.2	2.00m, 2.13m	24.1	2.11m	24.1	2.11m	24.2	2.08m, 2.12m	23.5	2.11m
12	127.8	5.58m	127.8	5.59m	128.1	5.66m	128.6	5.62m	123.0	5.49m
13	139.0		138.9		140.1		139.4		144.3	
14	42.2		42.3		42.2		42.2		42.3	
15	29.4	1.28m, 2.53m	29.3	1.35m, 2.56m	29.5	1.30m, 2.37m	29.4	1.47m, 2.52m	28.4	1.26m, 2.41m
16	26.9	2.12m, 3.28m	26.9	2.17m, 3.31m	26.5	2.08m, 3.17m	26.2	2.01m, 3.15m	23.9	1.95m,
17	48.4		48.5		48.4		48.7		47.1	
18	47.3	3.26s	47.3	3.27s	54.7	3.12s	54.6	3.00s	41.9	3.24m
19	73.5		73.5		72.8		72.8		46.3	1.31m, 1.83m
20	43.0	2.02m	43.0	2.03m	42.3	1.56m	42.8	1.44m	30.9	
21	24.8	1.27m, 2.66m	24.8	1.28m, 2.68m	27.1	1.41m, 2.14m	26.8	1.29m, 1.50m	34.1	1.18m, 1.44m
22	32.0	1.98m, 2.18m	32.0	1.98m, 2.18m	38.7	2.14m, 2.22m	37.8	1.93m, 2.13m	32.7	1.82m, 1.86m
23	64.6	3.78d (11.5), 4.34m	28.3	1.28s	64.4	3.78m, 4.39m	64.5	3.78m, 4.39m	28.1	1.37s
24	13.7	1.02s	16.9	1.13s	13.7	1.01s	13.7	1.03s	16.6	1.17s
25	16.2	1.08s	15.8	0.99s	16.2	0.98s	16.3	1.06s	15.7	0.88s
26	17.7	1.30s	17.6	1.28s	17.4	1.17s	17.6	1.28s	17.6	1.16s
27	24.4	1.72s	24.4	1.78s	24.8	1.77s	24.7	1.72s	26.3	1.35s
28	177.2		177.1		180.8		177.1		176.6	
29	29.8	1.45s	29.9	1.47s	27.2	1.50s	27.1	1.46s	33.3	0.98s
30	16.4	1.05d (7.5)	16.2	1.07d (10.0)	16.9	1.19d (6.5)	16.8	1.14d (5.0)	23.8	0.95s

[a]Data in parentheses are J values (in hertz).

3395 (OH), 2948, 1742 (C═O), 1643, 1454, 1056 (C—O—C), 886 cm^{-1}; ^1H NMR (C_5D_5N, 500 MHz) and ^{13}C NMR (C_5D_5N, 125 MHz) spectroscopic data, see Tables 1 and 2; HR-ESI-MS (positive ion mode) m/z:951.4887 ($[M + Na]^+$; calcd for $C_{47}H_{76}O_{18}Na$, 951.4929).

19α,23-Dihydroxyurs-12-en-28-oic acid 3β-O-β-D-glucuronopyranoside-6-O-methyl ester (3): white amorphous powder; $[\alpha]_D^{25}$ −11.0 (c 0.12, MeOH); IR (KBr) ν_{max} 3382 (OH), 2942, 1740 (C═O), 1693, 1644, 1455, 1046 (C—O—C), 887 cm^{-1}; ^1H NMR (C_5D_5N, 500 MHz) and ^{13}C NMR (C_5D_5N, 125 MHz) spectroscopic data, see Tables 1 and 2; HR-ESI-MS (negative ion mode) m/z 677.3869 ($[M - H]^-$; calcd for $C_{37}H_{57}O_{11}$, 677.3901).

19α,23-Dihydroxyurs-12-en-28-oic acid 3β-O-[β-D-glucuronopyranoside-6-O-methyl ester]-28-O-β-D-glucopyranosyl ester (4): white amorphous powder; $[\alpha]_D^{25}$ −13.2 (c 0.10, MeOH); IR (KBr) ν_{max} 3381 (OH), 2946, 1741 (C═O), 1648, 1462, 1057 (C—O—C), 882 cm^{-1}; ^1H NMR (C_5D_5N, 500 MHz) and ^{13}C NMR (C_5D_5N, 125 MHz) spectroscopic data, see Tables 1 and 2; HR-ESI-MS (positive ion mode) m/z 863.4405 ($[M + Na]^+$; calcd for $C_{43}H_{68}O_{16}Na$, 863.4405).

3β-O-[α-L-Arabinopyranosyl-(1→2)-β-D-glucuronic acid]-oleanolic acid 28-O-β-D-glucopyranosyl ester (5): white amorphous powder; $[\alpha]_D^{25}$ −12.1 (c 0.10, MeOH); IR (KBr) ν_{max} 3384 (OH), 2949, 1743 (C═O), 1693, 1644, 1449, 1038 (C—O—C), 889 cm^{-1}; ^1H NMR (C_5D_5N, 500 MHz) and ^{13}C NMR (C_5D_5N, 125 MHz) spectroscopic data, see Tables 1 and 2; HR-ESI-MS (positive ion mode) m/z 949.4729 ($[M + Na]^+$; calcd for $C_{48}H_{78}O_{16}Na$ 949.4772).

Acid Hydrolysis of Compounds 1−5. A solution of each compound (4 mg) dissolved in 1 N HCl (dioxane/H_2O, 1:1, 2.0 mL) was heated to 90 °C for 2 h. After cooling, the reaction mixture was neutralized with silver carbonate (10 mg), and the solvent was evaporated to dryness under N_2 and then extracted with $CHCl_3$ and H_2O. The aqueous layer was concentrated to dryness, the residue was dissolved in dry pyridine (0.2 mL), and then L-cysteine methyl ester hydrochloride in dry pyridine (0.06 M, 0.2 mL) was added. The mixture was reacted at 60 °C for 2 h, and 0.2 mL of (trimethylsilyl)-imidazole dissolved in dry pyridine was added. After being held at 60 °C for another 2 h, the reactant was partitioned with *n*-hexane and H_2O (0.1 mL, each). The *n*-hexane fraction was subjected to gas chromatographic analysis. The sugar residues in compounds **1−5** were identified by comparison with the standard references: D-glucose (t_R 10.49 min), L-glucose (t_R 11.10 min), D-glucuronic acid (t_R 9.21 min), L-glucuronic acid (t_R 9.66 min), D-arabinose (t_R 8.52 min), and L-arabinose (t_R 8.33 min).[13]

Assay for Testing the Protective Effects against Myocardial Cell Injury Induced by H_2O_2. H9c2 cells (1×10^5/well; Cell Bank of the Chinese Academy of Sciences Shanghai, China) were seeded into 96-well plates. After incubation with different concentrations of compounds **1−15** (12.5−200 μM) for 12 h, the cells were treated with 200 μM H_2O_2 for 24 h.[14,15] The cells in the control groups were treated with the same volume of phosphate-buffered saline (PBS). Cell viability was evaluated by 3-(4,5-dimethylthiazol-2-yl)-2,5-diphenyltetrazolium bromide (MTT) assay, which is based on the reduction of MTT by the mitochondrial dehydrogenase of intact cells to a purple formazan product. The quantity of formazan was determined by measuring the absorbance at 540 nm using an ELISA plate reader. The percentage cell viability was calculated as a ratio of the optical density (OD) value of the sample to the OD value of the control.[16] All experiments were done three times.

DPPH Radical Scavenging Capacity Assay. DPPH free radical scavenging activity of fractions and compounds was determined in

dx.doi.org/10.1021/jf4046667 | J. Agric. Food Chem. 2014, 62, 488−496

Table 2. NMR Spectroscopic Data for Sugar Moieties of Compounds 1−5 (in C_5D_5N)

	1		2		3		4		5	
no.	δ_C	δ_H	δ_C	δ_H	δ_C	δ_H	δ_C	δ_H	δ_C	δ_H
C_3−O−										
Ara-1	106.9	5.06d (7.0[a])	104.9	5.03d (7.0)					106.9	5.28d (6.0)
2	73.3	4.49m	81.1	4.66m					73.9	4.66m
3	74.9	4.14m	73.5	4.43m					74.4	4.28m
4	69.8	4.32m	68.4	4.44m					69.3	4.39m
5	67.2	4.35m, 3.79m	65.0	4.36m, 3.84m					67.2	4.47m, 3.87d (11.5)
Glc-1′			106.1	5.26d (9.5)						
2′			76.5	4.16m						
3′			78.3	4.26m						
4′			71.7	4.39m						
5′			78.3	3.88m						
6′			62.7	4.50m						
GlcA-1					106.6	5.31d (8.0)	106.5	5.31d (10.0)	105.5	5.09d (5.5)
2					75.6	4.15m	75.6	4.16m	83.7	4.27m
3					78.0	4.23m	78.0	4.23m	77.7	4.43m
4					73.3	4.52m	73.3	4.53m	73.4	4.61m
5					77.4	4.54m	77.4	4.54m	77.3	4.62m
6					171.0		170.9		173.1	
methyl-1					52.1	3.77s	52.1	3.78s		
C_{28}−O−										
Glc-1	95.9	6.43d (8.0)	95.9	6.43d (10.0)			96.0	6.39d (10.0)	95.9	6.43d (12.5)
2	74.2	4.29m	74.2	4.30m			74.2	4.30m	74.3	4.28m
3	79.1	4.37m	79.1	4.37m			79.1	4.37m	79.1	4.35m
4	71.1	4.46m	71.3	4.45m			71.4	4.44m	71.2	4.43m
5	79.4	4.12m	79.3	4.12m			79.3	4.12m	79.5	4.11m
6	62.2	4.62m	62.4	4.50m			62.5	4.54m, 4.48m	62.3	4.53m, 4.48m

[a]Data in parentheses are J values (in hertz). Ara refers to arabinose, GlcA refers to gluconic acid, and Glc refers to glucose.

triplicate according to the method proposed by Hatano.[17] In brief, 100 μL of tested fraction or compound at final concentrations (5−200 μM) in methanol was added to 100 μL of a 0.5 mM DPPH radical solution in methanol. The mixture was shaken vigorously and allowed to stand for 30 min in the dark. Vitamin E was considered as a positive control. A freshly prepared DPPH solution exhibits a deep purple color with absorption maximum at 517 nm with a spectrophotometer. The radical scavenging rate of free radical DPPH in percent (I%) was calculated in the following way:

$$I\% = (100 \times [1 - (A_{sample} - A_{blank})/A_{control}]$$

$A_{control}$ is the absorbance of the control reaction (containing all reagents except the test compound), A_{sample} is the absorbance of the test compound, and A_{blank} is the absorbance of blank sample.

Statistical Analysis. Data were expressed as the mean ± SD and evaluated using one-way ANOVA. The post hoc test was done with Student's Dunnett test. $p < 0.05$ was considered statistically significant. Calculations were performed using the SPSS 16.0 statistical package.

RESULTS AND DISCUSSION

The 50% EtOH extract of the aerial parts of *I. cornuta* was separated by repeated D101 resin CC and ODS CC to afford 5 new triterpenoid saponins, **1**−**5**, as well as 10 known ones, which were identified as 19α-hydroxyurs-12-en-28-oic acid 3β-*O*-α-L-arabinopyranosyl-(1→2)-β-D-glucuronopyranoside-6-*O*-methylester, **6**;[18] siaresinolic acid, **7**;[19] hederagenin-28-β-D-glucopyranoside, **8**;[20] hederacolchiside A, **9**;[21] ilexolic acid A, **10**;[22] 3β,23-dihydroxyurs-12-en-28-oic acid 28-*O*-β-D-glucopyranosyl ester, **11**;[23] cynarasaponin E, **12**;[24] cynarasaponin E methyl ester, **13**;[24] mateside, **14**;[25] and ilekudinoside D, **15**,[26] (Figure 1).

Compound **1** was obtained as a white powder. The molecular formula of $C_{41}H_{66}O_{14}$ was determined on the basis of its HR-ESI-MS $[M + Na]^+$ ion peak at m/z 805.4303 (calcd 805.4350). The ^{1}H NMR spectrum showed singlet resonances of five methyl groups at δ 1.72 (3H, s, Me-27), 1.45 (3H, s, Me-29), 1.30 (3H, s, Me-26), 1.08 (3H, s, Me-25), 1.02 (3H, s, Me-24) and one doublet methyl signal at δ 1.05 (3H, d, J = 7.5 Hz, Me-30), an olefinic proton signal at δ 5.58 (1H, m, H-12), and signals of a hydroxymethylene group at δ 4.34 (1H, m, H-23) and 3.78 (1H, d, J = 11.5 Hz, H-23), as well as a signal at δ 4.34 (1H, m, H-3). The ^{13}C NMR data, the downfield shift of C-3, and the upfield shift of C-28 suggested the presence of a bisdesmosidic saponin aglycone. The ^{1}H NMR data also indicated the presence of two sugar residues, which was inferred by the two anomeric proton signals at δ 5.06 (1H, d, J = 7.0 Hz, H-1 of arabinose) and δ 6.43 (1H, d, J = 8.0 Hz, H-1 of glucose), which correlated with δ_C 106.9 (C-1 of arabinose), 95.9 (C-1 of glucose), respectively, in the HSQC spectrum (Table 2). The types of sugar residues obtained from the acid hydrolysis of **1** were identified as L-arabinose and D-glucose by the GC analysis. The glycosidic side chain was located at C-28 of the aglycone, revealed by the HMBC correlation between δ_H 6.43 (H-1 of glucose) and δ_C 177.2 (C-28 of aglycone) (Figure 2). The β configuration of the glucopyranosyl group was confirmed on the basis of the large $^3J_{H\text{-}1,H\text{-}2}$ coupling constant. The location of another glycosidic unit, α-L-arabinopyranosyl, was determined to be attached at C-3, evidenced by the HMBC correlation between δ_H 4.34 (H-3 of aglycone) and δ_C 106.9 (C-1 of arabinose), as well as correlation between δ_H 5.06 (H-1 of arabinose) and δ_C 82.0 (C-3 of aglycone). The configuration of the arabinopyranosyl group was assigned as α on the basis of

dx.doi.org/10.1021/jf4046667 | J. Agric. Food Chem. 2014, 62, 488−496

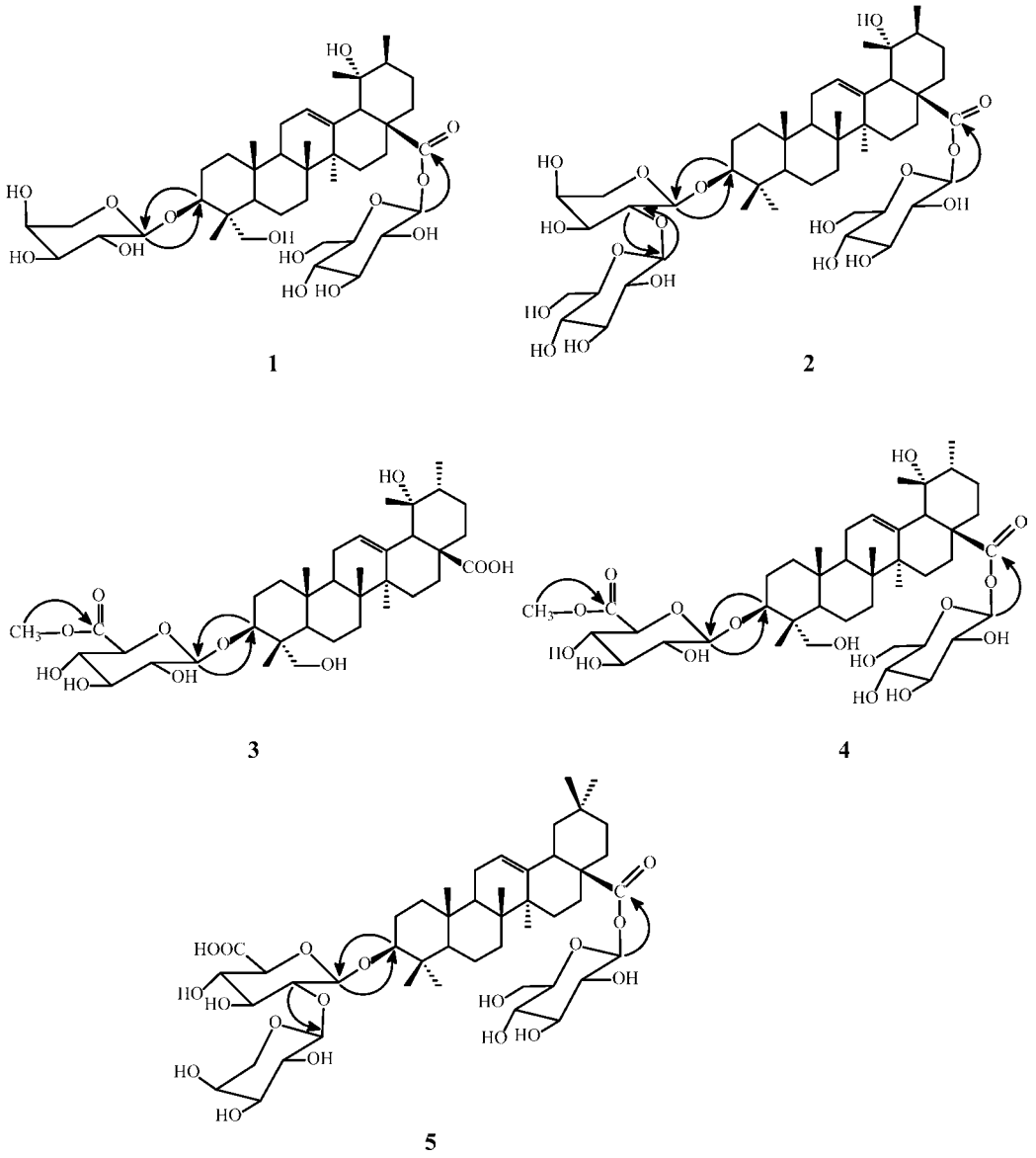

Figure 2. Key HMBC correlations for **1**−**5**.

the NOESY correlations between δ 5.06 (H-1 of arabinose) and δ 4.14 (H-3 of arabinose), 4.32 (H-4 of arabinose) (Figure 3). The ^{1}H and ^{13}C NMR spectral data of **1** were similar to those of 3β-*O*-α-L-arabinopyranosyl-19α,23-dihydroxyurs-12-en-28-oic acid 28-*O*-β-D-glucopyranosyl ester,[26] but showed differences for C-18 and C-22. Significant upfield shifts of the C-18 signal (−7.2 ppm) at δ 47.3 and C-22 signal (−5.9 ppm) at δ 32.0 were observed for compound **1**, which could be explained as the results of the γ-effect of the 30-β (axial) methyl group instead of a 30-*a* (equatorial) methyl group in the 3β,23-dihydroxyurs-12-en-28-oic acid moiety.[27] The β orientation of Me-30 was also confirmed by the NOESY correlations of Me-30 (δ_H 1.05) to both Me-29 (δ_H 1.45) and H-18 (δ_H 3.26) (Figure 3). The orientation of H-20 was determined to be α on the basis of the NOE information. Thus, compound **1** was identified as 3β-*O*-α-L-arabinopyranosyl-19α,23-dihydroxy-20α-urs-12-en-28-oic acid 28-*O*-β-D-glucopyranosyl ester.

Compound **2** was obtained as a white powder. The molecular formula was determined as $C_{47}H_{76}O_{18}$ on the basis of its HR-ESI-MS $[M + Na]^+$ ion peak at *m*/*z* 951.4887 (calcd 951.4929). The ^{1}H NMR spectrum showed singlet resonances of six tertiary methyl groups at δ 1.78 (3H, s, Me-27), 1.47 (3H, s, Me-29), 1.28 (3H, s, Me-26), 1.28 (3H, s, Me-23), 1.13 (3H, s, Me-24), and 0.99 (3H, s, Me-25), a doublet methyl signal at δ 1.07 (3H, d, J = 10.0 Hz, Me-30), and an olefinic proton signal at δ 5.59 (1H, m, H-12), as well as a signal at δ 3.27 (1H, dd, J = 15.0, 5.0 Hz, H-3). The ^{13}C NMR data and the downfield shift of C-3 and the upfield shift of C-28 indicated the presence of a bisdesmosidic saponin aglycone. The ^{1}H NMR spectroscopic data also indicated the presence of three sugar residues, which was inferred by three anomeric proton signals at δ 5.03 (1H, d, J = 7.0 Hz, H-1 of arabinose), δ 5.26 (1H, d, J = 9.5 Hz, H-1′ of glucose 1′), and δ 6.43 (1H, d, J = 10.0 Hz, H-1 of glucose 1), correlated with δ_C 104.9 (C-1 of arabinose), 106.1 (C-1′ of glucose 1′), and 95.9 (C-1 of glucose 1), respectively, in the HSQC spectrum (Table 2). The sugar residues were identified as L-arabinose and D-glucose by the GC analysis. The ^{1}H and ^{13}C NMR data of **2** were similar to those of brevicuspisaponin 3[28] except for the presence of additional signals attributed to one glucose moiety. The location of this

dx.doi.org/10.1021/jf4046667 | J. Agric. Food Chem. 2014, 62, 488−496

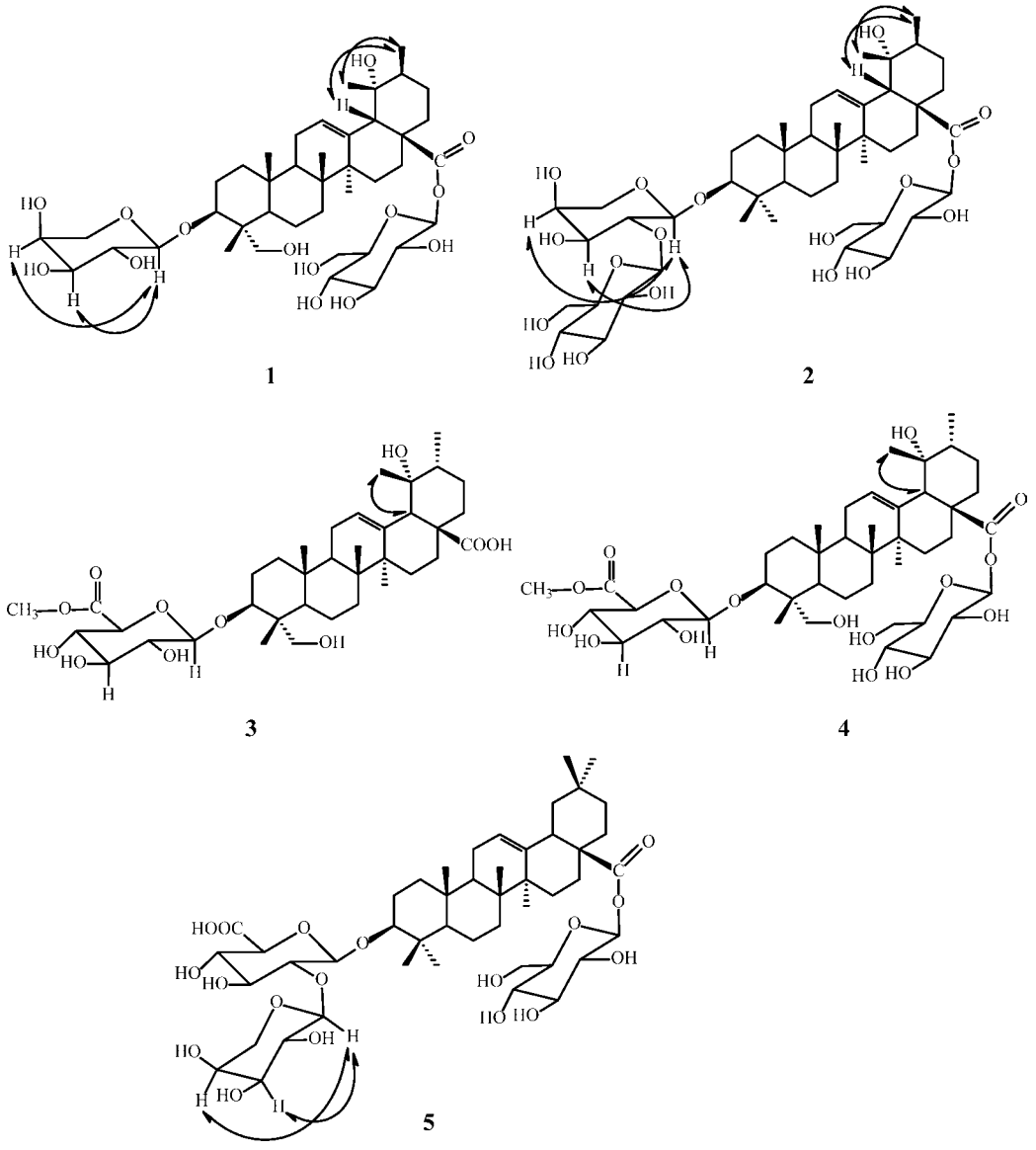

Figure 3. Key NOESY correlations for **1**−**5**.

glucose residue was determined at C-2 of the arabinose moiety, inferred by the downfield shift of C-2 of arabinose and HMBC correlation between δ_H 5.26 (H-1′ of glucose 1′) and δ_C 81.1 (C-2 of arabinose). Thus, the structure of compound **2** was established as 3*β*-*O*-*β*-D-glucopyranosyl-(1→2)-*α*-L-arabinopyranosyl-19-hydroxy-20*α*-urs-12-en-28-oic acid 28-*O*-*β*-D-glucopyranosyl ester.

Compound **3** was obtained as a white powder. The negative HR-ESI-MS of **3** showed a quasi-molecular ion peak at *m*/*z* 677.3869 ($[M - H]^-$, calcd 677.3901), indicating the molecular formula of $C_{37}H_{58}O_{11}$. The ^{1}H NMR spectrum showing singlet resonances of five tertiary methyl groups at δ 1.77 (3H, s, Me-27), 1.50 (3H, s, Me-29), 1.17 (3H, s, Me-26), 1.01 (3H, s, Me-24), 0.98 (3H, s, Me-25), a doublet methyl signal at δ 1.19 (3H, d, J = 6.5 Hz) corresponding to Me-30, an olefinic proton at δ 5.66 (1H, m, H-12), and hydroxymethylene group signals at δ 4.39, 3.78 (2H, m, H-23), as well as a proton signal at δ 4.36 (1H, m, H-3), suggested it contained an aglycone as 19*α*,23-dihydroxyurs-12-en-28-oic acid.[29] An anomeric proton was observed at δ_H 5.31 (1H, d, J = 8.0 Hz, H-1 of glucuronic acid), which showed HSQC correlation to the anomeric carbon at δ_C 106.6 (C-1 of glucuronic acid), indicating the presence of a sugar unit in the structure of compound **3**. The sugar residue obtained from the acid hydrolysis of **3** was identified as D-glucuronic acid by the GC analysis. The ^{1}H and ^{13}C NMR data of **3** were very similar to those of ilexasoside A,[30] except that it had an additional hydroxyl group. The downfield shift of C-23 signal (+36.3 ppm) at δ_C 64.4 suggested that the additional hydroxyl group was located at C-23, which was confirmed by the HMBC correlations of C-23 (δ_C 64.4) to Me-24 (δ_H 1.01) and H-3 (δ_H 4.36). Thus, compound **3** was identified as 19*α*,23-dihydroxyurs-12-en-28-oic acid 3*β*-*O*-*β*-D-glucuronopyranoside-6-*O*-methyl ester.

Compound **4** had a molecular formula of $C_{43}H_{68}O_{16}$, which showed a quasi-molecular ion peak ($[M + Na]^+$) at *m*/*z* 863.4405 (calcd 863.4405). The signals of two anomeric protons at δ_H 5.31 (1H, d, J = 10.0 Hz, H-1 of glucuronic acid) and 6.39 (1H, d, J = 10.0 Hz, H-1 of glucose), which correlated to the two anomeric carbon signals at δ_C 106.5 (C-1 of glucuronic acid) and δ_C 96.0 (C-1 of glucose), respectively, in the HSQC spectrum, suggested the presence of two sugar residues. The sugar residues were identified as D-glucuronic acid

dx.doi.org/10.1021/jf4046667 | J. Agric. Food Chem. 2014, 62, 488−496

Table 3. Protective Effects of Triterpenoidal Saponins from *Ilex cornuta* on H_2O_2-Induced H9c2 Cell Injury

	concentration[a]					
compd	0 μM	12.5 μM	25 μM	50 μM	100 μM	200 μM
1	69.78 ± 2.82	65.33 ± 1.65	73.38 ± 4.27	77.78 ± 0.43*	79.22 ± 5.55**	83.84 ± 4.44**
2	63.25 ± 1.25	54.41 ± 1.80	62.85 ± 2.64	65.22 ± 2.10	62.02 ± 2.89	62.61 ± 1.06
3	65.10 ± 2.45	68.91 ± 5.99	67.95 ± 2.39	65.53 ± 3.55	65.70 ± 3.72	63.29 ± 4.08
4	63.25 ± 1.25	65.86 ± 1.17	74.42 ± 1.39**	80.79 ± 2.61**	86.54 ± 3.76**	91.29 ± 4.60**
5	63.25 ± 1.25	60.38 ± 2.52	61.04 ± 1.53	68.28 ± 3.44	62.57 ± 0.28	65.46 ± 3.62
6	69.78 ± 2.82	74.39 ± 3.06	78.01 ± 4.58	82.00 ± 5.59	85.44 ± 1.08*	87.77 ± 3.02*
7	63.82 ± 3.94	68.33 ± 6.45	68.84 ± 7.13	64.70 ± 1.50	62.93 ± 4.39	69.19 ± 5.40
8	70.28 ± 2.78	67.74 ± 4.92	62.27 ± 2.43	63.87 ± 3.44	64.21 ± 4.95	64.27 ± 2.75
9	69.70 ± 5.48	63.06 ± 5.86	67.55 ± 6.95	60.61 ± 0.82	67.87 ± 1.21	66.99 ± 1.54
10	68.74 ± 3.86	63.53 ± 2.35	69.75 ± 2.98	69.80 ± 1.63	65.95 ± 4.52	62.54 ± 3.10
11	69.22 ± 4.18	63.54 ± 3.63	65.74 ± 5.28	63.86 ± 5.12	71.37 ± 0.49	72.32 ± 2.91
12	59.85 ± 1.18	62.76 ± 4.83	69.02 ± 3.07	68.27 ± 4.52	60.47 ± 2.98	66.21 ± 5.90
13	69.70 ± 5.48	70.06 ± 3.26	75.40 ± 2.42	83.23 ± 3.95	88.42 ± 4.71	89.34 ± 5.86*
14	69.78 ± 2.82	66.47 ± 5.50	69.88 ± 3.22	65.65 ± 4.72	65.79 ± 5.69	67.61 ± 6.81
15	70.28 ± 2.78	68.99 ± 4.15	67.81 ± 4.91	66.94 ± 1.17	68.12 ± 3.42	69.95 ± 1.01
vitamin E[b]	64.36 ± 2.18	65.39 ± 2.33	67.25 ± 1.94	68.17 ± 2.06	75.84 ± 1.88*	81.49 ± 1.96**

[a]*, $p < 0.05$, and **, $p < 0.01$, vs 0 μM group. [b]Positive control.

Table 4. Maximal Scavenging Rate of Compounds 1−15 against DPPH in Vitro

compd[a]	scavenging rate (200 μM)
1	21.06 ± 2.98
2	11.30 ± 0.34
3	8.49 ± 2.53
4	17.62 ± 1.19
5	15.34 ± 3.29
6	28.85 ± 2.13
7	18.32 ± 2.42
8	16.94 ± 0.53
9	20.53 ± 0.38
10	8.13 ± 3.64
11	9.72 ± 1.23
12	10.03 ± 5.11
13	21.43 ± 2.73
14	23.58 ± 3.18
15	11.86 ± 3.32
vitamin E	92.74 ± 0.70

[a]For compounds **1**−**15**, the test concentrations ranged from 5 to 200 μM; for vitamin E, the test concentration was 200 μM.

and D-glucose by the hydrolysis and GC analysis. The ^1H and ^{13}C NMR data of **4** were similar to those of **3** except for the presence of the additional signals corresponding to one glucose group. This glucose unit was attached to C-28 of the aglycone, evidenced by the downfield shift of C-28 and the HMBC correlation between δ_H 6.39 (H-1 of glucose) and δ_C 177.1 (C-28 of aglycone) (Figure 2). Both the glucopyranosyl and glucuronopyranosyl units existed in the form of β anomeric configuration, based on the observation of the large $^3J_{H\text{-}1,\ H\text{-}2}$ coupling constants. Thus, compound **4** was identified as 19α,23-dihydroxyurs-12-en-28-oic acid 3β-*O*-[β-D-glucuronopyranoside-6-*O*-methyl ester]-28-*O*-β-D-glucopyranosyl ester.

Compound **5** had a molecular formula of $C_{47}H_{74}O_{18}$ on the basis of its HR-ESI-MS $[M + Na]^+$ ion peak at m/z 949.4729 (calcd 949.4772). The ^1H and ^{13}C NMR data of **5** were similar to those of silphioside G[31] except for the presence of additional signals corresponding to one arabinose group. Compound **5** contained three sugar residues, which were identified as L-arabinose, D-glucuronic acid, and D-glucose by GC analysis. The arabinose group was located at the C-2 of the glucuronic acid unit, evidenced by the HMBC correlation between δ_H 5.28 (H-1 of arabinose) and δ_C 83.7 (C-2 of glucuronic acid). The β anomeric configuration of the glucopyranosyl unit was established on the basis of the observation of the large $^3J_{H\text{-}1,\ H\text{-}2}$ coupling constant. The anomeric configuration of the arabinopyranosyl unit was assigned to be α, deduced from the NOESY correlations among the signals at δ_H 5.28 (H-1 of arabinose), δ_H 4.28 (H-3 of arabinose), and δ_H 4.39 (H-4 of arabinose) (Figure 3). Therefore, compound **5** was identified as 3β-*O*-[α-L-arabinopyranosyl-(1→2)-β-D-glucuronic acid]-oleanolic acid 28-*O*-β-D-glucopyranosyl ester.

Protective Effects of the Isolates against H_2O_2-Induced Myocardial Cell Injury. Cardiovascular diseases may be caused by intracellular oxidative damage to biomolecules via reactive oxygen species (ROS).[32] A number of studies showed that antioxidants reduced oxidative stress-mediated cellular injury.[33] Among ROS, H_2O_2 readily crosses cellular membranes and gives rise to the highly reactive hydroxyl radical, which is the most reactive and induces severe damage to adjacent biomolecules.[34] The H_2O_2-mediated oxidative injury resulted in a significant decrease of mitochondrial respiration, glutathione, and protein thiol content and in an increased level of GSSG.[35] H_2O_2 has been used frequently in models of oxidative stress in H9c2 cardiomyocytes to investigate protective function.[36,37] The *I. cornuta* extract was reported to have the protective effect on myocardial ischemia.[38] In this study, the protective effects of compounds **1**−**15** against H_2O_2-induced myocardial cell injury were tested. As shown in Table 3, compounds **1**, **4**, **6**, and **13** (12.5−200 μM) significantly increased the viability of H9c2 induced by H_2O_2 in a dose-dependent manner, ranging from the concentrations at 12.5 to 200 μM. Compound **4** was shown to be the most efficient among the isolates. It increased the cell viability at a low concentration of 25 μM and was more efficient than vitamin E, which was used as the positive control. Compounds **1**, **6**, and **13** showed moderate protective effects. They significantly improved cell viability at a concentration of 200 μM. Previous studies have indicated that vitamin E inhibits peroxidative damage associated with ischemia and reperfu-

dx.doi.org/10.1021/jf4046667 | J. Agric. Food Chem. 2014, 62, 488−496

sion.[39,40] The triterpenoid saponins contained in *I. cornuta* might play a similar preventive role. Further studies are warranted to explore their potential.

DPPH Radical Scavenging Capacity Assay. The antioxidant activity bioassay of compounds **1**−**15** was tested by DPPH radical scavenging capacity assay. The maximal scavenging rates of compounds **1**−**15** are shown in Table 4; the scavenging rates of compounds **1**−**15** were <30% at a concentration of 200 μM. In other words, compounds **1**−**15** had no significant DPPH radical scavenging capacity over the concentration range from 5 to 200 μM. Combined with H_2O_2-induced myocardial cell injury experiment, these results indicated that the protective effects of the compounds against myocardial cell injury were not directly associated with their radical scavenging capacity. The mechanisms of the protective effects of the compounds on myocardial cell injury need to be further investigated.

■ ASSOCIATED CONTENT

Ⓢ Supporting Information

HR-ESI-MS and NMR spectra of compounds **1**−**5**. This material is available free of charge via the Internet at http://pubs.acs.org.

■ AUTHOR INFORMATION

Corresponding Author

*(Q.X.) Phone: 86-512-69561421. Fax: 86-512-65882089. E-mail: xuqiongming@suda.edu.cn.

Funding

This work was funded by the Priority Academic Program Development of Jiangsu Higher Education Institutions (PAPD).

Notes

The authors declare no competing financial interest.

■ ACKNOWLEDGMENTS

We sincerely thank Professor Hong-liang Jiang at Tongji School of Pharmacy, Huazhong University of Science and Technology, for determination of the MS spectral data and Dr. Jon Parcher at the University of Mississippi for helpful discussions.

■ REFERENCES

(1) Chau, C. F.; Wu, S. H. The development of regulations of Chinese herbal medicines for both medicinal and food uses. *Trends Food Sci. Technol.* **2006**, *17*, 313−323.

(2) Ahai, R. K. Iconographia Cormophytorum Sinicoru. *Beijing Sci.* **1985**, 641.

(3) Jiangsu Medical College. *Dictionary of Chinese Medicine*; Shanghai People's Press: Shanghai, China, 1975; pp 441−443.

(4) Qin, W. J.; Zhao, J. J.; Fukuyama, Y. Chemical constituent of the leaves of *Ilex corunta*. *Chin. Tradit. Herb. Drugs* **1988**, *19*, 434−439.

(5) Puangpraphant, S.; De Mejia, E. G. Saponins in yerba mate tea (*Ilex paraguariensis* A. St.-Hil) and quercetin synergistically inhibit iNOS and COX-2 in lipopolysaccharide-induced macrophages through NFκB pathways. *J. Agric. Food Chem.* **2009**, *57*, 8873−8883.

(6) Jiangsu New Medical College. *Dictionary of Chinese Herbal Medicines*; Shanghai Science and Technology Press: Shanghai, China, 1986; pp 441−443.

(7) Ouyang, M. A.; Yang, C. R.; Chen, Z. L.; Wang, H. Q. Triterpenes and triterpenoid glycosides from the leaves of *Ilex* kudincha. *Phytochemistry* **1996**, *41*, 871−877.

(8) Chen, X. Q.; Zan, K.; Yang, J.; Lai, M. X.; Wang, Q. A novel flavanone from *Ilex hainanensis* Merr. *Nat. Prod. Res.* **2009**, *23*, 442−447.

(9) Xie, J. B. Studies on phenolic acids from *Ilex purpurea* Hassk. *J. China Pharm. Univ.* **2002**, *33*, 76−77.

(10) Wu, T.; Cheng, Z.; Liu, H. Liposoluble components from leaves of *Ilex cornuta*. *Chin. Pharm. J.* **2005**, *40*, 1460−1464.

(11) Cai, H.; Griendling, K. K.; Harrison, D. G. The vascular NAD(P)H oxidases as therapeutic targets in cardiovascular diseases. *Trends Pharmacol. Sci.* **2003**, *24*, 471−478.

(12) Gugliucci, A. Antioxidant effects of *Ilex paraguariensis*: induction of decreased oxidability of human LDL in vivo. *Biochem. Biophys. Res. Commun.* **1996**, *224*, 338−344.

(13) Gao, L.; Zhang, L.; Liu, J. Y.; Cai, P. L.; Yang, S. L. New triterpenoid saponins from *Patrinia scabiosaefolia*. *Carbohydr. Res.* **2011**, *346*, 2881−2885.

(14) Konorev, E. A.; Kennedy, M. C.; Kalyanaraman, B. Cell-permeable superoxide dismutase and glutathione peroxidase mimetics afford superior protection against doxorubicin-induced cardiotoxicity: the role of reactive oxygen and nitrogen intermediates. *Arch. Biochem. Biophys.* **1999**, *368*, 421−428.

(15) Xu, S. M.; Wang, P. Y.; Ma, H. Y. Preparation of hypoxic surroundings with sodium dihionite for cell culture. *Acta Acad. Med. Mil. Tert.* **2005**, *27*, 359−360.

(16) Shi, M. F.; He, W. J.; Liu, Y. L.; Li, X. R.; Yang, S. L.; Xu, Q. M. Protective effect of total phenylethanoid glycosides from *Monochasma savatieri* Franch on myocardial ischemia injury. *Phytomedicine* **2013**, *20*, 1251−1255.

(17) Hatano, T.; Kagawa, H.; Yasuhara, T.; Okuda, T. Two new flavonoids and other constituents in licorice root: their relative astringency and radical scavenging effects. *Chem. Pharm. Bull.* **1988**, *36*, 2090−2097.

(18) Liao, L.; Zhou, X.; Liu, Y. L.; Xu, Q. M.; Li, X. R.; Yang, S. L. Four new triterpenoid saponins from *Ilex cornuta* and their cytotoxic activities. *Phytochem. Lett.* **2013**, *6*, 429−434.

(19) Mimaki, Y.; Fukushima, M.; Yokosuka, A.; Sashida, Y.; Furuya, S.; Sakagami, H. Triterpene glycosides from the roots of *Sanguisorba officinalis*. *Phytochemistry* **2001**, *57*, 773−779.

(20) Yu, J.; Liu, S.; Xuan, L. Two new lupene-type triterpenoids from the roots of *Liquidambar formosana*. *Nat. Prod. Res.* **2012**, *26*, 630−636.

(21) Li, W.; Ding, Y.; Sun, Y. N.; Yan, X. T.; Yang, S. Y.; Choi, C. W.; Kim, E. J.; Kang, H. K.; Kim, Y. H. Oleanane-type triterpenoid saponins from the roots of *Pulsatilla koreana* and their apoptosis-inducing effects on HL-60 human promyelocytic leukemia cells. *Arch. Pharmacal. Res.* **2013**, *36*, 768−774.

(22) Wang, L.; Zhang, C.; Layba, M.; Zhang, M. Triterpenes and sterols from *Nauclea latifolia*. *Chin. J. Chin. Mater. Med.* **2011**, *36*, 2511−2514.

(23) Yang, H.; Jeong, E. J.; Kim, J.; Sung, S. H.; Kim, Y. C. Antiproliferative triterpenes from the leaves and twigs of *Juglans sinensis* on HSC-T6 Cells. *J. Nat. Prod.* **2011**, *74*, 751−756.

(24) Xie, G. B.; Zheng, J.; Tu, P. F.; Liu, G. Q. Triterpene saponins from the leaves of *Ilex pernyi*. *Helv. Chim. Acta* **2008**, *91*, 1630−1639.

(25) Taketa, A. T.; Breitmaier, E.; Schenkel, E. P. Triterpenes and triterpenoid glycosides from the fruits of *Ilex paraguariensis*. *J. Braz. Chem. Soc.* **2004**, *15*, 205−211.

(26) Wu, Z. J.; Ouyang, M. A.; Wang, C. Z.; Zhang, Z. K.; Shen, J. G. Anti-tobacco mosaic virus (TMV) triterpenoid saponins from the leaves of *Ilex oblonga*. *J. Agric. Food Chem.* **2007**, *55*, 1712−1717.

(27) Hidaka, K.; Ito, M.; Matsuda, Y.; Kohda, H.; Yamasaki, K.; Yamahara, J.; Chisaka, T.; Kawakami, Y.; Sato, T.; Kagei, K. New triterpene saponins from *Ilex pubescens*. *Chem. Pharm. Bull.* **1987**, *35*, 524−529.

(28) Taketa, A. T. C.; Gondorf, M.; Breitmaier, E.; Schenke, E. P. New triterpene and triterpenoid glycosides from *Ilex brevicuspis*. *Rev. Bras. Cien. Farm.* **2002**, *38*, 155−161.

(29) Shu, J. C.; Liu, J. Q.; Chou, G. X.; Wang, Z. T. Two new triterpenoids from *Psidium guajava*. *Chin. Chem. Lett.* **2012**, *23*, 827−830.

(30) Wang, L.; Cai, Y.; Zhang, X. Q.; Fan, C. L.; Zhang, Q. W.; Lai, X. P.; Ye, W. C. New triterpenoid glycosides from the roots of *Ilex asprella*. *Carbohydr. Res.* **2012**, *349*, 39−43.
(31) Yoshizaki, K.; Murakami, M.; Fujino, H.; Yoshida, N.; Yahara, S. New triterpenoid saponins from fruit specimens of *Panax japonicus* collected in Toyama Prefecture and Hokkaido (2). *Chem. Pharm. Bull.* **2012**, *60*, 728−735.
(32) Fearon, I. M.; Faux, S. P. Oxidative stress and cardiovascular disease: novel tools give (free) radical insight. *J. Mol. Cell. Cardiol.* **2009**, *47*, 372−381.
(33) Yousuf, S.; Atif, F.; Ahmad, M.; Hoda, N.; Ishrat, T.; Khan, B.; Islam, F. Resveratrol exerts its neuroprotective effect by modulating mitochondrial dysfunctions and associated cell death during cerebral ischemia. *Brain Res.* **2009**, *1250*, 242−253.
(34) Valko, M.; Leibfritz, D.; Moncol, J.; Cronin, M. T.; Mazur, M.; Telser, J. Free radicals and antioxidants in normal physiological functions and human disease. *Int. J. Biochem. Cell Biol.* **2007**, *39*, 44−84.
(35) Sgobbo, P.; Pacelli, C.; Grattagliano, I.; Villani, G.; Cocco, T. Carvedilol inhibits mitochondrial complex I and induces resistance to H_2O_2-mediated oxidative insult in H9C2 myocardial cells. *Biochim. Biophys. Acta* **2007**, *1767*, 222−232.
(36) Hescheler, J.; Meyer, R.; Plant, S.; Krautwurst, D.; Rosenthal, W.; Schultz, G. Morphological, biochemical, and electrophysiological characterization of a clonal cell (H9c2) line from rat heart. *Circ. Res.* **1991**, *69*, 1476−1486.
(37) Yasuoka, C.; Ihara, Y.; Ikeda, S.; Miyahara, Y.; Kondo, T.; Kohno, S. Antiapoptotic activity of Akt is downregulated by Ca^{2+} in myocardiac H9c2 cells: evidence of Ca^{2+}-dependent regulation of protein phosphatase 2Ac. *J. Biol. Chem.* **2004**, *279*, 51182−51192.
(38) Liu, L. X.; Sun, Y.; Laura, T.; Liang, X. F.; Ye, H.; Zeng, X. X. Determination of polyphenolic content and antioxidant activity of kudingcha made from *Ilex kudingcha* C.J. Tseng. *Food Chem.* **2009**, *112*, 35−41.
(39) Yamamoto, M.; Shima, T.; Uozumi, T.; Sogabe, T.; Yamada, K.; Kawasaki, T. A possible role of lipid peroxidation in cellular damages caused by cerebral ischemia and the protective effect of alpha tocopherol administration. *Stroke* **1983**, *14*, 977−982.
(40) Fujimoto, S.; Mizoi, K.; Yoshimoto, T.; Suzuki, I. The protective effect of vitamin E on cerebral ischemia. *Surg. Neurol.* **1984**, *22*, 449−454.

JOURNAL OF AGRICULTURAL AND FOOD CHEMISTRY

Article

pubs.acs.org/JAFC

Assessment of Multi-mycotoxin Adsorption Efficacy of Grape Pomace

Giuseppina Avantaggiato,* Donato Greco, Anna Damascelli, Michele Solfrizzo, and Angelo Visconti

Institute of Sciences of Food Production (ISPA), National Research Council (CNR), Via Amendola 122/O, 70126 Bari, Italy

ABSTRACT: Grape pomace (pulp and skins) was investigated as a new biosorbent for removing mycotoxins from liquid media. In vitro adsorption experiments showed that the pomace obtained from Primitivo grapes is able to sequester rapidly and simultaneously different mycotoxins. Aflatoxin B_1 (AFB_1) was the most adsorbed mycotoxin followed by zearalenone (ZEA), ochratoxin A (OTA), and fumonisin B_1 (FB_1), whereas the adsorption of deoxynivalenol (DON) was negligible. AFB_1 and ZEA adsorptions were not affected by changing pH values in the pH 3−8 range, whereas OTA and FB_1 adsorptions were significantly affected by pH. Equilibrium adsorption isotherms obtained at different temperatures (5−70 °C) and pH values (3 and 7) were modeled and evaluated using the Freundlich, Langmuir, Sips, and Hill models. The goodness of the fits and the parameters involved in the adsorption mechanism were calculated by the nonlinear regression analysis method. The best-fitting models to describe AFB_1, ZEA, and OTA adsorption by grape pomace were the Sips, Langmuir, and Freundlich models, respectively. The Langmuir and Sips models were the best models for FB_1 adsorption at pH 7 and 3, respectively. The theoretical maximum adsorption capacities (mmol/kg dried pomace) calculated at pH 7 and 3 decreased in the following order: AFB_1 (15.0 and 15.1) > ZEA (8.6 and 8.3) > OTA (6.3−6.9) > FB_1 (2.2 and 0.4). Single- and multi-mycotoxin adsorption isotherms showed that toxin adsorption is not affected by the simultaneous presence of different mycotoxins in the liquid medium. The profiles of adsorption isotherms obtained at different temperatures and pH and the thermodynamic parameters ($\Delta G°$, $\Delta H°$, $\Delta S°$) suggest that mycotoxin adsorption is an exothermic and spontaneous process, which involves physisorption weak associations. Hydrophobic interactions may be associated with AFB_1 and ZEA adsorption, whereas polar noncovalent interactions may be associated with OTA and FB_1 adsorption. In conclusion, this study suggests that biosorption of mycotoxins onto grape pomace may be a reasonably low-cost decontamination method.

KEYWORDS: *biosorption, mycotoxins, grape pomace, adsorption isotherm models*

INTRODUCTION

Winemaking generates waste in the form of grape pomace that remains after grape has been pressed. On the basis of some estimates, approximately 20% of the grape total weight is waste, which translates to >8 million tons worldwide of grape pomace.[1] Removal of grape pomace is costly, and if it is not treated effectively, it poses a serious environmental problem.[2] Several processes have been suggested for utilization of pomace, including extraction of anthocyanins, citric acid, ethanol, and grape seed oil.[3] At present, grape pomace is mainly used for soil conditioning or as low-cost raw material for animal feed, especially for herbivores and in the dry season when pastures are scarce.[4,5] Grape pomace represents a potentially valuable source of phenolic antioxidants, which can have technological applications as feed additives and possible nutritional and health benefits.[6] The content of tannins in grape pomace reduces ruminal crude protein degradability, which may prevent bloat when cows are fed high-concentrate diets.[7] Dietary polyphenol-rich grape products were found effective in broiler chicks and piglets in improving the physiology and biochemistry of the gut, thus leading to better nutrient absorption and increased disease resistance.[8,9] The supplementation of human food with grape pomace and its use during some food-processing processes have been also attempted. In the form of dried, milled flour, grape pomace has been incorporated into bakery products to make cookies, cakes, or specialty breads, which showed higher contents of dietary fiber and phenolic compounds and enhanced antioxidant properties.[10,11]

Recently, an innovative winemaking procedure involving the use of grape pomace has been suggested as a corrective measure to reduce ochratoxin A (OTA) levels in must and wine.[12] The procedure proposed the repassage of contaminated musts or wines over grape pomaces having no or little OTA contamination, and it removed up to 65% of OTA within 24 h.[12] These findings supported the hypothesis that grape pomace has affinity for OTA adsorption.[12] The work did not study the mechanism for OTA adsorption by grape pomace or explore its effectiveness in adsorbing mycotoxins other than OTA, such as aflatoxin B_1 (AFB_1), zearalenone (ZEA), fumonisin B_1 (FB_1), and deoxynivalenol (DON). These fungal metabolites are the most commonly occurring mycotoxins, which can be found worldwide in food and feed. They can cause a variety of diseases (mycotoxicoses) in a wide range of susceptible animal species including humans.[13,14] They often co-occur, depending on the environmental and substrate conditions, and can lead to toxicological interactions (synergistic effects).[15] So far, only activated carbon has been found effective in adsorbing in vitro these mycotoxins.[16−19] However,

Received: September 2, 2013
Revised: December 20, 2013
Accepted: December 22, 2013
Published: December 22, 2013

ACS Publications © 2013 American Chemical Society

it is probably more suited to be used as an antidote for severe intoxication. The great variability in the results of long-term exposure experiments and its potential for also sequestering important nutrients diminishes its overall practical effectiveness for routine dietary inclusion.[18] Except for activated carbon, most substances (clays) used as mycotoxin binders to decontaminate mycotoxin-contaminated feeds fail in sequestering structurally different mycotoxins.[16,18] They appear to bind to only a limited group of mycotoxins (mainly aflatoxins) while showing very little or no binding to others. Therefore, feed additives acting as multi-mycotoxin binders are sought.

Due to the potential ability of grape pomace in binding OTA and its well-known health benefits, the objective of the present work was to explore the feasibility of using grape pomace as a low-cost biosorbent for mycotoxin decontamination. For the first time, this study examined the ability of grape pomace to adsorb simultaneously different mycotoxins from liquid media at physiological pH. The pomace obtained from a red grape variety (cv. Primitivo) was used for the adsorption study.

MATERIALS AND METHODS

Reagents and Samples. Mycotoxin standards (purity > 99%) were supplied by Sigma-Aldrich (Milan, Italy). All chemicals used were of analytical grade unless otherwise stated. All solvents (HPLC grade) were purchased from J. T. Baker (Deventer, The Netherlands). Water was of Milli-Q quality (Millipore, Bedford, MA, USA). Mycotoxin adsorption was studied at different pH values using different media (1 mmol/L), such as citrate buffers at pH 3, 4, and 5 and phosphate buffers at pH 6, 7, 8, and 9. Mycotoxin stock solutions of AFB_1, OTA, ZEA, and DON (1 mg/mL each) were prepared by dissolving solid commercial toxins in acetonitrile (HPLC grade). FB_1 stock solution (1 mg/mL) was prepared in acetonitrile/water (50:50, v/v). Stock solutions were stored in the dark at 4 °C. A multi-mycotoxin standard solution containing 200 μg/mL of each toxin (AFB_1, ZEA, FB_1, OTA, and DON) was prepared by mixing equal volumes of mycotoxin stock solutions. This solution or the mycotoxin stock solutions were properly diluted with buffers at different pH values to prepare the mycotoxin working solutions for adsorption experiments and calibrants.

Fermented grape pomace was obtained by manually processing grapes of a red grape variety (Primitivo) grown and harvested in Conversano (Apulia, Italy). Seeds and stems were manually separated and discarded, and the peel and pulp were oven-dried at 50 °C until constant weight. The dried material was ground into fine powder by a microfine grinder drive, MF10 Basic model (IKA-Werke GmbH & Co., KG/Germany), provided with a 0.5 mm interchangeable sieve (MF 0.5 model) for particle size filtering. OTA analysis of grape pomace was performed according to the method of Solfrizzo et al.[20] and showed the absence of toxin.

LC Analysis of Mycotoxins. DON, AFB_1, ZEA, and OTA were analyzed according to a UPLC method, which allowed the simultaneous determination of the toxins. The UPLC apparatus consisted of a Waters Acquity UPLC system (Milford, MA, USA). Data acquisition and instrument control were performed by Empower 2 software (Waters). The column used was a 100 mm × 2.1 mm i.d., 1.7 μm, Acquity UPLC BEH RP-18, with an Acquity UPLC column in-line filter (0.2 μm). Chromatographic separation of DON, AFB_1, ZEA, and OTA was achieved through a 13.5 min gradient delivery of a mixture of A (water/acetonitrile 85:15 v/v) and B (methanol/acetonitrile 50:50 v/v, containing 0.5% acetic acid) at a flow rate of 0.4 mL/min. The temperatures of the column and sample compartment were maintained at 40 and 15 °C, respectively. The injected volume was 5 μL in a partial loop with needle overfill mode. The UV absorption spectra of DON and AFB_1 were recorded in the range of 190−400 nm. UV absorbance data were collected with a bandwidth of 1.2 nm and without digital filtering, at wavelengths of 220 nm for DON and 350 nm for AFB_1. A LC UV chromatogram was acquired at 220 nm absorbance wavelength for the first 3 min and then at 350 nm. Fluorescence detection of AFB_1, ZEA, and OTA was carried out using a wavelength program with, respectively, excitation and emission wavelengths of 333 and 460 nm until 7.5 min for AFB_1 detection, then of 274 and 440 nm from 7.5 to 8.5 min for ZEA, and of 333 and 460 nm from 8.5 to 13.5 min for OTA. AFB_1 was detected by both UV and fluorometric detectors without postcolumn derivatization.

FB_1 was analyzed according to a HPLC method. The HPLC-FLD apparatus was an Agilent 1100 series (Agilent, Waldbronn, Germany) equipped with a binary pump, autosampler, column thermostat set at 30 °C, and spectrofluorometric detector with excitation and emission wavelengths set at 335 and 440 nm, respectively. The column was a 100 × 4.6 mm i.d., 2.6 μm, Kinetex core−shell particle with pentafluorophenyl stationary phase (Phenomenex, Torrance, CA, USA). The isocratic mobile phase consisted of the mixture water/methanol/acetonitrile (50:25:25, v/v/v) containing acetic acid (1%) and eluted at an 0.8 mL/min flow rate for 20 min. Prior to HPLC analysis, FB_1 samples were precolumn derivatized with *o*-phthaldialdehyde reagent, according to the method described by De Girolamo et al.[21]

LC methods were linear in the concentration range of 0.07−1.0 μg/mL (five mycotoxin levels) for DON; 0.007−1.0 μg/mL (seven mycotoxin levels) for AFB_1, ZEA, and OTA; and 0.05−5.0 μg/mL (eight mycotoxin levels) for FB_1. Calibrants were prepared in buffer at pH 3 and 7 and analyzed in triplicate. The coefficients of determination (R^2) were ≥0.996. The limits of quantitation were 70 ng/mL for DON, 7 ng/mL for ZEA, 0.7 ng/mL for OTA and AFB_1, and 50 ng/mL for FB_1 (S/N ratio = 10). These limits were 2−4 orders of magnitude below toxin concentration of the working solutions used for adsorption tests and safeguarded the ability to perform accurate LC measurements even when strong mycotoxin adsorption occurred (>90%).

Mycotoxin Adsorption Experiments. Grape pomace (pulp and skins) was weighed in a 4 mL silanized amber glass vial and suspended with an appropriate volume of (multi-)mycotoxin working solution in buffer. The suspension was vigorously mixed by vortex for a few seconds and then shaken in a thermostatically controlled shaker at constant temperature and 250 rpm speed. Adsorption studies were carried out for 90 min to ensure complete adsorption of mycotoxins. After the incubation period, the sample was allowed to settle, and 1 mL of suspension was transferred into an Eppendorf tube and centrifuged for 20 min at 18000*g* and 25 °C. Supernatant sample was split into two aliquots and analyzed for the residual mycotoxin content by HPLC for FB_1 and by UPLC for AFB_1, ZEA, OTA, and DON. Samples analyzed by UPLC were properly diluted by mixing 700 μL of the sample (in citrate or phosphate buffer solution) with 300 μL of a mixture of acetonitrile/methanol (1:2, v/v) containing acetic acid 1% and then filtered by microspin filter tubes 0.2 μm, RC/G (Grace Davison Discovery Science, Deerfield, IL, USA). A blank control was prepared using the mycotoxin working solution in buffer without grape pomace. This was subjected to the same test procedure and served as background control during the analysis to investigate the stability of toxins in the buffer solutions or any possible nonspecific adsorption. Chemical precipitation and losses of mycotoxins due to nonspecific adsorption were not detected.

Preliminary adsorption experiments were performed at constant temperature (37 °C) to determine the effect of various parameters (particle size, contact time, medium pH, and pomace dosage) on the adsorption of mycotoxins. Mycotoxin concentration was 1 μg/mL in all cases.

To study the effect of particle size on mycotoxin adsorption, five fractions of grape pomace were tested by quintuplicate independent adsorption experiments, at pH 7 and 0.5% w/v (5 mg/mL) dosage. The fractions (>500, 500−300, 300−100, 100−60, <60 μm) were obtained by sieving the dried ground material (>500 μm) and using woven wire test sieves (Endecotts, London, UK) with different nominal sizes of apertures placed in sequence.

To investigate the effect of contact time on the adsorption process, the grape pomace was tested at pH 7 and 0.1% w/v (1 mg/mL) dosage (triplicate independent experiments). Samples were withdrawn

Table 1. Isotherm Models and Equations Used To Analyze Experimental Adsorption Data

eq 2	Freundlich	$Q_{eq} = K_f C_{eq}^{1/n}$	K_f = constant related to capacity of the adsorbent for the mycotoxin n = adsorption intensity
eq 3	Langmuir	$Q_{eq} = Q_{max}[(K_L C_{eq})/(1 + K_L C_{eq})]$	Q_{max} = constant related to maximum mycotoxin uptake K_L = constant related to the energy of adsorption and affinity of the adsorbent
eq 4	Langmuir separation factor (R_L)[a]	$R_L = 1/(1 + K_L C_0)$	K_L = Langmuir constant C_0 = adsorbate initial concentration
eq 5	Sips	$Q_{eq} = (q_m a_s C_{eq}^{1/n})/(1 + a_s C_{eq}^{1/n})$	q_m = constant related to maximum mycotoxin uptake a_s = constant related to energy (affinity) of adsorption $1/n$ = index for the heterogeneity of binding sites[b]
eq 6	Hill	$Q_{eq} = (Q_{max} C_{eq}^{nH})/(K_D + C_{eq}^{nH})$	Q_{max} = constant related to maximum mycotoxin uptake K_D = Hill constant nH = Hill cooperativity coefficient of the binding interaction[c]

[a] R_L value indicates the adsorption nature: $R_L > 1$, unfavorable; $R_L = 1$, linear; $0 < R_L < 1$, favorable; $R_L = 0$, irreversible. [b] $1/n$ value indicates the heterogeneity of the adsorption sites ($0 < 1/n < 1$): $1/n < 1$, heterogeneous system; $1/n = 1$ material with relatively homogeneous binding sites. [c] $nH > 1$, positive cooperativity; $nH = 1$, no cooperativity; $nH < 1$, negative cooperativity.

at appropriate time intervals (1−120 min). Supernatant liquid portions were filtered by 0.2 μm syringe filter tubes (Sartorius Stedim Biotech, Goettingen, Germany) and analyzed for residual mycotoxin content.

To study the effect of pH on toxin adsorption, quintuplicate independent experiments were performed at different pH values (3−9), using 0.5% w/v (5 mg/mL) dosage. To investigate the desorption capacity of mycotoxins from grape pomace due to pH change, 10 mg of pomace was weighed into a 2 mL screw-cap test tube and mixed with 1 mL of mycotoxin working solution (pH 3), containing 1 μg/mL of each toxin (AFB_1, ZEA, OTA, FB_1, and DON) (1% w/v adsorbent dosage). Samples were incubated at 37 °C for 90 min in a rotary shaker (250 rpm). Then, they were centrifuged, and the supernatants were completely removed and analyzed for residual mycotoxin content to calculate mycotoxin adsorption. The adsorbent pellets were washed with 1 mL of buffer at pH 7 (30 min shaking), and then they were centrifuged and the supernatants analyzed to assess mycotoxin desorption. Desorption studies were performed in triplicate. Values for mycotoxin adsorption (pH 3) and desorption (pH 7) were calculated for each toxin and expressed in percent.

The effect of pomace dosage on toxin adsorption was investigated by equilibrium isotherms. Adsorption experiments were performed in triplicate, at constant pH (7 and 3), testing a fixed amount of toxins with different pomace dosages (0.05−3% w/v corresponding to 0.5−30 mg/mL). Adsorption data were expressed as percentage of mycotoxin adsorbed and plotted as a function of grape pomace dosage. Mycotoxin adsorption plots were fitted by the Langmuir model (Table 1).

Equilibrium Adsorption Isotherms. Three sets of adsorption isotherms were carried out at constant temperature and pH by testing a fixed amount of grape pomace with buffered solutions of mycotoxins at different toxin concentrations (0.05−5 μg/mL). Equilibrium isotherms were set up according to the results of preliminary adsorption experiments, using 90 min of contact time, a <500 μm particle size fraction, a 0.1% w/v (1 mg/mL) pomace dosage for AFB_1 and ZEA adsorption, and a 0.2% w/v (2 mg/mL) pomace dosage for OTA and FB_1 adsorption. Due to the inefficacy of grape pomace in adsorbing DON from liquid media, DON was excluded from this study. Isotherms consisted of 10 or more experimental points and were carried out in triplicate. The first set of isotherms (single-mycotoxin system) was conducted at constant temperature (37.0 ± 0.5 °C) and different pH values (3 and 7). These isotherms were used to calculate the parameters (maximum adsorption capacity, adsorption affinity, and heterogeneity of the adsorption process) related to the adsorptions of AFB_1, ZEA, OTA, and FB_1 onto grape pomace and the effect of pH on the adsorption. The second set of isotherms was conducted at constant pH (7) and different temperatures (5.0 ± 0.5, 37.0 ± 0.5, 50.0 ± 0.5, and 70.0 ± 0.5 °C). These isotherms allowed investigation of the influence of temperature change on the uptake of mycotoxins and calculation of the thermodynamic parameters ($\Delta G°$, $\Delta H°$, and $\Delta S°$) related to the mycotoxin adsorption. The third set of isotherms (multi-mycotoxin system) was carried out at constant temperature (37.0 ± 0.5 °C) and pH 7 using mycotoxin working solutions containing a pool of five mycotoxins, in the 0.05−5 μg/mL concentration range and in the 1:1 ratio. These multiple adsorption isotherms were performed to verify if the simultaneous presence of AFB_1, ZEA, OTA, FB_1, and DON can interfere with the adsorption process related to each toxin. The change for adsorption values due to the simultaneous presence of mycotoxins was evaluated by comparing adsorption isotherms and related parameters obtained by single- and multi-mycotoxin adsorption experiments carried out in the same experimental conditions.

Data Calculation and Curve Fitting. The amount of adsorbed mycotoxin was calculated as the difference between the amount of mycotoxin in the supernatant of the blank tubes with no grape pomace and the amount found in the supernatant of the experimental tubes with the pomace. This amount was related then to the quantity present in the supernatant of the blank tubes and expressed in percent. The amount of bound mycotoxin per unit mass of pomace was calculated using eq 1:

$$Q_{eq} = [(C_0 - C_{eq})V]/m \quad (1)$$

Q_{eq} = quantity of mycotoxin adsorbed per milligram of grape pomace (μg/mg); C_0 = concentration of mycotoxin in the supernatants of the blank tubes with no grape pomace (μg/mL); C_{eq} = residual mycotoxin concentration in the supernatant of the experimental tubes with grape pomace at equilibrium (μg/mL); V = volume of solution (mL); and m = mass of grape pomace (mg).

Adsorption isotherms were obtained by plotting the amount of mycotoxin adsorbed per unit of mass of adsorbent (Q_{eq}) against the concentration of the toxin in the external phase (C_{eq}), under equilibrium conditions ($Q_{eq} = f(C_{eq})$. These data were transferred to SigmaPlot (Systat.com, version 12.3) and fitted by the Langmuir, Freundlich, Sips, and Hill isotherm models (Table 1).[22−27] A dimensionless constant known as the separation factor (R_L) derived from the Langmuir equation (Table 1) was used to assess the favorability of adsorption.[25] The Gibbs free energy change ($\Delta G°$, kJ/mol), the standard enthalpy ($\Delta H°$, kJ/mol), and the standard entropy ($\Delta S°$, kJ/mol·K) were calculated according to the study performed by Ringot et al.[28] The SigmaPlot nonlinear regression method, which uses the Marquardt−Levenberg algorithm, was used as a viable tool to define the best-fitting relationship between a set of experimental data and the proposed isotherm models. Statistical analysis was performed using a factorial ANOVA with concentration (C_{eq}) or pomace dosage as categorical predictor variable and quantity of mycotoxin adsorbed (Q_{eq}) as dependent variable. The normality test (Kolmogorov−Smirnov test), the constant variance test (Spearman rank correlation), and the Durbin−Watson statistic test were used to test, respectively, for normally distributed population, constant variance assumption, and correlation between residuals. The threshold for significance level for normality and constant variance test was set at $p < 0.05$. The expected

dx.doi.org/10.1021/jf404179h | J. Agric. Food Chem. 2014, 62, 497−507

Table 2. Effect of Particle Size on AFB_1, ZEA, OTA, and FB_1 Adsorption by Grape Pomace

particle size (μm)	mycotoxin adsorption[a] (%), mean ± SD (n = 5)			
	AFB_1	ZEA	OTA	FB_1
>500	74.8 ± 0.7 a	63.1 ± 0.3 a	50.3 ± 1.8 a	26.3 ± 2.9 a
300−500	79.1 ± 1.2 b	69.0 ± 1.6 b	54.8 ± 2.8 b	26.6 ± 1.1 a
100−300	80.0 ± 1.4 b	69.2 ± 1.9 b	56.6 ± 1.6 b	27.5 ± 3.3 a
60−100	81.9 ± 0.3 c	69.5 ± 1.6 b	60.5 ± 0.7 c	27.5 ± 2.4 a
<60	80.2 ± 0.7 b	68.9 ± 0.8 b	58.9 ± 1.2 c	27.8 ± 1.6 a

[a]Values labeled with the same letters in a column are not significantly different (p < 0.05).

value of the Durbin−Watson statistic for random, independent, normally distributed residuals was 2. The coefficient of determination (R^2), the standard errors of the estimate (s_{ylx}), the residual sum of squares (SS_{res}), and the predicted residual error sum of squares (PRESS) were calculated to assess the fitness/suitability of the regression models. The isotherm models that provided the lowest SS_{res}, s_{ylx}, and PRESS and the highest R^2 were considered to give the closest fit.

RESULTS AND DISCUSSION

Effect of Particle Size. The effect of particle size on the mycotoxin adsorption process was studied using fractions with particle size ranging from >500 to <60 μm (Table 2). All fractions adsorbed significant amounts of AFB_1, ZEA, OTA, and FB_1, whereas DON adsorption was negligible. For most toxins, the coarse fraction yielded significantly lower adsorption values (75% AFB_1, 63% ZEA, 50% OTA, and 26% FB_1). These values slightly increased by decreasing particle size (<500 μm) and were constant in the range from 500 to <60 μm. Maximum adsorptions recorded in this range were 82% AFB_1, 70% ZEA, 61% OTA, and 28% FB_1. Therefore, the grape pomace fraction <500 μm was used for subsequent adsorption experiments.

Effect of Contact Time. The effect of contact time for the adsorption of mycotoxins by grape pomace was studied for a period of 2 h (Figure 1). From the kinetic experiments, the plot of mycotoxin adsorption versus time showed that the rate of AFB_1, ZEA, OTA, and FB_1 adsorption by grape pomace is fast at the initial stages of the contact period and then becomes slower near equilibrium. Half of the total adsorption occurred in <3 min, and maximum adsorption was reached in 15 min. No further changes in the adsorption were noted beyond the 15 min period up to 2 h (Figure 1). This finding is of significant importance in the toxin reduction by adsorption. A rapid uptake of toxins and establishment of equilibrium in a short period imply the efficacy of pomace for its use in reduction of toxin bioaccessibility in the gastrointestinal (GI) tract.

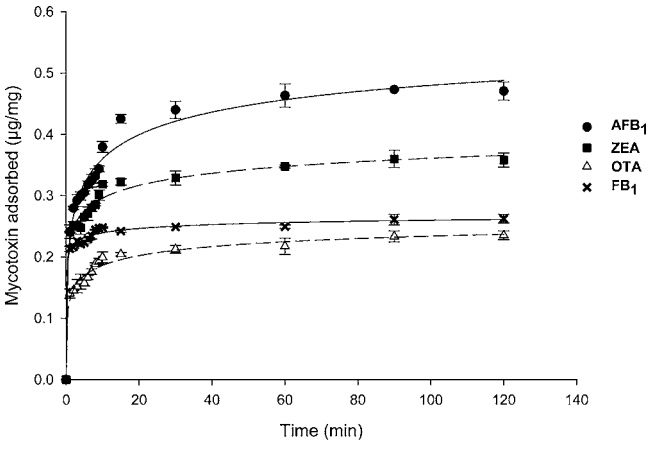

Figure 1. Effect of contact time on adsorption rate of AFB_1, ZEA, OTA, and FB_1 by grape pomace. Adsorption experiments were performed at constant pH (7) and temperature (37 °C), using 0.1% w/v pomace dosage and 1 μg/mL mycotoxin concentration.

Effect of pH. The removal of mycotoxins from aqueous medium through an adsorption process is, in most cases, highly dependent on the pH. Medium pH can affect the surface charge of adsorbents as well as the degree of ionization of toxins, and subsequently it can lead to a shift in reaction kinetics and equilibrium characteristics of the adsorption process. This is more important when the adsorption process involves electrostatic interactions. In general, the charge of the toxin depends on its pK_a. The toxin is mainly in protonated form at pH < pK_a and in deprotonated form at pH > pK_a. The effect of pH on AFB_1, ZEA, OTA, and FB_1 adsorption by grape pomace was different according to the degree of ionization of molecules (Table 3). AFB_1 is a non-ionizable molecule (Figure 2), and the

Table 3. Effect of pH on AFB_1, ZEA, OTA, and FB_1 Adsorption by Grape Pomace

pH	mycotoxin adsorption[a] (%), mean ± SD (n = 5)			
	AFB_1	ZEA	OTA	FB_1
3	83.2 ± 1.1 a	67.9 ± 1.3 a	67.6 ± 0.9 a	26.7 ± 2.1 a
4	83.0 ± 0.2 a	68.0 ± 0.8 a	65.4 ± 1.3 a	25.8 ± 2.9 a
5	83.4 ± 0.8 a	68.2 ± 1.4 a	62.2 ± 1.6 b	26.4 ± 2.4 a
6	84.6 ± 0.9 a	69.0 ± 1.3 a	62.3 ± 1.0 b	33.8 ± 5.2 b
7	82.0 ± 0.8 a	67.0 ± 0.9 a	61.3 ± 0.7 b	34.7 ± 2.8 b
8	82.6 ± 0.4 a	68.3 ± 1.0 a	62.4 ± 1.1 b	35.4 ± 0.6 b
9	83.0 ± 1.1 a	64.1 ± 1.8 b	60.7 ± 1.0 b	33.7 ± 1.1 b

[a]Values labeled with the same letters in a column are not significantly different (p < 0.05).

pK_a in water is not applicable. Therefore, a change of pH should not affect AFB_1 adsorption. Accordingly, grape pomace sequestered AFB_1 to the same extent in all pH ranges assayed in the study (Table 3). ZEA is a diphenolic compound with an estimated pK_a of 7.6,[29] so some amount of phenolate anion can be present in water near pH 7. ZEA adsorption was unaffected by pH in the range of 3−8 and slightly decreased at pH 9 (p < 0.05). OTA consists of a dihydroisocoumarin moiety linked through its 7-carboxyl group by an amide linkage to L-phenylalanine (Figure 2). The pK_a values are in the ranges of 4.2−4.4 and 7.0−7.3, respectively, for the carboxyl group of the phenylalanine moiety and the phenolic hydroxyl group of the isocoumarin part.[30] This indicates that, in aqueous solutions near pH 7, both the monoanion (OTA^-) and the dianion (OTA^{2-}) are present, whereas the protonated and uncharged toxin is present in acid solutions (pH <4). OTA adsorptions recorded at pH ≤4 were constant and significantly higher than those recorded at pH ≥5 (p < 0.05) (Table 3). This result

dx.doi.org/10.1021/jf404179h | J. Agric. Food Chem. 2014, 62, 497−507

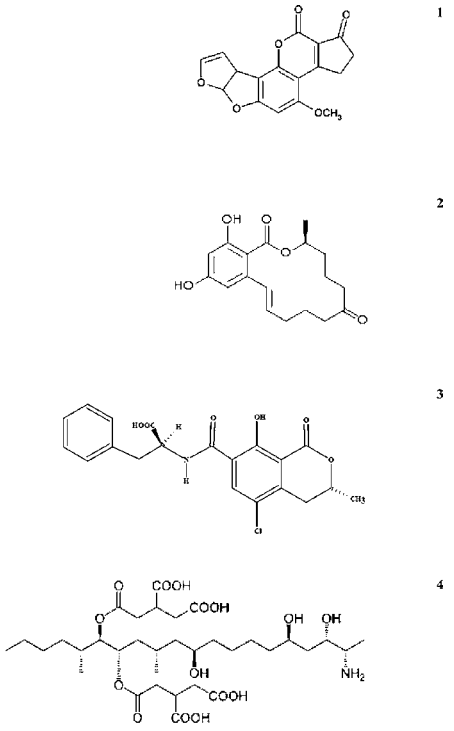

Figure 2. Structures of mycotoxins: **1**, AFB_1; **2**, ZEA; **3**, OTA; **4**, FB_1.

suggests that OTA adsorption is higher when it is in the uncharged form and slightly decreases when it is in the anionic form. Contrary to AFB_1, ZEA, and OTA, FB_1 is a more polar and water-soluble toxin, containing carboxylic, hydroxyl, and amino functional groups (Figure 2). No report concerning the pK_a of FB_1 is available in the literature.[31] The pK_a values for tricarballylic acid are 3.5, 4.6, and 5.8, and the aliphatic amine group should have a pK_a >9. Therefore, at pH between 6 and 9, FB_1 could be in the anionic form because of deprotonation of carboxylic groups, whereas it could be in the cationic form at pH <6 due to protonation of the amine group. FB_1 adsorption by grape pomace recorded at pH ≥6 was significantly higher than that recorded at pH ≤5 ($p < 0.05$) (Table 3). It seems that the anionic form of FB_1 contributes to adsorption by grape pomace, whereas the cationic form decreases such adsorption. During digestion, the pH of the food bolus is not constant but, depending on GI compartments, changes to a large extent. In monogastric animals, it ranges from 1.5−2.5 in the stomach to 5.5−6.0 in the intestinal lumen. Taking into account the findings of this study, it can be supposed that AFB_1 and ZEA adsorptions by grape pomace are stable within the pH range that can be found in the GI tract of monogastric animals, whereas pH change could affect FB_1 and OTA adsorptions to some extent. Hence, a desorption study was performed to assess if change of pH can cause release of the sequestered toxins. Mycotoxins were first adsorbed onto grape pomace at pH 3, and then the pellet containing the adsorbed mycotoxins was washed with a medium at pH 7. Adsorption and desorption values were, respectively, 94 and 4% for AFB_1; 87 and 10% for ZEA; 84 and 14% for OTA; and 16 and 45% for FB_1. These results suggest that grape pomace has high efficacy in adsorbing AFB_1, ZEA, and OTA at acid pH, and it is able to retain the adsorbed toxins when the pH rises to neutral values. FB_1 is sequestered poorly at pH 3, and almost half of the adsorbed toxin can be released when the pH of the medium changes from 3 to 7.

Effect of Adsorbent Dosage. AFB_1, ZEA, OTA, and FB_1 adsorption was significantly affected by the adsorbent dosage, and the percentage of mycotoxins removed from neutral or acid buffer solutions increased with increasing dosages of grape pomace (Figure 3). The Langmuir model provided good correlations for isotherm adsorption plots ($R^2 > 0.990$). AFB_1, ZEA, and OTA isotherms obtained at different pH values were comparable (Figure 3). Experimental values for AFB_1, ZEA, and OTA adsorption were in the ranges of 28−98, 21−94, and 6−94%, respectively. FB_1 adsorptions were significantly higher at pH 7 (17−44%) than at pH 3 (11−31%) (Figure 3). The Langmuir model allowed the calculation of the theoretically estimated maximum adsorption (Ads_{max}) and the C_{50},[32] which is the theoretically estimated adsorbent dosage to achieve a 50% reduction of the absorbable toxin (Table 4). The C_{50} could not be calculated for FB_1 at pH 3. For all toxins, Ads_{max} and C_{50} values were in accordance with the experimental values for mycotoxin adsorption shown in Figure 3. With these findings taken into account, it is not useful to increase the dosage of grape pomace beyond 4 mg/mL to sequester AFB_1, ZEA, and OTA from a 1 μg/mL or higher mycotoxin solutions. Therefore, for all of the subsequent isotherm experiments, grape pomace dosage was fixed at 1 mg/mL for AFB_1 and ZEA and at 2 mg/mL for OTA and FB_1.

Adsorption Isotherms (Single-Mycotoxin System). The adsorption isotherm is an invaluable curve describing the phenomenon governing the retention (or release) or mobility of a substance from the aquatic environments to a solid phase at a constant temperature and pH.[33] Its physicochemical parameters together with the underlying thermodynamic assumptions provide insight into the adsorption mechanism and surface properties as well as the degree of affinity of the adsorbents.[33] Several equations have been published to study the isotherm adsorption of mycotoxins to organic and inorganic adsorbent materials.[22,34] In this study, four adsorption models often reported in the literature were used to provide the best description of mycotoxin adsorption by grape pomace (Table 1). The nonlinear regression analysis method,[35] instead of the linear regression with transformed variables, was applied to assess the goodness of the fits and to calculate the parameters involved in the adsorption mechanism (Table 5). All adsorption models provided a good fit line to experimental adsorption data (small variance and $R^2 \geq 0.979$) (Table 5). The amount of mycotoxin adsorbed per unit mass of grape pomace increased gradually by increasing mycotoxin molecules in the working solution; thus, isotherms showed an exponential relationship and a typical L-1 (Langmuir) shape (Figure 4). This suggests that, in the experimental conditions of this study, the plateau was not reached and part of the capacity of the absorbent was occupied by the mycotoxins.

AFB_1 Adsorption Isotherms. AFB_1 adsorption by grape pomace yielded similar equilibrium isotherms at pH 3 and 7 (Figure 4). Experimental values for AFB_1 adsorption in percent varied in the range of 57−30%. The experimental values for maximum adsorption capacity recorded at pH 3 and 7 were, respectively, 1.53 ± 0.04 μg/mg (4.89 ± 0.12 mmol/kg) and 1.54 ± 0.05 μg/mg (4.94 ± 0.16 mmol/kg) (Figure 4). Among the tested isotherm equations, the better representation of the experimental results of the AFB_1 adsorption isotherms was obtained using the Sips and Hill models ($R^2 > 0.998$ and low error values) (Table 5). These equations are often found to be

dx.doi.org/10.1021/jf404179h | J. Agric. Food Chem. 2014, 62, 497−507

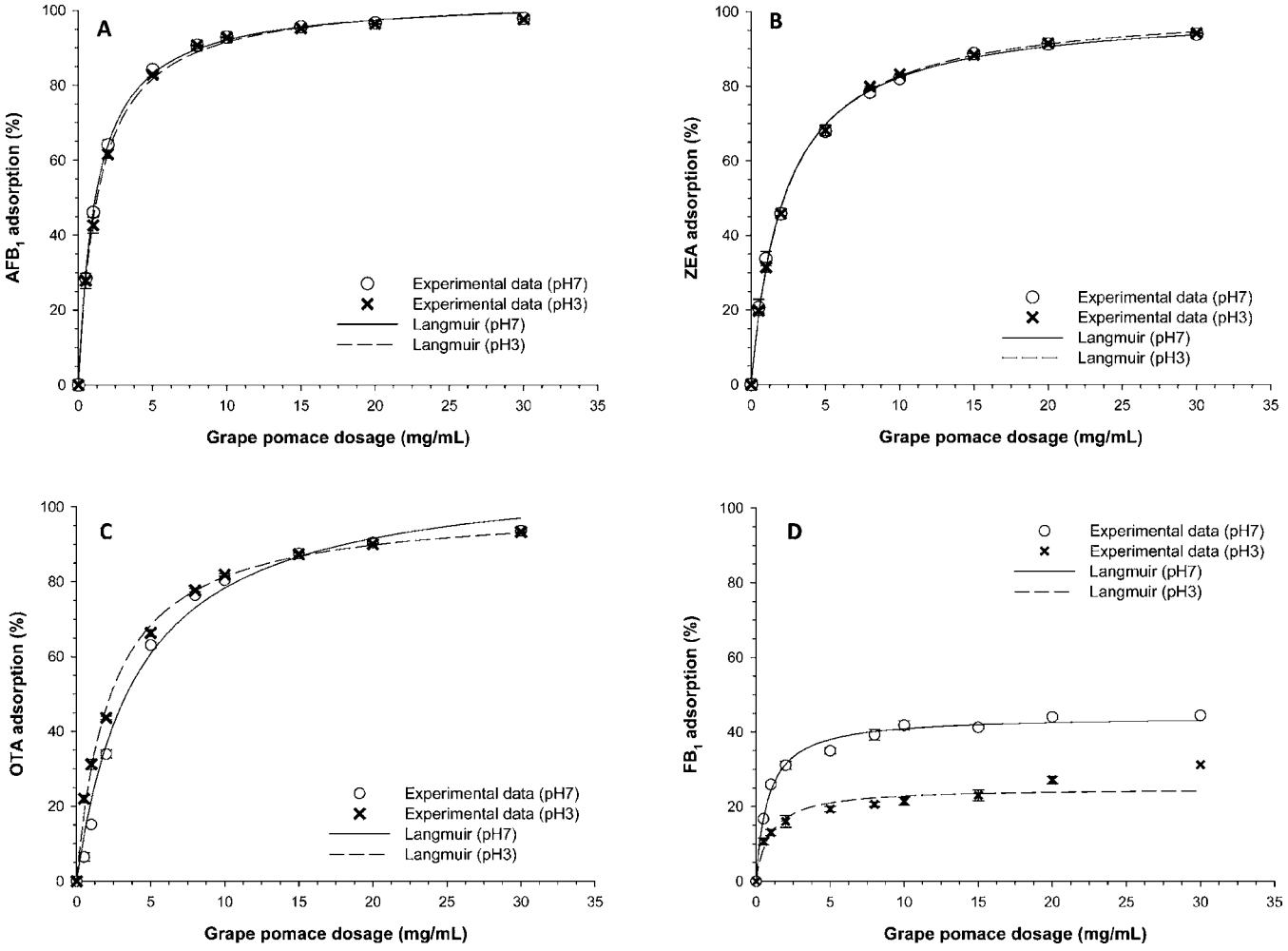

Figure 3. Effect of adsorbent dosage on (A) AFB_1, (B) ZEA, (C) OTA, and (D) FB_1 adsorption by grape pomace. Equilibrium adsorption isotherms were obtained at constant temperature (37 °C) and pH (3 and 7) by testing a fixed amount of toxins (1 μg/mL) with increasing adsorbent dosages (0.05−3% w/v).

Table 4. Theoretically Estimated Values for Maximum Adsorption (Ads_{max}) and Inclusion Rate of Grape Pomace To Obtain a 50% Reduction of the Absorbable Toxin (C_{50})[a]

	Ads_{max} (%)		C_{50} (mg/mL)	
toxin	pH 3	pH 7	pH 3	pH 7
AFB_1	103.9 ± 0.5	103.2 ± 0.3	1.4	1.2
ZEA	101.9 ± 0.5	100.7 ± 0.7	2.5	2.5
OTA	100.3 ± 0.9	100.2 ± 2.2	2.5	4.0
FB_1	22.8 ± 0.5	45.5 ± 0.4	nd	30.0

[a] Ads_{max} and C_{50} were calculated by fitting the adsorption isotherms in Figure 3 with the Langmuir isotherm model.

superior to either the Freundlich or Langmuir equation in correlations, as they were developed for adsorption on heterogeneous solids. The Sips isotherm (Table 1) is a combined form of the Langmuir and Freundlich expressions deduced for predicting the heterogeneous adsorption systems and circumventing the limitation of the rising adsorbate concentration associated with the Freundlich isotherm model.[26] At low adsorbate concentrations, it reduces to the Freundlich isotherm, whereas at high concentrations, it predicts a monolayer adsorption capacity characteristic of the Langmuir isotherm. The Hill model (Table 1) assumes that adsorption is a cooperative phenomenon, with the ligand binding ability at one site on the macromolecule, and may influence different binding sites on the same macromolecule.[27] The Sips and Hill models are mathematically equivalent[36] and provide same error values and coefficients of determination (Table 5). The $1/n$ exponent in the Sips model is analogous to the nH exponent in the Hill model. However, they have different meanings, $1/n$ being the heterogeneity factor of the adsorption and nH the cooperativity coefficient of the binding interaction. According to the Sips and Hill models, the theoretical maximum AFB_1 adsorption capacity was 4.73 ± 0.77 μg/mg (15.15 ± 2.47 mmol/kg) and 4.69 ± 0.55 μg/mg (15.02 ± 1.76 mmol/kg) at pH 3 and 7, respectively (Table 5). The constant a_s in the Sips equation is related to the energy and affinity of adsorption. The values for the a_s parameter in the Sips model were 0.17 ± 0.03 and 0.16 ± 0.02 mL/μg at pH 3 and 7, respectively (Table 5). The Sips exponent ($1/n$) was <1 in all cases, suggesting heterogeneous binding sites. Similarly, the Hill cooperativity coefficient (nH) was <1, indicating a negative cooperativity of the binding interaction. In conclusion, these findings suggest that the AFB_1 adsorption mechanism is heterogeneous and occurs at a finite (fixed) number of definite localized sites, which are nonequivalent, with lateral interaction (negative interaction) and steric hindrance between the AFB_1 adsorbed molecules.

dx.doi.org/10.1021/jf404179h | J. Agric. Food Chem. 2014, 62, 497−507

Table 5. Isotherm Model Parameters for the Adsorption of Mycotoxins by Grape Pomace at Different pH Values

		AFB_1		ZEA		OTA		FB_1	
model	parameter	pH 7	pH 3	pH 7	pH 3	pH 7	pH 3	pH 7	pH 3
Freundlich	K_f (±SE)	**0.65 ± 0.01**	**0.66 ± 0.01**	**0.42 ± 0.01**	**0.43 ± 0.01**	**0.18 ± 0.01**	**0.43 ± 0.01**	**0.16 ± 0.01**	**0.06 ± 0.01**
	$1/n$ (±SE)	**0.70 ± 0.01**	**0.70 ± 0.01**	**0.77 ± 0.02**	**0.76 ± 0.01**	**0.87 ± 0.02**	**0.77 ± 0.01**	**0.84 ± 0.03**	**0.45 ± 0.09**
	R^2	0.9974	0.9971	0.9888	0.9973	0.9939	0.9963	0.9910	0.9791
	SS_{res}	0.024	0.023	0.051	0.010	0.003	0.013	0.003	0.0004
	$s_{y/x}$	0.023	0.028	0.036	0.019	0.013	0.022	0.014	0.005
	PRESS	0.027	0.027	0.071	0.012	0.004	0.018	0.008	0.0006
Langmuir	Q_{max} (±SE)	**2.86 ± 0.07**	**3.02 ± 0.11**	**2.73 ± 0.20**	**2.65 ± 0.14**	**2.54 ± 0.47**	**2.79 ± 0.21**	**1.60 ± 0.19**	**0.13 ± 0.01**
	K_L (±SE)	**0.31 ± 0.01**	**0.29 ± 0.02**	**0.19 ± 0.02**	**0.20 ± 0.01**	**0.08 ± 0.02**	**0.19 ± 0.02**	**0.11 ± 0.02**	**0.99 ± 0.15**
	R^2	0.9976	0.9976	0.9916	0.9972	0.9935	0.9953	0.9941	0.9791
	SS_{res}	0.022	0.018	0.038	0.010	0.003	0.017	0.002	0.0008
	$s_{y/x}$	0.022	0.026	0.032	0.019	0.013	0.025	0.011	0.007
	PRESS	0.026	0.023	0.054	0.013	0.004	0.025	0.005	0.0010
Sips/Hill[a]	q_m (±SE)	**4.69 ± 0.55**	**4.73 ± 0.77**	**2.93 ± 0.70**	**4.78 ± 1.45**	**nc**[b]	**nc**	**1.17 ± 0.28**	**0.28 ± 0.11**
	a_s (±SE)	**0.16 ± 0.02**	**0.17 ± 0.03**	**0.17 ± 0.05**	**0.10 ± 0.03**			**0.16 ± 0.04**	**0.29 ± 0.17**
	$1/n = nH$ (±SE)	**0.85 ± 0.02**	**0.86 ± 0.03**	**0.98 ± 0.07**	**0.97 ± 0.04**			**1.09 ± 0.08**	**0.59 ± 0.09**
	R^2	0.9988	0.9985	0.9916	0.9980			0.9948	0.9829
	SS_{res}	0.011	0.012	0.038	0.008			0.002	0.0004
	$s_{y/x}$	0.016	0.020	0.032	0.017			0.011	0.005
	PRESS	0.013	0.014	0.061	0.010			0.006	0.0005

[a]The Sips and Hill models are mathematically equivalent and provide the same error values and adsorption parameters. [b]Does not converge.

ZEA Adsorption Isotherms. Isothermal adsorption of ZEA by grape pomace was not affected by pH (Figure 4). The experimental values for ZEA adsorption recorded at pH 3 and 7 were comparable and ranged from 38 to 20%. The experimental values for maximum adsorption capacity were 1.25 ± 0.03 μg/mg (3.91 ± 0.09 mmol/kg) and 1.12 ± 0.09 μg/mg (3.51 ± 0.27 mmol/kg) at pH 3 and 7, respectively. The Langmuir equation was found to be the best fitting isotherm model for ZEA adsorption (Table 5). At both pH values, the correlations obtained by this model were in excellent agreement with the experimental adsorption data and yielded comparable adsorption parameters (Table 5). The predicted maximum ZEA adsorption capacity was 2.65 ± 0.14 μg/mg (8.32 ± 0.44 mmol/kg) and 2.73 ± 0.20 μg/mg (8.58 ± 0.63 mmol/kg) at pH 3 and 7, respectively. The Langmuir K_L parameter, which is related to the free energy of adsorption, was 0.20 ± 0.01 and 0.19 ± 0.02 mL/μg at pH 3 and 7, respectively. These values suggest favorable ZEA adsorption by grape pomace. The favorability of ZEA adsorption was confirmed by the essential features of the Langmuir isotherm model, called the separation factor, R_L (Table 1).[25] At both pH values, this dimensionless factor ranged from 1.00 to 0.50 for the initial ZEA concentration values of 0.05−5.00 μg/mL. At all ZEA concentrations, R_L values were in the range of 0−1, which is indicative of favorable adsorption. In addition, the R^2 and error values demonstrate that the Sips and Hill models can also adequately fit ZEA adsorption data (Table 5). The Hill cooperativity coefficient (nH) was approximately 1, indicating no cooperativity of the binding interaction. Similarly, the heterogeneity factor ($1/n$) of the Sips isotherm equation was almost equal to 1. This implies that the Sips isotherm equation reduces to the Langmuir equation, and ZEA adsorption data are more of the Langmuir form rather than of the Freundlich form. In conclusion, these results are all indicative of a homogeneous adsorption process for ZEA by grape pomace.

OTA Adsorption Isotherms. Unlike AFB_1 and ZEA adsorptions, OTA adsorption was slightly affected by pH. The experimental values for OTA adsorption were 54−33% at pH 3 and 33−26% at pH 7. The related experimental values for maximum adsorption capacity were, respectively, 0.82 ± 0.08 μg/mg (2.04 ± 0.20 mmol/kg) and 0.64 ± 0.09 μg/mg (1.58 ± 0.22 mmol/kg) (Figure 4). At both pH values tested in the study, the Freundlich and Langmuir models provided a good fit line to experimental data (small variance and R^2 values >0.993), whereas the Hill and Sips models did not converge (Table 5). The latter models, exceeding the maximum number of repeated fit attempts before failure (200 iterations), provided inaccurate parameters. Maximum adsorption capacities were calculated by the Langmuir model and comparable at pH 3 and 7, being 2.79 ± 0.21 μg/mg (6.91 ± 0.52 mmol/kg) and 2.54 ± 0.47 μg/mg (6.29 ± 1.16 mmol/kg), respectively. Between the biparametric models, the Freundlich model was superior to the Langmuir model in fitting adsorption data. This may be explained by the binding process occurring under conditions outside the assumptions of the Langmuir model, and it suggests a heterogeneous binding mechanism. The Freundlich isotherm is the earliest known relationship describing the nonideal and reversible adsorption, not restricted to the formation of monolayer.[23] This empirical model can be applied to multilayer adsorption, with nonuniform distribution of adsorption heat and affinities over the heterogeneous surface. The Freundlich model provides no information on the monolayer adsorption capacity, in contrast to the Langmuir model. The heterogeneity index in the Freundlich model, $1/n$, gives information on the population of the binding sites and the adsorption intensity and is associated with the favorability of the binding process. A value of $1/n = 1$ suggests that the population of binding sites is homogeneous, whereas a value below unity implies favorability of the adsorption. At acid and neutral pH, the values computed for the Freundlich parameter $1/n$ were 0.77 ± 0.01 and 0.87 ± 0.02, respectively. These values were <1 and indicate

dx.doi.org/10.1021/jf404179h | J. Agric. Food Chem. 2014, 62, 497−507

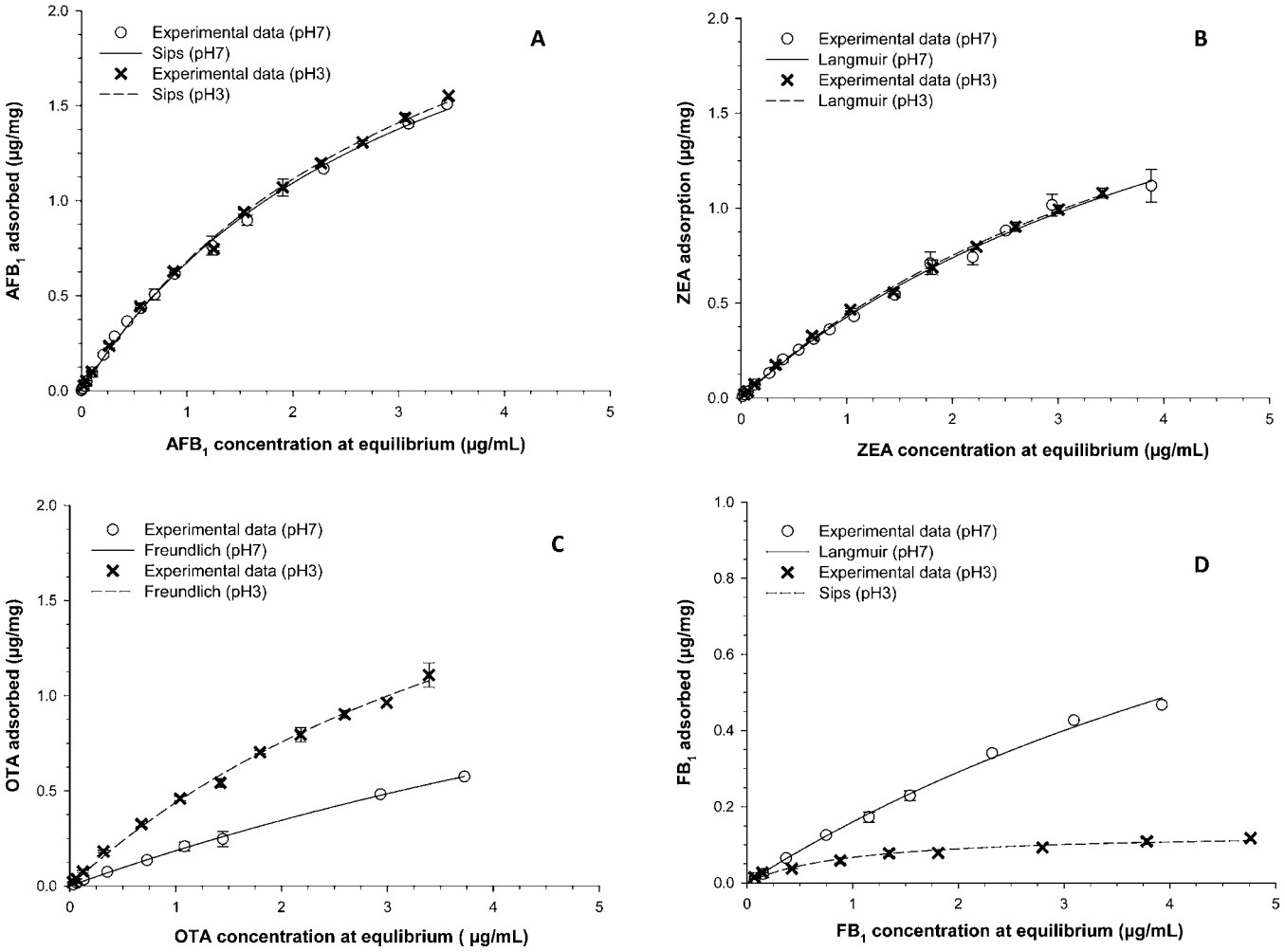

Figure 4. Effect of mycotoxin concentration on (A) AFB_1, (B) ZEA, (C) OTA, and (D) FB_1 adsorption by grape pomace. Equilibrium adsorption isotherms were obtained at constant temperature (37 °C) and pH (3 and 7) by testing a fixed amount of grape pomace with increasing toxin concentrations (0.05−5 μg/mL).

favorability for the OTA adsorption process. However, the $1/n$ parameter being estimated at pH 3 lower than at pH 7, it can be assumed that more binding sites or higher adsorption intensity can be found at acid pH than at neutral pH. Accordingly, the K_f Freundlich constant, which is attributed to affinity of the adsorbent, was 2-fold higher at pH 3 than at pH 7 (Table 5). In conclusion, increase of medium pH from 3 to 7 reduces the affinity of adsorption. The decreased affinity for OTA adsorption by grape pomace at pH 7 may be induced by the presence of an anionic form of the toxin, which probably leads to the repulsion between OTA molecules and negative charges that could be found on the adsorption surface. In agreement with these findings, OTA adsorption by negative charged surfaces (such as zeolites) has been found significantly higher at pH 3 than at pH 7 and 9.[30] The existence of a heterogeneous adsorption in the case of OTA suggests that different types of interaction can occur, such as hydrophobic and ionic forces.

FB_1 Adsorption Isotherms. Similarly to OTA adsorption, different mechanisms may be involved in FB_1 adsorption depending on pH and then on the degree of ionization of molecules. Highest adsorption was achieved at pH 7 (Figure 4). The experimental values for FB_1 adsorption were 30−5% at pH 3 and 25−22% at pH 7. The experimental values for maximum adsorption capacity recorded at these pH values were, respectively, 0.12 ± 0.01 μg/mg (0.16 ± 0.01 mmol/kg) and 0.54 ± 0.06 μg/mg (0.74 ± 0.08 mmol/kg) (Figure 4). With error and R^2 values reported in Table 5 taken into account, it was determined that the Langmuir model is the best isotherm model to fit the adsorption data at pH 7, whereas the Sips and Hill models produce better correlations at pH 3. The applicability of these isotherm models to the FB_1−grape pomace system implies that FB_1 adsorption is complex, and it confirms that more than one mechanism can be involved. In particular, monolayer adsorption (homogeneous adsorption) may exist at pH 7, whereas heterogeneous and lower adsorption can occur at pH 3. The predicted maximum adsorption capacities calculated by the Langmuir model at pH 7 and by the Sips/Hill models at pH 3 were 1.60 ± 0.19 μg/mg (2.22 ± 0.26 mmol/kg) and 0.28 ± 0.11 μg/mg (0.39 ± 0.15 mmol/kg), respectively (Table 5). In addition, at pH 7 the exponents in the Sips and Hill models were equal to 1. This suggests that the Sips model reduces to the Langmuir equation and the material holds relatively homogeneous binding sites. Moreover, no cooperativity in the binding interactions occurs when the adsorption system is at neutral pH, that is, when FB_1 has negative charges. At pH 3, FB_1 should be in the cationic form. Likely, the positive charge in the adsorbable molecules reduces the capacity and affinity of the adsorption and results in

dx.doi.org/10.1021/jf404179h | J. Agric. Food Chem. 2014, 62, 497−507

negative cooperativity of the binding process. Thus, it can be concluded that in aqueous solutions near the physiological pH (pH 7), FB_1 adsorption onto grape pomace is favored and occurs mainly by polar noncovalent interactions, such as electrostatic interactions or hydrogen bonds involving the carboxylic functional groups.

Multi-mycotoxin Adsorption Isotherms. In general, adsorbate−surface interactions complicate the adsorption in multicomponent systems.[37] Multi-mycotoxin systems have received less attention than single-mycotoxin systems, and multi-mycotoxin adsorption isotherms have never been described in the literature. Therefore, the adsorption of AFB_1, ZEA, OTA, and FB_1 by grape pomace was also studied by equilibrium adsorption isotherms using a five-component system. This system contained simultaneously AFB_1, ZEA, OTA, FB_1, and DON in equal ratios. Of course, these ratios are not reflected in the real world of natural contamination in which aflatoxin and fumonisin occur orders of magnitude apart. Multi-mycotoxin adsorption isotherms were obtained as in the single-mycotoxin adsorption system, testing the toxins at pH 7 and 37 °C. The adsorption parameters calculated for each toxin in the presence (five-mycotoxin system) and absence (single-mycotoxin system) of other mycotoxins are presented in Table 6. AFB_1 adsorption isotherm plots were fitted by the Sips/Hill models, because they produced better goodness of fit. ZEA, OTA, and FB_1 adsorption isotherms were well fitted by the Langmuir equation. For all mycotoxins considered in the study, the experimental values for mycotoxin adsorption obtained in the single- and multi-mycotoxin adsorption systems were comparable. Similarly, the predicted isotherm adsorption parameters calculated by these systems did not differ (Table 6). The effect of mycotoxin interactions on adsorption may be represented by the ratio of the adsorption capacity for one mycotoxin in the presence of the other mycotoxins, Q^{mix}, to the adsorption capacity for the same mycotoxin when it is present alone in the solution, Q^0. When $(Q^{mix}/Q^0) > 1$, adsorption is promoted by the presence of other mycotoxins; when $(Q^{mix}/Q^0) = 1$, there is no net interaction; and when $(Q^{mix}/Q^0) < 1$, adsorption is suppressed by other mycotoxins. As shown in Table 6, the values of Q^{mix}/Q^0 were all almost equal to 1. Therefore, it can be supposed that mycotoxin adsorption by grape pomace is not suppressed or enhanced by the presence of other mycotoxins in the experimental conditions. In conclusion, for the first time, this study proves that grape pomace can adsorb simultaneously AFB_1, ZEA, OTA, and FB_1 and that these mycotoxins did not compete for adsorption. Grape pomace shows the potential to be used as a broad-spectrum adsorbent material.

Table 6. Mycotoxin Adsorption Parameters Calculated for Mycotoxin Adsorption Isotherms Obtained by Single- and Multi-mycotoxin Adsorption Systems (37 °C, pH 7)

mycotoxin	parameter	single-mycotoxin system	multi-mycotoxin system	Q^{mix}/Q^{0a}
AFB_1	q_m[b]	4.69 ± 0.55	4.71 ± 0.28	0.99
	a_s[c]	0.16 ± 0.02	0.12 ± 0.07	
	$1/n$[d]	0.85 ± 0.02	0.78 ± 0.06	
ZEA	Q_{max}[e]	2.73 ± 0.20	2.72 ± 0.14	1.00
	K_L[f]	0.19 ± 0.02	0.21 ± 0.02	
OTA	Q_{max}	2.54 ± 0.47	2.59 ± 0.17	0.98
	K_L	0.08 ± 0.02	0.14 ± 0.01	
FB_1	Q_{max}	1.60 ± 0.19	1.51 ± 0.27	1.06
	K_L	0.11 ± 0.02	0.12 ± 0.02	

[a] Q^{mix} = adsorption capacity for one mycotoxin in the presence of other mycotoxins; Q^0 = adsorption capacity for one mycotoxin when it is present alone in the solution. [b] Sips parameter related to maximum adsorption capacity (μg/mg). [c] Sips parameter related to energy (affinity) of adsorption. [d] Sips index for the heterogeneity of binding sites. [e] Langmuir parameter related to maximum adsorption capacity (μg/mg). [f] Langmuir parameter related to the energy of adsorption and affinity of the adsorbent.

Thermodynamic Studies. In adsorption studies, both energy and entropy factors must be considered to determine what processes will occur spontaneously.[28] The Gibbs free energy change, $\Delta G°$ (kJ/mol), is the fundamental criterion of spontaneity. Reactions occur spontaneously at a given temperature if ΔG is a negative quantity. Thermodynamic parameters for AFB_1, ZEA, OTA, and FB_1 adsorption by grape pomace were calculated at pH 7 and at different temperatures (5, 37, 50, and 70 °C). For all toxins, experimental adsorption data and predicted maximum adsorption capacities calculated according to isotherm models decreased with an increase in temperature, indicating an exothermic process. Accordingly, the values for the equilibrium constant K^0 for the adsorption reaction decreased as the temperature rose (Table 7). This may be due to a tendency for the mycotoxin molecules to escape from the solid phase with an increase in temperature of the solution. The K^0 was used to calculate the standard Gibbs free energy of adsorption, $\Delta G°$.[28] The negative values of $\Delta G°$ in Table 7 are indicative of a spontaneous adsorption process with a high affinity of the mycotoxins to the surface of the grape pomace. Thermodynamic parameters ($\Delta H°$ and $\Delta S°$) were calculated according to the van't Hoff equation and were determined from the slope and intercept of the plots of ln K^0 versus $1/T$.[28] The plots obtained for all mycotoxins at four different temperatures gave good correlation ($R^2 \geq 0.985$) (data not shown). The values of $\Delta H°$ and $\Delta S°$ are presented in Table 7. $\Delta H°$ values for mycotoxin adsorption are negative, confirming the exothermic nature of the phenomenon. The magnitude of the $\Delta H°$ value gives an indication of the type of adsorption, which can be either physical or chemical.[38] Physisorption involves weak associations, which include hydrogen bonds, van der Waals, dipole−dipole, and induced dipole. Chemisorption implies a chemical reaction or sharing of electrons between the adsorbent and the adsorbate, such as covalent bonds. Physisorption is described as having an enthalpy of <20 kJ/mol, whereas chemisorption is generally >20 kJ/mol.[34] For all mycotoxins the value of enthalpy was <20 kJ/mol, indicating a physical adsorption phenomenon (Table 7). Physical adsorption requiring small energy allows the equilibrium to be attained rapidly and the process to be easily reversible. Interestingly, $\Delta S°$ values were positive for AFB_1 and ZEA adsorptions, but negative for OTA and FB_1 adsorptions (Table 7). The negative values of $\Delta S°$ for OTA and FB_1 adsorption may be understood in terms of restriction of the movement of the molecules on the surface (two dimensions), as compared to the bulk solution (three dimensions). The binding of OTA and FB_1 on grape pomace is thus only enthalpically driven. Generally, this situation corresponds to polar noncovalent interactions (benefit in enthalpy associated to a cost in entropy), such as electrostatic interactions or hydrogen bonds. At the pH value of this study (7.0 ± 0.5), OTA and

dx.doi.org/10.1021/jf404179h | J. Agric. Food Chem. 2014, 62, 497−507

Table 7. Thermodynamic Parameters for AFB_1, ZEA, OTA, and FB_1 Adsorption by Grape Pomace

toxin	temperature (K)	K^0	ln K^0	$\Delta G°$ (kJ/mol)	$\Delta H°$ (kJ/mol)	$\Delta S°$ (kJ/mol·K)
AFB_1	278	1270	7.15	−17.3	−7.2	34.0
	310	1124	7.02			
	323	775	6.65			
	343	731	6.59			
ZEA	278	673	6.51	−15.5	−8.94	22.2
	310	482	6.18			
	323	412	6.02			
	343	319	5.77			
OTA	278	394	5.98	−13.9	−14.7	−2.70
	310	238	5.47			
	323	170	5.14			
	343	118	5.77			
FB_1	278	431	6.07	−13.9	−17.4	−11.6
	310	160	5.07			
	323	294	5.68			
	343	79	4.37			

FB_1 are in the anionic form; thus, they may be involved in polar noncovalent interactions. On the contrary, positive $\Delta S°$ values for AFB_1 and ZEA adsorption process reflect an increase in the randomness at the solid/liquid interface and suggest hydrophobic interaction between the adsorbent and the adsorbate.[39−41] The positive entropy change may also be caused by the decrease in the number of water molecules surrounding both the adsorbent and the adsorbate molecules involved in the hydrophobic interaction. Generally, hydrophobic interactions are associated with a cost in enthalpy. In conclusion, the thermodynamic parameters calculated for adsorption of mycotoxins onto grape pomace give information about the type of the interaction involved in the adsorption process. At pH 7, hydrophobic interactions could be associated with AFB_1 and ZEA adsorption (small $\Delta H°$ and positive $\Delta S°$ values). Electrostatic interactions could explain the higher $\Delta H°$ and the negative $\Delta S°$ values calculated for OTA and FB_1 adsorption.

The present work shows that grape pomace can be used as a low-cost and healthy biosorbent for removing mycotoxins from liquid media. This is the first time that grape pomace has been tested as a multi-mycotoxin adsorbent. These findings show that a grape pomace prepared from a red grape variety (cv. Primitivo) is able to sequester, in different adsorption systems, AFB_1, ZEA, OTA, and FB_1. Contact time curves showed that the adsorption of mycotoxins by grape pomace is rapid, which is of significant importance in the toxin reduction by adsorption. Adsorption/desorption studies performed at physiological pH showed that mycotoxin adsorption by grape pomace is stable within the pH ranges that can be found in the GI tract of monogastric animals. For the first time, multi-mycotoxin adsorption isotherms were used to study the mechanism of mycotoxin adsorption by grape pomace and to calculate the adsorption and thermodynamic parameters. This work did not study the mycotoxin adsorption efficacy of pomaces obtained from different grape cultivars or different grape byproducts (such as stalks and seeds). Further studies are required to assess if the mycotoxin adsorption efficacy of grape pomace can be affected by the grape cultivar used to make wine, as well to understand which components are the active compounds for the adsorption process by grape pomace.

In conclusion, grape pomace is a sustainable source of bioactive compounds that may have a wide range of technological applications as biosorbent to decontaminate mycotoxin-contaminated foodstuffs. The use of grape pomace as a supplement in the formulation of food/feed products does not guarantee efficacy in sequestering mycotoxins, unless proper digestion or feeding experiments are performed. In addition to must, wine, and grape juice, grape pomace could be used to decontaminate mycotoxin-contaminated liquid foods, such as fruit juice. It is not expected to affect relevant quality parameters of the final products, apart from the color intensity and the enrichment in health-promoting phenolic content.

AUTHOR INFORMATION

Corresponding Author

*(G.A.) Phone: +39 080 5929348. Fax: +39 080 5929374. E-mail: giuseppina.avantaggiato@ispa.cnr.it.

Funding

This work was supported by the EC KBBE-2007-222690-2 MYCORED Project.

Notes

The authors declare no competing financial interest.

ABBREVIATIONS USED

AFB_1, aflatoxin B_1; ZEA, zearalenone; OTA, ochratoxin A; FB_1, fumonisin B_1; DON, deoxynivalenol; UPLC, ultraperformance liquid chromatography; GI, gastrointestinal

REFERENCES

(1) FAO-STAT. FAO statistical data base; http://www.fao.org (accessed February 2010).

(2) Inbar, Y.; Chen, Y.; Hadar, Y.; Verdonck, O. Composting of agricultural wastes for their use as container media—simulation of the composting process. *Biol. Wastes* **1988**, *26*, 247−59.

(3) Fontana, A. R.; Antoniolli, A.; Bottini, R. Grape pomace as a sustainable source of bioactive compounds: extraction, characterization, and biotechnological applications of phenolics. *J. Agric. Food Chem.* **2013**, *61*, 8987−9003.

(4) Mazza, G. Anthocyanins in grapes and grape products. *CRC Crit. Rev. Food Sci. Nutr.* **1995**, *35*, 341−371.

(5) Guemour, D.; Bannelier, C.; Dellal, A.; Gidenne, T. Nutritive value of sun-dried grape pomace, incorporated at a low level in complete feed for the rabbit bred under magrebian conditions. *World Rabbit Sci.* **2010**, *18*, 17−25.
(6) Pinelo, M.; Arnous, A.; Meyer, A. S. Upgrading of grape skins: significance of plant cell-wall structural components and extraction techniques for phenol release. *Trends Food Sci. Technol.* **2006**, *17*, 579−590.
(7) Mangan, J. L. Nutritional effects of tannins in animal feed. *Nutr. Res. Rev.* **1988**, *1*, 209−231.
(8) Viveros, A.; Chamorro, S.; Pizarro, M.; Arija, I.; Centeno, C.; Brenes, A. Effects of dietary polyphenol-rich grape products on intestinal microflora and gut morphology in broiler chicks. *Poult. Sci.* **2011**, *90*, 566−578.
(9) Sehm, J.; Lindermayer, H.; Dummer, C.; Treutter, D.; Pfaffl, M. W. The influence of polyphenol rich apple pomace or red-wine pomace diet on the gut morphology in weaning piglets. *J. Anim. Physiol. Anim. Nutr.* **2007**, *91*, 289−296.
(10) Hoye, C., Jr.; Ross, C. F. Total phenolic content, consumer acceptance, and instrumental analysis of bread made with grape seed flour. *J. Food Sci.* **2011**, *76*, 428−436.
(11) Mildner-Szkudlarz, S.; Bajerska, J.; Zawirska-Wojtasiaka, R.; Górecka, D. White grape pomace as a source of dietary fibre and polyphenols and its effect on physical and nutraceutical characteristics of wheat biscuits. *J. Sci. Food Agric.* **2013**, *93*, 389−395.
(12) Solfrizzo, M.; Avantaggiato, G.; Panzarini, G.; Visconti, A. Removal of ochratoxin A from contaminated red wines by repassage over grape pomaces. *J. Agric. Food Chem.* **2010**, *58*, 317−323.
(13) Richard, J. L. Some major mycotoxins and their mycotoxicoses-an overview. *Int. J. Food Microbiol.* **2007**, *119*, 3−10.
(14) Binder, E. M.; Tan, L. M.; Chin, L. J.; Handl, J.; Richard, J. Worldwide occurrence of mycotoxins in commodities, feeds and feed ingredients. *Anim. Feed Sci. Technol.* **2007**, *137*, 265−282.
(15) Grenier, B.; Oswald, I. P. Mycotoxin co-contamination of food and feed: meta-analysis of publications describing toxicological interactions. *World Mycotoxin J.* **2011**, *4*, 285−313.
(16) Avantaggiato, G.; Solfrizzo, M.; Visconti, A. Recent advances on the use of adsorbent materials for detoxification of *Fusarium* mycotoxins. *Food Addit. Contam.* **2005**, *22*, 379−388.
(17) Avantaggiato, G.; Havenaar, R.; Visconti, A. Assessment of the multi-mycotoxin-binding efficacy of a carbon/aluminosilicatebased product in an in vitro gastrointestinal model. *J. Agric. Food Chem.* **2007**, *55*, 4810−4819.
(18) Kolosova, A.; Stroka, J. Substances for reduction of the contamination of feed by mycotoxins: a review. *World Mycotoxin J.* **2011**, *4*, 225−256.
(19) EFSA (European Food Safety Authority). Review of mycotoxin-detoxifying agents used as feed additives: mode of action, efficacy and feed/food safety. Scientific report CFP/EFSA/FEEDAP/2009/01; http://www.efsa.europa.eu/en/supporting/doc/22e.pdf (accessed since Dec 8, 2009).
(20) Solfrizzo, M.; Panzarini, G.; Visconti, A. Determination of ochratoxin A in grapes, dried vine fruits, and winery by-products by high performance liquid chromatography with fluorometric detection and immunoaffinity cleanup. *J. Agric. Food Chem.* **2008**, *56*, 11081−11086.
(21) De Girolamo, A.; Pereboom-de Fauw, D.; Sizoo, E.; van Egmond, H. P.; Gambacorta, L.; Bouten, K.; Stroka, J.; Visconti, A.; Solfrizzo, M. Determination of fumonisins B_1 and B_2 in maize-based baby food products by HPLC with fluorometric detection after immunoaffinity column clean-up. *World Mycotoxin J.* **2010**, *3*, 135−146.
(22) Ringot, D.; Lerzy, B.; Chaplain, K.; Bonhoure, J. P.; Auclair, E.; Larondelle, Y. *In vitro* biosorption of ochratoxin A on the yeast industry by-products: comparison of isotherm models. *Bioresour. Technol.* **2007**, *98*, 1812−1821.
(23) Freundlich, H. M. F. Über die Adsorption in Lösungen. *Z. Phys. Chem.* **1906**, *57*, 385−470.
(24) Langmuir, I. The adsorption of gases on plane surface of glass, mica and platinum. *J. Am. Chem. Soc.* **1916**, *40*, 1361−1403.
(25) Weber, T. W.; Chakkravorti, R. K. Pore and solid diffusion models for fixed-bed adsorbers. *AIChE J.* **1974**, *20*, 228.
(26) Sips, R. On the structure of a catalyst surface. *J. Chem. Phys.* **1948**, *16*, 490−495.
(27) Hill, A. V. The possible effects of the aggregation of the molecules of haemoglobin on its dissociation curves. *J. Physiol. (London)* **1910**, *40*, iv−vii.
(28) Ringot, D.; Lerzy, B.; Bonhoure, J. P.; Auclair, E.; Oriol, E.; Larondelle, Y. Effect of temperature on *in vitro* ochratoxin A biosorption onto yeast cell wall derivatives. *Process Biochem.* **2005**, *40*, 3008−3016.
(29) Lemke, S. L.; Grant, P. G.; Phillips, T. D. Adsorption of zearalenone by organophilic montmorillonite clay. *J. Agric. Food Chem.* **1998**, *46*, 3789−3796.
(30) Daković, A.; Tomasevic-Canovic, M.; Rottinghaus, G.; Dondur, V.; Masic, Z. Adsorption of ochratoxin A on octadecyldimethyl benzyl ammonium exchanged-clinoptilolite-heulandite tuff. *Colloids Surf., B* **2003**, *30*, 157−165.
(31) Pietri, A.; Bertuzzi, T. Simple phosphate buffer extraction for the determination of fumonisins in masa, maize, and derived products. *Food Anal. Methods* **2012**, *5*, 1088−1096.
(32) Döll, S.; Dänicke, S.; Valenta, H.; Flachowsky, G. *In vitro* studies on the evaluation of mycotoxin detoxifying agents for their efficacy on deoxynivalenol and zearalenone. *Arch. Anim. Nutr.* **2004**, *58*, 311−324.
(33) Foo, K. Y.; Hameed, B. H. Insights into the modeling of adsorption isotherm systems. *Chem. Eng. J.* **2010**, *156*, 2−10.
(34) Grant, P. G.; Phillips, T. D. Isothermal adsorption of aflatoxin B_1 on HSCAS clay. *J. Agric. Food Chem.* **1998**, *46*, 599−605.
(35) Motulsky, K. J.; Ransnas, L. A. Fitting curves to data using nonlinear regression: a practical and nonmathematical review. *FASEB J.* **1987**, *1*, 365−374.
(36) Koopal, L. K.; van Riemsdijk, W. H.; de Wit, J. C. M.; Benedetti, M. F. Analytical isotherm equations for multicomponent adsorption to heterogeneous surfaces. *J. Colloid Interface Sci.* **1994**, *166*, 51−60.
(37) Seco, A.; Marzal, P.; Gabaldòn, C. Adsorption of heavy metals from aqueous solutions onto activated carbon in single Cu and Ni systems and in binary Cu-Ni, Cu-Cd and Cu-Zn systems. *J. Chem. Technol. Biotechnol.* **1997**, *68*, 23−30.
(38) Gatta, G. D. Determination of adsorption heats. *Thermochim. Acta* **1985**, *96*, 349−363.
(39) Manohar, D. M.; Anoop Krishnan, K.; Anirudhan, T. S. Removal of mercury(II) from aqueous solutions and chlor-alkali industry wastewater 2-mercaptobenzimidazole-clay. *Water Res.* **2002**, *36*, 1609−1619.
(40) Ho, Y. S. Removal of copper ions from aqueous solution by tree fern. *Water Res.* **2003**, *37*, 2323−2330.
(41) Kobya, M. Removal of Cr(VI) from aqueous solutions by adsorption onto hazelnut shell activated carbon: kinetic and equilibrium studies. *Bioresour. Technol.* **2004**, *91*, 317−321.

JOURNAL OF AGRICULTURAL AND FOOD CHEMISTRY

Article

pubs.acs.org/JAFC

Subcellular Distribution and Chemical Forms of Cadmium in Two Hot Pepper Cultivars Differing in Cadmium Accumulation

Junliang Xin and Baifei Huang*

Department of Safety and Environmental Engineering, Hunan Institute of Technology, Hengyang 421002, China

ABSTRACT: A greenhouse experiment was conducted to compare the subcellular distribution and chemical forms of cadmium (Cd) in roots, stems, leaves, and fruits between a low-Cd cultivar (Yeshengchaotianjiao, YCT) and a high-Cd cultivar (Jinfuzaohuangjiao, JFZ) of hot pepper (*Capsicum annuum* L.). The Cd concentrations in the root's subcellular fractions, and in all chemical forms in roots, were 1.85−4.88- and 1.84−4.90-fold higher, respectively, in YCT than in JFZ. Compared with JFZ, YCT had significantly lower Cd concentrations in the subcellular fractions (1.10−2.42-fold) of stems and leaves and in almost all chemical forms (1.17−2.97-fold) in the stems and leaves. Also, in fruits, the concentrations of Cd in the cell wall and soluble fractions were 1.18−2.24-fold significantly lower in YCT than in JFZ, and there were lower Cd concentrations (1.36−2.08-fold) in the chemical forms in YCT than in JFZ.

KEYWORDS: *hot pepper (Capsicum annuum L.), cadmium (Cd), subcellular distribution, chemical form, low-Cd cultivar*

INTRODUCTION

Cadmium (Cd) accumulation in agricultural soils as a result of industrial and agricultural activities has become a worldwide environmental problem.[1] Cadmium is readily taken up by the roots of crop plants and transported to edible plant parts because of its high mobility and bioavailability. Consequently, Cd-contaminated foodstuffs have become the major source of Cd intake by humans.[2] There are a variety of serious health risks associated with Cd intake, including lung cancer, osteoporosis, cardiovascular disease, and renal dysfunction.[3]

The accumulation of Cd in crops varies greatly not only among crop species but also among cultivars or genotypes within the same species.[4−6] Therefore, many researchers have suggested that the production of low-Cd cultivars could be useful tools in reducing the amount of Cd entering the human food chain.[2,7−9] However, the reasons for the variations in Cd uptake and accumulation among cultivars are still poorly understood.

There is some evidence that the subcellular distribution and chemical forms of Cd greatly affect the concentrations of free Cd ions in plant cells. Therefore, these factors can explain some of the differences in uptake and translocation of Cd among cultivars or genotypes.[10,11] Qiu et al. reported that the proportion of Cd bound to the cell walls was higher in a low-Cd cultivar than in a high-Cd cultivar of Chinese flowering cabbage (*Brassica parachinensis* L.).[12] However, the proportions of Cd bound to cell walls in the stems and young leaves were similar in low-Cd and high-Cd cultivars of water spinach (*Ipomoea aquatica* Forsk.).[13] Zhou et al. compared the chemical forms of Cd between low- and high-Cd genotypes of amaranth (*Amaranthus* spp.) and found that only the low-Cd genotype's stems had a lower proportion of Cd integrated into pectates and proteins.[14] In contrast, the shoots and roots of a low-Cd cultivar of Chinese flowering cabbage had higher proportions of Cd in the pectate/protein-integrated form, and lower proportions of Cd in the inorganic and other water-soluble forms, compared with a high-Cd cultivar.[12] Such studies have not yet provided consistent results regarding the differences in Cd uptake and storage among cultivars/species. Furthermore, these previous studies mainly focused on the roots, stems, and leaves of plants; there is little information available on other plant organs, including fruits, grains, or flowers.

Hot pepper (*Capsicum annuum* L.) is one of the most important vegetable crops worldwide. In China, hot pepper is cultivated on approximately 1.3 million hm^2 annually, producing 27 million tons of pepper.[15] It was reported that pepper has a medium tolerance to Cd, and accumulates Cd more readily in its fruits, when compared with the other two crops from the Solanaceae family, tomato (*Lycopersicon esculentum*) and aubergine (*Solanum melongena*).[16] Furthermore, the shoot portion of chili peppers maintained higher Cd uptake levels than the roots,[17] which is beneficial to the movement of Cd into fruits. Therefore, to minimize Cd accumulation in hot pepper fruits, it is extremely important to screen for low-Cd cultivars and elucidate the mechanisms for lower Cd accumulation. In our previous study, we identified some typical low- and high-Cd cultivars of hot pepper and found that the difference in fruit Cd concentrations between the low- and high-Cd cultivars was due to differences in Cd translocation rather than differences in Cd uptake by the roots.[18] However, the mechanisms of Cd translocation via the xylem or phloem to fruits, which are responsible for the differences in fruit Cd concentrations between low- and high-Cd cultivars, remained unclear. To study these mechanisms, we conducted a greenhouse pot experiment to investigate the subcellular distribution and chemical forms of Cd in the roots, stems, leaves, and fruits of two cultivars of hot pepper with different Cd accumulation characteristics.

Received: October 4, 2013
Revised: December 25, 2013
Accepted: December 30, 2013
Published: December 30, 2013

ACS Publications © 2013 American Chemical Society

dx.doi.org/10.1021/jf4044524 | J. Agric. Food Chem. 2014, 62, 508−515

The objectives of this study were to analyze the subcellular distribution, chemical forms, and amounts of Cd in various organs of a low-Cd cultivar and a high-Cd cultivar of hot pepper. We hypothesized that the subcellular distribution and chemical forms of Cd differ significantly among different tissues as well as between the low-Cd and high-Cd cultivars.

MATERIALS AND METHODS

Plant Materials. Two cultivars, Yeshengchaotianjiao (YCT) and Jinfuzaohuangjiao (JFZ), were selected from 30 hot pepper cultivars used in our previous study. The fruit Cd concentration in JFZ (0.19−3.22 mg kg^{-1} dry weight, DW) was 2.1−2.7-fold higher than that in YCT (0.07−1.54 mg kg^{-1}, DW) when grown in Cd-contaminated soils (0.28−2.69 mg kg^{-1}, DW).[18] Therefore, YCT and JFZ were identified as low-Cd and high-Cd cultivars, respectively.

Chemicals and Reagents. In the present study, 2-(*N*-morpholino)ethanesulfonic acid (MES), tris(hydroxymethyl)-aminomethane (Tris), and 1,4-dithioerythritol ($C_4H_{10}O_2S_2$, DTE) were purchased from Sigma (St. Louis, MO, USA). All other chemicals and reagents, except deionized water (d-H_2O), were of analytical grade and purchased from Guangzhou Chemical Regent Factory (Guangzhou, China).

Experimental Site and Soil. We conducted the pot experiment at the experimental garden of Hunan Institute of Technology (112°41′ E, 26°52′ N), Hunan Province, China. The experimental soil was collected from nearby farmland and was air-dried and ground to pass through a sieve with a 5 mm mesh size. The soil was a sandy loam, and its main physical and chemical properties were determined using the analytical methods described by Lu.[19] The soil pH, organic matter content, cation exchange capacity, total nitrogen, available P, available K, and total Cd were 6.42 g kg^{-1}, 19.3 g kg^{-1}, 91.0 mmol kg^{-1}, 1.6 g kg^{-1}, 103 mg kg^{-1}, 129 mg kg^{-1}, and 1.22 mg kg^{-1}, respectively. According to the Farmland Environmental Quality Evaluation Standards for Edible Agricultural Products (HJ 332-2006), the maximum level (ML) for Cd in soil is 0.3 mg kg^{-1}; therefore, the tested soil is considered as Cd-contaminated and served as a treatment (T1) without additional Cd^{2+} in this experiment. Two other Cd treatments (T2 and T3) consisted of soil with target Cd concentrations of 2.0 and 3.0 mg kg^{-1}, respectively, which were created by mixing T1 soil with appropriate amounts of Cd in the form of $Cd(NO_3)_2{\cdot}4H_2O$. Each of the T2 and T3 soils was placed in a large basin, watered, and left to equilibrate outdoors under a waterproof tarpaulin for approximately 6 months. This long period allowed for the equilibration of the various sorption mechanisms in the soils. For T2 and T3 treatments, the final soil total Cd concentrations were 2.02 and 3.26 mg kg^{-1}, respectively.

Experimental Design. The pot experiment was conducted in a greenhouse with an air temperature of 28−35 °C. Plastic pots (top diameter, 18 cm; bottom diameter, 13 cm; height, 15 cm) were filled with 3.0 kg (DW) of prepared soil. For each treatment, three pots (n = 3) were planted for each cultivar. The seeds were sown in the soil in the pots on March 10, 2013, and watered daily with tap water. The experiment was arranged in a completely randomized design. Within 15 days after germination, the seedlings were thinned to one per pot. A solid compound fertilizer (N/P/K = 15:15:15) was applied to the soil at the rate of 3.0 g pot^{-1} every 2 weeks. After the 120 day growth period, the plants were harvested. Fruits, leaves, stems, and roots were separately rinsed with tap water, and roots were desorbed for 15 min in ice-cold 5 mM $CaCl_2$ solution (5 mM MES-Tris, pH 6.0). All samples were thoroughly washed with deionized water, and the fresh weights were recorded. The fresh plant samples were divided into two portions: one for the analysis of the subcellular distribution of Cd and the other for the analysis of the chemical forms of Cd. Each portion was weighed (approximately 5 g), then immediately frozen in liquid N_2, and kept frozen until analyzed.

Separation of Tissue Fractions. Frozen plant samples were pretreated according to the method of Lozano-Rordriguez et al.[20] Each sample was homogenized in precooled extraction buffer (50 mM Tris-HCl, 250 mM sucrose, and 1.0 mM DTE, pH 7.5) with a chilled mortar and pestle.[21] The homogenate was sieved through nylon cloth (80 μm), and the liquid was squeezed from the residue. The residue on the cloth was washed twice with homogenization buffer and was designated fraction I (FI); it contained mainly cell walls and cell wall debris. The filtrate was centrifuged (Beckman JA-25.50 rotor, Fullerton, CA, USA) at 20000g for 45 min. The supernatant solution was referred to as the soluble fraction (including the vacuoles) and was designated fraction II (FII). The deposit was treated as the organelles (excluding the vacuoles) and was designated fraction III (FIII). All steps were performed at 4 °C. The subcellular fractions were dried at 70 °C to a constant weight and then digested at 145 °C for 24 h with an oxidative acid mixture of $HNO_3/HClO_4$ (2:1, v/v).

Extraction of Chemical forms of Cd. The chemical forms of Cd were determined using the method described by Wu et al.[10] Cd in different chemical forms was extracted by the specific solutions, in the following order: (1) 80% ethanol, which extracts inorganic Cd, giving priority to nitrate/nitrite, chloride, and aminophenol forms of Cd; (2) d-H_2O (Milli-Q, Millipore, Bedford, MA, USA), which extracts water-soluble Cd−organic acid complexes and $Cd(H_2PO_4)_2$; (3) 1 M NaCl, which extracts pectate- and protein-integrated Cd; (4) 2% acetic acid (HAc), which extracts undissolved Cd phosphates including $CdHPO_4$, $Cd_3(PO_4)_2$, and other Cd−phosphate complexes; and (5) 0.6 M HCl, which extracts Cd oxalate. Cd was not detected in residues because of its low concentration in the samples.

Frozen tissues were homogenized in extraction solution with a mortar and pestle, diluted at the ratio of 1:10 (w/v), and shaken for 22 h at 25 °C. Then, the homogenate was centrifuged at 5000g for 10 min, and the first supernatant was removed and transferred to a conical beaker. The sediment was resuspended twice in the same extraction solution, shaken for 2 h at 25 °C, and centrifuged at 5000g for 10 min, and the supernatant was collected. The three supernatants were pooled. The extraction procedure was the same for each of the five extraction solutions. Each of the pooled supernatant solutions was then evaporated on an electric plate at 70 °C to a constant weight and digested at 145 °C with an oxidative acid mixture of $HNO_3/HClO_4$ (2:1, v/v).

Chemical Analysis. The Cd concentrations in the digests were determined with an atomic absorption spectrophotometer (Shimadzu AA-6300C, Kyoto, Japan). A Certified Reference Material (CRM) of plant GBW07605 (provided by the National Research Center for CRM, China) was used for quality assurance and quality control (QA/QC) of the Cd analytical procedure.

Statistical Analysis. All Cd concentrations were calculated on the basis of the fresh weights of samples before separation or extraction. Data were statistically analyzed with the independent samples t test and least significant difference (LSD) test based on one-way ANOVA using Excel 2003 and SPSS 13.0. The data were checked for heteroscedasticity using Levene's test before the ANOVA was performed and showed no heteroscedasticity.

RESULTS

Effect of Soil Cd Concentrations on Plant Biomass. For both cultivars, there were no significant differences ($p > 0.05$) among the treatments in terms of the biomasses of roots, stems, and leaves (Table 1). However, the fruit biomass of JFZ in the T2 and T3 treatments was higher than that in the T1 treatment, and the fruit biomass of JFZ in the T2 treatment was significantly higher ($p < 0.05$) than that in the T1 treatment (Table 1). There was no significant difference ($p > 0.05$) in the fruit biomass of YCT among the three treatments (Table 1).

Subcellular Distribution of Cd. The subcellular distribution of Cd in fruits, leaves, stems, and roots of YCT (low-Cd cultivar) and JFZ (high-Cd cultivar) was analyzed by determining the Cd concentration in each of the different tissues. The Cd concentrations in the subcellular fractions of various tissues increased with increasing concentrations of Cd in the soil (Table 2). The concentrations of FI-Cd and FII-Cd in fruits were always significantly higher ($p < 0.01$ or $p < 0.05$)

dx.doi.org/10.1021/jf4044524 | J. Agric. Food Chem. 2014, 62, 508−515

Table 1. Biomass of Two Hot Pepper (*Capsicum annuum* L.) Cultivars, YCT and JFZ, under Different Cadmium (Cd) Treatments (T1−T3)

		biomass[a] (g FW)		
organ	cultivar	T1	T2	T3
fruit	YCT	10.9 ± 2.0	10.6 ± 1.2	9.2 ± 0.7
	JFZ	23.7 ± 6.7b	38.4 ± 7.6a	32.4 ± 7.0ab
leaf	YCT	41.2 ± 1.2	41.2 ± 1.6	39.6 ± 0.7
	JFZ	33.7 ± 1.4	31.0 ± 4.0	31.3 ± 3.0
stem	YCT	32.8 ± 2.7	35.1 ± 0.4	33.1 ± 0.6
	JFZ	19.1 ± 0.5	19.8 ± 1.6	19.2 ± 2.5
root	YCT	35.6 ± 4.3	39.6 ± 3.6	37.4 ± 2.8
	JFZ	36.2 ± 4.0	31.6 ± 1.7	31.6 ± 1.7

[a]Values are the mean ± SD (n = 3). Different letters in a row indicate significant difference at $p < 0.05$.

in JFZ than in YCT (Table 2). However, there were no significant differences ($p > 0.05$) in the concentrations of FIII-Cd in fruits between the two cultivars in all treatments (Table 2). In each treatment, the concentrations of FI-Cd, FII-Cd, and FIII-Cd in the leaves and stems of JFZ were significantly higher ($p < 0.01$ or $p < 0.05$) than those of their counterparts in the leaves and stems of YCT (Table 2). In contrast, the concentrations of FI-Cd, FII-Cd, and FIII-Cd in roots were always lower ($p < 0.01$) in JFZ than in YCT (Table 2).

In fruits, the majority of Cd was associated with FI, followed by FII and then FIII (Figure 1A). The proportions of FI-Cd in YCT fruit (46−51%) were lower than those in JFZ fruit (57−63%), but the proportions of FII-Cd and FIII-Cd in YCT fruit (27−30 and 22−24%, respectively) were slightly higher than those in JFZ fruit (22−26 and 15−18%, respectively). In leaves, most of the Cd was in FI (57−63% for YCT and 56−64% for JFZ), followed by FIII (20−28% for YCT and 23−24% for JFZ), and the smallest proportion of Cd was in FII (14−18% for YCT and 13−20% for JFZ) (Figure 1B).

In the stems, there were higher proportions of FI-Cd in YCT (71−75%) than in JFZ (63−70%) and lower proportions of FIII-Cd (13−15%) in YCT than in JFZ (18−21%) (Figure 1C). Furthermore, with increasing soil Cd concentrations, the proportions of FI-Cd decreased in both YCT (from 75 to 71%) and JFZ (from 70 to 63%), but the proportions of FII-Cd increased in both YCT (from 10 to 15%) and JFZ (from 10 to 19%). The proportions of FIII-Cd remained fairly constant (Figure 1C).

In roots, the largest proportion of Cd (77−82% for YCT and 82−87% for JFZ) was stored in FII, and the proportions of FII-Cd slightly increased as the soil Cd concentration increased in both cultivars (Figure 1D). In both cultivars, only small proportions of Cd (12−17% for YCT and 8−10% for JFZ) were bound to the cell wall, and even smaller proportions of Cd were partitioned into the organelles (5−6% for YCT and 4−8% for JFZ) (Figure 1D).

Chemical Forms of Cd. Overall, the concentrations of Cd in different chemical forms in various organs of hot pepper increased with increasing soil Cd concentrations (Table 3). In fruits, the concentrations of Cd in all chemical forms were consistently and significantly higher in JFZ ($p < 0.01$ or $p < 0.05$) than in YCT (Table 3), except there was no significant difference in the level of Cd extracted by 2% HAc between the two cultivars in the T2 treatment (Table 3). In addition, the Cd form extracted by 0.6 M HCl was not detected in fruits of either cultivar.

In leaves, the concentration of Cd extracted by 80% ethanol was higher in JFZ ($p < 0.05$) than in YCT in the T1 and T3

Table 2. Subcellular Distribution of Cadmium (Cd) in Different Organs of Low-Cd (YCT) and High-Cd (JFZ) Cultivars of Hot Pepper (*Capsicum annuum* L.)

			Cd concentration[a] (mg kg^{-1}, FW)			
subcellular fraction	treatment	cultivar	fruit	leaf	stem	root
cell wall (FI)	T1	YCT	0.02 ± 0.00*	0.34 ± 0.04**	0.52 ± 0.02*	0.39 ± 0.03**
		JFZ	0.05 ± 0.00	0.55 ± 0.04	0.75 ± 0.08	0.08 ± 0.01
	T2	YCT	0.04 ± 0.00*	0.55 ± 0.08**	0.79 ± 0.09*	0.60 ± 0.08**
		JFZ	0.08 ± 0.00	1.33 ± 0.15	1.03 ± 0.08	0.14 ± 0.02
	T3	YCT	0.06 ± 0.01**	1.21 ± 0.07**	1.46 ± 0.02*	0.97 ± 0.16**
		JFZ	0.11 ± 0.01	2.46 ± 0.25	1.61 ± 0.08	0.34 ± 0.00
soluble fraction (FII)	T1	YCT	0.01 ± 0.00**	0.10 ± 0.00**	0.07 ± 0.00**	1.76 ± 0.15**
		JFZ	0.02 ± 0.00	0.19 ± 0.01	0.11 ± 0.01	0.67 ± 0.11
	T2	YCT	0.02 ± 0.00**	0.15 ± 0.02** **	0.16 ± 0.00*	2.76 ± 0.06**
		JFZ	0.03 ± 0.00	0.31 ± 0.03	0.19 ± 0.01	1.48 ± 0.20
	T3	YCT	0.04 ± 0.00**	0.28 ± 0.03* *	0.31 ± 0.02**	6.64 ± 0.37**
		JFZ	0.05 ± 0.00	0.49 ± 0.08	0.48 ± 0.04	3.58 ± 0.22
organelle (FIII)	T1	YCT	0.01 ± 0.00ns	0.11 ± 0.02**	0.10 ± 0.01**	0.14 ± 0.01**
		JFZ	0.01 ± 0.00	0.23 ± 0.02	0.21 ± 0.03	0.07 ± 0.01
	T2	YCT	0.02 ± 0.00ns	0.27 ± 0.0**2	0.14 ± 0.01**	0.22 ± 0.02**
		JFZ	0.02 ± 0.00	0.53 ± 0.01	0.33 ± 0.01	0.10 ± 0.01
	T3	YCT	0.03 ± 0.00ns	0.43 ± 0.04**	0.27 ± 0.02	0.44 ± 0.07**
		JFZ	0.03 ± 0.00	0.87 ± 0.06	0.46 ± 0.07	0.18 ± 0.02

[a]Values shown are the mean ± SD, n = 3. ns, *, and ** indicate that the difference between the two cultivars in the same treatment is not significant, significant at $p < 0.05$, and significant at $p < 0.01$, respectively.

dx.doi.org/10.1021/jf4044524 | J. Agric. Food Chem. 2014, 62, 508−515

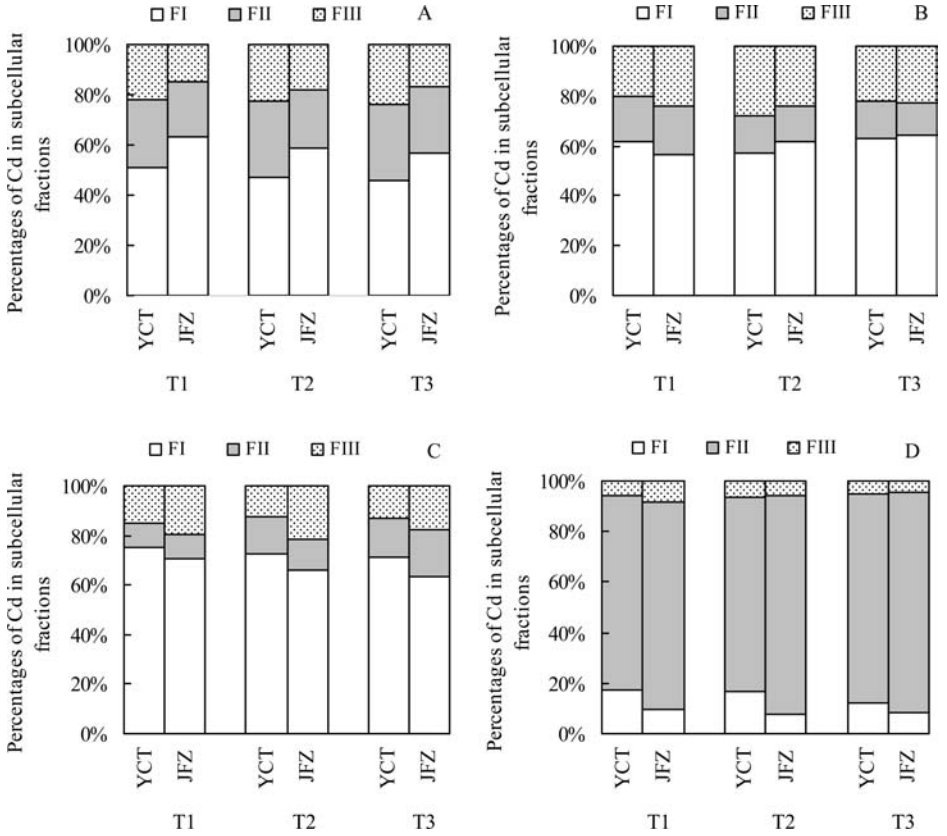

Figure 1. Percentages of cadmium (Cd) in subcellular fractions of fruits (A), leaves (B), stems (C), and roots (D) of hot pepper (*Capsicum annuum* L.) grown in soil with three different Cd concentrations. Cd percentage (%) = Cd concentration in fraction/(sum of Cd concentrations in all fractions) × 100.

treatments, but there was no significant difference ($p > 0.05$) between the two cultivars in the T2 treatment (Table 3). Also, the concentrations of Cd in other forms were always significantly higher in JFZ ($p < 0.05$ or $p < 0.01$) than in YCT (Table 3). In stems, the concentrations of Cd in all chemical forms were significantly higher in JFZ ($p < 0.05$ or $p < 0.01$) than in YCT, except for the chemical form extracted by d-H_2O in the T1 treatment (Table 3). In roots, the Cd concentration of each chemical form was significantly lower in JFZ ($p < 0.05$ or $p < 0.01$) than in YCT (Table 3).

In terms of the distribution of the different chemical forms of Cd, the Cd form extracted by 1 M NaCl accounted for the largest proportion of Cd in fruits, leaves, and stems, but the form extracted by 80% ethanol was the predominant form in roots (Figure 2). In addition, with increasing soil Cd concentrations, the proportion of the Cd form extracted by 1 M NaCl decreased in the leaves, stems, and roots, whereas those of the forms extracted by 0.6 M HCl, 2% HAc, and 80% ethanol markedly increased in the leaves, stems, and roots, respectively (Figure 2B–D). The proportions of each Cd form in the fruits were similar between YCT and JFZ (Figure 2A). However, in leaves, the proportions of the Cd form extracted by 80% ethanol were slightly higher in YCT (11–14%) than in JFZ (7–10%) in all treatments, but the proportions of the Cd form extracted by 1 M NaCl were lower in YCT than in JFZ in the T2 and T3 treatments (Figure 2B). In the stems and roots, the proportion of the Cd form extracted by 1 M NaCl was higher in YCT than in JFZ, whereas the proportion of the Cd form extracted by 80% ethanol was lower in YCT than in JFZ (Figure 2C). In most cases, the proportions of other forms of Cd extracted by d-H_2O, 2% HAc, or 0.6 M HCl in the stems, leaves, and roots were similar between YCT and JFZ.

DISCUSSION

The subcellular distribution of Cd has extremely important effects on the accumulation, migration, and detoxification of Cd in different species or cultivars.[12,13] In this study, most of the Cd (77–87%) in hot pepper roots was stored in the soluble fraction. The vacuole is a dynamic organelle that occupies as much as 90% of the total cell volume in some cell types.[22] Our results imply that the vacuole is the predominant sink for Cd in hot pepper. Similarly, Vázquez et al. reported that Cd was primarily associated with the vacuoles of bean roots, and no Cd was detected in the cell walls.[23] Wu et al.[10] reported that 51% of total Cd was present in the soluble fraction in barley roots, and a similar proportion of Cd was associated with the soluble fraction in rice roots, as reported by Yu et al.[11] Sequestration of Cd into the vacuole would greatly decrease its concentration in the cytosol, thereby preventing damage not only to organelles but also to many physiological and biochemical processes in the cells.

Plant cell walls, which are the first barrier protecting the protoplast against Cd toxicity, are mainly composed of polyose (including cellulose, hemicellulose, and pectin) and proteins, which provide functional groups, such as carboxyl, hydroxyl, amino, and aldehyde groups, on their surfaces to bind Cd ions and restrict their transport across the cell membrane.[1] Wang et al. reported that a large proportion of Cd (48.2–57.6%) in *Bechmeria nivea* (L.) Gaud. roots was bound to the cell walls.[24] However, in the present study, only a small proportion (8–

dx.doi.org/10.1021/jf4044524 | J. Agric. Food Chem. 2014, 62, 508–515

Table 3. Concentrations of Different Chemical Forms of Cadmium (Cd) in Two Hot Pepper (*Capsicum annuum* L.) Cultivars

			Cd concentration[a] (mg kg^{-1}, FW)			
extractant	treatment	cultivar	fruit	leaf	stem	root
80% ethanol	T1	YCT	0.01 ± 0.00**	0.07 ± 0.01*	0.05 ± 0.01**	1.16 ± 0.15**
		JFZ	0.01 ± 0.00	0.09 ± 0.01	0.13 ± 0.02	0.57 ± 0.08
	T2	YCT	0.01 ± 0.00**	0.12 ± 0.03ns	0.09 ± 0.01**	2.61 ± 0.23**
		JFZ	0.02 ± 0.00	0.14 ± 0.01	0.20 ± 0.01	1.20 ± 0.13
	T3	YCT	0.02 ± 0.00**	0.21 ± 0.01*	0.18 ± 0.02**	5.36 ± 0.24**
		JFZ	0.03 ± 0.00	0.25 ± 0.01	0.35 ± 0.03	2.84 ± 0.09
d-H_2O	T1	YCT	0.01 ± 0.00*	0.03 ± 0.00**	0.06 ± 0.01ns	0.28 ± 0.02**
		JFZ	0.02 ± 0.00	0.08 ± 0.01	0.06 ± 0.01	0.08 ± 0.01
	T2	YCT	0.02 ± 0.00**	0.06 ± 0.00**	0.09 ± 0.01*	0.39 ± 0.05**
		JFZ	0.04 ± 0.00	0.13 ± 0.01	0.11 ± 0.01	0.19 ± 0.01
	T3	YCT	0.04 ± 0.00**	0.09 ± 0.01**	0.17 ± 0.00*	0.90 ± 0.02**
		JFZ	0.06 ± 0.00	0.27 ± 0.04	0.26 ± 0.04	0.49 ± 0.07
1 M NaCl	T1	YCT	0.02 ± 0.00**	0.30 ± 0.02**	0.55 ± 0.04**	0.63 ± 0.07**
		JFZ	0.03 ± 0.00	0.54 ± 0.07	0.76 ± 0.02	0.21 ± 0.03
	T2	YCT	0.04 ± 0.01*	0.49 ± 0.05**	0.76 ± 0.09*	0.77 ± 0.12**
		JFZ	0.05 ± 0.01	1.00 ± 0.02	1.01 ± 0.09	0.30 ± 0.04
	T3	YCT	0.05 ± 0.00*	0.76 ± 0.05**	1.29 ± 0.08*	1.83 ± 0.09**
		JFZ	0.08 ± 0.01	1.73 ± 0.20	1.56 ± 0.08	0.67 ± 0.04
2% HAc	T1	YCT	0.01 ± 0.00*	0.03 ± 0.00**	0.01 ± 0.00**	0.02 ± 0.00**
		JFZ	0.01 ± 0.00	0.08 ± 0.01	0.03 ± 0.00	0.00 ± 0.00
	T2	YCT	0.01 ± 0.00ns	0.06 ± 0.00*	0.03 ± 0.00**	0.02 ± 0.01*
		JFZ	0.01 ± 0.00	0.11 ± 0.02	0.06 ± 0.00	0.01 ± 0.00
	T3	YCT	0.01 ± 0.00**	0.15 ± 0.01*	0.14 ± 0.01*	0.05 ± 0.00**
		JFZ	0.02 ± 0.00	0.25 ± 0.04	0.22 ± 0.04	0.01 ± 0.00
0.6 M HCl	T1	YCT	ND	0.07 ± 0.01*	0.03 ± 0.00**	0.01 ± 0.00*
		JFZ	ND	0.14 ± 0.03	0.04 ± 0.00	0.00 ± 0.00
	T2	YCT	ND	0.32 ± 0.05**	0.03 ± 0.00*	0.01 ± 0.00*
		JFZ	ND	0.61 ± 0.06	0.04 ± 0.00	0.00 ± 0.00
	T3	YCT	ND	0.65 ± 0.05**	0.11 ± 0.02*	0.10 ± 0.01**
		JFZ	ND	1.29 ± 0.16	0.17 ± 0.02	0.03 ± 0.00

[a]Values shown are the mean ± SD (n = 3). ND, not detected. ns, *, and ** indicate that the difference between the two cultivars in the same treatment is not significant, significant at $p < 0.05$, and significant at $p < 0.01$, respectively.

17%) of Cd was bound to the cell wall fraction in the roots of hot pepper. These conflicting results presumably reflect differences in experimental conditions and differences among species that have specific mechanisms and characteristics of Cd tolerance, uptake, translocation, and compartmentalization.

There was a higher Cd concentration in YCT's roots than in JFZ's roots, indicating that the low-Cd cultivar could retain more Cd in the root tissues. This may be associated with protection mechanisms by which excessive accumulation of a toxic substance will alleviate further uptake of that substance, such as NH_4-N in N-fixing symbiotic associations.[25] Similarly, a low-Cd water spinach cultivar accumulated more Cd in the roots than did a high-Cd cultivar.[13] However, Yu et al. reported that the root Cd concentration in a low-Cd rice cultivar was significantly lower than that in a high-Cd cultivar.[11] Therefore, the low Cd translocation from roots to aboveground parts in the low-Cd hot pepper cultivar, YCT, might be an additional mechanism to decrease uptake of Cd from the soil. Further research is needed to clarify this point.

When Cd is translocated from roots to aerial parts, the stem acts as a cation exchange column and, thus, it effectively reduces the amount of Cd that accumulates in leaves.[26] In the present study, a large proportion of Cd (63−75%) in stems was bound to the cell wall fraction. This could effectively reduce Cd accumulation in the cytoplasm and, hence, decrease the amount of Cd transported to the leaves. In addition, 56−64% of the total Cd in leaves was in the cell wall fraction. Therefore, large amounts of Cd were immobilized by the cell walls in stem and leaf tissues, thus decreasing the amount of Cd translocated to fruits. In the subcellular distribution of Cd between the two cultivars, YCT consistently had lower Cd concentrations in all three fractions of the stems and leaves and had a higher or similar proportion of Cd in FI, which contributed to the decrease of Cd mobility into the fruits from the stems and leaves. These attributes met the characteristics of a low-Cd cultivar. A high Cd concentration in the soluble fraction of rice leaves facilitates Cd translocation from leaves to grains.[11] Therefore, the reason for the high concentrations of Cd in fruits of JFZ might be that it has high concentrations of Cd in the FII of stem and leaf tissues.

A decrease in the concentration of free Cd in the cytosol of plants is one of the defense strategies against Cd toxicity and is achieved via various mechanisms.[10] The plant cell decreases the amount of Cd in the cytosol by sequestering Cd in subcellular

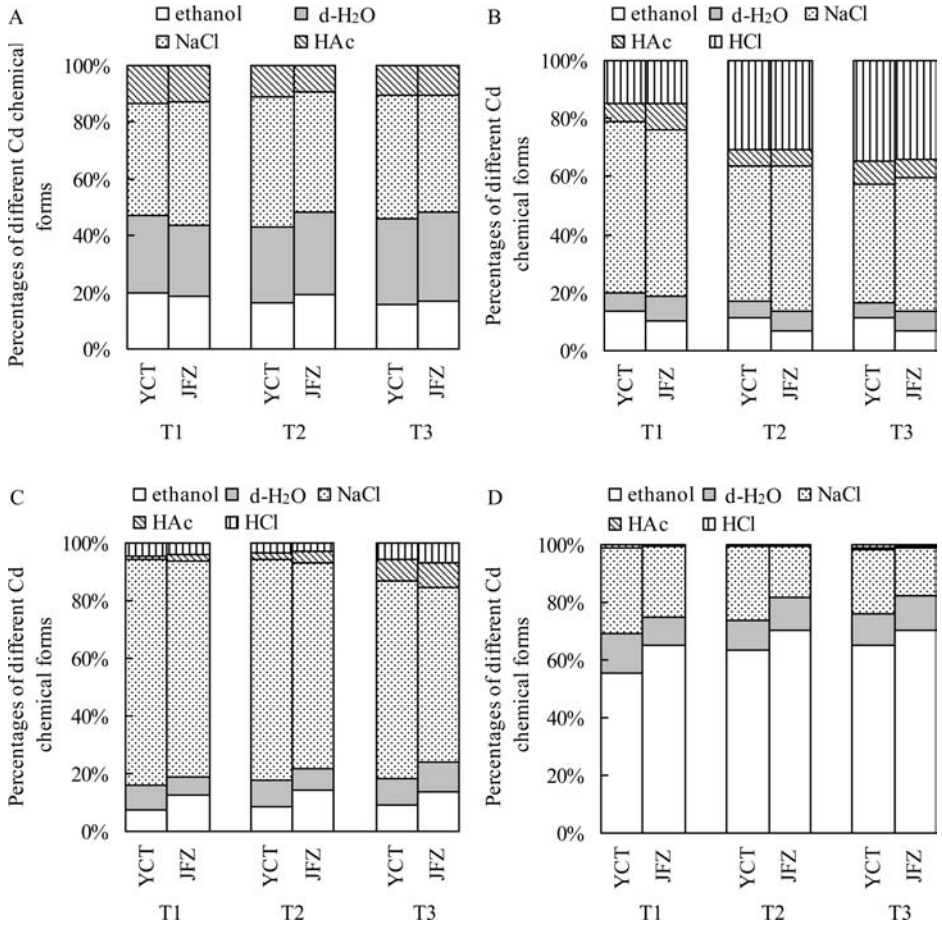

Figure 2. Percentages of different chemical forms of cadmium (Cd) in fruits (A), leaves (B), stems (C), and roots (D) of hot pepper (*Capsicum annuum* L.) grown in soil with three different Cd concentrations. Cd percentage (%) = Cd concentration in fraction/(sum of Cd concentrations in all fractions) × 100.

compartments. Our results showed that compared with YCT, JFZ accumulated a greater proportion of Cd in FI of fruits, thus reducing the proportion of Cd stored in FII. As a consequence, JFZ and YCT had similar concentrations of Cd in FIII of fruits. Also, the Cd concentrations in FIII of the stems and leaves were significantly higher in JFZ than in YCT, but the Cd concentrations in FIII of roots were significantly lower in JFZ than in YCT. However, the biomasses of stems, leaves, and roots did not decrease with increasing soil Cd concentrations in either cultivar. These results suggest that both cultivars are tolerant to Cd at the levels used in this experiment and that the Cd toxicity may be alleviated by sequestering Cd in cell walls. However, it is necessary to state that not all hot pepper cultivars have the same tolerance to Cd. León et al. reported that there were significant differences in tolerances to Cd^{2+} ions among pepper cultivars, and the tolerance to Cd is mainly dependent on the availability of nicotinamide adenine dinucleotide phosphate (NADPH) in pepper plants.[27] It was noteworthy that the highest proportion of Cd associated with organelles was generally in leaves, followed by fruits and then stems, and the lowest was in roots for both cultivars in all treatments. This may be because of the preferential accumulation of Cd in chloroplasts.[28]

The biological activity of Cd in plants is also dependent on its chemical forms, which can be extracted with various extractants.[10] For example, water-soluble Cd in inorganic forms (extracted by 80% ethanol) and organic forms (extracted by d-H_2O) migrate more readily than other forms and have strong negative effects on plant cells. Other forms of Cd, such as pectate/protein-integrated Cd (extracted by 1 M NaCl), insoluble cadmium phosphate (extracted by 2% HAc), and cadmium oxalate (extracted by 0.6 M HCl) are the least mobile and the least toxic to plant cells.[24] The largest proportion of Cd in roots of hot pepper was in the inorganic form, which is consistent with the highest proportion of Cd in FII. In root cells, Cd ions can induce phytochelatins (PCs) synthesis in the cytosol.[29,30] The PC−Cd complexes are sequestered into vacuoles by ATP-binding cassette transporters and can also be transported into vacuoles by heavy metal ATPases (e.g., HMA3) and proton/cation exchange transporters.[28] Thus, the amount of Cd^{2+} in the cytosol that can be loaded into the xylem by HMA2 and HMA4 and then translocated from root to shoot[31,32] is greatly decreased. In this sense, compartmentalization into the vacuoles may be crucial for Cd detoxification. Therefore, we can assume that more of the water-soluble Cd, extracted by 80% ethanol and d-H_2O from the roots, could be sequestered into vacuoles in YCT compared with that in JFZ. Also, the Cd concentration in the cytosol of root cells might not be higher in YCT than in JFZ. Further research is required to explore this point in detail. More importantly, HMA2 and HMA4 have been identified as key transporters mediating root-to-shoot Cd translocation via the xylem in rice.[31] Therefore, the Cd concentrations in aerial parts in the two hot pepper cultivars

dx.doi.org/10.1021/jf4044524 | J. Agric. Food Chem. 2014, 62, 508−515

might be strongly associated with that of the xylem sap, rather than that of the root's water-soluble form.

In the stems of YCT and JFZ, most of the Cd was integrated into pectates/proteins, and the Cd proportion in this form was higher in YCT than in JFZ; this might be partly related to the lower concentration of water-soluble Cd in the stem tissues of YCT. As a result, less Cd was translocated to leaves from the stem via the xylem in YCT than in JFZ. In leaves, most of the Cd was integrated with pectates/proteins, but the proportion of cadmium oxalate dramatically increased with higher soil Cd concentrations. The higher Cd concentrations in leaves might induce an increase in the production of oxalate to immobilize Cd and, thus, reduce Cd translocation to fruits via the phloem. Phloem-mediated transport might play a key role in delivering Cd to hot pepper fruits, and xylem-mediated Cd transport due to the transpiration of the fruits might also play an important role. Physiological experiments revealed that Cd is transported into seeds of grains mainly via the phloem in wheat and rice plants.[33,34] Analyses of different plant species have shown that the main Cd-ligand molecules in phloem sap are glutathione (GSH) and PCs.[35,36] Thus, it is assumed that in JFZ, which had higher Cd concentrations in fruits, a greater level of Cd translocation from the roots to aboveground parts via the xylem leads to higher levels of Cd in the stems and leaves (source organs). Subsequently, more Cd is available for transport from the source organs to sink organs (fruits) via the phloem, leading to higher Cd concentrations in fruits of JFZ than in fruits of YCT. Certainly, it is also possible that the greater Cd concentration in the xylem is transported directly into fruits after the xylem−phloem transfer, which may also cause more Cd accumulation in fruits.

The concentrations of all forms of Cd in fruits were lower in YCT than in JFZ, but the proportions of Cd in each form were similar in the two cultivars. Wu et al. reported that a Cd-sensitive barley genotype had higher Cd concentrations in inorganic and water-soluble forms, but lower concentrations of Cd in pectate/protein-integrated forms as compared with the Cd-resistant genotypes.[10] Because there were no differences in the proportions of Cd in each chemical form between YCT and JFZ and because the fruit biomass of the two cultivars did not decrease with increasing soil Cd concentrations, we assumed that the fruits of both hot pepper cultivars had a high tolerance to Cd at the levels used in these experiments.

In conclusion, our data support the hypothesis that there is a significant difference in the subcellular distribution and chemical forms of Cd among different tissues between the low-Cd and high-Cd hot pepper cultivars. Although most of the Cd is stored in the soluble fraction in roots of the two cultivars, the difference in the ability to translocate Cd from the roots to the stems is the main reason for the genotypic difference in Cd accumulation. In the stems, leaves, and fruits of both cultivars, the cell wall is the most crucial subcellular fraction for immobilization of Cd. Compared with the high-Cd cultivar, the low-Cd cultivar had lower concentrations of inorganic Cd (extracted by 80% ethanol), water-soluble Cd (extracted by d-H_2O), and pectate/protein-integrated Cd (extracted by 1 M NaCl) in both the stems and leaves; this resulted in less Cd being translocated from the stems and leaves to fruits via the phloem.

AUTHOR INFORMATION

Corresponding Author

*(B.H.) Phone: +84-734-3452095. Fax: +84-734-3452008. E-mail: huangbaifei@126.com.

Funding

This work was supported by the National Natural Science Foundation of China (Grants 41101303 and 41201320) and the Hunan Provincial Natural Science Foundation of China (Grants 11JJ6013 and 14JJ7082).

Notes

The authors declare no competing financial interest.

REFERENCES

(1) Fu, X.; Dou, C.; Chen, Y.; Chen, X.; Shi, J.; Yu, M.; Xu, J. Subcellular distribution and chemical forms of cadmium in *Phytolacca americana* L. *J. Hazard. Mater.* **2011**, *186*, 103−107.

(2) Grant, C. A.; Clarke, J. M.; Duguid, S.; Chaney, R. L. Selection and breeding of plant cultivars to minimize cadmium accumulation. *Sci. Total Environ.* **2008**, *390*, 301−310.

(3) Nawrot, T. S.; Staessen, J. A.; Roels, H. A.; Munters, E.; Cuypers, A.; Richart, T.; Ruttens, A.; Smeets, K.; Clijsters, H.; Vangronsveld, J. Cadmium exposure in the population: from health risks to strategies of prevention. *Biometals* **2010**, *23*, 769−782.

(4) Kuboi, T.; Noguchi, A.; Yazaki, J. Family-dependent cadmium accumulation in higher plants. *Plant Soil* **1986**, *92*, 405−415.

(5) Hocking, P. J.; McLaughlin, M. J. Genotypic variation in cadmium accumulation by seed of linseed, and comparison with seeds of some other crop species. *Aust. J. Agric. Res.* **2000**, *51*, 427−33.

(6) Wang, J.; Fang, W.; Yang, Z.; Yuan, J.; Zhu, Y.; Yu, H. Inter- and intraspecific variations of cadmium accumulation of 13 leafy vegetable species in a greenhouse experiment. *J. Agric. Food Chem.* **2007**, *55*, 9118−9123.

(7) Liu, J.; Qian, M.; Cai, G.; Yang, J.; Zhu, Q. Uptake and translocation of Cd in different rice cultivars and the relation with Cd accumulation in rice grain. *J. Hazard. Mater.* **2007**, *143*, 443−447.

(8) Liu, W.; Zhou, Q.; Sun, Y.; Liu, R. Identification of Chinese cabbage genotypes with low cadmium accumulation for food safety. *Environ. Pollut.* **2009**, *157*, 1961−1967.

(9) Xin, J.; Huang, B.; Yang, Z.; Yuan, J.; Dai, H.; Qiu, Q. Responses of different water spinach cultivars and their hybrid to Cd, Pb and Cd−Pb exposures. *J. Hazard. Mater.* **2010**, *175*, 468−476.

(10) Wu, F.; Dong, J.; Qian, Q. Q.; Zhang, G. P. Subcellular distribution and chemical form of Cd and Cd−Zn interaction in different barley genotypes. *Chemosphere* **2005**, *60*, 1437−1446.

(11) Yu, H.; Xiang, Z.; Zhu, Y.; Wang, J.; Yang, Z.; Yang, Z. Subcellular and molecular distribution of cadmium in two rice genotypes with different levels of cadmium accumulation. *J. Plant Nutr.* **2012**, *35*, 71−84.

(12) Qiu, Q.; Wang, Y.; Yang, Z.; Yuan, J. Effects of phosphorus supplied in soil on subcellular distribution and chemical forms of cadmium in two Chinese flowering cabbage (*Brassica parachinensis* L.) cultivars differing in cadmium accumulation. *Food Chem. Toxicol.* **2011**, *49*, 2260−2267.

(13) Xin, J.; Huang, B.; Yang, Z.; Yuan, J.; Zhang, Y. Comparison of cadmium subcellular distribution in different organs of two water spinach (*Ipomoea aquatica* Forsk.) cultivars. *Plant Soil* **2013**, *372*, 431−444.

(14) Zhou, Y.; Xue, M.; Yang, Z.; Gong, Y.; Yuan, J.; Zhou, C.; Huang, B. High cadmium pollution risk on vegetable amaranth and a selection for pollution-safe cultivars to lower the risk. *Front. Environ. Sci. Eng.* **2013**, *7*, 219−230.

(15) Xu, X.; Li, Y.; Wang, H. Present situation, development trend and countermeasures of pepper industry in China. *Chin. Agric. Sci. Bull.* **2008**, *24*, 332−338.

(16) Angelova, V. R.; Babrikov, T. D.; Ivanov, K. I. Bioaccumulation and distribution of lead, zinc, and cadmium in crops of Solanaceae family. *Commun. Soil Sci. Plant Anal.* **2009**, *40*, 2248−2263.

(17) Jidesh, C. V.; Kurumthottical, S. T. Selective retention of cadmium and lead in different parts of chilli (*Capsicum annuum* L.). *J. Trop. Agric.* **2000**, *38*, 51−54.
(18) Xin, J.; Huang, B.; Liu, A.; Zhou, W.; Liao, K. Identification of hot pepper cultivars containing low Cd levels after growing on contaminated soil: uptake and redistribution to the edible plant parts. *Plant Soil* **2013**, *373*, 415−425.
(19) Lu, R. *Soil and Agro-chemical Analysis Methods*; Agricultural Science and Technology Press: Beijing, China, 2000.
(20) Lozano-Rodriguez, E.; Hernàndez, L. E.; Bonay, P.; Carpena-Ruiz, R. O. Distribution of cadmium in shoot and root tissues. *J. Exp. Bot.* **1997**, *48*, 123−128.
(21) Weigel, H. J.; Jager, H. J. Subcellular distribution and chemical form of cadmium in bean plants. *Plant Physiol.* **1980**, *65*, 480−482.
(22) Pittman, J. K. Managing the manganese: molecular mechanisms of manganese transport and homeostasis. *New Phytol.* **2005**, *167*, 733−742.
(23) Vázquez, M. D.; Poschenrieder, C. H.; Barceló, J. Ultrastructural effects and localization of low cadmium concentrations in bean roots. *New Phytol.* **1992**, *120*, 215−226.
(24) Wang, X.; Liu, Y.; Zeng, G.; Chai, L.; Song, X.; Min, Z.; Xiao, X. Subcellular distribution and chemical forms of cadmium in *Bechmeria nivea* (L.) Gaud. *Environ. Exp. Bot.* **2008**, *62*, 389−395.
(25) Salvagiotti, F.; Cassman, K. G.; Specht, J. E.; Walters, D. T.; Weiss, A.; Dobermann, A. Nitrogen uptake, fixation and response to fertilizer N in soybeans: a review. *Field Crop Res.* **2008**, *108*, 1−13.
(26) Hardiman, R. T.; Jacoby, B. Absorption and translocation of Cd in bush beans (*Phaseolus vulgaris*). *Physiol. Plant.* **1984**, *61*, 670−674.
(27) León, A. M.; Palma, J. M.; Corpas, F. J.; Gómez, M.; Romero-Puertas, M. C.; Chatterjee, D.; Mateos, R. M.; del Río, L. A.; Sandalio, L. M. Antioxidative enzymes in cultivars of pepper plants with different sensitivity to cadmium. *Plant Physiol. Biochem.* **2002**, *40*, 813−820.
(28) Ramos, I.; Esteban, E.; Lucena, J. J.; Gárate, A. Cadmium uptake and subcellular distribution in plants of *Lactuca* sp. Cd-Mn interaction. *Plant Sci.* **2002**, *162*, 761−767.
(29) Hall, J. L. Cellular mechanisms for heavy metal detoxification and tolerance. *J. Exp. Bot.* **2002**, *53*, 1−11.
(30) Jemal, F.; Didierjean, L.; Ghrir, R.; Ghorbal, M. H.; Burkard, G. Characterization of cadmium binding peptides from pepper (*Capsicum annuum*). *Plant Sci.* **1998**, *137*, 143−154.
(31) Mendoza-Cózatl, D. G.; Jobe, T. O.; Hauser, F.; Schroeder, J. I. Long-distance transport, vacuolar sequestration, tolerance, and transcriptional responses induced by cadmium and arsenic. *Curr. Opin. Plant Biol.* **2011**, *14*, 554−562.
(32) Uraguchi, S.; Mori, S.; Kuramata, M.; Kawasaki, A.; Arao, T.; Ishikawa, S. Root-to-shoot Cd translocation via the xylem is the major process determining shoot and grain cadmium accumulation in rice. *J. Exp. Bot.* **2009**, *60*, 2677−2688.
(33) Herren, T.; Feller, U. Transport of cadmium via xylem and phloem in maturing wheat shoots: comparison with the translocation of zinc, strontium and rubidium. *Ann. Bot.* **1997**, *80*, 623−628.
(34) Tanaka, K.; Fujimaki, S.; Fujiwara, T.; Yoneyama, T.; Hayashi, H. Quantitative estimation of the contribution of the phloem in cadmium transport to grains in rice plants (*Oryza sativa* L.). *Soil Sci. Plant Nutr.* **2007**, *53*, 72−77.
(35) Van Belleghem, F.; Cuypers, A.; Semane, B.; Smeets, K.; Vangronsveld, J.; d'Haen, J.; Valcke, R. Subcellular localization of cadmium in roots and leaves of *Arabidopsis thaliana*. *New Phytol.* **2007**, *173*, 495−508.
(36) Mendoza-Cózatl, D. G.; Butko, E.; Springer, F.; Torpey, J. W.; Komives, E. A.; Kehr, J.; Schroeder, J. I. Identification of high levels of phytochelatins, glutathione and cadmium in the phloem sap of *Brassica napus*. A role for thiol-peptides in the long-distance transport of cadmium and the effect of cadmium on iron translocation. *Plant J.* **2008**, *54*, 249−259.

JOURNAL OF AGRICULTURAL AND FOOD CHEMISTRY

Article

pubs.acs.org/JAFC

High-Throughput Screening and Confirmation of 22 Banned Veterinary Drugs in Feedstuffs Using LC-MS/MS and High-Resolution Orbitrap Mass Spectrometry

Xufeng Wang,[‖] Yanghong Liu,[‖] Yijuan Su, Jianwen Yang, Kui Bian, Zongnan Wang, and Li-Min He*

National Reference Laboratory of Veterinary Drug Residues (SCAU), College of Veterinary Medicine, South China Agricultural University, Guangzhou 510642, China

Supporting Information

ABSTRACT: A new analytical strategy based on liquid chromatography−tandem mass spectrometry (LC-MS/MS) combined with accurate mass high-resolution Orbitrap mass spectrometry (HR-Orbitrap MS) was performed for high-throughput screening, confirmation, and quantification of 22 banned or unauthorized veterinary drugs in feedstuffs according to Bulletin 235 of the Ministry of Agriculture, China. Feed samples were extracted with acidified acetonitrile, followed by cleanup using solid-phase extraction cartridge. The extracts were first screened by LC-MS/MS in a single selected reaction monitoring mode. The suspected positive samples were subjected to a specific pretreatment for confirmation and quantification of analyte of interest with LC-MS/MS and HR-Orbitrap MS. Mean recoveries for all target analytes (except for carbofuran and chlordimeform, which were about 35 and 45%, respectively) ranged from 52.2 to 90.4%, and the relative standard deviations were <15% except for 20% for carbofuran. The decision limits (CCαs) for target analytes in formulated feed were between 2.6 and 23 μg/kg, and the detection capabilities (CCβs) were between 4.2 and 34 μg/kg. The method was successfully applied to screening of real samples obtained from local feed markets and confirmation of the suspected target analytes. It provides a high-throughput, sensitive, and reliable screening, identification, and quantification of banned veterinary drugs in routine monitoring programs of feedstuffs.

KEYWORDS: *screening, banned drugs, liquid chromatography-tandem mass spectrometry, confirmation, Orbitrap mass spectrometry, feedstuff*

INTRODUCTION

During the past decade, a large number of veterinary drugs have been widely used in the treatment of disease infection besides their use as growth promoters in farm animals. However, the increasing trend of abuse and illegal use of veterinary drugs as premixes and feed additives raises the risk of contamination of animal food and causes public panic. Therefore, in the European Community (EC), a series of regulations and directives have been issued to stringently regulate the appropriate use of veterinary drugs.[1] In Bulletin 235 of the Ministry of Agriculture (MOA), China, maximum residue limits (MRLs) of 96 veterinary drugs have also been laid down, 9 veterinary drugs without being detected in edible animal tissues, and 33 banned drugs in food-producing animals are regulated.[2] Great attention has been paid to the development and validation of various sensitive, specific, and reproducible analytical methods for simultaneously determining those registered veterinary drugs and banned drugs in various matrices such as edible animal tissues[3−5] and feedstuffs.[6,7]

Tandem mass spectrometry (MS/MS), using triple-quadrupole analyzer with electrospray ion (ESI) source, operated in selected reaction monitoring (SRM) mode, can provide accurate quantitative results, reliable identification, and confirmation. Thus, high-performance liquid chromatography coupled to triple-quadrupole mass spectrometry (LC-MS/MS) has become the predominant analysis technique in the detection of veterinary drug residues.[8−10] However, for a method to be deemed confirmatory in accordance with Commission Decision 2002/657/EC, identification of a target compound must meet the tolerances for the retention times, identification points (IPs), and relative ion ratios of the selected SRM transitions.[11] As for the latter, the relative intensities of the qualifier transition of some compounds (only limited fragment ions) are very weak no matter whether a standard or matrix is analyzed. As a result, the structural confirmation (the ion ratio of qualifier transition to quantifier transition) required in the system of IPs is unavailable in trace level of the target analyte. For example, in our routine monitoring of banned drugs in animal-derived foods and feeds, it has been observed that the intensity of a second "transition" (pair m/z parent > m/z product) is not strong enough in low level of a few compounds including but not limited to testosterone propionate, ronidazole, methaqualone, and trenbolone; higher 3:1 of signal-to-noise ratio (S/N) for the qualifier transition is difficult if the concentration of the analyte is below 1 ng/mL, so that the IPs rules defined in the Decision 2002/657/EC cannot be accomplished. More importantly, as for the routine monitoring of banned and illegal drugs in feeds and animal drinking water, the positive samples in fact are commonly very little. However, in cases when positive results are detected, the sample is required to be reanalyzed including a specific sample preparation (mandated in China). This implies that the two

Received: October 7, 2013
Revised: December 18, 2013
Accepted: December 23, 2013
Published: December 23, 2013

ACS Publications © 2013 American Chemical Society

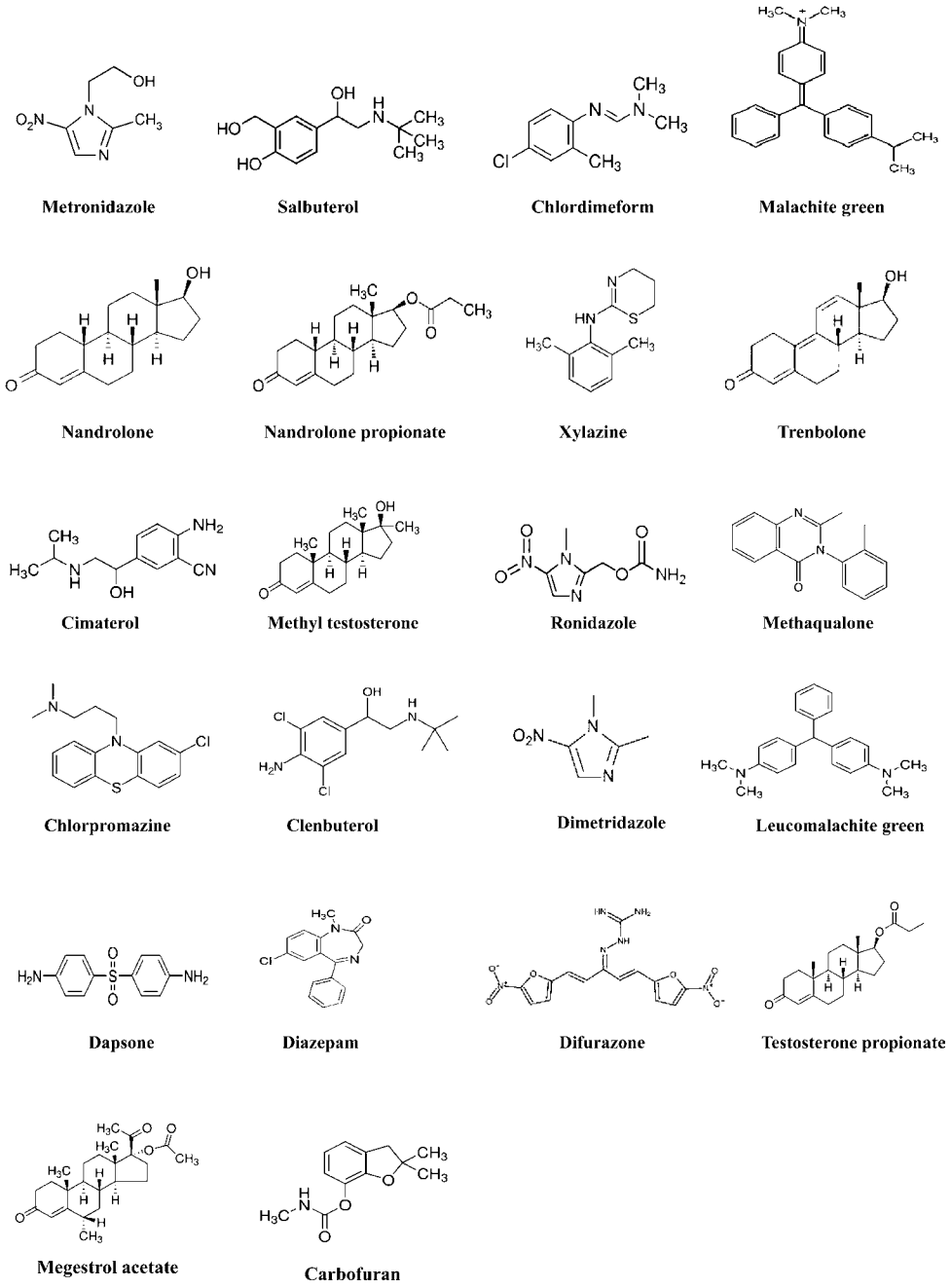

Figure 1. Chemical structures of 22 target compounds.

monitored transitions (in SRM mode) for each analyte are not necessary during multiresidue screening analysis by LC-MS/MS (only one transition). Thus, the acquired parameter settings are a simplification, and the number of monitoring analytes of interest may be double in a single selected reaction monitoring (S-SRM, a single ion pair monitoring) mode.

On the basis of the literature[12−15] and the descriptions above, a new idea for multiclass multiresidue analysis of veterinary drugs and banned substances in feedstuffs, animal drinking water, and animal-derived food is suggested. That is, one transition (the most abundant transition) in S-SRM mode is first adopted for high-throughput screening of target analytes in complex matrices. Then the suspected positive sample is subjected to a specific pretreatment for confirmation and quantification of the analyte of interest with LC-MS/MS and HR-Orbitrap MS in accordance with the accurate mass of precursor ion of target compound acquired in full scan mode. As an example, the present work aims at building up a high-throughput, sensitive, and efficient multiclass multiresidue approach for the screening and confirmation of 22 "no-tolerance" substances listed in Bulletin 235 of MOA, China, including metronidazole, salbutamol, chlordimeform, malachite green, nandrolone, nandrolone propionate, xylazine, trenbolone, cimaterol, methyl testosterone, ronidazole, methaqualone, chlorpromazine, clenbuterol, dimetridazole, leucomalachite green, dapsone, diazepam, difurazone, testosterone propionate, megestrol acetate, and carbofuran (Figure 1).

dx.doi.org/10.1021/jf404501j | J. Agric. Food Chem. 2014, 62, 516−527

Table 1. Mass Spectrometry Parameters of 22 Analytes and Their Mass Accuracy[a]

	LC-MS/MS			LC-LTQ-Orbitrap MS					
compound	DP (V)	quantifier ion m/z (CE, eV)	qualifier ion m/z (CE, eV)	elemental composition $[M + H]^+$	theoretical mass (Da) $[M + H]^+$	experimental mass (Da) $[M + H]^+$	mass error (ppm)	characteristic fragment ions[b] m/z (Da)	
metronidazole (A)	54	172.1 → 128.0 (19)	172.1 → 82.0 (38)	$C_6H_9N_3O_3$	172.0717	172.0716	−1.033	128.0453	82.0525
salbutamol (B)	60	240.0 → 148.0 (24)	240.0 → 221.9 (23)	$C_{13}H_{21}NO_3$	240.1594	240.1593	−1.083	148.0751	222.1485
chlordimeform (C)	70	197.2 → 117.1 (40)	197.2 → 125.1 (25)	$C_{10}H_{13}ClN_2$	197.0840	197.0839	−0.166	117.0572	152.0260
malachite green (D)	100	329.2 → 313.1 (40)	329.2 → 208.1 (38)	$C_{23}H_{24}N_2$	329.2012	329.2012	−0.715	208.1119	313.1696
nandrolone (E)	96	275.4 → 109.1 (36)	275.4 → 257.4 (24)	$C_{18}H_{26}O_2$	275.2006	275.2004	−0.533	257.1896	109.0648
nandrolone propionate (F)	102	331.3 → 109.2 (33)	331.3 → 275.4 (27)	$C_{21}H_{30}O_3$	331.2268	331.2265	−0.729	257.2896	239.1790
xylazine (G)	76	221.3 → 90.1 (30)	221.3 → 164.0 (35)	$C_{12}H_{16}N_2S$	221.1107	221.1106	−1.971	90.0372	164.0526
trenbolone (H)	130	271.3 → 199.2 (35)	271.3 → 253.3 (28)	$C_{18}H_{22}O_2$	271.1693	271.1691	−0.577	199.1116	253.1585
cimaterol (I)	55	220.2 → 202.0 (16)	220.2 → 160.2 (14)	$C_{12}H_{17}N_3O$	220.1444	220.1442	−1.175	202.1335	
methyl testosterone (J)	90	303.3 → 109.1 (37)	303.3 → 97.2 (37)	$C_{20}H_{30}O_2$	303.2319	303.2320	0.143	109.0642	285.2210
ronidazole (K)	40	201.0 → 140.0 (40)	201.0 → 110.1 (18)	$C_6H_8N_40_4$	201.0618	201.0617	−0.763	140.0452	110.0477
methaqualone (L)	90	251.2 → 132.1 (36)	251.2 → 91.2 (60)	$C_{16}H_{14}N_2O$	251.1179	251.1178	−0.556	132.0808	91.1815
chlorpromazine (M)	80	318.9 → 86.1 (30)	318.9 → 58.2 (60)	$C_{17}H_{19}ClN_2S$	319.1030	319.1029	0.020	274.0447	239.0758
clenbuterol (N)	48	277.1 → 203.0 (23)	277.1 → 259.0 (16)	$C_{12}H_{18}Cl_2N_2O$	277.0869	277.0868	−0.055	203.0134	259.0760
dimetridazole (O)	60	142.0 → 96.2 (25)	142.0 → 81.1 (35)	$C_5H_7N_3O_2$	142.0611	142.0610	−0.053	96.0681	112.0619
leucomalachite green (P)	100	331.4 → 239.1 (36)	331.4 → 316.1 (20)	$C_{23}H_{26}N_2$	331.2169	331.2167	−0.620	239.1791	316.1918
dapsone (Q)	80	249.2 → 156.1 (20)	249.2 → 108.1 (36)	$C_{12}H_{12}N_2O_2S$	249.0692	249.0691	−0.340	156.0112	108.0443
diazepam (R)	60	285.1 → 154.1 (38)	285.1 → 222.2 (38)	$C_{16}H_{13}ClN_2O$	285.0789	285.0784	−1.394	154.0416	222.1148
difurazone (S)	90	361.2 → 222.1 (26)	361.2 → 180.1 (30)	$C_{14}H_{12}N_6O_6$	361.0891	361.0886	−1.353	222.0619	180.0401
testosterone propionate (T)	113	345.3 → 109.1 (39)	345.3 →> 285.4 (25)	$C_{22}H_{32}O_3$	345.2424	345.2423	−0.757	109.0647	253.1947
megestrol acetate (U)	64	385.4 → 224.2 (35)	385.4 → 267.2 (26)	$C_{24}H_{32}O_4$	385.2373	385.2372	−0.405	267.1140	325.2159
carbofuran (V)	43	222.2 → 165.2 (18)	222.2 → 123.1 (31)	$C_{12}H_{15}NO_3$	222.1125	222.1124	−0.540	165.0980	197.7256

[a]DP represents declustering potential. $[M + H]^+$, precursor ion; CE, collision energy. [b]CE, 35 eV for cimaterol, methaqualone, clenbuterol, leucomalachite green and carbofuran; 30 eV for the other compounds.

MATERIALS AND METHODS

Chemicals. Methanol, acetonitrile, and formic acid (HPLC grade) were supplied by Fisher Scientific (Fair Lawn, NJ, USA). Ultrapure water was obtained by a Milli-Q Millipore system (Bedford, MA, USA). Acetone, ethyl acetate, and acetic acid, etc. (analytical reagent), were purchased from Guangzhou Chemical Reagent Factory. Solid phase extraction (SPE) cartridges including Oasis-HLB and Oasis-WCX (3 mL, 60 mg, Waters, Milford, MA, USA), SUPERCLEAN LC-18 cartridge (3 mL, 500 mg, Supelco, Bellefonte, PA, USA), HYPERSEP SCX (3 mL, 500 mg, Thermo Scientific and Technologies), and Poly-Sery MCX SPE (3 mL, 60 mg, CNW, Germany) were supplied from Shanghai ANPEL Scientific Instrument Co.

Preparation of Standards. The veterinary drug reference substances listed in Table 1 were of the highest available purity and were bought from Dr. Ehrenstorfer GmbH (Augsburg, Germany), China Institute of Veterinary Drugs Control (Beijing, China), and the National Institute of Control of Pharmaceutical and Biological Products (Beijing, China).

Individual stock standard solution (100−1000 μg/mL) was prepared by weighing each compound and then dissolving it in methanol, except for methaqualone and carbofuran standard solutions (100 μg/mL) purchased from Dr. Ehrenstorfer GmbH. They were stored in the dark at −20 °C for a maximum of 6 months. Multianalyte intermediate standard solution (0.050, 0.100, 0.500, 1.00, 5.00, 10.0, and 20.0 μg/mL) was prepared by pipetting appropriate individual standard solution and then diluting with methanol, respectively. Mixed standard working solution was prepared by diluting the multianalyte intermediate standard solution with a mixture of methanol/0.1% formic acid aqueous solution (10:90, v/v). The concentration of target analytes in the working standard solution ranged from 1.00 to 1000 ng/mL on the basis of the targeted concentration of the compound when added to the blank feed sample. Reconstitution solution was always prepared to dilute working standard solution and make a matrix-matched calibration curve.

Sample Collection. All kinds of feeds for pig, chicken, cattle, and aquatic product were collected from the local feedstuff markets and Quality Control and Inspection Center for Domestic Animal Product, MOA (Guangzhou, China). Prior to usage, feed samples were ground and passed through a 1 mm size sieve (16 mesh) and then stored at 4 °C. A previous analysis was conducted to ensure that they contained none of the studied analytes.

Sample Extract and Cleanup. Two grams of feed sample was accurately weighed into a 50 mL polypropylene centrifuge tube. For a spiked blank feed, the desired concentration levels (0.05, 0.25, 0.5, and 1.0 mg/kg for salbutamol, cimaterol, clenbuterol, and xylazine; 0.1, 0.5, 1.0, and 2.0 mg/kg for metronidazole, dimetridazole, difurazone, carbofuran, dapsone, methaqualone, diazepam, chlorpromazine, nandrolone 17-propionate, megestrol acetate, malachite green, and leucomalachite green; 0.2, 1.0, 2.0, and 4.0 mg/kg for ronidazole, chlordimeform, trenbolone, nandrolone, methyl testosterone, and testosterone propionate) were prepared, respectively, and these spiked samples were allowed to stand at room temperature in the dark for about 30 min before proceeding.

Twenty-four milliliters of acetonitrile and 1 mL of formic acid were added into the tube. The extraction was performed with an ultrasonic bath at 60 °C for 15 min and then centrifuged at 8000 rpm for 10 min at 4 °C. The supernatant was carefully decanted into another 50 mL tube, and the residue was re-extracted with 24 mL of acetontrile and 1 mL of formic acid. The mixture was then centrifuged at 8000 rpm for 10 min at 4 °C, the supernatant was decanted into the tube, and all of the organic

dx.doi.org/10.1021/jf404501j | J. Agric. Food Chem. 2014, 62, 516−527

extracts were combined into a 50 mL volumetric flask and diluted to the mark with 2% formic acid. Finally, 1 mL of sample extract solution was pipetted into a 10 mL tube and diluted with 2% formic acid to 5 mL for cleanup.

Five types of solid-phase extraction cartridges including Oasis HLB, WCX, LC-18, SCX, and MCX were evaluated. The cartridge was preconditioned with 3 mL of methanol, followed by 3 mL of water (WCX and SCX cartridge were further conditioned with 3 mL of 2% formic acid). Then, the sample extraction solution was loaded onto the cartridge and washed with 3 mL of 10% methanol aqueous solution. After the cartridge had been dried for 5 min under low vacuum, the analytes were eluted with 5 mL of methanol containing 5% ammonia (v/v), and the eluates were evaporated to near dryness under a gentle stream of nitrogen at 40 °C. The residues were reconstituted in 10% methanol in water containing 0.1% formic acid and filtered through a 0.22 μm filter before LC-MS/MS analysis.

LC-MS/MS Conditions. The chromatographic system was composed of an Agilent 1200 series high-performance liquid chromatography (LC) system, including a quaternary pump and an autosampler (Milford, MA, USA). The mass system included an Applied Biosystems API 4000 triple-quadrupole mass spectrometer with electrospray ionization interface and Analyst 1.5 software (Foster City, CA, USA).

The samples were analyzed using an Agilent ZORBAX SB-Aq (150 mm × 2.1 mm i.d., 3.5 μm) reversed-phase column (Torrance, CA, USA). The column temperature was kept at 35 °C. The mobile phase consisted of 0.1% formic acid aqueous solution (A) and acetonitrile (B). The detailed gradient elution program was as follows: 0−8.0 min, 4−55% B; 8.0−11 min, 55−95% B; 11−15 min, 95% B; 15−16 min, 4% B; 16−22 min, 4% B. An injection volume of 5 μL and a flow rate of 0.2 mL/min were used in LC-MS/MS analysis.

The mass analyses were performed using an ESI source in positive ionization mode. The operation conditions were as follows: ionspray voltage, 5.0 kV; source temperature, 550 °C; curtain gas (nitrogen), 20 psi; ion source gas 1, gas 2, and collision gas (nitrogen), 50, 55, and 6 psi, respectively. One SRM transition mode (for screening) and further SRM mode (for confirmation of the suspected positive findings) were carried out. The optimization of the main mass spectrometry parameters including collision energy (CE), declustering potential (DP), entrance potential (EP) and cell exit potential (CXP) values were optimized by flow injection analysis (FIA) for each compound. Table 1 shows the optimized parameter values and the single SRM transition used for screening and quantification of the 22 compounds.

LC-LTQ-Orbitrap MS Conditions. The LC system consisted of a Finnigan Surveyor LC system with a built-in degasser, autosampler, and pump (San Jose, CA, USA). The separation was performed on a Thermo Scientific Hypersil Gold (100 mm × 2.1 mm i.d., 3.5 μm) C_{18} column (Waltham, MA, USA), and the cartridge temperature was set at 35 °C. The same mobile phase composition and linear gradient program as for the LC-MS/MS analysis were used. The injection volume was 10 μL, and the flow rate was 0.25 mL/min.

Mass spectra were analyzed on a Finnigan LTQ-Orbitrap XL instrument with an ESI source (Thermo Electron, Bremen, Germany). Nitrogen was used as sheath gas (30 arbitrary units) and auxiliary gas (5 arbitrary units); helium served as the collision gas. Values of tube lens voltage and capillary voltage were set to 70 and 200 V, respectively. The scan event cycle used a full scan mass spectrum at a resolution of 30000 full width at half-maximum (fwhm at m/z 400). An external calibration for mass accuracy was performed using a mixture of caffeine, MRFA peptide, and Ultramark 1600 (Thermo Fisher Scientific Corp.) on the day of analysis. The mass spectrometric data were collected from m/z 65 to 500 in positive ion mode.

MetWorks 1.2 software (Waltham, MA, USA) was set to automatically identify target analytes by comparing the sample with the control. The mass tolerance and baseline window were set to 5 ppm and 40 s, respectively. An intensity ratio threshold of 5× and match threshold of 0.8 were set as limits to perform on the component-detected subtraction. LTQ-Orbitrap MS parameters and all of the analytes' elemental composition, theoretical mass (Da), experimental mass (Da), and characteristic fragment ions of precursor ion are shown in Table 1.

Validation Process. On the basis of the 2002/657/EC guidelines and the proposed new idea, in brief, the validation includes the high-throughput screening by LC-MS/MS and then the confirmation and quantification of the positive finding with LC-MS/MS and HR-Orbitrap MS. The performance characteristics of the developed LC-MS/MS method including specificity, decision limit (CCα) and detection capability (CCβ), recovery and precision, calibration curve, and stability were determined for validation purposes. The confirmation analysis of the suspected positive finding by HR-Orbitrap MS was also demonstrated.

Specificity. The specificity of the method was checked by analyzing 50 blank feed (30 formulated feeds and 20 premixes) samples from different species including pig, chicken, cattle, and fish to evaluate possible endogenous interferences.

CCα and CCβ. CCα is the lowest concentration at which a method can discriminate with a statistical certainty of $1 - \alpha$ that the analyte is present. In this case, CCα was established by the following: 20 blank matrix samples of feed (pig, chicken, cattle, and fish) were analyzed, and the S/N was calculated at the time window in which the analyte is expected. CCα values were defined as 3 times the S/N.

CCβ is the concentration at which the method is able to detect truly contaminated samples with a statistical certainty of $1 - \beta$. CCβ was calculated by analyzing 20 blank feed (pig, chicken, cattle, and fish) samples spiked with the analytes at CCα, and then the CCα value plus 1.64 times the corresponding standard derivation is equal to CCβ (β = 5%).

Recovery and Precision. Recovery and intraday precision (repeatability) were performed by the determination of the spiked blank feeds such as pig, chicken, cattle, and fish at the four concentration levels (six replicates at each level), respectively. For evaluation of interday precision (reproducibility), various blank feed samples were fortified with the same concentration levels during the three consecutive days. The final concentration of the spiked sample was determined by means of matrix-match standard curve. The recovery was calculated by the ratio of the concentration measured versus the concentration spiked in blank feed sample, whereas the precision was expressed as the relative standard deviation (RSD).

Calibration Curve. The matrix-matched calibration curves were prepared and used for quantification and testing the linearity of the developed method. Various blank feeds (pig, chicken, cattle, and fish) were pretreated according to the optimized extraction and cleanup procedures described above. The eluates from blank feeds were used to prepare a series of concentrations from 0.5 to 1000 ng/mL. The matrix-matched calibration curves were generated by using the peak area of analyte versus the corresponding concentration in the matrix solution. The acceptance criterion was that the coefficient of correlation (r^2) must be >0.99.

Stability. Instability of the analytes in stock solution or working standard solution may result in significant deviations of the detected results and thus exerts some influence on the accurate determination and confirmation of the target analytes. The stability of the 22 target analytes in the neat standard solution (10 μg/L) and the matrix-matched standard solution (10 μg/kg) at room temperature and 4 °C was assessed within 1 week. The measured values were compared to those of freshly prepared standard solutions.

RESULTS AND DISCUSSION

Optimization of Instrumental Conditions. The chromatographic conditions were investigated to gain overall optimum peak shape and resolution for the 22 analytes. Because the target compounds cover a wide diversity of polarities including polar compounds such as β-agonists, nitroimidazoles, and nonpolar compounds such as anabolic hormone esters, the mobile phase composition should be optimized to obtain higher sensitivity and resolution for major analytes. Numerous chromatographic runs were performed to test different mobile phases consisting of methanol or acetonitrile (as organic phase) and water with different percentages of formic acid (0.05, 0.1, and 0.2%, v/v). It

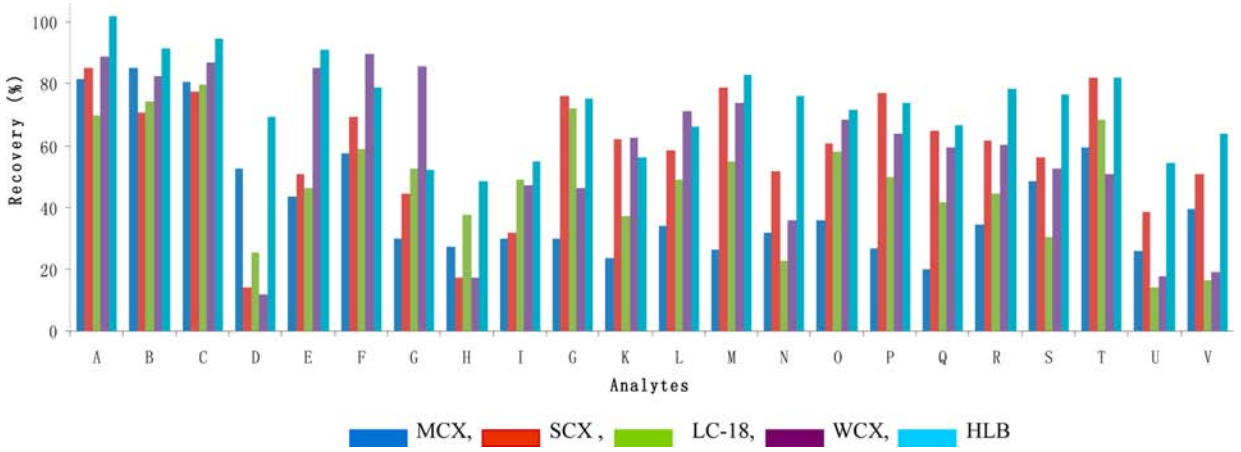

Figure 2. Recoveries of 22 analytes in the spiked formulated feed (0.5 mg/kg each) purified by different cartridges. Metronidazole (A), salbutamol (B), chlordimeform (C), malachite green (D), nandrolone (E), nandrolone propionate (F), xylazine (G), trenbolone (H), cimaterol (I), methyl testosterone (J), ronidazole (K), methaqualone (L), chlorpromazine (M), clenbuterol (N), dimetridazole (O), leucomalachite green (P), dapsone (Q), diazepam (R), difurazone (S), testosterone propionate (T), megestrol acetate (U), carbofuran (V).

was experimentally shown that acetonitrile provided better peak shape than methanol, and 0.1% formic acid in water gave the best overall peak sensitivity. Therefore, the system of acetonitrile and 0.1% formic acid aqueous solution was selected as the final mobile phase.

Four chromatographic columns (Thermo Hybrid golden C_{18}, CNW Athena C_{18}-WP (150 mm × 2.1 mm i.d., 3 μm), Agilent ZORBAX SB-Aq, and Phenomenex Luna C_{18} (150 mm × 2.0 mm i.d., 5 μm)) were used to evaluate their retention capabilities to the 22 target analytes. Under the optimized conditions, the separation of the analytes was performed on the Thermo Hybrid golden C_{18} chromatographic column, providing ideal analyte retention from 4 to 17 min, especially for those compounds with a similar polarity.

It should be mentioned that the properties of reconstitution solution before injection into the LC-MS/MS system were very important. Several different reconstitution solutions such as methanol, 10, 20, 30, 40, and 50% (v/v) methanol in water with 0.1% formic acid, and 10 mmol/L ammonium acetate solution were used to reconstitute the final extracts and dilute the mixed standard solution to prepare working standard solution. The results showed that the purified extracts reconstituted with methanol or 20, 30, 40 and 50% methanol aqueous solution containing 0.1% formic acid obtained broad and tailing peak shape and gave the drift of retention times. Conversely, not only good peak shape and constant retention time were obtained, but target analytes were also more stable when 10% methanol aqueous solution containing 0.1% formic acid was used as reconstitution solution.

Optimization of the main mass spectrometry parameters was achieved by FIA for each compound (0.5−10 μg/mL). The electrospray ion source operated in positive mode and a transition providing the highest signal was selected for each compound. The other optimized MS parameter values for screening and quantification are shown in Table 1.

For the confirmation of target analytes in the LTQ Orbitrap analyzer, the theoretical mass of each adduct ($[M + H]^+$) was previously calculated according to the elemental composition. The measurement of accurate mass obtained in full scan mode coupled to the characteristic ion fragmentations of precursor ion was used to confirm the presence of the target analyte and its molecular formula in suspected positive sample. A database including the elemental composition, the polarity of data acquisition, and expected adducts was established, and a high mass accuracy (below 5 ppm) was set as one of the identification criteria.

Extraction and Cleanup. The present work mainly aims at realizing a simultaneous detection for multiclass multiresidue target compounds. The performance of several generic extraction solvents and SPE cleanup cartridges has been evaluated. In the field of veterinary drug residue analysis, an extraction using acetonitrile followed by an SPE cleanup procedure is commonly used for multiple subclasses of veterinary drugs in feed,[16] meat,[17] milk,[18] and honey.[19] On the basis of these publications, methanol and acetonitrile were first used to extract the 22 target analytes from various feed matrices, and poor recoveries were obtained for the majority of the analytes. Therefore, organic solvent acidified with formic acid was used as extractive solvent.[6] The results show that acetonitrile acidified with formic acid could obtain extraction recoveries of >70% for all 22 analytes in feeds, especially >90% for β-agonists and nitroimidazoles; however, slightly lower recoveries for most analytes were obtained when methanol acidified with formic acid was used. To enhance the extraction yield of anabolic hormones while keeping the other recoveries within an acceptable range, a mixed solvent of acetonitrile, ethyl acetate, and formic acid (30:20:1, v/v/v) was further investigated. Regrettably, although much cleaner feed extracts and higher extraction recoveries for anabolic hormones were obtained, the recoveries of the other analytes were slightly decreased. Thus, acetonitrile acidified with formic acid was chosen as the final extraction solvent in the following experiments.

As far as the complex feed matrix is concerned, an additional cleanup step is generally required. Five SPE cartridges of HLB, WCX, LC-18, SCX, and MCX were used to purify and enrich the 22 analytes in feed extracts under their corresponding optimized conditions, respectively. High overall recoveries (>70%) for three β-agonists (salbutamol, cimaterol, and clenbuterol) in various feeds were obtained on the five types of cartridges, and slightly lower recoveries (>40%) for most analytes (except for metronidazole and chlordimeform, <20%) were obtained on Oasis HLB and WCX SPE cartridges. For most analytes poor recoveries (<40%) were obtained on the LC-18 and SCX SPE cartridges. Acceptable recoveries (>65% for 80% the compounds,

dx.doi.org/10.1021/jf404501j | J. Agric. Food Chem. 2014, 62, 516−527

Table 2. Sensitivity and Retention Time of Analyte by LC-MS/MS and LC-LTQ-Orbitrap MS

	LC-MS/MS						LC-LTQ-Orbitrap MS		
		SRM ion ratio[a] (%)							
compound	t_R (min)	solvent	matrix	concn[b] (μg/L)	CCα (μg/kg)	CCβ (μg/kg)	CCα (μg/kg)	CCβ (μg/kg)	t_R (min)
metronidazole (A)	7.4	0.17(12)	0.22(15)	0.1	11	13	4.9	8.2	6.1
salbutamol (B)	4.8	0.26(5.5)	0.23(7.2)	0.1	3.2	5.3	1.7	2.1	5.0
chlordimeform (C)	8.8	0.43(5.2)	0.39(4.5)	0.4	9.5	11	2.1	2.7	6.4
malachite green (D)	12.2	0.32(4.0)	0.28(5.8)	0.05	6.7	9.8	2.6	3.3	9.4
nandrolone (E)	14.2	0.81(1.9)	0.86(2.6)	0.2	14	20	6.0	7.9	11.9
nandrolone propionate (F)	17.3	0.38(5.0)	0.40(6.4)	0.2	11	16	3.1	4.4	16.4
xylazine (G)	9.1	0.29(5.5)	0.32(5.8)	0.1	5.4	7.4	2.3	2.9	6.5
trenbolone (H)	13.8	0.36(6.2)	0.38(7.8)	1.0	9.6	14	3.0	3.3	11.4
cimaterol (I)	5.1	0.52(8.0)	0.49(10)	0.05	3.5	4.7	1.5	2.0	5.0
methyl testosterone (J)	15.1	0.17(12)	0.13(15)	0.2	11	20	4.6	5.8	12.9
ronidazole (K)	8.3	0.55(6.2)	0.50(8.1)	1.0	13	19	5.5	7.3	6.8
methaqualone (L)	13.9	0.10(13)	0.13(18)	1.0	19	23	12	19	11.7
chlorpromazine (M)	11.4	0.20(5.5)	0.18(7.7)	0.05	4.4	5.9	1.2	1.5	9.0
clenbuterol (N)	9.2	0.22(4.8)	0.24(6.0)	0.5	2.6	4.2	1.3	2.0	6.7
dimetridazole (O)	8.1	0.37(8.0)	0.39(8.5)	0.2	8.0	10	2.4	3.2	6.7
leucomalachite green (P)	14.4	0.92(1.8)	0.91(4.4)	0.5	5.4	8.6	2.3	2.9	11.9
dapsone (Q)	10.9	0.65(3.0)	0.63(4.5)	0.1	5.3	7.2	1.3	1.8	8.9
diazepam (R)	14.8	0.22(15)	0.19(16)	0.5	6.4	9.0	1.7	2.5	12.8
difurazone (S)	10.8	0.79(3.0)	0.85(5.4)	0.1	4.5	6.2	1.9	2.5	8.4
testosterone propionate (T)	17.7	0.10(9.0)	0.13(12)	2.0	23	34	7.0	10	17.0
megestrol acetate (U)	16.2	0.88(3.5)	0.86(4.0)	0.05	4.6	6.7	1.0	1.3	14.7
carbofuran (V)	13.5	0.32(4.7)	0.37(6.0)	0.05	7.7	9.5	3.3	4.5	11.5

[a]Average of ion ratios obtained from the three levels spiked at 0.25, 0.5, and 2.5 mg/kg in solvent and matrix, respectively (data in parentheses are relative standard deviation). [b]Concentration of compound in mobile phase, when the intensity of confirmation transition is about 3 of signal-to-noise ratio.

Table 3. Recoveries of 22 Analytes for Spiked Formulated Feed Sample[a]

	spiked level (mg/kg)				intraday REC (%, n = 6)				intraday RSD (%, n = 6)					
compound	I	II	III	IV	I	II	III	IV	I	II	III	IV	interday REC (%, n = 72)	interday RSD (%, n = 72)
metronidazole (A)	0.1	0.5	1.0	2.0	63.6	64.7	52.4	56.9	8.3	2.1	3.5	11	59.4	9.8
salbutamol (B)	0.05	0.25	0.5	1.0	84.0	85.0	89.4	95.9	5.3	5.2	3.1	4.0	88.6	6.0
chlordimeform (C)	0.2	1.0	2.0	4.0	49.8	50.0	41.7	44.3	11	9.7	9.5	12	46.5	10
malachite green (D)	0.1	0.5	1.0	2.0	60.0	51.1	69.5	55.9	6.7	4.0	5.2	3.7	59.1	13
nandrolone (E)	0.2	1.0	2.0	4.0	62.7	60.4	66.0	59.4	5.7	3.6	5.7	2.4	62.1	4.7
nandrolone propionate (F)	0.1	0.5	1.0	2.0	64.8	68.1	66.2	75.7	9.2	6.4	6.3	8.0	68.7	7.2
xylazine (G)	0.05	0.25	0.5	1.0	66.4	63.2	67.4	67.3	8.7	6.7	6.2	10	66.1	3.0
trenbolone (H)	0.2	1.0	2.0	4.0	65.0	52.1	67.6	76.5	15	13	8.6	5.2	65.3	15
cimaterol (I)	0.05	0.25	0.5	1.0	82.3	86.0	80.8	104	8.9	8.5	4.9	2.8	88.3	12
methyl testosterone (J)	0.2	1.0	2.0	4.0	75.9	78.0	71.7	69.3	10	13	7.7	2.1	73.7	5.4
ronidazole (K)	0.2	1.0	2.0	4.0	74.7	76.9	77.2	75.2	7.4	6.7	3.6	3.2	76.0	1.8
methaqualone (L)	0.1	0.5	1.0	2.0	74.8	67.4	74.1	71.6	7.5	6.1	5.5	6.7	72.0	4.8
chlorpromazine (M)	0.1	0.5	1.0	2.0	62.2	58.6	59.3	64.4	8.4	7.0	9.7	8.7	61.1	4.5
clenbuterol (N)	0.05	0.25	0.5	1.0	85.4	84.8	87.8	79.8	6.0	3.2	5.1	1.8	84.5	4.1
dimetridazole (O)	0.1	0.5	1.0	2.0	88.9	91.5	87.4	93.7	4.8	2.4	2.9	2.1	90.4	3.2
leucomalachite green (P)	0.1	0.5	1.0	2.0	55.8	54.0	52.7	65.2	8.0	7.4	7.3	5.2	56.9	10
dapsone (Q)	0.1	0.5	1.0	2.0	50.5	52.1	55.4	50.9	5.5	2.6	3.1	4.6	52.2	4.4
diazepam (R)	0.1	0.5	1.0	2.0	77.5	78.9	73.4	85.5	6.0	6.7	11	4.5	78.8	6.4
difurazone (S)	0.1	0.5	1.0	2.0	51.6	52.3	51.7	55.9	4.7	2.9	5.1	5.2	52.9	3.9
testosterone propionate (T)	0.2	1.0	2.0	4.0	58.6	53.2	56.1	62.4	12	15	2.2	7.6	57.6	7.0
megestrol acetate (U)	0.1	0.5	1.0	2.0	82.4	81.1	84.2	81.9	5.9	5.3	4.8	3.1	82.4	1.8
carbofuran (V)	0.1	0.5	1.0	2.0	42.2	40.5	37.0	25.7	4.6	1.5	3.3	1.4	36.4	20

[a]REC, recovery; RSD, relative standard deviation.

dx.doi.org/10.1021/jf404501j | J. Agric. Food Chem. 2014, 62, 516−527

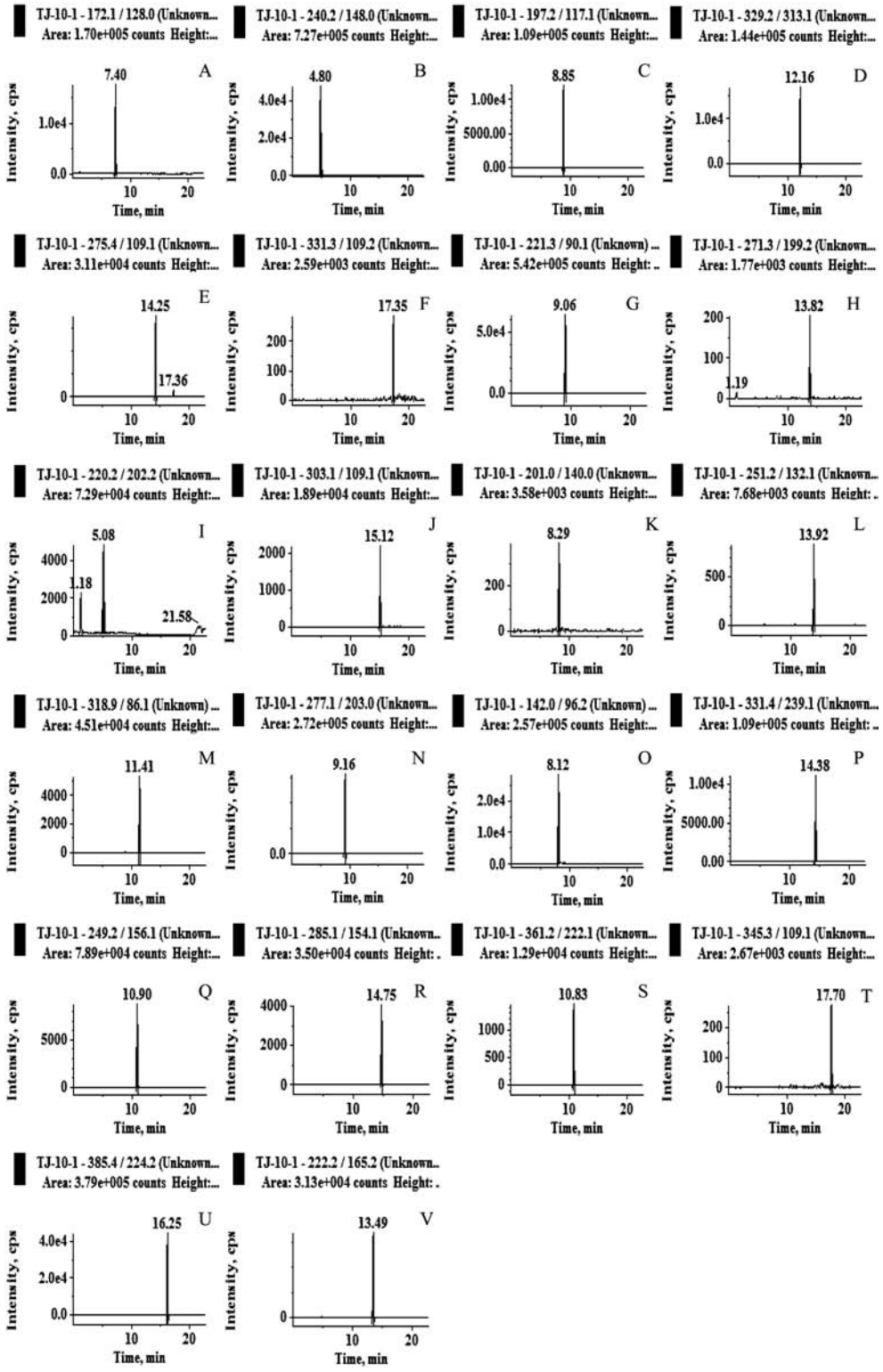

Figure 3. Typical S-SRM chromatograms of 22 analytes in the spiked formulated feed sample (0.5 mg/kg each). A–V identification as in Figure 2.

>50% for all 22 target analytes except for carbofuran and chlordimeform) were obtained on the Anpel MCX SPE cartridge. The recoveries of analytes of interest in spiking formulated feed purified by the five SPE cartridges are shown in Figure 2, demonstrating the higher absorptive capability of the MCX SPE cartridge relative to that of the other four SPE cartridges. Therefore, the MCX cartridge was selected for the following experiments. Further optimization of the loading, washing, and eluting solution for the MCX SPE cartridge was performed.

Because the acetontrile extraction solution was directly loaded on the MCX SPE cartridge, anabolic hormones were not well retained on the cartridge. When acetonitrile extracts were diluted with 2% formic acid before loading, good recoveries were obtained for most target analytes. In the washing step, methanol was first used, and some drugs were rinsed off. Finally, 10%

dx.doi.org/10.1021/jf404501j | J. Agric. Food Chem. 2014, 62, 516–527

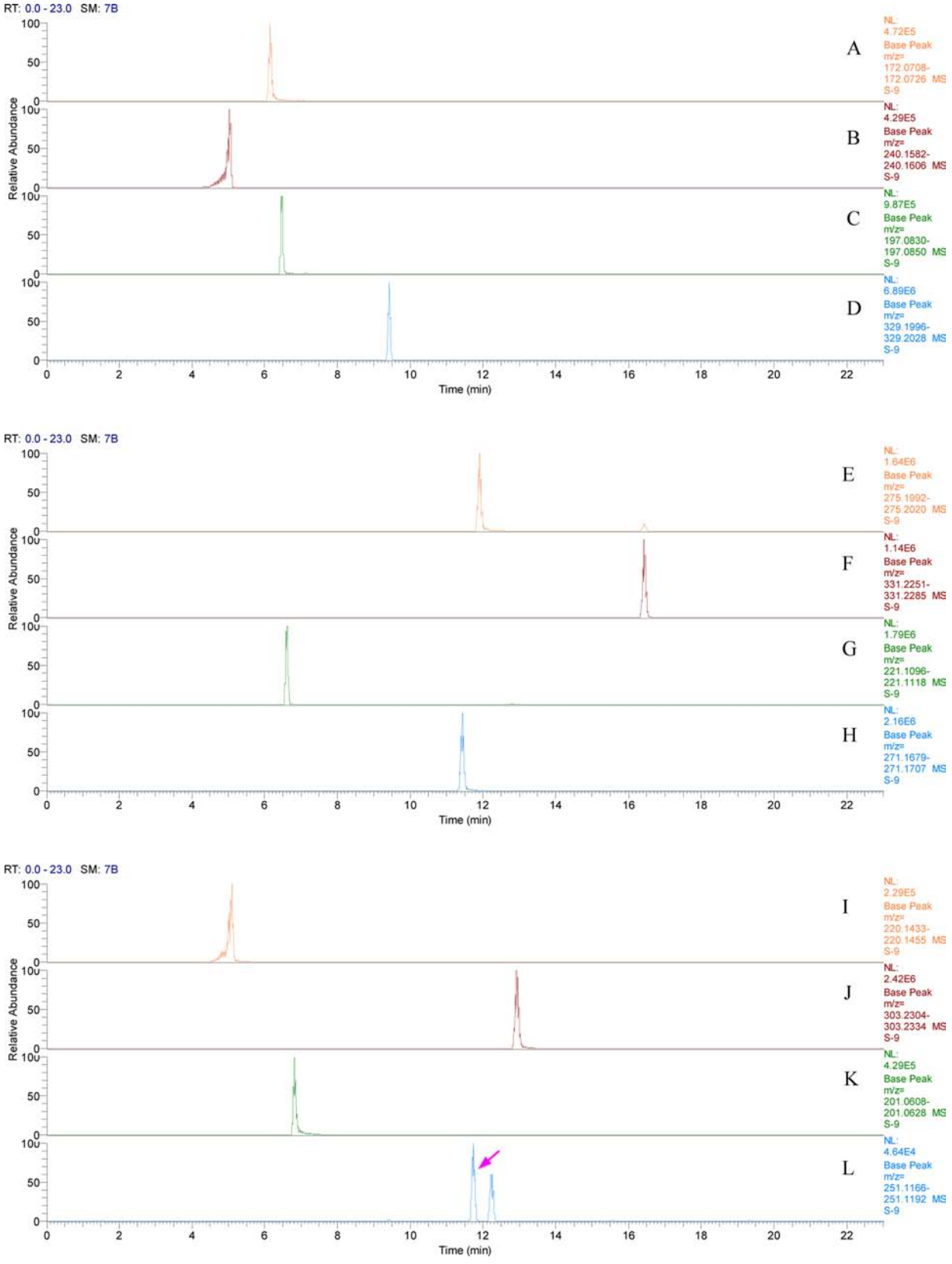

Figure 4. continued

dx.doi.org/10.1021/jf404501j | *J. Agric. Food Chem.* 2014, 62, 516−527

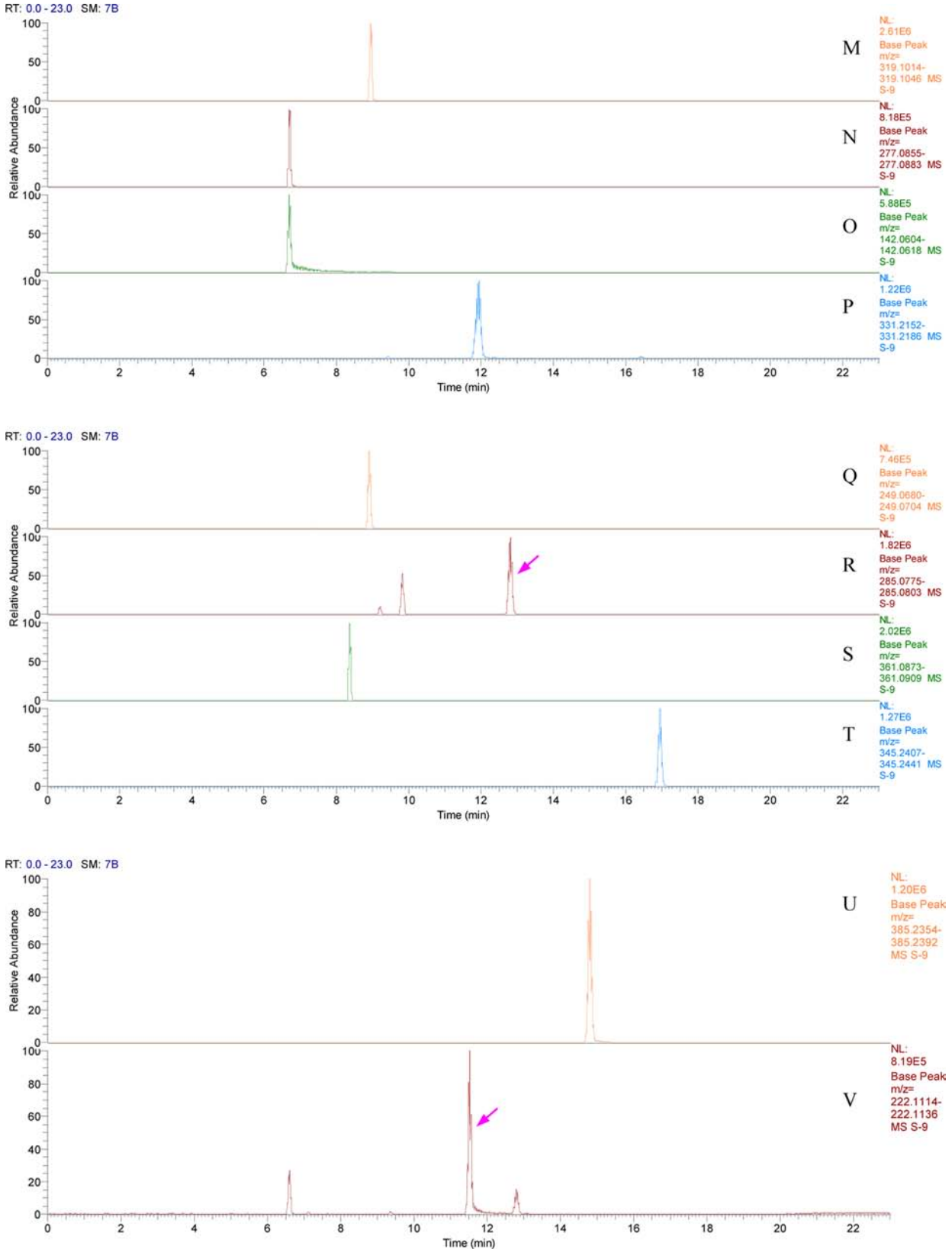

Figure 4. Accurate mass extracted ion chromatograms of 22 analytes in the spiked formulated feed sample (0.5 mg/kg each). A–V identification as in Figure 2.

methanol aqueous solution was selected as a proper washing solution. The selection of eluting solution was conducted between methanol and acetonitrile with different percentages of ammonium hydroxide. It was shown that 5% ammonium hydroxide in methanol could efficiently elute all target analytes on the cartridge and obtain fewer interferences.

dx.doi.org/10.1021/jf404501j | J. Agric. Food Chem. 2014, 62, 516–527

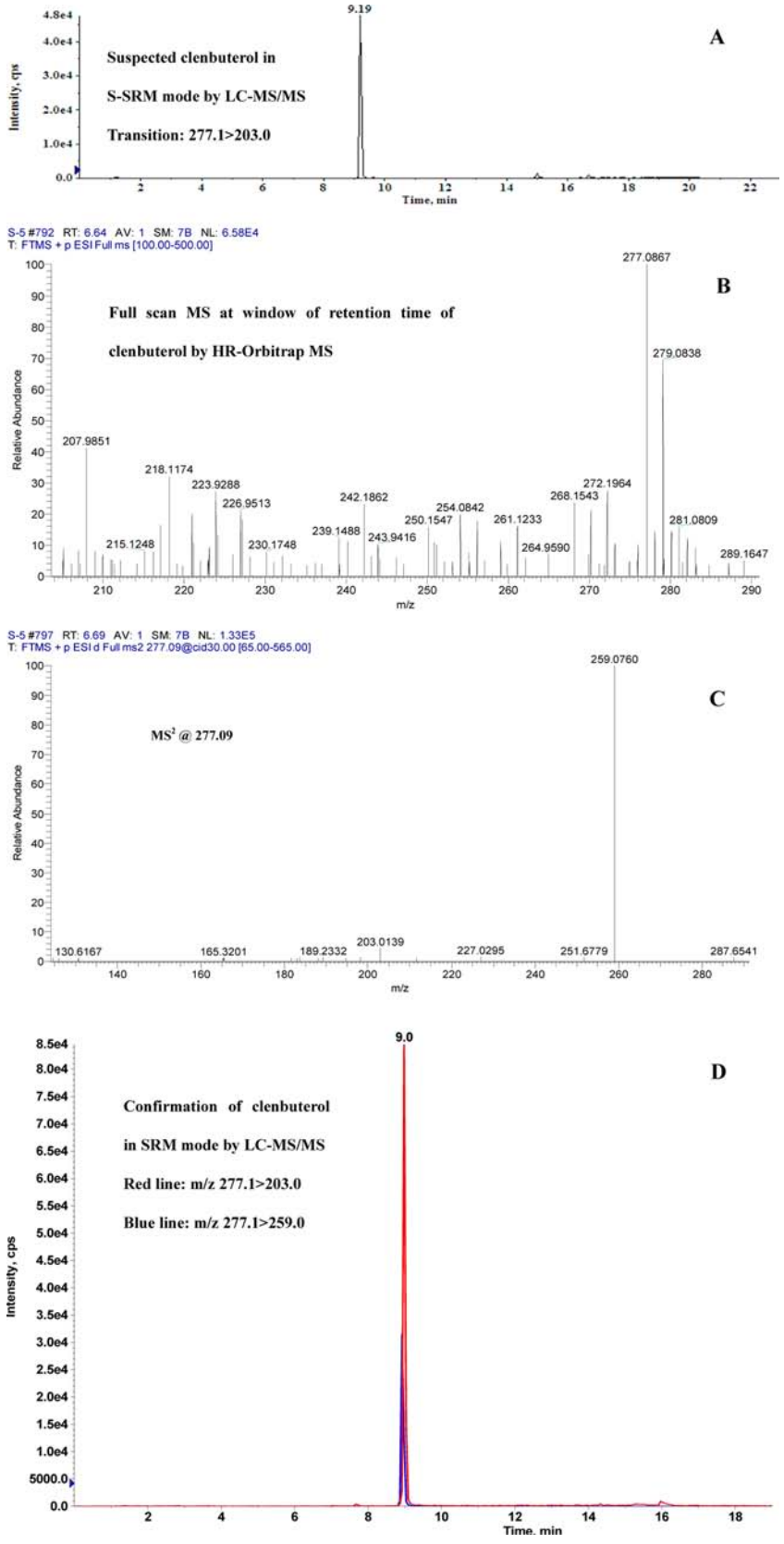

Figure 5. Demomstration of screening by LC-MS/MS and confirmation with LC-LTQ-Orbitrap MS in the cattle feed sample incurred by clenbuterol.

Method Validation. In accordance with Commission Decision 2002/657/EC, the performance characteristics of the proposed method based on LC-MS/MS analysis were validated as follows.

The selectivity was investigated by analyzing 50 blank pig, chicken, cattle, and fish feed samples to verify the absence of interfering substances. The results demonstrate that no interfering peaks within the 2.5% margin of the relative retention

dx.doi.org/10.1021/jf404501j | J. Agric. Food Chem. 2014, 62, 516−527

time of the 22 target analytes are detected in the single SRM chromatograms (Supporting Information, Figure S1).

As forbidden drugs used in feeds, the value of the limit should be as low as possible, as required by the Chinese government. To reveal weak intensity of qualifier transition of a certain compound in multiclass drugs analysis by LC-MS/MS in SRM mode, the ion abundance ratios of qualifier transition to quantifier transition of the studied analytes are shown in Table 2. The relative abundance ratios of testosterone propionate, methyl testosterone, and methaqualone were <15%, and those of metronidazole, chlorpromazine, and diazepam were about 20%. For obtaining 3 times the S/N ratio for confirmation transition of the compounds above, their corresponding concentration should be >1 μg/L. Thus, it is possible that the structural confirmation based on the relative abundance ratio in SRM mode is unavailable for certain compounds in the concentration levels required by the government. Under the conditions optimized in the proposed method, the values of CCα for the 22 compounds in various feeds ranged from 2.6 to 23 μg/kg, and the values of CCβ ranged from 4.2 to 34 μg/kg, suggesting the confirmation of these substances including but not limited to testosterone propionate, ronidazole, methaqualone, and trenbolone at <10 μg/kg in feeds is difficult by LC-MS/MS in SRM mode.

Accuracy (recovery) and precision (repeatability and within-laboratory reproducibility) were determined by processing independently the spiked feed samples at four different levels in three days (Table 3). The results show that the intraday recoveries for all target analytes were above 50% except chlordimeform and carbofuran (below 50 and 40%, respectively), and the intraday RSDs were all below 13%. The interday recoveries for most analytes were above 60%, and the interday RSDs were below 15% except for 19% carbofuran. The typical single SRM chromatograms of the spiked formulated feed sample are shown in Figure 3.

The linearity of the chromatographic response was evaluated with matrix-matched calibration curves at six concentration levels. The matrix-matched standard calibration curves showed good linearity in the ranges of 0.5−250 μg/mL for salbutamol, cimaterol, clenbuterol, and xylazine, 1.0−500 μg/mL for metronidazole, dimetridazole, difurazone, carbofuran, dapsone, methaqualone, diazepam, chlorpromazine, nandrolone 17-propionate, megestrol acetate, malachite green, and leucomalachite green, and 2.0−1000 μg/mL for trenbolone, nandrolone, methyltestosterone, testosterone propionate, ronidazole, and chlordimeform. The linear regression coefficients (r^2) of all the matrix-matched standard calibration curves were >0.99 (regression equations omitted).

Confirmation with LC-LTQ-Orbitrap MS. Because the confirmation of certain compounds using LC-MS/MS in SRM mode was unavailable according to Decision 2002/657/EC, the selectivity, sensitivity, and high-resolution mass behavior of the 22 target compounds using LC-LTQ-Orbitrap MS in full scan mode were evaluated. The blank feed matrices and spiked blank feeds in LC-MS/MS analysis were also subjected to analyses with LC-LTQ-Orbitrap MS. On the basis of the relative retention times, the 22 compounds in the spiked sample were identified efficiently in accordance with accurate mass provided by HR-Orbitrap MS, and no interfering peaks within the 2.5% margin of the relative retention time of the target analytes were detected. The typical extracted ion chromatograms of blank formulated feed are shown in Figure S2 (Supporting Information). The mean values of the mass measurements were all within 2 ppm of their theoretical m/z values at a mass resolving power of 30000 fwhm (Table 1). The results demonstrate that the confirmation of the spiked feed sample by HR-Orbitrap MS is reliable and feasible. The typical extracted ion chromatograms of the spiked formulated feed are shown in Figure 4.

The stability experiments revealed that the response factor of each compound remained almost constant in feed matrices for 2 days (room temperature) and 4 days (4 °C) and remained constant in neat solvent for 3 days (room temperature) and 6 days (4 °C), respectively. Therefore, the prepared samples should be injected within 2 days for good quantification. In addition, the mix standard stock solution should be used completely within 3 weeks.

Application to Real Samples. To evaluate the applicability of the proposed method, the analytical procedures described above were used to extract and determine 22 target analytes in 300 feed (including piglet, swine, poultry, cattle, and fish) samples collected from local feed markets. The real feed samples were first screened using LC-MS/MS in single SRM positive mode. The screening results showed that clenbuterol might be found in several cattle feed samples. These suspected positive samples were further confirmed by LC-MS/MS in SRM mode and also by means of accurate mass confirmation methodology of LC-LTQ-Orbitrap MS in full scan mode. Screening, confirmation, and quantification of clenbuterol in the incurred cattle feed based on this novel method are demonstrated in Figure 5. The screening analysis of the extracts of feed sample was carried out with LC-MS/MS in a single selected reaction monitoring mode. As shown in Figure 5A, the peak at a retention time of 9.2 min is detected in the channel of m/z 277.1/203.0. This suggested that there might be clenbuterol in this feed sample, so the extracts were subjected to further analysis by accurate mass HR-Orbitrap MS in full scan mode. In Figure 5B, the accurate monoisotopic mass of the $[M + H]^+$ ion of m/z 277.0868 is confirmed as clenbuterol, and in Figure 5C, clenbuterol is further proved by m/z 259.0760 and 203.0134 of specific fragment ions of m/z 277.0868. Finally, this positive cattle feed sample containing clenbuterol was reprepared with a specific procedure.[20] Briefly, after cleanup of extracts with the SCX cartridge, the eluates were evaporated to near dryness at 55 °C under a mild stream of nitrogen, dissolved in 10% methanol in water containing 0.1% formic acid, and filtered through a 0.22 μm filter. Then confirmation and quantification (simultaneously) by LC-MS/MS in selected reaction monitoring mode were carried out (Figure 5D). The identified result in accordance with the ratio of the qualifier transition to quantifier transition in LC-MS/MS analysis is consistent with the result of accurate mass confirmation by LC-LTQ-Orbitrap MS analysis. However, the HR-Orbitrap MS instrument is not cheap and can not be widely used in routine analytical laboratories registered with the government in China. Therefore, the high-throughput screening of multiclass drugs based on LC-MS/MS operated in a single SRM mode is feasible and recommendable in routine regulatory analysis. The suspected positive sample might be further identified by HR-Orbitrap MS for obtaining more reliable analysis if the confirmation with LC-MS/MS is poor.

In conclusion, a high-throughput, sensitive, and reliable screening and confirmative method using LC-MS/MS combined with accurate mass LC-LTQ-Orbitrap MS was first developed and validated for 22 banned and illicit drugs in feed matrices (Bulletin 235 of MOA, China). The multiclass screening analysis by LC-MS/MS operated in a single selected reaction monitoring mode is not only an intuitive and less time-consuming data process, but the number of monitoring analytes is also doubled

(in the same dwell time). For several suspected positive findings, accurate mass confirmation using LC-LTQ-Orbitrap MS can be an effective additional means of confirmation based on the ratios by LC-MS/MS in SRM mode.

■ ASSOCIATED CONTENT

Supporting Information

More details on the typical S-SRM chromatograms and accurate mass extracted ion chromatograms of 22 analytes in blank formulated feed (Figures S1 and S2). This material is available free of charge via the Internet at http://pubs.acs.org.

■ AUTHOR INFORMATION

Corresponding Author

*(L.-M.H.) Phone: 86-20-8528-0665. Fax: 86-20-8528-4896. E-mail: liminokhe@scau.edu.cn.

Author Contributions

‖X.W. and Y.L. contributed equally to this work.

Funding

This work was financially supported by the National Natural Science Foundation of China (No. 31072166) and the Veterinary Residues Fund of MOA, China (No. 12080).

Notes

The authors declare no competing financial interest.

■ ACKNOWLEDGMENTS

We thank Prof. Fang Binghu for facilitating preparation of the manuscript.

■ ABBREVIATIONS USED

CCα, decision limit; CCβ, detection capabilities; CE, collision energy; CID, collision-induced dissociation; CXP, cell exit potential; DP, declustering potential; EC, European Communities; EP, entrance potential; ESI, electrospray ion; FIA, flow injection analysis; fwhm, full width at half-maximum; HR-Orbitrap MS, high-resolution Orbitrap mass spectrometer; IPs, identification points; LC, high-performance liquid chromatography; LC-MS/MS, liquid chromatography−tandem mass spectrometry; MOA, Ministry of Agriculture; MRFA, tetrapeptide (Met-Arg-Phe-Ala); MRLs, maximum residue limits; RSD, relative standard deviation; S/N, signal-to-noise; SPE, solid phase extraction; SRM, selected reaction monitoring; S-SRM, single selected reaction monitoring

■ REFERENCES

(1) Council Directive 96/22/EC of 29 April 1996 concerning the prohibition on the use in stock-farming of certain substances having a hormonal or thyrostatic action and of β-agonists prohibits the use of certain substances for specific purposes in food-producing animals. *Off. J. Eur. Communities* **1996**, *L125*, 10.

(2) Bulletin 235, Ministry of Agriculture, People's Republic of China, 2002; p 27.

(3) Ishii, R.; Horie, M.; Chan, W.; MacNeil, J. Multi-residue quantitation of aminoglycoside antibiotics in kidney and meat by liquid chromatography with tandem mass spectrometry. *Food Addit. Contam. A* **2008**, *25*, 1509−1519.

(4) Olejnik, M.; Szprengier-Juszkiewicz, T.; Jedziniak, P. J. Multi-residue confirmatory method for the determination of twelve coccidiostats in chicken liver using liquid chromatography tandem mass spectrometry. *J. Chromatogr., A* **2009**, *29*, 8141−8148.

(5) Bittencourt, M. S.; Martins, M. T.; De Albuquerque, F. G.; Barreto, F.; Hoff, R. High-throughput multiclass screening method for antibiotic residue analysis in meat using liquid chromatography-tandem mass spectrometry: a novel minimum sample preparation procedure. *Food Addit. Contam. A* **2012**, *29*, 508−516.

(6) Mol, H. G.; Plaza-Bolanos, P.; Zomer, P.; de Rijk, T. C.; Stolker, A. A.; Mulder, P. P. Toward a generic extraction method for simultaneous determination of pesticides, mycotoxins, plant toxins, and veterinary drugs in feed and food matrixes. *Anal. Chem.* **2008**, *80*, 9450−9459.

(7) Boscher, A.; Guignard, C.; Pellet, T.; Hoffmann, L.; Bohn, T. Development of a multi-class method for the quantification of veterinary drug residues in feedingstuffs by liquid chromatography-tandem mass spectrometry. *J. Chromatogr., A* **2010**, *1217*, 6394−6404.

(8) Yang, Y.; Shao, B.; Zhang, J.; Wu, Y. N.; Duan, H. J. Determination of the residues of 50 anabolic hormones in muscle, milk and liver by very-high-pressure liquid chromatography-electrospray ionization tandem mass spectrometry. *J. Chromatogr., B* **2009**, *877*, 489−496.

(9) Herrmann, A.; Rosén, J.; Jansson, D.; Hellen, K. E. Evaluation of a generic multi-analyte method for detection of >100 representative compounds correlated to emergency events in 19 food types by ultrahigh-pressure liquid chromatography-tandem mass spectrometry. *J. Chromatogr., A* **2012**, *1235*, 115−124.

(10) Zhan, J.; Zhong, Y. Y.; Yu, X. J.; Peng, J. F.; Chen, S. B.; Yin, J. Y.; Zhang, J. J.; Zhu, Y. Multi-class method for determination of veterinary drug residues and other contaminants in infant formula by ultra performance liquid chromatography-tandem mass spectrometry. *Food Chem.* **2013**, *138*, 827−834.

(11) Commission Decision of 12 August 2002 implementing Council Directive 96/23/EC concerning the performance of analytical methods and the interpretation of results (2002/657/EC). *Off. J. Eur. Communities* **2002**, *L221*, 8.

(12) Kondrat, R. W.; McClusky, G. A.; Cooks, R. G. Multiple reaction monitoring in mass spectrometry/mass spectrometry for direct analysis of complex mixtures. *Anal. Chem.* **1978**, *50*, 2017−2021.

(13) Lau, J. H. W.; Khoo, C. S.; Murby, J. E. Determination of clenbuterol, salbutamol, and cimaterol in bovine retina by electrospray ionization-liquid chromatography-tandem mass spectrometry. *J. AOAC Int.* **2004**, *87*, 31−38.

(14) Fernández-Alba, A. R.; García-Reyes, J. F. UHPLC coupled with Fourier transform Orbitrap for residue analysis. *Trends Anal. Chem.* **2008**, *27*, 973−990.

(15) Nielen, M. W. F.; Lasaroms, J. J. P.; Mulder, P. P. J.; Hende, J.; Van Rhijn, J. A.; Groot, M. J. Multi residue screening of intact testosterone esters and boldenone undecylenate in bovine hair using liquid chromatography electrospray tandem mass spectrometry. *J. Chromatogr., B* **2006**, *830*, 126−134.

(16) Juan, C.; Igualada, C.; Moraguesa, F.; León, N.; Mañes, J. Development and validation of a liquid chromatography tandem mass spectrometry method for the analysis of beta-agonists in animal feed and drinking water. *J. Chromatogr., A* **2010**, *1217*, 6061−6068.

(17) Kaufmann, A.; Butcher, P.; Maden, K.; Widmer, M. Quantitative multiresidue method for about 100 veterinary drugs in different meat matrices by sub 2-micron particulate high-performance liquid chromatography coupled to time of flight mass spectrometry. *J. Chromatogr., A* **2008**, *1194*, 66−79.

(18) Stolker, A. A. M.; Rutgers, P.; Oosterink, E.; Lasaroms, J. J.; Peters, R. J.; Van Rhijn, J. A.; Nielen, M. W. Comprehensive screening and quantification of veterinary drugs in milk using UPLC-TOF-MS. *Anal. Bioanal. Chem.* **2008**, *391*, 2309−2322.

(19) Lopez, M. I.; Pettis, J. S.; Smith, I. B.; Chu, P. S. Multiclass determination and confirmation of antibiotic residues in honey using LC-MS/MS. *J. Agric. Food Chem.* **2008**, *56*, 1553−1559.

(20) He, L. M.; Su, Y. J.; Zeng, Z. L.; Liu, Y. H.; Huang, X. H. Determination of ractopamine and clenbuterol in feeds by gas chromatography-mass spectrometry. *Anim. Feed Sci. Technol.* **2007**, *132*, 316−323.

JOURNAL OF AGRICULTURAL AND FOOD CHEMISTRY

Addition/Correction

pubs.acs.org/JAFC

Correction to *Hericium erinaceus* (Lion's Mane) Mushroom Extracts Inhibit Metastasis of Cancer Cells to the Lung in CT-26 Colon Cancer-Transplanted Mice

Sung Phil Kim, Seok Hyun Nam,* and Mendel Friedman*

J. Agric. Food Chem. **2013**, *61* (20), 4898−4904. DOI: 10.1021/jf400916c

A corrected version of Figure 1 appears below.

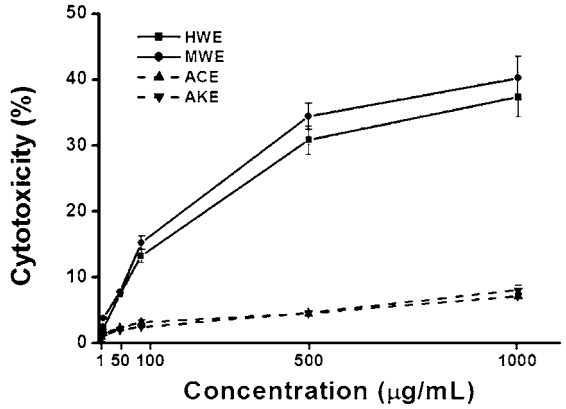

Figure 1. Cytotoxic effects of the four *H. erinaceus* extracts on murine colon carcinoma CT-26 cells. The cells were plated at a density of 1×10^5 cells/well in a 96-well microplate and then treated with various concentrations of each mushroom extract for 48 h. After incubation at 37 °C, cell death was determined using the MTT assay. ACE and AKE were used as the internal negative controls selected among the previously reported *H. erinaceus* extracts. Cytotoxicity was calculated according to the formula shown under Materials and Methods.

Published: January 2, 2014

ACS Publications © 2014 American Chemical Society

JOURNAL OF AGRICULTURAL AND FOOD CHEMISTRY

Review

pubs.acs.org/JAFC

Composition and Biological Activities of Hydrolyzable Tannins of Fruits of *Phyllanthus emblica*

Baoru Yang* and Pengzhan Liu

Food Chemistry and Food Development, Department of Biochemistry, University of Turku, FI-20014 Turku, Finland

ABSTRACT: Fruits of emblic leafflower have been used as food and traditional medicine in Asia. A wide range of biological activities have been shown in modern research suggesting potential of the fruits as healthy food and raw material for bioactive ingredients of food. Hydrolyzable tannins are among the major bioactive components of the fruits. Mucic acid gallate, mucic acid lactone gallate, monogalloylglucose, gallic acid, digalloylglucose, putranjivain A, galloyl-HHDP-glucose, elaeocarpusin, and chebulagic acid are the most abundant hydrolyzable tannins. The compositional profiles of tannins in the fruits vary depending on the cultivars as well as ripening stages. Fruits and tannin-rich extracts of fruits have shown antidiabetic, antimicrobial, anti-inflammatory, and immune-regulating activities in vitro and in animal studies. The fruits and fruit extracts have manifested protective effects on organs/tissues from damages induced by chemicals, stresses, and aging in animal models. The fruits and fruit extracts have potential in inhibiting the growth of cancer cells and reducing DNA damage induced by chemicals and radiation. Antioxidative activities are likely among the mechanisms of the biological activities and physiological effects. Human intervention/clinical studies are needed to investigate the bioavailability and metabolism of the tannins and to substantiate the health benefits in humans. Emblic leafflower may be a potential raw material for natural food preservatives.

KEYWORDS: *emblic leafflower, hydrolyzable tannins, elaeocarpusin, chebulagic acid, bioactive ingredients, nutraceuticals*

INTRODUCTION

The importance of food and diet in maintaining health and reducing the risk of chronic diseases is increasingly recognized. There is a fast-growing trend in the demand for foods with targeted health-promoting properties. The food industry is searching for new raw materials as sources of bioactive ingredients for foods and nutraceuticals.

Hydrolyzable tannins are derived by gallic acid (3,4,5-trihydroxybenzoic acid) being esterified to a core polyol, and the galloyl groups may be further esterified or cross-linked through dehydration to yield more complex hydrolyzable tannins.[1] Hydrolyzable tannins cover a wide group of compounds belonging to ellagitannins (esters of ellagic acid) and gallotannins (esters of gallic acid) that are present in many plant families. These compounds are gaining increasing attention of researchers in the areas of food and medicine because they are found to have a number of biological properties, including antioxidant, anticancer, antiatherosclerotic, antihepatotoxic, antibacterial, and anti-HIV replication activities.[2,3]

Emblic leafflower (*Phyllanthus emblica*) is a tropical fruit-bearing tree commonly planted in southern China, India, and other Asian countries. The fruits are consumed fresh and are also processed into food products in these regions. The fruits have been used in traditional medicines to treat various illnesses in Siddha, Sri Lanka, India, and China.[4] Recently, there has been increasing interest in the fruits as a raw material for food and nutraceuticals as well as bioactive ingredients of food and personal care products because of the traditional use and the biological activities shown in modern research. A wide array of biological activities and potential health benefits have been reported for emblic leafflower, including antioxidative, antidiabetic, antibacterial, hypolipidemic, anticancer, immunomodulatory, anti-inflammatory, and antiatherogenic properties as well as protective effects on the liver, gastric mucosa, and cardiovascular and nervous systems.[5−10] The materials studied are fresh fruits, fruit juice, and dried fruits, as well as extracts prepared with various solvents. The protocols applied in the studies carried out so far are mostly in vitro studies and animal experiments. Most of the studies have suggested that the phenolic compounds consisting of primarily hydrolyzable tannins of the fruits are the key bioactive components contributing to the beneficial effects. Several research groups have investigated the tannins of emblic leafflower fruits. This review summarizes the current literature on the compositional profile and the biological activities of hydrolyzable tannins of emblic leafflower fruits, juices, and various extracts of the fruits. The aim is to provide guidance for future research and application of this fruit as a source of bioactive ingredients of food.

HYDROLYZABLE TANNINS IN FRUITS OF *PHYLLANTHUS EMBLICA*

Hydrolyzable tannins are the dominating phenolic compounds of the fruits of *P. emblica*.[11,12] The tannin content is reported to be 4% of fresh weight in fruit[13] and 35% in dried fruit powder.[14] The highest content of tannins is found at the early development stage of the fruits.[15]

Tannins have been investigated in freeze-dried juice,[16] aqueous acetone (60%) extract of juice powder,[17,18] enzyme-aided water extract of fruits,[19] water extract of fresh fruits,[16]

Received: October 23, 2013
Revised: December 21, 2013
Accepted: December 26, 2013
Published: December 26, 2013

ACS Publications © 2013 American Chemical Society

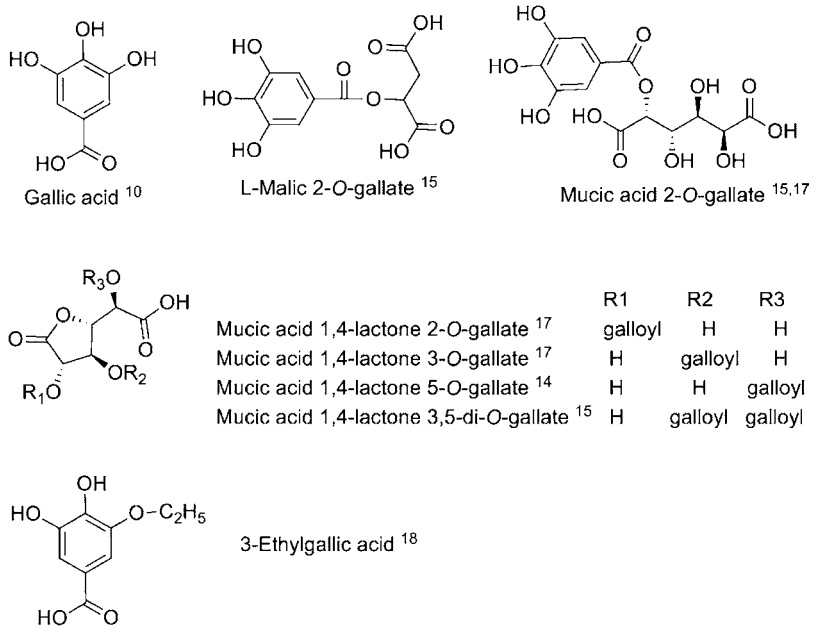

Figure 1. Simple esters and derivatives of gallic acid in *P. emblica* fruits.

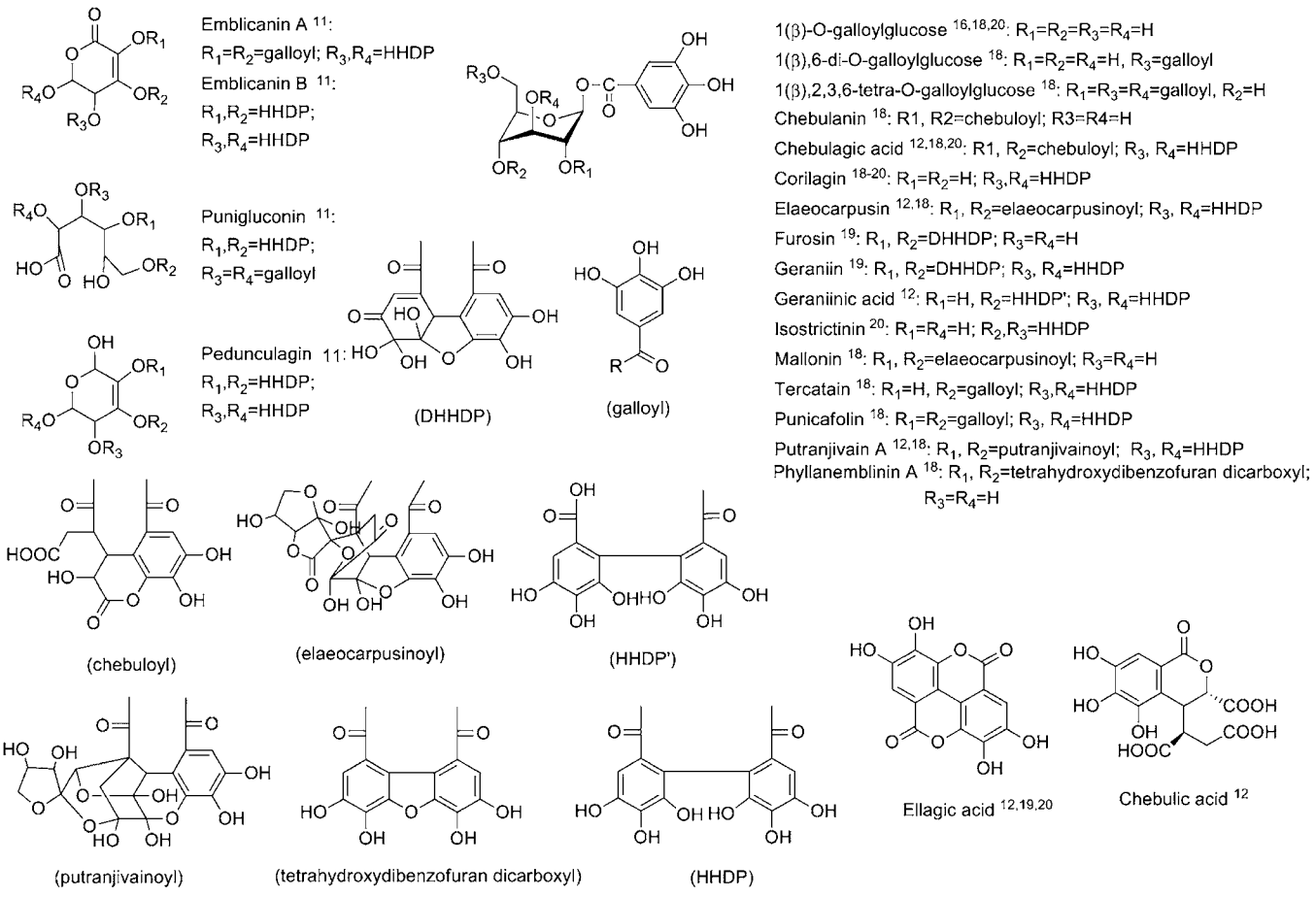

Figure 2. Hydrolyzable tannins in *P. emblica* fruits.

ethyl acetate extract of fresh fruits,[19] aqueous acetone (70%) extract of dried fruit powder,[20] aqueous methanol (60%) extract of dried fruits,[21] and methanol extract of dried fruits.[12] Both simple esters and derivatives of gallic acid (Figure 1) and large molecules of hydrolyzable tannins (Figure 2) have been reported in the fruits and juices of *P. emblica*.

Simple esters of gallic acid reported in *P. emblica* fruits and juices (Figure 1) include L-malic 2-*O*-gallate,[17] mucic acid 2-*O*-gallate,[17,19] mucic acid 1,4-lactone 2-*O*-gallate,[19] mucic acid 1,4-

dx.doi.org/10.1021/jf404703k | J. Agric. Food Chem. 2014, 62, 529−541

Table 1. Antioxidative, Radical-Scavenging, and Antiaging Activities of *P. emblica* (PE) Fruits and Fruit Extracts

target and method of study	fruits and extracts	dose	result	ref
DPPH, $O_2^{\bullet -}$, $OH^{\bullet}$, and NO radicals, in vitro	methanol extract of PE fruit		methanol extract of PE fruit exhibited the highest scavenging activity against DPPH, $O_2^{\bullet -}$, $OH^{\bullet}$, and NO radicals; the extract also significantly inhibited the oxidation of low-density lipoprotein (LDL) in vitro	7
$DPPH^{\bullet}$ radical, in vitro	gallic acid, ellagic acids, emblicanins A and B		all compounds showed activities in scavenging of $DPPH^{\bullet}$ radicals; emblicanins A and B showed highest activities	23
NO radicals, in vitro	methanolic extract of PE fruit		ethyl acetate fraction of methanolic extract of PE fruit showed strong NO-scavenging activity in vitro; gallic acid was found to be a major compound in the ethyl acetate fraction, and geraniin showed the highest NO-scavenging activity among the isolated compounds from the ethyl acetate fraction	24
oxidation of DNA, in vitro	free and bound phenolics of PE fruit		positive correlation between antioxidant activity and phenolic content was found ($R = 0.74$); gallic acid and tannic acid were identified as the major antioxidant components in phenolic fractions of PE; the extracts of PE also exhibited significant protection to DNA against oxidative damage	25
alcohol-induced oxidative changes in rats, in vivo	PE fruit extract (an aqueous fruit extract dry powder, including 49.5% tannins)	250 mg kg^{-1} BW per day for 60 days	PE fruit extract showed ameliorative effects against alcohol-induced oxidative changes in different organs of rats (erythrocyte membrane, plasma, liver, brain); the tannins present in PE fruit extract with antioxidant as well as NO-scavenging properties were suggested to contribute to these effects	26−30
ochratoxin-induced LPO in the kidney and liver of mice, in vivo	PE fruit aqueous extract	2 mg per animal per day for 45 days	significant reduction in the ochratoxin-induced LPO in liver and kidney of mouse were found	31
oxidative stress during aging process in rats, in vivo	SunAmla/ethyl acetate extract of PE fruit	40/10 mg kg^{-1} BW per day for 100 days	extract of PE fruit could attenuate age-related renal dysfunction and prevent age-related hyperlipidemia through attenuating oxidative stress in the aging process	19, 32

dx.doi.org/10.1021/jf404703k | J. Agric. Food Chem. 2014, 62, 529−541

lactone 3-*O*-gallate,[19] mucic acid 1,4-lactone 5-*O*-gallate,[16] and mucic acid 1,4-lactone 3,5-di-*O*-gallate.[17] Mucic acid 2-*O*-gallate, mucic acid 1,4-lactone 2-*O*-gallate, and mucic acid 1,4-lactone 5-*O*-gallate are found to be the major compounds of this group in juice powder.[17] 3-Ethylgallic acid was also isolated from the fruits.[20] Two isomers of mucic acid gallate and several isomers of mucic acid digallate, mucic acid lactone gallate, and mucic acid lactone digallate have been detected in the methanol extract of dried fruits of emblic leafflower.[12] Different isomers of mucic acid gallates, mucic acid digallates, and mucic acid lactone digallates tend to reach equilibrium in water solution, indicating the possible impact of sample handling and analytical procedures on the ratios between different isomers.[19] Methyl esters of mucic acid gallates, mucic acid 1,4-lactone gallates, and mucic acid 1,4-lactone-digallates have been identified in the fruit juice powder[17] and methanol extracts of whole fruits.[12] Examples of these compounds are mucic acid dimethyl ester 2-*O*-gallate, mucic acid 1-methyl ester 2-*O*-gallate, mucic acid 6-methyl ester 2-*O*-gallate, mucic acid 1,4-lactone 6-methyl ester 2-*O*-gallate, and mucic acid 1,4-lactone 6-methyl ester 5-*O*-gallate.[19] It has been suggested that most of the methyl esters found may have been artifacts generated during the separation process of multiple stages of column chromatography, although a small amount of methyl esters has been detected in an aqueous acetone extract of the juice powder.[19]

Figure 2 presents the structure of major gallotannins and ellagitannins found in the fruit and juice of emblic leafflower. Complex tannins have been investigated in an aqueous acetone extract of fruit juice powder.[18] 1(*β*)-*O*-, 1(*β*),6-di-*O*-, and 1(*β*),2,3,6-tetra-*O*-galloylglucose, corilagin, chebulanin, chebulagic acid, elaeocarpusin, punicafolin, tercatain, mallonin, putranjivain A, and phyllanemblinin A have been identified on the basis of mass spectrometric (MS) and nuclear magnetic resonance spectroscopic (NMR) spectra. In the same study, five other compounds named phyllanemblinins B, C, D, E, and F have been isolated and identified from leaves and branches, but not in the fruits, of *P. emblica*.[18] Isostrictinin is found in the aqueous acetone (70%) extract of dried fruit powder.[20]

In the study of Yang et al., the phenolic compounds in a methanol extract of dried fruits of *P. emblica* have been studied systematically by HPLC-DAD and HPLC-ESI(−)-MS combined with column chromatography.[12] A mucic acid gallate, three mucic acid lactone gallate isomers, a galloylglucose, gallic acid, a digalloylglucose, putranjivain A, a galloyl-HHDP-glucose, elaeocarpusin, and chebulagic acid are the most abundant compounds in the crude methanol extract of the fruits. In addition, 130 peaks are detected, of which 63 are identified/tentatively identified as simple gallic acid derivatives and derivatives of chebulic acid and chebuloylglucose, as well as ellagitannins and flavonoids. Neochebulagic acid, isomers of neochebuloyl galloylglucose (phyllanemblinins D, E, and F), punicalagin, geraniinic acid, ellagic acid glycosides, and quercetin glycosides are reported.[12]

Many hydrolyzable tannins have been reported in the fruits of *P. emblica*,[12] which remain to be identified by future research. In addition, some contradictory results have been reported concerning the identification of some hydrolyzable tannins in the fruits. For instance, according to Ghosal et al., the fruits of *P. emblica* contain two hydrolyzable tannins, emblicanin A (2,3-di-*O*-galloyl-4,6-(*S*)-hexahydroxydiphenoyl-2-ketogluconolactone) and emblicanin B (2,3,4,6-bis(*S*)-hexahydroxydiphenoyl-2-ketogluconolactone) (Figure 2).[11] However, Majeed et al. have suggested that the compounds identified as emblicanins A and B by Ghosal et al. are 1(*β*)-*O*-galloylglucose and mucic acid 1,4-lactone 5-*O*-gallate, respectively, according to the NMR spectra.[16] Thus, the presence of emblicanin A and emblicanin B needs confirmation by further studies. Both the origin of the samples and methods of sample preparation could influence the content and profile of hydrolyzable tannins. Corilagin, geraniin, chebulagic acid, and ellagic acid are found to be the major ellagitannins in both an enzyme-aided water extract and an ethyl acetate extract of fresh fruits of *P. emblica*.[19] Eleaocarpusin, a major compound in the water extract, is not detected in the ethyl acetate extract of the fruits. Furosin is more abundant in the ethyl acetate extract than in the enzyme-aided water extract.[19]

A recent study has shown clear differences in both the content and profile of tannins in the fruits of emblic leafflower of different origins in southern China.[12] Fruits of two cultivars from Guangxi province are richer sources of tannins than those of Tian Chuan emblic leafflower from Fujian province.[12] The fruits from Guangxi differ from those from Fujian also by higher proportions of ellagitannins and derivatives of chebulic acid and chebuloylglucose.[12]

HEALTH EFFECTS OF HYDROLYZABLE TANNINS OF *PHYLLANTHUS EMBLICA* FRUITS

Many studies have demonstrated that the *P. emblica* fruits and its extracts have beneficial effects on the health of human beings. Several studies have tested the compounds of purified hydrolyzable tannins; others used whole berries and extracts of different solvents. However, the hydrolyzable tannins were considered as the major bioactive compounds in the materials tested in most of the studies.

Antioxidant, Radical-Scavenging, and Antiaging Activities. An excess generation of free radicals is linked to many human diseases and early aging. Reactive oxygen species [ROS; superoxide anion radicals ($O_2^{\bullet -}$), hydroxyl radicals ($OH^{\bullet}$), and hydrogen peroxide (H_2O_2)] and reactive nitrogen species [RNS; nitric oxide (NO) and peroxynitrite ($ONOO^-$)] cause oxidation of lipids, proteins, and DNA, damage the structures and functions of cells, and lead to aging and development of diseases.[22]

Table 1 summarizes the literature on the antioxidative and radical-scavenging activities of *P. emblica* fruit or its extracts.

The free radical-scavenging activity of extracts and individual compounds of *P. emblica* fruits have been evaluated in vitro.[7,23−25] Methanol and aqueous extracts of the fruits have exhibited scavenging activity against 2,2-diphenylpicrylhydrazyl radical ($DPPH^{\bullet}$), $O_2^{\bullet -}$, $OH^{\bullet}$, and NO radicals[7,24] and inhibited the oxidation of low-density lipoprotein (LDL)[6] and DNA.[25] Emblicanins A and B are reported to have $DPPH^{\bullet}$-scavenging activity close to 10 times that of ascorbic acid and twice of that of gallic acid.[23] Geraniin has been identified as the compound with the highest NO-scavenging activity in an aqueous extract of *P. emblica* fruit.[24] Gallic acid and tannic acid are the major antioxidant components in phenolic fractions of *P. emblica* fruits according to both $DPPH^{\bullet}$-scavenging and reducing power assays.[25]

A series of studies have shown the ameliorative effects of a *P. emblica* fruit extract (a dried powder of aqueous fruit extract with a total content of tannins of 49.5% dry weight) against alcohol-induced oxidative changes in rats, suggesting tannins to be the major antioxidants in the extract.[26−30] Administration of the extract [250 mg kg^{-1} body weight (BW) per day] resulted in a significant ($p < 0.05$) reduction in NO levels, lipid

dx.doi.org/10.1021/jf404703k | J. Agric. Food Chem. 2014, 62, 529−541

Table 2. Effects of *P. emblica* (PE) Fruits and Fruit Extracts on Diabetes and Diabetic Complications

target and method of study	fruits and extracts	dose	result	ref
streptozotocin (STZ)-induced type 2 diabetes rats, in vivo	ethanolic extract of PE fruit	200 mg kg^{-1} BW for 45 days	significant reduction in blood glucose and significant increase in plasma insulin in diabetic rats	33
normal and diabetic human volunteers, clinical trial	PE fruit	1, 2, or 3 g PE fruit powder per day	decrease ($p < 0.05$) was found in fasting and 2 h postprandial blood glucose levels in both normal and diabetic subjects receiving PE powder; significant ($p < 0.05$) decreases were observed in TC and triglycerides in both normal and diabetic volunteers that were given either 2 or 3 g PE powder per day; the diabetic volunteers receiving 3 g of PE powder per day exhibited a significant ($p < 0.05$) decrease in total lipids; both normal and diabetic volunteers receiving 2 or 3 g of PE powder showed significant ($p < 0.05$) improvement in cholesterol levels	35
α-amylase and α-glucosidase, in vitro	extract of PE fruit		extract of PE fruit was able to inhibit α-amylase and α-glucosidase (IC_{50} value = 1.0 and 94.3 μg mL^{-1}, respectively)	7
fructose-induced metabolic syndrome in rat model	ethyl acetate extract of PE fruit	10 or 20 mg kg^{-1} BW per day for 2 weeks	ethyl acetate extract of PE fruit ameliorated the high fructose diet-induced hypertriacylglycerolemia and hypercholesterolemia	41
diabetic cataract, in vitro	PE fruit and an enriched fraction of PE fruit tannins		aqueous extract of PE fruit inhibited aldose reductase (AR) of rat lens and recombinant human AR with IC_{50} values of 0.72 and 0.88 mg mL^{-1}, respectively,	36
STZ-induced diabetic cataract in rats, in vivo	PE fruit and an enriched fraction of PE fruit tannins	0.2% diet	supplements of PE fruit and PE fruit tannins delayed cataract progression	37
diabetic neuropathy in rats, in vivo	aqueous extract of PE	250−1000 mg kg^{-1} per day	insulin in combination with PE extract not only attenuated the diabetic condition but also reduced neuropathic pain through modulation of oxidative−nitrosative stress in diabetic rats	38
diabetic-uremic patients, clinical trial	1:1 mixture of epigallocatechin-3-gallate and PE extract	100 mg of EGCG and 100 mg of PE extract 3 times per day	the mixture significantly improved antioxidant defense as well as diabetic and atherogenic indices in uremic patients with diabetes	39

dx.doi.org/10.1021/jf404703k | J. Agric. Food Chem. 2014, 62, 529−541

peroxidation (LPO), and the activities of Na^+/K^+- and Mg^{2+}-ATPases in erythrocyte membranes in alcohol-treated rats.[24] The extract showed hepatoprotective effects, reduced the contents of lipid peroxide and protein carbonyls, and restored the levels of enzymatic and nonenzymatic antioxidants in the liver[27,29] and the brain[30] of alcohol-treated rats. An ameliorative effect of a *P. emblica* aqueous extract on ochratoxin-induced LPO in the kidney and liver of mice is reported.[31]

Both an enzyme-aided water extract and a polyphenol-rich ethyl acetate extract of *P. emblica* fruits attenuated age-related renal dysfunction and prevented age-related hyperlipidemia by attenuating oxidative stress in the aging process of rats.[19,32] Oral administration of the fruit extract also significantly increased the hepatic peroxisome proliferator activated receptor α (PPARα) protein level and inhibited the levels of thiobarbituric acid-reactive substances (TBARS) in the serum, hepatic mitochondria, and kidney in aged rats.[19,32]

Effects on Sugar Metabolism, Diabetes, and Diabetic Complications. The antidiabetic activities of *P. emblica* fruits and fruit extracts have been studied in animal models and in humans (Table 2). Oral administration of an ethanol extract of the fruits (200 mg kg^{-1} BW for 45 days) resulted in a significant reduction in the plasma level of glucose and a significant increase in the plasma level of insulin in streptozotocin (STZ)-induced type 2 diabetic rats.[33] In addition, administration of the extract reduced total cholesterol (TC), VLDL-C, LDL-C, free fatty acid (FFA), and phospholipid (PL) levels in blood and increased the level of high-density lipoprotein (HDL) cholesterol.[33] Oral administration of an aqueous extract of *P. emblica* seeds reduced fasting glucose level and improved glucose tolerance in normal as well as subdiabetic and mildly diabetic rats.[34] Daily supplementation with 1, 2 or 3 g of *P. emblica* fruit powder for a period of 3 weeks significantly decreased ($p < 0.05$) fasting and 2 h postprandial levels of blood glucose as well as plasma lipid levels from baseline values in both normal subjects and diabetic patients.[33] The antidiabetic properties of *P. emblica* fruits and extracts are likely to be related to the inhibition of the activities of α-glucosidase and α-amylase, enzymes crucial for the digestion and absorption of dietary starch.[7]

Prolonged exposure to uncontrolled chronic hyperglycemia in diabetes results in complications including various microvascular and macrovascular diseases. Microvascular complications include neuropathy, nephropathy, and vision disorders. Macrovascular complications include heart disease, stroke, and peripheral vascular disease. Studies have shown that *P. emblica* and its tannins have beneficial effects on cataracts,[36,37] neuropathy,[38] and uremia[39] as complications of diabetes.

The studies of Suryanarayana's group have suggested that *P. emblica* fruits and the tannins of the fruits might be effective in delaying the development of diabetic cataracts in rats.[36,37] An aqueous extract of *P. emblica* fruit and a fraction rich in tannins of the fruits prevented activation of aldose reductase (AR) and also inhibited sugar-induced osmotic changes in the cultured lens of rat.[36] Neither *P. emblica* fruit nor its tannins showed any preventive effects on STZ-induced hyperglycemia as assessed by blood glucose and insulin levels in rats.[37] However, slit lamp microscopic observation indicated that these supplements delayed cataract progression. *P. emblica* fruit also prevented the aggregation and precipitation of lens proteins caused by hyperglycemia.[37]

Diabetic neuropathy is one of the most common microvascular complications, affecting >50% of diabetic patients. Tiwari et al. found that *P. emblica* fruits could correct functional, biochemical, and molecular defects in experimental diabetic neuropathy by targeting the inflammatory cascade mediated by oxido-nitrosative stress.[38] Treatment with an aqueous extract of the fruits (250−1000 mg kg^{-1} per day) significantly attenuated oxidative stress and the levels of nitrite and cytokines [tumor necrosis factor-α (TNF-α), interleukin-1β (IL-1β), and transforming growth factor- β1 (TGF-β1)] both in the serum and in the sciatic nerve in a dose-dependent manner in diabetic rats.[38] Oral administration of a mixture of epigallocatechin-3-gallate and *P. emblica* fruit extract for 3 months significantly improved the antioxidative defenses as well as the diabetic and atherogenic indices in uremic patients with diabetes.[39]

Metabolic syndrome is characterized by insulin resistance, dyslipidemia, and hypertension and is associated with increased morbidity and mortality from several prevalent diseases, such as diabetes, cancer, myocardial infarction, and stroke.[40] An ethyl acetate extract (polyphenol-rich fraction) of *P. emblica* fruit ameliorated the high fructose diet-induced hypertriacylglycerolemia and hypercholesterolemia in rats.[41]

Effects on Cardiovascular Health. Fruits and extracts of *P. emblica* have shown beneficial effects on different cardiovascular diseases (Table 3). Oxygen-derived free radicals play an important role in the initiation and progression of all clinical manifestations of ischemic heart disease. Myocardial cellular injury occurring during reperfusion of ischemic cells, known as ischemia-reperfusion injury, is primarily due to oxidative stress.[42] Studies have shown that antioxidants exert a protective effect against cardiac ischemia-reperfusion injury (IRI).[43,44]

Studies by Bhattcharya et al. and Rajak et al. have shown that tannin-rich extracts of *P. emblica* fruit can ameliorate the oxidative stress induced by IRI.[45,46] Oral administration of a *P. emblica* fruit extract enriched with emblicanins A and B (50 and 100 mg kg^{-1} BW twice per day for 14 days) significantly reversed the effects of IRI on superoxide dismutase (SOD), catalase (CAT), glutathione peroxidase (GPx), and LPO activities.[45] Similar results have been found in a study by Rajak et al.[46] Fresh *P. emblica* fruit homogenate (250−750 mg kg^{-1} per day) and saline were administered orally to Wistar albino rats for 30 days. There was a reduction in basal myocardial LPO, as evidenced by decreased TBARS levels, and an augmentation of myocardial endogenous antioxidants in the *P. emblica*-treated rats compared to those in the saline group. The results indicate that long-term *P. emblica* fruit administration improves myocardial adaptation by augmenting endogenous antioxidants and protecting the rat heart from oxidative stress associated with IRI.[46]

Anila and Vijayalakshmi separated flavonoids from *P. emblica* fruit by solvent extractions and silica gel column chromatography.[47] The ethyl acetate/methanol (50:50) fraction provided the maximum yield of flavonoids (789.4 mg from 1.9 kg of fresh fruit). The flavonoids were administered orally (10 mg kg^{-1} BW per day) to male albino rats fed a high-fat diet (coconut oil 15% and cholesterol 2%). After 90 days of treatment, significant decreases in lipid levels in serum and tissues were observed when compared with the control group.[47] Duan et al. studied the antiatherogenic effects of two soluble tannins, corilagin and its analogue Dgg16 (1,6-di-*O*-galloyl-β-D-glucose), isolated from *P. emblica* fruit. The results suggested that the two compounds are effective in inhibiting the progress of atherosclerosis by alleviating oxidation injury and by inhibiting

Table 3. Effects on Cardiovascular Health of *P. emblica* (PE) Fruits and Fruit Extracts

target and method of study	fruits and extracts	dose	result	ref
cardiac ischemia-reperfusion injury (IRI) in rats	emblicanin A and B enriched PE extract (prepared by eluting fresh PE juice though a Sephadex LH-20 column)	50 mg and 100 mg kg^{-1} BW twice per day for 14 days	the PE extract (50 mg and 100 mg kg^{-1} BW) significantly reversed the effects of IRI on SOD, CAT, GPx, and LPO activities	45
cardiac ischemia-reperfusion injury (IRI) in rats	fresh PE fruit homogenate	250−750 mg kg^{-1} per day for 30 days	PE administration improves myocardial adaptation by augmenting endogenous antioxidants and protects rat hearts from oxidative stress associated with IRI	46
rats fed a high-fat diet	flavonoids separated from PE fruit	10 mg kg^{-1} BW per day for 90 days	significant decreases in total cholesterol, triacylglycerol, phospholipids, and free fatty acid levels in serum and tissues were observed when compared with the control group	47
human umbilical vein endothelial cells, ECV-304, incubated with ox-LDL (50 mg/L), in vitro	tannins (corilagin/Dgg16) isolated from PE fruit	0.0001−0.1 mmol L^{-1}	corilagin and Dgg16 are effective in inhibiting the progress of atherosclerosis by alleviating oxidation injury and by inhibiting ox-LDL-induced VSMC proliferation	48
deoxycorticosterone acetate/1% NaCl high salt (DOCA/HS)-induced hypertension model rat	extract of PE	75−300 mg kg^{-1} BW per day for 5 weeks	extract of PE reduces oxidative stress, prevents development and progression of hypertension as well as cardiac and renal hypertrophy in DOCA/HS-induced hypertension via activation of endothelial nitric oxide synthase (eNOS) and endogenous antioxidants as well as regulation of serum NO and electrolyte levels	49

oxidized LDL-induced proliferation of vascular smooth muscle cell.[48]

Bhatia et al. investigated the antihypertensive effect of *P. emblica* fruit extract in a deoxycorticosterone acetate/1% NaCl high salt (DOCA/HS)-induced hypertension model in rat.[49] Hypertension was induced in rats by the DOCA/HS (20 mg kg^{-1}, sc) and, at the same time, these rats received cotreatment with different doses of an extract of *P. emblica* fruit with tannin content of 9.4% (75−300 mg kg^{-1} BW per day) for 5 weeks. The extract significantly decreased arterial blood pressure and heart rate as well as cardiac and renal hypertrophy in a dose-dependent fashion as compared to control rats treated with DOCA alone. Increased TBARS and decreased endogenous antioxidants activity in serum, heart, and kidney tissues of hypertensive rats were also normalized. These results demonstrate that the extract of *P. emblica* can prevent the development and progression of hypertension as well as cardiac and renal hypertrophy in DOCA/HS-induced hypertension via the activation of endothelial nitric oxide synthase (eNOS) and endogenous antioxidants as well as regulation of serum NO and electrolyte levels.[49]

Inflammation is involved in multiple aspects of the development of cardiovascular diseases.[50] Anti-inflammatory effects of PE fruits and extracts are among the mechanisms supporting vascular health.

Anticancer Activities. The anticancer effects of *P. emblica* fruit have been recently reviewed by Baliga and Dsouza.[9] They summarized that *P. emblica* fruit and its extracts can be used as (1) antineoplastic agents,[51,52] (2) radio-protective agents,[53,54] and (3) chemopreventive and chemomodulatory agents[55−59] to reduce the risk of cancers. The mechanism of the anticancer effects includes the following aspects: *P. emblica* fruit or its extracts (1) are scavengers of free radicals and decrease oxidation of lipids and other biomolecules; (2) can decrease the hepatic levels of phase I enzymes; (3) can increase the levels of glutathione *S*-transferase (GST), a phase II enzyme; (4) can decrease levels of ornithine decarboxylase; (5) can increase the levels of antioxidant enzymes; (6) have antimutagenic effects; (7) possess immunomodulatory effects; (8) can modulate the levels of proteins important in cell cycle progression; (9) can induce apoptosis of neoplastic cells; and (10) can prevent metastasis. Table 4 presents a list of studies related to the anticancer effects of *P. emblica* fruits and fruit extracts. Readers are referred to the paper recently published by Baliga and Dsouza for a thorough review on the topic.[9] A few points are worth noticing here. First, the inhibitory efficacy of *P. emblica* fruit extracts may differ between different cancer cell lines.[51] Second, the fruit extracts may work synergistically with some therapeutic cytotoxic agents (doxorubicin and cisplatin) inhibiting the growth of cancer cells.[51,52] Third, some short-term inhibitory effect has been recognized of aqueous extracts of *P. emblica* fruits on the growth of noncancer cells in vitro.[60]

Immune-Modulating and Anti-inflammatory Activities. Immune activation is an effective as well as protective approach against infectious diseases. Studies have shown that *P. emblica* fruits and fruit extracts have immune-modulating and anti-inflammatory activities (Table 5). A 90% ethanol extract of dry *P. emblica* fruits counter-acted the immune-suppressive effects of chromium(VI) compounds on lymphocytes[61] and macrophages[62] in vitro. The extract reduced the apoptosis and DNA fragmentation induced by chromium and relieved the suppressive effects of chromium on cell proliferation and production of IL-2 and γ-interferon (γ-IFN) of lymphocytes.[61]

Table 4. Cytotoxic Effects, Protective Effects against Clastogenicity, and Anticancer Activities of *P. emblica* (PE) Fruits and Fruit Extracts

subject and method of study	plant parts	dose	result	ref
human hepatocellular carcinoma (HepG2) and lung cancer cells (A549), in vitro	aqueous extract of PE fruit	4−48 μg mL^{-1} for A549/25−200 μg mL^{-1} for HepG2	PE extract demonstrated growth inhibitory activity, with a certain degree of selectivity between the two cancer cell lines tested; synergistic effects (CI < 1) between PE and doxorubicin as well as between PE and cisplatin were demonstrated on A549 and HepG2 cells at different dose levels	51
Vero cell line, in vitro; *Plasmodium falciparum* infected mice, in vivo	aqueous extract of PE	250 mg kg^{-1} BW per day (in vivo)	extract of PE exhibited interesting in vitro and in vivo antiplasmodial activity with good selectivity	52
Chinese hamster ovary (CHO) cell line	aqueous extract of PE fruit	50 μg mL^{-1}	aqueous extract of PE fruit caused 42% growth inhibition on CHO cells; aqueous extract of PE fruit did not significantly alter the colony-forming efficiency of CHO cells	60
chromosome aberrations (CA) on bone marrow cells induced by CsCl in mice	aqueous extract of PE fruit	685 mg kg^{-1} BW per day for 7 days	significantly reduced the frequency of CA on bone marrow cells induced by CsCl (125, 250, and 500 mg kg^{-1} BW) in Swiss albino mice	55
CA on bone marrow cells induced by nickel chloride in mice	aqueous extract of PE fruit	685 mg kg^{-1} BW per day for 7 days	significantly reduced the frequency of CA on bone marrow cells induced by nickel chloride in mice	56
CA on bone marrow cells induced by lead nitrate in mice	aqueous extract of PE fruit	685 mg kg^{-1} BW per day for 7 days	significantly reduced the frequency of CA on bone marrow cells induced by lead nitrate in mice	57
CA on bone marrow cells induced by aluminum sulfate in mice	aqueous extract of PE fruit	685 mg kg^{-1} BW per day for 7 days	significantly reduced the frequency of CA on bone marrow cells induced by aluminum sulfate in mice	58
mice exposed to 9 Gy of γ-radiation	aqueous extract of PE fruit	50−800 mg kg^{-1} BW per day for 7−30 days	the extract had radioprotective effects; the optimum dose was 100 mg kg^{-1} BW	54
mice exposed to 7 Gy of γ-radiation	fruit pulp of PE	2.5 g kg^{-1} BW for 10 days	administration of PE significantly increased the total leukocyte count, bone marrow viability, and level of hemoglobin; administration of PE significantly enhanced the activity of the various antioxidant enzymes and GST as well as glutathione system in the blood, and treatment with PE suppressed the elevation in lipid peroxides in the serum	53
hepatocarcinogenesis induced by NDEA in rats	aqueous extract of PE fruit	50−250 mg kg^{-1} BW per day for 20 weeks	extract of PE significantly inhibited hepatocarcinogenesis induced by NDEA in a dose-dependent manner	59

dx.doi.org/10.1021/jf404703k | J. Agric. Food Chem. 2014, 62, 529−541

Table 5. Anti-inflammatory and Immunomodulating Activities of *P. emblica* (PE) Fruits and Fruit Extracts

subject and method	plant parts	dose	result	ref
L-arginine induced acute pancreatitis in rats	PE fruit extract	100 mg kg^{-1} BW per day for 3, 7, 14, and 28 days	PE treatment was found to be beneficial for treating acute pancreatitis	65
carrageenan and cotton pellet induced acute and chronic inflammatory in rat paw	free and bound phenolic compounds from PE fruit (70% ethanol extract)	20 and 40 mg kg^{-1} BW for 6 days	in both acute and chronic inflammation, both free and bound phenolics of PE reduced inflammation	66
lymphocytes, in vitro	90% ethanol extract of PE dry fruit	10 μg^{-1} mg mL^{-1}	PE extract also inhibited apoptosis and DNA fragmentation induced by Cr, relieved immunosuppressive effects of Cr on lymphocyte proliferation, and restored IL-2 and γ-IFN production considerably; the results showed the fruit extract of PE had cytoprotective and immunomodulatory properties	61
chromium(VI) induced oxidative injury in murine macrophages, in vitro	70% ethanol extract of PE dry fruit	250 μg mL^{-1}	the presence of the PE extract enhanced cell survival, decreased free radical production, and maintained antioxidant levels close to those of the control cells; furthermore, chromium(VI) treatment resulted in decreased phagocytosis and γ-IFN production, which were restored by the PE extract	62
mice bearing Dalton's lymphoma ascites (DLA) tumor	PE fruit powder	20 mg kg^{-1} BW per day	PE enhanced natural killer (NK) cell activity and antibody-dependent cellular cytotoxicity (ADCC) in syngeneic BALB/c mice bearing DLA tumors	63
adjuvant induced arthritic (AIA) rat model	crude extract of PE	6.25−100 mg kg^{-1} BW	PE extract can cause immunosuppression in AIA rats	64

Treatment with *P. emblica* fruit extract increased the survival of cells and restored the phagocytosis and production of cytokines of murine macrophages treated with chromium(VI).[62] The cytoprotective and immune-modulating properties of the *P. emblica* extract were related to protection from oxidative damages induced by chromium treatment by scavenging the free radicals and by maintaining the antioxidative status as well as the levels of antioxidants and antioxidative enzymes.[61,62] Intake of *P. emblica* fruit powder enhanced natural killer (NK) cell activity and antibody-dependent cellular cytotoxicity (ADCC) in syngeneic BALB/c mice bearing Dalton's lymphoma ascites (DLA) tumors.[63] Adjuvant-induced arthritis (AIA) has been widely used as a model for rheumatoid arthritis (RA) and reactive arthritis. Crude water extracts of *P. emblica* fruit suppressed the immune response in AIA model in rats.[64]

The anti-inflammatory activities of *P. emblica* fruits or fruit extracts have been studied in animal models.[65,66] Acute pancreatitis is a rapidly developing inflammatory disease of the pancreas. A *P. emblica* fruit extract (tannin content $\geq$ 30% weight) has been reported to be effective in the treatment of arginine-induced acute pancreatitis in rats.[65] The administration of the extract lowered the serum levels of lipase and interleukin-10 in the arginine-treated rats. The nucleic acid content and rate of DNA synthesis in pancreatic tissue, pancreatic proteins, and pancreatic amylase content were significantly improved.[65] Muthuraman et al. studied the anti-inflammatory effects of extracts of free and bound phenolic compounds from *P. emblica* fruits in carrageenan- and cotton pellet-induced models of acute and chronic inflammation in rats at dose levels of 20 and 40 mg extract kg^{-1} body weight.[66] In both acute and chronic inflammation, both the free and bound phenolics of *P. emblica* reduced inflammation; at high doses, the effects of both fractions were comparable to treatment with diclofenac.[66] In this study, free phenolic compounds were extracted with 70% aqueous ethanol, acidified, and further extracted with ethyl acetate. The extract of bound phenolic compounds was prepared by extraction of fruits with sodium hydroxide (1 M) containing sodium borohydride (0.5%), followed by acidification with hydrochloride acid to pH 1.5.[66]

Ethanolic extract from *P. emblica* fruit and pyrogallol isolated from the extract were equally effective in inhibiting *Pseudomonas aeruginosa*-induced expression of the pro-inflammatory genes in bronchial epithelial cells in vitro. These results suggest that pyrogallol is a major bioactive compound responsible for the anti-inflammatory effect of the extracts of *P. emblica* fruit.[67]

Antimicrobial and Antidiarrheal Activity. The antimicrobial and cytotoxic activities of *P. emblica* fruits and fruit extracts have been studied by several research groups.[68−70] The antibacterial activity of the fruit extracts against 345 bacterial isolates belonging to 6 different genera of Gram-negative bacteria isolated from urine specimens was evaluated by Saeed and Tariq.[69] Aqueous infusion and decoction of *P. emblica* fruits exhibited potent antibacterial activity against *Escherichia coli*, *Klebsiella pneumoniae*, *Klebsiella ozaenae*, *Proteus mirabilis*, *Pseudomonas aeruginosa*, *Salmonella typhi*, *Salmonella paratyphi* A, *Salmonella paratyphi* B, and *Serratia marcescens*.[69] Saini et al. studied the protective effect of *P. emblica* fruit against *Klebsiella pneumoniae*-induced pneumonia in mice. The effect of short- (15 days) and long-term (30 days) feeding of *P. emblica* fruit powder in mice over the course of *K. pneumoniae* ATCC43816 infection in the lungs was studied in terms of bacterial colonization, macrophage activity, malondialdehyde (MDA)

and nitrite production in the bronchoalveolar lavage fluid.[70] TNF-α level in serum was also assessed. The results in the long-term feeding experimental model suggested that supplementation with *P. emblica* fruits might reduce bacterial colonization in the lung.[70] In addition to tannins, alkaloids were suggested to be among the antimicrobial compounds of *P. emblica* fruits.[71]

The methanol extract of *P. emblica* fruit showed a significant inhibitory effect on diarrhea in Wistar albino rats induced by castor oil and magnesium sulfate.[70] Oral administration of the extract (50−150 mg kg^{-1} BW) produced a significant dose-related reduction in gastrointestinal motility in charcoal meal tests in rats. The treatment also significantly inhibited the production of prostaglandin E_2 (PGE_2)-induced enteropooling.[72] The potential of *P. emblica* for the treatment of diarrhea has been investigated in mice and in isolated rabbit jejunum and guinea pig ileum.[73] Oral administration of 70% ethanol crude extract of *P. emblica* fruits inhibited castor oil-induced diarrhea and intestinal fluid accumulation in mice at 500−700 mg kg^{-1} BW. The results of the in vitro studies indicate that the *P. emblica* fruit extract possesses antidiarrheal and spasmolytic activities, possibly through the blockade of muscarinic receptors and Ca^{2+} channels.[73]

Hepato- and Gastroprotective Activities. *P. emblica* fruit and its extract have been shown to have potential in protecting the liver[74−77] and the gastric mucosa[10,78,79] from injuries induced by chemical agents in experimental models. Moreover, fruit of *P. emblica* may reverse CCl_4- and TAA-induced fibrosis in the liver in rat.[80,81]

Supplementation of *P. emblica* fruits decreased nitrosodiethylamine (NDEA)-induced hepatic apoptosis and autophagy via down-regulation of the Bax/Bcl-2 ratio and Beclin-1 expression.[74] Administration of an aqueous extract (2 mg/animal/day) of *P. emblica* fruits for 45 days along with ochratoxin significantly ameliorated ochratoxin-induced reduction in the content of DNA, RNA, and protein in the livers and kidneys in mice.[75] Oral administration with an extract of fresh *P. emblica* fruits (obtained by extraction with 50% ethanol) at a single dose of 25, 50, or 75 mg kg^{-1}, 4 h before ethanol treatment, enhanced liver cell recovery from the damage by ethanol and suppressed the ethanol-induced elevation in the levels of aspartate aminotransferase (AST), alanine aminotransferase (ALT), and IL-1β in rats.[76]

A hydroalcoholic (50%) extract of *P. emblica* fruit reversed fibrogenic events in the liver in rats[80] and showed a protective effect against antituberculosis (anti-TB) drug-induced liver toxicity in hepatocytes in vitro and in vivo.[77] In another study, *P. emblica* fruit reversed CCl_4- and TAA-induced prefibrogenic events in rat liver.[81]

Protective and healing properties of *P. emblica* fruit and its extracts against gastric ulceration have been studied mostly in animal models.[10,78,79]

Pretreatment with the butanol fraction of an aqueous extract of *P. emblica* fruit at a dose of 100 mg kg^{-1} BW per day, via oral administration to rats for 10 consecutive days, enhanced the secretion of gastric mucus and hexosamine ($p < 0.001$) in the context of indomethacin-induced ulceration in rats.[79] The morphological observation also suggested a protective effect of the extract on the stomach wall. Indomethacin treatment increased SOD and MDA levels in gastric tissue of rats but hardly affected the MDA or SOD levels in animals pretreated with the *P. emblica* fruit extract.[79] A methanolic extract of *P. emblica* fruits had significant gastroprotective and ulcer-healing effects, which might be due to its effects on both offensive and defensive mucosal factors.[78] A 95% ethanol extract of sun-dried *P. emblica* fruit (oral administration, 100 mg kg^{-1} per day) accelerated the healing process of indomethacin-induced ulcers in rats.[10] Biphasic activities were reported of an ethanolic extract of *P. emblica* fruits on gastric ulcers induced by nonsteroidal anti-inflammatory drug (NSAID) in mice, healing effects being observed at low dose but adverse effects at high dose.[82]

The hepato- and gastroprotective activities of *P. emblica* fruits and extracts are suggested to be related to the antioxidative and membrane-stabilizing activities.[77] Treatment with *P. emblica* fruit and extracts significantly preserved the expression of SOD and CAT and decreased the expression of inducible nitric oxide synthase (iNOS) and cytochrome P450 2E1 (CYP2E1) proteins in the liver of rats.[74,77] Antioxidant properties of *P. emblica* fruits and fruit extracts appeared to be among the primary factors responsible for the healing effects of the *P. emblica* extract on gastric ulcer.[78,79]

Analgesic and Antipyretic Activities and Effects on Nervous System and Skin. *P. emblica* fruits are traditionally used to treat disorders in the central nervous system (CNS).[83] Pretreatment with a hydroalcoholic extract of *P. emblica* fruits (500 and 700 mg kg^{-1} ip) increased the latency of seizures and reduced the cognitive deficits induced by kainic acid.[83] The extract suppressed the increase in TBARS and TNF-α levels and the decrease in reduced glutathione (GSH) level in the brain in kainic acid-treated rats, suggesting a possible role of antioxidant and anti-inflammatory activities in the neuroprotective effects of *P. emblica* fruit.[83] A memory-enhancing activity of orally adminstered *P. emblica* fruit was shown in mice.[84] The elevated plus maze and passive avoidance apparatus served as the exteroceptive behavioral models for testing memory. Diazepam-, scopolamine- and aging-induced amnesia served as the interoceptive behavioral models. *P. emblica* produced a dose-dependent improvement in memory scores in young and aged mice and reversed amnesia induced by scopolamine and diazepam and reduced cholinesterase activity in the brain.[84]

Some studies also suggest that *P. emblica* fruits possess antipyretic and analgesic activity, skin protective effects, and wound-healing effects.[83−88] A single oral dose of ethanol or aqueous extracts of *P. emblica* fruit (500 mg kg^{-1} BW, ip) led to a significant reduction in brewer's yeast-induced hyperthermia in rats.[85] Oral administration with the extracts also elicited inhibitory effects on the acetic acid-induced writhing response in mice, suggesting analgesic activity of the extracts.[85] *P. emblica* fruit effectively inhibited UVB-induced photoaging in human skin fibroblasts in vitro likely because of its strong ROS-scavenging ability.[86] Topical application of a 90% ethanol extract of dried fruit powder speded wound healing through the up-regulation of collagen expression and extracellular signal-regulated kinase (ERK1/2) signaling.[88]

Bioavailability of Hydrolyzable Tannins. The bioavailability of hydrolyzable tannins from various sources has been reviewed.[2,89] Most human studies have focused on pomegranate juice with punicalin and punicalagin being the major ellagitannins. Also, the ellagitannins of raspberries, strawberries, walnuts, and oak-aged wines have been studied. Dietary ellagitannins are hydrolyzed, releasing free ellagic acid, which is partly absorbed directly in the stomach and the proximal small intestine. After consumption of pomegranate juice by volunteers, the concentration of ellagic acid reached the maximum 33 ng/mL plasma 1 h after intake.[2] Ellagitanins

and free ellagic acid are metabolized to urolithins by the action of the microbiota in the distal part of the small intestine and the colon. After absorption, urolithins are converted to various derivatives of urolithin-3-*O*-glucuronide by the action of phase II enzymes.[89] The amount of urolithin A 3-*O*-glucuronide excreted in the urine corresponded to 3−17% of the intake of ellagitannins, depending on the sources.[89] Significant variations among individuals have been observed, mostly likely due to differences in the colonic microbiota. Some evidence obtained in Iberian pigs fed oak acorns suggested significant hepatic metabolism of urolithins and enterohepatic circulation of urolithin metabolites.[89] The tannins of emblic leafflower are a mixture of ellagitannins and gallotannins. The bioavailability and metabolism of tannins in emblic leafflower have not been reported. Further studies on these aspects would provide useful data for substantiating the physiological effects of these compounds in humans.

PERSPECTS FOR FUTURE RESEARCH

From a compositional point of view, the hydrolyzable tannins of emblic leafflower are a very complex mixture of over 100 compounds. Many compounds are either preliminarily identified or unidentified. Some contradictory identifications have been reported. Further research is necessary to provide a detailed characterization of the compounds in the tannin fraction of emblic leafflower. Most of the biological activities and physiological effects of the fruit and fruit extracts have been shown by in vitro studies or in animal models. The data from clinical and human intervention studies are extremely scanty. Ellagitannins and ellagic acid in food have been suggested to have low bioavailability due to the low absorption rate in the small intestine. Most of the dietary ellagitannins are metabolized to urolithins by the microbiota in the colon.[1] Urolithins are weaker antioxidants than ellagitannins. They are absorbed to the circulation and may accumulate in certain tissues as various derivatives with estrogenic or antiestrogenic activities. Therefore, it is also worth investigating the estrogenic and antiestrogenic effects of dietary supplementation of the tannin fraction of emblic leafflower in humans. Whereas many studies suggested that antioxidative activities are associated with most of the beneficial effects observed for the fruits and fruit extracts, the molecular biological mechanisms of the biological activities and physiological effects need further study. Extracts of emblic leafflower (*P. emblica*) fruits and hydrolyzable tannins isolated from some plant materials have been demonstrated to have effects on the expression of some genes related to various aspects of the biological activities. The approach of nutragenomic and metabolomic research shall be applied to investigate the effects of the fruits and extracts of *P. emblica* on the expression of genes and the metabolomes in humans of different genetic backgrounds and baseline metabolomic profiles. The current literature suggests strong antioxidative and antimicrobial activities of tannin-rich extracts of emblic leafflower fruits. Research shall be carried out to explore the potential of emblic leafflower fruit as a raw material for natural food preservatives.

AUTHOR INFORMATION

Corresponding Author

*(B.Y.) Phone: +358 2 333 6844. E-mail: bayang@utu.fi

Funding

We thank the Finnish Cultural Foundation and the Center of International Mobility CIMO (Finland) for financial support.

Notes

The authors declare no competing financial interest.

REFERENCES

(1) Hagerman, A. E. *Tannin Handbook*; Miami University: Oxford, OH, USA, 2002; www.users.muohio.edu/hagermae/.

(2) Landete, J. M. Ellagitannins, ellagic acid and their derived metabolites: a review about source, metabolism, functions and health. *Food Res. Int.* **2011**, *44*, 1150−1160.

(3) Larrosa, M.; García-Conesa, M. T.; Espín, J. C.; Tomás-Barberán, F. A. Ellagitannins, ellagic acid and vascular health. *Mol. Aspects Med.* **2010**, *31*, 513−539.

(4) Poltanov, E. A.; Shikov, A. N.; Dorman, H. J.; Pozharitskaya, O. N.; Makarov, V. G.; Tikhonov, V. P.; Hiltunen, R. Chemical and antioxidant evaluation of Indian gooseberry (*Emblica officinalis* Gaertn., syn. *Phyllanthus emblica* L.) supplements. *Phytother. Res.* **2009**, *23*, 1309−1315.

(5) Khan, K. H. Role of *Emblica officinalis* in medicine − a review. *Bot. Res. Int.* **2009**, *2*, 218−228.

(6) Krishnaveni, M.; Mirunalini, S. Therapeutic potential of *Phyllanthus emblica* (amla): the ayurvedic wonder. *J. Basic Clin. Physiol. Pharmacol.* **2010**, *21*, 93−105.

(7) Nampoothiri, S. V.; Prathapan, A.; Cherian, O. L.; Raghu, K. G.; Venugopalan, V. V.; Sundaresan, A. In vitro antioxidant and inhibitory potential of *Terminalia bellerica* and *Emblica officinalis* fruits against LDL oxidation and key enzymes linked to type 2 diabetes. *Food Chem. Toxicol.* **2011**, *49*, 125−131.

(8) Sabu, M. C.; Kuttan, R. Anti-diabetic activity of medicinal plants and its relationship with their antioxidant property. *J. Ethnopharmacol.* **2002**, *81*, 155−160.

(9) Baliga, M. S.; Dsouza, J. J. Amla (*Emblica officinalis* Gaertn), a wonder berry in the treatment and prevention of cancer. *Eur. J. Cancer Prev.* **2011**, *20*, 225−239.

(10) Bhattacharya, S.; Chaudhuri, S. R.; Chattopadhyay, S.; Bandyopadhyay, S. K. Healing properties of some Indian medicinal plants against indomethacin-induced gastric ulceration of rats. *J. Clin. Biochem. Nutr.* **2007**, *41*, 106−114.

(11) Ghosal, S.; Tripathi, V. K.; Chauhan, S. Active constituent of *Emblica officinalis*: part 1—the chemistry and antioxidant effects of two new hydrolyzable tannins, emblicanin A and B. *Indian J. Chem.* **1996**, *35B*, 941−948.

(12) Yang, B.; Kortesniemi, M.; Liu, P.; Salminen, J-P. Analysis of hydrolyzable tannins and other phenolic compounds in emblic leafflower (*Phyllanthus emblica* L.) fruits by high performance liquid chromatography-electrospray ionization mass spectrometry. *J. Agric. Food Chem.* **2012**, *60*, 8672−8683.

(13) Jacob, A.; Pandey, M.; Kapoor, S.; Saroja, R. Effect of the Indian gooseberry (amla) on serum cholesterol levels in men aged 35−55 years. *Eur. J. Clin. Nutr.* **1988**, *42*, 939−944.

(14) Wu, S. X.; Zhou, L. X. An edible value research of *Phyllenthus emblica* L. *Acad. J. Kunming Med. Coll.* **1996**, *17*, 22−23.

(15) Chen, G. Q.; Chen, J.; Hu, J. X.; Li, Q. H.; Su, Y. C. Study of composition changes of fruits of *Phyllanthus emblica* L. during ripening. *Chin. Wild Plant Resour.* **1995**, *2*, 31−33.

(16) Majeed, M.; Bhat, B.; Jadhav, A. N.; Srivastava, J. S.; Nagabhushanam, K. Ascorbic acid and tannins from *Emblica officinalis* Gaertn. fruits—a revisit. *J. Agric. Food Chem.* **2009**, *57*, 220−225.

(17) Zhang, Y. J.; Tanaka, T.; Yang, C.; Kouno, I. New phenolic constituents from the fruit juice of *Phyllanthus emblica*. *Chem. Pharm. Bull. (Tokyo)* **2001**, *49*, 537−540.

(18) Zhang, Y. J.; Abe, T.; Tanaka, T.; Yang, C. R.; Kouno, I. Phyllanemblinins A−F, new ellagitannins from *Phyllanthus emblica*. *J. Nat. Prod.* **2001**, *64*, 1527−1532.

(19) Yokozawa, T.; Kim, H. Y.; Kim, H. J.; Tanaka, T.; Sugino, H.; Okubo, T.; Chu, D. C.; Juneja, L. R. Amla (*Emblica officinalis* Gaertn.)

attenuates age-related renal dysfunction by oxidative stress. *J. Agric. Food Chem.* **2007**, *55*, 7744−7752.
(20) Zhang, L. Z.; Zhao, W. H.; Guo, Y. J.; Tu, G. Z.; Lin, S.; Xin, L. G. Studies on chemical constituents in fruits of Tibetan medicine—*Phyllanthus emblica*. *China J. Chin. Mat. Med.* **2003**, *28*, 940−943.
(21) Liu, X.; Cui, C.; Zhao, M.; Wang, J.; Luo, W.; Yang, B.; Jiang, Y. Identification of phenolics in the fruit of emblica (*Phyllanthus emblica* L.) and their antioxidant activities. *Food Chem.* **2008**, *109*, 909−915.
(22) Devasagayam, T. P.; Tilak, J. C.; Boloor, K. K.; Sane, K. S.; Ghaskadbi, S. S.; Lele, R. D. Free radicals and antioxidants in human health: current status and future prospects. *J. Assoc. Physicians India* **2004**, *52*, 794−804.
(23) Pozharitskaya, O. N.; Ivanova, S. A.; Shikov, A. N.; Makarov, V. G. Separation and evaluation of free radical-scavenging activity of phenol components of *Emblica officinalis* extract by using an HPTLC-DPPH* method. *J. Sep. Sci.* **2007**, *30*, 1250−1254.
(24) Kumaran, A.; Karunakaran, R. J. Nitric oxide radical scavenging active components from *Phyllanthus emblica* L. *Plant Foods Hum. Nutr.* **2006**, *61*, 1−5.
(25) Kumar, G. S; Nayaka, H.; Dharmesh, S. M.; Slimath, P. V. Free and bound phenolic antioxidants in amla (*Emblica officinalis*) and turmeric (*Curcuma longa*). *J. Food Compos. Anal.* **2006**, *19*, 446−452.
(26) Reddy, V. D.; Padmavathi, P.; Paramahamsa, M.; Varadacharyulu, N. Ch. Modulatory role of *Emblica officinalis* against alcohol induced biochemical and biophysical changes in rat erythrocyte membranes. *Food Chem. Toxicol.* **2009**, *47*, 1958−1963.
(27) Reddy, V. D.; Padmavathi, P.; Varadacharyulu, N. Ch. *Emblica officinalis* protects against alcohol-induced liver mitochondrial dysfunction in rats. *J. Med. Food* **2009**, *12*, 327−333.
(28) Reddy, V. D.; Padmavathi, P.; Paramahamsa, M.; Varadacharyulu, N. Ch. Amelioration of alcohol-induced oxidative stress by *Emblica officinalis* (amla) in rats. *Indian J. Biochem. Biophys.* **2010**, *47*, 20−25.
(29) Reddy, V. D.; Padmavathi, P.; Gopi, S.; Paramahamsa, M.; Varadacharyulu, N. Ch. Protective effect of *emblica officinalis* against alcohol-Induced hepatic injury by ameliorating oxidative stress in rats. *Indian J. Clin. Biochem.* **2010**, *25*, 419−424.
(30) Reddy, V. D.; Padmavathi, P.; Kavitha, G.; Gopi, S.; Varadacharyulu, N. Ch. *Emblica officinalis* ameliorates alcohol-induced brain mitochondrial dysfunction in rats. *J. Med. Food* **2011**, *14*, 62−68.
(31) Chakraborty, D.; Verma, R. Ameliorative effect of *Emblica officinalis* aqueous extract on ochratoxin-induced lipid peroxidation in the kidney and liver of mice. *Int. J. Occup. Environ. Med.* **2010**, *23*, 63−73.
(32) Yokozawa, T.; Kim, H. Y.; Kim, H. J.; Okubo, T.; Chu, D. C.; Juneja, L. R. Amla (*Emblica officinalis* Gaertn.) prevents dyslipidaemia and oxidative stress in the ageing process. *Br. J. Nutr.* **2007**, *97*, 1187−1195.
(33) Krishnaveni, M.; Mirunalini, S.; Karthishwaran, K.; Dhamodharan, G. Antidiabetic and antihyperlipidemic properties of *Phyllanthus emblica* Linn. (Euphorbiaceae) on streptozotocin induced diabetic rats. *Pak. J. Nutr.* **2010**, *9*, 43−51.
(34) Mehta, S.; Singh, R. K.; Jaiswal, D.; Rai, P. K.; Watal, G. Anti-diabetic activity of *Emblica officinalis* in animal models. *Pharm. Biol.* **2009**, *47*, 1050−1055.
(35) Akhtar, M. S.; Ramzan, A.; Ali, A.; Ahmad, M. Effect of amla fruit (*Emblica officinalis* Gaertn.) on blood glucose and lipid profile of normal subjects and type 2 diabetic patients. *Int. J. Food Sci. Nutr.* **2011**, *62*, 609−616.
(36) Suryanarayana, P.; Kumar, P. A.; Saraswat, M.; Petrash, J. M.; Reddy, G. B. Inhibition of aldose reductase by tannoid principles of *Emblica officinalis*: implications for the prevention of sugar cataract. *Mol. Vis.* **2004**, *10*, 148−154.
(37) Suryanarayana, P.; Saraswat, M.; Petrash, J. M.; Reddy, G. B. *Emblica officinalis* and its enriched tannoids delay streptozotocin-induced diabetic cataract in rats. *Mol. Vis.* **2007**, *13*, 1291−1297.
(38) Tiwari, V.; Kuhad, A.; Chopra, K. *Emblica officinalis* corrects functional, biochemical and molecular deficits in experimental diabetic neuropathy by targeting the oxido-nitrosative stress mediated inflammatory cascade. *Phytother. Res.* **2011**, *25*, 1527−1536.
(39) Chen, T. S.; Liou, S. Y.; Wu, H. C.; Tsai, F. J.; Tsai, C. H.; Huang, C. Y.; Chang, Y. L. Efficacy of epigallocatechin-3-gallate and amla (*Emblica officinalis*) extract for the treatment of diabetic-uremic patients. *J. Med. Food* **2011**, *14*, 718−723.
(40) Hwang, I. S.; Ho, H.; Hoffman, B. B.; Reaven, G. M. Fructose-induced insulin resistance and hypertension in rats. *Hypertension* **1987**, *10*, 512−516.
(41) Kim, H. Y.; Okubo, T.; Juneja, L. R.; Yokozawa, T. The protective role of amla (*Emblica officinalis* Gaertn.) against fructose-induced metabolic syndrome in a rat model. *Br. J. Nutr.* **2010**, *103*, 502−512.
(42) McCord, J. M. Oxygen-derived free radicals in postischaemic tissue injury. *N. Engl. J. Med.* **1985**, *312*, 159−163.
(43) Haramaki, N.; Packer, L.; Assadnazari, H.; Zimmer, G. Cardiac recovery during post-ischaemic reperfusion is improved by combination of vitamin E with dihydrolipoic acid. *Biochem. Biophys. Res. Commun.* **1993**, *196*, 1101−1107.
(44) Haramaki, N.; Aggrawal, S.; Kawabata, T.; Droy-Lefaix, M. T.; Packer, L. Effects of natural antioxidant *Ginkgo biloba* extract (EGb 761) on myocardial ischaemia-reperfusion injury. *Free Radical Biol. Med.* **1994**, *16*, 789−794.
(45) Bhattacharya, S. K.; Bhattacharya, D.; Sairam, K.; Ghosal, S. Effect of bioactive tannoid principles of *Emblica officinalis* on ischemia-reperfusion-induced oxidative stress in rat heart. *Phytomedicine* **2012**, *9*, 171−174.
(46) Rajak, S.; Banerjee, S. K.; Sood, S.; Dinda, A. K.; Gupta, Y. K.; Gupta, S. K.; Maulik, S. K. *Emblica officinalis* causes myocardial adaptation and protects against oxidative stress in ischemic-reperfusion injury in rats. *Phytother. Res.* **2004**, *18*, 54−60.
(47) Anila, L.; Vijayalakshmi, N. R. Flavonoids from *Emblica officinalis* and *Mangifera indica*-effectiveness for dyslipidemia. *J. Ethnopharmacol.* **2002**, *79*, 81−87.
(48) Duan, W. G; Yu, Y.; Zhang, L. Y. Antiatherogenic effects of *Phyllanthus emblica* associated with corilagin and its analogue. *Yakugaku Zasshi* **2005**, *125*, 587−591.
(49) Bhatia, J.; Tabassum, F.; Sharma, A. K.; Bharti, S.; Golechha, M.; Joshi, S.; Sayeed Akhatar, M.; Srivastava, A. K.; Arya, D. S. *Emblica officinalis* exerts antihypertensive effect in a rat model of DOCA-salt-induced hypertension: role of (p) eNOS, NO and oxidative stress. *Cardiovasc. Toxicol.* **2011**, *11*, 272−279.
(50) Libby, P. Inflammation and cardiovascular disease mechanisms. *Am. J. Clin. Nutr.* **2006**, *83*, S456−S460.
(51) Pinmai, K.; Chunlaratthanabhorn, S.; Ngamkitidechakul, C.; Soonthornchareon, N.; Hahnvajanawong, C. Synergistic growth inhibitory effects of *Phyllanthus emblica* and *Terminalia bellerica* extracts with conventional cytotoxic agents: doxorubicin and cisplatin against human hepatocellular carcinoma and lung cancer cells. *World J. Gastroenterol.* **2008**, *14*, 1491−1497.
(52) Pinmai, K.; Hiriote, W.; Soonthornchareonnon, N.; Jongsakul, K.; Sireeratawong, S.; Tor-Udom, S. *In vitro* and *in vivo* antiplasmodial activity and cytotoxicity of water extracts of *Phyllanthus emblica*, *Terminalia chebula*, and *Terminalia bellerica*. *J. Med. Assoc. Thai.* **2010**, *93*, S120−S126.
(53) Hari Kumar, K. B.; Sabu, M. C.; Lima, P. S.; Kuttan, R. Modulation of haematopoetic system and antioxidant enzymes by *Emblica officinalis* Gaertn and its protective role against γ-radiation induced damages in mice. *J. Radiat. Res.* **2004**, *45*, 549−555.
(54) Singh, I.; Sharma, A.; Nunia, V.; Goyal, P. K. Radioprotection of Swiss albino mice by *Emblica officinalis*. *Phytother. Res.* **2005**, *19*, 444−446.
(55) Ghosh, A.; Sharma, A.; Talukder, G. Relative protection given by extract of *Phyllanthus emblica* fruit and an equivalent amount of vitamin C against a known clastogen—caesium chloride. *Food Chem. Toxicol.* **1992**, *30*, 865−869.
(56) Dhir, H.; Roy, A. K.; Sharma, A.; Talukder, G. Modification of clastogenicity of lead and aluminium in mouse bone marrow cells by

dietary ingestion of *Phyllanthus emblica* fruit extract. *Mutat. Res.* **1990**, *241*, 305−312.
(57) Dhir, H.; Agarwal, K.; Sharma, A.; Talukder, G. Modifying role of *Phyllanthus emblica* and ascorbic acid against nickel clastogenicity in mice. *Cancer Lett.* **1991**, *59*, 9−18.
(58) Roy, A. K.; Dhir, H.; Sharma, A. Modification of metal-induced micronuclei formation in mouse bone marrow erythrocytes by *Phyllanthus* fruit extract and ascorbic acid. *Toxicol. Lett.* **1992**, *62*, 9−17.
(59) Jeena, K. J.; Joy, K. L.; Kuttan, R. Effect of *Emblica officinalis*, *Phyllanthus amarus* and *Picrorrhiza kurroa* on *N*-nitrosodiethylamine induced hepatocarcinogenesis. *Cancer Lett.* **1999**, *136*, 11−16.
(60) Sumantran, V. N.; Boddul, S.; Koppikar, S. J.; Dalvi, M.; Wele, A.; Gaire, V.; Wagh, U. V. Differential growth inhibitory effects of *W. somnifera* root and *E. officinalis* fruits on CHO cells. *Phytother. Res.* **2007**, *21*, 496−499.
(61) Sai Ram, M.; Neetu, D.; Yogesh, B.; Anju, B.; Dipti, P.; Pauline, T.; Sharma, S. K.; Sarada, S. K.; Ilavazhagan, G.; Kumar, D.; Selvamurthy, W. Cyto-protective and immunomodulating properties of amla (*Emblica officinalis*) on lymphocytes: an in-vitro study. *J. Ethnopharmacol.* **2002**, *81*, 5−10.
(62) Sai Ram, M.; Neetu, D.; Dipti, P.; Vandana, M.; Ilavazhagan, G.; Kumar, D.; Selvamurthy, W. Cytoprotective activity of amla (*Emblica officinalis*) against chromium(VI) induced oxidative injury in murine macrophages. *Phytother. Res.* **2003**, *17*, 430−433.
(63) Suresh, K.; Vasudevan, D. M. Augmentation of murine natural killer cell and antibody dependent cellular cytotoxicity activities by *Phyllanthus emblica*, a new immunomodulator. *J. Ethnopharmacol.* **1994**, *44*, 55−60.
(64) Ganju, L.; Karan, D.; Chanda, S.; Srivastava, K. K.; Sawhney, R. C.; Selvamurthy, W. Immunomodulatory effects of agents of plant origin. *Biomed. Pharmacother.* **2003**, *57*, 296−300.
(65) Sidhu, S.; Pandhi, P.; Malhotra, S.; Vaiphei, K.; Khanduja, K. L. Beneficial effects of *Emblica officinalis* in L-arginine-induced acute pancreatitis in rats. *J. Med. Food* **2011**, *14*, 147−155.
(66) Muthuraman, A.; Sood, S.; Singla, S. K. The antiinflammatory potential of phenolic compounds from *Emblica officinalis* L in rat. *Inflammopharmacology* **2010**, DOI: 10.1007/s10787-010-0041-9 (online).
(67) Nicolis, E.; Lampronti, I.; Dechecchi, M. C.; Borgatti, M.; Tamanini, A.; Bianchi, N.; Bezzerri, V.; Mancini, I.; Giri, M. G.; Rizzotti, P.; Gambari, R.; Cabrini, G. Pyrogallol, an active compound from the medicinal plant *Emblica officinalis*, regulates expression of pro-inflammatory genes in bronchial epithelial cells. *Int. Immunopharmacol.* **2008**, *8*, 1672−1680.
(68) Srikumar, R.; Jeya Parthasarathy, N. J.; Shankar, E. M.; Manikandan, S.; Vijayakumar, R.; Thangaraj, R.; Vijayananth, K.; Sheela Devi, R.; Rao, U. A. Evaluation of the growth inhibitory activities of *Triphala* against common bacterial isolates from HIV infected patients. *Phytother. Res.* **2007**, *21*, 476−480.
(69) Saeed, S.; Tariq, P. Antibacterial activities of *Emblica officinalis* and *Coriandrum sativum* against Gram negative urinary pathogens. *Pak. J. Pharm. Sci.* **2007**, *20*, 32−35.
(70) Saini, A.; Sharma, S.; Chhibber, S. Protective efficacy of *Emblica officinalis* against *Klebsiella pneumoniae* induced pneumonia in mice. *Indian J. Med. Res.* **2008**, *128*, 188−193.
(71) Rahman, S.; Akbor, M. M.; Howlader, A.; Jabbar, A. Antimicrobial and cytotoxic activity of the alkaloids of amlaki (*Emblica officinalis*). *Pak. J. Biol. Sci.* **2009**, *12*, 1152−1155.
(72) Perianayagam, J. B.; Narayanan, S.; Gnanasekar, G.; Pandurangan, A.; Raja, S.; Rajagopal, K.; Rajesh, R.; Vijayarajkumar, P.; Vijayakumar, S. G. Evaluation of antidiarrheal potential of *Emblica officinalis*. *Pharm. Biol.* **2005**, *43*, 373−377.
(73) Mehmood, M. H.; Siddiqia, H. S.; Gilani, A. H. The antidiarrheal and spasmolytic activities of *Phyllanthus emblica* are mediated through dual blockade of muscarinic receptors and Ca^{2+} channels. *J. Ethnopharmacol.* **2011**, *133*, 856−865.
(74) Chen, K. H.; Lin, B. R.; Chien, C. T.; Ho, C. H. *Emblica officinalis* Gaertn. attentuates *N*-nitrosodiethylamine-induced apoptosis, autophagy, and inflammation in rat livers. *J. Med. Food* **2011**, *14*, 746−755.
(75) Verma, R.; Chakraborty, D. Alterations in DNA, RNA and protein contents in liver and kidney of mice treated with ochratoxin and their amelioration by *Emblica officinalis* aqueous extract. *Acta Pol. Pharm.* **2008**, *65*, 3−9.
(76) Pramyothin, P.; Samosorn, P.; Poungshompoo, S.; Chaichantipyuth, C. The protective effects of *Phyllanthus emblica* Linn. extract on ethanol induced rat hepatic injury. *J. Ethnopharmacol.* **2006**, *107*, 361−364.
(77) Tasduq, S. A.; Kaisar, P.; Gupta, D. K.; Kapahi, B. K.; Maheshwari, H. S.; Jyotsna, S.; Johri, R. K. Protective effect of a 50% hydroalcoholic fruit extract of *Emblica officinalis* against anti-tuberculosis drugs induced liver toxicity. *Phytother. Res.* **2005**, *19*, 193−197.
(78) Sairam, K.; Rao, Ch. V.; Babu, M. D.; Kumar, K. V.; Agrawal, V. K.; K Goel, R. K. Antiulcerogenic effect of methanolic extract of *Emblica officinalis*: an experimental study. *J. Ethnopharmacol.* **2002**, *82*, 1−9.
(79) Bandyopadhyay, S. K.; Pakrashi, S. C.; Pakrashi, A. The role of antioxidant activity of *Phyllanthus emblica* fruits on prevention from indomethacin induced gastric ulcer. *J. Ethnopharmacol.* **2000**, *70*, 171−176.
(80) Tasduq, S. A.; Mondhe, D. M.; Gupta, D. K.; Baleshwar, M.; Johri, R. K. Reversal of fibrogenic events in liver by *Emblica officinalis* (fruit), an Indian natural drug. *Biol. Pharm. Bull.* **2005**, *28*, 1304−1306.
(81) Mir, A. I.; Kumar, B.; Tasduq, S. A.; Gupta, D. K.; Bhardwaj, S.; Johri, R. K. Reversal of hepatotoxin-induced pre-fibrogenic events by *Emblica officinalis* − a histological study. *Indian J. Exp. Biol.* **2007**, *45*, 626−629.
(82) Chatterjee, A.; Chattopadhyay, S.; Bandyopadhyay, S. K. Biphasic effect of *Phyllanthus emblica* L. extract on NSAID-induced ulcer: an antioxidative trail weaved with immunomodulatory effect. *Evidence Based Complement. Alternat. Med.* **2011**, DOI: 10.1155/2011/146808 (online).
(83) Golechha, M.; Bhatia, J.; Ojha, S.; Arya, D. S. Hydroalcoholic extract of *Emblica officinalis* protects against kainic acid-induced status epilepticus in rats: evidence for an antioxidant, anti-inflammatory, and neuroprotective intervention. *Pharm. Biol.* **2011**, *49*, 1128−1136.
(84) Vasudevan, M.; Parle, M. Memory enhancing activity of Anwala churna (*Emblica officinalis* Gaertn.): an Ayurvedic preparation. *Physiol. Behav.* **2007**, *91*, 46−54.
(85) Perianayagam, J. B.; Sharma, S. K.; Joseph, A.; Christina, A. J. Evaluation of anti-pyretic and analgesic activity of *Emblica officinalis* Gaertn. *J. Ethnopharmacol.* **2004**, *95*, 83−85.
(86) Adil, M. D.; Kaiser, P.; Satti, N. K.; Zargar, A. M.; Vishwakarma, R. A.; Tasduq, S. A. Effect of *Emblica officinalis* (fruit) against UVB-induced photo-aging in human skin fibroblasts. *J. Ethnopharmacol.* **2010**, *132*, 109−114.
(87) Kumar, M. S.; Kirubanandan, S.; Sripriya, R.; Sehgal, P. K. Triphala promotes healing of infected full-thickness dermal wound. *J. Surg. Res.* **2008**, *144*, 94−101.
(88) Sumitra, M.; Manikandan, P.; Gayathri, V. S.; Mahendran, P.; Suguna, L. *Emblica officinalis* exerts wound healing action through up-regulation of collagen and extracellular signal-regulated kinases (ERK1/2). *Wound Repair Regen.* **2009**, *17*, 99−107.
(89) Del Rio, D.; Rodriguez-Mateos, A.; Spencer, J. P.; Tognolini, M.; Borges, G.; Crozier, A. Dietary (poly)phenolics in human health: structures, bioavailability, and evidence of protective effects against chronic diseases. *Antioxid. Redox Signal.* **2013**, *18*, 1818−1892.

JOURNAL OF AGRICULTURAL AND FOOD CHEMISTRY

Review

pubs.acs.org/JAFC

Bioactivity and Potential Health Benefits of Licorice

Tzu-Chien Kao,[†] Chi-Hao Wu,[§] and Gow-Chin Yen*[,†,‡]

[†]Department of Food Science and Biotechnology, National Chung Hsing University, 250 Kuokuang Road, Taichung 402, Taiwan
[‡]Agricultural Biotechnology Center, National Chung Hsing University, 250 Kuokuang Road, Taichung 40227, Taiwan
[§]School of Nutrition and Health Sciences, Taipei Medical University, 250 Wu-Hsing Street, Taipei 110, Taiwan

ABSTRACT: Licorice is an herbal plant named for its unique sweet flavor. It is widely used in the food and tobacco industries as a sweetener. Licorice is also used in traditional Chinese medicine (TCM) and complementary medicine. Because the use of licorice has long been a part of TCM, the details of its therapeutic applications have been thoroughly established. In modern science, licorice is of interest because of its broad range of applications. Extracts of and compounds isolated from licorice have been well studied and biologically characterized. In this review, we discuss the nutraceutical and functional activities of licorice as well as those of the extracts of and the isolated compounds from licorice, including agents with anti-inflammatory activity, cell-protective abilities, and chemopreventive effects. The side effects of licorice are also enumerated. A comparison of the activities of licorice described by modern science and TCM is also presented, revealing the correspondence of certain characteristics.

KEYWORDS: *licorice, glycyrrhizic acid, 18β-glycyrrhetinic acid, biological function, safety*

INTRODUCTION

Licorice, also called liquorice, is the root or stem of *Glycyrrhiza glabra* (*G. glabra*), which has a sweet flavor. In China, licorice is called "gan cao". The ancient Greek physician Pedanius Dioscorides named licorice *γλυκύρριζα* (glukurrhiza), meaning "sweet root"; the first part of the word, "*γλυκύς*", (glukus) means "sweet", and the last part of the word "*ρίζα*" (rhiza) means "root" (Perseus digital library, http://www.perseus.tufts.edu/hopper/). Three plants are identified as licorice, *Glycyrrhiza glabra* (*G. glabra*), *Glycyrrhiza uralensis* Fisch. (*G. uralensis*), and *Glycyrrhiza inflata* Bat. (*G. inflata*).

Because of its sweet favor, licorice is used in a number of foods, most prominently condiments and confectionery. Condiments such as soy sauce and sweet chili sauce contain licorice powder to add a unique sweet flavor that might be referred to as mellow in English. Confectionery flavored with an extract of the roots of the licorice plant is also called licorice. Candies such as Red Vines and London drops are flavored with licorice. Tobacco manufacturers use a considerable amount of licorice in their products. Licorice block, powder, and extract can be used in tobacco for multiple purposes. According to Carmines et al.,[1] licorice is added to tobacco to enhance and harmonize the smoke flavor, reduce dryness in the mouth and throat, improve the moisture-holding characteristics of the tobacco to increase its stability and shelf life, act as a surface-active agent during the spraying process of the casing ingredients, improve the uniformity of the absorption of flavors, and minimize the rough smoke character by balancing the overall flavor profile of the tobacco smoke. Licorice is generally recognized as safe (GRAS, Report No. 28, Conclusion 2), which indicates that it does not represent a hazard to the public when used at typical levels and in a typical manner. Licorice is also a common and useful ingredient in cosmetics. In a clinical study, topical treatment with a gel containing 2% licorice extract led to a significant improvement in erythema, edema, and pruritus.[2] Licorice extracts are also used as skin depigmenting agents and are effective in the treatment of postinflammatory hyperpigmentation, including that caused by chemical peeling and laser therapy.[3] Licorice extract inhibits the rate-limiting first step of the oxidation of tyrosinase,[4] making it an effective treatment for melasma.[5] Furthermore, licorice extract is very useful in the treatment of aphthous ulcers;[6] even the deglycyrrhizinated form of licorice (DLG) has a similar positive effect.[7]

The application of licorice is not restricted to food, tobacco, and cosmetic use; this plant is also used in medicine. Licorice is considered to be an herbal remedy for many disorders. Nassiri et al.[8] characterized some of the traditional uses of licorice, including the treatment of wounds, diabetes, cough, and tuberculosis. In traditional Chinese medicine (TCM), licorice is one of the most frequently used herbs. Licorice is commonly used in herbal formulas to harmonize other ingredients and to carry the formula to the 12 regular meridians in TCM.[9] The compendium of Materia Medica (Bencao Gangmu) states that licorice can act as an effective antidote, a detoxicant, a beneficial agent in the development of bone and muscle, and a remedy for throat disorders and cough.[9] Licorice is also found in many TCM formulas for treating liver disease. Sho-saiko-to (TJ-9) is frequently used in Japan for liver disorders (e.g., chronic active hepatitis),[10] although this formula is from Xiao Chai Hu Tang (Minor Bupleurum Formula) in Shang Han Lun of TCM.[11]

Modern studies have demonstrated that the uses of licorice in TCM are viable. For example, Ma Huang Tang, a classic Chinese formula composed of Ephedra, Cassia twig, bitter apricot kernel, and prepared licorice, has recently been confirmed to be an effective remedy for pulmonary disorders such as colds, influenza, acute bronchitis, and bronchial asthma. The He group demonstrated that the direct effects of bitter apricot kernel

Received: November 3, 2013
Revised: December 17, 2013
Accepted: December 30, 2013
Published: December 30, 2013

ACS Publications © 2013 American Chemical Society

dx.doi.org/10.1021/jf404939f | *J. Agric. Food Chem.* 2014, 62, 542−553

and prepared licorice on the integral potency of the formula are nonsignificant. However, these two drugs have a significant synergetic effect when administered with Ephedra or Cassia twigs.[12] That study provides evidence that licorice can harmonize with the other ingredients in the formula, even though it may not be a primary effective ingredient. A gargle containing licorice has been shown to be an effective method for attenuating both the incidence and severity of postoperative sore throat,[13] providing scientific evidence corroborating the TCM-described effect of licorice. Because some of the healing effects described in TCM have been confirmed by modern medicine, an important question arises: which compound(s) in licorice mediate these effects?

BIOACTIVE COMPOUNDS IN LICORICE AND THEIR BIOLOGICAL FUNCTIONS

Glycyrrhizic Acid and 18β-Glycyrrhetinic Acid. The sweetness of licorice is derived from glycyrrhizic acid, also called glycyrrhizin (Figure 1A). Glycyrrhizic acid is a triterpenoid saponin glycoside and is 30−50 times as sweet as sucrose because glycyrrhizic acid can induce impulses from sugar receptor-containing cells at a concentration (3.0 mM) that is much lower than that of sucrose.[14] Furthermore, unlike the sugar substitute aspartame, glycyrrhizin maintains its sweetness after heating. Both sugar and glycyrrhizic acid taste sweet, but glycyrrhizic acid induces a lower onset sweet flavor than sugar, and its sweetness remains in the mouth for a longer period of time. Glycyrrhetinic acid (18α-glycyrrhetinic acid and 18β-glycyrrhetinic acid) is another triterpenoid in licorice (Figure 1A). Glycyrrhetinic acid can be obtained from the hydrolysis of glycyrrhizic acid. This process can be completed by presystemic metabolism by intestinal bacteria that perform glycolysis.[15] Human intestinal bacteria metabolize glycyrrhizic acid through the action of the glucuronidases of *Bacteroides* J-37 and *Eubacterium* sp. to yield 18β-glycyrrhetinic acid (18βGA).[16] Processing (Chinese Materia Medica) licorice by dry-roasting or honey-roasting[18] to obtain licorice preparata accelerates the hydrolysis of the sugar chains in the saponin and glycosidic flavonoid constituents.[17] Raw licorice and licorice preparata are both important agents in TCM, and each has a different function. Recent studies indicate that the anti-inflammatory activities[19] and neuroprotective effects[20] of roasted licorice may be more potent than those of raw licorice, in contrast to the characteristics described by TCM. Bencao Gangmu suggests that raw licorice can be used to treat the syndrome known as inflammation in modern medicine (Xie Huo in Chinese), and roasted licorice can be used for reinforcement (Bu Zhong in Chinese).[9] For example, roasted licorice is used in Buzhong Yiqi Tang instead of raw licorice, which suggests that glycyrrhizic acid and 18β-glycyrrhetinic acid may have distinct biological properties.

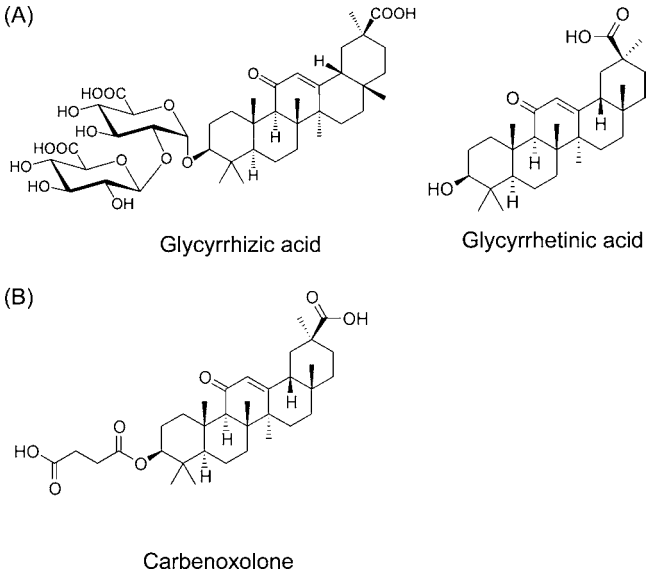

Figure 1. Chemical structures of glycyrrhizic acid and glycyrrhetinic acid (A) and the derivative of glycyrrhetinic acid; carbenoxolone (B) in licorice.

Because licorice has been used alone and as a component in many formulas to treat liver diseases, multiple mechanisms have been proposed for the hepatoprotective effects of glycyrrhizic acid and 18β-glycyrrhetinic acid. Both glycyrrhizic acid and 18β-glycyrrhetinic acid can protect rat hepatocytes from bile acid-induced cytotoxicity.[21] Recently, a beneficial effect of glycyrrhizic acid on hepatitis was demonstrated; the intravenous administration of glycyrrhizic acid decreases serum alanine transaminase (ALT) and necro-inflammation and fibrosis in the liver.[22] Many mechanisms are involved in the protective effects of glycyrrhizic acid and 18β-glycyrrhetinic acid. These mechanisms likely involve reduced AST (aspartate transaminase, also called GOT) and ALT (also called GPT) activities. The pregnane X receptor (PXR), as well as the cytochrome P450 family 3 subfamily A (CYP3A), can also be modulated by glycyrrhizic acid to protect against lithocholic acid-induced injury.[23] Both glycyrrhizic acid and 18β-glycyrrhetinic acid treatments can inhibit liver fibrosis,[24] which may lead to cancer.

In addition to liver protection, glycyrrhizic acid and 18β-glycyrrhetinic acid may be effective in the protection of other organs. Both glycyrrhizic acid and 18β-glycyrrhetinic acid have positive effects on brain damage induced by ischemia and 6-hydroxydopamine.[25] A recently study demonstrated that glycyrrhizic acid and 18β-glycyrrhetinic acid can penetrate the blood-brain barrier (BBB).[26] These findings indicate that glycyrrhizic acid and 18β-glycyrrhetinic acid are potent agents for the treatment of neural diseases, ischemic brain diseases, and Parkinson's disease. Glycyrrhizic acid also exhibits protective effects in the kidney; studies have demonstrated that glycyrrhizic acid protects against cisplatin-induced genotoxicity and nephrotoxicity.[27] Protective effects have also been observed with a renal hypoxia-reoxygenation model. However, 18β-glycyrrhetinic acid does not exhibit the same potential.[28] Glycyrrhizic acid seems to be effective against ischemic damage, including damage to the spinal cord,[28] myocardium,[29] liver,[30] and gut.[31]

Glycyrrhizic acid and 18β-glycyrrhetinic acid are considered inhibitors of inflammation induced by both bacterial and viral infection. Because inflammation is frequently triggered by bacteria or viral infection, antibacterial and antiviral activities are possible anti-inflammatory strategies. Glycyrrhizic acid can inhibit the replication of and infection by various viruses,[32] including severe acute respiratory syndrome (SARS)-associated coronavirus,[33] human immunodeficiency virus (HIV),[34] hepatitis A virus (HAV),[35] hepatitis B virus (HBV),[36] hepatitis C virus (HCV),[37] herpesviridae (varicella zoster virus, VZV),[38] herpes simplex virus 1 (HSV-1),[39] Epstein−Barr virus (EBV),[40] cytomegalovirus (CMV),[41] and influenza viruses, including H1N1[42] and H5N1.[43] Studies also indicate that glycyrrhizic acid inhibits the growth of *Helicobacter pylori*, and thus, this agent can be used in the treatment of gastric ulcers.[44] 18βGA has also been shown to be effective against clarithromycin-resistant

dx.doi.org/10.1021/jf404939f | J. Agric. Food Chem. 2014, 62, 542−553

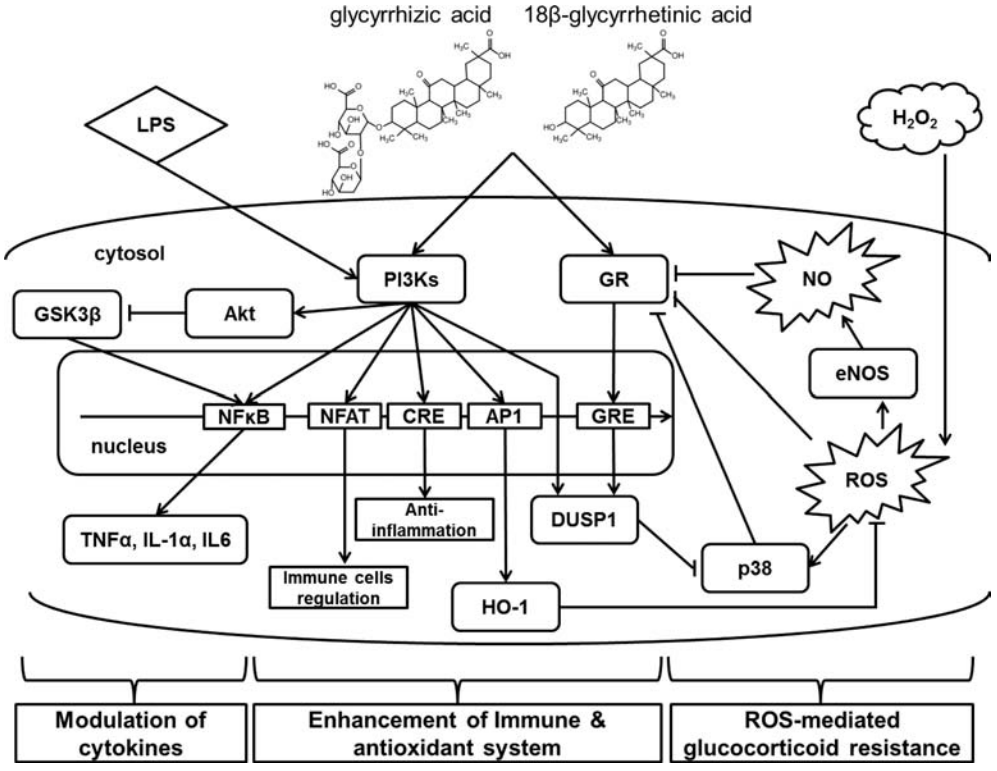

Figure 2. The proposed anti-inflammatory mechanism of glycyrrhizic acid and 18β-glycyrrhetinic acid. Glycyrrhizic acid and 18β-glycyrrhetinic acid can modulate PI3K signaling to upregulate the antioxidant system, leading to reduced intracellular ROS. Therefore, PI3K signaling also enhances GR signaling and modulates cytokines.[47,50]

strains of *H. pylori*.[45] Further studies have revealed that glycyrrhizic acid and 18β-glycyrrhetinic acid can modulate inflammation-related mechanisms. TCM often incorporates licorice to enhance the effect of other formulas that act as anti-inflammatory agents. Glycyrrhizic acid enhances the anti-inflammatory effect of licorice extract without glycyrrhizic acid.[46] Michaelis et al.[43] also demonstrated that glycyrrhizic acid can inhibit H5N1-induced pro-inflammatory gene expression without affecting the cytolytic activity of natural killer cells. These results indicate that glycyrrhizic acid might modulate inflammation by two methods of regulation, the inhibition of proinflammatory cytokines and the promotion of immune function. PI3K may play a role in this regulation. Glucocorticoids and the glucocorticoid receptor modulate inflammation very effectively, and glucocorticoids (e.g., dexamethasone) are used extensively in clinical treatment. There are several potential mechanisms for the involvement of glycyrrhizic acid and 18β-glycyrrhetinic acid in the induction of cortisone activity. Glycyrrhizic acid and 18β-glycyrrhetinic acid can activate glucocorticoid receptor (GR) signaling by binding to the GR[47] and inhibiting the activity of corticosteroid 11β-dehydrogenase isozyme 2 (11β-HSD2), which converts active cortisol into inactive cortisone.[48,49] Glycyrrhizic acid and 18β-glycyrrhetinic acid may also enhance GR signaling by eliminating intracellular oxidative stress.[50] Although glycyrrhizic acid can enhance glucocorticoid activity, it does not seem to increase glucocorticoid-induced side effects. For example, excessive glucocorticoid levels exert diverse effects on bone microstructure, integrity, and mineral metabolism.[51] Ramli et al.[52] demonstrated that glycyrrhizic acid has the potential to be used as an agent to protect bone against glucocorticoid-induced osteoporosis. High-mobility group box 1 (HMGB1), a nuclear component that functions extracellularly as a signaling molecule in acute and chronic inflammation, is inhibited by binding to glycyrrhizic acid.[53] Glycyrrhizic acid and 18β-glycyrrhetinic acid can modulate PI3K signaling to alleviate inflammation (Figure 2).[50] Altogether, these results suggest that glycyrrhizic acid and 18β-glycyrrhetinic acid have considerable potential for development as novel inflammation-modulating agents.

Glycyrrhizic acid and 18β-glycyrrhetinic acid also affect the biological mechanism of cancer formation. Glycyrrhizic acid may inhibit angiogenesis by targeting ERK signaling.[54] Glycyrrhizic acid also protects against UVB-induced carcinogenesis in the epidermis of SKH-1 hairless mice.[55] Because GA is effective against HCV-induced liver disorders, it also prevents hepatocarcinogenesis associated with hepatitis.[56,57] Glycyrrhetinic acid has a more potent anticarcinogenesis effect than glycyrrhizic acid. 18β-Glycyrrhetinic acid not only induces apoptotic cell death but also exhibits a synergistic toxic effect with antibiotics and anticancer drugs (e.g., camptothecin, mitomycin c, and doxorubicin).[58] Glycyrrhetinic acid, oleanolic acid, and ursolic acid have similar chemical structures and potent antiulcer activities.[59] Compounds whose chemical structures are similar to that of glycyrrhetinic acid also provide a satisfactory anticarcinogenesis outcome.[60] Many cancer cells are sensitive to treatment with glycyrrhetinic acid and its derivatives, including the human epithelial ovarian carcinoma cell lines OVCAR-3 and SK-OV-3,[61,62] the human prostate cancer cell lines DU145[63,64] and PC3, the human breast cancer cell line MCF7,[65,66] the human bladder cancer cell line NTUB1,[67] the human leukemia cell line HL60,[68] the human erythromyeloblastoid leukemia cell line K562,[69] the human colon cancer cell lines RKO and SW480,[70] the pancreatic cancer cell lines Panc1 and Panc28,[71] and many other cell lines. 18β-Glycyrrhetinic acid is more toxic than glycyrrhizic acid;

dx.doi.org/10.1021/jf404939f | J. Agric. Food Chem. 2014, 62, 542−553

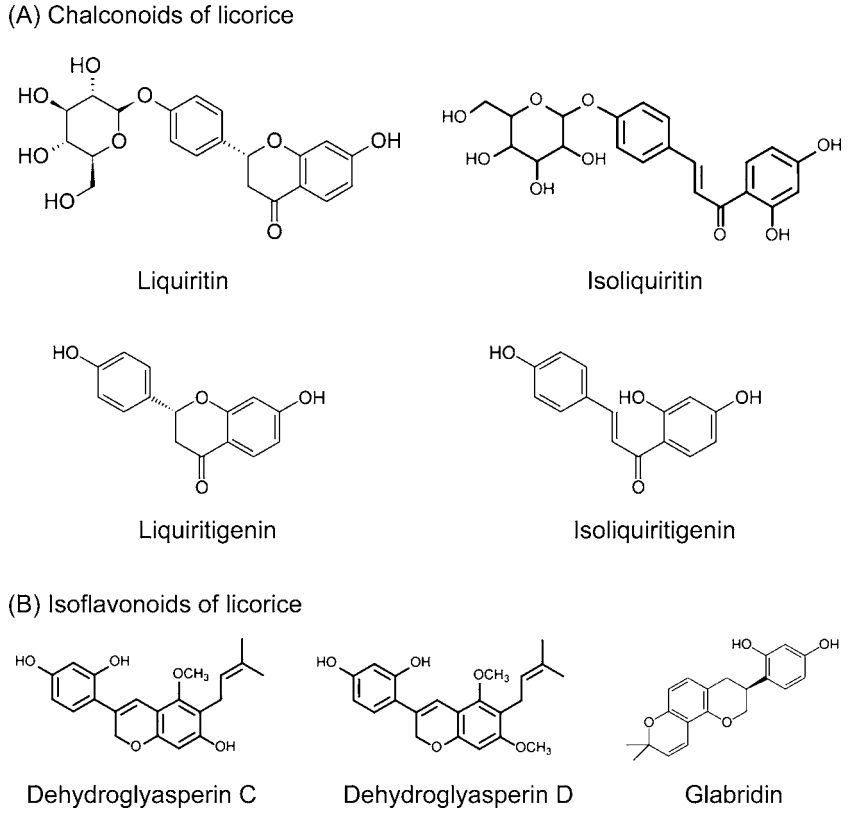

Figure 3. Chemical structures of the chalconoids (A) and the isoflavonoids (B) in licorice.

glycyrrhizic acid displays no obvious cell toxicity, even at 200 μM.[25,47,50]

Glycyrrhizic acid and glycyrrhetinic acid can bind to DNA[72] and RNA.[73] This behavior implies that glycyrrhizic acid and glycyrrhetinic acid may directly interfere with the pattern of transcription factors, the targeting of gene expression, and the interactions of DNA and RNA. This issue might be a promising research topic for understanding the biological functions of glycyrrhizic acid and glycyrrhetinic acid. On the basis of the above evidence, glycyrrhizic acid and 18β-glycyrrhetinic acid have distinct biological functions, which may be due to the differences in their chemical structures.

Liquiritin, Isoliquiritin, Liquiritigenin, and Isoliquiritigenin. Liquiritigenin and isoliquiritigenin are chalconoids of licorice; liquiritin and isoliquiritin are the glycone forms of liquiritigenin and isoliquiritigenin, respectively (Figure 3A). Although studies of the antioxidant abilities of liquiritin, isoliquiritin, liquiritigenin, and isoliquiritigenin are limited, these compounds are considered to be potent protective agents against cancer. These four compounds may have a potent antispasmodic effect.[74] Mai Men Dong Tang is a widely used licorice-containing TCM formula that is used to achieve tussive relief. Researchers believe that these four compounds play an important role in licorice's healing effects.[75] Because the chemical structures of these compounds are similar, the simultaneous study of all four compounds may facilitate the elucidation of the relationship between their biological effects and structure.

The biological functions of liquiritin are similar to those of glycyrrhizic acid. Liquiritin promotes neurite outgrowth in PC12 cells with nerve growth factor treatment,[76] suggesting its potential as a remedy for neurodegenerative diseases such as Alzheimer's disease or Parkinson's disease. Furthermore, liquiritin may exhibit an antidepressant-like effect in chronic variable stress-induced depression model rats by modulating oxidative stress.[77] Liquiritin also attenuates the induction of the RAGE/NFκB pathway in human umbilical vein endothelial cells (HUVECs) by advanced glycation end products (AGE), which may benefit patients with diabetes mellitus.[78] Liquiritin and glycyrrhizic acid can also stimulate immune responses,[79] enhance antioxidant enzymes such as superoxide dismutases (SOD), catalase, and glutathione peroxidase in mice focal cerebrum,[80] and might act as protective agents against epithelial injury in chronic obstructive pulmonary disease (COPD).[81] As with glycyrrhizic acid, liquiritin may bind to DNA.[82] Liquiritin may directly affect gene expression or other DNA-related mechanisms. Both liquiritin and glycyrrhizic acid are glycones or glycosides, functional groups that may be important for DNA binding, although this characterization has yet to be confirmed.

There are few studies of isoliquiritin listed in the PubMed database, and most are concerned with its isolation and identification. Isoliquiritin is thought to prevent angiogenesis and tube formation in granulomas[83] and may also have a potent antitussive effect.[84] Another possible application of isoliquiritin is skin depigmentation due to tyrosinase inhibition.[85] Research on isoliquiritin may be limited because of its lack of commercial availability.

Liquiritigenin is a well-known selective estrogen receptor β agonist[86] that has been implicated in the weight-reducing effects of licorice oil.[87] Liquiritigenin may facilitate the recovery of learning and memory deficits induced by amyloid beta Aβ(25−35)[88] and also help to enhance osteoblast function.[89] Both liquiritigenin and isoliquiritigenin are able to inhibit xanthine oxidase,[90] a promoting factor in many disorders. The IC_{50} values of these compounds are similar, 49.3 μM for liquiritigenin and 55.8 μM for isoliquiritigenin. Both liquiritigenin and isoliquir-

dx.doi.org/10.1021/jf404939f | J. Agric. Food Chem. 2014, 62, 542−553

itigenin display potential PPARγ activating activity,[91] suggesting their potential for use in recovery from metabolic syndrome. Isoliquiritigenin is also an inhibitor of aldose reductase, which suggests that it might be effective in treating diabetic complications.[92] In addition, both liquiritigenin and isoliquiritigenin are effective anti-inflammatory agents. Liquiritigenin inhibits iNOS and proinflammatory cytokines by blocking NFκB,[93] while isoliquiritigenin can influence the intercellular adhesion molecule-1 (ICAM-1) and the vascular cell adhesion molecule-1 (VCAM-1) to modulate inflammation.[94] In many cells and organs, liquiritigenin has a protective role against a number of injuries, including acetaminophen-induced rat liver damage,[95] cadmium-induced rat hepatoma Reuber H35 cell (H4IIE) damage,[96] D-galactosamine/lipopolysaccharide- or CCl_4-mediated rat hepatitis,[97] Aβ(25−35)-induced injury of rat hippocampal neurons,[98] and infection by *Candida albicans*.[99] Isoliquiritigenin also protects many cells and organs by inhibiting cisplatin-induced rat anorexia,[100] the hyperaggregability of platelets induced by diabetes,[101] and the accumulation of cyclic AMP in rat ventricular heart muscle[102] and by potently promoting neuronal health by inhibiting monoamine oxidase A and B,[103] among other mechanisms. In the liver, liquiritigenin can enhance bile secretion via a choleretic effect and can enhance the activity of transporters and phase II enzymes in the liver.[104] This effect is thought to be related to the antidote ability of licorice. In addition to increasing bile secretion, liquiritigenin might increase the rate of hepatic blood flow.[105] Liquiritigenin may also exhibit chemopreventive activity in liver cancer[106,107] and lung cancer.[108] The mechanisms by which liquiritigenin modulates chemoprevention might involve apoptotic molecular targets, such as cytochrome c, caspases,[109] matrix metalloproteinases (MMPs), PI3K, Akt,[110] and vascularization.[111] Notably, C8-prenylation of a flavonoid such as liquiritigenin may enhance the induction of H4IIE and C6 glioma cell apoptosis without affecting its antioxidative properties.[112] Isoliquiritigenin has been reported to inhibit lipoxygenase and prostaglandin E2 (PEG2),[113] induce cell cycle arrest in the human prostate cancer cell lines DU145 and LNCaP cells,[114] induce cell death in the human breast cancer cell line MCF7 at high concentration,[115] suppress pulmonary metastasis of mouse renal cell carcinoma,[116] inhibit human lung cancer cell growth,[117] inhibit colon cancer in ddY mice,[118,119] induce apoptosis in human MGC803 gastric cancer cells,[120] and activate the apoptosis in hepatoma cells[121,122] among other effects in cancer cell. Thus, liquiritigenin is a potent protectant in cells and organs, whereas isoliquiritigenin exhibits greater potential in cancer chemoprevention.

Liquiritigenin and isoliquiritigenin have also been applied in the treatment of cocaine addiction. Although the results are preliminary, liquiritigenin improved the selective molecular and behavioral disorders associated with cocaine use,[123] and isoliquiritigenin inhibited the dopamine release induced by cocaine.[124] This research has high practical value and is worth further study.

Dehydroglyasperin C and Dehydroglyasperin D. Dehydroglyasperin is an isoflavonoid isolated from licorice that has two isoforms, dehydroglyasperin C (DGC) and dehydroglyasperin D (DGD) (Figure 3B).[125] DGC and DGD are also classified as phenylflavonoids[126] and are strong antioxidants, although the potency of DGC is greater. Another phenylflavonoid, isoangustone A, was identified by Lee et al.[125] The antioxidant activity of isoangustone A is lower than that of DGD.[126]

DGC and DGD are potent ligands of peroxisome proliferator-activated receptor γ (PPARγ), which is thought to play a role in metabolic syndrome. Treatment with an ethanolic extract of licorice containing DGC and DGD prevents and ameliorates metabolic syndrome in diabetic KK-A^y and obese C57BL mice.[127] DGC is not only a ligand of PPARγ but also an activating factor of Nrf2 and detoxifying enzymes.[128] PI3K/Akt and Nrf2-Keap1 are also modulated by DGC to protect against glutamate-induced neuronal cell damage.[129] While DGC and DGD exhibit various potent activities, they are relatively newly isolated compounds in licorice, and further study of their biology and toxicity is needed.

Glabridin. Glabridin (Figure 3B) is a licorice isoflavonoid with antimicrobial[130] and antioxidant properties.[131] Because of its well-described antioxidant capabilities, glabridin is frequently used in studies of oxidative stress, including LDL oxidation.[132] The structure of glabridin is similar to that of estradiol-17β, and studies have shown that glabridin might modulate bone disorders in postmenopausal women[133] and increases in osteoblastic cell function.[134] Although glabridin is a potent antioxidant, brain penetration of glabridin through the BBB is altered by P-glycoprotein, which might limit the application of glabridin in central nervous system (CNS) diseases.[135]

The main application of glabridin might be cosmetics. The antioxidant ability of glabridin might help modulate anti-inflammatory mechanisms in skin tissue. Although clinical studies are lacking, some commercial formulations contain licorice extract and claim that glabridin is useful for skin depigmentation.[136] Glabridin and its derivatives[137] inhibit tyrosinase, and there have been reports of a reduction in UVB-induced pigmentation and erythema in brownish guinea pigs when glabridin was administered for three weeks after UVB irradiation.[138] As part of its potent anti-inflammatory activity, glabridin can inhibit inducible nitric oxide synthase (iNOS) expression[139] and upregulate manganese SOD, catalase, and paraoxonase 2 expression.[140]

Increasing evidence indicates that glabridin may be beneficial in the treatment of diabetes mellitus and related diseases. Licorice flavonoid oil (LFO, also called Kaneka glavonoid rich oil) contains glabridin as the bioactive flavonoid and suppresses abdominal fat accumulation and blood glucose levels in KK-A^y mice.[141] LFO can activate AMP-activated protein kinase (AMPK) and ameliorate the increases in fatty liver and in the triglyceride and cholesterol plasma levels induced by obesity.[142] LFO administered daily up to 1200 mg/day is considering safe in humans.[143] On the basis of this finding, LFO might be safe as a functional food. Glabridin also works as a cancer preventive agent. It blocks FAK/rho signaling in human nonsmall cell lung cancer A549 cells and inhibits the migration, invasion, and angiogenesis of A549 cells.[144] On the basis of these studies, uses of glabridin beyond cosmetics should be explored.

Carbenoxolone. Sodium carbenoxolone (also called carbenoxolone or CBX) is the 3-hemisuccinate of glycyrrhetinic acid and may be the best-known derivative of glycyrrhetinic acid (Figure 1B). As the disodium salt of the 3-*o*-hydrogen succinate, carbenoxolone is freely soluble in water.[145] The chemical structure of carbenoxolone is similar to that of glucocorticoids, and CBX can be used as an anti-inflammatory agent and an inhibitor of 11β-hydroxysteroid dehydrogenase type 1.[146] Sterol regulation is a very important characteristic of carbenoxolone, which is related to its effectiveness in the prevention of fatty liver.[147] Because of the regulatory ability of glucocorticoids, carbenoxolone might have a nootropic effect by improving verbal

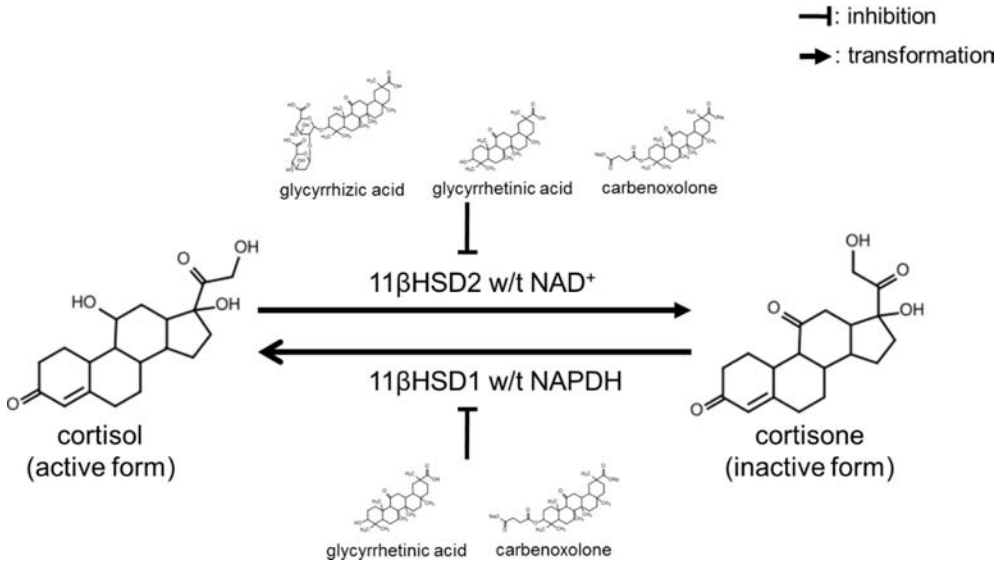

Figure 4. 11β-Hydroxysteroid dehydrogenase inhibition caused by glycyrrhizic acid, glycyrrhetinic acid, and carbenoxolone. There are two isoforms in humans, 11βHSD1 and 11βHSD2. 11βHSD2 converts biologically active cortisol into inactive cortisone, whereas 11βHSD1 converts inactive cortisone into active cortisol. Studies have shown that both glycyrrhizic acid and glycyrrhetinic acid can inhibit 11βHSD2, as can carbenoxolone. For 11βHSD1 inhibition, glycyrrhetinic acid and its derivative, carbenoxolone, may have greater potency than glycyrrhizic acid.

fluency and verbal memory in humans.[148] In TCM, Bencao Gangmu has been quoted as stating that licorice consumption may enhance memory. The best-known modern application of carbenoxolone is gastric ulcer treatment, which is based on the spironolactone,[149] and has good outcome in aphthous ulcers.[150]

Carbenoxolone is also a well-known gap junction inhibitor and is widely used in neuroscience research.[151] Gap junctions are also important in glutamate-induced neurotoxicity, and carbenoxolone can decrease the toxic effects of glutamate.[152] Carbenoxolone also protects against ischemic injury in skeletal muscle and the hippocampus resulting from gap junction inhibition.[153] Gap junctions are also related to pain control because the spinal cord glia exhibit extensive gap junctional connectivity, which is involved in the contralateral spread of excitation that results in mirror image pain.[154] Because carbenoxolone is an inhibitor of gap junctions, its application in pain relief is not unreasonable. Connexin gap junction proteins (Cx43 and Cx26) initiate brain metastatic lesion formation in association with the vasculature. Carbenoxolone can prevent tumor cell extravasation and blood vessel involvement.[155] Carbenoxolone is frequently used in cancer research to probe the relationship between gap junctions and cancer formation, such as in the study of the relationship between gap function and breast cancer metastasis or melanoma brain colonization.[155] Carbenoxolone is a useful agent for many research fields and is widely applied in clinical treatments.

SAFETY OF LICORICE

Although licorice is considered to be a nontoxic herb in TCM, some health concerns may be associated with the use of licorice. Clinical studies show that licorice may cause edema and apparent mineralocorticoid excess syndrome because glycyrrhizic acid and glycyrrhetinic acid can inhibit the activity of 11β-hydroxysteroid dehydrogenase type 2 (11β-HSD2),[48,49] which converts biologically active cortisol into the inactive compound cortisone, thereby preventing the overstimulation of the mineralocorticoid receptor by cortisol.[156] Mineralocorticoid overdose can lead to excessive sodium ion levels and the excretion of potassium ions, which may cause water retention and lead to hypertension. Excessive daily supplementation with licorice may cause low potassium levels due to licorice-induced hyperaldosteronism and may lead to hypertension and heart disease.[157] Licorice-induced hypertension can be reversed by stopping the intake of licorice-based products.[157] 11β-Hydroxysteroid dehydrogenase type 2 is inhibited by licorice, and licorice constituents can cause hypertonia and hypokalemia because of the associated change in potassium levels in the blood. Similar concerns are associated with the intake of carbenoxolone because it is a more potent inhibitor of 11βHSD2 (IC_{50}: 20−50 nM) than 11βHSD1 (IC_{50}: 1.8 μM)[49] (Figure 4). Potassium levels are also affected by digoxin,[158] which might act synergically with licorice intake. Some products use deglycyrrhizinated licorice (DGL) instead of raw licorice extract, which may reduce glycyrrhizic acid and glycyrrhetinic acid-induced side effects.

Excessive licorice intake may also influence the effects of other medicines. Glabridin may inhibit human cytochrome P450,[159] an important enzyme in drug metabolism and bioactivation.[160] Cytochrome P450 metabolizes warfarin (coumadin), an anticoagulant agent, into its inactive form,[161] and thus, licorice may increase warfarin clearance.[162] If treatment with warfarin is required, consulting a physician is strongly advised before consuming foods containing licorice.

Pregnant women should consider limiting their intake of licorice. Little research has examined the teratogenicity of licorice, but a single study has indicated that licorice may aggravate cyclophosphamide-induced body weight loss and malformations of fetuses by upregulating cytochrome P450 type 2B.[163] However, a study conducted in Korea indicated that women taking licorice for cough and cold control did not have an increased risk of stillbirths.[164] Licorice also increases estrogen levels in humans[165] and may increase the risk of estrogen-mediated cancer.[166] Licorice can potentially cause an antiandrogenic effect,[167,168] which may lead to erectile dysfunction. To avoid these side effects, careful intake of licorice-related food is highly advised.

dx.doi.org/10.1021/jf404939f | J. Agric. Food Chem. 2014, 62, 542−553

Table 1. In Vivo Biological Functions of Compounds in Licorice

biological function	species	targeting/mechanism	ref
		Glycyrrhizic Acid	
sugar substitute	*Phormia regina*	stimulates pyranose receptor site and furanose receptor site	14
hepatoprotection	human, rat, mice	liver necrosis ↓, mitochondrial permeability transition ↓, ROS ↓, cytochrome c ↓, HMGB1 ↓, harboring alpha2(I) collagen gene promoter	22, 21, 24, 30
nephroprotection	mice	antioxidant enzymes ↑	27
renal protection	rat	antioxidant enzymes ↑	28
cardio protection	rat	antioxidant enzymes ↑	29
gut protection	rat	mean arterial blood pressure ↓, NFκB ↓	31
antiosteoporosis	rat	11β-HSD1 dehydrogenase ↓	52
anticarcinogenesis	human, rat, mice	HCV-induced hepatocellular carcinogenesis ↓, ERK ↓, thymine dimer ↓, PCNA ↓, NFκB ↓, p53	56, 57, 54, 55
		Glycyrrhetinic Acid	
hepatoprotection	rat, mice	caspase 3/10 ↓, PARP ↓, JNK ↓, mitochondrial integrity ↑, ROS ↓, cytochrome c ↓, harboring alpha2(I) collagen gene promoter ↓, Smad3 ↓	21, 24
antiulcer	monkey	gastric PGE2 ↑	59
		Liquiritin	
antispasmodic	rat	muscle contraction ↓	74
antitussive	guinea pig	cough ↓	75
antidepression	rat	antioxidant enzymes ↑	77
promote immune	human	CD69 ↑	79
neuroprotection	mice	antioxidant enzymes ↑	80
		Isoliquiritin	
antispasmodic	rat	muscle contraction ↓	74
antitussive	guinea pig	cough ↓, ATP-sensitive potassium channel	75, 84
		Liquiritigenin	
hepatoprotection	rat	liver necrosis ↓, mortality ↓, hepatic blood flow rate ↑	95, 105
neuroprotection	rat	behavioral performance ↑, Notch2 ↓	88
antispasmodic	rat	muscle contraction ↓	74
antitussive	guinea pig	cough ↓	75
antidepression	rat	monoamine oxidase A and B ↓	103
anticocaine addiction	rat	hyperlocomotion ↓, CREB ↓, c-Fos ↓	123
antidote	rat	transporters activity ↑, phase-II enzymes ↑	104
anticarcinogenesis	mice	tumor growth ↓, apoptosis ↑, microvascular density ↓, VEGF ↓	107, 111
		Isoliquiritigenin	
antispasmodic	rat	muscle contraction ↓	74
antitussive	guinea pig	cough ↓	75
antidiabetes	rat	aldose reductase activity ↓	92
antianorexia	rat	5-HT2B antagonist	100
antiplatelet	platelet	cyclooxygenase activity ↓, lipoxygenase activity ↓, peroxidase activity ↓, acts as aldose reductase inhibitor	101
cardiotonic	rat	cyclic AMP ↑	102
antidepression	rat, mice	monoamine oxidase A and B ↓	103
anticarcinogenesis	mice	PGE2 ↓, platelet 12-lipoxygenase and 5-lipoxygenase ↓, immune ↑, direct cytotoxicity, iNOS ↓, preneoplastic aberrant crypt foci ↓, aberrant crypt focus formation ↓	113, 116, 118, 119
anticocaine addiction	rat	extracellular dopamine level ↓, GABA(B) receptor modulation	124
		Dehydroglyasperin C/Dehydroglyasperin D	
antidiabetes	mice	PPARγ ligand, spontaneously hypertension ↓	127
		Glabridin	
antiosteoporosis	rat	structure similar to estradiol-17β	133
antidiabetes	mice	body weight (gain) ↓, abdominal adipose tissues ↓, blood glucose level ↓, PPARγ ↑	141
antiobesity	rat	AMPK ↑	142
depigmentation	guinea pig	T1 and T3 tyrosinases ↓, ROS ↓, COX ↓	138
anti-inflammation	mice	NFκB ↓, ROS ↓	139

CONCLUSION

Licorice is extensively used in the TCM and appears as a component herb in about 60% of all TCM prescriptions. Numerous *in vitro* and *in vivo* studies have suggested healthful properties of licorice and its bioactive constituents such as glycyrrhizic acid, 18β-glycyrrhetinic acid, carbenoxolone, dehydroglyasperin C, and dehydroglyasperin D as well as some unique compounds such as glabridin, licoricidin, licorisoflavan A, and licochalcone A have potential beneficial effects in human diseases. These effects have been associated with the anti-inflammatory, antioxidative, antimicrobial, antivirus, and antidote properties of the compounds as summarized in Table 1.

dx.doi.org/10.1021/jf404939f | J. Agric. Food Chem. 2014, 62, 542−553

Although licorice intake may have some side effects in humans, all of these side effects should be reversible. With proper control of licorice intake, its health benefits outweigh its side effects. It is highly recommended that before beginning the regular intake of any food or medicine containing licorice and its related compounds, one should consult a traditional Chinese physician. In our opinion, licorice and the compounds isolated from this plant can be used as a complement to aid current medicines to reduce/eliminate side effects and improve the healing efficacy and outcome.

AUTHOR INFORMATION

Corresponding Author

*Tel: 886-4-2287-9755. Fax: 886-4-2285-4378. E-mail: gcyen@nchu.edu.tw.

Funding

This research work was supported in part by the National Science Council, NSC99-2628-B005-003-MY3, Taiwan, R.O.C., and by the Ministry of Education, Taiwan, R.O.C. under the ATU plan.

Notes

The authors declare no competing financial interest.

REFERENCES

(1) Carmines, E. L.; Lemus, R.; Gaworski, C. L. Toxicologic evaluation of licorice extract as a cigarette ingredient. *Food Chem. Toxicol.* **2005**, *43*, 1303−1322.

(2) Saeedi, M.; Morteza-Semnani, K.; Ghoreishi, M. R. The treatment of atopic dermatitis with licorice gel. *J. Dermatol. Treat.* **2003**, *14*, 153−157.

(3) Callender, V. D., St; Surin-Lord, S.; Davis, E. C.; Maclin, M. Postinflammatory hyperpigmentation: etiologic and therapeutic considerations. *Am. J. Clin. Dermatol.* **2011**, *12*, 87−99.

(4) Kim, Y. J.; Uyama, H. Tyrosinase inhibitors from natural and synthetic sources: structure, inhibition mechanism and perspective for the future. *Cell. Mol. Life Sci.* **2005**, *62*, 1707−1723.

(5) Sheth, V. M.; Pandya, A. G. Melasma: a comprehensive update: part II. *J. Am. Acad. Dermatol.* **2011**, *65*, 699−714 quiz 715.

(6) Burgess, J. A.; van der Ven, P. F.; Martin, M.; Sherman, J.; Haley, J. Review of over-the-counter treatments for aphthous ulceration and results from use of a dissolving oral patch containing glycyrrhiza complex herbal extract. *J. Contemp. Dent. Pract.* **2008**, *9*, 88−98.

(7) Das, S. K.; Das, V.; Gulati, A. K.; Singh, V. P. Deglycyrrhizinated liquorice in aphthous ulcers. *J. Assoc. Phys. India* **1989**, *37*, 647.

(8) Asl, M. N.; Hosseinzadeh, H. Review of pharmacological effects of Glycyrrhiza sp. and its bioactive compounds. *Phytother. Res.* **2008**, *22*, 709−724.

(9) Li, S. *Compendium of Materia Medica*; Foreign Languages Press: Beijing, 2003.

(10) Hirayama, C.; Okumura, M.; Tanikawa, K.; Yano, M.; Mizuta, M.; Ogawa, N. A multicenter randomized controlled clinical trial of Shosaiko-to in chronic active hepatitis. *Gastroenterol. Jpn.* **1989**, *24*, 715−719.

(11) Chang, C.-c. f. *Shang Han Lun*; Oriental Healing Arts Institute: Los Angeles, CA, 1981.

(12) He, Y.; Gai, Y.; Wu, X.; Wan, H. Quantitatively analyze composition principle of Ma Huang Tang by structural equation modeling. *J. Ethnopharmacol.* **2012**, *143*, 851−858.

(13) Agarwal, A.; Gupta, D.; Yadav, G.; Goyal, P.; Singh, P. K.; Singh, U. An evaluation of the efficacy of licorice gargle for attenuating postoperative sore throat: a prospective, randomized, single-blind study. *Anesth. Analg.* **2009**, *109*, 77−81.

(14) Ahamed, A.; Tsurumi, S.; Ozaki, M.; Amakawa, T. An artificial sweetener stimulates the sweet taste in insect: dual effects of glycyrrhizin in Phormia regina. *Chem. Senses* **2001**, *26*, 507−515.

(15) Ploeger, B.; Mensinga, T.; Sips, A.; Seinen, W.; Meulenbelt, J.; DeJongh, J. The pharmacokinetics of glycyrrhizic acid evaluated by physiologically based pharmacokinetic modeling. *Drug Metab. Rev.* **2001**, *33*, 125−147.

(16) Kim, D. H.; Lee, S. W.; Han, M. J. Biotransformation of glycyrrhizin to 18beta-glycyrrhetinic acid-3-*O*-beta-D-glucuronide by Streptococcus LJ-22, a human intestinal bacterium. *Biol. Pharm. Bull.* **1999**, *22*, 320−322.

(17) Kuwajima, H.; Taneda, Y.; Chen, W. Z.; Kawanishi, T.; Hori, K.; Taniyama, T.; Kobayashi, M.; Ren, J.; Kitagawa, I. Variation of chemical constituents in processed licorice roots: quantitative determination of saponin and flavonoid constituents in bark removed and roasted licorice roots. *Yakugaku Zasshi* **1999**, *119*, 945−955.

(18) Sung, M. W.; Li, P. C. Chemical analysis of raw, dry-roasted, and honey-roasted licorice by capillary electrophoresis. *Electrophoresis* **2004**, *25*, 3434−3440.

(19) Kim, K. R.; Jeong, C. K.; Park, K. K.; Choi, J. H.; Park, J. H.; Lim, S. S.; Chung, W. Y. Anti-inflammatory effects of licorice and roasted licorice extracts on TPA-induced acute inflammation and collagen-induced arthritis in mice. *J. Biomed. Biotechnol.* **2010**, *2010*, 709378.

(20) Hwang, I. K.; Lim, S. S.; Choi, K. H.; Yoo, K. Y.; Shin, H. K.; Kim, E. J.; Yoon-Park, J. H.; Kang, T. C.; Kim, Y. S.; Kwon, D. Y.; Kim, D. W.; Moon, W. K.; Won, M. H. Neuroprotective effects of roasted licorice, not raw form, on neuronal injury in gerbil hippocampus after transient forebrain ischemia. *Acta Pharmacol. Sin.* **2006**, *27*, 959−965.

(21) Gumpricht, E.; Dahl, R.; Devereaux, M. W.; Sokol, R. J. Licorice compounds glycyrrhizin and 18beta-glycyrrhetinic acid are potent modulators of bile acid-induced cytotoxicity in rat hepatocytes. *J. Biol. Chem.* **2005**, *280*, 10556−10563.

(22) Manns, M. P.; Wedemeyer, H.; Singer, A.; Khomutjanskaja, N.; Dienes, H. P.; Roskams, T.; Goldin, R.; Hehnke, U.; Inoue, H.; European, S. S. G. Glycyrrhizin in patients who failed previous interferon alpha-based therapies: biochemical and histological effects after 52 weeks. *J. Viral Hepat.* **2012**, *19*, 537−546.

(23) Wang, Y. G.; Zhou, J. M.; Ma, Z. C.; Li, H.; Liang, Q. D.; Tan, H. L.; Xiao, C. R.; Zhang, B. L.; Gao, Y. Pregnane X receptor mediated-transcription regulation of CYP3A by glycyrrhizin: a possible mechanism for its hepatoprotective property against lithocholic acid-induced injury. *Chem. Biol. Interact.* **2012**, *200*, 11−20.

(24) Moro, T.; Shimoyama, Y.; Kushida, M.; Hong, Y. Y.; Nakao, S.; Higashiyama, R.; Sugioka, Y.; Inoue, H.; Okazaki, I.; Inagaki, Y. Glycyrrhizin and its metabolite inhibit Smad3-mediated type I collagen gene transcription and suppress experimental murine liver fibrosis. *Life Sci.* **2008**, *83*, 531−539.

(25) Kao, T. C.; Shyu, M. H.; Yen, G. C. Neuroprotective effects of glycyrrhizic acid and 18beta-glycyrrhetinic acid in PC12 cells via modulation of the PI3K/Akt pathway. *J. Agric. Food Chem.* **2009**, *57*, 754−761.

(26) Tabuchi, M.; Imamura, S.; Kawakami, Z.; Ikarashi, Y.; Kase, Y. The blood-brain barrier permeability of 18beta-glycyrrhetinic acid, a major metabolite of glycyrrhizin in Glycyrrhiza root, a constituent of the traditional Japanese medicine yokukansan. *Cell. Mol. Neurobiol.* **2012**, *32*, 1139−1146.

(27) Arjumand, W.; Sultana, S. Glycyrrhizic acid: a phytochemical with a protective role against cisplatin-induced genotoxicity and nephrotoxicity. *Life Sci.* **2011**, *89*, 422−429.

(28) Yokozawa, T.; Liu, Z. W.; Chen, C. P. Protective effects of Glycyrrhizae radix extract and its compounds in a renal hypoxia (ischemia)-reoxygenation (reperfusion) model. *Phytomedicine* **2000**, *6*, 439−445.

(29) Haleagrahara, N.; Varkkey, J.; Chakravarthi, S. Cardioprotective effects of glycyrrhizic acid against isoproterenol-induced myocardial ischemia in rats. *Int. J. Mol. Sci.* **2011**, *12*, 7100−7113.

(30) Ogiku, M.; Kono, H.; Hara, M.; Tsuchiya, M.; Fujii, H. Glycyrrhizin prevents liver injury by inhibition of high-mobility group box 1 production by Kupffer cells after ischemia-reperfusion in rats. *J. Pharmacol. Exp. Ther.* **2011**, *339*, 93−98.

(31) Di Paola, R.; Menegazzi, M.; Mazzon, E.; Genovese, T.; Crisafulli, C.; Dal Bosco, M.; Zou, Z.; Suzuki, H.; Cuzzocrea, S. Protective effects of glycyrrhizin in a gut hypoxia (ischemia)-reoxygenation (reperfusion) model. *Intensive Care Med.* **2009**, *35*, 687−697.

(32) Fiore, C.; Eisenhut, M.; Krausse, R.; Ragazzi, E.; Pellati, D.; Armanini, D.; Bielenberg, J. Antiviral effects of Glycyrrhiza species. *Phytother. Res.* **2008**, *22*, 141−148.
(33) Cinatl, J.; Morgenstern, B.; Bauer, G.; Chandra, P.; Rabenau, H.; Doerr, H. W. Glycyrrhizin, an active component of liquorice roots, and replication of SARS-associated coronavirus. *Lancet* **2003**, *361*, 2045−2046.
(34) De Clercq, E. Current lead natural products for the chemotherapy of human immunodeficiency virus (HIV) infection. *Med. Res. Rev.* **2000**, *20*, 323−349.
(35) Crance, J. M.; Biziagos, E.; Passagot, J.; van Cuyck-Gandre, H.; Deloince, R. Inhibition of hepatitis A virus replication in vitro by antiviral compounds. *J. Med. Virol.* **1990**, *31*, 155−160.
(36) Takahara, T.; Watanabe, A.; Shiraki, K. Effects of glycyrrhizin on hepatitis B surface antigen: a biochemical and morphological study. *J. Hepatol.* **1994**, *21*, 601−609.
(37) Orlent, H.; Hansen, B. E.; Willems, M.; Brouwer, J. T.; Huber, R.; Kullak-Ublick, G. A.; Gerken, G.; Zeuzem, S.; Nevens, F.; Tielemans, W. C.; Zondervan, P. E.; Lagging, M.; Westin, J.; Schalm, S. W. Biochemical and histological effects of 26 weeks of glycyrrhizin treatment in chronic hepatitis C: a randomized phase II trial. *J. Hepatol.* **2006**, *45*, 539−546.
(38) Baba, M.; Shigeta, S. Antiviral activity of glycyrrhizin against varicella-zoster virus in vitro. *Antiviral Res.* **1987**, *7*, 99−107.
(39) Lampi, G.; Deidda, D.; Pinza, M.; Pompei, R. Enhancement of anti-herpetic activity of glycyrrhizic acid by physiological proteins. *Antiviral Chem. Chemother.* **2001**, *12*, 125−131.
(40) Lin, J. C. Mechanism of action of glycyrrhizic acid in inhibition of Epstein-Barr virus replication in vitro. *Antiviral Res.* **2003**, *59*, 41−7.
(41) Numazaki, K.; Nagata, N.; Sato, T.; Chiba, S. Effect of glycyrrhizin, cyclosporin A, and tumor necrosis factor alpha on infection of U-937 and MRC-5 cells by human cytomegalovirus. *J. Leukoc. Biol.* **1994**, *55*, 24−28.
(42) Pompei, R.; Flore, O.; Marccialis, M. A.; Pani, A.; Loddo, B. Glycyrrhizic acid inhibits virus growth and inactivates virus particles. *Nature* **1979**, *281*, 689−690.
(43) Michaelis, M.; Geiler, J.; Naczk, P.; Sithisarn, P.; Leutz, A.; Doerr, H. W.; Cinatl, J., Jr. Glycyrrhizin exerts antioxidative effects in H5N1 influenza A virus-infected cells and inhibits virus replication and pro-inflammatory gene expression. *PLoS One* **2011**, *6*, e19705.
(44) Chung, J. G. Inhibitory actions of glycyrrhizic acid on arylamine N-acetyltransferase activity in strains of Helicobacter pylori from peptic ulcer patients. *Drug Chem. Toxicol.* **1998**, *21*, 355−370.
(45) Krausse, R.; Bielenberg, J.; Blaschek, W.; Ullmann, U. In vitro anti-Helicobacter pylori activity of Extractum liquiritiae, glycyrrhizin and its metabolites. *J. Antimicrob. Chemother.* **2004**, *54*, 243−246.
(46) Uto, T.; Morinaga, O.; Tanaka, H.; Shoyama, Y. Analysis of the synergistic effect of glycyrrhizin and other constituents in licorice extract on lipopolysaccharide-induced nitric oxide production using knock-out extract. *Biochem. Biophys. Res. Commun.* **2012**, *417*, 473−478.
(47) Kao, T. C.; Shyu, M. H.; Yen, G. C. Glycyrrhizic acid and 18beta-glycyrrhetinic acid inhibit inflammation via PI3K/Akt/GSK3beta signaling and glucocorticoid receptor activation. *J. Agric. Food Chem.* **2010**, *58*, 8623−8629.
(48) Whorwood, C. B.; Sheppard, M. C.; Stewart, P. M. Licorice inhibits 11 beta-hydroxysteroid dehydrogenase messenger ribonucleic acid levels and potentiates glucocorticoid hormone action. *Endocrinology* **1993**, *132*, 2287−2292.
(49) Ma, X.; Lian, Q. Q.; Dong, Q.; Ge, R. S. Environmental inhibitors of 11beta-hydroxysteroid dehydrogenase type 2. *Toxicology* **2011**, *285*, 83−89.
(50) Kao, T. C.; Wu, C. H.; Yen, G. C. Glycyrrhizic acid and 18beta-glycyrrhetinic acid recover glucocorticoid resistance via PI3K-induced AP1, CRE and NFAT activation. *Phytomedicine* **2013**, *20*, 295−302.
(51) Iba, K.; Chiba, H.; Sawada, N.; Hirota, S.; Ishii, S.; Mori, M. Glucocorticoids induce mineralization coupled with bone protein expression without influence on growth of a human osteoblastic cell line. *Cell Struct. Funct.* **1995**, *20*, 319−330.
(52) Ramli, E. S.; Suhaimi, F.; Asri, S. F.; Ahmad, F.; Soelaiman, I. N. Glycyrrhizic acid (GCA) as 11beta-hydroxysteroid dehydrogenase inhibitor exerts protective effect against glucocorticoid-induced osteoporosis. *J. Bone Miner. Metab.* **2013**, *31*, 262−273.
(53) Mollica, L.; De Marchis, F.; Spitaleri, A.; Dallacosta, C.; Pennacchini, D.; Zamai, M.; Agresti, A.; Trisciuoglio, L.; Musco, G.; Bianchi, M. E. Glycyrrhizin binds to high-mobility group box 1 protein and inhibits its cytokine activities. *Chem. Biol.* **2007**, *14*, 431−441.
(54) Kim, K. J.; Choi, J. S.; Kim, K. W.; Jeong, J. W. The anti-angiogenic activities of glycyrrhizic acid in tumor progression. *Phytother. Res.* **2013**, *27*, 841−846.
(55) Cherng, J. M.; Tsai, K. D.; Yu, Y. W.; Lin, J. C. Molecular mechanisms underlying chemopreventive activities of glycyrrhizic acid against UVB-radiation-induced carcinogenesis in SKH-1 hairless mouse epidermis. *Radiat. Res.* **2011**, *176*, 177−186.
(56) Ikeda, K.; Arase, Y.; Kobayashi, M.; Saitoh, S.; Someya, T.; Hosaka, T.; Sezaki, H.; Akuta, N.; Suzuki, Y.; Suzuki, F.; Kumada, H. A long-term glycyrrhizin injection therapy reduces hepatocellular carcinogenesis rate in patients with interferon-resistant active chronic hepatitis C: a cohort study of 1249 patients. *Dig. Dis. Sci.* **2006**, *51*, 603−609.
(57) Ikeda, K. Glycyrrhizin injection therapy prevents hepatocellular carcinogenesis in patients with interferon-resistant active chronic hepatitis C. *Hepatol. Res.: Official J. Jpn. Soc. Hepatol.* **2007**, *37* (Suppl 2), S287−S293.
(58) Lee, C. S.; Kim, Y. J.; Lee, M. S.; Han, E. S.; Lee, S. J. 18beta-Glycyrrhetinic acid induces apoptotic cell death in SiHa cells and exhibits a synergistic effect against antibiotic anti-cancer drug toxicity. *Life Sci.* **2008**, *83*, 481−489.
(59) Farina, C.; Pinza, M.; Pifferi, G. Synthesis and anti-ulcer activity of new derivatives of glycyrrhetic, oleanolic and ursolic acids. *Farmaco* **1998**, *53*, 22−32.
(60) Csuk, R.; Schwarz, S.; Siewert, B.; Kluge, R.; Strohl, D. Synthesis and antitumor activity of ring A modified glycyrrhetinic acid derivatives. *Eur. J. Med. Chem.* **2011**, *46*, 5356−5369.
(61) Lee, C. S.; Yang, J. C.; Kim, Y. J.; Jang, E. R.; Kim, W.; Myung, S. C. 18beta-Glycyrrhetinic acid potentiates apoptotic effect of trichostatin A on human epithelial ovarian carcinoma cell lines. *Eur. J. Pharmacol.* **2010**, *649*, 354−361.
(62) Yang, J. C.; Myung, S. C.; Kim, W.; Lee, C. S. 18beta-glycyrrhetinic acid potentiates Hsp90 inhibition-induced apoptosis in human epithelial ovarian carcinoma cells via activation of death receptor and mitochondrial pathway. *Mol. Cell. Biochem.* **2012**, *370*, 209−219.
(63) Shetty, A. V.; Thirugnanam, S.; Dakshinamoorthy, G.; Samykutty, A.; Zheng, G.; Chen, A.; Bosland, M. C.; Kajdacsy-Balla, A.; Gnanasekar, M. 18alpha-glycyrrhetinic acid targets prostate cancer cells by down-regulating inflammation-related genes. *Int. J. Oncol.* **2011**, *39*, 635−640.
(64) Szpak, K.; Wybieralska, E.; Niedzialkowska, E.; Rak, M.; Bechyne, I.; Michalik, M.; Madeja, Z.; Czyz, J. DU-145 prostate carcinoma cells that selectively transmigrate narrow obstacles express elevated levels of Cx43. *Cell. Mol. Biol. Lett.* **2011**, *16*, 625−637.
(65) Sharma, G.; Kar, S.; Palit, S.; Das, P. K. 18beta-glycyrrhetinic acid induces apoptosis through modulation of Akt/FOXO3a/Bim pathway in human breast cancer MCF-7 cells. *J. Cell. Physiol.* **2012**, *227*, 1923−1931.
(66) Zhao, K.; Wang, W.; Guan, C.; Cai, J.; Wang, P. Inhibition of gap junction channel attenuates the migration of breast cancer cells. *Mol. Biol. Rep.* **2012**, *39*, 2607−2613.
(67) Lin, K. W.; Huang, A. M.; Hour, T. C.; Yang, S. C.; Pu, Y. S.; Lin, C. N. 18beta-Glycyrrhetinic acid derivatives induced mitochondrial-mediated apoptosis through reactive oxygen species-mediated p53 activation in NTUB1 cells. *Bioorg. Med. Chem.* **2011**, *19*, 4274−4285.
(68) Gao, Y.; Guo, X.; Li, X.; Liu, D.; Song, D.; Xu, Y.; Sun, M.; Jing, Y.; Zhao, L. The synthesis of glycyrrhetinic acid derivatives containing a nitrogen heterocycle and their antiproliferative effects in human leukemia cells. *Molecules* **2010**, *15*, 4439−4449.
(69) Song, D.; Gao, Y.; Wang, R.; Liu, D.; Zhao, L.; Jing, Y. Downregulation of c-FLIP, XIAP and Mcl-1 protein as well as depletion of reduced glutathione contribute to the apoptosis induction of glycyrrhetinic acid derivatives in leukemia cells. *Cancer Biol. Ther.* **2010**, *9*, 96−108.

(70) Chintharlapalli, S.; Papineni, S.; Abdelrahim, M.; Abudayyeh, A.; Jutooru, I.; Chadalapaka, G.; Wu, F.; Mertens-Talcott, S.; Vanderlaag, K.; Cho, S. D.; Smith, R., 3rd; Safe, S. Oncogenic microRNA-27a is a target for anticancer agent methyl 2-cyano-3,11-dioxo-18beta-olean-1,12-dien-30-oate in colon cancer cells. *Int. J. Cancer* **2009**, *125*, 1965−1974.
(71) Jutooru, I.; Chadalapaka, G.; Chintharlapalli, S.; Papineni, S.; Safe, S. Induction of apoptosis and nonsteroidal anti-inflammatory drug-activated gene 1 in pancreatic cancer cells by a glycyrrhetinic acid derivative. *Mol. Carcinog.* **2009**, *48*, 692−702.
(72) Nafisi, S.; Bonsaii, M.; Manouchehri, F.; Abdi, K. Interaction of glycyrrhizin and glycyrrhetinic acid with DNA. *DNA Cell Biol.* **2012**, *31*, 114−121.
(73) Nafisi, S.; Manouchehri, F.; Bonsaii, M. Study on the interaction of glycyrrhizin and glycyrrhetinic acid with RNA. *J. Photochem. Photobiol. B* **2012**, *111*, 27−34.
(74) Lee, K. K.; Omiya, Y.; Yuzurihara, M.; Kase, Y.; Kobayashi, H. Antispasmodic effect of shakuyakukanzoto extract on experimental muscle cramps in vivo: role of the active constituents of Glycyrrhizae radix. *J. Ethnopharmacol.* **2013**, *145*, 286−293.
(75) Kamei, J.; Saitoh, A.; Asano, T.; Nakamura, R.; Ichiki, H.; Iiduka, A.; Kubo, M. Pharmacokinetic and pharmacodynamic profiles of the antitussive principles of Glycyrrhizae radix (licorice), a main component of the Kampo preparation Bakumondo-to (Mai-men-dong-tang). *Eur. J. Pharmacol.* **2005**, *507*, 163−168.
(76) Chen, Z. A.; Wang, J. L.; Liu, R. T.; Ren, J. P.; Wen, L. Q.; Chen, X. J.; Bian, G. X. Liquiritin potentiate neurite outgrowth induced by nerve growth factor in PC12 cells. *Cytotechnology* **2009**, *60*, 125−132.
(77) Zhao, Z.; Wang, W.; Guo, H.; Zhou, D. Antidepressant-like effect of liquiritin from Glycyrrhiza uralensis in chronic variable stress induced depression model rats. *Behav. Brain Res.* **2008**, *194*, 108−113.
(78) Zhang, X.; Song, Y.; Han, X.; Feng, L.; Wang, R.; Zhang, M.; Zhu, M.; Jia, X.; Hu, S. Liquiritin attenuates advanced glycation end products-induced endothelial dysfunction via RAGE/NF-kappaB pathway in human umbilical vein endothelial cells. *Mol. Cell. Biochem.* **2013**, *374*, 191−201.
(79) Cheel, J.; Onofre, G.; Vokurkova, D.; Tumova, L.; Neugebauerova, J. Licorice infusion: Chemical profile and effects on the activation and the cell cycle progression of human lymphocytes. *Pharmacogn. Mag.* **2010**, *6*, 26−33.
(80) Sun, Y. X.; Tang, Y.; Wu, A. L.; Liu, T.; Dai, X. L.; Zheng, Q. S.; Wang, Z. B. Neuroprotective effect of liquiritin against focal cerebral ischemia/reperfusion in mice via its antioxidant and antiapoptosis properties. *J. Asian Nat. Products Res.* **2010**, *12*, 1051−1060.
(81) Guan, Y.; Li, F. F.; Hong, L.; Yan, X. F.; Tan, G. L.; He, J. S.; Dong, X. W.; Bao, M. J.; Xie, Q. M. Protective effects of liquiritin apioside on cigarette smoke-induced lung epithelial cell injury. *Fundam. Clin. Pharmacol.* **2012**, *26*, 473−483.
(82) Gao, W.; Li, K.; Yan, S.; Gao, X.; Hu, L. Effects of space flight on DNA mutation and secondary metabolites of licorice (Glycyrrhiza uralensis Fisch.). *Sci. China Ser. C Life Sci.* **2009**, *52*, 977−981.
(83) Kobayashi, S.; Miyamoto, T.; Kimura, I.; Kimura, M. Inhibitory effect of isoliquiritin, a compound in licorice root, on angiogenesis in vivo and tube formation in vitro. *Biol. Pharm. Bull.* **1995**, *18*, 1382−1386.
(84) Kamei, J.; Nakamura, R.; Ichiki, H.; Kubo, M. Antitussive principles of Glycyrrhizae radix, a main component of the Kampo preparations Bakumondo-to (Mai-men-dong-tang). *Eur. J. Pharmacol.* **2003**, *469*, 159−163.
(85) Fu, B.; Li, H.; Wang, X.; Lee, F. S.; Cui, S. Isolation and identification of flavonoids in licorice and a study of their inhibitory effects on tyrosinase. *J. Agric. Food Chem.* **2005**, *53*, 7408−7414.
(86) Mersereau, J. E.; Levy, N.; Staub, R. E.; Baggett, S.; Zogovic, T.; Chow, S.; Ricke, W. A.; Tagliaferri, M.; Cohen, I.; Bjeldanes, L. F.; Leitman, D. C. Liquiritigenin is a plant-derived highly selective estrogen receptor beta agonist. *Mol. Cell. Endocrinol.* **2008**, *283*, 49−57.
(87) Jungbauer, A.; Medjakovic, S. Phytoestrogens and the metabolic syndrome. *J. Steroid Biochem. Mol. Biol.* **2014**, *139*, 277−289.
(88) Liu, R. T.; Zou, L. B.; Fu, J. Y.; Lu, Q. J. Effects of liquiritigenin treatment on the learning and memory deficits induced by amyloid beta-peptide (25−35) in rats. *Behav. Brain Res.* **2010**, *210*, 24−31.
(89) Choi, E. M. Liquiritigenin isolated from Glycyrrhiza uralensis stimulates osteoblast function in osteoblastic MC3T3-E1 cells. *Int. Immunopharmacol.* **2012**, *12*, 139−43.
(90) Kong, L. D.; Zhang, Y.; Pan, X.; Tan, R. X.; Cheng, C. H. Inhibition of xanthine oxidase by liquiritigenin and isoliquiritigenin isolated from Sinofranchetia chinensis. *Cell. Mol. Life Sci.* **2000**, *57*, 500−505.
(91) Zhou, L.; Tang, Y. P.; Gao, L.; Fan, X. S.; Liu, C. M.; Wu, D. K. Separation, characterization and dose-effect relationship of the PPARgamma-activating bio-active constituents in the Chinese herb formulation 'San-Ao decoction'. *Molecules* **2009**, *14*, 3942−3951.
(92) Aida, K.; Tawata, M.; Shindo, H.; Onaya, T.; Sasaki, H.; Yamaguchi, T.; Chin, M.; Mitsuhashi, H. Isoliquiritigenin: a new aldose reductase inhibitor from glycyrrhizae radix. *Planta Med.* **1990**, *56*, 254−258.
(93) Kim, Y. W.; Zhao, R. J.; Park, S. J.; Lee, J. R.; Cho, I. J.; Yang, C. H.; Kim, S. G.; Kim, S. C. Anti-inflammatory effects of liquiritigenin as a consequence of the inhibition of NF-kappaB-dependent iNOS and proinflammatory cytokines production. *Br. J. Pharmacol.* **2008**, *154*, 165−173.
(94) Tanaka, S.; Sakata, Y.; Morimoto, K.; Tambe, Y.; Watanabe, Y.; Honda, G.; Tabata, M.; Oshima, T.; Masuda, T.; Umezawa, T.; Shimada, M.; Nagakura, N.; Kamisako, W.; Kashiwada, Y.; Ikeshiro, Y. Influence of natural and synthetic compounds on cell surface expression of cell adhesion molecules, ICAM-1 and VCAM-1. *Planta Med.* **2001**, *67*, 108−113.
(95) Kim, Y. W.; Ki, S. H.; Lee, J. R.; Lee, S. J.; Kim, C. W.; Kim, S. C.; Kim, S. G. Liquiritigenin, an aglycone of liquiritin in Glycyrrhizae radix, prevents acute liver injuries in rats induced by acetaminophen with or without buthionine sulfoximine. *Chem. Biol. Interact.* **2006**, *161*, 125−138.
(96) Kim, S. C.; Byun, S. H.; Yang, C. H.; Kim, C. Y.; Kim, J. W.; Kim, S. G. Cytoprotective effects of Glycyrrhizae radix extract and its active component liquiritigenin against cadmium-induced toxicity (effects on bad translocation and cytochrome c-mediated PARP cleavage). *Toxicology* **2004**, *197*, 239−251.
(97) Kang, H. E.; Kim, Y. W.; Sohn, S. I.; Baek, S. R.; Lee, J. W.; Kim, S. G.; Lee, I.; Lee, M. G. Pharmacokinetics of liquiritigenin and its two glucuronides, M1 and M2, in rats with acute hepatitis induced by d-galactosamine/lipopolysaccharide or CCl(4). *Xenobiotica* **2010**, *40*, 424−36.
(98) Liu, R. T.; Zou, L. B.; Lu, Q. J. Liquiritigenin inhibits Abeta(25−35)-induced neurotoxicity and secretion of Abeta(1−40) in rat hippocampal neurons. *Acta Pharmacol. Sin.* **2009**, *30*, 899−906.
(99) Lee, J. Y.; Lee, J. H.; Park, J. H.; Kim, S. Y.; Choi, J. Y.; Lee, S. H.; Kim, Y. S.; Kang, S. S.; Jang, E. C.; Han, Y. Liquiritigenin, a licorice flavonoid, helps mice resist disseminated candidiasis due to Candida albicans by Th1 immune response, whereas liquiritin, its glycoside form, does not. *Int. Immunopharmacol.* **2009**, *9*, 632−638.
(100) Takeda, H.; Sadakane, C.; Hattori, T.; Katsurada, T.; Ohkawara, T.; Nagai, K.; Asaka, M. Rikkunshito, an herbal medicine, suppresses cisplatin-induced anorexia in rats via 5-HT2 receptor antagonism. *Gastroenterology* **2008**, *134*, 2004−2013.
(101) Tawata, M.; Aida, K.; Noguchi, T.; Ozaki, Y.; Kume, S.; Sasaki, H.; Chin, M.; Onaya, T. Anti-platelet action of isoliquiritigenin, an aldose reductase inhibitor in licorice. *Eur. J. Pharmacol.* **1992**, *212*, 87−92.
(102) Wegener, J. W.; Nawrath, H. Cardiac effects of isoliquiritigenin. *Eur. J. Pharmacol.* **1997**, *326*, 37−44.
(103) Pan, X.; Kong, L. D.; Zhang, Y.; Cheng, C. H.; Tan, R. X. In vitro inhibition of rat monoamine oxidase by liquiritigenin and isoliquiritigenin isolated from Sinofranchetia chinensis. *Acta Pharmacol. Sin.* **2000**, *21*, 949−953.
(104) Kim, Y. W.; Kang, H. E.; Lee, M. G.; Hwang, S. J.; Kim, S. C.; Lee, C. H.; Kim, S. G. Liquiritigenin, a flavonoid aglycone from licorice, has a choleretic effect and the ability to induce hepatic transporters and phase-

II enzymes. *Am. J. Physiol. Gastrointest. Liver Physiol.* **2009**, *296*, G372−G381.
(105) Kang, H. E.; Chung, H. J.; Kim, H. S.; Lee, J. W.; Lee, M. G. Pharmacokinetic interaction between liquiritigenin (LQ) and DDB: increased glucuronidation of LQ in the liver possibly due to increased hepatic blood flow rate by DDB. *Eur. J. Pharm. Sci.* **2010**, *39*, 181−189.
(106) Zhang, S. P.; Zhou, Y. J.; Liu, Y.; Cai, Y. Q. Effect of liquiritigenin, a flavanone existed from Radix glycyrrhizae on pro-apoptotic in SMMC-7721 cells. *Food Chem. Toxicol.* **2009**, *47*, 693−701.
(107) Zhou, M.; Higo, H.; Cai, Y. Inhibition of hepatoma 22 tumor by Liquiritigenin. *Phytother. Res.* **2010**, *24*, 827−833.
(108) Jayaprakasam, B.; Doddaga, S.; Wang, R.; Holmes, D.; Goldfarb, J.; Li, X. M. Licorice flavonoids inhibit eotaxin-1 secretion by human fetal lung fibroblasts in vitro. *J. Agric. Food Chem.* **2009**, *57*, 820−825.
(109) Liu, C.; Wang, Y.; Xie, S.; Zhou, Y.; Ren, X.; Li, X.; Cai, Y. Liquiritigenin induces mitochondria-mediated apoptosis via cytochrome c release and caspases activation in HeLa cells. *Phytother. Res.* **2011**, *25*, 277−283.
(110) Xie, S. R.; Wang, Y.; Liu, C. W.; Luo, K.; Cai, Y. Q. Liquiritigenin inhibits serum-induced HIF-1alpha and VEGF expression via the AKT/mTOR-p70S6K signalling pathway in HeLa cells. *Phytother. Res.* **2012**, *26*, 1133−1141.
(111) Liu, Y.; Xie, S.; Wang, Y.; Luo, K.; Wang, Y.; Cai, Y. Liquiritigenin inhibits tumor growth and vascularization in a mouse model of HeLa cells. *Molecules* **2012**, *17*, 7206−7216.
(112) Watjen, W.; Weber, N.; Lou, Y. J.; Wang, Z. Q.; Chovolou, Y.; Kampkotter, A.; Kahl, R.; Proksch, P. Prenylation enhances cytotoxicity of apigenin and liquiritigenin in rat H4IIE hepatoma and C6 glioma cells. *Food Chem. Toxicol.* **2007**, *45*, 119−124.
(113) Yamamoto, S.; Aizu, E.; Jiang, H.; Nakadate, T.; Kiyoto, I.; Wang, J. C.; Kato, R. The potent anti-tumor-promoting agent isoliquiritigenin. *Carcinogenesis* **1991**, *12*, 317−323.
(114) Kanazawa, M.; Satomi, Y.; Mizutani, Y.; Ukimura, O.; Kawauchi, A.; Sakai, T.; Baba, M.; Okuyama, T.; Nishino, H.; Miki, T. Isoliquiritigenin inhibits the growth of prostate cancer. *Eur. Urol.* **2003**, *43*, 580−586.
(115) Maggiolini, M.; Statti, G.; Vivacqua, A.; Gabriele, S.; Rago, V.; Loizzo, M.; Menichini, F.; Amdo, S. Estrogenic and antiproliferative activities of isoliquiritigenin in MCF7 breast cancer cells. *J. Steroid Biochem. Mol. Biol.* **2002**, *82*, 315−322.
(116) Yamazaki, S.; Morita, T.; Endo, H.; Hamamoto, T.; Baba, M.; Joichi, Y.; Kaneko, S.; Okada, Y.; Okuyama, T.; Nishino, H.; Tokue, A. Isoliquiritigenin suppresses pulmonary metastasis of mouse renal cell carcinoma. *Cancer Lett.* **2002**, *183*, 23−30.
(117) Ii, T.; Satomi, Y.; Katoh, D.; Shimada, J.; Baba, M.; Okuyama, T.; Nishino, H.; Kitamura, N. Induction of cell cycle arrest and p21(CIP1/WAF1) expression in human lung cancer cells by isoliquiritigenin. *Cancer Lett.* **2004**, *207*, 27−35.
(118) Takahashi, T.; Takasuka, N.; Iigo, M.; Baba, M.; Nishino, H.; Tsuda, H.; Okuyama, T. Isoliquiritigenin, a flavonoid from licorice, reduces prostaglandin E2 and nitric oxide, causes apoptosis, and suppresses aberrant crypt foci development. *Cancer Sci.* **2004**, *95*, 448−453.
(119) Baba, M.; Asano, R.; Takigami, I.; Takahashi, T.; Ohmura, M.; Okada, Y.; Sugimoto, H.; Arika, T.; Nishino, H.; Okuyama, T. Studies on cancer chemoprevention by traditional folk medicines XXV. Inhibitory effect of isoliquiritigenin on azoxymethane-induced murine colon aberrant crypt focus formation and carcinogenesis. *Biol. Pharm. Bull.* **2002**, *25*, 247−250.
(120) Ma, J.; Fu, N. Y.; Pang, D. B.; Wu, W. Y.; Xu, A. L. Apoptosis induced by isoliquiritigenin in human gastric cancer MGC-803 cells. *Planta Med.* **2001**, *67*, 754−757.
(121) Hsu, Y. L.; Kuo, P. L.; Lin, L. T.; Lin, C. C. Isoliquiritigenin inhibits cell proliferation and induces apoptosis in human hepatoma cells. *Planta Med.* **2005**, *71*, 130−134.
(122) Hsu, Y. L.; Kuo, P. L.; Lin, C. C. Isoliquiritigenin induces apoptosis and cell cycle arrest through p53-dependent pathway in Hep G2 cells. *Life Sci* **2005**, *77*, 279−92.
(123) Jang, E. Y.; Hwang, M.; Yoon, S. S.; Lee, J. R.; Kim, K. J.; Kim, H. C.; Yang, C. H. Liquiritigenin decreases selective molecular and behavioral effects of cocaine in rodents. *Curr. Neuropharmacol.* **2011**, *9*, 30−34.
(124) Jang, E. Y.; Choe, E. S.; Hwang, M.; Kim, S. C.; Lee, J. R.; Kim, S. G.; Jeon, J. P.; Buono, R. J.; Yang, C. H. Isoliquiritigenin suppresses cocaine-induced extracellular dopamine release in rat brain through GABA(B) receptor. *Eur. J. Pharmacol.* **2008**, *587*, 124−128.
(125) Lee, Y. S.; Kim, S. H.; Kim, J. K.; Shin, H. K.; Kang, Y. H.; Park, J. H.; Lim, S. S. Rapid identification and preparative isolation of antioxidant components in licorice. *J. Sep. Sci.* **2010**, *33*, 664−671.
(126) Kim, H. J.; Seo, J. Y.; Suh, H. J.; Lim, S. S.; Kim, J. S. Antioxidant activities of licorice-derived prenylflavonoids. *Nutr. Res. Pract.* **2012**, *6*, 491−498.
(127) Mae, T.; Kishida, H.; Nishiyama, T.; Tsukagawa, M.; Konishi, E.; Kuroda, M.; Mimaki, Y.; Sashida, Y.; Takahashi, K.; Kawada, T.; Nakagawa, K.; Kitahara, M. A licorice ethanolic extract with peroxisome proliferator-activated receptor-gamma ligand-binding activity affects diabetes in KK-Ay mice, abdominal obesity in diet-induced obese C57BL mice and hypertension in spontaneously hypertensive rats. *J. Nutr.* **2003**, *133*, 3369−3377.
(128) Seo, J. Y.; Lee, Y. S.; Kim, H. J.; Lim, S. S.; Lim, J. S.; Lee, I. A.; Lee, C. H.; Yoon Park, J. H.; Kim, J. S. Dehydroglyasperin C isolated from licorice caused Nrf2-mediated induction of detoxifying enzymes. *J. Agric. Food Chem.* **2010**, *58*, 1603−1608.
(129) Kim, H. J.; Lim, S. S.; Park, I. S.; Lim, J. S.; Seo, J. Y.; Kim, J. S. Neuroprotective effects of dehydroglyasperin C through activation of heme oxygenase-1 in mouse hippocampal cells. *J. Agric. Food Chem.* **2012**, *60*, 5583−5589.
(130) Mitscher, L. A.; Park, Y. H.; Clark, D.; Beal, J. L. Antimicrobial agents from higher plants. Antimicrobial isoflavanoids and related substances from Glycyrrhiza glabra L. var. typica. *J. Nat. Prod.* **1980**, *43*, 259−269.
(131) Okada, K.; Tamura, Y.; Yamamoto, M.; Inoue, Y.; Takagaki, R.; Takahashi, K.; Demizu, S.; Kajiyama, K.; Hiraga, Y.; Kinoshita, T. Identification of antimicrobial and antioxidant constituents from licorice of Russian and Xinjiang origin. *Chem. Pharm. Bull. (Tokyo)* **1989**, *37*, 2528−2530.
(132) Belinky, P. A.; Aviram, M.; Mahmood, S.; Vaya, J. Structural aspects of the inhibitory effect of glabridin on LDL oxidation. *Free Radic. Biol. Med.* **1998**, *24*, 1419−1429.
(133) Somjen, D.; Katzburg, S.; Vaya, J.; Kaye, A. M.; Hendel, D.; Posner, G. H.; Tamir, S. Estrogenic activity of glabridin and glabrene from licorice roots on human osteoblasts and prepubertal rat skeletal tissues. *J. Steroid Biochem. Mol. Biol.* **2004**, *91*, 241−246.
(134) Choi, E. M. The licorice root derived isoflavan glabridin increases the function of osteoblastic MC3T3-E1 cells. *Biochem. Pharmacol.* **2005**, *70*, 363−368.
(135) Yu, X. Y.; Lin, S. G.; Zhou, Z. W.; Chen, X.; Liang, J.; Yu, X. Q.; Chowbay, B.; Wen, J. Y.; Duan, W.; Chan, E.; Li, X. T.; Cao, J.; Li, C. G.; Xue, C. C.; Zhou, S. F. Role of P-glycoprotein in limiting the brain penetration of glabridin, an active isoflavan from the root of Glycyrrhiza glabra. *Pharm. Res.* **2007**, *24*, 1668−1690.
(136) Leyden, J. J.; Shergill, B.; Micali, G.; Downie, J.; Wallo, W. Natural options for the management of hyperpigmentation. *J. Eur. Acad. Dermatol. Venereol.* **2011**, *25*, 1140−1145.
(137) Jirawattanapong, W.; Saifah, E.; Patarapanich, C. Synthesis of glabridin derivatives as tyrosinase inhibitors. *Arch. Pharm. Res.* **2009**, *32*, 647−654.
(138) Yokota, T.; Nishio, H.; Kubota, Y.; Mizoguchi, M. The inhibitory effect of glabridin from licorice extracts on melanogenesis and inflammation. *Pigment Cell Res.* **1998**, *11*, 355−361.
(139) Kang, J. S.; Yoon, Y. D.; Cho, I. J.; Han, M. H.; Lee, C. W.; Park, S. K.; Kim, H. M. Glabridin, an isoflavan from licorice root, inhibits inducible nitric-oxide synthase expression and improves survival of mice in experimental model of septic shock. *J. Pharmacol. Exp. Ther.* **2005**, *312*, 1187−1194.
(140) Yehuda, I.; Madar, Z.; Szuchman-Sapir, A.; Tamir, S. Glabridin, a phytoestrogen from licorice root, up-regulates manganese superoxide

dismutase, catalase and paraoxonase 2 under glucose stress. *Phytother. Res.* **2011**, *25*, 659−667.
(141) Nakagawa, K.; Kishida, H.; Arai, N.; Nishiyama, T.; Mae, T. Licorice flavonoids suppress abdominal fat accumulation and increase in blood glucose level in obese diabetic KK-A(y) mice. *Biol. Pharm. Bull.* **2004**, *27*, 1775−1778.
(142) Lee, J. W.; Choe, S. S.; Jang, H.; Kim, J.; Jeong, H. W.; Jo, H.; Jeong, K. H.; Tadi, S.; Park, M. G.; Kwak, T. H.; Man Kim, J.; Hyun, D. H.; Kim, J. B. AMPK activation with glabridin ameliorates adiposity and lipid dysregulation in obesity. *J. Lipid Res.* **2012**, *53*, 1277−1286.
(143) Aoki, F.; Nakagawa, K.; Kitano, M.; Ikematsu, H.; Nakamura, K.; Yokota, S.; Tominaga, Y.; Arai, N.; Mae, T. Clinical safety of licorice flavonoid oil (LFO) and pharmacokinetics of glabridin in healthy humans. *J. Am. Coll. Nutr.* **2007**, *26*, 209−218.
(144) Tsai, Y. M.; Yang, C. J.; Hsu, Y. L.; Wu, L. Y.; Tsai, Y. C.; Hung, J. Y.; Lien, C. T.; Huang, M. S.; Kuo, P. L. Glabridin inhibits migration, invasion, and angiogenesis of human non-small cell lung cancer A549 cells by inhibiting the FAK/rho signaling pathway. *Integr. Cancer Ther.* **2011**, *10*, 341−349.
(145) Lennon, G. G.; Lennard, M. To-day's Drugs. Carbenoxolone Sodium. *Br. Med. J.* **1964**, *1*, 1690−1691.
(146) Connors, B. W. Tales of a dirty drug: carbenoxolone, gap junctions, and seizures. *Epilepsy Curr.* **2012**, *12*, 66−68.
(147) Rhee, S. D.; Kim, C. H.; Park, J. S.; Jung, W. H.; Park, S. B.; Kim, H. Y.; Bae, G. H.; Kim, T. J.; Kim, K. Y. Carbenoxolone prevents the development of fatty liver in C57BL/6-Lep ob/ob mice via the inhibition of sterol regulatory element binding protein-1c activity and apoptosis. *Eur. J. Pharmacol.* **2012**, *691*, 9−18.
(148) Sandeep, T. C.; Yau, J. L.; MacLullich, A. M.; Noble, J.; Deary, I. J.; Walker, B. R.; Seckl, J. R. 11Beta-hydroxysteroid dehydrogenase inhibition improves cognitive function in healthy elderly men and type 2 diabetics. *Proc. Natl. Acad. Sci. U. S. A.* **2004**, *101*, 6734−6739.
(149) Doll, R.; Langman, M. J.; Shawdon, H. H. Treatment of gastric ulcer with carbenoxolone: antagonistic effect of spironolactone. *Gut* **1968**, *9*, 42−45.
(150) Porter, S. R.; Scully Cbe, C. Aphthous ulcers (recurrent). *Clin. Evid. (Online)* **2007**, *2007*, 1303.
(151) Davidson, J. S.; Baumgarten, I. M.; Harley, E. H. Reversible inhibition of intercellular junctional communication by glycyrrhetinic acid. *Biochem. Biophys. Res. Commun.* **1986**, *134*, 29−36.
(152) Ozog, M. A.; Siushansian, R.; Naus, C. C. Blocked gap junctional coupling increases glutamate-induced neurotoxicity in neuron-astrocyte co-cultures. *J. Neuropathol. Exp. Neurol.* **2002**, *61*, 132−141.
(153) Hosseinzadeh, H.; Nassiri Asl, M.; Parvardeh, S. The effects of carbenoxolone, a semisynthetic derivative of glycyrrhizinic acid, on peripheral and central ischemia-reperfusion injuries in the skeletal muscle and hippocampus of rats. *Phytomedicine* **2005**, *12*, 632−637.
(154) Spataro, L. E.; Sloane, E. M.; Milligan, E. D.; Wieseler-Frank, J.; Schoeniger, D.; Jekich, B. M.; Barrientos, R. M.; Maier, S. F.; Watkins, L. R. Spinal gap junctions: potential involvement in pain facilitation. *J. Pain* **2004**, *5*, 392−405.
(155) Stoletov, K.; Strnadel, J.; Zardouzian, E.; Momiyama, M.; Park, F. D.; Kelber, J. A.; Pizzo, D. P.; Hoffman, R.; VandenBerg, S. R.; Klemke, R. L. Role of connexins in metastatic breast cancer and melanoma brain colonization. *J. Cell Sci.* **2013**, *126*, 904−913.
(156) Hardy, R. S.; Raza, K.; Cooper, M. S. Endogenous glucocorticoids in inflammation: contributions of systemic and local responses. *Swiss Med. Weekly* **2012**, *142*, w13650.
(157) Ruiz-Granados, E. S.; Shouls, G.; Sainsbury, C.; Antonios, T., A salty cause of severe hypertension. *BMJ Case Rep.* **2012**, *2012*.
(158) Bielecka-Dabrowa, A.; Mikhailidis, D. P.; Jones, L.; Rysz, J.; Aronow, W. S.; Banach, M. The meaning of hypokalemia in heart failure. *Int. J. Cardiol.* **2012**, *158*, 12−17.
(159) Kent, U. M.; Aviram, M.; Rosenblat, M.; Hollenberg, P. F. The licorice root derived isoflavan glabridin inhibits the activities of human cytochrome P450S 3A4, 2B6, and 2C9. *Drug Metab. Dispos.* **2002**, *30*, 709−715.
(160) Guengerich, F. P. Cytochrome p450 and chemical toxicology. *Chem. Res. Toxicol.* **2008**, *21*, 70−83.
(161) Cavallari, L. H.; Limdi, N. A. Warfarin pharmacogenomics. *Curr. Opin. Mol. Ther.* **2009**, *11*, 243−251.
(162) Mu, Y.; Zhang, J.; Zhang, S.; Zhou, H. H.; Toma, D.; Ren, S.; Huang, L.; Yaramus, M.; Baum, A.; Venkataramanan, R.; Xie, W. Traditional Chinese medicines Wu Wei Zi (Schisandra chinensis Baill) and Gan Cao (Glycyrrhiza uralensis Fisch) activate pregnane X receptor and increase warfarin clearance in rats. *J. Pharmacol. Exp. Ther.* **2006**, *316*, 1369−1377.
(163) Park, D.; Yang, Y. H.; Choi, E. K.; Yang, G.; Bae, D. K.; Lee, S. H.; Kim, T. K.; Kyung, J.; Kim, D.; Choi, K. C.; Kim, Y. B. Licorice extract increases cyclophosphamide teratogenicity by upregulating the expression of cytochrome P-450 2B mRNA. *Birth Defects Res. B Dev. Reprod. Toxicol.* **2011**, *92*, 553−559.
(164) Choi, J. S.; Han, J. Y.; Ahn, H. K.; Ryu, H. M.; Kim, M. Y.; Chung, J. H.; Nava-Ocampo, A. A.; Koren, G. Fetal and Neonatal Outcomes in Women Reporting Ingestion of Licorice (Glycyrrhiza uralensis) during Pregnancy. *Planta Med.* **2013**, *79*, 97−101.
(165) Armanini, D.; Fiore, C.; Mattarello, M. J.; Bielenberg, J.; Palermo, M. History of the endocrine effects of licorice. *Exp. Clin. Endocrinol. Diabetes* **2002**, *110*, 257−261.
(166) Boucher, B. A.; Cotterchio, M.; Curca, I. A.; Kreiger, N.; Harris, S. A.; Kirsh, V. A.; Goodwin, P. J. Intake of phytoestrogen foods and supplements among women recently diagnosed with breast cancer in Ontario, Canada. *Nutr. Cancer* **2012**, *64*, 695−703.
(167) Zamansoltani, F.; Nassiri-Asl, M.; Sarookhani, M. R.; Jahani-Hashemi, H.; Zangivand, A. A. Antiandrogenic activities of Glycyrrhiza glabra in male rats. *Int. J. Androl.* **2009**, *32*, 417−422.
(168) Armanini, D.; Bonanni, G.; Mattarello, M. J.; Fiore, C.; Sartorato, P.; Palermo, M. Licorice consumption and serum testosterone in healthy man. *Exp. Clin. Endocrinol. Diabetes* **2003**, *111*, 341−343.

JOURNAL OF AGRICULTURAL AND FOOD CHEMISTRY

Letter

pubs.acs.org/JAFC

Does "Best Before" Date Embody Extra-Virgin Olive Oil Freshness?

ABSTRACT: Virgin olive oil (VOO) decays in quality properties during aging, so aged VOOs may have detectable undesirable sensory descriptors in comparison with oils recently extracted. For that reason, freshness has become a parameter of paramount importance to maintain the highest standard levels within the period indicated in the "best before" date. However, it is important to note that freshness of VOOs is not necessarily related to its sensory quality. Pigments have been suggested for tracing aging of VOO, and pyropheophytin *a* (PPP) seems to be the most promising molecule for this task. A predictive model has been used to estimate %PPP in VOO stored at different worldwide locations characterized with different temperatures. The recorded average temperatures, on a monthly basis, were inputs of the predictive model. The results show the influence of temperature in %PPP and how this molecule could serve as a better monitor of the storage period of VOOs. The initial value of %PPP in the oil could help to carry out the storage traceability. This information would be of interest for producers, sellers, and inspection agencies.

KEYWORDS: *virgin olive oil, freshness, pyropheophytin, storage*

Virgin olive oil (VOO), unlike red wines, decays in quality properties during aging due to oxidative processes, which decisively influences the consumer's preferences. Thus, an aged VOO may have detectable undesirable sensory descriptors in comparison with an olive oil recently extracted as long as both oils are produced from healthy and sound olives harvested at their optimum ripeness. These undesirable descriptors are mostly rancid notes, which are the result of a long and/or inadequate storage. However, sometimes VOOs are not produced entirely from healthy olives, but the batch of olives contains damaged olives that would be responsible for undesirable descriptors as those resulting from alcoholic and butyric fermentations of the olives. In this latter case, VOO may be characterized with sensory defects (e.g., fusty, musty, winey-vinegary) even if the oil is recently extracted.[1] As a consequence, sometimes aged oils from healthy olives may be of better quality than fresh oils obtained from damaged olives. This hypothetical comparison of oils illustrates how the relationship between freshness and quality is misleading because they are independent concepts. Thereby, freshness and sensory quality should not be mixed up as is commonly done by retailers and consumers. In fact, several compounds change in their concentration during VOO shelf life, but not all necessarily imply decay in aroma or taste properties.

It is unquestionable that freshness has become a parameter of paramount importance to maintain the highest standard levels, although freshness is not necessarily related to VOO sensory quality. Therefore, there is high interest in measuring freshness by chemical and objective methods to establish an appropriate "best before" date.

The methodologies to assess the freshness of oils should be separated from those evaluating sensory quality, for example, the sensory assessment or the profiles of volatile and phenolic compounds. Thus, the concept of freshness, which is intuitively associated with the time since olive oil processing, should be measured with chemical compounds that do not mislead to VOO underestimations or overestimations.[2]

Pigments have been suggested for tracing aging of VOOs[3] because their degradation process (e.g., pheophytinization of chlorophylls[4]) starts at the malaxation process of crushed olives and increases during olive oil storage.[5] Thus, pyropheophytin *a* (PPP) is formed from pheophytin *a* due to the loss of the carbomethoxy group in the C13 of the isocyclic ring of the chlorophyll structure.[5] The former compound, which is not quantified in VOOs produced under good manufacturing practices, has been revealed as a useful parameter for monitoring VOO degradation[4] as a consequence of inadequate temperatures during the storage of VOOs. This finding has awakened an interest in studying its kinetic performance with the aim of establishing a prediction model[3] for determining the "best before" date of VOOs by taking into account the temperature of the place of sale.

Although researchers have tried to demonstrate the usefulness of pigments for the assessment of the freshness,[6] these compounds actually have a merely casual relationship to the product age[2] because their concentration values are strongly influenced by the inadequate conditions of temperature during storage of any VOO in addition to the storage time. To increase the confusion, the only current regulation does not demand that the estimation for the "best before" date is calculated on the basis of the harvesting time of the olives (or the olive oil processing) but the bottling time,[7] although it is suggested that olive oil should be under "adequate storage condition" before bottling.

The term "adequate storage conditions" is relevant because, as previously mentioned, the percentage of PPPs increases after olives are crushed, and it depends on temperature. As a consequence, VOOs stored in a warm place would reach the limit (17% PPP) proposed in regulatory bodies of some countries[8−10] earlier than if they were stored in a cold place. Thus, the scientific support explaining the association of %PPP with freshness may have flaws because of the high dependence on temperature. Nevertheless, the determination of PPPs[11] can contribute to harmonize the parameter "best before" with the intuitive perception that consumers have for the freshness of VOOs.

A predictive mathematical model (Know-How, Utility model, MIT_TO-0022272) has been used to estimate %PPP in VOOs stored at any given temperature in darkness and with lack of oxygen.[3] The mathematical model has resulted from isokinetic

Received: October 22, 2013
Accepted: January 6, 2014
Published: January 6, 2014

 © 2014 American Chemical Society dx.doi.org/10.1021/jf405220d | *J. Agric. Food Chem.* 2014, 62, 554−556

Table 1. Evolution of %PPP[a] of a VOO (var. Arbequina; Initial %PPP = 0.26) That Had Been Stored in Five Cities at Their Average Temperatures (on a Monthly Basis) According to the Information Reported by The Weather Channel; Maximum Time (in Months) To Reach 17% PPP in the Same Cities but If EVOOs Had Been Bottled in the Production Place (Estepa, Spain) Several Months after Harvesting, and Obviously with Higher %PPP

	values of %PPP in the cities on their monthly average temperatures				
month and year	Estepa	Sacramento	Frankfurt	Adelaide	Johannesburg
January 2011	0.45	0.42	0.29	1.62	1.15
Februrary 2011	0.64	0.63	0.33	2.86	1.95
March 2011	0.92	0.96	0.44	3.79	2.69
April 2011	1.35	1.41	0.65	4.39	3.19
May 2011	1.90	2.19	0.99	4.80	3.52
June 2011	3.26	3.37	1.55	5.08	3.74
July 2011	5.17	5.03	2.22	5.35	3.96
August 2011	7.06	6.63	2.88	5.65	4.29
September 2011	8.09	7.84	3.27	6.00	4.82
October 2011	8.66	8.53	3.47	6.55	5.51
November 2011	8.86	8.81	3.55	7.25	6.25
December 2011	9.01	8.97	3.60	8.30	7.10
January 2012	9.22	9.14	3.63	9.67	8.01
Februray 2012	9.40	9.35	3.67	10.92	8.80
March 2012	9.69	9.68	3.79	11.85	9.55
April 2012	10.11	10.14	3.99	12.44	10.05
May 2012	10.67	10.92	4.34	12.85	10.38
June 2012	12.02	12.09	4.90	13.13	10.60
July 2012	13.94	13.76	5.56	13.40	10.82
August 2012	15.83	15.35	6.23	13.70	11.14
September 2012	16.86	16.56	6.62	14.05	11.67
October 2012	17.42	17.25	6.81	14.60	12.37
November 2012	17.62	17.54	6.90	15.30	13.10
December 2012	17.78	17.70	6.94	16.35	13.96
reaching 17% PPP at	21 months	21 months	>36 months	24 months	28 months

	then 17% PPP would be reached after VOO was storage in the cities for months				
if VOO is bottled in Estepa with %PPP =	Estepa	Sacramento	Frankfurt	Adelaide	Johannesburg
0.64	20	21	>36	24	27
1.35	18	20	>36	23	26
3.26	16	19	>36	20	24
7.06	14	16	34	13	16
8.66	12	10	30	12	13

[a]%PPP was determined by means of a mathematical model.[3]

studies of the formation and degradation of pigments at different temperatures, ranging from 15 to 120 °C, with various cultivars.[5] The predictive model can be used to estimate the trend of the percentages of pyropheophytin *a* in a given time−temperature frame.

Table 1 shows the results of applying the mathematical model expressed as %PPP during two years for the particular case of VOO var. Arbequina, which is the most globally distributed cultivar, in places where VOOs are usually sold. Thus, VOO was produced in Estepa (Spain) and its hypothetical sale places were Sacramento (USA) and Frankfurt (Germany) in the northern hemisphere and Adelaide (Australia) and Johannesburg (South Africa) in the southern hemisphere. The recorded average temperatures were considered for the application of the predictive model, which admits information in monthly, daily, and even hourly bases. All of the temperature values were collected from The Weather Channel.

Thus, VOO stored at a daily basis of average temperature of Sacramento would reach 17% PPP after 21 months, but this percentage would be reached sooner (at month 7) using the maximum average temperature. These results show that, in this case, VOO should be fully controlled and protected from daily temperatures if considering the limit of 17% PPP for freshness, although the oil can still be qualified as VOO according to IOC trade standards.[12] A very different situation is the hypothetical storage of the same VOO sample in Frankfurt, with the same monthly basis of average temperature, where winters and summers are much cooler, and VOO would be "fresh", in terms of %PPP, for more than 3 years and for around a year using the maximum average temperature. The behavior is similar in hypothetical places of the southern hemisphere (Adelaide and Johannesburg), although with the well-known change in the sequence of the seasons.

The main conclusion is that the initial value of %PPP should be supplied for a better monitoring of the storage period of VOOs. Several advantages would result from this information. Consumers would benefit from a better knowledge of the initial freshness of the olive oil (from the olive harvesting instead of the olive oil bottling). Producers and sellers would gain knowledge for selecting the best place of sale for each VOO,

dx.doi.org/10.1021/jf405220d | J. Agric. Food Chem. 2014, 62, 554−556

according to its initial %PPP and its predicted evolution. Finally, initial values of %PPP would also allow inspection agencies to carry out backward traceability of the storage conditions of VOOs by checking %PPP with the "best before" date at any moment.

Ramón Aparicio-Ruiz[†]
Ramon Aparicio*[,§]
Diego L. García-González[§]
[†]Department of Analytical Chemistry, Faculty of Pharmacy, University of Seville, Prof. García González 2, 41012 Sevilla, Spain
[§]Instituto de la Grasa (CSIC), Padre García Tejero 4, 41012 Sevilla, Spain

AUTHOR INFORMATION

Corresponding Author
*(R.A.) E-mail: aparicio@cica.es. Phone: +34 954 61 15 50. Fax: +34 954 61 67 90.

Notes
The authors declare no competing financial interest.

REFERENCES

(1) Morales, M. T.; Aparicio-Ruiz, R.; Aparicio, R. Chromatographic methodologies: compounds for olive oil odor issues. In *Handbook of Olive Oil: Analysis and Properties*, 2nd ed.; Aparicio, R., Harwood, J., Eds.; Springer Science + Business Media: New York, 2013; pp 261−309.
(2) Aparicio, R.; Morales, M. T.; García-González, D. L. Towards new instrumental approaches to understand sensory perception of olive oil. *Eur. J. Lipid Sci. Technol.* **2012**, *114*, 1114−1125.
(3) Aparicio-Ruiz, R.; Roca, M.; Gandul-Rojas, B. Mathematical model to predict the formation of pyropheophytin *a* in virgin olive oil during storage. *J. Agric. Food Chem.* **2012**, *60*, 7040−7049.
(4) Aparicio-Ruiz, R.; Minguez-Mosquera, M. I.; Gandul-Rojas, B. Thermal degradation kinetics of chlorophyll pigments in virgin olive oils. 1. Compounds of series *a*. *J. Agric. Food Chem.* **2010**, *58*, 6200−6208.
(5) Aparicio-Ruiz, R. *Characterization of the Thermodegradation Reactions of Chlorophyllic Pigments and Carotenoids in Virgin Olive Oils*. Ph.D. dissertation, University of Sevilla, Spain, 2008.
(6) Ayton, J.; Mailer, R. J.; Graham, K. *The Effect of Storage Conditions on Extra Virgin Olive Oil Quality*; RIRDC Publication 12/024; Rural Industries Research and Development Corporation (RIRDC): Canberra, Australia, 2012.
(7) Gazzetta Ufficiale della reuplica Italiana (GURI). *Norme sulla qualità e la transparenza della filiera degli oli di olive vergini*. Legge 14, 31 gennaio 2013, no. 9, pp 1−10.
(8) German Society for Fat Science (DGF). *Statement on the Applicability of Methods for the Determination of Pyropheophytin a and Isomeric Diacylglycerols in Virgin Olive Oils*, 2010.
(9) Standards Australia (SA). *AS5264-2011: Olive oils and olive-pomace oils*. Committee FT-034, 2011.
(10) South African National Standard (SANS). Working draft SANS 1377:2013. *Olive Oils and Pomace Olive Oils*; National Committee SABS, 2013.
(11) Gertz, C.; Fiebig, H. J. Pyropheophytin *a* − determination of thermal degradation products of chlorophyll *a* in virgin olive oil. *Eur. J. Lipid Sci. Technol.* **2006**, *108*, 1062−1065.
(12) International Olive Council (IOC). Document COI/T.15/NC No. 3/Rev. 6. Trade standards applying to olive oils and olive-pomace oils; Madrid, Spain, 2011.

JOURNAL OF AGRICULTURAL AND FOOD CHEMISTRY

Article

pubs.acs.org/JAFC

Inoculation of the Nonlegume *Capsicum annuum* (L.) with *Rhizobium* Strains. 1. Effect on Bioactive Compounds, Antioxidant Activity, and Fruit Ripeness

Luís R. Silva,*[,†] Jessica Azevedo,[†] Maria J. Pereira,[†] Lorena Carro,[‡,§] Encarna Velazquez,[‡,§] Alvaro Peix,[§,∥] Patrícia Valentão,[†] and Paula B. Andrade*[,†]

[†]REQUIMTE/Laboratório de Farmacognosia, Departamento de Química, Faculdade de Farmácia, Universidade do Porto, Rua de Jorge Viterbo Ferreira, No. 228, 4050-313 Porto, Portugal

[‡]Departamento de Microbiología y Genética, Universidad de Salamanca, Campus Miguel de Unamuno, s/n, 37007 Salamanca, Spain

[§]Unidad Asociada Grupo de Interacciones Planta-Microorganismo, Universidad de Salamanca-CSIC, Salamanca, Spain

[∥]Instituto de Recursos Naturales y Agrobiología, IRNASA-CSIC, Cordel de Merinas, 40-52, 37008 Salamanca, Spain

ABSTRACT: Pepper (*Capsicum annuum* L.) is an economically important agricultural crop and an excellent dietary source of natural colors and antioxidant compounds. The levels of these compounds can vary according to agricultural practices, like inoculation with plant growth-promoting rhizobacteria. In this work we evaluated for the first time the effect of the inoculation of two *Rhizobium* strains on *C. annuum* metabolites and bioactivity. The results revealed a decrease of organic acids and no effect on phenolics and capsaicinoids of leaves from inoculated plants. In the fruits from inoculated plants organic acids and phenolic compounds decreased, showing that fruits from inoculated plants present a higher ripeness stage than those from uninoculated ones. In general, the inoculation with *Rhizobium* did not improve the antioxidant activity of pepper fruits and leaves. Considering the positive effect on fruit ripening, the inoculation of *C. annuum* with *Rhizobium* is a beneficious agricultural practice for this nonlegume.

KEYWORDS: *Rhizobium spp., Capsicum annuum L., maturation, metabolites profile, bioactivity*

INTRODUCTION

Pepper (*Capsicum annuum* L.) is a member of the Solanaceae family, and its fruit is important as a vegetable food and spice.[1] It is a good source of vitamins C and E, provitamin A, carotenoids, tocopherols, flavonoids, and phenolic acids, compounds with well-known antioxidant properties.[1−3]

Although flavonoids and phenolic acids are considered separately from capsaicinoids, which provide pungency or "heat" to hot peppers,[4] it is known that the phenylpropanoid and capsaicinoid biosynthetic pathways may converge during pepper maturation.[5] The intake of these compounds is an important health-protecting factor, since they have been considered as beneficial for the prevention of widespread human diseases, including cancer and cardiovascular diseases, when taken daily in adequate amounts.[6]

Pepper fruits are recognized for their economic importance and nutritional value, being the second most consumed vegetable worldwide. Nevertheless, information concerning byproducts resulting from its production, namely, leaves, is scarce. This material may also be an interesting source of bioactive phytochemicals.

The increase of quality demanded by consumers requires specific agricultural practices, such as fertilization with products containing microorganisms.[7] The inoculation with plant growth-promoting rhizobacteria (PGPR) reducing the chemicals added to crops can improve not only the growth but also the quality of plants, since these microorganisms can mobilize nutrients to the plants, influence the plant hormonal balance, or produce microbial inhibitory compounds that preclude the growth of phytopathogens.[8] In the case of pepper, some bacteria have been reported as PGPR for different plants, as occurs with *Pseudomonas* and *Pantoea*.[9] Nevertheless, not all bacterial species can be used in biofertilization schemes when the fruits are raw consumed, those used for decades as plant biofertilizers being preferred. Within them, *Rhizobium*, widely known for its ability to establish symbiotic relationships with legume plants,[10] also has different plant growth-promoting mechanisms, being able to promote the development of nonlegumes.[8,11,12]

Some *Rhizobium* strains have a positive effect on pepper growth, since fruits from plants inoculated with them exhibited significantly higher fresh weight.[12] Moreover, the number of mature fruits in inoculated plants was higher than that in noninoculated ones, which could suggest that these fruits reach the maturation stage earlier. This is an important factor for the composition of fruits, since several biochemical, physiological, and structural modifications occur during fruit ripening and these changes determine the attributes of the fruit.[13] For example, a decline in phenolic compounds during maturation of *Capsicum* fruits has been reported.[14] These losses during fruit maturation may reflect the metabolic conversion to secondary phenolic compounds and degradation *via* enzyme action and

Received: October 16, 2013
Revised: December 31, 2013
Accepted: January 1, 2014
Published: January 9, 2014

ACS Publications © 2014 American Chemical Society

dx.doi.org/10.1021/jf4046649 | *J. Agric. Food Chem.* 2014, 62, 557−564

may indicate diversion of phenolic precursors from flavonoids to capsaicinoids.[15] Organic acids also contribute to fruit maturation, since the concentration of individual acids changed in pepper contributing to pepper fruit flavor.[16]

Although some work has been carried out about the changes in the chemical composition of pepper fruits after PGPR inoculation,[17] as far as we know there are no studies about the effect of rhizobial inoculation in the chemical composition of leaves and fruits of *C. annuum*, nor in their biological properties. Therefore the objectives of the present work were to compare the accumulation of bioactive compounds indicative of maturation, namely, phenolics and organic acids, in pepper leaves and fruits obtained after the inoculation with two PGPR *Rhizobium* strains with that of noninoculated material and its impact on their bioactivity.

MATERIALS AND METHODS

Standards and Reagents. All chemicals used were of analytical grade. The standard compounds were purchased from various suppliers. 5-*O*-Caffeoylquinic acid, quercetin-3-*O*-rutinoside, quercetin-3-*O*-rhamnoside, luteolin-7-*O*-glucoside, myricetin-3-*O*-rhamnoside, and apigenin-7-*O*-glucoside were from Extrasynthese (Genay, France). Caffeic, ferulic, sinapic, oxalic, malic, quinic, succinic, fumaric, acetic, citric, and aconitic acids, capsaicin, and dihydrocapsaicin were obtained from Sigma-Aldrich (St. Louis, MO, USA). 1,1-Diphenyl-2-picrylhydrazyl (DPPH$^{\bullet}$), β-nicotinamide adenine dinucleotide (NADH), phenazine methosulfate (PMS), nitrotetrazolium blue chloride (NBT), 5,5′-dithiobis(2-nitrobenzoic acid) (DTNB), sulfanilamide, acetylcholinesterase (AChE) from electric eel (type VI-s, lyophilized powder), acetylthiocholine iodide (ATCI), sodium nitroprusside dehydrate (SNP), and methanol were purchased from Sigma-Aldrich (St. Louis, MO, USA). N-(1-Naphthyl)ethylenediamine dihydrochloride and sulfuric acid were obtained from Merck (Darmstadt, Germany). Water was deionized using a Milli-Q water purification system (Millipore, Bedford, MA).

Plant Samples and Bacterial Strains. Samples of leaves and fruits used in this study were obtained from pepper var. "sweet Italian" plants inoculated with two fast-growing rhizobial strains, PETP01 and TVP08, and from uninoculated plants. These strains were isolated from *Trifolium pratense* and *Phaseolus vulgaris* nodules, respectively, presenting effective nodulation in their respective hosts.[12] PETP01 and TVP08 strains were identified in a previous work as *Rhizobium leguminosarum*, and they belong to different subphyla within this species following the analysis of the core *recA* and *atpD* genes and of two different symbiovars (trifolii and phaseoli, respectively), according to the analysis of the symbiotic *nodC* gene.[12]

Inoculation assays were performed as was previously described:[12] for plant inoculation, nonsterilized seeds were germinated in peat following the steps commonly used in the commercial process of seedling production and were irrigated from a bottom reservoir with water every 48 h and with commercial Hoagland's solution (Sigma Co., USA) every 8 days. Once placed on peat, each seed was inoculated with 1 mL of a suspension (2×10^8 cells/mL) of 5-day-old *Rhizobium* strains TPV08 and PETP01 grown on yeast-mannitol agar (YMA). Then, they were covered with vermiculite and germinated in darkness in a growth chamber at 24 °C, for seven days. Afterward, they were maintained in a plant growth chamber with mixed incandescent and fluorescent lighting (400 microeinsteins m^{-2} s^{-1}; 400 to 700 nm), programmed for a 16 h photoperiod, day−night cycle, with a constant temperature varying from 25 to 27 °C and 50−60% relative humidity. Uninoculated controls were kept under the same conditions.

After four weeks, 25 plants *per* treatment were used for a microcosm experiment, which was performed in a clayey soil collected at Salamanca (Spain), with neutral pH, 1.5−1.8% of organic matter, and 0.09−0.1 of N content. The seedling roots were flooded in bacterial suspensions containing 2×10^8 cells/mL during 4 h. Each plant was transplanted to a pot containing 2 kg of soil. Plants were irrigated from a bottom reservoir with water every 48 h and with commercial Hoagland's solution every 8 days. The plants were maintained during 10 weeks in a greenhouse illuminated with natural light in summer (night temperature ranging from 15 to 20 °C and day temperature ranging from 25 to 35 °C) with humidity control. At the end of the experiment, flowers and fruits were counted, fruits were harvested, and their fresh weight was measured.

Data related to the precocity of the pepper plants not published before are included in the present work.

Five plants *per* treatment were randomly selected and used for the chemical and biological analysis. They were frozen, lyophilized, and powdered (mean particle size lower than 910 μm), being divided into three aliquots, extracted, and analyzed separately for chemical composition and biological activity.

Phenolic Compounds. *Extraction.* *C. annuum* leaves and fruits (3 g) were extracted with 600 mL of boiling water during 15 min. The resulting extracts were filtered through a Büchner funnel, frozen, and lyophilized. The yield of extractions was 45.0 and 33.9% for fruits and leaves, respectively. The extracts were kept in a desiccator, in the dark, until analysis. Aqueous lyophilized extracts were redissolved in methanol and filtered through a PTFE membrane (0.45 μm).

Analysis by HPLC-DAD. The phenolic compounds were analyzed using a previously described procedure.[18] Briefly, each extract was analyzed on an analytical HPLC unit (Gilson), using a Spherisorb ODS2 (25.0 × 0.46 cm; 5 μm, particle size; Waters, Milford, MA) column. The solvent system used was a gradient of water:formic acid (19:1) (A) and methanol (B), starting with 5% methanol and installing a gradient to obtain 15% B at 3 min, 25% B at 13 min, 30% B at 25 min, 35% B at 35 min, 45% B at 39 min, 45% B at 42 min, 50% B at 44 min, 55% B at 47 min, 70% B at 50 min, 75% B at 56 min, and 80% B at 60 min, at a solvent flow rate of 0.9 mL/min. Detection was achieved with a Gilson diode array detector (DAD). Chromatograms were recorded at 280, 320, and 350 nm. The data were processed on Unipoint System software (Gilson Medical Electronics, Villiers-le-Bel, France). The compounds in each extract were identified by comparing their retention times and UV−vis spectra with those of authentic standards. Because standard was not commercially available, luteolin-7-*O*-(2-apiosyl-6-malonyl)-glucoside was quantified as luteolin-7-*O*-glucoside. Phenolic acids were determined at 320 nm and flavonoids at 350 nm. This procedure was performed in triplicate.

Capsaicinoids. *Extraction.* The method described by Estrada et al.[19] was used, with some modifications: 1.0 g of fruits and leaves was extracted with 10 mL of acetonitrile at 80 °C, for 4 h. The extract obtained was centrifuged at 4000 rpm for 5 min, and the supernatant was filtered. A 20 μL aliquot was used for each HPLC-DAD injection.

Analysis by HPLC-DAD. The samples were analyzed using an ACE3 C-18-AR column (150 × 4.6 mm, 3 μm particle size, Advanced Chromatography Technologies, Aberdeen, Scotland). The elution solvent was acetonitrile:water (60:40) at isocratic mode, flow rate of 1.0 mL/min, and a 35 min run.

Detection was achieved with a Gilson DAD, and chromatograms were registered at 280 nm. Spectral data from peaks were accumulated in the 200−400 nm range. The data were processed on Unipoint System software (Gilson Medical Electronics, Villiers-le-Bel, France). The compounds in each extract were identified by comparing their retention times and UV−vis spectra with those of external authentic standards (capsaicin and dihydrocapsaicin). Capsaicinoids quantification was achieved by measuring the absorbance at 280 nm in the chromatograms relative to external standards. This procedure was performed in triplicate.

Organic Acids. *Extraction.* Extraction of organic acids was performed according to a described procedure:[18] 0.1 and 1.0 g of lyophilized fruits and leaves, respectively, were mixed with 50 mL of H_2SO_4 0.01 N for 30 min under stirring (300 rpm). The obtained extracts were then filtered, evaporated to dryness under reduced pressure (40 °C), and redissolved in H_2SO_4 0.01 N.

HPLC−UV Analysis. The separation and quantification of organic acids were carried out according to the procedure described by Silva et al.[18] in an analytical HPLC unit (Gilson), using an ion exclusion Nucleogel Ion 300 OA (300 × 7.7 mm; Macherey-Nagel, Düren, Germany) column. Elution was performed in isocratic mode with

dx.doi.org/10.1021/jf4046649 | J. Agric. Food Chem. 2014, 62, 557−564

Table 1. Phenolic Composition of *C. annuum* Fruits and Leaves Inoculated with *Rhizobium* (mg/kg Lyophilized Material)[a]

	fruits			leaves		
phenolic compounds	control	PETP01	TVP08	control	PETP01	TVP08
5-*O*-caffeoylquinic acid	6.0 ± 0.1 a	0.5 ± 0.0 b	0.8 ± 0.0 b	68.0 ± 0.2 a	42.4 ± 0.1 b	46.1 ± 0.1 b
caffeic acid	53.7 ± 1.4 a	44.2 ± 2.8 b	14.0 ± 0.1 b	49.2 ± 1.3 a	80.5 ± 7.4 b	64.9 ± 1.2 b
sinapic acid	132.2 ± 0.0 a	16.9 ± 0.9 b	10.6 ± 0.7 b	nd	nd	nd
ferulic acid	nd	nd	nd	37.2 ± 2.0 a	73.6 ± 5.9 b	31.4 ± 2.9 a
luteolin-7-*O*-glucoside	13.5 ± 1.1 a	1.3 ± 0.0 b	2.5 ± 0.2 b	897.3 ± 5.4 a	810.3 ± 25.2 b	779.1 ± 6.4 b
quercetin-3-*O*-rutinoside	55.4 ± 0.8 a	3.6 ± 0.3 b	nd b	6.2 ± 0.8 a	6.3 ± 0.5 a	6.4 ± 0.6 a
apigenin-7-*O*-glucoside	nd	nd	nd	1027.5 ± 18.4 a	1090.4 ± 58.7 a	1086.2 ± 2.0 a
myricetin-3-*O*-rhamnoside	672.2 ± 6.7 a	228.2 ± 6.5 b	25.6 ± 2.3 b	nd	nd	nd
quercetin-3-*O*-rhamnoside	721.1 ± 7.8 a	591.5 ± 11.5 b	41.4 ± 2.0 b	nd	nd	nd
luteolin-7-*O*-(2-apiosyl-6-malonyl)-glucoside	468.4 ± 11.8 a	56.6 ± 0.4 b	10.8 ± 0.2 b	nd	nd	nd
total	2122.5	942.8	105.7	2085.4	2103.5	2014.1

[a]Values are expressed as mean ± standard deviation of three assays; nd, not detected. In the same line, different letters represent significant differences compared with the respective control ($p < 0.05$).

H_2SO_4 (0.01 N), at a flow rate of 0.2 mL/min. Detection was achieved with a UV detector set at 214 nm. Quantification of organic acids was achieved by measuring the absorbance recorded in the chromatograms relative to external standards. This procedure was performed in triplicate.

Antioxidant Activity. The aqueous lyophilized extracts prepared for phenolic compounds determination were used in the screening of the antioxidant activity. All determinations were made in a Multiskan Ascent plate reader (Thermo Electron Corporation).

DPPH• Assay. For each extract, a dilution series (five different concentrations) was prepared in a 96-well plate. The reaction mixtures in the sample wells consisted of 25 μL of extract (redissolved in methanol) and 200 μL of 150 mM methanolic DPPH•. The plate was incubated for 30 min at room temperature after addition of DPPH• solution, and the absorbance was determined at 515 nm.[20] Three experiments were performed in triplicate.

Nitric Oxide Assay. Antiradical activity was determined spectrophotometrically in a 96-wells plate reader. The reaction mixtures in each well consisted on 100 μL of extract dissolved in buffer (KH_2PO_4 100 mM, pH 7.4) and 100 μL of SNP (20 mM). The plates were incubated at room temperature for 60 min, under light. Griess reagent (1% sulfanilamide and 0.1% naphthylethylenediamine in 2% H_3PO_4) (100 μL) was then added, and 10 min later the absorbance of the chromophore formed during the diazotization of nitrite with sulfanilamide and subsequent coupling with naphthylethylenediamine was determined at 562 nm.[20] Three experiments were performed in triplicate.

Superoxide Radical Assay. Superoxide was generated by the NADH/PMS system, according to a described procedure: PMS reduced by NADH reacts with oxygen to produce $O_2^{\bullet-}$; this radical then reduces NBT to a formazan blue dye, which has an absorption maximum at 560 nm. [20] The reaction mixtures in the wells consisted on 50 μL of extract dissolved in buffer (KH_2PO_4 19 mM, pH 7.4), 50 μL of NADH (166 μM), 150 μL of NBT (43 μM), and 50 μL of PMS (2.7 μM). The rate of the reaction was assessed at 560 nm, during 2 min after PMS addition.[20] Three experiments were performed in triplicate.

AChE Inhibitory Activity. The aqueous lyophilized extracts were also used to assess AChE inhibition properties. Spectrophotometric determinations at 405 nm were performed in a Multiskan Ascent plate reader (Thermo Electron Corporation), based on Ellman's method, as previously described.[20] In each well the mixture consisted of 25 μL of ATCI (15 mM), 125 μL of DTNB (3 mM), 50 μL of buffer (50 mM Tris-HCl, pH 8, containing 0.1% BSA), and 25 μL of sample dissolved in buffer with 10% of methanol. The absorbance was read at 405 nm during 2 min. After this step, 25 μL of AChE (0.44 U/mL) was added and the absorbance was read again. The rates of reactions were calculated by Ascent Software version 2.6 (Thermo Labsystems Oy). The rate of the reaction before adding the enzyme was subtracted from that obtained after adding the enzyme in order to correct eventual spontaneous hydrolysis of substrate. [20] Three experiments were performed in triplicate.

Statistical Analysis. All data were recorded as mean ± standard deviation of triplicate determinations. Mean values were compared using one-way analysis of variance (one-way ANOVA) (Graph Pad Prism Version 5.00, GraphPad Software, Inc., San Diego, CA). Differences were considered significant for $p < 0.05$.

RESULTS AND DISCUSSION

Effect of *Rhizobium* Strains in the Growth of Pepper Plants. The inoculated plants were more precocious than noninoculated ones, displaying more rapid flowering and fruiting when they were inoculated with the two *Rhizobium* strains. In this way, the percentage of plants with flowers three weeks after transplanting was 80 and 100%, for the plants inoculated with strains TVP08 and PETP01, respectively, whereas only 60% of the noninoculated plants had flowers at this time. Also, seven weeks after transplanting, the percentage of plants with fruits was 50 and 60% for the plants inoculated with strains TVP08 and PETP01, respectively, whereas only 35% of the noninoculated plants had fruits at this time. These results showed that the inoculation with *Rhizobium* increased the precocity of pepper plants since the fruit production began earlier in inoculated plants. Therefore, pepper plants inoculated with *Rhizobium* strains TVP08 and PETP01 not only yielded more fruits, which have higher weight, than noninoculated plants, as was described before,[12] but also they are produced earlier. These results suggest that the inoculation has a direct effect on pepper fruit ripening, this being the first report about the ability of rhizobia to advance the fruit production of a nonlegume.

Phenolic Compounds. Phenolic compounds are plant secondary metabolites, which are synthesized by plants as a result of their adaptation to biotic and abiotic stress conditions.[1] They include flavonoids with antioxidant activity that may be beneficial for human health.[21,22]

The analysis of the aqueous extracts by HPLC-DAD allowed the identification of several phenolic compounds (Table 1). To evaluate the recovery of phenolic compounds, aliquots of known concentration of luteolin-7-*O*-glucoside standard solution were added to the samples and a recovery of 98% (±0.3) and 92% (±1.3) was obtained for leaves and fruits, respectively.

In pepper leaves hydroxycinnamic acids (5-*O*-caffeoylquinic, caffeic, and ferulic acids) and flavonoids (luteolin-7-*O*-gluco-

dx.doi.org/10.1021/jf4046649 | J. Agric. Food Chem. 2014, 62, 557−564

side, quercetin-3-*O*-rutinoside, and apigenin-7-*O*-glucoside) were identified (Table 1 and Figure 1A). These flavonoids have already been described in pepper leaves by Reigosa et al.[23] Several studies have already reported the fundamental role of luteolin and apigenin derivatives in the protection of cells (membranes, chlorophyll, and fragile organelles) from the damage caused by UV radiation.[1]

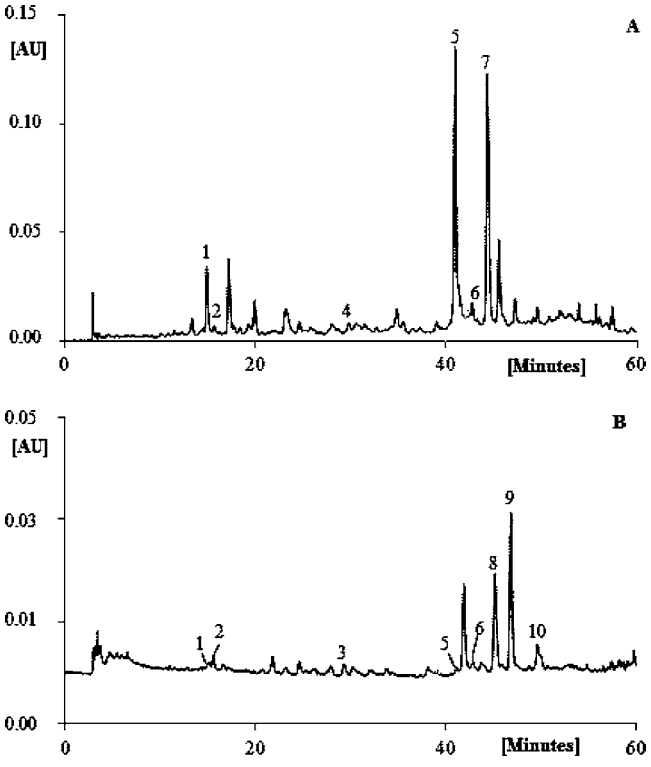

Figure 1. HPLC phenolic profile of *Capsicum annuum* (A) leaf control and (B) fruit control. Detection at 320 nm. Peaks: (1) 5-*O*-caffeoylquinic acid; (2) caffeic acid; (3) sinapic acid; (4) ferulic acid; (5) luteolin-7-*O*-glucoside; (6) quercetin-3-*O*-rutinoside; (7) apigenin-7-*O*-glucoside; (8) myricetin-3-*O*-rhamnoside; (9) quercetin-3-*O*-rhamnoside; (10) luteolin-7-*O*-(2-apiosyl-6-malonyl)-glucoside.

Pepper fruits showed a distinct phenolic profile, eight compounds being determined: 5-*O*-caffeoylquinic, caffeic, and sinapic acids, luteolin-7-*O*-glucoside, quercetin-3-*O*-rutinoside, myricetin-3-*O*-rhamnoside, quercetin-3-*O*-rhamnoside, and luteolin-7-*O*-(2-apiosyl-6-malonyl)-glucoside (Table 1 and Figure 1B). From these, only 5-*O*-caffeoylquinic acid and myricetin-3-*O*-rhamnoside were not previously described in pepper fruits.[1,2,15,24]

Quantitatively, the sum of the identified phenolic compounds in the three leaves samples was similar (Table 1). The major compound was apigenin-7-*O*-glucoside, corresponding to ca. 49, 52, and 54% of the total content in control sample and in the samples inoculated with strains PETP01 and TVP08, respectively. However, inoculation led to a significant increase of caffeic acid. Ferulic acid also increased significantly, but just in plants inoculated with the strain PETP01. On the contrary, the amounts of 5-*O*-caffeoylquinic acid and luteolin-7-*O*-glucoside were significantly higher in control leaves than in inoculated ones.

Regarding the fruits, the phenolic content decreased with the inoculation of both *Rhizobium* strains, especially with strain TVP08 (Table 1). Quercetin-3-*O*-rhamnoside was the main phenolic compound in all fruits. Although the inoculation with *Rhizobium* strains led to a significant decrease of the amounts of this compound, its relative content was higher in fruits from plants inoculated with strains PETP01 (about 60%) and TVP08 (almost 40%) than in control leaves, in which it represented 34% of total phenolics.

Several authors reported a decrease of phenolic compounds during ripening of several pepper varieties[15,25,26] due to their enzymatic degradation in secondary metabolism[15] and by the involvement in the structure of cell walls.[1] The decrease of phenolics in the fruits of plants inoculated with *Rhizobium* strains supports that the ripeness of these fruits is higher when the plants were inoculated with *Rhizobium* strains, mainly when the strain TVP08 was used. This result contrasts with that obtained by Amor et al.,[17] who did not find a decrease of phenolic compounds in pepper inoculated with *Azospirillum* and *Pantoea,* two bacteria considered as PGPR. Therefore, to our knowledge, this is the first report of a positive influence on fruit ripeness of the inoculation with *Rhizobium* PGPR strains of a nonlegume.

Capsaicinoids. Capsaicinoids are a group of alkaloids responsible for the pungent sensation caused by pepper fruits, capsaicin and dihydrocapsaicin being responsible for about 90% of the spiciness.[13]

HPLC-DAD analysis allowed the identification of two capsaicinoids (Table 2). To evaluate the recovery of capsaicinoids, aliquots of known concentration of capsaicin standard solution were added to the samples, a recovery of 80% (±7.3) and 77% (±3.0) being obtained for fruits and leaves, respectively.

In pepper leaves only capsaicin was detected (Table 2), ranging between 75.3 and 78.3 mg/kg. This contrasts with the results of Estrada et al.,[19] who also detected dyhidrocapsaicin in the leaves of other varieties of pepper in which the content of capsaicin was lower, ranging from 1 to 20 μg/g. No significant differences were found in the amounts of capsaicin of leaves from uninoculated and inoculated plants.

Besides capsaicin, dyhidrocapsaicin was also detected in the fruits. The total content of these capsaicinoids ranged between 275.2 and 309.2 mg/kg, capsaicin representing ca. 88.0% and dyhidrocapsaicin ca. 12.0%. As expected, these values are lower

Table 2. Capsaicinoids of *C. annuum* Fruits and Leaves Inoculated with *Rhizobium* (mg/kg Lyophilized Material)[a]

		fruits			leaves		
capsaicinoids	RT (min)	control	PETP01	TVP08	control	PETP01	TVP08
capsaicin	5.9	234.0 ± 17.0 a	277.3 ± 4.8 a	269.4 ± 9.0 a	78.3 ± 2.9 a	75.7 ± 2.7 a	75.3 ± 3.3 a
dihydrocapsaicin	9.7	41.2 ± 3.3 a	31.9 ± 3.5 a	33.2 ± 1.0 a	nd	nd	nd
total		275.2	309.2	302.6	78.3	75.7	75.3

[a]Values are expressed as mean ± standard deviation of three assays; RT, retention time; nd, not detected. In the same line, different letters represent significant differences compared with the respective control ($p < 0.05$).

dx.doi.org/10.1021/jf4046649 | J. Agric. Food Chem. 2014, 62, 557−564

Table 3. Organic Acids of *C. annuum* Fruits and Leaves Inoculated with *Rhizobium* (mg/kg Lyophilized Material)[a]

		fruits			leaves		
organic acids	RT (min)	control	PETP01	TVP08	control	PETP01	TVP08
oxalic	20.2	53711.3 ± 512.8 a	3169.8 ± 16.6 b	49257.6 ± 519.8 b	55292.7 ± 17.3 a	60640.7 ± 542.3 b	21542.2 ± 357.2 b
malic	36.4	21747.4 ± 1187.7 a	16780.1 ± 455.2 b	14785.6 ± 10.6 b	6438.7 ± 68.7 a	3194.8 ± 388.1 b	14785.6 ± 10.9 b
quinic	37.6	14349.1 ± 106.4 a	9182.8 ± 718.4 b	22680.2 ± 2638.0 b	4664.0 ± 29.8 a	4923.1 ± 42.9 b	4015.6 ± 18.5 b
succinic	47.4	35197.2 ± 380.0 a	24509.1 ± 1954.7 b	21805.6 ± 397.0 b	4892.9 ± 23.1 a	4746.3 ± 16.9 b	5307.4 ± 315.0 b
fumaric	61.6	13341.7 ± 199.9 a	6021.0 ± 112.8 b	6253.8 ± 170.7 b	5826.2 ± 261.1 a	4656.0 ± 227.5 b	6951.9 ± 321.2 b
citric	30.1	76786.0 ± 1701.3 a	95510.3 ± 378.2 b	99660.2 ± 46.1 b	30048.2 ± 873.1 a	31754.8 ± 205.9 b	7576.4 ± 846.8 b
acetic	51.5	55223.7 ± 8.9 a	58586.6 ± 1725.8 b	34560.8 ± 1391.9 b	106.8 ± 0.5 a	139.6 ± 0.8 b	122.0 ± 4.8 b
aconitic	24.3/43.8	1359.7 ± 78.5 a	185.6 ± 6.4 b	80.1 ± 3.3 b	16594.6 ± 47.2 a	16348.4 ± 83.4 b	16369.0 ± 1401.4 a
total		271716.1	213945.3	249083.9	123864.1	126403.7	76670.1

[a]Values are expressed as mean ± standard deviation of three assays. RT, retention time. In the same line, different letters represent significant differences compared with the respective control ($p < 0.05$).

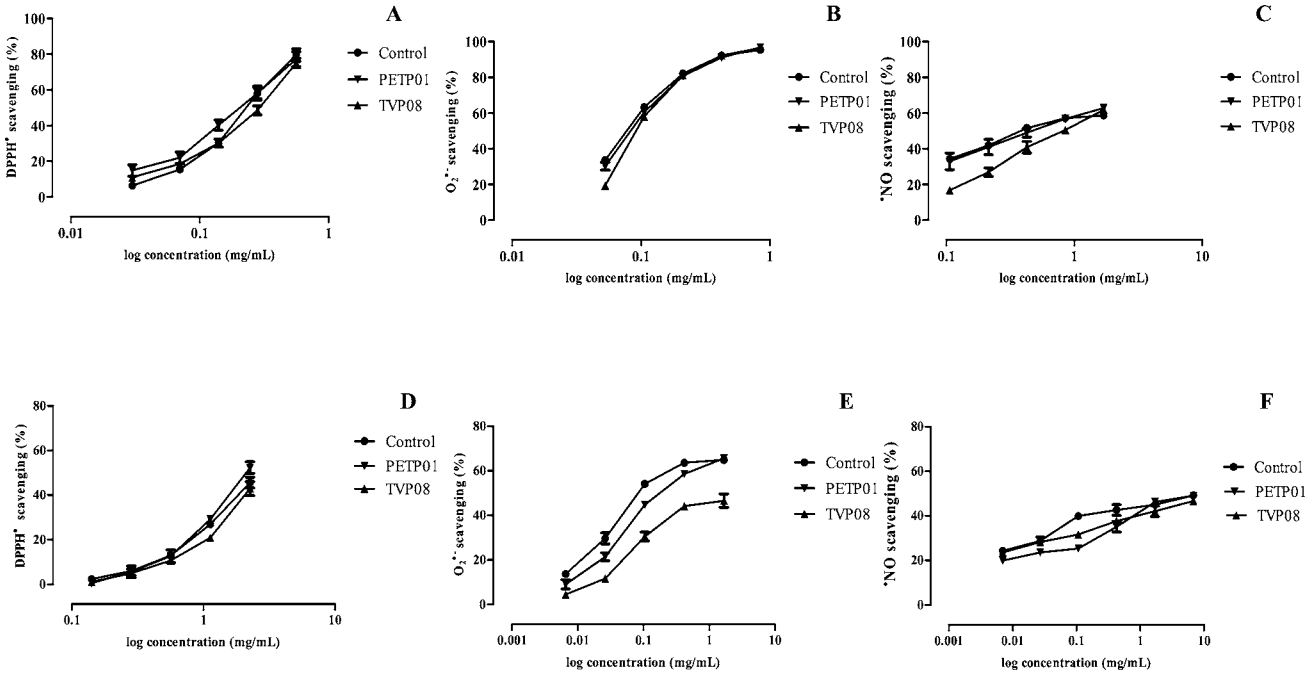

Figure 2. Effect of aqueous extracts of *C. annuum* leaves and fruits against (A, D) DPPH•, (B, E) superoxide radical ($O_2^{\bullet-}$), and (C, F) nitric oxide (•NO), respectively. Values show mean ± SE of three experiments performed in triplicate.

than those found on mature fruits from the spicy variety Jalapeño, in which levels of capsaicin and dyhidrocapsaicin ranging from 499−899 mg/kg to 540−989 mg/kg of dried material, respectively, were reported.[27]

Menichini et al.[13] observed that capsaicinoid amounts increase with ripening in *Capsicum chinense* Jacq. var. habanero, which is one of the most spicy varieties of pepper. In this study we also found a slight increase of capsaicin in peppers inoculated with *Rhizobium*. Nevertheless, the differences were not significant with respect to noninoculated ones, and in the case of dyhidrocapsaicin a decrease was even found. This was expected taking into account that a sweet variety ("sweet Italian") was analyzed in this study. This is the first study about the effect on content of capsaicinoids in leaves and fruits of *C. annuum* after the inoculation with *Rhizobium* spp. showing that it has not a significant effect in sweet peppers.

Organic Acids. Organic acids are primary metabolites, which can be found in great amounts in all plants, especially in fruits. Citric, malic, and tartaric acids are commonly found in fruits and berries, while oxalic acid is present in higher amounts in green leaves.[28]

The analysis of *C. annuum* fruits and leaves by HPLC−UV revealed a similar profile, composed of oxalic, malic, quinic, succinic, fumaric, citric, acetic, and aconitic acids (Table 3). To evaluate the recovery of organic acids, aliquots of a standard solution of fumaric acid with known concentration were added to the samples, 89 ± 0.9 and 81 ± 1.2% being recovered from fruits and leaves, respectively.

The total amount of organic acids in the leaves from control plants was lower than those from plants inoculated with PETP01 strain, but higher than in those from plants inoculated with TVP08 strain (Table 3).

In pepper leaves from all treatments oxalic acid was the main compound representing ca. 45, 48, and 28% from the total of the determined organic acids, in leaves of control, plants inoculated with strain PETP01, and those inoculated with strain TVP08, respectively (Table 3). The amounts of this acid together with quinic, citric, and acetic acids were significantly increased after the inoculation with strain PETP01, whereas it significantly decreased malic, succinic, fumaric, and aconitic acids. In the case of leaves from plants inoculated with strain TVP08 significant increases of malic, succinic, fumaric, and

dx.doi.org/10.1021/jf4046649 | J. Agric. Food Chem. 2014, 62, 557−564

Table 4. IC Values (mg/mL) Found with Extracts of *C. annuum* Fruits (IC_{25}) and Leaves (IC_{50}) in the Assays against DPPH•, Superoxide ($O_2^{\bullet-}$), and Nitric Oxide (•NO) Radicals and Acetylcholinesterase (AChE) Inhibition[a]

	fruits			leaves		
assay	control	PETP01	TVP08	control	PETP01	TVP08
DPPH•	1.047 (±0.040) a	0.991 (±0.051) a	1.345 (±0.076) b	0.234 (±0.199) a	0.193 (±0.042) a	0.294 (±0.013) a
$O_2^{\bullet-}$	0.020 (±0.002) a	0.033 (±0.003) a	0.075 (±0.005) a	0.080 (±0.023) a	0.085 (±0.082) a	0.093 (±0.057) b
•NO	0.010 (±0.002) a	0.039 (±0.005) b	0.013 (±0.001) a	0.377 (±0.003) a	0.466 (±0.003) a	0.806 (±0.001) b
AChE				2.570 (±0.218) a	2.685 (±0.226) a	3.492 (±0.044) b

[a]Values are expressed as mean + standard deviation of three assays. In the same line, different letters represent significant differences compared with the respective control ($p < 0.05$).

acetic acids were observed, while the content of oxalic, quinic, and citric acids was significantly reduced. Therefore, both strains had the same effect just in what concerns acetic acid content, which was significantly increased (Table 3).

The increased levels of malic acid in leaves from plants inoculated with TVP08 strain are in agreement with the results found for rice leaves inoculated with the PGPR bacterium *Herbaspirillum seropedicae* by Curzi et al.[29] This is the first report about the effect of the inoculation of *Rhizobium* in the organic acids composition of *C. annuum* leaves.

The organic acids qualitative profile of *C. annuum* fruits was similar to that of the leaves (Table 3), citric acid being the major organic acid in all samples, representing ca. 28% in control fruits and 45 and 40% in fruits from plants inoculated with strains PETP01 and TVP08, respectively. Succinic, acetic, and aconitic acids are described for the first time in this matrix, while all the others were already reported.[30] The inoculation with both *Rhizobium* strains led to the decrease of most of the organic acids in fruits, except citric acid; additionally, acetic and quinic acids increased when PETP01 and TVP08 strains were inoculated, respectively. These results are in agreement with those obtained with soybean, a legume, after the inoculation of *Bradyrhizobium*[31] and in pepper fruits after inoculation with other PGPR bacteria, such as *Azospirillum* sp. and *Pantoea* sp.[17] The concentrations of organic acids in sweet peppers change notably during ripening, a decrease of their total amounts being reported.[6,15,16] These authors reported that the concentration of malic acid decreases while that of citric acid increases considerably during the ripeness process. The same results were found in our study when the plants were inoculated with the two *Rhizobium*, strengthen the results obtained for phenolic compounds and showing a more advanced degree of ripeness in peppers from plants inoculated with *Rhizobium* strains.

Antioxidant Activity. Peppers are a good source of antioxidant compounds that can reduce harmful oxidation reactions in the human body, thus preventing various diseases associated with free radical oxidation, such as cardiovascular and neurological disorders and cancer.[2]

The antioxidant activity of the aqueous lyophilized extracts from *C. annuum* fruits and leaves was tested against DPPH•, superoxide ($O_2^{\bullet-}$), and nitric oxide (•NO) radicals. A concentration-dependent potential was observed in all assays (Figure 2).

As far we know, this is the first study about the antioxidant capacity of *C. annuum* leaves. The extract of leaves from plants inoculated with PETP01 strain revealed a tendency to be the most active against DPPH• radical (Table 4). In the assays against •NO and $O_2^{\bullet-}$ radicals the best results were obtained with the extract of leaves from control plants (Table 4). This result is in agreement with the phenolic composition of leaves, in which luteolin-7-*O*-glucoside and 5-*O*-caffeoylquinic acid (chlorogenic acid), two compounds with antioxidant potential,[32,33] were found in significant higher amounts in control leaves (Table 1). Although the contribution of other bioactive compounds not determined in the extracts cannot be discarded, the presence of higher amounts of luteolin-7-*O*-glucoside and 5-*O*-caffeoylquinic acid in control leaves may be linked to the higher antioxidant activities found in them. Comparing the results of the three assays performed, we can observe that the leaves' extracts were more active against superoxide radical. The scavenging of this reactive oxygen species is of great importance due to its potential to originate other reactive species that could be extremely deleterious to the cells.[34]

The extracts obtained from fruits followed the same pattern as those from the leaves. The extract of fruits from plants inoculated with PETP01 strain was the most active against DPPH• radical and that of fruits from plants inoculated with TVP08 strain the less effective, the differences being significant when compared to control (Figure 2D, Table 4). The extract from control fruits also showed a tendency to be the most active against •NO and $O_2^{\bullet-}$ (Table 4).

Conforti et al.[25] observed that more immature pepper fruits showed better antioxidant activity, due to the presence of higher amounts of phenolic compounds. Since the inoculation of pepper with *Rhizobium* anticipated the fruit ripening, a decrease in the antioxidant activity of fruits inoculated with *Rhizobium* was expected. Nevertheless, the inoculation with the PETP01 strain significantly increased the activity against DPPH•, decreasing only with the inoculation of the strain TVP08, which was the strain that more significantly advanced the ripening of pepper fruits. The inoculation does not significantly affect the activity against •NO and $O_2^{\bullet-}$ radicals.

Acetylcholinesterase (AChE) Inhibitory Activity. The search for natural matrices with capacity to inhibit AChE has increased due to their benefits in the treatment of Alzheimer's disease and other forms of dementia.[35]

In this study the inhibitory activity of aqueous extracts of *C. annuum* leaves was evaluated against AChE and a concentration-dependent activity was obtained (data not shown). Extract from control leaves was the most active (Table 4), and this result can be explained by the presence of various bioactive compounds, namely, flavonoids.[36]

The capacity of fruits' aqueous extracts to inhibit AChE was also assessed, but no effect was found for the tested concentrations. Despite the different composition, the same kind of phenolic compounds was found in both fruit and leaf extracts. As such, the absence of effect on AChE observed with the extracts prepared from fruits seems to suggest the interference of other nondetermined bioactive compounds.

In summary, the most relevant result obtained in this study is a positive effect on fruit ripening of pepper plants inoculated with two *Rhizobium* strains. The fruits from inoculated plants

had lower total levels of organic acids and phenolic compounds, pointing to a higher ripening stage than those from uninoculated ones. Data suggest that the application of nodulating rhizobacteria is a beneficial agricultural practice for this nonlegume, ensureing that they are optimal bacteria for biofertilization, with positive effects on production and fruit ripening, contributing to an increase in the consumption of this fruit, either as fruit or dietary supplement.

AUTHOR INFORMATION

Corresponding Author

*Tel: + 351 220 428 654. Fax: +351 226 093 390. E-mail: lmsilva@ff.up.pt (L.R.S.) or pandrade@ff.up.pt (P.B.A.).

Funding

The authors are grateful to Fundação para a Ciência e a Tecnologia (FCT) for Grant No. PEst-C/EQB/LA0006/2011.

Notes

The authors declare no competing financial interest.

ABBREVIATIONS USED

PGPR, plant growth-promoting rhizobacteria; DPPH$^{\bullet}$, 1,1-diphenyl-2-picrylhydrazyl radical; $O_2^{\bullet-}$, superoxide radical; $^{\bullet}$NO, nitric oxide; NADH, β-nicotinamide adenine dinucleotide; PMS, phenazine methosulfate; NBT, nitrotetrazolium blue chloride; DTNB, 5,5′-dithiobis(2-nitrobenzoic acid); AChE, acetylcholinesterase; ATCI, acetylthiocholine iodide; SNP, sodium nitroprusside dehydrate; HPLC, high-performance liquid chromatography; DAD, diode array detector

REFERENCES

(1) Materska, M.; Perucka, I. Antioxidant activity of the main phenolic compounds isolated from hot pepper fruit (*Capsicum annuum* L.). *J. Agric. Food Chem.* **2005**, *53*, 1750−1756.

(2) Sun, T.; Xu, Z.; Wu, C. T.; Janes, M.; Prinyawiwatkul, W.; No, H. K. Antioxidant activities of different colored sweet bell peppers (*Capsicum annuum* L.). *J. Food Sci.* **2007**, *72*, 98−102.

(3) Kim, J.-S.; Ahn, J.; Lee, S.-J.; Moon, B.; Ha, T.-Y.; Kim, S. Phytochemicals and antioxidant activity of fruits and leaves of Paprika (*Capsicum annuum* L., var. *Special*) cultivated in Korea. *J. Food Sci.* **2011**, *76*, C193−C198.

(4) Singh, S.; Jarret, R.; Russo, V.; Majetich, G.; Shimkus, J.; Bushway, R.; Perkins, B. Determination of capsinoids by HPLC-DAD in *Capsicum* species. *J. Agric. Food Chem.* **2009**, *57*, 3452−3457.

(5) Díaz, J.; Pomar, F.; Bernal, A.; Merino, F. Peroxidases and the metabolism of capsaicin in *Capsicum annuum* L. *Phytochem. Rev.* **1998**, *3*, 141−157.

(6) Navarro, J. M.; Flores, P.; Garrido, C.; Martinez, V. Changes in the contents of antioxidant compounds in pepper fruits at different ripening stages, as affected by salinity. *Food Chem.* **2006**, *96*, 66−73.

(7) Pascual, I.; Azcona, I.; Aguirreolea, J.; Morales, F.; Corpas, F. J.; Palma, J. M.; Rellán-Alvaréz, R.; Sánchez-Díaz, M. Growth, yeld, and fruit quality of pepper plants amended with two sanitized sewage sludges. *J. Agric. Food Chem.* **2010**, *58*, 6951−6959.

(8) Lugtenberg, B.; Kamilova, F. Plant-Growth-Promoting Rhizobacteria. *Annu. Rev. Microbiol.* **2009**, *63*, 541−556.

(9) Kang, S. H.; Cho, H. S.; Cheong, H.; Ryu, C. M.; Kim, J. F.; Park, S. H. Two bacterial entophytes eliciting both plant growth promotion and plant defense on pepper (*Capsicum annuum* L.). *J. Microbiol. Biotechnol.* **2007**, *17*, 96−103.

(10) Velázquez, A.; García-Fraile, P.; Ramírez-Bahena, M. H.; Rivas, R.; Martínez-Molina, E. Bacteria involved in nitrogen-fixing legume symbiosis: Current taxonomic perspective. In *Microbes for Legume Improvement*; Khan, M. S., Zaidi, A., Musarrat, J., Eds; Springer: Dordrecht, 2010; pp 1−25.

(11) Avis, T. J.; Gravel, V.; Antoun, H.; Tweddell, R. J. Multifaceted beneficial effects of rhizosphere microorganisms on plant health and productivity. *Soil Biol. Biochem.* **2008**, *40*, 1733−1740.

(12) García-Fraile, P.; Carro, L.; Robledo, M.; Ramírez-Bahena, M.-H.; Flores-Félix, J.-D.; Fernández, M. T.; Mateos, P. F.; Rivas, R.; Igual, J. M.; Martínez-Molina, E.; Peix, A.; Velázquez, E. Rhizobium promotes non-legumes growth and quality in several production steps: towards a biofertilization of edible raw vegetables healthy for humans. *PLoS One* **2012**, *7*, e38122.

(13) Menichini, F.; Tundis, R.; Bonesi, M.; Loizzo, M. R.; Conforti, F.; Statti, G.; De Cindio, B.; Houghton, P. J.; Menichini, F. The influence of fruit ripening on the phytochemical content and biological activity of *Capsicum chinense* Jacq. Cv Habanero. *Food Chem.* **2009**, *114*, 553−560.

(14) Sukrasno, N.; Yeoman, M. Phenylpropanoid metabolism during growth and development of *Capsicum frutescens* fruits. *Phytochemistry* **1993**, *32*, 839−844.

(15) Howard, L. R.; Talcott, S. T.; Brenes, C. H.; Villalon, B. Changes in phytochemical and antioxidant activity of selected pepper cultivars (*Capsicum* species) as influenced by maturity. *J. Agric. Food Chem.* **2000**, *48*, 1713−1720.

(16) Luning, P. A.; van der Vuurst de Vries, R.; Yuksel, D.; Ebbenhorst−Seller, T.; Wichers, H. J.; Roozen, J. P. Combined instrumental and sensory evaluation of flavor of fresh bell peppers (*Capsicum annuum*) harvested at three stages of maturity. *J. Agric. Food Chem.* **1994**, *42*, 2855−2861.

(17) Amor, F. M.; Serrano-Martínez, A.; Fortea, M. I.; Legua, P.; Núñez-Delicado, E. The effect of plant-associative bacteria (*Azospirillum* and *Pantoea*) on the fruit quality sweet pepper under limited nitrogen supply. *Sci. Hortic.* **2008**, *117*, 191−196.

(18) Silva, L. R.; Azevedo, J.; Pereira, M. J.; Valentão, P.; Andrade, P. B. Chemical assessment and antioxidant capacity of pepper (*Capsicum annuum* L.) seeds. *Food Chem. Toxicol.* **2013**, *53*, 240−248.

(19) Estrada, B.; Bernal, M. A.; Díaz, J.; Pomar, F.; Merino, F. Capsaicinoids in vegetative organs of *Capsicum annuum* L. in relation to fruiting. *J. Agric. Food Chem.* **2002**, *50*, 1188−1191.

(20) Oliveira, A. P.; Valentão, P.; Pereira, J. A.; Silva, B. M.; Tavares, F.; Andrade, P. B. *Ficus carica* L.: Metabolic and biological screening. *Food Chem. Toxicol.* **2009**, *47*, 2841−2846.

(21) Saxena, M.; Saxena, J.; Pradhan, A. Flavonoids and phenolic acids as antioxidants in plants and human health. *Int. J. Pharm. Sci. Rev. Res.* **2012**, *16*, 130−134.

(22) Padula, M. C.; Lepore, L.; Milella, L.; Ovesna, J.; Malafronte, N.; Martelli, G.; de Tommasi, N. Cultivar based selection and genetic analysis of strawberry fruits with high levels of health promoting compounds. *Food Chem.* **2013**, *140*, 639−646.

(23) Reigosa, M. J.; Souto, X. C.; González, L. Effect of phenolic compounds on the germination of six weeds species. *Plant Growth Regul.* **1999**, *28*, 83−88.

(24) Materska, M.; Piacente, S.; Stochmal, A.; Pizza, C.; Oleszek, W.; Perucka, I. Isolation and structure elucidation of flavonoid and phenolic acid glycosides from pericarp of hot pepper fruit *Capsicum annuum* L. *Phytochemistry* **2003**, *63*, 893−898.

(25) Conforti, F.; Statti, G. A.; Menichini, F. Chemical and biological variability of hot pepper fruits (*Capsicum annuum* var. *acuminatum* L.) in relation to maturity stage. *Food Chem.* **2007**, *102*, 1096−1104.

(26) Pérez-López, A. P.; Amor, F. M.; Serrano-Martínez, A.; Fortea, M.; Núnez-Delicado, E. Influence of agricultural practices on the quality of sweet pepper fruits as affected by the maturity stage. *J. Sci. Food Agric.* **2007**, *87*, 2075−2080.

(27) Topuz, A.; Dincer, C.; Özdemir, K. S.; Feng, H.; Kushad, M. Influence of different drying methods on carotenoids and capsaicinoids of paprika (Cv., jalapeno). *Food Chem.* **2011**, *129*, 860−865.

(28) Oliveira, A. P.; Pereira, J. A.; Andrade, P. B.; Valentão, P.; Seabra, R. M.; Silva, B. M. Organic acids composition of *Cydonia oblonga* Miller leaf. *Food Chem.* **2008**, *111*, 393−399.

(29) Curzi, M. J.; Ribaudo, C. M.; Trinchero, G. D.; Curá, J. A.; Pagano, E. A. Changes in the content of organic and amino acid and

ethylene production of rice plants in response to the inoculation with *Herbaspirillum seropedicae*. *J. Plant Interact.* **2008**, *3*, 163−73.
(30) López-Hernández, J.; Oruña-Concha, M. J.; Simal-Lozano, J.; Vázquez-Blanco, M. E.; González-Castro, M. J. Chemical composition of Padrón peppers (*Capsicum annuum* L.) grown in Galicia (N.W. Spain). *Food Chem.* **1996**, *51*, 557−559.
(31) Couto, C.; Silva, L. R.; Valentão, P.; Velázquez, E.; Peix, A.; Andrade, P. B. Effects induced by the nodulation with *Bradyrhizobium japonicum* on *Glycine max* (soybean) metabolism and antioxidant potential. *Food Chem.* **2011**, *127*, 1487−1495.
(32) Halliwell, B. Reactive species and antioxidants. Redox biology is a fundamental theme of aerobic life. *Plant Physiol.* **2006**, *141*, 312−322.
(33) Olthof, M. R.; Hollman, P. C. H.; Katan, M. B. Chlorogenic acid and caffeic acid are absorbed in humans. *J. Nutr.* **2001**, *131*, 66−71.
(34) Mikkelsen, R. B.; Wardman, P. Biological chemistry of reactive oxygen and nitrogen and radiation-induced signal transduction mechanisms. *Oncogene* **2003**, *22*, 5734−5754.
(35) Mukherjee, P. K.; Kumar, V.; Mal, M.; Houghton, P. J. Acetylcholinesterase inhibitors from plants. *Phytomedicine* **2007**, *14*, 289−300.
(36) Katalinic, M.; Rusak, G.; Barovic, J. D.; Sinko, G.; Jelic, D.; Antolovic, R.; Kovarik, Z. Structural aspects of flavonoids as inhibitors of human butyrylcholinesterase. *Eur. J. Med. Chem.* **2010**, *45*, 186−192.

JOURNAL OF AGRICULTURAL AND FOOD CHEMISTRY

Article

pubs.acs.org/JAFC

Inoculation of the Nonlegume *Capsicum annuum* L. with *Rhizobium* Strains. 2. Changes in Sterols, Triterpenes, Fatty Acids, and Volatile Compounds

Luís R. Silva,*[,†] Jessica Azevedo,[†] Maria J. Pereira,[†] Lorena Carro,[‡,§] Encarna Velazquez,[‡,§] Alvaro Peix,[§,∥] Patrícia Valentão,[†] and Paula B. Andrade*[,†]

[†]REQUIMTE/Laboratório de Farmacognosia, Departamento de Química, Faculdade de Farmácia, Universidade do Porto, Rua de Jorge Viterbo Ferreira, No. 228, 4050-313 Porto, Portugal

[‡]Departamento de Microbiología y Genética, Universidad de Salamanca, Campus Miguel de Unamuno, s/n, 37007 Salamanca, Spain

[§]Unidad Asociada Grupo de Interacciones Planta-Microorganismo, Universidad de Salamanca-CSIC, Salamanca, Spain

[∥]Instituto de Recursos Naturales y Agrobiología, IRNASA-CSIC, Cordel de Merinas, 40-52, 37008 Salamanca, Spain

ABSTRACT: Peppers (*Capsicum* spp.) are consumed worldwide, imparting flavor, aroma, and color to foods, additionally containing high concentrations of biofunctional compounds. This is the first report about the effect of the inoculation of two *Rhizobium* strains on sterols, triterpenes, fatty acids, and volatile compounds of leaves and fruits of pepper (*Capsicum annuum* L.) plants. Generally, inoculation with strain TVP08 led to the major changes, being observed a decrease of sterols and triterpenes and an increase of fatty acids, which are related to higher biomass, growth, and ripening of pepper fruits. The increase of volatile compounds may reflect the elicitation of plant defense after inoculation, since the content on methyl salicylate was significantly increased in inoculated material. The findings suggest that inoculation with *Rhizobium* strains may be employed to manipulate the content of interesting metabolites in pepper leaves and fruits, increasing potential health benefits and defense abilities of inoculated plants.

KEYWORDS: *Capsicum annuum L., plant-growth-promoting rhizobacteria, sterols, triterpenes, fatty acids, volatile compounds*

INTRODUCTION

The genus *Capsicum* belongs to the Solanaceae family and includes many species distributed by both sweet cultivars, mainly eaten as vegetables, and hot ones, often used as spice.[1] There is a plethora of dishes, pastas, and sauces to which peppers impart their particular color and flavor. Furthermore, peppers can be utilized at both ripe and unripe stages, although the former is preferred by European consumers.[2]

The increased production of peppers has created an economic and environmental burden that has led to the discarding of stems and leaves, even with nutraceutical potential. However, little information is available concerning specific phytochemicals or their functional value.

Within *Capsicum* genus, the most genetically diverse and economically important species corresponds to the common pepper (*Capsicum annuum* L.), whose varieties are cultivated worldwide. This species has become popular not only because of its morphological and genetic diversity, flavor, and aroma but also due to its beneficial properties for human health.[3] Actually, it is recognized for its excellent nutritional composition, containing proteins, fatty acids, and sugars, high levels of α- and β-carotene, β-cryptoxanthine, and other carotenoids, vitamin C, tocopherols, and phenolic compounds, mainly flavonoids like quercetin and luteolin derivatives.[3,4]

In plant tissues, the most abundant saturated fatty acids are palmitic and stearic, oleic, linoleic, and linolenic being the most common unsaturated ones.[5] The diet contains a mixture of different types of saturated (SFA), monounsaturated (MUFA), and ω-6 and ω-3 polyunsaturated (PUFA) fatty acids. Some fatty acids are primarily used for energy or storage (SFA and MUFA), and others, especially long-chain PUFAs, are used in cell membrane phospholipids and synthesis of lipid-derived mediators and as regulators of a number of cellular functions, including gene transcription.[6] PUFAs from the ω-6 family have important biological properties and are the biosynthetic precursors of eicosanoids (i.e., prostaglandins), having effects on cardiovascular diseases, triglyceride levels, and arthritis.[7]

Plant sterols are bioactive components of all vegetable foods. Phytosterols are cholesterol-like molecules found in most plant foods, with the highest concentrations occurring in vegetable oils. Plant materials contain free and esterified sterols that can be acylated, β-sitosterol, campesterol, and stigmasterol being the more abundant ones in nature. They are recognized to lower blood cholesterol, may provide protection against certain types of cancer, and present an immune-modulating activity.[8] The addition of plant sterols to the diet is suggested by health experts as a safe and effective way to reduce the risk of coronary heart disease,[9] and the short-term use of food supplements rich in these compounds is a safe and effective strategy, with or without statin therapy, among the majority of dyslipidemic patients with need for additional lipid-lowering (reviewed by Gupta et al.[10]).

Received: October 16, 2013
Revised: December 31, 2013
Accepted: January 1, 2014
Published: January 9, 2014

ACS Publications © 2014 American Chemical Society

dx.doi.org/10.1021/jf4046655 | *J. Agric. Food Chem.* 2014, 62, 565−573

Volatile compounds are released from leaves, flowers, and fruits into the atmosphere and from roots into the soil. The primary functions of volatile compounds are to defend plants against herbivores and pathogens, to attract pollinators, seed dispersers, and other beneficial animals and microorganisms, and to serve as signals in plant−plant communication.[11]

Currently the consumers demand high quality for raw consumed vegetables, such as pepper, and this implies a reduction of chemicals added to the crops that can be substituted by biological agents like fungi[12] and plant growth-promoting rhizobacteria (PGPR). These bacteria can enhance the plant growth by diverse mechanisms, such as mobilization of nutrients, production of siderophores that chelate iron and make it available to the plant roots, and synthesis of phytohormones.[13,14]

Rhizobia are generally regarded as microbial symbiotic partners of legumes and are mainly known for their role in the formation of nitrogen-fixing nodules.[15] Some of these bacteria have been explored with respect to their effect in the production of bioactive compounds in legumes.[16] Nevertheless, there are no data about the effect of rhizobia inoculation on the bioactive metabolites of nonlegumes. Part 1 of this study concerned the influence of the inoculation of two *Rhizobium* strains on the phenolic compounds, organic acids, capsaicinoids, and bioactivity of leaves and fruits of *C. annuum*.[17] Therefore, the aim of this second part was to evaluate the influence of the same strains on sterols, triterpenes, fatty acids, and volatiles composition.

MATERIALS AND METHODS

Standards and Reagents. All chemicals used were of analytical grade. The standard compounds were purchased from various suppliers: (*E*)-2-hexenal, camphene, α-pinene, linalool, camphor, β-caryophyllene, β-cyclocitral, (*Z*)-4-heptenal, (*E*,*Z*)-2,6-nonadienal, methyl salicylate, eugenol, hexanal, 1-octen-3-ol, benzyl alcohol, 6-methyl-5-hepten-2-one, 2-isobutyl-3-methoxypyrazine, benzaldehyde, *o*-guaiacol, β-sitosterol, campesterol, betulin, and stigmasterol were obtained from Sigma-Aldrich (St. Louis, MO, USA); fatty acid methyl esters kit were purchased from Supelco (Bellafonte, PA, USA), methyl jasmonate (internal standard), β-ionone, α-ionone, (*E*)-2-octenal, 2-methylbutanal, 3-methylbutanal, and heptanal from SAFC (St. Louis, MO, USA), and menthol and limonene from Fluka (Buchs, Switzerland). Methanol and acetonitrile were purchased from Sigma-Aldrich (St. Louis, MO, USA). Sodium sulfate anhydrous and isooctane were purchased from Panreac Química SA (Barcelona, Spain). Potassium hydroxide was from Pronalab (Lisboa, Portugal) and boron trifluoride (BF_3) 10% methanol solution from Supelco (Bellafonte, PA, USA). Water was deionized using a Milli-Q water purification system (Millipore, Bedford, MA).

Plant Samples and Bacterial Strains. The leaves and fruits of pepper were obtained in a previous experiment.[18] Nonsterilized seeds of peper var. "sweet italian" were germinated in peat, according to the steps usually applied in the commercial process of seedling production, and were irrigated from a bottom reservoir with water every 48 h and with commercial Hoagland's solution (Sigma Co., USA) every 8 days. Each seed was inoculated with 1 mL of a suspension (2×10^8 cells/mL) of 5-day-old *Rhizobium* strains TPV08 and PETP01 grown on yeast-mannitol agar (YMA). Then they were covered with vermiculite and germinated in the dark, in a growth chamber at 24 °C, for seven days. Afterward they were maintained in a growth chamber with fluorescent lighting 400−700 nm and 400 microeinsteins/m^2/s, set to a photoperiod of 16 h/day with temperature varying from 25 to 27 °C and 50−60% relative humidity. Uninoculated controls were kept under the same conditions.

After four weeks, 25 plants/treatment were used for a microcosm experiment, developed in a clayey soil (neutral pH, 1.5−1.8% of organic matter and 0.09−0.1 of N content). The seedling roots were flooded in bacterial suspensions containing 2×10^8 cells/mL during 4 h. Each plant was transplanted to a pot containing 2 kg of soil. Plants were irrigated from a bottom reservoir with water every 48 h and with commercial Hoagland's solution every 8 days. The plants were kept in a greenhouse illuminated with natural light (night temperature ranging from 15 to 20 °C and day temperature ranging from 25 to 35 °C) and humidity control, for 10 weeks. At the end of the experiment, flowers and fruits were counted, fruits were harvested, and their fresh weight was measured.

Five plants per treatment were then randomly selected. They were frozen, lyophilized, and powdered (mean particle size lower than 910 μm), being divided into three aliquots and analyzed separately.

Analysis of Sterols and Triterpenes. *Extraction and Alkaline Hydrolysis.* Alkaline hydrolysis was performed to obtain the free forms following the procedure described by Silva et al.[19] with some modifications. Briefly, 0.50 g of lyophilized fruits and 0.25 g of lyophilized leaves were saponified by refluxing with 20 mL of 0.5 M ethanolic KOH for 1 h at constant temperature (80 °C). The mixture was then centrifuged at 4000 rpm for 3 min, decanted, and transferred to a separation funnel to extract the unsaponifiable fraction with *n*-hexane (3 × 10 mL). The organic phase was evaporated to dryness in a rotary evaporator. The residue was dissolved in 1 mL of methanol and then filtered through a 0.45 μm PTFE membrane. This procedure was performed in triplicate.

HPLC-DAD Analysis. Compounds were determined using the method described by Silva et al.[19] The extracts were analyzed on an analytical HPLC unit (Gilson) coupled to a diode array detector (Gilson). The compounds in each extract were identified by comparing their retention times and UV spectra with those of authentic standards. Quantification was achieved by measuring the absorbance recorded at 205 nm relative to external standards. This procedure was performed in triplicate.

Analysis of Fatty Acids. *Extraction and Derivatization.* The extraction and derivatization procedures were performed according to Silva et al.[19] Briefly, esterified fatty acids in 40 and 100 mg of lyophilized fruits and leaves, respectively, were hydrolyzed with methanolic KOH and derivatized to their methyl ester forms with BF_3 (10%) methanolic solution. The methyl ester derivatives were extracted with isooctane, and anhydrous sodium sulfate was added to ensure the total absence of water. The resulting extract was evaporated to dryness under a stream of nitrogen and redissolved in 400 μL of isooctane. All assays were performed in triplicate.

GC−IT/MS Analysis. Quantification of fatty acids followed the work by Silva et al.[19] The thermal desorption was performed in a Varian CP-3800 gas chromatograph (USA) coupled to a VARIAN Saturn 4000 mass selective detector (USA), and a Saturn GC/MS workstation software version 6.8. A VF-5 ms (30 m × 0.25 mm × 0.25 μm, FactorFour) column from VARIAN was used in the analysis. The injector port was heated to 250 °C, and injections were performed in split mode with a ratio of 1:40. The carrier gas was helium C-60 (Gasin, Portugal), at a constant flow of 1 mL/min. The oven temperature was set at 40 °C for 1 min, then increased 5 °C/min to 250 °C, 3 °C/min to 300 °C, and held for 15 min. 1 μL of the extracts was analyzed in Full Scan mode. The components were identified according to their retention indices relative to C_8−C_{20} *n*-alkanes and mass spectra, which were compared with those of the NIST 05MS Library Database (Match and R. Match >80%), pure standards analyzed under the same conditions and the NIST Chemistry WebBook. The amounts of fatty acid methyl esters (FAMEs) present in the extract were calculated from the calibration curve of the respective FAME standard. The FAME values were then converted to the respective fatty acid contents. The assays were performed in triplicate.

Volatile Compounds Analysis. *Headspace Solid Phase Microextraction (HS-SPME).* HS-SPME was performed according to Silva et al.[19] Briefly, fruits (100 mg) and leaves (150 mg) of *C. annuum* were stirred (500 rpm) with 5 mL of water and 2 g of NaCl at 45 °C, for 5 min. A divinylbenzene/polydimethylsiloxane (DVB/PDMS) 65 μm fiber was then exposed to the headspace for 10 min, with agitation (250 rpm) at 45 °C.

Table 1. Sterols and Triterpenes Composition of *C. annuum* Fruits and Leaves, Uninoculated (Control) and Inoculated with PET01 and TVP08 Rhizobial Strains (mg/kg of Lyophilized Material)[a]

		fruits			leaves		
compounds	RT	control	PETP01	TVP08	control	PETP01	TVP08
betulin	2.4	117.8 ± 2.5 a	122.6 ± 2.6 a	110.2 ± 1.4 b	510.7 ± 15.1 a	508.3 ± 3.1 a	457.7 ± 11.0 b
β-sitosterol	8.4	36.4 ± 1.7 a	37.8 ± 1.8 a	27.2 ± 4.0 b	101.8 ± 6.8 a	170.2 ± 2.8 b	95.3 ± 8.3 a
campesterol	9.0	45.8 ± 3.1 a	44.7 ± 1.6 a	34.0 ± 1.0 b	162.6 ± 3.1 a	315.3 ± 7.9 b	183.2 ± 0.4 b
stigmasterol	9.9	1.2 ± 0.2 a	6.2 ± 0.4 b	4.1 ± 0.3 b	24.1 ± 0.2 a	31.8 ± 2.0 b	24.3 ± 0.3 a
total		201.2	211.3	175.5	799.2	1025.6	760.5

[a]Values are expressed as mean ± standard deviation of three assays. RT, retention time. Different letters in the same material and same row mean statistically significant differences ($p < 0.05$).

GC–IT/MS Analysis. The analysis of volatiles was performed as described by Silva et al.[19] The injector port was heated to 220 °C, and injections were performed in splitless mode. The carrier gas was helium C-60 (Gasin, Portugal), at a constant flow of 1 mL/min. Oven temperature was set at 40 °C (for 1 min), then increased 2 °C/min to 98 °C. All mass spectra were acquired in electron impact (EI) mode. Transfer line, manifold, and trap temperatures of the ion trap detector were set at 280, 50, and 180 °C, respectively. The emission current was 50 μA, and the electron multiplier was set in relative mode to auto tune procedure. The maximum ionization time was 25,000 μs, with an ionization storage level of 35–350 *m/z*. The analysis was performed in Full Scan mode. Compounds were identified according to their retention indices relative to C_8–C_{20} *n*-alkanes and mass spectra, which were compared with those of the NIST 05MS Library Database (Match and R. Match >80%), pure standards analyzed under the same conditions, NIST Chemistry Web-Book, and bibliography.[20−23] Each sample was analyzed in triplicate.

Statistical Analysis. All data were recorded as mean ± standard deviation of triplicate determinations. Mean values were compared by one-way analysis of variance (one-way ANOVA) (Graph Pad Prism Version 5.00, GraphPad Software, Inc., San Diego, CA). Differences were considered significant for $p < 0.05$.

Principal component analysis (PCA) was carried out using XLSTAT 2012 software. The PCA method shows similarities between samples projected on a plane and makes it possible to identify which variables determine these similarities and in what way.

RESULTS AND DISCUSSION

Profile of Sterols and Triterpenes. The analysis of the alkaline hydrolysis extracts by HPLC-DAD revealed a similar profile among *C. annuum* leaves, one triterpene (betulin) and three sterols (stigmasterol, campesterol, and β-sitosterol) being identified (Table 1). According to the literature, this is the first study about the sterols and triterpenes in *C. annuum* leaves. To evaluate the recovery of compounds, aliquots of betulin standard solution with known concentration were added to the samples, recoveries of 97% (±0.04) and 93% (±0.47) being obtained for fruits and leaves, respectively.

The total amounts of sterols and triterpenes in the leaves from all treatments ranged between 760.5 and 1025.6 mg/kg (Table 1). Concerning the effect of inoculation, we can observe a decrease of total compounds in the leaves from plants inoculated with strain TVP08, whereas those inoculated with strain PETP01 showed a total content higher than control. The decrease observed in leaves inoculated with TVP08 can be justified by higher use of these compounds (compared with PEPT01) in the synthesis of brassinosteroids during plant growth producing an increase in biomass.[24] Garcia-Freile et al.[18] reported a higher increase of plant weight with TVP08 than with PETP01.

Betulin was the main compound in the leaves of both inoculated and uninoculated plants, representing 64, 50, and 60% of the total content for control, PETP01, and TVP08, respectively (Table 1). A significant decrease of this compound was found in the leaves from plants inoculated with the strain TVP08 (Table 1), but no differences were found between the control leaves and those from plants inoculated with strain PETP01. The amounts of β-sitosterol and stigmasterol in leaves from plants inoculated with strain TVP08 were not affected, but campesterol content in these leaves was significantly higher. These three sterols significantly increased in leaves inoculated with strain PETP01.

The same four metabolites were found in the fruits of *C. annuum* (Table 1). As far as we know, with the exception of betulin, all compounds were already described in *C. annuum* fruits.[25,26] Besides these, Piironen et al.[25] reported the presence in *C. annuum* fruits of small amounts of brassicasterol, which was not found in the peppers analyzed in this study.

The amounts of sterols and triterpenes found in the fruits varied between 175.5 and 211.3 mg/kg (Table 1). As occurred in leaves, the total content increased when the plants were inoculated with the strain PETP01 and decreased when the strain TVP08 was used. Nevertheless, the amounts of stigmasterol were higher in fruits of inoculated plants.

Betulin was also the main compound in pepper fruits, representing 59, 58, and 63% of the identified metabolites in control fruits and in those inoculated with strains PETP01 and TVP08, respectively. As occurred in leaves, inoculation with strain TVP08 produced a significant decrease of betulin in pepper fruits. The amounts of stigmasterol increased significantly in both treatments. This is the first time that changes in the sterol content of *C. annuum* fruits is observed after *Rhizobium* inoculation. Nevertheless, differences were observed depending on the strain used for inoculation that can be related to the efficiency of each strain as PGPR, since strain TVP08 showed better characteristics (flower number, plant weight, and fruit size) in pepper production than PETP01.[18]

PGPR increase the vegetal growth through the synthesis of growth hormones, including brassinosteroids.[27] Indeed, the decrease of betulin and of some sterols (β-sitosterol and campesterol) in fruits from plants inoculated with the strain TVP08 can be justified because sterols are precursors and/or substrates of other biosynthetic pathways, such as the synthesis of brassinosteroids, involved in pepper production with an increase in the number of fruits.[24] As was previously reported, the pepper plants inoculated with the strain TVP08 presented higher fruit number[18] and these fruits were in a more advanced ripening stage than those from the other treatment (see part 1 of this work[17]).

Fatty Acids Profile. The fatty acids were determined by GC–IT/MS, which allowed the identification of 16 fatty acids in the fruits and leaves of *C. annuum* (Table 2). To evaluate the

dx.doi.org/10.1021/jf4046655 | J. Agric. Food Chem. 2014, 62, 565−573

Table 2. Fatty Acids Composition of *C. annuum* Fruits and Leaves, Uninoculated (Control) and Inoculated with PET01 and TVP08 Rhizobial Strains (mg/kg of Lyophilized Material)

		fruits[c]			leaves[c]		
fatty acid[a]	RT[b]	control	PETP01	TVP08	control	PETP01	TVP08
C12:0	24.8	nd a	nd a	nd a	112.6 (3.8) a	8.7 (0.8) b	10.4 (0.2) b
C13:0	27.2	nd a	nd a	nd a	21.2 (1.2) a	nd b	nd b
C14:0	29.5	148.6 (22.7) a	161.1 (8.3) a	666.1 (54.8) b	296.8 (16.0) a	70.4 (4.8) b	79.8 (5.2) b
C15:0	31.6	79.5 (6.7) a	137.9 (6.2) b	494.1 (28.8) b	122.3 (7.4) a	33.1 (2.0) b	43.1 (0.6) b
C16:0	33.6	2076.6 (120.4) a	2865.4 (52.3) b	6759.2 (343.1) b	14.0 (1.0) a	2.3 (0.1) b	3.4 (0.1) b
C16:1	33.1	222.1 (7.6) a	46.8 (2.0) b	144.3 (7.3) b	8.4 (0.1) a	7.4 (0.4) b	17.6 (0.8) b
C17:0	35.6	194.8 (10.9) a	216.4 (9.4) a	691.1 (4.9) b	228.1 (10.4) a	115.0 (10.2) b	110.4 (2.8) b
C18:0	37.4	1785.3 (102.6) a	2213.6 (45.2) b	6957.8 (220.5) b	2193.6 (146.9) a	197.3 (9.0) b	907.5 (33.4) b
C18:1c	36.9	1117.7 (80.7) a	1017.4 (7.0) b	1192.2 (9.8) a	1140.0 (60.6) a	846.2 (39.0) b	1234.9 (11.3) b
C18:1t	37.0	76.2 (5.8) a	nd b	74.2 (7.0) a	nd a	nd a	nd a
C18:2	36.8	1092.2 (79.5) a	1327.9 (36.0) b	1101.7 (22.7) a	210.1 (8.0) a	230.8 (10.4) b	268.7 (4.2) b
C20:0	40.8	296.5 (10.2) a	212.2 (10.4) b	1838.3 (3.3) b	623.4 (40.3) a	45.2 (2.0) b	248.5 (9.6) b
C21:0	42.5	61.5 (2.1) a	nd b	332.7 (2.2) b	92.5 (6.8) a	197.6 (16.5) b	48.7 (0.6) b
C22:0	44.1	212.0 (10.1) a	74.2 (3.6) a	1465.8 (140.4) b	554.0 (55.2) a	51.4 (2.6) b	194.9 (4.9) b
C23:0	46.2	110.4 (4.9) a	nd b	368.3 (30.7) b	120.2 (6.5) a	112.8 (3.5) a	46.0 (2.3) b
C24:0	48.7	143.9 (5.0) a	nd b	552.2 (8.1) b	192.2 (18.2) a	54.8 (1.7) b	49.2 (1.0) b
total		7617.3	8272.9	22638.0	5929.4	1973.0	3263.1
SFA		5109.1	5880.8	20155.6	4570.9	839.3	1741.9
MUFA		1339.8	1064.2	1306.5	1148.4	902.9	1252.5
PUFA		1168.4	1327.9	1175.9	210.1	230.8	268.7

[a]C12:0, lauric acid; C13:0, tridecanoic acid; C14:0, myristic acid; C15:0, pentadecanoic acid; C16:0, palmitic acid; C16:1, palmitoleic acid; C17:0, heptadecanoic acid; C18:0, stearic acid; C18:1c, oleic acid; C18:1t, elaidic acid; C18:2, linoleic acid; C20:0, arachidic acid; C21:0, heneicosanoic; C22:0, behenic acid; C23:0, tricosanoic acid; C24:0, lignoceric acid; SFA, saturated fatty acids; MUFA, monounsaturated fatty acids; PUFA, polyunsaturated fatty acids;. [b]RT, retention time (min). [c]Results are expressed as mean ± standard deviation of three determinations (mg/kg). Different letters in the same material and same row mean statistically significant differences compared with control sample ($p < 0.05$); nd, not detected.

fatty acids recovery, aliquots of oleic acid standard solution with known concentration were added to the samples, recovering 99% (±0.7) and 81% (±1.7) for fruits and leaves, respectively.

Whitaker[28] described the lipid composition of leaves from several species of the Solanaceae family, reporting the presence of five fatty acids in *C. annuum* leaves: palmitic (C16:0), palmitoleic (C16:1), stearic (C18:0), oleic (C18:1c), and linoleic (C18:2). The remaining fatty acids are being described in leaves for the first time.

The control leaves exhibited the highest total fatty acids content (5929.4 mg/kg). In inoculated samples, the concentrations corresponded to 1973.0 and 3263.1 mg/kg for leaves from plants inoculated with strains PETP01 and TVP08, respectively (Table 2). Stearic acid (C18:0) was the major one in control leaves (37% of total fatty acids), and oleic acid (C18:1c) was the main one in leaves inoculated with PETP01 (43%) and TVP08 strains (38%).

SFAs represent 43 to 77% of the total fatty acids contents (Table 2), stearic acid (C18:0) being the major one. Concerning unsaturated fatty acids, samples were richer in MUFAs (Table 2). Within this class, the main compound is oleic acid, ranging between 93 and 99% of MUFAs. In general, the inoculation with *Rhizobium* produced significant decreases in fatty acids content. However, significant increases of linoleic acid (C18:2) were observed in all inoculated treatments, of palmitoleic (C16:1) and oleic (C18:1c) acids in leaves inoculated with strain TVP08, and of heneicosanoic acid (C21:0) in those inoculated with strain PETP01.

In fruits of *C. annuum* 14 fatty acids were determined (Table 2). Pentadecanoic (C15:0), elaidic (C18:1t), heneicosanoic

Table 3. Volatile Composition of *C. annuum* Leaves, Uninoculated (Control) and Inoculated with PET01 and TVP08 Rhizobial Strains[a]

compounds	RI[b]	ID[c]	QI[d]	A^e/1000 control	PETP01	TVP08
			Aldehydes			
(*E*)-2-pentenal	758	MS (82/84)	55/83	218.1 (14.4) a	256.1 (5.7) b	167.6 (5.6) b
hexanal	808	S, MS (71/72)	41/55/67/82	nd a	nd a	nd a
(*E*)-2-hexenal	863	S, MS (75/77)	55/69/83/99	1312.0 (69.3) a	1231.0 (89.1) a	938.3 (79.5) b
(*Z*)-4-heptenal	900	S, MS (82/88)	55/67/84	252.7 (4.8) a	192.7 (4.2) b	119.1 (5.9) b
heptanal	909	S, MS (78/82)	55/70/81	129.8 (5.8) a	172.2 (14.4) b	95.4 (0.9) b
(*Z*)-2-heptenal	961	MS (81/87)	55/69/83	91.8 (1.1) a	202.4 (13.9) b	121.3 (4.8) b
benzaldehyde	975	S, MS (83/86)	77/105	569.0 (50.9) a	1314.5 (30.4) b	1977.0 (124.4) b
(*E*,*E*)-2,4-heptadienal	997	MS (80/81)	53/81	2189.3 (165.9) a	1639.5 (27.6) b	nd b
(*E*)-2-octenal	1068	S, MS (87/87)	55/70/83	439.9 (35.4) a	590.4 (39.8) b	268.1 (1.6) b
(*E*, *Z*)-2,6-nonadienal	1155	S, MS (80/81)	70/95/137/152	nd a	625.9 (31.8) b	396.7 (30.7) b
total aldehydes				5202.6	6224.7	4083.5
			Alcohols			
1-octen-3-ol	972	S, MS (75/84)	57/99	nd a	nd a	nd a
benzyl alcohol	1042	S, MS (85/87)	79/108	nd a	nd a	nd a
(*E*,*Z*)-3,6-nonadienol	1158	MS (82/86)	67/79	87.0 (5.1) a	97.1 (6.1) a	129.1 (12.8) b
total alcohols				87.0	97.1	129.1
			Ketones			
6-methyl-5-hepten-2-one	991	S, MS (68/86)	93/108	217.1 (20.1) a	299.8 (19.4) b	239.8 (13.3) a
(*E*,*E*)-3,5-octadien-2-one	1072	MS (80/82)	43/81/95	3531.5 (259.5) a	3030.0 (87.0) b	3205.5 (212.8) a
(*Z*)-jasmone	1292	MS (85/85)	77/131/164	421.1 (18.2) a	154.1 (8.0) b	391.2 (20.1) a
total ketones				4169.7	3483.9	3836.5
			Esters			
methyl salicylate	1200	S, MS (78/80)	92/120/152	31175.0 (2524.4) a	42920.0 (2121.3) b	54655.0 (3952.7) b
total esters				31175.0	42920.0	54655.0
			Monoterpenes			
linalool	1103	S, MS (85/85)	93/121	671.3 (48.2) a	1159.7 (100.8) b	1235.0 (55.2) b
menthol	1187	S, MS (85/89)	81	62.4 (4.0) a	57.0 (5.3) a	77.0 (5.0) b
total monoterpenes				733.7	1216.7	1312.0
			Norisoprenoids			
β-cyclocitral	1216	S, MS (84/85)	123/152	623.6 (18.1) a	803.3 (51.1) b	778.2 (35.9) b
α-ionone	1323	S, MS (85/86)	93/121	650.3 (34.4) a	nd b	359.9 (25.7) b
β-ionone	1387	S, MS (87/87)	177	1978.0 (142.8) a	2158.0 (4.2) b	3383.0 (325.3) b
β-ionone epoxide	1383	MS (89/89)	123/177	693.0 (13.3) a	1063.0 (69.3) b	1368.5 (65.8) b
total norisoprenoids				3944.9	4024.3	5889.6
			Miscellaneous Compounds			
2-isobutyl-3-methoxypyrazine	1176	S, MS (84/89)	151/124/94	731.6 (60.8) a	470.1 (32.5) b	425.3 (15.0) b
o-guaiacol	1087	S, MS (85/90)	81/109/124	917,9 (10,9) a	1559.0 (24.0) b	1349.0 (67.7) b
eugenol	1280	S, MS (84/87)	164/77/131	138.8 (1.4) a	81.8 (5.2) b	137.3 (4.1) a
total miscellaneous compounds				1788.3	2110.9	1911.6
Σ				47101.2	60077.6	71817.3

[a]Results are expressed as mean ± standard deviation of three determinations. Different letters in the same material and same row mean statistically significant differences compared with control sample ($p < 0.05$). [b]RI, retention index on VF-5 column. [c]ID = identification. S = identified by comparison with reference compounds; MS = tentatively identified by NIST05. [d]QI = quantification ions. [e]Area expressed as arbitrary units (standard deviation) of three assays; nd = not detected.

(C21:0), tricosanoic (C23:0), and lignoceric (C24:0) acids are described here for the first time in this matrix. The remaining fatty acids were already previously reported in fruits of *C. annuum*, palmitic (C16:0), stearic (C18:0), oleic (C18:1c), and linoleic (C18:2) acids being confirmed as the main ones.[28−30]

The total contents of fatty acids found in the analyzed fruits varied between 7617.3 and 22638.0 mg/kg (Table 2). The fatty acid profiles are mainly composed of SFAs, showing values that ranged between 67 and 89% of total compounds. Within the class of unsaturated fatty acids, control and fruits inoculated with TVP08 strain are richer in MUFAs, especially oleic acid (C18:1c), whereas the fruits inoculated with strain PETP01 are richer in PUFAs, linoleic acid being the only PUFA found.

In agreement with the results obtained by other authors,[28,30,31] palmitic (C16:0) and stearic (C18:0) acids were the main fatty acids in the fruits from all treatments: the first represented 27, 30, and 35% and the second 23, 31, and 27% of total amounts of fatty acids quantified in control and inoculated samples with strains TVP08 and PETP01, respectively.

The inoculated fruits showed a higher total content of fatty acids, those inoculated with the strain TVP08 having contents three times higher than controls (Table 2). Individually, the

dx.doi.org/10.1021/jf4046655 | J. Agric. Food Chem. 2014, 62, 565−573

Table 4. Volatile Composition of *C. annuum* Fruits, Uninoculated (Control) and Inoculated with PET01 and TVP08 Rhizobial Strains[a]

compounds	RI[b]	ID[c]	QI[d]	A^e/1000 control	PETP01	TVP08
			Aldehydes			
3-methylbutanal	663	S, MS (74/77)	41/44/58	80.5 (5.1) a	136.1 (3.7) b	67.5 (4.3) b
2-methylbutanal	672	S, MS (77/80)	41/57	85.1 (8.1) a	114.2 (5.2) b	50.1 (2.4) b
(*E*)-2-hexenal	863	S, MS (76/88)	55/69/83/99	239.3 (16.8) a	744.4 (5.6) b	562.8 (15.8) b
heptanal	909	S, MS (66/84)	55/70/81	nd a	25.8 (0.1) b	22.6 (0.9) b
benzaldehyde	975	S, MS (62/83)	77/105	14.9 (1.0) a	67.4 (0.9) b	nd
(*E*)-2-octenal	1068	S, MS (79/83)	55/70/83	68.6 (2.4) a	119.5 (2.2) b	268.1 (6.4) b
(*E*)-2-nonenal	1167	MS (82/84)	55/70/83	61.2 (1.7) a	267.1 (9.7) b	233.7 (6.7) b
total aldehydes				549.6	1474.5	1204.8
			Ketones			
6-methyl-5-heptene-2-one	991	S, MS (61/86)	93/108	35.7 (1.4) a	49.9 (2.9) b	32.7 (1.8) b
total ketones				35.7	49.9	32.7
			Esters			
hexyl isobutyrate	1115	MS (80/84)	43/55/71	147.8 (1.0) a	54.9 (2.0) b	8.2 (0.0) b
methyl salicylate	1200	S, MS (73/77)	92/120/152	9755.3 (64.8) a	30180.0 (658.3) b	22130.0 (2588) b
total esters				9903.1	30234.9	22138.2
			Monoterpenes			
α-pinene	941	S, MS (84/88)	92/93/136	40.4 (0.6) a	27.1 (2.6) b	13.0 (0.8) b
camphene	958	S, MS (70/84)	93	nd a	9.4 (1.0) b	7.7 (0.8) b
limonene	1036	S, MS (79/86)	68/93	92.9 (4.6) a	95.81 (2.2) b	35.7 (9.8) b
menthol	1187	S, MS (83/86)	81/95/123	46.1 (4.8) a	42.0 (2.6) b	17.1 (0.8) b
linalool	1103	S, MS (77/79)	55/71/93/121	916.1 (15.0) a	nd b	869.0 (17.8) b
camphor	1158	S, MS (73/80)	81/95/108	nd a	62.6 (2.1) b	32.7 (2.0) b
total monoterpenes				1095.5	236.9	975.2
			Sesquiterpenes			
β-caryophyllene	1330	S, MS (83/85)	161/189/204	24.7 (1.1) a	nd b	0.6 (0.1) b
α-bergamotene	1340	MS (84/89)	93/119/204	67.5 (1.7) a	54.5 (0.9) b	68.9 (3.6) b
α-himachalene	1362	MS (84/89)	41/93/94	160.9 (4.3) a	129.9 (3.9) b	63.7 (4.9) b
longifolene	1389	MS (84/85)	105/161/204	474.4 (26.3) a	596.9 (39.0) b	145.4 (8.9) b
total sesquiterpenes				727.5	781.3	278.6
			Norisoprenoids			
β-cyclocitral	1216	S, MS (81/84)	123/152	31.5 (1.9) a	42.7 (4.2) b	51.8 (10.4) b
β-ionone	1387	S, MS (85/85)	177	127.4 (1.5) a	nd b	80.4 (1.4) b
total norisoprenoids				158.9	42.7	132.2
			Miscellaneous Compounds			
2-*n*-pentylfuran	994	MS (83/86)	81	282.1 (12.2) a	375.6 (11.8) b	493.8 (4.1) b
2-isobutyl-3-methoxypyrazine	1183	S, MS (74/75)	94/124/151	2077.0 (1.4) a	1393.5 (31.8) b	1922.0 (16.5) b
total miscellaneous compounds				2359.1	1769.1	2415.8
$\sum$				14829.4	34589.3	27177.5

[a]Results are expressed as mean ± standard deviation of three determinations. Different letters in the same material and same row mean statistically significant differences compared with control sample ($p < 0.05$). [b]RI, retention index on VF-5 column. [c]ID = identification. S = identified by comparison with reference compounds; MS = tentatively identified by NIST05. [d]QI = quantification ions. [e]Area expressed as arbitrary units (standard deviation) of three assays; nd = not detected.

inoculation produced significant increases in several fatty acids, like pentadecanoic (C15:0), palmitic (C16:0), stearic (C18:0), and arachidic (C20:0), some of them with antimicrobial properties.[32] This effect is probably related to the maturation of the fruit since the highest increase was found in pepper fruits from plants inoculated with strain TVP08, with the higher potential in advancing fruit ripening (see part 1 of this work[17]). The fatty acids contents obtained in this work are similar to those found in peppers var. "green italian".[30] The increase of fatty acid contents, such as those of myristic (C14:0), palmitic (C16:0), stearic (C18:0), arachidic (C20:0), and behenic (C22:0) acids, has been reported in other fruits during ripening.[33]

Volatiles Profile. Although the volatile compounds in pepper fruits have already been studied, as far as we know, this is the first study on the volatile profile of the leaves, in which 26 compounds from several chemical classes were identified (Table 3).

The results showed that the leaves of plants inoculated with the two strains of *Rhizobium* (PETP01 and TVP08) are richer in these compounds than control material. All inoculated leaves showed higher levels of esters, namely, of methyl salicylate, which is the major volatile compound. Aldehydes are the second main class in control and in the material inoculated with PETP01 strain, (*E*,*E*)-2,4-heptadienal being the most abundant compound. Norisoprenoids were the second main class of

compounds in leaves inoculated with TVP08, β-ionone being the major volatile.

Leaves from plants inoculated with both strains PETP01 and TVP08 also exhibited increases of monoterpenes and miscellaneous compounds.

In *C. annuum* fruits 24 volatiles were characterized (Table 4), methyl salicylate and 2-isobutyl-3-methoxypyrazine being the main compounds in all analyzed samples. The identified compounds have been previously reported in pepper fruits,[34−39] with the exception of camphor and longifolene, which are described for the first time in fruits of *C. annuum*. Camphor, heptanal, and camphene were detected only in the fruits from inoculated plants (Table 4).

As occurred in leaves, the fruits from inoculated plants exhibited increased levels of aldehydes and esters; however, unlike the leaves, a decrease of monoterpenes, norisoprenoids, and 2-isobutyl-3-methoxypyrazine was observed (Table 4). Individually, all aldehydes increased with inoculation, except 3-methylbutanal, 2-methylbutanal, and benzaldehyde in the fruits from plants inoculated with TVP08 strain. The increase of volatiles like (*E*)-2-hexenal, (*E*)-2-octenal, and (*E*)-2-nonenal in fruits from inoculated plants can be associated with their intervention in plant defense, since these compounds are described as antimicrobials.[40] Concerning esters, the inoculated fruits showed significantly increased levels of methyl salicylate, a derivative of salicylic acid that may be accumulated at high levels in plants. Salicylic acid has been related, together with jasmonic acid, with systemic resistance (SAR) in plants,[14] and recently it has been reported that methyl salicylate is involved in long-distance communication and signal amplification in SAR.[41] Therefore, our results suggest that *Rhizobium* could elicit a long-distance systemic response *via* methyl salicylate, which is an unknown mechanism in PGPR to date.

PCA Analysis. The results obtained for volatiles, sterols, triterpenes, and fatty acids were analyzed by PCA to assess the influence of inoculation in their contents of the fruits and leaves more thoroughly. Figure 1 shows the projection of variables, grouped by chemical classes obtained for the three fruits and three leaves in the plane composed by principal axes F1 and F2, containing 84.5% of the total variance (Figure 1).

Fruits and leaves are clearly separated into the F1 axis; fruits are disposed in the negative section and leaves in the positive one. Leaves showed higher amounts in aldehydes, alcohols, ketones, norisoprenoids, triterpenes, esters, monoterpenes, sesquiterpenes, and sterols; on the other hand, fruits showed higher levels of miscellaneous compounds and fatty acids (Figure 1, Tables 1−4).

Control and fruits from plants inoculated with TVP08 are closely related due to their higher amounts of MUFA and miscellaneous compounds. Both samples are projected in the plane formed by negative F1 and positive F2 axes, 2-isobutyl-3-methoxypyrazine and oleic acid (C18:1c) being the main compounds (Figure 1, Tables 2 and 4).

The projection of fruit samples from plants inoculated with strain PETP01 is related to higher contents of PUFA, due to the higher linoleic acid (C18:2) content (Figure 1, Table 2).

The leaf samples from inoculated plants are projected in the plane formed by the F1 and F2 positive axes, while control leaves are projected into the plane formed by F1 positive and F2 negative axes (Figure 1). This separation may be due to the richness in SFA and ketones and lower contents of esters, monoterpenes, sesquiterpenes, and miscellaneous compounds in control sample (Tables 1 and 3).

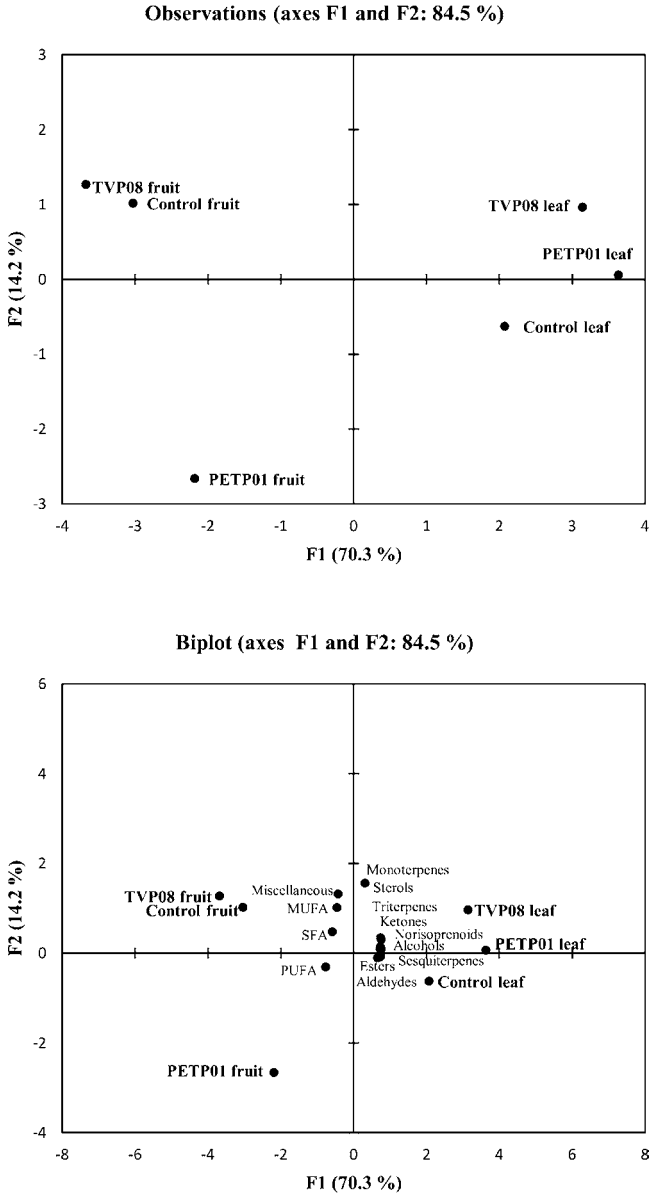

Figure 1. PCA of volatile compounds, sterols, triterpenes, and fatty acids in fruits and leaves of *C. annuum*: projection of volatile compounds (variables: total of monoterpenes, sesquiterpenes, aldehydes, ketones, alcohols, esters, norisoprenoids, miscellaneous compounds, sterols, triterpenes, and saturated (SFA), monounsaturated (MUFA), and polyunsaturated (PUFA) fatty acids; control leaf, PETP01 leaf, TVP08 leaf, control fruit, PETP01 fruit, and TVP08 fruit) in the plane composed by the principal axes F1 and F2.

In summary, the data obtained from sterol and fatty acids contents confirmed those obtained in part 1 of this work,[17] showing that the inoculation of *Rhizobium* has a positive effect on pepper fruit ripening. The increase of some primary and secondary metabolites in *C. annuum* materials by inoculation of PGPR may be beneficial to the plant, improving its nutritional value, which might contribute to an increase in the consumption of pepper. Moreover, the increase of content of volatile compounds, some of them involved in plant defense, was clearly demonstrated. Overall, the results of this work suggest that the inoculation with PGPR *Rhizobium* strains may be employed to manipulate the content of interesting

dx.doi.org/10.1021/jf4046655 | J. Agric. Food Chem. 2014, 62, 565−573

metabolites in pepper leaves and fruits, increasing the health benefits and the defense abilities of the plants.

AUTHOR INFORMATION

Corresponding Author

*Tel: + 351 220 428 654 Fax: +351 226 093 390. E-mail: lmsilva@ff.up.pt (L.R.S.) or pandrade@ff.up.pt (P.B.A.).

Funding

The authors are grateful to Fundação para a Ciência e a Tecnologia (FCT) for Grant No. PEst-C/EQB/LA0006/2011.

Notes

The authors declare no competing financial interest.

REFERENCES

(1) Materska, M.; Piacente, S.; Stochmal, A.; Pizza, C.; Oleszek, W.; Perucka, I. Isolation and structure elucidation of flavonoid and phenolic acid glycosides from pericarp of hot pepper fruit *Capsicum annuum* L. *Phytochemistry* **2003**, *63*, 893−898.

(2) Kollmannsberger, H.; Rodríguez-Burrezo, A.; Nitz, S.; Nuez, F. Volatile and capsaicinoid composition of ají (*Capsicum baccatum*) and rocoto (*Capsicum pubescens*), two Andean species of chile peppers. *J. Sci. Food Agric.* **2011**, *91*, 1598−1611.

(3) Topuz, A.; Ozdemir, F. Assessment of carotenoids, capsaicinoids and ascorbic acid composition of some selected pepper cultivars (*Capsicum annuum* L.) grown in Turkey. *J. Food Compos. Anal.* **2007**, *20*, 596−602.

(4) Sun, T.; Xu, Z.; Wu, C. T.; Janes, M.; Prinyawiwatkul, W.; No, H. K. Antioxidant activities of different colored sweet bell peppers (*Capsicum annuum* L.). *J. Food Sci.* **2007**, *72*, 98−102.

(5) Pérez-Gálvez, A.; Garrido-Fernández, J.; Mínguez-Mosquera, M. I.; Lozano-Ruiz, M.; Montero-de-Espinosa, V. Fatty acids composition of two new pepper varieties (*Capsicum annuum* L. cv. Jaranda and Jariza). Effetc of drying process and nutritional aspects. *J. Am. Oil Chem. Soc.* **1999**, *76* (2), 205−208.

(6) Mutanen, M. Comparison between dietary monounsaturated and polyunsaturated fatty acids as regards diet-related diseases. *Biomed. Pharmacother.* **1997**, *51*, 314−317.

(7) Gibney, M. J.; Vorster, H. H.; Kok, F. J. Introduction to Human Nutrition; Blackwell Science: Oxford, U.K., 2002; pp 100−113.

(8) Piironen, V.; Lindsay, D. G.; Miettinen, T. A.; Toivo, J.; Lampi, A. Plants sterols: biosynthesis, biological function and their importance to human nutrition. *J. Sci. Food Agric.* **2000**, *80*, 939−966.

(9) AbuMweis, S. S.; Jones, P. J. Cholesterol-lowering effect of plant sterols. *Curr. Atheroscler. Rep.* **2008**, *10*, 467−472.

(10) Gupta, A. K.; Savopoulos, C. G.; Ahuja, J.; Hatzitolios, A. I. Role of phytosterols in lipid-lowering: current perspectives. *QJM* **2011**, *104*, 301−308.

(11) Dudareva, N.; Negre, F.; Orlova, N.; Orlova, I. Plant volatiles: Recent advances and future perspectives. CRC Crit. *Rev. Plant Sci.* **2006**, *25*, 417−440.

(12) Sofo, A.; Milella, L.; Tataranni, G. Effects of *Trichoderma harzianum* strain T-22 on the growth of two *Prunus* rootstocks during the rooting phase. *J. Hortic. Sci. Biotechnol.* **2010**, *85*, 497−502.

(13) Bhattacharjee, R. B.; Singh, A.; Mukhopadhyay, S. N. Use of nitrogen-fixing bacteria as biofertiliser for non-legumes: prospects and challenges. *Appl. Microbiol. Biotechnol.* **2008**, *80*, 199−209.

(14) Lugtenberg, B.; Kamilova, F. Plant-growth-promoting rhizobacteria. *Annu. Rev. Microbiol.* **2009**, *63*, 541−556.

(15) Velázquez, A.; García-Fraile, P.; Ramírez-Bahena, M. H.; Rivas, R.; Martínez-Molina, E. Bacteria involved in nitrogen-fixing legume symbiosis: Current taxonomic perspective. In *Microbes for Legume Improvement*; Khan, M. S., Zaidi, A., Musarrat, J., Eds.; Springer: Dordrecht, 2010; pp 1−25.

(16) Couto, C.; Silva, L. R.; Valentão, P.; Velázquez, E.; Peix, A.; Andrade, P. B. Effects induced by the nodulation with *Bradyrhizobium japonicum* on *Glycine max* (soybean) metabolism and antioxidant potential. *Food Chem.* **2011**, *127*, 1487−1495.

(17) Silva, L. R.; Azevedo, J.; Pereira, M. J.; García, L.; Velazquez, E.; Peix, A.; Valentão, P.; Andrade, P. B. Inoculation of the Nonlegume *Capsicum annuum* (L.) with *Rhizobium* Strains. 1. Effect on Bioactive Compounds, Antioxidant Activity, and Fruit Ripeness. *J. Agric. Food Chem.* **2014**, DOI: 10.1021/jf4046649.

(18) García-Fraile, P.; Carro, L.; Robledo, M.; Ramírez-Bahena, M.-H.; Flores-Félix, J.-D.; Fernández, M. T.; Mateos, P. F.; Rivas, R.; Igual, J. M.; Martínez-Molina, E.; Peix, A.; Velázquez, E. *Rhizobium* promotes non-legumes growth and quality in several production steps: Towards a biofertilization of edible raw vegetables healthy for humans. *PLoS One* **2012**, *7*, e38122.

(19) Silva, L. R.; Azevedo, J.; Pereira, M. J.; Valentão, P.; Andrade, P. B. Chemical assessment and antioxidant capacity of pepper (*Capsicum annuum* L.) seeds. *Food Chem. Toxicol.* **2013**, *53*, 240−248.

(20) Zehentbauer, G.; Reineccius, G. A. Determination of key aroma components of Cheddar cheese using dynamic headspace dilution assay. *Flavour Fragrance J.* **2002**, *17*, 300−305.

(21) Flamini, G.; Cioni, P. L.; Morelli, I. Volatiles from leaves, fruits and virgin oil from *Olea europaea* cv. *olivastra seggianese* from Italy. *J. Agric. Food Chem.* **2003**, *51*, 1382−1386.

(22) Hognadottir, A.; Rouseff, R. L. Identification of aroma active compounds in orange essence oil using gas chromatography−olfactometry and gas chromatography−mass spectrometry. *J. Chromatogr. A* **2003**, *998*, 201−211.

(23) Leffingwell, J. C.; Alford, E. D. Volatile constituents of perique tobacco. Elec. J. Env. Agricult. *Food Chem.* **2005**, *4*, 899−915.

(24) Serna, M.; Hernández, F.; Coll, F.; Coll, Y.; Amorós, A. Brassinosteroid analogues effects on the yield and quality parameters of greenhouse-grown pepper (*Capsicum annuum* L.). *Plant Growth Regul.* **2012**, *68*, 333−342.

(25) Piironen, V.; Toivo, J.; Puupponen-Pimiä, R.; Lampi, A. Plant sterols in vegetables, fruits and berries. *J. Sci. Food Agric.* **2003**, *83*, 330−337.

(26) Han, J.; Yang, Y.; Feng, M. Contents of phytosterols in vegetables and fruits commonly consumed in China. *Biomed. Environ. Sci.* **2008**, *21*, 449−453.

(27) Avis, T. J.; Gravel, V.; Antoun, H.; Tweddell, R. J. Multifaceted beneficial effects of rhizosphere microorganisms on plant health and productivity. *Soil Biol. Biochem.* **2008**, *40*, 1733−1740.

(28) Whitaker, B. D. Fatty-acid composition of polar lipids in fruit and leaf chloroplasts of "16:3"- and "18:3"-plant species. *Planta* **1986**, *169*, 313−319.

(29) Orhan, I.; Eryilmaz, B.; Bingöl, F. A. comparative study on fatty acid contents of *Capsicum annuum* varieties. *Biochem. Syst. Ecol.* **2002**, *30*, 901−904.

(30) Guil-Guerrero, J. L.; Martínez-Guirado, C.; Rebolloso-Fuentes, M. M.; Carrique-Pérez, A. Nutrient composition and antioxidant activity of 10 pepper (*Capsicum annuum*) varieties. *Eur. Food Res. Technol.* **2006**, *224*, 1−9.

(31) Marion, J. E.; Dempsey, A. H. Fatty acids of pimiento pepper seed oil. *J. Am. Oil Chem. Soc.* **1964**, *41*, 548−549.

(32) Zheng, C. J.; Yoo, J. S.; Lee, T. G.; Cho, H. Y.; Kim, Y. H.; Kim, W. G. Fatty acids synthesis is a target for antibacterial activity of unsaturated fatty acids. *FEBS Lett.* **2005**, *579*, 5157−5152.

(33) Glew, R .H.; Ayaz, F. A.; Millson, M.; Huang, H. S.; Chuang, L T.; Sanz, C.; Golding, J. B. Changes in sugars, acids and fatty acids in naturally parthenocarpic date plum persimmon (*Diospyros lotus* L.) fruit during maturation and ripening. *Eur. Food Res. Technol.* **2005**, *221*, 113−118.

(34) Wu, C.; Liou, S. Effect of tissue disruption on volatile constituents of bell peppers. *J. Agric. Food Chem.* **1986**, *34*, 770−772.

(35) Ruth, S. M. V.; Roozen, J. P.; Cozijnsen, J. L. Volatile compounds of rehydrated French beans, bell peppers and leeks. Part 1. Flavour release in the mouth and in three mouth model system. *Food Chem.* **1995**, *53*, 15−22.

(36) Kim, I.; El-Aty, A. M. A.; Shin, H.; Lee, H.; Kim, I.; Shim, J. Analysis of volatile compounds in fresh healthy and diseased peppers (*Capsicum annuum*) using solvent free solid injection coupled with gas

chromatography-flame ionization detector and confirmation with mass spectrometry. *J. Pharm. Biomed. Anal.* **2007**, *45*, 487−494.
(37) Forero, M. D.; Quijano, C. E.; Pino, J. A. Volatile compounds of Chile pepper (*Capsicum annuum* L. var. *glabriusculum*) at two ripening stages. *Flavour Fragrance J.* **2008**, *24*, 25−30.
(38) Pino, J.; Fuentes, V.; Barrios, O. Volatile constituents of Cachucha peppers (*Capsicum Chinense* Jacq.) grown in Cuba. *Food Chem.* **2010**, *125*, 860−864.
(39) Kollmannsberger, H.; Rodríguez-Burrezo, A.; Nitz, S.; Nuez, F. Volatile and capsaicinoid composition of ají (*Capsicum baccatum*) and rocoto (*Capsicum pubescens*), two Andean species of chile peppers. *J. Sci. Food Agric.* **2011**, *91*, 1598−1611.
(40) Ryu, C.; Farag, M. A.; Hu, C.; Reddy, M. S.; Kloepper, J. W.; Paré, P. W. Bacterial volatiles induce systemic resistance in *Arabidopsis*. *Plant Physiol.* **2004**, *134*, 1017−1026.
(41) Shah, J.; Zeier, J. Long-distance communication and signal amplification in systemic acquired resistance. *Front. Plant Sci.* **2013**, *4*, 30 DOI: 10.3389/fpls.2013.00030.

JOURNAL OF AGRICULTURAL AND FOOD CHEMISTRY

Article

pubs.acs.org/JAFC

Profile and Antioxidant Activity of Phenolic Extracts from 10 Crabapples (*Malus* Wild Species)

Nan Li,[†] Junling Shi,*[,†,§,⊗] and Kun Wang[#]

[†]College of Food Science and Engineering, Northwest A&F University, 28 Xinong Road, Yangling, Shaanxi Province 712100, China

[§]School of Life Sciences, Northwestern Polytechnical University, 127 Youyi West Road, Xi'an, Shaanxi Province 710072, China

[⊗]Key Laboratory for Space Bioscience and Biotechnology, Northwestern Polytechnical University, 127 Youyi West Road, Xi'an, Shaanxi Province 710072, China

[#]Key Laboratory of the Use of Fruit Germplasm Resources, Ministry of Agriculture/Research Institute of Pomology, Chinese Academy Agricultural Sciences, Xingcheng, Liaoning 125100, China

ABSTRACT: Phenolic products are highly demanded by the food and cosmetics industries and consumers due to their high antioxidant activities. To evaluate the potential of crabapples (*Malus* wild species) in preparing phenolic extracts, fruits of 10 crabapples grown in China were separately extracted with 80% (v/v) ethanol and ethyl acetate and the phenolic profiles, polyphenol (PC) and flavonoid contents (FC), and antioxidant activities of the extracts were analyzed. Chlorogenic acid, (−)-epicatechin, rutin, hyperin, and phlorizin appeared as the major phenolic compounds in all phenolic extracts. Ethanol extracts had PC of 302.83−1265.94 mg GAE/100g and FC of 352.45−2351.74 mg RE/100g, being 4.17 and 4.49 times those obtained in ethyl acetate extracts and much higher than those previously reported in apples. *Malus* wild species appeared as rich sources of phenolic compounds with high antioxidant activity, especially when high chlorogenic acid and rutin contents are emphasized.

KEYWORDS: *wild apple, polyphenol, flavonoid, antioxidant activity*

INTRODUCTION

Phenolic compounds are of particular interest to food processors and consumers because they play a key role in preventing oxidation processes in human.[1,2] They are also highly valued as they possess high antioxidant activities.[3,4] Phenolic extracts are in high demand in the cosmetics and food industries due to their many functions promoting health benefits and preventing human diseases, such as reducing the occurrence of cancer,[5] anti-inflammation,[6−8] decreasing blood pressure,[9] resisting neurodegenerative disorders,[10] modulating gut microbial composition,[11] preventing obesity,[12] and protecting against acute oxidative damage.[13] Polyphenols derived from natural plants are used in edible oil, ham, cakes, chocolate, and other foods to prevent spoilage caused by oxidation and inhibit the generation of nitrosamines in these foods. Apple pomace is currently developed as a major source of phenolic compounds due to its high phenolic content and widespread occurrence in the world. To make apple trees more resistant to disease and suitable for diverse environments, *Malus* wild species are widely used as rootstocks in apple breeding besides being of importance in ecological diversity and use as an ornamental and economic *Malus* germplasm resource.[14]

Phenolic extracts are usually prepared using different solvents according to the solubility of the major phenolic compounds in the materials. Agourram et al. found 80% (v/v) aqueous acetone was more effective than 80% (v/v) aqueous methanol and 80% (v/v) aqueous ethanol in preparing phenolic extracts from fruit and vegetable byproducts.[15] However, Seo et al. found ethanol was more efficient in producing phenolic extracts from *Smilax china* L. leaf with higher antioxidant activity and total phenolic content than methanol, acetone, or water,[16] whereas Katalinić et al.[17] reported 80% (v/v) aqueous ethanol was efficient in the extraction of phenolic compounds from many plant materials. Eighty percent (v/v) aqueous methanol,[18] 80% (v/v) aqueous ethanol,[19] and 70% (v/v) aqueous acetone[20] have also been used to extract phenolic compounds from apples (*Malus*) and resulted in high phenolic containing extracts. From the toxicological point of view, ethanol and water are safer than methanol and other organic solvents.[21] However, it should be mentioned that ethyl acetate is normally used to prepare the phenolic extracts in the assays of obtaining phenolic profiles using high-performance liquid chromatography (RP-HPLC).[22−25] Furthermore, ethyl acetate is more efficacious with respect to aqueous ethanol in extracting carotenoids, and apples are known to be rich in this class of compounds. More importantly, these extraction solvents can be easily removed from the obtained phenolic extracts by evaporation, and thus there is opportunity to use these solvents to extract polyphenols for food, pharmaceutical, or cosmetics application.[26] In addition, the diversity in obtained phenolic profiles is theoretically expected when different extraction solvents are used in the preparation of phenolic extracts. However, this has not been comprehensively investigated before.

Received: October 9, 2013
Revised: December 25, 2013
Accepted: January 7, 2014
Published: January 7, 2014

ACS Publications © 2014 American Chemical Society

dx.doi.org/10.1021/jf404542d | *J. Agric. Food Chem.* 2014, 62, 574−581

Table 1. *Malus* Wild Species Analyzed, Skin Color Main Features, Dimensions, and Weights[a]

code	Chinese name	*Malus* wild species	skin color	dimensions (mm)	weight (g)
S1	Lijiangshandingzi	*Malus rockii* Rehder	deep red	21.8 ± 0.5	4.3 ± 0.3
S2	Xiaojinhaitang	*Malus xiaojinensis* Cheng et Jiang	yellow with small areas of bright red	21.0 ± 0.7	3.9 ± 0.5
S3	Huaguanhaitang	*Malus coronaria* (L.) Mill.	red with small areas of yellow	24.2 ± 0.3	7.3 ± 0.6
S4	Donghongguo	*Malus prunifolia* (Wild) Borkh.	deep red with small areas of yellow-green	42.7 ± 0.9	39.1 ± 1.1
S5	Sankuaishihaitang01	*Malus robusta* (Carr.) Rehd.	bright red with small areas of yellow	33.3 ± 0.7	12.8 ± 0.6
S6	Sankuaishihaitang02	*Malus robusta* (Carr.) Rehd.	deep red/green bicolor	33.4 ± 0.5	16.0 ± 0.4
S7	Xiaofanshanhaitang	*Malus robusta* (Carr.) Rehd.	bright red with small areas of yellow	32.0 ± 0.4	13.5 ± 0.5
S8	Balenghaitang	*Malus micromalus* (Carr.) Rehd.	bright red with small areas of yellow	32.5 ± 0.5	14.7 ± 0.4
S9	Pingdinghaitang	*Malus robusta* (Carr.) Rehd.	dark red with small areas of yellow	29.8 ± 0.7	11.9 ± 0.6
S10	Honghaitang	*Malus prunifolia* Mill.	bright pink red/bright yellow bicolor	27.2 ± 0.9	9.4 ± 0.5

[a]Means of 3 replicates ± standard errors or standard deviation.

Phenolic profiles of apple fruits have been extensively studied. Apple is found to be abundant in vitamin C,[27] flavonoids,[9] and polyphenols and has high antioxidant capacity.[4,28,29] Apple juice has been reported to have strong inhibitory activity on the proliferation of HL-60 human leukemia cells.[30] Belonging to *Malus* species, crabapples are supposed to possess similar nutrients, particularly phenolic compounds, as apples. However, no information of phenolic content and phenolic profiles of crabapples has been found in the literature.

To characterize the phenolic profile, phenolic contents, and antioxidant activity of different *Malus* wild species and to evaluate the potential of these species in producing phenolic extracts, 10 different crabapples grown in China were collected and analyzed. Ethanol and ethyl acetate were both used in aspects of the above characteristics to compare which is better in preparing phenolic extracts with high phenolic content and antioxidant activities.

MATERIALS AND METHODS

Chemicals. Folin−Ciocalteu reagent, 2,2-diphenyl-1-picrylhydrazyl (DPPH), 2,2′-azinobis(3-ethylbenzenothiazoline-6-sulfonic) (ABTS), 2,4,6-tri(2-pyridyl)-*s*-triazine (TPTZ), 6-hydroxy-2,5,7,8-teramethyl-chroman-2-carboxylic acid (Trolox), methanol, and phosphoric acid (HPLC grade) were obtained from Sigma Chemical Co. (St. Louis, MO, USA). Gallic acid, protocatechuic acid, (+)-catechin, chlorogenic acid, caffeic acid, (−)-epicatechin, *p*-coumaric acid, ferulic acid, rutin, hyperin, phlorizin, and quercetin (>98%) were purchased from Shanghai Winherb Medical Science Co., Ltd. (Shanghai, China). Ethanol, ethyl acetate, Na_2CO_3, $NaNO_2$, $AlCl_3$, NaOH, $K_2S_2O_8$, CH_3COONa, CH_3COOH, HCl, and $FeCl_3$ were from local reagent shops in Xi'an, China. All chemicals were of analytical grade. Water was prepared by purification with a Milli-Q water purification system (Millipore, Bedford, MA, USA).

Fruit of Crabapples. Fruits of 10 wild *Malus* species were collected from the garden of germplasm resources in Institute of Pomology, Chinese Academy of Agricultural Sciences (Xingcheng, Liaoning provionce). No manual protection was carried out during the whole growing season. All fruits were picked by hand at their ripeness season in September 2012 and immediately cooled and stored at −20 °C before the extraction and measurement were carried out within 1 month. The cross-sectional diameter of the fruits was measured using a vernier caliper (Xigong, Jiangsu, China). The main features of the analyzed fruits are reported in Table 1.

Blanching of Crabapple Fruits. The fruits of different wild *Malus* species were treated according to the method previously reported by McGhie et al.[19] and Lin et al.[31] with slight modification. In brief, 100 g of fruit was cut into slices in approximately 3 mm thickness. The slices were subjected to steam blanching for 1 min and then immediately taken out and placed in a refrigerator (Haier, Qingdao, China) for cooling.

Preparation of Phenolic Extracts. Eighty percent aqueous ethanol and ethyl acetate were separately used to extract the cooled crabapple slices according to the methods reported by Zhao et al.[32] and Kong et al.[33] with slight modification. Briefly, sliced and blanched crabapples were ground to a fine jam using a blender (Media, Foshan, China). A 5 g jam sample was weighed and then separately extracted with 25 mL of 80% aqueous ethanol and ethyl acetate. The extraction was conducted for 30 min at 20 °C in a Unique-1400A ultrasonic bath (Shumei, Kunshan, China) at a power of 250 W. After the extraction, centrifugation at 8000*g* was carried out for 10 min. The supernatant was collected, and the residue was extracted and centrifuged again two more times. The supernatants of each extraction solvent were combined and evaporated to dry powder using an R-210 vacuum rotary evaporator (Büchi, Flawil, Switzerland) at 40 °C. The dry residues were dissolved in 10 mL of 50% aqueous methanol and stored at −20 °C for measurements of polyphenol content, flavonoid content, antioxidant activity, and phenolic profiles by high-performance liquid chromatography (HPLC).

Measurement of Polyphenol and Flavonoid Contents. Measurement of polyphenol content (PC) was carried out using a modified colorimetric Folin−Ciocalteu method at 765 nm.[34] In summary, 0.2 mL of extract was mixed with 1.0 mL of deionized water and 1.0 mL of freshly prepared Folin−Ciocalteu reagent (diluted 10-fold in water). The mixing process was performed for 5 min before 0.8 mL of 7.5% (w/v) Na_2CO_3 solution was added. The above mixture was incubated at 25 °C in darkness for 30 min. Absorbance was obtained using a UVmini-1240 spectrophotometer (Shimadzu, Tokyo, Japan). A standard curve was created using gallic acid. Additional dilution was carried out when the measured absorbance value outranged the linear range of the standard curve. Results were expressed as milligrams of gallic acid equivalent per 100 g of fresh weight (mg GAE/100 g).

Flavonoid content (FC) was determined using the colorimetric method at 510 nm according to the method of Wolfe et al.[35] with slight modification. In brief, a 0.5 mL extract sample was mixed with 1.0 mL of deionized water and 0.15 mL of a 50 g/L $NaNO_2$ solution. After 5 min, 0.3 mL of $AlCl_3$ (100 g/L) was added. The mixture was incubated at 25 °C for 6 min, followed by the addition of 1.0 mL 1 mol/L NaOH before absorbance reading. A standard curve was made using rutin. Additional dilution was carried out when the measured absorbance value outranged the linear range of the standard curve. Results were expressed as milligrams of rutin equivalents per 100 g of fresh weight (mg RE/100 g).

Antioxidant Activity Assays. The DPPH assay was performed according to the method reported by Ma et al.[36] with minor modifications. A 50 μL extract was mixed with 2.0 mL of a 6.0×10^{-5} mol/L ethanol solution containing DPPH. After incubation at 25 °C for 30 min, the absorbance at 517 nm was read. A standard solution of Trolox was used to prepare a calibration curve. Results were expressed as micromoles of Trolox equivalent antioxidant capacity per 100 g ± SD fresh weight (μmol TE/100 g).

The ABTS assay was carried out according to the method described by Tai et al.[37] with slight modification. ABTS radical cation ($ABTS^{\bullet+}$)

was produced by reacting a 7 mmol/L ABTS solution with 140 mmol/L $K_2S_2O_8$, and the mixture was kept in the dark at room temperature for 12−16 h before use. For each assay, the above stored solution was freshly diluted with ethanol until the absorbance at 734 nm reached 0.700 ± 0.05. In the measurement, 25 μL of phenolic extract was allowed to react with 3.0 mL of $ABTS^{\bullet+}$ solution at 25 °C for 30 min. Then the absorbance was taken at 734 nm. Results wee reported as micromoles of Trolox equivalent antioxidant capacity per 100 g ± SD fresh weight (μmol TE/100 g).

The FRAP assay was performed according to the method described by Ma et al.[36] with slight modification. The stock solutions included 300 mmol/L acetate buffer (pH 3.6), 10 mmol/L TPTZ in 40 mmol/L HCl, and 20 mmol/L $FeCl_3$. A fresh working FRAP solution was prepared using the above stock solution in ratio of 25 mL of acetate buffer, 2.5 mL of TPTZ solution, and 2.5 mL of $FeCl_3$ solution. Twenty-five microliters of phenolic extract was allowed to react with 3.0 mL of fresh FRAP solution for 10 min at 37 °C. Readings of the colored product were taken at 593 nm. Results are reported as micromoles of Trolox equivalent antioxidant capacity per 100 g ± SD fresh weight (μmol TE/100 g).

Analysis of Phenolic Profiles. The phenolic profiles of phenolic extracts were measured using HPLC after a filtration through a 0.45 μm filter. The HPLC analysis was carried out using a Waters 600E HPLC system (Waters, Milford, MA, USA) equipped with a Waters 2487UV detector and a Waters Symmetry C18 reversed-phase column (250 × 4.6 mm, 5 μm). The mobile phase consisted of solvent A (methanol) and solvent B [water−phosphoric acid (pH 2.6)] using the following gradient program: 0−15 min, 15−25% solvent A; 15−25 min, 25% solvent A; 25−65 min, 25−75% solvent A; 65−70 min, 75−15% solvent A. All of the polyphenol and flavonoid standards were prepared in 50% methanol solution. The flow rate was kept constant at 1.0 mL/min throughout the measurement. The column temperature was set at 30 °C, and the injection volume was 5 μL. The UV detection wavelength was monitored at 280 nm because the phenolic extracts had obvious absorption peaks at 280 nm, but not at 320 and 350 nm. In addition, solely reading at 280 nm was also performed in phenolic analysis by Bhaskar et al.,[38] Łata et al.,[39] and Du et al.[40] Individual phenols and flavonoids in the sample were identified on the basis of comparison of their UV−vis spectra and retention times with the corresponding standards.

RESULTS AND DISCUSSION

Polyphenol and Flavonoid Contents. The PC and FC values obtained from ethanol extracts were significantly ($P < 0.01$) higher than those from ethyl acetate extracts (Figure 1). For wild *Malus* species of Xiaojin (*Malus xiaojinensis* Cheng et Jiang), the FC value obtained from ethanol extract was nearly 14-fold that obtained from ethyl acetate extract. A similar trend was also found by NurulMarian et al.[41] for *Barrington racemosa* leaves. Theoretically, different extraction solvents are greatly diverse in polarity, and therefore extracting abilities of different compounds are different.[33,42,43] Polyphenol and flavonoid are both polar due to their polyhydroxyl groups. Normally, the less polar solvents (ether, benzene, and chloroform) are effective in extracting aglycone flavonoids and more polar solvents (acetone, ethyl acetate, alcohol, and water) are effective in extracting glycoside flavonoids.[44] Also, phenolic compounds have higher solubility in higher polarity solvents,[45,46] such as ethanol. Ethyl acetate is comparatively more efficacious than aqueous ethanol in extracting carotenoids.[33] The higher values of PC and FC obtained in ethanol extracts than in ethyl acetate extracts illustrated that the phenolic and flavonoid compounds in crabapples are of high polarity.

In detail, PC values ranged from 302.83 to 1265.94 mg GAE/100 g (Figure 1A) with an average of 566.58 mg GAE/100 g (Table 2) for the ethanol extracts and from 62.96 to 215.21 mg GAE/100 g (Figure 1A) with an average of 135.97 mg GAE/100 g (Table 2) for ethyl acetate extracts. FC values ranged from 352.45 to 2351.74 mg RE/100 g (Figure 1B) with an average of 965.05 mg RE/100 g (Table 2) for ethanol extracts and from 83.77 to 369.21 mg RE/100 g (Figure 1B) with an average of 214.90 mg RE/100 g (Table 2) for ethyl acetate extracts. The average values of PC and FC in all ethanol extracts were 4.17- and 4.49-fold, respectively, of those in ethyl acetate extracts. Lijiang-shanjingzi (*Malus rockii* Rehder) had the highest values of PC and FC in both ethanol and ethyl acetate extracts, whereas Huaguan (*Malus coronaria* (L.) Mill.) had the lowest ones.

In addition, the HPLC data of total polyphenols were much lower than those obtained in Folin−Ciocalteu analysis. This is because the total amount of phenolic content was under-

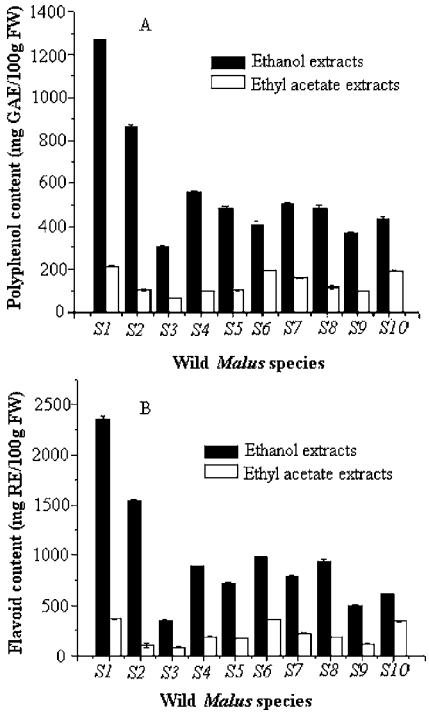

Figure 1. Polyphenol content (A) and flavonoid content (B) of 10 wild *Malus* species. Data are the means of three replicates ± standard deviation.

Table 2. Comparison of Polyphenol Contents and Antioxidant Activities of All *Malus* Wild Species Obtained in Different Solvent Extracts

	ethanol extracts[a]	ethyl acetate extracts[b]	ratio[c]
PC[d]	566.58 ± 91.19	135.97 ± 16.36	4.17
FC[e]	965.05 ± 184.70	214.90 ± 34.25	4.49
DPPH[f]	2110.07 ± 260.58	321.98 ± 46.33	6.55
ABTS[g]	5657.71 ± 974.14	1133.73 ± 157.30	4.99
FRAP[h]	3665.22 ± 773.60	556.74 ± 111.36	6.58

[a]Ethanol extracts: mean values ± standard errors of 10 crabapple samples in ethanol extracts. [b]Ethyl acetate extracts: mean values ± standard errors of 10 crabapple samples in ethyl acetate extracts. [c]Ratio: mean values of ethanol extracts/ethyl acetate extracts. Ratio >1 indicates that the ethanol extracts had more PC and FC and were more antioxidant. Ratio <1 indicates that the ethanol extracts had fewer PC and FC and were less antioxidant. [d]PC: phenolic content. [e]FC: flavonoid content. [f]DPPH: DPPH radical scavenging activity. [g]ABTS: ABTS radical scavenging activity. [h]FRAP: ferric reducing-antioxidant power.

dx.doi.org/10.1021/jf404542d | J. Agric. Food Chem. 2014, 62, 574−581

estimated in HPLC analysis at 280 nm and Folin−Ciocalteu data were increased due to the interference caused from other chemical components existing in the extracts, such as sugars and ascorbic acid.[47] Also, the Folin−Ciocalteu method gives different results in the semiquantification of polyphenols depending on the kind of prevalent classes of polyphenols present in the extracts.[48,49] However, the Folin−Ciocalteu procedure still provides a rapid and useful overall evaluation of the phenolic content of extracts.[50]

It should be mentioned that the PC values in ethanol extracts of the tested wild *Malus* species in the study were much higher than those reported for cultivated apple varieties, such as Fuji (167.11 mg GAE/100 g), EpagriCOOP24 (180.39 mg GAE/100 g), and EpagriF5P283 (233.57 mg GAE/100 g).[28] This is easy to understand because different varieties accumulate different quantities of polyphenols. However, the influence of environment may be another important contributor to the high value of phenolic contents in various *Malus* species. Environmental factors, such as climatic factors of soil type, sun exposure, rainfall, agronomic factors of biological culture, hydroponic culture, and fruit yield per tree, and the degree of ripeness affect the concentrations and proportions of different polyphenols in fruits.[51] The influence of agronomic factors can be verified by using principal component analysis (PCA) in the analysis of polyphenol indices in apple juice[52] and apple fruits.[53] Exposure to fungal infection is also an important role for the high accumulation of phenolic compounds in plants, such as resveratrol, to promote disease resistance.[54,55] Wild *Malus* species grow in various environments without any manual protection. Exposure to harsh environments and fungal infection might be another important reason for the high value of phenolic compounds in the wild *Malus* fruits used. In any case, it can be concluded that wild *Malus* species are good materials to prepare phenolic extracts.

Antioxidant Activity. *Radical-Scavenging Activity (DPPH and ABTS Assays).* Panels A and B of Figure 2 present the results of DPPH and ABTS assays, respectively. Consistent with that found in PC and FC, ethanol extracts had nearly 6-fold higher DPPH values and 5-fold higher ABTS values than ethyl acetate extracts on average. The higher values of DPPH and ABTS in ethanol extracts than in ethyl acetate extracts were also true for each wild *Malus* species. Also, similar to PC and FC, Lijiang-shanjingzi (*Malus rockii* Rehder) possessed the highest values of DPPH (3789.25 μmol TE/100 g) and ABTS (13056.68 μmol TE/100 g).

Ferric Reducing Antioxidant Power (FRAP Assay). Figure 2C shows that the FRAP values of ethanol extracts were significantly ($P < 0.01$) higher than those of ethyl acetate extracts. Particularly, the average FRAP value of ethanol extracts was almost 6 times higher than that in ethyl acetate extracts. For Xiaojin (*Malus xiaojinensis* Cheng et Jiang), the FRAP value of ethanol extract (6671.79 μmol TE/100 g) was nearly 54 times higher than that of ethyl acetate extract. Lijiang-shanjingzi (*Malus rockii* Rehder) still had the highest FRAP values in both ethanol extract (9356.14 μmol TE/100 g) and ethyl acetate extract (1181.94 mg GAE/100 g).

The antioxidant activity values obtained for most wild *Malus* species were significantly higher than that obtained in apple peel, from 1004.00 to 3877.73 μmol TE/100 g in DPPH assay, from 1225.53 to 4144.97 μmol TE/100 g in ABTS assay, and from 520.71 to 1160.58 μmol TE/100 g in FRAP assay,[4] even though apple peel had significantly higher antioxidant activity values than other parts of apple fruits.[4,19,50] In the present study, the antioxidant activity of whole fruits of wild *Malus* species, particularly Lijiang-shanjingzi (*Malus rockii* Rehder), was much higher than the reported value of apple peel, indicating *Malus* fruits are rich sources for preparing extracts with high antioxidant activities.

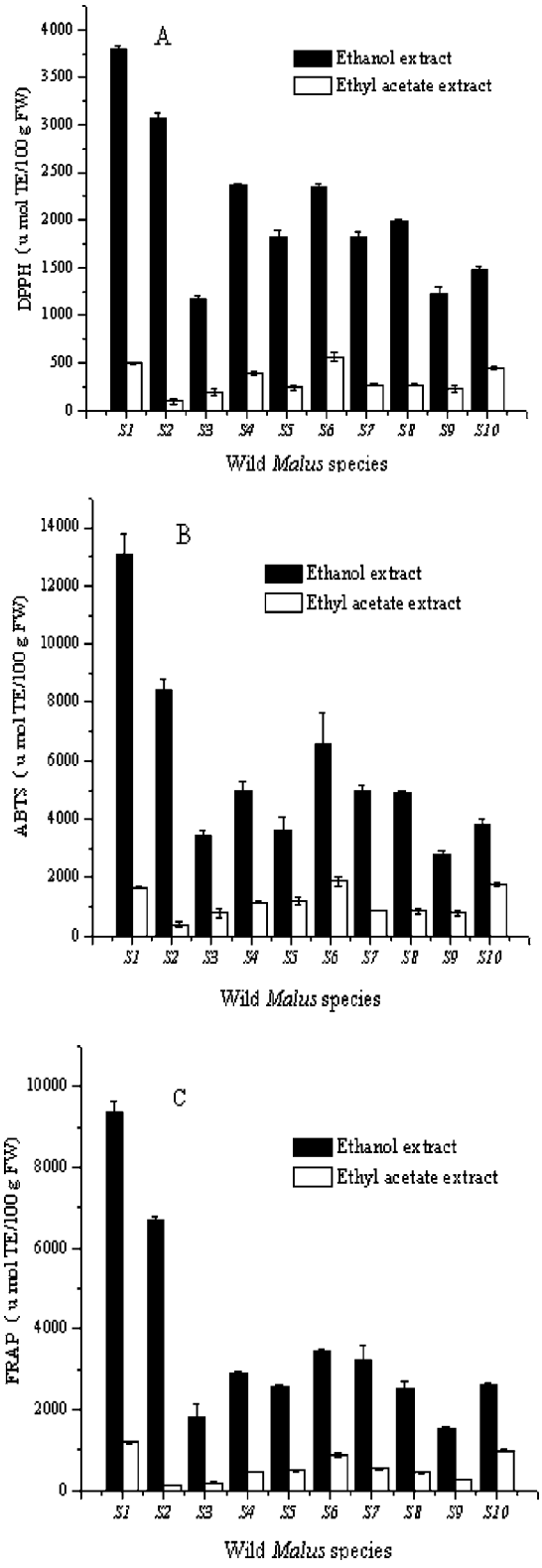

Figure 2. Antioxidant activities of 10 wild *Malus* species measured by DPPH (A), ABTS (B), and FRAP (C) assays. Data are the means of three replicates ± standard deviation.

dx.doi.org/10.1021/jf404542d | J. Agric. Food Chem. 2014, 62, 574−581

Table 3. Correlation Coefficients of PC, FC, DPPH, ABTS, and FRAP Values of Ethanol and Ethyl Acetate Extracts from All *Malus* Wild Species

	PC-E	FC-E	DPPH-E	ABTS-E	FRAP-E	PC-Ea	FC-Ea	DPPH-Ea	ABTS-Ea	FRAP-Ea
PC-E[c]	1									
FC-E[d]	0.974**[a]	1								
DPPH-E[e]	0.927**	0.970**	1							
ABTS-E[f]	0.944**	0.982**	0.953**	1						
FRAP-E[g]	0.975**	0.976**	0.940**	0.978**	1					
PC-Ea[h]	ns[b]	ns	ns	ns	ns	1				
FC-Ea[i]	ns	ns	ns	ns	ns	0.953**	1			
DPPH-Ea[j]	ns	ns	ns	ns	ns	0.792**	0.924**	1		
ABTS-Ea[k]	ns	ns	ns	ns	ns	0.774**	0.920**	0.954**	1	
FRAP-Ea[l]	ns	ns	ns	ns	ns	0.914**	0.973**	0.898**	0.917**	1

[a]**: significant at $p < 0.01$ level. [b]ns: nonsignificant. [c]PC-E: phenolic content in ethanol extracts. [d]FC-E: flavonoid content in ethanol extracts. [e]DPPH-E: DPPH radical scavenging activity in ethanol extracts. [f]ABTS-E: ABTS radical scavenging activity in ethanol extracts. [g]FRAP-E: ferric reducing-antioxidant power in ethanol extracts. [h]PC-Ea: phenolic content in ethyl acetate extracts. [i]FC-Ea: flavonoid content in ethyl acetate extracts. [j]DPPH-Ea: DPPH radical scavenging activity in ethyl acetate extracts. [k]ABTS-Ea: ABTS radical scavenging activity in ethyl acetate extracts. [l]FRAP-Ea: Ferric reducing-antioxidant power in ethyl acetate extracts.

Correlation Analysis. A correlation analysis was performed to investigate the relationship among PC, FC, DPPH, ABTS, and FRAP. The linear correlation coefficients are shown in Table 3. The results of PC and FC from ethanol extracts and ethyl acetate extracts were significantly and positively correlated with the antioxidant activity analysis values, including DPPH, ABTS, and FRAP. PC and FC were also significantly correlated with DPPH, ABTS, and FRAP for each used extraction solvent. Comparatively, the correlation between PC and antioxidant activity (DPPH, ABTS, and FRAP assays) was more significant (0.927, 0.944, and 0.975) in ethanol extracts, indicating more active polyphenols and flavonoids were extracted using ethanol. Although ethyl acetate is more efficacious than aqueous ethanol in extracting carotenoids, carotenoid content was reported to be negatively related to all of the antioxidant assays.[33] Therefore, aqueous ethanol is more efficacious for preparing phenolic extracts with high antioxidant activities than ethyl acetate.

Phenolic Profiles. Figure 3 shows the HPLC profiles at 280 nm of phenolic compounds of standards and of ethanol extract and ethyl acetate extract of Lijiang-shanjingzi (*Malus rockii* Rehder). Table 4 shows the obtained data of each phenol detected. It can be seen that the phenolic profiles differed when different extraction solvents were used. Chlorogenic acid, (−)-epicatechin, rutin, hyperin, and phlorizin were detected in both ethanol and ethyl acetate extracts of all tested wild *Malus* species. Caffeic acid, *p*-coumaric acid, and ferulic acid were detected in only some species. The occurrence of protocatechuic acid, (+)-catechin, and quercetin in the two different extracts was not consistent in some samples. Even for the same wild *Malus* species, the obtained phenolic profiles were different, which depends upon the extraction solvents used. For all tested species, the contents of chlorogenic acid and rutin were much higher in ethanol extracts than in ethyl acetate extracts.

It should be mentioned that phenolic profiles in HPLC analysis are not only related to the extraction solvents used but also depend on the wavelength used for measurement. Measurement of absorption at 280 nm is totally appropriate for monomeric and oligomeric proanthocyanidins, such as (+)-catechin and (−)-epicatechin, but not for the other individual compounds that have maximum absorbance at 369 nm (quercetin) and 320−340 nm (caffeic, *p*-coumaric acid, and ferulic acid). Valavanidis et al.[56] performed readings at 280, 320, and 350 nm and found that chlorogenic acid, catechin, procyanidins B1 and B2, and phloridzin were important polyphenol compounds in both organic and conventional apples. In the current study, reading was performed only at 280 nm using the external standard methods reported by Bhasker et al. in dietary fiber measurement,[38] Łata et al. in apple,[39] and Du et al. in jujubes.[40] The obtained data of caffeic acid, *p*-coumaric acid, and ferulic acid may be underestimated because 280 nm is

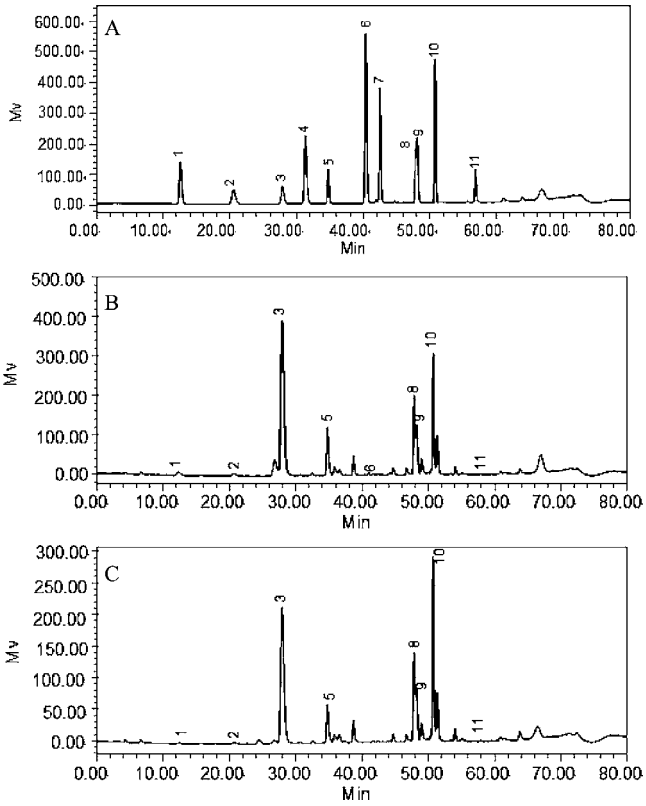

Figure 3. HPLC profiles at 280 nm of phenolic compounds of standards (A) and ethanol extract (B) and ethyl acetate extract (C) of Lijiang-shanjingzi (*Malus rockii* Rehder). Peaks: 1, protocatechuic acid; 2, (+)-catechin; 3, chlorogenic acid; 4, caffeic acid; 5, (−)-epicatechin; 6, *p*-coumaric acid; 7, ferulic acid; 8, rutin; 9, hyperin; 10, phlorizin; 11, quercetin.

dx.doi.org/10.1021/jf404542d | J. Agric. Food Chem. 2014, 62, 574−581

Table 4. Phenolic Compounds of Different *Malus* Wild Species[a]

parameter		mg/kg FW									
		S1	S2	S3	S4	S5	S6	S7	S8	S9	S10
protocatechuic acid	ethanol	2.00 ± 0.08	3.19 ± 0.14	ND[b]	13.36 ± 0.33	1.81 ± 0.03	5.73 ± 0.09	1.41 ± 0.10	2.01 ± 0.11	ND	4.96 ± 0.13
	ethyl acetate	0.41 ± 0.01	0.76 ± 0.00	0.21 ± 0.01	0.08 ± 0.00	ND	0.36 ± 0.02	2.38 ± 0.27	ND	0.03 ± 0.00	ND
(+)-catechin	ethanol	2.36 ± 0.06	6.34 ± 0.54	ND	33.94 ± 0.55	3.10 ± 0.20	10.74 ± 0.31	2.72 ± 0.02	2.95 ± 0.33	ND	7.30 ± 0.15
	ethyl acetate	4.01 ± 0.03	ND	ND	17.90 ± 1.22	3.61 ± 0.46	7.29 ± 0.41	6.46 ± 0.14	2.77 ± 0.47	0.72 ± 0.01	4.57 ± 0.27
chlorogenic acid	ethanol	160.35 ± 3.47	25.02 ± 0.47	337.84 ± 4.68	72.34 ± 2.04	129.39 ± 2.61	76.00 ± 2.13	84.56 ± 3.37	89.75 ± 2.22	65.97 ± 1.12	93.83 ± 2.28
	ethyl acetate	97.51 ± 1.07	13.69 ± 0.93	17.23 ± 0.32	3.12 ± 0.16	43.53 ± 0.88	34.73 ± 4.95	42.89 ± 1.23	37.20 ± 0.29	10.62 ± 0.32	21.16 ± 0.31
caffeic acid	ethanol	ND	ND	ND	0.14 ± 0.01	ND	ND	ND	ND	ND	0.28 ± 0.01
	ethyl acetate	ND	ND	ND	ND	ND	ND	0.94 ± 0.00	ND	ND	ND
(−)-epicatechin	ethanol	110.49 ± 2.13	7.67 ± 0.44	12.94 ± 0.15	111.80 ± 3.35	60.89 ± 0.69	175.93 ± 3.38	39.94 ± 2.30	59.25 ± 1.42	71.52 ± 1.38	123.18 ± 2.99
	ethyl acetate	55.71 ± 2.18	12.52 ± 0.72	5.01 ± 0.15	50.94 ± 1.76	41.36 ± 0.51	144.10 ± 7.36	35.45 ± 0.63	38.89 ± 1.40	40.34 ± 2.20	78.12 ± 1.25
p-coumaric acid	ethanol	0.09 ± 0.00	ND	ND	0.14 ± 0.00	0.08 ± 0.01	0.36 ± 0.00	0.06 ± 0.00	0.07 ± 0.00	0.02 ± 0.00	ND
	ethyl acetate	ND	0.67 ± 0.04	0.59 ± 0.07	ND	0.72 ± 0.04	0.09 ± 0.01	1.58 ± 0.0.03	0.49 ± 0.01	ND	ND
ferulic acid	ethanol	ND	0.30 ± 0.01	0.46 ± 0.03	ND	ND	ND	ND	ND	ND	0.88 ± 0.01
	ethyl acetate	ND	0.36 ± 0.02	0.78 ± 0.02	ND	ND	ND	1.27 ± 0.17	ND	ND	0.05 ± 0.00
rutin	ethanol	217.60 ± 6.72	184.73 ± 2.75	147.38 ± 3.30	81.89 ± 3.31	237.62 ± 2.00	112.59 ± 2.74	163.55 ± 3.48	222.12 ± 3.38	95.00 ± 2.55	303.72 ± 5.29
	ethyl acetate	103.70 ± 4.41	91.64 ± 5.17	12.87 ± 1.23	5.06 ± 0.09	72.81 ± 3.98	59.59 ± 1.35	51.29 ± 6.68	54.56 ± 2.78	0.71 ± 0.04	41.69 ± 1.97
hyperin	ethanol	17.59 ± 0.83	2.83 ± 0.21	23.10 ± 0.83	8.33 ± 0.21	14.44 ± 0.68	20.22 ± 0.66	12.27 ± 0.62	8.24 ± 0.35	2.77 ± 0.05	10.09 ± 0.62
	ethyl acetate	10.39 ± 0.48	5.00 ± 0.04	5.53 ± 0.01	2.68 ± 0.01	6.80 ± 0.13	17.19 ± 0.35	3.78 ± 0.07	3.71 ± 0.25	0.42 ± 0.03	4.61 ± 0.31
phlorizin	ethanol	115.09 ± 1.92	35.11 ± 1.96	71.77 ± 1.13	31.17 ± 1.04	31.84 ± 1.46	42.36 ± 0.44	30.69 ± 1.20	36.19 ± 1.50	17.63 ± 0.84	30.59 ± 0.84
	ethyl acetate	110.85 ± 1.29	41.74 ± 0.93	51.08 ± 1.47	12.54 ± 0.66	44.12 ± 0.16	68.55 ± 2.04	36.38 ± 1.29	30.70 ± 0.99	10.66 ± 0.41	34.77 ± 1.59
quercetin	ethanol	34.66 ± 1.37	12.92 ± 0.68	3.21 ± 0.17	4.74 ± 0.13	5.29 ± 0.52	1.88 ± 0.09	9.83 ± 0.28	6.52 ± 0.32	14.32 ± 0.75	2.59 ± 0.08
	ethyl acetate	11.16 ± 0.20	9.46 ± 0.22	11.34 ± 0.06	ND	4.44 ± 0.16	13.75 ± 0.98	15.05 ± 0.50	3.00 ± 0.16	ND	2.68 ± 0.07

[a]Mean ± SD; $n = 3$. [b]ND: not detected.

dx.doi.org/10.1021/jf404542d | J. Agric. Food Chem. 2014, 62, 574−581

not the maximum wavelength of these compounds. This might be one reason these phenolic compounds were occasionally and rarely detected in tested crabapples. For more precise analysis, readings should be performed at different wavelengths.

The obtained results were comparable with those reported by Łata et al.,[39] who performed HPLC analysis at 280 nm, the same as used in this study. They reported that chlorogenic acid, flavan-3-ols, rutin, and phloridzin presented the greatest amounts of phenolic compounds detected in whole apple fruits. Phloridzin is a dihydrochalcone and has been reported as the typical phenol in bark, leaves of apple trees, and apple fruits.[7,57] The similarity of the occurrence of phloridzin in apple and wild *Malus* species may be because they belong to the rose family known as Rosaceae. The obtained high content of chlorogenic acid in all wild *Malus* species was also consistent with previous results.[58] Comparatively, the chlorogenic acid, rutin, and phlorizin contents in all tested wild *Malus* species were higher than those reported in apples.

Inconsistent occurrence and low contents of caffeic acid, *p*-coumaric acid, and ferulic acidin in ethanol and ethyl acetate extracts of the tested wild *Malus* species might be because these compounds were not major phenolic compounds in Rosaceae, although they were abundant in wheat,[59] oat,[60−62] and rice.[63] This may be caused by the different regulations of phenolic metabolism in the plant family and grass family.

On the basis of the above results, it is concluded that fruits of wild *Malus* species are good sources for preparing phenolic extracts having high contents of chlorogenic acid, rutin, and phlorizin and having high antioxidant activity, indicating great potential in replacing apple pomace in producing phenolic extracts. In addition, extraction solvents had significant influence on the quality of phenolic extracts, and 80% ethanol was more effective than ethyl acetate in extracting phenolic compounds from wild *Malus* species.

AUTHOR INFORMATION

Corresponding Author

*(J.S.) Phone: +86 29 88460541. Fax: +86 29 88460541. E-mail: sjlshi2004@aliyun.com.

Funding

The work is partly supported by the Ministry of Agriculture of the People's Republic of China through funds for Agro-scientific Research in the Public Interest (No. 201003021).

Notes

The authors declare no competing financial interest.

REFERENCES

(1) Soto-Vaca, A.; Gutierrez, A.; Losso, J. N.; Xu, Z. M.; Finley, J. W. Evolution of phenolic compounds from color and flavor problems to health benefits. *J. Agric. Food Chem.* **2012**, *60*, 6658−6677.

(2) Bernal, J.; Mendiola, J. A.; Ibanez, E.; Cifuentes, A. Advanced analysis of nutraceuticals. *J. Pharm. Biomed. Anal.* **2011**, *55*, 758−774.

(3) Drogoudi, P. D.; Michailidis, Z.; Pantelidis, G. Peel and flesh antioxidant content and harvest quality characteristics of seven apple cultivars. *Sci. Hortic.* **2008**, *115*, 149−153.

(4) Vieira, F. G.; Borges, Gda. S.; Copetti, C.; Di Pietro, P. F.; Nunes, Eda. C.; Fett, R. Phenolic compounds and antioxidant activity of the apple flesh and peel of eleven cultivars grown in Brazil. *Sci. Hortic.* **2011**, *128*, 261−266.

(5) Ogimoto, I.; Shibata, A.; Fukuda, K. World Cancer Research Fund/American Institute of Cancer Research 1997 recommendations: applicability to digestive tract cancer in Japan. *Cancer Causes Control* **2000**, *11*, 9−23.

(6) Gonzalez, R.; Ballester, I.; Lopez-Posadas, R.; Suarez, M. D.; Zarzuelo, A.; Martinez-Augustin, O.; De Medina, F. Effects of flavonoids and other polyphenols on inflammation. *Crit. Rev. Food Sci.* **2011**, *51*, 331−362.

(7) Gonzalez-Gallego, J.; Garcia-Mediavilla, M. V.; Sanchez-Campos, S.; Tunon, M. J. Fruit polyphenols, immunity and inflammation. *Br. J. Nutr.* **2010**, *104*, S15−S27.

(8) Andre, C. M.; Greenwood, J. M.; Walker, E. G.; Rassam, M.; Sullivan, M.; Evers, D.; Perry, N. B.; Laing, W. A. Anti-inflammatory procyanidins and triterpenes in 109 apple varieties. *J. Agric. Food Chem.* **2012**, *60*, 10546−10554.

(9) Balasuriya, N.; Rupasinghe, H. P. V. Antihypertensive properties of flavonoid-rich apple peel extract. *Food Chem.* **2012**, *135*, 2320−2325.

(10) Ebrahimi, A.; Schluesener, H. Natural polyphenols against neurodegenerative disorders: potentials and pitfalls. *Ageing Res. Rev.* **2012**, *11*, 329−345.

(11) Hervert-Hernandez, D.; Goni, I. Dietary polyphenols and human gut microbiota: a review. *Food Rev. Int.* **2011**, *27*, 154−169.

(12) Sergent, T.; Vanderstraeten, J.; Winand, J.; Beguin, P.; Schneider, Y.-J. Phenolic compounds and plant extracts as potential natural anti-obesity substances. *Food Chem.* **2012**, *135*, 68−73.

(13) Espinosa, C.; Lopez-Jimenez, J. A.; Cabrera, L.; Larque, E.; Almajano, M. P.; Arnao, M. B.; Zamora, S.; Perez-Llamas, F. Protective effect of white tea extract against acute oxidative injury caused by adriamycin in different tissues. *Food Chem.* **2012**, *134*, 1780−1785.

(14) Tian, J.; Shen, H. X.; Zhang, J.; Song, T. T.; Yao, Y. C. Characteristics of chalcone synthase promoters from different leaf-color *Malus* crabapple cultivars. *Sci. Hortic.* **2011**, *129*, 449−458.

(15) Agourram, A.; Ghirardello, D.; Rantsiou, K.; Zeppa, G.; Belviso, S.; Romane, A.; Oufdou, K.; Giordano, M. Phenolic content, antioxidant potential, and antimicrobial activities of fruit and vegetable by-product extracts. *Int. J. Food Prop.* **2013**, *16*, 1092−1104.

(16) Seo, H.-K.; Lee, J.-H.; Kim, H.-S.; Lee, C.-K.; Lee, S.-C. Antioxidant and antimicrobial activities of *Smilax china* L. leaf extracts. *Food Sci. Biotechnol.* **2012**, *21*, 1723−1727.

(17) Katalinić, V.; Možina, S. S.; Skroza, D.; Generalić, I.; Abramovič, H.; Miloš, M.; Ljubenkov, I.; Piskernik, S.; Pezo, I.; Terpinc, P.; Boban, M. Polyphenolic profile, antioxidant properties and antimicrobial activity of grape skin extracts of 14 *Vitis vinifera* varieties grown in Dalmatia (Croatia). *Food Chem.* **2010**, *119*, 715−723.

(18) Lee, K. W.; Kim, Y. J.; Kim, D. O.; Lee, H. J.; Lee, C. Y. Major phenolics in apple and their contribution to the total antioxidant capacity. *J. Agric. Food Chem.* **2003**, *51*, 6516−6520.

(19) McGhie, T. K.; Hunt, M.; Barnett, L. E. Cultivar and growing region determine the antioxidant polyphenolic concentration and composition of apples grown in New Zealand. *J. Agric. Food Chem.* **2005**, *53*, 3065−3070.

(20) Vrhovsek, U.; Rigo, A.; Tonon, D.; Mattivi, F. Quantitation of polyphenols in different apple varieties. *J. Agric. Food Chem.* **2004**, *52*, 6532−6538.

(21) Oktay, M.; Gülçin, İ.; Küfrevioğlu, Ö. İ. Determination of in vitro antioxidant activity of fennel (*Foeniculum vulgare*) seed extracts. *LWT−Food Sci. Technol.* **2003**, *36*, 263−271.

(22) Erol, N. T. Determination of phenolic compounds from various extracts of green tea by HPLC. *Asian J. Chem.* **2013**, *25*, 3860−3862.

(23) Hosseinzadeh, R.; Khorsandi, K.; Hemmaty, S. Study of the effect of surfactants on extraction and determination of polyphenolic compounds and antioxidant capacity of fruits extracts. *PLoS One* **2013**, *8*, e57353.

(24) PerezIlzarbe, J.; Hernandez, T.; Estrella, I.; Vendrell, M. Cold storage of apples (cv. Granny Smith) and changes in phenolic compounds. *Z. Lebensm. Unters. Forsch. A* **1997**, *204*, 52−55.

(25) Valles, B. S.; Victorero, J. S.; Alonso, J. J. M.; Gomis, D. B. High-performance liquid chromatography of the neutral phenolic compounds of low molecular weight in apple juice. *J. Agric. Food Chem.* **1994**, *42*, 2732−2736.

(26) Roopchand, D. E.; Krueger, C. G.; Moskal, K.; Fridlender, B.; Lila, M. A.; Raskin, I. Food-compatible method for the efficient

extraction and stabilization of cranberry pomace polyphenols. *Food Chem.* **2013**, *141*, 3664−3669.
(27) Contreras-Calderón, J.; Calderón-Jaimes, L.; Guerra-Hernández, E.; García-Villanova, B. Antioxidant capacity, phenolic content and vitamin C in pulp, peel and seed from 24 exotic fruits from Colombia. *Food Res. Int.* **2011**, *44*, 2047−2053.
(28) Vieira, F. G.; Borges, Gda. S.; Copetti, C.; Gonzaga, L. V.; Nunes, Eda. C.; Fett, R. Activity and contents of polyphenolic antioxidants in the whole fruit, flesh and peel of three apple cultivars. *Arch. Latinoam. Nutr.* **2009**, *59*, 101−106.
(29) Rop, O.; Jurikova, T.; Sochor, J.; Mlcek, J.; Kramarova, D. Antioxidant capacity, scavenging radical activity and selected chemical composition of native apple cultivars from Central Europe. *J. Food Quality* **2011**, *34*, 187−194.
(30) Yoshizawa, Y.; Sakurai, K.; Kawaii, S.; Soejima, J.; Murofushi, N. Antiproliferative and antioxidant properties of crabapple juices. *Food Sci. Technol. Res.* **2004**, *10*, 278−281.
(31) Lin, L. Z.; Lei, F. F.; Sun, D. W.; Dong, Y.; Yang, B.; Zhao, M. M. Thermal inactivation kinetics of *Rabdosia serra* (Maxim.) Hara leaf peroxidase and polyphenol oxidase and comparative evaluation of drying methods on leaf phenolic profile and bioactivities. *Food Chem.* **2012**, *134*, 2021−2029.
(32) Zhao, B.; Hall, C. A. Antioxidant activity of raisin extracts in bulk oil, oil in water emulsion, and sunflower butter model systems. *J. Am. Oil Chem. Soc.* **2007**, *84*, 1137−1142.
(33) Kong, K. W.; Mat-Junit, S.; Aminudin, N.; Ismail, A.; Abdul-Aziz, A. Antioxidant activities and polyphenolics from the shoots of *Barringtonia racemosa* (L.) Spreng in a polar to apolar medium system. *Food Chem.* **2012**, *134*, 324−332.
(34) Yi, O. S.; Meyer, A. S.; Frankel, E. N. Antioxidant activity of grape extracts in a lecithin liposome system. *J. Am. Oil Chem. Soc.* **1997**, *74*, 1301−1307.
(35) Wolfe, K.; Wu, X. Z.; Liu, R. H. Antioxidant activity of apple peels. *J. Agric. Food Chem.* **2003**, *51*, 609−614.
(36) Ma, X. W.; Wu, H. X.; Liu, L. Q.; Yao, Q. S.; Wang, S. B.; Zhan, R. L.; Xing, S. S.; Zhou, Y. G. Polyphenolic compounds and antioxidant properties in mango fruits. *Sci. Hortic.* **2011**, *129*, 102−107.
(37) Tai, Z. G.; Cai, L.; Dai, L.; Dong, L. H.; Wang, M. F.; Yang, Y. B.; Cao, Q.; Ding, Z. T. Antioxidant activity and chemical constituents of edible flower of *Sophora viciifolia*. *Food Chem.* **2011**, *126*, 1648−1654.
(38) Bhaskar, J. J.; Mahadevamma, S.; Chilkunda, N. D.; Salimath, P. V. Banana (*Musa* sp. var. elakki bale) flower and pseudostem: dietary fiber and associated antioxidant capacity. *J. Agric. Food Chem.* **2012**, *60*, 427−432.
(39) Łata, B.; Trampczynska, A.; Paczesna, J. Cultivar variation in apple peel and whole fruit phenolic composition. *Sci. Hortic.* **2009**, *121*, 176−181.
(40) Du, L. J.; Gao, Q. H.; Ji, X. L.; Ma, Y. J.; Xu, F. Y.; Wang, M. Comparison of flavonoids, phenolic acids, and antioxidant activityof explosion-puffed and sun-dried jujubes (*Ziziphus jujuba* Mill.). *J. Agric. Food Chem.* **2013**, *61*, 11840−11847.
(41) NurulMarian, H.; Radzali, M.; Johari, R.; Syahida, A.; Maziah, M. Antioxidant activities of different aerial parts of putat (*Barringtonia racemosa* L.). *Malays. J. Biochem.* **2008**, *16*, 15−19.
(42) Liu, S. C.; Lin, J. T.; Wang, C. K.; Chen, H. Y.; Yang, D. J. Antioxidant properties of various solvent extracts from lychee (*Litchi chinenesis* Sonn.) flowers. *Food Chem.* **2009**, *114*, 577−581.
(43) Razali, N.; Mat-Junit, S.; Abdul-Muthalib, A. F.; Subramaniam, S.; Abdul-Aziz, A. Effects of various solvents on the extraction of antioxidant phenolics from the leaves, seeds, veins and skins of *Tamarindus indica* L. *Food Chem.* **2012**, *131*, 441−448.
(44) Mabry, T. J.; Markham, K. R.; Thomas, M. B. Reagents and procedures for the ultraviolet speetral analysisof flavonoids. *The Systematic Identificationof Flavonoids*; Springer Verlag: New York, 1970; 2240 pp.
(45) Siddhuraju, P.; Becker, K. Antioxidant properties of various solvent extracts of total phenolic constituents from three different agroclimatic origins of Drumstick tree (*Moringa oleifera* Lam.) leaves. *J. Agric. Food Chem.* **2003**, *51*, 2144−2155.
(46) Sultana, B.; Anwar, F.; Przybylski, R. Antioxidant activity of phenolic components present in barks of *Azadirachta indica*, *Terminalia arjuna*, *Acacia nilotica*, and *Eugenia jambolana* Lam. trees. *Food Chem.* **2007**, *104*, 1106−1114.
(47) Singleton, V. L.; Rossi, J. A., Jr. Colorimetry of total phenolics with phosphomolybdic−phosphotungstic acid reagents. *Am. J. Enol. Vitic.* **1965**, *16*, 144−158.
(48) Cheynier, V. Polyphenols in foods are more complex than often thought. *Am. J. Clin. Nutr.* **2005**, *81*, 223S−229S.
(49) Lee, J.; Rennaker, C. D. Influence of extraction methodology on grape composition values. *Food Chem.* **2011**, *126*, 295−300.
(50) Khanizadeh, S.; Tsao, R.; Rekika, D.; Yang, R.; Charles, M. T.; Vasantha Rupasinghe, H. P. V. Polyphenol composition and total antioxidant capacity of selected apple genotypes for processing. *J. Food Compos. Anal.* **2008**, *21*, 396−401.
(51) Kondakova, V.; Tsvetkov, I.; Batchvarova, R.; Badjakov, I.; Dzhambazova, T.; Slavov, S. Phenol compounds-qualitative index in small fruits. *Biotechnol. Biotechnol. Equip.* **2009**, *23*, 1444−1448.
(52) Guo, J.; Yue, T.; Yuan, Y.; Wang, Y. Chemometric classification of apple juices according to variety and geographical origin based on polyphenolic profiles. *J. Agric. Food Chem.* **2013**, *61*, 6949−6963.
(53) Cuthbertson, D.; Andrews, P. K.; Reganold, J. P.; Davies, N. M.; Lange, B. M. Utility of metabolomics toward assessing the metabolic basis of quality traits in apple fruit with an emphasis on antioxidants. *J. Agric. Food Chem.* **2012**, *60*, 8552−8560.
(54) Chang, X. L.; Heene, E.; Qiao, F.; Peter, N. The phytoalexin resveratrol regulates the initiation of hypersensitive cell death in *vitis* cell. *PLoS One* **2011**, *6*, e26405.
(55) Pont, V.; Pezet, R. Relation between the chemical structure and the biological activity of hydroxystilbenes against *Botrytis cinerea*. *J. Phytopathol.* **1990**, *130*, 1−8.
(56) Valavanidis, A.; Vlachogianni, T.; Psomas, A.; Zovoili, A.; Siatis, V. Polyphenolic profile and antioxidant activity of five apple cultivars grown under organic and conventional agricultural practices. *Int. J. Food Sci. Technol.* **2009**, *44*, 1167−1175.
(57) Dragovic-Uzelac, V.; Pospisil, J.; Levaj, B.; Delonga, K. The study of phenolic profiles of raw apricots and apples and their purees by HPLC for the evaluation of apricot nectars and jams authenticity. *Food Chem.* **2005**, *91*, 373−383.
(58) Huber, G. M.; Rupasinghe, H. P. V. Phenolic profiles and antioxidant properties of apple skin extracts. *J. Food Sci.* **2009**, *74*, C693−C700.
(59) Arranz, S.; Saura-Calixto, F. Analysis of polyphenols in cereals may be improved performing acidic hydrolysis: a study in wheat flour and wheat bran and cereals of the diet. *J. Cereal Sci.* **2010**, *51*, 313−318.
(60) Xu, J. G.; Tian, C. R.; Hu, Q. P.; Luo, J. Y.; Wang, X. D.; Tian, X. D. Dynamic changes in phenolic compounds and antioxidant activity in oats (*Avena nuda* L.) during steeping and germination. *J. Agric. Food Chem.* **2009**, *57*, 10392−10398.
(61) Peterson, D. M. Oat antioxidants. *J. Cereal Sci.* **2001**, *33*, 115−129.
(62) Peterson, D. M.; Emmons, C. L.; Hibbs, A. H. Phenolic antioxidants and antioxidant activity in pearling fractions of oat groats. *J. Cereal Sci.* **2001**, *33*, 97−103.
(63) Park, S.-Y.; Ha, S.-H.; Lim, S.-H.; Jung, J. Y.; Lee, S. M.; Yeo, Y.; Kim, J. K. Determination of phenolic acids in Korean rice (*Oryza sativa* L.) cultivars using gas chromatography-time-of-flight mass spectrometry. *Food Sci. Biotechnol.* **2012**, *21*, 1141−1148.

JOURNAL OF AGRICULTURAL AND FOOD CHEMISTRY

Article

pubs.acs.org/JAFC

Determination of Antioxidant Activity of Spices and Their Active Principles by Differential Pulse Voltammetry

Alberto Palma,[†] Mercedes Ruiz Montoya,*[,†] Jesús F. Arteaga,[‡] and Jose M. Rodríguez Mellado[§]

[†]Departamento de Ingeniería Química, Química Física y Química Orgánica, Facultad de Ciencias Experimentales, Campus de "El Carmen", Universidad de Huelva E-21071 Huelva, Spain

[‡]CIQSO—Centro para la Investigación en Química Sostenible y Departamento de Ingeniería Química, Química Física y Química Orgánica, Campus de "El Carmen", Universidad de Huelva, E-21071 Huelva, Spain

[§]Departamento de Química Física y Termodinámica Aplicada, Facultad de Ciencias CeiA3, Campus Universitario Rabanales, edificio Marie Curie, Universidad de Córdoba, E-14014 Córdoba, Spain

ABSTRACT: The anodic oxidation of mercury in the presence of hydrogen peroxide in differential pulse voltammetry (DPV) was used to determine the antioxidant (AO) character of radical scavengers. Hydroperoxide radical is formed at the potentials of the oxidation peak on mercury electrodes, such radical reacting with the antioxidants in different extension. The parameter C_{10} (antioxidant concentration at which the peak area decreases by 10%) is used to measure the scavenging activity of the individual antioxidants. To establish the scavenging activity of antioxidant mixtures as a whole, the parameter, μ_{10} as the reverse of V_{10}, V_{10} being the volume necessary to decrease the peak area in DPV by 10%, was selected. Higher μ_{10} values correspond to higher scavenging activity. The studies have been extended to aqueous extracts of some species. The results may be useful in explaining the effect of spices in vitro and in vivo studies.

KEYWORDS: *hydroperoxide radical, radical scavengers, antioxidant activity, spices, cinnamon, clove, numteg, oregano, thyme*

INTRODUCTION

Oxidative stress is defined as the excessive production of reactive oxygen species (ROS) and/or deficiency of the antioxidant cellular defense system. The ROS play a major role in causing antioxidant stress and damage to DNA, proteins, and lipids.[1] Free radical mediated cell damage has been implicated in the pathology of various human chronic diseases such as Alzheimer's, Parkinson's, Crohn's, and certain cancers.[2,3] In addition to endogenous antioxidant systems, a diet rich in antioxidant food products also protects DNA and increases resistance against oxidative stress. Spices may offer many health benefits and have been proven to counteract oxidative stress over in vitro and in vivo systems.[4,5]

Primary antioxidants (pro-oxidants) prevent the formation of free radicals,[6] particularly ROS. Secondary antioxidants (antioxidants with radical scavenging activity) interrupt the propagation of free radicals, inhibit the generation of ROS, and prevent the metabolic activation of carcinogens.[7,8] Tertiary antioxidants repair the damage from free radicals or eliminate damaged molecules.[9,10]

Direct and indirect methods have been proposed to evaluate the antioxidant activity of natural products.[11] Electrochemical measurements are a rapid proof to test the antioxidant capacity of many organic molecules[12,13] and to study the interaction between the antioxidant and ROS, as was observed for dihydropyridines and electrogenerated superoxide radical.[14,15]

Oxidation potentials of the peaks appearing in cyclic voltammetry have been used for comparison of the antioxidant action of compounds such as phenolic acids, flavonoids, and cinnamic acids.[16−18] The electrode more used was the glassy carbon electrode (GCE). Similarly, cyclic voltammetric measurements have been applied to the determination of the antioxidant capacity of wines.[17,18] The variation of the oxidation potential with the pH values can be provided, and measurements made at different pH values can be compared. Concentration is critical to the success of the technique. The area under the first voltammetric peak is a good estimate of phenol concentration with low oxidation potential and can be related to the antioxidant activity of the sample of wine. Other advantages are as follows: there is no need to measure the antioxidant capacity specific to each component, the sample preparation is simple and fast, and the sensitivity of the technique is sufficient for determination at physiological concentrations of antioxidants. Low oxidation potentials are associated with a greater facility of a given molecule for electrodonation, that is, acting as an antioxidant, with good correlation with other techniques such as the scavenging of the DPPH$^{\bullet}$ radical.[19]

The radical scavenging ability given by the DPPH$^{\bullet}$ assay was related to the reduction potential of DPPH$^{\bullet}$. Radicals such as ROO$^{\bullet}$ and OH$^{\bullet}$ exhibit much higher formal potentials than DPPH$^{\bullet}$ and can react with species with high oxidation potentials for which it is not possible to determine the antioxidant activity by the DPPH assay. There are some accepted methods for ROS, such as fluorometric assay for hydrogen peroxide,[20] ESR/EPR method, and so on.[20−24]

The anodic oxidation reaction of hydrogen peroxide was used in pioneering research to determine the antioxidant character of compounds in foods,[25−29] but some experimental problems led

Received: May 30, 2013
Revised: December 27, 2013
Accepted: December 28, 2013
Published: December 28, 2013

 © 2013 American Chemical Society

to a revision of this method.[30] Recently, Gorjanovic et al. and Potkonjak et al.[31−33] have developed polarographic criteria for antioxidant activity.

Sužnjević and co-workers[25] assessed that the anodic wave of H_2O_2 observed on mercury electrodes is due to the oxidation of Hg to Hg^{2+} and the subsequent formation of a mixed complex with HO_2^- and OH^- ions, as previously reported by Kikuchi and Murayama.[34] This led to the revision of the approach made in ref 30.

On the other hand, spices are commonly used to enrich flavor and aroma in cooking and to preserve food and also as components of a healthy diet. They are traditionally thought to have beneficial effects on health, and specific spices are used in traditional medicine as part of therapeutic formulations. Pharmacological studies on spices revealed a wide range of biological activities, including antioxidant, anti-inflammatory, antitumor, immunomodulatory, and antiradical activities.[35−37] Their antioxidant constituents are identified as responsible for the health-promoting properties of spices, such as antiatherosclerotic, anticancer, and anti-inflammatory activities.[38]

The aim of this work was, first, to revise the DPV method in light of the oxidation mechanism on mercury electrodes; second, to apply the studies to potential food antioxidants, namely, a number of bioactive compounds found in spices and condiments; and, third, to extend these studies to mixtures of antioxidants and to aqueous extracts of some species.

The compounds studied are mainly active principles of spices, seasonings, or drugs, belonging to the family of low molecular weight antioxidants, being aromatic phenolics and nonphenolics or cyclic and acyclic nonaromatic compounds: eugenol, carvacrol, cinnamaldehyde, thymol, sesamol, 3-hydroxycoumarin, salicylaldehyde, limonene, geraniol, vanillin, cinnamic acid, α- and β-pinene, 2,4- and 2,5-dihydroxybenzaldehydes, and gallic acid. The spices studied contain one or more of the above compounds.

MATERIALS AND METHODS

Materials. 3-Hydroxycoumarin, carvacrol, vanillin, and gallic acid were purchased from Aldrich (or Sigma-Aldrich), and the rest of chemicals were Merck analytical grade reagents. All of the reactants were used without further purification. Thyme, cinnamon, oregano, clove, and nutmeg were purchased in a grocery store and were of the Mercadona S.A. trademark.

Solutions of 0.1 M in both sodium carbonate and phosphoric acid at pH 10.5 were used as supporting electrolytes. The aqueous solutions were prepared with ultrapure water type I (resistivity = 18.2 MΩ·cm at 25 °C) obtained from a Millipore Simplicity system. The ionic strength was adjusted to 0.5 M with solid KNO_3, and the pH was adjusted with solid NaOH. Antioxidants were dissolved in ethanol, and the stock solution concentrations were 5×10^{-3} M. These solutions were stored in darkness at 277 K to avoid decomposition.

Aqueous extracts of thyme, cinnamon, oregano, clove, and nutmeg were obtained by adding 250 mg of the spice to 100 mL of deionized water, heating for 5 min at 95 °C, and filtering at room temperature. The DPPH assays of these filtrates were made directly, but they were 10-fold diluted for the H_2O_2 experiments. In this last case, the data reflected under Results and Discussion show the results corrected for the dilution.

Methods. *Electrochemical Measurements.* The concentration of hydrogen peroxide in the cell was 5×10^{-4} M, and the percentage of ethanol in the cell was 30%. Because the change in the ethanol content modifies the DPV peak area,[30] solutions were prepared with a fixed amount (6.9 mL) of supporting electrolyte, 100 μL of 5×10^{-2} M H_2O_2, variable volumes, V_{AO}, of the stock solution of antioxidant in ethanol, and the total volume was completed with $(3-V_{AO})$ mL of pure ethanol. Therefore, it was necessary to prepare a separate solution for each concentration of antioxidant, and the samples were not gradually added to the solution because of the undesirable decrease produced by the presence of ethanol, which depends on the ethanol content. One hundred microliters of H_2O_2 was added after the solutions were purged with purified nitrogen. For the experiments made with the aqueous extracts of spices, no ethanol was added, the overall volume being completed with water, and the measurements being referred to the signal obtained for H_2O_2 in the absence of ethanol.

Measurements were made on a CHI650A electrochemical workstation from IJCambria coupled to an EF-1400 controlled growth mercury electrode from BAS instruments, in the HMDE mode. The Hg drop area was 6.70×10^{-3} cm^2. The temperature was kept at 298 ± 0.1 K. All potentials were measured against an Ag|AgCl|KCl_{sat} electrode (BAS MF-2052). A platinum counter electrode, BAS MW-1034, was used. The parameters selected in the differential pulse voltammetry (DPV) were as follows: pulse amplitude, 0.05 V; pulse width, 0.05 s; and pulse period, 0.2 s.

The reproducibility of the measurements was ensured by repeating the experiments, and the standard deviations of the data were <5%.

Spectrophotometric Measurements. DPPH$^\bullet$ Radical Scavenging Assay. The maximum wavelength of the UV−visible absorption band of the DPPH$^\bullet$ is 515 nm, and the action of an AO causes the decrease of this band or its eventual disappearance through the reactions to give DPPH and AO$^\bullet$. The amount of antioxidant required to decrease the initial concentration of DPPH$^\bullet$ to 50% (efficient concentration or EC_{50}) is a measurement of the antioxidant activity. The reverse value, namely, antiradical power, ARP = $1/EC_{50}$, should be higher as the antioxidant is more efficient.

UV measurements were made on a Genesys 10 UV spectrophotometer from Thermo Electron Corp. with quartz cuvettes of 1.0 cm path length.

Different concentrations of antioxidants were added to DPPH$^\bullet$ methanolic solution. The initial DPPH$^\bullet$ concentration was 6×10^{-5} M. The DPPH$^\bullet$ concentration in the reaction medium was calculated from a calibration curve with the equation

$$\mathrm{Abs}_{515nm} = 12.195 c_{DPPH} - 0.0137$$

as determined by linear regression.

For the aqueous extracts of the spices, the ARP was referred to the weight of antioxidant required to decrease the initial concentration of DPPH$^\bullet$ to 50%, W_{50}, expressed in mg, the ARP value being ARP = $1/W_{50}$, in mg^{-1}.

RESULTS AND DISCUSSION

Kikuchi and Murayama[34] proposed that the anodic wave of H_2O_2 observed on mercury electrodes is due to the oxidation of Hg to Hg^{2+} and the subsequent formation of a mixed complex with HO_2^- and OH^- ions:

$$Hg \rightleftharpoons Hg^{2+} + 2e^-$$

$$Hg^{2+} + HO_2^- + HO^- \rightleftharpoons Hg(HO_2)(OH)$$

The formation of this complex was assessed by Sužnjević and co-workers[25] by titration of H_2O_2 with $HgCl_2$ in basic solutions. However, if the reactions shown in the above scheme were the only processes occurring at the electrode, no effect of the addition of antioxidants on the oxidation wave could be observed, because the antioxidants do not react with the mercury ions in the absence of hydrogen peroxide, at least under the experimental conditions of polarographic and voltammetric experiments.[39]

It could be claimed that antioxidants act by reacting with the dissociated hydrogen peroxide and thus decreasing the concentration of the complex, this producing a decrease in the polarographic limiting current (or in the DPV peak current) that can be related to the antioxidant activity. However, this implies that the antioxidant must react with H_2O_2 in the solution.

Experiments were made to check this possibility. As can be seen in Figure 1, linear sweep cyclic voltammograms of solutions of

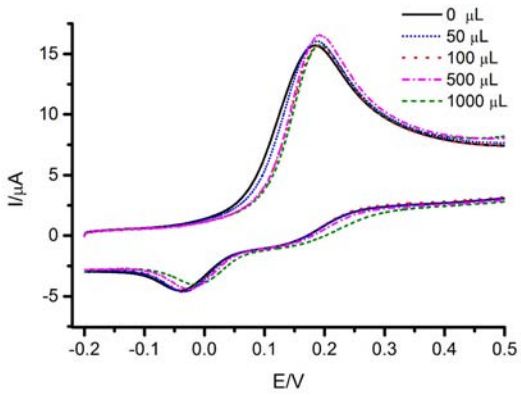

Figure 1. Linear sweep cyclic voltammograms on a glassy carbon electrode (IJCambria 38.5 mm^2) of 1 mM sesamol at pH 10.5 and different amounts of 5×10^{-2} M H_2O_2 solution added to a 10 mL final volume in the cell.

0.5 mM of the antioxidant sesamol were recorded at pH 10.5 in the absence and in the presence of increasing concentrations of hydrogen peroxide.

No effects on the oxidation wave were observed even at H_2O_2 concentrations 10 times higher than sesamol. In addition, the peak current of the oxidation peak of sesamol remained constant during 30 min, even at the maximum peroxide concentration used. Therefore, no reaction occurs involving these two reactants and, in conclusion, additional reactions must be considered.

Because the presence of radicals is needed to give an interaction with the antioxidants, the only possibility is that in the range of potentials of the oxidation peak on mercury electrodes such radicals are formed. It is evident that the electrode must play an important role in the electro-oxidation. This role could be viewed as the occurrence of adsorbed species on the electrode, the Gibbs energy of the adsorption processes decreasing the oxidation potential of hydrogen peroxide. In consequence, the simplified reaction scheme given in ref 30 must involve adsorbed species.

Another approach to the problem is to assume that radicals are produced after the formation of the mercury complex, probably through intramolecular electron transfers:

$$Hg \rightleftharpoons Hg^{2+} + 2e^-$$

$$Hg^{2+} + HO_2^- + HO^- \rightleftharpoons Hg(HO_2)(OH)$$

$$Hg(HO_2)(OH) \rightleftharpoons Hg + HO_2^{\bullet} + HO^{\bullet}$$

In this scheme, the last reaction must occur at trace levels in the absence of radical scavengers. The addition of increasing amounts of antioxidants must cause a shifting to the right of the last step by reaction with the radicals, and, consequently, the shifting to the right of the overall process. In this case, the addition of antioxidants must increase the limiting current of the dc wave (or the peak current of the DPV peak), in contradiction with the experimental findings.

It is known from decades ago[40] that the anodic oxidation of mercury involves both Hg(II) and Hg(I) ions in equilibrium with the complexes formed with chloride or bromide ions present in the solution. This takes place at potentials 0.1−0.2 V more positive than the peak here analyzed. This behavior is common to the redox processes of metal ions; that is, the electron transfers are one-electron, and the redox state of the ions increase, or decrease, in one unity.[41] Therefore, it seems reasonable to think that the Hg(I) ions are formed after the first one-electron transfer, and the following reactions could take place:

$$Hg \rightleftharpoons \frac{1}{2}Hg_2^{2+} + e^- \quad (1)$$

$$\frac{1}{2}Hg_2^{2+} \xrightarrow{e^-} Hg^{2+} \quad (2)$$

$$\frac{1}{2}Hg_2^{2+} \xrightarrow[+HO_2^-]{} Hg + HO_2^{\bullet} \quad (2')$$

$$Hg^{2+} + HO_2^- + HO^- \rightleftharpoons Hg(HO_2)(OH) \quad (3)$$

In the absence of AO, reaction 2′ takes place only at trace levels. When a radical scavenger is added, this species reacts with the hydroperoxide radical produced in reaction 2′ and decreases the available concentration of Hg(I) ion to give the Hg(II) ion and, consequently, the oxidation current. This scheme explains all of the experimental results obtained. First, the DPV peak area decreases as the antioxidant concentration increases from the value corresponding to a two-electron transfer (Hg oxidation to mercuric ions through mercurous ions followed by the complex formation) to the value corresponding to an EC one-electron transfer (Hg oxidation to mercurous ions followed by hydroperoxide radical and subsequent reaction with AO), that is, to a value not less than 50% of the original area. Second, the half-width of the DPV peak changes from the value corresponding to a two-electron process to the value corresponding to an EC one-electron process, as was experimentally found.[30]

The I-E relationships for the above-described process can be obtained by using the convective diffusion approximation and the steady-state conditions and the Nernst diffusion-layer approximation, but the equations for the limiting currents as a function of the AO concentration and the equilibrium and rate constants of reaction 2′ are complex and cannot be linearized. It is evident that the rate of such reaction must increase as the rate constant increases, and the decrease in limiting current (or in the area of DPV peak) must be higher at lower AO concentrations.

Therefore, the approach of Gorjanovic et al. and Potkonjak et al.[31−33] seems appropriate for the evaluation of the scavenging activity of antioxidants. In these papers, the slope of the linear part of the curve obtained by plotting the percentage of decrease of polarographic current versus the amount of individual compounds or volume of complex samples was used to express AO activity. This slope was found to be the most relevant and accurate way to express AO activity of samples with large differences in activity and was finally chosen as AO activity criteria. High correlations were reported between the slope and the content of total phenolics and AO activity determined by standard spectrophotometric assay such as FRAP, ABTS, and DPPH.

DPV is a differential technique, this implying that the parameter proportional to the concentration of the species that is oxidized or reduced at the electrode is the peak area.[40] Conversely, as the polarographic limiting current, the peak

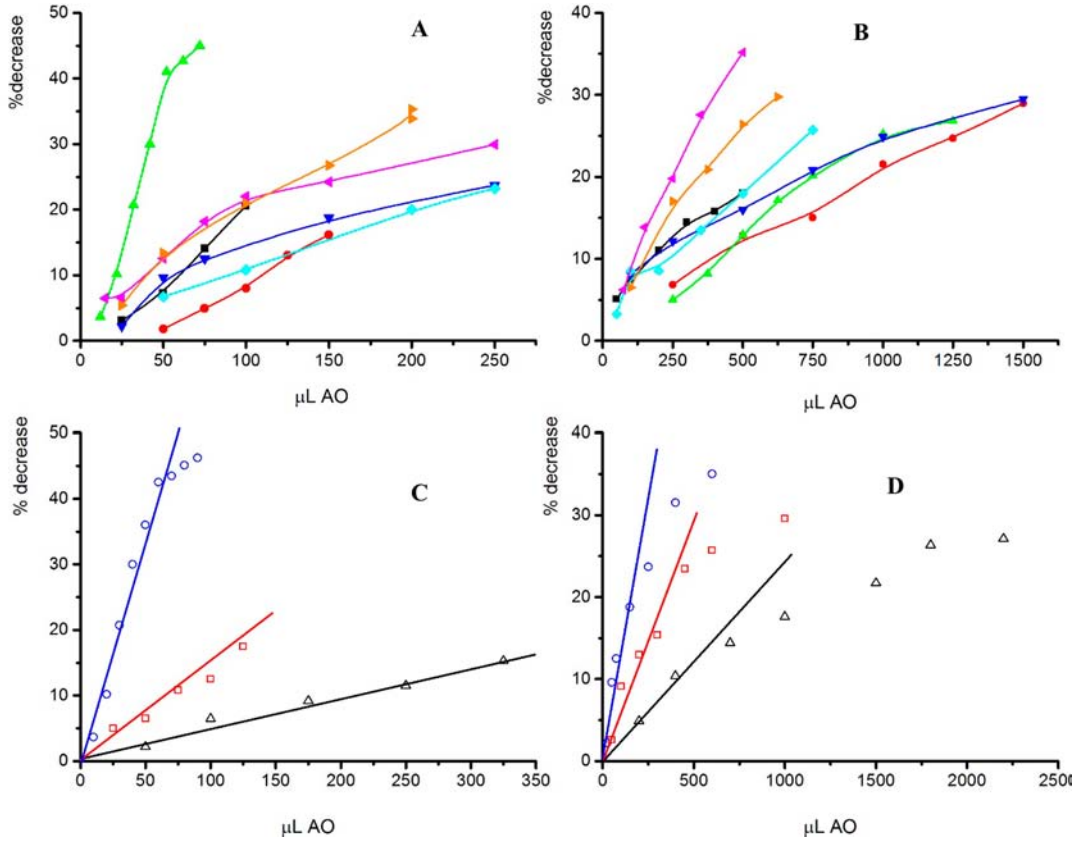

Figure 2. Dependencies of the DPV area of 5×10^{-4} M H_2O_2 after the addition of increasing amounts of antioxidants, relative to the area of the peak in the absence of antioxidant. (A) AO concentration = 5 mM: (green triangles) gallic acid; (magenta triangles) eugenol; (yellow triangles) 3-hydroxycoumarin; (black squares) 2,4-dihydroxybenzaldehyde; (purple triangles) carvacrol; (blue diamonds) cinnamaldehyde; (red circles) 2,5-dihydroxybenzaldehyde. (B) AO concentration = 5 mM: (magenta triangles) thymol; (yellow triangles) vanillin; (black squares) cinnamic acid; (purple triangles) salicylaldehyde; (blue diamonds) sesamol; (green triangles) limonene; (red circles) geraniol. (C) Gallic acid concentrations = (open triangles) 1 mM, (red outline squares) 3 mM, and (open circles) 5 mM. (D) Carvacrol concentrations = (open triangles) 1 mM, (red outline squares) 3 mM, and (open circles) 5 mM.

current depends on the reaction mechanism, at the same concentration, pH, temperature, and ionic strength. The half-width of the DPV peak changes with the AO addition, implying that there is a change in the oxidation mechanism and, so, the change of intensity reflects not only the dependence with the AO concentration but also this change in half-width. Therefore, the parameter to be tested is the DPV peak area.

Panels A and B of Figure 2 show the decrease of the peak area of the DP voltammograms of the DPV oxidation peak obtained for H_2O_2 in mercury electrodes after the addition of increasing amounts of several antioxidants.

Panels C and D of Figure 2 show the decrease of the peak area as a function of the added volume for two selected antioxidants and starting from different concentrations of antioxidant, to study the dependence on this parameter. From these graphs, it follows that the dependence of the decrease with the added volume is roughly linear at low percentages of decrease and is proportional to the initial antioxidant concentration. Therefore, this slope can be used as an AO activity criterion in the same way as in refs 31−33. The calculated slopes are given in Table 1.

To perform the experiments, different concentrations of antioxidants were used, because the more active antioxidants decrease the current below 10% at very low volumes added. Therefore, if this is the case, the essays were repeated after dilution of the antioxidant, allowing the addition of higher volumes and thus permitting a more accurate determination of the C_{10}, that is, the antioxidant concentration at which the area of the H_2O_2 oxidation peak decreases by 10%. The 10% decrease falls in the linear range of the plots shown in Figure 2.

As stated in a previous work,[30] the results obtained by using $1/C_{10}$, ARP, or voltammetric oxidation potentials (E_p) are quite different. Table 1 illustrates this. In this table, the ARP values of the previously essayed compounds have been taken from ref 30 (α- and β-pinene have been tested for this work), and the EP values were determined again for this work, being the same as found previously,[30] as expected.

From Table 1 it follows that there are compounds that do not exhibit measurable ARP or E_p values, but their scavenging activity can be evaluated using $1/C_{10}$. A part of these compounds consists of antioxidants of low scavenging activities. Other compounds such as 3-hydroxycoumarin, 2,4-dihydroxybenzaldehyde, or cinnamaldehyde showed very low ARP values and high oxidation potentials, but the corresponding $1/C_{10}$ values are high, indicating a high scavenging activity. In other cases such as carvacrol and vanillin or eugenol and sesamol, the ARP and the oxidation potentials have similar values, but the $1/C_{10}$ values are quite different. In fact, no evident correlation between ARP and $1/C_{10}$ or between E_p and $1/C_{10}$ has been found.

dx.doi.org/10.1021/jf404578a | J. Agric. Food Chem. 2014, 62, 582−589

Table 1. Values of $1/C_{10}$, Slopes of the Plots of the Decrease of the Peak Area versus the Added Volume, ARP, and Oxidation Potentials versus Ag/AgCl/KCl (3 M) Electrode for the Antioxidants Studied

antioxidant	slope[a]	$1/C_{10}$ (mM^{-1})	ARP[b]	E_p[c] (V)	μ_{10}[d] (mL^{-1})
gallic acid	0.440	102.108	8.500	0.274	45.530
eugenol	0.259	68.243	5.000	0.411	25.590
3-hydroxycoumarin	0.250	53.214		0.763	24.770
2,4-dihydroxybenzaldehyde	0.147	40.400		0.841	20.040
carvacrol	0.165	35.924	0.120	0.522	17.760
cinnamaldehyde	0.128	26.639		0.588	16.480
α-pinene	0.103	22.260	0.100		9.930
2,5-dihydroxybenzaldehyde	0.054	19.688	17.500	0.202	11.200
thymol	0.080	18.685	0.780	0.529	9.100
vainillin	0.067	14.580	0.110	0.584	8.800
cinnamic acid	0.059	14.470			6.590
salicylaldehyde	0.053	12.271		0.860	5.760
sesamol	0.056	12.048	5.500	0.343	5.760
β-pinene	0.035	9.435			4.280
geraniol	0.026	5.383			4.050
limonene	0.021	5.233			2.330

[a] ±1% = average of slope confidence interval. [b] ±0.5% = average of ARP confidence interval. [c] Confidence interval for E_p values was always < ±4 mV. [d] μ_{10} values at concentrations of 5 mM.

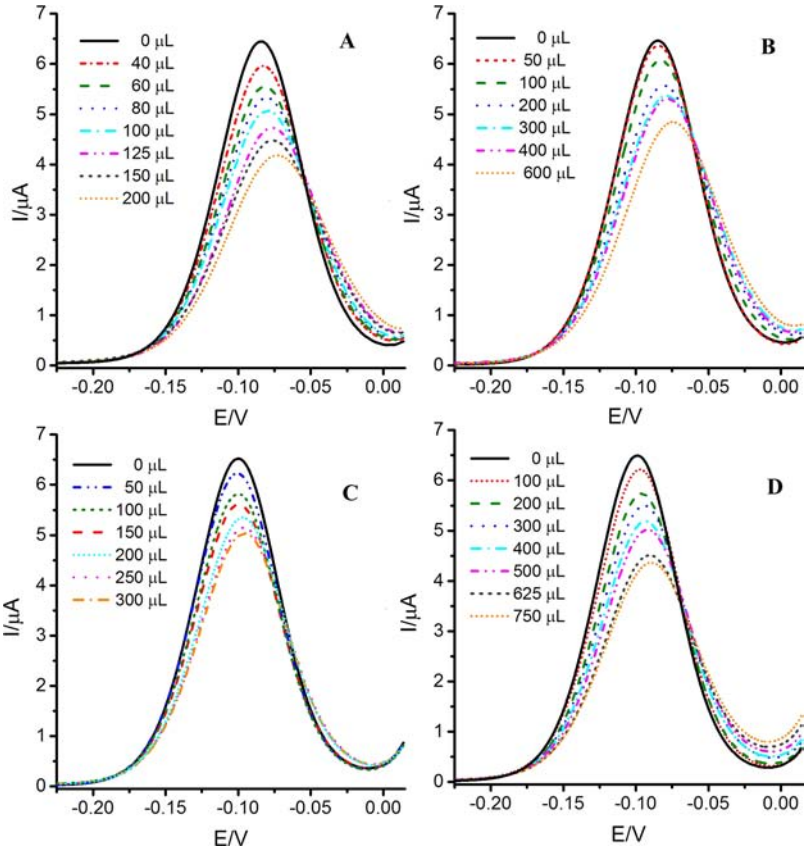

Figure 3. DPV voltammograms of 5×10^{-4} M H_2O_2 and different amounts of antioxidant mixture solution. pH 10.50. 30% ethanol in the medium. AO mixtures: (A) 2.5 mM eugenol + 2.5 mM limonene; (B) 0.5 mM eugenol + 0.75 mM thymol + 0.75 mM sesamol; (C) 0.5 mM eugenol + 0.75 mM thymol + 2 mM limonene; (D) 2.5 mM sesamol + 2.5 mM limonene.

It is known[19] that both ARP and oxidation potentials measure the capacity of a given compound to react with the DPPH• radical. The $1/C_{10}$ parameter is related to the interaction of the antioxidant with the ROS (hydroperoxide radicals).

The method can be easily extended to mixtures of n antioxidants because in this case reaction 2′ will consist of n parallel reactions. In this case, the goal is to establish the scavenging activity of the mixture as a whole, not the individual antioxidant activities. Because the added volume is proportional to the concentrations, the volume necessary to decrease the area of the H_2O_2 oxidation peak by 10%, V_{10}, must be related with the scavenging activity (more precisely,

dx.doi.org/10.1021/jf404578a | J. Agric. Food Chem. 2014, 62, 582−589

the reverse of V_{10}), equivalent to C_{10}. In this work $\mu_{10} = 1/V_{10}$ (expressed in mL^{-1}) is selected to express the antioxidant activity. In this way, higher μ_{10} values indicate higher scavenging activity. This parameter can be also used with individual antioxidants. Table 1 also lists the μ_{10} values corresponding to the antioxidants in the experiments made at concentrations of 5 mM.

Figure 3 shows the DP voltammograms of the H_2O_2 oxidation before and after the addition of increasing volumes of four antioxidant mixtures. Binary and ternary mixtures of antioxidants of high, medium, and low μ_{10} have been investigated. The concentrations were chosen to cover different proportions of compounds having low and high AO activities. As the volume added was increased, the DP peak decreases, and at a high enough volume of mixture added, the area of the peak becomes half of the original area (data not shown).

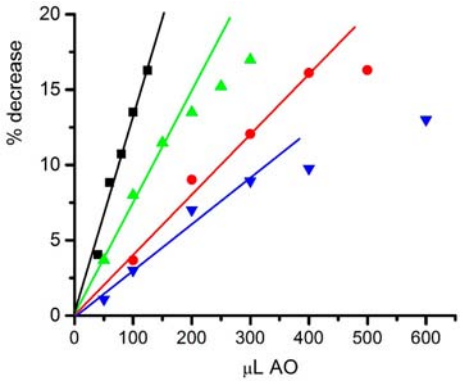

Figure 4. Dependencies of the DPV area of 5×10^{-4} M H_2O_2 after the addition of increasing amounts of antioxidant mixture solution, relative to the area of the peak in the absence of antioxidant. AO mixtures: (black squares) 2.5 mM eugenol + 2.5 mM limonene; (green triangles) 0.5 mM eugenol + 0.75 mM thymol + 2 mM limonene; (red circles) 2.5 mM sesamol + 2.5 mM limonene; (purple triangles) 0.5 mM eugenol + 0.75 mM thymol + 0.75 mM sesamol.

Figure 4 shows the dependence of the peak area of the DP voltammograms of the H_2O_2 oxidation after the addition of increasing volumes of antioxidant mixtures, relative to the area of the peak in the absence of antioxidant, for the same mixtures as in Figure 3.

From these data, the μ_{10} values can be obtained. Table 2 shows these values for a collection of mixtures of four antioxidants, mainly binary combinations.

The scavenging activities of the mixtures must be related, evidently, to the scavenging activities of the antioxidants used. Therefore, an antioxidant having high scavenging activity but in low concentration could contribute to the overall activity of the mixture in less grade than other antioxidants having lower activity, but present in greater concentration. Because the assumption in this work is that μ_{10} values are related with the scavenging activity, "expected" μ_{10} values have been calculated for each mixture from the individual μ_{10} values given in Table 1 and taking into account the concentration of each compound. The results of such calculations are given in Figure 5. The graph shows a correlation between experimental and calculated values. More precisely, there is a proportionality between both values, the slope obtained from the correlation being 1.06, that is, close to unity. This indicates that the μ_{10} parameter is a measure of the scavenging activity, being additive; that is, the overall μ_{10} value of a mixture is constituted by the sum of the μ_{10} values of the individual antioxidants.

Moreover, the proportionality shown in Figure 5 indicates that there are not synergistic effects in the mixtures, at least for the investigated mixtures, but this conclusion must be checked with a wider range of antioxidant mixtures.

The measurements were extended to the aqueous extracts of five spices. Figure 6 and Table 3 summarize the results. As can

Table 2. μ_{10} Values for Mixtures of Antioxidants[a]

mixture	eugenol	limonene	sesamol	thymol	vanillin	μ_{10}[b] (mL^{-1})
1	2.50	2.50	0	0	0	14.57
2	0	0.20	0	0.80	0	1.77
3	0	0.60	0	0.40	0	1.32
4	0	0.40	0	0.60	0	1.25
5	0	1.75	0	0	3.25	7.36
6	1.00	4.00	0	0	0	7.10
7	1.00	2.00	0	1.50	0	9.31
8	1.00	2.00	0	0	0	8.30
9	0	4.00	0	0	1.00	5.50
10	0	2.50	2.50	0	0	4.67
11	0.50	0	0.75	0.50	0	2.75

[a]Entries for each compound correspond to concentrations in millimolar for the mixture in question. [b]±1% = average of μ_{10} confidence interval.

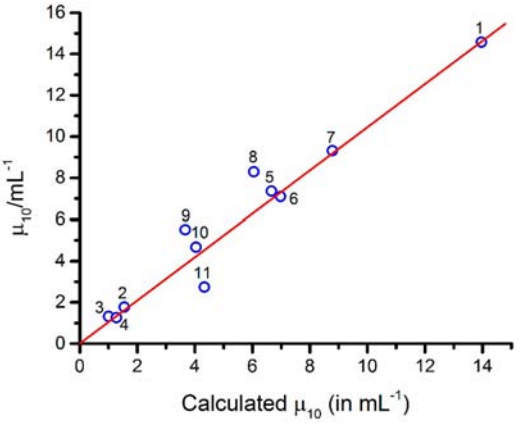

Figure 5. Correlation between experimental and calculated values of the μ_{10} parameter (see text) for the antioxidant mixtures shown in Table 2.

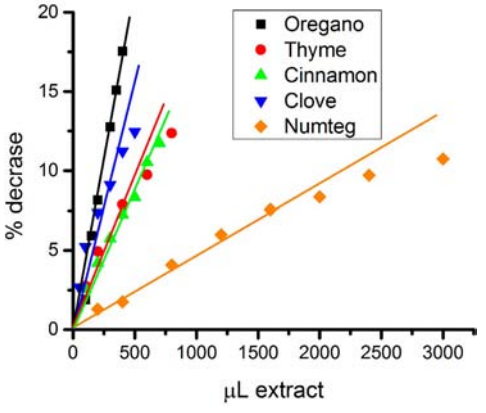

Figure 6. Dependencies of the DPV area of 5×10^{-4} M H_2O_2 after the addition of increasing amounts of aqueous extracts of spices, relative to the area of the peak in the absence of antioxidant.

dx.doi.org/10.1021/jf404578a | J. Agric. Food Chem. 2014, 62, 582−589

Table 3. V_{10} and μ_{10} Values, ARP, and Antioxidants Found in the Extracts for Aqueous Extracts of Spices[40]

spice	V_{10} (μL)	μ_{10} (mL^{-1})	ARP (mg^{-1})	main antioxidants	
oregano	23.10	43.29	5.25	*p*-cymene	12%
				thymol	5%
				carvacrol	49%
clove	32.40	30.86	16.23	*β*-caryophyllene	7%
				eugenol	83%
				acetyleugenol	8%
thyme	51.70	19.34	21.81	p-cymene	27%
				linalool	6%
				thymol	46%
cinnamon	56.80	17.61	16.02	*β*-caryophyllene	5%
				cinnamaldehyde	68%
				eugenol	7%
numteg	219.20	4.56	10.40	*α*-pinene	21%
				β-pinene	15%
				sabinene	19%
				terpinen-4-ol	4%

be seen, at low values of decrease, the plot shown in Figure 6 is roughly linear. From these experiments, μ_{10} values have been calculated for each extract and have been gathered in Table 3. In the table are also given the ARP values obtained from the DPPH$^{\bullet}$ experiments but not the oxidation potentials, because the voltammograms were complex and showed more than one oxidation peak.

In general, the sequence of μ_{10} values is related to the contents in antioxidants of the different spices, but it is important to note that such contents correspond to essential oils, not to aqueous extracts,[42] and the proportions must vary from one extraction mode to another. Nevertheless, when the spices are used as food condiments, they act essentially as aqueous extracts rather than nonaqueous essential oils.

AUTHOR INFORMATION

Corresponding Author

*(M.R.M.) Phone: +34 959 21 82 02. Fax: +34 959 21 99 83. E-mail: mmontoya@diq.uhu.es.

Funding

Financial support from Junta de Andalucía (Research Groups FQM-0198 and RNM-371) is gratefully acknowledged.

Notes

The authors declare no competing financial interest.

REFERENCES

(1) Barzilai, A.; Yamamoto, K. DNA damage responses to oxidative stress. *DNA Repair* **2004**, *3* (8−9), 1109−1115.

(2) Sies, H. Oxidative stress. Introductory remarks. In *Oxidative Stress*; Sies, H., Ed.; Academic Press: London, UK, 1985; pp 1−8.

(3) Halliwell, B.; Gutteridge, J. M. C. In *Free Radicals in Biology and Medicine*, 3rd ed.; Clarendron Press: Oxford, UK, 1989; pp 18−28.

(4) Ahmed, R. S.; Seth, V.; Banerjee, B. D. Influence of dietary ginger (*Zingiber officinales* Rosc) on oxidative stress induced by malathion in rats. *Food Chem. Toxicol.* **2000**, *38*, 443−450.

(5) Modak, M.; Dixit, P.; Londhe, J.; Ghaskadbi, S.; Paul, A.; Devasagayam, T. Indian herbs and herbal drugs used for the treatment of diabetes. *J. Clin. Biochem. Nutr.* **2007**, *40*, 163−173.

(6) Gutteridge, J. M.; Halliwell, B. Free radicals and antioxidants in the year 2000 − a historical look to the future. *Ann. N.Y. Acad. Sci.* **2000**, *899*, 136−144.

(7) Mukhtar, H.; Ahmad, N. Green tea in chemoprevention of cancer. *Toxicol. Sci.* **1999**, *52*, 111−117.

(8) Visioli, F.; Galli, C. Free radical-scavenging actions of olive oil phenolics. *Lipids* **1999**, *34*, S315.

(9) Brash, D. E.; Havre, P. A. New careers for antioxidants. *Proc. Natl. Acad. Sci. U.S.A.* **2002**, *99*, 13969−13971.

(10) Owuor, E. D.; Kong, A. T. Antioxidants and oxidants regulated signal transduction pathways. *Biochem. Pharmacol.* **2002**, *64*, 760−770.

(11) Antolovich, M.; Prenzler, P. D.; Patsalides, E.; McDonald, S.; Robards, K. Methods for testing antioxidant activity. *Analyst* **2002**, *127*, 183−198.

(12) Ortiz, M. E.; Núñez-Vergara, L. J.; Squella, J. A. Relative reactivity of dihydropyridine derivatives to electrogenerated superoxide ion in DMSO solutions: a voltammetric approach. *Pharm. Res.* **2003**, *20*, 292−296.

(13) Ortiz, M. E.; Núñez-Vergara, L. J.; Camargo, C.; Squella, J. A. Oxidation of Hantzsch 1,4-dihydropyridines of pharmacological significance by electrogenerated superoxide. *Pharm. Res.* **2004**, *21*, 428−435.

(14) Bollo, S.; Jara-Ulloa, P.; Finger, S.; Núñez-Vergara, L. J.; Squella, J. A. Scanning electrochemical microscopy (SECM) study of superoxide generation and its reactivity with 1,4-dihydropyridines. *J. Electroanal. Chem.* **2005**, *577*, 235−242.

(15) Yakovleva, K. E.; Kurzeev, S. A.; Stepanova, E. V.; Fedorova, T. V.; Kuznetsov, B. A.; Koroleva, O. V. Characterization of plant phenolic compounds by cyclic voltammetry. *Appl. Biochem. Microbiol.* **2007**, *43*, 661−668.

(16) Bortolomeazzi, R.; Sebastianutto, N.; Toniolo, R.; A. Pizzariello, A. Comparative evaluation of the antioxidant capacity of smoke flavouring phenols by crocin bleaching inhibition, DPPH radical scavenging and oxidation potential. *Food Chem.* **2007**, *100*, 1481−1489.

(17) Kilmartin, P. A.; Zou, H. L.; Waterhouse, A. L. Correlation of wine phenolic composition versus cyclic voltammetry response. *Am. J. Enol. Vitic.* **2002**, *53*, 294−302.

(18) Kilmartin, P. A.; Zou, H. L.; Waterhouse, A. L. A cyclic voltammetry method suitable for characterizing antioxidant properties of wine and wine phenolics. *J. Agric. Food Chem.* **2001**, *49*, 1957−1965.

(19) Arteaga, J. F.; Ruiz Montoya, M.; Palma, A.; Alonso Garrido, G.; Pintado, S.; Rodríguez Mellado, J. M. Comparison of the simple cyclic voltammetry (CV) and DPPH assays for the determination of antioxidant capacity of active principles. *Molecules* **2012**, *17*, 5126−5138.

(20) Rapoport, R.; Hanukoglu, I.; Sklan, D. A fluorimetric assay for hydrogen peroxide, suitable for NAD(P)H-dependent superoxide generating redox systems. *Anal. Biochem.* **1994**, *218*, 309−313.

(21) Moure, A.; Dominguez, H.; Parajo, J. C. Antioxidant properties of ultrafiltration-recovered soy protein fractions from industrial effluents and their hydrolysates. *Process Biochem.* **2006**, *41*, 447−456.

(22) Guo, H.; Kouzuma, Y.; Yonekura, M. Structures and properties of antioxidative peptides derived from royal jelly protein. *Food Chem.* **2009**, *113*, 238−245.

(23) Suetsuna, K.; Ukeda, H.; Ochi, H. Isolation and characterization of free radical scavenging activities peptides derived from casein. *J. Nutr. Biochem.* **2000**, *11*, 128−131.

(24) Ukeda, H.; Maeda, S.; Ishii, T.; Sawamura, M. Spectrophotometric assay for superoxide dismutase based on tetrazolium salt 3′-{1-[(phenylamino)-carbonyl]-3,4-tetrazolium}-bis(4-methoxy-6-nitro)-benzenesulfonic acid hydrate reduction by xanthine-xanthine oxidase. *Anal. Biochem.* **1997**, *251*, 206−209.

(25) Sužnjević, D. Ž.; Pastor, F. T.; Gorjanović, S. Ž. Polarographic study of hydrogen peroxide anodic current and its application to antioxidant activity determination. *Talanta* **2011**, *85*, 1398−1403.

(26) Gorjanović, S. Ž.; Novaković, M. M.; Potkonjak, N. I.; Leskošek-Čukalović, I.; Sužnjević, D. Ž. Application of a novel antioxidative

assay in beer analysis and brewing process monitoring. *J. Agric. Food Chem.* **2010**, *58*, 744−751.
(27) Gorjanović, S. Ž.; Novaković, M. M.; Potkonjak, N. I.; Sužnjević, D. Ž. Antioxidant activity of wines determined by a polarographic assay based on hydrogen peroxide scavenge. *J. Agric. Food Chem.* **2010**, *58*, 4626−4631.
(28) Gorjanović, S. Ž.; Novaković, M. M.; Vikosavijević, P. V.; Pastor, F. T.; Tešević, V. V.; Sužnjević, D. Ž. Polarographic assay based on hydrogen peroxide scavenging in determination of antioxidant activity of strong alcohol beverages. *J. Agric. Food Chem.* **2010**, *58*, 8400−8406.
(29) Novaković, M. M.; Stevanović, S. M.; Gorjanović, S. Ž.; Jovanovic, P. M.; Tešević, V. V.; Janković, M. A.; Sužnjević, D. Ž. Changes of hydrogen peroxide and radical-scavenging activity of raspberry during osmotic, convective, and freeze-drying. *J. Food Sci.* **2011**, *76*, C663−C668.
(30) Palma, A.; Ruiz Montoya, M.; Arteaga, J. F.; Rodríguez Mellado, J. M. Analysis of the interaction of radical scavengers with ROS electrogenerated from hydrogen peroxide. *J. Electrochem. Soc.* **2013**, *160*, H213−H218.
(31) Potkonjak, N. I.; Veselinović, D. S.; Novaković, M. M.; Gorjanović, S.; Pezo, L.; Sužnjević, D. Antioxidant activity of propolis extracts from Serbia: a polarographic approach. *Food Chem. Toxicol.* **2012**, *50*, 3614−3618.
(32) Gorjanović, S.; Komes, D.; Pastor, F. T.; Belščak-Cvitanović, A.; Pezo, L.; Hečimović, I.; Sužnjević, D. Antioxidant capacity of teas and herbal infusions: polarographic assessment. *J. Agric. Food Chem.* **2012**, *60*, 9573−9580.
(33) Gorjanović, S.; Alvarez-Suarez, J. M.; Novaković, M. M.; Pastor, F. T.; Pezo, L.; Battino, M.; Sužnjević, D. Comparative analysis of antioxidant activity of honey of different floral sources using recently developed polarographic and various spectrophotometric assays. *J. Food Compos. Anal.* **2013**, *30*, 13−18.
(34) Kikuchi, K.; Murayama, T. Polarographic anodic wave of hydrogen peroxide in alkaline solutions. *Bull. Chem. Soc. Jpn.* **1976**, *49*, 1554−1556.
(35) Cherng, J.; Chiang, W.; Chiang, L. Immunomodulatory activities of common vegetables and spices of umbelliferae and its related coumarins and flavonoids. *Food Chem.* **2008**, *106*, 944−950.
(36) Ho, S.; Tang, Y.; Lin, S.; Liew, Y. Evaluation of peroxynitrite-scavenging capacities of several commonly used fresh spices. *Food Chem.* **2010**, *119*, 1102−1107.
(37) Madsen, H. L.; Bertelsen, G. Spice as antioxidants. *Trends Food Sci. Technol.* **1995**, *6*, 271−277.
(38) Ringman, J. M.; Frautschy, S. A.; Cole, G. M.; Masterman, D. L.; Cummings, J. L. Potential role of the curry spice curcumin in Alzheimer's disease. *Curr. Alzheimer's Res.* **2005**, *2*, 131−136.
(39) McKillop, A.; Young, D. W. Oxidation of phenols and hydroquinones by mercury(II) trifluoroacetate and mercury(II) oxide. *Synth. Commun.* **1977**, *7*, 467−474.
(40) Behr, B.; Taraszewska, J. On the anodic oxidation of mercury in KCl solutions. *J. Electroanal. Chem.* **1968**, *19*, 373−384.
(41) Bard, A. J.; Faulkner, L. R. *Electrochemical Methods: Fundamentals and Applications*, 2nd ed.; Wiley: Hoboken, NJ, USA, 2000.
(42) Tomaino, A.; Cimino, F.; Zimbalatti, V.; Venuti, V.; Sulfaro, V.; De Pasquale, A.; Saija, A. Influence of heating on antioxidant activity and the chemical composition of some spice essential oils. *Food Chem.* **2005**, *89*, 549−554.

JOURNAL OF AGRICULTURAL AND FOOD CHEMISTRY

Article

pubs.acs.org/JAFC

New Method for the Extraction of Volatile Lipid Oxidation Products from Shrimp by Headspace−Solid-Phase Microextraction−Gas Chromatography−Mass Spectrometry and Evaluation of the Effect of Salting and Drying

Hugo A. L. Souza and Neura Bragagnolo*

Department of Food Science, Faculty of Food Engineering, University of Campinas, 13083-862 São Paulo, Brazil

Supporting Information

ABSTRACT: A new method based on headspace−solid-phase microextraction (HS−SPME) and gas chromatography−mass spectrometry (GC−MS) was developed, aimed at evaluating the formation of volatile lipid oxidation products (VLOPs) in shrimp during the salting and drying process. Of the four fibers evaluated, the fiber coated with divinylbenzene/carboxen/polydimethylsiloxane (DVB/CAR/PDMS) was the most adequate for the quantification of the VLOPs. The best analytical conditions were obtained by homogenization in an ultraturrax followed by extraction at 40 °C for 30 min. The optimized method allowed for the rapid and simple extraction of the VLOPs, with low detection (≤0.15 ng g^{-1}) and quantification (≤0.50 ng g^{-1}) limits and satisfactory precision (≤12.67%) and extraction efficiency (≥94.28%). The salting and drying negatively affected shrimp quality, reducing the fatty acid content and increasing the VLOPs, especially hexanal.

KEYWORDS: *volatile compounds, pacific white shrimp, Litopenaeus vannamei, method validation, arachidonic acid, eicosapentaenoic acid, docosahexaenoic acid*

INTRODUCTION

Shrimp represents about 15% of the fisheries commercialized throughout the world, being the most economically important international fishing and aquiculture product.[1] However, shrimp deteriorates easily; thus, it must be submitted to some kind of preservation method to increase its shelf life.[2] Among the preservation methods, salting followed by drying stands out because it allows for storage of the shrimp at room temperature for various days.[3]

Drying or dehydration is one of the oldest and most important unit operations in the food industry, which, by decreasing the water activity, reduces microbial growth and the speed of chemical and enzymatic reactions.[4] However, the addition of salt and application of heat can accelerate lipid oxidation, with the formation of products with off-flavors, and cause the loss of some nutritional properties.[5]

Despite its low lipid content (0.70−1.16 g/100 g), the lipid fraction of shrimp is rich in polyunsaturated fatty acids (PUFA), such as eicosapentaenoic acid (EPA, 20:5ω-3), docosahexaenoic acid (DHA, 22:6ω-3), and arachidonic acid (ARA, 20:4ω-6), making it highly susceptible to lipid oxidation.[6−8]

Various compounds are formed during lipid oxidation, and of these, those with the greatest impact on the sensory quality of foods are the short-chain volatile products formed from the β-cleavage of hydroperoxides.[9] In addition, analysis of these secondary lipid oxidation products presented good correlation with the more traditional analyses, such as the peroxide index (PI), the 2-thiobarbituric acid reactive substances (TBARS) test,[10,11] and the sensory analysis.[12]

Headspace−solid-phase microextraction (HS−SPME) is widely used in the analysis of volatile compounds in foods[13] and consists of the use of a fiber with a very small diameter covered by a stationary phase, which, upon being exposed to the headspace of a sample, adsorbs the volatile analytes, which are thermally desorbed directly in the gas chromatograph (GC) injector.[14,15] Among the advantages of SPME, short analysis time, absence of solvents, and high sensitivity and selectivity stand out, in relation to traditional techniques.[13]

Exhaustive extraction of the analytes does not occur during SPME, but equilibrium is formed between the sample and the stationary phase of the fiber. Various factors can affect this equilibrium, such as the type of stationary phase and the extraction time and temperature, and therefore, a careful study is required to establish a SPME method.[10,16]

Thus, the objective of the present work was to establish a headspace−solid-phase microextraction−gas chromatography−mass spectrometry (HS−SPME−GC−MS) method to quantify the volatile lipid oxidation products (VLOPs) in shrimp and, with the aid of this technique, evaluate the effect of processing on the lipid fraction of salted and salted, dried shrimp.

MATERIALS AND METHODS

Reagents and Materials. The alkane series (C_5−C_{24}) used to calculate the retention index was obtained from Polyscience (New Haven, CT). The standards used to identify and quantify the volatile compounds were pentanal, 2-methylpentanal [internal standard (IS)], hexanal, 1-penten-3-ol, heptanal, 2-pentylfuran, 1-pentanol, octanal, 1-hexanal, nonanal, 1-octen-3-ol, 1-heptanol, decanal, 1-octanol, and 2-octen-1-ol from Sigma Aldrich (St. Louis, MO). The purity of

Received: September 23, 2013
Revised: December 19, 2013
Accepted: December 19, 2013
Published: December 19, 2013

ACS Publications © 2013 American Chemical Society

standards varied from 95 to 99%. The fibers carboxen/polydimethylsiloxane (CAR/PDMS), divinylbenzene/carboxen/polydimethylsiloxane (DVB/CAR/PDMS), polyacrylate (PA), and polydimethylsiloxane/divinylbenzene (PDMS/DVB) were acquired from Supelco (Bellefonte, PA). A total of 37 saturated, monounsaturated, and polyunsaturated fatty acid methyl ester standards (C_4−C_{24}, Sulpeco 37-Component FAME Mix, catalog number 18919-1) were used to identify the fatty acids, and methyl undecanoate and methyl tricosanoate (Sigma Aldrich) were used to quantify the fatty acids. The reagents and solvents used were of analytical grade (Synth, Diadema, São Paulo, Brazil) or high-performance liquid chromatography (HPLC) grade (Fisher, Fair Lawn, NJ), and the water was purified by the Millipore Milli-Q system (Billerica, MA).

Samples. The volatile compound extraction method was optimized using salted and dried pacific white shrimp (*Litopenaeus vannamei*). The fresh and whole shrimp (1.0 kg with head and shell) was obtained from the local market in Campinas (São Paulo, Brazil) and was submitted to salting in boiling water (30% NaCl for 10 min) and drying in an air-circulating oven at 60 °C for 4 h. A new sample was prepared with fresh shrimp for each step of optimization.

To evaluate the effects of processing on the shrimp lipids, two new batches, each of 1.5 kg of fresh shrimp, were acquired from the same place with an interval of 1 week. Again, each batch was separated into three parts (500 g each, ∼25 shrimps), one fresh, another just salted, and the third salted and dried. The shrimp processing was identical to that used in the method optimization step. The moisture content was carried out according to the Association of Official Analytical Chemists (AOAC) method 950.46.[25] The moisture content of fresh samples was 75.75 ± 0.22 g/100 g at batch 1 and 76.41 ± 0.16 g/100 g at batch 2; the moisture content of salted shrimp was 63.68 ± 0.11 g/100 g at batch 1 and 62.34 ± 0.38 g/100 g at batch 2; and the moisture content of salted, dried shrimp was 50.84 ± 0.18 g/100 g at batch 1 and 47.57 ± 0.15 g/100 g at batch 2.

Optimization of the Analysis of the Volatiles by HS−SPME−GC−MS. To establish the method used to extract the volatile compounds by SPME, three factors that affect the extraction performance were evaluated in sequence: the type of stationary phase used to coat the fiber, the sample preparation method, and the extraction time/temperature binomial, using the best condition obtained in the previous step for the subsequent step.

Fibers coated with four different materials were tested to choose the best fiber for the above purpose: CAR/PDMS, DVB/CAR/PDMS, PA, and PDMS/DVB. The fibers were first conditioned according to the instructions of the manufacturer. The extraction procedure was carried out in the same way for all of the fibers (n = 6). The salted, dried shrimp (100 g) was peeled and ground, and 1 g of ground sample was placed in a vial [20 mL with a screw top and polytetrafluoroethylene (PTFE) septum, Supelco, Bellefonte, PA]. The vial was then incubated for 15 min at 40 °C, and then the fiber was exposed for 30 min to headspace (HS), followed by desorption directly in the injector for 1 min at 250 °C. After each desorption, the fibers were reconditioned for 10 min at 250 °C in a flow of He. The whole extraction step was carried out using an AOC-5000 autoinjector (Shimadzu, Kyoto, Japan).

Three sample preparation procedures were tested: in the first, 1 g of shrimp was sealed in a vial; in the second, 3 mL of ultrapure water was added to the shrimp (1 g), which was then sealed and homogenized in a vortex (Phoenix Luferco, São Paulo, Brazil) for 1 min; and in the third, 30 mL of ultrapure water was added to 10 g of sample in a beaker and homogenized in a high-speed ultraturrax (Jankel and Kunkel GmbH, Staufen, Germany) for 1 min at 12 000 rpm and 4 g of this mixture was placed in a vial and sealed. In the three cases, the volatiles were extracted in the same condition as that employed in the selection of the fiber (n = 3).

To evaluate the influence of time and temperature on the extraction of the volatile compounds by HS−SPME, analyses were carried out at 40, 60, and 80 °C for 15, 30, 60, and 120 min in random, independent trials using the fiber and sample preparation mode that gave the best results (n = 3).

GC−MS. The chromatographic analysis was carried out in GC coupled to mass spectrometer (MS, GCMS-QP2010 Ultra Shimadzu, Kyoto, Japan), equipped with a splitless injector at 250 °C, RTX-Wax capillary column (30 m × 0.25 mm inner diameter, 0.20 μm thick stationary phase, polyethylene glycol, Restek, Bellefonte, PA), workstation (GCMSSolution, Shimadzu, Kyoto, Japan), and ion source in the electron ionization (EI) mode at 70 eV and 250 °C, cutting the solvent after 1.1 min. The mass/charge (m/z) analyzer was quadrupole, operating in the scanning mode (SCAN = m/z 35−350) to identify the compounds and in the selected ion monitoring (SIM) mode for quantification. Helium was used as the carrier gas in the linear flow control mode with a constant column flow of 1.22 mL/min. The oven temperature program started at 30 °C for 5 min, followed by heating at 10 °C/min to 115 °C, maintaining at this temperature for 1 min, then heating at 30 °C/min to 220 °C, and maintaining at this temperature for 12 min, giving a total time of 30 min. The temperature program of the oven was based on the study by Shahidi and Pegg,[17] with changes in the initial and final temperatures.

The volatile compounds were identified by comparison of the mass spectra obtained for the samples to the mass spectra of the analytical standards under the same experimental conditions and those from the mass spectra library (Wiley9). In addition, an alkane series (C_5−C_{24}) was used to calculate the retention index (RI) for each compound with the RTX-Wax column[18] and compared to those found in the literature for columns with the same polarity.[19,20] The compounds that presented mass spectra similar to those in the library but differed from the literature with respect to the RI were considered to be tentatively identified.[21]

The VLOPs were quantified using analytical curves obtained with the respective standards added to the sample, using 2-methylpentanal as the IS in the SIM mode and the fragments that gave the best signal/noise ratio for each compound (Table 1).

Table 1. Standard RIs and Fragments Used To Quantify the VLOPs

peak	compound name	RI[a]	target fragment (m/z)	reference fragments (m/z)
1	pentanal	962	58	41; 44
IS[b]	2-methylpentanal	986	58	41; 43
2	hexanal	1069	56	41; 57
3	1-penten-3-ol	1156	57	29; 31
4	heptanal	1169	70	41; 57
5	2-pentylfuran	1214	81	82; 138
6	1-pentanol	1243	42	55; 70
7	octanal	1270	84	41; 56
8	1-hexanol	1341	56	42; 55
9	nonanal	1376	57	41; 56
10	1-octen-3-ol	1441	57	43; 72
11	1-heptanol	1447	70	55; 56
12	decanal	1487	57	55; 82
13	1-octanol	1551	56	55; 70
14	2-octen-1-ol	1606	57	43; 55

[a]RI = retention index. [b]IS = internal standard.

Validation. The optimized method for extracting the VLOPs (DVB/CAR/PDMS, ultraturrax, at 40 °C for 30 min) was submitted to validation by way of the following criteria: linearity, detection and quantification limits, repeatability, and recovery. Samples of salted, dried shrimp prepared on the same day as the analysis were used for validation.

The analytical curve was elaborated by the addition of external standards to the sample in the concentration range from 1 to 80 ng g^{-1} with the addition of 100 ng g^{-1} of 2-methylpentanal as the IS. The detection and quantification limits were calculated on the basis of the signal-to-noise ratio (S/N) with S/N = 3 and 10, respectively. Repeatability was expressed as the relative standard deviation (% RSD; n = 6). To calculate the recovery, samples were fortified with standards

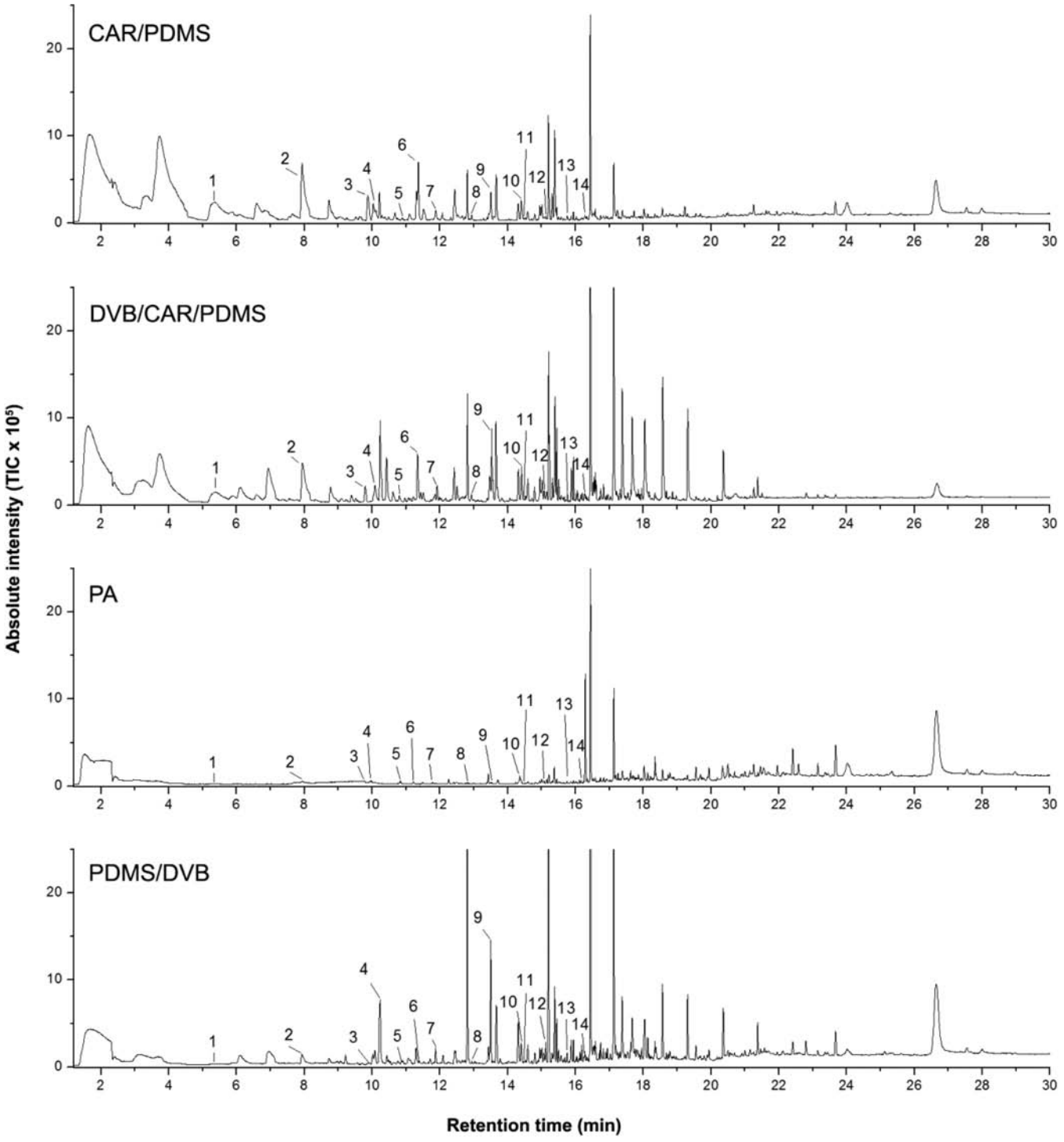

Figure 1. Chromatograms of the volatile compounds obtained from salted, dried shrimp by HS−SPME−GC−MS (scan m/z 35−350) according to the fiber used. Compounds are numbered according to Table 1.

in two levels (5 and 20 ng g^{-1}) and the response was subtracted from the mean result of not fortified samples (n = 6).

Fatty Acid Composition of the Shrimp Lipids. For the three samples of the two batches, the lipids were obtained according to the study by Folch et al.,[22] with the analyses being carried out in triplicate (n = 3). After extraction, the lipids (25 ± 1 mg) were converted into FAME according to Joseph and Ackman[23] and injected into GC using the hot needle technique for 5 s. The chromatograph used was the GC-2010 (Shimadzu, Kyoto, Japan) equipped with a split injector ($^1/_{50}$) at 250 °C, fused silica CP-SIL 88 capillary column (100 m × 0.25 mm inner diameter, 0.20 μm thick stationary phase, cyanopropyl, Chromopack, Middleburg, Netherlands), flame ionization detector at 260 °C, and workstation (GCSolution, Shimadzu, Kyoto, Japan). The temperature was programmed according to the study by Sancho et al.,[24] with H_2 as the carrier gas at a linear velocity of 34 cm/s and N_2 as the makeup gas at 30 mL/min. The fatty acids were identified by comparison of the retention times to those of the standards. Quantification was performed by internal standardization (11:0 and 23:0). The fatty acid concentrations were calculated according to the AOAC method,[25] and the results were expressed as milligrams of fatty acid per gram of lipid.

Statistical Analysis. The results were compared using the one-way analysis of variance (ANOVA) followed by Tukey's test in the case of

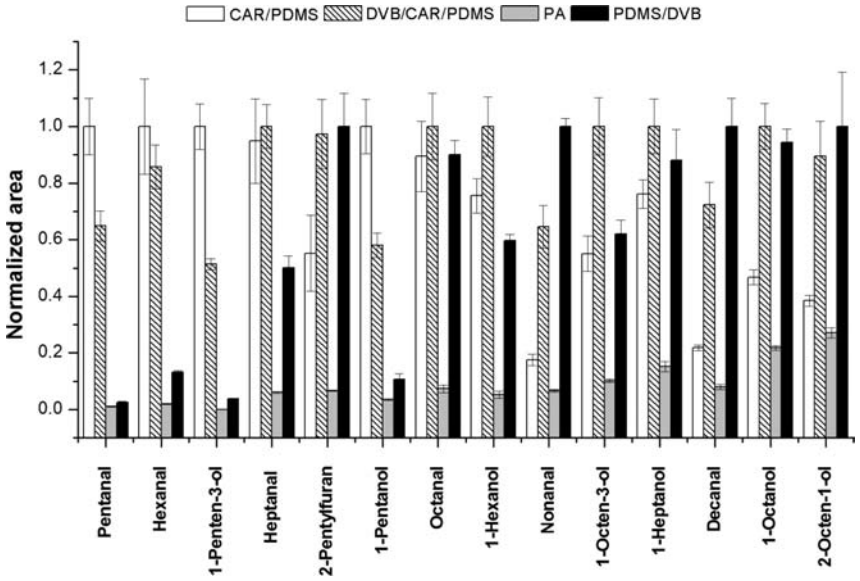

Figure 2. Effect of fiber coating in the extraction of VLOPs from salted, dried shrimp (obtained in the SIM mode; $n = 6$). Compounds are placed in order of increasing RI from left to right.

significant differences ($p < 0.05$). The ANOVA and the fit of the analytical curves were carried out with the aid of the Statistica 5.0 software (Statsoft, Tulsa, OK).

RESULTS AND DISCUSSION

Optimization of the HS–SPME Method. A total of 123 volatile compounds were found in the salted, dried shrimp (65 with the CAR/PDMS fiber, 64 with DVB/CAR/PDMS, 67 with PA, and 81 with PDMS/DVB; see Table S1 of the Supporting Information). Of those compounds, 14 (7 alcohols, 6 aldehydes, and 1 furan) could be classified as VLOPs (Table 1 and Figure 1).[26−28] Hexanal, heptanal, and 1-octen-3-ol were also found in cooked lobsters.[29,30] Dried shrimp of the species *Acetes chinensis* presented 1-penten-3-ol, 1-pentanol, 1-hexanol, and 1-octen-3-ol among their volatiles.[31]

The fiber coated with CAR/PDMS showed the best results for the VLOPs with the lowest RI values (Figure 2), whereas the fiber coated with PDMS/DVB presented the best results for the compounds with higher RI values, and the fiber coated with PA presented smaller areas for all of the compounds. However, the fiber coated with DVB/CAR/PDMS presented good results in a broader range of RI than the other fibers. Similar results were reported by Garcia-Esteban et al.,[32] where the CAR/PDMS fiber gave the best results for compounds with RI values below 980 and the DVB/CAR/PDMS fiber was better for compounds with higher RI values.

Thus, the DVB/CAR/PDMS fiber was considered to be the most adequate for the extraction of VLOPs from salted, dried shrimp. A total of 49 compounds were identified, and 15 were tentatively identified with this fiber, which are listed with their respective RI values in Table 2.

Sample preparation before SPME also influences the extraction yield of VLOP (Figure 3). Vortex homogenization with water resulted in the smallest area values and the highest RSD values (19.22% on average). The shrimp without water addition presented the largest areas for 2-pentylfuran, octanal, and 1-hexanol, whereas the shrimp homogenized with water in the ultraturrax showed the largest areas for 1-heptanol, 1-octanol, and 2-octen-1-ol. In these cases, no difference was observed for the areas between the other VLOPs. Nevertheless, the sample without water addition presented a mean RSD higher (8.47%) than that of the sample homogenized with water in the ultraturrax (2.34%). The difference in the results of the sample homogenized in the vortex and the ultraturrax can be attributed to the fact that, after a few minutes, the sample homogenized with vortex separated in two layers (liquid phase at the top and solid phase at the bottom). Probably, the liquid phase containing water hampered the volatile compounds to migrate to the headspace, leading to lower extraction; however, a homogeneous slurry was formed when the ultraturrax was used.

Both the temperature and the exposition time of the fiber in the HS of the sample significantly influenced the quantity of volatiles extracted. All of the VLOPs showed similar behavior to hexanal with the exception of pentanal, 1-penten-3-ol, and 1-pentanol. The increase in the temperature and extraction time provoked an increase in the area (Figure 4A). The five-carbon VLOPs (pentanal, 1-penten-3-ol, and 1-pentanol) probably did not interact with the fiber coating in the same way as the compounds with higher molecular masses, although their extraction was also affected by the time and temperature (see Figure S2 of the Supporting Information). The extraction time was not sufficient to reach equilibrium, which could take more than 5 h for the fiber used (DVB/CAR/PDMS). Moreover, long extraction times could cause the formation of a high amount of VLOPs, such as hexanal and nonanal,[33] while shorter extraction times make the analysis more acceptable for practical ends.[32]

After 30 min of extraction (Figure 4B), the RSD was lower, principally for the extractions at 40 and 80 °C, and no improvement in repeatability was achieved after this extraction time. Although the use of higher temperatures allowed for greater extraction of the volatile compounds, lower temperatures avoided the formation of VLOPs during extraction.[34,35] The use of lower temperatures (<50 °C) also allowed for better correlation with the sensory profile.[9]

Validation. The method (using DVB/CAR/PDMS fiber, homogenization with water using ultraturrax, and extraction at 40 °C for 30 min) showed good linearity for all of the VLOPs (the coefficient of determination varied from 0.9637 to 0.9978; Table 3). The detection limits varied from 0.03 to 0.15 ng g^{-1},

dx.doi.org/10.1021/jf404270f | J. Agric. Food Chem. 2014, 62, 590−599

Table 2. Volatile Compounds Obtained from Salted, Dried Shrimp by HS−SPME−GC−MS Using the Fiber DVB/CAR/PDMS

compound	RT[a] (min)	RI[b]	identification method
	Acids		
3-methylbutanoic acid	16.63	1659	MS + RI[c]
stearic acid	26.63	>2400	MS[d]
pentadecanoic acid	28.97	>2400	MS
	Alcohols		
1-butanol	9.47	1140	MS + RI
1-penten-3-ol[e]	9.77	1156	standard[f]
1-pentanol[e]	11.34	1243	standard
cyclopentanol	12.31	1302	MS + RI
1-hexanol[e]	12.89	1341	standard
2,6-dimethyl-1,7-octadiene-3,6-diol	14.05	1419	MS
1-octen-3-ol[e]	14.39	1441	standard
1-heptanol[e]	14.48	1447	standard
2,6-dimethyl-7-octen-2-ol	14.71	1463	MS + RI
1,5-octadien-3-ol	14.94	1478	MS + RI
2-ethyl-1-hexanol	15.00	1482	MS + RI
2,6-dimethyl-2,7-octadien-6-ol	15.65	1540	MS + RI
1-octanol[e]	15.75	1551	standard
2-(2-ethoxyethoxy)-ethanol	16.27	1608	MS + RI
2-octen-1-ol[e]	16.34	1618	standard
2-cycloocten-1-ol	16.74	1675	MS
1-octadecanol	23.67	>2400	MS
	Aldehydes		
2-methylbutanal	3.72	844	MS + RI
pentanal[e]	5.35	962	standard
hexanal[e]	7.93	1069	standard
heptanal[e]	10.02	1169	standard
4-heptenal	11.11	1230	MS + RI
octanal[e]	11.78	1270	standard
nonanal[e]	13.42	1376	standard
decanal[e]	15.07	1487	standard
benzaldehyde	13.37	1511	MS + RI
palmitaldehyde	19.55	2132	MS + RI
heptadecanal	21.26	2302	MS
	Cyclic Hydrocarbons		
ethylbenzene	8.73	1101	MS + RI
1,4-dimethylbenzene	9.04	1117	MS + RI
cyclododecane	11.05	1226	MS + RI
styrene	11.29	1241	MS + RI
1-methylnaphthalene	17.78	1779	MS
	Esters		
vinyl hexanoate	12.46	1312	MS + RI
2,2,4-trimethyl-1,3-pentanediol di-isobutyrate	17.89	1788	MS
di-isobutyl phthalate	23.15	>2400	MS
	Heterocyclic Compounds		
1-vinylaziridine	5.87	979	MS
2-pentylfuran[e]	10.84	1214	standard
2-methylpyrazine	11.50	1253	MS
2,5-dimethylpyrazine	12.40	1308	MS + RI
2-acetyl-1-pyrroline	12.66	1325	MS + RI
2-ethyl-6-methylpyrazine	13.38	1374	MS + RI
2,3,5-trimethylpyrazine	13.65	1392	MS + RI
3-ethyl-2,5-dimethylpyrazine	14.31	1436	MS + RI
2,6-diethylpyrazine	14.59	1454	MS + RI
2,3,5,6-tetramethylpyrazine	14.79	1468	MS + RI
3,5-diethyl-2-methylpyrazine	15.07	1486	MS + RI
pyrrole	15.31	1505	MS + RI
4-octadecylmorpholine	19.94	2177	MS
	Aliphatic Hydrocarbons		
decane	6.10	997	MS + RI
dodecane	10.60	1200	MS + RI

dx.doi.org/10.1021/jf404270f | J. Agric. Food Chem. 2014, 62, 590−599

Table 2. continued

compound	RT[a] (min)	RI[b]	identification method
	Aliphatic Hydrocarbons		
(3*E*)-3-tetradecene	11.21	1236	MS
5-methylenetridecane	13.77	1400	MS
1-pentadecene	15.69	1544	MS + RI
	Ketones		
1-hydroxyacetone	12.14	1291	MS + RI
2-nonanone	13.43	1377	MS + RI
2-undecanone	16.11	1589	MS + RI
2-pentadecanone	18.73	2018	MS + RI
o-aminoacetophenone	20.30	2216	MS + RI
	Others		
trimethylamine	1.62	616	MS + RI
methyl *N*-hydroxybenzenecarboximidate	17.13	1719	MS

[a]RT = retention time. [b]RI = retention index. [c]MS + RI = identified by comparison of the fragment to the library (Wiley9) and by the RI as compared to the literature. [d]MS = tentatively identified compound. [e]Compounds identified as VLOPs. [f]Standard = identity confirmed with the standard.

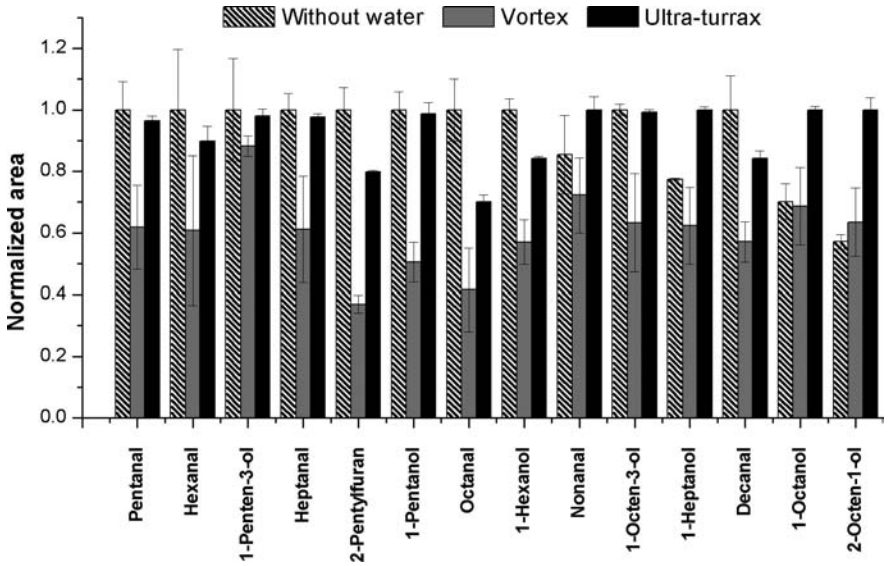

Figure 3. Effect of the sample preparation on the extraction of VLOPs from salted, dried shrimp with the fiber DVB/CAR/PDMS (n = 3).

and the quantification limits varied from 0.11 to 0.50 ng g^{-1}. The method showed satisfactory precision (RSD $\leq$ 12.67%) and efficiency (recovery $\geq$ 94.28%). The analytical curve was developed with low initial values (1 ng g^{-1}), because the VLOPs found in the salted, dried shrimp, according to the study by Buttery et al.,[36] have low thresholds (0.7−15 ng g^{-1}) but a great impact on the sensory characteristics, especially the aldehydes.

Effect of Processing on the Shrimp Fatty Acids. The ω-3 fatty acids represented the majority among the PUFAs of fresh shrimp (Table 4), and the fatty acids profiles were similar in both batches, with little differences in the eicosadienoic acid (20:2ω-6) and behenic acid (22:0). The predominant fatty acids in the shrimp lipids were palmitic acid (16:0), oleic acid (18:1ω-9), stearic acid (18:0), linoleic acid (18:2ω-6), DHA, and EPA.

Salting caused a reduction in five fatty acids in batch 1, whereas only four fatty acids were reduced in batch 2, but only the contents of ARA and DHA were reduced in both batches. After drying, the reduction in pentadecanoic acid (15:0), margaric acid (17:0), stearic acid (18:0), and EPA became significant for both batches in comparison to the fresh shrimp. In addition, processing reduced the total fatty acid content of the lipid fraction. A reduction in the fatty acid content after cooking was also observed in fish[24,37] and crab.[38]

According to Maulvault et al.,[38] the reduction in PUFAs during heat processing occurs because of their great susceptibility to oxidation at high temperatures. Although less frequent, a decrease in the SFA content can also occur during cooking.[24] The loss of PUFAs occurs mainly because of lipid oxidation and can be accelerated by both an increase in the temperature and the addition of salt (NaCl).[39] The main contribution of the increase in the temperature to fatty acid oxidation is due to the increase in the reaction rate.[40] The pro-oxidant effect of NaCl is attributed to an increase in the non-heme iron content in meats after cooking,[41] although this increase is mainly due to the liquid retention capacity of NaCl, because when cooked without salt, the non-heme iron is carried out because of liquid loss.[42] Another pro-oxidant mechanism of NaCl is due to the reduction in activity of the antioxidant enzymes.[43]

ARA, EPA, and DHA are fatty acids of great importance to human health and can be generated metabolically from essential fatty acids (linoleic and linolenic acids), although the conversion

dx.doi.org/10.1021/jf404270f | J. Agric. Food Chem. 2014, 62, 590−599

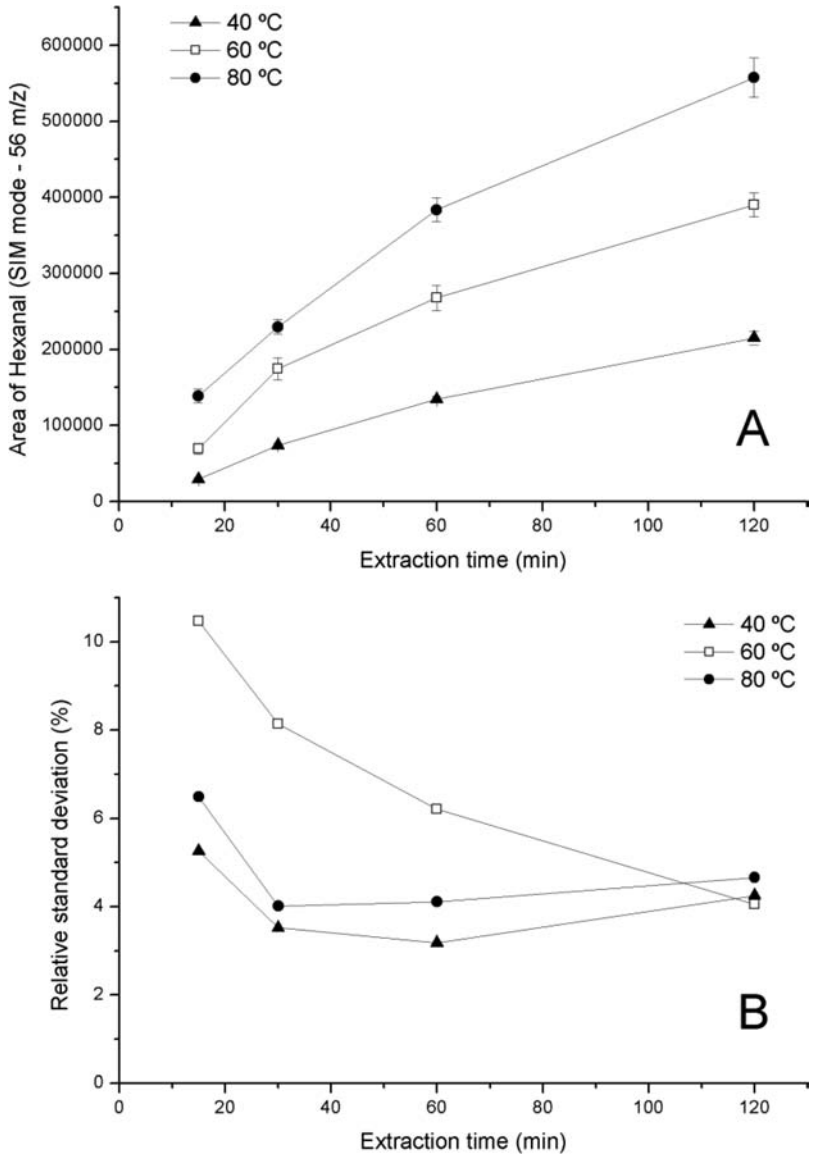

Figure 4. Effect of the time and temperature on (A) extraction of hexanal and (B) mean repeatability of the volatile compounds from salted, dried shrimp with the fiber DVB/CAR/PDMS (n = 3).

Table 3. Data of the Analytical Curve, Linearity, Detection and Quantification Limits, Precision, and Recovery of the Optimized Method

VLOPs[a]	slope	intercept	R^{2b}	linear range (ng g^{-1})	LOD[c] (ng g^{-1})	LOQ[d] (ng g^{-1})	repeatability (% RSD[e])	recovery of 5 ng (%)	recovery of 20 ng (%)
pentanal	0.0067	0.0025	0.9882	1−80	0.04 ± 0.01	0.15 ± 0.04	1.10	98.80 ± 3.40	100.52 ± 4.47
hexanal	0.0078	0.0155	0.9922	1−80	0.04 ± 0.01	0.13 ± 0.03	3.85	98.43 ± 3.82	99.85 ± 3.72
1-penten-3-ol	0.0145	−0.0243	0.9637	1−80	0.03 ± 0.01	0.11 ± 0.02	3.11	97.89 ± 2.10	101.77 ± 3.65
heptanal	0.0035	0.0010	0.9924	1−80	0.06 ± 0.01	0.21 ± 0.04	4.98	103.76 ± 2.58	97.41 ± 1.07
2-pentylfuran	0.0085	−0.0122	0.9898	1−80	0.06 ± 0.01	0.21 ± 0.05	5.24	101.77 ± 5.78	98.89 ± 6.82
1-pentanol	0.0051	−0.0036	0.9842	1−80	0.15 ± 0.01	0.50 ± 0.04	1.10	94.28 ± 2.49	103.00 ± 1.73
octanal	0.0019	−0.0014	0.9924	1−80	0.11 ± 0.03	0.36 ± 0.10	4.43	105.60 ± 9.29	98.39 ± 4.13
1-hexanol	0.0097	−0.0121	0.9964	1−80	0.03 ± 0.01	0.11 ± 0.02	4.23	99.23 ± 4.78	96.87 ± 6.28
nonanal	0.0038	0.0130	0.9787	1−80	0.04 ± 0.01	0.15 ± 0.03	4.49	102.38 ± 6.00	96.29 ± 4.56
1-octen-3-ol	0.0228	−0.0053	0.9978	1−80	0.05 ± 0.00	0.16 ± 0.01	2.60	97.36 ± 7.53	96.84 ± 5.03
1-heptanol	0.0051	−0.0085	0.9952	1−80	0.09 ± 0.02	0.29 ± 0.05	1.03	96.93 ± 3.83	96.11 ± 0.03
decanal	0.0015	−0.0009	0.9849	1−80	0.08 ± 0.03	0.26 ± 0.09	12.67	102.41 ± 4.75	99.14 ± 13.72
1-octanol	0.0039	−0.0051	0.9924	1−80	0.04 ± 0.01	0.14 ± 0.04	3.15	103.66 ± 7.28	97.33 ± 9.86
2-octen-1-ol	0.0034	−0.0104	0.9876	1−80	0.05 ± 0.01	0.16 ± 0.04	1.84	95.84 ± 5.13	98.85 ± 1.87

[a]VLOP = volatile lipid oxidation product. [b]R^2 = coefficient of determination. [c]LOD = limit of detection. [d]LOQ = limit of quantification. [e]RSD = relative standard deviation.

dx.doi.org/10.1021/jf404270f | J. Agric. Food Chem. 2014, 62, 590−599

Table 4. Fatty Acid Composition of the Lipids of Fresh and Processed Shrimp[a]

	fresh		salted		salted, dried	
fatty acids (mg g^{-1} of oil)	batch 1	batch 2	batch 1	batch 2	batch 1	batch 2
14:0	1.36 ± 0.06 ab	1.28 ± 0.04 b	1.24 ± 0.10 b	1.54 ± 0.09 ac	1.67 ± 0.05 c	1.53 ± 0.01 ac
15:0	8.89 ± 0.79 a	9.40 ± 0.13 a	8.39 ± 0.72 ab	8.79 ± 0.29 a	7.29 ± 0.27 b	7.21 ± 0.41 b
16:0	97.06 ± 3.90 a	90.17 ± 3.90 ab	81.41 ± 2.73 b	90.48 ± 3.45 ab	80.61 ± 5.14 b	85.90 ± 5.40 ab
16:1ω-9	5.39 ± 0.43 a	6.00 ± 0.51 ab	6.36 ± 0.19 ab	7.06 ± 0.27 b	6.14 ± 0.64 ab	7.11 ± 0.50 b
17:0	16.17 ± 1.66 a	14.90 ± 0.02 ab	13.34 ± 1.00 bd	13.06 ± 0.50 bcd	11.01 ± 0.20 c	11.67 ± 0.46 cd
17:1ω-6	0.70 ± 0.04 a	0.84 ± 0.04 ab	1.35 ± 0.07 c	0.83 ± 0.02 ab	0.79 ± 0.04 ab	0.85 ± 0.01 b
18:0	60.33 ± 2.99 a	55.17 ± 1.52 ab	51.48 ± 1.60 bd	51.02 ± 1.41 bcd	44.87 ± 3.13 c	46.83 ± 2.56 cd
18:1ω-9	84.58 ± 5.11 ab	79.75 ± 3.01 ab	78.16 ± 2.04 ab	86.52 ± 2.31 a	76.34 ± 4.56 b	87.02 ± 3.55 a
19:0	1.37 ± 0.02 a	1.28 ± 0.05 a	1.21 ± 0.09 a	1.15 ± 0.07 a	1.11 ± 0.04 a	1.17 ± 0.16 a
18:2ω-6	52.46 ± 2.74 ab	52.87 ± 1.52 ab	49.79 ± 1.47 a	56.18 ± 1.69 b	48.81 ± 3.45 a	54.29 ± 1.74 ab
20:0	1.28 ± 0.06 ab	1.45 ± 0.07 a	1.34 ± 0.07 ab	1.25 ± 0.03 bc	1.29 ± 0.04 ab	1.07 ± 0.08 c
20:1ω-9	2.04 ± 0.08 abc	1.82 ± 0.07 a	1.92 ± 0.14 ab	2.10 ± 0.02 bc	1.29 ± 0.13 ab	2.29 ± 0.07 c
18:3ω-3	2.25 ± 0.12 a	2.28 ± 0.13 a	2.21 ± 0.08 a	2.53 ± 0.06 a	2.40 ± 0.11 a	2.51 ± 0.25 a
20:2ω-6	5.49 ± 0.28 a	4.93 ± 0.13 ab	4.71 ± 0.14 bc	4.80 ± 0.11 bc	4.30 ± 0.08 c	5.22 ± 0.35 ab
22:0	1.42 ± 0.03 ab	1.73 ± 0.09 c	1.53 ± 0.05 ac	1.30 ± 0.05 b	1.46 ± 0.07 ab	1.41 ± 0.12 ab
20:4ω-6	26.43 ± 1.41 a	25.06 ± 0.80 ab	22.52 ± 0.42 bc	21.55 ± 0.30 cd	18.68 ± 1.05 e	19.72 ± 1.27 de
20:5ω-3	42.42 ± 2.28 a	41.17 ± 1.28 ab	39.98 ± 0.84 abd	37.45 ± 0.51 bd	32.58 ± 1.97 c	36.21 ± 1.68 cd
24:1ω-9	2.43 ± 0.19 a	2.41 ± 0.08 a	2.17 ± 0.09 a	2.12 ± 0.05 a	2.15 ± 0.17 a	3.57 ± 1.74 a
22:6ω-3	50.46 ± 1.59 ab	51.17 ± 1.45 a	47.15 ± 0.99 bc	44.07 ± 0.41 cd	42.31 ± 2.30 d	43.62 ± 0.80 cd
SFA	187.88 ± 9.50 a	175.38 ± 5.83 a	159.93 ± 6.36 a	168.59 ± 5.88 a	149.30 ± 8.92 a	156 ± 9.20 a
MUFA	95.14 ± 5.86 a	90.82 ± 3.71 a	89.97 ± 2.53 a	98.63 ± 2.67 a	87.34 ± 5.55 a	100 ± 5.87 a
PUFA	179.51 ± 8.42 a	177.48 ± 5.32 a	166.37 ± 3.93 a	166.58 ± 3.08 a	149.09 ± 8.95 a	131.58 ± 6.09 a
$\sum\omega$-3	95.13 ± 3.99 ab	94.62 ± 2.86 a	89.35 ± 1.91 ac	84.05 ± 0.98 c	77.30 ± 4.38 c	82.34 ± 2.73 bc
$\sum\omega$-6	84.38 ± 4.43 a	82.86 ± 2.46 a	77.02 ± 2.02 a	82.53 ± 2.10 a	71.79 ± 4.57 a	79.24 ± 3.36 a
total	462.53 ± 23.77 a	443.69 ± 14.86 b	416.28 ± 12.82 c	433.79 ± 11.63 d	385.73 ± 23.42 e	419 ± 21.17 f

[a]Values expressed as the mean ± standard deviation (n = 3). Different letters in the same line indicate significant difference between the values (p < 0.05). SFA, saturated fatty acids; MUFA, monounsaturated fatty acids; PUFA, polyunsaturated fatty acids; $\sum\omega$-3, PUFA ω-3; and $\sum\omega$-6, PUFA ω-6.

Table 5. VLOPs from Fresh and Processed Shrimp Obtained by HS−SPME−GC−MS[a]

	fresh		salted		salted, dried	
VLOP (ng g^{-1})	batch 1	batch 2	batch 1	batch 2	batch 1	batch 2
pentanal	ND[b]	ND[b]	7.07 ± 0.15 a	6.58 ± 0.40 a	7.37 ± 1.93 a	6.96 ± 0.38 a
hexanal	<0.13[c]	<0.13[c]	10.66 ± 1.50 a	13.58 ± 0.60 ab	15.00 ± 0.58 b	19.09 ± 0.98 c
1-penten-3-ol	5.45 ± 0.16 a	5.32 ± 0.45 a	4.97 ± 0.10 a	4.68 ± 0.16 a	7.03 ± 0.27 b	9.06 ± 0.27 c
heptanal	<0.21[c]	<0.21[c]	3.73 ± 0.10 a	5.49 ± 0.13 b	3.82 ± 0.27 a	5.36 ± 0.26 b
2-pentylfuran	1.45 ± 0.09 a	1.27 ± 0.01 a	1.91 ± 0.10 b	1.66 ± 0.08 ab	1.93 ± 0.15 b	2.07 ± 0.03 b
1-pentanol	3.89 ± 0.01 a	4.46 ± 0.09 a	12.23 ± 0.08 b	8.12 ± 0.49 ab	9.32 ± 2.39 b	10.38 ± 1.16 ab
octanal	<0.36[c]	<0.36[c]	3.65 ± 0.13 a	5.01 ± 0.24 b	3.63 ± 0.16 a	4.47 ± 0.16 b
1-hexanol	3.98 ± 0.07 a	3.69 ± 0.02 a	3.80 ± 0.01 a	4.40 ± 0.20 bc	3.24 ± 0.09 c	3.88 ± 0.07 a
nonanal	2.15 ± 0.11 a	1.97 ± 0.24 a	11.52 ± 0.07 b	16.57 ± 0.46 c	10.36 ± 0.49 b	17.02 ± 0.59 c
1-octen-3-ol	3.55 ± 0.11 a	4.40 ± 0.21 ab	5.46 ± 0.08 cd	4.60 ± 0.35 bc	5.36 ± 0.48 cd	6.21 ± 0.04 d
1-heptanol	2.01 ± 0.13 a	1.72 ± 0.03 ab	1.59 ± 0.01 b	1.87 ± 0.15 ab	1.16 ± 0.05 c	1.62 ± 0.04 b
decanal	1.81 ± 0.08 a	1.57 ± 0.12 a	5.58 ± 0.15 b	7.77 ± 0.42 c	5.48 ± 0.11 b	8.73 ± 0.14 c
1-octanol	6.42 ± 0.53 a	6.47 ± 0.32 a	2.56 ± 0.09 bc	3.17 ± 0.11 b	2.09 ± 0.13	2.71 ± 0.05 bc
2-octen-1-ol	1.83 ± 0.08 a	2.34 ± 0.09 b	1.29 ± 0.01 c	1.27 ± 0.03 c	1.30 ± 0.01 c	1.59 ± 0.03 d

[a]Values expressed as the mean ± standard deviation (n = 3). Different letters in the same line indicate significant difference between the values (p < 0.05). [b]ND = not detected (below the detection limits, 0.04 ng g^{-1}). [c]Below the quantification limit.

rate is very low, indicating the need for exogenous sources of these lipids.[44,45] Thus, the processing of shrimp negatively affected the nutritional value because it reduced the contents of these fatty acids in up to 29% for ARA, 23% for EPA, and 16% for DHA.

In comparison of the lipids of salted shrimp to those of salted, dried shrimp, there was no difference between them for any fatty acid simultaneously in both batches, indicating that the drying process did not significantly affect the lipids. In general, these results are in agreement with those by Ortiz et al.,[46] who observed that drying at 60 °C had little influence on the fish lipid profile, generating low oxidation indices.

Effect of Processing on Shrimp VLOPs. The two batches of fresh shrimp showed the same VLOP composition (Table 5), differing only with respect to 2-octen-1-ol. The only aldehydes with quantifiable contents in the fresh shrimp were nonanal and decanal. The main VLOP produced during processing was hexanal, as also verified by Shahidi and Pegg.[17] The salting process caused an increase in all of the aldehydes, as compared to the fresh shrimp, in addition to a reduction in 1-octanol and 2-octen-1-ol in both

batches as well as the contents of 1-pentanol and 2-pentylfuran in batch 1 but not in batch 2.

Drying caused an increase in hexanal and 1-penten-3-ol in both batches, plus an increase in 2-octen-1-ol just in batch 1. The formation of volatiles presented a behavior similar to the degradation of the fatty acids, where the salting process presented a greater oxidative effect than the drying process.

Of the VLOPs found in shrimp, only 1-penten-3-ol originated from the oxidation of ω-3 fatty acids, with pentanal, hexanal, 1-pentanol, 2-pentylfuran, 1-hexanol, 1-octen-3-ol, and 2-octen-1-ol being formed as from ω-6 fatty acids. Heptanal can be formed from both ω-6 and ω-9 fatty acids, and the other VLOPs are formed from ω-9 fatty acids.[26−28]

Despite a significant increase, 1-penten-3-ol was below its threshold, and hence, the oxidation of ω-3 fatty acids, despite forming VLOPs, was not sufficient to alter the sensory properties of the shrimp. However, the formation of hexanal, 1-octen-3-ol, octanal, nonanal, and decanal could have a negative impact on the aroma of the final product, because the contents of these compounds were above their respective thresholds.[36] Thus, the oxidation of ω-6 fatty acids showed a greater influence on the sensory quality of the shrimp than the oxidation of ω-3 fatty acids.

In conclusion, the type of fiber, sample preparation mode, and the time/temperature binomial during extraction all presented an influence on the extraction by HS−SPME. The best conditions to extract VLOPs from shrimp by HS−SPME consisted of homogenizing 1 g of sample in 3 mL of water using an ultraturrax and extracting the volatiles at 40 °C for 30 min with the fiber DVB/CAR/PDMS. This method was quick and practical and showed good repeatability, sensitivity, and efficiency. Heat processing and mainly the salting process caused a reduction in the content of fatty acids of the shrimp, especially in ARA, DHA, and EPA, as well as forming some VLOPs above their threshold values, showing an impact on the nutritional and sensory characteristics of the final product.

■ ASSOCIATED CONTENT

Ⓢ Supporting Information

Compounds obtained from salted, dried shrimp by HS−SPME−GC−MS using four fibers (CAR/PDMS, DVB/CAR/PDMS, PA, and PDMS/DVB) (Table S1), effect of the time and temperature on the extraction of (A) pentanal, (B) 1-penten-3-ol, and (C) 1-pentanol from salted, dried shrimp with the fiber DVB/CAR/PDMS (Figure S2). This material is available free of charge via the Internet at http://pubs.acs.org.

■ AUTHOR INFORMATION

Corresponding Author

*Telephone: +55-19-3521-2162. Fax: +55-19-3521-2153. E-mail: neurabragagnolo@gmail.com.

Funding

This research was supported by the State of São Paulo Research Foundation (FAPESP, Grant 09/54119-3) and the Brazilian National Research Council (CNPq).

Notes

The authors declare no competing financial interest.

■ REFERENCES

(1) Fisheries and Aquaculture Department, Food and Agriculture Organization of the United Nations (FAO). *Overview: Major Trends and Issues*; Fisheries and Aquaculture Department, FAO: Rome, Italy, 2013; ftp://ftp/fao.org/FI/STAT/summary/YB_Overview.pdf (accessed March 29, 2013).

(2) Chandrasekaran, M. Methods for preprocessing and freezing of shrimps—A critical evaluation. *J. Food Sci. Technol.* **1994**, *31*, 441−452.

(3) Kraemer, F. B.; Stussi, J. S. P.; Santos, N. N.; Sgarbi, D. B. D. G.; Clemente, S. C. D. S. Chemical−physical control in dried−salted shrimp comercialized in Rio de Janeiro state. *Rev. Bras. Cienc. Vet.* **2001**, *8*, 3.

(4) Barbosa-Canovas, G.; Ibarz, A. *Unit Operation in Food Engineering*; CRC Press: Boca Raton, FL, 2002; pp 572−623.

(5) Akoh, C. C.; Min, D. B. *Food Lipids: Chemistry, Nutrition, and Biotechnology*; Marcel Dekker: New York, 2002.

(6) Bragagnolo, N.; Rodriguez-Amaya, D. B. Total lipid, cholesterol, and fatty acids of farmed freshwater prawn (*Macrobrachium rosenbergii*) and wild marine shrimp (*Penaeus brasiliensis*, *Penaeus schimitti*, *Xiphopenaeus kroyeri*). *J. Food Compos. Anal.* **2001**, *14*, 359−369.

(7) Luzia, L. A.; Sampaio, G. R.; Castellucci, C. M. N.; Torres, E. A. F. S. The influence of season on the lipid profiles of five commercially important species of Brazilian fish. *Food Chem.* **2003**, *83*, 93−97.

(8) Simon, S. J. G. B.; Sancho, R. A. S.; Lima, F. A.; Cabral, C. C. V. Q.; Souza, T. M.; Bragagnolo, N.; Lira, G. M. Interaction between soybean oil and the lipid fraction of fried pitu prawn. *LWT—Food Sci. Technol.* **2012**, *48*, 120−126.

(9) Kamal-Eldin, A.; Pokorný, J. Lipid oxidation products and methods used for their analysis. In *Analysis of Lipid Oxidation*; Kamal-Eldin, A., Pokorný, J., Eds.; AOCS Press: Champaign, IL, 2005; pp 7−14.

(10) Iglesias, J.; Medina, I. Solid-phase microextraction method for the determination of volatile compounds associated to oxidation of fish muscle. *J. Chromatogr., A* **2008**, *1192*, 9−16.

(11) Mariutti, L. R. B.; Nogueira, G. C.; Bragagnolo, N. Solid phase microextraction−gas chromatography for the evaluation of secondary lipid oxidation products in chicken patties during long-term storage. *J. Braz. Chem. Soc.* **2009**, *20*, 1849−1855.

(12) Wu, T. C.; Sheldon, B. W. Flavor components and factors associated with the development of off-flavors in cooked turkey rolls. *J. Food Sci.* **1988**, *53*, 49−54.

(13) Wardencki, W.; Michulec, M.; Curylo, J. A review of theoretical and practical aspects of solid-phase microextraction in food analysis. *Int. J. Food Sci. Technol.* **2004**, *39*, 703−717.

(14) Arthur, C. L.; Pawliszyn, J. Solid-phase microextraction with thermal desorption using fused silica optical fibers. *Anal. Chem.* **1990**, *62*, 2145−2148.

(15) Roberts, D. D.; Pollien, P.; Milo, C. Solid-phase microextraction method development for headspace analysis of volatile flavor compounds. *J. Agric. Food Chem.* **2000**, *48*, 2430−2437.

(16) Zhang, Z. Y.; Pawliszyn, J. Headspace solid-phase microextraction. *Anal. Chem.* **1993**, *65*, 1843−1852.

(17) Shahidi, F.; Pegg, R. B. Hexanal as an indicator of the flavor deterioration of meat and meat products. *ACS Symp. Ser.* **1994**, *558*, 256−279.

(18) Vandendool, H.; Kratz, P. D. A generalization of retention index system including linear temperature programmed gas−liquid partition chromatography. *J. Chromatogr., A* **1963**, *11*, 463−471.

(19) Acree, H.; Arn, T. *Flavornet and Human Odor Space*; Cornell University: Geneva, NY, 2004; http://www.flavornet.org (accessed Aug 24, 2013).

(20) El-Sayed, A. M. *The Pherobase: Database of Insect Pherormones and Semiochemicals*, 2012; http://www.pherobase.com/database/kovats/kovats-index.php (accessed Aug 24, 2013).

(21) Garruti, D. S.; Franco, M. R. B.; Aparecida, M.; da Silva, A. P.; Janzantti, N. S.; Alves, G. L. Assessment of aroma impact compounds in a cashew apple-based alcoholic beverage by GGMS and GC−olfactometry. *LWT—Food Sci. Technol.* **2006**, *39*, 373−378.

(22) Folch, J.; Lees, M.; Stanley, G. H. S. A simple method for the isolation and purification of total lipides from animal tissues. *J. Biol. Chem.* **1957**, *226*, 497−509.

(23) Joseph, J. D.; Ackman, R. G. Capillary column gas chromatographic method for analysis of encapsulated fish oils and fish oil ethyl-esters—Collaborative study. *J. AOAC Int.* **1992**, *75*, 488−506.
(24) Sancho, R. A. S.; de Lima, F. A.; Costa, G. G.; Mariutti, L. R. B.; Bragagnolo, N. Effect of annatto seed and coriander leaves as natural antioxidants in fish meatballs during frozen storage. *J. Food Sci.* **2011**, *76*, C838−C845.
(25) Association of Official Analytical Chemists (AOAC). *Offical Methods of Analysis*; AOAC: Gaithersburg, MD, 1997.
(26) Genot, C.; Meynier, A.; Riaublanc, A. Lipid oxidation in emulsions. In *Lipid Oxidation*; Kamal-Eldin, A., Ed.; AOCS Press: Champaign, IL, 2003; pp 190−244.
(27) Choe, E.; Min, D. B. Mechanisms and factors for edible oil oxidation. *Compr. Rev. Food Sci. Food Saf.* **2006**, *5*, 169−186.
(28) Volden, J.; Bjelanovic, M.; Vogt, G.; Slinde, E.; Skaugen, M.; Nordvi, B.; Egelandsdal, B. Oxidation progress in an emulsion made from metmyoglobin and different triacylglycerols. *Food Chem.* **2011**, *128*, 854−863.
(29) Whitfield, F. B.; Freeman, D. J.; Last, J. H.; Bannister, P. A.; Kennett, B. H. Oct-1-en-3-ol and (5*Z*)-octa-1,5-dien-3-ol, compounds important in the flavor of prawns and sand-lobsters. *Aust. J. Chem.* **1982**, *35*, 373−383.
(30) Cadwallader, K. R.; Tan, Q.; Chen, F.; Meyers, S. P. Evaluation of the aroma of cooked spiny lobster tail meat by aroma extract dilution analysis. *J. Agric. Food Chem.* **1995**, *43*, 2432−2437.
(31) Lu, F.; Zhang, J. Y.; Liu, S. L.; Wang, Y.; Ding, Y. T. Chemical, microbiological and sensory changes of dried *Acetes chinensis* during accelerated storage. *Food Chem.* **2011**, *127*, 159−168.
(32) Garcia-Esteban, M.; Ansorena, D.; Astiasarán, I.; Ruiz, J. Study of the effect of different fiber coatings and extraction conditions on dry cured ham volatile compounds extracted by solid-phase micro-extraction (SPME). *Talanta* **2004**, *64*, 458−466.
(33) Gianelli, M. P.; Flores, M.; Toldrá, F. Optimisation of solid phase microextraction (SPME) for the analysis of volatile compounds in dry-cured ham. *J. Sci. Food Agric.* **2002**, *82*, 1703−1709.
(34) Ruiz, J.; Cava, R.; Ventanas, J.; Jensen, M. T. Headspace solid phase microextraction for the analysis of volatiles in a meat product: Dry-cured Iberian ham. *J. Agric. Food Chem.* **1998**, *46*, 4688−4694.
(35) Fratini, G.; Lois, S.; Pazos, M.; Parisi, G.; Medina, I. Volatile profile of Atlantic shellfish species by HS−SPME GC/MS. *Food Res. Int.* **2012**, *48*, 856−865.
(36) Buttery, R. G.; Turnbaugh, J. G.; Ling, L. C. Contribution of volatiles to rice aroma. *J. Agric. Food Chem.* **1988**, *36*, 1006−1009.
(37) Yagiz, Y.; Kristinsson, H. G.; Balaban, M. O.; Welt, B. A.; Ralat, M.; Marshall, M. R. Effect of high pressure processing and cooking treatment on the quality of Atlantic salmon. *Food Chem.* **2009**, *116*, 828−835.
(38) Maulvault, A. L.; Anacleto, P.; Lourenço, H. M.; Carvalho, M. L.; Nunes, M. L.; Marques, A. Nutritional quality and safety of cooked edible crab (*Cancer pagurus*). *Food Chem.* **2012**, *133*, 277−283.
(39) Jin, G. F.; He, L. C.; Zhang, J. H.; Yu, X.; Wang, J. M.; Huang, F. Effects of temperature and NaCl percentage on lipid oxidation in pork muscle and exploration of the controlling method using response surface methodology (RSM). *Food Chem.* **2012**, *131*, 817−825.
(40) Tan, C. P.; Man, Y. B. C.; Selamat, J.; Yusoff, M. S. A. Application of arrhenius kinetics to evaluate oxidative stability in vegetable oils by isothermal differential scanning calorimetry. *J. Am. Oil Chem. Soc.* **2001**, *78*, 1133−1138.
(41) Ahn, D. U.; Wolfe, F. H.; Sim, J. S. Three methods for determining nonheme iron in turkey meat. *J. Food Sci.* **1993**, *58*, 288−291.
(42) Kristensen, L.; Purslow, P. P. The effect of processing temperature and addition of mono- and di-valent salts on the heme−nonheme-iron ratio in meat. *Food Chem.* **2001**, *73*, 433−439.
(43) Lee, S. K.; Mei, L.; Decker, E. A. Influence of sodium chloride on antioxidant enzyme activity and lipid oxidation in frozen ground pork. *Meat Sci.* **1997**, *46*, 349−355.
(44) Salem, N.; Pawlosky, R.; Wegher, B.; Hibbeln, J. In vivo conversion of linoleic acid to arachidonic acid in human adults. *Prostaglandins, Leukotrienes Essent. Fatty Acids* **1999**, *60*, 407−410.
(45) Brenna, J. T.; Salem, N.; Sinclair, A. J.; Cunnane, S. C. α-Linolenic acid supplementation and conversion to ω-3 long-chain polyunsaturated fatty acids in humans. *Prostaglandins, Leukotrienes Essent. Fatty Acids* **2009**, *80*, 85−91.
(46) Ortiz, J.; Lemus-Mondaca, R.; Vega-Gálvez, A.; Ah-Hen, K.; Puente-Diaz, L.; Zura-Bravo, L.; Aubourg, S. Influence of air-drying temperature on drying kinetics, colour, firmness and biochemical characteristics of Atlantic salmon (*Salmo salar* L.) fillets. *Food Chem.* **2013**, *139*, 162−169.

JOURNAL OF AGRICULTURAL AND FOOD CHEMISTRY

Article

pubs.acs.org/JAFC

Quantitative Measurement of Major Secoiridoid Derivatives in Olive Oil Using qNMR. Proof of the Artificial Formation of Aldehydic Oleuropein and Ligstroside Aglycon Isomers

Evangelia Karkoula,[†] Angeliki Skantzari,[†] Eleni Melliou,[†,‡] and Prokopios Magiatis*[,†]

[†]Laboratory of Pharmacognosy and Natural Products Chemistry, Faculty of Pharmacy, University of Athens, Panepistimiopolis Zografou, 157 71 Athens, Greece

[‡]Olive Center, University of California—Davis, Davis, California 95616, United States

Supporting Information

ABSTRACT: A previously developed method for measurement of oleocanthal and oleacein in olive oil by quantitative ^{1}H NMR was expanded to include the measurement of the monoaldehydic forms of oleuropein and ligstroside aglycons. The method was validated and applied to the study of 340 monovarietal Greek and Californian olive oils from 23 varieties and for a 3-year period. A wide variation concerning the concentrations of all four secoiridoids was recorded. The concentration of each one ranged from nondetectable to 711 mg/kg and the sum of the four major secoiridoids (named as D3) ranged from nondetectable to 1534 mg/kg. Examination of the NMR profile of the olive oil extract before and after contact with normal or reversed stationary chromatography phase proved the artificial formation of the 5*S*,8*S*,9*S* aldehydic forms of oleuropein and ligstroside aglycon isomers during chromatography. Finally, methyl elenolate was identified for the first time as a minor constituent of olive oil.

KEYWORDS: *extra virgin olive oil, secoiridoids, oleuropein aglycon, ligstroside aglycon, quantitative NMR*

INTRODUCTION

Olive oil is a fundamental constituent of the traditional Mediterranean diet which is continuously attracting the interest of the scientific community for its health-protecting activities.[1−3] Among the numerous constituents of olive oil, the secoiridoid derivatives present an increasing potential for health protection, which tends to place olive oil in the interface between food and drugs.[4] A very important change in the European Union legislation with potentially very significant impact on the field of olive oil marketing and labeling is the recent recognition by EFSA of specific health claims related to the levels of specific phenolic compounds found in olive oil.[5] More specifically, hydroxytyrosol, tyrosol, and their derivatives have been correlated with protection from LDL oxidation, creating thus a new need for the accurate measurement of the levels of those compounds in olive oil. It is noteworthy that up to today there is no internationally accepted regulation concerning the method for their measurement because of several technical difficulties. It is well-known that the concentration of free hydroxytyrosol and tyrosol in olive oil is very low while their esterified derivatives are much more abundant.[6] Hydroxytyrosol is mainly present in the form of oleacein (3,4-DHPEA-EDA) and the monoaldehydic form of oleuropein aglycon (3,4-DHPEA-EA), while tyrosol is mainly present in the form of oleocanthal (*p*-HPEA-EDA) and the monoaldehydic form of ligstroside aglycon (*p*-HPEA-EA). All those four secoridoid derivatives possess significant biological activities, as previously summarized.[7] Especially oleocanthal and oleuropein aglycon have been very recently correlated with protection against Alzheimer's disease,[8,9] giving a new potential field for medical applications of olive oil. Although there are several works concerning the chromatographic analysis of those compounds (HPLC−UV or LCMS)[10−13] we have recently described[7] the reactivity of oleocanthal and oleacein with methanol and water, which are commonly and officially used for the extraction of polyphenols[14] and as constituents of the mobile phase during their analysis, leading to the formation of several artifacts and making the analysis very difficult. To overcome these problems that make the chromatographic analysis complicated and questionable, we recently developed a simple and rapid method using quantitative NMR (qNMR) and avoiding any interacting solvents as well as the need of chemically pure standards.[7] In the present work we have expanded the previous method to include all four major secoiridoid derivatives of hydroxytyrosol and tyrosol. Interestingly, during this study we recognized the instability of oleuropein and ligstroside aglycon when they come in contact with common normal or reversed stationery phases, leading to the artificial formation of isomers. In addition, during the isolation of olive oil constituents we identified a compound that is for the first time reported from a natural source. The qNMR method was applied to 340 olive oil samples, and the varieties presenting the highest concentrations of the studied compounds were recognized.

MATERIALS AND METHODS

Extra Virgin Olive Oil Samples. The commercial extra virgin olive oil (EVOO) samples used in the study were obtained from olives (*Olea europaea* L.) harvested and extracted in three seasons:

Received: October 1, 2013
Revised: December 22, 2013
Accepted: January 2, 2014
Published: January 2, 2014

ACS Publications © 2014 American Chemical Society

dx.doi.org/10.1021/jf404421p | *J. Agric. Food Chem.* 2014, 62, 600−607

November 2010−February 2011, October 2011−February 2012, and October 2012−February 2013. A total of 320 monovarietal commercial samples were obtained from Greece and 20 from California. In total, samples of 23 different varieties were included in the study. The olive oil production was performed in either two-phase or three-phase mills. All samples were provided by small-scale producers that could guarantee their monovarietal origin.

Olive Oil Extraction and Sample Preparation for NMR Analysis. Olive oil (5.0 g) was mixed with cyclohexane (20 mL) and acetonitrile (25 mL). The mixture was homogenized using a vortex mixer for 30 s and centrifuged at 4000 rpm for 5 min. A part of the acetonitrile phase (25 mL) was collected, mixed with 1.0 mL of a syringaldehyde (4-hydroxy-3,5-dimethoxybenzaldehyde) solution (0.5 mg/mL) in acetonitrile, and evaporated under reduced pressure using a rotary evaporator (Buchi, Switzerland).

Reference Compounds. Oleuropein aglycon and ligstroside aglycon were isolated from an olive oil extract prepared using the extraction method similar to that described above for sample preparation. The obtained extract was first fractionated using column chromatography, and then the fractions containing the two aglycons were purified with preparative TLC until maximum purity was achieved. In both cases, the mobile phase was prepared using mixtures of cyclohexane with ethyl acetate and silica gel as stationary phase. Details of the purification procedure are provided as Supporting Information. Each aglycon was obtained as an inseparable mixture of the 5*S*,8*R*,9*S* and 5*S*,8*S*,9*S* diastereomers in a ratio 3:1 and 4:1 for oleuropein and ligstroside aglycons, respectively. The ^{1}H NMR purity of both compounds (as a total of the two diastereomers in each case) was >98%. The identity of both compounds was undoubtedly defined by extensive 2D NMR study and comparison with literature data.[15−19] Syringaldehyde (98% purity) used as internal standard (IS) was purchased from Sigma-Aldrich (Steinheim, Germany). IS solution was prepared in acetonitrile at a concentration of 0.5 mg/mL and kept in a refrigerator. Prior to use the IS solution was left to come to room temperature. All NMR solvents used throughout the experiments were obtained by Sigma-Aldrich.

NMR Spectral Analysis. The residue of the above procedure was dissolved in $CDCl_3$ (750 μL) and an accurately measured volume of the solution (550 μL) was transferred to a 5 mm NMR tube. ^{1}H NMR spectra were recorded at 600 MHz (Bruker Avance600) or 400 MHz (Bruker DRX400). Typically, 50 scans were collected into 32K data points over a spectral width of 0−16 ppm with a relaxation delay of 1 s and an acquisition time of 1.7 s. Prior to Fourier transformation (FT) an exponential weighing factor corresponding to a line broadening of 0.3 Hz was applied. The spectra were phased corrected and integrated automatically using TopSpin software (Bruker). Where necessary, accurate integration was performed manually for the peaks of interest.

Calibration Curves and Quantitation. Calibration curves were prepared by addition of known quantities of isolated oleuropein aglycon or ligstroside aglycon to a selected olive oil, from cv. Adramytini, which is naturally free of secoiridoid derivatives, and following the above-described extraction and measurement method. The quantitation was based on the integration ratio between the aldehydic proton signal of syringaldehyde at 9.81 ppm and the aldehydic protons of oleuropein aglycon at 9.51 and 9.58 ppm and ligstroside aglycon at 9.49 and 9.55 ppm, respectively, for each pair of diastereomers.

Standard and Spiked Solutions. Stock standard solutions of oleuropein aglycon and ligstroside aglycon were prepared in acetonitrile at the 0.5 mg/mL level and were kept under refrigeration. Prior to use the stock solutions were allowed to come to room temperature. Spiked olive oil samples were prepared to give concentrations of both aglycons of 10, 20, 40, 80, 160, and 320 mg/kg by mixing appropriate volumes of the stock standard solutions with 5.0 g of olive oil of the variety Adramytini. The mixture was homogenized using a vortex mixer for 30 s and then extracted with cyclohexane (20 mL) and acetonitrile (as much as needed to become a total of 25 mL) as described above. A sample of Adramytini variety was selected as a blank because it was found that it did not contain oleuropein and ligstroside aglycons in detectable quantities and it did not give any interfering peaks at the chemical shift of the analytes.

Method Validation. The method was checked for the linearity, precision [calculated as the relative percent standard deviation (RSD %)], accuracy [evaluated as the relative percentage error (Er%), defined as (assayed concentration − nominal concentration)/(nominal concentration) × 100], and sensitivity [evaluated as the limits of detection (LOD) and quantitation (LOQ)].

Linearity. Spiked olive oil samples were prepared to give concentrations of oleuropein aglycon and ligstroside aglycon at 10, 20, 40, 80, 160, and 320 mg/kg and were analyzed for the determination of the linearity. The relationship of the integration ratio of the analytes versus the internal standard and the corresponding concentration of the spiked olive standards was determined by linear regression analysis.

Precision. The intraday precision was determined by analyzing five replicates of spiked olive oil samples at two concentration levels of both aglycons (80 and 160 mg/kg). The interday precision was assessed by analyzing spiked olive oil samples at two concentration levels, namely, 80 and 160 mg/kg levels, on five consecutive days.

Accuracy. Spiked olive oil samples at three concentration levels of both aglycons, 10, 80, and 160 mg/kg, were analyzed in order to determine the accuracy of the method.

Recovery. For the calculation of the recovery, spiked olive oil samples with concentrations of both analytes at the 160 mg/kg level (n = 5 for each analyte) were analyzed by employing the proposed extraction procedure. The recovery was calculated as the ratio of the response of both compounds in the spiked olive oil samples against that of the standards at the same levels and was expressed as the mean ± SD (standard deviation).

Limits of Detection and Quantitation. The LOD and LOQ were determined by running six blank samples of Adramytini olive oil and measuring the background response at the chemical shift of each analyte. Signal-to-noise (S/N) ratios of 3:1 and 10:1 were used for the calculation of the LOD and LOQ, respectively.

Isolation and Spectroscopic Identification of Methyl Elenolate. Methyl elenolate was isolated using column chromatography during the purification of the reference compounds as described above and in more details in the Supporting Information. The complete NMR data of methyl elenolate (^{1}H NMR, ^{13}C NMR) as well as the original 1D and 2D NMR spectra are provided in Supporting Information and were in accordance with literature data.[19,20]

RESULTS AND DISCUSSION

Purification of Oleuropein and Ligstroside Aglycons. In order to set up the qNMR method for the measurement of oleuropein and ligstroside aglycons it was necessary to obtain the target compounds in the maximum possible purity to be used as standards for the construction of the calibration curve. For this purpose usual chromatographic methodologies were followed either using normal or reversed stationary phases. In a first step the olive oil was extracted with acetonitrile and the ^{1}H NMR spectrum of the extract was recorded to ensure that the target compounds had been successfully extracted. Then the extract was submitted to column chromatography using silica gel as stationary phase and mixtures of cyclohexane with ethyl acetate as mobile phase. When both compounds were isolated, the ^{1}H NMR spectrum showed that each one contained 20−25% of the 5*S*,8*S*,9*S* isomer and 75−80% of the 5*S*,8*R*,9*S* isomer, identified by comparison with literature data.[17−19] However, when the spectra of the purified compounds were compared with the spectrum of the initial extract, surprisingly, we observed that the peaks corresponding to the 5*S*,8*S*,9*S* isomers were almost absent (Figure 1). The 5*S*,8*R*,9*R* isomer reported by Perez-Trujillo et al.[17] was not observed neither before nor after purification (and probably this is related with differences in olive variety or the followed extraction

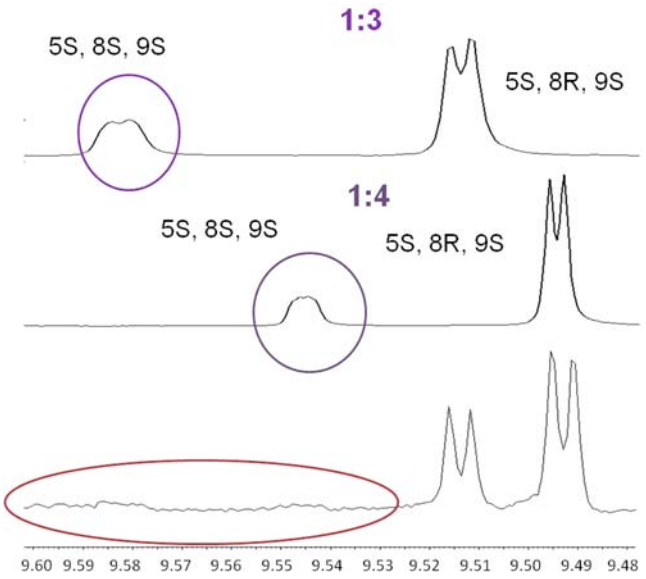

Figure 1. NMR region from 9.48 to 9.60 ppm showing the aldehyde protons of oleuropein and ligstroside aglycons. Top: Oleuropein aglycon after purification with normal-phase silica gel. Middle: Ligstroside aglycon after purification with normal phase silica gel. Bottom: Olive oil extract before submission to purification. The peaks of the 5*S*,8*S*,9*S* isomers of both aglycons are almost absent.

procedure). This observation led us to suppose the artificial formation of the minor isomers. Interestingly, the same was observed when the extract from another olive oil sample was submitted to reversed chromatography using RP-18 silica and a mixture of acetonitrile and water as mobile phase. In that case, the 5*S*,8*S*,9*S* isomers were observable before purification, but after purification, the ratio between the two isomers changed to 1:2 or 1:1 for ligstroside and oleuropein aglycons, respectively (Figure 2a,b).

To further study the role of the stationary phase in this isomerization, the following experiment was performed: A quantity of olive oil extract was diluted in a solvent (dichloromethane, cyclohexane, ethyl acetate, or mixtures of them) and added to a quantity of normal stationary phase and allowed to stand for 2 h. The same was performed with acetonitrile and water and reversed stationary phase. At the end, the mixture was filtered and evaporated and the residue was studied by NMR using $CDCl_3$. The comparison of the NMR profile of the treated and untreated olive oil extract showed that in all cases the percentage of the 5*S*,8*S*,9*S* isomers was significantly increased (Figure 3). The only combination that left the ratio unchanged was acetonitrile 100% with RP-18 silica. However, this combination was not useful for the purification of the target compounds. Although one previous work reports the purification of each isomer using Si 60 stationary phase,[19] in our hands it was obvious that it was not possible to purify oleuropein and ligstroside aglycons without isomerization using silica-based chromatography. Moreover, as it has been previously shown by LC−NMR, the two compounds are inseparable by HPLC.[17,18]

On the basis of the above observations, it is obvious that when oleuropein and ligstroside aglycons are needed for biological testing their diastereomeric purity cannot be safely determined by liquid chromatography methods. Any characterization of bioactivity should be accompanied by the isomer ratio as measured by NMR.

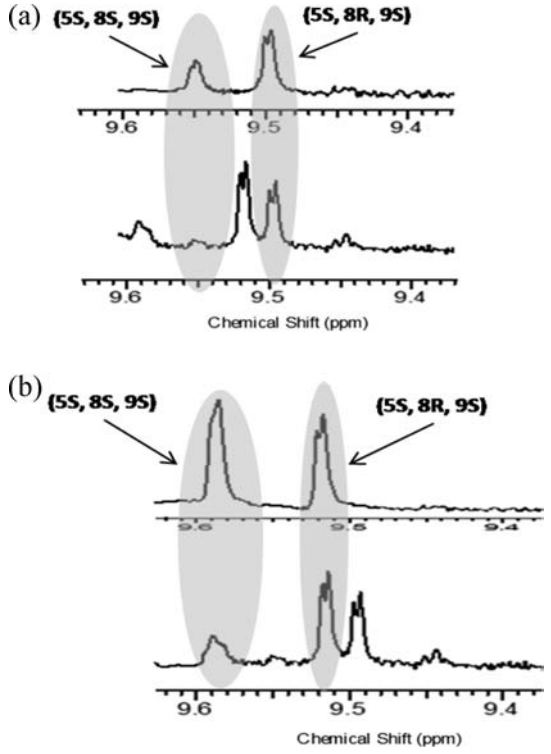

Figure 2. (a) Top: Ligstroside aglycon after purification with RP-18 and acetonitrile/water. Bottom: Olive oil extract before purification. (b) Top: Oleuropein aglycon after purification with RP-18 and acetonitrile/water. Bottom: Olive oil extract before purification.

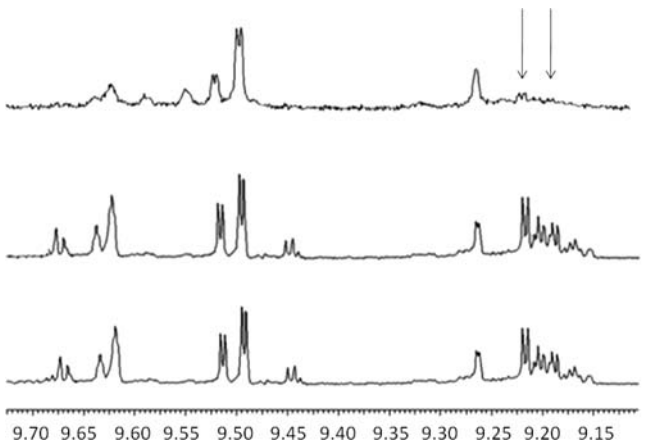

Figure 3. Oleocanthal and oleacein decomposition after contact with normal-phase silica gel. Top: NMR profile of the aldehydic region after contact with normal-phase silica gel. Middle: NMR profile of the aldehydic region after contact with reversed-phase silica gel and acetonitrile 100%. Bottom: NMR profile of the aldehydic region before contact with any stationary phase. The arrows show the strong reduction of the signals of oleocanthal and oleacein after contact with normal-phase silica gel. The signals of oleuropein and ligstroside aglycons are also reduced and new peaks corresponding to their isomers appear.

One additional observation based on the comparison of the NMR spectra of the olive oil extract before and after contact with normal phase silica (Figure 3) is that there is a significant percentage of decomposition of both oleocanthal and oleacein. This is a reasonable explanation for the low reported yield of both compounds when they are isolated by column

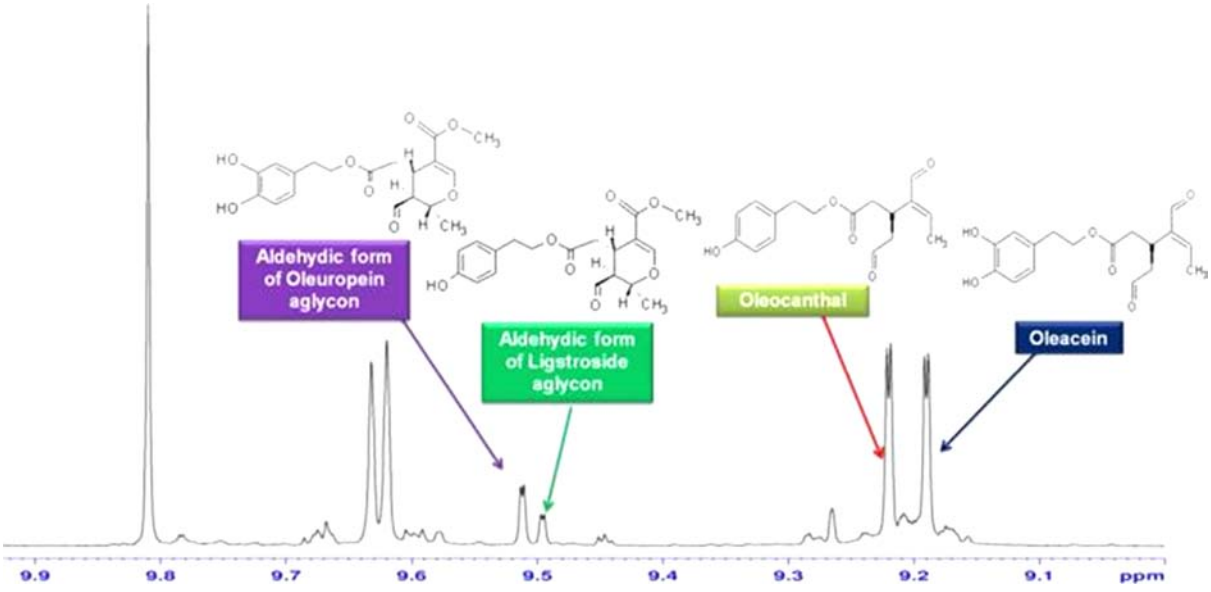

Figure 4. Typical NMR spectrum showing the peaks used for integration for each analyte.

chromatography. The mechanism of decomposition and the decomposition products were not studied.

Method Development. *Selection of Extraction Solvent.* The selection of acetonitrile as solvent for extraction of olive oil was based on the observation that it does not react with the two aglycons, as also described previously for the case of oleocanthal and oleacein.[7] It should be emphasized that methanol and/or water, which are commonly[17,18] and officialy[14] used for the extraction of phenolics from olive oil, react immediately with the dialdehydic form of oleocanthal or oleacein, leading to the corresponding acetals or hemiacetals.[7] A large number of compounds identified in HPLC−UV or LCMS chromatograms of olive oil extracts are obviously artifacts produced by that type of reaction. All those artifacts make the chromatograms much more complex and less reproducible and need to be reconsidered. For example, a recent study[13] quantified oleocanthal and oleacein with LC−MS/MS using external calibration curves prepared by dilution of standards in acetonitrile, although the analyzed olive oil extract was prepared using methanol. The proved reactivity of both compounds with methanol poses serious question about the reliability of such measurements. All hemiacetals or acetals produced during the extraction with methanol (and water) are not measured if the calibration is based on the MS/MS fragmentation of the dialdehydic forms and thus only a small part of unreacted oleocanthal or oleacein is finally measured, leading to questionable conclusions.

The two aglycons do not present such reactivity and this is possibly an explanation why they are often measured in higher levels than oleocanthal and oleacein. Moreover, one extraction with acetonitrile was sufficient for more than 85% recovery of all studied compounds. A second extraction achieved quantitative recovery but it was avoided to simplify the procedure. However, it should be noted that the exact percentage of recovery was not used for the calculations, because the final concentrations of the studied compounds in olive oil were calculated using calibration curves prepared by addition of pure compounds in olive oil originally free of both compounds.

Selection of Internal Standard and NMR Solvent. The choice of syringaldehyde as internal standard and of $CDCl_3$ as solvent for the NMR measurement was based on reasons explained previously.[7]

NMR Spectral Analysis of Target Compounds in Extra Virgin Olive Oil. The qNMR method was based on the observation that the ^1H NMR spectrum of olive oil acetonitrile extracts when recorded in $CDCl_3$ presented a very well resolved set of peaks corresponding to the aldehydic protons of the studied compounds between 9.1 and 9.8 ppm (Figure 4). This spectrum region in all the studied samples was clearly resolved, making feasible the integration of the corresponding peaks and their comparison with the peak of the internal standard. Oleuropein aglycon (3,4-DHPEA-EA) and ligstroside aglycon (*p*-HPEA-EA) were quantified by integrating doublets at 9.51and 9.49 ppm, respectively. Oleocanthal and oleacein were measured at 9.23 and 9.19 ppm, respectively, as previously described.[7]

The peaks of both aglycons did not present any overlapping in any studied sample recorded at 600 MHz or even at 400 MHz. The target peak of oleocanthal also did not present any overlapping at 600 MHz, but in some cases there was some overlapping observed at 400 MHz. The problem of overlapping was more significant for oleacein at 400 MHz but only in a few cases at 600 MHz (<3%). Even in those cases for the partially overlapped oleacein a good estimation of its quantity could be obtained. The overlapping problem can be overridden by 2D qNMR, which is currently under investigation.

Development of Calibration Curve. Since in our hands it was not possible to isolate oleuropein and ligstroside aglycons without the 5*S*,8*S*,9*S* isomer, it was obligatory to construct the calibration curve using the mixture of both isomers at a standard ratio. Since their difference is only one asymmetry center, it is reasonable to expect that their behavior during extraction will be similar and that the integration of the aldehyde proton of each isomer in the NMR spectrum in comparison with the internal standard will be the same. Under these conditions, the calibration curve was constructed by the addition of known quantities in a specifically selected olive oil sample which did not contain oleuropein or ligstroside

dx.doi.org/10.1021/jf404421p | J. Agric. Food Chem. 2014, 62, 600−607

aglycons. The sum of the integration of the two peaks corresponding to the aldehyde protons of each isomer of each compound was used as the response. The method was validated for accuracy, precision, and sensititvity.

Linearity. Good linearity was achieved for both analytes, as indicated by the equations listed in Table 1, for a concentration ranging from 10 to 320 mg/kg, with satisfactory correlation coefficients, r^2 (0.9991 and 0.991 for oleuropein and ligstroside aglycons, respectively.

Table 1. Linearity of the Oleuropein and Ligstroside Aglycons Determination in Olive Oil Samples

ratio	regression eq	correlation coeff, r^2
oleuropein aglycon/IS	$y = 336.5x - 8.66$	0.9991
ligstroside aglycon/IS	$y = 324.0x - 0.78$	0.991

Precision. The intraday precision, expressed as the relative standard deviation (RSD) ranged from 3.3 to 4.9% for the two analytes, as shown in Table 2. The interday precision ranged between 3.7 and 4.8% (Table 2). The RSD values are adequate and indicate the suitability of the method.

Table 2. Precision Data of the Oleuropein and Ligstroside Aglycons for Olive Oil Samples

	intraday precision (RSD%)		interday precision (RSD%)	
ratio	80 mg/L	160 mg/kg	80 mg/kg	160 mg/kg
oleuropein aglycon/IS	4.7	3.5	4.8	4.3
ligstroside aglycon/IS	4.9	3.3	4.8	3.7

Accuracy. The results for the accuracy are listed in Table 3 and are expressed as the relative percentage error (Er%). The estimated accuracy values with the proposed method are within acceptable levels for the two analytes. The obtained data indicate that the method could be considered as accurate.

Table 3. Accuracy Data of the Oleuropein and Ligstroside Aglycons Determination in Olive Oil Samples

	accuracy (Er%)		
ratio	10 mg/kg	80 mg/kg	160 mg/kg
oleuropein aglycon/IS	3.3	−2.9	0.70
ligstroside aglycon/IS	−9.3	−6.9	4.9

Recovery. The recoveries were found to be 85.5% (±3.5) and 85.8% (±3.1) for the 160 mg/kg levels for oleuropein and ligstroside aglycon, respectively, indicating acceptable recovery.

Sensitivity. The sensitivity of the method as presented by its limit of detection (LOD) and the limit of quantification (LOQ) were found to be 1 and 10 mg/kg, respectively, for both compounds, similarly with oleocanthal and oleacein as previously described.[7]

Isolation of Methyl Elenolate. During the isolation procedure of the four major secoiridoids, one additional minor constituent was also isolated and characterized. The ^{1}H NMR spectrum showed that it was a secoridoid derivative without a phenolic moiety. Examination of 1D and 2D NMR and MS data and comparison with literature data showed that it was the methyl ester of elenolic acid.[19,20] As in the case of oleuropein and ligstroside aglycons, methyl elenolate was isolated as a mixture of two diastereomers in a 1:4 ratio. The major one was identified as the 5*S*,8*R*,9*S* isomer by comparison with a synthetic methylated derivative of *epi*-elenolic acid.[20] The coupling constants of the major isomer were also in accordance with those described for the 5*S*,8*R*,9*S* isomer of oleuropein aglycon.[17] The main difference was the absence of the hydroxytyrosol moiety and its replacement by the methyl group. The minor diastereomer was identified as the 5*S*,8*S*,9*S* diastereomer of methyl elenolate described by Gariboldi et al.[19] as a synthetic product. As in the case of oleuropein and ligstroside aglycons, the formation of the minor isomer is most probably artificial (or artificially enhanced) due to the contact with the stationary phase during the chromatographic purification. This compound has been reported only as a synthetic derivative[19,20] and herein is reported for the first time as a constituent of olive oil.

Method Application. The developed method was applied to 340 samples of olive oil. The quantification results for each compound together with data about variety, geographic origin, and harvest time are provided as Supporting Information. The sum of the concentrations of the four compounds (named as D3) showed wide variation ranging from <1 to 1534 mg/kg (Figure 5). The highest recorded concentration of oleocanthal reached 711 mg/kg from cv. Koroneiki, while the concentration of oleacein was in almost all studied cases lower than that of oleocanthal (the highest recorded concentration for oleacein was 588 mg/kg). In total, among the Greek samples the highest concentration of the four secoiridoids were recorded in cv. Koroneiki from Aegean Islands (Paros, Antiparos), Messinia, Zakynthos, and Crete, and in cv. Throuba from Thassos Island (Table 4 and Supplementary Table 1, Supporting Information). Very interesting seems to be the case of olive oil samples from wild trees (Magnesia, Crete, Lakonia) showing very high oleocanthal content (Table 4 and Supplementary Table 1, Supporting Information). A map showing the main olive producing regions of Greece with the major variety in each region and the mean values of D3 has been constructed (Figure 6).

Concerning the two aglycons, their concentration in most studied cases was lower than that of oleocanthal and oleacein, and the previously described D1 index (sum of oleocanthal and oleacein) seems to have a dominating role in the total concentration of the secoiridoid derivatives. The concentration of the two aglycons in the Greek olive oil samples ranged from not detectable to 257 and 228 mg/kg for oleuropein and ligstroside aglycons, respectively. As shown in Figure 6, the sum of the four compounds is very well correlated with D1 as well as oleocanthal alone (supplementary Figure 9, Supporting Information), revealing the role of oleocanthal as the dominating factor at least among the Greek studied varieties. The highest recorded concentration of oleuropein aglycon (342 mg/kg) was recorded in a sample from cv. Mission from California, produced from green olives under stressed irrigation and low-temperature milling. The cv. Mission from California seems to be highly interesting, since in all studied samples the major secoiridoid was oleuropein aglycon. Moreover, in all Mission samples the concentration of oleocanthal and oleacein was lower than that of oleuropein and ligstroside aglycons, revealing that there are two distinct biosynthetic pathways leading to the domination of each group of compounds. It is apparent that regarding the phenolic secoiridoids of olive oil there are at least three different chemotypes: one with the domination of decarboxymethyl dialdehydic forms (oleocanthal,oleacein) (e.g., cv. Koroneiki, cv. Throuba, cv. Athenolia),

dx.doi.org/10.1021/jf404421p | J. Agric. Food Chem. 2014, 62, 600−607

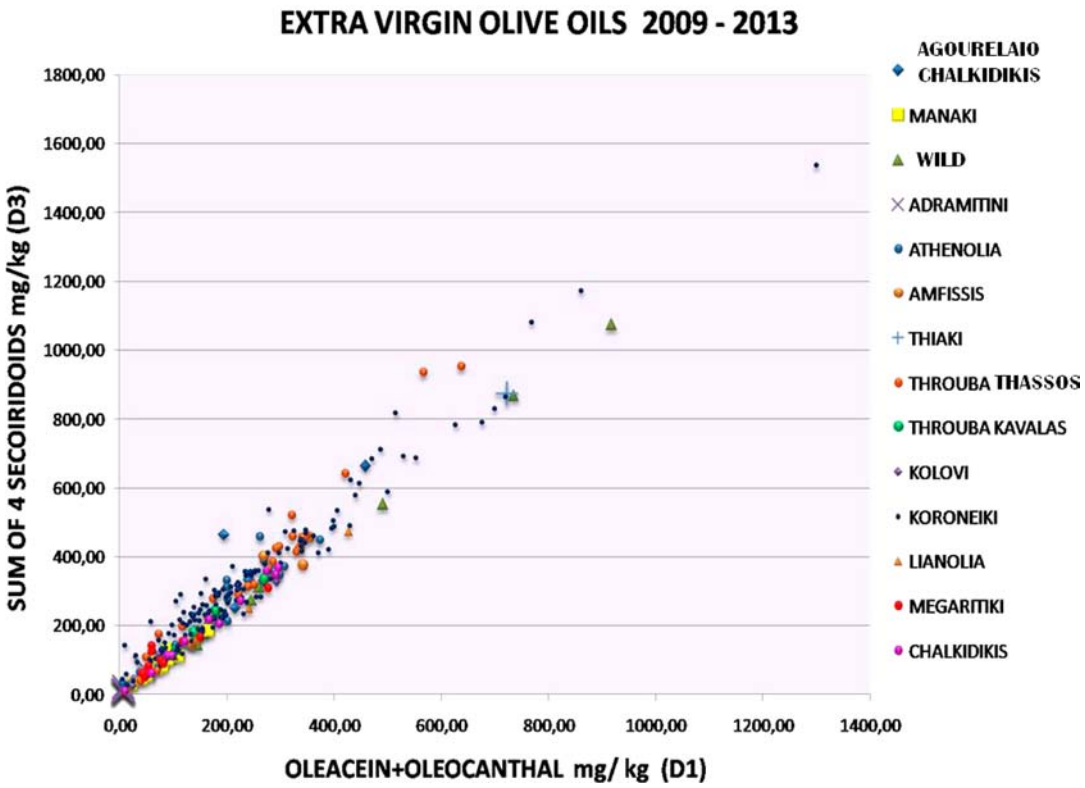

Figure 5. Distribution of oleocanthal, oleacein, oleuropein, and ligstroside aglycons concentrations among the studied Greek varieties.

Table 4. Top 15 Highest Concentration Greek Samples

cultivar	origin	harvest	oleocanthal, mg/kg	oleacein, mg/kg	oleuropein aglycon, mg/kg	ligstroside aglycon, mg/kg	D1,[a] mg/kg	D2[b]	D3,[c] mg/kg
Koroneiki	Paros	10/2012	711	588	120	114	1300	0.79	1534
Koroneiki	Antiparos[d]	10/2012	357	410	180	131	768	1.11	1080
Wild	Crete	10/2012	528	389	83	73	917	0.71	1075
Throuba	Thassos	10/2011	422	214	172	142	637	0.48	951
Throuba	Thassos	11/2011	515	51	139	228	566	0.08	933
Local	Zakynthos[d]	11/2012	559	185	80	93	745	0.31	919
Thiaki	Ithaki	11/2012	403	320	77	71	723	0.76	872
Wild	Lakonia	11/2012	631	103	108	25	735	0.15	868
Koroneiki	Zakynthos[d]	11/2012	423	297	68	74	720	0.67	863
Koroneiki	Zakynthos[d]	11/2012	415	284	64	64	699	0.65	828
Koroneiki	Paros	10/2012	417	98	257	40	516	0.22	814
Koroneiki	Messinia[d]	10/2012	393	283	52	58	676	0.69	788
Koroneiki	Antiparos[d]	11/2012	348	279	90	63	627	0.77	781
Koroneiki	Zakynthos[d]	11/2012	341	189	76	83	530	0.52	690
Koroneiki	Crete[d]	11/2012	284	268	78	52	553	0.90	684

[a]Oleacein + oleocanthal. [b]Oleacein/oleocanthal. [c]Sum of four secoiridoids. [d]Bottled samples.

one with the domination of monoaldehyde aglycons (e.g., cv. Mission), and one with the absence (or significantly reduced content) of both categories (e.g., cv. Adramytini, cv. Megaritiki) (supplementary Figure S1A–C, Supporting Information). However, we have also observed a number of samples with a different pattern presenting aldehyde peaks with significant intensity corresponding to not yet measured derivatives like oleuropein and ligstroside aglycon dialdehyde forms (supplementary Figure S1D, Supporting Information). The existence of varieties with other major secoiridoid derivatives makes necessary their exact identification and measurement. This is currently in progress as well as the expansion of the chemical database to other important varieties.

Although according to the European union legislation[21] all the studied samples were considered as extra virgin olive oils, the observed significant variation of the concentration of the bioactive polyphenolic secoiridoids confirms our previous conclusion[7] that there is need of a new type of classification of EVOO, especially related to possible health claims of those compounds.

Another observation that was further confirmed is that the ratio between oleocanthal and oleacein (index D2 = oleacein/oleocanthal) seems to be dependent on the olive tree variety, probably due to genetic reasons and independent of the olive mill procedure. Expanding our database[7] and including more samples (from 30 to 56 samples) coming only from cv.

dx.doi.org/10.1021/jf404421p | J. Agric. Food Chem. 2014, 62, 600–607

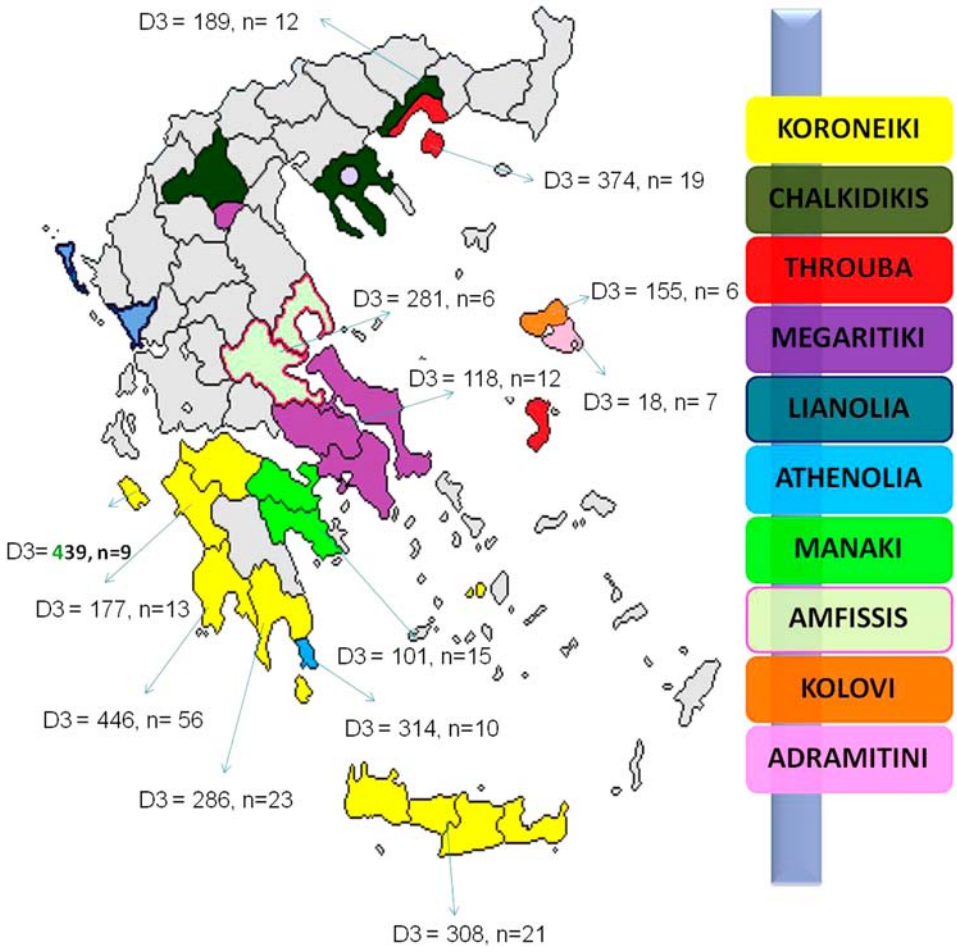

Figure 6. Map of the major olive oil producing regions of Greece showing the main variety cultivated/studied in each region and the mean D3 index for each region, *n* = number of studied samples.

Koroneiki from a narrow geographic region (Messinia) we observed that despite the variability of D1 (due to differences in harvest time or milling procedures), the correlation between oleocanthal and oleacein concentration was almost linear (R^2 = 0.71) and the mean D2 value was 0.50 ± 0.22 (supplementary Figure S8, Supporting Information). In contrast, in other varieties, for example Throuba Thassos (25 samples), the mean D2 value was significantly lower (0.29 ± 0.15) or, for Athenolia (20 samples, D2 = 0.31 ± 0.20), showed that the ratio between olacein and oleocanthal is mainly influenced by the tree variety.

Moreover, as previously reported for oleocanthal and oleacein, the highest levels of the two aglycons were also recorded in samples coming from early harvest showing again the positive correlation of the secoiridoid levels in olive oil with the low maturity index of the olive fruit.

As a final remark and based on the above observations, we would like to propose one more supplementary index, D3, as an addition to the previously described D1 and D2 indexes. Those indexes can be used for the support of health claims, since they are directly related with the European Union regulation[5] about the derivatives of hydroxytyrosol and tyrosol in olive oil. D1 and D3 are more accurate and specific than the commonly used total polyphenols index (expressed as gallic acid equivalent) and could become a new standard for the characterization of olive oil healthfulness.

■ ASSOCIATED CONTENT

Supporting Information

Isolation details for oleuropein and ligstroside aglycons; tables with the complete analysis of all the studied samples, including variety, geographic origin, harvest time, and analysis time; and methyl elenolate NMR spectra. This material is available free of charge via the Internet at http://pubs.acs.org.

■ AUTHOR INFORMATION

Corresponding Author

*Tel: +30-210-7274052. Fax: +30-210-7274594. E-mail magiatis@pharm.uoa.gr.

Notes

The authors declare no competing financial interest.

■ ACKNOWLEDGMENTS

The authors would like to thank Dan Flynn, Executive Director of UC Davis Olive Center for providing monovarietal samples of California olive oils and for supporting this study with critical advice and information. We also thank Berkeley Olive Grove for providing a collection of Mission samples; AGROCERT, G. Kasapidis, J. Paschalidis, and G. Baltopoulos for their assistance in collecting Greek olive oil samples; and J. Dallas for technical assistance in the UC Davis NMR facility.

REFERENCES

(1) Visioli, F.; Bernardini, E. Extra virgin olive oil's polyphenols: Biological activities. *Curr. Pharm. Des.* **2011**, *17*, 786−804.

(2) Pérez-Jiménez, F.; Ruano, J.; Perez-Martinez, P.; Lopez-Segura, F.; Lopez-Miranda, J. The influence of olive oil on human health: Not a question of fat alone. *Mol. Nutr. Food Res.* **2007**, *51*, 1199−1208.

(3) Frankel, E. N. Nutritional and biological properties of extra virgin olive oil. *J. Agric. Food Chem.* **2011**, *59*, 785−792.

(4) Keast R. S. J.; Han, Q.; Smith, A. B., III; Beauchamp, G. K.; Breslin, P.; Lin, J. Oleocanthal for treating pain. EP2583676, 2013.

(5) Scientific opinion on the substantiation of health claims related to polyphenols in olive and protection of LDL particles from oxidative damage. *EFSA J.* **2011**, *9*, 2033

(6) Brenes, M.; García, A.; García, P.; Garrido, A. Acid hydrolysis of secoiridoid aglycons during storage of virgin olive oil. *J. Agric. Food Chem.* **2001**, *49*, 5609−5614.

(7) Karkoula, E.; Skantzari, A.; Melliou, E.; Magiatis, P. Direct measurement of oleocanthal and oleacein levels in olive oil by quantitative ^{1}H NMR. Establishment of a new index for the characterization of extra virgin olive oils. *J. Agric. Food Chem.* **2012**, *60*, 11696−703.

(8) Grossi, C.; Rigacci, S.; Ambrosini, S.; Ed Dami, T.; Luccarini, I.; et al. The polyphenol oleuropein aglycone protects TgCRND8 mice against Aß plaque pathology. *PLoS ONE* **2013**, *8* (8), e71702 DOI: 10.1371/journal.pone.0071702.

(9) Abuznait, A. H.; Qosa, H.; Busnena, B. A.; El Sayed, K. A.; Kaddoumi, A. Olive-oil-derived oleocanthal enhances β-amyloid clearance as a potential neuroprotective mechanism against Alzheimer's disease: In vitro and in vivo studies. *ACS Chem. Neurosci.* **2013**, *19*, 973−82.

(10) Bendini, A.; Cerretani, L.; Carrasco-Pancorbo, A.; Gómez-Caravaca, A. M.; Segura-Carretero, A.; Fernández-Gutiérrez, A.; Lercker, G. Phenolic molecules in virgin olive oils: A survey of their sensory properties, health effects, antioxidant activity and analytical methods. An overview of the last decade. *Molecules* **2007**, *12*, 1679−1719.

(11) Beauchamp, G. K.; Keast, R. S. J.; Morel, D.; Lin, J.; Pika, J.; Han, Q.; Lee, C.; Smith, A. B.; Breslin, P. A. S. Phytochemistry: Ibuprofen-like activity in extra-virgin olive oil. *Nature* **2005**, *437*, 45−46.

(12) Impellizzeri, J.; Lin, J. A simple high-performance liquid chromatography method for the determination of throat-burning oleocanthal with probated antiinflammatory activity in extra virgin olive oils. *J. Agric. Food Chem.* **2006**, *54*, 3204−3208.

(13) Kanakis, P.; Termentzi, A.; Michel, T.; Gikas, E.; Halabalaki, M.; Skaltsounis, A. L. From olive drupes to olive oil. An HPLC-orbitrap-based qualitative and quantitative exploration of olive key metabolites. *Planta Med.* **2013**, *79*, 1576−1587.

(14) International Olive Council testing methods. Determination of biophenols in olive oil by HPLC. COI/T.20/Doc No. 29, November 2009.

(15) Montedoro, G.; Servilli, M.; Baldioli, M.; Selvaggini, R.; Miniati, E.; Macchioni, A. Simple and hydrolysable compounds in virgin olive oil. 3. Spectroscopic characterizations of the secoiridoid derivatives. *J. Agric. Food Chem.* **1993**, *41*, 2228−2234.

(16) Christophoridou, S.; Dais, P. Detection and quantification of phenolic compounds in olive oil by high resolution 1H nuclear magnetic resonance spectroscopy. *Anal. Chim. Acta* **2009**, *633*, 283−292.

(17) Pérez-Trujillo, M.; Gómez-Caravaca, A. M.; Segura-Carretero, A.; Fernández-Cutiérrez, A.; Parella, T. Separation and identification of phenolic compounds of extra virgin olive oil from *Olea europaea* L. by HPLC−DAD−SPE−NMR/MS. Identification of a new diasteroisomer of the aldehydic form of oleuropein aglycon. *J. Agric. Food Chem.* **2010**, *58*, 9129−9136.

(18) Christophoridou, S.; Dais, P.; Tseng, L. H.; Spraul, M. Separation and identification of phenolic compounds in olive oil by coupling high-performance liquid chromatography with postcolumn solid-phase extraction to nuclear magnetic resonance spectroscopy (LC−SPE−NMR). *J. Agric. Food Chem.* **2005**, *53*, 4667−4679.

(19) Gariboldi, P.; Jommi, G.; Verotta, L. Secoiridoids from *Olea europaea*. *Phytochemistry* **1986**, *25*, 865−869.

(20) Baggiolini, E. G.; Pizzolato, G.; Uskokovic, M. R. Stereocontrolled synthesis of 19-epiajmalicine from loganin aglucone. *Tetrahedron* **1988**, *44*, 3203−3208.

(21) EEC: Regulation No. 2568/1991. *Off. J. Eur. Communities July 11*, **1991**, L 248

JOURNAL OF AGRICULTURAL AND FOOD CHEMISTRY

Article

pubs.acs.org/JAFC

White Tea as a Promising Antioxidant Medium Additive for Sperm Storage at Room Temperature: A Comparative Study with Green Tea

Tânia R. Dias, Marco G. Alves, Gonçalo D. Tomás, Sílvia Socorro, Branca M. Silva,* and Pedro F. Oliveira*

CICS − UBI − Health Sciences Research Centre, University of Beira Interior, 6201-506 Covilhã, Portugal

ABSTRACT: Storage of sperm under refrigeration reduces its viability, due to oxidative unbalance. Unfermented teas present high levels of catechin derivatives, known to reduce oxidative stress. This study investigated the effect of white tea (WTEA) on epididymal spermatozoa survival at room temperature (RT), using green tea (GTEA) for comparative purposes. The chemical profiles of WTEA and GTEA aqueous extracts were evaluated by ^{1}H NMR. (−)-Epigallocatechin-3-gallate was the most abundant catechin, being twice as abundant in WTEA extract. The antioxidant power of storage media was evaluated. Spermatozoa antioxidant potential, lipid peroxidation, and viability were assessed. The media antioxidant potential increased the most with WTEA supplementation, which was concomitant with the highest increase in sperm antioxidant potential and lipid peroxidation decrease. WTEA supplementation restored spermatozoa viability to values similar to those obtained at collection time. These findings provide evidence that WTEA extract is an excellent media additive for RT sperm storage, to facilitate transport and avoid the deleterious effects of refrigeration.

KEYWORDS: *sperm, Camellia sinensis, white tea, green tea, epigallocatechin-3-gallate, reactive oxygen species, antioxidants*

INTRODUCTION

Tea (*Camellia sinensis* (L.)) is one of the world's most widely consumed beverages, and its medicinal properties have been widely explored.[1] It can be classified in three types: unfermented (green and white teas), partially fermented (oolong tea), and completely fermented (black tea).[2] To produce green tea (GTEA), freshly harvested leaves are steamed to inactivate polyphenol oxidase enzyme and then rolled and dried. Its chemical composition is very similar to that of the fresh tea leaf.[1] White tea (WTEA) is exclusively prepared from young tea leaves or buds, harvested before being fully opened. The tea materials are picked and immediately sent to be steamed and dried to prevent oxidation, frequently followed by polymerization.[3] Unfermented teas are known to have high polyphenolic content, mainly catechin derivatives, (−)-epigallocatechin 3-gallate (EGCG) being the most abundant and powerful antioxidant.[4] With respect to processing, there are very little differences between green and white teas, although several papers suggest that WTEA presents higher levels of antioxidants than GTEA.[5] Recently, antioxidant components have aroused great interest due to their ability to minimize the deleterious effects of reactive oxygen species (ROS) on a number of biological and pathological processes.[6] ROS are necessary for the normal physiological function of sperm,[7] although their concentration must be kept under strict control to avoid deleterious effects, such as damage to cell structures: lipids and membranes, proteins, and DNA.[8] It has been reported that ROS overproduction results in oxidative stress (OS), which is related to several problems that may end up in male subfertility or infertility.[9] In fact, spermatozoa are particularly vulnerable to such stress because ROS readily attack the polyunsaturated fatty acids (PUFA) of the cells membrane, initiating a self-propagating chain reaction. End-products of these lipid peroxidation reactions, such as malondialdehyde (MDA), are especially dangerous for cell viability.[10] Therefore, there is a growing interest in enlightening the role of ROS formation in sperm as they are responsible for lower sperm quality in freshly collected semen and poor quality of sperm after processing for usage in reproductive technologies, such as artificial insemination (AI), in vitro fertilization (IVF), or cryopreservation.[11]

The maintenance of mammalian sperm at room temperature (RT) for short-term periods is advantageous as the storage of sperm in a refrigerated environment induces a rapid decline in its viability.[12] Establishment of optimal composition for sperm storage is of extreme relevance, as these cells are highly dependent on the supply of exogenous substrates and, due to their high metabolic rates, produce elevated amounts of ROS.[12] The addition of GTEA polyphenols has proven to be of great significance on frozen−thawed spermatozoa motility.[13] Here, we aimed to investigate the possible protective effect of WTEA extract on epididymal spermatozoa survival at RT, using GTEA as a comparison reference.[14] For that purpose, the chemical profiles of WTEA and GTEA aqueous extracts were determined by using ^{1}H NMR as well as the antioxidant potential of storage media containing these extracts. Furthermore, the effect of both extracts on epididymal spermatozoa maintenance at RT during 24, 48, and 72 h was evaluated by determining the spermatozoa antioxidant potential, lipid peroxidation, and viability during that time frame.

Received: June 5, 2013
Revised: December 28, 2013
Accepted: December 28, 2013
Published: December 28, 2013

ACS Publications © 2013 American Chemical Society

dx.doi.org/10.1021/jf4049462 | *J. Agric. Food Chem.* 2014, 62, 608−617

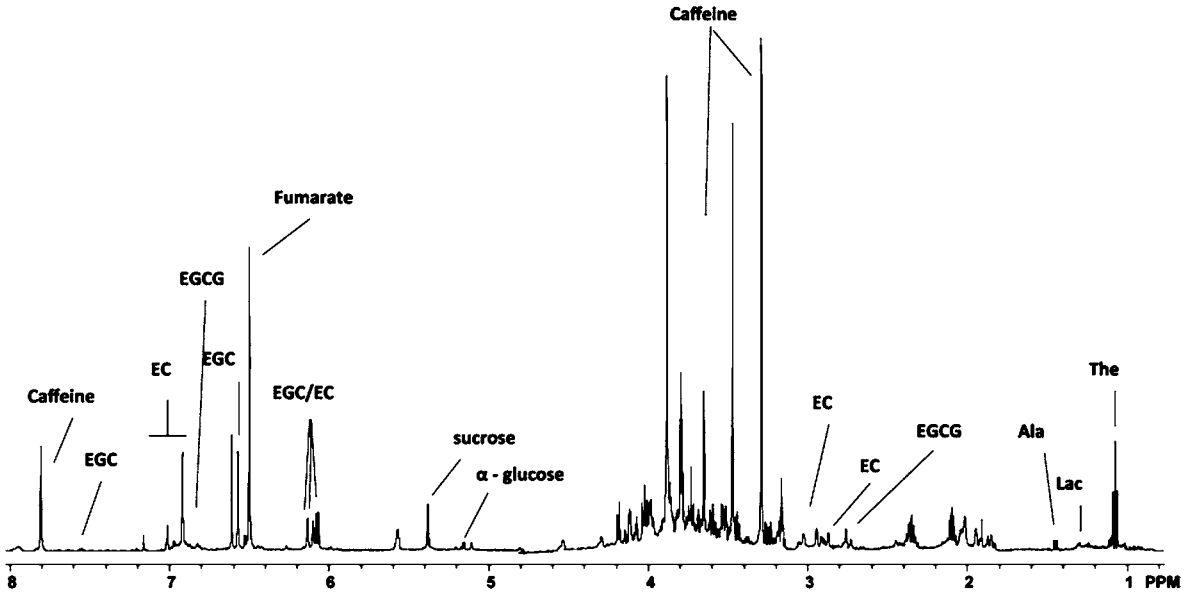

Figure 1. Representative ^{1}H NMR spectrum of WTEA extract showing the phytocomponent peak assignments: (EC) (−)-epicatechin; (EGC) (−)-epigallocatechin; (EGCG) (−)-epigallocatechin 3-gallate; (Ala) alanine; (The) theanine; (Lac) lactate.

MATERIALS AND METHODS

Chemicals. All chemicals were purchased from Sigma-Aldrich (St. Louis, MO, USA) unless specifically stated otherwise.

Tea Extracts. WTEA and GTEA were purchased on the Portuguese market (Diese, Bestlife - Comércio e Distribuição Lda., Portugal). Samples (n = 5) were subjected to infusion (1 g/100 mL distilled water; pH 5.5) at 100 °C during 3 min, according to the manufacturer's instructions. The resulting infusions were filtered with qualitative filter papers (catalog no. 516-0819, VWR, Leuven, France) in a vacuum system and freeze-dried overnight in a ScanVacCoolSafe Freeze-Dryer (Labogene, Lynge, Denmark). The mean extraction yields (g of lyophilized extract per 100 g of dried teas leaves) were 25% (for WTEA) and 20% (for GTEA). The lyophilized extracts were kept in a desiccator, protected from light, until analysis.

Proton Nuclear Magnetic Resonance (^{1}H NMR). ^{1}H NMR spectra were acquired as previously described.[15] Briefly, ^{1}H NMR spectra of WTEA and GTEA aqueous extracts dissolved in D_2O were acquired at 14.1 T, 25 °C, using a Bruker Avance 600 MHz spectrometer equipped with a 5 mm QXI probe and a z-gradient. ^{1}H NMR spectra were acquired with solvent suppression and a sweep width of 6 kHz, using a delay of 14 s, a water presaturation of 3 s, a pulse angle of 45°, an acquisition time of 3.5 s, and at least 128 scans. Sodium fumarate was added to the samples for quantification purposes (in a final concentration of 1 mM), because it does not exist in our tea extracts and was used as a reference (6.50 ppm), as routinely done in our laboratory,[16,17] to quantify the extract compounds whenever present in solution. The following coupling patterns, available in the literature,[18−23] were used to quantify the identifiable extract compounds (multiplet, ppm): L-theanine (triplet, 1.08); lactate (doublet, 1.33); alanine (doublet, 1.45); EGCG (doublet, 2.7); caffeine (singlet, 3.29); H1-α-glucose (doublet, 5.22); sucrose (doublet, 5.4); (−)-epigallocatechin (EGC) (singlet, 6.6); (−)-epicatechin (EC) (singlet, 7.0) (for a representative image see Figure 1). The relative areas of ^{1}H NMR resonances were quantified using the curve-fitting routine supplied with the NUTSproTM NMR spectral analysis program (Acorn, NMR Inc., Fremont, CA, USA).

Isolation of Epididymal Spermatozoa. The present study used six male 3-month-old Wistar rats, obtained from our accredited animal colony (Health Sciences Research Centre, University of Beira Interior) and maintained on ad libitum food and water in a constant room temperature (20 ± 2 °C) on a 12 h cycle of artificial lighting. Rats were fed a standard chow diet (4RF21 certificate, Mucedola, Italy). All animal experiments were performed according to the *Guide for the Care and Use of Laboratory Animals* published by the U.S. National Institutes of Health (NIH Publication 85-23, revised 1996) and the European directives for the care and handling of laboratory animals (Directive 86/609/EEC), after approbation by the National Ethics Committee of Animal Welfare.

Animals were anesthetized, by intraperitoneal injection of a mixture of 90 mg/kg of ketamine and 10 mg/kg of xylazine, and euthanized by cervical displacement. Cauda epididymis were isolated and immediately placed separately in 3 mL of a prewarmed (37 °C) Krebs−Ringer bicarbonate (TYH) medium (in mM: NaCl, 118.8; KCl, 4.78; $CaCl_2$, 1.71; KH_2PO_4, 1.19; $MgSO_4$, 1.19; $NaHCO_3$, 25; glucose, 5.56; sodium pyruvate, 1.01; sodium lactate, 29.2; plus 4.00 mg/mL BSA, 0.06 mg/mL potassium penicillin G and 0.05 mg/mL streptomycin sulfate), prepared on the day of the experiment, as described by Toyoda.[24] The two cauda epididymis of each animal were minced together with a scalpel blade, to allow sperm to disperse into the medium, and the suspension was then incubated for 1.5 h at 37 °C. The number of spermatozoa was determined using a hemocytometer, and 8×10^5 spermatozoa were placed in 300 μL of a control medium (in mM: NaCl, 96.66; KCl, 4.78; $CaCl_2$, 1.71; KH_2PO_4, 1.19; $MgSO_4$, 1.19; $NaHCO_3$, 4.15; D-glucose, 5.56; sodium pyruvate, 0.33; sodium lactate, 23.28; HEPES, 20.85; plus 4.00 mg/mL BSA, 0.06 mg/mL potassium penicillin G, 0.05 mg/mL streptomycin sulfate) as previously described.[25] Moreover, the same amount of spermatozoa was placed in four other media, with the same composition of the control group but containing additional concentrations of freeze-dried WTEA or GTEA aqueous extracts to a final concentration of 0.5 or 1 mg/mL. Subsequently, sperm suspensions were kept at acclimatized RT (22−23 °C) during 24, 48, and 72 h. These sperm suspensions were used for the FRAP, TBARS, and sperm viability assays, after being processed as described in each section.

Protein Quantification. After the 72 h of incubation, spermatozoa were separated from the storage media through centrifugation at 5000g for 15 min at 4 °C. Then, sperm pellets were washed with 100 μL of phosphate-buffered saline (PBS) solution (in mM: NaCl, 137; KCl, 2.7; Na_2HPO_4, 4.3; KH_2PO_4, 1.47; pH 7.4) and centrifuged again at 5000g for 15 min at 4 °C. Total proteins were isolated from the spermatozoa by the addition of an adequate amount of PBS, followed by a sonication for 15 min at 4 °C. Protein concentration was determined by Bio-Rad (Hemel Hempstead, UK) Bradford microassay according to the manufacturer's instructions. Sperm suspensions were used in FRAP and TBARS assays.

Ferric Reducing Antioxidant Power (FRAP) assay. The ferric reducing antioxidant power (FRAP) of the media samples and

dx.doi.org/10.1021/jf4049462 | J. Agric. Food Chem. 2014, 62, 608−617

spermatozoa pellets was performed according to the colorimetric method described by Benzie and Strain.[26] Briefly, working FRAP reagent was prepared by mixing acetate buffer (300 mM, pH 3.6), 2,4,6-tripyridyl-s-triazine (TPTZ) (10 mM in 40 mM HCl), and $FeCl_3$ (20 mM) in a 10:1:1 ratio (v/v/v); 180 μL of this reagent was mixed with 6 μL of each sample. The reduction of the Fe^{3+}−TPTZ complex to a colored Fe^{2+}−TPTZ complex by the samples was monitored immediately after addition of the sample and 40 min later, by measuring the absorbance at 595 nm using an Anthos 2010 microplate reader (Biochrom, Berlin, Germany). The antioxidant potential of the samples was determined against standards of ascorbic acid, which were processed in the same manner as the samples. Absorbance results were corrected by using a blank, with water instead of sample. The changes in absorbance values of test reaction mixtures were used to calculate FRAP values as described elsewhere.[26]

Thiobarbituric Acid Reactive Substances (TBARS) Assay. TBARS are formed as a byproduct of lipid peroxidation, which can be detected by the TBARS assay using thiobarbituric acid (TBA) as a reagent. This peroxidation reaction produces MDA, which reacts with TBA in conditions of high temperature and low pH, generating a pink complex that absorbs at 532 nm.[27] The TBARS assay was carried out according to the method described by Iqbal et al.,[28] with slight adaptations. Briefly, the reaction mixture in a total volume of 0.1 mL contained 0.01 mL of the sample, 0.01 mL of Tris-HCl buffer (150 mM, pH 7.1), 0.01 mL of ferrous sulfate (1.0 mM), 0.01 mL of ascorbic acid (1.5 mM), and 0.06 mL of H_2O. This mixture was incubated at 37 °C for 15 min. The reaction was stopped by the addition of 0.1 mL of trichloroacetic acid (10% w/v). Subsequently, 0.2 mL of thiobarbituric acid (0.375% w/v) was added, and all samples were incubated for 15 min at 100 °C. Finally, samples were subjected to centrifugation at 3000*g* for 10 min at 4 °C. The amount of MDA formed in each of the samples was estimated by measuring the optical density at 532 nm using a UV−vis spectrophotometer (Shimadzu, Kyoto, Japan) against a blank. The results were expressed as nanomoles of TBARS per milligram of protein.

Sperm Viability Evaluation. To assess sperm viability, an eosin/nigrosin staining was used because it is effective, simple, and, in addition to allowing sperm to be readily visualized, permits assessment of sperm membrane integrity. This method was performed with slight modifications of a method previously described.[29] A total of 5 μL of the sperm suspensions obtained as described above (see Isolation of Epididymal Spermatozoa) was mixed with 10 μL of 0.5% eosin/nigrosin stain and placed on a prewarmed glass microscope slide. Samples were analyzed at 0, 24, 48, and 72 h of the experiment. The number of viable and nonviable spermatozoa was determined by counting a total of 333 spermatozoa per slide in continuous random fields under a light microscope, with oil immersion (×1000 magnification), to determine the percentage of viable sperm, as previously described.[16] Live sperm remained white, whereas dead sperm stained pink, because the integrity of their plasma membrane was compromised, causing an increase in membrane permeability, which led to the uptake of the dye (Figure 5A).

Statistical Analysis. Statistical significance was assessed by two-way ANOVA, followed by Bonferroni post-test using GraphPad Prism 5 (GraphPad Software, San Diego, CA, USA). All data are presented as the mean ± SEM. Differences with $p < 0.05$ were considered statistically significant. Further analysis of the statistical power (SP) of differences of experimental data was evaluated with a one-tailed test assuming an α value of 0.05, which corresponds to a 0.95 confidence interval, as described by Levin,[30] using the software provided by http://www.dssresearch.com/KnowledgeCenter/toolkitcalculators/statisticalpowercalculators.aspx.

RESULTS

White Tea Extract Presents the Highest Content in Catechin Derivatives, Especially EGCG. Tea has been characterized by its high content in flavonoids,[31] such as catechin derivatives and other polyphenols,[32] which have biological and pharmaceutical properties that have been linked to beneficial effects on human health.[33]

The ^{1}H NMR data obtained from the aqueous extracts allowed the assignment of the following phytochemicals: three catechin derivatives, EC, EGC, and EGCG; one methylxanthine, caffeine; two free amino acids, L-theanine and alanine; two carbohydrates, glucose and sucrose; and one organic acid, lactate (for a representative image see Figure 1). As expected, the most abundant class of phytochemicals was the catechin family, representing 133 ± 14 and 91 ± 7 g/kg of WTEA and GTEA extracts, respectively. Among catechins, EGCG was the one present in the highest amount in both tea extracts, although in WTEA extract the quantity of this compound (82 ± 7 g/kg of WTEA extract) was nearly twice that verified in GTEA extract (42 ± 2 g/kg of GTEA extract). Concerning caffeine and sucrose, WTEA extract also demonstrated a larger amount (71 ± 8 and 60 ± 4 g/kg of WTEA extract, respectively) in comparison with GTEA (21 ± 3 and 26 ± 2 g/kg of GTEA extract, correspondingly). L-Theanine, alanine, and glucose were also present in considerable amounts, accounting for 19 ± 2, 0.7 ± 0.1, and 6 ± 1 g/kg of WTEA extract and 22 ± 1, 0.20 ± 0.04, and 11 ± 2 g/kg of GTEA extract, respectively (Table 1).

Table 1. White (WTEA) and Green Tea (GTEA) Extract Phytochemical Profiles As Determined by ^{1}H NMR Spectroscopy

	content[a] (g of compd/kg of tea extract)	
compound	WTEA	GTEA
glucose	6 ± 1.00	11 ± 2.00
sucrose	60 ± 4.00	26 ± 2.00
lactate	0.40 ± 0.01	0.46 ± 0.02
alanine	0.7 ± 0.10	0.20 ± 0.04
caffeine	71 ± 8.00	21 ± 3.00
L-theanine	19 ± 2.00	22 ± 1.00
EC[b]	5 ± 1.00	28 ± 2.00
EGC[c]	46 ± 6.00	21 ± 3.00
EGCG[d]	82 ± 7.00	42 ± 2.00

[a]Results are presented as the mean ± SEM (n = 5). [b]EC, (−)-epicatechin. [c]EGC, (−)-epigallocatechin. [d]EGCG, (−)-epigallocatechin 3-gallate.

In fact, (−)-epicatechin 3-gallate (ECG), (−)-catechin (C), and (−)-gallocatechin-3-gallate (GCG) were absent in our extracts. Generally, these polyphenols are minor tea components but sometimes are absent in tea extracts. For instance, Carvalho et al.[34] and Rusak et al.[35] have not found GCG and C, respectively, in tea extracts. Hence, the white and green tea qualitative phytochemical profiles obtained using ^{1}H NMR (Table 1) are in accordance with the phenolic and methylxanthine profiles obtained by HPLC-UV, HPLC-DAD, or HPLC-MS previously reported by Carvalho et al.,[34] Rusak et al.,[35] and Unachukwu et al.[36] The observed differences in the quantitative profile may be mainly due to the use of different extraction conditions (solvents, temperatures, times of extraction, and ratio leaves/water). Also, the natural variability of plants caused by edapho-climatic factors, harvesting techniques, or agricultural practices may contribute to these differences.

Storage Media Supplemented with White Tea Extract Have the Highest Antioxidant Potential. As the aqueous extracts of WTEA and GTEA demonstrated to be rich in

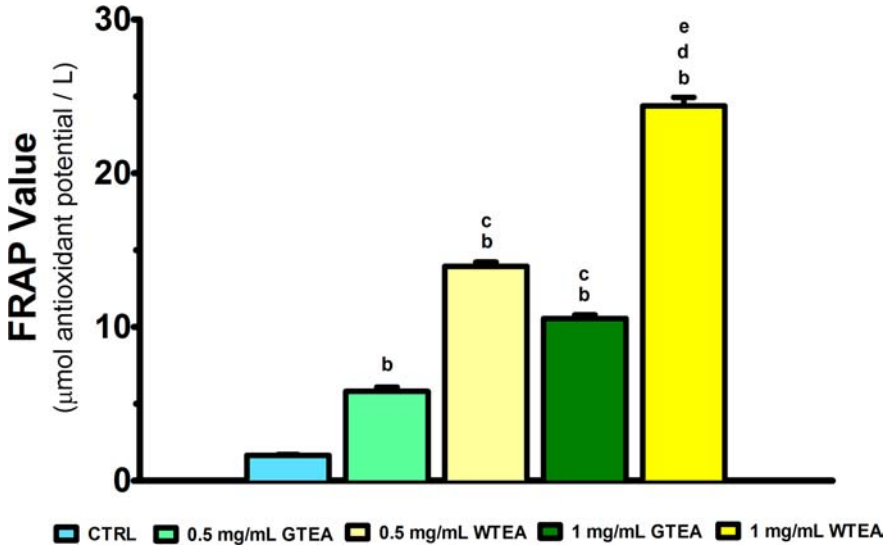

Figure 2. Ferric reducing antioxidant power (FRAP) of the epididymal spermatozoa storage media, control medium (CTRL), and media supplemented with freeze-dried WTEA or GTEA aqueous extracts to a final concentration of 0.5 or 1 mg/mL. The antioxidant power is expressed by the FRAP value (μmol of antioxidant potential/L). Results are presented as the mean ± SEM (n = 6). Significant results (p < 0.05) are indicated: b, versus CTRL; c, versus GTEA, 0.5 mg of GTEA extract/mL; d, versus WTEA, 0.5 mg of WTEA extract/mL; e, versus GTEA, 1 mg of GTEA extract/mL.

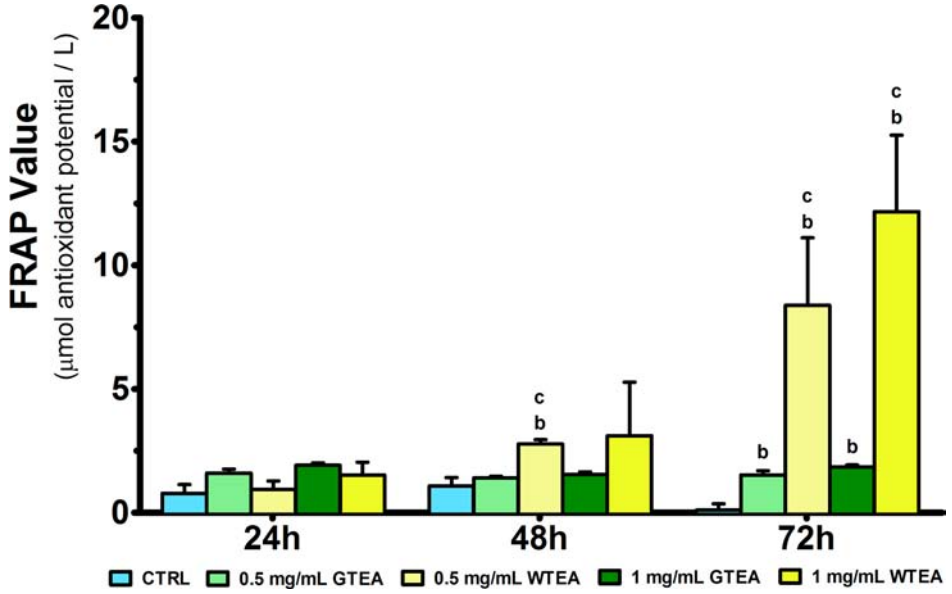

Figure 3. Ferric reducing antioxidant power (FRAP) of the epididymal spermatozoa stored in control medium (CTRL) and media supplemented with freeze-dried WTEA or GTEA aqueous extracts to a final concentration of 0.5 or 1 mg/mL, during the 24, 48, and 72 h of the experiment. The antioxidant power is expressed by the FRAP value in μmol of antioxidant potential/μg of protein and is presented as the mean ± SEM (n = 6). Significant results (p < 0.05) are indicated: b, versus CTRL; c, versus GTEA, 0.5 mg of GTEA extract/mL.

catechin derivatives, namely, EGCG, we performed a FRAP assay to evaluate the antioxidant potential of all experimental media supplemented with these extracts in comparison with the control media. The FRAP assay measures the potential of an antioxidant to reduce ferric(III) to ferrous(II) in a redox-linked colorimetric reaction that involves single electron transfer.[37] The reducing power of a compound/extract serves as a significant indicator of its potential antioxidant activity (FRAP value). The control medium showed a FRAP value of 1.64 ± 0.05 μmol of antioxidant potential/L (Figure 2). On the other hand, the FRAP value of the media supplemented with WTEA and GTEA revealed a dose-dependent reducing power (Figure 2), with significantly higher FRAP values relative to the control group during all of the experiments (SP = 100%). Comparing GTEA supplementation, the medium with 1 mg/mL of GTEA extract presented a significantly higher antioxidant potential compared to the medium with 0.5 mg of GTEA extract/mL (11 ± 0.2 vs 6 ± 0.3 μmol of antioxidant potential/L) (SP = 100%). In relation to WTEA, the FRAP value of the medium supplemented with 0.5 mg/mL of WTEA extract was 14 ± 0.3 μmol of antioxidant potential/L, which was significantly higher compared to the medium with the same concentration of GTEA extract (SP = 100%). Moreover, the medium containing 1 mg/mL of WTEA presented a significantly higher antioxidant potential of 24 ± 0.6 μmol of antioxidant potential/L in comparison with the medium supplemented with 0.5 mg/

dx.doi.org/10.1021/jf4049462 | J. Agric. Food Chem. 2014, 62, 608−617

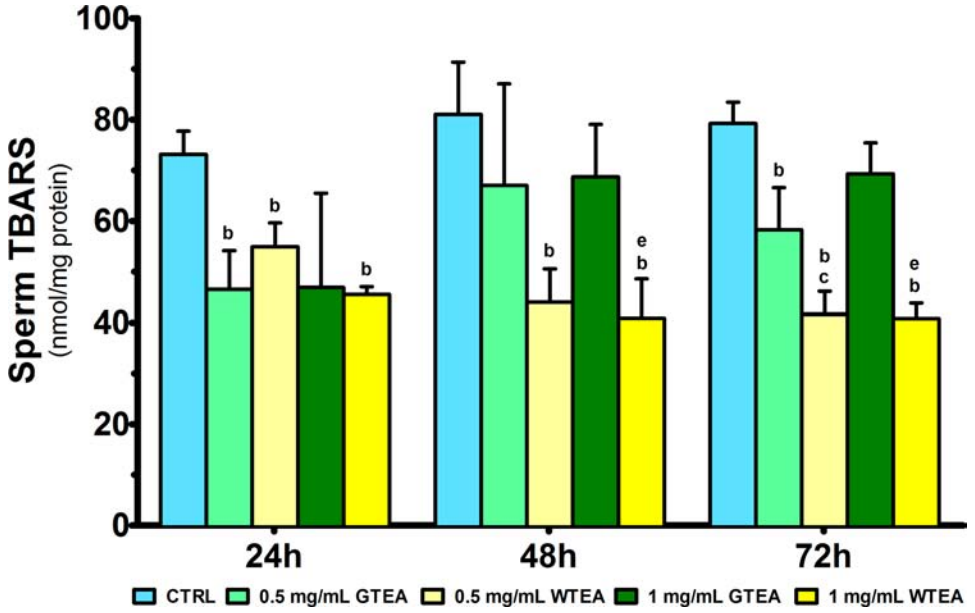

Figure 4. Sperm TBARS values produced in epididymal spermatozoa stored in control medium (CTRL) and media supplemented with freeze-dried WTEA or GTEA aqueous extracts to a final concentration of 0.5 or 1 mg/mL, during the 24, 48, and 72 h of the experiment. Results are expressed in nmol/mg of protein and are presented as the mean ± SEM ($n = 6$). Significant results ($p < 0.05$) are indicated: b, versus CTRL; c, versus GTEA, 0.5 mg of GTEA extract/mL; e, versus GTEA, 1 mg of GTEA extract/mL.

mL of WTEA extract and 1 mg/mL of GTEA extract (SP = 100%).

White Tea Extract Considerably Increases the Antioxidant Potential of Spermatozoa. Because the media supplemented with WTEA extract proved to have the highest antioxidant potential, we expected to verify the same profile in the antioxidant potential of the spermatozoa. Therefore, we also measured the antioxidant potential of the spermatozoa pellets at 24, 48, and 72 h with the FRAP assay. Accordingly, spermatozoa kept in control medium had always a lower antioxidant potential than spermatozoa stored in the media supplemented with WTEA and GTEA extracts, although these differences were statistically significant only after 48 and 72 h of storage, respectively (Figure 3). Indeed, at 48 h the spermatozoa stored in the medium with 0.5 mg of WTEA extract/mL presented a FRAP value of 2.8 ± 0.2 μmol of antioxidant potential/μg of protein, significantly higher than that of spermatozoa maintained in the control medium (1.1 ± 0.3) and in medium supplemented with 0.5 mg of GTEA extract/mL (1.4 ± 0.1) (SP = 100%). At 72 h, the FRAP values of spermatozoa maintained in media with 0.5 and 1 mg of GTEA extract/mL were 1.5 ± 0.2 (SP = 84%) and 1.8 ± 0.1 (SP = 100%) μmol of antioxidant potential/μg of protein, respectively, being significantly higher than that verified in the control group. At this time of incubation, the FRAP value determined for spermatozoa kept in the control medium was significantly lower than that at 48 h, reaching a value of 0.1 ± 0.3 μmol of antioxidant potential/μg of protein (SP = 100%) (Figure 3). In contrast, the antioxidant potentials of spermatozoa stored in the media supplemented with WTEA extract (0.5 and 1.0 mg of WTEA extract/mL) were remarkably higher than those observed at 48 h (8.4 ± 2.7 (SP = 99.9%) and 12.2 ± 3.1 (SP = 100%) μmol of antioxidant potential/μg of protein, respectively) and also than the FRAP value of the control group. Moreover, at 72 h there were no significant differences between both concentrations of the same extract.

Spermatozoa Lipid Peroxidation Is Significantly Reduced by White Tea Supplementation. During spermatozoa storage, ROS production is known to induce several deleterious effects[38] such as lipid peroxidation. Because spermatozoa antioxidant potential was increased after incubation with the tea extracts, we hypothesized that it could also decrease ROS production, thus decreasing lipid peroxidation. Therefore, we performed the TBARS assay to determine the levels of lipid peroxidation that occurred in spermatozoa during storage in the different media. Because ROS have extremely short half-lives, they are difficult to measure directly. Instead, several products induced by OS, such as TBARS, can be measured and used as an accurate indicator of OS.[39] Using the TBARS assay, it was possible to detect a significant decrease in lipid peroxidation in spermatozoa stored in media supplemented with WTEA and GTEA extracts. At 24 h, there was a significant decrease in lipid peroxidation from spermatozoa stored in the control medium (73 ± 4 nmol TBARS/mg protein) relative to the media containing 0.5 mg/mL of GTEA (47 ± 7 nmol TBARS/mg protein) and 0.5 and 1 mg/mL of WTEA (54.8 ± 4.7 and 46 ± 2 nmol TBARS/mg protein, respectively) (Figure 4) (SP = 100%). After 48 h, the lipid peroxidation significantly decreased from 81 ± 10 nmol TBARS/mg protein in the control group to 44 ± 6 and 41 ± 8 nmol TBARS/mg protein (SP = 100%) in the spermatozoa stored in the media supplemented with 0.5 and 1 mg of WTEA extract/mL, respectively (Figure 4). Moreover, the spermatozoa stored in the medium with 1 mg of WTEA extract/mL also presented significantly less lipid peroxidation than the spermatozoa maintained in the medium with 1 mg of GTEA extract/mL, which presented a value of 69 ± 10 nmol TBARS/mg protein (SP = 99.9%). At the end of the experiment (72 h), the control group presented a lipid peroxidation of 79 ± 4 nmol TBARS/mg protein that significantly decreased to 58 ± 8, 42 ± 5, and 41 ± 3 nmol TBARS/mg protein (SP = 100%) after storage in the media supplemented with 0.5 mg of GTEA extract/mL and 0.5 and 1 mg of WTEA extract/mL,

dx.doi.org/10.1021/jf4049462 | J. Agric. Food Chem. 2014, 62, 608−617

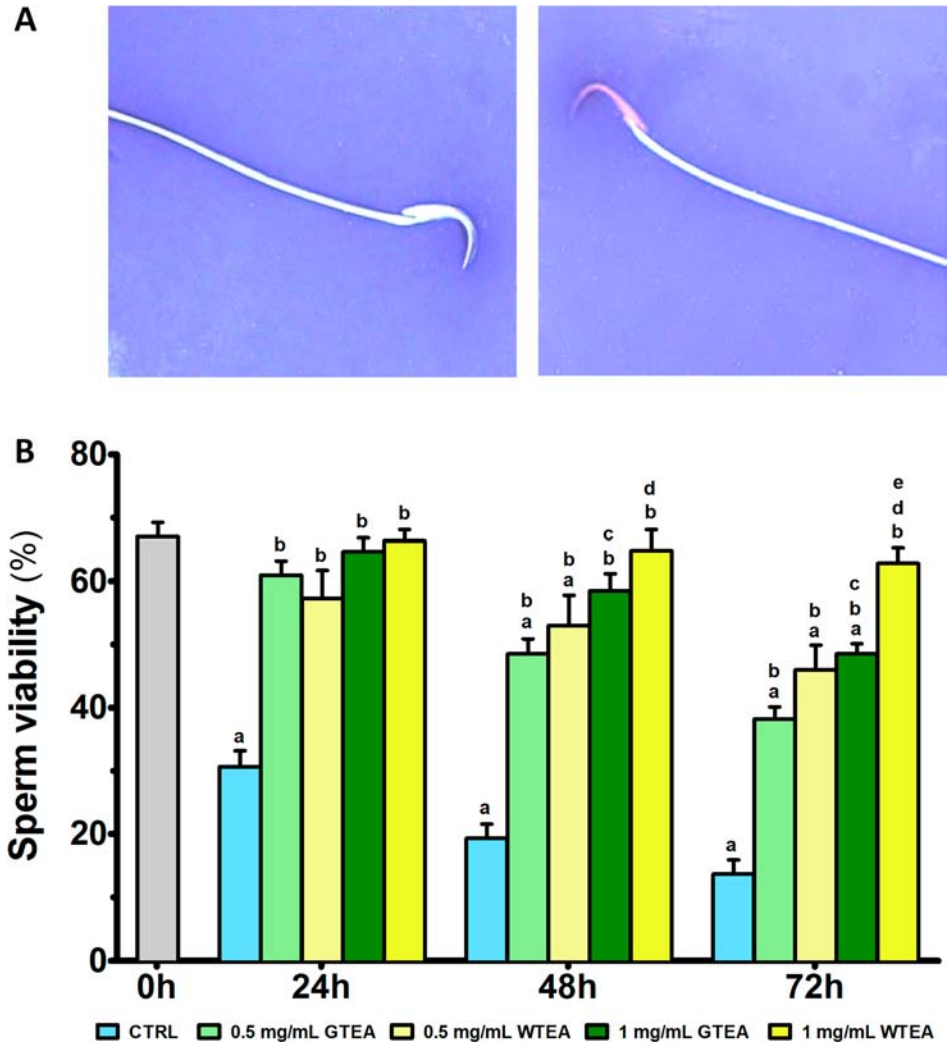

Figure 5. (A) Spermatozoa staining using eosin/nigrosin showing a viable (left) and a nonviable (right) cell. (B) Spermatozoa viability at collection time (0 h) and during the 3 day storage in control medium (CTRL) and media supplemented with freeze-dried WTEA or GTEA aqueous extracts to a final concentration of 0.5 or 1 mg/mL. Results are presented as the mean ± SEM (n = 6). Significant results (p < 0.05) are indicated: a, versus 0 h; b, versus CTRL; c, versus GTEA, 0.5 mg of GTEA extract/mL; d, versus WTEA, 0.5 mg of WTEA extract/mL; e, versus GTEA, 1 mg of GTEA extract/mL.

respectively. Additionally, lipid peroxidation in spermatozoa kept in the media with 0.5 and 1 mg of WTEA extract/mL were significantly lower than in spermatozoa stored in the media supplemented with 0.5 (SP = 99.5%) and 1 mg of GTEA extract/mL (SP = 100%), correspondingly.

White Tea Supplementation Increases Spermatozoa Viability after Room Temperature Storage. Sperm viability is one of the most important parameters to assess sperm quality.[40] Once the WTEA and GTEA supplementation significantly increased the antioxidant potential of storage media and spermatozoa and decreased spermatozoa lipid peroxidation, we hypothesized that sperm viability could be improved by these extracts. Therefore, we evaluated the sperm viability at the time of epididymal collection (0 h) and at 24, 48, and 72 h. At collection, sperm viability averaged 67 ± 2%. During spermatozoa storage at RT in control medium we observed that viability was continuously decreasing, presenting values of 31 ± 2, 19 ± 2, and 14 ± 1% at 24, 48, and 72 h, respectively (Figure 5B) and being significantly lower compared to viability at collection time (SP = 100%). There was a dose-dependent significant increase in viability, during the 3 day storage, in spermatozoa stored in media supplemented with both tea extracts when compared with the control. At 24 h, viability of spermatozoa kept in the media supplemented with any of the tea extracts was very similar to that observed at 0 h. At 48 h, viability of spermatozoa kept in the media with 0.5 mg/mL of GTEA or WTEA significantly decreased (49 ± 2 and 53 ± 5%, respectively) in comparison with that observed, 67 ± 2%, at the collection time (SP = 100%). Conversely, viability corresponding to the spermatozoa stored in the media with 1 mg/mL of GTEA or WTEA (59 ± 3 (SP = 100%) and 65 ± 3% (SP = 99.5%), respectively) was significantly higher than the viability verified in the media containing half the concentration of these extracts. The same profile was verified at 72 h of storage with the only exception that spermatozoa kept in 1 mg of WTEA extract/mL medium exhibited significantly higher viability of 63 ± 3% in relation to the spermatozoa kept in the medium with 1 mg of GTEA extract/mL, which was 49 ± 2% (SP = 100%), being in its turn significantly lower compared to the viability at 0 h (SP = 100%). Remarkably, spermatozoa maintained in the medium with 1 mg of WTEA extract/mL averaged a viability of 65%

dx.doi.org/10.1021/jf4049462 | J. Agric. Food Chem. 2014, 62, 608−617

throughout the experiment, a very similar value relative to viability at 0 h (Figure 5B).

DISCUSSION

Despite the similarities between GTEA and WTEA, the number of investigations studying the health benefits of WTEA is negligible compared to GTEA. Recently, WTEA aroused great interest among investigators due to its higher concentrations of tea polyphenols when compared to GTEA.[41] Thus, WTEA has been proven to have higher antioxidant activity than any other type of tea.[2,5] As expected, the WTEA extract we obtained was richer in this class of flavonoids than the GTEA extract, predominantly in EGCG (82 ± 7 g/kg of WTEA extract vs 42 ± 2 g/kg of GTEA extract), which is known as one of the most powerful antioxidants and the most pharmacologically active catechin derivative.[42] There are several pieces of evidence that EGCG has a positive impact in a variety of human diseases that is dependent on its concentration.[2,43,44] EGCG has been proven to have protective action against several deleterious effects of diseases by minimizing OS.[45]

Recently, it was reported that EGCG therapy protects against testicular ischemia-reperfusion injury through its antioxidant activity.[46] Importantly, it has been reported that for human spermatozoa maintained at 37 °C during 30 min, motility and viability can be improved by the addition of EGCG to the extracellular media at low concentrations.[47] In fact, our results showed that WTEA is very rich in EGCG, which represents 61.7% of the total catechin content, and the lower content in EGCG of GTEA may be reflected in the antioxidant properties of the extract.[41] In addition, caffeine content is also known to be higher in WTEA,[41] and our extract presented a remarkably high caffeine content (71 ± 8 g/kg of WTEA extract) when compared with the results obtained by other authors.[48] This phytochemical content difference, as well as the variation found between our GTEA extract composition and the ones verified by other authors,[34] could be due to the natural variability of the plants (caused by the influence of geographical origin, climate, and/or agricultural practices) and to differences in the extraction procedures (solvents, temperatures, times of extraction, and ratio of leaves to water) and analytical techniques.[35,49,50] Our WTEA extract also presented higher caffeine content compared to our GTEA extract (21 ± 3 g/kg of GTEA extract). This should be due to differences in leaf processing (e.g., the collection date and/or the type of leaves) to produce WTEA or GTEA, which have already been proven to influence the tea chemical composition.[41] Nevertheless, caffeine is described to stimulate lipolysis and interfere with glucose and fatty acid metabolism, thus having an important role in cellular metabolism.[51] The WTEA extract was also richer in the content of total sugars, which are known to be important substrates to cellular metabolism. Overall, our ^{1}H NMR results concerning WTEA and GTEA are in accordance with the phenolic and methylxanthine profiles obtained by HPLC-UV, HPLC-DAD, or HPLC-MS previously reported by Carvalho et al.,[34] Rusak et al.,[35] and Unachukwu et al.[36] Possible differences found in our quantitative profile compared to previous ones are certainly due to the reasons above-mentioned.

Spermatozoa present high metabolic rates that are in close association with elevated amounts of OS,[52] which is known as one of most relevant factors responsible for poor semen quality.[53] OS is associated with uncontrolled ROS production that, when it exceeds spermatozoa antioxidant capacity, becomes harmful, inducing membrane lipid peroxidation, compromising spermatozoa survival and fertilizing capacity.[54] Epididymal spermatozoa survival and maintenance are crucial for both natural and assisted reproduction.[55] The mammalian epididymis creates a unique microenvironment that helps in testicular spermatozoa maturation from an immotile immature state to fully fertile competent cells. Besides, it stores the fertile and viable spermatozoa in cauda epididymis until ejaculation. For that reason, spermatozoa from cauda epididymis are often used in assisted reproductive technologies. In fact, cryopreservation and refrigeration of spermatozoa have been highly debated, and it has been proposed that the maintenance of spermatozoa at RT for short-term periods can be an effective alternative to avoid the rapid decline of sperm viability after storage in a refrigerated environment.[12,56] Hence, there is a growing interest in the establishment of an optimal composition medium for RT sperm storage. Several media intended to improve spermatozoa survival at RT have been developed, but spermatozoa viability after storage in those media is still very low and far from the ideal.[12,57−60] A study using mouse sperm evaluated the effect of RT storage in various bicarbonate and phosphate-based media used for IVF or embryo culture, reporting that the low bicarbonate- and HEPES-containing media were able to better preserve spermatozoa in vitro.[12] The addition of substrates, such as glucose, further enhanced sperm survival, although the authors concluded that further tests concerning the addition of preserving agents are still required.[12,60] Studies using sperm from different mammalian origins preserved at RT in a saline-buffered storage medium also showed that supplementation with serum or egg yolk could greatly increase sperm survival and function.[57−59] At the same time those authors concluded that there was still a crucial requirement in controlling the ROS, which are more likely to be generated in an ambient temperature system, in the media in which the spermatozoa are suspended. Indeed, some studies have been made to assess the effect of tea catechins, which are known antioxidant agents, on sperm viability and survival.[13,47] In one of those studies, several concentrations of EGCG (1, 50, and 100 μM) were tested as a supplement of the storage media, and although the authors obtained encouraging results in the sperm fertilization ability of frozen−thawed sperm, they did not verify a significant increase in sperm survival after storage.[13]

Therefore, we hypothesized that WTEA extract could modulate some important functions such as antioxidant capacity and lipid peroxidation of spermatozoa, thus improving spermatozoa viability during RT storage. Using the FRAP assay, we verified that the media containing WTEA extract presented a higher antioxidant potential value, in a dose-dependent manner, than the media with GTEA extract, evidencing that the antioxidant potential is greatly increased by the addition of WTEA extract. The higher increase in the antioxidant potential of sperm after storage was verified in media with WTEA extract, and this is concomitant with the alteration measured for the media antioxidant potential. Indeed, the sperm antioxidant potential showed an increase over time with storage in WTEA supplemented media that is surely due to incorporation of antioxidant compounds present in the extract. The same profile was verified in sperm stored with GTEA extract in a much smaller extent, evidencing that WTEA extract is the one giving the best antioxidative potential.

One of the most important deleterious effects caused by OS is lipid peroxidation because mammalian spermatozoa are rich in PUFA that are highly vulnerable to OS.[10] When subjected to

high levels of OS, spermatozoa lipid membranes are oxidized, and the end-product of these reactions, MDA, can be measured by the TBARS assay. Our results showed that during the 3 day sperm storage at RT, WTEA extract was the most effective in decreasing the lipid peroxidation in spermatozoa. As WTEA extract presented a higher concentration of polyphenols, which are known to decrease lipid peroxidation in cells, it was expected that the media with WTEA extract presented a higher antioxidant potential and, consequently, a higher capacity to prevent lipid peroxidation. However, at 24 h, although there was a significant decrease in lipid peroxidation relative to the control group, there were no significant differences between storage with WTEA or GTEA. This is concordant with the sperm FRAP assay at 24 h that also showed no differences in the antioxidant potential of sperm stored with both tea extracts. This could be explained by ROS production, which is expected to increase over time and needs to be accompanied by the antioxidant defenses increase to control the amount of ROS. After 48 and 72 h, lipid peroxidation of sperm stored in the media supplemented with WTEA extract remained constant and similar to that observed at 24 h, whereas in sperm stored in the media containing GTEA extract the lipid peroxidation increased over time.

As our WTEA and GTEA extracts presented EGCG contents of 82 ± 7 g/kg of WTEA extract and 42 ± 2 g/kg of GTEA extract, these amounts reflect EGCG concentrations in the ranges of about 90−180 μM for WTEA and 45−90 μM for GTEA supplemented sperm storage media. Therefore, as our EGCG concentrations are in the same order of magnitude of those used in the study of Kaedei et al.[13] and, conversely to the data reported by those authors who were not able to verify a significant increase in the survival of sperm kept in the EGCG supplemented media, our results showed that tea supplementation highly improved spermatozoa survival, and this supports our idea that the synergistic effect between the tea components may be responsible for the positive effects observed in sperm viability. Additionally, our results support the effectiveness of WTEA extract in detriment to GTEA extract.

Male infertility is relatively common and affects about 50% of couples with fertility problems.[61] In most male patients with subfertility or infertility, the condition is due to loss of sperm function rather than the number of spermatozoa.[62] Therefore, spermatozoa viability is an essential parameter to evaluate sperm quality and male factor infertility. Supplementation of the storage media with tea extracts significantly increased sperm viability in a dose-dependent manner. OS is known to play a crucial role in the loss of functional competence, and when ROS production is significantly elevated, dysfunctional spermatozoa are produced.[63] A negative correlation between ROS production and sperm movement, evidencing the importance of ROS control in spermatozoa function, has also been reported.[64] High ROS levels are reported to be detrimental to fertility potential in natural and assisted conception,[65] and sperm capacitation is also known to be lost in the presence of high OS levels.[66] Therefore, the higher increase of sperm viability in spermatozoa stored in WTEA-supplemented media compared to spermatozoa stored in GTEA-supplemented media is certainly due to the higher polyphenolic content in WTEA extract and, consequently, to its higher antioxidant potential. Moreover, because the viability improvement was more effective with the highest dose of WTEA extract (1 mg/mL), we suggest that the best protection attained with the highest dose of WTEA extract may be responsible for the overall better results observed with this concentration.

In conclusion, WTEA is richer in antioxidants than other teas (black, oolong, and green teas),[2] and the addition of WTEA aqueous extract to the media can be a good, simple, and inexpensive strategy for sperm storage at RT. Our results strongly indicate that WTEA extract improves spermatozoa viability by increasing the spermatozoa and storage media antioxidant potential and decreasing spermatozoa lipid peroxidation. Moreover, the first hours of sperm preservation is crucial and marked by an increase in OS that can be counteracted by WTEA polyphenols. More studies will be needed to fully disclose the molecular mechanisms behind the results now reported. Nevertheless, the addition of WTEA aqueous extract to the standard sperm storage medium proved to be an excellent strategy for sperm storage at RT, which can reduce or even eliminate the limitations of the in vitro spermatozoa storage in a refrigerated environment and enable sperm transport for IVF or AI use.

AUTHOR INFORMATION

Corresponding Authors

*(B.M.S.) Phone: +351 275 329 077. Fax: +351 275 329 099. E-mail: bmcms@ubi.pt.

*(P.F.O.) Phone: +351 275 329 077. Fax: +351 275 329 099. E-mail: pfobox@gmail.com.

Funding

This work was supported by the Fundação para a Ciência e a Tecnologia − FCT (PTDC/QUI-BIQ/121446/2010 and PEst-C/SAU/UI0709/2011) cofunded by Fundo Europeu de Desenvolvimento Regional − FEDER via Programa Operacional Factores de Competitividade − COMPETE/QREN. T.R.D. was funded by Programa Operacional Regional do Centro 2007−2013 QREN (Programa Mais Centro). M.G.A. (SFRH/BPD/80451/2011) was funded by FCT. P.F.O. was funded by FCT through FSE and POPH funds (Programa Ciência 2008).

Notes

The authors declare no competing financial interest.

ABBREVIATIONS USED

AI, artificial insemination; BSA, bovine serum albumin; C, (−)-catechin; EC, (−)-epicatechin; ECG, (−)-epicatechin-3-gallate; EGC, (−)-epigallocatechin; EGCG, (−)-epigallocatechin-3-gallate; GCG, (−)-gallocatechin-3-gallate; FRAP, ferric reducing antioxidant power; GTEA, green tea; IVF, in vitro fertilization; MDA, malondialdehyde; OS, oxidative stress; PBS, phosphate-buffered saline; PUFA, polyunsaturated fatty acids; ROS, reactive oxygen and nitrogen species; RT, room temperature; TBA, thiobarbituric acid; TBARS, thiobarbituric acid reactive substances; TPTZ, 2,4,6-tripyridyl-s-triazine; TYH, Krebs−Ringer bicarbonate medium; WTEA, white tea

REFERENCES

(1) Moderno, P.; Carvalho, M.; Silva, B. Recent patents on *Camellia sinensis*: source of health promoting compounds. *Recent Pat. Food Nutr. Agric.* **2009**, *1*, 182−192.

(2) Dias, T. R.; Tomás, G.; Teixeira, N. F.; Alves, M. G.; Oliveira, P. F.; Silva, B. M. White tea (*Camellia sinensis* (L.)): antioxidant properties and beneficial health effects. *IJFS* **2013**, *2*, 1−15.

(3) Rusak, G.; Komes, D.; Likić, S.; Horžić, D.; Kovač, M. Phenolic content and antioxidative capacity of green and white tea extracts

depending on extraction conditions and the solvent used. *Food Chem.* **2008**, *110*, 852−858.
(4) Higdon, J. V.; Frei, B. Tea catechins and polyphenols: health effects, metabolism, and antioxidant functions. *Crit. Rev. Food Sci. Nutr.* **2003**, *43*, 89−143.
(5) Sharangi, A. Medicinal and therapeutic potentialities of tea (*Camellia sinensis* L.) − a review. *Food Res. Int.* **2009**, *42*, 529−535.
(6) Fiorentino, A.; D'Abrosca, B.; Pacifico, S.; Mastellone, C.; Piscopo, V.; Caputo, R.; Monaco, P. Isolation and structure elucidation of antioxidant polyphenols from quince (*Cydonia vulgaris*) peels. *J. Agric. Food Chem.* **2008**, *56*, 2660−2667.
(7) Hampl, R.; Drabkova, P.; Kandar, R.; Stepan, J. Impact of oxidative stress on male infertility. *Ceska Gynekol* **2012**, *77*, 241−245.
(8) Valko, M.; Leibfritz, D.; Moncol, J.; Cronin, M. T. D.; Mazur, M.; Telser, J. Free radicals and antioxidants in normal physiological functions and human disease. *Int. J. Biochem. Cell Biol.* **2007**, *39*, 44−84.
(9) Aitken, R. J.; De Iuliis, G. N.; Finnie, J. M.; Hedges, A.; McLachlan, R. I. Analysis of the relationships between oxidative stress, DNA damage and sperm vitality in a patient population: development of diagnostic criteria. *Hum. Reprod.* **2010**, *25*, 2415−2426.
(10) Mylonas, C.; Kouretas, D. Lipid peroxidation and tissue damage. *In Vivo* **1999**, *13*, 295−309.
(11) Guthrie, H.; Welch, G. Effects of reactive oxygen species on sperm function. *Theriogenology* **2012**, *78*, 1700−1708.
(12) Sato, M.; Ishikawa, A. Room temperature storage of mouse epididymal spermatozoa: exploration of factors affecting sperm survival. *Theriogenology* **2004**, *61*, 1455−1469.
(13) Kaedei, Y.; Naito, M.; Naoi, H.; Sato, Y.; Taniguchi, M.; Tanihara, F.; Kikuchi, K.; Nagai, T.; Otoi, T. Effects of (−)-epigallocatechin gallate on the motility and penetrability of frozen−thawed boar spermatozoa incubated in the fertilization medium. *Reprod. Domest. Anim.* **2012**, *47*, 880−886.
(14) Costa, R. M.; Magalhães, A. S.; Pereira, J. A.; Andrade, P. B.; Valentão, P.; Carvalho, M.; Silva, B. M. Evaluation of free radical-scavenging and antihemolytic activities of quince (*Cydonia oblonga*) leaf: a comparative study with green tea (*Camellia sinensis*). *Food Chem. Toxicol.* **2009**, *47*, 860−865.
(15) Alves, M. G.; Oliveira, P. J.; Carvalho, R. A. Substrate selection in hearts subjected to ischemia/reperfusion: role of cardioplegic solutions and gender. *NMR Biomed.* **2011**, *24*, 1029−1037.
(16) Rato, L.; Alves, M. G.; Dias, T. R.; Lopes, G.; Cavaco, J. E.; Socorro, S.; Oliveira, P. F. High-energy diets may induce a pre-diabetic state altering testicular glycolytic metabolic profile and male reproductive parameters. *Andrology* **2013**, *1*, 495−504.
(17) Alves, M. G.; Socorro, S.; Silva, J.; Barros, A.; Sousa, M.; Cavaco, J. E.; Oliveira, P. F. In vitro cultured human Sertoli cells secrete high amounts of acetate that is stimulated by 17β-estradiol and suppressed by insulin deprivation. *Biochim. Biophys.* **2012**, *1823*, 1389−1394.
(18) Govindaraju, V.; Young, K.; Maudsley, A. A. Proton NMR chemical shifts and coupling constants for brain metabolites. *NMR Biomed.* **2000**, *13*, 129−153.
(19) Ohno, A.; Oka, K.; Sakuma, C.; Okuda, H.; Fukuhara, K. Characterization of tea cultivated at four different altitudes using ^{1}H NMR analysis coupled with multivariate statistics. *J. Agric. Food Chem.* **2011**, *59*, 5181−5187.
(20) Uekusa, Y.; Kamihira, M.; Nakayama, T. Dynamic behavior of tea catechins interacting with lipid membranes as determined by NMR spectroscopy. *J. Agric. Food Chem.* **2007**, *55*, 9986−9992.
(21) Lee, J.-E.; Lee, B.-J.; Chung, J.-O.; Hwang, J.-A.; Lee, S.-J.; Lee, C.-H.; Hong, Y.-S. Geographical and climatic dependencies of green tea (*Camellia sinensis*) metabolites: a ^{1}H NMR-based metabolomics study. *J. Agric. Food Chem.* **2010**, *58*, 10582−10589.
(22) Peres, I.; Rocha, S.; Pereira, M. d. C.; Coelho, M.; Rangel, M.; Ivanova, G. NMR structural analysis of epigallocatechin gallate loaded polysaccharide nanoparticles. *Carbohydr. Polym.* **2010**, *82*, 861−866.
(23) Lee, J.-E.; Lee, B.-J.; Chung, J.-O.; Shin, H.-J.; Lee, S.-J.; Lee, C.-H.; Hong, Y.-S. ^{1}H NMR-based metabolomic characterization during green tea (*Camellia sinensis*) fermentation. *Food Res. Int.* **2011**, *44*, 597−604.
(24) Toyoda, Y. Studies on fertilization of mouse eggs in vitro. I. In vitro fertilization of eggs by fresh epididymal sperm. *Jpn. J. Anim. Reprod.* **1971**, *16*, 147−151.
(25) Quinn, P.; Barros, C.; Whittingham, D. Preservation of hamster oocytes to assay the fertilizing capacity of human spermatozoa. *J. Reprod. Fertil.* **1982**, *66*, 161−168.
(26) Benzie, I. F.; Strain, J. J. The ferric reducing ability of plasma (FRAP) as a measure of "antioxidant power": the FRAP assay. *Anal. Biochem.* **1996**, *239*, 70−76.
(27) Ohkawa, H.; Ohishi, N.; Yagi, K. Assay for lipid peroxides in animal tissues by thiobarbituric acid reaction. *Anal. Biochem.* **1979**, *95*, 351−358.
(28) Iqbal, M.; Sharma, S.; Rezazadeh, H.; Hasan, N.; Abdulla, M.; Athar, M. Glutathione metabolizing enzymes and oxidative stress in ferric nitrilotriacetate mediated hepatic injury. *Redox Rep.* **1996**, *2*, 385−392.
(29) Lopes, G.; Simões, A.; Ferreira, P.; Martins-Bessa, A.; Rocha, A. Differences in preservation of canine chilled semen using different transport containers. *Anim. Reprod. Sci.* **2009**, *112*, 158−163.
(30) Levin, Y. The role of statistical power analysis in quantitative proteomics. *Proteomics* **2011**, *11*, 2565−2567.
(31) Müller, N.; Ellinger, S.; Alteheld, B.; Ulrich-Merzenich, G.; Berthold, H. K.; Vetter, H.; Stehle, P. Bolus ingestion of white and green tea increases the concentration of several flavan-3-ols in plasma, but does not affect markers of oxidative stress in healthy non-smokers. *Mol. Nutr. Food Res.* **2010**, *54*, 1636−1645.
(32) Mao, J. T.; Nie, W. X.; Tsu, I. H.; Jin, Y. S.; Rao, J. Y.; Lu, Q. Y.; Zhang, Z. F.; Go, V. L. W.; Serio, K. J. White tea extract induces apoptosis in non-small cell lung cancer cells: the role of peroxisome proliferator-activated receptor-γ and 15-lipoxygenases. *Cancer Prev. Res.* **2010**, *3*, 1132−1140.
(33) Ferrara, L.; Montesano, D.; Senatore, A. The distribution of minerals and flavonoids in the tea plant (*Camellia sinensis*). *Farmaco* **2001**, *56*, 397−401.
(34) Carvalho, M.; Jerónimo, C.; Valentão, P.; Andrade, P. B.; Silva, B. M. Green tea: a promising anticancer agent for renal cell carcinoma. *Food Chem.* **2010**, *122*, 49−54.
(35) Rusak, G.; Komes, D.; Likić, S.; Horžić, D.; Kovač, M. Phenolic content and antioxidative capacity of green and white tea extracts depending on extraction conditions and the solvent used. *Food Chem.* **2008**, *110*, 852−858.
(36) Unachukwu, U. J.; Ahmed, S.; Kavalier, A.; Lyles, J. T.; Kennelly, E. J. White and green teas (*Camellia sinensis* var. *sinensis*): variation in phenolic, methylxanthine, and antioxidant profiles. *J. Food Sci.* **2010**, *75*, C541−C548.
(37) Li, Y.; Guo, C.; Yang, J.; Wei, J.; Xu, J.; Cheng, S. Evaluation of antioxidant properties of pomegranate peel extract in comparison with pomegranate pulp extract. *Food Chem.* **2006**, *96*, 254−260.
(38) de Lamirande, E.; Gagnon, C. Impact of reactive oxygen species on spermatozoa: a balancing act between beneficial and detrimental effects. *Hum. Reprod.* **1995**, *10*, 15−21.
(39) Pryor, W. A. The antioxidant nutrients and disease prevention − what do we know and what do we need to find out? *Am. J. Clin. Nutr.* **1991**, *53*, 391S−393S.
(40) WHO. *WHO Laboratory Manual for the Examination of Human Semen and Sperm-Cervical Mucus Interaction*; Cambridge University Press: Cambridge, UK, 1992; Vol. 4.
(41) Hilal, Y.; Engelhardt, U. Characterisation of white tea − comparison to green and black tea. *J. Verbrauch. Lebensm.* **2007**, *2*, 414−421.
(42) Singh, B. N.; Shankar, S.; Srivastava, R. K. Green tea catechin, epigallocatechin-3-gallate (EGCG): mechanisms, perspectives and clinical applications. *Biochem. Pharmacol.* **2011**, *82*, 1807−1821.
(43) Khan, N.; Mukhtar, H. Tea polyphenols for health promotion. *Life Sci.* **2007**, *81*, 519−533.

(44) Pan, T.; Jankovic, J.; Le, W. Potential therapeutic properties of green tea polyphenols in Parkinson's disease. *Drugs Aging* **2003**, *20*, 711−721.
(45) Higashi, N.; Kohjima, M.; Fukushima, M.; Ohta, S.; Kotoh, K.; Enjoji, M.; Kobayashi, N.; Nakamuta, M. Epigallocatechin-3-gallate, a green-tea polyphenol, suppresses Rho signaling in TWNT-4 human hepatic stellate cells. *J. Lab. Clin. Med.* **2005**, *145*, 316−322.
(46) Sugiyama, A.; Chiba, M.; Nakagami, T.; Kawano, S.; Sanada, Y.; Tajiri, T.; Toki, A. Beneficial effects of (−)-epigallocatechin gallate on ischemia-reperfusion testicular injury in rats. *J. Pediatr. Surg.* **2012**, *47*, 1427−1432.
(47) de Amicis, F.; Santoro, M.; Guido, C.; Russo, A.; Aquila, S. Epigallocatechin gallate affects survival and metabolism of human sperm. *Mol. Nutr. Food Res.* **2012**, *56*, 1655−1664.
(48) Almajano, M. P.; Carbo, R.; Jiménez, J.; Gordon, M. H. Antioxidant and antimicrobial activities of tea infusions. *Food Chem.* **2008**, *108*, 55−63.
(49) Friedman, M. Overview of antibacterial, antitoxin, antiviral, and antifungal activities of tea flavonoids and teas. *Mol. Nutr. Food Res.* **2007**, *51*, 116−134.
(50) Reto, M.; Figueira, M. E.; Filipe, H. M.; Almeida, C. M. Chemical composition of green tea (*Camellia sinensis*) infusions commercialized in Portugal. *Plant Foods Hum. Nutr.* **2007**, *62*, 139−144.
(51) Sugiura, C.; Nishimatsu, S.; Moriyama, T.; Ozasa, S.; Kawada, T.; Sayama, K. Catechins and caffeine inhibit fat accumulation in mice through the improvement of hepatic lipid metabolism. *J. Obes.* **2012**, *2012*, 510−520.
(52) Baumber, J.; Ball, B. A.; Gravance, C. G.; Medina, V.; Davies-Morel, M. The effect of reactive oxygen species on equine sperm motility, viability, acrosomal integrity, mitochondrial membrane potential, and membrane lipid peroxidation. *J. Androl.* **2000**, *21*, 895−902.
(53) Tuncer, P. B.; Bucak, M. N.; Sariozkan, S.; Sakin, F.; Yeni, D.; Cigerci, I. H.; Atessahin, A.; Avdatek, F.; Gundogan, M.; Buyukleblebici, O. The effect of raffinose and methionine on frozen/thawed Angora buck (*Capra hircus ancryrensis*) semen quality, lipid peroxidation and antioxidant enzyme activities. *Cryobiology* **2010**, *61*, 89−93.
(54) Tremellen, K. Oxidative stress and male infertility − a clinical perspective. *Hum. Reprod. Update* **2008**, *14*, 243−258.
(55) Silber, S. J. The use of epididymal sperm for the treatment of male infertility. *Baillieres Clin. Obstet. Gynaecol.* **1997**, *11*, 739−752.
(56) De Pauw, I.; Van Soom, A.; Mintiens, K.; Verberckmoes, S.; de Kruif, A. In vitro survival of bovine spermatozoa stored at room temperature under epididymal conditions. *Theriogenology* **2003**, *59*, 1093−1107.
(57) Cohen, J.; Fehilly, C.; Walters, D. Prolonged storage of human spermatozoa at room temperature or in a refrigerator. *Fertil. Steril.* **1985**, *44*, 254−262.
(58) Marín-Briggiler, C. I.; Tezon, J. G.; Miranda, P. V.; Vazquez-Levin, M. H. Effect of incubating human sperm at room temperature on capacitation-related events. *Fertil. Steril.* **2002**, *77*, 252−259.
(59) Vishwanath, R.; Shannon, P. Storage of bovine semen in liquid and frozen state. *Anim. Reprod. Sci.* **2000**, *62*, 23−53.
(60) Sato, M.; Ishikawa, A.; Nagashima, A.; Watanabe, T.; Tada, N.; Kimura, M. Prolonged survival of mouse epididymal spermatozoa stored at room temperature. *Genesis* **2001**, *31*, 147−155.
(61) Dohle, G. R.; Colpi, G. M.; Hargreave, T. B.; Papp, G. K.; Jungwirth, A.; Weidner, W. EAU guidelines on male infertility. *Eur. Urol.* **2005**, *48*, 703−711.
(62) Hull, M. G.; Glazener, C. M.; Kelly, N. J.; Conway, D. I.; Foster, P. A.; Hinton, R. A.; Coulson, C.; Lambert, P. A.; Watt, E. M.; Desai, K. M. Population study of causes, treatment, and outcome of infertility. *BMJ* **1985**, *291*, 1693−1697.
(63) Aitken, R. J.; Clarkson, J. S. Cellular basis of defective sperm function and its association with the genesis of reactive oxygen species by human spermatozoa. *J. Reprod. Fertil.* **1987**, *81*, 459−469.
(64) Koppers, A. J.; De Iuliis, G. N.; Finnie, J. M.; McLaughlin, E. A.; Aitken, R. J. Significance of mitochondrial reactive oxygen species in the generation of oxidative stress in spermatozoa. *J. Clin. Endocrinol. Metab.* **2008**, *93*, 3199−3207.
(65) Agarwal, A.; Saleh, R. A.; Bedaiwy, M. A. Role of reactive oxygen species in the pathophysiology of human reproduction. *Fertil. Steril.* **2003**, *79*, 829−843.
(66) Gomez, E.; Buckingham, D. W.; Brindle, J.; Lanzafame, F.; Irvine, D. S.; Aitken, R. J. Development of an image analysis system to monitor the retention of residual cytoplasm by human spermatozoa: correlation with biochemical markers of the cytoplasmic space, oxidative stress, and sperm function. *J. Androl.* **1996**, *17*, 276−287.

JOURNAL OF AGRICULTURAL AND FOOD CHEMISTRY

Article

pubs.acs.org/JAFC

Glycyrrhetinic Acid Suppressed NF-κB Activation in TNF-α-Induced Hepatocytes

Hong-Jhang Chen,[†] Shih-Pei Kang,[§] I-Jung Lee,[†] and Yun-Lian Lin*[,†,#]

[†]National Research Institute of Chinese Medicine, Ministry of Health and Welfare, Taipei, Taiwan

[§]Institute of Traditional Medicine, National Yang-Ming University, Taipei, Taiwan

[#]School of Pharmacy, National Taiwan University, Taipei, Taiwan

Supporting Information

ABSTRACT: Tumor necrosis factor-alpha (TNF-α) is a crucial inflammatory cytokine when hepatocytes are damaged. *Glycyrrhiza uralensis* Fisch. (Chinese licorice) has been widely used in Chinese herbal prescriptions for the treatment of liver diseases and as a food additive. Nuclear factor-kappa B (NF-κB) reporter gene assay in TNF-α-induced HepG2 was used as a screening platform. IκBα phosphorylation and p65 translocation were measured by Western blotting, and nitric oxide (NO) production and inducible nitric oxide synthase (*iNOS*) gene expression were further confirmed in rat primary hepatocytes. Results showed that TNF-α enhanced NF-κB activity was significantly attenuated by glycyrrhetinic acid in a concentration-dependent manner in the NF-κB reporter gene assay. Glycyrrhetinic acid decreased the gene expression of *iNOS* through inhibited IκBα phosphorylation and p65 translocation in protein level. Furthermore, NO production and *iNOS* expression were reduced by glycyrrhetinic acid in TNF-α-induced rat primary hepatocytes. These results suggest that glycyrrhetinic acid may provide hepatoprotection against chronic liver inflammation through attenuating NF-κB activation to alleviate the inflammation.

KEYWORDS: *TNF-α, hepatocytes, Glycyrrhiza uralensis, NF-κB, glycyrrhetinic acid*

INTRODUCTION

Chronic liver injury, resulting from viral infection, alcohol consumption, chemical substances, drugs, autoimmune diseases, and so on, induces liver fibrogenesis that can lead to the onset of cirrhosis or even hepatocellular carcinoma. When a liver is damaged, hepatocytes live in an inflammatory microenvironment. Liver inflammation can be induced by xenobiotic toxicity (such as alcohol and chemicals) or endogenous stimulation (such as LPS and cytokines). TNF-α, which is mainly released by Kupffer cells in the liver, has emerged as a key cytokine in various liver diseases.[1] TNF-α production is one of the earliest events in many types of liver injury, triggering the production of other cytokines that together recruit inflammatory cells, inducing hepatocyte apoptosis and initiating hepatic wound-healing response, including fibrogenesis. The involvement of TNF-α has been demonstrated in both acute and chronic alcoholic hepatitis[2] and in type B and C virus hepatitis.[3] Liver injury and fibrosis are reduced in TNF-$\alpha^{-/-}$ mice[4] and TNF receptor (TNFR)$1^{-/-}$ mice,[5] and liver fibrosis induced by carbon tetrachloride (CCl_4) is also alleviated in TNFR$1^{-/-}$ mice.[6] Therefore, TNF-α has been considered as a crucial inflammatory cytokine for liver injury and subsequent liver fibrosis. NF-κB, a major downstream of TNF-α, is permissive to α1(I) collagen expression and prevents apoptosis in activated hepatic stellate cells, which are key players in liver fibrosis. On the basis of this knowledge, inhibition of NF-κB is one important target for the therapeutic blockade of fibrogenesis.[7] NF-κB is a family of heterodimeric proteins including a proteolytic processing the p50 subunit as well as p65 subunit. NF-κB is ordinarily inactivated in a latent cytoplasmic form by association with various inhibitors such as IκBα. Dissociation of p65 from IκBα, through phosphorylation of IκBα followed by proteolysis via ubiquitination, is a prerequisite for p65 translocation.[8] NF-κB is a redox-sensitive transcription factor that regulates many genes related to inflammation, such as *iNOS*, interleukin-8 (*IL-8*), and cyclooxygenase-2 (*COX-2*) at the transcription level.[9]

The dried root of *Glycyrrhiza uralensis* Fisch. (Chinese licorice or *Gan-Cao* in Chinese) is widely used in traditional Chinese prescriptions[10] and as a flavoring additive in the food industry. Triterpenes such as glycyrrhizin (glycyrrhizic acid) and glycyrrhetinic acid, as well as flavonoids, such as neoliquiritin, liquiritigenin, and liquiritin, are two kinds of its major constituents.[11] Longyin decoction[12] and Sho-saiko-to[13] are famous Chinese prescriptions containing licorice for hepatoprotective effects. Glycyrrhizin, the major sweetening component, has been reported to exhibit hepatoprotective effects in different chemical-induced liver injury models. Tsuruoka et al. reported that glycyrrhizin (10.5 mg/kg, ip) suppresses increases in AST and ALT, inhibiting *iNOS* mRNA expression and protein, cell infiltration, and the degeneration of hepatocytes in the liver of concanavalin A-treated mice.[14] Lee et al. reported that glycyrrhizin (200 mg/kg, ip) alleviates CCl_4-induced liver injury by diminishing free radical toxic properties and down-regulating pro-inflammatory mediators.[15] Both glycyrrhizin and glycyrrhetinic acid exhibit protective effects on retrorsine-induced liver damage in rats,[16] inhibit Smad3-

Received: August 16, 2013
Revised: January 2, 2014
Accepted: January 4, 2014
Published: January 5, 2014

ACS Publications © 2014 American Chemical Society

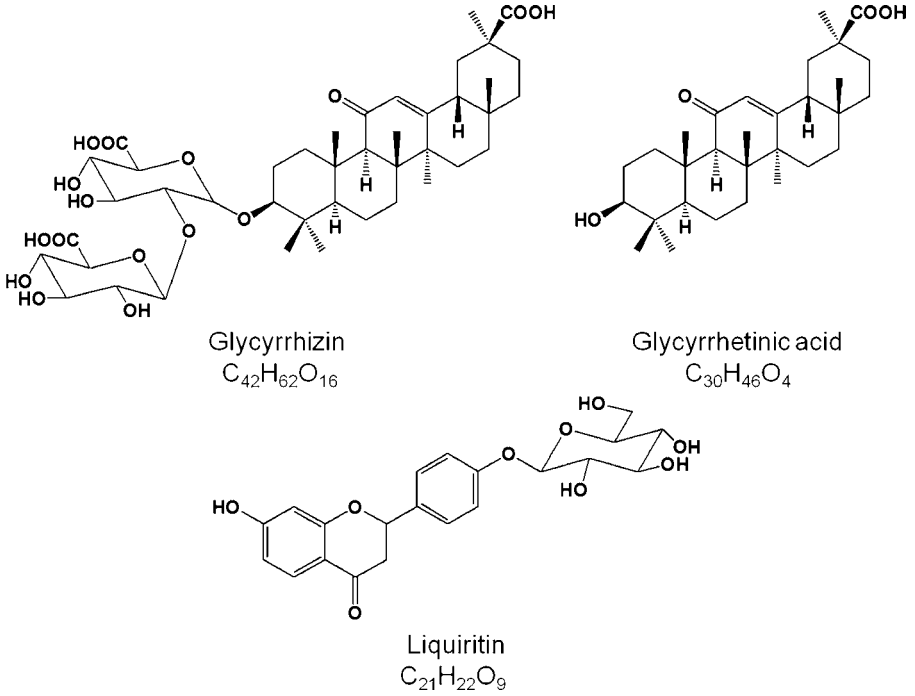

Figure 1. Structures of three major isolated pure compounds from *G. uralensis*.

mediated type I collagen gene transcription, and suppress experimental murine liver fibrosis.[17] Flavonoids from licorice have been reported to exhibit potent radical-scavenging activity.[18] A CO_2-supercritical licorice extract exhibited potent anti-inflammatory properties in LPS-induced IL-1β, -6, and -8 and TNF-α responses of macrophages.[19] Furthermore, two isoflavans, licoricidin and licorisoflavan A, isolated from the above supercritical licorice extract were potent inhibitors of the pro-inflammatory cytokine in the ex vivo human whole blood model, suggesting that these two isoflavans could be potential candidates for the development of a new therapy to prevent and/or treat periodontitis-associated tissue destruction.[20] However, the effects of licorice against endogenous stimulation such as TNF-α in hepatocytes are not clear.

The TNF-α-activated HepG2 cell model has been used for evaluating the translocation of the p65 of NF-κB subunits mediated by its inhibitor (IκBα) proteolysis.[21] The hepatoprotective effects of *G. uralensis* in TNF-α-induced HepG2 and rat primary hepatocyte inflammation were investigated in this study.

MATERIALS AND METHODS

Materials and Equipment. Silica gel (230−400 mesh) and Sephadex LH-20 (Amersham Biosciences, Uppsala, Sweden) were used for column chromatography. Solvents (analytical grade) were purchased from Merck (Darmstadt, Germany). Nuclear magnetic resonance (NMR) spectra were run in methanol-d_4 (Sigma-Aldrich Co., St. Louis, MO, USA) on a Varian unity INOVA-500 or VNMRS 600 (Varian, Palo Alto, CA, USA) using standard pulse sequences. Mass spectra (ESIMS) were recorded on a Finnigan MAT LCQ ion trap mass spectrometer system (Thermoquest, San Jose, CA, USA). Dulbecco's modified Eagle's medium (DMEM) and nonessential amino acids (NEAA) were purchased from Gibco BRL (Carlsbad, CA, USA). Fetal bovine serum (FBS) was purchased from Gibco BRL (Gaithersburg, MD, USA). pNF-κB-Luc was purchased from Stratagene (La Jolla, CA, USA). pCMV-β-gal was purchased from Life Technologies (Grand Island, NY, USA). Antiphospho-IκBα, antiphospho-IKKα/β, anti-p65, anti-lamin A/C, and anti-α-tubulin monoclonal antibodies were purchased from Cell Signaling (Danvers, MA, USA). HRP conjugated secondary antibodies were used. Pyrrolidine dithiocarbamate (PDTC) was purchased from Merck. All other chemicals used were of analytical grade and purchased from a commercial supplier (Sigma-Aldrich Co.).

Preparation of *G. uralensis* Extract and Isolation of Pure Compounds. *G. uralensis* was purchased from an herbal retailer in Taipei. A voucher herbarium specimen has been deposited at the Herbarium of National Research Institute of Chinese Medicine (NRICM) (NHP00917) and was identified by Dr. I-Jung Lee, herbarium leader of NRICM. The dried slices of *G. uralensis* (3 kg) were extracted at 60 °C by aqueous ethanol (80% ethanol/H_2O) overnight three times. The extract was concentrated with a vacuum rotary evaporator under reduced pressure and dried in a vacuum oven (491 g). The dried sample (GUE, about 16.4% yield based on dry raw materials) was sequentially partitioned with ethyl acetate (EtOAc) and *n*-butanol (BuOH) to give ethyl acetate- (GUE-EtOAc, 87.8 g, 2.93% of raw materials), *n*-butanol- (GUE-BuOH, 125.2 g, 4.17% of raw materials), and water- (GUE-H_2O, 265.3 g, 8.84% of raw materials) soluble fractions. The bioactive fraction, GUE-EtOAc, was chromatographed by silica gel column (5.5 × 60 cm) and eluted with an *n*-hexane/EtOAc gradient. The active fraction of 30−50% EtOAc elute was further purified over Sephadex LH-20 (3.8 × 40 cm, 50% EtOAc/MeOH elution) and then silica gel columns (2.8 × 30 cm, 30 or 40% EtOAc/*n*-hexane) to give glycyrrhetinic acid (0.024 g). The other two major components, glycyrrhizin (1.03 g) and liquiritin (1.35 g), were isolated from the BuOH subfraction by repeated Sephadex LH-20 column chromatography (Figure 1). All of the isolated compounds were mainly identified by 1D- and 2D-NMR and MS and further compared with an authentic sample, respectively (see the Supporting Information). For bioassay, the extracts and isolated pure compounds were all dissolved in dimethyl sulfoxide (DMSO) and diluted with a medium to give a final DMSO concentration of <0.1%. The vehicle control group contained 0.1% DMSO. Curcumin, a bioactive phenol compound from the Zingiberaceae family, was used as a positive control.[22,23]

Cell Culture. HepG2 cells were obtained from the Bioresource Collection and Research Center (BCRC, Food Industry Research and Development Institute, Hsinchu, Taiwan, no. 60025) and were cultured with DMEM containing 10% heat-inactivated FBS, 2% NEAA, and 2% glutamine in a 5% CO_2 incubator at 37 °C. Cells were

dx.doi.org/10.1021/jf405352g | J. Agric. Food Chem. 2014, 62, 618−625

detached with trypsin−EDTA solution. After washing, the cells were resuspended in fresh medium and used for subsequent experiments.

Cytotoxicity Assay. The assay of reduction of 3-(4,5-dimethylthiazol-2-yl)-2,5-diphenyltetrazolium bromide (MTT) was performed to evaluate the cytotoxicity of crude extract, subfractions, and isolated pure compounds. All test samples mentioned above were dissolved in DMSO, and the final concentration of DMSO was <0.1%; 0.1% DMSO was used as the control group.

Transfection and Reporter Assay. Transient transfection was conducted with Genejuice (Merck) according to the instructions of the manufacturer. HepG2 cells were seeded into 24-well plates at a density of 1×10^5 cells/well and cotransfected with the pNF-κB-Luc (0.2 μg/well) and pCMV-β-gal (0.02 μg/well). The total DNA amount was normalized with empty vectors in the transfection mixture. After transfection (24 h), the cells were cultured in FBS-free DMEM for the treatment of the test sample for 30 min and then incubated in TNF-α (10 ng/mL) for another 6 h. The total cells were harvested for luciferase assay. The luciferase assay was conducted using a 96-well luminometer with the dual luciferase substrate system (Promega, Madison, WI, USA). Relative luciferase activity was normalized to the β-gal assay and presented as the ratio of cells with and without TNF-α treatment. Each experiment was repeated at least three times.

mRNA Expression of *iNOS*, *COX-2*, and *IL-8* by Real-Time Polymerase Chain Reaction (PCR). HepG2 cells were seeded into 6-well plates at a density of 5×10^5 cells/well. After incubation overnight, cells were washed with PBS, and the medium was replaced with FBS-free DMEM. After 24 h of starvation, cells were pretreated with test samples for 6 h and then stimulated with TNF-α (10 ng/mL) for another 3 h. After washing with cold phosphate-buffered saline (PBS), the total RNA was prepared by TriPure isolation reagent (Roche, Mannheim, Germany) following the manufacturer's directions. After that, cDNA preparation and PCR were performed by a RevertAid First Strand cDNA synthesis kit (Fermentas, USA) according to the manufacturer's protocol. For real-time PCR, the amplification was carried out in a total volume of 20 μL containing 0.5 μM of each primer, 4 mM $MgCl_2$, 10 μL of SYBR Green Master (Roche), and 10 μL of 1:10 diluted cDNA. Real-time PCR was performed using the LightCycler480 (Roche), and PCR reactions were performed in duplicate and heated to 95 °C for 5 min, followed by 45 cycles of denaturation at 95 °C for 10 s, annealing at 55 °C for 10 s, and extension at 72 °C for 12 s. The sequences of primers for real-time PCR are listed in Table S1 (Supporting Information). Data are represented as the fold induction of inflammatory-related genes by TNF-α-induced compared to the spontaneous group. PDTC, a specific NF-κB inhibitor, was used as a positive control.[24]

Protein Preparation and Western Blotting. HepG2 cells were seeded into a 10 cm culture plate at a density of 2×10^6. After incubation overnight, cells were washed with PBS and the medium was replaced with FBS-free DMEM. After 24 h of starvation, cells were pretreated with test samples for 6 h and then stimulated with TNF-α (10 ng/mL) for another 30 min. The cells were washed twice with ice-cold PBS and then lysed in RIPA lysis buffer (20 mM Tris-HCl, 2 mM EDTA, 500 μM sodium orthovanadate, 10 μg/mL aprotinin, 10 mM NaF, 1% Triton X-100, and 0.1% SDS, pH 7.4) on ice for 20 min. The total cell lysates were clarified by centrifugation at 10000*g* for 30 min at 4 °C. The supernatants were collected for phosphor-IκBα assay.

For nuclear p65 assay, nuclear extraction was performed by a nuclear extraction kit (Millipore, Billerica, MA, USA). Briefly, HepG2 cells were lysed in ice-cold cytoplasmic lysis buffer and incubated on ice for 15 min. After centrifugation at 10000*g* for 5 min at 4 °C, the supernatants were discarded and the cell pellets resuspended with ice-cold cytoplasmic lysis buffer. After cytoplasma extraction by syringing with a 27 gauge needle, the supernatants were removed, and the remaining pellet consisted of the nuclear portion of the cell lysates. The nuclear pellet was suspended in ice-cold nuclear extraction buffer and incubated for 1 h. Nuclear proteins were harvested in the supernatant after centrifugation at 10000*g* for 10 min at 4 °C.

The protein contents of the supernatants were measured with the Bio-Rad Protein Assay Kit. Equal amounts (50 μg) of the samples were subjected to SDS-PAGE using 10% running gels and then transferred onto a PVDF membrane. The membrane was blocked with 5% nonfat milk in TBS-Tween buffer (25 mM Tris, 190 mM NaCl, and 0.5% Tween-20, pH 7.5) for 1 h at room temperature and subsequently incubated overnight at 4 °C with appropriate primary antibodies. After hybridization with the primary antibodies, the membrane was incubated with an HRP-labeled secondary antibody for 1 h. Following washing with TBS-Tween buffer, the membrane was developed with enhanced chemiluminescence (ECL) Western blotting reagents (Amersham Pharmacia Biotech). Immunoblot images were analyzed by ImageJ (NIH, USA).

Isolation and Culture of Primary Rat Hepatocytes. Isolation of rat hepatocytes from Sprague−Dawley (SD) rats was performed using the two-step collagenase perfusion method outlined in a previous study.[25] The isolated hepatocytes were cultured in Leibovitz L-15 medium supplemented with 10% FBS, 45 μg/mL penicillin G, and 50 μg/mL streptomycin in collagen-precoated 24-well plates (1×10^5 cells/mL) and incubated under 5% CO_2 in air at 37 °C.

Assay of NO Release. An NO release assay was carried out according to the method described by Chen et al.[26] Briefly, rat primary hepatocytes were seeded at 1×10^5 cells/well in a 96-well plate. After a washing with PBS, cells were pretreated with glycyrrhetinic acid (40 μM) for 6 h and then incubated with 10 ng/mL TNF-α for another 24 h. The supernatant (100 μL) was mixed with the same volume of Griess reagent (1% sulfanilamide in 5% phosphoric acid and 0.1% *N*-(1-naphthyl)ethylenediamine dihydrochloride in water) and incubated for 15 min in the dark. The absorbance of the water-soluble purplish-red product was read at 570 nm with an enzyme-linked immunosorbent assay (ELISA) reader. The amount of NO was calculated by a calibration curve established with 1.5−100 μM $NaNO_2$.

Statistical Analysis. Results are expressed as the mean ± standard deviation (SD) for three independent experiments. Differences between specific means were analyzed by one-way analysis of variance (ANOVA) using the SPSS system, vers. 11.0 (SPSS, Chicago, IL, USA). Group means were compared using one-way ANOVA followed by S−N−K test. p values of <0.05 were considered significant.

RESULTS

Extracts and Isolated Compounds of *G. uralensis* Attenuated the NF-κB Activation in TNF-α-Induced HepG2 Cells. The cytotoxicity of the extracts of *G. uralensis* were measured by MTT assay. Results showed that the ethanolic crude extract (GUE) and its subfractions have no direct cytotoxicity to HepG2 cells at the working concentrations (5−25 μg/mL) (Figure S1 in the Supporting Information). To determine the effect of *G. uralensis* on TNF-α-induced NF-κB activation, HepG2 cells were transfected with NF-κB *cis*-reporter plasmid, pNF-κB-Luc, which contains five repeats of NF-κB binding element GGGGACTTTCC in the enhancer element of the plasmid. Thereafter, cells were pretreated with or without 30 min GUE and its subfractions and then incubated with TNF-α (10 ng/mL) for 6 h. As shown in Figure 2, TNF-α significantly increased the NF-κB activation by a factor of 2.1 over the spontaneous control. GUE (25 μg/mL) treatment clearly attenuated the NF-κB activation induced by TNF-α with an $IC_{50} = 18.1 \pm 2.8$ μg/mL. In addition, GUE-EtOAc suppressed the activation of NF-κB at a lower concentration (10 μg/mL), but not in other subfractions. This result may imply that bioactive compounds exist in the EtOAc subfraction of GUE.

Under activity-guided fractionation to investigate the bioactive components in *G. uralensis*, glycyrrhetinic acid was isolated from GUE-EtOAc as an active compound. Two other major pure compounds were isolated from GUE-BuOH, named glycyrrhizin and liquiritin, for comparison. Figure 3 shows that glycyrrhetinic acid significantly decreased the activation of NF-

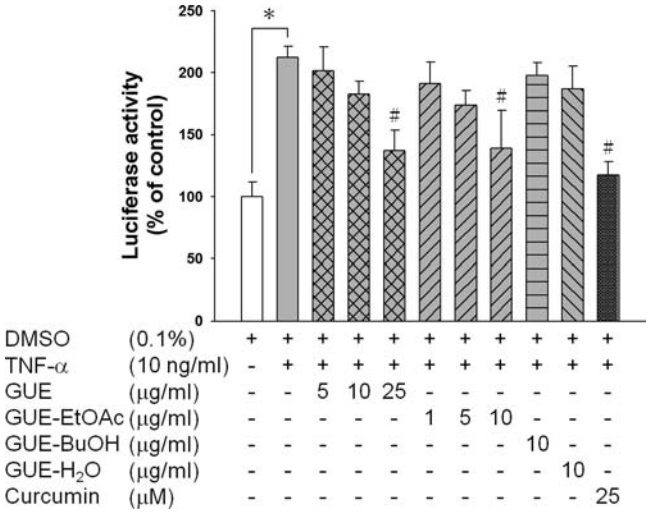

Figure 2. Effect of extracts of *G. uralensis* on the TNF-α-induced NF-κB activation in HepG2 cells. HepG2 cells were transiently cotransfected with pNF-κB-Luc and pCMV-β-gal for 24 h. The transfected cells were pretreated with or without test samples for 30 min, prior to 6 h of treatment with TNF-α (10 ng/mL). Spontaneous HepG2 cells acted as a negative control. Cells were then harvested, and luciferase activities were assessed with normalization by β-gal assay. Curcumin was used as a positive control. Data are presented as the mean ± SD of three independent experiments. *, $p < 0.05$, compared with the spontaneous control. #, $p < 0.05$, compared with the TNF-α-induced group.

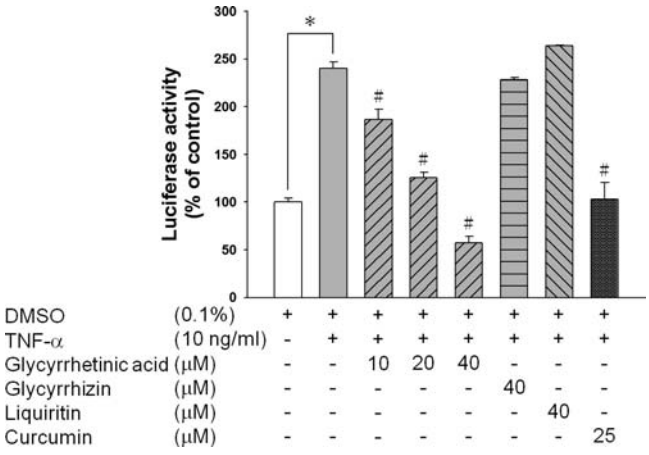

Figure 3. Effect of pure compounds isolated from *G. uralensis* on the activation of NF-κB in TNF-α-induced HepG2 cells. HepG2 cells were cotransfected with pNFκB-Luc and pCMV-β-gal for 24 h. The transfected cells were pretreated with or without various concentrations of pure compounds isolated from GUE for 30 min followed by TNF-α (10 ng/mL). After 6 h of incubation, the luciferase and β-gal activity assays were performed. The efficiency of transfection was normalized by β-gal activity. Curcumin was used as a positive control. Data are presented as the mean ± SD of three independent experiments. *, $p < 0.05$, compared with the spontaneous control. #, $p < 0.05$, compared with the TNF-α-induced group.

κB in a concentration-dependent manner (10−40 μM, $R = 0.898$, $p < 0.05$). However, glycyrrhizin and liquiritin have no effects in this NF-κB reporter gene assay even at a concentration of 40 μM. For a positive control, curcumin has an anti-inflammatory effect, as shown in the inhibition of NF-κB activation at 25 μM.

Glycyrrhetinic Acid Suppressed the Gene Expression of *iNOS* and *COX-2* but Not *IL-8* in TNF-α-Induced HepG2 Cells. To evaluate the expression of inflammatory genes in TNF-α-induced HepG2 cells, quantitative real-time PCR was performed. After prescreening of the gene expressions in TNF-α-induced HepG2 cells, *iNOS*, *COX-2*, and *IL-8* were selected as indicators for further experiments. As shown in Figure 4, HepG2 cells were stimulated with TNF-α (10 ng/mL) for 3 h, and the mRNA expressions of *iNOS*, *COX-2*, and *IL-8* were significantly enhanced compared with the spontaneous control (2.3-, 3.1-, and 4.3-fold, respectively). Glycyrrhetinic acid (40 μM) dramatically suppressed the mRNA expression of *iNOS* and *COX-2* by 57 and 53%, respectively. However, the mRNA expression of *IL-8* showed no significant changes in either glycyrrhetinic acid or curcumin in TNF-α-induced HepG2 cells.

Glycyrrhetinic Acid Suppressed the TNF-α-Induced Activation of NF-κB via Decreased Phosphorylation of IκBα and Translocation of p65. To explore whether glycyrrhetinic acid inhibition of *iNOS* expression is mediated by blocking the IκBα/NF-κB pathway, the protein levels of phospho-IκBα in cytosol and NF-κB p65 in the nucleus were analyzed by Western blotting. With or without pretreatment of glycyrrhetinic acid (40 μM) for 6 h, HepG2 cells were stimulated with TNF-α for 30 min. After TNF-α treatment, phosphorylation of IκBα in cytosol was apparently increased, because IκBα was degraded by ubiquitination. Thereby, NF-κB was activated (Figure 5A). Moreover, the translocation of p65 from cytosol into the nucleus revealed that the transcription factor, NF-κB, was activated in the nucleus (Figure 5B). Glycyrrhetinic acid suppressed the phosphorylation of Akt, inhibited the activation of IKK-α/β, and decreased the phosphorylation of IκBα, thereby inactivating NF-κB activity. PDTC, a specific inhibitor of NF-κB activation, inhibited the nuclear translocation of the NF-κB p65 subunit by reducing IκBα degradation and served as a positive control.

Glycyrrhetinic Acid Has an Anti-inflammatory Effect on TNF-α-Induced Rat Primary Hepatocytes. To clarify the anti-inflammatory effect on the liver ex vivo, the rat primary hepatocytes were stimulated by TNF-α and all samples were tested at noncytotoxic concentration as shown in Figure S2 (Supporting Information). NO is a molecular mediator of many physiological processes, including inflammation. After 24 h of rat primary hepatocyte stimulation by TNF-α, the nitrite concentration in the culture medium was measured as an indicator of NO production according to the Griess reaction. TNF-α (10 ng/mL) caused distinct increase of NO production compared to the spontaneous control (18.1 vs 10.7 μM, $p < 0.05$). As shown in Figure 6A, glycyrrhetinic acid significantly decreased NO production. Moreover, the biosynthesis gene, *iNOS*, was investigated at the transcription level by quantifying the mRNA level. TNF-α-induced *iNOS* expression was significantly reduced by 62% by glycyrrhetinic acid (Figure 6B). Curcumin served as the positive control showing anti-inflammatory effects in both NO production and *iNOS* expression.

DISCUSSION

In the present study, the NF-κB reporter gene assay was performed to evaluate the hepatoprotective qualities of *G. uralensis*. We demonstrated that glycyrrhetinic acid (a) attenuated the activation of NF-κB in a concentration-dependent manner (10−40 μM); (b) decreased the mRNA

dx.doi.org/10.1021/jf405352g | J. Agric. Food Chem. 2014, 62, 618−625

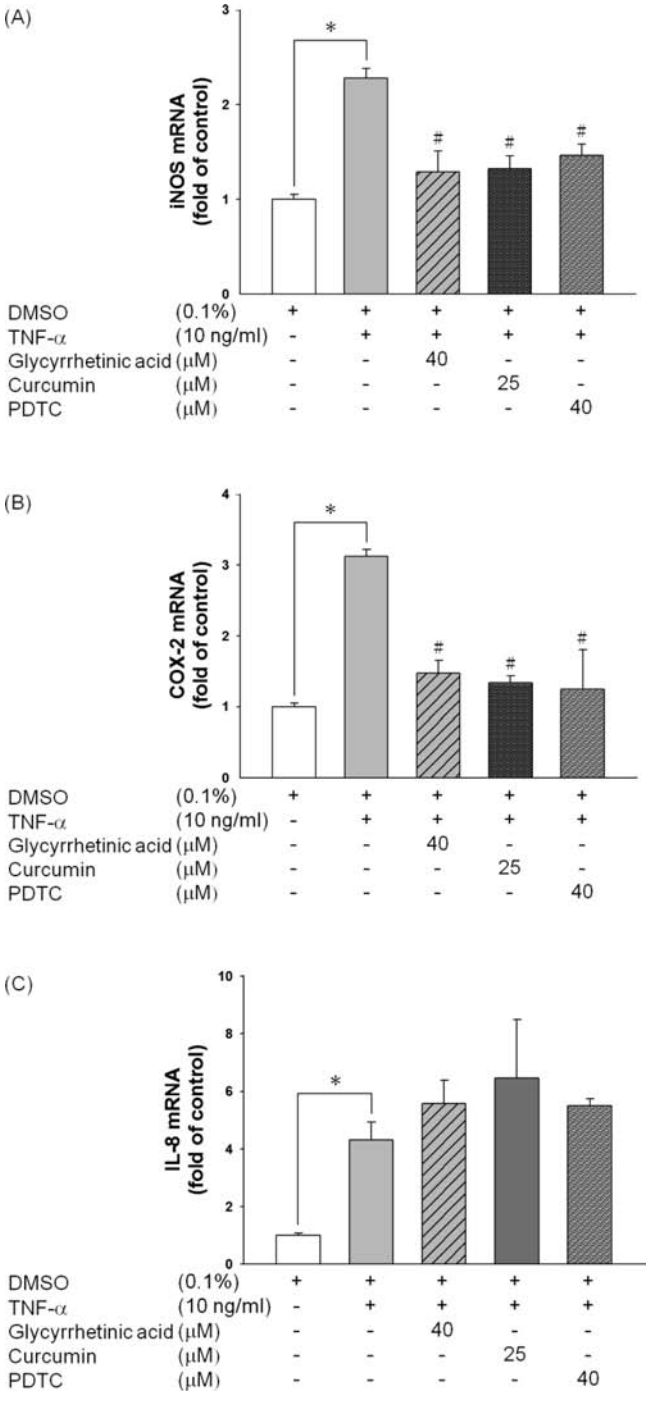

Figure 4. Effect of glycyrrhetinic acid on the mRNA expression of *iNOS* (A), *COX-2* (B), and *IL-8* (C) in TNF-α-induced HepG2 cells. HepG2 cells were pretreated with glycyrrhetinic acid (40 μM) for 6 h, followed by treatment with TNF-α (10 ng/mL) for 3 h. The expression of *iNOS*, *COX-2*, or *IL-8* mRNA was analyzed by quantitative real-time PCR. The level of *iNOS*, *COX-2*, or *IL-8* mRNA expression was normalized to *GAPDH*. Curcumin and PDTC were used as positive controls. Data are presented as the mean ± SD of three independent experiments. ∗, $p < 0.05$, compared with the spontaneous control. #, $p < 0.05$, compared with the TNF-α-induced group.

levels of *iNOS* and *COX-2*; (c) significantly inhibited the phosphorylation of IκBα and nuclear translocation of p65 in TNF-α-induced HepG2 cells; and (d) reduced NO production via suppression of *iNOS* expression in TNF-α-induced rat primary hepatocytes.

TNF-α is a pleiotropic cytokine triggering pro-inflammatory effects via NF-κB related pathways in various liver injuries. Therefore, therapeutic intervention in TNF-α/NF-κB signaling is technically feasible and could be of potential benefit in inflammatory liver disease.[27] Wu et al. reported that a *n*-hexane/ethanol (9:1; v/v) nonpolar extract of licorice inhibited LPS-induced nitrate oxide production in RAW 264.7 cells and also showed Nrf2-dependent transcriptionally active Nrf2-mediated antioxidant and induced phase II detoxifying agents genes in the Nrf2 knocked out mice.[28] Recently, Chen et al. reported that glycyrrhetinic acid (25 mg/kg, ig) protects the liver from CCl_4-induced oxidative stress through activation of the Nrf2 signaling, thereby reserving its hepatoprotective effect.[29] Furthermore, with chemical acute toxicity, endogenous factors, such as TNF-α and LPS, stimulate hepatocytes, causing chronic liver inflammation.[1,30] Ngan et al. reported that *Ginkgo biloba* revealed anti-inflammatory effects via activation of the PPARs transcriptional activity in TNF-α-induced HepG2 cell.[31] In our study, we focused on the role of *G. uralensis* in TNF-α-induced chronic liver inflammation. GUE and GUE-EtOAc attenuated the activation of NF-κB induced by TNF-α in a concentration-dependent manner with IC_{50} values of 18.1 ± 2.8 and 8.5 ± 3.2 μg/mL, respectively. Glycyrrhetinic acid, the bioactive compound isolated from GUE-EtOAc, showed suppression effects on NF-κB activation with an IC_{50} value of 14.3 ± 1.1 μM (~6.73 μg/mL) by reporter gene assay. A previous study demonstrated that glycyrrhetinic acid inhibited NF-κB activation in TNF-α-activated HUVEC cells.[32] Our findings provide evidence that glycyrrhetinic acid protects the liver from inflammation via inactivation of NF-κB signaling. Curcumin, as a positive control, has also been reported with hepatoprotective and anti-inflammatory effects via suppression of NF-κB activation both in vivo[22] and in vitro.[23]

The transcription factor NF-κB is important for the regulation of various genes involved in immune and acute phase inflammatory responses.[8] Most anti-inflammatory functional foods, such as mulberry leaf,[33] *Dunaliella salina* alga,[34] and *Magnolia officinalis*,[35], have been shown to suppress the expression of pro-inflammatory genes by inhibiting the NF-κB activation pathway. The NF-κB signal transduction pathway is directly engaged by the TNFR/Akt/IKK pathway with TNF-α stimulation.[36] Our study showed that glycyrrhetinic acid markedly suppressed NF-κB activation through the suppression of Akt phosphorylation and inhibition of IκBα phosphorylation, thereby inhibiting p65 translocation (Figures 3 and 5). These results are coincident with the effect of curcumin on NF-κB signaling.[37] The pro-inflammatory-related genes, inducible *iNOS*, *COX-2*, and *IL-8*, are downstream from NF-κB and are related to liver diseases. When a liver is damaged, *iNOS* is induced, followed by increased NO production, thereby decreasing the liver's detoxification ability and resulting in fibrosis or hepatitis.[38] COX-2 is a pro-inflammatory mediator that is correlated with chronic hepatitis, liver cirrhosis, and hepatocarcinogenesis.[39] IL-8, which is produced in response to stimulation by TNF-α, is a potent chemokine that may be implicated in infiltration of neutrophils causing acute hepatitis.[40] Our results showed that the mRNA expressions of *iNOS*, *COX-2*, and *IL-8* were significantly enhanced after being stimulated with TNF-α for 3 h in HepG2 cells. Glycyrrhetinic acid effectively suppressed mRNA expression of *iNOS* and *COX-2*, but not that of *IL-8* (Figure 4). Various transcription

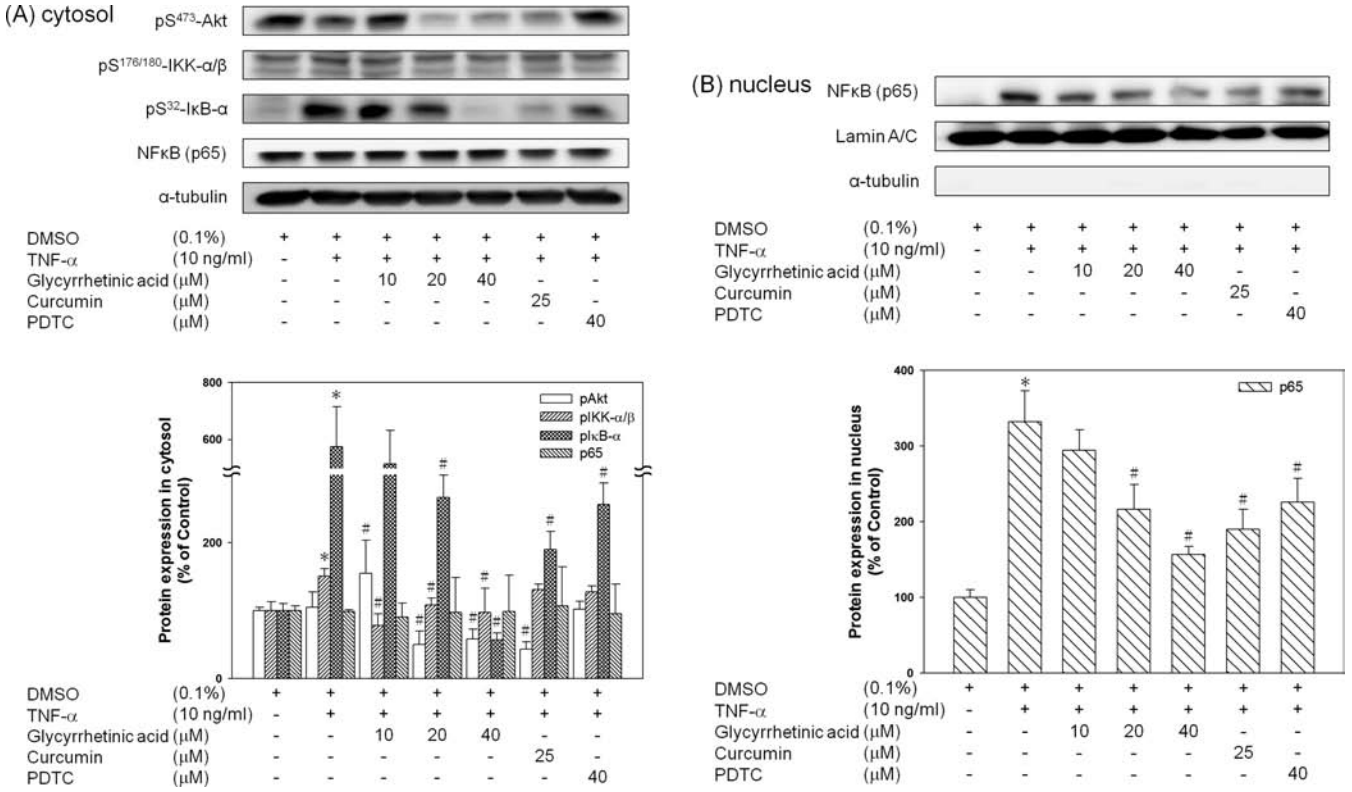

Figure 5. Effect of glycyrrhetinic acid on (A) TNFR/Akt/NF-κB signaling and (B) p65 translocation in TNF-α-induced HepG2 cells. HepG2 cells were pretreated glycyrrhetinic acid (40 μM) for 6 h, followed by treatment with TNF-α (10 ng/mL) for 30 min. The total cell lysate was collected to detect the levels of phospho-Akt, -IKKα/β, and -IκBα, and the nucleus lysate was collected to detect the level of p65 by Western blotting. Curcumin and PDTC were used as positive controls. Data are presented as the mean ± SD of three independent experiments. ∗, $p < 0.05$, compared with the spontaneous control. #, $p < 0.05$, compared with the TNF-α-induced group.

factors induced by TNF-α such as NF-κB and AP-1 modulate *IL-8* expression.[41] The effect of glycyrrhetinic acid on the regulation of AP-1 in TNF-α-induced hepatocytes is not clear and remains to be further investigated.

Although HepG2 is frequently used to replace primary human hepatocytes in in vitro models for various experiments, cell lines still have some restriction such as lack of phase I enzymes and thereby cannot reflect real organisms.[42] Therefore, we further isolated primary rat hepatocytes to confirm the effects of glycyrrhetinic acid on TNF-α-induced inflammation. Modulation of *iNOS* gene expression and suppression of NO production are important targets for anti-inflammatory properties in screening natural compounds.[43] Our results showed that glycyrrhetinic acid inhibited NO production and concomitantly suppressed *iNOS* expression at the mRNA level in primary hepatocytes (Figure 6). These results were also supported by the hepatoprotective property of *G. uralensis* in animal models.[44]

Glycyrrhizin and glycyrrhetinic acid are two major bioactive components in *G. uralensis*.[45] Glycyrrhizin, a glucuronide of glycyrrhetinic acid, is much more polar. It may hydrolyze in vivo to glycyrrhetinic acid, which is responsible for most of its pharmacological properties. Lin et al. reported that a 3 day pretreatment with either glycyrrhizin (200 mg/kg, ip) or glycyrrhetinic acid (10 mg/kg, ip) exhibited protective effects on retrorsine-induced liver damage in rats.[16] However, glycyrrhizin may have too high of a polarity to pass through the cell membrane. Therefore, it has not shown an effect on NF-κB activation in the in vitro study (Figure 3). Nonetheless, Wang et al. reported that both glycyrrhizin and glycyrrhetinic acid attenuate the generation of excessive NO, by suppressing the expression of pro-inflammatory genes via inhibition of NF-κB in a LPS-induced RAW 264.7 cell model.[46] This result may imply that glycyrrhizin cannot competitively inhibit the TNF receptor to inactive the NF-κB. Therefore, the suppression of NF-κB activation by glycyrrhizin may go through other pathways, such as the PI3K/Akt/GSK3β pathway.[47] Furthermore, roasted licorice extract inhibits acute inflammation more potently than raw licorice extract, and the glycyrrhetinic acid levels in licorice are increased after roasting.[48] Our results support this finding and suggest that glycyrrhetinic acid, an aglycone triterpene, may be a more potent inflammatory inhibitor than its glycoside, glycyrrhizin. Likewise, liquiritin, a glycoside of liquiritigenin with *O*-glucopyranosyl at C-4′ of the B-ring, has no effect in the reporter gene assay.

Our results suggest that glycyrrhetinic acid in *G. uralensis* contributed, at least partially, to its anti-inflammatory effect by inactivating NF-κB through decreasing phosphorylation of IκB and thereby inhibiting the translocation of p65. To our knowledge, this is the first study related to the inhibitory effect of TNF-α/NF-κB signaling in hepatocytes demonstrating the anti-inflammatory ability of glycyrrhetinic acid. These findings provide the molecular mechanisms for the hepatoprotective action of glycyrrhetinic acid against TNF-α-induced chronic inflammation and may be beneficial to the prevention of chronic liver injury.

dx.doi.org/10.1021/jf405352g | J. Agric. Food Chem. 2014, 62, 618−625

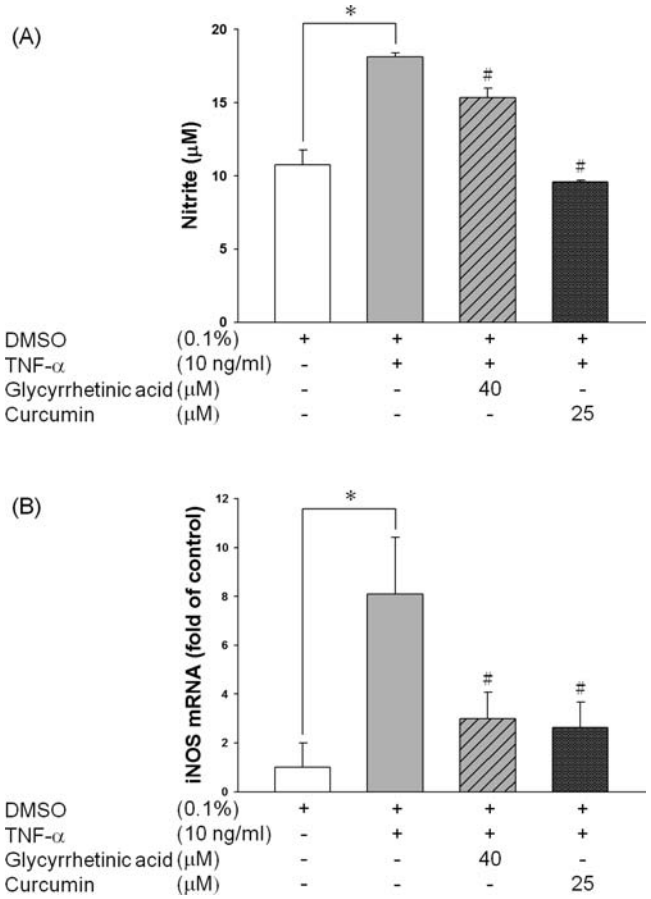

Figure 6. Effect of glycyrrhetinic acid on (A) NO production and (B) *iNOS* mRNA expression in TNF-α-induced rat primary hepatocytes. Rat primary cells were pretreated with glycyrrhetinic acid (40 μM) for 6 h. NO production and *iNOS* mRNA expression waere measured after TNF-α (10 ng/mL) treatment for 24 and 6 h, respectively. Curcumin was used as a positive control. Data are presented as the mean ± SD of three independent experiments. *, $p < 0.05$, compared with the spontaneous control. #, $p < 0.05$, compared with the TNF-α-induced group.

■ ASSOCIATED CONTENT

Ⓢ Supporting Information

Additional experimental details. This material is available free of charge via the Internet at http://pubs.acs.org.

■ AUTHOR INFORMATION

Corresponding Author

*(Y.-L.L.) Mailing address: National Research Institute of Chinese Medicine, Ministry of Health and Welfare, No. 155-1, Sec. 2, Linong St., Beitou District, Taipei 11221, Taiwan. Phone: +886-2-28201999, ext. 6531. Fax: +886-2-28250743. E-mail: yllin@nricm.edu.tw.

Funding

This work was supported by the National Science Council (NSC 99-2628-B-077-001-MY3) and the National Research Institute of Chinese Medicine (NRICM100-DMC-02) in Taiwan.

Notes

The authors declare no competing financial interest.

■ ABBREVIATIONS USED

DMSO, dimethyl sulfoxide; DMEM, Dulbecco's modified Eagle's medium; (FBS, fetal bovine serum; GUE, ethanolic extracts of *Glycyrrhiza uralensis*; iNOS, inducible nitric oxide synthase; IL-8, interleukin-8; NO, nitric oxide; NF-κB, nuclear factor-kappa B; PDTC, pyrrolidine dithiocarbamate; TNF-α, tumor necrosis factor-alpha; TNFR, TNF receptor

■ REFERENCES

(1) Tacke, F.; Luedde, T.; Trautwein, C. Inflammatory pathways in liver homeostasis and liver injury. *Clin. Rev. Allergy Immunol.* **2009**, *36*, 4−12.

(2) Tosello-Trampont, A. C.; Landes, S. G.; Nguyen, V.; Novobrantseva, T. I.; Hahn, Y. S. Kuppfer cells trigger nonalcoholic steatohepatitis development in diet-induced mouse model through tumor necrosis factor-alpha production. *J. Biol. Chem.* **2012**, *287*, 40161−40172.

(3) Brenndorfer, E. D.; Weiland, M.; Frelin, L.; Derk, E.; Ahlen, G.; Jiao, J.; Bode, J. G.; Sallberg, M. Anti-tumor necrosis factor alpha treatment promotes apoptosis and prevents liver regeneration in a transgenic mouse model of chronic hepatitis C. *Hepatology* **2010**, *52*, 1553−1563.

(4) Gäbele, E.; Froh, M.; Arteel, G. E.; Uesugi, T.; Hellerbrand, C.; Schölmerich, J.; Brenner, D. A.; Thurman, R. G.; Rippe, R. A. TNFα is required for cholestasis-induced liver fibrosis in the mouse. *Biochem. Biophys. Res. Commun.* **2009**, *378*, 348−353.

(5) Tarrats, N.; Moles, A.; Morales, A.; Garcia-Ruiz, C.; Fernandez-Checa, J. C.; Mari, M. Critical role of tumor necrosis factor receptor 1, but not 2, in hepatic stellate cell proliferation, extracellular matrix remodeling, and liver fibrogenesis. *Hepatology* **2011**, *54*, 319−327.

(6) Sudo, K.; Yamada, Y.; Moriwaki, H.; Saito, K.; Seishima, M. Lack of tumor necrosis factor receptor type 1 inhibits liver fibrosis induced by carbon tetrachloride in mice. *Cytokine* **2005**, *29*, 236−244.

(7) Hellerbrand, C.; Jobin, C.; Iimuro, Y.; Licato, L.; Sartor, R. B.; Brenner, D. A. Inhibition of NFκB in activated rat hepatic stellate cells by proteasome inhibitors and an IκB super-repressor. *Hepatology* **1998**, *27*, 1285−1295.

(8) Robinson, S. M.; Mann, D. A. Role of nuclear factor κB in liver health and disease. *Clin. Sci. (London)* **2010**, *118*, 691−705.

(9) Tilg, H.; Kaser, A.; Moschen, A. R. How to modulate inflammatory cytokines in liver diseases. *Liver Int* **2006**, *26*, 1029−1039.

(10) Zhiao, Z. Z.; Xiao, P. G. *Encyclopedia of Medicinal Plants 1*; Shanghai World Publishing: Shanghai, China, 2009; pp 436−441.

(11) Shin, Y. W.; Bae, E. A.; Lee, B.; Lee, S. H.; Kim, J. A.; Kim, Y. S.; Kim, D. H. In vitro and in vivo antiallergic effects of *Glycyrrhiza glabra* and its components. *Planta Med.* **2007**, *73*, 257−261.

(12) Wang, C.; Zhang, T.; Cui, X.; Li, S.; Zhao, X.; Zhong, X. Hepatoprotective effects of a chinese herbal formula, longyin decoction, on carbon-tetrachloride-induced liver injury in chickens. *Evidence-Based Complement. Alternat. Med.* **2013**, *2013*, 392743.

(13) Lee, J. K.; Kim, J. H.; Shin, H. K. Therapeutic effects of the oriental herbal medicine Sho-saiko-to on liver cirrhosis and carcinoma. *Hepatol. Res.* **2011**, *41*, 825−837.

(14) Tsuruoka, N.; Abe, K.; Wake, K.; Takata, M.; Hatta, A.; Sato, T.; Inoue, H. Hepatic protection by glycyrrhizin and inhibition of iNOS expression in concanavalin A-induced liver injury in mice. *Inflamm. Res.* **2009**, *58*, 593−599.

(15) Lee, C. H.; Park, S. W.; Kim, Y. S.; Kang, S. S.; Kim, J. A.; Lee, S. H.; Lee, S. M. Protective mechanism of glycyrrhizin on acute liver injury induced by carbon tetrachloride in mice. *Biol. Pharm. Bull.* **2007**, *30*, 1898−1904.

(16) Lin, G.; Nnane, I. P.; Cheng, T. Y. The effects of pretreatment with glycyrrhizin and glycyrrhetinic acid on the retrorsine-induced hepatotoxicity in rats. *Toxicon* **1999**, *37*, 1259−1270.

(17) Moro, T.; Shimoyama, Y.; Kushida, M.; Hong, Y. Y.; Nakao, S.; Higashiyama, R.; Sugioka, Y.; Inoue, H.; Okazaki, I.; Inagaki, Y. Glycyrrhizin and its metabolite inhibit Smad3-mediated type I collagen

gene transcription and suppress experimental murine liver fibrosis. *Life Sci.* **2008**, *83*, 531−539.
(18) Fu, Y.; Chen, J.; Li, Y. J.; Zheng, Y. F.; Li, P. Antioxidant and anti-inflammatory activities of six flavonoids separated from licorice. *Food Chem.* **2013**, *141*, 1063−1071.
(19) Bodet, C.; La, V. D.; Gafner, S.; Bergeron, C.; Grenier, D. A licorice extract reduces lipopolysaccharide-induced proinflammatory cytokine secretion by macrophages and whole blood. *J. Periodontol.* **2008**, *79*, 1752−1761.
(20) La, V. D.; Tanabe, S.; Bergeron, C.; Gafner, S.; Grenier, D. Modulation of matrix metalloproteinase and cytokine production by licorice isolates licoricidin and licorisoflavan A: potential therapeutic approach for periodontitis. *J. Periodontol.* **2011**, *82*, 122−128.
(21) Han, Y.; Brasier, A. R. Mechanism for biphasic rel A. NF-kappaB1 nuclear translocation in tumor necrosis factor alpha-stimulated hepatocytes. *J. Biol. Chem.* **1997**, *272*, 9825−9832.
(22) Wu, S. J.; Tam, K. W.; Tsai, Y. H.; Chang, C. C.; Chao, J. C. Curcumin and saikosaponin a inhibit chemical-induced liver inflammation and fibrosis in rats. *Am. J. Chin. Med.* **2010**, *38*, 99−111.
(23) Kuo, J. J.; Chang, H. H.; Tsai, T. H.; Lee, T. Y. Curcumin ameliorates mitochondrial dysfunction associated with inhibition of gluconeogenesis in free fatty acid-mediated hepatic lipoapoptosis. *Int. J. Mol. Med.* **2012**, *30*, 643−649.
(24) Brennan, P.; O'Neill, L. A. Effects of oxidants and antioxidants on nuclear factor kappa B activation in three different cell lines: evidence against a universal hypothesis involving oxygen radicals. *Biochim. Biophys. Acta* **1995**, *1260*, 167−175.
(25) Lin, Y. L.; Wu, C. H.; Luo, M. H.; Huang, Y. J.; Wang, C. N.; Shiao, M. S.; Huang, Y. T. In vitro protective effects of salvianolic acid B on primary hepatocytes and hepatic stellate cells. *J. Ethnopharmacol.* **2006**, *105*, 215−222.
(26) Chen, H. J.; Chung, C. P.; Chiang, W.; Lin, Y. L. Anti-inflammatory effects and chemical study of a flavonoid-enriched fraction from adlay bran. *Food Chem.* **2011**, *126*, 1741−1748.
(27) Liedtke, C.; Trautwein, C. The role of TNF and Fas dependent signaling in animal models of inflammatory liver injury and liver cancer. *Eur. J. Cell Biol.* **2012**, *91*, 582−589.
(28) Wu, T. Y.; Khor, T. O.; Saw, C. L.; Loh, S. C.; Chen, A. I.; Lim, S. S.; Park, J. H.; Cai, L.; Kong, A. N. Anti-inflammatory/anti-oxidative stress activities and differential regulation of Nrf2-mediated genes by non-polar fractions of tea *Chrysanthemum zawadskii* and licorice *Glycyrrhiza uralensis*. *AAPS J.* **2011**, *13*, 1−13.
(29) Chen, S.; Zou, L.; Li, L.; Wu, T. The protective effect of glycyrrhetinic acid on carbon tetrachloride-induced chronic liver fibrosis in mice via upregulation of Nrf2. *PLoS One* **2013**, *8*, e53662.
(30) Seki, E.; Schnabl, B. Role of innate immunity and the microbiota in liver fibrosis: crosstalk between the liver and gut. *J. Physiol.* **2012**, *590*, 447−458.
(31) Ngan, N. T.; Quang, T. H.; Tai, B. H.; Song, S. B.; Lee, D.; Kim, Y. H. Anti-inflammatory and PPAR transactivational effects of components from the stem bark of *Ginkgo biloba*. *J. Agric. Food Chem.* **2012**, *60*, 2815−2824.
(32) Chang, Y. L.; Chen, C. L.; Kuo, C. L.; Chen, B. C.; You, J. S. Glycyrrhetinic acid inhibits ICAM-1 expression via blocking JNK and NF-κB pathways in TNF-α-activated endothelial cells. *Acta Pharmacol. Sin.* **2010**, *31*, 546−553.
(33) Park, E.; Lee, S. M.; Lee, J.; Kim, J. H. Anti-inflammatory activity of mulberry leaf extract through inhibition of NF-κB. *J. Funct. Foods* **2013**, *5*, 178−186.
(34) Yang, D. J.; Lin, J. T.; Chen, Y. C.; Liu, S. C.; Lu, F. J.; Chang, T. J.; Wang, M.; Lin, H. W.; Chang, Y. Y. Suppressive effect of carotenoid extract of *Dunaliella salina* alga on production of LPS-stimulated pro-inflammatory mediators in RAW264.7 cells via NF-κB and JNK inactivation. *J. Funct. Foods* **2013**, *5*, 607−615.
(35) Lai, C. S.; Lai, Y. S.; Kuo, D. H.; Wu, C. H.; Ho, C. T.; Pan, M. H. Magnolol potently suppressed lipopolysaccharide-induced iNOS and COX-2 expression via downregulating MAPK and NF-κB signaling pathways. *J. Funct. Foods* **2011**, *3*, 198−206.
(36) Ozes, O. N.; Mayo, L. D.; Gustin, J. A.; Pfeffer, S. R.; Pfeffer, L. M.; Donner, D. B. NF-kappaB activation by tumour necrosis factor requires the Akt serine-threonine kinase. *Nature* **1999**, *401*, 82−85.
(37) Kim, K. H.; Lee, E. N.; Park, J. K.; Lee, J. R.; Kim, J. H.; Choi, H. J.; Kim, B. S.; Lee, H. W.; Lee, K. S.; Yoon, S. Curcumin attenuates TNF-alpha-induced expression of intercellular adhesion molecule-1, vascular cell adhesion molecule-1 and proinflammatory cytokines in human endometriotic stromal cells. *Phytother. Res.* **2012**, *26*, 1037−1047.
(38) Kanwar, J. R.; Kanwar, R. K.; Burrow, H.; Baratchi, S. Recent advances on the roles of NO in cancer and chronic inflammatory disorders. *Curr. Med. Chem.* **2009**, *16*, 2373−2394.
(39) Kwon, S. H.; Jeong, S. W.; Jang, J. Y.; Lee, J. E.; Lee, S. H.; Kim, S. G.; Kim, Y. S.; Cho, Y. D.; Kim, H. S.; Kim, B. S.; Jin, S. Y. Cyclooxygenase-2 and vascular endothelial growth factor in chronic hepatitis, cirrhosis and hepatocellular carcinoma. *Clin. Mol. Hepatol.* **2012**, *18*, 287−294.
(40) Goral, V.; Atayan, Y.; Kaplan, A. The relation between pathogenesis of liver cirrhosis, hepatic encephalopathy and serum cytokine levels: what is the role of tumor necrosis factor α? *Hepato-Gastroenterology* **2011**, *58*, 943−948.
(41) Roebuck, K. A.; Carpenter, L. R.; Lakshminarayanan, V.; Page, S. M.; Moy, J. N.; Thomas, L. L. Stimulus-specific regulation of chemokine expression involves differential activation of the redox-responsive transcription factors AP-1 and NF-κB. *J. Leukocyte Biol.* **1999**, *65*, 291−298.
(42) Wilkening, S.; Stahl, F.; Bader, A. Comparison of primary human hepatocytes and hepatoma cell line Hepg2 with regard to their biotransformation properties. *Drug Metab. Dispos.* **2003**, *31*, 1035−1042.
(43) Conforti, F.; Menichini, F. Phenolic compounds from plants as nitric oxide production inhibitors. *Curr. Med. Chem.* **2011**, *18*, 1137−1145.
(44) Yin, G.; Cao, L.; Xu, P.; Jeney, G.; Nakao, M.; Lu, C. Hepatoprotective and antioxidant effects of *Glycyrrhiza glabra* extract against carbon tetrachloride (CCl_4)-induced hepatocyte damage in common carp (*Cyprinus carpio*). *Fish Physiol. Biochem.* **2011**, *37*, 209−216.
(45) Wang, Y. C.; Yang, Y. S. Simultaneous quantification of flavonoids and triterpenoids in licorice using HPLC. *J. Chromatogr., B: Anal. Technol. Biomed. Life Sci.* **2007**, *850*, 392−399.
(46) Wang, C. Y.; Kao, T. C.; Lo, W. H.; Yen, G. C. Glycyrrhizic acid and 18β-glycyrrhetinic acid modulate lipopolysaccharide-induced inflammatory response by suppression of NF-κB through PI3K p110δ and p110γ inhibitions. *J. Agric. Food Chem.* **2011**, *59*, 7726−7733.
(47) Kao, T. C.; Shyu, M. H.; Yen, G. C. Glycyrrhizic acid and 18β-glycyrrhetinic acid inhibit inflammation via PI3K/Akt/GSK3β signaling and glucocorticoid receptor activation. *J. Agric. Food Chem.* **2010**, *58*, 8623−8629.
(48) Hwang, I. K.; Lim, S. S.; Choi, K. H.; Yoo, K. Y.; Shin, H. K.; Kim, E. J.; Yoon-Park, J. H.; Kang, T. C.; Kim, Y. S.; Kwon, D. Y.; Kim, D. W.; Moon, W. K.; Won, M. H. Neuroprotective effects of roasted licorice, not raw form, on neuronal injury in gerbil hippocampus after transient forebrain ischemia. *Acta Pharmacol. Sin.* **2006**, *27*, 959−965.

JOURNAL OF AGRICULTURAL AND FOOD CHEMISTRY

Article

pubs.acs.org/JAFC

Amphiphilic Chitosan Derivatives-Based Liposomes: Synthesis, Development, and Properties as a Carrier for Sustained Release of Salidroside

Hailong Peng,[†,‡] Wenjian Li,[†] Fangjian Ning,[†] Lihua Yao,[§] Mei Luo,[†,‡] Xuemei Zhu,[†] Qiang Zhao,[†] and Hua Xiong*[,†]

[†]State Key Laboratory of Food Science and Technology, Nanchang University, Nanchang, Jiangxi 330047, P.R. China

[‡]Department of Chemical Engineering, Nanchang University, Nanchang, Jiangxi 330031, P.R. China

[§]School of Life Science, Jiangxi Science & Technology Normal University, Nanchang, Jiangxi 330013, P.R. China

ABSTRACT: A novel amphiphilic chitosan derivative of *N*,*N*-dimethylhexadecyl carboxymethyl chitosan (DCMCs) was synthesized. The structure of DCMCs was confirmed via FT-IR and ^{1}H NMR, and the critical micelle concentration (CMC) was investigated by fluorescence spectroscopy. The results indicated that DCMCs has hydrophilic carboxyl and hydrophobic methylene groups and the CMC value was 23.00 mg·L^{-1}. The polymeric liposomes (DCMCs/cholesterol liposomes, DC-Ls) were developed, and its properties were evaluated. The DC-Ls exhibited multilamellar spheres with positive charge (+73.30 mV), narrow size distribution (PDI = 0.277), and good crystal properties. Salidroside was first to encapsulate into DC-Ls. Compared with traditional liposomes (phosphatidylcholine/cholesterol liposome, PC-Ls), DC-Ls showed higher encapsulation efficiency (82.46%) and slower sustained release rate. The in vitro salidroside release from DC-Ls was governed by two distinct stages (i.e., burst release and sustained release) and was dependent on the pH of the release medium. The case II transport and case I Fichian diffusion were the main release mechanisms for the entire release procedure. These results indicated that DC-Ls may be a potential carrier system for the production of functional foods that contain salidroside or other bioactive food ingredients.

KEYWORDS: *amphiphilic chitosan, liposomes, salidroside, sustained release, release mechanism*

INTRODUCTION

Because of a lipophilic and a hydrophilic group on the same molecules, polar lipids can be self-assembled and form self-organized traditional liposomes after interaction with water.[1] As an active agent's carrier, traditional liposomes have advantages, including biocompatible and biodegradable properties and targeting and protection of entrapped agents.[2] In addition, traditional liposomes are capable of entrapping both hydrophilic and hydrophobic agents.[3] Recently, traditional liposomes have been widely applied in pharmaceutical,[4] cosmetic,[5] nutrition, and food industries.[1,6,7] However, traditional liposomes exhibit notable defects on short circulation half-life in vitro, instability of the lipid, and a few certain chemical groups on the liposome surface. Hence, many efforts have been exerted to design sufficiently stable polymeric liposomes, which may be a promising carrier with good physical and thermal stability, excellent solubility, and high encapsulation efficiency.[8,9] For promoting the application of polymeric liposomes in the food industry, choosing the optimal food-grade biopolymers is a critical factor.

Chitosan (CS) is a natural polymer composed of randomly distributed β-(1−4)-linked D-glucosamine (deacetylated unit) and *N*-acetyl-D-glucosamine (acetylated unit).[10] CS has been widely used in several areas such as biomedical, pharmaceutical, and biotechnological fields as well as in the food industry because of its good properties such as nontoxicity, good biodegradability, and biocompatibility.[11−13] Among various food biopolymers for encapsulation and delivery systems, CS is one of the most popular polymers and has also been extensively investigated for its potential using in delivery of various nutrients.[14] However, CS is only soluble in aqueous acidic solutions below pH 6.5 but insoluble in neutral pH and physiological environments. Therefore, different chemical agents have been used to improve the CS solubility, and the formation of micelles has been confirmed. However, only a small section of the hydrophobic segment can conjugate to the CS backbone (substitution degree, DS < 10%) because of the limited solubility property.[15] Hence, the loading capacities of the micelles for hydrophobic bioactive agents are very low. Thus, CS derivatives were synthesized using the soluble CS (such as carboxymethyl chitosan, CMCs) as a necessary backbone.

Among these CS derivatives, amphiphilic CS derivatives with hydrophilic and lipophilic blocks have received extensive study.[15−17] The characteristics of amphiphilic CS derivatives are quite similar to that of polar lipids and surfactant complexes, which can form micelles via intra- or intermolecular association between hydrophobic moieties, and this process primarily minimizes interfacial free energy in contact with aqueous solvents.[13] Evidence has shown that amphiphilic CS derivatives have been applied to develop liposomes for drugs and genes delivery[8,9] because such polymeric liposomes exhibit higher stability in vivo/vitro and encapsulation efficiency.

Received: September 7, 2013
Revised: December 27, 2013
Accepted: December 29, 2013
Published: December 29, 2013

ACS Publications © 2013 American Chemical Society

dx.doi.org/10.1021/jf4039925 | *J. Agric. Food Chem.* 2014, 62, 626−633

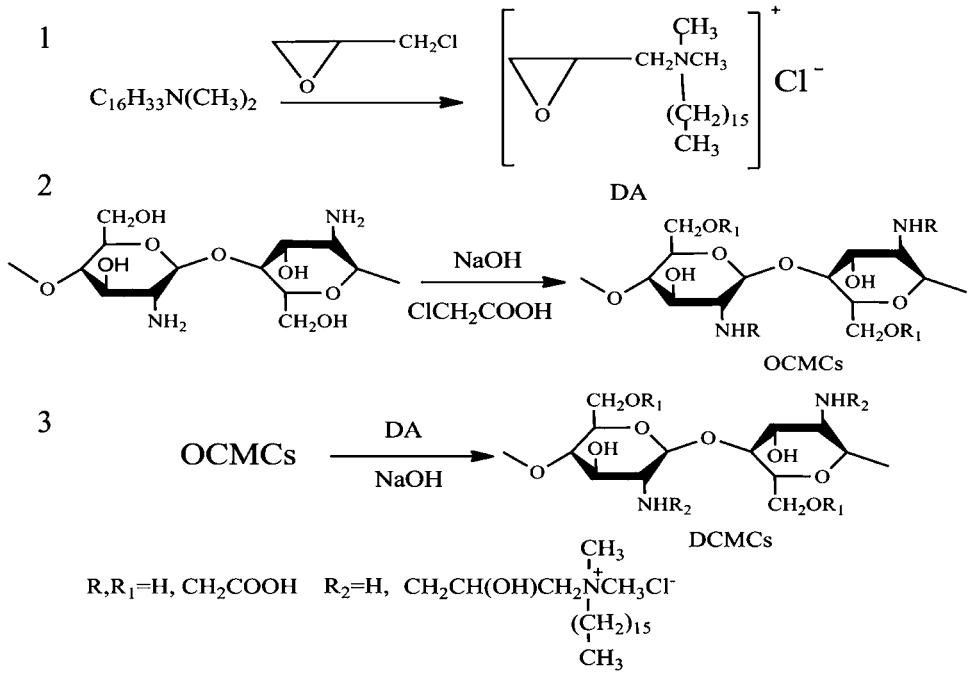

Figure 1. Schematic illustration of the synthesis process of DCMCs: (1) DA was synthesized using epoxychloropane and *N,N*-dimethylhexadecylamine; (2) OCMCs were synthesized using CS and monochloroacetic acid in an alkali environment; (3) DCMCs were then synthesized using OCMCs and DA in 2-propanol aqueous solution in an alkali environment.

However, to the best of our knowledge, the application of amphiphilic CS derivatives liposome in the food industry is rarely reported.

Salidroside has been widely used as a functional food for the various pharmacological actions such as antiaging, antioxidative, anticancer, and antidepressant activities.[18−20] Salidroside was widely applied in functional food industries in oral solution, powder, and capsule forms. The application of these forms has been significantly restricted because of the fluctuation of its concentration in blood, very high intake frequency, and poor oral bioavailability.[21,22] To overcome these drawbacks, traditional liposomes (phosphatidylcholine/cholesterol liposomes, PC-Ls) were developed to encapsulate salidroside.[21,22] However, PC-Ls suffer from various disadvantages such as instability in vivo/vitro environments and leaking of entrapped salidroside. On the basis of the advantages of amphiphilic CS derivatives, formulating a polymeric liposome by using amphiphilic CS derivatives for salidroside encapsulation may be an effective approach to overcome the above-mentioned problems.

In this study, the amphiphilic CS derivative (DCMCs) was synthesized. DCMCs were then used to develop liposomes with cholesterol (DC-Ls). As a functional food agent, salidroside was encapsulated first into DC-Ls. The physicochemical properties of DCMCs and DC-Ls were studied. Meanwhile, the encapsulation capacity and in vitro release properties of DC-Ls were also investigated.

EXPERIMENTAL PROCEDURES

Reagents and Materials. Salidroside (with 98.00% purity) was purchased from Dingsheng Pharmaceutical Technology Co., Ltd. (Hunan, China). Chitosan (CS) (300 KDa molecular weight, 90% deacetylation degree) was obtained from Lanji Technology Co., Ltd. (Shanghai, China). Epoxychloropane was purchased from Aladdin Chemistry Co., Ltd. (Shanghai, China). *N,N*-Dimethylhexadecylamine was purchased from Aoke Industrial Co., Ltd. (Shanghai, China). Cholesterol (Chol) and pyrene (with 99.00% purity) were purchased from Aladdin Chemistry Co., Ltd. (Shanghai, China). All other chemical agents used were of analytical grade.

Preparation of DCMCs. Figure 1 illustrates the synthesis procedure of DCMCs. Epoxychloropane (10 mg) and *N,N*-dimethylhexadecylamine (4 mg) were added into a flask and were reacted at 60 °C for 2 h with stirring. The residual epoxychloropane was then removed via reduced pressure distillation. The hexadecyl dimethylammonium chloride (DA) production was recrystallized using acetone and was washed with ether. CS (5 g) was subjected to swelling by using NaOH solutions (75 mL, 50 wt %) for 24 h in a flask. Monochloroacetic acid (5 g, 53 mmol) was dissolved in 25 mL of 2-propanol and then added dropwise into the flask containing CS for reaction of 24 h at room temperature. The pH of the reacted systems was adjusted to 7 using HCl (2.5 M). The product of *O*-carboxymethyl chitosan (OCMCs) was filtered and washed with ethanol. The production was then dialyzed for 3 days and was subsequently freeze-dried. OCMCs (5 g) were dissolved in an 2-propanol aqueous solution (100 mL, 2-propanol/deionized water = 1/3, V/V). In addition, DA was added slowly. The mixture was trickled with 10 mL of NaOH solution (42%, w/w) and reacted at 50 °C for 24 h with stirring. Finally, the solution was dialyzed for 3 days and lyophilized and the DCMCs were then obtained.

Structure Characterizations of DCMCs. The structure of DCMCs was determined via FT-IR and ^{1}H NMR. The FT-IR spectra of CS, OCMCs, and DCMCs were obtained using KBr pellets on a spectrophotometer (Nicolet 5700, Thermo Electron Corporation, Waltham, MA, USA) in the region of 400−4000 cm^{-1}. The ^{1}H NMR spectra of DCMCs were obtained using a spectrometer operated at 500 MHz (Bruker DPX300, Bruker Corporation, Karlsruhe, Germany) with D_2O as the solvent.

Substitution Degree (SD) of OCMCs. The SD of OCMCs was measured via the conductometric method.[23] OCMCs (0.1 g) was dissolved in an HCl solution (100 mL, 0.05 M) with mild stirring. The pH was adjusted to 2.0−2.2 by adding NaOH solution (0.1 M). The OCMCs solution was then titrated with NaOH solution (0.1 M) to pH 11.0−12.0. The typical titration curve was calculated, and the SD of OCMCs was measured based on the following equation:

$$SD = (V_2 - V_1) \times DD/(V_3 - V_2) \quad (1)$$

dx.doi.org/10.1021/jf4039925 | J. Agric. Food Chem. 2014, 62, 626−633

where SD is the OCMCs substitution degree and DD is the deacetylation degree of original CS. V_1, V_2, and V_3 are the consumed volume of NaOH in different linear sections of the titration curve.

Critical Micelle Concentration (CMC) of DCMCs. The CMC of DCMCs was investigated via fluorescence spectroscopy by using pyrene as a hydrophobic probe. A known volume of pyrene in acetone (6.0×10^{-6} M, 1 mL) was added to each of a series of 10 mL vials. Then 10 mL of various concentration of DCMCs (1.0×10^{-4}, 1.0×10^{-3}, 2.0×10^{-3}, 5.0×10^{-2}, 1.0×10^{-1}, and 1.0 mg·mL^{-1}) were added into each vial after acetone evaporation was complete. The fluorescence emission spectra were obtained using a fluorometer (F-4500, Hitachi, Tokyo, Japan) at an excitation wavelength of 339 nm, and the emission wavelength was 360−t450 nm for excitation spectra.

Preparation of DC-Ls. The DC-Ls were developed via thin-layer evaporation method.[9] DCMCs and cholesterol (Chol) (weight ratio 1/0.81, total lipids 90 mg) were dissolved in ethanol (15 mL) in a round-bottomed flask. The mixture was dried under reduced pressure by using an Eyela rotary evaporator (model N-1000; Eyela, Tokyo, Japan) at 40 °C under condition of N_2 environment to form a thin lipid film. The trace solvent was then removed by holding the lipid film at high vacuum overnight. The thin lipid film was hydrated by using deionized water (15 mL, with salidroside of 0.5 mg·mL^{-1}) and was then ultrasonicated using an ultrasonic processor (KQ-600B, Kun Shan Ultrasonic Instruments Co., Ltd., Jiangshu, China) at 25 °C for 30 min at 45 W to produce multilamellar liposomes (DC-Ls). For comparison, traditional PC-Ls were also prepared via the same procedures and conditions except egg yolk phosphatidylcholine (PC) replaced the DCMCs.

For verifying that DC-Ls have the capacity of forming multilamellar film structure, 25 mg of OA-Fe_3O_4 was also dissolved in ethanol (15 mL) with DCMCs and Chol, and other procedures were the same as that in the preparation of DC-Ls. The physical mixtures of DCMCs/Chol were prepared as follows: DCMCs/Chol (weight ratio 1/0.81) was mixed with chloroform, and the chloroform was then evaporated to obtain the dried physical mixtures of DCMCs/Chol.

Physicochemical Properties of DC-Ls. Transmission electron microscopy (TEM) images were obtained using JEOL (JEM-2010HR, Hitachi, Tokyo, Japan) with an operating voltage of 200 kV. X-ray diffraction (XRD) patterns were recorded using an XRD analyzer (D/max 2400, Rigaku Corporation, Tokyo, Japan) with a scattering angle range of 3−45°. DSC was performed using DSC equipment (Perkin-Elmer, Waltham, MA, USA) with a heating rate of 10 °C·min^{-1}. The average particle size was determined by a dynamic light scattering Zetasizer (Nano ZS90, Malvern Instruments, Worcester, UK). The ζ potential was measured using the Nano ZS90 zetasizer (DTS1060, Malvern Instruments) at 25 °C. The vibrating specimen magnetometer (VSM) (model 7407, Lakeshore, Westerville, OH, USA) was used to examine the magnetic properties of the DC-Ls.

Encapsulation Efficiency (EE) of DC-Ls. The Sephadex G_{25} column method was used to determine the salidroside EE in DC-Ls. A predetermined aliquot of salidroside loaded DC-Ls were first eluted through the Sephadex G_{25} column to remove free salidroside. The DC-Ls was dissolved in chloroform to destroy the liposomes structure. The trapped salidroside was extracted with deionized water and was then determined with high performance liquid chromatography (HPLC) (1100 series, Agilent Technologies Co., Ltd., Palo Alto, CA, USA) at a wavelength of 480 nm. The analytical column was a C_{18} column (5 μm, 4.6 mm × 150 mm, Waters Company, Milford, MA, USA). The mobile phase was a mixture of methanol/water (20:80, v/v) at a flow rate of 1.0 mL min^{-1}, and the injection volume was 20 μL at 25 °C. The EE of DC-Ls was determined using the equation below. EE test were performed in triplicate with data reported as the mean values.

$$\mathrm{EE}(\%) = (\text{salidroside loaded in DC-Ls/total salidroside added}) \times 100 \quad (2)$$

In Vitro Release of DC-Ls. First, 5 mL of salidroside loaded DC-Ls suspension were placed in dialysis bags and were suspended in 30 mL of simulated gastric fluid (SGF, pH 1.2), phosphate buffer saline (PBS, pH 7.0), and simulated intestinal fluid (SIF, pH 7.4), respectively. The release media was incubated at 37 ± 0.1 °C with stirring. At specified time intervals, 1 mL of the sample was taken and the same volume of fresh media was added to maintain a constant volume. The amount of salidroside release from DC-Ls was estimated via HPLC. All release tests were performed in triplicate, and the mean values were reported. The ingredients of simulated fluids were as follows:[24]

SGF (pH 1.2): NaCl (0.2 g), HCl (7 mL), and pepsin (3.2 g), pH was adjusted by NaOH to 1.2 ± 0.5.

SIF (pH 7.4): KH_2PO_4 (6.8 g), 0.2 N NaOH (190 mL), and pancreatin (10.0 g).

PBS (pH 7.0): 0.2 M KH_2PO_4 (250 mL), 0.2 M NaOH (145.5 mL), and H_2O (604.5 mL).

Release Mechanism of DC-Ls. The first-order, Higuchi, and Peppas models were used to fit the release data of salidroside from DC-Ls and were then used to investigate potential release mechanisms.

$$\text{first-order model: } \ln(1 - M_t/M_\infty) = -k_t \quad (3)$$

$$\text{Higuchi model: } M_t/M_\infty = k_t^{1/2} \quad (4)$$

$$\text{Peppas model: } \ln(M_t/M_\infty) = n \ln t + \ln k \quad (5)$$

where M_t/M_∞ is the fractional active agents release at time t, k is a constant incorporating the properties, and n gives an indication of the release mechanism. The correlation coefficient (R^2) is the linear relationship between salidroside release and time.

RESULTS AND DISCUSSION

Synthesis and Structural Characterization of DCMCs. A novel amphiphilically modified CS molecule with hydrophilic carboxyl and long hydrophobic methylene chains were synthesized. Detailed schemes for the DCMCs preparation are shown in Figure 1. FT-IR and ^{1}H NMR were performed to confirm the structural properties of DCMCs. The FT-IR spectra of CS, OCMCs, and DCMCs are shown in Figure 2A. In the FT-IR spectra of CS, the stretching vibrations at 3444.62 and 2927.73 cm^{-1} were attributed to the −OH and C−H groups, respectively. Meanwhile, the stretching vibration of C−O was found at 1092.96 cm^{-1}.[25] In the FT-IR spectra of OCMCs, the vibration absorption peaks were observed at 1575.94 and 1419.22 cm^{-1}, which indicates that carboxylate groups were successfully conjugated into CS.[26] In the FT-IR spectra of DCMCs, the characteristic stretching vibration absorption of long methylene chain was found at 2921.31 and 2853.49 cm^{-1}. Additionally, the appearance of new stretching vibration absorption at 721.55 cm^{-1} corresponds to the methylene planar rocking vibration. These results showed that the quaternary ammonium salt group was grafted into DCMCs. The DCMCs structure was further confirmed by the ^{1}H NMR spectra. In the ^{1}H NMR spectra of DCMCs (Figure 2B), the signal at δ 4.78, 1.72, 3.67, 3.65, 3.60, and 3.37 ppm were attributed to H-1, H-2, H-3, H-4, H-5, and H-6 of the D-glucosamine unit of DCMCs, respectively. The new signals at δ 0.91, 1.32−1.40, 3.25, 3.27, and 3.90 ppm were attributed to H-e, H-d, H-b, H-a, and H-c, which correspond to the proton assignment of long-chain alkyl of quaternary ammonium salt. The results of FT-IR and ^{1}H NMR confirmed that DCMCs were successfully synthesized, which was consistent with the previous report of Liang at el.[27]

Substitution Degree (SD) of OCMCs. A typical conductometric titration curve of OCMCs that consists of four linear branches is shown Figure 3. The excess HCl was neutralized using the volume of NaOH ($0-V_1$). (V_1-V_2) corresponds to the volume of NaOH that reacted with the

dx.doi.org/10.1021/jf4039925 | J. Agric. Food Chem. 2014, 62, 626−633

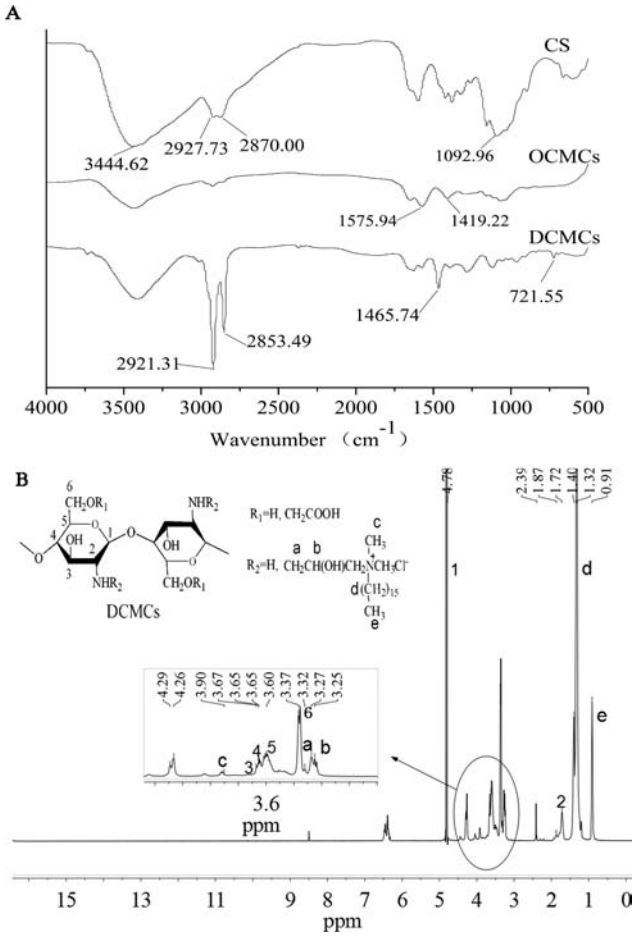

Figure 2. FT-IR spectra (A) of CS, OCMCs and DCMCs, and ^{1}H NMR spectra (B) of DCMCs.

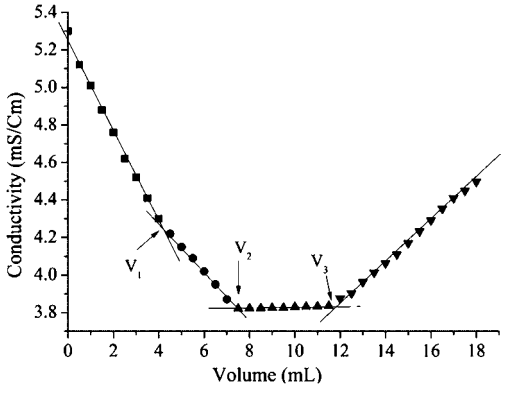

Figure 3. Conductimetric titration curve of OCMCs.

carboxymethyl groups of OCMCs. (V_2−V_3) represents the volume added to react with NH_3^+ of CS. The final volume (from V_3 to the end) indicated the excess amount of NaOH in the solution. The SD of OCMCs was determined according to eq 1, and the SD value was 70.00%. The results obtained in the current study was higher than that of the previous study.[23]

Critical Micelle Concentration (CMC) of DCMCs. For evaluation of the aggregation properties of DCMCs, the probe fluorescence technique was applied to determine the CMC by using pyrene as the fluorescence probe. Pyrene has a strong hydrophobic character with a very low solubility in water and tends to solubilize into the hydrophobic region of the micelles, thereby resulting in the fluorescence emission changes. Figure 4A shows the fluorescence emission spectra of pyrene in

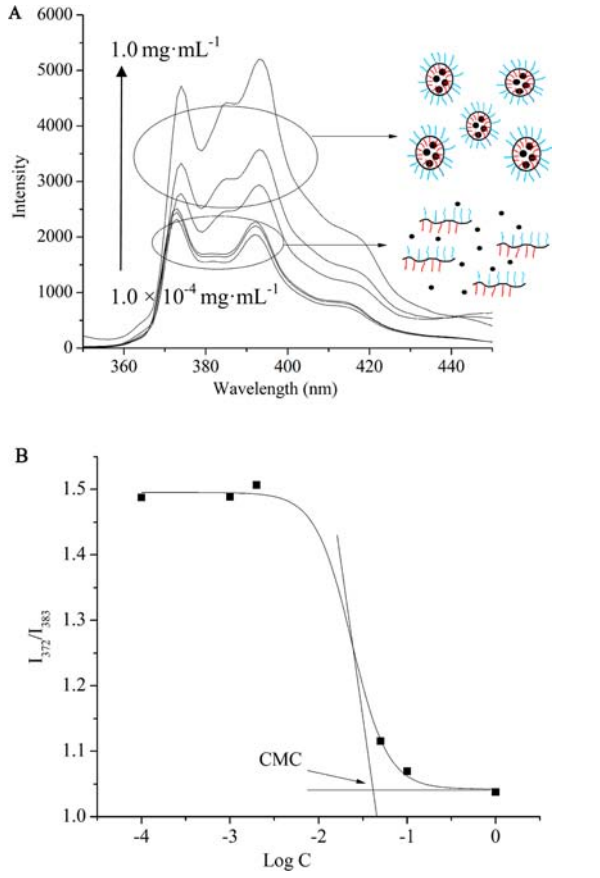

Figure 4. Fluorescence spectra of pyrene in different DCMCs concentrations (1.0×10^{-4}, 1.0×10^{-3}, 2.0×10^{-3}, 5.0×10^{-2}, 1.0×10^{-1}, and 1.0 mg·mL^{-1}) (A), and intensity ratio (I_{372}/I_{383}) versus the DCMCs concentration (B).

DCMCs solution with concentrations varying from 1.0×10^{-4} to 1.0 mg·mL^{-1}. The results indicated that the fluorescence intensity increased with increasing the concentration of DCMCs. The pyrene solubility in water is extremely low, and its dissolved fraction produces negligible fluorescence. When the concentration is above CMC, the hydrophobic phase (micelle core) was formed, which solubilizes pyrene and results in increased solution fluorescence. Plots of pyrene I_1 (372 nm /I_3 (383 nm) ratio versus logarithm of DCMCs concentration are shown in Figure. 4B. The scatters are fitted by using a Boltzmann function, which is expressed as following:

$$y = 1.29 + 0.52/[1 + e^{(x+1.88)/\Delta x}] \quad (6)$$

where y and x is the pyrene I_1/I_3 ratio and the DCMCs concentration logarithm, respectively. A common tangent can be obtained by determining the midpoint, which is obtained by using the second derivative of y ($y'' = 0$), and the CMC was defined as the crossover point of common tangent and flat tangent.[28] The CMC value of DCMCs was determined as approximately 23.00 mg·L^{-1}, which was lower than other similar CMCs-based micelle systems such as deoxycholic acid-*O*-carboxymethylated chitosan−folic acid conjugates and acylated CMCs.[29,30] These results indicated that DCMCs are capable of forming self-organized liposomes easily and are also

dx.doi.org/10.1021/jf4039925 | J. Agric. Food Chem. 2014, 62, 626−633

capable of maintaining their integrity even upon strong dilution.

Formulation of DC-Ls. Figure 5 illustrats the preparation processes of DC-Ls via the thin-layer evaporation method.

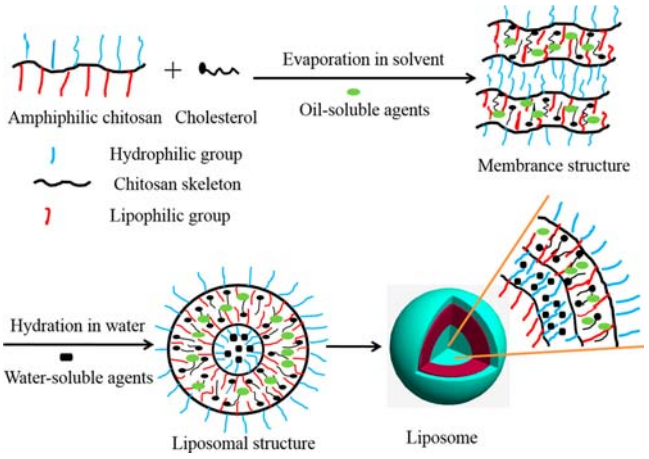

Figure 5. Schematic illustration of the formation process of DC-Ls. DCMCs and Chol (or with poorly water-soluble agents) were dissolved in an organic solvent, which was then completely removed, and the thin film was obtained. The thin film was hydrated using deionized water (or with water-soluble agents) and sonicated to obtain the liposomes. As a soluble agent, salidroside was dissolved in deionized water and used to hydrate the thin film and thus obtained the salidroside-load DC-Ls.

DCMCs and Chol were dissolved in organic solvents, and a thin film was obtained after removing the solvent via evaporation. The DC-Ls solution was obtained after hydration of thin film by adding an aqueous phase. The cross section of DC-Ls (Figure 5) showed that the hydrophilic heads of the DCMCs are oriented toward the water compartment, whereas the lipophilic tails are directed toward the center of the vesicle. Thus, the hydrophilic and lipophilic bioactive agents can be loaded into the water compartment and lipid section of DC-Ls, respectively.

Characterization of DC-Ls. The morphology and bilayer structure of DC-Ls were observed by TEM (Figure 6). The results indicated that DC-Ls exhibit a nearly spherical bubble with slight aggregation (Figure 6A,B). For verifying OA-Fe_3O_4 incorporated into DC-Ls, VSM was employed to study the magnetic properties of the DC-Ls@OA-Fe_3O_4. From the magnetic hysteresis loop of OA-Fe_3O_4 and DC-Ls@OA-Fe_3O_4 (Figure 7), it was found that the saturation magnetization of OA-Fe_3O_4 and DC-Ls@OA-Fe_3O_4 was 66.45 and 23.45 em$\mu\cdot g^{-1}$, respectively. These results (Figures 6C and 7) indicated that OA-Fe_3O_4 was encapsulated into DC-Ls with properties of core (OA-Fe_3O_4) and shell (DCMCs films) structure. Meanwhile, the multilamellar film structure was also found on the surface of OA-Fe_3O_4 nanoparticles (Figure 6D).

The particle size and ζ potential of DC-Ls were determined and are shown in Figure 8. The average size of DC-Ls was 32.21 nm with a narrow distribution (PDI = 0.277 < 0.5), and the ζ potential was approximately +73.30 mV. A previous study reported that the average size, PDI and ζ potential of the traditional liposomes (PC-Ls) were 604.00 nm, 0.36, and +7.50 mV,[21] respectively. These results indicated that DC-Ls has better properties than PC-Ls. Evidence has shown that nanocarriers with a small particle size (<200 nm) and positive

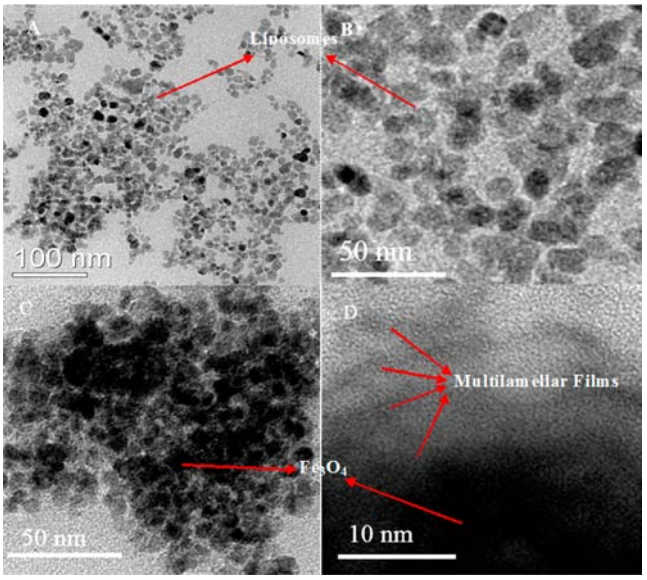

Figure 6. TEM images of DC-Ls and DC-Ls@OA-Fe_3O_4. DC-Ls exhibit a nearly spherical bubble shape with slight aggregation (A,B), DC-Ls@OA-Fe_3O_4 exhibit property of core (OA-Fe_3O_4) and shell (DMCMs films) structure (C,D), and multilamellar films can be seen on the surface of OA-Fe_3O_4 (D).

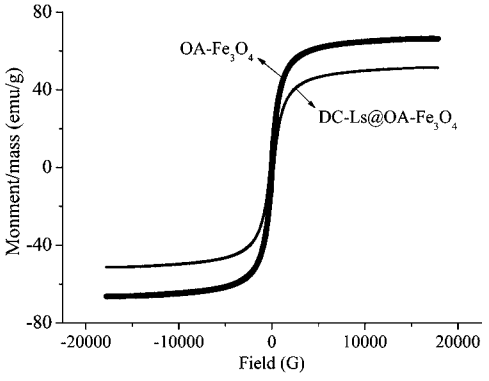

Figure 7. Magnetic hysteresis loop of OA-Fe_3O_4 and DC-Ls@OA-Fe_3O_4.

charge were not captured by the reticuloendothelial cell systems but were easily absorbed by the negatively charge cellular membrane.[31] Consequently, the bioavailability of bioactive agents can be improved after encapsulation into DC-Ls.

The XRD of DCMCs, Chol, DC-Ls, and DCMCs/Chol physical mixture were investigated, and the results are shown in Figure 9A. CS has the property of the crystal form II at 2θ = 20.5°. However, the crystal peaks of DCMCs at 2θ were sharply changed with shifting from 20.5° to 21.6°, and a new peak at 2θ of 5° appeared. These results indicated that DCMCs molecules have good crystal properties with a billayered lamellar structure.[32] The DCMCs peak of 21.6° and all Chol peaks disappeared for DCMCs/Chol physical mixture, which indicated that the interaction (i.e., hydrogen bonding and hydrophobic interactions) between DCMCs and Chol was occurred.[9] However, the peak at 20.9° appeared for DC-Ls after hydration, which suggested that DC-Ls can form lamellar-like structures as lipid.

The lipid physical state can change from an ordered gel phase to a disordered liquid-crystalline phase when temperature is

dx.doi.org/10.1021/jf4039925 | J. Agric. Food Chem. 2014, 62, 626−633

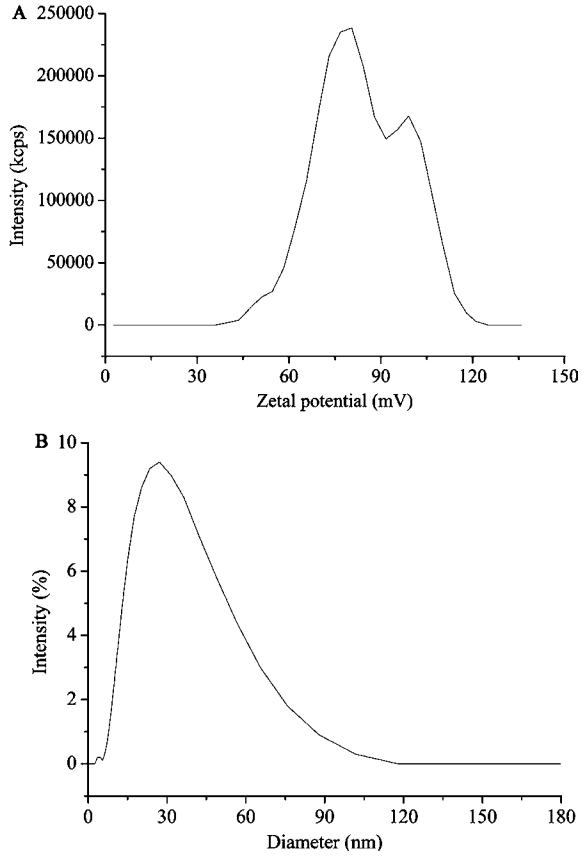

Figure 8. Size distribution (A) and ζ potential (B) of DC-Ls.

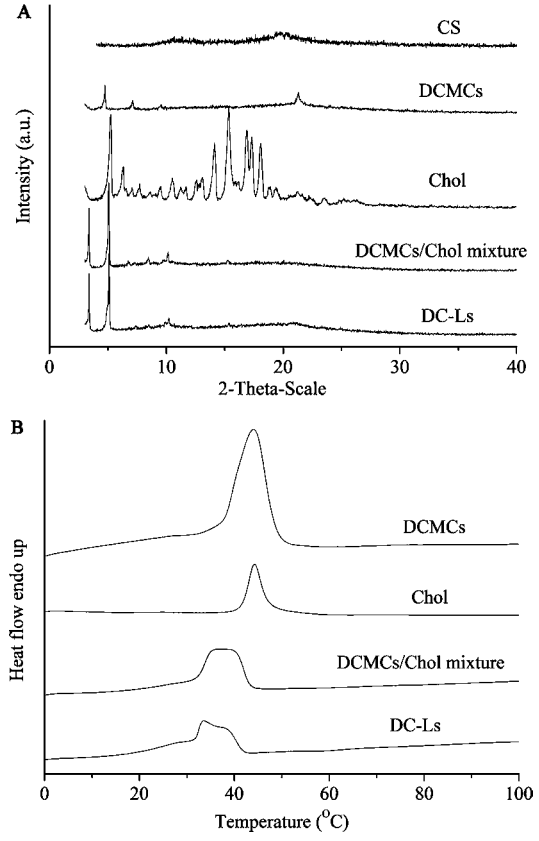

Figure 9. XRD (A) and DSC (B) spectra of DCMCs, Chol, DCMCs/Chol physical mixture, and DC-Ls.

changed. This change was defined as phase transition temperature (T_m). The DSC of DCMCs, DC-Ls, Chol, and DCMCs/Chol physical mixture was investigated and is shown in Figure 9B. The T_m values of Chol and DCMCs were 44.43 and 44.29 °C, respectively. However, the T_m of DCMCs/Chol physical mixture and DC-Ls decreased and the values were 37.50 and 33.61 °C, respectively. The results indicated that the structure of DCMCs was rearranged and interacted with Chol. The Chol interaction with DCMCs would increase the rigidity of the "fluid state" liposomal bilayers of DC-Ls, which results in good thermal stabilization.[33] The XRD and DSC results suggested that DC-Ls have the same physiochemical properties as that of PC-Ls.

Encapsulation Efficiency (EE) of DC-Ls. Compared with DC-Ls, PC-Ls of salidroside loading was also developed and the EE was only about 54.72%. Previous studies have also reported that the EE of salidroside loading in PC-Ls was lower than 60.00%.[21,22] Fortunately, the EE of salidroside in DC-Ls increased to 82.46%. The high EE (82.46%) may be attributed to the multilamellar structure of DC-Ls, which favored the formation of a high inner volume.[15] EE depends on the inner volume of liposomes for water-soluble compounds, thus, a large inner volume of DC-Ls results in a high EE.

Release of Salidroside from DC-Ls. The release of salidroside from salidroside solution (control sample), PC-Ls, and DC-Ls was investigated in PBS solutions (pH 7.0) (Figure 10A). The release of salidroside from the control solution occurred rapidly with a release rate of 86.44% after 6 h. As expected, the salidroside release from liposomes was slower than that in the control solution. The release rates were only about 38.38% and 30.77% for PC-Ls and DC-Ls after 6 h,

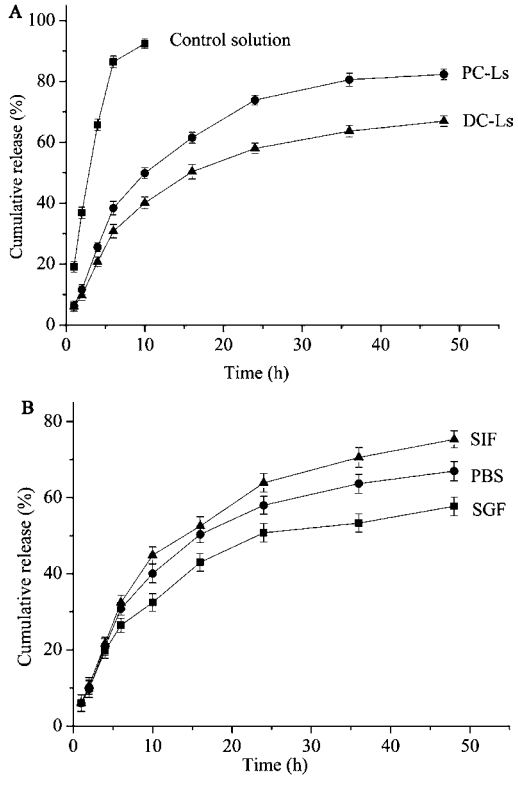

Figure 10. In vitro release of salidroside from control solution, PC-Ls, and DC-Ls in PBS solutions (A), and from DC-Ls in SGF, PBS, and SIF solutions (B), respectively. Data represent the mean ± SD (n = 3).

dx.doi.org/10.1021/jf4039925 | J. Agric. Food Chem. 2014, 62, 626−633

Table 1. Correlation Coefficients (R^2) and Release Exponent (n) of Different Models in SGF, PBS, and SIF Solution, Respectively[a]

		SGF solution		PBS solution		SIF solution	
model		stage 1	stage 2	stage 1	stage 2	stage 1	stage 2
First model	R^2	0.939	0.897	0.975	0.941	0.993	0.943
Higuchi model	R^2	0977	0908	0.984	0.951	0.989	0.933
Peppas model	R^2	0.983	0.948	0.987	0.979	0.995	0.964
	n	0.767	0.252	0.870	0.259	0.901	0.322

[a]Stage 1 and 2 is the burst (0−10 h) and sustained release (10−48 h) process, respectively.

respectively, and more interestingly, the release rate was 66.98% and 82.33% for DC-Ls and PC-Ls after 50 h, respectively. These results indicated that DC-Ls had a relatively longer release time than PC-Ls, which may be due to the high molar mass of DCMCs. Thus, DC-Ls can be used for sustained release of salidroside.

To further investigate the effect of gastrointestinal environment on salidroside release from DC-Ls, the solutions of SGF (pH 1.2), PBS (pH 7.0), and SIF (pH 7.4) were used as release media (Figure 10B). The results suggested that the release rate of salidroside from DC-Ls decreased with decreasing pH value. In the SGF solution, the H-bond between −COOH and −OH caused the aggregation of salidroside in the inner portion of DC-Ls. Moreover, the repulsive force between H^+ and the positive charge of liposomal surface made DC-Ls more stable. Consequently, the release rate of salidroside from DC-Ls was lower in the SGF solution. On the other hand, the positive charge on the surface of DC-Ls was partially neutralized with OH^- in the SIF solution, which leads to the destruction of DC-Ls and an improvement in the release rate of salidroside.

Release Mechanism of DC-Ls. Figure 10B shows that two stages were observed for the release of salidroside from DC-Ls. The first stage of release was initially rapid and was considered the burst release, which may be due to the unbound excess of salidroside on the DC-Ls surfaces. The second stage was a sustained release process. The burst release of salidroside may help to reach the effective concentration rapidly in plasma, whereas the sustained release would maintain the effective concentration in plasma for a long time. Thus, the bioavailability and biological half-life time of salidroside can be improved after loading into DC-Ls.

The amphiphilic CS derivatives have been used to develop liposome for drugs and genes delivery. However, the release mechanism is rarely reported. Thus, different kinetic models of first-order, Higuchi, and Peppas were used to fit the two release stages for further investigation of the probable DC-Ls release mechanism, and the results are shown in Table 1. It can be seen that the R^2 of Peppas model was highest among models. This finding indicated that Peppas is the most suitable model for describing the release kinetic of salidroside from DC-Ls. The value n of the Peppas model is characteristic for the release mechanism such as $n \leq 0.43$ for Case I Fichian diffusion, $0.43 < n < 0.85$ for anomalous behavior or non-Fickian transport, and $n \geq 0.85$ for case II transport.[34] The n values of DC-Ls were determined and are shown in Table 1. The results suggested that case II transport was the main release mechanism for stage 1 and case I Fichian diffusion for stage 2.

In conclusion, amphiphilic CS derivatives of DCMCs were successfully synthesized and the structure was confirmed via FT-IR and ^{1}H NMR. DCMCs have a self-assembling property with low CMC as the traditional lipid. DCMCs were used to develop liposomes with Chol (DC-Ls), which exhibits multilamellar structure with positive charge and narrow size distribution. Compared with traditional liposomes, DC-Ls have higher thermal stabilization and encapsulation efficiency. The release of salidroside from DC-Ls was initially burst release, followed by sustained release. Furthermore, the case II transport and case I Fichian diffusion were the main release mechanisms for the whole release process. In conclusion, DC-Ls may be a promising carrier system for the production of functional foods that contain salidroside or other bioactive food ingredients. However, further in vivo investigation is required to demonstrate the efficacy and safety of DC-Ls.

AUTHOR INFORMATION

Corresponding Author

*Phone: +86-791-6634810. Fax: +86-791-6634810. E-mail: huaxiong100@126.com.

Funding

This work was supported by the Planning Subject of "the Twelfth Five-Year-Plan" National Science and Technology for the Rural development of China (2013AA102203-05), and the National Natural Science Foundation of China (31160317, 21201098, 2126602, and 81360205)

Notes

The authors declare no competing financial interest.

REFERENCES

(1) Keller, B. C. Liposomes in nutrition. *Trends Food Sci. Technol.* **2001**, *12*, 25−31.

(2) Chun, J. Y.; Choi, M. J.; Min, S. G.; Weiss, J. Formation and stability of multiple-layered liposomes by layer-by-layer electrostatic deposition of biopolymers. *Food Hydrocolloids* **2013**, *30*, 249−257.

(3) Elizondo, E.; Moreno, E.; Cabrera, I.; Córdoba, A.; Sala, S.; Veciana, J.; Ventosa, N. Liposomes and other vesicular systems: structural characteristics, methods of preparation, and use in nanomedicine. *Prog. Mol. Biol. Trans. Sci.* **2011**, *104*, 1−52.

(4) Kuntsche, J.; Freisleben, I.; Steiniger, F.; Fahr, A. Temoporfin-loaded liposomes: physicochemical characterization. *Eur. J. Pharm. Sci.* **2010**, *40*, 305−315.

(5) Betz, G.; Aeppli, A.; Menshutina, N.; Leuenberger, H. In vivo comparison of various liposome formulations for cosmetic application. *Int. J. Pharm.* **2005**, *296*, 44−54.

(6) Liu, W. L.; Liu, W.; Liu, J. H.; Li, T.; Liu, C. M. Improved phyiscal and in vitro digestion stability of polyelectrolyte delivery system based on layer-by-layer self-assembled alginate−chitosan coated nanoliposomes. *J. Agric. Food Chem.* **2013**, *61*, 4133−4144.

(7) Liu, W. L.; Ye, A. Q.; Liu, C. M.; Liu, W.; Singh, H. Stability during in vitro digestion of lactoferrin-loaded liposomes prepared from milk-fat-globule-membrane-derived phospholipids. *J. Dairy Sci.* **2013**, *96*, 2061−2070.

(8) Su, W. Y.; Wang, H. J.; Wang, S.; Liao, Z. Y.; Kang, S. Y.; Peng, Y.; Han, L.; Chang, J. PEG/RGD-modified magnetic polymeric liposomes for controlled drug release and tumor cell targeting. *Int. J. Pharm.* **2012**, *426*, 170−181.

(9) Liang, X. F.; Wang, H. J.; Luo, H.; Tian, H.; Zhang, B. B.; Hao, L. J.; Teng, J. I.; Chang, J. Characterization of novel multifunctional cationic polymeric liposomes formed from octadecyl quaternized carboxymethyl chitosan/cholesterol and drug encapsulation. *Langmuir* **2008**, *24*, 7147−7153.
(10) Hoagland, P. D.; Parris, N. Chitosan/Pectin Laminated Films. *J. Agric. Food Chem.* **1996**, *44*, 1915−1919.
(11) Choi, A. J.; Kim, C. J.; Cho, Y. J.; Hwang, J. K.; Kim, C. T. Characterization of capsaicin-Loaded nanoemulsions stabilized with alginate and chitosan by self-assembly. *Food Bioprocess Technol.* **2011**, *4*, 1119−1126.
(12) Luo, Y. C.; Teng, Z.; Wang, Q. Development of Zein Nanoparticles Coated with Carboxymethyl Chitosan for Encapsulation and Controlled Release of Vitamin D3. *J. Agric. Food Chem.* **2012**, *60*, 836−843.
(13) Aranaz, I.; Harris, R.; Heras, A. Chitosan amphiphilic derivatives. Chemistry and applications. *Curr. Org. Chem.* **2010**, *14*, 308−330.
(14) Luo, Y.; Wang, Q. Recent advances of chitosan and its derivatives for novel applications in food science. *J. Food Process. Beverages* **2013**, *1*, 13.
(15) Huo, M. R.; Zhang, Y.; Zhou, J. P.; Zou, A. F.; Yu, D.; Wu, Y. P.; Li, J.; Li, H. Synthesis and characterization of low-toxic amphiphilic chitosan derivatives and their application as micelle carrier for antitumor drug. *Int. J. Pharm.* **2010**, *394*, 162−173.
(16) Liang, X. F.; Li, X. Y.; Chang, J.; Duan, Y. R.; Li, Z. H. Properties and evaluation of quaternized chitosan/lipid cation polymeric liposomes for cancer targeted gene delivery. *Langmuir* **2013**, *29*, 8683−8693.
(17) Choochottiros, C.; Yoksan, R.; Chirachanchai, S. Amphiphilic chitosan nanospheres: factors to control nanosphere formation and its consequent pH responsive performance. *Polymer* **2009**, *50*, 1877−1886.
(18) Zhang, L.; Yu, H. X.; Sun, Y.; Lin, X. F.; Chen, B.; Tan, T.; Cao, G. X.; Wang, Z. W. Protective effects of salidroside on hydrogen peroxide-induced apoptosis in SH-SY5Y human neuroblastoma cells. *Eur. J. Pharmacol.* **2007**, *564*, 18−25.
(19) Zhang, L.; Yu, H. X.; Zhao, X. C.; Lin, X. F.; Tan, C.; Cao, G. X.; Wang, Z. W. Neuroprotective effects of salidroside against beta-amyloid-induced oxidative stress in SH-SY5Y human neuroblastoma cells. *Neurochem. Int.* **2010**, *57*, 547−555.
(20) Hu, X. L.; Zhang, X. Q.; Qiu, S. F.; Yu, D. H.; Lin, S. X. Salidroside induces cell-cycle arrest and apoptosis in human breast cancer cells. *Biochem. Biophys. Res. Commun.* **2010**, *398*, 62−67.
(21) Fan, M. H.; Xu, S. Y.; Xia, S. Q.; Zhang, X. M. Effect of different preparation methods on physicochemical properties of salidroside liposomes. *J. Agric. Food Chem.* **2007**, *55*, 3089−3095.
(22) Fan, M. H.; Xu, S. Y.; Xia, S. Q.; Zhang, X. M. Preparation of salidroside nano-liposomes by ethanol injection method and in vitro release study. *Eur. Food Res. Technol.* **2008**, *227*, 167−17.
(23) Luo, Y. C.; Teng, Z.; Wang, X. G.; Wang, Q. Development of carboxymethyl chitosan hydrogel beads in alcohol−aqueous binary solvent for nutrient delivery applications. *Food Hydrocolloids* **2013**, *31*, 332−339.
(24) Feng, C.; Wang, Z. G.; Jiang, C. Q.; Kong, M.; Zhou, X.; Li, Y.; Cheng, X. J.; Chen, X. G. Chitosan/*o*-carboxymethyl chitosan nanoparticles for efficient and safe oral anticancer drug delivery: in vitro and in vivo evaluation. *Int. J. Pharm.* **2013**, *457*, 158−167.
(25) Peng, H. L.; Xiong, H.; Li, J. H.; Xie, M. Y.; Liu, Y. Z.; Bai, C. Q.; Chen, L. X. Vanillin cross-linked chitosan microspheres for controlled release of resveratrol. *Food Chem.* **2010**, *121*, 23−28.
(26) Liu, X. F.; Zhi, X. N.; Liu, Y. F.; Wu, B.; Sun, Z.; Shen, J. Effect of chitosan, *O*-carboxymethyl chitosan, and *N*-[(2-Hydroxy-3-*N*, *N*-dimethylhexadecyl ammonium)propyl] chitosan chloride on overweight and insulin resistance in a murine diet-induced obesity. *J. Agric. Food Chem.* **2012**, *60*, 3471−3476.
(27) Liang, X. F.; Wang, H. J.; Tian, H.; Luo, H.; Chang, J. Synthesis, structure and properties of novel quternized carboxymethyl chitosan with drug loading capacity. *Acta Phys.-Chim. Sin.* **2008**, *24*, 223−229.
(28) Yan, M.; Li, B.; Zhao, X. Determination of critical aggregation concentration and aggregation number of acid-soluble collagen from walleye pollock (*Theragra chalcogramma*) skin using the fluorescence probe pyrene. *Food Chem.* **2010**, *122*, 1333−1337.
(29) Wang, Y.; Yang, X.; Yang, J.; Wang, Y.; Chen, R.; Wu, J.; Liu, Y.; Zhang, N. Self-assembled nanoparticles of methotrexate conjugated *O*-carboxymethyl chitosan: preparation, characterization and drug release behavior in vitro. *Carbohydr. Polym.* **2011**, *86*, 1665−1670.
(30) Liu, K. H.; Chen, B. R.; Chen, S. Y.; Liu, D. M. Self-assembly behavior and doxorubicin-loading capacity of acylated carboxymethyl chitosans. *J. Phys. Chem. B* **2009**, *113*, 11800−11807.
(31) Pack, O. W.; Hoffman, A. S.; Pun, S.; Stayton, P. S. Design and development of polymers for gene delivery. *Nature Rev. Drug Discovery* **2005**, *4*, 581−593.
(32) Grant, J.; Tomba, J. P.; Lee, H.; Allen, C. Relationship between composition and properties for stable chitosan films containing lipid microdomains. *J. Appl. Polym. Sci.* **2007**, *103*, 3453−3460.
(33) Grit, M.; Zuidam, N. J.; Underberg, W. J. M.; Crommelin, D. J. A. Hydrolysis of partially saturated egg phosphatidylcholine in aqueous liposome dispersions and the effect of cholesterol incorporation on hydrolysis kinetics. *J. Pharm. Pharmacol.* **1993**, *45*, 490−495.
(34) Ritger, P. L.; Peppas, N. A. A simple equation for description of solute release II. Fickian and anomalous release from swellable devices. *J. Controlled Release* **1987**, *5*, 37−42.

JOURNAL OF AGRICULTURAL AND FOOD CHEMISTRY

Article

pubs.acs.org/JAFC

Concentration Variation and Molecular Characteristics of Soluble (1,3;1,6)-β-D-Glucans in Submerged Cultivation Products of *Ganoderma lucidum* Mycelium

Chung-Huang Wang,[†] Shu-Chen Hsieh,[†] Huei-Ju Wang,[§] Miaw-Ling Chen,[#] Bi-Fong Lin,[‡] Been-Huang Chiang,[†] and Ting-Jang Lu*[,†]

[†]Institute of Food Science and Technology, National Taiwan University, Taipei, Taiwan, Republic of China

[§]Department of Applied Science of Living, Chinese Culture University, Taipei, Taiwan, Republic of China

[#]Department of Nutrition and Health Sciences, Chang Jung Christian University, Tainan City, Taiwan, Republic of China.

[‡]Department of Biochemical Science and Technology, College of Life Science, National Taiwan University, Taipei, Taiwan, Republic of China

ABSTRACT: (1,3)-β-D-Glucans with (1,6)-β-D-glucosyl branches are bioactive polysaccharides in fruiting bodies and mycelia of *Ganoderma lucidum*, a mushroom used in traditional Chinese medicine. Submerged cultivation of mycelium is one of the more efficient means of generating polysaccharides from this fungus. Twelve mycelium samples examined in this study demonstrated the quantitative and qualitative molecular characteristics of soluble (1,3;1,6)-β-D-glucans. It was observed that the concentration of soluble (1,3;1,6)-β-D-glucan varied substantially from 1.3 to 79.9 mg/dL. (1,3;1,6)-β-D-Glucans also preserved their molecular characteristics with degrees of branching (DB) of 0.21−0.36 and molecular masses of 10^5−10^6 g/mol for those samples with substantial quantities of β-D-glucan. Using the high aggregating tendency of these molecules, (1,3;1,6)-β-D-glucans were successfully purified via fractional precipitation with 35% (v/v) ethanol. (1,3;1,6)-β-D-Glucan was proposed as a putative bioactive marker for immunomodulation because it was the most abundant polysaccharide in *G. lucidum* mycelium products to stimulate macrophage RAW 264.7 cells to release TNF-α.

KEYWORDS: *(1,3;1,6)-β-D-glucans, Ganoderma lucidum, degree of branching, molecular weight*

INTRODUCTION

Ganoderma lucidum, commonly known as Ling-Zhi and Reishi, is a medicinal mushroom that has long been a component of Oriental medicine. Polysaccharides are associated with the attributes of immunomodulating and antitumor activities of *Ganoderma*. Submerged fermentation of mycelium culture is one of the efficient means for producing *Ganoderma* polysaccharides.[1−3] Recently, as fermentation strategies have improved (e.g., fed-batch, pH-shift, or dissolved oxygen tension-shift), the maximum production of soluble (extracellular) polysaccharide has risen to higher yields from the range of 10−200 mg/dL[2−4] to reported yields of 259 mg/dL[5] and 1500 mg/dL.[6] However, not all *Ganoderma* polysaccharides are associated with immunoactivities. Therefore, using well-known bioactive polysaccharides as a quality marker during production is a more suitable strategy.

The β-D-glucans isolated from *G. lucidum* displayed high growth-inhibition activities against Sarcoma 180 solid tumors in mice[7] and enhanced regeneration of mouse bone marrow by protecting stem cells from irradiation damage.[8] Our previous study also confirmed that (1,3;1,6)-β-D-glucan was the major active polysaccharide from *G. lucidum* and showed significant tumor necrosis factor-α (TNF-α) releasing stimulation activity from human mononuclear cells (MNC).[9]

(1,3;1,6)-β-D-Glucans have been recognized as potent bioactive polysaccharides in mushrooms and fungi.[10−12] Several (1,3;1,6)-β-D-glucans and their conjugates have been commercialized for the clinical treatment of patients undergoing cancer therapy, such as those treated with schizophyllan, lentinan, grifolan, and Krestin (PSK, polysaccharide−protein complex).[13,14] In Japan, lentinan is prescribed to patients with gastric cancer, showing encouraging results in enhancing survival rates of patients.[15] (1,3)-β-D-Glucans are components of the fungal cell wall,[16,17] which can be recognized by specific cell-surface receptors, for example, dectin-1 in animal immunocytes[18,19] due to its pathogen-associated molecular pattern.[20] The interaction of (1,3)-β-D-glucans with immune cell receptors triggers a variety of immunological responses, leading to immunomodulation and antitumor activity. The distinct chemical structures of β-D-glucans provide various affinities toward these receptors.[21−23] It has been reported that the presence of (1,6)-linked side-chain branches on (1,3)-β-D-glucan increases the affinity of pattern recognition receptors[23] and dectin-1.[21] The activity plateau of these (1,3;1,6)-β-D-glucans showed a degree of branching (DB) ranging from 0.2 to 0.33.[10,24,25] Moreover, glucans with larger molecular weight may be required to cross-link spatially separated receptors and alter immunocyte function.[26]

There is limited information concerning the quantitative and qualitative molecular characteristics of soluble (1,3;1,6)-β-D-

Received: October 9, 2013
Revised: December 30, 2013
Accepted: January 4, 2014
Published: January 5, 2014

ACS Publications © 2014 American Chemical Society

glucans in submerged cultivation products of *G. lucidum*. Our preliminary study indicated that the concentration of soluble (1,3;1,6)-β-D-glucans varied substantially even under the same cultivating parameters. Twelve samples with different concentrations of (1,3;1,6)-β-D-glucans were selected to demonstrate this variance, and their DB and molecular weight data were also examined to understand their molecular characteristics.

MATERIALS AND METHODS

Submerged Cultivation Products of *Ganoderma lucidum* Mycelium. Twelve *G. lucidum* mycelium culture products from BCRC 36123 (Bioresource Collection and Research Center, Taiwan) kindly provided by Professor B. H. Chiang, Graduate Institute of Food Science and Technology, National Taiwan University, were used as samples in this study. The whole fermentation cultures were autoclaved and the mycelia removed by centrifugation. Only broth was used for analysis and coded S1−S2 and C1−C10, according to (1,3;1,6)-β-D-glucan concentration (in descending order). Samples S1 and S2 were products of static mycelium culturing with synthetic chemically defined medium (200 mL of medium consisted of 3% glucose, 2% malt extract, and 0.1% peptone with 10% mycelium inoculation) cultivated in customized 600 mL glass flasks (the inside diameters both of the bottom and of the broth surface were 14 cm) in a 28 °C incubator without aeration, illumination, and shaking. The harvest time was set when the mycelium mat fully covered the broth surface, which were 22 and 17 days for S1 and S2, respectively. Broth from three flasks was pooled for each sample. For comparison of the concentration variation of (1,3;1,6)-β-D-glucans in different samples, we designated S1 and S2 as references because they were cultured at the conditions (medium and temperature) suggested by BCRC and the cultivating conditions can be easily controlled. Samples C1−C10 were products from a commercial fermentor with leguminous composite medium [consisting of 2% glucose, 5% soybean (*Glycine max* L.), and 2% *Astragalus membranaceus*]. The fermentation was conducted in the dark, and the aeration rate, agitation speed, and inoculum size were 0.75 vvm, 50 rpm, and 10%, respectively, for 12 days. The fermentation temperature was at 30 °C for all of the C-samples except C6 and C7, for which 24 °C was used. Samples C1, C2, C6, and C7 were products of a 200 L customized pilot-scale manufacture fermentor (Grape King Inc., Taoyuan County, Taiwan) and others were of a 5 L fermentor (FB-6S, Firstek Scientific Co., Ltd., New Taipei City, Taiwan). No culture medium contained a detectable amount of (1.,3;1,6)-β-D-glucan (data not shown).

Preparation and Fractionation of Polysaccharides. The polysaccharides in the samples were obtained by precipitating polysaccharides in 4 volumes of 95% ethanol (Taiwan Tobacco and Wine Corp., Taipei, Taiwan) in a fermentation broth.

In this study, C2 was used to isolate (1,3;1,6)-β-D-glucans by using repeating fractional precipitation with ethanol. The polysaccharides of C2 were further separated into two fractions: (1,3;1,6)-β-D-glucans and C2-GRF (glucan-removed fraction). Ethanol was dripped into 3% (w/v) C2 polysaccharide aqueous solution with stirring; ethanol concentrations required for (1,3;1,6)-β-D-glucans and C2-GRF precipitation were 35 and 76% (v/v), respectively. After settling in a refrigerator overnight, the polysaccharide-precipitated fractions were collected by centrifugation (1500*g* for 15 min). The (1,3;1,6)-β-D-glucan fraction was precipitated three times to increase its purity.

Analytical Methods. *Content of Polysaccharides.* Polysaccharides were dispersed in 0.5 M NaOH and stirred at ambient temperature overnight until completely dissolved. The polysaccharide content of the sample was determined using a phenol−sulfuric acid method,[27] and glucose (Sigma Chemicals, St. Louis, MO, USA) was used as a standard (10−100 μg/mL).

Sugar Composition of Polysaccharides. The hydrolysis procedure used consisted of a combination of methanolysis and trifluoroacetic acid (TFA) hydrolysis. The polysaccharide sample (1−5 mg) was methanolyzed under vacuum in 1 mL of anhydrous 2 M HCl in absolute methanol in a sealed hydrolytic tube at 80 °C for 12 h. Next, the reagent was removed by evaporation, and the methyl glycosides generated during methanolysis were further hydrolyzed with 2 M TFA at 100 °C for 1.5 h. After removal of TFA by repeated evaporation under vacuum with HPLC grade distilled water, the sugars in the hydrolysate were analyzed by high-performance anion-exchange chromatography with pulsed amperometric detection (HPAEC-PAD). The HPAEC-PAD consisted of a Bioscan 817 Metrohm IC system (Metrohm, Herisau, Switzerland) including an IC pump 709, injection valve unit 812 with a 20 μL loop, and an electrochemical detector with a gold working electrode (E1 = 0.05 V, 0.48 s; E2 = 0.80 V, 0.18 s; E3 = −0.30 V, 0.36 s). A CarboPac PA1 (4 mm × 250 mm) analytical column (Dionex Corp., Sunnyvale, CA, USA) with a guard column (4 mm × 50 mm) was used. For separation of neutral monosaccharides, the eluent consisted of 19 mM NaOH containing 1 mM barium acetate applied at a flow rate of 0.5 mL/min. For separation of acidic monosaccharides (galacturonic acid and glucuronic acid), the eluent consisted of 75 mM NaOH, 150 mM sodium acetate, and 1 mM barium acetate applied at a flow rate of 1 mL/min. Data were collected and analyzed using Metrodata IC Net 2.1 software (Metrohm).

Concentration and Degree of Branching of (1,3;1,6)-β-D-Glucans. The concentration and the ratio of (1,6)-β-D-glucosyl branches of (1,3;1,6)-β-D-glucans were determined according to an enzymatic HPAEC-PAD method developed by Chang.[28] Samples (5 mg) were dissolved in 0.5 M NaOH and stirred at ambient temperature overnight. After addition of arabinose (Sigma) as an internal standard, the pH of the sample solution was adjusted to 4.5 by the addition of 1 M HCl, and the volume was filled to 5 mL with 50 mM sodium acetate buffer (pH 4.5) for use as the stock for enzymatic hydrolysis. A 1 mL sample aliquot was reacted with exo-(1,3)-β-D-glucanase (1 U; Megazyme, Wicklow, Ireland) and endo-(1,3)-β-D-glucanase (0.1 U, Megazyme) for 3 h at 40 °C, followed by boiling in water for 15 min to stop the enzymatic reaction. A 4 mL volume of ethanol (95%, v/v) was added to precipitate undigested polysaccharides. The supernatant was dried by vacuum evaporation and redissolved in distilled water. The glucose and gentiobiose released from the enzyme digestion were quantified by using HPAEC-PAD. The system conditions applied were identical to those described in identifying the sugar composition of polysaccharides above, except that isocratic elution was performed at 1 mL/min with 10 mM NaOH eluent containing 2 mM barium acetate.

The concentration and the DB of (1,3;1,6)-β-D-glucan in sample were calculated as follows:

$$\text{content of (1,3;1,6)-β-D-glucan in polysaccharide (mg/mg)} = (\text{Wt-Glc} \times 0.9 + \text{Wt-Gen} \times 0.95)/\text{Wt-Poly}$$

Wt-Glc and Wt-Gen are the calculated weights of glucose and gentiobiose in samples, respectively; 0.9 and 0.95 are factors to account for differences in molecular weight of a glucosyl monomer and gentiobiosyl (a dimer) bound in a polysaccharide, respectively, compared to the free form; and Wt-Poly is the weight of polysaccharide present in the stock solution for enzymatic hydrolysis. The weight of polysaccharide was determined by phenol−sulfuric acid.

$$\text{Wt-Glc} = \text{PA-Glc}/\text{PA-Is} \times \text{RF}_{\text{Glc}} \times \text{Wt-Is}$$

$$\text{Wt-Gen} = \text{PA-Gen}/\text{PA-Is} \times \text{RF}_{\text{Gen}} \times \text{Wt-Is}$$

PA-Glc, PA-Gen, and PA-Is denote peak areas of glucose, gentiobiose, and internal standard, respectively; RF_{Glc} and RF_{Gen} denote response factor of glucose and gentiobiose in chromatography, respectively; Wt-Is denotes the weight of internal standard present in the stock solution for enzymatic hydrolysis.

$$\text{DB (degree of branching)} = \text{Gen}/(\text{Glc} + \text{Gen})$$

Gen denotes mmol of gentiobiose = Wt-Gen/342.3, and Glc denotes mmol of glucose = Wt-Glc/180.2 (both denominators denote the formula for the weight of the compound).

Molecular Weight of (1,3)-β-D-Glucans and Their Polydispersity. Polysaccharides were dissolved in 0.5 M NaOH (2 mg/mL) overnight and then filtered through Whatman no. 5 filter paper (GE Healthcare, Florham Park, NJ, USA). Ascending gel filtration chromatography was

Table 1. Concentrations of Soluble (1,3;1,6)-β-D-Glucans and Polysaccharides and the Molecular Characteristics of (1,3;1,6)-β-D-Glucans in Submerged Cultivation Products of *Ganoderma lucidum* Mycelium[a]

				molecular characteristics of (1,3;1,6)-β-D-glucans			
code	(1,3;1,6)-β-D-glucan[b] (mg/dL)	polysaccharides (mg/dL)	(1,3;1,6)-β-D-glucan[b]/ polysaccharides (%)	degree of branching[b]	$M_n \times 10^4$ (g/mol)	$M_w \times 10^4$ (g/mol)	polydispersity (M_w/M_n)
C1	79.9 ± 3.9 a	322.6 ± 2.8a	24.8 ± 1.2 d	0.23 ± 0.01 e	47.0	69.1	1.5
C2	56.3 ± 2.4 b	235.0 ± 13.5b	24.0 ± 1.0 d	0.31 ± 0.01 cd	38.0	57.8	1.5
C3	33.0 ± 0.9 c	154.2 ± 13.5d	21.4 ± 0.6 e	0.33 ± 0.02 bc	29.2	64.9	2.2
C4	32.4 ± 0.4 c	116.2 ± 14.9 ef	27.8 ± 0.3 c	0.32 ± 0.01 c	79.1	101.8	1.3
C5	17.5 ± 0.8 d	101.3 ± 4.0 fg	17.2 ± 0.8 f	0.21 ± 0.01 e	11.0	42.1	3.8
S1	12.8 ± 0.4 e	26.4 ± 5.2i	48.4 ± 1.5 a	0.36 ± 0.01 a	22.6	41.3	1.8
S2	8.2 ± 0.5 f	24.2 ± 5.1i	33.9 ± 2.2 b	0.35 ± 0.03 ab	14.3	32.3	2.3
C6	6.7 ± 0.8 fg	117.4 ± 6.5e	5.7 ± 0.7 g	0.01 ± <0.01 g	0.2	0.8	3.9
C7	5.2 ± 0.2 g	126.5 ± 6.2e	4.1 ± 0.2 gh	0.08 ± 0.03 f	0.1	0.3	3.6
C8	2.6 ± 0.1 h	70.4 ± 8.8h	3.7 ± 0.2 h	0.29 ± 0.01 d	21.8	46.0	2.1
C9	1.9 ± 0.2 h	170.1 ± 9.9c	1.1 ± 0.1 i	0.10 ± 0.01 f	0.1	0.1	2.1
C10	1.3 ± 0.1 h	100.1 ± 5.9g	1.3 ± 0.1 i	0.08 ± 0.01 f	1.6	1.8	1.1

[a]Assays were performed in triplicate. Values are expressed as the mean ± SD. Data in the same column with different letters are significantly different ($p < 0.05$) by Duncan's test. [b]Determined by endo-, and exo-(1,3)-β-D-glucanase digestion and high-performance anion-exchange chromatography with pulsed amperometric detection (HPAEC-PAD).

performed on Toyopearl HW-65F gel (packing volume i.d. 2.6 cm × 90 cm; Tosoh, Tokyo, Japan), where 5 mL of sample was eluted with degassed eluent consisting of 100 mM NaOH and 50 mM NaCl (pH 13.0) at a flow rate of 0.5 mL/min. Fractions were collected in 4 mL volumes. The concentrations of polysaccharides and (1,3)-β-D-glucans in each fraction were determined.

The concentration of polysaccharides in each fraction was determined by using the phenol–sulfuric acid method. (1,3)-β-D-Glucan was measured by aniline blue fluorescence stain method, and the isolated (1,3;1,6)-β-D-glucans were used as a standard (5–30 μg/mL). The method described by Wood and Flucher[29] and Young and Jacobs[30] was adapted with some modifications.[28] Each 1 mL fraction aliquot was pipetted into a new tube. The pH of the solution was subsequently adjusted to 11.5 ± 0.1 by adding 2 M HCl, and the volume was filled to 2 mL by Na_2HPO_4–NaOH buffer (pH 11.5, containing 1 M NaCl). The sample aliquot was incubated with 0.2 mL of 0.1% (w/v) aniline blue (Ferak, Berlin, Germany) for 2 h at ambient temperature. The absorbance of the sample was measured on a Hitachi F4500 fluorescence spectrophotometer (Tokyo, Japan), with excitation and emission wavelengths set at 395 and 495 nm, respectively.

The molecular weight standards used for calibration were pullulans (Shodex, Standard P-82, Showa Denko, Kawasaki, Japan), with molecular weights of 5.9, 11.8, 47.3, 112, 212, 404, and 788 kDa. Additionally, blue dextran (Sigma) with an average molecular weight of 2000 kDa and glucose were used to determine the void volume and total permeation volume of the column, respectively.

TNF-α Release Activity. The murine macrophage cell line RAW 264.7 (Bioresource Collection and Research Center) was cultured in Dulbecco's modified Eagle's medium (Invitrogen, Grand Island, NY, USA) supplemented with 10% heat-inactivated fetal bovine serum (Invitrogen), high glucose (4.5 g/L), and 2 mM glutamine at 37 °C under 5% CO_2. Cells were seeded into 96-well culture plates (Nunc, Roskilde, Denmark) at a density of 1×10^4 cells/well and left to adhere for 3 h. After removal of the medium, cells were subsequently incubated in media containing each polysaccharide sample for 48 h. The concentrations of TNF-α in the cultured supernatants were assayed by DuoSet ELISA Development Systems (R&D Systems, Minneapolis, MN, USA) following the manufacturer's protocol.

Statistical Analysis. Statistical analysis was conducted by using SAS 9.3 software (SAS Institute, Cary, NC, USA). Data were determined to be significantly different ($p < 0.05$) by Duncan's test.

RESULTS AND DISCUSSION

Concentration Variation of Soluble (1,3;1,6)-β-D-Glucans. We developed an enzymatic HPAEC chromatographic method for (1,3;1,6)-β-D-glucan determination that can simultaneously measure the concentration and DB of the glucan in a *G. lucidum* fermentation broth with complicated composition. The concentration variation of soluble (1,3;1,6)-β-D-glucan in the broth was as large as the variance of the polysaccharide, a common quality index of broth (Table 1). The highest concentration (79.9 mg/dL) of soluble (1,3;1,6)-β-D-glucan was found in sample C1, which was 61 times the quantity found in sample C10 (1.3 mg/dL), although all samples were prepared by the same strain BCRC 36123. The results also showed that the mycelium of *G. lucidum* does not always generate substantial amounts of soluble (1,3;1,6)-β-D-glucans. Although (1,3)-β-D-glucans are the major class of structural polysaccharide found in the fungal cell wall and are required for normal development of fungi,[16,17,31] they are not always soluble and can be released into the broth, a common material for the food industry to produce *Ganoderma* products. In mature fungal cells, (1,3)-β-D-glucan is insoluble due to covalent linkages to chitin.[31] In response to environmental changes, such as medium composition, temperature, shaking speed, and cultivating volume, the fungal mycelia may alter its synthetic patterns to generate a more soluble component for greater water retention and cell wall flexibility. Despite a lack of data about (1,3;1,6)-β-D-glucans, many studies on *Ganoderma* spp. have indicated that small pellet size and short mycelium increased the production of extracellular *Ganoderma* polysaccharide.[32−36] In contrast to the morphology of mycelia, the amount of mycelia was not a major factor contributing to *Ganoderma* polysaccharide productivity.[32,37,38] We did not find a correlation between the concentration of (1.3;1,6)-β-D-glucans and the cultivating parameters (data not shown) in this study. This is worth further investigating in the future.

(1,3;1,6)-β-D-Glucan Percentage and Sugar Composition of Soluble Polysaccharides. To understand the relationship between yield of (1,3;1,6)-β-D-glucan and polysaccharides, the common marker for *Ganoderma* product

dx.doi.org/10.1021/jf404533b | J. Agric. Food Chem. 2014, 62, 634−641

Table 2. Sugar Composition of Soluble Polysaccharides from Submerged Cultivation Products of *Ganoderma lucidum* Mycelium[a]

	sugar composition (molar %)							
code	arabinose	fucose	galactose	glucose	mannose	rhamnose	xylose	galacturonic acid
C1	6.2 ± 0.2	6.1 ± 0.1	**25.4** ± 0.1	**25.1** ± 0.7	5.6 ± 0.3	3.2 ± 0.2	**10.5** ± 0.3	**17.1** ± 1.1
C2	5.1 ± 0.3	7.5 ± 0.3	**22.0** ± 0.3	**23.3** ± 0.2	5.7 ± 0.1	3.0 ± 0.1	**12.1** ± 0.3	**20.3** ± 1.2
C3	3.9 ± 0.5	8.9 ± 0.8	**15.4** ± 1.1	**22.1** ± 0.3	3.4 ± 0.2	5.0 ± 0.3	**13.5** ± 0.6	**27.2** ± 2.4
C4	3.9 ± 0.4	7.2 ± 0.6	**19.6** ± 0.3	**33.2** ± 1.4	4.9 ± 0.3	3.6 ± 0.7	8.4 ± 1.8	**18.6** ± 1.7
C5	7.6 ± 0.6	5.4 ± 0.3	**26.1** ± 2.0	**19.2** ± 0.2	4.7 ± 0.8	5.8 ± 0.5	7.9 ± 1.2	**22.3** ± 1.0
S1	trace		9.6 ± 0.2	**81.0** ± 0.1	7.1 ± 0.1	ND	2.4 ± 0.1	ND
S2	trace		6.2 ± 0.1	**84.9** ± 0.6	5.3 ± 0.1	ND	2.4 ± 0.1	ND
C6	2.9 ± 0.1	7.7 ± 0.2	**23.4** ± 0.2	**19.7** ± 0.1	8.2 ± 0.1	3.7 ± 0.1	**12.2** ± 0.1	**22.2** ± 0.5
C7	3.0 ± 1.1	**11.5** ± 0.1	**22.4** ± 1.4	6.2 ± 0.2	4.0 ± 0.4	4.3 ± 0.3	**15.8** ± 2.6	**31.8** ± 1.4
C8	8.5 ± 0.1	8.1 ± 0.2	**21.8** ± 0.3	**12.2** ± 0.2	2.6 ± 0.1	9.1 ± 0.2	12.8 ± 0.1	**23.9** ± 0.3
C9	9.1 ± 0.7	3.1 ± 0.4	**49.2** ± 0.6	5.3 ± 0.1	1.8 ± 0.5	7.5 ± 0.4	4.9 ± 1.3	**18.1** ± 0.8
C10	**19.5** ± 0.1	5.6 ± 0.3	**21.0** ± 0.1	**11.2** ± 0.3	1.5 ± 0.1	7.9 ± 0.5	10.4 ± 0.1	**22.3** ± 0.2

[a]The tested polysaccharide samples did not contain significant amounts of glucuronic acid. ND, not determined; trace, ratio was <1%.

quality, we analyzed the concentration of soluble polysaccharides and calculated its (1,3;1,6)-β-D-glucan percentage. The soluble polysaccharide concentration of samples from the composite (C) medium group ranged between 70.4 and 322.6 mg/dL with 4.6 times difference. By comparison, the reference groups S1 and S2 possessed far lower polysaccharide contents (26.4 and 24.2 mg/dL, respectively; Table 1) but much higher (1,3;1,6)-β-D-glucan percentage, revealing 48.4 and 33.9%, respectively, than that from samples fermented in the C medium group. The results demonstrate that samples with high polysaccharide concentration did not represent a high quantity of (1,3;1,6)-β-D-glucan. The lack of association between the yield of polysaccharide and (1,3;1,6)-β-D-glucan might come from the fact that the composite medium is also a source of soluble polysaccharide in *G. lucidum* mycelium products.

To confirm the assumption, we further analyzed the sugar composition profile of the soluble polysaccharide samples (Table 2). The results revealed that the glucose content of soluble polysaccharides of S1 and S2 reference groups accounted for 81.0 and 84.9%, respectively, with smaller amounts of galactose, mannose, and xylose and trace amounts of arabinose and fucose. Similar findings were also reported by Sone et al.[7] and Wagner et al.,[34] as glucose was universally observed as the dominant species in *Ganoderma* extracellular polysaccharide. For an alternate 10 samples from the C group, the molar ratio of glucose was in the range of 5.3 and 33.2%, far less than the corresponding ratios in S1 and S2. The ratios of galactose and galacturonic acid were substantially higher in the C group than in the reference group. This sugar composition ratio may be considered as an index of the presence of hemicellulose and pectic polysaccharides from higher plants. *Ganoderma* spp. are white-rot fungi and express several wood-degrading enzymes, for example, cellulases, lignin peroxidases, proteinase, and xylanase,[39] which hydrolyze composite media for mycelium growth. The partially degraded polysaccharides of leguminous plants used in the medium must be dissolved into the fermentation broth. A trend in the use of composite media, such as the use of food industrial waste material in *G. lucidum* mycelium culture, is reported in the literature;[40,41] therefore, adulteration of polysaccharide from the cultivating medium is inevitable. Therefore, the content of polysaccharide, a common index for mycelium quality, may not solely represent mycelium growth and the production of fungal polysaccharides.

Additionally, we also observed the content of glucan was not equal to the content of (1,3;1,6)-β-D-glucans in *Ganoderma* polysaccharides. For S1 and S2, the glucose contents of soluble polysaccharides (81.0 and 84.9%, respectively; Table 2) were higher than the contents of (1,3;1,6)-β-D-glucans (Table 1, 48.4 and 33.9%, respectively). This result indicated that *G. lucidum* generates different types of glucans aside from those with a β-(1,3)-linked backbone such as (1,3)-α-D-glucans,[42] β-D-galactoglucan with (1,4)-linked α-D-glucopyranosyl residues, highly branched mannoglucan with (1,3)-, (1,4)-, (1,6)-linked β-D-glucopyranosyl residues,[43] and (1,4)-α-D-glucans.[44] Therefore, specific methods for (1,3;1,6)-β-D-glucan determination are demanded for quality control, such as the one presented in this study or the one described by Danielson et al.[45]

Molecular Characteristics of Soluble (1,3;1,6)-β-D-Glucans. It has been reported that the molecular characteristics of soluble (1,3;1,6)-β-D-glucans are important to its biological function. We thus characterized several molecular characteristics. As shown in Table 1, DBs of soluble (1,3;1,6)-β-D-glucans in the majority of samples were in the range of 0.21−0.36, indicating that every 3−5 β-D-glucosyl residues in the (1,3)-linked backbone have a (1,6)-linked β-D-glucopyranosyl branch. The result was in accordance with the results reported by Sone et al.[7] showing that the DB of (1,3;1,6)-β-D-glucan from submerged fermentation of *G. lucidum* was approximately 0.31 (5/16), whereas that obtained from fruit body cold/hot water extraction had a DB in the range of 0.32−0.33. DBs of our samples also existed in the most bioactive DB range of (1,3;1,6)-β-D-glucans proposed by Bohn and BeMiller (i.e., 0.2−0.33).[10] Lentinan, a (1,3;1,6)-β-D-glucan with a DB of 0.2−0.3 from shiitake mushroom (*Lentinus edodes*), has been successfully administered as an antitumor adjuvant.[46]

The molecular weight of (1,3;1,6)-β-D-glucans reflect their solubility, stability in water, and rheological properties, concomitant with biological activity, although the structure−bioactivity relationship remains inconclusive.[12,47] The molecular mass of soluble (1,3;1,6)-β-D-glucans in samples with substantial quantities of β-D-glucan concentrated in the large molecular size range with M_n (number-average molecular weight) and M_w (weight-average molecular weight) of (11.0−

dx.doi.org/10.1021/jf404533b | J. Agric. Food Chem. 2014, 62, 634−641

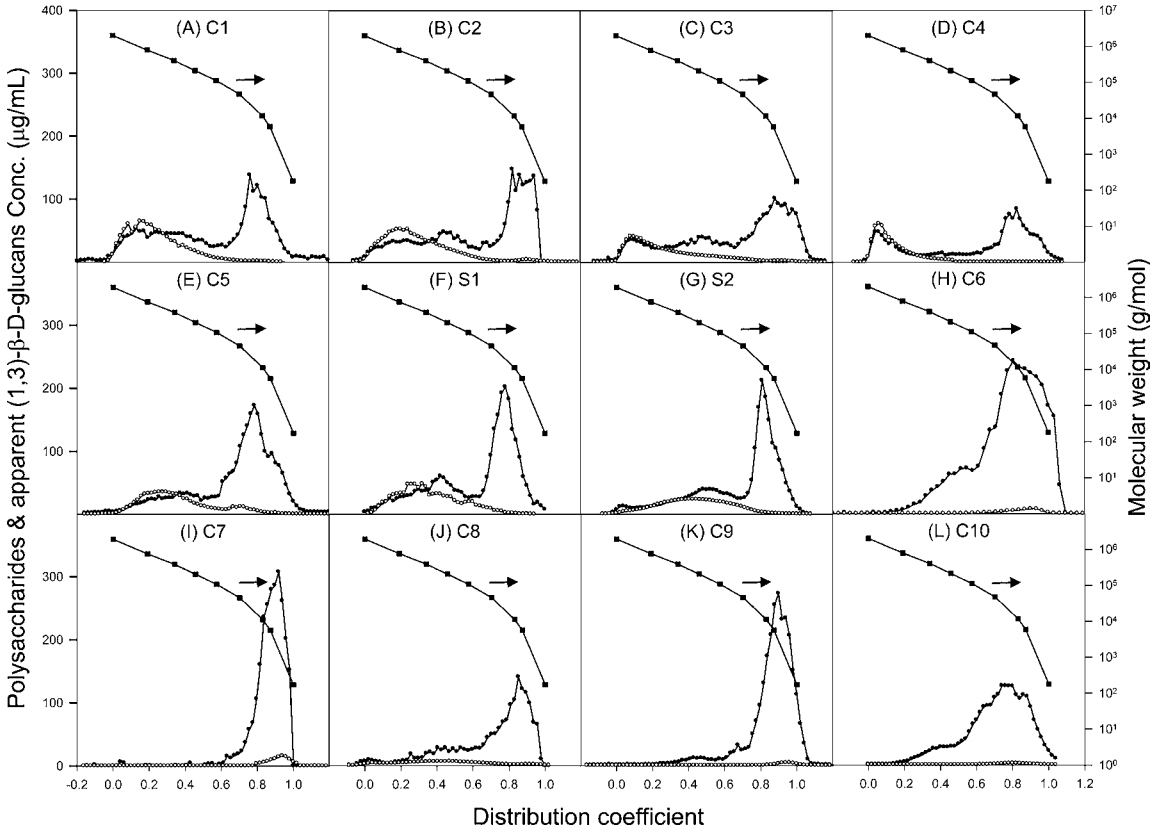

Figure 1. Chromatograms of molecular weight distribution of soluble polysaccharides (●) and (1,3)-*β*-D-glucans (○) from submerged cultivation products of *Ganoderma lucidum* mycelium. Pullulan standards and glucose were used to construct a standard curve (■) for molecular weight determination.

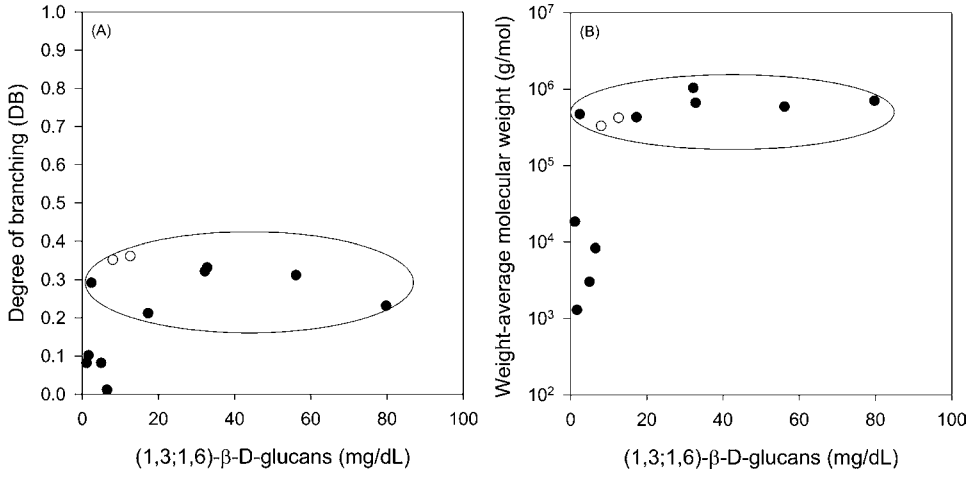

Figure 2. Scatter plot of the concentration versus degree of branching (A) and concentration versus molecular weight (B) of soluble (1,3;1,6)-*β*-D-glucans in submerged cultivation products of *Ganoderma lucidum* mycelium: (○) samples cultivated in synthetic chemically defined medium, including S1 and S2; (●) samples cultivated in composite medium containing polysaccharide matrix, including C1−C10.

79.1) × 10^4 and (32.3−101.8) × 10^4 g/mol, respectively (Table 1; Figure 1). The polydispersity (M_w/M_n), an index of the molecular weight distribution of polymers, of soluble (1,3;1,6)-*β*-D-glucans was in the range of 1.1−3.9. The molecular mass was consistent with the results from our previous study (2.08 × 10^6 g/mol)[9] as well as the previously reported value from fruiting bodies (6.3 × 10^4 g/mol).[43] Interesting, we also observed the molecular sizes of (1,3;1,6)-*β*-D-glucans were higher than the other types of polysaccharides in samples (Figure 1A−G), which could be considered useful information for isolating (1,3;1,6)-*β*-D-glucans from other polysaccharides in samples.

Subsequently, we plotted the relationship between concentration versus DB and molecular weight of (1,3;1,6)-*β*-D-glucans by using the collected data set. As shown in Figure 2, instead of spreading, both the DB and molecular weight distributions were consistently and similarly preserved for those samples with substantial quantities of (1,3;1,6)-*β*-D-glucan. This observation suggested that although the production of (1,3;1,6)-*β*-D-glucans could be altered by cultivation, the

dx.doi.org/10.1021/jf404533b | J. Agric. Food Chem. 2014, 62, 634−641

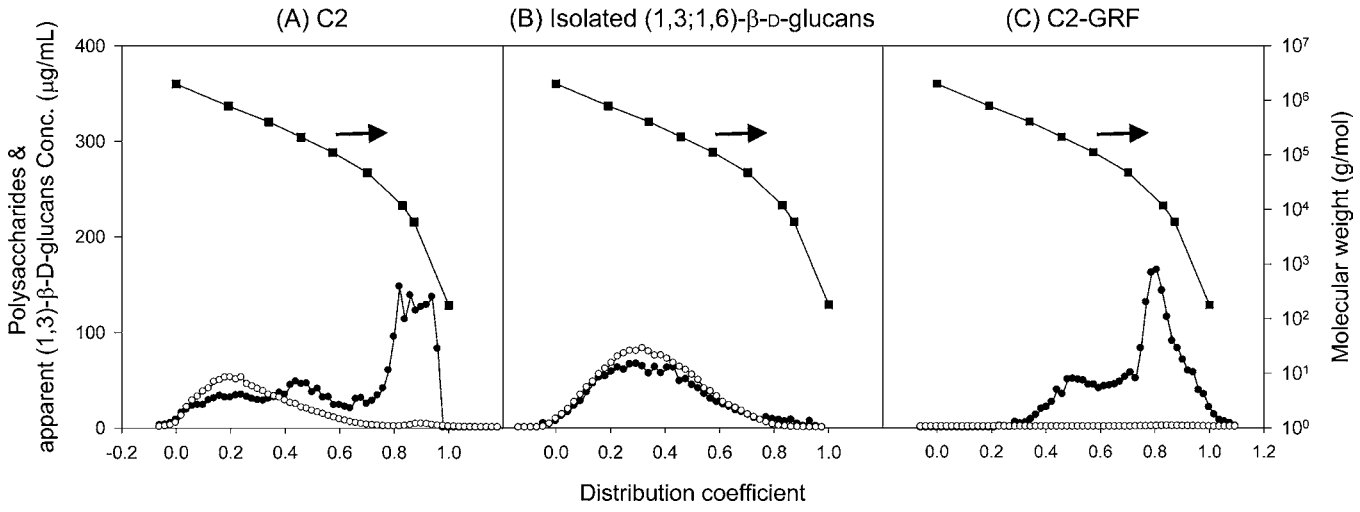

Figure 3. Chromatograms of molecular weight distribution of soluble polysaccharides (●) and (1,3)-β-D-glucans (○) from C2, a submerged cultivation product of *Ganoderma lucidum* mycelium (A), and its fraction after fractional precipitation with ethanol, isolated (1,3;1,6)-β-D-glucans (B) and C2-GRF [glucan-removed fraction (C)]. Pullulan standards and glucose were used to construct a standard curve (■) for molecular weight determination.

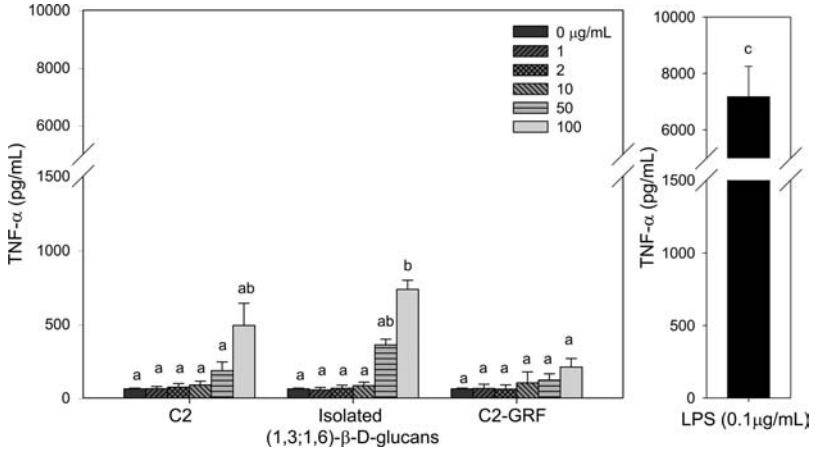

Figure 4. TNF-α releasing of RAW 264.7 treated with soluble polysaccharides from cultivation product of *Ganoderma lucidum* mycelium sample C2 and its isolated (1,3; 1,6)-β-D-glucans and glucan-removed fraction (C2-GRF). The error bars in the figure indicate standard deviation from three replicates. Data with different letters are determined to be significantly different ($p < 0.05$) by Duncan's test.

molecular structures of (1,3;1,6)-β-D-glucans displayed similar profiles. Therefore, we suggested this may be due to physiological homeostasis, which might be controlled by some metabolic pathways of *G. lucidum*. By contrast, (1,3)-β-D-glucans with lower DB (~0.1) and low molecular mass ($<10^4$ g/mol) were present in samples C6, C7, C9, and C10, which contained little (1,3;1,6)-β-D-glucan. It is known that linear (1,3)-β-D-glucans without branches are less soluble in water than those with branches. Sone et al. generated low-DB (0.06 and 0.04) glucans through alkali extraction from fruiting bodies of *G. lucidum*.[7] We surmise that most linear (1,3)-β-glucans are tightly attached to additional cell wall components and that autoclaving used in this study allowed for the collection of only a small portion of linear (1,3)-β-D-glucan. The concurrence of low molecular weight distribution and low DB may support the belief that glucans in samples C6, C7, C9, and C10 were fragments of the fungal cell wall caused by the autoclaving process.

Isolation and Immunoactivity Verification of (1,3;1,6)-β-D-Glucans. To further confirm the bioactivity and establish a method to purify (1,3;1,6)-β-D-glucans, fractional precipitation with ethanol was used whereby high molecular weight polysaccharides are precipitated by low concentrations of ethanol. Our results indicated that (1,3;1,6)-β-D-glucans could be isolated from a C2 sample by using 35% (v/v, final concentration) ethanol repeating precipitation. The purity of isolated (1,3;1,6)-β-D-glucans was 99.42 ± 4.82%, as determined by the enzymatic HPAEC method. The remaining polysaccharides in the 35% ethanol solution were collected by adding more ethanol to allow the concentration of ethanol to reach 76%. The percentage of (1,3;1,6)-β-D-glucans in the C2-GRF (glucan-removed fraction) was <1% on a carbohydrate basis. The high efficiency of (1,3;1,6)-β-D-glucan separation was a result of the high aggregation tendency of (1,3)-β-D-glucans,[47] although (1,3;1,6)-β-D-glucans and C2-GRF in the original polysaccharide solution overlapped with one another between the distribution coefficient range of 0.3−0.7 (Figure 3). A similar operation had been successfully performed for the isolation of (1,3;1,6)-β-D-glucans from fruiting bodies of *G. lucidum* in our previous study.[9]

On the basis of previous studies of the immunomodulating activities of (1,3;1,6)-β-D-glucans, the murine macrophage

dx.doi.org/10.1021/jf404533b | J. Agric. Food Chem. 2014, 62, 634−641

RAW 264.7 cell line was selected as a model for testing the TNF-α-stimulating activity of the polysaccharides. The original soluble polysaccharide of C2 and its fractions (1,3;1,6)-β-D-glucans and C2-GRF all displayed a trend in stimulating TNF-α release in RAW 264.7 cells (Figure 4). Isolated (1,3;1,6)-β-D-glucans displayed substantial stimulating activity in a dose-dependent manner at concentrations of 10, 50, and 100 μg/mL. The TNF-α stimulating activity was markedly less than that induced by lipopolysaccharide (LPS), suggesting a potentially beneficial effect for cytokine induction on innate immunity. Stimulating activities of (1,3;1,6)-β-D-glucans from *G. lucidum* and other distinct biological sources that trigger cytokine release from macrophage have been reported in the literature.[4,48−50] Therefore, (1,3;1,6)-β-D-glucans, rather than total polysaccharides, may be a more appropriate biological activity marker for the cultivation products of *G. lucidum* mycelium.

In conclusion, we reported quantitative data of concentration, degree of branching, and molecular weight distribution of soluble (1,3;1,6)-β-D-glucans in cultivation products of *G. lucidum* mycelium. (1,3;1,6)-β-D-Glucan was proposed to function as a biomarker because it was the most abundant polysaccharide in the stimulation of macrophage RAW 264.7 cell to release TNF-α in *G. lucidum* mycelium products. Indirect evidence was also provided demonstrating that polysaccharides from composite medium for submerged fermentation were included in the final mycelium products. The polysaccharide content was not well represented during the production of fungal polysaccharides. The large molecular size and degree of branching of the (1,3;1,6)-β-D-glucans were reserved for the mycelium products examined, as long as substantial quantities of the glucan were being produced. The cultivating factors that affected the production of soluble (1,3;1,6)-β-D-glucans should be further investigated. An understanding of the mechanisms of the fungal cell wall synthesis and related enzyme activities with the characteristics of soluble (1,3;1,6)-β-D-glucans may lead to improved design of optimum cultivation conditions necessary for efficient production.

AUTHOR INFORMATION

Corresponding Author

*E-mail: tjlu@ntu.edu.tw. Phone: 886-2-3366-4131. Mailing address: Institute of Food Science and Technology, National Taiwan University, No. 1, Sec. 4, Roosevelt Road, Taipei, Taiwan 10617, ROC. Fax: 886-2-2362-0849.

Funding

This study was supported by a grant from the National Science Council, Taiwan, Republic of China.

Notes

The authors declare no competing financial interest.

REFERENCES

(1) Elisashvili, V. Submerged cultivation of medicinal mushrooms: bioprocesses and products (review). *Int. J. Med. Mushrooms* **2012**, *14*, 211−239.

(2) Zhong, J. J.; Tang, Y. J. Submerged cultivation of medicinal mushrooms for production of valuable bioactive metabolites. In *Biomanufacturing*; Zhong, J. J., Ed.; Springer-Verlag: Berlin, Germany, 2004; Vol. 87, pp 25−59.

(3) Wagner, R.; Mitchell, D. A.; Sassaki, G. L.; Amazonas, M.; Berovic, M. Current techniques for the cultivation of *Ganoderma lucidum* for the production of biomass, ganoderic acid and polysaccharides. *Food Technol. Biotechnol.* **2003**, *41*, 371−382.

(4) Boh, B.; Berovic, M.; Zhang, J.; Lin, Z. B. *Ganoderma lucidum* and its pharmaceutically active compounds. In *Biotechnology Annual Review*; ElGewely, M. R., Ed.; Elsevier: Amsterdam, The Netherlands, 2007; Vol. 13, pp 265−301.

(5) Tang, Y. J.; Zhang, W.; Liu, R. S.; Zhu, L. W.; Zhong, J. J. Scale-up study on the fed-batch fermentation of *Ganoderma lucidum* for the hyperproduction of ganoderic acid and *Ganoderma* polysaccharides. *Process Biochem.* **2011**, *46*, 404−408.

(6) Papinutti, L. Effects of nutrients, pH and water potential on exopolysaccharides production by a fungal strain belonging to *Ganoderma lucidum* complex. *Bioresour. Technol.* **2010**, *101*, 1941−1946.

(7) Sone, Y.; Okuda, R.; Wada, N.; Kishida, E.; Misaki, A. Structures and antitumor activities of the polysaccharides isolated from fruiting body and the growing culture of mycelium of *Ganoderma lucidum*. *Agric. Biol. Chem.* **1985**, *49*, 2641−2653.

(8) Pillai, T. G.; Devi, P. U. Mushroom beta glucan: potential candidate for post irradiation protection. *Mutat. Res.−Genet. Toxicol. Environ. Mutagen.* **2013**, *751*, 109−115.

(9) Chang, Y. W.; Lu, T. J. Molecular characterization of polysaccharides in hot-water extracts of *Ganoderma lucidum* fruiting bodies. *J. Food Drug Anal.* **2004**, *12*, 59−67.

(10) Bohn, J. A.; BeMiller, J. N. (1→3)-β-D-glucans as biological response modifiers: a review of structure-functional activity relationships. *Carbohydr. Polym.* **1995**, *28*, 3−14.

(11) Wasser, S. P. Medicinal mushrooms as a source of antitumor and immunomodulating polysaccharides. *Appl. Microbiol. Biotechnol.* **2002**, *60*, 258−274.

(12) Chen, J. Z.; Seviour, R. Medicinal importance of fungal β-(1→3), (1→6)-glucans. *Mycol. Res.* **2007**, *111*, 635−652.

(13) Mizuno, T. The extraction and development of antitumor-active polysaccharides from medicinal mushrooms in Japan (review). *Int. J. Med. Mushrooms* **1999**, *1*, 9−29.

(14) Ooi, V. E. C.; Liu, F. Immunomodulation and anti-cancer activity of polysaccharide-protein complexes. *Curr. Med. Chem.* **2000**, *7*, 715−729.

(15) Nakano, H.; Namatame, K.; Nemoto, H.; Motohashi, H.; Nishiyama, K.; Kumada, K.; Kanagawa Lentinan Res, G. A multi-institutional prospective study of lentinan in advanced gastric cancer patients with unresectable and recurrent diseases: effect on prolongation of survival and improvement of quality of life. *Hepato-Gastroenterology* **1999**, *46*, 2662−2668.

(16) Bowman, S. M.; Free, S. J. The structure and synthesis of the fungal cell wall. *Bioessays* **2006**, *28*, 799−808.

(17) Osherov, N.; Yarden, O. The cell wall of filamentous fungi. In *Cellular and Molecular Biology of Filamentous Fungi*; Borkovich, K. A., Ebbole, D. J., Eds.; ASM Press: Washington, DC, 2010; pp 224−237.

(18) Brown, G. D.; Gordon, S. Fungal β-glucans and mammalian immunity. *Immunity* **2003**, *19*, 311−315.

(19) Brown, G. D.; Gordon, S. Immune recognition of fungal β-glucans. *Cell. Microbiol.* **2005**, *7*, 471−479.

(20) Janeway, C. A. The immune-system evolved to discriminate infectious nonself from noninfectious self. *Immunol. Today* **1992**, *13*, 11−16.

(21) Adams, E. L.; Rice, P. J.; Graves, B.; Ensley, H. E.; Yu, H.; Brown, G. D.; Gordon, S.; Monteiro, M. A.; Papp-Szabo, E.; Lowman, D. W.; Power, T. D.; Wempe, M. F.; Williams, D. L. Differential high-affinity interaction of Dectin-1 with natural or synthetic glucans is dependent upon primary structure and is influenced by polymer chain length and side-chain branching. *J. Pharmacol. Exp. Ther.* **2008**, *325*, 115−123.

(22) Goodridge, H. S.; Reyes, C. N.; Becker, C. A.; Katsumoto, T. R.; Ma, J.; Wolf, A. J.; Bose, N.; Chan, A. S. H.; Magee, A. S.; Danielson, M. E.; Weiss, A.; Vasilakos, J. P.; Underhill, D. M. Activation of the innate immune receptor Dectin-1 upon formation of a 'phagocytic synapse'. *Nature* **2011**, *472*, 471−475.

(23) Mueller, A.; Raptis, J.; Rice, P. J.; Kalbfleisch, J. H.; Stout, R. D.; Ensley, H. E.; Browder, W.; Williams, D. L. The influence of glucan polymer structure and solution conformation on binding to (1→3)-β-

D-glucan receptors in a human monocyte-like cell line. *Glycobiology* **2000**, *10*, 339−346.
(24) Miyazaki, T.; Oikawa, N.; Yadomae, T.; Yamada, H.; Yamada, Y.; Hsu, H. Y.; Ito, H. Relationship between the chemical-structure and anti-tumor activity of glucans prepared from *Grifora-umbellata*. *Carbohydr. Res.* **1979**, *69*, 165−170.
(25) Bae, I. Y.; Kim, H. W.; Yoo, H. J.; Kim, E. S.; Lee, S.; Park, D. Y.; Lee, H. G. Correlation of branching structure of mushroom β-glucan with its physiological activities. *Food Res. Int.* **2013**, *51*, 195−200.
(26) Lowe, E.; Rice, P.; Ha, T. Z.; Li, C. F.; Kelley, J.; Ensley, H.; Lopez-Perez, J.; Kalbfleisch, J.; Lowman, D.; Margl, P.; Browder, W.; Williams, D. A (1→3)-β-D-linked heptasaccharide is the unit ligand for glucan pattern recognition receptors on human monocytes. *Microb. Infect.* **2001**, *3*, 789−797.
(27) Dubois, M.; Gilles, K. A.; Hamilton, J. K.; Rebers, P. A.; Smith, F. Colorimetric method for determination of sugars and related substances. *Anal. Chem.* **1956**, *28*, 350−356.
(28) Chang, Y. W. Characteristics and determination of (1→6) branched (1→3)-β-D-glucans in *Ganoderma lucidum*. Doctoral Dissertation, National Taiwan University, 2003.
(29) Wood, P. J.; Fulcher, R. G. Specific interaction of aniline blue with (1→3)-β-D-glucan. *Carbohydr. Polym.* **1984**, *4*, 49−72.
(30) Young, S. H.; Jacobs, R. R. Sodium hydroxide-induced conformational change in schizophyllan detected by the fluorescence dye, aniline blue. *Carbohydr. Res.* **1998**, *310*, 91−99.
(31) Wessels, J. G. H. Wall growth, protein excretion and morphogenesis in fungi. *New Phytol.* **1993**, *123*, 397−413.
(32) Tang, Y. J.; Zhong, J. J. Fed-batch fermentation of *Ganoderma lucidum* for hyperproduction of polysaccharide and ganoderic acid. *Enzyme Microb. Technol.* **2002**, *31*, 20−28.
(33) Fang, Q. H.; Tang, Y. J.; Zhong, J. J. Significance of inoculation density control in production of polysaccharide and ganoderic acid by submerged culture of *Ganoderma lucidum*. *Process Biochem.* **2002**, *37*, 1375−1379.
(34) Wagner, R.; Mitchell, D. A.; Sassaki, G. L.; Amazonas, M. Links between morphology and physiology of *Ganoderma lucidum* in submerged culture for the production of exopolysaccharide. *J. Biotechnol.* **2004**, *114*, 153−164.
(35) Kim, H. M.; Park, M. K.; Yun, J. W. Culture pH affects exopolysaccharide production in submerged mycelial culture of *Ganoderma lucidum*. *Appl. Biochem. Biotechnol.* **2006**, *134*, 249−262.
(36) Ding, Z.; Wang, Q.; Peng, L.; Zhang, L.; Gu, Z.; Shi, G.; Zhang, K. Relationship between mycelium morphology and extracellular polysaccharide production of medicinal mushroom *Ganoderma lucidum* in submerged culture. *J. Med. Plants Res.* **2012**, *6*, 2868−2874.
(37) Fang, Q. H.; Zhong, J. J. Effect of initial pH on production of ganoderic acid and polysaccharide by submerged fermentation of *Ganoderma lucidum*. *Process Biochem.* **2002**, *37*, 769−774.
(38) Hsieh, C.; Tseng, M. H.; Liu, C. J. Production of polysaccharides from *Ganoderma lucidum* (CCRC 36041) under limitations of nutrients. *Enzyme Microb. Technol.* **2006**, *38*, 109−117.
(39) Rai, R. D.; Kamal, S.; Singh, S. K. Effect of wheat bran supplementation to the sawdust substrate on mycelial growth rate and production of extracellular degradative enzymes by the medicinal Reishi mushroom *Ganoderma lucidum* (W.Curt.:Fr.) Lloyd (Aphyllophoromycetideae). *Int. J. Med. Mushrooms* **2004**, *6*, 375−382.
(40) Yang, H. L.; Zhang, L. Changes in some components of soymilk during fermentation with the basidiomycete *Ganoderma lucidum*. *Food Chem.* **2009**, *112*, 1−5.
(41) Fazenda, M. L.; Seviour, R.; McNeil, B.; Harvey, L. M. Submerged culture fermentation of "higher fungi": the macrofungi. In *Advances Applied Microbiology*; Laskin, A. L., Sariaslani, S., Eds.; Elsevier Academic Press: San Diego, CA, USA, 2008; Vol. 63, pp 33−103.
(42) Chen, J. H.; Zhang, L. N.; Nakamura, Y.; Norisuye, T. Viscosity behavior and chain conformation of a (1→3)-α-glucan from *Ganoderma lucidum*. *Polym. Bull.* **1998**, *41*, 471−478.
(43) Bao, X. F.; Wang, X. S.; Dong, Q.; Fang, J. N.; Li, X. Y. Structural features of immunologically active polysaccharides from *Ganoderma lucidum*. *Phytochemistry* **2002**, *59*, 175−181.
(44) Peng, Y. F.; Zhang, L. N.; Zeng, F. B.; Kennedy, J. F. Structure and antitumor activities of the water-soluble polysaccharides from *Ganoderma tsugae* mycelium. *Carbohydr. Polym.* **2005**, *59*, 385−392.
(45) Danielson, M. E.; Dauth, R.; Elmasry, N. A.; Langeslay, R. R.; Magee, A. S.; Will, P. M. Enzymatic method to measure β-1,3-β-1,6-glucan content in extracts and formulated products (GEM assay). *J. Agric. Food Chem.* **2010**, *58*, 10305−10308.
(46) Sasaki, T.; Takasuka, N. Further study of the structure of lentinan, an anti-tumor polysaccharide from *Lentinus edodes*. *Carbohydr. Res.* **1976**, *47*, 99−104.
(47) Sletmoen, M.; Stokke, B. T. Review: Higher order structure of (1,3)-β-D-glucans and its influence on their biological activities and complexation abilities. *Biopolymers* **2008**, *89*, 310−321.
(48) Mizuno, M.; Minato, K.; Kawakami, S.; Tatsuoka, S.; Denpo, Y.; Tsuchida, H. Contents of anti-tumor polysaccharides in certain mushrooms and their immunomodulating activities. *Food Sci. Technol. Res.* **2001**, *7*, 31−34.
(49) Schepetkin, I. A.; Quinn, M. T. Botanical polysaccharides: macrophage immunomodulation and therapeutic potential. *Int. Immunopharmacol.* **2006**, *6*, 317−333.
(50) Godfrey, C.; Wing, C.; Daniel, S. The effects of β-glucan on human immune and cancer cells. *J. Hematol. Oncol.* **2009**, *2*, 25.

JOURNAL OF AGRICULTURAL AND FOOD CHEMISTRY

Article

pubs.acs.org/JAFC

Beneficial Effects of Camellia Oil (*Camellia oleifera* Abel.) on Ketoprofen-Induced Gastrointestinal Mucosal Damage through Upregulation of HO-1 and VEGF

Yu-Ting Cheng,[†] Shu-Li Wu,[†] Cheng-Ying Ho,[†] Shang-Ming Huang,[†] Chun-Lung Cheng,[§] and Gow-Chin Yen*[,†,‡]

[†]Department of Food Science and Biotechnology, National Chung Hsing University, 250 Kuokuang Road, Taichung 402, Taiwan

[‡]Agricultural Biotechnology Center, National Chung Hsing University, 250 Kuokuang Road, Taichung 40227, Taiwan

[§]Food Technology and Precessing Section, Animal Industry Department, Council of Agriculture, Executive Yuan, Taipei 10014, Taiwan

ABSTRACT: Nonsteroidal anti-inflammatory drugs, such as ketoprofen, are generally used to treat pain and inflammation and as pyretic agents in clinical medicine. However, the usage of these drugs may lead to oxidative injury to the gastrointestinal mucosa. Camellia oil (*Camellia oleifera* Abel.) is commonly used in Taiwan and China as cooking oil. Traditional remedies containing this oil exert beneficial health effects on the bowel, stomach, liver, and lungs. However, the effects of camellia oil on ketoprofen-induced oxidative gastrointestinal mucosal lesions remain unknown. The objective of this study was to evaluate the effect of camellia oil on ketoprofen-induced acute gastrointestinal ulcers. The results showed that treatment of Int-407 cells with camellia oil (50−75 μg/mL) not only increased the levels of heme oxygenase-1 (HO-1), glutathione peroxidase (GPx), and superoxide dismutase (SOD) mRNA expression but also increased vascular endothelial growth factor (VEGF) and prostaglandin E_2 (PGE_2) protein secretion, which served as a mucosal barrier against gastrointestinal oxidative injury. Moreover, Sprague−Dawley (SD) rats treated with camellia oil (2 mL/kg/day) prior to the administration of ketoprofen (50 mg/kg/day) successfully inhibited COX-2 protein expression, inhibited the production of interleukin-6 (IL-6) and nitrite oxide (NO), reversed the impairment of the antioxidant system, and decreased oxidative damage in the gastrointestinal mucosa. More importantly, pretreatment of SD rats with camellia oil strongly inhibited gastrointestinal mucosal injury induced by ketoprofen, which was proved by the histopathological staining of gastrointestinal tissues. Our data suggest that camellia oil exerts potent antiulcer effects against oxidative damage in the stomach and intestine induced by ketoprofen.

KEYWORDS: *gastrointestinal ulcer, ketoprofen, camellia oil, antioxidant enzyme, VEGF, HO-1*

1. INTRODUCTION

Nonsteroidal anti-inflammatory drugs (NSAIDs), such as ketoprofen and indomethacin, are generally used to alleviate swelling and pain of rheumatoid arthritis and other inflammatory diseases in clinical medicine. Despite their benefits as anti-inflammatory agents, these drugs may cause peptic ulcers.[1,2] Currently, peptic ulcers caused by mucosal damage are a common digestive disease in the United States and it affects approximately 500000 individuals per year.[3] The major causes of peptic ulcers include gastric acid, pepsin, bile salts, consumption of alcohol and tobacco, *Helicobacter pylori* infection, and NSAIDs. Musumba et al.[4] indicated that NSAID users have a higher risk of peptic ulcers than those with *Helicobacter pylori* infection. Thus, it is imperative to search for novel compounds that may help to prevent ulceration of the gastrointestinal tract.

Digestive diseases, including peptic ulcers, are associated with mucosal lipid peroxidation and oxidative damage.[5] Proton pump inhibitors (PPIs), such as lansoprazole, are usually used to cure gastric and duodenal ulcers.[6,7] Some reports have indicated that lansoprazole can also reverse the effects of diclofenac, indomethacin, ketoprofen, and piroxicam on the mucosal content of lipid peroxidation products (malondialdehyde, MDA), glutathione (GSH), and myeloperoxidase (MPO).[6−8] Therefore, the up-regulated activity of antioxidant enzymes may play an important role against oxidative stress in gastrointestinal mucosa.[9,10] Recent evidence indicates that heme oxygenase-1 (HO-1) breaks down heme to biliverdin and carbon monoxide, which has antioxidative effects in addition to mitigating inflammation, controlling cell growth, and eliminating cell death.[11] Guo et al.[12] suggested that the upregulation of HO-1 expression may reduce inflammation and tissue injury caused by reactive oxygen species (ROS) in the gastrointestinal tract. We recently found that catechin effectively inhibits ketoprofen-induced oxidative damage by upregulating HO-1 in Int-407 cells, which might play a key role in the prevention of NSAIDs-induced gastrointestinal injury.[13] These results suggest that HO-1 expression induced by pharmacological modulators may be a novel means of increasing gastrointestinal protection.

Ketoprofen is one of the most common NSAIDs. Some reports have indicated that photodegradation products of ketoprofen by sunlight or UV-irradiated are associated with oxidative stress-induced peptic ulcer.[2,14] de la Lastra et al.[14] reported that the gastrointestinal toxicity of ketoprofen in rats

Received: October 15, 2013
Revised: December 29, 2013
Accepted: December 30, 2013
Published: December 30, 2013

ACS Publications © 2013 American Chemical Society

was due to stimulation of cyclooxygenase-2 (COX-2) enzyme production and nitric oxide (NO) synthase in gastric mucosal lesions. Liu et al.[2] indicated that pro-inflammatory mediators, such as NO and interleukin-6 (IL-6), were generated by upregulation of COX-2 expression following ketoprofen treatment in Sprague−Dawley (SD) rats. Therefore, reduction of excess NO and IL-6 production as well as inhibition of COX-2 enzyme expression may be associated with the prevention and treatment of ketoprofen-induced inflammatory disease in the gastrointestinal mucosa.

Camellia oil (obtained from tea seed, *Camellia oleifera* Abel.) is generally used as cooking oil in Taiwan and China and usually consists of an abundance of unsaturated fatty acids, vitamins, and various antioxidant factors. The naturally occurring active compounds in tea seeds are different from those in other types of oil seeds.[15,16] Camellia oil is also traditionally used as a remedy for bowel, stomach, and burn injuries in China. Chen et al.[17] indicated that the saponin in tea seed could lower the triglyceride, cholesterol, and low density-lipoprotein levels in the blood of rats. Our previous study indicated that administration of camellia oil strongly prevented the liver injuries induced by carbon tetrachloride (CCl_4).[18] However, the role of camellia oil on acute gastrointestinal ulcers induced by ketoprofen remains unknown. The objective of this study was to evaluate the effects of camellia oil on the activities of antioxidant enzymes and on ketoprofen-induced acute gastrointestinal oxidative damage.

2. MATERIALS AND METHODS

2.1. Materials. *S*(+)-Ketoprofen and 3-(4,5-dimethyl-thiazol-2-yl)-2,5-diphenyltetrazolium bromide (MTT) were purchased from Sigma Chemical Co. (St. Louis, MO, USA). Basal Medium Eagle (BME/EBSS), bovine serum, trypsin-EDTA (T/E), L-glutamine, and penicillin/streptomycin (PS) were purchased from Gibco (Grand Island, NY, USA). The Trizol RNA isolation kit was purchased from Life Technologies (Rockville, MD, USA). Primers, dNTPs, reverse transcriptase, and Taq polymerase for RT-PCR were purchased from Gibco BRL (Cergy Pontoise, France). All chemicals and solvents used were of the highest purity available. The camellia oil was obtained from the Hsin-I Country Farmer'S Association (Nantou, Taiwan).

2.2. Cell Culture and Treatment. The human intestinal Int-407 cell line (BCRC 60022) was obtained from the Bioresource Collection and Research Center (BCRC) of the Food Industry Research and Development Institute (Hsinchu, Taiwan). The cells were cultured in complete medium (90% BME/EBSS, 10% bovine serum, and 1% penicillin/streptomycin) at 37 °C, under humidified 5% CO_2 incubator. The cells were detached with T/E (0.1% trypsin, 10 mM EDTA) solution and split weekly. The solution of camellia oil was prepared in DMSO, and according to the method described by Jang et al.,[19] The control group received DMSO only and the concentration of DMSO used for the experiments was lower than in 0.1% (v/v).

2.3. Wound Scratch Assay. The human Int-407 cells were cultured to 90% confluence in 6-well tissue culture plates. A wound phenomenon was made by scratching the cells with a sterile 200 μL pipet tip and removing floating cells with PBS. Next, camellia oil (prepared in DMSO) was added to the complete medium at 25, 50, and 75 μg/mL (final concentrations) for 24 h. Cell migration was monitored and recorded under a phase contrast microscope. The cell migration ability was calculated using the following equation: migration area = [migration area $_{(treated)}$/migration area $_{(control)}$].

2.4. Animal Treatment Procedures. Six-week-old (175−200 g) male SD rats were obtained from BioLASCO Co. (Taipei, Taiwan). Each rat was raised at 22 ± 2 °C, under 65−70% relative humidity on a 12/12 h light/dark cycles. The animals were fed a LabDiet 5001 Rodent Diet (24% protein, 5% fat, 5% fiber) (Nestle Purina, St. Louis, MO). All animal trial protocols were based on the National Institutes of Health (NIH) guidelines. These experiments were approved by the Institutional Animal Care and Use Committee (IACUC) of the National Chung Hsing University (approval no. 100-21). The compounds were orally administered as in the previous methods.[13,20] Briefly, the animals received an oral administration of camellia oil (1, 2, and 4 mL/kg/day) for 3 weeks. The control group received soybean oil (Sigma, St. Louis, MO, USA) only. On the 21st day, all animals were orally administrated with ketoprofen (50 mg/kg) and were sacrificed using CO_2 after 24 h.

2.5. Preparation of Gastrointestinal Mucosal Homogenate. Extraction of the gastrointestinal mucosa was carried out according to a previously reported method with some modifications.[21] Briefly, gastrointestinal mucosa was homogenized in 1.15% potassium chloride (KCl) buffer. The tissue samples were centrifuged at 10000g for 10 min (4 °C) to obtain a homogenate of gastrointestinal mucosa. Finally, aliquots of the homogenate were collected and preserved at −80 °C for the subsequent assay.

2.6. Measurement of Antioxidant Enzymes. The activities of GSH peroxidase (GPx), glutathione reductase (GRd), catalase, and GSH S-transferase (GST) antioxidant enzymes were assayed according to previously reported methods.[18,22] The GSH and the GSH/GSSG ratio were measured using a commercial kit (Cayman Chemical Co., Ann Arbor, MI, USA). SOD activity was assayed using a SOD assay kit-WST (Dojindo Molecular Technologies Inc., Gaithersburg, MD, USA) as specified by the manufacturer.

2.7. Measurement of Nitric Oxide (NO). The levels of NO were assayed according to a previously reported method.[23] Briefly, a gastrointestinal mucosal homogenate solution was mixed with the same volume of Griess reagent (5% phosphoric acid, 1% sulfanilamide, and 0.1% naphthyl ethylenediamine dihydrochloride) and incubated at room temperature for 10 min. The concentration of nitrite was measured by determining the optical density (OD) at 550 nm and calculated with a standard curve generated by Sodium nitrite.

2.8. Enzyme-Linked Immunosorbent Assay (ELISA). Int-407 cells were grown to 90% confluence in 6-well tissue culture plates and then added to the complete medium with camellia oil (prepared in DMSO) at 25, 50, and 75 μg/mL (final concentrations) for 24 h. The supernatants of Int-407 cells grown in conditioned medium and rat gastrointestinal mucosa protein samples was then harvested to be assayed for PGE_2 (Cayman Chemical Company, Ann Arbor, MI, USA), VEGF (Invitrogen, Carlsbad, CA, USA), and IL-6 (eBioscience, San Diego, CA, USA) secretion using a specific ELISA kit as indicated by the manufacturer's instructions.

2.9. RNA Extraction and Reverse Transcription-Polymerase Chain Reaction (RT-PCR). The mRNA expression levels of GPx, HO-1, and SOD were determined by RT-PCR. Total RNA was prepared using the TRIzol method (Life Technologies, Rockville, MD) following the manufacturer's instructions. The following sense and antisense primer sequences used for RT-PCR analysis were: GPx, 5′-GCA GAG CCG GGG ACA AGA GAA-3′ (forward) and 5′-CTG CTC TTT CTC TCC ATT GAC′-3 (reverse); HO-1, 5′-AAG ATT GCC CAG AAA GCC CTG GAC-3′ (forward) and 5′-AAC TGT CGC CAC CAG AAA GCT GAG-3′ (reverse); SOD, 5′-TAC ACC CAG ATG AAC GAG C-3′ (forward) and 5′-AGG AAC TTC TCA AAG TTC CAG GA-3′ (reverse); 18S, 5′-TTG GAG GGC AAG TCT GGT G-3′ (forward) and 5′-CCG TCC CAA GAT CCA ACT A-3′ (reverse). The amplification products were determined by electrophoresis on a 1.8% agarose gel containing 0.06 mg/L ethidium bromide. The gel was then photographed under UV transillumination. The results are expressed as ratios after normalization of the gene signal to the corresponding 18S or β-actin signal in each sample.

2.10. Pathological Histology Studies. The gastrointestinal tissues were fixed in formaldehyde (10%) and processed for histopathological studies according to the standard method and stained by hematoxylin/eosin (H&E) solutions. The pathological features of the gastrointestinal inner surface were scored as described by de la Lastra et al.[24] as follows: score 0 = no lesions; score 1 = vasodilatation or erythema; score 2 = 1−10 scattered small ulcers (<5 mm); score 3 = more than 10 scattered small ulcers (<5 mm); score 4 = 1−10 scattered medium ulcers (5−10 mm); score 5 = more than 10 scattered medium ulcers (5−10 mm); score 6 = 1−5 longitudinal ulcers (>10 mm); score 7 = more than five longitudinal ulcers (>10 mm).

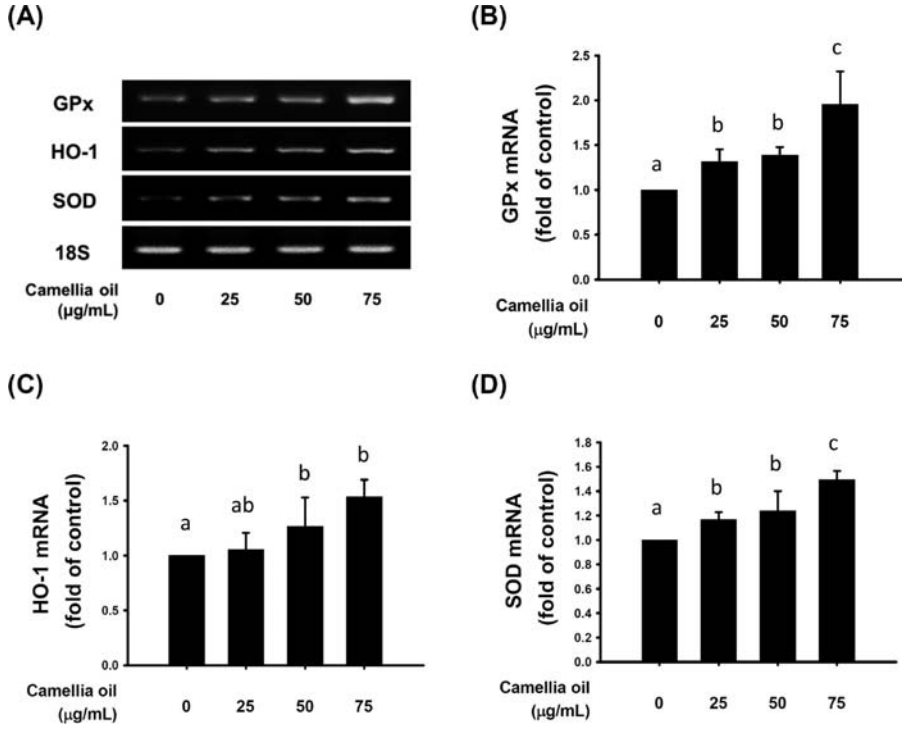

Figure 1. Effect of camellia oil on GPx, HO-1, and SOD mRNA expression in Int-407 cells. The cells were treated with camellia oil at 25, 50, and 75 μg/mL for 12 h, and the levels of GPx, HO-1, and SOD mRNA expression were analyzed by RT-PCR. The results are presented as the mean ± SD for $n = 3$. Each group with different letter subscripts is significantly different ($p < 0.05$).

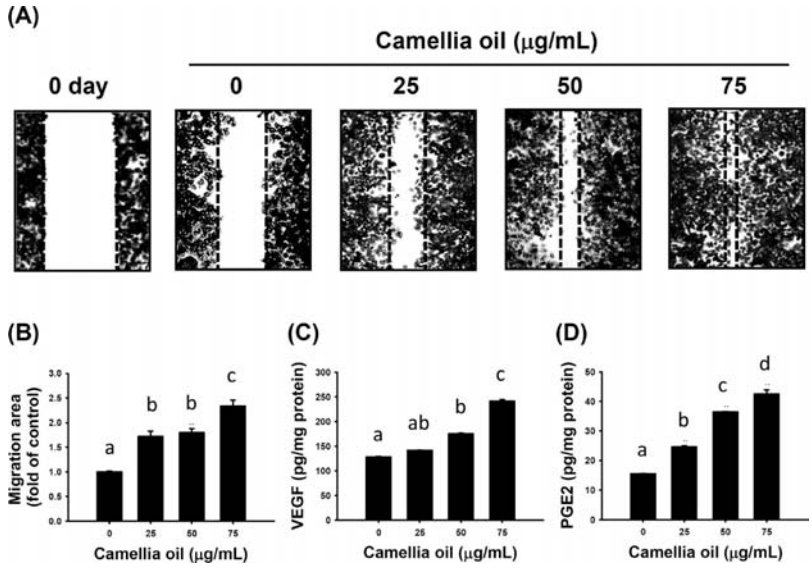

Figure 2. Effect of camellia oil on wound healing in Int-407 cells. (A) The cells were treated with camellia oil (25, 50, and 75 μg/mL) for 24 h, and a migration assay was performed to evaluate the wound-healing effects of camellia oil in Int-407 cells. (B) Graphical representation of cell migration ability. (C,D) Cells were treated with camellia oil at 25, 50, and 75 μg/mL for 24 h, and the production of VEGF and PGE_2 was analyzed by ELISA. The results are presented as the mean ± SD for $n = 3$. Each group with different letter subscripts is significantly different ($p < 0.05$).

2.11. Immunohistochemical (IHC) Staining. For IHC staining of VEGF and HO-1 was determined following a previously reported method.[25] Briefly, the tissue sections were blocked with StartingBlock blocking buffers prior to incubation with an anti-VEGF or anti-HO-1 antibody. Finally, the tissue sections were incubated with Envision-labeled polymer reagent containing peroxidase-conjugated anti-IgG at room temperature, followed by detection with a 3,3-diaminobenzidine tetrahydrochloride solution and hematoxylin.

2.12. Statistical Analysis. The statistical analysis was carried out using analysis of variance (ANOVA) according to the SAS User's Guide. Duncan's multiple range test was used to determine the significant differences ($p < 0.05$) between the means.

3. RESULTS

3.1. Effects of Camellia Oil on GPx, HO-1, and SOD mRNA Expression in Int-407 Cells. It has been suggested that upregulation of antioxidant enzyme activities may play an important role on cytoprotection against oxidative stress. In the present study, the induction effect of camellia oil on the activity

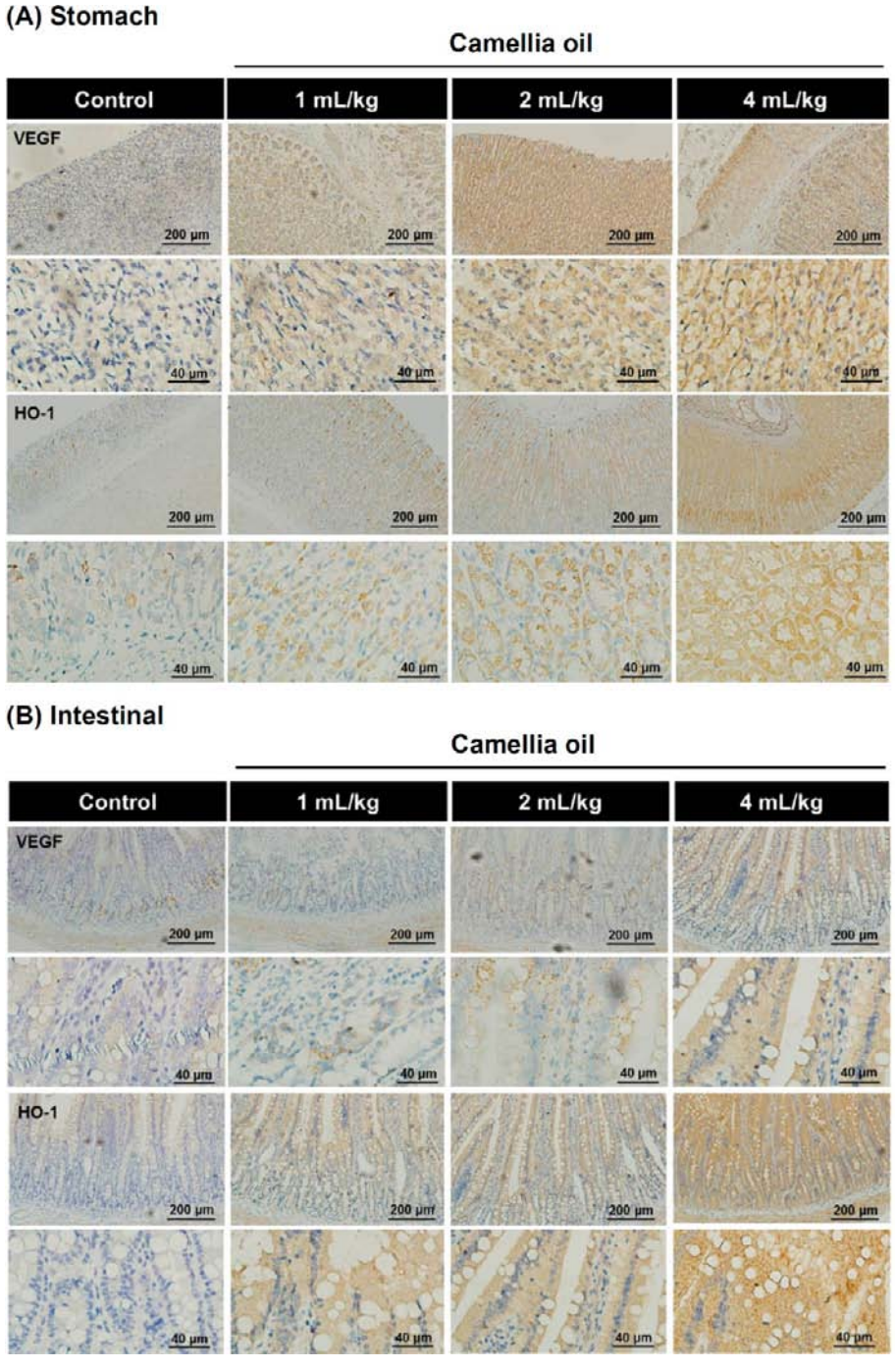

Figure 3. Immunohistochemical analysis of VEGF and HO-1 in the gastrointestinal mucosa induced by oral administration of camellia oil. SD rats were orally administered camellia oil (1, 2, and 4 mL/kg/day) for 21 days, and VEGF and HO-1 expression levels were examined by immunohistochemical analysis. VEGF and HO-1 protein expression in the gastrointestinal mucosa is represented by brown color.

of antioxidant enzymes was evaluated, including GPx, HO-1, and SOD. Int-407 cells treated with camellia oil at 25, 50, and 75 μg/mL for 12 h showed a dose-dependent increase in the mRNA expression of the antioxidant enzymes GPx, HO-1, and SOD, which reached a maximum at 75 μg/mL. Moreover, in the cells treated with camellia oil at 75 μg/mL for 12 h, the mRNA expression levels of GPx, HO-1, and SOD were increased by 1.80, 1.53, and 1.49-fold, respectively, compared with the control group (Figure 1, $p < 0.05$). These results suggest that camellia oil may potentially prevent oxidative stress-induced gastrointestinal injury.

3.2. Effect of Camellia Oil on Wound Healing in Vitro and in Vivo. In the wound-healing assay, Int-407 cells were treated with various concentrations (25, 50, and 75 μg/mL) of camellia oil for 24 h. As shown in Figure 2A,B, the 75 μg/mL concentration exhibited the greatest effect on cell motility after 24 h of incubation relative to the control group ($p < 0.05$). VEGF (vascular endothelial growth factor) and prostaglandins play key roles in maintaining gastrointestinal mucosal integrity.[26,27] As shown in Figure 2C,D, treatment of the cells with camellia oil at 25, 50, and 75 μg/mL for 24 h led to a dose-dependent increase in VEGF and PGE_2 production. Moreover, some reports have

dx.doi.org/10.1021/jf404614k | J. Agric. Food Chem. 2014, 62, 642−650

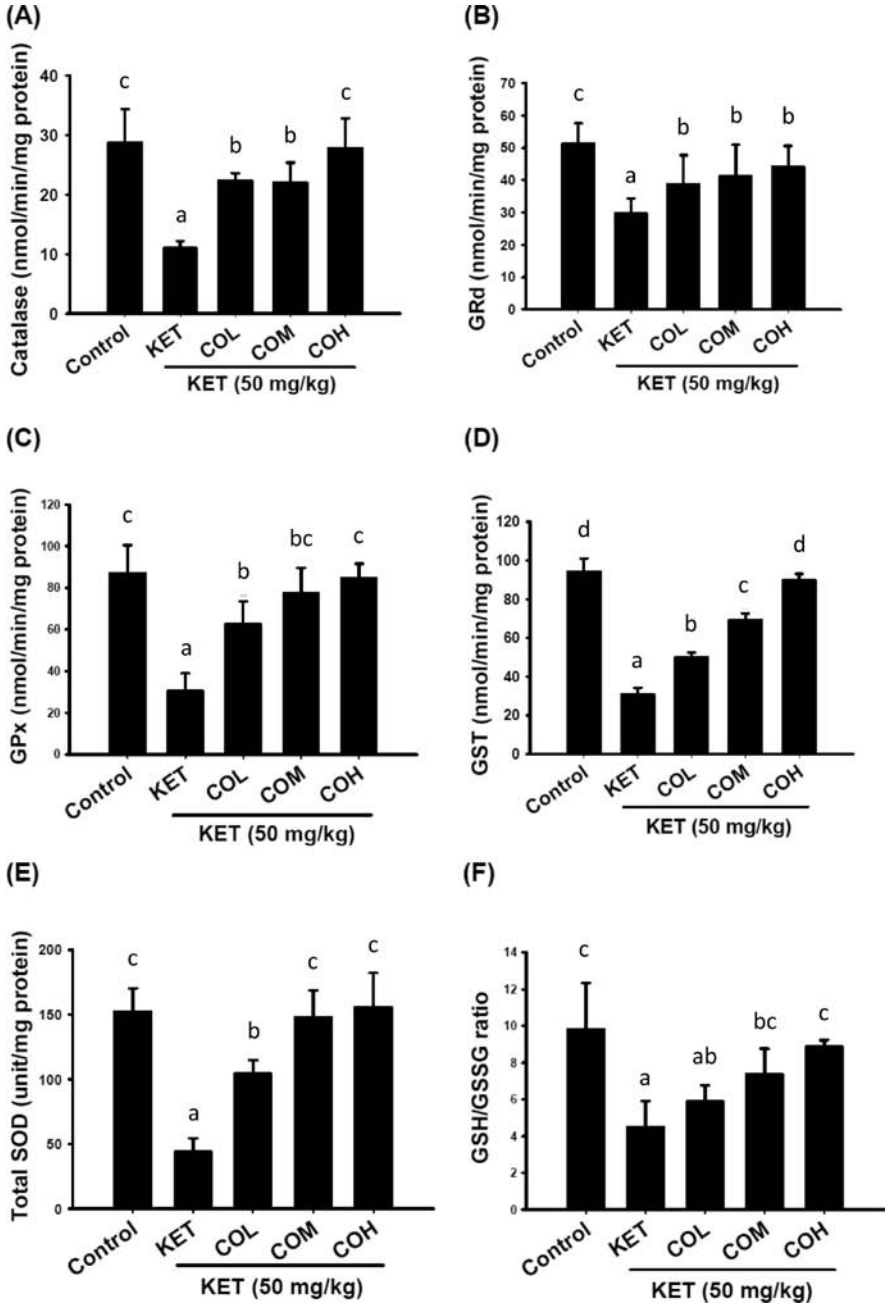

Figure 4. Effect of camellia oil on ketoprofen-induced changes in the activity levels of (A) catalase, (B) GRd, (C) GPx, (D) GST, (E) SOD, and the ratio of (F) GSH/GSSG in the gastrointestinal mucosa of SD rats. The animals were orally administered camellia oil (1, 2, and 4 mL/kg/day) for 21 consecutive days, and ketoprofen was then orally administered to all animals for 1 day. The data are presented as the mean ± SD for $n = 6$. Each group with different letter subscripts is significantly different ($p < 0.05$). KET, 50 mg ketoprofen/kg BW; COL, 1 mL camellia oil/kg BW; COM, 2 mL camellia oil/kg BW; COH, 4 mL camellia oil/kg B.W.

suggested that VEGF might prevent gastric mucosal injury by upregulation of HO-1 expression.[27,28] In vitro, Int-407 cells treated with camellia oil at 25, 50, and 75 μg/mL exhibited a dose-dependent increase in HO-1 mRNA expression as well as VEGF production (Figures 1C and 2C). More importantly, the administration of camellia oil to animals at 1, 2, and 4 mL/kg for 21 days had significant effects on VEGF and HO-1 protein expression in the stomach (Figure 3A) and intestinal (Figure 3B) mucosa, as determined by immunohistochemical analysis. These results suggest that the induction of VEGF and HO-1 by camellia oil might play a key role in the regulation of wound healing.

3.3. Effect of Camellia Oil on Ketoprofen-Induced Changes in Catalase, GRd, GPx, GST, and SOD Activities As Well as the GSH/GSSG Ratio in Gastrointestinal Mucosa. As shown in Figure 4, the treatment of SD rats with ketoprofen (50 mg/kg) resulted in a significant ($p < 0.05$) reduction in the activity of catalase, GRd, GPx, GST, and SOD as well as a reduction in the GSH/GSSH ratio in the gastrointestinal mucosa. However, oral administration of camellia oil (1, 2, and 4 mL/kg/day) exhibited a significant dose-dependent reversal of the impairment of the antioxidant enzyme system in the gastrointestinal mucosa compared with the ketoprofen-induced group ($p < 0.05$). The results indicate that camellia oil could

dx.doi.org/10.1021/jf404614k | J. Agric. Food Chem. 2014, 62, 642−650

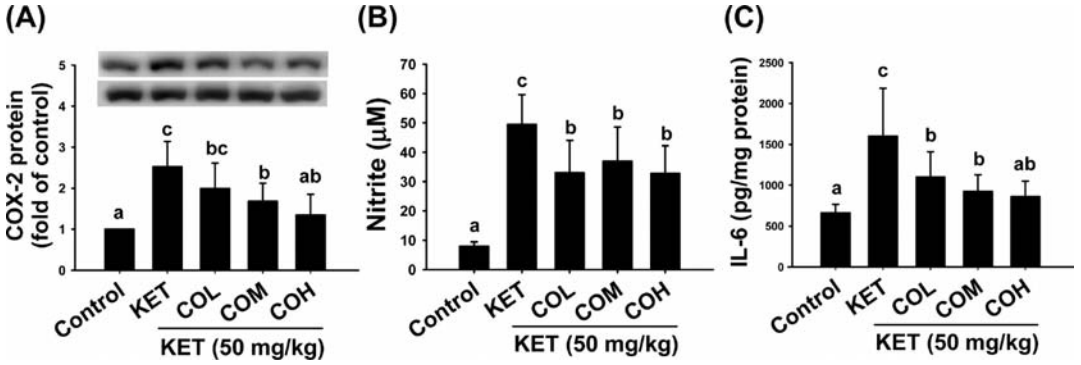

Figure 5. Effect of camellia oil on ketoprofen-induced changes in the levels of COX-2, NO, and IL-6 expression in rat gastrointestinal mucosal tissue. The animals were orally administered camellia oil (1, 2, and 4 mL/kg) for 21 consecutive days, and ketoprofen was then orally administered to all animals for 1 day. The data are presented as the mean ± SD for $n = 6$. Each group with different letter subscripts is significantly different ($p < 0.05$). KET, 50 mg ketoprofen/kg BW; COL, 1 mL camellia oil/kg BW; COM, 2 mL camellia oil/kg BW; COH, 4 mL camellia oil/kg BW.

reverse the impairment of the antioxidant system induced by ketoprofen in the gastrointestinal mucosa of SD rats.

3.4. Effect of Camellia Oil on Ketoprofen-Induced Changes in COX-2, NO, and IL-6 Expression Levels in the Gastrointestinal Mucosa. As shown in Figure 5A, treatment of rats with ketoprofen showed a significant ($p < 0.05$) increase in the level of COX-2 protein expression that was partly reduced by pretreatment with camellia oil (1, 2, and 4 mL/kg/day). NO and IL-6 are potent mediators of gastrointestinal mucosal inflammation caused by a wide variety of inflammatory stimuli such as toxic chemicals, viruses, and drugs. As shown in Figure 5B, NO production was abrogated by camellia oil in ketoprofen-treated SD rats ($p < 0.05$). As shown in Figure 5C, IL-6 production in animals treated with camellia oil (1, 2, and 4 mL/kg/day) was significantly inhibitory ($p < 0.05$), compared with the ketoprofen-induced group. However, no significant ($p < 0.05$) difference was found between any of dose-dependent manner. These results indicate that camellia oil might have the potential to protect patients with inflammation-associated gastrointestinal ulcers.

3.5. Pathological Histology of the Gastrointestinal Tract. The protective effects of camellia oil against oxidative injury to the gastrointestinal mucosa were investigated by hematoxylin/eosin staining. As shown in Figure 6, treatment of animals with ketoprofen at 50 mg/kg/day caused acute gastrointestinal injury as well as concavity of the gastrointestinal surface. The gastrointestinal tissues showed cloudy, swelled areas of variable size as well as necrosis and lymphocyte infiltration in the central zone and midzone. However, animals pretreated with camellia oil at 1, 2, and 4 mL/kg/day for 3 weeks prior to the administration of ketoprofen (50 mg/kg/day) showed decreased incidence of gastrointestinal mucosal injury.

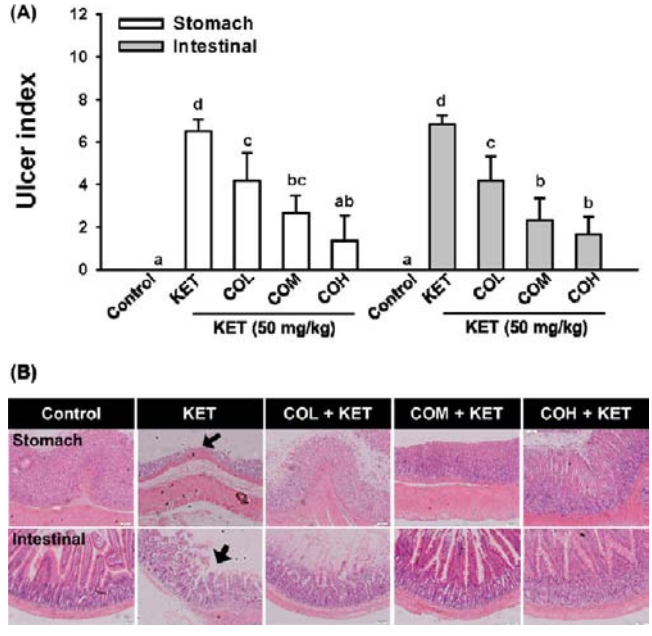

Figure 6. Effect of camellia oil on ketoprofen-induced gastrointestinal mucosal damage in SD rats. (A) Histological injury score of the gastrointestinal mucosa after different doses of camellia oil in rats treated with ketoprofen. (B) The morphology of ketoprofen-induced gastrointestinal ulcers in SD rats pretreated with or without camellia oil for 21 d. Gastrointestinal damage is indicated with an arrow. The data are presented as the mean ± SD for $n = 6$. Each group with different letter subscripts is significantly different ($p < 0.05$). KET, 50 mg ketoprofen/kg BW; COL, 1 mL camellia oil/kg BW; COM, 2 mL camellia oil/kg BW; COH, 4 mL camellia oil/kg BW. Hematoxylin/eosin staining, 100×.

4. DISCUSSION

Camellia oil has been reported to have positive health effects and is used as a traditional remedy for stomachache. Several studies have suggested that vegetable oils (corn, olive, and sunflower oils) strongly inhibit gastrointestinal injuries induced by NSAID.[20] Similar to olive oil, camellia oil is rich in oleic acid, which plays a key role in protection against ulcerogenesis.[18] In the preliminary test (data not shown), our data found that methanol extract of camellia oil revealed the highest antioxidant activity (127.48 μM trolox/g extract) as determined by trolox equivalent antioxidant capacity (TEAC). The similar antioxidant activity was also obtained by the oxygen radical absorbance capacity (ORAC) assay; it was the equal of 1.27 mM trolox/g extract. Moreover, methanol extract of camellia oil had the highest α-tocopherol (303.09 μg/g oil) and total phenolics (12.61 mg gallic acid/g extract) content as compare to soybean oil at concentrations of 24.27 (μg/g oil) and 1.72 (mg gallic acid/g extract), respectively. Chen et al.[17] have demonstrated that administration of camellia oil could lower triglyceride, cholesterol, and low density-lipoprotein levels in the blood of rats. Moreover, we reported that two major active compounds in camellia oil, sesamin, and novel compound B (2,5-bis-benzo[1,3] dioxol-5-yl-tetrahydro-furo[3,4-*d*][1,3]dioxine) could effectively prevent carbon tetrachloride (CCl_4)-induced liver oxidative

dx.doi.org/10.1021/jf404614k | J. Agric. Food Chem. 2014, 62, 642−650

damage in rats.[18] However, the protective effect of camellia oil against injury of the gastrointestinal mucosa induced by ketoprofen remains unknown. Thus, the objective of this study was designed to study the effects of camellia oil on the activities of antioxidant enzymes against ketoprofen-induced acute gastrointestinal damage.

NSAIDs such as ketoprofen are commonly used to treat inflammatory pain and as pyretic agents in clinical medicine. Despite their benefits, these drugs may cause peptic ulcer.[2] Our previous study indicated that ketoprofen causes gastrointestinal ulcers through a variety of mechanisms, including increased mucosal lipid peroxidation and oxidative damage as well as decreased gastric mucus secretion in rats.[13] Therefore, reducing oxidative stress and/or upregulating antioxidant enzymes may be effective approaches for preventing and treating gastrointestinal ulcers induced by ketoprofen. GPx, SOD, and, HO-1 are important antioxidant enzymes in the human body that have been shown to act as metal ion chelators and effective scavengers for ROS and reactive carbonyl species (RCS).[11,12,29] As shown in Figure 1, camellia oil (75 μg/mL) strongly increased GPx, SOD, and HO-1 mRNA expression in Int-407 cells. Some reports have indicated that gastrointestinal isoenzyme-GPx is the mainly important gastric enzyme because it serves as a barrier against hydroperoxide formed during xenobiotic metabolism.[30] Kirkby and Adin[11] indicated that HO-1 breaks down heme to biliverdin and carbon monoxide, which can protect gastrointestinal cell against oxidative damage. Guo et al.[12] reported that the upregulation of of HO-1 expression may reduce inflammation and tissue injury caused by ROS in the stomach and intestine. Our previous study showed that catechin effectively prevented injury of Int-407 cells induced by ketoprofen with upregulating HO-1 expression through the Nrf2 pathway.[13] These results suggest that camellia oil inhibits oxidative injury of the gastrointestinal mucosa induced by ketoprofen through upregulating antioxidant enzymes, especially HO-1.

Another approach for protection against ketoprofen-induced gastrointestinal mucosal damage may involve the upregulation of neovascularization in the gastrointestinal mucosal tissue. Neovascularization, which is the generation of new capillaries by sprouting of pre-existing microvessels, is under stringent control and normally occurs during embryonic and postembryonic development, the reproductive cycle, and wound repair.[27,28] Taupin and Podolsky[31] also indicated that enhanced stomach epithelial cell migration may be an effective approach for the treatment of stomach ulcers. VEGF is one of the most important factors for gastrointestinal mucosal reconstruction, mucosal defense, and ulcer healing.[27] Sofalcone is used to treat gastrointestinal ulcers and protects the gastric mucosa. Shibuya et al.[28] indicated that sofalcone might prevent gastric mucosal injury through the upregulation of VEGF production mediated via the Nrf2/HO-1 pathways. Similar to VEGF, prostaglandins play an important role in maintaining gastrointestinal mucosal integrity, which controls most gastric mucosa defense, and resolving inflammation.[26,27] Megias et al.[32] indicated that HO-1 modulated PGE_2 production in osteoarthritic chondrocytes. Similarly, our results showed that treatment with camellia oil (25−75 μg/mL) not only increased the levels of HO-1, VEGF, and PGE_2 expression but also enhanced the migration of human Int-407 cells (Figures 1C and 2). Furthermore, the VEGF and HO-1 protein levels in the stomach and intestinal mucosa of animals pretreated with camellia oil at 1, 2, and 4 mL/kg for 21 days were upregulated as evidenced by immunohistochemical analysis (Figure 3). These results indicate that camellia oil may serve as barrier against ketoprofen-induced gastrointestinal mucosal injury, which may aid mucosal repair.

Proton pump inhibitors (PPIs), such as lansoprazole, are usually used to treat gastric and duodenal ulcers.[6,7] Many studies have suggested that administration of lansoprazole can reverse the effects of diclofena, ketoprofen, indomethacin, and piroxicam on the mucosal content of GSH, MDA, and myeloperoxidase (MPO).[6−8] Similarly, our results indicated that camellia oil caused a significant ($p < 0.05$) dose-dependent reversal of the impairment of the antioxidant system during ketoprofen-induced gastrointestinal mucosal injury (Figure 4). To further investigate the protective effects of camellia oil against gastrointestinal injury in vivo induced by ketoproten in relation to antioxidant systems, SD rats were orally administered lansoprazole followed by gavage with ketoprofen. Our results showed that administration of lansoprazole (30 mg/kg) inhibited lipid peroxidation and reversed the reduction in the activities of GRd, GPx, GSH, and the GSH/GSSG ratio induced by ketoprofen (data not shown). These results suggest that camellia oil could reverse the impairment of the antioxidant enzymes activity in the gastrointestinal mucosa of SD rats induced by ketoprofen.

On the other hand, numerous studies have indicated that the gastrointestinal toxicity of *S*(+)-ketoprofen in rats is due to stimulation of the production of COX-2 and NO synthase in gastric mucosal lesions.[2,33,34] Pawlik et al.[35] suggested that proinflammatory mediators, such as IL-6 and NO, are produced by COX-2. Erkan et al.[36] indicated that COX-2 plays a key role in the stepwise process that ultimately causes gastric cancer. Blandizzi et al.[8] reported that administration of lansoprazole prevented gastric mucosal injury caused by indomethacin, piroxicam, or ketoprofen by reducing COX-2 mRNA expression in SD rats. As shown in Figure 5, the administration of camellia oil to animals at 2 mL/kg/day reduced COX-2 protein expression as well as the production of NO and IL-6 in SD rats treated with ketoprofen. Moreover, the camellia oil group was no difference ($p < 0.05$) in food, water intake, and body weight compared with the levels in the control group and the ketoprofen-treated group (data not shown). More importantly, we found that administration of camellia oil (2 mL/kg/day) strongly prevented the ketoprofen-induced gastrointestinal mucosal damage, as demonstrated by the histopathological (H&E) staining of gastrointestinal tissues (Figure 6). Odabasoglu et al.[20] indicated that animals treated with vegetable oils (corn, olive, and sunflower oils) at 2 mL/kg strongly inhibited indomethacin-induced gastric injuries in vivo. Furthermore, the animal dose of camellia oil was further extrapolated to a human equivalent dose following the calculated of Freireich et al.[37] The result suggests that oral administration of camellia oil at 2 mL/kg is approximately equivalent in human dose to 0.3 mL/kg. Overall, these data indicate that camellia oil may offer a potential therapeutic approach for inflammation-associated disorders such as gastrointestinal ulcers.

In conclusion, we demonstrated that intestinal epithelial cells treated with camellia oil (50−75 μg/mL) not only exhibited increased levels of GPx, HO-1, and SOD mRNA expression but also exhibited increased VEGF and PGE_2 protein expression, which might serve as barrier against gastrointestinal mucosal oxidative injury. Moreover, the administration of camellia oil at 2 mL/kg/day strongly inhibited the ketoprofen-induced gastrointestinal mucosal damage in SD rats. These results confirm the health-promoting effects of camellia oil, which exhibits potent antiulcer effects against oxidative damage in the stomach and intestine induced by ketoprofen.

AUTHOR INFORMATION

Corresponding Author

*Phone: 886-4-2287-9755. Fax: 886-4-2285-4378. E-mail: gcyen@nchu.edu.tw.

Funding

This research work was supported by the Council of Agriculture, Taiwan, under grant 100AS-3.1.4-FD-Z1(6).

Notes

The authors declare no competing financial interest.

ACKNOWLEDGMENTS

We thank Dr. J. W. Liao of the Graduate Institute of Veterinary Pathobiology for his technical assistance on histological examination.

ABBREVIATIONS USED

CCl_4, carbon tetrachloride; CAT, catalase; COX, cyclooxygenase; GSH, glutathione; GSSG, glutathione disulfide; GPx, glutathione peroxidase; GRd, glutathione reductase; HO-1, heme oxygenase-1; Int-407 cells, intestinal-407 cells; NSAIDs, nonsteroidal anti-inflammatory drugs; PGE_2, prostaglandin E_2; NO, nitric oxide; NQO1, NAD(P)H:(quinone-acceptor) oxidoreductase 1; Nrf2, nuclear factor erythroid 2-related factor 2; ROS, reactive oxygen species; SD rats, Sprague−Dawley rats; SOD, superoxide dismutase; VEGF, vascular endothelial growth factor

REFERENCES

(1) Rainsford, K. D. Profile and mechanisms of gastrointestinal and other side effects of nonsteroidal anti-inflammatory drugs (NSAIDs). *Am. J. Med.* **1999**, *107*, 27S−35S discussion 35S−36S.

(2) Liu, S.; Mizu, H.; Yamauchi, H. Photoinflammatory responses to UV-irradiated ketoprofen mediated by the induction of ROS generation, enhancement of cyclooxygenase-2 expression, and regulation of multiple signaling pathways. *Free Radical Biol. Med.* **2011**, *48*, 772−780.

(3) Smith, J. W.; Mathis, T.; Benns, M. V.; Franklin, G. A.; Harbrecht, B. G.; Larson, G. Socioeconomic disparities in the operative management of peptic ulcer disease. *Surgery* **2013**, *154*, 672−678 discussion 678−679..

(4) Musumba, C.; Pritchard, D. M.; Pirmohamed, M. Review article: cellular and molecular mechanisms of NSAID-induced peptic ulcers. *Aliment. Pharmacol. Ther.* **2009**, *30*, 517−531.

(5) van der Vliet, A.; Bast, A. Role of reactive oxygen species in intestinal diseases. *Free Radical Biol. Med.* **1992**, *12*, 499−513.

(6) Chandranath, S. I.; Bastaki, S. M.; Singh, J. A comparative study on the activity of lansoprazole, omeprazole and PD-136450 on acidified ethanol- and indomethacin-induced gastric lesions in the rat. *Clin. Exp. Pharmacol. Physiol.* **2002**, *29*, 173−180.

(7) Fornai, M.; Natale, G.; Colucci, R.; Tuccori, M.; Carazzina, G.; Antonioli, L.; Baldi, S.; Lubrano, V.; Abramo, A.; Blandizzi, C.; Del Tacca, M. Mechanisms of protection by pantoprazole against NSAID-induced gastric mucosal damage. *Naunyn Schmiedeberg's Arch. Pharmacol.* **2005**, *372*, 79−87.

(8) Blandizzi, C.; Fornai, M.; Colucci, R.; Natale, G.; Lubrano, V.; Vassalle, C.; Antonioli, L.; Lazzeri, G.; Del Tacca, M. Lansoprazole prevents experimental gastric injury induced by non-steroidal anti-inflammatory drugs through a reduction of mucosal oxidative damage. *World J. Gastroenterol.* **2005**, *11*, 4052−4060.

(9) Devasagayam, T. P.; Tilak, J. C.; Boloor, K. K.; Sane, K. S.; Ghaskadbi, S. S.; Lele, R. D. Free radicals and antioxidants in human health: current status and future prospects. *J. Assoc. Physicians India* **2004**, *52*, 794−804.

(10) Surh, Y. J. Cancer chemoprevention with dietary phytochemicals. *Nature Rev. Cancer* **2003**, *3*, 768−780.

(11) Kirkby, K. A.; Adin, C. A. Products of heme oxygenase and their potential therapeutic applications. *Am. J. Physiol.: Renal Physiol.* **2006**, *290*, F563−F571.

(12) Guo, X.; Shin, V. Y.; Cho, C. H. Modulation of heme oxygenase in tissue injury and its implication in protection against gastrointestinal diseases. *Life Sci.* **2001**, *69*, 3113−3119.

(13) Cheng, Y. T.; Wu, C. H.; Ho, C. Y.; Yen, G. C. Catechin protects against ketoprofen-induced oxidative damage of the gastric mucosa by up-regulating Nrf2 in vitro and in vivo. *J. Nutr. Biochem.* **2013**, *24*, 475−483.

(14) de la Lastra, C. A.; Nieto, A.; Martin, M. J.; Cabre, F.; Herrerias, J. M.; Motilva, V. Gastric toxicity of racemic ketoprofen and its enantiomers in rat: oxygen radical generation and COX-expression. *Inflammation Res.* **2002**, *51*, 51−57.

(15) Yu, Y. S.; Ren, S. X.; Tan, K. Y. Study on climatic regionalization and layer and belt distribution of oiltea camellia quality in China. *J. Nat. Res.* **1999**, *14*, 123−127.

(16) Lee, C. P.; Yen, G. C. Antioxidant activity and bioactive compounds of tea seed (*Camellia oleifera* Abel.) oil. *J. Agric. Food Chem.* **2006**, *54*, 779−784.

(17) Chen, L. F.; Qiu, S. H.; Peng, Z. H. Effects of sasanguasaponin on blood lipids and subgroups of high density lipoprotein cholesterol in hyper lipoidemia rat models. *Pharmacol. Clin. Chin. Mater. Med.* **1998**, *14*, 13−16.

(18) Lee, C. P.; Shih, P. H.; Hsu, C. L.; Yen, G. C. Hepatoprotection of tea seed oil (*Camellia oleifera* Abel.) against CCl4-induced oxidative damage in rats. *Food Chem. Toxicol.* **2007**, *45*, 888−895.

(19) Jung, E.; Lee, J.; Baek, J.; Jung, K.; Huh, S.; Kim, S.; Koh, J.; Park, D. Effect of *Camellia japonica* oil on human type I procollagen production and skin barrier function. *J. Ethnopharmacol.* **2007**, *112*, 127−31.

(20) Odabasoglu, F.; Halici, Z.; Cakir, A.; Halici, M.; Aygun, H.; Suleyman, H.; Cadirci, E.; Atalay, F. Beneficial effects of vegetable oils (corn, olive and sunflower oils) and alpha-tocopherol on anti-inflammatory and gastrointestinal profiles of indomethacin in rats. *Eur. J. Pharmacol.* **2008**, *591*, 300−306.

(21) Mutlu-Turkoglu, U.; Erbil, Y.; Oztezcan, S.; Olgac, V.; Toker, G.; Uysal, M. The effect of selenium and/or vitamin E treatments on radiation-induced intestinal injury in rats. *Life Sci.* **2000**, *66*, 1905−1913.

(22) Hsu, C. L.; Hsu, C. C.; Yen, G. C. Hepatoprotection by freshwater clam extract against CCl4-induced hepatic damage in rats. *Am. J. Chin. Med.* **2010**, *38*, 881−894.

(23) Fang, S. C.; Hsu, C. L.; Yen, G. C. Anti-inflammatory effects of phenolic compounds isolated from the fruits of *Artocarpus heterophyllus*. *J. Agric. Food Chem.* **2008**, *56*, 4463−4468.

(24) de la Lastra, C. A.; Nieto, A.; Motilva, V.; Martin, M. J.; Herrerias, J. M.; Cabre, F.; Mauleon, D. Intestinal toxicity of ketoprofen-trometamol vs its enantiomers in rat. Role of oxidative stress. *Inflammation Res.* **2000**, *49*, 627−632.

(25) Wu, C. H.; Huang, S. M.; Yen, G. C. Silymarin: a novel antioxidant with antiglycation and antiinflammatory properties in vitro and in vivo. *Antioxid. Redox Signaling* **2011**, *14*, 353−366.

(26) Wallace, J. L. Prostaglandins, NSAIDs, and gastric mucosal protection: why doesn't the stomach digest itself? *Physiol. Rev.* **2008**, *88*, 1547−1565.

(27) Tarnawski, A. S.; Ahluwalia, A. Molecular mechanisms of epithelial regeneration and neovascularization during healing of gastric and esophageal ulcers. *Curr. Med. Chem.* **2012**, *19*, 16−27.

(28) Shibuya, A.; Onda, K.; Kawahara, H.; Uchiyama, Y.; Nakayama, H.; Omi, T.; Nagaoka, M.; Matsui, H.; Hirano, T. Sofalcone, a gastric mucosa protective agent, increases vascular endothelial growth factor via the Nrf2-heme-oxygenase-1 dependent pathway in gastric epithelial cells. *Biochem. Biophys. Res. Commun.* **2010**, *398*, 581−584.

(29) Husain, K.; Mejia, J.; Lalla, J.; Kazim, S. Dose response of alcohol-induced changes in BP, nitric oxide and antioxidants in rat plasma. *Pharmacol. Res.* **2005**, *51*, 337−343.

(30) Brigelius-Flohe, R. Tissue-specific functions of individual glutathione peroxidases. *Free Radical Biol. Med.* **1999**, *27*, 951−965.

(31) Taupin, D.; Podolsky, D. K. Trefoil factors: initiators of mucosal healing. *Nature Rev. Mol. Cell Biol.* **2003**, *4*, 721−732.
(32) Megias, J.; Guillen, M. I.; Clerigues, V.; Rojo, A. I.; Cuadrado, A.; Castejon, M. A.; Gomar, F.; Alcaraz, M. J. Heme oxygenase-1 induction modulates microsomal prostaglandin E synthase-1 expression and prostaglandin E(2) production in osteoarthritic chondrocytes. *Biochem. Pharmacol.* **2009**, *77*, 1806−1813.
(33) Kuwano, T.; Nakao, S.; Yamamoto, H.; Tsuneyoshi, M.; Yamamoto, T.; Kuwano, M.; Ono, M. Cyclooxygenase 2 is a key enzyme for inflammatory cytokine-induced angiogenesis. *FASEB J.* **2004**, *18*, 300−310.
(34) Adhikary, B.; Yadav, S. K.; Bandyopadhyay, S. K.; Chattopadhyay, S. Role of the COX-independent pathways in the ulcer-healing action of epigallocatechin gallate. *Food Funct.* **2011**, *2*, 338−347.
(35) Pawlik, M.; Pajdo, R.; Kwiecien, S.; Ptak-Belowska, A.; Sliwowski, Z.; Mazurkiewicz-Janik, M.; Konturek, S. J.; Pawlik, W. W.; Brzozowski, T. Nitric oxide (NO)-releasing aspirin exhibits a potent esophagoprotection in experimental model of acute reflux esophagitis. Role of nitric oxide and proinflammatory cytokines. *J. Physiol. Pharmacol.* **2011**, *62*, 75−86.
(36) Erkan, G.; Gonul, I. I.; Kandilci, U.; Dursun, A. Assessment of COX-2 expression presence and severity by immunohistochemical method in patients with chronic active gastritis and intestinal metaplasia. *Turk. J. Gastroenterol.* **2012**, *23*, 478−484.
(37) Freireich, E. J.; Gehan, E. A.; Rall, D. P.; Schmidt, L. H.; Skipper, H. E. Quantitative comparison of toxicity of anticancer agents in mouse, rat, hamster, dog, monkey, and man. *Cancer Chemother. Rep.* **1966**, *50*, 219−244.

JOURNAL OF AGRICULTURAL AND FOOD CHEMISTRY

Article

pubs.acs.org/JAFC

Synthesis of All Stereoisomers of 3,3′-Dimethoxy-7,7′-epoxylignane-4,4′-diol and Their Plant Growth Inhibitory Activity

Hisashi Nishiwaki, Kumiko Nakayama, Yoshihiro Shuto, and Satoshi Yamauchi*

Faculty of Agriculture, Ehime University, 3-5-7 Tarumi, Matsuyama, Ehime 790-8566, Japan

Supporting Information

ABSTRACT: All stereoisomers of 3,3′-dimethoxy-7,7′-epoxylignane-4,4′-diol were synthesized to examine the effect of stereochemistry on their plant growth inhibitory activity using lettuce and Italian ryegrass. The effect of structural modifications such as dehydroxylation, methoxylation and hydroxylation at the 9- and 9′-positions of the lignans on the activity was also studied. Most of the epoxylignanes showed higher plant growth inhibitory potency against ryegrass than against lettuce, and the inhibitory activity varied depending on the configurations of each position of the tetrahydrofuran ring (7-, 7′-, 8-, and 8′-positions of the epoxylignanes). Among the 9,9′-position-modified derivatives, the dehydroxy derivatives showed the highest potency. These results suggested that the plant growth inhibitory activity should be influenced by the structure of the epoxylignanes.

KEYWORDS: *3,3′-dimethoxy-7,7′-epoxylignane-4,4′-diol, lignan, plant growth inhibitory activity, lettuce, Italian ryegrass*

INTRODUCTION

Lignans widely distributed in plants exert various biological activities such as anticancer and antioxidant activities.[1] Lariciresinol, which is a trisubstituted tetrahydrofuran lignan, has also interesting biological activities including phytotoxic activity. Our previous study of the effect of the stereochemistry of lariciresinol on plant growth regulatory activity against lettuce (*Lactuca sativa* L.) and Italian ryegrass (*Lolium multiflorum* Lam.) demonstrated that the phytotoxic activity of lariciresinol depended on its stereochemistry, that is, the importance of both the 8*S* absolute configuration and the 7,8′-*trans* relative configuration for high activity.[2] It is undoubted that lignans other than lariciresinol should also show potent phytotoxic activity, as reported for diayangambin and dihydrodiconiferyl alcohol,[3,4] and that the structural modification as well as the absolute structure of lignans should influence their phytotoxicity, but data regarding the phytotoxicity of lignans, especially in-depth discussion of the relationship between their stereochemistry and activity, are less available.

Herein we focused on the relationship between the stereochemistry of 3,3′-dimethoxy-7,7′-epoxylignane-4,4′-diol compounds, which are tetrasubstituted tetrahydrofuran lignans (Figure 1), and their plant growth regulatory activity. In addition, the effect of the structural modifications at the 9- and 9′-positions such as dehydroxylation, methoxylation and hydroxylation on the activity was also studied. Some of these lignans have been isolated and named as follows: (−)-verrucosin, **1** (**1-H**, (−)-odoratisol);[5,6] (+)-verrucosin, **4** (**2-H**);[7] (+)-fragransin A2, **7** (**3-H**);[7] (+)-*neo*-olivil, **9** (**3-OH**);[8] (+)-saucernetin diol, **13** (**5-H**);[9,10] (−)-*neo*-olivil, **18** (**6-OH**);[11] (−)-machilin-I, **22** (**8-H**);[12] nectandrin B, **25** (**9-H**);[7] and tetrahydrofuroguaiacin B, **28** (**10-H**).[10] The syntheses of **1**,[13] **7**,[13] and **13**[14,15] have been achieved, and the conversion from glucoside to **27** (**9-OH**) has been reported.[16] The other stereoisomers were synthesized for the first time in this project. In our previous studies, the constructions of all stereochemistries of 7,7′-epoxylignane have been established,[17−19] and these synthetic methods were modified to provide the stereoisomers of 3,3′-dimethoxy-7,7′-epoxylignane-4,4′-diol. This research would contribute to the collation of stereoisomer libraries of natural products.

MATERIALS AND METHODS

Chemicals. The synthetic scheme is shown in Figure 2. Reagents used for the syntheses were purchased from Wako Pure Chemical Industries, Ltd. (Osaka, Japan), Nacalai Tesque, Inc. (Kyoto, Japan), Tokyo Chemical Industry Co., Ltd. (Tokyo, Japan), and Aldrich Chemical Co (Milwaukee, WI, USA). Melting points were uncorrected. Optical rotations were measured on a SEPA-200 instrument (Horiba Ltd., Kyoto, Japan). NMR data were obtained using a Bruker AVANCE III 500 spectrometer (Bruker BioSpin K.K., Kanagawa, Japan). EIMS data were measured with a JMS-MS700 V spectrometer (JEOL Ltd., Tokyo, Japan). The silica gel used was Wakogel C-300 (Wako, 200−300 mesh). The numbering of compounds follows the nomenclature of lignans.[20] Information for compounds **1**, **4**, **7**, **9**, **10**, **12**, **13**, **15**, **16**, **18**, **19**, **22**, **25**, **27**, and **28** (**1-H**−**10-H**, **3-OH**, **4-OH**, **5-OH**, **6-OH**, and **9-OH**), which has been published,[5−8,10,11,13,14,16,21] was placed in the Supporting Information.

(7S,7′R,8S,8′S)-4,4′-Dibenzyloxy-3,3′-dimethoxy-7,7′-epoxylignane-9,9′-diol, ***31****:* colorless oil; $[\alpha]^{20}_{D}$ −18 (*c* 1.2, $CHCl_3$); ^{1}H NMR (500 MHz, $CDCl_3$) δ 2.23 (1H, m, H-8′), 2.55 (1H, m, H-8), 2.65−3.00 (1H, br, OH), 3.08 (1H, dd, *J* = 10.3, 9.9 Hz, H-9a), 3.18−3.48 (1H, br, OH), 3.30 (1H, dd, *J* = 10.3, 4.7 Hz, H-9b), 3.55 (1H, dd, *J* = 9.6, 9.0 Hz, H-9′a), 3.72 (1H, dd, *J* = 9.6, 3.4 Hz, H-9′b), 3.84 (3H, s, 3-OCH_3), 3.88 (3H, s, 3′-OCH_3), 4.47 (1H, d, *J* = 9.4 Hz, H-7′), 5.09 (1H, d, *J* = 8.7 Hz, H-7), 5.11 (2H, s, CH_2OPh), 5.14 (2H, s, CH_2OPh), 6.82 (2H, s, H-5, H-6), 6.84 (1H, d, *J* = 8.3 Hz, H-5′), 6.89 (1H, s, H-2), 6.92 (1H, dd, *J* = 8.3, 1.9 Hz, H-6′), 7.04 (1H, d, *J* = 1.9 Hz, H-2′), 7.27−7.30 (2H, m, BnO), 7.33−7.37 (4H, m, BnO), 7.40−7.43 (4H, m, BnO); ^{13}C NMR (125 MHz, $CDCl_3$) δ 50.9 (C-8), 54.9 (C-8′), 56.0 (C-9′), 56.1 (C-9), 63.0 (OCH_3), 63.7 (OCH_3), 71.10 (OCH_2Ph), 71.13 (OCH_2Ph), 81.2 (C-7), 82.5 (C-7′), 110.4 (C-2′), 110.8 (C-2), 113.9 (C-5), 114.0 (C-5′), 118.7 (C-6′), 119.0 (C-6),

Received: October 15, 2013
Revised: December 21, 2013
Accepted: December 22, 2013
Published: December 22, 2013

ACS Publications © 2013 American Chemical Society

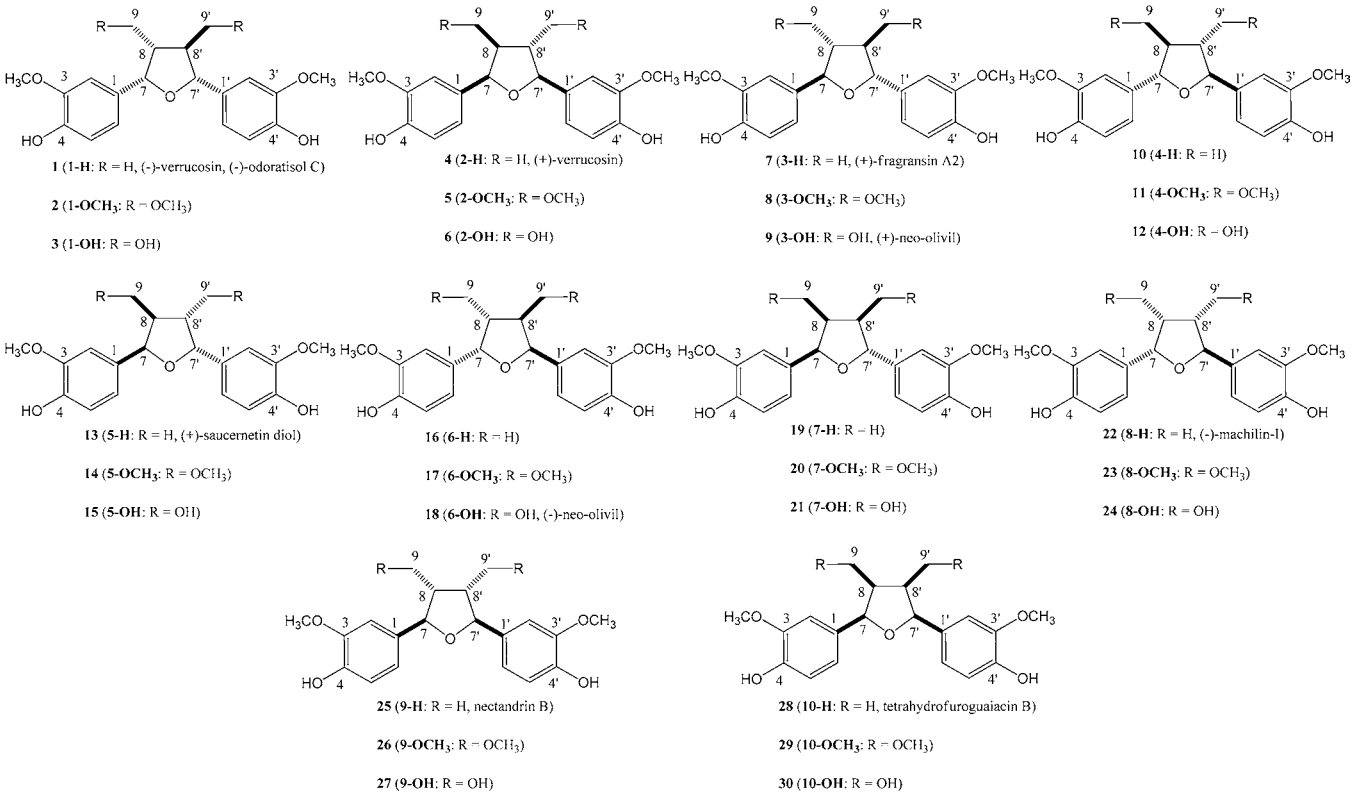

Figure 1. Chemical structures of the epoxylignanes synthesized in the present study.

127.26 (OBn), 127.33 (OBn), 127.86 (OBn), 127.88 (OBn), 128.53 (OBn), 128.55 (OBn), 132.1 (C-1), 133.2 (C-1′), 137.0 (OBn), 137.1 (OBn), 147.7 (C-4), 148.1 (C-4′), 149.5 (C-3), 149.8 (C-3′). Anal. Found: C, 73.38%; H, 6.60%. Calcd for $C_{34}H_{36}O_7$: C, 73.36%; H, 6.52%.

(7R,7′S,8R,8′R)-4,4′-Dibenzyloxy-3,3′-dimethoxy-7,7′-epoxylignane-9,9′-diol, ***32:*** colorless oil; $[\alpha]^{20}_D$ +18 (*c* 1.6, $CHCl_3$); NMR data agreed with those of **31**.

(7S,7′R,8S,8′S)-3,3′,9,9′-Tetramethoxy-7,7′-epoxylignane-4,4′-diol, ***2 (1-OCH3):*** colorless oil; $[\alpha]^{20}_D$ −21 (*c* 1.1, $CHCl_3$); ^{1}H NMR (500 MHz, $CDCl_3$) δ 2.37 (1H, m, H-8′), 2.63 (1H, m, H-8), 2.97 (1H, dd, *J* = 9.3, 5.8 Hz, H-9a), 3.07−3.10 (1H, overlapped, H-9b), 3.08 (3H, s, 9-OCH_3), 3.36 (3H, s, 9′-OCH_3), 3.51 (1H, dd, *J* = 9.5, 5.2 Hz, H-9′a), 3.55 (1H, dd, *J* = 9.5, 5.4 Hz, H-9′b), 3.86 (3H, s, 3-OCH_3), 3.90 (3H, s, 3′-OCH_3), 4.72 (1H, d, *J* = 8.0 Hz, H-7′), 5.10 (1H, d, *J* = 7.3 Hz, H-7), 5.70 (1H, s, ArOH), 5.74 (1H, s, ArOH), 6.89−6.92 (4H, m, H-2, H-5, H-5′, H-6), 6.99 (1H, dd, *J* = 8.2, 1.9 Hz, H-6′), 7.01 (1H, d, *J* = 1.9 Hz, H-2′); ^{13}C NMR (125 MHz, $CDCl_3$) δ 46.7 (C-8), 50.6 (C-8′), 55.85 (9-OCH_3), 55.90 (9′-OCH_3), 58.6 (3′-OCH_3), 59.0 (3-OCH_3), 73.1 (C-9′, C-9), 81.6 (C-7), 82.7 (C-7′), 109.3 (C-2′), 109.5 (C-2), 114.0 (C-5), 114.2 (C-5′), 119.3 (C-6′), 119.5 (C-6), 130.9 (C-1), 133.5 (C-1′), 144.7 (C-4), 145.2 (C-4′), 146.2 (C-3), 146.5 (C-3′); MS (EI) *m*/*z* 404 (M^+, 34), 175 (100); HRMS (EI) *m*/*z* calcd for $C_{22}H_{28}O_7$ (M^+) 404.1835, found 404.1834.

(7S,7′R,8S,8′S)-3,3′-Dimethoxy-7,7′-epoxylignane-4,4′,9,9′-tetraol, ***3 (1-OH):*** colorless oil; $[\alpha]^{20}_D$ −20 (*c* 1.4, MeOH); ^{1}H NMR (500 MHz, CD_3OD) δ 1.28 (2H, s, OH), 2.28 (1H, m, H-8′), 2.56 (1H, m, H-8), 3.16 (1H, dd, *J* = 10.4, 10.0 Hz, H-9a), 3.22 (1H, dd, *J* = 10.4, 5.1 Hz, H-9b), 3.64 (1H, dd, *J* = 11.0, 6.1 Hz, H-9′a), 3.71 (1H, dd, *J* = 11.0, 4.7 Hz, H-9′b), 3.85 (3H, s, 3-OCH_3), 3.89 (3H, s, 3′-OCH_3), 4.65 (1H, d, *J* = 8.6 Hz, H-7′), 5.10 (1H, d, *J* = 7.9 Hz, H-7), 6.78 (1H, d, *J* = 8.1 Hz, H-6), 6.80−6.85 (2H, m, H-2, H-5), 6.95−6.97 (2H, m, H-5′, H-6′), 7.10 (1H, s, H-2′); ^{13}C NMR (125 MHz, $CDCl_3$) δ 50.5 (C-8), 54.2 (C-8′), 54.89 (OCH_3), 54.91 (OCH_3), 60.5 (C-9′), 61.0 (C-9), 76.2 (C-7), 77.1 (C-7′), 98.9 (C-2′), 99.1 (C-2), 102.5 (C-5), 102.7 (C-5′), 106.1 (C-6′), 106.3 (C-6), 115.2 (C-1), 116.9 (C-1′), 127.4 (C-4), 127.8 (C-4′), 128.8 (C-3), 129.1 (C-3′); MS (EI) *m*/*z* 376 (M^+, 51), 224 (71), 193 (81), 176 (100), 151 (62), 137 (69); HRMS (EI) *m*/*z* calcd for $C_{20}H_{24}O_7$ (M^+) 376.1522, found 376.1515.

(7R,7′S,8R,8′R)-3,3′,9,9′-Tetramethoxy-7,7′-epoxylignane-4,4′-diol, ***5 (2-OCH3):*** colorless oil; $[\alpha]^{20}_D$ +21 (*c* 0.2, $CHCl_3$); NMR data agreed with those of **2**.

(7R,7′S,8R,8′R)-3,3′-Dimethoxy-7,7′-epoxylignane-4,4′,9,9′-tetraol, ***6 (2-OH):*** colorless oil; $[\alpha]^{20}_D$ +20 (*c* 0.1, MeOH); NMR data agreed with those of **3**.

(7R,7′R,8S,8′S)-4,4′-Dibenzyloxy-3,3′-dimethoxy-7,7′-epoxylignane-9,9′-diol, ***33:*** colorless oil; $[\alpha]^{20}_D$ +46 (*c* 2.6, $CHCl_3$); ^{1}H NMR (500 MHz, $CDCl_3$) δ 2.19 (2H, m, H-8, H-8′), 3.44 (2H, dd, *J* = 9.1, 8.8 Hz, H-9a, H-9′a), 3.63 (2H, d, *J* = 9.1 Hz, H-9b, H-9′b), 3.84 (6H, s, OCH_3), 4.22 (2H, br s, OH), 4.66 (2H, d, *J* = 9.0 Hz, H-7, H-7′), 5.09 (4H, s, OCH_2Ph), 6.76 (2H, dd, *J* = 8.3, 1.9 Hz, H-6, H-6′), 6.82 (2H, d, *J* = 8.3 Hz, H-5, H-5′), 6.92 (2H, d, *J* = 1.9 Hz, H-2, H-2′), 7.24−7.27 (2H, m, OBn), 7.30−7.33 (4H, m, OBn), 7.38−7.66 (4H, m, Bn); ^{13}C NMR (125 MHz, $CDCl_3$) δ 56.1 (OCH_3), 57.0 (C-8, C-8′), 62.6 (C-9, C-9′), 71.1 (OCH_2Bn), 83.1 (C-7, C-7′), 110.0 (C-2, C-2′), 113.9 (C-5, C-5′), 118.7 (C-6, C-6′), 127.3 (OBn), 127.6 (OBn), 127.8 (OBn), 128.5 (OBn), 134.6 (C-1), 134.8 (C-1′), 137.0 (Bn), 147.9 (C-4, C-4′), 149.8 (C-3, C-3′). Anal. Found: C, 73.40%; H, 6.53%. Calcd. for $C_{34}H_{36}O_7$: C, 73.36%; H, 6.52%.

(7S,7′S,8R,8′R)-4,4′-Dibenzyloxy-3,3′-dimethoxy-7,7′-epoxylignane-9,9′-diol, ***34:*** colorless oil; $[\alpha]^{20}_D$ −49 (*c* 0.9, $CHCl_3$); NMR data agreed with those of **33**.

(7R,7′R,8S,8′S)-3,3′,9,9′-Tetramethoxy-7,7′-epoxylignane-4,4′-diol, ***8 (3-OCH3):*** colorless crystals; mp 129−130 °C; $[\alpha]^{20}_D$ +29 (*c* 0.8, $CHCl_3$); ^{1}H NMR (500 MHz, $CDCl_3$) δ 2.38 (2H, m, H-8, H-8′), 3.33 (6H, s, 9-OCH_3, 9′-OCH_3), 3.45 (2H, dd, *J* = 9.5, 4.5 Hz, H-9a, H-9′a), 3.50 (2H, dd, *J* = 9.5, 5.0 Hz, H-9b, H-9′b), 3.89 (6H, s, 3-OCH_3, 3′-OCH_3), 4.96 (2H, d, *J* = 7.8 Hz, H-7, H-7′), 5.65 (2H, s, 4-OH, 4′OH), 6.87 (2H, d, *J* = 8.2 Hz, H-5, H-5′), 6.90 (2H, dd, *J* = 8.2, 1.5 Hz, H-6, H-6′), 7.00 (2H, d, *J* = 1.5 Hz, H-2, H-2′); ^{13}C NMR (125 MHz, $CDCl_3$) δ 51.2 (C-8, C-8′), 56.0 (9-OCH_3, 9′-OCH_3), 59.0 (3-OCH_3, 3′-OCH_3), 72.4 (C-9, C-9′), 82.8 (C-7, C-7′), 108.8 (C-2, C-2′), 114.1(C-5, C-5′), 119.3(C-6, C-6′), 134.4 (C-1, C-1′),

dx.doi.org/10.1021/jf4046396 | J. Agric. Food Chem. 2014, 62, 651−659

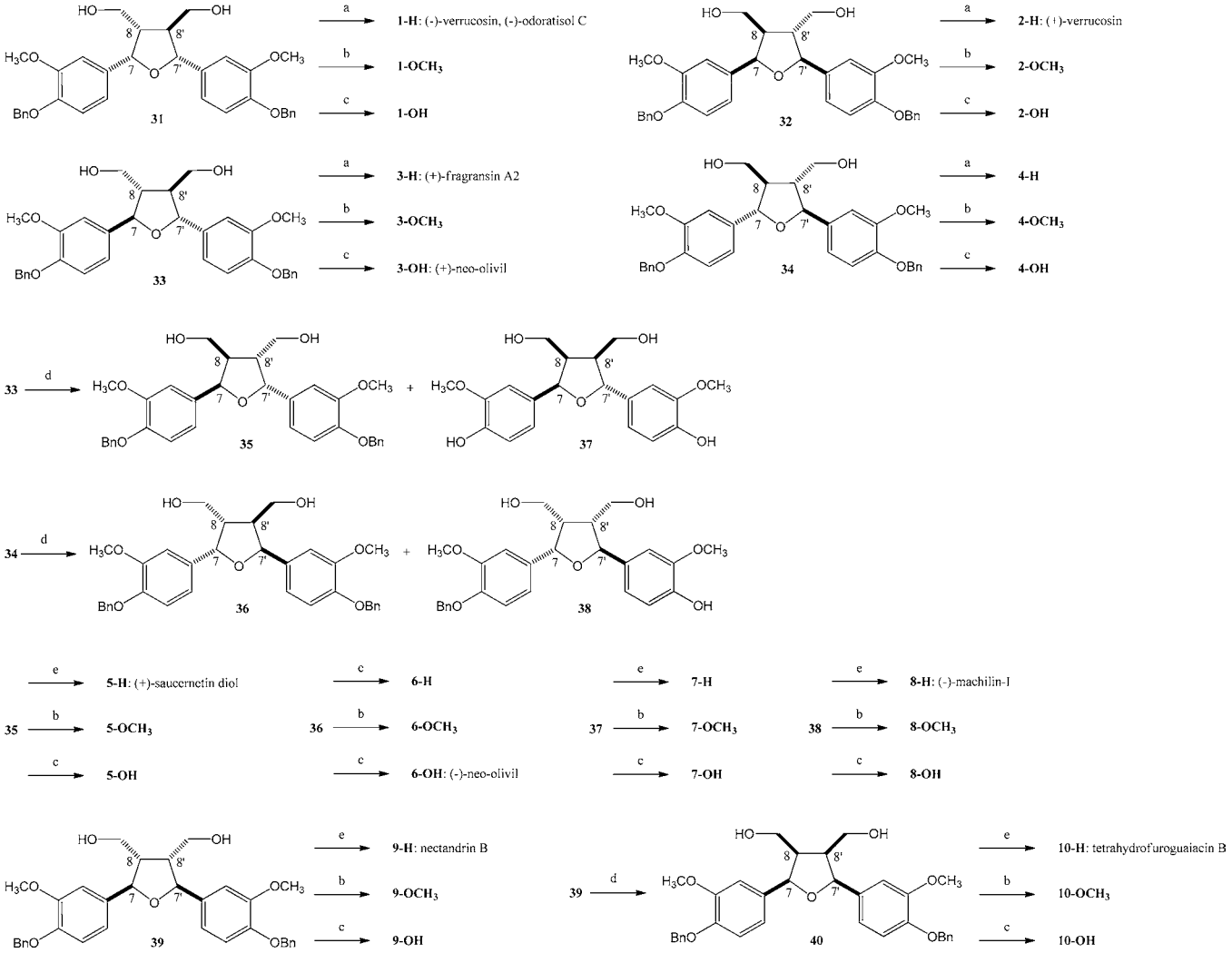

Figure 2. Synthetic schemes: (a) (1) MsCl, Et_3N, CH_2Cl_2, rt, 30 min; (2) $NaBH_4$, HMPA, 60 °C, 1.5 h; (3) H_2, 5% Pd/C, EtOAc, ambient temperature, 2 h (3 steps, **1-H**, 57%; **2-H**, 60%; **3-H**, 43%; **4-H**, 48%). (b) (1) NaH, MeI, THF, rt, 3 h; (2) H_2, 5% Pd/C, ambient temperature, 5 h (2 steps, **1-OCH$_3$**, 65%; **2-OCH$_3$**, 62%; **3-OCH$_3$**, 51%; **4-OCH$_3$**, 48%; **5-OCH$_3$**, 50%; **6-OCH$_3$**, 51%; **7-OCH$_3$**, 44%; **8-OCH$_3$**, 46%; **9-OCH$_3$**, 35%; **10-OCH$_3$**, 32%). (c) H_2, 5% Pd/C, EtOAc, ambient temperature, 6 h (**1-OH**, 59%; **2-OH**, 65%; **3-OH**, 64%; **4-OH**, 70%; **5-OH**, 57%; **6-OH**, 61%; **7-OH**, 73%; **8-OH**, 73%; **9-OH**, 46%; **10-OH**, 58%). (d) (1) MsCl, Et_3N, CH_2Cl_2, rt, 30 min; (2) NaI, DBU, DMF, 80 °C, 30 min; (3) $BH_3{\cdot}SMe_2$, THF, rt, 1 h, and then saturated aqueous $NaHCO_3$, 30% aqueous H_2O_2 (3 steps, **35**, 13%; **37**, 15%; **36**, 15%; **38**, 16%; **40**, 23%). (e) (1) MsCl, Et_3N, CH_2Cl_2, rt, 30 min; (2) super-H, THF, rt for **5-H**–**9-H**, 60 °C for **10-H**, 2.5 h; (3) H_2, 5% Pd/C, EtOAc, ambient temperature, 4 h (3 steps, **5-H**, 27%; **6-H**, 24%; **7-H**, 12%; **8-H**, 15%; **9-H**, 24%; **10-H**, 13%).

145.0 (C-4, C-4′), 146.6 (C-3, C-3′); MS (EI) m/z 404 (M^+, 51), 175 (100); HRMS (EI) m/z calcd for $C_{22}H_{28}O_7$ (M^+) 404.1835, found 404.1833.

*(7S,7′S,8R,8′R)-3,3′,9,9′-Tetramethoxy-7,7′-epoxylignane-4,4′-diol, **11** (**4-OCH$_3$**):* colorless crystals; mp 130–131 °C; $[\alpha]^{20}_D$ −29 (c 0.4, $CHCl_3$); NMR data agreed with those of **8**.

*(7R,7′R,8R,8′R)-4,4′-Dibenzyloxy-3,3′-dimethoxy-7,7′-epoxylignane-9,9′-diol, **35**, and (7R,7′R,8R,8′S)-4,4′-dibenzyloxy-3,3′-dimethoxy-7,7′-epoxylignane-9,9′-diol, **37**:* **35**, colorless oil; $[\alpha]^{20}_D$ +44 (c 1.3, $CHCl_3$); ^{1}H NMR (500 MHz, $CDCl_3$) δ 2.50–2.70 (2H, br, OH), 2.67 (2H, m, H-8, H-8′), 3.03–3.10 (2H, m, H-9a, H-9′a), 3.46 (2H, br d, J = 8.0 Hz, H-9b, H-9′b), 3.87 (6H, s, OCH_3), 5.12 (4H, s, OCH_2Ph), 5.48 (2H, d, J = 6.8 Hz, H-7, H-7′), 6.77 (2H, d, J = 8.4 Hz, H-5, H-5′), 6.84–6.86 (4H, m, H-2, H-2′, H-6, H-6′), 7.29–7.30 (2H, m, OBn), 7.34–7.36 (4H, m, OBn), 7.41–7.43 (4H, m, OBn); ^{13}C NMR (125 MHz, $CDCl_3$) δ 49.1 (C-8, C-8′), 56.1 (OCH_3), 62.6 (C-9, C-9′), 71.2 (OCH_2Ph), 82.5 (C-7, C-7′), 110.1 (C-2, C-2′), 114.1 (C-5, C-5′), 118.4 (C-6, C-6′), 127.28 (OBn), 127.33 (OBn), 127.9 (OBn), 128.5 (OBn), 133.6 (C-1, C-1′), 137.1 (OBn), 147.7 (C-4, C-4′), 149.7 (C-3, C-3′); MS (EI) m/z 556 (M^+, 1.5), 91 (100); HRMS (EI) m/z calcd for $C_{34}H_{36}O_7$ (M^+) 556.2462, found 556.2470. **37**, colorless oil; $[\alpha]^{20}_D$ +66 (c 1.1, $CHCl_3$); ^{1}H NMR (500 MHz, $CDCl_3$) δ 2.70 (2H, m, H-8, H-8′), 2.78 (2H, br s, OH), 3.28 (1H, br d, J = 10.2 Hz, H-9a), 3.60 (1H, dd, J = 10.2, 10.2 Hz, H-9b), 3.72–3.85 (2H, m, H-9′), 3.85 (3H, s, OCH_3), 3.88 (3H, s, OCH_3), 4.91 (1H, d, J = 9.0 Hz, H-7′), 5.12 (2H, s, OCH_2Ph), 5.13 (2H, s, OCH_2Ph), 5.43 (1H, d, J = 4.7 Hz, H-7), 6.78 (1H, dd, J = 8.3, 1.6 Hz, H-6), 6.82–6.86 (3H, m, H-5, H-5′, H-6′), 6.90 (1H, d, J = 1.8 Hz. H-2), 6.95 (1H, d, J = 1.6 Hz, H-2′), 7.27–7.30 (2H, m, OBn), 7.33–7.36 (4H, m, OBn), 7.41–7.42 (4H, m, OBn); ^{13}C NMR (125 MHz, $CDCl_3$) δ 48.4 (C-8), 54.3 (C-8′), 56.09 (OCH_3), 56.11 (OCH_3), 59.8 (C-9′), 59.9 (C-9), 71.18 (OCH_2Ph), 71.23 (OCH_2Ph), 81.0 (C-7), 83.0 (C-7′), 109.6 (C-2′), 109.7 (C-2), 114.2 (C-5), 114.3 (C-5′), 117.9 (C-6′), 118.4 (C-6), 127.28 (OBn), 127.34 (OBn), 127.8 (OBn), 127.9 (OBn), 128.5 (OBn), 132.4 (C-1), 135.7 (C-1′), 137.15 (OBn), 137.18 (OBn), 147.4 (C-4), 147.9 (C-4′), 149.8 (C-3), 150.0 (C-3′); MS (EI) m/z 556 (M^+, 0.3), 137 (31), 91 (100); HRMS (EI) m/z calcd for $C_{34}H_{36}O_7$ (M^+) 556.2462, found 556.2467.

*(7S,7′S,8S,8′S)-4,4′-Dibenzyloxy-3,3′-dimethoxy-7,7′-epoxylignane-9,9′-diol, **36**, and (7S,7′S,8S,8′R)-4,4′-dibenzyloxy-3,3′-dimethoxy-7,7′-epoxylignane-9,9′-diol, **38**:* **36**, colorless oil; $[\alpha]^{20}_D$ −44

dx.doi.org/10.1021/jf4046396 | J. Agric. Food Chem. 2014, 62, 651–659

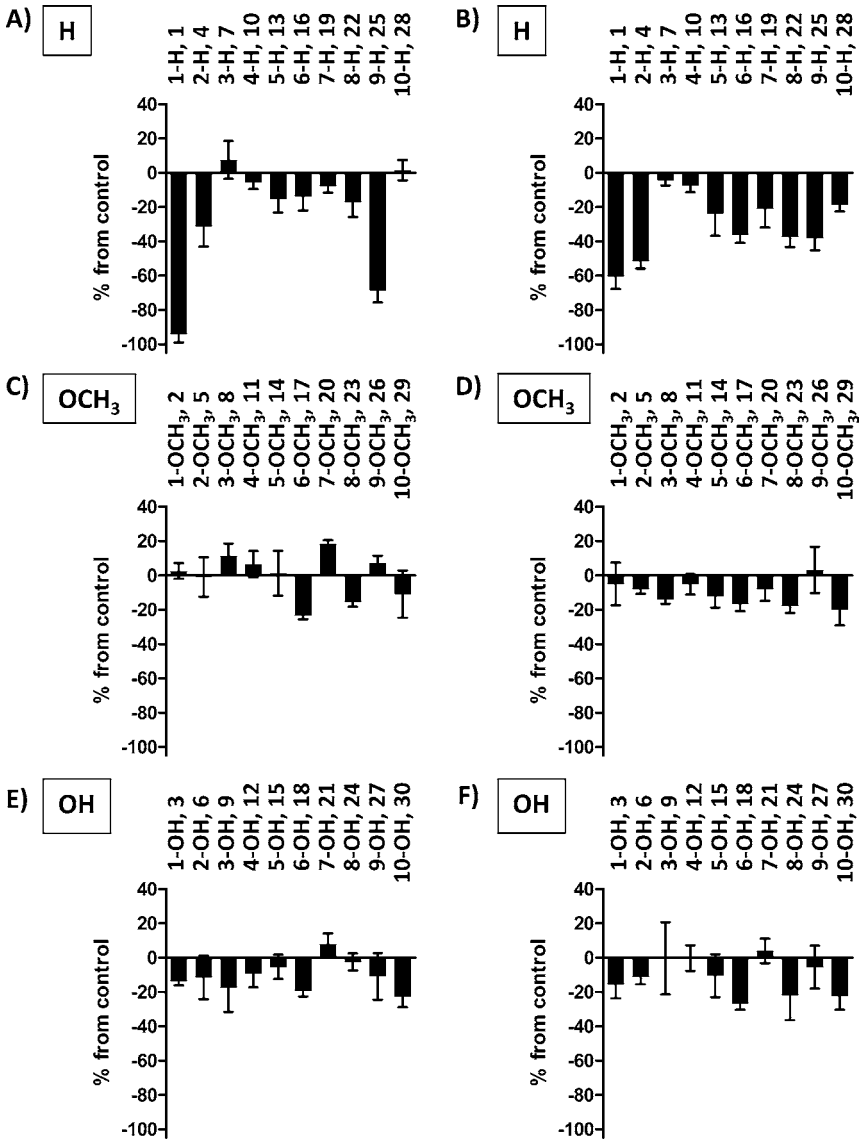

Figure 3. Plant growth inhibitory activity (percent from control) of test chemicals against root (A, C, E) and shoot (B, D, F) of lettuce when applied at the concentration of 1×10^{-3} M. Data are presented as the mean ± standard error of the mean.

(*c* 1.1, $CHCl_3$). **38**, colorless oil; $[\alpha]^{20}_D$ −66 (*c* 1.2, $CHCl_3$). NMR data of **36** and **38** agreed with those of **35** and **37**, respectively.

(7R,7′R,8R,8′R)-3,3′,9,9′-Tetramethoxy-7,7′-epoxylignane-4,4′-diol, ***14 (5-OCH$_3$):*** colorless oil; $[\alpha]^{20}_D$ +21 (*c* 0.2, $CHCl_3$); ^{1}H NMR (500 MHz, $CDCl_3$) δ 2.73 (2H, m, H-8, H-8′), 2.85 (2H, dd, *J* = 9.4, 6.7 Hz, H-9a, H-9′a), 3.13 (2H, dd, *J* = 9.4, 2.6 Hz, H-9b, H-9′b), 3.16 (6H, s, 9-OCH_3, 9′-OCH_3), 3.90 (6H, s, 3-OCH_3, 3′-OCH_3), 5.54 (2H, d, *J* = 6.6 Hz, H-7, H-7′), 5.57 (2H, s, ArOH), 6.84 (2H, dd, *J* = 8.2, 1.5 Hz, H-6, H-6′), 6.89−6.90 (4H, m, H-2, H-2′, H-5, H-5′); ^{13}C NMR (125 MHz, $CDCl_3$) δ 45.4 (C-8, C-8′), 56.0 (9-OCH_3, 9′-OCH_3), 58.7 (3-OCH_3, 3′-OCH_3), 71.9 (C-9, C-9′), 82.4 (C-7, C-7′), 109.0 ((C-2, C-2′), 114.0 (C-5, C-5′), 119.3 (C-6, C-6′), 132.3 (C-1, C-1′), 144.7 (C-4, C-4′), 146.3 (C-3, C-3′); MS (EI) *m*/*z* 404 (M^+, 14), 210 (100), 194 (53), 175 (94); HRMS (EI) *m*/*z* calcd for $C_{22}H_{28}O_7$ (M^+) 404.1835, found 404.1831.

(7S,7′S,8S,8′S)-3,3′,9,9′-Tetramethoxy-7,7′-epoxylignane-4,4′-diol, ***17 (6-OCH$_3$):*** colorless oil; $[\alpha]^{20}_D$ −20 (*c* 0.1, $CHCl_3$); NMR data agreed with those for **14**.

(7R,7′R,8R,8′S)-3,3′,9,9′-Tetramethoxy-7,7′-epoxylignane-4,4′-diol, ***20 (7-OCH$_3$):*** colorless oil; $[\alpha]^{20}_D$ +39 (*c* 0.2, $CHCl_3$); ^{1}H NMR (500 MHz, $CDCl_3$) δ 2.67 (1H, m, H-8′), 2.74 (1H, m, H-8), 3.09 (1H, dd, *J* = 9.8, 5.3 Hz, H-9a), 3.12 (3H, s, 9-OCH_3), 3.21 (1H, dd, *J* = 9.8, 4.1 Hz, H-9b), 3.30 (3H, s, 9′-OCH_3), 3.44 (1H, dd, *J* = 9.3, 5.8 Hz, H-9′a), 3.62 (1H, dd, *J* = 9.3, 8.5 Hz, H-9′b), 3.895 (3H, s, 3-OCH_3), 3.899 (3H, s, 3′-OCH_3), 4.98 (1H, d, *J* = 8.5 Hz, H-7′), 5.44 (1H, d, *J* = 6.2 Hz, H-7), 5.56 (1H, s, ArOH), 5.57 (1H, s, ArOH), 6.83 (1H, dd, *J* = 8.1, 1.5 Hz, H-6), 6.85−6.91 (3H, m, H-5, H-5′, H-6′), 6.95 (1H, d, *J* = 1.5 Hz, H-2), 7.03 (1H, d, *J* = 1.5 Hz, H-2′); ^{13}C NMR (125 MHz, $CDCl_3$) δ 46.2 (C-8), 51.7 (C-8′), 56.0 (9-OCH_3, 9′-OCH_3), 58.5 (3-OCH_3), 58.8 (3′-OCH_3), 69.3 (C-9), 70.5 (C-9′), 82.7 (C-7′), 83.6 (C-7), 108.5 (C-2′), 109.1 (C-2), 113.8 (C-5), 114.1 (C-5′), 119.20 (C-6′), 119.23 (C-6), 131.8 (C-1), 135.4 (C-1′), 145.1 (C-4, C-4′), 146.3 (C-3), 146.7 (C-3′); MS (EI) *m*/*z* 404 (M^+, 28), 210 (51), 207 (63), 175 (100); HRMS (EI) *m*/*z* calcd for $C_{22}H_{28}O_7$ (M^+) 404.1835, found 404.1836.

(7R,7′R,8R,8′S)-3,3′-Dimethoxy-7,7′-epoxylignane-4,4′,9,9′-tetraol, ***21 (7-OH):*** colorless oil; $[\alpha]^{20}_D$ +56 (*c* 0.1, MeOH); ^{1}H NMR (500 MHz, CD_3OD) δ 2.71 (2H, m, H-8, H-8′), 3.53 (1H, dd, *J* = 11.5, 8.8 Hz, H-9), 3.68 (1H, dd, *J* = 11.5, 4.5 Hz, H-9), 3.80−3.92 (2H, overlapped, H-9′, H-9′), 3.85 (3H, s, 3-OCH_3), 3.88 (3H, s, 3′-OCH_3), 4.98 (1H, d, *J* = 8.5 Hz, H-7′), 5.47 (1H, d, *J* = 5.4 Hz, H-7), 6.77−6.83 (3H, m, H-5, H-5′, H-6), 6.86 (1H, dd, *J* = 8.3, 1.8 Hz, H-6′), 6.97 (1H, d, *J* = 1.4 Hz, H-2), 7.01 (1H, d, *J* = 1.8 Hz, H-2′); ^{13}C NMR (125 MHz, CD_3OD) δ 55.4 (C-8, C-8′), 56.46 (3-OCH_3), 56.51 (3′-OCH_3), 60.0 (C-9), 60.5 (C-9′), 83.1 (C-7′), 84.7 (C-7), 110.88 (C-2′), 110.94 (C-2), 116.0 (C-5), 116.2 (C-5′), 119.8 (C-6′),

dx.doi.org/10.1021/jf4046396 | J. Agric. Food Chem. 2014, 62, 651−659

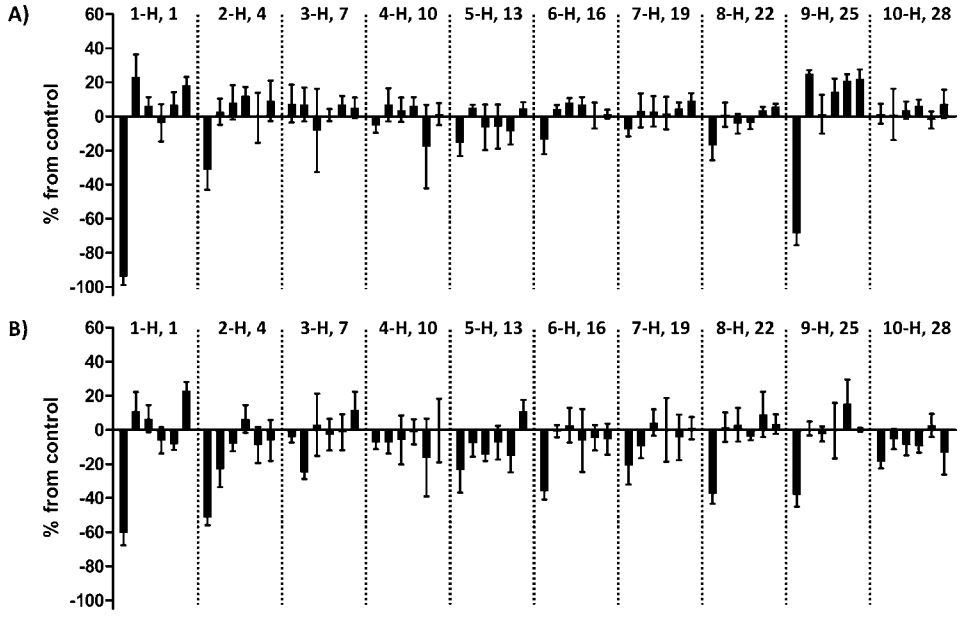

Figure 4. Plant growth inhibitory activity (percent from control) of **1-H**−**10-H** against root (A) and shoot (B) of lettuce when applied at concentrations from 1×10^{-3} to 1×10^{-8} M (from left to right for each compound). The plant growth activity of the commercial herbicide, diuron, was as follows: for root (1×10^{-3}−1×10^{-8} M), −48.5 ± 1.78%, −37.6 ± 1.48%, −9.9 ± 3.05%, −2.8 ± 5.09%, −8.2 ± 4.04%, and 0.0 ± 7.85%; for shoot (1×10^{-3}−1×10^{-8} M), −29.9 ± 5.09%, −23.7 ± 1.06%, +7.8 ± 6.67%, +13.9 ± 6.24,% +8.1 ± 6.24%, and +9.0 ± 1.55%. Data are presented as the mean ± standard error of the mean.

120.2 (C-6), 132.3 (C-1), 135.6 (C-1′), 146.8 (C-4), 147.3 (C-4′), 148.9 (C-3), 149.2 (C-3′); MS (EI) *m*/*z* 376 (M^+, 49), 193 (79), 175 (86), 151 (100), 137 (84); HRMS (EI) *m*/*z* calcd for $C_{20}H_{24}O_7$ (M^+) 376.1522, found 376.1519.

(7S,7′S,8S,8′R)-3,3′,9,9′-Tetramethoxy-7,7′-epoxylignane-4,4′-diol, ***23 (8-OCH$_3$):*** colorless oil; $[\alpha]^{20}_D$ −39 (*c* 0.2, $CHCl_3$); NMR data agreed with those of **20**.

(7S,7′S,8S,8′R)-3,3′-Dimethoxy-7,7′-epoxylignane-4,4′,9,9′-tetraol, ***24 (8-OH):*** colorless oil; $[\alpha]^{20}_D$ −56 (*c* 0.1, MeOH); NMR data agreed with those of **21**.

(7R,7′S,8S,8′R)-4,4′-Dibenzyloxy-3,3′-dimethoxy-7,7′-epoxylignane-9,9′-diol, ***39:*** colorless crystals; mp 79−80 °C (MeOH); ^{1}H NMR (500 MHz, $CDCl_3$) δ 2.57 (2H, m, H-8, H-8′), 3.19 (2H, br s, OH), 3.75 (2H, dd, *J* = 11.4, 2.6 Hz, H-9, H-9′), 3.87 (6H, s, OCH_3), 3.89 (2H, dd, *J* = 11.4, 3.9 Hz, H-9, H-9′), 4.62 (2H, d, *J* = 7.3 Hz, H-7, H-7′), 5.14 (4H, s, OCH_2Ph), 6.85 (2H, d, *J* = 8.3 Hz, H-5, H-5′), 6.89 (2H, dd, *J* = 8.3, 1.8 Hz, H-6, H-6′), 6.99 (2H, d, *J* = 1.8 Hz), 7.28−7.30 (2H, m, OBn), 7.34−7.37 (4H, m, OBn), 7.42−7.43 (4H, m, OBn); ^{13}C NMR (125 MHz, $CDCl_3$) δ 51.6 (C-8, C-8′), 56.0 (OCH_3), 60.4 (C-9, C-9′), 71.1 (OCH_2Ph), 82.1 (C-7, C-7′), 110.4 (C-2, C-2′), 114.0 (C-5, C-5′), 118.8 (C-6, C-6′), 127.3 (OBn), 127.8 (OBn), 128.5 (OBn), 134.3 (C-1, C-1′), 137.1 (OBn), 148.0 (C-4, C-4′), 149.8 (C-3, C-3′). Anal. Found: C, 73.40%; H, 6.34%. Calcd for $C_{34}H_{36}O_7$: C, 73.36%; H, 6.52%.

(7R,7′S,8S,8′R)-3,3′,9,9′-Tetramethoxy-7,7′-epoxylignane-4,4′-diol, ***26 (9-OCH$_3$):*** colorless oil; ^{1}H NMR (500 MHz, $CDCl_3$) δ 2.61 (2H, m, H-8, H-8′), 3.34 (6H, s, 9-OCH_3, 9′-OCH_3), 3.50 (2H, dd, *J* = 9.5, 5.0 Hz, H-9a, H-9′s), 3.57 (2H, dd, *J* = 9.5, 6.3 Hz, H-9b, H-9′b), 3.84 (6H, s, 3-OCH_3, 3′-OCH_3), 4.82 (2H, d, *J* = 6.6 Hz, H-7, H-7′), 5.71 (2H, s, 4-OH, 4′-OH), 6.87 (2H, d, *J* = 8.0 Hz, H-5, H-5′), 6.92 (2H, dd, *J* = 8.0, 1.8 Hz, H-6, H-6′), 6.96 (2H, d, *J* = 1.8 Hz, H-2, H-2′); ^{13}C NMR (125 MHz, $CDCl_3$) δ 49.0 (C-8, C-8′), 55.8 (9-OCH_3, 9′-OCH_3), 58.9 (3-OCH_3, 3′-OCH_3), 70.6 (C-9, C-9′), 82.9 (C-7, C-7′), 109.3 (C-2, C-2′), 114.2 (C-5, C-5′), 119.4 (C-6, C-6′), 134.0 (C-1, C-1′), 145.1 (C-4, C-4′), 146.5 (C-3, C-3′); MS (EI) *m*/*z* 404 (M^+, 30), 210 (73), 194 (54), 175 (100), 151 (52); HRMS (EI) *m*/*z* calcd for $C_{22}H_{28}O_7$ (M^+) 404.1835, found 404.1835.

(7R,7′S,8R,8′S)-4,4′-Dibenzyloxy-3,3′-dimethoxy-7,7′-epoxylignane-9,9′-diol, ***40:*** colorless oil; ^{1}H NMR (500 MHz, $CDCl_3$) δ 2.75 (2H, br s, OH), 2.90 (2H, m, H-8, H-8′), 3.35 (2H, dd, *J* = 11.2, 3.7 Hz, H-9a, H-9′a), 3.43 (2H, dd, *J* = 11.2, 9.9 Hz, H-9b, H-9′b), 3.88 (6H, s, OCH_3), 5.11 (2H, d, *J* = 6.9 Hz, H-7, H-7′), 5.14 (4H, s, OCH_2Ph), 6.87 (4H, s, H-5, H-5′, H-6, H-6′), 6.95 (2H, s, H-2, H-2′), 7.28−7.31 (2H, m, OBn), 7.34−7.37 (4H, m, OBn), 7.42−7.44 (4H, m, OBn); ^{13}C NMR (125 MHz, $CDCl_3$) δ 48.0 (C-8, C-8′), 56.0 (OCH_3), 60.9 (C-9, C-9′), 71.2 (OCH_2Ph), 80.9 (C-7, C-7′), 109.9 (C-2, C-2′), 114.1 (C-5, C-5′), 118.2 (C-6, C-6′), 127.3 (OBn), 127.9 (OBn), 128.6 (OBn), 132.1 (C-1, C-1′), 137.1 (OBn), 147.5 (C-4, C-4′), 149.6 (C-3, C-3′); MS (EI) *m*/*z* 556 (M^+, 0.4), 91 (100); HRMS (EI) *m*/*z* calcd for $C_{34}H_{36}O_7$ (M^+) 556.2462, found 556.2464.

(7R,7′S,8R,8′S)-3,3′,9,9′-Tetramethoxy-7,7′-epoxylignane-4,4′-diol, ***29 (10-OCH$_3$):*** colorless oil; ^{1}H NMR (500 MHz, $CDCl_3$) δ 2.85 (2H, m, H-8, H-8′), 3.03 (2H, dd, *J* = 9.6, 6.1 Hz, H-9a, H-9′a), 3.05 (6H, s, 9-OCH_3, 9′-OCH_3), 3.26 (2H, dd, *J* = 9.6, 6.2 Hz, H-9b, H-9′b), 3.91 (6H, s, 3-OCH_3, 3′-OCH_3), 5.17 (2H, d, *J* = 7.0 Hz, H-7, H-7′), 5.59 (2H, s, 4-OH, 4′-OH), 6.91 (2H, d, *J* = 8.1 Hz, H-5, H-5′), 6.97 (2H, dd, *J* = 8.1, 1.4 Hz, H-6, H-6′), 7.07 (2H, d, *J* = 1.4 Hz, H-2, H-2′); ^{13}C NMR (125 MHz, $CDCl_3$) δ 46.5 (C-8, C-8′), 55.9 (9-OCH_3, 9′-OCH_3), 58.4 (3-OCH_3, 3′-OCH_3), 70.2 (C-9, C-9′), 81.5 (C-7, C-7′), 109.5 (C-2, C-2′), 113.9 (C-5, C-5′), 119.5 (C-6, C-6′), 131.2 (C-1, C-1′), 144.6 (C-4, C-4′), 146.1 (C-3, C-3′); MS (EI) *m*/*z* 404 (M^+, 32), 175 (100); HRMS (EI) *m*/*z* calcd for $C_{22}H_{28}O_7$ (M^+) 404.1835, found 404.1831.

(7R,7′S,8R,8′S)-3,3′-Dimethoxy-7,7′-epoxylignane-4,4′,9,9′-tetraol, ***30 (10-OH):*** colorless oil; ^{1}H NMR (500 MHz, CD_3OD) δ 2.91 (2H, m, H-8, H-8′), 3.29 (2H, dd, *J* = 11.2, 4.2 Hz, H-9a, H-9′a), 3.44 (2H, dd, *J* = 11.2, 10.2 Hz, H-9b, H-9′b), 4.84 (6H, s, OCH_3), 5.13 (2H, d, *J* = 6.9 Hz, H-7, H-7′), 6.82 (2H, d, *J* = 8.1 Hz, H-5, H-5′), 6.89 (2H, dd, *J* = 8.1, 1.7 Hz, H-6, H-6′), 7.02 (2H, d, *J* = 1.7 Hz, H-2, H-2′); ^{13}C NMR (125 MHz, CD_3OD) δ 49.4 (C-8, C-8′), 56.4 (OCH_3), 61.4 (C-9, C-9′), 82.6 (C-7, C-7′), 111.1 (C-2, C-2′), 116.1 (C-5, C-5′), 120.0 (C-6, C-6′), 131.9 (C-1, C-1′), 146.9 (C-4, C-4′), 148.9 (C-3, C-3′); MS (EI) *m*/*z* 376 (M^+, 43), 224 (54), 193 (81), 175 (100), 151 (66), 137 (69); HRMS (EI) *m*/*z* calcd for $C_{20}H_{24}O_7$ (M^+) 376.1522, found 376.1523.

Evaluation of Plant Growth Inhibitory Activity. For all of the synthesized epoxylignane derivatives, their plant growth inhibitory activities were evaluated using lettuce (*L. sativa* L., green-wave (Takii Seed Co. Ltd., Kyoto, Japan)) and Italian ryegrass (*L. multiflorum* Lam., wase-fudo (Takii Seed Co. Ltd., Kyoto, Japan)), according to our earlier paper.[2] Briefly, 30 seeds of each plant were placed on a filter paper (in a 90 mm Petri dish) moisturized with 3 mL of water

dx.doi.org/10.1021/jf4046396 | J. Agric. Food Chem. 2014, 62, 651−659

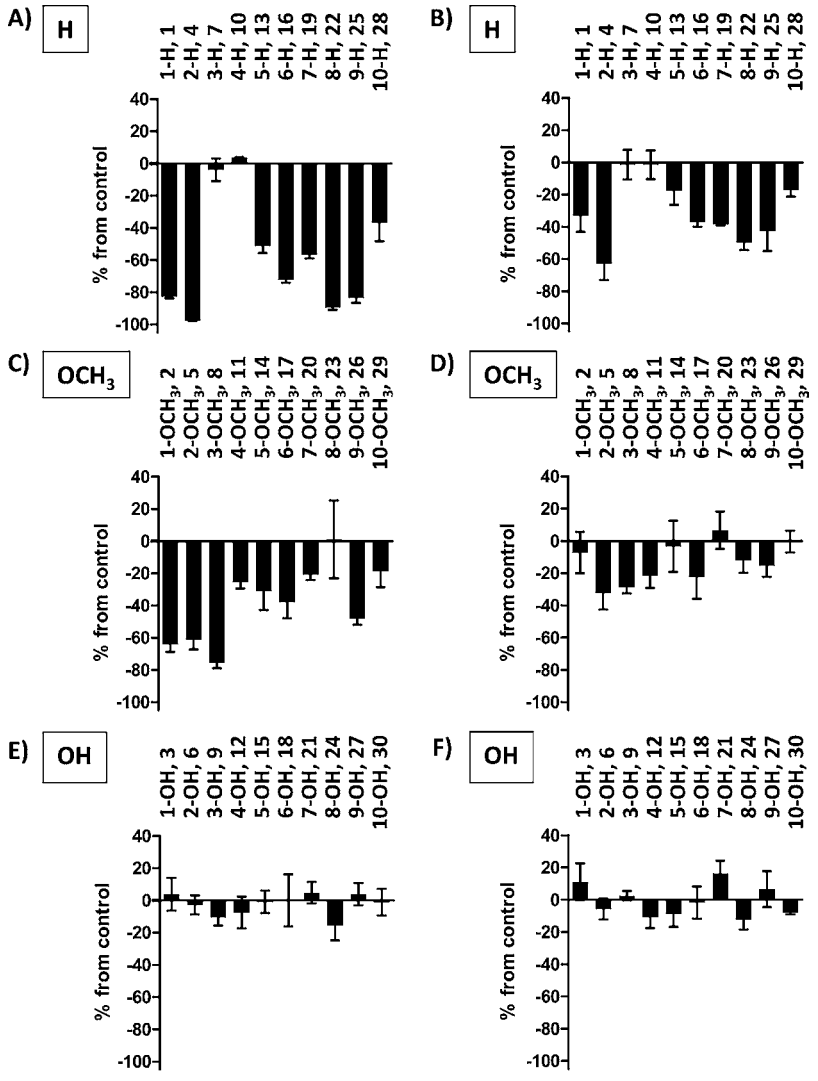

Figure 5. Plant growth inhibitory activity (percent from control) of test chemicals against root (A, C, E) and shoot (B, D, F) of ryegrass when applied at the concentration of 1×10^{-3} M. Data are presented as the mean ± standard error of the mean.

containing each sample at the concentration of 1.0 mM. After they were incubated in the dark at 20 °C for 3 and 5 days for lettuce and grass, respectively, the lengths of their roots and shoots were measured using a ruler. Experiments were performed in triplicate, and statistical analyses were conducted by one-way ANOVA followed by Tukey's multiple-comparison test using PRISM software (Graphpad Software, San Diego, CA, USA).

For compounds **1-H** and **2-H**, the germination rates of lettuce and grass seeds were recorded 3 days after seeding.

■ RESULTS AND DISCUSSION

The intermediates **31**−**34** and **39** were synthesized according to the previously described method with modification.[17−19] The mesylation of the two hydroxyl groups, followed by reduction, gave dimethyl compounds. To obtain **1-H**, **2-H**, **3-H**, and **4-H**, $NaBH_4$ in hexamethylphosphoramide (HMPA) was employed for the corresponding mesylates. On the other hand, lithium triethylborohydride (superhydride) was used for reduction of mesylate from the intermediate **39**, giving **9-H**. To prepare the intermediates **35** and **37**, compound **33** was selected as a starting compound. After conversion of **33** to the corresponding conjugated diene by elimination, hydroboration was tried to give two stereoisomers **35** and **37**. By the same procedure, **36** and **38** were obtained from diol **34**. The intermediate **40** was obtained by the isomerization of **39** using elimination followed by hydroboration. The intermediates **35**−**38** and **40** were subjected to mesylations followed by superhydride reductions, giving **5-H**, **6-H**, **7-H**, **8-H**, and **10-H**, respectively.

Among 10 stereoisomers of **H**-type epoxylignane (**1-H**−**10-H**), the compounds with the configurations of 7*S*,7′*R*,8*R*,8′*R* (**1-H**) and 7*R*,7′*S*,8*R*,8′*S* (**9-H**) suppressed the growth of lettuce root to −94 and −69%, respectively, whereas the other stereoisomers showed less activity (from −25 to +7.5%) (Figure 3A). Against the lettuce shoot (Figure 3B), −60 and −52% inhibitions relative to the control were observed for **1-H** and **2-H**, respectively. On the other hand, **5-H**, **6-H**, **7-H**, **8-H**, and **9-H** suppressed the shoot growth moderately (from −20 to −40%), but statistically insignificant relative to the control. The application of **3-H**, **4-H**, and **10-H** did not influence the lettuce shoot growth. With these results taken together, **1-H** showed the highest potency against lettuce. Introduction of the methoxy and hydroxyl groups to the 9 and 9′ carbon atoms (**1-OCH_3**−**10-OCH_3** and **1-OH**−**10-OH**) induced the absolute values of the growth rate below 25% (Figure 3C−F), demonstrating that the modification of the 9 and 9′ carbon atoms with the methoxy and hydroxyl groups influences the

dx.doi.org/10.1021/jf4046396 | J. Agric. Food Chem. 2014, 62, 651−659

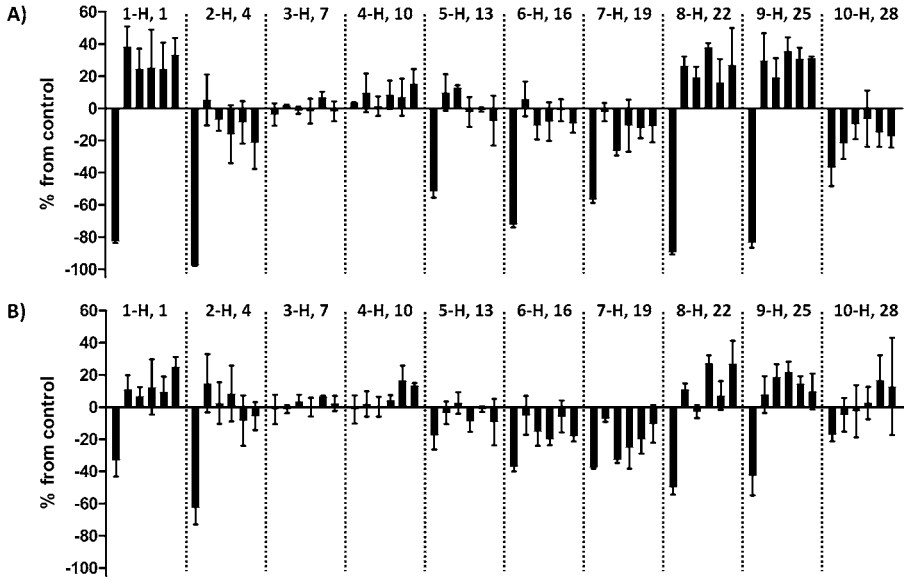

Figure 6. Plant growth inhibitory activity (precent from control) of **1-H**−**10-H** against root (A) and shoot (B) of ryegrass when applied at concentrations from 1×10^{-3} to 1×10^{-8} M (from left to right for each compound). The plant growth activity of the commercial herbicide, diuron, was as follows: for root (1×10^{-3}−1×10^{-8} M), −78.2 ± 3.79%, −49.8 ± 2.47%, −21.8 ± 8.69%, −4.83 ± 1.29%, −0.02 ± 6.1%3, and −9.70 ± 8.83%; for shoot (1×10^{-3}−1×10^{-8} M), −66.7 ± 8.15%, −32.9 ± 6.29%, −24.1 ± 8.59%, −21.9 ± 3.19%, −15.8 ± 5.54%, and −25.4 ± 5.52%. Data are presented as the mean ± standard error of the mean.

activity adversely. At the dose-dependent assay for evaluating the influence on the lettuce growth of the **H**-type epoxylignane compounds, the compounds did not influence the root growth at the diluted concentrations (Figure 4A). The inhibitory activity of **2-H** against the lettuce shoot decreased depending on the dilution of the concentration, but no significant activity was observed for the other compounds at the tested concentrations (Figure 4B).

Ryegrass root was found to be more sensitive to the epoxylignanes than lettuce root (Figure 5). Among the **H**-type epoxylignanes, not only the compounds **1-H** and **9H**, which were active to the lettuce root, but also **2-H**, **5-H**, **6-H**, **7-H**, and **8-H** suppressed the growth of the grass root below −50%, whereas **3-H** and its enantiomer **4-H**, which have the configuration of all *R* and all *S*, respectively, did not show any inhibitory activity (Figure 5A). Among these epoxylignanes, compound **2-H** with the 7*R*,7′*S*,8*S*,8′*S* configuration was the most potent compound, which could suppress the growth of the root almost completely at 1×10^{-3} M. The order of the sensitivity of the grass shoot to the **H**-type epoxylignanes was likely to be similar to that of the sensitivity of the grass root, although the sensitivity of the shoot was relatively less than that of the root (Figure 5A vs 5B). Introduction of the methoxy group induced less activity except the compounds with the configuration of all *R* and all *S*; especially the inhibitory activity of the all *R* configuration compound **3-H**, which showed no activity to the grass shoot, was strengthened up to −76% from control by attaching the methoxy group (**3-OCH$_3$**, Figure 5C). The inhibitory activity against the grass shoot of the compounds having the methoxy group was weak (Figure 5D). The compounds having the hydroxyl group did not influence the growth of grass root as well as shoot (Figure 5E,F). At the dose-dependent assay for evaluating the influence on the grass of the **H**-type epoxylignane compounds, compounds **1-H**, **8-H**, and **9-H** showed a promotive effect on the growth of grass root at diluted concentrations (Figure 6).

The phytotoxicity of all stereoisomers of lariciresinol has been evaluated in our previous paper,[2] in which (−)-lariciresinol and its 7*S*,8*S*,8′*R* stereoisomer have been found to inhibit the growth of Italian ryegrass as well as suppress the germination of the ryegrass seed to some extent. The most potent compound in the present study, **2-H**, inhibited the root growth of ryegrass almost completely, demonstrating that lariciresinol, which suppressed the growth of ryegrass root to around 50%, was less potent than **2-H**. Lariciresinol has the hydroxyl group at the 9-position, and all of the **OH**-type epoxylignanes in the present study were slightly potent, suggesting that hydrophilic features of the compounds having a hydroxyl group at the 9-position should be adverse to the root growth of ryegrass. Because the substitution patterns on the epoxylignanes synthesized in this study are basically different from that of lariciresinol, the effects of the conformations of each compound on the phytotoxicity were not compared.

The germination rate of the lettuce seed applied by **1-H**, which showed the highest inhibitory activity against the lettuce root (Figure 3), was 92.5 ± 1.12% (mean ± SEM, $n = 3$), which was almost the same as the control (95.7 ± 2.15%, $n = 3$). Also, the germination rate of the ryegrass seed applied by **2-H**, which almost completely suppressed the growth of the ryegrass root (Figure 5), was 87.3 ± 2.07% ($n = 3$), which was a little smaller than that of the control (94.7 ± 2.78%, $n = 3$), suggesting that these potent epoxylignanes should not suppress the germination process of the seed, unlike lariciresinol,[2] but influence the development and growth process other than germination. Because the inhibitory effects of the compounds on the shoot of both lettuce and grass were similar (in Figures 3B and 5B, **3-H** and **4-H** were ineffective, but the others suppressed the growth to some degree), the target sites would be the same in both species, although the mode of action of these compounds remains unknown.

Among the epoxylignanes that have been isolated in the previous studies, the antifungal activity[5] and disruption of ion homeostasis of (−)-verrucosin (**1-H**)[22] have been reported.

dx.doi.org/10.1021/jf4046396 | J. Agric. Food Chem. 2014, 62, 651−659

Nectandrin B (**9-H**) was found to activate AMP-activated protein kinase[10,23] and endothelial nitric-oxide synthase phosphorylation,[24] to show neuroprotective effects,[25,26] antifungal,[27] and glucocorticoid receptor binding activity,[28] and to inhibit proliferation,[29,30] hydroxysteroid dehydrogenase,[30] aromatase,[30] topoisomerase,[31] melanin biosynthesis,[32] prostaglandin,[33] and platelet aggregation induction.[34] Tetrahydrofuroguaiacin B (**10-H**) also activated AMP-activated protein kinase.[10] The target sites in the plants of the epoxylignanes synthesized in the present study are still unclear, but the targets should strictly recognize the stereochemistry of the compounds, and the affinity to the target sites may be different among the stereoisomers, because these stereoisomers should have the same physicochemical properties such as hydrophobicity (Clog P) and acidity (pK_a), indicating that the potency of the systemic translocation to the target site would be similar.

In summary, stereoisomers of tetrasubstituted tetrahydrofuran type epoxylignanes were synthesized to evaluate their plant growth inhibitory activity, and it was suggested that the structures of these epoxylignanes should be strictly recognized by the targets in the plants. As seen in the recent reviews for lignans,[35,36] studies on the effect of its fine chemical structure of lignans on their biological activities should be performed routinely. To retrieve the information of the target sites of the epoxylignanes, the structure−activity relationship results in the present study should be useful, and the probe compound will be designed on the basis of the stereochemical structure of the highest potency compound in the future.

■ ASSOCIATED CONTENT

Supporting Information

Additional experimental details. This material is available free of charge via the Internet at http://pubs.acs.org.

■ AUTHOR INFORMATION

Corresponding Author

*(S.Y.) Phone: +81-89-946-9846. Fax: +81-89-977-4364. E-mail: syamauch@agr.ehime-u.ac.jp.

Funding

Part of this study was performed at the INCS (Johoku station) of Ehime University. We are grateful to Marutomo Co. for financial support.

Notes

The authors declare no competing financial interest.

■ REFERENCES

(1) Finefield, J. M.; Sherman, D. H.; Kreitman, M.; Williams, R. M. Enantiomeric natural products: occurrence and biogenesis. *Angew. Chem., Int. Ed.* **2012**, *51*, 4802−4836.

(2) Nishiwaki, H.; Kumamoto, M.; Shuto, Y.; Yamauchi, S. Stereoselective syntheses of all stereoisomers of lariciresinol and their plant growth inhibitory activities. *J. Agric. Food Chem.* **2011**, *59*, 13089−13095.

(3) Rimando, A.; Dayan, F. E.; Mikell, J. R.; Moraes, R. M. Phytotoxic lignans of *Leucophyllum frutescens*. *Nat. Toxins* **1999**, *7*, 39−43.

(4) Carillo, P.; Cozzolino, C.; D'Abrosca, B.; Nacca, F.; DellaGreca, M.; Fiorentio, A.; Fuggi, A. Effects of the allelochemicals dihydrodiconiferyl alcohol and lariciresinol on metabolism of *Lactuca sativa*. *Open Bioact. Compd. J.* **2010**, *3*, 18−24.

(5) Sartorelli, P.; Young, M. C. M.; Kato, M. J. Antifungal lignans from the arils of *Virola oleifera*. *Phytochemistry* **1998**, *47*, 1003−1006.

(6) Giang, P. M.; Son, P. T.; Matsunami, K.; Otsuka, H. New neolignans and lignans from vietnamese medicinal plant *Machilus odoratissima* Nees. *Chem. Pharm. Bull.* **2006**, *54*, 380−383.

(7) Hattori, M.; Hada, S.; Kawata, Y.; Tezuka, Y.; Kikuchi, T.; Namba, T. New 2,5-bis-aryl-3,4-dimethyltetrahydrofuran lignans from the aril of *Myristica fragrans*. *Chem. Pharm. Bull.* **1987**, *35*, 3315−3322.

(8) Schöttner, M.; Reiner, J.; Tayman, F. K. (+)-*neo*-Olivil from roots of *Urtica dioica*. *Phytochemistry* **1997**, *46*, 1107−1109.

(9) Rao, K. V.; Oruganty, R. S. An improved method for the isolation of the lignan constituents of *Saururus cernuus* by reverse phase column chromatography. *J. Liq. Chromatogr. Relat. Technol.* **1997**, *20*, 3121−3134.

(10) Nguyen, P. H.; Le, T. V. T.; Kang, H. W.; Chae, J.; Kim, S. K.; Kwon, K.; Seo, D. B.; Lee, S. J.; Oh, W. K. AMP-activated protein kinase (AMPK) activators from *Myristica fragrans* (nutmeg) and their anti-obesity effect. *Bioorg. Med. Chem. Lett.* **2010**, *20*, 4128−4131.

(11) Hernandez, A.; Pascual, C.; Valverde, S. Neo-olivil, a new lignan from *Thymus longiflorus*. *Phytochemistry* **1981**, *20*, 181−182.

(12) Shimomura, H.; Sashida, Y.; Oohara, M. Lignan from *Machilus thunbergii*. *Phytochemistry* **1988**, *27*, 634−636.

(13) Kim, H.; Wooten, C. M.; Park, Y.; Hong, J. Stereoselective synthesis of tetrahydrofuran lignans via $BF_3.OEt_2$-promoted reductive deoxygenation/epimerization of cyclic hemiketal: synthesis of (−)-odoratisol C, (−)-futokadsurin A, (−)-veraguensin, (+)-fragransin A2, (+)-gabelgin, and (+)-talaumidin. *Org. Lett.* **2007**, *9*, 3965−3968.

(14) Hanessian, S.; Reddy, G. J.; Chahal, N. Total synthesis and stereochemical confirmation of manassantin A, B, and B_1. *Org. Lett.* **2006**, *8*, 5477−5480.

(15) Kim, H.; Kasper, A. C.; Moon, E. J.; Park, Y.; Wooten, C. M.; Dewhirst, M. W.; Hong, J. Nucleophilic addition of organozinc reagents to 2-sulfonyl cyclic ethers: stereoselective synthesis of manassantins A and B. *Org. Lett.* **2009**, *11*, 89−92.

(16) Kraus, R.; Spiteller, G. Lignanglucoside aus wurzeln von *Urtica dioica*. *Liebigs Ann. Chem.* **1990**, 1205−1213.

(17) Yamauchi, S.; Okazaki, M.; Akiyama, K.; Sugahara, T.; Kishida, T.; Kashiwagi, T. First enantioselective synthesisof (−)- and (+)-virgatusin, tetra-substituted tetrahydrofuran lignan. *Org. Biomol. Chem.* **2005**, *3*, 1670−1675.

(18) Yamauchi, S.; Nakato, T.; Tsuchiya, M.; Akiyama, K.; Maruyama, M.; Sugahara, T.; Kishida, T. Use of the benzyl mesylate for the synthesis of tetrahydrofuran lignan: syntheses of 7,8-*trans*, 7′,8′-*trans*, 7,7′-*cis*, and 8,8′-*cis*-virgatusin stereoisomers. *Biosci., Biotechnol., Biochem.* **2007**, *71*, 2248−2255.

(19) Nakato, T.; Yamauchi, S.; Tago, R.; Akiyama, K.; Maruyama, M.; Sugahara, T.; Kishida, T.; Koba, Y. Syntheses and antimicrobial activity of tetrasubstituted tetrahydrofuran lignan stereoisomers. *Biosci., Biotechnol., Biochem.* **2009**, *73*, 1608−1617.

(20) Moss, G. P. Nomenclature of lignans and neolignans (IUPAC recommendations 2000). *Pure Appl. Chem.* **2000**, *72*, 1493−1523.

(21) Chaurasia, V. N.; Wichtl, M. Phenylpropane und lignane aus der wurzel von *Urtica dioica*. *Dtsch. Apoth. Ztg.* **1986**, *126*, 1559−1563.

(22) Akiyama, K.; Tone, J.; Yamauchi, S.; Sugahara, T.; Maruyama, M.; Kakinnuma, Y. Disruption of ion homeostasis by verrucosin and a related compound. *Biosci., Biotechnol., Biochem.* **2011**, *75*, 1000−1002.

(23) Nguyen, P. H.; Kang, H. W.; Le, T. V. T.; Chae, J.; Kim, S. K.; Kwon, K. I.; Lim, S. I.; Oh, W. K. Simple process for the decrease of myristicin content from *Myristica fragrans* (nutmeg) and its activity with AMP-activated protain kinase (AMPK). *J. Food Biochem.* **2011**, *35*, 1715−1722.

(24) Hien, T. T.; Oh, W. K.; Nguyen, P. H.; Oh, S. J.; Lee, M. Y.; Kang, K. W. Nectandrin B activates endothelial nitric-oxide synthase phosphorylation in endothelial cells: role of the AMP-activated protein kinase/estrogen receptor α/phosphatidylinositol 3-kinase/Akt pathway. *Mol. Pharmacol.* **2011**, *80*, 1166−1178.

(25) Na, C. S.; Hong, S. S.; Choi, Y.-H.; Lee, Y. H.; Hong, S. H.; Lim, J.-Y.; Kang, B. H.; Park, S.-Y.; Lee, D. Neuroprotective effects of constituents of *Eragrostis ferruginea* against a β-induced toxicity in PC 12 cells. *Arch. Pharm. Res.* **2010**, *33*, 999−1003.

(26) Zhai, H.; Inoue, T.; Moriyama, M.; Esumi, T.; Mitsumoto, Y.; Fukuyama, Y. Neuroprotective effects of 2,5-diaryl-3,4-dimethyltetrahydrofuran neolignans. *Biol. Pharm. Bull.* **2005**, *28*, 289−293.

(27) Cho, J. Y.; Choi, G. J.; Son, S. W.; Jang, K. S.; Lim, H. K.; Lee, S. O.; Sung, N. D.; Cho, K. Y.; Kim, J.-C. Isolation and antifungal activity of lignans from *Myristica fragrans* against various plant pathogenic fungi. *Pest Manag. Sci.* **2007**, *63*, 935−940.
(28) Davis, R. A.; Carroll, A. R.; Duffy, S.; Avery, V. M.; Guymer, G. P.; Forster, P. I.; Quinn, R. J. Endiandrin A, a potent glucocorticoid receptor binder isolated from the Australian plant *Endiandra anthropophagorum*. *J. Nat. Prod.* **2007**, *70*, 1118−1121.
(29) Lee, J. W.; Choi, Y. H.; Yoo, M. Y.; Choi, S. U.; Hong, K.-S.; Lee, B. H.; Yon, G. H.; Ryu, S. Y. Inhibitory effects of the seed extract of Myristicae semen on the proliferation of human tumor cell line (II). *Kor. J. Pharmacog.* **2006**, *37*, 206−211.
(30) Filleur, F.; Le Bail, J. C.; Duroux, J. L.; Simon, A.; Chulia, A. J. Antiproliferative, anti-aromatase, anti-17β-HSD and antioxidant activity of lignans isolated from *Myristica argentea*. *Planta Med.* **2001**, *67*, 700−704.
(31) Li, G.; Lee, C.-S.; Woo, M.-H.; Lee, S.-H.; Chang, H.-W.; Son, J.-K. Lignans from the bark of *Machilus thunbergii* and their DNA topoisomerases I and II inhibition and cytotoxicity. *Biol. Pharm. Bull.* **2004**, *27*, 1147−1150.
(32) Li, G.; Ju, H. K.; Chang, H. W.; Jahng, Y.; Lee, S.-H.; Son, J.-K. Melanin biosynthesis inhibitors from the bark of *Machilus thunbergii*. *Biol. Pharm. Bull.* **2003**, *26*, 1039−1041.
(33) Sadhu, S. K.; Okuyama, E.; Fujimoto, H.; Ishibashi, M. Separation of *Leucas aspera*, a medicinal plant of Bangladesh, guided by prostaglandin inhibitory and antioxidant activities. *Chem. Pharm. Bull.* **2003**, *51*, 595−598.
(34) Wang, B.-G.; Hong, X.; Li, L.; Zhou, J.; Hao, X.-J. Chemical constituents of two Chinese Magnoliaceae plants, *Tsoongiodendron odorum* and *Manglietiastrum sinicum*, and their inhibition of platelet aggregation. *Planta Med.* **2000**, *66*, 511−515.
(35) Satake, H.; Ono, E.; Murata, J. Recent advances in the metabolic engineering of lignan biosynthesis pathways for the production of transgenic plant-based foods and supplements. *J. Agric. Food Chem.* **2013**, *61*, 11721−11729.
(36) DellaGreca, M.; Zuppolini, S.; Zarrelli, A. Isolation of lignans as seed germination and plant growth inhibitors from Mediterranean plants and chemical synthesis of some analogues. *Phytochem. Rev.* **2013**, *12*, 717−731.

JOURNAL OF AGRICULTURAL AND FOOD CHEMISTRY

Article

pubs.acs.org/JAFC

Isolation of Megaritolactones and Other Bioactive Metabolites from 'Megaritiki' Table Olives and Debittering Water

Evgenia Mousouri, Eleni Melliou, and Prokopios Magiatis*

Department of Pharmacognosy and Natural Products Chemistry, Faculty of Pharmacy, University of Athens, Panepistimiopolis Zografou, GR-15771 Athens, Greece

Supporting Information

ABSTRACT: 'Megaritiki' is an olive cultivar widely used in Greece for the production of low polyphenol olive oil and table olives. To investigate possible metabolic differentiation in comparison with other varieties, the composition of 'Megaritiki' olive fruits and wastewaters from the debittering procedure was studied. Moreover, the recovery of bioactive metabolites from wastewater using adsorption resin was studied to exploit this byproduct. Metabolites in fruits and wastewaters were monitored using NMR spectroscopy. The major constituents of wastewater were hydroxytyrosol-4-*O*-glucoside, 11-methyl-oleoside, hydroxytyrosol, and tyrosol but not oleuropein. Furthermore, wastewater afforded rengyoxide and rengyoside B, which are for the first time isolated from olives. The final edible olives, besides hydroxytyrosol and tyrosol, contained rengyoxide and cleroindicin C, which are the first isolated from the species, haleridone for the first time isolated from edible olives, and four metabolites, which are the first reported as natural products, megaritodilactone, megaritolactonic acid, methyl ester of megaritolactonic acid B, and megaritolactonol.

KEYWORDS: *Olea europaea, 'Megaritiki', table olives, iridoid, qNMR*

INTRODUCTION

Table olives are used as a typical part of the Mediterranean diet since antiquity. They contain a large number of minor constituents[1] with interesting bioactivities, which are mainly dependent on the olive variety and the followed debittering process.[2,3] In general, olive fruits undergo a debittering procedure that removes totally or partially the natural bitterness that is mainly due to oleuropein, **1**. A few years ago, we performed a screening of the major table olive varieties found in the Greek market, and we identified varieties with high oleuropein, **1**, and/or hydroxytyrosol, **2**, content in the final edible product.[3] Both compounds have important antioxidant activities, and they have been correlated with protection from LDL oxidation.[4] The role of hydroxytyrosol and oleuropein derivatives has been recently recognized by the European Union for olive oil but not yet for edible olives. A significant observation[3] concerning the olive debittering method was that the use of dry salt and not brine can lead to table olives with high oleuropein content and potentially increased health protecting properties. However, one of the varieties that had been included in the previous study and that had been treated with dry salt without giving high oleuropein content was cv. 'Megaritiki'. This fact had been initially attributed to a possible metabolic differentiation of that specific variety without further study.

Meanwhile, we studied extensively the olive oil produced by the major olive oil producing varieties in Greece, and again we found that the olive oil from cv. 'Megaritiki' presented very low concentration of secoiridoid derivatives (oleocanthal, oleacein, oleuropein aglycone, and ligstroside aglycone).[5] This specific variety is widely cultivated in regions like Attica for the production of both table olives and olive oil (dual use variety). The olive oil of that cultivar is known in the market as a low bitterness oil, which is in accordance with the low recorded content of the usual secoiridoid derivatives responsible for pungency and bitterness. Moreover, the table olives from that variety belong to a group of cultivars that require traditionally little processing to debitter, indicating that oleuropein levels in the untreated fruit of this variety are lower comparatively to others. A simple method, known since antiquity for the debittering of this variety, is crushing and placement for a few days in water. The olives produced with this method are traditionally known as "klastades".

All of the above observations led us to investigate that specific variety for possible metabolic differentiation. For this purpose, we studied the initial metabolic profile of the untreated olive fruits for the presence of oleuropein, and in a next step we studied the major compounds recovered from the debittering wastewater, and finally we studied the chemical constituents of the final edible product (Figure 1).

MATERIALS AND METHODS

General Experimental Procedures. NMR spectra were recorded on Avance 600 (with cryoprobe) and DRX400 spectrometers (Bruker, Rheinstetten, Germany); chemical shifts are expressed in ppm downfield from TMS. Column chromatography was performed on columns containing Si gel 60 (40−63 μm) (Merck, Darmstadt, Germany). Thin layer chromatography (TLC) was performed on plates coated with Si gel 60 F_{254} Merck, 0.25 mm. For HPLC−MS analysis, the column used was a 150 mm × 2.0 mm i.d., 5 μm, PolymerX RP-1 (Phenomenex, Torrance, CA). Samples (5 μL) were dissolved in methanol and injected onto HPLC−MS. A standard

Received: October 17, 2013
Revised: December 30, 2013
Accepted: January 2, 2014
Published: January 2, 2014

ACS Publications © 2014 American Chemical Society

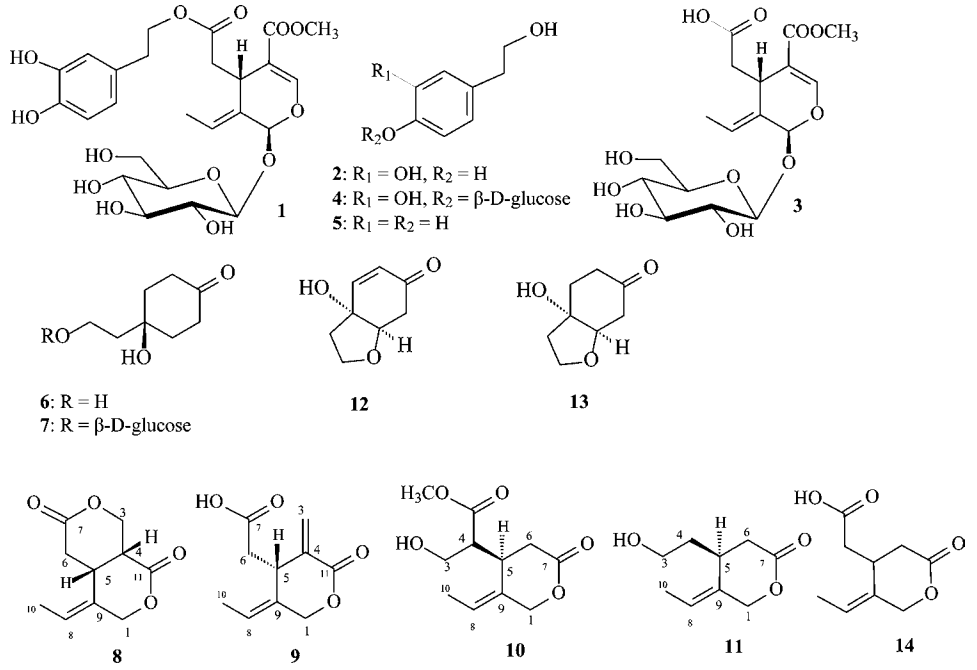

Figure 1. Structures of compounds **1**−**14**.

reverse phase linear gradient with acidified water (0.1% formic acid) and acetonitrile was run over 30 min at a flow rate of 250 μL/min, and the eluent was monitored for negative anions by a LTQ Orbitrap (Thermo Fisher Scientific, Waltham, MA) operated in the centroided mode. Source parameters were 5.5 kV spray voltage, capillary temperature of 275 °C, and nitrogen sheath gas setting of 20 mL/min. Data were acquired at a resolution setting of 60 000 fwhm with the lockmass feature, which typically results in a mass accuracy <2 ppm.

Preparation of Table Olives. Olives of the 'Megaritiki' cultivar used in this study were collected in August, October, and November 2011 from Salamina island. The olives collected in November were water-cured according to a traditional method of debittering as follows: olive fruits (3 kg) were soaked in water (3 L) for 1 day, and the second day each olive was removed, incised, and subsequently added to water (3 L). The water was replaced daily for 5 days. At the end of the sixth day, water-cured olives were placed in brine (salt solution of 10% NaCl) and stored until further analysis. Debittering wastewaters were stored separately for each day at −20 °C until analysis.

Sample Preparation for NMR Analysis. The fruits were collected and analyzed in the same day. The fruits were first washed with water, and then the stone and the flesh were separated and mashed using a laboratory blender. The olive flesh (10 g) was extracted with 25 mL of a MeOH/H_2O mixture (4:1) in a supersonic bath for 45 min. The supernatant was separated from the flesh by centrifugation at 3400*g* for 10 min. Next, 25 mL of hexane was added for oil removal, agitated for 30 s, and then the methanol extract was separated by subsequent centrifugation at 3400*g* for 3 min. The volume of the methanol phase was measured, and 1/20 of the extract was used for NMR analysis. The appropriate volume of methanol extract was mixed with 0.5 mL of the internal standard solution (0.5 mg of syringaldehyde/mL in acetonitrile) and evaporated under reduced pressure at 40 °C.

Quantitative NMR Analysis of Oleuropein Content. The dry extract was dissolved in 600 μL of CD_3OD. ^{1}H NMR spectra were recorded at 400 MHz. 32 scans were collected, and the spectra were phased corrected and integrated automatically using TopSpin software (Bruker). The quantitation was based on the integration ratio between the aldehydic proton signal of syringaldehyde at 9.75 ppm and the proton of oleuropein appearing at 5.91 ppm. Calibration curve of oleuropein was prepared at seven different concentrations ranging between 70 and 4500 μg in tube. The solutions for the construction of the calibration curve were prepared by mixing appropriate volumes of a stock solution of pure oleuropein (Extrasynthese, Genay, France) (1 mg/mL in MeOH) with 0.5 mL of the internal standard solution (0.5 mg of syringaldehyde/mL in acetonitrile) and evaporation under reduced pressure at 40 °C. The equation used for the quantitation of oleuropein in tube was $y = 0.512x + 0.0904$, with $r^2 = 0.995$.

Study of the Debittering Wastewaters. *Treatment with Resins.* After filtration through filter paper, wastewater from each day was separately passed through a column containing adsorption resin. A column of 3.5 cm diameter filled with 250 g of Amberlite XAD-4 resin (Rohm and Haas, Philadelphia, PA) (BV = 375 mL), was used. The feeding flow rate was 750 mL/h (2 BV/h). The resin total feeding duration was 2 h. The procedure above refers to 1.5 L of wastewater. After the adsorption, the subsequent regenerating procedure consisted of three steps. The first one included resin wash by water until the water effluent was colorless. Afterward, the resin was regenerated by eluting the metabolites with methanol (500 mL). The methanol extract was evaporated to dryness and was used for subsequent analysis. Finally, the resin was washed again by water (500 mL). After these three steps, the resin was ready to be used again.

Monitoring. The debittering procedure was monitored using thin layer chromatography (TLC) and ^{1}H NMR spectroscopy. More specifically, 20 mg of the dry methanol extract from each day of the debittering procedure was dissolved in 600 μL of CD_3OD, and ^{1}H NMR spectra were recorded at 400 MHz. The appearance, increase, or decrease from day to day of characteristic peaks corresponding to 11-methyl oleoside, **3** (5.95 ppm), hydroxytyrosol-4-*O*-β-D-glucoside, **4** (7.09 ppm), hydroxytyrosol, **2** (6.53 ppm), and tyrosol, **5** (7.02 ppm), were monitored.

Isolation. The extracts were combined, and low pressure column chromatography was performed on them leading to the isolation of five compounds. Three of them were already known, and the other two were for the first time isolated from olives. The structures of the already known compounds were identified using NMR spectroscopy, and the structure elucidation of the other two compounds was achieved both with NMR spectroscopy and with MS spectrometry.

A part (2.30 g) of the total extract (7.78 g) was placed into a 5 cm diameter column filled with silica gel 60 Merck (40−63 μm) up to 20 cm height. The eluent flowed through the column under low pressure. The column was eluted collecting fractions of 20 mL according to the following gradient: 1% (25 fractions), 2% (55 fractions), 3% (57

dx.doi.org/10.1021/jf404685h | J. Agric. Food Chem. 2014, 62, 660−667

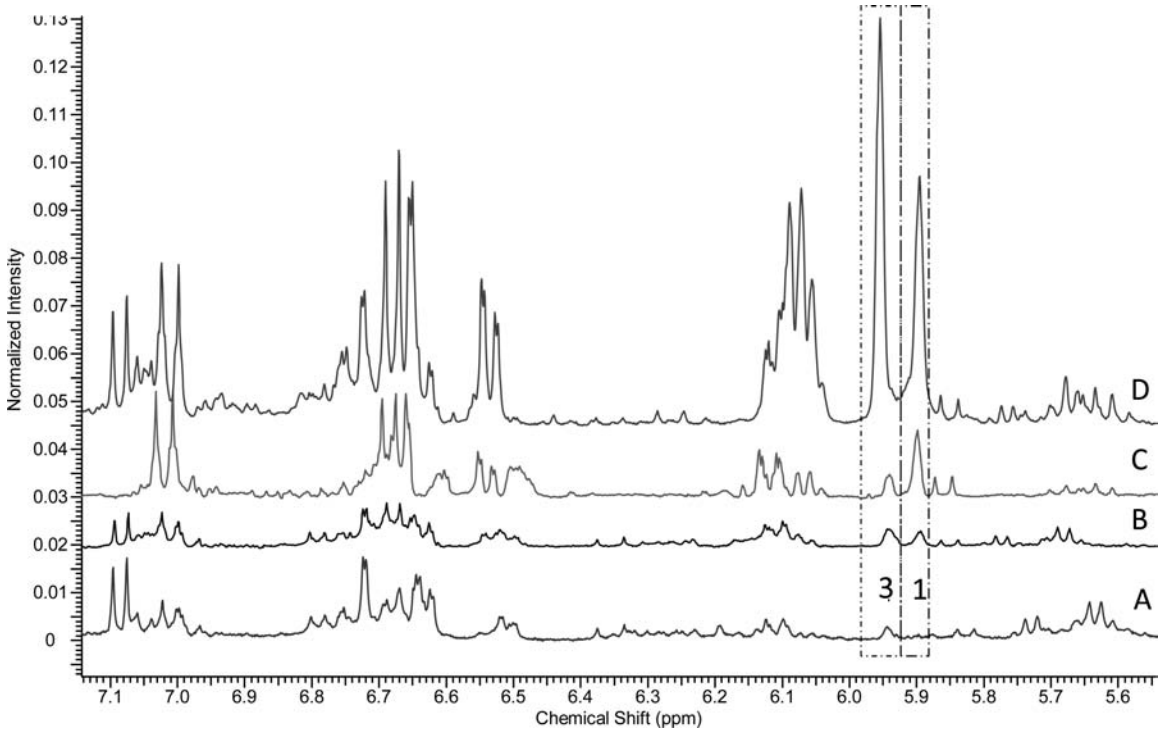

Figure 2. Monitoring of oleuropein in unprocessed olives of cv. 'Megaritiki' by quantitative ^{1}H NMR. (A) 'Megaritiki', November; (B) 'Megaritiki', October; (C) 'Megaritiki', August; (D) 'Throuba Thassos', November. **1**, oleuropein; **3**, 11-methyl oleoside. Spectra are normalized according to the contained internal standard peak (not shown).

fractions), 4% (19 fractions), 5% (21 fractions), 6% (29 fractions), 7% (26 fractions), 8% (63 fractions), 10% (45 fractions), 20% (20 fractions), and 50% (25 fractions) MeOH in CH_2Cl_2. The obtained fractions were pooled using TLC (migration solvent 90:10 CH_2Cl_2:MeOH) to give 32 final fractions. Fractions 8 and 9−14 afforded rengyoxide, **6**[6] (29.9 mg), and hydroxytyrosol, **2**[7] (43.6 mg), respectively. Fraction 19 was rechromatographed on a preparative TLC plate Merck (migration system 80:20 CH_2Cl_2/MeOH) to give rengyoside B, **7**[8] (6.8 mg), hydroxytyrosol-4-*O*-*β*-D-glucoside, **4**[9] (12.4 mg), and 11-methyl oleoside, **3** (14 mg).[10] Other fractions containing the above compounds were extensively rechromatographed leading to a total yield of hydroxytyrosol (30 mg/g of total extract), hydroxytyrosol-4-*O*-*β*-D-glucoside (82 mg/g), and 11-methyl oleoside (25 mg/g).

Study of the Olive Flesh. *Extraction and Resin Treatment.* Six months after the brine addition, 1 kg of the debittered olives was extracted at room temperature with water (2 × 0.5 L) in a supersonic bath for 1 h. The water extract (1 L) was treated in the same way as the wastewater above to lead to an enriched extract. It was passed through a column of 3.5 cm diameter filled with 250 g of XAD-4 resin (BV = 375 mL). The feeding flow rate was 750 mL/h (2 BV/h). The resin total feeding duration was 1.3 h. The procedure above refers to 1.0 L of wastewater. The resin regeneration procedure was exactly the same as the corresponding for the case of the wastewater treatment described above. The MeOH eluent was evaporated under reduced pressure at 40 °C.

Isolation. The enriched extract of the olive flesh was fractionated with low pressure column chromatography, and this separation procedure led to the identification of nine compounds. Two of the isolated compounds were already known, three were for the first time isolated from table olives, and the other four are for the first time reported as natural compounds. The dry MeOH extract (1.98 g) was chromatographed under low pressure on a column similar to that above filled with silica gel 60 Merck (40−63 μm) up to 20 cm height. The volume of the collected fractions was 20 mL, and the solvent gradient was 1% (40 fractions), 2% (66 fractions), 3% (28 fractions), 4% (60 fractions), 5% (15 fractions), 6% (25 fractions), 7% (30 fractions), 8% (13 fractions), 10% (25 fractions), 20% (25 fractions), and 50% (25 fractions) MeOH in CH_2Cl_2. The obtained fractions were merged using TLC (migration solvent 90:10 CH_2Cl_2/MeOH) to afford 27 final fractions. From fractions 4, 5, 6, and 8 were isolated the four new compounds, megaritodilactone, **8** (1.2 mg), megaritolactonic acid, **9** (2 mg), megaritolactonic acid B methyl ester, **10** (3 mg), and megaritolactonol, **11** (3 mg) respectively, after rechromatography on preparative TLC (migration systems 10:50:40 CH_2Cl_2/hexane/EtOAc, 80:20 EtOAc/cyclohexane, 96.5:3.5 CH_2Cl_2/MeOH, and 96:4 CH_2Cl_2/MeOH, respectively). Fraction 12 was purified using preparative TLC to give tyrosol, **5**[7] (30 mg), and two compounds first isolated from olives: halleridone (rengyolone), **12**[6] (9.7 mg), and cleroindicin C, **13**[11] (16.1 mg). Finally, fraction 15 was rechromatographed on silica gel 60 Merck (40−63 μm) with CH_2Cl_2/MeOH (from 100:0 to 95:5 gradient) leading to the isolation of hydroxytyrosol, **2** (119 mg), and rengyoxide, **6** (78.4 mg).

*Megaritodilactone, **8**.* White amorphous solid. ^{1}H NMR ($CDCl_3$) δ: 1.74 (3H, d, J = 7.2 Hz, CH_3-10), 2.29 (1H, dd, J = 16.9, 12.1 Hz, H-6b), 2.84 (1H, dd, J = 16.9, 5.7 Hz, H-6a), 3.11 (1H, m, H-4), 3.51 (1H, dt, J = 11.8, 6.4 Hz, H-5), 4.46 (1H, dd, J = 11.8, 4.6 Hz, H-3b), 4.77 (1H, d, J = 13.4 Hz, H-1b), 4.80 (1H, d, J = 13.4 Hz, H-1a), 4.94 (1H, dd, J = 11.8, 3.1 Hz, H-3a), 5.71 (1H, q, J = 7.2 Hz, H-8). ^{13}C NMR ($CDCl_3$) δ: 13.3 (C-10), 29.9 (C-5), 32.8 (C-6), 37.6 (C-4), 66.64 (C-3), 71.04 (C-1), 125.17 (C-8), 130.1 (C-9), 167.9 (C-7), 169.7 (C-11). HR-ESI−MS: m/z 195.0716 $[M - H]^-$, $[C_{10}H_{12}O_4 - H]^-$, calcd 195.0657.

*Megaritolactonic Acid, **9**.* White amorphous solid. ^{1}H NMR ($CDCl_3$) δ: 1.75 (3H, dd, J = 7.0, 1.5 Hz, CH_3-10), 2.65 (1H, dd, J = 15.6, 7.3 Hz, H-6a), 2.70 (1H, dd, J = 15.6, 7.3 Hz, H-6b), 4.12 (1H, t, J = 7.6 Hz, H-5), 4.58 (1H, d, J = 12.9 Hz, H-1b), 4.97 (1H, dt, J = 12.9, 1.5 Hz, H-1a), 5.715 (1H, q, J = 6.8 Hz, H-8), 5.72 (1H, s, H-3b), 6.41 (1H, s, H-3a). ^{13}C NMR ($CDCl_3$) δ: 12.8 (CH_3-10), 36.3 (C-5), 38.1 (C-6), 71.5 (C-1), 125.5 (C-8), 128.8 (C-3), 129.1 (C-9), 136.3 (C-4), 165.0 (C-11), 173.3 (C-7). HR-ESI−MS: m/z 195.0702 $[M - H]^-$, $[C_{10}H_{12}O_4 - H]^-$, calcd 195.0657.

*Megaritolactonic Acid B Methyl Ester, **10**.* White amorphous solid. ^{1}H NMR ($CDCl_3$) δ: 1.75 (3H, dd, J = 6.9, 1.4 Hz, CH_3-10), 2.67

dx.doi.org/10.1021/jf404685h | J. Agric. Food Chem. 2014, 62, 660−667

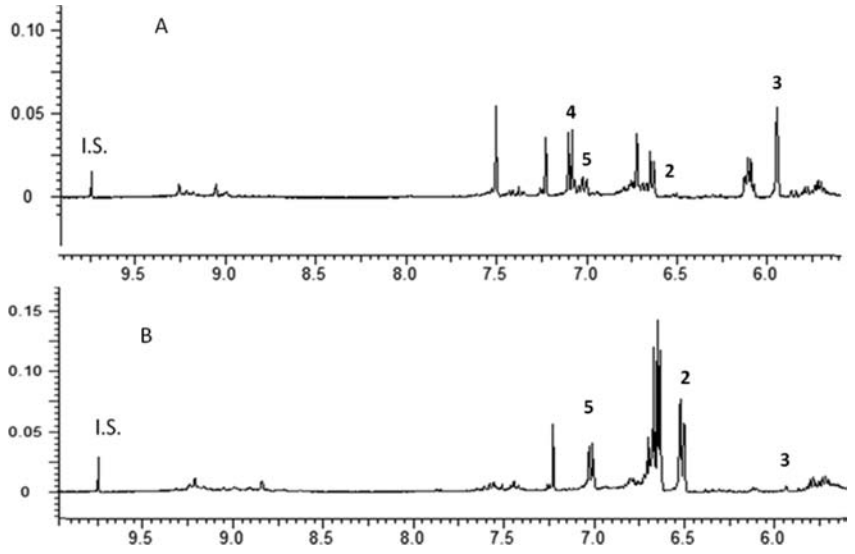

Figure 3. Monitoring of debittering evolution with ^{1}H NMR. **2**, hydroxytyrosol; **3**, 11-methyl oleoside; **4**, hydroxytyrosol-4-*O*-glucoside; **5**, tyrosol. (A) First day. (B) Sixth day.

(1H, dd, *J* = 16.4, 7.0 Hz, H-6a), 2.77 (1H, dd, *J* = 16.4, 6.7 Hz, H-6b), 2.90 (1H, q, *J* = 6.6 Hz, H-4), 3.32 (1H, q, *J* = 7.2 Hz, H-5), 3.73 (1H, t, *J* =7.8 Hz, H-3a), 3.75 (3H, s, CH_3O-12), 3.80 (1H, t, *J* = 5.3 Hz, H-3b), 4.51 (1H, d, *J* = 12.5 Hz, H-1a), 4.82 (1H, d, *J* = 12.5 Hz, H-1b), 5.78 (1H, q, *J* = 6.7 Hz, H-8). ^{1}H NMR (acetone-d_6) δ: 1.73 (3H, d, *J* = 7.7 Hz, CH_3-10), 2.61 (1H, dd, *J* = 15.9/7.2 Hz, H-6a), 2.82 (1H, dd, *J* = 15.9, 6.7 Hz, H6b), 2.99 (1H, q, *J* = 6.9 Hz, H-4), 3.32 (1H, q, *J* = 6.9 Hz, H-5), 3.67 (3H, s, CH_3O-12), 3.72 (1H, dd, *J* = 10.5, 6.4 Hz, H-3a), 3.79 (1H, dd, *J* = 10.5, 7.5 Hz, H-3b), 4.44 (1H, d, *J* = 12.3 Hz, H-1a), 4.82 (1H, d, *J* = 12.8 Hz, H-1b), 5.78 (1H, q, *J* = 7.0 Hz, H-8). ^{13}C NMR (acetone-d_6) δ: 12.7 (C-10), 31.2 (C-5), 32.1 (C-6), 50.1 (C-4), 50.9 (C-12), 60.6 (C-3), 71.8 (C-1), 126.9 (C-8), 133.4 (C-9), 171.5 (C-7), 173.7 (C-11). HR-ESI−MS: *m*/*z* 227.0915 $[M - H]^-$, $[C_{11}H_{15}O_5 - H]^-$, calcd 227.0919.

*Megaritolactonol, **11***. White amorphous solid, $[\alpha]^{20}_D$ +8° (*c* 0.15, MeOH). ^{1}H NMR ($CDCl_3$) δ: 1.66 (1H, m, H-4a), 1.74 (3H, d, *J* = 6.8 Hz, H-10), 1.86 (1H, m, H-4b), 2.58 (1H, dd, *J* = 15.9, 5.9 Hz, H-6a), 2.72 (1H, dd, *J* = 15.9, 6.5 Hz, H-6b), 3.14 (1H, m, H-5), 3.72 (2H, t, *J* = 6.3 Hz, H-3), 4.58 (1H, d, *J* = 12.9 Hz, H-1a), 4.77 (1H, d, *J* = 12.9 Hz, H-1b), 5.62 (1H, q, *J* = 7.0 Hz, H-8). ^{13}C NMR ($CDCl_3$) δ: 13.6 (C-10), 29.6 (C-5), 35.5 (C-6), 37.1 (C-4), 60.1 (C-3), 72.2 (C-1), 124.2 (C-8), 133.4 (C-9), 172.5 (C-7). HR-ESI−MS: *m*/*z* 169.0870 $[M - H]^-$, $[C_9H_{14}O_3 - H]^-$, calcd 169.0864.

RESULTS AND DISCUSSION

Oleuropein Monitoring in Untreated Olives. The initial target was to monitor the presence of oleuropein, **1**, in the untreated olive fruit of cv. 'Megaritiki'. For this purpose, a simple method for the measurement of oleuropein was developed using quantitative ^{1}H NMR. Using the integration ratio between the internal standard and the characteristic peak of oleuropein at 5.91 ppm, we constructed a calibration curve, which was used to measure quantitatively the levels of oleuropein in the olive fruit. The method was applied in the untreated fruits of cv. 'Megaritiki' at three different stages of ripeness as well as in cv. 'Throuba Thassos' well-known[3] for producing oleuropein at harvest time. As it is presented in Figure 2, the peak of oleuropein in the case of cv. 'Megaritiki' at usual harvest time (mid November, half green-half violet color) was almost absent corresponding to a concentration lower than 0.15 mg/g. In contrast, cv. 'Throuba Thassos' at the same harvest time and maturity stage presented significantly higher concentration of 9.1 mg/g, which is comparable with the usually measured levels of oleuropein in untreated olives.[12] When the cv. 'Megaritiki' olives were studied in August (fully unripe), oleuropein was present in higher levels (3.2 mg/g) than in November as expected, showing that the variety has the capability to biosynthesize oleuropein. In early October, the oleuropein level had been already reduced to 0.55 mg/g, showing a gradual but early oleuropein catabolism. In contrast with oleuropein, the peak of 11-methyl oleoside, **3**, was higher at harvest time than that of oleuropein showing that in the case of cv. 'Megaritiki', the hydrolysis of oleuropein is activated much earlier than in other varieties, leading to a fruit that at harvest time has very low content of oleuropein. The peak of methyl oleoside at 5.95 ppm was clearly distinguished from that of oleuropein and was used for its monitoring. Several other characteristic compounds (such as hydroxytyrosol, **2**, hydroxytyrosol-4-*O*-glucoside, **4**, tyrosol, **5**, maslinic acid, etc.) could be simultaneously quantitated by combination of 1D and 2D qNMR, but this is a subject of a separate work. The characteristic peak for the measurement of oleuropein was not overlapping with signals from other major constituents as confirmed by extensive 2D NMR experiments. The observation of the very low content in untreated 'Megaritiki' olives offers an explanation why the debittered olives with dry salt did not contain oleuropein in contrast with cv. 'Throuba Thassos', which after debittering with the same method contained high amounts of oleuropein.[3] Moreover, this finding shows that specific cultivars like 'Megaritiki' present technological advantages concerning the removal of bitterness because oleuropein is already naturally hydrolyzed and the main bitter compound needing to be removed is 11-methyl oleoside. This compound is very soluble in water and can be easily dissolved out of the olive flesh simply by contact with water as explained below. A similar case of an olive cultivar in which the oleuropein level is very low at harvest time due to earlier activation of glucosidase and esterase has also been reported in cv. Dhokar from Tunisia,[12] but most probably there are also many other cultivars with similar behavior.

Study of the Debittering Process with Water. To study the evolution of the debittering process, table olives were prepared, according to a traditional water-curing method for 6 days, and the composition of the wastewater resulting from the

dx.doi.org/10.1021/jf404685h | J. Agric. Food Chem. 2014, 62, 660−667

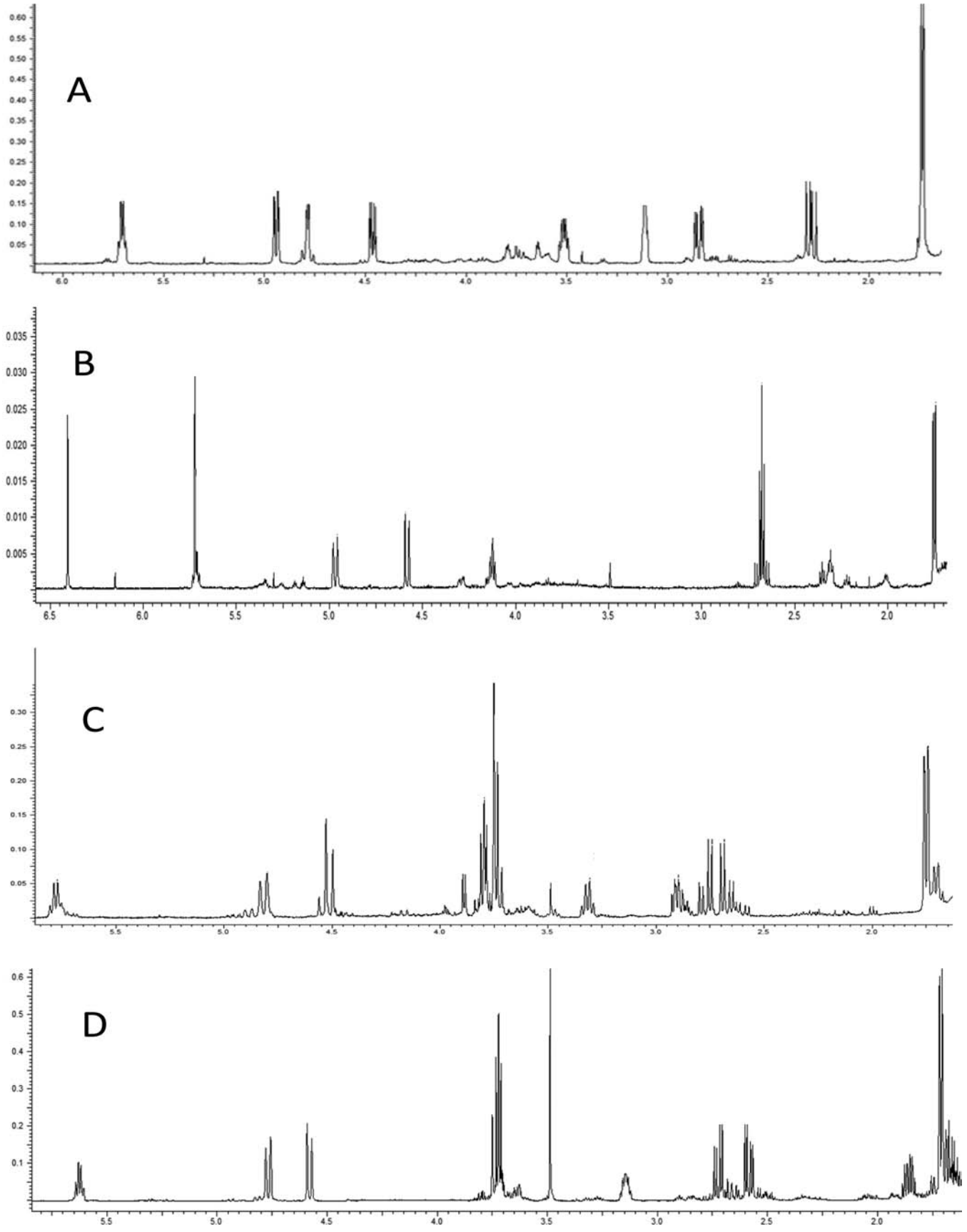

Figure 4. ^{1}H NMR spectra of compounds **8**–**11**. (A) **8**, (B) **9**, (C) **10**, (D) **11**.

debittering procedure as well as that of the final edible olive fruits was determined. To facilitate this study, we applied a method for the recovery of metabolites from wastewater and then we monitored them using NMR spectroscopy. More

dx.doi.org/10.1021/jf404685h | J. Agric. Food Chem. 2014, 62, 660–667

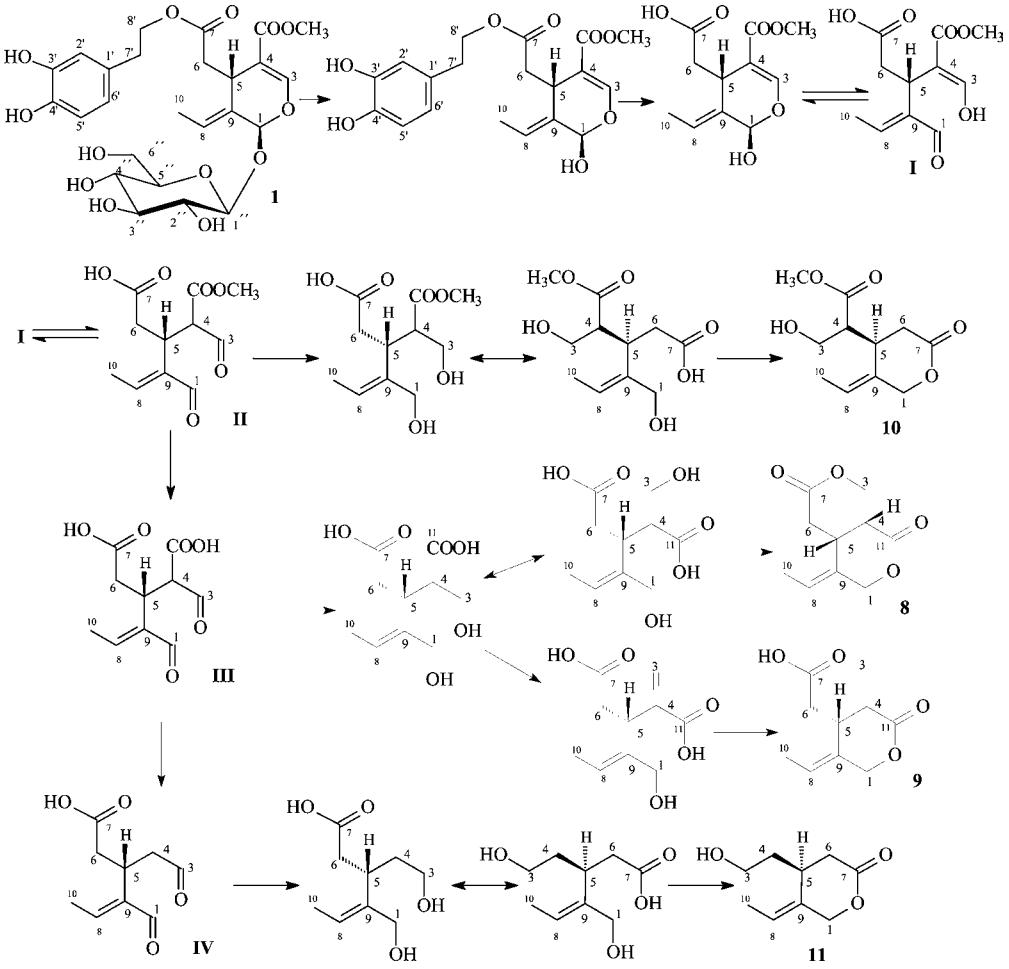

Figure 5. Proposed biosynthetic pathway of compounds **8**−**11**.

specifically, we used a method similar to that developed a few years ago for the recovery of bioactive compounds from the olive mill wastewater.[13] In the current case, the debittering water was treated with adsorption resin XAD-4, and the adsorbed compounds were desorbed using a polar solvent such as methanol. The methanol extract was analyzed by TLC chromatography and NMR. This study showed that the major components of this specific wastewater are the bioactive metabolites: hydroxytyrosol, **2**, 11-methyl oleoside, **3**, hydroxytyrosol-4-*O*-glucoside, **4**, and tyrosol, **5**, but not oleuropein, **1**. It is very interesting that the diffusion of each compound from the flesh to the debittering water was very different (Figure 3). Characteristically, 11-methyl oleoside was almost completely removed after the first two days, while hydroxytyrosol started to appear only after the third day. Additionally, the chemical analysis of the wastewater afforded two metabolites, rengyoxide, **6**, and rengyoside B, **7**, which are for the first time isolated from olives. Rengyoxide has been previously isolated from plants of the families Oleaceae (*Forsythia suspensa*),[6] Bignoniaceae,[14] Verbenaceae (*Clerodendrum indicum*),[11] Scrophulariaceae,[15] and Plantaginaceae.[16] Rengyoside B has been previously isolated from several Bignoniaceae (e.g., *Markhamia stipulata*)[17] and from *Forsythia suspensa* (Oleaceae).[8]

Study of Metabolites Identified in the Final Treated Product. The early hydrolysis of oleuropein in cv. 'Megaritiki' led us to assume that the olive flesh should be rich in compounds deriving from the breakdown of the oleuropein secoiridoid skeleton. In particular, the less hydrophilic derivatives should stay in the flesh until the stage of the final edible product. Indeed, the water extract of the final olive flesh after enrichment with adsorption on XAD4 resin and several chromatographic purification steps led to the isolation of: two metabolites that are for the first time isolated from this species, rengyoxide, **6**, and cleroindicin C, **13**, one that is for the first time isolated from the edible fruit (rengyolone, **12**) and four new natural products. The new natural products are all lactone derivatives coming from the skeleton of oleuropein after hydrolysis of the hydroxytyrosol moiety, cleavage of the glycosidic bond, removal or not of the carbomethoxy group, and subsequent reactions of reduction and/or dehydration and final lactonization. Their common characteristics prompted us to name them as megaritolactones. Currently, it is not known if they are common or not in other edible olive varieties.

Structure Elucidation of New Compounds. Megaritolactonol, **11**, was isolated as an amorphous solid with molecular formula corresponding to $C_9H_{14}O_3$. The ^{1}H NMR profile (Figure 4A) was very closely related to that of (5-ethylidene-2-oxo-tetrahydropyran-4-yl) acetic acid, **14**, which had been described as a semisynthetic derivative[18] and isolated[13] in significant quantities from olive mill wastewater as a breakdown product of the secoiridoid skeleton of oleuropein after hydrolysis of the glycosidic bond and removal of the hydroxytyrosol moiety. The most characteristic signal revealing the similarity with lactone **14** is the methyl group observed as a

dx.doi.org/10.1021/jf404685h | J. Agric. Food Chem. 2014, 62, 660−667

doublet at 1.74 ppm, which is attached to the exocyclic double bond observed as a quadruplet at 5.62 ppm. Moreover, two pairs of geminal protons H-1a,b and H-6a,b at 4.77/4.58 and 2.72/2.58, respectively, and one methine at 3.14 ppm (H-5) comprised the six-membered lactone ring, similar to lactone **14**. The presence of the lactone was confirmed by the carbonyl observed at 172.5 ppm. The main difference from lactone **14** is the side chain attached at position 5. While in the case of lactone **14** the side chain was ethanoic acid, in the case of compound **11** the side chain consisted of one oxygenated methylene at 3.72 ppm and one aliphatic methylene observed as two multiplets at 1.65 and 1.86 ppm. Sequential COSY correlations between H-6a,b/H-5, H-5/H-4a,b, H-4a,b/H-3 confirmed the positioning and the structure of the side chain. The structure was confirmed by the HMBC spectrum where the most important correlations were between H-1a,b and carbonyl C-7 and between H-5 with both the double bond carbon C-8 and the carbonyl C-7. The NOE correlation between H-8 and H-1 revealed the orientation of the methyl group of the double bond as depicted in Figure 1. On the basis of the above description, it was clear the compound **11** was a δ-lactone with one ethylidene and one ethanol side chain for which we propose the name megaritolactonol. The absolute stereochemistry was deduced from the biosynthetic pathway (Figure 5).

Compound **10** was isolated as an amorphous solid with molecular formula $C_{11}H_{16}O_5$. The ^{1}H NMR profile of **9** (Figure 4B) showed many similarities with **11**, making it obvious that it was also a δ-lactone with one ethylidene group. The methyl group on the exocyclic double bond, two pairs of geminal protons, and one methine (3.32 ppm, H-5) bearing a side chain in combination with the carbonyl at 171.5 ppm made clear that **10** belonged to the same family of megaritolactones. The main difference from **11** was the size and the substitution pattern of the side chain. The side chain of **10** contained an oxygenated methylene H-3a,b at 3.73/3.80 ppm, one methine at 2.90 ppm (H-4), and a carbomethoxy group. In the COSY spectrum, H-3a,b was correlated with the methine at 2.90 ppm, and this methine (H-4) was correlated with the second methine at 3.32 ppm (H-5) belonging to the lactone ring. In the HMBC spectrum, both H-3, H-5 and the methoxy group were correlated with the carbonyl at 173.7 ppm, showing that the side chain of **10** consisted of a 2-yl-3-hydroxypropanoic acid methyl ester. The side chain was attached at the same position as in the case of **11**. The NOE spectrum showed also the same orientation for the methyl group of the ethylidene moiety. The absolute stereochemistry was also based on the biosynthetic pathway starting from the oleuropein secoiridoid skeleton as discussed below. Compound **10** was named as the methyl ester of megaritolactonic acid B.

Compound **9** was also obtained as a white amorphous solid with molecular formula $C_{10}H_{12}O_4$. Compound **9** showed also significant similarities with lactone **14** as well as **10** and **11** (Figure 4C). In comparison with **14**, the main difference was the presence of an exomethylene double bond observed as two singlets at 6.41 and 5.72 ppm and the absence of one pair of geminal protons. On the other hand, all of the other signals of the ethylidene group, the ethanoic acid side chain, and the oxygenated methylene of the lactone group were observed as expected. The third member of the megaritolactone family was also a product coming from the breakdown of oleuropein skeleton after hydrolysis, reduction, dehydration, and lactonization as explained in the biosynthetic pathway scheme (Figure 5). The exact placement of the exomethylene group was determined through the HMBC spectrum where the geminal protons of the double bond showed a ^3J correlation with conjugated lactone carbonyl at 165 ppm and the methine carbon C-5 at 36.3 ppm. H-5 showed also critical correlations with both the lactone and the carboxylic carbonyls as well as the ethylidene double bond and the oxygenated methylene of the lactone ring. The lactone carbonyl was clearly discriminated from the carboxylic carbonyl through its correlation with the oxygenated methylene H-1a,b. The orientation of the methyl group was also the same as in **10** and **11**, highlighting their common biosynthetic origin. The orientation of the ethanoic acid side chain was opposite in comparison with **10** and **11** because the lactonization occurred between C-11 and C1 and not between C-1 and C-7 as in the case of **10** and **11**. In the case of **11**, C-11 is not present due to decarboxylation, while in the case of **10** C-11 is blocked as a methyl ester and cannot participate in the formation of the lactone. Compound **9** was named megaritolactonic acid.

The corresponding compound coming from the lactonization between C1 and C7 can be obtained in the case where C-11 is blocked as a methyl ester. It could be considered as a dehydration derivative of **10** leading to an exomethylene double bond on the side chain and not on the ring. This compound has been originally isolated from 'Throuba Thassos' table olives.[19] Although it has not yet been isolated from 'Megaritiki' olives, its existence is reported herein to strengthen the discussion about the biosynthesis of the olive lactones and the possible occurrence of similar compounds in other table olives cultivars.

The last member of the megaritolactones family **9** had a molecular formula $C_{10}H_{12}O_4$. It was a compound closely related to megaritolactonic acid with the difference that the alcohol at position 3 was not dehydrated as in the case of **9** but lactonized with the carboxyl at C-7. This compound contained two δ-lactone rings, and for this reason was named megaritodilactone. It presented all of the expected HMBC correlations, and more significantly the oxygenated methylene H-3 was correlated not only with C-11 and C-5 (as in **9**) but also with C-7 due to the formation of the second lactone ring. As in all of the previous compounds, the orientation of the methyl group was the same. Concerning the fusion between the two rings, it was found to be cis based on the small coupling constants of H-4 with H-5, H-3a, and H-3b, 6.4, 3.1, and 4.6 Hz, respectively. H-5 has clearly an axial orientation based on the large coupling constant with H-6b (12.1 Hz), and consequently H-4 has an equatorial orientation leading to a cis fusion between the two lactone rings (Figure 4D).

The proposed biosynthetic pathway (Figure 5) leading to megaritolactones starts from oleuropein (or ligstroside) first by hydrolysis of the glycosidic bond and then by hydrolysis of the ester at position 7. The obtained form I through keto−enol tautomerism leads to the key compound II. Reduction of aldehydes at positions 1 and 3 and subsequent lactonization between alcohol at position 1 and carboxyl at position 7 leads to **10**. Compound II after hydrolysis of the methyl ester at position 11 gives compound III from which starts the biosynthesis of **9** and **8**. Reduction of aldehydes at positions 1 and 3, dehydration of alcohol 3 to double bond, and lactonization between positions 1 and 11 leads to **9**. In the case of **8**, the biosynthesis occurs through double lactonization, between positions 1 and 11 and between 3 and 7. Compound III after decarboxylation leads to compound IV, which after reduction of the two aldehydes at positions 1 and 3 and

dx.doi.org/10.1021/jf404685h | J. Agric. Food Chem. 2014, 62, 660−667

subsequent lactonization between positions 1 and 7 leads to **11**. In all cases, the absolute configuration at position 5 is already determined by the configuration of the corresponding carbon of oleuropein, which remains unchanged.

In conclusion, 'Megaritiki' table olives and debittering wastewater are useful sources of polyphenols and secoiridoids with unique structural characteristics. Quantitative NMR is a very useful tool for the rapid and easy measurement of key compounds in complex mixtures such as the olive extracts.

■ ASSOCIATED CONTENT

Supporting Information

NMR spectra of new compounds and compounds for the first time reported from table olives. This material is available free of charge via the Internet at http://pubs.acs.org.

■ AUTHOR INFORMATION

Corresponding Author

*Tel.: +30-210-7274052. Fax: +30-210-7274594. E-mail: magiatis@pharm.uoa.gr.

Notes

The authors declare no competing financial interest.

■ ACKNOWLEDGMENTS

We would like to thank Dr. Maria Nikolantonaki for recording NMR and MS spectra at University of California, Davis.

■ REFERENCES

(1) Boskou, D. Phenolic compounds in olives and olive oil. In *Olive Oil: Minor Constituents and Health*, 1st ed.; Boskou, D., Ed.; CRC Press: New York, 2008; pp 12−36.

(2) Charoenprasert, S.; Mitchell, A. Factors influencing phenolic compounds in table olives (*Olea europaea*). *J. Agric. Food Chem.* **2012**, *60*, 7081−7095.

(3) Zoidou, E.; Melliou, E.; Gikas, E.; Tsarbopoulos, A.; Magiatis, P.; Skaltsounis, A.-L. Identification of Throuba Thassos, a traditional Greek table olive variety, as a nutritional rich source of oleuropein. *J. Agric. Food Chem.* **2010**, *58*, 46−50.

(4) Scientific Opinion on the substantiation of health claims related to polyphenols in olive and protection of LDL particles from oxidative damage. *EFSA J.* **2011**, *9*, 2033.

(5) Karkoula, E.; Skantzari, A.; Melliou, E.; Magiatis, P. Direct measurement of oleocanthal and oleacein levels in olive oil by quantitative ^{1}H NMR. Establishment of a new index for the characterization of extra virgin olive oils. *J. Agric. Food Chem.* **2012**, *60*, 11696−11703.

(6) Endo, K.; Hikino, H. Structures of rengyol, rengyoxide, and rengyolone, new cyclohexylethane derivatives from *Forsythia suspensa* fruits. *Can. J. Chem.* **1984**, *62*, 2011−2014.

(7) Park, C. H.; Kim, K. H.; Lee, I. K.; Lee, S. Y.; Choi, S. U.; Lee, J. H.; Lee, K. R. Phenolic constituents of *Acorus gramineus*. *Arch. Pharm. Res.* **2011**, *34*, 1289−1296.

(8) Seya, K.; Endo, K.; Hikino, H. Structures of rengyosides A, B and C, three glucosides of *Forsythia suspensa* fruits. *Phytochemistry* **1989**, *28*, 1495.

(9) Bianco, A.; Mazzei, R. A.; Melchion, C.; Romeo, G.; Scarpati, M. L.; Soriero, A. Microcomponents of olive oil-III. Glucosides of 2 (3,4-dihydroxy- phenyl) ethanol. *Food Chem.* **1998**, *63*, 461−464.

(10) Zhang, Y. J.; Liu, Y. Q.; Pu, X. Y.; Yang, C. R. Iridoidal glycosides from *Jasminum sambac*. *Phytochemistry* **1995**, *38*, 899−903.

(11) Tian, J.; Zhao, Q. S.; Zhang, H. J.; Lin, Z. W.; Sun, H. D. New cleroindicins from *Clerodendrum indicum*. *J. Nat. Prod.* **1997**, *60*, 766−768.

(12) Jemai, H.; Bouaziz, M.; Sayadi, S. Phenolic composition, sugar contents and antioxidant activity of tunisian sweet olive cuitivar with regard to fruit ripening. *J. Agric. Food Chem.* **2009**, *57*, 2961−2968.

(13) Agalias, A.; Magiatis, P.; Skaltsounis, A. L.; Mikros, E.; Tsarbopoulos, A.; Gikas, E.; Spanos, I.; Manios, T. A new process for the integrated management of olive oil mill waste water, recovering natural antioxidants. *J. Agric. Food Chem.* **2007**, *55*, 2671−2676.

(14) Su, Y. Q.; Shen, Y. H.; Tang, J.; Zhang, W. D. Chemical constituents of *Incarvillea mairei* var. *Grandiflora*. *Chem. Nat. Compd.* **2010**, *46*, 109−111.

(15) Abdullahi, H.; Nyandat, E.; Galeffi, C.; Messana, I.; Nicoletti, M.; Bettolo, G. B. Cyclohexanols of *Halleria lucida*. *Phytochemistry* **1986**, *25*, 2821−2824.

(16) Breton, J. L.; Llera, L. D.; Navarro, E.; Trujillo, J. Photochemical synthesis of halleridone, hallerone, rengyol and derivatives. *Tetrahedron* **1987**, *43*, 4447−4451.

(17) Kanchanapoom, T.; Kasai, R.; Yamasaki, K. Phenolic glycosides from *Markhamia stipulata*. *Phytochemistry* **2002**, *59*, 557−563.

(18) Gil, M.; Haidour, A.; Ramos, J. L. Two glutaric acid derivatives from olives. *Phytochemistry* **1998**, *49*, 1311−1315.

(19) Zoidou, E.; Agalias, A.; Magiatis, P.; Skaltsounis, A. L. New iridoid derivatives from table olives cv. 'Throuba Thassos' and olive mill waste waters. *Planta Med.* **2008**, *74*, 1081−1082.

JOURNAL OF AGRICULTURAL AND FOOD CHEMISTRY

Article

pubs.acs.org/JAFC

Protection of Feruloylated Oligosaccharides from Corn Bran against Oxidative Stress in PC 12 Cells

Sheng-wen Yao,[†,∥] Xiao-xiao Wen,[‡,∥] Ru-qing Huang,[†,∥] Rong-rong He,[#] Shi-yi Ou,*[,†] Wei-zai Shen,*[,‡] Cai-huan Huang,[†] and Xi-chun Peng[†]

[†]Department of Food Science and Engineering, [‡]Scool of Medicine, and [#]College of Pharmacy, Jinan University, Guangzhou 510632, Guangdong, China

Supporting Information

ABSTRACT: Feruloylated oligosaccharides (FOs) were prepared by autoclaving corn bran in oxalic acid (0.6%) solution, and their protection effects against oxidative stress in pheochromocytoma cells (PC 12) cells were investigated. The FOs samples, which comprised a mixture of feruloylated mono- and dipentoses with 4.88% bound ferulic acid (FA), as well as xylose, arabinose, galactose, and glucose amounting to 46.43, 40.46, 3.76, and 8.68% of the total sugars, respectively, were prepared by autoclaving the pretreated corn bran in 0.6% oxalic acid and then further separated. Antioxidant activity was tested by 1,1-diphenyl-2-picrylhydrazyl radical 2,2-diphenyl-1-(2,4,6-trinitrophenyl)hydrazyl (DPPH) scavenging and oxygen radical absorbance capacity (ORAC) methods. Oxidative stress was induced by H_2O_2 in PC 12 neuronal cell culture model. The results showed that FOs exhibited higher antioxidant activity than free ferulic acid, with an IC_{50} value of 11 versus 128 μM for DPPH and an ORAC value of 4.77 versus 2.62 μmol Trolox/μmol. Tetrazolium blue assay showed that the addition of FOs with an FA concentration >50 μM significantly increased cell viability after treatment with H_2O_2. Flow cytometry analysis showed that the addition of FOs at concentrations of 800, 200, and 50 μM significantly decreased the apoptosis rate at the sub-G0 phase from 37.5 to 12.7, 16.2, and 20.9% ($P < 0.01$), respectively. FOs also significantly decreased the malonic dialdehyde content and lactate dehydrogenase (LDH) activity, but increased superoxide dismutase activity in PC 12 cells treated with H_2O_2 and prevented the damage of cellular membranes by decreasing the release of LDH to the cultures. The addition of FA at 800 μM showed an effect similar to that of FOs at 200 μM. Therefore, the FOs prepared from corn bran are potential functional ingredients for protection against oxidative stress.

KEYWORDS: *feruloylated oligosaccharides, corn bran, antioxidative stress, PC 12 cells*

INTRODUCTION

Oxidative stress is caused by an imbalance between the production of reactive species (peroxides and oxygen radicals) and the scavenging ability of the organism to destroy these species.[1] Oxidative stress can damage the macromolecules in cells and tissues, resulting in membrane damage, fragmentation, or random cross-linking of molecules, such as DNA, enzymes, and structural proteins, and can even lead to cell death induced by DNA fragmentation and lipid peroxidation. Thus, oxidative stress has a crucial role in the development of cancer, neurodegenerative disorders, cardiovascular diseases, Alzheimer's disease, diabetes, and autoimmune disorders.[2,3]

Ferulic acid, an antioxidant ubiquitously existing in plant tissues,[4] protects DNA against Cu^{2+}/GSH-induced oxidation,[5] has therapeutic effects on hydrogen peroxide-induced oxidative stress in nucleus pulposus cells,[6] and restores activity at the antioxidant level in alloxan-induced mice.[7] Corn (*Zea mays*) ranks first among the crops in the world. Corn bran, produced at a yield of 60−70 g/kg after milling, contains the highest content of ferulic acid (28−31 g/kg of ferulic acid) among fiber sources.[8] However, ferulic acid in corn bran is only slightly bioavailable in rats.[9] Zhao et al. fed rats a diet containing 5% refined corn bran for 10 days and found that only 0.4−0.5% of the ingested ferulic acid was recovered in rat urine, whereas 81% of the ingested ferulic acid was excreted through the rat feces within 3 days after ingestion.[9] Thus, the ferulic acid of corn bran would show very low bioavailability in humans when corn bran is eaten unprocessed.

Feruloylated oligosaccharides (FOs), which comprise a bound form of ferulic acid and oligosaccharides, possess the physiological functions of both ferulic acid and oligosaccharides. The ferulic acid in FOs acts as a novel antioxidant, whereas oligosaccharides increase water solubility, and their combination may result in the synergistic antioxidant activities of FOs[10,11] and may act as a new potential antioxidant for the prevention of oxidative stress. Corn bran contains a high amount of ferulic acid and hemicellulose (approximately 700 g/kg) but <10 g/kg level of lignin.[8] These characteristics make corn bran an ideal source for the preparation of FOs compared with other brans.

FOs prepared from corn bran have good antioxidant activity in the lipid oxidation of rapeseed−fish oil-in-water emulsions[12] and human low-density lipoprotein (LDL) autoxidation system by $CuSO_4$[13] and showed stronger antioxidant activity than free ferulic acid.[14] However, studies on the protective effect against oxidative stress in cells by FOs are lacking.

Received: October 31, 2013
Revised: December 24, 2013
Accepted: December 24, 2013
Published: December 24, 2013

ACS Publications © 2013 American Chemical Society

In this research, FOs were prepared from corn bran by autoclaving in a 0.6% oxalic acid solution for 30 min and were tested for their prevention of oxidative stress in H_2O_2-injured pheochromocytoma cells (PC 12).

MATERIALS AND METHODS

Materials and Chemicals. Corn bran and PC 12 cells were provided by Shandong Xiwang Group Co. Ltd. (Zouping, Shandong, China) and the College of Medicine, Jinan University, Guangzhou, China, respectively. Dulbecco's modified Eagle medium (DMEM) with horse serum, fetal bovine serum, and trypsin were purchased from Gibco BRL (Grand Island, NY, USA). Tetrazolium blue (MTT), RNase A, nitrotetrazolium blue chloride, 1,1-diphenyl-2-picrylhydrazyl radical 2,2-diphenyl-1-(2,4,6-trinitrophenyl)hydrazyl (DPPH), monosaccharides, and Trolox [(±)-6-hydroxy-2,5,7,8-tetramethylchroman-2-carboxylic acid] were purchased from Sigma-Aldrich Co. (St. Louis, MO, USA). 2,2′-Azobis(2-methylpropionamidine) dihydrochloride (AAPH) and fluorescein (FL) sodium were purchased from Wako Pure Chemical Industries, Ltd. (Japan). Amberlite XAD-2 was from Beijing North Real Science and Technology Development Co. Ltd. (Beijing, China). Test kits for the determination of malonic dialdehyde (MDA), lactate dehydrogenase (LDH), and superoxide dismutase (SOD) were from Nanjing Jiancheng Biological Engineering Research Center (Nanjing, China). Heat-stable α-amylase (EC 3.2.1.1, from *Bacillus licheniformis*, 120,000 units/g), alcalase (EC 3.4.21.62, from *B. licheniformis*, 2.4 units/g), and amyloglucosidase (EC 3.2.1.3, from *Aspergillus niger*, 300 units/g) were purchased from Novo Nordisk (Bagsvaerd, Denmark).

All other reagents were of analytical grade.

Preparation of FOs from Corn Bran. Corn bran was oven-dried at 105 °C for 6 h and then ground to pass a 45-mesh sieve. The dried corn bran (2000 g) was then destarched and deproteinized in a 30 L biological reactor (Zhenjiang East Bioengineering Co., Zhenjiang, Jiangsu Province, China) by heat-stable α-amylase, amyloglucosidase, and protease, sequentially, and the water-insoluble dietary fiber was separated by a basket centrifuge as pretreated corn bran.[15]

FOs were prepared according to our previous method.[16] The pretreated corn bran was suspended in 10 volumes of oxalic acid (0.6%) solution, autoclaved at 120 °C for 30 min, cooled, and filtered using 200-mesh nylon cloth and further ultrafiltered at 5 kDa using a Pellicon XL 50 cassette and a Labscale TFF system. The filtrate was loaded on an Amberlite XAD-2 (filtrate/resin, 2:1) column and eluted with 10 volumes of deionized water to remove the oxalic acid and some non-FOs; 5 volumes of ethanol at 50% was used to elute the FOs. The eluents then were vacuum-concentrated to approximately 70% moisture content.

The bound ferulic acid content and relative contents of different FOs were determined by HPLC, and the species of FOs were identified by HPLC-MS or MS alone. The average degree of polymerization (DP) was calculated as the total content of sugars divided by the content of reducing sugars, and the monosaccharides in FOs were determined using an ion chromatograph.

Oxygen Radical Absorbance Capacity (ORAC)-FL Assay. The assay was conducted in three replicates using the procedure described by Davalos et al.[17] with some modifications. Phosphate-buffered saline (PBS) at 75 mM (pH 7.4, 20 μL), FOs (26.8 μM based on ferulic acid, 20 μL), and FL at 20 μL (63 nM, final concentration) were placed in the microplate well. The mixture was then pre-incubated for 15 min at 37 °C. The AAPH solution at 140 μL (12.8 mM, final concentration) was added rapidly using a multichannel pipet. The microplate was immediately placed in the reader, and an automated ORAC assay was then performed on a Labsystems Fluoroskan Ascent plate reader (Labsystems Co.) with fluorescent filters (Infinite F200, excitation wavelength, 485 nm; emission wavelength, 527 nm) described in our previous study.[18] Trolox (20 μM) was used as a standard, and ferulic acid (50.29 μM) was used as a control. The final results were calculated on the basis of the difference in the area under the fluorescein decay curve between the AAPH control and the samples.

DPPH Assay. A 0.5 mM solution of DPPH in ethanol was prepared. Subsequently, 2 mL of this solution was mixed with different concentrations of FOs or ferulic acid in a test tube and incubated for 30 min at room temperature (in three replicates). The residual DPPH was determined by absorbance at 517 nm. The DPPH radical scavenging activity (%) was calculated as $[(A_0 - A_1/A_0) \times 100]$, where A_0 is the absorbance of the control and A_1 is the absorbance of the FOs or ferulic acid.

Cell Culture. The PC 12 cell line was cultivated in DMEM supplemented with 10% heat-inactivated fetal bovine serum, 5% fetal bovine serum, and 1% antibiotic mixture comprising penicillin and streptomycin, in a 5% CO_2 humidified atmosphere at 37 °C. Growth medium was replaced once every 2−3 days. PC 12 cells were seeded in flat-bottom 96-well plates (100 μL/plate) at a density of 6×10^4 cells/mL and then incubated in a Forma MIP-332 CO_2 incubator (Sanyo Electric Medica System, Tokyo, Japan) overnight, until all cells adhered to the wall.

Effect of Hydrogen Peroxide on the Viability of PC 12 Cells. The cell culture media were replaced with 100 μL/plate DMEM complete media, which contained H_2O_2 at concentrations of 0, 0.25, 0.4, 0.5, 0.8, 1.0, 1.6, and 2.0 mM, and incubated at 37 °C in a humidified atmosphere of 5% CO_2/95% air for 4 h. The culture media were removed, the cells were washed once with DMEM and incubated in DMEM (100 μL/plate). The MTT reagent (10 μL) was then added to the cells with continuous shaking for 2 min, followed by 4 h of incubation at 37 °C. The liquid was then carefully removed by pipets, 100 μL of dimethyl sulfoxide was added to dissolve the formazan crystal, and the absorbance at 570 nm was measured with a Safire 2 microplate reader (Tecan, Switzerland). The absorbance of the control cells was assumed to be 100%, and the results were expressed as the percentages of reduced MTT, in that

$$\text{cell viability (\%)} = (1 - A_{570}\ \text{of}\ H_2O_2\ \text{treatment}/A_{570}\ \text{of the control}) \times 100\%$$

Protective Effects of FOs against Oxidative Stress in PC 12 Cells. The cell culture medium was replaced with 100 μL/plate DMEM complete media, which contained 0, 25, 50, 100, 200, 400, 800, and1600 μM FOs (based on ferulic acid), and incubated at 37 °C in a humidified atmosphere of 5% CO_2/95% air for 12 h. Subsequently, 10 μL of H_2O_2 was added after pre-incubation with FOs for different times to reach a final concentration 0.8 mM, after which culturing was performed for another 4 h. PBS at 10 μL was added then to the treatment without the addition of H_2O_2 and FOs as a control.

Cell viability was determined with six replicates using the MTT method, as previously mentioned. In the following research, the low, middle, and high levels of FOs at 50, 200, and 800 μM, respectively, were used for determining the apoptosis rate by flow cytometry method, the contents of MDA, and the activities of SOD and LDH using the test kits. Morphological observation was conducted using a Leica DM IRBE inverted microscope (Heidelberg, Germany).

Flow Cytometry Method. The cells were centrifuged at 10000*g* for 5 min and thoroughly washed with PBS at room temperature. Cells were collected and fixed overnight using 70% ethanol at −4 °C. Cells were subsequently washed and resuspended in DNA staining solution, which contained propidium iodide (100 μg/mL) and RNase A (250 IU/mL), for 30 min. Analysis of cells was done by flow cytometry using a BD FACSAria flow cytometer. The data were analyzed with BD FACS Diva software (all from BD Biosciences, Franklin Lakes, NJ, USA). The apoptosis rate and percentage of the cells at different phases were also calculated.

Effect of FOs on MDA Content and the Activities of SOD and LDH in H_2O_2-Injured PC 12 Cells. Cells were suspended in PBS at 0 °C at the end of the culture and then completely crushed using a Scientz-IID Ultrasonic cell crusher (Ningbo Scientz Biotechnology Polytron Technologies Inc., Zhejiang province, China) until no intact cells were observed under the microscope. MDA content and the activities of LDH and SOD in cells and cultures were determined using

dx.doi.org/10.1021/jf404841c | J. Agric. Food Chem. 2014, 62, 668−674

commercially available kits from Nanjing Jiancheng Bioengineering Co. (Nanjing, China), as previously described.[15]

Determination of Ferulic Acid, Reducing Sugars, Total Sugars, and Monosaccharide Composition in FOs. FOs were hydrolyzed using 10 volumes of NaOH (1.0 M) as previously described.[19] Reducing sugars were determined using the DNS method, and total sugars were determined using the DNS method after the FOs were acid-hydrolyzed by 1 M H_2SO_4 at 100 °C for 3 h according to the method used by Van den Borne et al.[20] Monosaccharides in the acid hydrolysates were determined using an ICS-2500 model (Sunnyvale, CA, USA) ion chromatogram equipped with an ED50A pulsed amperometric detector. The column used was a Dionex PA 10 (250 mm, 5 μm) and kept at 30 °C. The samples at 10 μL were injected and eluted using 10.0 mol/L NaOH at a flow rate of 0.25 mL/min. A mixture of monosaccharides at a concentration of 8 μmol/L was used as a standard.

Identification of FOs in Oxalic Acid Hydrolysates. The analysis of FOs was performed in an Agilent 1100 HPLC equipped with quaternary pumps, a 4000Q TRAP mass spectrometer (Applied Biosystem Sciex), and an electrospray ionization source (ESI, Thermo Scientific) or an atmospheric pressure chemical ionization (APCI) ion source. Samples (10 μL) were separated on an Agilent Eclipse XDB-C_{18} column (2.1 mm × 150 mm, 5 μm) using 0.01% formic acid (A) and methanol (B) as mobile phase for the following stepwise gradient elution time scale: at 0−5 min, A:B = 90:10 (v/v); 5.1−20 min, A:B = 75:25; 20.1−25 min, A:B = 68:32; and 25.1−35 min, A:B = 90:10. The flow rate was 0.3 mL/min, and the column temperature was set at 23 °C. ESI-positive or -negative ions (H^+) were used to determine the molecular weight of the components in the hydrolysates. Full-scan MS was conducted using APCI-MS.

Statistical Analysis. Data were analyzed using SPSS 13.0 software.

RESULTS

Chemical Composition of Oxalic Acid Hydrolysates. Ferulic acid, reducing sugars, and total sugars (based on dry pretreated corn bran) at 15.6, 158.3, and 532.2 mg/g, respectively, were recovered in the hydrolysates after autoclaving the pretreated corn bran in 0.6% oxalic acid for 30 min. When the hydrolysates were separated and purified sequentially by ultrafiltration and Amberlite XAD-2, 204.8 mg/kg solids was obtained, of which the contents of total sugars, reducing sugars, and bound ferulic acid were 959.4, 315.2, and 48.8 mg/kg, respectively. Therefore, the average DP of the purified product, which was used as FOs in the following study, was approximately 3.0 (959.4/315.2). The monosaccharides existing in FOs include xylose, arabinose, galactose, and glucose, which amount to 46.43, 40.46, 3.76, and 8.68% of the total sugars, respectively.

Two main FOs, compounds **1** and **2** (at a concentration of 9:1 according to their peak areas in HPLC), were separated by HPLC at 314 nm. The results of APCI-MS and LC-MS indicated that the molecular weight of compound **1** is 326, with an m/z 327.3 $[M + H^+]$ and an m/z 325.4 $[M - H^+]$. Compound **1** can be tentatively regarded as feruloylated arabinose (MW = 194 + 150 − 18) according to the linkage type reported previously in corn bran.[10] Compound **2** has an m/z 459.5 $[M + H^+]$ and an m/z 457.6 $[M - H^+]$ in APCI-MS, indicating that its molecular weight is 458. Thus, compound **2** is supposed to be an FO comprising two molecules of pentose, and the linkage type would be (5-*O*-ferulic acid-α-L-arabinose)-1,3-xylose according to the structure of polysaccharide in corn bran.[10] A trace amount of ferulic acid was also detected, but no other species of FOs were detected after oxalic acid hydrolysis and purification using Amberlite XAD-2 resin.

The FOs we prepared from corn bran have the same structure as thaose prepared from wheat bran. The latter have been approved by U.S. FDA as wheat bran extract (GRAS Notice 000343),[21] which has an average DP 3−8 and bound ferulic acid content of 1−3%, suggesting that the samples we prepared following this standard, but with higher ferulic acid content. In the next research, the samples (mixture of FOs and oligosaccharides) were used for testing the antioxidant activity in vitro and in an in vitro cell culture (PC 12) study.

Scavenging Capacity of FOs against DPPH Free Radical and Their ORAC. The scavenging capacity of FOs and free ferulic acid against DPPH free radical was investigated at concentrations of 0, 25, 50, 100, 200, 400, 800, and 1600 μM (based on ferulic acid). FOs showed higher scavenging capacity for DPPH free radical than free ferulic acid at all tested concentrations (Figure 1), especially at concentrations <400

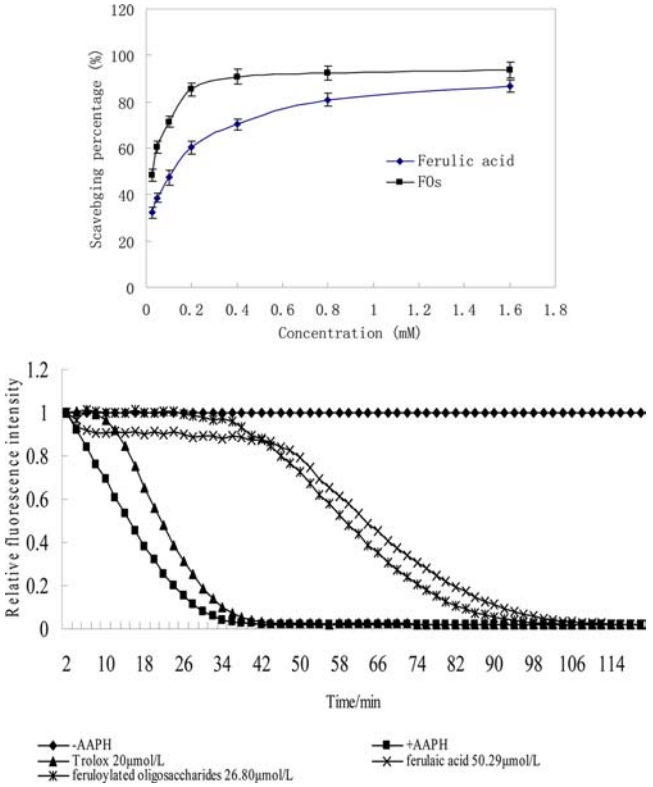

Figure 1. Scavenging capacity of FOs for DPPH free radicals (top) and their fluorescence extinction curves (bottom).

μM. At 1.6 mM, the DPPH free radical scavenging capacity of FOs was 93.80%. The IC_{50} values (the concentration for scavenging 50% of DPPH free radical) of FOs and free ferulic acid were 0.011 and 0.128 mM, by the extrapolated method.

The extent of the antioxidant capability of FOs was also evaluated by the ORAC method. Both FOs and ferulic acid showed the capacity to postpone the fluorescence extinction. The ORAC value was calculated as the ratio of the area under the fluorescence decay curve, with 20 μM Trolox as a standard. The ORAC value for FOs is 4.77 μmol Trolox/μmol, which was 1.8 times higher than that of ferulic acid (2.62 μmol Trolox/μmol). These findings are in accordance with previously reported results, which indicated that FOs exhibit higher antioxidant activity than ferulic acid in vitro.[10]

Effect of FOs on the Viability and Apoptosis of PC 12 Cells. H_2O_2 injured the PC 12 cells in a dose-dependent manner (Table 1), and probit analysis using the SPSS 13.0

dx.doi.org/10.1021/jf404841c | J. Agric. Food Chem. 2014, 62, 668−674

Table 1. Effects of H_2O_2 on PC 12 Cell Viability

H_2O_2 (mmol/L)	A_{570}[a]	cell inhibition rate (%)
0	0.770 ± 0.008	0.00
0.25	0.642 ± 0.005	16.83 ± 0.19
0.4	0.554 ± 0.004	28.11 ± 0.30
0.5	0.471 ± 0.007	38.80 ± 0.73
0.8	0.356 ± 0.006	53.91 ± 0.58
1.0	0.282 ± 0.007	63.38 ± 0.73
1.6	0.172 ± 0.004	77.58 ± 0.31
2.0	0.088 ± 0.007	88.56 ± 0.81

[a]Means ± SD (n = 6).

program showed that the IC_{50} value was 0.8 mM. In the following study, 0.8 mM H_2O_2 was used on PC 12 cells to test the protective effect of FOs against oxidative stress.

The MTT assay showed a significant protection in PC 12 cells when the cells were pretreated with FOs ($P < 0.05$ at 50 μM and $P < 0.01$ at ≥100 μM). The protective effect was dose dependent. The viability of the PC 12 cells significantly ($P < 0.05$) increased after the addition of FOs at concentrations of 50 μM ($P < 0.05$) or higher ($P < 0.01$, Table 2). When the concentration reached 800 μM, the cell viability increased from 53.91% (without the addition of FOs) to 81.91% (Table 2).

Table 2. Effects of Feruloylated Oligosaccharides Added 12 h before Injury by 0.8 mM H_2O_2 on Cell Viability of PC 12 Cells

FO concn (FA; μM)	A[a]	cell viability (%)
0	0.356 ± 0.006	53.91 ± 0.58
1600	0.475 ± 0.007[c]	78.69 ± 2.34[c]
800	0.493 ± 0.003[c]	81.91 ± 1.57[c]
400	0.441 ± 0.004[c]	70.46 ± 1.12[c]
200	0.407 ± 0.006[c]	65.82 ± 1.04[c]
100	0.383 ± 0.005[c]	60.44 ± 1.68[c]
50	0.336 ± 0.004[b]	55.73 ± 0.68[b]
25	0.325 ± 0.010	53.80 ± 1.46

[a]Means ± SD (n = 6). [b]$P < 0.05$ vs 0.8 mM H_2O_2 treatment alone. [c]$P < 0.01$ vs 0.8 mM H_2O_2 treatment alone.

Obvious morphological changes of the cells were observed after H_2O_2 treatment. Cells in the control (without H_2O_2 treatment) grew well with regular shapes (fusiform), uniform sizes, and clear borders (Figure 2). After treatment with 0.8 mM H_2O_2, the cells became round and distorted, the synapse shortened, and the cell border remained clear. When the H_2O_2 concentration reached 1.6 mM, cell distortion became apparent and the cell borders became obscure. After the addition of FOs into the cell culture with H_2O_2 treatment, cells grew better, the number of adhered cells increased, the number of round cells decreased, and cell synapse recovered normally. The addition of 800 μM ferulic acid improved the growth of PC 12 cells in a manner similar to that obtained with the addition of FOs at 200 μM (Figure 2).

The administration time of FOs also affected the viability of the PC 12 cells. Cells were pre-incubated with different concentrations of FOs and ferulic acid before treatment with H_2O_2, and cell viability was determined after culturing for another 4 h after H_2O_2 treatment. Increasing the time difference between the addition of FOs and hydrogen peroxide increased the cell viability in all of the treatments, including treatments involving FOs and ferulic acid (Table 3). FOs were

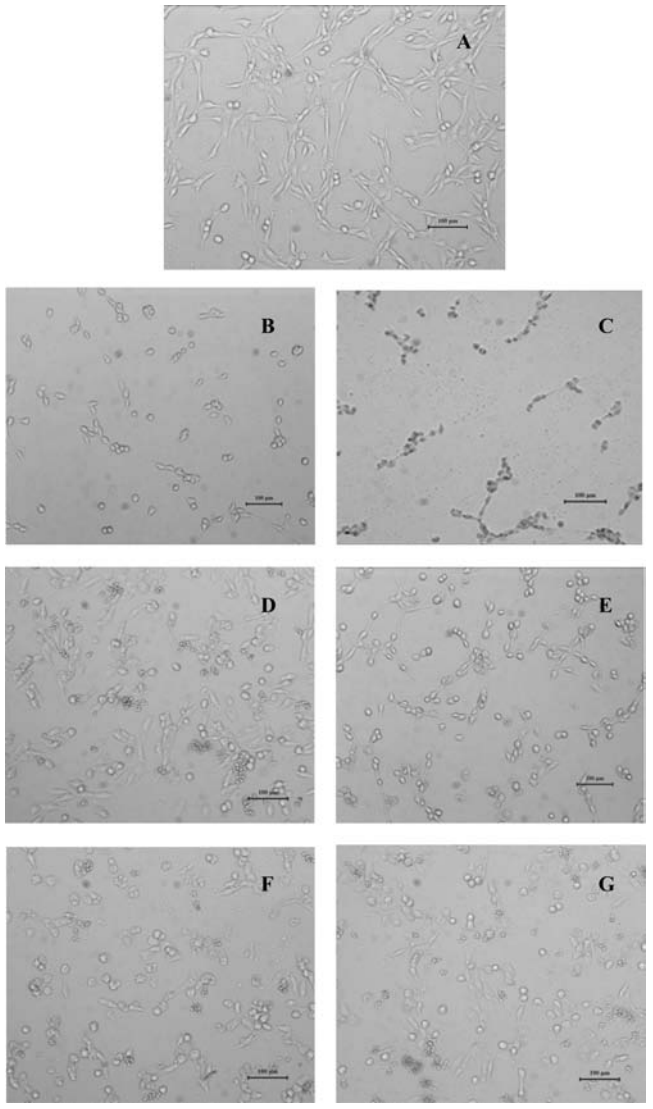

Figure 2. Effect of H_2O_2 treatment on the morphology of PC 12 cells under reverse-phase microscope: (A) control; (B, C) treatment with H_2O_2 at 0.8 and 1.6 mM; (D−F) addition of FOs at 800, 200, and 50 μM (on the basis of FA) to the treatment with 0.8 mM H_2O_2; (G) addition of ferulic acid at 800 μM to the treatment with 0.8 mM H_2O_2.

more efficient for preventing oxidative stress and have restoring capacity for antioxidant activity, resulting in an increase in the viability of the PC 12 cells after H_2O_2 treatment (Tables 2 and 3).

The effect of H_2O_2 treatment on apoptosis (Figure 3) was investigated using the flow cytometry method. After incubation with H_2O_2 at concentrations of 0.4, 0.8, and 1.6 mM for 4 h, apoptosis peaks were observed at the sub-G0 phase, and the apoptosis rates were 19.6 ± 0.6, 37.5 ± 1.1, and 46.2 ± 1.3%, respectively (n = 6), which were significantly higher ($P < 0.01$) than the control (8.2 ± 0.2%). Moreover, the rate of cells in G0/G1 phase was significantly reduced to 61.2% ($P < 0.05$), 59.6% ($P < 0.01$), and 58.1% ($P < 0.01$), at concentrations of 0.4, 0.8, and 1.6 mM, respectively, compared with 67.5% in the control. The rate of the cells in the S phase significantly increased to 35.8, 37.3, and 38.2% ($P < 0.01$) at concentrations of 0.4, 0.8, and 1.6 mM, respectively, compared with the control (31.2%). After the addition of FOs at 800, 200, and 50 μM, the apoptosis rates at sub-G0 phase decreased to 12.7 ± 0. 3, 16.2

dx.doi.org/10.1021/jf404841c | J. Agric. Food Chem. 2014, 62, 668−674

Table 3. Effects of Pre-incubation Time of Feruloylated Oligosaccharides before Addition of 0.8 μM H_2O_2 on the Viability of PC 12 Cells in 4 h

group	pretreatment time of FOs before the addition of H_2O_2[a]			
	0 h	6 h	12 h	24 h
0.8 mM H_2O_2	50.54 ± 2.56	52.15 ± 2.31	54.14 ± 2.48	53.52 ± 3.18
0.8 mM H_2O_2 + 800 μM (FA) FOs	68.89 ± 2.23	72.99 ± 1.65[b]	81.54 ± 2.17[bc]	84.72 ± 1.83[bc]
0.8 mM H_2O_2 + 200 μM (FA) FOs	57.10 ± 2.31	65.71 ± 2.09[b]	71.73 ± 2.15[bc]	72.51 ± 2.31[bc]
0.8 mM H_2O_2 + 50 μM (FA) FOs	53.97 ± 2.09	60.14 ± 2.26[b]	63.58 ± 2.57[b]	61.37 ± 3.14[b]
0.8 mM H_2O_2 + 800 μM FA	62.08 ± 2.60	69.44 ± 2.99[b]	74.36 ± 2.53[bc]	75.03 ± 2.59[bc]

[a]Means ± SD (n = 3). [b]P < 0.05 vs the group of no pre-incubation of FOs (0 h). [bc]P < 0.05 vs the group of no pre-incubation of FOs for 6 h.

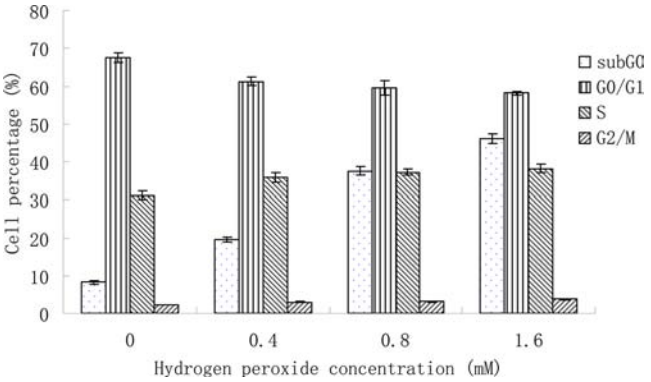

Figure 3. Effects of H_2O_2 on apoptosis rate and cell cycle of PC 12 cells.

Table 5. Effects of FOs on the Activities of SOD and LDH and the Content of MDA in PC 12 Cells Injured by H_2O_2

group	SOD[a] (IU/mg)	LDH[a] (IU/L)	MDA[a] (nmol/mg)
control	205.36 ± 7.17	350.08 ± 45.68	0.14 ± 0.02
0.8 mM H_2O_2	98.75 ± 6.92[b]	1343.01 ± 133.37[b]	1.22 ± 0.10[b]
0.8 mM H_2O_2 + 800 μM FOs	180.98 ± 3.04[d]	573.71 ± 36.34[d]	0.27 ± 0.02[d]
0.8 mM H_2O_2 + 200 μM FOs	147.46 ± 3.95[d]	923.95 ± 42.44[d]	0.70 ± 0.04[d]
0.8 mM H_2O_2 + 50 μM FOs	119.34 ± 6.25[d]	1218.21 ± 77.34[c]	1.08 ± 0.07[c]
0.8 mM H_2O_2 + 800 μM FA	158.61 ± 3.74[d]	1023.84 ± 40.36[d]	0.58 ± 0.04[d]

[a]Means ± SD (n = 3). [b]P < 0.01 vs control group. [c]P < 0.05 vs H_2O_2 injury group. [d]P < 0.01 vs H_2O_2 injury group.

± 0.6, and 20.9 ± 0.8%, significantly lower (P < 0.01) than that obtained from treatment with 0.8 mM H_2O_2 alone (Table 3). The addition of 800 μM ferulic acid showed an effect similar to that of 200 μM FO (Table 4).

Effect of FOs on MDA Content and Activities of SOD and LDH of PC 12 Cells after Injury by H_2O_2. H_2O_2 treatment significantly (P < 0.01) increased the activities of LDH and MDA contents in PC 12 cells by 3.84 and 8.71 times, respectively, compared with cells in the control (Table 5), whereas H_2O_2 significantly decreased the activity of SOD by 2.05 times. The addition of FOs significantly decreased the MDA content and LDH activity, but significantly increased SOD activity compared with the group treated with H_2O_2 alone (Table 5). FOs at 800 μM resulted in an MDA content and LDH activity of only 1.9 and 1.6 times higher than the control, and the SOD activity was restored to 88.2% of the activity in normal cells (calculated from Table 5). Ferulic acid at the 800 μM level also decreased MDA content and LDH activity and increased SOD activity, compared with the group treated with hydrogen peroxide alone. However, ferulic acid showed antioxidant activity in PC 12 cells only at a concentration equivalent to 200 μM FOs (Table 5).

DISCUSSION

Corn bran contains high amounts of ferulic acid and hemicellulose, which makes it a suitable source for the preparation of FOs. However, our previous research indicated that enzymatic hydrolysis is not an efficient way to prepare FOs from corn bran. When a mixture of enzymes containing Viscozyme L and xylanase was used to hydrolyze the pretreated corn bran at pH 5.5 and 45 °C for 24 h, only 25.4% of ferulic acid (including bound and free) and 30.0% of sugars were released.[22] In the current study, autoclaving the pretreating corn bran in 0.6% oxalic acid for 30 min can release nearly 50% of ferulic acid and reducing sugars. Approximately 20% of the target products (FOs), which contain 4.88% bound ferulic acid, were obtained. The composition and structures of FOs were similar to those in wheat bran extract,[21] which indicates that corn bran FOs can be a commercially functional ingredient.

PC 12 cells, a rat pheochromocytoma cell line, have been extensively used as a tool for studying the functions of

Table 4. Effects of FOs on Apoptosis Rate of PC 12 Cells Injured by H_2O_2

group	phase of cell cycle[a] (%)			apoptosis rate (%) sub-G0
	G0/G1	S	G2/M	
control	67.5 ± 1.2	31.5 ± 0.8	3.9 ± 0.2	8.2 ± 0.2
0.8 mM H_2O_2	59.7 ± 0.9[b]	36.8 ± 1.0[b]	3.5 ± 0.3	35.3 ± 1.1[b]
0.8 mM H_2O_2 + 800 μM (FA) FOs	63.8 ± 1.1[d]	32.4 ± 0.9[d]	3.8 ± 0.1	12.7 ± 0.3[d]
0.8 mM H_2O_2 + 200 μM (FA) FOs	61.9 ± 1.0[d]	33.7 ± 1.1[d]	4.4 ± 0.3	16.2 ± 0.6[d]
0.8 mM H_2O_2 + 50 μM (FA) FOs	60.9 ± 0.9[c]	35.0 ± 0.9[c]	4.1 ± 0.2	20.9 ± 0.8[d]
0.8 mM H_2O_2 + 800 μM FA	61.2 ± 0.9[d]	34.1 ± 1.1[d]	4.7 ± 0.5	16.4 ± 0.6[d]

[a]Means ± SD (n = 6). [b]P < 0.01 vs control group. [c]P < 0.05 vs H_2O_2 injury group. [d]P < 0.01 vs H_2O_2 injury group.

dx.doi.org/10.1021/jf404841c | J. Agric. Food Chem. 2014, 62, 668−674

neurotrophic factors and neuronal differentiation.[23] H_2O_2 can induce apoptosis in many different cell types and has been extensively used as an inducer of oxidative stress in in vitro models. The injury of PC 12 cells by H_2O_2 has been often used to screen neuroprotective drugs.[24,25] In this study, LDH and SOD activities and MDA content were used to evaluate the protective effects of FOs against oxidative stress in PC 12 cells induced by H_2O_2. LDH is a stable cytoplasmic enzyme present in all cells, and the release of intracellular enzymes can be used to evaluate the release of cellular contents into the plasma and the damage to cellular membranes.[26] Peroxidative damage has often been expressed in terms of MDA content, and SOD was considered an enzyme for protection against oxidative damage.[15]

The results showed that FOs prepared from corn bran can significantly decrease the content of MDA and the LDH activity, but significantly increase SOD activity in PC 12 cells injured by H_2O_2. Thus, cell growth is restored. An increase in the number of dead or plasma membrane-damaged cells results in an increase in LDH activity in the culture.[24] FOs can also decrease the release of LDH to the medium (Table 6), suggesting that FOs can mitigate the cell membrane damage induced by H_2O_2.

Table 6. Effects of FOs on the Activities of SOD and LDH and the Content of MDA in the Cultures

group	SOD (IU/mg)	LDH (IU/L)	MDA (nmol/mL)
control	29.01 ± 1.15	311.64 ± 15.43	1.15 ± 0.16
0.8 mM H_2O_2	12.39 ± 0.88[a]	1372.35 ± 70.84[a]	2.40 ± 0.18[a]
0.8 mM H_2O_2 + 800 μM (FA) FOs	25.91 ± 0.67[c]	510.83 ± 38.97[c]	1.35 ± 0.13[c]
0.8 mM H_2O_2 + 200 μM (FA) FOs	18.91 ± 1.14[c]	895.59 ± 41.18[c]	1.78 ± 0.14[c]
0.8 mM H_2O_2 + 50 μM (FA) FOs	14.66 ± 0.51[b]	1128.19 ± 78.35[c]	2.07 ± 0.12[b]
0.8 mM H_2O_2 + 800 μM FA	21.31 ± 1.04[c]	874.53 ± 40.24[c]	1.64 ± 0.12[c]

[a] $P < 0.01$ vs control group. [b] $P < 0.05$ vs H_2O_2 injury group. [c] $P < 0.01$ vs H_2O_2 injury group.

PC 12 cells can be induced to differentiate to neuron-like cells by nerve growth factor and other factors,[23] and, thus, whether or not FOs can act as neuroprotective agents to prevent or mitigate neurodegenerative disorders should be investigated.

In summary, FOs with structure similar to that of the wheat bran extracts can be prepared from corn bran by autoclaving in 0.6% oxalic acid for 30 min. FOs showed higher capacity than ferulic acid for protection against oxidative stress, which involves scavenging free radicals, and decreasing the apoptosis rate and membrane damage induced by H_2O_2 in PC 12 cells.

■ ASSOCIATED CONTENT

Supporting Information

Additional figure. This material is available free of charge via the Internet at http://pubs.acs.org.

■ AUTHOR INFORMATION

Corresponding Authors

*(S.O.) E-mail: tosy@jnu.edu.cn. Phone: +86-13640210646. Fax: +86-20-85226630.

*(W.S.) E-mail: tshenwz@jnu.edu.cn. Phone: +86-13503011588.

Author Contributions

‖S.Y., X.W., R.H. contributed equally to this work.

Funding

The present work was cofunded by the National Natural Science Fund (31071596), Jinan University (11613419), and the Science and Technology Council of Guangdong (2012A080800013).

Notes

The authors declare no competing financial interest.

■ ABBREVIATIONS USED

AAPH, 2,2-azobis(2-amidinopropane) dihydrochloride; DMEM, Dulbecco's modified Eagle medium; DP, degree of polymerization; DPPH, 1,1-diphenyl-2-picrylhydrazyl radical 2,2-diphenyl-1-(2,4,6-trinitrophenyl)hydrazyl; FA, ferulic acid; FBS, fetal bovine serum; FL, sodium fluorescein; FO(s), feruloylated oligosaccharide(s); LDH, lactate dehydrogenase; MDA, malondialdehyde; MTT, Tetrazolium blue; ORAC, oxygen radical absorbance capacity; PBS, phosphate-buffered saline; PC 12, pheochromocytoma cells; SOD, superoxide dismutase; Trolox, 6-hydroxy-2,5,7,8-tetramethylchroman-2-carboxylic acid

■ REFERENCES

(1) Pohanka, M. Role of oxidative stress in infectious diseases. A review. *Folia Microbiol.* **2013**, *58*, 503−513.

(2) Ratnam, D. V.; Ankola, D. D.; Bhardwaj, V.; Sahana, D. K.; Kumar, M. N. V. R. Role of antioxidants in prophylaxis and therapy: a pharmaceutical perspective. *J. Controlled Release* **2006**, *113*, 189−207.

(3) Taverne, Y. J. H. J.; Bogers, A. J. J. C.; Duncker, D. J.; Merkus, D. Reactive oxygen species and the cardiovascular system. *Oxid. Med. Cell. Longevity* **2013**, article ID 862423, 15.

(4) Ou, S. Y.; Kwok, K. C. Review: Ferulic acid: pharmaceutical functions, preparation and applications in foods. *J. Sci. Food Agric.* **2004**, *84*, 1261−1269.

(5) Nabi, G.; Liu, Z. Q. Ferulic and coumaric acids: application to release oxidative stress of dna and methyl linoleate. *J. Food Biochem.* **2012**, *36*, 38−45.

(6) Cheng, Y. H.; Yang, S. H.; Yang, K. C.; Chen, M. P.; Lin, F. H. The effects of ferulic acid on nucleus pulposus cells under hydrogen peroxide-induced oxidative stress. *Process Biochem.* **2011**, *46*, 1670−1677.

(7) Ramar, M.; Manikandan, B.; Raman, T.; Priyadarsini, A.; Palanisamy, S.; Velayudam, M.; Munusamy, A.; Prabhu, N. M.; Vaseeharan, B. Protective effect of ferulic acid and resveratrol against alloxan-induced diabetes in mice. *Eur. J. Pharmacol.* **2012**, *690*, 226−235.

(8) Rose, D. J.; Inglett, G. E.; Liu, S. X. Utilisation of corn (*Zea mays*) bran and corn fiber in the production of food components. *J. Sci. Food Agric.* **2010**, *90*, 915−924.

(9) Zhao, Z. H.; Egashira, Y.; Sanada, H. Phenolic antioxidants richly contained in corn bran are slightly bioavailable in rats. *J. Agric. Food Chem.* **2005**, *53*, 5030−5035.

(10) Ou, J. Y.; Sun Z. Feruloylated oligosaccharides: structure, metabolism and function. *J. Funct. Foods* **2013**, DOI: 10.1016/j.jff.2013.09.028.

(11) Veenashri, B. R.; Muralikrishna, G. In vitro antioxidant activity of xylo-oligosaccharides derived from cereal and millet brans − a comparative study. *Food Chem.* **2011**, *126*, 1475−1481.

(12) Bauer, J. L.; Harbaum-Piayda, B.; Stöckmann, H.; Schwarz, K. Antioxidant activities of corn fiber and wheat bran and derived extracts. *LWT−Food Sci. Technol.* **2013**, *50*, 132−138.

(13) Ohta, T.; Semboku, N.; Kuchii, A.; Egashira, Y.; Sanada, H. Antioxidant activity of corn bran cell-wall fragments in the LDL oxidation system. *J. Agric. Food Chem.* **1997**, *45*, 1644−1648.
(14) Ohta, T.; Yamasaki, S.; Egaehira, Y.; Sanada, H. Antioxidative activity of corn bran hemicellulose fragments. *J. Agric. Food Chem.* **1994**, *42*, 663−060.
(15) Ou, S. Y.; Jackson, G. M.; Jiao, X.; Chen, J.; Wu, J. Z.; Huang, X. S. Protection against oxidative stress in diabetic rats by wheat bran feruloyl oligosaccharides. *J. Agric. Food Chem.* **2007**, *55*, 3191−3195.
(16) Huang, R. Q.; Ou, S. Y. Effects of oxalic acid-autoclaving treatment and surfactants on preparation feruloylatedated oligosaccharides from maize bran. *J. Chinese Inst. Food Sci. Technol.* **2012**, *12*, 71−75.
(17) Davalos, A.; GoMez-CordoveS, C.; Bartolome, B. Extending applicability of the oxygen radical absorbance capacity (ORAC-fluorescein) assay. *J. Agric. Food Chem.* **2004**, *52*, 48−54.
(18) Yao, N.; Lan, F.; He, R. R.; Kurihara, H. Protective effects of bilberry (*Vaccinium myrtillus* L.) extract against endotoxin-induced uveitis in mice. *J. Agric. Food Chem.* **2010**, *58*, 4731−4736.
(19) Zhao, S. Q.; Yao, S. W.; Ou, S. Y.; Lin, J.; Wang, Y.; Peng, X. C.; Li, A. J.; Yu, B. Preparation of ferulic acid from corn bran: its improved extraction and purification by membrane separation. *Food Bioprod. Process.* **2013**, DOI: 10.1016/j.fbp.2013.09.004.
(20) van den Borne, J. J. G. C.; Kabel, M. A.; Briens, M.; van der Poel, A. F. B.; Hendriks, W. H. Effects of pretreatment of wheat bran on the quality of protein-rich residue for animal feeding and on monosaccharide release for ethanol production. *Bioresour. Technol.* **2012**, *124*, 446−454.
(21) GRAS Notice 000343, http://www.accessdata.fda.gov/scripts/fcn/gras_notices/grn000343.pdf.
(22) Zhu, Y. J.; Ou, S. Y. Preparation of ferulic acid and oligosaccharides from maize bran by ferulic esterase in combination with xylanase, cellulose and Viscozyme L. *Food Res. Dev.* **2007**, *28*, 68−71.
(23) Zhou, T.; Xu, B. N.; Que, H. P.; Lin, Q. X.; Lv, S. H.; Liu, S. J. Neurons derived from PC 12 cells have the potential to develop synapse with primary neurons from rat cortex. *Acta Neur. Exp.* **2006**, *66*, 105−112.
(24) Hong, H.; Liu, G. Q. Protection against hydrogen peroxide-induced cytotoxicity in PC 12 cells by scutellarin. *Life Sci.* **2004**, *74*, 2959−2973.
(25) Prabhu, B. M.; Medina-Bolivar, F.; Condori, J.; Sivakumar, G.; Srivatsan, M. Neuroprotective effect of peanut hairy root extract against oxidative stress in PC 12 derived neurons. *J. Med. Active Plants* **2013**, *1*, 125−133.
(26) Ramos, D.; Martins, E. G.; Viana-Gomes, D.; Casimiro-Lopes, G.; Salerno, V. P. Biomarkers of oxidative stress and tissue damage released by muscle and liver after a single bout of swimming exercise. *Appl. Physiol. Nutr. Metab.* **2013**, *38*, 507−511.

JOURNAL OF AGRICULTURAL AND FOOD CHEMISTRY

Article

pubs.acs.org/JAFC

Algal Sterols are as Effective as β-Sitosterol in Reducing Plasma Cholesterol Concentration

Jingnan Chen,*[,†] Rui Jiao,[§] Yue Jiang,[‡] Yanlan Bi,[†] and Zhen-Yu Chen[#]

[†]Lipids Technology and Engineering, School of Food Science and Engineering, Henan University of Technology, Lianhua Road, Zhengzhou, Henan, China

[§]Department of Food Science and Engineering, Jinan University, Guangzhou, China

[‡]School of Food Science and Technology, Jiangnan University, Wuxi, China

[#]Food and Nutritional Sciences Programme, School of Life Sciences, The Chinese University of Hong Kong, Shatin, NT, Hong Kong, China

Supporting Information

ABSTRACT: The present study examined the cholesterol-lowering activity of sterol extract (SE) derived from alga *Schizochytrium* sp. and its interaction with gene expression of transporters, receptors, and enzymes involved in cholesterol absorption and metabolism. GC-MS analyses found that SE was a mixture of various sterols including lathosterol, ergosterol, stigmasterol, 24-ethylcholesta-5,7,22-trienol, stigmasta-7,24(24[1])-dien-3β-ol, and cholesterol. Results showed that SE at doses of 0.06 and 0.30 g/kg diet were able to decrease plasma cholesterol concentration by 19.5 and 34%, respectively, compared with the control, in hamsters maintained on a 0.1% high-cholesterol diet. SE at a dose of 0.30 g/kg diet was as effective as β-sitosterol in reducing plasma total cholesterol (TC). SE-induced reduction in plasma TC was accompanied by down-regulation of intestinal acyl-CoA:cholesterol acyltransferase 2 (ACAT2) and hepatic 3-hydroxy-3-methylglutaryl-CoA (HMG-CoA) reductase and up-regulation of hepatic low-density lipoprotein (LDL) receptor. Addition of SE to the diet increased the excretion of total fecal sterols. It was concluded that SE possessed the same cholesterol-lowering activity as β-sitosterol and the underlying mechanisms were mediated by increasing sterol excretion and decreasing cholesterol absorption and synthesis.

KEYWORDS: *algal sterol, β-sitosterol, cholesterol, ACAT2, LDL receptor, HMG-CoA-reductase*

INTRODUCTION

Cardiovascular disease is the major cause of human mortality. It has been shown that total plasma cholesterol (TC) and low-density lipoprotein cholesterol (LDL-C) are positively, whereas high-density lipoprotein cholesterol (HDL-C) is negatively, correlated with coronary heart disease. The three basic principles associated with cholesterol-lowering functional foods are to reduce cholesterol absorption, decrease cholesterol synthesis, and increase cholesterol catabolism by converting cholesterol to bile acids for elimination via the bile duct. Cholesterol absorption is mediated by actions of intestinal Niemann-Pick C1 like 1 (NPC1L1), acyl-CoA:cholesterol acyltransferase (ACAT-2), microsomal triglyceride protein (MTP), and ATP-binding cassette transporters (ABCG5/8).[1] Cholesterol synthesis is regulated by 3-hydroxy-3-methylglutaryl-CoA (HMG-CoA) reductase, whereas low-density lipoprotein (LDL) receptor mediates cholesterol removal from the circulation. Elimination of excessive cholesterol in the liver is mediated by cholesterol-7a-hydroxylase CYP7A1, which converts cholesterol to bile acids.[2] In this connection, cholesterol homeostasis is maintained by sterol-responsive element-binding protein 2 (SREBP2) and hepatic liver X receptor-α (LXRα) with the former regulating the gene expression of LDL receptor and HMG-CoA reductase and the latter governing the gene expression of CYP7A1.[1,2]

Microalgae are a new source of functional foods because they are rich in lipids, proteins, chlorophyll, carotenoids, vitamins, minerals, and pigments as well sterols. It is known that plant sterols cannot be absorbed and are capable of reducing plasma TC concentration by inhibiting cholesterol absorption.[3−7] However, no study has addressed the effect of algal sterols on plasma TC. We have previously examined the cholesterol-lowering activity of the lipid extracts of alga *Schizochytrium* sp., finding algal lipids were capable of lowering plasma TC and LDL-C; the two fatty acids, namely, docosahexaenoic acid (22:6n-3, DHA) and docosapentaenoic acid (22:5n-3, DPA), in the lipid extract were partially accountable for such activity.[8,9] We herewith speculate that sterols in the algal lipid extract are also possible cholesterol-lowering active ingredients. The present study was therefore the first time (i) to characterize the sterol profile of alga *Schizochytrium* sp; (ii) to compare the cholesterol-lowing activity of algal sterols with that of β-sitosterol; and (iii) to investigate its cholesterol-lowering activity as well as its interaction with gene expression of sterol transporters, proteins, and receptors involved in cholesterol metabolism.

MATERIALS AND METHODS

Preparation of Algal Sterol Extract (SE). Algal total lipids were prepared as we previously described.[8] Algal lipid (50 g) was weighed in a 1 L round-bottom flask followed by the addition of 500 mL of 1 M

Received: November 4, 2013
Revised: December 29, 2013
Accepted: December 31, 2013
Published: December 31, 2013

ACS Publications © 2013 American Chemical Society

NaOH in 90% ethanol. The sample was subjected to saponification by refluxing under a gentle stream of N_2 for 2 h at 90 °C. After the mixture was cooled to the room temperature, 200 mL of double-distilled H_2O was added. The total sterols were extracted into 200 mL of cyclohexane followed by centrifugation at 2500 rpm for 10 min. The process was repeated three times. The cyclohexane layer was pooled and evaporated using a rotary evaporator at 40 °C. The resultant SE was weighed and saved for the animal feeding study described below.[8]

GC-MS Analysis of SE. Sterol-TMS derivatives were prepared, and GC-MS analysis was performed in a fused silica capillary column (SACTM-5, 30 m × 0.25 mm, i.d.; Supelco, Inc., Bellefonte, PA, USA) fitting in a 6890N gas−liquid chromatograph coupled with a 7683B injector and an Agilent 5975 inert mass selective detector (Agilent Technologies Inc., Palo Alto, CA, USA) with a full scan mode (m/z 50−550). Helium was used as a carrier gas at a flow rate of 1 mL/min. The column temperature was set at 290 °C and held for 10 min followed by programming to 300 °C at the rate of 5 °C/min and being held for 20 min. MS interface temperature was set at 280 °C, and the ion source was set at 230 °C. The electron ionization energy was 70 eV. A typical GC chromatogram of SE is shown in Figure 1. Individual TMS sterols were identified according to their retention times of authentic standards and specific characteristics of mass spectra as previously published.[10−13] The characteristic spectrum of each sterol was shown in Supplementary Figure 1.

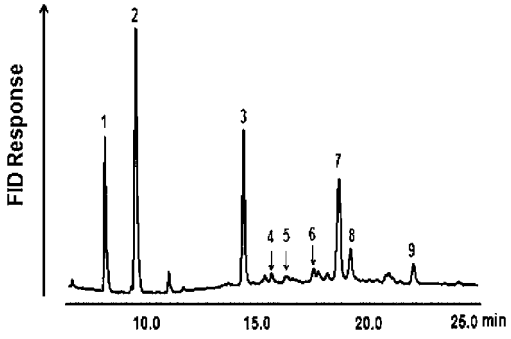

Figure 1. Gas−liquid chromatogram profiles of algal sterol extract (SE). Peaks: 1, squalene; 2, 5α-cholestane (internal standard); 3, cholesterol; 4, lathosterol; 5, ergosterol; 6, stigmasterol; 7, 24-ethylcholesta-5,7,22-trienol; 8, stigmasta-7,24(24^1)-dien-3β-ol; 9, unknown.

Diets. The four diets were prepared as previously described.[8] Casein, mineral mix, and vitamin mix were purchased from Harlan Teklad (Madison, WI, USA), and lard was purchased from the local market. DL-Methionine and cholesterol were purchased from Sigma Chemical (St. Louis, MO, USA). The control diet (CTL) was formulated by mixing 508 g of cornstarch, 242 g of casein, 50 of lard, 119 g of sucrose, 40 g of mineral mix, 20 g of vitamin mix, 1 g of DL-methionine, and 1 g of cholesterol. The other three experimental diets were prepared by adding 0.06 g of SE derived from 10 g of algal lipids (SE1), 0.30 g of SE derived from 50 g of algal lipids (SE5), and 0.30 g of β-sitosterol (ST), respectively, into 1 kg of basal diet (Table 1). The powered diets were gelatinized with a gelatin solution (20 g/L) in a ratio of 200 g of diet per liter and were cut into 10 g cubes and stored frozen at −20 °C before the hamsters were fed.

Hamsters. Male golden hamsters (*Mesocricetus auratus*; body weights = 110−130 g) were randomly divided into four groups (n = 10/group) and fed one of the four diets for 5 weeks. Diets and water were given ad libitum. Body weights were recorded, and the fecal samples per cage were collected weekly. Blood (0.5 mL) was obtained from the retro-orbital sinus into a heparinized capillary tube at the end of weeks 0, 3, and 5 following food deprivation for 14 h overnight and light anesthesia, using a mixture of ketamine, xylazine, and saline (v/v/v, 4:1:5).[14] Following the last blood sample collection at week 5, all of the hamsters were sacrificed by carbon dioxide suffocation. The liver, heart, kidney, testis, epididymal and perirenal adipose tissue, and aorta were removed, washed in saline, and weighed. The first 10 cm of duodenum was discarded, and the next 30 cm of the small intestine was kept. All tissue samples were flash frozen in liquid nitrogen and stored at −80 °C until analysis. The entire experimental procedure was approved by the Animal Experimental Ethical Committee, Chinese University of Hong Kong.

Table 1. Composition (Grams per Kilogram Diet) of the Control Diet (CTL) and Three Experimental Diets Supplemented with 0.06 g of Sterol Extract (SE1), 0.30 g of Sterol Extract (SE5), and 0.30 g of β-Sitosterol (ST) per Kilogram of Diet

	CTL	SE1	SE5	ST
corn starch	508	508	508	508
casein	242	242	242	242
sucrose	119	119	119	119
lard	50	50	50	50
mineral mix	40	40	40	40
vitamin mix	20	20	20	20
DL-methionine	1	1	1	1
SE	0	0.06	0.30	0
ST	0	0	0	0.30

Measurement of Plasma Lipoproteins. Plasma TC, HDL-C, non-HDL-C, and triacylglycerols (TG) were measured using the commercially available enzymatic kits from Infinity (Waltham, MA, USA) and Stanbio Laboratories (Boerne, TX, USA), respectively.[14] To quantify plasma HDL-C, very low-density lipoprotein (VLDL) and LDL were first precipitated using a commercial kit containing phosphotungstic acid and magnesium chloride (Stanbio Laboratories). HDL-C in the supernatant was measured similarly as done for TC. Non-HDL-C was calculated by deducting HDL-C from TC. The apparent cholesterol absorption was calculated by the equation [cholesterol intake − (excretion of cholesterol + microbial neutral and acidic sterols)]/cholesterol intake].

Quantification of Organ Cholesterol. Cholesterol in the liver was determined as we previously described.[15,16] The 300 mg liver sample was homogenized with 5α-cholestane being added as an internal standard. The total liver lipids were extracted into a solvent mixture of methanol/chloroform (2:1, v/v). After evaporation of the solvent, the total lipid extract was mildly saponified. The free cholesterol in the extract was converted to its trimethylsilyl ether (TMS) derivative before the GC analysis.

Fecal Sterol Analysis. Fecal sterols were analyzed as we described previously.[14] The total fecal output from each hamster was collected, freeze-dried, and then ground into powder. The fecal powder sample of about 300 mg was weighed with the addition of 5α-cholestane and hyodeoxycholic acid as internal standards for quantification of fecal neutral and acidic sterols, respectively. Total fecal neutral sterols were extracted into cyclohexane and then converted to their TMS derivatives. The total acidic sterols in aqueous phase were saponified, extracted, and converted to their corresponding TMS derivatives. Both neutral and acidic sterol TMS derivatives were run in a fused silica capillary column (SAC-5, 30 m × 0.25 mm, i.d.; Supelco, Bellefonte, PA, USA) using a Shimadzu GC-14 B gas−liquid chromatograph equipped with a flame

Table 2. Sterol Composition of Algal Lipids Derived from *Schizochytrium* sp.

sterol	% total sterol extract
squalene	20.69
cholesterol	27.67
lathosterol	1.23
ergosterol	2.54
stigmasterol	4.82
24-ethylcholesta-5,7,22-trienol	32.62
stigmasta-7,24(24^1)-dien-3β-ol	7.47
others	2.96

dx.doi.org/10.1021/jf404955n | J. Agric. Food Chem. 2014, 62, 675−681

ionization detector (Kyoto, Japan). Total neutral sterols were the sum of cholesterol and its microbial metabolites, namely, coprostanol, coprostanone, and dihydrocholesterol, whereas fecal total acidic sterols were the sum of primary and secondary bile acids including cholic, chenodeoxycholic, lithocholic, deoxycholic, and ursocholic acids.

Real-Time PCR Analysis. mRNA of liver SREBP-2, LDL receptor, HMG-CoA reductase, LXRα, CYP7A1, and intestinal NPC1L1, ABCG5/8, ACAT2, and MTP was measured as we described previously.[14] In brief, total RNA was extracted and then converted to its complementary DNA. Real-time PCR analysis was carried out on a Fast Real-time PCR System 7500 (Applied Biosystems). Primers and TaqMan probes were used for real-time PCR analysis of liver GAPDH, CYP7A1, HMG-CoA reductase, LDL receptor, SREBP-2, LXRα[14] and intestinal NPC1L1, ABCG5, ABCG8, ACAT2, MTP, and 18S with SYBR green being used as fluorophore.[17−19]

Statistics. All data are presented as the mean ± standard deviation (SD). The significance of difference was assessed using ANOVA. Differences were considered significant when the P value was <0.05. The post hoc LSD test was carried out to detect any significant difference between the two group means using SigmaStat Advisory Statistical Software.

RESULTS

SE Composition. Dry powder of alga *Schizochytrium* sp. was rich in lipids (49.80%).[8] It was found that algal lipids contained 0.66% SE by weight. The GC-MS analysis demonstrated that SE was a mixture of squalene, cholesterol, lathosterol, ergosterol, stigmasterol, 24-ethylcholesta-5,7,22-trienol, and stigmasta-7,24-(24^1)-dien-3β-ol with 24-ethylcholesta-5,7,22-trienol accounting for 32.62% and squalene accounting for 20.69% with cholesterol being about 27.67% (Table 2).

Food Intake and Body and Organ Weights. The food intake among the four groups was in the range of 10.14−11.00 g daily. The SE1 group had lesser food intake than the control

Table 3. Change in Food Intake, Body Weight, and Relative Organ Weights in Hamsters Fed the Control (CTL) and Three Experimental Diets Supplemented with 0.06 g of Sterol Extract (SE1), 0.30 g of Sterol Extract (SE5), and 0.30 g of β-Sitosterol (ST) per Kilogram of Diet[a]

	CTL	SE1	SE5	ST	P
food intake	11.00 ± 0.57a	10.14 ± 0.43b	10.76 ± 0.58ab	10.63 ± 0.60ab	0.14
body wt (g)					
initial	110.6 ± 6.8ab	107.5 ± 7.9b	113.0 ± 5.4ab	115.0 ± 6.6a	0.08
final	112.2 ± 7.6ab	108.5 ± 5.3b	115.5 ± 7.6a	116.1 ± 3.3a	0.04
relative organ wt (%)					
liver	5.56 ± 0.41a	5.42 ± 0.26ab	5.41 ± 0.45ab	5.19 ± 0.22b	0.17
heart	0.45 ± 0.05a	0.46 ± 0.04a	0.43 ± 0.04ab	0.40 ± 0.06b	0.03
testis	3.39 ± 0.23ab	3.54 ± 0.30a	3.38 ± 0.31ab	3.22 ± 0.26b	0.12
kidney	1.03 ± 0.17	1.04 ± 0.15	1.04 ± 0.08	1.02 ± 0.05	0.97
epididymal fat	2.05 ± 0.46	1.89 ± 0.27	1.93 ± 0.38	1.84 ± 0.39	0.70
perirenal fat	1.36 ± 0.25a	1.08 ± 0.18b	1.28 ± 0.36ab	1.15 ± 0.15ab	0.90

[a]Data are expressed as the mean ± SD; n = 10 each group. Means in the same row with different letters differ significantly at P < 0.05.

Table 4. Changes in Plasma Total Cholesterol (TC), Total Triacylglycerols (TG), High-Density Lipoprotein Cholesterol (HDL-C), Non-HDL-Cholesterol (non HDL-C), TC:HDL-C in Hamsters Fed the Control (CTL) Diet and Four Experimental Diets Supplemented with 0.06 g of Sterol Extract (SE1), 0.30 g of Sterol Extract (SE5), and 0.30 g of β-Sitosterol (ST) per Kilogram of Diet[a]

	CTL	SE1	SE5	ST	P
			Week 0		
TC (mg/dL)	149.87 ± 13.05	149.37 ± 14.43	150.16 ± 21.00	148.60 ± 15.69	1.00
TG (mg/dL)	84.03 ± 23.08	78.19 ± 26.60	71.46 ± 21.62	70.16 ± 19.52	0.57
HDL-C (mg/dL)	51.37 ± 15.06	50.42 ± 7.72	50.22 ± 7.10	53.35 ± 7.57	0.28
non-HDL-C (mg/dL)	97.81 ± 29.387	98.95 ± 18.66	99.94 ± 19.34	95.25 ± 19.49	0.84
non-HDL-C:HDL-C	1.91 ± 1.13	1.90 ± 0.52	1.92 ± 0.39	1.98 ± 0.55	0.74
TC:HDL-C	2.91 ± 1.13	2.90 ± 0.52	2.92 ± 0.39	2.98 ± 0.55	0.75
			Week 3		
TC (mg/dL)	260.43 ± 21.13a	233.54 ± 35.47ab	205.28 ± 32.93b	247.28 ± 31.77a	<0.01
TG (mg/dL)	158.30 ± 38.59a	95.31 ± 21.02b	96.52 ± 26.25b	145.42 ± 42.48a	<0.01
HDL-C (mg/dL)	123.45 ± 9.96a	90.53 ± 22.11b	91.68 ± 20.00b	123.17 ± 14.77a	<0.01
non-HDL-C (mg/dL)	136.99 ± 15.37ab	140.78 ± 31.34a	113.59 ± 38.99b	123.04 ± 26.83ab	0.27
non-HDL-C:HDL-C	1.11 ± 0.13bc	1.62 ± 0.52a	1.53 ± 0.52ab	1.05 ± 0.43c	0.01
TC:HDL-C	2.11 ± 0.13bc	2.62 ± 0.52a	2.53 ± 0.52ab	2.05 ± 0.43c	0.01
			Week 5		
TC (mg/dL)	292.98 ± 23.60a	235.95 ± 60.13b	194.42 ± 35.87c	204.91 ± 36.21bc	<0.01
TG (mg/dL)	247.14 ± 40.63	145.62 ± 57.66	220.47 ± 72.43	152.61 ± 42.62	0.15
HDL-C (mg/dL)	124.01 ± 23.85a	113.83 ± 32.38a	82.03 ± 11.66b	85.30 ± 17.92b	<0.01
non-HDL-C (mg/dL)	168.97 ± 9.86a	122.11 ± 55.15b	112.39 ± 35.16b	119.61 ± 34.77b	0.01
non-HDL-C:HDL-C	1.43 ± 0.40	1.10 ± 0.42	1.40 ± 0.48	1.43 ± 0.41	0.37
TC:HDL-C	2.43 ± 0.40	2.10 ± 0.42	2.40 ± 0.48	2.43 ± 0.41	0.37

[a]Values are means ± SD, n = 10. Means in a row for a given week with different letters differ significantly, P < 0.05.

dx.doi.org/10.1021/jf404955n | J. Agric. Food Chem. 2014, 62, 675−681

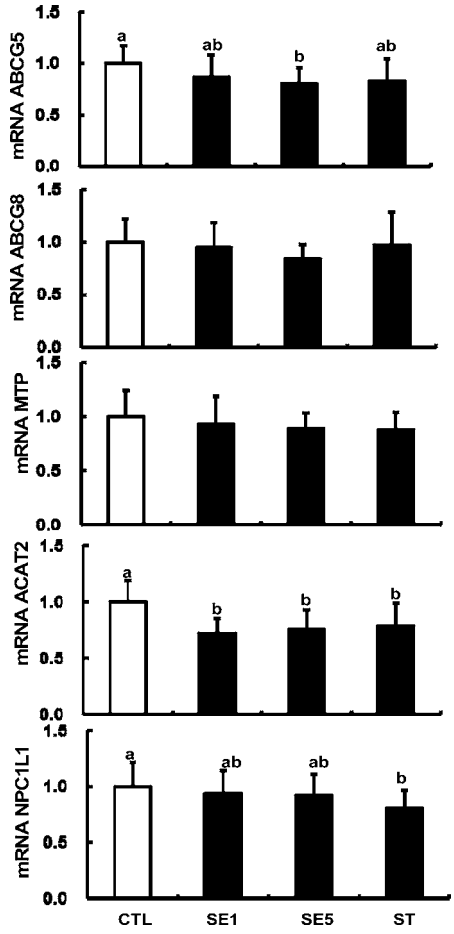

Figure 2. Effect of 0.06 g of sterol extract (SE1), 0.30 g of sterol extract (SE5), and 0.30 g of β-sitosterol (ST) per kilogram diet on intestinal Niemann-Pick C1 like 1 (NPC1L1), acyl coenzyme A:cholesterol acyltransferase 2 (ACAT2), microsomal triacylglycerol transport protein (MTP), and ATP binding cassette transporters (ABCG5 and ABCG8) in hamsters fed a high-cholesterol diet. Data are normalized with cyclophilin. Values are expressed as means ± SD (n = 10) with those for the control group being arbitrarily taken as one. Means with different letters differ significantly, $P < 0.05$.

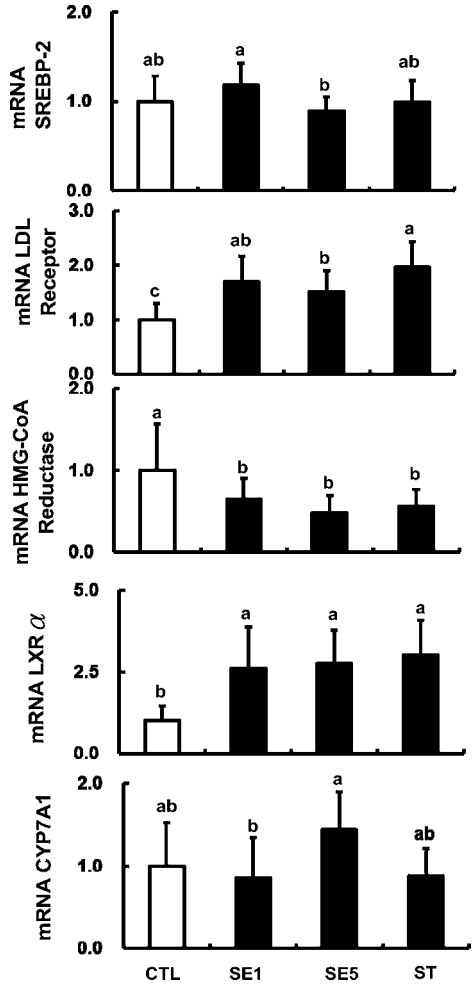

Figure 3. Effect of 0.06 g of sterol extract (SE1), 0.30 g of sterol extract (SE5), and 0.30 g of β-sitosterol (ST) per kilogram diet on mRNA levels of hepatic sterol regulatory element-binding protein-2 (SREBP-2), liver X receptor (LXRα), 3-hydroxy-3-methylglutaryl-CoA (HMG-CoA) reductase, LDL receptor, and cholesterol-7α-hydroxylase (CYP7A1) in hamsters fed a high-cholesterol diet. Data are normalized with GAPDH. Values are expressed as means ± SD (n = 10) with those for the control group being arbitrarily taken as one. Means with different letters differ significantly, $P < 0.05$.

hamsters. The SE1 group had lighter initial and final body weights compared with the ST hamsters (Table 3). However, no significant differences were seen among the other three groups. The sizes of liver, heart, and testis in the ST group were smaller compared with the control group. No significant differences in the kidney and epididymal fat pad were seen among the four groups. The SE1 group had a smaller perirenal fat pad compared with the control (Table 3).

Plasma Lipid Profile. There was no difference in plasma lipoprotein profiles among the four groups at week 0 (Table 4). At the end of week 3, plasma TC in group SE5 was significantly decreased compared with the other three groups (SE5, 205.28 mg/dL; CTL, 260.43 mg/dL; SE1, 233.54 mg/dL; ST, 248.28 mg/dL). Plasma TG in groups SE1 and SE5 was significantly lower compared with that in the other two groups. Non-HDL-C concentration in the SE5 group was significantly decreased compared with the SE1 group, whereas HDL-C concentration was lower in groups SE1 and SE5 compared with that in the control and ST groups (Table 4). At the end of week 5, plasma TC in SE1, SE5, and ST was significantly lower than that in the control (SE5, 194.42 mg/dL; CTL, 292.98 mg/dL; SE1, 235.95 mg/dL; ST, 204.91 mg/dL). Among the three experimental groups, SE5 had the lowest plasma TC concentration followed by the ST group. With regard to non-HDL-C, addition of SE and ST to the diet significantly reduced its concentration compared with the control hamsters. Both SE5 and ST groups had HDL-C concentration lower than the control group.

Liver Cholesterol. No significant differences in hepatic cholesterol concentrations were seen among the four groups (data not shown).

mRNA Analyses of Intestinal ABCG5, ABCG8, NPC1L1, MTP, and ACAT2. Real-time PCR analyses demonstrated that dietary SE and β-sitosterol had no effect on the gene expression of ABCG8 and MTP (Figure 2). With regard to intestinal ABCG5, only the SE5 group demonstrated down-regulation compared with the control. In contrast, addition of SE and ST to diets could down-regulate the mRNA of intestinal ACAT2. ST also down-regulated the mRNA of intestinal NPC1L1. Although SE1 and SE5 showed a trend of down-regulation of intestinal NPC1L1, no significant difference was seen compared with the control (Figure 2).

mRNA Analysis of SREBP-2, HMG-CoA Reductase, LDL Receptor, LXRα, and CYP7A1. The real-time PCR analyses demonstrated that SE1, SE5, and β-sitosterol had no effect on

dx.doi.org/10.1021/jf404955n | J. Agric. Food Chem. 2014, 62, 675−681

Table 5. Fecal Excretion of Total Neutral Sterols and Total Acidic Sterols (Milligrams/Hamster/Day) in Hamsters Fed the Control (CTL) Diet and Three Experimental Diets Supplemented with 0.06 g of Sterol Extract (SE1), 0.30 g of Sterol Extract (SE5), and 0.30 g of β-Sitosterol (ST) per Kilogram of Diet, Respectively, at Week 1[a]

	CTL	SE1	SE5	ST	*P*
fecal neutral sterols					
coprostanol	0.39 ± 0.14b	0.40 ± 0.02b	0.62 ± 0.20a	0.49 ± 0.13ab	<0.01
coprostanone	0.03 ± 0.01a	0.03 ± 0.01a	0.02 ± 0.00ab	0.01 ± 0.00b	0.02
cholesterol	0.13 ± 0.04b	0.15 ± 0.04b	0.26 ± 0.08a	0.14 ± 0.03b	<0.01
dihydrocholesterol	0.11 ± 0.04c	0.15 ± 0.02b	0.16 ± 0.04b	0.18 ± 0.03a	<0.01
total cholesterol and its microbial metabolites	**0.66 ± 0.21c**	**0.73 ± 0.06c**	**1.06 ± 0.25a**	**0.82 ± 0.10b**	**<0.01**
campersterol	0.02 ± 0.01b	0.03 ± 0.01a	0.03 ± 0.01a	0.04 ± 0.01a	<0.01
stigmasterol	0.03 ± 0.01c	0.04 ± 0.01b	0.06 ± 0.01a	0.04 ± 0.00b	<0.01
β-sitosterol	0.03 ± 0.02c	0.05 ± 0.01b	0.13 ± 0.03a	0.12 ± 0.02a	<0.01
squalene	ND	0.01 ± 0.00	0.05 ± 0.01	ND	
lathosterol	ND	0.00 ± 0.00	0.01 ± 0.00	ND	
ergosterol	ND	0.01 ± 0.00	0.02 ± 0.01	ND	
24-ethylcholesta-5,7,22-trierol	ND	0.01 ± 0.00	0.12 ± 0.02	ND	
stigmasta-7,24(24′)-dien-3β-ol	ND	0.01 ± 0.00	0.01 ± 0.00	ND	
fecal acidic sterols					
lithocholic	0.28 ± 0.05	0.29 ± 0.10	0.27 ± 0.11	0.25 ± 0.07	0.78
deoxycholic	0.19 ± 0.05	0.21 ± 0.09	0.19 ± 0.08	0.18 ± 0.05	0.89
chenodeoxycholic	0.29 ± 0.11	0.23 ± 0.08	0.23 ± 0.11	0.20 ± 0.06	0.31
cholic acid	0.27 ± 0.15b	0.40 ± 0.13b	0.95 ± 0.83a	0.33 ± 0.13b	0.01
ursodeoxycholic	0.18 ± 0.07b	0.17 ± 0.07b	0.15 ± 0.06b	0.38 ± 0.03a	<0.01
total	**1.22 ± 0.36**	**1.29 ± 0.38**	**1.80 ± 0.90**	**1.35 ± 0.23**	**0.91**

[a]Values are expressed as means ± SD, $n = 10$. Means at the same row with different letters differ significantly, $P < 0.05$.

mRNA level of SREBP-2 and CYP7A1. However, SE1, SE5, and β-sitosterol all up-regulated LDL receptor and mRNA LXRα, whereas they all down-regulated HMG-CoA reductase (Figure 3).

Cholesterol Balance and Excretion of Fecal Neutral and Acidic Sterols. The individual neutral and acidic sterols in the feces at weeks 1 and 5 were quantified (Tables 5 and 6). In week 1, group SE5 had significantly higher fecal excretion of cholesterol and its major microbial metabolite coprostanol as well as total fecal neutral sterols. SE5 hamsters also excreted greater cholic acid than other three groups. In week 5, SE5 excreted a greater amount of cholesterol compared with the other three groups. Excretions of total fecal neutral sterols in both SE5 and ST groups were greater than those of the control hamsters. SE and ST groups had an increasing trend in the excretion of fecal total acidic sterols; however, no significant difference between the control and the three experimental groups was seen.

Total intake of cholesterol was compared with its excretion of neutral and acidic sterols (Table 7). Net cholesterol equivalent retained was calculated by difference between the intake and excretion of cholesterol and both its neutral and acidic metabolites. It was clear that at week 1, SE and ST demonstrated a trend of decreasing the apparent cholesterol absorption. At the end of week 5, the inhibition of the apparent cholesterol absorption by both SE and ST became more significant compared with that of the control group.

DISCUSSION

The present study clearly demonstrated that SE of alga *Schizochytrium* sp. possessed cholesterol-lowering activity. Addition of 0.06 and 0.30 g of SE to 1 kg of diet was able to decrease plasma TC concentration by 19.5 and 34%, respectively, in hamsters fed a 0.1% high-cholesterol diet. The reason for choosing 0.06 g/kg diet as the first dose was that it was equivalent to the amount present in 1% algal lipids, which was added to the diet and showed a cholesterol-lowering activity in a previous study.[8] The rationale for choosing 0.30 g SE/kg diet as the second dose was that this dose was used in most research studies on phytosterols. It was clear that SE reduced plasma cholesterol concentration in a dose-dependent manner. The present result supports the hypothesis that, in addition to DPA n-3 and DHA, SE in alga *Schizochytrium* sp. may also be the active ingredient accountable for the cholesterol-lowering activity of algal lipid extract observed in the previous studies.[8,9]

The hypocholesterolemia effect of SE was comparable to that of β-sitosterol (Table 4), which is commonly used as a cholesterol-lowering functional plant sterol added to foods such as margarine and vegetable oil.[5] As a health supplement, phytosterols including β-sitosterol can lower blood cholesterol concentration and reduce the risk of heart diseases.[20,21] The cholesterol-lowering activity of phytosterols is mediated by their inhibition of cholesterol absorption in the digestive tract through its competition with cholesterol for transporter NPL1L1.[22−26] Additionally, numerous studies have investigated the potential applications of β-sitosterol as blood cholesterol-lowering agents not only for pharmaceutical formulations but also for use as a food ingredient, and their effectiveness and safety have also been demonstrated.[27] The present results clearly demonstrated that algal sterols were as effective as β-sitosterol in reducing plasma cholesterol concentration, most likely mediated by decreasing cholesterol absorption (Tables 4−7). GC-MS analyses found that SE was a mixture of several sterols, lathosterol, ergosterol, stigmasterol, 24-ethylcholesta-5,7,22-trienol, and stigmasta-7,24-(24[1])-dien-3β-ol. In this connection, two questions remain unanswered. First, it is unknown which sterol species is responsible for SE's cholesterol-lowering activity. Second, if two or more sterol species are the active ingredients, it will be interesting to know whether they have any synergistic effect on plasma TC.

Table 6. Fecal Excretion of Total Neutral Sterols and Total Acidic Sterols (Milligrams/Hamster/Day) in Hamsters Fed the Control (CTL) Diet and Three Experimental Diets Supplemented with 0.06 g of Sterol Extract (SE1), 0.30 g of Sterol Extract (SE5), and 0.30 g of β-Sitosterol (ST) per Kilogram of Diet, Respectively, at Week 5[a]

	CTL	SE1	SE5	ST	*P*
fecal neutral sterols					
coprostanol	0.39 ± 0.05b	0.49 ± 0.09ab	0.45 ± 0.06ab	0.53 ± 0.13a	0.19
coprostanone	0.04 ± 0.01	0.07 ± 0.03	0.06 ± 0.03	0.05 ± 0.02	0.49
cholesterol	0.22 ± 0.04b	0.23 ± 0.07b	0.32 ± 0.08a	0.20 ± 0.05b	0.05
dihydrocholesterol	0.11 ± 0.02a	0.11 ± 0.03a	0.06 ± 0.01b	0.12 ± 0.02a	<0.01
total cholesterol and its neutral metabolites	**0.76 ± 0.08b**	**0.90 ± 0.12ab**	**0.89 ± 0.10a**	**0.91 ± 0.19a**	**0.05**
campersterol	0.00 ± 0.00b	0.00 ± 0.00b	0.03 ± 0.01a	0.01 ± 0.00b	<0.01
stigmasterol	0.03 ± 0.00	0.04 ± 0.01	0.04 ± 0.01	0.03 ± 0.01	0.11
β-sitosterol	0.01 ± 0.00c	0.02 ± 0.00c	0.10 ± 0.02b	0.27 ± 0.05a	<0.01
squalene	ND	0.02 ± 0.00	0.06 ± 0.01	ND	
lathosterol	ND	0.01 ± 0.00	0.04 ± 0.02	ND	
ergosterol	ND	0.01 ± 0.00	0.02 ± 0.00	ND	
24-ethylcholesta-5,7,22-trierol	ND	0.02 ± 0.00	0.22 ± 0.05	ND	
stigmasta-7,24(24′)-dien-3β-ol	ND	0.00 ± 0.00	0.09 ± 0.02	ND	
fecal acidic sterols					
lithocholic	0.73 ± 0.04	0.85 ± 0.20	0.71 ± 0.18	0.79 ± 0.36	0.76
deoxycholic	0.33 ± 0.12	0.44 ± 0.11	0.41 ± 0.09	0.44 ± 0.19	0.57
chenodeoxycholic	0.20 ± 0.03b	0.19 ± 0.09b	0.35 ± 0.10a	0.26 ± 0.15ab	0.11
cholic acid	0.47 ± 0.02b	0.66 ± 0.16a	0.68 ± 0.12a	0.56 ± 0.08ab	0.06
ursodeoxycholic	0.07 ± 0.06b	0.04 ± 0.01b	0.08 ± 0.01b	0.36 ± 0.04a	<0.01
total	**1.80 ± 0.18**	**2.18 ± 0.46**	**2.22 ± 0.45**	**2.41 ± 0.81**	**0.41**

[a]Values are expressed as means ± SD, $n = 10$. Means at the same row with different superscript letters differ significantly, $P < 0.05$.

Table 7. Total Cholesterol Intake, Fecal Excretion of Total Sterols (Milligrams/Hamster/Day), and Cholesterol Balance in Hamsters Fed the Control (CTL) Diet and Three Experimental Diets Supplemented with SE1, SE5, and ST, Respectively[a]

	CTL	SE1	SE5	ST	*P*
Week 1					
total fecal cholesterol and neutral metabolites	0.66 ± 0.21c	0.73 ± 0.06bc	1.06 ± 0.25a	0.82 ± 0.10b	<0.01
total fecal acidic sterol excretion	1.22 ± 0.36	1.29 ± 0.38	1.33 ± 0.51	1.35 ± 0.23	0.91
cholesterol intake (mg)	10.09 ± 0.68	9.57 ± 0.30	10.07 ± 0.55	9.67 ± 0.28	0.13
apparent cholesterol retention	8.21 ± 1.11	7.55 ± 0.41	7.68 ± 1.08	7.50 ± 0.39	0.19
apparent cholesterol aborption (%)	81.30 ± 6.69a	78.89 ± 3.29ab	76.26 ± 7.62b	77.56 ± 2.76ab	0.09
Week 5					
total fecal cholesterol and neutral metabolites	0.76 ± 0.08b	0.90 ± 0.12ab	0.89 ± 0.10b	0.91 ± 0.19a	0.05
total fecal acidic sterol excretion	1.79 ± 0.16	2.18 ± 0.46	2.22 ± 0.45	2.41 ± 0.81	0.41
cholesterol intake (mg)	11.58 ± 0.45	10.71 ± 0.21	11.00 ± 1.20	10.51 ± 0.42	0.23
apparent cholesterol retention	9.03 ± 0.31a	7.63 ± 0.59	7.89 ± 1.34b	7.19 ± 0.65	0.03
apparent cholesterol aborption (%)	77.97 ± 1.32a	71.24 ± 3.99b	71.72 ± 5.42b	68.41 ± 5.83b	0.02

[a]Values are means ± SD, $n = 10$. Means in a row for a given week with different letters differ significantly, $P < 0.05$.

The real-time PCR analyses demonstrated that SE could affect the gene expression of intestinal ACAT2. On the one hand, SE behaved like β-sitosterol, which could down-regulate the ACAT2 mRNA level. ACAT2 is an essential enzyme in intestinal cholesterol absorption because it catalyzes the reaction of converting cholesterol to cholesteryl ester before cholesterol can be packed into chylomicrons via lymphatic system to blood. Previous studies found that β-sitosterol was poorly esterified by ACAT2.[28,29] On the other hand, SE did not behave like β-sitosterol as it did not significantly affect, whereas β-sitosterol could down-regulate, the mRNA of intestinal NPC1L1. Cholesterol absorption in the intestine is a very complex process and requires several transporters. NPC1L1 is responsible for carrying free cholesterol in the lumen to enterocytes.[30] As SE contained cholesterol, it was therefore speculated that SE had two confronting factors. The cholesterol in SE could up-regulate, whereas the other sterols could down-regulate, the gene expression of intestinal NPC1L1, and therefore no effect of SE on the gene expression of intestinal NPC1L1 was seen.

The real-time PCR analyses demonstrated that SE could down-regulate the gene expression of HMG-CoA reductase, whereas it could up-regulate that of hepatic LDL receptor. This was consistent with the observation in the previous study that algal lipids down-regulated the mRNA of HMG-CoA reductase.[8] As expected, SE behaved like β-sitosterol to modulate these genes as they are structurally similar. It is known that HMG-CoA reductase is a key enzyme involved in cholesterol synthesis, whereas LDL receptor is responsible for the removal of LDL-cholesterol from circulation. The present results clearly suggest that algal sterols are one of the active ingredients also partially accountable for the cholesterol-lowering activity of alga *Schizochytrium* sp., possibly mediated by down-regulation of HMG-CoA reductase and up-regulation of LDL receptor in addition to down-regulation of intestinal ACAT2.

In conclusion, the present study was the first time to demonstrate that algal SE had a cholesterol-lowering activity comparable to that of β-sitosterol. Cholesterol-lowering activity of algal SE was mediated by down-regulation of intestinal ACAT2 and hepatic HMG-CoA reductase but up-regulation of LDL receptor. Acting like β-sitosterol, SE increased the excretion of total sterols and decreased cholesterol absorption. Together with the results in our previous study,[9] it was concluded that DPA n-3, DHA, and sterols were all active ingredients accountable for the cholesterol-lowering activity of alga *Schizochytrium* sp. The whole investigation clearly showed that alga *Schizochytrium* sp. could be further explored as a cholesterol-lowering functional food.

■ ASSOCIATED CONTENT

Supporting Information

Mass spectra of eight sterols. This material is available free of charge via the Internet at http://pubs.acs.org.

■ AUTHOR INFORMATION

Corresponding Author

*(J.C.) E-mail: chenjingnan813@hotmail.com. Phone: +86-371-67758022. Fax: +86- 371-67758022.

Funding

This study was supported by the Doctor Grant of Henan Technology University (No. 2013BS038).

Notes

The authors declare no competing financial interest.

■ REFERENCES

(1) Chen, Z. Y.; Jiao, R.; Ma, K. Y. Cholesterol-lowering nutraceuticals and functional foods. *J. Agric. Food Chem.* **2008**, *56*, 8761−8773.

(2) Chen, Z. Y.; Ma, K. Y.; Liang, Y.; Peng, C.; Zuo, Y. Role and classification of cholesterol-lowering functional foods. *J. Funct. Food* **2011**, *3*, 61−69.

(3) Andersson, S. W.; Skinner, J.; Ellegard, L. Intake of dietary plant sterols is inversely related to serum cholesterol concentration in men and women in the EPIC Norfolk population: a cross-sectional study. *Eur. J. Clin. Nutr.* **2004**, *58*, 1378−1385.

(4) Kim, S. K.; Ta, Q. V. Potential benefical effects of marine algal sterols on human health. *Adv. Food Nutr. Res.* **2011**, *64*, 191−198.

(5) Law, M. Plant sterols and stanol margarine and health. *West. J. Med.* **2000**, *173*, 43−47.

(6) Plat, J.; van Onselen, E. N.; van Heugten, M. M.; Mensink, R. P. Effects on serum lipids, lipoproteins and fat soluble antioxidant concentrations of consumption frequency of margarines and shortenings enriched with plant stanol esters. *Eur. J. Clin. Nutr.* **2000**, *54*, 671−677.

(7) Plat, J.; Mensink, R. P. Plant stanol and sterol esters in the control of blood cholesterol levels: mechanism and safety aspects. *Am. J. Cardiol.* **2005**, *96*, 15−22.

(8) Chen, J. N.; Jiang, Y.; Ma, K. Y.; Chen, F.; Chen, Z. Y. Microalga decreases plasma cholesterol by down-regulation of intestinal NPC1L1, hepatic LDL receptor, and HMG-CoA reductase. *J. Agric. Food Chem.* **2011**, *59*, 6790−6797.

(9) Chen, J. N.; Jiang, Y.; Liang, Y. T.; Tian, X. Y.; Peng, C.; Ma, K. Y.; Liu, J.; Huang, Y.; Chen, Z. Y. DPA n-3, DPA n-6 and DHA improve lipoprotein profiles and vascular function in hamsters fed a high cholesterol diet. *Atherosclerosis* **2012**, *221*, 397−404.

(10) Markus, S.; Walter, V. Investigation of unsaponifiable matter of plant oils and isolation of eight phytosterols by means of high-speed counter-current chromatography. *J. Chromatogr., A* **2012**, *1237*, 96−105.

(11) Haas, D.; Morgenthaler, J.; Lacbawan, F.; Long, B.; Runz, H.; Garbade, S. F.; Zschocke, J.; Kelley, R. I.; Okun, J. G.; Hoffmann, G. F.; Muenke, M. Abnormal sterol metabolism in holoprosencephaly: studies in cultured lymphoblasts. *J. Med. Genet.* **2007**, *44*, 298−305.

(12) Weete, J. D.; Kim, H.; Gandhi, S. R.; Wang, Y.; Dute, R. Lipids and ultrastructure of *Thraustochytrium* sp. ATCC 26185. *Lipids* **1997**, *32*, 839−845.

(13) Yang, B. R.; Koponen, J.; Tahvonen, R.; Kallio, H. Plant sterols in seeds of two species of *Vaccinium* (*V. myrtillus* and *V. vitis-idaea*) naturally distributed in Finland. *Eur. Food Res. Technol.* **2003**, *216*, 34−38.

(14) Ma, K. Y.; Yang, N.; Jiao, R.; Peng, C.; Guan, L.; Huang, Y.; Chen, Z. Y. Dietary calcium decreases plasma cholesterol by down-regulation of intestinal NPC1L1 and MTP and up-regulation of CYP7A1 and ABCG 5/8 in hamsters. *Mol. Nutr. Food Res.* **2011**, *55*, 247−258.

(15) Lam, C. K.; Chen, J. N.; Cao, Y.; Yang, L.; Wong, Y. M.; Yeung, S. Y.; Yao, X.; Huang, Y.; Chen, Z. Y. Conjugated and non-conjugated octadecaenoic acids affect differently intestinal acyl coenzyme A:cholesterol acyltransferase activity. *Atherosclerosis* **2008**, *198*, 85−93.

(16) Chan, P. T.; Fong, W. P.; Cheung, Y. L.; Huang, Y.; Ho, W. K.; Chen, Z. Y. Jasmine green epicatechins are hypolipidemic in hamsters fed a high fat diet. *J. Nutr.* **1999**, *129*, 1094−1101.

(17) Alasek, M. A. J.; Repa, J. J.; Quan, G.; Dietschy, J. M.; Turley, S. D. Inhibiting intestinal NPC1L1 activity prevents diet-induced increase in biliary cholesterol in Golden Syrian hamsters. *Am. J. Physiol. Gastrointest. Liver. Physiol.* **2008**, *295*, 813−822.

(18) Field, F. J.; Born, E.; Mathur, S. N. Stanol esters decrease plasma cholesterol independently of intestinal ABC sterol transporters and Niemann-Pick C1-like 1 protein gene expression. *J. Lipid Res.* **2004**, *45*, 2252−2259.

(19) Qin, B.; Qiu, W.; Avramoglu, R. K.; Adeli, K. Tumor necrosis factor-α induces intestinal insulin resistance and stimulates the overproduction of intestinal apolipoprotein B48-containing lipoproteins. *Diabetes* **2007**, *56*, 450−461.

(20) Plat, J.; Brufau, G.; Dallinga-Thie, G. M.; Dasselaar, M.; Mensink, R. P. A plant stanol yogurt drink alone or combined with a low-dose stains lowers serum triacylglycerol and non-HDL-choleterol in metabolic syndrome patients. *J. Nutr.* **2009**, *139*, 1143−1149.

(21) Klingberg, S.; Ellegård, L.; Johansson, I.; Hallmans, G.; Weinehall, L.; Andersson, H.; Winkvist, A. Inverse relation between dietary intake of naturally occurring plant sterols and serum cholesterol in northern Sweden. *Am. J. Clin. Nutr.* **2008**, *87*, 993−1001.

(22) Ostlund, R. E., Jr.; Lin, X. Regulation of cholesterol absorption by phytosterols. *Curr. Atheroscler. Rep.* **2006**, *8*, 487−491.

(23) Jones, P. J.; AbuMweis, S. S. Phytosterols as functional food ingredients: linkages to cardiovascular disease and cancer. *Curr. Opin. Clin. Nutr. Metab. Care* **2009**, *12*, 147−151.

(24) Vanhanen, H. T.; Miettinen, T. A. Effects of unsaturated and saturated dietary plant sterols on their serum contents. *Clin. Chim. Acta* **1992**, *205*, 97−107.

(25) Gylling, H.; Miettinen, T. A. Effects of inhibiting cholesterol absorption and synthesis on cholesterol and lipoprotein metabolism in hypercholesterolemic non-insulin-dependent diabetic men. *J. Lipid Res.* **1996**, *37*, 1776−1785.

(26) Becker, M.; Staab, D.; Bergmann, K. V. Treatment of severe familial hypercholesterolemia in childhood with sitosterol and sitostanol. *J. Pediatr.* **1993**, *122*, 292−296.

(27) Kritchevsky, D.; Chen, S. C. Phytosterols−health benefits and potential concerns: a review. *J. Nutr. Res.* **2005**, *25*, 413−428.

(28) Swell, L.; Trout, E. C., Jr.; Field, H., Jr.; Treadwell, C. R. Absorption of H3-β-sitosterol in the lymph fistula rat. *Proc. Soc. Exp. Biol. Med.* **1959**, *100*, 140−142.

(29) Bhattacharyya, A. K.; Lopez, L. A. Absorbability of plant sterols and their distribution in rabbit tissues. *Biochim. Biophys. Acta* **1979**, *574*, 146−153.

(30) Altmann, S. W.; Davis, H. R.; Zhu, L. J.; Yao, X.; Hoos, L. M.; Tetzloff, G.; Iyer, S. P.; Maguire, M.; Golovko, A.; Zeng, M.; Wang, L.; Murgolo, N.; Graziano, M. Niemann-Pick C1 like 1 protein is critical for intestinal cholesterol absorption. *Science* **2004**, *303*, 1201−1204.

JOURNAL OF AGRICULTURAL AND FOOD CHEMISTRY

Article

pubs.acs.org/JAFC

Dual-Component System Dimethyl Sulfoxide/LiCl as a Solvent and Catalyst for Homogeneous Ring-Opening Grafted Polymerization of ε-Caprolactone onto Xylan

Xue-Qin Zhang,[†] Ming-Jie Chen,[†] Chuan-Fu Liu,*[,†] and Run-Cang Sun[†,‡]

[†]State Key Laboratory of Pulp and Paper Engineering, South China University of Technology, Guangzhou 510640, People's Republic of China

[‡]Institute of Biomass Chemistry and Technology, Beijing Forestry University, Beijing 100083, People's Republic of China

ABSTRACT: The preparation of xylan-*graft*-poly(ε-caprolactone) (xylan-*g*-PCL) copolymers was investigated by homogeneous ring-opening polymerization (ROP) in a dual-component system containing Lewis base LiCl and strong polar aprotic solvent dimethyl sulfoxide (DMSO). DMSO/LiCl acted as solvent, base, and catalyst for the ROP reaction. The effects of the parameters, including the reaction temperature, molar ratio of ε-caprolactone (ε-CL) to anhydroxylose units (AXU) in xylan, and reaction time, on the degree of substitution (DS) and weight percent of PCL side chain (W_{PCL}) were investigated. The results showed that xylan-*g*-PCL copolymers with low DS in the range of 0.03−0.39 were obtained under the given conditions. The Fourier transform infrared spectroscopy (FTIR), ^{1}H nuclear magnetic resonance (NMR), ^{13}C NMR, ^{1}H−^{1}H correlation spectroscopy (COSY), and ^{1}H−^{13}C correlation two-dimensional (2D) NMR [heteronuclear single-quantum coherence (HSQC)] characterization provided more evidence of the attachment of side chains onto xylan. Only one ε-CL was confirmed to be attached onto xylan with each side chain. Integration of resonances assigned to the substituted C_2 and C_3 in the HSQC spectrum also indicated 69.23 and 30.77% of PCL side chains attached to AXU at C_3 and C_2 positions, respectively. Although the attachment of PCL onto xylan led to the decreased thermal stability of xylan, the loss of unrecovered xylan fractions with low molecular weight because of the high solubility of xylan in DMSO/LiCl resulted in the increased thermal stability of the samples. This kind of xylan derivative has potential application in environmentally friendly and biodegradable materials considering the good biodegradability of xylan and PCL.

KEYWORDS: *xylan, ε-caprolactone, DMSO/LiCl, ring-opening polymerization*

INTRODUCTION

Hemicelluloses, the second most abundant class of renewable and biodegradable polysaccharides found in nature after cellulose, account for on average about 20−35% of most plant materials.[1,2] Because of the easy availability, good biodegradability, biocompatibility, and renewability, low price, and good mechanical properties, much attention has been paid to the use of hemicelluloses to produce performance biomaterials, biofuels, and platform biochemicals with increased environmental awareness and the development of green chemistry.[3,4]

Xylan-type hemicelluloses are the main hemicellulosic components of cell walls of hardwoods and grasses. As heterogeneous polymers with low molecular weight, they possess backbone chains of β-(1 → 4)-D-xylopyranose units and are branched by short carbohydrate chains.[5] Besides xylose, xylans may also contain arabinose, glucuronic acid or its 4-*O*-methyl ether, and acetic, ferulic, and *p*-coumaric acids. Usually, mostly the α-L-arabinofuranosyl residue may attach to some of the C_3 positions of the xylan backbone as the principal substituent and also carry minor amounts of 4-*O*-methlglucuronic or α-1,2-linked glucuronic acid residues, which are mainly linked to the C_2 positions of the xylan backbone.[6] In addition, there can be *O*-acetyl substitution on the backbone.[1]

Recently, much attention has been focused on the use of lignocellulosic biomass and its components.[7] In comparison to cellulose and lignin, the exploiting of hemicelluloses was paid little attention until the last decade. Because of their inherent low molecular weight and heterogeneous structure, chemical modification of hemicelluloses becomes an important way to prepare material with the desired properties.[8,9] In comparison to heterogeneous functionalization, homogeneous functionalization is simple and the degree of substitution (DS) of the products can be easily controlled and reproduced.[10−12] Because of the excellent biodegradability, biocompatibility, and permeability, considerable efforts have been paid to aliphatic polyesters,[13] among which poly(ε-caprolactone) (PCL) is one of the most important polyesters. PCL is a tough, flexible, and crystalline polymer with a low glass transition temperature (about −60 °C) and melting point (60 °C).[14−17] Ring-opening polymerization (ROP) of ε-caprolactone (ε-CL) is the most common way to prepare PCL, which can be accomplished in melt or in solution, catalyzed with 4-dimethylaminopyridine (DMAP), stannous octoate [$Sn(Oct)_2$], LiCl, or other catalysts.[18−20] However, because of the cytotoxicity and difficulties in the removal of the catalyst from the resulting polymers, the use of $Sn(Oct)_2$ and DMAP has been limited in many cases. LiCl, a very economic and

Received: August 14, 2013
Revised: January 3, 2014
Accepted: January 3, 2014
Published: January 3, 2014

ACS Publications © 2014 American Chemical Society

almost nontoxic chemical, could effectively catalyze the ROP reaction.[19]

The novel dissolution systems for lignocelluloses and their components received much attention because of the complexity of the plant cell walls. Dimethyl sulfoxide (DMSO)/LiCl was proposed as a novel dual-component system containing a Lewis base and strong polar aprotic solvent for the dissolution and pretreatment of plant materials.[21,22] In the present study, the DMSO/LiCl system was investigated as the reaction medium for the ROP reaction of ε-CL onto xylan. The physicochemical properties of xylan derivatives were characterized with Fourier transform infrared spectroscopy (FTIR), ^{1}H nuclear magnetic resonance (NMR), ^{13}C NMR, ^{1}H−^{1}H correlation spectroscopy (COSY), ^{1}H−^{13}C correlation two-dimensional (2D) NMR [heteronuclear single-quantum coherence (HSQC)], scanning electron microscopy (SEM), and thermal analysis.

MATERIALS AND METHODS

Materials. Xylan with a xylose content of over 85% was purchased from Yuan-Ye Biological Technology Co., Ltd. (Shanghai, China). LiCl with a purity of 97% was provided by Kermel Chemical Reagent Co., Ltd. (Tianjin, China). DMSO with 99.5% purity and ε-CL with 99% purity were supplied by Aladdin Reagent Co. (Shanghai, China). All chemicals were of analytical reagent grade and directly used without further purification.

Preparation of Xylan-*g*-PCL Copolymers in DMSO/LiCl. A series of xylan-*g*-PCL copolymers were prepared in dual-component system DMSO/LiCl under the conditions in Table 1. Dry xylan (0.33 g, 0.005 mol of hydroxyl group in xylan) was added to 20 mL of DMSO/LiCl (6 wt % LiCl) in a 50 mL dried three-neck flask. The mixture was agitated with magnetic stirring at 80 °C for about 2 h under the protection of nitrogen to achieve a homogeneous solution. Then, the required quantities of ε-CL [the molar ratio of ε-CL to anhydroxylose units (AXU) in xylan were 1:1, 4:1, 8:1, 12:1, and 20:1] were added at 80, 90, 100, 110, and 120 °C, respectively. The reaction was carried out under the protection of nitrogen with magnetic stirring for 3, 6, 12, 24, and 48 h, respectively. After the required time, the resulting solution was cooled to room temperature. The solid residues after precipitation into 150 mL of ethanol were filtered out, washed thoroughly with ethanol and dichloromethane to eliminate DMSO, LiCl, ε-CL, and byproducts, and then dried in vacuum for 48 h at 50 °C.

Table 1. Detailed Structural Factors of Xylan-*g*-PCL Copolymers Obtained under Various Conditions in DMSO/LiCl

sample	temperature (°C)	time (h)	ε-CL/AXU	DS	W_{PCL} (%)
1	80	24	4:1		
2	90	24	4:1	0.04	3.34
3	100	24	4:1	0.20	14.73
4	110	24	4:1	0.18	13.45
5	120	24	4:1	0.09	7.21
6	100	24	1:1	0.04	3.34
7	100	24	8:1	0.21	15.35
8	100	24	12:1	0.23	16.57
9	100	24	20:1	0.39	25.20
10	100	3	8:1	0.03	2.53
11	100	6	8:1	0.07	5.70
12	100	12	8:1	0.15	11.47
13	100	48	8:1	0.21	15.35

Film Preparation and Physical Property Determination. The xylan-*g*-PCL copolymer sample (0.3 g) was dissolved in 10 mL of deionized water. The solution was poured onto a polystyrene dish (9 × 9 cm) and allowed to dry at ambient temperature to obtain xylan-*g*-PCL film. The film thickness was measured using a micrometer (Lorentzen and Wettre; precision = 1 μm) at five different locations, and the mean value was used for the measurements of stress strength, tensile strain, and elasticity modulus on a universal tensile machine (DRK101).

Scheme 1. Grafting Copolymerization of PCL onto the Xylan Backbone in DMSO/LiCl

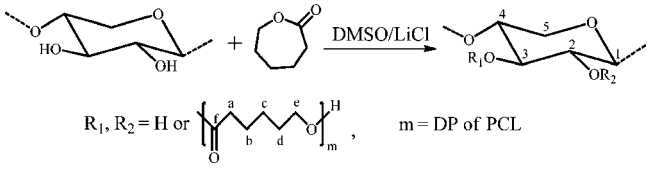

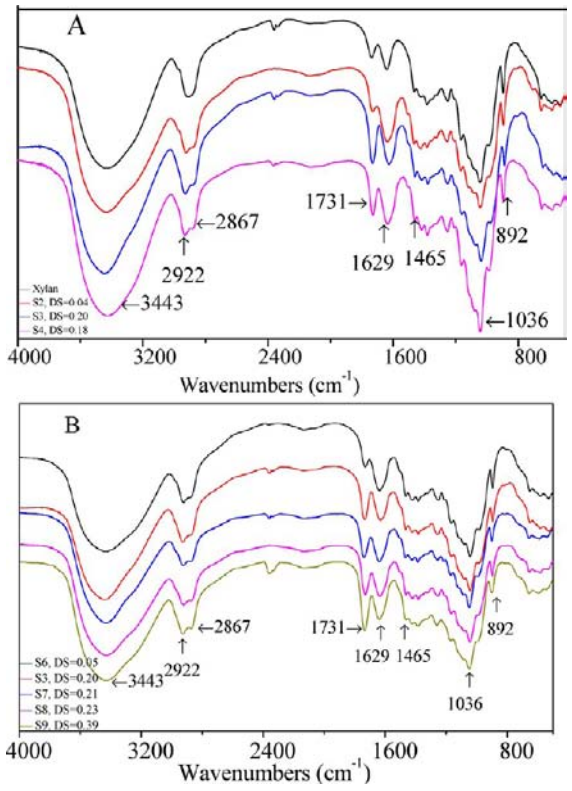

Figure 1. FTIR spectra of unmodified xylan and xylan-*g*-PCL copolymers obtained with an increased reaction temperature (A) from 90 °C (sample 2) to 100 °C (sample 3) and 110 °C (sample 4) and increased molar ratio of ε-CL to AXU (B) from 1:1 (sample 6), 4:1 (sample 3), 8:1 (sample 7), 12:1 (sample 8), and 20:1 (sample 9).

Detailed Physicochemical Characterization. FTIR spectra of the unmodified xylan and xylan-*g*-PCL copolymers were recorded on a Bruker spectrophotometer (TENSOR 27, Switzerland) from finely ground samples (1%) in KBr pellets in the range of 4000−500 cm^{-1}. The ^{1}H NMR, ^{13}C NMR, ^{1}H−^{1}H COSY, and HSQC spectra of unmodified xylan and xylan-*g*-PCL copolymers were recorded from 40 mg samples in 0.5 mL of DMSO-d_6 on a Bruker Avance III 400 M spectrometer (Germany) with a 5 mm multinuclear probe. For the ^{1}H NMR analysis, the detailed collecting and processing parameters were listed as follows: number of scans, 11; receiver gain, 62; acquisition time, 4.0894 s; relaxation delay, 1.0 s; pulse width, 11.0 s; spectrometer frequency, 400.13 MHz; and spectral width, 8012.8 Hz. For the ^{13}C NMR analysis, the detailed collecting and processing parameters were listed as follows: number of scans, 1932; receiver gain, 1440; acquisition time, 1.2583 s; relaxation delay, 1.5 s; pulse width, 12.0 s; spectrometer frequency, 100.61 MHz; and spectral width, 26 041.7 Hz. For the ^{1}H−^{1}H COSY analysis, the detailed collecting and processing parameters were listed as follows: number of scans, 16; receiver gain, 355; acquisition time, 0.4588 s; relaxation delay, 2.0 s; pulse width, 8.5 s;

dx.doi.org/10.1021/jf4036047 | J. Agric. Food Chem. 2014, 62, 682−690

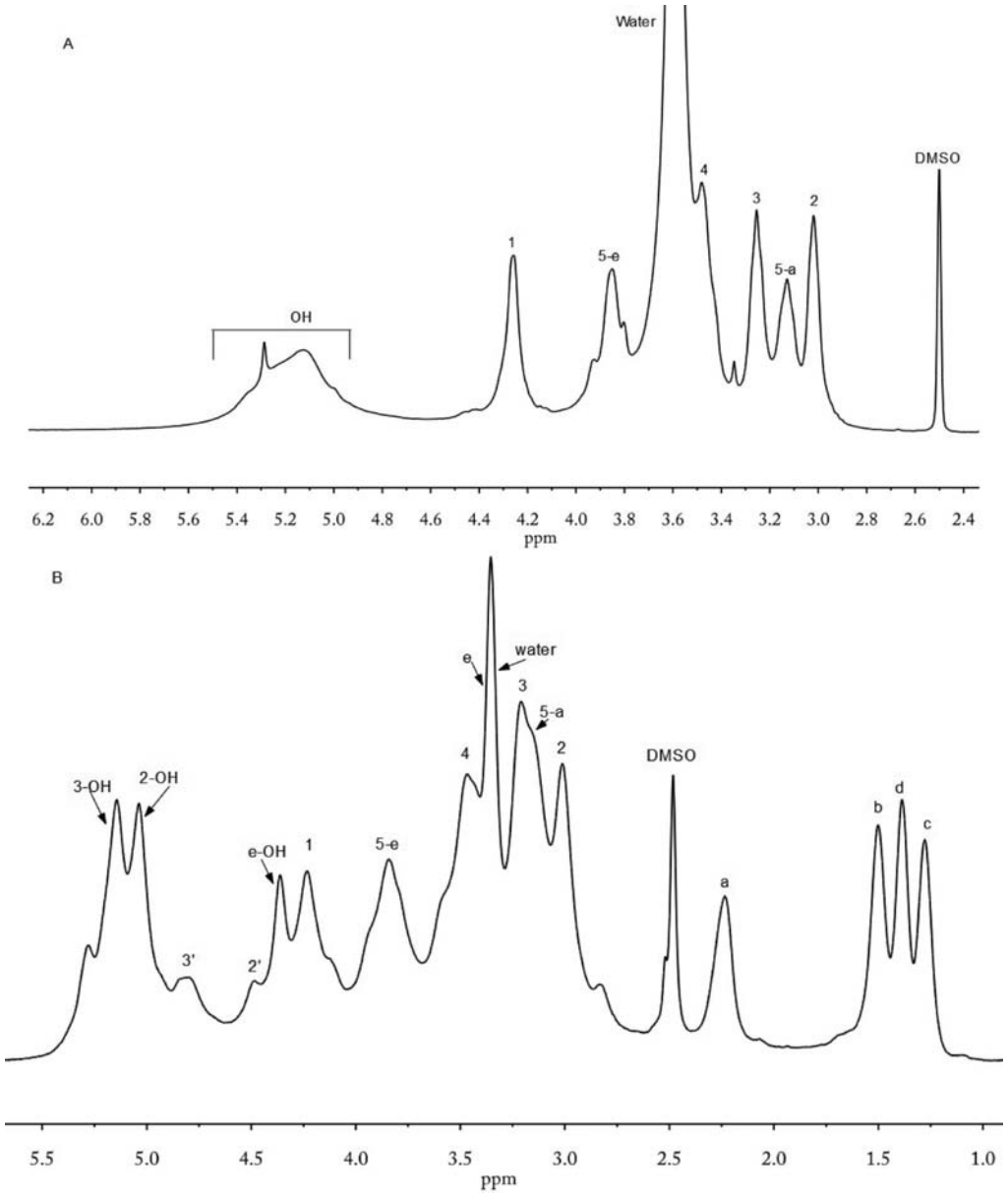

Figure 2. ^{1}H NMR spectra of unmodified xylan (A) and xylan-*g*-PCL copolymer sample 9 (B).

spectrometer frequency, 400.13/400.13 MHz; and spectral width, 2231.1/2231.1 Hz. For the ^{1}H−^{13}C HSQC analysis, the detailed collecting and processing parameters were listed as follows: number of scans, 20; receiver gain, 879; acquisition time, 0.1645 s; relaxation delay, 2.0 s; pulse width, 8.5 s; spectrometer frequency, 400.13/100.61 MHz; and spectral width, 3113.3/22 727.3 Hz. The detailed structural factors of xylan-*g*-PCL copolymers, including DS and weight percent of PCL side chains (W_{PCL}), were calculated from the integral area of the resonances assigned to the characteristic protons from AXU (H_1) and the attached PCL (the methylene protons). The thermal stability of the samples was performed using thermogravimetric analysis (TGA) and derivative thermogravimetry (DTG) using a Q500 theromgravimetric analyzer (TA Instruments, New Castle, DE). The apparatus was continually flushed with nitrogen. The sample between 9 and 11 mg was heated from 30 to 600 °C at a heating rate of 10 °C/min. The surface morphology was examined by SEM on a field emission scanning electron microscope (LEO 1530 VP, LEO, Germany). The samples for SEM were prepared by casting a few solids onto a mica sheet followed by gold plating.

RESULTS AND DISCUSSION

Effects of Reaction Conditions on the DS of Xylan-*g*-PCL Copolymers. Xylan-*g*-PCL copolymers were synthesized via homogeneous ROP of *ε*-CL onto xylan in DMSO/LiCl. Scheme 1 illustrates the ROP reaction of *ε*-CL with the hydroxyl groups of AXU in xylan in DMSO/LiCl. The preparation conditions and the detailed structural factors of xylan-*g*-PCL copolymers are shown in Table 1. The ROP reaction was easily achieved in DMSO/LiCl at 100 °C, and the xylan derivatives with DS of 0.20 were obtained within 24 h. However, the reaction occurred much more difficultly at higher or lower temperatures and even did not occur at 80 °C. The optimum reaction temperature for the ROP reaction in DMSO/LiCl was 100 °C. Clearly, the increase of the derivatizing reagent dosage and reaction time had favorable effects on the ROP reaction because of the increased molecule collisions of *ε*-CL with reactive hydroxyl groups. An enhancement of the molar ratio of *ε*-CL to AXU in xylan from 1:1 to 20:1 resulted in an increase in DS from

dx.doi.org/10.1021/jf4036047 | J. Agric. Food Chem. 2014, 62, 682−690

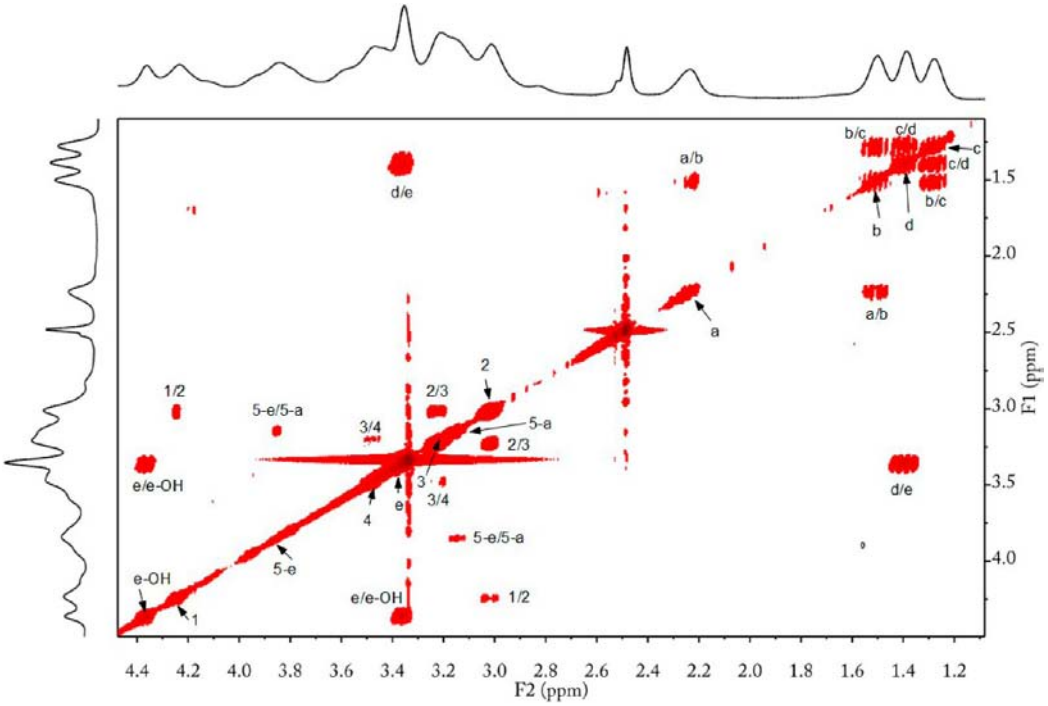

Figure 3. $^{1}H-^{1}H$ COSY spectrum of xylan-*g*-PCL copolymer sample 9.

0.04 to 0.39, and an increasing reaction time from 3 to 48 h led to an improvement of DS from 0.03 to 0.21. The similar results of the ROP reaction of ε-CL onto cellulose were reported in ionic liquid 1-*N*-butyl-3-methylimidazolium chloride ([Bmim]Cl) with DMAP and $Sn(Oct)_2$ as catalysts at 130 °C.[18] The higher DS of cellulose-*g*-PCL (0.09−2.41) was probably due to the higher temperature in [Bmim]Cl and more hydroxyl groups available in cellulose. Because the ROP reaction of ε-CL onto xylan is acid- or base-catalyzed, in the present study, the favorable effect of Lewis base LiCl in strong polar aprotic solvent DMSO resulted in the occurrence of the ROP reaction of ε-CL with the hydroxyl groups in xylan at relatively low temperatures. This dual-component system acted as a solvent, base, and catalyst in the preparation of xylan-*g*-PCL copolymers. Similarly, the dissolution of the plant whole cell wall was reported in this system, because of the favorable effects on the destruction of hydrogen bonds extensively present in the cell wall.[23,24]

FTIR. Figure 1 illustrated the FTIR spectra of unmodified xylan and xylan-*g*-PCL copolymers obtained with an increased reaction temperature (A) and molar ratio of ε-CL to AXU (B). The absorbances at 3443, 2922, 1731, 1629, 1465, 1036, and 892 cm^{-1} in the spectrum of unmodified xylan are previously reported.[23] In comparison, the spectra of xylan-*g*-PCL copolymers provided evidence for the ROP reaction by showing changes of two important bands at 2867 cm^{-1} for CH_2 stretching and 1731 cm^{-1} for C═O stretching.[24] The intensities of these two bands increased with the increment of the reaction temperature and the molar ratio of ε-CL to AXU, corresponding to the slight changes of DS in Table 1.

^{1}H NMR, $^{1}H-^{1}H$ COSY, ^{13}C NMR, and HSQC. Figure 2 illustrates the ^{1}H NMR spectra of unmodified xylan (A) and xylan-*g*-PCL copolymer sample 9 (B; DS of 0.39). In spectrum A, the proton signals at 4.90−5.50 ppm originated from the hydroxyl groups in AXU.[25] The strong signals at 3.59 and 2.50 ppm relate to water and DMSO, respectively. The signals at 4.26, 3.02, 3.25, 3.48, 3.85, and 3.13 ppm originated from the protons at H_1, H_2, H_3, H_4, H_{5e}, and H_{5a} of AXU, respectively.[26] In comparison, spectrum B provided evidence of the attachment of PCL side chains onto xylan. The methylene proton signals of the attached PCL could be observed at 3.36 ppm (−C$\underline{H}_2$OH, e, end unit), 2.24 ppm (−COC$\underline{H}_2$−, a), 1.50 ppm (−C$\underline{H}_2$−, b), 1.38 ppm (−C$\underline{H}_2$−, d), and 1.28 ppm (−C$\underline{H}_2$−, c).[18] The signal for the hydroxyl group at the end of PCL side chains (−CH_2O$\underline{H}$, e−OH) after the ROP reaction was present at 4.36 ppm. Unexpectedly, there was no signal for the methylene proton at the e position in the repeating unit of PCL (−C$\underline{H}_2$−O−, e), indicating probably only one ε-CL attached onto xylan with each side chain. As expected, no carboxyl proton was found in spectrum B, suggesting the absence of homopolymers of ε-CL and the formation of xylan−PCL ester. To confirm the correct assignment of the primary signals, the $^{1}H-^{1}H$ COSY spectrum of xylan-*g*-PCL copolymer sample 9 was collected, as illustrated in Figure 3. To avoid the overlapping of the primary signals, the COSY spectrum is shown at higher contour levels to provide the well-resolved correlations. As shown in Figure 3, the moderate cross-correlations in the lower left corner for H_1/H_2, H_2/H_3, H_3/H_4, and H_{5e}/H_{5a} were clearly observed. More importantly, the strong cross-correlations for PCL side chains in the upper right corner for a/b, b/c, c/d, and d/e and that in the lower left corner for e/e−OH provided the primary proton signals in PCL. Beside the cross-correlation at δ_H/δ_H of 3.36/1.38 ppm, there were no other cross-correlations of the methylene proton at the d position, indicating the absence of the PCL repeating unit. This result was consistent with ^{1}H NMR analysis, confirming that only one ε-CL was attached onto xylan with each side chain; that is, the degree of polymerization (DP) of the side chain was only 1.

On the basis of the typical proton signals from PCL side chains and AXU in xylan, the DS and weight percent of PCL side chains in Table 1 were calculated with the integral area of the resonances of the corresponding protons according to the following equations:

dx.doi.org/10.1021/jf4036047 | J. Agric. Food Chem. 2014, 62, 682−690

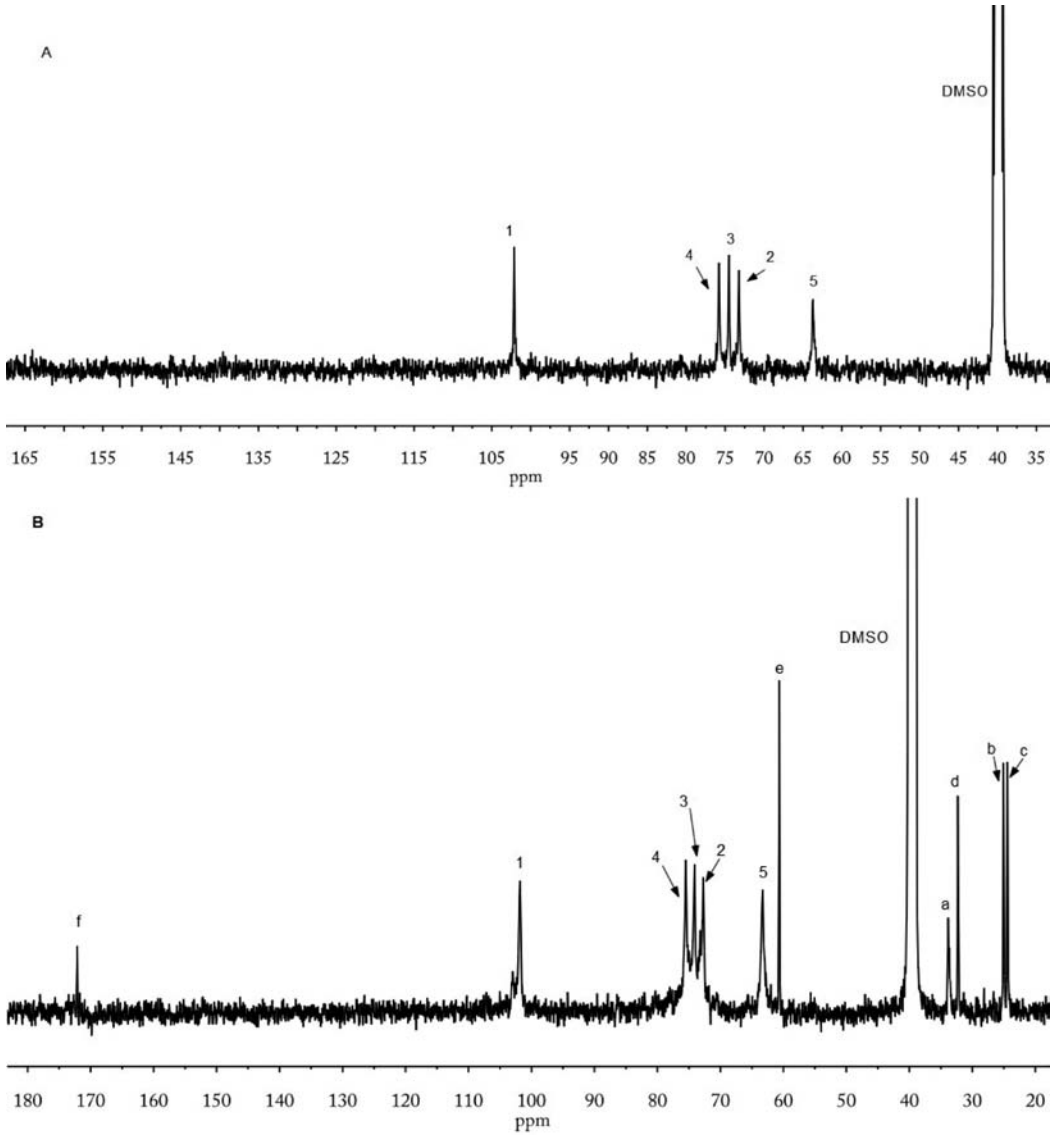

Figure 4. ^{13}C NMR spectra of unmodified xylan (A) and xylan-*g*-PCL copolymer sample 9 (B).

$$\mathrm{DS} = \frac{\text{terminal CL}}{\text{AXU}} = \frac{Ia/2}{I_{H_1}} \quad (1)$$

$$W_{\mathrm{PCL}} = \frac{114\mathrm{DS}}{132 + 114\mathrm{DS}} \times 100\% \quad (2)$$

where DS is the degree of substitution of PCL, W_{PCL} is the weight percent of PCL side chains, AXU is anhydroxylose unit, 114 g/mol is the molar mass of ε-CL, and 132 g/mol is the molar mass of an AXU.

As shown in Table 1, the data calculated from ^{1}H NMR confirmed the attachment of PCL onto xylan. However, the length of PCL side chains was only 1, which was less than that (2.29−3.05) attached onto cellulose in ionic liquid [Bmim]Cl.[18] The differences of the ROP reaction of ε-CL onto xylan and cellulose were probably due to the different chemistries of xylan and cellulose. Cellulose is a linear chain polymer with three reactive hydroxyls on each anhydroglucose unit (AGU), while xylan is heterpolysaccharide with two reactive hydroxyls on each AXU of the backbone and branched with different groups. Cellulose comparatively allows for slightly longer side chains than xylan, resulting in the high DP of PCL attached.

Figure 4 shows the ^{13}C NMR spectra of the unmodified xylan (A) and xylan-*g*-PCL copolymer sample 9 (B; DS of 0.39). The five major signals at 102.1, 75.8, 74.5, 73.2, and 63.7 ppm are attributed to C_1, C_4, C_3, C_2, and C_5, respectively, of AXU in xylan.[25] The signal at 172.1 ppm observed in spectrum B is assigned to the carbonyl group (f position in PCL), indicating the successful attachment of PCL onto xylan, corresponding to the results from FTIR analysis. Moreover, the signals at 33.7 ppm (a), 32.3 ppm (d), 25.0 ppm (b), 24.4 ppm (c), and 60.6 ppm (e) correspond to the methylene carbons of the attached PCL side chains,[18] suggesting that the ROP reaction of ε-CL onto xylan does occur in DMSO/LiCl.

Two-dimensional ^{1}H−^{13}C HSQC is a powerful tool for qualitative and quantitative analyses of chemical structures. It could provide more detailed information of signals overlapped in ^{1}H and ^{13}C NMR spectra. In the present study, unmodified xylan (A) and xylan-*g*-PCL copolymer sample 9 (B; DS of 0.39) were characterized with HSQC spectroscopy to better understand the xylan-*g*-PCL structure and further confirm the attachment of PCL on xylan. The HSQC spectra are illustrated in Figure 5 at a relatively low contour level to exhibit the primary

dx.doi.org/10.1021/jf4036047 | J. Agric. Food Chem. 2014, 62, 682−690

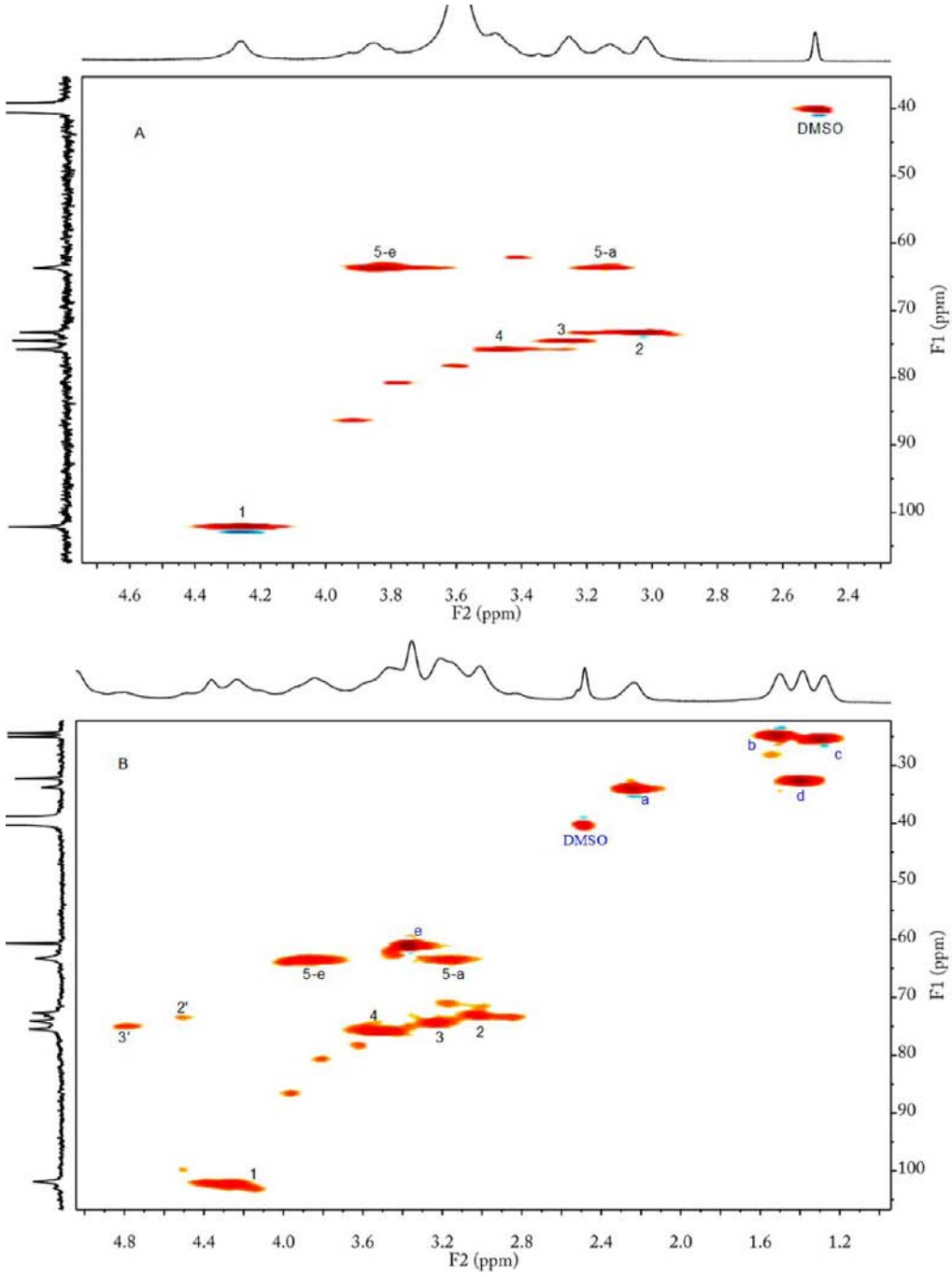

Figure 5. HSQC spectra of unmodified xylan (A) and xylan-*g*-PCL copolymer sample 9 (B).

signals, both substituted and unsubstituted. In spectrum A, the six strong correlations at δ_H/δ_C of 4.26/102.1, 3.02/73.2, 3.25/74.5, 3.48/75.8, 3.85/63.7, and 3.13/63.7 ppm are related to C_1-H_1, C_2-H_2, C_3-H_3, C_4-H_4, $C_{5e}-H_{5e}$, and $C_{5a}-H_{5a}$, respectively, in xylan. The weak correlations at δ_H/δ_C of 3.78/80.8, 3.60/78.3, 3.91/86.4, and 3.41/62.2 ppm are attributed to C_2-H_2, C_3-H_3, C_4-H_4, and C_5-H_5 in α-L-arabinofuranosyl residues.[26] Typically, methylene signals in the PCL side chain are shown in the aliphatic region as strong $^1H-^{13}C$ correlations. The strong correlations at δ_H/δ_C of 2.24/33.7, 1.50/25.0, 1.28/24.4, 1.38/32.3, and 3.36/60.6 ppm in spectrum B are assigned to the methylene group at a, b, c, d and e positions of PCL, respectively. The presence of these strong correlations indicated that the PCL side chains were successfully introduced into xylan. More importantly, the changes of the correlations belonging to the polysaccharides indicated the detailed ROP reaction on AXU. The strong signals, especially C_2 and C_3, indicated that most of xylan was unsubstituted, corresponding to the relatively low DS (0.39). The two important weak correlations at δ_H/δ_C of 4.49/73.6 and 4.79/75.0 ppm are due to substituted C_2 and C_3,[27] respectively, indicating that the attachment of PCL occurred at C_2 and C_3 positions of AXU. Clearly, more PCL side chains were attached to C_3 than to C_2. The resonances assigned to substituted and unsubstituted C_2 and C_3 were integrated to quantitatively compare the ROP reactivity of hydroxyl groups at C_2 and C_3 in DMSO/LiCl, and the results indicated that 69.23 and 30.77% of PCL side chains were attached to C_3 and C_2 positions of AXU, respectively.

dx.doi.org/10.1021/jf4036047 | J. Agric. Food Chem. 2014, 62, 682−690

In addition, the HSQC spectrum indicated that the proton signal at C_1 was not overlapped with other signals after the ROP reaction, whereas that at C_4 was overlapped with methylene at the e position from PCL, C_3 and C_5 from AXU, and C_3 from arabinofuranose. Similarly, the proton signal at the a position had less overlapped signals than other positions. Therefore, H_1 and methylene at the a position were selected as the typical proton signals in the DS calculation in the present study.

Thermal Analysis. The thermal properties of unmodified xylan and xylan-*g*-PCL copolymers were investigated using TGA and DTG, and the TGA/DTG curves are illustrated in Figure 6.

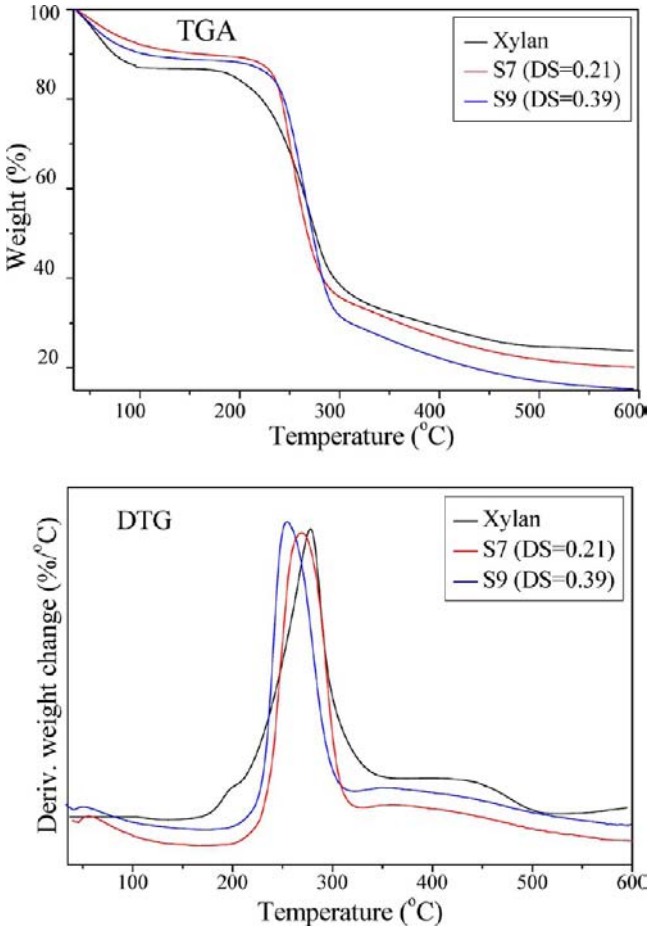

Figure 6. TGA/DTG curves of xylan and xylan-*g*-PCL copolymer samples 7 and 9.

In TGA curves, unmodified xylan began to decompose at 180 °C, while xylan-*g*-PCL copolymer samples 7 (DS of 0.17) and 9 (DS of 0.39) began to decompose at 220 and 235 °C, respectively. At 50% weight loss, the decomposition temperature occurred at 270 °C for unmodified xylan, 275 °C for sample 7, and 278 °C for sample 9. These data implied that the thermal stability of xylan increased after the ROP reaction in DMSO/LiCl. It is interesting that the pyrolysis residues at 600 °C for unmodified xylan and samples 7 and 9 were 28, 24, and 16%, respectively, indicating the decreased contents of inorganic salts in the samples after modification in DMSO/LiCl under the selected conditions, which was really different from that of cellulose regenerated from ionic liquids.[28] DTG means the degradation rate and can be used to compare the thermal stability between the samples.[29] In DTG curves, the small peak at about 185 °C in unmodified xylan disappeared after modification, indicating that the low-molecular-weight xylan was not recovered after the ROP reaction under the selected conditions, which was probably due to the high solubility of the dual-component system containing a strong polar aprotic solvent and Lewis base. The primary peak in DTG curves showed the maximum degradation rate at 270 °C for unmodified xylan, 260 °C for sample 7, and 255 °C for sample 9. These data suggested that the attachment of PCL onto xylan led to the decrease of thermal stability of xylan, especially with the increased DS of xylan-*g*-PCL copolymers, which implied that the increased thermal stability of xylan after modification was probably due to the loss of unrecovered low-molecular-weight fractions in xylan. The TGA/DTG curves of unmodified xylan and xylan-*g*-PCL copolymers indicated that the ROP reaction actually led to the reduction in thermal stability of xylan.

SEM and Physical Properties. The surface morphologies of unmodified xylan and the dried xylan-*g*-PCL copolymer samples 6 (DS of 0.04), 7 (DS of 0.17), 8 (DS of 0.23), and 9 (DS of 0.39) were examined by SEM, as shown in Figure 7. Unmodified xylan exhibited a rough and irregular surface with different sizes of agglomerates and blocks. The dissolution, modification, and regeneration of xylan destroyed the blocks, and the morphology of xylan-*g*-PCL copolymer samples changed from an irregular surface with blocks to relatively less rough surface. With the increased DS, the surface of the xylan derivatives gradually became regular and homogeneous, resulting in a more compact structure with decreased agglomerates, which was probably due to the attached PCL side chains on the xylan backbone. In addition, hemicelluloses from plant biomass are known to be non-film-forming polymers.[30] The rough and irregular surface with different sizes of agglomerates and blocks of unmodified xylan was probably responsible for the cracks and shrinkage during the failed film forming. Unexpectedly, the easily film-forming capability of xylan-*g*-PCL copolymers was found in comparison to that of unmodified xylan. The film from xylan-*g*-PCL copolymer sample 9 exhibited a flat and smooth surface. In addition, the film with a thickness ranging from 20 to 30 μm exhibited a relatively low tensile strength, and the stress strength, tensile strain, and elasticity modulus were 17.8 MPa, 5.33%, and 532.8 MPa, respectively.

In conclusion, the xylan-*g*-PCL copolymers were successfully prepared by the homogeneous ROP reaction in DMSO/LiCl under the given mild conditions. The dual-component system, containing a Lewis base LiCl and strong polar aprotic solvent DMSO, acted as a solvent, base, and catalyst for the ROP reaction. The results showed xylan-*g*-PCL copolymers with a low DS in the range of 0.03−0.39 were obtained under the given conditions. The FTIR and NMR characterization provided more evidence of the occurrence of the ROP reaction and the attachment of PCL side chains onto xylan. The results also indicated that only one ε-CL was confirmed to be attached onto xylan with each side chain. A total of 69.23 and 30.77% of PCL side chains were attached to C_3 and C_2 positions of AXU, respectively. Thermal analysis indicated that the attachment of PCL onto xylan led to the decreased thermal stability of xylan; however, the loss of unrecovered xylan fractions with a low molecular weight resulted in the increased thermal stability of the samples. The smooth surface of derivatived xylan was obtained with increased DS. Considering the good biodegradability of xylan and PCL, this kind of xylan derivative has potential application in environmentally friendly and biodegradable materials, such as edible food packaging film.

dx.doi.org/10.1021/jf4036047 | J. Agric. Food Chem. 2014, 62, 682−690

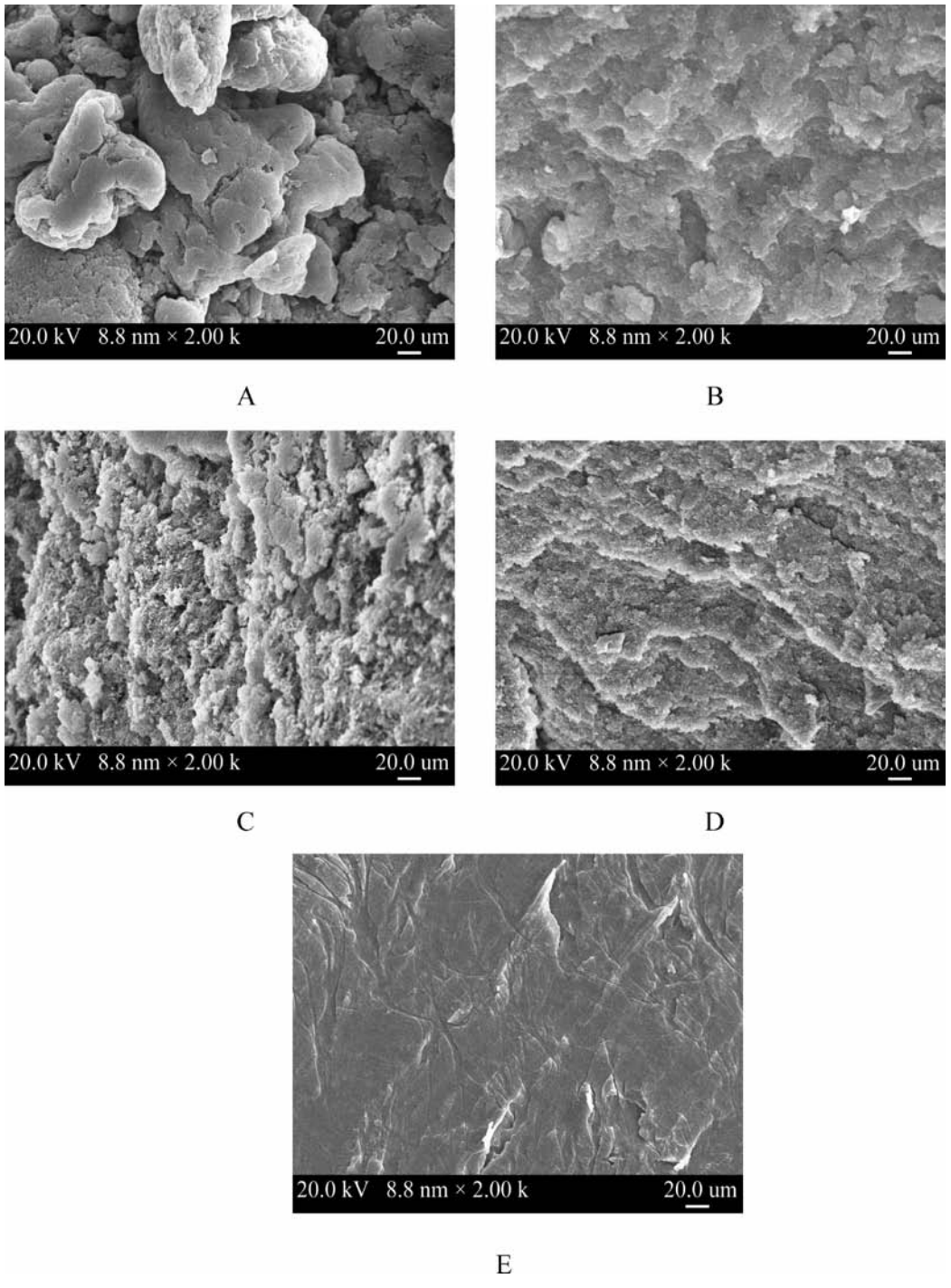

Figure 7. Scanning electron microscope images of unmodified xylan (A), xylan-*g*-PCL copolymers (sample 6, DS of 0.04, B; sample 7, DS of 0.21, C; and sample 8, DS of 0.23, D), and the xylan-*g*-PCL film (sample 9, DS of 0.39, E).

AUTHOR INFORMATION

Corresponding Author

*Telephone: 86-20-87111735. Fax: 86-20-87111861. E-mail: chfliu@scut.edu.cn.

Funding

This work was financially supported by the National Natural Science Foundation of China (31170550), the Program for New Century Excellent Talents in University (NCET-11-0154), and the Fundamental Research Funds for the Central Universities.

Notes

The authors declare no competing financial interest.

REFERENCES

(1) Saha, B. Hemicellulose bioconversion. *J. Ind. Microbiol. Biotechnol.* **2003**, *30*, 279−291.

(2) Ebringerová, A.; Heinze, T. Xylan and xylan derivatives—Biopolymers with valuable properties. 1. Naturally occurring xylans structures, isolation procedures and properties. *Macromol. Rapid Commun.* **2000**, *21*, 542−556.

(3) Gabrielii, I.; Gatenholm, P. Preparation and properties of hydrogels based on hemicellulose. *J. Appl. Polym. Sci.* **1998**, *69*, 1661−1667.

(4) Heinze, T.; Koschella, A.; Ebringerová, A. Chemical functionalization of xylan: A short review. In *Hemicelluloses: Science and Technology*; Gatenholm, P., Tenkanen, M., Eds.; American Chemical Society (ACS):

Washington, D.C., 2003; ACS Symposium Series, Vol. *864*, Chapter 20, pp 312−325.
(5) Ebringerová, A.; Hromádková, Z.; Heinze, T. Hemicellulose. In *Polysaccharides I*; Heinze, T., Ed.; Springer: Berlin, Germany, 2005; Vol. *186*, pp 1−67.
(6) Puls, J.; Schröder, N.; Stein, A.; Janzon, R.; Saake, B. Xylans from oat spelts and birch kraft pulp. *Macromol. Symp.* **2005**, *232*, 85−92.
(7) El Seoud, O. A.; Koschella, A.; Fidale, L. C.; Dorn, S.; Heinze, T. Applications of ionic liquids in carbohydrate chemistry: A window of opportunities. *Biomacromolecules* **2007**, *8*, 2629−2647.
(8) Belmokaddem, F.-Z.; Pinel, C.; Huber, P.; Petit-Conil, M.; Da Silva Perez, D. Green synthesis of xylan hemicellulose esters. *Carbohydr. Res.* **2011**, *346*, 2896−2904.
(9) Sun, R.; Fang, J. M.; Tomkinson, J. Stearoylation of hemicelluloses from wheat straw. *Polym. Degrad. Stab.* **2000**, *67*, 345−353.
(10) Liu, C.-F.; Zhang, A.-P.; Li, W.-Y.; Yue, F.-X.; Sun, R.-C. Homogeneous modification of cellulose in ionic liquid with succinic anhydride using *N*-bromosuccinimide as a catalyst. *J. Agric. Food Chem.* **2009**, *57*, 1814−1820.
(11) Marson, G. A.; El Seoud, O. A. A novel, efficient procedure for acylation of cellulose under homogeneous solution conditions. *J. Appl. Polym. Sci.* **1999**, *74*, 1355−1360.
(12) Nawaz, H.; Casarano, R.; El Seoud, O. A. First report on the kinetics of the uncatalyzed esterification of cellulose under homogeneous reaction conditions: A rationale for the effect of carboxylic acid anhydride chain length on the degree of biopolymer substitution. *Cellulose* **2012**, *19*, 199−207.
(13) Habibi, Y.; Goffin, A. L.; Schiltz, N.; Duquesne, E.; Dubois, P.; Dufresne, A. Bionanocomposites based on poly(ε-caprolactone)-grafted cellulose nanocrystals by ring-opening polymerization. *J. Mater. Chem.* **2008**, *18*, 5002−5010.
(14) Lonnberg, H.; Fogelstrom, L.; Berglund, M.; Malmstrom, E.; Hult, A. Surface grafting of microfibrillated cellulose with poly(ε-caprolactone)—Synthesis and characterization. *Eur. Polym. J.* **2008**, *44*, 2991−2997.
(15) Lonnberg, H.; Fogelstrom, L.; Zhou, Q.; Hult, A.; Berglund, L.; Malmstrom, E. Investigation of the graft length impact on the interfacial toughness in a cellulose/poly(ε-caprolactone) bilayer laminate. *Compos. Sci. Technol.* **2011**, *71*, 9−12.
(16) Lonnberg, H.; Zhou, Q.; Brumer, H.; Teeri, T. T.; Malmstrom, E.; Hult, A. Grafting of cellulose fibers with poly(ε-caprolactone) and poly(L-lactic acid) via ring-opening polymerization. *Biomacromolecules* **2006**, *7*, 2178−2185.
(17) Hou, Q.; Grijpma, D. W.; Feijen, J. Preparation of porous poly(ε-caprolactone) structures. *Macromol. Rapid Commun.* **2002**, *23*, 247−252.
(18) Guo, Y. Z.; Wang, X. H.; Shen, Z. G.; Shu, X. C.; Sun, R. C. Preparation of cellulose-*graft*-poly(ε-caprolactone) nanomicelles by homogeneous ROP in ionic liquid. *Carbohydr. Polym.* **2013**, *92*, 77−83.
(19) Xie, W.; Chen, D.; Fan, X.; Li, J.; Wang, P. G.; Cheng, H. N.; Nickol, R. G. Lithium chloride as catalyst for the ring-opening polymerization of lactide in the presence of hydroxyl-containing compounds. *J. Polym. Sci., Polym. Chem.* **1999**, *37*, 3486−3491.
(20) Wang, Z. D.; Zheng, L. C.; Li, C. C.; Zhang, D.; Xiao, Y. N.; Guan, G. H.; Zhu, W. X. A novel and simple procedure to synthesize chitosan-*graft*-polycaprolactone in an ionic liquid. *Carbohydr. Polym.* **2013**, *94*, 505−510.
(21) Wang, Z.; Yokoyama, T.; Chang, H.-m.; Matsumoto, Y. Dissolution of beech and spruce milled woods in LiCl/DMSO. *J. Agric. Food Chem.* **2009**, *57*, 6167−6170.
(22) Wang, Z.; Yokoyama, T.; Matsumoto, Y. Dissolution of ethylenediamine pretreated pulp with high lignin content in LiCl/DMSO without milling. *J. Wood Chem. Technol.* **2010**, *30*, 219−229.
(23) Ayoub, A.; Venditti, R. A.; Pawlak, J. J.; Sadeghifar, H.; Salam, A. Development of an acetylation reaction of switchgrass hemicellulose in ionic liquid without catalyst. *Ind. Crops Prod.* **2013**, *44*, 306−314.
(24) Labet, M.; Thielemans, W. Improving the reproducibility of chemical reactions on the surface of cellulose nanocrystals: ROP of ε-caprolactone as a case study. *Cellulose* **2011**, *18*, 607−617.
(25) Cao, X. F.; Sun, S. N.; Peng, X. W.; Zhong, L. X.; Sun, R. C. Synthesis and characterization of cyanoethyl hemicelluloses and their hydrated products. *Cellulose* **2013**, *20*, 291−301.
(26) Wen, J. L.; Xiao, L. P.; Sun, Y. C.; Sun, S. N.; Xu, F.; Sun, R. C.; Zhang, X. L. Comparative study of alkali-soluble hemicelluloses isolated from bamboo (*Bambusa rigida*). *Carbohydr. Res.* **2011**, *346*, 111−120.
(27) Evtuguin, D. V.; Tomas, J. L.; Silva, A. M. S.; Neto, C. P. Characterization of an acetylated heteroxylan from *Eucalyptus globulus* Labill. *Carbohyd. Res.* **2003**, *338*, 597−604.
(28) Lan, W.; Liu, C. F.; Yue, F. X.; Sun, R. C.; Kennedy, J. F. Ultrasound-assisted dissolution of cellulose in ionic liquid. *Carbohydr. Polym.* **2011**, *86*, 672−677.
(29) Nadji, H.; Diouf, P. N.; Benaboura, A.; Bedard, Y.; Riedl, B.; Stevanovic, T. Comparative study of lignins isolated from Alfa grass (*Stipa tenacissima* L.). *Bioresour. Technol.* **2009**, *100*, 3585−3592.
(30) Goksu, E. I.; Karamanlioglu, M.; Bakir, U.; Yilmaz, L.; Yilmazer, U. Production and characterization of films from cotton stalk xylan. *J. Agric. Food Chem.* **2007**, *55*, 10685−10691.

JOURNAL OF AGRICULTURAL AND FOOD CHEMISTRY

Article

pubs.acs.org/JAFC

Treatment and Biotransformation of Highly Polluted Agro-industrial Wastewater from a Palm Oil Mill into Vermicompost Using Earthworms

Su Lin Lim,[†] Ta Yeong Wu,*[,†] and Charles Clarke[‡]

[†]Chemical Engineering Discipline, School of Engineering and [‡]School of Science, Monash University, Jalan Lagoon Selatan, Bandar Sunway, 46150, Selangor Darul Ehsan, Malaysia

ABSTRACT: In this laboratory-scale study, earthworms were introduced as biodegraders of palm oil mill effluent (POME), which is a wastewater produced from the wet process of palm oil milling. POME was absorbed into amendments (soil or rice straw) in different ratios as feedstocks for the earthworm, *Eudrilus eugeniae*. The presence of earthworms led to significant increases in pH, electrical conductivity, and nutrient content but decreases in the C/N ratio (0.687−75.8%), soluble chemical oxygen demand (19.7−87.9%), and volatile solids (0.687−52.7%). However, earthworm growth was reduced in all treatments by the end of the treatment process. Rice straw was a better amendment/absorbent relative to soil, with a higher nutrient content and greater reduction in soluble chemical oxygen demand with a lower C/N ratio in the vermicompost. Among all treatments investigated, the treatment with 1 part rice straw and 3 parts POME (w/v) (RS1:3) produced the best quality vermicompost with high nutritional status.

KEYWORDS: *cleaner production, rice straw, soil, wastewater treatment, organic fertilizer, Eudrilus eugeniae, palm oil mill effluent (POME), vermicomposting*

INTRODUCTION

Agro-industries play a major role in the global economy, especially in developing countries. Developing nations often rely on a combination of subsistence farming and formal and/or informal agro-industries for income generation, yet associated health risks and environmental pollution can have a great impact on these nations. Due to the unsafe disposal of untreated agro-industry wastes in the form of solid wastes or effluents, clean water supplies are polluted, productive potential is exhausted, and health risks around the region are gravely increased.

Malaysia is one of the leading global producers and exporters of palm oil. The Malaysian palm oil industry is growing rapidly and is quickly becoming a significant agricultural industry in this country. However, the production of large amounts of crude palm oil leads to the generation of a greater amount of agro-industrial wastewater or palm oil mill effluent (POME). The wet process of palm oil milling consumes a large amount of water. It is estimated that POME is generated at nearly 3 times the rate of crude palm oil.[1] In Malaysia, approximately 44 million tonnes of POME was generated during oil palm processing in 2008. As the Malaysian palm oil industry continues to grow, the amount of POME generated is expected to increase annually.[2] POME is a brown slurry, containing 95−96% water, 0.6−0.7% residual oil, and 4−5% solids (mainly organic). POME is characterized by a high biochemical oxygen demand (BOD) (25000 mg/L) and chemical oxygen demand (COD) (53630 mg/L) and contains 8370 mg/L oil and grease, 43635 mg/L total solids, 19020 mg/L suspended solids, and a high concentration of organic nitrogen.[3] One of the disposal options for POME is a ponding system, which is used by >85% of palm oil mills in Malaysia. This treatment method is proven to be economically viable, but it accumulates large amounts of sludge, causes uncontrollable release of greenhouse gases, and requires large areas of land. Furthermore, it was reported that this disposal option allows the lowest utilization of renewable resources.[2] Other conventional POME treatment processes are aerobic and anaerobic digestions, physiochemical treatments, and membrane treatments. However, biological processes such as aerobic and anaerobic digestion are inefficient ways to treat POME due to its colloidal nature (suspended solids), low pH, and high BOD and COD loadings.[3]

In many countries, waste management systems are undergoing changes due to the threat of global climate change and other environmental issues.[4] Waste management systems are also influenced by socio-economic, political, and environmental factors, including population growth, consumption patterns, and technological development of waste systems.[5] Recently, numerous studies have examined the "zero waste" concept. Waste treatment technologies such as composting give rise to opportunities for resource recovery and production of nutrient-rich organic fertilizer and soil conditioner from the waste.[6] Thus, vermicomposting could be used as an alternative treatment method for managing POME. In this process, earthworms and micro-organisms convert organic wastes into a useful product known as vermicompost.[7] Earthworms affect the soil biological activity through organic matter decomposition and nutrient mineralization. They are the important drivers for substrate conditioning, whereas microbes are responsible for the biochemical degradation of organic matter. Among all of the different species of earthworms, epigeic earthworms are the most suitable for the vermicomposting process. Epigeic earthworms

Received: September 24, 2013
Revised: December 25, 2013
Accepted: December 27, 2013
Published: December 27, 2013

ACS Publications © 2013 American Chemical Society

dx.doi.org/10.1021/jf404265f | J. Agric. Food Chem. 2014, 62, 691−698

are litter dwellers and live in or near the soil surface. These species feed on decaying organic matter and have high reproduction rates. Examples of epigeic earthworms are *Eisenia fetida*, *Eisenia andrei*, *Eudrilus eugeniae*, and *Perionyx excavatus*.[8,9] Epigeic earthworms are also less susceptible to toxicity than endogeic or anecic earthworms.[10] In the reported study, *E. eugeniae* was used because it is able to decompose organic wastes rapidly and it is a suitable species for vermicomposting in tropical countries.[8] Compared to compost, vermicompost is produced in less time and has greater fertilizer value with a higher humus content and less phytotoxicity.[7] A study conducted by Coria-Cayupán et al.[11] showed that vermicompost application increased the yield of lettuce without significant loss in food nutritional value. Additionally, vermicompost can be used for soil remediation purposes, such as degradation of pesticides.[12] According to Hait and Tare,[13] vermicomposting is a cost-effective, energy-saving, and zero-discharge process. However, several factors such as moisture content, pH, temperature, and aeration need to be monitored closely during the vermicomposting process because earthworms are involved. The surrounding conditions need to be favorable for the earthworms to break down organic wastes.[9] Nevertheless, the utilization of earthworms to stabilize solid wastes has been well documented. Vermicomposting of wastes such as animal manure, sewage sludge, agricultural wastes, and industrial wastes showed that it is an efficient technology for waste management.[9,14] This process can also be performed at any scale, from small-scale household vermicomposting to community or pilot-scale vermicomposting.[9] Pilot-scale vermicomposting has been attempted on paper mill and dairy industry sludges and on pineapple wastes by Elvira et al.[15] and Mainoo et al.,[16] respectively. Both studies showed that the pilot-scale vermicomposting process is feasible. However, there were differences between the end products produced at the laboratory scale and the pilot scale. For example, Elvira et al. found that the pilot-scale trials yielded better quality vermicompost than the laboratory-scale trials.[15]

Thus far, no studies have been conducted on the vermicomposting of POME because vermicomposting is generally used in solid waste management. Wastewaters (for example, swine and urban wastewaters) are usually treated using a vermifiltration process, which is adapted from a traditional vermicomposting system.[17,18] However, the present study shows that it is possible to treat POME if it is mixed with an appropriate ratio of amendments, which act as absorbents of wastewater. In this study, rice straw and soil were used as amendments to achieve a conducive physical and chemical environment in which the earthworms could thrive. POME was absorbed into the amendments to produce a suitable solid feedstock for the growth and reproduction of the earthworms. The addition of amendments also improved the C/N ratio of the initial organic wastes, making the POME more suitable for decomposition by the earthworms.[19] Therefore, the aim of this study was to assess the potential of using *E. eugeniae* to treat and biotransform POME into organic fertilizer after absorption of wastewater into amendments.

MATERIALS AND METHODS

Epigeic Earthworms and Collection of Organic Waste. *E. eugeniae* worms were obtained from ESI Agrotech, Malaysia. Stock earthworms were cultured and developed in the laboratory under ambient temperature on partially decomposed papaya and cow dung. POME was obtained from Hulu Langat Palm Oil Mill, Selangor, Malaysia, and kept in the refrigerator (at 4 °C) before being used as a feedstock in vermicomposting. As mentioned earlier, rice straw and soil were used as amendments. The rice straw was obtained from a paddy field in Sekinchan, Selangor, Malaysia, and experimental soil was a locally mixed peat moss soil obtained from Peat Organic (M) Sdn Bhd, Selangor, Malaysia. The initial chemical characteristics of POME, rice straw, and soil are given in Table 1.

Table 1. Chemical Characteristics of POME, Rice Straw, and Soil (Means ± SD, n = 3)

parameter	POME	rice straw	soil
pH	4.51 ± 0.01	7.17 ± 0.03	4.65 ± 0.04
electrical conductivity (μS/cm)	1396 ± 21	908 ± 6	1645 ± 7
C/N	15.94 ± 1.17	47.36 ± 2.11	52.59 ± 2.67
Ca (g/kg dry wt)	0.51 ± 0.00	4.97 ± 0.35	9.90 ± 0.15
K (g/kg dry wt)	1.73 ± 0.42	13.19 ± 0.04	5.73 ± 0.85
Mg (g/kg dry wt)	0.61 ± 0.01	1.45 ± 0.14	3.77 ± 0.74
P (g/kg dry wt)	0.26 ± 0.00	1.34 ± 0.09	0.42 ± 0.04
volatile solids (g/kg dry wt)		751.6 ± 13.5	806.8 ± 23.8
COD (mg/L)	65667 ± 1803		

Experimental Design. Rice straw or soil amendments (200 g) were mixed with POME in three different ratios, namely, 1:1, 1:2, and 1:3 w/v (amendment:POME) (Table 2). The initial chemical characteristics of all treatments are given in Table 3. The amendments with different volumes of POME were then placed in rectangular plastic containers (17 cm × 14 cm × 12 cm). A 1:4 (w/v) treatment ratio was not attempted because earthworm mortality was observed at the initial stage of vermicomposting. Furthermore, the POME was not absorbed fully into the amendments (especially soil) in the 1:4 (w/v) treatment. Control bins (without earthworms) were also set up for all ratios investigated. Waste mixtures were turned periodically for 2 weeks to eliminate anaerobic conditions and remove any volatile gases potentially toxic to earthworms.[20] After 2 weeks, 10 nonclitellate *E. eugeniae* (~0.60 g each) were selected from the stock culture and released into each experimental container. The experimental containers were kept in triplicate for each treatment. Periodic sprinkling with water maintained moisture content at approximately 75% throughout the vermicomposting process. Experimental containers were placed in a dark laboratory at a temperature of 25 ± 2 °C.

Table 2. Description of the Different Treatments Used for the Vermicomposting Experiment

treatment in w/v	treatment description
RS1:1	1 part rice straw:1 part POME
RS1:2	1 part rice straw:2 parts POME
RS1:3	1 part rice straw:3 parts POME
S1:1	1 part soil:1 part POME
S1:2	1 part soil:2 parts POME
S1:3	1 part soil:3 parts POME

The vermicomposting process was conducted for 6 weeks. In each experimental container, the changes in earthworm biomass were measured at the beginning and the end of vermicomposting process to reduce the stress on the earthworms due to changing environmental conditions.[21] Earthworms were hand-sorted and then washed with distilled water to remove any adhering materials from their bodies. The live weights of the earthworms were measured, and no correction for gut content was applied to any of the data.

Approximately 10 g of homogenized wet substrates (free from earthworms, hatchlings, and cocoons) was collected for analysis on the first and final days of vermicomposting. The samples were oven-dried at 60 °C for 48 h, ground in a blender, and stored in polythene bags (at 4 °C) for further chemical analysis.

Table 3. Initial Chemical Characteristics of the Different Treatments (Means ± SD, $n = 3$)[a]

treatment in w/v	pH	EC (μS/cm)	P (g/kg dry wt)	K (g/kg dry wt)	Ca (g/kg dry wt)	Mg (g/kg dry wt)	C/N ratio
RS1:1	6.77 ± 0.21 a	719 ± 86 a	1.42 ± 0.25 ab	6.19 ± 1.38 ab	6.26 ± 1.15 a	2.40 ± 0.05 a	46.90 ± 2.15 a
RS1:2	7.17 ± 0.08 b	827 ± 18 b	2.18 ± 0.13 c	9.03 ± 0.09 b	10.80 ± 1.60 b	3.20 ± 0.26 ab	35.67 ± 1.90 bc
RS1:3	6.96 ± 0.04 ab	898 ± 48 b	1.70 ± 0.27 bc	12.38 ± 0.07 c	11.15 ± 1.20 b	3.48 ± 0.42 ab	31.61 ± 4.36 c
S1:1	5.19 ± 0.02 c	853 ± 24 b	0.91 ± 0.21 a	5.93 ± 1.25 a	17.51 ± 1.85 c	4.36 ± 1.08 b	50.07 ± 0.98 a
S1:2	5.17 ± 0.03 c	1055 ± 9 c	1.40 ± 0.10 ab	6.27 ± 1.33 ab	15.09 ± 0.86 c	4.66 ± 0.87 b	46.60 ± 1.46 a
S1:3	5.50 ± 0.01 d	1313 ± 45 d	1.03 ± 0.04 ab	6.07 ± 1.24 ab	22.46 ± 0.82 d	6.49 ± 0.05 c	43.37 ± 7.30 ab

[a]Mean values followed by different letters are statistically different (ANOVA; Tukey's test, $P < 0.05$).

Table 4. Initial and Final Soluble Chemical Oxygen Demand (sCOD) and Volatile Solids (VS) of Different Treatments (Means ± SD, $n = 3$)[a]

	sCOD (mg/L)			VS (g/kg dry wt)		
		final			final	
treatment in w/v	initial	vermicompost	control	initial	vermicompost	control
RS1:1	46400 ± 4525 bc	20000 ± 1131 a	127967 ± 1168 a	790.0 ± 17.1 a	373.4 ± 71.0 a	570.7 ± 86.2 a
RS1:2	50000 ± 1697 bc	18800 ± 2828 a	130000 ± 5091 a	808.4 ± 9.5 ab	434.7 ± 22.5 a	506.0 ± 18.2 a
RS1:3	52800 ± 2263 c	6400 ± 1131 b	140000 ± 18102 a	809.0 ± 45.7 ab	449.7 ± 10.6 a	628.8 ± 34.1 a
S1:1	37333 ± 2013 a	27200 ± 3394 ac	44800 ± 2263 b	838.3 ± 13.6 ab	818.3 ± 3.3 b	885.0 ± 49.5 b
S1:2	42667 ± 1665 ab	33600 ± 4525 cd	64800 ± 4525 b	844.4 ± 11.5 ab	838.6 ± 12.2 b	844.6 ± 15.9 b
S1:3	52800 ± 2884 c	42400 ± 2263 d	45600 ± 2263 b	864.6 ± 25.6 b	829.3 ± 9.0 b	826.7 ± 33.0 b

[a]Mean value followed by different letters is statistically different (ANOVA; Tukey's test, $P < 0.05$). Statistical analysis was carried out separately for initial, vermicompost and control values.

Vermicompost Analysis. The electrical conductivity (EC) and pH of the vermicompost in 1:10 (w/v) aqueous solution (deionized water) were measured using digital conductivity and pH meters, respectively.[22] Total organic carbon (TOC) was determined using the partial oxidation method.[23] Total Kjeldahl nitrogen (TKN) was measured using the micro-Kjeldahl method.[24] Total calcium, magnesium, and potassium were measured with the ignition method using an atomic absorption spectrophotometer following sample digestion with concentrated H_2SO_4 and concentrated H_2O_2.[25] Total phosphorus was determined using the colorimetric method following sample digestion with concentrated HNO_3 and concentrated HCl.[26] The soluble COD (sCOD) was analyzed in 1:10 (w/v) aqueous solution using the reactor digestion method (Hach method 8000).[1] The volatile solids (VS) content (loss on ignition) was obtained by combusting the dried samples in a furnace at 550 °C for 2 h.[13] The microstructures of the vermicompost were determined using a variable-pressure scanning electron microscope (VP-SEM), Hitachi S3400N-II, from Japan.

Statistical Analysis. One-way ANOVA was used to analyze the differences within vermicomposting and control treatments. Tukey's b test was also performed to identify the homogeneous type of treatments for the various parameters. IBM SPSS Statistics (version 20) was used for data analysis. All results reported in this study are significant at the $P < 0.05$ level.

RESULTS AND DISCUSSION

sCOD and VS of Vermicompost. sCOD is an important indicator of wastewater organic load. More sCOD was removed in treatments inoculated with earthworms than in those without earthworms (controls) (Table 4). The results suggest that, by feeding on the solid fractions of the POME, earthworms were responsible for the removal of the organic load in wastewater.[17] Earthworms secrete gut enzymes that help to reduce the chemical compounds in wastewater that cannot be decomposed by microbes alone.[27] In fact, Zhao et al.[28] suggested that, with the help of microorganisms, earthworms could accelerate the decomposition of organic wastes by favoring the breakdown of excreted polysaccharides. There was also a significant difference in sCOD removal when different amendments were used. The ranges of sCOD removal for earthworm treatments amended with rice straw and soil were 56.9−87.9 and 19.7−27.1%, respectively. The higher percentages of sCOD removal in treatments amended with rice straw can be explained by the higher decomposition rate of organic matter by the earthworms and microorganisms.[17] Khwairakpam and Bhargava[22] reported that COD was reduced by 29−73% during vermicomposting of sewage sludge. In comparison, conventional POME treatment using aerobic and anaerobic digestion is usually able to reduce the COD of POME by >95%.[2] Although the vermicomposting process could not remove the same amount of COD as the conventional biological method, it managed to transform POME into an organic fertilizer for agricultural purposes (Table 5). The sCOD removal was highest in the RS1:3 treatment, which was statistically different from the other treatments ($P < 0.05$).

Figure 1 shows a linear relationship between sCOD and VS for treatments amended with rice straw and soil. The sCOD and VS of the initial feedstocks and final vermicomposts were represented well by linear equations, with R^2 values of 0.8826 and 0.7414 for treatments amended with rice straw and soil, respectively. As shown in Figure 1, the slope of the equation demonstrates large differences between the two amendments. The slope for treatments amended with soil was higher, as there was a minimal decrease in VS content relative to the treatments amended with rice straw during vermicomposting process. Similar to sCOD removal, higher VS reduction was observed in treatments amended with rice straw relative to those amended with soil. In general, more VS reduction was also observed in the vermicomposts relative to controls for all treatments (Table 4). The decrease in VS is an indication of decomposition, substrate mineralization, and compost maturity.[13] VS reduction in the vermicomposts in treatments amended with rice straw (44.4−52.7%) and soil (0.7−4.1%) was also statistically different ($P < 0.05$). Hait and Tare[29] also showed decreases in volatile solids in waste-activated sludge during the vermicomposting process. The higher rate of VS reduction in POME treatments amended with rice straw showed that the

dx.doi.org/10.1021/jf404265f | J. Agric. Food Chem. 2014, 62, 691−698

Table 5. Final Chemical Characteristics of Different Treatments (Means ± SD, $n = 3$)[a]

treatment in w/v	pH		EC (μS/cm)		P (g/kg dry wt)		K (g/kg dry wt)		Ca (g/kg dry wt)		Mg (g/kg dry wt)		C/N ratio	
	vermicompost	control	vermicompost	control	vermicompost	control	vermicompost	control	vermicompost	control	vermicompost	control	vermicompost	control
RS1:1	8.26 ± 0.08 a	8.44 ± 0.28 a	1189 ± 132 a	597 ± 140 a	5.79 ± 1.37 a	2.54 ± 0.26 a	20.04 ± 1.63 a	11.77 ± 0.42 a	27.70 ± 1.00 a	19.90 ± 0.20 a	6.26 ± 0.77 ab	3.43 ± 0.38 a	11.34 ± 0.90 a	20.92 ± 1.24 a
RS1:2	7.98 ± 0.36 a	6.54 ± 0.25 b	1734 ± 17 b	2130 ± 57 b	5.15 ± 0.61 a	3.00 ± 0.35 ab	20.27 ± 1.68 a	11.63 ± 1.80 a	19.18 ± 1.82 b	13.73 ± 1.17 b	5.32 ± 0.53 ab	4.60 ± 0.82 ab	16.37 ± 0.60 a	22.15 ± 2.06 a
RS1:3	8.46 ± 0.10 a	9.09 ± 0.20 a	1437 ± 64 a	1141 ± 151 c	6.29 ± 0.74 a	3.55 ± 0.31 b	21.35 ± 0.45 a	10.07 ± 1.25 a	24.25 ± 2.34 ab	17.25 ± 2.76 ab	6.88 ± 0.77 ab	6.19 ± 0.00 c	9.64 ± 0.20 a	20.36 ± 3.07 a
S1:1	5.08 ± 0.08 b	5.77 ± 0.40 c	1240 ± 65 a	1564 ± 132 d	1.83 ± 0.44 b	0.34 ± 0.04 d	8.10 ± 2.03 bc	4.71 ± 1.00 b	20.68 ± 0.56 b	27.83 ± 1.87 cd	4.76 ± 0.65 a	5.86 ± 0.76 bc	49.60 ± 2.30 b	50.54 ± 2.62 b
S1:2	5.63 ± 0.32 c	5.45 ± 0.14 c	1359 ± 74 a	2009 ± 185 b	1.24 ± 0.30 b	1.63 ± 0.13 c	10.70 ± 0.03 b	6.60 ± 0.45 b	21.39 ± 1.19 b	27.04 ± 0.20 c	7.63 ± 0.85 b	5.66 ± 0.08 bc	46.28 ± 4.51 bc	54.96 ± 3.97 b
S1:3	5.79 ± 0.05 c	6.05 ± 0.37 bc	1682 ± 4 b	2050 ± 122 b	1.48 ± 0.12 b	3.40 ± 0.32 ab	5.38 ± 0.18 c	6.15 ± 0.43 b	29.39 ± 4.19 a	32.15 ± 1.02 d	7.04 ± 0.93 ab	5.83 ± 0.20 bc	41.86 ± 1.29 c	55.77 ± 3.15 b

[a]Mean values followed by different letters are statistically different for each parameter (ANOVA; Tukey's test, $P < 0.05$). Statistical analysis was carried out separately for vermicompost and control values.

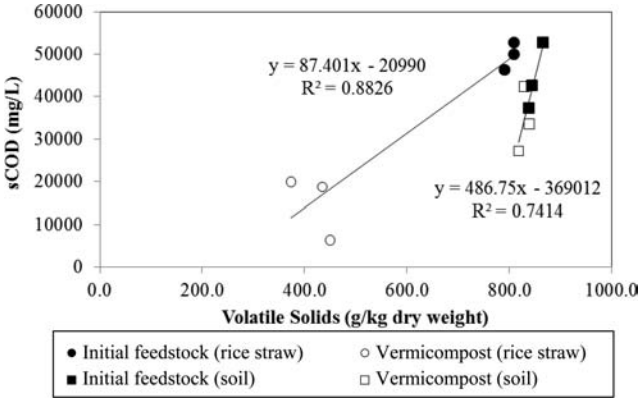

Figure 1. sCOD content (mg/L) against volatile solids (g/kg dry wt) of the treatments amended with rice straw and soil.

earthworms were consuming and breaking down these wastes at a much higher rate.[22]

pH of Vermicompost. The pH shifted toward alkaline conditions except in treatment S1:1, which showed no significant difference from the initial sampling (Tables 3 and 5). The shift in pH could be attributed to degradation of short-chain fatty acids and intensive mineralization of nitrogen by microbes.[25] A similar increase in pH was also observed by Shak et al.[30] and Tognetti et al.[31] Final pH ranged between 5.08 and 5.79 for treatments using soil as an amendment, but the final pH in the rice straw treatments ranged between 7.98 and 8.46. There was a significant difference between the rice straw and the soil treatments ($P < 0.05$). According to Singh and Suthar,[32] the difference in pH when different amendments were used was mainly due to variation in amendment quality, which affected the mineralization process and the intermediate species produced during the vermicomposting process.

Electrical Conductivity of Vermicompost. EC describes the soluble salt level in an organic amendment and is a good indicator of the applicability of vermicompost for agricultural purposes.[33] In this study, EC increased significantly in all vermicomposts. Control treatments also had higher final EC values, except in the RS1:1 treatment as compared to initial feedstocks (Tables 3 and 5). The loss of organic matter and release of minerals in the form of cations during vermicomposting are the main reasons for the EC increase.[20,34] Cations such as potassium, magnesium, and calcium are contributors to EC in vermicomposts,[35] which explains the higher EC in all treatments. The percentage of increase in EC also depends on the extent of organic matter mineralization under favorable experimental conditions.[29] The EC of the final vermicomposts did not exceed the threshold value of 3000 μS/cm, indicating that they can be safely applied as agronomic fertilizers.[33]

C/N Ratio of Vermicompost. The C/N ratio is used as an indicator of stabilization and mineralization of organic waste during the vermicomposting process.[36] The C/N ratio decreased for both the controls and the vermicomposts when POME was absorbed into rice straw. The treatments with earthworms showed a larger reduction in the C/N ratio relative to the treatments without earthworms (control) (Tables 3 and 5). Decreases in the C/N ratios in vermicomposts and controls using rice straw as an amendment ranged from 54.1 to 75.8% and from 35.6 to 55.4%, respectively. The greater reduction in the vermicompost C/N ratio relative to the control was due to the mineralization process caused by both the earthworms and microorganisms.[19] This is because earthworms release carbon as CO_2

during respiration and produce mucus and nitrogen excrements, thus increasing the nitrogen content.[37] Additionally, during a successful vermicomposting process, organic wastes are generally transformed into more stable, complex organic forms that resemble humic substances through the activity of microbial populations and earthworms.[9] However, there were no significant differences between initial and final products in the POME amended with soil treatment (Tables 3 and 5). Soil consumption rates are dependent on the earthworm species, the organic matter content of the feedstock, and the quality of the soil.[38] *E. eugeniae* is an epigeic earthworm that feeds on biodegradable waste; thus, *E. eugeniae* prefers fresh organic materials to soil.[9] Additionally, rice straw is rich in cellulose, which could increase the carbon mineralization rate during vermicomposting due to colonization by cellulose-decomposing fungi, contributing to the lower C/N ratio as compared to soil. The presence of earthworms is known to increase cellulolytic fungal populations and cellulase activity.[39] The lowest C/N ratio was observed in RS1:3 (9.64), followed by RS1:1 (11.34) and RS1:2 (16.37). There were no statistical differences between the treatments amended with rice straw. However, the C/N ratios were significantly different between the rice straw and soil amendments ($P < 0.05$). A final C/N ratio of approximately 10−15 is often taken as an indication of humic material formation and enhanced stability of treated organic wastes.[40] Thus, it is possible for the vermicomposts derived from rice straw and POME to be used as organic fertilizers.

Phosphorus, Potassium, Calcium, and Magnesium in Vermicompost. After 6 weeks of vermicomposting, all vermicomposts had higher phosphorus contents (43.7−308%), with the exception of the S1:2 treatment. Control treatments (except S1:1) also showed increases in phosphorus content, but the percentage increases were generally lower than those observed in vermicomposts (Tables 3 and 5). Similarly, there was a significant increase in potassium for all vermicomposts except in treatment of S1:3. Potassium content was highest in RS1:3 (21.35 g/kg) and lowest in S1:3 (5.38 g/kg) (Table 5). Higher percentage increases were observed in vermicomposts containing rice straw relative to those containing soil. The phosphorus and potassium contents in the rice straw and the soil treatments were statistically different ($P < 0.05$). Both Hait and Tare[29] and John Paul et al.[19] reported similar results during vermicomposting of waste-activated sludge and municipal solid waste, respectively.

Increases in calcium in the vermicomposts were observed in RS1:1 (342%), as well as RS1:3 (117%) and RS1:2 (77.6%) (Tables 3 and 5). A significant increase in calcium was also reported by other researchers using the earthworm *E. eugeniae* in a vermicomposting process.[22,41] However, the opposite was found in treatments using soil as an amendment, in which calcium increased more in the control relative to the vermicomposts. There are contradicting reports regarding the final calcium content obtained from different feedstocks. For example, Liu and Price[42] also reported a greater increase in calcium content for composts (30.8−171.4%) as compared to vermicomposts (10.3−53.8%) when spent coffee grounds were used as a feedstock. In contrast, Raphael and Velmourougane[41] reported a greater increase in calcium content in vermicomposts relative to composts with coffee pulp as a feedstock. The richness of organic wastes used is important in determining the final calcium level in vermicomposts.[43]

Magnesium content was higher in all vermicomposts and controls than in initial feedstocks, except S1:3 treatment for control. Generally, the increase in magnesium was more prominent in vermicomposts than controls (Tables 3 and 5). The maximum increase in magnesium content in vermicomposts occurred in the treatments RS1:1 (161%), RS1:3 (97.7%), RS1:2 (66.3%), S1:2 (63.7%), S1:1 (9.17%), and S1:3 (8.47%). Other researchers have reported an increase in magnesium content during the vermicomposting process. For example, Raphael and Velmourougane[41] reported an increase in magnesium (210%) during vermicomposting of coffee pulp amended with farmyard manure. Similarly, Liu and Price[42] reported a 50% increase in magnesium during vermicomposting of spent coffee grounds. Currently, there is no known contribution of earthworms to magnesium metabolism. Therefore, it is postulated that fungal and microalgal hyphae, which easily colonize freshly deposited earthworm casts, contribute to magnesium content in the vermicomposts.[43] Statistically, only treatment S1:1 was significantly different ($P < 0.05$) from the S1:2 treatment.

In general, the overall increase in nutrient contents (phosphorus, potassium, calcium, and magnesium) in the vermicompost can be explained by the reduction in weight of the feedstock material during the vermicomposting process.[21,44] According to Garg et al.,[34] the concentration effect was caused by the degradation of organic matter, which reduced the volume of feedstock due to the release of CO_2. In addition, the total nutrient contents in the vermicompost were generally higher than in the control, implying that the earthworms accelerated the decomposition of organic matter.

Earthworm Biomass. The biomass of earthworms in all treatments had decreased by the end of the vermicomposting process (Figure 2). There were no significant differences

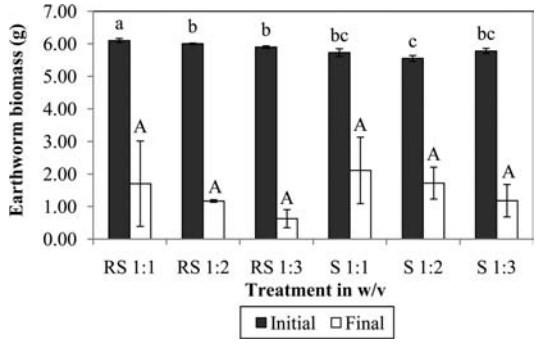

Figure 2. Initial and final earthworm biomass (g) of different treatments. Lower and uppper case letters indicate significant difference ($P < 0.05$) between initial and final earthworm biomass, respectively.

in total earthworm biomass among the different treatments ($P < 0.05$). The number of earthworms also decreased in all treatments. The highest sCOD removal rates (Table 4) and lowest C/N ratios in final vermicomposts (Table 5) were observed in the treatments amended with rice straw, indicating the possibility of food shortage after 6 weeks of the vermicomposting process. Food shortage caused the earthworms to lose weight, leading to the observed reduction in biomass and to earthworm fatality. Moreover, earthworms lost weight at a rate that depended on the quantity and nature of their indigestible substrates.[20] Degradation of the feedstock during vermicomposting could also result in environmental changes that would increase earthworm mortality. For example, a breakdown of polysaccharides could alter the structure of the feedstock, reducing the water retention capacity.[14] Additionally, Liu and Price[42] reported that high EC, low oxygen availability,

dx.doi.org/10.1021/jf404265f | J. Agric. Food Chem. 2014, 62, 691−698

and high levels of harmful organic compounds during vermicomposting were the reasons for poor earthworm survival rates. On the other hand, treatments amended with soil showed only a marginal reduction in sCOD and no significant decrease in the C/N ratio in final vermicomposts, indicating low organic matter ingestion rates by the earthworms. This was also corroborated by the higher levels of VS in treatments amended with soil. Thus, the decrease in earthworm biomass in treatments amended with soil was most likely due to the feedstock quality and its palatability.[38] In general, different amendments exhibit different chemical profiles that affect earthworm growth patterns differently. Therefore, the use of rice straw as an amendment provides a more conducive environment (i.e., easily metabolized organic matter and lower concentrations of growth-retarding substances for earthworms) relative to soil.[14] Shak et al.[30] also came to the conclusion that growth of *E. eugeniae* was closely associated with feed quality.

Physical Structure of Waste Mixture and Vermicompost. As a comparison of initial waste mixture (Figure 3a)

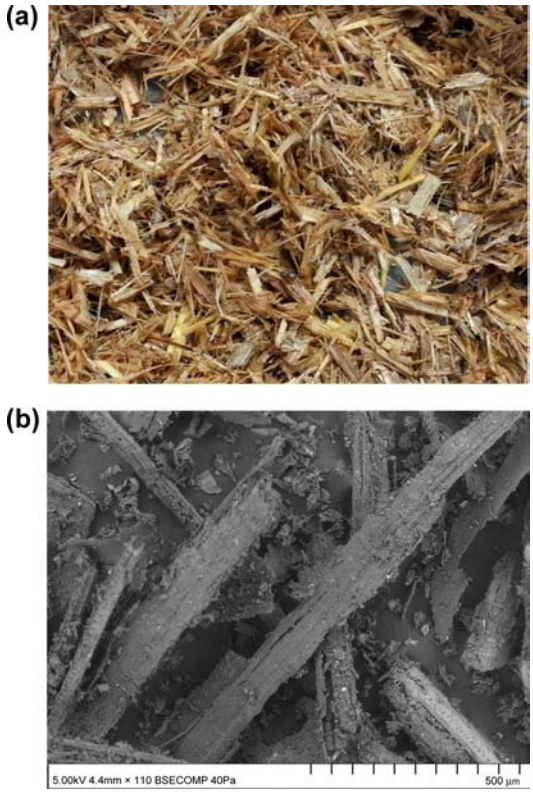

Figure 3. Photography (a) and scanning electron microscopy (b) images of waste mixture of RS1:3 treatment.

and the vermicompost obtained from RS1:3 (Figure 4a), the latter had finer granular structure and was darker in color. The vermicompost was also odorless after 6 weeks of vermicomposting. These observations were similar to those in previous studies conducted by Lim et al.[25] and Yadav and Garg.[45] However, some rice straw residues could still be observed in the final vermicompost (Figure 4a), suggesting that the initial waste mixture was not completely digested by the earthworms. Thus, the duration of the vermicomposting process could be extended to ensure complete biotransformation of rice straw into organic fertilizer.

Scanning electron microscopy (SEM) images of the initial waste mixture and final vermicompost in treatment RS 1:3

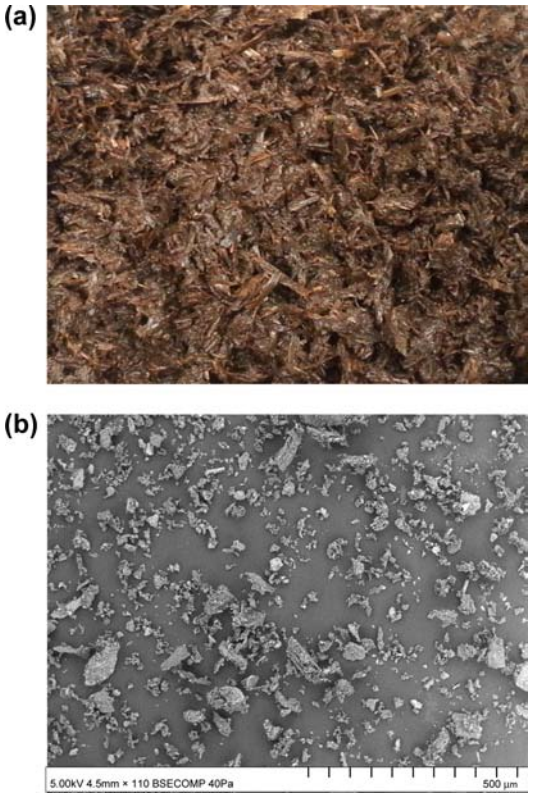

Figure 4. Photography (a) and scanning electron microscopy (b) images of vermicompost of RS1:3 treatment after 6 weeks of vermicomposting process.

are shown in Figures 3b and 4b, respectively. The SEM image revealed that the initial waste mixture was characterized by long fibers (Figure 3b). After the vermicomposting process, the vermicompost exhibited a distinct physical appearance that was more fragmented and porous (Figure 4b). The observations indicate that the long fibers of the rice straw present in the initial state were digested and fragmented by the earthworms, leading to a larger surface area in the vermicompost.[28]

Conclusions. This study demonstrates that vermicomposting enables the treatment and biotransformation of POME (and amendment) into mature organic fertilizer with higher nutrient contents than feedstock materials. Rice straw was proven to be a better absorbent for POME relative to soil because vermicomposts that were produced from the POME amended with rice straw had higher nutrient contents and sCOD removal rates but lower VS contents and C/N ratios. Among all of the waste mixtures, RS1:3 had the greatest reduction in sCOD (87.9%) and produced superior quality vermicompost with the lowest C/N ratio (9.64), but considerably high levels of phosphorus (6.29 g/kg), potassium (21.35 g/kg), calcium (24.25 g/kg), and magnesium (6.88 g/kg). The present results suggest that the vermicomposting process can be considered a viable waste treatment technology for POME that is amended with rice straw. This process utilized organic wastes to produce organic fertilizer or vermicompost, suitable for agronomic application. The vermicompost produced could also be used for soil remediation purposes.

AUTHOR INFORMATION

Corresponding Author

*(T.Y.W.) Phone: +60 3 55146258. Fax: +60 3 55146207. E-mail: wu.ta.yeong@monash.edu or tayeong@hotmail.com.

Funding

This research was supported by the Department of Higher Education, Malaysia, under Fundamental Research Grant Scheme (FRGS/1/2013/STWN03/MUSM/02/1). In addition, we thank Monash University, Sunway campus, for providing Su Lin Lim with a Ph.D. scholarship.

Notes

The authors declare no competing financial interest.

REFERENCES

(1) Wu, T. Y.; Mohammad, A. W.; Jahim, J. M.; Anuar, N. Optimized reuse and bioconversion from retentate of pre-filtered palm oil mill effluent (POME) into microbial protease by *Aspergillus terreus* using response surface methodology. *J. Chem. Technol. Biotechnol.* **2009**, *84*, 1390−1396.

(2) Wu, T. Y.; Mohammad, A. W.; Jahim, J. M.; Anuar, N. Pollution control technologies for the treatment of palm oil mill effluent (POME) through end-of-pipe processes. *J. Environ. Manage.* **2010**, *91*, 1467−1490.

(3) Wu, T. Y.; Mohammad, A. W.; Jahim, J. M.; Anuar, N. A holistic approach to managing palm oil mill effluent (POME): biotechnological advances in the sustainable reuse of POME. *Biotechnol. Adv.* **2009**, *27*, 40−52.

(4) Nouri, J.; Nouri, N.; Moeeni, M. Development of industrial waste disposal scenarios using life-cycle assessment approach. *Int. J. Environ. Sci. Technol.* **2012**, *9*, 417−424.

(5) Zaman, A. U. Life cycle assessment of pyrolysis-gasification as an emerging municipal waste treatment technology. *Int. J. Environ. Sci. Technol.* **2013**, *10*, 1029−1038.

(6) Zaman, A. U. Identification of waste management development drivers and potential emerging waste treatment technologies. *Int. J. Environ. Sci. Technol.* **2013**, *10*, 455−464.

(7) Sim, E. Y. S.; Wu, T. Y. The potential reuse of biodegradable municipal solid wastes (MSW) as feedstocks in vermicomposting. *J. Sci. Food Agric.* **2010**, *90*, 2153−2162.

(8) Domínguez, J. State-of-the-art and new perspectives on vermicomposting research. In *Earthworm Ecology*, 2nd ed.; Edwards, C. A., Ed.; CRC Press: Boca Raton, FL, USA, 2004; pp 401−424.

(9) Yadav, A.; Garg, V. K. Industrial wastes and sludges management by vermicomposting. *Rev. Environ. Sci. Biotechnol.* **2011**, *10*, 243−276.

(10) Suthar, S. Toxicity of methyl parathion on growth and reproduction of three ecologically different tropical earthworms. *Int. J. Environ. Sci. Technol.* **2013**, DOI: 10.1007/s13762-012-0154-3.

(11) Coria-Cayupán, Y. S.; Pinto, M. I. S.; Nazareno, M. A. Variations in bioactive substance contents and crop yields of lettuce (*Lactuca sativa* L.) cultivated in soils with different fertilization treatments. *J. Agric. Food Chem.* **2009**, *57*, 10122−10129.

(12) Delgado-Moreno, L.; Peña, A. Organic amendments from olive cake as a strategy to modify the degradation of sulfonylurea herbicides in soil. *J. Agric. Food Chem.* **2007**, *55*, 6213−6218.

(13) Hait, S.; Tare, V. Vermistabilization of primary sewage sludge. *Bioresour. Technol.* **2011**, *102*, 2812−2820.

(14) Suthar, S. Vermicomposting potential of *Perionyx sansibaricus* (Perrier) in different waste materials. *Bioresour. Technol.* **2007**, *98*, 1231−1237.

(15) Elvira, C.; Sampedro, L.; Benítez, E.; Nogales, R. Vermicomposting of sludges from paper mill and dairy industries with *Eisenia andrei*: a pilot-scale study. *Bioresour. Technol.* **1998**, *63*, 205−211.

(16) Mainoo, N. O. K.; Barrington, S.; Whalen, J. K.; Sampedro, L. Pilot-scale vermicomposting of pineapple wastes with earthworms native to Accra, Ghana. *Bioresour. Technol.* **2009**, *100*, 5872−5875.

(17) Tomar, P.; Suthar, S. Urban wastewater treatment using vermibiofiltration system. *Desalination* **2011**, *282*, 95−103.

(18) Wu, T. Y.; Mohammad, A. W.; Lim, S. L.; Lim, P. N.; Hay, J. X. W. Recent advances in the reuse of wastewaters for promoting sustainable development. In *Wastewater Reuse and Management*; Sharma, S. K., Sanghi, R., Eds.; Springer: Dordrecht, The Netherlands, 2013; pp 47−103, DOI: 10.1007/978-94-007-4942-9_3.

(19) John Paul, J. A.; Karmegam, N.; Daniel, T. Municipal solid waste (MSW) vermicomposting with an epigeic earthworm, *Perionyx ceylanensis* Mich. *Bioresour. Technol.* **2011**, *102*, 6769−6773.

(20) Gupta, R.; Garg, V. K. Stabilization of primary sewage sludge during vermicomposting. *J. Hazard. Mater.* **2008**, *153*, 1023−1030.

(21) Hanc, P.; Pliva, P. Vermicomposting technology as a tool for nutrient recovery from kitchen bio-waste. *J. Mater. Cycles Waste Manage.* **2013**, *15*, 431−439.

(22) Khwairakpam, M.; Bhargava, R. Vermitechnology for sewage sludge recycling. *J. Hazard. Mater.* **2009**, *161*, 948−954.

(23) Walkley, A.; Black, I. A. An examination of the Degtjareff method for determination soil organic matter and a proposed modification of the chromic acid titration method. *Soil Sci.* **1934**, *37*, 29−38.

(24) Shaw, J.; Beadle, L. C. A simplified ultra-micro Kjedahl method for estimation of protein and total nitrogen in fluid samples of less than 1.0 μL. *J. Exp. Biol.* **1949**, *26*, 15−23.

(25) Lim, S. L.; Wu, T. Y.; Sim, E. Y. S.; Lim, P. N.; Clarke, C. Biotransformation of rice husk into organic fertilizer through vermicomposting. *Ecol. Eng.* **2012**, *41*, 60−64.

(26) John, M. K. Calorimetric determination of phosphorus in soil and plant materials with ascorbic acid. *Soil Sci.* **1970**, *109*, 214−220.

(27) Sinha, R. K.; Bharambe, G.; Chaudhari, U. Sewage treatment by vermifiltration with synchronous treatment of sludge by earthworms: a low-cost sustainable technology over conventional systems with potential for decentralization. *Environmentalist* **2008**, *28*, 409−420.

(28) Zhao, L.; Wang, Y.; Yang, J.; Xing, M.; Li, X.; Yi, D.; Deng, D. Earthworm-microorganism interactions: a strategy to stabilize domestic wastewater sludge. *Water Res.* **2010**, *44*, 2572−2582.

(29) Hait, S.; Tare, V. Optimizing vermistabilization of waste activated sludge using vermicompost as bulking material. *Waste Manage.* **2011**, *31*, 502−511.

(30) Shak, K. P. Y.; Wu, T. Y.; Lim, S. L.; Lee, C. A. Sustainable reuse of rice residues as feedstocks in vermicomposting for organic fertilizer production. *Environ. Sci. Pollut. Res.* **2014**, *21*, 1349−1359.

(31) Tognetti, C.; Mazzarino, M. J.; Laos, F. Improving the quality of municipal organic waste compost. *Bioresour. Technol.* **2007**, *98*, 1067−1076.

(32) Singh, D.; Suthar, S. Vermicomposting of herbal pharmaceutical industry solid wastes. *Ecol. Eng.* **2012**, *39*, 1−6.

(33) Lazcano, C.; Gomez-Brandon, M.; Dominguez, J. Comparison of the effectiveness of composting and vermicomposting for biological stabilization of cattle manure. *Chemosphere* **2008**, *72*, 1013−1019.

(34) Garg, V. K.; Suthar, S.; Yadav, A. Management of food industry waste employing vermicomposting technology. *Bioresour. Technol.* **2012**, *126*, 437−443.

(35) Fornes, F.; Mendoza-Hernández, D.; García-de-la-Fuente, R.; Abad, M.; Belda, R. M. Composting versus vermicomposting: a comparative study of organic matter evolution through straight and combined processes. *Bioresour. Technol.* **2012**, *118*, 296−305.

(36) Fernández-Gómez, M. J.; Díaz-Raviña, M.; Romero, E.; Nogales, R. Recycling of environmentally problematic plant wastes generated from greenhouse tomato crops through vermicomposting. *Int. J. Environ. Sci. Technol.* **2013**, *10*, 697−708.

(37) Lim, P. N.; Wu, T. Y.; Sim, E. Y. S.; Lim, S. L. The potential reuse of soybean husk as feedstock of *Eudrilus eugeniae* in vermicomposting. *J. Sci. Food Agric.* **2011**, *91*, 2637−2642.

(38) Curry, J. P.; Schmidt, O. The feeding ecology of earthworms − a review. *Pedobiologia* **2007**, *50*, 463−477.

(39) Pramanik, P.; Chung, Y. R. Changes in fungal population of fly ash and vinasse mixture during vermicomposting by *Eudrilus eugeniae* and *Eisenia fetida*: documentation of cellulose isozymes in vermicompost. *Waste Manage.* **2011**, *31*, 1169−1175.

(40) Macci, C.; Masciandaro, G.; Ceccanti, B. Vermicomposting of olive oil mill wastewaters. *Waste Manage. Res.* **2010**, *28*, 738−747.

(41) Raphael, K.; Velmourougane, K. Chemical and microbiological changes during vermicomposting of coffee pulp using exotic (*Eudrilus eugeniae*) and native earthworm (*Perionyx ceylanesis*) species. *Biodegradation* **2011**, *22*, 497−507.

(42) Liu, K.; Price, G. W. Evaluation of three composting systems for the management of spent coffee grounds. *Bioresour. Technol.* **2011**, *102*, 7966−7974.
(43) Suthar, S. Recycling of agro-industrial sludge through vermitechnology. *Ecol. Eng.* **2010**, *36*, 1028−1036.
(44) Hait, S.; Tare, V. Transformation and availability of nutrients and heavy metals during integrated composting-vermicomposting of sewage sludges. *Ecotox. Environ. Saf.* **2012**, *79*, 214−224.
(45) Yadav, A.; Garg, V. K. Feasibility of nutrient recovery from industrial sludge by vermicomposting technology. *J. Hazard. Mater.* **2009**, *168*, 262−268.

JOURNAL OF AGRICULTURAL AND FOOD CHEMISTRY

Article

pubs.acs.org/JAFC

Effect of Oxidation of Dietary Proteins with Performic Acid on True Ileal Amino Acid Digestibility As Determined in the Growing Rat

Shane M. Rutherfurd,* Carlos A. Montoya, and Paul J. Moughan

Riddet Institute, Massey University, Palmerston North, New Zealand

ABSTRACT: The study examined the impact of oxidation with performic acid on the true ileal amino acid digestibility (TIAAD) of seven dietary protein sources. TIAAD of both the unoxidized and oxidized protein sources was determined in the growing rat and compared. After oxidation, TIAAD was 30 and 58% higher across amino acids ($P < 0.001$) for the more poorly digestible protein sources, zein and blood meal respectively, 6−16% lower ($P < 0.05$) for the more highly digestible protein sources (casein, soy protein isolate, and beef muscle protein), and generally unchanged (<2% difference) for the more moderately digested protein sources (lactalbumin and gelatin). Overall, the change in TIAAD after oxidation was negatively correlated ($P < 0.001$, $r = -0.90$) with the TIAAD prior to oxidation, most likely as a result of the balance between two processes, protein denaturation resulting in increased digestion and indigestible limit peptide formation resulting in decreased digestion.

KEYWORDS: *performic acid, oxidation, digestibility, protein, ileal*

INTRODUCTION

During the processing or prolonged storage of foods, dietary nutrients are susceptible to oxidative damage. The oxidation of dietary lipids has been studied extensively, and protein oxidation in the context of age-related diseases has also received some attention.[1,2] However, oxidation as it pertains to dietary proteins has been largely ignored by the scientific community.[3] Several different oxidative reactions in proteins are believed to occur during food processing, which include the formation of carbonyl groups and the oxidation of thiol groups to sulfenic acids, sulfinic acids, and disulfides. As an example, it has been reported that in processed foods, even those that undergo relatively mild processing such as infant formulas, soy protein isolate (SPI), and egg white powder, between 23 and 64% of the methionine present may be oxidized to methionine sulfoxide or methionine sulfone.[4,5] In addition, cross-linking can also occur via the formation of disulfide bonds and dityrosine bonds[6,7] and reactions of the side chains of several amino acids (for example, lysine, histidine, methionine, and phenylalanine) with the products of lipid peroxidation.[8]

Studies on the oxidation of food proteins have largely focused on the presence of oxidized derivatives such as carbonyl, sulfhydryl, and dityrosine groups and the effect these derivatives have on protein functionality. However, given that it is well-known that the chemical modification of proteins during processing can greatly affect their subsequent digestion in the gastrointestinal tract (for example, the Maillard reaction with lysine)[9] and because dietary protein sources can be substantially oxidized during processing,[4−8] it is important to have an understanding of the impact of protein oxidative damage on protein digestion in the gastrointestinal tract. However, to date, little published work has focused on the impact of oxidation on the digestion of dietary proteins, and of those studies that have been published, all have used in vitro digestion models[10−13] where the in vitro digestion findings are often extrapolated to digestion in the gastrointestinal tract. However, given that in vitro digestion models are simplistic and provide only approximations of gastrointestinal digestion, such extrapolations must be viewed with caution. Ideally, the impact of oxidation on protein digestion should be evaluated using animal or human models. To the authors' knowledge, no such in vivo studies have been reported in the literature. Consequently, the aim of the present study was to conduct a preliminary examination of the impact of oxidation on the true ileal amino acid digestibility of dietary protein sources using both highly and poorly digestible dietary protein sources. To that end, performic acid was used to oxidize the proteins, and true ileal amino acid digestibility determined in the growing rat was used as a measure of the extent of digestion. True ileal amino acid digestibility is measured as the difference between the amino acid content of the diet and the amino acid content of digesta collected from the end of the small intestine (terminal ileum), corrected for the presence of endogenous amino acids (amino acids derived from nondietary proteins present in the gut lumen, for example, mucins, digestive enzymes, microbial protein). Performic acid is a powerful oxidizing agent and was used to allow investigation at the boundaries of the extent of oxidation likely to occur during food manufacture.

MATERIALS AND METHODS

Chemicals. Soy protein isolate (SPI, Supro 670) was obtained from Columbit NZ Ltd., Auckland, New Zealand, zein from Sigma-Aldrich Chemicals (St Louis, MO), gelatin (GB25 standard) from Gelita NZ Ltd., Christchurch, New Zealand, and blood meal from Denver Stockfeeds, Palmerston North, New Zealand. Casein and lactalbumin were obtained from Fonterra Group Ltd., New Zealand, and for beef muscle protein, lean ground beef was obtained from a

Received: July 23, 2013
Revised: December 9, 2013
Accepted: December 13, 2013
Published: January 8, 2014

ACS Publications © 2014 American Chemical Society

dx.doi.org/10.1021/jf403146u | J. Agric. Food Chem. 2014, 62, 699−707

local supermarket. All of the original protein sources (unoxidized) were also ground and freeze-dried prior to inclusion in the diets. Vitamin and mineral mixes for the rat diets were obtained from Plant and Food Research Ltd., Palmerston North, New Zealand. Laboratory rats were obtained from the Small Animal Production Unit, Massey University, Palmerston North, New Zealand.

Oxidized Protein Sources and Diets. The unoxidized protein sources were used as controls. They contained no detectable methionine sulfone, methionine sulfoxide, or cysteic acid and underwent no form of oxidation treatment. The latter controls, which were effectively "untreated", were designated "unoxidized" protein sources. Each protein source was oxidized using performic acid.[14] Performic acid was prepared by adding one part hydrogen peroxide (30%) to nine parts formic acid (98%). The solution was then mixed and left at room temperature for 30 min before being cooled to 0 °C. Approximately 200 g of each protein source was incubated in 1.5 L of performic acid at 0 °C overnight. Hydrogen bromide (450 mL) was then very slowly added to the protein−performic acid mixture on ice to reduce the performic acid to formic acid. The pH of each protein solution was then slowly adjusted with sodium hydroxide until the protein precipitated. The precipitated protein was filtered and washed with water using a Buchner funnel to remove any residual formic acid. The washed precipitate was then freeze-dried and finely ground, ready for chemical analysis and incorporation into the experimental diets.

Fourteen semisynthetic powdered diets were formulated containing one of the seven protein sources (casein, SPI, beef muscle protein, gelatin, blood meal, lactalbumin, or zein) or their oxidized counterparts. Each experimental diet was formulated to contain 100 g/kg crude protein. The diets also contained 50 g/kg purified cellulose, 50 g/kg soybean oil, 100 g/kg sucrose, 50 g/kg vitamin mix, and 50 g/kg mineral mix. The vitamin and mineral mixes were proprietary mixes formulated to meet the requirements of the growing rat for vitamins and minerals in the final diets.[15] All diets met the nutritional requirements of the growing rat for all nutrients except protein.[15] Titanium dioxide (3 g/kg) was included in each diet as an indigestible marker. Wheat starch was used to make each diet up to its total weight of 1 kg.

Animal Trial. Ethics approval for the animal trial was obtained from the Animal Ethics Committee, Massey University, Palmerston North, New Zealand.

Two hundred and twenty-four Sprague−Dawley male rats (204 ± 1.3 g, mean ± standard error, body weight) were housed individually in stainless steel wire-bottom cages in a room maintained at 22 ± 2 °C, with a 12 h light/dark cycle. For the first 13 days of the trial, the rats received the diets containing the unoxidized protein sources only, such that there were 32 rats allocated to each unoxidized protein source. The rats were fed using a frequent (hourly) feeding regimen as described by Rutherfurd and Moughan,[16] and water was available at all times. On the final day of the study, the rats were reallocated to the diets such that half the rats in each treatment group (i.e., receiving one of the unoxidized protein sources during the first 13 days of the study) received the diet containing the corresponding oxidized protein source. The diets containing the oxidized protein sources were fed only on the final day as the amount of oxidized protein source material was limited. Approximately 5 h after the first meal, the rats were killed by asphyxiation with carbon dioxide gas followed by cervical dislocation and digesta carefully sampled from the terminal ileum as described by Rutherfurd and Moughan.[16] To ensure there was sufficient digesta material for all of the chemical analyses, digesta samples were pooled across randomly selected pairs of rats within each treatment group, to give eight samples each per oxidized and unoxidized protein source and then freeze-dried and stored at −20 °C ready for chemical analysis.

Chemical Analysis. The crude protein content of the unoxidized and oxidized protein sources was determined as the total nitrogen content multiplied by 6.25. Total nitrogen was determined using the Dumas method on a LECO analyzer (LECO Corp., St. Joseph, MI, USA).

Amino acid contents were determined as described by Rutherfurd et al.[17] Briefly, amino acids in the ileal digesta and diets were hydrolyzed using 6 M glass-distilled HCl containing 0.1% phenol for 24 h at 110 ± 2 °C in evacuated sealed tubes before undergoing C18 reversed-phase HPLC (Agilent 1200 HPLC system) with precolumn derivatization with *o*-phthalaldehyde and detection by fluorescence (excitation λ 338 nm; emission λ 450 nm). Norvaline was used as an internal standard. Tryptophan in the protein sources was determined by alkali hydrolysis (4.5 M NaOH containing 5% (w/v) of maltodextrin at 110 °C for 20 h), followed by neutralization and C18 reversed-phase HPLC on an Agilent 1100 HPLC system and detected using absorbance at 280 nm. For the tryptophan analysis, 5-methyltryptophan was used as an internal standard, and tryptophan concentration values were corrected for the recovery of the internal standard. Cysteine is most commonly determined as cysteic acid using amino acid analysis following performic acid oxidation. Therefore, bcause cysteic acid was present in the oxidized protein sources and would consequently interfere with the determination of cysteine in the corresponding diets and digesta, cysteine was not determined as part of the present study. When appropriate, the weight of each amino acid was calculated using free amino acid molecular weights.

The titanium dioxide content of the diets and digesta samples was determined following the method of Short et al.[18] Briefly, samples were ashed at 500 °C in a muffle furnace before being digested in 60% (v/v) sulfuric acid. The mixture was then incubated with 30% hydrogen peroxide and the absorbance read at 405 nm.

Data Analysis. Ileal amino acid flows were calculated using the following equation:

$$\begin{aligned}&\text{ileal amino acid flow (mg/kg dry matter intake (DMI))}\\&\quad=\text{ileal amino acid content (mg/kg DM)}\\&\qquad\times\frac{\text{diet titanium (mg/kg DM)}}{\text{ileal titanium (mg/kg DM)}}\end{aligned}\tag{1}$$

True ileal amino acid digestibility (TIAAD) was calculated using the following equation (units are mg/kg DMI):

$$\begin{aligned}\text{TIAAD (\%)}=[&\text{dietary AA intake}-(\text{ileal AA flow}\\&-\text{endogenous AA flow})]/\text{dietary AA intake}\times 100\end{aligned}\tag{2}$$

Endogenous AA flow is based on average endogenous amino acid flows for growing rats of a similar age and body weight as those used in the present work and as reported by Rutherfurd and Moughan[19] determined using the enzyme hydrolyzed protein (casein)/ultrafiltration method.[20,21]

The percentage difference in true ileal amino acid digestibility after oxidation was calculated as follows (units are %):

$$\begin{aligned}\text{difference (\%)}=\Big[&(\text{TIAAD}_{\text{oxidized protein source}}\\&-\text{TIAAD}_{\text{unoxidized protein source}})\\&/\text{TIAAD}_{\text{unoxidized protein source}}\Big]\times 100\end{aligned}\tag{3}$$

Statistical Analysis. The true ileal amino acid digestibilities of the unoxidized and oxidized protein sources were compared statistically using one-way ANOVA (GLM procedure)[22] for each protein source separately. The correlation between the percentage difference in true ileal amino acid digestibility before and after oxidation and the true ileal amino acid digestibility of the unoxidized protein sources was analyzed by simple correlation using the CORR procedure of SAS.[22]

RESULTS

The mean daily food intakes of the rats consuming the diets containing the unoxidized protein sources on the penultimate day of the study were 6.5 ± 0.15, 15.3 ± 0.61, 12.6 ± 0.62, 19.0 ± 0.65, 19.7 ± 0.36, 6.3 ± 0.65, and 9.7 ± 0.31 g for the rats receiving the zein-, SPI-, lactalbumin-, beef muscle protein-,

Table 1. Mean[a] Amino Acid[b] Composition (Grams per Kilogram Protein) of the Unoxidized (unox) and Oxidized (oxid) Protein Sources

	casein		soy protein isolate		beef muscle protein		gelatin		blood meal		lactalbumin		zein		overall CV[c] (%)
	unox	oxid	unox	oxid	unox	oxid	unox	oxid	unox	oxid	unox	oxid	unox	oxid	
aspartic acid	72.8	76.7	103.7	111.3	70.0	74.2	70.3	67.1	88.1	91.1	89.5	122.3	64.1	67.1	5.5
threonine	40.3	42.4	32.8	33.2	33.4	34.4	25.3	26.1	40.7	39.8	34.1	33.5	28.1	27.7	4.0
serine	54.5	58.1	46.3	45.7	28.8	34.2	36.5	35.6	35.4	36.1	30.8	27.5	56.3	54.6	5.8
glutamic acid	227.7	246.8	171.7	173.5	117.7	128.3	123.4	127.7	68.3	68.7	135.4	139.5	290.8	287.4	6.0
glycine	19.2	19.0	37.4	38.8	33.1	40.0	291.3	306.9	33.7	33.5	13.9	12.5	16.5	12.1	3.3
alanine	35.5	33.3	37.6	41.9	47.0	52.5	110.6	115.5	67.9	65.9	42.8	42.5	108.1	109.5	3.3
valine	67.3	67.1	42.4	49.0	42.7	46.6	28.9	30.4	72.1	77.7	45.0	46.8	43.5	44.3	3.7
methionine	29.1	0.0	11.1	0.0	25.2	0.5	10.3	0.0	14.3	0.0	20.0	0.0	17.3	0.0	2.7
isoleucine	51.7	52.1	41.6	47.6	38.6	45.9	25.5	27.3	16.6	17.6	42.3	44.5	43.7	41.4	4.3
leucine	97.5	108.6	74.6	83.4	67.7	82.5	37.1	39.6	104.1	113.7	102.8	98.1	231.4	243.4	3.3
tyrosine	59.9	0.0	35.4	0.0	25.8	0.6	8.5	0.0	22.7	0.6	26.8	0.4	56.0	0.7	9.3
phenylalanine	53.7	55.8	49.0	53.7	32.1	39.0	25.5	26.0	60.1	60.8	29.4	29.6	81.7	78.6	6.5
histidine	32.5	41.6	24.1	21.8	31.7	8.7	9.2	6.0	50.7	29.7	13.6	4.3	14.8	1.9	5.7
lysine	83.9	86.5	57.6	55.7	72.0	83.7	39.5	46.1	72.2	69.7	77.8	75.5	2.4	2.2	4.5
arginine	37.7	39.3	70.0	67.0	56.3	69.0	100.2	106.7	35.5	35.2	24.3	23.8	18.2	17.9	3.7
tryptophan	85.7	0.0	12.1	0.0	11.4	0.0	0.6	0.0	13.5	0.0	23.9	0.0	2.4	0.0	8.2

[a]Analyses was conducted in duplicate. [b]Cysteine and proline were not determined. [c]CV, coefficient of variation.

Table 2. Mean (n = 8) True Ileal Amino Acid[a] Digestibility (TIAAD) of Unoxidized and Performic Acid-Oxidized Lactalbumin

	TIAAD (%)				
	unoxidized	oxidized	overall SE[b]	significance[c]	difference[d] (%)
aspartic acid	76.3	86.9	2.65	*	14
threonine	71.4	70.3	4.46	NS	
serine	79.6	70.8	4.75	NS	
glutamic acid	82.7	89.0	2.11	NS	
alanine	89.4	88.7	1.98	NS	
valine	85.1	84.8	2.56	NS	
isoleucine	90.1	90.1	1.80	NS	
leucine	93.1	91.8	1.45	NS	
phenylalanine	91.1	87.8	2.27	NS	
histidine	85.4	69.7	5.44	NS	
lysine	91.3	90.3	1.60	NS	
arginine	85.5	76.4	3.77	NS	
mean digestibility[e]	85.1	86.6			

[a]Methionine, cysteine, tyrosine, and tryptophan were not included in the analysis because they were destroyed during the oxidation process. [b]Overall standard error of the unoxidized and oxidized lactalbumin. [c]NS, not significant, $P > 0.05$; *, $0.05 > P > 0.01$. [d]Difference was calculated according to eq 3. [e]Mean true ileal amino acid digestibility across all examined amino acids.

casein-, blood meal-, and gelatin-based basal diets, respectively. The mean daily weight gains of the rats over the last 7 days of the study were −0.5 ± 0.09, 2.6 ± 0.28, 5.9 ± 0.31, 4.5 ± 0.45, 4.2 ± 0.19, −0.1 ± 0.15, and −0.5 ± 0.12 g for the rats allocated to the zein-, SPI-, lactalbumin-, beef muscle protein-, casein-, blood meal-, and gelatin-based basal diets, respectively. One rat allocated to the oxidized blood meal-based diet died during the study, but all the remaining rats appeared to be healthy throughout the study. The rats fed the zein-, blood meal-, and gelatin-based diets lost weight over the last 7 days of the study, and this likely reflects the poor amino acid balance and relatively lower feed intake for the rats on the latter diets compared to the animals receiving the diets containing SPI, lactalbumin, beef muscle protein, or casein. Although it has been reported that feed intake can affect true ileal amino acid digestibility, at least in piglets,[23] the extent of the latter effect is reported to be small (<3% over a feed intake range of 30−60 g/kg bodyweight). Consequently, in light of the latter finding and also because the dietary treatments were compared only within protein source (oxidized vs unoxidized), any impact on true ileal amino acid digestibility due to the lower feed intakes for the rats receiving the unoxidized and oxidized zein-, blood meal-, and gelatin-based diets was deemed to be insignificant in the context of the present study.

The amino acid compositions of the unoxidized and oxidized protein sources are presented in Table 1. The main observation was that the concentrations of methionine, tyrosine, and tryptophan in the seven protein sources after performic acid treatment were 0−0.5, 0−0.7, and 0 g/kg protein, respectively, indicating that the latter amino acids were almost completely chemically modified. Given that performic acid is a powerful oxidizing agent, it was assumed that any reduction in the

dx.doi.org/10.1021/jf403146u | J. Agric. Food Chem. 2014, 62, 699−707

Table 3. Mean (n = 8) True Ileal Amino Acid[a] Digestibility (TIAAD) of Unoxidized and Performic Acid-Oxidized Gelatin

	TIAAD (%)				
	unoxidized	oxidized	overall SE[b]	significance[c]	difference[d] (%)
aspartic acid	82.6	80.7	2.20	NS	
threonine	85.4	86.8	2.45	NS	
serine	86.1	86.9	1.82	NS	
glutamic acid	87.5	89.7	1.26	NS	
alanine	91.7	93.1	0.85	NS	
valine	89.6	90.1	1.48	NS	
isoleucine	93.6	91.5	1.13	NS	
leucine	89.7	90.6	1.39	NS	
phenylalanine	92.6	92.5	1.14	NS	
histidine	73.0	89.6	4.02	*	23
lysine	93.9	93.2	0.87	NS	
arginine	96.5	95.9	0.63	NS	
mean digestibility[e]	88.5	90.1			

[a]Methionine, cysteine, tyrosine, and tryptophan were not included in the analysis because they were destroyed during the oxidation process. [b]Overall standard error of the unoxidized and oxidized gelatin. [c]NS, not significant, $P > 0.05$; * $0.05 > P > 0.01$. [d]Difference was calculated according to eq 3. [e]Mean true ileal amino acid digestibility across all examined amino acids.

Table 4. Mean (n = 8) True Ileal Amino Acid[a] Digestibility (TIAAD) of Unoxidized and Performic Acid-Oxidized Blood Meal

	TIAAD (%)				
	unoxidized	oxidized	overall SE[b]	significance[c]	difference[d] (%)
aspartic acid	54.4	78.0	4.81	**	43
threonine	63.7	81.3	4.08	*	28
serine	64.2	81.0	4.16	*	26
glutamic acid	58.8	79.0	4.22	**	34
alanine	65.2	84.2	2.87	**	29
valine	64.8	88.5	3.12	***	37
isoleucine	76.6	85.9	2.80	*	12
leucine	65.3	89.3	2.72	***	37
phenylalanine	69.1	88.5	2.81	***	28
histidine	70.0	87.9	2.79	***	26
lysine	66.2	84.7	2.91	***	28
arginine	66.5	83.8	2.83	***	26
mean digestibility[e]	65.4	84.4			

[a]Methionine, cysteine, tyrosine, and tryptophan were not included in the analysis because they were destroyed during the oxidation process. [b]Overall standard error of the unoxidized and oxidized blood meal. [c]*, $0.05 > P > 0.01$; **, $0.01 > P > 0.001$; ***, $P < 0.001$. [d]Difference was calculated according to eq 3. [e]Mean true ileal amino acid digestibility across all examined amino acids.

amount of the determined amino acids present in the protein sources after performic acid treatment was due to the oxidation of those amino acids. Oxidation appeared to be incomplete for methionine in beef muscle protein (2.1% of the original methionine was present after oxidation) and for tyrosine in beef muscle protein, blood meal, lactalbumin, and zein (1.2−2.4% of the original tyrosine was present after oxidation). The recovery of histidine after performic acid oxidation was also low for beef muscle protein, gelatin, blood meal, lactalbumin, and zein with recoveries of 27, 65, 59, 31, and 13%, respectively. The recoveries of all of the remaining determined amino acids were virtually complete, suggesting that no modification of the latter amino acids occurred during performic acid oxidation, although it is possible that oxidized amino acids were present but that any altered amino acids reverted back to their parent form during HCl hydrolysis.

True ileal amino acid digestibility was determined for both the unoxidized and oxidized protein sources, and these data are presented in Tables 2−8. Digestibility values for glycine were omitted because the enzyme-hydrolyzed protein (casein)/ultrafiltration method used to determine endogenous ileal amino acids flows, which are in turn used to calculate true ileal amino acid digestibility, underestimates endogenous ileal flows for glycine because a significant amount of the endogenous glycine in the gastrointestinal tract is conjugated to bile salts, the latter of which are excluded from the endogenous protein fraction during ultrafiltration of the digesta.[16] For almost all of the amino acids examined in lactalbumin (Table 2) and gelatin (Table 3), histidine being the exception for gelatin and aspartic acid being the exception for lactalbumin, there was no difference ($P > 0.05$) between true ileal amino acid digestibility of the protein sources prior to and after treatment with performic acid. However, for the oxidized lactalbumin, the true ileal amino acid digestibility values obtained for one replicate were quite different from the others within the treatment group. The digestibility values for the latter replicate, which were not outliers based on the Grubb test and were therefore not excluded from the statistical analysis, may explain why large

dx.doi.org/10.1021/jf403146u | J. Agric. Food Chem. 2014, 62, 699−707

Table 5. Mean (n = 8) True Ileal Amino Acid[a] Digestibility (TIAAD) of Unoxidized and Performic Acid-Oxidized Zein

	TIAAD (%)				
	unoxidized	oxidized	overall SE[b]	significance[c]	difference[d] (%)
aspartic acid	47.7	83.9	3.18	***	76
threonine	42.6	81.3	3.88	***	91
serine	45.4	85.5	3.13	***	88
glutamic acid	49.6	90.8	2.68	***	83
alanine	86.9	93.1	3.07	NS	
valine	54.5	91.5	2.77	***	68
isoleucine	47.8	90.3	3.03	***	89
leucine	53.8	94.4	2.45	***	75
phenylalanine	53.0	92.1	2.54	***	74
histidine	45.1	64.8	7.27	NS	
arginine	57.9	88.2	3.55	***	53
mean digestibility[e]	53.1	86.9			

[a]Methionine, cysteine, tyrosine, and tryptophan were not included in the analysis because they were destroyed during the oxidation process. Lysine was not determined because the lysine content of zein is negligible. [b]Overall standard error of the unoxidized and oxidized zein. [c]NS, not significant, $P > 0.05$; ***, $P < 0.001$. [d]Difference was calculated according to eq 3. [e]Mean true ileal amino acid digestibility across all examined amino acids.

Table 6. Mean (n = 8) True Ileal Amino Acid[a] Digestibility (TIAAD) of Unoxidized and Performic Acid-Oxidized Beef Muscle Protein

	TIAAD (%)				
	unoxidized	oxidized	overall SE[b]	significance[c]	difference[d] (%)
aspartic acid	86.0	60.4	2.52	***	−30
threonine	88.3	55.1	2.88	***	−38
serine	91.4	70.4	2.18	***	−23
glutamic acid	91.2	79.8	1.52	***	−12
alanine	94.2	85.5	0.89	***	−9
valine	93.2	81.5	1.33	***	−13
isoleucine	94.6	83.7	1.10	***	−12
leucine	94.6	86.7	1.00	***	−8
phenylalanine	94.4	87.0	0.98	***	−8
histidine	95.0	65.2	2.18	***	−31
lysine	94.5	89.9	0.70	***	−5
arginine	94.2	90.4	0.77	***	−4
mean digestibility[e]	92.6	78.0			

[a]Methionine, cysteine, tyrosine, and tryptophan were not included in the analysis because they were destroyed during the oxidation process. [b]Overall standard error of the unoxidized and oxidized beef muscle protein. [c]***, $P < 0.001$. [d]Difference was calculated according to eq 3. [e]Mean true ileal amino acid digestibility across all examined amino acids.

numerical differences observed between the true ileal amino acid digestibility for the unoxidized and oxidized lactalbumin were not statistically significant. For blood meal (Table 4) and zein (Table 5), true ileal amino acid digestibility was higher ($P > 0.05$) after treatment with performic acid for all of the amino acids for blood meal and for all of the amino acids except alanine and histidine for zein. For beef muscle protein (Table 6), SPI (Table 7), and casein (Table 8), true ileal amino acid digestibility was lower ($P > 0.001$) after treatment with performic acid for all of the amino acids examined, with the exception of serine for casein. Overall, treatment with performic acid led to an increase in the mean true ileal amino acid digestibility across amino acids of 63% for zein (Table 5) and 29% for blood meal (Table 4), a decrease in the mean true ileal amino acid digestibility across amino acids of 16% for beef muscle protein (Table 6), 15% for SPI (Table 7), and 6% for casein (Table 8) and had little effect on the mean true ileal amino acid digestibility of lactalbumin (Table 2) and gelatin (Table 3).

A correlation analysis was also conducted comparing true ileal amino acid digestibility prior to performic acid treatment and the percentage change in true ileal amino acid digestibility after performic acid treatment across the seven protein sources for each of the amino acids individually and across all amino acids collectively. A negative correlation ($P < 0.01$, $r = -0.90$ to -0.98) was observed for each of the amino acids individually and also for the amino acids collectively. True ileal amino acid digestibility prior to performic acid treatment and the percentage change in true ileal amino acid digestibility after performic acid treatment were plotted for all of the amino acids collectively, and a quadratic model fitted the data well ($P < 0.001$, adjusted $R^2 = 0.90$; Figure 1).

DISCUSSION

Performic acid is a powerful oxidizing agent and was chosen in the present study to provide conditions that would lead to extensive, but defined, modifications of selected amino acids, namely, cysteine, methionine, tyrosine, and tryptophan.[24] In the

dx.doi.org/10.1021/jf403146u | J. Agric. Food Chem. 2014, 62, 699−707

Table 7. Mean (n = 8) True Ileal Amino Acid[a] Digestibility (TIAAD) of Unoxidized and Performic Acid-Oxidized Soy Protein Isolate

	TIAAD (%)				
	unoxidized	oxidized	overall SE[b]	significance[c]	difference[d] (%)
aspartic acid	88.2	78.5	0.86	***	−11
threonine	85.0	54.6	1.94	***	−36
serine	92.7	69.5	1.17	***	−25
glutamic acid	94.4	79.8	0.69	***	−15
alanine	91.4	77.8	1.97	***	−15
valine	90.8	79.0	1.06	***	−13
isoleucine	92.7	84.6	0.77	***	−9
leucine	91.1	86.8	0.97	***	−5
phenylalanine	94.3	88.8	0.60	***	−6
histidine	96.0	68.4	2.31	***	−29
lysine	99.1	85.3	1.17	***	−14
arginine	96.9	88.6	0.57	***	−9
mean digestibility[e]	92.7	78.5			

[a]Methionine, cysteine, tyrosine, and tryptophan were not included in the analysis because they were destroyed during the oxidation process. [b]Overall standard error of the unoxidized and oxidized soy protein isolate. [c]***, $P < 0.001$. [d]Difference was calculated according to eq 3. [e]Mean true ileal amino acid digestibility across all examined amino acids.

Table 8. Mean (n = 8) True Ileal Amino Acid[a] Digestibility (TIAAD) of Unoxidized and Performic Acid-Oxidized Casein

	TIAAD (%)				
	unoxidized	oxidized	overall SE[b]	significance[c]	difference[d] (%)
aspartic acid	90.2	78.6	1.22	***	−13
threonine	88.2	80.4	1.30	***	−9
serine	77.3	75.7	1.60	NS	
glutamic acid	89.7	85.3	0.95	***	−5
alanine	92.1	81.3	0.94	***	−12
valine	91.6	87.8	0.74	***	−4
isoleucine	87.5	83.2	1.05	***	−5
leucine	96.5	91.8	0.48	***	−5
phenylalanine	98.4	94.0	0.40	***	−4
histidine	99.3	95.9	0.51	***	−3
lysine	96.5	92.5	0.42	***	−4
arginine	95.2	91.8	0.72	***	−4
mean digestibility[e]	91.9	86.5			

[a]Methionine, cysteine, tyrosine, and tryptophan were not included in the analysis because they were destroyed during the oxidation process. [b]Overall standard error of the unoxidized and oxidized casein. [c]NS, not significant, $P > 0.05$; ***, $P < 0.001$. [d]Difference was calculated according to eq 3. [e]Mean true ileal amino acid digestibility across all examined amino acids.

presence of performic acid, cysteine is oxidized to cysteic aci [25] and any disulfide bonds present will be inevitably broken, which will in turn cause the affected proteins to unfold.[26] Methionine is quantitatively oxidized to methionine sulfone in the presence of performic acid,[25,27] tyrosine undergoes halogenation, and the indole ring of tryptophan is destroyed.[28] In the present study, the oxidation of methionine, tyrosine, and tryptophan was evaluated on the basis of the disappearance of the original amino acids after performic acid treatment rather than quantitation of the modified amino acids themselves. The negligible recoveries of methionine, tyrosine, and tryptophan after performic acid treatment, as determined using conventional amino acid analysis, suggest that the latter amino acids were almost completely modified. In addition, the poor recoveries of histidine suggest that this amino acid also was modified, at least to some degree. The concentrations of cysteine in the unoxidized and oxidized protein sources were not determined because cysteine is commonly determined following performic acid oxidation of the protein, and any unoxidized cysteine oxidized to cysteic acid as part of the amino acid analysis procedure would not be distinguishable from cysteic acid present due to the original performic acid treatment used to chemically modify the dietary protein sources. However, given that cysteine is particularly sensitive to oxidation, it is likely that performic acid treatment would have resulted in the complete oxidation of cysteine to cysteic acid in the oxidized protein sources.[29]

The protein sources used in the present study were chosen to represent both poorly and highly digestible protein sources. Zein and blood meal were poorly digestible (mean digestibility across amino acids was 53 and 65% for zein and blood meal, respectively), lactalbumin and gelatin were digested to an intermediate degree (mean digestibility across amino acids was 85 and 88% for lactalbumin and gelatin, respectively), and casein, beef muscle protein, and SPI were the most digestible proteins (mean digestibility across amino acids ranged from 92

dx.doi.org/10.1021/jf403146u | J. Agric. Food Chem. 2014, 62, 699−707

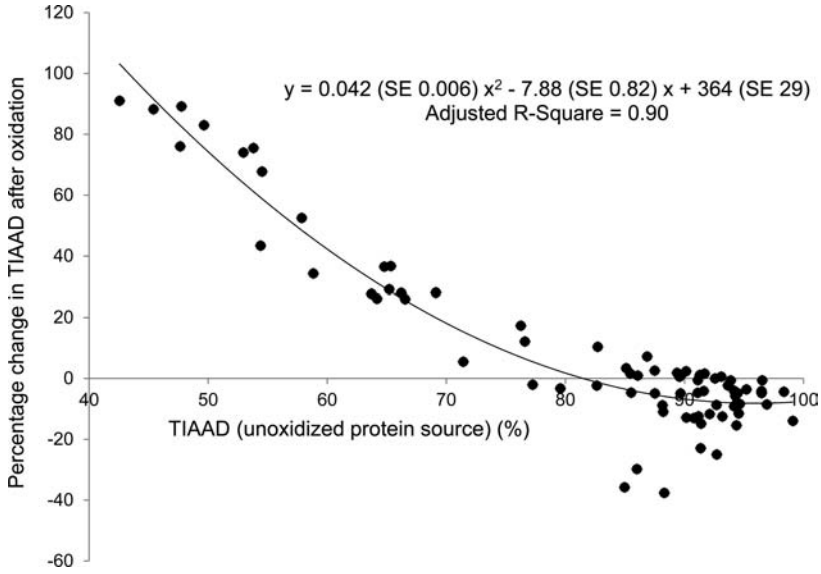

Figure 1. Relationship between the true ileal amino acid digestibility (TIAAD) of the seven protein sources prior to oxidation and the percentage change in TIAAD after oxidation. Methionine, cysteine, tyrosine, tryptophan, and histidine were not included in the analysis because they were destroyed (or partially destroyed in the case of histidine) during the oxidation process. Percentage change (%) was calculated according to eq 3. The differences within individual amino acids for each protein source are presented in Tables 2−8.

to 93% for the latter three protein sources). Interestingly, for the poorly digested protein sources, performic acid treatment led to a quantitatively large increase in the overall true ileal amino acid digestibility, whereas for the moderately digested proteins performic acid treatment had little impact on true ileal amino acid digestibility and for the highly digested protein sources true ileal amino acid digestibility generally decreased after performic acid treatment.

The rate and extent to which dietary proteins are digested in the gastrointestinal tract are dependent on many factors including the structure of the dietary protein, the presence of antinutritional factors, digesta viscosity, and enzyme to substrate ratio within the gastrointestinal tract. In the context of the present study protein structure is likely to have had the greatest impact on the extent of protein digestion. Proteins possess primary (the amino acid sequence), secondary (α-helix and β-sheet), and tertiary (the three-dimensional folding of the protein chain) structures, all of which can affect the efficacy of proteases in the digestive tract. Given the range of cleavage site specificities of the proteases in the gastrointestinal tract, it is expected that primary structure would have only a relatively minor influence on the overall extent of protein digestion in the small intestine. In contrast, the presence of secondary and tertiary structures in dietary proteins may be of greater significance for digestion. Deshpande and Damodaran[30] demonstrated that by changing the tertiary structure, but not the secondary structure, using heat treatment, the in vitro digestion of phaseolin was markedly increased. Samadi et al.[31] reported a strong correlation between the ratio of α-helix to β-sheet structures in heated canola meal proteins and the digestion of protein in the bovine rumen and intestine. Moreover, Carbonaro et al.[32] reported a strong inverse correlation between in vitro digestibility and the relative amount of β-sheets across a range of unprocessed and processed protein-containing foods. The latter workers suggested that the β-sheet structure present in the unprocessed foods and the intermolecular β-sheet aggregates induced by processing negatively affected digestibility and indeed were major factors in this regard.

In the present study, the performic acid oxidation would be expected to denature the proteins, leading to an increase in the digestibility of the protein source overall. However, for highly digestible proteins such as those present in casein and SPI, any increase in digestibility due to denaturation will be small. While for poorly digested proteins, the increase in digestibility will be much greater. In the present study, performic acid oxidation led to a marked increase in the true ileal amino acid digestibility of zein and blood meal, both of which were poorly digested prior to oxidation.

The proteolytic endopeptidases such as pepsin, trypsin, and chymotrypsin do not cleave proteins at random but rather cleave peptides adjacent to specific amino acids. For example, pepsin has a preference for large uncharged residues, whereas trypsin is specific for arginine and lysine and chymotrypsin has a preference for hydrophobic, preferably aromatic, residues.[33] When amino acids within a protein source are chemically modified, proteases present in the gastrointestinal tract are often less effective, leading to the presence of relatively large indigestible peptides (limit peptides) at the terminal ileum, which would in turn lead to lower true ileal amino acid digestibility.[34]

Although denaturation of the dietary proteins may explain the increase in true ileal amino acid digestibility for zein and blood meal, it does not explain the decrease in the true ileal amino acid digestibility of casein, SPI, and beef muscle protein. Conversely, although the formation of limit peptides may explain the decrease in the true ileal amino acid digestibility of casein, SPI, and beef muscle protein, it does not explain the increase in true ileal amino acid digestibility for zein and blood meal. Consequently, it is hypothesized that the change in true ileal amino acid digestibility of the dietary protein sources after performic acid oxidation observed in the present study was due to the relative contribution of the two opposing processes: (1) increased digestion due to the denaturation of the proteins and (2) decreased digestibility due to the formation of indigestible

limit peptides. It is hypothesized that denaturation was the predominant factor for zein and blood meal and that the presence of limit peptides was the predominant factor for casein, SPI, and beef muscle protein. For lactalbumin and gelatin, it is conjectured that the relative contributions of the two opposing factors were similar. Although the analysis of digesta material for the presence of limit peptides can be carried out using LC-MS, the latter analysis is not trivial and therefore was not done as part of this preliminary study. However, more work in this area is warranted.

It is also possible that oxidation of the dietary protein sources affected the endogenous protein secretion into the gastrointestinal tract, which could in turn affect the determination of true ileal amino acid digestibility given that endogenous ileal amino acid flows were used to correct apparent ileal amino acid digestibility values to true values. However, in the present study, modulation of the endogenous ileal amino acid flows due to alimentation with oxidized versus unoxidized protein sources did not appear to be a factor. The evidence for this is given below. Zein contains negligible amounts of lysine and tryptophan, and as such the total ileal flows of the latter two amino acids for the rats given the unoxidized and oxidized zein-based diets were equivalent to endogenous ileal flows. The endogenous ileal lysine and tryptophan flows were not different ($P > 0.05$) between the unoxidized and oxidized zein (313 ± 30.1 and 327 ± 35.1 mg/kg DMI for lysine in the unoxidized and oxidized zein, respectively, and 171 ± 16.7 and 203 ± 13.4 mg/kg DMI for tryptophan in the unoxidized and oxidized zein, respectively). Similarly for gelatin, which is almost completely devoid of tryptophan, the endogenous ileal tryptophan flows were not different between the unoxidized (321 ± 15.6 mg/kg DMI) and oxidized (299 ± 19.7 mg/kg DMI) gelatins.

The present study represents a preliminary investigation into the impact of oxidation of proteins on protein digestion using an in vivo (rat) model. Only the net effects of oxidation on true ileal amino acid digestibility were examined, and as a result the mechanisms by which performic acid oxidation altered protein digestion can only be surmised. Nevertheless, the results suggest that protein oxidation affected protein digestion in the gastrointestinal tract, possibly by more than one mechanism, most likely (1) denaturation of the protein and (2) formation of limit peptides, and that the overall effect of oxidation on digestibility as a whole is a result of the balance of these individual effects. The study provides insights as to how oxidation affects the digestion of proteins in the gastrointestinal tract, and further studies elucidating the structural changes that take place in proteins in relation to true ileal amino acid digestibility and using oxidation conditions relevant to those used for the processing of food proteins are warranted.

AUTHOR INFORMATION

Corresponding Author

*(S.M.R.) Mailing address: Riddet Institute, Massey University, Private Bag 11222, Palmerston North, New Zealand. Phone: +64 6 3505894. Fax: +64 6 3505655. E-mail: s.m.rutherfurd@massey.ac.nz.

Funding

The work was supported by a Centre of Research Excellence fund from the Tertiary Education Commission and the Ministry of Education, New Zealand.

Notes

The authors declare no competing financial interest.

ACKNOWLEDGMENTS

We acknowledge Maggie L. Zou, Russell K. Richardson, and Chanapha Sawatdeenaruenat for their expertise in conducting the chemical analyses.

REFERENCES

(1) Stadtman, E. R.; Berlett, B. S. Reactive oxygen-mediated protein oxidation in aging and disease. *Chem. Res. Toxicol.* **1997**, *10*, 485−494.

(2) Davies, M. J.; Dean, R. T. *Radical-Mediated Protein Oxidation: From Chemistry to Medicine*; Oxford Science Publications, Oxford University Press: Oxford, UK, 2003.

(3) Lund, M. N.; Heinonen, M.; Baron, C. P.; Estévez, M. Protein oxidation in muscle foods: a review. *Mol. Nutr. Food Res.* **2011**, *55*, 83−95.

(4) Todd, J. M.; Marable, N. L.; Kehrberg, N. L. Methionine sulphoxide determination after alkaline hydrolysis of amino acid mixtures, model protein systems, soy products and infant formulas. *J. Food Sci.* **1984**, *49*, 1547−1551.

(5) Hayashi, R.; Suzuki, F. Determination of methionine sulphoxide in protein and food by hydrolysis with *p*-toluenesulfonic acid. *Anal. Biochem.* **1985**, *149*, 521−528.

(6) Bhoite-Solomon, V.; Kessler-Icekson, G.; Shaklai, N. Peroxidative crosslinking of myosins. *Biochem. Int.* **1992**, *26*, 181−189.

(7) Lund, M. N.; Luxford, C.; Skibsted, L. H.; Davies, M. J. Oxidation of myosin by heme proteins generates myosin radicals and protein cross-links. *Biochem. J.* **2008**, *410*, 565−574.

(8) Singh, H. Modification of food proteins by covalent crosslinking. *Trends Food Sci. Technol.* **1991**, *2*, 196−200.

(9) Rutherfurd, S. M.; Moughan, P. J. Application of a new method for determining digestible reactive lysine to variably heated protein sources. *J. Agric. Food Chem.* **1997**, *45*, 1582−1586.

(10) Sun, W.; Cui, C.; Zhao, M.; Zhao, Q.; Yang, B. Effect of composition and oxidation of proteins on their solubility, aggregation and proteolytic susceptibility during processing of Cantonese sausage. *Food Chem.* **2011**, *124*, 336−341.

(11) Sun, W.; Zhao, M.; Yang, B.; Zhao, H.; Cui, C. Oxidation of sarcoplasmic proteins during processing of Cantonese sausage in relation to their aggregation behaviour and *in vitro* digestibility. *Meat Sci.* **2011**, *88*, 462−467.

(12) Zamora, R.; Hidalgo, F. J. Inhibition of proteolysis in oxidized lipid-damaged proteins. *J. Agric. Food Chem.* **2001**, *49*, 6006−6011.

(13) Liu, G.; Xiong, Y. L. Electrophoretic pattern, thermal denaturation, and in vitro digestibility of oxidized myosin. *J. Agric. Food Chem.* **2000**, *48*, 624−630.

(14) Rutherfurd, S. M.; Gilani, G. S. Amino acid analysis. *Curr. Protoc. Protein Sci.* **2009**, *58*, 11.9.1−11.9.37.

(15) National Research Council. Nutrient requirement of the laboratory rat. In *Nutrient Requirements of Laboratory Animals*, 4th ed.; National Academy of Sciences: Washington, DC, 1995.

(16) Rutherfurd, S. M.; Moughan, P. J. The rat as a model animal for the growing pig in determining ileal amino acid digestibility in soya and milk proteins. *J. Anim. Physiol. Anim. Nutr.* **2003**, *87*, 292−300.

(17) Rutherfurd, S. M.; Bains, K.; Moughan, P. J. Proteinaceous foods of India and the supply of available lysine. *Br. J. Nutr.* **2012**, *108*, S59−S68.

(18) Short, F. J.; Gorton, P.; Wiseman, J.; Boorman, K. N. Determination of titanium dioxide added as an inert marker in chicken digestibility studies. *Anim. Feed Sci. Technol.* **1996**, *59*, 215−221.

(19) Rutherfurd, S. M.; Moughan, P. J. The digestible amino acid composition of several milk proteins − application of a new bioassay. *J. Dairy Sci.* **1998**, *81*, 909−917.

(20) Moughan, P. J.; Darragh, A. J.; Smith, W. C.; Butts, C. A. Perchloric and trichloroacetic acids as precipitants of protein in

endogenous ileal digesta from the rat. *J. Sci. Food Agric.* **1990**, *52*, 13−21.
(21) Butts, C. A.; Moughan, P. J.; Smith, W. C. Endogenous amino acid flow at the terminal ileum of the rat determined under conditions of peptide alimentation. *J. Sci. Food Agric.* **1991**, *55*, 175−187.
(22) *SAS User's Guide: Statistics*, version 9.3; SAS Institute Inc.: Cary, NC, 2009.
(23) Goerke, M.; Eklund, M.; Sauer, N.; Rademacher, M.; Piepho, H. P.; Börner, C.; Mosenthin, R. Effect of feed intake level on ileal digestibilities of crude protein and amino acids in diets for piglets. *J. Sci. Food Agric.* **2012**, *92*, 1261−1266.
(24) Thompson, E. O. P. Modification of tyrosine during performic acid oxidation. *Biochim. Biophys. Acta* **1954**, *15*, 440−441.
(25) Manneberg, M.; Lahm, H.-W.; Fountoulakis, M. Quantification of cysteine residues following oxidation to cysteic acid in the presence of sodium azide. *Anal. Biochem.* **1995**, *231*, 349−353.
(26) Simpson, R. J. Performic acid oxidation of proteins. *Cold Spring Harbor Protocols*; Cold Spring Harbor Laboratory Press: Cold Spring Harbor, NY, USA, 2007.
(27) Chowdhury, S. K.; Eshraghi, J.; Wolfe, H.; Forde, D.; Hlavac, A. G.; Johnston, D. Mass spectrometry identification of amino acid transformations during oxidation of peptides and proteins: modifications of methionine and tyrosine. *Anal. Chem.* **1995**, *67*, 390−398.
(28) Ozols, J. Amino acid analysis. *Methods Enzymol.* **1990**, *182*, 587−601.
(29) Berlett, B. S.; Stadtman, E. R. Protein oxidation in aging disease, and oxidative stress. *J. Biol. Chem.* **1997**, *272*, 20313−20316.
(30) Deshpande, S. S.; Damodaran, S. Heat-induced conformational-changes in phaseolin and its relation to proteolysis. *Biochim. Biophys. Acta* **1989**, *998*, 179−188.
(31) Samadi; Theodoridou, K.; Yu, P. Detect the sensitivity and response of protein molecular structure of whole canola seed (yellow and brown) to different heat processing methods and relation to protein utilization and availability using ATR-FT/IR molecular spectroscopy with chemometrics. *Spectrochim. Acta A: Mol. Biomol. Spectrosc.* **2013**, *105*, 304−313.
(32) Carbonara, M.; Maselli, P.; Nucara, A. Relationship between digestibility and secondary structure of raw and thermally treated legume proteins: a Fourier transform infrared (FT-IR) spectroscopic study. *Amino Acids.* **2012**, *43*, 911−921.
(33) BRENDA (Braunschweig Enzyme Database) enzyme portal; http://www.brenda-enzymes.org (accessed 2013).
(34) Moughan, P. J.; Gall, M. P. J.; Rutherfurd, S. M. Absorption of lysine and deoxyketosyllysine in an early Maillard browned casein by the growing pig. *J. Agric. Food Chem.* **1996**, *44*, 1520−1525.

JOURNAL OF AGRICULTURAL AND FOOD CHEMISTRY

Article

pubs.acs.org/JAFC

Distribution and Speciation of Iron and Zinc in Grain of Two Wheat Genotypes

Tristan Eagling,[†] Andrew L. Neal,[†] Steve P. McGrath,[†] Susan Fairweather-Tait,[‡] Peter R. Shewry,[†] and Fang-Jie Zhao*[,§]

[†]Rothamsted Research, Harpenden, Hertfordshire AL5 2JQ, U.K.

[‡]Norwich Medical School, University of East Anglia, Norwich NR4 7TJ, U.K.

[§]State Key Laboratory of Crop Genetics and Germplasm Enhancement, College of Resources and Environmental Sciences, Nanjing Agricultural University, Nanjing 210095, China

Supporting Information

ABSTRACT: This study aimed to determine differences among wheat cultivars in the distribution and speciation of Fe and Zn in grain milling fractions. Cultivars with higher Fe and Zn concentrations in the wholemeal flour were found to contain higher concentrations in the white flour. Soluble Fe and Zn were extracted and analyzed by size exclusion−inductively coupled plasma mass spectrometry. Fe speciation varied between milling fractions with a low molecular weight (LMW) complex likely to be Fe−deoxymugenic acid/nicotianamine being the predominant extractable Fe species in white flour, accounting for approximately 85% of the extractable Fe. Bran fractions had a lower amount of LMW-Fe form but more as soluble Fe−phytate and an unidentified high molecular weight peak. In the white flour fraction soluble Zn was found to be present mainly as a LMW peak likely to be Zn−nicotianamine complex. Soluble Fe−phytate was found in the white flour fraction of a high-Fe cultivar but not in a low-Fe cultivar.

KEYWORDS: *wheat, iron, zinc, speciation, phytic acid, nicotianamine, deoxymugenic acid*

INTRODUCTION

Iron (Fe) and zinc (Zn) deficiencies are associated with increased mortality and morbidity. Populations in developing countries are at a disproportional risk, in part due to a greater reliance on less nutrient dense foods such as cereals.[1] One proposed approach to reducing Fe and Zn deficiencies is through biofortification, including the breeding of cereals with higher concentrations of Fe and Zn.[2,3] However, essential minerals are under tight homeostatic control within the grain as they are required at an adequate level for germination without causing toxicity.[4] Therefore, a greater understanding of how Fe and Zn are distributed within the grain is required.

The majority of wheat products consumed in the diet are produced after milling of the grain to yield white flour. This consists almost entirely of the starchy endosperm, while the bran, which contains the aleurone layer, embryo, and outer layers of the grain (pericarp and testa), is largely discarded.[5] However, the concentrations of Fe and Zn in the endosperm are much lower than those in the bran.[6] It is therefore important that biofortification strategies also consider the localization of minerals within the grain if the end products are to have increased nutritional benefits.

Variation in the concentrations of total Fe and Zn in whole grain of wheat genotypes has been widely reported. For example, a recent study of 130 cultivars grown on the same site showed that the concentrations of Fe and Zn ranged from 28 to 51 and from 13 to 35 mg/kg, respectively.[7] Other studies have shown even greater variation; analyses of lines grown in France showed variation of 19−58 and 14−35 mg/kg for Fe and Zn, respectively,[8] while in Asian wheat varieties the concentration of Fe ranged from 23 to 49 mg/kg [9] and of Zn from 25 to 56 mg/kg.[10] Variation from 4 to 16 mg/kg of Fe and from 5 to 16 mg/kg of Zn has also been reported for white flour of Chinese wheat cultivars.[11] Although this range of genotypic variation is encouraging from a plant breeding perspective, it is not clear whether the variation is consistent between different fractions of the grain and, in particular, whether the variation reported for whole grain is reflected in white flour from the same genotypes.

In addition to concentration and localization, the speciation of Fe and Zn is also an important factor in determining grain nutritional quality. Fe and Zn are present in plants as various chemical species, which may vary in their bioavailability. The nonprotein amino acid nicotianamine [2(*S*),3′(*S*),3″(*S*)-*N*-[*N*-(3-amino-3-carboxypropyl)-3-amino-3-carboxypropyl]-azetidine-2-carboxylic acid, NA] complexes both Fe and Zn [12] and is involved in the transport of these minerals via the phloem and subsequent loading into the seed, as well as in the detoxification of free minerals.[13] Recently 2′-deoxymugineic acid (DMA), which is biosynthesized from NA, has also been shown to play a role in the phloem transport of Fe and is thought to be the predominant Fe chelator in the phloem sap of rice.[14,15] Complexes of Fe and Zn with NA and DMA are present in rice grain,[15] especially in the transgenic lines overexpressing NA synthase (NAS) genes,[16] indicating that

Received: July 30, 2013
Revised: December 24, 2013
Accepted: January 1, 2014
Published: January 1, 2014

ACS Publications © 2014 American Chemical Society

they may also play a role in Fe and Zn storage. Elevated levels of NA in rice seed have also been shown to improve Fe and Zn bioavailability using both mouse and Caco-2 cell models.[12,17,18] However, to date there is no report of NA- or DMA-bound Fe or Zn in wheat grain.

Most of the Fe, Zn, and other minerals in cereal grain are complexed by phytic acid [inositol hexakisphosphate (IP_6)], resulting in salts known as phytates, which may be insoluble or soluble depending on the degree of metal bonding to phosphate groups.[19,20] However, it has recently been reported that Zn may not be complexed by phytate in barley embryos and is instead associated with S (as a proxy for thiol groups) and therefore likely to be bound to proteins.[21] There is also evidence that some of the soluble Fe in cereal grains is bound to inositol pentaphosphate (IP_5), a partially dephosphorylated soluble form of IP_6.[21,22] Since nonruminant animals (including humans) lack phytases, minerals complexed with IP_6 are unavailable for uptake.[23] Phytate has therefore been regarded as an "anti-nutrient". However, soluble forms of phytate-complexed Fe such as monoferric phytate (Fe−IP_6) and Fe−IP_5 have been suggested to have some degree of bioavailability.[19,22] By contrast, Zn bound to phytates is thought to be insoluble, being made up of heterometal salts and/or Zn_5IP_6 and therefore not bioavailable.[20]

Identifying and quantifying Fe and Zn species in cereals remains a technical challenge. Size-exclusion chromatography coupled with inductively coupled plasma mass spectrometry (SEC−ICP-MS) has been used to identify a soluble form of Fe complexed with phytate in barley embryos [21] and Fe and Zn complexed with NA and/or DMA in rice endosperm.[12,18] The presence of NA−Zn and DMA−Zn complexes in the low molecular weight (LMW) peak eluded from SEC was further confirmed by electrospray ionization mass spectrometry.[18] However, little is known about Fe and Zn speciation within wheat grain. The objective of this study was therefore to determine genotypic differences in the total concentrations and speciation of extractable Fe and Zn in different milling fractions of wheat, particularly white flour.

MATERIALS AND METHODS

Grain Materials. Analyses were initially performed on grain samples of six wheat cultivars selected on the basis of previous results which showed high Fe concentrations in three cultivars (Rialto, San Pastore, Tiger) and low Fe concentrations in the other three cultivars (Crousty, Rialto, Riband).[7] The six cultivars were grown at three European sites (Martonvásár, Hungary; Saxham, UK; Choryn, Poland) in 2007, as described by Shewry et al.[24] Climate and soil conditions of all three sites are reported by Shewry et al.[24] Grain samples from replicated plots at each site were pooled for each cultivar, giving rise to a total of 18 grain samples (6 cultivars grown at 3 sites). In addition, Rialto (a high-Fe cultivar) and Riband (a low-Fe cultivar) were grown in a field trial on a farm of Rothamsted Research, U.K., in 2010, in three replicated plots (1.8 × 10 m) in a completely randomized block design. Standard farm practices and fertilization (176 kg N/ha split into two applications) were followed. All grain samples were stored in a cold room at 4 °C prior to analysis.

Milling. Grain was dried at ambient temperature and the water content was raised to 15% before milling. Wholemeal samples were produced using a Perten Laboratory Mill 3100 (Des Plaines, IL) (with 0.5 mm sieve). White flour and bran fractions were prepared using a Brabender Quadrumat Junior Mill (Duisburg, Germany). The flour samples from the Brabender mill were sieved (150 μm mesh) to remove contaminating bran. Grain from the replicated field plots of Riband and Rialto was combined and 2.5 kg sample each was milled using a Bühler MLU-202 mill (Urzwil, Switzerland) to produce 10 milling fractions. These comprised six white flour fractions: three breaks (B1−B3) which are obtained sequentially and three reductions (R1−R3). These vary in purity, with the first break (B1) and reduction (R1) corresponding to the purest starchy endosperm tissue and the third break (B3) and reduction (R3) the least pure. The remaining four fractions are the bran fractions, which are then separated into offal flour, bran flour, coarse offal, and coarse bran.

Total Mineral Analysis. Mineral concentrations were determined using inductively coupled plasma optical emission spectrometry (ICP-OES, Perkin-Elmer Optima 7500 DV, Waltham, MA). A 500 mg portion (oven-dried at 80 °C for 4 h) of each sample was digested in ultrapure HNO_3 and $HClO_4$ (87:13% v/v) in triplicate using digestion blocks (200 °C, 12 h) (Eurotherm MBB151, Durrington, UK). Working conditions for ICP-OES wereas follows: RF power 1.5 kW, auxilary gas (Ar) flow rate 0.2 L/min, carrier gas (Ar) flow 0.85 L/min. Blank and certified reference materials (CRM, BCR-189, wheat wholemeal flour and NIST1568a, rice flour) were included in each batch of analyses, and the values for the CRM were within <5% of the certified values for Fe and Zn. Signal drift was corrected by measuring a standard solution every 10−20 samples.

Extraction of Soluble Fe and Zn. All samples were extracted in a Tris-HCl buffer solution as described by Persson et al.[21] with some modifications. Preliminary experiments showed that grinding with quartz sand using a pestle and mortar, as reported by Persson et al.,[21] released contaminating Fe which bound to the samples; therefore, the grinding step was omitted in our study. To enhance extraction a longer extraction at an elevated temperature was used (18 h, 37 °C). This longer extraction was used because preliminary tests showed a higher extraction rate for Fe and Zn in endosperm compared with the 1 h extraction used by Persson et al.[21] However, it is possible that this longer extraction could result in a higher degree of digestion of phytate by phytase activity in the aleurone layer. Briefly, 140 mg of flour fractions or 70 mg of bran fractions was extracted with 7 mL of Tris-HCl buffer (50 mM, pH 7.5) in sterile vials with gentle shaking (120 rpm). Samples were then centrifuged (21 000*g*, 10 min) to remove the solid phase before being filtered through 0.2 μm sterile filters (Minisart). Total concentrations of Fe and Zn in the extracts were determined using inductively coupled plasma mass spectrometry (ICP-MS; Agilent 7500ce, Agilent Technologies, Palo Alto, CA) with the following conditions: RF power 1.5 kW, carrier gas 0.85 L/min, nebulizer pump speed 0.2 L/min, H_2 gas 6 mL/min. All samples were measured with three technical replicates. A standard of 10 μg/L Fe and Zn and a blank were used to monitor signal stability.

Iron and Zinc Speciation. All analyses were performed on an HPLC (Agilent 1100 Series, Agilent Technologies, Waltham, MA) coupled to ICP-MS (Agilent 7500ce, Agilent Technologies, Waltham, MA). A Superdex 75 10/300 GL size exclusion column (glass, 10 × 300 mm, 13 μm cross-linked agarose/dextran, Amersham Biosciences) was used with an optimum separation range between 0.7 and 70 kDa. The mobile phase was Tris-HCl buffer (50 mM, pH 7.5), pumped through the column isocratically at 0.47 mL/min at a controlled temperature of 18 °C. The sample injection volume was 100 μL. After HPLC molecular size exclusion separation, the solution was measured sequentially by a UV detector at the wavelength of 214 nm and then by ICP-MS. ICP-MS was set up with the following conditions: RF power 1.5 kW, carrier gas 0.85 L/min, nebulizer pump speed 0.2 L/min, and collision/reaction gas H_2 3 mL/min and He 2 mL/min. Due to the low levels of Fe in the white flour samples the analyses were performed on ^{56}Fe, which is the most abundant isotope (91.8 atom %). H_2 and He were used as the collision/reaction gas as this prevented any polyatomic inference on this isotope. Molecular size calibration was achieved using a range of standard compounds varying in molecular size, including apoprotein (6.6 kDa), cytochrome *c* (12.4 kDa), vitamin B_{12} (1.35 kDa), triglycine (0.19 kDa), and glycine (0.075 kDa) (all from Sigma-Aldrich). The UV absorption was first measured. For cytochrome *c* and vitamin B_{12}, Fe and Co, respectively, were also measured by ICP-MS following UV detection. The delay in the retention time from the UV absorption peak to the ICP-MS signal peak was 0.6 min. A log−linear regression curve was derived from the plot of molecular size versus retention time (based on the ICP-MS

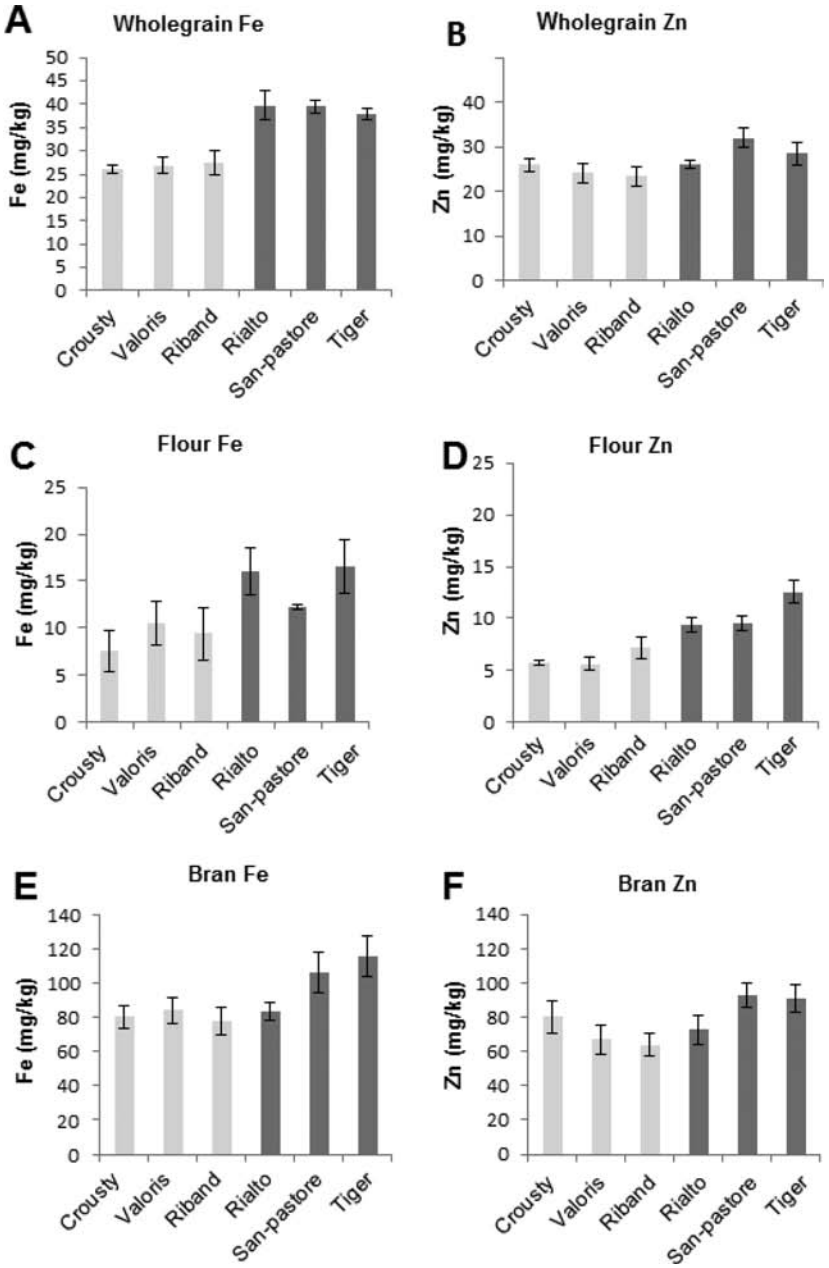

Figure 1. The concentrations of Fe and Zn in wholemeal, bran and white flour fractions of six wheat cultivars. Data are means (mg/kg dm ± SE) of materials grown in field trials at three sites (Hungary, Poland, UK) in 2007.

signal peak). A 100 μL aliquot of 20 mM EDTA/50 mM Tris-HCl buffer (pH 7.5) was injected between flour samples to remove residual metals adsorbed to the column. This wash was repeated twice after bran fractions due to the higher levels of Fe and Zn in the samples. A more thorough wash with 100 μL of pepsin (1 mg/mL), phytase (2 mg/mL), NaCl (0.5 M), and acetic acid (10%) (all from Sigma-Aldrich), at a flow rate of 0.2 mL/min at 36 °C, was performed between batches of samples. Finally, 10 mM EDTA/50 mM Tris-HCl buffer (pH 7.5) was run through the column for 40 min each day to remove any residual metals retained by the column. All speciation analysis was performed within 6 months of milling, as longer term storage may have an effect on phytate levels and therefore speciation.[23]

Ash Content. Ash contents of milling fractions were determined using the AACC-approved Method 08-12.[25]

Phytic Acid Content. Phytic acid analysis was performed using a commercially available kit (K-PHYT 12/12 Megazyme) as per the manufacturer's instructions.

Statistical Analysis. For the Rothamsted trial comparing the cultivars Rialto and Riband, one-way analysis of variance (ANOVA) was performed using GenStat (13th ed.; VSN, Hemel Hempstead, UK). For the multisite trials comparing six cultivars, ANOVA was not performed because replicated samples were bulked. Instead, correlation analyses between the Fe and Zn concentrations in the wholemeal and white flour samples were performed.

RESULTS

Concentrations of Fe and Zn in Whole Grain, Bran and Flour Fractions. Figure 1 shows the concentrations of Fe and Zn in the white flour and bran samples of six wheat cultivars grown on three European sites (in Hungary, Poland, UK). It was observed that cultivar differences were generally consistent across the three sites, and therefore, only the mean data (±SE across the three sites) are presented in Figure 1. Cultivars Rialto, San Pastore, and Tiger contained higher

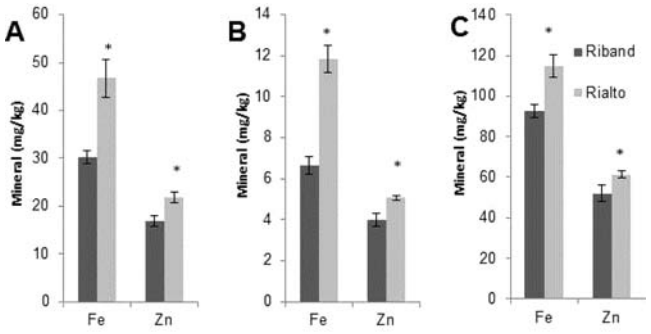

Figure 2. The concentrations of Fe and Zn in (A) wholemeal, (B) white flour, and (C) bran fractions of the cultivars Rialto and Riband grown at Rothamsted in 2010. Data are means ± SE of three biological replicates, and * represents significant difference at $p < 0.05$ according to ANOVA.

concentrations of Fe in the wholemeal than cultivars Crousty, Valoris, and Riband. This cultivar difference was generally maintained for the concentrations of Fe in both bran and white flour. Notably, the mean concentrations of Fe were 43% higher in the wholemeal samples and 43% higher in the white flour of the high-Fe cultivars when compared to the low-Fe cultivars. Similarly, the mean concentrations of Zn were 16% higher in the wholemeal samples and 58% higher in the white flour of the high-Fe cultivars when compared to the low-Fe cultivars. Among the six cultivars across the three sites, the concentrations of Fe and Zn of white flour were found to correlate significantly with those of the wholemeal ($r = 0.54$ and 0.48 for Fe and Zn, respectively; $p < 0.05$). There were also significant correlations between Fe and Zn concentrations in the wholemeal ($r = 0.60$, $p < 0.01$), bran ($r = 0.49$, $p < 0.05$), and white flour ($r = 0.61$, $p < 0.01$).

Figure 2 shows the concentrations of Fe and Zn in grain of Rialto and Riband grown at Rothamsted in 2010. Rialto had significantly ($p < 0.05$) higher concentrations of Fe and Zn than Riband, in wholemeal (by 54% and 29%, respectively), bran (by 24% and 18%), and white flour (by 80% and 26%). It is notable that the difference in the concentration of Fe was greatest in the white flour fraction. These differences were broadly similar to the data from the multisite trials (Figure 1).

Speciation of Fe and Zn in the Soluble Extracts from White Flour. Figures 3 and 4 show SEC−ICP-MS analyses of the Fe and Zn species in the Tris-HCl extractable fraction of white flour from the samples of Riband (low Fe) and Rialto (high Fe) grown at Rothamsted in 2010. The flour extracts of both cultivars showed two unidentified high molecular weight (HMW) forms of Fe (at 20 ± 0.4 and >70 kDa, respectively). A medium molecular weight (MMW, 5.0 ± 0.1 kDa) peak of Fe was identified in the extracts of Rialto, but not in Riband. Further analysis of this peak using He and O_2 as the collision/reaction gases and measuring P as ^{47}PO and Fe as ^{57}Fe showed that the 5 kDa ^{57}Fe peak coeluted with ^{47}PO (Supplementary

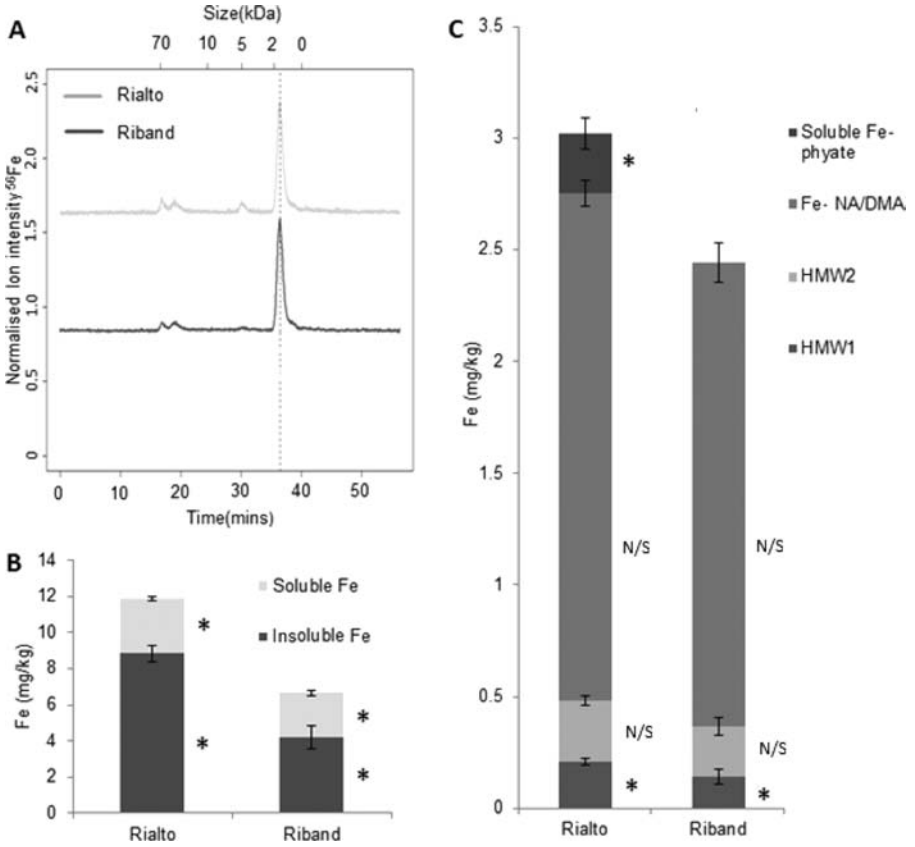

Figure 3. Determination of Fe speciation in white flour fractions of Rialto and Riband. (A) SEC−ICP-MS chromatograms (averages of three biological replicates). All samples were extracted in 50 mM Tris HCl at pH 7.5. (B) Soluble and insoluble Fe. (C) Quantification of soluble Fe species from relative peak areas on SEC−ICP-MS data and total soluble Fe by ICP-MS. Data in parts B and C represent means ± SE of three replicates; * indicates significant ($p < 0.05$) difference between the two cultivars for the individual Fe form and N/S connotes no significant difference.

dx.doi.org/10.1021/jf403331p | J. Agric. Food Chem. 2014, 62, 708−716

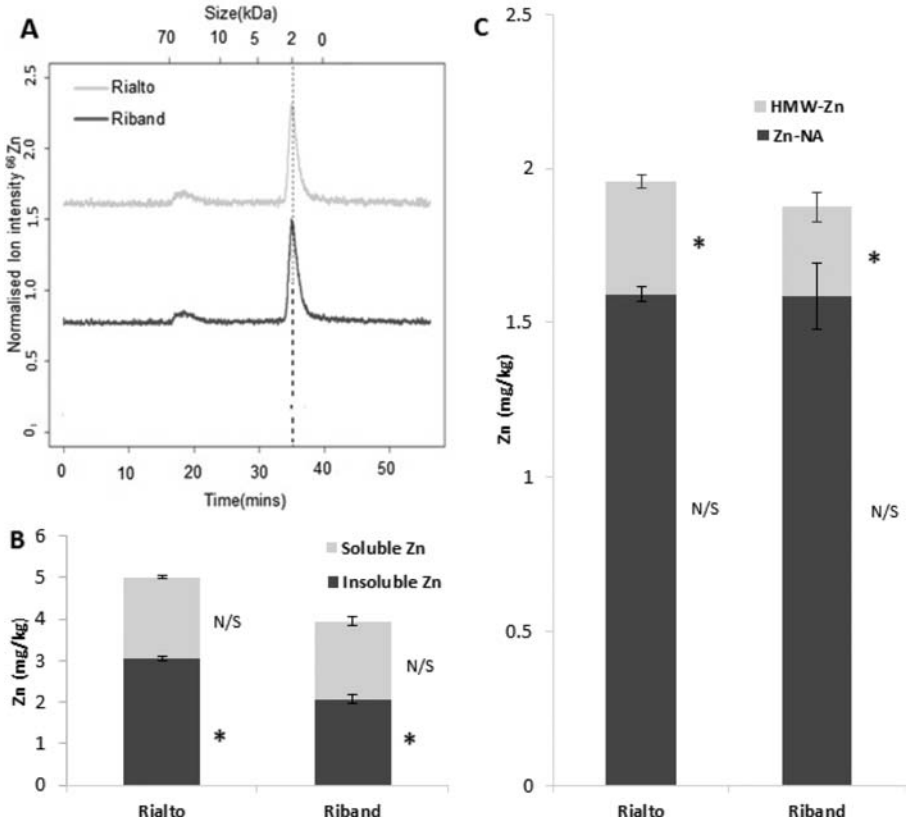

Figure 4. Determination of Zn speciation in white flour fractions of Rialto and Riband. (A) SEC−ICP-MS chromatograms (averages of three biological replicates). All samples were extracted in 50 mM Tris HCl at pH 7.5. (B) Soluble and insoluble Zn. (C) Quantification of soluble Zn species from relative peak areas on SEC−ICP-MS and total soluble Zn by ICP-MS. Data in parts B and C represent means ± SE of three replicates; * indicates significant ($p < 0.05$) difference between the two cultivars for the individual Zn form and N/S connotes no significant difference.

Figure 1, Supporting Information). We therefore tentatively consider this peak to be soluble Fe−phytate (possibly Fe−IP_6 and/or Fe−IP_5), as it has a similar composition to a peak identified as a soluble Fe−phytate oligomer in the extracts of barley embryo.[21]

The extracts of Riband and Rialto contained similar amounts of a low molecular weight (LMW, 1.5 ± 0.1 kDa) peak of Fe, which has no coelution of P (Supplementary Figure 1, Supporting Information). This LMW peak eluted at the same time as a standard of Fe−DMA; however, the retention time was also very similar to that of Fe−NA (Supplementary Figure 2, Supporting Information). Similarly, previous studies[12,18] using SEC−ICP-MS and ES-MS have shown that the LMW peak in the extract of rice endosperm contains both Fe−DMA and Fe−NA. For comparison, a rice endosperm sample was extracted and analyzed with the same method, and the LMW peak identical to that in wheat flour extracts was found (Supplementary Figure 2, Supporting Information). In contrast, Fe−citrate can be ruled out as the possible Fe−chelate form for the LMW peak, as it eluted at a much smaller size (Supplementary Figure 2, Supporting Information). On the basis of retention time matching and the similarity to previous studies on rice,[12,18] we tentatively consider the LMW peak to represent a mixture of Fe−DMA and Fe−NA.

SEC−ICP-MS also identified a LMW Zn complex (1.9 ± 0.2 kDa) in the extracts of white flour (Figure 4a) that was of a similar size to a peak identified in rice using SEC−ICP-MS.[18] On the basis of this report and on comparison with Zn−NA and Zn−DMA standards, which eluted at 1.9 and 2.5 kDa respectively (Supplementary Figure 3, Supporting Information), we tentatively identified the LMW peak as Zn−NA, although further investigation is needed to determine its exact identity.

The concentrations of soluble Fe differed significantly between the two cultivars ($p < 0.05$), with Rialto having 23% more soluble Fe than Riband (Figure 3B), but the total concentrations of soluble Zn (sum of both LMW Zn and Zn associated with HMW compounds) were not significantly different (Figure, 4B). Most of the soluble Fe and Zn were bound to LMW complexes and the total amounts of LMW Fe and LMW Zn did not differ significantly between the two cultivars (Figures 3C and 4C).

As a percentage, insoluble Fe made up the majority of the total Fe in the white flour, accounting for 74.6% in Rialto and 62.5% in Riband (Figure 3B). Fe−NA/DMA was the largest soluble fraction of Fe, making up 19.3% of the total Fe in Rialto and 32.1% in Riband. Soluble Fe−phytate accounted for 2% of the total Fe in Rialto, while HMW peaks accounted for 4.1% in Rialto and 5.8% in Riband. Insoluble Zn also made up the majority of the total Zn in the white flour, accounting for 60.7% in Rialto and 52.5% in Riband (Figure 4B). Zn−NA was the largest soluble fraction of Zn, accounting for 31.8% of the total Zn in Rialto and 40% in Riband, while HMW Zn peaks accounted for 7.3% in Rialto and 7.4% in Riband.

Fe Speciation in Milling Fractions. Figure 5 shows the speciation of Fe in soluble extracts of 10 milling fractions from Bühler mill for both Riband (low Fe) and Rialto (high Fe) grown in the Rothamsted trial. The break fractions B1−B3 and

dx.doi.org/10.1021/jf403331p | J. Agric. Food Chem. 2014, 62, 708−716

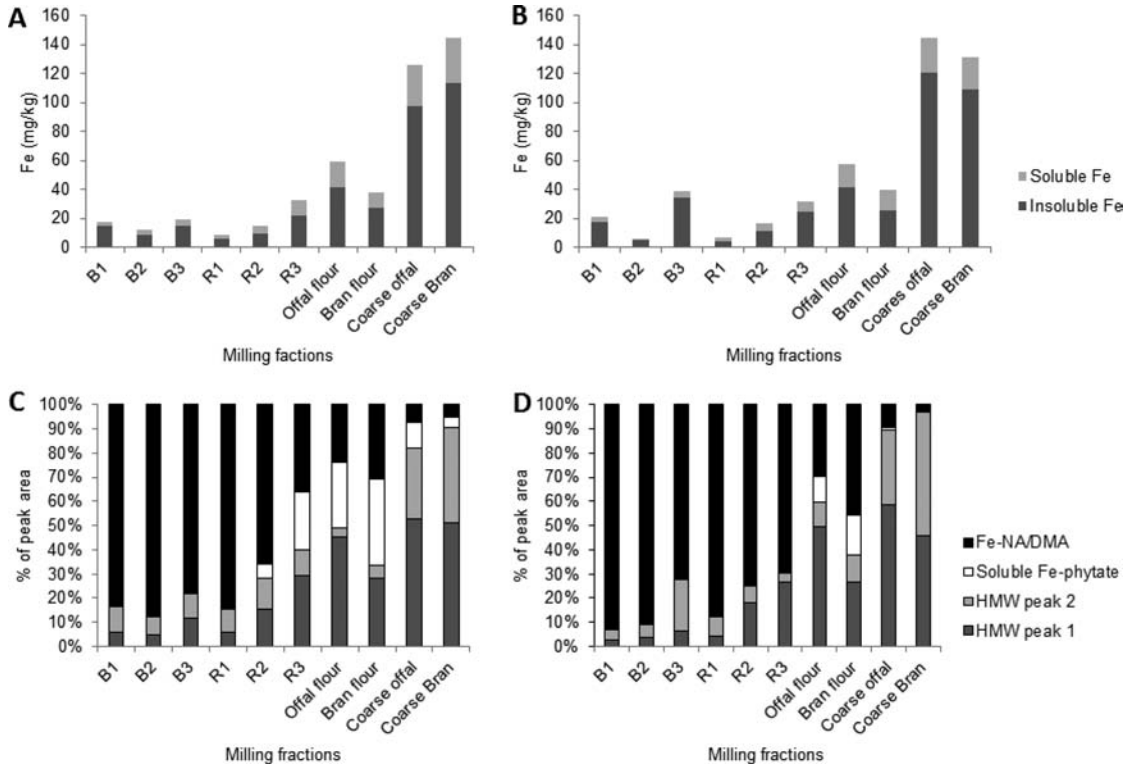

Figure 5. Quantification of the Fe forms in different milling fractions of Rialto (A, C) and Riband (B, D) from the Rothamsted trial. Parts A and B show the concentrations of different Fe forms and parts C and D the relative proportions of soluble Fe species in the total soluble Fe. Results are means of two technical replicates. The standard deviation of the method was less than 0.5% by analysis of five replicate samples of bran flour from Rialto.

Table 1. Extraction Yield, Ash Content, and Phytic Acid Content of 10 Milling Fractions from Bühler Mill

	B1	B2	B3	R1	R2	R3	offal flour	bran flour	coarse offal	coarse bran
					Extraction Yield (%)					
Rialto	6.1	9.1	1.5	47.6	5.9	1.8	2.1	2.5	7.2	16.3
Riband	8.1	9.4	1.8	42.1	9.2	3.0	2.1	3.1	7.1	14.0
					Ash Content (%)[a]					
Rialto	0.2	0.4	0.7	0.4	0.7	1.3	1.3	1.5	6.1	4.6
Riband	0.3	0.5	1.8	0.4	0.7	1.1	1.3	1.7	6.3	4.9
					Phytic Acid (g/100 g of dry matter)[a]					
Rialto	0.10	0.07	0.02	0.08	0.23	0.76	0.29	0.45	2.83	2.04
Riband	0.03	0.014	0.08	0.03	0.13	0.36	0.42	0.36	2.31	2.05

[a]Mean of three replicates.

the reduction fractions R1−R3 correspond to white flour, with R1 accounting for 47.6% and 42.1% of the total mass in Rialto and Riband, respectively (Table 1). The R1 and B1 fractions have very low ash and phytate contents (Table 1) and are therefore considered to represent the purest starchy endosperm fraction derived from the central part of the grain.[26] Ash content, an indicator of bran contamination, decreases closer to the center of the grain. A similar effect is observed with phytic acid content (Table 1).

The total concentrations of Fe (Figure 5A,B) varied greatly between the six flour fractions (R1, R2, R3, B1, B2, and B3), from 9 to 32 mg/kg in Rialto and 5 to 35 mg/kg in Riband, respectively. The differences were even greater between the six flour and four bran/offal (offal flour, bran flour, coarse offal and coarse bran) fractions, with a 26-fold difference in Fe concentration between the R1 and coarse offal fractions from Riband. The speciation of Fe in soluble extracts also differed between the flour fractions and bran/offal fractions, with LMW complexes being the predominant soluble form of Fe in flour (Figure 5C,D). By contrast, Fe bound to HMW components was the predominant form in bran/offal.

The main difference observed between the milling fractions from the two cultivars was in the amount of soluble Fe−phytate (Figures 5C,D). These results agree with the data in Figure 3A, showing that soluble Fe−phytate was present in the white flour extracts of Rialto but not of Riband. In addition, more soluble Fe−phytate was present in the bran fractions, especially the offal fractions, of Rialto compared to Riband.

The calculated amounts of soluble Fe species in whole grains of Rialto and Riband are given in Table 2, based on the yields of the milling fractions and the SEC−ICP-MS analyses. This shows that the concentration of soluble Fe−phytate was over 5-fold higher in Rialto than in Riband, although this form still represents only a small percentage of the total grain Fe (1.6%). The contents of LMW Fe (likely to be Fe−NA and/or Fe−DMA) were similar in the two cultivars but it represented a

dx.doi.org/10.1021/jf403331p | J. Agric. Food Chem. 2014, 62, 708−716

Table 2. Quantification of Forms of Fe in Grain of Rialto and Riband, Based on Analyses of Milling Fractions and Whole Grain

	Fe species in whole grain[a]						
	Fe-HMW1	Fe-HMW2	soluble Fe−phytate	Fe−NA/DMA	insoluble Fe	sum	total Fe determined by ICP-OES[b]
Rialto (mg/kg)	4.1	2.9	0.7	2.3	33.1	43.1	46.7
%	9.6	6.7	1.6	5.3	76.7		
Riband (mg/kg)	3.8	3.3	0.12	2.5	24.2	33.8	30.3
%	11.2	9.6	0.38	7.3	71.4		
technical error (%)[c]	0.5	0.5	0.2	0.4			

[a]The total concentrations and percentages of each form of Fe were calculated on the basis of the peak relative area on SEC−ICP-MS and total soluble Fe determined by ICP-MS for each milling fraction and the proportions of the milling fractions (Table 1). [b]Total Fe determined by ICP-OES of whole grain. [c]Technical error was determined by analyzing five replicate samples of Rialto bran.

higher percentage of the total Fe in Riband. The concentration of insoluble Fe in Rialto was 36% higher than that in Riband (Table 2).

DISCUSSION

The initial aim of our study was to establish if there was a relationship between the total concentrations of Fe and Zn in whole grain and in white flour of wheat. There is evidence that the loading of minerals, such as Fe and Zn, into the starchy endosperm is highly regulated and occurs independently of loading into the outer layers that constitute the bran.[27,28] Consequently, the concentrations of minerals in the white flour may not reflect those in whole grain, which is dominated by the minerals stored in the outer layers (especially the aleurone) and the embryo. Our results (Figures 1 and 2) show that cultivars with higher concentrations of Fe and Zn in whole grain also tend to have higher concentrations of these minerals in the white flour, although the concentrations in the white flour are much lower than those in the whole grain. Therefore, for biofortification purposes, the rankings of wholegrain and white flour Fe and Zn concentrations among wheat cultivars are likely to be reasonably consistent.

The second aim of our study was to determine Fe and Zn speciation in the soluble extracts of wheat flour and to investigate if they differ between a high-Fe (Rialto) and a low-Fe (Riband) cultivar. Tris-HCl buffer-soluble Fe accounted for 25−37% and 23−29%, respectively, of the total Fe in white flour (Figure 3) and whole grain (Table 2). The high-Fe cultivar (Rialto) had a larger concentration of soluble Fe than the low-Fe cultivar Riband; however, when this concentration was expressed as a percentage of the total Fe, the cultivar difference was the reverse. Compared to Fe, Zn appeared to be more soluble in white flour, accounting for 39−48% of the total Zn (Figure 4).

SEC−ICP-MS analyses showed the presence of HMW, MMW, and LMW peaks of Fe and Zn (Figures 3 and 4). The LMW Fe in wheat is likely to be a mixture of Fe−NA and Fe−DMA, whereas Zn−NA appears to be the only form of soluble Zn in the endosperm in both rice and wheat (Supplementary Figures 2 and 3, Supporting Information). This is in agreement with other studies which have shown that Zn binds more favorably with NA [29] and Zn−NA was the only Zn−chelate in the phloem sap of rice.[14] Proportionally, LMW Fe increased from the bran to the endosperm fraction and was quantitatively the most important species in the soluble extracts of white flour, suggesting that NA/DMA may also play an important role in the storage of Fe in the endosperm of wheat. However, there was no significant difference in the proportion of this Fe form between the two cultivars. Zn−NA was also the most important soluble Zn species in the white flour extracts, with no significant difference between the two cultivars being observed.

The most notable difference between the two cultivars was the presence of Fe bound to soluble phytate, which appeared as MMW complexes in the white flour of the high-Fe cultivar (Rialto) but not of the low-Fe cultivar (Riband) (Figure 3). The highest concentrations of soluble Fe−phytate were found in the offal and bran flour fractions, with Rialto having higher concentrations than Riband (Figure 5). One explanation for the difference between the two cultivars could be premature sprouting of Rialto, which is known to be prone to prematurity amylase production. This is supported by the determination of the Hagberg falling number (HFN), which was lower for Rialto than for Riband (112.3 ± 10.0 compared to 217.0 ± 23.3, $p < 0.05$). Although HFN measures the activity of amylase on starch, the synthesis of phytase also occurs during germination.[30] Increased phytase activity could therefore be responsible for the higher soluble phytate in Rialto. We found no evidence of soluble forms of phytate−Zn in white flour (Figure 4) or other milling fractions (data not shown), which is in agreement with analyses of barley embryos.[21] Another factor which needs to be considered is how each cultivar responds to shear forces during the milling process, as milling of hard (e.g., Rialto) and soft (e.g. Riband) wheat may result in different amounts of aleurone tissue being present in the white flour fractions, especially the late break and reduction fractions (i.e., B3, R3). In particular, white flour from hard wheat cultivars contains more aleurone material, especially the break fractions (B1−B3).[26] The degree to which this would affect our data is not known, but the observation that the R2 and R3 fractions of the hard wheat Rialto contained more ash, phytate, and soluble Fe−phytate (Table 1, Figure 5) is consistent with the presence of aleurone tissue.

In addition to the complexes with soluble phytate and NA/DMA, Fe and Zn are also bound to HMW compounds (Figures 3−5, Table 2). The identification of these peaks is challenging. HMW1 is excluded from the size exclusion column, suggesting that it is in excess of 70 kDa in size and could represent any complexes above this size. HMW2 also elutes very close to HMW1. The Fe storage protein ferritin may contribute to these peaks as it is a soluble complex of subunits of mass 40−44 kDa.[31] However, ferritin is present in low abundance in cereals (1−3% of total Fe).[32,33] Therefore, it is possible that these peaks are also made up of other large Fe-containing complexes (e.g., soluble proteins). Previous studies using high resolution secondary ion mass spectroscopy (NanoSIMS) have shown the presence of Fe in the cytoplasm surrounding the starch granules in starchy endosperm cells of wheat grain, suggesting a possible association of Fe with proteins.[34] Our results also show that these HMW forms are present in higher concentrations in bran

fractions than in the white flour; the former are more protein rich than the latter.[26]

Very little is known about the insoluble forms of Fe and Zn in wheat, which in the case of Fe make up 76.7% in Rialto and 71.4% in Riband of the total amount under our extraction conditions. In the outer fractions at least part of this is probably bound to insoluble phytate,[35] while another proportion may be bound to tannic acid, which is present in the outer layers of the grain and forms both soluble and insoluble complexes with Fe.[19]

The results from this study demonstrate the usefulness of SEC−ICP-MS in the speciation of Fe and Zn in wheat flour. This information is likely to be important for understanding the factors that influence the bioavailability of the minerals and will allow for more targeted breeding strategies for improved mineral content and speciation in wheat grain.

■ ASSOCIATED CONTENT

Supporting Information

Chromatogram demonstrating coelution between Fe and P in the soluble phytate peak (Supplementary Figure 1), chromatogram providing evidence comparing LMW peaks from wheat and rice extracts to NA and DMA standards for Fe (Supplementary Figure 2) and Zn (Supplementary Figure 3), and distribution of Zn in the different milling fractions of Buhler mill in Riband and Rialto (Supplementary Figure 4). This material is available free of charge via the Internet at http://pubs.acs.org.

■ AUTHOR INFORMATION

Corresponding Author

*E-mail: Fangjie.zhao@njau.edu.cn. Phone: +86 (0) 2584396509. Fax: +86 (0)2584399551.

Funding

T.E. is supported by a Ph.D. studentship from the Biotechnology and Biological Sciences Research Council of the UK and by HarvestPlus Project 8055 "Optimising the quality, species and availability of Fe in modern bread wheat cultivars in order to prevent global Fe deficiencies". Rothamsted Research receives strategic funding from the Biotechnological and Biological Sciences Research Council (BBSRC).

Notes

The authors declare no competing financial interest.

■ ACKNOWLEDGMENTS

We thank Prof. Zoltan Bedo and Br Mariann Rakszegi of the Centre for Agricultural Research, Agricultural Institute, Hungarian Academy of Sciences (Martonvasar, Hungary) for providing wheat samples produced under the EU FP6 HEALTHGRAIN project and Prof. Jian Feng Ma (Okayama University, Japan) for providing nicotianamine.

■ REFERENCES

(1) Allen, L.; de Benoist, B.; Dary, O.; Hurrell, R. *Guidelines on Food Fortification with Micronutrients*; World Health Organization: Geneva, Switzerland, 2006; p 375.

(2) Cakmak, I. Enrichment of cereal grains with zinc: Agronomic or genetic biofortification? *Plant Soil* **2008**, *302*, 1−17.

(3) Zhao, F. J.; Shewry, P. R. Recent developments in modifying crops and agronomic practice to improve human health. *Food Policy* **2011**, *36*, S94−S101.

(4) Morrissey, J.; Guerinot, M. L. Iron uptake and transport in plants: The good, the dad, and the ionome. *Chem. Rev.* **2009**, *109*, 4553−4567.

(5) Cakmak, I.; Kalayci, M.; Kaya, Y.; Torun, A. A.; Aydin, N.; Wang, Y.; Arisoy, Z.; Erdem, H.; Yazici, A.; Gokmen, O.; Ozturk, L.; Horst, W. J. Biofortification and localization of zinc in wheat grain. *J. Agric. Food Chem.* **2010**, *58*, 9092−9102.

(6) Zhang, Y. Q.; Shi, R. L.; Rezaul, K. M.; Zhang, F. S.; Zou, C. Q. Iron and zinc concentrations in grain and flour of winter wheat as affected by foliar application. *J. Agric. Food Chem.* **2010**, *58*, 12268−12274.

(7) Zhao, F. J.; Su, Y. H.; Dunham, S. J.; Rakszegi, M.; Bedo, Z.; McGrath, S. P.; Shewry, P. R. Variation in mineral micronutrient concentrations in grain of wheat lines of diverse origin. *J. Cereal Sci.* **2009**, *49*, 290−295.

(8) Oury, F. X.; Leenhardt, F.; Remesy, C.; Chanliaud, E.; Duperrier, B.; Balfourier, F.; Charmet, G. Genetic variability and stability of grain magnesium, zinc and iron concentrations in bread wheat. *Eur. J. Agron.* **2006**, *25*, 177−185.

(9) Ihsanullah; Qureshi, I. M. J.; Khattak, T. N.; Akhtar, J. Determination of iron in different types of wheat flours. *Inter. J. Agric. Biol.* **2002**, *4*, 297−299.

(10) Morgounov, A.; Gomez-Becerra, H. F.; Abugalieva, A.; Dzhunusova, M.; Yessimbekova, M.; Muminjanov, H.; Zelenskiy, Y.; Ozturk, L.; Cakmak, I. Iron and zinc grain density in common wheat grown in Central Asia. *Euphytica* **2007**, *155*, 193−203.

(11) Tang, J. W.; Zou, C. Q.; He, Z. H.; Shi, R. L.; Ortiz-Monasterio, I.; Qu, Y. Y.; Zhang, Y. Mineral element distributions in milling fractions of Chinese wheats. *J. Cereal Sci.* **2008**, *48*, 821−828.

(12) Lee, S.; Jeon, U. S.; Lee, S. J.; Kim, Y. K.; Persson, D. P.; Husted, S.; Schjorring, J. K.; Kakei, Y.; Masuda, H.; Nishizawa, N. K.; An, G. Iron fortification of rice seeds through activation of the nicotianamine synthase gene. *Proc. Natl. Acad. Sci. U. S. A.* **2009**, *106*, 22014−22019.

(13) Colangelo, E. P.; Guerinot, M. L. Put the metal to the petal: Metal uptake and transport throughout plants. *Curr. Opin. Plant Biol.* **2006**, *9*, 322−330.

(14) Nishiyama, R.; Kato, M.; Nagata, S.; Yanagisawa, S.; Yoneyama, T. Identification of Zn−nicotianamine and Fe−2′-deoxymugineic acid in the phloem sap from rice plants (*Oryza sativa* L.). *Plant Cell Physiol.* **2012**, *53*, 381−390.

(15) Bashir, K.; Ishimaru, Y.; Nishizawa, N. K. Iron uptake and loading into rice grains. *Rice* **2010**, *3*, 122−130.

(16) Masuda, H.; Ishimaru, Y.; Aung, M. S.; Kobayashi, T.; Kakei, Y.; Takahashi, M.; Higuchi, K.; Nakanishi, H.; Nishizawa, N. K. Iron biofortification in rice by the introduction of multiple genes involved in iron nutrition. *Sci. Rep.* **2012**, *2*.

(17) Zheng, L. Q.; Cheng, Z. Q.; Ai, C. X.; Jiang, X. H.; Bei, X. S.; Zheng, Y.; Glahn, R. P.; Welch, R. M.; Miller, D. D.; Lei, X. G.; Shou, H. X., Nicotianamine, a novel enhancer of rice iron bioavailability to humans. *PLoS One* **2010**, *5*.

(18) Lee, S.; Persson, D. P.; Hansen, T. H.; Husted, S.; Schjoerring, J. K.; Kim, Y. S.; Jeon, U. S.; Kim, Y. K.; Kakei, Y.; Masuda, H.; Nishizawa, N. K.; An, G. Bio-available zinc in rice seeds is increased by activation tagging of nicotianamine synthase. *Plant Biotechnol. J.* **2011**, *9*, 865−873.

(19) Engle-Stone, R.; Yeung, A.; Welch, R.; Glahn, R. Meat and ascorbic acid can promote Fe availability from Fe−phytate but not from Fe−tannic acid complexes. *J. Agric. Food Chem.* **2005**, *53*, 10276−10284.

(20) Simpson, C. J.; Wise, A. Binding of zinc and calcium to inositol phosphates (phytate) in vitro. *Br. J. Nutr.* **1990**, *64*, 225−232.

(21) Persson, D. P.; Hansen, T. H.; Laursen, K. H.; Schjoerring, J. K.; Husted, S. Simultaneous iron, zinc, sulfur and phosphorus speciation analysis of barley grain tissues using SEC−ICP-MS and IP−ICP-MS. *Metallomics* **2009**, *1*, 418−426.

(22) Sandberg, A. S.; Brune, M.; Carlsson, N. G.; Hallberg, L.; Skoglund, E.; Rossander-Hulthen, L. Inositol phosphates with different numbers of phosphate groups influence iron absorption in humans. *Am. J. Clin. Nutr.* **1999**, *70*, 240−246.

(23) Schlemmer, U.; Frolich, W.; Prieto, R. M.; Grases, F. Phytate in foods and significance for humans: Food sources, intake, processing, bioavailability, protective role and analysis. *Mol. Nutr. Food Res.* **2009**, *53*, S330−S375.
(24) Shewry, P. R.; Piironen, V.; Lampi, A. M.; Edelmann, M.; Kariluoto, S.; Nurmi, T.; Fernandez-Orozco, R.; Ravel, C.; Charmet, G.; Andersson, A. A. M.; Aman, P.; Boros, D.; Gebruers, K.; Dornez, E.; Courtin, C. M.; Delcour, J. A.; Rakszegi, M.; Bedo, Z.; Ward, J. L. The HEALTHGRAIN wheat diversity screen: Effects of genotype and environment on phytochemicals and dietary fiber components. *J. Agric. Food Chem.* **2010**, *58*, 9291−9298.
(25) AACC. *Approved Methods of the AACC*, 10th ed.. American Association of Cereal Chemists: St. Paul, MN, 2000.
(26) Greffeuille, V.; Abecassis, J.; Bar L'Helgouach, C.; Lullien-Pellerin, V. Differences in the aleurone layer fate between hard and soft common wheats at grain milling. *Cereal Chem.* **2005**, *82*, 138−143.
(27) Borg, S.; Brinch-Pedersen, H.; Tauris, B.; Holm, P. B. Iron transport, deposition and bioavailability in the wheat and barley grain. *Plant Soil* **2009**, *325*, 15−24.
(28) Stomph, T. J.; Choi, E. Y.; Stangoulis, J. C. R. Temporal dynamics in wheat grain zinc distribution: Is sink limitation the key? *Ann. Bot.* **2011**, *107*, 927−937.
(29) von Wiren, N.; Klair, S.; Bansal, S.; Briat, J. F.; Khodr, H.; Shioiri, T.; Leigh, R. A.; Hider, R. C. Nicotianamine chelates both Fe-III and Fe-II. Implications for metal transport in plants. *Plant Physiol.* **1999**, *119*, 1107−1114.
(30) Greiner, R.; Konietzny, U. Phytase for food application. *Food Technol. Biotechnol.* **2006**, *44*, 125−140.
(31) Lukac, R. J.; Aluru, M. R.; Reddy, M. B. Quantification of ferritin from staple food crops. *J. Agric. Food Chem.* **2009**, *57*, 2155−2161.
(32) Reddy, M. B.; Lukac, R.; Maneesha, A. The quantitation of ferritin in the seeds of staple crops: ELISA method development. *FASEB J.* **2008**, *22*.
(33) Hoppler, M.; Zeder, C.; Walczyk, T. Quantification of ferritin-bound iron in plant samples by isotope tagging and species-specific isotope dilution mass spectrometry. *Anal. Chem.* **2009**, *81*, 7368−7372.
(34) Moore, K. L.; Zhao, F. J.; Gritsch, C. S.; Tosi, P.; Hawkesford, M. J.; McGrath, S. P.; Shewry, P. R.; Grovenor, C. R. M. Localisation of iron in wheat grain using high resolution secondary ion mass spectrometry. *J. Cereal Sci.* **2012**, *55*, 183−187.
(35) Bohn, L.; Josefsen, L.; Meyer, A. S.; Rasmussen, S. K. Quantitative analysis of phytate globoids isolated from wheat bran and characterization of their sequential dephosphorylation by wheat phytase. *J. Agric. Food Chem.* **2007**, *55*, 7547−7552.

JOURNAL OF AGRICULTURAL AND FOOD CHEMISTRY

Article

pubs.acs.org/JAFC

Type and Amount of Lipids Influence the Molecular and Textural Properties of a Soy Soft Pretzel

Amber L. Simmons,[†,‡] Ian R. Kleckner,[§] and Yael Vodovotz*[,†,∥]

[†]Interdisciplinary Ph.D. Program in Nutrition, The Ohio State University, 223 Animal Sciences Building, 2029 Fyffe Road, Columbus, Ohio 43210, United States

[§]Department of Psychology, Northeastern University, 125 Nightingale Hall, 360 Huntington Avenue, Boston, Massachusetts 02115, United States

[∥]Department of Food Science and Technology, The Ohio State University, 110 Parker Food Science and Technology Building, 2015 Fyffe Court, Columbus, Ohio 43210, United States

Supporting Information

ABSTRACT: Altering baked goods by the addition of nutrient-rich ingredients, such as soy and ground almonds, affects the water and lipid distribution of the product and, subsequently, its final quality. Here, we studied how three lipid sources, shortening, canola oil, and ground almonds, affected texture and water distribution in a baked soy pretzel and the molecular mobility in the dough. Pretzel crumb from all formulations exhibited 40−43% moisture with a little more than half present as "freezable" water. Firmness and chewiness decreased with increased shortening and canola oil, whereas firmness and chewiness increased with additional almonds. In contrast, neither springiness nor cohesiveness was affected by the lipid quantity or source. Finally, magnetic resonance imaging of the soy pretzel dough revealed two or three populations of dough components that have distinct molecular mobilities. With increased lipid content, the mobility of each population increased in magnitude and heterogeneity. Interestingly, almonds had the smallest effect on the molecular mobility of the dough but had the largest effect on textural properties. These results provide quantitative insight into the mechanisms by which the lipid source can influence molecular properties that have textural implications for bakery products.

KEYWORDS: *soy, lipid, almond, physical properties, bread, magnetic resonance, pretzel*

INTRODUCTION

In order to deliver bioactive compounds in soy bread and related bakery products,[1−3] we must understand the interactions between the macromolecular constituents. Herein, we focus on the key plasticizing components in a soy soft pretzel,[4] water and lipids, and their influence on the texture of dough and the final product.

Lipids serve an essential structural role in the production of bakery products, such as soft pretzels. The amphipathic properties of lipids lubricate the gluten strands and adsorb to the gas−lipid interface of gas cells, allowing for the bubbles to develop and be evenly distributed in the crumb.[5] Solid fat (traditionally lard, now more commonly shortening) promotes a lighter, more homogeneous crumb than liquid oil (for a review, see the study by Pareyt et al.[6]). Oil does not adhere to the surface of gas cells as well as solid fat, and therefore, oil promotes a less consistent distribution of gas cells and gluten in the dough. An unrefined lipid source, for example, ground nuts, is unique in that it is composed of mostly unsaturated oils but is present in a solid matrix. It was hypothesized that oil from ground nuts can participate in molecular interactions that promote the growth of gas cells and serve the essential role of lipids in the developing crumb.

As a representative unrefined lipid source for use in these studies, ground almonds were selected. Almonds were chosen because of their natural β-glucosidase activity driving the conversion of soy isoflavones to aglycones and, thereby, potentially promoting the absorption of these phytochemicals.[4,8] Accordingly, the soy soft pretzel formulation used in these experiments contained about 25 mg of soy isoflavone aglycone equivalents per 59 g of pretzel, and a soy pretzel made with 5.5% ground, raw almonds doubled the amount of aglycones in the pretzel (more than 25% aglycones).[4] It was hypothesized that ground almonds could be substituted for shortening in a soy pretzel while maintaining favorable crumb texture. As a comparison, in addition to using shortening and almond lipid sources, canola oil was selected as a commonly used, refined, pure lipid source with a similar triglyceride profile as almonds.[7]

Several prior studies have examined the effects of the type and amount of lipid on the crumb texture of bread. A reciprocal relationship has been established between consumer acceptability and crumb firmness, since increased crumb firmness is an indicator of bread staling.[9] Because of the role of shortening in facilitated gas formation and structural support of the gas cells in bakery products,[6] it was hypothesized that its incorporation would result in the softest crumb compared to pretzel rolls made with canola oil or ground almonds. Describing the state of the water and its interaction within the matrix will help

Received: August 8, 2013
Revised: December 19, 2013
Accepted: January 7, 2014
Published: January 7, 2014

ACS Publications © 2014 American Chemical Society

dx.doi.org/10.1021/jf403531f | J. Agric. Food Chem. 2014, 62, 717−724

elucidate the mechanisms by which the type, amount, and source of lipid modulate physical properties of the crumb.

Using thermogravimetric analysis (TGA), the total quantity of water in the crumb as well as the relative binding strength of the water to the macromolecules in the matrix can help determine the locational and functional relationship between the lipid and the matrix, as well as how the lipid ingredients modulate the interactions between the water and macromolecule.[10] Additionally, differential scanning calorimetry (DSC) reveals the compartmentalization of water into "freezable" water (FW) and "unfreezable" water (UFW), which is useful in determining the susceptibility of the products to staling and frozen storage shelf life.[11,12] In a prior study using magnetic resonance imaging (MRI), Lodi et al. did not observe large differences in the water states between soy bread and soy bread containing almonds,[13] but it is unknown how the different lipid components affect the water properties in the dough or the physical attributes of the baked product.

Only two studies, to our knowledge, have investigated the use of nuts as the lipid source in bread. Oliete et al.[29] and Gómez et al.[33] produced bread with almond, hazelnut, peanut, or walnut pastes at 5, 10, and 15% in the absence of other added lipid. They demonstrated that different types and amounts of nut pastes discretely affect dough rheology,[33] as well as the firmness, chewiness, cohesiveness, and resilience of the bread.[29] However, it is unknown how ground almonds would affect texture in a soy bread matrix or the mechanisms by which the lipids participate in intermolecular interactions with water.

To assess the physiochemical effects of lipid constituents on a soy soft pretzel, pretzel rolls were prepared with 0, 2.9, or 6.0% lipid from shortening, canola oil, or ground almonds. To study the dough, pretzel dough was prepared with 2.9 or 10% of shortening, canola oil, or ground almonds. The crumb was subsequently assessed for texture and water distribution, and dough was assessed for water mobility. We hypothesized that the addition of ground almonds would attenuate the negative effects of the crumb texture that are associated with oil because of the differences in the distributions of water and lipid in the pretzel roll.

MATERIALS AND METHODS

Pretzel Preparation. Soft pretzel rolls with 16.2% soy ingredients (dry weight) were produced on the basis of the protocol by Simmons et al.[1,4] and soy bread patent[14] with the ingredients in Table S1 of the Supporting Information. Formulations included 0, 2.9, or 6.0% lipid from shortening, ground almonds, or canola oil; none of the formulations included more than one of these lipid sources. Almonds contain approximately 50% fat by weight,[7] and therefore, to achieve the traditional lipid amount, 2.9% lipid, a soy bakery product required 5.5% ground almonds (w/w). The pretzel inherently contained 1.9 ± 0.2% endogenous lipid from the other ingredients.[4]

To make the sponge, activated yeast, 43% of the total wheat flour, the wheat gluten, and the dough conditioner were combined with 45% of the total water in a standing mixer (Kitchen Aid, St. Joseph, MI) on a low setting with the beater attachment. The sponge was proofed at about 43 °C at 100% humidity (CM2000 Combination Module, InterMetro Industries Corp, Wilkes-Barre, PA). The remaining ingredients, except lipid, were added, and the dough was stirred with the dough hook attachment, first on low until ingredients were moistened and then on medium–high. After about 5 min, the lipid source was added. The dough was then stirred until it sheeted (about 5 min more). Pretzel rolls were formed by rolling 71.0 g of dough into slightly oblong balls (pretzel rolls were formed instead of the traditional twisted shape to produce congruent samples of crumb for textural analysis). Stickier formulations were dusted lightly with wheat flour to facilitate roll formation. Balls were submerged in 1.0% sodium hydroxide solution at 60–65 °C for 60 s and placed in the center of a lightly greased mini loaf pan. Rolls were proofed for 25 min (43 °C and 100% humidity) and then baked at 149 °C for 16 min in a convection oven (Jet-Air oven, JA14, Doyon, Linière, Québec, Canada). Rolls were cooled on wire racks, stored in plastic bags overnight, and analyzed the following day. At least four pretzel rolls were prepared and analyzed per batch. Analysis of all of the parameters of pretzel rolls made from 2.9% shortening from two different batches prepared on 2 different days showed that the variability between samples of different batches was similar to the variability between samples of the same batch. Therefore, one batch was prepared for each of the other variables.

Quantification of Total Water, FW, and UFW. The moisture content and water desorption patterns were assessed using TGA (Thermogravimetric Analyzer Q5000, TA Instruments, New Castle, DE). Samples of pretzel crumb (15–20 mg) were subjected to a linear heat ramp from room temperature to 200 °C at 10 °C/min. Under the assumption that weight loss resulted solely from water evaporation,[15] the weight of the sample at 150 °C was subtracted from the initial weight to yield the moisture content. The derivative of the thermogravimetric analysis curve (dTG) was calculated by Advantage for the Q Series, version 2.8.0.394 (TA Instruments–Waters LLC, New Castle, DE).

The amount of FW was quantified using DSC. Pretzel crumb (10–15 mg) was placed in a hermetically sealed stainless-steel pan with an O-ring (PerkinElmer, Waltham, MA). The temperature was lowered to −50 °C, held isothermally for 2 min, and then increased linearly at 5 °C/min to 150 °C. The peak near 0 °C was integrated to yield the change of enthalpy (ΔH) associated with the phase transition from ice to water. The latent heat of fusion of water (333 J/g) was used to quantify the amount of FW in the dough sample.[16,17] Subsequently, the amount of FW was subtracted from the amount of total water to yield UFW.

Textural Profile Analysis (TPA). Pretzel rolls were sliced into two adjacent 2.5 cm cubes that included pretzel crumb free of crust (electric carving knife, Toastmaster, St. Louis, MO). Each cube of pretzel crumb was subjected to a double compression test to 40% compression at a crosshead speed of 100 mm/min (Instron Universal Texture Analyzer 5542, Instron, Norwood, MA). Firmness, springiness, chewiness, and cohesiveness of the pretzel crumb were calculated using Bluehill 2 software, version 2.17 (Instron, Norwood, MA).[18] Firmness was reported as the maximum force at the first compression. Cohesiveness was calculated as the ratio of the energy to maximum load during the second compression to that at the first compression. At least five samples were analyzed per treatment.

Dough Preparation for MRI. Dough was prepared by combining 189.6 g of wheat flour, 57.6 g of soy flour, 19.2 g of soy milk powder, 4.6 g of wheat gluten, 0.6 g of dough conditioner, 5.0 g of salt, 20.0 g of sugar, and 188.5 g of water (yeast was omitted to avoid changes in the sample during image acquisition). The dough was then divided into 6 × 75 g portions to ensure that the only difference between dough samples was the added lipid. Subsequently, lipid was added to produce six formulations: 1.6 g for 2.9% shortening or canola oil, 5.1 g for 10.0% shortening or canola oil, 3.3 g for 2.9% ground almonds, or 10.4 g for 10.0% ground almonds. Lipid was incorporated by kneading by hand, and then dough was placed in 6 g glass vials. Vials were capped and then sealed with Parafilm M (Bemis Co., Neenah, WI) to prevent moisture equilibration.

Proton Intensity and T_2-Weighed Images. MRI scans were performed the same day that the dough was prepared. The experiments were performed at ambient temperature on a 4.7 T/40 cm magnet controlled by a Bruker Avance Console (Bruker Biospin, Billerica, MA). The instrument was equipped with a 260 mm inner diameter gradient coil and a 200 mm inner diameter proton volume radio-frequency coil. For an intensity reference, a phantom was prepared by combining water and deuterated water at a proportion that resulted in an intensity similar to that of an average dough sample. Both the dough sample and the phantom were placed inside the coil.

For all images acquired, the voxel size was 234.375 × 234.375 μm with a 5 mm slice thickness (i.e., 0.275 mm^3 per voxel). Each of five slices used 256 × 128 voxels for a 60.0 × 30.0 mm field of view. The proton intensity images were T_1-weighed, using a multi-slice FLASH pulse sequence with two averages (Bruker, Billerica, MA); there was a 0.5 s repetition time (TR), a 2.6 ms echo time (TE), and a 32° flip angle. The T_2 images were acquired using a multi-slice, multi-echo (MSME) Carr−Purcell−Meiboom−Gill (CPMG) pulse sequence (Bruker, Billerica, MA) with a 90° flip angle and a 5 s TR, with TE of 10, 20, 35, 55, 75, 95, 115, 135, 150, and 160 ms. The set of 10 images in the echo series were used to estimate T_2 values for each voxel by fitting intensity(TE) = amp × exp(−TE/T_2) + offset, where intensity(TE) is the observed intensity of the voxel in the image with echo time TE, amp is the amplitude of the T_2 decay curve, T_2 is the T_2 of the decay curve, and offset is the intensity at infinite TE (the magnitude of the noise). These fits yielded T_2 maps for each formulation and were the focus of additional analyses.

The program ImageJ (version 1.46r; http://rsbweb.nih.gov/ij) was used to prepare T_2 histograms using a region of interest analysis of the T_2 spatial maps. For each formulation, a circular region of interest was drawn within the edges of the dough image in each slice to avoid edge effects. Each T_2 histogram contained 200 bins between 0 and 50 ms (0.25 ms per bin) with 3228 voxels per five slices, for a total of 16 140 voxels per formulation.

T_2 histograms were analyzed using a deconvolution analysis programmed in MATLAB (The Mathworks, Natick, MA). In this analysis, the T_2 histogram of each formulation was fit to a sum of one, two, or three Gaussian curves to quantify distinct populations of T_2 values in the sample. Each Gaussian curve was modeled as counts(T_2) = amp × exp(−((T_2 − μ)^2)/(2σ^2))/($\sigma\sqrt{(2\pi)}$), where counts(T_2) is the number of counts in the T_2 histogram, amp is the amplitude of the Gaussian curve, μ is the mean T_2 value for the population, and σ is the standard deviation in T_2 value for the population. The fitted parameters were amp, μ, and σ. For the two-population deconvolution analysis, the observed data, counts$_{obs}$(T_2), were fit to the simulated curve counts$_{tot}$(T_2) = counts$_A$(T_2, amp$_A$, μ_A, σ_A) + counts$_B$(T_2, amp$_B$, μ_B, σ_B). For the three-population deconvolution analysis, observed data were fit to counts$_{tot}$(T_2) = counts$_A$(T_2, amp$_A$, μ_A, σ_A) + counts$_B$(T_2, amp$_B$, μ_B, σ_B) + counts$_C$(T_2, amp$_C$, μ_C, σ_C). Population fractions were calculated using numerical integrals of fitted counts(T_2) curve of each population compared to the numerical integral of the observed data curve counts$_{obs}$(T_2). Confidence intervals for each fitted parameter (amp, μ, and σ for each population) and for the population fractions were estimated using 1000 iterations of Monte Carlo bootstrapping from residuals.[19]

Statistical Analysis. For quantity of total moisture, FW, and UFW as well as texture properties, statistical analysis was performed to fit the model Y = lipid type + lipid amount + (lipid type × lipid amount), where Y is the parameter at hand, lipid type is shortening, almonds, or canola oil, lipid amount is 2.9 or 6.0%, and lipid type × lipid amount is the interaction between the two variables. Analysis of variance and least-squares means for the (lipid type × lipid amount) interaction were calculated using SAS 9.1 (SAS Institute, Cary, NC). Statistical significance was evaluated with an α of 0.05; the Bonferroni correction was used where appropriate. Average ± standard deviation is reported throughout the text.

RESULTS AND DISCUSSION

Moisture Content, FW, and UFW. Soy soft pretzel rolls were produced with lipid from shortening, canola oil, and ground almonds at two different levels and assessed for total moisture content, percent FW, and percent UFW. All pretzels contained 41.9 ± 4.3% total moisture, while FW comprised 58.7 ± 2.6% of the total water. There were no statistical differences in total moisture content or percent FW or UFW between the formulations (p > 0.09). Because the same amount of water was added to all of the soy pretzel formulations and almonds have only about 5% moisture,[7] this observation suggests that there were little to no differences in water migration, distribution between the crust and crumb, or evaporation from the crust during baking.

Water desorption as determined by TGA occurred in a biphasic manner for the shortening and almond samples and a monophasic manner in canola oil samples and samples without added lipid (Figure 1 and Table 1). The absence of the peak at

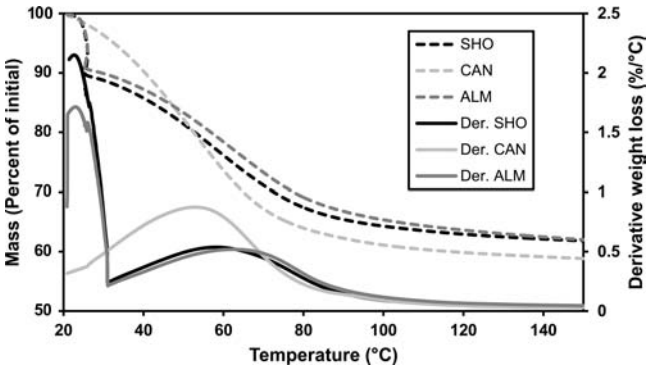

Figure 1. Example water desorption patterns from samples with 6.0% added lipid measured using TGA. Black lines represent samples made with shortening; dark gray lines represent samples made with ground almonds; and light gray lines represent samples made with canola oil. Dashed lines show the mass of the sample as a function of the temperature, whereas solid lines show the derivative of the weight loss curve. SHO, shortening; CAN, canola oil; and ALM, ground almonds.

Table 1. Peak Rate of Water Loss during Heating of Soy Pretzel Crumb

type of lipid	amount added (%)	dTG1 (°C)	dTG2 (°C)
no added lipid	0.0	N/A	64.2 ± 7.9 b
shortening	2.9	23.7 ± 1.5 a	64.1 ± 2.5 b
shortening	6.0	23.8 ± 2.1 a	63.5 ± 4.8 b
almond	2.9	23.1 ± 0.2 a	63.3 ± 2.5 b
almond	6.0	25.8 ± 4.9 a	65.1 ± 2.7 b
canola oil	2.9	N/A	55.7 ± 3.6 c
canola oil	6.0	N/A	53.8 ± 2.5 c

the lower temperature range (23−40 °C) in the canola oil samples and samples without added lipid suggests that (1) water loosely bound to the matrix exhibited a vaporization temperature lower than room temperature and quickly evaporated during sample preparation and/or (2) water did not exist in the fraction that was more easily removed. Also, in the water desorption thermograms, there was a peak near 60 °C that represented the majority of the water evaporation for all formulations (Figure 1 and Table 1). The temperature of this peak was similar for the shortening samples, almond samples, and samples without added lipid (approximately 60−68 °C) but was lower for the canola oil samples (51−59 °C; p < 0.05 when comparing canola oil samples to other samples; differences in peak temperatures between 2.9% canola oil and 6.0% canola oil samples were not statistically significant). Because the water evaporated at different temperatures, this suggests that canola oil caused different interactions between the water and macromolecular structures, such as starch, lipids, and proteins, as observed historically (Pareyt et al.,[6] and references within).

Both the physical state of the lipid and the chemical composition of the lipids likely contributed to the disparity in water desorption patterns observed in the samples with canola

oil. Specifically, the melting points of the individual triglycerides within each lipid ingredient can dictate both lipid−lipid interactions (such as the size and distribution of fat crystals[20]) and interactions between the lipid and other macromolecules. Shortening is about 19% saturated fat and forms solid lipid crystals that reduce surface tension at the oil−water interface and promote air incorporation and gas cell stabilization during baking.[6] On the other hand, canola oil is less than 10% saturated fat and liquid at room temperature, thereby contributing a much more uniform triglyceride profile and very little emulsification properties; it is expected that water would be associated with fewer microenvironments within the matrix.

Almond as a lipid source differs drastically from shortening and canola oil in that part of the lipid provided by ground almonds is bound in the nut matrix and not involved in macromolecular interactions with the other ingredients. For example, more mastication of almonds led to a greater *in vivo* bioaccessibility of lipid and less lipid in the feces;[21] therefore, it is expected that the lipid bound in the almonds within the food matrix is also inaccessible to its surrounding environment. It is interesting to note that ground almonds also promoted the diphasic water desorption pattern, despite the low percentage of saturated fat (about 7% compared to shortening at about 19%[7]). Almonds contain polysaccharide-rich cell wall material[22] that likely promoted water−lipid−protein interaction during proofing and baking, although the extent of the endogenous emulsifying properties of almond has yet to be explored.

This is the first study, to our knowledge, showing that different sources and amounts of lipid did not lead to differences in the partitioning of water into FW and UFW compartments in the pretzel formulations studied. Consistent with these results, Matuda et al. did not observe a change in UFW in dough with and without shortening when investigating the effects of vegetable shortening and different dough conditioners in French bread dough.[23] These results are also consistent with findings by Lodi and Vodovotz that showed that the addition of almond to soy bread (both formulations contained shortening) led to only small temperature differences in the peak rates of water loss in a similar TGA experiment.[24] Together, these results demonstrate that the soy matrix can accommodate ground almonds with or without shortening but not canola oil without drastically altering water content, water state, or water desorption patterns.

Texture Analysis. This soy pretzel formulation contained 16.2% soy ingredients (dry weight; see Table S1 of the Supporting Information) and, consequently, less gluten, more protein, more fiber, and more water (for optimal workability[2]) compared to a wheat pretzel without soy. The changes in the macromolecular composition and microscale ingredient interactions led to changes in texture when comparing bakery products made with or without soy ingredients, including firmness and chewiness.[25,26] However, the role of the lipid component in modulating textural properties of a soy-based bakery product had not been explored.

In Figure 2, the firmness, chewiness, and cohesiveness of the pretzel rolls are illustrated relative to the properties of the 2.9% shortening product. The values for the 2.9% shortening product were firmness, 9.37 ± 1.63 N; chewiness, 57.8 ± 9.6 N; and cohesiveness, 0.62 ± 0.03 (ratio). The springiness values were 7.83 ± 0.66 mm, with no difference between formulations ($p > 0.05$). Although it was expected that the canola oil products would be firmer and chewier than the shortening products

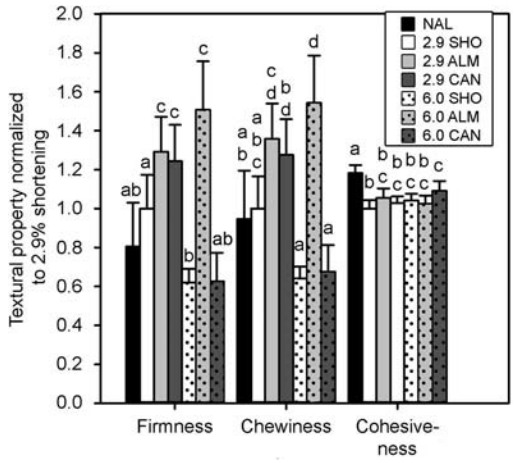

Figure 2. Textural properties of the pretzel rolls, including firmness, springiness, chewiness, and cohesiveness. The actual values were normalized to the 2.9% shortening pretzel roll (the traditional formulation; i.e., values obtained for the 2.9% shortening formulation were set to 1.0). Formulations with no added lipid (NAL) are black bars; formulations with 2.9% added lipid are solid white or gray bars; and formulations with 6.0% shortening have black dots. Shortening (SHO) samples are white; almond (ALM) samples are light gray; and canola oil (CAN) samples are dark gray. Different letters above the bars indicate statistical significance for each property. Error bars are standard deviations across five independent measurements.

because of their inability to promote gas cell development,[6] less than a 25% increase in firmness was observed when ground almonds or canola oil was used in place of 2.9% shortening (Figure 2). The presence of polar lipids (e.g., soy lecithin) in the soy ingredients perhaps attenuated changes in gas cell formation[27] compared to crumb of a wheat product without soy. An increase in the lipid content to 6.0% lipid caused a 40% decrease in firmness for both the shortening and, unexpectedly, the canola oil products. Baldwin et al. proposed that shortening melts during proofing and baking, thereby providing a constant source of lubrication for bubble formation and strengthening for air retention; perhaps the high amount of lipid in the 6.0% canola pretzel roll provided ample lipid for coating growing gas cells during proofing, while the soy ingredients aided in gas cell stabilization.[28] Additionally, large, inhomogeneous gas cells would also exhibit low degrees of firmness. The gas cell size was not quantified here but may be important in future studies. The higher amount of almond did not soften the crumb, corroborating TGA and water mobility data and suggesting that the lipid in the almond is bound within the nut matrix. Similarly, although the lipid is more accessible in an almond paste compared to ground almonds, an increase in firmness and chewiness was also observed with the addition of different kinds of nut pastes to wheat bread likely because of other components of the nut.[29]

The springiness and cohesiveness of the crumb were similar between all formulations (Figure 2). Similarly, no practical changes were observed in springiness when comparing wheat and soy bread,[25] suggesting that springiness is very resilient to such changes in bread formulation. The cohesiveness values were similar to what has been reported previously in soy, and these values were greater than wheat bread.[25] Similar to the trends observed with firmness, chewiness was increased slightly in formulations with ground almonds and canola oil at 2.9% (Figure 2). Moreover, at 6.0% added lipid, pretzels made with

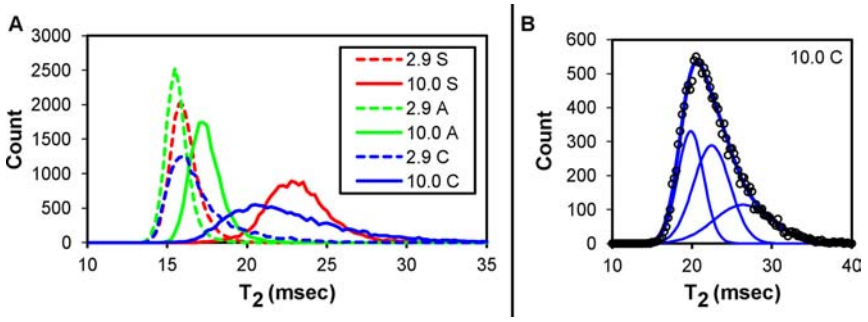

Figure 3. T_2 histograms from each formulation reveal that each formulation has a different magnitude and heterogeneity of T_2 values, reflecting different molecular level mobilities of the dough. (A) Each formulation is shown overlaid. (B) Deconvolution analysis quantifies the population fraction, mean T_2, and heterogeneity in T_2 for each of 2−3 subpopulations in each formulation. The results for the 10.0% canola oil formulation are shown here. Results for all formulations are listed in Table 2. Figures for the other formulations are in Figures S4−S6 of the Supporting Information.

shortening and canola oil exhibited a slight although not statistically significant decrease in chewiness, likely because of a more airy structure. In contrast, pretzels made with 6.0% lipid from ground almonds were chewier than all other formulations (89.2 ± 14.1 N versus 78.5 ± 10.5 N or less). Collectively, these data show that (1) both 2.9% canola oil and increasing amounts of ground almonds led a greater force requirement to deform the product and, because deformations are equally reversible with all formulations, more total force would be required to chew the product, (2) addition of more than twice the traditional amount of shortening provides a softer, less chewy crumb, and, interestingly, (3) addition of greater amounts of canola oil, for example 6.0%, reversed the increase in firmness and chewiness seen at 2.9% canola oil, perhaps because of very large air bubbles.

Proton Intensity and T_2-Weighted Images of Pretzel Dough. MRI allows for the spatial resolution of water content and water mobility within a sample[13,30] and can provide insight into the molecular properties and interactions between ingredients. Proton density-weighed images minimize the effects of T_2 relaxation and correlate with the water content of the dough at each voxel. Because the dough samples had equal amounts of added water, it was expected that these images would be similar, as was observed (see Figure S1 of the Supporting Information). In all samples, the water appeared to be evenly distributed in the dough on a centimeter scale. However, the mottled appearance indicates that the water content of each voxel is slightly different from neighboring voxels. This mirrors what was seen previously in MRI images of non-yeasted wheat and soy dough.[30]

T_2-weighed images reported the mobilities of protons from water, lipids, carbohydrates, and proteins in the dough. T_2 histograms revealed that each formulation had a different magnitude and heterogeneity of T_2 values, reflecting different molecular level mobilities of the dough (Figure 3A). There are several noteworthy features of these results. First, the T_2 values in all three 2.9% lipid formulations (shortening, canola oil, and ground almonds) exhibited similar T_2 values, suggesting that their proton mobilities were similar. However, when more lipid was used (i.e., the 10% lipid formulations), the mean T_2 increased, which implies that the protons were more mobile, the deviation in T_2 increased, which implies that there were greater differences in the mobilities of the protons in the sample, and the samples appeared increasingly different from one another. Moreover, samples with canola oil and shortening exhibited much greater shifts in average and standard deviation T_2 upon higher lipid addition compared to the almond samples. This is likely due to the inaccessibility of the almond lipid to the dough matrix environment, as was observed in TGA. Mechanistically, one possible explanation for the observation that adding more lipid increased the molecular mobility of the dough is that water droplets became larger (i.e., more like mobile bulk water than less mobile bound water) because of the immiscibility between the water and lipid.

Moreover, the T_2 histogram from each formulation suggests that there were several populations of T_2 values, which were quantified using a deconvolution analysis (Figure 3B and Table 2). From this analysis, the shortening and almond formulations each revealed two populations of T_2 values, whereas the canola oil formulations both revealed three populations of T_2 values. Each population is likely important because it made up a significant fraction of the observed protons (i.e., the smallest population was 25%). Unfortunately, assigning the molecular identity of these populations (e.g., water, lipid, or carbohydrate) could not be accomplished with these data alone. However, on the basis of the changes of the proton relaxometry during baking of bread dough, Engelsen et al. labeled the two proton populations with the longest relaxation times as starch-bound water and protons that are diffusing between starch, protein, and water.[31] In contrast, Lodi et al. observed a peak from not just water protons but also lipid protons in MRI images of baked soy bread.[13] Careful assignment of these populations may be important in future studies. In any event, the range of T_2 values observed here was more broad than those in soy and soy−almond bread,[24] indicating that molecular mobilities of this dough were much less homogeneous than the molecular mobilities of baked bread.

Taken together, these MRI data support that, with increased lipid content, the average proton mobility both increased and became more heterogeneous across voxels. This is consistent with increasing size of the components (e.g., water and fat) within each 0.275 mm^3 voxel, such that with greater lipid content, some voxels were more water or more lipid than when there was a smaller percentage of fat.

These MRI experiments have several limitations. First, the T_2 values presented here result from fitting a mono-exponential function to the T_2 decay curve at each voxel. However, each voxel likely contained a mixture of molecules with different T_2 values, and thus, the T_2 decay curve is best described by a multi-exponential function. Unfortunately, these multiple T_2 values cannot be determined using these data because the temporal resolution was too low to trust the fitted parameters from a multi-exponential function. Thus, the T_2 values reported here are influenced by all of the molecules within each voxel, and the

Table 2. Populations (Denoted P_A, P_B, and P_C) from Deconvolution Analysis of T_2 Histograms

	population A			population B			population C		
formulation	P_A (%)	mean T_2 (ms)	deviation in T_2 (ms)	P_B (%)	mean T_2 (ms)	deviation in T_2 (ms)	P_C (%)	mean T_2 (ms)	deviation in T_2 (ms)
2.9% shortening	58.8 [52.5, 75.7][a]	15.77 [15.76, 15.80]	0.61 [0.59, 0.65]	40.7 [23.4, 47.0]	16.53 [16.42, 17.02]	1.01 [0.84, 1.05]	0		
10% shortening	60.8 [39.2, 88.0]	22.60 [22.47, 22.80]	1.48 [1.32, 1.61]	38.3 [10.8, 60.1]	24.13 [23.54, 26.05]	2.13 [1.43, 2.33]	0		
2.9% almond	55.7 [47.0, 64.2]	15.43 [15.41, 15.45]	0.51 [0.49, 0.54]	44.0 [35.5, 52.5]	15.81 [15.74, 15.91]	0.86 [0.82, 0.91]	0		
10% almond	66.9 [48.4, 84.8]	17.07 [17.04, 17.17]	0.74 [0.67, 0.78]	32.5 [14.5, 51.4]	18.15 [17.73, 18.83]	1.06 [0.76, 1.18]	0		
2.9% canola	37.5 [23.8, 56.3]	15.59 [15.52, 15.76]	0.71 [0.62, 0.78]	36.7 [15.2, 52.7]	16.68 [16.38, 17.28]	1.00 [0.68, 1.15]	25.1 [16.0, 33.3]	18.96 [18.28, 19.87]	2.04 [1.51, 2.33]
10% canola	33.2 [20.8, 52.4]	19.83 [19.66, 20.25]	1.61 [1.40, 1.78]	41.2 [16.7, 59.2]	22.46 [21.84, 23.64]	2.30 [1.59, 2.67]	25.8 [11.3, 39.8]	26.37 [24.76, 28.96]	3.64 [2.47, 4.23]

[a]95% confidence intervals computed from Monte Carlo error analysis.

distributions shown here reflect deviations in the molecular composition of the voxels. Second, small air bubbles in the samples could have an effect on the results in a manner that depends upon the magnetic susceptibility difference between the air in the bubble and the surrounding medium, the size of the bubble, and the read-out gradient strength.[33] To minimize bubble formation, yeast was not added to the samples for MRI experiments, yet it is possible that different formulations led to discernible differences in the size and distribution of air bubbles in the sample. Further experiments are required to quantify potential artifacts because of air bubbles and how these potential artifacts may differ across samples. Third, images based on magnitude data were used to calculate T_2 values; fitting magnitude data to a decay curve can result in an overestimate of the decay time.[34] With that in mind, these results must be analyzed relatively and not absolutely.

Molecular insight into textural properties has been achieved with nuclear magnetic resonance (NMR) and MRI on baked bread, including work by Engelsen et al.,[31] Seow and Teo,[32] Lodi et al.,[13] and Bosmans et al.[35,36] However, quantitative analyses have not yet been performed to predict the texture of the bread from molecular properties of the dough. Dough made with high amounts of shortening or canola oil exhibited the longest T_2 relaxation times, and pretzel rolls baked from similar formulations also exhibited the lowest degrees of firmness and chewiness. Similarly, upon increasing levels of ground almonds, both T_2 relaxation times and textural properties exhibited only relatively small changes compared to changes induced by added shortening or added canola oil. Future experiments can shed light on the role of relaxometry of the protons (especially water) and the textural consequences of the baked product. Engelsen et al. developed a model to predict the degree of staling in bread from T_2 relaxation behavior of protons in freshly baked bread.[31] It is theoretically possible to adapt this model to dough to identify formulations that have favorable shelf stability.

In conclusion, the substitution of 100% oil for shortening has historically led to a decrease in the quality of bread crumb;[6] however, a denser and chewier crumb is an asset for soft pretzels. The pretzel matrix can easily accommodate a significant amount of soy while still remaining consumer-acceptable,[1] and this work has shown that pretzels can accommodate different types and levels of lipids, although a sensory evaluation is needed to confirm consumer acceptability (and is planned as part of a future study). The different types (shortening, canola oil, and ground almonds) and levels (2.9 and 6.0%) of added lipid did not affect the total moisture content or compartmentalization of FW and UFW. However, the water in samples with higher lipid exhibited greater proton mobility, as seen with MRI. The lipid in the ground almond appeared to be bound in the solid nut matrix, thereby attenuating added-lipid-induced changes in water mobility, firmness, and chewiness of the crumb compared the observed changes in these properties with increased shortening and canola oil. These findings emphasize that the source of the lipid can influence molecular properties and have consequential textural implications. The details of these relationships can aid functional food development in baked goods.

■ ASSOCIATED CONTENT

Supporting Information

MRI intensity images of one axial slice from each sample (Figure S1), MRI T_2-weighted images using a 10 ms echo time

of one axial slice from each sample (Figure S2), MSME method was used to acquire images, and the multi-echoes were used to calculate T_2 values (Figure S3), shortening (Figure S4) and almond (Figure S5) formulations yield T_2 histograms that are well-described by two populations of T_2 values but not one population, canola oil formulations yield T_2 histograms that are well-described by three populations of T_2 values but neither one nor two populations (Figure S6), and ingredients used in pretzel rolls (Table S1). This material is available free of charge via the Internet at http://pubs.acs.org.

AUTHOR INFORMATION

Corresponding Author

*Telephone: 614-247-7696. Fax: 614-292-0218. E-mail: vodovotz.1@osu.edu.

Present Address

‡Amber L. Simmons: Department of Medicine, Boston University, 650 Albany Street, Boston, Massachusetts 02118, United States.

Notes

The authors declare no competing financial interest.

ACKNOWLEDGMENTS

The authors thank Dr. Amir Abduljalil for help with acquiring the MRI images and data analysis.

ABBREVIATIONS USED

DSC, differential scanning calorimetry; dTG, derivative of the weight loss as represented in the thermogram; FW, "freezable" water; UFW, "unfreezable" water; MRI, magnetic resonance imaging; TE, echo time; TGA, thermogravimetric analysis; TR, repetition time

REFERENCES

(1) Simmons, A. L.; Miller, C. K.; Clinton, S. K.; Vodovotz, Y. A comparison of satiety, glycemic index, and insulinemic index of wheat-derived soft pretzels with or without soy. *Food Funct.* **2011**, *2*, 678−683.

(2) Zhang, Y. C.; Albrecht, D.; Bomser, J.; Schwartz, S.; Vodovotz, Y. Isoflavone profile and biological activity of soy bread. *J. Agric. Food Chem.* **2003**, *51*, 7611−7616.

(3) Ahn-Jarvis, J.; Clinton, S. K.; Riedl, K. M.; Vodovotz, Y.; Schwartz, S. J. Impact of food matrix on isoflavone metabolism and cardiovascular biomarkers in adults with hypercholesterolemia. *Food Funct.* **2012**, *3*, 1051−1058.

(4) Simmons, A. L.; Chitchumroonchokchai, C.; Vodovotz, Y.; Failla, M. L. Isoflavone retention during processing, bioaccessibility, and transport by Caco-2 cells: Effects of source and amount of fat in a soy soft pretzel. *J. Agric. Food Chem.* **2012**, *60*, 12196−12203.

(5) Brooker, B. The role of fat in the stabilisation of gas cells in bread dough. *J. Cereal Sci.* **1996**, *24*, 187−198.

(6) Pareyt, B.; Finnie, S. M.; Putseys, J. A.; Delcour, J. A. Lipids in bread making: Sources, interactions, and impact on bread quality. *J. Cereal Sci.* **2011**, *54*, 266−279.

(7) United States Department of Agriculture (USDA). *USDA National Nutrient Database for Standard Reference*; USDA: Washington, D.C., 2011; http://ndb.nal.usda.gov/ (accessed July 31, 2013).

(8) Izumi, T.; Piskula, M. K.; Osawa, S.; Obata, A.; Tobe, K.; Saito, M.; Kataoka, S.; Kubota, Y.; Kikuchi, M. Human nutrition and metabolism soy isoflavone aglycones are absorbed faster and in higher amounts than their glucosides in humans. *J. Nutr.* **2000**, *130*, 1695−1699.

(9) Chinachoti, P.; Vodovotz, Y. *Bread Staling*; CRC Press: Boca Raton, FL, 2000.

(10) Fessas, D.; Schiraldi, A. Water properties in wheat flour dough II: Classical and knudsen thermogravimetry approach. *Food Chem.* **2005**, *90*, 61−68.

(11) Baik, M.-Y.; Chinachoti, P. Moisture redistribution and phase transitions during bread staling. *Cereal Chem.* **2000**, *77*, 484−488.

(12) Vittadini, E.; Vodovotz, Y. Changes in the physicochemical properties of wheat- and soy-containing breads during storage as studied by thermal analyses. *J. Food Sci.* **2003**, *68*, 2022−2027.

(13) Lodi, A.; Abduljalil, A. M.; Vodovotz, Y. Characterization of water distribution in bread during storage using magnetic resonance imaging. *Magn. Reson. Imaging* **2007**, *25*, 1449−1458.

(14) Vodovotz, Y.; Ballard, C. Compositions and processes for making high soy protein-containing bakery products. U.S. Patent 7,592,028, 2009.

(15) Fessas, D.; Schiraldi, A. Water properties in wheat flour dough I: Classical thermogravimetry approach. *Food Chem.* **2001**, *72*, 237−244.

(16) Davies, R.; Webb, T. Calorimetric determination of freezable water in dough. *Chem. Ind.* **1969**, *16*, 1138−1139.

(17) Nilufer, D.; Boyacioglu, D.; Vodovotz, Y. Functionality of soymilk powder and its components in fresh soy bread. *J. Food Sci.* **2008**, *73*, C275−281.

(18) Bourne, M. *Food Texture and Viscosity: Concept and Measurement*, 2nd ed.; Elsevier Science: Amsterdam, Netherlands, 2002; p 427.

(19) Motulsky, H.; Christopoulos, A. *Fitting Models to Biological Data Using Linear and Nonlinear Regression: A Practical Guide to Curve Fitting*; Oxford University Press: Cary, NC, 2003; p 108.

(20) Carr, N. O.; Daniels, N. W. R.; Frazier, P. J. Lipid interactions in breadmaking. *Crit. Rev. Food Sci. Nutr.* **1992**, *31*, 237−258.

(21) Cassady, B. A.; Hollis, J. H.; Fulford, A. D.; Considine, R. V; Mattes, R. D. Mastication of almonds: Effects of lipid bioaccessibility, appetite, and hormone response. *Am. J. Clin. Nutr.* **2009**, *89*, 794−800.

(22) Dourado, F.; Barros, A.; Mota, M.; Coimbra, M. A; Gama, F. M. Anatomy and cell wall polysaccharides of almond (*Prunus dulcis* D. A. Webb) seeds. *J. Agric. Food Chem.* **2004**, *52*, 1364−1370.

(23) Matuda, T. G.; Parra, D. F.; Lugão, A. B.; Tadini, C. C. Influence of vegetable shortening and emulsifiers on the unfrozen water content and textural properties of frozen French bread dough. *LWT—Food Sci. Technol.* **2005**, *38*, 275−280.

(24) Lodi, A.; Vodovotz, Y. Physical properties and water state changes during storage in soy bread with and without almond. *Food Chem.* **2008**, *110*, 554−561.

(25) Simmons, A. L.; Smith, K. B.; Vodovotz, Y. Soy ingredients stabilize bread dough during frozen storage. *J. Cereal Sci.* **2012**, *56*, 232−238.

(26) Serventi, L.; Sachleben, J.; Vodovotz, Y. Soy addition improves the texture of microwavable par-baked pocket-type flat doughs. *J. Therm. Anal. Calorim.* **2011**, *106*, 117−121.

(27) Erazo-Castrejón, S. V; Doehlert, D. C.; D'Appolonia, B. L. Application of oat oil in breadbaking. *Cereal Chem.* **2001**, *78*, 243−248.

(28) Baldwin, R. R.; Johansen, R. G.; Keogh, W. J.; Titcomb, S. T.; Cotton, R. H. Continuous bread baking: The role that fat plays. *Cereal Sci. Today* **1963**, *8*, 273−276 284, 296.

(29) Oliete, B.; Gomez, M.; Pando, V.; Fernandez-Fernandez, E.; Caballero, P. A.; Ronda, F. Effect of nut paste enrichment on physical characteristics and consumer acceptability of bread. *Food Sci. Technol. Int.* **2008**, *14*, 259−269.

(30) Simmons, A. L.; Vodovotz, Y. The effects of soy on freezable bread dough: A magnetic resonance study. *Food Chem.* **2012**, *135*, 659−664.

(31) Engelsen, S.; Jensen, M.; Pedersen, H.; Norgaard, L.; Munck, L. NMR-baking and multivariate prediction of instrumental texture parameters in bread. *J. Cereal Sci.* **2001**, *33*, 59−69.

(32) Seow, C. C.; Teo, C. H. Staling of starch-based products: A comparative study by firmness and pulsed NMR measurements. *Starch/Staerke* **1996**, *48*, 90−93.

(33) Wills, S. Quantitation of bubbles using magnetic resonance imaging. M.Sc. Thesis, University of Cambridge, Cambridge, U.K., 2000; http://www.inference.phy.cam.ac.uk/saw27/part3project.pdf.

(34) van der Weerd, L.; Vergeldt, F. J.; de Jager, P. A.; van As, H. Evaluation of algorithms for analysis of NMR relaxation decay curves. *Magn. Reson. Imaging* **2000**, *18* (9), 1151−1158.
(35) Bosmans, G. M.; Lagrain, B.; Deleu, L. J.; Fierens, E.; Hills, B. P.; Delcour, J. A. Assignments of proton populations in dough and bread using NMR relaxometry of starch, gluten, and flour model systems. *J. Agric. Food Chem.* **2012**, *60* (21), 5461−5470.
(36) Bosmans, G. M.; Lagrain, B.; Ooms, N.; Fierens, E.; Delcour, J. A. Biopolymer interactions, water dynamics, and bread crumb firming. *J. Agric. Food Chem.* **2013**, *61* (19), 4646−4654.

JOURNAL OF AGRICULTURAL AND FOOD CHEMISTRY

Article

pubs.acs.org/JAFC

Preparation of a Capsaicin-Loaded Nanoemulsion for Improving Skin Penetration

Jee Hye Kim,[†,‡] Jung A Ko,[†,‡] Jun Tae Kim,[§] Dong Su Cha,[∥] Jin Hun Cho,[⊥] Hyun Jin Park,*[,†] and Gye Hwa Shin*[,†]

[†]College of Life Sciences & Biotechnology, Korea University, Anam-dong, Seongbuk-gu, Seoul 136-701, Korea

[§]Department of Food Science and Technology, Keimyung University, Daegu 704-701, Korea

[∥]Functional Food Research Center, Korea University, Anam-dong, Seongbuk-gu, Seoul 136-701, Korea

[⊥]Coway Cosmetics R&D Center, Gasan-dong, Geumcheon-gu, Seoul 153-803, Korea

ABSTRACT: Capsaicin o/w nanoemulsions with enhanced skin permeation were successfully prepared by controlling the ratios of the surfactant mixtures, oleoresin capsicum as the oil phase, and aqueous phase. Oleoresin capsicum contains 22.67 mg/g of capsaicin, which is an active and oil-soluble ingredient. Nonionic surfactants, Tween 80 and Span 80, were used to optimize the weight ratio of surfactant mixtures (85.98:14.02) by calculating the hydrophile−lipophile balance (HLB) value. The optimal processing conditions for stable nanoemulsions were investigated by using a ternary phase diagram. The mean droplet size of nanoemulsions ranged from 20 to 62 nm. Skin permeation studies were performed using a Franz diffusion cell. The permeation profiles and confocal laser scanning microscopy (CLSM) images supported that capsaicin nanoemulsion could well permeate all skin layers from the stratum corneum to the dermis. The selected nanoemulsions showed great potential as transdermal delivery carriers for enhancing the permeation of core materials.

KEYWORDS: *nanoemulsion, capsaicin, skin penetration, confocal microscopy, HLB value*

INTRODUCTION

Capsaicin (*trans*-8-methyl-*N*-vanillyl-6-nonenamide), the primary active ingredient of chili pepper, is a pungent and lipid soluble compound.[1] Capsaicin has been extensively used as a therapeutic agent for various diseases such as cancer, inflammation, cardiovascular disease, stroke, neurodegenerative disorder, and dermatological disease due to its excellent pharmacological activity.[2−6] However, capsaicin has shown two contradictory physiological effects. First, capsaicin stimulates the nervous system and induces intense pain in mammalian tissues, but its strong pungency has limited its clinical applications. Second, capsaicin has great antinociceptive and anti-inflammatory effects even if it excites the desensitization of nociceptors by depleting the neurotransmitter substance P and other sensory neuropeptides.[7]

Especially, transdermal delivery system of capsaicin has received considerable attention in the pharmaceutical and medical fields due to the antinociceptive and anti-inflammatory functions of capsaicin.[8,9] Compared to an oral drug delivery system, a transdermal delivery system provides various advantages such as avoidance of hepatic first-pass metabolism, reduction of side effects, and improvement in drug solubility.[10] The challenge of skin penetration is to overcome the stratum corneum, (SC) which is highly hydrophobic and rich in proteins. Hydrophobic drugs, however, are not favorable to hydrophilic viable epidermis and dermis layer in deeper stage.[11] To date, various transdermal delivery systems have been investigated for improving transdermal transport through the epidermal barrier. In order to enhance the skin penetration of drugs, nanocarrier delivery systems have been extensively investigated in various formulations such as nanoparticles, solid lipid nanoparticle (SLN), nanostructured lipid carrier (NLC), liposomes, microemulsions, and noisomes.[12−18] For improved transdermal delivery, carrier materials should be biocompatible, biodegradable, and easily excreted from the body as well as capable of sustaining the active core ingredient until reaching the target site without causing skin irritation during skin penetration.

As an effective transdermal carrier systems, nanoemulsion appears an attractive and competitive system due to many benefits such as easy manufacturing, small droplet size (20−200 nm), high thermodynamic stability, and enhanced solubilization for hydrophobic ingredients.[10,11] It has been shown that the active ingredients in an emulsion can enhance skin penetration through the large surface area of the emulsion system, the low surface tension of the whole system, and the low interfacial tension of the o/w droplets.[19] Because of their small size (less than 100 nm), nanoemulsions can easily penetrate the skin surface.[10]

The aim of this study is to investigate the optimum condition of capsaicin-loaded nanoemulsion formulations for topical application. In order to compare the quantitative permeability of the capsaicin nanoemulsion with that of a capsaicin-free ethanol solution, skin permeation studies were conducted using a synthetic membrane similar to human skin. In addition, ex vivo permeation study was performed using pig skins to demonstrate that capsaicin can penetrate through the whole pig skin layers, which consist of the stratum corneum, epidermis,

Received: September 20, 2013
Revised: November 27, 2013
Accepted: January 7, 2014
Published: January 7, 2014

ACS Publications © 2014 American Chemical Society

and dermis. Confocal laser scanning microscopy (CLSM) images were examined to verify that the capsaicin-loaded nanoemulsion fully penetrated the whole skin layers in both in vitro and ex vivo permeation studies.

MATERIALS AND METHODS

Chemicals. Span 80 and Tween 80, used as surfactant, were purchased from Samchun Pure Chemical (Seoul, Korea). Oleoresin capsicum was purchased in pungency ratings of 500,000 Scoville Heat Units (SHU) from EVESA (Madrid, Spain). Since oleoresin capsicum is an oil extraction from a fruit of *Capsicum* species and consists of mainly capsaicin, oleoresin capsicum was used as the oil phase. Strat-M membrane was purchased from Merck KGaA (Darmstadt, Germany), and Nile red was purchased from Sigma-Aldrich (St. Louis, MO, USA). HPLC-grade methanol and acetonitrile were used for HPLC analysis.

Skin. The flank area of a pig skin sample (700 μm thick as measured using dermatome) was obtained from Micropig (Medi Kinetics Co. Ltd., Pyeongtaek, Korea). All skin samples were prepared less than 1 mm thick to allow following confocal microscope study. The skin samples prepared were carefully washed with a phosphate buffered saline (PBS) solution, stored at −20 °C, and used within 1 week for the ex vivo skin permeation experiments.

Capsaicin Contents in Oleoresin Capsicum. Oleoresin capsicum is an extract of chili pepper that contains capsaicin as a primary active ingredient. The accurate amount of capsaicin in the nanoemulsion was determined by measuring the capsaicin contents in oleoresin capsicum by high performance liquid chromatography (HPLC) consisting of a pump (model 2690, Waters, Milford, MA, USA), a photodiode array detector (model 996, Waters), and a Kromasil C18 column (250 mm × 4.6 mm; EKA Chemicals AB, Bohus, Sweden). The mobile phase was a mixture of isocratic methanol−water (70:30 v/v), and the flow rate was 1 mL/min at room temperature. The injection volume was 10 μL, and the column effluent was monitored at a wavelength of 280 nm for capsaicin.

Preparation of Capsaicin Nanoemulsion. Capsaicin nanoemulsion was prepared using hot homogenization and high pressure homogenization. Tween 80 and Span 80 were mixed in various ratios, and the surfactant mixture was added to distilled water with magnetic stirring at 75 °C for 30 min. The surfactant and water mixing solution was added into oleoresin capsicum, which was preheated to 75 °C. The mixture of surfactant, water, and oil was homogenized using an Ultra-Turrax T 25 basic homogenizer (IKA-Werke, Staufen, Germany) at 12,000 rpm for 5 min, followed by size reduction using high pressure homogenization (model: M-110P Microfluidizer, Microfluidics, Newton, MA, USA) under 1,000 bar pressure.

Screening of Hydrophile−Lipophile balance (HLB) Value. The HLB value of surfactant was screened to determine the best ratio of surfactant mixture.[20] As nonionic surfactant, Span 80 (sorbitan monooleate, HLB value of 4.3) and Tween 80 (polyoxyethylene sorbitan monooleate, HLB value of 15) were chosen, and various mixtures of Span 80 and Tween 80 were prepared to determine the optimum ratio. The HLB values of the surfactant mixtures (HLB_{mix}) were calculated using the weight fraction of Tween 80 and Span 80 according to the following equation:

$$HLB_{mix} = f_A\ HLB_A + f_B\ HLB_B \quad (1)$$

where HLB_A and HLB_B are the HLB values for Tween 80 and Span 80, respectively, and f_A and f_B are the weight fractions of Tween 80 and Span 80, respectively. Phase separation and size distribution of the nanoemulsions were considered to determine the optimum condition.

Ternary Phase Diagrams. To delineate ternary phase diagrams, the stability of the prepared formulations was monitored at room temperature for 1 month. The formulations, in which no phase separation, flocculation, and sedimentation were observed, were selected as stable nanoemulsions. In the selected formulations, the droplet size of nanoemulsions was not changed significantly over one month and the PDI value was also maintained less than 0.3. The formulations were found to maintain isotropic, transparent properties during the observation period.

Measurement of Droplet Size, Polydispersity Index (PDI), and Zeta Potential. The mean droplet size, PDI, and zeta potential of nanoemulsions were measured using nano size analyzer (Malvern Zetasizer Nano ZS; Malvern Instruments, Malvern, U.K.). Three milliliters of capsaicin nanoemulsion diluted in 40 times Milli-Q water was added to polystyrene latex cells, and the mean droplet size, PDI, and zeta potential were measured at 25 °C with a detector angle of 90°, and wavelength of 633 nm. Each sample was measured at least three times, and the average values were used.

Morphology of Nanoemulsions. The morphology of the nanoemulsions was investigated using a TECNAI G2 F30 transmission electron microscope (Philips-FEI, Eindhoven, Holland). For transmission electron microscopy (TEM) sample preparation, approximately 10 μL of the nanoemulsion was dropped onto carbon-coated grids for 30 s and the excess was drawn off with membrane filter paper. This step was performed three times. The grid was stained with uranyl acetate and dried overnight at room temperature. The images were obtained using TEM in the high angle annular dark field (HAADF) micrograph mode.

Skin Penetration Experiments. A synthetic membrane (Strat-M) was used to mimic human skin. The skin penetration studies were performed using a vertical modified amber glass Franz diffusion cell (Daihan Labtech, Gyeonggi-do, South Korea) with an effective diffusion area of 2.27 cm^2 and a receptor volume of 15.9 mL. The skin sample was sandwiched between the donor and receiver compartments, which were then securely fastened with a clip. The receiver compartment was filled with 20% ethanol in PBS solution and continuously stirred at 600 rpm at 37 ± 1 °C for 1 h to equilibrate the skin. After equilibration, 1 mL of the nanoemulsion or the capsaicin in a 40% ethanol aqueous solution (control) was dropped slowly on the donor compartment to cover the nanoemulsions on the skin surface. The receptor medium (1 mL) was withdrawn at fixed intervals (1, 2, 3, 6, 9, 12, and 24 h) and analyzed by HPLC to evaluate skin penetration. To fill the withdrawn amount, 1 mL of hydro ethanolic solution was added to the receptor medium.

HPLC Analysis of the Cumulative Amount of the Nanoemulsion Penetrating the Skin. The capsaicin content was analyzed by reversed phase HPLC using the more sensitive fluorometric detector rather than the photodiode detector so that even a trace of capsaicin permeating the skin into the receptor solution could be detected.[21] For capsaicin, the excitation wavelength was 270 nm and the emission wavelength was 330 nm. The HPLC system consisted of a model 2690 pump (Waters, Milford, MA, USA), a model 717 auto sampler (Waters), a fluorescence detector (Waters), and a Symmetry C18 column (100 Å, 5 μm, 4.6 mm × 150 mm, Waters). The mobile phase was an isocratic acetonitrile−water mixture (70:30 v/v), and the flow rate was 1 mL/min at room temperature.

Permeation Data Analysis. The cumulative amount of capsaicin permeation per unit of skin surface area (Q_t/S) was calculated using eq 2:[22,23]

$$Q_t = V_r C_t + \sum_{i=0}^{t-1} V_s C_i \quad (2)$$

where C_t and C_i are the capsaicin concentrations of the receiver solution at each sampling time and for the ith sample, respectively, while V_r and V_s are the volumes of the receiver solution and the sample, respectively.

The flux of capsaicin permeation at steady state (J_{ss}) was calculated from the slope of the linear portion of the graph plotted between cumulative capsaicin permeation per unit of skin surface area (Q_t/S) and time (t) as follows (eq 3):

$$J_{ss} = \frac{\Delta Q_t}{\Delta t \times S} \quad (3)$$

The permeability coefficient (K_p) was calculated by dividing J_{ss} by the initial concentration of capsaicin in the donor compartment (C_0) as follows (eq 4):

$$K_p = \frac{J_{ss}}{C_0} \quad (4)$$

Enhancement ratio (E_r) was calculated by dividing the J_{ss} of the respective formulation with the J_{ss} of the control formulation as follows (eq 5):

$$E_r = \frac{J_{ss} \text{ of formulation}}{J_{ss} \text{ of control}} \quad (5)$$

CLSM Studies for Optical Images of ex Vivo Skin Penetration. Fluorescent dye (Nile red, 0.1% w/w) was incorporated in the selected nanoemulsions to study skin penetration using CLSM. Nile red could be mixed well with capsaicin due to its similar lipophilicity to capsaicin.[32] The skin from the flank area of the pig was used for ex vivo skin permeation studies. The skin samples were thawed at room temperature and rehydrated in PBS solution for 30 min before the experiments. The skin permeation studies were performed for 24 h by using a vertical modified amber glass Franz diffusion cell as described above. After the ex vivo skin permeation experiments, the skin surface was gently rinsed with 50% ethanol and wiped. The skin was placed between a slide glass and a coverslip and examined using CLSM (LSM 5 Exciter, Carl Zeiss, Jena, Germany). The skin sample was scanned from the skin surface (0 μm) to a depth of 32 at 1 μm intervals. The skin was inspected under a 20× objective lens (EC Plan-NEOFLUAR 20x/0.50 M27). The detecting wavelength was 543 nm. CLSM images were recorded and further processed using LSM Image Browser software, version 4.2.0.121 (CarlZeiss Microimaging, Gottingen, GMBH).

CLSM Images from Cryotome-Sectioned Skin. After the final sampling interval of 24 h for the ex vivo skin permeation experiments, the skin was washed with 50% ethanol and stored at −20 °C. The skin samples were cut into small pieces and sectioned vertically to a thickness of 30 μm by using a cryotome (Leica Cryostat CM 3505S, Wetzlar, Germany). The permeation of the fluorescence dye incorporated into the capsaicin nanoemulsion was qualitatively observed using CLSM (LSM 5 Exciter, Carl Zeiss, Jena, Germany). The skin was inspected under a 10× objective lens (EC Plan-NEOFLUAR 10x/0.30 M27). The images were obtained in differential interference contrast (DIC) mode, fluorescence mode, and merge mode.

Statistical Analysis. All data were statistically analyzed using analysis of variance (ANOVA). Statistical Package for the Social Science (SPSS, Version 20.0, SPSS Inc., Chicago, IL, USA) was used for this analysis. Duncan's multiple range tests were used to determine the statistical significance among the means at 95% significant level.

RESULTS AND DISCUSSION

Screening of Optimal Surfactant Mixtures. Before the screening of surfactant mixtures, the concentration of capsaicin in oleoresin capsicum was measured by HPLC. Oleoresin capsicum contains 22.67 mg/g of capsaicin (data not shown). The selection of the best emulsifier is really crucial to enhance the emulsion stability. The ratios of nonionic surfactant mixtures were studied to determine the most stable and size controllable nanoemulsion with a droplet size optimal for efficient topical delivery of capsaicin. In this experiment, various ratios of Span 80 (HLB value 4.3) and Tween 80 (HLB value 15) were selected to prepare the nonionic surfactant mixtures. The optimal HLB_{mix} was determined when the nanoemulsion with a surfactant mixture having an appropriate HLB value also showed the smallest droplet size and a low PDI (less than 0.3). The droplet size distribution and phase separation were also considered. Results from a previous study suggested that surfactants with higher HBL values formed more stable o/w emulsion than surfactants with lower HLB values; thus, HLB values ranging from 9 to 15 were chosen to screen the optimum condition. We selected an HLB value of 13.5 for oleoresin capsicum because the nanoemulsion showed the smallest droplet size with the lowest PDI as shown in Figure 1. Nanoemulsions using higher hydrophilic surfactant showed smaller particle sizes than those using lower hydrophilic surfactant. According to our screening of the HLB value for oleoresin capsicum, the weight ratio of Tween 80 to Span 80 was fixed at 85.98:14.02.

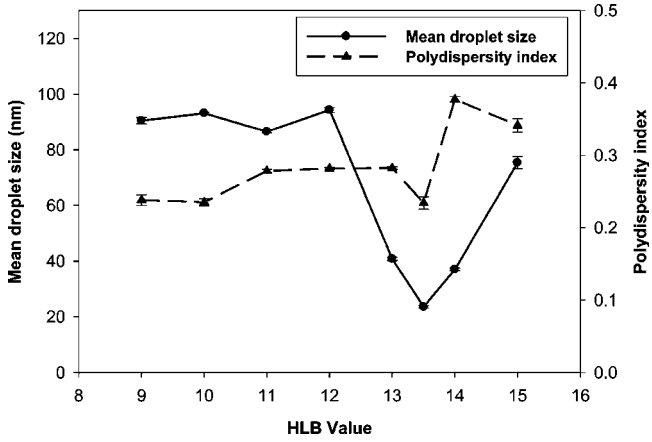

Figure 1. Droplet size and polydispersity index of nanoemulsions depending on the surfactant HLB value. Data are plotted as the mean ± standard deviation (n = 3).

Ternary Phase Diagram. To determine the best formulation of capsaicin-loaded nanoemulsion, we constructed a ternary phase diagram that consisted of various ratios of water, oleoresin capsicum, and a fixed surfactant mixture of Tween 80 and Span 80 at a weight ratio of 85.98:14.02 ($surfactant_{mix}$), respectively. In Figure 2, the area I indicates the optimal process conditions for fine and uniform sized nanoemulsions. The droplet size and zeta potential of nanoemulsions ranged from 20.26 to 62.98 nm and from −19.9 to −8.8 mV, respectively. Any phase separation was not observed until 30 days of storage for this region. Table 1 showed the formulations and characteristics such as droplet size, PDI, and zeta potential of nanoemulsions indicated in the area I. The droplet size of nanoemulsions was dependent on the ratio of oil to surfactant. In most case, droplet size of nanoemulsions decreased with lower oil to surfactant ratio. When the ratio of oil to surfactant was 1:1, the droplet size was around 63 to 64 nm and not statistically significant ($P < 0.05$) while the droplet size was around 20 nm when the ratio of oil to surfactant was 1:3. In contrast, area II nanoemulsions were not formed homogeneously and showed high PDI values (>0.3). For the remainder of the regions, immediate phase separation was obserbed. Our observations indicated that nanoemulsion regions were not identified when the aqueous phase was below 50%. The optimal nanoemulsion formulations were found to be in the range of more than 50% of water, less than 18% of oleoresin capsicum, and 15.4%−33.3% of $surfactant_{mix}$ with treatment of a high pressure homogenization.

Optimal Formulation and Stability Study of the Nanoemulsions. Based on the HLB value and the phase study, the nanoemulsion formulations that had oil/$surfactant_{mix}$ ratios of 1:1, 1:1.3, 1:1.5, 1:2, and 1:3 were selected for the following penetration studies. Figure 3 represents the profile for the change in droplet size and PDI value of nanoemulsion formulations (NE-1 to NE-13) in which the oil and $surfactant_{mix}$ ratio ranged from 1:1 to 1:3. The formulations of the selected nanoemulsions were stable and showed a controlled droplet size ranging from 20.26 to 62.98 nm. As the surfactant concentration increased, the droplet size tended to become smaller, but PDI

dx.doi.org/10.1021/jf404220n | J. Agric. Food Chem. 2014, 62, 725−732

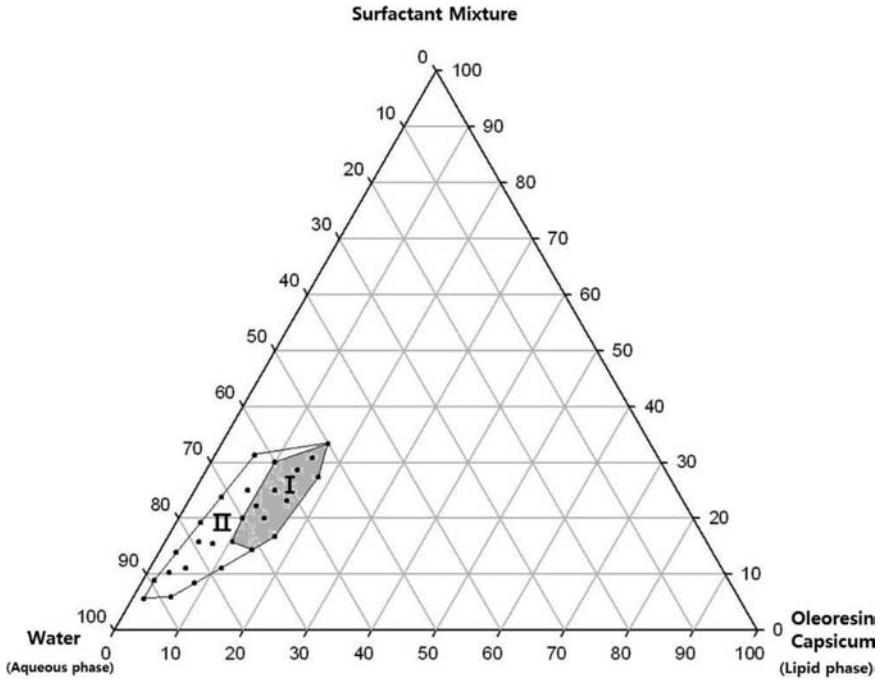

Figure 2. Ternary phase diagram of nanoemulsions composed of oleoresin capsicum, the mixed surfactant (Tween 80/Span 80), and aqueous phase. Area I depicts the conditions in which fine and homogeneous nanoemulsions could be formed.

Table 1. Characteristics of the Nanoemulsion Formulations[a]

	mixing ratio		composition (% w/w)					
form no.[b]	oil:surfactant	water	oil	surfactant	water	droplet size (nm)	PDI	zeta potential (mV)
NE-1	1:1	4	16.7	16.7	66.7	62.98 ± 0.49 e[c]	0.26 ± 0.02	−15.0 ± 1.48 abcd
NE-2		5	14.3	14.3	71.4	64.27 ± 0.10 e	0.27 ± 0.01	−16.8 ± 2.17 abc
NE-3	1:1.5	3	18.2	27.3	54.5	48.20 ± 0.80 d	0.25 ± 0.04	−12.7 ± 0.44 bcd
NE-4		4	15.4	23.1	61.5	47.16 ± 0.15 d	0.23 ± 0.01	−11.0 ± 0.87 cd
NE-5		5	13.3	20.0	66.7	48.31 ± 1.64 d	0.26 ± 0.00	−9.2 ± 1.46 d
NE-6		7	10.5	15.8	73.7	41.71 ± 0.76 c	0.25 ± 0.00	−8.8 ± 1.02 d
NE-7	1:2	3	16.7	33.3	50.0	31.70 ± 4.27 b	0.22 ± 0.02	−18.8 ± 3.70 ab
NE-8		3.5	15.4	30.8	53.8	34.56 ± 2.68 b	0.21 ± 0.01	−16.3 ± 1.03 abc
NE-9		4	14.3	28.6	57.1	30.92 ± 2.21 b	0.22 ± 0.00	−11.7 ± 2.15 cd
NE-10		5	12.5	25.0	62.5	25.13 ± 2.40 a	0.25 ± 0.01	−19.9 ± 4.20 a
NE-11		6	11.1	22.2	66.7	23.46 ± 0.10 a	0.27 ± 0.01	−16.9 ± 0.82 abc
NE-12		7	10.0	20.0	70.0	24.62 ± 0.65 a	0.23 ± 0.03	−10.7 ± 0.47 cd
NE-13	1:3	6	10.0	30.0	60.0	20.26 ± 0.43 a	0.27 ± 0.02	−12.7 ± 2.55 bcd

[a]Data are plotted as the mean ± standard deviation (n = 3). [b]Formulation number. [c]Different letters indicate a significant difference at $P < 0.05$ by Duncan's multiple range test.

and zeta potential were not correlated with the amount of surfactant. A smaller droplet size might have a larger the surface area, so that more surfactant would be required to cover particles.[24] When we fixed the ratio of oil and surfactant, the droplet size of nanoemulsion was decreased by adding more aqueous phase.

Morphology of Capsaicin-Loaded Nanoemulsions. Figure 4 shows the TEM images of the nanoemulsions (NE-13). The droplet size of NE-13 was approximately 20 nm in TEM images, and this was consistent with our previous results obtained by using a size analyzer. The droplets were spherical and showed a uniform emulsion droplet distribution.

Penetration Profiles of Different Formulation of Nanoemulsion. One of the main barriers for skin penetration is the lipophilic stratum corneum (SC) layer. It is well-known that it is difficult for hydrophilic substances and high molecular weight vesicles to penetrate the SC. On the other hand, hydrophobic substances easily get into the SC layer but they also have some limitation to penetrate the next epidermis layer which has a hydrophilic feature.[25] Therefore, it needs to be delivered in both hydrophilic and hydrophobic barriers with special formulation vesicles to penetrate all layers of the skin. The effect of different compositions of nanoemulsions on skin permeation was investigated using the synthetic membrane that is considered the standard model for in vitro transdermal diffusion studies replacing human or animal skin. Reproducibility of results is enhanced by using this synthetic membrane as compared with using animal skin. Figure 5 shows the permeation profiles of capsaicin-loaded nanoemulsions and a control sample. The concentration of capsaicin in nanoemulsion ranged from 2.08 to 3.45 mg/g whereas the capsaicin concentration of control was 2.64 mg/g. All nanoemulsion samples continuously

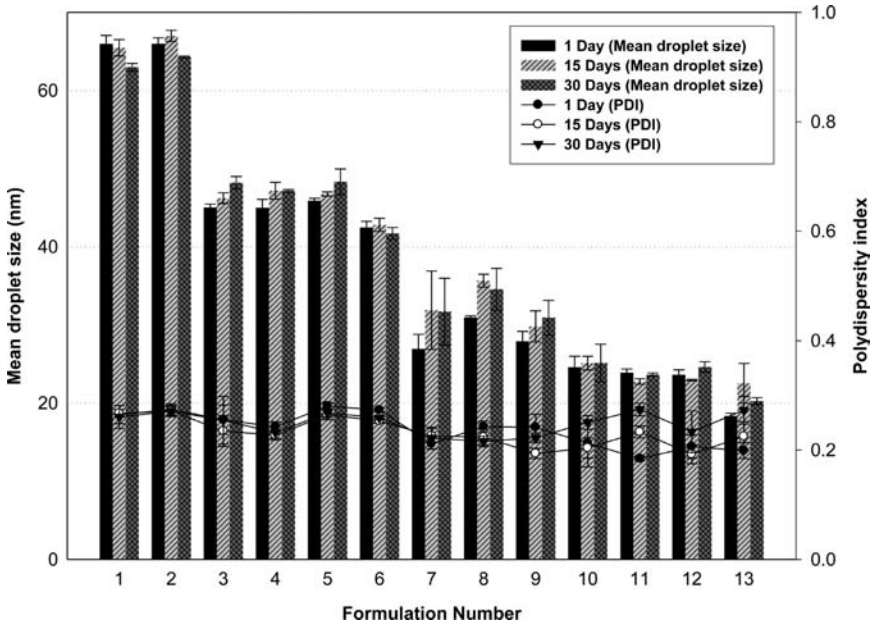

Figure 3. Droplet size profiles of nanoemulsion formulations for 30 days. Data are plotted as the mean ± standard deviation (n = 3).

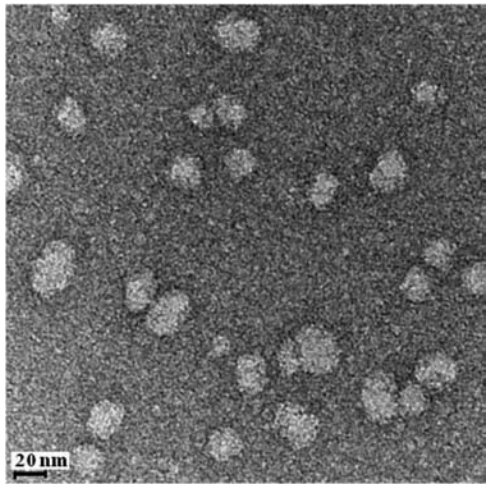

Figure 4. The morphology of the capsaicin-loaded nanoemulsion (NE-13) with TEM micrograph in the high-angle annular dark field (HAADF) micrograph mode.

permeated the membrane over time. NE-1 showed the highest cumulative capsaicin permeated amounts whereas NE-13 showed the lowest permeated amounts, which were not statistically significant ($P > 0.05$) with those of the control at the all sampling time as shown in Figure 5. Cumulative capsaicin permeated amounts of NE-4 and NE-9 were not statistically significant ($P > 0.05$) until 8 h and were significantly ($P < 0.05$) higher at 12 and 24 h compared to the control. Only NE-1 showed statistical significance ($P < 0.05$) in the capsaicin permeated amounts with other formulations including the control throughout all the time. Cumulative permeation of NE-1 was steeply increased for the initial time (until 6 h) and was slowly increased over time. This phenomenon could be explained by capsaicin-incorporated nanoemulsion being highly accumulated in the receptor fluid, which could affect the permeation flux and delay the capsaicin penetration since the sink condition limit might have been reached. However, many factors may affect the diffusion phenomenon for skin membrane permeation such as sink condition, sampling frequency, experiment duration, type of membrane sample, or membrane materials.[24] It has been reported that infrequent sampling increases drug concentration in the receptor chamber and sink condition (<10%) could rise over the limited state.[26] Thus, in our case, the sampling frequency and experimental duration of 24 h could also account for the slower cumulative permeation observed after 12 h.

The permeation parameters such as permeation flux (J_{ss}), permeability coefficient (K_p), and enhancement ratio (E_r) are summarized in Table 2. The permeation flux of the nanoemulsions ranged from 10.597 μg/cm^2 h to 21.251 μg/cm^2 h. The highest permeation flux was obtained in NE-1, while the lowest permeation flux was observed in NE-13. Except for NE-13, the permeation flux of the nanoemulsions was higher than that of control (12.864 μg/cm^2 h) by about 30% to 65%. However, the permeation flux and permeability coefficient of most of the nanoemulsion formulations were not statistically significant ($P > 0.05$) compared to those of the control except NE-1 as shown in Table 2. The enhancement ratio (E_r) of the nanoemulsions ranged from 0.849 for NE-13 to 1.658 for NE-1. The enhancement ratio of the nanoemulsions was statistically significant ($P < 0.05$) compared to that of the control except NE-13. The enhancement ratios of the nanoemulsions were also higher than that of the control sample, except for NE-13. It has been reported that the manner of skin penetration depends on various physiological properties including size, composition, and surface charge of the vesicles, the HLB value, and the type of surfactant, as well as the presence of a penetration enhancer.[27] In general, the skin penetration should be fast and higher with smaller droplet size. However, the highest penetration flux was obtained with NE-1 containing larger mean droplet size of 62.98 nm and the lowest penetration flux was obtained with NE-13 containing smaller droplet size of 20.26 nm. The skin penetration might be highly dependent on the amount of surfactant because thermodynamic activity of core in nanoemulsion increased at the lower concentration of surfactant.[28] NE-1 contains the least amount of surfactant in the formulations and showed the highest penetration flux. Based on the permeation profiles, NE-1 showed the best nanoemulsion

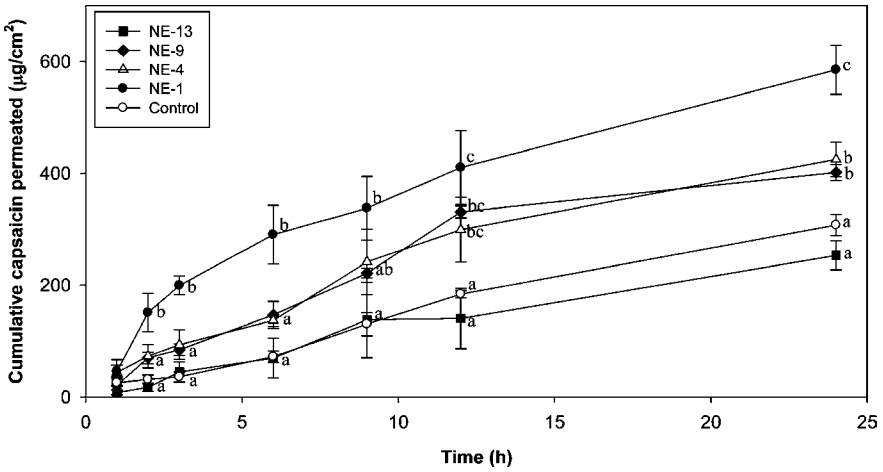

Figure 5. Permeation profiles of capsaicin from capsaicin-loaded nanoemulsion formulations through a synthetic membrane similar to human skin. The control sample was a 40% ethanol solution of capsaicin (mean ± SD, n = 3). Different letters at the same time indicate a significant difference at $P < 0.05$ by Duncan's multiple range test.

Table 2. Permeability Parameters of Different Formulations[a]

form. no.[b]	J_{ss} (μg/cm^2 h)	K_p ($\times 10^2$ cm/h)	enhancement ratio (E_r)
NE-13	10.597 ± 1.239 a[c]	0.509 ± 0.060 a	0.849 ± 0.168 a
NE-9	16.873 ± 0.861 b	0.811 ± 0.041 b	1.321 ± 0.051 b
NE-4	16.759 ± 0.847 b	0.805 ± 0.041 b	1.312 ± 0.052 b
NE-1	21.251 ± 1.826 c	1.021 ± 0.088 c	1.658 ± 0.091 c
control	12.864 ± 1.140 ab	0.618 ± 0.055 ab	1.000 ± 0.000 a

[a]The control sample was 40% ethanol solution of capsaicin (mean ± SD, n = 3). [b]Formulation number. [c]Different letters indicate a significant difference at $P < 0.05$ by Duncan's multiple range test.

formulation for improved skin penetration and was, therefore, selected for optical image observation using CLSM.

CLSM. Images derived from CLSM were used to show the permeation pathway of active compounds through the skin layer. This method provides multidepth images that parallel the skin surface without any physical sectioning.[29] While the conventional method of studying skin penetration relies on classical sectioning processes that can destroy the skin membrane structures, CLSM is noninvasive and allows the observation of the skin penetration pathways of active compounds without

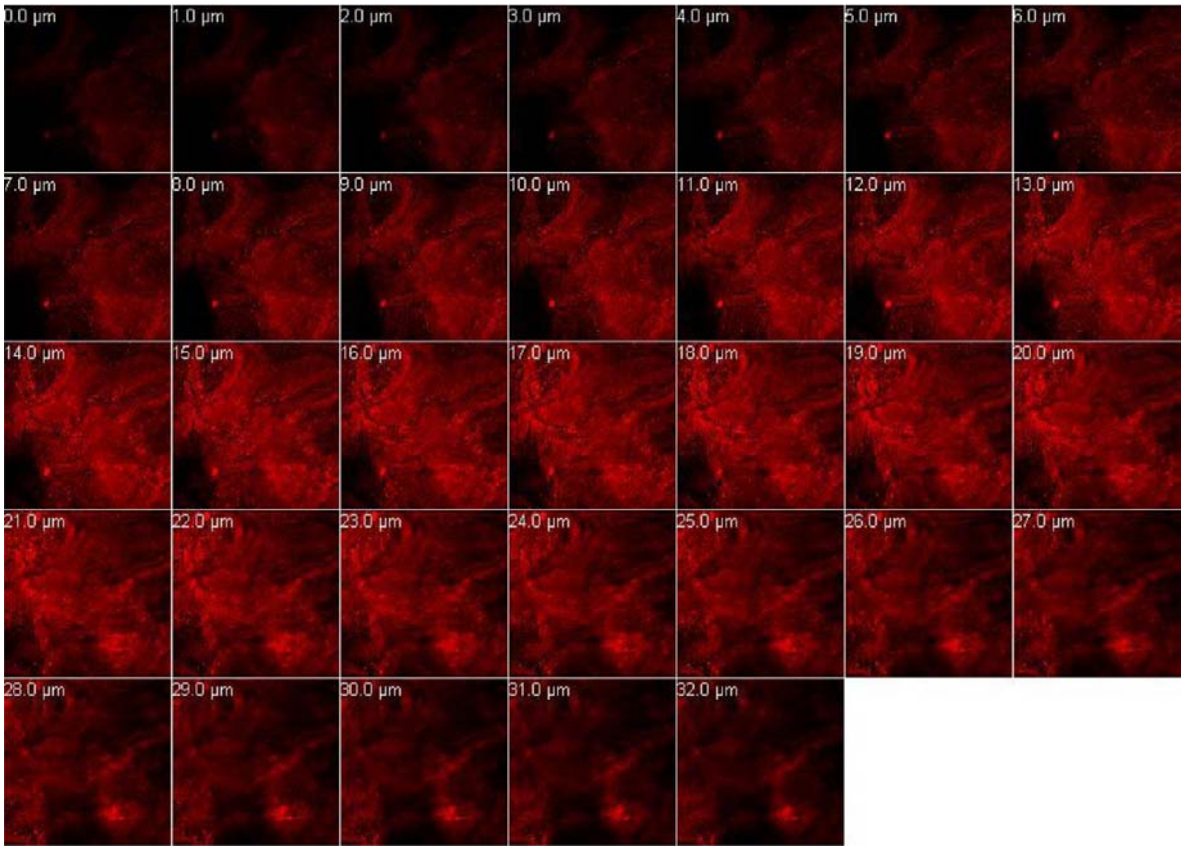

Figure 6. Confocal laser scanning microscopy (CLSM) images for penetration of capsaicin-loaded nanoemulsion (NE-1) into the pig skin. Nile red (0.1% w/w) was used as a fluorescence dye, and the detection wavelength was 543 nm.

inflicting tissue damage.[30,31] To obtain images using CLSM, the skin thickness was not more than 700 μm from SC to dermis so that the laser could penetrate all skin layers. The fluorescence dye, Nile red (0.1% w/w), was used as model compound for observation of capsaicin-loaded NE-1 permeation pathway. Nile red has the ability to emit strong fluorescence, and its lipophilicity (log P = 3.10) is similar to capsaicin (log P = 3.81).[32] The fluorescence intensity indirectly indicates the amount of permeated capsaicin. Figure 6 shows 32 fluorescence images that parallel the skin surface (z direction images). The first skin surface image did not show strong fluorescence intensity compared with other images because of rinsing the skin sample with 50% ethanol in sample preparation. However, we could observe a clear fluorescence image of penetrated capsaicin nanoemulsion until 32 μm depth in other images. The strongest fluorescent spot was observed near the hair follicles. Capsaicin nanoemulsion can penetrate and accumulate in the skin well through the hair follicles as shown in Figure 6. Because the thickness of the stratum corneum is 10−20 μm, these images indicated that capsaicin-loaded NE-1 permeated stratum corneum and epidermis.

CLSM Images of Cryotome-Sectioned Skin. Vertical sectioning of pig skin using the cryotome was performed to ensure and visualize the permeation profile through the skin layers. Figure 7 shows CLSM images of Nile red in 40% ethanol

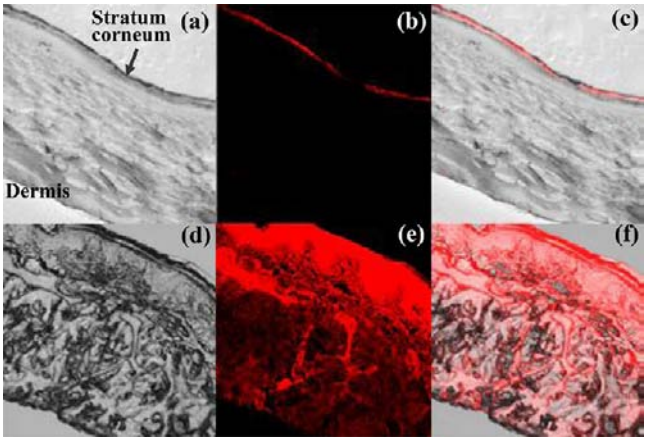

Figure 7. Confocal laser scanning microscopy (CLSM) images of cryotome-sectioned pig skin of (a, b, c) Nile red in 40% ethanol and (d, e, f) capsaicin-loaded nanoemulsion (NE-1) permeation in differential interference contrast mode (a, d), fluorescence mode (b, e), and merge mode (c, f). Sample thickness is 700 μm. Images of the same area were obtained in fluorescence mode (420−720 nm and 580−720 nm).

(control) and capsaicin-loaded nanoemulsion (NE-1) permeating into pig skin layers consisting of stratum corneum, epidermis, and dermis. Nile red in 40% ethanol could not permeate even the stratum corneum layer, and any fluorescence intensity was not observed in Figure 7a. However, capsaicin-loaded nanoemulsion (NE-1) could successfully penetrate the skin layers, and strong fluorescence intensity was observed through the whole skin layers from stratum corneum to dermis. The stratum corneum layer (10−20 μm thick) shows the strongest fluorescence intensity while the dermis layer shows less fluorescence intensity. Although it gradually decreased from stratum corneum to dermis, the red fluorescence intensity was observed through all skin layers up to 700 μm thick. This result indicates that capsaicin-loaded nanoemulsions have a great potential as a transdermal delivery carrier for the effective penetration through all skin layers.

AUTHOR INFORMATION

Corresponding Author

*Hyun Jin Park: tel, 82-2-3290-4149; fax, 82-2-953-5892; e-mail, hjpark@korea.ac.kr. Gye Hwa Shin: tel, 82-2-3290-4149; fax, 82-2-953-5892; e-mail, winnie19@gmail.com.

Author Contributions

‡Authors contributed equally to this work.

Funding

This research was supported by the Basic Science Research Program through the National Research Foundation of Korea (NRF) funded by the Ministry of Education (NRF-2013R1A1A2008490) and Coway cosmetics R&D center.

Notes

The authors declare no competing financial interest.

REFERENCES

(1) Hayman, M.; Kam, P. C. A. Capsaicin: A review of its pharmacology and clinical applications. *Curr. Anaesth. Crit. Care* **2008**, *19*, 338−343.

(2) Molina-Torres, J.; Garcia-Chavez, A.; Ramirez-Chavez, E. Antimicrobial properties of alkamides present in flavoring plants traditionally used in Mesoamerica: Affinin and capsaicin. *J. Ethnopharmacol.* **1999**, *64*, 241−248.

(3) Ghosh, A. K.; Basu, S. Fas-associated factor 1 is a negative regulator in capsaicin induced cancer cell apoptosis. *Cancer Lett.* **2010**, *287*, 142−149.

(4) Manzini, S.; Perretti, F.; Benedetti, L. D.; Pradelles, P.; Maggi, C. A.; Geppetti, P. A comparison of bradykinin- and capsaicin-induced myocardial and coronary effects in isolated perfused heart of the guinea pig: involvement of substance P and calcitonin gene-related peptide release. *J. Pharmacol.* **1989**, *97*, 303−312.

(5) Xu, X.; Wang, P.; Zhao, Z.; Cao, T.; He, H.; Luo, Z.; Zhong, J.; Gao, F.; Zhu, Z.; Li, L.; Yan, Z.; Chen, J.; Ni, Y.; Liu, D.; Zhu, Z. Activation of transient receptor potential Vanilloid 1 by dietary capsaicin delays the onset of stroke in stroke-prone spontaneously hypertensive rats. *Stroke* **2011**, *42*, 3245−3251.

(6) Hautkappe, M.; Roizen, M. F.; Toledano, A. Review of the effectiveness of capsaicin for painful cutaneous disorders and neural dysfunction. *Clin. J. Pain* **1998**, *14*, 97−106.

(7) Bevan, S.; Szolcsányi, J. Sensory neuron-specific actions of capsaicin: mechanisms and applications. *Trends Pharmacol. Sci.* **1990**, *11*, 330−333.

(8) Mousseau, D. D.; Sun, X.; Larson, A. A. An antinociceptive effect of capsaicin in the adult mouse mediated by the NH2-terminus of substance P1. *J. Pharmacol. Exp. Ther.* **1994**, *268*, 785−990.

(9) Kim, C. S.; Kawada, T.; Kim, B. S.; Han, I. S.; Choe, S. Y.; Kurata, T.; Yu, R. Capsaicin exhibits anti-inflammatory property by inhibiting IkB-a degradation in LPS-stimulated peritoneal macrophages. *Cell. Signalling* **2003**, *15*, 299−306.

(10) Shakeel, F.; Shafiq, S.; Haq, N.; Alanazi, F. K.; Alsarra, I. A. Nanoemulsions as potential vehicles for transdermal and dermal delivery of hydrophobic compounds: an overview. *Expert Opin. Drug Delivery* **2012**, *9*, 953−974.

(11) Prow, T. W.; Grice, J. E.; Lin, L. L.; Faye, R.; Butler, M.; Becker, W.; Wurm, E. M.; Yoong, C.; Robertson, T. A.; Soyer, H. P.; Roberts, M. S. Nanoparticles and microparticles for skin drug delivery. *Adv. Drug Delivery Rev.* **2011**, *63*, 470−491.

(12) Kim, S.; Kim, J. C.; Sul, D.; Hwang, S. W.; Lee, S. H.; Kim, Y. H.; Tae, G.; Kim, J. Nanoparticle formulation for controlled release of capsaicin. *Nanosci. Nanotechnol.* **2011**, *11*, 4586−4591.

(13) Schlupp, P.; Blaschke, T.; Kramer, K. D.; Holtje, H. -D.; Mehnert, W.; Schafer-Korting, M. Drug release and skin penetration from solid lipid nanoparticles and a base cream: A systematic approach

from a comparison of three glucocorticoids. *Skin Pharmacol. Physiol.* **2011**, *24*, 199−209.
(14) Li, B.; Ge, Z. Q. Nanostructured lipid carriers improve skin permeation and chemical stability of Idebenone. *AAPS PharmSciTech* **2012**, *13*, 276−283.
(15) El Maghraby, G. M.; Barry, B. W.; Williams, A. C. Liposomes and skin: From drug delivery to model membranes. *Eur. J. Pharm. Sci.* **2008**, *34*, 203−222.
(16) Yaw, B. H.; Yong, H. L.; Tzy, M. L.; Ren, J. W.; Yi, H. T.; Pao, C. W. Transdermal delivery of capsaicin derivative-sodium nonivamide acetate using microemulsions as vehicles. *Int. J. Pharm.* **2008**, *349*, 206−211.
(17) Kong, M.; Park, H. J.; Feng, C.; Lin, H.; Cheng, X.; Chen, X. Construction of hyaluronic acid noisome as functional transdermal nanocarrier for tumor therapy. *Carbohydr. Polym.* **2013**, *94*, 634−641.
(18) Choi, A. Y.; Kim, C. T.; Park, H. Y.; Kim, H. O.; Lee, N. R.; Lee, K. E.; Gwak, H. S. Pharmacokinetic characteristics of capsaicin-loaded nanoemulsions fabricated with alginate and chitosan. *J. Agric. Food Chem.* **2013**, *61*, 2096−2102.
(19) Bouchemal, K.; Briançon, S.; Perrier, E.; Fessi, H. Nano-emulsion formulation using spontaneous emulsification: solvent, oil and surfactant optimization. *Int. J. Pharm.* **2004**, *280*, 241−251.
(20) Kong, M.; Chen, X.; Park, H. J. Design and investigation of nanoemulsified carrier based on amphiphile-modified hyaluronic acid. *Carbohydr. Polym.* **2011**, *83*, 462−469.
(21) Saria, A.; Lembeck, F.; Skofitsch, G. Determination of capsaicin in tissues and separation of capsaicin analogues by high-performance liquid chromatography. *J. Chromatogr.* **1981**, *208*, 41−46.
(22) Kong, M.; Chen, X.; Kwon, D. K.; Park, H. J. Investigations on skin permeation of hyaluronic acid based nanoemulsion as transdermal carrier. *Carbohydr. Polym.* **2011**, *86*, 837−843.
(23) Shakeel, F.; Ramadan, W. Transdermal delivery of anticancer drug caffeine from water-in-oil nanoemulsions. *Colloids Surf., B* **2009**, *75*, 356−362.
(24) Choi, A. J.; Kim, C. J.; Cho, Y. J.; Hwang, J. K.; Kim, C. T. Effects of surfactants on the formation and stability of capsaicin loaded nanoemulsions. *Food Sci. Biotechnol.* **2009**, *18*, 1161−1172.
(25) Bolzinger, M.; Briançon, S.; Pelletier, J.; Chevalier, Y. Penetration of drugs through skin, a complex rate-controlling membrane. *Curr. Opin. Colloid Interface Sci.* **2012**, *17*, 156−165.
(26) Ng, S. F.; Rouse, J. J.; Sanderson, F. D.; Meidan, V.; Eccleston, G. M. Validation of a static franz diffusion cell system for in vitro permeation studies. *AAPS PharmSciTech* **2010**, *11*, 1432−1441.
(27) Aripin, N. F. K.; Hashim, R.; Heidelberg, T.; Kweon, D. K.; Park, H. J. Effect of vesicle's membrane packing behaviour on skin penetration of model lipophilic drug. *J. Microencapsulation* **2013**, *30*, 265−273.
(28) Chen, H.; Chang, X.; Weng, T.; Zhao, X.; Gao, Z.; Yang, Y.; Xu, H.; Yang, X. A study of microemulsion systems for transdermal delivery of triptolide. *J. Controlled Release* **2004**, *98*, 427−436.
(29) Meidan, V. M. Methods for quantifying intrafollicular drug delivery: a critical appraisal. *Expert Opin. Drug Delivery* **2010**, *7*, 1095−1108.
(30) Breternitz, M.; Flach, M.; Präßler, J.; Elsner, P.; Fluhr, J. W. Acute barrier disruption by adhesive tapes is influenced by pressure, time and anatomical location: integrity and cohesion assessed by sequential tape stripping; a randomized, controlled study. *Br. J. Dermatol.* **2007**, *156*, 231−240.
(31) Nehal, K. S.; Dan, G.; Rajadhyasha, M. Skin imaging with reflectance confocal microscopy. *Semin. Cutaneous Med. Surg.* **2008**, *27*, 37−43.
(32) Akihito, M.; Yusaku, I.; Kenji, K.; Tohko, I.; Tomohiro, H.; Kyoko, O.; Asami, S.; Masataka, N.; Shiho, S.; Hidehiko, Y.; Susumu, Y.; Makoto, T.; Tatsuo, W. Lipophilicity of capsaicinoids and capsinoids influences the multiple activation process of rat TRPV1. *Life Sci.* **2006**, *79*, 2303−2310.

JOURNAL OF AGRICULTURAL AND FOOD CHEMISTRY

Article

pubs.acs.org/JAFC

Heat-Induced Aggregation of Whey Proteins in Aqueous Solutions below Their Isoelectric Point

Leonardo Cornacchia,*[,†] Cécile Forquenot de la Fortelle,[†,§] and Paul Venema[§]

[†]Nutricia Research, Uppsalalaan 12, 3584 CT Utrecht, The Netherlands

[§]Laboratory of Physics and Physical Chemistry of Foods, Department of Agrotechnology and Food Sciences, Wageningen University, Bornse Weilanden 9, 6708 WG Wageningen, The Netherlands

Supporting Information

ABSTRACT: Processing beverages containing high concentrations of globular proteins represents a technological challenge due to their instability during heating caused by protein aggregation and gelation. Aggregation of whey protein mixtures was investigated in aqueous model systems at pH 3.5, 4.0, and 4.5 at heating conditions resembling conventional industrial treatment (90 °C for 30 s). The extent of aggregation progressively decreased moving away from the p*I*. Protein aggregates became smaller and had a more open structure compared to higher pH values. Significant loss of protein dispersibility occurred at pH 4.0 and 4.5 above the denaturation *T* of whey protein (~70 °C), at which aggregation was caused by intermolecular hydrophobic interactions. Accessible thiol groups were detected in the heat-treated systems, with a higher intensity at higher pH and increasing extent of aggregation. Intermolecular −S−S− bonding played only a minor role in the aggregation at all conditions studied.

KEYWORDS: *whey protein, aggregation, thiol reactivity, surface hydrophobicity*

INTRODUCTION

The use of whey proteins in beverages represents an important opportunity due to their high nutritive and biological values,[1] which can fulfill the dietary requirements of various categories of individuals (e.g., the elderly and the frail).[2] However, the production of stable whey protein-based nutritional beverages is a great technological challenge. Processing (i.e., thermal treatment to ensure microbial safety) and product formulation affect protein solubility, which can lead to turbidity and/or sedimentation[3,4] or compromise manufacturing due to fouling of the heating equipment during pasteurization/sterilization processes.[5] To reduce the effect of the heat load the whey protein undergoes, whey-based beverages can be formulated at acidic pH (below pH 4.6) as, for their microbial safety, a milder thermal treatment compared to pH-neutral recipes is possible.[6]

Whey protein of bovine milk is a mix of globular proteins (*β*-lactoglobulin, *β*-LG, 50%; *α*-lactalbumin, *α*-LA, 20%; bovine serum albumin, BSA, 5%; immunoglobulins, IGs, 10%; lactoferrin, LF, 2.5%; lactoperoxidase, LP, 0.5%) with a high level of secondary, tertiary, and in some cases quaternary structure.[7] Far from their isoelectric point (p*I*), proteins have a net charge that leads to electrostatic repulsion, resulting in stable protein solutions.[8,9] At the p*I* (*β*-LG, p*I* = 5.1; *α*-LA, p*I* = 4.3; BSA, p*I* = 4.1) where the net charge of the proteins equals zero, the electrostatic repulsive forces are minimal, and intermolecular interactions, such as hydrophobic interaction and hydrogen bonds, may lead to aggregation.[9−11]

The solubility of whey proteins is highly dependent on the modification of the protein structure caused by heat treatment. Native globular proteins unfold upon heating and, depending on the balance of attractive and repulsive interactions, can form aggregates or gels with various structures (i.e., opaque particulates or transparent filaments).[9,12,13] When whey proteins are heated in an aqueous solution, the globular structure progressively unfolds, exposing hydrophobic groups and free thiol groups (when present, as in the case of *β*-LG and BSA) which are normally buried in the interior of the native protein molecule away from the protein−water interface. The exposed hydrophobic domains are driven toward their association, thereby leading to noncovalent protein aggregation (physical aggregation). At the same time, reactive −SH groups can lead to intermolecular covalent cross-linking (chemical aggregation) via oxidation or, as thiolate groups $-S^-$, via sulfhydryl/disulfide interchange reactions. The −S−S− bridges can also rearrange within the same molecule via an intraprotein thiol−disulfide exchange reaction (i.e., disulfide bond shuffling).[14,15] As Ako et al.[16] pointed out, aggregation and gelation of denatured whey proteins can even occur at conditions of strong electrostatic repulsion.

The mechanism of heat-induced aggregation and gelation of whey proteins has been extensively studied for model systems at neutral pH[4,17−20] or at high acidity (pH ~2), where fine-stranded fibrillar structures are formed.[12,21,22] At intermediate pH values, near the p*I*, the structural characteristics of particulate *β*-LG gels have been studied. It was found that between pH 4.05 and 5.55, *β*-LG heated at 60 °C for 24 h formed particulate aggregates without evidence for fibrillar structures. However, near the p*I*, spherical crystalline structures, called spherulites, can be formed by fibrillar structures growing radially from a central amorphous nucleus.[13] Recently, *β*-LG close to the p*I* was thoroughly investigated as a way to obtain

Received: October 4, 2013
Revised: December 21, 2013
Accepted: December 23, 2013
Published: December 23, 2013

ACS Publications © 2013 American Chemical Society

stable dispersions of spherical protein particles, called microgels.[23,24] Furthermore, micrometer-size highly-dense spherical whey protein particles were prepared[25,26] by heat-induced gelation of whey protein solutions dispersed as droplets in water-in-oil emulsions.

Although the literature has provided an in-depth characterization of the structures formed when β-LG is heated in aqueous solutions around the p*I*, the mechanism of aggregation of whey protein mixtures at moderately acidic conditions (3.5 < pH < 4.5) has received less attention.

Therefore, in this study we chose to focus on whey protein aggregation and dispersibility at heating conditions resembling the manufacturing of acidic beverages. The relevance of intermolecular disulfide bonds and hydrophobic interactions on the heat-induced aggregation of whey protein isolate in aqueous solutions at pH 3.5, 4.0, and 4.5 was investigated. The microstructure of the systems was also characterized. The results of this study contribute to a better understanding of the mechanism leading to whey protein instability at acidic pH and can be used to develop novel strategies for improving the stability and processability of concentrated whey protein aqueous formulations.

MATERIALS AND METHODS

Materials. A commercial whey protein isolate (BiPRO, Davisco Foods International Inc., Le Sueur, MN, USA) was used. The protein content was 92.84% (w/w) (all percentages used are w/w, unless stated otherwise) protein on a wet basis (N × 6.25), as measured by Dumas nitrogen analysis (Thermo Fisher Scientific Inc., Flash 4000 N/Protein Analyzer, Waltham, MA, USA).

All salts and reagents used for the thiol reactivity and the hydrophobicity study were of reagent grade. HPLC grade chemicals were used for ζ-potential measurements, transmission electron microscopy (TEM), and electrophoresis experiments.

Preparation of Protein Solutions. Protein solutions were freshly prepared for each set of experiments, similar to methods reported in the literature.[16,27] Protein powder was dispersed in demineralized water to obtain a homogeneous stock solution of 25%. The concentrated protein solution was stirred at room temperature for 3 h and stored overnight to allow for complete hydration of the protein. The next day, the 25% solution (approximately 400 mL) was transferred into a 3.5 kDa cutoff dialysis tubing (35 mm dry SnakeSkin, Thermo Scientific, Rockford, IL, USA) and dialyzed against 10 L of demineralized water for 2 h. After washing with demineralized water, the dialysis tubing was transferred into 10 L containing 3% of 12 kg mol^{-1} polyethylene glycol (PEG) (Sigma-Aldrich, Steinheim, Germany) solution, and the dialysis was continued for 24 h. The overall preparation was performed at 4 °C, and after dialysis no sign of bacterial growth was observed. Addition of PEG was necessary to compensate for osmotic pressure, thereby avoiding bursting of the dialysis tube. After dialysis, the concentration of the protein in the dialyzed solution was determined by the UV absorbance at 280 nm (kinetics spectrophotometer, LKB Biochron, Ultrospec K 4053, Cambridge, UK) using calibration curves prepared by dissolving known amounts of whey protein. At the dialysis conditions used in this study, the final protein concentration was approximately 14%. This stock solution was divided into various aliquots, and the pH was adjusted to pH 3.5, 4.0, and 4.5 using 2 N HCl. Finally, the solutions were diluted to the different protein concentrations (1, 5, and 10%).

Mineral and Lactose Contents. The concentrations of Ca, Cl, P, K, Mg, Mn, Na, and lactose were measured in the nondialyzed and dialyzed solutions with the same protein concentration. Minerals were analyzed by inductively coupled plasma atomic emission spectroscopy (ICP-OES) (iCAP 6300, Thermo Fisher Scientific Inc.), whereas lactose was determined by high-performance anion-exchange chromatography (HPAEC) and pulsed electrochemical detection (PED) (Dionex ICS-5000, Thermo Scientific, Sunnyvale, CA, USA).

Protein Dispersibility after Heat Treatment. Whey protein dispersibility before and after heat treatment was measured in 1, 5, and 10% protein solutions at pH 3.5, 4.0, and 4.5. Solutions with a volume of 15 mL were transferred into sealed screw-capped glass test tubes and heated in a water bath at 92 °C. The temperature increase of the sample was monitored with a thermocouple inserted in a reference tube containing 15 mL of deionized water.

The initial temperature of the sample was 20 °C, and heat treatment was immediately stopped when the sample temperature had reached 50, 60, 70, 80, or 90 °C. All of these temperatures were reached within 5 min. One of the samples was held at 90 °C for 30 s (this latter heat treatment is indicated as 90* °C). After heat treatment, the test tubes were cooled to room temperature using running tap water. This heating protocol was chosen to mimic temperature treatments of acidic formulations on liquid processing lines. At the end of the heat treatment protein aggregates were removed by centrifuging the samples at 3500*g* for 30 min using a refrigerated centrifuge (Biofuge Fresco, Heraeus Sepatech GmbH, Osterode, Germany).

The supernatant was filtered through a 0.2 μm pore size syringe filter (Minisart; Sartorius Stedim Biotech GmbH, Goettingen, Germany), and the protein concentration was analyzed by Dumas.

The dispersibility was expressed as the percentage of the protein concentration in the supernatant, relative to the initial total protein concentration of the solution. The heat treatment was repeated in three replicate experiments, and values were reported as an average and standard deviation.

Accessibility of Thiol Groups. The accessibility of the free thiol groups in protein was determined by their reactivity with 5,5′-dithiobis(2-nitrobenzoic acid) (DTNB; Sigma-Aldrich, Inc., St. Louis, MO, USA) according to the method described by Ellman,[28] adapted for the composition of the system.[19]

A 0.1 M sodium citrate at pH 3.5, 4.0, and 4.5 buffer containing 1 mM ethylenediaminetetraacetic acid (EDTA; Sigma-Aldrich, Inc.) was prepared and diluted 1:1 with demineralized water. Ellman's reagent was prepared by dissolving 8 mg of DTNB (Sigma-Aldrich, Inc.) in 2 mL of buffer. The reaction mix for the analysis of accessible reactive thiol groups was prepared by adding 2.5 mL of reaction buffer to 50 μL of Ellman's reagent solution and 250 mL of protein solution (or protein gels) and was left to react overnight. After complete reaction, solutions were spun at 16000*g* for 100 min at 20 °C (Biofuge Fresco, Heraeus Sepatech GmbH, Osterode, Germany) to remove the aggregates. The supernatant was collected, and the reactive thiol concentration was measured spectrophotometrically at 412 nm and determined using an extinction coefficient of 13600 M^{-1} cm^{-1}.[4,28−30] This method is based on the quantification of *p*-nitrothiophenol derived from the equimolar reaction between DTNB and −SH. Blank samples were prepared by replacing 250 μL of protein solutions with 250 μL of reaction buffer. The heat treatment was repeated in three replicated experiments, and values were reported as an average and standard deviation.

Surface Hydrophobicity. Surface hydrophobicity was determined using the fluorescent probe 1-(anilino)-naphthalene-8-sulfonate (ANS) (Sigma-Aldrich, Inc.), according to the method described by Monahan, German, and Kinsella.[4] Protein solutions of 1, 5, and 10% at pH 3.5, 4.0, and 4.5 were heat treated as described above and centrifuged at 3500*g* for 30 min at 20 °C, and the protein concentration in the supernatant was measured by Dumas.

ANS [10% (w/v)] was dissolved in dimethyl sulfoxide (DMSO) (Sigma-Aldrich, Inc.) and diluted in 30 mM citrate buffer (pH 4.0) to obtain a stock solution containing 0.5% (w/v) ANS; 0.2 mL of the 0.5% (w/v) ANS solution was added to 0.3 mL of supernatant and diluted with 30 mM citrate buffer (pH 4.0) to a final volume of 3 mL. Samples were analyzed by a fluorescence spectrometer (LS50B; Perkin-Elmer, Norwalk, CT, USA), with an emission wavelength from 400 to 580 nm, an excitation wavelength at 350 nm, and both slits widths (emission and excitation) at 4 nm, as described in the literature.[31] Surface hydrophobicity was expressed as the value at the maximum emission wavelength (475 nm) and normalized relative to protein concentration. The background signal as caused by the presence of dispersed aggregates in systems with no added ANS was

found to be negligible relative to the signal when ANS was added (<1%).

Microscopy. The microstructure of 10% whey protein systems was observed by transmission electron microscopy (TEM) (JEM-1011/100 kV, JEOL, Tokyo, Japan), using the negative staining method. Systems at pH 3.5, 4.0, and 4.5 were diluted 100-fold with the appropriate buffer (citrate buffer, pH 3.5, 4.0, and 4.5) for the control samples (no heat treatment) and 1000-fold for the heat-treated samples (90* °C for pH 3.5 and 4.5 and 70 °C for pH 4.0, where a gel was formed at 90* °C).

A drop of diluted protein solution was deposited on a 400-mesh Formvar/carbon-coated copper grid (Electron Microscopy Sciences, Washington, PA, USA) and dried with filter paper. After 2 min, the sample was stained for 15 s with one drop of 2% uranyl acetate (Merck) and then dried with filter paper. The grid was left to dry completely for 15 min before analysis.

Electrophoresis. After heat treatment at 20, 50, 60, 70, 80, 90, and 90* °C, the 10% whey protein solutions were analyzed by polyacrylamide gel electrophoresis (Midi Criterion system, Bio-Rad Laboratories B.V., Veenendaal, The Netherlands). Native PAGE and SDS-PAGE experiments under reducing and nonreducing conditions were performed using stain-free precast 8−16% gradient gels (Criterion TGX, Bio-Rad Laboratories B.V.).

Care was taken to avoid overloading of the gels; therefore, 15 μg of protein was loaded on each well. The running buffer was prepared from 10× premixed Tris/glycine electrophoresis buffer (25 mM Tris, 192 mM glycine, pH 8.3, Bio-Rad) or from 10× Tris/glycine/SDS (25 mM Tris, 192 mM glycine, 0.1% SDS, pH 8.3, Bio-Rad) according to procedures described by the manufacturer.

To investigate the mechanisms of protein aggregation and the composition of protein aggregates[32] the following experimental approach was used:

- Native-PAGE was used as a control.
- For native-PAGE under reducing conditions, 10 mM dithiothreitol (DTT) solution was added to the sample buffer to investigate the presence of intermolecular disulfide bridges in the aggregates.
- In SDS-PAGE, SDS disrupts aggregates connected by noncovalent interactions; therefore, this method was used to determine the influence of noncovalent interactions on aggregation.
- For SDS-PAGE under reducing conditions, DTT (10 mM) was added to the SDS sample buffer to determine the influence of both intermolecular −S−S− bridging and noncovalent interactions on aggregation.

Gels were stained with 10 mL of Coomassie (Brilliant) Blue R-250 (Bio-Rad) for 30 min and destained in a solution of 40% (w/v) methanol, 10% (w/v) acetic acid, and 50% (w/v) demineralized water. Gels were scanned with a ChemiDoc XRS system (Bio-Rad), and the protein bands were quantified using Quantity One 4.6.5 software (Bio-Rad). Values were normalized for each protein fraction by using α-LA (>85% purity, Sigma-Aldrich), β-LG (>90% purity, Sigma-Aldrich), and BSA (>98% purity, Sigma-Aldrich) standards. Protein concentrations were obtained using

$$C_U = (C_S/I_S)I_U$$

where, C_U and C_S are the concentrations, whereas I_S and I_U are the measured intensities of the unknown sample (U) and reference (S), respectively. The heat treatment of each system was performed in duplicate, and the heat-treated samples were run on two different lanes in the same gel. The average values of band intensity calculated from all of the previous were then quantified with a calibration curve obtained on a different gel (five concentrations in three replicates) and corrected according to the band intensity of an internal standard.

The concentrations of α-LA, β-LG, and BSA in the WPI were obtained by analyzing unheated aqueous solutions containing whey protein by SDS-PAGE. The relative concentrations of α-LA, β-LG, and BSA derived from a calibration curve were 24.0 ± 0.3, 68.0 ± 1.0, and 3.0 ± 0.2%, respectively.

RESULTS AND DISCUSSION

Effect of Dialysis on Minerals and Lactose. The data for nondialyzed and dialyzed protein dispersions obtained by ICP-OES (for minerals) and HPAEC-PED (for lactose) are compared in Table 1. Nondialyzed protein solutions contained only residual amounts of lactose and minerals. At the conditions used in the present study, dialysis did not lead to a significant loss of minerals, but reduced the lactose content 10-fold. This shows that most of the ions are present as counterions or associated with the protein structure (e.g., Ca^{2+} in α-LA).

Table 1. Compositional Data for 10% (w/w) Whey Protein Solutions before and after Dialysis through a 3.5 kDa Cutoff Membrane

element	control	3.5 kDa dialyzed system	unit
Ca	9	9	mg/100 g
Cl	1	0	mg/100 g
P	5	5	mg/100 g
K	3	2	mg/100 g
lactose	5.43	0.55	μg/mL
Mg	1	1	mg/100 g
Mn	0.005	0.003	mg/100 g
Na	54	50	mg/100 g

ζ-Potential and Visual Appearance. The ζ-potential of dialyzed whey protein solutions was measured upon titration with 1 M HCl from pH 7 to 2 using Zetasizer Nano cells (DTS1060, Malvern Instruments Inc., Worcestershire, UK), and the p*I* of the whey protein mix was determined. p*I* was reached around pH 4.8 (Supporting Information, Figure S1).

The whey protein solutions showed an increased turbidity as the pH was close to the p*I*. The visual appearance of the 5 and 10% freshly prepared whey protein samples at pH 4.5, 4.0, or 3.5 are shown in Figure 1. After 2 h at room temperature (Figure 1), the 5% whey protein samples at pH 4.5 phase-separated into an opaque protein-rich white sediment and a (protein-depleted) clear top layer. Less extensive separation was observed in the 10% whey protein samples at pH 4.5. No macroscopic phase separation was observed at pH 4.0 or 3.5, showing a cloudy or translucent appearance, respectively. At pH 4.5, close to the isoelectric point, the whey protein molecules form (reversible upon pH change) aggregates that

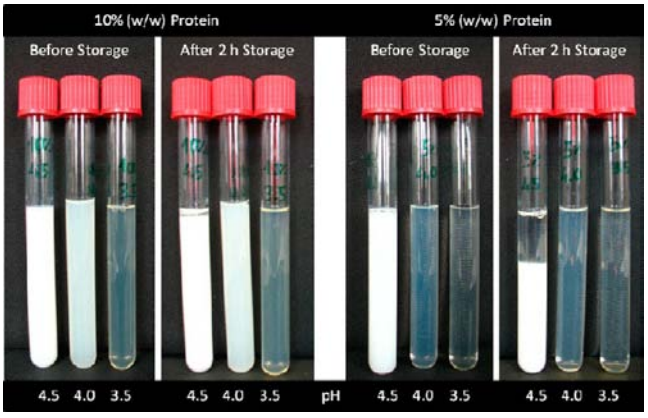

Figure 1. Whey protein solutions, 10 and 5% (w/w), at pH 4.5, 4.0, and 3.5, before and after 2 h of storage at room temperature.

dx.doi.org/10.1021/jf404456q | J. Agric. Food Chem. 2014, 62, 733−741

are large enough to be prone to sedimentation. This is often ascribed to the interactions between non-native protein fractions present in the whey protein isolate powders.[33,34]

Whey Protein Dispersibility. The results obtained for the protein dispersibility on systems containing 1, 5, and 10% protein are shown in Figure 2. In line with previous work,[8] a limited dispersibility of unheated whey protein at pH 4.5 was found. Dispersibility in the non-heat-treated systems was 93.88 ± 0.71, 93.22 ± 3.79, and 90.15 ± 1.26% at 1, 5, and 10% protein, respectively. This loss of dispersibility is in line with the visual observations described in the previous section.

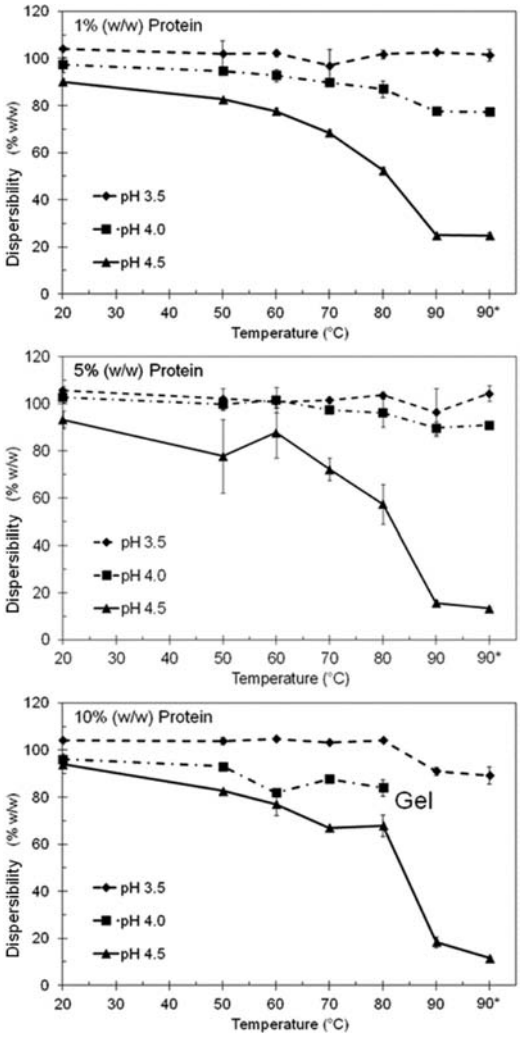

Figure 2. Dispersibility of 1, 5, and 10% (w/w) whey protein solutions at pH 4.5, 4.0, and 3.5 as a function of heat treatment.

At increasing temperature, the protein dispersibility progressively decreased until a sharp decrease occurred above 70 °C. This temperature is close to the peak of whey protein denaturation curve as measured by differential scanning calorimetry by Potes et al.[35]

According to the pathway suggested by Lumry,[36] upon heating, native proteins undergo structural changes, which can be followed by (irreversible) non-native protein association to form aggregates. Aggregation affects protein dispersibility so that protein clusters precipitate as they exceed a critical size[37] or are able to form a stable microgel.

The lower pH values investigated gave significantly higher dispersibility. The 1 and 5% protein systems at pH 3.5 did not lead to any significant dispersibility loss when heated from 20 °C to 90* °C. At higher protein concentration (10% protein), however, a limited loss in dispersibility (∼10%) was observed. A similar trend was observed for systems at pH 4.0. In this latter case 10% protein systems showed a lower dispersibility between 50 and 80 °C (dispersibility of ∼80%) and formed a gel at 90 °C.

At pH values between pH 3.5 and 4.5 a significant effect of the pH of the system on protein dispersibility was found. At all protein concentrations and heat treatments studied, the protein dispersibility increased progressively as the pH was decreasing below the p*I*. This is due to the higher net positive charge on the protein surface at low pH (Supporting Information, Figure S1), which leads to a stronger intermolecular electrostatic repulsion.

Accessibility of Thiol Groups. During the heating of whey protein, the formation of intermolecular disulfide bridges has been found to occur as a result of thiol−disulfide exchange reactions or oxidation. As explained by Visschers and de Jongh[15] and De Wit,[38] this process is driven by free sulfhydryl groups located on the cysteine of β-LG and BSA and is regulated by its pK_a (≈8.3), with the thiolate ion ($-S^-$) being the reactive species. Moreover, reactive thiols should be free from steric hindrance and be exposed and accessible to complete the reaction.[39]

In this study, the concentration of accessible thiol groups was monitored in 10% whey protein systems at pH 3.5, 4.0, and 4.5 during heating from 20 to 90 °C. To evaluate the accessibility of thiol groups, the reaction mixes in which the DTNB was allowed to react with proteins were buffered at pH 4.0 for all three systems (Figure 3A) and at pH 3.5, 4.0, 4.5 (Figure 3B). As shown in Figure 3A, the concentration of accessible thiol groups in the three different systems followed the same trend. No thiol groups were accessible to react with DTNB below 80 °C. As the proteins formed aggregates above the denaturation temperature, molecular rearrangement might have led to the exposure of the thiol groups to the solvent or to an open structure that allowed diffusion of DTNB (as already postulated by McGuffey et al.[19]). This implies the presence of accessible thiol groups. The experiment conducted in the three different buffer mixes (Figure 3B) revealed a pH-dependent accessibility of thiols on the protein aggregates. Again, reactive free thiol goups were detected with DTNB, and systems at pH 4.5 showed higher residual thiol group reactivity than systems at pH 4.0 and 3.5 (0.425 ± 0.003, 0.953 ± 0.014, and 4.134 ± 0.019 nmol/mg protein, in systems heated at 90* °C at pH 3.5, 4.0, and 4.5, respectively). As this might be due both to the increased reactivity of thiols to DTNB with increasing pH and to the different structural reorganization of the aggregates resuspended in different buffers, an additional experiment was performed. Solutions at the same concentration of free cysteine (0.4 mM) in citrate buffers at pH 3.5, 4.0, and 4.5 were tested with DTNB. Results showed values of absorbance that increased with increasing pH 3.5 < pH 4.0 < pH 4.5 (Supporting Information, Figure S2). However, the increased absorbance due to the sole effect of pH was significantly lower than the combined effect of pH and structural rearrangement observed for heat-treated (aggregated) whey proteins.

Therefore, it can be concluded that free thiol groups were accessible to DTNB only above 80 °C, when protein unfolding and aggregation occurred. Furthermore, the thiol accessibility

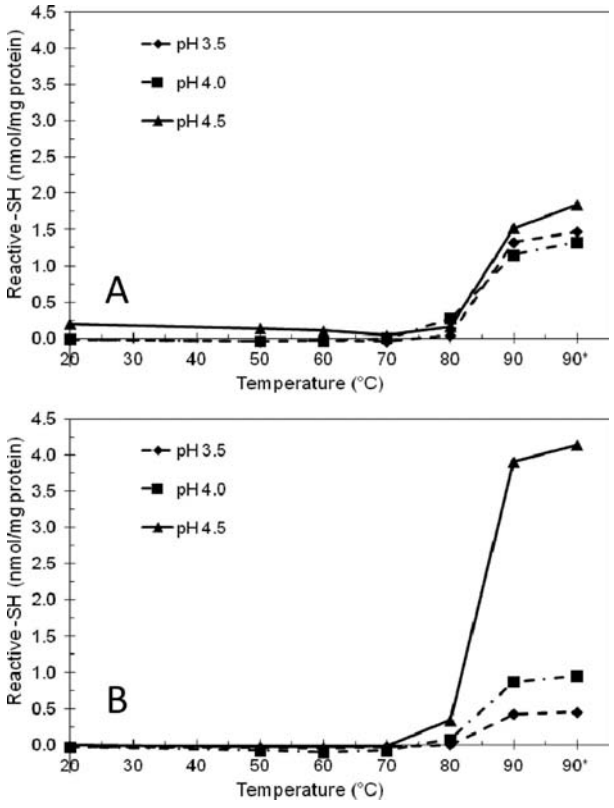

Figure 3. Temperature-dependent thiol group concentration of 10% whey protein solutions at pH 4.5, 4.0, and 3.5: (A) reaction with DTNB performed in citrate buffer, pH 4.0; (B) reaction with DTNB performed in citrate buffer, pH 3.5, 4.0, and 4.5.

increased rapidly with increasing pH from pH 3.5 to 4.5, whereas their reactivity was only slightly enhanced by increasing the pH from pH 3.5 to 4.5. This in agreement with earlier results[30,40] where the presence of exposed reactive of thiol groups was observed at acidic pH, in acid-induced cold-set gels of whey proteins. However, Alting et al.[41] observed a decrease of detectable thiol groups when aggregation was caused by a long heating period (>6 h). A long heat treatment might induce a compacting of the aggregate structure, which was not detected during the short heating time used in this study.

Surface Hydrophobicity. Heating globular proteins (such as whey proteins) causes conformational changes (denaturation), which can lead to the exposure of hydrophobic sites that are buried inside the native structure of the protein and are inaccessible to the surrounding.[42] Hydrophobicity is one of the major factors controlling intermolecular association of proteins, which results in the formation of (soluble or insoluble) aggregates.[43] Hence, studying the evolution of exposed hydrophobicity as a function of heating can provide useful information on the mechanism regulating whey protein aggregation and the impact on dispersibility. Here we assume that even if large aggregates are present, a discussion of the hydrophobicity on a molecular level is still meaningful.

The effect of pH and heating on whey protein hydrophobicity in 1, 5, and 10% protein solutions, as determined using the aromatic probe ANS, is reported in Figure 4. Independent of protein concentration, systems at pH 4.5 showed the lowest fluorescence intensity (<100 AU). The limited accessibility of hydrophobic patches at this pH might be

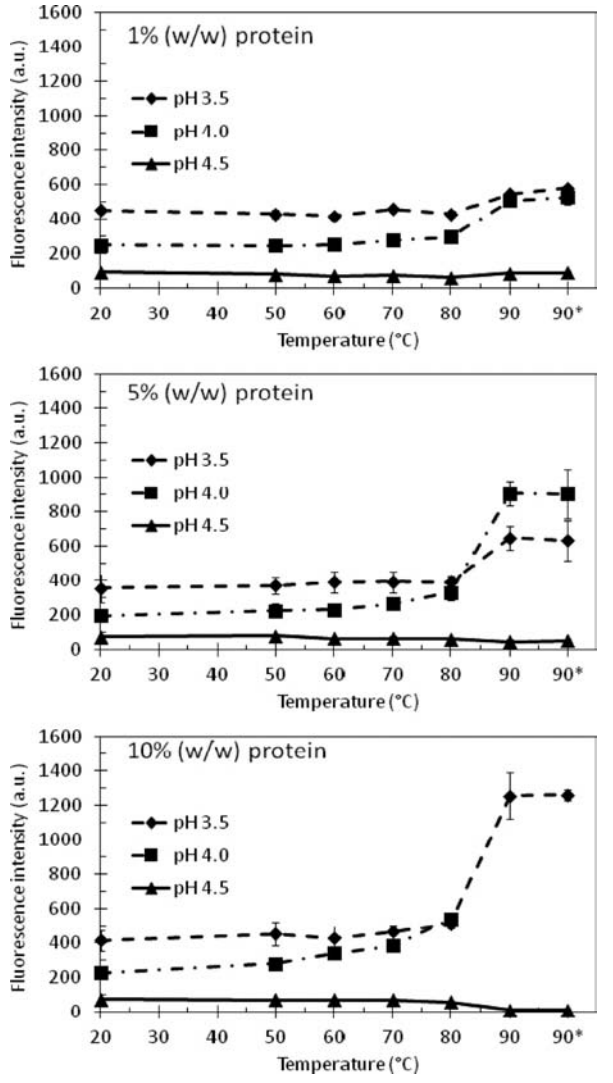

Figure 4. Heat-induced surface hydrophobicity change in whey protein systems. Surface hydrophobicity was expressed as the fluorescence value at the maximum emission wavelength (475 nm) per gram of protein.

explained with the formation of native octamers of β-LG[44] and compact structure of calcium binding (holo) α-LA, which hindered the interaction between hydrophobic sites and ANS.

Surface hydrophobicity progressively increased by decreasing the pH. Non-heat-treated systems at pH 3.5 showed an initial hydrophobicity (20 °C) equal to 451.65 ± 19.27, 354.25 ± 79.89, and 413.70 ± 57.37 au, whereas systems at pH 4.0 showed an initial hydrophobicity equal to 254.54 ± 16.72, 197.33 ± 11.18, and 228.67 ± 6.64 au, respectively, at 1, 5, and 10% protein concentrations. These different values might be explained with the partial dissociation of native β-LG octamers to form monomers with a higher accessibility of hydrophobic patches, and the loose structure of (apo) α-LA (decreasing pH below p*I*, α-LA reversibly loses its structure-stabilizing Ca^{2+}).[45]

The hydrophobicity of protein solutions at pH 3.5 and 4.0 increased more than linearly with protein concentrations at temperatures >70 °C. The 10% WPI solutions at pH 4.0 showed gelation at 90 °C, making the measurement of the hydrophobicity impossible. The increasing hydrophobicity with increasing heat treatment was also observed by Moro et al.[42] in

dx.doi.org/10.1021/jf404456q | J. Agric. Food Chem. 2014, 62, 733−741

a similar study on interactions between WPC and ANS in aqueous systems treated at 85 °C for periods from 0 to 60 min.

The change of surface hydrophobicity in the various systems closely followed the behavior observed for dispersibility. As pointed out earlier,[43] a low hydrophobicity leads to a higher dispersibility in an aqueous environment. Accordingly, the present study showed that the loss of dispersibility can be explained with the increasing surface hydrophobicity, which resulted in the formation of insoluble whey protein aggregates.

Microstructure. TEM images showed significant differences in the microstructure of 10% whey protein solutions at pH 3.5, 4.0, and 4.5 both before and after heat treatment (Figure 5). Aggregates were present in the samples before heat

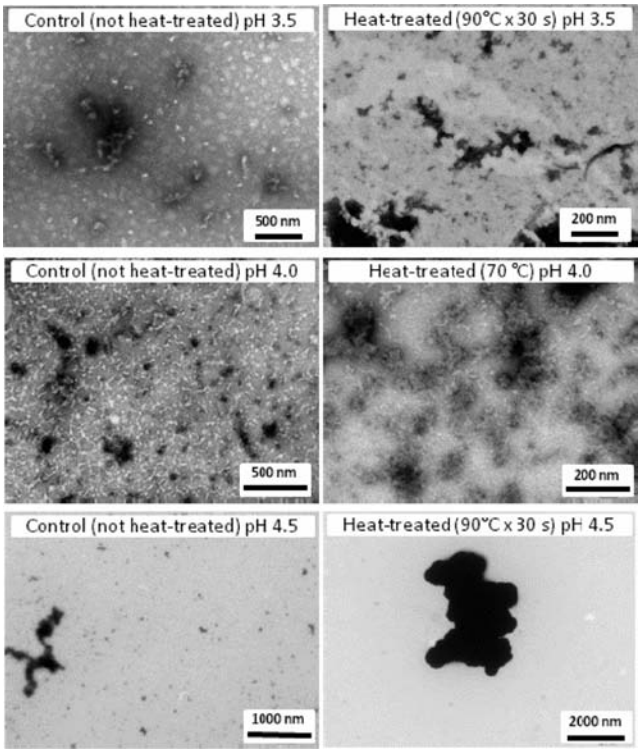

Figure 5. TEM micrographs showing untreated 10% (w/w) whey protein solutions at pH 3.5, 4.0, and 4.5 (left) and after heat treatment (right).

treatment. This was expected for systems at pH 4.0 and 4.5 due to their turbid appearance and reduced dispersibility. At pH 3.5, further away from the p*I*, unheated samples were translucent and the dispersibility was high (~100%); however, still some large aggregates were present. These can be attributed to the structural changes (i.e., denaturation) occurring during the production of the whey protein powder. In Figure 5, the three different morphologies of the systems are shown. At pH 4.0 the size and the distribution of the aggregates were more homogeneous than at pH 3.5 and 4.5. The pH 3.5 system showed that larger aggregates coexist with smaller aggregates, whereas at pH 4.5, larger aggregates (~1000 nm) could be observed. The larger aggregates seem to result from the aggregation of smaller spherical particles and are surrounded by numerous smaller (<100 nm) aggregates.

After heat treatment at 90* °C, the pH 3.5 systems showed an increased number of aggregates compared to the nonheated system. As shown in Figure 5, a few large aggregates (~200−400 nm) are surrounded by a number of smaller aggregates (~10−50 nm). This particle size distribution can explain the dispersibility value for the heat-treated pH 3.5 system (89.29 ± 3.66%). Whereas small aggregates (~10−50 nm) remained dispersed, large aggregates (~200−400 nm) precipitated, causing a ~10% dispersibility loss.

Heat-treated systems at pH 4.0 could be analyzed by TEM only before reaching the gelation temperature. Figure 5 shows the TEM results for pH 4.0 systems heated at 70 °C. The TEM picture gives an impression of the structure immediately before the formation of a gel network, with the presence of spherical particles with a radius of ~50 nm.

Heat-induced (90* °C) aggregation of systems at pH 4.5 resulted in the formation of large aggregates (size ~2000 × 4000 nm), which seem to result from the association of spherical smaller aggregates. No indication for the presence of single smaller aggregates was found. Similar structures were described by Jung et al.[46] for β-LG systems at pH 5.8 and by Sullivan et al.[47] using TEM and SEM, respectively.

PAGE. To investigate the mechanism leading to heat-induced aggregation and the relative contribution of the α-LA, β-LG, and BSA to aggregation, the water dispersible fractions of thermally treated 10% whey protein solutions were analyzed by native PAGE, native PAGE under reducing conditions (DTT), SDS-PAGE, and SDS-PAGE under reducing conditions (SDS + DTT) (Figure 6). The three major protein bands (α-LA, β-LG, and BSA) were observed after electrophoresis. The gels were scanned and the protein concentrations quantified on the basis of the intensity of the bands. Results of the intensity analysis are summarized in Figure 7.

Analysis of gels showed that the aggregation of α-LA, β-LG, and BSA was negligible in all of the systems heated to 80 °C. Samples heat-treated at 90 and 90* °C showed significant differences depending on pH and type of electrophoresis used. As observed in Figure 7 the concentration (%) of α-LA, β-LG, and BSA on native PAGE was reduced compared to the control at all pH values (pH 3.5: α-LA = 28.35 ± 8.50, 19.05 ± 8.52; β-LG = 38.13 ± 14.58, 27.86 ± 12.01; BSA = 46.79 ± 27.36, 22.07 ± 5.01. pH 4.0: α-LA = 23.44 ± 0.31, 21.22 ± 6.01; β-LG = 38.26 ± 0.15, 34.56 ± 12.13; BSA = 53.87 ± 12.04, 50.20 ± 1.57. pH 4.5: α-LA = 16.27 ± 1.50, 9.65 ± 2.13; β-LG = 22.02 ± 1.15, 13.40 ± 0.73; BSA = 101.32 ± 20.52, 57.91 ± 18.13, at 90 and 90* °C, respectively). This set of data shows that the amount of aggregated protein increased with increasing heating time and at pH 4.5, thus implying a more extensive aggregation close to the p*I* (in line with the results for dispersibility). The contributions of the various whey protein fractions in the formation of aggregates were proportional to their concentrations in the initial solution. By analyzing the data from native PAGE (Figure 7), in the aggregation at the three different pH values, α-LA, β-LG, and BSA participated in the following proportions at 90 °C: 28.50 ± 1.15, 69.89 ± 2.37, 1.60 ± 1.45. α-LA, β-LG, and BSA participated in the following proportions at 90*: 27.69 ± 1.33, 69.93 ± 1.79, 2.38 ± 0.88. At these temperatures, systems at pH 3.5 also aggregated into small clusters (SA band on the top of the gel in Figure 6). The SA band progressively reduced with increasing pH due to the larger size of the aggregates, which hindered their transport through the gel.

Unfortunately, the relevance of intermolecular disulfide bonds on aggregation and the relative contributions of α-LA, β-LG, and BSA could not be quantitatively determined on DTT-PAGE for systems at pH 4.0 and 4.5. This was due to the presence of a smeared band between 70 and 30 kDa, which

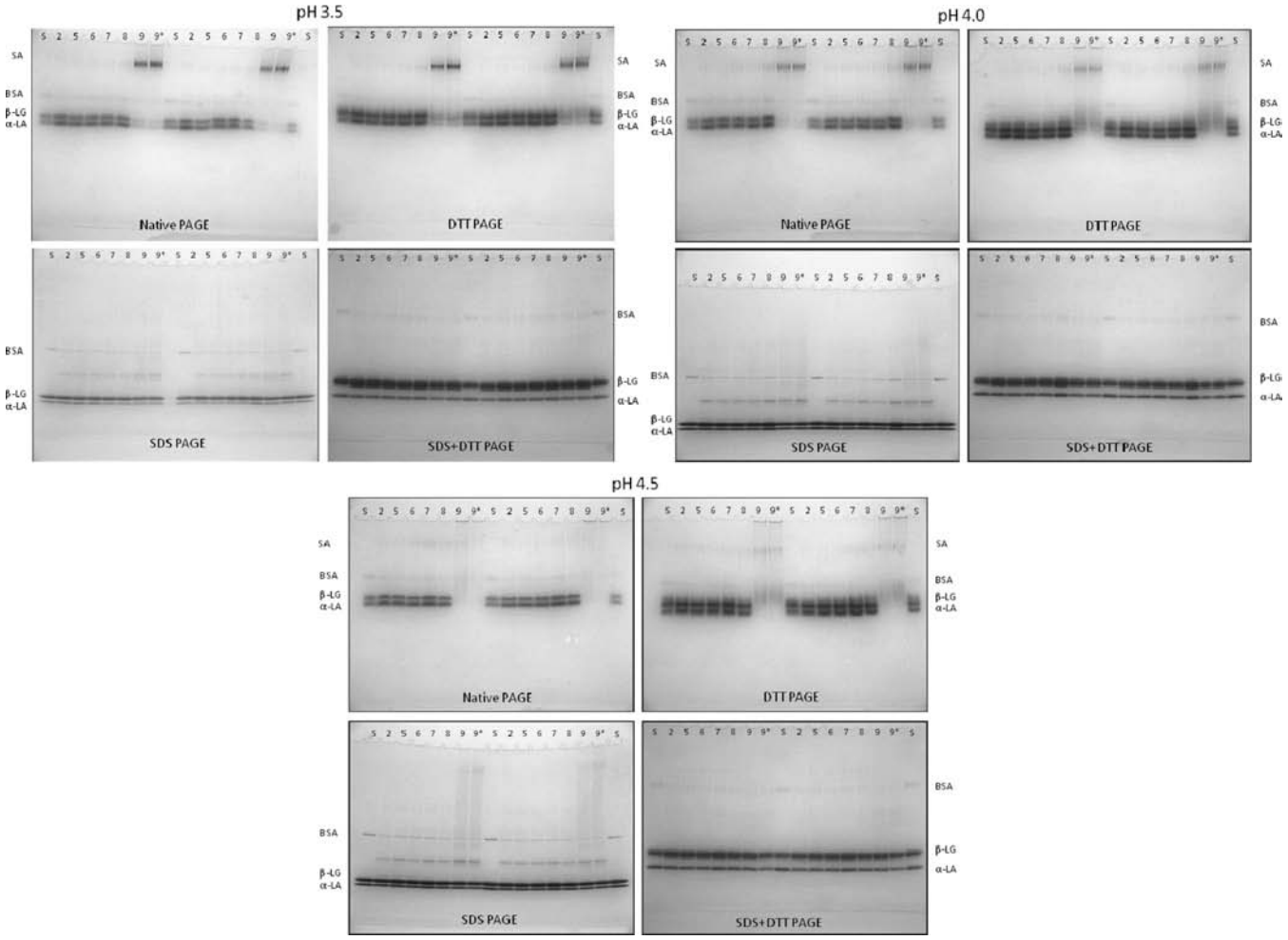

Figure 6. PAGE of dispersed fractions obtained from 10% (w/w) protein solutions. Electrophoresis was performed under native, reducing (DTT), denaturing (SDS), and denaturing and reducing (SDS + DTT) conditions. Lanes: S, standard; 2–9*, heat-treated samples (20, 50, 60, 70, 80, and 90 °C and 90 °C × 30 s).

could not be appropriately analyzed by the imaging software. However, the DTT-PAGE gels revealed that reducing the intermolecular S–S– bridges minimally affected the breakdown of aggregates into the various whey protein fractions. Interestingly, the smeared band visible between 70 and 30 kDa in systems heated at 90 and 90* °C suggests the presence of small aggregates derived from the breakdown of larger aggregates due to the reduction of –S–S– bridges caused by DTT.

SDS-PAGE and SDS-PAGE + DTT highlighted a complete recovery of all the protein fractions when hydrophobic bonds were disrupted. The only exception was BSA, which was partially lost as aggregates. Thus, hydrophobic interactions seem to be the dominating aggregation mechanism. Conversely, the covalent aggregation due to disulfide bonding was negligible; only DTT-PAGE seemed to indicate association of small aggregates via –S–S– bridges.

This result confirms the trend observed by Hoffmann and van Mil,[18] who postulated an increasing importance of noncovalent interactions in heat-treated (65 °C for various time periods) β-LG systems when the pH was closer to the p*I* (the pH range studied was 8–6). Moreover, Surroca et al.[48] excluded the formation of intermolecular –S–S– bridges in β-LG systems at pH 4.6 in the early stages of heat-induced aggregation (68.5 °C). However, despite the reduced reactivity of thiol groups at acidic pH, the formation of intermolecular disulfide bonds in acid-induced gels of heat-denatured whey proteins was observed earlier.[30,40,41,49] These authors postulated that the disulfide bond formation was favored by the effective concentration of thiol groups, which were placed in close proximity upon the physical aggregation of the protein. Accordingly, association driven by hydrophobic interactions was observed by Galani[50] for β-LG at pH 6.7, where intermolecular –S–S– bonds were also detected. In the same study, the noncovalent association was reported to be temperature dependent and maximal at 90–100 °C. Lupano, Renzi, and Romera[27] reported the lack of intermolecular –S–S– bonds in WPC gels obtained by heating (87 °C for 45 min) 10% protein solutions at pH 3.5 and 4.0. However, the same authors highlighted the presence of –S–S– bonds in gels obtained at pH 4.25.

The PAGE confirmed the limited contribution of covalent disulfide bridging in heat-induced whey protein aggregates at moderately acidic conditions and clearly highlighted the hydrophobic interactions as the driving mechanism behind the aggregation effect as the predominant association force. However, residual activity of free thiols was responsible for the association of intermediate-size whey protein clusters at pH 4.0 and 4.5.

dx.doi.org/10.1021/jf404456q | J. Agric. Food Chem. 2014, 62, 733–741

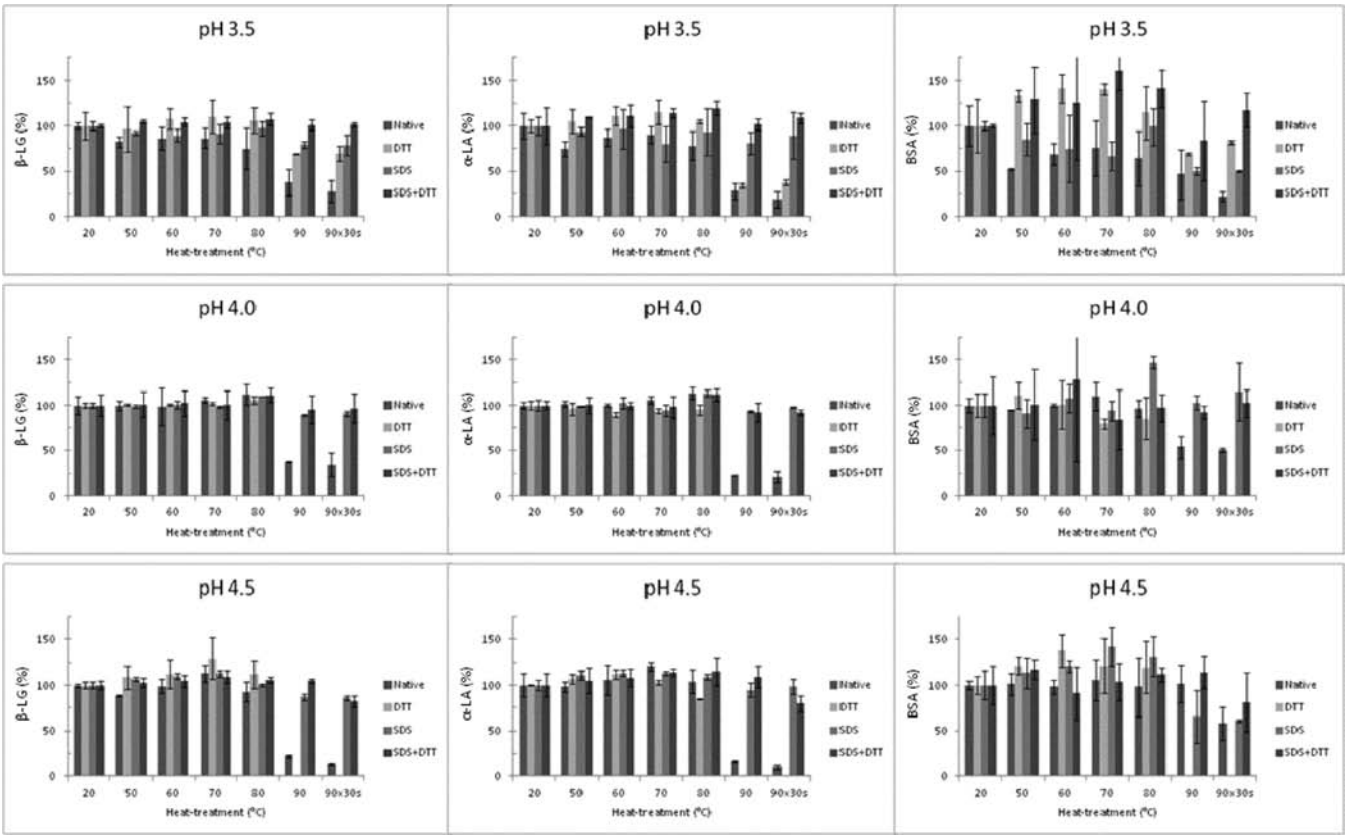

Figure 7. Concentration (%, w/w) of α-LA, β-LG, and BSA after heat treatment (20, 50, 60, 70, 80, and 90 °C and 90 °C × 30 s) in 10% (w/w) whey protein systems determined by native, DTT, SDS, and SDS + DTT electrophoresis. Data of DTT PAGE are missing for pH 4.0 and 4.5 systems treated at 90 and 90 °C × 30 s.

In conclusion, the association of whey protein isolate solutions is controlled by complicated mechanisms that are influenced by both pH and heat treatment. Close to the p*I*, the reduced intermolecular electrostatic repulsions facilitated the association of protein molecules, which caused a loss of protein dispersibility. Unfolding of the globular whey protein structure upon heating in aqueous systems between pH 3.5 and 4.5 showed that noncovalent hydrophobic interactions were the driving mechanism for aggregation, whereas intermolecular disulfide bridging contributed only in a limited way to the aggregation mechanism.

Microscopic and macroscopic observations revealed that the extent of aggregation was limited further away from the p*I* (i.e., pH 3.5), where aggregates were small and had a more open structure.

■ ASSOCIATED CONTENT

Ⓢ Supporting Information

Figures S1 and S2. This material is available free of charge via the Internet at http://pubs.acs.org.

■ AUTHOR INFORMATION

Corresponding Author

*(L.C.) Phone: +31 30 2095000. E-mail: leonardo.cornacchia@danone.com. Fax: +31 30 2100436.

Funding

This work is supported by NanoNextNL, a micro- and nanotechnology consortium of the Government of The Netherlands and 130 partners.

Notes

The authors declare no competing financial interest.

■ REFERENCES

(1) Smithers, G. W. Whey and whey proteins—from 'gutter-to-gold'. *Int. Dairy J.* **2008**, *18*, 695−704.

(2) Wolfe, R. R.; Miller, S. L.; Miller, K. B. Optimal protein intake in the elderly. *Clin. Nutr.* **2008**, *27*, 675−684.

(3) LaClair, C. E.; Etzel, M. R. Ingredients and pH are key to clear beverages that contain whey protein. *J. Food Sci.* **2010**, *75*, C21−C27.

(4) Monahan, F. J.; German, J. B.; Kinsella, J. E. Effect of pH and temperature on protein unfolding and thiol/disulfide interchange reactions during heat-induced gelation of whey proteins. *J. Agric. Food Chem.* **1995**, *43*, 46−52.

(5) Belmar-Beiny, M. T.; Fryer, P. J. Preliminary stages of fouling from whey protein solutions. *J. Dairy Res.* **1993**, *60*, 467−483.

(6) Simpson, R. *Engineering Aspects of Thermal Food Processing*; CRC Press: Boca Raton, FL, USA, 2010.

(7) de Wit, J. Nutritional and functional characteristics of whey proteins in food products. *J. Dairy Sci.* **1998**, *81*, 597−608.

(8) Pelegrine, D.; Gasparetto, C. Whey proteins solubility as function of temperature and pH. *LWT−Food Sci. Technol.* **2005**, *38*, 77−80.

(9) Nicolai, T.; Britten, M.; Schmitt, C. β-Lactoglobulin and WPI aggregates: formation, structure and applications. *Food Hydrocolloids* **2011**, *25*, 1945−1962.

(10) De Wit, J.; Kessel, T. v. Effects of ionic strength on the solubility of whey protein products. A colloid chemical approach. *Food Hydrocolloids* **1996**, *10*, 143−149.

(11) Majhi, P. R.; Ganta, R. R.; Vanam, R. P.; Seyrek, E.; Giger, K.; Dubin, P. L. Electrostatically driven protein aggregation: β-lactoglobulin at low ionic strength. *Langmuir* **2006**, *22*, 9150−9159.

(12) Langton, M.; Hermansson, A.-M. Fine-stranded and particulate gels of β-lactoglobulin and whey protein at varying pH. *Food Hydrocolloids* **1992**, *5*, 523−539.
(13) Bromley, E.; Krebs, M.; Donald, A. Mechanisms of structure formation in particulate gels of β-lactoglobulin formed near the isoelectric point. *Eur. Phys. J. E* **2006**, *21*, 145−152.
(14) Creamer, L. K.; Bienvenue, A.; Nilsson, H.; Paulsson, M.; van Wanroij, M.; Lowe, E. K.; Anema, S. G.; Boland, M. J.; Jiménez-Flores, R. Heat-induced redistribution of disulfide bonds in milk proteins. 1. Bovine β-lactoglobulin. *J. Agric. Food Chem.* **2004**, *52*, 7660−7668.
(15) Visschers, R. W.; de Jongh, H. H. Disulphide bond formation in food protein aggregation and gelation. *Biotechnol. Adv.* **2005**, *23*, 75−80.
(16) Ako, K.; Nicolai, T.; Durand, D.; Brotons, G. Micro-phase separation explains the abrupt structural change of denatured globular protein gels on varying the ionic strength or the pH. *Soft Matter* **2009**, *5*, 4033−4041.
(17) Roefs, S. P.; Kruif, K. G. A model for the denaturation and aggregation of β-lactoglobulin. *Eur. J. Biochem.* **1994**, *226*, 883−889.
(18) Hoffmann, M. A.; van Mil, P. J. Heat-induced aggregation of β-lactoglobulin: role of the free thiol group and disulfide bonds. *J. Agric. Food Chem.* **1997**, *45*, 2942−2948.
(19) McGuffey, M. K.; Otter, D. E.; van Zanten, J. H.; Foegeding, E. A. Solubility and aggregation of commercial α-lactalbumin at neutral pH. *Int. Dairy J.* **2007**, *17*, 1168−1178.
(20) Tolkach, A.; Kulozik, U. Reaction kinetic pathway of reversible and irreversible thermal denaturation of β-lactoglobulin. *Lait* **2007**, *87*, 301−315.
(21) Aymard, P.; Nicolai, T.; Durand, D.; Clark, A. Static and dynamic scattering of β-lactoglobulin aggregates formed after heat-induced denaturation at pH 2. *Macromolecules* **1999**, *32*, 2542−2552.
(22) Akkermans, C.; Venema, P.; van der Goot, A. J.; Gruppen, H.; Bakx, E. J.; Boom, R. M.; van der Linden, E. Peptides are building blocks of heat-induced fibrillar protein aggregates of β-lactoglobulin formed at pH 2. *Biomacromolecules* **2008**, *9*, 1474−1479.
(23) Phan-Xuan, T.; Durand, D.; Nicolai, T.; Donato, L.; Schmitt, C.; Bovetto, L. On the crucial importance of the pH for the formation and self-stabilization of protein microgels and strands. *Langmuir* **2011**, *27*, 15092−15101.
(24) Schmitt, C.; Bovay, C.; Vuilliomenet, A.-M.; Rouvet, M.; Bovetto, L.; Barbar, R.; Sanchez, C. Multiscale characterization of individualized β-lactoglobulin microgels formed upon heat treatment under narrow pH range conditions. *Langmuir* **2009**, *25*, 7899−7909.
(25) Sağlam, D.; Venema, P.; de Vries, R.; van Aelst, A.; van der Linden, E. Relation between gelation conditions and the physical properties of whey protein particles. *Langmuir* **2012**, *28*, 6551−6560.
(26) Sağlam, D.; Venema, P.; De Vries, R.; Sagis, L.; Van der Linden, E. Preparation of high protein micro-particles using two-step emulsification. *Food Hydrocolloids* **2011**, *25*, 1139−1148.
(27) Lupano, C. E.; Renzi, L. A.; Romera, V. Gelation of whey protein concentrate in acidic conditions: effect of pH. *J. Agric. Food Chem.* **1996**, *44*, 3010−3014.
(28) Ellman, G. L. Tissue sulfhydryl groups. *Arch. Biochem. Biophys.* **1959**, *82*, 70−77.
(29) Shimada, K.; Cheftel, J. C. Sulfhydryl group/disulfide bond interchange reactions during heat-induced gelation of whey protein isolate. *J. Agric. Food Chem.* **1989**, *37*, 161−168.
(30) Alting, A. C.; Hamer, R. J.; de Kruif, C. G.; Visschers, R. W. Formation of disulfide bonds in acid-induced gels of preheated whey protein isolate. *J. Agric. Food Chem.* **2000**, *48*, 5001−5007.
(31) Gasymov, O. K.; Glasgow, B. J. ANS fluorescence: Potential to augment the identification of the external binding sites of proteins. *Biochim. Biophys. Acta (BBA)−Proteins Proteomics* **2007**, *1774*, 403−411.
(32) Zhou, P.; Liu, X.; Labuza, T. P. Moisture-induced aggregation of whey proteins in a protein/buffer model system. *J. Agric. Food Chem.* **2008**, *56*, 2048−2054.
(33) Schmitt, C.; Bovay, C.; Rouvet, M.; Shojaei-Rami, S.; Kolodziejczyk, E. Whey protein soluble aggregates from heating with NaCl: physicochemical, interfacial, and foaming properties. *Langmuir* **2007**, *23*, 4155−4166.
(34) Donato, L.; Schmitt, C.; Bovetto, L.; Rouvet, M. Mechanism of formation of stable heat-induced β-lactoglobulin microgels. *Int. Dairy J.* **2009**, *19*, 295−306.
(35) Potes, N.; Kerry, J. P.; Roos, Y. H. Oil as reaction medium for glycation, oxidation, denaturation, and aggregation of whey protein systems of low water activity. *J. Agric. Food Chem.* **2013**, *61*, 3748−3756.
(36) Lumry, R.; Eyring, H. Conformation changes of proteins. *J. Phys.Chem.* **1954**, *58*, 110−120.
(37) Wang, W.; Nema, S.; Teagarden, D. Protein aggregation—pathways and influencing factors. *Int. J. Pharm.* **2010**, *390*, 89−99.
(38) De Wit, J. Thermal behaviour of bovine β-lactoglobulin at temperatures up to 150 C. A review. *Trends Food Sci. Technol.* **2009**, *20*, 27−34.
(39) Cecil, R. The role of sulfur in proteins. In *The Proteins, Composition, Structure, And Function*; Neurath, H., Ed.; Academic Press: New York, 1963; Vol. 1, pp 379−476.
(40) Alting, A. C.; Weijers, M.; de Hoog, E. H.; van de Pijpekamp, A. M.; Cohen Stuart, M. A.; Hamer, R. J.; de Kruif, C. G.; Visschers, R. W. Acid-induced cold gelation of globular proteins: effects of protein aggregate characteristics and disulfide bonding on rheological properties. *J. Agric. Food Chem.* **2004**, *52*, 623−631.
(41) Alting, A. C.; Hamer, R. J.; de Kruif, C. G.; Paques, M.; Visschers, R. W. Number of thiol groups rather than the size of the aggregates determines the hardness of cold set whey protein gels. *Food Hydrocolloids* **2003**, *17*, 469−479.
(42) Moro, A.; Gatti, C.; Delorenzi, N. Hydrophobicity of whey protein concentrates measured by fluorescence quenching and its relation with surface functional properties. *J. Agric. Food Chem.* **2001**, *49*, 4784−4789.
(43) Nakai, S. Structure-function relationships of food proteins: with an emphasis on the importance of protein hydrophobicity. *J. Agric. Food Chem.* **1983**, *31*, 676−683.
(44) Verheul, M.; Pedersen, J. S.; Roefs, S. P.; de Kruif, K. G. Association behavior of native β-lactoglobulin. *Biopolymers* **1999**, *49*, 11−20.
(45) Boye, J. I.; Alli, I. Thermal denaturation of mixtures of α-lactalbumin and β-lactoglobulin: a differential scanning calorimetric study. *Food Res. Int.* **2000**, *33*, 673−682.
(46) Jung, J.-M.; Savin, G.; Pouzot, M.; Schmitt, C.; Mezzenga, R. Structure of heat-induced β-lactoglobulin aggregates and their complexes with sodium dodecyl sulfate. *Biomacromolecules* **2008**, *9*, 2477−2486.
(47) Sullivan, S. T.; Khan, S. A.; Eissa, A. S. Whey proteins: functionality and foaming. *Whey Process., Funct. Health Benefits* **2009**, *82*, 99.
(48) Surroca, Y.; Haverkamp, J.; Heck, A. Towards the understanding of molecular mechanisms in the early stages of heat-induced aggregation of β-lactoglobulin AB. *J. Chromatogr., A* **2002**, *970*, 275−285.
(49) Alting, A. C.; Hamer, R. J.; de Kruif, C. G.; Visschers, R. W. Cold-set globular protein gels: interactions, structure and rheology as a function of protein concentration. *J. Agric. Food Chem.* **2003**, *51*, 3150−3156.
(50) Galani, D. Heat-induced denaturation and aggregation of β-lactoglobulin: kinetics of formation of hydrophobic and disulphide-linked aggregates. *Int. J. Food Sci. Technol.* **1999**, *34*, 467−476.

JOURNAL OF AGRICULTURAL AND FOOD CHEMISTRY

Article

pubs.acs.org/JAFC

Preparation and Physicochemical Properties of Whole-Bean Soymilk

Hsin-Yu Kuo,[†] Shih-Hsin Chen,[‡] and An-I Yeh*[,†]

[†]Graduate Institute of Food Science and Technology, National Taiwan University, 1 Roosevelt Road, Section 4, Taipei 10617, Taiwan

[‡]Department of Food Science, National Ilan University, Ilan, 1 Shen-Lung Road, Section 1I-Lan 260, Taiwan

ABSTRACT: Whole-bean soymilk has been prepared by using media-milling. Some characteristics of media-milled soymilk have been determined and compared with filtered soymilk (similar to commercial ones) and whole-bean soymilk prepared by blending. There existed particles in the nano/submicrometer scale in both media-milled and filtered soymilk. The particles in blended soymilk were greater than 1 μm. Media-milled soymilk was the most stable among three samples, even after autoclaving. Solid recovery (98.44 ± 0.16%), viscosity (160.59 ± 4.26 cps), dietary fiber (22.68 ± 0.97% on dry basis), total polyphenol recovery (95.15 ± 7.09%), and isoflavone content (4.42 ± 0.03 mg/g dry solid) of media-milled samples were greater than those of filtered ones. Aglycones, the most bioactive form of isoflavone, in autoclaved media-milled soymilk were more than 2-fold those in autoclaved filtered soymilk. With almost no okara generated, the media-milled soymilk retained fiber in soybeans which would be beneficial to human health.

KEYWORDS: *soymilk, media milling, isoflavone, whole bean*

INTRODUCTION

Soymilk, an aqueous extract of soybeans, is a traditional beverage consumed for centuries in Asia. Soymilk provides high-quality proteins and essential fatty acids containing no cholesterol, gluten, and lactose. Thus, it is a good dietary protein source for general consumers or vegetarians and is a suitable substitute of cow's milk for lactose-intolerant populations.[1] In addition, there exist various biologically active phytochemicals such as isoflavones, polyphenols, phytate, saponins, lecithin, phytosteroids, and tocopherol.[2] Isoflavones, a plant derived phytoestrogen, have caught considerable attention due to its biological activities including antioxidation and prevention of cardiovascular diseases, type 2 diabetes, cancers, osteoporosis, as well as relief of menopausal syndromes.[3−8] Isoflavones can be divided into three types, daidzein, genistein, and glycitein, and each type consists of four different chemical forms which are β-glucoside, 6″-*O*-acetyl-β-glucoside, 6″-*O*-malonyl-β-glucoside, and aglycone.[9] During soymilk production, some processes such as soaking, grinding, filtering, and heating result in loss of isoflavones to different degrees.[10,11] These processes generally result in high loss of glucoside and malonylglucoside but increase in aglycone.[11−13]

Via traditional methods, soymilk is produced after soaked soybeans are ground and filtered.[14] To process 1 kg soybean for soymilk manufacture, about 8−10 kg water are added and about 0.3 kg of okara (dry basis) is generated.[15,16] Okara is rich in protein (25.4−28.4%), oil (9.3−10.9%), dietary fiber (52.8−58.1%), and isoflavone (0.14%).[17,18] Jackson et al.[11] have found that the proportion of aglycone in okara is greater than that in soymilk. However, okara is generally considered as waste. It putrefies very quickly due to high water activity, which results in an issue of plant management for commercial production. Whole-bean soymilk can retain original nutrients and is environmentally friendly.

A media mill is derived from a stirred ball mill which is utilized to produce nano/submicrometer particles via a top-down concept and has been applied in paint and pharmaceutical industries. During media-milling, material is comminuted among the stirring media, the grinding chamber wall, and the material itself by friction, impact, compression, and shearing forces.[19] Yeh et al.[20] have revealed that media-milling can significantly decrease crystallinity and average particle size (to submicrometer scale) and effectively enhance the enzymatic hydrolysis of microcrystalline cotton cellulose. Nano/submicrometer corn starch has been prepared by using media-milling and exhibits unique pasting properties.[21] Media-milling appears to be an attractive method for utilizing whole edible materials.

The objectives of this study were to explore the feasibility of preparing whole-bean soymilk by using media-milling and to understand the physicochemical properties of media-milled soymilk.

MATERIALS AND METHODS

Samples. Soybean (Kaohsiung no. 1 cultivar, moisture content 9.24 ± 0.13%) was provided by the Kaohsiung District Agricultural Research and Extension Station and was stored at 4 °C until use.

Soybean Flour Preparation. Soybeans were milled in a commercial pulverizing machine (RT-04, Hsin An Instrument Co. Ltd., Taipei, Taiwan) for 1−2 min through a 20-mesh sieve.

Soymilk Preparation. Soybeans (60 g) were soaked in deionized water (440 g) overnight at 4 °C and then ground by using a laboratory blender (MX-7012S, Waring Laboratory Science, New Hartford, CT, USA) for 3−4 min. The soybean slurry was used to prepare filtered, blended, and media-milled soymilk.

Filtered Soymilk (FS). The soybean slurry was filtered through a double-layered cheese cloth. The filtrate was designated as filtered soymilk, which was similar to the commercial products in Taiwan. The pulp was considered as okara.

Received: October 4, 2013
Revised: December 3, 2013
Accepted: December 31, 2013
Published: December 31, 2013

ACS Publications © 2013 American Chemical Society

Blended Soymilk (BS). The soybean slurry was further minced by using a high-speed blender (PT 3100, Kinematica, Lucerne, Switzerland) at 2000 rpm for 10 min to obtain the blended soymilk. As no okara was produced, its composition was similar to whole soybeans.

Media-Milled Soymilk (MS). The media-milled soymilk was prepared by using a media mill (Minipur, Netzsch-Feinmahltechnik GmbH, Germany) with a driving motor of 0.94 kW. Media (0.8 mm, yttria-stabilized tetragonal zirconia, YTZ) at 70% v/v filling ratio was loaded in the milling chamber (200 mL). The soybean slurry was loaded into a jacket-cooling tank and then fed at a flow rate of 350 mL/min into the milling chamber by a circulating pump. The agitation speed was set at 3000 rpm, and the milling was conducted for 60 min. During milling, particles smaller than the gap (0.30 mm) of the media separator were driven back to the stirred tank for cooling by the circulation system. The temperature of the soymilk was maintained below 30 °C during milling.

Generally, soymilk is cooked or autoclaved before consumption. To minimize the effect of concentration, the solid contents of three soymilks were adjusted to 7% (w/w) and then heated by an autoclave (TM-325, Tomin Medical Equipment Co. Ltd., Taipei, Taiwan) at 121 °C for 3 min.[22] The effects of heating on pH, viscosity, and stability of soymilk were explored.

Particle Size Distribution (PSD). Particle size distribution of samples was measured by using a laser diffraction particle size analyzer (LS 230, Beckman Coulter, Fullerton, CA) with a detection range of 0.04−2000 μm. The instrument was calibrated with deionized water. All samples were diluted 10-fold with deionized water and vortexed for 10 s. Average diameters of particles were obtained using the following equations.

by volume

$$D_V = \sum_i \frac{n_i d_i^4}{n_i d_i^3}$$

by number

$$D_N = \sum_i \frac{n_i d_i}{n_i}$$

where n_i was the number of i particle with diameter of d_i. All of the measurements were done in triplicate, and the average data were reported.

Morphology. Morphology of suspended particles in soymilk was examined by optical microscope (OM) (model TS100, Nikon Co., Tokyo, Japan) and scanning electron microscope (SEM) (Hitachi S-800, Hitachi Co. Ltd., Tokyo, Japan). Diluted samples (1%, w/w) were used for OM observation. For SEM, critical-point drying was used to prepare samples. Ten-fold diluted soymilk (FS, BS, or MS, 1 mL) was mixed with 9 mL of acetone and then evaporated to 1 mL at 60 mmHg. After repeating the replacement process in triplicate, solids were suspended in 5 mL of acetone. The suspension was further dried using liquid CO_2 in a critical-point drying apparatus (Hitachi HCP-2, Hitachi Co. Ltd., Tokyo, Japan) at 31.1 °C and 73.9 bar. After being dried, the sample was attached on a SEM stub using double-backed cellophane tape. The stub and sample were coated with gold−palladium and then were examined and photographed at 20 kV.

Viscosity. A rheometer (AR 2000ex, TA Instruments, New Castle, NJ, USA) was employed to measure the viscosity of soymilk. Soymilk (30 mL) was transferred into a concentric cylinder system with a procedure of FLOW. The viscosity of soymilk was measured at 25 °C using steady mode with a shear rate at 100 s^{-1}. In addition, the solid content of MS was adjusted to 7, 8, 9, and 10% (w/w) for understanding the effect of solid content on the viscosity of MS.

pH. The pH of sample was determined by using a pH meter (SP-2200, Suntex Instrument Co., Ltd., Taipei, Taiwan).

Stability. The stability of soymilk was determined by using a demixing tester (LUMiCheck, L.U.M. GmbH, Berlin, Germany). About 3 mL of sample was loaded into the sample cell. The intensity of light (870 nm) backscattered from the tilted bottom of the cell was detected every 5 min for 12 h. The stability was expressed by the difference (ΔI_{t-0}) in the light intensity at time of t (I_t) and initial state (0 min) (I_0) along with time. A positive ΔI_{t-0} indicates the occurrence of precipitation. Once floating or foaming occurred, ΔI_{t-0} drops with time. For a stable suspension, ΔI_{t-0} does not change significantly with time.

Composition Analysis. After freeze-drying, the lyophilized powder of soymilk was used for composition analysis. The contents of moisture, ash, crude fat, crude protein, and dietary fiber (including soluble, insoluble, and total fiber) were determined according to the methods of the Association of Official Analytical Chemists (AOAC).[23]

Total Polyphenol Content. The content of total polyphenol was determined according to the method of Xu and Chang.[24] Soybean flour and lyophilized soymilk powders (0.5 g) were extracted with 5 mL of acetone/water (50/50, v/v), and the mixture was stirred at 300 rpm for 3 h. After centrifuging at 3000 rpm for 10 min, the supernatant was collected. The precipitate was extracted again via the procedures described above. Both supernatants were combined and added with 50% acetone to be 10 mL and stored at 4 °C in the dark until analysis.

The total polyphenol content was determined by a Folin−Ciocalteu assay[25] using gallic acid as a standard.[26] The mixture of 50 μL sample solution, 3 mL of distilled water, 250 μL of Folin−Ciocalteu's reagents solution, and 750 μL of 7% sodium carbonate (Na_2CO_3) were vortexed and incubated for 8 min in the dark at 25 °C. Then, 950 μL of distilled water was added. The mixture was left in the dark for reaction for 2 h at 25 °C. The absorbance was measured at 765 nm. The total polyphenol content was obtained against the calibration curve of gallic acid and expressed as gallic acid equivalents (mg of GAE/g of dry sample or mg of gallic acid/100 g undiluted soymilk). The calibration curve of gallic acid was established with concentration of 12.5−1000 μg/mL.

Isoflavone Content. *Isoflavone Extraction.* The extraction procedure was conducted according to the method described by Murphy et al.[27] Soymilk samples were freeze-dried and sieved through a 60-mesh (for FS and MS) or 20-mesh (for BS) sifter. Lyophilized powder (1.0 g) was extracted with 10 mL of acetonitrile, 7 mL of deionized water, and 2 mL of 0.1 N HCl by stirring (400 rpm) at room temperature for 2 h and then filtered through Whatman no. 1 filter paper. The filtrate was evaporated to remove solvent at vacuum conditions and then was dissolved in 2 mL of 80% methanol. The solution was seeped through a 0.45 μm nylon syringe filter. Fluorescein (1000 μg/mL) was added into filtrate as an internal standard with a ratio of fluorescein solution to a sample solution of 1:9 (v/v). After being analyzed by using HPLC, the content of isoflavone was calculated using an internal standard method reported by Kao and Chen.[28] A calibration curve is required to quantitatively determine the concentration of isoflavone by utilizing the internal standard method. To establish calibration curves, each individual isoflavone compound was dissolved in 80% methanol at a concentration of 1000 μg/mL, which was further diluted at different concentrations (3.125, 6.25, 12.5, 25, 50, 100, 200 μg/mL) as standard solutions. Filtration and addition of fluorescein solution were conducted as described above for HPLC analysis.

HPLC Analysis. The high-performance liquid chromatography (HPLC) method[9] with minor modification was employed to determine the content of isoflavones. The HPLC used was equipped with a C18 column (4.6 mm × 250 mm, YMC-Pack ODS-AM, S-5 μm, YMC Co., Tokyo, Japan), a UV−vis detector (UV-2075 Plus, Jasco, Tokyo, Japan), and a chromatography data processor (EC 2000, Analab Co., Taipei, Taiwan). Linear concentration gradient in mobile phase was conducted by using two solutions: (A) 0.1% glacial acetic acid in deionized H_2O and (B) 0.1% glacial acetic acid in acetonitrile. After a 20 μL sample was injected into the column, a percentage of solvent B was increased from 15% to 20% in 20 min, successively increased to 24% in 10 min, and held for 4 min then further increased to 35% in 10 min and held for 8 min, and finally reduced to 15% in 5 min and held for 3 min. The total time was 60 min. The flow rate of the mobile phase was 1.0 mL/min.

Statistical Analysis. Data were reported as the mean of measurements in triplicate. One-way analysis of variance (ANOVA)

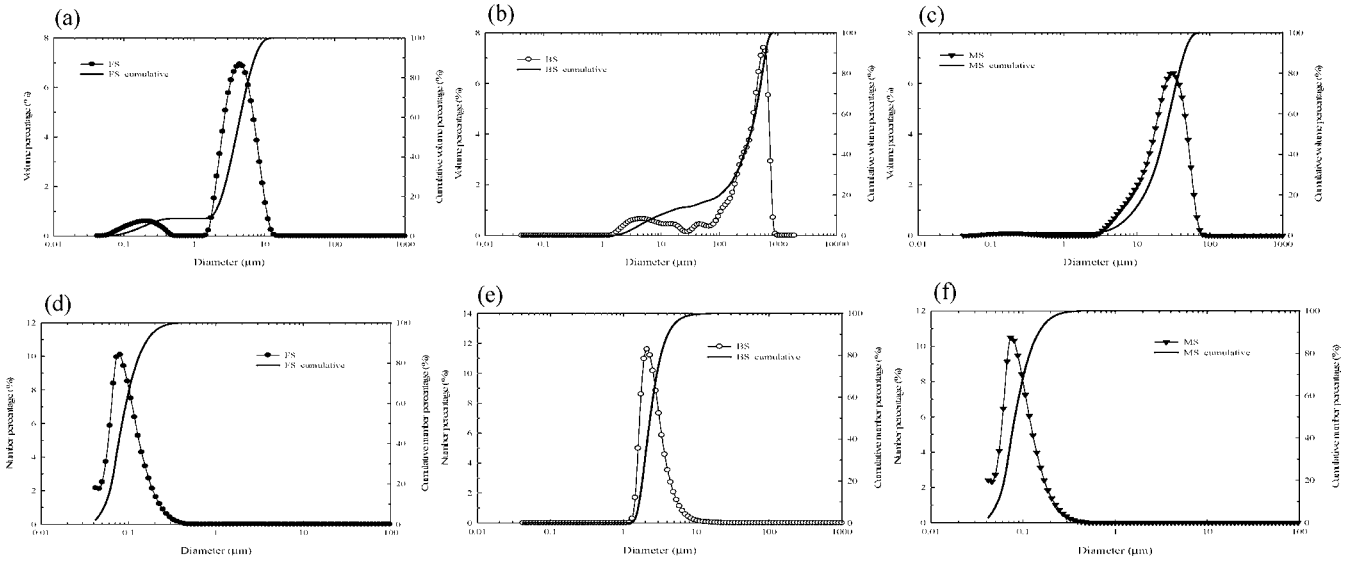

Figure 1. Particle size distribution: (a−c) volume and (d−f) number of (a,d) filtered (FS), (b,e) blended (BS), and (c,f) media-milled (MS) soymilk.

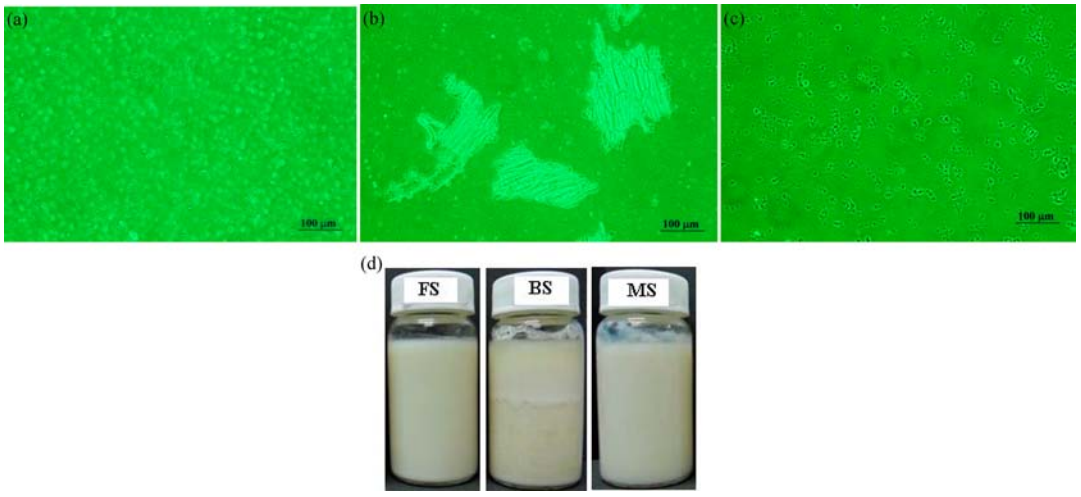

Figure 2. (a−c) Optical microscopic observation and (d) appearance of (a) filtered (FS), (b) blended (BS), and (c) media-milled (MS) soymilk

was used to determine the significance of treatment using the Statistical Analysis System (SAS version 9.1; SAS Institute Inc., Cary, NC), followed by a Duncan's new multiple range test. Differences were considered as statistically significant when the P value was <0.05.

RESULTS AND DISCUSSION

Particle Size Distribution (PSD). FS exhibited a bimodal distribution in terms of volume with a volume-mean diameter of 4.40 ± 2.39 μm and largest particle of 16.4 μm (Figure 1a), which was similar to the data in the literature.[14,29] Small particles ranged from 0.042 to 0.571 μm, and large particles ranged from 1.321 to 16.4 μm. The percentage of small particles was 8.8%. The presence of a two particle range might induce instability of soymilk. The particle size distribution in terms of number provided the evidence that almost all the particles (99.93%) were smaller than 1 μm with a number-mean diameter of 0.103 ± 0.086 μm. The percentage of the number of particles smaller than 0.1 μm was about 65% (Figure 1d). The grinding generated ultrafine particles, and the removal of large particles by filtration resulted in high percentage of nanoparticles. That was similar to commercial soymilk in Taiwan. BS exhibited similar bimodal size distribution (in volume) but with a much greater volume-mean diameter of 348 ± 227 μm (Figure 1b) and with most of particles ranging from 100 to 1000 μm. Because of fast precipitation, particles greater than 1000 μm were not detected during size measurement. The largest particle was about 905 μm, and there were no particles smaller than 1 μm (Figure 1e). Media-milling resulted in a skewed particle size distribution in terms of volume (Figure 1c) with a volume-mean diameter of 26.6 ± 14.6 μm. Apparently, there existed very few particles smaller than 1 μm. Thus, the size distribution was monomodal. Most of the particles ranged from 2.313 to 87.9 μm. The presence of larger particles in MS was due to greater content in fiber. The monomodal size distribution might let the product exhibit reasonable stability. Nevertheless, the size distribution (Figure 1f) in terms of number was similar to that of FS with most of particles (99.97%) smaller than 1 μm. The number-mean diameter was 0.099 ± 0.095 μm with 68% of particles smaller than 0.1 μm. The data indicated that media-milling resulted in a soymilk similar to FS in terms of particle size.

Morphology. FS appeared to be well dispersed (Figure 2a) due to the removal of coarse particles by filtration. Nonetheless, there existed unbroken cell walls or fibers (about 200−300 μm)

dx.doi.org/10.1021/jf404465w | J. Agric. Food Chem. 2014, 62, 742−749

in BS (Figure 2b). The force exerted by the high-speed blender was not adequate to break the fibrillar structure. Media-milling did break soybean structure down to the nano/submicrometer scale (Figure 2c). There was no precipitation observed for FS and MS (Figure 2d), but precipitation occurred remarkably in BS. The morphology of three samples were further examined by using a scanning electron microscope (SEM). Both FS (Figure 3a,b) and MS (Figure 3e,f) exhibited similar

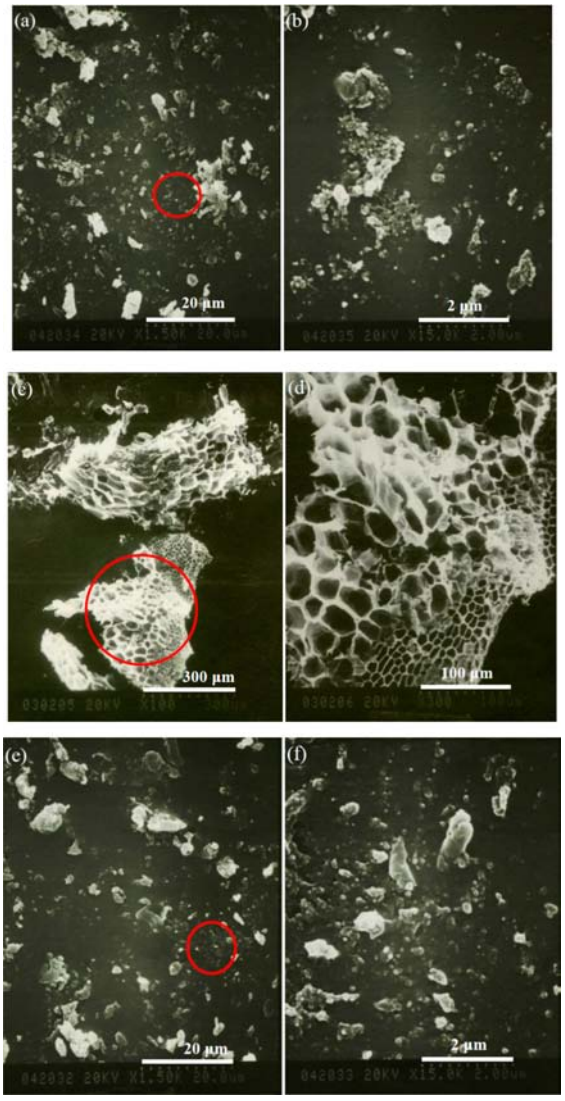

Figure 3. SEM micrographs of (a) filtered, (c) blended, and (e) media-milled soymilk. (b,d,f) Enlargement of circle portion in (a), (c), and (e), respectively.

morphology and particle size. Although there were some particles greater than 1 μm, most particles were smaller than 1 μm (Figure 3b,f). In BS, there were large particles (greater than 300 μm) which appeared to be cell walls (Figure 3c,d). SEM confirmed the presence of nano/submicrometer particles in FS and MS.

Physical Properties. As described previously, a constant percentage (10.89% db) of soybean was used to prepare all soymilk samples. The solid contents in BS (10.61%) and MS (10.72%) were similar due to retaining the whole soybean with minimum okara. The solid content in FS was 8.24%, indicating a solid loss more than 20%. The filtration resulted in more okara and low solid recovery (75.67 ± 0.74%), which was close to that (74.48%) reported by Wang and Murphy.[10] The viscosity (160.59 ± 4.26 cps) of MS was about 38-fold of that (4.22 ± 0.02 cps) of FS, probably due to greater content in solid and fiber, which have been shown to exhibit high swelling power[30] and water retention capacities[31] as well as viscosity. Because of fast precipitation, the viscosity of BS was not determined. The solid content did affect the viscosity of MS (Figure 4). The viscosity of MS was increased linearly with

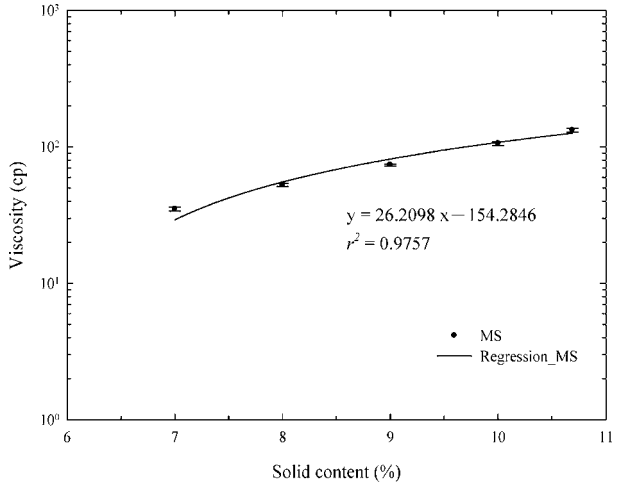

Figure 4. Viscosity versus solid content of media-milled (MS) soymilk.

solid content with a coefficient of determination (r^2) of 0.98. Calculated from Figure 4, the viscosity of MS at 8.24% solid was 61.68 cps, which was much greater than that of FS. The data indicated that the presence of fiber resulted in high viscosity. Via media-milling, less soybean was needed to achieve similar viscosity of FS.

Heating or autoclaving are required in commercial processes. To minimize the effect of solid content on the properties measured, the solid contents of all the samples were adjusted to about 7% before autoclaving. Both solid content and pH were not significantly altered by autoclaving (Table 1). The viscosity

Table 1. Solid Content, Viscosity, and pH[a] of Filtered (FS), Blended (BS), and Media-Milled (MS) Soymilk[b] before and after Autoclaving

sample	autoclaving[c]	solid content (%)	viscosity[d] (cp)	pH
FS	before	7.04 ± 0.02a	2.91 ± 0.08c	6.44 ± 0.03b
	after	7.07 ± 0.02a	4.26 ± 0.07c	6.53 ± 0.04a
BS	before	7.00 ± 0.08a	NA[e]	6.50 ± 0.04ab
	after	7.04 ± 0.04a		6.56 ± 0.04a
MS	before	7.02 ± 0.01a	35.03 ± 1.18b	6.44 ± 0.01b
	after	7.05 ± 0.07a	38.97 ± 1.50a	6.50 ± 0.01ab

[a]Mean ± standard deviation (n = 3). Values in the same column with different lowercase letters (in a, b ,and c) were significantly different by Duncan's new multiple range test (p < 0.05). [b]The concentration of soybean slurry using to soymilk production was 10.89%. [c]Soymilks were adjusted to 7% (w/w) before autoclaving for minimizing the effect of solid content. [d]Viscosity was measured at shear rate 100 s^{-1}. [e]NA, not available. Viscosity of blended sample was undetectable due to fast precipitation.

dx.doi.org/10.1021/jf404465w | J. Agric. Food Chem. 2014, 62, 742−749

of both FS and MS were increased after autoclaving, probably due to denaturation of protein. After autoclaving, FS exhibited a viscosity of 4.26 cps, which was close to that of heated soymilk (3.56 cps) measured by Toda et al.[14] and were greater than those (1.77−2.55 cps) of soymilks produced from six soybean cultivar.[32] The viscosity of MS (38.97 ± 1.50 cP) was much greater than that of FS due to higher content of dietary fibers.

The stability of soymilk was elucidated by the change in the backscattered-light intensity difference ($\Delta I_{t\text{-}0\ min}$) with time (Figure 5). Without heat treatment, there existed a rapid increase in $\Delta I_{t\text{-}0\ min}$ (Figure 5a) for BS during 95 min, which indicated the occurrence of fast precipitation. Then, $\Delta I_{t\text{-}0\ min}$ reached a plateau, probably due to the completion of precipitation. Nevertheless, autoclaving resulted in a continuous increase in $\Delta I_{t\text{-}0\ min}$ (Figure 5b) showing slow precipitation. The data illustrated that BS was not stable and was not appropriate for commercial use. FS was more stable than BS. The $\Delta I_{t\text{-}0\ min}$ of FS slightly decreased at the beginning, then increased gradually, but increased remarkably after 500 min (Figure 5a) due to precipitation. MS appeared to be the most stable among three samples. There existed a slight decrease in $\Delta I_{t\text{-}0\ min}$ in 300 min. Afterward, the change in $\Delta I_{t\text{-}0\ min}$ was minimum, which indicated the stability of MS due to high viscosity and fine particles. Autoclaving reduced the floating and made both FS and MS be more stable. Heating has been shown to improve the stability of soymilk.[29]

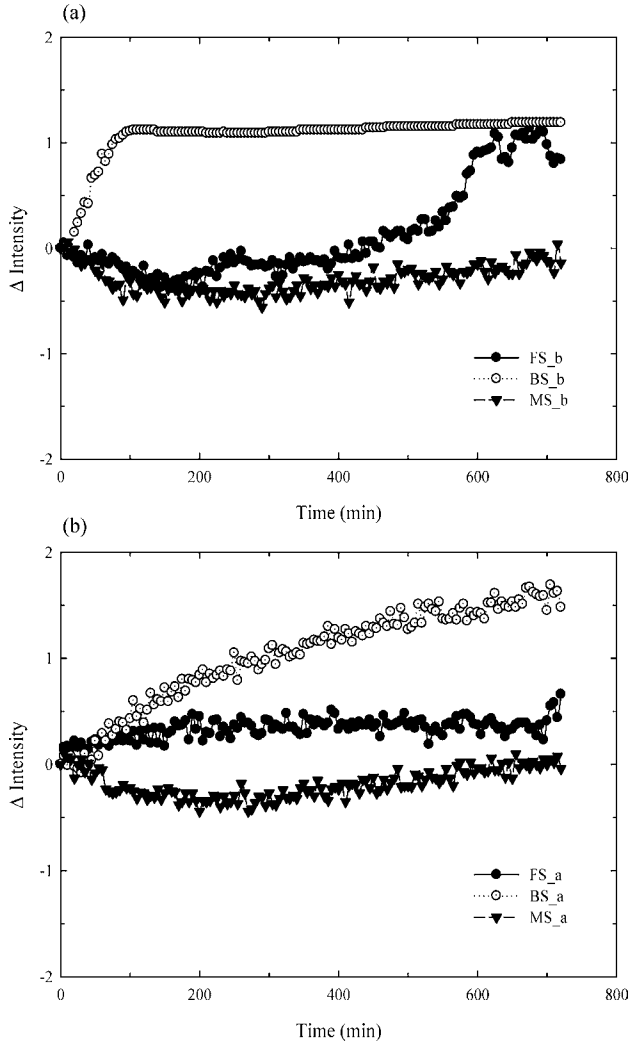

Figure 5. Stability of filtered (FS), blended (BS), and media-milled (MS) soymilk (a) before and (b) after autoclaving.

Composition Analysis. There was no okara during processing, and the compositions of BS and MS were similar to those of soybean flour in terms of crude protein, total dietary fiber, and ash (Table 2). The data of total dietary fiber were close to those (21.1−23.2%) reported by Van der Riet et al.,[17] who pointed out that the dietary fiber content in okara ranged from 52.8 to 58.1% (composed by 40.2−43.6% of insoluble dietary fiber). FS was high in crude fat but low in total dietary fiber (including insoluble and soluble fiber). Compared with soybean flour, MS appeared to have higher content of soluble dietary fiber (4.65 ± 0.79%), probably due to intensive shearing forces during media-milling.

Total Polyphenol Content. The total polyphenol content in soybean flour was 3.30 ± 0.12 mg GAE/g dry solid. In other words, there were 35.94 mg GAE in a 100 g mixture of water and soybean flour. The measurements were slightly greater than literature data (2.15−2.99 mg GAE/g).[33,34] On the basis of the weight of dry solid, FS exhibits the most total polyphenol content among three samples (Table 3). Most of phenolic compounds were not removed by filtration and were reserved in the product.[33,34] Thus, it was reasonable to obtain a high amount of polyphenol in FS. Although BS and MS exhibited similar composition and solid content, MS had higher total polyphenol content than BS. Autoclaving resulted in 7−11% (including three samples) loss of polyphenol due to thermal effect.[33,34] However, on the basis of 100 g of soymilk for general consumption, MS had the highest total polyphenol content among three samples due to highest solid content. Compared with soybean flour, media-milling resulted in the greatest recovery of total polyphenol due to no okara produced and full breakage of the fibrous structure of soybeans by shearing forces. The results were similar to the impact of severe processes (such as steam explosion and high-pressure steam-

Table 2. Proximate Compositions[a] of Soybean Flour, and Filtered (FS), Blended (BS), and Media-Milled (MS) Soymilk Being Autoclaved and Lyophilized

component (%)	flour	FS	BS	MS
crude fat	18.82 ± 0.08b	21.62 ± 1.19a	17.37 ± 0.26c	19.53 ± 0.72b
crude protein	30.91 ± 0.32a	30.84 ± 0.15a	30.19 ± 0.91a	30.20 ± 0.13a
total dietary fiber	22.21 ± 0.60a	5.81 ± 1.02b	21.34 ± 0.69a	22.68 ± 0.97a
insoluble dietary fiber	18.84 ± 1.42a	1.83 ± 0.42b	17.89 ± 0.11a	18.04 ± 1.76a
soluble dietary fiber	3.37 ± 0.82a	3.98 ± 0.60a	3.45 ± 0.58a	4.65 ± 0.79a
ash	6.20 ± 0.07b	7.10 ± 0.02a	6.21 ± 0.01b	6.19 ± 0.04b

[a]All data were presented as percentage (%) on dry weight basis as the mean ± standard deviation (n = 3). Values in the same row with different lowercase letters (in a, b, and c) were significantly different by Duncan's new multiple range test (p < 0.05).

Table 3. Total Polyphenol Content and Recovery[a] of Filtered (FS), Blended (BS), and Media-Milled (MS) Soymilk before and after Autoclaving

sample[b]	mg GAE/g dry solid[c]	mg GAE/100 g soymilk	recovery (%)[d]
FS_b	3.42 ± 0.05a	28.21 ± 0.40c	78.49 ± 1.11c
BS_b	2.69 ± 0.25d	28.54 ± 2.62c	79.39 ± 7.28c
MS_b	3.19 ± 0.24b	34.21 ± 2.55a	95.15 ± 7.09a
FS_a	3.06 ± 0.11bc	25.23 ± 0.89d	70.22 ± 2.47d
BS_a	2.49 ± 0.04e	26.43 ± 0.38d	75.53 ± 1.06d
MS_a	2.94 ± 0.24c	31.51 ± 2.55b	87.65 ± 7.10b

[a]Mean ± standard deviation (n = 3).Values in the same column with different lowercase letters (in a−e) were significantly different by Duncan's new multiple range test ($p < 0.05$). [b]The suffix "b" means "before autoclaving"; "a" means "after autoclaving". [c]GAE, gallic acid equivalents. [d]Recovery (%) = (total polyphenol in 100 g soymilk/35.94 mg GAE) × 100%

ing) generating considerable breakdown of lignocelluloses structure, depolymerization of lignin (a category of phenolic derivates), and defibration and increasing in water-soluble phenolic compounds.[33,35,36]

Isoflavone Content. Isoflavone is a major bioactive compound in soybeans and related products. There were almost no aglycone and low acetylglucoside in soybean flour (Table 4). Processes resulted in the loss of total isoflavone. Compared with soybean flour, the contents of glucoside, malonylglucoside, and acetylglucoside in FS, BS, and MS were significantly decreased. Nevertheless, the content of aglycone in three samples increased and MS yielded the most aglycone. Grinding might raise the activity of β-glucosidase(glucan endo-1,6-β-glucosidase)[37,38] and thus resulted in an increase in unconjugated aglycone (daidzein, genistein, and glycitein). As reported in the literature,[11,33] heating resulted in the loss of isoflavone. After autoclaving, the loss of total isoflavone contents in three samples ranged from 10 to 13%. Autoclaving affected the profile of four categories of isoflavone. Malonylglucoside and aglycone were reduced, but glucoside was increased. Acetylglucoside was not affected significantly. The phenomena were similar to those reported in the literature.[10,33,34,39,40] Among three samples, the percentage of loss of aglycone in FS was the highest (about 65%). This might be the reason why the content of aglycone in commerical soymilk was low. The content of aglycone in MS was the greatest one among three samples, which would be beneficial to human health.

As the price of crops has appreciated in recent years, yield would be a key factor on choosing appropriate process. The total isoflavone conserved in autoclaved FS, BS, and MS from the starting materials was 44.95, 61.09, and 65.83%, respectively. The low recovery of isoflavone in FS was due to the discarding of okara in which there was about one-third of total isoflavone of soybeans and a high proportion of aglycone,[11] probably due to low solubility of aglycone (about 3 μM for geistein and 10 μM for daidzein) in pure water.[41] High recovery of agyclone in MS indicated that media-milling could preserve resources.

Aglycone has been found to exhibit the highest bioavailability among isoflavones.[42,43] Genistein has been found to exhibit more antioxidation capacity than daidzein.[12] In addition, it is the major compound for the chemopreventive efficacy of soy[44] and has been found to exhibit anticancer effects via in vitro and in vivo studies.[8,45] The rise in the content of genistein in MS might increase the health benefits of the product. To decrease serum cholesterol levels and to prevent coronary heart disease (CVD), the USFDA has recommended a daily intake of 25 g of soy protein[46] with about 87.5 mg of isoflavones,[47−51] which is near the daily isoflavones consumption (40−80 mg/day) by Asian people.[52] To achieve a similar purpose, the daily consumption of three soymilks would be 311.72 mL of FS, 229.24 mL of BS, or 212.43 mL of MS. It appeared that the utilization of media-milling could save the use of soybean and thus reduce the cost of production.

Table 4. Isoflavone Contents[a] of Soybean Flour, Lyophilized Filtered (FS), Blended (BS), and Media-Milled (MS) Soymilk

	FS		BS		MS		
isoflavone (mg/g)	unautoclaved	autoclaved	unautoclaved	autoclaved	unautoclaved	autoclaved	flour
Glucoside							
daidzin	0.11 ± 0.00cd	0.46 ± 0.02b	0.13 ± 0.01c	0.52 ± 0.02a	0.10 ± 0.00d	0.45 ± 0.00b	0.44 ± 0.03b
genistin	0.18 ± 0.00c	0.47 ± 0.06ab	0.18 ± 0.00c	0.54 ± 0.06a	0.12 ± 0.00c	0.52 ± 0.01a	0.45 ± 0.05b
glycitin	0.04 ± 0.00d	0.10 ± 0.01a	0.04 ± 0.00d	0.08 ± 0.01c	0.04 ± 0.00d	0.09 ± 0.01bc	0.10 ± 0.01ab
Malonylglucoside							
daidzin	1.61 ± 0.00c	1.26 ± 0.11d	1.80 ± 0.05b	1.16 ± 0.11d	1.76 ± 0.02b	1.25 ± 0.05d	2.73 ± 0.11a
genistin	1.02 ± 0.00c	0.75 ± 0.03de	1.11 ± 0.03b	0.69 ± 0.07e	1.15 ± 0.01b	0.78 ± 0.02d	1.60 ± 0.09a
glycitin	0.16 ± 0.00b	0.08 ± 0.02c	0.14 ± 0.02b	0.08 ± 0.01c	0.16 ± 0.00b	0.10 ± 0.01c	0.21 ± 0.02a
Acetylglucoside							
daidzin	0.06 ± 0.00b	0.06 ± 0.01b	0.06 ± 0.00b	0.05 ± 0.01b	0.05 ± 0.01b	0.06 ± 0.00b	0.11 ± 0.01a
genistin	0.002 ± 0.000d	0.03 ± 0.01b	0.004 ± 0.000d	0.04 ± 0.00a	0.002 ± 0.000d	0.03 ± 0.00ab	0.01 ± 0.00c
glycitin	0.007 ± 0.000d	0.03 ± 0.01b	0.02 ± 0.00c	0.02 ± 0.00c	0.002 ± 0.001d	0.03 ± 0.00a	0.04 ± 0.00a
Aglycone							
daidzein	0.37 ± 0.00b	0.16 ± 0.03d	0.32 ± 0.01b	0.26 ± 0.04c	0.59 ± 0.02a	0.34 ± 0.01b	0.04 ± 0.00e
genistein	0.19 ± 0.00b	0.02 ± 0.01d	0.17 ± 0.00b	0.12 ± 0.03c	0.33 ± 0.03a	0.13 ± 0.00c	0.04 ± 0.00d
glycitein	0.04 ± 0.00b	0.03 ± 0.01c	0.02 ± 0.00c	0.02 ± 0.01c	0.10 ± 0.01a	0.05 ± 0.01b	0.006 ± 0.001d
total	3.79 ± 0.01cd	3.41 ± 0.22e	4.01 ± 0.10c	3.60 ± 0.35de	4.42 ± 0.03b	3.84 ± 0.09cd	5.74 ± 0.22a

[a]All data were presented as milligram per gram of dry solid as the mean ± standard deviation (n = 3). Values in the same row with different lowercase letters (in a−e) were significantly different by Duncan's new multiple range test ($p < 0.05$).

dx.doi.org/10.1021/jf404465w | J. Agric. Food Chem. 2014, 62, 742−749

AUTHOR INFORMATION

Corresponding Author

*Phone: +886-2-3366-4121. Fax: +886-2-2362-0849. E-mail: yehs@ntu.edu.tw.

Funding

This study (project no. NSC-101−2221-E-002−182-MY2) has been financially supported by National Science Council of the Republic of China.

Notes

The authors declare no competing financial interest.

ABBREVIATIONS USED

ANOVA, analysis of variance; AOAC, association of official analytical chemists; BS, blended soymilk; cm, centimeter; FS, filtered soymilk; g, gram; GAE, gallic acid equivalents; h, hour; kg, kilogram; min, minute; mL, milliliter; μm, micrometer; MS, media-milled soymilk; nm, nanometer; rpm, rounds per minute; SAS, statistical analysis system; SEM, scanning electron microscopy; USFDA, U.S. Food and Drug Administration; UV−vis, ultraviolet−visible; YTZ, yttria-stabilized tetragonal zirconia

REFERENCES

(1) Kulkarni, D. S.; Kapanoor, S. S.; Girigouda, K.; Kote, N. V.; Mulimani, V. H. Reduction of flatus-inducing factors in soymilk by immobilized α-galactosidase. *Biotechnol. Appl. Biochem.* **2006**, *45*, 51−57.

(2) Kang, J.; Badger, T. M.; Ronis, M. J. J.; Wu, X. Non-isoflavone phytochemicals in soy and their health effects. *J. Agric. Food Chem.* **2010**, *58*, 8119−8133.

(3) Anderson, J. J. B.; Garner, S.C. The effects of phytoestrogens on bone. *Nutr. Res. (N. Y.)* **1997**, *17*, 1617−1632.

(4) Setchell, K. D. R. Phytoestrogens: the biochemistry, physiology, and implications for human health of soy isoflavones. *Am. J. Clin. Nutr.* **1998**, *68*, 1333S−1346S.

(5) Setchell, K. D. R.; Cassidy, A. Dietary isoflavones: biological effects and relevance to human health. *J. Nutr.* **1999**, *129*, 758S−767S.

(6) Messina, M.; Hughes, C. Efficacy of soyfoods and soybean isoflavone supplements for alleviating menopausal symptoms is positively related to initial hot flush frequency. *J. Med. Food* **2003**, *6*, 1−11.

(7) Prakash, D.; Upadhyay, G.; Singh, B. N.; Singh, H. B. Antioxidant and free radical-scavenging activities of seeds and agri-wastes of some varieties of soybean (*Glycine max*). *Food Chem.* **2007**, *104*, 783−790.

(8) Banerjee, S.; Li, Y.; Wang, Z.; Sarkar, F. H. Multi-targeted therapy of cancer by genistein. *Cancer Lett.* **2008**, *269*, 226−242.

(9) Wang, H. J.; Murphy, P. A. Isoflavone content in commercial soybean foods. *J. Agric. Food Chem.* **1994**, *42*, 1666−1673.

(10) Wang, H. J.; Murphy, P. A. Mass balance study of isoflavones during soybeanprocessing. *J. Agric. Food Chem.* **1996**, *44*, 2377−2383.

(11) Jackson, C. J. C.; Dini, J. P.; Lavandier, C.; Rupasinghe, H. P. V.; Faulkner, H.; Poysa, V.; Buzzell, D.; DeGrandis, S. Effects of processing on the content and composition of isoflavones during manufacturing of soy beverage and tofu. *Process Biochem.* **2002**, *37*, 1117−1123.

(12) Ishihara, M.; Singh, H.; Chung, G.; Tam, C. Content, composition and antioxidant activity of isoflavones in commercial and homemade soymilk and tofu. *J. Sci. Food Agric.* **2007**, *87*, 2844−2852.

(13) Villares, A.; Rostagno, M. A.; García-Lafuente, A.; Guillamón, E.; Martínez, J. A. Content and profile of isoflavones in soy-based foods as a function of the production process. *Food Bioprocess Technol.* **2011**, *4*, 27−38.

(14) Toda, K.; Chiba, K.; Ono, T. Effect of components extracted form okara on the physicochemical properties of soymilk and tofu texture. *J. Food Sci.* **2007**, *72*, C108−C113.

(15) Wang, H. L.; Cavins, J. F. Yield and acid composition of fractions obtained during tofu production. *Cereal Chem.* **1989**, *66*, 359−361.

(16) Khare, S. K.; Jha, K.; Gandhi, A. P. Citric acid production from okara (soy-residue) by solid-state fermentation. *Bioresour. Technol.* **1995**, *54*, 323−325.

(17) Van der Riet, W. B.; Wight, A. W.; Cilliers, J. J. L.; Datal, J. M. Food chemical investigation of tofu and its byproduct okara. *Food Chem.* **1989**, *34*, 193−202.

(18) Erdman, J. W., Jr.; Badger, T. M.; Lampe, J. W.; Setchell, K. D. R.; Messina, M. Not all soy products are created equal: caution needed in interpretation of research results. *J. Nutr.* **2004**, *134*, 1229S−1233S.

(19) Shinohara, K.; Golman, B.; Uchiyama, T.; Otani, M. Fine-grinding characteristics of hard materials by attrition mill. *Powder Technol.* **1999**, *103*, 292−296.

(20) Yeh, A. I.; Huang, Y. C.; Chen, S. H. Effect of particle size on the rate of enzymatic hydrolysis of cellulose. *Carbohydr. Polym.* **2010**, *79*, 192−199.

(21) Chen, C. J.; Shen, Y. C.; Yeh, A. I. Physico-chemical characteristics of media-milled corn starch. *J. Agric. Food Chem.* **2010**, *58*, 9083−9091.

(22) Lo, W. Y. L.; Steinkraus, K. H.; Hand, D. B. Heat sterilization of bottled soymilk. *Food Technol.* **1968**, *22*, 129−131.

(23) *Official Methods of Analysis of AOAC International*, 19th ed.; AOAC International: Gaithersburg, MD, 2012.

(24) Xu, B. J.; Chang, S. K. C. Total phenolic content and antioxidant properties of Eclipse black beans (*Phaseolus vulgaris* L.) as affected by processing methods. *J. Food Sci.* **2008**, *73*, H19−H27.

(25) Singleton, V. L.; Orthofer, R.; Lamuela-Raventos, R. M. Analysis of total phenols and other oxidation substrates and antioxidants by means of Folin−Ciocalteu reagent. *Method. Enzymol.* **1999**, *299*, 152−178.

(26) Xu, B. J.; Chang, S. K. C. A comparative study on phenolic profiles and antioxidant activities of legumes as affected by extraction solvents. *J. Food Sci.* **2007**, *72*, S159−S166.

(27) Murphy, P. A.; Barua, K.; Hauck, C. C. Solvent extraction selection in the determination of isoflavones in soy foods. *J. Chromatogr., B* **2002**, *777*, 129−138.

(28) Kao, T. H.; Chen, B. H. An improved method for determination of isoflavones in soybean powder by liquid chromatography. *Chromatographia* **2002**, *56*, 423−430.

(29) Malaki Nik, A.; Tosh, S.; Poysa, V.; Woodrow, L.; Corredig, M. Physicochemical characterization of soymilk after step-wise centrifugation. *Food Res. Int.* **2008**, *41*, 286−294.

(30) Córdoba, A.; del Mar Camacho, M.; Martinez-Navarrete, N. Rheological behaviour of an insoluble lemon fibre as affected by stirring, temperature, time and storage. *Food Bioprocess Technol.* **2012**, *5*, 1083−1092.

(31) Espinosa-Martos, I.; Rupérez, P. Indigestible fraction of okara from soybean: composition, physicochemical properties and in vitro fermentability by pure cultures of *Lactobacillus acidophilus* and *Bifidobacterium bifidum*. *Eur. Food Res. Technol.* **2009**, *228*, 685−693.

(32) Achouri, A.; Boye, J. I.; Zamani, Y. Soybean variety and storage effects on soymilk flavor and quality. *Int. J. Food Sci. Technol.* **2008**, *43*, 82−90.

(33) Xu, B.; Chang, S. K. C. Total phenolics, phenolic acids, isoflavones, and anthocyanins and antioxidant properties of yellow and black soybeans as affected by thermal processing. *J. Agric. Food Chem.* **2008**, *56*, 7165−7175.

(34) Xu, B.; Chang, S. K. C. Isoflavones, flavan-3-ols, phenolic acids, total phenolic profiles, and antioxidant capacities of soy milk as affected by ultrahigh-temperature and traditional processing methods. *J. Agric. Food Chem.* **2009**, *57*, 4706−4717.

(35) Fernández-Bolaños, J.; Felizón, B.; Brenes, M.; Guillén, R.; Heredia, A. Hydroxytyrosol and tyrosol as the main compounds found in the phenolic fraction of steam-exploded olive stones. *J. Am. Oil Chem. Soc.* **1998**, *75*, 1643−1649.

(36) Castro, E.; Conde, E.; Moure, A.; Falqué, E.; Cara, C.; Ruiz, E.; Domínguez, H. Antioxidant activity of liquors from steam explosion of *Oleaeuropea* wood. *Wood Sci. Technol.* **2008**, *42*, 579−592.
(37) Pandjaitan, N.; Hettiarachchy, N.; Ju, Z. Y. Enrichment of genistein in soy protein concentrate with *β*-glucosidase. *J. Food Sci.* **2000**, *65*, 403−407.
(38) Prabhakaran, M. P.; Perera, C. O. Effect of extraction methods and UHT treatment conditions on the level of isoflavones during soymilk manufacture. *Food Chem.* **2006**, *99*, 231−237.
(39) Kao, T. H.; Lu, Y. F.; Hsieh, H. C.; Chen, B. H. Stability of isoflavone glucosides during processing of soymilk and tofu. *Food Res. Int.* **2004**, *37*, 891−900.
(40) Huang, H.; Liang, H.; Kwok, K. C. Effect of thermal processing on genistein, daidzein and glycitein content in soymilk. *J. Sci. Food Agric.* **2006**, *86*, 1110−1114.
(41) Stancanelli, R.; Mazzaglia, A.; Tommasini, S.; Calabrò, M. L.; Villari, V.; Guardo, M.; Ficarra, P.; Ficarra, R. The enhancement of isoflavones water solubility by complexation with modified cyclodextrins: a spectroscopic investigation with implications in the pharmaceutical analysis. *J. Pharm. Biomed. Anal.* **2007**, *44*, 980−984.
(42) Izumi, T.; Piskula, M. K.; Osawa, S.; Obata, A.; Tobe, K.; Saito, M.; Kataoka, S.; Kubota, Y.; Kikuchi, M. Soy Isoflavone aglycones are absorbed faster and inhigher amounts than their glucosides in humans. *J. Nutr.* **2000**, *130*, 1695−1699.
(43) Setchell, K. D. R.; Brown, N. M.; Desai, P.; Zimmer-Nechemias, L.; Wolfe, B. E.; Brashear, W. T.; Kirschner, A. S.; Cassidy, A.; Heubi, J. E. Bioavailability of pure isoflavones in healthy humans and analysis of commercial soy isoflavone supplements. *J. Nutr.* **2001**, *131*, 1362S−1375S.
(44) Ullah, M. F.; Ahmad, A.; Zubair, H.; Khan, H. Y.; Wang, Z.; Sarkar, F. H.; Hadi, S. M. Soy isoflavone genistein induces cell death in breast cancer cells through mobilization of endogenous copper ions and generation of reactive oxygen species. *Mol. Nutr. Food Res.* **2011**, *55*, 553−559.
(45) Farina, H. G.; Pomies, M.; Alonso, D. F.; Gomez, D. E. Antitumor and antiangiogenic activity of soy isoflavone genistein in mouse models of melanoma and breast cancer. *Oncol. Rep.* **2006**, *16*, 885−891.
(46) Food and Drug Administration. Food labeling, health claims, soy protein, and coronary heart disease. *Fed. Regist.* **1999**, *64*, 57700−57733.
(47) Nagata, C. Ecological study of the association between soy product intake and mortality form cancer and heart disease in Japan. *Int. J. Epidemiol.* **2000**, *29*, 832−836.
(48) Ho, S. C.; Woo, J. L. F.; Leung, S. S. F.; Sham, A. L. K.; Lam, T. H.; Janus, E. D. Intake of soy products is associated with better plasma lipid profiles in the Hong Kong Chinese population. *J. Nutr.* **2000**, *130*, 2590−2593.
(49) Dai, Q.; Shu, X. O.; Jin, F.; Potter, J. D.; Kushi, L. H.; Teas, J.; Gao, Y. T.; Zheng, W. Population-based case-control study of soyfood intake and breast cancer risk in Shanghai. *Br. J. Cancer* **2001**, *85*, 372−378.
(50) Ho, S. C.; Woo, J.; Lam, S.; Chen, Y.; Sham, A.; Lau, J. Soy protein consumption and bone mass in early postmenopausal Chinese women. *Osteoporosis Int.* **2003**, *14*, 835−842.
(51) Messina, M.; Nagata, C.; Wu, A. H. Estimated Asian adult soy protein and isoflavone intakes. *Nutr. Cancer* **2006**, *55*, 1−12.
(52) Herman, C.; Adlercreutz, T.; Goldin, B. R.; Gorbach, S. L.; Höckerstedt, K. A. V.; Watanabe, S.; Hämäläinen, E. K.; Markkanen, M. H.; Mäkelä, T. H.; Wähälä, K. T.; Hase, T. A.; Fotsis, T. Soybean phytoestrogen intake and cancer risk. *J. Nutr.* **1995**, *125*, 757S−770S.

JOURNAL OF AGRICULTURAL AND FOOD CHEMISTRY

Article

pubs.acs.org/JAFC

The Polyphenol Extract from *Sechium edule* Shoots Inhibits Lipogenesis and Stimulates Lipolysis via Activation of AMPK Signals in HepG2 Cells

Cheng-Hsun Wu,[†,‡,§,+] Ting-Tsz Ou,[∥,+] Chun-Hua Chang,[∥] Xiao-Zong Chang,[⊥] Mon-Yuan Yang,[∥] and Chau-Jong Wang*[,∥,#]

[†]Department of Anatomy, China Medical University, Taichung 40402, Taiwan

[‡]Department of Biochemistry, China Medical University, Taichung 40402, Taiwan

[§]Department of Medical Research, China Medical University Hospital, Taichung 40402, Taiwan

[∥]Institute of Biochemistry and Biotechnology, Chung Shan Medical University, Taichung 40201, Taiwan

[⊥]Department of Medical Technology, Cishan Hospital, Kaohsiung 84247, Taiwan

[#]Department of Medical Research, Chung Shan Medical University Hospital, Taichung 40201, Taiwan

ABSTRACT: Fatty liver may have implications for metabolic syndrome, such as obesity, hypertension, and diabetes. Therefore, the development of pharmacological or natural agents to reduce fat accumulation in the liver is an important effort. The *Sechium edule* shoots have already been verified to decrease serum lipids and cholesterol and prevent atherosclerosis. However, how *Sechium edule* shoots modulate hepatic lipid metabolism is unclear. This study was designed to investigate the effects and mechanisms of polyphenol extracts (SPE) of *Sechium edule* shoots in reducing lipid accumulation in oleic acid-treated HepG2 cells. We found that water extracts (SWE) of *Sechium edule* shoots could decrease serum and hepatic lipid contents (e.g., triacylglycerol and cholesterol). Furthermore, SWE and SPE through the AMPK (AMP-activating protein kinase) signaling pathway could decrease lipogenic relative enzymes, such as FAS (fatty acid synthase), HMGCoR (HMG-CoA reductase), and SREBPs (sterol regulatory element binding proteins), and increase the expression of CPT-I (carnitine palmitoyltransferase I) and PPARα (peroxisome proliferators activated receptor α), which are critical regulators of hepatic lipid metabolism. These observations suggested that *Sechium edule* shoots have potential for developing health foods for preventing and remedying fatty liver.

KEYWORDS: *SPE (polyphenol extracts of Sechium edule shoots), SWE (water extracts of Sechium edule shoots), AMPK, FAS, HMGCoR, SREBPs*

INTRODUCTION

Excessive lipid may accumulate in liver,[1] leading to obesity-associated fatty liver disease (FLD).[2] Fatty liver is closely associated with life-style-related diseases such as hyperlipidemia, hypertension, arteriosclerosis, type 2 diabetes mellitus, and cancer.[3,4] Fatty liver has a strong positive relationship to outbreaks of hepatitis, cirrhosis, and cancer.[5] The fat that accumulates can cause inflammation and scarring in the liver. At its most severe, nonalcoholic fatty liver disease (NAFLD) can progress to liver failure.[6] Therefore, prevention and treatment of lipid accumulation in liver are relevant to health promotion.

Previous research showed that the hepatic TG (triacylglycerol) content is significantly correlated with plasma TG levels and fat mass in humans.[7] As we know, the hepatic TG availability is controlled by the balance between FAS and oxidation in the liver.[8] The underlying cause of fat accumulation in NAFLD is mostly due to the synthesis of fatty acids and inhibition of fatty acid oxidation.[9] Several recent studies have demonstrated transcriptional regulation of the gene for the enzymes of synthesis of fatty acids, including FAS (fatty acid synthase) and glycerol-3-phosphate acyltransferase (GPAT), by sterol regulatory element binding proteins (SREBPs).[10,11] Activation of FAS through modulation of SREBP-1 has been reported in human breast cancer.[12] The transcription factor peroxisome proliferators activated receptor (PPAR) is expressed at very low levels in the liver, and overexpression of this transcription factor in the liver leads to hepatic adipose accumulation with the expression of several adipogenic genes in the liver.[13] SREBP-1 can modulate the enzymes of lipid production, such as FAS and GPAT, and can affect the formation of fatty acids and TG. In addition, SREBP-1 not only regulates the formation rate of TG but also determines whether TG can be released from the liver.[14,15] SREBP-2 regulates the generation of cholesterol metabolism-related proteins such as HMG-CoA reductase (HMGCoR) and low density lipoprotein receptor (LDLR).[16,17] SREBP plays an important role in the process of controlling the formation of fatty liver. PPARs are the sensors of in vivo lipids. They control the related gene, carnitine palmitoyltransferase (CPT), in lipid oxidation and thus play a role in regulating lipid metabolism, which controls

Received: October 14, 2013
Revised: December 25, 2013
Accepted: December 30, 2013
Published: December 30, 2013

ACS Publications © 2013 American Chemical Society

almost all aspects in fatty acid metabolism.[18] AMP-activating protein kinase (AMPK) phosphorylates and inactivates a number of metabolic enzymes involved in ATP-consuming cellular events including fatty acid and cholesterol synthesis, involving FAS[19] and HMGCoR.[20] The activation of the AMPK pathway is necessary to prevent fat accumulation.

The *Sechium edule* shoots contain many nutritional components including flavonoids, which are known as a powerful polyphenol and antioxidant.[21] It is useful as a complementary treatment for arteriosclerosis and hypertension and as a diuretic and anti-inflammatory remedy.[22,23] It has already been verified to decrease serum lipid and cholesterol and prevent atherosclerosis.[22] However, how components of *Sechium edule* shoots modulate hepatic lipid metabolism is unclear.

We examined the effect of the SWE and SPE on hepatic hypolipidemia. Human HepG2 cells were treated with indicated concentrations of SWE and SPE in the presence of OA for 24 h. We used this model to elucidate whether SWE and SPE prevents lipid accumulation in hepatic cells.

MATERIALS AND METHODS

Materials. Leaves of fresh *Sechium edule* shoots were collected in Nantou County, located in central Taiwan. The 3-(4, 5-dimethylthiazol-zyl)-2, 5-diphenylterazolium bromide (MTT) and oleic acid were purchased from Sigma-Aldrich (St. Louis, MO, U.S.A.). GPx, SOD, and SREBP antibodies were obtained from Santa Cruz Biotechnology (CA, U.S.A.). Anti-pThr172-AMPK and anti-AMPK antibodies were purchased from Cell Signaling Technology (Beverly, MA, U.S.A). Anti-β-actin, anti-FAS, anti-SREBP-1, anti-GPAT, anti-HMGCoR, SREBP-2, anti-LDLR, and anti-catalase antibodies were purchased from Sigma-Aldrich.

Preparation of SWE and SPE. Fresh leaves were chopped and air-dried under shade and milled to a coarse powder. The powder was used for the preparation of water extracts (SWE) and phenolic extracts (SPE). The powder (20 g) was then subjected to maceration with sufficient volume of distilled water (1000 mL) for 4 °C for 24 h. Then the aqueous extract was filtered and lypophilized to get the yield of 17.24%. For preparation of the SPE, 100 g of dried powder of *Sechium edule* was submerged in 300 mL of ethanol and heated at 50 °C for 3 h. The extract was filtered and thereafter lyophilized under reduced pressure at room temperature. The powder was then resuspended in 500 mL of 50 °C distilled water, followed by extraction with 180 mL of ethyl acetate three times, redissolved in 250 mL of distilled water, stored at 70 °C overnight, and lyophilized. The presence and proportion of the main constituents of SPE were then analyzed by HPLC.

HPLC (High Performance Liquid Chromatography) Analysis. HPLC was performed with a Hitachi HPLC system (Hitachi, Danbury, CT, USA), which consisted of a pump (L-6200A), an ultraviolet detector (L-4250), and the Hitachi D-7000 HPLC System Manager program. A reported procedure was used for analyzing the phenolic acids, using a Mightysil RP-18 GP 250 column (Kanto, Tokyo, Japan) and two mobile phase solvent: solvent A, acetic acid/water (2:98, v/v), and solvent B, 0.5% acetic acid in water/acetonitrile (50:50, v/v). The flow rate was 1 mL/min. The gradient for the separation was 100% solvent A at 0 min, 70% solvent A and 30% solvent B at 5 min, 65% solvent A and 35% solvent B at 50 min, 60% solvent A and 40% solvent B at 55 min, 0% solvent A and 100% solvent B at 60 min, followed by a 5 min postrun with HPLC grade water. Phenolic acids were detected at 260 nm.

Cell Culture. Human HepG2 cells obtained from the American Type Culture Collection were maintained in DMEM supplemented with 10% fetal calf serum, 100 U/mL penicillin, 100 μg/mL streptomycin, and 2 mM L-glutamine and kept at 37 °C in a humidified atmosphere of 5% CO_2. Cells were grown to 70% confluence and then incubated in serum-free medium for 24 h before treatments. To induce FA (fatty acid) overloading, HepG2 cells at 70% confluence were exposed to a long-chain oleic acid (OA). OA/BSA complex was prepared as reported previously.[24] Stock solutions of 1 M OA prepared in culture medium containing 1% BSA were diluted in culture medium to obtain the desired final concentrations. The OA/BSA complex solution was sterile-filtered through a 0.22 μm pore membrane filter and stored at −20 °C.

Cytotoxicity Assay. HepG2 cells were seeded at a density of 1×10^6 cells/mL in 24-well plates and incubated with oleic acid, SPE, and SWE at various concentrations for 24 h. Thereafter, the medium was removed and 3-(4,5-dimethylthiazol-2-yl)-2,5-diphenyltetrazolium bromide (MTT, 0.5 mg/mL) was added to incubate for 4 h. The viable cells were directly proportional to the production of formazan. Following dissolution in isopropanol, the absorbance was read at 563 nm with a spectrophotometer (Beckman DU640).

Nile Red Stain. HepG2 cells were seeded in 6-well plates (3×10^6 cells/mL) and treated with 0.6 mM oleic acid and different concentrations of SPE and SWE for 24 h. After the cells were washed twice with PBS, they were fixed with 4% formaldehyde for 30 min and then stained with 40 μg of Nile red solution for 30 min at room temperature. Lipid-bound Nile red fluorescence was observated using inverted fluorescence microscopy.

Preparation of Protein Extract of HepG2 Cells. The proteins of cells were harvested in cold RIPA (radioimmunoprecipitation assay) buffer [1% NP-40 (nonyl phenoxypolyethoxylethanol), 50 mM Tris-base, 0.1% SDS, 0.5% deoxycholic acid, 150 mM NaCl, pH 7.5] containing leupeptin (17 μg/mL) and sodium orthovanadate (10 μg/mL). The cell mixture was vortexed at 4 °C for 4 h. All mixtures were then centrifuged at 12 000 rpm at 4 °C for 10 min, and the protein contents of the supernatants were determined with the Coomassie blue total protein reagent (Kenlor Industries, Inc., USA) using bovine serum albumin as the standard.

Western Blot Analysis. Equal amounts of protein samples (50 μg) were subjected to SDS−polyacrylamide gel electrophoresis and electrotransferred to nitrocellulose membranes (Millipore, Bedford, MA, USA). Membranes were blocked with 5% nonfat milk powder with 0.05% Tween 20 in PBS and then incubated with the first antibody at 4 °C overnight. Thereafter, membranes were washed three times with 0.05% Tween 20 in PBS and incubated with the anti-mouse secondary antibody conjugated to horseradish peroxidase (GE Healthcare, Little Chalfont, Buckinghamshire, U.K.). Bands were detected and revealed by enhanced chemiluminescence using ECL Western blotting detection reagents and exposed ECL hyperfilm in FUJFILM Las-3000 (Tokyo, Japan). Protein quantitation was determined by densitometry using the FUJFILM-Multi Gauge V2.2 software.

Statistical Analysis. Results are reported as the mean ± standard deviation of three independent experiments and statistical comparisons were evaluated by one-way analysis of variance (ANOVA). *P* values less than 0.05 were considered statistically significant.

RESULTS

SWE and SPE Content Assay. The single-ring type of polyphenol compounds (gallic acid, GA) were used to determine the standard content of total polyphenol. The results show (Table 1) that in SWE, the single-ring polyphenol compounds were 4.41% ± 0.02% polyphenol (using gallic acid as the standard), 3.32% ± 0.17% flavonoids (using quercetin and naringenin as the standard), 26.73% ± 2.18% carbohydrate, 4.67% ± 1.46% protein, and 3.25% ± 1.611% lipid.

The analysis of SPE revealed that it contained 17.74% ± 0.05% total polyphenol (using gallic acid as the standard) and 21.10% ± 0.28% flavonoids (using quercetin and naringenin as the standard). The presence and proportion of the main constituents of SPE were then analyzed by HPLC (Figure 1). For the standardization of SPE, the presence of protocatechuic acid (3.56% ± 0.14%), gallocatechin gallate (11.06% ± 0.18%), caffeic acid (4.42% ± 0.25%), rutin (1.14% ± 0.13%), quercetin

dx.doi.org/10.1021/jf404611a | J. Agric. Food Chem. 2014, 62, 750−759

Table 1. Components of SWE and SPE (polyphenol extracts) of *Sechium edule* Shoots

	SWE (%)	SPE (%)
polyphenol (gallic acid as STD)	4.41 ± 0.02	17.74 ± 0.05
flavonoid	3.32 ± 0.17	21.10 ± 0.28
flavone and flavonol	1.54 ± 0.07	4.52 ± 0.07
flavanone and flavanonol	1.78 ± 0.10	16.58 ± 0.21
carbohydrate	26.73 ± 2.18	
protein	4.67 ± 1.46	
lipid	3.25 ± 1.11	

(3.71% ± 0.32%), and naringenin (11.28% ± 1.12%) was confirmed in the SPE.

The Effect of SWE and SPE on Cell Viability of HepG2 Cells. Using different concentrations of SWE and SPE to treat HepG2 cells, after 24 h, we analyzed cell viability. Figure 2A,B showed that from the result of MTT, the drug lethal dose (IC_{50}) of SWE was more than 5 mg/mL and that of SPE was 2.32 mg/mL respectively. This experiment focuses on the premise that intracellular lipid accumulation will not cause any damage to cells. So the follow-up experiment used concentrations of 1 and 5 mg/mL SWE and 0.5 and 1 mg/mL SPE for treatment of HepG2 cells.

Inhibition of OA-Induced Lipid Accumulation by SWE and SPE in HepG2 Cells. The above results showed that the cell growth condition was good, and cell survival rates remained at 100%. Our preliminary work has demonstrated that cell viability is unaffected at a concentration of 0.6 mM OA. Thus, we used 0.6 mM OA and SWE (1 and 5 mg/mL) and SPE (0.5 and 1 mg/mL) to culture HepG2 cells in order to observe the fat accumulation. Figure 3A is the result of using Nile red fluorescent staining to show that fat accumulation altered the red fluorescence with change in fat in cytoplasm in a dose dependent manner. Next, using Nile red staining and flow cytometric analysis to detect the intensity of fluorescence (Figure 3B), we found that the intensity of fluorescence was proportional to fat content. Then, we quantified the intracellular fat content (Figure 3C). The fat content of HepG2 was 2.1 times higher ($*p < 0.05$) than the control group after exposure to OA. SWE treatment of cells at doses of 1 or 5 mg/mL resulted in a reduction of lipid content (92.1% and 84.25%) compared with the OA group ($*p < 0.05$). Treatment with SPE, also reduced lipid content about 88.1% and 83.21% ($*p < 0.05$) compared with the OA group. These results showed that SWE and SPE had the effect of inhibiting intracellular fat accumulation. SPE was more efficient than SWE in causing this effect.

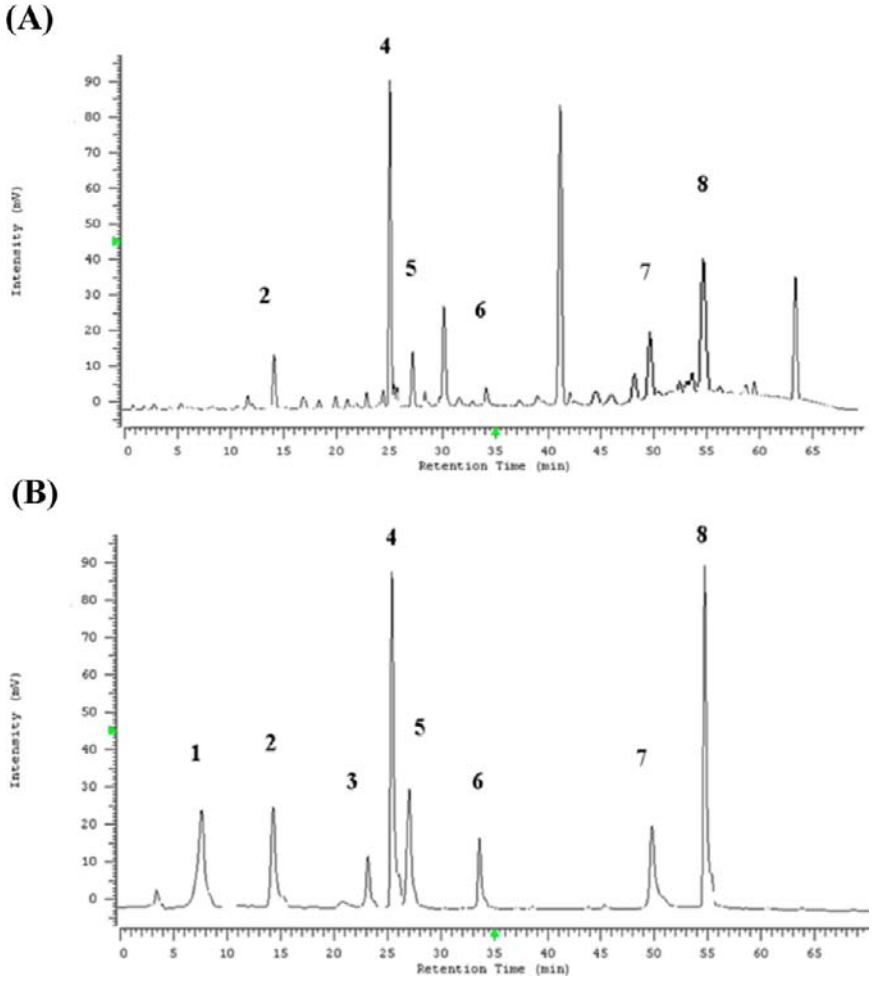

Figure 1. The HPLC chromatogram of SPE (polyphenol extracts of *Sechium edule* shoots). (A) HPLC chromatogram of free polyphenols from SPE (10 mg/mL, 10 μL). (B) HPLC chromatogram of eight kinds of standard polyphenols (1 mg/mL; 10 μL). Peaks: (1) gallic acid; (2) protocatechuic acid; (3) catechin; (4) gallocatechin gallate; (5) caffeic acid; (6) rutin; (7) quercetin; (8) naringenin.

dx.doi.org/10.1021/jf404611a | J. Agric. Food Chem. 2014, 62, 750−759

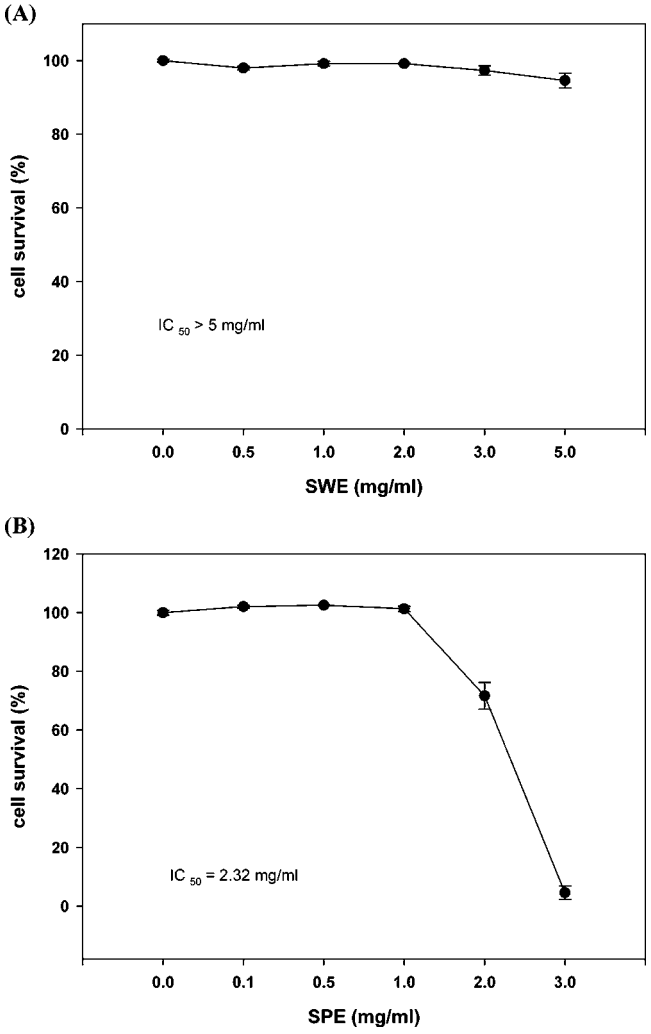

Figure 2. The cytotoxicity effects of SWE (water extracts of *Sechium edule* shoots) and SPE (polyphenol extracts of *Sechium edule* shoots) on human hepatocarcinoma cell line. HepG2 cells were treated with various concentrations of SWE (A) or SPE (B) for 24 h. Viability of HepG2 cells was determined by the MTT assay. The results are presented as mean ± SD of two independent experiments.

Effect of SWE and SPE on the Expression of TG Synthesis Related Proteins. Figure 4A shows that cells that were induced by OA had 1.24 times the expression of FAS. When compared with the control group, in cells that were exposed to 1 or 5 mg/mL SWE, the expression of FAS was 1.08 and 1.03 times, respectively. Figure 4A shows that cells that were induced by OA had 1.28 times the expression of SREBP-1. When compared with the control group, after exposure to 1 or 5 mg/mL SWE, the expression of SREBP-1 was 1.21 and 1.11 times, respectively. GPAT is the rate-determining enzyme of triglyceride synthesis. Figure 4A also reveals that the expression of GPAT induced by OA was 1.25 times. When compared with the control group, after cells were exposure to 1 or 5 mg/mL SWE, the expression of GPAT was 1.22 and 1.03 times, respectively. Figure 4B shows that cells induced by OA had the expression of FAS 1.26 times. After exposure to 0.5 or 1.0 mg/mL SPE, the expression of FAS was 1.09 and 0.687 times, respectively. SWE and SPE reduced the expression of FAS in HepG2 cells in a dose dependent manner after induction by OA.

Figure 4B shows that cells induced by OA had 1.31 times the expression of SREBP-1. After exposure to 0.5 or 1.0 mg/mL SPE, the expression of SREBP-1 was 1.17 and 1.13 times, respectively. SWE and SPE reduced the expression of FAS in HepG2 cells in a dose-dependent manner after induction by OA. Figure 4B also reveals that the expression of GPAT was induced 1.29 times by OA. When compared with the control group, after cells were exposed to 0.5 or 1 mg/mL SPE, the expression of GPAT was 0.98 and 0.91 times respective. Both SWE and SPE reduced the expression of GPAT in HepG2 cells after induced by OA, and the response was dose-dependent. From those data, we can validate that, through the inhibition of those transcription factors, SWE and SPE may regulate the synthesis of triglycerides.

Effect of SWE and SPE on the Expression of Cholesterol Synthesis Related Proteins. HMGCoR is the rate-determining enzyme of cholesterol synthesis. To test whether the reduction of lipid accumulation in both SWE- and SPE-treated HepG2 cells is accompanied by changes in cholesterol biosynthesis, Western Blots were performed. As seen in Figure 5A,B, the expression of HMGCoR, SREBP-2, and LDL-R were remarkably decreased by SWE (1 or 5 mg/mL) or SPE (0.5 or 1 mg/mL) treatment compared with the OA-treated group. From those data, we can validate that, through the inhibition of those transcription factors and LDLR, SWE and SPE may regulate the synthesis of cholesterol (Figure 5).

Effect of SWE and SPE on the Expression of Fatty Acid Oxidation Related Proteins. CPT-1 is an enzyme in the body that helps change fat to energy. In this study, the results have shown that SWE or SPE treatment increases the expression of PPARα and CPT-1 compared with that in the OA group in HepG2 cells (Figure 6). Thus, through the stimulation of those transcription factors, SWE and SPE were shown to increase the oxidation of fatty acids.

Effect of SWE and SPE on the Phosphorylation of AMPK. AMPK is an important regulator in the metabolism mechanism for sugar and fat. In Figure 7A, when cells were treated with 1 or 5 mg/mL SWE, the expression of p-AMPK was significantly increased 1.33- and 1.40-fold respectively, compared with that in the OA group. We further observed that the ratio of AMPK/p-AMPK was increased ($*p < 0.05$, $**p < 0.001$), indicating that SWE can activate AMPK. In Figure 7B, the expression of p-AMPK was significantly increased 1.29- and 1.32-fold after treatment with 0.5 or 1 mg/mL SPE in HepG2 cells. We also observed that the p-AMPK/AMPK ratio had an upward trend. With those results, we prove that SWE and SPE can activate AMPK and, hence, reduce lipid synthesis in cells.

DISCUSSION

The liver plays an essential role in lipid metabolism via regulating lipogenesis and oxidative stress.[23] Excessive lipid accumulation in liver may progress to steatohepatitis.[2] The mechanism study is well-known in oleic acid-induced human hepatoma HepG2 cells model. Here, we attempted to examine the hypolipidemia effect and possible mechanism of SWE or SPE on hepatic lipid metabolism. Previous reports indicated that a regulation of hepatic LDLR and HMGCoR activity could be observed in HepG2 cells.[25,26] The fat accumulation in NAFLD is mostly due to the synthesis of fatty acids and inhibition of fatty acid oxidation.[27] Generally, hepatic hypolipidemic mechanisms are highly associated with expression of lipogenic enzymes, cholesterol biosynthesis, fatty

dx.doi.org/10.1021/jf404611a | J. Agric. Food Chem. 2014, 62, 750−759

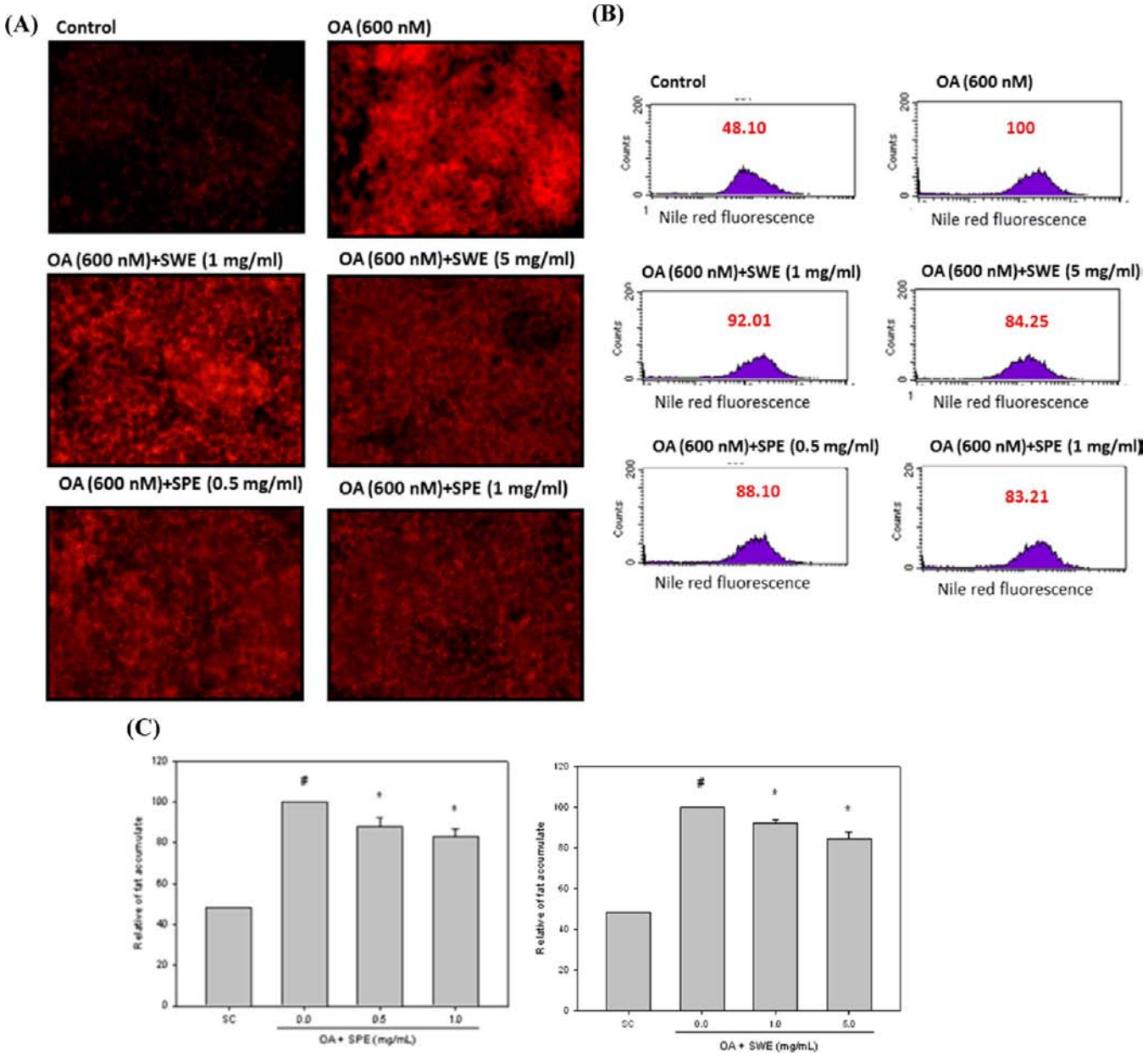

Figure 3. Effects of SWE (water extracts of *Sechium edule* shoots) or SPE (polyphenol extracts *of Sechium edule* shoots) on intracellular lipid accumulation in HepG2 cells. Cells are cotreated with oleic acid (OA) 0.6 mM and various concentrations of SWE or SPE for 24 h. (A) After culturing, cells were fixed with formalin and stained with Nile red and (B) analyzed by flow cytometry. (C) Quantitative assessment of the percentage of lipid accumulation; data represent the average of three independent experiments ± SD. SC indicates an internal control of cell stained with Nile red; 0 indicates an induced control of cells treated with oleic acid only. #$p < 0.05$ compared with the SC group; *$p < 0.05$ compared with the OA-induced group.

acid β-oxidation, and TG biosynthesis in HepG2 cells. In our present study, the hypolipidemic mechanisms of SWE and SPE were related to expression of lipogenic enzymes (SREBP-1 and FAS), cholesterol biosynthesis (HMGCoR, SREBP-2, and LDL-R), fatty acid β-oxidation (PPAR-α and CPT-1), and TG biosynthesis (GPAT) in OA-induced HepG2 cells.

AMPK is a multisubunit enzyme recognized as a major regulator of lipid biosynthetic pathways due to its role in the phosphorylation and inactivation of key enzymes such as FAS.[28] Studies demonstrated that polyphenolic extracts from plants can activate AMPK and inhibit FAS expression by preventing SREBP-1 translocation to the nuclei.[29−31]

Polyphenols are widely found in *Sechium edule* shoots.[32] In this study, we found that both SWE and SPE contained total polyphenols about 7.73% and 38.84%, respectively. These concentrations were sufficient to lower lipid levels in the liver.[33] Therefore, both SWE and SPE have great ability to activate AMPK and then reduce protein expression of SREBP-1, leading to inhibition of hepatic lipogenesis. Our data showed that AMPK plays a pivotal role in the hypolipid effect, and both SWE and SPE can augment AMPK activation (Figure 7). SREBP-1 is a key lipogenic transcription factor regulating the gene expression of lipogenic enzymes and is dedicated to the synthesis and uptake of fatty acids and triacylglycerol.[31,34] Our data showed that the expression of SREBP-1 and its

dx.doi.org/10.1021/jf404611a | J. Agric. Food Chem. 2014, 62, 750−759

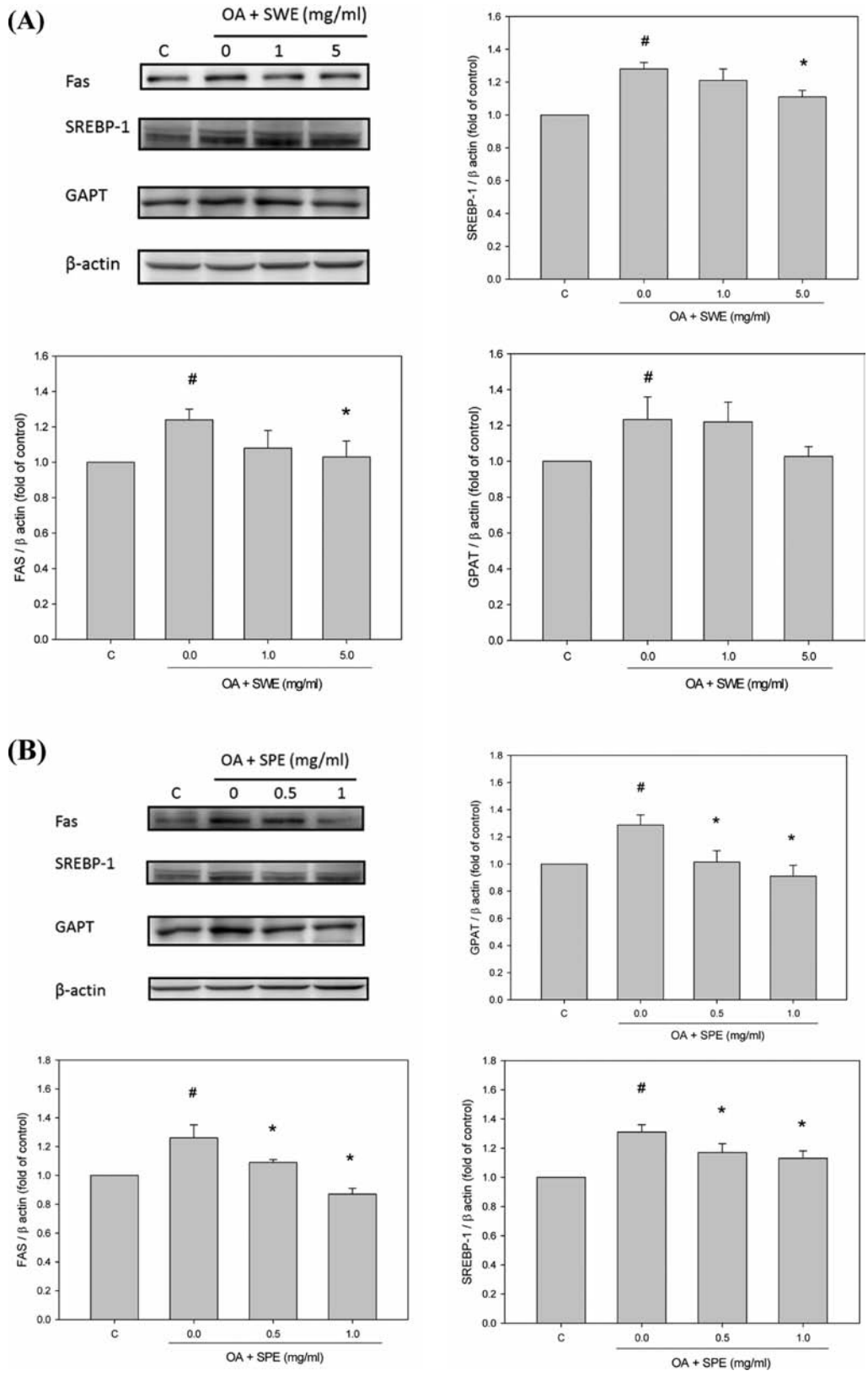

Figure 4. Treatment of SWE (water extracts of *Sechium edule* shoots) and SPE (polyphenol extracts of *Sechium edule* shoots) decreased fatty acid biosynthesis relative protein expression in OA (oleic acid)-induced HepG2 cell. Cells were coexposed to OA (0.6 mM) and various doses of SWE (A) or SPW (B) for 24 h. The FAS, SREBP-1, and GPAT protein levels were also examined under the same conditions. The numbers below the panels represent quantification of the immunoblot by densitometry. #$p < 0.05$ compared with a control group; *$p < 0.05$ compared with OA-induced group.

dx.doi.org/10.1021/jf404611a | *J. Agric. Food Chem.* 2014, 62, 750−759

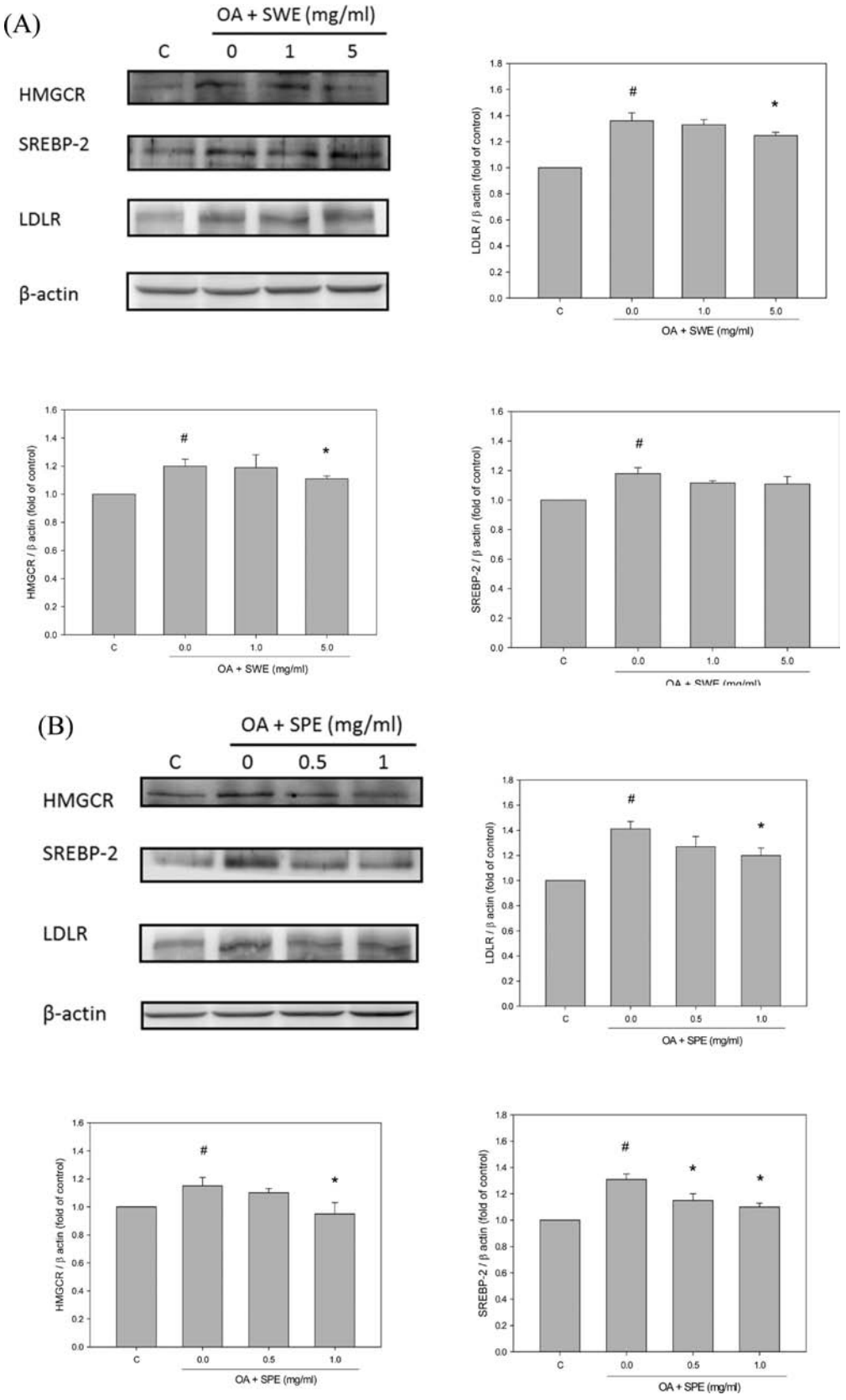

Figure 5. Treatment of SWE (water extracts of *Sechium edule* shoots) and SPE (polyphenol extracts of *Sechium edule* shoots) decreased cholesterol biosynthesis related protein expression in OA (oleic acid)-induced HepG2 cell. Cells were coexposed to OA (0.6 mM) and various doses of SWE (A) or SPE (B) for 24 h. The HMGCoR, SREBP-2, and LDLR protein levels were also examined under the same conditions. The numbers below the panels represent quantification of the immunoblot by densitometry. #$p < 0.05$ compared with control group. *$p < 0.05$ compared with OA-induced group.

dx.doi.org/10.1021/jf404611a | *J. Agric. Food Chem.* 2014, 62, 750−759

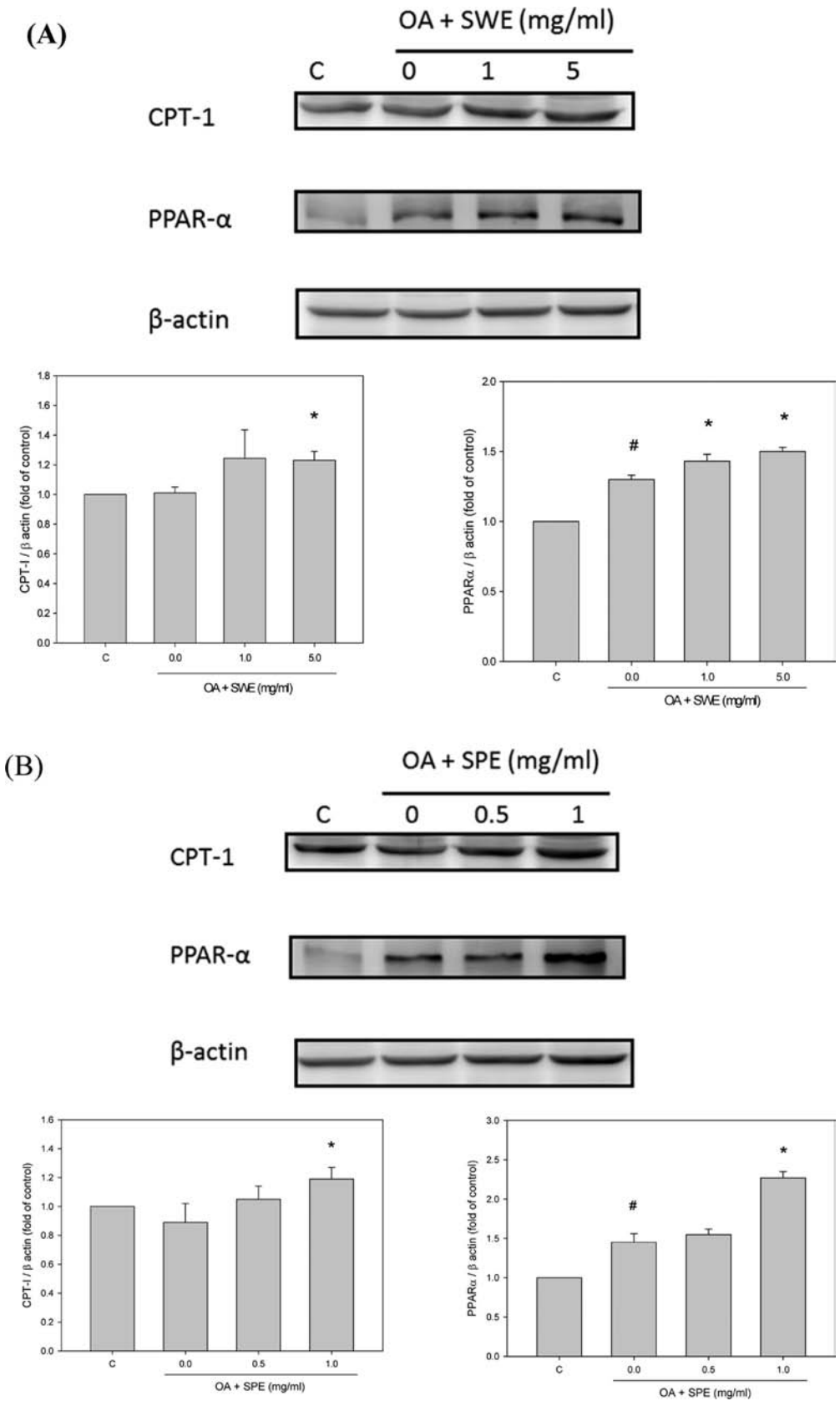

Figure 6. Treatment with SWE (water extracts of *Sechium edule* shoots) and SPE (polyphenol extracts of *Sechium edule* shoots) increased fatty acid oxidation related protein expression in OA (oleic acid)-induced HepG2 cell. Cells were coexposed to OA (0.6 mM) and various doses of SWE (A) or SPE (B) for 24 h. CPT-1 and PPARα were detected by Western blot analysis under the same conditions. The numbers below the panels represent quantification of the immunoblot by densitometry. #$p < 0.05$ compared with control group; *$p < 0.05$ compared with OA-induced group.

dx.doi.org/10.1021/jf404611a | *J. Agric. Food Chem.* 2014, 62, 750−759

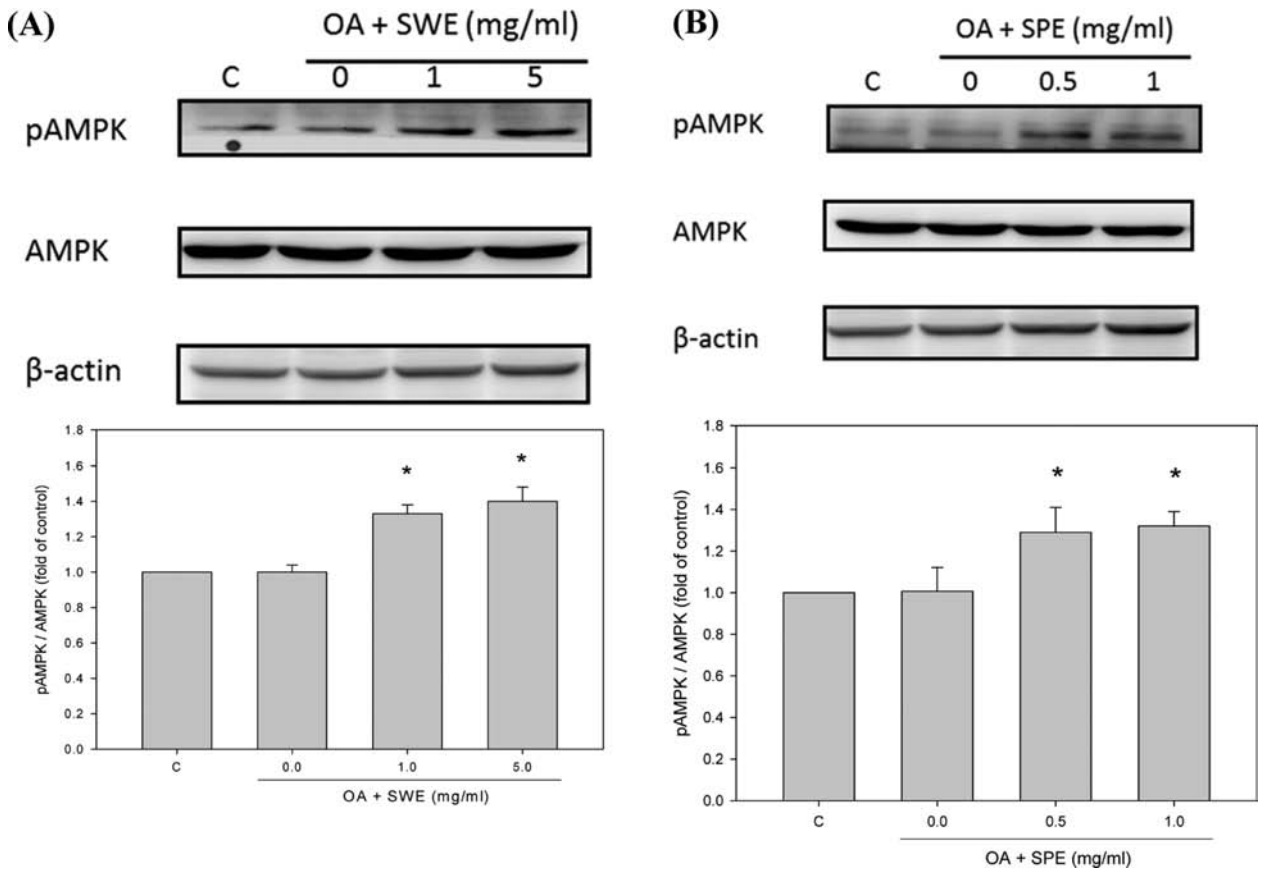

Figure 7. Treatment of SWE (water extracts of *Sechium edule* shoots) and SPE (polyphenol extracts of *Sechium edule* shoots) increased AMP-activated protein kinase (AMPK) phosphorylation protein expression in OA (oleic acid)-induced HepG2 cell. Cells were coexposed to OA (0.6 mM) and various doses of SWE (A) or SPE (B) for 24 h. AMPK phosphorylation (pThr172-AMPK) was detected by Western blot analysis under the same conditions. The numbers below the panels represent quantification of the immunoblot by densitometry. *$p < 0.05$ compared with OA-induced group.

downstream factors, FAS and GAPT, were reduced in response to SWE or SPE treatment in HepG2 cells (Figure 4). Another recent study suggests that AMPK mediates a decrease in SREBP-1 expression.[29] Consequently, our data suggest that the ability of SWE and SPE to decrease FAS and GAPT expression may occur through AMPK activation and SREBP-1 suppression.

In addition increase of hepatic lipogenesis by activation of SREBP-1 may contribute to the development of chemically induced fatty liver.[35] AMPK phosphorylates and inhibits SREBP-1 activity to attenuate hepatic steatosis,[36] whereas SREBP-2 primarily controls cholesterol homeostasis by activating genes required for cholesterol synthesis and uptake.[37] Our data corroborated these results (Figure 5 and Figure 7). Similarly, AMPK inhibits in vitro lipogenesis in hepatocytes through the downregulation of the cleavage processing and transcriptional activity of SREBP.[36] PPAR-α is highly expressed in the liver where it activates genes involved in β-oxidation of fatty acids.[38] In our study, both SWE and SPE treatment result in an increased expression of PPAR-α in OA-induced lipid accumulation cells.

In conclusion, the current study identifies that SWE and SPE can reduce lipid accumulation. We also propose that AMPK is pivotal in closing the anabolic pathway and promoting catabolism by down regulating the activity of key enzymes in lipid metabolism, such as HMGCoR and FAS. Both SWE and SPE can suppress fat accumulation of the liver and could be developed as a potential therapeutic treatment in order to reduce the formation of a fatty liver.

AUTHOR INFORMATION

Corresponding Author

*Tel: +886-4-24730022, ext. 11670. Fax: +886-4-2324-8167. Mailing address: No.110, Sec. 1, Jianguo N. Rd., South District, Taichung, Taiwan 402. E-mail: wcj@csmu.edu.tw.

Author Contributions

[+]C.-H.W. and T.T.O. contributed equally to this work and therefore share first authorship.

Funding

This work was supported by a National Science Council Grant NSC99-2321-B-040-001), Taiwan.

Notes

The authors declare no competing financial interest.

REFERENCES

(1) Fabbrini, E.; Sullivan, S.; Klein, S. Obesity and nonalcoholic fatty liver disease: Biochemical, metabolic, and clinical implications. *Hepatology* **2010**, *51*, 679−89.

(2) Evans, R. M.; Barish, G. D.; Wang, Y. X. PPARs and the complex journey to obesity. *Nat. Med.* **2004**, *10*, 355−61.

(3) Brooks, S. C., 3rd; Brooks, J. S.; Lee, W. H.; Lee, M. G.; Kim, S. G. Therapeutic potential of dithiolethiones for hepatic diseases. *Pharmacol. Ther.* **2009**, *124*, 31−43.

(4) Wu, C. H.; Lin, M. C.; Wang, H. C.; Yang, M. Y.; Jou, M. J.; Wang, C. J. Rutin inhibits oleic acid induced lipid accumulation via reducing lipogenesis and oxidative stress in hepatocarcinoma cells. *J. Food Sci.* **2011**, *76*, T65−72.
(5) Corrao, G.; Torchio, P.; Zambon, A.; D'Amicis, A.; Lepore, A. R.; di Orio, F. Alcohol consumption and micronutrient intake as risk factors for liver cirrhosis: A case-control study. The Provincial Group for the study of Chronic Liver Disease. *Ann. Epidemiol.* **1998**, *8*, 154−9.
(6) Musso, G.; Gambino, R.; Cassader, M.; Pagano, G. A meta-analysis of randomized trials for the treatment of nonalcoholic fatty liver disease. *Hepatology* **2010**, *52*, 79−104.
(7) Hartz, A. J.; Rupley, D. C., Jr.; Kalkhoff, R. D.; Rimm, A. A. Relationship of obesity to diabetes: Influence of obesity level and body fat distribution. *Prev. Med.* **1983**, *12*, 351−7.
(8) Chan, D. C.; Watts, G. F.; Ng, T. W.; Hua, J.; Song, S.; Barrett, P. H. Measurement of liver fat by magnetic resonance imaging: Relationships with body fat distribution, insulin sensitivity and plasma lipids in healthy men. *Diabetes, Obes. Metab.* **2006**, *8*, 698−702.
(9) Duval, C.; Muller, M.; Kersten, S. PPARalpha and dyslipidemia. *Biochim. Biophys. Acta* **2007**, *1771*, 961−71.
(10) Heemers, H.; Maes, B.; Foufelle, F.; Heyns, W.; Verhoeven, G.; Swinnen, J. V. Androgens stimulate lipogenic gene expression in prostate cancer cells by activation of the sterol regulatory element-binding protein cleavage activating protein/sterol regulatory element-binding protein pathway. *Mol. Endocrinol.* **2001**, *15*, 1817−28.
(11) Reddy, J. K.; Rao, M. S. Lipid metabolism and liver inflammation. II. Fatty liver disease and fatty acid oxidation. *Am. J. Physiol.: Gastrointest. Liver Physiol.* **2006**, *290*, G852−8.
(12) Magana, M. M.; Koo, S. H.; Towle, H. C.; Osborne, T. F. Different sterol regulatory element-binding protein-1 isoforms utilize distinct co-regulatory factors to activate the promoter for fatty acid synthase. *J. Biol. Chem.* **2000**, *275*, 4726−33.
(13) Magana, M. M.; Osborne, T. F. Two tandem binding sites for sterol regulatory element binding proteins are required for sterol regulation of fatty-acid synthase promoter. *J. Biol. Chem.* **1996**, *271*, 32689−94.
(14) Matsusue, K.; Haluzik, M.; Lambert, G.; Yim, S. H.; Gavrilova, O.; Ward, J. M.; Brewer, B., Jr.; Reitman, M. L.; Gonzalez, F. J. Liver-specific disruption of PPARgamma in leptin-deficient mice improves fatty liver but aggravates diabetic phenotypes. *J. Clin. Invest.* **2003**, *111*, 737−47.
(15) Shimano, H.; Horton, J. D.; Shimomura, I.; Hammer, R. E.; Brown, M. S.; Goldstein, J. L. Isoform 1c of sterol regulatory element binding protein is less active than isoform 1a in livers of transgenic mice and in cultured cells. *J. Clin. Invest.* **1997**, *99*, 846−54.
(16) Engelking, L. J.; Kuriyama, H.; Hammer, R. E.; Horton, J. D.; Brown, M. S.; Goldstein, J. L.; Liang, G. Overexpression of Insig-1 in the livers of transgenic mice inhibits SREBP processing and reduces insulin-stimulated lipogenesis. *J. Clin. Invest.* **2004**, *113*, 1168−75.
(17) Yahagi, N.; Shimano, H.; Hasty, A. H.; Matsuzaka, T.; Ide, T.; Yoshikawa, T.; Amemiya-Kudo, M.; Tomita, S.; Okazaki, H.; Tamura, Y.; Iizuka, Y.; Ohashi, K.; Osuga, J.; Harada, K.; Gotoda, T.; Nagai, R.; Ishibashi, S.; Yamada, N. Absence of sterol regulatory element-binding protein-1 (SREBP-1) ameliorates fatty livers but not obesity or insulin resistance in Lep(ob)/Lep(ob) mice. *J. Biol. Chem.* **2002**, *277*, 19353−7.
(18) Briggs, M. R.; Yokoyama, C.; Wang, X.; Brown, M. S.; Goldstein, J. L. Nuclear protein that binds sterol regulatory element of low density lipoprotein receptor promoter. I. Identification of the protein and delineation of its target nucleotide sequence. *J. Biol. Chem.* **1993**, *268*, 14490−6.
(19) Schoonjans, K.; Watanabe, M.; Suzuki, H.; Mahfoudi, A.; Krey, G.; Wahli, W.; Grimaldi, P.; Staels, B.; Yamamoto, T.; Auwerx, J. Induction of the acyl-coenzyme A synthetase gene by fibrates and fatty acids is mediated by a peroxisome proliferator response element in the C promoter. *J. Biol. Chem.* **1995**, *270*, 19269−76.
(20) Zhou, G.; Myers, R.; Li, Y.; Chen, Y.; Shen, X.; Fenyk-Melody, J.; Wu, M.; Ventre, J.; Doebber, T.; Fujii, N.; Musi, N.; Hirshman, M. F.; Goodyear, L. J.; Moller, D. E. Role of AMP-activated protein kinase in mechanism of metformin action. *J. Clin. Invest.* **2001**, *108*, 1167−74.
(21) Oliaro-Bosso, S.; Calcio Gaudino, E.; Mantegna, S.; Giraudo, E.; Meda, C.; Viola, F.; Cravotto, G. Regulation of HMGCoA reductase activity by policosanol and octacosadienol, a new synthetic analogue of octacosanol. *Lipids* **2009**, *44*, 907−16.
(22) Chandrasekaran, C. V.; Vijayalakshmi, M. A.; Prakash, K.; Bansal, V. S.; Meenakshi, J.; Amit, A. Review Article: Herbal Approach for Obesity Management. *Am. J. Plant Sci.* **2012**, *3*, 1003−14.
(23) Wellen, K. E.; Hotamisligil, G. S. Inflammation, stress, and diabetes. *J. Clin. Invest.* **2005**, *115*, 1111−9.
(24) Cousin, S. P.; Hugl, S. R.; Wrede, C. E.; Kajio, H.; Myers, M. G., Jr.; Rhodes, C. J. Free fatty acid-induced inhibition of glucose and insulin-like growth factor I-induced deoxyribonucleic acid synthesis in the pancreatic beta-cell line INS-1. *Endocrinology* **2001**, *142*, 229−40.
(25) Kong, W.; Wei, J.; Abidi, P.; Lin, M.; Inaba, S.; Li, C.; Wang, Y.; Wang, Z.; Si, S.; Pan, H.; Wang, S.; Wu, J.; Li, Z.; Liu, J.; Jiang, J. D. Berberine is a novel cholesterol-lowering drug working through a unique mechanism distinct from statins. *Nat. Med.* **2004**, *10*, 1344−51.
(26) Lu, N.; Li, Y.; Qin, H.; Zhang, Y. L.; Sun, C. H. Gossypin up-regulates LDL receptor through activation of ERK pathway: a signaling mechanism for the hypocholesterolemic effect. *J. Agric. Food Chem.* **2008**, *56*, 11526−32.
(27) Zhang, S.; Zheng, L.; Dong, D.; Xu, L.; Yin, L.; Qi, Y.; Han, X.; Lin, Y.; Liu, K.; Peng, J. Effects of flavonoids from *Rosa laevigata* Michx fruit against high-fat diet-induced non-alcoholic fatty liver disease in rats. *Food Chem.* **2013**, *141*, 2108−16.
(28) Carling, D. The AMP-activated protein kinase cascade–a unifying system for energy control. *Trends Biochem. Sci.* **2004**, *29*, 18−24.
(29) Kemp, B. E.; Stapleton, D.; Campbell, D. J.; Chen, Z. P.; Murthy, S.; Walter, M.; Gupta, A.; Adams, J. J.; Katsis, F.; van Denderen, B.; Jennings, I. G.; Iseli, T.; Michell, B. J.; Witters, L. A. AMP-activated protein kinase, super metabolic regulator. *Biochem. Soc. Trans.* **2003**, *31*, 162−8.
(30) Hwang, J. T.; Park, I. J.; Shin, J. I.; Lee, Y. K.; Lee, S. K.; Baik, H. W.; Ha, J.; Park, O. J. Genistein, EGCG, and capsaicin inhibit adipocyte differentiation process via activating AMP-activated protein kinase. *Biochem. Biophys. Res. Commun.* **2005**, *338*, 694−9.
(31) Auger, C.; Teissedre, P. L.; Gerain, P.; Lequeux, N.; Bornet, A.; Serisier, S.; Besancon, P.; Caporiccio, B.; Cristol, J. P.; Rouanet, J. M. Dietary wine phenolics catechin, quercetin, and resveratrol efficiently protect hypercholesterolemic hamsters against aortic fatty streak accumulation. *J. Agric. Food Chem.* **2005**, *53*, 2015−21.
(32) Flores, E. M. [The chayote, *Sechium edule* Swartz (Cucurbitaceae)]. *Rev. Biol. Trop.* **1989**, *37* (Suppl 1), 1−54.
(33) Ribeiro Rde, A.; de Barros, F.; de Melo, M. M.; Muniz, C.; Chieia, S.; Wanderley, M. d. G.; Gomes, C.; Trolin, G. Acute diuretic effects in conscious rats produced by some medicinal plants used in the state of Sao Paulo, Brasil. *J. Ethnopharmacol.* **1988**, *24*, 19−29.
(34) Winder, W. W.; Hardie, D. G. AMP-activated protein kinase, a metabolic master switch: Possible roles in type 2 diabetes. *Am. J. Physiol.* **1999**, *277*, E1−10.
(35) You, M.; Fischer, M.; Deeg, M. A.; Crabb, D. W. Ethanol induces fatty acid synthesis pathways by activation of sterol regulatory element-binding protein (SREBP). *J. Biol. Chem.* **2002**, *277*, 29342−7.
(36) Li, Y.; Xu, S.; Mihaylova, M. M.; Zheng, B.; Hou, X.; Jiang, B.; Park, O.; Luo, Z.; Lefai, E.; Shyy, J. Y.; Gao, B.; Wierzbicki, M.; Verbeuren, T. J.; Shaw, R. J.; Cohen, R. A.; Zang, M. AMPK phosphorylates and inhibits SREBP activity to attenuate hepatic steatosis and atherosclerosis in diet-induced insulin-resistant mice. *Cell Metab.* **2011**, *13*, 376−88.
(37) Jung, E. J.; Kwon, S. W.; Jung, B. H.; Oh, S. H.; Lee, B. H. Role of the AMPK/SREBP-1 pathway in the development of orotic acid-induced fatty liver. *J. Lipid Res.* **2011**, *52*, 1617−25.
(38) Rakhshandehroo, M.; Knoch, B.; Muller, M.; Kersten, S. Peroxisome proliferator-activated receptor alpha target genes. *PPAR Res.* **2010**, *2010*, No. 612089.

JOURNAL OF AGRICULTURAL AND FOOD CHEMISTRY

Article

pubs.acs.org/JAFC

Mechanism for Starch Granule Ghost Formation Deduced from Structural and Enzyme Digestion Properties

Bin Zhang, Sushil Dhital, Bernadine M. Flanagan, and Michael J. Gidley*

Centre for Nutrition and Food Sciences, Queensland Alliance for Agriculture and Food Innovation, The University of Queensland, St. Lucia, Brisbane, Queensland 4072, Australia

Supporting Information

ABSTRACT: After heating in excess water under little or no shear, starch granules do not dissolve completely but persist as highly swollen fragile forms, commonly termed granule "ghosts". The macromolecular architecture of these ghosts has not been defined, despite their importance in determining characteristic properties of starches. In this study, amylase digestion of isolated granule ghosts from maize and potato starches is used as a probe to study the mechanism of ghost formation, through microstructural, mesoscopic, and molecular scale analyses of structure before and after digestion. Digestion profiles showed that neither integral nor surface proteins/lipids were crucial for control of either ghost digestion or integrity. On the basis of the molecular composition and conformation of enzyme-resistant fractions, it was concluded that the condensed polymeric surface structure of ghost particles is mainly composed of nonordered but entangled amylopectin (and some amylose) molecules, with limited reinforcement through partially ordered enzyme-resistant structures based on amylose (for maize starch; V-type order) or amylopectin (for potato starch; B-type order). The high level of branching and large molecular size of amylopectin is proposed to be the origin for the unusual stability of a solid structure based primarily on temporary entanglements.

KEYWORDS: *starch granule ghosts, gelatinization, α-amylase, enzyme-resistant fraction, glucan conformation, polymer entanglement*

INTRODUCTION

Many agriculture and food biopolymers are assembled in an ordered or crystalline form in nature to confer stability and minimize hydration-driven swelling in the native environment. However, once these molecules or assemblies are heated above the relevant melting temperature, most become soluble, at least initially. Examples include many proteins and polysaccharides. Starch, however, is an exception, as when native semicrystalline granules are heated above their characteristic melting temperature under little or no shear, they swell and release some lower molecular weight components, but do not dissolve completely. Most applications of starch in food and industrial processes involve a heating step in the presence of water, which disrupts the ordered arrangement of polymers within granules (termed gelatinization). Gelatinized starches typically contain a mixture of solubilized polymers (mainly leached amylose and amylopectin molecules with low molecular weight) and residual granular structure (also termed (fragments of) granule "ghosts").[1] The importance of starch granule ghosts in determining the properties of cooked starches is often underestimated in studies that treat gelatinized starch as a fully dissolved polymer solution, like other biopolymer solutions such as agar and gelatin.[2,3] The presence of the large (10−200 μm) macromolecular architecture of granule ghosts within an otherwise homogeneous polymer system can affect molecular processes, such as phase separation, and contribute to functional properties of starches that play important roles in texture and mouthfeel (e.g., viscosity, rheology, and tribology).[2]

Numerous studies of the structural changes associated with starch gelatinization have been reported,[4−8] but the factors that contribute to the stability of granule ghost structures are still not clear. Various approaches have been used to understand the robustness of granule ghosts, including selective extraction of surface nonpolysaccharide components, treatment of ghosts with protein-degrading enzymes, and the study of waxy maize mutants with variable (low) amylose contents.[2,9] On the basis of these studies, it has been hypothesized that ghost formation is due to the cross-linking of amylose chains and/or long amylopectin branches (previously presumed to be by double helices), modulated by surface nonpolysaccharide components.[2,9] However, direct experimental testing of this hypothesis has not been reported yet. Due to the lack of detectable ordered structure in granule ghosts[1] (e.g., crystallinity from X-ray diffraction, helical order, or regularity of amylopectin clusters from small-angle X-ray scattering), physical techniques used to study the intermolecular interaction of biopolymers, such as wide- and small-angle X-ray scattering, differential scanning calorimetry (DSC), ^{13}C nuclear magnetic resonance (NMR), and Fourier transform infrared (FTIR) spectrometry, may provide limited insight into the mechanism of ghost formation and stabilization. We have recently shown, however, that there is a fraction of granule ghosts that is relatively resistant to enzymatic digestion.[10] In this work we hypothesize that such enzyme-resistant fractions may be important in providing stabilizing structure to granule ghosts. We have therefore studied the susceptibility of granule ghosts toward enzymatic hydrolysis and investigated the macromolecular and ordered structures present in undigested residues as a probe of local structures that may be important in the formation and structure of ghosts.

Received: October 18, 2013
Revised: December 18, 2013
Accepted: January 1, 2014
Published: January 1, 2014

ACS Publications © 2014 American Chemical Society

Although there is some enzyme-resistant material present in granule ghosts formed under low shear cooking conditions from both maize and potato starches, high shear cooked starches are almost 100% digested, suggesting that granule ghosts are structurally different from high shear cooked starches.[10] In this study, amylase digestion is used as a probe to investigate the structure of granule ghosts isolated from maize and potato, two commonly used commercial starches with different ghost profiles (e.g., size and integrity), as exemplars. On the basis of the concept that the enzyme-resistant fraction is important for maintaining ghost integrity, at least three hypotheses for the underlying structural basis for enzyme resistance can be proposed: (a) the multimicrometer structure of granule ghosts acts as a barrier to limit enzyme access; (b) cross-linking or dense entanglement of amylose and/or amylopectin branches limits enzyme action; or (c) proteins and lipids associated with the granule may contribute to either barrier or local cross-linking mechanisms. To test these hypotheses, in this study morphological parameters of ghosts and digested remnants have been studied with different microscopic techniques, the molecular structure evolution during amylase digestion of granule ghosts has been monitored by ^{1}H NMR spectroscopy and size exclusion chromatography (SEC), and the conformation of polymers within ghosts and enzyme-resistant residues has been determined by ^{13}C CP/MAS NMR. On the basis of the data obtained, mechanisms for starch granule ghost formation and stability are discussed.

EXPERIMENTAL PROCEDURES

Materials. Maize starch (MS) was purchased from Penford Australia Ltd. (Lane Cove, NSW, Australia), and potato starch (PS) was from Sigma-Aldrich. (St. Louis, MO, USA). Porcine pancreatic α-amylase (A3176, activity = 23 unit/mg) and other chemicals were obtained from Sigma-Aldrich.

Depletion of Proteins and Lipids from Granule Surfaces. Treatment of starch granule slurries (20% w/v) with sodium dodecyl sulfate (SDS, 2% w/v) at 20 °C for 30 min was used to extract surface proteins and lipids.[9] Extracted granules were isolated by centrifugation and washed with >10 volumes of cold deionized water until no foaming was observed in the washings. Despite the extensive washing, some SDS was retained by the granules as shown by the increase in sodium and sulfur contents after treatment (Supporting Information, Table S1).

Preparation of Cooked Starch and Granule Ghosts. Starch granule aqueous slurry (10 mL, 0.5% w/v) in a 50 mL centrifuge tube (with a magnetic stirrer, 3 mm × 8 mm) was heated to 100 °C on a hot plate stirrer at a stirring rate of 1500 rpm for 30 min ("high shear cooking") and designated "cooked starch". Granule ghosts were isolated from maize and potato starches following an adaptation of a method reported previously.[1,2] Starch (200 mg) was suspended in a small amount of cold water and then poured into hot water (95 °C, 40 mL). The dilute suspension (0.5% w/v starch) was kept at 95 °C for 30 min at a low stirring rate (250 rpm, "low shear cooking") and then centrifuged (30 °C, 2000*g* for 15 min). The supernatant was removed, and the spun ghosts were washed twice by resuspension in hot water (90 °C) with gentle manual stirring followed by centrifugation. Ghost yield was defined as the weight ratio of freeze-dried pellet to initial starch. The washed ghosts were finally resuspended in excess water for microscopy and in vitro digestion. For SEC, NMR, and scanning electron microscopy (SEM) measurements, starch samples were precipitated by absolute ethanol and dried under pressured nitrogen gas overnight.

Microscopy. Light microscopy was performed using a Zeiss Axio microscope (Oberkochen, Germany). One drop of fresh granule ghost suspension was placed on a glass slide and stained with 2% iodine solution, and the images were recorded by AxioCam ERc5s camera (Zeiss). For confocal microscopy, the staining procedure of fresh granule ghosts with Nile Blue was adapted from the method described by Schirmer et al.[11] Aqueous suspensions of granule ghosts (0.5 mL) and 40 μL of aqueous Nile Blue solution (0.1 g/100 mL; N0766, Sigma-Aldrich) were transferred into 2 mL microcentrifuge tubes. After thorough mixing by repeated pipetting up and down, the stained solutions were incubated at 20 °C for 3 h. For confocal microscopic observation, the stained suspensions were dropped into the cavity of glass slides, sealed with a coverslip, and then observed using an LSM 700 confocal laser scanning microscope (CLSM, Zeiss). Excitation was at 639 nm with a diode laser operating at 2% of power capacity, and the emitted light was detected at an interval wavelength of 640−700 nm. Images of optical sections of granule ghosts were recorded with ZEN 2011 software (Zeiss). For SEM, ethanol-dried samples were thinly spread onto circular metal stubs covered with double-sided adhesive carbon tape and then platinum coated in a sputter coater. Images of the granule ghosts were acquired with a JEOL 6300 scanning electron microscope (JEOL Ltd., Tokyo, Japan) under an accelerating voltage of 5 kV.

Particle Size Distribution. Particle size analysis was carried out using a Malvern Mastersizer Hydro 2000MU (Malvern Instruments Ltd., Malvern, UK) following the method of Dhital et al.[12] A refractive index of 1.34 was used for granule ghost size calculation. The starch samples were added to circulating water until an obscuration of >10% was recorded.

In Vitro Starch Digestion. In vitro starch digestion was performed with porcine pancreatic α-amylase, from the method described by Zhang, Dhital, and Gidley[10] with slight modifications. Starch samples (50 mg, dry basis) were digested with 2.5 units of α-amylase in 30 mL of sodium acetate buffer (0.2 M, pH 6.0) in a shaking water bath at 37 °C. Aliquots (0.2 mL) were removed at different intervals, mixed with 1.0 mL of 95 °C water, and then boiled for 10 min to inactivate enzymes. The reducing sugar value was measured by the Nelson−Somogyi method.[13] The maltose equivalent released (%) was calculated using the following equation (eq 1). Results were expressed as means with standard deviations of at least duplicate measurements.

$$\text{maltose equivalent released (\%)} = \frac{\text{total wt of equivalent maltose in supernatant}}{\text{dry wt of starch}} \times 100 \quad (1)$$

Size Exclusion Chromatography. The fully branched and debranched size distribution of starch molecules during the course of in vitro digestion was obtained from an SEC system (Agilent 1100, Agilent Technologies, Waldbronn, Germany) equipped with a refractive index detector (RID-10A, Shimadzu, Kyoto, Japan) following the methods of Cave et al.[14] and Hasjim et al.[15] SEC samples were prepared following the method described elsewhere[15] and then injected into the following series of columns: precolumn, Gram30, Gram3000 (PSS, Mainz, Germany) for the fully branched distribution, and precolumn, Gram100, Gram 1000 for debranched distribution. The molecular size distribution data were plotted as SEC weight distribution, $w(\log V_h)$, against the hydrodynamic radius (R_h/nm). For linear polymers of uniform geometry, the size and molecular weight (or equivalently the degree of polymerization, DP) are uniquely related, and hence the size distribution can be processed to a molecular weight distribution using the Mark−Houwink equation.[14,16] SEC calibration was performed using pullulan standards with molecular weights ranging from 342 to 1.66 × 10^6 Da (PSS, Mainz, Germany). The standards were dissolved in the SEC eluent and injected into the branched and debranched SEC setups to provide universal calibration curves to relate elution volume with R_h. Because of the calibration range, the R_h values above the upper limit of the standards available (~50 nm) are only semiquantitative. The amylose content can also be calculated as the ratio of the area under the curve (AUC) of the debranched SEC distribution curves for the larger branches to the total AUC for all branches.[17] The amylose contents of maize and potato starches determined in this way were 23.3 ± 1.0 and 18.3 ± 0.4% respectively.

^{1}H Nuclear Magnetic Resonance Spectroscopy. The degree of branching (DB) of starch molecules during the course of in vitro digestion was measured on a Bruker Avance NMR spectrometer (Bruker Biospin, Rheinstetten, Germany), operating at a Larmor

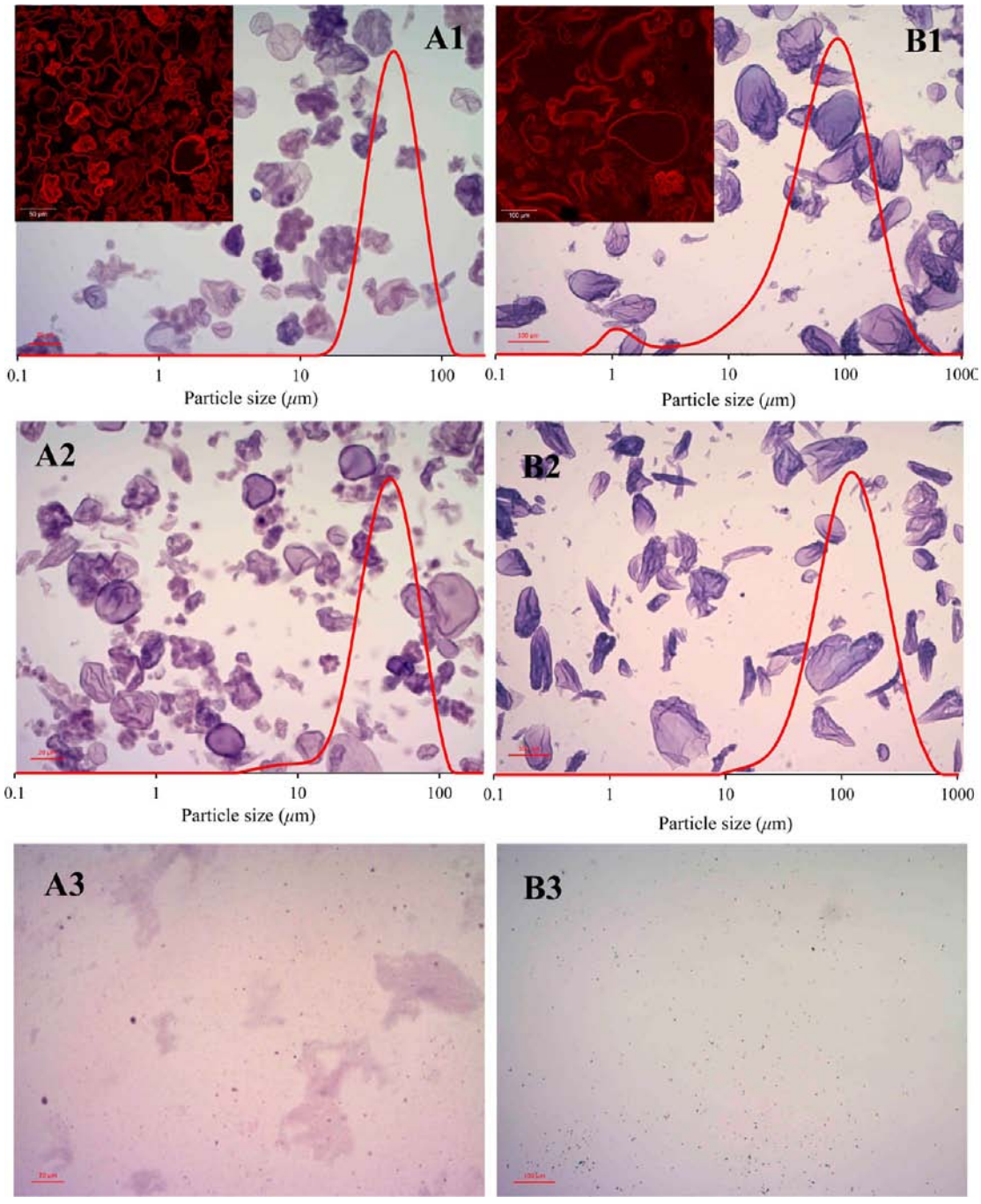

Figure 1. Light micrographs and particle size distribution of fresh granule ghosts (A, maize, scale bar = 20 μm; B, potato, scale bar = 100 μm) with/without SDS pretreatment or high shear force (1, without any treatment; 2, with SDS pretreatment; 3, with high shear force treatment after ghost formation). Insets in panels A1 and B1 are confocal microscopy images after staining with Nile Blue.

frequency of 750 MHz for ^{1}H, equipped with a TXI5z probe following the method of Tizzotti et al.[18] ^{1}H NMR spectra were recorded at 333 K with an 8 μs 90° pulse, a repetition time of 15.98 s (composed of an acquisition time of 3.98 s and a relaxation delay of 12 s), and 128 scans. The addition of a very low amount of TFA-d_1 to the medium causes the exchangeable protons of the starch hydroxyl groups and of the residual water to shift to higher frequency, leading to clear and well-defined ^{1}H NMR spectra.[18] DB is obtained using eq 2

$$\mathrm{DB}\ (\%) = \frac{I_{\alpha\text{-}(1,6)}}{I_{\alpha\text{-}(1,4)} + I_{\alpha\text{-}(1,6)}} \times 100 \qquad (2)$$

where $I_{\alpha\text{-}(1,4)}$ and $I_{\alpha\text{-}(1,6)}$ are the ^{1}H NMR integrals of internal α-(1,4) and α-(1,6) linkages at ∼5.12 and ∼4.78 ppm, respectively.

^{13}C CP/MAS Nuclear Magnetic Resonance Spectroscopy. Starch samples were examined using a solid-state ^{13}C CP/MAS NMR spectrometer (Bruker MSL-300, Rheinstetten, Germany) at a ^{13}C frequency of 75.46 MHz. Approximately 200 mg of sample was packed in a 4 mm diameter, cylindrical, partially stabilized zirconium oxide rotor with a KelF end-cap. The rotor was spun at 5 kHz at the magic angle (54.7°). The 90° pulse width was 5 μs, and a contact time of 1 ms was used for all samples with a recycle delay of 3 s. The spectral width was 38 kHz; acquisition time, 50 ms; time domain points, 2L; transform size, 4K; and line broadening, 50 Hz. At least 2400 scans were accumulated for each spectrum. In the case of the 3 h digestion residues of maize and potato ghosts, it was necessary to collect 20000 scans, as only 50 mg was available. Spectra were referenced to external adamantine and were

dx.doi.org/10.1021/jf404697v | J. Agric. Food Chem. 2014, 62, 760−771

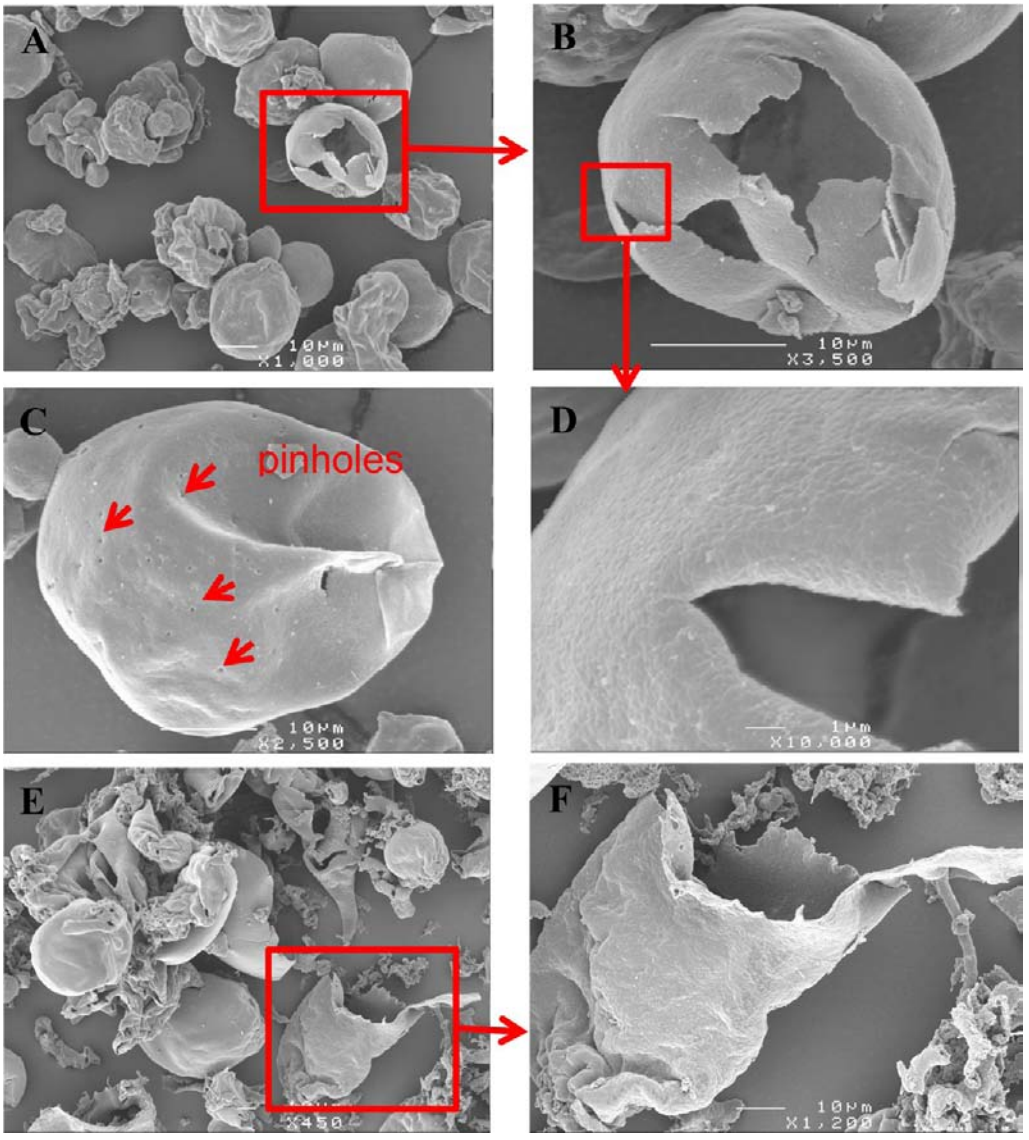

Figure 2. SEM micrographs of ethanol-precipitated granule ghosts (A–D, maize; E and F, potato).

analyzed by resolving the spectra into ordered and amorphous subspectra and calculating the relative areas as described previously.[19] When percentage order is calculated, freeze-dried starches are compared with freeze-dried amorphous standards, and samples precipitated with ethanol are compared with ethanol-precipitated amorphous standards.

RESULTS AND DISCUSSION

Microscopic Structure of Granule Ghosts. Fresh granule ghosts from maize and potato starches were isolated by centrifugation following the method reported by Debet and Gidley.[2] This method ensures full gelatinization and maximum swelling (for most normal starches) when starch is heated at 95 °C for 30 min in excess water. The risks of retrogradation from leached amylose and shear degradation are minimized by the low starch concentration (<1% w/v) and low stirring rate during ghost preparation respectively.[20] Light microscopy and particularly confocal microscopy suggest that ghost particles are essentially hollow with a surface "skin" composed of apparently densely packed starch (Figure 1A1,B1). Granule ghosts have characteristic microscopic features depending on their botanical and genetic origins.[21] Fresh maize ghosts showed complex shapes and surface folds, but appeared overall fairly spherical, typically with a particle size between 15 and 35 μm (Figure 1A1). In contrast, potato ghosts have a wide range of particle sizes (typically 50–150 μm) with more ellipsoidal shapes and significant amounts of granule fragments (Figure 1B1). Expansion is so extensive that the resultant potato ghosts (ca. 4 times expansion in original diameter, i.e., ca. 64-fold increase in granular volume) are more fragile and sensitive to shear force, compared with maize ghosts (increasing only ca. 2 times in diameter) even under the low shear conditions used in ghost preparation. This is not surprising because potato starch contains an appreciable amount of phosphate monoester groups,[22] which are negatively charged and linked to potato amylopectin molecules. The resulting charge repulsion effect helps to untangle the individual branches and extends the degree of granule swelling.[23] Maize ghosts frequently appeared to have more localized regions of folds and wrinkles (Figure 1A1,B1, insets), which may trap undispersed starch polymers.[3]

The morphology of granule ghosts was also investigated using CLSM after being stained by Nile Blue, a water-soluble basic oxazine dye, which is one of the most suitable fluorescent staining agents for both granular and gelatinized starches in the absence of

dx.doi.org/10.1021/jf404697v | J. Agric. Food Chem. 2014, 62, 760–771

proteins.[11] CLSM micrographs of granule ghosts show isolated balloon-like structures, lacking their original contents (Figure 1A1,B1 insets). The skins of maize ghosts appear to be thicker and more substantial and do not show much deterioration or collapse, compared with potato ghosts (Figure 1A1,B1 insets).

To visualize structure at higher resolution, fresh ghosts were precipitated with absolute ethanol, dried with N_2 gas, and examined by SEM. Although syneresis occurring during ethanol precipitation can reduce the roughness of surfaces,[24] the sizes of granule ghosts visualized by electron microscopy (Figure 2) are in agreement with the fresh ghosts (Figure 1) observed by light microscopy. Walls of the ghosts, especially those from maize, did not show much deterioration or collapse, which is consistent with CLSM images (Figure 1A1). Surface pinholes were visible in some ethanol-precipitated ghost particles (Figure 2C) and were of approximately the same size as before cooking (0.1−0.3 μm).[25] Potato ghosts (Figure 2E,F) showed a spongier and more open structure and evidence for deterioration/fracture, probably due to the comparatively thinner walls of these more expanded hollow particles.

Starch granules, in addition to amylose and amylopectin, contain small quantities of minor components, such as lipids and proteins. The proportion of these components depends on the botanical origin and the degree of purification during extraction.[21] SDS can be used to solubilize at least some proteins and lipids from the surface of starch granules (see Supporting Information, Table S1).[9] The extraction of lipids/proteins from the granule interior is difficult, requiring more disruptive methods such as stringent extractions at higher temperatures, chaotropic agents, or starch-degrading enzymes.[9] SDS washing of granules prior to ghost formation resulted in reduced ghost integrity (or robustness), especially for potato (Figure 1A2,B2). As granule ghosts with SDS pretreatment have more irregular shapes (some rod-like shapes for potato), it is not appropriate to assess the particle size by laser scatting techniques. These results are consistent with a previous study in which surface proteins and lipids were found to be a determinant of ghost robustness rather than ghost formation.[2] Shearing results in fragmentation of heated starch granules and facilitates the development of a homogeneous matrix.[26] The multimicrometer structure of ghosts can be efficiently disrupted by Ultraturrax homogenization (20000 rpm for 1 min), resulting in a dispersion of smaller particles and dissolved polymer molecules (Figure 1A3,B3).

α-Amylase Digestion. For the range of starches examined here and previously, both surface nonpolysaccharide material and polysaccharide chains themselves appear to be linked with ghost formation and/or resultant integrity.[1,2,9] The roles of the multimicrometer structure (hypothesis a) and surface proteins/lipids (hypothesis c) during ghost formation were tested by breaking down the ghost particles by high-speed homogenization or extracting surface components by SDS at room temperature, respectively, with enzyme digestion being used as a structure/function probe. According to our previous findings, there is some enzyme-resistant fraction present in granule ghosts after α-amylase and amyloglucosidase digestion, individually and in combination, compared with high-shear-cooked starch.[10] We suggest that the most enzyme-resistant fractions may play an important role in maintaining ghost integrity.

The kinetic profiles of granule ghost digestion were monitored by measuring the reducing sugar released at specific intervals during digestion with a low amount of α-amylase (Figure 3). In addition, the influence of maltose on the kinetics of α-amylase was also investigated (see the Supporting Information, Figure S1), to confirm that the end products (i.e., malto-oligosaccharides) do not inhibit further α-amylase digestion under the conditions used.[27] For both maize and potato ghost samples, pretreatment with SDS or post treatment by shearing did not change digestion behaviors markedly, but cooking with high shearing to prevent ghost formation resulted in a small increase in digestibility, particularly after 3 h of digestion (Figure 3A,B). When the yield of enzyme-resistant fraction was quantified by weight, the high-shear-cooked starches were found to be almost completely digested after 3 h, particularly for potato (isolated yields of 2.1 ± 0.3% for cooked maize and 0.2 ± 0.2% for cooked potato). Starch gelatinization disrupts structural features (e.g., semicrystalline structure, original surface organization) that otherwise slow down enzyme action, and can cause surface rupture at stress points.[3] Digestion profiles suggest that SDS-extractable proteins/lipids are not crucial for control of either ghost digestion or ghost integrity. The skins of many ghosts appear incomplete, with cracks and openings on the micrometer scale and additional small (~20 nm) pores (particularly for maize starch) and fine particles (~400 nm, particularly for potato starch)[3,28] Therefore, we propose that the formation of enzyme−substrate complexes, rather than the access of the enzyme to the granule ghost skin, primarily determines the rate-limiting step of enzyme digestion. Evidence that surface nonpolysaccharide components alone are not sufficient to restrict swelling and affect resultant ghost formation also comes from a previous comparison of swelling profiles for a wide range of starches from different botanical origins.[9] This is logical, as starch polymers are the dominant components in ghosts.[2]

For maize and potato starches, temperatures of structural disorganization (as monitored by loss of birefringence or DSC)

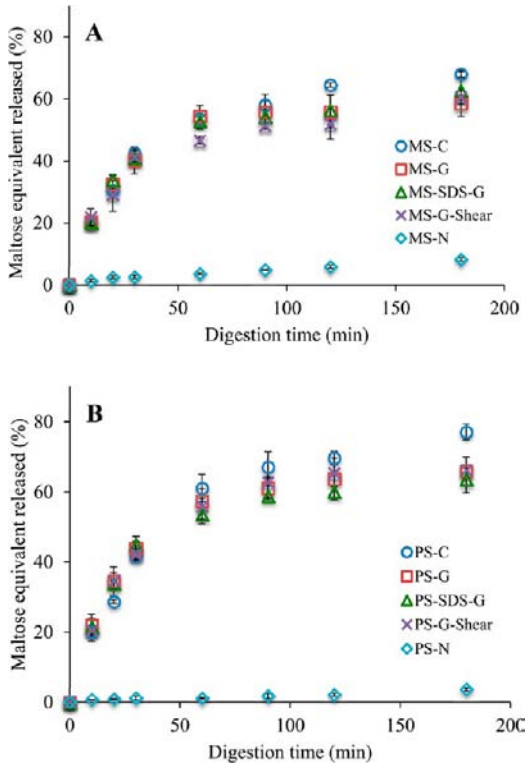

Figure 3. Amylase digestion profiles of granule ghosts (A, maize; B, potato). N, native starch; C, cooked starch prepared under high shear condition; G, granule ghosts; SDS-G, granule ghosts with SDS pretreatment; Shear, with high shear treatment.

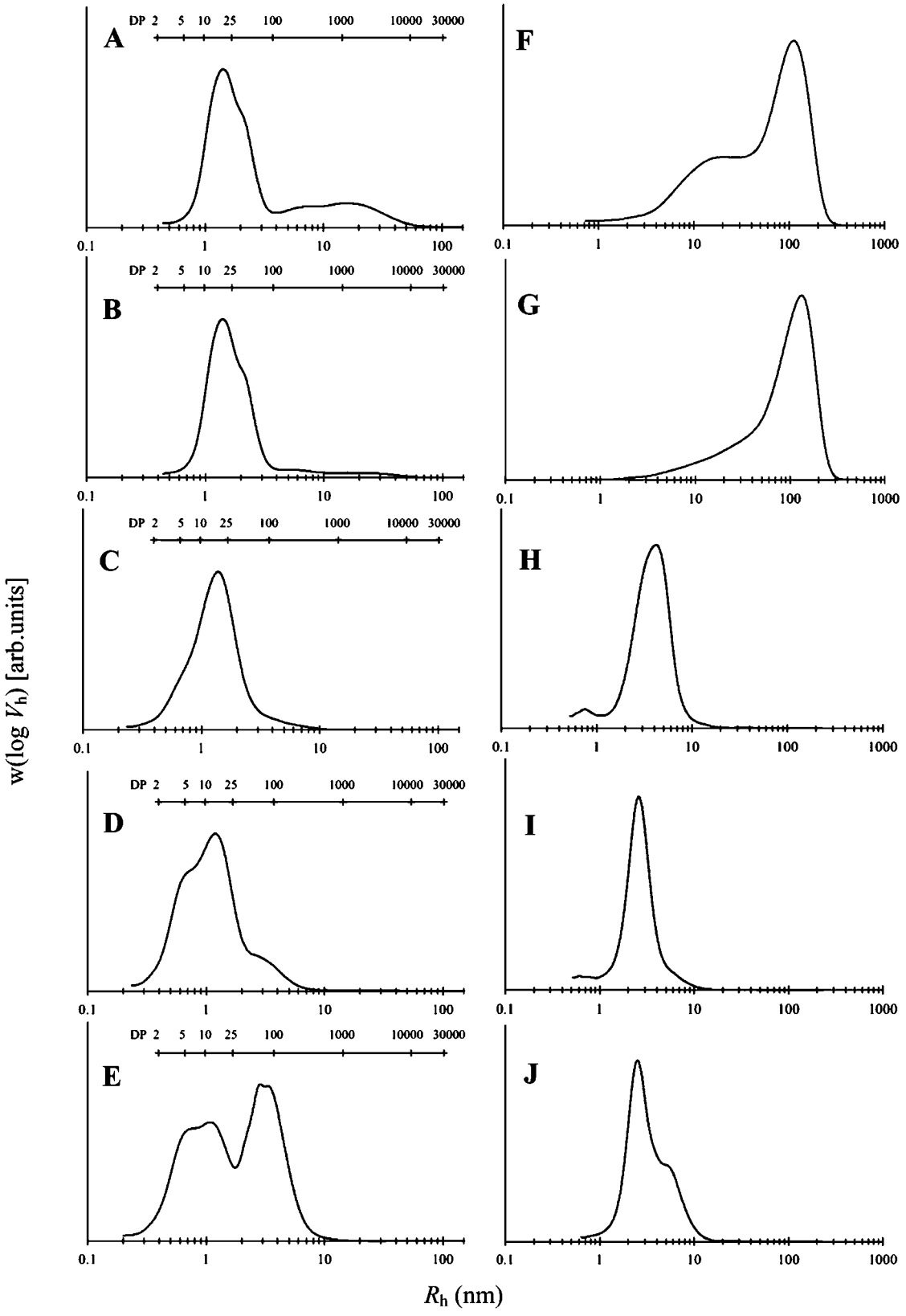

Figure 4. Size distributions of debranched (A–E) and whole (F–J) molecules from maize starch (A and F) and granule ghosts (B and G) after α-amylase hydrolysis for (C and H) 20, (D and I) 60, and (E and J) 180 min.

are relatively similar, yet swelling profiles show major differences.[29] However, once swollen, the digestibilities of potato and maize granule ghosts are comparable (Figure 3), but in both cases for starch cooked under shear, the maltose equivalents released are ca. 10% higher than for ghost samples after 3 h of hydrolysis, suggesting some structural differences between high-shear-cooked starch and granule ghosts. Up to now,[1] no direct evidence of any carbohydrate ordered structure has been found

dx.doi.org/10.1021/jf404697v | J. Agric. Food Chem. 2014, 62, 760–771

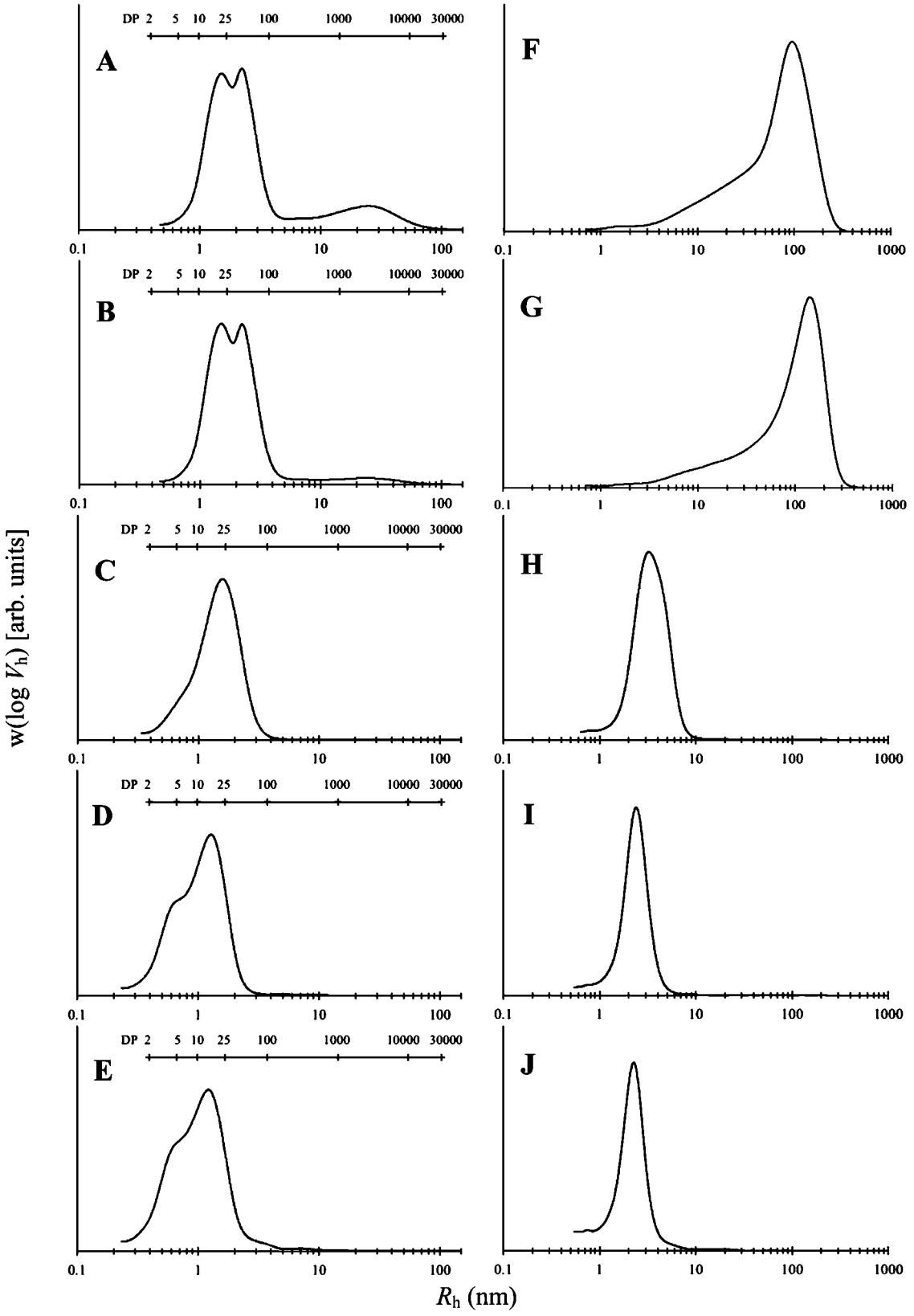

Figure 5. Size distributions of debranched (A–E) and whole (F–J) molecules from potato starch (A and F) and granule ghosts (B and G) after α-amylase hydrolysis for (C and H) 20, (D and I) 60, and (E and J) 180 min.

for ghosts by X-ray scattering/diffraction, ^{13}C NMR, or DSC (e.g., Supporting Information Figure S2). For starch that has been solubilized and then become insoluble by retrogradation, the driving force is typically double-helix formation and subsequent crystallization, but there is currently no evidence that these structures exist in granule ghosts, which have never been solubilized. The possible reasons could be that either the double-helical order is present within ghosts but lower than the

dx.doi.org/10.1021/jf404697v | J. Agric. Food Chem. 2014, 62, 760–771

detection limit of measurement techniques or the polymer chains are just physically entangled without any fixed conformation in the skins of ghosts.

Molecular Structures Present in Granule Ghosts and Their Evolution during Amylase Digestion. Molecular size distribution of whole maize and potato starch molecules (Figures 4F and 5F, respectively) and chain length distributions of enzymatically debranched maize and potato starch samples (Figures 4A and 5A) were characterized using SEC. The fully branched SEC weight distribution of the whole molecules of the two starches showed an amylopectin peak (R_h between 40 and 300 nm, peak R_h = ∼100 nm) and a shoulder for amylose molecules stretching from R_h of 1 to 40 nm. However, some hybrid components could also be present, such as molecules that are highly branched like amylopectin but with molecular size similar to that of amylose and also amylopectin molecules with extra-long branches.[30] The debranched SEC weight distribution can be empirically divided into two regions representing amylopectin branches (single-lamella branches, peak R_h ∼1.5 nm or DP ∼12; trans-lamella branches, peak R_h ∼2.5 nm or DP ∼50) and amylose branches (R_h ∼3.5−80 nm, DP ∼100−30000).[15,31] Amylose molecules are typically smaller than amylopectin and tend to leach out from granules during swelling, as shown by amylose contents of maize (8.4%) and potato (6.7%) ghosts, which are much lower than the starting starches (Figures 4B and 5B). Comparison of Figures 4F/5F with Figures 4G/5G shows that ghost formation is accompanied by loss of the lower molecular size molecules, again consistent with the amylose content results. During ghost formation, 15.1 and 38.8% of amylopectin (calculated from the amylose content of both granules and ghosts and the isolated yields of ghosts, see the Supporting Information) is leached out of maize and potato granules, respectively, suggesting that either a proportion of ghosts do not survive the cooking process or that amylopectin molecules are leached alongside amylose. Despite differences in particle size and robustness, ghosts from maize and potato starch have similar fully branched and debranched molecular size distributions (Figures 4B,G and 5B,G).

The debranched and fully branched SEC weight distributions of maize and potato ghosts and their evolution during amylase digestion are shown in Figures 4 and 5, and DB values calculated from ^{1}H NMR spectra are summarized in Table 1. DB values increase with digestion time, consistent with branched residues being less susceptible to digestion than nonbranched residues, and potato DB values reach higher levels, suggesting a difference in the relative enzyme susceptibility of nonbranched residues between maize and potato ghosts. The size distribution of whole starch molecules reveals that both amylose and amylopectin were quickly degraded to smaller molecules with a single R_h peak (∼4 nm for maize; ∼3 nm for potato) apparent within 20 min of digestion. The remnant small molecules were mainly degraded amylopectin and possibly contain some linear polymers, consistent with the fact that α-amylase is an endoacting enzyme and likely to cleave α-1,4 linkages largely at random locations and also in line with the increased DB values during digestion (Table 1). The corresponding chain length distributions showed fewer changes of the degraded amylopectin together with a clear loss of longer amylose branches (R_h >10 nm, DP >500) (Figures 4C and 5C), suggesting that α-amylase tends to cleave amylopectin molecules into clusters (which provide a barrier to enzyme access and hence prevent preferential digestion of intercluster amylopectin molecules[32]) and that digestion within clusters occurs at random. At the beginning of digestion (20 min), there was a gradual degradation of starch molecules as the peaks of both whole and debranched distributions were slightly shifted to lower R_h regions (Figures 4 and 5D,F,I,J). In addition, it is noteworthy that the debranched chain distributions of 3-h-digested maize ghosts had bimodal peaks, whereas those from potato ghosts showed only one peak at R_h ∼1.5 nm with a shoulder that diminishes in size without changing shape (Figures 4E and 5E). The bimodal peaks of maize ghost residues are designated highly branched α-limit dextrin (peak observed at R_h ∼1 nm) and longer chain polymers (R_h peak ∼3.4 nm) respectively, which are consistent with their whole molecule distributions and DB values (Figures 4E,J; Table 1). Clusters of branching points within starch molecules will slow the amylase action because of steric hindrance. It is noteworthy that some long-chain polymers (DP >100) survived, presumably from degraded amylose in original maize ghost particles. Cuevas et al.[33] also found that the hot-water-insoluble fractions in waxy rice starch contained DP ≥100 chains, which were absent in the hot-water-soluble fractions. However, these long-chain components were not found for the potato ghosts with the same digestion time and similar digestion extents (Figure 3), in agreement with the higher DB values, compared with that of maize residues (Table 1). Furthermore, the α-limit dextrin peak indicates that whole amylopectin present in the ghosts is reduced in size by α-amylase to ∼2.5 nm remnant molecules, which is consistent with previous results.[15,31]

Table 1. DB Values (Number of Branching Points as a Percentage of the Total Number of Glucosidic Linkages) of Maize and Potato Ghosts and Their Evolution during Amylase Digestion

sample[a]	DB (%)	sample[a]	DB (%)
MS	2.81	PS	2.11
MS-G	3.02	PS-G	2.17
MS-G-20	7.81	PS-G-20	4.82
MS-G-60	8.57	PS-G-60	12.75
MS-G-180	7.35	PS-G-180	11.95

[a]MS, maize starch; PS, potato starch; G, granule ghosts; 20, 60, and 180 represent hydrolysis for 20, 60, and 180 min, respectively.

Conformation of Ghost Residues after Enzyme Digestion. The macromolecular architecture of an apparently amorphous matrix such as granule ghosts is critical to their formation and stability. For starch granules, Biliaderis et al.[34] proposed a three-phase model incorporating two distinct types of amorphous materials, that is, nonordered intercrystalline and bulk amorphous matrix, together with the crystalline domains of amylopectin clusters, accounting for order−disorder phase transitions of starch gelatinization. However, there is no reason to suppose that the same amorphous structures exist after gelatinization. As a probe of molecular conformation, molecular order (single helices, double helices) at short distance scale solid-state CP/MAS NMR spectra were recorded before and after enzyme digestion.

The ^{13}C CP/MAS NMR spectra of maize and potato ghosts prepared by freeze-drying or ethanol precipitation produce distinct NMR spectra (Figure 6A). Regardless of the botanical origin of starch, when the starches from the two drying methods are intensity matched at 84 ppm (Figure 6A), there is a difference in intensity between 92 and 100 ppm. By instead matching the intensity of a freeze-dried ghost spectrum, and an ethanol-precipitated ghost spectrum in the 92−100 ppm region, and then

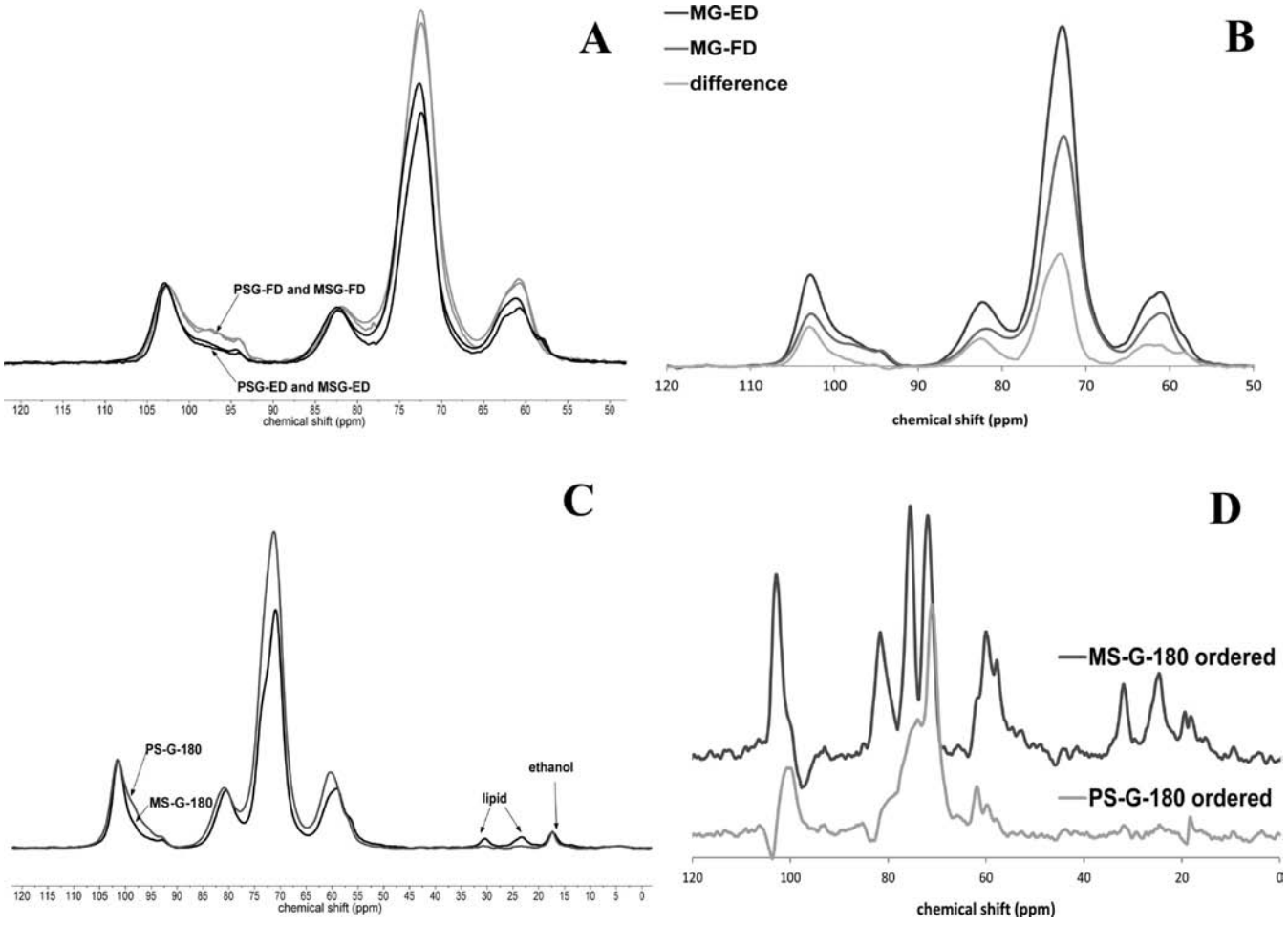

Figure 6. ^{13}C NMR spectra: (A) maize and potato ghosts with freeze-drying (FD) or ethanol-drying (ED); (B) maize ghosts with freeze- or ethanol-drying; (C) digestion residues from maize and potato ghosts. Separation of ^{13}C NMR spectra into ordered subspectra: (D) digestion residues from maize and potato ghosts. MS, maize starch; PS, potato starch; G-180, granule ghost hydrolysis for 180 min.

subtracting the two spectra, a spectrum of V-type helices is revealed (Figure 6B). Spectra of all ethanol-precipitated ghosts clearly indicated the presence of V-type helices with peaks for C1 at 102.9 ppm and C4 at 81.5 ppm.[35] After 3 h of enzyme digestion, the resistant material was recovered by ethanol precipitation to separate it from the large amount of low molecular weight digestion products. NMR spectra (Figure 6C) therefore showed intensity consistent with V-type helices with peaks at 102.9 and 81.5 ppm. The ordered subspectra (Figure 6D) were obtained by matching the intensity at 84 ppm of the 3 h digestion residues and an ethanol-dried amorphous maize starch standard and subtracting one from the other. Although there is no obvious order present when the total spectrum of 3-h-digested potato ghost is compared with the amorphous standard, upon subtraction of the two spectra it becomes apparent that a small amount of B-type double helices (13 ± 2%) is found for the potato ghost digestion residue with peaks at 100.3 and 99.5 ppm.[35−38] In contrast, the spectrum of the 3 h digestion residue from maize ghosts shows more V-type (19 ± 2%) than the standard and the starting ghost material. As shown in Figure 6A,B, ghosts (residues) isolated by ethanol precipitation have some V-type character. Consistent with this, digestion residues from both maize and potato starch ghosts have a signal for ethanol in the NMR spectrum (Figure 6C, 17 ppm). However, there are clearly also signals for lipids in the 3 h digestion residue from maize ghosts (Figure 6C, 33 and 23 ppm), and similar levels of ethanol peaks for both maize and potato 3 h digestion residues (Figure 6C, 17 ppm) can be detected.[39] We therefore propose that the enzyme-resistant V-type helices found in the digestion residue from maize ghosts are due to amylose−lipid complexes either present in the starting granule or formed during gelatinization and/or digestion processes.[40]

Proposed Mechanism for Granule Ghost Formation. At the early stage of heat/moisture-induced starch swelling, even at lower temperatures than those required for crystallite melting, amylose and a small amount of amylopectin molecules can leach out of granules.[41] Crystallite melting,[4] driven by double-helix dissociation,[5] causes granule swelling essentially by replacing hydrogen bonds between amylopectin chains with hydrogen bonds to water molecules,[42] thereby allowing swelling of high molecular weight amylopectin. Swelling behavior is primarily a property of amylopectin,[43] a main molecular component of ghosts, whereas amylose acts both as a diluent and as an inhibitor of swelling, especially in the presence of lipids/proteins, which can form insoluble complexes with amylose.[42,44] An intact amylopectin surface is thought to form a continuous layer surrounding internal starch granule components.[3,28] At certain critical stress points of granules, swelling eventually ruptures the envelope (e.g., Figure 2F), presumably by breakdown of the molecular interactions that holds the granule surface together. On the basis of the high level of enrichment of high molecular size amylopectin, we suggest that molecular interaction between

amylopectin units is responsible for the surface integrity of ghost particles. It has previously been shown by both small-angle and wide-angle X-ray scattering that there is no detectable crystalline or lamellar order in barley starch ghosts.[1] This lack of detectable organizational structure was further extended in this study through both DSC, which showed no detectable melting endotherms (Supporting Information, Figure S2), and solid state ^{13}C NMR, which showed only amorphous features for both maize and potato freeze-dried ghost samples (Figure 6A). However, it is possible that a small amount of cross-linking through, for example, double helices could be present below detection levels of the X-ray, NMR, and DSC techniques. The finding that there is a small amount of an enzyme-resistant fraction in maize (3.8 ± 0.3%, calculated by weight of 3 h digestion residue) and potato (1.5 ± 0.4%) starch ghosts suggests the possibility that this fraction provides a cross-linking or other stabilizing function in otherwise amorphous granule ghost structures.

From NMR (Figure 6) and SEC (Figures 4 and 5) results, the enzyme-resistant fraction of maize ghosts is enriched in amylose with 19% of the sample in a lipid-complexed single-helical form, and the enzyme-resistant portion of potato ghosts is enriched in amylopectin branches/clusters with 13% of the sample present as B-type double helices. In the case of maize, no evidence has been found for the presence of any potentially cross-linking double helices within ghosts, suggesting that double helices are not necessary to provide structure to ghost particles. Although the V-type helices from amylose−lipid complexes are not responsible for cross-linking starch chains as they involve only a single starch chain, they may help to rigidify segments of amylose within maize ghosts. Potato ghosts are more highly swollen and more sensitive to shear than maize ghosts, probably due to the repulsion effect from negatively charged phosphate groups during swelling. Despite similar amylose contents and enzyme digestibility to maize starch ghosts, the enzyme-resistant fraction from potato ghosts is qualitatively different, being based on amylopectin and containing at least some double helices. Normally, B-type double helices would be expected to be formed more readily from amylose and thereby potentially act to cross-link starch polymers. SEC data (Figure 5E,J) for potato ghost enzyme-resistant residue, however, show that it contains predominantly amylopectin, consistent with largely intra-amylopectin double helices formed from adjacent branches, although cross-linking between amylopectin molecules cannot be ruled out. The presence of double helices in enzyme-resistant fractions of potato but not maize starch ghosts is consistent with the fact that the chain length distribution of amylopectin from potato is longer than that of maize (Figures 4A and 5A), and the absence of V-type helices is consistent with the much lower lipid content of potato compared to maize starch.[45] However, it should be noted that the amount of double helices is low (~13% calculated for the 3 h digestion residue, corresponding to ~0.2% based on total starch ghost explaining why it cannot be detected in non-enzyme-treated ghosts) and, therefore, not likely to be a primary mechanism for ghost formation.

On the basis of the lack of detectable ordered structure in intact ghosts, and the low level of order within the small fraction of ghosts that are enzyme resistant, it is apparent that the stable structure of ghosts is derived primarily from simple entanglement of nonordered polymers, particularly amylopectin. The highly branched primary structure and very high molecular size of amylopectin (Figure 5) mean that each molecule can be involved in a large number of temporary entanglements, the sum of which can result in an effectively permanent multimicrometer structure. Small amounts of amylose molecules may also be important to hold amylopectin molecules together by physical entanglements (e.g., maize and potato ghosts) and strengthen the cross-linking entanglements between amylopectin molecules. For example, starches from waxy maize lines with variable low levels of amylose formed granule ghosts with yield and integrity dependent on amylose content.[2] Surface proteins and lipids can also affect ghost properties. For those starches (e.g., wheat and maize) that have restricted swelling due to surface proteins/lipids,[9] ghosts prepared from SDS-treated granules show greater expansion due to the removal of constraining proteins and lipids, leading to a greater extent of swelling before sufficient cross-linking interactions occur to prevent dissolution.

In conclusion, the high molecular weight and highly branched primary structure of amylopectin will lead to many dynamic entanglements, which in combination seem to be sufficient to retain a stable ghost structure. The formation of ghosts as a consequence of extensive swelling of granules following gelatinization suggests that entanglements are formed during the swelling process, explaining why stable hydrated nonordered starch structures starting from preisolated amylopectin have not been reported. The proposed mechanism for granule ghost formation not only confirms that double helices are not necessary to strengthen ghost structure but also raises the question as to how enzyme-resistant fractions could be formed from an essentially amorphous (entangled) starch matrix. Crystallinity alone does not always lead to an increase in enzyme resistance, and almost amorphous high-amylose starches can provide high yields of resistant fraction, although it has generally been accepted that crystallinity must play some role in determining enzyme resistance.[46−48]

■ ASSOCIATED CONTENT

Ⓢ Supporting Information

Methods and results of protein contents and mineral compositions, the influence of maltose on the kinetics of α-amylase digestion, the DSC thermograms of ghost and their digestion residue samples. This material is available free of charge via the Internet at http://pubs.acs.org.

■ AUTHOR INFORMATION

Corresponding Author

*(M.J.G.) Phone: +61 7 3365 2145. Fax: +61 7 3365 1177. E-mail: m.gidley@uq.edu.au.

Notes

The authors declare no competing financial interest.

■ ACKNOWLEDGMENTS

We thank Dr. Fred Warren for the DSC data and fruitful discussions and Dr. Jovin Hasjim and Sarah Chung for their technical assistance with SEC measurement. We also acknowledge the facilities and the technical assistance of Dr. Kim Sewell, Australian Microscopy and Microanalysis Research Facility at the Centre for Microscopy and Microanalysis, The University of Queensland.

■ ABBREVIATIONS USED

AUC, area under the curve; CLSM, confocal laser scanning microscopy; DB, degree of branching; DP, degree of polymerization; DSC, differential scanning calorimetry; FTIR, Fourier transform infrared; MS, maize starch; NMR, nuclear magnetic

resonance; PS, potato starch; R_h, hydrodynamic radius; SDS, sodium dodecyl sulfate; SEC, size exclusion chromatography; SEM, scanning electron microscopy

REFERENCES

(1) Prentice, R. D. M.; Stark, J. R.; Gidley, M. J. Granule residues and ghosts remaining after heating A-type barley-starch granules in water. *Carbohydr. Res.* **1992**, *227*, 121−130.

(2) Debet, M. R.; Gidley, M. J. Why do gelatinized starch granules not dissolve completely? Roles for amylose, protein, and lipid in granule "ghost" integrity. *J. Agric. Food Chem.* **2007**, *55*, 4752−4760.

(3) Atkin, N. J.; Abeysekera, R. M.; Robards, A. W. The events leading to the formation of ghost remnants from the starch granule surface and the contribution of the granule surface to the gelatinization endotherm. *Carbohydr. Polym.* **1998**, *36*, 193−204.

(4) Donovan, J. W. Phase transitions of the starch-water system. *Biopolymers* **1979**, *18*, 263−275.

(5) Cooke, D.; Gidley, M. J. Loss of crystalline and molecular order during starch gelatinization: origin of the enthalpic transition. *Carbohydr. Res.* **1992**, *227*, 103−112.

(6) Cameron, R. E.; Donald, A. M. A small-angle X-ray-scattering study of starch gelatinization in excess and limiting water. *J. Polym. Sci., Part B: Polym. Phys.* **1993**, *31*, 1197−1203.

(7) Jenkins, P. J.; Donald, A. M. Gelatinisation of starch: a combined SAXS/WAXS/DSC and SANS study. *Carbohydr. Res.* **1998**, *308*, 133−147.

(8) Fannon, J. E.; BeMiller, J. N. Structure of corn starch paste and granule remnants revealed by low-temperature scanning electron-microscopy after cryopreparation. *Cereal Chem.* **1992**, *69*, 456−460.

(9) Debet, M. R.; Gidley, M. J. Three classes of starch granule swelling: Influence of surface proteins and lipids. *Carbohydr. Polym.* **2006**, *64*, 452−465.

(10) Zhang, B.; Dhital, S.; Gidley, M. J. Synergistic and antagonistic effects of α-amylase and amyloglucosidase on starch digestion. *Biomacromolecules* **2013**, *12*, 1945−1954.

(11) Schirmer, M.; Hochstotter, A.; Jekle, M.; Arendt, E.; Becker, T. Physicochemical and morphological characterization of different starches with variable amylose/amylopectin ratio. *Food Hydrocolloids* **2013**, *32*, 52−63.

(12) Dhital, S.; Shrestha, A. K.; Gidley, M. J. Relationship between granule size and in vitro digestibility of maize and potato starches. *Carbohydr. Polym.* **2010**, *82*, 480−488.

(13) Nelson, N. A photometric adaptation of the Somogyi method for the determination of glucose. *J. Biol. Chem.* **1944**, *153*, 375−380.

(14) Cave, R. A.; Seabrook, S. A.; Gidley, M. J.; Gilbert, R. G. Characterization of starch by size-exclusion chromatography: the limitations imposed by shear scission. *Biomacromolecules* **2009**, *10*, 2245−2253.

(15) Hasjim, J.; Lavau, G. C.; Gidley, M. J.; Gilbert, R. G. In vivo and in vitro starch digestion: are current in vitro techniques adequate? *Biomacromolecules* **2010**, *11*, 3600−3608.

(16) Clay, P. A.; Gilbert, R. G. Molecular-weight distributions in free-radical polymerizations. 1. Model development and implications for data interpretation. *Macromolecules* **1995**, *28*, 552−569.

(17) Vilaplana, F.; Hasjim, J.; Gilbert, R. G. Amylose content in starches: toward optimal definition and validating experimental methods. *Carbohydr. Polym.* **2012**, *88*, 103−111.

(18) Tizzotti, M. J.; Sweedman, M. C.; Tang, D.; Schaefer, C.; Gilbert, R. G. New ^{1}H NMR procedure for the characterization of native and modified food-grade starches. *J. Agric. Food Chem.* **2011**, *59*, 6913−6919.

(19) Tan, I.; Flanagan, B. M.; Halley, P. J.; Whittaker, A. K.; Gidley, M. J. A method for estimating the nature and relative proportions of amorphous, single, and double-helical components in starch granules by C-13 CP/MAS NMR. *Biomacromolecules* **2007**, *8*, 885−891.

(20) Gidley, M. J.; Bulpin, P. V. Aggregation of amylose in aqueous systems: the effect of chain-length on phase-behavior and aggregation kinetics. *Macromolecules* **1989**, *22*, 341−346.

(21) Obanni, M.; BeMiller, J. N. Ghost microstructures of starch from different botanical sources. *Cereal Chem.* **1996**, *73*, 333−337.

(22) Kasemsuwan, T.; Jane, J. L. Quantitative method for the survey of starch phosphate derivatives and starch phospholipids by P-31 nuclear magnetic resonance spectroscopy. *Cereal Chem.* **1996**, *73*, 702−707.

(23) Swinkels, J. J. M. Composition and properties of commercial native starches. *Starch/Staerke* **1985**, *37*, 1−5.

(24) Bowler, P.; Evers, A. D.; Sargent, J. Dehydration artifacts in gelatinized starches. *Starch-Starke* **1987**, *39*, 46−49.

(25) Fannon, J. E.; Hauber, R. J.; BeMiller, J. N. Surface pores of starch granules. *Cereal Chem.* **1992**, *69*, 284−288.

(26) Langton, M.; Hermansson, A. M. Microstructural changes in wheat-starch dispersions during heating and cooling. *Food Microstruct.* **1989**, *8*, 29−39.

(27) Robertson, G. H.; Wong, D. W. S.; Lee, C. C.; Wagschal, K.; Smith, M. R.; Orts, W. J. Native or raw starch digestion: a key step in energy efficient biorefining of grain. *J. Agric. Food Chem.* **2006**, *54*, 353−365.

(28) Atkin, N. J.; Abeysekera, R. M.; Cheng, S. L.; Robards, A. W. An experimentally-based predictive model for the separation of amylopectin subunits during starch gelatinization. *Carbohydr. Polym.* **1998**, *36*, 173−192.

(29) Jane, J. L.; Chen, Y. Y.; Lee, L. F.; McPherson, A. E.; Wong, K. S.; Radosavljevic, M.; Kasemsuwan, T. Effects of amylopectin branch chain length and amylose content on the gelatinization and pasting properties of starch. *Cereal Chem.* **1999**, *76*, 629−637.

(30) Vilaplana, F.; Gilbert, R. G. Two-dimensional size/branch length distributions of a branched polymer. *Macromolecules* **2010**, *43*, 7321−7329.

(31) Witt, T.; Gidley, M. J.; Gilbert, R. G. Starch digestion mechanistic information from the time evolution of molecular size distributions. *J. Agric. Food Chem.* **2010**, *58*, 8444−8452.

(32) Shrestha, A. K.; Blazek, J.; Flanagan, B. M.; Dhital, S.; Larroque, O.; Morell, M.; Gilbert, E. P.; Gidley, M. J. Molecular, mesoscopic and microscopic structure evolution during amylase digestion of maize starch granules. *Carbohydr. Polym.* **2012**, *90*, 23−33.

(33) Cuevas, R. P.; Gilbert, R. G.; Fitzgerald, M. A. Structural differences between hot-water-soluble and hot-water-insoluble fractions of starch in waxy rice (*Oryza sativa* L.). *Carbohydr. Polym.* **2010**, *81*, 524−532.

(34) Biliaderis, C. G.; Page, C. M.; Maurice, T. J.; Juliano, B. O. Thermal characterization of rice starches: a polymeric approach to phase-transitions of granular starch. *J. Agric. Food Chem.* **1986**, *34*, 6−14.

(35) Gidley, M. J.; Bociek, S. M. Molecular organization in starches: a ^{13}C CP/MAS NMR study. *J. Am. Chem. Soc.* **1985**, *107*, 7040−7044.

(36) Gidley, M. J.; Bociek, S. M. C-13 CP/MAS NMR studies of amylose inclusion complexes, cyclodextrins, and the amorphous phase of starch granules: Relationships between glycosidic linkage conformation and solid-state C-13 chemical-shifts. *J. Am. Chem. Soc.* **1988**, *110*, 3820−3829.

(37) Veregin, R. P.; Fyfe, C. A.; Marchessault, R. H. C-13 CP/MAS NMR study of the polypivalolactone polymorphs. *Macromolecules* **1986**, *19*, 2379−2383.

(38) Horii, F.; Yamamoto, H.; Hirai, A.; Kitamaru, R. Structural study of amylose polymorphs by cross-polarization magic-angle spinning, C-13-NMR spectroscopy. *Carbohydr. Res.* **1987**, *160*, 29−40.

(39) Snape, C. E.; Morrison, W. R.; Maroto-Valer, M. M.; Karkalas, J.; Pethrick, R. A. Solid state C-13 NMR investigation of lipid ligands in V-amylose inclusion complexes. *Carbohydr. Polym.* **1998**, *36*, 225−237.

(40) Zhang, B.; Huang, Q.; Luo, F. X.; Fu, X. Structural characterizations and digestibility of debranched high-amylose maize starch complexed with lauric acid. *Food Hydrocolloids* **2012**, *28*, 174−181.

(41) Gallant, D. J.; Bouchet, B.; Baldwin, P. M. Microscopy of starch: evidence of a new level of granule organization. *Carbohydr. Polym.* **1997**, *32*, 177−191.

(42) Srichuwong, S.; Jane, J.-l. Physicochemical properties of starch affected by molecular composition and structures: a review. *Food Sci. Biotechnol.* **2007**, *16*, 663−674.

(43) Tester, R. F.; Morrison, W. R. Swelling and gelatinization of cereal starches. 1. Effects of amylopectin, amylose, and lipids. *Cereal Chem.* **1990**, *67*, 551−557.
(44) Morrison, W. R.; Tester, R. F.; Snape, C. E.; Law, R.; Gidley, M. J. Swelling and gelatinization of cereal starches. 4. Some effects of lipid-complexed amylose and free amylose in waxy and normal barley starches. *Cereal Chem.* **1993**, *70*, 385−391.
(45) Vasanthan, T.; Hoover, R. A comparative-study of the composition of lipids associated with starch granules from various botanical sources. *Food Chem.* **1992**, *43*, 19−27.
(46) Shrestha, A. K.; Ng, C. S.; Lopez-Rubio, A.; Blazek, J.; Gilbert, E. P.; Gidley, M. J. Enzyme resistance and structural organization in extruded high amylose maize starch. *Carbohydr. Polym.* **2010**, *80*, 699−710.
(47) Htoon, A.; Shrestha, A. K.; Flanagan, B. M.; Lopez-Rubio, A.; Bird, A. R.; Gilbert, E. P.; Gidley, M. J. Effects of processing high amylose maize starches under controlled conditions on structural organisation and amylase digestibility. *Carbohydr. Polym.* **2009**, *75*, 236−245.
(48) Chanvrier, H.; Uthayakumaran, S.; Appelqvist, I. A. M.; Gidley, M. J.; Gilbert, E. P.; Lopez-Rubio, A. Influence of storage conditions on the structure, thermal behavior, and formation of enzyme-resistant starch in extruded starches. *J. Agric. Food Chem.* **2007**, *55*, 9883−9890.

JOURNAL OF AGRICULTURAL AND FOOD CHEMISTRY

Article

pubs.acs.org/JAFC

Volatile Compounds as Markers of Tofu (Soybean Curd) Freshness during Storage

Seonmi Lee, Heera Cho, and Kwang-Geun Lee*

Department of Food Science and Biotechnology, Dongguk University—Seoul, 26, 3-Ga, Pil-dong, Chung-gu, Seoul 100-715, Republic of Korea

ABSTRACT: Volatile compounds in packed and unpacked commercial tofu were extracted by solid phase microextraction fibers and analyzed by gas chromatography−mass spectrometry. The tofu samples were stored at 4 °C for 15 days to measure freshness and quality changes during storage. Totals of 41 and 35 volatile compounds were identified from packed tofu and unpacked tofu, respectively. Peak area ratio (PAR) of hexanal in packed tofu increased from 11.44 (day 0) to 496.30 (day 9) and finally decreased to 11.06 on day 15 of storage. PAR of ethanol and 1-hexanol increased from 5.41 and 0.76 (day 1) to 66.93 (day 9) and 47.46 (day 15), respectively. Changes in these volatiles in unpacked tofu were similar to those in packed tofu. The results show that hexanal, ethanol, and 1-hexanol are characteristic volatile compounds for providing quantitative and qualitative information regarding deterioration of tofu.

KEYWORDS: *volatile compounds, tofu, storage, freshness, HS-SPME, GC-MS*

INTRODUCTION

Tofu (soybean curd) is a healthy, popular, and traditional soy food in Asian diets, as it is rich in protein, calcium, B-vitamins, iron, and magnesium.[1] Tofu is becoming more popular in other countries because isoflavones in soybean are very beneficial to human health.[2] However, tofu is very perishable and has a short shelf life of 2−3 days.[3] Tofu is very sensitive to microbial growth even under refrigeration due to its high moisture content (>80%) and neutral pH (5.8−6.2).[4−6] Mass production of tofu is currently carried out in Korea through a pasteurizing process at a low temperature and packaging in sealed containers. Tofu is distributed by a cold-chain system. Sales of tofu increased rapidly from $336 million (2004) to $414 million (2008) in Korea. The cold-chain system provides easy handling of tofu and improves its storability.[7] Nevertheless, the only way to check the freshness of leftover tofu is to look at the expiration date on the label or smell the tofu. A few studies have investigated the development of a freshness indicator for tofu.[8]

Many studies have been conducted on the volatile compounds in fermented tofu and other soybean products. However, these studies were restricted to volatile compounds of fermented soybean products such as Thai thua nao, Chinese sufu, and Korean doenjang.[9−13] Among the volatiles, hexanal, ethanol, and 1-hexanol are found in all fermented tofu. In particular, hexanal contributes a disagreeable green grass-like aroma to tofu and soy milk.[14,15] The content of hexanal in the nonfermented tofu is higher than that in fermented tofu. This phenomenon suggests that fermentation may remove the undesirable green grass flavor from soybean products[16,17] and indicates that volatile compounds in tofu could be a durable index chemical to determine the quality of tofu during storage.

The typical methods for extracting volatile compounds from tofu are simultaneous distillation extraction, supercritical fluid extraction, and solid phase microextraction (SPME).[13,18,19] SPME has recently replaced older techniques for volatile analysis as it is fast and less labor intensive.[20] In addition, the SPME method is a solvent-free technique and is relatively inexpensive.[21] SPME coupled with gas chromatography−mass spectrometry (GC-MS) was adopted in this study.

Few studies have investigated changes in volatile compounds of fresh commercial tofu during storage.[18,22] The objective of our study was to investigate the changes in volatile compounds in commercial tofu using the SPME method and GC-MS during storage. Analyses of volatiles and microbial contamination were carried out to evaluated the freshness and quality change in tofu. The relationship between tofu freshness and volatile compounds was determined.

MATERIALS AND METHODS

Materials. Two types of tofu, a packed tofu and an unpacked tofu, were purchased at a commercial market in Korea. In Korea the market for tofu is divided into packed and unpacked tofu. The packed tofu selected in this study is the first in market share in Korea. The unpacked tofu was also selected due to higher market share in Korean traditional market. Petri film was used for microbiological analysis (3M, St. Paul, MN, USA). The C_8−C_{20} alkanes for calculating the retention indices (RI) were purchased from Aldrich Chemical Co. (St. Louis, MO, USA). Three kinds of SPME fibers with different coats were purchased from Supelco Inc. (Bellefonte, PA, USA); they were polydimethylsiloxane (PDMS, 100 μm film thickness), Carboxen−polydimethylsiloxane (CAR-PDMS, 75 μm film thickness), and polydimethylsiloxane−divinylbenzene (PDMS-DVB, 65 μm film thickness).

Sample Preparation and Storage Condition. The tofu was cut into cubed samples (5 cm ×5 cm ×3 cm) and placed in a plastic container with 160 mL of sterile purified water. Tofu was classified according to temperature and storage day. The samples were stored at 4 °C for 15 days.

Microbiological Analysis. Ten grams of sample was mixed with 90 mL of buffered peptone water (0.1%) in a sterile stomacher bag.

Received: October 29, 2013
Revised: January 3, 2014
Accepted: January 6, 2014
Published: January 6, 2014

ACS Publications © 2014 American Chemical Society

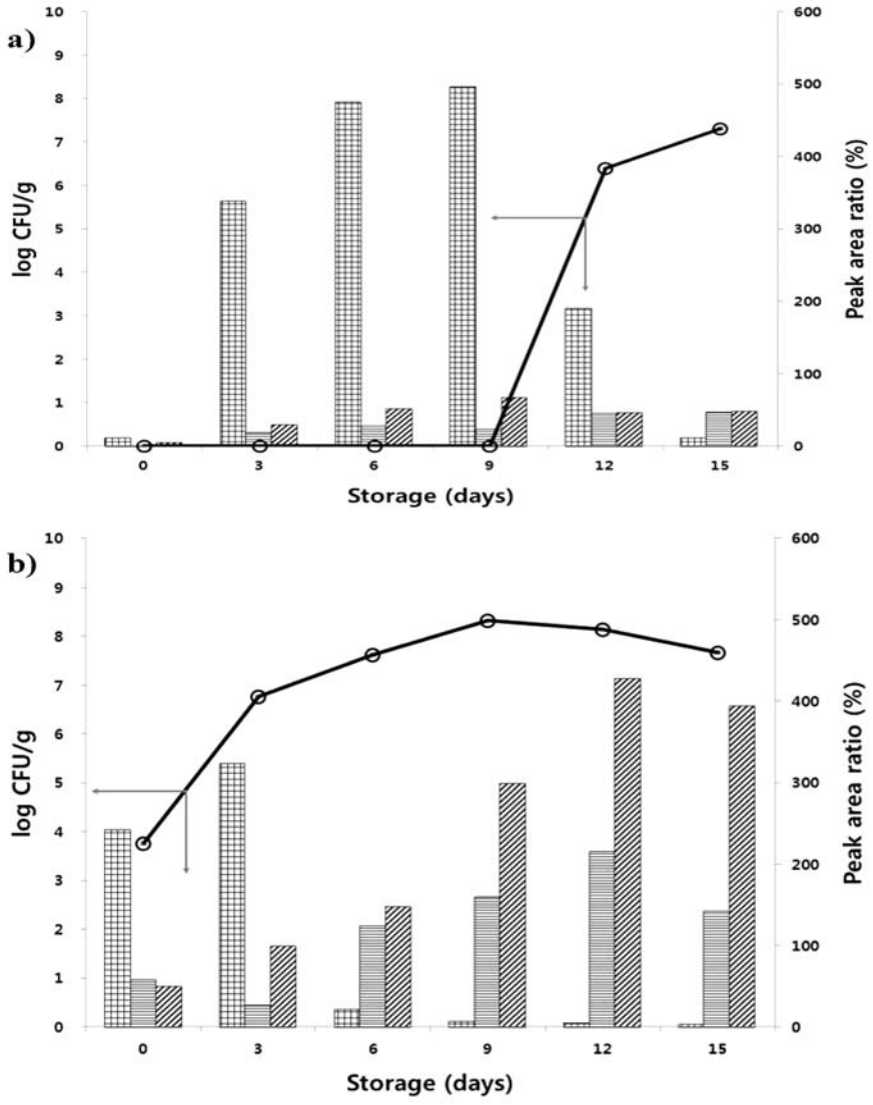

Figure 1. Relationship between microbial growth and peak area ratio of volatile compounds in packed tofu (a) and unpacked tofu (b) during storage at 4 °C. Bars represent, from left to right in each group, hexanal, 1-hexanol, and ethanol.

The mixture was blended for 1 min using a Stomacher Lab Blender (Bag mixer model, Inter Science), serially (1:10) diluted with buffered peptone water (0.1%), and plated on Petri film (3M). The Petri film was incubated at 37 °C for 48 h, and total bacterial counts were carried out.

Volatile Compound Analysis. The ground samples (2.5 g) were mixed with 2.5 mL of tofu soaking water, and the mixtures were placed into a 15 mL headspace vials (Supelco). The headspace vials were sealed with a polypropylene hole cap and PTFE/silicone septa (Supelco). Then they were pre-equilibrated for 21 min at 46 °C in a thermostatic bath. Before the volatile compound extraction, 20 μL (1 ppm) of internal standard (1,2-dichlorobenzene) was added to the sample solution. Samples were analyzed using headspace-SPME-GC-MS.

Three fibers were tested and compared: PDMS (100 μm film thickness), CAR-PDMS (75 μm film thickness), and PDMS-DVB (65 μm film thickness). Each fiber was preconditioned in the injector of the GC system according to the conditions provided by the manufacturer.

The selected fiber (CAR-PDMS (75 μm film thickness) fiber) was pushed through the vial septum of the prepared sample. The fiber was pushed out of the housing and exposed to the headspace (3 cm in depth) at 46 °C for 14 min. After extraction, the fiber was pulled into the housing, and the SPME device was removed from the vial and inserted into the injection port of a gas chromatograph (GC) for thermal desorption of the analysis (4 cm in depth). The fiber was desorbed for 10 min at 230 °C to eliminate any residual volatile compounds.

GC-MS analysis was performed using an Agilent 6890 gas chromatograph with a 5975 mass spectrometry detector (Agilent Technologies Inc., Palo Alto, CA, USA) equipped with a DB-WAX column (30 m length × 0.32 mm i.d × 0.25 μm film thickness; J&W Scientific, Folsom, CA, USA). The analytical conditions were as follows: inlet temperature, 220 °C; column head pressure, 14.14 psi; splitless time, 1 min; helium carrier gas flow rate, 1.3 mL/min; oven temperature, held at 40 °C for 4 min, raised at 5 °C/min to 185 °C, and held for 20 min. Mass spectra were generated in the electron impact mode (MSEI) at 70 eV and an ion source temperature of 230 °C. The total ion chromatograms acquired via GC-MS was used for peak area integration. Agilent MSD Chemstation software (G1701BA ver.D.02.00) was used for data acquisition.

Compound Identification and Quantification. The volatile compounds were positively identified by comparing Kovats retention indices (KI)[23] and the MS fragmentation patterns with those of reference compounds or with mass spectra in the Wiley 275 mass spectral database (Hewlett-Packard, Palo Alto, CA, USA) and previously reported KIs. The KIs of the unknown compounds were determined via sample injection with a homologous series of alkanes (C_8−C_{20}). The GC-MS conditions were the same as described above. To quantify volatiles, the samples were run in duplicate, and the integrated areas based on the total ion chromatograms were normalized to the areas of the internal standard and averaged. The relative volatile concentrations

dx.doi.org/10.1021/jf404847g | J. Agric. Food Chem. 2014, 62, 772−779

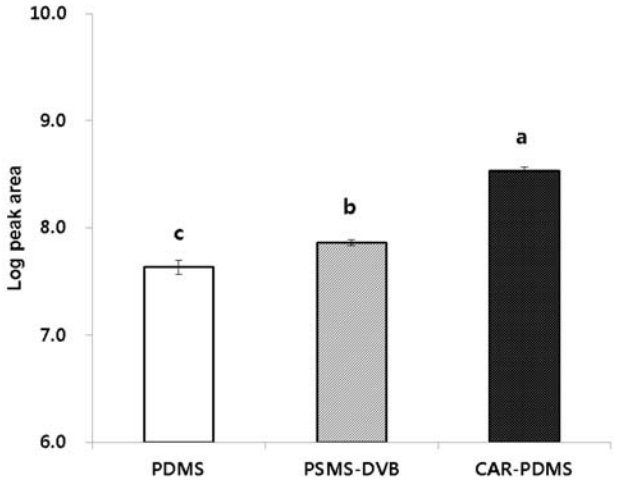

Figure 2. Effect of the SPME fiber on extraction of total volatile compounds from tofu (values sharing a common letter are not significantly different; $p \leq 0.05$).

in the tofu samples were determined by comparison with the concentration of the internal standard (1,2-dichlorobenzene), assuming a response factor of 1.

Statistical Analysis. SPME fiber screening statistics were conducted using the Statistical Analysis System (SAS) software ver. 9.2 (SAS Institute, Cary, NC, USA).

RESULTS AND DISCUSSION

Microbiological Analysis. Figure 1 shows the microbial population and volatiles of packed and unpacked tofu during the storage period at 4 °C. The initial colony-forming units (CFUs) of aerobic mesophilic microorganisms (total bacterial count) of packed tofu and unpacked tofu were different. No microorganisms were detected until storage day 9 for packed tofu. Then, their level reached 7.29 log CFU/g at day 15. The initial number of microbial flora in unpacked tofu was 3.76 log CFU/g, which was much higher than that of packed tofu. The number of microbial flora ranged from 3.76 to 7.67 log CFU/g in unpacked tofu for all storage days. The maximum log CFU/g in unpacked tofu was found after 9 days of storage. The unpacked tofu had rapidly growing microbial flora compared with that in the packed tofu because it was exposed to air without any packaging material. In Korea the microbial (aerobic mesophilic microorganisms) count exceeding the safe level is approximately 6−7 log CFU/g.[8] However, coli form should be <1 log CFU/g in tofu.[24]

Selection of SPME Fiber. Three fibers, PDMS (100 μm film thickness), PDMS-DVB (65 μm film thickness), and CAR-PDMS (75 μm film thickness), were evaluated to analyze total volatiles in tofu. The effects of the various PDMS, PDMS-DVB, and CAR-PDMS fibers on extraction of the volatile compounds in packed tofu are shown in Figure 2. The sum of peak area of each volatile was significantly higher in CAR-PDMS than that in

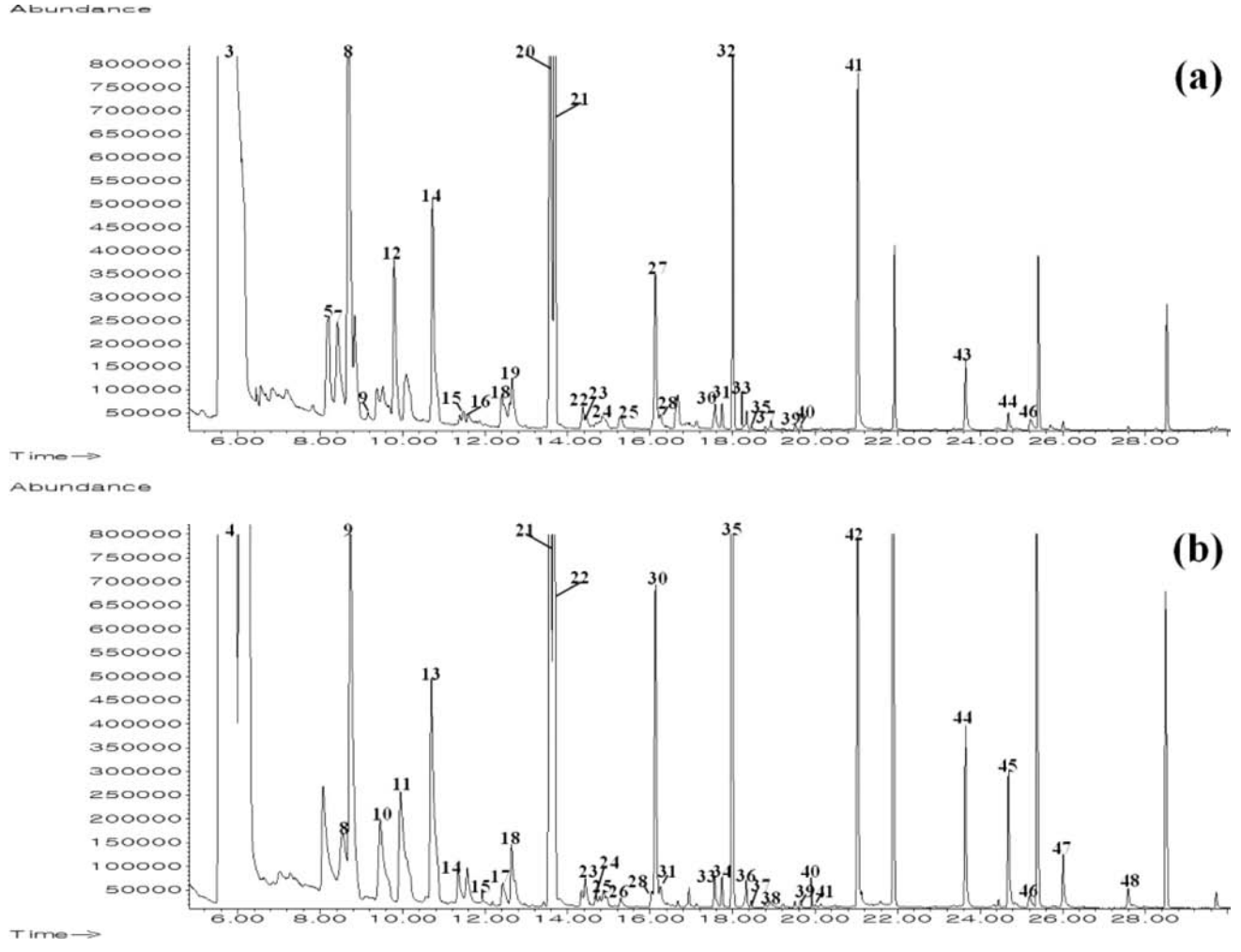

Figure 3. Gas chromatography−mass spectrometry chromatogram of packed tofu (a) and unpacked tofu (b) on day 0 at 4 °C.

dx.doi.org/10.1021/jf404847g | J. Agric. Food Chem. 2014, 62, 772−779

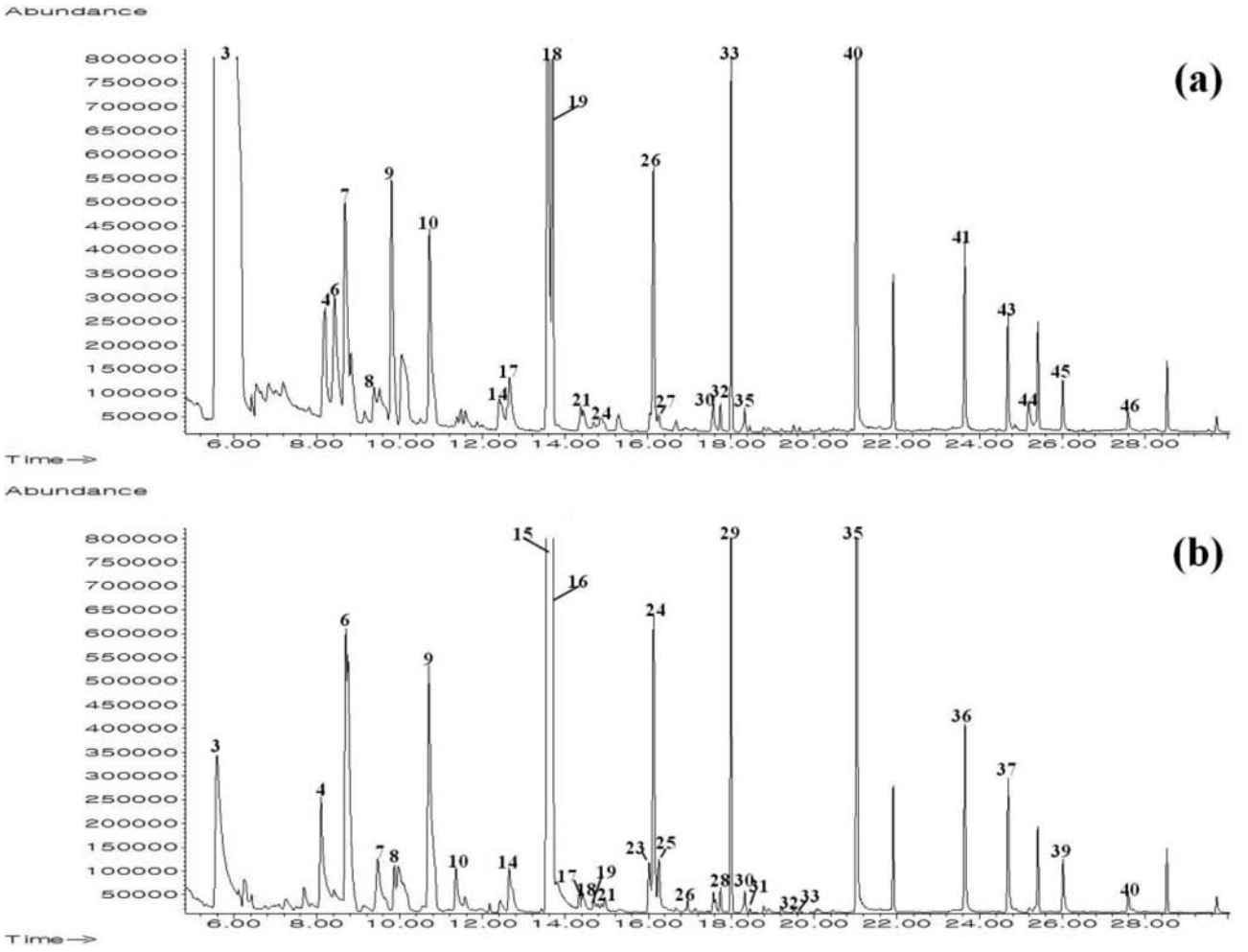

Figure 4. Gas chromatography−mass spectrometry chromatogram of packed tofu (a) and unpacked tofu (b) on day 6 at 4 °C.

the other fibers ($p \leq 0.05$). Thus, CAR-PDMS was selected to analyze the tofu volatiles.

Changes in Tofu Volatile Compounds. Volatile compounds were analyzed by GC-MS using a SPME method to measure freshness and quality changes in the packed and unpacked tofu. Figures 3, and 4, 5 show GC-MS chromatograms in the two types of tofu at days 0, 6, 15 (4 °C), respectively. Volatile chemicals in the GC-MS chromatograms were clearly separated in the packed and unpacked tofu. The major peaks in tofu were hexanal (peak 3 in both tofus) and 1-hexanol (peak 18 in the packed and peak 15 in the unpacked) (Figure 4). As shown in Table 1, 42 volatile compounds were identified in packed tofu during storage for 15 days at 4 °C, including 6 acids, 17 alcohols, 9 aldehydes, 1 alkane, 1 aromatic compound, 2 furans, 3 ketones, and 3 miscellaneous compounds. Thirty-five volatile compounds were identified in unpacked tofu, including 5 acids, 16 alcohols, 6 aldehydes, 1 alkane, 1 aromatic compound, 2 furans, 2 ketones, and 2 miscellaneous compounds during storage for 15 days at 4 °C (Table 2).

Alcohols were the largest class of volatile compounds in both packed and unpacked tofu. Seventeen and 16 alcohols were identified in packed and unpacked tofu, respectively, including ethanol, 1-penten-3-ol, 3-methyl-1-butanol, 1-pentanol, (*Z*)-2-penten-1-ol, 1-hexanol, (*Z*)-3-hexen-1-ol, 3-octanol, (*E*)-2-hexen-1-ol, 1-octen-3-ol, 1-heptanol, benzenemethanol, 2,3-butanediol, 1-octanol, 1,2-propanediol, and 1*H*-indol-5-ol. 1-Hexanol and 1-octen-3-ol were key compounds that yield a green bean flavor.[24] The peak area ratio (PAR) of 1-hexanol increased from 0.76 to 47.46 in packed tofu and from 58.05 to 215.24 in unpacked tofu as the storage was extended. The PAR of 1-octen-3-ol increased from 0.21 to 10.16 in packed tofu and from 8.67 to 14.24 in unpacked tofu, but it was not dramatically increased compared to that of hexanol.

Ethanol increased steadily in accordance with increasing storage. The PAR of ethanol increased from 5.41 to 66.93 in packed tofu during 9 storage days. However, the PAR of ethanol in unpacked tofu was 49.46 and increased to 428.18 at storage day 12. In contrast, pleasant odors such as 1-octanol (rosy-like odor) and 3-octanol (melon, herbaceous, nutty, citrus-like odor) in packed tofu were detected until storage day 3, but they were not detected after day 6. 1-Octanol and 3-octanol were detected in unpacked tofu until storage days 9 and 15, respectively. The PARs of 1-octanol and 3-octanol were 0.36 and 0.71, respectively, at days 9 and 15 of storage. The trend in the change in alcohols in the two types of tofu was different during storage. The PARs of nine alcohols increased in packed tofu. However, those of the other eight alcohols decreased and were not detected at day 3 or later. The PARs of the 14 alcohols increased during storage in the unpacked tofu, but 3 alcohols, 1-octanol, benzenemethanol, and 1,2-propanediol, were not detected at days 12, 15, and 3, respectively.

Six acids, including benzeneacetic acid, acetic acid, butanoic acid, propionic acid, hexanoic acid, and benzoic acid, were identified in packed and unpacked tofu except for propionic acid.

dx.doi.org/10.1021/jf404847g | *J. Agric. Food Chem.* 2014, 62, 772−779

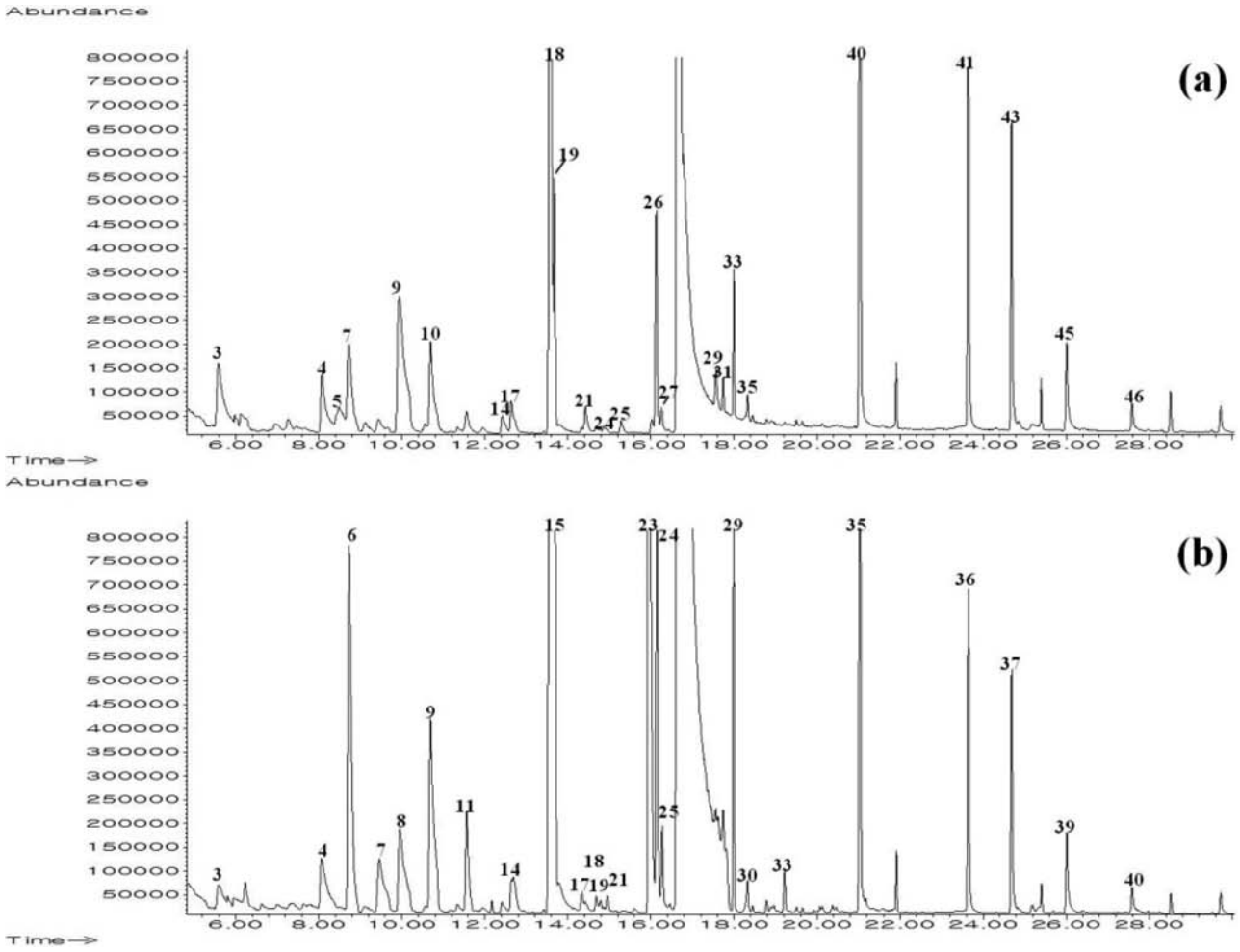

Figure 5. Gas chromatography−mass spectrometry chromatogram of packed tofu (a) and unpacked tofu (b) on day 15 at 4 °C.

The benzeneacetic acid and butanoic acid levels were relatively high among acids in both tofus. In accordance with a previous study, hexanoic acid was found in mold-fermented sufu, soybean milk, and soybean paste. This acid is derived from the oxidation of hexanal.[12,25,26] However, in our study, hexanoic acid was detected in both tofus only during early storage. Butanoic acid and acetic acid result from hydrolysis of soybean lipids.[27] Several acids have been described as having a cheesy odor, including butanoic acid (cheesy, sweaty, sharp, sour, rancid) and hexanoic acid (cheesy, pungent, rancid, sour, sweaty, fatty).[9] The various acids were observed more in fermented or deteriorated tofu than those in fresh tofu. In particular, unpacked tofu had higher levels of benzeneacetic acid and acetic acid than packed tofu.

Nine aldehydes, including hexanal, heptanal, (*E*)-2-hexanal, octanal, (*E*)-2-heptenal, nonanal, (*E*)-2-octenal, benzaldehyde, and 2, 4-decadienal, were identified in packed tofu. Six aldehydes, including hexanal, heptanal, (*E*)-2-heptenal, nonanal, 3-hydroxybutanal, and benzaldehyde, were also found in unpacked tofu. Benzaldehyde (cherry or almond-like odor) and 2,4-decadienal (potato chip-like odor) are favorable odors of aldehyde compounds.[28,29] Hexanal is one of the important volatile compounds of tofu, but it contributes a disagreeable green grass-like odor to tofu.[14] It was reported that the content of hexanal in tofu decreased markedly during storage,[16] and fermented soybean pastes and tofu had large amounts of hexanoic acid, a derivative of hexanal.[12] In accordance with those early studies, it is inferred that hexanal can be used as a freshness indicator of tofu. A high concentration of hexanal was found in the fresh tofu, indicating that it had not deteriorated. The PAR of hexanal increased from 11.44 (initial day) to 496.30 (day 9) and finally decreased to 11.06 (day 15) in packed tofu. It increased from 242.27 (initial day) to 324.04 (day 9) in unpacked tofu and then decreased to 2.87 (day 15). Previous study reported that hexanal contributes to the green and grassy odor of the raw material of tofu.[17] From these results, we assumed that the undesirable green grass-like flavor decreased during deterioration.

2-Ethylfuran and 2-pentylfuran were identified in both packed tofu and unpacked tofu. 2-Pentylfuran has been recognized to have a grassy or green bean aroma.[30] Formation of furan is due to sugar dehydration of fragmentation in the Maillard reaction.[30] Three ketones, including 2-heptanone, 3-hydroxy-2-butanone, and 2,3-octanedione, were identified from packed tofu. Among them, 2-heptanone, which possesses a spicy, fruity, cinnamon-like odor, has been reported in mold-fermented sufu, cooked soybean, fermented soybean paste, soybean milk, chungkuk-jang, and natto.[9,26,28,31] However, 2-heptanone was not found in unpacked tofu.

In conclusion, the objectives of the present study were to analyze the profile of the volatile compounds in packed and unpacked tofu during storage at 4 °C. Among the SPME fibers, the CAR-PDMS fiber was the most suitable to extract the volatile compounds in tofu; 42 and 40 volatile compounds were identified from packed and unpacked tofu, respectively.

dx.doi.org/10.1021/jf404847g | *J. Agric. Food Chem.* 2014, 62, 772−779

Table 1. Changes in Volatile Compounds of Packed Tofu during Storage at 4°C

peak	volatile compound[a]	t_R[b] (min)	RI[c]	ID[d]	peak area ratio[e] after storage for 0 days	3 days	6 days	9 days	12 days	15 days
acids (6)										
7	benzeneacetic acid	8.68	1185	MS	1.23	12.48	21.33	21.1	17.13	9.71
25	acetic acid	15.99	1449	RI, MS, Co-GC	ND[f]	ND	ND	ND	ND	0.68
33	butanoic acid	18.01	1529	RI, MS	0.34	10.88	9.03	11.89	3.79	6.77
34	propionic acid	18.27	1540	MS, Co-GC	0.01	ND	ND	ND	ND	ND
44	hexanoic acid	25.22	1848	RI, MS, Co-GC	0.02	1.21	1.63	1.39	ND	ND
46	benzoic acid	27.59	1965	MS, Co-GC	0.04	0.09	0.82	1.30	1.46	1.56
alcohols (17)										
1	ethanol	2.85	931	RI, MS, Co-GC	5.41	29.31	51.4	66.93	46.62	48.16
4	1-penten-3-ol	8.21	1170	RI, MS	0.31	2.92	10.30	9.46	15.81	6.54
10	1-pentanol	10.73	1257	RI, MS, Co-GC	0.43	8.64	12.76	11.59	10.69	8.90
15	(*E*)-2-penten-1-ol	12.43	1315	RI, MS	1.16	0.56	ND	ND	ND	ND
17	(*Z*)-2-penten-1-ol	12.65	1323	RI, MS	0.10	2.03	4.28	3.62	2.19	2.79
18	1-hexanol	13.57	1350	RI, MS	0.76	19.02	27.97	23.54	45.36	47.46
20	(*Z*)-3-hexen-1-ol	14.37	1364	RI, MS	0.03	ND	ND	ND	ND	ND
22	3-octanol	14.67	1396	RI, MS, Co-GC	0.01	0.34	ND	ND	ND	ND
26	1-octen-3-ol	16.13	1455	RI, MS, Co-GC	0.21	6.79	10.16	7.52	9.59	9.35
27	1-heptanol	16.25	1459	RI, MS, Co-GC	0.02	0.68	0.96	1.11	1.02	1.46
28	2-ethylhexanol	17.13	1492	RI, MS	3.49	0.28	ND	ND	ND	ND
31	(*E*)-2-hepten-1-ol	17.62	1512	RI,MS	ND	ND	ND	ND	ND	4.69
32	benzenemethanol	17.75	1518	MS	0.03	0.77	0.93	1.39	ND	ND
36	1-octanol	18.79	1562	RI, MS, Co-GC	0.05	0.14	ND	ND	ND	ND
38	2,3-butanediol	19.22	1579	RI, MS	0.02	0.87	ND	ND	ND	ND
39	1,2-propanediol	19.52	1591	RI, MS	0.01	0.26	ND	ND	ND	ND
41	1*H*-indol-5-ol	23.65	1774	MS	0.08	4.85	6.34	2.68	22.17	15.27
aldehydes (9)										
3	hexanal	5.60	1076	RI, MS, Co-GC	11.44	338.72	475.66	496.30	190.29	11.06
6	heptanal	8.42	1177	RI, MS	0.32	13.95	12.66	9.95	ND	ND
8	(*E*)-2-hexenal	9.38	1207	RI, MS	0.08	2.66	4.42	5.12	5.56	ND
12	octanal	11.47	1282	RI, MS, Co-GC	0.06	ND	ND	ND	ND	ND
14	2-heptenal	12.40	1314	RI, MS	0.09	1.02	2.78	2.73	1.88	1.56
21	nonanal	14.44	1389	RI, MS, Co-GC	0.03	1.19	2.36	1.85	1.90	1.82
24	(*E*)-2-octenal	15.30	1421	RI, MS	0.03	0.55	1.30	1.56	0.90	0.79
30	benzaldehyde	17.58	1510	MS, Co-GC	0.04	0.63	1.29	1.63	ND	ND
42	2,4-decadienal	24.40	1808	RI, MS	0.14	ND	ND	ND	ND	ND
alkane (1)										
35	2,6,10,14-tetramethylpentadecane	18.34	1543	MS	0.03	0.64	0.99	ND	1.39	ND
aromatic compound (1)										
45	4-phenylbenzene	26.01	1886	MS	ND	1.13	1.87	0.72	3.56	4.42
furans (2)										
2	2-ethylfuran	3.01	970	RI, MS	2.16	111.35	189.68	182.11	113.91	118.33
9	2-pentylfuran	9.80	1223	RI, MS	0.54	18.19	24.04	21.88	20.75	22.27
ketones (3)										
5	2-heptanone	8.40	1176	RI, MS	ND	ND	ND	ND	ND	4.05
11	3-hydroxy-2-butanone	11.39	1279	RI, MS	0.03	1.86	ND	ND	ND	ND
16	2,3-octanedione	12.60	1321	RI, MS	0.02	1.08	ND	ND	ND	ND
miscellaneous compounds (3)										
19	3-ethyl-2-methyl-1,3-hexadiene	14.84	1403	MS	0.05	0.72	ND	ND	ND	ND
23	1*H*-pyrrole	17.57	1510	RI, MS, Co-GC	ND	ND	ND	ND	ND	5.43
29	dimethyl sulfoxide	18.92	1567	RI, MS	0.01	0.30	ND	ND	ND	ND

[a]Compounds by order of their Kovats indices in a chemical class. [b]Retention time on DB-WAX column for GC-MS. [c]Retention index (RI) based on identified compound retention times calculated from a linear equation between each pair of straight-chain alkanes (C_8–C_{20}). [d]Identification method: RI, agrees with RI in the literature; MS, compared with NIST 08 Mass Spectral Database; Co-GC, identification based on co-injection with authentic compounds. [e]Peak area of each compound/peak area of internal standard. [f]ND, not determined.

dx.doi.org/10.1021/jf404847g | J. Agric. Food Chem. 2014, 62, 772−779

Table 2. Changes in the Volatile Compounds of Unpacked Tofu during Storage at 4°C

peak	volatile compound[a]	t_R[b] (min)	RI[c]	ID[d]	peak area ratio[e] after storage for 0 days	3 days	6 days	9 days	12 days	15 days
acids (5)										
6	benzeneacetic acid	8.64	1183	MS	47.96	24.90	22.87	26.02	33.05	21.95
23	acetic acid	15.92	1446	RI, MS, Co-GC	ND[f]	0.85	2.02	40.72	34.41	38.12
29	butanoic acid	18.01	1529	RI, MS	9.27	10.37	10.04	8.04	8.33	8.99
38	hexanoic acid	25.20	1847	RI, MS, Co-GC	0.78	0.60	ND	ND	ND	ND
40	benzoic acid	27.60	1965	MS, Co-GC	1.07	0.93	0.89	0.96	1.03	1.18
alcohols (16)										
1	ethanol	2.86	932	RI, MS, Co-GC	49.46	98.94	147.98	299.39	428.18	394.13
4	1-penten-3-ol	8.27	1152	RI, MS	4.15	7.80	8.33	9.82	10.28	6.45
7	3-methyl-1-butanol	9.59	1215	RI, MS	4.45	6.10	4.97	5.68	5.61	6.12
9	1-pentanol	10.77	1258	RI, MS, Co-GC	0.84	11.30	15.93	19.04	20.30	14.79
14	(*Z*)-2-penten-1-ol	12.68	1324	RI, MS	2.16	3.01	3.22	3.71	3.77	3.49
15	1-hexanol	13.59	1358	RI, MS	58.05	27.02	123.66	159.64	215.24	142.83
17	(*Z*)-3-hexen-1-ol	14.35	1364	RI, MS	0.14	0.23	1.05	1.16	2.16	0.93
19	3-octanol	14.67	1396	RI, MS, Co-GC	0.41	0.52	0.61	0.69	0.70	0.71
21	(*E*)-2-hexen-1-ol	14.96	1407	RI, MS	ND	ND	0.74	0.94	1.18	0.82
24	1-octen-3-ol	16.11	1454	RI, MS, Co-GC	8.67	8.81	10.34	12.97	13.05	14.24
25	1-heptanol	16.25	1459	RI, MS, Co-GC	1.07	0.97	2.42	4.37	3.55	3.26
28	benzenemethanol	17.75	1518	MS	0.87	0.82	0.82	0.99	1.04	ND
32	1-octanol	18.79	1561	RI, MS, Co-GC	0.13	0.24	0.35	0.36	ND	ND
33	2,3-butanediol	19.22	1579	RI, MS	0.43	1.26	1.21	1.92	1.16	1.37
34	1,2-propanediol	19.52	1591	RI, MS	0.25	ND	ND	ND	ND	ND
36	1*H*-indol-5-ol	23.65	1774	MS	7.00	6.83	5.57	6.62	8.95	8.78
aldehydes (6)										
3	hexanal	5.61	1076	RI, MS, Co-GC	242.27	324.04	21.05	7.04	5.33	2.87
5	heptanal	8.42	1177	RI, MS	11.27	6.41	ND	ND	ND	ND
12	(*E*)-2-heptenal	12.38	1313	RI, MS	0.42	1.19	ND	ND	ND	ND
18	nonanal	14.47	1389	RI, MS, Co-GC	0.45	1.80	1.37	1.03	ND	0.73
22	3-hydroxybutanal	15.24	1419	RI, MS	0.26	ND	ND	ND	ND	ND
27	benzaldehyde	17.58	1510	MS, Co-GC	1.13	ND	ND	ND	ND	ND
alkane (1)										
31	2,6,10,14-tetramethylpentadecane	18.46	1543	MS	0.17	0.95	0.99	ND	ND	ND
aromatic compound (1)										
39	4-phenylbenzene	26.02	1886	MS	1.80	2.20	1.76	2.45	2.19	3.03
furans (2)										
2	2-ethylfuran	3.01	970	RI,MS	96.38	42.97	ND	ND	ND	ND
8	2-pentylfuran	9.70	1220	RI, MS	7.02	11.53	7.47	7.88	8.43	9.22
ketones (2)										
10	3-hydroxy-2-butanone	11.46	1281	RI, MS	1.62	2.42	2.67	6.94	2.21	ND
13	2,3-octanedione	12.57	1320	RI, MS	0.76	ND	ND	ND	ND	ND
miscellaneous compounds (2)										
16	3-ethyl-2-methyl-1,3-hexadiene	14.82	1401	MS	0.80	ND	ND	ND	ND	ND
20	1*H*-pyrrole	17.57	1510	RI, MS, Co-GC	ND	0.87	0.57	0.73	0.61	ND

[a]Compounds by order of their Kovats indices in a chemical class. [b]Retention time on DB-WAX column in GC-MS. [c]Retention index (RI) based on identified compound retention times calculated from a linear equation between each pair of straight-chain alkanes (C_8–C_{20}). [d]Identification method: RI agrees with RIs in the literature; MS, compared with NIST 08 Mass Spectral Database; Co-GC, identification based on co-injection with authentic compounds. [e]Peak area of each compound/peak area of internal standard. [f]ND, not determined.

Hexanal, ethanol, and 1-hexanol were characteristic volatile compounds that provided quantitative and qualitative information regarding the deterioration of tofu. Volatile compounds could be a useful indicator to determine the overall edibility of food such as tofu. Currently, this approach is being applied to more diverse foods to determine their edibility.

dx.doi.org/10.1021/jf404847g | J. Agric. Food Chem. 2014, 62, 772−779

AUTHOR INFORMATION

Corresponding Author

*(K.-G.L.) Phone: 82-2-2260-3370. Fax: 82-2-2285-3370. E-mail: kwglee@dongguk.edu.

Funding

This study was supported by the R&D Convergence Center Support Program, Ministry for Food, Agriculture, Forestry, and Fisheries, Republic of Korea.

Notes

The authors declare no competing financial interest.

REFERENCES

(1) Shin, I. S.; Han, J. S.; Choi, K. D.; Chung, D. H.; Choi, G. P.; Ahn, J. Effect of isothiocyanates from horseradish (Armoracia rusticana) on the quality and shelf life of tofu. *Food Control* **2010**, *21*, 1081−1086.

(2) Wang, H. J.; Murphy, P. A. Isoflavone content in commercial soybean foods. *J. Agric. Food Chem.* **1994**, *42*, 1666−1673.

(3) Kim, M.; Son, S. I. Evaluation of microbiological, physicochemical and sensory qualities of chitosan tofu during storage. *J. Food Quality* **2004**, *27*, 27−40.

(4) Asharaf, H. R.; White, M.; Klubek, B. Microbiological survey of tofu sold in a rural Illinois country. *J. Food Prot.* **1999**, *62*, 1050−1053.

(5) Tuitemwong, K.; Fung, D. Y. C. Microbiological study of tofu. *J. Food Prot.* **1991**, *54*, 212−216.

(6) van Kooij, J. A.; de Boer, E. A survey of the microbiological quality of commercial tofu in The Netherlands. *Int. J. Food Microbiol.* **1985**, *2*, 349−354.

(7) Kwon, H. R.; Choi, K. H. Changes in physico and biochemical quality of packed tofu during cold storage. *Appl. Sci.* **1999**, *7*, 73−79.

(8) Shin, H. Y.; Ku, K. J.; Park, S. K.; Song, K. B. Use of freshness indicator for determination of freshness and quality change of tofu during storage. *J. Korean Soc. Appl. Biol. Chem.* **2006**, *49*, 158−162.

(9) Chung, H. Y. Volatile flavor components in red fermented soybean (*Glycine max*) curds. *J. Agric. Food Chem.* **1999**, *47*, 1803−1809.

(10) Dajanta, K.; Apichartsrangkoon, A.; Chukeatirote, E. Volatile profiles of thua nao, a Thai fermented soy product. *Food Chem.* **2001**, *125*, 464−470.

(11) Hwan, C. H.; Chou, C. C. Volatile components of the Chinese fermented soya bean curd as affected by the addition of ethanol in ageing solution. *J. Sci. Food Agric.* **1999**, *79*, 243−248.

(12) Lee, S. J.; Ahn, B. Comparison of volatile components in fermented soybean pastes using simultaneous distillation and extraction (SDE) with sensory characterization. *Food Chem.* **2009**, *114*, 600−609.

(13) Liu, Y.; Miao, Z.; Guan, W.; Sun, B. Analysis of organic volatile flavor compounds in fermented stinky tofu using SPME with different fiber coatings. *Molecules* **2012**, *17*, 3708−3722.

(14) Ames, J. M.; Macleod, G. Volatile components of an unflavored textured soy protein. *J. Food Sci.* **1984**, 1552−1565.

(15) Kobayashi, A.; Tsuda, Y.; Hirata, N.; Kubota, K.; Kitamura, K. Aroma constituents of soybean [*Glycine max* (L.) Merril] milk lacking lipoxygenase isozymes. *J. Agric. Food Chem.* **1995**, *43*, 2449−2452.

(16) Moy, Y. S.; Lu, T. J.; Chou, C. C. Volatile components of the enzyme-ripened sufu, a Chinese traditional fermented product of soy bean. *J. Biosci. Bioeng.* **2012**, *113*, 196−201.

(17) Sugawara, E.; Ito, T.; Odagiri, S.; Kubota, K.; Kobayashi, A. Comparison of volatile compositions of odor components of natto and cooked soybeans. *Agric. Biol. Chem.* **1985**, *49*, 311−317.

(18) Lee, S. H.; Kim, Y. T.; Shon, M. Y.; Han, S. Y.; Park, J. R.; Park, S. K. Major components of fermented tofu prepared with different molds and coagulants. *Food Sci. Biotechnol.* **2001**, *11*, 93−98.

(19) Chung, H. Y.; Fung, P. K.; Kim, J. S. Aroma impact components in commercial plain sufu. *J. Agric. Food Chem.* **2005**, *53*, 1684−1691.

(20) Sides, A.; Robards, K.; Helliwell, S.; An, M. Changes in the volatile profile of oats induced by processing. *J. Agric. Food Chem.* **2001**, *49*, 2125−2130.

(21) Boue, S. M.; Shih, B. Y.; Carter-Wientjes, C. H.; Cleveland, T. E. Identification of volatile compounds in soybean at various developmental stages using solid phase microextraction. *J. Agric. Food Chem.* **2003**, *51*, 4873−4876.

(22) Matsui, K.; Takaki, S.; Shimada, K.; Hajika, M. Effects of anaerobic processing of soybean seeds on properties of tofu. *Biosci., Biotechnol., Biochem.* **2011**, *75*, 1174−1176.

(23) Kovats, E. Gas chromatographic characterization of organic substances in the retention index system. *Adv. Chromatogr.* **1965**, *1*, 229−247.

(24) KFDA, Korean Food Code, 2011; p 5132.

(25) Arai, S. M.; Suzuki, H.; Fujimaki, M.; Sakurai, Y. Studies on flavor components in soybean. Part 2. Phenolic acids in defatted soybean flour. *Agric. Biol. Chem.* **1996**, *30*, 863−868.

(26) Wilkens, W. F.; Lin, F. M. Gas chromatographic and mass spectral analyses of soybean milk volatile. *J. Agric. Food Chem.* **1970**, *18*, 333−336.

(27) Han, B. Z.; Rombouts, F. M.; Nout, M. J. R. A Chinese fermented soybean food. *Int. J. Food Microbiol.* **2001**, *65*, 1−10.

(28) Chung, H. Y. Volatile components in fermented soybean (*Glycine max*) curds. *J. Agric. Food Chem.* **2000**, *47*, 2690−2696.

(29) Mookherjee, B. D.; Deck, R. E.; Chang, S. S. Food flavor changes, relationship between monocarbonyl compounds and flavor of potato chips. *J. Agric. Food Chem.* **1965**, *13*, 113−134.

(30) Fors, S. Sensory properties of volatile Maillard reaction products and related compounds: a literature review. In *The Maillard Reaction in Foods and Nutrition*; Waller, G. R., Feather, M. S., Eds.; ACS Symposium Series 215; American Chemical Society: Washington, DC, 1983; pp 185−286.

(31) Tanaka, T.; Muramatsu, K.; Kim, H. R.; Watanabe, T.; Takeyasu, M.; Kanai, Y.; Kiuchi, K. Comparison of volatile compounds from chungkuk-jang and itohiki-natto. *Biosci., Biotechnol., Biochem.* **1998**, *62*, 1440−1444.

JOURNAL OF AGRICULTURAL AND FOOD CHEMISTRY

Article

pubs.acs.org/JAFC

Topoisomerase II-Targeting Properties of a Grapevine-Shoot Extract and Resveratrol Oligomers

Simone A. Baechler,[†] Anika Schroeter,[†] Martina Dicker,[†] Pablo Steinberg,[§] and Doris Marko*[,†]

[†]Department of Food Chemistry and Toxicology, University of Vienna, Waehringerstrasse 38, A-1090 Vienna, Austria

[§]Institute for Food Toxicology and Analytical Chemistry, University of Veterinary Medicine Hannover, Bischofsholer Damm 15, D-30173 Hannover, Germany

ABSTRACT: Grapevine-shoot extracts (GSE), containing *trans*-resveratrol and resveratrol oligomers, are commercially available as food supplements. Considering the topoisomerase-targeting properties of *trans*-resveratrol, the question of whether GSE affect these enzymes, thereby potentially causing DNA damage, was addressed. In a decatenation assay, GSE potently suppressed the catalytic activity of topoisomerase IIα ($\geq$5 μg/mL). The resveratrol oligomers ϵ-viniferin, r2-viniferin, and hopeaphenol, isolated from GSE, were also identified as topoisomerase IIα inhibitors. In the in vivo complexes of enzyme to DNA (ICE) bioassay, neither GSE, r2-viniferin, nor hopeaphenol affected the level of enzyme–DNA intermediates in A431 cells, thus representing catalytic inhibitors rather than topoisomerase poisons. GSE caused moderate DNA strand breaks ($\geq$25 μg/mL) in the comet assay. Taken together, GSE presumably acts as a catalytic inhibitor of topoisomerase II with r2-viniferin and hopeaphenol as potentially contributing constituents. However, the increase of FPG-sensitive sites points to an additional mechanism that may contribute to the DNA-damaging properties of GSE constituents.

KEYWORDS: *grapevine-shoot extract, resveratrol oligomers, topoisomerase II, DNA damage*

INTRODUCTION

Resveratrol (*trans*-3,5,4′-trihydroxystilbene) is a natural polyphenol found in grapes (*Vitis vinifera*), berries, peanuts, and red wine.[1,2] This plant phytoalexin has been associated with health benefits due to its antioxidant, anti-inflammatory, and antitumorigenic properties.[2−5] These activities are mediated through its interaction with multiple cell signaling pathways including several receptors, kinases, and cyclooxygenases.[5,6] Recently, topoisomerase II has been identified as another target for *trans*-resveratrol.[7,8] Due to the claimed beneficial health effects of resveratrol such as cardioprotection and cancer prevention,[5,9] the intake of dietary supplements consisting of grape-derived complex mixtures is increasing.[5]

The grapevine-shoot extract (GSE) used in this study contains high amounts of *trans*-resveratrol (7.7%) and resveratrol oligomers (29.4%) such as ϵ-viniferin, r2-viniferin, and hopeaphenol (Figure 1; see Materials and Methods), which are biosynthesized by the plants via oxidative coupling.[10,11] GSE has been shown to exert antiproliferative, pro-apoptotic, and antioxidant properties, partially exceeding the effects expected for *trans*-resveratrol.[11−13] Thus, it might be presumed that individual polyphenols present in the extract act synergistically.[11] Although data regarding the biological activity of resveratrol oligomers are quite limited, it has been reported that hopeaphenol, r2-viniferin, and ϵ-viniferin possess potent antiproliferative effects in different tumor cell lines.[14−17] Furthermore, these resveratrol oligomers have been identified, besides *trans*-resveratrol and miyabenol C, as growth-inhibiting compounds present in GSE in an activity-guided isolation.[10] Because *trans*-resveratrol has been shown to interact with human topoisomerase II,[7,8] the question arises whether GSE, rich in stilbenes, exhibits topoisomerase-II-inhibiting activity, thereby potentially contributing to its antiproliferative effects.

Topoisomerases are ubiquitous enzymes maintaining the topology of DNA within the cell.[18] Thus, they are essential during replication, transcription, chromosome segregation, and cell division, because these processes demand an alteration of DNA topology.[19−21] During their catalytic cycle, they generate transient DNA strand breaks by forming a covalent enzyme–DNA intermediate, called a "cleavable complex", to release torsional stress.[22] Two distinct topoisomerase II isozymes, α and β, are present in mammals. Despite their high sequence homology, they are encoded on different genes and exhibit differences in their cellular expression and function. Expression of topoisomerase IIα is tightly linked to cell proliferation, whereas IIβ is constitutively expressed.[23,24] Because topoisomerases are essential for cell proliferation, they are important targets of clinically used anticancer and antibacterial drugs.[22,23,25] However, in the present work we focused exclusively on the inhibition of human topoisomerase II. Two classes of inhibitors are distinguished by their mode of action. Topoisomerase poisons are able to stabilize the covalent enzyme–DNA intermediate and by doing so enhance the levels of cleavable complexes, whereas catalytic inhibitors act on many different steps in the catalytic cycle of topoisomerases.[19,22,25,26] Topoisomerase poisons exert cytotoxic properties by causing DNA strand breaks after collision of replication or transcription machineries with the stabilized cleavable complex. In contrast, catalytic inhibitors block the overall catalytic activity of the enzyme, leading to inhibition of tumor cell proliferation.[19,27]

Received: June 5, 2013
Revised: December 22, 2013
Accepted: December 26, 2013
Published: December 26, 2013

ACS Publications © 2013 American Chemical Society

dx.doi.org/10.1021/jf4046182 | *J. Agric. Food Chem.* 2014, 62, 780−788

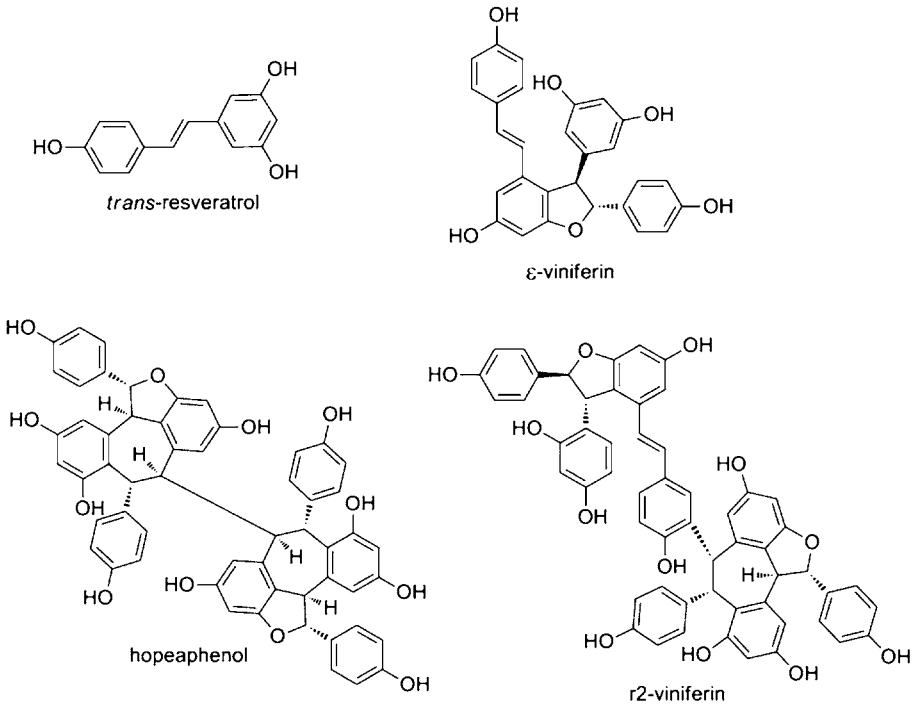

Figure 1. Chemical structures of *trans*-resveratrol and the resveratrol oligomers tested in this study.

In the present study, the question of whether GSE and several of its resveratrol oligomers possess topoisomerase II inhibitory properties, leading to DNA damage, was addressed. Because topoisomerase inhibitors mediate antiproliferative effects, possible therapeutic benefits in chemotherapy should be revealed. Therefore, we determined the ability of GSE to interact with human topoisomerase II in a cell-free decatenation assay and compared it with that of its constituents resveratrol, *ε*-viniferin, r2-viniferin, and hopeaphenol. By measuring the ability of topoisomerase II to decatenate circulated kinetoplast DNA, both classes of topoisomerase inhibitors are detected in a decatenation assay. Therefore, an ICE bioassay was additionally performed in human epidermoid carcinoma cells, which selectively detects topoisomerase poisons by separating cleavable complexes from free enzyme. Because inhibition of these essential enzymes might lead to an enhanced DNA strand break rate, the impact of GSE and its resveratrol oligomers on DNA integrity was measured via single-cell gel electrophoresis (comet assay).

MATERIALS AND METHODS

Chemicals and Recombinant Enzymes. The GSE vineatrol30 was kindly provided by Breko GmbH (Bremen, Germany) and Actichem (Montauban, France), which develop and produce this extract in cooperation. Vineatrol30 included 7.7% resveratrol, 14.6% *ε*-viniferin, 3.4% ampelopsin A, 1.8% hopeaphenol, 2.4% iso-*trans*-*ε*-viniferin, 1.6% vitisin A (r2-viniferin), 2.5% vitisin B (r-viniferin), 0.6% piceatannol, and 2.5% miyabenol C. Taken together, 37.1% of vineatrol30 consists of resveratrol and resveratrol oligomers. According to the manufacturer Actichem, at the present time the identities of compounds making up 62.9% of the extract remain unknown, but the presence of further polyphenols can definitely be discarded. *ε*-Viniferin (90% purity), r2-viniferin (>93% purity), and hopeaphenol (95% purity) were kindly provided by Actichem. Resveratrol and etoposide (ETO) were purchased from Sigma-Aldrich Chemie GmbH (Taufkirchen, Germany) and cell culture media and supplements from GIBCO Invitrogen Life Technologies (Karlsruhe, Germany), Sigma-Aldrich Chemie GmbH, and SARSTEDT AG & Co. (Nuembrecht, Germany). Recombinant topoisomerase II*α* was generously provided by Prof. Boege (Duesseldorf, Germany).

Cell Culture and Incubation. The human epidermoid carcinoma cell line A431 was obtained from the German Collection of Microorganisms and Cell Cultures (DSMZ, Braunschweig, Germany). A431 cells were cultivated in minimum essential medium (MEM, 4.5 g/L glucose, without sodium pyruvate), containing 10% (v/v) heat-inactivated fetal calf serum (FCS), 1% (v/v) penicillin/streptomycin, and 1% (v/v) L-glutamine. Cells were cultured at 37 °C in a humidified 5% CO_2 atmosphere and routinely tested for mycoplasma contamination. Cell passages between 10 and 25 were used to perform the experiments.

GSE was dissolved in dimethyl sulfoxide, whereas solutions of resveratrol, r2-viniferin, *ε*-viniferin, and hopeaphenol were prepared with 70% (v/v) ethanol on ice. Aliquots of the stock solutions were stored at −80 °C and added to the incubation media just before the experiments, thus resulting in the corresponding final concentrations of the test compounds and 1% (v/v) DMSO and ethanol. However, final concentrations of the solvents of 3.3% were present in the decatenation assay. All tests were carried out in the presence of catalase (100 U/mL) to prevent hydrogen peroxide generation in the cell culture media.

Decatenation Assay. The catalytic activity of topoisomerase II was measured with kinetoplast DNA from *Crithidia fasciculata* (kDNA) (TopoGen, Port Orange, FL, USA). kDNA (250 ng) was incubated at 37 °C for 60 min in a final volume of 30 μL topoisomerase II assay buffer (50 mM Tris-HCl, pH 7.9, 120 mM KCl, 10 mM $MgCl_2$, 1 mM ATP, 0.5 mM DTT, 0.5 mM EDTA, and 0.03 mg/mL BSA) in the presence or absence of 40 ng of topoisomerase II*α*. The reaction was stopped by the addition of $^1/_{10}$ volume of 1 mg/mL proteinase K in 10% (w/v) SDS and incubated for 30 min at 37 °C. Gel electrophoresis was conducted at 4.5 V/cm in 1% (w/v) agarose gels with a Tris acetate/EDTA buffer (40 mM Tris, 1 mM EDTA, pH 8.5, 20 mM acetic acid). The gel was stained with ethidium bromide solution (10 μg/mL) for 20 min. The fluorescence of ethidium bromide was measured with a LAS4000 digital imaging system (Fujifilm, Duesseldorf, Germany).

Isolating in Vivo Complexes of Enzyme to DNA (ICE) Bioassay. The ICE bioassay was performed with slight modifications as previously described.[28] Three million A431 cells were seeded in

dx.doi.org/10.1021/jf4046182 | J. Agric. Food Chem. 2014, 62, 780−788

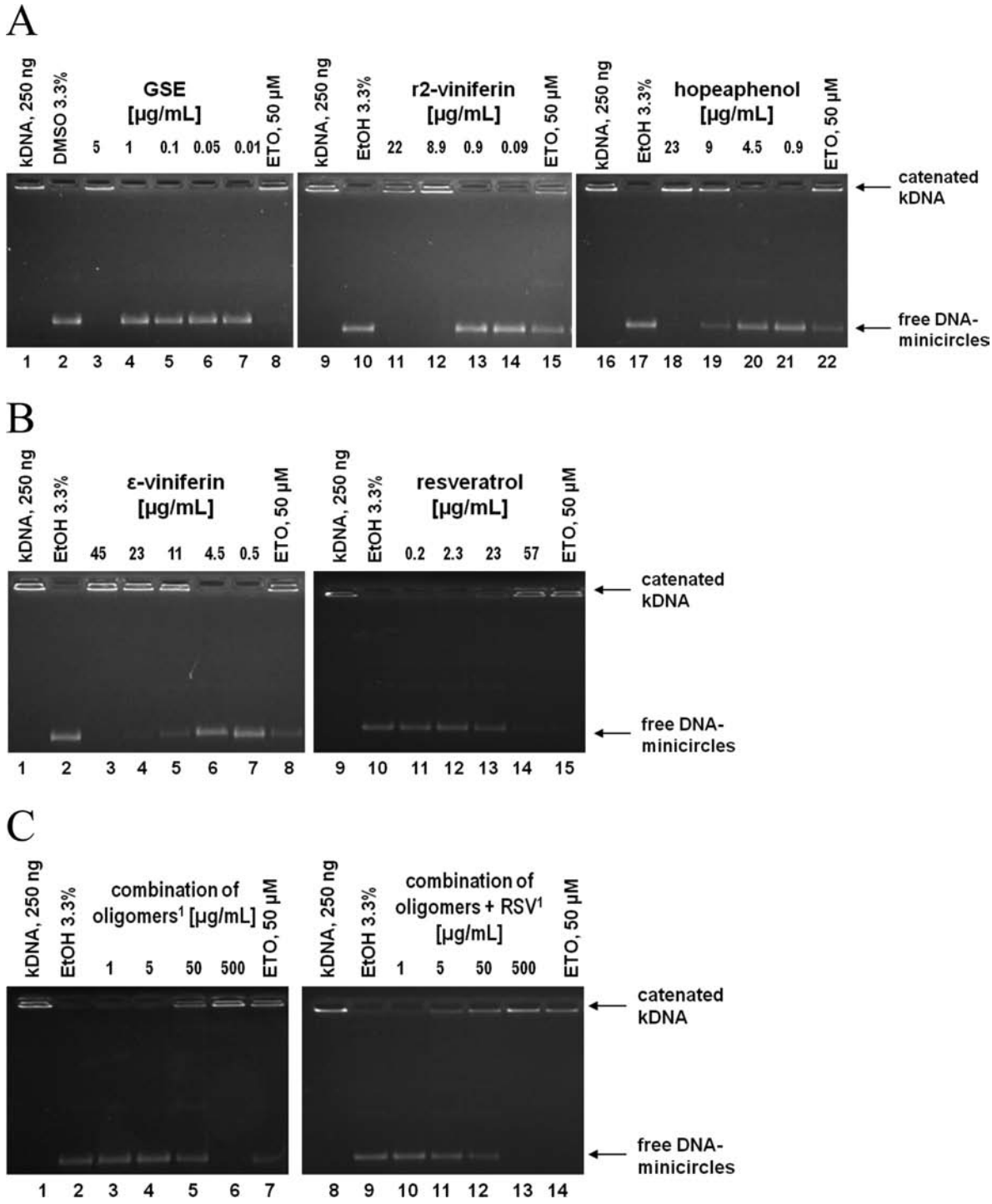

Figure 2. Impact of GSE and resveratrol oligomers on the catalytic activity of topoisomerase IIα using a decatenation assay. Topoisomerase IIα was exposed to increasing concentrations of the compounds for 60 min at 37 °C. A representative gel of three experiments with similar outcomes is shown. The topoisomerase II poison etoposide (ETO) was used as positive control. (A) Lanes: 1, 9, and 16, kDNA (250 ng); 2, 10, and 17, kDNA + topoisomerase IIα + respective solvent control (3.3%); 3−7, 11−14, and 18−21, kDNA + topoisomerase IIα + test compound; 8, 15, and 22, kDNA + topoisomerase IIα + ETO. (B) Lanes: 1 and 9, kDNA (250 ng); 2 and 10, kDNA + topoisomerase IIα + EtOH (3.3%); 3−7 and 11−14, kDNA + topoisomerase IIα + test compound; 8 and 15, kDNA + topoisomerase IIα + ETO. (C) Lanes: 1 and 8, kDNA (250 ng); 2 and 9, kDNA + topoisomerase IIα + EtOH (3.3%); 3−6 and 10−13, kDNA + topoisomerase IIα + test compounds; 7 and 14, kDNA + topoisomerase IIα + ETO.

Petri dishes (diameter = 15 cm) and allowed to grow for 72 h to achieve a cell confluence of ∼80%. Cells were incubated with the solvent control or the test compounds for 1 h under serum-free conditions. The topoisomerase II poison etoposide (ETO), which is clinically used as a chemotherapeutic drug, was included as a positive control. Thereafter, cells were harvested and lysed in 6 mL of TE buffer (10 mM Tris, pH 8.0, 1 mM EDTA, 1% (w/v) *N*-laurylsarcosyl sodium salt). Cell lysates (4 mL) were layered onto a cesium chloride gradient in polyallomer tubes (14 mL; SW40, Beckman Coulter GmbH, Krefeld, Germany). After centrifugation at 100000*g* for 24 h at 20 °C, the gradient was fractionated and slot-blotted onto nitrocellulose membranes. Immunodetection was performed by using

dx.doi.org/10.1021/jf4046182 | *J. Agric. Food Chem.* 2014, 62, 780−788

specific polyclonal antibodies (Santa Cruz Biotechnology, Heidelberg, Germany). Chemoluminescent signals (LumiGLO, Cell Signaling Technology, Beverly, MA, USA) were analyzed with a LAS4000 digital imaging system (Fujifilm). The DNA content of the single fractions was measured with a NanoDrop2000 spectrophotometer (PeqLab Biotechnologie GmbH, Erlangen, Germany). The intensity of the chemoluminescent signals was integrated using the software Multi Gauge V3.2 (Fujifilm). The resulting arbitrary light units of the DNA-containing fractions were normalized to the respective DNA content and plotted as test over control (T/C, %).

Comet Assay. Single-cell gel electrophoresis was performed according to the method of Gedik et al.[29] as previously described by Pelka et al.[30] Three hundred thousand A431 cells were seeded in Petri dishes (diameter = 5.5 cm) and allowed to grow for 48 h prior to drug treatment (cell confluence = ∼60−70%). Cells were exposed to the corresponding solvent controls (DMSO or ethanol (70%, v/v) or the test compounds for 1 h in serum-free medium. Irradiation with UV light for 2 min was included in the testing as a positive control. Cells were harvested, and cell viability was determined by trypan blue exclusion. An equivalent volume of trypan blue solution (0.4%; Sigma-Aldrich Chemie GmbH) was added to 50 μL of cell solution. Whereas viable cells are able to exclude the dye, dead cells are stained dark blue. Cell viability was determined as percentage of total viable cells (unstained) per total cells (stained and unstained). After centrifugation of aliquots containing 30000 cells at 425*g* for 10 min, the pellet was resuspended in 65 μL of low-melting agarose and layered onto microscope slides. After the solidification of agarose, the slides were immersed overnight at 4 °C in lysis solution (89 mL of lysis buffer [2.5 mM NaCl, 100 mM EDTA, and 10 mM Tris-HCl, pH 10, 1% (w/v) *N*-laurylsarcosyl sodium salt], 10 mL of DMSO, and 1 mL of Triton X-100).

Treatment with the enzyme formamidopyrimidine-DNA-glycosylase (FPG) was conducted to detect FPG-sensitive base modifications. Samples were incubated with a 1:3000 dilution of the enzyme (New England Biolabs, Vienna, Austria) in FPG buffer (40 mM HEPES, 0.1 M KCl, 0.5 mM EDTA, pH 8, 0.2 mg/mL BSA) for 30 min at 37 °C. Alkaline treatment (300 mM NaOH, 1 mM EDTA, pH 13.5) was performed for 20 min at 4 °C and was followed by a horizontal gel electrophoresis (25 V, 300 mA) for another 20 min at 4 °C. After neutralization, samples were stained with ethidium bromide. Fluorescence was detected with a Zeiss Axioskop (λ_{ex} = 546 ± 12 nm; λ_{em} > 590 nm), and tail intensity (intensity of the DNA in the comet tail calculated as a percentage of overall DNA intensity) was analyzed by scoring 50 images per slide with CometIV software (Perceptive Instruments, Suffolk, UK).

Statistical Analysis. Data were expressed as the mean ± SD. After analysis of the variance of the results (ANOVA), differences between single groups were determined by Student's *t* test using the software Origin 9 (OriginLab, Northampton, MA, USA).

RESULTS

Topoisomerase II-Targeting Properties of GSE and Several of Its Constituents. In preliminary experiments r2-viniferin, ε-viniferin, and hopeaphenol were tested in the concentration ranges 0.9−18, 0.5−44.5, and 0.9−18 μg/mL, respectively, whereby the growth-inhibiting effect of r2-viniferin and hopeaphenol became statistically significant after 48 h at a concentration ≥4.5 μg/mL and that of ε-viniferin at a concentration ≥27 μg/mL (E. Nevo-Koch, unpublished observations). To elucidate the molecular mode of action leading to the observed antiproliferative effects of GSE and the resveratrol oligomers, the impact of these compounds on topoisomerase II activity was investigated within the same concentration range using a decatenation assay. Resveratrol was also included in the testing for comparison reasons (Figure 2). Whereas kDNA in its catenated form cannot enter an agarose gel (Figure 2A, lanes 1, 9, and 16), single DNA minicircles released from the catenated network by catalytically active topoisomerase II will migrate into the gel (Figure 2A, lanes 2, 10, and 17). GSE showed potent topoisomerase II-inhibiting properties, completely blocking the enzyme at a concentration of 5 μg/mL, as no migrating minicircles were detected. This inhibitory concentration of the extract contains 0.7 μg/mL ε-viniferin, 0.4 μg/mL *trans*-resveratrol, 0.09 μg/mL hopeaphenol, and 0.08 μg/mL r2-viniferin. A possible contribution of these single compounds to the topoisomerase-II-inhibiting properties of the extract was further determined in the decatenation assay. All tested resveratrol oligomers were found to inhibit the catalytic activity of topoisomerase IIα. The resveratrol tetramer r2-viniferin possessed the strongest inhibiting properties entirely suppressing enzyme activity at concentrations ≥8.9 μg/mL. Hopeaphenol also exhibited a moderate topoisomerase II-targeting potency and inhibited the enzyme at concentrations ≥4.5 μg/mL. Exposure to 23 μg/mL hopeaphenol led to a complete inhibition of the catalytic activity of topoisomerase IIα. The resveratrol dimer ε-viniferin exerted the lowest inhibitory properties of all resveratrol oligomers tested by equimolar comparison, slightly affecting the catalytic activity of topoisomerase IIα at a 11 μg/mL concentration and reaching entire suppression of enzyme activity at 45 μg/mL (Figure 2B,D). Resveratrol itself caused almost complete inhibition of the catalytic activity of topoisomerase IIα at a concentration of 57 μg/mL. The topoisomerase poison ETO (50 μM) was used as a positive control (Figure 2A, lanes 8, 15, and 22).

Possible additive or synergistic effects of resveratrol and its oligomers were further investigated by combination experiments (Figure 2C). Concentrations of the single oligomers in the combination were chosen equivalent to their amounts in the extract. Indicated concentrations refer to the combination of oligomers present in 1, 5, 50, or 500 μg/mL GSE. The combination of r2-viniferin, hopeaphenol, and ε-viniferin showed an inhibition of topoisomerase II activity in concentrations equivalent to 50−500 μg/mL GSE. Addition of resveratrol increased the inhibitory properties of the combination, slightly inhibiting enzyme activity at concentrations equivalent to 5 μg/mL. Although the combination experiments revealed that resveratrol as well as its oligomers contribute to the effects of the GSE, neither of the two combinations reached the strong inhibitory effect of the extract.

To investigate whether the topoisomerase II targeting properties of GSE and its constituents also unfold within human epidermoid carcinoma cells, the ICE bioassay was performed (Figure 3). This technique allows identification of topoisomerase poisons, as the enzyme is detected while being covalently linked to DNA. Incubation of A431 cells with increasing concentrations of GSE for 1 h did not enhance the level of stabilized topoisomerase IIα−DNA intermediates, as no topoisomerase IIα signal was detected in the DNA-rich fractions (Figure 3A). In contrast, a strong signal for topoisomerase IIα was observed for the topoisomerase II poison ETO (50 μM), used as a positive control.

The tetramers r2-viniferin and hopeaphenol, which led to a potent inhibition of catalytic activity of topoisomerase II in the cell-free system, as well as resveratrol, were also tested in the ICE bioassay. As it showed only weak inhibitory effects on topoisomerase IIα, the resveratrol dimer ε-viniferin was not included in the cellular testing. The immunoblots of the DNA-containing fractions and the results of the quantification (Figure 3B) indicate that none of the constituents were able to increase the amount of covalent topoisomerase II−DNA

dx.doi.org/10.1021/jf4046182 | J. Agric. Food Chem. 2014, 62, 780−788

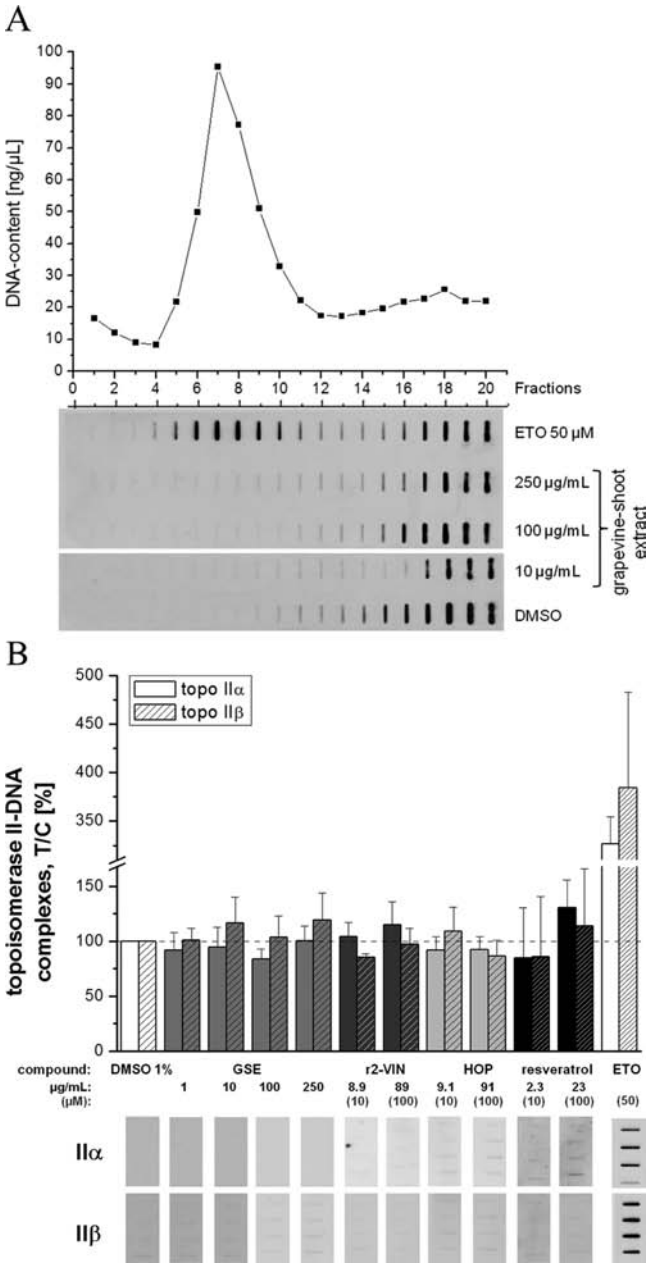

Figure 3. Effect of the GSE on the stabilization of covalent topoisomerase II–DNA intermediates in A431 cells. (A) Using the ICE bioassay, free enzyme was separated from DNA-linked protein via ultracentrifugation in a cesium chloride gradient. DNA content of the single fractions is exemplarily plotted for the positive control etoposide (ETO). On the bottom, representative immunoblots after detection of topoisomerase IIα of three independent experiments with similar outcome are shown. (B) Quantification of the amount of stabilized topoisomerase II–DNA intermediates in the DNA-containing fractions. Results are calculated as test over control with respect to DNA content × 100 (T/C, %) and represent the mean ± SD of three independent experiments. Representative immunoblots of the DNA-containing fractions used for quantification are shown for both topoisomerase II isoforms.

complexes. Thus, the level of cleavable complexes was not significantly increased after incubation of A431 cells with the GSE, resveratrol, r2-viniferin, and hopeaphenol, even at the highest tested concentrations of 250, 23, 89, and 91 μg/mL, respectively, when compared to the solvent control. Moreover, no differences could be observed between the topoisomerase isoforms IIα and IIβ. However, a slight, yet not significant, increase of covalent topoisomerase IIα–DNA complexes was observed after incubation with 23 μg/mL resveratrol, possibly indicating weak topoisomerase II poisoning activities.

Induction of DNA Strand Breaks by GSE and Several of Its Constituents. Because topoisomerase inhibitors might cause torsional stress within cells, they could affect DNA integrity. Thus, the DNA strand-breaking potential of GSE and resveratrol oligomers was investigated in A431 cells by single-cell gel electrophoresis under alkaline conditions (Figure 4A). Treatment with the DNA repair enzyme FPG was included in the testing to detect FPG-sensitive sites, which are indicative of oxidative DNA damage. Cell viability exceeded 80% throughout the experiment (Figure 4B).

The incubation of A431 cells with GSE for 1 h was found to significantly enhance the level of DNA strand breaks in the cells. At the highest tested concentration of 25 μg/mL GSE, a tail intensity of ∼2.5% was reached. In contrast, resveratrol, r2-viniferin, and hopeaphenol showed no impact on DNA integrity in A431 cells after this incubation period. FPG treatment led to an increased DNA strand break rate for the GSE and the tetramers at the highest tested concentration (GSE, 25 μg/mL; r2-viniferin and hopeaphenol, 45 μg/mL). In the case of GSE and hopeaphenol, the FPG-sensitive sites were significantly increased when compared to the samples not exposed to FPG. Furthermore, a tail intensity of almost 6% was reached after a FPG treatment by GSE, whereas the effects after incubation with r2-viniferin (3.5%) and hopeaphenol (4.5%) were less pronounced. In contrast, resveratrol did not increase the level of FPG-sensitive sites.

DISCUSSION

The potential health-enhancing properties of *trans*-resveratrol have prompted numerous studies to identify the cellular mechanisms and potential target molecules involved.[2,4,5] Several studies showed topoisomerase I- and II-inhibiting properties of this stilbene possibly contributing to its antiproliferative effects.[31−33] Recently, it has been reported to act as a topoisomerase II poison in human carcinoma cells, affecting chromosome segregation during mitosis.[8,34] Whereas topoisomerase poisons trap the enzyme when it is covalently bound to DNA, catalytic topoisomerase inhibitors interact with the enzymes in a noncovalent bound state.[26] Thus, *trans*-resveratrol has been reported to induce micronuclei and affect chromosome segregation in proliferating cells, probably due to its topoisomerase-poisoning effects.[34] GSE has been shown to possess biological properties similar to those of *trans*-resveratrol, as antiproliferative, pro-apoptotic, and antioxidant effects have been described.[11−13] Because GSE was shown to be more potent regarding cell growth inhibition than *trans*-resveratrol itself, it was suggested that *trans*-resveratrol and its oligomers may act synergistically.[12,35] In the present study we investigated whether GSE possesses topoisomerase-II-inhibitory properties similar to those of *trans*-resveratrol resulting in DNA damage and thereby contributing to its antiproliferative effects. A431 cells were used because in a preliminary screening of human tumor cells the antiproliferative effect of the resveratrol oligomers was significant in this cell line (E. Nevo-Koch, unpublished observations). Therefore, A431 cells were considered to be particularly adequate to study the mechanisms underlying the growth-inhibiting effects of these compounds.

dx.doi.org/10.1021/jf4046182 | J. Agric. Food Chem. 2014, 62, 780−788

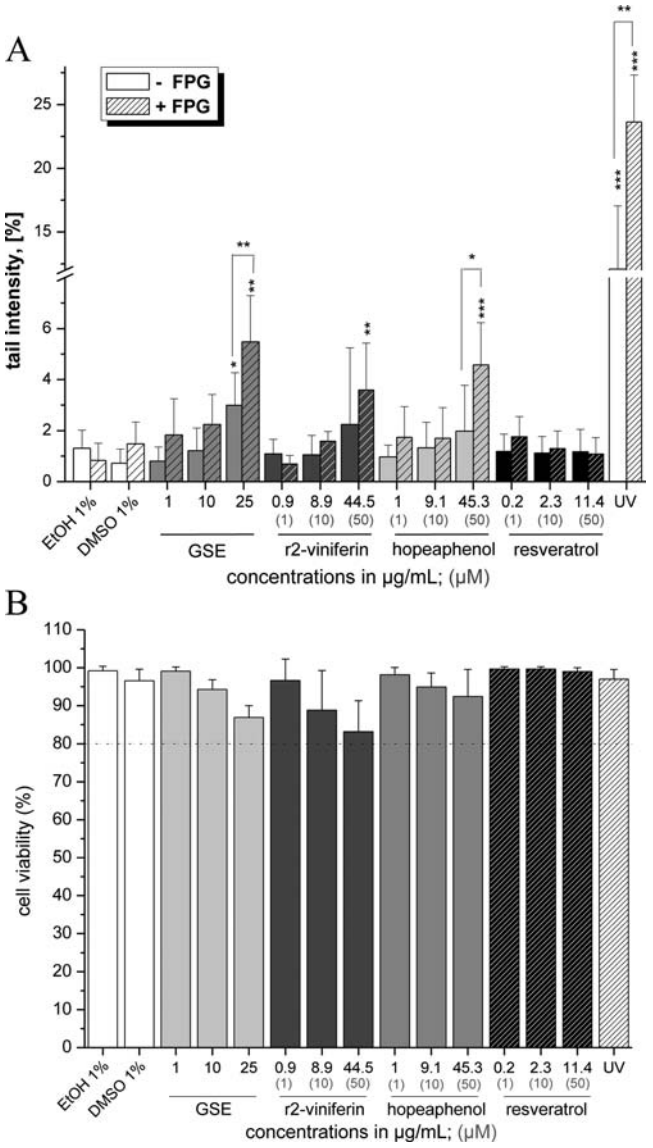

Figure 4. Impact of the GSE and resveratrol oligomers on DNA integrity in A431 cells determined by single-cell gel electrophoresis (comet assay). Cells were treated with the extract or the single compounds for 1 h in serum-free medium. (A) Results are given as the mean ± SD of tail intensities (%) from at least three separate experiments, each performed in duplicate. Dashed bars display additional treatment with the enzyme FPG to detect FPG-sensitive sites indicative for oxidative stress. Irradiation with UV light was used as a positive control. Significances are calculated by Student's *t* test (∗, $p < 0.05$; ∗ ∗, $p < 0.01$; ∗∗∗, $p < 0.001$) and either refer to the corresponding solvent control or indicate significant differences between FPG-treated and untreated samples. (B) Cell viability was determined by trypan blue exclusion. Results were calculated as the number of vital cells over total cell number, and data are presented as the mean ± SD.

GSE was found to be a potent catalytic inhibitor of topoisomerase IIα, suppressing enzyme activity at a concentration of 5 μg/mL. Thus, GSE, containing 0.4 μg/mL *trans*-resveratrol, exhibits stronger topoisomerase II-targeting effects than the stilbene, which showed almost complete inhibition of topoisomerase IIα activity at 23 μg/mL. These results are in line with previous studies, which reported an IC_{50} value for topoisomerase II inhibition by resveratrol of 15.0 μg/mL,[36] whereas complete suppression of enzyme activity was observed with 27.4 μg/mL.[7] The higher potency of GSE in inhibiting topoisomerase II activity could be due to additive or synergistic effects of *trans*-resveratrol and the individual resveratrol oligomers present in the extract. The resveratrol oligomers ε-viniferin, r2-viniferin, and hopeaphenol have been identified as biologically active constituents of GSE, contributing to its antiproliferative effect in A431 cells.[10] To elucidate whether these oligomers might be responsible for the topoisomerase II inhibition by GSE, their potential to inhibit this enzyme was investigated. All tested resveratrol oligomers inhibited the catalytic activity of purified topoisomerase II, whereas the tetramers r2-viniferin and hopeaphenol exhibited a stronger inhibitory potency than the resveratrol dimer ε-viniferin at equimolar concentrations. This is in accordance with previous findings showing that ε-viniferin exhibits only a limited inhibitory activity on tumor cell progression in the cell cycle and apoptotic death compared to *trans*-resveratrol.[13,35] Yet, none of the tested oligomers alone seems to be responsible for the entire effect of the GSE, because much higher concentrations than those present in the extract were needed to block topoisomerase II activity. Furthermore, we addressed the question of whether topoisomerase II inhibition by GSE might be due to additive or synergistic effects of *trans*-resveratrol and its active resveratrol oligomers. A combination of the oligomers corresponding to their amounts present in the extract revealed that r2-viniferin, hopeaphenol, and ε-viniferin are not exclusively responsible for the topoisomerase II inhibition by GSE. When resveratrol was included in the combination experiment, enzyme activity was suppressed at lower concentrations, suggesting that resveratrol has a considerable impact on the topoisomerase II-inhibitory properties of GSE. Nevertheless, the potent suppression of enzyme activity by GSE cannot be explained by resveratrol and the herein tested resveratrol oligomers alone. Therefore, we suggest that other constituents, which have not been identified up to now, may substantially contribute to the strong topoisomerase II-targeting effects of GSE. In this context it should be noted that the identity of compounds making up 62.9% of the extract remain unknown and that no further polyphenols besides resveratrol and its oligomers listed under Materials and Methods are present in GSE.

Depending on their mode of action, topoisomerase inhibitors can be divided into two classes. Whereas catalytic inhibitors of topoisomerase II may prevent the enzyme from binding to DNA or block ATP binding prior to DNA cleavage, topoisomerase poisons stabilize the covalent enzyme−DNA intermediate.[26] In a further approach, we investigated whether GSE or the resveratrol oligomers act as a topoisomerase II poison in human tumor cells. Neither the GSE, resveratrol nor the tetramers r2-viniferin and hopeaphenol significantly increased the amount of topoisomerase II−DNA intermediates in human epidermoid carcinoma cells. This indicates that GSE rather acts as a pure catalytic inhibitor of topoisomerase II and not as a topoisomerase II poison. Although *trans*-resveratrol has previously been reported to poison topoisomerase II,[8] the level of cleavable complexes was not significantly increased under our conditions. However, a slight, yet not significant increase of covalent topoisomerase IIα−DNA complexes was observed at the highest tested concentration of 23 μg/mL. These controversial findings might be due to differences in the concentration range as well as variation between the used cell lines. Thus, the resveratrol concentration present in the GSE (~19 μg/mL in 250 μg/mL GSE) seems to be insufficient to

dx.doi.org/10.1021/jf4046182 | J. Agric. Food Chem. 2014, 62, 780−788

stabilize covalent topoisomerase II−DNA intermediates in human epidermoid cancer cells. However, the lack of topoisomerase poisoning of GSE despite containing *trans*-resveratrol could also be explained by other constituents of the extract acting as catalytic inhibitors. Because the resveratrol oligomers r2-viniferin and hopeaphenol did not poison topoisomerase II, they might present catalytic inhibitors, possibly restraining topoisomerase II poisons in the GSE from stabilizing the cleavable complex. This is the case of anthocyanins and anthocyanin-rich extracts, which are known to suppress the stabilization of topoisomerase−DNA complexes of chemotherapeutics by acting as catalytic topoisomerase inhibitors.[37,38] It also has to be considered that other extract constituents might exhibit a higher binding affinity to topoisomerases, thereby blocking the active site of the enzyme.

So far, we cannot rule out that the lack of topoisomerase poisoning in A431 cells is due to the fact that resveratrol or its tetramers are quickly biotransformed into inactive metabolites. Furthermore, the tetramers might not reach the nucleus in concentrations necessary to stabilize the cleavable complex. Thus, the bioactivity of resveratrol metabolites and cellular uptake of resveratrol tetramers are subjects of our ongoing studies.

As expected for catalytic inhibitors of topoisomerase II, only weak DNA strand-breaking properties were observed for GSE. Resveratrol has been reported to increase phosphorylation of H2AX by topoisomerase II poisoning after a long incubation time.[7] H2AX becomes rapidly phosphorylated at DNA strand break sites to form γH2AX foci and holds a key position in DNA repair processes. Thus, phosphorylation of H2AX presents a sensitive marker for DNA double-strand breaks.[39] However, the effects of GSE may not be explained by *trans*-resveratrol, as no increase of DNA strand break rate was observed by *trans*-resveratrol after a short incubation time. In addition to the enhanced DNA strand break rate, FPG-sensitive sites were detected after GSE treatment. Because r2-viniferin and hopeaphenol also increased the level of FPG-sensitive sites, it might be assumed that they account for the oxidative DNA damage observed with GSE. These results suggest that mechanisms other than topoisomerase inhibition are likely to be responsible for the detected DNA strand-breaking properties of GSE and the resveratrol tetramers. Thus, the resveratrol tetramers as well as the GSE might cause a shift towards pro-oxidative processes regarding the intracellular redox balance. The detection of FPG-sensitive sites was unexpected, as GSE and r2-viniferin have been reported to exhibit antioxidant rather than pro-oxidant properties.[11,40,41] However, *trans*-resveratrol has been shown to act as a pro-oxidant in the presence of copper ions, which has been proposed to be an important mechanism underlying its anticancer properties.[42,43] Besides *trans*-resveratrol, other pro-oxidant compounds might be present in the extract, causing oxidative stress and oxidative DNA damage.[11]

Inhibition of the catalytic activity of topoisomerase II might cause a delay in cell cycle progression, mainly in the S phase, resulting in cell cycle arrest or cell death.[36,44,45] Resveratrol is known to inhibit cell cycle progression of different cancer cells by blocking cells in the S phase.[7,13,46] Moreover, GSE has been demonstrated to affect cell cycle progression by causing a delay in the early S phase.[13,47] The accumulation of cells in the S phase could be topoisomerase-mediated, as has been shown for *trans*-resveratrol.[8] Thus, topoisomerase inhibition may account (at least in part) for the reported antiproliferative effects of *trans*-resveratrol[48,49] and GSE.[11,12]

Taken together, our results show that GSE has potent topoisomerase-II-inhibiting properties, acting as a catalytic inhibitor rather than a poison. Thus, inhibition of topoisomerase II might possibly contribute to the antiproliferative effects of the GSE. No study regarding the bioavailability of the individual resveratrol oligomers in laboratory animals or humans has been published up to now. On the basis of their structure, it is probable that they will reach a biologically relevant concentration only in the epithelium of the gastrointestinal tract. Because they can exert a pronounced antiproliferative effect in tumor cell lines in the lower micromolar concentration range, they may be useful in combination with cytostatic agents to treat gastrointestinal tumors such as colorectal carcinomas.

AUTHOR INFORMATION

Corresponding Author

*(D.M.) Phone: +43 (0) 1 4277 708 00. Fax: +43 (0) 1 4277 708 99. E-mail: doris.marko@univie.ac.at.

Notes

The authors declare no competing financial interest.

ABBREVIATIONS USED

A431, human epidermoid carcinoma cell line; ETO, etoposide; FPG, formamidopyrimidine−DNA−glycosylase; GSE, grapevine-shoot extract; HOP, hopeaphenol; ICE, isolating in vivo complexes of enzyme to DNA; kDNA, kinetoplast DNA; r2-VIN, r2-viniferin; RSV, resveratrol

REFERENCES

(1) Harikumar, K. B.; Aggarwal, B. B. Resveratrol: a multitargeted agent for age-associated chronic diseases. *Cell Cycle* **2008**, *7*, 1020−1035.

(2) Baur, J. A.; Sinclair, D. A. Therapeutic potential of resveratrol: the in vivo evidence. *Nat. Rev. Drug Discovery* **2006**, *5*, 493−506.

(3) Feng, Y.-H.; Zhou, W.-L.; Wu, Q.-L.; Li, X.-Y.; Zhao, W.-M.; Zou, J.-P. Low dose of resveratrol enhanced immune response of mice. *Acta Pharmacol. Sin.* **2002**, *23*, 893−897.

(4) Delmas, D.; Aires, V.; Limagne, E.; Dutartre, P.; Mazue, F.; Ghiringhelli, F.; Latruffe, N. Transport, stability, and biological activity of resveratrol. *Ann. N.Y. Acad. Sci.* **2011**, *1215*, 48−59.

(5) Smoliga, J. M.; Baur, J. A.; Hausenblas, H. A. Resveratrol and health − a comprehensive review of human clinical trials. *Mol. Nutr. Food Res.* **2011**, *55*, 1129−1141.

(6) Bishayee, A. Cancer prevention and treatment with resveratrol: from rodent studies to clinical trials. *Cancer Prev. Res.* **2009**, *2*, 409−418.

(7) Leone, S.; Cornetta, T.; Basso, E.; Cozzi, R. Resveratrol induces DNA double-strand breaks through human topoisomerase II interaction. *Cancer Lett. (Shannon, Irel.)* **2010**, *295*, 167−172.

(8) Leone, S.; Basso, E.; Polticelli, F.; Cozzi, R. Resveratrol acts as a topoisomerase II poison in human glioma cells. *Int. J. Cancer* **2012**, *131*, E173−E178.

(9) Bradamante, S.; Barenghi, L.; Villa, A. Cardiovascular protective effects of resveratrol. *Cardiovasc. Drug Rev.* **2004**, *22*, 169−188.

(10) Macke, S.; Jerz, G.; Empl, M. T.; Steinberg, P.; Winterhalter, P. Activity-guided isolation of resveratrol oligomers from a grapevine-shoot extract using countercurrent chromatography. *J. Agric. Food Chem.* **2012**, *60*, 11919−11927.

(11) Mueller, C.; Ullmann, K.; Wilkens, A.; Winterhalter, P.; Toyokuni, S.; Steinberg, P. Potent antioxidative activity of vineatrol 30 grapevine-shoot extract. *Biosci., Biotechnol., Biochem.* **2009**, *73*, 1831−1836.

(12) Billard, C.; Izard, J.-C.; Roman, V.; Kern, C.; Mathiot, C.; Mentz, F.; Kolb, J.-P. Comparative antiproliferative and apoptotic effects of resveratrol, ε-viniferin and vine-shots derived polyphenols (vineatrols) on chronic B lymphocytic leukemia cells and normal human lymphocytes. *Leukemia Lymphoma* **2002**, *43*, 1991−2002.
(13) Marel, A.-K.; Lizard, G.; Izard, J.-C.; Latruffe, N.; Delmas, D. Inhibitory effects of *trans*-resveratrol analogs molecules on the proliferation and the cell cycle progression of human colon tumoral cells. *Mol. Nutr. Food Res.* **2008**, *52*, 538−548.
(14) Ohyama, M.; Tanaka, T.; Ito, T.; Iinuma, M.; Bastow, K. F.; Lee, K.-H. Antitumor agents 200.1 cytotoxicity of naturally occurring resveratrol oligomers and their acetate derivatives. *Bioorg. Med. Chem. Lett.* **1999**, *9*, 3057−3060.
(15) Kim, H. J.; Chang, E. J.; Bae, S. J.; Shim, S. M.; Park, H. D.; Rhee, C. H.; Park, J. H.; Choi, S. W. Cytotoxic and antimutagenic stilbenes from seeds of *Paeonia lactiflora*. *Arch. Pharmacal Res.* **2002**, *25*, 293−299.
(16) Zghonda, N.; Yoshida, S.; Araki, M.; Kusunoki, M.; Mliki, A.; Ghorbel, A.; Miyazaki, H. Greater effectiveness of ε-viniferin in red wine than its monomer resveratrol for inhibiting vascular smooth muscle cell proliferation and migration. *Biosci., Biotechnol., Biochem.* **2011**, *75*, 1259−1267.
(17) Huang, K. S.; Lin, M.; Cheng, G. F. Anti-inflammatory tetramers of resveratrol from the roots of *Vitis amurensis* and the conformations of the seven-membered ring in some oligostilbenes. *Phytochemistry* **2001**, *58*, 357−362.
(18) Wang, J. C. DNA topoisomerases. *Annu. Rev. Biochem.* **1996**, *65*, 635−692.
(19) Pommier, Y. Drugging topoisomerases: lessons and challenges. *ACS Chem. Biol.* **2013**, *8*, 82−95.
(20) Deweese, J. E.; Osheroff, N. The DNA cleavage reaction of topoisomerase II: wolf in sheep's clothing. *Nucleic Acids Res.* **2009**, *37*, 738−748.
(21) Champoux, J. J. DNA topoisomerases: structure, function, and mechanism. *Annu. Rev. Biochem.* **2001**, *70*, 369−413.
(22) McClendon, A. K.; Osheroff, N. DNA topoisomerase II, genotoxicity, and cancer. *Mutat. Res.* **2007**, *623*, 83−97.
(23) Pommier, Y.; Leo, E.; Zhang, H.; Marchand, C. DNA topoisomerases and their poisoning by anticancer and antibacterial drugs. *Chem. Biol.* **2010**, *17*, 421−433.
(24) McClendon, A. K.; Rodriguez, A. C.; Osheroff, N. Human topoisomerase iiα rapidly relaxes positively supercoiled DNA: implications for enzyme action ahead of replication forks. *J. Biol. Chem.* **2005**, *280*, 39337−39345.
(25) Nitiss, J. L. Targeting DNA topoisomerase II in cancer chemotherapy. *Nat. Rev. Cancer* **2009**, *9*, 338−350.
(26) Larsen, A. K.; Escargueil, A. E.; Skladanowski, A. Catalytic topoisomerase II inhibitors in cancer therapy. *Pharmacol. Ther.* **2003**, *99*, 167−181.
(27) Fortune, J. M.; Osheroff, N. Merbarone inhibits the catalytic activity of human topoisomerase IIα by blocking DNA cleavage. *J. Biol. Chem.* **1998**, *273*, 17643−17650.
(28) Kalfalah, F. M.; Mielke, C.; Christensen, M. O.; Baechler, S.; Marko, D.; Boege, F. Genotoxicity of dietary, environmental and therapeutic topoisomerase II poisons is uniformly correlated to prolongation of enzyme DNA residence. *Mol. Nutr. Food Res.* **2011**, *55*, S127−S142.
(29) Gedik, C. M.; Ewen, S. W. B.; Collins, A. R. Single-cell gel electrophoresis applied to the analysis of UV-C damage and its repair in human cells. *Int. J. Radiat. Biol.* **1992**, *62*, 313−320.
(30) Pelka, J.; Gehrke, H.; Rechel, A.; Kappes, M.; Hennrich, F.; Hartinger, C. G.; Marko, D. DNA damaging properties of single walled carbon nanotubes in human colon carcinoma cells. *Nanotoxicology* **2011**, *7*, 2−20.
(31) Hwangbo, K.; Zheng, M. S.; Kim, Y.-J.; Im, J.-Y.; Lee, C.-S.; Woo, M.-H.; Jahng, Y.; Chang, H.-W.; Son, J.-K. Inhibition of DNA topoisomerases I and II of compounds from *Reynoutria japonica*. *Arch. Pharmacal Res.* **2012**, *35*, 1583−1589.
(32) Webb, M. R.; Ebeler, S. E. Comparative analysis of topoisomerase IB inhibition and DNA intercalation by flavonoids and similar compounds: structural determinates of activity. *Biochem. J.* **2004**, *384*, 527−541.
(33) Jo, J.-Y.; Gonzalez de Mejia, E.; Lila, M. A. Effects of grape cell culture extracts on human topoisomerase II catalytic activity and characterization of active fractions. *J. Agric. Food Chem.* **2005**, *53*, 2489−2498.
(34) Basso, E.; Fiore, M.; Leone, S.; Degrassi, F.; Cozzi, R. Effects of resveratrol on topoisomerase II-α activity: induction of micronuclei and inhibition of chromosome segregation in CHO-K1 cells. *Mutagenesis* **2013**, *28*, 243−248.
(35) Colin, D.; Lancon, A.; Delmas, D.; Lizard, G.; Abrossinow, J.; Kahn, E.; Jannin, B.; Latruffe, N. Antiproliferative activities of resveratrol and related compounds in human hepatocyte derived HepG2 cells are associated with biochemical cell disturbance revealed by fluorescence analyses. *Biochimie* **2008**, *90*, 1674−1684.
(36) Jo, J.-Y.; Gonzalez de Mejia, E.; Lila, M. A. Catalytic inhibition of human DNA topoisomerase II by interactions of grape cell culture polyphenols. *J. Agric. Food Chem.* **2006**, *54*, 2083−2087.
(37) Esselen, M.; Barth, S. W.; Winkler, S.; Baechler, S.; Briviba, K.; Watzl, B.; Skrbek, S.; Marko, D. Anthocyanins suppress the cleavable complex formation by irinotecan and diminish its DNA strand breaking activity in the colon of Wistar rats. *Carcinogenesis* **2013**, *34*, 835−840.
(38) Esselen, M.; Boettler, U.; Teller, N.; Bachler, S.; Hutter, M.; Rufer, C. E.; Skrbek, S.; Marko, D. Anthocyanin-rich blackberry extract suppresses the DNA-damaging properties of topoisomerase I and II poisons in colon carcinoma cells. *J. Agric. Food Chem.* **2011**, *59*, 6966−6973.
(39) Bonner, W. M.; Redon, C. E.; Dickey, J. S.; Nakamura, A. J.; Sedelnikova, O. A.; Solier, S.; Pommier, Y. γH2AX and cancer. *Nat. Rev. Cancer* **2008**, *8*, 957−967.
(40) Romain, C.; Gaillet, S.; Carillon, J.; Vide, J.; Ramos, J.; Izard, J.-C.; Cristol, J.-P.; Rouanet, J.-M. Vineatrol and cardiovascular disease: beneficial effects of a vine-shoot phenolic extract in a hamster atherosclerosis model. *J. Agric. Food Chem.* **2012**, *60*, 11029−11036.
(41) Jang, M. H.; Piao, X. L.; Kim, H. Y.; Cho, E. J.; Baek, S. H.; Kwon, S. W.; Park, J. H. Resveratrol oligomers from *Vitis amurensis* attenuate β-amyloid-induced oxidative stress in PC12 cells. *Biol. Pharm. Bull.* **2007**, *30*, 1130−1134.
(42) Hadi, S. M.; Ullah, M. F.; Azmi, A. S.; Ahmad, A.; Shamim, U.; Zubair, H.; Khan, H. Y. Resveratrol mobilizes endogenous copper in human peripheral lymphocytes leading to oxidative DNA breakage: a putative mechanism for chemoprevention of cancer. *Pharm. Res.* **2010**, *27*, 979−988.
(43) Zheng, L.-F.; Wei, Q.-Y.; Cai, Y.-J.; Fang, J.-G.; Zhou, B.; Yang, L.; Liu, Z.-L. DNA damage induced by resveratrol and its synthetic analogues in the presence of Cu(II) ions: mechanism and structure-activity relationship. *Free Radical Biol. Med.* **2006**, *41*, 1807−1816.
(44) Kallio, M.; Lahdetie, J. Effects of the DNA topoisomerase II inhibitor merbarone in male mouse meiotic divisions in vivo: cell cycle arrest and induction of aneuploidy. *Environ. Mol. Mutagen.* **1997**, *29*, 16−27.
(45) Stewart, N.; Hicks, G. G.; Paraskevas, F.; Mowat, M. Evidence for a second cell cycle block at G2/M by p53. *Oncogene* **1995**, *10*, 109−115.
(46) Tyagi, A.; Singh, R. P.; Agarwal, C.; Siriwardana, S.; Sclafani, R. A.; Agarwal, R. Resveratrol causes Cdc2-tyr15 phosphorylation via ATM/ATR-Chk1/2-Cdc25C pathway as a central mechanism for S phase arrest in human ovarian carcinoma Ovcar-3 cells. *Carcinogenesis* **2005**, *26*, 1978−1987.
(47) Colin, D.; Gimazane, A.; Lizard, G.; Izard, J.-C.; Solary, E.; Latruffe, N.; Delmas, D. Effects of resveratrol analogs on cell cycle progression, cell cycle associated proteins and 5-fluorouracil sensitivity in human derived colon cancer cells. *Int. J. Cancer* **2009**, *124*, 2780−2788.

(48) Cui, J.; Sun, R.; Yu, Y.; Gou, S.; Zhao, G.; Wang, C. Antiproliferative effect of resveratrol in pancreatic cancer cells. *Phytother. Res.* **2010**, *24*, 1637−1644.
(49) Signorelli, P.; Ghidoni, R. Resveratrol as an antiproliferative agent for cancer. *Oxid. Stress Dis.* **2006**, *20*, 57−83.

JOURNAL OF AGRICULTURAL AND FOOD CHEMISTRY

Article

pubs.acs.org/JAFC

Effects of Anthocyanidins and Anthocyanins on the Expression and Catalytic Activities of CYP2A6, CYP2B6, CYP2C9, and CYP3A4 in Primary Human Hepatocytes and Human Liver Microsomes

Alzbeta Srovnalova,[†,#] Michaela Svecarova,[†,#] Michaela Kopecna Zapletalova,[‡,#] Pavel Anzenbacher,[‡] Petr Bachleda,[§] Eva Anzenbacherova,*[,∥] and Zdenek Dvorak*[,†]

[†]Department of Cell Biology and Genetics, Regional Centre of Advanced Technologies and Materials, Faculty of Science, Palacky University, Slechtitelu 11, 783 71 Olomouc, Czech Republic

[‡]Institute of Pharmacology, Faculty of Medicine and Dentistry, Palacky University, Hnevotinska 3, 775 15 Olomouc, Czech Republic

[§]Second Department of Surgery, University Hospital Olomouc, I. P. Pavlova 6, 775 20 Olomouc, Czech Republic

[∥]Institute of Medical Chemistry and Biochemistry, Faculty of Medicine and Dentistry, Palacky University, Hnevotinska 3, 775 15 Olomouc, Czech Republic

ABSTRACT: Anthocyanidins and anthocyanins are pharmacologically active constituents of various berry fruits, such as blueberry and cranberry. These compounds are also contained in massively used nutritional supplements based on extracts or dry matter from berry fruits. The current study evaluated the effects of anthocyanidins and anthocyanins on the expression and catalytic activity of major drug-metabolizing enzymes CYP2C9, CYP2A6, CYP2B6, and CYP3A4 in primary cultures of human hepatocytes and human liver microsomes. Expression of mRNA was quantified by qRT-PCR. Expression of proteins was evaluated by Western blotting and immunochemiluminescence. The catalytic activity of CYP enzymes was measured by HPLC using specific enzyme substrates. Tested anthocyanidins (6) and anthocyanins (21) did not induce the expression of mRNA and protein of CYP2C9, CYP2A6, CYP2B6, and CYP3A4 genes in human hepatocytes. Catalytic activities of CYP2C9, CYP2A6, CYP2B6, and CYP3A4 enzymes were inhibited by all anthocyanidins to different extents (e.g., delphinidin inhibits CYP3A4 by >90% at 100 μM with IC_{50} = 32 μM). Of 21 anthocyanins tested, only cyanidin-3-*O*-rhamnoside (CYP3A4 by >75% at 100 μM with IC_{50} = 44 μM) and two glycosides of delphinidin significantly inhibited examined cytochromes P450. It may be concluded that in the ranges of common ingestion of either food or dietary supplement an induction or significant inhibition of CYP2C9, CYP2A6, CYP2B6, and CYP3A4 activity is most probably not expected.

KEYWORDS: *anthocyans, cytochrome P450, food−drug interactions, human hepatocytes, xenobiotics*

INTRODUCTION

The anthocyans (in Greek *anthos* means flower and *kyanos* means blue) are widespread natural flavonoids that occur in all tissues of higher plants (flowers, leaves, roots, stems, fruits, and vegetables) as water-soluble vacuolar pigments. They have significant roles in the animal kingdom in pollination and seed dispersal.[1] The stability and color of anthocyans depend on the pH and the occurrence of chelating metal ions.[2] The structural differences between anthocyans are the number of the hydroxyl groups; the degree of methylation of −OH groups; the number, nature, and position of sugar attachments; and the number and nature of aliphatic or aromatic acids fixed to sugars in the molecule.[3] The most common sugars are glucose, galactose, and rhamnose.[4] Anthocyans comprise two types of compounds, that is, anthocyanins and anthocyanidins, which are aglycon (sugar-free) backbones of anthocyanins (for structures see Table 1). Anthocyanins are found in plant foods including cereals, tubers, roots, pulses, etc., and also in beverages and dietary supplements.[5] The most common anthocyanidins in higher plants include cyanidin, delphinidin, malvidin, pelargonidin, peonidin, and petunidin.[1,5] The anthocyans are important for their various health benefits.[4,6] They play an important role in obesity and diabetes control, neuronal and cardiovascular disease prevention, and improvement of visual and brain functions.[5] Anthocyans display a plethora of biological effects, including antiproliferative,[7] antiapoptotic,[8] antitumor,[9] antimutagenic,[10] antioxidant,[11] antiradical,[12] and nitric oxide inhibitory effects.[13]

Despite numerous studies of anthocyan biological activities, a systematic study focused on the interactions between anthocyans and drug-metabolizing cytochromes P450 was not carried out yet. Because common foods, beverages, and food supplements contain various natural or synthetic xenobiotics, including anthocyans, a phenomenon of food−drug interactions emerged. Dietary xenobiotics can interfere with drug-metabolizing enzymes and may cause their inhibition or induction. Indeed, we recently described the activation of the aryl hydrocarbon receptor (AhR) and induction of drug-metabolizing CYP1A1 in human cancer cell lines and human hepatocytes by anthocyanidin pelargonidin[14] and by anthocyanins pelargonidin-3-*O*-rutinoside and cyanidin-3,5-*O*-diglucoside.[15] In the current study, we have evaluated the effects of 21 anthocyanins and 6 anthocyanidins on the main drug-metabolizing cytochromes P450, those being CYP2A6,

Received: October 16, 2013
Revised: December 20, 2013
Accepted: January 5, 2014
Published: January 6, 2014

ACS Publications © 2014 American Chemical Society

Table 1. Chemical Structures of Anthocyanins and Anthocyanidins

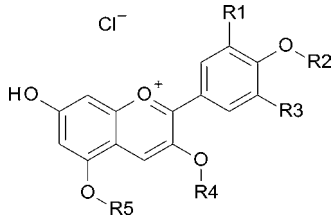

		R1	R2	R3	R4	R5
		Anthocyanins				
PEL-1	pelargonidin-3,5-di-*O*-glucoside chloride	H	H	H	glucoside	glucose
PEL-2	pelargonidin-3-*O*-rutinoside chloride	H	H	H	rutinoside	H
DEL-1	delphinidin-3-*O*-glucoside chloride	OH	H	OH	glucoside	H
DEL-2	delphinidin-3-*O*-rutinoside chloride	OH	H	OH	rutinoside	H
DEL-3	delphinidin-3,5-di-*O*-glucoside chloride	OH	H	OH	glucoside	glucose
DEL-4	delphinidin-3-*O*-sambubioside chloride	OH	H	OH	sambubioside	H
DEL-5	delphinidin-3-*O*-rhamnoside chloride	OH	H	OH	rhamnoside	H
MAL-1	malvidin-3-*O*-glucoside chloride	OCH_3	H	OCH_3	glucoside	H
MAL-2	malvidin-3,5-di-*O*-glucoside chloride	OCH_3	H	OCH_3	glucoside	glucose
MAL-3	malvidin-3-*O*-galactoside chloride	OCH_3	H	OCH_3	galactoside	H
CYA-1	cyanidin-3-*O*-glucoside chloride	OH	H	H	glucoside	H
CYA-2	cyanidin-3-*O*-rutinoside chloride	OH	H	H	rutinoside	H
CYA-3	cyanidin-3,5-di-*O*-glucoside chloride	OH	H	H	glucoside	glucose
CYA-4	cyanidin-3-*O*-sophoroside chloride	OH	H	H	sophoroside	H
CYA-5	cyanidin-3-*O*-arabinoside chloride	OH	H	H	arabinoside	H
CYA-6	cyanidin-3-*O*-rhamnoside chloride	OH	H	H	rhamnoside	H
CYA-7	cyanidin-3-*O*-galactoside chloride	OH	H	H	galactoside	H
CYA-8	cyanidin-3-*O*-sambubioside chloride	OH	H	H	sambubioside	H
CYA-9	cyanidin-3-*O*-lathyroside chloride	OH	H	H	lathyroside	H
		Anthocyanidins				
	pelargonidin chloride	H	H	H	H	H
	cyanidin chloride	OH	H	H	H	H
	delphinidin chloride	OH	H	OH	H	H
	petunidin chloride	OCH_3	H	OH	H	H
	malvidin chloride	OCH_3	H	OCH_3	H	H
	peonidin chloride	OCH_3	H	H	H	H

CYP2B6, CYP2C9, and CYP3A4. We measured (i) induction = expression of CYPs at the levels of mRNA and protein in primary cultures of human hepatocytes and (ii) inhibition = catalytic activity of CYPs in human liver microsomes. Tested anthocyanins did not induce CYP2A6, CYP2B6, CYP2C9, and CYP3A4 in primary human hepatocytes. On the other hand, CYP3A4 activity was inhibited by all anthocyanidins tested (with delphinidin at a concentration of 100 μM down to 8% of the original activity). The inhibition of CYP2C9 by anthocyanidins was prominent with pelargonidin and peonidin only, whereas CYP2A6 and CYP2B6 were not inhibited. Of the anthocyanins tested, only cyanidin-3-*O*-rhamnoside inhibited activities of all CYP isoforms examined, with the strongest effect on CYP3A4 activity (inhibition down to 25% of the control).

MATERIALS AND METHODS

Compounds and Reagents. Dimethyl sulfoxide (DMSO), rifampicin (RIF), and hygromycin B were purchased from Sigma-Aldrich (Prague, Czech Republic). The following anthocyanins and anthocyanidins were purchased from Extrasynthese (Lyon, France): peonidin-3-*O*-glucoside chloride (PEO-1), peonidin-3-*O*-rutinoside chloride (PEO-2), pelargonidin-3,5-di-*O*-glucoside chloride (PEL-1), pelargonidin-3-*O*-rutinoside chloride (PEL-2), delphinidin-3-*O*-glucoside chloride (DEL-1), delphinidin-3-*O*-rutinoside chloride (DEL-2), delphinidin-3,5-di-*O*-glucoside chloride (DEL-3), delphinidin-3-*O*-sambubioside chloride (DEL-4), delphinidin-3-*O*-rhamnoside chloride (DEL-5), malvidin-3-*O*-glucoside chloride (MAL-1), malvidin-3,5-di-*O*-glucoside chloride (MAL-2), malvidin-3-*O*-galactoside chloride (MAL-3), cyanidin-3-*O*-glucoside chloride (CYA-1), cyanidin-3-*O*-rutinoside chloride (CYA-2), cyanidin-3,5-di-*O*-glucoside chloride (CYA-3), cyanidin-3-*O*-sophoroside chloride (CYA-4), cyanidin-3-*O*-arabinoside chloride (CYA-5), cyanidin-3-*O*-rhamnoside chloride (CYA-6), cyanidin-3-*O*-galactoside chloride (CYA-7), cyanidin-3-*O*-sambubioside chloride (CYA-8), cyanidin-3-*O*-lathyroside chloride (CYA-9), cyanidin chloride (CYA), delphinidin chloride (DEL), malvidin chloride (MAL), peonidin chloride (PEO), petunidin chloride (PET), and pelargonidin chloride (PEL). Luciferase lysis buffer and P450-Glo CYP1A1 assay were from Promega (www.promega.com; Hercules, CA, USA). Oligonucleotide primers used in RT-PCR reactions were from Invitrogen. LightCycler FastStart DNA Master^{PLUS} SYBR Green I was from Roche Diagnostic Corp. (Intes Bohemia, Czech Republic). Cryopreserved human liver microsomes (pooled) were purchased from Biopredic International (Rennes, France). Microsomes were obtained under approval of the local ethics committee and in accordance with the ethic regulations of the country of origin (France). They were from 20 males and 6 females with a protein content of 25 mg/mL; the CYP1A1/2, CYP2A6, CYP2B6, CYP2C9, CYP2C19, CYP2E1, and CYP3A4/5 enzyme activities were verified prior to the experiment.

For determination of CYP activities, testosterone (CYP3A4), coumarin (CYP2A6), 7-ethoxy-4-(trifluoromethyl)coumarin (CYP2B6), and diclofenac (CYP2C9) as well as respective metabolites

dx.doi.org/10.1021/jf404643w | J. Agric. Food Chem. 2014, 62, 789−797

7-hydroxy-4-(trifluoromethyl)coumarin and 7-hydroxycoumarin were supplied by Sigma-Aldrich; 6β-hydroxytestosterone was from Ultrafine (Manchester, UK), and 4-hydroxydiclofenac was supplied by BD Biosciences (San Jose, CA, USA).

All other chemicals were of the highest quality commercially available.

Human Hepatocytes. Human hepatocytes (six different primary cultures) were obtained from two sources: (i) human liver obtained from multiorgan donors LH44 (F, 57 years), LH45 (M, 46 years), LH46 (M, 37 years), LH47 (M, 47 years), and LH49 (M, 38 years); tissue acquisition protocol was in accordance with the requirements issued by the local ethical commission in the Czech Republic; (ii) long-term human hepatocytes in monolayer batch HEP220670 (F, 64 years) (Biopredic International, Rennes, France). Hepatocytes were treated in a serum-free medium for 24 or 48 h with the tested compounds, RIF (10 μM), and/or vehicle (DMSO; 0.1% v/v). Cultures were maintained at 37 °C and 5% CO_2 in a humidified incubator.

Quantitative Reverse Transcriptase Polymerase Chain Reaction (qRT-PCR). Total RNA was isolated using TRI reagent, and cDNA was synthesized according to the common protocol, using M-MLV reverse transcriptase F-572 (Finnzymes) and random hexamers 3801 (Takara). qRT-PCR was carried out on a Light Cycler apparatus 480 II (Roche Diagnostic Corp., Prague, Czech Republic). The levels of CYP2A6, CYP2B6, CYP2C9, CYP3A4, and GAPDH mRNAs were determined as described elsewhere.[16] The measurements were performed in triplicates. Gene expression levels were normalized to glyceraldehyde-3-phosphate dehydrogenase (GAPDH), a housekeeping gene. Data were processed according to the delta−delta method.

Protein Detection and Western Blotting. Total protein extracts were prepared, and they were subjected to SDS-PAGE separation and Western blot transfer. The blots were probed with antibodies against CYP2A6 (mouse monoclonal; sc-53615, F16 P2 D8), CYP2B6 (rabbit polyclonal; sc-67224, H-110), CYP2C9 (goat polyclonal; sc-23436, C-21), CYP3A4 (mouse monoclonal; sc-53850, HL3), and β-actin (goat polyclonal; sc-1616, I-19), all purchased from Santa Cruz Biotechnology (Santa Cruz, CA, USA). Chemiluminescent detection was performed using horseradish peroxidase-conjugated secondary antibody and an Amersham (GE Healthcare) ECL kit.

Enzyme Activities of CYP2A6, CYP2B6, CYP2C9, and CYP3A4 in Human Liver Microsomes. Activities of individual CYP isoforms were measured according to published protocols.[17] The following microsomal CYP activities were tested: CYP3A4, testosterone 6β-hydroxylation; CYP2A6, coumarin 7-hydroxylation; CYP2B6, 7-ethoxy-4-(trifluoromethyl)-coumarin 7-deethylation; and CYP2C9 activity, diclofenac 4′-hydroxylation.

Reaction mixtures of individual determinations contained, for determination of CYP2A6, CYP2B6, or CYP2C9 activity, 35 pmol P450 and for determination of CYP3A4 activity, the amount of microsomal fraction with 100 pmol of P450. All reaction mixtures were buffered by 100 mM K/PO_4 (pH 7.4) and contained a NADPH generating system consisting of isocitrate dehydrogenase (9 U/mlL), $NADP^+$ (0.5 mM), isocitric acid (4 mM), and $MgSO_4$ (5 mM). Final concentrations of substrates in the corresponding reaction mixtures were as follows: CYP2A6, coumarin (10 μM); CYP2B6, 7-ethoxy-4-(trifluoromethyl)coumarin (15 μM); CYP2C9, diclofenac (16 μM); CYP3A4, testosterone (100 μM). Aqueous stock solutions of anthocyanins were 1 mM (pH 6.7); anthocyanidins of the same concentration were dissolved in aqueous solution of pH 3.5. For detailed description of the incubations, see the previous papers.[14,15] For each enzyme assay, a preliminary experiment was done to determine the K_M and V_{max} for a given enzyme reaction and to obtain the values of substrate concentrations suitable for the inhibition experiments. Inhibition experiments were routinely performed with six concentrations of the tested compound (0, 10, 20, 40, 80, and 100 μM in the reaction mixture). All determinations were done in triplicates. The effects of anthocyans on CYP activities were determined according to methods indicated above by HPLC using the Prominence system (Shimadzu, Kyoto, Japan). Sigma Plot v. 10.0 (Systat, Chicago, IL, USA) was used for plotting the results. The inhibition was expressed as the relative activity (control, 100%) remaining after addition of the respective inhibitor.

RESULTS

Effects of Anthocyanidins on the Expression of CYP2A6, CYP2B6, CYP2C9, and CYP3A4 in Human Hepatocytes. Six major anthocyanidins (i.e., cyanidin, peonidin, petunidin, pelargonidin, delphinidin, malvidin) were examined in three different primary cultures of human hepatocytes (i.e., LH44, LH45, HEP220670). Cells were incubated with tested compounds (50 μM), model panel CYP2/3 inducer rifampicin (RIF; 10 μM), and DMSO (0.1% v/v) as vehicle for control. The duration of the treatments was 24 and 48 h for mRNA and protein analyses, respectively. Rifampicin strongly induced CYP3A4 mRNA in all human hepatocyte cultures, LH44 (117-fold), LH45 (55-fold), and HEP220670 (45-fold). Consistently, CYP3A4 protein was strongly induced by rifampicin in all human hepatocyte cultures. None of the anthocyanidins tested induced the expression of CYP3A4 mRNA (Figure 1) or protein (Figure 2) in any of the three cultures used. Similarly, no induction of CYP2B6 mRNA and protein was observed for tested anthocyanidins. Strong induction of CYP2B6 protein and mRNA was achieved by rifampicin, yielding the inductions of mRNA by factors of 9-, 15-, and 22-fold, in cultures LH44, LH45, and HEP220670, respectively (Figures 1 and 2). The expression of CYP2C9 mRNA was increased by rifampicin by factors of 3-, 2-, and 48-fold, in cultures LH44, LH45, and HEP220670 (Figure 1), respectively, whereas the level of CYP2C9 protein was not significantly increased by rifampicin (Figure 2). The lack of CYP2C9 protein induction and weak CYP2C9 mRNA induction (LH44, LH45) by rifampicin is probably due to high constitutive levels of CYP2C9 in human hepatocytes. None of the anthocyanidins tested induced the expression of CYP2C9 mRNA (Figure 1) or protein (Figure 2) in any human hepatocyte culture. Rifampicin induced CYP2A6 mRNA in all human hepatocyte cultures, LH44 (3-fold), LH45 (4-fold), and HEP220670 (18-fold). Cyanidin, malvidin, delphinidin, and petunidin increased CYP2A6 mRNA levels, but the effects were not systematic in all hepatocyte cultures and occurred rather randomly, perhaps due to interindividual metabolic profiles (Figure 1). Rifampicin also induced CYP2A6 protein, whereas the tested anthocyanins had no systematic effects on CYP2A6 protein level in human hepatocyte cultures (Figure 2).

Effects of Anthocyanins on the Expression of CYP2A6, CYP2B6, CYP2C9, and CYP3A4 in Human Hepatocytes. In the next series of experiments, the effects of 21 anthocyanins (for details see Materials and Methods) were tested in four different human hepatocyte cultures (LH45, LH46, LH47, LH49). For this purpose, hepatocytes were incubated for 24 and 48 h with tested compounds (50 μM), rifampicin (RIF; 10 μM), and vehicle (DMSO; 0.1% v/v). Rifampicin significantly induced CYP2A6 (3-, 4-, 8-, 5-fold), CYP2B6 (9-, 15-, 25-, 14-fold), CYP2C9 (3-, 2-, 5-, 2-fold), and CYP3A4 (117-, 55-, 121-, 13-fold) mRNAs in all human hepatocyte cultures. None of the anthocyanins tested induced CYP2B6, CYP2C9, or CYP3A4 mRNAs. Similarly as in the case of anthocyanidins, the expression of CYP2A6 mRNA was increased by some anthocyanins, but these effects were not reproducible between individual human hepatocyte cultures (Figure 3). The data from Western blot analyses of CYP3A4 and CYP2B6 proteins were consistent with those at mRNA level. Whereas rifampicin strongly induced CYP3A4 and CYP2B6 proteins, the tested anthocyanins had no effects (Figure 4). Rifampicin strongly induced CYP2A6 protein, but the tested anthocyanins had no

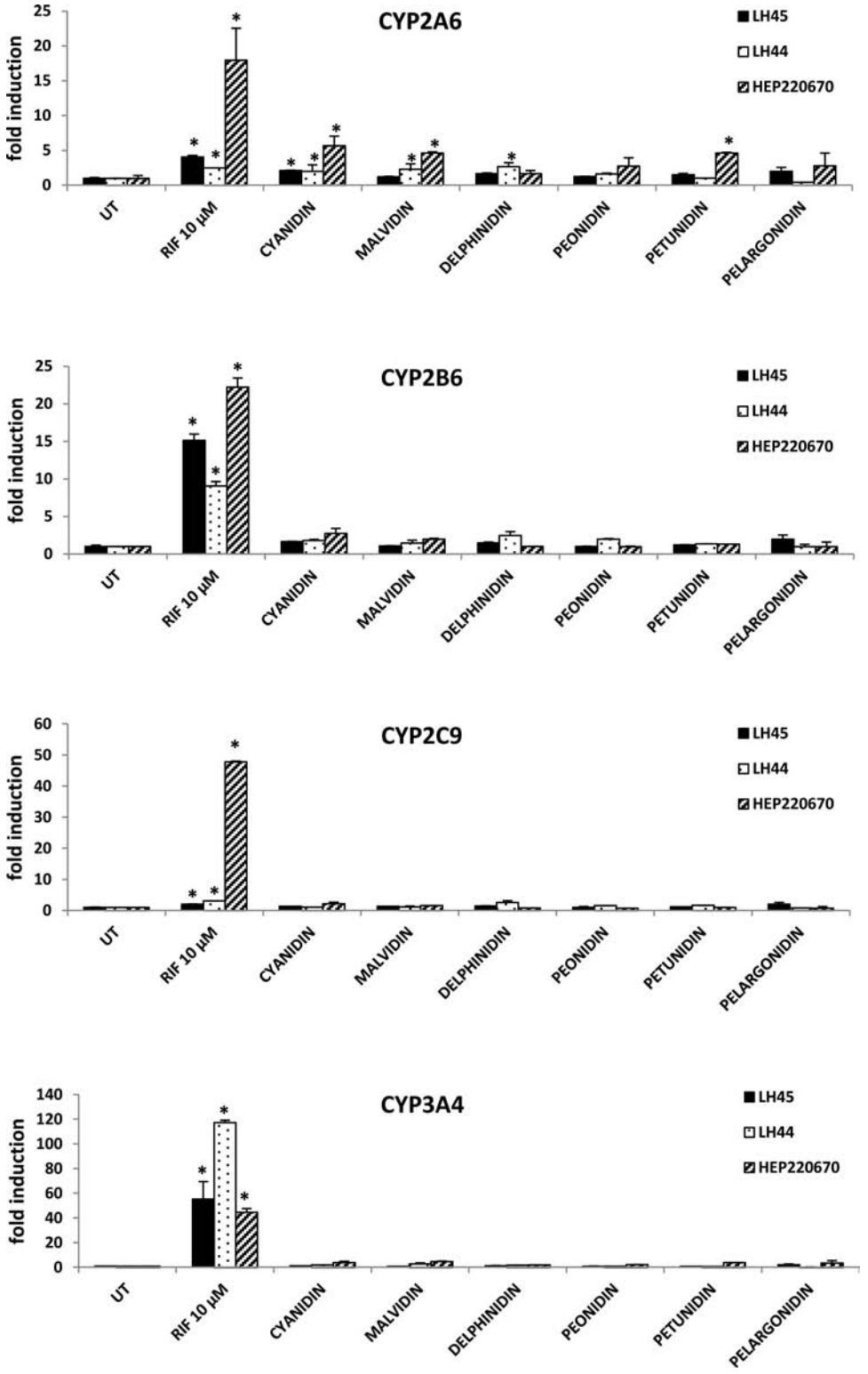

Figure 1. Effects of anthocyanidins on the expression of CYP2A6, CYP2B6, CYP2C9, and CYP3A4 mRNAs in human hepatocytes. Primary human hepatocyte cultures (LH44, LH45, HEP220670) were incubated for 24 h with cyanidin (50 μM), peonidin (50 μM), petunidin (50 μM), pelargonidin (50 μM), delphinidin (50 μM), malvidin (50 μM), rifampicin (10 μM), and DMSO (0.1% v/v) as a vehicle for control. Bar graphs show RT-PCR analyses of CYP2A6, CYP2B6, CYP2C9, and CYP3A4 mRNAs. The data are the mean from triplicate measurements and are expressed as a fold-induction as compared to DMSO-treated cells. The data were normalized per GAPDH mRNA levels. ∗, value is significantly different from DMSO-treated cells ($p < 0.05$) as determined by Student's t test.

effects, and CYP2A6 protein was not detectable in cells incubated with anthocyanins. The levels of CYP2C9 protein were not significantly and systematically altered either by rifampicin or by tested anthocyanins (Figure 4).

Effects of Anthocyanidins and Anthocyanins on Catalytic Activities of CYP2A6, CYP2B6, CYP2C9, and CYP3A4 in Human Liver Microsomes. Enzyme activities were examined with anthocyanidins (and anthocyanins) in

dx.doi.org/10.1021/jf404643w | J. Agric. Food Chem. 2014, 62, 789−797

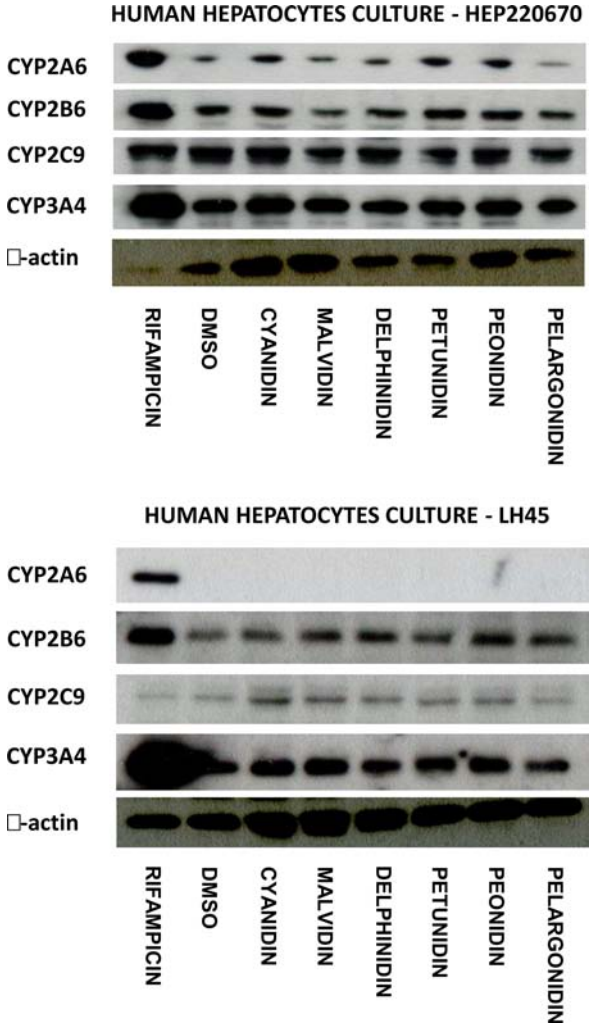

Figure 2. Effects of anthocyanidins on the expression of CYP2A6, CYP2B6, CYP2C9, and CYP3A4 proteins in human hepatocytes. Primary human hepatocytes cultures (LH44, LH45, HEP220670) were incubated for 48 h with cyanidin (50 μM), peonidin (50 μM), petunidin (50 μM), pelargonidin (50 μM), delphinidin (50 μM), malvidin (50 μM), rifampicin (10 μM), and DMSO (0.1% v/v) as a vehicle for control. Western blots show analyses of CYP2A6, CYP2B6, CYP2C9, and CYP3A4 proteins. As a loading control, the blots were probed to β-actin (data not shown).

concentrations of 0, 10, 20, 40, 80, and 100 μM. The most prominent inhibitions of CYP activities were observed for CYP3A4 (testosterone 6-β-hydroxylation) and CYP2C9 (diclofenac 4′-hydroxylation). The enzyme activity of CYP3A4 was inhibited by at least down to 50% with all six anthocyanidins tested. The most prominent inhibitory effects were observed with delphinidin (down to 9% of the control value by 100 μM delphinidin with IC_{50} = 32 μM) and petunidin and peonidin (down to about 20% of the control at 100 μM; the IC_{50} values reached 31 μM for petunidin and 36 μM for peonidin). Pelargonidin inhibited this activity down to 35% at 100 μM concentration with IC_{50} = 55 μM. Inhibition of CYP3A4 activity by malvidin and cyanidin did not reach 50% of control value (Figure 5; top left).

Significant inhibition of CYP2C9 was attained by pelargonidin, peonidin (down to 25−30% of the control value with 100 μM, IC_{50} = 25 and 21 μM) and petunidin (100 μM, IC_{50} = 61 μM), whereas cyanidin did not inhibit CYP2C9 enzyme activity (Figure 5; top right). All anthocyanidins tested inhibited the CYP2A6 enzyme activity (coumarin 4-hydroxylation), albeit to different extents. The strongest inhibition was attained by delphinidin, where the activity was inhibited down to 75% at the 100 μM concentration (Figure 5; bottom left). All other anthocyanidins exhibited concentration-dependent, however much lower, degrees of inhibition. Concentration-dependent inhibition of CYP2B6 activity (7-ethoxy-4-(trifluoromethyl) coumarin O-deethylation) was observed with all anthocyanidins. On the other hand, the extent of inhibition was not greater than 20% only (Figure 5; bottom right).

Interestingly, among the anthocyanins (i.e., the respective glycosides of anthocyanidins) CYA-6 (cyanidin-3-*O*-rhamnoside chloride) inhibited activities of all CYP isoforms examined with the strongest effects on the CYP3A4 activity (down to 25% of the control at 100 μM with IC_{50} = 44 μM). The CYP2C9, CYP2A6, and CYP2B6 activities were inhibited by CYA-6 down to 40% of the initial enzyme activity (Figure 6). Besides CYA-6, the CYP3A4 activity was inhibited also by DEL-2 (delphinidin-3-*O*-rutinoside; down to 35% at 100 μM, IC_{50} = 67 μM), whereas other anthocyanins inhibited the CYP activities to lower extents; a more prominent decrease in the enzyme activity was observed for CYP2B6 and CYA-2 (to 45% at 100 μM) and for CYP2C9 with DEL-1 (to 55% at 100 μM concentration).

DISCUSSION

Metabolism of xenobiotics, including drugs, may be influenced by the presence of second xenobiotic, producing a phenomenon of drug−drug interaction. Because many natural and synthetic xenobiotics originate from food, a phenomenon of food−drug interactions was established. A mechanistic base for food−drug interaction may be either inhibition or induction of drug-metabolizing enzymes by xenobiotics. Therefore, in the current study, we have examined the effects of common dietary anthocyanidins (6) and anthocyanins (21) on the expression and catalytic activity of cytochromes P450 CYP2A6, CYP2B6, CYP2C9, and CYP3A4. The major findings of the study are that (i) tested anthocyans (i.e., both the anthocyanidins and anthocyanins) do not induce CYP2A6, CYP2B6, CYP2C9, and CYP3A4 mRNAs and proteins in primary human hepatocytes and that (ii) all of the anthocyanidins did inhibit the CYP3A4 activity; among anthocyanins, the enzyme activity of this isoform was also inhibited the most, although not so largely as with the anthocyanidin aglycons.

Xenobiotic-mediated induction of cytochromes P450 CYP2A6, CYP2B6, CYP2C9, and CYP3A4 is controlled by various transcriptional regulators, including xenoreceptors (e.g., pregnane X receptor, PXR; constitutive androstane receptor, CAR), nuclear receptors (e.g., retinoic acid receptors, RARs; retinoid X receptors, RXRs; liver X receptor, LXR; farnesoid X receptor, FXR; vitamin D receptor, VDR), and receptors for steroid hormones (e.g., glucocorticoid receptor, GR; estrogen receptor, ER).[18] The activators of listed receptors are therefore usually inducers of CYP2 and CYP3 genes, and vice versa. Importantly, xenoreceptors and steroid and nuclear receptors are important transcriptional regulators of many genes, involved in energy metabolism, cells growth, differenciation, immunity, etc. Activation of these receptors by xenobiotics often leads to so-called endocrine disruption, besides from CYP gene induction. In addition, induction of drug-metabolizing CYPs by xenobiotics may cause chemically induced cell damage or carcinogenesis. Overall, the finding that 27 dietary anthocyans are not inducers of human CYP2A6, CYP2B6,

dx.doi.org/10.1021/jf404643w | J. Agric. Food Chem. 2014, 62, 789−797

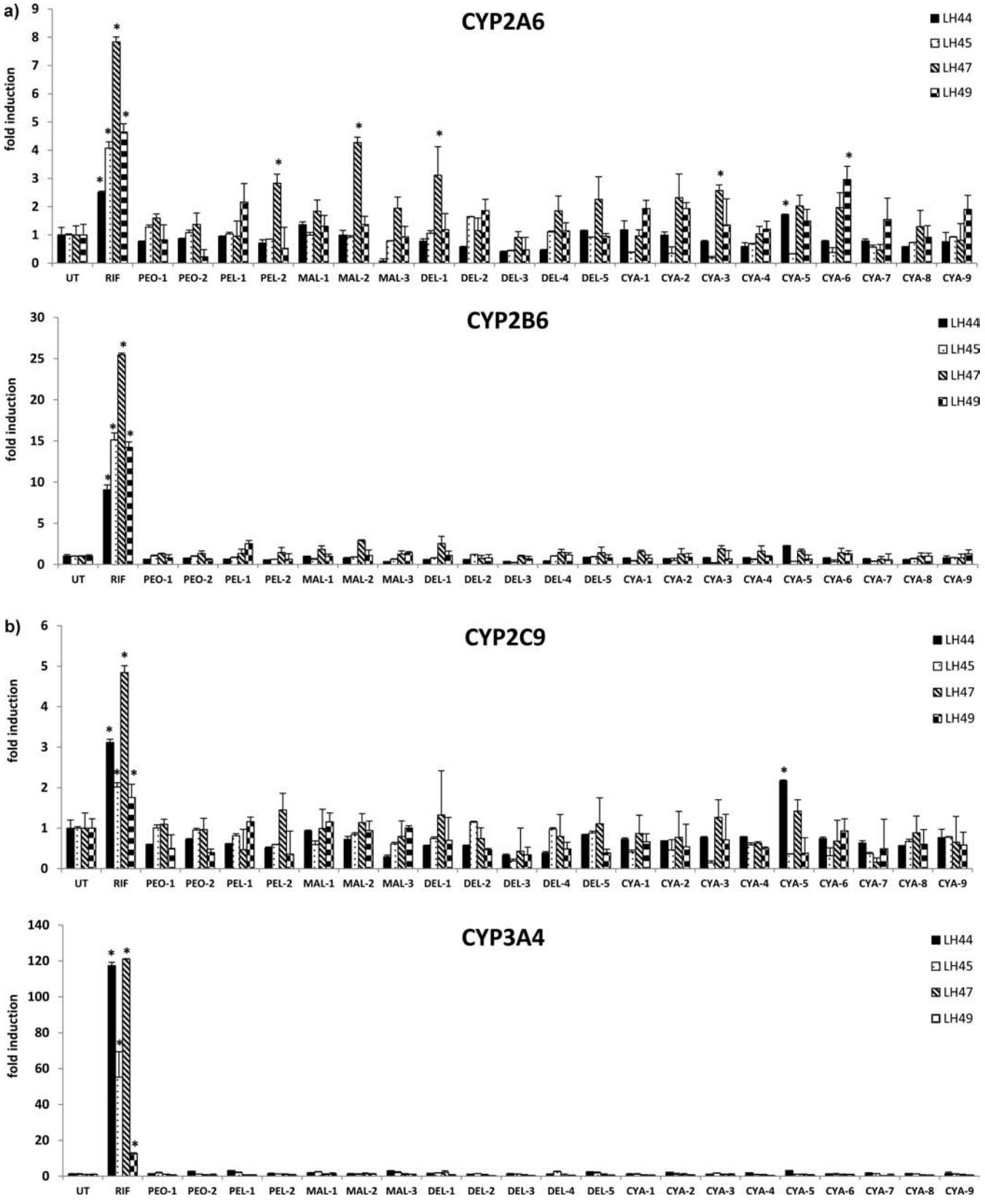

Figure 3. Effects of anthocyanins on the expression of CYP2A6, CYP2B6, CYP2C9, and CYP3A4 mRNAs in human hepatocytes. Primary human hepatocytes cultures (LH44, LH45, LH47, LH49) were incubated for 24 h with 21 different anthocyanins (for details see Materials and Methods), each at a concentration of 50 μM, rifampicin (10 μM), and DMSO (0.1% v/v) as a vehicle for control. Bar graphs show RT-PCR analyses of CYP2A6, CYP2B6, CYP2C9, and CYP3A4 mRNAs. The data are the mean from triplicate measurements and are expressed as a fold-induction as compared to DMSO-treated cells. The data were normalized per GAPDH mRNA levels. ∗, value is significantly different from DMSO-treated cells ($p < 0.05$) as determined by Student's t test.

dx.doi.org/10.1021/jf404643w | J. Agric. Food Chem. 2014, 62, 789−797

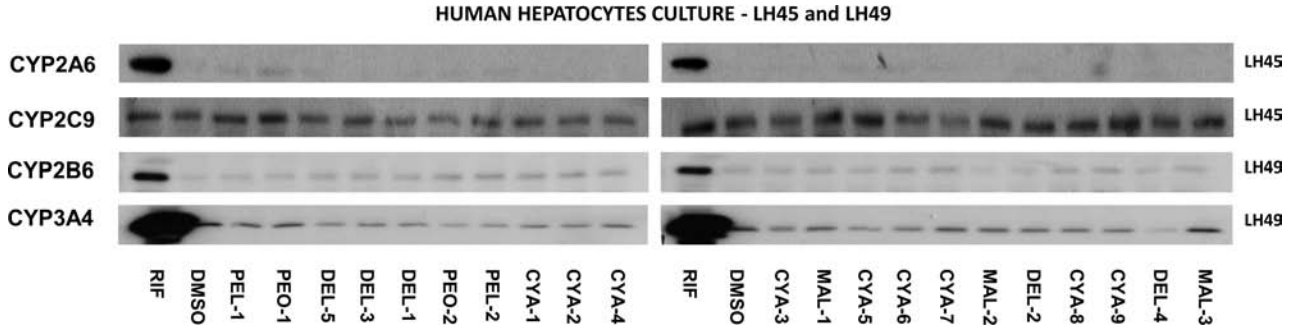

Figure 4. Effects of anthocyanins on the expression of CYP2A6, CYP2B6, CYP2C9, and CYP3A4 proteins in human hepatocytes. Primary human hepatocytes cultures (LH44, LH45, LH47, LH49) were incubated for 48 h with 21 different anthocyanins (for details see Materials and Methods), each at a concentration of 50 μM, rifampicin (10 μM), and DMSO (0.1% v/v) as a vehicle for control. Representative Western blots show analyses of CYP2A6, CYP2B6, CYP2C9, and CYP3A4 proteins in human hepatocytes cultures LH45 and LH49. Similar profiles were observed in cultures LH44 and LH47. As a loading control, the blots were probed to β-actin (data not shown).

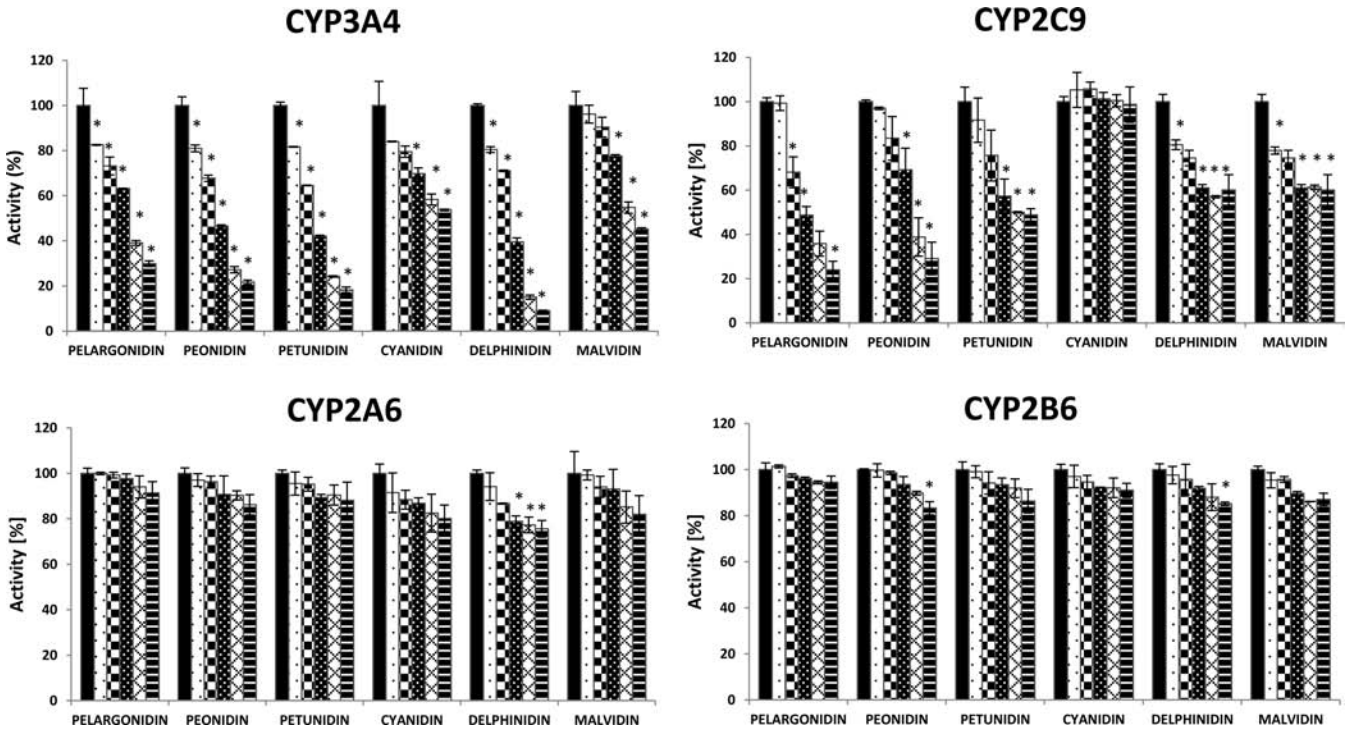

Figure 5. Effects of anthocyanidins on catalytic activities of CYP2A6, CYP2B6, CYP2C9, and CYP3A4 proteins in human liver microsomes. Inhibition of catalytic activities is expressed as the activity remaining relative to control (100%, without anthocyanidin) in percent. Concentration of respective anthocyanidins in the reaction mixture was 0, 10, 20, 40, 80, and 100 μM. For experimental details, see Materials and Methods. *, value significantly different from control ($p < 0.05$).

CYP2C9, and CYP3A4 is of positive value, with regard to massive use of anthocyan-containing foods and products in alimentation and herbal medicine.

However, the anthocyans were able to inhibit the marker activities of CYP enzymes to a significant extent. In particular, CYP3A4 activity was inhibited by all anthocyanidins tested and at least with two anthocyanins (CYA-6 and DEL-2) to 25 and 35% at 100 μM, respectively. In other cases, the decrease of enzyme activity has exceed 50% only exceptionally, as in case of CYP2C9 with pelargonidin and peonidin (25−30% at 100 μM) and to 40% with cyanidin glycoside (CYA-6).

Interestingly, the ability of anthocyanidins to inhibit an enzyme activity is not directly reflected in properties of corresponding anthocyanins. For example, it is the delphinidin that inhibits the CYP3A4 enzyme activity the most (Figure 5), but the most prominent inhibition of the same activity was observed with a cyanidin glycoside (CYA-6). However, cyanidin aglycon (i.e., the anthocyanidin) inhibited the CYP to a much lesser extent (Figure 5). Hence, it seems that the ability of an anthocyanin to inhibit a particular CYP enzyme is given by the molecule as a whole; in other words, it cannot be simply derived from the property of the respective aglycon (anthocyanidin). The fact that it is the activity of CYP3A4 that is influenced the most by an interaction with an anthocyan molecule is clearly in line with the relative openness, accessibility, and flexibility of the active site of this enzyme, which is known to accommodate molecules with different sizes and properties.[19−21] The most important question is the relevance of these interactions to human nutrition. The concentrations of anthocyans and anthocyanidins as well as anthocyanins in plasma may reach the micromolar range after ingestion of tens of milligrams of fruit. However, the level may

dx.doi.org/10.1021/jf404643w | J. Agric. Food Chem. 2014, 62, 789−797

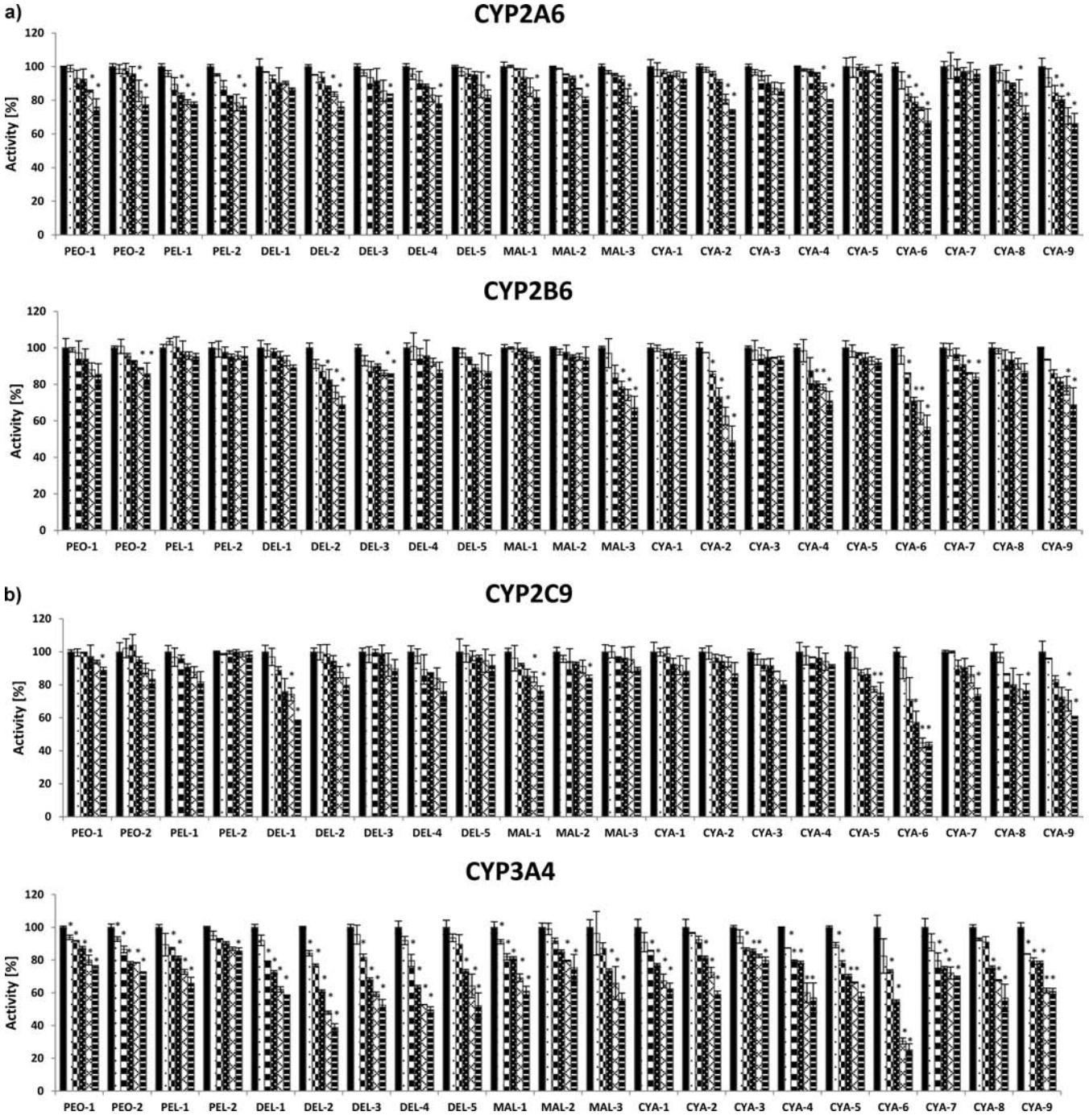

Figure 6. Effects of anthocyanins on catalytic activities of CYP2A6, CYP2B6, CYP2C9, and CYP3A4 proteins in human liver microsomes. Inhibition is expressed as in Figure 5; for abbreviations, see Compounds and Reagents. Anthocyanin concentrations were 0, 10, 20, 40, 80, and 100 μM. $*$, value significantly different from control ($p < 0.05$).

be much higher when a dietary supplement is taken or, more generally, at the site of action. However, it may be concluded that, in the ranges of common ingestion of either food or a dietary supplement, an induction or significant inhibition of, for example, CYP3A4 activity is most probably not expected.

AUTHOR INFORMATION

Corresponding Authors

*(Z.D.) E-mail: moulin@email.cz. Phone: +420-58-5634903. Fax: +420-58-5634901.

*(E.A.) E-mail: eva.anzenbacherova@upol.cz. Phone: +420-58-5632321. Fax: +420-58-5632302.

Author Contributions

#A.S., M.S., and M.K.Z. contributed equally.

Funding

Our laboratories are supported by Grant GACR 303/12/G163 from the Grant Agency of the Czech Republic, by a grant from the Czech Ministry of Health, IGA NT/13591, Operational Program Research and Development for Innovations - European Regional Development Fund (CZ.1.05/2.1.00/03.0058), and by student grants from Palacky University Olomouc, PrF-2013-002

and LF-2013-007. The infrastructural part of this work has been supported by Project CZ.1.05/2.1.00/01.0030 (BIOMEDREG).

Notes

The authors declare no competing financial interest.

■ ABBREVIATIONS USED

AhR, aryl hydrocarbon receptor; CAR, constitutive androstane receptor; CYP, cytochrome P450; ER, estrogen receptor; FXR, farnesoid X receptor; GR, glucocorticoid receptor; LXR, liver X receptor; PXR, pregnane X receptor; RARs, retinoic acid receptors; RXRs, retinoid X receptors; VDR, vitamin D receptor

■ REFERENCES

(1) Kong, J. M.; Chia, L. S.; Goh, N. K.; Chia, T. F.; Brouillard, R. Analysis and biological activities of anthocyanins. *Phytochemistry* **2003**, *64*, 923−933.

(2) Castaneda-Ovando, A.; Pacheco-Hernandez, M. D.; Paez-Hernandez, M. E.; Rodriguez, J. A.; Galan-Vidal, C. A. Chemical studies of anthocyanins: a review. *Food Chem.* **2009**, *113*, 859−871.

(3) Galvano, F.; La Fauci, L.; Lazzarino, G.; Fogliano, V.; Ritieni, A.; Ciappellano, S.; Battistini, N. C.; Tavazzi, B.; Galvano, G. Cyanidins: metabolism and biological properties. *J. Nutr. Biochem.* **2004**, *15*, 2−11.

(4) Zhang, Y.; Vareed, S. K.; Nair, M. G. Human tumor cell growth inhibition by nontoxic anthocyanidins, the pigments in fruits and vegetables. *Life Sci.* **2005**, *76*, 1465−1472.

(5) Tsuda, T. Dietary anthocyanin-rich plants: biochemical basis and recent progress in health benefits studies. *Mol. Nutr. Food Res.* **2012**, *56*, 159−170.

(6) Kaume, L.; Howard, L. R.; Devareddy, L. The blackberry fruit: a review on its composition and chemistry, metabolism and bioavailability, and health benefits. *J. Agric. Food Chem.* **2012**, *60*, 5716−5727.

(7) Fernandes, I.; Faria, A.; Azevedo, J.; Soares, S.; Calhau, C.; De Freitas, V.; Mateus, N. Influence of anthocyanins, derivative pigments and other catechol and pyrogallol-type phenolics on breast cancer cell proliferation. *J. Agric. Food Chem.* **2010**, *58*, 3785−3792.

(8) Shih, P. H.; Yeh, C. T.; Yen, G. C. Effects of anthocyanidin on the inhibition of proliferation and induction of apoptosis in human gastric adenocarcinoma cells. *Food Chem. Toxicol.* **2005**, *43*, 1557−1566.

(9) Kamei, H.; Hashimoto, Y.; Koide, T.; Kojima, T.; Hasegawa, M. Anti-tumor effect of methanol extracts from red and white wines. *Cancer Biother. Radiopharm.* **1998**, *13*, 447−452.

(10) Deguchi, T.; Yoshimoto, M.; Ohba, R.; Ueda, S. Antimutagenicity of the purple pigment, hordeumin, from uncooked barley bran-fermented broth. *Biosci., Biotechnol., Biochem.* **2000**, *64*, 414−416.

(11) Ghiselli, A.; Nardini, M.; Baldi, A.; Scaccini, C. Antioxidant activity of different phenolic fractions separated from an Italian red wine. *J. Agric. Food Chem.* **1998**, *46*, 361−367.

(12) Espin, J. C.; Soler-Rivas, C.; Wichers, H. J.; Garcia-Viguera, C. Anthocyanin-based natural colorants: a new source of antiradical activity for foodstuff. *J. Agric. Food Chem.* **2000**, *48*, 1588−1592.

(13) Wang, J.; Mazza, G. Inhibitory effects of anthocyanins and other phenolic compounds on nitric oxide production in LPS/IFN-γ-activated RAW 264.7 macrophages. *J. Agric. Food Chem.* **2002**, *50*, 850−857.

(14) Kamenickova, A.; Anzenbacherova, E.; Pavek, P.; Soshilov, A. A.; Denison, M. S.; Anzenbacher, P.; Dvorak, Z. Pelargonidin activates the AhR and induces CYP1A1 in primary human hepatocytes and human cancer cell lines HepG2 and LS174T. *Toxicol. Lett.* **2013**, *218*, 253−259.

(15) Kamenickova, A.; Anzenbacherova, E.; Pavek, P.; Soshilov, A. A.; Denison, M. S.; Zapletalova, M.; Anzenbacher, P.; Dvorak, Z. Effects of anthocyanins on the AhR-CYP1A1 signaling pathway in human hepatocytes and human cancer cell lines. *Toxicol. Lett.* **2013**, *221*, 1−8.

(16) Vrzal, R.; Knoppova, B.; Bachleda, P.; Dvorak, Z. Effects of oral anorexiant sibutramine on the expression of cytochromes P450s in human hepatocytes and cancer cell lines. *J. Biochem. Mol. Toxicol.* **2013**, *27*, 515−521.

(17) Chang, T. K.; Waxman, D. J. Catalytic assays for human cytochrome P450: an introduction. *Methods Mol. Biol.* **2006**, *320*, 73−83.

(18) Monostory, K.; Dvorak, Z. Steroid regulation of drug-metabolizing cytochromes P450. *Curr. Drug Metab.* **2011**, *12*, 154−172.

(19) Anzenbacherova, E.; Bec, N.; Anzenbacher, P.; Hudecek, J.; Soucek, P.; Jung, C.; Munro, A. W.; Lange, R. Flexibility and stability of the structure of cytochromes P450 3A4 and BM-3. *Eur. J. Biochem./FEBS* **2000**, *267*, 2916−2920.

(20) Ekroos, M.; Sjogren, T. Structural basis for ligand promiscuity in cytochrome P450 3A4. *Proc. Natl. Acad. Sci. U.S.A.* **2006**, *103*, 13682−13687.

(21) Hendrychova, T.; Anzenbacherova, E.; Hudecek, J.; Skopalik, J.; Lange, R.; Hildebrandt, P.; Otyepka, M.; Anzenbacher, P. Flexibility of human cytochrome P450 enzymes: molecular dynamics and spectroscopy reveal important function-related variations. *Biochim. Biophys. Acta* **2011**, *1814*, 58−68.

JOURNAL OF AGRICULTURAL AND FOOD CHEMISTRY

Article

pubs.acs.org/JAFC

Lipid Rafts and *Fas*/*FasL* Pathway May Involve in Elaidic Acid-Induced Apoptosis of Human Umbilical Vein Endothelial Cells

Huan Rao,[†] Li-Xin Ma,[‡] Ting-Ting Xu,[†] Jing Li,[†] Ze-Yuan Deng,*[,†] Ya-Wei Fan,[†] and Hong-Yan Li[†]

[†]State Key Laboratory of Food Science and Technology, Institute for Advanced Study, Nanchang University, Nanchang, Jiangxi 330047, P.R. China

[‡]Institute of Chronic and Noncommunicable Disease Control and Prevention, Shijiazhuang Center for Disease Control and Prevention, Shijiazhuang, Hebei 050019, P.R. China

ABSTRACT: Our previous study showed that *trans*-fatty acids can cause apoptosis of endothelial cells through the caspase pathway and the mitochondrial pathway. The objective of this study was to explore how *trans*-fatty acids activate the caspase pathway, whether there exist specific receptors induced apoptosis by comparing normal cells and non-rafts cells treated with elaidic acid (9*t*18:1) and oleic acid (9*c*18:1), respectively. Compared to normal cells treated with 9*t*18:1, the cell viability increased by 13% and the number of apoptotic cells decreased by 3% in non-rafts cells treated with 9*t*18:1 ($p < 0.05$), and the expression levels of pro-apoptotic proteins such as caspase-3, -8, -9, Bax, and Bid decreased, and expression of antiapoptotic protein Bcl-2 increased ($p < 0.05$). In addition, *Fas*/*FasL* expression in cell membrane decreased significantly ($p < 0.05$). In conclusion, the lipid rafts and *Fas*/*FasL* pathway may involve in 9*t*18:1-induced apoptosis of human umbilical vein endothelial cells.

KEYWORDS: *trans-fatty acid, lipid raft, human umbilical vein endothelial cells, receptor, apoptosis*

INTRODUCTION

trans-Fatty acids (TFAs) have been reported to promote vascular diseases mainly by promoting apoptosis and inflammation of vascular endothelial cells (ECs).[1] Excessive apoptosis of ECs is the start of endothelial dysfunction and the development of cardiovascular disease. Epidemiological and animal studies have shown that a high intake of TFAs raise the level of serum low-density lipoprotein (LDL) and triglyceride (TG) and cause vascular endothelial injury. It can also increase expression of the soluble intercellular adhesion molecule (SICAM)-1, soluble vascular cell adhesion molecule (SVCAM)-1, and E-selectin, which are important mediators in the process of inflammation.[2] TFAs induce endothelial cell apoptosis through the caspase pathway[3] and promote release of endothelial inflammatory cytokines.[1] However, it is unknown how the pathway is activated and whether there exist specific receptors at the cell membranes.

Over the past decade, many studies have shown the existence of particular microdomains at the cell membranes: lipid rafts, which are rich in cholesterol and sphingolipids and play many important roles in cell signal transduction.[4,5] Apoptosis is a genetically controlled mechanism of cell death and can be mediated by the death receptor pathway as well as the mitochondrial pathway.[6] There are a number of membrane receptors and channels located in lipid rafts which promote apoptosis when activated.[7] Caveolin-1 is a main protein which exhibits several functional domains in which the caveolin scaffolding domain involves in signaling pathways by the interaction with proteins.[8]

There have been few references about the relationship between lipid rafts and TFAs based on our knowledge. However, several studies have shown that polyunsaturated fatty acids, such as eicosapentaenoic acid (EPA) and docosahexaenoic acid (DHA), can change the component of lipid rafts.[9−11] DHA was also found to change the lipid rafts regulation of interleukin receptor signaling pathway.[12,13] n-3 polyunsaturated fatty acids regulated downstream signaling, activation of T cells, activation of transcription, and secretion of cytokines by changing the structure of lipid rafts, which provided evidence for n-3 polyunsaturated fatty acids in the prevention of colon cancer.[14] Iwona et al.[15] reported that 9*c*11*t*-conjugated linoleic acid (CLA) changed cell membrane structure and then interfered with intracellular transport of epidermal growth factor receptor and its related signaling pathway, both functionally associated with lipid raft properties. Therefore, we supposed that TFAs as a kind of fatty acids might have similar connection with lipid rafts. It is interesting to know if TFAs alter vascular cell lipid rafts and stimulate cell membrane receptor proteins and activate downstream signaling pathways in the process of cell dysfunction. The aim of this study was to determine whether lipid rafts play a key role in cell dysfunction caused by TFAs and its receptor proteins activate caspase pathway.

MATERIALS AND METHODS

Chemicals and Reagents. Dulbecco Modified Eagles Medium (DMEM) and fetal bovine serum (FBS) were obtained from Gibco Life Technologies (Carlsbad, USA). Anti-p21, anti-cyclin-dependent kinase (CDK) 4, anti-CDK2, anti-cyclinD1, and anticaspase-3, -8, and -9 antibodies were purchased from Santa Cruz Biotechnology (Santa Cruz, USA). Anti-p53, anti-Bax, and anti-Bcl-2 antibodies were obtained from Anbo Biotechnology (California, USA). Methyl-β-

Received: October 28, 2013
Revised: December 23, 2013
Accepted: December 23, 2013
Published: December 23, 2013

ACS Publications © 2013 American Chemical Society

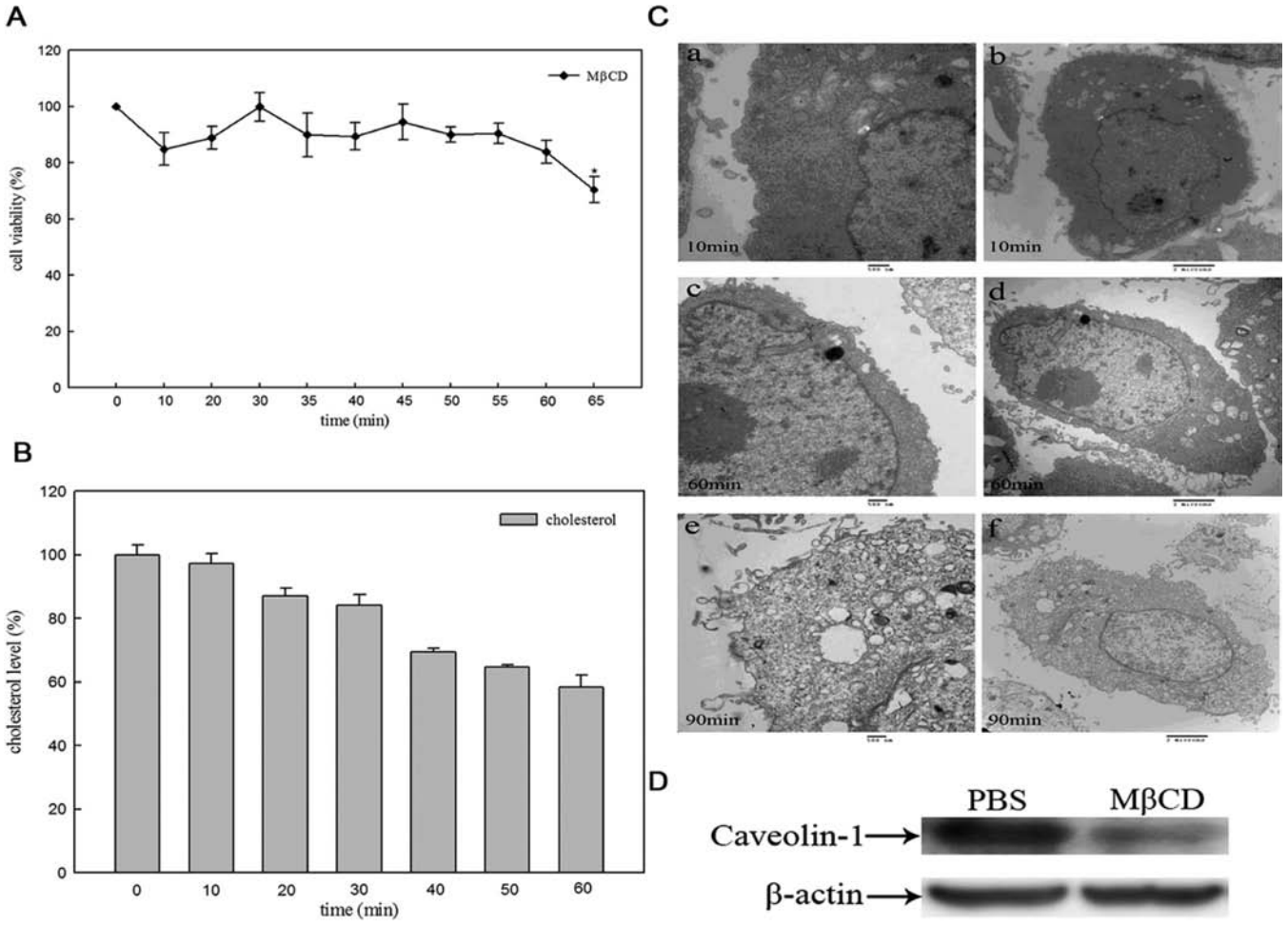

Figure 1. The reasonable time for HUVECs treated with MβCD. (A) Effects of MβCD on HUVECs viability in different time points. HUVECs were treated with 10 mM MβCD in 10, 20, 30, 35, 40, 45, 50, 55, 60, and 65 min. Data are expressed as the mean of five individual experiments ± SD * $p < 0.05$. (B) The levels of cholesterol in cell membrane on different MβCD action time. Cholesterol levels were negatively correlated with the time. (C) The ultrastructure of HUVEC observed by transmission electron microscope after treatment with MβCD for 10, 60, and 90 min: (a) 10 min (magnification of 25000×), (b) 10 min (magnification of 12000×), (c) 60 min (magnification of 20000×), (d) 60 min (magnification of 12000×), (e) 90 min (magnification of 20000×), (f) 90 min (magnification of 8000×). (D) Western blot analysis of caveolin-1 before and after MβCD treatment for 50 min.

cyclodextrin (MβCD) was from Aladdin (Shanghai, China). Elaidic and oleic acid (98.5% purity) were purchased from Sigma (Boston, USA). All other chemicals were of reagent grade or better.

Cell Culture and TFA Treatment. Human umbilical vein endothelial cells (HUVECs, College of Medical Sciences, Nanchang University) were maintained in DMEM supplemented with 10% fetal bovine serum, 1% penicillin, and 1% streptomycin at 37 °C in a humidified atmosphere of 5% CO_2 and 90% air. The cells were divided into six groups: control group (treated with 0.1 M PBS), elaidic acid group (treated with 100 μmol/L 9*t*18:1 for 24 h), oleic acid group (treated with 100 μmol/L 9*c*18:1 for 24 h), MβCD group (treated with 10 mmol/L MβCD), MβCD + elaidic acid group (incubated with 100 μmol/L9*t*18:1 for 24 h after treated with 10 mmol/L MβCD), and MβCD + oleic acid group (incubated with 100 μmol/L 9*c*18:1 for 24 h after treated with 10 mmol/L MβCD).

Cytotoxicity Assay of MβCD. HUVECs in logarithm period were seeded at a density of 2×10^4–5×10^4 cells/ml into 96-well microculture plates after centrifugation and were cultured at 37 °C in humidified air with 5% CO_2. HUVECs were treated with 10 mmol/L MβCD for 10, 20, 30, 40, 45, 50, 55, 60, and 65 min, respectively, and then 20 μL methyl thiazol tetrazolium (MTT) solution (5 mg/mL) was added to each well and incubated at 37 °C in humidified air with 5% CO_2 for 4 h. Afterward, the medium with MTT was removed, 150 μL dimethyl sulfoxide (DMSO) was added into each well, and after shaking the plates for about 10 min, the cell pellet was resuspended. Detection and quantification of the formazan crystals was performed by a micro plate reader (Thermo, Finland) at 490 nm.

Assay of Cholesterol Efflux. To investigate the effect of 10 mmol/L MβCD on cholesterol level in cell membranes, a cholesterol assay kit (Ke Da Hong Wei, Beijing, China) was used to detect the cholesterol level in cell membranes after being treated with MβCD for different times following the instruction of the manufacturer. Cholesterol ester was decomposed into free cholesterol by cholesterol esterase, and free cholesterol was oxidized by cholesterol oxidase. Hydrogen peroxide was generated during the reaction and catalyzed by peroxidase. Chromogenic substance has a maximum absorption peak at 550 nm.

Observation of HUVECs with Transmission Electron Microscope. After HUVECs were treated with 10 mmol/L MβCD for 10, 60, and 90 min, respectively. Cells were collected and fixed with 2.5% glutaraldehyde overnight. After washed in 0.1 M PBS (3 × 5 min), the cells were post fixed with 1% OsO4 for 1 h, followed by dehydration with a graded acetone series (30, 70, 90, and 2 × 100%, each for 30 min). The specimens were then embedded in resin and polymerized at 35 °C for 24 h and 60 °C for 12 h. The specimens were cut by an ultrathin microtome. The sections were collected on copper grids, stained with 0.5% lead citrate for 10 min, and rinsed with water. The

dx.doi.org/10.1021/jf404834e | J. Agric. Food Chem. 2014, 62, 798–807

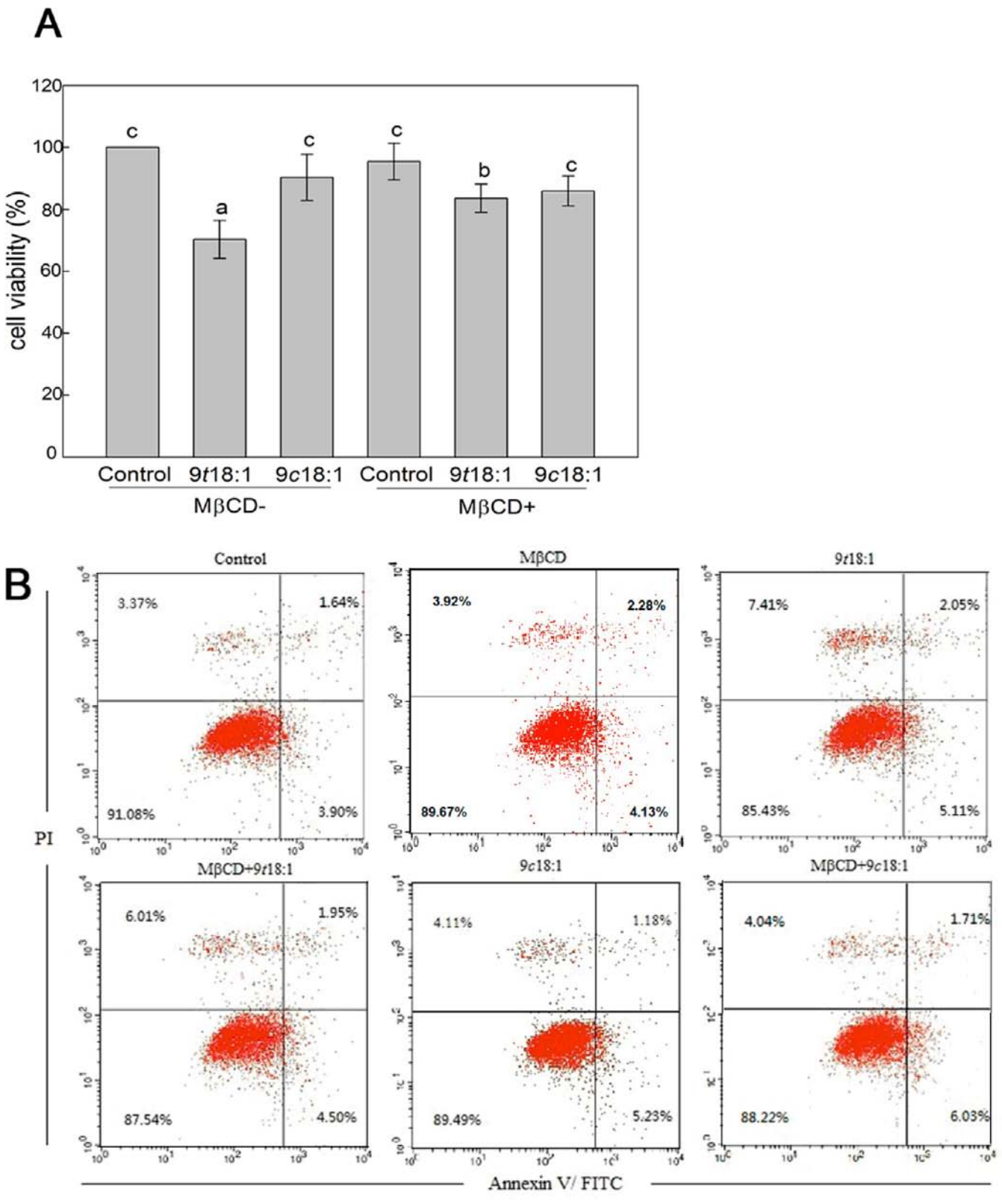

Figure 2. continued

dx.doi.org/10.1021/jf404834e | J. Agric. Food Chem. 2014, 62, 798−807

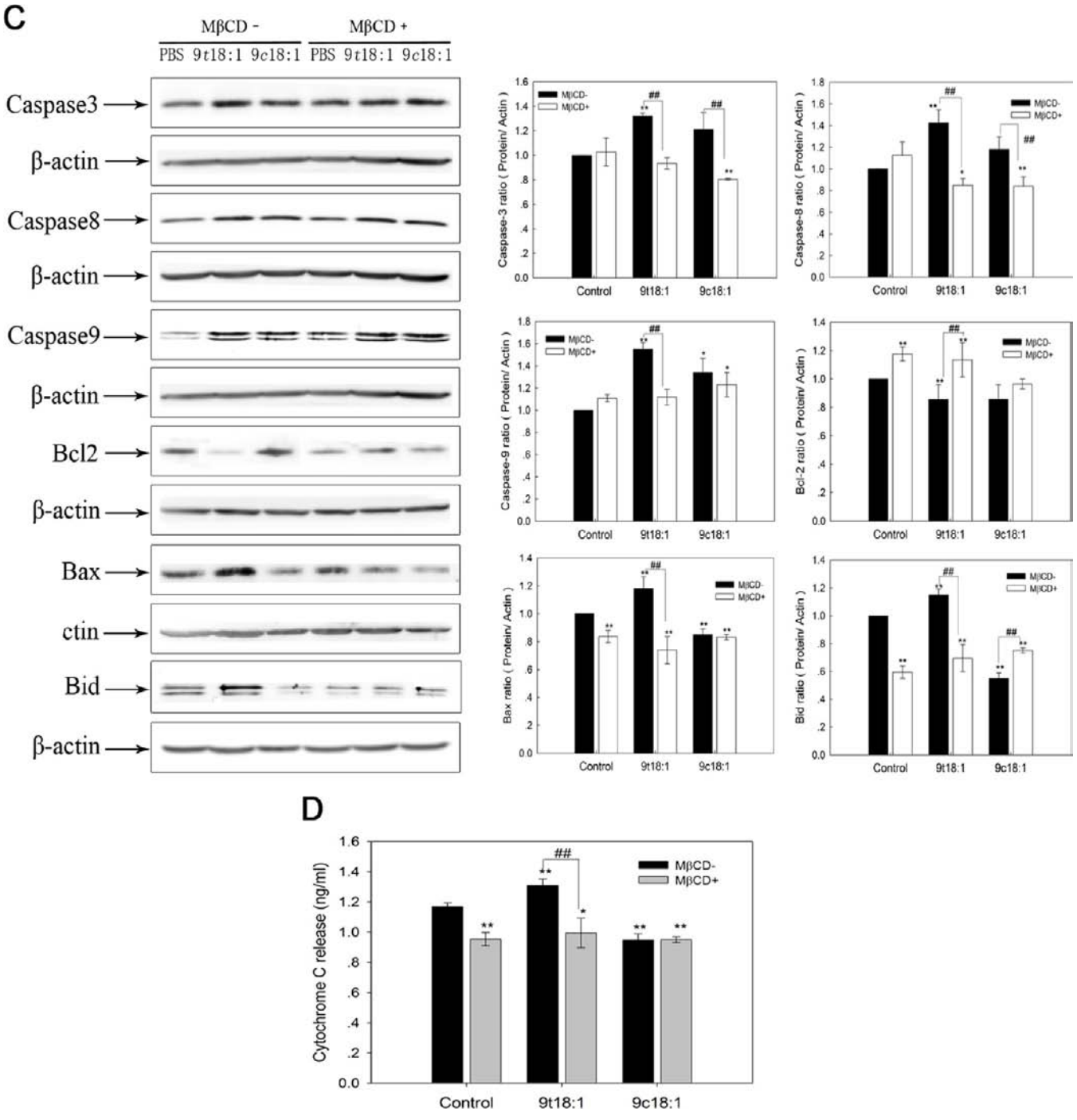

Figure 2. Effect of TFA on apoptosis of MβCD treated or nontreated HUVECs. (A) The effect of 9*t*18:1 and 9*c*18:1 on viability of MβCD treated and nontreated HUVECs. HUVECs were treated or nontreated with MβCD for 50 min and then cultured with 9*t*18:1 or 9*c*18:1 for 24 h. (B) Apoptosis detection by flow cytometry. Cells were treated as (A) labeled with PI and Annexin V-FITC and then were analyzed by flow cytometry. The histograms represent the data obtained by flow cytometry. In upper quadrants: right, percentage of cells labeled with PI; left, percentage of cells labeled with PI and Annexin V. In lower quadrants: right, percentage of cells labeled with Annexin V; left, percentage of viable cells. (C) Western blot analysis of caspase-3, -8, -9, Bcl-2, Bax, and Bid in different groups. (D) Cytochrome C release rate with different treatments detected by ELISA kit. Data are expressed as the mean of 3−5 individual experiments ± SD * $p < 0.05$, ** $p < 0.01$, compared with the control group. # $p < 0.05$, ## $p < 0.01$, 9*t*18:1 group compared with the MβCD + 9*t*18:1 group, 9*c*18:1 group compared with the MβCD + 9*c*18:1 group.

images of these sections were made by transmission electron microscope.

Cell Viability Assay. Briefly, at the end of the incubation, the media were removed and MTT added in each well for 4 h incubation. Then DMSO was added and shaken gently for 10 min so that the precipitation was completely dissolved. Absorbance was recorded at 490 nm using a micro plate reader (Spectra max190, Molecular Devices, California).

Apoptosis Detection by Flow Cytometry. Cells were collected from each group and 100 μL of binding buffer added to suspend the cells. The cells were then collected by centrifugation and washed twice with PBS. Then 5 μL of fluorescein isothiocyanate (FITC) and 5 μL of propidium iodide (PI) were added to the mixture and incubated in the

dx.doi.org/10.1021/jf404834e | J. Agric. Food Chem. 2014, 62, 798−807

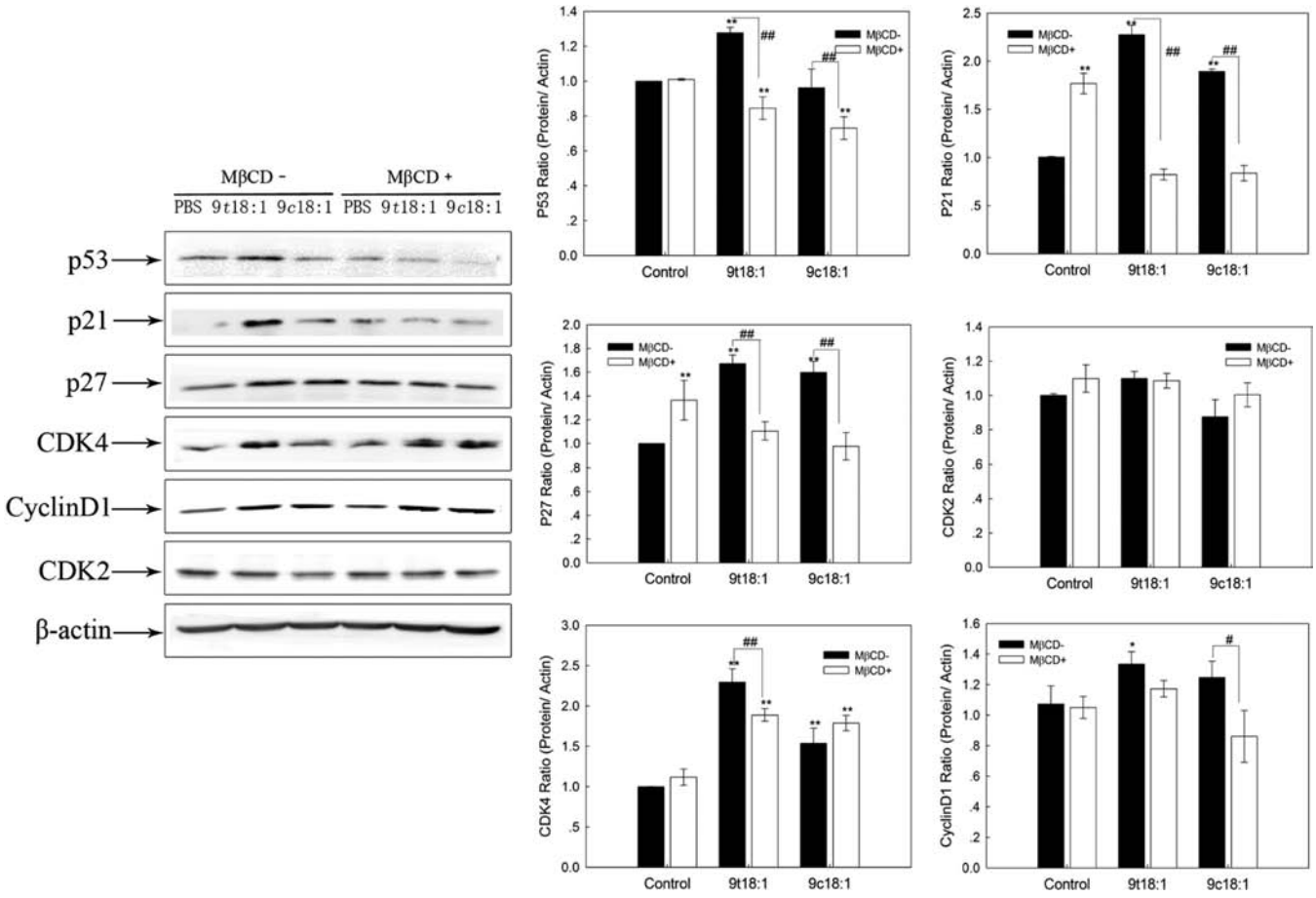

Figure 3. Western blot analysis of p53, p21, p27, CDK4, CyclinD1, and CDK2. Data are expressed as the mean of three individual experiments ± SD * $p < 0.05$, ** $p < 0.01$, compared with the control group. # $p < 0.05$, ## $p < 0.01$, 9*t*18:1 group compared with the M*β*CD + 9*t*18:1 group, 9*c*18:1 group compared with the M*β*CD + 9*c*18:1 group.

dark for 10−15 min at room temperature. Apoptosis of the cells was detected by flow cytometry within 1 h after the addition of 500 μL of binding buffer.

Western Blot Analysis of Apoptosis-Related Proteins. Total cell lysates were extracted by RIPA buffer on ice. After centrifugation at 20000*g* for 15 min, supernatant was taken and stored at −70 °C until use. Protein (80 μg) was mixed with loading buffer and denatured by boiling for 5 min. The proteins were separated by SDS-PAGE and then transferred to a nitrocellulose membrane. After blocking with 5% nonfat milk, membranes were then incubated with anticaspase-3, -8, and -9, anti-Bcl_2, anti-Bax, and anti-Bid antibodies overnight at 4 °C, followed by incubation with horseradish peroxidase-conjugated secondary antibodies at room temperature for 1 h. Finally, protein bands were visualized by enhanced chemiluminescence (ECL) detection system (Kang Wei, Beijing, China).

Immunofluorescence of Fas. Briefly, cells were fixed with 4% paraformaldehyde for 15 min and 0.5% Triton X-100 in PBS for 20 min. Cells were blocked with goat serum for 1 h and then incubated overnight at 4 °C with anti-Fas antibody (1:100). Subsequently, cells were incubated with goat antirabbit FITC antibody (1:200) for 1 h at room temperature and incubated with 40, 6-diamidino-2-phenylindole (DAPI), to label nuclei, for 5 min in a dark space. Images were acquired with a fluorescence microscope (Olympus, Japan).

Measurement of Cytochrome C Level. Treated cells were washed with cold PBS twice and homogenized in cold lysis buffer containing 1 mmol/L DTT and 0.5 mmol/L PMSF on ice for 40 min and then centrifuged at 10000 rpm at 4 °C for 2 min. The supernatants were used for the measurement of cytochrome C using ELISA kit (Senxiong Biotechnology, Shanghai, China).

Determination of Fatty Acids by Gas Chromatography. Total lipids were extracted from $4-6 \times 10^7$ cells using chloroform/methanol (1:1, v:v). Fatty acids were then methylated using sodium methoxide and analyzed by a gas chromatograph equipped with a flame ionization detector (model 6890 N, Agilent Technologies, Shanghai, China). Peaks were identified by their retention times relative to standards FAME mixture (no. 463).

Statistical Analysis. Data are expressed as mean ± SD. Statistical analysis was performed by one-way ANOVA followed by Student's *t*-test using SPSS.15.0 software. $p < 0.05$ was indicative of significant difference.

RESULTS

Treatment Time of M*β*CD in HUVECs. M*β*CD is a time-dependent reagent which could extract cholesterol of cell and perturb the function of lipid rafts. The reasonable treatment time of M*β*CD (10 mmol/L) in HUVECs without cytotoxicity should be determined. As shown in Figure 1 A, cell viability decreased by 30% within 65 min treatment. Cholesterol levels (Figure 1B) dropped to 60% after treatment with M*β*CD for 1 h. Although the longer the treatment time with M*β*CD and the better extract efficiency of cholesterol, cells membranes were more seriously damaged with the increased treatment time. As shown in Figure 1C, there was almost no injury to the cells when the treatment times were less than 60 min, but obvious damages were found after 60 min, such as morphological changes, cytoplasm leakage, and increased cavities. To ensure the normal physiological conditions of cells, the reasonable

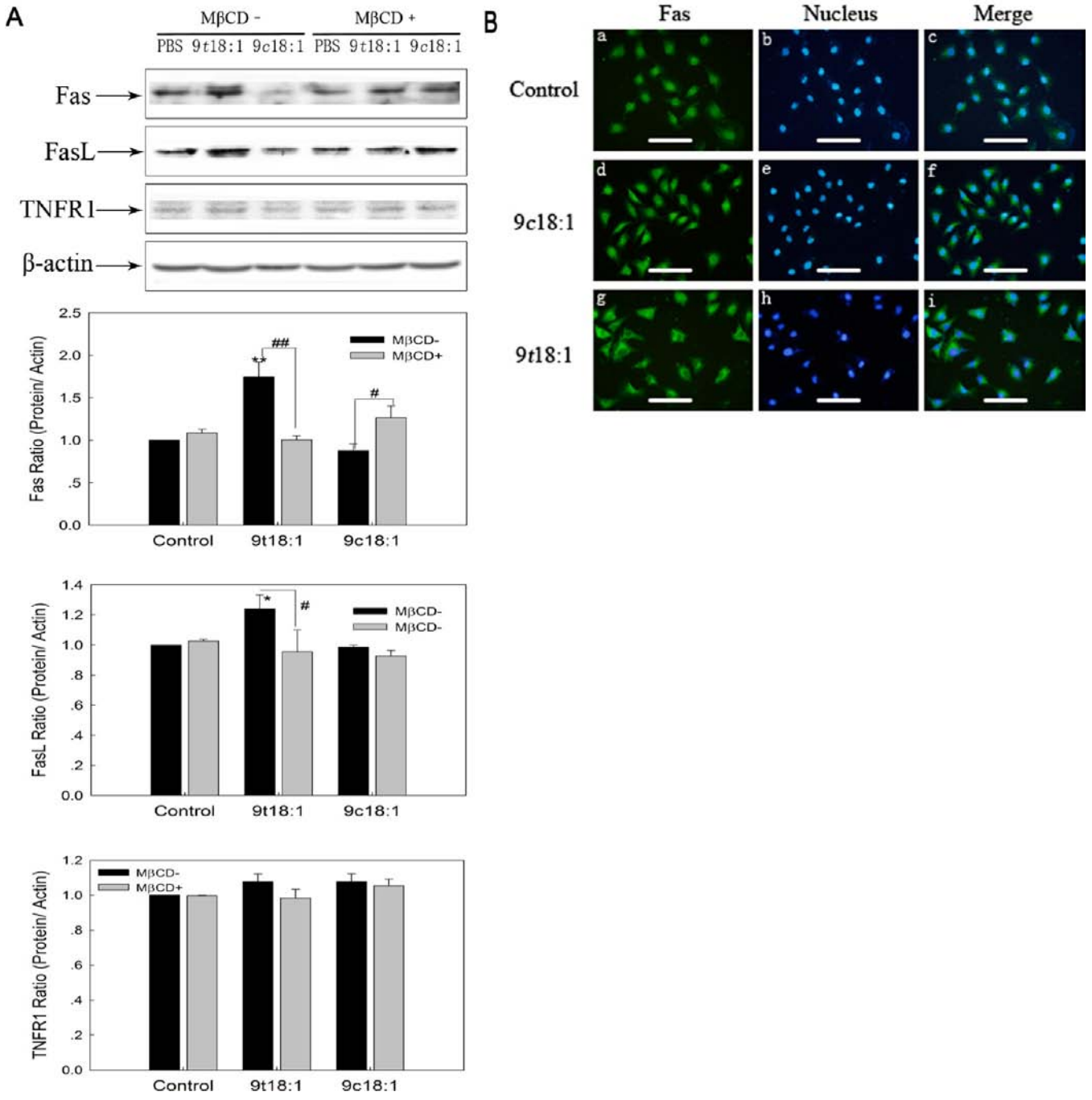

Figure 4. (A) The expression of Fas and its ligand (FasL). Data are expressed as the mean of three individual experiments ± SD * $p < 0.05$, ** $p < 0.01$, compared with the control group. # $p < 0.05$, ## $p < 0.01$, 9*t*18:1 group compared with the M*β*CD + 9*t*18:1 group, 9*c*18:1 group compared with the M*β*CD + 9*c*18:1 group. (B) Visualization of Fas in HUVECs. Micrographs show the Fas (light green), nucleus (light blue), and the overlapping of images (merge) of the studied cells.

treatment time of M*β*CD should be within 60 min. We also examined the effect of M*β*CD on lipid rafts in 50 min by determining the expression of cavelin-1, one of important makers of lipid rafts. A significant decrease in cavelin-1 expression was observed (Figure 1D). The results suggest that M*β*CD may interrupt the function of lipid rafts.

Effect of M*β*CD on TFA-Induced Apoptosis of HUVECs. MTT assay and flow cytometry were performed to examine the effect of TFA on cell viability and apoptosis of HUVECs. The cell viability rate in M*β*CD + elaidic acid group increased significantly (from 70% to 84%), and the M*β*CD + oleic acid group had no obvious changes (Figure 2A). In the M*β*CD treated groups, the number of apoptotic cells which incubated with 9*t*18:1 dropped significantly by nearly 3% (the early apoptosis decreased from 5.11% to 4.50% and late apoptosis dropped to 1.5%), while the apoptotic cells of 9*c*18:1 group slightly increased when compared with non-M*β*CD treated group (Figure 2B).

To determine whether lipid rafts play an important role in cell apoptosis after TFA supplementation, we compared the expression levels of apoptosis-related proteins between M*β*CD treated and nontreated cells. In the M*β*CD + elaidic acid group,

dx.doi.org/10.1021/jf404834e | J. Agric. Food Chem. 2014, 62, 798−807

Table 1. Effect of Different Treatments on Fatty Acid Composition of HUVECs[a]

	% of total fatty acids					
fatty acids in lipid fractions	control	MβCD	elaidic acid	MβCD + elaidic acid	oleic acid	MβCD + oleic acid
∑SFA	31.58 ± 0.12[c]	33.34 ± 4.76[c]	21.13 ± 0.20[a]	19.03 ± 0.72[a]	23.97 ± 0.33[b]	24.82 ± 0.07[b]
∑cisMUFA	54.29 ± 0.12[b]	53.59 ± 3.00[b]	42.14 ± 0.06[a]	42.99 ± 0.47[a]	66.36 ± 0.41[c]	64.48 ± 1.17[c]
∑PUFA	13.60 ± 0.00[b]	12.45 ± 1.78[b]	8.52 ± 0.36[a]	9.00 ± 0.35[a]	9.16 ± 0.01[a]	10.24 ± 1.24[a]
∑TFA	0.53 ± 0.01[a]	0.62 ± 0.02[a]	28.21 ± 0.62[b]	28.98 ± 0.84[b]	0.51 ± 0.07[a]	0.45 ± 0.01[a]
9t18:1	0.30 ± 0.01[a]	0.37 ± 0.03[a]	27.50 ± 0.67[b]	28.29 ± 0.88[b]	0.38 ± 0.02[a]	0.35 ± 0.01[a]
9c18:1	36.29 ± 0.27[b]	36.23 ± 0.95[b]	26.25 ± 0.11[a]	27.09 ± 0.23[a]	50.72 ± 0.21[bc]	48.12 ± 1.44[c]
∑n-3 PUFA	7.54 ± 0.03[b]	6.79 ± 1.06[b]	4.48 ± 0.34[a]	4.37 ± 0.24[a]	4.72 ± 0.05[a]	5.00 ± 0.05[a]
∑n-6 PUFA	5.89 ± 0.06[b]	5.67 ± 0.72[b]	3.76 ± 0.06[a]	4.27 ± 0.64[a]	4.16 ± 0.08[a]	4.93 ± 1.21[ab]

[a]Mean values ± SD (n = 3.. Values in the same row with different letters for each species show significant differences ($p < 0.05$. ∑SFA, total saturated fatty acids; ∑cis MUFA, total cis monounsaturated fatty acids; ∑trans, total trans fatty acids; ∑PUFA, total polyunsaturated fatty acids; ∑n-3 PUFA, total n-3 polyunsaturated fatty acids; ∑n-6 PUFA, total n-6 polyunsaturated fatty acids.

the expression of caspase-3, -8, -9, and Bax was down-regulated and Bcl-2 was up-regulated when compared with elaidic acid group and control group (Figure 2C). Furthermore, the release of cytochrome C from the mitochondria to cytosol decreased (Figure 2D), perhaps due to the down-regulated expression of Bid. The expression levels of pro-apoptotic proteins decreased significantly in MβCD + oleic acid group compared with control group, while expression levels of some proteins including Bax, Bcl-2, and caspase-9 almost unchanged between the MβCD + oleic acid group and the oleic acid group (Figure 2C). These results indicate that lipid rafts had greater impact on the elaidic acid group than on the oleic acid group.

Effect of MβCD on TFA-Induced Cell Cycle Changes in HUVECs. As shown in Figure 3, in non-MβCD treated groups, elaidic acid significantly increased the expression of p53, p21, and p27 in comparison with other groups. The expression levels of p21 and p27 also increased in 9*c*18:1 group compared with control group. It has been reported that p21 and p27 could induce cell cycle arrest in G1 phase and G2/M phase through inhibition of CDK4-cyclin D1 and CDK2-cyclin E activity (18, 19). However, the expression of CDK4 and cyclin D1 increased significantly ($p < 0.05$) and CDK2 expression did not change significantly ($p > 0.05$).

In MβCD treated HUVECs, 9*t*18:1 supplementation resulted in a down-regulation of p53, p21, p27, and CDK4-cyclin D1 compared with 9*t*18:1 group. It should be pointed out that expression of p53 decreased significantly compared with control group, but CDK2 had no significant changes compared with other groups. Similar data were obtained with 9*c*18:1.

Effect of MβCD on TFA-Induced Expression of Apoptosis Receptors. As shown in Figure 4A, Fas and TNFR1, two apoptosis receptors located in lipid rafts, were investigated. The expressions of Fas and its ligand (FasL) were significantly increased in the elaidic acid group and unchanged in the oleic acid group, while they returned to normal levels in the MβCD + elaidic acid group and slightly increased in the MβCD + oleic acid group. The expression of TNFR1 had no significant change in each group ($p < 0.05$).

As shown in Figure 4B, both Fas and its ligand (FasL) were highly expressed on the cell membranes of 9*t*18:1 stimulated HUVECs The death domain with each other together formed tripolymers and activated the apoptosis pathway.

Effect of MβCD on Absorption of Fatty Acids in HUVECs. The levels of 9*t*18:1 in elaidic acid group and 9*c*18:1 in the oleic acid group significantly increased in comparison with control group ($p < 0.05$, Table 1). The results showed that the cells had obvious absorption of fatty acids. However, there were no significant differences between control and MβCD groups or between elaidic acid and MβCD + elaidic acid groups. Only did 9c18:1 level decrease in the MβCD + oleic acid group compared with the oleic acid group. The results indicated that lipid rafts had little effect on elaidic acid absorption but a slight effect on oleic acid absorption.

DISCUSSION

Lipid Rafts Could Involve in Elaidic Acid-Induced Apoptosis of HUVECs. TFAs resulted in systemic inflammation, insulin resistance, and adiposity resistance. Both randomized trials and observational studies demonstrated that TFAs consumption led to endothelial dysfunction.[16] Previous studies have shown that several dietary fatty acids had an effect on both cell membranes and gene transcription.[17,18] Qiu et al.[3] showed that TFAs led to endothelial cell apoptosis through the caspase pathway and the mitochondria. However, they did not report how TFAs activated the caspase pathway. It remains unknown whether there are specific receptor-induced apoptosis or what roles cell membranes play during this process. Apoptosis was a genetically controlled mechanism of cell death with a number of specific biochemical and morphological changes, including membrane blebbing, chromatin condensation, cytoplasmic condensation, and internucleosomal fragmentation of DNA. It could be mediated by death receptor pathway as well as the mitochondria pathway.[19]

Lipid rafts were specific membrane microdomains which were rich in cholesterols and sphingolipids.[4] Lipid rafts appeared to be involved in many biological events such as synthetic traffic, cell skeletal reconstruction, and signal transduction.[5] MβCD was the most common drug that interferes with lipid rafts; its mechanism of action was to remove or disturb the specificity of membrane cholesterol. Treatment with 10 mmol/L of MβCD within 60 min did not cause significant changes in both morphology (Figure 1C) and physiology (Figure 1A) of HUVECs. The content of cholesterol and expression level of cavelin-1 in cell membrane decreased significantly (Figure 1B,D). These results indicated that treatment with 10 mmol/L of MβCD within 60 min successfully destroy lipid rafts on cell membrane. The 9*t*18:1 treatment decreased cell viability, increased apoptosis, and resulted in down-regulation of Bcl-2 and up-regulation of the pro-apoptotic proteins such as Bax, Bid, caspase-3, caspase-8, and caspase-9. However, when lipid rafts of the endothelial cells were destroyed, the expression levels of these pro-apoptotic proteins were decreased and antiapoptotic protein (Bcl-2) was increased in 9*t*18:1-induced apoptosis. These results have for

dx.doi.org/10.1021/jf404834e | J. Agric. Food Chem. 2014, 62, 798−807

the first time demonstrated that lipid rafts could influence on 9*t*18:1-induced apoptosis of HUVECs.

Taken together, we have for the first time shown that fatty acids especially TFAs act on HUVECs by affecting lipid rafts. However, whether apoptotic receptors were destroyed or fatty acids were less absorbed remained unclear. Therefore, we conducted fatty acids composition analysis in the study. It was found that there was no significant difference in the level of fatty acids between elaidic acid group and MβCD + elaidic acid group, but the level of 9c18:1 in MβCD + oleic acid group decreased significantly ($p < 0.05$). We proposed that the absorption of 9t18:1 was not affected by lipid rafts, and the apoptotic receptor was the key point of apoptosis. The decreased absorption of 9c18:1 in MβCD + oleic acid group might be due to the decline of fatty acid translocase, a receptor localized in lipid rafts and nonraft plasma membrane, with an ability to help the uptake of required long-chain fatty acids for normal biological function of cells.[20]

Fas/FasL Pathway May Involve in 9*t*18:1-Induced Apoptosis of HUVECs. Two apoptosis receptors, Fas and tumor necrosis factor receptor (TNFR) 1, were located in lipid rafts. Fas (also known as CD95 or APO-1) was a type I glycosylated 45 kD membrane protein that belonged to the TNF family and transmitted a suicide signal to the cell upon binding of its ligand (FasL), a highly conserved, 40 kD glycoprotein.[21] TNFR1 was also a kind of apoptotic receptor.[22] Fas/FasL system was a critical signal pathway involved in apoptosis regulation in several cell types[23] and could be activated by many factors, such as drugs,[24] oxidative stress,[25] and other stimuli. Loss of integrity of lipid rafts by drugs could diminish CD95-mediated caspase-8 activation and apoptosis.[26,27] The activation of CD95 linked with its translocation into the lipid rafts. Lang et al.[28] reported that CD95 signaling was triggered by the interaction between active/inactive CD95 species and lipid rafts. A number of studies have demonstrated the importance of formation and internalization of CD95-containing raft in CD95-induced apoptosis of different kinds of human cells.[29,30] Zhang et al.[31] using a reconstituted system, found that the Fas/FasL interaction between membranes creates submicrometer membrane microdomains, and the cells then reveal various apoptosis features.

Treatment of elaidic acid increased the apoptosis of HUVECs. The result of immunofluorescence analysis (Figure 4B) showed that Fas clustered on lipid rafts when HUVECs were stimulated by 9*t*18:1. However, the expression levels of Fas and FasL significantly decreased in nonrafts cells after 9*t*18:1 treatment where cell apoptosis was inhibited. These results indicated that the Fas/FasL pathway might be involved in elaidic acid-induced apoptosis of HUVECs.

In conclusion, we proposed a possible molecular mechanism involved in 9*t*18:1-induced apoptosis and cell-cycle arrest in HUVECs (Figure 5). Lipid rafts and Fas/FasL pathway could play an important role in 9*t*18:1-induced apoptosis. Fas receptor and its ligand clustered in the lipid raft and then started the apoptosis program after 9*t*18:1 stimulated HUVECs. Then caspase-8 was activated when the signal was received that the apoptosis receptor (Fas/FasL) transmitted. The high expression of caspase-8 could increase the expression of Bid and Bax and decrease the expression of Bcl-2 and lead to release of mitochondrial cytochrome C. The mitochondrial cytochrome C which released to the cytoplasm would activate caspase-9 and then activate its downstream protein caspase-3. In addition, p53 as a critical pro-apoptotic protein and cell cycle

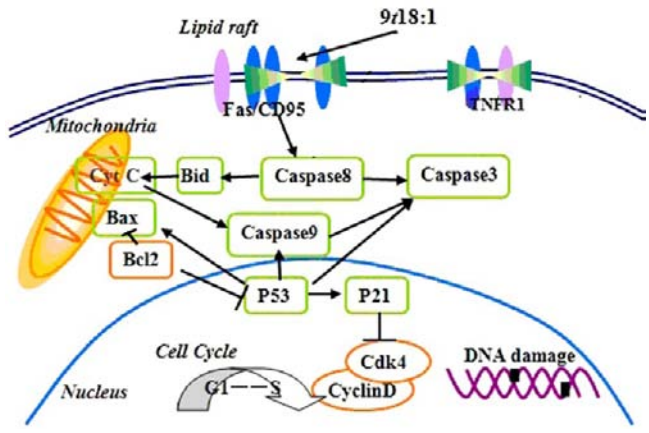

Figure 5. The proposed molecular mechanisms involved in 9*t*18:1-induced apoptosis and cell-cycle arrest in HUVECs.

protein was highly expressed after being treated with 9*t*18:1. The high expression of p53 increased the caspase-9 and other pro-apoptotic protein like Bax. p53 could also activate the expression of p21 and then interfere with the cell cycle.

9*t*18:1 Affects G1/S Phase in Cell Cycle. Cells in the long term evolution have developed detection mechanisms to ensure correct DNA replication and cell cycle distribution, and these critical control stages were often called cell cycle checkpoints or restriction points. There were three major cell cycle checkpoints, namely G1/S phase, G2/M phase, and the spindle assembly checkpoint. In the process of cell cycle regulation, the control point of G1/S phase was the key point of signal transmission and integration into the nucleus and the process of cell proliferation.

The human tumor suppressor protein p53 was critical for the transcriptional activation of a series of proteins involved in cell cycle control and apoptosis. p53 played its control on the cell cycle primarily through the G1/S checkpoint [32] and also regulated the G2/M checkpoint.[33] Activation of p53 in response to a variety of stimuli was associated with an increase in its protein levels and post-translational modifications, which induced the activation of a number of genes like p21 and p27, leading to cell cycle arrest.[34] CDK4 as a checkpoint regulates cell cycle in G1/S phase. In general, increased expression of p21 could enhance the inhibitory effect on CDKs and weaken CDK4-cyclinD1 regulation in the G1/S phase, resulting in G1 arrest and incomplete cell mitosis.[35] Compared to the control, 9*t*18:1 induced significant increases in the expression levels of p53, p21, and p27 ($p < 0.05$) and the expression level of CDK4-cyclinD1 increased in 9*t*18:1 group. When nonraft cells were exposed to 9*t*18:1, p53, p21, and p27 protein levels decreased and CDK4-cyclinD1 level also decreased compared with that in the 9*t*18:1 group, but they were still higher than that of the control. Whether this phenomenon is the result of self-regulation or of other mechanisms needs to be further investigated.

AUTHOR INFORMATION

Corresponding Author

*E-mail: zeyuandeng@hotmail.com. Fax: +86 791 88304402.

Funding

This study was supported by a National Natural Science Foundation of China, the Research Program of State Key Laboratory of Food Science and Technology (SKLF-TS-

200921), Ph.D. Subject Fund from Education Department (201136 011200 04), Natural Science Fund of Jiangxi Province (20114BAB2 14016).

Notes

The authors declare no competing financial interest.

■ ACKNOWLEDGMENTS

We thank Dr. Deming Gong for editing the manuscript.

■ ABBREVIATIONS USED

FBS, fetal bovine serum; FITC, fluorescein isothiocyanate; HDL, high-density lipoprotein; HUVECs, human umbilical vein endothelial cells; ICAM-1, intercellular adhesion molecule; LDL, low-density lipoprotein; MβCD, methyl-β-cyclodextrin; MTT, methyl thiazol tetrazolium; PI, propidium iodide; TFAs, *trans*-fatty acids

■ REFERENCES

(1) Mozaffarian, D. Trans fatty acids—effects on systemic inflammation and endothelial function. *Atheroscler. Suppl.* **2006**, *7*, 29−32.

(2) Ascherio, A. Trans fatty acids and blood lipids. *Atheroscler. Suppl.* **2006**, *7*, 25−27.

(3) Qiu, B.; Hu, J. N.; Liu, R.; Fan, Y. W.; Li, J.; Li, Y.; Deng, Z. Y. Caspase pathway of elaidic acid 9t-C18:1-induced apoptosis in human umbilical vein endothelial cells. *Cell Biol. Int.* **2012**, *36*, 255−260.

(4) Calder, P. C.; Yaqoob, P. Lipid Rafts—Composition, Characterization, and Controversies. *J. Nutr.* **2007**, *37*, 545−547.

(5) George, K. S.; Wu, S. Lipid raft: a floating island of death or survival. *Toxicol. Appl. Pharmacol.* **2012**, *259*, 311−319.

(6) Lee, Y.; Gustafsson, Å. B. Role of apoptosis in cardiovascular disease. *Apoptosis* **2009**, *14*, 536−548.

(7) Lemaire-Ewing, S.; Lagrost, L.; Néel, D. Lipid rafts: A signaling platform linking lipoprotein metabolism to atherogenesis. *Atherosclerosis* **2012**, *221*, 303−310.

(8) Xu, Y.; Buikema, H.; Gilst, W. H.; Henning, R. H. Caveolae and endothelial dysfunction: filling the caves in cardiovascular disease. *Eur. J. Pharmacol.* **2008**, *585*, 256−260.

(9) Stulnig, T. M.; Huber, J.; Leitinger, N.; Imre, E.-M.; Angelisová, P.; Nowotny, P.; Waldhäusl, W. Polyunsaturated eicosapentaenoic acid displaces proteins from membrane rafts by altering raft lipid composition. *J. Biol. Chem.* **2001**, *276*, 37335−37340.

(10) Li, Q.; Wang, M.; Tan, L.; Wang, C.; Ma, J.; Li, N.; Li, Y.; Xu, G.; Li, J. Docosahexaenoic acid changes lipid composition and interleukin-2 receptor signaling in membrane rafts. *J. Lipid Res.* **2005**, *46*, 1904−1913.

(11) Chen, W.; Jump, D. B.; Esselman, W. J.; Busik, J. V. Inhibition of cytokine signaling in human retinal endothelial cells through modification of caveolae/lipid rafts by docosahexaenoic acid. *Invest. Ophthalmol. Visual Sci.* **2007**, *48*, 18−26.

(12) Kim, W.; Fan, Y.-Y.; Barhoumi, R.; Smith, R.; McMurray, D. N.; Chapkin, R. S. n-3 Polyunsaturated fatty acids suppress the localization and activation of signaling proteins at the immunological synapse in murine CD4$^+$ T cells by affecting lipid raft formation. *J Immunol.* **2008**, *181*, 6236−6243.

(13) Fan, Y.-Y.; Ly, L. H.; Barhoumi, R.; McMurray, D. N.; Chapkin, R. S. Dietary docosahexaenoic acid suppresses T cell protein kinase Cθ lipid raft recruitment and IL-2 production. *J. Immunol.* **2004**, *173*, 6151−6160.

(14) Turk, H. F.; Chapkin, R. S. Membrane lipid raft organization is uniquely modified by n-3 polyunsaturated fatty acids. *Prostaglandins, Leukotrienes Essent. Fatty Acids* **2013**, *88*, 43−47.

(15) Grądzka, I.; Sochanowicz, B.; Brzóska, K.; Wójciuk, G.; Sommer, S.; Wojewódzka, M.; Gasińska, A.; Degen, C.; Jahreis, G.; Szumiel, I. *cis*-9,*trans*-11-Conjugated linoleic acid affects lipid raft composition and sensitizes human colorectal adenocarcinoma HT-29 cells to X-radiation. *Biochim. Biophys. Acta* **2013**, *1830*, 2233−2242.

(16) Micha, R.; Mozaffarian, D. Trans fatty acids: effects on cardiometabolic health and implications for policy. *Prostaglandins, Leukotrienes Essent. Fatty Acids* **2008**, *79*, 147−152.

(17) Feller, S. E.; Gawrisch, K. Properties of docosahexaenoic-acid-containing lipids and their influence on the function of rhodopsin. *Curr. Opin. Struct. Biol.* **2005**, *15*, 416−422.

(18) Roach, C.; Feller, S. E.; Ward, J. A.; Shaikh, S. R.; Zerouga, M.; Stillwell, W. Comparison of cis and trans fatty acid containing phosphatidylcholines on membrane properties. *Biochemistry* **2004**, *43*, 6344−6351.

(19) Hengartner, M. O. The biochemistry of apoptosis. *Nature* **2000**, *407*, 770−776.

(20) Eyre, N. S.; Cleland, L. G.; Tandon, N. N.; Mayrhofer, G. Importance of the carboxyl terminus of FAT/CD36 for plasma membrane localization and function in long-chain fatty acid uptake. *J. Lipid Res.* **2007**, *48*, 528−542.

(21) Rao-Bindal, K.; Zhou, Z.; Kleinerman, E. S. MS-275 sensitizes osteosarcoma cells to Fas ligand-induced cell death by increasing the localization of Fas in membrane lipid rafts. *Cell Death Dis.* **2012**, *3*, e369.

(22) Poggi, M.; Kara, I.; Brunel, J.-M.; Landrier, J.-F.; Govers, R.; Bonardo, B.; Fluhrer, R.; Haass, C.; Alessi, M. C.; Peiretti, F. Palmitoylation of TNF alpha is involved in the regulation of TNF receptor 1 signalling. *Biochim. Biophys. Acta* **2013**, *1833*, 602−612.

(23) Walczak, H.; Krammer, P. H. The CD95 APO-1/Fas and the TRAIL APO-2L apoptosis systems. *Exp. Cell Res.* **2000**, *256*, 58−66.

(24) Liu, W.-H.; Chang, L.-S. Fas/FasL-dependent and -independent activation of caspase-8 in doxorubicin-treated human breast cancer MCF-7 cells: ADAM10 down-regulation activates Fas/FasL signaling pathway. *Int. J. Biochem. Cell Biol.* **2011**, *43*, 1708−1719.

(25) Anathy, V.; Roberson, E.; Cunniff, B.; Nolin, J. D.; Hoffman, S.; Spiess, P.; Guala, A. S.; Lahue, K. G.; Goldman, D.; Flemer, S. Oxidative processing of latent Fas in the endoplasmic reticulum controls the strength of apoptosis. *Mol. Cell. Biol.* **2012**, *32*, 3464−3478.

(26) Grassmé, H.; Cremesti, A.; Kolesnick, R.; Gulbins, E. Ceramide-mediated clustering is required for CD95-DISC formation. *Oncogene* **2003**, *22*, 5457−5470.

(27) Grassmé, H.; Schwarz, H.; Gulbins, E. Molecular mechanisms of ceramide-mediated CD95 clustering. *Biochem. Biophys. Res. Commun.* **2001**, *284*, 1016−1030.

(28) Lang, I.; Fick, A.; Schäfer, V.; Giner, T.; Siegmund, D.; Wajant, H. Signaling active CD95 receptor molecules trigger co-translocation of inactive CD95 molecules into lipid rafts. *J. Biol. Chem.* **2012**, *287*, 24026−24042.

(29) Eramo, A.; Sargiacomo, M.; Ricci-Vitiani, L.; Todaro, M.; Stassi, G.; Messina, C. G.; Parolini, I.; Lotti, F.; Sette, G.; Peschle, C. CD95 death-inducing signaling complex formation and internalization occur in lipid rafts of type I and type II cells. *Eur. J. Immunol.* **2004**, *34*, 1930−1940.

(30) Gajate, C.; Mollinedo, F. The antitumor ether lipid ET-18-OCH3 induces apoptosis through translocation and capping of Fas/CD95 into membrane rafts in human leukemic cells. *Blood* **2001**, *98*, 3860−3863.

(31) Zhang, L.; Kaizuka, Y.; Hanagata, N. Imaging of Fas−FasL membrane microdomains during apoptosis in a reconstituted cell−cell junction. *Biochem. Biophys. Res. Commun.* **2012**, *422*, 298−304.

(32) Kano, H.; Arakawa, Y.; Takahashi, J. A.; Nozaki, K.; Kawabata, Y.; Takatsuka, K.; Kageyama, R.; Ueba, T.; Hashimoto, N. Over-expression of RFT induces G1-S arrest and apoptosis via p53/p21Waf1 pathway in glioma cell. *Biochem. Biophys. Res. Commun.* **2004**, *317*, 902−908.

(33) Ikeda, M.; Okamoto, I.; Tamura, K.; Satoh, T.; Yonesaka, K.; Fukuoka, M.; Nakagawa, K. Down-regulation of survivin by ultraviolet C radiation is dependent on p53 and results in G_2-M arrest in A549 cells. *Cancer Lett.* **2007**, *248*, 292−298.

(34) Lavin, Ma.; Gueven, N. The complexity of p53 stabilization and activation. *Cell Death Differ.* **2006**, *13*, 941−950.

(35) Koljonen, V.; Tukiainen, E.; Haglund, C.; Böhling, T. Cell cycle control by p21, p27 and p53 in merkel cell carcinoma. *Anticancer Res.* **2006**, *26*, 2209−2212.

JOURNAL OF AGRICULTURAL AND FOOD CHEMISTRY

Article

pubs.acs.org/JAFC

Characterization of the Surface Properties of Wheat Spikelet Components Grown under Different Regimens and the Biocontrol Yeast *Cryptococcus flavescens*

Christopher A. Dunlap* and David A. Schisler

Crop Bioprotection Research Unit, National Center for Agricultural Utilization Research, Agricultural Research Service, U.S. Department of Agriculture, 1815 North University Street, Peoria, Illinois 61604, United States

Supporting Information

ABSTRACT: Surface properties play an important role in plant−microbe interactions and determine if microbial propagules adhere to the surface of a plant. Fusarium head blight is an important disease of wheat that is initiated by the pathogen colonizing the wheat head. To better understand how surface properties of wheat may affect disease development and spray applications, the surface properties of wheat (*Triticum aestivum* L.) spikelet components were characterized under different environmental growing regimes. In addition, the surface properties of the biocontrol yeast *Cryptococcus flavescens* OH 182.9, which has been shown to effective in managing Fusarium head blight, were characterized. Wheat samples grown in a greenhouse environment were compared with samples produced in the field for two wheat cultivars. The results show changes occurring in the surface energy parameters and estimates of roughness during this period between the two cultivars. In general, the greenhouse samples were more hydrophobic than those grown in the field. The surface properties of the biocontrol yeast *C. flavescens* OH 182.9 were determined from contact angles on microbial lawns and revealed the cells were hydrophobic with a free energy of aggregation of −86.3 mJ/m^2 in water.

KEYWORDS: *wheat, spikelet, greenhouse, field, anthesis, Cryptococcus*

INTRODUCTION

The surfaces of the aerial parts of terrestrial plants frequently are covered by a waxy cuticle, which mediates the interactions between the plant and the environment. The chemical and physical properties of these surfaces determine the nature of these interactions. These properties play an important role in plant−microorganism interactions by influencing the likelihood of a microbial propagule adhering to the plant and subsequently colonizing the surface. In the case of the wheat disease Fusarium head blight (FHB), these propagules are ascospores and macroconidia of *Gibberella zeae*, the primary causal agent of FHB in North America. In addition, it is also important to understand how propagules of some beneficial microorganisms interact and adhere to the plant surface, such as applied biological control agents.

In previous work, our laboratory isolated the basidiomycetous yeast *Cryptococcus flavescens* OH 182.9 (NRRL Y-30216) from anthers of flowering wheat heads.[1] Research has demonstrated the yeast's efficacy in reducing FHB and its associated mycotoxin production in greenhouse and field settings[2,3] when assayed alone or in combination with other biocontrol agents.[4,5] Wheat is primarily vulnerable to FHB when favorable (warm and wet) weather conditions coincide with the period of anthesis when wheat florets open for flowering.[6] Little is known about the surface properties of wheat heads during this period when the pathogen must adhere and colonize the plant. Understanding the physicochemical properties of the wheathead are important, because adhering to the plant surface is the first step in the infection process both for the plant pathogen and for the beneficial biocontrol organism.

Although several studies have characterized the surface properties of the leaves of wheat,[7−9] no studies could be found that characterized the surface properties of the wheat spikelet. The wheat spikelet is the prevalent location for infection onset,[10,11] and the glume and lemma make up the bulk of the surface area (see Figure 1). It is also not known if any significant surface property alterations occur during the period of anthesis, which may make the plant more vulnerable to colonization. In addition, no studies have examined the impact of growing regimen on the surface properties of wheat spikelets grown in a greenhouse versus field-grown plants. This is important because many crop protection products are first tested in the greenhouse before taken to the field.

Knowledge of these physicochemical properties of the spikelet surface is also important for developing formulations of sprayable pest control products. Understanding how a spray droplet interacts with the target surface can help in guiding formulation decisions. These surface properties are also needed as parameters for accurate spray droplet adhesion models such as the model of Forster, which incorporates spray droplet size, velocity, surface angle, dynamic surface tension, and leaf contact angle measurements.[12] These models can help guide decisions

Received: September 19, 2013
Revised: January 2, 2014
Accepted: January 11, 2014
Published: January 12, 2014

ACS Publications This article not subject to U.S. Copyright. Published 2014 by the American Chemical Society

dx.doi.org/10.1021/jf404181f | J. Agric. Food Chem. 2014, 62, 809−815

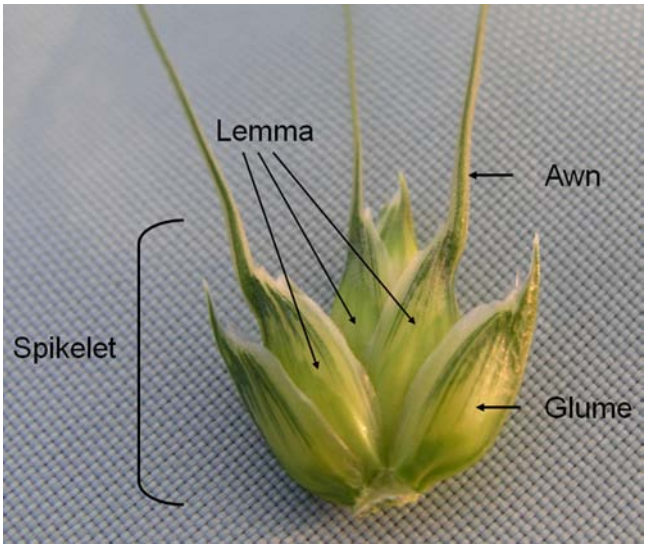

Figure 1. Anatomy of a wheat spikelet.

when developing new formulations or application technology for a specific crop system.

The goal of this study was to characterize the surface properties of the wheat spikelet components around the period of anthesis under greenhouse- and field-growing regimens. An additional goal was to characterize the surface properties of the biocontrol yeast antagonist *C. flavescens* OH 182.9.

MATERIALS AND METHODS

Wheat Samples. Field trials were conducted in Peoria, IL, USA, in 2009. Soft red winter wheat cultivar Freedom (moderately resistant to FHB) and Pioneer Brand 2545 (susceptible to FHB) were grown using standard agronomic conditions.[13] Whole wheat heads were cut from plots at split boot (early Feekes 10.1), out of boot (Feekes 10.5), and flowering (Feekes 10.5.1) and at 4, 8, and 12 days after flowering. Heads were stored in zip-lock bags on ice until analysis. For greenhouse growth of wheat seedlings, experiments were conducted in a climate-controlled greenhouse with temperatures that ranged from 17 to 20 °C at night and from 25 to 28 °C during the day. Natural sunlight was supplemented with high-pressure sodium lights for 14 h/day. Each experimental unit consisted of two plants of the chosen cultivar grown in a 19 cm diameter plastic pot. Each pot contained air-steam pasteurized (60 °C for 30 min) potting mix (Terra-lite Redi-earth mix, W. R. Grace, Cambridge, MA, USA), and plants were grown in a growth chamber (25 °C, 14 h photoperiod, 600 μmol/[m^2/s]) for 7−8 weeks prior to transfer to greenhouse benches. Pots were fertilized after 1 week and weekly thereafter with 50 mL of a solution containing 1.25 g/L Peters 20−20−20 (Grace-Sierra Horticultural Products, Milpitas, CA, USA) and 0.079 g/L iron chelate (Sprint 330, Becker Underwood, Inc., Ames, IA, USA). From approximately 1 week to 3 weeks after transferring plants to the greenhouse, wheat heads were harvested at the same physiologic stage of development as used for the field-grown wheat.

Contact Angle Measurements on Wheat Tissues. To determine the contact angle of glume or lemma tissues, samples were removed from a wheat spikelet and affixed to a microscope slide using double-sided tape. The location on the wheat head of spikelet samples was randomly chosen with at least three samples from each of the top, middle, or bottom third of the head. Four liquids were tested on each type of sample: deionized water, formamide, methyleneiodide, and acetone/water (1:1). Acetone, formamide, and methyleneiodide were obtained from Sigma-Aldrich (St. Louis, MO, USA) in the highest purity available. The water was provided by a Barnstead Easypure II reverse osmosis system. Contact angles were determined using an FTA4000 video drop shape analysis system (First Ten Angstroms, Portsmouth, VA, USA). A droplet of 5 μL was deposited onto the sample and the image recorded every 100 ms for 15 s. Under this time regimen, the droplets reached equilibrium. The droplet images were analyzed using software provided by the instrument manufacturer. The images were fit to a nonspherical model. A minimum of 10 replicate samples was tested for each sample and each liquid.

Production of *C. flavescens* OH 182.9. A pure culture of *C. flavescens* OH 182.9 (NRRL Y-30216) was initiated on one-fifth strength tryptic soy broth agar (TSBA, Difco Laboratories, Detroit, MI, USA) from a 10% glycerol stock stored at −80 °C. After growth at 25 °C for 24 h, cells from a plate were used to inoculate starter cultures of the strain. Starter cultures were produced in nonbaffled, 125 mL Erlenmeyer flasks containing 25 mL of liquid medium (SDCL)[14] that was incubated at 250 rpm, 2.5 cm orbit, and 25 °C for 24 h. A test culture was then initiated by inoculating it to an initial optical density (OD) of approximately 0.100 at 620 nm wavelength light (A620) using starter culture cells. Test cultures were incubated as described for starter cultures and harvested after 48 h of growth.

Contact Angle Measurements on *C. flavescens* OH 182.9. A microbial lawn of *C. flavescens* OH 182.9 was produced using a modified version of a previously described procedure.[15] Briefly, a 5 mL suspension of the production culture containing (~1 × 10^8 cfu/mL) was filtered in a 15 mL vacuum filtration unit utilizing a 25 mm, 0.22 μm pore, GVWP membrane, both from Millipore Inc. (Billerica, MA, USA). The membranes are hydrophilic and low protein binding and made of polyvinylidene fluoride. The membrane was prewetted and rinsed with deionized water. The sample was added to the filter, vacuum was initiated, and the solution was allowed to remain on the filtering apparatus for 30 min. Under these conditions, the microbial lawn/membrane would clog the filtering process and only about 1 mL of water would have been removed. The remaining liquid was carefully removed with a pipet. The membrane was allowed to slowly dry for 3 h in a Petri dish before measurements were conducted. The membrane was secured to a microscope slide using double-sided tape to provide a stable platform. Contact angles were determined and analyzed as previously described for the wheat components.

Filtering Experiments. To determine the propensity of *C. flavescens* OH 182.9 to clog a filter membrane, we measured the time needed to clog or completely filter a solution of *C. flavescens* OH 182.9 cells. Three solutions were prepared using 8 mL of cell suspension (~1 × 10^8 cfu/mL) in spent culture media combined with either 2 mL of water or 2 mL of 100 mM ethylene glycol bis(2-aminoethylether)-*N*,*N*,*N*′,*N*′-tetraacetic acid (EGTA), pH 8.0, or 2 mL of 100 mM 2-({2-[bis(carboxymethyl)amino]ethyl}(carboxymethyl)-amino) acetic acid (EDTA), pH 8.0. The solution was filtered in a 15 mL vacuum filtration unit utilizing a 25 mm, 0.22 μm pore, GVWP membrane, both from Millipore Inc. The vacuum pressure was provided by a building-wide system and averaged ~95 mbar. The membrane was prewetted with deionized water. The sample was added to the filter, vacuum was initiated, and the time to complete clogging or until all of the water was removed was assessed visually. The tests were run on three individual cultures with two or more technical replicates of each.

Microscopy. Photomicrographs of cells of *C. flavescens* in culture were taken using an Olympus BX60 system light microscope equipped with Nomarski optics and an Olympus DP70 digital camera (Melville, NY, USA).

RESULTS AND DISCUSSION

Contact Angle Measurements on Greenhouse-Grown Wheat Spikelets. The contact angles of three liquids were determined for the wheat spikelet components (glume and lemma) for samples immediately before and after anthesis for two wheat cultivars grown under a greenhouse-growing regimen. The measurements were conducted on two different wheat cultivars, Freedom and Pioneer Brand 2545 (Table S1 in the Supporting Information). The choice of these two wheat

varieties is based on the cultivar Freedom being moderately resistant to FHB and Pioneer Brand 2545 being susceptible to FHB. Both tissue types have been identified as potential infection sites of the FHB pathogen.[10,16] The results are reported in Figure 2A. The results show no significant differences between the two wheat cultivars under these conditions. In addition, for each cultivar, the glume and lemma show no significant differences among themselves under these conditions. Observing the change in water contact angle as a function of time, the means trend toward higher contact angles from the split boot stage to day 8 (post anthesis). The most notable difference from the time course is observed in the lemma from the Freedom strain at the split boot stage and day 8 (post anthesis) and is statistically significant ($P < 0.05$).

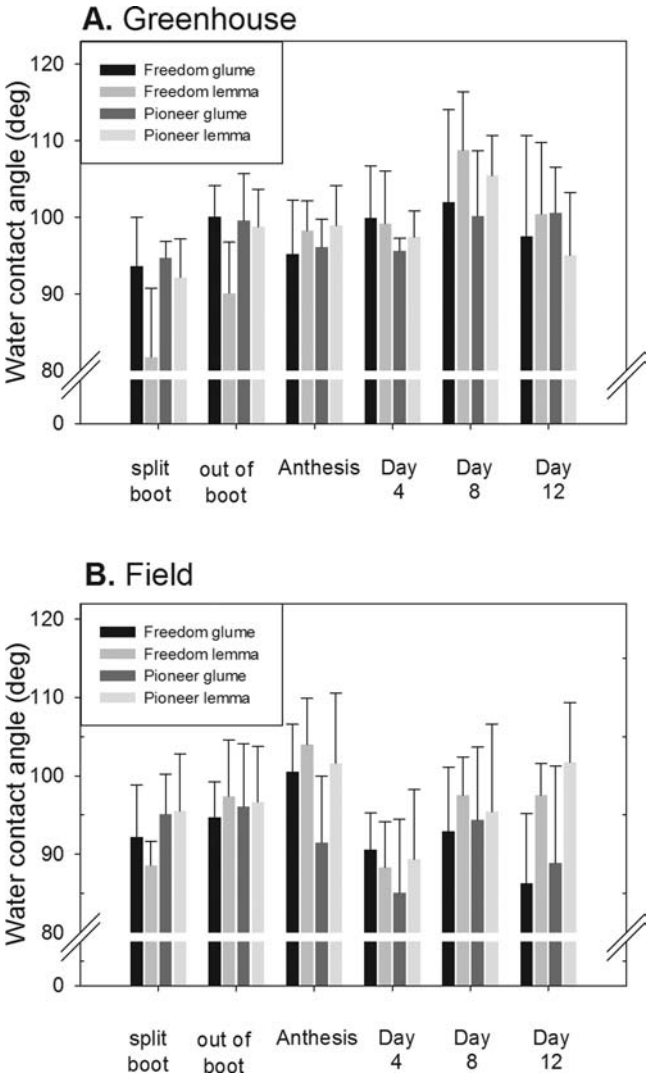

Figure 2. (A) Water contact angles of the glume and lemma of two wheat varieties (Freedom and Pioneer) grown (A) in a greenhouse and (B) in the field at different stages of growth. Error bars are ±1 SD.

Contact Angle Measurements on Field-Grown Wheat Spikelets. The contact angles were determined for the wheat spikelet components for the two wheat varieties grown in field plots (Table S2 in the Supporting Information). The field-grown samples exhibited much more variation and differences between the strains. The only significant difference ($P < 0.05$) between the strains for a specific tissue and time was between the lemma at the split boot stage. Comparisons of tissue type for a specific strain and time showed three significant differences. These include the Pioneer cultivar at anthesis and day 12 and Freedom at day 12. From an analysis of the time course, the most notable difference is that all of the conditions, except Pioneer lemma, are significantly different between anthesis and day 4 (post anthesis). Weather during the field trials was uneventful with two moderate precipitation events occurring on day 2 (post anthesis, 29 mm) and the evening of day 8 (post anthesis, 24 mm), daily temperature highs and lows are included in supplemental Figure S1. Previous studies on wheat leaves reported a much higher water contact angle than we observed on the wheat head. Early studies report wheat leaves have a water contact angle in excess of 130°,[8] whereas a more recent study reported a wheat leaf water contact angle of 165°.[9]

Comparing the results between greenhouse- and field-grown plants shows the field-grown plants tend to be less hydrophobic than the greenhouse plants. In cereals, a variety of agronomic traits have been identified to be altered when produced in greenhouse versus the field environment,[17−19] but only limited studies could be found that identify changes in surface properties or ultrastructure of plant surfaces under these regimens.[20,21] These results suggest surface properties may affect studies comparing greenhouse- and field-grown plant traits. This may be one of the causes of the variation in performance microbial biocontrol products in greenhouse environments versus field environments.[3,22]

Surface Energy Calculations for Wheat Spikelet Components. The contact angles were used to calculate the surface free energy using the Owens−Wendt method (geometric mean),[23] which uses the contact angle of a polar (water) and apolar (methyleneiodide) liquid to calculate the dispersive and polar components of surface energy. The results for the greenhouse-grown plants are reported in Figure 3A. The two wheat varieties show a distinct difference in surface energy for the post anthesis time points. The results for the field-grown plants are reported in Figure 3B. The field results do not reveal any distinct patterns; the largest change occurs in the Pioneer glume sample between anthesis and day 4 with a change of 5.1 dyn/cm ($P < 0.05$).

Water/Acetone Contact Angle Measurements. The contact angle of a acetone/water, 1:1 (v/v), solution has been used to estimate the surface roughness of various leaves.[24] This measurement is also required as a parameter in the spray droplet adhesion model.[12] The results for the greenhouse-grown samples are reported in Figure 4A. The contact angles range in value from 68° to 84°. The results identify differences between individual samples, but there are no clear trends in the data. The acetone/water contact angles of the field-grown samples are reported in Figure 4B. As before, the field-grown samples show a greater diversity in the observed contact angles, which range in value from 73° to 95°. There are no significant differences between the tissue types, although both surfaces show changes occurring at or immediately after anthesis. The two cultivars show significant differences before anthesis and become comparable post anthesis. One possible attribute in plants that could produce differences in roughness is variation in the trichomes. Trichomes are small fine outgrowths on the surface plant parts. Variation in trichome distribution has been reported in pigeonpeas (*Cajanus* spp.) for plants grown in the greenhouse versus field-grown plants.[20] Alternatively, wax

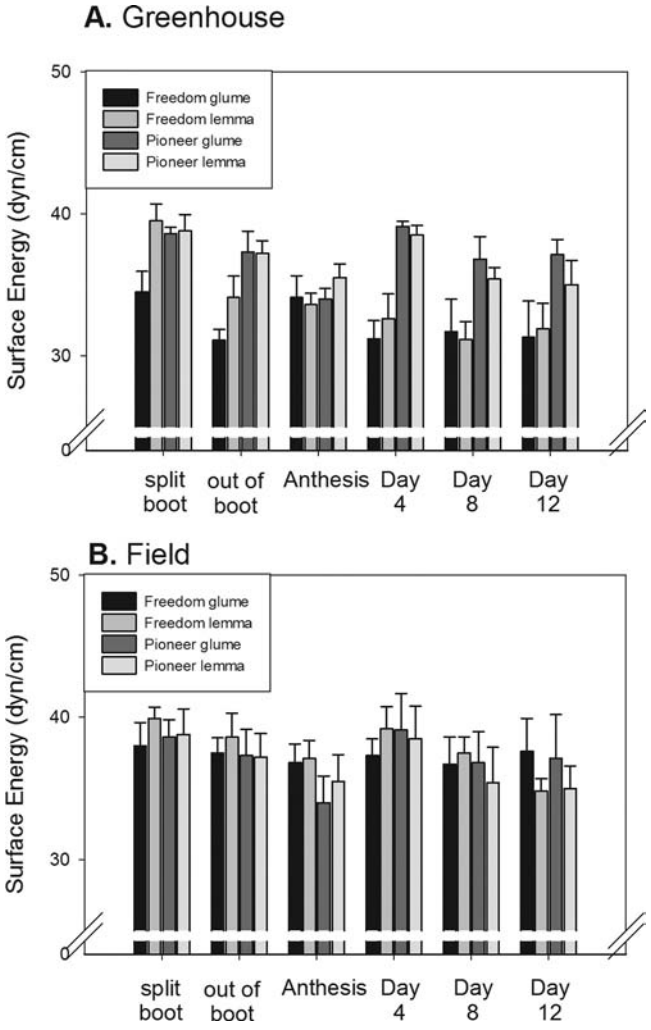

Figure 3. Surface energy of the glume and lemma of two wheat varieties (Freedom and Pioneer) grown (A) in a greenhouse and (B) in the field at different stages of growth. Surface energy was calculated from water and methyleneiodide contact angles using the Owens–Wendt method (geometric mean).[23] Error bars are ±1 SD.

morphology and ultrastructure have been correlated with surface roughness on wheat leaves.[8]

Contact Angle Measurements on *Cryptococcus flavescens* OH 182.9. To determine the surface properties of microorganisms, they are typically prepared by capturing them on a filter membrane and drying them to a uniform state.[25] This method was used to generate samples for our biocontrol antagonist *C. flavescens*. The contact angles were determined for three liquids, two polar (water and formamide) and one apolar (methyleneiodide). The contact angles are reported in Table 1.

The contact angles were then used to derive the surface energy parameters for the *C. flavescens* lawn. The contact angles were used to calculate the surface free energy using the Owens–Wendt method (geometric mean),[23] which uses the contact angle of a polar and an apolar liquid to calculate the dispersive and polar components of surface energy. In addition, surface free energy was determined using the VCG method,[26] which requires two polar liquids and one apolar liquid. The VCG method also calculates the dispersive and polar components of surface energy, but further refines the estimate by separating the polar fraction into Lewis acid and base

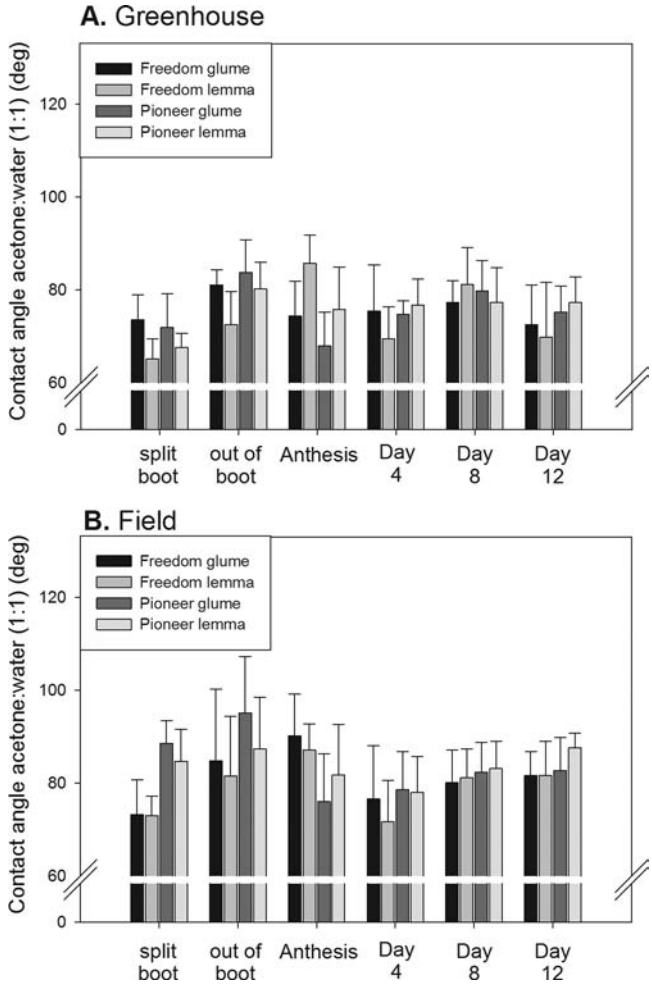

Figure 4. Acetone/water (1:1) contact angles of the glume and lemma of two wheat varieties (Freedom and Pioneer) grown (A) in a greenhouse amd (B) in the field at different stages of growth. Error bars are ±1 SD.

Table 1. Contact Angles and Surface Energy Parameters for *C. flavescens* OH 182.9

(A) Contact Angles		
compound	$\theta \pm$ SD	
water	94.3 ± 5.3	
formamide	53.2 ± 3.7	
methyleneiodide	40.5 ± 1.1	
(B) Surface Energy Parameters		
method	geometric mean[a]	VCG[b]
γ_{total}	39.8	40.1
γ^{disp}	39.4	40.1
γ^{polar}	0.4	0
γ^{+}		1.1
γ^{-}		0

[a]Reference 23. [b]Reference 26.

components. The calculated results for the surface energy parameters are reported in Table 1. The calculated surface energy parameters for *C. flavescens* are at the high end of the range reportedly observed in microorganisms.[27]

Microbial surface hydrophilicity or hydrophobicity can be described by calculating the free energy of aggregation (ΔG_{mwm}) in aqueous solution, where m is microbe and w is

dx.doi.org/10.1021/jf404181f | J. Agric. Food Chem. 2014, 62, 809–815

water.[28−30] The free energy of aggregation is a measure of the interactions between two of the same particles (two cells of *C. flavescens*), immersed in a liquid (water). A microbial surface is characterized as hydrophobic when ΔG_{mwm} is <0 or as hydrophilic when ΔG_{mwm} is >0. If the change in free energy is positive ($\Delta G_{mwm} > 0$), it is energetically unfavorable to bring the particles together and the particles do not aggregate in aqueous solution. Likewise, if the change in free energy is negative ($\Delta G_{mwm} < 0$), it is energetically favorable to bring the particles together and the particles readily aggregate in aqueous solution. The free energy of aggregation is the sum of the Lifschitz−van der Waals interaction free energy and polar interaction free energy, which can be written in terms of their component surface tensions.

$$\Delta G_{mwm} = -2\left(\sqrt{\gamma_m^{LW}} - \sqrt{\gamma_w^{LW}}\right)^2 - 4\left(\sqrt{\gamma_m^+\gamma_m^-} + \sqrt{\gamma_w^+\gamma_w^-} - \sqrt{\gamma_m^+\gamma_w^-} - \sqrt{\gamma_m^-\gamma_w^+}\right) \quad (1)$$

Calculation of the free energy of aggregation for cells of *C. flavescens* in aqueous solution yielded a value of −86.3 mJ/m^2. This would classify the surfaces of these cells as hydrophobic, because the interaction between cells is energetically favorable. Interestingly, this is inconsistent with observations in our laboratory that the cells do not readily aggregate in aqueous solution. Figure 5 shows the yeast cells at the typical harvest

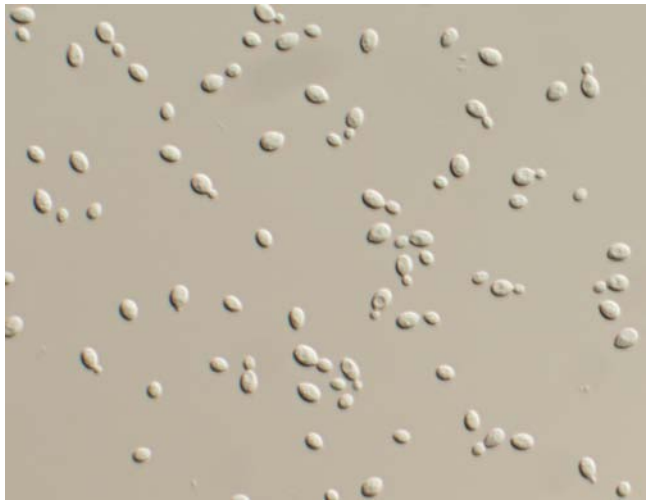

Figure 5. Micrograph of cells of *C. flavescens* OH 189.2 at the time of harvest.

time (early stationary phase), and they demonstrate no inclination to aggregate. It is important to note that this treatment of free energy of aggregation does not account for electrostatic interactions. Therefore, one possible explanation for the difference in calculated versus observed properties is that electrostatic interactions are an important contribution to surface free energy and that the repulsive nature of like charges (same charge on each cell) is able to keep the cells from aggregating.

Another possible explanation for the inconsistent results between the measured surface properties of the microbial lawn and their behavior in solution is the cells in the microbial lawn are in a different state from the cells in solution. One observation supporting this possibility is the previously reported ability of the cells to rapidly clog a filter membrane.[31] This suggests cells have the ability change properties during the filtering of the solution. Although it is tempting to speculate this maybe the result of a quorum sensing or concentration-dependent phenomenon, there are no laboratory observations to support this theory. The cells can be highly concentrated through centrifugation, and they are still readily dispersible back into solution. Scanning electron micrographs of the microbial lawns on a filter membrane show the cells have an extracellular polymer connecting each other.[31] Given the rapid rate of filter clogging (∼30 s), it is not feasible for the cells to produce the compound quickly enough to respond to the changes in environmental conditions. This suggests the compound is already made and excreted when needed or is already made and activated/altered with another small molecule when needed.

It has long been known that multivalent cations, specifically calcium, can promote cell to cell aggregation via bridging of anionic cell surface polymers.[32,33] To explore if multivalent ions could play a role in the current system, we used divalent chelators during filtration to reduce the bioavailability of divalent ions in the culture supernatant. The common divalent chelators EDTA and EGTA have been used study cell to cell aggregation in other systems.[34] To determine if divalent ions played a role in preventing filtration, we added EDTA or EGTA to a final concentration of 20 mM before filtering. The results of the experiment are somewhat qualitative given the nature of the experiment. The control sample with *C. flavescens* only quickly clogged the filter (∼1 min) and allowed only ∼1 mL of a total of 6 mL of the water to be removed. Allowing the material to stay under vacuum overnight (∼16 h) yielded no additional water removal. Whereas both the EGTA- and EDTA-amended solutions stopped noticeable filtering in (∼1 min) also, an extended period of time (8−16 h) on the vacuum resulted in complete water removal. These results suggest calcium or other divalent ions play a role in the phenomena, but are not the sole determining variable.

This is the first study to characterize the surface of wheat spikelets under different environmental growth regimens and to do so through the important period of anthesis. Overall, these results suggest the surface properties and surface ultrastructure of the glume and lemma are experiencing only minor changes during anthesis for these cultivars, because only some are statistically significant. However, small changes have the potential to alter the ability of microorganisms to adhere to these surfaces.[35] It has previously been shown that these properties can alter the binding of pathogen conidia to wheat surface.[9,36] In addition, these properties also play a role in preharvest sprouting, by regulating ear wetting through water repellency.[7] These data can also be used to optimize pest control formulations for improved delivery and retention to the wheat head. This is accomplished by incorporating these parameters into spray droplet adhesion models, such as the model of Forster, which incorporates spray droplet size, velocity, surface angle, dynamic surface tension, and leaf contact angle measurements.[12] These models allow the user to predict the size of spray droplets needed to ensure adhesion to the target.

■ ASSOCIATED CONTENT

Supporting Information

Tables S1 and S2 and Figure S1. This material is available free of charge via the Internet at http://pubs.acs.org.

AUTHOR INFORMATION

Corresponding Author

*(C.A.D.) Phone: (309) 861-6339. E-mail: christopher.dunlap@ars.usda.gov.

Funding

Studies were made possible, in part, by a grant from the U.S. Wheat and Barley Scab Initiative. Any opinions, findings, conclusions, or recommendations expressed in this publication are those of the author(s) and do not necessarily reflect the view of the U.S. Department of Agriculture. The mention of firm names or trade products does not imply that they are endorsed or recommended by the USDA over other firms or similar products not mentioned.

Notes

The authors declare no competing financial interest.

REFERENCES

(1) Khan, N. I.; Schisler, D. A.; Boehm, M. J.; Slininger, P. J.; Bothast, R. J. Selection and evaluation of microorganisms for biocontrol of *Fusarium* head blight of wheat incited by *Gibberella zeae*. *Plant Dis.* **2001**, *85* (12), 1253−1258.

(2) Khan, N. I.; Schisler, D. A.; Boehm, M. J.; Lipps, P. E.; Slininger, P. J. Field testing of antagonists of Fusarium head blight incited by *Gibberella zeae*. *Biol. Control* **2004**, *29* (2), 245−255.

(3) Schisler, D. A.; Khan, N. I.; Boehm, M. J.; Slininger, P. J. Greenhouse and field evaluation of biological control of Fusarium head blight on durum wheat. *Plant Dis.* **2002**, *86* (12), 1350−1356.

(4) Kolombet, L. V.; Starshov, A. A.; Schisler, D. Biological efficiency *Trichoderma asperellum* GJS 03-35 and yeast *Cryptococcus nadoensis* OH 182.9 as biocontrol agents against fusarium head blight of wheat. *Mikol. Fitopatol.* **2005**, *39* (5), 80−88.

(5) Yuen, G. Y.; Jochum, C. C.; Halley, S. A.; Sweets, L. E.; Kirk, W.; Schisler, D. A. In *2010 Uniform Biological Control Trials − Preliminary Results*; The 2010 National Fusarium Head Blight Forum, Milwaukee, WI; Canty, S., Clark, A., Anderson-Scully, A., Ellis, D., Sanford, D. V., Eds.; University of Kentucky: Lexington, KY, USA, 2010; pp 112−115.

(6) De Wolf, E. D.; Madden, L. V.; Lipps, P. E. Risk assessment models for wheat Fusarium head blight epidemics based on within-season weather data. *Phytopathology* **2003**, *93* (4), 428−435.

(7) King, R. W.; Von Wettstein-Knowles, P. Epicuticular waxes and regulation of ear wetting and pre-harvest sprouting in barley and wheat. *Euphytica* **2000**, *112* (2), 157−166.

(8) Netting, A. G.; von Wettstein-Knowles, P. The physico-chemical basis of leaf wettability in wheat. *Planta* **1973**, *114* (4), 289−309.

(9) Stosch, A. K.; Solga, A.; Steiner, U.; Oerke, E. C.; Barthlott, W.; Cermann, Z. Efficiency of self-cleaning properties in wheat (*Triticum aestivum* L.). *J. Appl. Bot. Food Qual.* **2007**, *81* (1), 49−55.

(10) Pritsch, C.; Muehlbauer, G. J.; Bushnell, W. R.; Somers, D. A.; Vance, C. P. Fungal development and induction of defense response genes during early infection of wheat spikes by *Fusarium graminearum*. *Mol. Plant−Microbe Interact.* **2000**, *13* (2), 159−169.

(11) Boenisch, M. J.; Schäfer, W. *Fusarium graminearum* forms mycotoxin producing infection structures on wheat. *BMC Plant Biol.* **2011**, *11*, 110.

(12) Forster, W. A.; Kimberley, M. O.; Zabkiewicz, J. A. A universal spray droplet adhesion model. *Trans. Am. Soc. Agric. Eng.* **2005**, *48* (4), 1321−1330.

(13) Schisler, D. A.; Khan, N. I.; Boehm, M. J.; Lipps, P. E.; Slininger, P. J.; Zhang, S. Selection and evaluation of the potential of choline-metabolizing microbial strains to reduce Fusarium head blight. *Biol. Control* **2006**, *39* (3), 497−506.

(14) Slininger, P. J.; Dunlap, C. A.; Schisler, D. A. Polysaccharide benefits dry storage survival of the biocontrol agent *Pseudomonas fluorescens* S11:P:12 effective against several maladies of stored potatoes. *Biocontrol Sci. Technol.* **2010**, *20* (3), 227−244.

(15) Busscher, H. J.; Weerkamp, A. H.; Van Der Mei, H. C.; van Pelt, A. W.; de Jong, H.; Arends, J. Measurement of the surface free energy of bacterial cell surfaces and its relevance to adhesion. *Appl. Environ. Microbiol.* **1984**, *48* (5), 980−983.

(16) Ribichich, K. F.; Lopez, S. E.; Vegetti, A. C. Histopathological spikelet changes produced by *Fusarium graminearum* in susceptible and resistant wheat cultivars. *Plant Dis.* **2000**, *84* (7), 794−802.

(17) Pinkard, E. A.; Patel, V.; Mohammed, C. Chlorophyll and nitrogen determination for plantation-grown Eucalyptus nitens and *E. globulus* using a non-destructive meter. *For. Ecol. Manag.* **2006**, *223* (1−3), 211−217.

(18) Bahrani, J.; McVetty, P. B. E. Relationship of seed quality traits for greenhouse-grown versus field-grown high erucic acid rapesseed: Is seed quality trait selection for greenhouse-grown seed worthwhile? *Can. J. Plant Sci.* **2008**, *88* (3), 419−423.

(19) Zeller, S. L.; Kalinina, O.; Brunner, S.; Keller, B.; Schmid, B. Transgene × environment interactions in genetically modified wheat. *PLoS One* **2010**, *5* (7), e11405.

(20) Romeis, J.; Shanower, T. G.; Peter, A. J. Trichomes on pigeonpea [*Cajanus cajan* (L.) Mill sp.] and two wild *Cajanus* spp. *Crop Sci.* **1999**, *39* (2), 564−569.

(21) Louro, R.; Santiago, L.; dos Santos, A.; Machado, R. Ultrastructure of *Eucalyptus grandis* × *E. urophylla*; plants cultivated ex vitro in greenhouse and field conditions. *Trees − Struct. Funct.* **2003**, *17* (1), 11−22.

(22) Serfling, A.; Wirsel, S. G. R.; Lind, V.; Deising, H. B. Performance of the biocontrol fungus *Piriformospora indica* on wheat under greenhouse and field conditions. *Phytopathology* **2007**, *97* (4), 523−531.

(23) Lehr, C. M.; Bouwstra, J. A.; Bodde, H. E.; Junginger, H. E. A surface energy analysis of mucoadhesion: contact angle measurements on polycarbophil and pig intestinal mucosa in physiologically relevant fluids. *Pharm. Res.* **1992**, *9* (1), 70−75.

(24) Forester, W. A.; Zabkiewicz, J. A. In *Improved Method for Leaf Surface Roughness Characterization*, Proceedings of the 6th International Symposium of Adjuvants for Agrochemicals, Renkum, The Netherlands; Ruiter, H. d., Ed.; SURfaPLUS: Wageningen, The Netherlands, 2001; pp 113−118.

(25) van der Mei, H. C.; Weerkamp, A. H.; Busscher, H. J. Assessment of microbial cell surface hydrophobicity. In *Microbial Cell Surface Analysis: Structural and Physiochemical Methods*; Mozes, N., Handley, P. S., Busscher, H. J., Rouxhet, P. G., Eds.; VCH Publishers: New York, 1991.

(26) van Oss, C. J.; Chaudhury, M. K.; Good, R. J. Monopolar surfaces. *Adv. Colloid Interface Sci.* **1987**, *28* (1), 35−64.

(27) Sharma, P. K.; Rao, K. H. Analysis of different approaches for evaluation of surface energy of microbial cells by contact angle goniometry. *Adv. Colloid Interface Sci.* **2002**, *98* (3), 341−463.

(28) Strevett, K. A.; Chen, G. Microbial surface thermodynamics and applications. *Res. Microbiol.* **2003**, *154* (5), 329−335.

(29) van der Mei, H. C.; Bos, R.; Busscher, H. J. A reference guide to microbial cell surface hydrophobicity based on contact angles. *Colloids Surf., B* **1998**, *11* (4), 213−221.

(30) van Oss, C. J.; Chaudhury, M. K.; Good, R. J. Interfacial Lifshitz-van der Waals and polar interactions in macroscopic systems. *Chem. Rev.* **1988**, *88*, 927−941.

(31) Dunlap, C. A.; Schisler, D. A. Fluidized-bed drying and storage stability of *Cryptococcus flavescens* OH 182.9, a biocontrol agent of Fusarium head blight. *Biocontrol Sci. Technol.* **2010**, *20* (5), 465−474.

(32) Hoygaard Bruus, J.; Halkjaer Nielsen, P.; Keiding, K. On the stability of activated sludge flocs with implications to dewatering. *Water Res.* **1992**, *26* (12), 1597−1604.

(33) Mahoney, E. M.; Varangu, L. K.; Cairns, W. L.; Kosaric, N.; Murray, R. G. E. The effect of calcium on microbial aggregation during uasb reactor start-up. *Water Sci. Technol.* **1987**, *19* (1−2), 249−260.

(34) Grotenhuis, J. T. C.; Van Lier, J. B.; Plugge, C. M.; Stams, A. J. M.; Zehnder, A. J. B. Effect of ethylene glycol-bis(β-aminoethyl ether)-*N*,*N*-tetraacetic acid (EGTA) on stability and activity of methanogenic granular sludge. *Appl. Microbiol. Biotechnol.* **1991**, *36* (1), 109−114.

(35) Lindow, S. E.; Brandl, M. T. Microbiology of the phyllosphere. *Appl. Environ. Microbiol.* **2003**, *69* (4), 1875−1883.

(36) Zelinger, E.; Hawes, C. R.; Gurr, S. J.; Dewey, F. M. Attachment and adhesion of conidia of *Stagonospora nodorum* to natural and artificial surfaces. *Physiol. Mol. Plant Pathol.* **2006**, *68* (4−6), 209−215.

JOURNAL OF AGRICULTURAL AND FOOD CHEMISTRY

Article

pubs.acs.org/JAFC

Fate and Uptake of Pharmaceuticals in Soil–Plant Systems

Laura J. Carter,[†] Eleanor Harris,[‡] Mike Williams,[§] Jim J. Ryan,[#] Rai S. Kookana,[§] and Alistair B. A. Boxall*[,†]

[†]Environment Department, University of York, Heslington, York, U.K. YO10 5DD

[‡]Cranfield University, Cranfield, Bedford, U.K. MK43 0AL

[§]CSIRO Land and Water, Waite Campus, Adelaide, South Australia, Australia 5064

[#]EHS Technical CoE, GlaxoSmithKline, Ware, U.K. SG12 0DP

Supporting Information

ABSTRACT: Pharmaceuticals have been detected in the soil environment where there is the potential for uptake into crops. This study explored the fate and uptake of pharmaceuticals (carbamazepine, diclofenac, fluoxetine, propranolol, sulfamethazine) and a personal care product (triclosan) in soil–plant systems using radish (*Raphanus sativus*) and ryegrass (*Lolium perenne*). Five of the six chemicals were detected in plant tissue. Carbamazepine was taken up to the greatest extent in both the radish (52 μg/g) and ryegrass (33 μg/g), whereas sulfamethazine uptake was below the limit of quantitation (LOQ) (<0.01 μg/g). In the soil, concentrations of diclofenac and sulfamethazine dropped below the LOQ after 7 days. However, all pharmaceuticals were still detectable in the pore water at the end of the experiment. The results demonstrate the ability of plant species to accumulate pharmaceuticals from soils with uptake apparently specific to both plant species and chemical. Results can be partly explained by the hydrophobicity and extent of ionization of each chemical in the soil.

KEYWORDS: *plant uptake, pharmaceuticals, fate, soil, bioavailability, carbamazepine, diclofenac, fluoxetine, propranolol, sulfamethazine, triclosan*

INTRODUCTION

Worldwide, pharmaceutical use has been on the increase for the past century[1−3] and will continue to increase into the future with the development of new medicines to cure recently discovered diseases as well as previously untreatable conditions. Following use by the patient, active pharmaceutical ingredients (APIs) and their metabolites are excreted to the sewerage system. They are then typically transported to a wastewater treatment works, where, depending on their molecular structure and physicochemical properties, they can be either degraded by biological treatment processes or released to the environment in effluents or sorb to sludge.[4−8] The soil environment will therefore be exposed to APIs and their metabolites when sludge from treatment processes is applied to land as an agricultural fertilizer or when soil is irrigated with reclaimed wastewater effluent.[9−13] While only a few studies have explored the occurrence of APIs in the soil environment, available data indicate that a range of API classes, including nonsteroidal anti-inflammatory drugs, antidepressants, anticonvulsants, and antibacterial agents do occur in soils in concentrations up to the low mg/kg level.[9−15]

Because of detection of pharmaceuticals in soils, concerns have been raised over the potential for these substances to be taken up into human food items and to pose a risk to human health.[16,17] A number of studies have demonstrated the uptake of pharmaceuticals used in human and veterinary medicine into plants.[16−24] Studies have explored the uptake and translocation of a variety of APIs with a particular focus on the antidepressant drug fluoxetine and antibacterial chemicals including sulfamethazine, sulfamethoxazole, and trimethoprim into numerous plant species including root and shoot crops such as soybean, lettuce, and carrot.

Many of the previous plant uptake studies have been done at unrealistic exposure concentrations. Studies typically have looked at uptake only with no attempt being made to understand the temporal fate of the pharmaceutical in soil matrices. Without understanding the dynamics of the distribution and fate of the pharmaceuticals in the soil, it is difficult to establish relationships between the properties of pharmaceuticals and uptake. This study was therefore initiated to explore the fate, distribution, and uptake of a range of pharmaceuticals in soil–plant systems. This work consisted of a fate study (with no plants) and an uptake study performed on two crop species with five pharmaceuticals and an antimicrobial personal care product. The compounds were selected to cover a diverse range of physicochemical properties (Table 1).

MATERIALS AND METHODS

Analytical grade carbamazepine (>98% purity), diclofenac (>98% purity), fluoxetine (>98% purity), propranolol (>99% purity), sulfamethazine (>99% purity), and triclosan (>97% purity) were obtained from Sigma-Aldrich (Sydney, Australia). Deuterated forms of selected study compounds (carbamazepine-d_{10} (99.8% purity), diclofenac-d_4 (98.5% purity), fluoxetine-d_5 (99.4% purity), propranolol-d_7 (99.6% purity), and triclosan-d_3 (98.6% purity) were purchased

Received: September 24, 2013
Revised: January 7, 2014
Accepted: January 9, 2014
Published: January 9, 2014

ACS Publications © 2014 American Chemical Society

Table 1. Selected Properties of Test Chemicals

test chemical	therapeutic use	chemical formula	molecular weight (g/mol)	pK_a	log K_{ow} [a]	log D_{ow} [b]
carbamazepine	anticonvulsant	$C_{15}H_{12}N_2O$	236.27	N/A	2.5	N/A
diclofenac	anti-inflammatory	$C_{14}H_{11}Cl_2NO_2$	296.15	4.0	4.5	2.30
fluoxetine	antidepressant	$C_{17}H_{18}F_3NO$	309.33	10.1	4.1	0.19
propranolol	beta-blocker	$C_{16}H_{21}NO_2$	259.34	9.5	3.5	0.19
sulfamethazine	antibacterial	$C_{12}H_{14}N_4O_2S$	278.32	7.4	0.9	0.87
triclosan	antimicrobial	$C_{12}H_7Cl_3O_2$	289.54	8.1	4.8	4.80

[a]Un-ionized form of the drugs; [b]at pH 6.25.

from TLC Pharmachem (Vaughan, Canada) for use as internal standards in the chemical analyses.

Tepko soil (obtained from near Tepko township in South Australia) was used for both the plant uptake and fate studies (pH 6.25, EC 0.09 dS/cm, OC 1%, CEC 5.2 cmol(+)/kg, 0.6% moisture, clay 8%, 3% silt and 89% sand). The soil was not cropped and had not previously received biosolid or wastewater applications. Test soil was obtained from the top 10 cm depth and prior to testing was air-dried and then sieved to 2 mm to ensure homogeneity.

Ryegrass seeds (*Lolium perenne*, Guard variety) were obtained from Seed Services (SARDI, South Australian Research and Development Institute) and radish seeds (*Raphanus sativus*, Cherry belle variety) were from Mr Fothergills (Sydney, Australia).

Fate Study. For each study chemical, duplicate pots of soil (200 ± 5 g) were spiked with aliquots of 1 g/L (in acetone) solution to give a nominal concentration of test compound of 10 mg/kg. This concentration, which is higher than concentrations expected in the environment, was chosen to enable detection of the study compounds in the soil pore water. Following spiking, soil was mixed by hand to ensure a homogeneous distribution of the test chemicals; pots were then left for 2 h in a fume cupboard to evaporate off any solvent. Blank control pots were also prepared. Plants were omitted from fate study pots because previous research has demonstrated that the presence of plants results in no significant differences in compound dissipation in soils either by uptake or enhanced degradation and therefore would not significantly influence our fate study.[17] Pots were then kept in controlled conditions (14 h light (23 °C) 10 h dark (15 °C)) until time of sampling. Moisture content adjustments were made on a daily basis, by addition of deionized water (DI), to ensure levels remained at 60% of the soil maximum water holding capacity (MWHC) (for methods see Supporting Information, section 1.1). Sampling points were 0 h, 1, 3, 7, 14, 40 days. At each sampling point, duplicate pots were removed, and the soil pore water was extracted. Extractions were done by taking 2 × 25 g portions of soil from each pot and placing these on top of a glass wool insert in 2 × 25 mL disposable plastic syringes. Syringes were placed in plastic centrifuge tubes and centrifuged at 3500 rpm for 45 min. The resulting pore water collected in the two centrifuge tubes for each single sample was combined into one sample and centrifuged again at 15 000 rpm for an additional 30 min and then transferred to vials ready for analysis. Soil samples (sampled directly from the fate pots) were also taken and stored at −20 °C for later analysis.

Uptake of Pharmaceuticals into Plants. Plastic pots containing 500 ± 5 g and 200 ± 5 g were prepared for use in uptake studies with radish and ryegrass respectively. Pots were prepared in triplicate for each pharmaceutical and plant type and spiked as per the fate study to give a final soil concentration of 1 mg/kg. This concentration, which is at the high end of reported concentrations for pharmaceuticals in soil and at the lower end of concentrations used in previous uptake studies, was chosen to maximize the likelihood of detection in plant tissue while maintaining a degree of realism. Solvent and blank controls were also prepared in triplicate. Soils were then left for 48 h to equilibrate before a total of 6 and 16 seeds were initially added to each pot for radish and ryegrass respectively, which were then lightly covered in test soil.

Plants were left to grow for 6 weeks in a growth chamber under the same conditions as the pots in the fate study. Pots were arranged in a randomized order (specific positions were determined based on a random number generator in Microsoft Excel). A similar watering regime to that used in the fate study was adopted to maintain moisture levels at 60% of the MWHC. After 50% germination (when the seedling was visible through the soil), plants were fed Ruakura nutrient solution, where 5 mL was applied per 250 g soil twice weekly (for three weeks) instead of the DI water. After 3 weeks, addition of nutrient solution continued with one 5 mL application of nutrient solution per 250 g of soil per week (for nutrient solution preparation, see Supporting Information, section 1.2). When 80−90% of plants had germinated (approximately day 11), the radish plants were thinned to leave behind three seedlings. This was to ensure maximum for growth potential in order to gather enough biomass for the chemical analysis.

At harvest, loose soil was removed from around the radish plant to allow for the intact removal of the whole radish. The radish plant was thoroughly rinsed in deionized water to remove any soil residues, patted dry with paper towel, weighed, and divided up into root and above ground biomass, and these were then reweighed separately. For the ryegrass, after the maximum height of the plants from each treatment was measured, the above ground plant material was cut away, rinsed in DI water, patted dry, and then weighed. All plant samples were cut into smaller pieces and then freeze-dried and stored at −20 °C until extraction for residue analysis. Soil was also taken from the plant pots, at the end of the uptake study, for analysis.

Pharmaceutical Analysis. *Extraction from Soil and Plant Material.* Pharmaceutical compounds were extracted from soils and plants using validated methods chosen for their high percentage recoveries (Supporting Information, section 1.3). Prior to plant and soil extractions, 1 mg/g of deuterated stable isotope standard was added to their respective samples (100 μg/L stock solution in acetone). Since stable isotopes were unavailable for sulfamethazine, control plants and control soil samples were spiked with a known amount of sulfamethazine to determine recoveries. For the soil extraction (i.e., soil taken directly from the pots), 5 mL of methanol was added to 1 g of soil (wet weight) and 1 g of sand. After addition of the solvent, the test tubes were vortexed for 1 min and then ultrasonicated for 15 min. Lastly, the tubes were centrifuged for 30 min at 1500 rpm, and the supernatant was removed. The extraction process was repeated with a further addition of 5 mL of methanol and then 5 mL of acetone. The supernatants from the three extractions were combined and then evaporated to dryness before being reconstituted in 1 mL of methanol, sonicated for 5 min and then transferred into LC-MS/MS vials for analysis.

For the plant extractions, sand (1 g) was added to 1 ± 0.1 g of plant material for each of the samples and 5 mL of extraction solvent (70:30 acetonitrile/Milli-Q water solution) was then added to the test tube. After addition of the solvent, the test tubes were vortexed for 1 min and then ultrasonicated for 15 min. The samples were then centrifuged for 30 min at 1500 rpm, and the supernatant was removed and the process was repeated for two further extractions. The combined extracts (15 mL) were diluted with Milli-Q to make a maximum solvent concentration of 10%, and the extract was then applied to an Oasis HLB (Waters Corporation) 6 mL 200 mg solid phase extraction (SPE) cartridge that had been preconditioned with Milli-Q water and methanol. The cartridges were left to dry under a vacuum, washed with 10% methanol in Milli-Q water, and eluted with 2× methanol (3 mL) and 1× dichloromethane (3 mL). The eluates were combined and evaporated to dryness under a nitrogen stream and reconstituted in 1

mL of methanol. Lastly, the test tubes were sonicated for 5 min ready for the extract to be transferred into LC-MS/MS vials.

LC-MS/MS Analysis. Cleaned-up extracts were analyzed for the pharmaceuticals by LC-MS/MS using a ThermoFinnigan TSQ Quantum Discovery Max (Thermo Electron Corporation). HPLC separation was performed with a Kinetex C18 100 × 2.1 mm i.d. (2.6 μm particle size) column (Phenomenex, USA) with a mobile phase flow rate of 0.3 mL/min. The mobile phase composition consisted of two eluents which were (A) formic acid (0.1%) and (B) acetonitrile using a binary gradient program over 12 min. The relative flow of 0.1% formic acid was 95% for 2 min, 20% after 3 min, 2% at 4 min, and held for 3 min until 7 min before returning to 95% by 9.5 min. MS/MS analysis was undertaken using atmospheric pressure electrospray ionization (ESI) in both positive and negative ionization modes. Spray voltage was 5000 V, and source collision induced dissociation was −12 V in positive ESI and −4000 and 10 V for negative ESI, with the ESI capillary line maintained at 350 °C and collision gas (Ar) pressure set at 1.5 mTorr. More details of the analytical method pertaining to each compound are summarized in Supporting Information, section 1.4. Qualitative and quantitative analysis of compounds was based on retention time, multiple reaction monitoring (MRM) of two product ions, and the ratios between the product ions.

Isotopes were used to account for recovery (loss of analytes during sample preparation and matrix effects); however, isotopes were unavailable for sulfamethazine. Sulfamethazine spiked matrix samples were extracted and run throughout the analysis and compared with sulfamethazine standards in a clean matrix to determine the extent of ion suppression or enhancement. Lower limits of quantitation (LOQs) were derived using guidelines proposed by the USEPA.[25]

Data Analysis. *Soil Degradation.* Concentrations of pharmaceuticals in soil and pore water were plotted against time of sampling. Where there was a significant difference in concentration to that measured at 0 days (for methods see Statistical Analysis section), three kinetic models were used to fit the data: a simple first-order degradation kinetic (SFO; eq 1) model, a first-order multicompartment model (FOMC; eq 2),[26] and a biexponential first-order model (BFO; eq 3).[27] Model parameters were optimized according to recommendations by FOCUS using the least-squares method with Microsoft Excel Add-Inn Solver.[27]

$$C_t = C_0 e^{-kt} \quad (1)$$

$$C_t = C_0(1 + \beta t)^{-\alpha} \quad (2)$$

$$C_t = C_{t1} + C_{t2} = C_{01} e^{(-k1t)} + C_{02} e^{(-k2t)} \quad (3)$$

where C_t is the concentration of pharmaceutical remaining in soil (μg/g) after t (days), C_0 is the initial concentration of pharmaceutical (μg/g), k is the rate of degradation (day^{-1}), β is the location parameter, α is a shape parameter determined by coefficient of variation k values. For eq 3, $C_{t1} + C_{t2}$ is the total amount of pharmaceutical applied at time t = 0 (in two compartments), C_{01} and C_{02} is the amount of chemical applied to compartment 1 and 2 respectively, and k_1 and k_2 are independent decay rate constants for compartments 1 and 2 respectively. Models used specific to each pharmaceutical, parameter, and measurement to assess the goodness of fit for the optimized parameters are outlined in Supporting Information, section 1.5. For SFO and FOMC model fits, the time it took for a 50 or 90% decline in the concentration of the pharmaceutical (DT_{50}, DT_{90}) could then be calculated from the model fits (Supporting Information, section 1.5.1). For BFO models, no analytical solution exists to calculate degradation end points.

Uptake Factors. Measured concentrations for each of the pharmaceuticals taken up by the radish and ryegrass were used to calculate soil and pore water-based uptake factors (UFs). UFs were derived using concentrations in the soil, pore water, and plant material (eqs 4−6).

$$UF_{soil} = \frac{C_p}{C_s} \quad (4)$$

$$UF_{pore\ water} = \frac{UF_{soil}}{K_d} \quad (5)$$

$$K_d = \frac{C_s}{C_{pw}} \quad (6)$$

where UF_{soil} is the soil-based UF, $UF_{pore\ water}$ is the soil pore water-based UF, C_p is the concentration in plant material, C_s is the concentration associated with the soil particles (i.e., total soil concentration corrected for the concentration in the pore water), C_{pw} is the concentration in the pore water, and K_d is the average soil sorption coefficient for each pharmaceutical calculated across seven sampling points in the fate study.

Statistical Analysis. Statistical analysis of the data was performed using Sigma Plot (v.11.0). A one-way ANOVA (significance level 0.05) was employed to assess differences in plant biomass (dry weight) between plants grown under treated soil and controls. Additionally, a one-way ANOVA (p = 0.05) was employed to assess any differences in concentration of the pharmaceuticals in the soil and pore water over 40 day exposures, with additional comparisons between sampling points assessed by Holm−Sidak pairwise comparison. To determine which pharmaceuticals showed a significant difference in concentration between radish leaf and ryegrass, t test's were performed. Prior to all tests, the data were tested for normality and equal variance by performing a Shapiro−Wilk and Levene−Mediane test, respectively.

RESULTS AND DISCUSSION

Fate Study. Over 40 days, average K_d values ranged from 0.99 to 121.88 L/kg and increased in the order of sulfamethazine < carbamazepine < fluoxetine < diclofenac < propranolol < triclosan (Table 2). Some of the study compounds persisted in the soil throughout the 40 day uptake period, while others were readily dissipated (Figure 2; Table 3). There was no significant difference between measured concentrations at 0 and 40 days for carbamazepine (p = 0.026), fluoxetine (p = 0.162), and propranolol (p = 0.757). Triclosan dissipated from the soil after 14 days (p = 0.004). Concentrations of diclofenac (p = 0.032) and sulfamethazine (p = 0.013) significantly decreased after 1 day and were undetectable after 3 days. The dissipation rates of these three compounds was fast (0.06−1.4 day^{-1}; Table 3); compound degradation followed single first-order kinetics, and corresponding DT_{50} values were 0.5, 0.99, and 11.55 days for diclofenac, sulfamethazine, and triclosan respectively.

The persistent nature of carbamazepine, fluoxetine, and propranolol is consistent with previous research findings.[9,28−30] The observed degradation of triclosan is also consistent with previous research which has suggested a half-life of 18 days.[31] Results presented in this study show that in less than 40 days only 10% of the applied triclosan remained in the soil (Supporting Information, section 1.5). This is probably due to the transformation of triclosan to methyl triclosan.[13,32] Previous fate studies have also shown that diclofenac is not persistent and readily biodegradable from soils as a result of chemical mineralization.[15,33] The half-life observed in this study (0.5 days) is therefore comparable to previous findings of <5 days[33] and considerably faster than observations by Xu et al.,[34] who reported DT_{50}'s ranging from 3.1 days (loamy sand) to 20.4 days (silty loam) (Table 3). Dissipation of sulfamethazine has been observed in previous research, although the average half-life was longer at 18.6 days than reported in this study (Table 3).[35]

Even though diclofenac and sulfamethazine were not detectable in whole soil extracts after 3 days, detectable concentrations of these chemicals in the pore water were seen

dx.doi.org/10.1021/jf404282y | J. Agric. Food Chem. 2014, 62, 816−825

Table 2. Average Soil Concentrations Measured at the End of the Experiment from Soils Collected from the Plant Pots, Soil–Water Partition Distribution Coefficients (K_d) Values Calculated during Fate Study and Calculated Uptake Factors (UF) for Ryegrass, Radish Bulb, and Leaf[a]

pharmaceutical	radish soil (μg/g)	ryegrass soil (μg/g)	soil K_d (L/kg: average 21 days)	ryegrass UF_{soil}	radish leaf UF_{soil}	radish bulb UF_{soil}	ryegrass $UF_{pore\ water}$	radish leaf $UF_{pore\ water}$	radish bulb $UF_{pore\ water}$
carbamazepine	0.71	0.46	7.85	65.26	60.59	8.28	8.31	7.71	1.05
diclofenac	0.07	0.05	12.40	6.82	11.53	5.39	0.55	0.93	0.43
fluoxetine	0.47	0.55	8.39	0.08	0.10	0.36	0.01	0.011	0.043
propranolol	0.16	0.21	79.44	11.04	0.91	1.20	0.14	0.011	0.015
sulfamethazine	<LOQ	0.01	0.99	<LOQ	<LOQ	<LOQ	<LOQ	<LOQ	<LOQ
triclosan	9.31	0.05	121.88	37.59	0.10	0.12	0.31	0.0008	0.001

[a]Plant concentrations used for calculations are on a dry weight basis.

Table 3. Summary Statistics from Soil and Pore Water Dissipation Modeling[a]

	pore water					soil				
pharmaceutical	model	DT_{50} (days)	DT_{90} (days)	rate constants	r^2	model	DT_{50} (days)	DT_{90} (days)	rate constants	r^2
carbamazepine	*b*	>40	>40			*b*	>40	>40		
diclofenac	FOMC	19.65	2.57×10^3	$\alpha = 0.79$, $\beta = 0.34$	0.88	SFO	0.50	1.64	(1.4)	0.99
fluoxetine	*b*	>40	>40			*b*	>40	>40		
propranolol	*b*	>40	>40			*b*	>40	>40		
sulfamethazine	BFO			C01 = 91 C02 = 9 $k_1 = 0.85$ $k_2 = 0.017$	0.99	SFO	0.99	3.29	(0.7)	0.99
triclosan	*b*	>40	>40			SFO	11.55	38.38	(0.06)	0.97

[a]More detailed table including model fit provided in Supporting Information, section 1.5. [b]No significant difference between 0 and 40 day measured concentrations; therefore, data were not modeled to determine degradation rates.

for the full duration of the fate study (Figure 2). By 40 days, concentrations of all test chemicals remaining in the pore water decreased in the order carbamazepine > fluoxetine > sulfamethazine > propranolol > triclosan > diclofenac (Figure 2). With the exception of sulfamethazine on 0 days, carbamazepine concentrations were consistently the highest in the pore water (1321–3129 μg/L) over 40 days (Figure 2). Sulfamethazine concentrations were initially high (2932–6502 μg/L); however after 1 day, concentrations dropped to 832–2683 μg/L, after which they decreased at a slower rate. Unlike soil dissipation, pore water dissipation did not follow first-order kinetics. Models instead included first-order multicompartment model (FOMC; eq 2)[26] and a biexponential first-order model (BFO; eq 3) (Table 3). Pore water concentrations decreased significantly in the diclofenac ($p = 0.016$) and sulfamethazine studies ($p = < 0.001$) resulting in DT_{50}'s < 20 days (Table 3) in comparison to DT_{50}'s for the remaining compounds of >40 days. While triclosan dissipated rapidly from the soil, pore water concentrations were not significantly different at any of the sampling points over 40 days ($p = 0.266$).

Plant Uptake. Plants contain ion channels and enzymes which could also be potentially targeted by pharmaceuticals and may initiate a response such as inhibition in the transport of essential elements required for plant growth for example.[36] Previous research has highlighted the potential for pharmaceuticals to induce toxic effects on plants.[22] Dose response relationships with plants grown under triclosan treatment have been noted starting at 0.44 mg/L in hydroponic studies[24] and low observed effect concentrations (LOECs) seen at 0.74 mg/kg after plant growth in quartz sand.[37] In this study, however, no observed effect on plant growth was noted for any of the treatments in comparison to the controls ($p = 0.08–0.966$) for both radish and ryegrass, probably due to the more realistic exposure concentrations that were used. This is in support of previous research where concentrations of carbamazepine in root tissue ranging between 202–426 μg/kg yielded no observed effect on ryegrass aerial plant growth (Supporting Information, section 1.6).[38]

Previous research has demonstrated metabolism of carbamazepine within the bean and leaf.[17,39] Therefore, in our study it is possible there may have been some transformation of parent compounds; however potential metabolite products were not quantified, and the results presented focus on the parent compounds. Five of the six test chemicals were taken up in detectable quantities into radish and ryegrass (Table 2; Figure 1). The degree of uptake varied across pharmaceuticals and plant species. With the exception of propranolol, greater uptake into radish was seen after combining the concentrations in the bulb and leafy parts compared to ryegrass. For both radish and ryegrass, carbamazepine was taken up to the greatest extent with measured concentrations of up to 52 μg/g dwt in radish leaf (Figure 1). While sulfamethazine was taken up by both plants, this was consistently below the LOQ (Supporting Information, section 1.4.1). Therefore, both radish leaf and radish bulb accumulated chemicals in the order of carbamazepine > triclosan > diclofenac > propranolol > fluoxetine, whereas chemicals accumulated in the ryegrass in the order of carbamazepine > propranolol > triclosan > fluoxetine > diclofenac (Figure 1).

In the propranolol exposure, there was very high uptake into the ryegrass, but this was not mirrored in the radish leaf where concentrations were some 16 times lower ($t_{(4)} = 6.38$, $p = 0.003$) (Figure 1). For the remaining pharmaceuticals, concentrations in the radish leaf and ryegrass were not significantly different (carbamazepine $t_{(4)} = 2.28$, $p = 0.09$;

dx.doi.org/10.1021/jf404282y | J. Agric. Food Chem. 2014, 62, 816–825

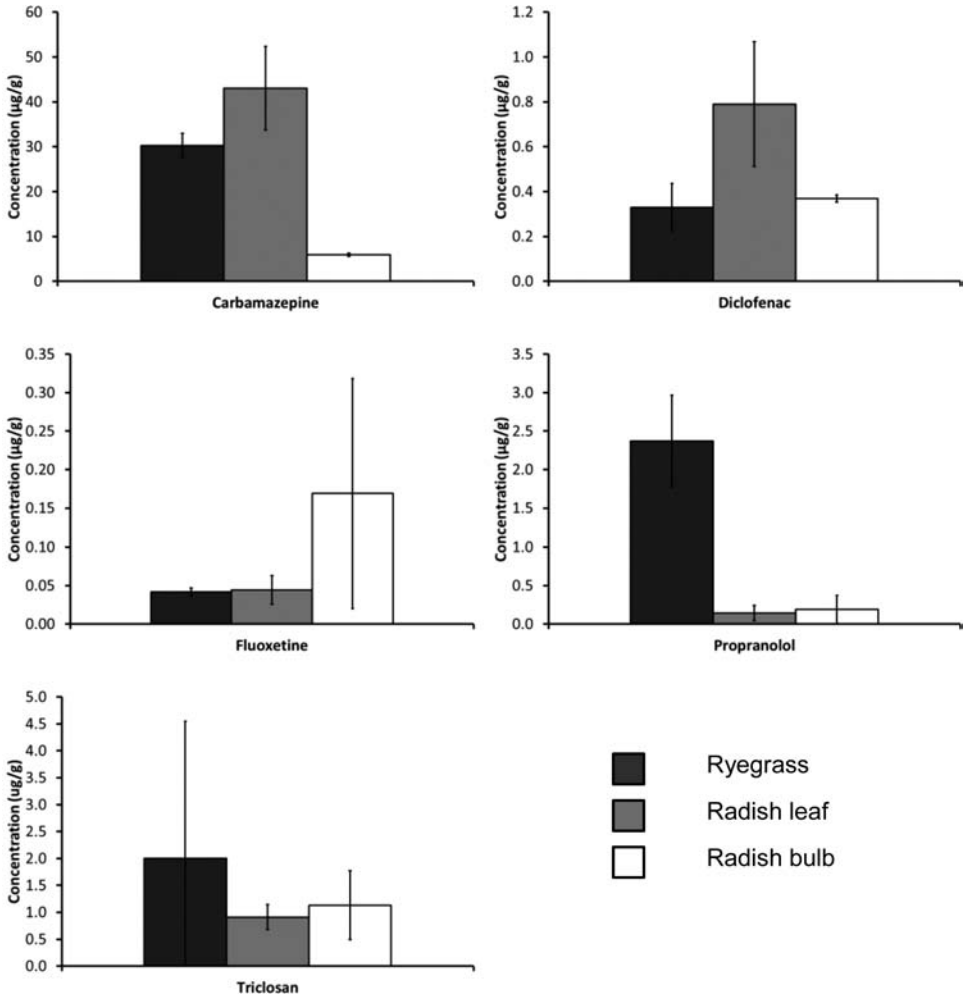

Figure 1. Uptake of carbamazepine, diclofenac, fluoxetine, propranolol, and triclosan into ryegrass, radish leaf, and radish bulb after plants were grown from seed in pharmaceutically spiked soil for 40 days. Average concentrations (dry weight) provided with error bars representing the standard error. Sulfamethazine uptake was below LOQ.

diclofenac $t_{(4)} = 2.69$, $p = 0.06$; fluoxetine $t_{(4)} = 0.24$, $p = 0.82$; triclosan $t_{(4)} = 0.34$, $p = 0.75$).

Greater fluoxetine uptake into the roots was observed in this study (170 ng/g dwt) in comparison to research by Wu et al.[17] where fluoxetine root concentrations were <22.2 ± 5.3 ng/g after exposure via biosolids application. The amended soil concentration in the Wu et al.[17] study was lower (0.07 mg/kg) than the current study, whereas in an earlier study Redshaw and colleagues saw fluoxetine uptake by *Brassicaceae* tissue cultures from a hydroponic setup comparable to the results from our study at 0.26−0.49 µg/g.[23]

Uptake Factors. The greatest UF_{soil} values for the ryegrass, radish leaf, and radish bulb were obtained in the carbamazepine treatments, with values of 65.3, 60.6, and 8.28, respectively (Table 2). In comparison, relatively small UF_{soil} values were found for fluoxetine (0.08−0.36) (Figure 1). Calculated $UF_{pore\ water}$ range between 0.01−8.31, 0.0008−7.71, and 0.001−1.05 for the ryegrass, radish leaf, and radish bulb respectively (Table 2). Similar to UF_{soil} carbamazepine exposure resulted in the highest $UF_{pore\ water}$ in the ryegrass, radish leaf, and radish bulb. Triclosan had the lowest $UF_{pore\ water}$ in the radish leaf (0.0008) and bulb (0.001), whereas fluoxetine had the lowest $UF_{pore\ water}$ in ryegrass (0.01).

In comparison to results generated from field experiments (via biosolid application) for carbamazepine uptake into roots and shoots, the results presented in this study are just over double those observed in the field study.[21] Specifically for triclosan, work by Karnjanapiboonwong et al.[40] found greater UFs between the soil and the root in the pinto bean (*Phaseolus vulgaris*), which ranged between 9 and 12, in comparison to UF_{soil} (0.12) and $UF_{pore\ water}$ (0.001) values generated in this study for the radish root. However, in the ryegrass exposure the triclosan UF_{soil} is considerably larger in the present study at 37.6, demonstrating that plant uptake is dependent on both species and compound; such factors are discussed in more detail below.

Potential Factors Influencing the Uptake of Pharmaceuticals. Plant uptake is thought to be heavily dependent on the physicochemical characteristics of the chemical, including Henry's Law constant, water solubility, and octanol−water partition coefficient.[41−44] Dissociation constants are important because they can describe whether a chemical is neutral or ionizable at environmentally relevant pH values. A clear distinction has been made between the plant uptake of neutral chemicals and chemicals that are ionized (electrically charged), and separate models exist to predict uptake of chemicals in both these forms.[45] However, it is important to note the total

dx.doi.org/10.1021/jf404282y | J. Agric. Food Chem. 2014, 62, 816−825

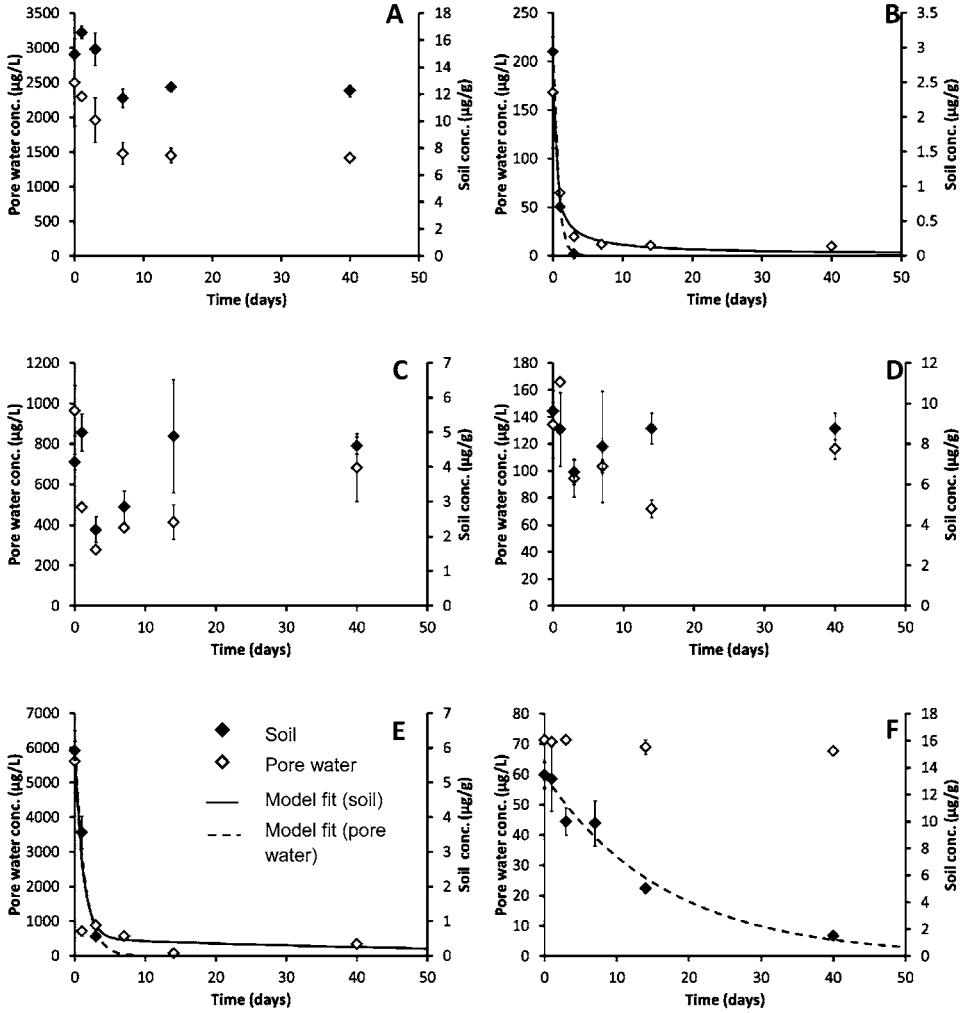

Figure 2. Average measured soil (closed) and pore water (open) concentrations during fate study (40 days) for test pharmaceuticals: carbamazepine (A), diclofenac (B), fluoxetine (C), propranolol (D), sulfamethazine (E), and triclosan (F). Best model fit provided by dashed line for soil and a solid line for pore water where necessary and error bars represent standard error of mean.

concentration in a plant cell comprises neutral, ionic, and complexed forms of a compound.[45] In this study, carbamazepine was the only neutral chemical, whereas the remaining pharmaceuticals were ionizable (Table 1).

For neutral chemicals, hydrophobicity (usually expressed as log K_{ow}) has been postulated to be the most important property involved in the uptake of chemicals into a plant from the soil medium[46] as the degree of uptake appears to be proportional to the octanol–water partition coefficient.[47,48] Briggs et al.[47] proposed that plant uptake of neutral chemicals can be represented by a Gaussian distribution (bell-shaped curve) where maximum translocation of chemicals can be seen at a log K_{ow} ~1.78 in comparison to particularly hydrophobic (high log K_{ow}) and hydrophilic (low log K_{ow}) chemicals which are taken up to a lesser extent.

Carbamazepine is hydrophilic in nature preferring to reside in the aqueous phase rather than attached to the soil particles as demonstrated by the low K_d values discussed above (Table 2). The high concentrations in pore water for the carbamazepine exposure may have played a crucial role in the large amount of uptake observed. However, the consistently high carbamazepine uptake into leafy parts of the plants (<52 μg/g) can more likely be attributable to the log K_{ow} of this neural compound which is similar to the K_{ow} values where maximum uptake of neutral organics is observed.[47] Greater carbamazepine concentrations were noted in the leaf material in comparison to the roots (Figure 1; Table 2) which is in agreement with previous research findings.[17,19,21,38] It appears that the uptake of carbamazepine is passive and not restricted by root membranes. The relatively low hydrophobicity of carbamazepine enables it to be transported by mass flow from the roots and concentrate in the mature and older leaves.[19]

Even though triclosan is slightly ionized at the test soil pH of 6.19 (1.2%), most of the compound will be in the nonionized form. The un-ionized molecule has a log K_{ow} of 4.80, so the low observed uptake for triclosan can be also explained by the fact that it falls on the upper tail of the Gaussian distribution.[47] Small radish $UF_{pore\ water}$ (0.0008–0.001) and UF_{soil} (0.10–0.12) values for triclosan uptake demonstrate that particularly hydrophobic chemicals are not taken up to a great extent in the plant material.

Similar to triclosan, only a small proportion of sulfamethazine (5.8%) would be in the ionized form. On the basis of the Gaussian distribution,[47] the neutral form of sulfamethazine (log K_{ow} of 0.9) would not be expected to enter the root system; it is therefore not surprising that concentrations of sulfamethazine were below the LOQ and that UFs could not be calculated. The rapid dissipation from the soil in the first of the study 3 days

dx.doi.org/10.1021/jf404282y | J. Agric. Food Chem. 2014, 62, 816–825

may have also contributed to the lack of detection of sulfamethazine in plant tissue (Figure 2).

Diclofenac, fluoxetine, and propranolol are expected to be extensively ionized in the test soil (>99%). Previous research demonstrates that plant uptake of the dissociated species of an ionizable compound is lower compared to the un-ionized species.[49,50] As demonstrated in Figure 1, there was up to 600 times less uptake of diclofenac, fluoxetine, and propranolol in the ryegrass in comparison to the neutral pharmaceutical carbamazepine. Specifically for diclofenac, the large ionization combined with the results from the fate study which show extensive dissipation from both the soil and pore water and low measured concentrations can probably explain the minimal uptake of diclofenac into the radish and ryegrass.

Previous research findings demonstrate that some pharmaceuticals have a tendency to accumulate in the roots with the roots acting as a sink for hydrophobic neutral compounds.[17,24] In general, organic chemicals with log K_{ow} > 4 are expected to have high potential for root retention and low translocation capacity.[44] Even though diclofenac and fluoxetine have log K_{ow} > 4 (Table 1), this is in their un-ionized form. As both diclofenac and fluoxetine are extensively ionized at test soil pH log K_{ow} is not applicable and thus cannot explain plant uptake. However log D_{ow} (pH corrected log K_{ow}) could be a better descriptor for ionized chemicals as our results show a general increase in log D_{ow} corresponds to an increase in $UF_{pore\ water}$ and UF_{soil}. For example, fluoxetine and propranolol have low log D_{ow} values (Table 1) and smaller $UF_{pore\ water}$ (<0.14) than diclofenac ($UF_{porewater}$ < 0.93) at log D_{ow} 2.3.

Similar to other studies, our results found differences in uptake between the two crop species.[16,21] Differences may be explained by factors such as degree of root growth, transpiration rates, and the size and shape of the leaf material. Differences in plant lipid contents may also be important as this can affect the sorption of hydrophobic chemicals.[51,52] The reported lipid content of perennial ryegrass ranges between 2−4%,[53] whereas radish bulbs only contain trace amounts of lipid which may explain the lower observed uptake of carbamazepine, diclofenac, and propranolol in the radish (Figure 1). However, similarly to results in the Wu et al.[21] study, differences in plant uptake behavior could not be solely attributable to differences in lipid content between plants.

On the basis of the results presented, the factors that affect the uptake of pharmaceuticals into plants include physicochemical properties of the pharmaceuticals, species type including lipid content, and distribution between above and below ground plant. Previous work has also highlighted that plant uptake can vary between a mixture and single compound exposure,[54] and additional research has also demonstrated that soil properties and the application of biosolids or wastewater irrigation can also affect plant uptake.[17,21,55−57] Interestingly, the persistence of pharmaceuticals in soil can also be influenced by the presence of biosolids, which can ultimately affect plant uptake as well.[29] Therefore to conclude, the uptake of chemicals into plants is a complex process governed by a combination of soil, plant, and chemical factors. However on the whole, the uptake behavior observed in this study makes sense based on the knowledge from previous research.

Human Exposure. Uptake into plants, especially edible crops, may represent an important exposure pathway of these chemicals into the food chain and thus present a risk to humans and livestock which feed on them.[16,58−60] An acceptable daily intake (ADI) value can be used to calculate the amount of a substance, for example, pharmaceuticals, that can be consumed by a human without resulting in appreciable risk to health. For a full explanation of calculated methods to determine the risk to humans from consuming contaminated crops from results in the present study see Supporting Information, section 1.7.

Results show that if all crops consumed were grown in soil containing the selected pharmaceuticals, then humans would not consume levels greater than the ADI for any of the pharmaceuticals in this study (Table 4). It should also be noted that all crops eaten must be grown in the contaminated soil as our analysis assumed radish leaf and bulb to be representative of all above and below ground crops consumed, which is not currently the case. A safety factor of 100 was also applied to the minimum therapeutic dose to calculate the ADI, and for a large proportion of the population this is not needed, which would make the actual ADI higher than the current threshold.

Table 4. Results from a Comparison of Acceptable Daily Intake (ADI) Values for Study Chemicals and Theoretical Crop Concentration (Based on Measured Soil Concentrations and UF_{soil} Calculated in This Study) Shown As a Percentage of ADI[a]

		ryegrass	radish
	soil (mg/kg)	% of ADI in 359.5 g crop	% of ADI in 159 g crop
carbamazepine	0.0065[b]	3.81	0.21
diclofenac	0.00054[c]	0.18	0.06
fluoxetine	0.0067[c]	0.09	0.19
propranolol	0.0004[d]	0.20	0.01
triclosan	0.019[b]	83.80	0.12

[a]With exception of sulfamethazine as plant concentrations were below LOQ. Ryegrass was used as a representative above ground crop species and radish as a representative below ground crop species. [b]Measured soil concentration reference = Duran-Alverez et al., 2009. [c]Measured soil concentration reference = Dalkmann et al., 2012. [d]Measured soil concentration reference = Vazquez-Roig et al., 2012.[10,14,15]

To date, the health risks from pharmaceuticals in drinking water have been reviewed, and several papers have also computed levels in crops fit for human consumption.[16,61,62] For fluoxetine, a comparison of measured concentrations in drinking water and predicted no effect concentrations in children yielded a ratio of 2.8×10^{-4}, which would infer the risk to humans drinking water contaminated with fluoxetine would be minimal. Indeed, for all APIs evaluated, approximate margins of safety for potential exposures ranged from 30 to 38000.[61] Presently, the risk to humans in terms of contaminated crops is therefore similar to drinking water exposures, in that it is highly unlikely.

However, an important note for the future is that with the growing demand for alternative irrigation resources in water stressed regions and projected increases in the application of sewage sludge on land, pharmaceutical loadings in soil will inevitably increase. The threat posed by pharmaceuticals taken up into crops may therefore be of more concern in the future than based on current exposure levels.

In conclusion, radish and ryegrass can take up a variety of pharmaceuticals and personal care products from spiked soil. On the basis of current exposure levels, however, this uptake does not pose a risk to humans consuming crop grown in contaminated soil. Using a combination of fate study and plant uptake data, it is clear that relationships between plant uptake

and the available fraction of the chemical are key. While a chemical may have a log K_{ow} that fits within the Gaussian distribution correlating with a high propensity for uptake, this clearly is not the only property influencing uptake into plants. The ionizable state of the chemical together with its potential for degradation may result in diminishing concentrations in the soil matrix. The fraction available for uptake may therefore be very small, and, correspondingly, the measured concentrations in the plant material will also be minimal. Interestingly, fate studies data show that while a chemical may dissipate from the soil it can still remain in the pore water. This may hold wider implications for risk assessments and screening techniques as chemicals present in the pore water may still be bioavailable for uptake into an organism.

Our results demonstrate that in some circumstances uptake and distribution of pharmaceuticals and personal care products in a plant can be related to hydrophobicity (K_{ow}) and generally follows a Gaussian distribution, although this is not always the case. The results presented here would suggest that there are different drivers responsible for the uptake between different plant species. It is instructive to note that pharmaceuticals are predominantly ionizable organic chemicals, and in contrast to neutral organics, this is a characteristic that is likely to affect their partitioning behavior in terms of bioavailability, plant uptake, and molecular interaction with soil matrices of variable pH. It therefore may be important to question previous assumptions on plant uptake, and specific models may be required to accurately predict plant uptake which account for species differences, distribution of chemicals in the plant, chemical properties, and the fate of the pharmaceutical in different soil matrices.

■ ASSOCIATED CONTENT

Supporting Information

Detailed information on preparation of nutrient stock solution, LC-MS/MS methods, parameters for dissipation modeling, and human exposure calculations. This material is available free of charge via the Internet at http://pubs.acs.org.

■ AUTHOR INFORMATION

Corresponding Author

*E-mail: alistair.boxall@york.ac.uk.

Funding

The work presented here is part of a BBSRC Ph.D. Case Award in collaboration with GlaxoSmithKline.

Notes

The authors declare no competing financial interest.

■ ACKNOWLEDGMENTS

The authors would like to gratefully acknowledge Sheridan Martin (CSIRO) who provided valuable input to the study.

■ REFERENCES

(1) Community prescribing in the UK. The Association of the British Pharmaceutical Industry (ABPI): London, 2012; http://www.abpi.org.uk/industry-info/knowledge-hub/medicines/Pages/community-prescribing.aspx#fig1 (accessed March 25, 2012).

(2) Top-line market data. Intercontinental Medical Statistics (IMS Health): Danbury, CT, 2012; http://www.imshealth.com/portal/site/ims/menuitem.5ad1c081663fdf9b41d84b903208c22a/?vgnextoid=fbc65890d33ee210VgnVCM10000071812ca2RCRD&vgnextfmt=default (accessed March 25, 2012).

(3) National statistics. Prescriptions dispensed in the community: England, Statistics for 2000 to 2010. National Health Service (NHS): London, 2011; https://catalogue.ic.nhs.uk/publications/prescribing/primary/pres-disp-com-eng-2000-10/pres-disp-com-eng-2000-10-rep.pdf; (accessed March 25, 2012).

(4) Stackelberg, P.; Furlong, E.; Meyer, M.; Zaugg, S.; Henderson, A.; Reissman, D. Persistence of pharmaceutical compounds and other organic wastewater contaminants in a conventional drinking-water treatment plant. *Sci. Total Environ.* **2004**, *329*, 99−113.

(5) Gobel, A.; Thomsen, A.; McArdell, C.; Joss, A.; Giger, W. Occurrence and sorption behavior of sulfonamides, macrolides, and trimethoprim in activated sludge treatment. *Environ. Sci. Technol.* **2005**, *39*, 3981−3989.

(6) Joss, A.; Keller, E.; Alder, A.; Gobel, A.; McArdell, C.; Ternes, T.; Siegrist, H. Removal of pharmaceuticals and fragrances in biological wastewater treatment. *Water Res.* **2005**, *39*, 3139−3152.

(7) Gomez, M.; Bueno, M.; Lacorte, S.; Fernandez-Alba, A.; Aguera, A. Pilot survey monitoring pharmaceuticals and related compounds in a sewage treatment plant located on the Mediterranean coast. *Chemosphere* **2007**, *66*, 993−1002.

(8) Kim, S.; Cho, J.; Kim, I.; Vanderford, B.; Snyder, S. A. Occurrence and removal of pharmaceuticals and endocrine disruptors in South Korean surface, drinking, and waste waters. *Water Res.* **2007**, *41*, 1013−1021.

(9) Kinney, C.; Furlong, E.; Werner, S.; Cahill, J. Presence and distribution of wastewater-derived pharmaceuticals in soil irrigated with reclaimed water. *Environ. Toxicol. Chem.* **2006**, *25*, 317−326.

(10) Durán-Alvarez, J.; Becerril-Bravo, E.; Castro, V.; Jiménez, B.; Gibson, R. The analysis of a group of acidic pharmaceuticals, carbamazepine, and potential endocrine disrupting compounds in wastewater irrigated soils by gas chromatography-mass spectrometry. *Talanta* **2009**, *78*, 1159−1166.

(11) Golet, E.; Xifra, I.; Siegrist, H.; Alder, A.; Giger, W. Environmental exposure assessment of fluoroquinolone antibacterial agents from sewage to soil. *Environ. Sci. Technol.* **2003**, *37*, 3243−3249.

(12) Redshaw, C.; Cooke, M.; Talbot, H.; McGrath, S.; Rowland, S. Low biodegradability of fluoxetine HCl, diazepam and their human metabolites in sewage sludge-amended soil. *J. Soils Sediments* **2008**, *8*, 217−230.

(13) Butler, E.; Whelan, M.; Sakrabani, R.; van Egmond, R. Fate of triclosan in field soils receiving sewage sludge. *Environ. Pollut.* **2012**, *167*, 101−109.

(14) Vazquez-Roig, P.; Segarra, R.; Blasco, C.; Andreu, V.; Pico, Y. Determination of pharmaceuticals in soils and sediments by pressurized liquid extraction and liquid chromatography tandem mass spectrometry. *J. Chromatogr., A* **2010**, *1217*, 2471−2483.

(15) Dalkmann, P.; Broszat, M.; Siebe, C.; Willaschek, E.; Sakinc, T.; Huebner, J.; Amelung, W.; Grohmann, E.; Siemens, J. Accumulation of pharmaceuticals, *Enterococcus*, and resistance Genes in soils irrigated with wastewater for zero to 100 years in Central Mexico. *PLoS One* **2012**, *7* (9), e45397.

(16) Boxall, A.; Johnson, P.; Smith, E.; Sinclair, C.; Stutt, E.; Levy, L. Uptake of veterinary medicines from soils into plants. *J. Agric. Food Chem.* **2006**, *54*, 2288−2297.

(17) Wu, C.; Batt, A.; Witter, J.; Fang, M.; Czajkowski, K. Uptake of pharmaceutical and personal care products by soybean plants from soils applied with biosolids and irrigated with contaminated water. *Environ. Sci. Technol.* **2010**, *44*, 6157−6161.

(18) Dolliver, H.; Kumar, K.; Gupta, S. Sulfamethazine uptake by plants from manure-amended soil. *J. Environ. Qual.* **2007**, *36*, 1224−1230.

(19) Shenker, M.; Harush, D.; Ben-Ari, J.; Chefetz, B. Uptake of carbamazepine by cucumber plants - A case study related to irrigation with reclaimed wastewater. *Chemosphere* **2011**, *82*, 905−910.

(20) Holling, C.; Bailey, J.; Heuvel, B.; Kinney, C. Uptake of human pharmaceuticals and personal care products by cabbage (*Brassica campestris*) from fortified and biosolids-amended soils. *J. Environ. Monit.* **2012**, *14*, 3029−3036.

(21) Wu, C.; Spongberg, A.; Witter, J.; Sridhar, B. Transfer of wastewater associated pharmaceuticals and personal care products to crop plants from biosolids treated soil. *Ecotoxicol. Environ. Saf.* **2012**, *85*, 104−109.
(22) Kong, W.; Liang, Y.; Zhang, J.; Smith, F.; Yang, A. Uptake of oxytetracycline and its phytotoxicity to alfalfa (*Medicago sativa* L.). *Environ. Pollut.* **2007**, *147*, 187−193.
(23) Redshaw, C.; Wootton, V.; Rowland, S. Uptake of the pharmaceutical fluoxetine hydrochloride from growth medium by *Brassicaceae*. *Phytochemistry* **2008**, *69*, 2510−2516.
(24) Herklotz, P.; Gurung, P.; Heuvel, B.; Kinney, C. Uptake of human pharmaceuticals by plants grown under hydroponic conditions. *Chemosphere* **2010**, *78*, 1416−1421.
(25) *Revised Assessment of Detection and Quantiftation Approaches EPA-821-B-04-005*; United States Environment Protection Agency (USEPA): Washington, DC, 2004.
(26) Gustafson, D.; Holden, L. R. Nonlinear pesticide dissipation in soil: a new model based on spatial variability. *Environ. Sci. Technol.* **1990**, *24*, 1032−1038.
(27) *Guidance Document on Estimating Persistence and Degradation Kinetics from Environmental Fate Studies on Pesticides in EU Registration*; The forum for co-ordination of pesticide fate models and their use (FOCUS), European Union, 2006; http://focus.jrc.ec.europa.eu/ (accessed November 28, 2013).
(28) Williams, C.; Williams, C.; Adamsen, E. Sorption-desorption of carbamazepine from irrigated soils. *J. Environ. Qual.* **2006**, *35*, 1779−1783.
(29) Monteiro, S.; Boxall, A. Factors affecting the degradation of pharmaceuticals in agricultural soils. *Environ. Toxicol. Chem.* **2009**, *28*, 2546−2554.
(30) Drillia, P.; Stamatelatou, K.; Lyberatos, G. Fate and mobility of pharmaceuticals in solid matrices. *Chemosphere* **2005**, *60*, 1034−1044.
(31) Ying, G.-G.; Yu, X.-Y.; Kookana, R. Biological degradation of triclocarban and triclosan in a soil under aerobic and anaerobic conditions and comparison with environmental fate modelling. *Environ. Pollut.* **2007**, *150*, 300−305.
(32) Waria, M.; O'Connor, G.; Toor, G. Biodegradation of triclosan in biosolids-amended soils. *Environ. Toxicol. Chem.* **2011**, *30*, 2488−2496.
(33) Al-Rajab, A.; Sabourin, L.; Lapen, D.; Topp, E. The non-steroidal anti-inflammatory drug diclofenac is readily biodegradable in agricultural soils. *Sci. Total Environ.* **2010**, *409*, 78−82.
(34) Xu, J.; Wu, L.; Chang, A. Degradation and adsorption of selected pharmaceuticals and personal care products (PPCPs) in agricultural soils. *Chemosphere* **2009**, *77*, 1299−305.
(35) Accinelli, C.; Koskinen, W.; Becker, J.; Sadowsky, M. Environmental fate of two sulfonamide antimicrobial agents in soil. *J. Agric. Food Chem.* **2007**, *55*, 2677−2682.
(36) Williams, R.; Cook, J. Exposure to Pharmaceuticals Present in the Environment. *Ther. Innovation Regul. Sci.* **2007**, *41*, 133−141.
(37) Reiss, R.; Lewis, G.; Griffin, J. An ecological risk assessment for triclosan in the terrestrial environment. *Environ. Toxicol. Chem.* **2009**, *28*, 1546−1556.
(38) Winker, M.; Clemens, J.; Reich, M.; Gulyas, H.; Otterpohl, R. Ryegrass uptake of carbamazepine and ibuprofen applied by urine fertilization. *Sci. Total Environ.* **2010**, *408*, 1902−1908.
(39) Dordio, A.; Belo, M.; Martins Teixeira, D.; Palace Carvalho, A.; Dias, C.; Pico, Y.; Pinto, A. Evaluation of carbamazepine uptake and metabolism by *Typha* spp., a plant with potential use in phytotreatment. *Bioresour. Technol.* **2011**, *102*, 7827−7834.
(40) Karnjanapiboonwong, A.; Chase, D.; Canas, J.; Jackson, W.; Maul, J.; Morse, A.; Anderson, T. Uptake of 17 alpha-ethynylestradiol and triclosan in pinto bean, *Phaseolus vulgaris*. *Ecotoxicol. Environ. Saf.* **2011**, *74*, 1336−1342.
(41) Briggs, G.; Bromilow, R.; Evans, A.; Williams, M. Relationships between lipophilicity and the distribution of non-ionized chemicals in barley shoots following uptake by the roots. *Pestic. Sci.* **1983**, *14*, 492−500.
(42) Bacci, E.; Calamari, D.; Gaggi, C.; Vighi, M. Bioconcentration of organic-chemical vapors in plant-leaves - Experimental measurements and correlation. *Environ. Sci. Technol.* **1990**, *24*, 885−889.
(43) Trapp, S.; Matthies, M.; Scheunert, I.; Topp, E. Modeling the bioconcentration of organic-chemicals in plants. *Environ. Sci. Technol.* **1990**, *24*, 1246−1252.
(44) Duarte Davidson, R.; Jones, K. Screening the environmental fate of organic contaminants in sewage sludge applied to agricultural soils: II. The potential for transfers to plants and grazing animals. *Sci. Total Environ.* **1996**, *185* (1−3), 59−70.
(45) Trapp, S. Plant uptake and transport models for neutral and ionic chemicals. *Environ. Sci. Pollut. Res.* **2004**, *11*, 33−39.
(46) Hellström, A. Uptake of Organic Pollutants in Plants. Department of Environmental Assessment Swedish University of Agricultural Sciences: Uppsala, Sweden, 2004; http://info1.ma.slu.se/IMA/Publikationer/internserie/2004-01.pdf.
(47) Briggs, G.; Bromilow, R.; Evans, A. Relationships between lipophilicity and root uptake and translocation of non-ionized chemicals by barley. *Pestic. Sci.* **1982**, *13*, 495−504.
(48) Paterson, S.; Mackay, D.; McFarlane, C. A model of organic-chemical uptake by plants from soil and the atmosphere. *Environ. Sci. Technol.* **1994**, *28*, 2259−2266.
(49) Trapp, S. Modelling uptake into roots and subsequent translocation of neutral and ionisable organic compounds. *Pest. Manag. Sci* **2000**, *56*, 767−778.
(50) Briggs, G. G. Theoretical and experimental relationships between soil adsorption, octanol-water partition coefficients, water solubilities, bioconcentration factors, and the parachor. *J. Agric. Food Chem.* **1981**, *29*, 1050−1059.
(51) Orita, N. Root uptake of organic contaminants into plants: Species differences. All Graduate Theses and Dissertations. Paper 1287. M.S. Thesis, Civil and Environmental Engineering Department, Utah State University: Logan, UT, 2012; http://digitalcommons.usu.edu/cgi/viewcontent.cgi?article=2282&context=etd.
(52) Bromilow, R.; Chamberlain, K. *Principles Governing Uptake and Transport of Chemicals in Plant Contamination*; Trapp, S., Mc Farlane, J. C., Eds.; Lewis/CRC Press: Boca Raton, FL, USA, 1995; pp 37−68.
(53) Mir, P.; Bittmann, S.; Hunt, D.; Entz, T.; Yip, B. Lipid content and fatty acid composition of grasses sampled on different dates through the early part of the growing season. *Can. J. Anim. Sci.* **2006**, *86*, 279 −290.
(54) Tanoue, R.; Sato, Y.; Motoyama, M.; Nakagawa, S.; Shinohara, R.; Nomiyama, K. Plant uptake of pharmaceutical chemicals detected in recycled organic manure and reclaimed wastewater. *J. Agric. Food Chem.* **2012**, *60*, 10203−10211.
(55) Chiou, C.; Sheng, G.; Manes, M. A partition-limited model for the plant uptake of organic contaminants from soil and water. *Environ. Sci. Technol.* **2001**, *35*, 1437−1444.
(56) Harris, C.; Sans, W. Absorption of organochlorine insecticide residues from agricultural soils by root crops. *J. Agric. Food Chem.* **1967**, *15*, 861−863.
(57) Topp, E.; Scheunert, I.; Attar, A.; Korte, F. Factors affecting the uptake of ^{14}C-labeled organic-chemicals by plants from soil. *Ecotoxicol. Environ. Saf.* **1986**, *11*, 219−228.
(58) Zohair, A.; Salim, A.-B.; Soyibo, A.; Beck, A. Residues of polycyclic aromatic hydrocarbons (PAHs), polychlorinated biphenyls (PCBs) and organochlorine pesticides in organically-farmed vegetables. *Chemosphere* **2006**, *63*, 541−553.
(59) Zhang, F.-Q.; Wang, Y.-S.; Lou, Z.-P.; Dong, J.-D. Effect of heavy metal stress on antioxidative enzymes and lipid peroxidation in leaves and roots of two mangrove plant seedlings (*Kandelia candel* and *Bruguiera gymnorrhiza*). *Chemosphere* **2007**, *67*, 44−50.
(60) Sridhara Chary, N.; Kamala, C. T.; Samuel Suman, R. D. Assessing risk of heavy metals from consuming food grown on sewage irrigated soils and food chain transfer. *Ecotoxicol. Environ. Saf.* **2008**, *69*, 513−524.
(61) Schwab, B.; Hayes, E.; Fiori, J.; Mastrocco, F. J.; Roden, N. M.; Cragin, D.; Meyerhoff, R. D.; D'Aco, V. J.; Anderson, P. D. Human

pharmaceuticals in US surface waters: A human health risk assessment. *Regul. Toxicol. Pharmacol.* **2005**, *42*, 296−312.
(62) Bruce, G.; Pleus, R.; Snyder, S. Toxicological relevance of pharmaceuticals in drinking water. *Environ. Sci. Technol.* **2010**, *44*, 5619−5626.

NOTE ADDED AFTER ASAP PUBLICATION

Due to a production error, this article published January 17, 2014 with an incorrect version of Figure 1. The correct version published January 21, 2014.

JOURNAL OF AGRICULTURAL AND FOOD CHEMISTRY

Article

pubs.acs.org/JAFC

Minor Polar Compounds in Extra Virgin Olive Oil: Correlation between HPLC-DAD-MS and the Folin-Ciocalteu Spectrophotometric Method

Stefano Alessandri,[†,§] Francesca Ieri,*[,†,‡] and Annalisa Romani[†,‡]

[†]Department of Statistic, Informatics and Applications "G. Parenti" (DiSIA), University of Florence, Viale Morgagni, 59 - 50134 Firenze (FI), Italy

[‡]Phytolab Laboratory, University of Florence, via Ugo Schiff 6, 50019 Sesto Fiorentino (FI), Italy

[§]CERM—Centro di Ricerca di Risonanze Magnetiche, Via Luigi Sacconi, 6, 50019 Sesto Fiorentino (Florence), Italy

Supporting Information

ABSTRACT: Minor polar compounds of 88 extra virgin olive oils were analyzed by HPLC-DAD-MS (high-performance liquid chromatography—diode array detector—mass spectrometry) and by the Folin-Ciocalteu (FC) spectrophotometric method, to validate and evaluate, for olive oils, the linear association between FC and HPLC data. The Pearson correlation coefficients were calculated between HPLC and FC results. The highest, positive R were related with deacetoxyoleuropein aglycone (R = 0.93) and oleuropein aglycone (R = 0.93) as single compounds and with the sum of orthodiphenols (R = 0.94) and the sum of all compounds (R = 0.95), showing that both estimations of total phenols content are reliably correlated, regardless for the absolute contents and are independent of the relative composition of the phenolic fraction. On the other hand the HPLC quantifications of apigenin and lignans showed no significant correlation with FC. These results, supported also by principal component analysis, may suggest caution about the interpretation of FC results to compare olive oils with very different phenolic profiles.

KEYWORDS: *polyphenols quantification in olive oils, biophenolic minor polar compounds, analytical methods, secoiridoids, lignans*

INTRODUCTION

The definition of quality of extra virgin olive oil (EVOO) is currently based on commodity specifications and on the assessment of its organoleptic characteristics and health properties. These properties are mainly due to the presence of antioxidants, among them minor polar compounds (MPCs). Both simple and complex phenolic antioxidants are detectable in the minor polar fraction of EVOO: 5-hydroxytyrosol, tyrosol derivatives,[1−3] secoiridoids, and lignans.[4,5] Single biophenols, such as hydroxytyrosol and oleuropein aglycone, are endowed with potent antioxidant and cardioprotective activity.[6−9] Either in vitro[10−12] or in animal models,[13] olive oil phenolic compounds inhibit low-density lipoprotein (LDL) oxidation in a concentration-dependent way, and an extract of EVOO containing phenolic compounds can inhibit NF-kB (nuclear factor κ-light-chain-enhancer of activated B cells) activation, reducing the risk of coronary heart diseases.[14]

The phenolic compound concentration in EVOO depends on several factors such as cultivar[15−17] and agronomic and technological aspects of production.[18−20] Phenolic compounds are correlated to the olive oil stability.[21,22] Molecules containing an orthodiphenolic group (e.g., oleuropein aglycone and derivatives) are thought to be the main responsible for the olive oil resistance to oxidations,[23] and a method of assessing oil stability is based on the evaluation of biophenols over time.[24]

Currently, the two most commonly used methods to evaluate polyphenolic content of olive oil are the well-known Folin-Ciocalteu (FC) colorimetric assay[25−28] and high-performance liquid chromatography (HPLC). FC is a simple and highly efficient procedure, but it is limited by a low specificity.[27,28] HPLC is sensitive and specific, but it is very time-consuming and requires special expertise and a laboratory.[29−31] Recently, also the correlation of polyphenolic content with the extinction coefficient at 225 nm (K 225) was studied, mainly to estimate the sensorial attribute of bitterness[32,33] or bitterness and pungent[34] on a chemical basis.

The FC spectrophotometric method quantifies the total content of polyphenols as gallic acid.[9,35] For wine and other water-based systems FC is well-established and was deeply discussed and compared with different methods.[36,37] On the contrary, in the scientific literature specifically concerning olive oil analysis, to date there are no papers comparing the FC result with the evaluation of phenol content by chromatographic separation followed by their quantification, although both kinds of result may be reported and indirectly correlated.[38−41]

Furthermore this reagent has been considered by some authors[27,28] as nonspecific to phenolic compounds, because it can be reduced by nonphenolic compounds,[42] and this analytical method has been proposed as more appropriate to evaluate the reducing capacity than to determine the total phenolic content.

Therefore, consistent information about FC validation by reliable analytical protocols is currently lacking for olive oil quality assessment. The International Olive Oil Council (IOC)

Received: July 15, 2013
Revised: December 23, 2013
Accepted: January 9, 2014
Published: January 9, 2014

ACS Publications © 2014 American Chemical Society

Table 1. Linear Correlation between Biophenols Identified and Quantified by HPLC-DAD and Total Biophenols Obtained by the Spectrophotometric Folin-Ciocalteu (FC) Method[a]

1	2	3	4	5	6	7
variable	mean (mg/kg)	stand. deviat. (mg/kg)	*n*	homog. of slopes, Pr > F	Pearson correl. coeff.	prob > |*r*| under H0:Rho=0
(1.1) All Data: Correlations Calculated on LS-Means Adjusted Data and Means and Standard Deviations Calculated on Original Data						
lignans	103.45	45.69	88	0.8263	−0.08	0.4616
apigenin	0.29	0.43	88		0.19	0.0736
luteolin aglycone	2.53	1.87	88	0.8702	0.60	<0.0001
elenolic acid derivatives	50.23	41.56	88	0.5365	0.61	<0.0001
elenolic acid	40.32	21.61	88	0.9188	0.74	<0.0001
tyrosol	5.13	5.49	88	0.0003	0.64	<0.0001
oleocanthal	45.23	21.20	41	0.2817	0.68	<0.0001
5-hydroxytyrosol	3.97	5.51	88	0.0034	0.80	<0.0001
deacetoxyoleuropein aglycone	76.34	62.15	88	0.1231	0.93	<0.0001
oleuropein aglycone	44.08	34.34	88	0.6262	0.93	<0.0001
secoiridoid derivatives without oleocanthal	33.54	19.89	41	0.5004	0.75	<0.0001
secoiridoid derivatives	77.46	46.46	88	<0.0001	0.90	<0.0001
sum of flavonoids	2.82	2.14	88	0.9527	0.56	<0.0001
sum of orthodiphenols	120.42	92.32	88	0.2436	0.94	<0.0001
total sum	403.80	145.24	88	0.4433	0.95	<0.0001
total sum (oleocanthal quantified)	379.31	99.76	41	0.3622	0.79	<0.0001
FC	248.67	140.86	88			
(1.2) Cultivar = Frantoio/Correggiolo/Leccino/Moraiolo, Original Data						
lignans	107.03	20.10	20		−0.07	0.7652
apigenin	0.36	0.51	20		0.03	0.9081
luteolin aglycone	4.64	1.00	20		0.29	0.2095
elenolic acid derivatives	55.56	17.57	20		0.25	0.2967
elenolic acid	30.25	10.54	20		0.46	0.0397
tyrosol	2.17	0.53	20		−0.46	0.0435
5-hydroxytyrosol	1.24	0.78	20		0.61	0.0039
deacetoxyoleuropein aglycone	83.06	39.02	20		0.60	0.0053
oleuropein aglycone	36.41	15.74	20		0.56	0.0102
secoiridoid derivatives	79.75	20.59	20		0.69	0.0009
sum of flavonoids	5.00	1.39	20		0.22	0.3485
sum of orthodiphenols	119.46	53.73	20		0.60	0.0053
total sum	400.47	96.65	20		0.56	0.0095
FC	250.44	60.28	20			
(1.3) Cultivar = Seggianese, Original Data						
lignans	49.77	8.86	12		−0.02	0.9401
apigenin	0.05	0.02	12		−0.01	0.9650
luteolin aglycone	1.09	0.51	12		0.62	0.0301
elenolic acid derivatives	16.13	5.33	12		0.29	0.3521
elenolic acid	31.76	4.26	12		0.00	0.9978
tyrosol	5.89	2.61	12		−0.13	0.6810
5-hydroxytyrosol	9.29	5.94	12		−0.29	0.3625
deacetoxyoleuropein aglycone	118.66	35.70	12		0.45	0.1376
oleuropein aglycone	45.79	5.86	12		0.67	0.0180
secoiridoid derivatives	126.52	18.19	12		0.67	0.0178
sum of flavonoids	1.15	0.50	12		0.65	0.0212
sum of orthodiphenols	164.46	35.47	12		0.53	0.0759
total sum	404.96	48.84	12		0.72	0.0089
FC	239.58	24.96	12			
(1.4) Cultivar = Taggiasca, Original Data						
lignans	130.83	40.11	22		0.15	0.5188
apigenin	0.05	0.01	22		0.33	0.1358
luteolin aglycone	0.92	0.64	22		0.16	0.4883
elenolic acid derivatives	36.24	18.55	22		0.40	0.0624
elenolic acid	31.35	23.94	22		0.44	0.0398
tyrosol	7.16	7.31	22		0.64	0.0013
5-hydroxytyrosol	2.07	5.74	22		0.69	0.0003
deacetoxyoleuropein aglycone	15.62	30.18	22		0.66	0.0007

dx.doi.org/10.1021/jf403104a | J. Agric. Food Chem. 2014, 62, 826−835

Table 1. continued

1 variable	2 mean (mg/kg)	3 stand. deviat. (mg/kg)	4 *n*	5 homog. of slopes, Pr > F	6 Pearson correl. coeff.	7 prob > |r| under H0:Rho=0
(1.4) Cultivar = Taggiasca, Original Data						
oleuropein aglycone	11.59	16.26	22		0.88	<0.0001
secoiridoid derivatives	46.36	30.95	22		0.54	0.0096
sum of flavonoids	0.97	0.64	22		0.17	0.4606
sum of orthodiphenols	27.21	43.69	22		0.77	<0.0001
total sum	282.18	93.35	22		0.79	<0.0001
FC	118.86	66.45	22			

[a]In the first section of the table (1.1) all data are considered, while in the following sections three subsets are separately analyzed: (1.2) oils from typical Tuscan varieties, traditionally mixed together; (1.3) oils from Seggianese variety; and (1.4) oils from Taggiasca variety. In column 1 the single compounds and the sums of chemically related compounds are listed. The mean, the standard deviation, and the number of observations are reported in Columns 2−4, respectively. Column 5 shows the *F* values of the homogeneity-of-slopes test. Column 6 shows the Pearson correlation coefficients between each HPLC-DAD and the FC value, followed by Column 7, where the corresponding significance test is reported. Many samples show values under the detection limit for apigenin and make the homogeneity of slopes test unreliable.

itself adopts the HPLC method[43] but gives also a provisional approval[44] to a method for the colorimetric determination of *o*-diphenols, based on sodium molibdate dehydrate and 370 nm absorbance,[45] thus confirming the need of both analytical approaches and the importance of making them as interchangeable as possible.

The purpose of this work is to evaluate, in EVOO analysis, the correlation of FC's results with the results by HPLC-DAD-MS (high-performance liquid chromatography−diode array detector−mass spectrometry), focusing also on the relationship between the single molecules or classes of MPCs quantified by HPLC, and the corresponding FC results, and aiming to a consistent interpretation of FC results, for olive oils characterized by very different phenolic profiles.

MATERIALS AND METHODS

Sampling. Eighty-eight commercial EVOOs were selected and analyzed. They were crushed during the years 2002, 2003, 2004, 2005, 2006, and 2008 at the technological maturity of the olives and derived from the following Italian cultivars and provinces or homogeneous mixtures of cultivars, according to the tradition of their cultivation area: Carboncella (Rieti), Frantoio (Livorno), Leccino (Rieti), Leccio del Corno (Florence), Madonna dell'Impruneta (Florence), Mignolo (Livorno), Moraiolo (Livorno), Pendolino (Firenze), Seggianese (Grosseto), Taggiasca (Imperia), a mixture from Siena of Frantoio, Moraiolo, Leccino, and Pendolino, a mixture from Florence of Frantoio, Moraiolo, Leccino, and Correggiolo, and a mixture of Frantoio, Moraiolo, and Leccino. The observations were distributed as shown in the reported graphs. All oils were stored at room temperature in bottles capped with nitrogen after crushing and were analyzed within one month.

The cultivars Frantoio, Moraiolo, Leccino, Leccio del Corno, Pendolino, and Seggianese are known to be characterized by high contents of secoiridoidic derivatives.[15−17,46] On the contrary Taggiasca, a Ligurian cultivar of extreme interest, and Carboncella, a cultivar from the Lazio Region, are characterized by high levels of lignans and low levels of total MPCs.[47] For this reason, a subset of 41 observations, including mainly the cultivars of the first group, was more deeply analyzed, and oleocanthal, one of the secoiridoidic derivatives, was also quantified.

Sample Preparation and Chemical Analyses. A volume of 50 mL of each sample was extracted with 150 mL of EtOH−H_2O (70:30 v/v), where the water was acidified with formic acid (pH = 2.5). Defatting with *n*-hexane was carried out to remove the lipid fraction. The hydroalcholic extract was concentrated under reduced pressure (around 0.25 atm) to dryness with a Rotavapor (BÜCHI Labortechnik AG), dissolved with 2 mL of extraction solvent, and analyzed by HPLC using an HP-1100 liquid chromatograph equipped with a DAD detector and an HP 1100 MSD quadrupole mass spectrometer with an API-electrospray interface (Agilent Technologies, Palo Alto, CA, USA).

Reagents, Standards, and Solvents. Solvents for the HPLC-DAD-MS analyses were of analytical grade and were purchased from Sigma (St. Louis, MO, USA). Water was purified by a Milli-Q Plus system from Millipore (Milford, MA, USA). The following commercial compounds were used: tyrosol, oleuropein, luteolin, and apigenin (Extrasynthèse, France) and 5-hydroxytyrosol (Cayman Chemical Ltd., United States). FC reagent was purchased from Sigma (St. Louis, MO).

HPLC-DAD-MS. The adopted HPLC method was similar to the method previously reported.[22] It is more time-consuming than the SSOG (Stazione Sperimentale Oli e Grassi) method in terms of sample preparation and time analysis but is more detailed, allowing the determination at different wavelengths (240, 280, and 350 nm) of single molecules belonging to different subclasses. In detail, the LiChrosorb RP18 (Merk Hibar) column, 250 mm × 4.6 mm (5 μm), was used. The eluents were H_2O at pH 3.2 by formic acid (0.035% v/v) (A) and acetonitrile (B). The analyses were performed by a multistep linear solvent gradient as follows: 0−23 min, gradient 0−11% B; 23−33 min, isocratic 11% B; 33−45 min, gradient 11−13% B; 45−49 min, isocratic 13% B; 49−59 min, gradient 13−20% B; 59−72 min, isocratic 20% B; 72−74 min, gradient 20−25% B; 74−79 min, isocratic 25% B; 79−89 min, gradient 25−35% B; 89−92 min, isocratic 35% B; 92−100 min, gradient 35−45% B; 100−103 min, isocratic 45% B; 103−107 min, gradient 45−100% B; 107−110 min, isocratic 100% B. Total time of analysis 110 min, oven temperature 26 °C; flow rate 0.8 mL min^{-1}. The operative conditions of the electrospray ionization/mass spectrometry (ESI-MS) detector were: capillary voltage from 3000 to 3500 V, working in negative ionization, with a variable fragmentor potential in the range of 80−150 V. MS spectra were acquired from m/z 100−800. MPCs (minor polar compounds) were identified by comparison with pure standards, isolated compounds, UV spectra, relative retention time, and mass spectra in ESI. A detailed presentation of the method of identification is provided (see the Supporting Information). Lignans were identified and analyzed as described in Mulinacci et al.[47] For a subset of 41 observations oleocanthal was also quantified according to Beauchamp et al.[8] The single compounds were quantified with HPLC-DAD using a four-point regression curve constructed with the following standards: tyrosol, luteolin, and oleuropein (Extrasynthèse, France), 5-hydroxytyrosol (Cayman Chemical Ltd., United States). Calibration curves with a $r^2 \geq 0.9998$ were used. Tyrosol and lignans concentrations were calculated at 280 nm using tyrosol as the reference compound. 5-Hydroxytyrosol was calculated at 280 nm using a 5-hydroxytyrosol standard. The flavonoids were evaluated at 350 nm and using luteolin as an external standard. The secoiridoids were calculated at 280 nm using oleuropein as the reference compound; elenolic acid and elenolic acid derivatives were evaluated at 240 nm using oleuropein as the

reference compound at the same wavelength. In all cases actual concentrations of derivatives were calculated after applying corrections for changes in molecular weight: knowing the molecular weight of each compound (MW_x), their actual concentration was obtained by applying a multiplication factor of MW_x/MW_y, where MW_y is the molecular weight of the specific reference compound. The compounds evaluated by HPLC-DAD-MS were 5-hydroxytyrosol, tyrosol, deacetoxyoleuropein aglycone, oleocanthal, lignans as acetoxypinoresinol, oleuropein aglycone, a group of other secoiridoidic derivatives, luteolin, apigenin, and elenolic acid. Elenolic acid is not a phenolic compound, but it is a hydrolysis product of its polyphenols esters; therefore it was included. Biophenols were extracted and fractionated aiming at the total recovery of all MPCs, thus pointing to a reliable estimate of their total content. All of the samples were analyzed in triplicate, and the standard deviation was <5%. The limits of detection (LOD) were found to be 0.20 mg kg^{-1} for luteolin and 0.33 mg kg^{-1} for tyrosol, oleuropein, and 5-hydroxytyrosol. A signal-to-noise ratio of 3:1 was used for the calculation of the LOD.

The MPCs that were identified and quantified (Table 1) belong to five classes characterized by different functional groups: simple phenols (tyrosol, 5-hydroxytyrosol), ortho-diphenols (oleuropein aglycone, deacetoxyoleuropein aglycone), oleocanthal and other secoiridoidic derivatives, lignans (acetoxypinoresinol and pinoresinol, hereafter referred to as "lignans"), flavonoids (luteolin and apigenin, hereafter referred to as "flavonoids"), and molecules without the phenolic group (elenolic acid and its derivatives). For this reason the relationship of the FC value with two groups of compounds was also considered, and the sum of the flavonoids (luteolin and apigenin) and of the orthodiphenols (oleuropein aglycone and deacetoxyoleuropein aglycone) was calculated, together with the total sum.

Folin-Ciocalteu Assay. The total phenolic content by the FC method was determined according to the analytical protocol described by Singleton et al.[26] The method was adapted for oils as follows: 2.5 g of EVOO was diluted with 5 mL of *n*-hexane and extracted two times by 2 min of vortex and 5 min of centrifugation (4500 rpm) with 5 mL of CH_3OH-H_2O (80:20 v/v). A portion of 1 mL of the extract was added to 0.25 mL of FC reagent, 1.5 mL of Na_2CO_3 (20% w/v), in a 10 mL volumetric flask reaching the final volume with purified water. Each sample was stored for 45 min at the controlled temperature of 25 °C, and the spectrophotometric analysis was performed at λ = 725 nm. The final result, expressed in mg/kg of gallic acid, was obtained through a calibration curve with range from 1 to 15 μg mL^{-1} (R^2 = 0.9985).

Statistical Analysis. The Pearson correlation coefficient and its corresponding significance was calculated between every single HPLC determination and the total phenolic content quantified by FC (FC in tables and graphs) and discussed. The same was done for the sums of compounds described formerly.

Correlation analysis was applied to the whole data set and to every Cultivar*Year subset. The variable labeled "Cultivar" included also the mixtures of cultivars described formerly. The Cultivar*Year subsets of data were included in calculation as replications. The consistency of the correlations was evaluated by the homogeneity-of-slopes analysis. For this reason two linear models were adopted and tested. The models included each HPLC result as a response variable, the Cultivar*Year combination as grouping variable, the FC result as covariate or as regressor, and contributor to the continuous-by-class effects (to test the homogeneity of slopes). Least squares means (LS-means) were computed for each Cultivar*Year subset, and the data were adjusted accordingly, before calculating again and evaluating correlations, to minimize the Cultivar*Year variations. Data belonging to Cultivar*Year subsets with less than four oils are shown in graphs but were not included in statistical calculations. Data were also explored by principal component analysis (PCA).

The programs for the statistical and graphical processing were developed in SAS 9.3 executing on the Linux 3.9.10-100.fc17.x86_64 platform.

RESULTS AND DISCUSSION

MPCs are present in very different quantities in the oils under study (Table 1, Columns 2 and 3, Figures 1−4). This is consistent with the expected profiles of the cultivar that were considered.[15−17,46,47]

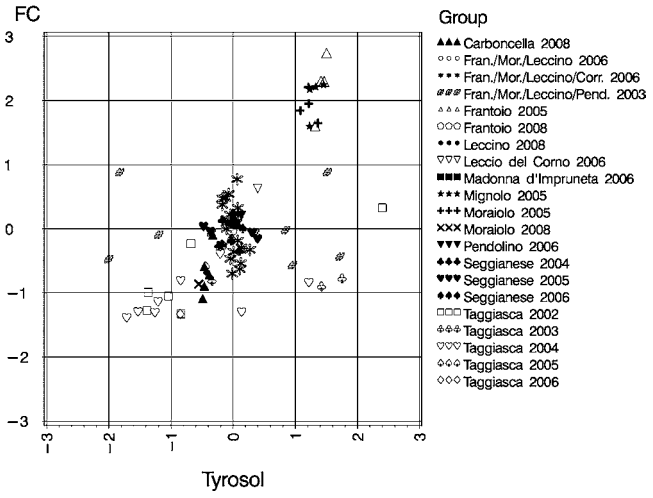

Figure 1. Correlation between the concentration of total polyphenols by the Folin-Ciocalteu (FC) spectrophotometric method (mg/kg of gallic acid) and the concentration of tyrosol (mg/kg) determined by HPLC-DAD-MS. All values are standardized. The values of the *X*-axis variable are adjusted for the Cultivar*Year group: the least-squares means were computed for each Cultivar*Year subset, and the data were adjusted accordingly.

Secoiridoidic derivatives showed a UV−vis spectrum similar to that of oleuropein, and the MS spectrum recorded in the negative ion mode exhibited the signal at 377 *m*/*z*, corresponding to the quasi-molecular ion of the aglycone of oleuropein.

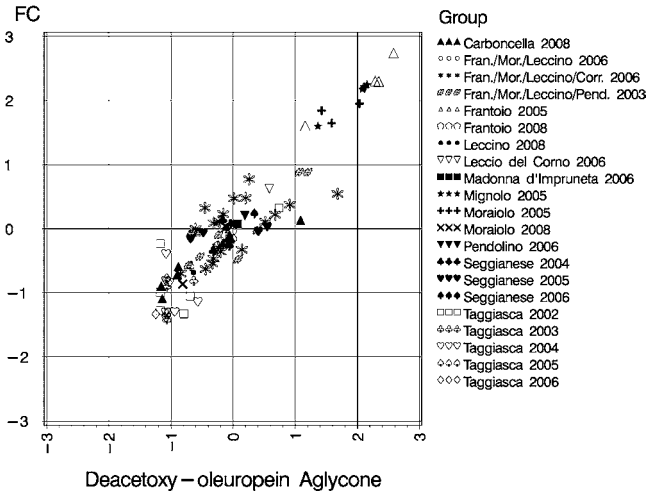

Figure 2. Correlation between the concentration of total polyphenols by the FC spectrophotometric method (mg/kg of gallic acid) and the corrected concentration of deacetoxyoleuropein aglycone (mg/kg) determined by HPLC-DAD-MS. All values are standardized. The values of the *X*-axis variable are adjusted for the Cultivar*Year group: the least-squares means were computed or each Cultivar*Year group, and the data were adjusted accordingly.

dx.doi.org/10.1021/jf403104a | J. Agric. Food Chem. 2014, 62, 826−835

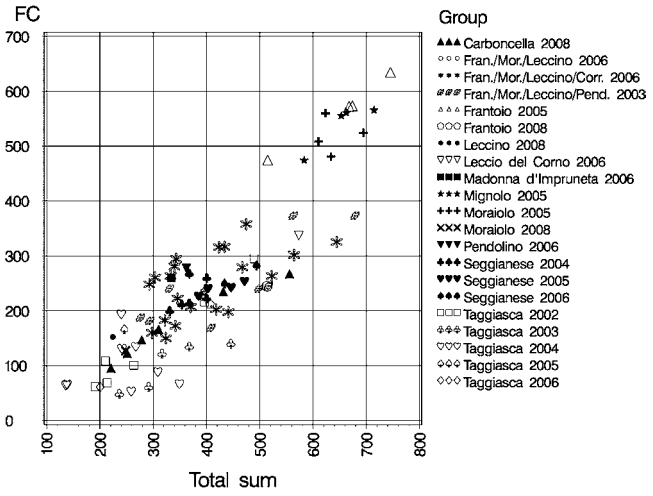

Figure 3. Correlation between the concentration of total polyphenols by the FC spectrophotometric method (mg/kg of gallic acid) and the sum of corrected concentrations (mg/kg) of all compounds determined by HPLC-DAD-MS. Values are not standardized nor corrected for the Cultivar*Year group.

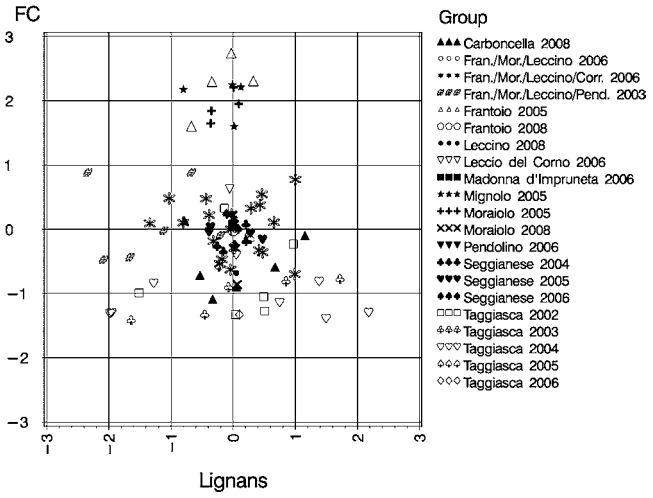

Figure 4. Correlation between the concentration of total polyphenols by the FC spectrophotometric method (mg/kg of gallic acid) and the corrected concentration (mg/kg) of lignans determined by HPLC-DAD-MS. All values are standardized. The values of the *X*-axis variable are adjusted for the Cultivar*Year group: the least-squares means were computed for each Cultivar*Year group, and the data were adjusted accordingly.

The homogeneity-of-slopes results show that 5-hydroxytyrosol, tyrosol, and the secoiridoidic derivatives (oleocanthal included), are not reliably correlated with FC (Table 1 Column 5); that is, the linear relationships between these variables and FC are significantly different in the different Cultivar*Year subsets. This kind of relationship is made clear by the tyrosol graph (Figure 1) where the scatters of the single Cultivar*Year subsets have very different shapes and orientations. The apigenin contents are generally too low to be detected by the method adopted, but, in those cultivars with appreciable apigenin contents (Moraiolo 2005, Frantoio 2005, and the three mixtures of Tuscan cultivars) apigenin shows no reliable (nor significant) linear relationship (data not shown) between its HPLC-DAD and FC quantifications (Table 1). The detection limit, evaluated for apigenin in all analyzed extracts, is 0.2 mg/kg. The estimate of the detection limits were based on a signal-to-noise ratio of 3:1 of the minor component.

All of the remaining variables show opposite results (Table 1, Column 5) and, from this point of view, perform reliably and can be divided in four groups (Table 1, Columns 6 and 7): those having a highly significant and strong positive correlation ($R > 0.90$) with FC, those having a significant but weaker correlation ($0.71 \geq R > 0.65$), those showing an intermediate position ($0.90 \geq R > 0.70$), and those having no significant correlation with FC or a Pearson correlation coefficient significant but less or equal than 0.65.

The highest significant correlations were scored by the ortho-diphenols deacetoxyoleuropein aglycone ($R = 0.93$, Figure 2) and oleuropein aglycone ($R = 0.93$) as single compounds and by the their sum ($R = 0.94$), and by the sum of all compounds ($R = 0.95$, Figure 3) .

By contrast the lowest correlation ($R = -0.08$, non-significant) was related to lignans (Figure 4), followed by the sum of flavonoids ($R = 0.56$), luteolin aglycone ($R = 0.60$), and elenolic acid derivatives ($R = 0.61$). The fact that lignans reliably show no significant linear relationship between the HPLC and the FC values could mean that these molecules do not react properly with the Folin reagent, due to the absence of functional groups, like the catechol group, that can more effectively exchange with the reagent.

The inconsistency of hydroxytyrosol and tyrosol (Figure 1, Table 1, part 1.1 Column 5, parts 1.2−1.4 Columns 6 and 7), is possibly related to the variation of their concentration due to their antioxidant capacity and to the opportunity to be easily produced by hydrolysis from the secoiridoidic molecules containing them. They play a transient role as intermediate products between the reserve of secoiridoidic compounds and the redox systems where their antioxidative power may be spent. This makes the quantification of hydroxytyrosol and tyrosol less meaningful than the quantification of their source-compounds.

Oleocanthal, shows a constant, positive ($R = 0.68$) correlation with the FC result within the subset of data where it was quantified.

These results can be better explained if we consider also the eigenvalues and the eigenvectors (Table 2) derived from the PCA. The first principal component explains about 58% of the total variance, the second principal component explains about 12%, and the third principal component explains about 10%. The eigenvalues indicate that three to five components provide a good summary of the data, with three components accounting for about 81% of the total variance and five components explaining about 92%.

The first component reflects the overall performance of almost all variables since the first eigenvector shows approximately equal loadings on almost all of them, with two remarkable exceptions: lignans and apigenin (Table 2, part 2.2, and Figure 5, top left graph). Notably, the highest positive loadings involve FC, deacetoxyoleuropein aglycone and oleuropein aglycone. The second eigenvector, on the contrary has the highest loadings on the variables lignans (positive) and flavonoids (negative). Here FC and diphenols (deacetoxyoleuropein aglycone and oleuropein aglycone) shows extremely low loadings. The third eigenvector has a very high positive loading on lignans and flavonoids, but low and negative loadings on FC and diphenols. The loadings on the first three components of the secoiridoidic derivatives are similar to those of diphenols and FC.

Table 2. Principal Component Analyses for the Whole Data Set and of Subsets of Data[a]

Principal Component Analysis				
2.1 eigenvalues of the correlation matrix				
	variance	difference	proportion	cumulative
(2.1.1) Whole Data Set (88 Observations)				
1	6.42583856	5.07681623	0.5842	0.5842
2	1.34902233	0.20375469	0.1226	0.7068
3	1.14526764	0.43290408	0.1041	0.8109
4	0.71236356	0.25746016	0.0648	0.8757
5	0.4549034	0.0414	0.917	
(2.1.2) Frantoio/Correggiolo/Leccino/Moraiolo (20 Observations)				
1	4.99275459	2.65789372	0.4539	0.4539
2	2.33486087	1.01127592	0.2123	0.6661
3	1.32358495	0.55421307	0.1203	0.7865
4	0.76937188	0.29806635	0.0699	0.8564
5	0.47130553	0.0428	0.8993	
(2.1.3) Seggianese (12 Observations)				
1	4.69783725	1.36442951	0.4271	0.4271
2	3.33340774	1.79537764	0.303	0.7301
3	1.53803009	0.956166	0.1398	0.8699
4	0.5818641	0.20224121	0.0529	0.9228
5	0.37962288	0.0345	0.9573	
(2.1.4) Taggiasca (22 Observations)				
1	4.58124187	2.79274735	0.4165	0.4165
2	1.78849452	0.54660056	0.1626	0.5791
3	1.24189396	0.16857105	0.1129	0.692
4	1.07332291	0.09337712	0.0976	0.7895
5	0.97994579	0.0891	0.8786	

(2.2) Loadings					
variables	Prin1	Prin2	Prin3	Prin4	Prin5
(2.2.1) Whole Data Set (88 Observations)					
FC	0.377908	0.060257	−0.097702	−0.048492	0.175224
lignans	−0.033733	0.595712	0.605264	0.040033	−0.016278
apigenin	0.115629	−0.619152	0.526068	0.017164	0.077797
luteolin aglycone	0.278545	−0.369038	0.340743	−0.081912	0.063569
elenolic acid derivatives	0.281991	0.172359	0.249899	−0.375483	−0.642241
elenolic acid	0.290918	0.261645	0.143286	−0.281026	0.656556
tyrosol	0.275888	0.136391	0.104335	0.759859	0.09624
5-hydroxytyrosol	0.345924	−0.018633	−0.075394	0.386478	−0.297333
deacetoxyoleuropein aglycone	0.371676	0.029584	−0.184013	−0.117001	−0.078041
oleuropein aglycone	0.380166	0.049035	−0.112277	−0.036448	−0.070261
secoiridoid derivatives	0.349988	−0.039524	−0.291959	−0.16526	0.081867
(2.2.2) Frantoio/Correggiolo/Leccino/Moraiolo (20 Observations)					
FC	0.323024	0.188681	0.31815	−0.201279	0.635907
lignans	0.099002	−0.514707	−0.267574	0.205685	0.483611
apigenin	−0.088499	0.563651	−0.101186	0.134028	−0.179126
luteolin aglycone	0.026685	0.560764	−0.00227	0.388131	0.361546
elenolic acid derivatives	0.309284	0.06127	−0.544047	0.098957	−0.184541
elenolic acid	0.363198	0.015498	−0.377349	0.154906	0.150884
tyrosol	−0.234682	−0.202373	0.277542	0.804922	−0.031342
5-hydroxytyrosol	0.336959	−0.142273	0.408336	−0.042571	−0.189997
deacetoxyoleuropein aglycone	0.411746	−0.000194	0.103765	0.217751	−0.186711
oleuropein aglycone	0.421893	−0.028994	−0.052863	0.11485	−0.237868
secoiridoid derivatives	0.365507	0.035862	0.348183	0.066824	−0.116603
(2.2.3) Seggianese (12 Observations)					
FC	−0.197868	0.365956	0.327697	−0.148753	−0.589054
lignans	0.368396	0.268868	−0.09343	0.026954	−0.238528
apigenin	−0.178651	−0.34511	0.496743	0.179754	−0.123877
luteolin aglycone	−0.108294	0.467378	−0.005308	−0.520835	0.334693
elenolic acid derivatives	0.246071	0.444568	0.022318	0.044685	0.015809
elenolic acid	0.196759	−0.120978	0.628041	−0.457842	−0.049772
tyrosol	0.417184	0.164604	0.156494	0.197105	0.002708

dx.doi.org/10.1021/jf403104a | J. Agric. Food Chem. 2014, 62, 826−835

Table 2. continued

(2.2) Loadings					
variables	Prin1	Prin2	Prin3	Prin4	Prin5
(2.2.3) Seggianese (12 Observations)					
5-hydroxytyrosol	0.369345	−0.02818	0.323587	0.078431	0.567242
deacetoxyoleuropein aglycone	−0.44198	0.031465	0.138954	−0.049452	0.341918
oleuropein aglycone	−0.164435	0.373635	0.303538	0.643085	0.092642
secoiridoid derivatives	−0.386498	0.274743	0.039095	0.030719	0.136993
(2.2.4) Taggiasca (22 Observations)					
FC	0.424645	0.077516	−0.163097	0.121437	0.154697
lignans	0.079033	0.530581	0.065152	0.212233	−0.548382
apigenin	0.172257	0.28604	0.218343	−0.586854	0.293131
luteolin aglycone	0.063638	0.330183	0.566244	0.542014	0.114133
elenolic acid derivatives	0.243016	0.368883	−0.106666	−0.430256	−0.353642
elenolic acid	0.105848	0.477029	−0.517548	0.143527	0.366158
tyrosol	0.304047	−0.175278	−0.371018	0.24387	0.012508
5-hydroxytyrosol	0.39156	−0.278892	−0.012396	0.065719	−0.286226
deacetoxyoleuropein aglycone	0.400456	−0.205672	0.27034	−0.134756	−0.206795
oleuropein aglycone	0.448472	−0.084486	−0.054353	0.115581	0.041383
secoiridoid derivatives	0.319675	−0.007895	0.328282	−0.031687	0.436693

[a]Sections 2.1.1 and 2.2.1: all data; Sections 2.1.2 and 2.2.2: oils from typical Tuscan varieties, mixed together according to tradition; Sections 2.1.3 and 2.2.3: oils from Seggianese variety; Sections 2.1.4 and 2.2.4: oils from Taggiasca variety.

In short, the first component (58% of the variance) is the only one having a high positive loading on FC and shows that the compounds under study can be considered as positively correlated with the FC variable, though with major quantitative differences (apigenin) and with a clear exception: lignans. The second and the third component, accounting for 23% of variance, are not correlated with FC and show mainly the relationship between lignans and flavonoids.

The statistical analysis was repeated including only the typical Tuscan mixture of Frantoio, Correggiolo, Leccino, and Moraiolo cultivar (Table 1 part 1.2, Table 2 parts 2.1.2 and 2.2.2, and Figure 5, top right graph), the Seggianese cultivar (Table 1 part 1.3, Table 2 parts 2.1.3 and 2.2.3, and Figure 5, bottom left graph) and Taggiasca cultivar (Table 1 part 1.4, Table 2 parts 2.1.4 and 2.2.4, and Figure 5, bottom right graph).

If the results including only the mixture of Frantoio, Correggiolo, Leccino, and Moraiolo are compared with those of the whole data set, they show weaker correlation (20 observations scoring $R = 0.56$ between FC and total phenol content by HPLC) but similar trends. This subset of oils shows an estimated total phenols content of 250 mg/kg by FC and 400 mg/kg by HPLC, with lignans contributing for 27% (107 mg/kg, vs 103 mg/kg of the whole data set) and deacetoxyoleuropein aglycone and oleuropein aglycone for 30% (119 mg/kg, vs 120 mg/kg of the whole data set). The results of PCA also suggest that this subset of data closely resembles the whole data set: in the space of the first two components, accounting for 67% of total variance, almost all HPLC variables are grouped together with FC except lignans and flavonoids that show opposite loadings along the second component.

Also for the Taggiasca subset (22 observations) in the space of the first two components (58% of total variance) FC, diphenols and phenols are grouped together but not with lignans and flavonoids.

This pattern is less clear in the Seggianese subset, including only 12 observations, where anyway oleuropein aglycone can be seen close to FC, while lignans and apigenin show an opposite trend.

The total phenol content of the Seggianese cultivar was estimated as 240 mg/kg by FC and 405 mg/kg by HPLC-DAD, with lignans contributing for 12% (50 mg/kg) and deacetoxyoleuropein aglycone and oleuropein aglycone for 41% (164 mg/kg).

The total phenol content of the Taggiasca cultivar was estimated 119 mg/kg by FC and 282 mg/kg by HPLC-DAD, with lignans contributing for 46% (131 mg/kg) and deacetoxyoleuropein aglycone and oleuropein aglycone for 10% (27 mg/kg). Interestingly, the correlations between the two results (FC and total by HPLC) were $R = 0.72$ for Seggianese and $R = 0.79$ for Taggiasca.

This suggests that the FC and HPLC-DAD estimations of total phenols content are reliably correlated, regardless for the absolute contents, and are independent of the relative composition of the phenolic fraction. The FC reagent seems to react poorly with lignans and flavonoids, while an opposite behavior is shown with stable orthodiphenols. The strong specific reactivity of FC reagent with catechol group in oils, and a weaker reactivity with other functional groups, typical of the polyphenols family, suggests caution about interpretation of FC results for olive oils characterized by very different phenolic profiles.

Considering the complexity of MPCs in olive oil, the current, single FC assay may not be the best choice to characterize the phenolic composition of an oil sample. Choosing an appropriate phenolic assay depends on what kind of information is required. For example the total phenol content estimated by the FC assay may be useful to determine the approximate actual content of phenolics, but this amount may be do not correspond directly to the organoleptic property of bitterness, or to specific health properties such as the total antioxidant power, both of them so important to oil qualification. Furthermore the total antioxidant power depends also on compounds that, according to our findings, are not properly intercepted by the FC assay. Therefore RP-HPLC and the identification and quantification of single MPC currently cannot be easily replaced by any simpler test. On the other

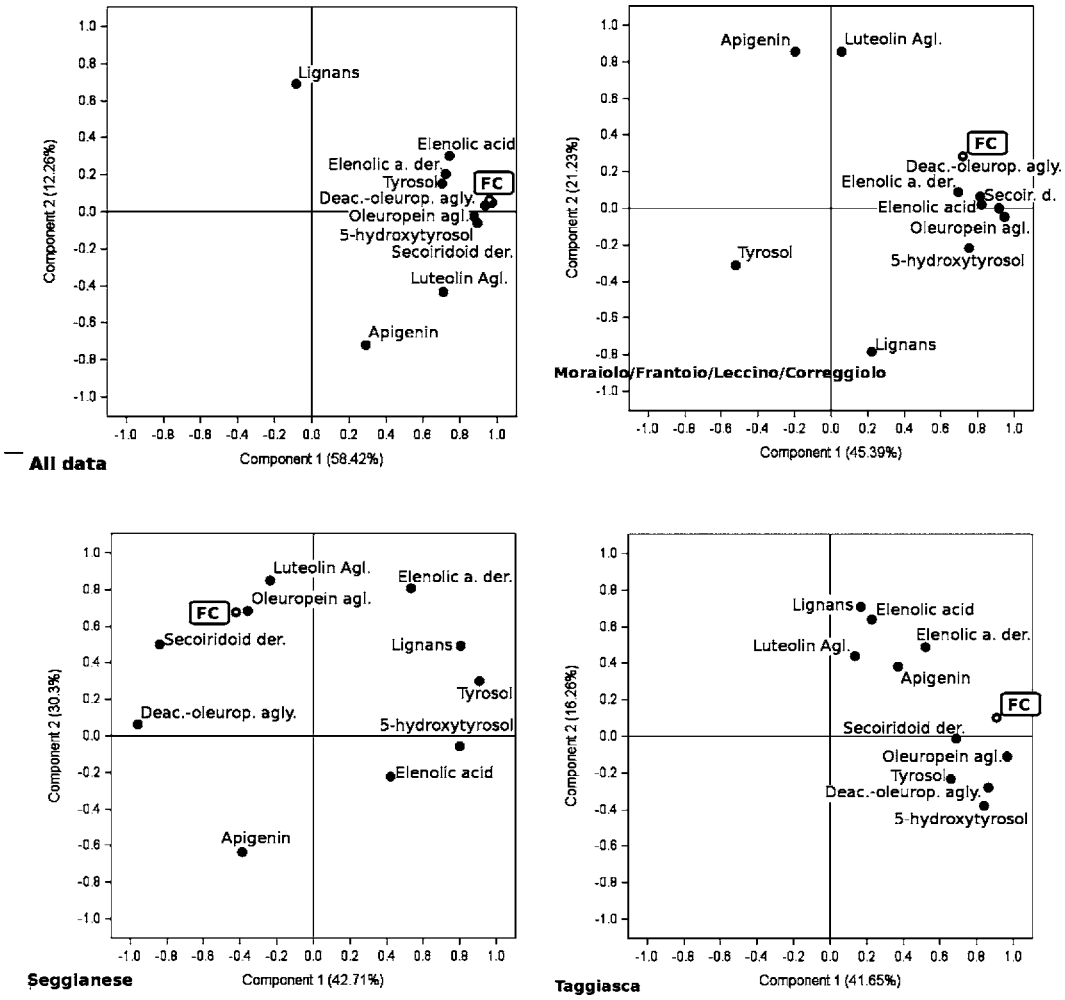

Figure 5. Loading plots of the concentrations of total polyphenols by FC spectrophotometric method and of the single compounds determined by HPLC-DAD-MS, in the space defined by the first two principal components. Top left graph: the whole data set is considered (88 observations, 71% of total variance explained). Top right graph: the principal component analysis is limited to a subset of data, including only a typical Tuscan mixture of varieties (20 observations, 67% of total variance explained). Bottom left graph: the principal component analysis is limited to a subset of data, including only Seggianese variety (12 observations, 73% of total variance explained). Bottom right graph: the principal component analysis is limited to a subset of data, including only Taggiasca variety (22 observations, 58% of total variance explained). FC stands for Folin-Ciocalteu.

hand there is a strong need for simple and reliable methods for olive oil quality assessing.

■ ASSOCIATED CONTENT

Supporting Information

Chromatogram of an EVOO extract of cv Seggianese, main constituents identified in EVOO extract and their method of identification, UV−vis and MS spectra of the oleuropein aglycone with a secoiridoid derivative, and structures of olive oil main MPCs. This material is available free of charge via the Internet at http://pubs.acs.org.

■ AUTHOR INFORMATION

Corresponding Author

*Tel.: +390554573676. E-mail: francesca.ieri@unifi.it.

Notes

The authors declare no competing financial interest.

■ ACKNOWLEDGMENTS

The authors are grateful to Ente Cassa di Risparmio di Firenze for supplying part of the instrumentation used for this research.

■ ABBREVIATIONS USED

EVOO, extra virgin olive oil; FC, Folin-Ciocalteu; IOC, International Olive Oil Council; SSOG, Stazione Sperimentale Oli e Grassi

■ REFERENCES

(1) Montedoro, G.; Servili, M.; Baldioli, M.; Miniati, E. Simple and hydrolyzable phenolic compounds in virgin olive oil. 2. Initial characterization of the hydrolyzable fraction. *J. Agric. Food Chem.* **1992**, *40*, 1577−1580.

(2) Angerosa, F.; D'Alessandro, N.; Konstantinou, P.; Di Giacinto, L. GC-MS evaluation of phenolic compounds in virgin olive oil. *J. Agric. Food Chem.* **1995**, *43*, 1802−1807.

(3) Okogeri, O.; Tasioula-Margari, M. Changes occurring in phenolic compounds and alpha-tocopherol of virgin olive oil during storage. *J. Agric. Food Chem.* **2002**, *50*, 1077−1080.

(4) Brenes, M.; Garcia, A.; Garsia, P.; Rios, J. J.; Carrido, A. Phenolic compounds in Spanish olive oils. *J. Agric. Food Chem.* **1999**, *47*, 3535−3540.

(5) Owen, R. W.; Mier, W.; Giacosa, A.; Hull, W. E.; Spiegelhalder, B.; Bartsch, H. Phenolic and lipid components of olive oil: identification of lignans as major components of olive oil. *Clin. Chem.* **2000**, *46*, 976−988.

(6) Visioli, F.; Galli, C. Biological properties of olive oil phytochemicals. *Crit. Rev. Food Sci.* **2002**, *42*, 209−221.
(7) Covas, M. I.; Ruiz-Gutíerrez, V.; De la Torre, R.; Kafatos, A.; Lamuela-Raventos, R. M.; Osada, J.; Owen, R. W.; Visioli, F. Minor components of olive oil: evidence to date of health benefits in humans. *Nutr. Rev.* **2006**, *64*, 20−30.
(8) Beauchamp, G. K.; Keast, R. S. J.; Morel, D.; Lin, J.; Pika, J.; Han, Q.; Lee, C. H.; Smith, A. B.; Breslin, P. A. S. Ibuprofen-like activity in extra-virgin olive oil. *Nature* **2005**, *437*, 45−46.
(9) Rosenblat, M.; Volkova, N.; Coleman, R.; Almagor, Y.; Aviram, M. Antiatherogenicity of extra virgin olive oil and its enrichment with green tea polyphenols in the atherosclerotic apolipoprotein-E-deficient mice: enhanced macrophage cholesterol efflux. *J. Nutr. Biochem.* **2008**, *19*, 514−523.
(10) Visioli, F.; Bellomo, G.; Montedoro, G.; Galli, C. Low density lipoprotein oxidation is inhibited in vitro by olive oil constituents. *Atherosclerosis* **1995**, *117*, 25−32.
(11) Fito, M.; Covas, M. I.; Lamuela-Raventos, R. M.; Vila, J.; Torrents, L.; De la Torre, C.; Marrugat, J. Protective effect of olive oil and its phenolic compounds against low density lipoprotein oxidation. *Lipids* **2000**, *35*, 633−638.
(12) Franconi, F.; Coinu, R.; Carta, S.; Urgeghe, P. P.; Ieri, F.; Mulinacci, N.; Romani, A. Antioxidant effect of two virgin olive oils depends on the concentration and composition of minor polar compounds. *J. Agric. Food Chem.* **2006**, *54*, 3121−3125.
(13) Visioli, F.; Galli, C.; Plasmati, E.; Viappiani, S.; Hernandez, A.; Colombo, C.; Sala, A. Olive oil hydroxytyrosol prevents passive smoking-induced oxidative stress. *Circulation* **2000**, *102*, 2169−2171.
(14) Brunelleschi, S.; Bardelli, C.; Amoruso, A.; Gunella, G.; Ieri, F.; Romani, A.; Malorni, W.; Franconi, F. Minor polar compounds extra-virgin olive oil extract (MPC-OOE) inhibits NF-kappaB translocation in human monocyte/macrophages. *Pharmacol. Res.* **2007**, *56*, 542−549.
(15) Flamini, G.; Coini, P. L.; Morelli, I. Volatiles from leaves, fruits, and virgin oil from Olea europaea cv. Olivastra Seggianese from Italy. *J. Agric. Food Chem.* **2003**, *51*, 1382−1386.
(16) Pinelli, P.; Galardi, C.; Mulinacci, N.; Vincieri, F. F.; Cimato, A.; Romani, A. Minor polar compound and fatty acid analyses in monocultivar virgin olive oils from Tuscany. *Food Chem.* **2003**, *80*, 331−336.
(17) Kalua, C. M.; Allen, M. S.; Bedgood, D. R., Jr.; Bishop, A. G.; Prenzler, P. D. Discrimination of olive oils and fruits into cultivars and maturity stages based on phenolic and volatile compounds. *J. Agric. Food Chem.* **2005**, *53*, 8054−8062.
(18) Amirante, P.; Catalano, P.; Amirante, R.; Clodoveo, M. L.; Montel, G. L.; Leone, A.; Tamborrino, A. Prove sperimentali di estrazione di oli da olive snocciolate (Experimental tests of olive oil extraction from depitted olives). *Olivo Olio* **2002**, *6*, 16−22.
(19) Servili, M.; Selvaggini, R.; Esposto, S.; Taticchi, A.; Montedoro, G.; Morozzi, G. Health and sensory properties of virgin olive oil hydrophilic phenols: agronomic and technological aspects of production that affect their occurrence in the oil. *J. Chromatogr., A* **2004**, *1054*, 113−127.
(20) Mulinacci, N.; Giaccherini, C.; Innocenti, M.; Romani, A.; Vincieri, F. F.; Marotta, F.; Mattei, A. Analysis of extra virgin olive oils from stoned olives. *J. Sci. Food Agric.* **2005**, *85*, 662−670.
(21) Del Carlo, M.; Sacchetti, G.; Di Mattia, C.; Compagnone, D.; Mastrocola, D.; Liberatore, L.; Cichelli, A. Contribution of the Phenolic Fraction to the Antioxidant Activity and Oxidative Stability of Olive Oil. *J. Agric. Food Chem.* **2004**, *52*, 4072−4079.
(22) Romani, A.; Lapucci, C.; Cantini, C.; Ieri, F.; Mulinacci, N.; Visioli, F. Evolution of Minor Polar Compounds and Antioxidant Capacity during Storage of Bottled Extra Virgin Olive Oil. *J. Agric. Food Chem.* **2007**, *55*, 1315−1320.
(23) Cinquanta, L.; Esti, M.; La Notte, E. Evolution of phenolic compounds in virgin olive oil during storage. *J. Am. Oil Chem. Soc.* **1997**, *74*, 1259−1264.
(24) Hrncirik, K.; Fritsche, S. Relation between the endogenous antioxidant system and the quality of extra virgin olive oil under accelerated storage condition. *J. Agric. Food Chem.* **2005**, *53*, 2103−2190.
(25) Singleton, V. L.; Rossi, J. A., Jr. Colorimetry of total phenolics with phosphomolybdic-phosphotungstic acid reagents. *Am. J. Enol. Viticult.* **1965**, *16*, 144−158.
(26) Singleton, V. L.; Orthofer, R.; Lamuela-Raventos, R. M. Analysis of total phenols and other oxidation substrates and antioxidants by means of the Folin-Ciocalteu reagent. *Methods Enzymol.* **1999**, *299*, 152−178.
(27) Huang, D.; Ou, B.; Prior, R. L. The chemistry behind antioxidant capacity assays. *J. Agric. Food Chem.* **2005**, *53*, 1841−1856.
(28) Magalhães, L. M.; Segundo, M. A.; Reis, S.; Lima, J. L. F. C.; Rangel, A. Automatic method for the determination of Folin-Ciocalteu reducing capacity in food products. *J. Agric. Food Chem.* **2006**, *54*, 5241−5246.
(29) Alessandri, S.; Cimato, A.; Mattei, A.; Modi, G. Characterization of olive oils from Tuscany according to harvesting time, by means of their phenols contents. *Boll. Chim. Igienisti Sci.* **1992**, *43*, 141−161.
(30) Romani, A.; Mulinacci, N.; Pinelli, P.; Vincieri, F. F.; Cimato, A. Polyphenolic content in five tuscany cultivars of Olea europaea L. *J. Agric. Food Chem.* **1999**, *47*, 964−967.
(31) Romani, A.; Pinelli, P.; Mulinacci, N.; Galardi, C.; Vincieri, F. F.; Liberatore, L.; Cichelli, A. HPLC and HRGC analyses of polyphenols and secoiridoids in olive oil. *Chromatographia* **2001**, *53*, 279−284.
(32) Garcia-Mesa, J. A.; Mateos, R. Direct Automatic Determination of Bitterness and Total Phenolic Compounds in Virgin Olive Oil Using a pH-Based Flow-Injection Analysis System. *J. Agric. Food Chem.* **2007**, *55*, 3863−3868.
(33) Beltrán, G.; Ruano, M. T.; Jiménez, A.; Uceda, M.; Aguilera, M. P. Evaluation of Virgin Olive Oil Bitterness by Total Phenol Content Analysis. *Eur. J. Lipid Sci. Tech.* **2007**, *108*, 193−197.
(34) Inarejos-Garcia, A. M.; Androulaki, A.; Salvador, M. D.; Fregapane, G.; Tsimidou, M. Z. Discussion on the objective evaluation of virgin olive oil bitterness. *Food Res. Int.* **2009**, *42*, 279−284.
(35) Gimeno, E.; Castellote, A. I.; Lamuela-Raventós, R. M.; De la Torre, M. C.; López-Sabater, M. C. The effects of harvest and extraction methods on the antioxidant content (phenolics, α-tocopherol, and β-carotene) in virgin olive oil. *Food Chem.* **2002**, *78*, 207−211.
(36) De Beer, D.; Harbertson, J. F.; Kilmartin, P. A.; Roginsky, V.; Barsukova, T.; Adams, D. O.; Waterhouse, A. L. Phenolics: A Comparison of Diverse Analytical Methods. *Am. J. Enol. Viticult.* **2004**, *55*, 389−400.
(37) Costa, R. M.; Magalhães, A. S.; Pereira, J. A.; Andrade, P. B.; Valentão, P.; Carvalho, M.; Silva, B. M. Evaluation of free radical-scavenging and antihemolytic activities of *Cydonia oblonga* leaf. A comparative study with green tea (*Camellia sinensis*). *Food Chem. Toxicol.* **2009**, *47*, 860−865.
(38) Ocakoglu, D.; Tokatli, F.; Ozen, B.; Korel, F. Distribution of simple phenols, phenolic acids and flavonoids in Turkish monovarietal extra virgin olive oils for two harvest years. *Food Chem.* **2009**, *113*, 401−410.
(39) Klen, T. J.; Vodopivec, B. M. Optimisation of olive oil phenol extraction conditions using a high-power probe ultrasonication. *Food Chem.* **2012**, *134*, 2481−2488.
(40) Pizarro, M. L.; Becerra, M.; Sayago, A.; Beltrán, M.; Beltrán, R. Comparison of different extraction methods to determine phenolic compounds in virgin olive oil. *Food Anal. Methods* **2013**, *6*, 123−132.
(41) Inarejos-García, A. M.; Santacatterina, M.; Salvador, M. D.; Fregapane, G.; Gómez-Alonso, S. PDO virgin olive oil quality—Minor components and organoleptic evaluation. *Food Res. Int.* **2010**, *43*, 2138−2146.
(42) Magalhães, L. M.; Segundo, M. A.; Reis, S.; Lima, J. L. F. C. Methodological aspects about in vitro evaluation of antioxidant properties. *Anal. Chim. Acta* **2008**, *613*, 1−19.
(43) Determination of Biophenols in Olive Oils by HPLC, COI/T.20/DOC. 29; International Olive Council: Madrid, 2009.

(44) Identification and Quantification of Phenolics in Olive Oil, Decision No. Dec-17/97-V; International Olive Council: Madrid, 2009.
(45) Cert, A.; Romero, A.; Cert, R. Colorimetric Method for the Determination of O-diphenolic Compounds in Olive Oils, Revised Method; International Olive Council: Madrid, December 2007; http://www.internationaloliveoil.org/documents/viewfile/3857-testing12eng.
(46) Rotondi, A.; Alfei, B.; Maglia, M.; Pannelli, G. Influence of genetic matrix and crop year on chemical and sensory profiles of Italian monovarietal extra-virgin olive oils. *J. Sci. Food Agric.* **2010**, *90*, 2641−2648.
(47) Mulinacci, N.; Giaccherini, C.; Ieri, F.; Romani, A.; Vincieri, F. F. Evaluation of lignans and free and linked hydroxy-tyrosol and tyrosol in extra virgin olive oil after hydrolysis processes. *J. Sci. Food Agric.* **2006**, *86*, 757−764.

JOURNAL OF AGRICULTURAL AND FOOD CHEMISTRY

Article

pubs.acs.org/JAFC

Inhibitory Effects of the Leaves of Loquat (*Eriobotrya japonica*) on Bone Mineral Density Loss in Ovariectomized Mice and Osteoclast Differentiation

Hui Tan,[†] Syoko Furuta,[†] Toshiro Nagata,[†] Koichiro Ohnuki,[§] Taiki Akasaka,[#] Bungo Shirouchi,[⊥] Masao Sato,[⊥] Ryuichiro Kondo,[†] and Kuniyoshi Shimizu*[,†]

[†] Department of Agro-environmental Sciences, Faculty of Agriculture, Kyushu University, 6-10-1 Hakozaki, Higashi-ku, Fukuoka 812-8581, Japan

[§] Department of Biological and Environmental Chemistry, Kinki University, Kayanomori 11-6, Iizuka, Fukuoka 820-8555, Japan

[#] Center for Advanced Instrumental and Educational Supports, Faculty of Agriculture, Kyushu University, 6-10-1 Hakozaki, Higashi-ku, Fukuoka 812-8581, Japan

[⊥] Department of Bioscience and Biotechnology, Faculty of Agriculture, Kyushu University, 6-10-1, Hakozaki, Higashi-ku, Fukuoka 812-8581, Japan

Supporting Information

ABSTRACT: The loquat, *Eriobotrya japonica* Lindl. (Rosaceae), is a small tree native to Japan and China that is widely cultivated for its succulent fruit. Its leaves are used as an ingredient of a tasty tea called "Biwa cha" in Japanese. The anti-osteoporosis effects of the leaves of loquat in vitro and in vivo have been investigated. After 15 days of feeding normal diet or diet supplemented with 5% loquat leaves, the body weight, viscera weights, and bone mineral density (BMD) of both groups of eight ovariectomized (OVX) mice were compared. The result showed that the loss of BMD in loquat-fed mice was significantly prevented in three parts of the body, especially in the trabecular bone of the head ($P < 0.05$), abdomen ($P < 0.01$), and lumbar ($P < 0.05$) compared to the control group. No hypertrophy in the uterus by the loquat leaves diet was observed. The effect of the extract (447.25 g) prepared from the dried leaves of loquat (2.36 kg) was further studied on RANKL-induced osteoclast differentiation and cell viability. The extract suppressed the differentiation of osteoclasts under 50, 125, 250, and 500 μg/mL. Through bioactivity-guided fractionation, ursolic acid (**1**) was isolated and inhibited osteoclast differentiation under 4 and 10 μg/mL. It was concluded that loquat leaves possess the potential to suppress ovariectomy-induced bone mineral density deterioration.

KEYWORDS: *tea, osteoporosis, Eriobotrya japonica, osteoclast differentiation, ursolic acid*

INTRODUCTION

Biwa (Japanese) is a flowering plant known as loquat, *Eriobotrya japonica*, and belongs to the Rosaceae family. It probably had its origin in southeastern China and has been cultivated in Japan since ancient times. It is widely cultivated for its succulent fruit. Its leaves are used as the ingredient of tasty teas called as "Biwa cha" in Japanese. It has been reported that the extracts of the leaves from *E. japonica* exerted an antiobesity effect through regulation of plasma lipid and adiponectin levels in mice and adipogenic transcription factors PPARγ and C/EBPα in 3T3-L1 adipocytes.[1] Also, the leaves of *E. japonica* were reported to have a potent inhibitory effect on the inflammatory mediator via the attenuation of NF-κB translocation to the nucleus.[2] *E. japonica* significantly delayed carcinogenesis induced by peroxynitrite (initiator) and TPA (promoter), and its potency was comparable to that of a green tea polyphenol, (−)-epigallocatechin 3-*O*-gallate, in the same assay.[3]

Osteoporosis is a growing public health problem, affecting millions of people worldwide.[4] It is a major growing health problem for elderly women associated with ovarian hormone deficiency following menopause and is by far the most common cause of age-related bone loss in women.[5] Decreased bone density and the resulting bone dysfunction greatly affect the quality of life, because the bone is a supporting organ, hematopoietic tissue, and immune tissue.[6] This imbalance of bone remodeling is caused by excess osteoclast activity. Osteoclasts are large multinucleated cells, which can resorb bone. These multinucleated cells express known markers, including tartrate-resistant acid phosphatase (TRAP),[7] a glycosylated monomeric metalloenzyme expressed in mammals, that is highly expressed in osteoclasts associated with osteoblast migration to bone resorption sites. This initiates osteoblast differentiation, proliferation, and activation.[8]

Hormone replacement therapy (HRT) is a treatment for the prevention of bone loss and for restoring the rate of bone resorption and formation.[9] However, long-term HRT may increase a patient's risk of developing breast cancer, endometrial cancer, thromboembolic events, or vaginal

Received: June 26, 2013
Revised: December 28, 2013
Accepted: January 9, 2014
Published: January 9, 2014

ACS Publications © 2014 American Chemical Society

bleeding.[10] Therefore, because of women's reluctance to comply with HRT, safer ingredients originating from foods or beverages such as tea are needed for the treatment or prevention of menopausal symptoms, such as osteoporosis.

As far as we know, the antiosteoporosis effect of the leaves of *E. japonica* has not yet been investigated. The objective of this study was to investigate the effect of the leaves of *E. japonica* on the bone mineral density (BMD) of ovariectomized mice and RANKL-induced osteoclast differentiation and to identify the active substance.

MATERIALS AND METHODS

Chemicals. *E. japonica* (Thunb.) Lindl. (Rosaceae) was obtained from Japan in 2010, and a voucher specimen (No. EJ001) has been deposited in the Laboratory of Systematic Forest and Forest Products Sciences (Kyushu University, Fukuoka, Japan). All leaves were air-dried and powdered mechanically. Methanol and water extracts of the leaves of loquat were prepared with three times extraction at room temperature. Mice (C57BL/6JJc1) used for the experiment were purchased from Clea Co. (Osaka, Japan). RAW 264.7 macrophage cells were purchased from the Riken Bioresource Center Cell Bank (Tsukuba, Japan). Minimal essential medium, alpha modification (α-MEM medium), was from Gibco BRL (Grand Island, NY, USA); fetal bovine serum (FBS) and antibiotics—antimycotics were obtained from Gibco and Invitrogen (Carlsbad, CA, USA), respectively. Receptor activator of NF-κB (RANKL) from *Escherichia coli* was purchased from PeproTech EC (London, UK), and tumor necrosis factor alpha (TNF-α) was obtained from Roche Molecular Biochemicals (Mannheim, Germany). TRAP staining kit 387-A was obtained from Sigma-Aldrich (St. Louis, MO, USA). Oleic acid was obtained from Wako (Osaka, Japan). Dimethyl sulfoxide (DMSO) was also obtained from Wako.

Animals and Diets. Sixteen 12-week-old female mice were bilaterally ovariectomized at 11 weeks of age. Groups of four mice were randomly housed in one animal cage. The animal room was conditioned at 23 ± 1 °C and illuminated according to a 12 h light/dark cycle (light on at 8:00 a.m. and off at 8:00 p.m.). All animals were allowed free access to distilled water and fed ad libitum. AIN-76 diets with (loquat group) or without the leaves of loquat (control group) were used on the basis of the diet reported by the American Institute of Nutrition Ad Hoc Committee on Standards for Nutritional Studies.[11] This diet was composed on the basis of the average energy intake for Japanese 40−49-year-old women with a slight modification of protein, fat, and carbohydrate weight.[12] The total calorie count in both groups' diets was the same. The main diet ingredients were vitamins, minerals, DL-glutamin, choline bitartrate, cellulose, casein, safflower oil, starch, and sucrose (Table 1).

Animal Experiment Protocol. At the beginning of the experiment, the mice were acclimated for 6 days by feeding the control diets to both groups. Then the 16 mice were randomly divided into two groups (n = 8 each), and (1) the control group was fed the modified AIN-76 diet and (2) the loquat group was fed the modified AIN-76 diet incorporating 5% leaves of loquat. The treatment continued to the 22nd day, and then the mice were sacrificed and dissected. The body weights and food intakes of all animals were measured every day. The handling and sacrificing of all animals were carried out in accordance with nationally prescribed guidelines, and ethical approval for the studies was granted by the Animal Care and Use Committee of Kyushu University (Authorization A22-234-0).

Table 1. Compositions of the AIN-76 Diet in the Control Group and Loquat Group

composition	percentage (%)	
	control group	loquat group
vitamins	1.0	1.0
minerals	3.5	3.5
DL-glutamine	0.3	0.3
choline bitartrate	0.2	0.2
cellulose	5.0	2.69
casein	20.6	20.29
safflower oil	12.71	12.53
corn starch	15.49	15.56
leaves of loquat powder	0	5.0
sucrose	41.15	38.93

X-ray CT Scan. On the 21st day of the diet regimen, each mouse underwent a computed tomography (CT) scan. BMD was measured by a computerized tomography scanner (X-ray CT) (La Theta, Aloka Co. Tokyo) at a scan pitch of 5 mm for mouse body parts. The BMD of the head, chest, abdomen, and lumbar (including the trabecular bone, cortical bone, and whole) were analyzed.

Anatomy. At the end of the experiment, the mice were euthanized with pentobarbital sodium at 50 mg/kg body weight, and the liver, uterus, kidney, spleen, brain, and fat mass (fat around the kidney and fat around the uterus) were carefully removed and weighed.

Cell Cultures. Cells of the murine macrophage cell line RAW 264.7 were maintained in α-MEM with 10% FBS and 1% antibiotics. For the osteoclastogenesis experiments, cells were cultured in a 96-well plate at the density of 6×10^3 cells/well, and after 24 h, the adherent cells were cocultured with an additional α-MEM medium + 10% FBS + 1% antibiotics containing cytokines (40 ng/mL RANKL and 10 ng/mL TNF-α). Samples at appropriate concentrations were dissolved into DMSO (v/v, 0.1% in each well) and added into each well. The cells were then cultured for 4 days.

Assay for Osteoclastic TRAP Activity. The protocol for the assay of osteoclastic TRAP activity was as follows. After the cell culture period, the media were removed and adherent cells were fixed in 37% formaldehyde mixed with acetone and citrate solution (8:65:25, v/v/v) for 3 min and then washed with water. The cells were then stained for TRAP with the TRAP staining kit 387-A according to the manufacturer's instructions: the cells were stained with a fast garnet GBC base solution mixed with sodium nitrite solution, naphthol AS-BI phosphoric solution, acetate solution, and tartrate solution. After 1 h of staining in the dark, the stained cells were washed with water and colored by hematoxylin solution for 2 min and then rinsed with 0.1 N NaOH. The number of TRAP-positive multinucleated cells in each well was counted. Oleic acid was used as a positive control based on reference.[13]

Assay for Cell Proliferation. Cell viability was evaluated using a 3-(4,5-dimethylthiazol-2-yl)-2,5-diphenyl tetrazolium bromide (MTT) assay. RAW cells (1×10^5 cells/well) were seeded into 96-well plates for 24 h. Samples at appropriate concentrations were dissolved in DMSO (v/v, 0.1% in each well) and added into each well for another 24 h. After culturing, the cells were treated with 5 μL of MTT (final concentration = 5 mg/mL dissolved in phosphate buffer solution) for 4 h, and the precipitated dye was solubilized by isopropanol (with 0.04 N HCl). The absorbance at 570 nm was measured.

Extraction and Isolation. For the extraction and isolation of bioactive principles, 5.10 kg of fresh leaves of loquat was freeze-dried and ground into powder, and the resulting 2.36 kg of the dried leaves of loquat were extracted with methanol (35 L) and evaporated. Then, 447.25 g of methanol extract was obtained (yield = 18.95%). First, a part of the methanol extract (234.22 g) was separated by silica gel column chromatography (20 cm i.d. × 50 cm, 4.49 kg of Wakogel C-200) and eluted with an n-hexane/EtOAc solvent system [10:0 (11 L), 9.8:0.2 (2 L), 9.7:0.3 (2 L), 9.6:0.4 (2 L), 9.5:0.5 (2 L), 9:1 (2 L), 8.5:1.5 (11 L), 8:2 (8 L), 7:3 (5 L), 6.5:3.5 (12 L), 6:4 (5 L), 5.5:4.5 (2.5 L), 5:5 (6.5 L), 4:6 (3 L), 3:7 (3 L), 2:8 (2 L), 0:10 (2 L), and methanol 100% (13 L)] to yield 14 fractions. The remaining part of the methanol extract (213.03 g) was applied to column chromatography again (20 cm i.d. × 50 cm, 4.21 kg of Wakogel C-200) and eluted with an n-hexane/EtOAc solvent system [10:0 (10 L), 9:1 (5 L), 8.5:1.5 (5 L), 8:1.5 (5 L), 8:2 (7 L), 7.5:2.5 (6 L), 7:3 (5 L), 6.5:3.5 (5 L), 6:4 (5 L), 5.5:4.5 (5 L), 5:5 (5 L), 4:6 (5 L), 3:7 (5 L), 2:8 (5 L), 1:9 (5 L), 0:10 (14 L), and methanol 100% (10 L)] to yield 14 fractions. On the basis of the TLC results, twice-separated fractions were combined into nine fractions [Fr. 1 (17.58 g), Fr. 2 (8.37 g), Fr. 3

dx.doi.org/10.1021/jf402735u | J. Agric. Food Chem. 2014, 62, 836−841

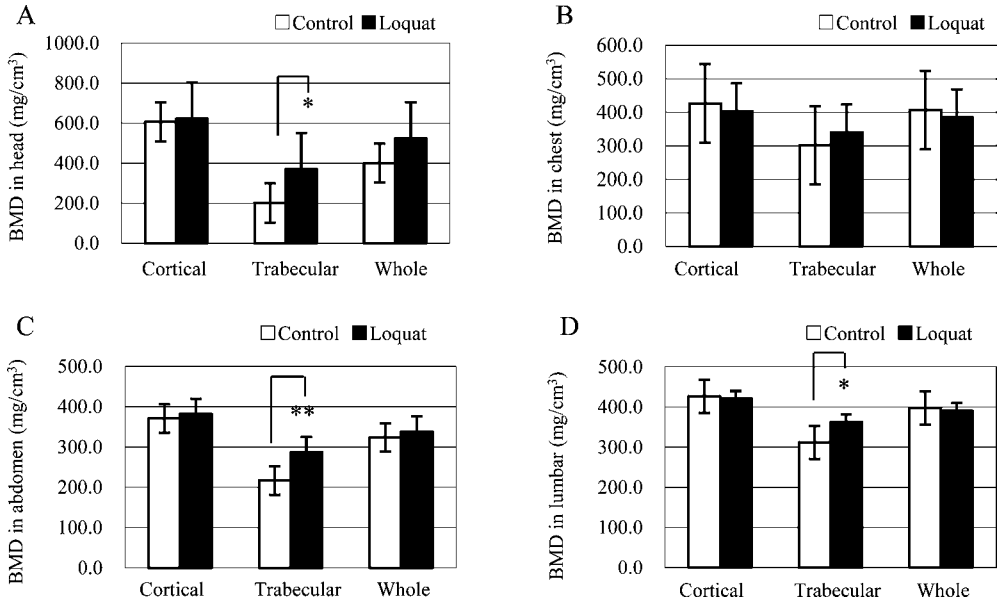

Figure 1. Effect of diet with or without the leaves of loquat on the bone mineral density (BMD) of the head (A), chest (B), abdomen (C), and lumbar (D) in OVX mice. Data showed ± SD (n = 8); Student's t test: (*) $P < 0.05$; (**) $P < 0.01$.

(4.86 g), Fr. 4 (7.55 g), Fr. 5 (12.46 g), Fr. 6 (13.34 g), Fr. 7 (14.44 g), Fr. 8 (14.03 g), and Fr. 9 (366.45 g)]. On the basis of bioactivity-guided fractionation on osteoclastic TRAP activity, Fr. 4 (7.10 g) was subjected to further separation. Fraction 4 was applied to silica gel column chromatography (6 cm i.d. × 120 cm, 963 g of Wakogel C-200) and eluted with an *n*-hexane/EtOAc solvent system [10:0 (1 L), 9:1 (1.5 L), 8:2 (1.5 L), 7:3 (1.5 L), 6.8:3.2 (1 L), 6.5:3.5 (1 L), 6.2:3.8 (1 L), 6:4 (1 L), 5:5 (1 L), 2.5:8.5 (1 L), and methanol 100% (2 L)] to give eight fractions. The amount of each fraction was shown as Fr. 4-1 (74.11 mg), Fr. 4-2 (3.79 mg), Fr. 4-3 (17.52 mg), Fr. 4-4 (74.16 mg), Fr. 4-5 (85.29 mg), Fr. 4-6 (1.18 g), Fr. 4-7 (1.04 g), and Fr. 4-8 (4.79 g). Further fractionation procedures were applied only to Fr. 4-7, due to its highest osteoclastic TRAP inhibitory activity. Fraction 4-7 (989.1 mg) was applied to a Sephadex LH 20 column (5 cm i.d. × 50 cm, Sephadex amount = 100 g) and eluted with MeOH/$CHCl_3$ (500 mL) to give eight fractions: Fr. 4-7-1, Fr. 4-7-2, Fr. 4-7-3, Fr. 4-7-4, Fr. 4-7-5, Fr. 4-7-6, Fr. 4-7-7, and Fr. 4-7-8. The 15 mg of fraction 4-7-6 (see the HPLC chromatogram in the Supporting Information, Figure S1) dissolved in methanol was separated by recycling preparative HPLC (LC- 9204, Japan Analytical Industry Co., Tokyo, Japan). The total injection amount was 3 mL, with the flow rate at 5 mL/min; mobile phase was methanol 95% + water 5%, and the column was an Inertsil ODS-3 (20 × 250 mm, GL Science, Toyko, Japan) with detection for absorbance at 210 nm to give compound **1** (6.27 mg) (see the Supporting Information, Figure S2). To verify the purity, the isolated compound **1** was confirmed by HPLC (see the Supporting Information, Figure S3). HPLC chromatograms for individual fractions (Fr. 1−9, Fr. 4-1, 4-3−4-8, Fr. 4-7-1−4-7-8) and methanol extract were also studied (see the Supporting Information, Figure S4).

GC-MS and NMR Identification. For the gas chromatography−mass spectrometry (GC-MS), compound **1** (white solid) was treated with trimethylsilyldiazomethane (Tokyo Chemical Industry, Tokyo, Japan) in a solution of benzene (20% ethanol) for 30 min at room temperature and then subjected to a GC-MS analysis. Conditions were as follows: column temperature, 260 °C for 60 min; injection temperature, 250 °C; detector temperature, 300 °C; column, DB-5 capillary column, 0.25 mm i.d. × 30 m; helium rate, 1.4 mL/min; injection volume, 1 μL; split ratio, 5:1; m/z range, 50−600. EI/MS m/z (relative intensity %): 470 (3), 412 (3), 262 (100), 233 (6), 203 (97), 189 (24), 133 (75), 119 (27). Then compound **1** was dissolved in DMSO-d_6 and identified by ^{1}H NMR and ^{13}C NMR as ursolic acid (**1**) (optical rotation $[\alpha]_D^{24}$ +31.3 (methanol, c 0.117). The above data were compared with the literature[14] (see the Supporting Information, Figure S5).

Statistical Analysis. All values are expressed as means ± SD. The significance of differences between means for two groups was determined by Student's t test. Differences were considered significant at (*)$P < 0.05$ and (**)$P < 0.01$.

RESULTS

Effect of the Leaves of Loquat on Body Weight and the Weight of Each Organ. The two groups of mice showed no significant difference in body weight or viscera weights; notably, their uterine weights were the same. This outcome suggests that the leaves of loquat did not influence the actions of estrogen or its receptors; it also indicates that there is no potential side effect caused by unexpected estrogenic activity.

Effect of the Leaves of Loquat on BMD of Various Body Parts. We investigated the effect of the leaves of loquat on the BMD of various body parts of mice and found that the loss of BMD in the trabecular cells of head, abdomen, and lumbar parts was inhibited after treatment with the diet containing the leaves of loquat compared to the control group. As shown in Figure 1, the BMD of the loquat group was significantly higher in the trabecular bone of the head, abdomen, and lumbar.

Effect of the Extracts Prepared from the Leaves of Loquat on Osteoclast Differentiation. To determine the effect of the extracts prepared from the leaves of loquat on osteoclast differentiation, we applied water extract or methanol extract with various concentrations to RAW 264.7 cells. As shown in Figure 2, the multinucleated osteoclast-like cells were significantly inhibited by the methanol extract in a dose-dependent manner (**, $P < 0.01$). Under these concentrations, the methanol extract did not affect the cell viability of RAW 264.7 cells, suggesting that the methanol extract of the leaves of loquat inhibited osteoclast differentiation specifically without any cytotoxicity. It should be noted that the water extract showed no influence on osteoclast differentiation up to 500 μg/mL.

dx.doi.org/10.1021/jf402735u | J. Agric. Food Chem. 2014, 62, 836−841

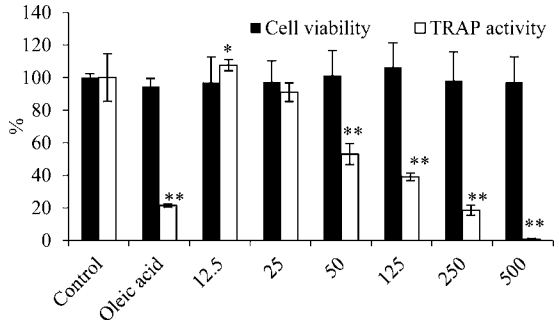

Figure 2. Effect of methanol extract of the leaves of loquat on osteoclast differentiation and cell viability of each concentration on RAW 264.7 cells. Oleic acid (50 μg/mL) was used as a positive control. The concentrations of methanol extract of the leaves of loquat were 12.5, 25, 50, 125, 250, and 500 μg/mL. Data showed ± SD (n = 3). Student's t test against control: (*) $P < 0.05$; (**) $P < 0.01$.

Effect of Subfractions Prepared from Methanol Extract of the Leaves of Loquat by Chromatography on Osteoclast Differentiation. We examined the effects of the nine fractions separated from the methanol extract on osteoclast differentiation. Under the concentration of 20 μg/mL, Fr. 4 showed significant osteoclast differentiation inhibitory activity with less cytotoxicity (Figure 3A), so it was further fractionated into eight fractions (Fr. 4-1−4-8), and their effects on osteoclast differentiation activity under 20 μg/mL were examined. As shown in Figure 3B, fraction 4-7 significantly inhibited the osteoclast differentiation; other fractions had less effect. In light of the search for bioactive principles, we applied Fr. 4-7 to further fractionation procedures and evaluated their effects on osteoclast differentiation. Among the eight fractions (Fr. 4-7-1−4-7-8), Fr. 4-7-6 showed significant inhibitory activity Figure 3C).

Effect of an Isolated Compound on Osteoclast Differentiation. Fraction 4-7-6 was further separated by recycling preparative HPLC to give compound **1**. Compound **1** was identified as ursolic acid (**1**) (Figure 4B). Ursolic acid (**1**) inhibited osteoclast differentiation in a dose-dependent manner shown in Figure 4A. We concluded that ursolic acid (**1**) should be the major principle for antiosteoclast activity of the leaves of loquat.

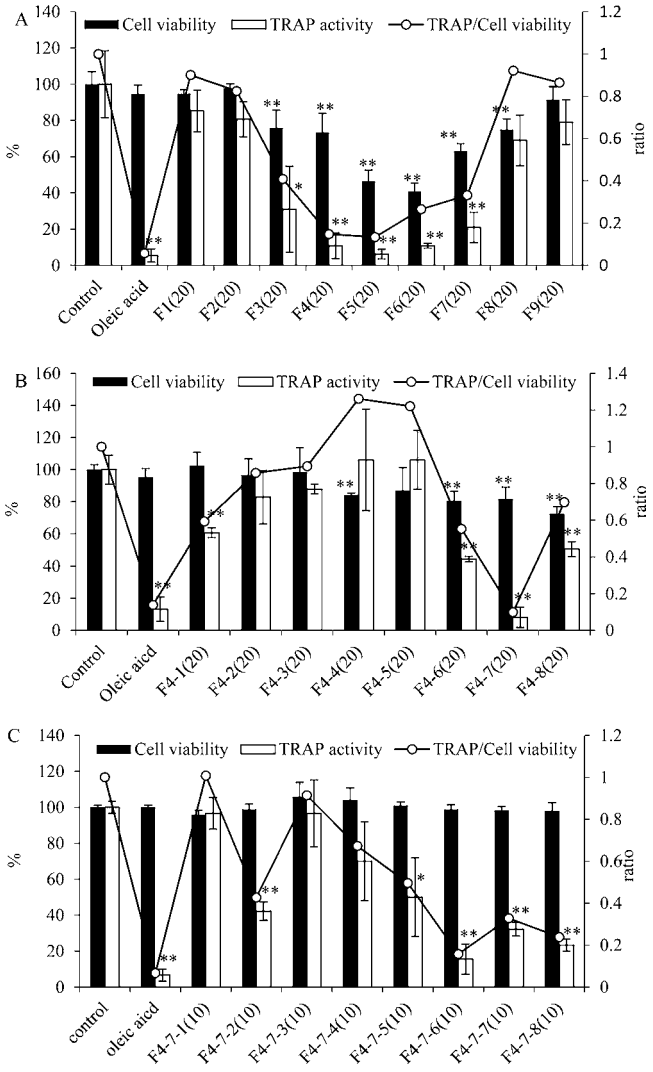

Figure 3. Effect of subfractions separated from methanol extract (A), Fr. 4 (B) and Fr. 4-7 (C) on osteoclast differentiation and cell viability on RAW 264.7 cells. Oleic acid (50 μg/mL) was used as a positive control. The concentration of subfractions separated from methanol extract and Fr. 4 was 20 μg/mL, and the concentration of subfractions separated from Fr. 4-7 was 10 μg/mL. Data showed means ± SD (n = 3). Student's t test against control: (*) $P < 0.05$; (**) $P < 0.01$.

DISCUSSION

Ovariectomized animal models (OVX) have been widely used to study preventive treatments for postmenopausal osteoporosis with estrogen insufficiency.[15] In OVX animals, as in postmenopausal women, bone loss induced by ovarian deficiency results mainly from trabecular bone loss.[15] In the present study, the administration of the leaves of loquat had a significant preventive effect against BMD loss of trabecular bone in OVX mouse compared to the control, especially in the head, abdomen, and lumbar. However, there is no obvious effect on the weight of the uterus and other organs in ovariectomized mice, indicating that the mechanism of the preventive effect of bone loss is not related to estrogenic activity.[7]

The loss of bone mass and the deterioration of bone microstructure have been linked to an imbalance between bone formation and bone resorption.[16] Here we found that the methanol extract of the leaves of loquat significantly inhibited the expression of multinucleated osteoclast cells, which are responsible for bone resorption, by evaluating the TRAP activity of osteoclast cells. Dose-dependent inhibitory effects of the extract on the differentiation of the osteoclasts without any cytotoxicity were observed.

The leaves of loquat exhibit significant in vivo and in vitro bone preventive activity; thus, it will be of interest to further investigate bioactive compounds. By using a bioactivity-guided fractionation judged by bioassay using RAW 264.7 cells, the effects of subfractions prepared from methanol extract on osteoclast differentiation at different concentrations were screened; the most significant bioactive fractions were tracked and further fractionated. One bioactive compound separated from bioactive fractions, ursolic acid (**1**), showed osteoclast differentiation inhibitory activity dose-dependently. On the basis of previous study on the leaves of loquat, pentacyclic triterpene acids make up the greatest percentage of secondary metabolites. Ursolic acid (**1**) accounted for >50% of the quantified triterpene fraction.[17] The yield of ursolic acid (**1**) extracted by methanol is higher than that by water due to its

dx.doi.org/10.1021/jf402735u | J. Agric. Food Chem. 2014, 62, 836−841

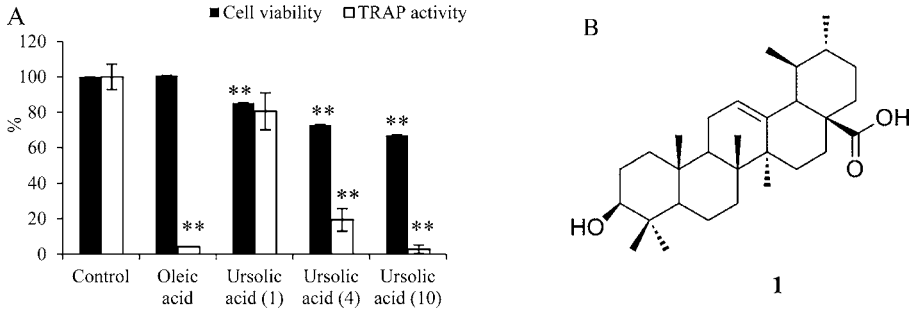

Figure 4. Effect of ursolic acid (**1**) on osteoclast differentiation and cell viability on RAW 264.7 cells (A) and chemical structure of ursolic acid (**1**) (B). Oleic acid (50 μg/mL) was used as a positive control. The concentrations were 1 μg/mL (2.19 μM), 4 μg/mL (8.77 μM), and 10 μg/mL (21.9 μM). Data showed ± SD (n = 3). Student's t test against control: (*) $P < 0.05$; (**) $P < 0.01$.

relatively low polarities.[18] In our study, through quantified study by HPLC, the percentage of ursolic acid in methanol extract of loquat leaves is nearly 33%, and the percentage of ursolic acid in the dried loquat leaves is 6.25% (see the Supporting Information Figure S4 and Table 1). A number of studies have demonstrated ursolic acid (**1**) can indeed suppress multiple molecular targets that play a pivotal role in anticancer potential, anti-inflammatory in vitro, and in vivo human clinical trials.[19−21] However, more detailed investigations are needed to completely understand its exact mode of action against different diseases. There are few reports of ursolic acid (**1**) in the study of osteoporosis diseases. Lee et al. observed that ursolic acid (**1**) has bone-forming activity in an in vivo mouse calvarial bone formation model. Also, ursolic acid (**1**) stimulates osteoblast differentiation and mineralization with the induction of osteoblast-specific gene expressions.[22] However, no study focused on the inhibitory activity of ursolic acid (**1**) on osteoclast differentiation. We found that ursolic acid (**1**) inhibited osteoclast differentiation with an IC_{50} value of 3.49 μM.

To the best of our knowledge, the present study is the first to report the effect of the leaves of loquat in the treatment of osteoporosis. Our results showed that the leaves of loquat in the diet could prevent BMD loss in OVX mice. Ursolic acid (**1**) is responsible for the osteoclast differentiation inhibitory activity. In conclusion, the leaves of loquat should be a functional ingredient of tea for the prevention and treatment of osteoporosis.

■ ASSOCIATED CONTENT

Supporting Information

TLC, HPLC, and recycling preparative HPLC chromatogram of Fr. 4-7-6; HPLC chromatogram of compound **1**, fraction (Fr. 1−9, 4-1, 4-3−4-8, 4-7-1−4-7-8) and methanol extract; quantified data for ursolic acid in fraction 4, 4-7, 5, 6, 7 and methanol extract. This material is available free of charge via the Internet at http://pubs.acs.org.

■ AUTHOR INFORMATION

Corresponding Author

*(K.S.) Phone/fax: +81 092 642 3002. E-mail: shimizu@agr.kyushu-u.ac.jp.

Funding

The costs of publication were supported in part by the Research Grant for Young Investigators of Faculty of Agriculture, Kyushu University.

Notes

The authors declare no competing financial interest.

■ REFERENCES

(1) Oh, J.; Min, O.-J.; Kim, H. A.; Kim, Y. J.; Baek, H. Y.; Rhyu, D. Y. Effect of *Eriobotrya japonica* on adipogenesis and body weight. *Appl. Biol. Chem.* **2011**, *54*, 382−387.

(2) Cha, D. S.; Eun, J. S.; Jeon, H. Anti-inflammatory and antinociceptive properties of the leaves of *Eriobotrya japonica*. *J. Ethnopharmacol.* **2011**, *134*, 305−312.

(3) Ito, H.; Kobayashi, E.; Li, S. H.; Hatano, T.; Sugita, D.; Kubo, N.; Shimura, S.; Itoh, Y.; Tokuda, H.; Nishino, H.; Yoshida, T. Antitumor activity of compounds isolated from leaves of *Eriobotrya japonica*. *J. Agric. Food Chem.* **2002**, *50*, 2400−2403.

(4) Meryl, S. L. *Metabolic Bone Disease in Text Book of Rheumatology*, 5th ed.; W. B. Saunders: London. UK, 1997; pp 1563−72.

(5) Shirwaikar, A.; Khan, S.; Kamariya, Y. H.; Patel, B. D.; Gajera, F. P. Medicinal plants for the management of postmenopausal osteoporosis: a review. *Open Bone J.* **2010**, *2*, 1−13.

(6) Tanaka, T.; Tang, H. T.; Yu, F. N.; Michihara, S.; Uzawa, Y.; Zaima, N.; Moriyama, T.; Kawamura, Y. Kudzu (*Pueraria lobata*) vine ethanol extract improve ovariectomy-induced bone loss in female mice. *J. Agric. Food Chem.* **2011**, *59*, 13230−13237.

(7) Das, S. K.; Ren, R.; Hashimoto, T.; Kanazawa, K. Fucoxanthin induces apoptosis in osteoclast-like cells differentiated from RAW 264.7 cells. *J. Agric. Food Chem.* **2010**, *58*, 6090−6095.

(8) Sheu, T.-J.; Schwarz, E. M.; Martinez, D. A.; O'Keefe, R. J.; Rosier, R. N.; Zuscik, M. J.; Puzas, J. E. A phage display technique identifies a novel regulator of cell differentiation. *J. Biol. Chem.* **2003**, *278*, 438−443.

(9) Yogesh, H. S.; Chandrashekhar, V. M.; Katti, H. R.; Ganapaty, S.; Raqhavendra, H. L.; Gowda, G. K.; Goplakhrishna, B. Anti-osteoporotic activity of acqueous-methanol extract of *Berberis aristata* in ovariectomized rats. *J. Ethnopharmacol.* **2011**, *134*, 334−338.

(10) Genunt, H. K.; Baylink, D. J.; Gallagher, J. C. Estrogens in the prevention of osteroporosis in postmenopausal women. *Am. J. Obstet. Gynecol.* **1989**, *161*, 1841−1846.

(11) American Institute of Nutrition.. Report of the American Institute of Nutrition Ad Hoc Committee on Standards for Nutritional Studies. *J. Nutr.* **1977**, *107*, 1340−1348.

(12) The Ministry of Health, Labor and Welfare. *National Nutrition Health Investigation*, 2008.

(13) Cornish, J.; MacGibbon, A.; Lin, J-M; Watson, M.; Callon, K. E.; Tong, P. C.; Dunford, J. E.; Does, Y. V. D.; Williams, G. A.; Grey, A. B.; Naot, D.; Reid, L. R. Modulation of osteoclastogenesis by fatty acids. *Endocrinology* **2008**, *149*, 5688−5695.

(14) Silval, M. G. V.; Vieira, Í.G.P.; Mendes, F. N. P.; Albuquerque, I. L.; dos Santos, R. N.; Silva, F. O.; Morais, S. M. Variation of ursolic acid content in eight *Ocimum* species from northeastern Brazil. *Molecules* **2008**, *13*, 2482−2487.

(15) Kalu, D. N. The ovariectomized rat model of postmenopausal bone loss. *Bone Miner.* **1991**, *15*, 175−191.

(16) Szulc, P.; Delmas, P. D. Biochemical markers of bone turnover in men. *Calcif. Tissue Int.* **2001**, *69*, 229−234.
(17) Rollinger, J. M.; Kratschmar, D. V.; Schuster, D.; Pfisterer, P. H.; Gumy, C.; Aubry, E. M.; Brandstötter, S.; Stuppner, H.; Wolber, G.; Odermatt, A. 11β-Hydroxysteroid dehydrogenase 1 inhibiting constituents from *Eriobotrya japonica* revealed by bioactivity-guided isolation and computational approaches. *Bioorg. Med. Chem.* **2010**, *18*, 1507−1515.
(18) Xia, E.-Q.; Wang, B. W.; Xu, X. R.; Zhu, L.; Song, Y.; Li, H. B. Microwave-assisted extraction of oleanolic acid and ursolic acid from *Ligustrum lucidum* ait. *Int. J. Mol. Sci.* **2011**, *12*, 5319−5329.
(19) Patlolla, J. M.; Rao, C. V. Triterpenoids for cancer prevention and treatment: current status and future prospects. *Curr. Pharm. Biotechnol.* **2012**, *13*, 147−155.
(20) Shanmugam, M. K.; Dai, X. Y.; Kumar, A. P.; Tan, B. K. H.; Sethia, G.; Bishayeee, A. Ursolic acid in cancer prevention and treatment: molecular targets, pharmacokinetics and clinical studies. *Biochem. Pharmacol.* **2013**, *85*, 1579−1587.
(21) Laszczyk, M. N. Pentacyclic triterpenes of the lupane, oleanane and ursane group as tools in cancer therapy. *Planta Med.* **2009**, *75*, 1549−1560.
(22) Lee, S. U.; Park, S. J.; Kwak, H. B.; Oh, J.; Min, Y. K.; Kim, H. S. Anabolic activity of ursolic acid in bone: stimulating osteoblast differentiation *in vitro* and inducing new bone formation *in vivo*. *Pharmacol. Res.* **2008**, *58*, 290−296.

JOURNAL OF AGRICULTURAL AND FOOD CHEMISTRY

Article

pubs.acs.org/JAFC

Effect of Alcoholic Fermentation on the Carotenoid Composition and Provitamin A Content of Orange Juice

Isabel Cerrillo,[†] Blanca Escudero-López,[†] Dámaso Hornero-Méndez,[§] Francisco Martín,[†,‡] and María-Soledad Fernández-Pachón*[,†]

[†]Área de Nutrición y Bromatología, Departamento de Biología Molecular e Ingeniería Bioquímica, Universidad Pablo de Olavide, Carretera de Utrera Km 1, E-41013 Sevilla, Spain

[§]Departamento de Fitoquímica de Alimentos, Instituto de la Grasa−CSIC, Avenida Padre García Tejero 4, E-41012 Sevilla, Spain

[‡]CIBER de Diabetes y Enfermedades Metabólicas Asociadas (CIBERDEM), Universidad Pablo de Olavide, Carretera de Utrera Km 1, E-41013 Sevilla, Spain

ABSTRACT: Orange juice is considered a rich source of carotenoids, which are thought to have diverse biological functions. In recent years, a fermentation process has been carried out in fruits resulting in products that provide higher concentrations of bioactive compounds than their original substrates. The aim of this study was to evaluate the effect of a controlled alcoholic fermentation process (15 days) on the carotenoid composition of orange juice. Twenty-two carotenoids were identified in samples. The carotenoid profile was not modified as result of the fermentation. Total carotenoid content and provitamin A value significantly increased from day 0 (5.37 mg/L and 75.32 RAEs/L, respectively) until day 15 (6.65 mg/L and 90.57 RAEs/L, respectively), probably due to a better extractability of the carotenoids from the food matrix as a result of processing. Therefore, the novel beverage produced could provide a rich source of carotenoids and exert healthy effects similar to those of orange juice.

KEYWORDS: *orange juice, alcoholic fermentation, carotenoids, β-cryptoxanthin, provitamin A, bioactive compounds, LC-MS (APCI)*

INTRODUCTION

Orange juice is among the most consumed fruit juices worldwide. Orange juice accounts for 60% of all Western Europe consumption of fruit juices and juice-based drinks. In the United States, this juice is the most popular juice per capita, being consumed at 5 times the rate of Americans' second choice, apple juice.[1] Orange juice is considered a rich source of bioactive compounds beneficial for human health, such as ascorbic acid, flavonoids, and carotenoids. Numerous epidemiological and intervention studies have provided evidence to support that orange consumption may reduce the risk of cardiovascular diseases and cancer.[2,3]

Carotenoids are an important group of natural pigments, responsible for the coloring of most fruits and vegetables such as oranges, red peppers, watermelons, carrots, and tomatoes.[4] These compounds are minor constituents in cereal grains.[5] Nearly 750 naturally occurring carotenoids have been identified, and this number continues to rise.[6] Orange juice has one of the most complex carotenoid profiles reported in any fruit.[7] From a nutritional and physiological standpoint, orange juice carotenoids are thought to have diverse biological functions and actions, such as antioxidant capacity,[8] provitamin A activity,[9] macular protection,[10] bone health,[11] and anticarcinogenic effect.[12]

The increasing interest in these pigments has prompted the development of numerous analytical methods for characterizing carotenoids in orange juice[7] and other foods[13] and has prompted research into adequate production conditions and technological treatments to maintain or enhance carotenoid composition and subsequent application in the food industry.[14] Many studies have examined the effect of processing such as pulsed electric fields, thermal treatment, high pressure, refrigerated storage, or ultrafrozen on the carotenoid content of different types of orange juice, determining the optimal technological conditions to preserve the potential healthy effect of the resulting product.[15] It has been recently found that fermentation might improve the profile of bioactive compounds in fruits and vegetables, so a fermentation process has been carried out in fruits (pomenagrate,[16] mulberry,[17] apple[18]) and vegetables (red sorghum,[19] onion[20]), resulting in products that provide higher concentration of bioactive compound content than the substrate. Accordingly, it would be interesting to analyze the effect of a controlled fermentation process on the carotenoid composition of orange juice. On the other hand, this orange fermented product contains a moderate amount of alcohol. Numerous studies have demonstrated that moderate alcoholic consumption produces positive effects on plasma lipid profile, coagulation system, and the atherosclerotic process.[21] Therefore, healthy effects of dietary bioactive compounds and moderate alcohol consumption would also act synergistically in a potential beverage based on a controlled alcoholic fermentation of orange juice.

Therefore, the aim of this study was to evaluate the effect of the controlled alcoholic fermentation on the carotenoid composition of orange juice with a special emphasis on the provitamin A content. Furthermore, this novel orange juice beverage would suggest a new way to commercialize orange

Received: June 28, 2013
Revised: January 10, 2014
Accepted: January 13, 2014
Published: January 13, 2014

ACS Publications © 2014 American Chemical Society

dx.doi.org/10.1021/jf404589b | J. Agric. Food Chem. 2014, 62, 842−849

and the possibility of providing the consumer with a new potentially healthful beverage that could extend the supply of other similar drinks with higher alcohol content, such as wine, beer, or cider.

MATERIALS AND METHODS

Samples. The company Grupo Hespérides Biotech S.L. carried out the controlled alcoholic fermentation by using a novel process (patent WO2012/066176A120120524). A commercial pasteurized orange juice made from *Citrus sinensis* L. var. Navel late (Huelva, Spain) was used as starting material. The criteria for selection of this orange juice were the compositional homogeneity, microbiological stability, and organoleptic quality. These aspects are necessary for adequate development of the fermentation process and consumer acceptance of the final product. The yeast strain *Pichia kluyveri* var. *kluyveri* (Saccharomycetaceae family), isolated by Grupo Hespérides Biotech S.L. from the natural microbiota present in the orange fruit, was used as the inoculum. This yeast was selected for producing a low alcohol percentage (0.8−1.2% v/v) in the final product. The fermentation was carried out in a PVC tank (5 L) at 20 °C for 15 days in repose. Before sample collection, the fermentation liquid was agitated and mixed by the use of magnetic agitator to promote sample homogenization. Samples were aseptically collected on alternate days throughout the fermentation period (days 0, 1, 3, 5, 7, 9, 11, 13, and 15) and immediately stored at −20 °C until analysis. Two simultaneous fermentation processes were performed under identical conditions. Table 1 summarizes the quality parameters in both orange juice and fermented product: pH, tritatable acidity (TA), total glucids (reducing and nonreducing sugar), total soluble solids (TSS) (°Brix), pulp content (%), and alcohol (% v/v).[22]

Table 1. Quality Parameters of Orange Juice before and after Fermentation

quality parameter[a]	orange juice	fermented orange juice
pH	3.48 ± 0.20	3.43 ± 0.20
TA[b] (g citric acid/L)	8.48 ± 0.02	8.85 ± 0.02
total glucids (g/L)	78.20 ± 5.64	53.70 ± 4.65
reducing sugars (g/L)	48.50 ± 3.63	24.70 ± 2.13
nonreducing sugars (g/L)	29.70 ± 2.01	29.00 ± 2.51
TSS[c] (°Brix)	11.00 ± 0.50	10.00 ± 0.50
% pulp	12.00 ± 2.00	8.00 ± 0.50
alcohol (% v/v)	0.00	0.87 ± 0.01

[a]Values are expressed as the mean ± standard deviation. [b]TA, titratable acidity. [c]TSS, total soluble solids.

Chemicals and Reagents. HPLC grade methanol and acetone were supplied by BDH Prolabo (VWR International Eurolab, S.L., Barcelona, Spain). Diethyl ether containing 7 ppm of butylated hydroxytoluene (BHT) was purchased from Scharlau S.L. (Barcelona, Spain). HPLC grade deionized water was produced with a Milli-Q 50 system (Millipore Iberica S.A., Madrid, Spain). The remaining reagents were all of analytical grade and purchased from Sigma-Aldrich Química S.A. (Madrid, Spain).

Carotenoid Extraction. Carotenoid pigments were extracted from the nonfermented and fermented orange juice samples using the method of Mínguez-Mosquera and Hornero-Méndez[23] with some modifications. Briefly, an aliquot (10 mL) of a previously shaken sample was centrifuged at 10000*g* and 4 °C for 10 min to collect the solids in suspension. The pellet containing the carotenoid pigments was extracted with acetone (3 mL) containing 0.5% (w/v) BHT and centrifuged at 5000*g* and 4 °C for 5 min. The extraction step was repeated once, and both extracts were combined and dried under a nitrogen stream in a round-capped 15 mL polypropylene centrifuge tube. A saponification step was included to simplify the complexity of the HPLC carotenoid profiles by hydrolyzing the carotenoid acyl esters naturally present in orange juice. The dried extract was dissolved in 3 mL of diethyl ether and 0.5 mL of 20% (w/v) KOH/MeOH was added, followed by a reaction period of 20 min with intermittent agitation. After the addition of 3 mL of distilled water, samples were centrifuged at 5000*g* and 4 °C for 5 min to separate organic (upper) and aqueous (lower) phases. The supernatant was collected, dried under a nitrogen stream, and kept under the inert atmosphere at −30 °C until chromatographic analysis. Before the analysis, samples were dissolved in 0.5 mL of acetone and centrifuged at 12000*g* and 4 °C for 5 min. All operations were carried out under dimmed light to prevent isomerization and photodegradation of carotenoids.

Pigment Identification. Routine procedures were used to identify the carotenoids, using a combination of different experiments: separation and isolation of pigments by TLC and cochromatography (TLC and HPLC) with pure standards, analysis of the UV−visible and mass spectra, comparison with values in the literature,[4,24−28] and chemical test for 5,6-epoxy groups. Samples of *β*-carotene (*β*,*β*-carotene), antheraxanthin (5,6-epoxy-5,6-dihydro-*β*,*β*-carotene-3,3′-diol), *β*-cryptoxanthin (*β*,*β*-caroten-3-ol), zeaxanthin (*β*,*β*-carotene-3,3′-diol), lutein (*β*,*ε*-carotene-3,3′-diol), violaxanthin (5,6:5′,6′-diepoxy-5,6:5′,6′-tetrahydro-*β*,*β*-carotene-3,3′-diol), and neoxanthin (5′,6′-epoxy-6:7-didehydro-5,6:5′,6′-tetrahydro-*β*,*β*-carotene-3,5,3′-triol) were isolated and purified from natural sources (*Capsicum annuum* and *Mentha arvensis*).[23] 5,8-Epoxy-carotenoids, such as mutatoxanthin (5,8-epoxy-5,8-dihydro-*β*,*β*-carotene-3,3′-diol), auroxanthin (5,8:5′,8′-diepoxy-5,8:5′,8′-tetrahydro-*β*,*β*-carotene-3,3′-diol), luteoxanthin (5,6:5′,8′-diepoxy-5,6:5′,8′-tetrahydro-*β*,*β*-carotene-3,3′-diol), and neochrome (5′,8′-epoxy-6,7-didehydro-5,6:5′,8′-tetrahydro-*β*,*β*-carotene-3,5,3′-triol) were prepared from the corresponding 5,6-epoxy parent pigments (antheraxanthin, violaxanthin, and neoxanthin) by controlled treatment with diluted HCl. Latochrome (5′,8′-epoxy-5,6,5′,8′-tetrahydro-*β*,*β*-carotene-3,5,6,3′-tetrol) and karpoxanthin (5,6-dihydro-*β*,*β*-carotene-3,3′,5,6-tetrol) were only tentatively identified due to the lack of pure standards. The tentative identification of *Z* isomers of lutein and mutatoxanthin was based on the presence and relative intensity ($\%A_B/A_{II}$) of the *cis* peak at about 330−340 nm in the UV−visible spectrum; a reduced fine structure and small hypsochromic shift in λ_{max} with respect to the all-*E* counterpart; and the chromatographic behavior in the C18 HPLC column, showing a slightly greater retention of *Z* than the all-*E* isomer.[28]

Carotenoid Analysis and Quantification by HPLC. Carotenoid pigments were analyzed by reversed-phase HPLC using a method previously developed[23] with slight modifications. Briefly, the method uses a C18 reversed-phase column (Mediterranea SEA18, 20 × 0.46 cm i.d., 3 *μ*m particle size; Teknokroma S.C.L., Barcelona, Spain) and a binary gradient elution system of acetone−deionized water at a flow of 1.0 mL/min. The mobile phase started at 75% acetone and rose linearly to 95% within 10 min and continued isocratically for 7 min, then changing to 100% within 3 min and maintaining this composition for 3 min. The injection volume was 10 *μ*L, and detection was carried out simultaneously at 402, 424, and 450 nm (1.2 nm spectral resolution and 10 scan/s scanning speed), to detect and quantify the diverse family of citrus carotenoids characterized as having different chromophores. The column and sample compartment were maintained at 25 and 15 °C, respectively. HPLC analyses were performed with a Waters 2695E Alliance quaternary pump equipped with a Waters 2998 diode array detector and were controlled with Empower2 data acquisition software (Waters Corp., Milford, MA, USA). Pigments were quantified in the saponified extracts by using calibration curves (six to eight concentration levels) prepared with standard stock solutions for each carotenoid in the concentration range of 5−100 *μ*g/mL. Calibration curves were constructed by plotting the peak area at 402 nm (for auroxanthin and *ζ*-carotene), 424 nm (for neochrome and luteoxanthin), and 450 nm (for mutatoxanthin, zeaxanthin, lutein, *β*-cryptoxanthin, and *β*-carotene) versus the pigment concentration. Latochrome and karpoxanthin were quantified by using the calibration curve of neochrome and zeaxanthin, respectively. The *Z* isomers were quantified by using the calibration curve of the all-*E* isomer. Concentration values were calculated as milligrams of pigment per liter of juice.

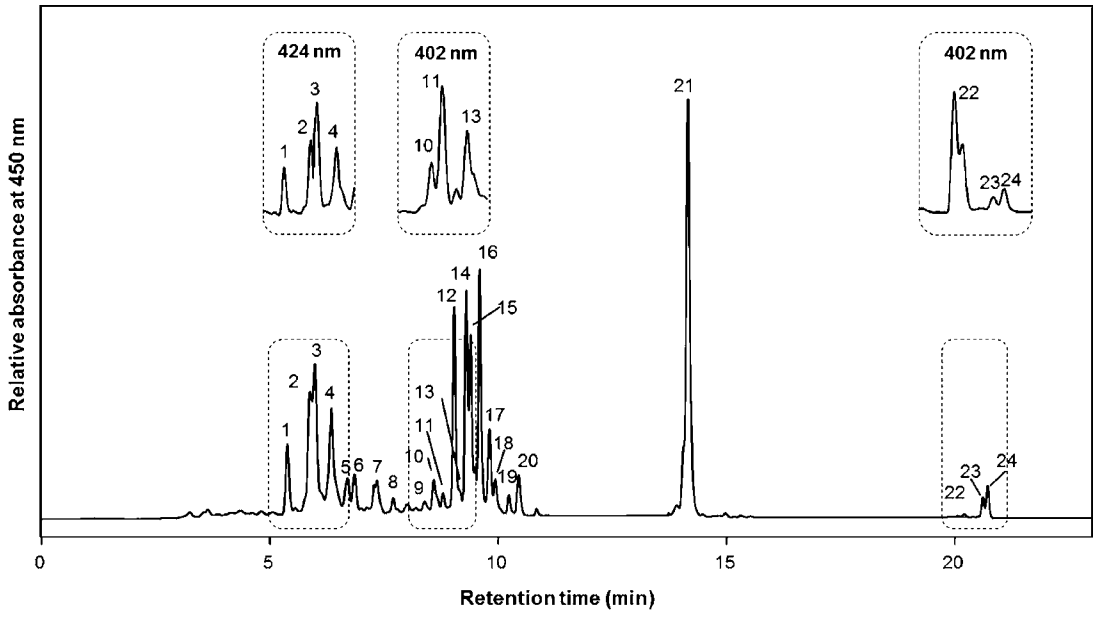

Figure 1. C18 reversed-phase HPLC chromatogram obtained for a saponified carotenoid extract prepared from the orange juice used for fermentation. See text for chromatographic conditions. Peak identification and characterization are given in Table 2.

Table 2. Chromatographic and Spectral Characteristics of the Carotenoid Pigments Present in the Orange Juice Used for Fermentation

		UV−visible spectrum					
peak	carotenoid	t_R (min)	λ_{max} (nm) in HPLC mobile phase	λ_{max} (nm) according to the lit.[b]	% III/II	epoxide test	LC-MS (APCI) m/z $[M + H]^+$
1	latochrome[a]	5.38	401, 424, 450	398, 422, 448; ethanol	100	−	619
2	karpoxanthin[a]	5.86	424, 450, 476	419, 443,472; ethanol	94	−	nd[c]
3	neochrome	6.05	401, 424, 450	398, 421, 448; acetone	88	−	601
4	karpoxanthin isomer[a]	6.31	423, 448, 476	419, 443,472; ethanol	94	−	nd
5	neochrome isomer	6.71	399, 421, 446	400, 423, 448; acetone	87	−	601
6	karpoxanthin isomer[a]	6.87	422, 445, 471	419, 443, 472; ethanol	90	−	nd
7	not identified (lutein-like chromophore)	7.27	420, 442, 469		nd	−	nd
8	not identified	7.37	420, 442, 465		nd	−	nd
9	luteoxanthin	8.57	397, 420, 446	400, 423, 448; acetone	105	+	601
10	auroxanthin epimer 1	8.68	384, 403, 427	377, 398, 423; acetone	94	−	601
11	auroxanthin epimer 2	8.79	384, 403, 427	377, 398, 423; acetone	94	−	601
12	mutatoxanthin epimer 1	9.03	411, 430, 457	409, 428, 456; ethanol	87	−	585
13	auroxanthin epimer 3	9.18	384, 403, 427	377, 398, 423; acetone	94	−	601
14	mutatoxanthin epimer 2	9.31	411, 430, 457	409, 428, 456; ethanol	85	−	585
15	(all-*E*)-zeaxanthin	9.40	426, 452, 480	430, 452, 479; acetone	20	−	569
16	(all-*E*)-lutein	9.61	424, 449, 476	422, 445, 474; ethanol	65	−	569
17	(*Z*)-mutatoxanthin[a]	9.82	328, 405, 425, 449	na[d]		−	585
18	(*Z*)-mutatoxanthin[a]	9.95	328, 404, 426, 448	na		−	585
19	(9*Z*)-lutein	10.23	330, 424, 443, 470	330, 422, 444, 474; ethanol	63	−	569
20	(13*Z*)-lutein	10.45	334, 422, 444, 472	332, 422, 442, 472; ethanol	54	−	569
21	*β*-cryptoxanthin	14.15	428, 454, 480	428, 450, 478; ethanol	18	−	553
22	*ζ*-carotene	20.27	380, 401, 425	378, 400, 425; hexane	100	−	541
23	(all-*E*)-*α*-carotene	20.61	422, 446, 475	424, 448, 476; acetone	55	−	537
24	(all-*E*)-*β*-carotene	20.72	430, 454, 480	429, 452, 478; acetone	15	−	537

[a]Tentative identification. [b]Britton et al.[6] [c]nd, not determined. [d]na, not available.

Provitamin A carotenoid content was expressed as retinol activity equivalents per liter of juice (RAEs/L) following the method of Scott and Rodríguez-Amaya,[29] with 1 RAE corresponding to 12 *μ*g of (all-*E*)-*β*-carotene or 24 *μ*g of *Z* isomers of *β*-carotene or any other carotenoid containing one unsubstituted *β*-ring.

Carotenoid Analysis and Quantification by Liquid Chromatography−Mass Spectrometry (LC-MS (APCI+)). LC-MS was performed by coupling a chromatographic system with a Micromass ZMD4000 mass spectrometer equipped with a single-quadrupole analyzer (Micromass Ltd., Manchester, UK) and an atmospheric

dx.doi.org/10.1021/jf404589b | J. Agric. Food Chem. 2014, 62, 842−849

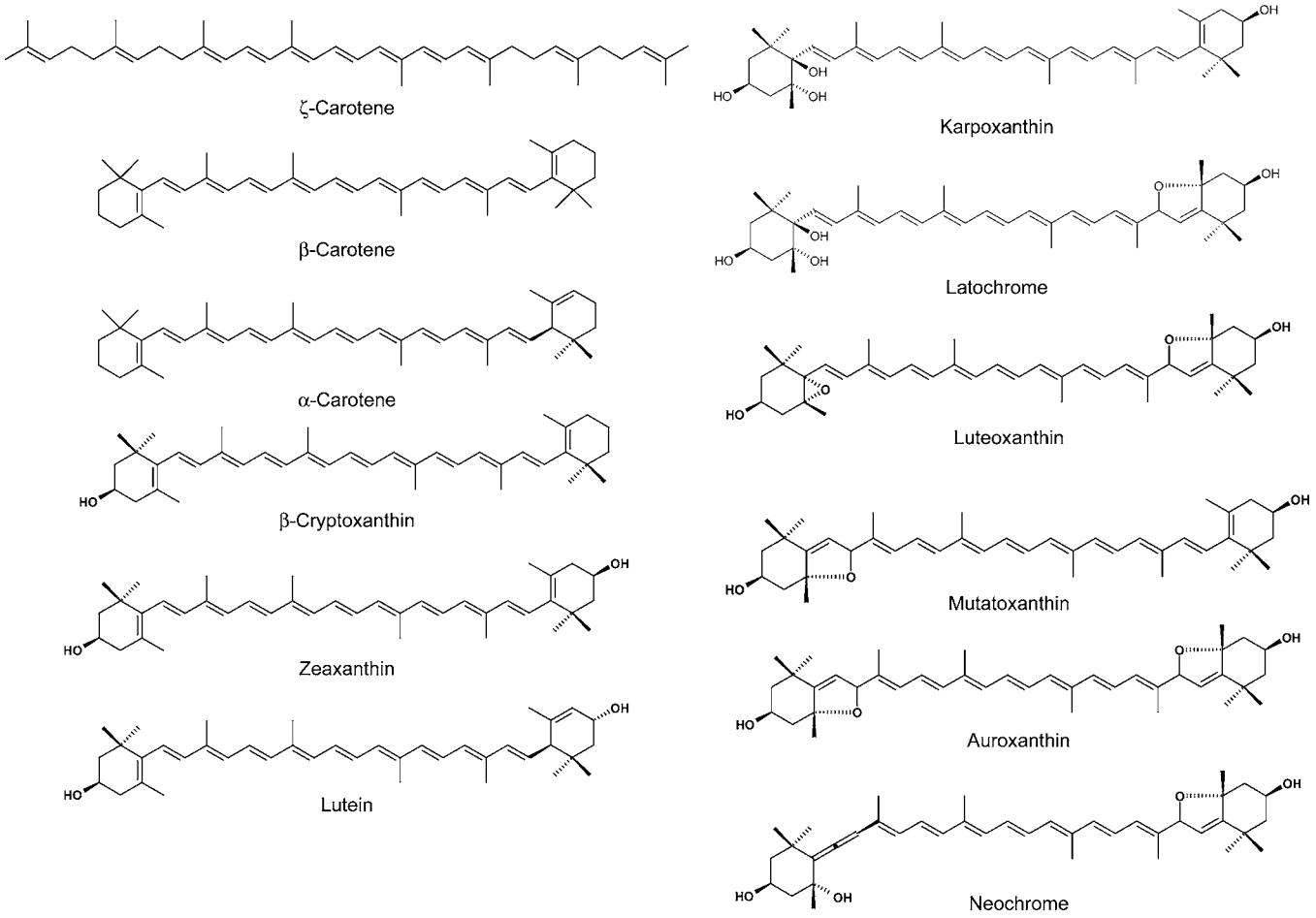

Figure 2. Chemical structures of the carotenoid pigments present in the orange juice used for fermentation.

pressure chemical ionization (APCI) probe. The system was controlled with MassLynx 3.2 software (Micromass Ltd., Manchester, UK). MS conditions were as follows: positive ion mode (APCI+); source temperature, 150 °C; probe temperature, 400 °C; corona voltage, 3.7 kV; high-voltage lens, 0.5 kV; and cone voltage, 30 V. Nitrogen was used as the desolvation and cone gas at 300 and 50 L/h, respectively. Mass spectra were acquired within the m/z 300−1200 range. The chromatographic conditions were as described above for carotenoid analysis and quantification.

Statistical Analysis. The fermentation process was performed in duplicate, and all samples were analyzed in triplicate. Results are expressed as the mean ± standard deviation. Analysis of variance (one-way ANOVA; Duncan's test) was applied to establish significant differences between the values of carotenoid and provitamin A carotenoid content obtained during the fermentation. A probability value of $p < 0.05$ was considered as the criteria for significance. These analyses were carried out by SPSS15.0 software (SPSS Inc., Chicago, IL, USA).

RESULTS AND DISCUSSION

Carotenoid Composition of Orange Juice Used in the Fermentation. Figure 1 depicts the chromatogram corresponding to the carotenoid profile present in the orange juice used in the fermentation process, and Table 2 summarizes the chromatographic and spectroscopic data (UV−visible and mass spectra). Twenty-two carotenoids, including some *Z* geometrical isomers, were identified in the saponified extracts of the orange juice. The carotene fraction was composed of *β*-carotene, *α*-carotene, and *ζ*-carotene, whereas the xanthophyll group was more complex, being composed of zeaxanthin, lutein, *β*-cryptoxanthin, and several carotenoids containing 5,8-epoxy groups in their structure (neochrome, mutatoxanthin, luteoxanthin, auroxanthin, and latochrome), which are respectively derived from neoxanthin, antheraxanthin, violaxanthin, and latoxanthin by the rearrangement of 5,6-epoxy groups under acidic conditions.[30] Figure 2 depicts the chemical structures of these pigments. Several geometric isomers corresponding to *Z* isomers of mutatoxanthin and lutein were also identified. Latochrome was only tentatively identified due to the lack of a pure standard. The $[M + H]^+$ value (m/z 619) was consistent with the formula $C_{40}H_{58}O_5$ (MW = 618.4284) and the presence of at least three to four hydroxy groups, explaining the higher polarity (shorter retention time) with respect to neochrome. The UV−visible absorption maxima at 401, 424, and 450 nm were in agreement with a chromophore of eight conjugated double bonds (as in the case of luteoxanthin) and with the presence of a 5,8-epoxy group, as supported by the negative results of the epoxide test. These data were in accordance with Meléndez-Martínez et al., who reported that numerous authors had erroneously identified latoxanthin (5′,6′-epoxy-5,6,5′,6′-tetrahydro-*β*,*β*-carotene-3,5,6,3′-tetrol) and its 5,8-epoxy derivative, latochrome, as neoxanthin in citrus fruit.[31] The presence of latochrome in orange juice was previously reported by Gross et al.,[32] but no further identification work has been carried out in this vegetable product. The UV−visible spectra of latoxanthin (417, 440, 468 nm, %I II/II = 95, in ethanol) and latochrome (398, 422, 448 nm, % III/II = 95, in ethanol) are highly similar to the spectra

dx.doi.org/10.1021/jf404589b | J. Agric. Food Chem. 2014, 62, 842−849

Table 3. Evolution in the Carotenoid Composition and Provitamin A Content of Orange Juice during the Fermentation Process

	concentration[a] (mg/L) at a fermentation time of								
carotenoid	0 days	1 day	3 days	5 days	7 days	9 days	11 days	13 days	15 days
latochrome	0.15 ± 0.00a	0.13 ± 0.01b	0.15 ± 0.00a	0.15 ± 0.00a	0.16 ± 0.00ac	0.17 ± 0.00de	0.17 ± 0.01cd	0.18 ± 0.01e	0.18 ± 0.00e
karpoxanthin	0.22 ± 0.01ab	0.21 ± 0.01a	0.23 ± 0.01ab	0.23 ± 0.00bc	0.26 ± 0.02cd	0.27 ± 0.01de	0.28 ± 0.01de	0.29 ± 0.01e	0.29 ± 0.00e
neochrome	0.37 ± 0.01a	0.32 ± 0.02b	0.37 ± 0.02a	0.41 ± 0.02ac	0.42 ± 0.04c	0.45 ± 0.01cd	0.44 ± 0.01cd	0.47 ± 0.02cd	0.46 ± 0.01d
karpoxanthin isomer	0.23 ± 0.01ab	0.21 ± 0.01a	0.24 ± 0.01ab	0.23 ± 0.00ab	0.26 ± 0.01bc	0.27 ± 0.01cd	0.29 ± 0.01d	0.27 ± 0.02cd	0.29 ± 0.00d
neochrome isomer	0.10 ± 0.00ab	0.09 ± 0.00a	0.10 ± 0.00ab	0.11 ± 0.00b	0.12 ± 0.01bc	0.12 ± 0.00cd	0.13 ± 0.00cd	0.12 ± 0.01cd	0.13 ± 0.00d
karpoxanthin isomer	0.10 ± 0.00abc	0.10 ± 0.00a	0.10 ± 0.00ab	0.10 ± 0.00a	0.11 ± 0.00bcd	0.11 ± 0.00d	0.12 ± 0.00d	0.11 ± 0.01cd	0.12 ± 0.00d
luteoxanthin	tr[b]	tr	tr	tr	tr	tr	tr	tr	tr
auroxanthin epimer 1	0.65 ± 0.03a	0.55 ± 0.04b	0.67 ± 0.05ac	0.74 ± 0.03cde	0.71 ± 0.00acd	0.81 ± 0.02ef	0.78 ± 0.04de	0.86 ± 0.07f	0.86 ± 0.03f
auroxanthin epimer 2	0.43 ± 0.01a	0.38 ± 0.02b	0.44 ± 0.03a	0.44 ± 0.01a	0.51 ± 0.05cd	0.53 ± 0.00 cd	0.54 ± 0.01d	0.49 ± 0.03c	0.55 ± 0.02d
mutatoxanthin epimer 1	0.29 ± 0.01a	0.25 ± 0.01b	0.29 ± 0.01a	0.28 ± 0.01a	0.32 ± 0.03c	0.33 ± 0.00cd	0.34 ± 0.01cd	0.36 ± 0.02d	0.36 ± 0.00d
auroxanthin epimer 3	0.31 ± 0.01a	0.26 ± 0.02b	0.31 ± 0.03a	0.30 ± 0.02ab	0.33 ± 0.03ac	0.34 ± 0.00ac	0.32 ± 0.01ac	0.35 ± 0.05ac	0.36 ± 0.02c
mutatoxanthin epimer 2	0.32 ± 0.01a	0.29 ± 0.01b	0.32 ± 0.01a	0.32 ± 0.00a	0.36 ± 0.03c	0.37 ± 0.00c	0.38 ± 0.02cd	0.40 ± 0.01d	0.40 ± 0.00d
(all-*E*)-zeaxanthin	0.40 ± 0.02ac	0.36 ± 0.02ab	0.39 ± 0.02a	0.33 ± 0.02b	0.43 ± 0.03cd	0.44 ± 0.00de	0.47 ± 0.02e	0.47 ± 0.01e	0.47 ± 0.00e
(all-*E*)-lutein	0.30 ± 0.01a	0.27 ± 0.02b	0.30 ± 0.01a	0.27 ± 0.00ab	0.32 ± 0.02cd	0.34 ± 0.00de	0.35 ± 0.02de	0.36 ± 0.00e	0.36 ± 0.00e
(*Z*)-mutatoxanthin	0.13 ± 0.00a	0.11 ± 0.00b	0.13 ± 0.00a	0.13 ± 0.00a	0.14 ± 0.01c	0.15 ± 0.00cd	0.15 ± 0.00cd	0.16 ± 0.00d	0.16 ± 0.00d
(*Z*)-mutatoxanthin	0.05 ± 0.00ab	0.04 ± 0.00a	0.05 ± 0.00ab	0.05 ± 0.00abc	0.05 ± 0.00bcd	0.05 ± 0.00cde	0.06 ± 0.00de	0.06 ± 0.00de	0.06 ± 0.00e
(9*Z*)-lutein	0.02 ± 0.00abc	0.02 ± 0.00a	0.02 ± 0.00ab	0.02 ± 0.00a	0.02 ± 0.00bcd	0.02 ± 0.00cd	0.02 ± 0.00d	0.02 ± 0.00d	0.03 ± 0.00d
(13*Z*)-lutein	0.09 ± 0.00ab	0.08 ± 0.00a	0.09 ± 0.00ab	0.09 ± 0.00a	0.10 ± 0.00bc	0.10 ± 0.00c	0.11 ± 0.01c	0.10 ± 0.01c	0.11 ± 0.00c
β-cryptoxanthin	0.71 ± 0.03ab	0.66 ± 0.04a	0.70 ± 0.04ab	0.72 ± 0.02ab	0.77 ± 0.05bc	0.80 ± 0.02cd	0.85 ± 0.03d	0.81 ± 0.07cd	0.85 ± 0.01d
ζ-carotene	0.37 ± 0.02a	0.36 ± 0.01a	0.36 ± 0.03a	0.35 ± 0.00a	0.42 ± 0.02b	0.43 ± 0.01bc	0.46 ± 0.00c	0.44 ± 0.04bc	0.46 ± 0.01c
(all-*E*)-α-carotene	0.04 ± 0.00acd	0.04 ± 0.00ab	0.04 ± 0.00abc	0.04 ± 0.00b	0.04 ± 0.00cde	0.04 ± 0.00def	0.05 ± 0.00f	0.05 ± 0.00ef	0.05 ± 0.00ef
(all-*E*)-β-carotene	0.08 ± 0.00ab	0.07 ± 0.00ab	0.08 ± 0.00ab	0.07 ± 0.00a	0.08 ± 0.00bc	0.09 ± 0.00cd	0.09 ± 0.00d	0.09 ± 0.00cd	0.09 ± 0.00cd
total carotenoid content	5.37 ± 0.21a	4.82 ± 0.31b	5.38 ± 0.32a	5.41 ± 0.17a	5.94 ± 0.41c	6.28 ± 0.12 cd	6.41 ± 0.23d	6.47 ± 0.28d	6.65 ± 0.07d
provitamin A (RAEs/L)[c]	75.32 ± 3.58ab	71.27 ± 3.86a	74.38 ± 4.40ab	74.46 ± 2.24ab	81.86 ± 5.82bc	86.07 ± 3.32cd	90.70 ± 3.97d	86.32 ± 7.98cd	90.57 ± 1.53d

[a]The values are the mean of three determinations ± standard deviation. Values with different letters (a–f) in the same row are significantly different ($p < 0.05$) as determined by Duncan's test. [b]tr, traces. [c]Provitamin A content calculated according to Scott and Rodríguez-Amaya.[29]

dx.doi.org/10.1021/jf404589b | J. Agric. Food Chem. 2014, 62, 842–849

of neoxanthin (418, 442, 471 nm, % III/II = 85, in ethanol) and neochrome (398, 421, 448 nm, % III/II = 80, in ethanol), respectively. This similarity and their analogous chromatographic behaviors would likely explain the misidentification of these pigments in citrus fruit. For this reason, a complete experimental characterization is essential for their unambiguous identification. In addition, three peaks (eluting at 5.86, 6.31, and 6.87 min) with λ_{max} at 419, 443, and 472 nm (% III/II = 90) were detected, consistent with a chromophore of nine conjugated double bonds plus a β-end ring.[30] The negative epoxide test result and the shorter retention time with respect to the dihydroxylated xanthophylls (lutein and zeaxanthin) supported the tentative identification of these pigments as karpoxanthin (5,6-dihydro-β,β-carotene-3,3′,5,6-tetrol) isomers. Unfortunately, no mass spectra could be recorded for these minor chromatographic peaks. Nevertheless, given that latochrome is the 5,8-epoxy derivative of karpoxanthin, it can be conjectured that karpoxanthin was present.

Table 3 reports the carotenoid profile and content of the samples. In relation to the quantitative analysis of carotenoids in the orange juice, auroxanthin (1.39 mg/L; sum of three epimers) and β-cryptoxanthin (0.71 mg/L) were the most abundant xanthophylls among the 22 carotenoid pigments identified in this study. As mentioned before, auroxanthin derived from violaxanthin under the acidic conditions of orange juice. These observations were in agreement with previous studies reporting β-cryptoxanthin and violaxanthin as the major carotenoids in orange juice.[4,33] Luteoxanthin, the intermediate product between violaxanthin and auroxanthin, was detected in trace amounts. (all-*E*)-Zeaxanthin, ζ-carotene, and (all-*E*)-lutein were present at 0.40, 0.37, and 0.30 mg/L, respectively. Two epimers of mutatoxanthin (8*R* and 8*S*) were detected in orange juice with concentrations of 0.29 and 0.32 mg/L, which derived from antheraxanthin, their 5,6-epoxy precursor, originally present in the fresh juice. Geometric carotenoid isomers were detected in minor concentrations in orange juice, including (9*Z*)- and (13*Z*)-lutein and two (*Z*)-mutatoxanthin isomers, were found at concentrations ranging from 0.02 to 0.13 mg/L. The carotenoid composition of characterized orange juice was similar to other studies,[7] but comparisons of the carotenoid profiles of orange juices are notoriously difficult. Their composition depends on the variety of the fruit, climate, stage of maturity, industrial processing, and storage conditions, among other factors. Mouly et al. were able to use the carotenoid profile to identify the geographic origin (cultivation and/or production) of orange juice samples.[34]

Effect of Alcoholic Fermentation on the Carotenoid Composition of Orange Juice. A limited number of authors have evaluated the effect of fermentation on carotenoid composition in other fruits and vegetables, and the results reported are diverse. Fermentation of carrot slices resulted in carrot chips with higher α-carotene content.[35] Fermented sweet potatoes presented higher β-carotene concentration than the starting product.[36] Grape must showed increased neoxanthin, violaxanthin, and luteoxanthin contents and decreased α-carotene content during alcoholic fermentation.[37] Koh et al. did not find significant variation in lycopene content of tomato juice after fermentation.[38] The type of microorganism used and the duration of the fermentation process could explain these differences. In contrast, the influence of fermentation on the content of other bioactive compounds has been widely studied. Fermentation of onion led to an increase in flavononoid metabolites and its consequent biological activity enhancement.[39] Fermented chickpeas showed a higher total phenolic content than the unstarted product,[40] and fermentation of red sorghum increased the flavonoid content in the final product.[19]

Our results show that the carotenoid profile at the end of the fermentation process was similar to that of the nonfermented orange juice, with no apparent degradation and/or transformation of carotenoids associated with the processing (Table 3). Carotenoids containing 5,6-epoxy groups were already converted into the corresponding carotenoid 5,8-epoxy derivatives in the nonfermented juice due to the close contact of the pigments with the organic acids naturally present in the starting material (commercial orange juice). In addition, the fact that no increase in *Z* isomer content was observed during the fermentation suggests that the applied conditions were very smooth and did not affect the integrity of the pigment structures. Hence, the 5,8-epoxy carotenoids and *Z* isomers in the fermented orange juice would have been formed during the industrial production of the commercial orange juice, including the pasteurization. Auroxanthin (1.77 mg/L; sum of three epimers) and β-cryptoxanthin (0.85 mg/L) also were the most abundant pigments in fermented orange juice (at the end of the process). The sum of the epimers of mutatoxanthin reached a remarkable value of 0.76 mg/L. (all-*E*)-Zeaxanthin, ζ-carotene, neochrome, and (all-*E*)-lutein were quantified at similar amounts (0.47, 0.45, 0.46, and 0.36 mg/L, respectively). Karpoxanthin and one of its isomer reached a final content of 0.29 mg/L. The other pigments also were detected in minor concentrations (0.03−0.18 mg/L) in fermented orange juice, as in orange juice (Table 3).

As a general trend, the concentration of all individual carotenoids were significantly higher ($p < 0.05$) after 15 days of the fermentation processing with respect to the original juice. The total carotenoid content, expressed as the sum of individual carotenoid concentrations, showed a significantly higher value ($p < 0.05$) after the fermentation period (6.65 mg/L) when compared with the initial content (5.37 mg/L), these data being similar to those reported by Lee and Coates (5.70 mg/L).[41] Because de novo biosynthesis of carotenoids is not possible after the processing of orange juice, a feasible explanation for their apparent increase in concentration during fermentation may be due to the occurrence of some changes in the internal structure of the suspended solids, in which the pigments are integrated, enhancing their extractability during the analytical procedure. This aspect is of particular interest because it would indirectly indicate an increased bioaccessibility of the carotenoids in the fermented juice, so that further research should be carried out to confirm this hypothesis.

Carotenoids have been implicated in several biological processes including cardiovascular protection,[42] immune responses,[43] antioxidant activity,[44] or bone metabolism.[11] Humans need to acquire carotenoids through their diet because they are not able to synthesize them de novo.

According to our results, fermentation of orange juice induces an apparent increase of carotenoid content, so the fermented orange juice could be considered as a good source of these bioactive compounds and may have potentially beneficial effects already tested in orange juice. In addition, there is a remarkable presence of carotenoids with provitamin A activity (β-carotene, α-carotene, and β-cryptoxanthin) in the samples, because these compounds have also been assigned with important biological activities (antioxidant capacity, reducing the risk of atherosclerosis process).[44,45] The provitamin A value obtained in the present study for the starting orange juice

(75.32 RAEs/L) was similar to those reported by Meléndez-Martínez (9.69−94.8 RAEs/L) for different types of commercial orange juice marketed in Spain.[46] As observed for the individual carotenoids, provitamin A content was significantly higher ($p < 0.05$) in the fermented juice (at day 15 of processing) (90.57 RAEs/L) than in original substrate (75.32 RAEs/L) (Table 3). Some of the most relevant carotenoids with biological activities related with human health (lutein, β-cryptoxanthin, and β-carotene) showed a significantly higher content after fermentation, as indicated above. Consequently, the increase in the carotenoid extractability observed in the fermented orange juice should be considered as an advantage with respect to the original juice.

In summary, a potential novel beverage of fermented orange juice may be a rich source of carotenoids and provitamin A compounds, which could exert healthy effects similarly to the original orange juice. Moreover, the controlled alcoholic fermentation would be of great interest to the citrus industry due to the recent interest in the development of innovative practices to meet the demand for natural products rich in bioactive compounds by the consumer, in consonance with their increasing concern about diet and health. In vivo and intervention studies are currently being performed to evaluate the bioavailability of the bioactive compounds of this novel orange drink and its potential effects derived from both the bioactive compounds and the low alcoholic degree. Subsequently, the assessment of its sensory characteristics and consumer acceptance is also necessary.

AUTHOR INFORMATION

Corresponding Author

*(M.-S.F.-P.) Phone: 34 954977613: Fax: 34 954349813. E-mail: msferpac@upo.es.

Funding

This study was supported by funding from the Ministerio de Ciencia e Innovación (Spanish government, Project AGL2010-14850/ALI) and the Consejería de Economía, Innovación, Ciencia y Empleo (Junta de Andalucía, Projects P08-AGR-03477 and P09-AGR4814, and Grupo PAI BIO311). The Research Project grant of B.E.-L. is supported by the Junta de Andalucía. D.H.-M. is member of the IBERCAROT Network 112RT0445 financed by CYTED.

Notes

The authors declare no competing financial interest.

ACKNOWLEDGMENTS

We are grateful to Grupo Hespérides Biotech S.L. for providing the samples and to Richard Davies for editorial assistance.

REFERENCES

(1) U.S. Department of Agriculture. Economic Research Service. Food availability spread sheets; http://www.ers.usda.gov/data/foodconsumption/FoodAvailspreadsheets.htm#fruitju (accessed Jan 23, 2012).

(2) Morand, C.; Dubray, C.; Milenkovic, D.; Lioger, D.; Martin, J. F.; Scalbert, A.; Mazuret, A. Hesperidin contributes to the vascular protective effects of orange juice: a randomized crossover study in healthy volunteers. *Am. J. Clin. Nutr.* **2011**, *93*, 73−80.

(3) Rech-Franke, S. I.; Guecheva, T. N.; Henriques, J. A.; Prá, D. Orange juice and cancer chemoprevention. *Nutr. Cancer* **2013**, 1−11.

(4) Britton, G.; Hornero-Méndez, D. Carotenoids and colour in fruit and vegetables. In *Phytochemistry of Fruit and Vegetables*; Tomás-Barberán, F. A., Robins, R. J., Eds.; Clarendon Press: Oxford, UK, 1997; pp 11−27.

(5) Fratianni, A.; Giuzio, L.; Di Criscio, T.; Zina, F.; Panfili, G. Response of carotenoids and tocols of durum wheat in relation to water stress and sulfur fertilization. *J. Agric. Food Chem.* **2013**, *61*, 2583−2590.

(6) Britton, G.; Liaanen-Jensen, S.; Pfander, H. *Carotenoid Handbook*; Birkhäuser Verlag: Basel, Switzerland, 2004.

(7) Meléndez-Martínez, A. J.; Vicario, I. M.; Heredia, F. J. Review: analysis of carotenoids in orange juice. *J. Food Compos. Anal.* **2007**, *20*, 638−649.

(8) Franke, A. A.; Cooney, R. V.; Henning, S. M.; Custer, L. J. Bioavailability and antioxidant effects of orange juice components in humans. *J. Agric. Food Chem.* **2005**, *53*, 5170−5178.

(9) Meléndez-Martínez, A. J.; Vicario, I. M.; Heredia, F. J. Rapid assessment of vitamin A activity through objective color measurements for the quality control of orange juices with diverse carotenoid profiles. *J. Agric. Food Chem.* **2007**, *55*, 2808−2815.

(10) Mozaffarieh, M.; Sacu, S.; Wedrich, A. The role of the carotenoids, lutein and zeaxanthin, in protecting against age-related macular degeneration: a review based on controversial evidence. *Nutr. J.* **2003**, *11*, 2−20.

(11) Sugiura, M.; Nakamura, M.; Ogawa, K.; Ikoma, Y.; Ando, F.; Shimokata, H.; Yano, M. Dietary patterns of antioxidant vitamin and carotenoid intake associated with bone mineral density: findings from post-menopausal Japanese female subjects. *Osteoporosis Int.* **2011**, *22*, 143−152.

(12) Chatterjee, M.; Roy, K.; Janarthan, M.; Das, S.; Chatterjee, M. Biological activity of carotenoids: its implications in cancer risk and prevention. *Curr. Pharm. Biotechnol.* **2012**, *13*, 180−190.

(13) Rivera, S. M.; Vilaró, F.; Zhu, C.; Bai, C.; Farré, G.; Christou, P.; Canela-Garayoa, R. Fast quantitative method for the analysis of carotenoids in transgenic maize. *J. Agric. Food Chem.* **2013**, *61*, 5279−285.

(14) Alferez, F.; Pozo, L. V.; Rouseff, R. R.; Burns, J. K. Modification of carotenoid levels by abscission agents and expression of carotenoid biosynthetic genes in 'Valencia' sweet orange. *J. Agric. Food Chem.* **2013**, *61*, 3082−3089.

(15) Stinco, C. M.; Fernández-Vázquez, R.; Escudero-Gilete, M. L.; Heredia, F. J.; Meléndez-Martínez, A. J.; Vicario, I. M. Effect of orange juice's processing on the color, particle size, and bioaccessibility of carotenoids. *J. Agric. Food Chem.* **2012**, *60*, 1447−1455.

(16) Mena, P.; Ascacio-Valdés, J. A.; Gironés-Vilaplana, A.; Del Rio, D.; Moreno, D. A.; García-Viguera, C. Assessment of pomegranate wine lees as a valuable source for the recovery of (poly)phenolic compounds. *Food Chem.* **2014**, *145*, 327−334.

(17) Pérez-Gregorio, M. R.; Regueiro, J.; Alonso-González, E.; Pastrana-Castro, L. M.; Simal-Gándara, J. Influence of alcoholic fermentation process on antioxidant activity and phenolic levels from mulberries (*Morus nigra* L.). *LWT−Food Sci.Technol.* **2011**, *44*, 1793−1801.

(18) Ajila, C. M.; Brar, S. K.; Verma, M.; Tyagi, R. D.; Valéro, J. R. Solid-state fermentation of apple pomace using *Phanerocheate chrysosporium* − liberation and extraction of phenolic antioxidants. *Food Chem.* **2011**, *126*, 1071−1108.

(19) Svensson, L.; Sekwati-Monang, B.; Lutz, D. L.; Schieber, A.; Ganzle, M. G. Phenolic acids and flavonoids in nonfermented and fermented red sorghum (*Sorghum bicolor* (L.) Moench). *J. Agric. Food Chem.* **2012**, *58*, 9214−9220.

(20) Yang, E. J.; Kim, S. I.; Park, S. Y.; Bang, H. Y.; Jeong, J. H.; So, J. H.; Rhee, I. K.; Song, K. S. Fermentation enhances the in vitro antioxidative effect of onion (*Allium cepa*) via an increase in quercetin content. *Food Chem. Toxicol.* **2012**, *50*, 2042−2048.

(21) Wang, J. J.; Tung, T. H.; Yin, W. H.; Huang, C. M.; Jen, H. L.; Wei, J.; Young, M. S. Effects of moderate alcohol consumption on inflammatory biomarkers. *Acta Cardiol.* **2008**, *63*, 65−72.

(22) Office Internationale de la Vigne & du Vin. *Recueil des Mèthodes Internationales d'analyse des Vins*; OIV: Paris, France, 1990.

(23) Mínguez-Mosquera, M. I.; Hornero-Méndez, D. Separation and quantification of the carotenoid pigments in red peppers (*Capsicum annuum* L), paprika and oleoresin by reversed-phase HPLC. *J. Agric. Food Chem.* **1993**, *41*, 1616−1620.
(24) Foppen, F. H. Tables for identification of carotenoid pigments. *Chromatogr. Rev.* **1971**, *14*, 133−298.
(25) Davies, B. H. Carotenoids. In *Chemistry and Biochemistry of Plant Pigments*; Goodwin, T. W., Ed.; Academic Press: London, UK, 1976; Vol. 2, pp 38−165.
(26) Britton, G. General carotenoid methods. In *Methods in Enzymology*; Law, J. H., Rilling, H. C., Eds.; Academic Press: New York, 1985; Vol. 111, pp 113−149.
(27) Davies, B. H.; Köst, H. P. Carotenoids. In *CRC Handbook of Chromatography Plant Pigments*; Köst, H. P., Ed.; CRC Press: Boca Raton, FL, 1988; Vol. 1, pp 3−183.
(28) Britton, G. UV/visible spectroscopy. In *Carotenoids*; Britton, G., Liaaen-Jensen, S., Pfander, H., Eds.; Birkhäuser: Basel, Switzerland, 1995; Vol. 1B: Spectroscopy, pp 13−62.
(29) Scott, K. J.; Rodriguez-Amaya, D. Pro-vitamin A carotenoid conversion factors: retinol equivalents − fact or fiction? *Food Chem.* **2000**, *69*, 125−127.
(30) Gross, J. Carotenoids. In *Pigments in Fruits*; Food Science and Technology Series of Monographs; Schweigert, B. S., Ed.; Academic Press: London, UK, 1987; pp 87−186.
(31) Meléndez-Martínez, A. J.; Britton, G.; Vicario, I. M.; Heredia, F. J. Does the carotenoid neoxanthin occur in orange juice? *Food Chem.* **2008**, *107*, 49−54.
(32) Gross, J.; Carmon, M.; Lifshitz, A.; Sklarz, B. Structural elucidation of some orange juice carotenoids. *Phytochemistry* **1975**, *14*, 249−252.
(33) Gama, J. J. T.; Sylos, C. M. Major carotenoid composition of Brazilian Valencia orange juice: identification and quantification by HPLC. *Food Res. Int.* **2005**, *38*, 899−903.
(34) Mouly, P. P.; Gaydou, E. M.; Lapierre, L.; Corsetti, J. Differentiation of several geographical origins in single strength Valencia orange juice using quantitative comparison of carotenoid profiles. *J. Agric. Food Chem.* **1999**, *47*, 4038−4045.
(35) Sulaeman, A.; Keeler, L.; Taylor, S. L.; Giraud, D. W.; Driskell, J. A. Carotenoid content, physicochemical, and sensory qualities of deep-fried carrot chips as affected by dehydration/rehydration, antioxidant, and fermentation. *J. Agric. Food Chem.* **2001**, *49*, 3253−3261.
(36) Panda, S. H.; Ray, R. C. Lactic acid fermentation of β-carotene rich sweet potato (*Ipomoea batatas* L.) into lacto-juice. *Plant Foods Hum. Nutr.* **2007**, *62*, 65−70.
(37) Guedes de Pinho, P.; Silva Ferreira, A. C.; Mendes Pinto, M.; Gomez Benitez, J.; Hogg, T. A. Determination of carotenoid profiles in grapes, musts, and fortified wines from Douro varieties of *Vitis vinifera*. *J. Agric. Food Chem.* **2001**, *49*, 5484−5488.
(38) Koh, J. H.; Kim, Y.; Oh, J. H. Chemical characterization of tomato juice fermented with bifidobacteria. *J. Food Sci.* **2010**, *75*, C428−C432.
(39) Millet, A.; Lamy, E.; Jonas, D.; Stintzing, F.; Mersch-Sundermann, V.; Merfort, I. Fermentation enhances the biological activity of *Allium cepa* bulb extracts. *J. Agric. Food Chem.* **2012**, *60*, 2148−2156.
(40) Wei, X.; Luo, M.; Xu, L.; Zhang, Y.; Lin, X.; Kong, P.; Liu, H. Production of fibrinolytic enzyme from *Bacillus amyloliquefaciens* by fermentation of chickpeas, with the evaluation of the anticoagulant and antioxidant properties of chickpeas. *J. Agric. Food Chem.* **2011**, *59*, 3957−3963.
(41) Lee, H. S.; Coates, G. A. Effect of thermal pasteurization on Valencia orange juice color and pigments. *Food Sci. Technol.* **2003**, *36*, 153−156.
(42) Tavani, A.; Negri, E.; D'Avanzo, B.; La Vecchia, C. β-Carotene intake and risk of nonfatal acute myocardial infarction in women. *Eur. J. Epidemiol.* **1997**, *13*, 631−637.
(43) Fernández-García, E.; Carvajal-Lérida, I.; Jarén-Galán, M.; Garrido-Fernández, J.; Pérez-Gálvez, A.; Hornero-Méndez, D. Carotenoids bioavailability from foods: from plant pigments to efficient biological activities. *Food Res. Int.* **2012**, *46*, 438−450.
(44) Tsuchihashi, H.; Kigoshi, M.; Iwatsuki, M.; Niki, E. Action of β-carotene as an antioxidant against lipid peroxidation. *Arch. Biochem. Biophys.* **1995**, *1*, 137−147.
(45) Kritchevsky, S. B.; Tell, G. S.; Shimakawa, T.; Dennis, B.; Li, R.; Kohlmeier, L.; Steere, E.; Heiss, G. Provitamin A carotenoid intake and carotid artery plaques: the atherosclerosis risk in communities study. *Am. J. Clin. Nutr.* **1998**, *68*, 726−733.
(46) Meléndez-Martínez, A. J.; Vicario, I. M.; Heredia, F. J. Provitamin A carotenoids and ascorbic acid contents of the different types of orange juices marketed in Spain. *Food Chem.* **2007**, *101*, 177−184.

JOURNAL OF AGRICULTURAL AND FOOD CHEMISTRY

Article

pubs.acs.org/JAFC

Antioxidant Activity of Phenolics in Leaves of Three Red Pepper (*Capsicum annuum*) Cultivars

Woo-Ri Kim,[†] Eun Ok Kim,[†] Kyungsu Kang,[†] Sarangerel Oidovsambuu,[†] Sang Hoon Jung,[†] Byung Sup Kim,[‡] Chu Won Nho,[†] and Byung-Hun Um*[,†]

[†]Functional Food Center, Korea Institute of Science and Technology (KIST) Gangneung Institute, Gangneung 210-340, Korea

[‡]Department of Plant Science, Gangneung-Wonju National University, Gangneung 210-702, Korea

ABSTRACT: The antioxidant properties and phenolic profiles were first investigated in this paper on the leaves of three red pepper cultivars, Blackcuban (BCPL), Hongjinju (HPL), and Yeokgang-hongjanggun (YHPL). Of the ethanol extract of the three cultivars, BCPL showed potent antioxidant activities against the 1,1-diphenyl-2-picrylhydrazyl radical (DPPH) and the 2,2-azinobis(3-ethylbenzothiazoline-6-sulfonic acid) (ABTS) radical. Nine antioxidative compounds from the red pepper leaves were isolated and identified as one polyamine phenolic conjugate, *N*-caffeoylputrescine (**1**); three chlorogenic acid derivatives, 5-*O*-caffeoylquinic acid (**2**), 5-*O*-caffeoylquinic acid methyl ester (**4**), and 5-*O*-caffeoylquinic acid butyl ester (**9**); one anthocyanin, delphinidin-3-[4-*trans*-coumaroyl-L-rhamnosyl(1→6)glucopyranoside]-5-*O*-glucopyranoside (**3**); and four flavone glycosides, luteolin-7-*O*-apiofuranosyl(1→2)glucopyranoside (**5**), luteolin-7-*O*-glucopyranoside (**6**), apigenin 7-*O*-apiofuranosyl(1→2)-glucopyranoside (**7**), apigenin-7-*O*-glucopyranoside (**8**). **1** and **3** had the greatest potential for radical-scavenging activity and HepG2 cells protecting effect against oxidative stress. BCPL exhibited the highest content of **1** and **3**. Of the three cultivars BCPL may be considered a good source of antioxidants.

KEYWORDS: *Capsicum annuum, red pepper leaves, phenolic compounds, anthocyanin, antioxidant effects*

INTRODUCTION

Recently, researchers have actively studied new sources to provide safe natural antioxidant additives for foods and cosmetics. This is, in part, because some synthetic antioxidants commonly used to preserve food and cosmetic base materials, such as butylated hydroxyanisole (BHA), butylated hydroxytoluene (BHT), and *tert*-butylhydroquinone (TBHQ), are suspected to be toxic.[1] Thus, there is a need to identify newer antioxidants that can scavenge several free radicals and prevent multiple diseases, including cancer, atherosclerosis, diabetes, inflammation, and aging.[2,3] Natural antioxidants have become the target of many studies searching for sources of potentially safe, effective, and cheap antioxidants.[4]

Pepper (*Capcicum annuum* L.), belonging to the plant family Solanaceae, is the most highly consumed worldwide season-free vegetable. In Korea, it is the most important spice in food, as it is one of the most important ingredients in kimchi, which is a traditional fermented food.[5] The red pepper fruit contains a high amount of provitamin A (*β*-carotene and *β*-cryptoxanthin).[6] With respect to flavonoids, most studies have concentrated only on flavonoid aglycones (quercetin and luteolin) obtained after hydrolysis of red pepper fruits.[7]

Red pepper consumption and research have primarily focused on its fruits. Traditionally, however, red pepper leaves have also been eaten as cooked vegetables after blanching in hot water. Red pepper leaves can be a good source of food and cosmeceutical materials, including antioxidants. Recently, red pepper leaves have been reported to have antimutagenic, antioxidant, antimicrobial, and tyrosinase inhibitory activities.[8] In addition, two flavonoids, apigenin and apigenin 7-*O*-apiofuranosyl(1→2)glucopyranoside, have been identified in pepper leaves.[9]

The present research aimed to investigate phenolic compound profiles and antioxidant properties in the red pepper leaves of three cultivars, Blackcuban (BCPL), Hongjinju (HPL), and Yeokgang-hongjanggun (YHPL). The isolation and identification of phenolic compounds from the red pepper leaves of three cultivars, as well as the evaluation of antioxidant properties (through DPPH and ABTS radical-scavenging activity) and HepG2 cells protecting effects against *tert*-butyl hydroperoxide (*t*-BHP) induced oxidative stress are reported in this paper.

MATERIALS AND METHODS

Plant Materials. Leaves of three red pepper cultivars (BCPL, HPL, and YHPL) were obtained from the Department of Plant Science at Gangneung-Wonju National University in Gangneung, Gangwondo, Korea. Seeds of three red pepper cultivars were sowed and cultured in a glass house (20−30 °C) for 60 days. The cultured seedlings were transplanted on May 24, 2011, and cultivated in the fields under an experimental vinyl house (20−35 °C) of Gangneung-Wonju National University in Gangneung. After 90 days of cultivation, the full-grown leaves were collected. The fresh pepper leave samples were immediately stored at −20 °C until analysis.

General Procedure. 1,1-Diphenyl-2-picrylhydrazyl radical (DPPH), 2,2-azinobis(3-ethylbenzothiazoline-6-sulfonic acid) (ABTS), and potassium persulfate for ABTS, as well as Folin−Ciocalteu's phenol reagent, trolox, quercetin, tannic acid, gallic acid, trifluoroacetic acid (TFA), and formic acid, were purchased from Sigma Chemicals (St. Louis, MO, USA). Analytical grade acetonitrile

Received: July 10, 2013
Revised: October 1, 2013
Accepted: October 2, 2013
Published: October 2, 2013

ACS Publications © 2013 American Chemical Society

and distilled HPLC grade water were purchased from Fisher Scientific (Pittsburgh, PA, USA). Column chromatography was performed over silica gel (Merck, Darmstadt, Germany), Sephadex LH-20 (Pharmacia, Uppsala, Sweden), and Amberlite XAD-7 (Sigma Chemicals). Sodium carbonate anhydrous (Na_2CO_2) and aluminum chloride ($AlCl_3$) were purchased from Shinyo Pure Chemical Co. Ltd. (Osaka, Japan).

UV−vis absorption spectra were measured on a Synergy HT Multimicroplate reader (Bio-Tek instrument, Winooski, VT, USA). The preparative HPLC separations were performed using a JASCO PU-2086 Plus pump, an MD-2015 detector, a Rheodyne injector with a 2 mL sample loop, and an FC204 fraction collector (Gilson Scientific Ltd., Luton, Bedfordshire, UK). ^1H and ^{13}C nuclear magnetic resonance (NMR) spectra were acquired on a Varian Unity INOVA 500 spectrometer for the 1D and 2D NMR experiments in CD_3OD. The chemical shifts are expressed in parts per million (ppm), and the coupling constants are in hertz (Hz). An Agilent LC-MS (Agilent Technologies, Waldbronn, Germany) equipped with UV detectors, quaternary pump, and quadrupole LC-MS 6120 was used with ChemStation as the operation system program.

Radical-Scavenging Activity (Offline Spectrophotometric $ABTS^+$ and $DPPH^+$ Assay). ABTS radical-scavenging activity of the test extracts and compounds were determined using an $ABTS^+$ decolorization assay according to the method of Argoti et al.[10] with minor modifications. To the ABTS liquid substrate system was added 2.45 mM potassium persulfate in a stoichiometric ratio of 1:0.5 (v/v). The mixture was allowed to stand in the dark at room temperature for 8 h. Then, the nine purified compounds (100 μL) were allowed to react with 100 μL of the ABTS radical solution. The reaction mixture was incubated for 5 min at room temperature in dark conditions, and the absorbance was measured at 734 nm. The change in absorbance with respect to the control (containing $ABTS^+$ solution only without the sample, expressed as 100% free radicals) was calculated as the IC_{50} value. The known antioxidants ascorbic acid and trolox were used as positive controls.

The free radical-scavenging activity of the test extracts and compounds were determined by the DPPH assay.[10] Briefly, the reaction mixture was contained in an ethanol solution of DPPH (100 μL) and purified phenolic compounds of three different concentrations (100 μL). The reaction mixture was incubated for 1 h at room temperature in dark conditions, and the absorbance was measured at 517 nm. IC_{50} values against three radical-scavenging activities were determined by regression analysis of the results obtained at three different concentrations of the sample. Ascorbic acid and trolox were used as positive controls.

Measurement of Total Phenolics and Flavonoids Content. Total phenolics was determined using the reported method.[11] A 20 μL sample aliquot of extract or gallic acid/tannic acid standard (50−500 μg/mL) was mixed with distilled water (1.58 mL) followed by 2 N Folin−Ciocalteau's reagent (20 μL). After the mixture had been vortexed and incubated at room temperature for 5 min, 20% sodium carbonate solution (100 μL) was added. Samples were vortexed and kept at room temperature for 30 min. Absorbance of the blue solution was recorded at 730 nm. The total phenolic content was expressed as milligrams of gallic acid equivalent (mg GAE/g) and tannic acid equivalent (mg TAE/g) per gram of sample.

Total flavonoid content was determined by the aluminum chloride colorimetric method using quercetin as a standard.[12] Briefly, the extracts were dissolved in EtOH. Then, the sample solution (100 μL) was mixed with an aqueous solution of 2% aluminum chloride (100 μL). After 5 min of incubation at ambient temperature, the absorbance of the supernate was measured at 435 nm. The total flavonoid content was expressed as milligrams of quercetin equivalents per gram of sample.

Screening of Antioxidant Activity with Online HPLC-ABTS System. To test the antioxidant activity of the extracts directly, the online HPLC-ABTS screening system was applied. This system consisted of an Agilent 1200 analysis HPLC system (Agilent Technologies, Santa Clara, CA, USA) fitted with an additional pump to supply the ABTS radical solution. For the ABTS radical reagent, a 2 mM ABTS stock solution containing 3.5 mM potassium persulfate was prepared in water and diluted 8-fold in HPLC grade water. This solution was incubated overnight in darkness at room temperature for radical stabilization. Antioxidant capacity was measured according to the previous method.[13]

Briefly, 10 μL of three cultivars of pepper leaf extract solutions was injected into the online HPLC-ABTS system. The individual compounds were separated with a column (Kromasil 100-5 C18, 250 × 4.6 mm, 5 μm) in the solvent system of 0.1% TFA in acetonitrile (A) and 0.1% TFA in water (B) with a 1 mL/min flow rate. The gradient conditions were as follows: 0−10 min, 20% A; 10−30 min, 20−50% A; and then returning to the initial conditions. The column was kept at 25 °C during the entire sequence. The ABTS radical solution was supplied with a flow rate of 0.5 mL/min. The chromatogram was recorded at 330 and 530 nm as a positive peak, and the visible detector was set at 734 nm to measure the decrease of ABTS radicals as a negative peak. The data were analyzed by ChemStation software (Agilent Technology).

Extraction and Isolation of Anthocyanin and Phenolics from Red Pepper Leaves. The leaves (1 kg) of three different red pepper cultivars were extracted three times with EtOH containing 0.1% HCl in a dark environment during 24 h at room temperature. The acidic ethanol solvent was evaporated under reduced pressure to afford the BCPL (76.10 g), HPL (49.99 g); and YHPL (45.27 g) extracts.

The BCPL extract was resuspended in water containing 0.1% HCl and was partitioned with *n*-hexane (*n*-Hex), methylene chloride (CH_2Cl_2), ethyl acetate (EtOAc), *n*-butanol (*n*-BuOH), and water (H_2O). All fractions were then concentrated in vacuo (*n*-Hex fraction, 11.1 g; CH_2Cl_2 fraction, 3.06 g; EtOAc fraction, 3.56 g; *n*-BuOH fraction, 29.69 g; H_2O fraction, 24.77 g). The EtOAc fraction was chromatographed by a preparative HPLC system (Waters prep-HPLC, Hydrosphere C18 column (250 × 20 mm, 5 μm)) eluting with an ACN/0.1% FA in H_2O (10:0 to 100:0, v/v) gradient condition. Three fractions were obtained as follows: A (0.31 g), B (0.16 g), and C (0.27 g). The A and B fractions were purified by the preparative HPLC system (JASCO PU-2086 Plus pump, MD-2015 detector); compound **4** (1.62 mg) and compound **9** (5.80 mg) were obtained, respectively. The C fraction was chromatographed by the preparative HPLC system to yield three subfractions (EA-C-1−EA-C-3). Subfractions EA-C-1 (60 mg), EA-C-2 (27.5 mg), and EA-C-3 (86.95 mg) were further chromatographed by the same purification procedure on preparative HPLC and yielded a pure compound **7** (3.37 mg) and compound **8** (80 mg). The purple *n*-BuOH fraction (3 g) was chromatographed for anthocyanin by Amberlite XAD-7 column chromatography eluting with acidic MeOH containing 0.1% HCl/H_2O (40:60 to 70:30) to yield two fractions (Bu-A and Bu-B). The Bu-B fraction (1.2 g) was chromatographed by the preparative HPLC system to yield two subfractions (Bu-B-1 and Bu-B-2). Subfraction Bu-B-1 (84.2 mg) was rechromatographed by Sephadex LH-20 column chromatography eluting with MeOH containing 0.1% TFA, and a pure compound **1** (21.76 mg) and compound **3** (32 mg) were separated.

The extracts of HPL and YHPL were not isolated as the same chemical components from the HPLC chromatogram, and the LC-MS data of HPL and YHPL as BCPL are presented in Figure 2. The YHPL extract was resuspended to isolate the compounds except for the same chemical components of BCPL in water. It was partitioned three times with *n*-Hex, CH_2Cl_2, EtOAc, *n*-BuOH, and H_2O. All fractions were then concentrated in vacuo (*n*-Hex fraction, 16.14 g; CH_2Cl_2 fraction, 5.76 g; EtOAc fraction, 1.7 g; *n*-BuOH fraction, 10.26 g; H_2O fraction, 14.0 g). The EtOAc fraction was purified by the preparative HPLC system, and compound **2** (56.66 mg) and compound **5** (7.83 mg) were obtained. The H_2O fraction (2 g) was fractionated using vacuum liquid chromatography with silica-C18. Elution was carried out successively with solvents of increasing nonpolar MeOH/H_2O (5:95 to 100:0, v/v) to afford compound **6** (4.08 mg).

Cell Culture and Cell Viability Assay. Human hepatoma HepG2 cells were obtained from the American Type Culture Collection (Manassas, VA, USA). HepG2 cells were maintained in Dulbecco's modified Eagle's medium (DMEM) supplemented with 10% fetal bovine serum (FBS, Hyclone, Logan, UT, USA), 100 units/mL penicillin, and 100 μg/mL streptomycin. The cells were cultured in a

humidified atmosphere of 5% CO_2 at 37 °C. For chemical treatments, HepG2 cells were cultured in DMEM without FBS to reduce direct interaction between the phytochemicals and FBS. Protective activities of the isolated compounds from the three pepper cultivar leaves against *t*-BHP-induced cell death were measured using the cell viability assay as previous described.[14]

Briefly, HepG2 cells (1×10^4 cells/well) were plated in 96-well plates and incubated for 24 h. Cells were then preincubated with the isolated (10−20 μg/mL) compounds from three pepper cultivar leaves and epigallocatechin gallate (EGCG, 10 μM) in serum-free DMEM for 24 h. Cells were washed with Dulbecco's phosphate-buffered saline (DPBS) and treated with *t*-BHP (250 μM) in serum-free DMEM for 3 h. Then, cell viability was measured using the EZ-Cytox Cell Viability Assay Kit (Daeil Lab Service, Seoul, Korea).

Quantification of Phenolics by HPLC. The nine phenolic compounds isolated from red pepper leaves of the three different cultivars were quantified by an HPLC method. HPLC analysis was performed with an Agilent 1200 HPLC system consisting of a binary pump (G1312A), autosampler (G1367B), diode array detector (G1315D), and degasser (D1379B). The separation of each compound was carried out on a Kromasil 100-5 C18 column (250 × 4.6 mm, 5 μm) with 1 mL/min flow rate in a solvent system of acetonitrile containing 0.1% TFA (A) and water containing 0.1% TFA (B). The gradient condition used was as follows: 0−10 min, 20% A; 10−30 min, 20−50% A; and then returning to the initial conditions. The chromatogram was detected at 330 nm. Calibration curves were constructed with each compound in a range of 0.1−1000 μg/mL. A high linearity ($r^2 > 0.999$) was obtained for each standard curve.

Statistical Analysis. Data were expressed as the mean ± standard deviation (SD). Statistical analysis included one-way analysis of variance (ANOVA) followed by Tukey's Honestly Significant Difference (HSD) test, and Pearson correlation test for correlation between variables were performed using IBM SPSS statistics 21. p values <0.05 were considered statistically significant.

RESULTS AND DISCUSSION

Radical Scavenging Activity of the Extracts of Three Red Pepper Cultivar Leaves. The antioxidative activities of the ethanol extracts from the pepper leaves of three different cultivars (BCPL, HPL, and YHPL) were evaluated by DPPH and ABTS assay with ascorbic acid and trolox as standards. As shown in Table 1, the DPPH radical-scavenging activity (IC_{50}) of BCPL was 49.2 ± 6.1 μg/mL, lower than that of YHPL (54.3 ± 4.5 μg/mL) or HPL (62.2 ± 3.4 μg/mL). Similarly, the ABTS radical-scavenging activity (IC_{50}) of BCPL was 26.2 ± 3.2 μg/mL, lower than that of YHPL (33.7 ± 3.9 μg/mL) or HPL (41.9 ± 3.1 μg/mL). Therefore, the order of antioxidant effects by radical-scavenging activity of the three red pepper leaves was BCPL > YHPL > HPL.

Table 1. Radical-Scavenging Activity of the Extracts of Three Pepper Cultivar Leaves[a]

	radical-scavenging activity IC_{50} (μg/mL)	
extract	DPPH	$ABTS^+$
BCPL	49.2 ± 6.1b	26.2 ± 3.2b
HPL	62.2 ± 3.4a	41.9 ± 3.1a
YHPL	54.3 ± 4.5ab	33.7 ± 3.9ab
ascorbic acid	1.3 ± 0.2c	0.3 ± 0.1c
trolox	1.6 ± 0.6c	0.3 ± 0.0c

[a]Values represent the means ± SD from triplicate experiments. Different letters in the same column denote a significant difference according to Tukey's test, $p < 0.05$.

Content of Total Phenolics and Total Flavonoids. Folin−Ciocalteu's assay is a frequently used screening method for the measurement of the antioxidant capacity of food products and dietary supplements. The total phenolic content of ethanol extracts from three red pepper leaves was assayed by the Folin-Ciocalteu method using gallic acid and tannic acid as standards, and the result is presented in Figure 1A. Total phenolic content of BCPL was the highest, 6.5 ± 0.8 mg GAE/g (6.4 ± 0.6 mg TAE/g), for fresh weight. HPL was found to be 4.4 ± 0.1 mg GAE/g (4.3 ± 0.1 mg TAE/g), and YHPL had the lowest at 4.3 ± 0.1 mg GAE/g (4.1 ± 0.1 mg TAE/g). Ku et al.[8] recently reported that the total phenolic content in pepper leaves of 13 commercial cultivars ranged from 2.31 ± 0.07 to 5.16 ± 0.09 mg GAE/g. These data are consistent with our results.

The total flavonoid content of three pepper leaves was evaluated by aluminum chloride colorimetric assay. The content was expressed as milligrams of quercetin equivalents (mg/g) of fresh weight. As shown in Figure 1B, total flavonoid content ranged from 2.4 ± 0.1 mg/g in HPL to 2.7 ± 0.2 mg/g in YHPL. However, no significant difference was observed among the three cultivars studied (BCPL, HPL, and YHPL). Thus, the order of total phenolics content of three red pepper leaves was found to be BCPL > HPL > YHPL. On the other hand, the order of total flavonoid content was found to be YHPL > BCPL > HPL.

Online HPLC−$ABTS^+$ Assays as Activity Guide. To investigate the major compounds and to measure their ABTS radical-scavenging activity, the ethanol extracts of the three red pepper cultivar leaves were subjected to the online HPLC−$ABTS^+$ screening system.[15] This methodology allows rapid pinpointing of antioxidants in complex mixtures through postcolumn mixing of separated analytes with radical solutions. The resulting reduction signal was detected as a negative peak by an absorbance detector (at 734 nm for $ABTS^+$ scavenging activity). After this online radical-scavenging screening of the extracts, it was easy to detect the active components present in each extract. Without isolation by the online HPLC−$ABTS^+$ assay system, peaks 1, 2, and 4 would have been easily overlooked because of their small quantity (Figure 2). These compounds were negligible in HPLC chromatogram at 330 nm, but it was very active in the online HPLC-$ABTS^+$ assay system. Hence, the online ABTS assay system was an efficient method for the purification of antioxidants based on activity-guided chromatographic separation and isolation from natural resources. As shown in Figure 2, the BCPL chemical components were almost similar to HPL, but YHPL was different from BCPL and HPL. In addition, the anthocyanin from the chromatogram at 530 nm existed only for BCPL. Therefore, this indicated that major and minor antioxidants (peaks 1−9) were isolated using preparative HPLC and open column chromatography.

Isolation and Identification of Anthocyanin and Phenolic Compounds. To identify peaks 1, 3, 4, and 7−9 of the HPLC chromatogram of the BCPL extract and peaks 1, 2, 5, and 6 of the HPLC chromatogram of the YHPL extract, we partitioned with *n*-Hex, CH_2Cl_2, EtOAc, *n*-BuOH, and H_2O. The EtOAc and *n*-BuOH fractions of BCPL and EtOAc and H_2O fraction of YHPL were subjected to silica gel RP-C18 chromatography and reverse phase preparative-HPLC. The resulting compounds **1**−**9** were isolated from BCPL and YHPL (Figure 3). Compounds **1**−**9** were characterized and identified by UV and ESI-MS, as well as 1D and 2D NMR. The spectral data of compounds **1**−**9** agreed with earlier published data: compound **1**,[16] compound **2**,[15] compound **3**,[17] compound **4**,[18]

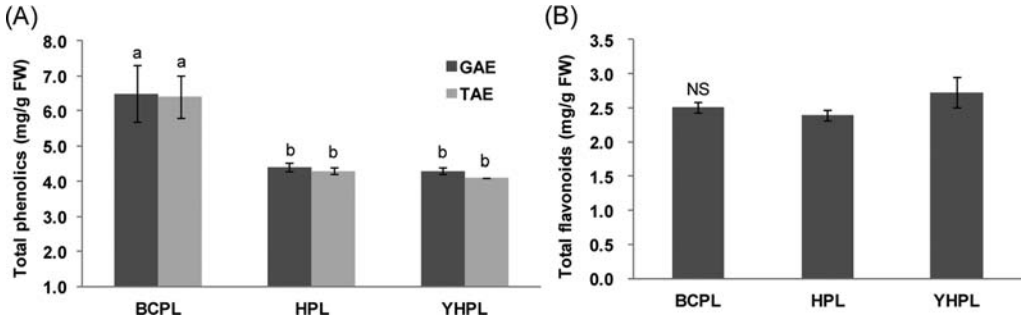

Figure 1. Total phenolic (A) and flavonoid contents (B) of three red pepper cultivar leaves. The total phenolic content was expressed as gallic acid equivalent (GAE) and tannic acid equivalent (TAE). The total flavonoid content was expressed as quercetin equivalents. BCPL, Blackcuban; HPL, Hongjinju; YHPL, Yeokgang-hongjanggun; FW, fresh weight. Each bar represent the mean ± SD from triplicate experiments. Different letters in the bar denote a significant difference according to Tukey's test, $p < 0.05$.

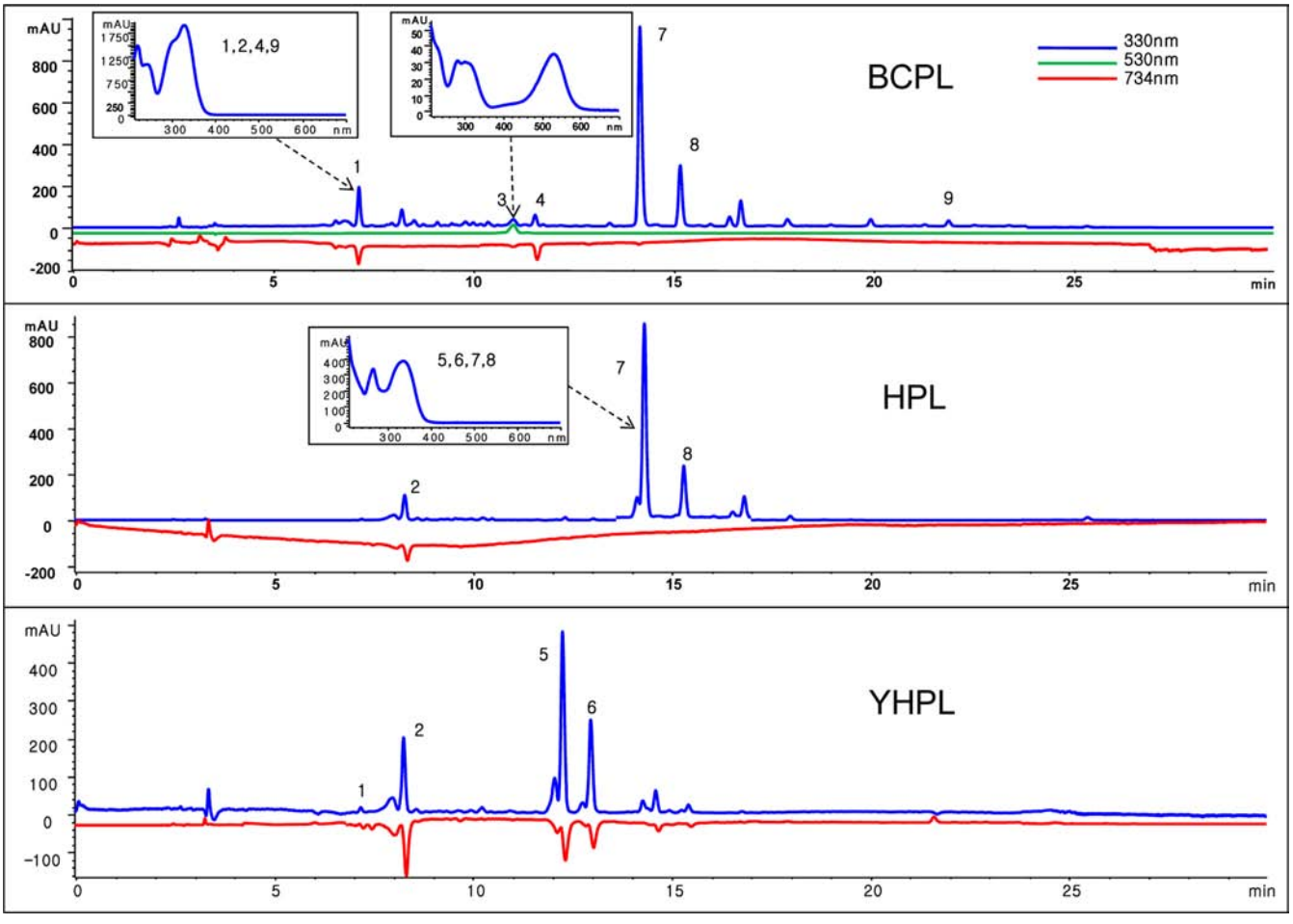

Figure 2. Chromatogram and UV spectrum of the online HPLC-DAD-ABTS screening system. The ethanol extracts from red pepper leaves of three different cultivars, Blackcuban (BCPL), Hongjinju (HPL), and Yeokgang-hongjanggun (YHPL), were analyzed with an HPLC system, and the eluates from the HPLC column were reacted with ABTS radical reagent. The analytes were detected at 330 and 530 nm as a positive peak, and their ABTS radical-scavenging activity was recorded at 734 nm as a negative peak.

compound **5**,[19,20] compound **6**,[21] compound **7**,[22] compound **8**,[13] and compound **9**.[21] The structural characteristics of isolated phenolics **1**−**9** are detailed below.

*N-Caffeoylputrescine (**1**):* apricot powder; ESI-MS *m*/*z* 251 $[M + H]^+$; ^{1}H NMR (500 MHz, CD_3OD) δ 7.39 (1H, d, J = 15.6 Hz, H-7), 7.00 (1H, d, J = 1.9 Hz, H-6), 6.90 (1H, dd, J = 8.2 Hz, 1.9 Hz, H-2), 6.76 (1H, d, J = 8.1 Hz, H-3), 6.37 (1H, d, J = 15.6 Hz, H-8), 3.34 (2H, d, J = 6.4 Hz, H-11), 2.96 (1H, t, J = 7.2 Hz, 7.2 Hz, H-14), 1.70 (2H, m, H-13), 1.63 (2H, m, H-12); ^{13}C NMR (125 MHz, CD_3OD) δ 169.6 (C-9), 148.9 (C-4), 146.8 (C-5), 142.4 (C-7), 128.1 (C-1), 122.2 (C-2), 118.2 (C-8), 116.4 (C-3), 115.0 (C-6), 40.5 (C-14), 39.6 (C-11), 27.6 (C-12), 25.9 (C-13).

*5-O-Caffeoylquinic acid (**2**):* pale yellow powder; ESI-MS *m*/*z* 355 $[M + H]^+$; ^{1}H NMR (500 MHz, CD_3OD) δ 7.52 (1H, d, J = 15.9 Hz, H-7′), 7.04 (1H, d, J = 1.8 Hz, H-2′), 6.94 (1H, dd, J = 8.2 Hz, 1.7 Hz, H-6′), 6.78 (1H, d, J = 8.2 Hz, H-5′), 6.22 (1H, *d*, J = 15.9 Hz, H-8′), 5.28 (1H, dd, J = 11.7 Hz, 7.4

dx.doi.org/10.1021/jf403006c | J. Agric. Food Chem. 2014, 62, 850−859

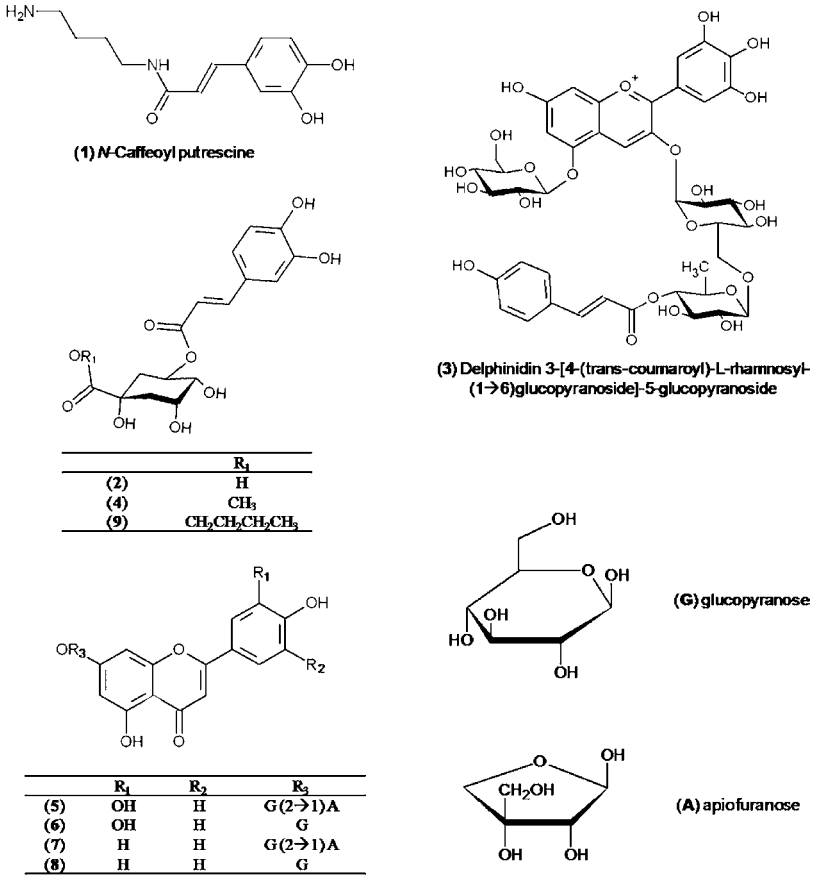

	R_1
(2)	H
(4)	CH_3
(9)	$CH_2CH_2CH_2CH_3$

	R_1	R_2	R_3
(5)	OH	H	G(2→1)A
(6)	OH	H	G
(7)	H	H	G(2→1)A
(8)	H	H	G

Figure 3. Chemical structures of phenolic compounds (**1**–**9**) isolated from red pepper leaves. **1**, *N*-Caffeoyl putrescine; **2**, 5-*O*-caffeoylquinic acid; **3**, delphinidin-3-[4-(*trans*-coumaroyl)-L-rhamnosyl(1→6)glucopyranoside]-5-*O*-glucopyranoside; **4**, 5-*O*-caffeoylquinic acid methyl ester; **5**, luteolin-7-*O*-apiofuranosyl(1→2)glucopyranoside; **6**, luteolin-7-*O*-glucopyranoside; **7**, apigenin-7-*O*-apiofuranosyl(1→2)glucopyranoside; **8**, apigenin-7-*O*-glucopyranoside; **9**, 5-*O*-caffeoylquinic acid butyl ester.

Hz, H-3), 4.14 (1H, t, *J* = 3.6 Hz, 3.6 Hz, H-5), 3.74 (1H, dd, *J* = 7.0 Hz, 2.6 Hz, H-4), 2.19 (2H, m, H-2), 2.01 (2H, m, H-6); ^{13}C NMR (125 MHz, CD_3OD) δ 175.4 (C-7), 168.3 (C-9′), 149.6 (C-4′), 147.2 (C-7′), 146.7 (C-3′), 127.5 (C-1′), 123.0 (C-6′), 116.5 (C-5′), 115.0 (C-2′), 114.9 (C-8′), 76.1 (C-1), 72.4 (C-4), 72.0 (C-3), 70.3 (C-5), 38.0 (C-6), 37.8 (C-2).

Delphinidin 3-[4-trans-coumaroyl-L-rhamnosyl(1→6)-glucopyranoside]-5-O-glucopyranoside (3): amorphous purple powder; ESI-MS *m*/*z* 920 $[M + H]^+$; ^{1}H NMR (500 MHz, CD_3OD) δ 8.86 (1H, s, H-4), 7.76 (2H, s, H-2′, H-6′), 7.56 (1H, d, *J* = 15.9 Hz, H-7′′′′′, 7.40 (2H, d, *J* = 8.6 Hz, H-2′′′′′, H-6′′′′′), 6.98 (1H, s, H-8), 6.97 (1H, s, H-6), 6.80 (2H, d, *J* = 8.6 Hz, H-3′′′′′, H-5′′′′′), 6.24 (1H, s, H-8′′′′′), 5.52 (1H, d, *J* = 7.8 Hz, H-1‴), 5.19 (1H, d, *J* = 7.8 Hz, H-1″), 4.90 (1H, m, H-4′′′′), 4.70 (1H, s, H-1′′′′), 4.05 (1H, m, H-6‴), 3.94 (1H, m, H-6″), 3.87 (1H, m, H-3′′′′), 3.85 (1H, d, *J* = 3.3 Hz, H-5‴), 3.81 (1H, d, *J* = 3.8 Hz, H-2‴), 3.80 (1H, m, H-6″), 3.79 (1H, m, H-2′′′′), 3.77 (1H, m, H-5′′′′), 3.71 (1H, s, H-6″), 3.70 (1H, m, H-2″), 3.63 (1H, m, H-5″), 3.60 (1H, m, H-3″), 3.59 (1H, m, H-4″), 3.48 (1H, m, H-4‴), 1.00 (3H, d, *J* = 6.3 Hz, H-6′′′′); ^{13}C NMR (125 MHz, CD_3OD) δ 169.7 (C-9′′′′′), 169.2 (C-7), 164.4 (C-2), 157.0 (C-9), 156.6 (C-5), 147.7 (C-4′), 147.4 (C-4′′′′′), 146.2 (C-3), 145.8 (C-3′), 145.7 (C-5′), 133.3 (C-4), 131.5 (C-2′′′′′), 131.4 (C-6′′′′′), 127.26 (C-1′′′′′), 117.2 (C-3′′′′′, C-5′′′′′), 116.92 (C-7′′′′′), 114.9 (C-8′′′′′), 113.2 (C-3′, C-6′), 112.9 (C-10), 112.8 (C-1′), 105.7 (C-6), 102.9 (C-1″), 102.1 (C-1″), 101.9 (C-1′′′′), 97.2 (C-8), 78.38 (C-3‴), 77.8 (C-5″), 77.7 (C-3″), 77.4 (C-5‴), 75.2 (C-4′′′′), 74.6 (C-2″), 74.2 (C-2‴), 71.9 (C-2′′′′), 71.2 (C-4‴), 70.7 (C-4″), 70.3 (C-3′′′′), 67.6 (C-5′′′′), 66.9 (C-6‴), 61.9 (C-6″), 18.15 (C-6′′′′).

5-O-Caffeoylquinic acid methyl ester (4): oale yellow powder; ESI-MS *m*/*z* 369 $[M + H]^+$; ^{1}H NMR (500 MHz, CD_3OD) δ 7.52 (1H, d, J = 15.9 Hz, H-7′), 7.04 (1H, d, J = 2.1 Hz, H-5′), 6.95 (1H, dd, *J* = 8.2 Hz, 2.1 Hz, H-6′), 6.78 (1H, d, *J* = 8.2 Hz, H-2′), 6.22 (1H, d, *J* = 15.9 Hz, H-8′), 5.27 (1H, m, H-3), 4.15 (1H, m, H-5), 3.73 (1H, dd, *J* = 7.3 Hz, 3.1 Hz, H-4), 3.69 (3H, s, H-9), 2.21 (2H, m, H-6), 2.16 (2H, m, H-2); ^{13}C NMR (125 MHz, CD_3OD) δ 175.3 (C-7), 168.3 (C-9′), 149.7 (C-4′), 147.2 (C-7′), 146.9 (C-3′), 127.7 (C-1′), 123.0 (C-6′), 116.5 (C-2′), 115.0 (C-5′), 114.9 (C-8′), 75.5 (C-1), 72.8 (C-4), 72.4 (C-3), 70.0 (C-5), 52.7 (C-9), 38.0 (C-6), 37.6 (C-2).

Luteolin-7-O-apiofuranosyl(1→2)glucopyranoside (5): brown powder; UV (MeOH) λ_{max} 210, 253, 262sh, 348 nm; ESI-MS *m*/*z* 581 $[M + H]^+$; ^{1}H NMR (500 MHz, DMSO-d_6) δ 7.45 (1H, dd, *J* = 8.4 Hz, 2.2 Hz, H-6′), 7.42 (1H, d, *J* = 2.2 Hz, H-2′), 6.89 (1H, d, *J* = 8.3 Hz, H-5′), 6.76 (1H, s, H-8), 6.75 (1H, s, H-3), 6.42 (1H, d, *J* = 2.2 Hz, H-6), 5.35 (1H, s, H-1‴), 5.19 (1H, d, *J* = 7.3 Hz, H-1″), 3.91 (1H, d, *J* = 9.3 Hz, H-4‴), 3.73 (1H, m, H-2‴), 3.70 (1H, d, *J* = 10.4 Hz, H-6″), 3.66 (1H, d, *J* = 9.3 Hz, H-4‴), 3.51 (1H, d, *J* = 9.2 Hz, H-2″), 3.48 (1H, s, H-5″), 3.47 (1H, m, H-6″), 3.31 (1H, m, H-4″), 3.29 (1H, m, H-5‴), 3.25 (1H, m, H-3″); ^{13}C NMR (125 MHz, DMSO-d_6) δ 181.9 (C-4), 169.8 (C-9), 164.5 (C-2), 162.1 (C-7), 156.9 (C-5), 150.1 (C-3′), 145.7 (C-4′), 121.2 (C-1′), 119.0 (C-6′),

dx.doi.org/10.1021/jf403006c | J. Agric. Food Chem. 2014, 62, 850−859

115.8 (C-5′), 113.2 (C-2′), 108.4 (C-1‴), 105.3 (C-10), 102.9 (C-3), 99.1 (C-6), 97.7 (C-1″), 94.4 (C-8), 79.4 (C-2‴), 76.8 (C-5″), 76.2 (C-2‴), 75.9 (C-2″), 73.8 (C-5‴), 72.8 (C-3″), 69.6 (C-4″), 64.1 (C-4‴), 60.4 (C-6″).

*Luteolin-7-O-glucopyranoside (**6**):* brown powder; ESI-MS m/z 449 $[M + H]^+$; ^{1}H NMR (500 MHz, CD_3OD) δ 7.42 (1H, s, H-2′), 7.41 (1H, d, J = 4.5 Hz, H-6′), 6.90 (1H, d, J = 8.3 Hz, H-5′), 6.79 (1H, s, H-8), 6.60 (1H, s, H-3), 6.49 (1H, s, H-6), 6.49 (1H, s, H-7), 5.07 (1H, d, J = 6.7 Hz, H-1″), 3.94 (1H, d, J = 11.8 Hz, H-6″), 3.73 (1H, m, H-6″), 3.55 (1H, m, H-5″), 3.51 (1H, m, H-3″), 3.50 (1H, m, H-2″), 3.42 (1H, m, H-4″); ^{13}C NMR (125 MHz, CD_3OD) δ 184.1 (C-4), 167.0 (C-2), 164.9 (C-7), 162.9 (C-5), 159.0 (C-9), 151.3 (C-3′), 147.2 (C-4′), 123.4 (C-1′), 120.5 (C-2′), 116.8 (C-5′), 114.2 (C-6′), 107.2 (C-10), 104.1 (C-3), 101.6 (C-1″), 101.1 (C-6), 96.0 (C-8), 78.4 (C-5″), 77.9 (C-3″), 74.7 (C-2″), 71.3 (C-4″), 62.4 (C-6″).

*Apigenin 7-O-apiofuranosyl(1→2)glucopyranoside (**7**):* yellow powder; UV (MeOH) λ_{max} 210, 268, 340 nm; ESI-MS m/z 565 $[M + H]^+$; ^{1}H NMR (500 MHz, CD_3OD) δ 7.89 (2H, d, J = 8.7 Hz, H-2′, H-6′), 6.93 (2H, d, J = 9.0 Hz, H-3′, H-5′), 6.81 (1H, dd, J = 2.0 Hz, 15.0 Hz, H-8), 6.66 (1H, d, J = 1.2 Hz, H-3), 6.48 (1H, d, J = 16.5 Hz, 2.0 Hz, H-6), 5.46 (1H, d, J = 1.6 Hz, H-1‴), 5.15 (1H, d, J = 7.3 Hz, H-1″), 4.04 (1H, d, J = 9.7 Hz, H-4‴), 3.95 (1H, t, J = 1.5 Hz, 1.5 Hz, H-2‴), 3.93 (1H, m, H-6″), 3.82 (1H, d, J = 9.6 Hz, H-4‴), 3.71 (1H, m, H-6″), 3.68 (1H, m, H-2″), 3.66 (1H, m, H-3″), 3.54 (1H, m, H-5″), 3.54 (2H, m, H-5‴), 3.41 (1H, t, J = 9.2 Hz, 9.2 Hz, H-4″); ^{13}C NMR (125 MHz, CD_3OD) δ 184.1 (C-4), 168.1 (C-9), 166.9 (C-2), 164.0 (C-7), 163.0 (C-4′), 159.0 (C-5), 129.6 (C-2′, C-6′), 123.2 (C-1′), 117.0 (C-3′, C-5′), 110.9 (C-1‴), 107.2 (C-10), 104.2 (C-3), 101.1 (C-6), 100.1 (C-1″), 95.9 (C-8), 80.7 (C-3‴), 78.6 (C-2″), 78.4 (C-3‴), 78.3 (C-5″), 78.1 (C-2‴), 75.4 (C-4‴), 71.2 (C-4″), 65.8 (C-5‴), 62.5 (C-6″).

*Apigenin-7-O-Glucopyranoside (**8**):* yellow powder; ESI-MS m/z 433 $[M + H]^+$; ^{1}H NMR (500 MHz, CD_3OD) δ 7.89 (2H, d, J = 8.3 Hz, H-2′, H-6′), 6.93 (2H, d, J = 8.3 Hz, H-3′, H-5′), 6.82 (1H, s, H-8), 6.66 (1H, s, H-3), 6.49 (1H, s, H-6), 5.08 (1H, d, J = 6.1 Hz, H-1″), 3.94 (1H, d, J = 11.7 Hz, H-6″), 3.72 (1H, m, H-6″), 3.55 (1H, m, H-5″), 3.51 (1H, m, H-3″), 3.50 (1H, m, H-2″), 3.41 (1H, m, H-4″); ^{13}C NMR (125 MHz, CD_3OD) δ 184.1 (C-4), 166.9 (C-2), 165.0 (C-7), 163.1 (C-5), 163.0 (C-4′), 159.1 (C-9), 129.8 (C-2′, C-6′), 123.1 (C-1′), 117.0 (C-3′, C-5′), 107.1 (C-10), 104.1 (C-3), 101.7 (C-1″), 101.1 (C-6), 96.0 (C-8), 78.2 (C-5″), 77.8 (C-3″), 74.6 (C-2″), 71.3 (C-4″), 62.4 (C-6″).

*5-O-Caffeoylquinic acid butyl ester (**9**):* pale yellow powder; ESI-MS m/z 411 $[M + H]^+$; ^{1}H NMR (500 MHz, CD_3OD) δ 7.52 (1H, d, J = 15.9 Hz, H-7′), 7.04 (1H, d, J = 2.0 Hz, H-5′), 6.95 (1H, dd, J = 8.2 Hz, 2.0 Hz, H-6′), 6.78 (1H, d, J = 8.2 Hz, H-2′), 6.21 (1H, d, J = 15.9 Hz, H-8′), 5.26 (1H, m, H-3), 4.14 (1H, m, H-5), 3.75 (1H, dd, J = 7.0 Hz, 2.7 Hz, H-4), 2.22 (2H, d, J = 5.4, H-2), 2.17 (2H, m, H-9), 1.99 (2H, m, H-6), 1.61 (2H, m, H-11), 1.34 (2H, m, H-12), 0.89 (3H, t, J = 7.4 Hz, 7.4 Hz, H-13); ^{13}C NMR (125 MHz, CD_3OD) δ 175.0 (C-7), 168.1 (C-9′), 149.7 (C-4′), 147.3 (C-7′), 146.9 (C-3′), 127.6 (C-1′), 123.0 (C-6′), 116.5 (C-2′), 115.0 (C-5′), 114.9 (C-8′), 75.5 (C-1), 72.4 (C-4), 72.1 (C-3), 70.1 (C-5), 38.0 (C-2), 37.9 (C-6), 37.6 (C-9), 31.6 (C-10), 20.0 (C-11), 14.1 (C-12).

All of these compounds (**1**–**9**) were identified for the first time in this paper as constituents of pepper leaves, except for compound **7**.[9] Compound **1** has been found in the leaves of *Nicotiana tabacum* and yellow bell pepper,[16,23] and compounds **2**, **4**, and **8** have been isolated from *Ligularia fischeri* var. *spiciformis* Nakai, *Lonicera confuse*, *B. parviflora*, *Euphorbia ebracteolata*, and leaves of *Lonicera japonica*, *Erigeron breviscapus*, and *Sarcandra glabra*.[13,18] Compound **3** has been isolated from eggplant.[17] In addition, compound **5** has been isolated from celery seeds, celery husk, *Campanula patula*, *Centaurea cyanus*, hot pepper fruits, *Astragalus eremophilys*, and *Astragalus vogelii*,[24,25] and compound **7** has been isolated from *Crotalaria podocarpa*, *Conocaryum calleryanum*, and *Artabotrys hexapetalus* and leaves of *Capsicum annuum*.[9,22,26] Finally, compounds **6** and **9** have been isolated from the leaves of *Codonopsis nervosa* and *Elsholtzia rugulosa*, flowers of *Ligustrum lucidum*, and leaves of *Callicarpa nudiflora*.[21,27−30]

Antioxidant Activities of Anthocyanin and Phenolic Compounds Isolated from Three Red Pepper Cultivar Leaves. The antioxidant activities of the isolated compounds **1**−**9** were assayed using the different assay systems: (1) scavenging activity of free radicals based on chemical trapping using DPPH and ABTS assay methods; (2) protective activity of compounds against *t*-BHP-induced HepG2 cell death.

The free radical chain reaction is widely accepted as a common mechanism of lipid peroxidation. Radical scavengers may directly quench and react with peroxide radicals to terminate peroxidation chain reactions. Assays based upon the use of DPPH and $ABTS^+$ are the most popular spectrophotometric methods for the determination of the antioxidant capacity of foods, beverages, and vegetable extracts.[31] In the DPPH assay, the stable DPPH in alcoholic solution reduces to the yellow diphenylpicrylhydrazine due to the formation of the nonradical from DPPH by accepting an electron or hydrogen radical in the presence of an antioxidant. The DPPH radical-scavenging activities of nine phenolic compounds isolated from red pepper leaves are shown in Table 2. Most of the phenolic compounds significantly scavenged the DPPH radical in a dose-dependent manner. Among the nine phenolics, compounds **3** (IC_{50} = 3.5 ± 0.4 μM) and **1** (IC_{50} = 4.8 ± 0.0 μM) showed the highest DPPH free radical-scavenging activity, of which

Table 2. Radical-Scavenging Activity of the Phenolic Compounds Isolated from Red Pepper Leaves[a]

		radical-scavenging activity IC_{50} (μM)	
no.	compound	$DPPH^+$	$ABTS^+$
1	*N*-caffeoylputrescine	4.8 ± 0.0f	9.2 ± 0.8f
2	5-*O*-caffeoylquinic acid	37.0 ± 3.4d	68.1 ± 1.7bc
3	delphinidin-3-[4-(*trans*-coumaroyl)-L-rhamnosyl-(1→6) glucopyranoside]-5-*O*-glucopyranoside	3.5 ± 0.4f	4.4 ± 0.3f
4	5-*O*-caffeoylquinic acid methyl ester	20.4 ± 1.1e	38.0 ± 0.8e
5	luteolin-7-*O*-apiofuranosyl-(1→2)-glucopyranoside	18.8 ± 1.5e	76.2 ± 8.6b
6	luteolin-7-*O*-glucopyranoside	39.5 ± 4.7cd	61.4 ± 8.7cd
7	apigenin-7-*O*-apiofuranosyl(1→2) glucopyranoside	>200a	133.9 ± 3.0a
8	apigenin-7-*O*-glucopyranoside	153.7 ± 13.2b	63.9 ± 4.4cd
9	5-*O*-caffeoylquinic acid butyl ester	51.7 ± 0.7c	55.6 ± 0.5d
	ascorbic acid	7.4 ± 1.1f	1.7 ± 0.6g
	trolox	6.4 ± 2.4f	1.2 ± 0.0g

[a]Values represent means ± SD from triplicate experiments. Different alphabet letters in the same column denote a significant difference according to Tukey's test, $p < 0.05$.

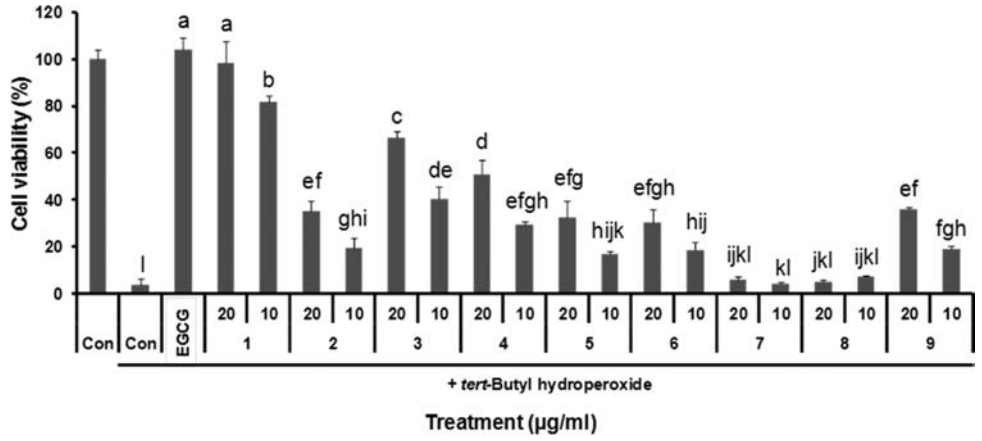

Figure 4. Protective effects of the compounds from pepper leaves against HepG2 cell death induced by *tert*-butyl hydroperoxide (*t*-BHP). Each bar represents the mean ± SD from triplicate experiments. Different letters over the bars denote a significant difference according to Tukey's test, $p < 0.05$. **1**, *N*-caffeoylputrescine; **2**, 5-*O*-caffeoylquinic acid; **3**, delphinidin-3-[4-(*trans*-coumaroyl)-L-rhamnosyl(1→6)glucopyranoside]-5-*O*-glucopyranoside; **4**, 5-*O*-caffeoylquinic acid methyl ester; **5**, luteolin-7-*O*-apiofuranosyl(1→2)glucopyranoside; **6**, luteolin-7-*O*-glucopyranoside; **7**, apigenin-7-*O*-apiofuranosyl(1→2)glucopyranoside; **8**, apigenin-7-*O*-glucopyranoside; **9**, 5-*O*-caffeoylquinic acid butyl ester.

activities were stronger than that of ascorbic acid (IC_{50} = 7.4 ± 1.1 μM) and trolox (IC_{50} = 6.4 ± 2.4 μM), but was not statistically significant. The scavenging activities of the remaining compounds were in the following order: **5** > **4** > **2** ≥ **6** ≥ **9** > **8** > **7**. The scavenging effects on the ABTS radical also showed marked differences according to the compounds (Table 2). Among them, the highest inhibition effects on the ABTS radical cation were found in compounds **3** (IC_{50} = 4.4 ± 0.3 μM) and **1** (IC_{50} = 9.2 ± 0.8 μM), similar to the results obtained from the DPPH assay. Meanwhile, the antioxidant effects for the ABTS radical scavenging of two phenolic compounds were lower than those of ascorbic acid (IC_{50} =1.7 ± 0.6 μM) and trolox (IC_{50} = 1.2 ± 0.0 μM), a well-known antioxidant. The scavenging activities of the remaining compounds were in the following order: **4** > **9** ≥ **6** ≥ **8** ≥ **2** ≥ **5** > **7**. In previous research, the radical-scavenging activities by DPPH assay of compounds **2**,[10] **6**,[11] and **8**[32] have been similarly reported with results of compounds isolated from pepper leaves as 54.8 ± 1.4, 37.9 ± 1.6, and 44.7 μM, respectively.

The in vitro ability to protect HepG2 cells from oxidative damage was evaluated for the isolated nine compounds (Figure 4). The protective effects of the compounds against oxidative stress were evaluated; *t*-BHP treatment for 3 h significantly decreased cell viability (3.8 ± 2.4%) compared to the control (100 ± 4.0%). Pretreatments using the compounds (10 and 20 μg/mL) increased cell viability in a dose-dependent manner. Particularly, compounds **1**, **3**, and **4** enhanced cell viability up to 98.3 ± 9.2, 66.4 ± 2.9, and 50.8 ± 6.1% at a concentration of 20 μg/mL, respectively. Table 3 summarizes the correlation between DPPH and ABTS radical-scavenging activity and HepG2 cells protective effect. A positive correlation ($p < 0.05$) was observed between DPPH and ABTS radical-scavenging activity, whereas a negative correlation ($p < 0.01$) was observed between DPPH and ABTS radical-scavenging activity and the protective effect of the compounds in the cell culture system. These results suggest that the cell protective effect was exerted through a radical-scavenging mechanism. Most of the phenolic compounds expected from compounds **7** and **8** isolated from red pepper leaves had potent protective effects against *t*-BHP-induced HepG2 cell death, as well as scavenging activity on DPPH and ABTS radicals. Therefore, **1** and **3** of the phenolic compounds included in red pepper leaves are potent free radical scavengers and may be considered an excellent source of antioxidants.

Table 3. Correlation of Bioactivities of Each Compound[a]

	correlation coefficient (*r*)		
	DPPH	ABTS	cell protective effect
DPPH		0.774*	−0.772**
ABTS			−0.832**
cell protective effect			

[a]Correlation is significant at (*) $p < 0.05$ level or (**) $p < 0.01$ level.

Phenolic Contents in Three Red Pepper Cultivar Leaves. The content of nine phenolic compounds in three red pepper cultivar leaves was determined by HPLC analysis. As shown in Table 4, red pepper leaves of different cultivars contain different ratios and types of polyphenols. The sums of identified phenolic compounds **1**−**9** of BCPL, HPL, and YHPL are 6.23 ± 0.68, 4.16 ± 0.15, and 2.76 ± 0.13 mg/g, respectively (Table 4), which correspond to the total phenolic contents of the three extracts (Figure 1). The most abundant phenolic compound found in BCPL was compound **7** (3.53 ± 0.28 mg/g fresh weight), representing approximately 57% of the total phenolics composition, followed by **3** (0.86 ± 0.01 mg/g) > **1** (0.77 ± 0.05 mg/g) > **4** (0.34 ± 0.16 mg/g) > **6** (0.04 ± 0.01 mg/g) > **5** (0.02 ± 0.00 mg/g), and **9** (0.02 ± 0.01 mg/g). Furthermore, the main phenolic compounds in HPL were **7** (3.28 ± 0.09 mg/g), **2** (0.36 ± 0.02 mg/g), and **8** (0.26 ± 0.01 mg/g), representing approximately 79, 8.7, and 6.3% of the total phenolic composition, respectively. In contrast to BCPL and HPL, the major phenolic compounds of YHPL were **5** (1.83 ± 0.09 mg/g) and **6** (0.37 ± 0.01 mg/g), representing 66 and 13.3% of the total phenolics, respectively, followed by **2** (0.26 ± 0.01 mg/g) and **1** (0.26 ± 0.02 mg/g) > **7** (0.06 ± 0.00 mg/g). Therefore, flavonoid **7** was the main component in BCPL and HPL, whereas flavonoids **5** and **6** were the predominant constituents in YHPL. Anthocyanin **3** was found only in BCPL.

Compound **3** was identified for the first time from pepper leaves. Anthocyanins have been categorized as the most important group of water-soluble natural pigment in crops

Table 4. Content of Phenolic Compounds in the Leaves of Three Red Pepper Cultivars[a]

cultivar	content (mg/g FW)									
	1	2	3	4	5	6	7	8	9	sum[b]
BCPL	0.77 ± 0.05a	nd	0.86 ± 0.01	0.34 ± 0.16	0.02 ± 0.00b	0.04 ± 0.01b	3.53 ± 0.28a	0.65 ± 0.16	0.02 ± 0.01	6.23 ± 0.68a
HPL	0.12 ± 0.02c	0.36 ± 0.02	nd	0.01 ± 0.00	0.10 ± 0.01b	0.03 ± 0.00b	3.28 ± 0.09a	0.26 ± 0.01	nd	4.16 ± 0.15b
YHPL	0.26 ± 0.02b	0.26 ± 0.01	nd	nd	1.83 ± 0.09a	0.37 ± 0.01a	0.06 ± 0.00b	nd	nd	2.78 ± 0.13c

[a]Values represent the mean ± SD from triplicate experiments. Different letters in the same column denote a significant difference according to Tukey's test, $p < 0.05$. FW, fresh weight; total, sum of nine compound contents; nd, not detected. **1**, *N*-caffeoylputrescine; **2**, 5-*O*-caffeoylquinic acid; **3**, delphinidin-3-[4-(*trans*-coumaroyl)-L-rhamnosyl(1→6)glucopyranoside]-5-*O*-glucopyranoside; **4**, 5-*O*-caffeoylquinic acid methyl ester; **5**, luteolin-7-*O*-apiofuranosyl(1→2)glucopyranoside; **6**, luteolin-7-*O*-glucopyranoside; **7**, apigenin-7-*O*-apiofuranosyl(1→2)glucopyranoside; **8**, apigenin-7-*O*-glucopyranoside; **9**, 5-*O*-caffeoylquinic acid butyl ester. [b]Values represent the sum of the phenolic components 1−9.

such as fruits, vegetables, and flowers.[33−35] These natural pigments are beneficial to the food industry due to their good properties as food colorants and beneficial human health effects, such as antioxidant, anti-inflammatory, anticancer, antidiabetic, and antiartherogenic properties.[11,33] Compound **2** is well-known as a treatment material for its antihistamine, antiviral, antioxidative activity, and DNA-protective activity.[13,36,37] Compound **6** is reported on for its antiproliferative, anti-LDL oxidative, and cytotoxic activity, as well as its gelatinase and collagenase inhibition, antifeedant activity, and anti-HBV activity.[38−43] Compound **7** is well-known as a treatment material for its anticomplement, anti-inflammatory, liver protection, and antibacterial activities.[44−46] Compound **8** is well-known as a treatment material as an antifungal, cytotoxic, antibacterial, and anti-HIV agent.[47−49] Finally, compound **9** is well-known as a treatment material due to its antibacterial nature.[50] Thus, they represent an effective antioxidant source for commercial food and pharmaceutical uses due to their content, disease treatment, and strong radical-scavenging activities.

Individual and total phenolic compounds showed significant differences in cultivars, and BCPL was observed to have the highest phenolic content for compounds **1** and **3**, as well as the highest antioxidant capacity (DPPH, IC_{50} = 49.2 ± 6.1 μg/mL; and ABTS, IC_{50} = 26.2 ± 3.2 μg/mL). On the basis of the above findings, it is suggested that strong antioxidant activities of BCPL of red pepper leaves were related with high contents of compounds **1** and **3**. These results indicate that compounds **1** and **3** may be important factors for the quality of red pepper leaves. Future studies are required to evaluate the various beneficial health effects of phenolic compounds isolated, as well as for red pepper leaves in vitro and in vivo.

AUTHOR INFORMATION

Corresponding Author

*(B.-H.U.) Phone: +82-33-650-3601. Fax.: +82-33-650-3629. E-mail: albertum@kist.re.kr.

Funding

This work was supported by an intramural grant (2Z03850) from the Korea Institute of Science and Technology, Gangneung Institute.

Notes

The authors declare no competing financial interest.

ACKNOWLEDGMENTS

We appreciate the assistance of Dr. H. L. Eum and Prof. S. J. Hong in the department of Plant Science, Gangneung-Wonju National University in Gangneung, Gangwondo, Korea, in obtaining the plant material.

REFERENCES

(1) Gharavi, N.; Haggarty, S.; El-Kadi, A. O. S. Chemoprotective and carcinogenic effects of tert-butylhydroquinone and its metabolites. *Curr. Drug Metab.* **2007**, *8*, 1−7.

(2) Crozier, A.; Jaganath, I. B.; Clifford, M. N. Dietary phenolics: chemistry, bioavailability and effects on health. *Nat. Prod. Rep.* **2009**, *26*, 1001−1043.

(3) Skrovankova, S.; Misurcova, L.; Machu, L. Antioxidant activity and protecting health effects of common medicinal plants. *Adv. Food Nutr. Res.* **2012**, *67*, 75−139.

(4) Dimitrios, B. Sources of natural phenolic antioxidants. *Trends Food Sci. Technol.* **2006**, *17*, 505−512.

(5) Ku, K. M.; Kang, Y. H. Quinone reductase inductive activity of *Capsicum annuum* leaves and isolation of the active compounds. *J. Korean Soc. Appl. Biol. Chem.* **2010**, *53*, 709−715.
(6) Minguez-Mosquera, M. I.; Hornero-Mendez, D. Separation and quantification of the carotenoid pigments in red peppers (*Capsicum annuum* L.), paprika, and oleoresin by reversed-phase HPLC. *J. Agric. Food Chem.* **1993**, *41*, 1616−1620.
(7) Lee, Y.; Howard, L. R.; Villalon, B. Flavonoids and antioxidant activity of fresh pepper (*Capsicum annuum*) cultivars. *J. Food Sci.* **1995**, *60*, 473−476.
(8) Ku, K. M.; Kim, H. S.; Kim, B. S.; Kang, Y. H. Antioxidant activities and antioxidant constituents of pepper leaves from various cultivars and correlation between antioxidant activities and antioxidant constituents. *J. Appl. Biol. Chem.* **2009**, *52*, 70−76.
(9) Choi, J. G.; Hur, J. M.; Cho, H. W.; Park, J. C. Phenolic compounds from *Capsicum annuum* leaves showing radical scavenging effect. *Saengyak Hakhoechi* **2007**, *38*, 258−262.
(10) Argoti, J. C.; Linares-Palomino, P. J.; Salido, S.; Ramirez, B.; Insuasty, B.; Altarejos, J. On-line activity screening for radical scavengers from *Baccharis chilco*. *Chem. Biodiversity* **2013**, *10*, 189−197.
(11) Ben, H. A.; Trigui, M.; Culioli, G.; Blache, Y.; Jaoua, S. Antioxidant constituents from *Lawsonia inermis* leaves: isolation, structure elucidation and antioxidative capacity. *Food Chem.* **2011**, *125*, 193−200.
(12) Quettier-Deleu, C.; Gressier, B.; Vasseur, J. Phenolic compounds and antioxidant activities of buckwheat (*Fagopyrum esculentum* Moench) hulls and flour. *J. Ethnopharmacol.* **2000**, *72*, 35−42.
(13) Wang, J.; Wang, N.; Yao, X.; Kitanaka, S. Caffeoyl quinic acid derivatives from *Bidens parviflora* and their antihistamine release activities. *Zhongcaoyao* **2006**, *37*, 966−970.
(14) Kang, K.; Jho, E. H.; Lee, H. J. *Youngia denticulata* protects against oxidative damage induced by *tert*-butylhydroperoxide in HepG2 cells. *J. Med. Food* **2011**, *14*, 1198−1207.
(15) Shang, Y. F.; Kim, S. M.; Song, D. G.; Pan, C. H.; Lee, W. J.; Um, B. H. Isolation and identification of antioxidant compounds from *Ligularia fischeri*. *J. Food Sci.* **2010**, *75*, C530−C535.
(16) Mizusaki, S.; Tanabe, Y.; Noguchi, M. New aromatic amide, caffeoylputrescine from callus tissue culture of *Nicotiana tabacum*. *Agric. Biol. Chem.* **1970**, *34*, 972−973.
(17) Ichiyanagi, T.; Kashiwada, Y.; Shida, Y.; Ikeshiro, Y.; Kaneyuki, T.; Konishi, T. Nasunin from eggplant consists of cis-trans isomers of delphinidin 3-[4-(*p*-coumaroyl)-L-rhamnosyl (1→6)glucopyranoside]-5-glucopyranoside. *J. Agric. Food Chem.* **2005**, *53*, 9472−9477.
(18) Zhang, W.; Thi, B. T. H.; Chen, W.; Kong, D.; Li, H. Studies on structure and activity of phenolic compounds from *Erigeron breviscapus*. *Zhongguo Yaoxue Zazhi. (Beijing, China)* **2002**, *37*, 579−582.
(19) Harborne, J. B. *Comparative Biochemistry of the Flavonoids*; Academic: New York, 1967; 383 pp.
(20) Materska, M.; Piacente, S.; Stochmal, A.; Pizza, C.; Oleszek, W.; Perucka, I. Isolation and structure elucidation of flavonoid and phenolic acid glycosides from pericarp of hot pepper fruit *Capsicum annuum* L. *Phytochemistry (Elsevier)* **2003**, *63*, 893−898.
(21) Lee, J. Y.; Moon, S. O.; Kwon, Y. J.; Rhee, S. J.; Park, H. R.; Choi, S. W. Identification and quantification of anthocyanins and flavonoids in mulberry (*Morus* sp.) cultivars. *Food Sci. Biotechnol.* **2004**, *13*, 176−184.
(22) Wanjala, C. C. W.; Majinda, R. R. T. Flavonoid glycosides from *Crotalaria podocarpa*. *Phytochemistry* **1999**, *51*, 705−707.
(23) Park, S.; Jeong, W. Y.; Lee, J. H. Determination of polyphenol levels variation in *Capsicum annuum* L. cv. Chelsea (yellow bell pepper) infected by anthracnose (*Colletotrichum gloeosporioides*) using liquid chromatography-tandem mass spectrometry. *Food Chem.* **2012**, *130*, 981−985.
(24) Perrone, A.; Masullo, M.; Plaza, A.; Hamed, A.; Piacente, S. Flavone and flavonol glycosides from *Astragalus eremophilus* and *Astragalus vogelii*. *Nat. Prod. Commun.* **2009**, *4*, 77−82.
(25) Lin, L. Z.; Lu, S.; Harnly, J. M. Detection and quantification of glycosylated flavonoid malonates in celery, chinese celery, and celery seed by LC-DAD-ESI/MS. *J. Agric. Food Chem.* **2007**, *55*, 1321−1326.
(26) Li, T. M.; Li, W. K.; Yu, J. G. Flavonoids from *Artabotrys hexapetalus*. *Phytochemistry* **1997**, *45*, 831−833.
(27) Long, F.; Deng, L.; Chen, Y. Study on the chemical constituents in the flowers of *Ligustrum lucidum*. *Huaxi Yaoxue Zazhi* **2011**, *26*, 97−100.
(28) Liu, B.; Deng, A. J.; Yu, J. Q.; Liu, A. L.; Du, G. H.; Qin, H. L. Chemical constituents of the whole plant of *Elsholtzia rugulosa*. *J. Asian Nat. Prod. Res.* **2012**, *14*, 89−96.
(29) Aga, E. b.; Li, H. j.; Chen, J.; Li, P. Chemical constituents from the aerial parts of *Codonopsis nervosa*. *Zhongguo Tianran Yaowu* **2012**, *10*, 366−369.
(30) Gao, F.; Wang, H.; Ye, W.; Zhao, S. Chemical constituents from the leaves of *Callicarpa nudiflora*. *Zhongguo Yaoke Daxue Xuebao* **2010**, *41*, 120−123.
(31) Ak, T.; Gulcin, I. Antioxidant and radical scavenging properties of curcumin. *Chem.−Biol. Interact.* **2008**, *174*, 27−37.
(32) Nazemiyeh, H.; Bahadori, F.; Delazar, A. Antioxidant phenolic compounds from the leaves of *Erica arborea* (Ericaceae). *Nat. Prod. Res.* **2008**, *22*, 1385−1392.
(33) Wang, H.; Cao, G.; Prior, R. L. Oxygen radical absorbing capacity of anthocyanins. *J. Agric. Food Chem.* **1997**, *45*, 304−309.
(34) Clifford, M. N. Anthocyanins − nature, occurrence and dietary burden. *J. Sci. Food Agric.* **2000**, *80*, 1063−1072.
(35) Cooper-Driver, G. A. Contributions of Jeffrey Harborne and co-workers to the study of anthocyanins. *Phytochemistry* **2001**, *56*, 229−236.
(36) Xu, J. G.; Hu, Q. P.; Liu, Y. Antioxidant and DNA-protective activities of chlorogenic acid isomers. *J. Agric. Food Chem.* **2012**, *60*, 11625−11630.
(37) Zhang, Y.; Shi, S. Method for extracting and purifying high-purity antiviral active caffeoyl quinic acid components from Chinese medicine *Cynara*. *Central South Univ., People's Rep. China* **2010**, 10.
(38) Garritano, S.; Pinto, B.; Giachi, I.; Pistelli, L.; Reali, D. Assessment of estrogenic activity of flavonoids from Mediterranean plants using an in vitro short-term test. *Phytomedicine* **2005**, *12*, 143−147.
(39) Gupta, P.; Yadav, D. K.; Siripurapu, K. B.; Palit, G.; Maurya, R. Constituents of *Ocimum sanctum* with antistress activity. *J. Nat. Prod.* **2007**, *70*, 1410−1416.
(40) Harinantenaina, L.; Matsunami, K.; Otsuka, H. Chemical and biologically active constituents of *Pteris multifida*. *J. Nat. Med.* **2008**, *62*, 452−455.
(41) Mohammed, M. M. D.; Chen, M.; Zhai, L.; Ali, I. N. The cytotoxic activity of *Linum grandiflorum* leaves. *Eur. J Chem.* **2010**, *1*, 110−114.
(42) Tian, Y.; Sun, L. M.; Liu, X. Q.; Li, B.; Wang, Q.; Dong, J. X. Anti-HBV active flavone glucosides from *Euphorbia humifusa* Willd. *Fitoterapia* **2010**, *81*, 799−802.
(43) Chen, Y. Y.; Pan, Q. D.; Li, D. P. New pregnane glycosides from *Brucea javanica* and their antifeedant activity. *Chem. Biodiversity* **2011**, *8*, 460−466.
(44) Babenko, N. A.; Shakhova, E. G. Effects of *Chamomilla recutita* flavonoids on age-related liver sphingolipid turnover in rats. *Exp. Gerontol.* **2006**, *41*, 32−39.
(45) Cottiglia, F.; Loy, G.; Garau, D. Antimicrobial evaluation of coumarins and flavonoids from the stems of *Daphne gnidium* L. *Phytomedicine* **2001**, *8*, 302−305.
(46) Pieroni, A.; Pachaly, P. An ethnopharmacological study on common privet (*Ligustrum vulgare*) and phillyrea (*Phillyrea latifolia*). *Fitoterapia* **2000**, *71*, 89−94.
(47) Tang, R.; Chen, K.; Cosentino, M.; Lee, K. H. Anti-AIDS agents. 12. Apigenin-7-*O*-*β*-D-glucopyranoside, an anti-HIV principle from *Kummerowia striata*. *Bioorg. Med. Chem. Lett.* **1994**, *4*, 455−458.
(48) Guelcemal, D.; Alankus-Caliskan, O.; Karaalp, C.; Oers, A. U.; Ballar, P.; Bedir, E. Phenolic glycosides with antiproteasomal activity

from *Centaurea urvillei* DC. subsp. *urvillei*. *Carbohydr. Res.* **2010**, *345*, 2529−2533.
(49) Chen, W. Q.; Song, Z. J.; Xu, H. H. A new antifungal and cytotoxic C-methylated flavone glycoside from *Picea neoveitchii*. *Bioorg. Med. Chem. Lett.* **2012**, *22*, 5819−5822.
(50) Xu, D. d.; Jiang, X. Z.; Gao, Y.; Zheng, W.; He, M.; Gao, Q. P. Chemical constituents of effective fraction of honeysuckle on inhibition of *Escherichia coli* biofilms. *Zhongguo Shiyan Fangjixue Zazhi* **2012**, *18*, 122−125.

JOURNAL OF AGRICULTURAL AND FOOD CHEMISTRY

Article

pubs.acs.org/JAFC

Oral Administration of *Lactobacillus fermentum* I5007 Favors Intestinal Development and Alters the Intestinal Microbiota in Formula-Fed Piglets

Hong Liu,[†] Jiang Zhang,[†] Shihai Zhang,[†] Fengjuan Yang,[†] Phil A. Thacker,[‡] Guolong Zhang,[§] Shiyan Qiao,[†] and Xi Ma*[,†]

[†]State Key Laboratory of Animal Nutrition, China Agricultural University, No. 2, Yuanmingyuan West Road, Beijing 100193, China

[‡]Department of Animal and Poultry Science, University of Saskatchewan, 51 Campus Drive, Saskatoon, Saskatchewan, Canada

[§]Department of Animal Science, Oklahoma State University, Stillwater, Oklahoma, United States

ABSTRACT: The present study was conducted to evaluate the effects of early administration of *Lactobacillus fermentum* I5007 on intestinal development and microbial composition in the gastrointestinal tract using a neonatal piglet model. Full-term 4 day old piglets, fed with milk replacer, were divided into a control group (given placebo of 0.1% peptone water) and a *L. fermentum* I5007 group (dosed daily with 6×10^9 CFU/mL *L. fermentum* I5007). The experiment lasted 14 days. On day 14, a significant increase in the jejunum villous height (583 ± 33 vs 526 ± 18) and increases in the concentrations of butyrate (7.55 ± 0.55 vs 5.33 ± 0.39) and branched chain fatty acids in the colonic digesta were observed in piglets in the *L. fermentum* I5007 treatment ($P < 0.05$). mRNA expression of IL-1β (1.29 ± 0.29 vs. 0.62 ± 0.07) in the ileum were lower after 14 days of treatment with *L. fermentum* I5007. Denaturing gradient gel electrophoresis (DGGE) revealed that *L. fermentum* I5007 affected the colonic microbial communities on day 14 and, in particular, reduced numbers of *Clostridium sp.* *L. fermentum* I5007 play a positive role in gut development in neonatal piglets by modulating microbial composition, intestinal development, and immune status. *L. fermentum* I5007 may be useful as a probiotic for application in neonatal piglets.

KEYWORDS: *intestinal metabolism, Lactobacillus fermentum I5007, gut microbiota, neonatal piglets*

INTRODUCTION

Before birth, the gastrointestinal tract of the fetus is sterile, and during the initiation of the birth process and thereafter, acquisition of microbes is ongoing and time-dependent.[1,2] Many factors affect the composition of the microbiota in the intestinal tract before the gut finally gets a dense and stable population as an adult.[3] Early colonization with beneficial bacteria could help establish an effective ecosystem and bring about maturity in the physical structure of the gut.[4,5]

Probiotic and prebiotic administration during the neonatal period can improve gut function by improving the intestinal immune status and maintaining microbial balance during gastrointestinal disturbances.[5,6] Although progress has been made in disclosing the mechanisms through which probiotics act on the intestinal immunity and microbial composition of clinical models, knowledge about the interaction between probiotics and intestinal microbial metabolism, as well as microbial composition in healthy animals and humans, is lacking.

Lactobacilli are normal inhabitants of the gastrointestinal tract in humans and other mammals, and have been intensively studied during the past decades for their probiotic properties in both clinical and animal models.[7−9] *Lactobacillus fermentum* I5007 was initially isolated in our lab from the colonic mucosa of healthy weaning piglets, identified by the Institute of Microbiology Chinese Academy of Sciences (Beijing, China), and was shown to possess many characteristics of an excellent probiotic, including gastric acid and bile tolerance, high adhesion to CaCo-2 cells, competitive exclusion against pathogen invasion, and alleviation of weaning stress in piglets.[10−12] Our previous study has conferred the optimum dosage (about 10^{10} CFU/d *L. fermentum* I5007) for improving growth performance and diarrhea incidence in the neonatal period in piglets (data not published). However, the exact role of these lactobacilli in the intestine during the neonatal period in vivo is still unknown.

In contrast to rodent models, the size of the newborn piglet easily allows for clinically relevant nutritional interventions, and the ontogeny and anatomy of the gastrointestinal tract are more similar to those of human infants.[13,14] The present study evaluated the effects of an early introduction of an exogenous *L. fermentum* I5007 strain to gut metabolism and maturation, as well as the indigenous microbiota and their metabolic products, which will determine any implications of *L. fermentum* I5007 for pediatric nutrition.

MATERIALS AND METHODS

Chemicals. Rogosa Sharpe medium, Luria−Bertani agar, ampicillin, metaphosphoric acid, and peptone were all purchased from ZSGB-Bio Company (Beijing, China) while Agarose was provided from Gene Company LTD (Hong Kong, China). Skim milk, phosphate buffer saline, ampule, and hematoxylin−eosin were purchased from Huaxing-Bio Company (Beijing, China). Polyacrylamide gels, Tris-acetate-

Received: July 25, 2013
Revised: January 2, 2014
Accepted: January 9, 2014
Published: January 9, 2014

 © 2014 American Chemical Society

EDTA buffer, formamide, and urea were obtained from Premedical Lab (Beijing, China).

Ethics Statement. The experimental protocol was approved by the China Agriculture University Institutional Animal Care and Use Ethical Committee (Beijing, China).

Bacterial Strain, Growth, and Storage Conditions. *L. fermentum* I5007 was cultured on sterile Man Rogosa Sharpe medium at 37 °C for 24 h in an anaerobic environment, followed by centrifugation at 5000*g* for 10 min at 4 °C. The cells were resuspended in reconstituted skim milk (20% w/v) and immediately freeze-dried. The freeze-dried powder containing 6×10^9 colony forming units (CFU)/g was stored in sealed packets at a temperature of 4 °C until used.

Piglets and Treatment. A total of thirty-six, full-term crossbred (Large White sires × Landrace dams) piglets obtained from four litters were used in this study. The piglets were delivered vaginally at the Langzhong Bei Pig Husbandry Training Farm (Beijing, China) and allowed colostrum for 48 h after birth. After colostrum consumption, the piglets were individually housed in stainless steel pens located over a totally slotted floor in a temperature (33 ± 1 °C) and relative humidity (65−70%) controlled room programmed to deliver a light:dark cycle of 16:8 h. On the third day of life, piglets were trained to suckle from bottles filled with milk replacer (Rosalac Instant, Bonilait Proteins, France, dry matter 89%, lactose 45%, protein 21.5%, fat 18.7%, ash 9.8%, lysine 1.7%; vitamins and minerals meet the nutrient requirements), and the milk replacer was dissolved in warm boiled water (w/v 1:4.5) to provide the same level of nutrients as sow-reared piglets. The fresh liquid milk replacer was fed to piglets individually from the feeder six times daily (2, 6, 10, 14, 18, and 22 h). The feeders were cleaned each time before adding the new fresh milk replacer, and the remaining milk was measured. The formula did not contain any antibiotics or other medicine.

On day 4 (equivalent to the first day of the experiment), piglets were allocated to one of two treatments (the *L. fermentum* I5007 group and the control group) balanced for litter of origin and body weight (initial body weight of 2.00 ± 0.31 kg). Each piglet in the *L. fermentum* I5007 group was orally administered 6×10^9 CFU *L. fermentum* I5007 dissolved in 3 mL of 0.1% of peptone water once a day for 14 days while the piglets in the control group were given the same volume of 0.1% peptone water.

Sample Collection. The health status was recorded for each piglet, and the occurrence of diarrhea was visually assessed each afternoon according to the method of Hart and Dobb.[15] Scores were 0 = normal, firm feces; 1 = possible slight diarrhea; 2 = definitely unformed, moderately fluid feces; or 3 = very watery and frothy diarrhea. The occurrence of diarrhea was defined as maintaining score of 3 for one day (monitor time: 10:00 a.m. and 16:00 p.m.). Diarrhea incidence was calculated according to the equation where diarrhea incidence (%) = n (numbers piglets of diarrhea) × days (the diarrhea duration)/n (the total number of experiment piglets) × days (the whole experiment days) × 100%.

After being weighed on the morning of the days 7 and 14 of the experiment (equivalent to 11 and 18 days of age), 6 healthy piglets closest to the average body weight balanced for litter of origin from each treatment were euthanized with electricity and their abdominal cavities were opened to remove the gastrointestinal tract. The small intestine was carefully dissected from the mesentery, and 2 cm segments were obtained from the jejunum (the middle of the small intestine). The intestinal segments were placed in neutral formalin for histological analysis. Additional segments 15 cm long, taken from the jejunum, were rinsed with cold 0.01 M sterile PBS (pH 7.4) and blotted dry on filter paper. Jejunal mucosa from the jejunum was obtained by gently scraping the mucosal layer using a glass microscope slide, 0.5 g of mucosal scrapings from each piglet was collected into a sterile Eppendorf tube (Axygen Inc., Union City, California), and 1 mL of 0.01 M PBS containing 2 mg/mL protease inhibitor supplied by the Huaxingbochuang Institute (Beijing, China) was added to each tube. Each sample was centrifuged at 3500*g* for 10 min at 4 °C after being homogenized (T10, IKA Works, Staufen, Germany). The supernatant was harvested and stored at −20 °C for analysis of disaccharidase activities. The colonic digesta were used for pH measurements and then gently squeezed into sterile Eppendorf tubes, frozen in liquid nitrogen, and subsequently stored at −80 °C until processing. Two digesta samples per treatment ($n = 6$) were randomly selected and pooled as three new samples (with equal wet weight) until needed for further genomic DNA isolation.

Intestinal Morphology and Enzyme Activities. Samples from jejunal segment were embedded in paraffin and cut into serial sections (5 μm). Five nonsuccessive sections of each sample were selected and stained with hematoxylin−eosin for identification. Five well oriented villi (determined as the distance between the crypt openings and the end of the villi) and their associated crypt (measured from the crypt-villous junction to the base of the crypt) per section were selected and measured under an Olympus Light Microscope (CK-40, Olympus, Tokyo, Japan) at 40× magnification. The means of these measurements were calculated to yield a single value per piglet. These procedures were conducted by an observer unaware of the treatment assignment. Myeloperoxidase (MPO), as an indicator of neutrophil infiltration, was determined in ileal segment on day 14. The activities of the disaccharidase (lactase, maltase, sucrase) and MPO were determined according to assay kit instructions (Nanjingjiancheng, Nanjing, China). One unit of specific MPO activity was defined as that degrading 1 μmol of hydrogen peroxide per min, and data were expressed as units of MPO per gram of tissue. The disaccharidase activities were expressed as units per milligram of protein, and the amount of protein of samples was determined using a commercially available bicinchoninic acid kit (Thermo, Rockford, IL, USA).

RNA Isolation and RT-PCR. Total RNA was isolated from the ileal segments using a RNeasy Mini Kit (Qiagen, Hilden, Germany). The purity was determined by the ratio of A_{260}:A_{280} using a NanoDrop spectrophotometer (P330, Implen, Germany), and then the quality was checked with 1% agarose gel electophoresis. The extracted RNA was converted into first-strand cDNA by reverse transcription of 1 μg of total RNA using a PrimeScript First Strand cDNA Synthesis Kit (Takara, Dalian, China) according to the manufacturer's protocol and stored at −80 °C. Real-time PCR was performed on an Applied Biosystems 7500 Real-Time PCR System (Applied Biosystems, Singapore) using SYBR Green PCR Master Mix (Takara, Dalian, China). The sequences of PCR primer for target genes were as follows: forward 5′-CCTCCTCCCAGGCCTTCTGT-3′, reverse 5′-GGGCCAGCCAGCACTAGAGA-3′ for IL-1β;[16] forward 5′-AGT-TTTCCTGCTTTCTGCAGC T-3′, reverse 5′-TGGCATCGAAGT-TCTGCACT-3′ for IL-8;[17] forward 5′-ATGGGCGACTTGTTG-CTGAC-3′, reverse 5′-CACAGGGCAGAAATTGATGACA-3′ for IL-10;[18] forward 5′-CCCAAGGACTCAGATCATCG-3′, reverse 5′-ATACCCACTCTGCCATTGGA-3′ for TNF-α;[16] forward 5′-CAT-CACCATCGGCAACGA-3′, reverse 5′-GCGTAGAGGTCCTTC-CTGATGT-3′ for β-actin.[19] Quantification of target mRNA was conducted using a relative standard curve generated by a serial dilution (1:10) covering the appropriate concentration range. The reaction was conducted in a total volume of 10 μL, and the process included predenaturation for 30 s at 95 °C, and then 40 cycles of 5 s at 95 °C, 30 s at 60 °C, and 40 s at 72 °C for the target genes. For the porcine β-actin gene, the annealing temperature was set at 58 °C. The relative gene expression was determined for the two treatments on day 14. All reactions were performed in triplicate. The mRNA expression is expressed as the ratio between the target gene and β-actin gene expression.

Colonic Short Chain Fatty Acid Concentrations and pH Value. The pH in the colonic digesta was determined for each sample, and the concentrations of short chain fatty acids were determined by a gas chromatographic method following the procedures of Franklin et al.[20] with modification. About 1.5 g of thawed digesta was suspended in 1.5 mL of distilled water in a screw-capped tube (Axygen Inc., Union City, CA). The entire sample was centrifuged at 15000*g* at 4 °C for 10 min. After that, 1 mL of suspernatant was transferred into an ampule and mixed with 200 μL of metaphosphoric acid (HPO_3). The ampules were placed in an ice bath for 30 min and then centrifuged again for 10 min. The sample was injected into a HP 6890 series gas chromatograph (Hewlett-Packard, Palo Alto, CA) equipped with a HP

19091N-213 column 30.0 m × 0.32 mm i.d. (Agilent, Palo Alto, CA. The injector and detector temperatures were 185 and 210 °C, respectively.

DNA Isolation, PCR-Denaturing Gradient Gel Electrophoresis (DGGE), and Identification of Fragments Extracted from the Gels. The extraction of DNA from colonic digesta for denaturing gradient gel electrophoresis was performed using a QIAamp Stool Mini-Kit (Qiagen, Hilden, Germany). The concentration of extracted DNA was measured using a NanoDrop spectrophotometer (P330, Implen, Germany). The bacterial universal V3 region of the 16S rDNA gene was amplified according to Muyzer et al.[21] The PCR products were analyzed by electrophoresis on 1.2% (w/v) agarose gel in SYBR Green I (Sigma, St. Louis, MO) to verify that a single product of the expected size was obtained.

DGGE was performed for separation of PCR amplicons in 8% (w/v) polyacrylamide gels with a vertical gradient of denaturants between 35 and 60% (100% denaturing solution was defined as 40% (v/v) formamide and 7 M urea). For each sample, the same concentration of DNA was loaded to one lane of the gel. Electrophoresis was initiated by prerunning for 5 min at 200 V and then for 16 h at 85 V in 0.5× Tris-acetate-EDTA buffer at a constant temperature of 60 °C in a DCode System Apparatus (Bio-Rad, Hercules, CA). The DGGE gel was stained by SYBR green I (Sigma, St. Louis, MO) for 15 min at room temperature, photographed with a Gel Doc XR$^+$ System (Bio-Rad, Hercules, CA), and analyzed with Quantity One Basic 4.6.6 Software for Windows (Bio-Rad, Hercules, CA).

Interesting bands in the DGGE profiles were excised with a sterile needle, reamplified, and purified with a Takara Mini Best DNA Fragment Purification Kit (Takara, Dalian, China) according to the manufacturer's protocol. The PCR products were cloned into the vector pMD-19T according to the manufacturer's instructions and transformed into *Escherichia coli* DH5α cells via chemical transformation. The transformants were grown on Luria−Bertani agar in the presence of 100 μg/mL ampicillin. The positive recombinants were screened and identified by PCR and sent for sequencing. Homology searches were performed using the BLAST program in the NCBI database (http://blast.ncbi.nlm.nih.gov/).

Statistical Analysis. Statistical analyses were performed using the Analysis of Variance (ANOVA) procedures of the Statistical Analysis Systems Statistical Software Package Version 8.02 (SAS Institute, Cary, NC). Each piglet served as an experimental unit. Differences at $P < 0.05$ were considered significant, and $P < 0.1$ was considered to be indicative of a trend.

RESULTS

Performance, Jejunum Morphology, and Enzyme Activities. The average daily weight gain during days 8 to 14 and the whole experiment period was 26.9% and 24.3% higher for piglets in the *L. fermentum* I5007 treatment compared with the control ($P < 0.05$, Table 1). Diarrhea incidence was lower in piglets fed *L. fermentum* I5007 compared with the control (1.19 vs 2.98%). During the second week, two piglets in the control treatment died on days 10 and 13 separately due to serious diarrhea.

Maturation of the intestine was assessed by changes in intestinal morphology and the activity ofthe disaccharidases, lactase, sucrase, and maltase in the jejunum (Table 2). In jejunum, villous height on day 14 was higher in *L. fermentum* I5007 piglets compared with the control piglets ($P < 0.05$), while disaccharidase activities on either day 7 or 14 did not differ due to treatment as well as the MPO activity in ileal segment on day 14.

Digesta Metabolites. Table 3 shows the concentrations of short chain fatty acids and pH values determined in the colonic digesta. Short chain fatty acid concentrations were not different between the two treatments measured on day 7. However, on day 14, the concentrations of branched chain fatty acids (isobutyric acid and isovaleric acid) and butyric acid were

Table 1. Effects of *L. fermentum* I5007 on Piglet Growth Performance and Diarrhea Incidence[a]

items	control	*L. fermentum* I5007
initial body wt (kg)	1.99 ± 0.09	2.01 ± 0.08
body wt at day 7 (kg)	2.67 ± 0.09	2.78 ± 0.08
body wt at day 14 (kg)	4.11 ± 0.24	4.60 ± 0.13
wt gain (g/day)		
1−7 days	97 ± 5	110 ± 5
8−14 days	196 ± 23 b	250 ± 10 a
1−14 days	148 ± 13 b	184 ± 6 a
diarrhea incidence (%)	2.98	1.19

[a]All data are means ± SEM. Means within the same row that have no common letters are significantly different ($p < 0.05$); $n = 10$, the control group; $n = 12$, *L. fermentum* I5007 group respectively.

Table 2. Jejunum Structure and Enzyme Activities of *L. fermentum* I5007 Treated Piglets and the Control[a]

items	control	*L. fermentum* I5007
	Day 7	
villus height (μm)	431 ± 31	436 ± 43
crypt depth (μm)	151 ± 32	143 ± 12
lactase (U/mg protein)	172 ± 20	211 ± 13
maltase (U/mg protein)	96 ± 17	140 ± 22
sucrase (U/mg protein)	100 ± 15	92 ± 15
	Day 14	
villus height (μm)	526 ± 18 b	583 ± 33 a
crypt depth (μm)	148 ± 11	172 ± 23
lactase (U/mg of protein)	190 ± 22	185 ± 19
maltase (U/mg of protein)	87 ± 4	104 ± 11
sucrase (U/mg of protein)	122 ± 17	83 ± 16
MPO (U/g of tissue)	0.24 ± 0.02	0.23 ± 0.01

[a]All data are means ± SEM. Means within the same row that have no common letters are significantly different ($p < 0.05$); $n = 6$.

Table 3. pH Values and Short Chain Fatty Acid Concentrations in Colonic Digesta Obtained from the Control and *L. fermentum* I5007 Treated Piglets[a]

items	control	*L. fermentum* I5007
	Day 7	
pH	6.46 ± 0.14	6.37 ± 0.07
acetic acid (mmol/kg)	27.03 ± 3.68	26.19 ± 2.82
propionic acid (mmol/kg)	6.73 ± 0.96	7.13 ± 1.23
butyric acid (mmol/kg)	5.62 ± 1.11	4.99 ± 0.17
pentanoic acid (mmol/kg)	2.32 ± 0.39	2.16 ± 0.91
isobutyric acid (mmol/kg)	0.87 ± 0.27	0.72 ± 0.21
isovaleric acid (mmol/kg)	1.10 ± 0.36	1.19 ± 0.24
	Day 14	
pH	6.41 ± 0.05	6.27 ± 0.05
acetic acid (mmol/kg)	40.00 ± 4.47	45.91 ± 4.90
propionic acid (mmol/kg)	15.08 ± 1.54	14.14 ± 1.51
butyric acid (mmol/kg)	5.33 ± 0.39 b	7.55 ± 0.55 a
pentanoic acid (mmol/kg)	2.51 ± 0.38	2.32 ± 0.33
isobutyric acid (mmol/kg)	0.63 ± 0.11 b	0.95 ± 0.08 a
isovaleric acid (mmol/kg)	1.32 ± 0.13 b	1.82 ± 0.16 a

[a]All data are means ± SEM. Means within the same row that have no common letters are significantly different ($p < 0.05$); $n = 6$.

higher in piglets fed *L. fermentum* I5007 than the control treatment ($P < 0.05$). Piglets treated with the *L. fermentum* I5007 tended to exhibited a lower pH ($P = 0.06$) on day 14 (6.27 vs 6.41).

Cytokine Expression. Both inflammatory and anti-inflammatory cytokines in the intestinal tissue were measured at the end of the experiment to assess the effects of feeding *L. fermentum* I5007 on modulations of the immune response (Figure 1). The expression of the inflammatory cytokine IL-1β

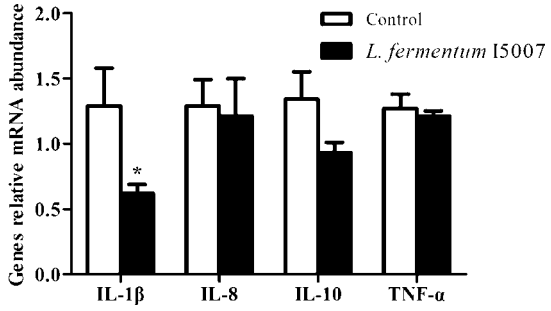

Figure 1. mRNA expression of relevant cytokines in ileal segments. Effects of the *L. fermentum* I5007 on IL-1β, IL-8, IL-10, and TNF-α mRNA expression in the ileal segment of piglets on day 14. Data are means ± SEM ($n = 6$). Significant differences between control and *L. fermentum* I5007 treated piglets: * $p < 0.05$.

mRNA was observed to be lower in piglets in the *L. fermentum* I5007 treatment compared with the control treatment ($P = 0.05$) on day 14. The expression of the anti-inflammatory cytokine IL-10 also tended to be lower in *L. fermentum* I5007 treated piglets ($P = 0.09$), while IL-8 and TNF-α mRNA expression did not differ between the two treatments (Figure 1).

Colon Microbiota Profiles Generated by PCR-DGGE and Sequence Analysis of DGGE Bands. Analysis of the DGGE fingerprints revealed no significant differences between the treatments in band numbers on day 7 or 14 of the experiment (Table 4). Simpson's index of diversity and Dice's

Table 4. Effects of *L. fermentum* I5007 on the Microbial Communities in the Colon of Piglets as Indicated by the Number of Bands, Simpson's Index of Diversity, and Dice's Coefficient of Similarity, as Calculated from the DGGE[a]

items	control	*L. fermentum* I5007
	Day 7	
number of bands	12.33 ± 1.76	16.67 ± 2.33
Simpson's index of diversity	1.04 ± 0.06	1.47 ± 0.07
Dice's coeff of similarity	31.57 ± 6.67	38.47 ± 3.24
	Day 14	
number of bands	16.67 ± 0.67	17.33 ± 0.33
Simpson's index of diversity	1.19 ± 0.02 b	1.27 ± 0.01 a
Dice's coeff of similarity	43.67 ± 2.84 b	55.13 ± 1.54 a

[a]All data are means ± SEM. Means within the same row that have no common letters are significantly different ($p < 0.05$); $n = 6$.

coefficient of similarity were not different on day 7. In contrast, Simpson's index of diversity and Dice's coefficient of similarity were increased in piglets in the *L. fermentum* I5007 treatment compared with the control treatment on day 14 ($P < 0.05$ Table 4). The bands which differed between the two groups were excised from the gels and their species identified by sequence analysis. The sequences of excised DGGE bands are available in the EMBL database under accession numbers HF559182−HF559188. These are summarized in Table 5. On

Table 5. Clone Relatives to Sequences Retrieved from the DGGE bands of Colonic Digesta

band no.	closest relative in GenBank	% similarity
1	*Clostridium clostridioforme*	100
2	*Clostridium symbiosum*	100
3	*Clostridium sp.*	100
4	*Clostridium sp.*	100
5	uncultured *Clostridiales bacterium*	99
6, 8	*Latobacillus fermentum* I5007	100
7	uncultured bacterium	98

day 7, high individual variation was observed compared with the profile shown on day 14 and the microbial populations became more similar within groups over time. Different bands between two treatments on day 14 were excised from the profile, and a relative decrease of the *Clostridium*-like phenotype was observed in the *L. fermentum* I5007 group. The *L. fermentum* I5007 strain could only be detected in the *L. fermentum* I5007 group (99% indentity with pure *L. fermentum* I5007 strain) and was not present in control piglets on either day 7 or 14 (bands 6, 8, Figure 2).

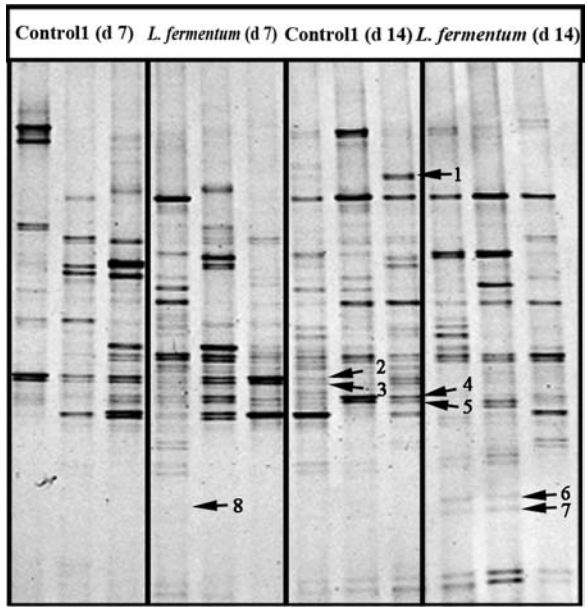

Figure 2. Bacterial diversity of the colonic microbiota of *L. fermentum* I5007 treated piglets and the control. DGGE fingerprints of PCR products of the V3 region of 16S rDNA from colonic digesta from piglets. Arrows (1 to 8) indicate excised bands that were different between the treated group and the control, followed by being reamplified (see Table 5); $n = 3$.

DISCUSSION

In the present study, neonatal piglets were selected as the model and the effects of *L. fermentum* I5007 were evaluated during a two-week intervention period. A significant increase in villous height in the jejunum was observed on day 14, indicating a certain rapid maturation of the intestines. The increase in villous height demonstrated improved architecture

dx.doi.org/10.1021/jf403288r | J. Agric. Food Chem. 2014, 62, 860−866

and active sites between the luminal digesta and the epithelium, which might result in an increased digestive and absorptive ability.[22] Siggers et al.[5] observed that a combination of probiotics supplemented into neonate formulas could increase the villous height. This result was also supported by the work conducted by Wang et al.,[12] which revealed that *L. fermentum* I5007 enhanced the level of mucosal proteins involved in energy metabolism, cell structure, and mobility in the jejunum in weaning piglets. The jejunum is the main organ for nutrient absorption, and therefore it is reasonable that the beneficial effects of *L. fermentum* I5007 could be mediated via improving the physiological structure of the jejunum. In the present study, lactase, maltase, and sucrase activities were not affected by *L. fermentum* I5007. Siggers et al.[5] also observed that a combination of probiotics supplemented into neonate formulas did not increase disaccharidase activities compared with the control. Our findings show that intervening with desirable microbes at an early age and shifting the microbiota toward a more beneficial composition is a good strategy to maintain a healthy gut and impact later succession of microbiota.[23,24]

To further illuminate whether the effects of *L. fermentum* I5007 were mediated through immune regulation, both pro-inflammatory and anti-inflammatory cytokine mRNA abundance were determined in ileum. IL-1β, mostly considered as a sensitive pro-inflammatory cytokine as the occurrence of host lesions,[25] was observed to have lower mRNA expression after 14 days of *L. fermentum* I5007 administration compared with piglets in the control group. However, myeloperoxidase, which has been considered related to inflammatory response, was not observed significantly different between the two treatments, which indicated that *L. fermentum* I5007 introduction did not irrigate disturbance in intestine. IL-10 is associated with T_{H2} cell or T_{reg} cell stimulation and usually is used as a marker for anti-inflammatory effects,[26] and it tended to be lower in the *L. fermentum* I5007 treatment, which was in accordance with the IL-1β expression, while IL-8 and TNF-α expression were not changed. Thus, the beneficial effects of exogenous strain of *L. fermentum* I5007 could be at least partly mediated via effects on immune modulation. In addition, our results were strengthened by some recent research related to the pathogen invasion in piglets that have been challenged.[27,28]

Short chain fatty acids are the major end products from the fermentation processes of gut microbiota in the large intestine and play an important role in the maintenance of colonic function such as improving barrier function, inhibiting adherence of pathogens, and contributing to energy utilization.[29−32] It is known that changes in the concentration and proportion of individual short chain fatty acids are consistent with changes in bacterial populations.[33−37] Our results showed that oral administration of *L. fermentum* I5007 not only increased the concentration of butyrate and the branched chain fatty acids but also decreased *Clostridium* strains accompanied by a lowered pH in the colonic digesta, which were consistent with the findings conducted by Hu et al.,[35] who found that increase in butyrate-producing bacteria or probiotics as *L. fermentum* can be related to the reduction of *Clostridiales sp*. Butyrate has been proved associated with positive effects on pathogen control and gut barrier function,[38,39] especially colonic energy utilization, cell proliferation in the gastrointestinal tract, and stabilization of the luminal pH in rodent animals.[36,38−41] Recently, via in vivo experiments, it also has been reported that butyrate is capable of reducing the incidence of *Clostridium spp.* and coliform induced opportunistic infection, and the reduction of these opportunistic putrefactive bacteria has been suspected of reducing the probability of pathophysiology disorders.[38,42] Thus, it is reasonable to assume that the growth performance and intestinal health were also improved via impact on intestinal metabolism. However, the exact role and its pathway of the branched chain fatty acids are still poorly understood.

The microbial ecosystem in the colon is complex and sophisticated.[33] *L. fermentum* I5007 administration increased Simpson's index of diversity measured using DGGE analysis. This revealed that the population got more complex and diverse by supplementation of the *L. fermentum* I5007 strain. A more diverse population could allow a more stable ecology when facing environmental disruptions.[43,44] This may be the potential reason for the low incidence of diarrhea in the *L. fermentum* I5007 treatment. In addition, the increase in Dice's coefficient of similarity within the *L. fermentum* I5007 treatment in the second week indicated that the microbial profile within this group tended to be more uniform. However, the whole profile revealed that administered *L. fermentum* I5007 could only make a minor change in the total microbial population. These findings were supported by the work conducted by Fuentes et al.[45] and Rauch and Lynch,[6] both of whom observed that administration of lactobacilli could shape the gastrointestinal niche and facilitate colonization by a diversity of beneficial bacterial species, but not alter the overall bacteria structure.

After *L. fermentum* I5007 was introduced, no statistical differences were observed between the two groups for any parameters measured during the first week. We speculated that it would take more than one week for the introduction of the exogenous strain to fully interact with the bacterial community for the newborn piglets. The development of the gut microbiota after intervention should be regarded as a gradual and complex process, not only as a succession in the ecological sense but influenced by microbial and host interactions, including strain adhesion, colonization, and proliferation as well as bacterial-host communication.[3,46] In addition, due to the immature gut in neonates, the intestinal environment may have undergone turbulence and high dynamics while establishing a new and steady profile. Here the results showed that the profiles were more uniform on day 14 compared with day 7, and the microbiota and concentrations of metabolic products in piglets in the *L. fermentum* I5007 treatment were significantly different from those in the control on day 14. Furthermore, *L. fermentum* I5007 was found in the treated group on days 7 and 14 in colonic digesta, which demonstrated that *L. fermentum* I5007 can tolerate the gastric acid and bile from the small intestine and inhabit the lower gastrointestinal tract. The above-mentioned findings suggest that *L. fermentum* I5007 exerts its function promptly after initial introduction, but the significant changes in microbial composition and metabolism were time dependent and occur during the following week.

In conclusion, our study indicated that after early introduction of *L. fermentum* I5007, the structure of the neonatal piglets' microbial composition and their metabolism as well as immune status could be manipulated, while promoting communities more resilient and putatively beneficial to gut homeostasis. The effects are exerted at an early stage following introduction, which suggests that *L. fermentum* I5007 could be used as a probiotic for application in the neonatal period in piglets. As for the limitations of the study, in our opinion, increased amount of experimental animals will help to reduce

the impact of individual differences among animals; in addition, further research will be performed to reveal the mechanism of *L. fermentum* I5007 favors on intestinal development.

AUTHOR INFORMATION

Corresponding Author

*Fax: (8610) 62733688. Phone: (8610) 62733588-1112. E-mail: maxi@cau.edu.cn.

Funding

This study was financially supported by the National Natural Science Foundation of China (No. 30930066), the National Basic Research Program of China (973 Program, No. 2012CB124702, 2013CB117302).

Notes

The authors declare no competing financial interest.

REFERENCES

(1) Fanaro, S.; Chierici, R.; Guerrini, P.; Vigi, V. Intestinal microflora in early infancy: composition and development. *Acta Paediatr.* **2003**, *92*, 48−55.

(2) Tiihonen, K.; Ouwehand, A. C.; Rautonen, N. Human intestinal microbiota and healthy ageing. *Ageing Res. Rev.* **2010**, *9*, 107−116.

(3) Mackie, R. I.; Sghir, A.; Gaskins, H. R. Developmental microbial ecology of the neonatal gastrointestinal tract. *Am. J. Clin. Nutr.* **1999**, *69*, 1035S−1045S.

(4) Bezkorovainy, A. Probiotics: determinants of survival and growth in the gut. *Am. J. Clin. Nutr.* **2001**, *73*, 399S−405S.

(5) Siggers, R. H.; Siggers, J.; Boye, M.; Thymann, T.; Molbak, L.; Leser, T.; Jensen, B. B.; Sangild, P. T. Early administration of probiotics alters bacterial colonization and limits diet-induced gut dysfunction and severity of necrotizing enterocolitis in preterm pigs. *J. Nutr.* **2008**, *138*, 1437−1444.

(6) Rauch, M.; Lynch, S. V. Probiotic manipulation of the gastrointestinal microbiota. *Gut Microbes* **2010**, *1*, 335−338.

(7) Livingston, M.; Loach, D.; Wilson, M.; Tannock, G. W.; Baird, M. Gut commensal *Lactobacillus reuteri* 100-23 stimulates an immunoregulatory response. *Immunol. Cell Biol.* **2009**, *88*, 99−102.

(8) Hoffmann, M.; Rath, E.; Hölzlwimmer, G.; Quintanilla-Martinez, L.; Loach, D.; Tannock, G.; Haller, D. *Lactobacillus reuteri* 100-23 transiently activates intestinal epithelial cells of mice that have a complex microbiota during early stages of colonization. *J. Nutr.* **2008**, *138*, 1684−1691.

(9) Schultz, M.; Linde, H. J.; Lehn, N.; Zimmermann, K.; Grossmann, J.; Falk, W.; Schölmerich, J. Immunomodulatory consequences of oral administration of *Lactobacillus rhamnosus* strain GG in healthy volunteers. *J. Dairy Res.* **2003**, *70*, 165−173.

(10) Wang, A.; Yu, H.; Gao, X.; Li, X.; Qiao, S. Influence of *Lactobacillus fermentum* I5007 on the intestinal and systemic immune responses of healthy and E. coli challenged piglets. *Antonie van Leeuwenhoek* **2009**, *96*, 89−98.

(11) Li, X.; Yue, L.; Guan, X.; Qiao, S. The adhesion of putative probiotic lactobacilli to cultured epithelial cells and porcine intestinal mucus. *J. Appl. Microbiol.* **2008**, *104*, 1082−1091.

(12) Ma, X.; He, P.; Sun, P.; Han, P. Lipoic acid: an immunomodulator that attenuates glycinin-induced anaphylactic reactions in a rat model. *J. Agric. Food Chem.* **2010**, *58*, 5086−5092.

(13) Snoeck, V.; Huyghebaert, N.; Cox, E.; Vermeire, A.; Saunders, J.; Remon, J. P.; Verschooten, F.; Goddeeris, B. Gastrointestinal transit time of nondisintegrating radio-opaque pellets in suckling and recently weaned piglets. *J. Controlled Release* **2004**, *94*, 143−153.

(14) Siggers, R. H.; Siggers, J.; Thymann, T.; Boye, M.; Sangild, P. T. Nutritional modulation of the gut microbiota and immune system in preterm neonates susceptible to necrotizing enterocolitis. *J. Nutr. Biochem.* **2011**, *22*, 511−521.

(15) Song, P.; Zhang, R.; Wang, X.; He, P.; Tan, L.; Ma, X. Dietary grape-seed procyanidins decreased post-weaning diarrhea by modulating intestinal permeability and suppressing oxidative stress in rats. *J. Agric. Food Chem.* **2011**, *59*, 6227−6232.

(16) Ye, L.; Tuo, W.; Liu, X.; Simister, N. E.; Zhu, X. Identification and characterization of an alternatively spliced variant of the MHC class I-related porcine neonatal Fc receptor for IgG. *Dev. Comp. Immunol.* **2008**, *32*, 966−979.

(17) Weber, T.; Ziemer, C.; Kerr, B. Effects of adding fibrous feedstuffs to the diet of young pigs on growth performance, intestinal cytokines, and circulating acute-phase proteins. *J. Anim. Sci.* **2008**, *86*, 871−881.

(18) Paulin, S. M.; Jagannathan, A.; Campbell, J.; Wallis, T. S.; Stevens, M. P. Net replication of Salmonella enterica serovars Typhimurium and Choleraesuis in porcine intestinal mucosa and nodes is associated with their differential virulence. *Infect. Immun.* **2007**, *75*, 3950−3960.

(19) Collado-Romero, M.; Arce, C.; Ramírez-Boo, M.; Carvajal, A.; Garrido, J. J. Quantitative analysis of the immune response upon *Salmonella typhimurium* infection along the porcine intestinal gut. *Vet. Res.* **2010**, *41*, 23.

(20) Franklin, M.; Mathew, A.; Vickers, J.; Clift, R. Characterization of microbial populations and volatile fatty acid concentrations in the jejunum, ileum, and cecum of pigs weaned at 17 vs 24 days of age. *J. Anim. Sci.* **2002**, *80*, 2904−2910.

(21) Muyzer, G.; De Waal, E. C.; Uitterlinden, A. G. Profiling of complex microbial populations by denaturing gradient gel electrophoresis analysis of polymerase chain reaction-amplified genes coding for 16S rRNA. *Appl. Environ. Microbiol.* **1993**, *59*, 695−700.

(22) Burrin, D. G.; Stoll, B.; Jiang, R.; Chang, X.; Hartmann, B.; Holst, J. J.; Greeley, G. H.; Reeds, P. J. Minimal enteral nutrient requirements for intestinal growth in neonatal piglets: how much is enough? *Am. J. Clin. Nutr.* **2000**, *71*, 1603−1610.

(23) Bennet, R.; Eriksson, M.; Nord, C.; Zetterström, R. Suppression of aerobic and anaerobic faecal flora in newborns receiving parenteral gentamicin and ampicillin. *Acta Paediatr.* **1982**, *71*, 559−562.

(24) Collins, M. D.; Gibson, G. R. Probiotics, prebiotics, and synbiotics: approaches for modulating the microbial ecology of the gut. *Am. J. Clin. Nutr.* **1999**, *69*, 1052S−1057S.

(25) Kabir, A.; Aiba, Y.; Takagi, A.; Kamiya, S.; Miwa, T.; Koga, Y. Prevention of *Helicobacter pylori* infection by lactobacilli in a gnotobiotic murine model. *Gut* **1997**, *41*, 49−55.

(26) Bron, P. A.; van Baarlen, P.; Kleerebezem, M. Emerging molecular insights into the interaction between probiotics and the host intestinal mucosa. *Nat. Rev. Microbiol.* **2012**, *10*, 66−90.

(27) Liu, P.; Piao, X.; Kim, S. W.; Wang, L.; Shen, Y.; Lee, H. S.; Li, S. Effects of chito-oligosaccharide supplementation on the growth performance, nutrient digestibility, intestinal morphology, and fecal shedding of Escherichia coli and Lactobacillus in weaning pigs. *J. Anim. Sci.* **2008**, *86*, 2609−2618.

(28) Li, J.; Li, D.; Xing, J.; Cheng, Z.; Lai, C. Effects of beta-glucan extracted from Saccharomyces cerevisiae on growth performance, and immunological and somatotropic responses of pigs challenged with Escherichia coli lipopolysaccharide. *J. Anim. Sci.* **2006**, *84*, 2374−2381.

(29) Bellier, R.; Gidenne, T. Consequences of reduced fibre intake on digestion, rate of passage and caecal microbial activity in the young rabbit. *Br. J. Nutr.* **1996**, *75*, 353−364.

(30) Walter, J.; Britton, R. A.; Roos, S. Host-microbial symbiosis in the vertebrate gastrointestinal tract and the Lactobacillus reuteri paradigm. *Proc. Natl. Acad. Sci. U.S.A.* **2011**, *108*, 4645−4652.

(31) Sakata, T.; Inagaki, A. Organic acid production in the large intestine: implication for epithelial cell proliferation and cell death. In *Gut Environment of Pigs*; Piva, A., Bach Knudsen, K. E., and Lindberg, J. E., Eds.; Nottingham University Press: Nottingham, 2001; pp 85−94.

(32) Galfi, P.; Bokori, J. Feeding trial in pigs with a diet containing sodium n-butyrate. *Acta Vet. Hung.* **1990**, *38*, 3−17.

(33) Martins dos Santos, V.; Müller, M.; De Vos, W. M. Systems biology of the gut: the interplay of food, microbiota and host at the mucosal interface. *Curr. Opin. Biotechnol.* **2010**, *21*, 539−550.

(34) Schwiertz, A.; Taras, D.; Schäfer, K.; Beijer, S.; Bos, N. A.; Donus, C.; Hardt, P. D. Microbiota and SCFA in lean and overweight healthy subjects. *Obesity* **2009**, *18*, 190−195.
(35) Maynard, C. L.; Elson, C. O.; Hatton, R. D.; Weaver, C. T. Reciprocal interactions of the intestinal microbiota and immune system. *Nature* **2012**, *489*, 231−241.
(36) Hu, J.-L.; Nie, S.-P.; Min, F.-F.; Xie, M.-Y. Polysaccharide from seeds of *Plantago asiatica* L. increases short-chain fatty acid production and fecal moisture along with lowering pH in mouse colon. *J. Agric. Food Chem.* **2012**, *60*, 11525−11532.
(37) Niemi, P.; Aura, A.-M.; Maukonen, J.; Smeds, A. I.; Mattila, I.; Niemela, K.; Tamminem, T.; Faulds, C. B.; Buchert, J.; Poutanen, K. Interactions of a lignin-rich fraction from brewer's spent grain with gut microbiota in vitro. *J. Agric. Food Chem.* **2013**, *61*, 4754−4762.
(38) Guilloteau, P.; Martin, L.; Eeckhaut, V.; Ducatelle, R.; Zabielski, R.; Van Immerseel, F. From the gut to the peripheral tissues: the multiple effects of butyrate. *Nutr. Res. Rev.* **2010**, *23*, 366−384.
(39) Raqib, R.; Sarker, P.; Bergman, P.; Ara, G.; Lindh, M.; Sack, D. A.; Islam, K. M. N.; Gudmundsson, G. H.; Andersson, J.; Agerberth, B. Improved outcome in shigellosis associated with butyrate induction of an endogenous peptide antibiotic. *Proc. Natl. Acad. Sci. U.S.A.* **2006**, *103*, 9178−9183.
(40) Roediger, W. Utilization of nutrients by isolated epithelial cells of the rat colon. *Gastroenterology* **1982**, *83*, 424−429.
(41) Inagaki, A.; Sakata, T. Dose-dependent stimulatory and inhibitory effects of luminal and serosal n-butyric acid on epithelial cell proliferation of pig distal colonic mucosa. *J. Nutr. Sci. Vitaminol.* **2005**, *51*, 156−160.
(42) Timbermont, L.; Lanckriet, A.; Dewulf, J.; Nollet, N.; Schwarzer, K.; Haesebrouck, F.; Ducatelle, R.; Van Immerseel, F. Control of Clostridium perfringens-induced necrotic enteritis in broilers by target-released butyric acid, fatty acids and essential oils. *Avian Pathol.* **2010**, *39*, 117−121.
(43) Hooper, L. V.; Macpherson, A. J. Immune adaptations that maintain homeostasis with the intestinal microbiota. *Nat. Rev. Immunol.* **2010**, *10*, 159−169.
(44) Shanahan, F. Probiotics in perspective. *Gastroenterology* **2010**, *139*, 1808−1812.
(45) Fuentes, S.; Egert, M.; Jiménez-Valera, M.; Ramos-Cormenzana, A.; Ruiz-Bravo, A.; Smidt, H.; Monteoliva-Sanchez, M. Administration of *Lactobacillus casei* and *Lactobacillus plantarum* affects the diversity of murine intestinal lactobacilli, but not the overall bacterial community structure. *Res. Microbiol.* **2008**, *159*, 237−243.
(46) Isolauri, E.; Sütas, Y.; Kankaanpää, P.; Arvilommi, H.; Salminen, S. Probiotics: effects on immunity. *Am. J. Clin. Nutr.* **2001**, *73*, 444S−450S.

termination process can involve combination reactions of the resulting free radicals including production of ether dimers.

Oleic acid (OA), a monounsaturated 18-carbon fatty acid, is the major ingredient of virgin olive oil or any other type of olive oil, and a free radical mechanism for thermal dimerization/oligomerization is very plausible when OA is the starting material. An example of a possible autoxidation mechanism is shown below, with an ether linkaged dimer (PM1) as an end product.

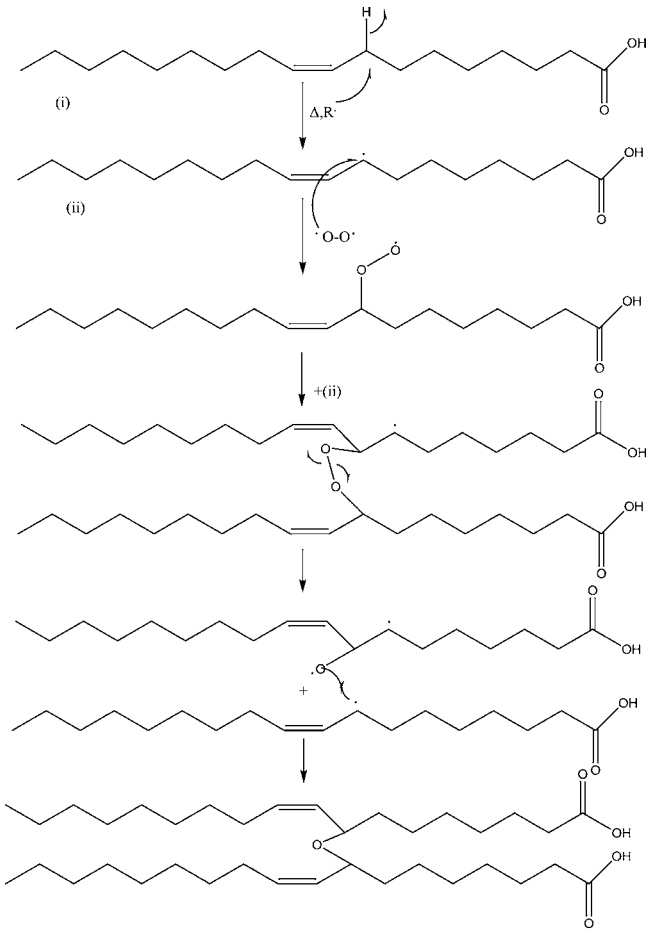

PM1

Many different structural isomers are possible as a result of head-to-head or head-to-tail alignment of the starting material, as well as many possible positional and geometrical isomers of the double bond.[10]

It has previously been shown that virgin olive oil becomes a strong hemagglutinin against human red blood cells when heated open in air. The dimer of oleic acid has been characterized as one of the major molecules responsible for the effect.[7,9] In this paper an effort is made to investigate if any other byproduct molecules, formed as a result of the virgin olive oil heating process, are associated with hemagglutination abilities and to characterize them structurally.

MATERIALS AND METHODS

Materials. HPLC grade solvents and fatty acids were obtained from Sigma (St. Louis, MO, USA). The lipid standards were obtained from Larodan Fine Chemicals (Malmo, Sweden).

Hemagglutination Assays. Human red blood cells (RBCs) were washed twice with 1 mM phosphate-buffered saline (0.85%)−0.01% sodium azide (pH 7.4). The hemagglutination assays were performed as previously discussed by Patrikios et al.[9] The plates were read at half-hour intervals by observing the bottoms of the wells. The first row of wells served as control. Hemagglutination activity was recognized as the settling of cells in contrast to flowing in the control wells. Titer is expressed as the highest dilution of test samples that still gives agglutination. Specific titer is defined as titer per milligram lipid per milliliter.

Thin-Layer Chromatography. Silica gel G plates (20 × 20 cm) (Macherey-Nagel, GmbH & Co., Germany) were prewashed in the developing solvent system (heptane/diethyl ether/acetic acid, 55:45:1, v/v/v) and activated by heating for 1 h at 120 °C under vacuum (15 mm). Sample (20−30 μg, 0.5 mg/mL in chloroform/methanol (1: 1 v/v)) was spotted onto silica gel plates using 2 mL Microcap pipets (Blaubrand, Germany). The plates were dried using a hand-dryer (cool setting) for 5 min before development. The chromatography chamber was saturated with solvent system vapor for 30 min before development of plates. The plates were developed until the solvent front was about 2 cm from the top, removed and air-dried for 30 min, and visualized in iodine vapor. For sample extraction from the plates the bands were visualized by a strip exposed to iodine. Each band was scraped off and eluted with chloroform/methanol (1:1 v/v).[11]

Heated Extra Virgin Olive Oil Preparation. Virgin olive oil was heated at 130 °C (an average cooking temperature) for 24 h in a metal heating block (USA/Scientific, Olala, FL, USA) in glass tubes open to air. Standard oleic (OA) and ricinoleic acid (RA) (Sigma) were also treated as above.

Preparation of Extra Virgin Olive Oil Dispersions. Dispersions were prepared by diluting the samples to 0.5 mg/mL PBS-N. The lipid extract dispersions were filtered through LC PVDF Acrodisc membranes (0.2 μm, Gelman) to remove particulate matter.

Table 1. R_f Values of the Components of OA, RA, and Virgin Olive Oil, Unheated and Heated (24 h at 130 °C), on Silica Gel TLC Plates in Isooctane/Isopropyl Alcohol/Acetic Acid (95:5:1, v/v/v)

	R_f values of components[a]			
item	monomer	dimer	trimer	specific activity[b]
OA	0.52			0
heated OA	0.87[c]			0
		0.30		2.3×10^3
		0.28		7.3×10^2
		0.26		
			0.18	1.0×10^4
RA	0.62			0
heated RA	0.92			0
		0.33		1.2×10^2
		0.24		7.2×10^2
			0.17	1.0×10^3
virgin olive oil	0.65			0
heated virgin olive oil	0.65			0
		0.31		7.5×10^2
		0.25		7.3×10^2
			0.19	1.0×10^3

[a]Identification of the components of the fractions was by comparison with R_f values of the components of standard commercial monomer, linear dimer, and trimer (Emery). [b]The concentration was approximately 0.5 mg/mL. Specific titer is defined as titer per mg lipid per mL. [c]The R_f value of the heated OA monomer differs from the R_f value of the nonheated OA monomer because the molecular structure is affected during heating at 130 °C for 24 h (mostly at the double-bond position in the fatty acid chain), probably due to formation of positional and/or geometrical isomers.

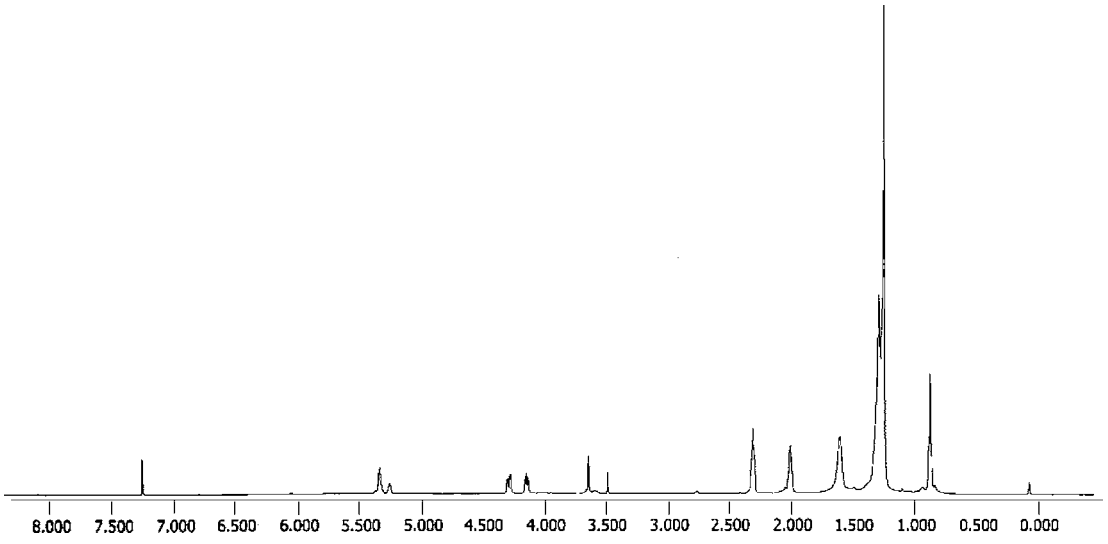

Figure 1. ^{1}H NMR spectrum of virgin olive oil sample heated at 130 °C for 24 h open in air and esterified with CH_2N_2. The ester was obtained in $CDCl_3$ solvent at ambient temperature using an INOVA Varian 600 MHz spectrometer.

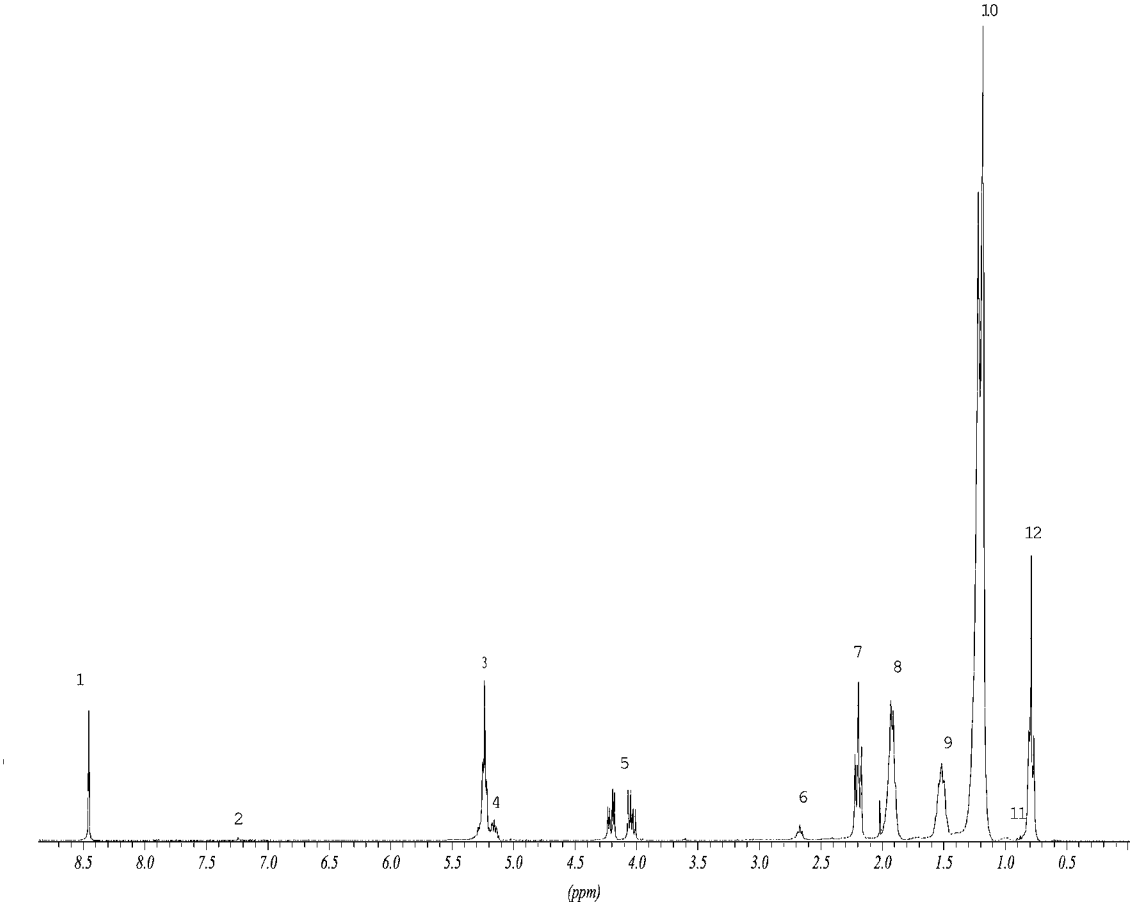

Figure 2. ^{1}H NMR spectrum of refined virgin olive oil in $CDCl_3$ solvent. The spectrum was obtained at ambient temperature using a Bruker 300 MHz spectrometer.

Synthesis of Fatty Acid Methyl Esters. The methyl esters were prepared according to a standard protocol.[9]

Light Microscopy. A Cytovision Analyzer (Applied Image Co) was used for photographs, attached to a microscope (Zeiss Axioskop). Agglutinated cells were taken from microtiter plates that were titered and allowed to develop for approximately 30 min. The following preparations were used: (1) untreated human RBCs; (2) active lipid extract from heated virgin olive oil (1 mg/mL); (3) unheated virgin olive oil preparations (1 mg/mL). All samples were dissolved in PBS-N. Fresh human RBCs were washed once with citrate because the cells retain their shape much better in citrate than in PBS and, therefore, allow better photographs to be taken. It should be noted that cells washed in citrate will maintain their integrity for only approximately 2 h.

Nuclear Magnetic Resonance Spectroscopy. $CDCl_3$ (99.5%) ampules were purchased from Merck (Darmstadt, Germany) and ultraprecision NMR tubes from Peypin (France) and Wilmad 535-5 mm

dx.doi.org/10.1021/jf403745x | J. Agric. Food Chem. 2014, 62, 867−874

Table 2. ^{1}H NMR Chemical Shifts of Virgin Olive Oil in $CDCl_3$ Solvent

peak	δ	proton	assignment
1	8.45	pyrazine	
2	7.27	$CHCl_3$	
3	5.29	CH═CH	all unsaturated fatty acids
4	5.15	CHOCOR	glycerol (triacylglycerols)
5	4.19	CH_2OCOR	glycerol (triacylglycerols)
6	2.76	CH═CHCH_2CH═CH	linoleyl and linolenyl
7	2.2	CH_2COOH	all acyl chains
8	2.02	CH_2CH═CH	all unsaturated fatty acids
9	1.6	CH_2CH_2COOH	all acyl chains
10	1.2	$(CH_2)_n$	all acyl chains
11	0.95	$CH_2CH_2CH_2CH_3$	linolenyl
12	0.85	CH═CHCH_2CH_3	all acids except linolenyl

(Spintec-Rototec). The high-resolution spectra in $CDCl_3$ were obtained using Bruker 300 AC and Varian INOVA 600 instruments. All data were collected using pulse sequences and phase cycling routines provided in the Bruker and Varian libraries of pulse programs. ^{1}H NMR spectra in the Bruker instrument were recorded using the following acquisition parameters: pulse width (PW), 3.0 μs; spectral width (SW), 2513 Hz; data size (TD), 32K; recycling delay (RD), 1.0 s; number of transients (NS), 16; and digital resolution, 0.076 Hz pt^{-1}. DQF-COSY and ^{1}H−^{13}C HSQC spectra experiments were performed with gradients at 600 MHz. The ^{1}H sweep width was 9820 at 600 MHz. Typically homonuclear proton spectra were acquired with 4096 data points in t_2, 16−64 scans, 256−512 complex points in t_1, and relaxation delay of 1−1.5 s. Data were processed and analyzed with the v-NMR software package from Varian. Spectra were zero-filled two times and apodized with a square sine-bell function shifted by $\pi/2$ in both dimensions. The ^{1}H−^{13}C HSQC spectrum was recorded with 1024 data points in t_2, 16 scans per increment, 128 complex points in t_1, and a relaxation delay of 1 s. The ^{13}C spectral width was 20000 Hz.

Mass Spectrometry. Mass spectra were obtained with a TSQ 7000 Finnigan MAT spectrometer using electron spin ionization (ESI) and spray voltage (4.5 kV). The sheath gas pressure (N_2) during the experiment was 35 psi and the capillary temperature, 200 °C. Samples were dissolved in a mixture of $CH_3OH/CHCl_3$.

RESULTS AND DISCUSSION

The approach by which oils and foodstuffs in general are manufactured, processed, cooked, and used affects their nutritional value and safety.

Many studies in the literature have discussed the oxidation products of olive oil. In 2002 Patrikios and in 2003 Patrikios et al. reported the hemaglutinating properties of oxidation and thermal degradation products of lipid extracts isolated from heat-processed foodstuffs including virgin olive oil.[8,9] In the present study we focused on the molecular structure of another possible specific molecule that is possibly formed in the virgin olive oils under the above conditions and which promotes hemagglutinating activity with human RBCs.

Thin-layer chromatography on silica gel, in a system that discriminates by the number of carboxyl groups (free fatty acids are released from glycerol after the sample heating preparation process), was used to resolve the components of the heated virgin olive oil (Table 1). Bands were cut out, eluted, and titered against human RBCs. The identification of the components of the fraction was carried out by comparison with R_f values of the components of a heated sample of oleic acid, ricinoleic acid (RA), and standard commercial monomer, dimer and trimer (Emery). A portion of byproducts in the heated virgin olive oil sample showed the same R_f values as the corresponding R_f values of the monomeric, oligomeric, and polymeric byproducts of the heated sample of OA, RA, and the commercial oligomers. As reported by Patrikios, this might be the result of hydrolysis, which can take place under heat processing in air, of the triacylglycerols,

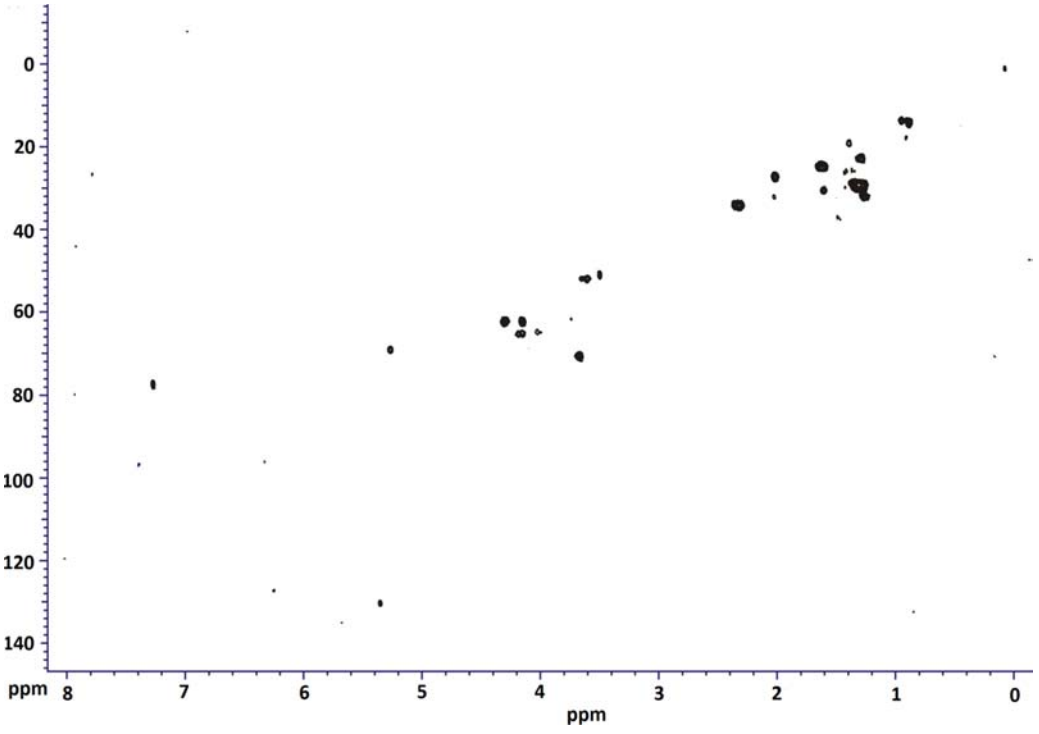

Figure 3. 2D NMR spectrum of HSQC virgin oil sample heated at 130 °C for 24 h open in air and esterified with CH_2N_2. The ester was obtained in $CDCl_3$ solvent at ambient temperature using an INOVA Varian 600 MHz.

dx.doi.org/10.1021/jf403745x | J. Agric. Food Chem. 2014, 62, 867−874

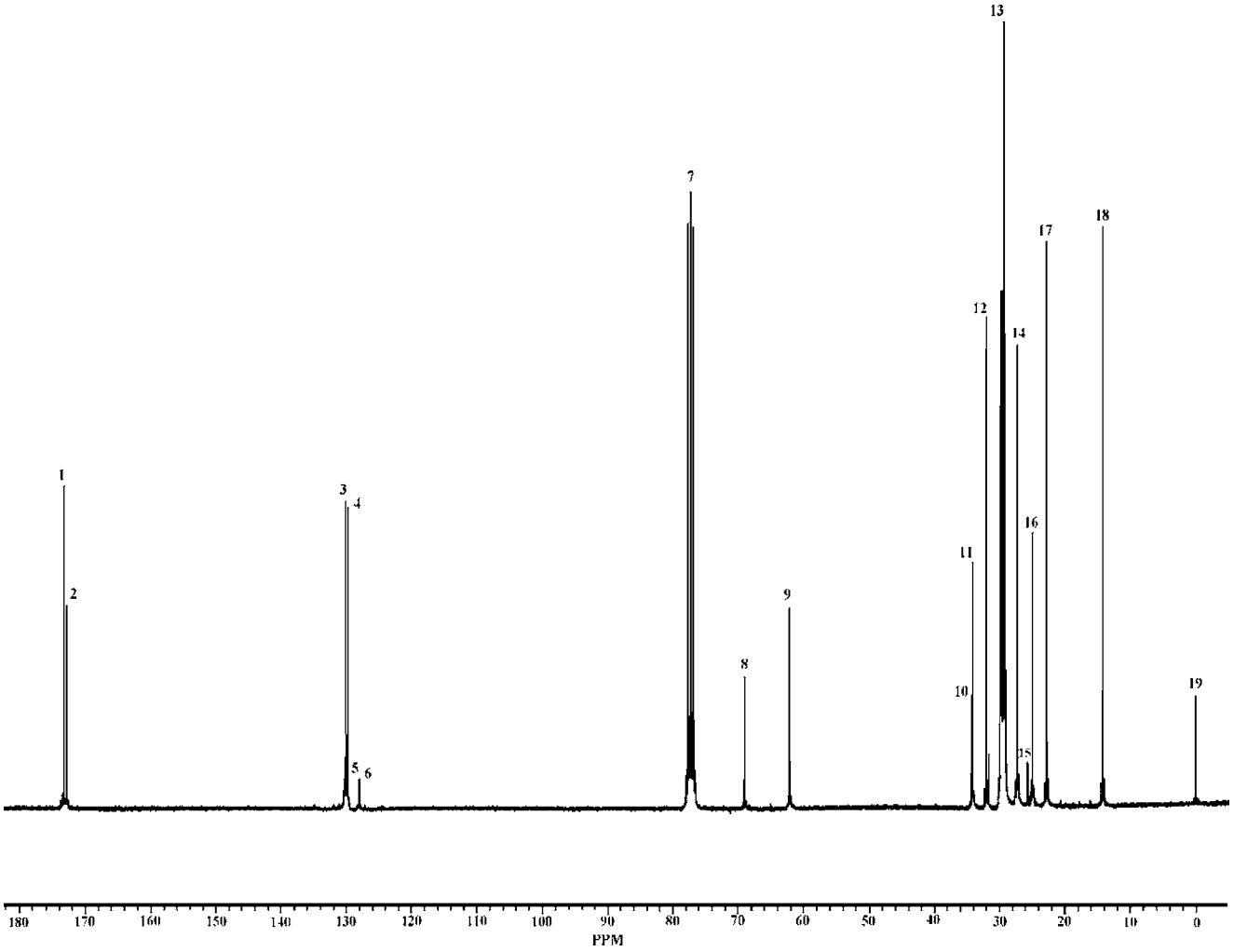

Figure 4. ^{13}C NMR spectrum of virgin olive oil in $CDCl_3$ solvent. The spectrum was obtained at ambient temperature using a Bruker 300 MHz spectrometer.

Table 3. ^{13} C NMR Chemical Shifts of Virgin Olive Oil in $CDCl_3$ Solvent

peak	δ	carbon	compound
1	173.26	C-1, sn-1,3	triacylglycerols
2	172.81	C-1, sn-2	triacylglycerols
3	129.98	C-10	oleyl
4	129.67	C-9	oleyl
5	128.06	C-10	linoleyl
6	127.86	C-12	linoleyl
7	77.01	$CDCl_3$	solvent
8	68.92	CHO−, sn-2	triacylglycerols
9	62.18	CH_2O−, sn-1,3	triacylglycerols
10	34.18	C-2, sn-2	all acyl chains
11	34.02	C-2, sn-1,3	all acyl chains
12	31.88	ω3	saturated, n-9 and n-6 acids
13	29.1−29.8	$(CH_2)_n$	all acyl chains
14	27.16	allylic: C-8−C-11 oleyl, C-8−C-14 linoleyl	
15	25.81	diallylic: C-11 linoleyl, C-11−C-14 linolenyl	
16	24.84	C-3	all acyl chains
17	22.65	ω2	all acyl chains
18	14.15	ω1 ($-CH_3$)	all acyl chains
19	0	TMS	

releasing oleic acid, which after free radical formation and oxidation can result in dimerization, oligomerization, and polymerization.[9] The TLC shows two spots with slightly different R_f values for dimers. One of the dimer molecules with

dx.doi.org/10.1021/jf403745x | J. Agric. Food Chem. 2014, 62, 867−874

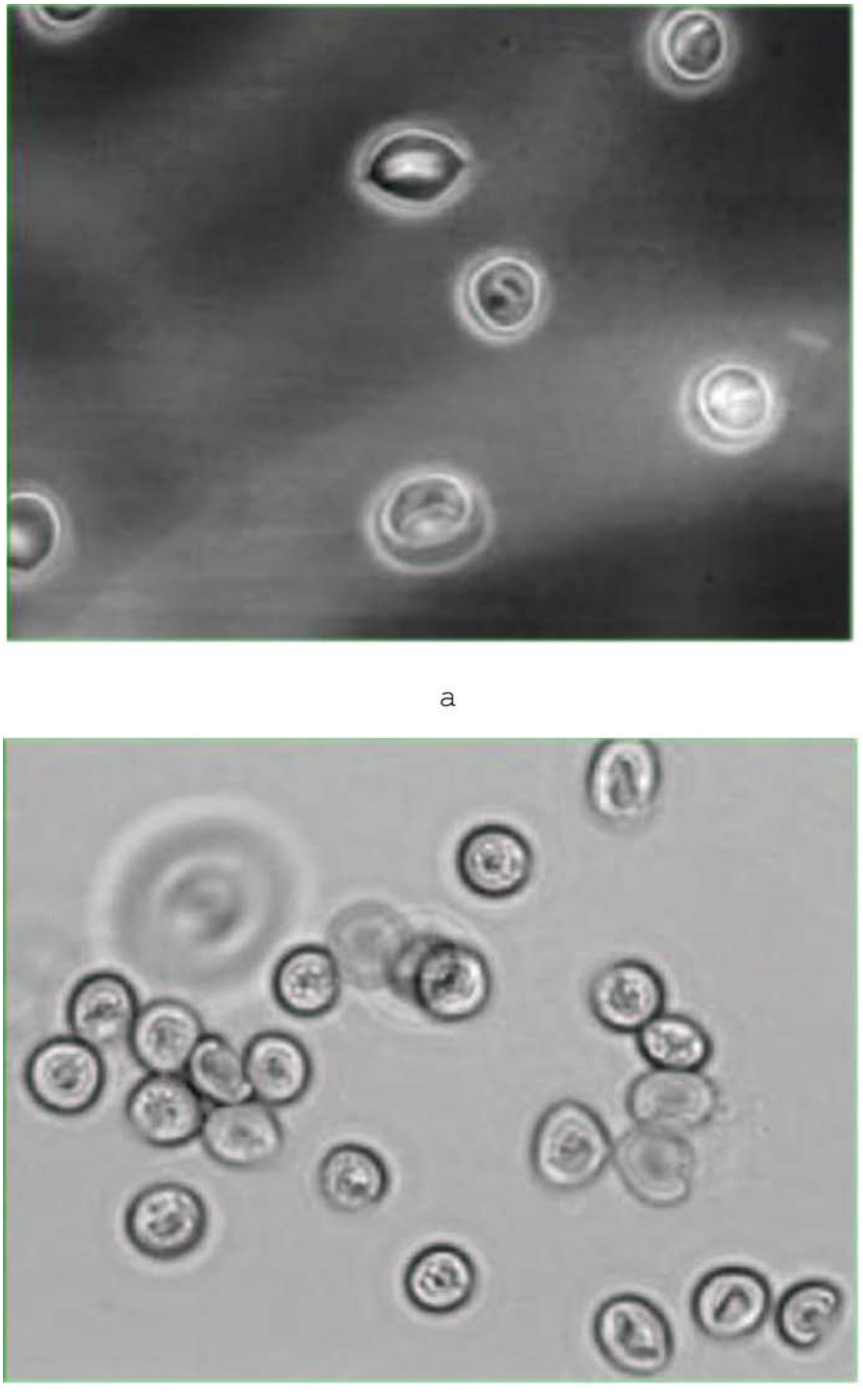

Figure 5. Light micrographs of human erythrocytes in citrate buffer (pH 7.4): (a) with unheated virgin olive oil; (b) with the isolated virgin olive oil oligomer preparation (1.0 mg/mL).

R_f 0.31 was characterized by Patrikos et al. as a linear dimer of oleic acid (dioleyl), dimerized by −C−C− linkage.[9] This dimer was shown to be associated with strong hemagglutinating properties against human RBCs. The second dimer formed with R_f 0.25 is now characterized as an ether-linked unsaturated dimer and is also shown to be associated with hemagglutinating properties against human RBC.

A spot with about the same R_f is observed when commercial RA was treated under the same conditions (Table 1). The ^{1}H NMR spectrum of the compound is shown in Figure 1. To characterize it, several ^{1}H NMR spectra from virgin olive oil samples originated from different countries were obtained. A representative one is shown in Figure 2. The sample was run in $CDCl_3$ and using a known amount of pyrazine in case a

dx.doi.org/10.1021/jf403745x | J. Agric. Food Chem. 2014, 62, 867−874

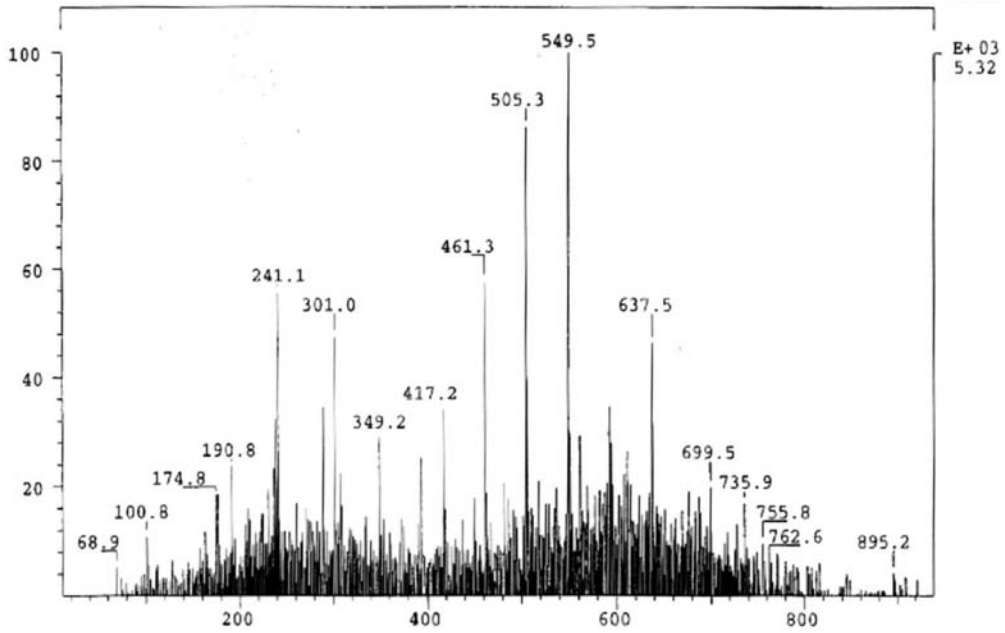

Figure 6. MS spectrum of virgin olive oil sample heated at 130 °C for 24 h open in air and esterified with CH_2N_2. The MS spectrum was obtained using a TSQ 7000 Finnigan MAT spectrometer and electron spin ionization with spray voltage (4.5 kV).

Table 4. Major Mass Spectrum (MS) Peaks (m/e) and Their Interpretation

peak m/e	interpretation
637.5	the ether dimer has an m/e 606 the sample was dissolved in $CH_3OH/CHCl_3$ CH_3OH has an m/e 32 606 + 32 = **638**
549.5	$2[CH_3C{=}OH]^+ = 44 \times 2 = 88$ 637.5 − 88 = **549.5**
505.5	$[CH_3C{=}OH]^+ = 44$ 549.5 − 44 = **505.5**
461.3	$[CH_3C{=}OH]^+ = 44$ 505.5 − 44 = **461.5**
417.2	$[CH_3C{=}OH]^+ = 44$ 461.3 − 44 = **417.3**

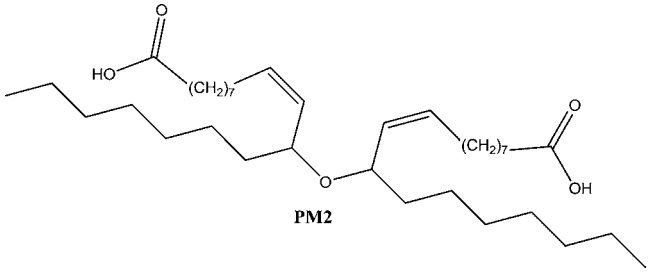

PM2

quantitative result was necessary. This method was developed in two previous publications by Mavromoustakos et al.[12,13]

As can be observed in the representative spectrum shown in Figure 2, the peaks are almost identical with those reported by Sacchi et al. and are shown in Table 2.[14] All olive oils analyzed were missing the peaks in the region of 3.5−3.7 ppm observed for the sample under investigation. We made an effort to characterize these peaks. First, we have drawn several plausible structures and used NMR databases to simulate the spectrum. A compound that gave a ^{1}H NMR spectrum similar to the experimental was PM2 (esterified).

The peak at 3.5 ppm corresponds to a methoxy group, whereas the peak at 3.65−3.7 ppm corresponds to C<u>H</u>−O−CH. HSQC experiment is in agreement with this assignment. C−H correlation between the two critical peaks at the region of 3.5−3.7 ppm and the corresponding peaks centered at 50 ppm were observed in HSQC spectrum (Figure 3). ^{13}C NMR spectra of virgin olive oils are lacking peaks in the region of 50 ppm (Figure 4 and Table 3), in agreement with data obtained by Sacchi.[14] The 2D COSY spectrum showed a correlation between the assigned peaks as C<u>H</u>−O−C<u>H</u> with C<u>H$_2$</u> as expected.

Panels a and b of Figure 5 show human RBCs that were mixed with unheated virgin olive oil and with the isolated oligomer preparation, respectively. As seen in Figure 5b, mixtures of chains and rosettes were observed by light microscopy (LM), but no lysis or fusion was apparent. Agglutination was found to involve cell clumping and to be time-dependent. The agglutination activity, which we observed, most likely is due to a partial insertion of the dimer/oligomer formed into red cell membrane in a way that links red cell without affecting membrane dynamics and permeability properties.

ESI mass spectroscopy of the oligomer isolated from the heated sample of virgin olive oil after methylation suggests the possible existence of the proposed dimer, an acyclic "hydro" dimer that contains two *cis* and/or *trans* double bonds and ether linkages at the 8, 9, 10, and 11 carbons between two aliphatic (hydrocarbon) chains. The interpretations of all major peaks in the Figure 6 mass spectrum are shown in Table 4. In particular, the peak at 637.5 has a molecular weight very close to that of PM1 + CH_3OH (CH_3OH was used as a dilution solvent along with $CHCl_3$). The peak at 549.5 is 88 units smaller and may correspond to a dimer without two positively charged ions of m/e 88 $2[CH_3C{=}OH]^+$. Interestingly, the most intense peaks observed in the spectrum differ from the ones with higher m/e by 44.

dx.doi.org/10.1021/jf403745x | J. Agric. Food Chem. 2014, 62, 867−874

We concluded that virgin olive oil can undergo oligomerization through free radical mechanism of the oleic acid and autoxidation when heated at 130 °C for 24 h open in air. Subsequently, dioleyl or oligomers are formed by a direct linkage of the accumulated free radicals or by an intermediated peroxy radical formation (through autoxidation reaction).[7] Thus, when virgin olive oil is consistently heated open in air it can possibly undergo nutritional damage with a possible direct but as yet unknown effect on human health.

AUTHOR INFORMATION

Corresponding Author

*(I.S.P.) Mail: School of Medicine, European University Cyprus, 6 Diogenes Street, 2404 Engomi, P.O. Box 22006, 1516 Nicosia, Cyprus. Phone: 00-357-99097856. E-mail: i.patrikios@euc.ac.cy.

Author Contributions

Both authors interpreted the data. I.S.P. drafted the report tables and figures, and all authors critically revised and approved the final version. I.S.P. was responsible for the laboratory experiments, and T.M. was responsible for the NMR and GC-MS experiments. Both I.S.P. and T.M. performed the literature search, and both contributed to the structural elucidation of the active molecule and the rationale of the involved biochemical mechanisms. Both authors vouch for the accuracy and completeness of the data, and both authors read and approved the final manuscript.

Funding

This work was supported by a grant from the Research Promotion Foundation of Cyprus, RPF 06/99.

Notes

The authors declare no competing financial interest.

ACKNOWLEDGMENTS

We thank the Cyprus Institute of Neurology and Genetics for hosting the project. We also acknowledge E. Siapi for obtaining MS spectrum and Simona Golic Grdadolnik, who obtained some of NMR spectra. We especially thank Elsa Tsartsidou for her contribution in the preparation of the tables.

REFERENCES

(1) Frankel, E. N. Lipid oxidation. *Prog. Lipid Res.* **1980**, *19*, 1−22.
(2) Conroy, N. H. Polymerization of unsaturated fatty acids. U.S. Patent 3,632,822, 1969.
(3) Cowan, J. C. Dimer acids. *J. Am. Oil Chem. Soc.* **1962**, *39*, 534−545.
(4) Leonard, E. C. Dimer acids. In *Kirk-Othmer: Encyclopedia of Chemical Technology*, 3rd ed.; Wiley Interscience: Hoboken, NJ, USA, 1979; pp 768−782.
(5) Leonard, E. C. *The Dimer Acids*; Hunko Sheffield Chemical: Memphis, TN, USA, 1975; pp 1−112.
(6) Myers, L. D.; Goebel, C. G.; Barrett, F. O. Process for polymerizing unsaturated fatty acids. U.S. Patent 3,076,003, 1960.
(7) Patrikios, I. S.; Britton, O'N.; Bing, D. K.; Russell, C. S. Heating unsaturated fatty acids in air produces hemagglutinins. *Biochim. Biophys. Acta* **1994**, *1212*, 225−234.
(8) Patrikios, I. S. Lipid extracts isolated from heat processed food show a strong agglutinating activity against human red blood cells. *Food Res. Int.* **2002**, *35* (6), 535−540.
(9) Patrikios, I. S.; Patsalis, P. C. Monounsaturaded fatty acid oligomerization is responsible for the agglutination activity of heated virgin olive oil. *Food Res. Int.* **2003**, *36*, 480−489.
(10) McMahon, D. H.; Crowell, E. P. Characterization of products from clay-catalyzed polymerization of tall oil fatty acids. *J. Am. Oil Chem. Soc.* **1974**, *51*, 522−527.
(11) Kates, M. *Techniques in Lipidology*; North Holland/American Elsevier: New York, 1986.
(12) Mavromoustakos, T.; Zervou, M.; Theodoropoulou, E.; Panagiotopoulos, D.; Bonas, G.; Day, M.; Helmis, A. ^{13}C NMR analysis of the triacylglycerol composition of Greek virgin olive oils. *Magn. Reson. Chem.* **1997**, *35*, S3−S7.
(13) Mavromoustakos, T.; Zervou, M.; Bonas, G.; Kolocouris, A.; Petrakis, P. A. Novel analytical method to detect adulteration of virgin olive oil by other oils. *J. Am. Oil. Chem. Soc.* **2000**, *77* (4), 405−411.
(14) Sacchi, R.; Addeo, F.; Paolillo, L. ^{1}H and ^{13}C NMR of virgin olive oil. An overview. *Magn. Reson. Chem.* **1997**, *35*, S1333−S145.

The mammalian target of rapamycin (mTOR) is one of the major growth regulatory pathways controlled by AMPK. The mTOR pathway plays a major role in proliferation, angiogenesis, and metastasis of NSCLC and other cancers. The target on mTOR signaling pathways is extensively investigated for cancer chemotherapy including NSCLC.[10] Moreover, AMPK controlled lipid metabolism at transcriptional and post-translational levels. AMPK phosphorylates and inactivates metabolic enzyme acetyl-CoA carboxylase (ACC) that is involved in regulating de novo biosynthesis of fatty acid and cholesterol. Phosphorylated ACC led to the decrease of malonyl-CoA levels, thus stimulating mitochondrial carnitine palmitoyltransferase 1 (CPT1) and promoting fatty acid oxidation. Moreover, AMPK inhibits transcription factor SREBP1c, which controls the entire fatty acid synthetic pathway or directly inhibits the expression of fatty acid synthase (FASN).[11]

Rhododendron formosanum Hemsl. (Ericaceae) is an evergreen broad-leafed tree native to Taiwan and ubiquitously distributed from 800 to 2000 m. The vegetation exhibits a unique pattern and forms pure dominant vegetation.[12,13] We studied whether *R. formosanum* exhibited pharmacological activities for NSCLC and investigated its bioactive phytochemical constituents. Our results indicated that treatment of NSCLC cells with *R. formosanum* had a very potent inhibitory effect on cellular growth.

MATERIALS AND METHODS

Materials. The leaves of *R. formosanum* were collected after flowering in April 2010 and July 2010 at the Dasyueshan site (24°14′6.49″ N, 120°57′7.29″ E at 1911 m asl). Ursolic acid, oleanolic acid, betulinic acid, 4′,6-diamidino-2-phenylindole (DAPI), 3-[4,5-dimethylthylthiazol-2-yl]-2,5-diphenyltetrazolium (MTT), and propidium iodide (PI) were purchased from Sigma Chemical Co. (St. Louis, MO, USA). The antibody for LKB1 was purchased from Santa Cruz Biotechnology (Santa Cruz, CA, USA). Primary antibody against phospho-AMPK (Thr 172), AMPK, Bcl-2, Bax, caspase-9, caspase-3, FASN, phospho-ACC (Ser 79), mTOR, phospho-mTOR (Ser 2448), and phospho-p70S6k (Thr 389) were purchased from Cell Signaling Technology (Beverly, MA, USA). β-Actin antibody was purchased from Sigma Chemical Co. HRP-conjugated goat anti-rabbit IgG and goat anti-mouse IgG were obtained from Millipore (Billerica, MA, USA). Methanol (MeOH), *n*-hexane, dichloromethane (DCM), *n*-butanol (BuOH), and ethyl acetate (EA) were purchased form Seedchem Co. (Melbourne, Australia). Silica gel 60 was purchased from Merck KGaA (Darmstadt, Germany).

Plant Collection, Chemical Extraction, and Isolation. The leaves of *R. formosanum* were air-dried for chemical analysis. The air-dried and powdered leaves of *R. formosanum* (5.5 kg) were extracted with MeOH for 3 days at room temperature (three times), and the combined extracts were concentrated in vacuo (under 35 °C) to obtain a dark green gum (1540 g), which was suspended in H_2O and partitioned sequentially with DCM, EA, and BuOH. The EA extract (3.5 g) was subjected to column chromatography on silica gel using *n*-hexane, *n*-hexane−EA, and EA−MeOH mixtures of increasing polarity for elution to furnish 10 fractions.

Quantification of Ursolic Acid, Oleanolic Acid, and Betulinic Acid in RFL-EA-2 and RFL-EA-3 Fractions. The EA fractions of *R. formosanum* were prepared at concentration of 1 mg/mL in MeOH. The samples were passed through 0.22 μm filters (Millipore) and placed in sample vials for liquid chromatography (LC) analysis. LC mass analysis for the quantification of betulinic acid, oleanolic acid, and ursolic acid was carried out with an Atlantis T3 RP-18 column (150 × 2.1 mm; 3 μm; Waters, Milford, MA, USA). In each case the injection volume was 5 mL. The column was eluted with buffer A (distilled water/acetonitrile/formic acid; 95/5/0.1, v/v/v) and buffer B (acetonitrile/formic acid; 100/0.1, v/v) at a flow rate of 0.25 mL/min at 25 °C. The column was eluted initially with 100% buffer A, followed by a linear increase in buffer B to 30% from 0 to 5 min, and maintained in 30% buffer B for another 5 min. From 10 to 20 min, a linear increase in buffer B to 80% was carried out, and the column was maintained in 80% buffer B for another 10 min. The column was further eluted with a linear increase in buffer B to 95% from 30 to 40 min. The column was finally equilibrated with buffer A for 10 min. Quantification of the triterpenoids in EA fraction was performed in the ion monitoring mode selected. Both positive and negative ionization mode MS analyses were undertaken. The molecular ion peaks and mass spectra recorded were compared to those of reference substances. Analysis was carried out using data-dependent MS/MS scanning from m/z 100 to 1000. The temperature of the ion source was maintained at 100 °C, the dry temperature was 365 °C, and the desolvation gas, N_2, had a flow rate of 12 L/min. Product ion scans for mass were performed by low-energy collision (20 eV) using argon as the collision gas. All liquid chromatography−electrospray ionization−tandem mass spectrometry (LC-ESI-MS/MS) data were processed by Bruker Daltonics data analysis software (version 4.0). All chemicals were prepared at a concentration range of 0.01−1000 μg/mL. Quantification of triterpenoids was performed with the selected ion monitoring (SIM) mode. The separated $[M - H]^-$ ion chromatogram was selected at m/z 455 for the specific parent ion of triterpenoids. The linearity of the calibration curves was demonstrated by the good determination of coefficients (r^2) obtained for the regression line. Good linearity was achieved over the calibration range, with all coefficients of correlation >0.995. All samples were freshly prepared. The mean values for the regression equation were $y = 6 \times 10^7x + 1 \times 10^7$ ($r^2 = 0.9997$) for betulinic acid, $y = 552577x + 5 \times 10^7$ ($r^2 = 0.9983$) for oleanolic acid, and $y = 353895x + 3 \times 10^7$ ($r^2 = 0.9985$) for ursolic acid. The limits of quantification (LOQ) and determination (LOD), defined as signal-to-noise ratios of 3:1 and 10:1, were in the ranges 0.01−0.1 and 0.1 mg/mL, respectively.

Cell Lines and Cell Culture. Both A549 cells (human lung adenocarcinoma cell line) and H460 cells (human non-small-cell lung cancer cell line) were used in the study and were acquired from the American Type Culture Collection. A549 cells were cultured in DMEM (Invitrogen, Carlsbad, CA, USA), and H460 cells were cultured in RPMI-1640 (Invitrogen) supplemented with 10% fetal bovine serum (FBS, 10%) (Invitrogen), streptomycin (100 μg/mL), and penicillin (100 IU/mL) (Invitrogen) in a humidified incubator at 37 °C with 5% CO_2.

Cell Viability Assay. To measure the cell viability, A549 cells or H460 cells were incubated on the 96-well cell culture cluster (1×10^4 cells/well). MTT stock solution was prepared at a conentration of 5 mg/mL in PBS, and working solution (500 μg/mL) was diluted from stock solution. The medium was removed from each well, and 100 μL of MTT working solution was added for 1 h at 37 °C. When the crystals had formed, the solution was removed and 80 μL of DMSO was aded to dissolve the crystals. Finally, OD 570 nm was used to detect the absorbance by the ELISA reader. MTT assay was done as described previously.[14]

Western Blot Analysis. Cells (2×10^6) were seeded onto the 10 cm cell culture dish overnight and treated with ursolic acid (30 μM) for 0, 12, 24, and 48 h. After treatment, cells were collected in a 1.5 mL eppendorf and lysed in the lysis buffer (0.1% SDS, 1% NP-40, 10 g/mL leupeptin, 1% sodium deoxycholate, 1 mM PMSF, 10 mM Tris-HCl, pH 7.5, 150 mM NaCl, and 10 g/mL aprotinin). Each protein sample was extracted and quantified by using a Bio-Rad protein assay kit, and each group took 50 μg of total proteins to run SDS-PAGE, following transfer to the PVDF membrane. Western Blot was done as described previously.[15] The results were analyzed and quantified by using Image J software.

Cell Cycle and Apoptosis Analysis. A549 cells (5×10^5) were cultured in a 6 cm cell culture dish for 24 h and then treated with ursolic acid (10−30 μM) for 24 and 48 h. After treatment, cells were harvested in a 15 mL tube, washed with PBS, resuspended in PBS, and fixed in 2 mL of 70% ethanol at 20 °C overnight. The cell cycle state and apoptosis was determined by using PI staining as reported previously.[15]

Fluorescence Microscopy. After treatment with ursolic acid (30 μM) for 48 h, A549 cells were fixed by 70% ethanol at −4 °C for 6 h or overnight. Cells were stained with DAPI (1 μg/mL DAPI, 0.1% Triton X-100) at room temperature for 15 min. The morphology of cell nuclei

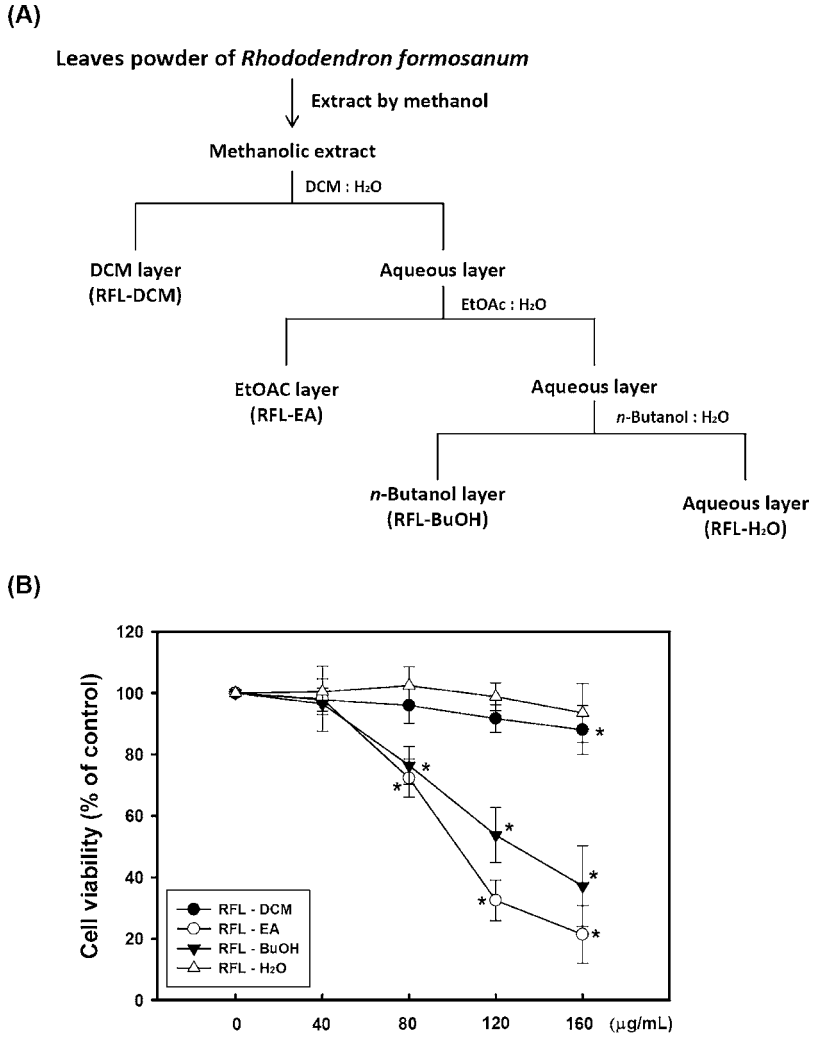

Figure 1. Antiproliferation activities of different fractions from *R. formosanum*. (A) Leaf powder of *R. formosanum* was extracted by methanol and partitioned into four fractions including dichloromethane, ethyl acetate, *n*-butanol, and water to get RFL-DCM, RFL-EA, RFL-BuOH, and RFL-H_2O fractions. (B) A549 cells were treated with the four fractions (40−160 μg/mL) for 24 h. Cell viability was then determined using the MTT assay. This experiment was repeated three times. The data represent the mean ± SD. Values were significantly different from the control group: ∗, $P < 0.05$.

was observed by Nikon TE2000-U fluorescence microscope at 400× magnification. Fluorescence microscopy was done as described previously.[16]

RNA Interference Suppression of LKB1. A549 cells were transfected with LKB1 small interfering RNA (siRNA) using siRNA transfection reagent (Santa Cruz Biotechnology) and incubated for 6 h. The LKB1 siRNA was obtained from Santa Cruz Biotechnology (sc-25816).

Statistical Analysis. Data were presented as the mean ± SD of at least three independent experiments. For statistical analysis, the independent Student's *t* test was used to compare the continuous variables between two groups, and the chi-squared test was applied for comparison of the dichotomous variables. An asterisk indicates that the values were significantly different from the control (∗, $P < 0.05$).

RESULTS

***R. formosanum* Induced NSCLC A549 Cell Growth Inhibition.** To evaluate the bioactive phytochemical constituents of *R. formosanum*, we extracted with methanol and separated the methanol extract into dichloromethane (RFL-DCM), ethyl acetate (RFL-EA), *n*-butanol (RFL-BuOH), and water (RFL-H_2O) fractions (Figure 1A). We next examined the antiproliferative activity of *R. formosanum* extracts on NSCLC A549 cells. Among these *R. formosanum* extracts, RFL-EA was the most effective in our assay (Figure 1B). Further fractionation of the RFL-EA by column chromatography was used to analyze the detailed bioactive phytochemical constituents (Figure 2A). Our study demonstrated that fractions 2 and 3 from the RFL-EA extract (RFL-EA-2, RFL-EA-3) possessed the strongest antiproliferative activity against A549 cells (Figure 2B). The morphology variations of *R. formosanum*-treated A549 cells were investigated by microscopic inspection. After treatment with different concentrations of RFL-EA-2 or RFL-EA-3 for 48 h, apoptotic bodies were observed in A549 cells (Figure 2C). These results may provide a rationale for the potential use of *R. formosanum* against NSCLC.

Comparative Study of the Phytochemical Constituents of RFL-EA-2 and RFL-EA-3. The HPLC fingerprint chromatogram was established to analyze the detailed phytochemical constituents of RFL-EA-2 and RFL-EA-3. Figure 3A shows the HPLC fingerprint chromatogram for the mixture of ursolic acid, oleanolic acid, and betulinic acid. As shown in Figure 3B, RFL-EA-3 contains ursolic acid, oleanolic acid, and betulinic acid. Interestingly, our results revealed that ursolic acid was the most abundant constituent in RFL-EA-2 and RFL-EA-3 (Table 1).

dx.doi.org/10.1021/jf404243p | J. Agric. Food Chem. 2014, 62, 875−884

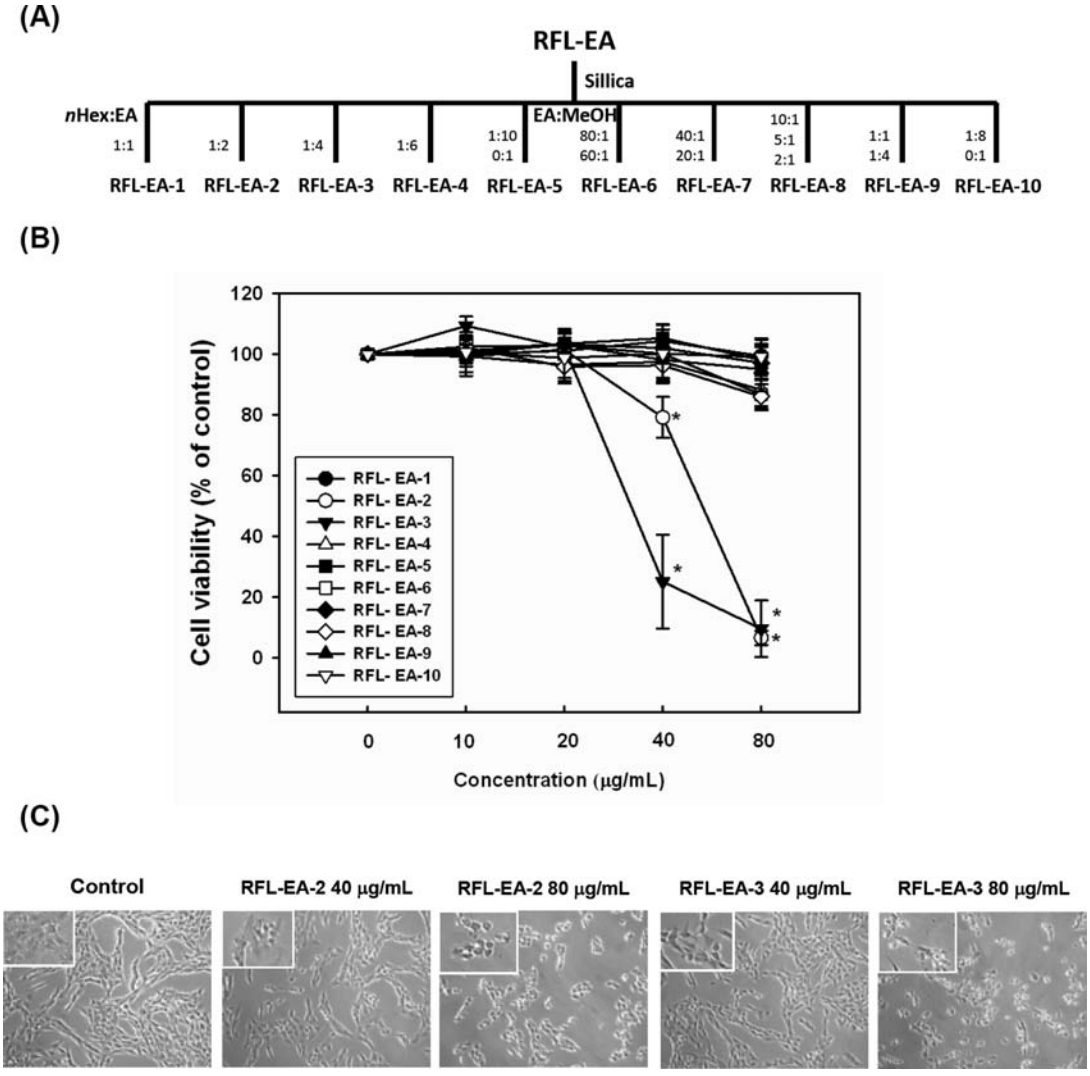

Figure 2. Antiproliferation activities of different RFL-EA fractions against NSCLC A549 cells. (A) RFL-EA was injected into a silica column and eluted with *n*-hexane, ethyl actate, and methanol at different combination rates to get 10 fractions. (B) A549 cells were treated with the 10 fractions (10−80 μg/mL) for 24 h. Cell viability was then determined using the MTT assay. This experiment was repeated three times. The data represent the mean ± SD. Values were significantly different from the control group: ∗, $P < 0.05$. (C) A549 cells were treated with RFL-EA-2 (40−80 μg/mL) and RFL-EA-3 (40−80 μg/mL) for 24 h, and cell morphology was observed by photomicroscope.

Effect of Oleanolic Acid, Ursolic Acid, and Betulinic Acid on NSCLC Cell Proliferation. The potential antiproliferative activities of oleanolic acid, ursolic acid, and betulinic acid were evaluated using the MTT assay. A549 and H460 cells were treated with various concentrations of ursolic acid (Figure 4A), oleanolic acid (Figure 4B), and betulinic acid (Figure 4C) for 24 and 48 h. Among these constituents, ursolic acid and betulinic acid exhibited potent cytotoxic effects on NSCLC cells (Figure 4). Because ursolic acid was the most abundant constituent and exhibited potent cytotoxic effects, we chose ursolic acid for the subsequent experiments.

Ursolic Acid Induces NSCLC Cell Apoptosis. To test whether ursolic acid could induce apoptosis, apoptosis and morphology variations were investigated by microscopic inspection. After treatment with different concentrations of ursolic acid for 48 h, apoptotic bodies were observed in A549 cells (Figure 5A). We next elucidated whether ursolic acid induced chromatin condensation in A549 cells. After 30 μM ursolic acid treatment, chromatin condensation was seen in A549 cells, as evidenced by staining with DAPI (Figure 5B). To further confirm ursolic acid-induced A549 cell apoptosis, flow cytometric analysis was performed. After treatment with various concentrations of ursolic acid for 24 and 48 h, A549 cells underwent apoptosis (Figure 5C). Apoptosis-related modulators were studied by Western blot analysis. Treatment with 30 μM ursolic acid increased the cleavages of caspase-3 and caspase-9 (Figure 5D). Moreover, there was a marked increase of pro-apoptotic protein Bax and a marked decrease of anti-apoptotic protein Bcl-2 in ursolic acid-treated A549 cells (Figure 5E). These results indicated that ursolic acid induced apoptosis in NSCLC cells.

Ursolic Acid Decreases Protein Synthesis via the Up-regulation of AMPK Activity in NSCLC Cells. Abnormalities in the AMPK function have emerged as an important pathway implicated in cancer development.[9] We examined whether ursolic acid was involved in the regulation of AMPK. Figure 6A indicates that ursolic acid stimulated AMPK phosphorylation in a time-dependent manner, whereas AMPK activation resulted in marked inhibition of mTOR and p70S6K in a time-dependent manner (Figure 6B). Our studies suggest that the phosphor-

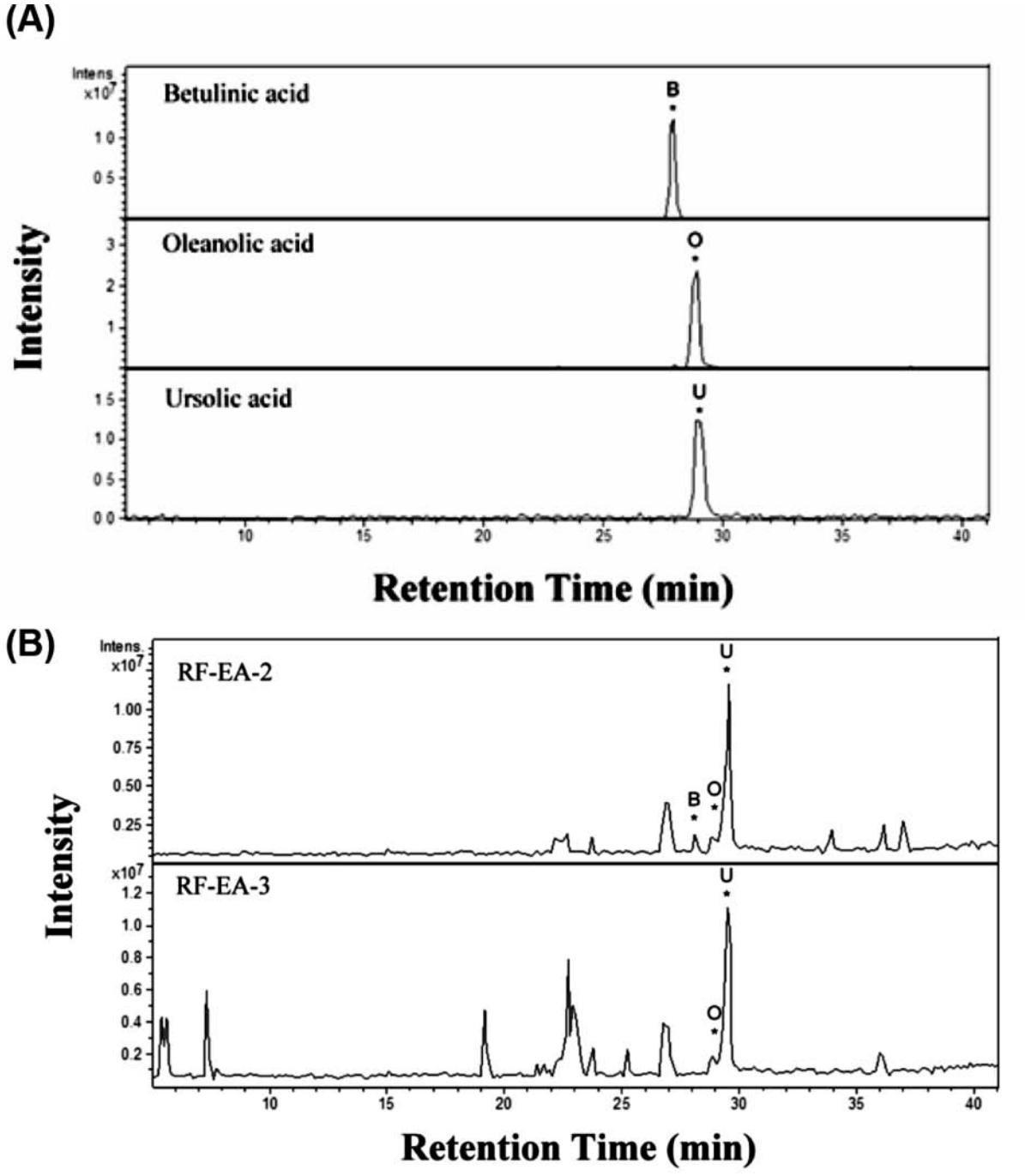

Figure 3. Quantification of triterpenoids by LC-ESI-MS/MS analysis. (A) Individual standard triterpenoids including betulinic acid (B), oleanolic acid (O), and ursolic acid (U) were subjected to LC-ESI-MS/MS analysis for chemical identification and quantification. Panel B shows quantification of the betulinic acid, oleanolic acid, and ursolic acid from RFL-EA-2 and RFL-EA-3 fractions.

Table 1. Concentration of Betulinic, Oleanolic, and Ursolic Acid in the Fractions RF-EA-2 and RF-EA-3

	concentration (μg/mg)	
	RF-EA-2	RF-EA-3
betulinic acid	0.37	<0.1
oleanolic acid	2.55	1.88
ursolic acid	550.2	528.2

ylation of AMPK is required for ursolic acid to decrease protein synthesis in NSCLC cells.

Ursolic Acid Inhibits Lipogenesis through Activation of AMPK in NSCLC Cells. AMPK negatively regulated the activities of lipogenic enzymes FASN and ACC. We next examined reduction of FASN expression and ACC activity in ursolic acid-treated A549 cells. Our result indicated that ursolic acid decreased the expression of FASN and increased ACC phosphorylation in a time-dependent manner (Figure 6C). Our results suggested that ursolic acid suppressed lipogenesis through modulation of AMPK activity.

Ursolic Acid Induces AMPK Phosphorylation via an LKB1-Dependent Pathway. The canonical target of LKB1 is AMPK.[6] To further investigate whether ursolic acid induced

dx.doi.org/10.1021/jf404243p | J. Agric. Food Chem. 2014, 62, 875−884

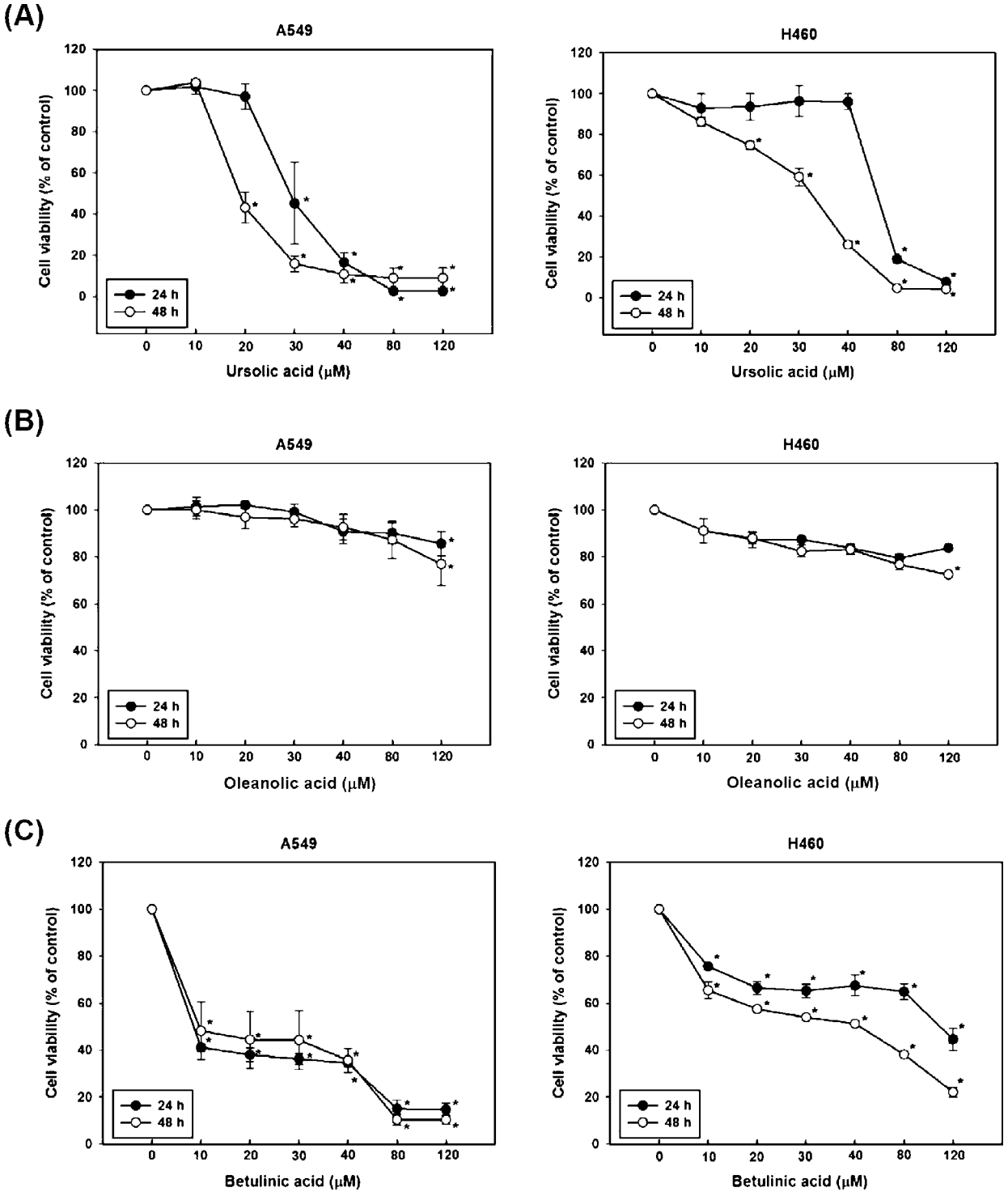

Figure 4. Antiproliferation effect of ursolic acid, oleanolic acid, and betulinic acid against NSCLC cells. A549 cells and H460 cells were treated with (A) ursolic acid, (B) oleanolic acid, and (C) betulinic acid at concentrations of 10−160 μM for 24 or 48 h. Cell viability was then determined using the MTT assay. This experiment was repeated three times. The data represent the mean ± SD. Values were significantly different from the control group: ∗, $P < 0.05$.

AMPK phosphorylation via an LKB1-dependent pathway, LKB1 siRNA was used to inhibit LKB1 expression in A549 cells. After treatment with ursolic acid, an increasing level of phosphorylated AMPK was observed; however, under LKB1 siRNA transfection, despite the addition of ursolic acid, AMPK phosphorylation was reduced (Figure 6D). Our results showed that the activation of AMPK by ursolic acid treatment might occur via an LKB1-dependent pathway.

DISCUSSION

The present study has clearly evaluated the bioactive constituents of *R. formosanum* and investigated the antiproliferative activity on NSCLC. We extracted *R. formosanum* with dichloromethane

dx.doi.org/10.1021/jf404243p | J. Agric. Food Chem. 2014, 62, 875−884

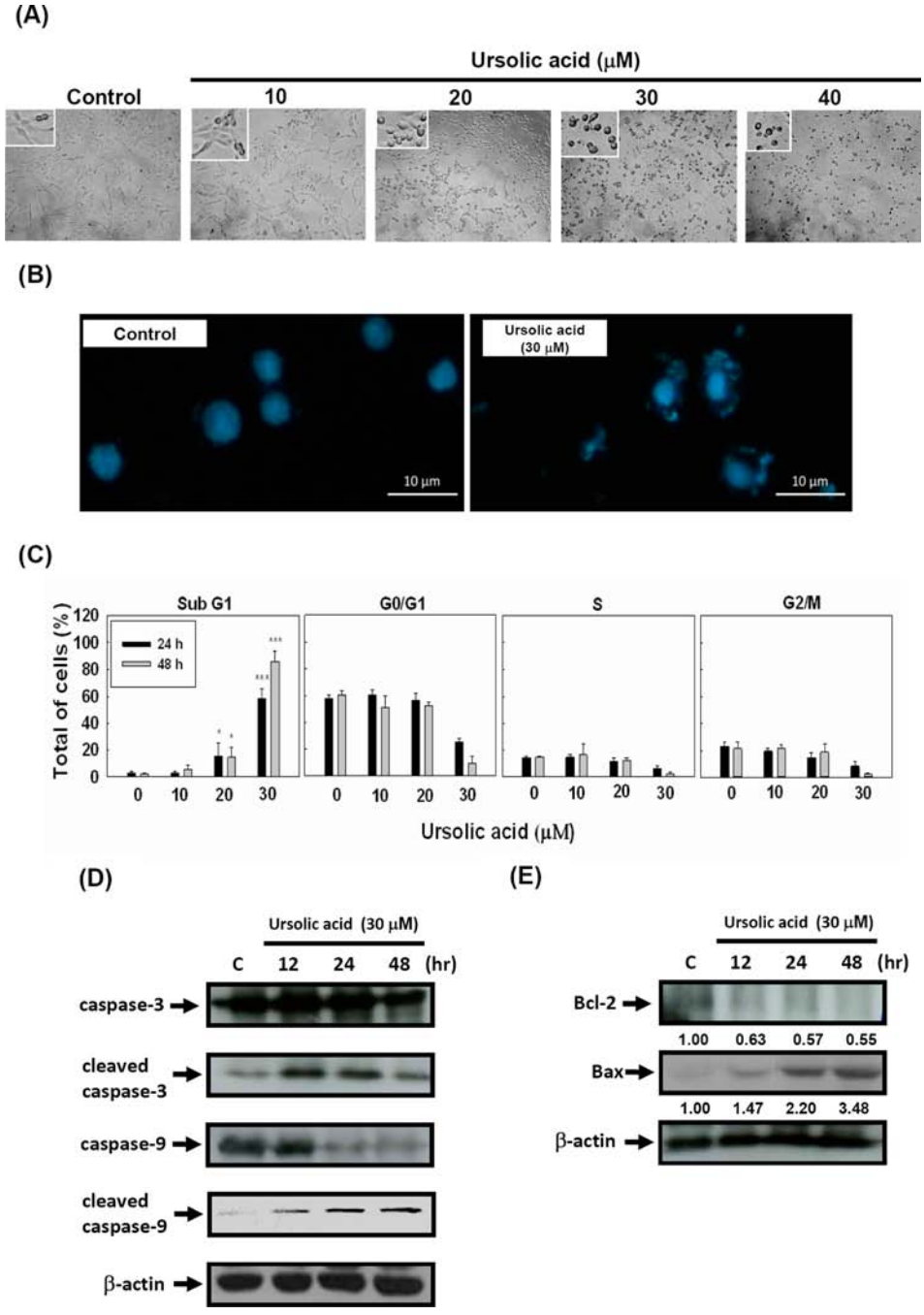

Figure 5. Ursolic acid induced A549 cell apoptosis. (A) A549 cells were incubated with ursolic acid (10−40 μM) for 24 h, and morphology was observed by photomicroscope; (B) the morphology of cell nuclei was observed by fluorescence microscope. (C) To observe cell cycle statements and apoptosis levels, cell were stained with PI and measured by flow cytometry. (D) A549 cells were treated with ursolic acid (30 μM) for the indicated time. Cells were then harvested and lysed for the detection of caspase-3, cleaved caspase-3, caspase-9, cleaved caspase-9, and β-actin. (E) A549 cells were treated with ursolic acid (30 μM) for the indicated times. Cells were then harvested and lysed for the detection of Bcl-2, Bax, and β-actin. Western blot data presented are representative of those obtained in at least three separate experiments. The values below the figures represent change in protein expression of the bands normalized to β-actin.

(RFL-DCM), ethyl acetate (RFL-EA), *n*-butanol (RFL-BuOH), and water (RFL-H_2O). RFL-EA possesses the most effective bioactivity in our cell viability assay. Moreover, our study also demonstrated that fractions 2 and 3 from the RFL-EA extract (RFL-EA-2, RFL-EA-3) showed the greatest antiproliferative effect on NSCLC cells. In our previous study, 18 known compounds were isolated from the 6 fractions obtained by column chromatography from the methanolic extract of *R. formosanum* leaves.[13] In this study, the major components of RFL-EA-2 and RFL-EA-3 were ursolic acid, oleanolic acid, and betulinic acid. Among the three constituents, ursolic acid was the most abundant compound in RFL-EA-2 and RFL-EA-3. Interestingly, our results also revealed that ursolic acid possessed the most efficient antiproliferative effect on NSCLC cells.

Ursolic acid is a natural pentacyclic triterpene acid, which exists in elder flower, apples, lavender, peppermint rosemary, basil, bilberries, cranberries, thyme, oregano, hawthorn, prunes, and medicinal herbs. Because ursolic acid is relatively nontoxic,

dx.doi.org/10.1021/jf404243p | J. Agric. Food Chem. 2014, 62, 875−884

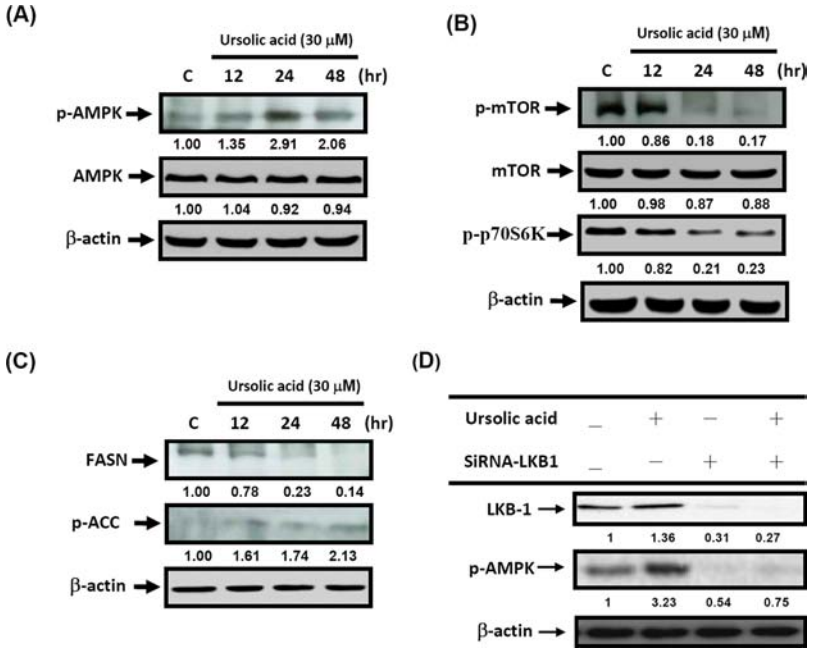

Figure 6. Ursolic acid decreases general mRNA translation and the activity of fatty acid synthesis via activation of AMPK. (A) A549 cells were treated with ursolic acid (30 μM) for the indicated times. Cells were then harvested and lysed for the detection of phosphorylated AMPK (Thr 172), AMPK, and β-actin. (B) A549 cells were treated with ursolic acid (30 μM) for the indicated times. Cells were then harvested and lysed for the detection of phosphorylated mTOR (Ser 2448), mTOR, phosphorylated p70S6K, and β-actin. (C) A549 cells were treated with ursolic acid (30 μM) for the indicated times. Cells were then harvested and lysed for the detection of FASN, phospho-ACC (Ser79), and β-actin. (D) A549 cells were transfected with 50 nmol/L LKB1-siRNA using Oligofectamine. A total of 24 h after transfection, cells were treated with ursolic acid (30 μM) for 24 h. After harvesting, cells were lysed and prepared for Western blotting analysis using antibodies against LKB-1, phosphorylated AMPK (Thr 172), and β-actin. Western blot data presented are representative of those obtained in at least three separate experiments. The values below the figures represent change in protein expression of the bands normalized to β-actin.

there is a growing interest in the elucidation of the pharmacological activities. Several papers reported that ursolic acid has many health benefits including hepatoprotective, anti-inflammatory, and anticancer effects.[17−19] Ursolic acid possesses strong anticancer activity against several cancers of the prostate,[20] breast,[21] lung,[22] pancreas,[23] ovary,[24] colon,[25] and bladder.[26] In the present study, we focused on the antineoplastic effect of ursolic acid on NSCLC cells. These findings suggested that ursolic acid is a potent anticancer agent.

Induction of cell apoptosis is thought to be the principal mechanism by which anticancer drugs kill cells. Ursolic acid has been reported to induce apoptosis through calcium-dependent activation of sphingomyelinase.[27,28] To confirm whether the cytotoxic effect of ursolic acid was due to apoptosis in NSCLC cells, phenotypic characteristics, cell cycle analysis, and Western blotting were used in the present study. Our results indicate that ursolic acid induced cleavages of caspase-9 and caspase-3 and also attenuated the expression of Bcl-2, indicating that ursolic acid induced apoptosis via a caspase-dependent pathway. The Bcl-2 family of proteins plays a crucial role in the mitochondrial pathway of apoptosis. The ratio between Bcl-2 and Bax proteins has been suggested as a primary event in determining the sensitivity to the mitochondrial pathway of apoptosis. Bax translocation to the mitochondria and insertion into the membrane induces cytochrome *c* and other apoptogenic factor release that subsequently activates caspase-3, leading to downstream apoptotic responses.[29] From the above results, we suggest that the enhancement of Bax and the attenuation of Bcl-2 a might be the important molecular pathway that is involved in ursolic acid-induced apoptosis in A549 cells.

Recent studies have focused on the potential of targeting cellular metabolic pathways that may be altered during NSCLC tumorigenesis and progression. AMPK has recently been considered as a critical energy-sensing serine/threonine kinase in the regulation of cellular metabolism. The activation of AMPK switches on catabolic pathways that generate ATP while switching off ATP-consuming processes. Recently, our group and others have reported that sustained AMPK activation inhibits cancer cell growth and proliferation and induces cancer cell apoptosis.[15,30] These findings are given that cancer cell DNA replication, mitosis, cell growth, and proliferation are all ATP-consuming processes. In this study, ursolic acid induced growth inhibition and apoptosis in NSCLC A549 cells, and activation of AMPK may contribute to the process. Similarly, Zheng et al. suggested that activation of AMPK by ursolic acid contributes to growth inhibition and apoptosis in human bladder cancer T24 cells.[31] Son et al. reported that ursolic acid induced apoptosis in HepG2 cells via AMPK activation and GSK3β phosphorylation.[32] Lee et al. found that ursolic acid potentiated cell cycle arrest and UVR-induced apoptosis in skin melanoma cells via AMPK activation.[33] These studies are consistent with our findings here that AMPK activation by ursolic acid induced A549 cell apoptosis. However, how AMPK activation induces A549 cell apoptosis needs further study. Our study provides evidence that ursolic acid may be a potential cancer chemopreventive agent for NSCLC, and AMPK might be the key mechanism for its action.

Targeting the mTOR pathway may lead to the development of novel drugs for cancers. Many laboratories and pharmaceutical companies have focused intensely on developing approaches to block the mTOR pathway. particularly due to the fact that the

mTOR pathway plays such a crucial role in cancer biology. The intervention of some target proteins will lower mTOR activity; for example, activation of AMPK results in decreased mTOR signaling and, in turn, inhibition of protein synthesis and cellular growth.[14,15,34] The present data show that ursolic acid inhibits protein synthesis via the AMPK−mTOR pathway.

In conclusion, *R. formosanum* is an endemic species distributed widely in Taiwan. The pharmacological activities of *R. formosanum* have not yet been fully explained. To the best of our knowledge, the antineoplastic activity of *R. formosanum* has not been explored in previous studies. In this study, we have investigated the chemical constituents and antineoplastic activity of *R. formosanum* against NSCLC cells. On the basis of these studies, it is tempting to propose that *R. formosanum* could be developed as an antineoplastic agent for NSCLC.

AUTHOR INFORMATION

Corresponding Author

*(C.-H.C.) Mail: Academia Sinica, Chair Professor and Director, Research Center for Biodiversity and Graduate Institute of Ecology and Evolutionary Biology, Room 720, 7F, Lifu Hall, China Medical University, 91 Hsueh-Shih Road, Taichung 40402, Taiwan. E-mail: choumasa@mail.cmu.edu.tw. Phone: +886-4-2205-3366, ext. 1633. Fax: +886-4-2207-1500.

Funding

This study was financially supported by grants from the National Science Council of Taiwan (NSC101-2811-B-039-013, NSC101-2621-B-039-001, NSC102-2313-B-039-001, and NSC102-2811-B-039-005) to C.-H.C.

Notes

The authors declare no competing financial interest.

ACKNOWLEDGMENTS

Technical assistance with chemical data analyses from the Instrument Analysis Centers at the China Medical University and National Chung Hsing University is greatly appreciated.

ABBREVIATIONS USED

ACC, acetyl-CoA carboxylase; AMPK, AMP-activated protein kinase; BuOH, *n*-butanol; DAPI, 4′,6-diamidino-2-phenylindole; DCM, dichloromethane; DR, death receptor; EA, ethyl acetate; FASN, fatty acid synthase; FBS, fetal bovine serum; LC, liquid chromatography; MeOH, methanol; mTOR, mammalian target of rapamycin; MTT, 3-(4,5-dimethylthiazol-2-yl)-2,5-diphenyltetrazolium bromide; NSCLC, non-small-cell lung carcinoma; PI, propidium iodide; PS, phosphatidylserine

REFERENCES

(1) Siegel, R.; Naishadham, D.; Jemal, A. Cancer statistics 2012. *CA Cancer J. Clin.* **2012**, *62*, 10−29.

(2) Askoxylakis, V.; Thieke, C.; Pleger, S. T.; Most, P.; Tanner, J.; Lindel, K.; Katus, H. A.; Debus, J.; Bischof, M. Long-term survival of cancer patients compared to heart failure and stroke: a systematic review. *BMC Cancer* **2010**, *10*, 105.

(3) Green, D. R.; Reed, J. C. Mitochondria and apoptosis. *Science* **1998**, *281*, 1309−1312.

(4) Riedl, S. J.; Salvesen, G. S. The apoptosome: signalling platform of cell death. *Nat. Rev. Mol. Cell Biol.* **2007**, *8*, 405−413.

(5) Carretero, J.; Medina, P. P.; Pio, R.; Montuenga, L. M.; Sanchez-Cespedes, M. Novel and natural knockout lung cancer cell lines for the LKB1/STK11 tumor suppressor gene. *Oncogene* **2004**, *23*, 4037−4040.

(6) Mu, J.; Brozinick, J. T., Jr.; Valladares, O.; Bucan, M.; Birnbaum, M. J. A role for AMP-activated protein kinase in contractionand hypoxia-regulated glucose transport in skeletal muscle. *Mol. Cell* **2001**, *7*, 1085−1094.

(7) Hardie, D. G. AMP-activated protein kinase: a cellular energy sensor with a key role in metabolic disorders and in cancer. *Biochem. Soc. Trans.* **2011**, *39*, 1−13.

(8) Hadad, S. M.; Baker, L.; Quinlan, P. R.; Robertson, K. E.; Bray, S. E.; Thomson, G.; Kellock, D.; Jordan, L. B.; Purdie, C. A.; Hardie, D. G.; Fleming, S.; Thompson, A. M. Histological evaluation of AMPK signalling in primary breast cancer. *BMC Cancer* **2009**, *9*, 307.

(9) Kim, I.; He, Y. Y. Targeting the AMP-activated protein kinase for cancer prevention and therapy. *Front. Oncol.* **2013**, *3*, 175.

(10) Alayev, A.; Holz, M. K. mTOR signaling for biological control and cancer. *J. Cell. Physiol.* **2013**, *228*, 1658−1664.

(11) Russo, G. L.; Russo, M.; Ungaro, P. AMP-activated protein kinase: a target for old drugs against diabetes and cancer. *Biochem. Pharmacol.* **2013**, *86*, 339−350.

(12) Krishna, V.; Chang, C. I.; Chou, C. H. Two isomeric epoxysitosterols from *Rhododendron formosanum*: ^{1}H and ^{13}C NMR chemical shift assignments. *Magn. Reson. Chem.* **2006**, *44*, 817−819.

(13) Chou, S. C.; Krishna, V.; Chou, C. H. Hydrophobic metabolites from *Rhododendron formosanum* and their allelopathic activities. *Nat. Prod. Commun.* **2009**, *4*, 1189−1192.

(14) Shieh, J. M.; Chen, Y. C.; Lin, Y. C.; Lin, J. N.; Chen, W. C.; Chen, Y. Y.; Ho, C. T.; Way, T. D. Demethoxycurcumin inhibits energy metabolic and oncogenic signaling pathways through AMPK activation in triple-negative breast cancer cells. *J. Agric. Food Chem.* **2013**, *61*, 6366−6375.

(15) Lin, V. C.; Tsai, Y. C.; Lin, J. N.; Fan, L. L.; Pan, M. H.; Ho, C. T.; Wu, J. Y.; Way, T. D. Activation of AMPK by pterostilbene suppresses lipogenesis and cell-cycle progression in p53 positive and negative human prostate cancer cells. *J. Agric. Food Chem.* **2012**, *60*, 6399−6407.

(16) Liu, L. C.; Tsao, T. C.; Hsu, S. R.; Wang, H. C.; Tsai, T. C.; Kao, J. Y.; Way, T. D. EGCG inhibits transforming growth factor-β-mediated epithelial-to-mesenchymal transition via the inhibition of Smad2 and Erk1/2 signaling pathways in nonsmall cell lung cancer cells. *J. Agric. Food Chem.* **2012**, *60*, 9863−9873.

(17) Takeoka, G.; Dao, L.; Teranishi, R.; Wong, R.; Flessa, S.; Harden, L.; Edwards, R. Identification of three triterpenoids in almond hulls. *J. Agric. Food Chem.* **2000**, *48*, 3437−3439.

(18) Tang, X.; Gao, J.; Chen, J.; Fang, F.; Wang, Y.; Dou, H.; Xu, Q.; Qian, Z. Inhibition of ursolic acid on calcium-induced mitochondrial permeability transition and release of two proapoptotic proteins. *Biochem. Biophys. Res. Commun.* **2005**, *337*, 320−324.

(19) Andersson, D.; Liu, J. J.; Nilsson, A.; Duan, R. D. Ursolic acid inhibits proliferation and stimulates apoptosis in HT29 cells following activation of alkaline sphingomyelinase. *Anticancer Res.* **2003**, *23*, 3317−3322.

(20) Kassi, E.; Papoutsi, Z.; Pratsinis, H.; Aligiannis, N.; Manoussakis, M.; Moutsatsou, P. Ursolic acid, a naturally occurring triterpenoid, demonstrates anticancer activity on human prostate cancer cells. *J. Cancer Res. Clin. Oncol.* **2007**, *133*, 493−500.

(21) Yeh, C. T.; Wu, C. H.; Yen, G. C. Ursolic acid, a naturally occurring triterpenoid, suppresses migration and invasion of human breast cancer cells by modulating c-Jun N-terminal kinase, Akt and mammalian target of rapamycin signaling. *Mol. Nutr. Food Res.* **2010**, *54*, 1285−1295.

(22) Hsu, Y. L.; Kuo, P. L.; Lin, C. C. Proliferative inhibition, cell-cycle dysregulation, and induction of apoptosis by ursolic acid in human non-small cell lung cancer A549 cells. *Life Sci.* **2004**, *75*, 2303−2316.

(23) Li, J.; Liang, X.; Yang, X. Ursolic acid inhibits growth and induces apoptosis in gemcitabine-resistant human pancreatic cancer via the JNK and PI3K/Akt/NF-kappaB pathways. *Oncol. Rep.* **2012**, *28*, 501−510.

(24) Song, Y. H.; Jeong, S. J.; Kwon, H. Y.; Kim, B.; Kim, S. H.; Yoo, D. Y. Ursolic acid from *Oldenlandia diffusa* induces apoptosis via activation of caspases and phosphorylation of glycogen synthase kinase 3 beta in SK-OV-3 ovarian cancer cells. *Biol. Pharm. Bull.* **2012**, *35*, 1022−1028.

(25) Wang, J.; Liu, L.; Qiu, H.; Zhang, X.; Guo, W.; Chen, W.; Tian, Y.; Fu, L.; Shi, D.; Cheng, J.; Huang, W.; Deng, W. Ursolic acid simultaneously targets multiple signaling pathways to suppress

proliferation and induce apoptosis in colon cancer cells. *PLoS One* **2013**, *8*, e63872.
(26) Zheng, Q. Y.; Li, P. P.; Jin, F. S.; Yao, C.; Zhang, G. H.; Zang, T.; Ai, X. Ursolic acid induces ER stress response to activate ASK1-JNK signaling and induce apoptosis in human bladder cancer T24 cells. *Cell. Signal.* **2013**, *25*, 206−213.
(27) Andersson, D.; Liu, J. J.; Nilsson, A.; Duan, R. D. Ursolic acid inhibits proliferation and stimulates apoptosis in HT29 cells following activation of alkaline sphingomyelinase. *Anticancer Res.* **2003**, *23*, 3317−3322.
(28) Lauthier, F.; Taillet, L.; Trouillas, P.; Delage, C.; Simon, A. Ursolic acid triggers calcium-dependent apoptosis in human Daudi cells. *Anticancer Drugs* **2000**, *11*, 737−745.
(29) Fesik, S. W. Promoting apoptosis as a strategy for cancer drug discovery. *Nat. Rev. Cancer* **2005**, *5*, 876−885.
(30) Russo, G. L.; Russo, M.; Ungaro, P. AMP-activated protein kinase: a target for old drugs against diabetes and cancer. *Biochem. Pharmacol.* **2013**, *86*, 339−350.
(31) Zheng, Q. Y.; Jin, F. S.; Yao, C.; Zhang, T.; Zhang, G. H.; Ai, X. Ursolic acid-induced AMP activated protein kinase (AMPK) activation contributes to growth inhibition and apoptosis in human bladder cancer T24 cells. *Biochem. Biophys. Res. Commun.* **2012**, *419*, 741−747.
(32) Son, H. S.; Kwon, H. Y.; Sohn, E. J.; Lee, J. H.; Woo, H. J.; Yun, M.; Kim, S. H.; Kim, Y. C. Activation of AMP-activated protein kinase and phosphorylation of glycogen synthase kinase3 β mediate ursolic acid induced apoptosis in HepG2 liver cancer cells. *Phytother. Res.* **2013**, *27*, 1714−1722.
(33) Lee, Y. H.; Wang, E.; Kumar, N.; Glickman, R. D. Ursolic acid differentially modulates apoptosis in skin melanoma and retinal pigment epithelial cells exposed to UV-VIS broadband radiation. *Apoptosis* **2013**, DOI: 10.1007/s10495-013-0962-z.
(34) Lin, J. N.; Lin, V. C.; Rau, K. M.; Shieh, P. C.; Kuo, D. H.; Shieh, J. C.; Chen, W. J.; Tsai, S. C.; Way, T. D. Resveratrol modulates tumor cell proliferation and protein translation via SIRT1-dependent AMPK activation. *J. Agric. Food Chem.* **2010**, *58*, 1584−1592.

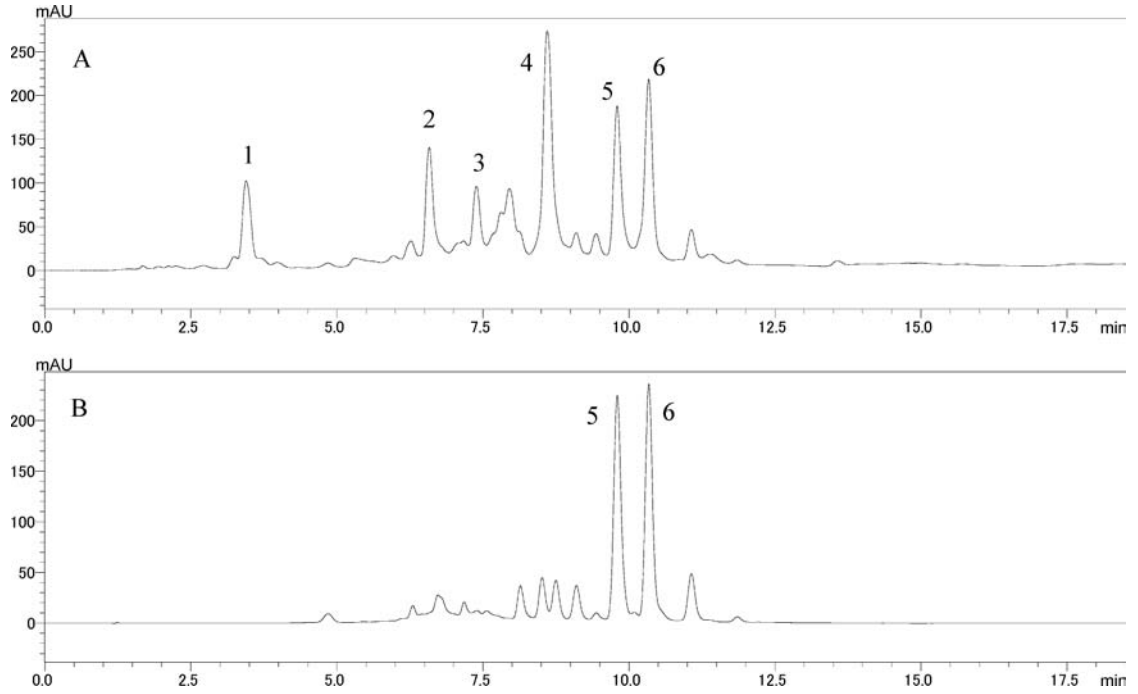

Figure 1. UFLC chromatograms of *Perilla* leaf extract: (A) 280 nm, (B) 520 nm; (1) caffeic acid; (2) luteolin 7-*O*-diglucuronide; (3) apigenin 7-*O*-diglucuronide; (4) rosmarinic acid; (5) shisonin; (6) malonylshisonin.

serum (FBS), antibiotic−antimycotic 100X, bovine serum albumin (BSA) were supplied by Equitech-bio (Kerrville, TX, USA), Invitrogen (Grand Island, NY, USA) and Jackson ImmunoResearch Laboratories (West Grove, PA, USA), respectively. All the reagents in the study were of analytical grade.

Ultrafast Liquid Chromatography (UFLC). A Shimadzu UFLC system equipped with two LC-20AD pumps and a SPD-M20A detector was used to analyze test samples. The analysis was performed on a Shim-pack XR ODS column, 2.2 μm (3.0 mm i.d. × 100.0 mm). The mobile phase was composed of (A) 20% methanolic solution containing 0.5% TFA and (B) 70% methanolic solution containing 0.5% TFA. The injection volume was 1 μL, and the analytical temperature was set at 40 °C.The UFLC elution conditions were as follows: 0.0% B (0−0.50 min); 0 → 30.0% B (0.50−1.00 min); 30.0 → 50.0% B (1.00−6.00 min); 50.0 → 70.0% B (6.00−11.50 min); 70.0 → 100.0% B (11.50−13.00 min); holding 100% B for further 2.00 min. The flow rate was 0.50 mL/min.

Preparation of *Perilla* Leaf Extract. The red *Perilla* leaves, 2.4 kg, harvested in September 2012, were first smashed by a muller. They were then immersed in 5 L of 10% acetic acid solution and extracted by a modified extractor. After extraction in triplicate with 5 L of 10% acetic acid, the total extraction solution arrived at 15.6 L. Amberlite XAD-7 resin (46.7 cm × 5.7 cm inner diameter) was filled with the above solution. Three liters of 1% TFA−80% methanol eluent was collected and evaporated to dryness (11.1 g).

The *Perilla* leaf extract obtained above was analyzed by UFLC. As shown in Figure 1A main six peaks were distributed in the UFLC chromatogram at a wavelength of 280 nm. Peaks 5 and 6 were also detected at a wavelength of 520 nm and determined as anthocyanins (S and MS, Figure 1B) (see also Table 1). These six peaks isolated were identified as the following compounds by UV spectra, mass spectra, and previous literature. (1) Caffeic acid:[16−18] λ_{max} = 322 nm, m/z 179 ($[M - H]^-$). (2) Luteolin 7-*O*-diglucuronide:[16] λ_{max} = 347 nm, 265 nm, m/z 639 ($[M + H]^+$). (3) Apigenin 7-*O*-diglucuronide:[16] λ_{max} = 336 nm, 266 nm, m/z 623 ($[M + H]^+$). (4) Rosmarinic acid:[16−18] λ_{max} = 329 nm, m/z 359 ($[M - H]^-$). (5) Shisonin:[16] λ_{max} = 523 nm, m/z 757 ($[M + H]^+$). (6) Malonylshisonin:[16,19] λ_{max} = 524 nm, 278 nm, m/z 843 ($[M + H]^+$).

Supramolecular Formation and Rosmarinic Acid Extract Isolation. Figure 2 shows the process of supramolecular formation and RA extraction from *Perilla* leaf. *Perilla* leaf extract (2.0 g), dissolved by 50% aqueous methanol solution (10.0 mL), was neutralized with $NH_3 \cdot H_2O$ (2.0 mL). After the solution was dried by a vacuum, flavocommelin (Fc; 612.0 mg/12.0 mL) and magnesium acetate aqueous solution (Mg^{2+}; 714.0 mg/5.0 mL) were added into the above residue. The reaction solution was mixed thoroughly for 20 min. After the solution was evaporated with a rotary evaporator, 8.0 mL of water and 56.0 mL of ethanol were added in order to form a precipitate at −20 °C overnight. The precipitation step was repeated two times. The supernatant and precipitate were separated by centrifugation (3000 rpm × 10 min) and evaporated to dryness. Both the dried supernatant and precipitate were kept in a desiccator with $CaCl_2$ for several days, yielding 1.7 and 1.5 g, respectively.

The supernatant described above (50.3 mg) was dissolved in 12.0 mL of 1% TFA aqueous solution, followed by the addition of 4.0 mL of ethyl acetate for extraction. The extraction procedure was repeated three times (12.0 mL of ethyl acetate extract). The ethyl acetate layer and water layer were evaporated to dryness in a vacuum, yielding 10.5 ± 0.5 mg and 44.3 ± 2.9 mg, respectively.

Table 1. Identification of UFLC Peaks of *Perilla* Leaf Extract Using a PDA Detector of UFLC and Mass Spetra Analysis[a]

peak no.	t_R (min)	UV λ_{max} (nm)	molecular ion (m/z)	compound identification	refs
1	3.2	322	179 $[M - H]^-$	caffeic acid	19−21
2	5.5	347, 265	639 $[M + H]^+$	luteolin 7-*O*-diglucuronide	19
3	6.8	336, 266	623 $[M + H]^+$	apigenin 7-*O*-diglucuronide	19
4	9.2	329	359 $[M - H]^-$	rosmarinic acid	19−21
5	11.6	523	757 $[M + H]^+$	shisonin	19
6	12.4	524, 278	843 $[M + H]^+$	malonylshisonin	19, 22

[a]Liquid chromatography/electrospray ionization quadrupole time-of-flight mass spectrometry (LC/ESI-Q-TOF-MS) analysis was conducted using an Acquity UPLC/Xevo QTof MS system (Waters Corporation).

dx.doi.org/10.1021/jf404318j | J. Agric. Food Chem. 2014, 62, 885−892

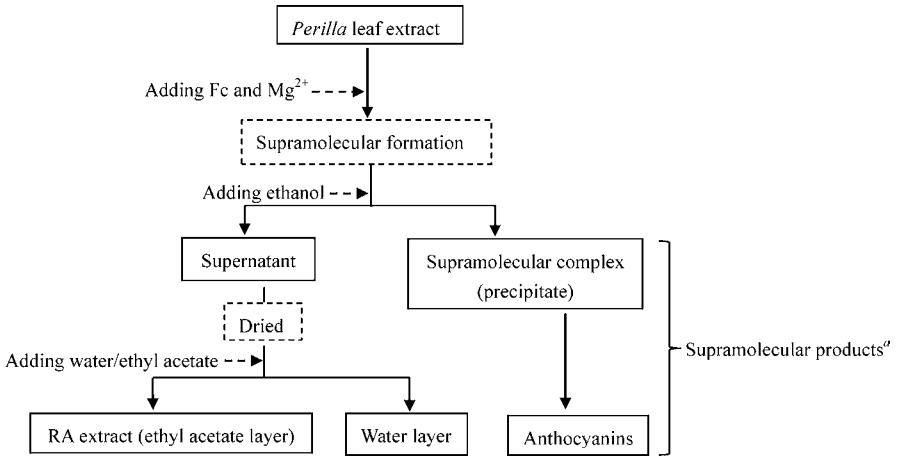

Figure 2. Rosmarinic acid extract and anthocyanins isolated from *Perilla* leaf extract by supramolecular formation. [a]Supramolecular products are supernatant and supramolecular complex obtained by supramolecluar formation, and the related extracts such as RA extract, water layer, and anthocyanins described above.

Total Phenolics (TP). TP was determined by a previous method reported by Cheplick et al.[20] Absorbance was monitored at 725 nm. Gallic acid (10, 25, 40, 60, 80 μg/mL) was used to establish a standard curve. TP was expressed as gallic acid equivalent (GAE) of a test sample.

DPPH Radical Scavenging Activity (DRSA). DRSA was determined using a previously reported method.[18] A sample solution (0.25 mL) was added into a tube with 0.10 M acetic acid buffer (0.25 mL, pH 5.5). The above solution was mixed with methanol (0.25 mL) and DPPH (0.25 mL, 0.4 mM in methanol). The reaction stood for 30 min in a dark place. DPPH absorbance was measured at 517 nm. Trolox and BHT were used as the standard chemicals. The calculation of DPPH radical scavenging activity (%) was carried out according to eq 1.

$$\text{scavenging activity}(\%) = (A_{\text{control}} - A_{\text{sample}})/A_{\text{control}} \times 100 \quad (1)$$

The SC_{50} value which represents the concentration of sample that caused 50% scavenging was determined by GraphPad PRISM 5 from the obtained scavenging activity values.

β-Hexosaminidase Release from the RBL-2H3 Cell Line. β-Hexosaminidase release from the RBL-2H3 cell line (supplied by RIKEN BioResource Center Cell Bank, Ibaraki, Japan) was determined using a previous method with some modifications.[21] The RBL-2H3 cells in a base medium (D-MEM containing 10% FBS and 1% antibiotic−antimycotic 100X) were dispensed into a 24−well plate (2.5×10^5 cells/well), followed by an incubation at 37 °C in 5% CO_2 atmosphere for one night. The cells were washed by PBS (1 mL) and incubated with 500 μL of antibody solution (mouse monoclonal anti-dinitrophenyl antibody, 50 ng/mL in base medium) for 2 h sensitization. A test sample solution of 490 μL was added to each well after washing two times with 500 μL of modified Tyrode's buffer (MT buffer, Tyrode's salt solution containing 1 g/L BSA and 4.76 g/L HEPES). The MT buffer instead of the sample was added into the well as the control. The test samples, dissolved in DMSO, were diluted with MT buffer (final DMSO concentration = 0.1%). After 10 min incubation, albumin dinitrophenyl (10 μL, final concentration = 50 ng/mL) was added to each well. The cells evoked allergic reactions for 30 min (degranulation). The microplate was cooled at 0 °C for 10 min to terminate the reactions. After transference of supernatant (50 μL) into a 96-well plate, 100 μL of *p*-nitrophenyl-2-acetamide-2-deoxy-β-D-glucopyranoside (3.3 mM) in 0.1 M citric acid buffer (pH 4.5) was added into each well with an incubation at 37 °C for 25 min. Finally, 100 μL of glycine buffer (pH 10.0, 2 M) was added and β-hexosaminidase release was quantitatively calculated by the amount of *p*-nitorophenol release from the substrate with a microplate reader at 405 nm. The calculation was carried out using eqs 2 and 3 below. In "blank", spontaneous β-hexosaminidase release from cells was checked in the condition without antibody or samples. In "total", total amount of β-hexosaminidase release from the cells was confirmed by lysing the cells with 0.1% TritonX-100 in MT buffer. In "control", the amount of β-hexosaminidase released from cells was determined in the condition without a sample. In "sample", the amount of β-hexosaminidase released from cells was determined in the condition with a sample added.

$$\text{ratio of } \beta\text{-hexosaminidase release } (\%) = \frac{(\text{OD}_{\text{control}} \text{ or } \text{OD}_{\text{sample}} - \text{OD}_{\text{blank}})}{(\text{OD}_{\text{total}} - \text{OD}_{\text{blank}})} \times 100 \quad (2)$$

$$\beta\text{-hexosaminidase release } (\%) = \frac{\text{OD}_{\text{sample}} - \text{OD}_{\text{blank}}}{\text{OD}_{\text{control}} - \text{OD}_{\text{blank}}} \times 100 \quad (3)$$

The ratio of β-hexosaminidase release (%) of "control" was between 25% and 38%.

α-Glucosidase Activity. α-Glucosidase activity was assessed according to a previous report.[11] A sample solution (50 μL) was mixed with α-glucosidase solution (100 μL, 1 U/mL) in a 96-well plate. After preincubation at 25 °C for 10 min, the reaction was initiated by adding 50 μL of *p*-nitrophenyl-α-D-glucopyranoside (5 mM) in 0.1 M PBS (pH 6.9). The mixed solution was shook at 25 °C for 5 min. At the beginning and the end of the reaction, absorbance at 405 nm was measured by a microplate reader. In control, PBS instead of the sample was added into the well. The α-glucosidase inhibition (%) was calculated by eq 4.

$$\text{inhibition } (\%) = (\triangle A_{\text{control}} - \triangle A_{\text{sample}})/\triangle A_{\text{control}} \times 100 \quad (4)$$

The sample concentration that causes 50% inhibition (IC_{50} value) was calculated from α-glucosidase inhibition by GraphPad PRISM 5.

Statistical Analysis. Statistical analysis was carried out by GraphPad PRISM 5 with Newman−Keuls test (one-way ANOVA). The value represents mean ± standard deviation (SD) in triplicate at least. Significant differences of values were statistically $p < 0.05$.

RESULTS AND DISCUSSION

Separation of RA Extract by Supramolecular Formation. There are many resources of RA in nature as biologically active substances. So, isolation techniques have been developed so far. For example, RA was purified up to 38.8%, yielding 43.8% from 1 g of the crude sample by a Sephadex LH-20[22] column, after response surface optimized

dx.doi.org/10.1021/jf404318j | J. Agric. Food Chem. 2014, 62, 885−892

Table 2. RA Extract and Anthocyanins Separated from *Perilla* Leaf Extract by Supramolecular Formation[a]

		purity (%)		yield (%)	
sample	weight (g)	RA	anthocyanins	RA	anthocyanins
Perilla leaf extract	2.0[b]	21.2	27.5		
supernatant	1.7	16.3	6.5	79.5	18.9
RA extract	10.5 ± 0.5[c]	62.9 ± 4.5	1.2 ± 0.2	82.9 ± 5.6	3.9 ± 0.3
water layer	44.3 ± 2.9[c]	1.0 ± 0.1	5.9 ± 0.6	1.6 ± 0.1	79.9 ± 1.8
supramolecular complex	1.5	1.5	18.7	7.4	71.4
anthocyanins	15.6 ± 1.2[d]	ND[e]	95.5 ± 2.5	ND	83.9 ± 2.3

[a]Each value represents mean ± SD in triplicate. [b]Weight of *Perilla* leaf extract for supramolecular formation. [c]Amount of sample (mg) was obtained by water/ethyl acetate extraction from 50.3 mg of supernatant. [d]Amount of anthocyanin (mg) obtained from 94.9 mg of supramolecular complex. [e]Not detected.

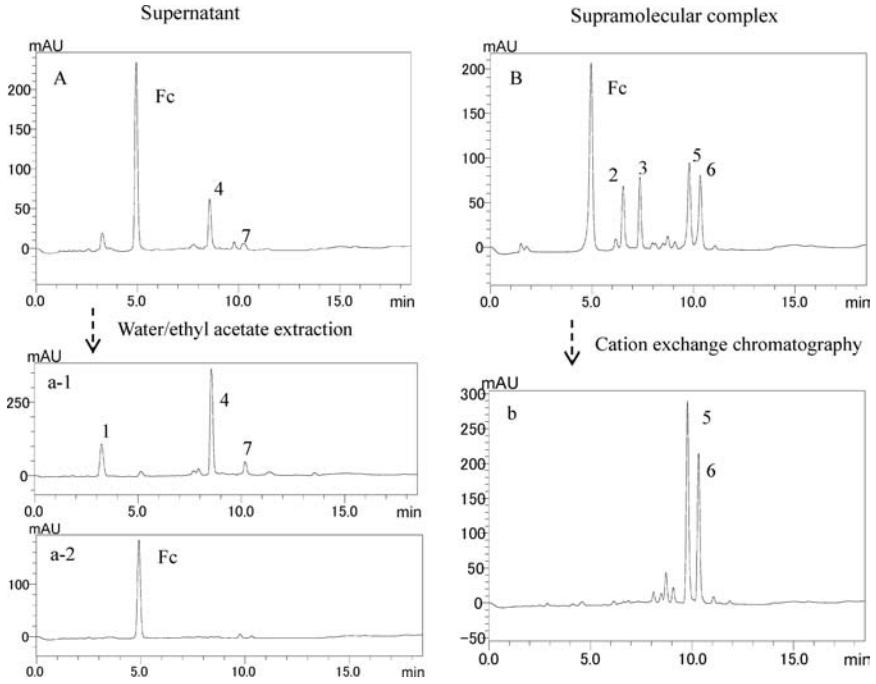

Figure 3. UFLC chromatograpms of rosmarinic acid extract from supernatant and anthocyanin from supramolecular complex after supramolecular formation (280 nm): (A) supernatant; (B) supramolecular complex; (a-1) RA extract; (a-2) water layer; (b) anthocyanins. (1) Caffeic acid. (2) Luteolin 7-*O*-diglucuronide. (3) Apigenin 7-*O*-diglucuronide. (4) Rosmarinic acid. (5) Shisonin. (6) Malonylshisonin. (7) Rosmarinic acid methyl ester.

extraction from *Melissa officinalis* leaves. Phenolics and RA were purified with macroporous resins (HP-20 and Amberlite XAD-7HP)[23] from *Rabdosia serra* (MAXIM.) HARA leaf, yielding highly concentrated RA (112.5 mg with 62.9% purity for HP-20 and 95.7 mg with 58.8% purity for Amberlite XAD-7HP).

In this experiment, crude extracts (11.1 g) of *Perilla* leaves immersed in 10% acetic acid contained anthocyanins (27.5% purity, MS and S mainly) and RA (21.2% purity) with caffeic acid, luteolin 7-*O*-diglucuronide, and apigenin 7-*O*-diglucuronide (Figure 1A). Figure 2 shows the scheme of practical separation of RA extract and *Perilla* anthocyanins by applying the supramolecular formation technique. Through supramolecular formation of anthocyanins in *Perilla* leaf extract (2.0 g) and adding Fc (612.0 mg) and Mg^{2+} (714.0 mg), RA-containing supernatant (1.7 g) was excluded from the supramolecular complex (precipitate, 1.5 g). Thus, purity of RA in the supernatant was 16.3%, including excess amount of Fc in the supernatant. If Fc content is omitted from the calculation of the purity, purity of RA would be 53.4%, compared with the initial purity of RA (21.2%). RA extract (yield 10.5 ± 0.5 mg, purity 62.9 ± 4.5%) was easily purified and isolated from an ethyl acetate layer through partitioning of water and ethyl acetate from 50.3 mg of supernatant by excluding Fc (Table 2) because RA was able to dissolve in ethyl acetate but Fc could not be dissolved in it at all. With the solubility difference between RA and Fc in ethyl acetate, RA extract, 390.4 mg (purity of 60.9%), could be isolated in ethyl acetate layer with a fairly high purity from 1.5 g of supernatant as a typical example of large scale of purification. Moreover, Fc could be recycled after usage in the experiment.

On the other hand, as supramolecular formation, supramolecular complex (Figure 3B) including anthocyanins (MS and S mainly) and unexpected flavonoids (luteolin 7-*O*-diglucuronide and apigenin 7-*O*-diglucuronide) was precipitated by ethanol, which is supported by the report on the alumina complex formation published by Asada et al.[15] In the supramolecular complex, 15.6 mg of anthocyanins (Figure 3b, 95.5 ± 2.5% purity) has been successfully isolated from the supramolecular complex (94.9 mg), after excluding neutral

chemicals such as Fc and flavonoids (Table 2). Thus, by supramolecular technique, both rosmarinic acid and anthocyanins could be easily isolated from *Perilla* leaf extract.

With supramolecular technology, fairly pure rosmarinic acid (60.9%) and highly pure malonylshisonin and shisonin (95.5%), which have various biological activities,[2−9] as well as RA extract are possible for large scale purifications to supply the extracts and the pure chemicals to the food industry.

Antioxidant Activities of Supramolecular Products. Polyphenols possess biologically beneficial activities and are frequently utilized as antioxidant,[18] antiallergic,[24] and antidiabetic[20] reagents. Phenolics in *Perilla* leaves are well-known compounds, owing to their potent antioxidant activities and other bioactivities.[4−9] In our study, *Perilla* leaf extract, Fc, and supramolecular products (Figure 2) were tested for antioxidant and other biological activities. Total phenolics (TPs) as an antioxidant activity were 433.9 ± 58.6 mg/g gallic acid equivalent (GAE) for RA extract, 116.9 ± 2.7 mg/g GAE for supernatant, 170.7 ± 8.2 mg/g GAE for supramolecular complex, and 4.1 ± 1.3 mg/g GAE for Fc (Table 3). Fc, with only one hydroxyl group on the A-ring, hardly contributed to high TP. RA extract exhibited the highest TP, more than two times higher than *Perilla* leaf extract (215.2 ± 2.9 mg/g GAE). It is suggested that TP of RA extract isolated from *Perilla* leaf extract using the supramolecular technique showed the greatest TP. Moreover, the TP of standard RA (711.8 ± 5.3 mg/g GAE) was higher than that of RA extract. The TP of RA extract was calculated to be 61.0% of standard RA. Therefore TP of RA extract was interpreted by the purity of RA (62.9 ± 4.5%) in the extract. Compared with the previous report, RA extract and *Perilla* leaf extract have a higher TP than the extracts of oregano, chocolate mint, and other Lamiaceae family herbs.[11]

Table 3. Total Phenolics of *Perilla* Leaf Extract, Fc, and Supramolecular Products[a]

sample	total phenolics (mg/g GAE)[b]
Perilla leaf extract	215.2 ± 2.9
Fc	4.1 ± 1.3
supernatant	116.9 ± 2.7
RA extract	433.9 ± 58.6
water layer	47.6 ± 1.6
supramolecular complex	170.7 ± 8.2
anthocyanins	189.8 ± 9.8
standard RA	711.8 ± 5.3

[a]Each value represents mean ± SD in triplicate. [b]Total phenolics expressed as gallic acid equivalent (GAE).

DPPH radical scavenging activity (DRSA) is widely applied in assessment of antioxidant activities of plant extracts. A dose-dependent capability of DRSA was observed for *Perilla* leaf extract and supramolecular products (Table 4). RA extract exhibited DRSA at 88.3 ± 0.7% at a concentration of 10 μg/mL while the other supramolecular products exhibited scavenging activity below 50%. RA extract exhibited the highest DRSA with an SC_{50} value of 5.5 ± 0.2 μg/mL (concentration of sample that causes 50% scavenging of free radicals as shown in eq 1), which was more than two times higher DRSA than *Perilla* leaf extract (SC_{50} value, 10.8 ± 0.1 μg/mL) and supernatant (SC_{50} value, 21.7 ± 0.3 μg/mL). Standard RA (SC_{50} value, 4.6 ± 0.2 μg/mL) exhibited higher DRSA than RA extract (SC_{50} value, 5.5 ± 0.2 μg/mL), which is consistent with the results for TP. It has been reported that polyphenols are good antioxidants because phenolic hydroxyl groups are able to provide hydrogen to hydroxyl radical, superoxide radical, and other reactive free radicals.[25] Comparing DRSA of RA extract with those of the reference chemicals it demonstrated that RA extract exhibited similar DRSA to Trolox and higher than BHT (Table 4).

As many inflammations (induced by TNF-α, IL-6, and other sources) of animal cells including human are triggers of diabetes and cancer,[26] anti-inflammatory activities, which can be linked with free radical scavenging activity, of polyphenols including flavonoids and phenylpropanoids have been reported.[24] Polyphenolic compounds also provide anticarcinogenic, antimutagenic, and cardioprotective activities, as a consequence of their strong antioxidant properties.[27] Polyphenols could be good resources for suppressing allergy[24] and treating hyperglycemia associated with type 2 diabetes.[20] Because of the observation of high total phenolics, as well as strong DPPH radical elimination ability, among supramolecular products, we expected that effective antiallergic activity would be observed and hyperglycemia could be suppressed by α-glucosidase inhibition.

Antiallergic Activities of Supramolecular Products on the Suppression of β-Hexosaminidase Release from the RBL-2H3 Cell Line. The lower release of β-hexosaminidase, biomarkers of the RBL-2H3 cell line, is necessary to elicit an antiallergenic response while the RBL-2H3 cell line is applied as a typical model for the research on mast cell excretion and screening for antiallergic phytochemicals.[28] Shimoda et al.[21]

Table 4. DPPH Radical Scavenging Activity of *Perilla* Leaf extract, Fc, and Supramolecular Products[a]

	scavenging activity (%)					
sample (μg/mL)	2.5	5	10	15	20	SC_{50}[b] (μg/mL)
Perilla leaf extract	10.7 ± 1.2	23.4 ± 2.0	48.8 ± 0.2 e	71.7 ± 1.6	87.0 ± 0.3	10.8 ± 0.1 c
Fc	NI[c]	NI	NI	NI	NI	>25
supernatant	NI	10.2 ± 0.9	23.5 ± 0.9 f	35.9 ± 0.1	50.5 ± 0.6	21.7 ± 0.3 e
RA extract	21.1 ± 3.9	48.0 ± 2.2	88.3 ± 0.7 b	89.7 ± 0.5	89.8 ± 0.1	5.5 ± 0.2 a
water layer	NI	NI	2.5 ± 0.2 h	6.1 ± 0.5	11.7 ± 2.1	>25
supramolecular complex	7.8 ± 0.6	8.9 ± 0.6	22.7 ± 0.3 f	36.9 ± 0.3	61.1 ± 0.4	17.6 ± 0.2 d
anthocyanins	5.7 ± 0.5	9.0 ± 1.4	20.8 ± 0.5 g	35.8 ± 0.8	45.8 ± 0.8	23.2 ± 0.4 f
standard RA	32.3 ± 0.6	58.3 ± 1.0	90.6 ± 0.7 a	90.9 ± 0.7	92.5 ± 0.5	4.6 ± 0.1 a
Trolox	24.7 ± 0.7	53.4 ± 0.9	85.3 ± 0.7 c	91.6 ± 1.7	94.4 ± 0.3	5.1 ± 0.1 a
BHT	14.0 ± 0.6	41.5 ± 2.9	76.2 ± 0.9 d	84.5 ± 0.6	87.0 ± 0.4	6.6 ± 0.3 b

[a]Each value represents mean ± SD in triplicate. Means with different letters are significantly different ($p < 0.05$). [b]SC_{50} value which represents the concentration of sample that caused 50% scavenging was calculated from scavenging activity values. [c]No inhibition detected.

reported β-hexosaminidase release suppression by extracts of *Perilla* leaf (*Perilla frutescens*), Japanese butterbur (*Petasites japonicas*, Compositae), and tien-cha (*Rubus suavissimus*). These extracts have a potency for the prevention of pollennosis, seasonal allergic rhinitis, and other allergic reactions.[29−31] Therefore, *Perilla* leaf extract is becoming more popular in the Japanese market as a folk medicine. However, they did not show the efficient extraction technique of RA extract with great activities.

In this paper, the antiallergic activities of *Perilla* leaf extract, Fc, and supramolecular products, such as supramolecular complex, supernatant, RA extract, anthocyanins, and water layer, were assessed by β-hexosaminidase release suppression of RBL-2H3 cells (Figure 4). The concentrations of 50% β-

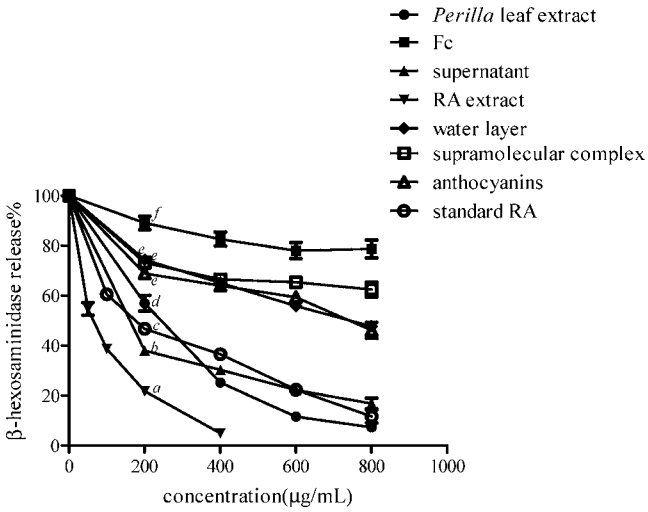

Figure 4. Antiallergic activities of supramolecular products on β-hexosaminidase release suppression from the RBL-2H3 cell line. Each value represents mean ± SD in quadruplicate.

hexosaminidase release inhibition of standard RA, *Perilla* leaf extract, supernatant, and RA extract were mainly 136.7 ± 12.6 μg/mL, 208.4 ± 20.0 μg/mL, 81.1 ± 23.3 μg/mL, and 52.9 ± 6.7 μg/mL (IC_{50} values), respectively. The suppression of β-hexosaminidase release was dose-dependent. In our study, RA extract suppressed β-hexosaminidase release 3.9 times and 2.6 times more than *Perilla* leaf extract and standard RA, respectively, and exhibited the highest antiallergic activity among the supramolecular products. Also, it is suggested that other compounds as well as RA in RA extract may contribute to antiallergic activity.

RA is reported to possess anti-inflammatory and antiallergic effect and inhibit seasonal allergic rhinoconjunctivitis.[31,32] RA suppresses inflammatory activity by the decrease of IgE and COX-2 levels.[5] Therefore, efficient isolation of pure RA and RA extract that has higher antiallergic activity than RA itself is desired in current food and drug markets. Supramolecular formation and solvent partition technique may offer the possibility of the development of new drugs.

In the UFLC chromatogram (Figure 3a-1), caffeic acid (t_R = 3.2 min) and rosmarinic acid methyl ester (RA-me, t_R = 10.2 min) were found in RA extract as minor components besides RA. The β-hexosaminidase release inhibitory result gave IC_{50} values of caffeic acid and RA-me (synthesized by us) of 132.0 ± 3.6 μg/mL and 9.9 ± 0.8 μg/mL, respectively. This result showed that RA-me exhibited higher inhibitory activity than standard RA. In RA extract the content of RA and RA-me was 62.9% and 6.9% respectively. At IC_{50} of RA extract (52.9 μg/mL), it was calculated as 33.3 μg/mL for RA and 3.7 μg/mL for RA-me, respectively, which contributed to 43% β-hexosaminidase release inhibition as an additive effect. Therefore, RA-me, as a component in RA extract, contributed to high β-hexosaminidase release inhibitory activity besides RA. We found the greatest activity of RA-me in RA extract and supernatant as a minor component. So, although the purity of RA (16.3%) in supernatant is a bit lower than that of RA in leaf extract (21.2%), supernatant showed greater values of IC_{50} than that of leaf extract because of not only increasing of Fc in supernatant as the impurity but also increasing of RA-me by the selective isolation with supramolecular technique and solvent partition technique.

Yun et al.[24] reported that curcumin, with the highest potential to suppress β-hexosaminidase release among 25 polyphenols, was around 4 times greater than RA. In contrast, RA-me found in RA extract was 13.8 times higher than RA. Therefore, RA-me can suppress β-hexosaminidase release more effectively than curcumin.

In conclusion, RA extract isolated by supramolecular technique showed effective antiallergic activity. We clarified that RA-me, as a minor component in RA extract, contributed to high antialleric activity with RA as an additive effect.

α-Glucosidase Inhibitory Activities of Supramolecular Products. α-Glucosidase inhibitors, alleviating postprandial hyperglycemia, would have potential to manage diabetes. *Perilla* leaf extract, Fc, and supramolecular products were examined for inhibition effects of α-glucosidase. RA extract inhibited the greatest α-glucosidase activity (IC_{50} of 0.23 ± 0.01 mg/mL) among the supramolecular products (Table 5). Furthermore,

Table 5. α-Glucosidase Inhibitory Activity of *Perilla* Leaf Extract, Fc, and Supramolecular Products

sample	IC_{50}[a] (mg/mL)
Perilla leaf extract	0.42 ± 0.01 a
Fc	5.60 ± 0.23 e
supernatant	0.42 ± 0.01 a
RA extract	0.23 ± 0.01 a
water layer	2.74 ± 0.21 d
supramolecular complex	1.54 ± 0.04 b
anthocyanins	1.99 ± 0.01 c
standard RA	0.95 ± 0.01 b

[a]IC_{50} values were calculated from dose−response curves of α-glucosidase inhibition. Each value represents mean ± SD in triplicate. Means with different letters are significantly different ($p < 0.05$).

RA extract inhibited α-glucosidase activity 4.1 times and 1.8 times higher than standard RA (IC_{50} value, 0.95 ± 0.01 mg/mL) and *Perilla* leaf extract (IC_{50} value, 0.42 ± 0.01 mg/mL), respectively, while RA is reported to be a better research target on α-glucosidase inhibitory activity.[11] Moreover, RA extract exhibited α-glucosidase inhibitory activity higher than 4,5-dicaffeoylquinic acid (IC_{50}, 0.46 mg/mL), as an effective α-glucosidase inhibitor, isolated from flower buds of *Tussilago farfara* L.[33] and coffee bean.[34] Therefore, RA extract has potential to suppress hyperglycemia by inhibiting α-glucosidase activity.

The α-glucosidase inhibitory activity result showed that IC_{50} values of caffeic acid and RA-me were 3.46 ± 0.18 mg/mL and 0.44 ± 0.01 mg/mL, respectively. It showed that RA-me

exhibited greater α-glucosidase inhibitory activity than standard RA. We concluded that RA extract containing RA-me and other minor components as unknown compounds besides RA contributed to high α-glucosidase inhibitory activity, especially unknown compounds might highly contribute to the activity. We found that RA-me and other minor compounds with high α-glucosidase inhibitory activity were contained in RA extract and supernatant. So, although the purity of RA (16.3%) in supernatant was a bit lower than that of RA in leaf extract (21.2%), supernatant showed the same IC_{50} value of α-glucosidase inhibitory activity with that of leaf extract because of not only increasing of Fc in supernatant as the impurity but also increasing of RA-me and other minor compounds by the selective isolation with supramolecular technique and solvent partition technique (Table 5).

Moreover, in the *Perilla* leaf extracted by 10% acetic acid, RA-me was not detected in our experiment though Kang et al.[17] characterized RA-me as one phenolic phytochemical in *Perilla frutescens*. Therefore, we surmise it to be an artificial compound in *Perilla* leaf extract. The generated RA-me and other minor components in RA extract potently contributed to antiobesity activity by inhibiting α-glucosidase activity. Clarification of the minor components contributing to α-glucosidase inhibitory activity is under investigation.

Through supramolecular formation, RA-containing supernatant was excluded by supramolecular complex and RA extract (62.9 ± 4.5% purity) with potent biological activities was obtained. The obtained RA extract had exhibited the three great activities of DPPH radical scavenging, antiallergy effects, and α-glucosidase inhibition. Antiallergic activity and α-glucosidase inhibition of RA extract were greater than those of standard RA. This study shows that RA and other minor components in RA extract contributed both activities of antiallergy effects and α-glucosidase inhibition. We will discuss molecular mechanisms of the activities in detail by linking with the interaction of biologically important chemicals after identification of these active compounds. In conclusion, the RA extract isolated from *Perilla* leaf extract by supramolecular formation and solvent extraction has potential applications in managing diabetes mellitus and other chronic and degenerative diseases. This is the first report on RA extract with potent antioxidant, antiallergic, and α-glucosidase inhibitory activity separated from *Perilla* leaf extract using the supramolecular formation and partition technique.

AUTHOR INFORMATION

Corresponding Author

*E-mail: tamura@ag.kagawa-u.ac.jp. Phone: +81-87-891-3104. Fax: +81-87-891-3021.

Funding

This work was supported by Monbukagakusho Scholarship, provided by Japanese Ministry of Education, Culture, Sports, Science and Technology.

Notes

The authors declare no competing financial interest.

ABBREVIATIONS USED

DPPH, 2,2-diphenyl-1-picrylhydrazyl; DRSA, DPPH radical scavenging activity; Fc, flavocommelin; GAE, gallic acid equivalent; MS, malonylshisonin; RA, rosmarinic acid; RA-me, rosmarinic acid methyl ester; S, shisonin; TP, total phenolics; UFLC, ultrafast liquid chromatography

REFERENCES

(1) Chang, H. H.; Chen, C. S.; Lin, J. Y. Dietary perilla oil lowers serum lipids and ovalbumin-specific IgG1, but increase total IgE levels ovalbumin challenged mice. *Food Chem. Toxicol.* **2009**, *47*, 848−854.

(2) Tamura, H.; Yamagami, A. Antioxidative activity of monoacylated anthocyanins isolated from Muscat Bailey A grape. *J. Agric. Food Chem.* **1994**, *42*, 1612−1615.

(3) Tsuda, T.; Shiga, K.; Ohshima, K.; Kawakishi, S.; Osawa, T. Inhibition of lipid peroxidation and the active oxygen radical scavenging effect of anthocyanin pigments isolated from *Phaseolus vulgaris* L. *Biochem. Pharmacol.* **1996**, *56*, 1033−1039.

(4) Sanbongi, C.; Takano, H.; Osakabe, N.; Sasa, N.; Natsume, M.; Yanagisawa, R.; Inoue, K.; Sadakane, K.; Ichinose, T.; Yoshikawa, T. Rosmarinic acid in perilla extract inhibits allergic inflammation induced by mite allergen, in a mouse model. *Clin. Exp. Allergy* **2004**, *34*, 971−977.

(5) Oh, H. A.; Park, C. S.; Ahn, H. J.; Park, Y. S.; Kim, H. M. Effect of *Perilla frutescens* var. *acuta* Kudo and rosmarinic acid on allergic inflammatory reactions. *Exp. Biol. Med.* **2011**, *236* (1), 99−106.

(6) Meng, L.; Lozano, Y. F.; Gaydou, E. M.; Li, B. Antioxidant activities of polyphenols extracted from *Perilla frutescens* varieties. *Molecules* **2009**, *14*, 133−140.

(7) Kim, E. K.; Lee, S. J.; Lim, B. O.; Jeon, Y. J.; Song, M. D.; Park, T. K.; Lee, K. H.; Kim, B.; Lee, S. R.; Moon, S. H.; Jeon, B. T.; Park, P. J. Antioxidative and neuroprotective effects of enzymatic extracts from leaves of *Perilla frutescens* var. *japonica*. *Food Sci. Biotechnol.* **2008**, *17*, 279−286.

(8) Ueda, H.; Yamazaki, C.; Yamazaki, M. Inhibitory effect of *Perilla* leaf extract and luteolin on mouse skin tumor promotion. *Biol. Pharm. Bull.* **2003**, *26*, 560−563.

(9) Kim, M.-J.; Kim, H. K. Perilla leaf extract ameliorates obesity and dyslipidemia induced by high-fat diet. *Phytother. Res.* **2009**, *23* (12), 1685−1690.

(10) McCue, P. P.; Shetty, K. Inhibitory effects of rosmarinic acid extracts on porcine pancreatic amylase *in vitro*. *Asia Pac. J. Clin. Nutr.* **2004**, *13*, 101−106.

(11) Kwon, Y. I.; Vattem, D. A.; Shetty, K. Evaluation of clonal herbs of Lamiaceae species for management of diabetes and hypertension. *Asia Pac. J. Clin. Nutr.* **2006**, *15*, 107−118.

(12) Takeda, K.; Yanagisawa, M.; Kifune, T.; Kinoshita, T.; Timberlake, C. F. A blue pigment complex in flowers of *Salvia patens*. *Phytochemistry* **1994**, *35*, 1167−1169.

(13) Kondo, T.; Yoshida, K.; Nakagawa, A.; Kawai, T.; Tamura, H.; Goto, T. Structural basis of blue-colour development in flower petals from *Commelina communis*. *Nature* **1992**, *358*, 515−518.

(14) Mori, M.; Kondo, T.; Yoshida, K. Cyanosalvianin, a supramolecular blue metalloanthocyanin, from petals of *Salvia uliginosa*. *Phytochemistry* **2008**, *69*, 3151−3158.

(15) Asada, T.; Tamura, H. Isolation of bilberry anthocyanindin 3-glycosides bearing *ortho*-dihydroxyl groups on the B ring by forming an aluminum complex and their antioxidant activity. *J. Agric. Food Chem.* **2012**, *60*, 10634−10640.

(16) Meng, L.; Lozano, Y.; Bombarda, I.; Gaydou, E. M.; Li, B. Polyphenol extraction from eight *Perilla frutescens* cultivars. *C. R. Chim.* **2009**, *12*, 602−611.

(17) Kang, N. S.; Lee, J. H. Characterization of phenolic phytochemicals and quality changes related to the harvest times from the leaves of Korean purple perilla (*Perilla frutescens*). *Food Chem.* **2011**, *124*, 556−562.

(18) Lee, J. H.; Park, K. H.; Lee, M.-H.; Kim, H.-T.; Seo, W. D.; Kim, J. Y.; Baek, I.-Y.; Jang, D. S.; Ha, T. J. Identification, characterization, and quantification of phenolic compounds in the antioxidant activity-containing fraction from the seeds of Korean perilla (*Perilla frutescens*) cultivars. *Food Chem.* **2013**, *136*, 843−852.

(19) Kondo, T.; Tamura, H.; Yoshida, K.; Goto, T. Structure of malonylshisonin, a genuine pigment in purple leaves of *Perilla ocimoides* L. var. *crispa* Benth. *Agric. Biol. Chem.* **1989**, *53*, 797−800.

(20) Cheplick, S.; Kwon, Y.-I.; Bhowmik, P.; Shetty, K. Phenolic-linked variation in strawberry sultivars for potential dietary manage-

ment of hyperglycemia and related complications of hypertension. *Bioresour. Technol.* **2010**, *101*, 404−413.
(21) Shimoda, H.; Tanaka, J.; Yamada, E.; Morikawa, T.; Kasajima, N.; Yoshikawa, M. Anti Type I allergic property of Japanese Butterbur extract and its mast cell degranulation inhibitory ingredients. *J. Agric. Food Chem.* **2006**, *54*, 2915−2920.
(22) Kim, S.; Yun, E. J.; Bak, J. S.; Lee, H.; Lee, S. J.; Kim, C. T.; Lee, J.-H.; Kim, K. H. Response surface optimized extraction and chromatographic purification of rosmarinic acidfrom *Melissa officinalis* leaves. *Food Chem.* **2010**, *121*, 521−526.
(23) Lin, L.; Zhao, H.; Dong, Y.; Yang, B.; Zhao, M. Macroporous resin purification behavior of phenolics and rosmarinic acid form *Rabdosia serra* (MAXIM.) HARA leaf. *Food Chem.* **2012**, *130*, 417−424.
(24) Yun, S. S.; Kang, M. Y.; Park, J. C.; Nam, S. H. Comparison of anti-allergenic activities of various polyphenols in cell assays. *J. Appl. Biol. Chem.* **2010**, *53* (3), 139−146.
(25) Valentao, P.; Fernandes, E.; Carvalho, F.; Andrade, P. B.; Seabra, R. M.; Bastos, M. L. Hydroxyl radical and hypochlorous acid scavenging activity of small centaury (*Centaurium erythraea*) infusion. A comparative study with green tea (*Camellia sinensis*). *Phytomedicine* **2003**, *10* (6−7), 517−522.
(26) Nair, H.; Sung, B.; Yadav, V. R.; Kannappan, R.; Chaturvedi, M. M.; Aggarwal, B. B. Delivery of anti-inflammatory nutraceuticals by nanoparticles for the prevention and treatment of cancer. *Biochem. Pharmacol.* **2010**, *80*, 1833−1843.
(27) Urquiaga, I.; Leighton, F. Plant polyphenol antioxidants and oxidative stress. *Biol. Res.* **2000**, *33*, 55−64.
(28) Aketani, S.; Teshima, R.; Umezawa, Y.; Sawada, J. Correlation between cytosolic calcium concentration and degranulation in RBL-2H3 cells in the presence of various concentrations of antigen-specific IgEs. *Immunol. Lett.* **2001**, *75* (3), 185−189.
(29) Ukai, K.; Amesara, R.; Sakakura, Y. Clinical study of Tien cha candy on nasal allergy. *Oto-Rhino-Laryngol (Tokyo)* **1995**, *38*, 519−532 in Japanese.
(30) Makino, T.; Furuta, Y.; Fujii, H.; Nakagawa, T.; Wakushima, H.; Saito, K.; Kano, Y. Effect of oral treatment of *Perilla frutescens* and its constituents on Type-I allergic in mice. *Biol. Pharm. Bull.* **2001**, *24* (10), 1206−1209.
(31) Takano, H.; Osakabe, N.; Sanbongi, C.; Yanagisawa, R.; Inoue, K.; Yasuda, A.; Natsume, M.; Baba, S.; Ichiishi, E.; Yoshikawa, T. Extract of *Perilla Frutescens* enriched for rosmarinic acid, a polyphenolic phytochemical, inhibits seasonal allergic rhinoconjunctivitis in humans. *Exp. Biol. Med.* **2004**, *229*, 247−254.
(32) Osakabe, N.; Takano, H.; Sanbongi, C.; Yasuda, A.; Yanagisawa, R.; Inoue, K.; Yoshikawa, T. Anti-inflammatory and anti-allergic effect of rosmarinic acid (RA); inhibition of seasonal allergic rhinoconjunctivities (SAR) and its mechanism. *Biofactors* **2004**, *21*, 127−131.
(33) Gao, H.; Huang, Y.; Gao, B.; Xu, P.; Inagaki, C.; Kawabata, J. α-Glucosidase inhibitory effect by the flower buds of *Tussilago farfara L.* *Food Chem.* **2008**, *106*, 1195−1201.
(34) Clifford, M. N. Coffee bean dicaffeoylquinic acids. *Phytochemistry* **1986**, *25* (7), 1767−1769.

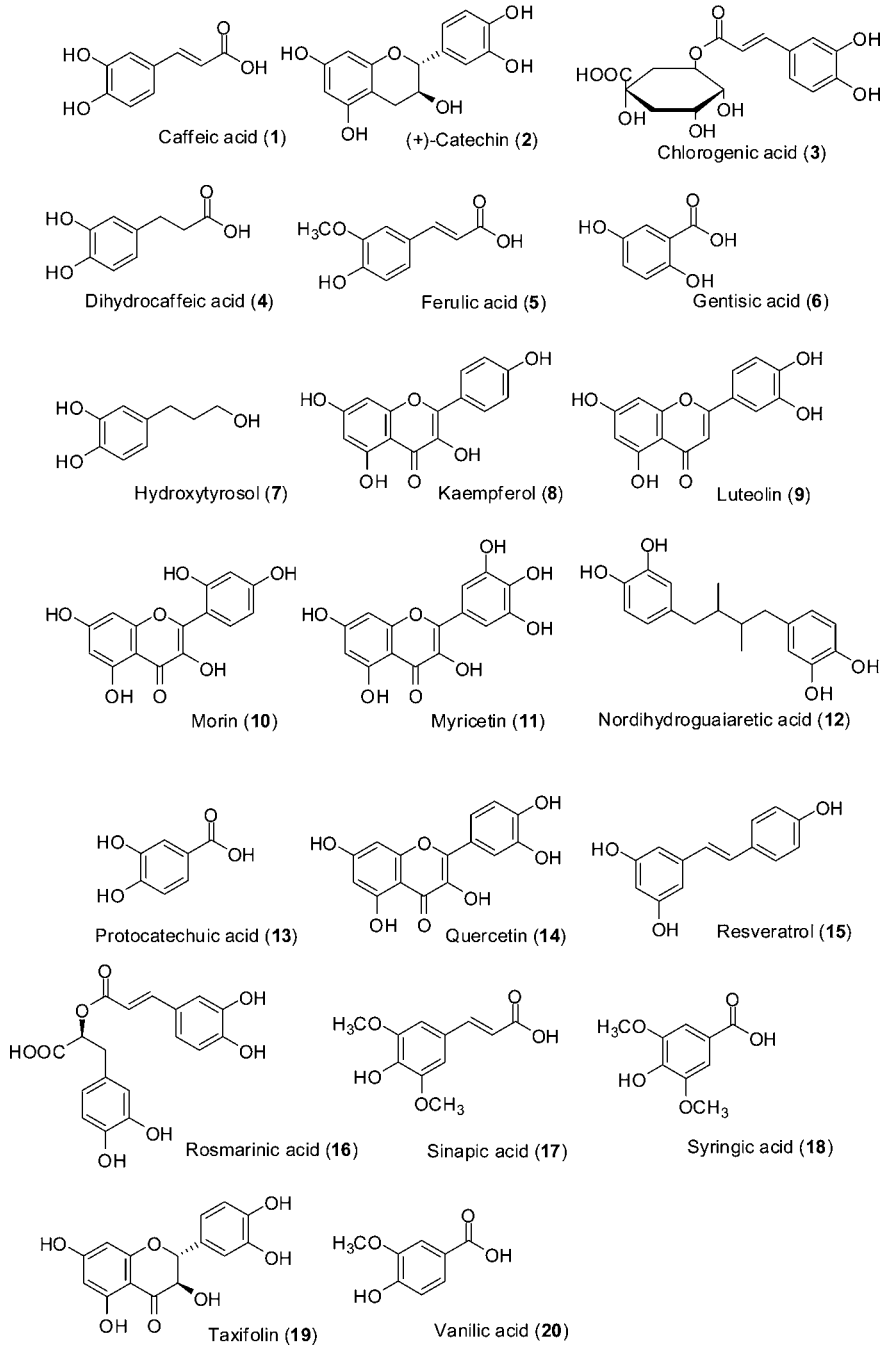

Figure 1. Chemical structures of the polyphenols and related phenols investigated for MetMb reduction.

MO). Vanillic acid (purity > 96%) was purchased from Wako Pure Chemicals (Osaka, Japan). Kaempferol (purity > 97%) and taxifolin (purity > 96%) were obtained from Funakoshi (Tokyo, Japan). All solvents [extra pure grade or high-performance liquid chromatography (HPLC) grade] were obtained from Nacalai Tesque. Nuclear magnetic resonance (NMR) spectra were obtained from an ECS-400 spectrometer (JEOL, Tokyo, Japan) using the pulse sequences of the manufacturer. High-resolution mass spectrometric data were obtained using a XEVO QtofMS spectrometer (Waters Japan, Tokyo, Japan) in negative electrospray ionization (ESI) mode. A PU-2089 low-pressure gradient system (JASCO, Tokyo, Japan) equipped with a MD-2018 photodiode array (PDA) detector was employed for analytical HPLC. PDA data were analyzed using ChromNAV, version 1.8 (JASCO). A LC-6AD system (Shimadzu, Kyoto, Japan) equipped with a UV-970 detector (JASCO) was used for preparative HPLC.

Preparation of MbO_2 and MetMb. MbO_2 was prepared using the method reported previously.[9] MetMb solution was prepared from a stock solution of MbO_2. Potassium hexacyanoferrate (III) (2 mg) was added to a solution of MbO_2 (120 μmol/L) in a phosphate buffer (pH 7.4, 3 mL) at 23 °C. After gentle stirring for 0.5 min, the solution was desalted 3 times at 14000*g* for 6 min at 4 °C with an Amicon Ultra-0.5, Ultracel-10 ultrafiltration membrane (Merck Millipore, Cork, Ireland) using phosphate buffer. The final residual solution (ca. 0.5 mL) was diluted with buffer, yielding 120 μmol/L MetMb solution (3 mL). The purity and concentration of the MetMb solution were confirmed with a UVmini 1240 ultraviolet−visible (UV−vis) spectrometer (Shimadzu).[17]

Measurement of MetMb Reduction and MbO_2 Oxidation. To a 96-well microplate, 50 mmol/L phosphate buffer (pH 7.4, 140 μL), 120 μmol/L MetMb or MbO_2 in the same buffer (150 μL), and an appropriate amount of test samples (polyphenols, their products, or L-

dx.doi.org/10.1021/jf404357h | J. Agric. Food Chem. 2014, 62, 893−901

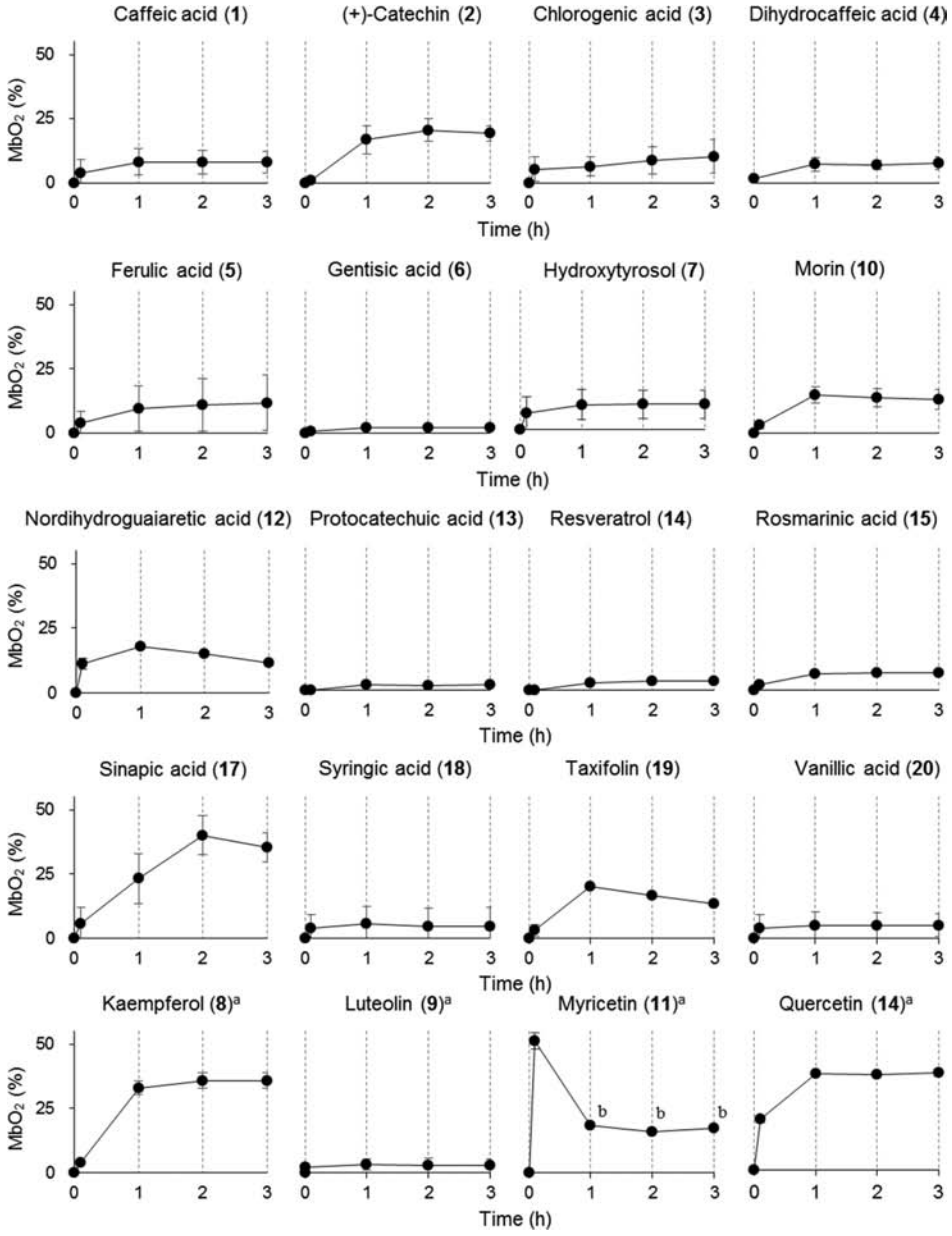

Figure 2. Effects of phenols (600 or 300 μmol L^{-1}) on MetMb reduction. Results are expressed as the mean ± standard deviation (SD) (n = 6). (a) Activity of kaempferol, luteolin, myricetin, and quercetin was measured at 300 μmo/L because their solubilities are below 600 μmol/L. (b) Data on myricetin after 1 h are low of accuracy because of the dark brown color of the solution mixture.

ascorbic acid) in dimethyl sulfoxide (DMSO) (10 μL) were subsequently added. The microplate was incubated at 37 °C in a Multiskan GO microplate reader (Thermo Fisher Scientific, Yokohama, Japan) for 3 h, and absorbance at 500 and 582 nm was measured at 1 h intervals. At the beginning and end of the experiment, visible spectra (450−650 nm) were obtained with the same microplate reader. MbO_2 and MetMb concentrations in the well were calculated by the following equation based on the absorption spectra of 60 μmol/L pure MbO_2 or MetMb: MbO_2 (μmol/L) = $(89.7A_{582}) - (32.9A_{500})$, where A_{500} and A_{582} refer to absorbance at 500 and 582 nm, respectively. Redox conversion efficiency between MetMb and MbO_2 was expressed as a percentage calculated by the MbO_2 concentration relative to the initial concentrations (60 μmol/L) of each MbO_2 and MetMb.

HPLC and Liquid Chromatography−Mass Spectrometry (LC−MS) Analyses of Quercetin Products during MetMb Reduction. At 1 h intervals, an aliquot (5 μL) was removed from the above-mentioned reaction with quercetin (300 μmol/L) and the reaction products were analyzed under the following conditions: column, a 250 × 4.6 mm inner diameter, 5 μm, Cosmosil $5C_{18}$-AR-II (Nacalai Tesque); flow rate, 1.0 mL/min; solvent A, 1% acetic acid in water; solvent B, acetonitrile; gradient conditions, linear gradient from 5 to 100% solvent B (40 min); and detection, absorbance at 280 nm. The concentration of each product in the reaction mixture was calculated using the following calibration equations: quercetin, Y (μmol/L) = $0.70X \times 10^{-3} + 0.15$ (range for Y, 50−300 μmol/L); product I, Y (μmol/L) = $3.62X \times 10^{-4} + 2.39$ (range for Y, 1−1000 μmol/L); product II, Y (μmol/L) = $1.02X \times 10^{-3} + 1.64$ (range for Y, 10−1000 μmol/L); product III, Y (μmol/L) = $3.59X \times 10^{-4} + 8.94$ (range for Y, 10−1000 μmol/L), where X represents the peak area at 280 nm. The MS data for each product was obtained by LC−MS. An additional aliquot (5 μL) was also taken after 1 and 3 h for the analysis of products I−III, and the analyses were carried out under the following conditions: separation conditions, column, a 250 × 4.6 mm inner diameter, 5 μm, Cosmosil $5C_{18}$-AR-II (Nacalai Tesque); flow rate, 0.5 mL/min; solvent A, 1% acetic acid in ultrapure water, solvent

dx.doi.org/10.1021/jf404357h | J. Agric. Food Chem. 2014, 62, 893−901

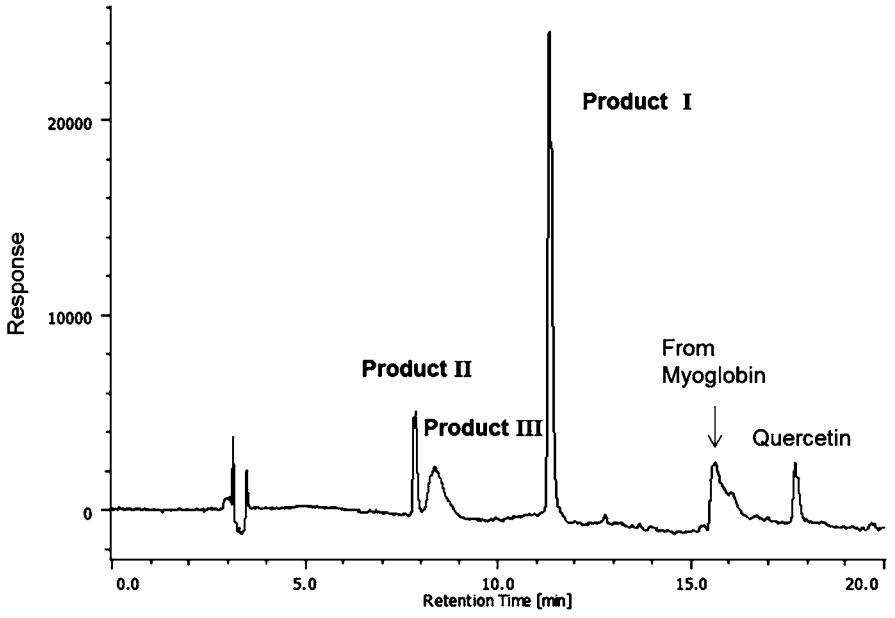

Figure 3. HPLC profile for the reaction of quercetin and MetMb at 2 h.

B, acetonitrile (LC−MS grade, Merck, Darmstadt, Germany); gradient conditions, linear gradient from 5 to 100% solvent B (80 min); and MS conditions, mode, negative ESI; capillary voltage, 2.4 kV; cone voltage, 40 V; source temperature, 150 °C; desolvation temperature, 500 °C; cone gas flow rate, 50 L/h; desolvation gas flow rate, 1000 L/h, MS^E low collision energy, 6 V; and MS^E high collision energy, 20−30 V. The elemental composition of each peak compound was calculated from the high-resolution MS data of the deprotonated molecular ion using MassLynx software, version 4.1 (Waters).

Preparation and Structure Elucidation of Quercetin Oxidation Products I−III. To a solution of quercetin (50 mg) in acetonitrile (50 mL) and water (50 mL) was added 90 mg of $FeCl_3 \cdot 6H_2O$ and the solution was stirred at 37 °C for 1 h. The solution was passed through a short column of Chelex100 (10 g), and the eluate was evaporated *in vacuo*. The residue obtained was purified by preparative HPLC under the following conditions: column, a 250 × 20 mm inner diameter, 5 μm, Cosmosil $5C_{18}$-AR-II (Nacalai Tesque); flow rate, 9.0 mL/min; solvent, 0.1% trifluoroacetic acid in 85:15 (v/v) water/acetonitrile. All eluates from 18−24 min were collected and evaporated to give product I (**21**, 40 mg). Product I (**21**): HR-ESIMS (m/z) $[M - H]^-$, calcd for $C_{15}H_9O_8$, 317.0297; found, 317.0284. UV λ_{max} (acetonitrile/H_2O/acetic acid), 325 (sh), 292 nm. ^1H NMR (acetone-d_6) δ: 7.64 (1H, d, J = 2.4 Hz), 7.57 (1H, dd, J = 8.1 and 1.8 Hz), 6.92 (1H, d, J = 8.1 Hz), 6.13 (1H, brd, J = 1.2 Hz), 6.12 (1H, brd, J = 1.2 Hz) [6.13 (2H, brs)]. Products II (**22**, 1 mg) and III (**23**, 7 mg) were also isolated after oxidizing quercetin (55 mg) for 2 h with $FeCl_3 \cdot 6H_2O$ (99 mg) in acetonitrile−water [1:1 (v/v), 100 mL] at room temperature. Purification was carried out as follows: The reaction solution was passed through a Chelex100 column (10 g), and the eluate was purified by preparative HPLC after evaporation. Two peaks (14−16 and 22−25 min) were collected and evaporated to give products II (**22**) and III (**23**), respectively. Product II (**22**) (protocatechuic acid): ESIMS (m/z) 153 $[M - H]^-$ (100%). UV λ_{max} (acetonitrile/H_2O/acetic acid), 292, 260 nm. ^1H NMR (DMSO-d_6) δ: 8.30 (1H, br s), 7.31 (1H, d, J = 1.8 Hz), 7.26 (1H, J = 8.2 and 1.8 Hz), 6.76 (1H, J = 8.2 Hz). Product III (**23**) (2,4,6-trihydroxyphenylglyoxylic acid): ESIMS (m/z), 193 $[M - H]^-$ (40%), 195 (40%), 177 (50%), 153 (100%). UV λ_{max} (acetonitrile/H_2O/acetic acid), 292 nm. ^1H NMR (DMSO-d_6) δ: 5.62 (2H, s).

HPLC Analysis of the Reactions of Products I−III with MetMb. To each well of a microplate, 140 μL of 50 mmol/L phosphate buffer (pH 7.4), 10 μL of the appropriate concentration of each product in DMSO, and 150 μL of 120 μmol/L of MetMb or MbO_2 in the same buffer were added. The plate was incubated at 37 °C, and absorption at 582 and 500 nm was obtained at 1 h intervals. At the same intervals, aliquots (5 μL) were taken and injected into the HPLC unit. Analysis of the reaction products I−III was carried out under the following conditions: column, a 250 × 4.6 mm inner diameter, 5 mm, Cosmosil $5C_{18}$-AR-II (Nacalai Tesque); flow rate, 1.0 mL/min; solvent A, 1% acetic acid in water; solvent B, acetonitrile; linear gradient from 5 to 100% solvent B (40 min); and detection, absorbance at 280 nm. The concentration of each product in the reaction mixture was calculated using the above-mentioned equations.

RESULTS AND DISCUSSION

MetMb Reduction by Polyphenols. Ascorbic acid is known to potently reduce MetMb; however, the precise concentration required for this reduction *in vitro* has not yet been reported. First, we examined the effect of the ascorbic acid concentration (60−2400 μmol/L) on MetMb (60 μmol/L) in pH 7.4 phosphate buffer. The results obtained showed that 600 μmol/L ascorbic acid reduced MetMb gradually, forming MbO_2 equivalent to 80% of the initial amount of MetMb after 3 h at 37 °C. Therefore, these conditions were employed in experiments using 20 kinds of polyphenols and related phenolic compounds (Figure 1). Figure 2 shows the MetMb reduction

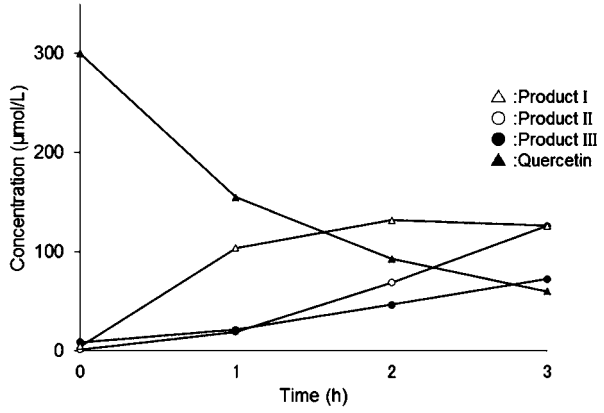

Figure 4. Time-course analytical data for products I−III in the reaction of quercetin and MetMb.

dx.doi.org/10.1021/jf404357h | J. Agric. Food Chem. 2014, 62, 893−901

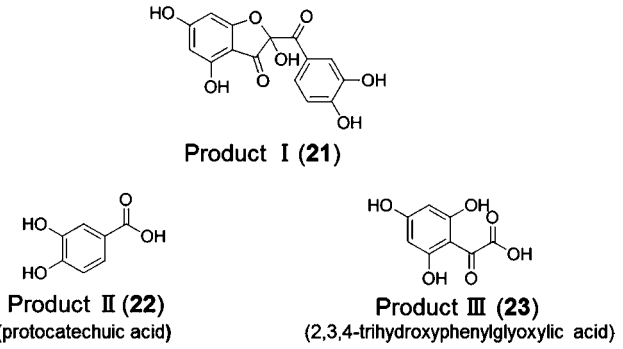

Figure 5. Chemical structures of products I–III.

and MbO_2 formation by the polyphenols. The data are shown in percentage of MbO_2 in total myoglobins, which was calculated on the basis of absorbance at 500 and 582 nm of each 60 μmol/L pure MbO_2 and MetMb.[18] Although most polyphenols showed weak reducing activity as reductants, sinapic acid (**17**) (600 μmol/L) exhibited apparent potency, followed by catechin (**2**), nordihydroguaiaretic acid (**12**), taxifolin (**19**), morin (**10**), and ferulic acid (**5**). Unfortunately, the activity of some flavonoid polyphenols could not be measured at this concentration because of insolubility. Therefore, the activity of 300 μmol/L of these flavonoids [kaempferol (**8**), luteolin (**9**), myricetin (**11**), and quercetin (**14**)] was measured; the results are illustrated in the lower part of Figure 2. As shown there, kaempferol (**8**), quercetin (**14**),

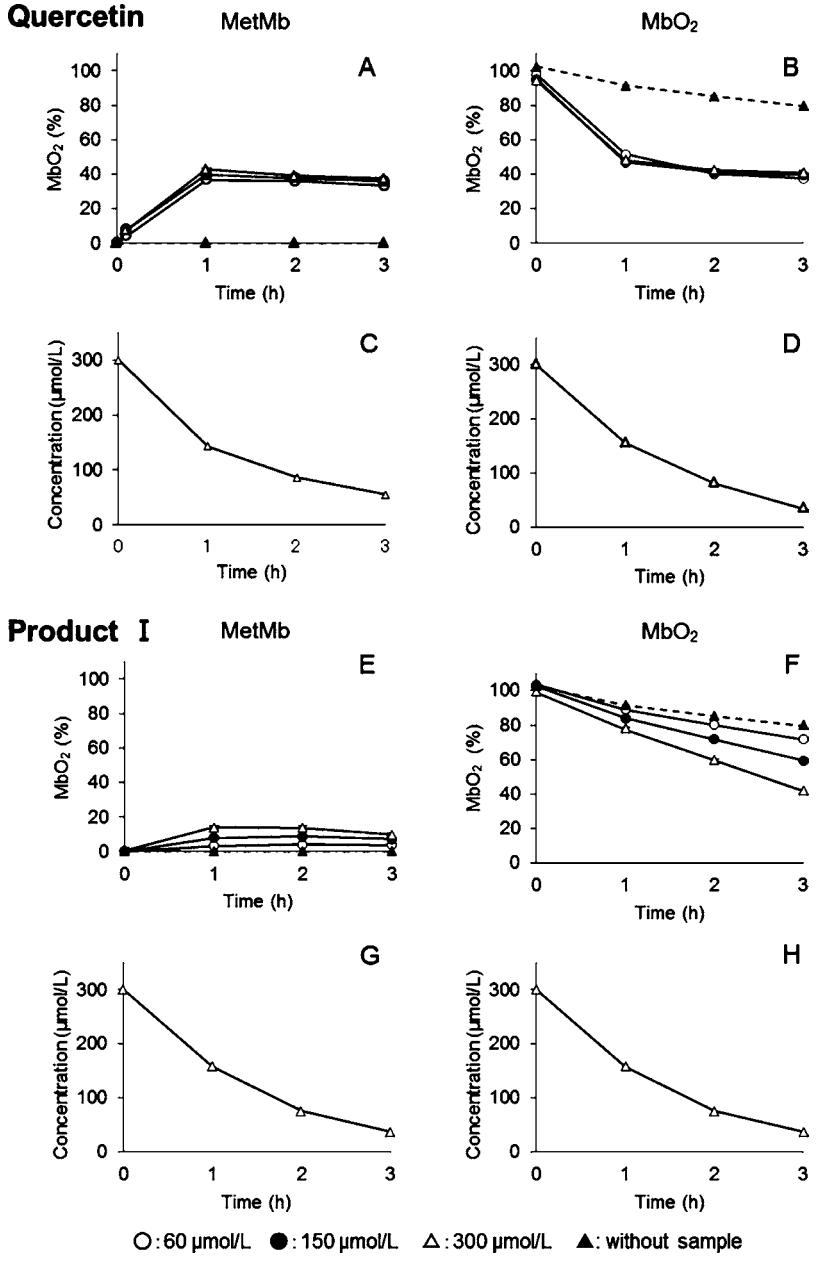

Figure 6. MetMb reduction andMbO_2 oxidation of quercetin and product I and changes in concentrations of quercetin and product I in the reaction solutions. Panels A and E refer to MetMb reduction. Panels B and F refer to MbO_2 oxidation. Panels C and G express concentration changes during MetMb reduction. Panels D and H express concentration changes during MbO_2 oxidation to MetMb. Data are expressed as the mean ± SD; note that most SD values are smaller than the symbols used in the graph.

dx.doi.org/10.1021/jf404357h | J. Agric. Food Chem. 2014, 62, 893–901

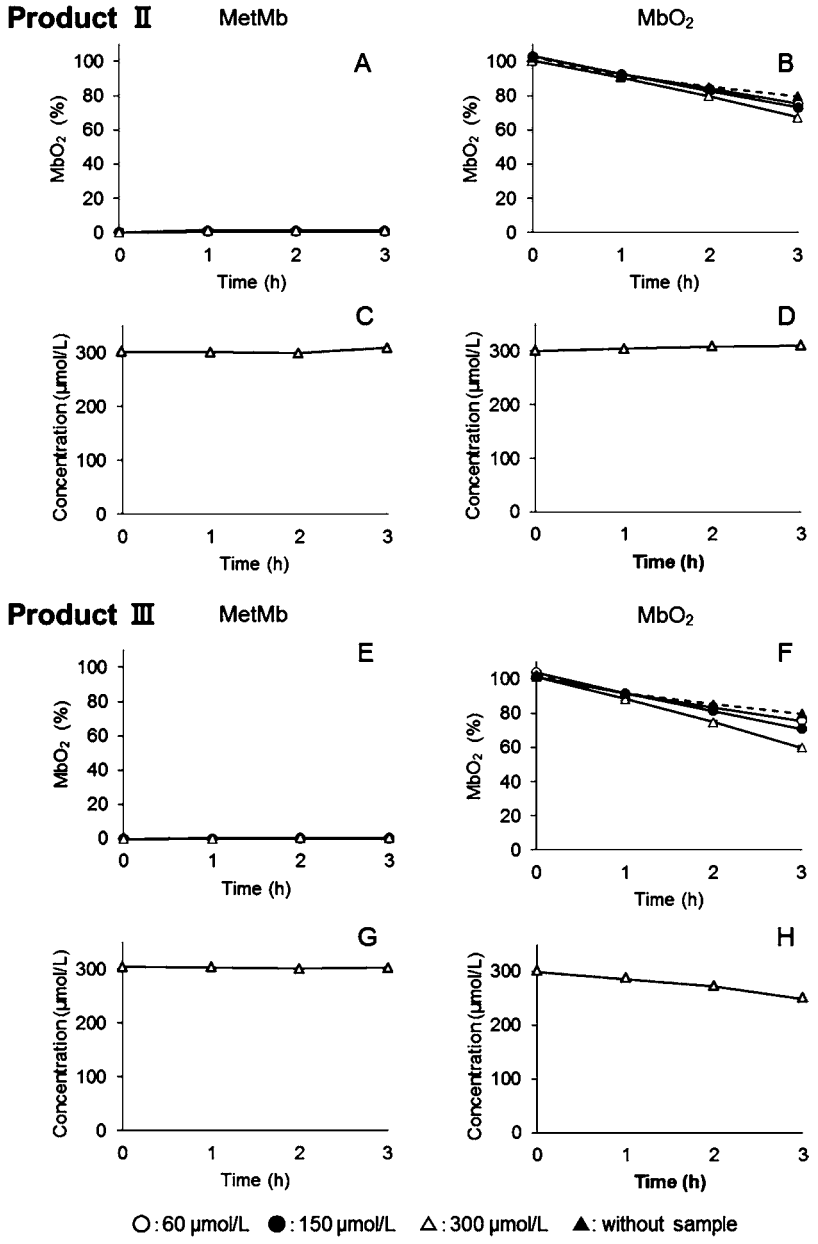

Figure 7. MetMb reduction and MbO_2 oxidation of products II and III and changes in concentrations of products II and III in the reaction solutions. Panels A and E refer to MetMb reduction. Panels B and F refer to MbO_2 oxidation. Panels C and G express concentration changes during MetMb reduction. Panels D and H express concentration changes during MbO_2 oxidation to MetMb. Data are expressed as the mean ± SD; note that most SD values are smaller than the symbols used in the graph.

and myricetin (**11**) showed apprant reducing activity even at this lower concentration. These compounds are flavonols, and flavonols are known to be potent antioxidants[19] with low reduction potential[20] relative to other flavonoids. Next, we undertook a chemical investigation of the high reducing activity of the flavonol, quercetin (**14**).

HPLC Analysis of Quercetin Products during MetMb Reduction. On the basis of redox principles, quercetin should be oxidized during MetMb reduction. We carried out a time-course analysis of the MetMb reducing reaction of quercetin by HPLC. Figure 3 shows analytical results at 2 h. In the HPLC profile, three noticeable peaks were observed at retention times of 7.8, 8.3, and 11.3 min, in addition to quercetin (17.8 min). The time course of the formation of these reaction products is summarized in Figure 4. Figure 4 shows three new compounds (products I–III) coinciding with the decrease in quercetin levels during the reaction. The formation of product I was faster than that of products II and III, indicating that product I was the first oxidation product from quercetin and that products II and III were secondary products, possibly derived from product I. The MetMb reduction was completed by 1 h, and the produced MbO_2 remained at the same concentration (the bottom–right panel of Figure 2). Product I reached a plateau after 2 h, while products II and III continued to increase and quercetin decreased over 3 h. These results suggested that quercetin was largely responsible for MetMb reduction, while the other products probably contributed to the maintenance of MbO_2 levels.

Identification of Products I–III from Quercetin. To identify the structures of products I–III, we applied various

dx.doi.org/10.1021/jf404357h | J. Agric. Food Chem. 2014, 62, 893–901

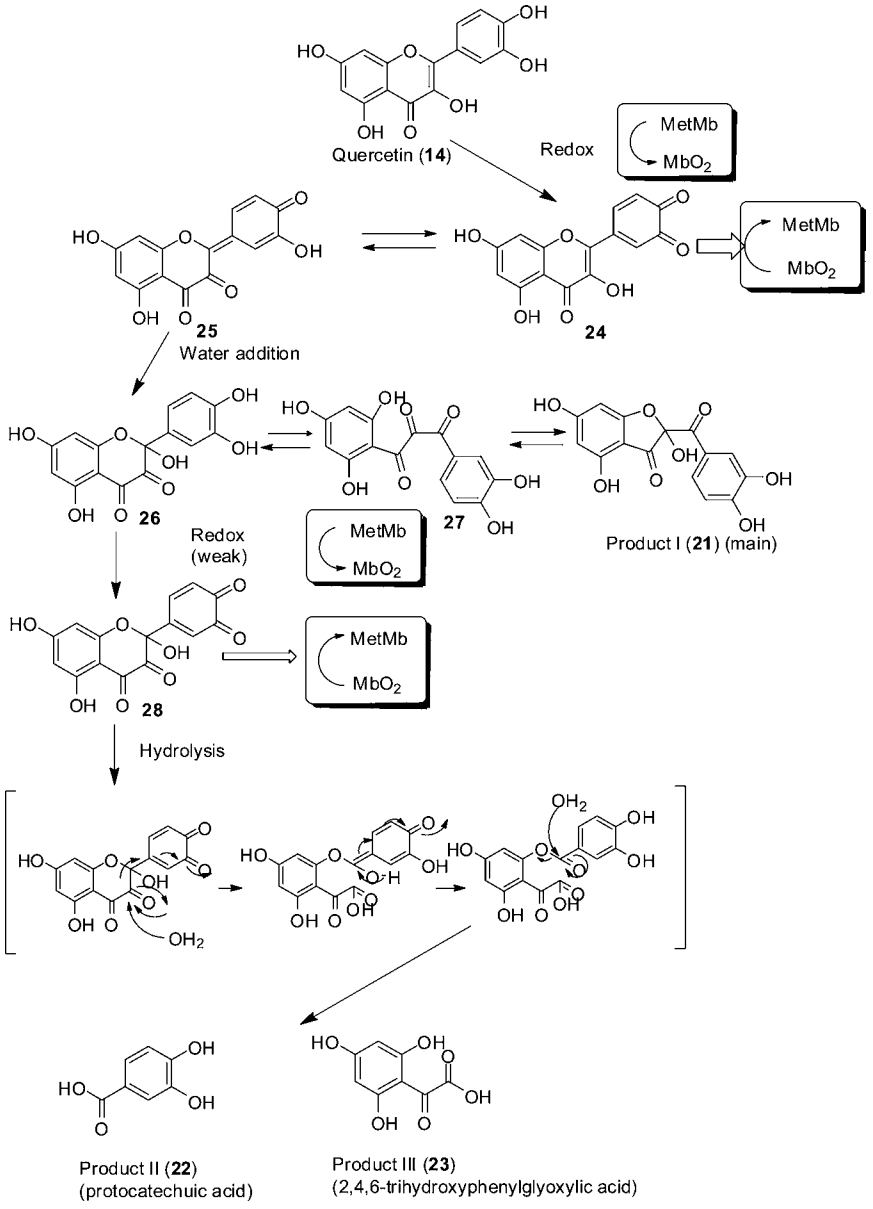

Figure 8. Proposed mechanism for MbO_2 production from MetMb by quercetin.

chemical reagents to quercetin. We found that oxidation by ferric chloride afforded better results than other oxidation reagents. Treatment of quercetin with ferric chloride in acetonitrile and water gave a mixture of the same products as observed in the MetMb reduction. The products were purified by preparative HPLC using an ODS column to give products I–III. ^{1}H NMR, UV, and MS analysis of these products revealed that they are products of oxidation and oxidative degradation of quercetin. The structures of these products are shown in Figure 5. Products II (**22**) (protocatechuic acid) and III (**23**) (2,4,6-trihydroxyphenylglyoxylic acid) were previously identified from peroxidase oxidation of quercetin, and their UV spectra were identical with the reported values.[21] Although product I was also identified previously from the oxidation of quercetin[22−24] and the structure is tentatively identified as product I (**21**) in Figure 5, it may exist as a tautomer because HPLC of product I showed two slightly split peaks; however, the corresponding pure forms could not be isolated under the analytical conditions because of their rapid conversion to each other. Also, the chemical shifts of the ^{1}H NMR signals for 6 and 8 positions were observed at slightly different values depending up the on concentration. Tautomerism in product I has been reported by several groups,[22,23,25−27] but the observed UV spectrum of product I suggested that it exists mainly as structure I (**21**) (Figure 5).

Effect of Quercetin and Its Oxidation Products on the Redox State of Mb. The effects of three isolated quercetin oxidation products on the redox state of Mb were examined and compared to quercetin. Results for the change in the concentration of MbO_2 in the presence of 60−300 μmol/L quercetin are shown in Figure 6. Panels A and B of Figure 6 show that quercetin oxidizes MbO_2 and reduces the MetMb concentration independently; both reactions converged to ca. 40% MbO_2. Although quercetin and Mb seemed to be under redox equilibrium, quantitative analysis of the reaction mixture (panels C and D of Figure 6) showed that quercetin decreased continuously after reaching equilibrium. These results indicate that the oxidation products identified also influence the redox

dx.doi.org/10.1021/jf404357h | J. Agric. Food Chem. 2014, 62, 893−901

state of Mb. Panels E−H of Figure 6 and panels A−H of Figure 7 show the redox activity of these products toward MbO_2 and MetMb, and their concentration changes during the reaction. As shown in panels E and F of Figure 6, product I also oxidizes MbO_2 and reduces MetMb, but efficiency is much lower than quercetin in both cases. Products II and III have negligible oxidative activity toward MbO_2 and no reductant activity toward MetMb (panels A, B, E, and F of Figure 7). These results for the redox relation between myoglobins and these products were confirmed by HPLC analysis of products I−III in the reaction mixture (panels G and H of Figure 6 and panels C, D, G, and H of Figure 7). As shown in panels G and H of Figure 6, the concentration of product I (300 μmol/L) was decreased with myoglobins, revealing that product I influences the redox reactions with myoglobins. On the other hand, treatment of products II and III with MetMb and MbO_2 shows a negligible change in the concentration, indicating that products II and III are stable under these reaction conditions and do not strongly influence the redox state of Mb.

Proposed Mechanism for MetMb Reduction by Quercetin. We proposed a mechanism for MetMb reduction by quercetin *in vitro* (Figure 8). First, quercetin reduces MetMb to produce bright red MbO_2; however, oxidized quercetin drivatives, including the B-ring quinone (**24**), enhance MbO_2 oxidation. It has been found that electrophilic compounds, such as α,β-unsaturated aldehydes enhanced MbO_2 oxidation.[28] These electrophiles were indicated to react with Mb at nucleophilic amino acid residues, destabilizing MbO_2.[29] Quinone derivatives of polyphenols also have the same electrophilic tendency[30,31] to alter the tertiary structure of proteins, such as MbO_2, which is rich in nucleophilic amino acid residues, such as histidine and lysine.[32] Polyphenols are potent antioxidants bearing catechol moieties, which during oxidation afford *ortho*-quinone derivatives, and some polyphenols afford quinone derivatives that accumulate in the system.[33,34] To date, no quinone derivative has been isolated from quercetin or related flavonols, but several water adducts have been identified.[24,35,36] These results suggested that water addition to the oxidized flavonols is fast and quickly yields phenolic compounds that prevent quinone−protein interactions. As illustrated in Figure 8, one molecule of water is added to a tautomer of the quinone (**25**) and affords product I (**21**) via water adducts **26** and **27**, which has a catechol moiety that can reduce MetMb. Although reduction by product I (**21**) also produces another quinone derivative **28** that may oxidize MbO_2, its efficiency is much lower than that of quercetin. In addition to its low redox activity, product I (**21**) is converted to products II (**22**) and III (**23**) via oxidation and subsequent hydrolysis. Thus, products II (**22**) and III (**23**) exhibit almost no redox activity toward MetMb or MbO_2. These properties are also supported by the higher reduction potential of product II (E_7 of 0.60 V)[37] and that of quercetin (E_7 of 0.33 V).[38] From the results of this investigation, we propose that most of the predominant MetMb-reducing activity of quercetin and related flavonols is because of their high propensity to reduce MetMb combined with the rapid conversion of their oxidized products, which destabilize MbO_2, to redox-stable compounds.

The results of this investigation showed that some polyphenols were applicable to reduce MetMb to bright red MbO_2. The bright red color is very important to maintain the freshness and quality of meat and meat-derived foods. The proposed reduction mechanism of one of polyphenols, quercetin, have revealed high potential for application of polyphenols to maintain the fresh meat color as reductants and also to develop a new color-maintaining technique for meat foods based on the redox chemistry of polyphenols.

■ ASSOCIATED CONTENT

Supporting Information

Figure for the concentration effect on MetMb reduction by L-ascorbic acid. This material is available free of charge via the Internet at http://pubs.acs.org.

■ AUTHOR INFORMATION

Corresponding Author

*Telephone/Fax: +81-88-656-7244. E-mail: masuda.ias@tokushima-u.ac.jp.

Funding

Financial support was from the Japan Society for the Promotion of Science (KAKENHI 23500939).

Notes

The authors declare no competing financial interest.

■ REFERENCES

(1) Mancini, A. R.; Hunt, C. M. Current research in meat color. *Meat Sci.* **2005**, *71*, 100−121.

(2) McMillin, K. W. Where is MAP going? A review and future potential of modified atmosphere packaging for meat. *Meat Sci.* **2008**, *80*, 42−65.

(3) Samejima, K. Meat processing method. In *Science of Meat*; Okita, A., Ed.; Asakura: Tokyo, Japan, 1996; Chapter 7.2, pp 141−157.

(4) Faustman, C.; Sun, Q.; Mancini, R.; Suman, S. P. Myoglobin and lipid oxidation interactions: Mechanistic bases and control. *Meat Sci.* **2010**, *86*, 86−94.

(5) Okita, A. Development of good taste by aging. In *Science of Meat*; Okita, A., Ed.; Asakura: Tokyo, Japan, 1996; Chapter 4.2, pp 71−87.

(6) Jakobsen, G.; Bertelsen, G. The use of CO_2 in packaging of fresh red meats and its effect on chemical quality changes in the meat: A review. *J. Muscle Foods* **2002**, *13*, 143−168.

(7) Morrissey, E. R.; Jacob, R. H.; Pluske, J. M. Perception of red brown colour by consumer. *Proceedings of the 54th International Congress of Meat Science and Technology*; Helsinki, Finland, Aug 10−15, 2008; Session 9, http://www.icomst.helsinki.fi/ICoMST2008 (accessed Dec 28, 2013).

(8) O'Keeffe, M.; Hood, D. E. Biochemical factors influencing metmyoglobin formation on beef from muscles of differing colour stability. *Meat Sci.* **1982**, *7*, 209−228.

(9) Masuda, T.; Inai, M.; Miura, Y.; Masuda, A.; Yamauchi, S. Effect of polyphenols on oxymyoglobin oxidation: Prooxidant activity of polyphenols in vitro and inhibition by amino acids. *J. Agric. Food. Chem.* **2013**, *61*, 1097−1104.

(10) Fox, J. B.; Keyser, S.; Nicholas, R. A. Pyridine catalysis of ascorbate reduction of metmyoglobin. *J. Food Sci.* **1975**, *40*, 435.

(11) Tukahara, K.; Yamamoto, Y. Kinetic studies on the reduction of metmyoglobins by ascorbic acid. *J. Biochem.* **1983**, *93*, 15−22.

(12) Ashida, S.; Naguchi, F. S.; Sato, R. Development of a spectrophotometric assay system for evaluating reducibility of water-soluble substances. *Food Sci. Technol. Res.* **2004**, *10*, 432−436.

(13) Mordente, A.; Martorana, G. E.; Santini, S. A.; Miggiano, D. A. G.; Petti, T.; Giardina, B.; Battino, M.; Littarru, P. G. Antioxidant effect of coenzyme Q on hydrogen peroxide-activated myoglobin. *Clin. Invest.* **1993**, *71*, S92−S96.

(14) Romero, F. J.; Ordoňez, I.; Arduini, A.; Cadenas, E. The reactivity of thiols and disulfides with different redox states of myoglobin. Redox and addition reaction and formation of thiyl radical intermediates. *J. Biol. Chem.* **1992**, *3*, 1680−1688.

(15) Khalife, H. K.; Lupidi, G. Reduction of hypervalent states of myoglobin and hemoglobin to their ferrous forms by thymoquinone:

The role of GSH, NADH and NADPH. *Biochim. Biophys. Acta* **2008**, *1780*, 627−637.
(16) Decker, E. A.; Can, W. K. M.; Livisay, S. A.; Butterfield, D. A.; Faustman, C. Interactions between carnosine and the different redox states of myoglobin. *J. Food Sci.* **1995**, *60*, 1201−1204.
(17) Bowen, W. J. The absorption spectra and extinction coefficients of myoglobin. *J. Biol. Chem.* **1949**, *179*, 235−245.
(18) American Meat Science Association (AMSA). *Meat Color Measurement Guidelines*; AMSA: Champaign, IL, 2012; Section X, pp 59−65.
(19) Rice-Evans, C.; Miller, N. J.; Paganga, G. Structure−antioxidant activity relationships of flavonoids and phenolic acids. *Free Radical Biol. Med.* **1996**, *20*, 933−956.
(20) Jovanovic, S. V.; Steenken, S.; Hara, Y.; Simic, M. G. Reduction potentials of flavonoid and model phenoxyl radicals. Which ring in flavonoids is responsible for antioxidant activity? *J. Chem. Soc., Perkin Trans. 2* **1996**, 2497−2504.
(21) Takahama, U.; Hirota, S. Deglucosidation of quercetin glucosides to the aglycone and formation of antifungal agents by peroxidase-dependent oxidation of quercetin on browning of onion scales. *Plant Cell Physiol.* **2000**, *41*, 1021−1029.
(22) Jørgensen, L. V.; Cornett, C.; Justesen, U.; Skibsted, L. H.; Dragsted, L. O. Two-electron electrochemical oxidation of quercetin and kaempferol changes only the flavonoid C-ring. *Free. Radical Res.* **1998**, *29*, 339−350.
(23) Jungbluth, G.; Rühling, I.; Ternes, W. Oxidation of flavonols with Cu(II), Fe(II) and Fe(III) in aqueous media. *J. Chem. Soc., Perkin Trans. 2* **2000**, 1946−1952.
(24) Jungbluth, G.; Ternes, W. HPLC separation of flavonols, flavones and oxidized flavonols with UV-, DAD-, electrochemical and ESI-ion trap MS detection. *Fresenius' J. Anal. Chem.* **2000**, *367*, 661−666.
(25) Krishnamachari, V.; Levine, L. H.; Paré, P. W. Flavonoid oxidation by the radical generator AIBN: A unified mechanism for quercetin radical scavenging. *J. Agric. Food Chem.* **2002**, *50*, 4357−4363.
(26) Zhou, A.; Kikandi, S.; Sadik, O. A. Electrochemical degradation of quercetin: Isolation and structural elucidation of the degradation products. *Electrochem. Commun.* **2007**, *9*, 2246−2255.
(27) Zhou, A.; Sadik, O. A. Comparative analysis of quercetin oxidation by electrochemical, enzymatic, autoxidation, and free radical generation techniques: A mechanistic study. *J. Agric. Food Chem.* **2008**, *56*, 12081−12091.
(28) Faustman, C.; Liebler, D. C.; McClure, T. D.; Sun, Q. α,β-Unsaturated aldehydes accelerate oxymyoglobin oxidation. *J. Agric. Food Chem.* **1999**, *47*, 3140−3144.
(29) Alderton, A. L.; Faustman, C.; Liebler, D. C.; Hill, D. W. Induction of redox instability of bovine myoglobin by addition with 4-hydroxyl-2-nonenal. *Biochemistry* **2003**, *42*, 4398−4405.
(30) Bitter, S. When quinones meet amino acids: Chemical, physical and biological consequences. *Amino Acids* **2006**, *30*, 205−224.
(31) Hullell, R. F.; Finot, P. A.; Cuo, J. L. Protein−polyphenol reactions 1. Nutritional and metabolic consequences of the reaction between oxidized caffeic acid and the lysine residues of casein. *Br. J. Nutr.* **1982**, *47*, 191−211.
(32) *Protein Knowlegebase (UniportKB)*; http://www.uniprot.org/uniprot/P68082 (accessed Dec 28, 2013).
(33) Sawai, Y.; Moon, J.-H.; Sakata, K.; Watanabe, N. Effects of structure on radical-scavenging abilities and antioxidative activities of tea polyphenols: NMR analytical approach using 1,1-diphenyl-2-picrylhydrazyl radicals. *J. Agric. Food Chem.* **2005**, *53*, 3598−3604.
(34) Masuda, T.; Inaba, Y.; Takeda, Y. Antioxidant mechanism of carnosic acid: Structure identification of two oxidation products. *J. Agric. Food Chem.* **2001**, *49*, 5560−5565.
(35) Awad, H. M; Boersma, M. G.; Boeren, S.; van Bladeren, P. J.; Vervoot, J.; Rietjens, M. C. M. Structure−activity study on the quinone/quinone methide chemistry of flavonoids. *Chem. Res. Toxicol.* **2001**, *14*, 398−408.
(36) Hvattum, E.; Stenstrøm, T.; Eleberg, D. Study of the reaction products of flavonoids with 2,2-diphenyl-1-picrylhydrazyl using liquid chromatography coupled with negative electrospray ionization tandem mass spectrometry. *J. Mass Spectrom.* **2004**, *39*, 1570−1581.
(37) Lien, E. J.; Ren, S.; Bui, H.-H.; Wang, R. Quantitative structure−activity relationship analysis of phenolic antioxidants. *Free Radical Biol. Med.* **1999**, *26*, 285−294.
(38) Pietta, P.-G. Falvonoids as antioxidants. *J. Nat. Prod.* **2000**, *63*, 1035−1042.

300 HR was obtained from Amersham Biosciences. Other chemicals and reagents were of analytical grade.

Extraction and Purification. The pulp tissues of *L. chinensis* (500 g) were defatted with ethanol for 8 h and then extracted with water (1:20, w/v) at 85 °C for 3 h. This process was repeated three times. After centrifugation at 3018*g* for 10 min, the supernatant was concentrated and precipitated with 95% ethanol (2 times volume) at 4 °C for 12 h. The precipitate was then dissolved in distilled water and intensively dialyzed for 2 days against distilled water (cutoff M_w 3500 Da). After concentration, the solution was deproteinized with Sevag reagent ($CHCl_3$/BuOH = 4:1, v/v) for 15 min, and the procedure was repeated seven times. Finally, the extracts were centrifuged to remove insoluble material, and the supernatant was lyophilized as the crude polysaccharide (LCP50).

The crude polysaccharide was dissolved in distilled water and fractionated on a DEAE-cellulose-52 column (5.0 × 70.0 cm) equilibrated with distilled water with a linear gradient from 0 to 1.0 M NaCl at a flow rate of 0.7 mL/min. All of the fractions were assayed for carbohydrate content by using the phenol−sulfuric acid method, and one sharp peak was pooled, dialyzed, concentrated, and further purified by a Sephadex G-100 column (1.6 × 80.0 cm) and Sephacryl S-300 HR (1.2 × 100.0 cm) eluting with water, to afford a purified polysaccharide (LCP50W).

General Analysis. The carbohydrate content was determined according to the phenol−sulfuric acid method using glucose as a standard.[14] Sulfate content was measured according to the referenced method.[15] Uronic acid content was determined by the carbazole−sulfuric acid method using glucuronic acid as a standard.[16] Fourier transform infrared (FT-IR) spectroscopy was recorded using a Tensor 27 Bruker instrument. The sample was ground with KBr powder and then pressed into pellets for FT-IR measurement in the frequency range of 4000−500 cm^{-1}.[6] Optical rotation was measured using a Jasco Polarimeter model P-1020 at 23 °C.

Determination of Homogeneity and Number-Average Molecular Weight. The homogeneity and number-average molecular weight of LCP50W were determined on a Waters Acquity UPLC system equipped with a TSK-SW4000 column and an evaporative light scattering detector (ELSD). The sample solution (10 mL, 1.0 mg/mL) was injected each run, with water as the mobile phase at a flow rate of 0.3 mL/min. The linear regression was calibrated with T-series dextran standards (M_w = 5 × 10^6, 2 × 10^5, 7 × 10^4, 1 × 10^4, and 3 × 10^3 Da).[17]

Chemical Composition Determination. LCP50W (5 mg) was hydrolyzed for 6 h at 110 °C with 2 mL of 2 M TFA. Excess acid was removed through codistillation with MeOH. High-performance anion-exchange chromatography with pulsed amperometric detection (HPAEC-PAD) was used for identification and quantification of the monosaccharides. The diluted sample was passed through a 0.45 μm filter and injected into the HPAEC-PAD system (Dionex-5500, Dionex Corp., Canada).[18] LCP50W (30 mg) was partially hydrolyzed with 0.05 M TFA at 100 °C for 6 h, and TFA was removed by evaporation. The hydrolysate was dialyzed against distilled water for 48 h in a dialysis bag with a 3500 Da cutoff. The fraction outside the dialysis bag was collected and evaporated to dryness (fraction 1). The fraction in the dialysis bag was dried by evaporation under reduced pressure and then hydrolyzed with 0.5 M TFA. The hydrolysate was also dialyzed against distilled water for 48 h. The fraction out of the dialysis bag (fraction 2) and the fraction in the dialysis bag (fraction 3) were collected and evaporated to dryness, respectively. Fractions 1, 2, and 3 were hydrolyzed with 2 M TFA at 110 °C for 6 h and then analyzed by HPAEC-PAD.[6]

Periodate Oxidation and Smith Degradation Analysis. LCP50W (15 mg) was dissolved in distilled water, and then 15 mM $NaIO_4$ (25 mL) was added into the solution. Thirty milliliters of the solution was drawn at 6 h intervals in the dark 4 °C and then diluted to 5 mL with the water and measured in a spectrophotometer at 223 nm.[19] The reaction was completed after 84 h, and ethylene glycol (0.2 mL) was added to the solution to decompose the excess reagent. Consumption of HIO_4 was measured according to a spectrophotometric method,[20] and the production of formic acid was determined by titration with 0.060 M NaOH. The reaction mixture was dialyzed against distilled water, and the nondialysate was reduced with $NaBH_4$ (30 mg) for 24 h. The pH was adjusted to 6.0 with 0.1 M HOAc, and then the solution was dialyzed. The nondialysate was lyophilized and hydrolyzed with 2 M TFA at 110 °C for 6 h. Finally, the products were acetylated and analyzed by GC.[7]

Methylation and GC-MS Analysis. LCP50W (20 mg) was methylated six times according to the method described by Hakomori.[21] Complete methylation was confirmed by the disappearance of the OH band (3200−3700 cm^{-1}) in the IR spectrum. The methylated products were hydrolyzed, reduced, and acetylated. The resulting alditol acetates were analyzed by GC-MS.[22] Linkages were identified according to the relative retention time and fragmentation patterns. The monosaccharide molar ratio was calibrated using the peak areas and response factor in GC.

NMR Spectroscopy. LCP50W (60 mg) was dried in a vacuum oven (70 °C) for 6 h, and then the dried sample was dissolved in 2 mL of D_2O and lyophilized. This procedure was repeated three times to completely replace H with D, and the sample was finally dissolved in D_2O for 3 h before NMR analysis. ^{13}C NMR and ^{1}H NMR spectra were recorded on a Bruker AMX 500 FT spectrometer (Bruker, Germany).

Ultrastructure of LCP50W. A scanning electron microscope (SEM) image of LCP50W was obtained by means of an environmental scanning electron microscope (ESEM, Philips XL-30, Philips-FEI Co., Eindhoven, The Netherlands). The dried powder sample was placed on a specimen holder fixed with double-side adhesive tapes and then sputtered with gold powder using a sputter coater. The sample was observed with 1000-, 5000-, 10000-, and 30000-fold magnification at an accelerating potential of 5.0 kV under a high-vacuum condition.

Animals and Cells. Kunming mice (grade II, SCXK 2011-2015, 20−25 g, 6−8 weeks old) were obtained from the Experimental Animal Center, Sun Yat-sen University, China. Animals were acclimatized for at least 7 days prior to use and maintained in a temperature-controlled environment (22 ± 2 °C) with a 12 h light−dark cycle and with free access to water and standard rodent chow.

YAC-1 lymphoma cell line was obtained from The Cell Bank of Type Culture Collection of Chinese Academy of Sciences (Shanghai, China). It was maintained in RPMI 1640 medium supplemented with 100 IU/mL penicillin, 100 μg/mL streptomycin, and 10% FBS at 37 °C under humidified air with 5% CO_2.

Splenic Lymphocyte Proliferation Assay. The assay for splenic lymphocyte proliferation was performed by MTT method.[23] Briefly, spleens were aseptically removed from sacrificed mice with scissors and forceps in cold phosphate-buffered saline (PBS) and then minced in aseptic PBS. The splenocytes were obtained by pressing spleen tissue through nylon mesh filters. The removal of blood cells in the splenocyte suspension was carried out by washing the cells with Tris-NH_4Cl three times. The isolated splenocytes were counted by trypan blue exclusion with viability of >95%, and then they were placed into the 96-well flat-bottom microplates at 5 × 10^6 cells/mL in RPMI 1640 medium with or without LCP50W. The groups that combined with Con A were cotreated with Con A (5 μg/mL), whereas the negative control was treated with RPMI 1640 medium only. Each group was repeated in three wells. The cells were incubated at 37 °C under 5% CO_2 for 48 h, and then 20 μL of MTT (5 mg/mL) was added to each well, with further incubation for another 4 h. After removal of MTT by centrifugation at 1811*g* for 5 min at 4 °C, the formazan precipitate was solubilized in DMSO (200 μL/well). Splenic lymphocyte proliferation was measured by determining the optical density (OD) at 570 nm using multifunctional microplate reader (Boteng, USA).

Natural Killer (NK) Cell Cytotoxicity Assay. Lymphocytes from each mouse were prepared as effector cells, whereas YAC-1 cells were used as target cells. In brief, the effector cells (1 × 10^7 cells/mL) were incubated for 48 h with LCP50W ranging from 3.9 to 250 μg/mL. Then the same volume of YAC-1 cells (2 × 10^5 cells/mL, effector cells/target cells = 50:1) was added to the wells of 96-well round-bottom microwell plates in the sample group. In addition, the wells that had only added effector cells or target cells were respectively taken as effector and target cells control groups. Each group was repeated in three wells. After 4 h of incubation, the MTT method was used to

detect NK cell activity. The OD value at 570 nm for each well was measured using a multifunctional microplate reader (Boteng, USA). The percentage of NK cell cytotoxicity was calculated from the formula

$$\text{NK cell cytotoxicity} = [1 - (OD_S - OD_E)/OD_T] \times 100\%$$

where OD_S refers to the OD value of test sample, OD_E refers to the OD value of effector cell control, and OD_T refers to the OD value of target cell control.[24]

Measurement of Th1/Th2 Cytokines. The levels of cytokines IFN-γ and IL-4 (especially secreted by Th1 and Th2 cells, respectively) were determined using sandwich ELISA kits. Briefly, lymphocytes from each mouse were prepared as described above, and then they were placed into the 24-well flat-bottom microplates at 5×10^6 cells/mL in RPMI 1640 medium with or without LCP50W, in which concentrations were 3.9, 15.6, and 62.5 μg/mL respectively. Meanwhile, all wells were in the presence of Con A (5 μg/mL). Each group was repeated in three wells. After incubation for 48 h, the lymphocyte supernatant was collected by centrifugation at 906*g* for 15 min. The cytokine concentrations were assayed according to the cytokine ELISA protocol from the manufacturer's instructions.[25]

Determination of Th1/Th2 Specific Transcription Factors.[26] Lymphocytes were prepared as described above, and then they were placed into the 6-well flat-bottom microplates at 5×10^6 cells/mL in RPMI 1640 medium with or without LCP50W, in which concentrations were 3.9, 15.6, and 62.5 μg/mL, respectively. All wells were in the presence of Con A (5 μg/mL). Each group was repeated in three wells. After incubation for 48 h, the lymphocytes were collected by centrifugation at 1811*g* for 5 min. The collected lymphocytes were homogenized using Trizol reagent, and then chloroform was added to remove proteins. Isopropanol was used to precipitate total RNA. RNA pellets were dissolved in 20 μL of diethylpyrocarbonate (DEPC)-treated water. Total RNA was converted into cDNA using a Veriti 96-well thermal cycler (Applied Biosystems), and cDNA was amplified by PrimeScript One Step RT-PCR kit ver. 2. Primers were designed and synthesized by Shanghai Sangon Biotech. The sequences of specific primers are listed in Table 1.

Table 1. Primers Used in This Study

primer	sequence (5′−3′)	product size (bp)
mouse T-bet forward	GCCAGGGGAACCGCTTATATG	136
mouse T-bet reverse	GACGATCATCTGGGTCACATTGT	
mouse GATA-3 forward	TCTGGAGGAGGAACGCTAATGG	408
mouse GATA-3 reverse	GAACTCTTCGCACACTTGGAGACTC	
mouse β-actin forward	ATGTTTGAGACCTTCAACAC	491
mouse β-actin reverse	CACGTCACTTCATGATGG	

The reaction conditions were as follows: 50 °C/30 min for reverse transcription, 94 °C/2 min for initial denaturation, amplification for 30 cycles (94 °C/30 s for denaturation, 58 °C/30 s for annealing, and 72 °C/40 s for extension), and hold at 4 °C. PCR products (5 μL) were analyzed by electrophoresis in a 1.5% agarose gel for 30 min. Then the electrophoresis bands were observed by gel imager (Bio-Rad Corp., Hercules, CA USA), and photographs were taken. Image analysis software (Image J) was applied to analyze the DNA bands. The gray value of β-actin was taken as the standard one, and the results were represented by the ratios of gray values of transcription factor T-bet or GATA-3 to β-actin.

Determination of Cell Cycle Distribution. Lymphocytes from each mouse were prepared as described above, and then they were placed into the 24-well flat-bottom microplates at 5×10^6 cells/well in RPMI 1640 media with or without LCP50W, in which concentrations were 7.8, 31.2, and 125 μg/mL, respectively. The positive control was treated with Con A (5 μg/mL), whereas the negative control was treated with RPMI 1640 only. Each group was repeated in three wells. After incubation for 48 h, the lymphocytes were collected by centrifugation at 1811*g* for 5 min. The collected lymphocytes were fixed by cold 70% ethanol (10% FBS) at 4 °C for 8 h. The fixed cells were rinsed by PBS and then dyed by PI dye solution for 15 min. The dyed cells were filtered through 300 mesh nylon mesh and finally analyzed by a FACScan Flow cytometer (BD) with ModFit LT 4.0 software.

Statistical Analysis. The results are expressed as the means ± SD of data obtained from triplicate experiments. Statistical analysis was performed by independent *t* test in Statistical Analysis software SPSS 11.5, and $P < 0.05$ was regarded as statistically significant.

RESULTS AND DISCUSSION

Isolation, Purification, Determination of Molecular Weight, and Composition of LCP50W. After hot water extraction and ethanol precipitation, the crude polysaccharide (8.54 g) was obtained from pulp tissues of *L. chinensis*. After purification via DEAE-cellulose 52, Sephadex G-100, and Sephacryl S-300 HR column chromatography, the profile of LCP50W appeared as a single and symmetrical sharp peak, which was detected by the phenol−sulfuric acid method. The yield of LCP50W from the crude polysaccharide was calculated to be 55.6%. It also exhibited a single and symmetrical peak in HPLC-GPC analysis, which showed its homogeneity based on the distribution of molecular weight. Its molecular weight was determined as 4.72×10^4 Da according to the retention time. The total carbohydrate content of LCP50W was measured to be 98.2% (w/w), and the *m*-hydroxybiphenyl colorimetric test

Table 2. Monosaccharide Composition and Molar Ratio of LCP50W

	molar ratios				
	rhamnose	arabinose	galactose	glucose	mannose
LCP50W	2.45	5.78	1.00	4.58	1.32
fraction 1	nd	1.00	nd[a]	nd	nd
fraction 2	1.12	nd	1.00	nd	0.97
fraction 3	1.00	nd	nd	4.32	nd
Smith degradation	2.33	nd	1.00	nd	1.17

[a]nd, not detected.

Table 3. Methylation Analysis of LCP50W

methylated sugar	retention time (min)	molar ratio	mass fragments (*m*/*z*)	linkage pattern
2,3,5-Me_3-Ara	12.56	3.17	43, 45, 71, 87, 101, 117, 129, 161	T→
3,4-Me_2-Rha	14.02	0.96	87, 129, 131, 189	1→2
2,4-Me_2-Rha	14.92	0.98	43, 75, 85, 117, 131, 189	1→3
2,4,6-Me_3-Man	15.89	1.25	45, 87, 101, 118, 161, 234, 277	1→3
2,3,4-Me_3-Glc	16.84	1.13	87, 99, 101, 117, 129, 161	1→6
2,4,6-Me_3-Gal	17.33	1.09	43, 45, 87, 101, 117, 129, 161	1→3
3,4-Me_2-Glc	18.15	3.03	99, 101, 129, 149, 208, 234	1→2,6

dx.doi.org/10.1021/jf404752c | J. Agric. Food Chem. 2014, 62, 902−911

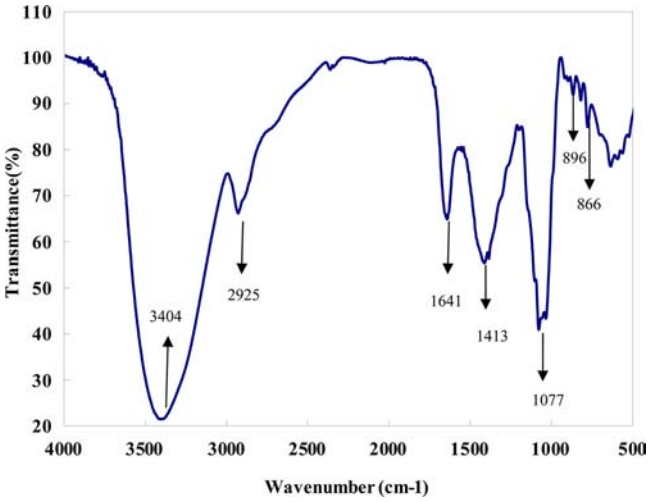

Figure 1. FI-IR spectrum of LCP50W.

was negative. LCP50W did not contain any sulfate esters. The uronic acid content of LCP50W was below the detection limit. The optical rotation of LCP50W was $[\alpha]_D^{20} = -35°$ (c 1.0, 23 °C, H_2O).

Structural Characterization of LCP50W. The monosaccharide composition of LCP50W is presented in Table 2. Five monosaccharides, rhamnose, arabinose, galactose, glucose, and mannose, were identified in the hydrolysate of LCP50W, and their ratios were 2.45:5.78:1.00:4.58:1.32 by HPAEC-PAD analysis. The component of fraction 3 in Table 2 showed that rhamnose and glucose may be the backbone of the structure of LCP50W. The analysis results of fractions 1 and 2 indicated that the branched structure of LCP50W was composed of rhamnose, galactose, and mannose and terminated with arabinose. The periodate-oxidized products were fully hydrolyzed and analyzed by HPAEC-PAD after periodate oxidation. The results shown in Table 2 indicate that there were rhamnose, galactose, and mannose in the oxidation products. The presence of rhamnose, galactose, and mannose revealed that some residues of rhamnose, galactose, and mannose were (1→3)-linked, (1→2,3)-linked, (1→2,4)-linked, (1→3,4)-linked, or (1→2,3,4)-linked, which could not be oxidized, respectively. There was no arabinose or glucose in the oxidation products (Table 2). It could be inferred that linkages of arabinose and glucose were (1→), (1→2), (1→6), and (1→2,6), which might be oxidized to produce glycerol.[27,28]

Methylation and GC-MS Analysis of LCP50W. Methylation analysis by GC-MS was used to provide more structural information for LCP50W. Seven homogeneous peaks of the fully methylated alditol acetates were obtained from GC-MS analysis. The results showed the presence of seven components, namely, 2,3,5-Me_3-Ara, 3,4-Me_2-Rha, 2,4-Me_2-Rha, 2,4,6-Me_3-Man, 2,3,4-Me_3-Glc, 2,4,6-Me_3-Gal, and 3,4-Me_2-Glc in a molar ratio of 3.17:0.96:0.98:1.25:1.13:1.09:3.03 (Table 3). According to their retention times, by comparison with mass spectrum patterns from the literature, and on the basis of the standard data in the CCRC Spectral Database for PMAAs, the linkages of D-galactose and L-mannose were deduced as (1→3), the linkage of L-arabinose was deduced as (1→), the linkages of D-glucose were deduced as (1→2) and (1→2,6), and the linkages of L-rhamnose were deduced as (1→2) and (1→3). These results showed a good correlation between terminal and branched residues. The molar ratio of these residues agreed overall with the monosaccharide composition of LCP50W described as above.

IR Spectroscopy and NMR Analysis. The infrared spectrum of LCP50W revealed the purified product's major functional groups and the chemical bonds (Figure 1). In the FT-IR spectrum, the characteristic bands in the regions of 3404, 2925, and 1641 cm^{-1} belonged to O−H bending, C−H bending, and associated water, respectively. The band at 1413 cm^{-1} was due to C−O bending; the bands at 1024−1154 cm^{-1} indicated pyranose. The characteristic absorptions at 866 and 896 cm^{-1} indicated that α- and β-configurations present simultaneously. Any signals corresponding to sulfate ester were not found in FT-IR spectrum of LCP50W. There was no absorption at 1740 cm^{-1}, indicating no existence of uronic acid in the polysaccharide structure.[14,29]

The spectra of ^{13}C NMR and ^{1}H NMR of LCP50W are shown in Figure 2. Signals of LCP50W in ^{13}C NMR and ^{1}H NMR spectra were assigned on the basis of the monosaccharide analysis, linkage analysis, and chemical shifts.[6,19,30−34] The resonances in the region of 95.0−110.0 ppm in ^{13}C NMR were attributed to the anomeric carbon atoms of D-galactose, D-glucose, L-rhamnose, L-mannose, and L-arabinose. The peaks at 95.9 ppm corresponded to C-1 of (1→3)-linked α-L-Man unit, 97.5 ppm corresponded to C-1 of (1→6)-linked α-D-Glc unit, 98.5 ppm corresponded to C-1 of (1→2)-linked α-LRha unit, 99.7 ppm corresponded to C-1 of (1→3)-linked α-D-Gal unit, 101.6 ppm corresponded to C-1 of (1→2,6)-linked α-D-Glc unit, 107.5 ppm corresponded to C-1 of (1→3)-linked β-L-Rha unit, and 109.2 ppm corresponded to C-1 of (1→)-linked α-L-Ara unit. The ^{1}H NMR spectrum contained seven signals at δ 5.23, 5.17, 5.13, 5.09, 5.07, 4.99, and 4.85 for the anomeric protons, indicating that seven residues, designated (1→)-linked α-L-Ara, (1→3)-linked α-L-Man, (1→3)-linked α-D-Gal, (1→2)-linked α-L-Rha, (1→2,6)-linked α-D-Glc, (1→6)-linked α-D-Glc, and (1→3)-linked β-L-Rha units, respectively, were present in LCP50W (Table 4). The results also indicated that the backbone was composed of (1→2,6)-linked α-D-glucopyranosyl residues, which branched at O-6. By means of ^{13}C and ^{1}H NMR spectra, the entire assignment of the ^{13}C and ^{1}H chemical shifts of LCP50W was achieved and is presented in Table 4.

On the basis of the results of HPAEC-PAD, GC-MS and NMR, the backbone of LCP50W should contain (1→3)-linked β-L-rhamnopyranosyl residues, (1→6)-linked α-D-glucopyranosyl residues, and (1→2,6)-linked α-D-glucopyranosyl residues, which branched at O-6. The three branches consisted of (1→2)-linked α-L-rhamnopyranosyl residues, (1→3)-linked α-D-galactopyranosyl residues, and (1→3)-linked α-L-mannopyranosyl residues, terminated with (1→)-linked α-L-arabinopyranosyl residues, respectively. From the aforementioned results, the repeating structural unit of LCP50W could be as shown in Figure 3.

Ultrastructure. Figure 4 presents scanning electron micrographs (SEM) of LCP50W at magnifications of 1000, 5000, 10000, and 30000. SEM observations revealed that the ultrastructure of LCP50W was mainly composed of a surface with a sheet-like appearance and randomly distributed ovoid-shape particles, with diameters of approximately 2.5 μm. These might be due to the branches and network structures of the polysaccharide.

Effect of LCP50W on Splenic Lymphocyte Proliferation. The spleen combines the innate and adaptive immune system in a uniquely organized way, which has become the most important organ for antibacterial and antifungal immune

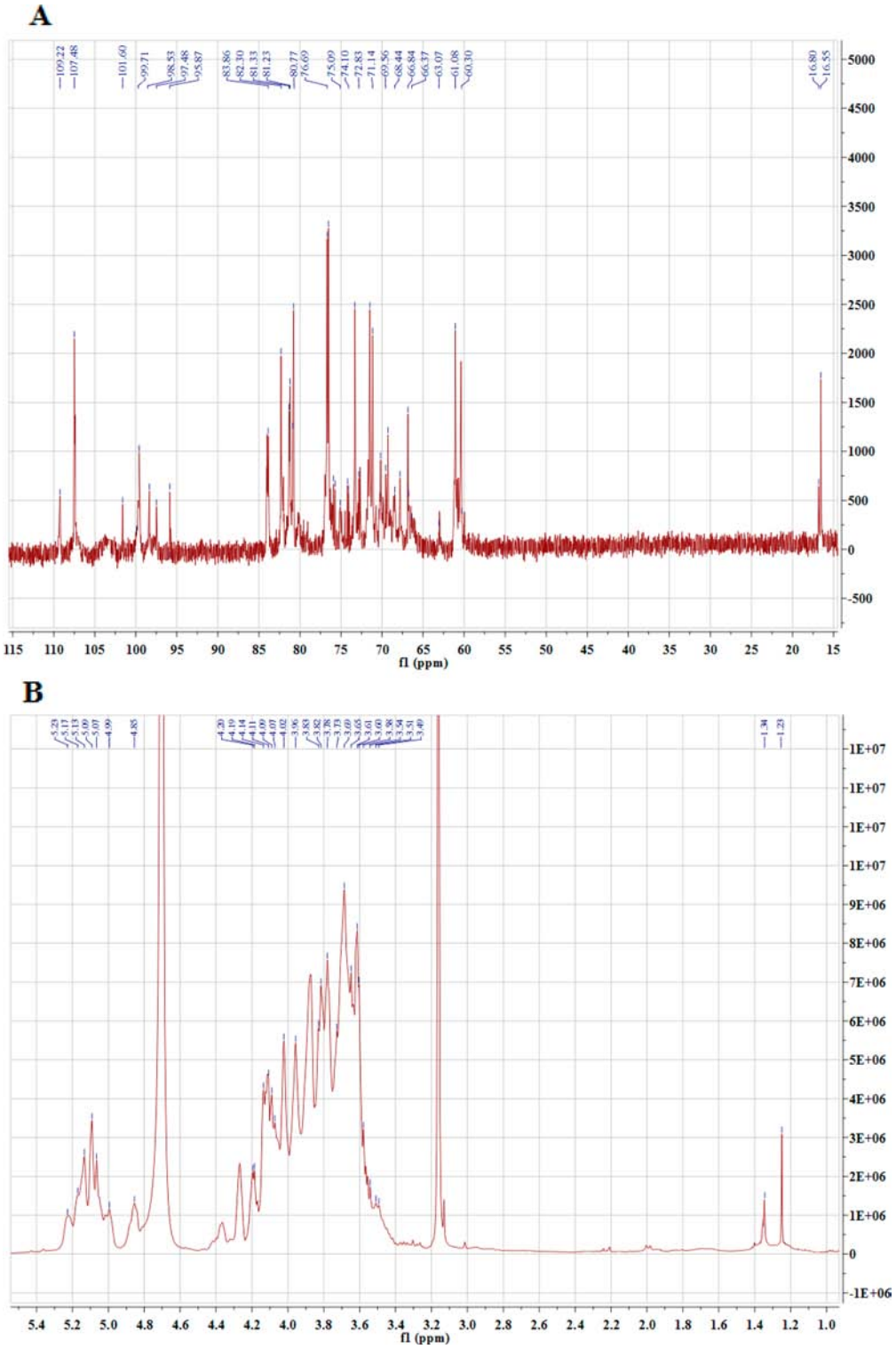

Figure 2. (A) ^{13}C NMR spectrum and (B) ^{1}H NMR spectrum of LCP50W.

reactivity. Therefore, the spleen has been an ideal tissue to be studied in immune research.[35] To investigate the general activity of LCP50W on immune cells, the effect on splenic lymphocyte proliferation was investigated, and the results are presented as Figure 5. LCP50W (3.9−125 μg/mL) significantly promoted the proliferation of splenic lymphocytes in a concentration-dependent manner. When used in combination with Con A, LCP50W also caused a significant stimulation of the proliferation of splenic lymphocytes. These results indicated that LCP50W had the potential of promoting the lymphocyte proliferation alone or along with Con A.

Effect of LCP50W on NK Cell Cytotoxicity. NK cells are another important group of immune cells, serving as effector lymphocytes of the innate immune system that control several types of tumors and microbial infections by limiting their spread and subsequent tissue damage.[36] In Figure 6, we could find that LCP50W promoted the cytotoxicity of NK cells at

dx.doi.org/10.1021/jf404752c | J. Agric. Food Chem. 2014, 62, 902−911

Table 4. Chemical Shifts of Resonances in the ^{13}C and ^{1}H NMR Spectra of LCP50W

	chemical shift (ppm)						
sugar residue	C1/H1	C2/H2	C3/H3	C4/H4	C5/H5	C6/H6	CH_3
α-L-Ara(1→	109.2/5.23	81.2/4.20	74.5/3.95	83.9/4.14	66.8/3.73		
→3)-β-L-Rha(1→	107.5/4.85	76.5/4.19	82.3/3.65	76.7/4.07	73.3/3.78		16.6/1.23
→2,6)-α-D-Glc(1→	101.6/5.07	76.7/4.02	69.4/3.82	75.1/3.58	63.1/3.73	75.7/3.95	
→3)-α-D-Gal(1→	99.7/5.13	70.7/3.60	80.8/4.11	69.6/3.83	75.7/4.09	66.4/4.02	
→2)-α-L-Rha(1→	98.5/5.09	81.3/3.69	68.4/4.18	70.2/4.02	69.3/3.82		16.8/1.34
→6)-α-D-Glc(1→	97.5/4.99	72.8/3.83	74.1/3.54	71.5/3.51	70.2/3.78	61.1/3.96	
→3)-α-L-Man(1→	95.9/5.17	76.7/4.11	69.6/3.85	67.8/3.61	71.1/3.65	60.3/3.82	

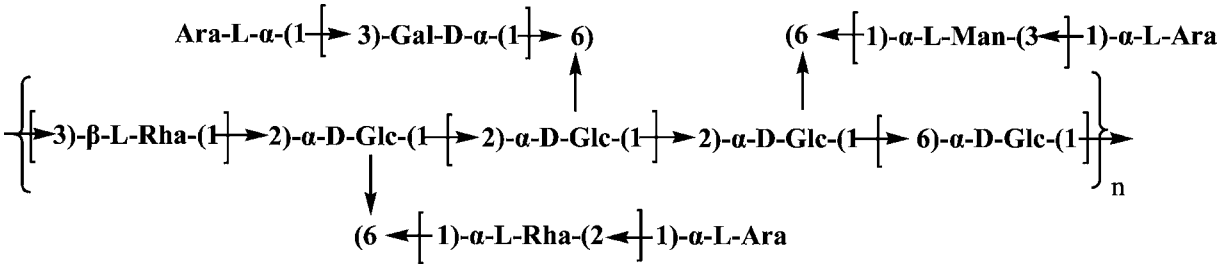

Figure 3. Predicted structure of the repeating unit of LCP50W.

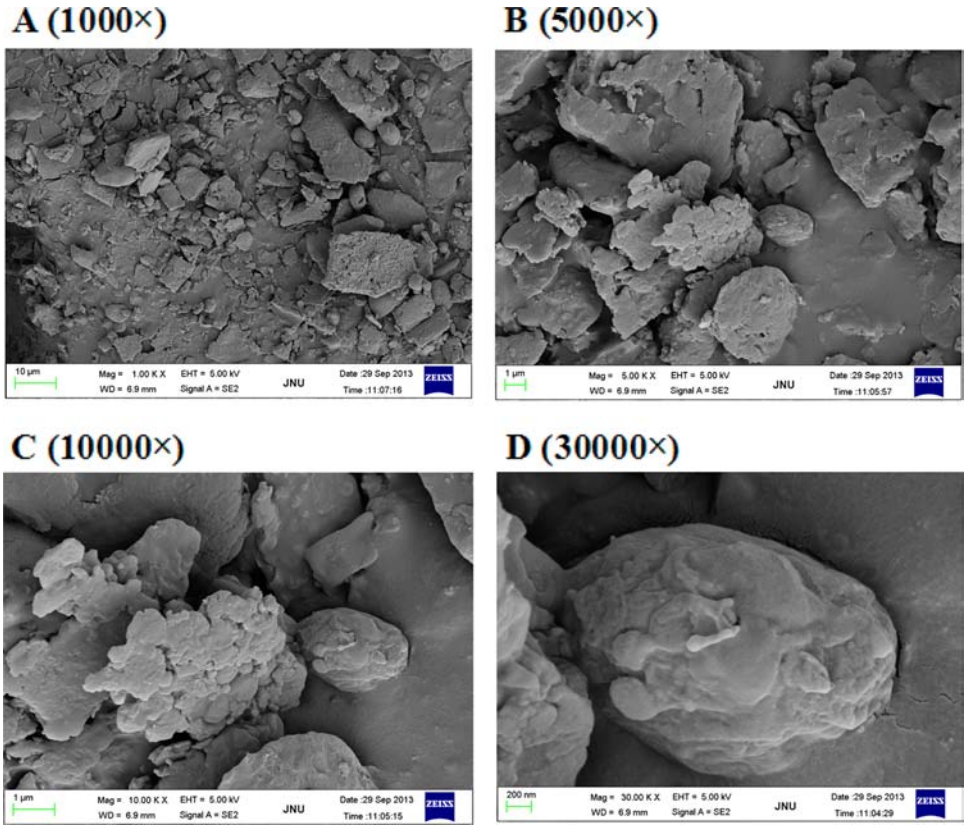

Figure 4. SEM images of LCP50W: (A) morphology of LCP50W at 1000×, scale bar = 10 μm; (B) morphology of LCP50W at 5000×, scale bar = 1 μm; (C) morphology of LCP50W at 10000×, scale bar = 1 μm; (D) morphology of LCP50W at 30000×, scale bar = 200 nm.

concentrations of 3.9−250 μg/mL, which showed a concentration-dependent manner.

Effect of LCP50W on Secretion of Cytokines IFN-γ and IL-4. From the results of LCP50W on the proliferation of lymphocytes and cytotoxicity of NK cells, we could get the initial conclusion that LCP50W had the potential of immune enhancement. To further explore its immunomodulatory mechanism, we investigated the secretion levels of IFN-γ and IL-4, which are hallmark cytokines of Th1 and Th2 cells, respectively.[37] The two cytokines are often mutually exclusive in immune response. IFN-γ secreted by Th1 cells could inhibit the proliferation of Th2 cells, whereas IL-4 secreted by Th2 cells in turn may suppress the proliferation of Th1 cells. As shown in Figure 7A, LCP50W (3.9−62.5 μg/mL) boosted the secretion of IFN-γ but significantly inhibited that of IL-4 (Figure 7B) in a concentration-dependent manner.

dx.doi.org/10.1021/jf404752c | J. Agric. Food Chem. 2014, 62, 902−911

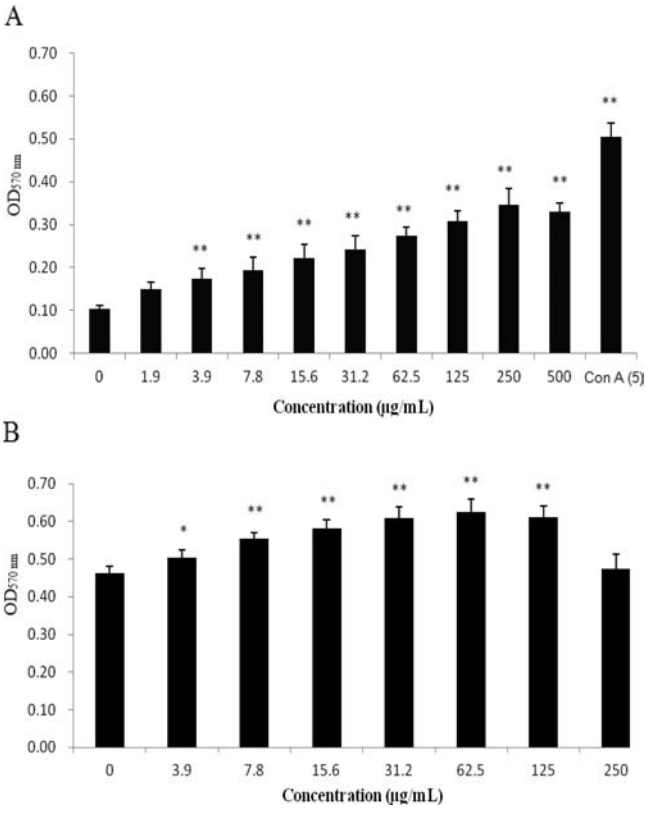

Figure 5. Effect of LCP50W on splenic lymphocyte proliferation: (A) LCP50W; (B) LCP50W + Con A. Values are expressed as the means ± SD obtained from triplicate experiments. Statistical analysis was performed by independent *t* test in Statistical Analysis software SPSS 11.5. *, $P < 0.05$, and **, $P < 0.01$, versus the negative control.

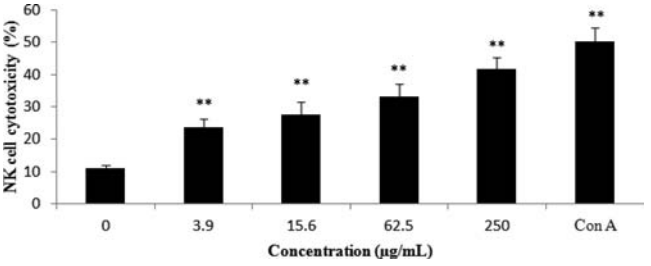

Figure 6. Effect of LCP50W on NK cell cytotoxicity. Values are expressed as the means ± SD obtained from triplicate experiments. Statistical analysis was performed by independent *t* test in Statistical Analysis software SPSS 11.5. **, $P < 0.01$, versus the negative control.

Effect of LCP50W on Expression of Transcription Factors T-bet and GATA-3. The effect of LCP50W on the release of IFN-γ and IL-4 suggested that its stimulation of mice immune function might be mediated by influencing Th1/Th2 balance. For exploring the mechanism, the transcription factors T-bet and GATA-3, which are specific transcription factors of Th1 and Th2 cells, were further investigated. T-bet, which belongs to the Tbr1 subfamily of the T box gene family, is a 530 amino acid protein with a 189 amino acid T box DNA-binding domain. T-bet is a Th1-specific transcription factor that plays a central role in Th1 development, which transactivates the IFN-γ gene, induces IFN-γ production, and redirects polarized Th2 cells into the Th1 pathway.[38] GATA-3 belongs to the GATA family of zinc finger proteins, which was selectively expressed in differentiating and effector Th2 cells. GATA-3 is required for

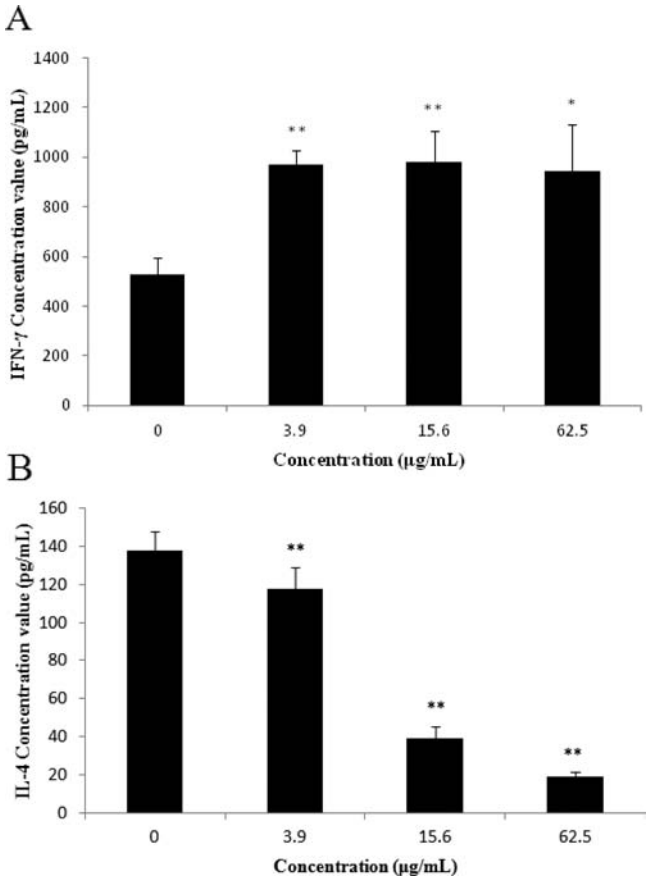

Figure 7. Effect of LCP50W on secretion of IFN-γ (A) and IL-4 (B). Values are expressed as the means ± SD obtained from triplicate experiments. Statistical analysis was performed by independent *t* test in Statistical Analysis software SPSS 11.5. *, $P < 0.05$, and **, $P < 0.01$, versus the negative control.

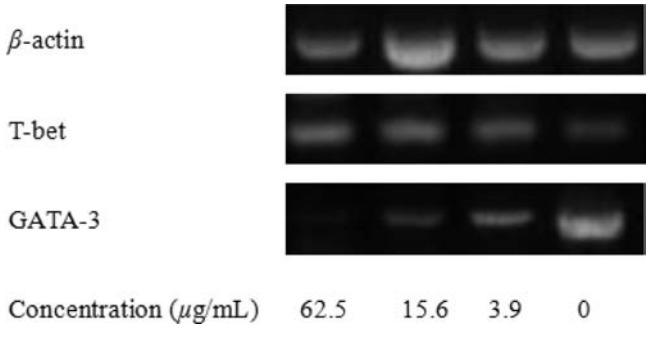

Figure 8. Effect of LCP50W on expression of T-bet and GATA-3. The electrophoresis bands were observed by gel imager, and photos were taken as above, where β-actin was taken as the standard.

Table 5. Effect of LCP50W on T-bet/GATA-3 Expression (Means ± SD, $n = 3$)[a]

concn (μg/mL)	GATA-3/β-actin (%)	T-bet/β-actin (%)
0	62.28 ± 3.43	17.35 ± 1.58
3.9	40.23 ± 4.37**	22.82 ± 3.70
15.6	17.60 ± 1.41**	26.86 ± 5.40*
62.5	6.17 ± 1.40**	52.81 ± 7.59**

[a]*, $P < 0.05$, and **, $P < 0.01$, versus the negative control(without LCP50W).

dx.doi.org/10.1021/jf404752c | J. Agric. Food Chem. 2014, 62, 902−911

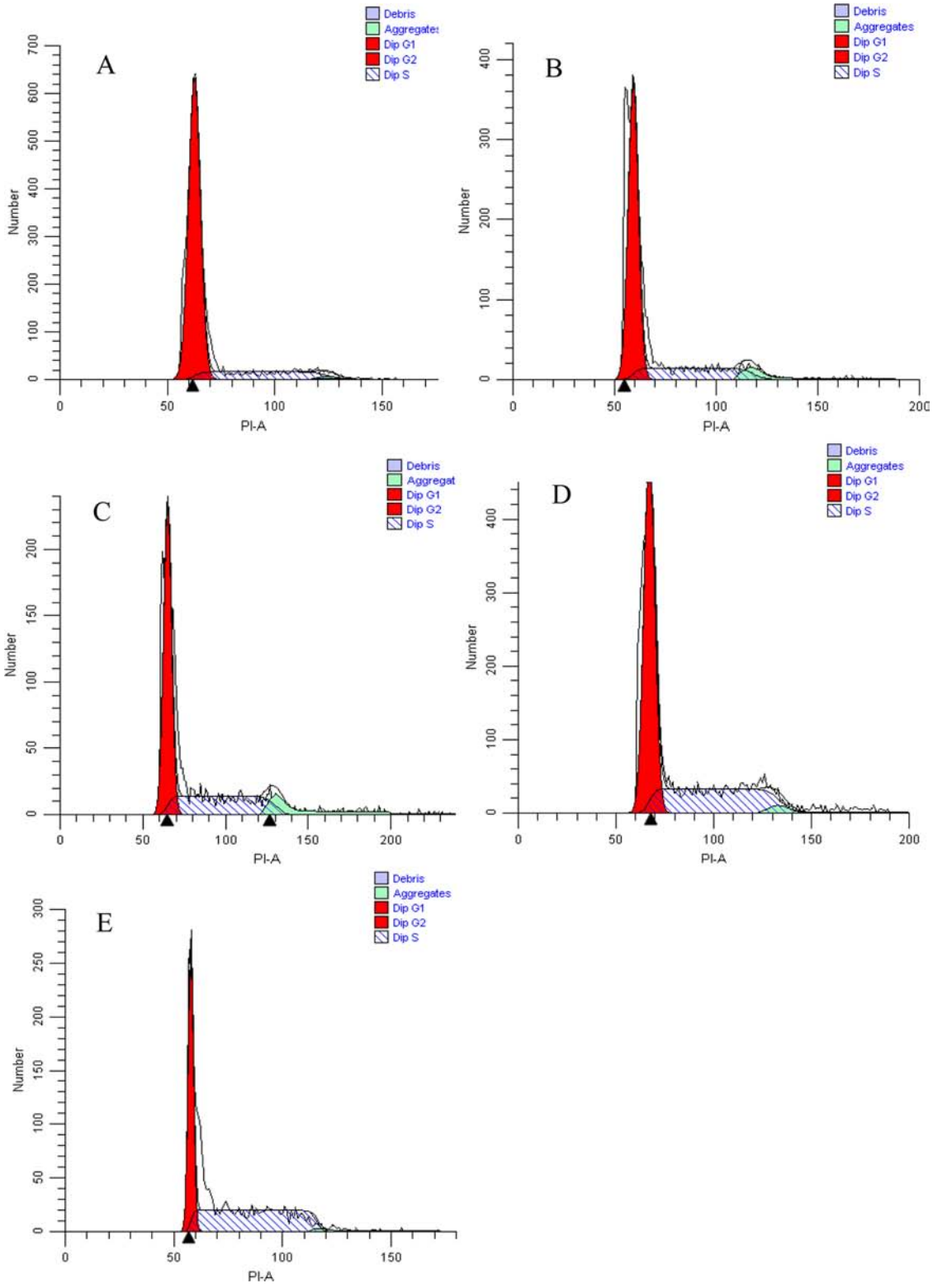

Figure 9. Effect of LCP50W on lymphocyte cell cycle: (A) 0 μg/mL; (B) 7.8 μg/mL; (C) 31.2 μg/mL; (D) 125 μg/mL; (E) Con A 5 μg/mL. Data were analyzed by a BD FACScan Flow with ModFit LT 4.0 software.

the transcription of all Th2 cytokine genes, and the loss of Th2 cytokine gene expression in Th1 cells is at least in part a consequence of the down-regulation of GATA-3. GATA-3 appears therefore to be a potent transactivator of the IL-4 promoter.[39] The results shown in Figure 8 indicated that LCP50W (3.9−62.5 μg/mL) inhibited the expression of GATA-3 but enhanced that of T-bet. The DNA bands were further analyzed by image analysis software Image J, and results are represented in Table 5 by the ratios of gray values of transcription factor T-bet or GATA-3 to β-actin. LCP50W showed significant up-regulation of T-bet at concentrations of 15.6 and 62.5 μg/mL and noticeable down-regulation of

dx.doi.org/10.1021/jf404752c | J. Agric. Food Chem. 2014, 62, 902−911

Table 6. Effect of LCP50W on Lymphocyte Cell Cycle (Means ± SD, $n = 3$)[a]

concn (μg/mL)	G0/G1 (%)	S (%)
0	84.03 ± 0.69	16.37 ± 1.36
7.8	73.06 ± 1.16**	26.94 ± 1.16**
31.2	59.93 ± 2.95**	40.07 ± 2.95**
125	56.30 ± 4.11**	43.7 ± 4.11**
Con A	45.21 ± 3.43**	54.78 ± 3.43**

[a]**, $P < 0.01$, versus the negative control (without LCP50W).

GATA-3 at 3.9, 15.6, and 62.5 μg/mL, respectively, when compared to the negative control.

Effect of LCP50W on Lymphocyte Cell Cycle. For analysis at DNA level, flow cytometry was used to analyze lymphocyte cell cycle distribution. The results obtained by ModFit LT 4.0 software demonstrated that LCP50W promoted spleen cells into the S phase (Figure 9). Data were further performed by independent t test in Statistical Analysis software SPSS 11.5, which are presented in Table 6. LCP50W (7.8, 31.2, and 125 μg/mL) significantly promoted spleen cells into the S phase in a concentration-dependent manner, which was consistent with the results in Figure 5A.

In conclusion, a novel water-soluble polysaccharide (LCP50W) isolated from the pulp tissues of *L. chinensis* contained five monosaccharides, D-galactose, D-glucose, L-rhamnose, L-mannose, and L-arabinose. Particularly, our research proposes for the first time the mechanism of immunomodulation of *L. chinensis* polysaccharide (LCP50W). This novel polysaccharide in vitro could promote the proliferation of lymphocytes, NK cell cytotoxicity, and the development of cell cycle toward the S phase. LCP50W boosted the secretion of Th1 cytokine IFN-γ but inhibited the secretion of Th2 cytokine IL-4; it enhanced the expression of T-bet but inhibited the expression of GATA-3. In addition, in vitro study demonstrated that LCP50W had the potential of enhancing the immune functions of mice, which may be mediated by influencing Th1/Th2 balance. Further research is necessary to elucidate the mechanism of LCP50W's immunomodulation on subpopulations of Th1/Th2 cells.

AUTHOR INFORMATION

Corresponding Authors

*(L.S.) Phone: +86-20-85228205. Fax: +86-20-85224766. E-mail: tsly@jnu.edu.cn.

*(R.Y.) Phone: +86-20-85220386. Fax: +86-20-85224766. E-mail: tyrm@jnu.edu.cn.

Author Contributions

‖Y.J. and L.H. contributed equally to this work.

Notes

The authors declare no competing financial interest.

REFERENCES

(1) Mahattanatawee, K.; Manthey, J. A.; Luzio, G.; Talcott, S. T.; Goodner, K.; Baldwin, E. A. Total antioxidant activity and fiber content of select Florida-grown tropical fruits. *J. Agric. Food Chem.* **2006**, *54*, 7355−7363.

(2) Zhang, R. F.; Zeng, Q. S.; Deng, Y. Y.; Zhang, M. W.; Wei, Z. C.; Zhang, Y.; Tang, X. J. Phenolic profiles and antioxidant activity of litchi pulp of different cultivars cultivated in southern China. *Food Chem.* **2013**, *136*, 1169−1176.

(3) Chyau, C. C.; Ko, P. T.; Chang, C. H.; Mau, J. L. Free and glycosidically bound aroma compounds in lychee (*Litchi chinensis* Sonn). *Food Chem.* **2003**, *80*, 387−392.

(4) Kong, F. L.; Zhang, W. Z.; Kuang, R. B.; Yu, S. J.; Chi, J. W.; Wei, Z. C. Antioxidant activities of different fractions of polysaccharide purified from pulp tissue of litchi (*Litchi chinensis* Sonn.). *Carbohydr. Polym.* **2010**, *81*, 612−616.

(5) Kong, F. L.; Zhang, M. W.; Liao, S. T.; Yu, S. J.; Chi, J. W.; Wei, Z. C. Antioxidant activity of polysaccharide-enriched fractions extracted from pulp tissue of *Litchi chinensis* Sonn. *Molecules* **2010**, *15*, 2152−2165.

(6) Hu, X. Q.; Huang, Y. Y.; Dong, Q. F.; Song, L. Y.; Yuan, F.; Yu, R. M. Structure characterization and antioxidant activity of a novel polysaccharide isolated from pulp tissues of *Litchi chinensis*. *J. Agric. Food Chem.* **2011**, *59*, 11548−11552.

(7) Yang, B.; Wang, J. S.; Zhao, M. M.; Liu, Y.; Wang, W.; Jiang, Y. M. Identification of polysaccharides from pericarp tissues of litchi (*Litchi chinensis* Sonn.) fruit in relation to their antioxidant activities. *Carbohydr. Res.* **2006**, *341*, 634−638.

(8) Yi, Y.; Zhang, M. W.; Liao, S. T.; Zhang, R. F.; Deng, Y. Y.; Wei, Z. C.; Tang, X. J.; Zhang, Y. Structural features and immunomodulatory activities of polysaccharides of longan pulp. *Carbohydr. Polym.* **2012**, *87*, 636−643.

(9) Yang, X. B.; Lv, Y.; Tian, L. M.; Zhao, Y. Composition and systemic immune activity of the polysaccharides from an herbal tea (*Lycopus lucidus* Turcz). *J. Agric. Food Chem.* **2010**, *58*, 6075−6080.

(10) Wang, M. C.; Jiang, C. X.; Ma, L. P.; Zhang, Z. J.; Cao, L.; Liu, J.; Zeng, X. X. Preparation, preliminary characterization and immunostimulatory activity of polysaccharide fractions from the peduncles of *Hovenia dulcis*. *Food Chem.* **2013**, *138*, 41−47.

(11) Li, W. W. *Studies on Extraction and Purification of Litchi Polysaccharides and Researches on Their Immunomodulatory Activities*; Huazhong Agricultural University, Wuhan, China, 2009.

(12) Chen, W. Y. *Litchi Pulp Polysaccharide Extracted by Ultrasound Microwave and Enzymolysis and Its Analysis of Biological Activity*; Huazhong Agricultural University, Wuhan, China, 2011.

(13) Li, X. H.; Li, F. S.; Wei, W.; Wu, N. N. Studies on the immunomodulatory effects of *Litchi* polysaccharides. *Shizhen Guoyi Guoyao* **2008**, *19*, 2119−2120.

(14) Yuan, F.; Yu, R. M.; Yin, Y.; Shen, J. R.; Dong, Q. F.; Zhong, L.; Song, L. Y. Structure characterization and antioxidant activity of a novel polysaccharide isolated from *Ginkgo biloba*. *Int. J. Biol. Macromol.* **2010**, *46*, 436−439.

(15) Therho, T. T.; Hartiala, K. Method for determination of the sulfate content of glycosamino glycans. *Anal. Biochem.* **1971**, *41*, 471−476.

(16) Bitter, T.; Muir, H. M. A modified uronic acid carbazole reaction. *Anal. Biochem.* **1962**, *4*, 330−334.

(17) Han, X. Q.; Chan, B. C. L.; Dong, C. X.; Yang, Y. H.; Ko, C. H.; Yue, G. G. L.; Chen, D.; Han, Q. B. Isolation, structure characterization, and immunomodulating activity of a hyperbranched polysaccharide from the fruiting bodies of *Ganoderma sinense*. *J. Agric. Food Chem.* **2012**, *60*, 4276−4281.

(18) Yu, R. M.; Yang, W.; Song, L. Y.; Yan, C. Y.; Zhang, Z.; Zhao, Y. Structural characterization and antioxidant activity of a polysaccharide from the fruiting bodies of cultured *Cordyceps militaris*. *Carbohydr. Polym.* **2007**, *70*, 430−436.

(19) Linker, A.; Evans, L. R.; Impallomeni, G. The structure of a polysaccharide from infectious strains of *Burkholderia cepacia*. *Carbohydr. Res.* **2001**, *335*, 45−54.

(20) Aspinall, G. O.; Ferrier, R. J. A pectrophtomertc method for the determination of periocate consumed during the oxidation of carbohydrateds. *Chem. Ind.* **1957**, *7*, 1216−1221.

(21) Hakomori, S. A rapid premethylation of glycolipid, and polysaccharide catalyzed by methylsulfinyl carbanion in dimethyl sulfoxide. *J. Biochem.* **1964**, *55*, 205−208.

(22) Peng, Q.; Song, J. J.; Lv, X. P.; Wang, Z. F.; Huang, L. J.; Du, Y. G. Structural characterization of an arabinogalactan-protein from the fruits of *Lycium ruthenicum*. *J. Agric. Food Chem.* **2012**, *60*, 9424−9429.

(23) Chen, R. Z.; Liu, Z. Q.; Zhao, J. M.; Chen, R. P.; Meng, F. L.; Zhang, M.; Ge, W. C. Antioxidant and immunobiological activity of water-soluble polysaccharide fractions purified from *Acanthopanax senticosu*. *Food Chem.* **2011**, *127*, 434−440.
(24) Yuan, H. M.; Song, J. M.; Li, X. G.; Li, N.; Liu, S. Enhanced immunostimulatory and antitumor activity of different derivatives of κ-carrageenan oligosaccharide from *Kappaphycus striatum*. *J. Appl. Phycol.* **2011**, *23*, 59−65.
(25) Orsatti, C. L.; Missima, F.; Pagliarone, A. C.; Sforcin, J. M. Th1/Th2 cytokines' expression and production by propolis-treated mice. *J. Ethnopharmacol.* **2010**, *129*, 314−318.
(26) Zhao, J. Z.; Xie, Y. Q.; Qian, C. Y.; Li, L.; Jiang, R. F.; Kan, H. D.; Chen, R. Z.; Song, W. M. Imbalance of Th1 and Th2 cells in cardiac injury induced by ambient fine particles. *Toxicol. Lett.* **2012**, *208*, 225−231.
(27) Qiao, D. L.; Liu, J.; Ke, C. L.; Sun, Y.; Ye, H.; Zeng, X. X. Structural characterization of polysaccharides from *Hyriopsis cumingii*. *Carbohydr. Polym.* **2010**, *82*, 1184−1190.
(28) Asker, M. M.; Shawky, B. T. Structural characterization and antioxidant activity of an extracellular polysaccharide isolated from *Brevibacterium otitidis* BTS 44. *Food Chem.* **2010**, *123*, 315−320.
(29) Zhu, Z. Y.; Liu, N.; Si, C. L.; Liu, Y.; Ding, L. N.; Jing, C.; Liu, A. J.; Zhang, Y. M. Structure and anti-tumor activity of a high-molecular-weight polysaccharide from cultured mycelium of *Cordyceps gunnii*. *Carbohydr. Polym.* **2012**, *88*, 1072−1076.
(30) Bi, H. T.; Gao, T. T.; Li, Z. H.; Ji, L.; Yang, W.; Iteku, B. J.; Liu, E. X.; Zhou, Y. F. Structural elucidation and antioxidant activity of a water-soluble polysaccharide from the fruit bodies of *Bulgaria inquinans* (Fries). *Food Chem.* **2013**, *138*, 1470−1475.
(31) Pan, D.; Wang, L. Q.; Chen, C. H.; Teng, B. S.; Wang, C. D.; Xu, Z. X.; Hu, B. W.; Zhou, P. Structure characterization of a novel neutral polysaccharide isolated from *Ganoderma lucidum* fruiting bodies. *Food Chem.* **2012**, *135*, 1097−1103.
(32) Yu, R. M.; Wang, L.; Zhang, H.; Zhou, C. X.; Zhao, Y. Isolation, purification and identification of polysaccharides from cultured *Cordyceps militaris*. *Fitoterapia* **2004**, *75*, 662−666.
(33) Wu, Y.; Ai, L. Z.; Wu, J. H.; Cui, S. W. Structural analysis of a pectic polysaccharide from boat-fruited sterculia seeds. *Int. J. Biol. Macromol.* **2013**, *56*, 76−82.
(34) Zhang, H.; Li, W. J.; Nie, S. P.; Chen, Y.; Wang, Y. X.; Xie, M. Y. Structural characterization of a novel bioactive polysaccharide from *Ganoderma atrum*. *Carbohydr. Polym.* **2012**, *88*, 1047−1054.
(35) Mebius, R. E.; Kraal, G. Structure and function of the spleen. *Nature* **2005**, *5*, 606−616.
(36) Vivier, E.; Tomasello, E.; Baratin, M.; Walzer, T.; Ugolini, S. Functions of natural killer cells. *Nat. Immunol.* **2008**, *9*, 503−510.
(37) Mosmann, T. R.; Coffman, R. L. TH1 and TH2 cells: different patterns of lymphokine secretion lead to different functional properties. *Annu. Rev. Immunol.* **1989**, *7*, 145−173.
(38) Szabo, S. J.; Kim, S. T.; Costa, G. L.; Zhang, X. K.; Fathman, C. G.; Glimcher, C. G. A novel transcription factor, T-bet, directs Th1 lineage commitment. *Cell* **2000**, *100*, 655−669.
(39) Zheng, W. P.; Flavell, R. A. The transcription factor GATA-3 is necessary and sufficient for Th2 cytokine gene expression in CD4 T cells. *Cell* **1997**, *89*, 587−596.

Table 1. Primers and Probes Used in Real-Time PCR

gene name		sequence	length (mer)	product length (bp)
renin	-F	5′-GTCCTGTGGGTGTGTATA-3′	18	175
	-R	5′-GAGCAAGATTCGTCCAAA-3′	18	
	-P	5′-(FAM) TCTGGGCTACACGGCTCTCA (eclipse)-3′	20	
Agtr2	-F	5′- CAACGTGTTACTTTGGAA-3′	18	70
	-R	5′-CGGGTAATTCTGTTCTTC-3′	18	
	-P	5′-(FAM) AACATCTGCTGAAGACCAATAGCT (eclipse)-3′	24	
Ace	-F	5′- CCAACGAGTTAGAAGAGTA-3′	19	124
	-R	5′-GCCATTATATTTGTCAGATCA-3′	21	
	-P	5′-(FAM) TCCAGTGACAGACAAGTGCCA (eclipse)-3′	21	
Agtr1a	-F	5′-CAGTCAGAGGTGAATACA-3′	18	132
	-R	5′-AGAGGTAAACATACATTGC-3′	19	
	-P	5′-(FAM) ATTCCATACAGTCTGCCTTGCTCT (eclipse)-3′	24	
β-actin	-F	5′-TATGAGGGTTACGCGCTCCC-3′	20	146
	-R	5′-TCTTTAATGTCACGCACGATTTCC-3′	24	
	-P	5′-(FAM) CCTGCGTCTGGACCTGGCTGGC (eclipse)-3′	22	
GAPDH	-F	5′- TGGTCTACATGTTCCAGTATGACT-3′	24	134
	-R	5′- CCATTTGATGTTAGCGGGATCTC-3′	23	
	-P	5′-(FAM) CCACGGCAAGTTCAACGGCACAGT (eclipse)-3′	24	

protein, was provided by Shanghai Science Peptide Biological Technology Corp. The purity and molecular mass of the synthesized peptide were verified by HPLC and mass spectrometry, respectively. All the products used were dissolved in 0.9% saline to be administered to the rats.

In Vitro ACE Inhibitory Activity Assay. The assay was conducted using a previously reported HPLC method.[7]

Animal Ware. This study was carried out in strict accordance with the recommendations from the Guide for the Care and Use of Laboratory Animals of the National Institutes of Health. The protocol was approved by the Committee on the Ethics of Animal Experiments of Jilin University. All surgery was performed under ether, and all efforts were made to minimize suffering. The protocol conformed to guidelines for the humane care of animals.[14] A total of 30 male SHRs (purchased from Vital River Laboratories), aged 9−10 weeks and weighing 220−270 g, were used in the course of this study. The SHRs were housed in temperature-controlled rooms (22 ± 2 °C) with 12 h light/dark cycles, where spontaneously hypertensive rats could consume tap water and standard diets ad libitum. All SHRs were acclimatized for 3 days with diet before the experiment. The 30 SHRs were assigned to 5 groups: 0.9% saline for the negative group, 10 mg/kg of body mass of captopril for the positive group, and three treatment groups, i.e., 2 mg/kg of body mass of RVPSL for low dose, 10 mg/kg of body mass of RVPSL for medium dose, and 50 mg/kg of body mass of RVPSL for high dose. The rats from the negative group, positive group, and treatment groups were orally administered 1 mL of the corresponding solution from 7:30 a.m. to 8:00 a.m. every day for 4 weeks.

Blood Pressure Measurement. The blood pressure of the SHRs was measured by the tail-cuff method.[15] Before measurement, the rats were kept at 39 °C for 2−3 min to make the pulsation of the tail artery detectable using a blood pressure monitor (model BP-2010A, Softron Co., Tokyo, Japan). The tail cuff was connected to a cylinder of compressed air through an arrangement of inlet and outlet valves that permitted inflation and deflation of the cuff at a constant rate. The systolic blood pressure (SBP) and the diastolic blood pressure (DBP) of the rats were measured by the tail-cuff method before administration and also 5, 10, 15, and 20 h postadministration. Moreover, to guarantee the reliability of the measurements, we established a training period of 4 days before the actual trial time, and during this period the rats were accustomed to the procedure. All measurements were performed by the same person in a quiet environment.

Isolation of RNA from the Rats' Kidneys. Kidney tissues of the spontaneously hypertensive rats that were stored in an ultra-low-temperature freezer at −80 °C (Haier, Beijing, China) were homogenized with a tissue homogenizer under liquid nitrogen conditions. The total RNA of the SHRs' kidneys was isolated using the SV total RNA isolation system Z3105 according to the manufacturer's product instructions (Promega Corp., Beijing, China). The RNA purity and concentration were determined by the A260/A280 ratio (UV2550, Shimadzu, Japan).

Single-Strand cDNA Synthesis. Transcriptor first-strand cDNA was synthesized from 1 μg of RNA using the First Strand cDNA synthesis kit for RT-PCR. A 1 μg portion of total RNA was added to a thin-wall PCR tube on ice, and then 2 μL of 60 μM random hexamer primers was added. RNA-free water was added to a total volume of 13 μL. A 40 μL aliquot of transcriptor reverse transcriptase reaction buffer, 0.5 μL of protector ribonuclease (RNase) inhibitor, 2 μL of deoxynucleotide mix, and 0.5 μL of transcriptor reverse transcriptase were added subsequently to the thin-wall tube, and the contents were incubated at 25 °C for 10 min followed by 55 °C for another 30 min. The reaction was stopped by heating at 85 °C for 5 min. The reaction tube was placed on ice and then stored at −20 °C for an RT-PCR study.

RT-PCR. Real-time PCR was performed for renin, Ang, ACE, AT1 receptor, AT2 receptor, and the housekeeping gene glyceraldehyde 3-phosphate dehydrogenase (GAPDH) using the Premix Ex Taq kits on an ABI 7500 real-time PCR system. The primers were ordered from Takara China (Dalian, Liaoning, China). The results are shown in Table 1. PCR reactions were carried out in a 20 μL solution consisting of 2 μL of cDNA template (50 ng), 10 μL of Premix Ex Taq (Probe qPCR), 0.4 μL of forward primer (10 μM), 0.4 μL of reverse primer (10 μM), 0.8 μL of probe solution, 0.4 μL of ROX reference dye II, and 6.0 μL of PCR water. Thermal cycling was initiated with 30 s of denaturation at 95 °C and then by 40 repeats of 5 s at 95 °C and 30 s at 60 °C for melting curve analysis and cooling. The entire process was performed according to the guidelines of the ABI 7500 instrument (Life Technologies Corp., Grand Island, NY). The quantification of a target gene was expressed as the relative expression ratio of the target gene (i.e., ACE, renin, Ang, AT1 receptor, and AT2 receptor) in a sample versus that of a control in contrast to the housekeeping gene GAPDH.

Assay of Serum Ang and Aldosterone Concentrations. The serum Ang I, Ang II, and aldosterone concentrations were determined with the iodine angiotensin I radioimmunoassay kit, iodine angiotensin II radioimmunoassay kit, and iodine aldosterone radioimmunoassay kit, respectively. The above-mentioned samples were measured with an SN-6105 γ RIA counter (Beijing Tayasaf Science & Technology Co., Ltd., Beijing, China) within 20 min after the reaction was stopped. Test samples and standards were measured in duplicate. All of the

processes were implemented according to the aforementioned guidelines of the manufacturers.

Statistical Analysis. Values are expressed as the means ± SD. Statistical comparisons between groups were performed using one-way analysis of variance (ANOVA) followed by Student's *t* test. *p* values of <0.05 were considered significant.

RESULTS AND DISCUSSION

Effects of RVPSL on the SBP and DBP of the SHRs in 4 Weeks. There were no mortalities and no significant differences in the final body mass among the experimental SHRs during the 4 weeks. The results demonstrated that the oral administration of saline to SHRs did not lower the values of the SBP and DBP (Figure 1). On the contrary, the SBPs of

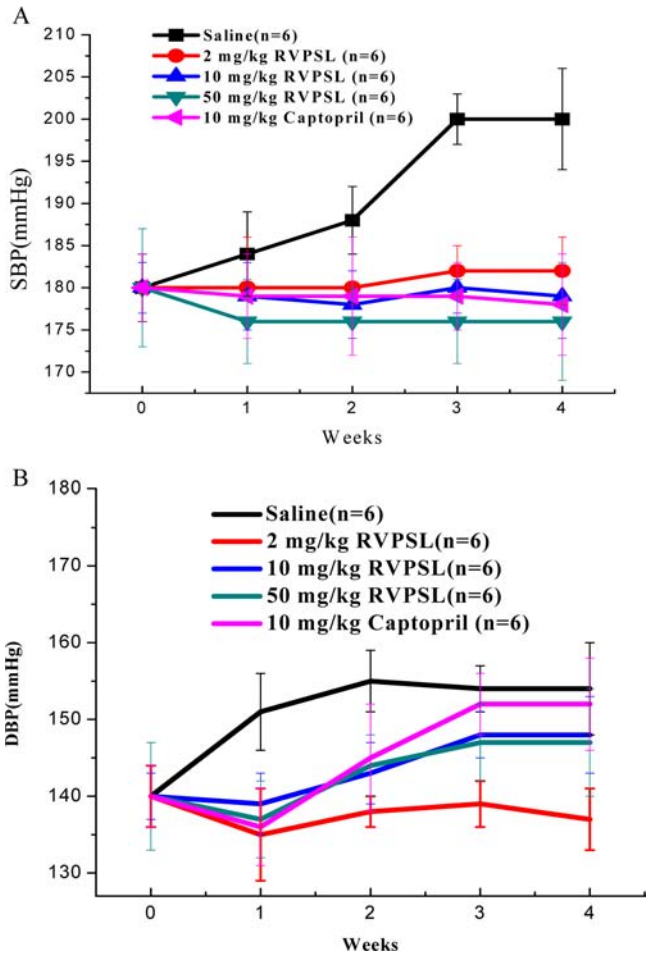

Figure 1. Antihypertensive effects of RVPSL in SHRs: (A) change in the SBP after administration for 4 weeks and (B) change in the DBP after administration for 4 weeks. Each value is expressed as the mean ± SD. A *p* value of <0.05 (*) is considered statistically significant by one-way ANOVA.

SHRs administered saline as the negative group increased from 180 ± 7 to 200 ± 9 mmHg. However, the SBPs of SHRs administered different concentrations of RVPSL as the treatment groups decreased. RVPSL caused a significant dose-dependent decrease in SBP in these animals from the first week until the fourth week. Moreover, the greatest decreases of SBP were obtained when the SHRs were administered 50 mg/kg RVPSL. From the third week after the oral administration with peptide RVPSL, the SBP of the positive control group and that of the treatment groups were significantly lower than that of the negative group.

However, the reduction of DBP in the treatment groups was not significantly higher than that of the negative group from the first week to the fourth week. Some researchers suggested that orally administered bioactive peptide decreased the blood pressure of the SHRs[16] and also demonstrated that the antihypertensive activity of bioactive peptide was blocked by a CCK1 antagonist. In this context, we performed further studies to evaluate the mechanism of antihypertensive peptide derived from egg protein.

Effects of RVPSL on Renin mRNA Expression of the Kidney. Relative renin mRNA levels of the kidney were detected by real-time PCR and quantified as shown in Figure 2A in contrast to GAPDH, which remained stable in comparison to *β*-actin in our study. The expression was analyzed on the fourth week, when a decrease in the treatment group with oral administration of RVPSL (50 mg/kg) and in the positive control group (captopril) was found in contrast to the negative control group (saline). Renin can cleave the substrate angiotensinogen to form Ang I, which is later converted to Ang II. Ang II raises blood pressure by a number of actions: the most important ones being vasoconstriction, sympathetic nervous stimulation, increased aldosterone biosynthesis, and renal actions. Angiotensin II-converting enzyme inhibitors presumably stimulate renin secretion by interrupting angiotensin II feedback inhibition. To some extent, the decrease of renin may contribute to the low production of Ang I and Ang II.

Effects of RVPSL on ACE mRNA Expression of the Kidney. Relative ACE mRNA levels of the kidney were detected by real-time PCR and quantified as shown in Figure 2B in comparison to GAPDH. The expression was also analyzed on the fourth week. A significant decrease in the treatment group with oral administration of RVPSL (50 mg/kg) and in the positive group was found compared to the negative group, but there was no significant difference between the treatment group and the positive group. The results demonstrated that captopril and egg white peptide RVPSL exhibited high activity against ACE in vivo. The antihypertensive effects of captopril and RVPSL were thought to be correlated with their inhibition of ACE activity, which was reflected in our study by the decrease in the mRNA expression of ACE in the kidney for the positive group and RVPSL-treated groups. Consequently, the production of Ang II converted by ACE from Ang I was decreased by the effects of the captopril and/or RVPSL administration. The captopril and the peptide RVPSL are potent inhibitors of angiotensin I-converting enzyme, which is responsible for the conversion of angiotensin I to angiotensin II.

Effects of RVPSL on AT1 and AT2 Receptor mRNA Expression of the Kidney. Relative AT1 receptor and AT2 receptor mRNA levels of the kidney were measured by real-time PCR as shown in parts C and D, respectively, of Figure 2 and compared to the housekeeping gene GAPDH. On the basis of the expression analysis after oral administration for 4 weeks, the results revealed that a significant decrease of AT1 in the treatment group and the positive control group occurred in comparison with the negative control group. However, the AT2 receptor was highly expressed in the treatment group and positive group in contrast to the negative control group. The AT1 receptor seemed to have functions opposite those of the AT2 receptor. Some researchers also demonstrated that the

dx.doi.org/10.1021/jf405189y | J. Agric. Food Chem. 2014, 62, 912−917

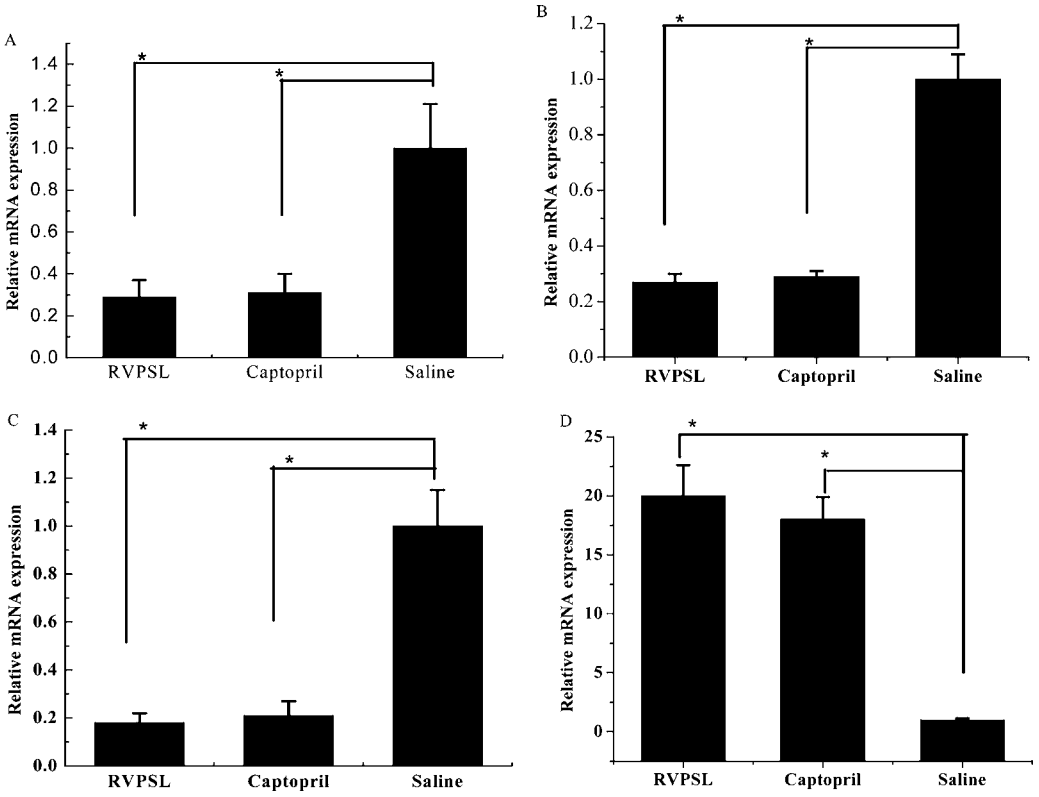

Figure 2. Effect of RVPSL on major RAS components in the SHR kidney: (A) change in relative renin mRNA levels, (B) change in relative ACE mRNA levels, (C) change in relative mRNA levels of the AT1 receptor, and (D) change in the relative mRNA levels of the AT2 receptor . Each value is expressed as the mean ± SD. A p value of <0.05 (*) is considered statistically significant by one-way ANOVA.

AT2 receptors appeared to antagonize the actions of the AT1 receptor.[17]

Effects of RVPSL on the Concentrations of RAS Components of the Serum. The concentrations of serum Ang I, renin, Ang II, and aldosterone were investigated and quantified with an RIA counter and are shown in Figure 3. Compared to the negative group, the serum renin levels of the positive group and high-dose treatment group (50 mg/kg) were significantly lower by 37% and 44% (Figure 3A), respectively. Ang II levels and aldosterone levels of the positive group and high-dose treatment group also declined significantly (Figure 3B,C) in comparison with the negative group. Thus, the peptide RVPSL reduced the blood pressure in combination with the ACE inhibitor or/and renin inhibitor. Although the expression levels of the serum renin of the positive and high-dose treatment groups decreased, the Ang I levels of the positive group and treatment group were not reduced significantly (Figure 3D). Our study on the SHRs gave results similar to those described in another report.[1] In addition, there was no significant difference between the positive group and the high-dose treatment group in the serum Ang I, renin, aldosterone, and Ang II concentrations. In our earlier work, the peptide from egg white protein was shown to have an in vitro ACE inhibition activity with an IC_{50} value of 20 μM,[7] which prompted us to further investigate the in vivo antihypertensive effect of the peptide and explore the corresponding expression of major RAS components in the SHRs. We found that the peptide RVPSL (50 mg/kg) from egg white protein significantly decreased the SBPs of SHRs by 24 mmHg in comparison to the negative group. Miguel[15,18] also evaluated the effects of the hydrolysate of egg white on the short- and long-term arterial blood pressure and suggested that the hydrolysis of egg white with pepsin may be a practical procedure to produce functional bioactive peptides with antihypertensive activity. Ovokinin, a peptide that was hydrolyzed by chymotrypsin from OA 359-364, was found to be able to significantly lower the systolic blood pressure in the SHRs in a dose-dependent manner, when administered orally.[11] Besides, three novel peptides, IQW, IRW, and LKP purified from the ovotransferrin, also exhibited potent activity against ACE based on the quantitative structure−activity relationship of tri- and dipeptides with angiotensin-converting enzyme inhibitory activity.[19] Moreover, IQW was stable against the digestive enzymes.[20] Since the process and pathological characteristics of the SHRs' hypertension are very similar to those of human hypertension,[1] SHRs have generally been used to conduct initial studies on in vivo antihypertensive effects of bioactive peptides. While much is known about diet and physical activity linked to high blood pressure, less is known about the effects of the gene expression level on individual components of RAS in tissues that are responsible for predisposition to cardiovascular disease.[21−24] In this context, we evaluated the mRNA levels of renin, ACE, and AT1 receptor in the rat kidney and found they were significantly reduced. On the contrary, the mRNA level of AT2 receptor in the kidney was upregulated in the treatment group (50 mg/kg) and positive control group compared to the negative group. For the AT1 receptor, the mRNA levels of the positive group and high-dose treatment group (50 mg/kg RVPSL) were decreased significantly. In comparison to that of the negative group, mRNA levels of the AT2 receptor were significantly increased by 20- and 16-fold for the positive group and treatment group (50 mg/kg), respectively. In addition, the

dx.doi.org/10.1021/jf405189y | J. Agric. Food Chem. 2014, 62, 912−917

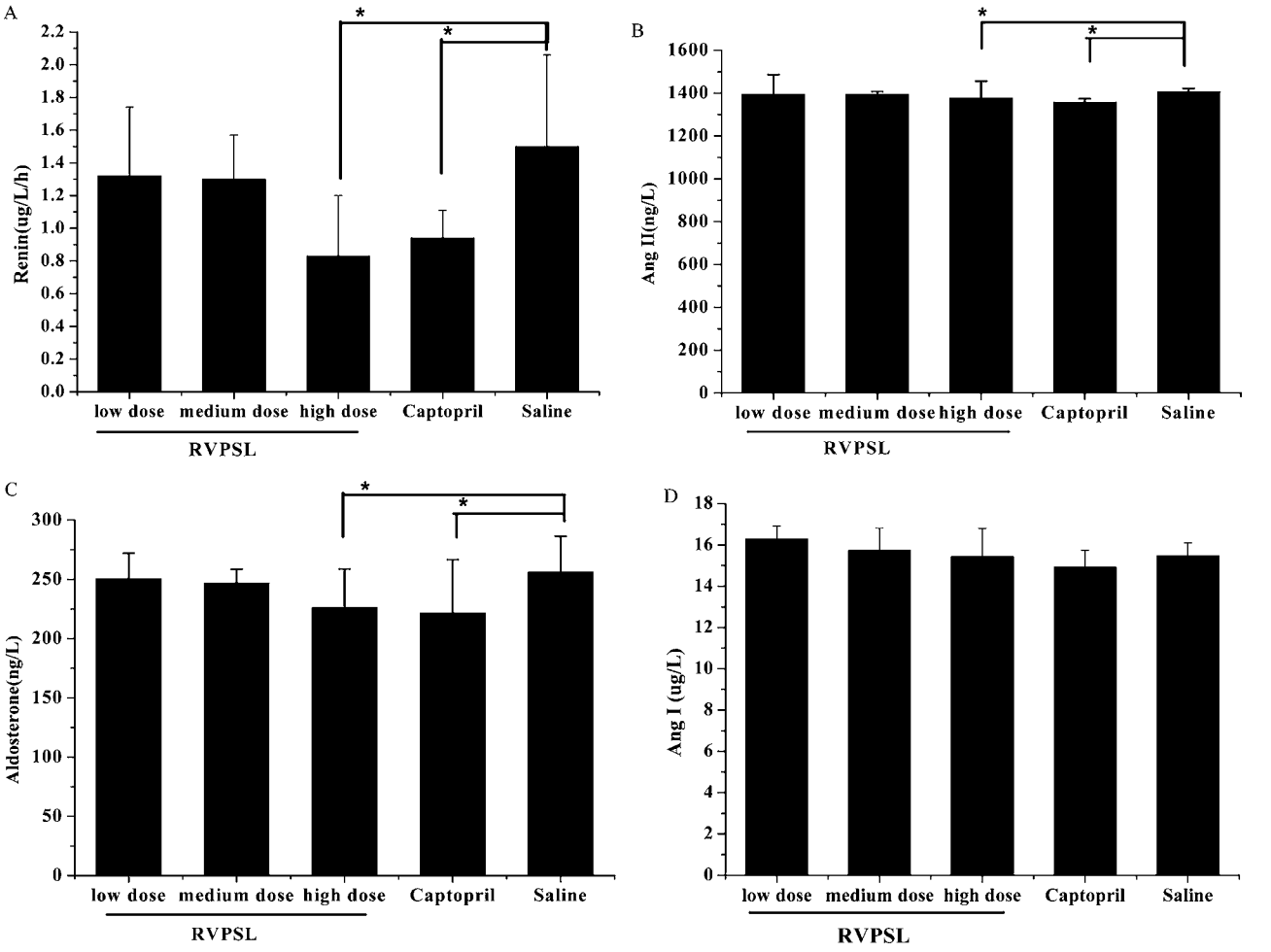

Figure 3. Effects of RVPSL on major RAS components in the serum of SHRs: (A) change in serum renin concentrations, (B) change in serum Ang I concentrations, (C) change in serum Ang II concentrations, and (D) change in serum aldosterone concentrations. Each value is expressed as the mean ± SD. A p value of <0.05 (*) is considered statistically significant by one-way ANOVA.

concentrations of renin, Ang II, and aldosterone in the serum increased significantly in comparison to those of the negative group.

In summary, the current work demonstrated clearly, for the first time, that the peptide RVPSL derived from the egg white significantly decreased the SBP of SHRs in 4 weeks. Also, our results indicated that the peptide RVPSL affected the expression of major RAS components by downregulating the renin, ACE, Ang II, and AT1 receptor while upregulating the AT2 receptor in the kidney or serum of SHRs.

AUTHOR INFORMATION

Corresponding Author

*E-mail: ljb168@sohu.com.

Funding

This work was supported in part by the China Scholarship Council (CSC), the National Natural Science Foundation of China (Grants 31071577 and 31271907), and the Jilin University Graduate Core Curriculum Project (Grant 2012JC008).

Notes

The authors declare no competing financial interest.

ABBREVIATIONS USED

ACE, angiotensin-converting enzyme; Ang I, angiotensin I; Ang II, angiotensin II; AT1, angiotensin type 1; AT2, angiotensin type 2; CCK, cholecystokinin; CVD, cardiovascular disease; DBP, diastolic blood pressure; GAPDH, glyceraldehyde 3-phosphate dehydrogenase; HHL, hippuryl-L-histidyl-L-leucine; HA, hippuric acid; TFA, trifluoroacetic acid; RNase, ribonuclease; RIA, radioimmune assay; RAS, renin−angiotensin system; SHRs, spontaneously hypertensive rats; SBP, systolic blood pressure

REFERENCES

(1) Lu, J.; Sawano, Y.; Miyakawa, T.; Xue, Y.-L.; Cai, M.-Y.; Egashira, Y.; Ren, D.-F.; Tanokura, M. One-week antihypertensive effect of ile-gln-pro in spontaneously hypertensive rats. *J. Agric. Food Chem.* **2011**, *59* (2), 559−563.

(2) Welderufael, F. T.; Gibson, T.; Methven, L.; Jauregi, P. Chemical characterisation and determination of sensory attributes of hydrolysates produced by enzymatic hydrolysis of whey proteins following a novel integrative process. *Food Chem.* **2012**, *134* (4), 1947−1958.

(3) Patchett, A. A.; Harris, E.; Tristram, E. W.; Wyvratt, M. J.; Wu, M. T.; Taub, D.; Peterson, E. R.; Ikeler, T. J.; Tenbroeke, J.; Payne, L. G.; Ondeyka, D. L.; Thorsett, E. D.; Greenlee, W. J.; Lohr, N. S.; Hoffsommer, R. D.; Joshua, H.; Ruyle, W. V.; Rothrock, J. W.; Aster, S. D.; Maycock, A. L.; Robinson, F. M.; Hirschmann, R.; Sweet, C. S.; Ulm, E. H.; Gross, D. M.; Vassil, T. C.; Stone, C. A. A new class of

angiotensin-converting enzyme-inhibitors. *Nature* **1980**, *288* (5788), 280−283.
(4) Vijayaraghavan, P. K.; Narasinga Rao, B. S. Action of duck's egg white ovomucoid on tryptic hydrolysis of casein in vitro. *Nature* **1953**, *172* (4390), 1152−3.
(5) Ferreira, S. H.; Bartelt, D. C.; Greene, L. J. Isolation of bradykinin-potentiating peptides from bothrops-jararaca venom. *Biochemistry* **1970**, *9* (13), 2583−&.
(6) Yang, R. Q.; Zou, Y.; Yu, N. J.; Gu, Z. X. Accumulation and identification of angiotensin-converting enzyme inhibitory peptides from wheat germ. *J. Agric. Food Chem.* **2011**, *59* (8), 3598−3605.
(7) Liu, J. B.; Yu, Z. P.; Zhao, W. Z.; Lin, S. Y.; Wang, E. L.; Zhang, Y.; Hao, H.; Wang, Z. Z.; Chen, F. Isolation and identification of angiotensin-converting enzyme inhibitory peptides from egg white protein hydrolysates. *Food Chem.* **2010**, *122* (4), 1159−1163.
(8) Huang, W.-H.; Sun, J.; He, H.; Dong, H.-W.; Li, J.-T. Antihypertensive effect of corn peptides, produced by a continuous production in enzymatic membrane reactor, in spontaneously hypertensive rats. *Food Chem.* **2011**, *128* (4), 968−973.
(9) Wu, J. P.; Ding, X. L. Hypotensive and physiological effect of angiotensin converting enzyme inhibitory peptides derived from soy protein on spontaneously hypertensive rats. *J. Agric. Food Chem.* **2001**, *49* (1), 501−506.
(10) Liu, L. L.; Liu, L. Y.; Lu, B. Y.; Xia, D. Z.; Zhang, Y. Evaluation of antihypertensive and antihyperlipidemic effects of bamboo shoot angiotensin converting enzyme inhibitory peptide in vivo. *J. Agric. Food Chem.* **2012**, *60* (45), 11351−11358.
(11) Fujita, H.; Sasaki, R.; Yoshikawa, M. Potentiation of the antihypertensive activity of orally administered ovokinin, a vaso-relaxing peptide derived from ovalbumin, by emulsification in egg phosphatidylcholine. *Biosci., Biotechnol., Biochem.* **1995**, *59* (12), 2344−2345.
(12) Marques, C.; Amorim, M. M.; Pereira, J. O.; Pintado, M. E.; Moura, D.; Calhau, C.; Pinheiro, H. Bioactive peptides—are there more antihypertensive mechanisms beyond ace inhibition? *Curr. Pharm. Des.* **2012**, *18* (30), 4706−4713.
(13) Cushman, D. W.; Cheung, H. S. Spectrophotometric assay and properties of the angiotensin-converting enzyme of rabbit lung. *Biochem. Pharmacol.* **1971**, *20* (7), 1637−48.
(14) Kilkenny, C.; Browne, W.; Cuthill, I. C.; Emerson, M.; Altman, D. G. Animal research: reporting in vivo experiments: the arrive guidelines. *Br. J. Pharmacol.* **2010**, *160* (7), 1577−1579.
(15) Miguel, M.; Lopez-Fandino, R.; Ramos, M.; Aleixandre, A. Short-term effect of egg-white hydrolysate products on the arterial blood pressure of hypertensive rats. *Br. J. Nutr.* **2005**, *94* (5), 731−737.
(16) Tavares, T.; Sevilla, M. A.; Montero, M. J.; Carron, R.; Malcata, F. X. Acute effect of whey peptides upon blood pressure of hypertensive rats, and relationship with their angiotensin-converting enzyme inhibitory activity. *Mol. Nutr. Food Res.* **2012**, *56* (2), 316−324.
(17) Bomback, A. S.; Toto, R. Dual blockade of the renin-angiotensin-aldosterone system: beyond the ace inhibitor and angiotensin-ii receptor blocker combination. *Am. J. Hypertens.* **2009**, *22* (10), 1032−1040.
(18) Miguel, M.; Lopez-Fandino, R.; Ramos, M.; Aleixandre, A. Long-term intake of egg white hydrolysate attenuates the development of hypertension in spontaneously hypertensive rats. *Life Sci.* **2006**, *78* (25), 2960−2966.
(19) Wu, J. P.; Aluko, R. E. Quantitative structure-activity relationship study of bitter di- and tri-peptides including relationship with angiotensin I-converting enzyme inhibitory activity. *J. Pept. Sci.* **2007**, *13* (1), 63−69.
(20) Majumder, K.; Wu, J. P. Purification and characterisation of angiotensin I converting enzyme (ACE) inhibitory peptides derived from enzymatic hydrolysate of ovotransferrin. *Food Chem.* **2011**, *126* (4), 1614−1619.
(21) Crackower, M. A.; Sarao, R.; Oudit, G. Y.; Yagil, C.; Kozieradzki, I.; Scanga, S. E.; Oliveira-dos-Santos, A. J.; da Costa, J.; Zhang, L. Y.; Pei, Y.; Scholey, J.; Ferrario, C. M.; Manoukian, A. S.; Chappell, M. C.; Backx, P. H.; Yagil, Y.; Penninger, J. M. Angiotensin-converting enzyme 2 is an essential regulator of heart function. *Nature* **2002**, *417* (6891), 822−828.
(22) Staessen, J. A.; Li, Y.; Richart, T. Oral renin inhibitors. *Lancet* **2006**, *368* (9545), 1449−1456.
(23) Burnier, M.; Brunner, H. R. Angiotensin II receptor antagonists. *Lancet* **2000**, *355* (9204), 637−645.
(24) Kokubu, T.; Ueda, E.; Fujimoto, S.; Hiwada, K.; Kato, A.; Akutsu, H.; Yamamura, Y.; Saito, S.; Mizoguch, T. Peptide inhibitors of the renin-angiotensin system. *Nature* **1968**, *217* (5127), 456−457.

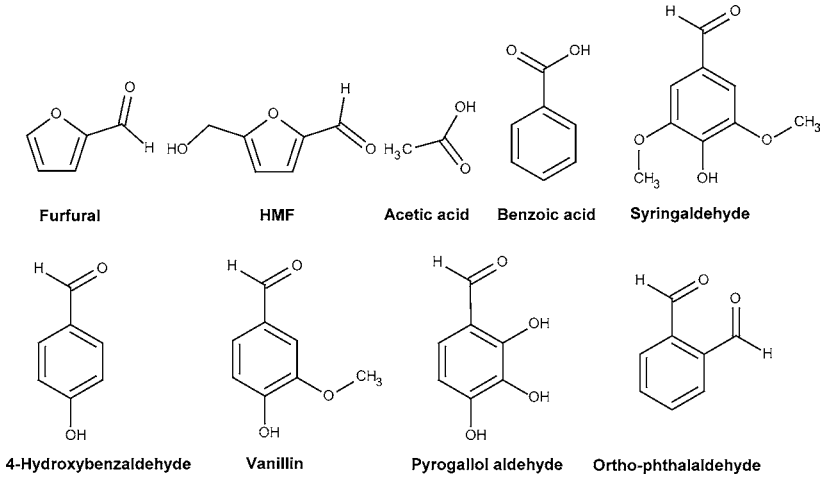

Figure 1. Carbonyl compounds tested for their inhibitory activity on alcoholic fermentation by *Saccharomyces cerevisiae*.

correlation between the structural features of carbonyl compounds and their biological activities will help to understand inhibition of biofuel production. Therefore, we are using QSAR modeling to assess this inhibition on ethanolic fermentation in our research.

In this study, the inhibitory effects of selected aldehydes and acids (Figure 1) on ethanolic fermentation by *Saccharomyces cerevisiae* were investigated. The objective of this study was to identify the specific molecular descriptors that correlate the molecular structure of carbonyl compounds to their inhibitory activity. The quantitative information on carbonyl inhibition was evaluated on the basis of the initial rate of glucose consumption and the final ethanol yield. The alcohol dehydrogenase (ADH) activity in response to vanillin inhibition was determined from the batch fermentation results. Effects of acetic acid and benzoic acid on alcoholic fermentation were also studied with and without pH control. Using those data, the correlation between the inhibition efficiency and carbonyl molecular descriptors was established.

MATERIALS AND METHODS

Chemicals. Glycerol, 4-hydroxybenzaldehyde, 4-hydroxy-3-methoxybenzaldehyde (vanillin), and 2,3,4-trihydroxybenzaldehyde (pyrogallol aldehyde) were purchased from Acros Organics (Morris Plains, NJ, USA). 3,5-Dimethoxy-4-hydroxybenzaldehyde (syringaldehyde) was purchased from Aldrich (Milwaukee, WI, USA). *o*-Phthalaldehyde was purchased from Pickering Laboratories (Mountain View, CA, USA). Benzoic acid and glucose (anhydrous) were purchased from Alfa Aesar (Ward Hill, MA, USA). Vanillyl alcohol and vanillic acid were purchased from Fluka (Milwaukee, WI, USA). Acetic acid, NaOAc, NaCl, KCl, $MgCl_2$, and $CaCl_2$ were purchased from Fisher Scientific (Fair Lawn, NJ, USA). All chemical reagents were of chromatographic grade. Stock solutions of aldehydes (1.0 M) were prepared in ethanol (Sigma-Aldrich, St. Louis, MO, USA), and stock solutions of carboxylic acids (1.0 M) were prepared in deionized water. All stocks were kept at 4 °C before use.

Calculation of Physicochemical Descriptor. The physicochemical properties of model inhibitory compounds were calculated using open software MarvinSketch for the hydrophobicity (log *P*), steric parameter, and molecular refractivity. The E_{LUMO}, E_{HOMO} and dipole moment (u), were calculated using PM6 semiempirical methods (GaussView 5.0). Together, the molecular electrophilicity index (ω) was calculated by using the equation[15,18]

$$\omega = \frac{\mu^2}{2\eta} = \frac{E_{HOMO}{}^2 + 2E_{HOMO}E_{LUMO} + E_{LUMO}{}^2}{4(E_{LUMO} - E_{HOMO})}$$

where μ is the molecular chemical potential and η is the molecular hardness.

Yeast Strain, Culture, and Fermentation. *S. cerevisiae* (baker's yeast, Fleischmann's) was precultured in a YPG liquid medium composed of 10 g/L yeast extract, 20 g/L peptone, and 20 g/L glucose at 30 °C. After 12−15 h, the yeast was harvested and concentrated by centrifugation. The harvested yeast was washed at least twice with sterile water before it was inoculated for batch fermentation. The initial yeast innoculation was 2.0 g/L in fermentation. Batch fermentation was performed in 125 mL serum bottles with 60 mL of 2% (w/w) glucose only at 30 °C, with an initial pH at 6.0 and a shaking speed at 165 rpm for 48 h. No additional nutrients were added in the fermentation medium. The glucose solution was sterilized by filtration through a 0.2 μm sterile filter (VWR, Suwanee, GA, USA). Carbonyl compounds or salts were added into the glucose solution individually from their stock solutions or powders before sterilization. Samples were taken from the fermentation at various time points (1, 3, 6, 9, 12, 24, and 48 h) and centrifuged to collect the supernantant for identification and quantitation by HPLC. Yeast biomass concentration of each data point was measured by UV−vis spectrophotometry at 600 nm. All fermentations were carried out in duplicate. To examine the pH effects of acetic acid and benzoic acid on fermentation, acids were added to the glucose solution from their stock soltuions, and the pH was adjusted with 10% NaOH before sterilization. The resulting pH of the fermentation medium for individual carbonyl compounds was 5.3 (5.0 mM *o*-phthalaldehyde), 4.8 (5.0 mM pyrogallol aldehyde), 5.0 (5.0 mM syringaldehyde), 5.2 (5.0 mM 4-hydroxybenzaldehyde), 5.0 (5.0 mM vanillin), and 5.9 (glucose control), respectively. To examine the effects of inorganic and organic salts on fermentation, we added 27.5 mM NaCl, KCl, $MgCl_2$, and $CaCl_2$ and 50 mM NaOAc individually to 2% glucose solution for batch fermentation. No additional nutrients were added to the fermentation medium. The fermentation conditions were kept the same as above.

The initial consumption rate of glucose (R_S) was calculated on the basis of the sugar consumed in the first 3 h of fermentation [$R_S = (C_0 - C_t)/t$)], where C_0 and C_t were the sugar concentrations at 0 and *t* h, respectively.

The inhibition efficiency *E* (%) of carbonyl compound on fermentation was calculated using the decreased gluocse consumption rate

$$E\ (\%) = \frac{R_{SC} - R_S}{R_{SC}} \times 100$$

where R_{SC} is the initial glucose consumption rate without inhibitor.

HPLC Analysis. Glucose, ethanol, and glycerol were quantitated with a Shimadzu (LC-20A) HPLC system consisting of an autosampler, LC-20AD pump, and RID-10A detector, with a 300 mm × 7.8 mm i.d., 9 μm, Aminex HPX-87P column and a 30 mm × 4.6 mm i.d. guard column of the same material (Bio-Rad, Hercules,

dx.doi.org/10.1021/jf405711f | J. Agric. Food Chem. 2014, 62, 918−926

CA, USA). The mobile phase was composed of 5 mM sulfuric acid running isocratic at 0.6 mL/min. The temperature of the column was maintained at 45 °C throughout the run.

Vanillin, vanillyl alcohol, and vanillic acid were separated and quantitated on the same HPLC system mentioned above with a diode array detector at 254 nm (SPD-M20A). The column for separation was a 250 mm × 4.6 mm i.d., 5 μm, C30 Carotenoid column (Waters, Milford, MA, USA). The mobile phase was acetonitrile/water/formic acid (20:80:1, v/v/v) at 0.6 mL/min, and the temperature of the column was maintained at 30 °C.

Yeast Alcohol Dehydrogenase Activity Assay. To examine the alcohol dehydrogenase (ADH) enzyme activity in response to vanillin inhibition during the batch fermentation, yeast cells were collected at 0, 6, and 9 h of fermentation time with the addition of 0, 2.5, 5.0, 10, and 25 mM vanillin. Samples in 5 mL aliquots were first centrifuged at 2100 rpm for 10 min and then washed with deionized water and centrifuged in an Eppendorf centrifuge 5415R at 13000 rpm for 5 min. The cell pellets were then resuspended in a Y-PER yeast protein extraction reagent (Thermo Fisher Scientific, Rockford, IL, USA) and lysed at room temperature for 20 min with a gentle vortex. The Halt protease inhibitor cocktail (Thermo Fisher Scientific) was added to the lysed solution to prevent protein degradation. The lysed cells were centrifuged in an Eppendorf centrifuge 5415R at 13,000 rpm for 10 min to remove the cell debris, and the supernatant was collected for ADH enzyme activity assays.

The total protein concentration of the supernatant was determined using the Quick Start Bradford dye reagent (Bio-Rad), measuring at 595 nm using bovine serum albumin (BSA) as the reference standard. The ADH enzyme activity was measured on the basis of method described previously by Vallee and Hoch.[19] Briefly, 1.3 mL of 50 mM, pH 8.8, sodium pyrophosphate buffer, 0.1 mL of 95% ethanol, and 1.5 mL of 15 mM cofactor nicotinamide adenine dinucleotide (NAD+) (Sigma-Aldrich) were mixed fresh. The reaction was started by adding 0.1 mL of cell extract (lysate) to the solution. The reaction rate was then measured for 6 min at 340 nm for the change of NAD^+. One unit of ADH activity was defined as the amount of enzyme required to catalyze the conversion of 1.0 μmol of ethanol to acetaldehyde per minute, at pH 8.8 and 25 °C.

Statistical Analysis and Structure−Inhibition Relationships. The data results of carbonyl compound inhibition on glucose consumption and ethanol production were analyzed using one-way analysis of variance (ANOVA) (Excel 2007, Microsoft Office). A p value of <0.05 was considered to be significant. Statistical calculation of correlations between physicochemical parameters and inhibiton efficiency was carried out by regression analysis using Excel 2007 (Microsoft Office). The statistical values include n, the number of observations; s, the stardard error of the estimate; r^2, the coefficient of determination; F, the Fisher statistic; and p, the signficance. A value of $p < 0.05$ indicated that the correlation was significant.

RESULTS AND DISCUSSION

Effects of Aldehydes on Alcoholic Fermentation. The inhibitory effects of different carbonyl compounds on alcoholic fermentation were observed when vanillin, syringaldehyde, 4-hydroxybenzaldehyde, pyrogallol aldehyde, and *o*-phthalaldehyde (all 5.0 mM) were added to the yeast fermentation using glucose as the substrate. Syringaldehyde, pyrogallol aldehyde, and *o*-phthalaldehyde showed significant inhibition on both the glucose consumption rate and ethanol productivity, whereas furfural, HMF, and 4-hydroxybenzaldehyde showed no inhibition on the final ethanol yields. Specifically, pyrogallol aldehyde and *o*-phthalaldehyde reduced the initial glucose consumption rate by 60 and 89%, respectively, and also decreased the final ethanol yield by 60 and 99%, respectively (Figure 2). Although syringaldehyde did not reduce the final ethanol yield (0.40 g/g), it decreased the initial glucose consumption rate by 31%. Interestingly, it was observed that vanillin, syringaldehyde, and 4-hydroxybenzaldehyde could

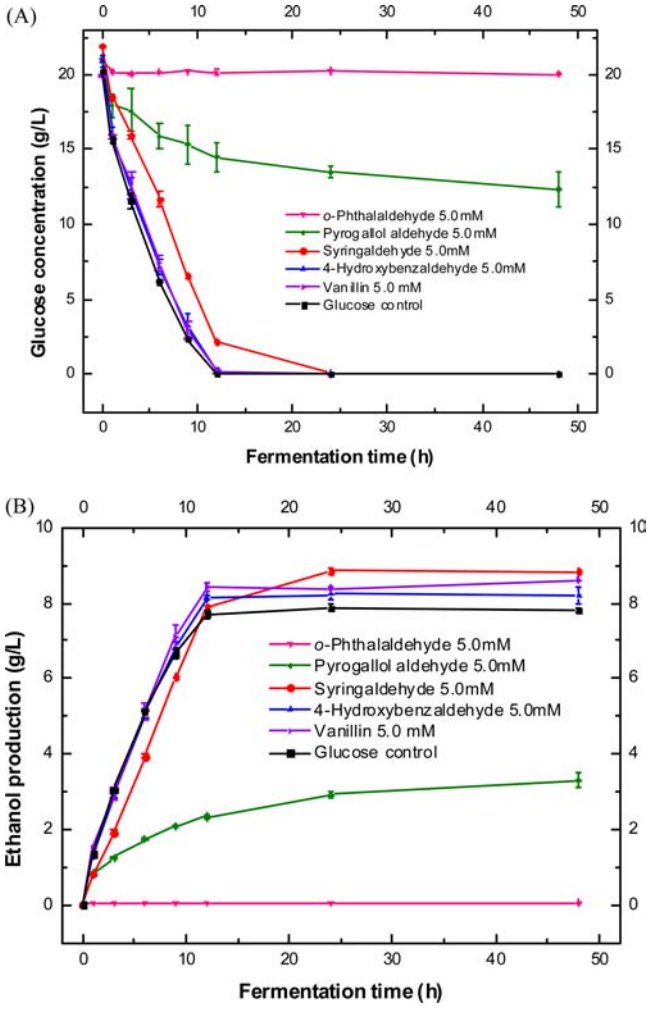

Figure 2. Effects of aldehydes on (A) glucose consumption and (B) ethanol production by *S. cerevisiae*.

increase the ethanol yields by 11, 4, and 1%, respectively, which are similar to those by furfural and HMF in our previous study.[20] These results were in good agreement with reports in the literature that ethanol or butanol yields could be improved by the addition of weak inhibitors.[21−24]

Glucose was completely consumed at 12 h with the addition of vanillin and 4-hydroxybenzaldehyde, similar to the control (without addition of any selected compounds). The addition of *o*-phthalaldehyde and pyrogallol aldehyde resulted in partial consumption of glucose even at 48 h. With the addition of syringaldehyde, the glucose uptake was delayed but completed at 24 h. The initial glucose consumption rates (0.32, 1.15, and 1.98 g/L/h) with the addition of *o*-phthalaldehyde, pyrogallol aldehyde, and syringaldehyde were closely matched to their volumetric ethanol productivity (0.02, 0.42, and 0.42 g/L/h). We performed an ANOVA for both glucose consumption rates and ethanol yields. Statistical analysis showed significant inhibition from *o*-phthalaldehyde, pyrogallol aldehyde, and syringaldehyde. Judging from the initial glucose consumption rate, the inhibitory activity on yeast fermentation was ranked as *o*-phthalaldehyde > pyrogallol aldehyde > syringaldehyde > furfural, HMF, vanillin > 4-hydroxybenzaldehyde.

We believe that the inhibitory activity of these aldehydes is related to the chemical environment of their reactive carbonyl groups (C═O). Previously, various molecular descriptors have

dx.doi.org/10.1021/jf405711f | J. Agric. Food Chem. 2014, 62, 918−926

Table 1. Physicochemical Descriptors of Carbonyl Compounds and Their Inhibitory Activity

inhibitor	log P	E_{LUMO} (eV)	E_{HOMO} (eV)	dipole (Debye)	MR	ω	inhibition efficiency E (%)
HMF	−0.10	−0.79	−9.74	4.50	31.73	3.10	17.2
furfural	0.75	−0.82	−9.95	3.50	2 5.03	3.17	16.1
vanillin	1.22	−0.77	−8.90	4.05	41.09	2.91	16.4
syringaldehyde	1.07	−0.82	−8.82	5.50	47.55	2.88	31.1
4-hydroxybenzaldehyde	1.38	−0.71	−9.58	2.77	34.62	2.98	1.30
pyrogallol aldehyde	1.43	−0.83	−9.19	5.66	38.58	2.98	60.0
o-phthalaldehyde	1.44	−1.50	−10.01	5.21	39.23	3.73	88.9

Table 2. Regression Analysis between Inhibition Efficiency and Molecular Descriptors

eq	regression	n	r^2	s	F	p
1	$E = -0.541 - 0.979\ E_{LUMO}$	7	0.74	0.171	14.31	0.013
2	$E = -0.607 + 0.21$dipole	7	0.55	0.225	6.16	0.056
3	$E = -1.723 + 0.655\omega$	7	0.55	0.225	6.22	0.055
4	$E = 0.096 + 0.227 \log P$	7	0.17	0.31	1.01	0.360

been widely used to characterize chemical reactivity of quinones, unsaturated esters, and phenols.[25−27] These molecular descriptors typically include hydrophobicity (log P, octanol/water partition coefficient), molar refractivity, dipole moment, energy of the lowest unoccupied molecular orbital (E_{LUMO}), energy of the highest occupied molecular orbital (E_{HOMO}), and electrophilicity index (ω).[15,16]

Carbonyl Reactivity and Quantitative Structure−Inhibition Relationship (QSIR). The inhibition efficiency of carbonyl compounds on yeast fermentation was correlated with several molecular descriptors as summarized in Table 1. Significant correlation (r^2 = 0.74, p = 0.013) has been found between E_{LUMO} and the inhibition efficiency (E) of aldehydes (eq 1). E_{LUMO} is a global parameter that indicates the electrophilic reactivity of a molecule.[25,28] The E_{LUMO} of *o*-phthalaldehyde showed the most negative value of −1.50 eV; *o*-phthalaldehyde also was the most inhibitory compound to yeast fermentation (Table 1). Linear regression analysis found the dipole moment and ω were weakly correlated to the inhibitory efficiency (eqs 2 and 3, Table 2). The dipole moment is a measure of the polarity of the molecule.[29] Pyrogallol aldehyde showed the highest dipole moments (5.66 D), and it was the second most inhibitory compound among the tested carbonyl compounds. The electrophilicity index (ω) is defined by the square of its electronegativity divided by its chemical hardness.[18] *o*-Phthalaldehyde showed the highest electrophilicity index (3.73), but its overall weak correlation with inhibitory efficiency (E) was probably due to the E_{HOMO} value. No correlation was found between E_{HOMO} and inhibitory efficiency. Another global parameter, log P, which measured the hydrophobicity of a molecule,[28] showed a poor correlation to inhibitory efficiency in regression eq 4 (Table 2). Previously, Zaldivar et al.[30,31] reported that the toxicity of aldehydes and organic acids on ethanolic fermentation by *Escherichia coli* LY01 was directly related to hydrophobicity. However, the difference may come from the use of a different microorganism and a difference in calculation methods; we used sugar consumption instead of bacterial growth in calculating inhibition.

Studies in the literature have proposed that the chemical reactivity of aldehydes contributed to the inhibition.[31] This hypothesis was supported by the observation that the addition of bisulfite reduced the toxicity of acid hydrolysates.[32] However, few studies have quantitated the chemical reactivity of aldehydes or correlated their reactivity to fermentation inhibition. Here, we quantitated the carbonyl reactivity by calculating their molecular descriptors and correlating the electrophilicity to the inhibitory activity of carbonyl compounds. Table 1 summarizes the inhibitory effects and physicochemical descriptors of carbonyl compounds; the E_{LUMO} correlated best with the inhibition efficiency (E), which could be described as a QSAR model:

$$E = -0.541 - 0.979E_{LUMO}$$

This indicates that carbonyl compounds with higher negative E_{LUMO} values would have higher inhibitory effects. E_{LUMO} typically serves as one of the reactivity parameters for molecular electrophilicity.[26] Carbonyl compounds, as electrophiles, could react with biological macromolecules (protein and DNA) by Michael addition[15] or Schiff base formation,[33] and their inhibitory effects have been related to strong electrophilic reactivity.[34] Our results support using E_{LUMO} to indicate the inhibitory effects of carbonyl compounds on alcoholic fermentation. Consequently, we have identified E_{LUMO}, one of the molecular descriptors, as a reliable, perhaps global parameter that correlates carbonyl compound electrophilicity to inhibition. Obviously, more work to build the QSAR model with a larger number of carbonyl compounds on ethanol and butanol fermentation in *S. cerevisiae* and *Clostridium acetobutylicum* will fine-tune the model and make it more accurate in predicting the structure−inhibitory activity of carbonyl compounds in biomass hydrolysate.

The fact that pyrogallol aldehyde and *o*-phthalaldehyde exhibited inhibition on the final ethanol yield was probably attributed to their strong electrophilic reactivity toward the biological nucleophilic sites. However, the addition of weak inhibitors including furfural, HMF, 4-hydroxybenzaldehyde, vanillin, and syringaldehyde indeed enhanced the final ethanol yield; in particular, vanillin had the highest enhancement. Thus, we used vanillin as a model compound to further examine the effect of weak inhibitors on ethanol (as well as glycerol) production with *S. cerevisiae*.

Effects of Vanillin Concentration on Alcoholic Fermentation. To examine the tolerance of yeast to vanillin, we added various amounts of vanillin (2.5, 5.0, 10, 25 mM) to yeast fermentation (Figure 3). The pH of the medium decreased to 5.3, 5.0, 4.8, and 4.7, respectively. The results showed that vanillin at 25 mM significantly inhibited the final ethanol yield by 63%, whereas at 2.5, 5, and 10 mM it increased

dx.doi.org/10.1021/jf405711f | J. Agric. Food Chem. 2014, 62, 918−926

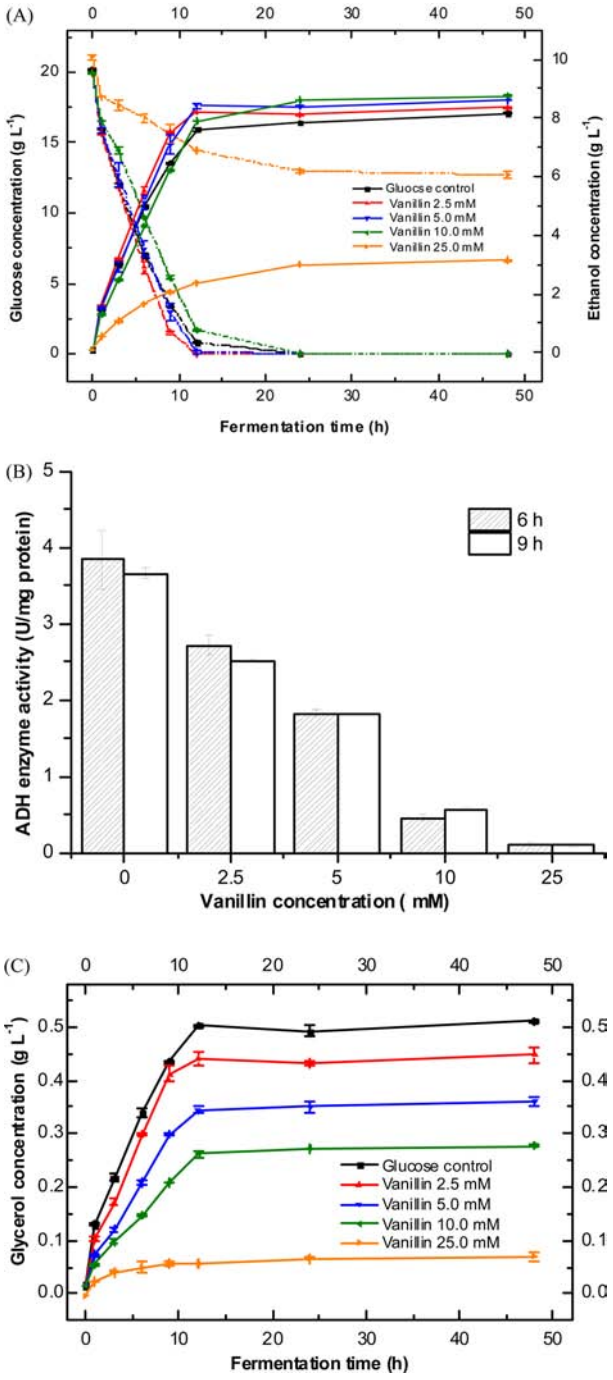

Figure 3. Effects of vanillin on (A) glucose consumption, (B) ADH enzyme specific activity, and (C) glycerol production in fermentation by *S. cerevisiae*.

the final ethanol yield by 3.2, 6.7, and 8.7%, respectively. This indicated a concentration-dependent activity: At low concentrations (2.5, 5, and 10 mM) there was nearly complete glucose consumption within 12 h. However, high concentration (25 mM) inhibited glucose consumption significantly and stopped glucose usage at 24 h. Previously, it was reported that the less inhibitory activities of furfural and HMF were from detoxification by microbes that converted them to alcohols.[35,36] In this study, we observed that vanillin could be reduced to vanillyl alcohol (major product) and oxidized to vanillic acid (minor product) at the same time under the tested conditions. The conversion yields were also dose-dependent; at low concentration (2.5 mM), the yield of vanillyl alcohol was 96.6% and that of vanillic acid, 3.4%. At high concentration (5.0 and 10 mM), the yields of vanillyl alcohol were 71.4 and 59.5%, respectively, and the yields of vanillin acid were 1.4 and 0.7%, respectively. The enzymes responsible for converting vanillin to vanillyl alcohol and vanillic acid probably were alcohol dehydrogenase (ADH) and aldehyde dehydrogenase (ALDH).[37] The higher conversion yield (95% at 2.5 mM vanillin) of vanillyl alcohol was related to higher ADH enzyme activity in the anaerobic conditions, because the NAD^+-dependent ADH activity was typically 10-fold higher than ALDH activity in aerobic condition.[38] The increase of vanillin concentration would decrease the ADH and ALDH enzyme activities, which probably explains why both vanillyl alcohol and vanillic acid yields decreased with increasing vanillin concentration. Consequently, we examined the ADH activity in cell extract at 6 and 9 h of fermentation with various amounts of added vanillin (Figure 3B). The results showed ADH activity decreased significantly with the increase of vanillin concentration. The ADH activity dropped significantly at 6 h of fermentation from 3.85 U/mg to 2.72, 1.83, 0.46, and 0.11 U/g, respectively, with vanillin at 0, 2.5, 5.0, 10.0, and 25.0 mM. A positive correlation has been found between the vanillyl conversion yield and ADH activity ($y = 0.0569x - 2.6473$, $r^2 = 0.90$). At 9 h of fermentation, the ADH activity dropped similarly with increasing vanillin concentration (Figure 3B).

Addition of vanillin decreased the glycerol yield in yeast fermentation as compared to the control (Figure 3C). The glycerol yield decreased by 12.3, 29.6, 45.7, and 82.7%, respectively, with vanillin at 2.5, 5.0, 10.0, and 25 mM. Glycerol, another major byproduct in yeast fermentation, is produced by the reduction of dihydroxyacetone phosphate to glycerol 3-phosphate (G3P) and then dephosphorylation to glycerol.[39,40] The formation of glycerol maintains the redox balance and removes the extra NADP and NAD.[39] The decrease of glycerol yield was probably related to the reducing activities of the yeast cells, which acted as an alternative redox sink for reoxidizing NADH/NADPH. As a result, the ethanol yield increased in the presence of low concentrations of vanillin (2.5, 5.0, and 10 mM) (Figure 3C). The addition of vanillin also decreased the pH of the fermentation medium (5.3−4.7). This could also potentially contribute to the increase in ethanol yield and the decrease in glycerol yield.[41] However, the control experiments did not show a pH effect on glycerol yield within the pH range examined.

Effects of Acetic Acid and Benzoic Acid on Alcoholic Fermentation. Acetic acid and benzoic acid have been implicated as potential inhibitors from lignocellulosic biomass pretreatment.[42,43] To examine whether acids or their salts play a role in the fermentation inhibition, we first added various amounts of acetic acid into yeast fermentation with the initial pH adjusted at 6 (Figure 4A). The results showed that acetate (25, 50, 100, and 150 mM) did not inhibit ethanol production and glucose consumption at pH 6; contrarily, the final ethanol yield increased by 3%, and the glucose consumption rate increased by 20%. On the other hand, acetate (25, 50, 100, and 150 mM) inhibited the yeast growth and reduced the final biomass by 10, 20, 30, and 38% (Figure 4B). Interestingly, the beginning of the stationary phase was shifted earlier, from 12 h (the control) to 6 h. Glycerol production was also inhibited by acetate; the final glycerol concentration was reduced from 0.53 to 0.3, 0.25, 0.22, and 0.22 g/L, respectively.

dx.doi.org/10.1021/jf405711f | J. Agric. Food Chem. 2014, 62, 918−926

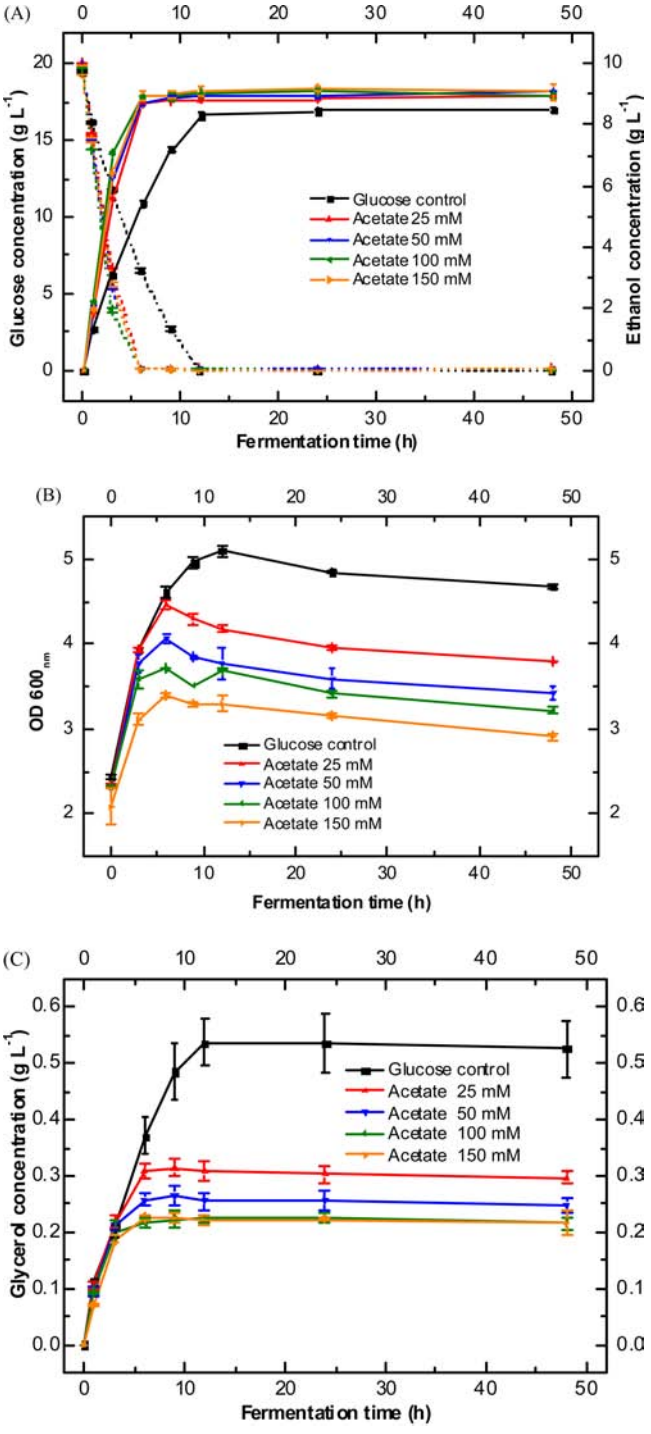

Figure 4. Effects of acetate on ethanol yields, yeast biomass, and glycerol production in fermentation by *S. cerevisiae*.

Acetic or benzoic acid inhibition was found to be pH-dependent. Without pH adjustment, the addition of 5.0 mM benzoic acid resulted in pH 3.3 in the fermentation medium. The glucose consumption was significantly inhibited, and the final ethanol yield was reduced by 89% when compared to the glucose control (Figure 5). The addition of 50 mM acetic acid resulted in pH 3.0, the glucose consumption was significantly inhibited, and the ethanol final yield was reduced by 94% when compared to the control. At pH 4.0, the acetic acid inhibited the volumetric ethanol productivity, but not the final ethanol yield. The volumetric ethanol productivity was reduced from

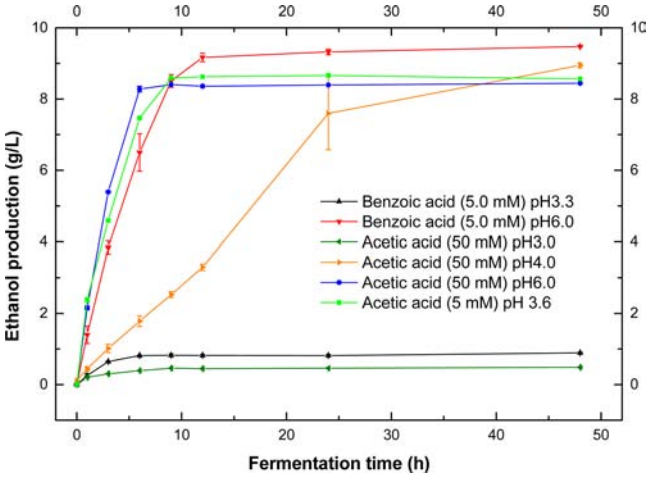

Figure 5. Effect of acetic acid and benzoic acid with and without pH control on fermentation by *S. cerevisiae*.

1.04 to 0.31 g/L/h. When the pH was adjusted to 6, the acetic acid and benzoic acid changed to their corresponding salts (acetate and benzoate). Both appeared to have no inhibitory activity on the final ethanol yield (Figure 5). Actually at pH 6.0, benzoate and acetate increased the final ethanol yields by 16 and 3%, respectively.

These results suggest that the inhibitory effect of acetic acid and benzoic acid are pH-dependent. The inhibition by these weak organic acids at low pH probably came from their undissociated forms. It is believed that the addition of weak organic acids has a significant impact on the growth energetics of fermenting microorganisms.[24,44] When a weak acid was present in the fermentation medium, a low medium pH value (especially lower than the pK_a value of the acids added) increased the fraction of undissociated forms of the acids, which diffused into the cells and decreased the intracellular pH. To maintain a constant pH, the cell must pump out the proton using a plasma membrane ATPase. Consequently, if the diffusion rate exceeded the transport capacity of the plasma membrane, acidification of the cells occurred, which led to the inhibition of both cell growth and ethanol production. Benzoic acid and acetic acid have pK_a values of 4.2 and 4.8, respectively. At a medium pH of 3.0, both acids were present in their undissociated forms; this could cause significant inhibition on fermentation. The pH dependence of weak acid inhibition was also reported on cofermentation of glucose and xylose by genetically engineered *S. cerevisiae*,[43] where the inhibition by acetic acid could be removed by adjusting the pH.

To examine if lowering the medium pH affected the fermentation, we also compared the effect of 5 and 50 mM acetic acid on fermentation without pH control (Figure 5). Addition of 5 mM acetic acid decreased the medium pH to 3.6, whereas it showed no inhibition on either glucose consumption or final ethanol yield. This indicated that it was the concentration of the undissociated form of acetic acid, rather than the medium pH, which led to the inhibition. A similar result was observed before, in which the specific growth rate of *S. cerevisiae* in batch culture did not decrease as the medium pH decreased from 5 to 3.[24]

To examine whether the beneficial effect of acetate on glucose consumption rate was specifically related to acetate or to commonly used inorganic or organic salts, we added 27.5 mM NaCl, KCl, $MgCl_2$, and $CaCl_2$ and 50 mM NaOAc to the

dx.doi.org/10.1021/jf405711f | J. Agric. Food Chem. 2014, 62, 918−926

fermentation. The results showed that all added salts improved the final ethanol yields slightly (Figure 6). The addition of KCl

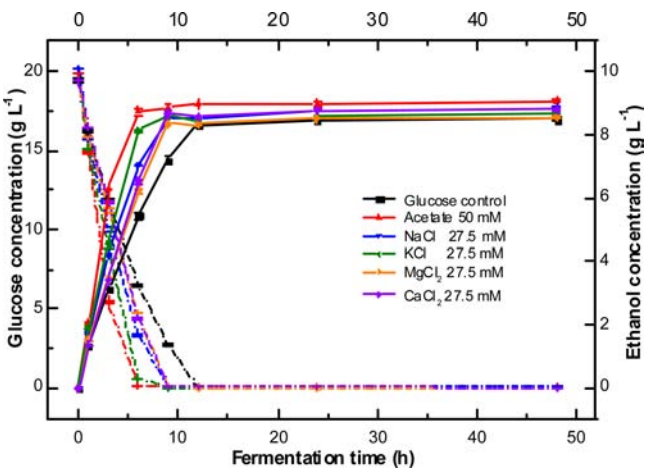

Figure 6. Effects of various salts on ethanol production by *S. cerevisiae*.

and $CaCl_2$ increased the ethanol yields by 2.0 and 3.5%, respectively, whereas NaCl and $MgCl_2$ increased the ethanol yield by <1%. More interestingly, the glucose consumption rates were increased significantly as compared to the control; addition of NaOAc, NaCl, KCl, $MgCl_2$, and $CaCl_2$ increased the glucose initial consumption rates by 88, 33, 39, 7, and 1%, respectively. It was likely that acetate activated the cell membrane permeability and increased glucose consumption.[45,46] Consequently, the time for complete glucose consumption was reduced from 12 to 9 h. A similar observation was reported on ethanolic fermentation by *Zymomonas mobilis*, where chloride salts enhanced ethanol production.[46] The improvement of glucose consumption with inorganic or organic salts could be valuable in the fermentation of biomass hydrolysate, because it would eliminate the requirement to remove the salts generated from biomass pretreatment in hydrolysate conditioning stages, and the presence of salts in biomass hydrolysate could be beneficial to alcoholic fermentation.

Glucose Respiration and Anaerobic Fermentation. In yeast metabolism, glucose consumption takes place via respiration or anaerobic fermentation. The culture conditions typically control the prevailing pathways. Repression of respiration under high glucose concentration resulting in aerobic fermentation, is known as the Crabtree effect. However, we carried out all of the fermentation experiments under facultative anaerobic conditions in 125 mL serum bottles; the Crabtree effect, therefore, was not expected to be significant in our study. Statistical analysis of the results indicated that furfural, HMF, syringaldehyde, pyrogallol aldehyde, and *o*-phthalaldehyde showed significant inhibition ($p < 0.05$) on volumetric ethanol productivity (Q_{EtOH}), which indirectly suggests that these carbonyl compounds inhibit anaerobic fermentation. The analysis also showed a significant inhibitory effect of syringaldehyde, pyrogallol aldehyde, and *o*-phthalaldehyde on the glucose consumption rate (R_S), which was related to both respiration and anaerobic fermentation. However, the exact effect of carbonyl compounds on glucose respiration could not be estimated in this study. As for the effect of acetate on alcoholic fermentation, the volumetric ethanol productivity increased by >79%, but the yeast biomass decreased by 10–38%. This suggested that acetate had a stimulatory effect on anaerobic fermentation and an inhibitory effect on respiration (biomass yield typically was related to sugar respiration).

In summary, effects of aldehydes and carboxylic acids on ethanolic fermentation have been quantitated on the basis of glucose consumption rate and final ethanol yield. With an attempt to build a structure–inhibition relationship of carbonyl compounds on fermentation, we have identified that E_{LUMO} is a very good global parameter to correlate the molecular structure of carbonyl compounds to their inhibitory effects. The study also revealed that the addition of vanillin (<10 mM) changed the glycerol pathway to an ethanol pathway and decreased glycerol yields in fermentation. In addition, fermentation inhibition by acetic and benzoic acids was found to be pH-dependent. The inorganic and organic salts showed the potential to enhance glucose consumption rates and final ethanol yields by activating the membrane permeability of yeast. Future work will be focused on building the QSAR model for ethanol and butanol fermentation with a larger number of carbonyl compounds.

■ ASSOCIATED CONTENT

Supporting Information

Table S1 and Figures S1 and S2. This material is available free of charge via the Internet at http://pubs.acs.org.

■ AUTHOR INFORMATION

Corresponding Author

*(M.T.) E-mail: mtu@auburn.edu. Fax: +1 (334) 844-1084. Phone: +1 (334) 844-8829.

Funding

We appreciate the support of this study, partially, by grants from the U.S. Department of Energy (DE-EE0003115) and the National Science Foundation (NSF-CBET 1254899).

Notes

The authors declare no competing financial interest.

■ ACKNOWLEDGMENTS

We are grateful to Dr. Thomas Webb for his comments and critical proofreading of the manuscript.

■ REFERENCES

(1) Office of the Biomass Program (EERE/DOE), Biomass program multi-year program plan; http://www1.eere.energy.gov/biomass/pdfs/mypp_april_2012.pdf (accessed Sept 3, 2013).

(2) Schepf, R.; Yacobucci, B. D. Renewable fule standard (RFS): overview and issues; http://www.fas.org/sgp/crs/misc/R40155.pdf (accessed Sept 3, 2013).

(3) Himmel, M. E.; Ding, S. Y.; Johnson, D. K.; Adney, W. S.; Nimlos, M. R.; Brady, J. W.; Foust, T. D. Biomass recalcitrance: engineering plants and enzymes for biofuels production. *Science* **2007**, *315*, 804–807.

(4) Lynd, L. R.; Weimer, P. J.; van Zyl, W. H.; Pretorius, I. S. Microbial cellulose utilization: fundamentals and biotechnology. *Microbiol. Mol. Biol. Rev.* **2002**, *66*, 506–577.

(5) Carter, B.; Squillace, P.; Gilcrease, P. C.; Menkhaus, T. J. Detoxification of a lignocellulosic biomass slurry by soluble polyelectrolyte adsorption for improved fermentation efficiency. *Biotechnol. Bioeng.* **2011**, *108*, 2053–2060.

(6) Nichols, N. N.; Dien, B. S.; Cotta, M. A. Fermentation of bioenergy crops into ethanol using biological abatement for removal of inhibitors. *Bioresour. Technol.* **2010**, *101*, 7545–7550.

(7) Lau, M. W.; Gunawan, C.; Dale, B. E. The impacts of pretreatment on the fermentability of pretreated lignocellulosic

biomass: a comparative evaluation between ammonia fiber expansion and dilute acid pretreatment. *Biotechnol. Biofuels* **2009**, *2*, 30.
(8) Luo, C. D.; Brink, D. L.; Blanch, H. W. Identification of potential fermentation inhibitors in conversion of hybrid poplar hydrolyzate to ethanol. *Biomass Bioenerg.* **2002**, *22*, 125−138.
(9) Nichols, N. N.; Sharma, L. N.; Mowery, R. A.; Chambliss, C. K.; van Walsum, G. P.; Dien, B. S.; Iten, L. B. Fungal metabolism of fermentation inhibitors present in corn stover dilute acid hydrolysate. *Enzyme Microb. Technol.* **2008**, *42*, 624−630.
(10) Chen, S. F.; Mowery, R. A.; Castleberry, V. A.; van Walsum, G. P.; Chambliss, C. K. High-performance liquid chromatography method for simultaneous determination of aliphatic acid, aromatic acid and neutral degradation products in biomass pretreatment hydrolysates. *J. Chromatogr., A* **2006**, *1104*, 54−61.
(11) Sharma, L. N.; Nichols, N. N.; Becker, C.; Chambliss, C. K. Analytical characterization of fermentation inhibitors in biomass pretreatment samples using liquid chromatography, UV-visible spectroscopy, and tandem mass spectrometry. In *Biofuels: Methods and Protocols*; Mielenz, J. R., Ed.; Methods in Molecular Biology 581; Springer Protocols: Berlin, Germany, 2010; pp 125−143.
(12) Agblevor, F. A.; Fu, J.; Hames, B.; McMillan, J. D. Identification of microbial inhibitory functional groups in corn stover hydrolysate by carbon-13 nuclear magnetic resonance spectroscopy. *Appl. Biochem. Biotechnol.* **2004**, *119*, 97−120.
(13) Almeida, J. R. M.; Modig, T.; Petersson, A.; Hahn-Hagerdal, B.; Liden, G.; Gorwa-Grauslund, M. F. Increased tolerance and conversion of inhibitors in lignocellulosic hydrolysates by *Saccharomyces cerevisiae*. *J. Chem. Technol. Biotechnol.* **2007**, *82*, 340−349.
(14) Clark, T. A.; Mackie, K. L. Fermentation inhibitors in wood hydrolysates derived from the softwood *Pinus-radiata*. *J. Chem. Technol. Biotechnol.* **1984**, *34*, 101−110.
(15) Schwobel, J. A. H.; Wondrousch, D.; Koleva, Y. K.; Madden, J. C.; Cronin, M. T. D.; Schuurmann, G. Prediction of Michael-type acceptor reactivity toward glutathione. *Chem. Res. Toxicol.* **2010**, *23*, 1576−1585.
(16) Schwobel, J. A. H.; Koleva, Y. K.; Enoch, S. J.; Bajot, F.; Hewitt, M.; Madden, J. C.; Roberts, D. W.; Schutz, T. W.; Cronin, M. T. D. Measurement and estimation of electrophilic reactivity for predictive toxicology. *Chem. Rev.* **2011**, *111*, 2562−2596.
(17) Perkins, R.; Fang, H.; Tong, W. D.; Welsh, W. J. Quantitative structure-activity relationship methods: perspectives on drug discovery and toxicology. *Environ. Toxicol. Chem.* **2003**, *22*, 1666−1679.
(18) Parr, R. G.; Von Szentpaly, L.; Liu, S. B. Electrophilicity index. *J. Am. Chem. Soc.* **1999**, *121*, 1922−1924.
(19) Vallee, B. L.; Hoch, F. L. Zinc, a component of yeast alcohol dehydrogenase. *Proc. Natl. Acad. Sci. U.S.A.* **1955**, *41*, 327−338.
(20) Xie, R.; Tu, M. B.; Wu, Y. N.; Taylor, S. Reducing sugars facilitated carbonyl condensation in detoxification of carbonyl aldehyde model compounds for bioethanol fermentation. *RSC Adv.* **2012**, *2*, 7699−7707.
(21) Ezeji, T.; Qureshi, N.; Blaschek, H. P. Butanol production from agricultural residues: impact of degradation products on *Clostridium beijerinckii* growth and butanol fermentation. *Biotechnol. Bioeng.* **2007**, *97*, 1460−1469.
(22) Palmqvist, E.; Almeida, J. S.; Hahn-Hagerdal, B. Influence of furfural on anaerobic glycolytic kinetics of *Saccharomyces cerevisiae* in batch culture. *Biotechnol. Bioeng.* **1999**, *62*, 447−454.
(23) Wahlbom, C. F.; Hahn-Hagerdal, B. Furfural, 5-hydroxymethyl furfural, and acetoin act as external electron acceptors during anaerobic fermentation of xylose in recombinant *Saccharomyces cerevisiae*. *Biotechnol. Bioeng.* **2002**, *78*, 172−178.
(24) Taherzadeh, M. J.; Niklasson, C.; Liden, G. Acetic acid − friend or foe in anaerobic batch conversion of glucose to ethanol by *Saccharomyces cerevisiae*? *Chem. Eng. Sci.* **1997**, *52*, 2653−2659.
(25) Chan, K.; O'Brien, P. J. Structure-activity relationships for hepatocyte toxicity and electrophilic reactivity of alpha,beta-unsaturated esters, acrylates and methacrylates. *J. Appl. Toxicol.* **2008**, *28*, 1004−1015.
(26) Chan, K.; Jensen, N.; O'Brien, P. J. Structure-activity relationships for thiol reactivity and rat or human hepatocyte toxicity induced by substituted *p*-benzoquinone compounds. *J. Appl. Toxicol.* **2008**, *28*, 608−620.
(27) Cronin, M. T. D.; Schultz, T. W. Structure-toxicity relationships for phenols to *Tetrahymena pyriformis*. *Chemosphere* **1996**, *32*, 1453−1468.
(28) Cronin, M. T. D.; Schultz, T. W. Development of quantitative structure-activity relationships for the toxicity of aromatic compounds to *Tetrahymena pyriformis*: comparative assessment of the methodologies. *Chem. Res. Toxicol.* **2001**, *14*, 1284−1295.
(29) Eroglu, E.; Turkmen, H. A DFT-based quantum theoretic QSAR study of aromatic and heterocyclic sulfonamides as carbonic anhydrase inhibitors against isozyme, CA-II. *J. Mol. Graph. Model.* **2007**, *26*, 701−708.
(30) Zaldivar, J.; Ingram, L. O. Effect of organic acids on the growth and fermentation of ethanologenic *Escherichia coli* LY01. *Biotechnol. Bioeng.* **1999**, *66*, 203−210.
(31) Zaldivar, J.; Martinez, A.; Ingram, L. O. Effect of selected aldehydes on the growth and fermentation of ethanologenic *Escherichia coli*. *Biotechnol. Bioeng.* **1999**, *65*, 24−33.
(32) Mcmillan, J. D. Conversion of hemicellulose hydrolyzates to ethanol. In *Enzymatic Conversion of Biomass for Fuels Production*; Himmel, M. E., Baker, J. O., Overend, R. P., Eds.; ACS Symposium Series 566; American Chemical Society: Washington, DC, 1994; pp 411-437.
(33) Karabunarliev, S.; Mekenyan, O. G.; Karcher, W.; Russom, C. L.; Bradbury, S. P. Quantum-chemical descriptors for estimating the acute toxicity of electrophiles to the fathead minnow (*Pimephales promelas*): an analysis based on molecular mechanisms. *Quant. Struct.−Act. Relat.* **1996**, *15*, 302−310.
(34) Mccarthy, T. J.; Hayes, E. P.; Schwartz, C. S.; Witz, G. The reactivity of selected acrylate esters toward glutathione and deoxyribonucleosides in-vitro − structure-activity-relationships. *Fundam. Appl. Toxicol.* **1994**, *22*, 543−548.
(35) Koopman, F.; Wierckx, N.; de Winde, J. H.; Ruijssenaars, H. J. Identification and characterization of the furfural and 5-(hydroxymethyl)furfural degradation pathways of *Cupriavidus basilensis* HMF14. *Proc. Natl. Acad. Sci. U.S.A.* **2010**, *107*, 4919−4924.
(36) Liu, Z. L.; Moon, J. A novel NADPH-dependent aldehyde reductase gene from *Saccharomyces cerevisiae* NRRL Y-12632 involved in the detoxification of aldehyde inhibitors derived from lignocellulosic biomass conversion. *Gene* **2009**, *446*, 1−10.
(37) Modig, T.; Liden, G.; Taherzadeh, M. J. Inhibition effects of furfural on alcohol dehydrogenase, aldehyde dehydrogenase and pyruvate dehydrogenase. *Biochem. J.* **2002**, *363*, 769−776.
(38) Kometani, T.; Sakai, Y.; Urai, H.; Goto, M.; Matsuno, R. Effect of aeration conditions on aldehyde dehydrogenase activity in yeast cultivation. *J. Ferment. Bioeng.* **1998**, *86*, 617−619.
(39) Michnick, S.; Roustan, J. L.; Remize, F.; Barre, P.; Dequin, S. Modulation of glycerol and ethanol yields during alcoholic fermentation in *Saccharomyces cerevisiae* strains overexpressed or disrupted for GPD1 encoding glycerol 3-phosphate dehydrogenase. *Yeast* **1997**, *13*, 783−793.
(40) Guo, Z. P.; Zhang, L. A.; Ding, Z. Y.; Shi, G. Y. Minimization of glycerol synthesis in industrial ethanol yeast without influencing its fermentation performance. *Metab. Eng.* **2011**, *13*, 49−59.
(41) Gonzalez, R.; Quiros, M.; Morales, P. Yeast respiration of sugars by non-*Saccharomyces* yeast species: a promising and barely explored approach to lowering alcohol content of wines. *Trends Food Sci. Technol.* **2013**, *29*, 55−61.
(42) Pereira, R. S.; Mussatto, S. I.; Roberto, I. C. Inhibitory action of toxic compounds present in lignocellulosic hydrolysates on xylose to xylitol bioconversion by *Candida guilliermondii*. *J. Ind. Microbiol. Biotechnol.* **2011**, *38*, 71−78.
(43) Casey, E.; Sedlak, M.; Ho, N. W. Y.; Mosier, N. S. Effect of acetic acid and pH on the cofermentation of glucose and xylose to ethanol by a genetically engineered strain of *Saccharomyces cerevisiae*. *FEMS Yeast Res.* **2010**, *10*, 385−393.

(44) Verduyn, C.; Postma, E.; Scheffers, W. A.; Vandijken, J. P. Effect of benzoic-acid on metabolic fluxes in yeasts − a continuous-culture study on the regulation of respiration and alcoholic fermentation. *Yeast* **1992**, *8*, 501−517.
(45) Soma, M. K.; Savadogo, A.; Barro, N.; Thonart, P.; Traore, A. S. Effect of minerals salts in fermentation process using mango residues as carbon source for bioethanol production. *Asian J. Ind. Eng.* **2011**, *3*, 29−38.
(46) Kirk, L. A.; Doelle, H. W. The effects of potassium and chloride-ions on the ethanolic fermentation of sucrose by *Zymomonas-mobilis* 2716. *Appl. Microbiol. Biotechnol.* **1992**, *37*, 88−93.

89Grx is therefore potentially useful for biotechnological applications.

MATERIALS AND METHODS

Materials. *C. sorokiniana* T-89 (isolated from the paddy field of Chiayi, Taiwan) was provided by Dr. Tan-Chi Huang. The restriction enzymes, *Nde*I and *Xho*I, were purchased from NEB (New England BioLabs, U.S.A.). β-Hydroxyethylene disulfide [HED, $(HOCH_2CH_2)_2S_2$], as a low molecular weight substrate, was purchased from Sigma-Aldrich-Fluka (St. Louis, MO). Glutathione reductase (GR), NADPH, and glutathione (GSH) were obtained from Sigma (St. Louis, MO). The High-speed Plasmid Mini Kit and Gel/PCR DNA Fragments Extraction Kit were purchased from Geneaid (Geneaid Biotech, Bade City, Taiwan). Protein molecular mass markers were obtained from Fermentas (Canada).

RNA Extraction and cDNA Synthesis. Total RNA of *C. sorokiniana* T-89 was prepared using RNAzol RT (Molecular Research Center). The mRNA was then purified using Oligotex mRNA Mini kit (Qiagen, U.S.A.). The cDNA was carried out using the 5′/3′ RACE kit (Roche, Germany).

Cloning of *C. sorokiniana* T-89 Grx Gene and Its Mutant Forms. After total RNA was extracted from *C. sorokiniana* T-89, the cDNA was synthesized for sequencing analysis. Gene-specific primers of CsT-89Grx were designed on the basis of the RNA sequencing analysis information of *C. sorokiniana* T-89. The full length Grx gene from *C. sorokiniana* T-89 was amplified by polymerase chain reaction (PCR) using gene-specific primers, and the CsT-89 Grx gene was obtained using *C. sorokiniana* T-89 cDNA as a template. The forward primer Grx-F (5′-GGAATTC*CATATG*AGCGCGGCCAAG-CAGCTGG-3′) and the reverse primer Grx-R (5′-CCGC*TCGAG*GAGCACGCCGGCATTGCGCAGCAT-3′) were incorporated with the cloning sites of *Nde*I and *Xho*I (in italics), respectively. After digestion with *Nde*I and *Xho*I, the CsT-89Grx DNA fragment was ligated into a pET-20b(+) expression vector (Novagen, Germany), which was previously treated with the same restriction enzymes. Consequently, the recombinant pET-20b_CsT-89Grx plasmid was transformed into the cloning host *E. coli* DH5α (GeneMark, Taiwan). The site-directed mutagenesis of CsT-89Grx active sites (C25A and C28A) were constructed using the QuikChange Site-Directed Mutagenesis Kit (Agilent Technologies, U.S.A.). The mutant primers were designed to replace cysteine by alaline (in italics) as follows: CsT-89GrxC25A-F (5′- AGCAAGACC-TAC*GC*GCCTTACTGCGTG-3′), CsT-89GrxC25A-R (5′-CACGCAGTAAGG*CGC*GTAGGTCTTGCT-3′); CsT-89Grx C28A-F (5′-TACTGCCCTTAC*GC*GGTGAAGGGCAAG-3′), CsT-89GrxC28A-R (5′-CTTGCCCTTCAC*CGC*GTAAGGG-CAGTA-3′); and CsT-89GrxC25,28A-F (5′-TTTAGCAA-GACCTC*GC*GCCTTAC*GC*GGTGAAGGGCAAGCGG-3′), CsT-89Grx C25,28A-R (5′-CCGCTTGCCCTTCAC*CGC*G-TAAGG*CGC*GTAGGTCTTGCTAA A-3′).

Bioinformatic Analysis of CsT-89Grx. The protein sequence of CsT-89Grx was analyzed using protein−protein BLAST in NCBI (http://www.ncbi.nlm.nih.gov/). The molecular mass and pI of the encoded protein were computed using ExPASy (http://www.expasy.ch/tools/protparam.html). The multiple amino acid sequence alignment of CsT-89Grx was compared using ClustalW2 (http://www.ebi.ac.uk/Tools/clustalw2/index.html).

Expression and Purification of Recombinant CsT-89Grx. For recombinant CsT-89Grx (rCsT-89Grx) expression, *E. coli* BL21(DE3) (Novagen, Germany) was used as the expression host. The BL21(DE3) containing pET-20b_CsT-89Grx was grown until OD_{600} 0.4 at 37 °C in LB broth with ampicillin (100 μg/mL). Thereafter, the recombinant protein was induced by adding isopropyl thio-β-D-galactoside (IPTG) to a final concentration of 0.4 mM. Protein induction was performed at 28 °C for 4 h before cell harvesting. The cells were lysed in BugBuster Protein Extraction Reagent (Novagen, Germany). The crude protein lysate was obtained after 10 000*g* centrifugation for 15 min. The rCsT-89Grx was purified using BD TALON Superflow Resin, which was used for the purification of polyhistidine-tagged protein (BD Biosciences Clontech, U.S.A.). The purified enzyme was desalted using a Protein Desalting Spin Column following affinity purification (Pierce, U.S.A.). The recombinant protein was analyzed using 16% Tricine sodium dodecyl sulfate polyacrylamide gel electrophoresis (Tricine SDS-PAGE).[28]

Protein Quantitation and Enzyme Activity Assay. Protein concentrations were quantified according to Bradford's [29] method using bovine serum albumin as the standard. Grx activity was assayed using the HED method.[30] The reaction mixture consisted of 50 mM of Tris-Cl (pH 7.4), 0.6 μg of GR, 0.3 mM of HED, 0.2 mM of NADPH, 0.8 mM of GSH, and 0.1 μg of rCsT-89Grx in a total volume of 500 μL. Briefly, the disulfide bond was spontaneously formed between HED and GSH within 2 min, and the reaction was subsequently commenced by adding 0.1 μg of rCsT-89Grx. Activity was monitored on the basis of the decrease in NADPH absorbance at 340 nm. One unit of activity was defined as the enzyme necessary to deplete 1 μmol of NADPH per minute. The value was calculated by $(\Delta A340 \times V)/(\min \times 6.2)$, where V indicates the cuvette volume in milliliters, and 6.2 is the millimolar extinction coefficient for NADPH.[30]

Biochemical Characterization of the Recombinant CsT-89Grx. The activities of CsT-89Grx under various conditions were studied using the described HED assay. The optimal pH and temperature, stability of pH and temperature, kinetic analysis as well as the effects of metal ions, chemical reagents, and inhibitors were studied. For the optimal pH of CsT-89Grx, the activity of the enzyme over the pH range of 3.0 to 11.0 was measured using a 50 mM acetate buffer (pH 3.0−6.0), a 50 mM Tris-HCl buffer pH (pH 7.0−9.0), and a 50 mM glycine-NaOH buffer (pH 10.0−11.0) at 30 °C. Optimal enzyme activities were also tested at various temperatures (15 to 60 °C) at pH 8.5 in 50 mM Tris-HCl buffer. To analyze thermal tolerance, the enzyme was incubated at various temperatures from 4 to 100 °C for 1 h, and residual activity was analyzed in 50 mM Tris-HCl buffer (pH 8.5) at 50 °C. The pH stability of CsT-89Grx was investigated at different pH values (pH 3, 5, 7, 9, and 11) and at optimum pH and temperature. The kinetic analyses of the purified CsT-89Grx with different concentrations of HED (0.06 mM to 0.2 mM) were conducted under the optimum pH and temperature conditions. To study the effects of various metal ions (NaCl, $MgCl_2$, $MnCl_2$, $CaCl_2$, $CoCl_2$, $CuSO_4$, $ZnCl_2$, and $FeCl_3$) on the enzyme, 1 or 10 mM of the metal ions and CsT-89Grx was preincubated in 50 mM Tris-HCl (pH 8.5) at 37 °C for 30 min. The mixture was then analyzed for enzyme activity under optimal conditions. The effects of chemical reagents and inhibitors on enzyme activity were measured. Chemical reagents and inhibitors, including urea, ethylenediaminetetraacetic acid (EDTA), sodium dodecyl disulfate (SDS), dithiotheretiol (DTT), phenylmethanesulfony fluoride

(PMSF), and iodoactamide, were incubated with the enzyme for 30 min at 37 °C in 50 mM Tris-HCl (pH 8.5). Residual activity was determined at 50 °C in 50 mM Tris-HCl buffer (pH 8.5). Enzyme activity without treatment was defined as 100%.

RESULTS AND DISCUSSION

Cloning of Grx Gene from *C. sorokiniana* T-89 and Sequence Analysis. *C. sorokiniana* T-89 isolated from a paddy field in Chiayi, Taiwan, belonged to the heat-tolerant *Chlorella species* because it could grow well up to 38 °C.[31] Cultures of *C. sorokiniana* T-89 at different growth stages were used for RNA extraction, and mRNA was converted to cDNA for sequence analysis. The contig data of sequences were obtained using the Illuina sequencing system. Contigs were predicted for their function via sequence alignment using NCBI BLAST. Among the sequence data, Grx was identified. The forward and reverse specific primers of CsT-89Grx were designed on the basis of sequence alignment using NCBI BLAST. Using *C. sorokiniana* T-89 cDNA as template, the 321 bp DNA fragment encoding the Grx protein was amplified by PCR. CsT-89Grx was further constructed into pET-20b(+) and was confirmed to have the correct sequence by DNA sequencing.

Using the ExPASy Compute pI/MW program, the theoretical molecular mass and pI of CsT-89Grx were computed as 11.4 and 8.97 kDa, respectively. The bioinformatics of CsT-89Grx was analyzed using the NCBI protein-BLAST program. According to the data analysis, the predicted active sites of CsT-89Grx were Cys^{25} and Cys^{28}, and the conserved redox active site CPYC motif suggested that CsT-89Grx belonged to the dithiol superfamily.[26,32,33] The residues of Lys^{22}, Cys^{25}, Tyr^{27}, Arg^{69}~Pro^{72}, and Gly^{83}~Asp^{86} were predicted to be the putative GSH binding sites (Figure 1).

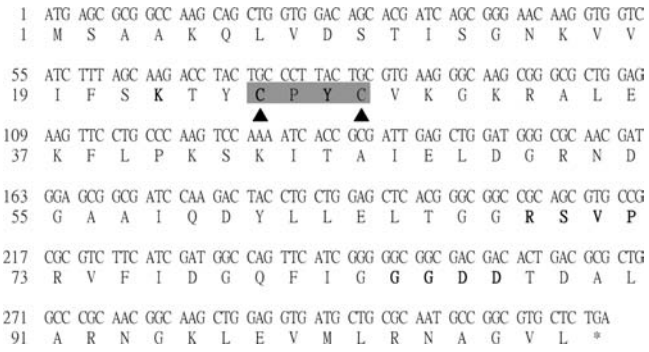

Figure 1. Deduced nucleotide and amino acid sequence of *C. sorokiniana* T-89 glutaredoxin (CsT-89Grx). The stop codon is shown in asterisks. The predicted active sites of CsT-89Grx, Cys^{25}, and Cys^{28} are shown as black triangles, and the putative conserved CPYC motif is indicated by a gray block. The putative GSH-binding sites are composed of Lys^{22}, Cys^{25}, Tyr^{27}, Arg^{69}~Pro^{72}, and Gly^{83}~Asp^{86}, as presented by bold letters.

Moreover, multiple amino acid sequence alignments of Grx containing *C. sorokiniana* T-89 (in this study), *Aspergillus fumigates* Af293 (XP_750359.1), *Chlamydomonas reinhardtii* (XP_001694001.1), *E. coli* (AAA23936.1), *Homo sapiens* (NP_002055.1), *Saccharomyces cerevisiae* S288c (NP_009895.1), and *Taiwanofungus camphorates* (ABY58974.1) were also conducted. Despite low sequence similarity (CsT-89Grx shared 53% identity with CrGrx, 44% with AfGrx, 43% with TcGrx, 36% with HsGrx and ScGrx, and 27% with EcGrx), the active site (CPYC motif) and GSH-binding sites were highly conserved (Figure 2).

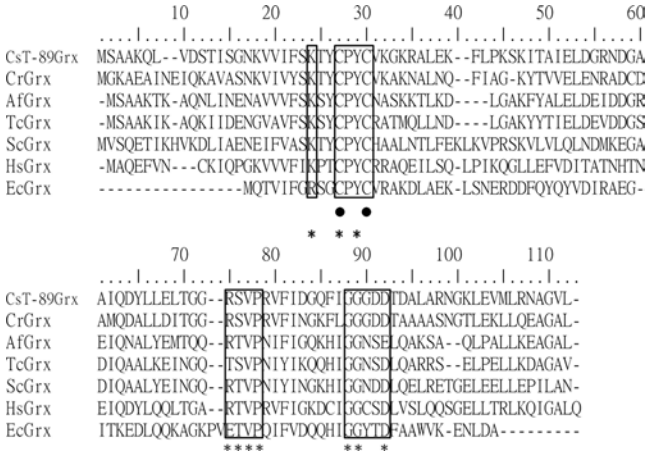

Figure 2. Multiple amino acid sequence alignments of CsT-89Grx with diverse organisms using the ClustalW2 program. Accession numbers and abbreviations of the sequences: *Chlorella sorokiniana* T-89 (CsT-89Grx, this study), *Chlorella variabilis* (CvGrx, EFN57573.1), *Aspergillus fumigates* Af293 (AfGrx, XP_750359.1), *Chlamydomonas reinhardtii* (CrGrx, XP_001694001.1), *Escherichia coli* (EcGrx, AAA23936.1), *Homo sapiens* (HsGrx, NP_002055.1), *Saccharomyces cerevisiae* S288c (ScGrx, NP_009895.1), and *Taiwanofungus camphorates* (TcGrx, ABY58974.1). The conserved residual amino acids are displayed in the black box.

Expression and Purification of Recombinant CsT-89Grx. The DNA fragment of 321 bp of CsT-89Grx was amplified by PCR using the specific primers (Grx-F/Grx-R) and cloned into the pET-20b(+) expression vector, as described in the Materials and Methods. The result was analyzed by 16% Tricine SDS-PAGE (Figure 3). After induction by IPTG, the rCsT-89Grx containing the 6-His tag was overexpressed in *E.*

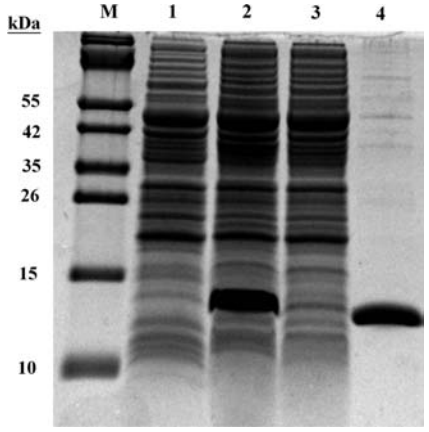

Figure 3. Expression and purification of the recombinant CsT-89Grx in the *E. coli* expression system. The total protein and purified enzyme were analyzed with 16% Tricine SDS-PAGE followed by Coomassie blue staining. Lane 1, crude soluble extract from Bl21(DE3) with pET-20b(+); lane 2, crude soluble extract from Bl21(DE3) expressing CsT-89Grx containing the 6-His tag; lane 3, pass-through protein from TALON Co^{2+} column; lane 4, the purified CsT-89Grx by TALON Co^{2+} column; and lane M is a PageRuler Prestained protein marker (Fermentas).

dx.doi.org/10.1021/jf405213h | J. Agric. Food Chem. 2014, 62, 927−933

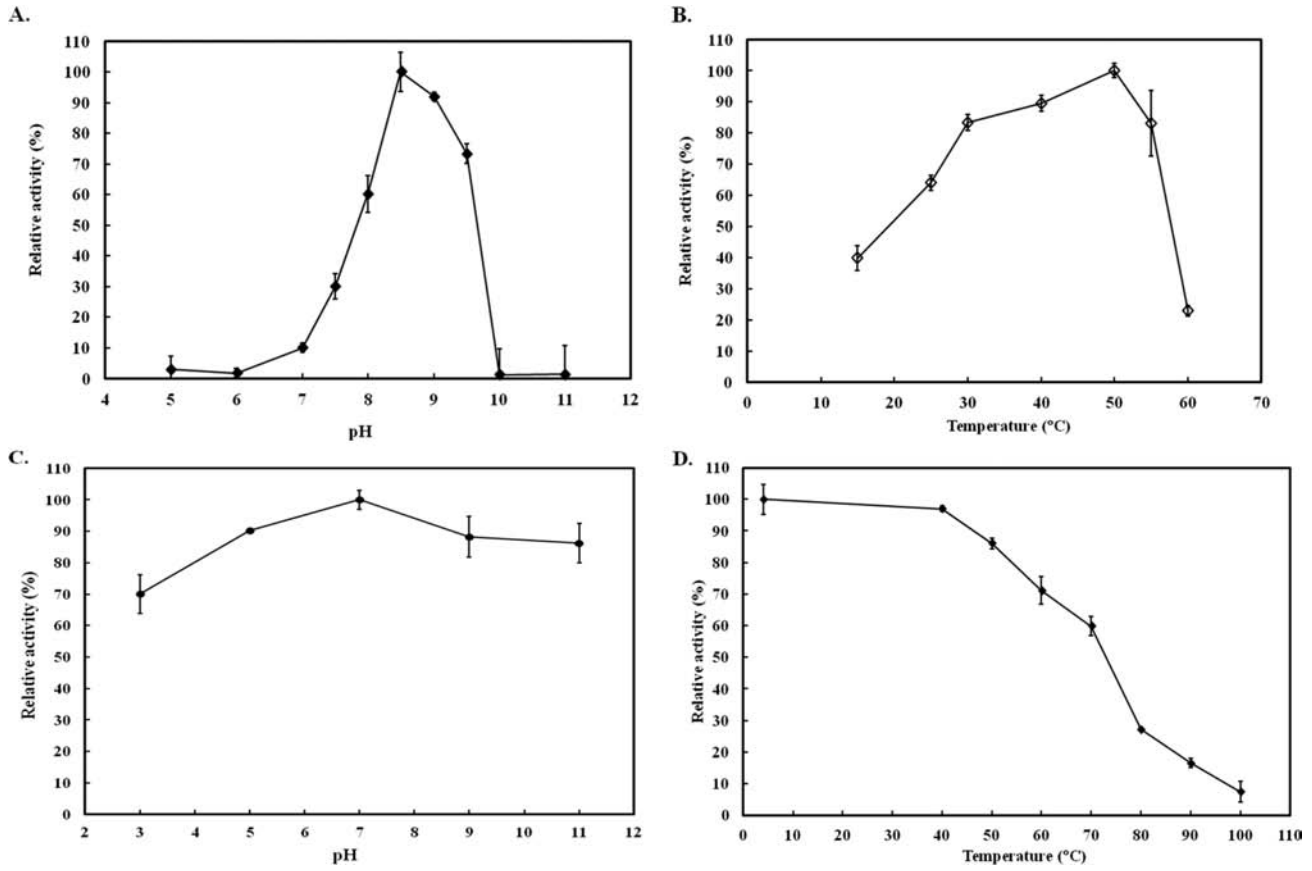

Figure 4. Effect of pH and temperature on purified CsT-89Grx using HED assay. (A) Optimal pH of CsT-89Grx measured at different pH values (pH 5 to 11). Activity at pH 8.5 corresponds to 100%. (B) Optimal temperature of CsT-89Grx measured from 15 to 60 °C. Activity at 50 °C corresponds to 100%. (C) Effect of pH on the stability of CsT-89Grx. Purified CsT-89Grx was incubated at 37 °C from 50 mM acetate buffer (pH 3, 5), 50 mM Tris-HCl (pH 7, 9), and 50 mM glycine-NaOH (pH 11) for 1 h. (D) Thermal stability of the purified CsT-89Grx. Enzyme was incubated at pH 7.4, 50 mM Tris-HCl buffer at different temperatures (4 to 100 °C) for 1 h. Grx activity was monitored on the basis of the decrease in NADPH absorbance at 340 nm.

Table 1. Kinetic Parameters of CsT-89Grx and the Published Grxs from Other Organisms

		CsT-89Grx	EcGrx1[a]	ScGrx1[b]	CrGrx1[c]	HsGrx1[d]	TcGrx[e]
HED	K_m (mM)	0.17 ± 0.02	3.0	0.12	0.34	1.07	0.57
	k_{cat} (min^{-1})	3566.8 ± 269.94	6900	132	1800	490	1633.0
	k_{cat}/K_m	20982 ± 390.26	2300	1100	5294	458	2864.9

[a] The reaction mixture, 100 mM Tris-Cl, pH 8.0, 6 mg/mL yeast glutathione reductase (GR), 1 mM GSH, 0.7 mM HED, 0.2 mM NADPH, 0.1 mg/mL bovine serum albumin (BSA), and 2 mM EDTA, was incubated at 25 °C for the enzyme activity measurements.[35] [b] The reaction mixture, 100 mM Tris−HCl, pH 7.4, 6 μg/mL GR, 1 mM GSH, HED (0.03 to 2.2 mM), 0.2 mM NADPH, 0.1 mg/mL BSA, and 2 mM EDTA, was incubated at 30 °C for 3 min for the enzyme activity measurements.[36] [c] The reaction mixture contained: 50 μmol Tris-Cl, pH 8.0, 1 μmol EDTA, 0.5 μmol GSH, 3.8 μg yeast GR, 0.2 μmol NADPH, 50 μg BSA, (0.1−2 mM) HED, in a final volume of 0.5 mL.[37] [d] The reaction mixture contained: 100 mM potassium phosphate, pH 7.0, 1 mM EDTA, 1 mM GSH, 6 μg/mL yeast GR, 240 μM NADPH, 0.1 mg/mL BSA, and 0.1−3 mM HED.[38] [e]The reaction mixture, 100 mM Tris-Cl, pH 7.4, 0.8 mM GSH, 0.6 μg GR, 0.2 mM NADPH, and 0.3 mM to 2.4 mM HED in a final volume of 100 μL, was incubated at 25 °C for 2 min for the enzyme activity measurements.[32]

coli BL21(DE3) (Figure 3, lane 2). A molecular mass of approximately 12 kDa of the purified rCsT-89Grx was also shown in the gel and was consistent with the expected size of rCsT-89Grx, including the 6-His tag (Figure 3, lane 4).

Effects of pH and Temperature on the Purified CsT-89Grx. The effects of pH and temperature on the purified rCsT-89Grx were evaluated using the HED assay. The optimal pH of rCsT-89Grx was determined at pH 8.5. High activity was observed in a broad temperature range from 30 to 55 °C (>80% relative activity of maximum activity), and the optimum activity was observed at 50 °C (Figure 4A,B). Meanwhile, the stability of pH and temperature on the rCsT-89Grx was investigated. After preincubation under different pH conditions for 1 h, over 70% residual activity of CsT-89Grx was detected in a broad pH range from 3 to 11, which suggested stability at a broad pH range (Figure 4C). Analysis of the stability of CsT-89Grx at the temperature range of 4 to 100 °C showed relative stability below 70 °C (>50% of residual activity) and even at 80 °C for 1 h, with approximately 30% of CsT-89Grx activity retained (Figure 4D). Ken et al. [32] reported that the residual activity of TcGrx remained at approximately 50% at 100 °C for 8.5 min. The Grx from *Ipomoea batatas* maintained 60% activity after heating at 80 °C for 16 min.[34] Compared with TcGrx and *Ipomoea batatas* glutaredoxin, CsT-89Grx retained 70% activity

dx.doi.org/10.1021/jf405213h | J. Agric. Food Chem. 2014, 62, 927−933

under 100 °C for 8.5 min and 80 °C for 30 min (data not shown). These results suggested that the recombinant CsT-89Grx is the most heat-stable Grx reported.

Kinetic Parameters of the Purified CsT-89Grx. The kinetic analysis of rCsT-89Grx was illustrated with the Lineweaver−Burk plot. The kinetic parameters K_m (0.17 mM), k_{cat} (3566.9 min^{-1}), and k_{cat}/K_m (20 982 min^{-1} mM^{-1}) were calculated. The kinetic parameters of CsT-89Grx were compared with those of Grx from other organisms, including *E. coli*,[35] *Saccharomyces cerevisiae*,[36] *Chlamydomonas reinhardtii*,[37] *Taiwanofungus camphorates*,[32] and *Homo sapiens*.[38] The rCsT-89Grx showed that a relatively lower K_m corresponds to a higher k_{cat} value, and the highest k_{cat}/K_m value compared with Grx from other organisms. These results suggested that rCsT-89Grx had the highest catalytic efficiency in reducing the disulfide bond (Table 1).

Effects of Metal Ions and Chemical Reagents on the Purified CsT-89Grx. The effects of metal ions and chemical reagents on the activities of rCsT-89Grx are presented in Table 2. Metal ions, such as Na^+, Mg^{2+}, Mn^{2+}, and Ca^{2+}, displayed no significant effect on enzyme activity. The activity was slightly decreased by 1 mM Co^{2+} (retaining 89% relative activity) and was significantly inhibited by 10 mM Co^{2+} (loss of 65.4% relative activity). The activity of rCsT-89Grx was sharply reduced by treatment with Cu^{2+}, Zn^{2+}, and Fe^{3+}. Meanwhile, the activity of rCsT-89Grx was unaffected by 1 or 5 mM of EDTA, which suggested that rCsT-89Grx was not a metalloenzyme (Table 3).

Table 2. Effects of Metal Ions on the Activities of the Purified CsT-89Grx

metal ions	concentration	relative activity (%)
none		100
Na^+	1 mM	93.2 ± 3.3
	10 mM	104.6 ± 6.2
Mg^{2+}	1 mM	84.0 ± 3.6
	10 mM	99.3 ± 4.5
Mn^{2+}	1 mM	92.4 ± 8.0
	10 mM	109.1 ± 4.7
Ca^{2+}	1 mM	81.2 ± 6.2
	10 mM	109.5 ± 4.0
Co^{2+}	1 mM	89.1 ± 14.2
	10 mM	34.6 ± 2.7
Cu^{2+}	1 mM	9.4 ± 9.0
	10 mM	7.7 ± 3.9
Zn^{2+}	1 mM	5.0 ± 3.9
	10 mM	2.4 ± 1.6
Fe^{3+}	1 mM	21.0 ± 7.0
	10 mM	1.5 ± 1.7

Recombinant CsT-89Grx was incubated with different chemical reagents to investigate their effects on its activity. Residual activity was measured following the HED assay. As shown in Table 3, the activity of rCsT-89Grx was significantly reduced by 1 or 5 mM SDS treatment. After treatment with 1 and 4 M urea, enzyme activity was reduced to approximately 23.3 and 60%, respectively. DTT is a strong reducing agent frequently used to reduce the disulfide bonds of proteins.[39] Unexpectedly, CsT-89Grx activity was slightly decreased following preincubation with 5 mM DTT. This result suggested that DTT might affect either the activity of GR or GSSG (glutathione, oxidized form).[40,41] Indeed, DTT did not influence the activity of rCsT-89Grx after being removed from the reaction. PMSF, an irreversible inhibitor, slightly affected the activity of CsT-89Grx at 5 mM. The result suggested that PMSF might influence serine, which is a GSH-binding site, thus causing part of the charge change for serine.

Table 3. Effects of Chemicals on the Activities of the Purified CsT-89Grx

chemicals	concentration	relative activity (%)
none		100
EDTA	1 mM	103.1 ± 7.0
	5 mM	100 ± 6.3
SDS	1 mM	37.1 ± 4.2
	5 mM	23.8 ± 11.8
Urea	1 M	76.7 ± 7.6
	4 M	40.0 ± 5.2
iodoacetamide	1 mM	68.1 ± 0.9
	5 mM	49.3 ± 4.1
PMSF	1 mM	96.4 ± 6.7
	5 mM	89.8 ± 5.7
DTT	1 mM	94.0 ± 12.3
	5 mM	68.9 ± 3.0
removing DTT[a]	1 mM	101.1 ± 4.4
	5 mM	98.7 ± 4.8

[a]The purified CsT-89Grx was preincubated with DTT for 30 min at 37 °C in 50 mM Tris-HCl (pH 8.5). DTT was then removed from the reaction solution by a protein desalting spin column. The residual activity was determined at 50 °C in 50 mM Tris-HCl buffer (pH 8.5).

Active Site Identification by Site-Directed Mutagenesis. According to the sequence analyses, only two cysteine (putative active sites, Cys^{25} and Cys^{28}) appeared in CsT-89Grx. Moreover, CsT-89Grx belonged to the dithiol superfamily, and its reaction mechanism is presumably catalyzed by dithiol−disulfide exchange via the coupling of −SH groups to GR and NADPH.[20,42] This finding suggested that no disulfide bond appeared in the active site of CsT-89Grx. On the basis of the bioinformatics analysis, the active site of CsT-89Grx was predicted to be the Cys^{25} and Cys^{28}. As expected, the CsT-89Grx activity was destroyed by iodoacetamide (Table 3). The CsT-89Grx retained 68.1 and 49.3% activity in 1 and 5 mM iodoacetamide, respectively. To confirm the active sites, site-directed mutagenesis of the putative active sites Cys^{25} and Cys^{28} was performed (Supplemental Data). The single mutation C25A and C28A and the double mutation C25,28A retained 1.63, 12.87, and 1.5% activity, respectively (Table 4). The above analyses suggested that the Cys25 and Cys28 of CsT-89Grx acted as active sites and served an important function in the antioxidant activity of rCsT-89Grx.

In conclusion, we obtained a novel, highly active recombinant Grx enzyme with strong antioxidation capacity

Table 4. Specific Activity of rCsT-89Grx and Mutant Forms

protein	specific activity[a] (unit/mg)	relative activity (%)
rCsT-89Grx	259.3 ± 6.35	100
rCsT-89Grx ^{C25A}	4.23 ± 7.75	1.63 ± 2.99
rCsT-89Grx ^{C28A}	33.37 ± 3.48	12.87 ± 1.34
rCsT-89Grx ^{C25,28A}	3.88 ± 2.81	1.50 ± 1.08

[a]Since the enzyme activities of mutant forms were not detected under the same condition of wild type, the specific activity analyses were carried out with 100 ng rCsT-89Grx and 1 μg mutant forms, respectively.

dx.doi.org/10.1021/jf405213h | J. Agric. Food Chem. 2014, 62, 927−933

from *C. sorokiniana* T-89. The thiol/disulfide oxidoreductase, Grx, from *C. sorokiniana* T-89 was successfully expressed in the *E. coli* expression system. On the basis of the biochemical analyses, CsT-89Grx exhibited the highest activity at 50 °C and pH 8.5. CsT-89Grx displayed high heat stability and can adapt to a broader pH range for catalytic reactions. These biochemical properties suggest that the recombinant CsT-89Grx is potentially useful for biotechnological applications such as natural foods and pharmaceuticals. CsT-89Grx presented the highest catalytic efficiency (k_{cat}/K_m) in reducing the disulfide bond compared with Grx from other organisms. The above conclusions are possible reasons why *C. sorokiniana* T-89 can grow well at temperatures up to 38 °C, thus aiding in the scavenging of oxidative stress. Moreover, *C. sorokiniana* T-89 can be useful as a functional food.

■ ASSOCIATED CONTENT

Supporting Information

Site-directed mutagenesis of the putative active sites Cys^{25} and Cys^{28}. This material is available free of charge via the Internet at http://pubs.acs.org.

■ AUTHOR INFORMATION

Corresponding Authors

*E-mail: Shawjf@isu.edu.tw. Fax:886-7-657-7051. Tel.:886-7-657-7001 (J.-F.S.).

*E-mail: yuting@dragon.nchu.edu.tw. Fax: 886-4-2285-9329. Tel.: 886-4-2284-0338, ext. 7021 (Y.-T.C.).

Funding

This research was partially supported by the Ministry of Education, Taiwan, R.O.C.

Notes

The authors declare no competing financial interest.

■ ACKNOWLEDGMENTS

The authors thank Dr. Tan-Chi Huang for providing *C. sorokiniana* T-89.

■ REFERENCES

(1) Liu, K.; Li, J.; Qiao, H.; Lin, A.; Wang, G. Immobilization of *Chlorella sorokiniana* GXNN 01 in alginate for removal of N and P from synthetic wastewater. *Bioresour. Technol.* **2012**, *114*, 26−32.

(2) Robert, A. K.; Larry, L. B. Microalgae as food and supplement. *Crit. Rev. Food Sci. Nutr.* **1991**, *30*, 555−573.

(3) Spolaore, P.; Joannis-Cassan, C.; Elie Duran, E.; Isambert, A. Commercial applications of microalgae. *J. Biosci. Bioeng.* **2006**, *101*, 87−96.

(4) Suarez, E. R.; Kralovec, J. A.; Grindley, T. B. Isolation of phosphorylated polysaccharides from algae: the immunostimulatory principle of *Chlorella pyrenoidosa*. *Carbohydr. Res.* **2010**, *345*, 1190−1204.

(5) Ko, S. C.; Kim, D.; Jeon, Y. J. Protective effect of a novel antioxidative peptide purified from a marine *Chlorella ellipsoidea* protein against free radical-induced oxidative stress. *Food Chem. Toxicol.* **2012**, *50*, 2294−2302.

(6) Jeong, H.; Hye Jin Kwon, H. J.; Kim, M. K. Hypoglycemic effect of *Chlorella vulgaris* intake in type 2 diabetic Goto-Kakizaki and normal Wistar rats. *Nutr. Res. Pract.* **2009**, *3*, 23−30.

(7) Schepetkin, I. A.; Quinn, M. T. Botanical polysaccharides: macrophage immunomodulation and therapeutic potential. *Int. Immunopharmacol.* **2006**, *6*, 317−333.

(8) Cherng, J. Y.; Shih, M. F. Improving glycogenesis in streptozocin (STZ) diabetic mice after administration of green algae *Chlorella*. *Life Sci.* **2006**, *78*, 1181−1186.

(9) Tanaka, K.; Yamada, A.; Noda, K.; Shoyama, Y.; Kubo, C.; Nomoto, K. Oral administration of a unicellular green algae, *Chlorella vulgaris*, prevents stress-induced ulcer. *Planta Med.* **1997**, *63*, 465−466.

(10) Gonzfilez, L. E.; Cafiizares, R. O.; Baena, S. Efficiency of ammonia and phosphorus removal from a colombian agroindustrial wastewater by the microalgae *Chlorella vulgaris* and *Scenedesmus dimorphus*. *Bioresour. Technol.* **1997**, *60*, 259−262.

(11) Kang, M. S.; Sim, A. J.; Chae, H. J. *Chlorella* as a functional biomaterial. . *Korean J. Biotechnol. Bioeng.* **2004**, *19*, 1−11.

(12) Roos, G.; Messens, J. Protein sulfenic acid formation: from cellular damage to redox regulation. *Free Radical Biol. Med.* **2011**, *51*, 314−326.

(13) Storz, G.; Imlay, J. A. Oxidative stress. *Curr. Opin. Microbiol.* **1999**, *2*, 188−l94.

(14) Peltoniemi, M. J.; Rytilä, P. H.; Harju, T. H.; Soini, Y. M.; Salmenkivi, K. M.; Ruddock, L. W.; Kinnula, V. L. Modulation of glutaredoxin in the lung and sputum of cigarette smokers and chronic obstructive pulmonary disease. *Respir. Res.* **2006**, *7*, 133−143.

(15) Saeed, U.; Durgadoss, L.; Valli, R. K.; Joshi, D. C.; Joshi, P. G.; Ravindranath, V. Knockdown of cytosolic glutaredoxin 1 leads to loss of mitochondrial membrane potential: implication in neurodegenerative diseases. *PLoS One* **2008**, *3*, e2459−e2474.

(16) Berndt, C.; Lillig, C. H.; Holmgren, A. Thiol-based mechanisms of the thioredoxin and glutaredoxin systems: implications for diseases in the cardiovascular system. *Am. J Physiol. Heart Circ. Physiol.* **2007**, *292*, H1227−H1236.

(17) Flohé, L. Changing paradigms in thiology: from antioxidant defense toward redox regulation. *Methods Enzymol.* **2010**, *473*, 1−39.

(18) Cox, A. G.; Christine, C.; Winterbourn, C. C.; Hampton, M. B. Mitochondrial peroxiredoxin involvement in antioxidant defence and redox signaling. *Biochem. J.* **2010**, *425*, 313−325.

(19) Aslund, F.; Nordstrand, K.; Berndt, K. D.; Nikkola, M.; Bergman, T.; Ponstingl, H.; Jornvall, H.; Otting, G.; Holmgren, A. Glutaredoxin-3 from *Escherichia coli*. *J. Biol. Chem.* **1996**, *271*, 6736−6745.

(20) Meyer, Y.; Buchanan, B. B.; Vignols, F.; Reichheld, J. P. Thioredoxins and glutaredoxins: unifying elements in redox biology. *Annu. Rev. Genet.* **2009**, *43*, 335−367.

(21) Meyer, Y.; Siala, W.; Bashandy, T.; Riondet, C.; Vignols, F.; Reichheld, J. P. Glutaredoxins and thioredoxins in plants. *Biochim. Biophys. Acta* **2008**, *1783*, 589−600.

(22) Rouhier, N.; Couturier, J.; Johnson, M. K.; Jacquot, J. P. Glutaredoxins: roles in iron homeostasis. *Trends Biochem. Sci.* **2010**, *35*, 43−52.

(23) Sha, S.; Minakuchi, K.; Higaki, N.; Sato, K.; Ohtsuki, K.; Kurata, A.; Yoshikawa, H.; Kotaru, M.; Masumura, T.; Ichihara, K.; Tanaka, K. Purification and characterization of glutaredoxin (thioltransferase) from rice (*Oryza sativa* L.). *J. Biochem.* **1997**, *121*, 842−848.

(24) Lillig, C. H.; Berndt, C.; Holmgren, A. Glutaredoxin systems. *Biochim. Biophys. Acta* **2008**, *1780*, 1304−1317.

(25) E. Herrero, E.; de la Torre-Ruiz, M. A. Monothiol glutaredoxins: a common domain for multiple functions. *Cell. Mol. Life Sci.* **2007**, *64*, 1518−1530.

(26) Nordstrand, K.; Åslund, F.; Holmgren, A.; Otting, G.; Berndt, K. D. NMR structure of *Escherichia coli* glutaredoxin 3-glutathione mixed disulfide complex: implications for the enzymatic mechanism. *J. Mol. Biol.* **1999**, *286*, 541−552.

(27) Fitzgerald, L. A.; Zhang, Y.; Lewis, G.; Van Etten, J. L. Characterization of a monothiol glutaredoxin encoded by *Chlorella* virus PBCV-1. *Virus Genes* **2009**, *39*, 418−426.

(28) Schägger, H. Tricine−SDS-PAGE. *Nat. Protoc.* **2006**, *1*, 16−22.

(29) Bradford, M. A rapid and sensitive method for the quantitation of microgram quantities of protein utilizing the principle of protein-dye binding. *Anal. Biochem.* **1976**, *72*, 248−254.

(30) Holmgren, A.; Aslund, F. Glutaredoxin. *Methods Enzymol.* **1995**, *252*, 283−292.

(31) Kessler, E. Physiological and biochemical contributions to the taxonomy of the genus *Chlorella*. VII. The thermophily of *Chlorella vulgaris* f. tertia Fott et Nováková. *Arch. Mikrobiol.* **1972**, *87*, 243−248.

(32) Ken, C. F.; Lin, C. Y.; Jiang, Y. C.; Wen, L.; Lin, C. T. Cloning, expression, and characterization of an enzyme possessing both glutaredoxin and dehydroascorbate reductase activity from *Taiwanofungus camphorate*. *J. Agric. Food Chem.* **2009**, *57*, 10357−10362.
(33) Gallogly, M. M.; Starke, D. W.; Mieyal, J. J. Mechanistic and kinetic details of catalysis of thiol−disulfide exchange by glutaredoxins and potential mechanisms of regulation. *Antioxid. Redox Signaling* **2009**, *11*, 1059−1081.
(34) Chi, X. W.; Lin, C. T.; Jiang, Y. C.; Wen, L.; Lin, C. T. A dithiol glutaredoxin cDNA from sweet potato (*Ipomoea batatas* [L.] Lam): enzyme properties and kinetic studies. *Plant Biol.* **2012**, *14*, 659−665.
(35) Vlamis-Gardikas, A.; Aslund, F.; Spyrou, G.; Bergman, T.; Holmgren, A. Cloning, overexpression, and characterization of glutaredoxin 2, an atypical glutaredoxin from *Escherichia coli*. *J. Biol. Chem.* **1997**, *272*, 11236−11243.
(36) Discola, K. F.; de Oliveira, M. A.; Cussiol, R. J. R.; Monteiro, G.; Bárcena, J. A.; Porras, P.; Padilla, C. A.; Guimarães, B. G.; Netto, L. E. S. Structural aspects of the distinct biochemical properties of glutaredoxin 1 and glutaredoxin 2 from *Saccharomyces cerevisiae*. *J. Mol. Biol.* **2009**, *385*, 889−901.
(37) Gao, X. H.; Zaffagnini, M.; Bedhomme, M.; Michelet, L.; Cassier-Chauvat, C.; Decottignies, P.; Lemaire, S. D. Biochemical characterization of glutaredoxins from *Chlamydomonas reinhardtii*: kinetics and specificity in deglutathionylation reactions. *FEBS Lett.* **2010**, *584*, 2242−2248.
(38) Johansson, C.; Lillig, C. H.; Holmgren, A. Human mitochondrial glutaredoxin reduces S-glutathionylated proteins with high affinity accepting electrons from either glutathione or thioredoxin reductase. *J. Biol. Chem.* **2004**, *279*, 7537−7543.
(39) Cleland, W. W. Dithiothreitol, a new protective reagent for SH groups. *Biochemistry* **1964**, *3*, 480−482.
(40) Rendón, J. L.; del Arenal, I. P.; Guevara-Flores, A.; Uribe, A.; Plancarte, A.; Mendoza-Hernández, G. Purification, characterization and kinetic properties of the multifunctional thioredoxin-glutathione reductase from *Taenia crassiceps* metacestode (cysticerci). *Mol. Biochem. Parasitol.* **2004**, *133*, 61−69.
(41) Ates, B.; Ercal, B. C.; Manda, K.; Abraham, L.; Ercal, N. Determination of glutathione disulfide levels in biological samples using thiol−disulfide exchanging agent, dithiothreitol. *Biomed. Chromatogr.* **2009**, *23*, 119−123.
(42) Holmgren, A. Thioredoxin and glutaredoxin systems. *J. Biol. Chem.* **1989**, *264*, 13963−13966.

form.[15] However, there were no reports on how antibacterial and antioxidant activities of tea polyphenols changed after nanoliposomal encapsulation. In addition, chitosan−tripolyphosphate nanoparticles could improve the stability of (−)-epigallocatechin gallate in alkaline solution.[16] However, the changes in the stability of tea polyphenol encapsulated in nanoliposomal were not clear when exposed to an alkaline solution.

To improve alkaline media stability of tea polyphenols, the methodology of combining ethanol injection methods with DHPM was adopted to prepare TPN. The physicochemical characteristics of TPN under optimal conditions were described in detail, such as morphology, particle size, size distribution, zeta potential, entrapment efficiency, and sustaining release. The stability under alkaline environment and release profiles of tea polyphenol encapsulated in nanoliposome was studied. Besides, biological activities (in vitro antioxidant activity (DPPH free radical scavenging assay and ferric reducing/antioxidant power) and in vitro antibacterial activity) of TPN were also investigated.

MATERIALS AND METHODS

Materials. Tea polyphenol (98%) was purchased from Hangzhou Gosun Biotechnologies Co., Ltd. (Hangzhou, China). The main compositions of tea polyphenol were flavanols (EGCG (50.44%), EGC (13.76%), DL-C (4.56%), EC (4.98%), GCG (2.02%), and ECG (13.84%)), anthocyanins, flavonoids and phenolic acids. Phospholipid 90G (phosphatidylcholine content = 96.6%) was provided by Lipoid GmbH (Ludwigshafen, Germany). Cholesterol (MKBF1936 V) was obtained from Sigma-Aldrich Chemical Co. (St. Louis, MO, USA) Ethanol, Tween 80, methanol, and other reagent chemicals were all of analytical grade.

Preparation of TPN by Ethanol Injection−DHPM Method. First, according to the method of Fan et al.[17] with modifications, TPN was prepared by an ethanol injection method under the optimum conditions as follows. Phospholipid, cholesterol, Tween 80, and tea polyphenols were mixed in a mass ratio of 8:1.2:2:1. The mixture (40 mg/mL phospholipid) was well dissolved in absolute ethanol and quickly injected into the same volume of phosphate-buffered saline (PBS; pH 6.0, 0.05 M). Then, it was stirred vigorously and kept for half an hour. The aqueous phase immediately became milky, which is a result of liposome formation (20 mg/mL phospholipid). Then, the liposomal system was transferred to a rotary evaporator and lowered into a 45 °C water bath. Ethanol was removed under reduced pressure during the hydration reaction.

Second, according to our previous method,[12−14,18] tea polyphenol liposomes (40 mg/mL phospholipid) obtained were applied to a microfluidizer (M-110, Microfluidic Corp., Newton, MA, USA) at room temperature, which works on the principle of dividing a pressurized stream into two parts, passing each part through a fine orifice and impacting or colliding the parts against each other in the interaction chamber, at a pressure of 120 MPa for one cycle, and then TPN (40 mg/mL phospholipid) was obtained. TPN was used for the following experiments without further purification.

Physicochemical Characterizations and Morphology of TPN. Physicochemical characterizations of TPN, including determination of tea polyphenol content, entrapment efficiency, particle size, size distribution, and zeta potential, were determined as follows.

Preparation of standard curve was conducted according to the method of Lu et al.[2] The reference standard of tea polyphenol was weighed precisely and dissolved in absolute ethanol to form 5, 10, 15, 20, 30, 40, 50, and 60 μg/mL standard solutions. The absorbances of these solutions were determined at 275 nm by taking ethanol as a blank. The linear regression of absorbance on concentration was made, and the regression equation was calculated; the standard curve was $y = 0.0228x + 0.0317$, $R^2 = 0.9999$.

Determination of entrapment efficiency was conducted according to the methods of Yang et al.[12] and Fan et al.[17] with few modifications. The encapsulation efficiency of nanoliposome was determined by using the dialysis technique to separate the nonentrapped tea polyphenol from liposomes. Five milliliters of tea polyphenol liposomal dispersion was placed into a dialysis bag of cellulose membrane (MW cutoff 10000, Shanghai Huamei Biochemistry Ltd., Shanghai, China) and immersed in 100 mL of PBS (pH 6.0, 0.05 M) for 8 h, with mild stirring, and phosphate buffer was refreshed every 2 h. The rest of the dispersion remaining in the dialysis bag after 8 h was placed into a 500 mL brown capacity bottle and diluted with absolute ethanol. After 30 min of sonication, aiming to break down the nanoliposome, the sample was cooled to room temperature, and then the tea polyphenol content was determined using a spectrophotometer at 275 nm and calculated according to a calibration curve. The entrapment efficiency (EE) was calculated from eq 1:

$$\mathrm{EE}\,(\%) = (W_{\mathrm{en}}/W_{\mathrm{total}}) \times 100\% \quad (1)$$

W_{en} is the weight of tea polyphenol encapsulated in nanoliposomes, and W_{total} is the initial weight of tea polyphenol added in the preparation.

The size distribution of TPN was measured by a dynamic laser light scattering method at 25 °C using a Nicomp 380 ZLS (Santa Barbara, CA, USA), according to our previous method.[18] The intensity was detected at an angle of 90°. Samples were diluted 10-fold with Milli-Q water before measurement. Mean particle sizes were calculated as the average of at least triplicate measurements.

The zeta potential values of TPN were measured using the Nicomp 380 ZLS according to our previous method.[18] Samples were diluted 10-fold in Milli-Q water before analysis. Zeta potentials were calculated as the average of at least triplicate measurements. Each individual zeta potential measurement was calculated from the mean of at least 10 readings from each sample.

According to our previous method[18] with modifications, the morphology observations were performed with an AFM (Agilent 5500, Agilent Technologies, Santa Clara, CA, USA). The TPN was diluted and made to a final lipid concentration (8 μg/mL). Diluted sample (10 uL) was deposited onto a freshly cleaved mica surface and subsequently dried in a desiccator.

In Vitro Antioxidation. The free radical scavenging capacity was determined according to the method of our previous work[12] with minor modifications. The free radical scavenging activities of TPN and tea polyphenol solution were assayed using a relatively stable free radical, DPPH. An amount of 0.1 mL of the test samples (50, 75, 100, and 125 μg/mL of TPN and pure tea polyphenol solution) was added into 2.3 mL of anhydrous ethanol. After they had been mixed vigorously, 1.6 mL of 60 μg/mL DPPH solution was added. The redox reaction was carried out at room temperature for 20 min, and the free radical scavenging activities of TPN and tea polyphenol solution were quantified by determining the change of absorbance at 517 nm. The control solution contained the same amount of blank nanoliposome and DPPH radical. The blank solution included the same amount of blank nanoliposome and 3.9 mL of anhydrous ethanol. DPPH radical scavenging activity was evaluated by using eq 2:

$$\text{radical scavenging activity}\,(\%) = (A - B)/(A - C) \times 100\% \quad (2)$$

A is the absorbance of control solution after reaction, B is the absorbance of the samples after the reaction, and C is the absorbance of the blank solution.

The FRAP of TPN was determined according to the methods of Benzie and Strain[19] and Patel et al.[20] with modifications. Briefly, 4.8 mL of FRAP reagent, prepared freshly and warmed at 37 °C, was mixed with 0.2 mL of the samples at different dilute times. FRAP reagent contained 2.5 mL of a 10 mmol/L 2,4,6-tris(2-pyridyl)-s-triazine (TPTZ) solution in 40 mmol/L HCl plus 2.5 mL of 20 mmol/L $FeCl_3 \cdot 6H_2O$ and 25 mL of 0.3 mol/L acetate buffer of pH 3.6. The reaction took place at a temperature of 37 °C for 10 min. Once the reaction was completed, the value of absorbance in a UV−vis spectrophotometer was recorded at 593 nm against blank. A blank

solution contained 4.8 mL of FRAP reagent solution and an appropriate volume of blank nanoliposome, and it was incubated under the same conditions as the rest of the samples. Aqueous solutions of gallic acid (0.2 mL) with concentrations in the range of 10−80 μg/mL were combined in a test tube with 4.8 mL of reagent solution, and they were incubated under the same conditions as the rest of the samples. The absorbance of gallic acid solutions was then determined at 593 nm, respectively, with PBS as blank. The linear regression of absorbance on concentration was made and its equation was calculated. The regression equation of the standard curve was $y = 0.0197x - 0.0348$, $R^2 = 0.9998$. The FRAP of TPN was expressed as the equivalent content of gallic acid, using above regression equation of the standard curve.

Antimicrobial Activity. It was found in our preliminary experiment that the turbidity of liposomes prepared by ethanol injection was much higher than that of nanoliposomes prepared by ethanol injection in combination with DHPM, which was not suitable for in vitro antibacterial activity experiments. Consequently, the antibacterial activity of TPN was conducted in this study, by taking tea polyphenol solution as a control group. The inhibition zone of tea polyphenol before and after nanoliposome encapsulation was determined by diffusion technique (disc method), according to method of Liolios et al.[21] with few modifications. The tests were conducted against four common food pathogenic bacteria: *Staphylococcus aureus* (ATCC6538), *Escherichia coli* (ATCC8739), *Salmonella typhimurium* (ATCC14028), and *Listeria monocytogenes* (ATCC19115). The experiments were repeated three times, and the results (mm of zone of inhibition) were expressed as average values.

Minimum inhibitory concentration and minimum bactericidal concentration determinations were conducted according to Wattanasatcha et al.'s[22] method. Four food pathogenic bacteria were grown in LB at 37 °C until a total bacterial count of 10^8 cfu/mL was reached. Then, the obtained bacterial suspension was used for evaluating the minimum inhibitory concentration and minimum bactericidal concentration of each test compound.

The minimum inhibitory concentrations of tea polyphenol solution and TPN were determined by using the broth dilution method. To each test, 1.5 mL of tea polyphenol solution and TPN (concentration range of 39−5000 μg/mL) was added in 1.5 mL of sterile (121 °C for 15 min) broth in the test tubes, respectively. Then, the tubes were inoculated with 200 μL of the above bacterial suspension, mixed, and incubated at 37 °C for 24 h before the turbidity of the broth recorded at 600 nm. The lowest concentration at which no growth occurred in either tube was taken as the MIC. After the MIC was determined, the tubes that did not show an increase in turbidity at 24 h were streaked on LB agar plates and incubated for 24 h at 37 °C to check for bacterial growth/survival. Each experiment was performed in triplicate.

In Vitro Drug Release. In vitro drug release from TPN was performed in 50 mM PBS (pH 6.0), which was used in the preparation of TPN, according to Lu et al.'s[2] method with slight modifications, by taking tea polyphenol solution as a control group. An amount of 2 mL of TPNs was loaded in a dialysis bag with the cutoff size of 10 kDa before being placed into 200 mL of PBS (kept constant at 37 ± 0.5 °C and stirred at 100 rpm). At predetermined time intervals (0.5, 1, 2, 4, 6, 8, 10, 12, and 24 h), the content of tea polyphenol in the samples were determined as described above.

Stability in Alkaline Solution. Tea polyphenol is unstable in alkali solution, and its half-life would significantly decrease due to the alkaline environment. The stability of TPN under alkaline conditions (pH 7.4) could mimic the pH environment present in intestinal or other fluids such as plasma. Therefore, a stability study, under alkaline conditions (pH 7.4), could provide a useful guide for oral administration application of TPN. The detailed process of alkali stability was conducted according to Dube et al.'s[16] method with modifications. A suspension of TPN in 50 mM potassium hydrogen phosphate buffer (pH 7.4) was prepared. The final concentration of tea polyphenol present in the suspensions was 200 μg/mL, and then it was incubated at 37 °C for a set period. The absorbance of TPN in alkaline solution (pH 7.4) was determined at 430 nm to determine oxidation contents of tea polyphenol.[23] Free tea polyphenol without being encapsulated, at a similar concentration of 200 μg/mL, was used as a control in parallel experiments and was subjected to the same treatment as the nanoliposome preparations.

Statistical Analysis. All experiments were done in at least triplicate. The values are expressed as means ± standard deviation (SD). Data were subjected to statistical analysis using SPSS software version 18.0. Differences were considered significant at $p < 0.05$.

RESULTS AND DISCUSSION

Characterization and Morphology of TPN. Characterizations of TPN, including entrapment efficiency, particle size, polydispersity index, and zeta potential, will be discussed in detail in this work. The surface morphology of TPN was observed by atomic force microscope. The entrapment efficiency and drug load values are key points for potential applications of the liposomal system. The entrapment efficiency and drug load of TPN under the optimum conditions were 78.5 ± 5 and 8.5 ± 0.5%, respectively. The entrapment efficiency of tea polyphenol nanolipsome in this work was different from that in previous papers.[2,7,8] Gulseren and Corredig[7] reported that the entrapment efficiency of tea polyphenol-bearing nanoliposome using high-pressure homogenization was 58.3%. The entrapment efficiency of TPN prepared by the thin film ultrasonic dispersion method was 60.3%.[2] Tea polyphenols and vitamin E-loaded nanoscale complex liposome using reverse-phase evaporation method exhibited 50.81% entrapment efficiency.[8] In addition, the drug load of tea polyphenol nanolipsome in this work was similar to that of Lu et al.[2] (6.0%).

To determine the particle size of TPNs, their mean particle size and polydispersity index were measured by using a dynamic laser light scattering method. Tea polyphenol nanolipsome exhibited smaller size (66.8 ± 7.6 nm) than previous results[2,7−9] and had a narrow polydispersity index (0.213 ± 0.046). TPN prepared with milk fat globule membrane phospholipids, using a high-pressure homogenizer, showed lager mean sizes (>100 nm);[7] TPN obtained by thin film ultrasonic dispersion method were 160.4 nm with a polydispersity index of 0.28;[2] and the tea polyphenol nanoscale complex liposome showed 202.8 nm (mean sizes) and 0.296 (polydispersity index).[8] In a preliminary experiment, a thin film dispersion method was also attempted to prepare tea polyphenol liposome, but it was difficult to wash membrane from the wall of the rotary flask and difficult to spontaneously form liposome when the tea polyphenol was 5 mg/mL. Hence, an ethanol injection method, without the membrane washing off process, was used to prepare tea polyphenol liposome. The mean particle size of tea polyphenol liposome prepared by the ethanol injection method was 496 nm, which was not in nanoscale. In our previous research, we also found that DHPM treatment containing strong mechanical forces could significantly reduce the particle size of liposome.[12,24] In addition, the zeta potential of TPN under the optimum conditions was −6.16 mv (pH 6.0), which was lower than those of Gulseren and Corredig[7] (−12 mv, pH 5.0) and Lu et al.[2] (−67.2 mv, pH 6.62). Liposomes are mainly composed of cholesterol and phospholipids. The different value of zeta potential of liposome was probably attributed to variations in competence and property of phospholipids. There are two main viewpoints on whether the zeta potential value could directly decide its shelf life. The suspension with greater zeta potential is more likely to be stable, which was due to the charged particles repelling one another and thus overcoming the natural tendency to

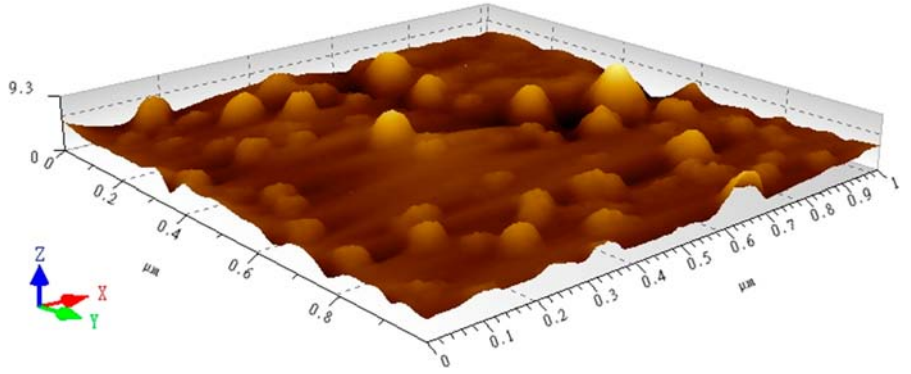

Figure 1. AFM micrograph of tea polyphenol nanoliposome.

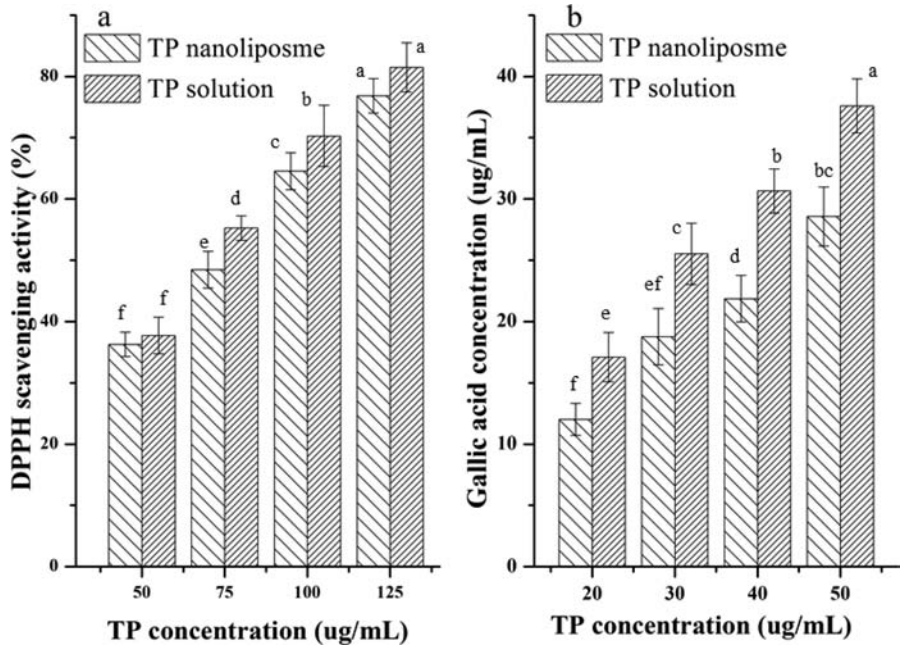

Figure 2. (a) DPPH free radical scavenging capacity and (b) ferric reducing/antioxidant power (FRAP) of tea polyphenol solution and nanoliposme at various concentrations.

aggregate.[25] However, it was also deemed in some studies that even at low zeta potential values (i.e., close to 0), liposomes might remain stable.[26] According to the research studies of Lu et al.[2] and Makino et al.,[26] it can be concluded that the zeta potential value was not a direct indicator of the stability of liposome. Consequently, the shelf life of liposome depended not just on its zeta potential value. In this work, two vital indicators of liposome (entrapment efficiency and particle size) indicated that DPHM combined with ethanol injection methods was suitable for preparing TPN.

As presented in Figure 1, 1 μm × 1 μm scans were captured, showing the morphology of TPN was mainly spherical defined shapes (indicated by the arrows). TPNs maintained a spherical and well-defined shape (common characteristic of nanoliposome), which was in agreement with the morphology observed by transmission electron microscopy.[2] According to AFM photographs, most of the TPN was well distributed, which is in agreement with a narrow size distribution obtained by DLS (shown in Figure S1 in the Supporting Information). Furthermore, the sizes of nanoliposomes obtained through AFM were close to mean sizes measured by a dynamic laser light scattering method, which was consistent with results of Maherani et al.[27]

Nanoliposome is a new technology for the encapsulation and delivery of bioactive agents. It is generally acknowledged that the performance of bioactive agents could be enhanced by nanoliposomes, improving their solubility and bioavailability and in vitro and in vivo stability, as well as preventing their unwanted interactions with other molecules.[28] In addition, their smaller mean diameters could be helpful in enhancing their bioavailability.[12] This study examined how the bioactivity of TPN varied. In vitro antibacterial activity and in vitro antioxidant activity of TPN will be discussed in detail in the following text.

In Vitro Antioxidation. To date, it is still not clear how the in vitro antioxidant activity of tea polyphenols after nanoliposome encapsulation changed. There are different types of antioxidant methods used to estimate in vitro antioxidant activity of tea polyphenols before and after nanoliposome encapsulation. The DPPH free radical scavenging capacity assay and ferric reducing/antioxidant power (FRAP) assay were chosen to represent organic solvent and aqueous phase environments, respectively.

dx.doi.org/10.1021/jf402886s | J. Agric. Food Chem. 2014, 62, 934−941

The stable DPPH radical is a widely used scavenging model for evaluating the free radical scavenging ability of natural compounds. The effect of antioxidants on DPPH radical scavenging was attributed to their hydrogen-donating ability. It is shown in Figure 2a that both tea polyphenol solution and TPN had concentration-dependent antioxidant activities toward DPPH free radical scavenging capacity. No significant differences in DPPH free radical scavenging capacity of the same concentration of tea polyphenol were found before and after nanoliposome encapsulation. The DPPH scavenging activities of the tea polyphenol solution in 50, 75, 100, and 125 μg/mL were 37.7 ± 3.0, 55.2 ± 1.9, 70.2 ± 5.2, and 81.4 ± 4.0%, respectively, with an equal or higher DPPH scavenging power of TPN (36.2 ± 2.0, 48.4 ± 3.1, 64.5 ± 3.0, and 76.8 ± 2.8%, respectively).

Alterations in DPPH radical scavenging activity of antioxidants were reported by other authors after gum arabic–maltodextrin particle,[29] liposome,[30] and placebo chitosan microsphere[31] encapsulation. Peres et al.[29] demonstrated that free catechin and gum arabic–maltodextrin particles loaded with catechin exhibited similar DPPH quenching abilities in all tested concentrations and deemed that the loading method preserved the original antioxidant properties of the catechin. Niu et al.[30] reported that the DPPH radical scavenging activity of liposomal curcumin was higher than that of free curcumin. It was ascribed to the polarity of different environments. Curcumin is a hydrophobic core material, so it would be entrapped in the liposomal bilayer, the polarity of which is much lower than that of sodium phosphate buffer, and the DPPH molecule has a highly hydrophobic nature; it is likely that the DPPH radical is scavenged by curcumin inside liposome.[30] Weerakody et al.[31] reported that lipoic acid encapsulated in placebo chitosan microspheres exhibited lower DPPH radical scavenging activity as compared to free lipoic acid, which could be attributed to an incomplete extraction of the encapsulated lipoic acid due to structural interactions. In this work, nanoliposome encapsulation did not reduce the DPPH radical scavenging capacity of tea polyphenol. It was probably explained by the main reagent in the DPPH radical scavenging system being alcohol. Nanoliposome would be demulsified by high concentrations of alcohol. Tea polyphenol encapsulated in liposome aqueous phase was exposed homogeneously into the DPPH system, after alcohol demulsification. Therefore, compared with tea polyphenol solution, TPN exhibited an equal or lower DPPH radical scavenging activity. In our previous study, it was also found that the DPPH radical scavenging activity of vitamin C was not significantly altered by nanoliposome encapsulations.[12]

The FRAP assay was developed to measure reducing power in plasma,[19] but the assay has been adapted to measure antioxidant activity of tea polyphenols.[32] The FRAP assay is quick and simple to perform, and the reaction is reproducible and linearly related to the molar concentration of the antioxidant present.[19] It is based on the reduction, which is monitored by measuring the change of absorbance at 593 nm. At low pH, a colorless ferric complex (Fe^{3+}–tripyridyltriazine) changes to a blue ferrous complex (Fe^{2+}–tripyridyltriazine) by the action of electron-donating antioxidants.[19] Figure 2b shows that both tea polyphenol solution and TPN have concentration-dependent antioxidant activity toward ferric reducing/antioxidant assay. Nevertheless, the ferric reducing/antioxidant power of tea polyphenol was reduced by nanoliposome encapsulations. In the current study, we found that the ferric reducing/antioxidant power of TPN was significantly lower than that of tea polyphenol solution. The FRAP values of the tea polyphenol solution at 20, 30, 40, and 50 μg/mL were equivalent to 17.1 ± 2.0, 25.5 ± 2.5, 30.6 ± 1.8, and 37.6 ± 2.2 μg/mL gallic acid, respectively, which are higher FRAP values than those of TPN (12.0 ± 1.3, 18.7 ± 2.3, 21.9 ± 1.9, and 28.6 ± 2.4 μg/mL gallic acid, respectively).

It was reported by some researchers that the antioxidant activity measured by the FRAP assay was reduced by many encapsulations (solid lipid matrix, chitosan microspheres, novel polymer–polyphenol beads).[20,31,33] Patel et al.[20] reported that the lower FRAP value of epigallocatechin gallate in the novel polymer–polyphenol beads at an initial stage of 2 h was probably hindered by bead encapsulation, compared with free epigallocatechin gallate. Weerakody et al.[31] also found that the antioxidant activity by FRAP assay of lipoic acid encapsulated in chitosan microspheres was much lower than the same concentration of free lipoic acid, which was probably due to structural interaction between chitosan matrix and lipoic acid. Donsì et al.[33] reported that the antioxidant activities by FRAP assay of the encapsulated resveratrol and curcumin in a solid lipid matrix were much lower than those of resveratrol and curcumin that were not encapsulated. In this study, the FRAP assay of tea polyphenol was decreased by nanoliposome encapsulation. This was probably due to the fact that most of the tea polyphenol was encapsulated in the nanoliposome aqueous phase. Therefore, donating electron capacity of tea polyphenol encapsulated in nanoliposome would be influenced by phospholipid bilayer membranes, which resulted in a low antioxidant activity that was evaluated by the FRAP value of TPN.

In Vitro Antibacterial Activity of TPN. It was not clear how the in vitro antibacterial activity of tea polyphenol changed after nanoliposome encapsulation. To evaluate the variation in antibacterial activity of tea polyphenol after nanoliposome encapusulation, four common food pathogenic bacteria (*S. aureus*, *E. coli*, *S. typhimurium*, and *L. monocytogenes*) were used to determine the antimicrobial activities of tea polyphenol before and after encapsulation of nanoliposomes. The inhibition zones of tea polyphenol solution and nanoliposome are shown in Figure 3. The inhibition zones of tea polyphenol solution for *S. aureus*, *E. coli*, *S. typhimurium*, and *L. monocytogenes* were 21.3 ± 1.3, 19.7 ± 0.5, 19.7 ± 1.2, and 19.3 ± 0.9 mm, respectively, whereas TPN exhibited smaller inhibition zones for *S. aureus*, *E. coli*, *S. typhimurium*, and *L.*

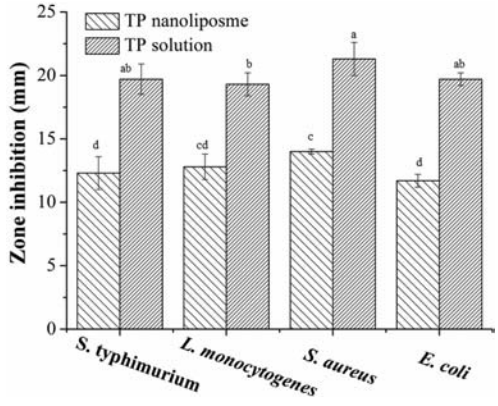

Figure 3. Antimicrobial activities (mm of zone inhibition) of tea polyphenol solution and nanoliposme.

monocytogenes (14.0 ± 0.2, 11.7 ± 0.5, 12.3 ± 1.3, and 12.8 ± 1.0 mm, respectively). The minimum inhibitory concentrations of tea polyphenol solution for *S. aureus*, *E. coli*, *S. typhimurium*, and *L. monocytogenes* were 0.078, 0.312, 0.078, and 0.039 mg/mL, respectively, and minimum bactericidal concentrations were 0.312, 0.312, 0.312, and 0.312 mg/mL, respectively. Compared with tea polyphenol solution, TPN exhibited higher minimum inhibitory concentrations (1.25, 1.25, 1.25, and 0.625 mg/mL, respectively) and minimum bactericidal concentrations (2.5, >2.5, 2.5, and 2.5 mg/mL, respectively). It could be concluded from the above that the antibacterial activity of tea polyphenol was decreased by nanoliposome encapsulation.

Low antibacterial activity of tea polyphenol nanoliposome in this work could be explained by the photograph of tea polyphenol solution and TPN incubated in a broth for 24 h (Figure S2 in the Supporting Information). With the concentration increasing from 0.078 to 2.5 mg/mL, the color of both tea polyphenol solution and nanolipsome in the broth became deeper and deeper. However, the color of tea polyphenol solution in the broth was much deeper than that of TPN in broth. Red sediments were found in tea polyphenol solution in the broth, and they became larger with increasing concentration (indicated by the arrows). Red circles were also formed on the walls of the test tube, which was due to the red sediments in the broth. However, no red sediments and circles were observed in all various concentrations of TPN samples. The cause for the sediment phenomenon could be probably attributed to the tea polyphenol. Catechins as the main components in tea polyphenol would react with proteins present in the broth and form various complexes with protein, thus resulting in the formation of sediments.[34] TPN possessing high entrapment efficiency (78.5%) could prevent tea polyphenol incorporated into the aqueous cores from being released into the broth, interacting with proteins in the broth solution and forming sediments. Tea polyphenol solution could interact with the protein (in the broth) and form sediment, but there were large portions of antibacterial compositions still in the broth. The nonencapsulated portion of tea polyphenol in nanoliposome would also interact with protein, but the nonencapsulated portion in nanoliposome was too small to form obvious sediment. In addition, the content of encapsulated tea polyphenol released from nanoliposome during 24 h of incubation in broth was very low, which was also confirmed by the following sustained release profiles of TPN. Resident antibacterial ingredients remaining in broth in the TPN sample were much lower than that in the control group (tea polyphenol solution). Consequently, liposomal encapsulation could reduce the antibacterial activity of tea polyphenols.

There have been some reports on encapsulation technologies that could alter the antibacterial activity of biological agents, but there were no uniform viewpoints on how the antibacterial activity of biological agents varied after encapsulation. According to previous papers, there were no consensus opinions on whether encapsulation technology could enhance or reduce the antibacterial activity of biological substances.[21,22] In Liolios et al.'s[21] study, all tested compounds from the essential oil presented enhanced antimicrobial activity after the liposomal encapsulation, even only 4.16% entrapment efficiency. According to Liolios et al.,[21] the dramatically increased antimicrobial activity by liposomal encapsulation was probably due to PC−liposomes interacting with cells in many ways (intermembrane transfer, contact release, absorption, fusion, phagocytosis); the mechanism of interaction depends on the cell type (cell wall/membrane composition), as well as the liposome membrane physicochemical characteristics; the use of liposomal formulation improves the cellular transport and releases the active component inside the cell. However, Wattanasatcha et al.[22] reported that minimum inhibitory concentration and minimum bactericidal concentration of *P. aeruginosa* were increased by nanosphere encapsulation, which means that the action of thymol toward this bacterial strain is somewhat retarded when the material is encapsulated. Wattanasatcha et al.[22] deemed that it was probably due to the ethylcellulose/methylcellulose shell being nondegradable under the experimental condition, and it is speculated that diffusion of the hydrophobic thymol molecules from the spheres is prior to their action on the bacteria. In the present study, we found that nanoliposome encapsulation reduced the antibacterial activity of tea polyphenols. This was probably due to the high viscidity, which made it difficult for tea polyphenols to diffuse into the agar. In addition, slight amounts of tea polyphenols released from the nanolipsome after encapsulation also result in lower antibacterial activity.

In Vitro Drug Release of TPN. Liposomes have the property of prolonging the residence time of the drugs in the blood, releasing the drugs slowly in vivo. An in vitro release model in this work was expected to partly reflect properties of prolonging the residence time in vivo of liposome, which was an important factor of liposome potential applications. The in vitro drug release profiles of tea polyphenol solution and TPN were obtained and are shown in Figure 4. Rapid tea polyphenol

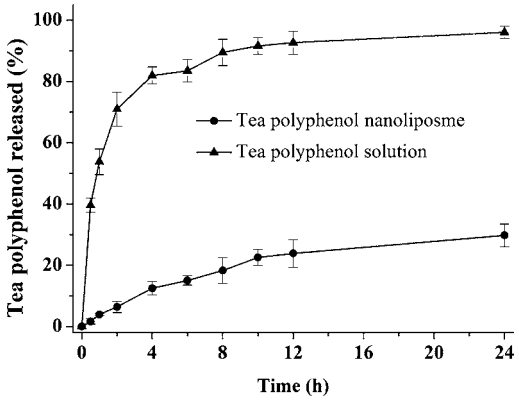

Figure 4. In vitro release of tea polyphenol from tea polyphenol solution and nanoliposme.

diffusion was observed in tea polyphenol solution before 2 h, and nearly 70% of tea polyphenol diffuses across the dialysis membrane. After that, the tea polyphenol diffusion rate from tea polyphenol solution dropped, and reached a maximum content of 92.6 ± 3.8% at 12 h. This was similar to Zhou et al.'s[5] result that 81% of tea polyphenol solution diffused across the dialysis membrane after 4 h and reached a maximum content (near 95%) at 12 h. Compared with tea polyphenol solution, nanoliposome obviously slowed the release of tea polyphenol. TPNs had a continued release rate, with only 6.4 ± 1.9% of tea polyphenol released in 2 h and reaching a maximum content of 23.9 ± 4.5% in 12 h. Then they exhibited a very slow release of 29.8 ± 3.7% after 24 h. It could be concluded from the above that TPN has a sustained release profile.

There were some reports that encapsulation methods or carrier systems such as nanoliposomes prepared by the thin film ultrasonic dispersion method,[2] chitosan-coated nanoparticles,[3]

high-pressure antisolvent coprecipitation,[4] and complex coacervation core micelles[5] could enhance the sustained release profile of tea polyphenols. Various carrier systems exhibited different sustained release capacities of tea polyphenols. In the Lu et al.[2] study, TPN also exhibited a sustained profile, but the sustained capacity was lower than that in this work. The sustained release rate reached nearly 25% after 2 h, and within 12 h, the cumulative release increased to about 70%.[2] The burst effect of tea polyphenols from chitosan-coated tea polyphenols nanoparticles was observed in 6 h, in which 30−40% of the drug was released from nanoparticles.[3] Sosa et al.'s[4] results showed that green tea encapsulation using high-pressure antisolvent coprecipitation exhibited a release of nearly 30% of the drug in 20 h, and no significant release was observed from 20 to 90 h. Zhou et al.[5] demonstrated that complex coacervation core micelles had a sustained release capacity, and the complex coacervation core micelles continuously released tea polyphenol, until it was completely released at 14 h (97%). In this work, the sustained release behavior of nanoliposomes is presumably due to the high probability of tea polyphenols being incorporated into the aqueous cores inside the bilayers, which overcomes a burst release, whereas the variant sustained capacity of liposomes was probably attributed to their difference in entrapment efficiency, encapsulation method, and membrane structure.

Stability under Alkaline Solution. Tea catechins incubating at slightly alkaline pH, similar to the small intestine, showed a rapid decline in the concentrations of tea catechins,[35] and their half-life was significantly reduced by alkaline media.[36] Consequently, the stability experiment of TPN under alkaline pH (pH 7.4), which mimics the environment present in the intestinal tract or other fluids such as plasma, is necessary to carry out. Tea polyphenols are easily oxidized, which is due to their abundance of various sensitive ingredients such as chemically unstable catechins and theaflavins. Tea catechins readily undergo oxidation and form quinone oxidized products,[16] and their oxidation products are a brown color possessing a peak area at 430 nm.[23] Therefore, the stability of tea polyphenol solutions and tea polyphenol encapsulated in nanoliposome could be measured by the absorbance of oxidation products.

Changes in absorbance at 430 nm of 200 μg/mL tea polyphenol solution and tea polyphenol in nanoliposome in PBS (50 mM 7.4) were recorded with increasing time from 0 to 24 h. The variations in absorbance and color of tea polyphenol solution and TPN are shown in Figure 5. Both tea polyphenol solution and TPN at 0 h showed low absorbance at 430 nm (0.083 ± 0.01 and 0.062 ± 0.01), and then the absorbance increased to 1.304 ± 0.075 and 0.827 ± 0.068, respectively, at 24 h, whereas the absorbance of TPN at the same incubation time was much lower than that of tea polyphenol solution. For example, after incubation for 4 h, the absorbances at 430 nm of tea polyphenol solution and TPN were 0.613 ± 0.061 and 0.357 ± 0.044, respectively. In addition, the absorbance differences between the two samples were increasing. The difference was 0.138 at 1 h and increased to 0.477 at 24 h. In addition, we could observe that both tea polyphenol solution and TPN became browner over time. The brown color of tea polyphenol solution at the same incubation time was much darker than that of TPN. This was consistent with absorbance alteration. Both absorbance and color alteration reflected that nanoliposome encapsulation could decrease the degradation rate of tea polyphenol and improve the stability of tea

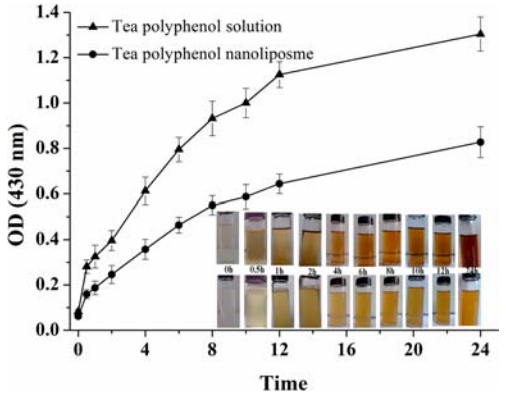

Figure 5. Stability profiles of tea polyphenol solution and nanoliposome in 50 mM potassium hydrogenphosphate buffer, pH 7.4 (37 °C), at an initial concentration of 200 μg/mL. (Inset) Photograph of tea polyphenol solution and nanoliposome incubated at 50 mM potassium hydrogenphosphate buffer, pH 7.4 (37 °C), for a set period.

polyphenols in an alkaline solution. This was similar to Fang et al.'s[15] report that liposomes could provide stable retention of epigallocatechin gallate in the medium. Encapsulation of tea catechins in chitosan−tripolyphosphate nanoparticles enhanced their stability in potassium hydrogen phosphate buffer (pH 7.4), which was also observed.[16]

Several factors, including pH, oxygen level, and concentration of epigallocatechin gallate, could affect the stability of epigallocatechin gallate.[37] It was reported that tea catechins became much less stable[38] and tea polyphenol became more sensitive to degradation with reducing concentrations[37] and when the pH increased from an acid pH to an alkaline pH. In this work, nanoliposome encapsulations' ability to protect tea polyphenols was probably attributed to hindering two important factors (oxygen levels and concentration of tea polyphenol), which could obviously affect the stability of tea polyphenols. Tea polyphenols encapsulated in nanoliposome were isolated with extra membrane environments, so little oxygen could interact with tea polyphenol. In addition, due to the slow release ratio of tea polyphenols, the concentration of tea polyphenols in nanoliposome might remain at a high value and the degradation rate of tea polyphenols was much slower than that of tea polyphenol solution. In this study, the stability of tea polyphenols against alkaline media was significantly improved by nanoliposome using a combination ethanol injection method with DHPM. Although the antioxidant and antimicrobial activities of TPN were not improved after encapsulation of polyphenol in the liposome, the sustaining property was obviously enhanced.

■ ASSOCIATED CONTENT

Ⓢ Supporting Information

Particle size distribution of tea polyphenol nanoliposome; photograph of tea polyphenol solution and tea polyphenol nanoliposome incubated in broth for 24 h. This material is available free of charge via the Internet at http://pubs.acs.org.

■ AUTHOR INFORMATION

Corresponding Authors

*(W.L.) Phone: +86 791 88305872 (8106). Fax: +86 791 88334509. E-mail: liuwei@ncu.edu.cn.

*(C.L.) Fax: +86-791-8334509. E-mail: liuchengmei@aliyun.com.

Funding

This study was supported financially by the National Natural Science Foundation of China (No. 21266021) and the Research Program of State Key Laboratory of Food Science and Technology, Nanchang University (No. SKLF-ZZB-201311).

Notes

The authors declare no competing financial interest.

REFERENCES

(1) Sajilata, M.; Bajaj, P. R.; Singhal, R. Tea polyphenols as nutraceuticals. *Crit. Rev. Food Sci. Nutr.* **2008**, *7*, 229−254.

(2) Lu, Q.; Li, D.-C.; Jiang, J.-G. Preparation of a tea polyphenol nanoliposome system and its physicochemical properties. *J. Agric. Food Chem.* **2011**, *59*, 13004−13011.

(3) Liang, J.; Li, F.; Fang, Y.; Yang, W.; An, X.; Zhao, L.; Xin, Z.; Cao, L.; Hu, Q. Synthesis, characterization and cytotoxicity studies of chitosan-coated tea polyphenols nanoparticles. *Colloids Surf. B: Biointerfaces* **2011**, *82*, 297−301.

(4) Sosa, M. V.; Rodriguez-Rojo, S.; Mattea, F.; Cismondi, M.; Cocero, M. J. Green tea encapsulation by means of high pressure antisolvent coprecipitation. *J. Supercrit. Fluids* **2011**, *56*, 304−311.

(5) Zhou, H.; Sun, X.; Zhang, L.; Zhang, P.; Li, J.; Liu, Y.-N. Fabrication of biopolymeric complex coacervation core micelles for efficient tea polyphenol delivery via a green process. *Langmuir* **2012**, *28*, 14553−14561.

(6) Elabbadi, A.; Jeckelmann, N.; Haefliger, O. P.; Ouali, L. Complexation/encapsulation of green tea polyphenols in mixed calcium carbonate and phosphate micro-particles. *J. Microencapsul.* **2011**, *28*, 1−9.

(7) Gulseren, I.; Corredig, M. Storage stability and physical characteristics of tea polyphenol bearing nanoliposomes prepared with milk fat globule membrane phospholipids. *J. Agric. Food Chem.* **2013**, *61*, 3242−3251.

(8) Ma, Q. H.; Kuang, Y. Z.; Hao, X. Z.; Gu, N. Preparation and characterization of tea polyphenols and vitamin e loaded nanoscale complex liposome. *J. Nanosci. Nanotechnol.* **2009**, *9*, 1379−1383.

(9) Gülseren, İ.; Guri, A.; Corredig, M. Encapsulation of tea polyphenols in nanoliposomes prepared with milk phospholipids and their effect on the viability of HT-29 human carcinoma cells. *Food Digestion* **2012**, *3*, 36−45.

(10) Fang, Z.; Bhandari, B. Encapsulation of polyphenols − a review. *Trends Food Sci. Technol.* **2010**, *21*, 510−523.

(11) Liu, W.; Liu, J.; Xie, M.; Liu, C.; Liu, W.; Wan, J. Characterization and high-pressure microfluidization-induced activation of polyphenoloxidase from Chinese pear (*Pyrus pyrifolia* Nakai). *J. Agric. Food Chem.* **2009**, *57*, 5376−5380.

(12) Yang, S.; Liu, W.; Liu, C.; Liu, W.; Tong, G.; Zheng, H.; Zhou, W. Characterization and bioavailability of vitamin c nanoliposomes prepared by film evaporation-dynamic high pressure microfluidization. *J. Dispers. Sci. Technol.* **2012**, *33*, 1608−1614.

(13) Liu, W.; Liu, W. L.; Liu, C. M.; Liu, J. H.; Yang, S. B.; Zheng, H. J.; Lei, H. W.; Ruan, R.; Li, T.; Tu, Z. C. Medium-chain fatty acid nanoliposomes for easy energy supply. *Nutrition* **2011**, *27*, 700−706.

(14) Liu, W.-L.; Liu, W.; Liu, C.-M.; Yang, S.-B.; Liu, J.-H.; Zheng, H.-J.; Su, K.-M. Medium-chain fatty acid nanoliposomes suppress body fat accumulation in mice. *Br. J. Nutr.* **2011**, *106*, 1330−1336.

(15) Fang, J. Y.; Lee, W. R.; Shen, S. C.; Huang, Y. L. Effect of liposome encapsulation of tea catechins on their accumulation in basal cell carcinomas. *J. Dermatol. Sci.* **2006**, *42*, 101−109.

(16) Dube, A.; Ng, K.; Nicolazzo, J. A.; Larson, I. Effective use of reducing agents and nanoparticle encapsulation in stabilizing catechins in alkaline solution. *Food Chem.* **2010**, *122*, 662−667.

(17) Fan, M.; Xu, S.; Xia, S.; Zhang, X. Preparation of salidroside nano-liposomes by ethanol injection method and in vitro release study. *Eur. Food Res. Technol* **2008**, *227*, 167−174.

(18) Liu, W.; Liu, J.; Liu, W.; Li, T.; Liu, C. Improved physical and in vitro digestion stability of a polyelectrolyte delivery system based on layer-by-layer self-assembly alginate−chitosan-coated nanoliposomes. *J. Agric. Food Chem.* **2013**, *61*, 4133−4144.

(19) Benzie, I. F. F.; Strain, J. The ferric reducing ability of plasma (FRAP) as a measure of "antioxidant power": the FRAP assay. *Anal. Biochem.* **1996**, *239*, 70−76.

(20) Patel, A. R.; Nijsse, J.; Velikov, K. P. Novel polymer−polyphenol beads for encapsulation and microreactor applications. *Soft Matter* **2011**, *7*, 4294−4301.

(21) Liolios, C.; Gortzi, O.; Lalas, S.; Tsaknis, J.; Chinou, I. Liposomal incorporation of carvacrol and thymol isolated from the essential oil of *Origanum dictamnus* L. and in vitro antimicrobial activity. *Food Chem.* **2009**, *112*, 77−83.

(22) Wattanasatcha, A.; Rengpipat, S.; Wanichwecharungruang, S. Thymol nanospheres as an effective anti-bacterial agent. *Int. J. Pharm.* **2012**, *434*, 360−365.

(23) Oszmianski, J.; Cheynier, V.; Moutounet, M. Iron-catalyzed oxidation of (+)-catechin in model systems. *J. Agric. Food Chem.* **1996**, *44*, 1712−1715.

(24) Liu, W.; Liu, W.; Liu, C.; Liu, J.; Zheng, H.; Yang, S.; Su, J. Preparation and evaluation of easy energy supply property of medium-chain fatty acids liposomes. *J. Microencapsul.* **2011**, *28*, 783−790.

(25) Heurtault, B.; Saulnier, P.; Pech, B.; Proust, J.-E.; Benoit, J.-P. Physico-chemical stability of colloidal lipid particles. *Biomaterials* **2003**, *24*, 4283−4300.

(26) Makino, K.; Yamada, T.; Kimura, M.; Oka, T.; Ohshima, H.; Kondo, T. Temperature-and ionic strength-induced conformational changes in the lipid head group region of liposomes as suggested by zeta potential data. *Biophys. Chem.* **1991**, *41*, 175−183.

(27) Maherani, B.; Arab-Tehrany, E.; Kheirolomoom, A.; Cleymand, F.; Linder, M. Influence of lipid composition on physicochemical properties of nanoliposomes encapsulating natural dipeptide antioxidant L-carnosine. *Food Chem.* **2012**, *134*, 632−640.

(28) Mozafari, M. R. Nanoliposomes: preparation and analysis. *Methods Mol. Biol.* **2010**, *605*, 29−50.

(29) Peres, I.; Rocha, S.; Gomes, J.; Morais, S.; Pereira, M. C.; Coelho, M. Preservation of catechin antioxidant properties loaded in carbohydrate nanoparticles. *Carbohydr. Polym.* **2011**, *86*, 147−153.

(30) Niu, Y.; Ke, D.; Yang, Q.; Wang, X.; Chen, Z.; An, X.; Shen, W. Temperature-dependent stability and DPPH scavenging activity of liposomal curcumin at pH 7.0. *Food Chem.* **2012**, *135*, 1377−1382.

(31) Weerakody, R.; Fagan, P.; Kosaraju, S. L. Chitosan microspheres for encapsulation of α-lipoic acid. *Int. J. Pharm.* **2008**, *357*, 213−218.

(32) Chan, E.; Lim, Y.; Chew, Y. Antioxidant activity of *Camellia sinensis* leaves and tea from a lowland plantation in Malaysia. *Food Chem.* **2007**, *102*, 1214−1222.

(33) Donsì, F.; Sessa, M.; Mediouni, H.; Mgaidi, A.; Ferrari, G. Encapsulation of bioactive compounds in nanoemulsion-based delivery systems. *Proc. Food Sci.* **2011**, *1*, 1666−1671.

(34) He, Q.; Lv, Y.; Yao, K. Effects of tea polyphenols on the activities of α-amylase, pepsin, trypsin and lipase. *Food Chem.* **2007**, *101*, 1178−1182.

(35) Record, I. R.; Lane, J. M. Simulated intestinal digestion of green and black teas. *Food Chem.* **2001**, *73*, 481−486.

(36) Su, Y. L.; Leung, L. K.; Huang, Y.; Chen, Z.-Y. Stability of tea theaflavins and catechins. *Food Chem.* **2003**, *83*, 189−195.

(37) Sang, S.; Lee, M.-J.; Hou, Z.; Ho, C.-T.; Yang, C. S. Stability of tea polyphenol (−)-epigallocatechin-3-gallate and formation of dimers and epimers under common experimental conditions. *J. Agric. Food Chem.* **2005**, *53*, 9478−9484.

(38) Zhu, Q. Y.; Zhang, A.; Tsang, D.; Huang, Y.; Chen, Z.-Y. Stability of green tea catechins. *J. Agric. Food Chem.* **1997**, *45*, 4624−4628.

without any detectable regeneration of β-carotene from its radical cation.[8]

It is accordingly of interest to study ET to carotenoid radical cations from a series of plant phenolates, with decreasing reduction potentials resulting in increasing driving force for ET. Such a kinetic study should further explore whether the fundamental ET reaction of eq 4 in an antioxidant interaction in membranes will enter the inverted region for increasing driving force where the rate of ET according to the Marcus theory decreases. Such an inverted region for the rate of ET now has been recognized for other types of bimolecular ET reactions and may for antioxidant regeneration have important biological consequences for controlling oxidative stress and also for design of functional foods with sensitive nutrients.[9−19] We have selected β-carotene, lycopene, zeaxanthin, astaxanthin, and canthaxanthin as a series of carotenoids of general food interest for our studies together with the selection of plant phenols shown in Figure 1, all of which are known to be important plant-based antioxidants in human nutrition or used for antioxidant protection of food emulsions. A large difference in antioxidative activity has been noted for rather small changes in molecular structure in homologue series of natural plant phenols also with a positive effect on human health as taylored by increasing hydrophobicity.[20,21]

2. MATERIALS AND METHODS

2.1. Chemicals. *all-trans*-β-Carotene (β-Car) was purchased from Sigma-Aldrich Chemical Co. (St. Louis, MO). *all-trans*-Lycopene was extracted from tomato juice and purified according to the procedure described by Zhang et al.[22] Astaxanthin, canthaxanthin, and zeaxanthin sealed in ampules under argon were supplied by Roche A/S (Hvidovre, Denmark). *m*-Hydroxybenzoic acid (≥99%), vanillic acid (≥97%), *p*-coumaric acid (≥98%), syringic acid (≥95%), caffeic acid (≥98%), and rutin (≥94%) were also purchased from Sigma-Aldrich. Quercetin (≥98%) was purchased from Fluka Biochemika (Buchs, Switzerland). Methanol of high-performance liquid chromatography (HPLC) grade (J&K Scientific Ltd., Beijing, China) was used as received. Chloroform (>99.0%, Beijing Chemical Works, Beijing, China) was purified before use by being passed through an alumina column (AR, Tianjin Fuchen Chemical Plant, Tianjin, China). Solutions of phenolates were prepared by addition 1 or 2 equiv of tetramethylammonium hydroxide (97%, Sigma-Aldrich) to the phenols dissolved in neutral chloroform/methanol (9:1, v/v) solutions.

2.2. Laser Flash Photolysis. The laser flash photolysis apparatus has been described elsewhere.[8] Briefly, the excitation laser pulses at 532 nm (4 mJ/pulse, 7 ns, 10 Hz) were supplied by a Nd^{3+}:YAG laser (Quanta-Ray PRO-230; Spectra Physics, Santa Clara, CA), and the probe light was provided by a xenon lamp (CW 300 W). The optical path length of the flow cuvette (~30 mL) used for laser flash photolysis was 5 mm. The near-infrared kinetics probed at 900 nm for β-carotene radical cation (β-$Car^{\bullet+}$) was detected with a photodiode (model S3071, Hamamatsu Photonics, Hamamatsu, Japan) attached to a Trivista spectrograph monochromator (Princeton Instruments, Trenton, NJ), and the kinetic traces were stored and averaged with a digital storage oscilloscope (bandwidth 600 MHz; Teledyne LeCroy WaveSurfer 64Xs, Chestnut Ridge, NY) connected to a personal computer. For kinetic analyses, the time evolution profiles of the optical density change (ΔOD) upon pulsed excitation were fitted to a two- or three-exponential model function as previously described.[2,8] The concentration of β-carotene was 50 μM. Solution samples were used immediately after preparation under reduced light conditions. All of the measurements were carried out in a thermostated room (23 ± 1 °C). The decay kinetics for carotenoid radical cations was found independent of dissolved oxygen upon a comparison between air-saturated and degassed solutions.

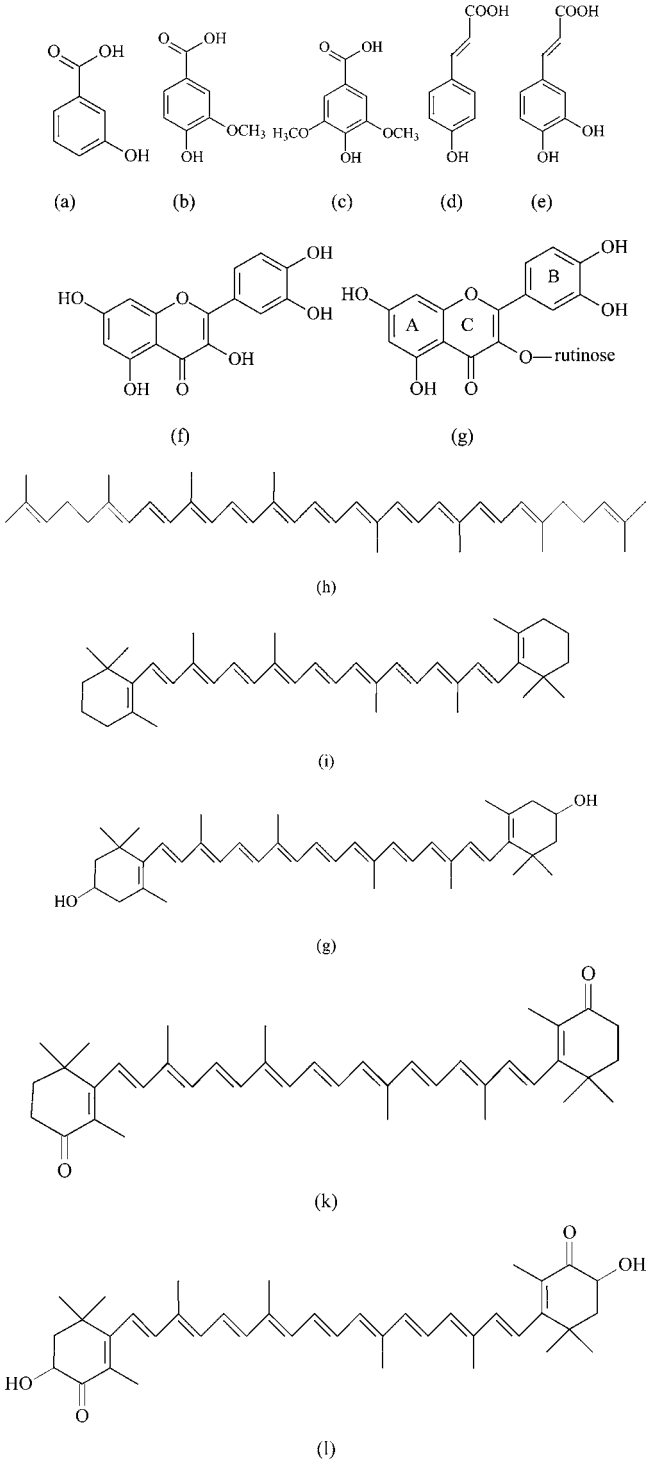

Figure 1. Molecular structures of (a) *m*-hydroxybenzoic acid, (b) vanillic acid, (c) syringic acid, (d) *p*-coumaric acid, (e) caffeic acid, (f) rutin, (g) quercetin, (h) lycopene, (i) β-carotene, (g) zeaxanthin, (k) canthaxanthin, and (l) astaxanthin.

3. RESULTS AND DISSCUSSION

Carotenoids modulate oxidative stress in membranes and cellular structures through ET to oxidizing radicals.[3] The fate of carotenoid radical cations formed under such conditions of oxidative stress have previously been followed in real time kinetic studies using fast spectroscopic techniques for homogeneous solutions, and their effect on lipid oxidation

dx.doi.org/10.1021/jf404725v | J. Agric. Food Chem. 2014, 62, 942−949

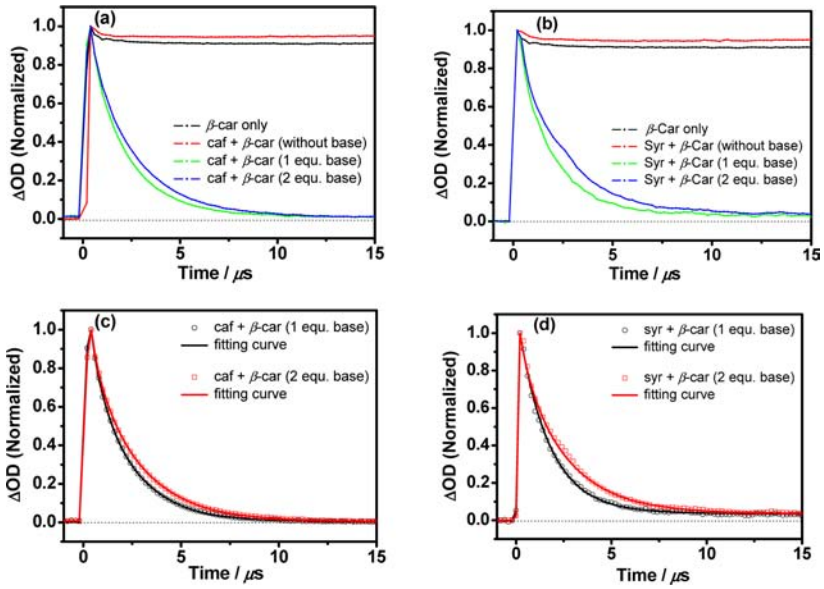

Figure 2. Normalized transient absorption probed at 900 nm for chloroform/methanol (9:1, v/v) solutions of (a) caffeic acid (100 μM) and (b) syringic acid (100 μM) with β-carotene (50 μM) following 7 ns flash excitation at 532 nm, and parameter fitting for caffeic acid (c) and syringic acid (d) using two exponentials for addition of 1 equiv of base and three exponentials for addition of 2 equiv of base.

Table 1. Second-Order Rate Constants for the Reaction of Radical Cations of β-Carotene, Lycopene, and Zeaxanthin with Phenolic Acids in the Presence of 1 or 2 equiv of Base to Plant Phenol Based on Experiment As Shown in Figure 2 for β-Carotene, All at 23 °C

	β-carotene			lycopene			zeaxanthin		
		k_4/ L·mol^{-1}·s^{-1}			k_4/L·mol^{-1}·s^{-1}			k_4/L·mol^{-1}·s^{-1}	
compd	E^a/V	1 equiv of base	2 equiv of base	E^a/V	1 equiv of base	2 equiv of base	E^a/V	1 equiv of base	2 equiv of base
m-hydroxybenzoic adid	0.01	8.0×10^8	7.2×10^8	−0.07	5.7×10^8	5.9×10^8	−0.02	1.3×10^9	1.3×10^9
vanillic acid	0.11	2.8×10^9	2.0×10^9	0.03	1.2×10^9	1.3×10^9	0.08	2.1×10^9	2.3×10^9
p-coumaric acid	0.17	3.7×10^9	3.3×10^9	0.09	1.8×10^9	1.9×10^9	0.14	3.2×10^9	3.1×10^9
syringic acid	0.35	6.3×10^9	4.2×10^9	0.27	2.0×10^9	1.6×10^9	0.32	3.3×10^9	3.1×10^9
caffeic acid	0.39	5.0×10^9	4.2×10^9	0.31	1.1×10^9	1.5×10^9	0.36	3.0×10^9	1.9×10^9
rutin	0.61	3.4×10^9	2.0×10^9	0.53	1.9×10^9	1.8×10^9	0.58	3.2×10^9	2.7×10^9
quercetin	0.74	2.0×10^9	1.4×10^9	0.66	1.3×10^9	1.2×10^9	0.71	2.5×10^9	2.1×10^9

[a] $E = E^{\ominus}_{\text{Car}^{\bullet+}} - E^{\ominus}_{\text{phenol}}$ with $E^{\ominus}_{\text{phenol}}$ based on ref 16 and $E^{\ominus}_{\text{Car}^{\bullet+}}$ based on ref 17.

have been evaluated in liposomes as a model for membranes.[2,7] Carotenoids have thus been found to form an antioxidant network according to their tendency of reduction of their one-electron-oxidized forms but also to undergo regeneration reactions by other antioxidants such as polyphenols when available as electron donors, leading to antioxidant synergism between different carotenoids and between carotenoids and polyphenols.[7,14]

Carotenoid radical cations were generated as in our previous studies using laser flash photolysis in homogeneous chloroform/methanol (9:1, v/v) as an electron-withdrawing solvent.[2] The fate of the β-carotene radical cation was followed using transient absorption spectroscopy at 900 nm in the absence or presence of one of the plant phenols shown in Figure 1 with and without base added as shown in Figure 2 for caffeic acid and syringic acid. The β-carotene radical decays only slowly even in the presence of a plant phenol in the absence of base. However, addition of 1 or 2 equiv of base in the presence of a plant phenol induces rapid decay, which for 1 equiv of base is described by a biexponential decay curve and for 2 equiv of base requires a triexponential fitting as can be seen in Figure 2. Similar results were obtained for the other plant phenols investigated (data not shown), and an analysis of the numerical values for the multiexponential decay curves showed in all cases that one exponential term dominated with a larger amplitude contribution. Other minor components in the exponential decay curves may be due to interference from the laser or to parallel or sequential reactions as previously noted for reactions of β-carotene radical cations with (iso)flavonoids and their glycosides.[2] The rate constant for the dominant decay reaction of β-carotene radical cations by each of the seven plant phenols investigated can be found in Table 1 for conditions with both 1 and 2 equiv of base added after conversion to second-order rate constants. Similar results were obtained for lycopene and zeaxanthin, for which the second-order rate constants are also presented in Table 1. For none of these carotenoids did the decay of the radical cation induced by base alone interfere with the reduction of the radical cation by the plant phenolate. In contrast, under alkaline conditions, the radical cation of astaxanthin and canthaxanthin decayed rapidly. The first-order rate constants for decay of carotenoid radical cations formed by laser flash photolysis in the absence of phenolates are for all five carotenoids collected in Table 2. For astaxanthin and canthaxanthin, the observed first-order rate constants are

dx.doi.org/10.1021/jf404725v | J. Agric. Food Chem. 2014, 62, 942−949

Table 2. Observed First-Order Rate Constants for Decay of Carotenoid Radical Cation in 9:1 (v/v) Chloroform/Methanol with Tetramethylammonium Hydroxide as Base Following 532 nm Photolysis at 23 °C

	k_{obsd}/s^{-1}	
compd (10 μM)	$[OH^-]$ = 20 μM	$[OH^-]$ = 40 μM
β-carotene	1.7×10^4	2.5×10^4
lycopene	1.3×10^4	1.4×10^4
zeaxanthin	4.7×10^4	5.1×10^4
canthaxanthin	5.1×10^5	7.0×10^5
astaxanthin	5.9×10^5	1.5×10^6

larger by more than a factor of 10 than for zeaxanthin, lycopene, and especially β-carotene. Accordingly, under the actual experimental conditions, the reaction of the radical cations of the two ketocarotenoids with the plant phenols became slower than the reaction with the solvent. This observation of a rapid reduction of these carotenoid radicals by the alkaline solvent is in agreement with the previous identification of the keto group as important for electron transfer to astaxanthin and canthaxanthin radical cations.[7]

The first-order rate constants for decay of the carotenoid radical cations were assigned to the reaction of eq 4 in which a carotenoid is regenerated by ET from the phenolate.[2,7] Notably, the phenolate (≥100 μM) was for all experimental conditions in large excess compared to the radical cations, which were only formed as a minor fraction of the total concentration of the carotenoid (50 μM) during laser flash photolysis. This large excess provides pseudo-first-order conditions for the reactions with phenolates following the laser flash photolysis. The pseudo-first-order rate constants determined as shown in Figure 2 for β-carotene by exponential fitting were found to depend linearly on the concentration of excess plant phenol, in agreement with a second-order reaction as shown in Figure 3 for caffeic acid and syringic acid reacting

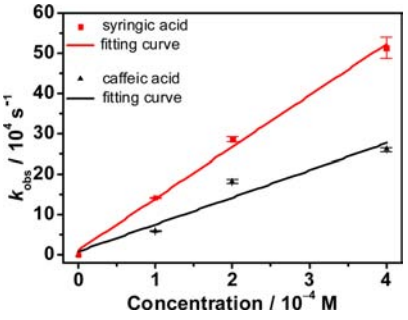

Figure 3. Dependence of the observed first-order rate constant for reduction of β-carotene (50 μM) radical cation on the concentration of caffeic acid and syringic acid in the presence of 1 equiv of base in chloroform/methanol (9:1, v/v) solution at 23 °C. Linear regression for up to 4.0×10^{-4} M provides the second-order rate constants of Table 1.

with β-carotene for up to 400 μM phenolate. For a higher concentration of plant phenolate, deviations from this simple second-order reaction were noted with indications of rate saturation at higher phenol concentrations (data not shown), as also noted previously for the puerarin dianion reacting with carotenoid radical cations.[7] The pseudo-first-order rate constants determined for lycopene and zeaxanthin by the same procedure as for β-carotene were likewise converted to second-order rate constants and are included in Table 1 for further discussion. The second-order rate constants calculated from the observed pseudo-first-order rate constants and included in Table 1 for further discussion are all based on the conditions used for the experiment of Figure 2.

The plant phenols were found not to react directly with the β-carotene radical cation despite a large driving force. The values of E of Table 1 are based on the reduction potentials determined in aqueous solution of pH 7.0[16]

$$\varphi\text{-}O^{\bullet} + e^- + H^+ \rightarrow \varphi\text{-}OH \quad (5)$$

and $E^{\ominus}$ = 1.06 V for reduction of the radical cation of β-carotene, 0.98 V for lycopene, and 1.03 V for zeaxanthin as determined for aqueous conditions.[17] However, deprotonation of the plant phenols studied (Figure 1) resulted in each case in a rapid reaction even following reaction with only 1 equiv of base as for *m*-hydroxybenzoic acid:

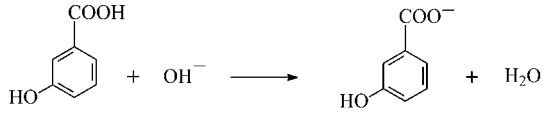

(6)

The deprotonation of the neutral phenols is suggested to facilitate formation of an encounter complex with the radical cation. The deprotonation of the plant phenol will mainly occur at the more acidic carboxylic group ($pK_a \approx 3$) rather than at the phenol group ($pK_a \approx 8$). However, the equilibrium, although shifted to the left

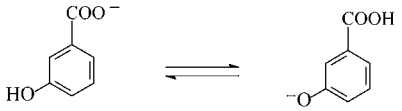

(7)

may be important for ET to the radical cation in the encounter complex.

The values of the second-order rate constants for ET from the plant phenol to the radical cation of β-carotene, lycopene, and zeaxanthin increase in the chloroform/methanol binary solvent for increasing driving force to a certain rate close to the diffusion limit for bimolecular reactions;[18] see Figure 4 for β-carotene, Figure 5 for lycopene, and Figure 6 for zeaxanthin. However, for a continuing increase in driving force, the rate constants decrease for all these carotenoid radical cations. Such a bell-shaped dependence on the driving force for the rate of ET was predicted by the Marcus theory for ET[9] and was later confirmed experimentally for a number of processes, including

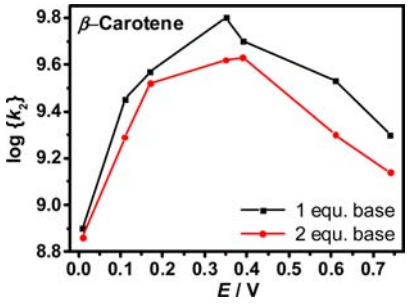

Figure 4. Logarithm of the second-order rate constant for electron transfer to β-carotene radical cation from plant phenolate in the presence of 1 or 2 equiv of base in chloroform/methanol (9:1, v/v) at 23 °C as a function of the driving force for ET ($E = E^{\ominus}_{\beta\text{-Car}^{\bullet+}} - E^{\ominus}_{\text{phenol}}$). For identification of phenols, see Table 1.

dx.doi.org/10.1021/jf404725v | J. Agric. Food Chem. 2014, 62, 942−949

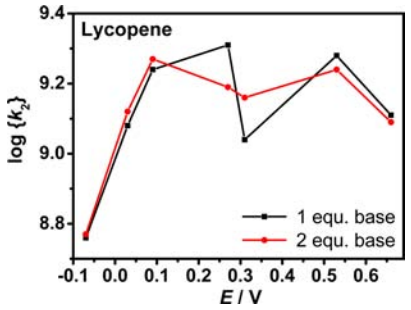

Figure 5. Logarithm of the second-order rate constant for electron transfer to lycopene radical cation from plant phenolate in the presence of 1 or 2 equiv of base in chloroform/methanol (9:1, v/v) at 23 °C as a function of the driving force for ET ($E = E^{\ominus}_{\beta\text{-Car}^{\bullet+}} - E^{\ominus}_{\text{phenol}}$). For identification of phenols, see Table 1.

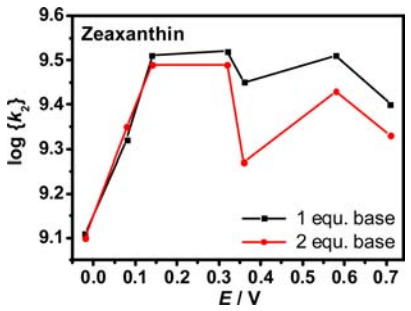

Figure 6. Logarithm of the second-order rate constant for electron transfer to zeaxanthin radical cation from plant phenolate in the presence of 1 or 2 equiv of base in chloroform/methanol (9:1, v/v) at 23 °C as a function of the driving force for ET ($E = E^{\ominus}_{\text{Zea}^{\bullet+}} - E^{\ominus}_{\text{phenol}}$). For identification of phenols, see Table 1.

ET from phenolate ions.[10−14] Accordingly, we analyzed the rate data on the basis of the Marcus theory.[9,14] The rate of ET is controlled by the driving force ($-\Delta G^{\circ}_{\text{ET}}$), a matrix coupling element (V), and the reorganization energy (λ) for the reaction:[14,19]

$$k_{\text{ET}} = \sqrt{\frac{4\pi^3}{h^2\lambda RT}}\, V^2 \exp -\left\{\frac{(\Delta G^{\circ} + \lambda)^2}{4\lambda RT}\right\} \tag{8}$$

The plot of Figure 7 is based on a reorganization of eq 8 and yields $\lambda = 0.41 \pm 0.03$ and 0.40 ± 0.03 eV from the slope of the linear regression lines for the reorganization energy for ET from the plant phenols to the β-carotene radical cation in the presence of 1 or 2 equiv of base, respectively.[23] The matrix coupling element has the value $V = 5.85$ cm^{-1} for the plant phenols with 1 equiv of base added and $V = 5.10$ cm^{-1} for 2 equiv of base. For lycopene, similar plots gave $\lambda = 0.33 \pm 0.04$ eV and $V = 4.53$ cm^{-1} and $\lambda = 0.34 \pm 0.05$ eV and $V = 4.40$ cm^{-1} for 1 and 2 equiv of base, respectively. For zeaxanthin the values were $\lambda = 0.39 \pm 0.04$ eV and $V = 6.03$ cm^{-1} and $\lambda = 0.38 \pm 0.04$ eV and $V = 5.24$ cm^{-1} for 1 and 2 equiv of base, respectively. The values for the relative coupling elements represent the coupling between each of the carotenoid radical cations and the plant phenolates investigated. For the three carotenoids, the driving force, $-\Delta G^{\circ}_{\text{ET}}$, increases for the same series of phenolates reacting with radical cations as β-carotene > zeaxanthin > lycopene, in agreement with the increasing maximal rate for ET observed in experiments (β-carotene > zeaxanthin > lycopene) and an increasing calculated reorganization energy, λ, in agreement with the Marcus theory. λ

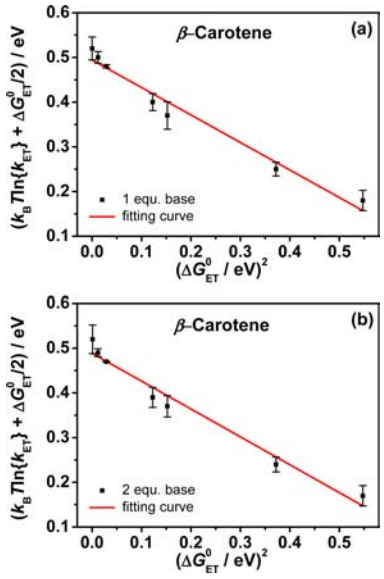

Figure 7. Marcus plot for reduction of β-carotene radical cation by plant phenolate in chloroform/methanol (9:1, v/v) at 23 °C in the presence of 1 (a) and 2 (b) equiv of base.

decreases for decreasing $E^{\ominus}$ for the carotenoid, but is independent of the charge on the phenolate. In contrast, V decreases with increasing charge on the phenolate.

The regeneration of β-carotene following laser flash photolysis shows a pattern similar to the bell-shaped relationship seen in Figure 4 for the rate of ET. The highest degree of protection of the β-carotene, defined as

$$\text{protection} = \frac{\Delta\text{OD(absence of phenol)} - \Delta\text{OD(presence of phenol)}}{\Delta\text{OD(absence of phenol)}} \times 100 \tag{9}$$

in which ΔOD is the relative steady-state absorbance at 500 nm following bleaching of β-carotene, is found for caffeic acid and syringic acid, as can be seen in Figures 8 and 9. Both for less

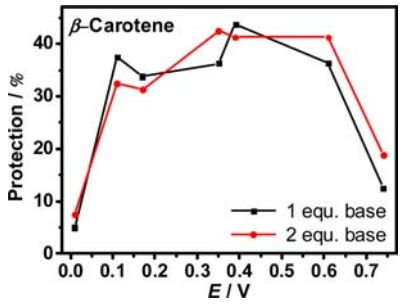

Figure 8. Fraction of β-carotene regenerated by plant phenol in the presence of 1 or 2 equiv of base for 50 μM β-carotene and 100 μM phenol in chloroform/methanol (9:1, v/v) following 7 ns flash photolysis at 532 nm and 23 °C as a function of the driving force for ET ($E = E^{\ominus}_{\beta\text{-Car}^{\bullet+}} - E^{\ominus}_{\text{phenol}}$). For identification of phenols, see Table 1.

reducing and for more reducing plant phenol than caffeic acid and syringic acid, the degree of protection decreases. For both lycopene and zeaxanthin, the same similarity between the dependence of protection of carotenoid and rate of regeneration of carotenoid was found. This dependence of protection of β-carotene through regeneration of β-carotene

dx.doi.org/10.1021/jf404725v | J. Agric. Food Chem. 2014, 62, 942−949

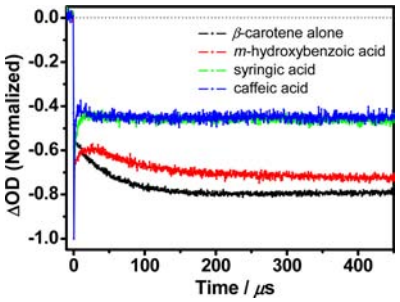

Figure 9. Slow bleaching of β-carotene in chloroform/methanol (9:1, v/v) at 23 °C following laser flash photolysis at 532 nm as monitored at 500 nm in the absence or presence of plant phenol and 2 equiv of base.

through ET according to eq 4 was further confirmed by inspection of the spectral changes of the β-carotene/phenolate solutions subjected to photolysis; see Figure 10. β-Carotene is bleached by irradiation at 532 nm, a wavelength where none of the plant phenols absorb light, to a certain degree depending on the nature of the plant phenol present in reactions providing no spectral evidence for formation of β-carotene/phenol adducts as was seen for catechins.[8] The recovery of β-carotene following photolysis as followed by transient absorption at 500 nm (Figure 10 d) is seen to occur on a time scale similar to that of the decay of the radical cation (Figure 2) with a half-life around 1 μs corresponding to $k \approx 10^6$ s^{-1}. The fast regeneration of β-carotene is, however, followed by a slower bleaching as is evident in Figure 9, in agreement with previous findings.[24]

The maximal protection of β-carotene approaches 50% as is seen for caffeic acid and syringic acid. The protection of lycopene by the same plant phenols was found to be slightly better, while the protection of zeaxanthin was found to be comparable to the protection of β-carotene. This observation is in agreement with the detection of a slow secondary bleaching of β-carotene in electron-withdrawing solvents initiated by a solvent radical formed in the initial photobleaching of β-carotene in a 1:1 ratio.[24] For the chloroform/methanol mixture as solvent, $CHCl_3^{\bullet-}$ as the initially formed solvent radical was previously found to be converted to $CHCl_2^{\bullet}$ prior to reaction with β-carotene, resulting in the secondary and slower bleaching.[24]

The reactions of Scheme 1 show the coupling between the primary photobleaching and the slower bleaching of β-carotene

Scheme 1

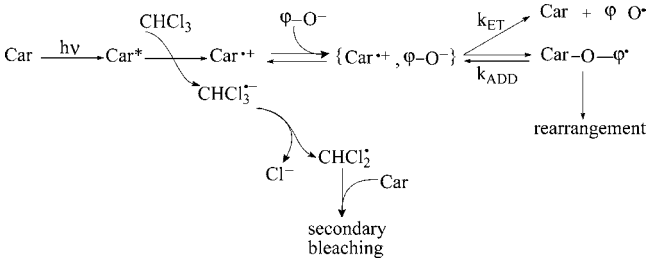

in chloroform/methanol in the presence of plant phenolates. The maximal protection against photobleaching of β-carotene provided by the plant phenolates reacting most efficiently in ET reactions only approaches 50% as is seen in Figure 8. This observation seems to indicate that the plant phenolates are not involved in the secondary bleaching, but only in the primary bleaching. The β-carotene radical cation formed in the primary bleaching reaction may react with a plant phenolate to form a precursor complex for further reaction. Such precursor complexes are often indicated in ET reactions, and their formation may, for some combinations of electron donors and electron acceptors, be rate determining, while, for other combinations, the subsequent reaction of the encounter complex controls the rate.[19] For the ET from the plant phenolate to the carotenoid radical cations, the reaction of the encounter complex seems to be rate determining; see Figures

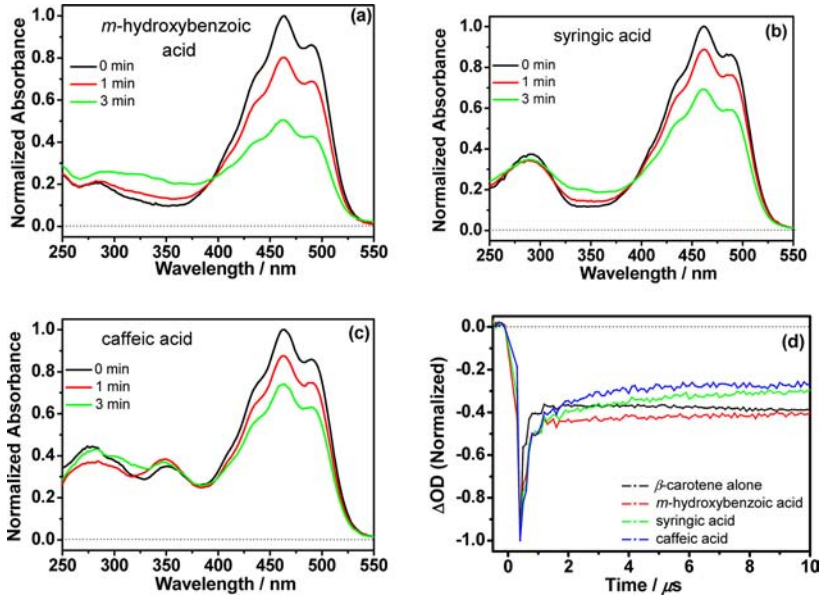

Figure 10. Steady-state absorption spectra of β-carotene (50 μM) in the presence of 100 μM *m*-hydroxybenzoic acid (a), syringic acid (b), or caffeic acid (c) in chloroform/methanol (9:1, v/v) at 23 °C in the presence of 2 equiv of base before and after laser flash photolysis at 532 nm for the indicated time. (d) Normalized recovery of β-carotene bleaching followed at 500 nm for 10 μs in the presence of *m*-hydroxybenzoic acid, syringic acid, and caffeic acid each in the presence of 2 equiv of base.

dx.doi.org/10.1021/jf404725v | J. Agric. Food Chem. 2014, 62, 942−949

4−6, since the rate depends on the driving force for ET and does not level off for increasing driving force, but continues to decrease. Other factors such as an increasing edge-to-edge distance of the encounter complex may, however, also contribute to the decreasing rate for the increasing driving force for the actual series of plant phenols.

A reaction competitive with ET from the phenolate in the encounter complex to the radical cation formed during the primary bleaching may explain the correlation between k_{ET} and the degree of protection of β-carotene. Such a competing reaction may involve a reversible adduct formation as shown in Scheme 1, which for some strongly reducing plant phenols may involve further rearrangements as was seen for the tea catechins and β-carotene.[8] For the plant phenolates investigated in the present study, adducts formed with carotenoids may not react further as they are not seen as stable products. However, it remains unexplained why the phenolate dianion reacts with a rate comparable to or even slower than the phenolate monoanion; see Table 1. However, a single negative charge seems to facilitate formation of the encounter complex, and intramolecular proton transfer equilibria as shown in eq 7 may be involved. Such equilibria may specifically be involved for caffeic acid as a simple plant phenol with two phenol groups in the *ortho* position, decreasing the rate for the reactions of the cations of lycopene and zeaxanthin with the anions of caffeic acid. The small difference in the matrix coupling constant corresponds to a large difference in rates between the reaction of monoanions and dianions. Notably, the rates are comparable for a driving force below the reorganization energy for the two series of phenolates for all three carotenoids, while the difference increases above the reorganization energy, with the monoanion reacting faster; see Figure 4.

Regeneration of lipophilic carotenoids from their radical cations as formed in membranes during oxidative stress by hydrophilic plant phenolates seems to involve an encounter complex, the formation of which depends on electrostatic forces. This encounter complex may react through at least two reaction channels. One reaction involves ET and leads to immediate regeneration of the carotenoids, while the other leads to adduct formation and for some polyphenols to further degradation of the carotenoids. The ET channel is fast, but for increasing driving force above the reorganization energy for ET, inverted region effects as described by the Marcus theory are recognized. As a consequence, the most reducing phenolic antioxidants may not be the most efficient in regeneration of carotenoids and may even show antioxidant antagonism.[1,21] This aspect may also be worth considering when foods or beverages colored by carotenoids need an antioxidant protection agent against light-induced bleaching.

AUTHOR INFORMATION

Corresponding Authors

*E-mail: jpzhang@chem.ruc.edu.cn. Phone: +86-10-62516604.
*E-mail: ls@food.ku.dk. Phone: +45 3533 3221.

Funding

Support from the Danish Research Council for Technology and Production to L.H.S. as Grant 09-065906/FTP: Redox Communication in the Digestive Tract and from the Fundamental Research Funds for The Central Universities to J.-P.Z. is acknowledged.

Notes

The authors declare no competing financial interest.

ACKNOWLEDGMENTS

Dr. Ran Liang is thanked for helpful comments.

ABBREVIATIONS USED

Car, carotenoid; β-Car, β-carotene; Lyc, *all-trans*-lycopene; Zea, zeaxanthin; ET, electron transfer

REFERENCES

(1) Skibsted, L. H. Carotenoids in antioxidant networks. Colorants or radical scavengers. *J. Agric. Food Chem.* **2012**, *60*, 2409−2417.

(2) Liang, R.; Chen, C. H.; Han, R. M.; Zhang, J. P.; Skibsted, L. H. Thermodynamic versus kinetic control of antioxidant synergism between β-carotene and (iso)flavonoids and their glycosides in liposomes. *J. Agric. Food Chem.* **2010**, *58*, 9221−9227.

(3) Martínez, A.; Vargas, R.; Galano, A. What is important to prevent oxidative stress? A theoretical study on electron-transfer reactions between carotenoids and free radicals. *J. Phys. Chem. B* **2009**, *113*, 12113−12120.

(4) Martínez, A.; Vargas, R.; Galano, A. Theoretical study study of the chemical fate of adducts formed through free radical addition reactions to carotenoids. *Theor. Chem. Acc.* **2010**, *127*, 595−603.

(5) Böhm, F.; Edge, R.; Truscott, G. Interactions of dietary carotenoids with activated (singlet) oxygen and free radicals: potential effects for human health. *Mol. Nutr. Food Res.* **2012**, *56*, 205−216.

(6) Chen, C. H.; Han, R. M.; Liang, R.; Fu, L. M.; Zhang, J. P.; Skibsted, L. H. Direct observation of the β-carotene reaction with hydroxyl radical. *J. Phys. Chem. B* **2011**, *115*, 2082−2089.

(7) Han, R. M.; Chen, C. H.; Tian, Y. X.; Zhang, J. P.; Skibsted, L. H. Fast regeneration of carotenoids from radical cations by isoflavonoid dianions: importance of the carotenoid keto group for electron transfer. *J. Phys. Chem. A* **2010**, *114*, 126−132.

(8) Song, L. L.; Liang, R.; Li, D. D.; Xing, Y. D.; Han, R. M.; Zhang, J. P.; Skibsted, L. H. β-Carotene radical cation addition to green tea polyphenols. Mechanism of antioxidant antagonism in peroxidizing liposomes. *J. Agric. Food Chem.* **2011**, *59*, 12643−12651.

(9) Marcus, R. A. Electron transfer reactions in chemistry. Theory and experiment. *Rev. Mod. Phys.* **1993**, *65*, 599−610.

(10) Turró, C.; M. Zaleski, J.; M. Karabatsos, Y.; G. Nocera, D. Bimolecular electron transfer in the Marcus inverted region. *J. Am. Chem. Soc.* **1996**, *118*, 6060−6067.

(11) Thanasekaran, P.; Rajendran, T.; Rajagopal, S.; Srinivasan, C.; Ramaraj, R.; Ramamurthy, P.; Venkatachalapathy, B. Marcus inverted region in the photoinduced electron transfer reactions of ruthenium(II)−polypyridine complexes with phenolate ions. *J. Phys. Chem. A* **1997**, *101*, 8195−8199.

(12) Weng, Y. X.; Chan, K. C.; Tzeng, B. C.; Che, C. M. Effect of laser intensity on the determination of intermolecular electron transfer rate constants—observation of Marcus inverted region in photoinduced back electron transfer reactions. *J. Chem. Phys.* **1998**, *109*, 5948−5956.

(13) Fukuzumi, S.; Ohkubo, K.; Imahori, H.; M. Guldi, D. Driving force dependence of intermolecular electron-transfer reactions of fullerenes. *Chem.—Eur. J.* **2003**, *9*, 1585−1593.

(14) Hong, J.; A. Kharenko, O.; Fan, J. F.; Xie, F.; K. Petros, A.; R. Gibney, B.; Y. Ogawa, M. Evidence that a miniature Cu^{I} metalloprotein undergoes collisional electron transfer in the inverted Marcus region. *Angew. Chem., Int. Ed.* **2006**, *45*, 6137−6140.

(15) Liang, J.; Tian, Y.-X.; Yang, F.; Zhang, J. P.; Skibsted, L. H. Antioxidant synergism between carotenoids in membranes. Astaxanthin as a radical transfer bridge. *Food Chem.* **2009**, *115*, 1437−1442.

(16) Simić, A.; Manojlović, D.; Šegan, D.; Todorović, M. Electrochemical behavior and antioxidant and prooxidant activity of natural phenolics. *Molecules* **2007**, *12*, 2327−2340.

(17) Burke, M.; Edge, R.; Land, E. J.; Mcgarvey, D. J; Truscott, T. G. One-electron reduction potentials of dietary carotenoid radical cations in aqueous micellar environment. *FEBS Lett.* **2001**, *500*, 132−136.

(18) Li, W. B.; Gandra, N.; Courtney, S. N.; Gao, R. M. Singlet oxygen production upon two-photon excitation of TiO_2 in chloroform. *ChemPhysChem* **2009**, *10*, 1789−1793.
(19) Imahori, H.; Yamada, H.; Guldi, D. M.; Endo, Y.; Shimomura, A.; Kundu, S.; Yamada, K.; Okada, T.; Sakata, Y.; Fukuzumi, S. Comparison of reorganization energies for intra- and intermolecular electron transfer. *Angew. Chem., Int. Ed.* **2002**, *41*, 2344−2347.
(20) Shahidi, F.; Zhong, Y. Lipophilised epigallocatechin gallate (EGCG) derivatives and their antioxidant potential in food and biological systems. *Food Chem.* **2012**, *131*, 22−30.
(21) Shahidi, F.; Zhong, Y. Revisiting the polar paradox theory: a critical overview. *J. Agric. Food Chem.* **2011**, *59*, 3499−3504.
(22) Zhang, J. P.; Chen, C. H.; Koyama, Y.; Nagae, H. Vibrational relaxation and redistribution in the $2A_g^-$ state of *all-trans*-lycopene as revealed by picosecond time-resolved absorption spectroscopy. *J. Phys. Chem. B* **1998**, *102*, 1632−1640.
(23) Zhang, W.; Wang, Y. W.; Hu, R.; Ai, X. C.; Zhang, J. P.; Hou, J. H. Mechanism of primary charge photogeneration in polyfluorene copolymer/fullerene blends and influence of the donor/acceptor lowest unoccupied molecular orbital level offset. *J. Phys. Chem. C* **2013**, *117*, 735−749.
(24) Tian, Y. X; Han, R. M.; Zhang, J. P.; Skibsted, L. H. Effect of polar solvents on *β*-carotene radical precursor. *Free Radical Res.* **2008**, *42*, 281−286.

MATERIALS AND METHODS

Dynamic in Vitro Gastrointestinal Model. TIM-1, a dynamic in vitro gastrointestinal model, was originally described by Minekus et al.[5,6] For a schematic diagram of TIM-1, see Verwei et al.[15] This gastric small-intestinal model comprises four connected compartments that represent the stomach, duodenum, jejunum, and ileum, respectively. Each compartment consists of a glass outer wall with a flexible inner wall. The flexible wall is surrounded by water at 37 °C, which is used to squeeze the flexible walls and mix the chyme, simulating peristaltic movements in the gastrointestinal tract. The jejunal and ileal compartments are connected with semipermeable hollow-fiber membranes to remove digested products and especially fat-soluble compounds that were incorporated into mixed micelles.[6−8] The pH values, as well as the gastric emptying and small-intestinal passage of the food, are computer-controlled according to preset curves based on information on human in vivo conditions.[6]

TIM-1 Experimental Design. Two diets that had already been tested in vivo[14] were each evaluated using TIM-1. The difference between the two diets was the food matrix where the β-carotene was incorporated, with one diet containing vegetables high in β-carotene (mixed diet) and the second diet containing vegetables low in β-carotene but supplemented with β-carotene in salad dressing oil (oil diet). The frozen diets were defrosted at 4 °C for ∼16 h before the experiment and were homogenized to mimic the process of chewing by human teeth, to increase experimental consistency and to minimize mixing errors as only a limited amount could be introduced in the gastric compartment. A portion of the diet was put into the gastric compartment of TIM-1. During digestion, the total filtrate (bioaccessible fraction) was collected in 30-min fractions during the first 2 h and hourly fractions until the end of the experiment at 6 h. The total ileal efflux was collected hourly during the 6 h experiment. At the end of the experiment, the residues from the gastric, jejunal, and ileal compartments were collected. The ileal efflux and residues were analyzed to determine the non-bioaccessible fraction. Possibly present β-carotene content in the bile and pancreatic solutions was also analyzed. The samples were stored at −20 °C until β-carotene analysis by HPLC.

Feeding Sample. The feeding sample consisted of 120.0 g of the homogenized diet and was introduced into the gastric compartment together with 50.0 g of gastric juice, 5 g of amylase, and 37 g of water.[6,8] The 120.0 g of the mixed diet contained 498 μg of β-carotene (90% as *trans*-β-carotene), and 120.0 g of the oil diet contained 220 μg of β-carotene (98% as *trans*-β-carotene) (Table 1). A capsule containing 47.0 μg of [$^{13}C_{10}$]β-carotene was introduced into TIM-1 immediately after putting the feeding sample in the gastric compartment.

The β-carotene in the oil diet originated from supplemental β-carotene (85%) and from vegetables and fruits (15%). The supplemental β-carotene in the oil suspension was added to salad dressing for the oil diet (all-*trans* β-carotene, 30% suspension in vegetable oil, Hoffmann-La Roche, Switzerland). Both diets were typical Western diets with respect to the contribution of carbohydrates, proteins, and fats to the energy intake (57%, 13%, and 30%, respectively). Both diets were prepared as duplicate diets during a previously conducted diet-controlled study in humans.[14] Each of the duplicate diets was pooled, homogenized, mixed thoroughly with 2.5 mL of 20% butylhydroquinone (t-BHQ) per kilogram of food, and stored at −20 °C until analysis.

Table 1. Values of Energy, Macronutrients, Fiber, Retinol, and Carotenoids of Two Diets per 100 g Wet Weight[a]

	mixed diet	oil diet
energy (kJ)	584	570
fat (g)	4.7	4.3
protein (g)	4.9	4.8
carbohydrates (g)	17.5	18.2
fiber (g)	1.7	1.6
retinol (μg)	12	13
total β-carotene in salad dressing oil (μg)	<1	156
total β-carotene in vegetables and fruits (μg)	415	28
trans-β-carotene (μg)	373	180
cis-β-carotene (μg)	42	4
α-carotene (μg)	75	3
β-cryptoxanthin (μg)	8	12
lutein (μg)	84	37
zeaxanthin (μg)	8	8

[a]Values of energy and carbohydrates were calculated. The mixed diet contained vegetables high in β-carotene, and the oil diet contained vegetables low in β-carotene supplemented with synthetic β-carotene in salad dressing oil. For the in vitro study, the feeding sample consisted of 120.0 g of the homogenized diet.

Chemical Analysis of β-Carotene in the Feeding Sample. Samples of each homogenized diet (4.0 g each) were extracted in duplicate using a mixture of methanol, tetrahydrofuran (THF), and dichloromethane (45:45:10 v/v/v). The resulting extract was saponified at room temperature overnight using a 1.5 mol/L potassium hydroxide ethanolic solution supplemented with sodium ascorbate, disodium sulfide, and glycerol. Then the mixture was extracted using diisopropyl ether, which was subsequently washed three times with water. Part of the resulting extract was evaporated to dryness and redissolved in HPLC mobile phase. The resulting solution was analyzed for β-carotene using reversed-phase HPLC with diode array detection.[16,17] These analyses were performed for quality control at two laboratories (Food Analysis Laboratory at TNO, Zeist and at Human Nutrition, Wageningen University). Results from both analyses were similar.

Chemical Analysis of β-Carotene in Jejunal and Ileal Filtrates. Samples of 1000 μL each were vortex mixed with an equal volume of ethanol containing tocol as an internal standard (IS). This mixture was extracted with a 2-fold volume of hexane using vortex mixing for 2 min. Part of the resulting extract was evaporated to dryness and redissolved in eluent. The resulting solution was analyzed for β-carotene and IS using reversed-phase HPLC-diode array detection.[16] The limit of precision of the known value of IS was 5%. These analyses were performed at the Food Analysis Laboratory at TNO, Zeist.

Chemical Analysis of β-Carotene in Ileal Efflux and Residues. The ileal efflux and residues had more complex and less dissoluble matrices than the filtrates and consisted of supernatants and pellets. The concentrations of carotenoids in the ileal efflux and residues were measured at the division of Human Nutrition, Wageningen University. The supernatants of both ileal efflux and residues were treated according to the procedure described by Khan et al.[17] Briefly, the pellets of both ileal efflux and residues were extracted in duplicate in the presence of anhydrous sodium sulfate (4.0 g) and calcium

dx.doi.org/10.1021/jf403312v | J. Agric. Food Chem. 2014, 62, 950−955

carbonate (0.5 g), with 20 mL of THF containing 0.01% t-BHT after using a tissue grinder. The extract was filtered through a glass funnel fitted with Whatman paper no. 54. The residue was twice re-extracted with 20 mL of THF. The extract was evaporated to dryness, redissolved in methanol/THF (1:1 v/v %) containing 0.01% t-BHT, transferred into a 25.0 mL volumetric flask, and made up to volume. An amount of 25 μL was injected into the HPLC system for analysis. Within-run and between-run coefficients of variation for β-carotene were 2.6% and 7.1%, respectively.

Labeled β-Carotene in the Capsule and Measurement of Isotopic Enrichment in Filtrates. The concentration of β-carotene in the capsules was analyzed by HPLC with absorbance detection according to the method described by Khan et al.[17] The capsule contained 47.0 (±0.8) μg [12,13,14,15,20,12′,13′,14′,15′,20′-$^{13}C_{10}$]-β-carotene in sunflower oil (>82% oleic acid and >9% linoleic acid; Hozol; Contined BV, Bennekom, The Netherlands). The $^{13}C_{10}$-labeled β-carotene was synthesized at ARC Laboratories (Apeldoorn, The Netherlands) as described previously[18] (isotopic incorporation >99%, isomeric purity >93% all-*trans*, chemical purity >98%). The capsules were designed for oil solutions and were made from bovine gelatin (Capsugel, Bornem, Belgium).

The first experiment of each diet was analyzed for isotopic enrichment in the filtrates. The degree of isotopic enrichment of β-carotene with [$^{13}C_{10}$]β-carotene in filtrates was measured by using liquid chromatography-atmospheric pressure chemical ionization-mass spectrometry (APCI LC−MS) as described previously.[19,20] β-Carotene and [$^{13}C_{10}$]β-carotene were monitored in negative ion mode at mass-to-charge ratios (m/z) 536 and 546, respectively.[20] Isotopic enrichment of β-carotene in the filtrates was the proportion of labeled β-carotene to total β-carotene. These analyses were performed at the University of Illinois.

Calculations. The β-carotene bioaccessibility, the amount of bioaccessible β-carotene in μg per 100 μg of β-carotene available for digestion, was expressed as a fraction of β-carotene feeding and was calculated by the formula

$$\frac{\mu g\ \beta\text{-carotene}_{filtrates}}{\mu g\ \beta\text{-carotene}_{feeding} + \beta\text{-carotene}_{endogenous}} \times 100$$

where β-carotene$_{filtrates}$ is the total β-carotene in the jejunal and ileal filtrate, β-carotene$_{feeding}$ is the β-carotene in the feeding sample and comprises the β-carotene in 120.0 g of the diet and a capsule with 47 μg of labeled β-carotene, and β-carotene$_{endogenous}$ is the β-carotene content in the bile and pancreatic solutions secreted into the duodenal compartment.

The recovery (%) (mass balance) of β-carotene was calculated by the formula

$$\frac{\beta\text{-carotene}_{filtrates} + \beta\text{-carotene}_{ileal\ efflux} + \beta\text{-carotene}_{residues}}{\beta\text{-carotene}_{feeding} + \beta\text{-carotene}_{endogenous}} \times 100$$

where β-carotene$_{ileal\ efflux}$ is the β-carotene content in the total material delivered from the ileal compartment, and β-carotene$_{residues}$ is the total β-carotene in the residues of stomach, duodenum, and ileum.

The proportion of isotopic enrichment (IE) of β-carotene with [$^{13}C_{10}$]β-carotene was calculated by IE in filtrates divided by IE in feeding sample and multiplied by 100.

RESULTS

The endogenous β-carotene content of the bile and pancreatic juice used in TIM-1 was below the detection limit in all runs. There were no other sources of β-carotene than the feeding samples. The results with the mixed diet are based on triplicate experiments. The results with the oil diet are based on duplicate experiments since one experiment failed due to a defective hollow-fiber membrane unit. Because of the high recovery in both oil diet runs and similar bioaccessibilities, these duplicate runs were regarded as representative.

The bioaccessibility of β-carotene, determined by collection of all the filtrates, was 28.2 μg/100 μg β-carotene from the mixed diet and 53.4 μg/100 μg β-carotene from the oil diet (Table 2 and Figure 1). The recovery of β-carotene was 92% and 105% in the two runs with the oil diet and 88%, 94%, and 104% in the three runs with the mixed diet (Table 2).

Table 2. β-Carotene Amounts, Bioaccessibility of β-Carotene, and the Recovery of β-Carotene with the Two Diets in TIM-1 over 6 h[a]

	β-carotene in mixed diet			β-carotene in oil diet	
	run 1	run 2	run 3	run 1	run 2
feeding					
diet (μg)	498	498	498	220	220
capsule (μg)	47	47	47	47	47
endogenous (μg)	nd	nd	nd	nd	nd
filtrates					
jejunal filtrate (μg)	95.6	83.5	80.3	76.3	80.5
ileal filtrate (μg)	73.7	73.0	55.5	65.4	62.8
ileal efflux (μg)	264.2	312.0	233.6	34.8	44.9
residues					
residue of stomach and duodenum (μg)	31.7	27.4	67.9	44.0	62.9
residue of jejunum and ileum (μg)	48.2	69.7	40.1	25.8	29.7
bioaccessibility (μg β-carotene/100 μg β-carotene)[b]	31.1	28.7	24.9	53.1	53.7
recovery (%)[c]	94.2	103.8	87.6	92.3	105.2

[a]The mixed diet contained vegetables high in β-carotene, and the oil diet contained vegetables low in β-carotene supplemented with synthetic β-carotene in salad dressing oil. nd = not detected. [b]The β-carotene bioaccessibility is the amount bioaccessible β-carotene in μg per 100 μg of β-carotene available for digestion and is calculated as (μg β-carotene in filtrates)/(μg β-carotene from feeding + endogenous) × 100. [c]Recovery (%) = (β-carotene in filtrates + ileal efflux + residues)/(β-carotene from feeding + endogenous) × 100.

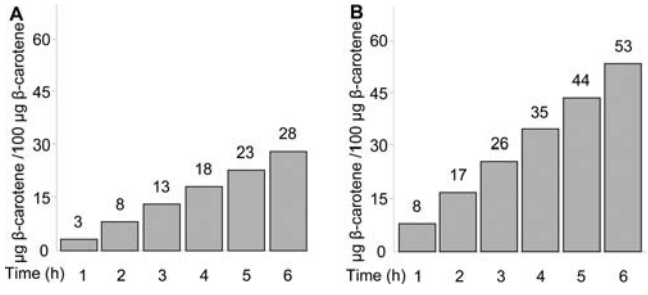

Figure 1. Cumulative β-carotene in filtrates expressed as a percentage of feeding to time after the runs (n = 3) with the mixed diet (A) and with the oil diet (B) after the runs (n = 2) in TIM-1 during 6 h.

dx.doi.org/10.1021/jf403312v | J. Agric. Food Chem. 2014, 62, 950−955

The isotopic enrichments of β-carotene in the feeding sample compared with the isotopic enrichment of β-carotene in the filtrates varied over time from 85% to 122% in the jejunal filtrates and from 79% to 139% in the ileal filtrates (Table 3).

Table 3. Proportion of Isotopic Enrichment of β-Carotene with [$^{13}C_{10}$]β-Carotene in Filtrates Compared with That of the Feeding Sample for the Two Diets in TIM-1 over 6 h

	mixed diet (%)	oil diet (%)
jejunal filtrate 0−3 h	85	106
jejunal filtrate 3−6 h	111	122
ileal filtrate 0−3 h	112	79
ileal filtrate 3−6 h	139	85
weighted average filtrate 0−6 h[a]	113	99

[a]The measured β-carotene levels in jejunal filtrates were slightly higher than in ileal filtrates (Table 2).

Averaged over 6 h, the isotopic enrichment of β-carotene in the filtrate for the oil diet was closer to the theoretical value of 100% than for the mixed diet (99% v 113%). This difference in isotopic enrichment was expected because the oil diet with supplemental β-carotene was more comparable with the matrix of labeled β-carotene in the feeding sample than was the β-carotene in vegetables in the mixed diet. In the TIM-1 run with the mixed diet, the isotopic enrichment in the jejunal filtrate was lower than in the ileal filtrate, which indicates that micellarization of labeled β-carotene in the jejunal compartment lagged behind that in the ileal compartment. In contrast, the opposite was seen in the TIM-1 run with the oil diet, where micellarization of labeled β-carotene was faster in the jejunal compartment than in the ileal compartment. The isotopic enrichment increased over time in both jejunal and ileal filtrates, which means that the labeled β-carotene was not equally distributed over time in the bioaccessible fractions. Labeled β-carotene either did not fully equilibrate with the β-carotene in the food matrix or else followed a different micellarization pattern.

DISCUSSION

This in vitro gastrointestinal model appears useful for determination of the effects of food matrices on the bioaccessibility of β-carotene from foods, especially when fat-soluble nutrients compete for uptake in mixed micelles.

Comparing the Bioaccessibilities of β-Carotene from Both Diets. The mixed diet represented a healthy diet with high amounts of cooked vegetables and fruits. The oil diet was representative of a diet low in vegetables and fruits but high in food items fortified with β-carotene, such as those regularly consumed in industrialized societies (e.g., margarine). The oil diet and the mixed diet contained β-carotene in the physiological dose range and were designed according to the guidelines of 'good nutrition' from the Dutch Nutrition Board in The Hague, The Netherlands. Both diets were typical western diets with respect to the contribution of carbohydrates, proteins, and fats to the energy intake (57%, 13%, and 30%, respectively). The β-carotene amount in the oil diet was not the same as in the mixed diet; however, this was also the situation in the in vivo study.[14] The absorption efficiency of β-carotene is regarded constant as long as the β-carotene consumption is within physiological ranges.[1,2,21] Furthermore, the mixed diet contained a higher amount of β-carotene than the oil diet but had a lower amount bioaccessible β-carotene compared to the oil diet; in contrast, the oil diet contained a lower amount of β-carotene than the mixed diet but had a higher amount bioaccessible β-carotene compared to the mixed diet.

Bioaccessibility of β-carotene was 28 μg/100 μg β-carotene (or 28%) from the mixed diet and 53 μg/100 μg β-carotene (or 53%) from the oil diet. So, the bioaccessibility of labeled and dietary β-carotene from the oil diet was 1.9-fold higher than from the mixed diet. This 1.9-fold enhancement in apparent absorption between two diets was also found in the in vivo study.[14]

Although in absolute terms results of β-carotene bioaccessibility using TIM-1 are not strictly comparable with in vivo experiments, the differences in β-carotene bioaccessibilities between food matrices are still comparable with absorption estimates in humans. Thus, TIM-1 cannot be used for predicting absorption in vivo, but the system is a useful tool for measuring differences in bioaccessibility of β-carotene between various food matrices.

Comparing the Bioaccessibilities of β-Carotene Measured Using Other Models. Bioaccessibility of β-carotene from various meals, fruits, and vegetables have been reported using other in vitro digestion models. Garrett et al.[22] developed an in vitro digestion model based on the method of Miller et al.,[23] which simulates human gastric and pancreatic digestion as static duo-compartments. Our result of 28% bioaccessibility of β-carotene from the mixed diet is slightly higher than the reported bioaccessibility of β-carotene from meals. For example, the micellarization of β-carotene was 12−18% from a baby food meal of carrots, spinach, and chicken,[22] 16% from a meal of mango and chicken,[24] 16% from stir-fried meal of spinach, carrots, and tomato paste,[25] and 18% from a salad meal of spinach, tomato, carrot, and lettuce.[26]

Several other studies have used the same in vitro method for single fruits or vegetables. From orange and kiwi, the micellarization of β-carotene was 34% and 47%, respectively.[27] From mango, the micellarization of β-carotene was 25−39%; from mango with milk and sugar, 37−48%; from papaya, 31−34%; and from papaya with milk and sugar, 41−44%.[28] The micellarization of β-carotene from carrot was 14% for carrot juice,[29] 17% from processed carrots,[30] 20% from raw carrots,[31] and 33% from stir-fried carrots.[31] From other vegetables, the micellarization of β-carotene was 17% from maize,[32] 17% from boiled spinach,[29] 30% from spinach puree,[33] 30% from spinach,[27] 29% from tomatoes,[34] 30% from boiled cassava,[35,36] 45% from sweet potato,[27] 54% from broccoli,[27] and 57% from courgette.[34] Our result of 28% is comparable to these as our study included a mix of different cooked vegetables and fruits.

Hedrén et al.[37] developed a similar static duo-compartmental in vitro model, which estimates the maximum amount of carotenoids released, but not necessarily micellarized. Using this other in vitro model, the percentages of accessible β-carotene in homogenized, raw carrots were 21% and 30% and from cooked carrots were 27% and 39%, without and with addition of oil, respectively.[37] Another study by Hedrén et al.[38] showed accessible β-carotene was 39% from sweet potato, 64% from pumpkin, and 47% from cassava, which were all cooked with sunflower oil. Three other studies with this method showed a bioaccessibility of β-carotene of 19% from boiled pumpkin,[39] 74% from boiled carrot,[39] and when cooked with vegetable oil, 11−22% from various processed sweet potato,[40] 21% from sweet potato, and 39% from pumpkin.[41] Our results of 28% and 53% are also comparable with the results from this in vitro method.

dx.doi.org/10.1021/jf403312v | J. Agric. Food Chem. 2014, 62, 950−955

Although these other models are temperature- and pH-controlled, they are not representative of the continuously changing variables during passage through the stomach and the small intestine. For general prediction of micellarization of β-carotene, these models are adequate. However, TIM-1 allows for the closest simulation to date of in vivo dynamic physiological processes occurring within the lumen of the stomach, duodenum, jejunum, and ileum of humans. Furthermore, TIM-1 has as major advantage that the model allows for the collection of samples during the process of digestion without disturbing or temporarily stopping the experiment and thereby allows studying the digestion process in time.

Extrinsic Labeled β-Carotene vs Time of Both Diets. When using any extrinsic labeling technique in absorption studies, the assumption must be made that the label fully mixes with the compound and equally distributes in the lumen of the small intestine. This means that in each time period of the digestion process, the isotopic enrichment of β-carotene in the filtrates should be the same as in the diet. However, during the 6 h of the TIM-1 experiment, the isotopic enrichments of β-carotene in the ileal filtrate in mixed diet runs increased and in oil diet runs decreased compared with the jejunal filtrate, which indicates discrimination for micellarization. This enrichment pattern can be explained by retarded equilibration in the mixed diet run, where the labeled β-carotene is bound and captured by the complex matrix and available later in time for digestion than in the oil diet. The isotopic enrichment of β-carotene with [$^{13}C_{10}$]β-carotene in filtrates was not constant over time. This implies that the labeled β-carotene behaved differently from the β-carotene incorporated into the matrices of vegetables and fruits high in β-carotene and behaved differently from the matrix of supplemental β-carotene in oil. The labeled β-carotene dissolved in oil was not equally distributed over time in the bioaccessible fractions, which means that during the experiment, it did not fully mix with dietary β-carotene. As suggested by the average filtrate over 6 h for the oil diet, which was 99%, the extrinsic labeling technique could be used to measure absorption in vivo if the matrix of the homogenized diet were comparable with the oily matrix of extrinsic labeled β-carotene. However, the different isotopic enrichments of β-carotene in the ileal filtrate and jejunal filtrate in the oil diet suggested different micellarization patterns for dietary β-carotene in oil and labeled β-carotene in oil.

Additional experiments are required to confirm and explain this result, which may be influenced by dissolving of the capsule, and to investigate the reproducibility of the measured isotopic enrichments in these samples with very low amounts of labeled and unlabeled β-carotene.

The advantage of this TIM-1 dynamic model is that it can address mixing effects and partitioning effects of labeled fat-soluble compounds during the digestion process. Therefore, this in vitro model could provide significant value for checking assumptions in distribution of labeled compounds in in vivo labeling studies.

In summary, the food matrix effects on bioaccessibility of β-carotene could be measured using TIM-1 and were consistent with in vivo data. The labeled β-carotene either did not fully equilibrate with the β-carotene in the food matrix or else followed a different micellarization pattern. The application of extrinsically labeled β-carotene was not confirmed.

AUTHOR INFORMATION

Corresponding Author

*Tel: +31 630345010. E-mail: Carolien.VanLooBouwman@hotmail.com.

Funding

We acknowledge grant support from the Dutch Dairy Association and from the National Institutes of Health in the United States (R01 CA101052).

Notes

The authors declare no competing financial interest.

ACKNOWLEDGMENTS

We thank Hans Kooijman at TNO for performing the runs in TIM-1 and Tineke van Roekel-Jansen at Wageningen University for performing many analyses.

REFERENCES

(1) U.S. Institute of Medicine. *Dietary reference intakes for vitamin A, vitamin K, arsenic, boron, chromium, copper, iodine, iron, manganese, molybdenum, nickel, silicon, vanadium, and zinc*; National Academy Press: Washington, DC. 2001; pp 82−161.

(2) Food and Agriculture Organization /World Health Organization Joint Expert Consultation. *Vitamin and mineral requirements in human nutrition*, 2nd ed.; WHO Press: Geneva. 2004; pp 17−44.

(3) van het Hof, K.; West, C. E.; Weststrate, J. A.; Hautvast, J. G. Dietary factors that affect the bioavailability of carotenoids. *J. Nutr.* **2000**, *130*, 503−506.

(4) Veda, S.; Platel, K.; Srinivasan, K. Enhanced bioaccessibility of β-carotene from yellow-orange vegetables and green leafy vegetables by domestic heat processing. *Int. J. Food Sci. Technol.* **2010**, *45*, 2201−2207.

(5) Minekus, M. *Development and validation of a dynamic model of the gastrointestinal tract*. Doctoral thesis, University of Utrecht, Utrecht, the Netherlands. May 28, 1998; pp 1−174.

(6) Minekus, M.; Marteau, P.; Havenaar, R.; Huis in 't Veld, J. H. J. A multicompartmental dynamic computer-controlled model simulating the stomach and small intestine. *ATLA, Altern. Lab. Anim.* **1995**, *23*, 197−209.

(7) Minekus, M.; Lelieveld, J.; van den Berg, H. A dynamic model of the stomach and small intestine to study the bio-accessibility of carotenoids from vegetables and the effect of processing. In *Abstracts of the Bioavailability Congress, Interlaken, Switzerland, 2001*; pp 111.

(8) Minekus, M.; Jelier, M.; Xiao, J.-Z.; Kondo, S.; Iwatsuki, K.; Kokubo, S.; Bos, M.; Dunnewind, B.; Havenaar, R. Effect of partially hydrolyzed guar gum (PHGG) on the bioaccessibility of fat and cholesterol. *Biosci. Biotechnol. Biochem.* **2005**, *69*, 932−938.

(9) Gervais, R.; Gagnon, F.; Kheadr, E. E.; Van Calsteren, R.-M.; Farnworth, E. R.; Fliss, I.; Chouinard, P. Y. Bioaccessibility of fatty acids from conjugated linoleic acid-enriched milk and milk emulsions studied in a dynamic in vitro gastrointestinal model. *Int. Dairy J.* **2009**, *19*, 574−581.

(10) Arkbåge, K.; Verwei, M.; Havenaar, R.; Witthoft, C. Bioaccessibility of folic acid and (6S)-5-methyltetrahydrofolate decreases after addition of folate-binding protein to yogurt as studied in a dynamic in vitro gastrointestinal model. *J. Nutr.* **2003**, *133*, 3678−3683.

(11) Verwei, M.; Freidig, A. P.; Havenaar, R.; Groten, J. P. Predicted serum folate concentrations based on in vitro studies and kinetic modeling are consistent with measured folate concentrations in humans. *J. Nutr.* **2006**, *136*, 3074−3078.

(12) Deat, E.; Blanquet-Diot, S.; Jarrige, J.-F.; Denis, S.; Beyssac, E.; Alric, M. Combining the dynamic TNO-gastrointestinal tract system with a Caco-2 cell culture model: Application to the assessment of lycopene and α-tocopherol bioavailability from a whole food. *J. Agric. Food Chem.* **2009**, *57*, 11314−11320.

(13) Richelle, M.; Sanchez, B.; Tavazzi, I.; Lambelet, P.; Bortlik, K.; Williamson, G. Lycopene isomerisation takes place within enterocytes during absorption in human subjects. *Br. J. Nutr.* **2010**, *103*, 1800−1807.
(14) Van Loo-Bouwman, C. A.; Naber, T. H. J.; van Breemen, R. B.; Zhu, D.; Dicke, H.; Siebelink, E.; Hulshof, P. J. M.; Russel, F. G. M.; Schaafsma, G.; West, C. E. Vitamin A equivalency and apparent absorption of β-carotene in ileostomy subjects using a dual-isotope dilution technique. *Br. J. Nutr.* **2010**, *103*, 1836−1843.
(15) Verwei, M.; Arkbage, K.; Havenaar, R.; van den Berg, H.; Withoft, C.; Schaafsma, G. Folic acid and 5-methyltetrahydrofolate in fortified milk are bioaccessible as determined in a dynamic in vitro gastrointestinal model. *J. Nutr.* **2003**, *133*, 2377−2383.
(16) Broekmans, W. M. R.; Berendschot, T. T. J. M.; Klöpping-Ketelaars, I. A. A.; de Vries, A. J.; Goldbohm, R. A.; Tijburg, L. B. M.; Kardinaal, A. F. M.; van Poppel, G. Macular pigment density in relation to serum and adipose tissue concentrations of lutein and serum concentrations of zeaxanthin. *Am. J. Clin. Nutr.* **2002**, *76*, 595−603.
(17) Khan, N. C.; West, C. E.; de Pee, S.; Bosch, D.; Phuong, H. D.; Hulshof, P. J. M.; Khoi, H. H.; Verhoef, H.; Hautvast, J. G. A. J. The contribution of plant foods to the vitamin A supply of lactating women in Vietnam: a randomized controlled trial. *Am. J. Clin. Nutr.* **2007**, *85*, 1112−1120.
(18) Lugtenburg, J.; Creemers, A. F. L.; Verhoeven, M. A.; van Wijk, A. A. C.; Verdegem, P. J. E.; Monnee, M. C. F.; Jansen, F. J. H. M. Synthesis of ^{13}C labeled carotenoids and retinoids. *Pure Appl. Chem.* **1999**, *71*, 2245−2251.
(19) van Breemen, R. B.; Nikolic, D.; Xu, X.; Xiong, Y.; van Lieshout, M.; West, C. E.; Schilling, A. B. Development of a method for quantification of retinol and retinyl palmitate in human serum using high-performance liquid chromatography-atmospheric pressure chemical ionization-mass spectrometry. *J. Chromatogr. A* **1998**, *794*, 245−251.
(20) Zhu, D.; Wang, Y.; Pang, Y.; Liu, A.; Guo, J.; Bouwman, C. A.; West, C. E.; van Breemen, R. B. Quantitative analyses of β-carotene and retinol in serum and feces in support of clinical bioavailability studies. *Rapid Commun. Mass. Spectrom.* **2006**, *20*, 2427−2432.
(21) Food and Agriculture Organization /World Health Organization. Requirements of vitamin A, iron, folate and vitamin B_{12}. FAO/WHO Joint Expert Consultation. *FAO Food and Nutrition Series*, no. 23; FAO: Rome, 1988; pp 16−32.
(22) Garrett, D. A.; Failla, M. L.; Sarama, R. J. Development of an in vitro digestion method to assess carotenoid bioavailability from meals. *J. Agric. Food Chem.* **1999**, *47*, 4301−4309.
(23) Miller, D. D.; Schricker, B. R.; Rasmussen, R. R.; van Campen, D. An in vitro method for estimation of iron availability from meals. *Am. J. Clin. Nutr.* **1981**, *34*, 2248−2256.
(24) Ornalas-Paz, J.; De, J.; Failla, M. L.; Yahia, E. M.; Gardea-Bejar, A. Impact of the stage of ripening and dietary fat on in vitro bioaccessibility of β-carotene in 'Ataulfo' mango. *J. Agric. Food Chem.* **2008**, *56*, 1511−1516.
(25) Garrett, D. A.; Failla, M. L.; Sarama, R. J. Estimation of carotenoid bioavailability from fresh stir-fried vegetables using an in vitro digestion/caco-2 cell culture model. *J. Nutr.* **2000**, *11*, 574−580.
(26) Huo, T.; Ferruzzi, M. G.; Schwartz, S. J.; Failla, M. L. Impact of fatty acyl composition and quantity of triglycerides on bioaccessibility of dietary carotenoids. *J. Agric. Food Chem.* **2007**, *55*, 8950−8957.
(27) O'Connell, O. F.; Ryan, L.; O'Brien, N. M. Xanthophyll carotenoids are more bioaccessible from fruits than dark green vegetables. *Nutr. Res.* **2007**, *27*, 258−264.
(28) Veda, S.; Platel, K.; Srinivasan, K. Varietal differences in the bioaccessibility of β-carotene from mango (*Mangifera indica*) and papaya (*Carica papaya*) fruits. *J. Agric. Food Chem.* **2007**, *55*, 7931−7935.
(29) Reboul, E.; Richelle, M.; Perrot, E.; Desmoulins-Malezet, C.; Pirisi, V.; Borel, P. Bioaccessibility of carotenoids and vitamin E from their main dietary sources. *J. Agric. Food Chem.* **2006**, *54*, 8749−8755.
(30) Failla, M. L.; Thakkar, S. K.; Kim, J. Y. In vitro bioaccessibility of β-carotene in orange fleshed sweet potato (*Ipomoea batatas, Lam.*). *J. Agric. Food Chem.* **2009**, *57*, 10922−10927.
(31) Veda, S.; Kamath, A.; Platel, K.; Begum, K.; Srinivasan, K. Determination of bioaccessibility of β-carotene in vegetables by in vitro methods. *Mol. Nutr. Food Res.* **2006**, *50*, 1047−1052.
(32) Thakkar, S. K.; Failla, M. L. Bioaccessibility of pro-vitamin A carotenoids is minimally affected by non pro-vitamin A xanthophylls in maize (*Zea mays sp.*). *J. Agric. Food Chem.* **2008**, *56*, 11441−11446.
(33) Ferruzzi, M. G.; Failla, M. L.; Schwartz, S. J. Assessment of degradation and intestinal cell uptake of carotenoids and chlorophyll derivatives from spinach puree using an in vitro digestion and Caco-2 human cell model. *J. Agric. Food Chem.* **2001**, *49*, 2082−2089.
(34) Ryan, L.; O'Connell, O.; O'Sullivan, L.; Aherne, S. A.; O'Brien, N. M. Micellarisation of carotenoids from raw and cooked vegetables. *Plant Foods Hum. Nutr.* **2008**, *63*, 127−133.
(35) Thakkar, S. K.; Maziya-Dixon, B.; Dixon, A. G. O.; Failla, M. L. β-Carotene micellarization during in vitro digestion and uptake by caco-2 cells is directly proportional to β-carotene content in different genotypes of cassava. *J. Nutr.* **2007**, *137*, 2229−2233.
(36) Thakkar, S. K.; Huo, T.; Maziya-Dixon, B.; Failla, M. L. Impact of style of processing on retention and bioaccessibility of β-carotene in cassava (*Manihot esculanta, Crantz*). *J. Agric. Food Chem.* **2009**, *57*, 1344−1348.
(37) Hedrén, E.; Diaz, V.; Svanberg, U. Estimation of carotenoid accessibility from carrots determined by an in vitro digestion method. *Eur. J. Clin. Nutr.* **2002**, *56*, 425−430.
(38) Hedrén, E.; Mulokozi, G.; Scanberg, U. In vitro accessibility of carotenes from green leafy vegetables cooked with sunflower oil or red palm oil. *Int. J. Food Sci. Nutr.* **2002**, *53*, 445−453.
(39) Priyadarshani, A. M. B.; Chandrika, U. G. Content and in-vitro accessibility of pro-vitamin A carotenoids from Sri Lankan cooked non-leafy vegetables and their estimated contribution to vitamin A requirements. *Int. J. Food Sci. Nutr.* **2007**, *58*, 659−667.
(40) Bengtsson, A.; Alminger, M. L.; Svanberg, U. In vitro bioaccessibility of β-carotene from heat-processed orange-fleshed sweet potato. *J. Agric. Food Chem.* **2009**, *57*, 9693−9698.
(41) Mulokozi, G.; Hedren, E.; Svanberg, U. In vitro accessibility and intake of β-carotene from cooked green leafy vegetables and their estimated contribution to vitamin A requirements. *Plant Foods Hum. Nutr.* **2004**, *59*, 1−9.

mobilization, are synthesized only after seed germination,[24,25] revealing that P34 may possess different biological activity. Structurally, the thiol proteases of the papain family possessed highly conserved catalytic triad (Cys-His-Asn) residues and three disulfide bonds.[26] Compared with these thiol proteases, a Gly37 replaced the highly conserved catalytic Cys in P34; of the three disulfides, two were present in P34 (Cys68-Cys108 and Cys171-Cys224). However, one of the three disulfides in other thiol proteases existed as Cys34 and Asn77 in P34, so it was suggested that the Cys34 near Gly37 should be a free thiol and act as the active-site residue.[23,24] Until now, only one protein was reported to be similar to P34, which was a 31 kDa thiol protease (SPE31) isolated from the seeds of a legume plant (*Pachyrizhus erosus*), and they were considered to form a unique subfamily within the papain family.[27] However, the substrates of P34 and SPE31 were not clear yet.

Several members of the papain protease family have been reported in allergenic reaction, such as fecal dust mite allergen Der 1p[28] and archtype papain thiol protease.[29] And it was considered that the destructive proteolytic activity of these thiol proteases might be a significant factor in the allergenicity.[30] Bd 30K (257 AARs), an allergenic soybean protein, was first identified by Ogawa et al., and considered as similar protein to P34 owing to their identical N-terminal amino acid sequences and amino acid compositions.[31,32] However, the Arg46, Ser75, Gln80, and Phe203 of P34 were replaced by the Ser46, Cys75, His80, and Glu203 of Bd 30K (NCBI database). Two studies reported that there were two spots for P34 and Bd 30K on the two-dimensional electrophoresis gel,[30,33] revealing that P34 and Bd 30K might be two different proteins with similar biological activities. Many studies reported that P34/Bd 30K had high specificity to interact with soybean OBs,[5,12,22−24,34] very similar to the interaction between protease and its substrate. The interaction between P34/Bd 30K and soybean OBs was clarified as the disulfide bond between P34/Bd 30K and 24 kDa oleosin.[5]

In fact, the best way to confirm one protease is directly mixing it with its substrate. Sewekow et al. reported a method for the purification of P34 by hydrophobic interaction chromatography, and a key buffer of 0.1 M sodium carbonate (pH > 11.0) was used.[35] Ogawa et al. reported a method for the purification of Bd 30K, and sodium dodecylsulfate (SDS, 4%) and heat treatment (98 °C, 10 min) were used.[32] According to the present study, P34 and Bd 30K (assumed as the proteases) are already denatured at pH 11.0 and also denatured when exposed to SDS and/or high temperature. It is considered that a method for bioactive P34/Bd 30K purification is a great challenge at the present stage. In this study, some properties (specificity, optimal pH, and temperature) of the proteases of 24 and 18 kDa oleosins, and oleosin hydrolysis in soybean germination were examined, and the high relationship between the proteases and P34/Bd 30K was also discussed. It is considered that this study is very meaningful for designing better processing methods for the soybean OB extraction and the enzyme-assisted aqueous extraction of soybean oil.

MATERIALS AND METHODS

Materials. Soybean Nannong 88−31 (moisture content, 9%), harvested in August, 2011, was used. It was stored at 4 °C until use. This study was conducted from March, 2012 to June, 2013, and the behaviors of oleosin hydrolysis were consistent in this period. One study reported that the structure of glycinin, which was purified from soybean stored at 4 °C for 18 months, did not show significant changes compared to the purified glycinin from soybean stored in a −20 °C freezer.[36] These showed that the data in the study should be acceptable. All reagents were purchased from Sigma-Aldrich Trading Co., Ltd. or of analytical reagent grade. Precision Plus Protein All Blue (Bio-Rad, USA), including 250, 150, 100, 75, 50, 37, 25, 15, and 10 kDa proteins, was used as the protein marker.

Raw Soymilk Preparation. Soybean (20 g) was soaked in deionized (DI) water at 4 °C for 18 h. The soaking water was poured off, and the soaked soybeans were washed with fresh DI water three times. DI water, precooled in 4 °C refrigerator, was added to make the total weight of 200 g. This mixture was ground in a Waring blender (18 000 rpm, MJ-60BE01B, Midea) for 2 min and filtered through four layers of gauze to obtain raw soymilk (about pH 6.8).

Oil Bodies (OBs) Extracted by pH 6.8, 8.0, 9.5, and 11.0 at 4 °C. This was conducted with the method by Chen and Ono[34] with the modification that the temperature was controlled at 4 °C. Sucrose was added into raw soymilk to make the concentration of 20% (w/w) and mixed well in 4 °C refrigerator. A total of 40 g of raw soymilk (20% sucrose) was added into the first centrifuge tube. The residual raw soymilk was adjusted to pH 8.0 by 2 M NaOH, and 40 g was added into the second centrifuge tube. The residual raw soymilk was adjusted to pH 9.5, and 40 g was added into the third centrifuge tube. The residual raw soymilk was adjusted to pH 11.0, and 40 g was added into the fourth centrifuge tube. Then they were treated by centrifugation (25,000*g*, 30 min; 4 °C). The supernatant of pH 6.8 system was collected (termed pH 6.8 supernatant), stored in 4 °C refrigerator and used for the experiment below. The floating fractions were collected, dispersed into 39 g of sucrose solution (20%, w/w), and adjusted to corresponding pH, respectively. They were mixed well and treated by centrifugation (25,000*g*, 30 min; 4 °C). Then the collection of floating fraction, dispersion into sucrose solution (20%, w/w), pH adjustment, and centrifugation as above was repeated twice. The floating fractions obtained were dispersed into DI water with oil concentrations of 40 mg/mL. The four suspensions were all adjusted to pH 6.5. Each suspension (7 mL) was incubated in 35 °C water bath for 0, 0.5, 1, 3, 6, and 9 h, and 1 mL of suspension was collected and cooled in one ice water bath, respectively. The obtained OB suspensions (1 mL) were defatted by diethyl ether with the method by Tzen et al.[37] Briefly, three milliliters of diethyl ether (4 °C) was added, thoroughly mixed for 30 min and centrifuged (15,000*g*, 5 min; 4 °C). The upper diethyl ether was removed, and the procedure was repeated one more time. The residual diethyl ether was allowed to evaporate in a hood combined with fan blowing, which was conducted in ice water bath. The residual aqueous solution was well mixed. The protein concentration of pH 6.8 extracted OBs was determined by the micro-Kjeldahl method, and 0.5 mL of the defatted sample (well mixed) was diluted with Tricine-SDS-PAGE sample buffer to make the protein concentration of 2 mg/mL. The other three defatted samples (pH 8.0, 9.5 and 11.0), which had lower protein concentrations, were mixed with the same volume of sample buffer above. This method, different from the traditional method, was beneficial for examining the protein release behaviors from OBs.

Effect of pH 6.8 Supernatant on pH 11.0 Extracted OBs. A total of 7 mL of the pH 11.0 extracted OB suspension (pH 6.5, 4 °C) was added into 30 mL of pH 6.8 supernatant obtained above. They were stirred in ice water bath for 30 min and centrifuged (25,000*g*, 30 min; 4 °C). The floating fraction was carefully collected and dispersed well into 7 mL of DI water, and stored in 4 °C refrigerator (termed the first OBs). The supernatant was collected carefully with syringe and mixed in ice water bath for 30 min with another 7 mL of fresh pH 11.0 extracted OB suspension. It was treated by centrifugation (25,000*g*, 30 min; 4 °C). Then the collection of supernatant fraction, and its mixing with 7 mL of fresh pH 11.0 extracted OB suspension followed by centrifugation was repeated three more times, and floating fraction (OBs) and supernatant (termed the fifth supernatant) were obtained by the last centrifugation. The floating fraction was dispersed into 7 mL of DI water (4 °C) and termed the fifth OBs. The protein concentrations of the fifth supernatant and pH 6.8 supernatant were determined by bicinchoninic acid assay with bovine serum albumin as standard, and diluted with SDS-PAGE sample buffer to make the

concentrations of 20 mg/mL. The first and fifth OBs were incubated in 35 °C water bath for 0, 0.5, 1, 3, 6, and 9 h, and 1 mL of suspension was collected and cooled in an ice water bath. Then they were treated as above for Tricine-SDS-PAGE analysis.

Soybean Germination. In order to simulate the natural soybean germination, 20 g of soybeans was washed and soaked in tap water for 9 h at room temperature. A food-grade plastic container, without cover, was used for the soybean germination, and there were many holes on its bottom and walls. The tap water was poured off, and the soybeans were uniformly placed on the container bottom. The boiled tap water (room temperature) was sprayed on the soybean for about 2 min, and a preservative film (with artificially small holes) was used to cover the container for germination (1, 2, 4, 6, and 8 days). Everyday the soybeans was sprayed with boiled tap water (room temperature) four times (at 8:00, 12:00, 16:00, and 20:00). In the soybean germination, the room temperature was within the range of 21−33 °C. DI water, precooled in 4 °C refrigerator, was added into the germinated soybeans to make total weight of 200 g. It was ground for 2 min and filtered through four layers of gauze to obtain raw germinated soymilk. Sucrose was added into raw germinated soymilk to make a concentration of 25% (w/w) and mixed well. Raw germinated soymilk (6.5 mL; 25% sucrose, w/w) was added into the first ultracentrifuge tube. The residual raw germinated soymilk was adjusted to pH 8.0, and 6.5 mL was added into the second ultracentrifuge tube. The residual was adjusted to pH 9.5, and 6.5 mL was added into the third ultracentrifuge tube. The three tubes were all preplaced in the ice water bath. Then 3 mL of 20% (w/w) sucrose solution was carefully layered on the top of the raw germinated soymilk in the three tubes. These were treated by ultracentrifugation (197,000*g*, 1 h; 4 °C), and solid OB pad was formed on the top of 20% sucrose solution. The OB pad was carefully taken out and rinsed by DI water (4 °C). The residual DI water was carefully absorbed by filter paper. The OB pad was weighed, and 5-fold of DI water (4 °C) was added to disperse it well. Then it was defatted as above. The protein concentration of the defatted sample (pH 6.8 extracted OBs from 1 d germinated soybean) was determined by the micro-Kjeldahl method, and 0.5 mL of the defatted sample was diluted with Tricine-SDS-PAGE sample buffer to make the protein concentration of 2 mg/mL. The other defatted samples (pH 8.0, pH 9.5; 2, 4, 6, and 8 d germinated soybean), which had lower protein concentrations, were all diluted with the same volume of sample buffer above and used for Tricine-SDS-PAGE analysis.

Effects of Temperature and pH on Oleosin Hydrolysis. pH 6.8 extracted OB suspension (pH 6.5), without repeated washing as above, was used to examine the effect of temperature on oleosin hydrolysis. A total of 15 mL of suspension was incubated in 20, 30, 35, 40, 50, and 60 °C water baths, respectively. After 0, 0.5, 1, 3, 6, and 9 h, 1 mL of suspension was collected and cooled in ice water bath. In addition, 15 mL of pH 6.8 extracted OB suspension was respectively adjusted to pH 4.0, 5.0, 6.0, 6.5, 7.0, 8.0, 9.0, 10.0, and 11.0, and all incubated in 35 °C water bath. After 0, 0.5, 1, 3, 6, and 9 h, 1 mL of suspension was collected and cooled in ice water bath. The obtained OB suspensions (1 mL) were treated as above for Tricine-SDS-PAGE analysis. These experiments were conducted two times and showed the same trend.

SDS-PAGE. SDS-PAGE was conducted with the method by Laemmli with the concentrations of the stacking and separating gels being 5% and 12.5%, respectively.[38] 2-Mercaptoethanol was added into the samples (pH 6.8 supernatant and the fifth supernatant) to the concentration of 2% (v/v) and heated for 3 min in a boiling water bath. Then 10 μL of each sample was loaded into a sample well. SDS-PAGE was performed at 15 mA for about 2 h. The gel was stained by using Coomassie Brilliant Blue G-250.

Tricine-SDS-PAGE. Tricine-SDS-PAGE was conducted according to the method by Schagger.[39] The concentrations of stacking and separating gels were 4% and 16%, respectively. 2-Mercaptoethanol (no 2-mercaptoethanol for nonreducing Tricine-SDS-PAGE) was added into the samples above to the concentration of 2% (v/v), and samples were heated for 3 min in a boiling water bath. Then 20 μL of each sample was loaded into a sample well, and the samples were electrophoresed at constant voltage of 30 mV until all samples entered into the stacking gel and then at constant voltage of 100 mV until end. The gel was stained using Coomassie Brilliant Blue G-250.

Two-Dimensional Electrophoresis. The pH 6.8 and 8.0 extracted OB suspensions obtained without strict temperature control were desalted by dialysis against DI water (4 °C) and lyophilized. The lyophilized OBs were extracted with acetone at 4 °C. After stirred for 30 min, the homogenate was filtered through one layer of filter paper, and the protein fraction was recovered. This was repeated two more times to remove neutral lipids. Then it was further defatted by chloroform/methanol (2/1, v/v) three times. Finally, the protein obtained was placed in the hood to allow the organic solvent evaporated.

The two-dimensional electrophoresis was performed according to the Bio-Rad manufacturer's instructions. One hundred and fifty micrograms of protein obtained above was thoroughly dissolved in 125 μL of 2-D electrophoresis sample preparation solution (7 M urea, 2 M thiourea, 2% (w/v) CHAPS, 75 mM DTT, 0.2% (w/v) ampholyte 3−10, 0.001% bromophenol blue), assisted by vortexing and ultrasonic treatment. It was loaded onto a linear IPG gel strip (pH 3−10, 7 cm, Bio-Rad, USA) and allowed to hydrate for 16 h at 20 °C. The first dimensional isoelectric focusing (IEF) was conducted at 40 kVh using Protean IEF Cell (Bio-Rad Laboratories). After IEF, the IPG strip was reduced and alkylated with DTT (20 mg/mL) and iodoacetamide (25 mg/mL) in equilibration buffer (6 M urea, 2% (w/v) SDS, 0.375 M Tris-HCl, pH 8.8 and 20% (w/v) glycerol) for 15 min. After rinsed by SDS-PAGE electrode buffer, it was transferred onto the SDS-PAGE separating gel, covered with low melting point agarose and subjected to the second dimensional SDS-PAGE. The gel was stained by Coomassie Brilliant Blue G-250.

MALDI-TOF/TOF MS. The protein spots were excised from the Coomassie Brilliant Blue G-250 stained gel, washed in distilled water, and destained completely in a 30% acetonitrile (v/v) containing 100 mM NH_4HCO_3. After a 100% acetonitrile washing, the destained gel piece was placed into reducing solution (10 μL of 100 mM DTT, 90 μL of 100 mM NH_4HCO_3) for 30 min at 56 °C. After a 100% acetonitrile washing, 70 μL of 100 mM NH_4HCO_3 and 30 μL of 200 mM iodoacetic acid were added and incubated for 20 min in dark. After a 100% acetonitrile washing again, 5 μL (10 μg/mL) of trypsin (Promega, V5111) was added and put into 4 °C refrigerator for 30 min. Then 25 mM NH_4HCO_3 solution was added. The peptides were generated after 20 h incubation at 37 °C. The solution containing peptides was collected and concentrated at 30 °C to get dry powder. A total of 3 μL of 0.1% trifluoroacetic acid (v/v) was used to dissolve dry powder. In the final step before MALDI-TOF/TOF analysis, the sample was prepared by mixing 0.7 μL of the sample and 0.7 μL of 4-hydroxy-α-cyanocinnamic acid (matrix) on a MALDI target and air-dried. All mass spectra were obtained with an ultrafleXtreme MALDI-TOF/TOF (Bruker Daltonics, Germany) and were analyzed by flexAnalysis software provided by Bruker Daltonics Corp. Protein identification was performed by searching plant proteins in the latest version of the NCBInr database.

RESULTS AND DISCUSSION

Oleosin Hydrolysis of pH 6.8 Extracted OBs. The pH 6.8 extracted OB suspension (pH 6.5) was incubated in a 35 °C water bath for 0, 0.5, 1, 3, 6, and 9 h. Figure 1 reveals that 24 kDa oleosin shows an apparent molecular weight (MW) of 24 kDa, 18 kDa oleosin shows an apparent MW of 16 kDa, and 16 kDa oleosins (two bands) show apparent MWs of 13−14 kDa on Tricine-SDS-PAGE gel. The bands of 24 and 18 kDa oleosins gradually became weak with increasing incubation time, while the bands of lipoxygenase, β-conglycinin, γ-conglycinin, β-amylase, glycinin, Bd 30K, and P34 did not change. The band of 16 kDa oleosin 1 gradually became dense with increasing incubation time and merged with the band of 16 kDa oleosin 2. Band 1 already appeared in the freshly extracted OBs, gradually became dense before 3 h, and became

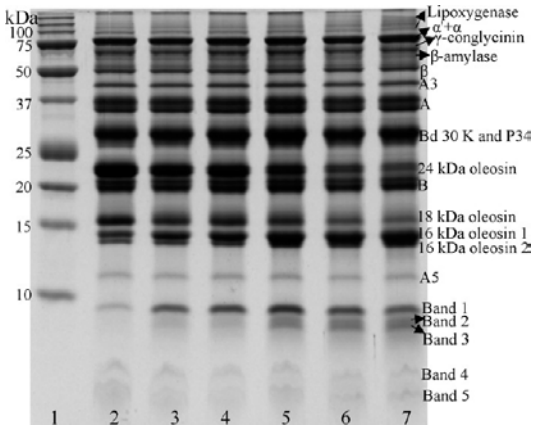

Figure 1. 24 and 18 kDa oleosin hydrolysis in the pH 6.8 extracted OB suspension (pH 6.5) incubated at 35 °C. Lane 1, marker; lanes 2−7, OB suspension incubated for 0, 0.5, 1, 3, 6, and 9 h, respectively. α', α, and β are the subunits of β-conglycinin; A3, A, and A5 are acidic polypeptides of glycinin; and B is the basic polypeptides of glycinin.

weak after 3 h. Bands 2 and 3 weakly appeared after 0.5−1 h and gradually became dense after 1 h. Bands 4−5 already appeared in the freshly extracted OBs (similar to band 1) and did not show a clear trend with increasing incubation time. The total intensities of 24, 16, and 13−14 kDa band and bands 1−5 on lanes 2−7 were analyzed by Image Lab Software (Bio-Rad, USA), and they were almost the same; 13−14 kDa band on lane 7 was matched to 24 kDa oleosins (P29530 and P29531), 18 kDa oleosin (C3VHQ8), and 16 kDa oleosins (C6SZ13 and gil35657640) by MALDI-TOF/TOF MS. The apparent MWs of bands 1−3 and bands 4−5 were respectively determined as around 9 and 3−4 kDa by Image Lab Software with the standard on lane 1, indicating that bands 1−3 should be the small hydrolyzed products of 24 kDa oleosins (P29530 and P29531), while bands 4−5 might be the small hydrolyzed products of 18 kDa oleosin (C3VHQ8). Different from bands 1−3, bands 4−5 did not show a clear trend with increasing incubation time, and it was considered that this should result from the smaller MWs of bands 4−5, which were highly possible to be removed in the gel treatment (fixing, staining and destaining). These results clearly showed: (1) the proteases, which had high specificities for 24 and 18 kDa oleosins, were existed in the pH 6.8 extracted OBs; (2) the proteases did not hydrolyze the extrinsic proteins and also were unlikely to hydrolyze 16 kDa oleosins 1 and 2; (3) the large hydrolyzed products of 24 and 18 kDa oleosins contributed to the 13−14 kDa band by the incubation of pH 6.8 extracted OB suspension (pH 6.5); (4) bands 1−3 (around 9 kDa) should be the small hydrolyzed products of 24 kDa oleosin, while bands 4−5 might be the small hydrolyzed products of 18 kDa oleosin; (5) the proteases should cleave specific peptide bonds of 24 and 18 kDa oleosins to form limited hydrolyzed products (13−14 kDa band and bands 1−5, Figure 1).

The results above showed that the proteases of 24 and 18 kDa oleosins exactly existed of the pH 6.8 extracted OBs, which contained many OB extrinsic proteins as well as OB intrinsic proteins. On one hand, it was very hard to consider that lipoxygenase (enzyme for lipid), β-conglycinin (storage protein), γ-conglycinin (storage protein), β-amylase (enzyme for amylose), and glycinin (storage protein) could hydrolyze oleosins. On the other hand, it was reported that oleosin could act as a bifunctional enzyme that had both monoacylglycerol acyltrasferase and phospholipase activities,[40] caleosin could act as peroxygenase to produce peroxidized polyunsaturated fatty acids,[41] and steroleosin, also named as sterol dehydrogenase, could dehydrogenate phytosterol into its ketone-containing derivative,[42] indicating that OB intrinsic proteins had enzymatic activities on different lipid species, but not on protein. Therefore, it was considered that P34 and Bd 30K (or some Tricine-SDS-PAGE undetectable proteins) might be the proteases of 24 and 18 kDa oleosins.

Effect of pH 6.8 Supernatant on pH 11.0 Extracted OBs. It was highly possible that the proteases were the OB extrinsic proteins. As stated above, pH 6.8 extracted OBs were obtained as a floating fraction from raw soymilk by centrifugation. It was considered that some of the proteases might still remain in the pH 6.8 supernatant. In addition, it was reported that soybean OBs without extrinsic proteins could be obtained by pH 11.0 extraction. Therefore, an experiment was designed to eliminate the possibility that OB intrinsic proteins, lipoxygenase, β-conglycinin, γ-conglycinin, β-amylase, and glycinin could hydrolyze 24 and 18 kDa oleosins. The protein in 30 mL of pH 6.8 supernatant was absorbed by the pH 11.0 extracted OB suspension (pH 6.5, 4 °C) five times (7 mL each time), and the first and fifth OBs were obtained.

Figure 2 shows the protein compositions of the pH 6.8 supernatant (lane 2) and the fifth supernatant (lane 3). For the

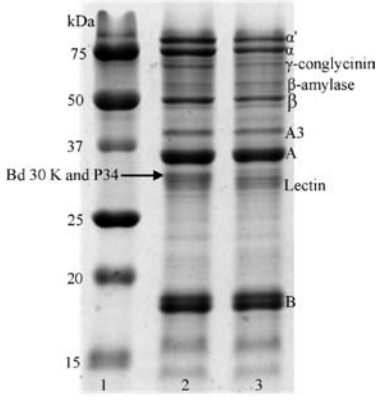

Figure 2. SDS-PAGE profiles of the pH 6.8 supernatant and the fifth supernatant. Lane 1, marker; lane 2, the pH 6.8 supernatant; lane 3, the fifth supernatant.

detectable protein bands, it is found that the band indicated by an arrow (lane 2), identified as P34 and Bd 30K by MALDI-TOF/TOF MS, is almost disappeared for the fifth supernatant (lane 3). For the first OBs, 24 and 18 kDa oleosins are respectively hydrolyzed to about 48% and 64% by 9 h incubation (Figure 3a,c). For the fifth OBs, 24 and 18 kDa oleosins are not hydrolyzed (Figure 3b,d). The detectable protein composition of the fifth OBs (Figure 3b) is almost the same as that of the first OBs (Figure 3a). However, the band indicated by an arrow in Figure 3a is obviously denser than the corresponding one in Figure 3b. The band in Figure 3a is matched to P34, Bd 30K, and caleosin, while the one in Figure 3b is matched to caleosin by MALDI-TOF/TOF MS. These results clearly revealed: (1) the proteases of 24 and 18 kDa oleosins were the OB extrinsic proteins; (2) 24 and 18 kDa oleosins still could be hydrolyzed even after exposed to pH 11.0; (3) the hydrolysis of 24 and 18 kDa oleosins was not happened in the absence of P34 and Bd 30K (or some Tricine-SDS-PAGE undetectable proteins). These results also made us

dx.doi.org/10.1021/jf405382w | J. Agric. Food Chem. 2014, 62, 956−965

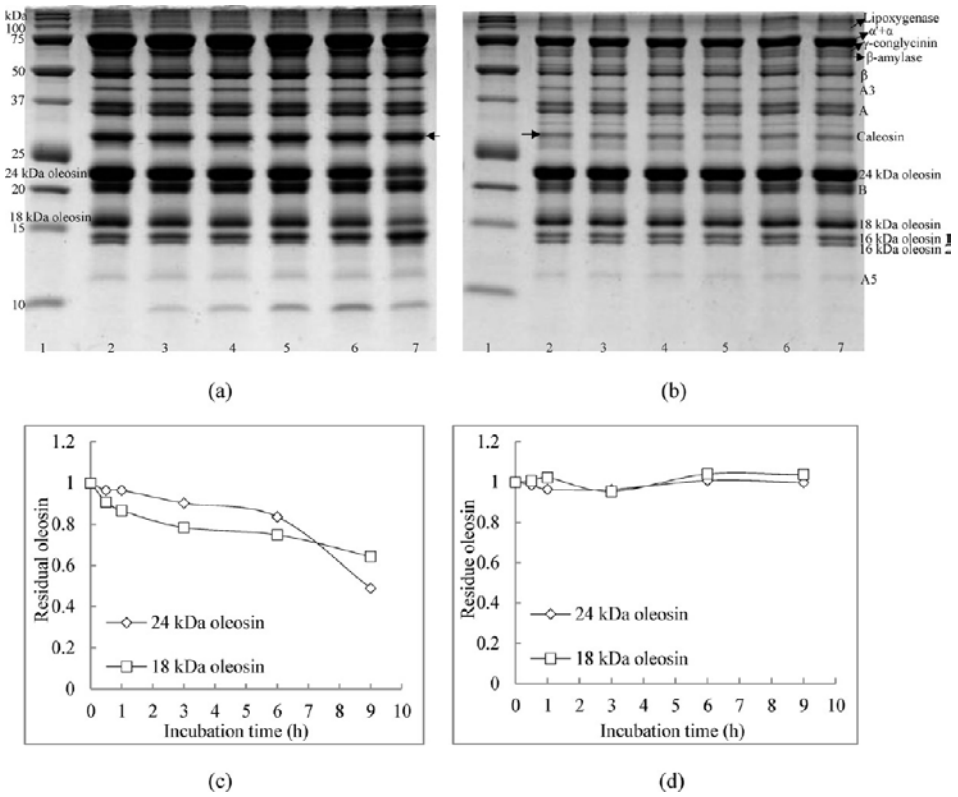

Figure 3. (a) Tricine-SDS-PAGE profile of the first OBs incubated at 35 °C. (b) The Tricine-SDS-PAGE profile of the fifth OBs incubated at 35 °C. Lane 1, marker; lanes 2−7, the fifth OBs incubated for 0, 0.5, 1, 3, 6, and 9 h, respectively. (c) The effect of incubation time on the hydrolysis of 24 and 18 kDa oleosins in the first OBs. (d) The effect of incubation time on the hydrolysis of 24 and 18 kDa oleosins in the fifth OBs.

realize that it was the OB extrinsic proteins, not the microbial spoilage, that was responsible for the oleosin hydrolysis.

Oleosin Hydrolysis in the pH 6.8, 8.0, 9.5, and 11.0 Extracted OBs. The results above exactly revealed that the proteases were the OB extrinsic proteins. Chen and Ono reported that more and more extrinsic proteins were released from OBs with increasing alkaline pH.[34] It was considered that the proteases might also show the similar trend. And it is well-known that protease must keep its natural conformation to possess its proteolytic activity and must contact its substrate to express its proteolytic activity. Therefore, OBs were obtained by pH 6.8, 8.0, 9.5, and 11.0 extractions, respectively. Lanes 2 in Figure 4a−d show the protein compositions of pH 6.8, 8.0, 9.5, and 11.0 extracted OBs before incubation. Different from the other extrinsic proteins, considerable amounts of Bd 30 K/P34 are remained in the pH 8.0 (lane 2, Figure 4b) and pH 9.5 (lane 2, Figure 4c) extracted OBs. There are two bands near the position of P34 and Bd 30K for the pH 11.0 extracted OBs (lane 2, Figure 4d), and they are matched to caleosins by MALDI-TOF/TOF MS.[5]

pH 6.8, 8.0, 9.5, and 11.0 extracted OBs were dispersed into DI water, respectively. All of them were adjusted to pH 6.5, and incubated in 35 °C water bath for 0, 0.5, 1, 3, 6, and 9 h (Figure 4a−d). The band intensities of 24 and 18 kDa oleosins were analyzed by Image Lab Software (Bio-Rad, USA). Figure 4e shows that the residual 24 kDa oleosin of pH 6.8 extracted OBs is decreased to 43% by 9 h incubation, followed by pH 8.0 (53%) and 9.5 (74%) extracted OBs, and the 24 kDa oleosin of pH 11.0 extracted OBs is unlikely to be hydrolyzed. Figure 4f shows that the residual 18 kDa oleosin of pH 6.8 extracted OBs is decreased to 45% by 9 h incubation, while the 18 kDa oleosin of pH 8.0, 9.5, and 11.0 extracted OBs is slightly or unlikely to be hydrolyzed. It was interesting that high proteolytic activity of 24 kDa oleosin-hydrolyzing protease was remained, but very low proteolytic activity of 18 kDa oleosin-hydrolyzing protease was remained in the suspension (pH 6.5) of pH 8.0 extracted OBs. In addition, obvious proteolytic activity of 24 kDa oleosin-hydrolyzing protease was still remained in the suspension (pH 6.5) of pH 9.5 extracted OBs. These clearly revealed that the interaction between 24 kDa oleosin and its protease was strong to alkaline pH. In our previous research, it was confirmed that all of P34 and Bd 30K were bound to 24 kDa oleosin by disulfide bonds (SS).[5] Together with the P34 and Bd 30K behavior in the pH 6.8, 8.0, 9.5, and 11.0 extracted OBs, it showed: (1) some of the disulfide bonds were weak to alkaline pH, but some of the disulfide bonds were strong to alkaline pH; (2) P34 and Bd 30K had high relationship with the proteases of 24 kDa and 18 kDa oleosins. In addition, it was considered that P34 and Bd 30K were different proteins owing to their four different amino acid residues (NCBI database) and their behaviors on the two-dimensional electrophoresis gel.[30,33] Therefore, it was considered that P34 and Bd 30K might be bound to 24 kDa oleosin through disulfide bonds with different bond energies. In order to confirm this hypothesis, two-dimensional electrophoresis was conducted for the proteins of pH 6.8 and 8.0 extracted OBs. Figure 5 shows that there are two spots (PX1 and PX2) resolved for the P34 and Bd 30K.[30,33] This further made us realize that P34 and Bd 30K should be different proteins. Unluckily, both of PX1 and PX2 were matched to P34 and Bd 30K by MALDI-TOF/TOF MS, which should be resulted from their high homologies with each other. According to their amino acid sequences (NCBI

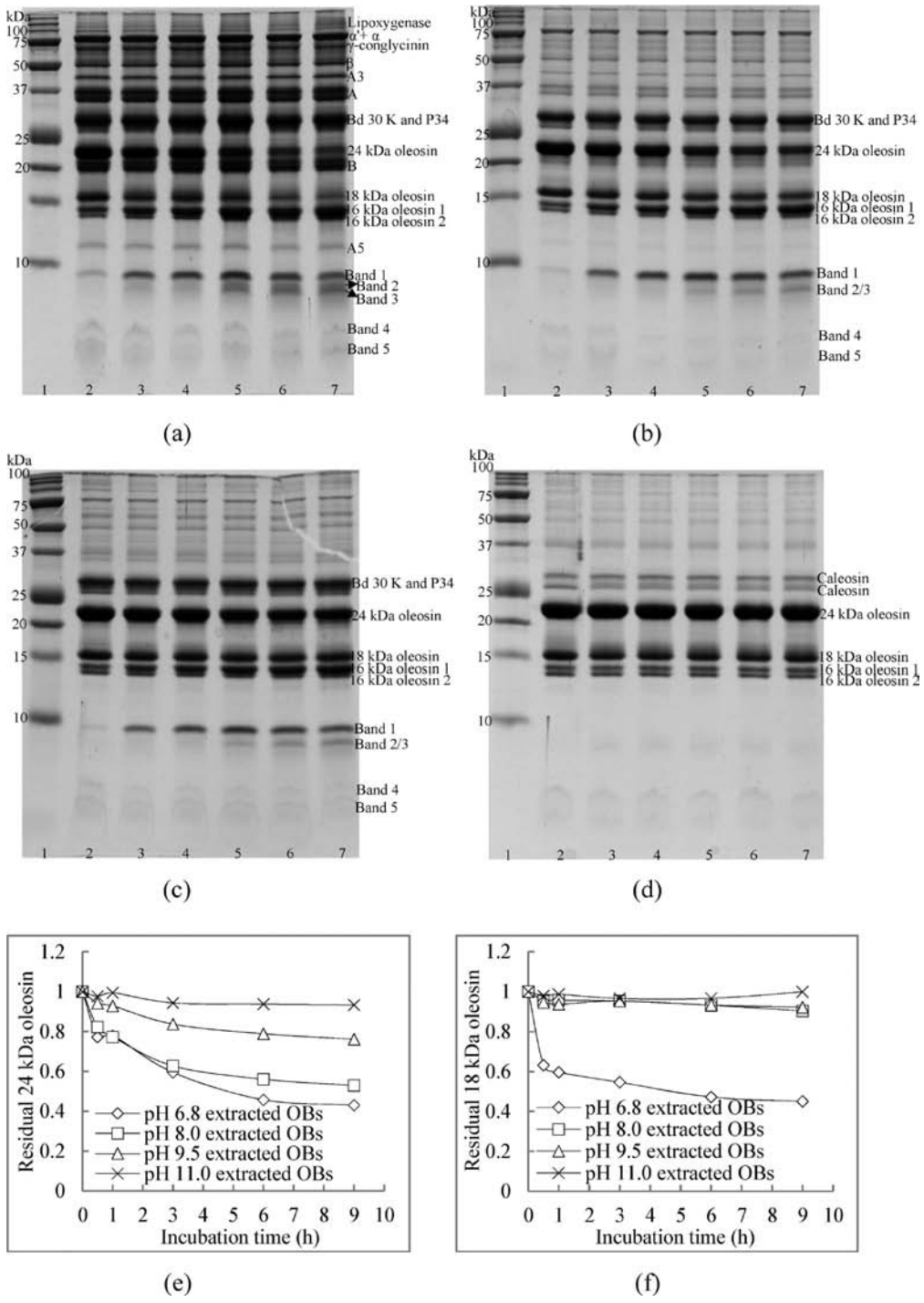

Figure 4. Tricine-SDS-PAGE profile of pH 6.8 (a), 8.0 (b), 9.5 (c), and 11.0 (d) extracted OB suspensions (pH 6.5) incubated at 35 °C. Lane 1, marker; lanes 2−7, OB suspension incubated for 0, 0.5, 1, 3, 6, and 9 h, respectively. (e) The 24 kDa oleosin hydrolysis in pH 6.8, 8.0, 9.5, and 11.0 extracted OB suspensions (pH 6.5) incubated for 0, 0.5, 1, 3, 6, and 9 h. (f) The 18 kDa oleosin hydrolysis in pH 6.8, 8.0, 9.5, and 11.0 extracted OB suspensions (pH 6.5) incubated for 0, 0.5, 1, 3, 6, and 9 h.

database), Bd 30K was more acidic than P34. Therefore, PX1 and PX2 could be preliminarily matched to P34 and Bd 30K, respectively. It is found that the PX2/PX1 intensity ratio of pH 8.0 extracted OBs is obviously larger than that of pH 6.8 extracted OBs (Figure 5), exactly revealing that PX1 (possibly P34) has weak resistance to alkaline pH, while PX2 (possibly Bd 30K) has strong resistance to alkaline pH. This is greatly consistent with the protease behaviors on the hydrolysis of 24 and 18 kDa oleosins.

Because both P34 and Bd 30K were interacted with 24 kDa oleosin by disulfide bonds, the behavior of the interaction in the incubation of pH 6.8 extracted OBs could be examined by nonreducing Tricine-SDS-PAGE (Figure 6a) combined with its corresponding reducing Tricine-SDS-PAGE (Figure 6b). The band intensities (24 kDa oleosin; 18 kDa oleosin; 16 kDa oleosin 1 + 16 kDa oleosin 2 + large hydrolyzed products of 24 and 18 kDa oleosins; band 1) were analyzed by Image Lab Software (Bio-Rad, USA). It was found that 24 kDa oleosin

dx.doi.org/10.1021/jf405382w | J. Agric. Food Chem. 2014, 62, 956−965

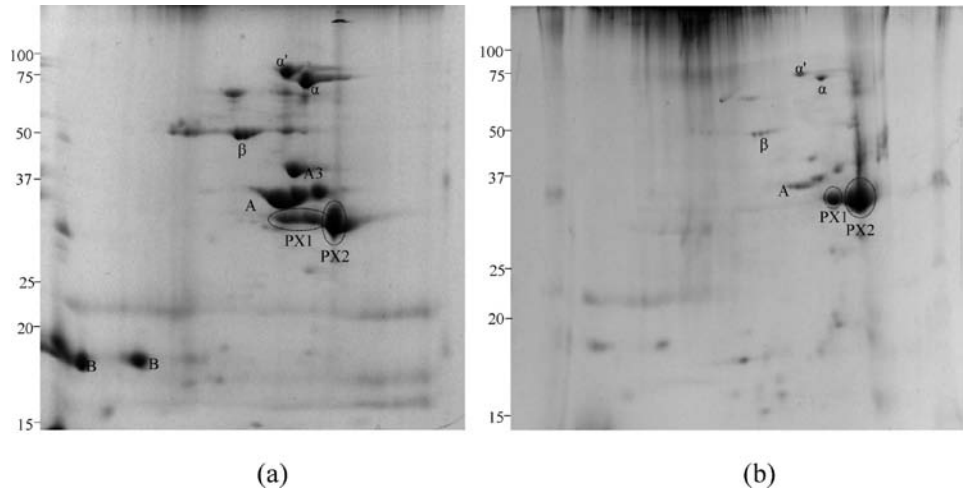

Figure 5. Protein profiles of pH 6.8 (a) and 8.0 (b) extracted OBs by two-dimensional electrophoresis. Both of PX1 and PX2 were matched to Bd 30K and P34 by MALDI-TOF/TOF MS.

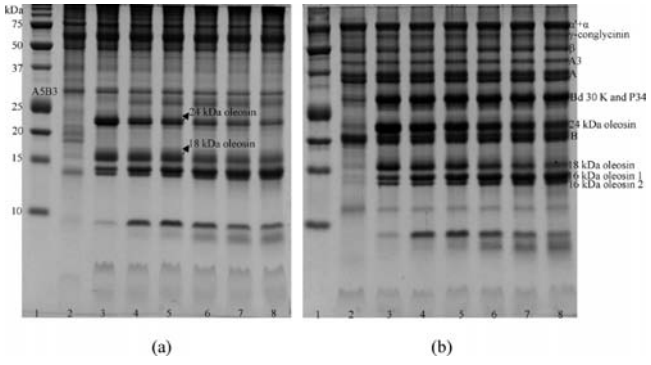

Figure 6. Nonreducing (a) and reducing (b) tricine-SDS-PAGE profiles of pH 6.8 extracted OB suspension (pH 6.5) incubated at 40 °C. Lane 1, marker; lane 2, raw soymilk; lanes 3−8, OB suspension incubated for 0, 0.5, 1, 3, 6, and 9 h, respectively.

bands in the nonreducing condition were weaker than their corresponding ones in the reducing condition, while the other three were almost the same as each other. Figure 6a shows that a thin band is located at the position of P34 and Bd 30K, and it is matched to one subunit of glycinin and caleosin by MALDI-TOF/TOF MS. These revealed that P34 and Bd 30K were always bound to 24 kDa oleosin by disulfide bonds in the incubation, very similar to the interaction between enzyme and its substrate in the reaction system that enzyme was less than its substrate. In addition, if Bd 30K and P34 were not the proteases, the Bd 30K/P34-SS-polypeptides (13−14 kDa) or the Bd 30K/P34-SS-polypeptides (around 9 kDa) might be produced in the incubation, meaning that the 13−14 kDa band or the band around 9 kDa in the nonreducing condition (Figure 6a) should be less than the corresponding one in the reducing condition (Figure 6b). However, this is unlikely happened in Figure 6.

Therefore, one hypothesis was suggested as below: PX1 (the protease of 18 kDa oleosin) was not only bound to 24 kDa oleosin by disulfide bond, but also interacted with 18 kDa oleosin by noncovalent molecular interactions for hydrolyzing 18 kDa oleosin, which might be able to weaken bond energy of the disulfide bond above; PX2 (the protease of 24 kDa oleosin) was just bound to 24 kDa oleosin without interaction with 18 kDa oleosin. As a result, PX1 was easily removed from OBs, while PX2 was difficult to remove by alkaline pH.

According to the UniProtKB database, 24 kDa oleosin (P29530) is divided into three parts: N-terminal (76 AARs), hydrophobic central domain (54 AARs) and C-terminal (96 AARs); 24 kDa oleosin (P29531) is also divided into three parts: N-terminal (57 AARs), hydrophobic central domain (72 AARs), and C-terminal (94 AARs). The hydrophobic central domain is buried in the TAGs matrix of OBs, while N- and C-terminals are exposed to the exterior. Both of P34 and Bd 30K have 257 AARs, so it is highly possible that P34/Bd 30K can interact with 18 kDa oleosin by noncovalent molecular interactions in addition to the disulfide bond with 24 kDa oleosin. Therefore, it was considered that the hypothesis above was reasonable and acceptable.

Oleosin in Germinated Soybean. If 24 kDa oleosin was hydrolyzed in soybean germination, it meant that its protease must be bound to OBs for the 24 kDa oleosin hydrolysis. In addition, the results above clearly showed that 24 kDa oleosin-hydrolyzing protease was still bound to OBs even at pH 8.0 and 9.5. Therefore, it was considered that the pH 6.8, 8.0, and 9.5 extracted OBs from germinated soybean should contain the 24 kDa oleosin-hydrolyzing protease if the assumption above was correct.

Soybean was naturally germinated for 1, 2, 4, 6, and 8 d, and OBs of each germinated soybean were extracted by pH 6.8, 8.0, and 9.5, respectively. Figure 7 shows that almost all of the 24 kDa oleosin is hydrolyzed by 4 d germination. If 24 kDa oleosin-hydrolyzing protease was detectable protein by Tricine-SDS-PAGE, it should appear not only in Figure 7, but also in Figures 1−6. As a result, P34/Bd 30K should be the most possible protein as the protease of 24 kDa oleosin.

Figure 7e shows that four protein bands (6−9) remained for the OBs of 8 d germinated soybean. By MALDI-TOF/TOF MS, band 6 was matched to several lipoxygenase isoforms, band 7 was not matched to any proteins, band 8 was matched to P34, Bd 30K, and caleosin, and band 9 was matched to 24 kDa oleosins (P29530 and P29531). These results revealed (1) 24, 18, and 16 kDa oleosins were all hydrolyzed in soybean germination, showing a different trend from the extracted OBs of ungerminated soybean; (2) Bd 30K and P34 were always bound to the extracted OBs from germinated soybean even when all oleosins were hydrolyzed. The mechanism for the 16

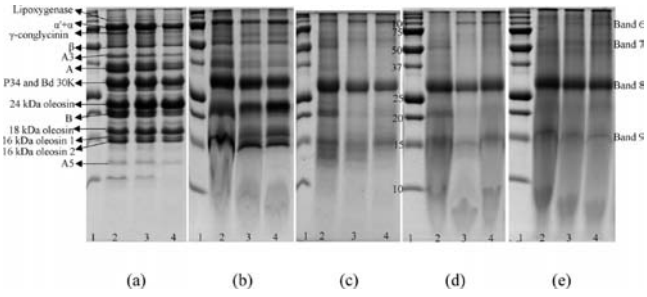

Figure 7. Protein profiles of pH 6.8, 8.0, and 9.5 extracted OBs from germinated soybean by Tricine-SDS-PAGE. (a) 1 d germinated soybean. (b) 2 d germinated soybean. (c) 4 d germinated soybean. (d) 6 d germinated soybean. (e) 8 d germinated soybean. Lane 1, marker; lanes 2–4, pH 6.8, 8.0, and 9.5 extracted OBs, respectively.

kDa oleosin hydrolysis needed further researches, which should be closely correlated with the germination.

Effects of Temperature and pH on Oleosin Hydrolysis. The pH 6.8 extracted OB suspensions (pH 6.5) were respectively put into 20, 30, 35, 40, 50, and 60 °C water baths and incubated for 0, 0.5, 1, 3, 6, and 9 h. The hydrolysis behaviors of 24 and 18 kDa oleosins (analyzed by Image Lab Software) at different temperatures are shown in Figure 8a,b, clearly revealing that 35–50 °C is the optimal temperature range for the hydrolysis of 24 and 18 kDa oleosins, while 60 °C can denature the proteases. This showed that the proteases of 24 and 18 kDa oleosins had the similar resistances to temperature.

The pH 6.8 extracted OB suspensions were respectively adjusted to pH 4.0, 5.0, 6.0, 6.5, 7.0, 8.0, 9.0, 10.0, and 11.0, and incubated in 35 °C water bath for 0, 0.5, 1, 3, 6, and 9 h. Figure 8c,d show that pH 6.0–6.5 is the optimal pH range for the hydrolysis of 24 and 18 kDa oleosins. The hydrolysis of 24 kDa oleosin was gradually slowed down from pH 6.5 to 10.0 and almost completely inhibit at pH 11.0. Different from 24 kDa oleosin, the hydrolysis of 18 kDa oleosin was greatly inhibited at pH ≥8.0, agreeing with the results in Figure 4. Therefore, it was considered that pH ≥11.0 or ≥60 °C might be better for the extraction of soybean OBs, while the combination of pH 6.0–6.5 and 35–50 °C might be better for the enzyme-assisted aqueous extraction of soybean oil.

In all, this study showed that the proteases (OB extrinsic proteins) in the pH 6.8 extracted OBs had high specificity to hydrolyze 24 and 18 kDa oleosins, and they should cleave specific peptide bonds to form limited hydrolyzed products (13–14 kDa band and bands 1–5, Figure 1). In addition, the optimal temperature and pH of the proteases were respectively

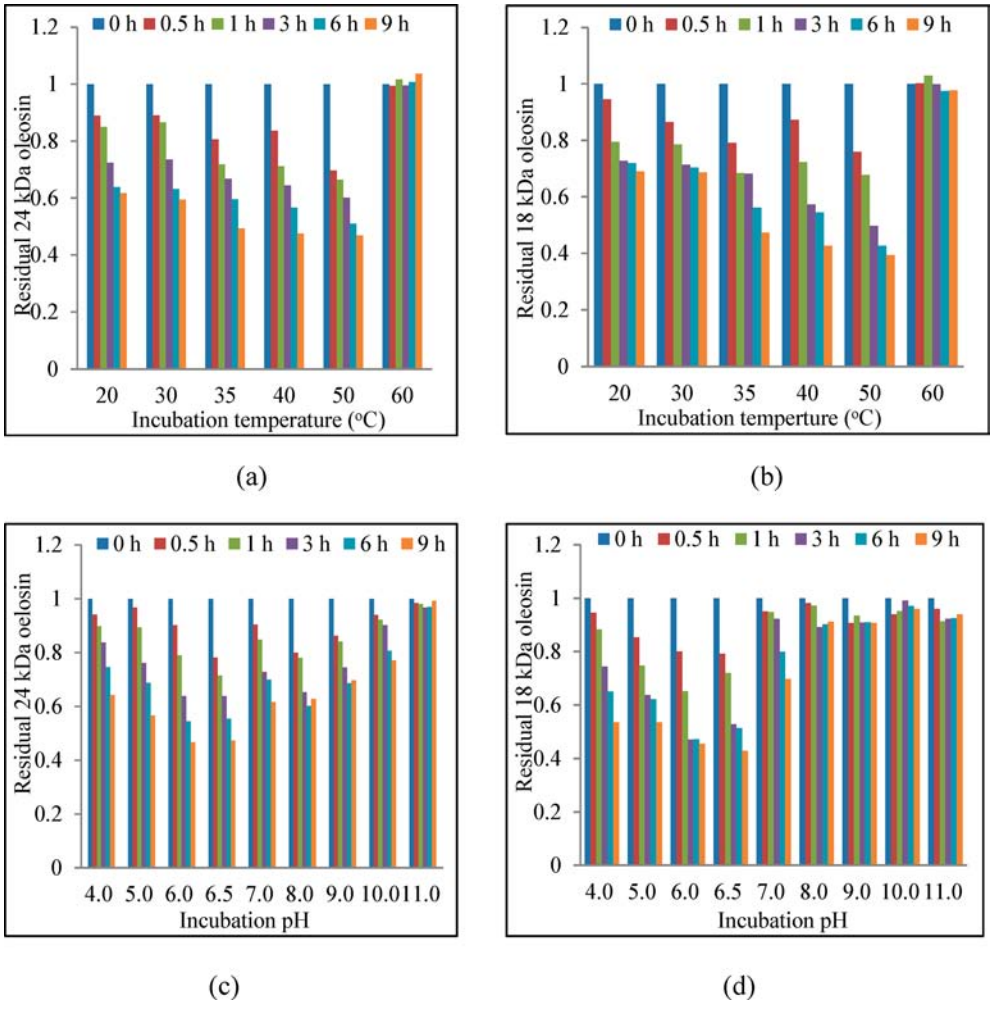

Figure 8. Effects of temperature (a, b) and pH (c, d) on the hydrolysis of 24 (a, c) and 18 kDa (b, d) oleosins in the pH 6.8 extracted OB suspensions.

dx.doi.org/10.1021/jf405382w | J. Agric. Food Chem. 2014, 62, 956–965

clarified as in the ranges of 35−50 °C and 6.0−6.5, and 60 °C or pH 11.0 could denature them. Different from the extracted OBs from ungerminated soybean, 16 kDa oleosin was also hydrolyzed in soybean germination in addition to 24 and 18 kDa oleosins. Although this study did not show direct evidence for confirming the proteases, all results in this study showed a high possibility that P34 and Bd 30K were the proteases of 24 and 18 kDa oleosins. For further research, it is considered that the respective purification of the bioactive Bd 30K and P34 (a great challenge at present stage) and their effects on oleosin hydrolysis should be examined. At last, it is suggested that some Tricine-SDS-PAGE undetectable proteins should be also considered in further studies.

AUTHOR INFORMATION

Corresponding Author

*Phone: 0510-85917812. Fax: 0510-85329091. E-mail: yfhua@jiangnan.edu.cn.

Funding

We gratefully acknowledge the financial support received from Natural Science Foundation of China (31301496), Fundamental Research Fund of Ministry of Education (2050205), Natural Science Foundation of China (31201380), Natural Science Foundation of Jiangsu Province, PR China (BK2011151), and a Project Funded by the Priority Academic Program Development of Jiangsu Higher Education Institutions.

Notes

The authors declare no competing financial interest.

REFERENCES

(1) Huang, A. H. C. Oil bodies and oleosins in seeds. *Annu. Rev. Plant Physiol. Plant Mol. Biol.* **1992**, *43*, 177−200.

(2) Shimada, T.; Shimada, T.; Takahashi, H.; Fukao, Y.; Hara-Nishimura, I. A novel role for oleosins in freezing tolerance of oilseeds in *Arabidopsis thaliana*. *Plant J.* **2008**, *55*, 798−809.

(3) Hsieh, K.; Huang, A. H. C. (2004) Endoplasmic reticulum, oleosins, and oils in seeds and tapetum cells. *Plant Physiol.* **2004**, *136*, 3427−3434.

(4) Lin, L. J.; Liao, P. C.; Yang, H. H.; Tzen, J. T. C. Determination and analyses of the N-termini of oil body proteins, steroleosin, caleosin and oleosin. *Plant Physiol. Biochem.* **2005**, *43*, 770−776.

(5) Zhao, L.; Chen, Y.; Cao, Y.; Kong, X.; Hua, Y. The integral and extrinsic bioactive proteins in the aqueous extracted soybean oil bodies. *J. Agric. Food Chem.* **2013**, *61*, 9727−9733.

(6) Iwanaga, D.; Gray, D. A.; Fisk, I. D.; Decker, E. A.; Weiss, L.; McClements, D. J. Extraction and characterization of oil bodies from soy beans: A natural source of pre-emulsified soybean oil. *J. Agric. Food Chem.* **2007**, *55*, 8711−8716.

(7) Marcoux, D.; Gorkiewicz-Petkow, A.; Hirsch, R.; Korting, H. C. Dry skin improvement by an oleosome emulsion as carrier for sphingolipid. *J. Am. Acad. Dermatol.* **2004**, *293*.

(8) Deckers, H. M.; Van Rooijen, G.; Boothe, J.; Goll, J.; Moloney, M. M. Products for topical applications comprising oil bodies; assignee: Sembiosys Genetics Inc.; U.S. Patent US6,599,513, 2003.

(9) Kapchie, V. N.; Wei, D.; Hauck, C.; Murphy, P. Enzyme-assisted aqueous extraction of oleosomes from soybeans (*Glycine Max*). *J. Agric. Food Chem.* **2008**, *56*, 1766−1771.

(10) Iwanaga, D.; Gray, D.; Decker, E. A.; Weiss, J.; McClements, D. J. Stabilization of soybean oil bodies using protective pectin coatings formed by electrostatic deposition. *J. Agric. Food Chem.* **2008**, *56*, 2240−2245.

(11) Chen, B.; McClements, D. J.; Gray, D. A.; Decker, E. A. Physical and oxidative stability of pre-emulsified oil bodies extracted from soybeans. *Food Chem.* **2012**, *132*, 1514−1520.

(12) Wu, N.; Huang, X.; Yang, X.; Guo, J.; Yin, S.; He, X.; Wang, L.; Zhu, J.; Qi, J.; Zheng, E. In vitro assessment of the bioaccessibility of fatty acids and tocopherol from soybean oil body emulsions stabilized with ι-carrageenan. *J. Agric. Food Chem.* **2012**, *60*, 1567−1575.

(13) Campbell, K. A.; Glatz, C. E. Mechanisms of aqueous extraction of soybean oil. *J. Agric. Food Chem.* **2009**, *57*, 10904−10912.

(14) Fernandez, D. E.; Qu, R.; Huang, A. H. C.; Staehelin, L. A. Immunogold localization of the L3 protein of maize lipid bodies during germination and seedling growth. *Plant Physiol.* **1988**, *86*, 270−274.

(15) Murphy, D. J.; Cummins, I.; Kang, A. S. Immunocytochemical and biochemical studies of the mobilization of storage oil-bodies and proteins in germinating cotyledons of oilseed rape, *Brassica napus*. *J. Sci. Food Agric.* **1989**, *48*, 209−223.

(16) Radetzky, R.; Langheinrich, U. (1994) Induction of accumulation and degradation of the 18.4 kDa oleosin in a triacylglycerol-storing cell culture of anise (*Pimpinella anisum* L.). *Planta.* **1994**, *194*, 1−8.

(17) Herman, E. M. The cell and molecular biology of seed oil bodies. In *Seed development and germination*; Kigel, J., Gallili, G., Eds.; Marcel Dekker: New York, 1995; pp 194−214.

(18) Tzen, J. T. C.; Peng, C. C.; Cheng, D. J.; Chen, E. C.; Chiu, J. M. A new method for seed oil body purification and examination of oil body integrity following germination. *J. Biochem.* **1997**, *121*, 762−768.

(19) Vandana, S.; Bhatla, S. C. Evidence for the probable oil body association of a thiol-protease, leading to oleosin degradation in sunflower seedling cotyledons. *Plant Physiol. Biochem.* **2006**, *44*, 714−723.

(20) Rudolph, M.; Feussner, I.; Korner, M.; Feussner, K.; Berndt, E.; Meler, M.; Horung, E.; Feussner, I. The lipoxygenase-dependent oxygenation of lipid body membranes is promoted by a patatin-type phospholipase in cucumber cotyledons. *J. Exp. Bot.* **2011**, *62*, 749−760.

(21) Matsui, K.; Hijiya, K.; Tabuchi, Y.; Kajiwara, T. Cucumber cotyledon lipoxygenase during postgerminative growth. Its expression and action on lipid bodies. *Plant Physiol.* **1999**, *119*, 1279−1287.

(22) Herman, E. M. Immunogold-localization and synthesis of an oil body membrane protein in developing soybean seeds. *Planta* **1987**, *172*, 336−345.

(23) Kalinski, A.; Weisemann, J. M.; Matthews, B. F.; Herman, E. M. Molecular cloning of a protein associated with soybean seed oil bodies that is similar to thiol proteases of the papain family. *J. Biol. Chem.* **1990**, *265* (23), 13843−13848.

(24) Kalinski, A.; Melroy, D. L.; Dwivedi, R. S.; Herman, E. M. A soybean vacuolar protein (P34) related to thiol proteases is synthesized as a glycoprotein precursor during seed maturation. *J. Biol. Chem.* **1992**, *267*, 12068−12076.

(25) Toyooka, K.; Okamoto, T.; Minamikawa, T. Mass transport of proform of a KDEL-tailed cysteine proteinase (SH-EP) to protein storage vacuoles by endoplasmic recticulum-derived vesicle is involved in protein mobilization in germinating seeds. *J. Cell Biol.* **2000**, *148*, 453−463.

(26) Wenig, K.; Chatwell, L.; von Pawel-Rammingen, U.; Bjorck, L.; Huber, R.; Sondermann, P. Structure of the streptococcal endopeptidase IdeS, a cysteine proteinase with strict specificity for IgG. *Proc. Natl. Acad. Sci. U.S.A.* **2004**, *101*, 17371−17376.

(27) Zhang, M.; Wei, Z.; Chang, S.; Teng, M.; Gong, W. Crystal structure of a papain-fold protein without the catalytic residue: a novel member in the cysteine proteinase family. *J. Mol. Biol.* **2006**, *358*, 97−105.

(28) Yasuhara, T.; Takai, T.; Yuuki, T.; Okudaira, H.; Okumura, Y. Biologically active recombinant forms of a mojor house dust mite group 1 allergen Der f 1 with full activities of both cysteine protease and IgE binding. *Clin. Exp. Allergy* **2001**, *31*, 116−124.

(29) Soto-Mera, M. T.; Lopez-Rico, M. R.; Filgueira, J. F.; Villamil, E.; Cidras, R. Occupational allergy to papain. *Allergy* **2000**, *55*, 983−984.

(30) Herman, E. M.; Helm, R. M.; Jung, R.; Kinney, A. J. Genetic modification removes an immunodominant allergen from soybean. *Plant Physiol.* **2003**, *132*, 36−43.
(31) Ogawa, T.; Bando, N.; Tsuji, H.; Okajima, H.; Nishikawa, K.; Sasaoka, K. Investigation of the IgE-binding proteins in soybean by immunoblotting with the sera of the soybean sensitive patients with atopic dermatitis. *J. Nutr. Sci. Vitaminol.* **1991**, *37*, 555−565.
(32) Ogawa, T.; Tsuji, H.; Bando, N.; Kitamura, K.; Zhu, Y.; Hirano, H.; Nishikawa, K. Identification of the soybean allergenic protein, *Gly* m Bd 30K, with the soybean seed 34-kDa oil-body-associated protein. *Biosci. Biotechnol. Biochem.* **1993**, *57* (6), 1030−1033.
(33) Natarajan, S.; Xu, C.; Bae, H.; Caperna, T. J.; Garrett, W. M. Proteomic analysis of allergen and antinutritional proteins in wild and cultivated soybean seeds. *J. Plant Biochem. Biotechnol.* **2006**, *15*, 103−108.
(34) Chen, Y.; Ono, T. Simple extraction method of non-allergenic intact soybean oil bodies that are thermally stable in an aqueous medium. *J. Agric. Food Chem.* **2010**, *58*, 7402−7407.
(35) Sesekow, E.; Kessler, L. C.; Seidel-Morgenstern, A.; Rothkotter, H. Isolation of soybean protein P34 from oil bodies using hydrophobic interaction chromatography. *BMC Biotechnol.* **2008**, *8*, 27.
(36) Hou, D. H. J.; Chang, S. K. C. Structural characteristics of purified glycinin from soybeans stored under various conditions. *J. Agric. Food Chem.* **2004**, *52*, 3792−3800.
(37) Tzen, J. T. C.; Huang, A. H. C. Surface structure and properties of plant seed oil bodies. *J. Cell Biol.* **1992**, *117*, 327−335.
(38) Laemmli, U. K. Cleavage of structural proteins during the assembly of the head of bacteriophage T4. *Nature.* **1970**, *227*, 680−685.
(39) Schagger, H. Tricine-SDS-PAGE. *Nat. Protocols* **2006**, *1*, 16−22.
(40) Parthibane, V.; Rajakumari, S.; Venkateshwari, V.; Lyappan, R.; Rajasekharan, R. Oleosin is bifunctional enzyme that has both monoacylglycerol acyltransferase and phospholipase activities. *J. Biol. Chem.* **2012**, *287*, 1946−1954.
(41) Hanano, A.; Burcklen, M.; Flenet, M.; Ivancich, A.; Louwagie, M.; Garin, J.; Blee, E. Plant seed peroxygenase is an original heme-oxygenase with an EF-hand calcium binding motif. *J. Biol. Chem.* **2006**, *281*, 33140−33151.
(42) Lin, L. J.; Tai, S. S.; Peng, C. C.; Tzen, J. T. Steroleosin, a sterol-binding dehydrogenase in seed oil bodies. *Plant Physiol.* **2002**, *128*, 1200−1211.

Table 1. UHPLC/ESI-MS/MS Parameters and Method Performance for Analysis of Pesticide Residues in Brewed Tea

Pesticides	Ionization	Q1 Mass (amu)	Q3 Mass[a] (amu)	DP (V)	EP (V)	CE (V)	CE[b] (V)	CXP (V)	Brewed tea			
									Retention time[c] (min)	Overall Recovery[d] (%)	Intermediate precision[e] (%)	Measurement uncertainty[f] (%)
1[g]	2	3	4	6	7	8	9	10	11	12	13	14
Abamectin $B1_a$	$[M + H]^+$	890.5	305.2	111.0	10	37	37	30	6.60	97.9	7.5	15.0
		890.5	567.3	111.0	10	21		28				
		890.5	113.2	111.0	10	69		14				
Acetochlor	$[M + H]^+$	270.1	224.1	66.0	10	15	15	14	5.41	101.3	6.3	12.6
		270.1	148.1	66.0	10	29		20				
		270.1	133.1	66.0	10	47		16				
Aclonifen[h]	$[M + H]^+$	265.0	182.2	101.0	10	41	41	24	5.53	97.8	19.4	39.0
		265.0	217.9	101.0	10	35		22				
		265.0	194.1	101.0	10	27		18				
Aldicarb	$[M + NH_4]^+$	208.1	116.1	26.0	10	13	13	16	3.94	99.5	8.5	17.2
		208.1	88.9	26.0	10	25		16				
		208.1	70.0	26.0	10	21		14				
Aldicarb sulfone	$[M + NH_4]^+$	240.1	86.0	51.0	10	31	31	20	2.55	102.2	6.1	12.3
		240.1	148.1	51.0	10	21		14				
		240.1	76.0	51.0	10	19		30				
Aldicarb sulfoxide	$[M + H]^+$	207.1	132.1	86.0	10	11	11	16	1.76	98.5	7.7	15.5
		207.1	88.9	86.0	10	21		14				
		207.1	41.0	86.0	10	49		18				
Anilofos	$[M + H]^+$	369.0	198.9	76.0	10	21	21	14	5.59	102.5	7.5	18.3
		369.0	125.0	76.0	10	47		8				
		369.0	171.0	76.0	10	29		12				
Azaconazole	$[M + H]^+$	300.0	159.1	76.0	10	41	**27**	10	4.51	100.0	8.5	17.0
		300.0	231.0	76.0	10	25		14				
		300.0	89.1	76.0	10	97		34				
Benoxacor[i]	$[M + H]^+$	260.0	149.1	76.0	10	29	29	22	5.09	102.8	12.5	26.0
		260.0	134.1	76.0	10	43		12				
		260.0	120.0	76.0	10	49		14				
Bitertanol	$[M + H]^+$	338.2	99.2	61.0	10	23	23	12	5.26	100.7	8.2	16.5
		338.2	70.0	61.0	10	31		26				
		338.2	43.1	61.0	10	59		16				
Bromuconazole	$[M + H]^+$	376.0	159.1	91.0	10	37	37	10	5.04	100.0	9.2	18.7
		376.0	70.0	91.0	10	31		28				
		376.0	89.0	91.0	10	123		12				
Butafenacil	$[M + NH_4]^+$	492.0	331.0	46.0	10	33	**15**	34	5.42	103.7	8.4	18.3
		492.0	180.0	46.0	10	61		18				
		492.0	348.8	46.0	10	23		18				
Butocarboxim	$[M + H]^+$	191.1	75.0	1.0	10	15	15	16	3.73	97.6	12.9	25.8
		191.1	47.0	1.0	10	39		12				
		191.1	41.1	1.0	10	35		6				
Butocarboxim sulfoxide	$[M + H]^+$	207.1	75.0	86.0	10	21	21	30	1.61	98.3	7.8	15.7
		207.1	132.2	86.0	10	13		6				
		207.1	43.1	86.0	10	31		16				
Cadusafos	$[M + H]^+$	271.1	159.0	81.0	10	21	**12**	10	5.74	97.7	7.1	14.4
		271.1	130.9	81.0	10	33		16				
		271.1	97.0	81.0	10	49		12				
Carbaryl	$[M + H]^+$	202.1	145.1	91.0	10	17	17	18	4.47	101.8	7.4	15.4
		202.1	127.1	91.0	10	43		16				
		202.1	117.0	91.0	10	33		16				
Carbendazim	$[M + H]^+$	192.1	160.2	106.0	10	25	**13**	16	3.43	102.4	3.9	8.8
		192.1	132.0	106.0	10	45		18				
		192.1	104.9	106.0	10	49		14				
Carbendazim d_4 (IS)	$[M + H]^+$	196.1	164.1	66.0	10	29	**21**	22	3.41			
Carbetamide	$[M + H]^+$	237.1	192.0	76.0	10	13	13	14	3.82	102.6	7.3	14.7
		237.1	118.1	76.0	10	19		16				
		237.1	120.2	76.0	10	23		8				
Carbofuran	$[M + H]^+$	222.2	165.1	81.0	10	19		20	4.36	102.7	4.2	8.9
		222.2	**123.0**	81.0	10	31	**20**	14				
		222.2	55.1	81.0	10	37		20				
Carbofuran d_3 (IS)	$[M + H]^+$	225.1	123.1	96.0	10	33	33	14	4.35			
Carfentrazone-ethyl	$[M + H]^+$	412.0	345.8	141.0	10	33	**29**	18	5.50	102.8	8.4	16.8
		412.0	365.9	141.0	10	25		28				
		412.0	383.8	141.0	10	21		30				
Chlorantraniliprole	$[M + H]^+$	484.0	452.9	66.0	10	23	23	28	4.72	97.7	14.2	28.5
		484.0	285.9	66.0	10	19		22				
		484.0	112.1	66.0	10	95		16				

dx.doi.org/10.1021/jf404123h | J. Agric. Food Chem. 2014, 62, 966−983

Table 1. continued

Pesticides	Ionization	Q1 Mass (amu)	Q3 Mass[a] (amu)	DP (V)	EP (V)	CE (V)	CE[b] (V)	CXP (V)	Brewed tea: Retention time[c] (min)	Brewed tea: Overall Recovery[d] (%)	Brewed tea: Intermediate precision[e] (%)	Brewed tea: Measurement uncertainty[f] (%)
1[g]	2	3	4	6	7	8	9	10	11	12	13	14
Chlorbromuron[h]	$[M + H]^+$	293.0	125.0	101.0	10	51	51	16	5.09	108.9	**28.9**	**58.3**
		293.0	63.0	101.0	10	101		12				
		293.0	62.1	101.0	10	23		12				
Chloridazon[i,l]	$[M + H]^+$	222.0	51.0	116.0	10	93	93	20	3.44	100.3	9.7	19.5
		222.0	64.9	116.0	10	53		14				
		222.0	104.0	116.0	10	37		12				
Chlorimuron-ethyl	$[M + H]^+$	414.9	186.1	86.0	10	29	**15**	24	3.61	90.5	8.4	21.9
		414.9	184.8	86.0	10	37		10				
		414.9	82.9	86.0	10	65		16				
Chloroxuron	$[M + H]^+$	291.1	72.2	106.0	10	31	**19**	16	5.01	100.2	8.6	17.3
		291.1	46.1	106.0	10	49		20				
		291.1	30.7	106.0	10	109		12				
Chlortoluron	$[M + H]^+$	213.1	72.0	66.0	10	37	**15**	14	4.42	100.3	5.6	11.6
		213.1	46.1	66.0	10	29		20				
		213.1	56.0	66.0	10	71		6				
Clodinafop-propargyl	$[M + H]^+$	350.0	265.9	121.0	10	23	**15**	26	5.60	103.1	10.1	21.8
		350.0	91.2	121.0	10	43		8				
		350.0	238.1	121.0	10	35		24				
Cloquintocet-mexyl	$[M + H]^+$	336.1	238.0	76.0	10	25	**11**	14	6.06	99.6	8.2	16.6
		336.1	191.9	76.0	10	41		22				
		336.1	179.1	76.0	10	45		18				
Clothianidin[i]	$[M + H]^+$	250.0	169.1	61.0	10	21	21	16	3.33	100.5	9.1	18.6
		250.0	132.0	61.0	10	27		22				
		250.0	112.9	61.0	10	37		46				
Cyanofenphos[l]	$[M + H]^+$	304.1	275.9	51.0	10	19	19	30	5.74	103.9	11.9	24.3
		304.1	157.0	51.0	10	33		24				
		304.1	120.2	51.0	10	31		10				
Cyazofamid[i]	$[M + H]^+$	325.9	107.9	46.0	10	21	21	16	5.44	100.6	**20.1**	42.4
		325.9	109.1	46.0	10	21		16				
		325.9	44.1	46.0	10	43		6				
Cycloxydim	$[M + H]^+$	326.1	280.0	111.0	10	21	21	32	4.86	94.7	11.7	29.7
		326.1	180.0	111.0	10	29		26				
		326.1	101.1	111.0	10	33		22				
Cycluron	$[M + H]^+$	199.2	89.0	86.0	10	23	**15**	10	4.44	98.0	7.3	14.7
		199.2	72.0	86.0	10	33		12				
		199.2	69.1	86.0	10	31		16				
Cyromazin[i]	$[M + H]^+$	167.1	42.9	76.0	10	57	57	18	1.42	**79.5**	9.2	18.4
		167.1	68.1	76.0	10	49		14				
		167.1	60.2	76.0	10	29		24				
Demeton-S-methyl sulfone[k]	$[M + H]^+$	263.0	169.0	111.0	10	23	23	10	2.98	100.7	7.2	15.4
		263.0	127.0	111.0	10	37		14				
		263.0	109.0	111.0	10	41		12				
Demeton-S-methyl sulfoxide[k]	$[M + H]^+$	247.1	169.0	86.0	10	21	**13**	4	2.51	97.1	6.8	13.6
		247.1	127.0	86.0	10	37		16				
		247.1	105.0	86.0	10	21		12				
Desmedipham	$[M + H]^+$	301.1	182.0	116.0	10	15	**19**	10	4.92	103.2	7.4	15.0
		301.1	136.2	116.0	10	35		8				
		301.1	65.1	116.0	10	77		26				
Dialifor	$[M + NH_4]^+$	411.1	187.0	46.0	10	19	19	12	5.84	102.5	9.8	20.3
		411.1	208.1	46.0	10	29		16				
		411.1	394.0	46.0	10	9		28				
Diclocymet	$[M + H]^+$	313.0	173.1	116.0	10	25	25	24	5.42	102.4	11.7	25.0
		313.0	137.1	116.0	10	47		12				
		313.0	102.0	116.0	10	63		12				
Diethofencarb	$[M + H]^+$	268.2	226.1	61.0	10	17	**23**	14	5.01	101.5	8.7	17.5
		268.2	124.1	61.0	10	45		14				
		268.2	152.0	61.0	10	31		20				
Difenoconazole	$[M + H]^+$	406.0	251.0	136.0	10	39	**22**	26	5.55	99.7	9.6	19.5
		406.0	337.0	136.0	10	25		26				
		406.0	188.0	136.0	10	49		26				
Dimethametryn	$[M + H]^+$	256.1	186.1	121.0	10	31		30	5.43	101.3	7.1	16.4
		256.1	**91.0**	121.0	10	43	**31**	14				
		256.1	96.1	121.0	10	45		12				

dx.doi.org/10.1021/jf404123h | J. Agric. Food Chem. 2014, 62, 966−983

Table 1. continued

Pesticides	Ionization	Q1 Mass (amu)	Q3 Mass[a] (amu)	DP (V)	EP (V)	CE (V)	CE[b] (V)	CXP (V)	Brewed tea			
									Retention time[c] (min)	Overall Recovery[d] (%)	Intermediate precision[e] (%)	Measurement uncertainty[f] (%)
1[g]	2	3	4	6	7	8	9	10	11	12	13	14
Dimethomorph	$[M + H]^+$	388.1	300.9	76.0	10	31	**17**	16	4.82	97.2	14.7	29.6
		388.1	165.2	76.0	10	45		10				
		388.1	152.2	76.0	10	99		20				
Dimetilan	$[M + H]^+$	241.1	72.0	86.0	10	21	**14**	12	3.40	101.4	6.3	12.9
		241.1	196.0	86.0	10	15		14				
		241.1	55.9	86.0	10	71		12				
Dimoxystrobin	$[M + H]^+$	327.1	205.2	91.0	10	15	**11**	14	5.31	102.4	6.7	13.7
		327.1	116.0	91.0	10	29		14				
		327.1	58.0	91.0	10	45		8				
Diniconazole	$[M + H]^+$	326.1	70.0	136.0	10	37	**31**	28	5.40	99.2	9.7	19.5
		326.1	43.0	136.0	10	105		16				
		326.1	159.1	136.0	10	47		20				
Dioxacarb	$[M + H]^+$	224.1	123.0	96.0	10	25	25	16	3.53	102.6	7.2	16.6
		224.1	167.1	96.0	10	15		10				
		224.1	95.1	96.0	10	39		12				
Dipropetryn	$[M + H]^+$	256.1	144.1	101.0	10	41		14	5.52	101.7	7.1	16.5
		256.1	**214.2**	101.0	10	29	**17**	22				
		256.1	102.0	101.0	10	53		12				
Diuron	$[M + H]^+$	233.1	72.0	56.0	10	35	35	28	4.58	100.8	9.7	19.5
		233.1	133.0	56.0	10	55		18				
		233.1	74.1	56.0	10	107		14				
Dodemorph	$[M + H]^+$	282.2	116.0	106.0	10	31	**21**	16	9.21	**79.8**	9.3	18.6
		282.2	98.0	106.0	10	39		14				
		282.2	41.2	106.0	10	73		16				
Emamectin B_{1a}	$[M + H]^+$	886.4	158.2	41.0	10	47	**33**	18	**6.87**	82.9	8.6	17.4
		886.4	82.1	41.0	10	49		10				
		886.4	126.0	41.0	10	49		14				
Epoxiconazole	$[M + H]^+$	330.0	121.0	91.0	10	29	**19**	24	5.09	100.9	7.8	16.0
		330.0	123.1	91.0	10	31		8				
		330.0	90.9	91.0	10	49		20				
Ethiofencarb	$[M + H]^+$	226.1	107.1	86.0	10	25	25	14	4.57	90.2	10.0	22.4
		226.1	164.1	86.0	10	13		10				
		226.1	76.9	86.0	10	49		16				
Ethiofencarb sulfone	$[M + NH_4]^+$	275.0	107.2	76.0	10	27		14	3.35	102.5	10.2	20.8
		275.0	**201.1**	76.0	10	17	17	0				
		275.0	77.0	76.0	10	79		32				
Ethiofencarb sulfoxide	$[M + H]^+$	242.1	107.0	76.0	10	29	**15**	18	3.06	109.2	11.4	22.9
		242.1	77.0	76.0	10	67		32				
		242.1	78.9	76.0	10	53		32				
Ethiprole[j]	$[M + H]^+$	398.1	352.0	126.0	10	29	29	26	4.81	100.0	17.5	36.4
		398.1	256.0	126.0	10	53		16				
		398.1	351.4	126.0	10	29		24				
Ethirimol[k]	$[M + H]^+$	210.1	140.1	56.0	10	33	**21**	20	3.93	90.4	9.8	19.7
		210.1	98.1	56.0	10	39		14				
		210.1	43.0	56.0	10	71		16				
Ethoprop	$[M + H]^+$	243.1	131.0	86.0	10	29	**23**	14	5.20	96.6	6.6	13.7
		243.1	97.0	86.0	10	51		12				
		243.1	43.0	86.0	10	41		10				
Etofenprox	$[M+NH_4]^+$	394.2	177.3	31.0	10	21	**18**	18	7.17	100.9	**22.4**	46.2
		394.2	359.1	31.0	10	17		26				
		394.2	106.9	31.0	10	65		12				
Etoxazole	$[M + H]^+$	360.1	141.1	101.0	10	49	**22**	14	6.46	100.4	9.3	18.7
		360.1	304.0	101.0	10	27		34				
		360.1	57.2	101.0	10	43		12				
Fenamidone	$[M + H]^+$	312.1	91.9	81.0	10	33	**19**	10	5.11	101.7	7.9	15.9
		312.1	236.1	81.0	10	25		20				
		312.1	65.0	81.0	10	49		14				
Fenazaquin	$[M + H]^+$	307.1	57.0	91.0	10	35	**23**	14	6.52	98.9	11.5	24.9
		307.1	161.2	91.0	10	25		18				
		307.1	91.1	91.0	10	93		20				
Fenhexamid	$[M + H]^+$	302.0	97.1	106.0	10	33	33	20	5.11	104.7	12.0	25.1
		302.0	55.0	106.0	10	61		14				
		302.0	143.1	106.0	10	47		14				
Fenoxanil	$[M + NH_4]^+$	346.0	302.0	36.0	10	23	23	28	5.51	103.1	7.3	16.2
		346.0	86.0	36.0	10	39		36				
		346.0	189.1	36.0	10	43		20				

dx.doi.org/10.1021/jf404123h | J. Agric. Food Chem. 2014, 62, 966−983

Table 1. continued

Pesticides	Ionization	Q1 Mass (amu)	Q3 Mass[a] (amu)	DP (V)	EP (V)	CE (V)	CE[b] (V)	CXP (V)	Brewed tea: Retention time[c] (min)	Brewed tea: Overall Recovery[d] (%)	Brewed tea: Intermediate precision[e] (%)	Brewed tea: Measurement uncertainty[f] (%)
1[g]	2	3	4	6	7	8	9	10	11	12	13	14
Fenpropidin	$[M + H]^+$	274.2	147.2	76.0	10	39	**29**	8	**5.86**	91.6	11.4	23.7
		274.2	116.9	76.0	10	73		16				
		274.2	86.0	76.0	10	41		10				
Fenpropimorph	$[M + H]^+$	304.2	147.3	76.0	10	45	**28**	14	7.45	92.4	7.1	14.4
		304.2	116.9	76.0	10	81		16				
		304.2	91.0	76.0	10	113		12				
Fenpyroximate[k]	$[M + H]^+$	422.1	366.0	126.0	10	27	**9**	36	6.42	100.1	9.6	20.6
		422.1	135.0	126.0	10	45		20				
		422.1	107.2	126.0	10	81		12				
Fentrazamide	$[M + H]^+$	350.1	154.1	111.0	10	17	17	16	5.71	104.0	8.1	18.4
		350.1	83.0	111.0	10	35		16				
		350.1	196.9	111.0	10	13		24				
Fluazifop-butyl	$[M + H]^+$	384.1	282.1	121.0	10	31	**17**	18	6.17	101.1	9.0	18.1
		384.1	328.1	121.0	10	25		30				
		384.1	91.0	121.0	10	49		10				
Flubendiamide	$[M + H]^+$	683.0	407.9	126.0	10	13	13	26	5.40	103.3	12.3	27.1
		683.0	273.9	126.0	10	37		20				
		683.0	255.9	126.0	10	83		16				
Flucarbazone	$[M + NH_4]^+$	414.0	130.2	46.0	10	35	35	18	3.10	**55.7**	**27.8**	**63.4**
		414.0	115.0	46.0	10	49		18				
		414.0	72.9	46.0	10	49		30				
Fluoxastrobin	$[M + H]^+$	460.1	428.1	91.0	10	23	23	32	5.28	103.4	10.3	20.6
		460.1	187.9	91.0	10	49		12				
		460.1	75.0	91.0	10	129		10				
Flutolanil	$[M + H]^+$	324.1	262.0	111.0	10	27	**17**	14	5.33	102.8	7.2	14.4
		324.1	242.0	111.0	10	35		12				
		324.1	65.0	111.0	10	63		30				
Flutriafol	$[M + H]^+$	302.1	70.0	96.0	10	25	**17**	14	4.41	100.5	7.3	15.2
		302.1	122.9	96.0	10	37		16				
		302.1	75.0	96.0	10	110		32				
Forchlorfenuron	$[M + H]^+$	248.0	129.0	31.0	10	27	**18**	14	4.46	99.9	9.3	19.0
		248.0	93.0	31.0	10	49		18				
		248.0	111.1	31.0	10	47		14				
Fosthiazate	$[M + H]^+$	284.0	104.0	86.0	10	33	**16**	24	4.47	102.3	6.2	12.6
		284.0	228.2	86.0	10	17		22				
		284.0	199.9	86.0	10	25		10				
Fuberidazole[i]	$[M + H]^+$	185.1	157.1	96.0	10	33	**19**	14	3.81	96.4	6.5	14.5
		185.1	156.1	96.0	10	43		22				
		185.1	65.0	96.0	10	49		14				
Furathiocarb	$[M + H]^+$	383.1	195.2	121.0	10	29	**13**	18	6.13	100.9	7.2	14.5
		383.1	167.0	121.0	10	39		22				
		383.1	162.1	121.0	10	49		16				
Griseofulvin[i]	$[M + H]^+$	354.0	68.9	86.0	10	41	41	10	4.46	99.5	12.5	25.2
		354.0	286.2	86.0	10	25		20				
		354.0	166.1	86.0	10	27		14				
Haloxyfop[i]	$[M + H]^+$	362.0	316.0	121.0	10	29	29	36	3.87	**50.5**	**22.5**	46.7
		362.0	91.0	121.0	10	43		16				
		362.0	287.8	121.0	10	39		28				
3-Hydroxycarbofuran	$[M + NH_4]^+$	255.1	163.1	46.0	10	27		16	3.36	101.7	8.8	18.9
		255.1	**220.1**	46.0	10	17	17	12				
		255.1	181.2	46.0	10	23		18				
Imazamethabenz-methyl	$[M + H]^+$	289.1	144.1	66.0	10	49	**30**	10	4.04	101.0	8.6	17.3
		289.1	86.2	66.0	10	33		18				
		289.1	229.1	66.0	10	29		22				
Imidacloprid	$[M + H]^+$	256.1	209.1	81.0	10	25	25	24	3.45	98.5	11.7	23.5
		256.1	174.9	81.0	10	29		22				
		256.1	84.0	81.0	10	25		12				
Indoxacarb[j]	$[M + H]^+$	528.0	248.9	141.0	10	25	25	28	5.83	102.6	11.2	22.9
		528.0	292.9	141.0	10	21		20				
		528.0	203.0	141.0	10	49		20				
Ipconazole	$[M + H]^+$	334.1	70.1	76.0	10	33	33	12	5.53	100.0	9.2	18.5
		334.1	43.1	76.0	10	127		6				
		334.1	125.1	76.0	10	53		8				
Iprovalicarb	$[M + H]^+$	321.2	119.1	91.0	10	35	**11**	16	5.03	101.5	7.6	15.2
		321.2	91.1	91.0	10	73		14				
		321.2	116.2	91.0	10	31		14				

dx.doi.org/10.1021/jf404123h | J. Agric. Food Chem. 2014, 62, 966−983

Table 1. continued

Pesticides	Ionization	Q1 Mass (amu)	Q3 Mass[a] (amu)	DP (V)	EP (V)	CE (V)	CE[b] (V)	CXP (V)	Brewed tea			
									Retention time[c] (min)	Overall Recovery[d] (%)	Intermediate precision[e] (%)	Measurement uncertainty[f] (%)
1[g]	2	3	4	6	7	8	9	10	11	12	13	14
Isocarbamide	$[M + H]^+$	186.1	86.9	86.0	10	25	25	14	3.34	99.3	10.1	20.3
		186.1	44.0	86.0	10	49		18				
		186.1	130.1	86.0	10	19		14				
Isoprocarb	$[M + H]^+$	194.2	94.9	86.0	10	23	23	18	4.68	98.9	7.0	14.8
		194.2	137.1	86.0	10	13		14				
		194.2	77.0	86.0	10	49		32				
Isoxadifen-ethyl	$[M + H]^+$	296.1	232.2	111.0	10	25	25	16	5.50	103.6	8.2	18.0
		296.1	263.1	111.0	10	17		20				
		296.1	204.0	111.0	10	35		14				
Isoxathion	$[M + H]^+$	314.0	105.0	111.0	10	23	23	12	5.86	101.3	8.9	18.2
		314.0	285.9	111.0	10	15		16				
		314.0	114.9	111.0	10	47		16				
Linuron[k,i]	$[M + H]^+$	249.0	160.0	101.0	10	27	27	16	5.02	102.7	14.9	29.9
		249.0	182.1	101.0	10	23		18				
		249.0	133.0	101.0	10	47		18				
Mandipropamid	$[M + H]^+$	413.1	329.1	111.0	10	21	22	22	4.99	101.5	10.2	20.7
		413.1	328.5	111.0	10	21		22				
		413.1	357.1	111.0	10	15		24				
Mepanipyrim	$[M + H]^+$	224.1	105.9	91.0	10	37	**31**	12	5.31	101.9	7.5	18.0
		224.1	77.0	91.0	10	49		16				
		224.1	42.2	91.0	10	49		16				
Mephosfolan	$[M + H]^+$	270.0	139.9	91.0	10	33	**21**	16	3.99	100.5	8.3	16.7
		270.0	74.9	91.0	10	29		30				
		270.0	59.9	91.0	10	69		14				
Methabenzthiazuron	$[M + H]^+$	222.1	164.9	71.0	10	27		18	4.37	100.3	6.9	13.9
		222.1	**150.1**	71.0	10	45	**37**	20				
		222.1	124.1	71.0	10	45		28				
Methidathion[k]	$[M + H]^+$	302.9	145.1	91.0	10	13	13	20	5.00	104.4	8.8	17.7
		302.9	85.0	91.0	10	31		18				
		302.9	58.0	91.0	10	47		26				
Methiocarb	$[M + H]^+$	226.1	169.2	76.0	10	15	15	16	4.96	102.0	8.2	16.7
		226.1	120.9	76.0	10	27		20				
		226.1	122.1	76.0	10	33		16				
Methiocarb sulfone	$[M + NH_4]^+$	275.1	122.1	46.0	10	35	35	16	3.76	100.2	8.1	16.4
		275.1	201.1	46.0	10	19		20				
		275.1	107.1	46.0	10	49		12				
Methiocarb sulfoxide[k]	$[M + H]^+$	242.1	185.2	111.0	10	21	**10**	12	3.24	95.3	12.9	26.0
		242.1	122.0	111.0	10	39		14				
		242.1	170.2	111.0	10	35		14				
Methomyl	$[M + H]^+$	163.1	87.9	41.0	10	15	15	10	2.77	101.2	6.7	13.4
		163.1	106.0	41.0	10	17		14				
		163.1	58.0	41.0	10	31		22				
Methoxyfenozide	$[M + H]^+$	369.1	149.2	131.0	10	25	**19**	14	5.25	101.8	8.9	17.9
		369.1	313.3	131.0	10	13		32				
		369.1	91.1	131.0	10	65		22				
Metolcarb	$[M + H]^+$	166.1	109.0	51.0	10	15	15	16	4.14	99.6	7.1	15.0
		166.1	93.9	51.0	10	45		16				
		166.1	64.8	51.0	10	59		30				
Metosulam	$[M + H]^+$	419.0	175.0	116.0	10	33	33	12	3.57	92.6	12.6	25.2
		419.0	176.0	116.0	10	37		12				
		419.0	140.0	116.0	10	75		10				
Metoxuron	$[M + H]^+$	229.1	72.0	111.0	10	27	**15**	12	3.93	100.2	7.4	15.1
		229.1	46.0	111.0	10	33		18				
		229.1	56.0	111.0	10	71		12				
Mexacarbate[k]	$[M + H]^+$	223.1	151.1	86.0	10	35	**20**	20	5.12	101.9	6.4	13.0
		223.1	166.2	86.0	10	23		22				
		223.1	136.2	86.0	10	53		18				
Molinate[i]	$[M + H]^+$	188.2	126.0	41.0	10	21	21	18	5.22	89.6	13.6	27.4
		188.2	55.0	41.0	10	39		22				
		188.2	83.0	41.0	10	27		18				
Monocrotophos[k]	$[M + H]^+$	224.1	126.9	71.0	10	23	**17**	16	2.76	98.0	6.8	13.7
		224.1	193.1	71.0	10	13		10				
		224.1	98.0	71.0	10	19		12				
Napropamide	$[M + H]^+$	272.1	129.1	86.0	10	23	**14**	18	5.23	100.5	6.9	13.9
		272.1	171.2	86.0	10	29		18				
		272.1	58.0	86.0	10	43		6				

dx.doi.org/10.1021/jf404123h | J. Agric. Food Chem. 2014, 62, 966−983

Table 1. continued

Pesticides	Ionization	Q1 Mass (amu)	Q3 Mass[a] (amu)	DP (V)	EP (V)	CE (V)	CE[b] (V)	CXP (V)	Brewed tea			
									Retention time[c] (min)	Overall Recovery[d] (%)	Intermediate precision[e] (%)	Measurement uncertainty[f] (%)
1[g]	2	3	4	6	7	8	9	10	11	12	13	14
Naptalam	$[M + H]^+$	292.1	144.1	91.0	10	15	15	14	3.24	**29.7**	**32.8**	**68.4**
		292.1	149.0	91.0	10	33		20				
		292.1	256.1	91.0	10	37		18				
Neburon	$[M + H]^+$	275.0	88.0	106.0	10	25	**21**	20	5.47	101.8	8.9	19.4
		275.0	56.9	106.0	10	39		24				
		275.0	114.1	106.0	10	23		24				
Ofurace	$[M + H]^+$	282.1	254.0	111.0	10	19	**13**	26	4.55	102.7	7.0	14.0
		282.1	160.1	111.0	10	37		22				
		282.1	236.1	111.0	10	23		22				
Oxadixyl[k]	$[M + H]^+$	279.1	219.0	91.0	10	17	**11**	24	4.05	102.9	5.6	11.3
		279.1	132.2	91.0	10	47		18				
		279.1	133.2	91.0	10	31		18				
Oxamyl	$[M + NH_4]^+$	237.1	71.9	21.0	10	25	25	30	2.60	100.7	5.8	12.2
		237.1	90.0	21.0	10	13		16				
		237.1	56.0	21.0	10	49		24				
Oxamyl oxime	$[M + H]^+$	163.1	72.0	61.0	10	21	21	16	1.76	98.7	6.2	12.5
		163.1	89.9	61.0	10	27		18				
		163.1	115.1	61.0	10	21		16				
Oxycarboxine[k]	$[M + H]^+$	268.1	175.1	91.0	10	23	**15**	18	3.87	101.8	7.0	14.8
		268.1	147.1	91.0	10	35		14				
		268.1	192.9	91.0	10	19		18				
Paclobutrazol	$[M + H]^+$	294.1	69.9	86.0	10	25	**17**	28	4.86	101.3	8.8	18.3
		294.1	43.1	86.0	10	111		18				
		294.1	124.9	86.0	10	51		16				
Pencycuron	$[M + H]^+$	329.1	125.0	96.0	10	39	**19**	16	5.79	100.1	9.4	19.6
		329.1	89.1	96.0	10	99		16				
		329.1	99.0	96.0	10	89		14				
Penoxsulam	$[M + H]^+$	484.0	195.1	146.0	10	41	41	30	3.62	94.0	7.6	16.1
		484.0	443.8	146.0	10	35		26				
		484.0	164.1	146.0	10	49		20				
Picolinafen	$[M + H]^+$	377.0	238.1	146.0	10	45	45	24	6.05	99.8	17.4	34.9
		377.0	255.9	146.0	10	33		10				
		377.0	283.9	146.0	10	27		28				
Picoxystrobin	$[M + H]^+$	368.0	145.1	111.0	10	33	**19**	20	5.58	104.5	9.4	20.3
		368.0	204.9	111.0	10	15		18				
		368.0	102.0	111.0	10	93		20				
Piperophos	$[M + H]^+$	354.1	170.9	96.0	10	31	**19**	8	5.90	100.6	7.1	14.3
		354.1	255.0	96.0	10	21		12				
		354.1	143.0	96.0	10	45		14				
Pretilachlor	$[M + H]^+$	312.1	252.1	81.0	10	23	**10**	26	5.96	101.1	6.0	12.2
		312.1	176.2	81.0	10	39		24				
		312.1	147.0	81.0	10	49		20				
Primisulfuron-methyl[j]	$[M + H]^+$	468.9	253.9	81.0	10	29	29	26	3.96	93.7	11.6	28.2
		468.9	199.0	81.0	10	33		10				
		468.9	437.1	81.0	10	19		46				
Prodiamine[i]	$[M + H]^+$	351.1	250.2	31.0	10	41	41	26	6.09	100.0	15.5	31.1
		351.1	266.8	31.0	10	27		30				
		351.1	290.8	31.0	10	25		24				
Propamocarb	$[M + H]^+$	189.2	102.0	46.0	10	25	25	14	2.19	**75.4**	11.6	24.8
		189.2	74.0	46.0	10	37		16				
		189.2	144.2	46.0	10	19		14				
Propoxur	$[M + H]^+$	210.1	110.9	76.0	10	23	**16**	12	4.33	101.3	4.5	9.9
		210.1	168.1	76.0	10	13		22				
		210.1	65.0	76.0	10	49		26				
Pymetrozine	$[M + H]^+$	218.1	105.0	91.0	10	27	**19**	22	2.57	87.4	7.3	14.6
		218.1	77.9	91.0	10	49		18				
		218.1	79.0	91.0	10	47		18				
Pyraclostrobin	$[M + H]^+$	388.1	194.0	81.0	10	19	**10**	10	5.71	104.4	8.3	16.6
		388.1	163.1	81.0	10	33		16				
		388.1	104.1	81.0	10	85		22				
Pyraflufen-ethyl	$[M + H]^+$	413.0	338.7	136.0	10	29	**27**	22	5.58	101.2	13.2	26.8
		413.0	253.1	136.0	10	45		14				
		413.0	288.9	136.0	10	43		40				
Pyridalyl[k,i]	$[M + H]^+$	489.8	109.0	126.0	10	43	43	12	7.72	88.8	**39.8**	**81.0**
		489.8	183.1	126.0	10	27		10				
		489.8	204.1	126.0	10	31		22				

dx.doi.org/10.1021/jf404123h | J. Agric. Food Chem. 2014, 62, 966−983

Table 1. continued

Pesticides	Ionization	Q1 Mass (amu)	Q3 Mass[a] (amu)	DP (V)	EP (V)	CE (V)	CE[b] (V)	CXP (V)	Brewed tea: Retention time[c] (min)	Brewed tea: Overall Recovery[d] (%)	Brewed tea: Intermediate precision[e] (%)	Brewed tea: Measurement uncertainty[f] (%)
1[g]	2	3	4	6	7	8	9	10	11	12	13	14
Pyridaphenthion	$[M + H]^+$	341.1	188.9	141.0	10	30	**23**	22	5.16	99.8	9.6	19.3
		341.1	92.1	141.0	10	57		12				
		341.1	205.0	141.0	10	31		28				
Pyridate	$[M + H]^+$	379.1	206.9	76.0	10	23	**18**	10	7.23	87.7	**22.1**	45.4
		379.1	76.9	76.0	10	75		18				
		379.1	56.9	76.0	10	41		22				
Pyrifenox	$[M + H]^+$	295.0	93.0	106.0	10	37	**19**	10	5.33	101.2	9.1	18.2
		295.0	92.6	106.0	10	79		34				
		295.0	67.1	106.0	10	83		14				
Pyrimethanil	$[M + H]^+$	200.1	107.0	91.0	10	35	35	14	5.01	101.1	7.3	16.5
		200.1	82.0	91.0	10	37		18				
		200.1	42.0	91.0	10	49		18				
Pyriproxyfen	$[M + H]^+$	322.1	96.0	81.0	10	23	**13**	12	6.22	102.8	9.3	21.9
		322.1	78.0	81.0	10	81		32				
		322.1	51.0	81.0	10	111		22				
Pyroquilon	$[M + H]^+$	174.2	132.1	61.0	10	33	33	20	3.77	98.2	8.1	16.2
		174.2	117.0	61.0	10	47		16				
		174.2	89.0	61.0	10	77		14				
Pyroxsulam	$[M + H]^+$	435.1	195.1	121.0	10	41	**27**	14	3.09	88.5	14.9	29.9
		435.1	194.1	121.0	10	57		14				
		435.1	82.0	121.0	10	93		12				
Quinoxyfen	$[M + H]^+$	308.0	197.0	51.0	10	47	**35**	26	6.13	99.4	9.9	24.6
		308.0	214.0	51.0	10	49		22				
		308.0	272.0	51.0	10	39		30				
Quizalofop[i]	$[M + H]^+$	345.0	299.0	61.0	10	27	27	38	3.69	**41.2**	**31.0**	**63.6**
		345.0	90.9	61.0	10	43		18				
		345.0	270.8	61.0	10	35		30				
Quizalofop-ethyl	$[M + H]^+$	373.0	298.9	126.0	10	29	**17**	34	5.96	101.2	12.1	24.6
		373.0	270.9	126.0	10	35		28				
		373.0	90.9	126.0	10	49		18				
Schradan[j]	$[M + H]^+$	287.1	135.2	116.0	10	39	**21**	12	3.18	88.3	13.2	26.5
		287.1	242.1	116.0	10	19		24				
		287.1	44.0	116.0	10	69		10				
Simeconazole	$[M + H]^+$	294.1	70.1	71.0	10	27	27	12	4.95	99.4	7.9	15.9
		294.1	135.1	71.0	10	29		8				
		294.1	73.1	71.0	10	47		10				
Spinosyn A	$[M + H]^+$	732.3	142.1	186.0	10	41	41	20	**7.58**	83.2	7.8	16.5
		732.3	98.1	186.0	10	93		22				
		732.3	98.6	186.0	10	71		16				
Spinosyn D	$[M + H]^+$	746.3	142.1	186.0	10	43	43	20	**8.16**	80.3	12.3	25.8
		746.3	98.5	186.0	10	75		12				
		746.3	98.2	186.0	10	101		18				
Spirodiclofen	$[M + H]^+$	411.1	71.0	136.0	10	33	33	12	6.79	100.7	11.6	23.4
		411.1	312.9	136.0	10	17		16				
		411.1	43.0	136.0	10	49		16				
Spiromesifen	$[M + NH_4]^+$	388.2	273.1	51.0	10	21	**9**	26	6.69	100.1	8.9	19.1
		388.2	255.1	51.0	10	39		26				
		388.2	187.0	51.0	10	43		26				
Spirotetramat	$[M + H]^+$	374.2	302.0	81.0	10	25	25	30	4.93	96.2	11.1	22.3
		374.2	216.1	81.0	10	47		22				
		374.2	330.2	81.0	10	25		26				
Spiroxamine	$[M + H]^+$	298.2	144.1	86.0	10	31	**17**	16	**6.62**	81.3	7.0	14.7
		298.2	100.2	86.0	10	43		42				
		298.2	58.1	86.0	10	67		24				
Sulfentrazone	$[M + H]^+$	386.9	306.9	146.0	10	31	31	18	4.16	102.7	8.4	17.0
		386.9	273.2	146.0	10	41		28				
		386.9	307.9	146.0	10	31		32				
Tebufenozide	$[M + H]^+$	353.2	133.1	86.0	10	33		20	5.46	101.6	8.8	18.4
		353.2	**297.1**	86.0	10	13	**23**	32				
		353.2	105.0	86.0	10	59		40				
Tebufenpyrad	$[M + H]^+$	334.1	145.1	121.0	10	39	**31**	18	6.01	97.5	10.1	23.0
		334.1	117.0	121.0	10	49		10				
		334.1	147.2	121.0	10	37		18				
Tebupirimfos	$[M + H]^+$	319.1	277.0	51.0	10	21	**11**	22	6.31	98.9	8.9	21.4
		319.1	153.2	51.0	10	39		16				
		319.1	230.9	51.0	10	39		20				

dx.doi.org/10.1021/jf404123h | J. Agric. Food Chem. 2014, 62, 966−983

Table 1. continued

Pesticides	Ionization	Q1 Mass (amu)	Q3 Mass[a] (amu)	DP (V)	EP (V)	CE (V)	CE[b] (V)	CXP (V)	Brewed tea: Retention time[c] (min)	Brewed tea: Overall Recovery[d] (%)	Brewed tea: Intermediate precision[e] (%)	Brewed tea: Measurement uncertainty[f] (%)
1[g]	2	3	4	6	7	8	9	10	11	12	13	14
Tepraloxydim[i]	$[M + H]^+$	342.1	250.1	61.0	10	19	19	34	3.57	**145.0**	10.7	21.5
		342.1	250.2	61.0	10	19		28				
		342.1	166.1	61.0	10	33		18				
Tetraconazole	$[M + H]^+$	374.0	161.0	126.0	10	51	51	10	5.14	100.9	7.7	15.7
		374.0	69.9	126.0	10	37		28				
		374.0	89.0	126.0	10	109		18				
Thiabendazole	$[M + H]^+$	202.1	175.0	51.0	10	39	**25**	18	3.71	103.6	4.3	11.0
		202.1	131.2	51.0	10	47		26				
		202.1	65.0	51.0	10	61		14				
Thiabendazole d_4 (IS)	$[M + H]^+$	206.1	179.1	131.0	10	39	39	18	3.69			
Thiacloprid	$[M + H]^+$	253.0	126.1	101.0	10	33	**20**	12	3.88	99.6	9.0	18.0
		253.0	89.9	101.0	10	49		12				
		253.0	99.0	101.0	10	49		12				
Thiamethoxam	$[M + H]^+$	292.0	210.9	76.0	10	19		18	3.06	99.9	8.8	18.9
		292.0	**181.0**	76.0	10	33	33	18				
		292.0	132.1	76.0	10	33		8				
Thiazopyr	$[M + H]^+$	397.0	376.9	146.0	10	31	**26**	36	5.71	102.9	7.5	15.1
		397.0	334.9	146.0	10	39		40				
		397.0	61.0	146.0	10	49		28				
Thiodicarb	$[M + H]^+$	355.0	88.0	106.0	10	23	23	16	4.23	98.1	10.6	21.3
		355.0	108.1	106.0	10	23		14				
		355.0	73.0	106.0	10	73		14				
Thiofanox[j]	$[M + Na]^+$	241.1	184.2	76.0	10	17	17	18	4.50	95.8	9.1	19.2
		241.1	97.9	76.0	10	19		12				
		241.1	106.0	76.0	10	21		22				
Thiofanox sulfone	$[M + NH_4]^+$	268.1	57.1	51.0	10	19	19	4	3.55	103.6	8.3	17.5
		268.1	76.1	51.0	10	17		10				
		268.1	41.1	51.0	10	55		6				
Thiofanox sulfoxide	$[M + H]^+$	235.1	103.9	46.0	10	15	15	12	3.09	102.1	6.5	14.3
		235.1	57.1	46.0	10	29		14				
		235.1	63.9	46.0	10	41		12				
Tolfenpyrad	$[M + H]^+$	385.1	198.2	106.0	10	35	35	14	5.97	98.1	11.0	22.2
		385.1	197.0	106.0	10	35		12				
		385.1	91.1	106.0	10	75		12				
Tolylfluanid[i]	$[M + H]^+$	346.9	237.9	106.0	10	17	17	26	5.76	96.6	10.3	25.6
		346.9	137.0	106.0	10	35		18				
		346.9	136.6	106.0	10	67		18				
Tralkoxydim	$[M + H]^+$	330.2	284.1	86.0	10	19	**15**	28	5.10	**120.6**	8.8	17.9
		330.2	138.0	86.0	10	31		14				
		330.2	96.1	86.0	10	45		20				
Trichlorfon	$[M + H]^+$	256.9	127.1	101.0	10	29	29	18	3.19	100.5	13.1	26.4
		256.9	220.8	101.0	10	17		24				
		256.9	109.0	101.0	10	31		10				
Tricyclazole[k]	$[M + H]^+$	190.0	163.1	111.0	10	33	**24**	16	3.61	96.5	10.3	20.6
		190.0	136.0	111.0	10	43		18				
		190.0	109.0	111.0	10	51		14				
Trietazine	$[M + H]^+$	230.1	99.0	101.0	10	35	**30**	22	5.36	100.0	6.9	13.9
		230.1	42.9	101.0	10	49		18				
		230.1	202.2	101.0	10	29		10				
Trifloxysulfuron	$[M + H]^+$	438.0	182.1	106.0	10	29	**14**	26	3.55	90.2	10.8	21.7
		438.0	257.0	106.0	10	29		28				
		438.0	176.2	106.0	10	47		18				
Triforine[j,l]	$[M + H]^+$	434.8	389.8	71.0	10	19	19	12	4.53	99.0	10.2	20.5
		434.8	98.0	71.0	10	49		10				
		434.8	82.8	71.0	10	91		12				
Trimethacarb[k]	$[M + H]^+$	194.2	137.2	86.0	10	17		18	4.68	101.0	6.8	13.6
		194.2	**122.1**	86.0	10	37	37	16				
		194.2	107.0	86.0	10	53		12				
Zinophos[i]	$[M + H]^+$	249.0	97.0	51.0	10	41	41	12	4.87	97.8	12.0	26.1
		249.0	193.1	51.0	10	21		26				
		249.0	220.8	51.0	10	17		24				

dx.doi.org/10.1021/jf404123h | J. Agric. Food Chem. 2014, 62, 966−983

Table 1. continued

Pesticides	Ionization	Q1 Mass (amu)	Q3 Mass[a] (amu)	DP (V)	EP (V)	CE (V)	CE[b] (V)	CXP (V)	Brewed tea: Retention time[c] (min)	Brewed tea: Overall Recovery[d] (%)	Brewed tea: Intermediate precision[e] (%)	Brewed tea: Measurement uncertainty[f] (%)
1[g]	2	3	4	6	7	8	9	10	11	12	13	14
Zoxamide	$[M + H]^+$	336.0	187.0	131.0	10	33	**19**	20	5.68	104.5	11.7	24.5
		336.0	159.1	131.0	10	49		22				
		336.0	204.0	131.0	10	25		22				

[a] Bold and underlined are the second transition that is used for quantification.
[b] Collision energy (bold and underlined) was attenuated to avoid the saturation of the detector at the highest concentration level of the calibration curve. Transitions in the corresponding row were used for quantification.
[c] Retention time may vary from column-to-column. Bold and underlined are pesticides whose retention time drifted within a batch run.
[d] Bold and underlined are pesticides with recoveries not in the range of 81 to 110 %.
[e] Bold and underlined are pesticides intermediate precision > 20 %.
[f] Bold and underlined are pesticides MU > 50 %.
[g] Column number.
[h] Method performance was based on two spike levels, i.e. 240.0 and 400.0 μg/kg due to its poor sensitivity.
[i] Method performance was based on three spike levels, i.e. 90.0, 240.0 and 400.0 μg/kg due to its poor sensitivity.
[j] Pesticides have a relatively low solubility in methanol. Stock solution was prepared in 1000.0 μg /mL.
[k] Pesticides have a relatively low solubility in methanol. Stock solution was prepared in 2000.0 μg /mL.
[l] An Ion with Cl^{37} was selected as a precursor ion.

MATERIALS AND METHODS

Materials and Reagents. For the pesticide residue transfer rate study, 44 dried tea leaf samples, which had tested positive for one or more pesticides, were obtained from a 2011 targeted survey program under the Food Safety Action Plan in Canada. All samples (50 g per samples) were well blended in CFIA contract laboratories prior to shipment to the Calgary Laboratory for the study. For method development and validation, blank samples of tea leaves (pesticide free), including Earl Grey, oolong, green tea, herbal tea and orange pekoe, were obtained from local markets. Tea bags were cut and emptied into mixing bowls, then mixed to create a composite. Loose tea leaf samples (200−500 g per sample) were blended using a food blender. All samples were stored at room temperature.

Ammonium acetate (reagent grade and LC-MS grade) and LC-MS acetonitrile (Chromasolv, 2.5 L) were purchased from Sigma-Aldrich Corp. (Canada). ENVIRO CLEAN extraction columns (6.0 g of anhydrous magnesium sulfate ($MgSO_4$) and 1.5 g of sodium acetate, 50 mL centrifuge tubes) and ENVIRO CLEAN extraction columns ((900 mg of $MgSO_4$, 150 mg C_{18}, and 300 mg of primary−secondary amine (PSA), 15 mL centrifuge tubes) or (900 mg of $MgSO_4$, 150 mg of graphitized black carbon, and 300 mg of PSA, 15 mL centrifuge tubes)) were obtained from United Chemical Technologies, Inc. (Bristol, PA, USA). Acetic acid (glacial acetic acid, reagent grade, 99.7%), acetonitrile (distilled in glass), and methanol (distilled in glass) were obtained from Caledon Laboratories Ltd. (Canada). Water (18.2 MΩ·Cm) used for reagent and sample preparation was from a Barnstead Nanopure system (Thermo Scientific, USA). Pesticide standards (Table 1, column 1) were obtained from EQ Laboratories Inc. (USA), Riedel-de Haen AG (Germany), or Chem Service (USA). Internal standards carbendazim-d_4 and carbofuran-d_3 were purchased from EQ Laboratories Inc. (USA), and thiabendazole-d_4 was from Chemical Synthesis Services (Northern Ireland). LC vials were Mini-UniPrep syringeless filter devices with polypropylene housing and PVDF 0.45 μm membrane (Whatman Inc., USA).

UHPLC/ESI-MS/MS Parameters. The LC/ESI-MS/MS system utilized was an Agilent 1200 SL (Agilent, Germany) coupled with an API 5000 LC/MS/MS system (Applied Biosystem, Canada). The system was controlled using Analyst 1.5 software.

Mobile phase B was acetonitrile, and mobile phase A was 10 mM ammonium acetate with 2% acetonitrile in water. The column oven temperature was set at 35 °C, and the autosampler temperature was set at 5 °C.

Core−Shell Particles Column. The core−shell particles or UHPLC column utilized was a Kinetex C_{18}, 100 mm × 2.1 mm, 2.6 μm column (Phenomenex, USA). Injection volume was 3 μL, and total run time was 12 min. The UHPLC gradient profile is shown in Table 2.

MS/MS Conditions. The ion source was a TurboIonSpray or Turbo V electrospray ion source in positive mode. Pause time between mass ranges was 5 ms. Specific mass spectrometric parameters such as dwell time, declustering potential (DP), entrance potential (EP), collision energy (CE), collision cell exit potential (CXP), and multiple reaction monitoring transitions (MRM or Q1 and Q3) are listed in Table 1. Parameters including DP, EP, CE, and CXP were optimized using the Quantitative Optimization bundled with the Analyst software by infusing each individual pesticide standard (10 or 50 μg/L) into the mass spectrometer. The syringe pump (Harvard Apparatus, USA) flow rate was set at 10 μL/min for infusion. Scheduled MRM was set according to the retention time of pesticides using a MRM detection window of 100 s. The total scan time was 1.6211 s, and the duration was 11 min. Other general mass spectrometric parameters are shown in Table 2.

Table 2. UHPLC Gradient Profiles and MS Parameters

Kinetex C_{18}, 2.6 μm			
Total time	Flow rate (μl/min)	A (%)	B (%)
0.0	300	92	8
4.0	300	10	90
8.0	300	10	90
9.0	500	0	100
9.5	500	0	100
10.0	500	92	8
12.0	300	92	8

API 5000 parameters	
Collision gas (CAD)	7
Curtain gas (CUR)	25
Ion source gas 1 (GS1)	60
Ion source gas 2 (GS2)	60
IonSpray voltage (IS)	5000
Temperature	550

Preparation of Standard Solutions. Individual pesticide standard stock solutions were generally prepared at a concentration of 4000.0 μg/mL in methanol. Due to its poor solubility in methanol, carbendazim was prepared at 200.0 μg/mL, and a few pesticides were prepared at 1000.0 or 2000.0 μg/mL (Table 1, column 1). Internal standard stock solution including carbofuran-d_3, carbendazim-d_4, and

dx.doi.org/10.1021/jf404123h | J. Agric. Food Chem. 2014, 62, 966−983

Table 3. Pesticide Residue Transfer Rate Simulation and Analytical Range Determination

Lowest concentration in brewed tea

A							
Brewed tea (μg/L)							
0.4	0.15	L	(amount of hot water for brewing)				
	0.06	μg	0.2	(transfer rate)			
			0.3	μg	0.005	kg	(dried tea leaves to brew)
					60.0	μg/kg	
					Tea leaves (μg/kg)		

B							
Brewed tea (μg/L)							
0.4	0.15	L	(amount of hot water for brewing)				
	0.06	μg	1	(transfer rate)			
			0.06	μg	0.005	kg	(dried tea leaves to brew)
					12.0	μg/kg	
					Tea leaves (μg/kg)		

Highest concentration in dried tea leaves

C							
Tea leaves (μg/kg)							
1200	0.005	kg	(dried tea leaves to brew)				
	6.0	μg	0.2	(transfer rate)			
			1.2	μg	0.15	L	(amount of hot water for brewing)
					8.0	μg/L	
					Brewed tea (μg/L)		

D							
Tea leaves (μg/kg)							
1200	0.005	kg	(dried tea leaves to brew)				
	6.0	μg	1	(transfer rate)			
			6.0	μg	0.15	L	(amount of hot water for brewing)
					40.0	μg/L	
					Brewed tea (μg/L)		

thiabendazole-d_4 was prepared at 100.0 μg/mL. Intermediate pesticide standard mix working solutions were prepared at 10.0 μg/mL. Stock and intermediate solutions were stored at −20 °C.

Dried Tea Leaves. A six-level pesticide standard mix working solution was prepared by transferring 0.1, 0.5, 2.0, 4.0, 6.0, and 10.0 mL of 10.0 μg/mL intermediate working solution into six separate 50 mL volumetric flasks and making up to volume with methanol. This resulted in 0.02, 0.1, 0.4, 0.8, 1.2, and 2.0 μg/mL standard solutions, which were used to construct matrix-matched standard calibration curves. Internal standard working solution (2.0 μg/mL) was prepared from their respective stock in a mixture of acetonitrile and methanol (50:50, v/v). All working solutions were stored at 4 °C.

Brewed Tea. A six-level pesticide standard mix working solution was prepared by transferring 0.1, 0.5, 2.0, 4.0, 6.0, and 10.0 mL of 10.0 μg/mL intermediate working solution into six separate 50 mL volumetric flasks and making up to volume with methanol. This resulted in 0.02, 0.1, 0.4, 0.8, 1.2, and 2.0 μg/mL standard solutions, which were used to construct matrix-matched standard calibration curves. Four-level sample spike pesticide standard working solutions were prepared by transferring 2.0, 6.0, 10.0, and 16.0 mL of 10.0 μg/mL intermediate working solution into separate 50 mL volumetric flasks and making up to volume with methanol. This resulted in 0.4, 1.2, 2.0, and 3.2 μg/mL standard solutions, which were used for sample fortification. Internal standard working solution (0.8 μg/mL) was prepared from their stock in a mixture of acetonitrile and methanol (50:50, v/v). All working solutions were stored at 4 °C.

Preparation of Reagent Solutions. Acetonitrile/acetic acid (99 + 1, v/v) was prepared by mixing 990 mL of acetonitrile with 10 mL of acetic acid. Ammonium acetate solution (0.1 M) was prepared by weighing 7.7 g of ammonium acetate and dissolving in 800 mL of water. After transfer into a 1000 mL volumetric flask, the solution was made up to volume with water. Solvent buffer was a mixture of 0.1 M ammonium acetate and methanol (50 + 50, v/v).

Sample Preparation and Extraction Procedure. *Dried Tea Leaves.* Sample extraction and cleanup procedures followed the buffered QuEChERS method.[7] An incurred tea sample (5.0 g/sample) was weighed into individual 50 mL polypropylene centrifuge tubes (VWR International, Canada). To each tube was added 250 μL of 2.0 μg/mL internal standard working solution (100.0 μg/kg equivalent in samples) and 15 mL of water. Tubes were capped, and the contents were mixed and allowed to stand for the purpose of hydration. After 30 min of hydration at room temperature, 15 mL of acetonitrile/acetic acid (99 + 1, v/v) was added to individual samples and mixed, followed by the addition of 1.5 g of sodium acetate anhydrous and 6.0 g of magnesium sulfate anhydrous. The centrifuge tubes were capped, and all samples were shaken for 1 min using a Geno/Grinder 2010 at 1500 rpm (SPEX SamplePrep, USA) and then were centrifuged at 3000 rpm (~2100*g*) for 3 min using an Allegra 6 centrifuge (Beckman Coulter Inc., USA). Supernatants were transferred (7 mL/sample) into individual 15 mL polypropylene centrifuge tubes that contained 900 mg of $MgSO_4$, 150 mg of graphitized black carbon, and 300 mg of PSA. The centrifuge tubes were capped, shaken for 45 s by hand, and centrifuged at 3000 rpm (~2100*g*) for 3 min. Three milliliters of supernatant (1 g sample/3 mL) was transferred into individual 5 mL Pyrex brand centrifuge tubes, precalibrated with 1 mL volume accuracy (VWR International, Canada). Each of the sample extracts was evaporated to 0.1−0.2 mL, which took approximately 45 min, using an N-EVAP nitrogen evaporator (Organomation Associates Inc., USA) at 30 °C under a stream of nitrogen. The extracts were made up to 0.5 mL with methanol, vortexed for 30 s, and then made up to 1.0 mL with 0.1 M ammonium acetate and vortexed again for 30 s. One hundred microliters of each extract was transferred into a Mini-UniPrep vial (Whatman Inc., USA), and 500 μL of solvent buffer (a mixture of 0.1 M ammonium acetate/methanol, 50 + 50, v/v) was added. The vials were capped, vortexed for 30 s, and pressed to filter. Sample extracts were injected to the UHPLC/ESI-MS/MS. All dried tea leaves (incurred samples) were analyzed in duplicate.

Brewed Tea. Dried tea leaves were brewed as follows. Five grams of dried tea leaves were weighed into a 250 mL Erlenmeyer flask, to which 150 mL of boiling water (distilled) was added. The sample was swirled to mix after 3 and 6 min with a total brewing time of 10 min. After the brewing process, the brewed tea samples were cooled by immersing the flask in cold water (~7 °C) for 20 min. Then, 10 mL of brewed tea was subsampled into individual 50 mL polypropylene centrifuge tubes (VWR International, Canada) for the QuEChERS extraction and cleanup. For the fortification experiment, 100 μL of each four-level sample spike pesticide standard working solution was added into four centrifuge tubes to provide 4.0, 12.0, 20.0, and 32.0 μg/L pesticide equivalents in samples. To each tube was added 100 μL of 0.8 μg/mL internal standard working solution (8.0 μg/kg equivalent in samples). After 10 min at room temperature, 10 mL of acetonitrile/acetic acid (99 + 1, v/v) was added to individual samples and mixed for 45 s, followed by the addition of 1.5 g of sodium acetate anhydrous and 6.0 g of magnesium sulfate anhydrous. Four to six samples were processed at a time and shaken immediately by hand to avoid clumping. All samples were then shaken for 1 min using Geno/Grinder 2010 at 1500 rpm (SPEX SamplePrep, USA) and were centrifuged at 3000 rpm (~2100*g*) for 3 min using an Allegra 6 centrifuge (Beckman Coulter Inc., USA). Supernatants were transferred (5 mL/sample) into individual 15 mL polypropylene centrifuge tubes (VWR International, Canada) that contained 900 mg of $MgSO_4$, 150 mg of C_{18}, and 300 mg of PSA. The centrifuge tubes were capped, shaken for 45 s by hand, and centrifuged at 3000 rpm (~2100*g*) for 3 min. Two and half milliliters of supernatant was transferred into individual 5 mL Pyrex brand centrifuge tubes, precalibrated with 1 mL volume accuracy (VWR International, Canada). Each of the sample extracts was evaporated to 0.1 − 0.2 mL, which took approximately 30−45 min, using an N-EVAP nitrogen evaporator (Organomation Associates Inc., USA) at 30 °C under a stream of nitrogen. The extracts were made up to 0.5 mL with methanol, vortexed for 30 s, and then made up to 1.0 mL with 0.1 M ammonium acetate and vortexed again for 30 s. Five hundred microliters of each extract was transferred into a Mini-UniPrep vial (Whatman Inc., USA), and the vials were capped, vortexed for 30 s, and pressed to filter. Sample extracts were injected on an UHPLC/ESI-MS/MS system. All brewed tea (incurred) were analyzed in duplicate.

Preparation of Matrix-Matched Calibration Standards and Calculation. *Dried Tea Leaves.* Matrix-matched calibration standards were prepared by adding standards and internal standards to blank sample extracts after sample extraction and cleanup. A blank tea sample (5.0 g/sample) was weighed into a 50 mL centrifuge tube, and the

dx.doi.org/10.1021/jf404123h | J. Agric. Food Chem. 2014, 62, 966−983

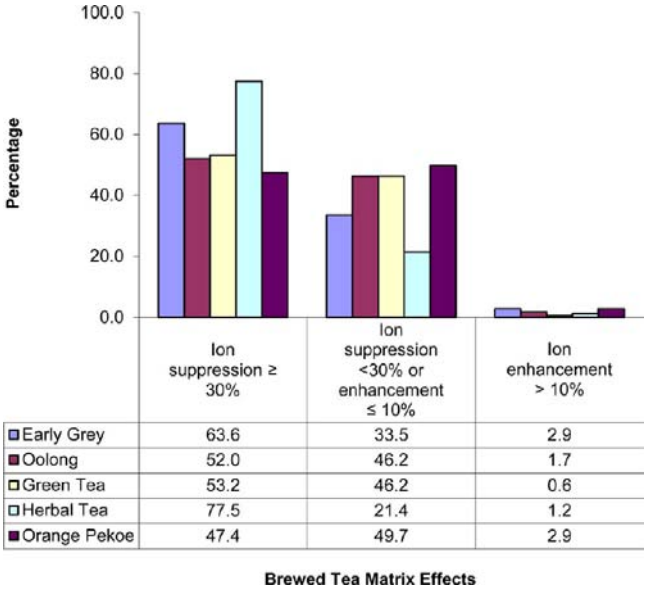

Figure 1. UHPLC/ESI-MS/MS matrix effects. The 172 pesticides were prepared in matrix extracts (a total of 5 brewed tea matrices) and solvent buffer at a concentration of 8.0 μg/kg equivalent in sample.

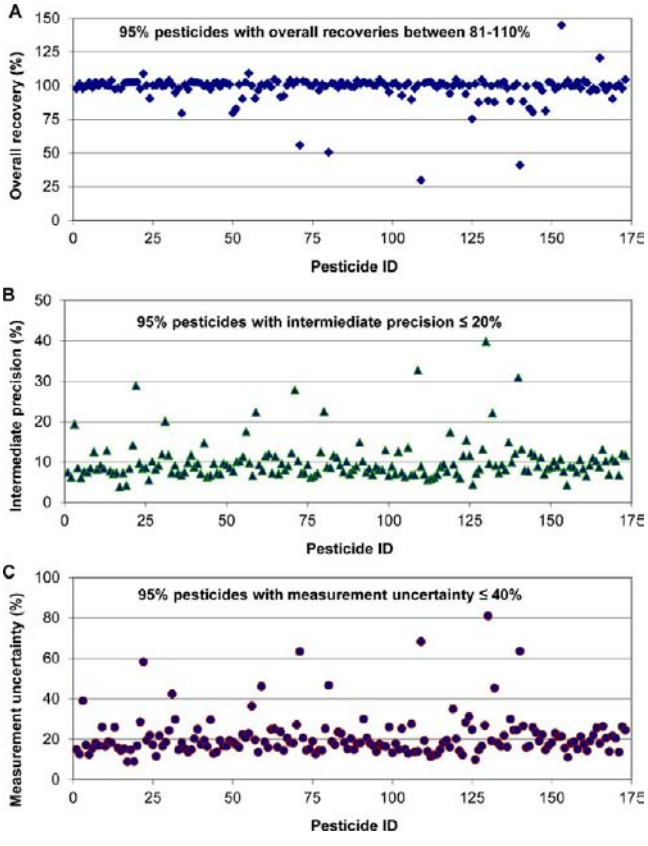

Figure 2. UHPLC/ESI-MS/MS method performance for analysis of 172 pesticides in brewed tea: (A) overall recovery; (B) intermediate precision; (C) measurement uncertainty.

sample was processed through the extraction procedure as described above for dried tea leaves. Two hundred and fifty microliters of each six-level pesticide standard mix working solution was added into each of six blank sample extracts, providing 5.0, 25.0, 100.0, 200.0, 300.0, and 500.0 μg/kg per standard equivalent in samples. Then, 50 μL of 2.0 μg/mL internal working solution was added to each sample

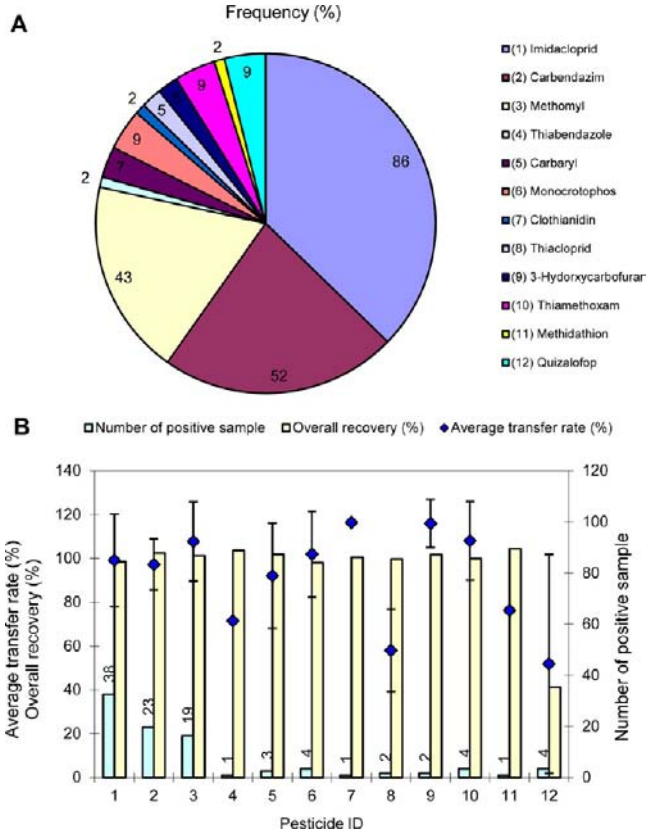

Figure 3. (A) Frequency (%) of 12 pesticides found in 44 incurred samples. (B) Number of positive samples, average transfer rate (%), and overall recovery in brewed tea (%). Pesticides: (1) imidacloprid; (2) methomyl; (3) carbendazim; (4) thiabendazole; (5) carbaryl; (6) monocrotophos; (7) clothianidin; (8) thiacloprid; (9) 3-hydroxycarbofuran; (10) thiamethoxam; (11) methidathion; (12) quizalofop.

(100.0 μg/kg equivalent in samples). The extracts were made up to 0.5 mL with methanol, vortexed for 30 s, made up to 1.0 mL volume with 0.1 M ammonium acetate and then vortexed again for 30 s. The extracts were diluted six times using the solvent buffer prior to UHPLC/ESI-MS/MS injection.

Brewed Tea. Matrix-matched calibration standards were prepared by adding standards and internal standards to blank sample extracts after sample extraction and cleanup. A blank brewed tea sample (10.0 mL/sample) was weighed into a 50 mL centrifuge tube, and the sample was processed through the extraction procedure as described above for brewed tea. Fifty microliters of each six-level pesticide standard mix working solution was transferred into six separate blank sample extracts, providing 0.4, 2.0, 8.0, 16.0, 24.0, and 40.0 μg/L per standard equivalent in samples. Then, 25 μL of 0.8 μg/mL internal working solution was added to each sample (8.0 μg/L equivalent in samples). The extracts were made up to 0.5 mL with methanol, vortexed for 30 s, made up volume to 1.0 mL with 0.1 M ammonium acetate, and then vortexed again for 30 s. Five hundred microliters of each extract was transferred into a Mini-UniPrep vial (Whatman Inc., USA), and the vials were capped, vortexed for 30 s, and pressed to filter. Sample extracts were analyzed using UHPLC/ESI-MS/MS.

To compensate for matrix effects, the oolong tea was used as the standard matrix to prepare matrix-matched calibration standards in both dried tea leaves and brewed tea.

Matrix-matched standard calibration curves for each individual pesticide were constructed using MultiQuant. Concentration, (μg/kg or μg/L (ppb)) versus the ratio (analyte area/IS area) of each individual pesticide was plotted. Deuterium-labeled standards carbendazim-d_4, carbofuran-d_3, and thiabendazole-d_4 were used as internal standards for their respective native compounds for quantification. Other pesticides

dx.doi.org/10.1021/jf404123h | J. Agric. Food Chem. 2014, 62, 966−983

Table 4. Pesticide Residue Transfer Rates (%) from Dried Tea Leaves to Brewed Tea Determined Using UHPLC/ESI-MS/MS

Pesticide names		Methomyl			Carbendazim			Thiabendazole			Carbaryl			Monocrotophos			Clothianidin			Thiacloprid			3-Hydroxycarbo-furan			Imidacloprid			Thiamethoxam			Methidathion			Quizalofop		
Pesticide classification or activity		Insecticides			Fungicides			Fungicides			Acaricides, Insecticides, Plant growth regulators			Acaricides, Insecticides			Insecticides			Insecticides			Carbofuran metabolite			Insecticides			Insecticides			Insecticides			Herbicides		
Tea		Tea leaves	Brewed tea		Tea leaves	Brewed tea		Tea leaves	Brewed tea		Tea leaves	Brewed tea		Tea leaves	Brewed tea		Tea leaves	Brewed tea		Tea leaves	Brewed tea		Tea leaves	Brewed tea		Tea leaves	Brewed tea		Tea leaves	Brewed tea		Tea leaves	Brewed tea		Tea leaves	Brewed tea	
Sample ID	Duplicate	Concentration (μg/kg)	Concentration (μg/L)	Transfer rate (%)	Concentration (μg/kg)	Concentration (μg/L)	Transfer rate (%)	Concentration (μg/kg)	Concentration (μg/L)	Transfer rate (%)	Concentration (μg/kg)	Concentration (μg/L)	Transfer rate (%)	Concentration (μg/kg)	Concentration (μg/L)	Transfer rate (%)	Concentration (μg/kg)	Concentration (μg/L)	Transfer rate (%)	Concentration (μg/kg)	Concentration (μg/L)	Transfer rate (%)	Concentration (μg/kg)	Concentration (μg/L)	Transfer rate (%)	Concentration (μg/kg)	Concentration (μg/L)	Transfer rate (%)	Concentration (μg/kg)	Concentration (μg/L)	Transfer rate (%)	Concentration (μg/kg)	Concentration (μg/L)	Transfer rate (%)	Concentration (μg/kg)	Concentration (μg/L)	Transfer rate (%)
1	1	33.6	1.1		19.2	0.5		298.0	5.8		64.9	1.5													243.0	6.9					78.0	1.7				
	2	36.2	1.1		19.0	0.5		289.0	6.2		65.3	1.6													236.0	7.7					75.6	1.7				
	Mean	34.9	1.1	**94.1**	19.1	0.5	**73.8**	293.5	6.0	**61.3**	65.1	1.5	**70.7**												239.5	7.3	**91.5**				76.8	1.7	**65.4**			
2	1																																153.0	5.7	
	2																																138.0	4.7	
	Mean																																145.5	5.2	**107.1**
3	1				31.2	0.9																			93.1	2.8										
	2				31.4	0.8																			88.0	3.3										
	Mean				31.3	0.8	**77.6**																		90.6	3.1	**101.4**									
4	1													37.4	0.8					18.1	0.4					66.1	2.5		125.0	3.0						
	2													33.7	1.0					18.7	0.4					69.8	2.8		125.0	3.7						
	Mean													35.6	0.9	**73.8**				18.4	0.4	**61.1**				68.0	2.7	**117.2**	125.0	3.4	**80.5**					
5	1	16.1	0.6		18.0	0.5																			158.7	3.8										
	2	16.9	0.6		15.4	0.5																			165.0	4.4										
	Mean	16.5	0.6	**103.6**	16.7	0.5	**89.8**																		161.9	4.1	**76.0**									
6	1				23.6	0.7																			82.6	1.7										
	2				26.3	0.6																			75.8	1.9										
	Mean				25.0	0.7	**82.4**																		79.2	1.8	**67.2**									
7	1	195.0	4.2		56.5	1.4					46.5	1.0								110.5	1.5				3400.0	96.5										
	2	206.0	4.3		53.0	1.6					43.0	0.9								113.5	1.4				3355.0	101.0										
	Mean	200.5	4.2	**63.4**	54.8	1.5	**81.4**				44.8	1.0	**63.7**							112.0	1.4	**38.3**				3377.5	98.7	**87.7**									
8	1	13.3	0.4		13.1	0.4																			86.2	3.0										
	2	13.3	0.4		12.9	0.3																			81.1	3.1										
	Mean	13.3	0.4	**90.2**	13.0	0.4	**85.4**																		83.7	3.1	**109.9**									
9	1	122.7	3.9		35.5	0.8																			459.0	10.7										
	2	120.7	4.2		27.7	0.8																			405.0	10.8										
	Mean	121.7	4.0	**99.3**	31.6	0.8	**78.8**																		432.0	10.8	**74.7**									
10	1				39.1	1.0																			109.0	2.9										
	2				40.7	1.0																			103.0	2.8										
	Mean				39.9	1.0	**74.8**																		106.0	2.9	**80.9**									
11	1	160.0	6.1		73.0	2.0																			201.0	4.6										
	2	183.0	6.2		74.3	2.0																			201.0	5.4										
	Mean	171.5	6.2	**107.9**	73.7	2.0	**81.1**																		201.0	5.0	**74.6**									
12	1	34.1	1.3																																		
	2	31.0	1.3																																		
	Mean	32.6	1.3	**118.9**																																	
13	1																								62.3	1.8										
	2																								77.7	1.5										
	Mean																								70.0	1.7	**71.8**									
14	1	13.7	0.4		25.9	0.8																			172.0	5.4										
	2	12.3	0.4		29.7	0.8																			162.0	5.6										
	Mean	13.0	0.4	**92.3**	27.8	0.8	**81.5**																		167.0	5.5	**98.7**									
15	1	12.3	0.5		17.8	0.6																			87.0	3.3										
	2	12.9	0.5		15.7	0.6																			82.3	2.7										
	Mean	12.6	0.5	**116.7**	16.8	0.6	**112.8**																		84.7	3.0	**105.3**									
16	1																								112.0	3.6										
	2																								121.0	3.6										
	Mean																								116.5	3.6	**92.2**									
17	1				104.0	3.0																			159.0	4.5										
	2				107.0	2.7																			155.0	3.7										
	Mean				105.5	2.8	**80.0**																		157.0	4.1	**78.1**									
18	1										45.5	2.0																									
	2										75.2	2.2																									
	Mean										60.4	2.1	**102.4**																								
19	1	313.7	8.7		33.0	0.9																			1503.3	38.1										
	2	323.7	9.0		31.0	0.9																			1576.7	39.8										
	Mean	318.7	8.8	**83.0**	32.0	0.9	**85.8**																		1540.0	38.9	**75.8**									
20	1				102.0	2.4								25.1	0.7										38.7	1.2										
	2				102.0	2.7								24.9	0.7										44.5	1.1										
	Mean				102.0	2.6	**75.3**							25.0	0.7	**79.2**									41.6	1.1	**81.5**									
21	1				28.1	0.7																			164.0	5.4										
	2				27.1	0.8																			143.0	6.4										
	Mean				27.6	0.7	**78.8**																		153.5	5.9	**115.1**									
22	1																																108.0	0.9	
	2																																126.0	1.1	
	Mean																																117.0	1.0	**24.7**
23	1				28.5	0.8																			73.2	2.5										
	2				28.3	0.6																			59.2	2.5										
	Mean				28.4	0.7	**74.5**																		66.2	2.5	**114.7**									
24	1																																134.0	0.5	
	2																																132.0	0.6	
	Mean																																133.0	0.5	**11.6**

dx.doi.org/10.1021/jf404123h | J. Agric. Food Chem. 2014, 62, 966−983

Table 4. continued

Pesticide names		Methomyl			Carbendazim			Thiabendazole			Carbaryl			Monocrotophos			Clothianidin			Thiacloprid			3-Hydroxycarbofuran			Imidacloprid			Thiamethoxam			Methidathion			Quizalofop		
Pesticide classification or activity		Insecticides			Fungicides			Fungicides			Acaricides, Insecticides, Plant growth regulators			Acaricides, Insecticides			Insecticides			Insecticides			Carbofuran metabolite			Insecticides			Insecticides			Insecticides			Herbicides		
Tea		Tea leaves	Brewed tea		Tea leaves	Brewed tea		Tea leaves	Brewed tea		Tea leaves	Brewed tea		Tea leaves	Brewed tea		Tea leaves	Brewed tea		Tea leaves	Brewed tea		Tea leaves	Brewed tea		Tea leaves	Brewed tea		Tea leaves	Brewed tea		Tea leaves	Brewed tea		Tea leaves	Brewed tea	
Sample ID	Duplicate	Concentration (μg/kg)	Concentration (μg/L)	Transfer rate (%)	Concentration (μg/kg)	Concentration (μg/L)	Transfer rate (%)	Concentration (μg/kg)	Concentration (μg/L)	Transfer rate (%)	Concentration (μg/kg)	Concentration (μg/L)	Transfer rate (%)	Concentration (μg/kg)	Concentration (μg/L)	Transfer rate (%)	Concentration (μg/kg)	Concentration (μg/L)	Transfer rate (%)	Concentration (μg/kg)	Concentration (μg/L)	Transfer rate (%)	Concentration (μg/kg)	Concentration (μg/L)	Transfer rate (%)	Concentration (μg/kg)	Concentration (μg/L)	Transfer rate (%)	Concentration (μg/kg)	Concentration (μg/L)	Transfer rate (%)	Concentration (μg/kg)	Concentration (μg/L)	Transfer rate (%)	Concentration (μg/kg)	Concentration (μg/L)	Transfer rate (%)
25	1																									210.0	8.1										
	2																									234.0	8.4										
	Mean																									222.0	8.3	**111.6**									
26	1	125.0	3.2																							527.0	15.7										
	2	128.0	3.2																							498.0	15.3										
	Mean	126.5	3.2	**75.4**																						512.5	15.5	**99.8**									
27	1																									60.7	2.2										
	2																									58.3	1.7										
	Mean																									59.5	1.9	**97.3**									
28	1	123.8	3.9		63.6	1.5																				149.0	2.8										
	2		4.2		54.4	1.7																				172.0	3.1										
	Mean	123.8	4.0	**97.7**	59.0	1.6	**80.8**																			160.5	2.9	**54.9**									
29	1	719.0	17.4		42.5	1.4																	59.0	2.0		6546.0	221.0										
	2	694.0	16.4		31.5	1.4																	65.5	1.9		5478.0	280.0										
	Mean	706.5	16.9	**71.7**	37.0	1.4	**110.7**																62.3	1.9	**92.8**	6012.0	250.5	**125.0**									
30	1													96.3	2.7											38.0	1.0		230.0	8.5								
	2													97.7	2.8											34.5	1.0		239.0	9.0								
	Mean													97.0	2.7	**84.9**										36.3	1.0	**82.8**	234.5	8.8	**112.2**						
31	1	121.0	3.3																							86.5	1.7										
	2	119.0	3.5																							87.2	2.0										
	Mean	120.0	3.4	**85.3**																						86.9	1.8	**63.0**									
32	1																																	139.0	1.9	
	2																																	147.0	1.4	
	Mean																																	143.0	1.6	**34.4**
33	1				30.6	0.8																				99.5	2.7										
	2				39.4	1.0																				106.0	3.1										
	Mean				35.0	0.9	**78.0**																			102.8	2.9	**84.4**									
34	1				63.4	1.9								87.0	3.2		114.1	3.2								52.9	1.6		177.4	5.6								
	2				64.6	1.9									3.4		99.4	3.9								58.8	1.7		191.8	6.4								
	Mean				64.0	1.9	**88.8**							87.0	3.3	**111.6**	106.8	3.6	**99.8**							55.9	1.7	**89.4**	184.6	6.0	**97.7**						
35	1	15.0	0.4																							58.6	1.7										
	2	-	0.4																							66.3	1.5										
	Mean	15.0	0.4	**82.5**																						62.5	1.6	**76.6**									
36	1																									226.0	7.6										
	2																									290.0	6.9										
	Mean																									258.0	7.2	**84.2**									
37	1																									81.0	1.9		62.7	1.5								
	2																									68.8	2.3		56.4	1.7								
	Mean																									74.9	2.1	**84.1**	59.6	1.6	**80.1**						
38	1	166.4	4.6		27.5	0.7																				738.0	15.0										
	2	-	4.8		26.6	0.7																				704.0	15.3										
	Mean	166.4	4.7	**85.1**	27.1	0.7	**76.0**																			721.0	15.1	**62.9**									
39	1	23.9	0.9		142.5	3.7																				54.1	1.3										
	2	23.6	0.8		128.0	4.2																				49.9	1.3										
	Mean	23.8	0.9	**107.4**	135.3	4.0	**87.7**																			52.0	1.3	**72.4**									
40	1	23.5	0.9																							118.1	3.1										
	2	22.0	0.8																							117.5	3.2										
	Mean	22.8	0.8	**106.2**																						117.8	3.2	**80.3**									
41	1																									252.0	6.2										
	2																									291.0	6.6										
	Mean																									271.5	6.4	**70.9**									
42	1																									99.7	2.1										
	2																									92.7	2.0										
	Mean																									96.2	2.0	**63.5**									
43	1																									288.2	4.9										
	2																									289.4	5.1										
	Mean																									288.8	5.0	**51.6**									
44	1	509.0	12.0		33.7	0.8																	24.3	0.8		1731.0	32.9										
	2	477.0	12.5		27.7	0.9																	18.7	0.7		1231.0	34.1										
	Mean	493.0	12.2	**74.5**	30.7	0.8	**81.6**																21.5	0.8	**106.0**	1481.0	33.5	**67.8**									
Average transfer rate (%)				**92.4**			**83.4**			**61.3**			**78.9**			**87.4**			**99.8**			**49.7**			**99.4**			**84.9**			**92.6**			**65.4**			**44.5**		
RSD (%)				**16.8**			**12.0**						**26.1**			**19.2**						**32.5**			**9.4**			**21.3**			**16.6**						**96.2**		
Overall method recovery (%), brewed tea				**101.2**			**102.4**			**103.6**			**101.8**			**98.0**			**100.5**			**99.6**			**101.7**			**98.5**			**99.9**			**104.4**			**41.2**		
Overall method recovery (%), tea leaves				**105.0**			**106.2**			**101.2**			**92.7**			**94.4**			**94.5**			**94.4**			**96.9**			**89.8**			**92.0**			**95.5**			**-**		

used carbofuran-d_3 as an internal standard for quantification. In general, the quadratic function was applied to the calibration curves based on the line of best fit. $1/x$ weighting was used to improve the accuracy for quantification of pesticide residues at low concentration. Responses for the unknown concentration or fortified samples were compared to the curves to calculate the amount of pesticide residues (μg/kg or μg/L (ppb)) in samples. Matrix-matched calibration standards were prepared fresh for each batch of samples.

Method Validation. The method for brewed tea was validated by a nested experimental design, described elsewhere.[8] The main factors of variances associated with method performance or measurement uncertainties of an in-house validated method are concentrations or

dx.doi.org/10.1021/jf404123h | J. Agric. Food Chem. 2014, 62, 966−983

Table 5. Pesticide Ion Ratios from Dried Tea Leaves and Brewed Tea Determined by UHPLC/ESI-MS/MS

Sample ID	Duplicate	Methomyl				Carbendazim				Thiabendazole				Carbaryl				Monocrotophos				Clothianidin			
		163.1→87.9 (T_1), 163.1→106.0 (T_2), 163.1→58.0 (T_3)				192.1→160.2 (T_1), 192.1→132.0 (T_2), 192.1→104.9 (T_3)				202.1→175.0 (T_1), 202.1→131.2 (T_2), 202.1→65.0 (T_3)				202.1→145.1 (T_1), 202.1→127.1 (T_2), 202.1→117.0 (T_3)				224.1→126.9(T_1), 224.1→193.1 (T_2), 224.1→98.0 (T_3)				250.0→169.1(T_1), 250.0→132.0 (T_2), 250.0→112.9 (T_3)			
		Tea leaves		Brewed tea		Tea leaves		Brewed tea		Tea leaves		Brewed tea		Tea leaves		Brewed tea		Tea leaves		Brewed tea		Tea leaves		Brewed tea	
		T_2/T_1	T_3/T_1	T_2/T_1	T_3/T_1	T_2/T_1	T_3/T_1	T_2/T_1	T_3/T_1	T_2/T_1	T_3/T_1	T_2/T_1	T_3/T_1	T_2/T_1	T_3/T_1	T_2/T_1	T_3/T_1	T_2/T_1	T_3/T_1	T_2/T_1	T_3/T_1	T_2/T_1	T_3/T_1	T_2/T_1	T_3/T_1
1	1	0.75	0.33	0.75	0.32	1.15	0.82	1.41	1.13	2.78	1.90	3.09	2.22	0.23	0.26	0.29	0.28								
	2	0.75	0.32	0.77	0.33	1.28	0.83	1.63	1.09	2.62	1.92	3.13	2.18	0.24	0.26	0.25	0.25								
	Mean	0.75	0.33	0.76	0.33	1.21	0.83	1.52	1.11	2.80	1.91	3.11	2.20	0.24	0.26	0.27	0.27								
2	1																								
	2																								
	Mean																								
3	1					1.09	0.86	1.29	0.92																
	2					1.27	0.97	1.82	1.07																
	Mean					1.18	0.92	1.46	1.00																
4	1																	1.26	0.83	1.35	0.82				
	2																	1.23	0.75	1.28	0.85				
	Mean																	1.25	0.79	1.32	0.84				
5	1	0.77	0.34	0.72	0.33	1.26	1.01	1.56	0.90																
	2	0.80	0.28	0.82	0.38	1.53	1.08	1.27	0.87																
	Mean	0.79	0.31	0.77	0.35	1.40	1.05	1.42	0.89																
6	1					1.29	1.08	1.31	1.18																
	2					1.24	1.03	1.43	1.00																
	Mean					1.27	1.06	1.37	1.09																
7	1	0.77	0.32	0.78	0.32	1.22	0.93	1.40	1.00					0.24	0.27	0.23	0.27								
	2	0.82	0.33	0.72	0.31	1.25	0.99	1.30	1.08					0.28	0.20	0.25	0.25								
	Mean	0.80	0.33	0.74	0.32	1.24	0.96	1.35	1.04					0.26	0.24	0.24	0.26								
8	1	0.64	0.26	0.75	0.30	1.35	0.86	1.34	1.10																
	2	0.81	0.34	0.68	0.31	1.28	0.83	1.62	1.04																
	Mean	0.73	0.30	0.72	0.31	1.32	0.85	1.48	1.07																
9	1	0.77	0.30	0.73	0.33	1.11	0.93	1.58	1.00																
	2	0.72	0.32	0.73	0.32	1.15	0.90	1.50	1.08																
	Mean	0.75	0.31	0.73	0.33	1.13	0.92	1.54	1.04																
10	1					1.08	0.79	1.43	1.01																
	2					1.30	1.03	1.45	1.06																
	Mean					1.19	0.91	1.44	1.04																
11	1	0.71	0.30	0.72	0.31	1.22	0.91	1.28	0.99																
	2	0.75	0.31	0.71	0.31	1.27	0.86	1.39	1.06																
	Mean	0.73	0.31	0.72	0.31	1.25	0.89	1.34	1.03																
12	1	0.75	0.32	0.72	0.31																				
	2	0.75	0.29	0.76	0.34																				
	Mean	0.75	0.31	0.74	0.33																				
13	1																								
	2																								
	Mean																								
14	1	0.84	0.30	0.74	0.31	1.28	0.92	1.40	1.14																
	2	0.73	0.31	0.78	0.33	1.23	0.83	1.39	1.09																
	Mean	0.79	0.31	0.76	0.32	1.26	0.88	1.40	1.12																
15	1	0.73	0.32	0.74	0.31	1.32	0.97	1.54	1.09																
	2	0.74	0.31	0.74	0.30	1.52	0.88	1.39	0.95																
	Mean	0.74	0.32	0.74	0.31	1.42	0.93	1.47	1.02																
16	1																								
	2																								
	Mean																								
17	1					1.21	0.94	1.42	1.05																
	2					1.22	0.89	1.43	1.04																
	Mean					1.22	0.92	1.43	1.05																
18	1													0.28	0.26	0.22	0.37								
	2													0.22	0.25	0.21	0.36								
	Mean													0.24	0.26	0.22	0.37								
19	1	0.83	0.33	0.76	0.31	1.34	0.90	1.48	0.95																
	2	0.75	0.31	0.73	0.31	1.29	0.93	1.43	0.95																
	Mean	0.79	0.32	0.75	0.31	1.32	0.92	1.46	0.95																
20	1					1.24	0.91	1.36	0.98									1.25	0.80	1.28	0.84				
	2					1.26	0.92	1.40	0.97									1.24	0.79	1.21	0.75				
	Mean					1.25	0.92	1.38	0.98									1.25	0.80	1.25	0.80				
21	1					1.17	0.83	1.35	0.83																
	2					1.27	0.88	1.28	1.14																
	Mean					1.22	0.86	1.32	0.99																
22	1																								
	2																								
	Mean																								
23	1					1.24	0.93	1.37	0.93																
	2					1.09	0.76	1.38	1.03																
	Mean					1.17	0.85	1.38	0.98																
24	1																								
	2																								
	Mean																								
25	1																								
	2																								
	Mean																								
26	1	0.80	0.32	0.71	0.30																				
	2	0.77	0.32	0.71	0.32																				
	Mean	0.79	0.32	0.71	0.31																				
27	1																								
	2																								
	Mean																								
28	1	0.75	0.30	0.74	0.32	1.28	0.95	1.49	1.09																
	2	0.75	0.31	0.76	0.32	1.30	1.00	1.45	0.97																
	Mean	0.75	0.31	0.75	0.32	1.29	0.98	1.47	1.03																
29	1	0.77	0.31	0.75	0.32	1.26	1.04	1.33	1.03																
	2	0.74	0.31	0.74	0.32	1.37	1.23	1.34	1.03																
	Mean	0.76	0.31	0.75	0.32	1.32	1.14	1.34	1.03																
30	1																	1.27	0.83	1.29	0.81				
	2																	1.33	0.78	1.29	0.83				
	Mean																	1.30	0.81	1.29	0.82				
31	1	0.81	0.31	0.75	0.31																				
	2	0.69	0.31	0.74	0.31																				
	Mean	0.75	0.31	0.75	0.31																				
32	1																								
	2																								
	Mean																								
33	1					1.28	0.93	1.48	0.96																
	2					1.27	0.91	1.28	0.98																
	Mean					1.28	0.92	1.38	0.97																
34	1					1.32	0.95	1.29	0.98									1.23	0.76	1.29	0.79	0.92	0.35	1.00	0.75
	2					1.28	1.00	1.43	1.08											1.30	0.79	0.85	0.35	0.80	0.66
	Mean					1.30	0.98	1.36	1.03									1.23	0.76	1.30	0.79	0.89	0.35	0.90	0.71
35	1	0.83	0.40	0.75	0.30																				
	2	-	-	0.74	0.33																				
	Mean	0.83	0.40	0.75	0.32																				
36	1																								
	2																								
	Mean																								
37	1																								
	2																								
	Mean																								
38	1	0.77	0.30	0.74	0.31	1.31	1.02	1.44	1.04																
	2	-	-	0.75	0.32	1.37	0.93	1.42	0.98																
	Mean	0.77	0.30	0.75	0.32	1.34	0.96	1.43	1.01																

Sample ID	Duplicate	Clothianidin				Thiacloprid				3-Hydroxycarbo-furan				Imidacloprid				Thiamethoxam				Methidathion				Quizalofop			
		250.0→169.1(T_1), 250.0→132.0 (T_2), 250.0→112.9 (T_3)				253.0→126.1(T_1), 253.0→89.9 (T_2), 253.0→99.0 (T_3)				225.1→163.1(T_1), 225.1→220.1 (T_2), 225.1→181.2 (T_3)				256.1→209.1(T_1), 256.1→174.9 (T_2), 256.1→84.0 (T_3)				292.0→210.9 (T_1), 292.0→181.0 (T_2), 292.0→132.1 (T_3)				302.9→145.1(T_1), 302.9→85.0 (T_2), 302.9→58.0 (T_3)				345.0→299.0 (T_1), 345.0→90.9 (T_2), 345.0→270.8 (T_3)			
		Tea leaves		Brewed tea		Tea leaves		Brewed tea		Tea leaves		Brewed tea		Tea leaves		Brewed tea		Tea leaves		Brewed tea		Tea leaves		Brewed tea		Tea leaves		Brewed tea	
		T_2/T_1	T_3/T_1	T_2/T_1	T_3/T_1	T_2/T_1	T_3/T_1	T_2/T_1	T_3/T_1	T_1/T_2	T_3/T_2	T_1/T_2	T_3/T_2	T_2/T_1	T_3/T_1	T_2/T_1	T_3/T_1	T_1/T_2	T_3/T_2	T_1/T_2	T_3/T_2	T_2/T_1	T_3/T_1	T_2/T_1	T_3/T_1	T_2/T_1	T_3/T_1	T_2/T_1	T_3/T_1
1	1													1.19	0.32	0.96	0.36					0.68	0.19	0.76	0.20				
	2													1.25	0.30	0.81	0.31					0.66	0.21	0.62	0.20				
	Mean													1.22	0.31	0.89	0.34					0.67	0.20	0.69	0.20				
2	1																									0.55	0.36	0.37	0.41
	2																									0.54	0.41	0.37	0.41
	Mean																									0.55	0.39	0.37	0.41
3	1													1.03	0.30	0.72	0.38												
	2													1.05	0.32	0.71	0.30												
	Mean													1.04	0.31	0.72	0.34												
4	1					0.51	0.46	0.57	0.49					1.10	0.30	0.73	0.25	0.43	0.43	0.42	0.33								
	2					0.51	0.35	0.63	0.45					0.97	0.29	0.65	0.33	0.48	0.43	0.42	0.35								
	Mean					0.51	0.41	0.60	0.47					1.04	0.30	0.69	0.29	0.46	0.43	0.42	0.34								
5	1													1.07	0.24	0.74	0.30												
	2													0.97	0.26	0.71	0.31												
	Mean													1.02	0.25	0.73	0.31												
6	1													0.96	0.25	0.91	0.24												
	2													0.93	0.29	0.68	0.36												
	Mean													0.95	0.27	0.80	0.30												
7	1					0.58	0.46	0.56	0.44					0.98	0.26	0.96	0.29												
	2					0.58	0.43	0.53	0.42					0.99	0.27	0.94	0.28												
	Mean					0.58	0.45	0.55	0.43					0.99	0.27	0.95	0.29												
8	1													1.14	0.29	0.75	0.38												
	2													1.28	0.32	0.88	0.35												
	Mean													1.21	0.31	0.82	0.37												
9	1													1.06	0.24	0.92	0.35												
	2													1.04	0.28	0.90	0.33												
	Mean													1.05	0.26	0.91	0.34												
10	1													1.13	0.25	1.02	0.40												
	2													1.05	0.27	0.76	0.43												
	Mean													1.09	0.26	0.89	0.42												
11	1													1.08	0.26	1.03	0.32												
	2													1.08	0.26	0.89	0.33												
	Mean													1.08	0.26	0.96	0.33												
12	1																												
	2																												
	Mean																												
13	1													0.96	0.32	0.73	0.41												
	2													0.97	0.36	0.69	0.31												
	Mean													0.97	0.34	0.71	0.36												
14	1													1.01	0.30	0.97	0.34												
	2													1.05	0.30	0.81	0.32												
	Mean													1.03	0.30	0.89	0.33												
15	1													0.93	0.24	0.77	0.32												
	2													1.07	0.28	0.72	0.42												
	Mean													1.00	0.26	0.75	0.37												
16	1													1.36	0.36	0.93	0.46												
	2													1.00	0.26	0.90	0.39												
	Mean													1.18	0.31	0.92	0.43												
17	1													1.08	0.27	0.70	0.31												
	2													1.02	0.26	0.75	0.31												
	Mean													1.04	0.27	0.73	0.31												
18	1																												
	2																												
	Mean																												
19	1													0.98	0.28	1.02	0.31												
	2													0.92	0.25	1.00	0.31												
	Mean													0.95	0.27	1.01	0.31												
20	1													1.11	0.34	0.92	0.48												
	2													0.99	0.30	0.70	0.41												
	Mean													1.05	0.32	0.81	0.45												
21	1													1.01	0.24	0.99	0.40												
	2													1.11	0.30	0.79	0.36												
	Mean													1.06	0.27	0.89	0.38												
22	1																									0.64	0.64	0.35	0.59
	2																									0.60	0.58	0.32	0.53
	Mean																									0.62	0.61	0.34	0.56
23	1													0.92	0.26	1.04	0.32												
	2													1.30	0.30	0.91	0.46												
	Mean													1.11	0.28	0.98	0.39												
24	1																									0.56	0.52	0.38	0.52
	2																									0.61	0.42	0.36	0.54
	Mean																									0.59	0.47	0.37	0.53
25	1													1.09	0.35	0.85	0.36												
	2													1.02	0.29	0.88	0.33												
	Mean													1.06	0.32	0.87	0.35												
26	1													1.05	0.33	0.93	0.37												
	2													1.10	0.33	0.96	0.38												
	Mean													1.08	0.33	0.95	0.38												
27	1													1.08	0.38	0.94	0.42												
	2													1.05	0.34	1.13	0.37												
	Mean													1.07	0.36	1.04	0.40												
28	1													1.05	0.26	0.99	0.29												
	2													1.07	0.28	1.00	0.33												
	Mean													1.06	0.27	1.00	0.31												
29	1									0.95	0.53	0.87	0.49	0.99	0.29	0.93	0.30												
	2									0.94	0.50	0.87	0.51	1.06	0.28	0.94	0.33												
	Mean									0.95	0.52	0.87	0.50	1.03	0.29	0.94	0.32												
30	1													1.13	0.31	0.90	0.45	0.50	0.49	0.46	0.36								
	2													1.08	0.35	0.86	0.41	0.49	0.40	0.46	0.35								
	Mean													1.11	0.33	0.88	0.42	0.50	0.45	0.46	0.36								
31	1													1.19	0.36	1.05	0.45												
	2													1.27	0.36	0.97	0.43												
	Mean													1.23	0.36	1.01	0.44												
32	1																									0.57	0.46	0.40	0.54
	2																									0.57	0.46	0.46	0.49
	Mean																									0.57	0.46	0.43	0.52
33	1													1.31	0.37	1.02	0.39												
	2													1.24	0.26	1.01	0.30												
	Mean													1.28	0.32	1.02	0.36												
34	1													1.08	0.33	0.83	0.29	0.54	0.45	0.42	0.34								
	2													1.03	0.31	0.82	0.31	0.48	0.40	0.47	0.37								
	Mean													1.06	0.32	0.83	0.30	0.51	0.43	0.45	0.36								
35	1													1.33	0.32	1.00	0.37												
	2													1.12	0.26	1.18	0.37												
	Mean													1.23	0.29	1.09	0.37												
36	1													1.16	0.27	1.03	0.39												
	2													1.07	0.30	1.14	0.33												
	Mean													1.12	0.29	1.09	0.36												
37	1													1.06	0.27	1.15	0.44	0.48	0.42	0.51	0.37								
	2													1.12	0.38	0.84	0.38	0.60	0.52	0.51	0.37								
	Mean													1.09	0.33	1.00	0.41	0.54	0.47	0.51	0.37								
38	1													1.03	0.26	0.92	0.32												
	2													1.10	0.28	1.03	0.35												
	Mean													1.07	0.27	0.98	0.34												

dx.doi.org/10.1021/jf404123h | J. Agric. Food Chem. 2014, 62, 966−983

Table 5. continued

Sample ID	Duplicate	Methomyl				Carbendazim				Thiabendazole				Carbaryl				Monocrotophos				Clothianidin				Thiacloprid				3-Hydroxycarbofuran				Imidacloprid				Thiamethoxam				Methidathion				Quizalofop			
		163.1→87.9 (T_1), 163.1→106.0 (T_2), 163.1→58.0 (T_3)				192.1→160.2 (T_1), 192.1→132.0 (T_2), 192.1→104.9 (T_3)				202.1→175.0 (T_1), 202.1→131.2 (T_2), 202.1→65.0 (T_3)				202.1→145.1 (T_1), 202.1→127.1 (T_2), 202.1→117.0 (T_3)				224.1→126.9(T_1), 224.1→193.1 (T_2), 224.1→98.0 (T_3)				250.0→169.1(T_1), 250.0→132.0 (T_2), 250.0→112.9 (T_3)				253.0→126.1(T_1), 253.0→89.9 (T_2), 253.0→99.0 (T_3)				225.1→163.1(T_1), 225.1→220.1 (T_2), 225.1→181.2 (T_3)				256.1→209.1(T_1), 256.1→174.9 (T_2), 256.1→84.0 (T_3)				292.0→210.9 (T_1), 292.0→181.0 (T_2), 292.0→132.1 (T_3)				302.9→145.1(T_1), 302.9→85.0 (T_2), 302.9→58.0 (T_3)				345.0→299.0 (T_1), 345.0→90.9 (T_2), 345.0→270.8 (T_3)			
		Tea leaves				Brewed tea				Tea leaves				Brewed tea				Tea leaves				Brewed tea				Tea leaves				Brewed tea				Tea leaves				Brewed tea				Tea leaves				Brewed tea				Tea leaves				Brewed tea			
		T_2/T_1	T_3/T_1	T_2/T_1	T_3/T_1	T_2/T_1	T_3/T_1	T_2/T_1	T_3/T_1	T_2/T_1	T_3/T_1	T_2/T_1	T_3/T_1	T_2/T_1	T_3/T_1	T_2/T_1	T_3/T_1	T_2/T_1	T_3/T_1	T_2/T_1	T_3/T_1	T_2/T_1	T_3/T_1	T_2/T_1	T_3/T_1	T_2/T_1	T_3/T_1	T_2/T_1	T_3/T_1	T_1/T_2	T_3/T_2	T_1/T_2	T_3/T_2	T_2/T_1	T_3/T_1	T_2/T_1	T_3/T_1	T_2/T_1	T_3/T_1	T_2/T_1	T_3/T_1	T_2/T_1	T_3/T_1	T_2/T_1	T_3/T_1	T_2/T_1	T_3/T_1	T_2/T_1	T_3/T_1	T_2/T_1	T_3/T_1
39	1	0.71	0.30	0.75	0.33	1.24	0.94	1.35	0.97																									1.20	0.32	1.10	0.36												
	2	0.78	0.32	0.77	0.33	1.31	1.01	1.37	0.98																									1.18	0.34	1.10	0.45												
	Mean	0.75	0.31	0.76	0.33	1.28	0.98	1.36	0.98																									1.19	0.33	1.10	0.42												
40	1	0.80	0.33	0.78	0.34																													1.07	0.34	0.98	0.37												
	2	0.72	0.31	0.80	0.35																													1.07	0.25	0.91	0.28												
	Mean	0.76	0.32	0.79	0.35																													1.07	0.30	0.95	0.33												
41	1																																	1.11	0.35	0.98	0.41												
	2																																	1.05	0.34	0.95	0.38												
	Mean																																	1.08	0.35	0.97	0.40												
42	1																																	1.18	0.32	0.95	0.31												
	2																																	1.17	0.30	0.86	0.38												
	Mean																																	1.18	0.31	0.91	0.35												
43	1																																	1.04	0.31	0.93	0.38												
	2																																	1.07	0.30	1.05	0.34												
	Mean																																	1.06	0.31	0.99	0.36												
44	1	0.75	0.29	0.73	0.33	1.55	1.07	1.55	1.00																					0.87	0.59	0.91	0.55	1.02	0.27	0.92	0.26												
	2	0.80	0.31	0.74	0.31	1.40	0.98	1.56	1.06																					0.85	0.67	0.87	0.57	1.10	0.33	0.88	0.26												
	Mean	0.78	0.30	0.74	0.32	1.48	1.03	1.56	1.03																					0.86	0.63	0.89	0.56	1.06	0.30	0.90	0.26												

spike levels of analytes, matrix effects, day-to-day variation, and within-day variation of the method. The last two factors are designated the intermediate precision. In this study, there were a total of five brewed teas, that is, Earl Grey, oolong, green tea, herbal tea, and orange pekoe. For each matrix, samples were spiked at four levels, that is, 4.0, 12.0, 20.0, and 32.0 μg/L, in triplicate. Spike experiments were repeated on two different days or by each of two analysts. Overall recovery, intermediate precision, and measurement uncertainty were calculated using a combined algorithm that consisted of SAS codes (SAS software release 9.1, SAS Institute Inc., USA) along with a Microsoft Excel (Microsoft Office 2002) workbook.

RESULTS AND DISCUSSION

Experimental Design. To study pesticide residue transfer rates from dried tea leaves to brewed tea, a two-stage experiment was deliberately designed. First, tea leaves were brewed, and then the resulting tea was analyzed for pesticide residues. Five grams of dried tea leaves and 150 mL of hot water were used in the brewing process. Data from a few preliminary experiments showed this combination increased method sensitivity or decreased detection limits to low parts per billion. This allowed us to use a 10 mL subsample of brewed tea, a typical QuEChERs sample size, to quantify a pesticide at a concentration as low as 12.0 μg/kg in dried tea leaves. The thermohydrolysis, which may induce the loss of certain pesticides, was not investigated in the current study because we were concerned with the concentrations or amounts of pesticides in brewed tea after the brewing process. The study on thermohydrolysis would be of value, especially for investigation of the production of additional pesticide metabolites.

In general, the amounts of incurred pesticides in dried tea leaves, including green tea, oolong tea, and black tea, ranged from 5.0 to 500.0 μg/kg (ppb), as being confirmed by the previous year's monitoring program results, and some residues were as high as a few millligram per kilogram (ppm). The challenge was to quantify pesticides at parts per billion concentration levels in both dried tea leaves and brewed tea, especially after the brewing process. Some published studies have reported transfer rates for a few pesticides from tea leaves to brewed tea.[4−6] These studies were performed at relatively high residue concentrations, that is, parts per million levels, and for a very limited number of pesticides. In the current study, we utilized a highly sensitive UHPLC/ESI-MS/MS system with an appropriate experiment design to analyze up to 172 pesticides at parts per billion concentration levels to understand the transfer rates of a broad spectrum of pesticide residues. The API 5000 LC/MS/MS system used had an analytical range from 1.0 to 100.0 μg/L in solvent buffer (concentration in vials) for most pesticides studied, which was equivalent to 0.4 μg/L to 40.0 μg/kg in brewed tea as a result of a factor of 2.5 times concentration from brewed tea to final sample extracts.

Assuming a pesticide residue will transfer with a rate between 20 and 100%, Table 3 presents four scenarios of the lowest or highest concentration of an incurred pesticide that could possibly be detected in tea leaves or brewed tea when following the procedure described under Materials and Methods. For example, if a pesticide has a transfer rate of 20%, the lowest concentration of a pesticide in tea leaves that can be detected in brewed tea (Table 3A) is 60 μg/kg; and a transfer rate of 100% leads to as low as 12.0 μg/kg in tea leaves (Table 3B). In these cases, when the amount of a pesticide in dried tea leaves happens to be over 40 μg/L in brewed tea (Table 3D), the sample size (tea leaves) can be reduced to fit its level in the range of 0.4−40.0 μg/kg for quantification. Basically, the experiment was designed to detect pesticides in a range from 12.0 to 1200.0 μg/kg in tea leaves when a 100% transfer rate was assumed.

QuEChERS. Pesticides were extracted from dried tea leaves (5 g/sample) and brewed tea (10.0 mL/sample) following the buffered QuEChERS method[7] or AOAC Official Method 2007.01.[9] The complete procedure consisted of three steps including the first step, extraction with acetonitrile containing 1% acetic acid, $MgSO_4$, and sodium acetate; and the second step, cleanup by dispersive solid-phase extraction (d-SPE) using $MgSO_4$, PSA, and graphitized black carbon for dried tea leaves or $MgSO_4$, PSA, and C_{18} for brewed tea. Graphitized black carbon helps to remove some pigments such as catechins and chlorophyll from tea leaves while leaving polar pesticides behind in the acetonitrile extract. It should be mentioned that the final extracts were still relatively dark in color, especially for black tea. The third step comprised concentration, reconstitution, and filtration. Concentration and reconstitution served as an additional cleanup step to remove particles or pigments, which were precipitated out during the process. Extracts were diluted six times for tea leaves, and no dilution was used for brewed tea (filtered to remove particles) prior to UHPLC/ESI-MS/MS injections. The QuEChERS method proved to be a practical extraction procedure for UHPLC/ESI-MS/MS analysis of pesticide residues in tea.

Matrix Effects. The matrix could either enhance or suppress ionization of pesticides during the electrospray process. Its effects might vary from sample to sample and ultimately affect the UHPLC/ESI-MS/MS quantitative results. Previous experiments indicated that the matrix effects were significant in tea leaves,

dx.doi.org/10.1021/jf404123h | J. Agric. Food Chem. 2014, 62, 966−983

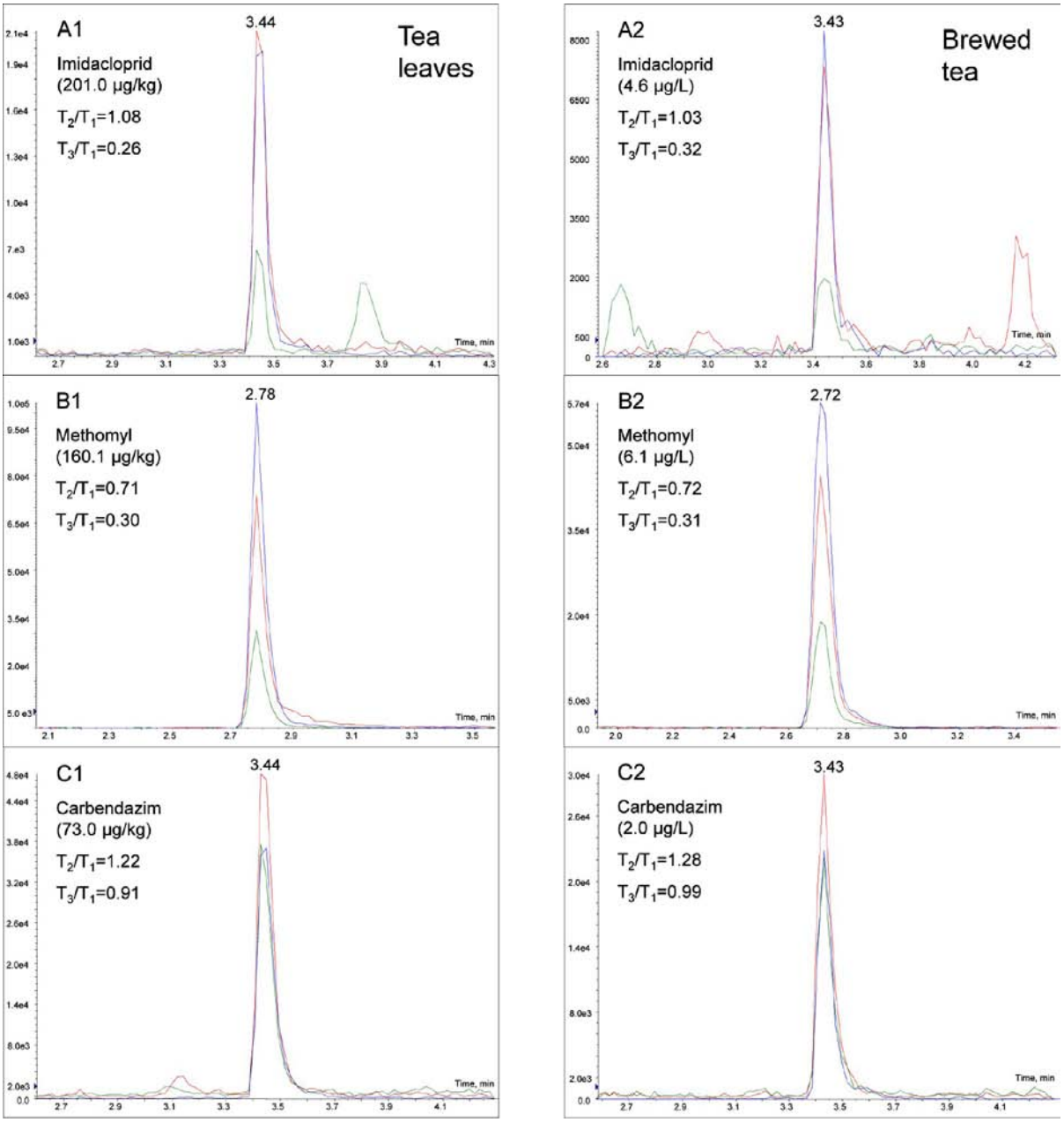

Figure 4. Examples of UHPLC/ESI-MS/MS chromatograms of three common incurred pesticides from one tea and its corresponding brew tea for quantification and confirmation. Imidacloprid transitions: 256.1→209.1 (T_1), 256.1→174.9 (T_2), and 256.1→84.0 (T_3). Methomyl transitions: 163.1→87.9 (T_1), 163.1→106.0 (T_2), and 163.1→58.0 (T_3). Carbendazim transitions: 192.1→160.2 (T_1), 192.1→132.0 (T_2), and 192.1→104.9 (T_3).

and only 8−16% of the pesticides showed ion suppression of <30% or enhancement ≤10%.[7] Matrix effects in brewed tea were evaluated by comparing the responses of pesticides in sample extracts to those pesticide standards prepared in solvent buffer at the same concentration, for example, 8.0 μg/L equivalent in samples. Between 21.4 and 49.7% of the pesticides in brewed tea showed ion suppression of <30% or enhancement ≤10% in brewed tea (Figure 1). Therefore, to quantify pesticides in both tea leaves and brewed tea for the purpose of studying the transfer rates, oolong tea was chosen as a standard or reference matrix for all samples to prepare matrix-matched standard calibration curves to compensate for matrix effects during quantification or to cancel out matrix effects when pesticide transfer rates were calculated.

Quantification and Method Performance. LC/ESI-MS/MS analysis of pesticide residues in tea leaves has been reported elsewhere,[7] and the UHPLC/ESI-MS/MS method was revalidated when a core−shell column replaced the conventional C_{18} column in this study (data not shown). With the core−shell column method for dried tea leaves, 87% of the pesticides had recoveries between 81 and 110%, 94% had an intermediate precision ≤20%, and 89% showed measurement uncertainty ≤40%. The method performance of UHPLC/ESI-MS/MS was very comparable to that of LC/ESI-MS/MS, which was published in 2011.[7]

The UHPLC/ESI-MS/MS analysis of pesticides in brewed tea was a newly developed method and was therefore fully validated according to a nested design[10] to evaluate method performance characteristics including accuracy expressed as overall recovery, intermediate precision, and measurement uncertainty (MU). Four factors, that is, concentrations or spike levels of pesticides,

dx.doi.org/10.1021/jf404123h | J. Agric. Food Chem. 2014, 62, 966−983

matrix effects, day-to-day variation, and within-day variation, were included in the evaluation. Method performance results are summarized in Table 1 and are illustrated in Figure 2. About 95% of the pesticides had recoveries between 81 and 110%, intermediate precision ≤20%, and measurement uncertainty ≤40%. In general, 97% of the pesticides demonstrated MU ≤ 50%, which was a recommended default value in European Union (EU) Document SANCO/12495/2011 for pesticide analysis and enforcement decisions (MRL exceedances).[11] Therefore, the UHPLC/ESI-MS/MS along with QuEChERs served as a practical tool for quantifying pesticide residues in brewed tea.

Pesticide Transfer Rates. Among the 172 pesticides studied, 12 were detected in 44 known-incurred dried tea leaves. Of these pesticides, imidacloprid, carbendazim, and methomyl were the three most frequently found pesticides (Figure 3A). Most of the incurred samples had concentrations of <100 μg/kg in tea leaves, but in one sample imidacloprid concentrations reached as high as 6012 μg/kg (Table 4). The results for quizalofop were not quantitative because of its large measurement uncertainty (>50%). The 12 identified pesticides represented different classes of pesticides such as insecticides, fungicides, and acaricides. All pesticides, in both tea leaves and brewed tea, were confirmed according to the criteria of ion ratios and retention times (Tables 1 and 5) in 2002/657/EC.[12] Because the method recoveries of 11 pesticides (quizalofop not included) in tea leaves and brewed tea were around 100% (Figure 3B and Table 4) and a standard matrix (i.e., oolong tea) was used to overcome matrix effects, the transfer rates presented in Table 4 should reflect accurate percentages for those pesticides that were transferred from dried tea leaves to brewed tea after the brewing process. The variations in transfer rates are most likely as a result of the differences in tea samples. For example, the transfer rate of imidacloprid ranged from 51.6 to 125.0% (average = 84.9%), that for carbendazim ranged from 73.8 to 112.8% (average = 83.4%), and that for methomyl ranged from 63.3 to 118.9% (average = 92.4%) depending on individual samples of the type of tea (Table 4). The overall average transfer rates of 11 pesticides (quizalofop not included) ranged from 49.7 to 99.8%. The 11 identified pesticides were LC-amenable pesticides; therefore, their physicochemical properties might be attributed to their relatively high transfer rates.

Conclusion. This paper presented a practical approach to study pesticide residue transfer rates from dried tea leaves to brewed tea. UHPLC/ESI-MS/MS with a core−shell column was demonstrated to be a fast tool (12 min analytical run time) to analyze 172 pesticides in both tea leaves and brewed tea. Twelve pesticides were detected in 44 known incurred tea samples. Imidacloprid, carbendazim, and methomyl were the three most frequently found pesticides among 12 pesticides. Transfer rates of 11 pesticides (quizalofop not included) ranged from 49.7 to 99.8%. The pesticide residues were likely transferred from tea leaves to brewed tea during the brewing process and may therefore pose a risk to consumers. This study has underscored the importance of establishing an adequate monitoring program for pesticide residues in dried tea leaves with appropriate maximum residue limits.

AUTHOR INFORMATION

Corresponding Author

*(J.W.) Phone: (403) 338-5273. Fax: (403) 338-5299. E-mail: jian.wang@inspection.gc.ca.

Notes

The authors declare no competing financial interest.

ACKNOWLEDGMENTS

We are grateful to Dr. Greg Appleyard and Willis Chow, Calgary Laboratory, Canadian Food Inspection Agency, for comments and review on this paper.

REFERENCES

(1) FAO. Current situation and medium term outlook for tea; http://www.fao.org/fileadmin/templates/est/COMM_MARKETS_MONITORING/Tea/Documents/IGG_20/12-CRS7-CurrentSit_01.pdf (accessed Aug 7, 2013).

(2) Cabrera, C.; Artacho, R.; Gimenez, R. Beneficial effects of green tea − a review. *J. Am. Coll. Nutr.* **2006**, *25*, 79−99.

(3) Taylor, S. Tea: types, production, and trade. In *Encyclopedia of Food Sciences and Nutrition*; Caballero, B., Finglas, P., Trugo, L., Eds.; Academic Press: Oxford, UK, 2003; pp 5737−5743.

(4) Manikandan, N.; Seenivasan, S.; Ganapathy, M. N. K.; Muraleedharan, N. N.; Selvasundaram, R. Leaching of residues of certain pesticides from black tea to brew. *Food Chem.* **2009**, *113*, 522−525.

(5) Sharma, A.; Gupta, M.; Shanker, A. Fenvalerate residue level and dissipation in tea and in its infusion. *Food Addit. Contam., Part A* **2008**, *25*, 97−104.

(6) Gupta, M.; Shanker, A. Persistence of acetamiprid in tea and its transfer from made tea to infusion. *Food Chem.* **2008**, *111*, 805−810.

(7) Wang, J.; Chow, W.; Leung, D. Applications of LC/ESI-MS/MS and UHPLC QqTOF MS for the determination of 141 pesticides in tea. *J. AOAC Int.* **2011**, *94*, 1685−1714.

(8) Wang, J.; Leung, D. Determination of 142 pesticides in fruit- and vegetable-based infant foods using liquid chromatography electrospray ionization tandem mass spectrometry and estimation of measurement uncertainty. *J. AOAC Int.* **2009**, *92*, 279−301.

(9) AOAC Official Method 2007.01. Pesticide residues in foods by acetonitrile extraction and partitioning with magnesium sulfate gas chromatography/mass spectrometry and liquid chromatography/tandem mass spectrometry. First Action, 2007.

(10) Wang, J.; Wotherspoon, D. Determination of pesticides in apples by liquid chromatography with electrospray ionization tandem mass spectrometry and estimation of measurement uncertainty. *J. AOAC Int.* **2007**, *90*, 550−567.

(11) Method validation and quality control precedures for pesticide residues analysis in food and feed. Document No. SANCO/12495/2011 Supersedes Document No. SANCO/10684/2009 Implemented by 01/01/2012; http://www.crl-pesticides.eu/library/docs/allcrl/AqcGuidance_Sanco_12495_2011_upload2.pdf, 2012 (accessed Aug 4, 2013).

(12) 2002/657/EC, Commission Decision of 12 August 2002 implementing Council Directive 96/23/EC concerning the performance of analytical methods and the interpretation of results. *Off. J. Eur. Communities* **2002**, *L221*, 8−36.

NOTE ADDED AFTER ASAP PUBLICATION

After this paper was published ASAP on January 15, 2014, an error under Sample Preparation and Extraction Procedure, Brewed Tea, was noted. The equivalency of the internal standard working solution has been changed with the posting of January 16, 2014.

Drug Administration,[20] and therefore they represent a suitable alternative as chemical preservatives to be used on fruits and other food products.

Methyl cinnamate (MC), a methyl ester of cinnamic acid, is one of the major volatile components of strawberry aroma produced and released during fruit maturation.[21,22] Its antimicrobial activity against common phytopathogenic fungi has been tested under in vitro conditions.[23,24] Most recently, the successful incorporation of MC into edible films has been reported.[25] In the present work MC was used in combination with carvacrol (C; the major component of EOs from oregano and thyme), for which antibacterial and antifungal properties have been widely studied. Therefore, the development of an alginate coating containing MC in combination with C has been proposed in this study to improve the antimicrobial activity of C as well as to overcome the negative impact of the strong odor of C on the sensory properties of strawberries. However, although EOs have a positive effect on extending fruit shelf life, the concentrations needed in edible coatings to have an effective antimicrobial property may have a negative effect on barrier-mechanical and optical properties of the coating and therefore affect its performance and acceptability.

The aim of this work was to optimize the antimicrobial and physical properties of alginate coatings containing C and MC for their potential application on fresh strawberries and other perishable fruits. Response surface methodology (RSM) was used as an effective statistical technique for simultaneously investigating and optimizing the response variables.

MATERIALS AND METHODS

Materials and Preparation of Alginate Coating Solution. Food grade sodium alginate (Keltone LV, ISP, San Diego, CA, USA) was the primary ingredient use in the edible coating formulations. Glycerol (Starwest Botanicals Inc., Rancho Cordova, CA, USA) was added as plasticizer to provide good flexibility to the coatings. C and MC were purchased from Sigma-Aldrich (St. Louis, MO, USA).

Coating solutions were prepared by dissolving sodium alginate powder (2% w/v) in distilled water while heating on a stirring hot plate for 15 min at 70 °C until the mixture became clear. Then, 1.5% (w/v) glycerol was added to the solution and stirred for 5 min. Finally, C and MC (active compounds) were incorporated into the solution a little at the time and homogenized with a Polytron 3000 (Kinematica, Luzern, Switzerland) for 10 min at 4000 rpm. Because of the insolubility of MC in water, MC was previously dissolved in ethanol (40% w/w) at 40 °C under stirring at 220 rpm for 5 min.

Antimicrobial Properties of Coating Solutions. An overlay diffusion[26] test was performed as a qualitative test for antimicrobial activity of coatings against *E. coli* and *B. cinerea*. Frozen cultures of *E. coli* O157:H7 (strain RM 1484, original designation SEA13B88), obtained from the U.S. Food and Drug Administration, were streaked on tryptic soy agar (TSA) plate and incubated overnight at 37 °C. One isolated colony was restreaked on TSA and then incubated at 37 °C for 24 h. This was followed by inoculating one isolated colony into 5 mL of trypticase soy broth (TSB) and incubating it at 37 °C for 24 h, under agitation. The microbial broth was then serially diluted (10×) in 0.1% peptone water. Afterward, 100 μL of 10^5 colony-forming units (CFU/mL) was uniformly spread onto TSA plates and left to dry for 5 min at room temperature. Plates were divided into three or four even areas on the basis of the compound concentrations, and a 10 mm diameter filter paper, aseptically cut in the shape of a disk, was placed at the center of each area. Then, 20 μL of each solution was placed on top of the filter paper. The plates were incubated at 37 °C for 24 h. The inhibition radius around the filter paper (colony-free perimeter) was measured in triplicate with a digital caliper (Neiko Tools, Ontario, CA, USA), and the inhibition area was then calculated in square millimeters.

Botrytis cinerea was isolated from small pieces of surface tissue cut from molded strawberries. The molded pieces were placed in a 500 mL flask, and 0.05% Tween 80 was added until the pieces were completely covered. The flask was cupped and shaken for 10 min; after that, the solution was serially diluted (10×) with 0.05% v/v Tween 80. Aa aliquot of 100 μL was spread onto potato dextrose agar (PDA, with 100 mg of chloramphenicol in 1 L media plates) plates and stored for 3−5 days at room temperature. Cultures were then restreaked into PDA plates and incubated at room temperature for 6 days. Spores from day 6 cultures were harvested in 10 mL of 0.05% Tween 80 solution, which was vortexed for several minutes until uniform spore suspension was obtained. The inoculum's concentration was adjusted to 10^5 spores/mL using a hemocytometer. Then, 100 μL of the final inoculum was plated and evenly spread onto PDA plates and left to dry for 5 min. The plates, in triplicate, were divided into three and four areas; at the center of each area, 20 μL of each coating solution were placed on top of a 10 mm diameter filter paper. The inhibition radius and area around the filter paper were measured and calculated, as those for the overlay test on *E. coli*, after 4 days at room temperature.

Viscosity. The viscosity of the solutions was measured using a Brookfield Digital Rheometer (model DV − III+, Brookfield Engineering Laboratories, Middleboro, MA, USA) with a SC4-21 spindle (0.66 mm diameter, 1.23 mm long) set at 125 rpm constant rotation speed. Eight milliliters of solution at 40 °C was used for the measurement, immediately after the incorporation of EOs. Five viscosity readings were made for each coating solution from 1 to 5 min at constant shear rate (116.25 1/s) and temperature (40 °C).

Turbidity. Turbidity studies of the solution, previously warmed at 40 °C, were determined with an HI 88703 turbidity meter (Hanna Instruments, Carrollton, TX, USA). Ten milliliters of each solution was placed into transparent glass cuvettes for this assay, and measurements unit were expressed as nephelometric turbidity units (NTU).

Whitish Index (W_i). The color of the alginate coating solution was measured using a Konica Minolta spectrophotometer (CM508D, Konica−Minolta Inc., Ramsey, NJ, USA) under a standard white reflector plate. CIE L^*, a^*, b^* color coordinates, obtained from the reflection spectra of the samples using a D65 illuminant/10° observer angle, were used to calculate the whitish index as $W_i = 100 - [(100 - L^*)^2 + a^{*2} + b^{*2}]^{1/2}$.[27]

Experimental Design. To optimize the antimicrobial and physical properties of alginate coating, a full factorial design (FFD) was used as a first step to determine which independent variables, between C and MC, influenced the most the antimicrobial activity against *B. cinerea* and *E. coli* (responses). Levels of C and MC, ranging from 0.25 to 1.25% (w/w) (Table 1), were selected on the basis of preliminary tests

Table 1. Levels of the Variables Used in FFD 2^2

	levels % (w/w)		
independent variable	−1	0	+1
carvacrol	0.25	0.75	1.25
methyl cinnamate	0.25	0.75	1.25

on antimicrobial activity. A 2^2 factorial design was replicated three times to obtain more precise estimates of the effects as well as to analyze the variation at each treatment combination.

After the concentrations of the variables had been selected, on the basis of their effect on antimicrobial activity, a RSM was run for evaluating the antimicrobial activity against *E. coli* and *B. cinerea*, viscosity, turbidity, and whitish index (W_i) of the coating, to determine the concentrations of the independent factors that optimize coating characteristic for its potential application on fresh strawberries. A central composite design (CCD), characterized by 11 experimental points (4 star points, 4 cube points, and 3 central points), was selected for this purpose. Three replicates of each experimental condition were carried out, and the mean values were stated as observed responses. Experimental runs were randomized to minimize the effects of unexpected variability in the observed responses. It was assumed that a

dx.doi.org/10.1021/jf4042886 | J. Agric. Food Chem. 2014, 62, 984−990

second-order response function was fitted for relating the responses to the independent variables:

$$Y = \beta_0 + \sum \beta_i x_i + \sum \beta_{ii} x_i^2 + \sum \beta_{ij} x_i x_j$$

Y is the dependent variable and, β_0, β_i, β_{ii}, and β_{ij} are constant coefficients of intercept, linear, quadratic, and interaction terms, respectively. X_i, X_i^2, and X_{ij} represent linear, quadratic, and interactive effects of independent factors, respectively. The coefficients of the independent variables in the model were estimated by multiple regressions and evaluated by analysis of variance (ANOVA).

ANOVA was used to compare the control (alginate-based coating without antimicrobial) with the coating formulations (with antimicrobials) generated by the CCD for viscosity, turbidity, and W_i.

Tukey's means-comparison test was applied at a significance level of 0.05 to determine differences among treatments. The Minitab 14 statistical package was used to perform data analysis, experimental design matrix, and optimization procedure (Minitab Inc., USA).

Multiple Responses Optimization. After the elaboration of response surface models, a multicriteria methodology was used for the simultaneous optimization of the significant response variables. The Derringer function (desirability function) is the most currently used methodology to find optimal compromises between the total number of responses taken into account.[28,29] Each estimated response variable was transformed into a dimensionless individual desirability value (d_i) using the desirability function of the statistical program. The desirability function included the minimum and maximum acceptable values of each response. The values of d_i vary in the interval $0 \leq d_i \leq 1$, increasing as the desirability of the corresponding response increases. This transformation makes it possible to combine the results obtained from responses localized in different regions because they were measured on different orders of magnitude.

The individual desirabilities were then combined to give an overall desirability (D) by using a geometric mean equation

$$D = \sqrt[m]{d_1 d_2 \ldots d_m}$$

where m is the number of responses studied in the optimization process.

The simultaneous optimization process aimed to find the levels of the factors that demonstrated the maximum overall desirability.

RESULTS AND DISCUSSION

Full Factorial Design (FFD). Five combinations of C and MC were generated from the FFD. A preliminary antifungal test against *B. cinerea* was made for the five solutions (containing the five combinations of active compounds) with and without the addition of calcium chloride. Indeed, as a coating agent, alginate is commonly used in combination with $CaCl_2$ because of its ability to form strong gels upon cross-linking reaction.

Results indicated that solutions with $CaCl_2$ had poor inhibition of fungus growth (Table 2). It was previously reported that the physical properties of the gel adversely affected the release of low molecular weight compounds.[31] The calcium alginate gel is characterized by a typical egg-box structure in which the guluronic acid of alginate molecule can be linked to a similar region in another alginate molecule by means of calcium ions.[30] Therefore, the poor antifungal activity of alginate gels containing $CaCl_2$ could be related to the limited release of C and MC from the gel structure. On the basis of this result, a sodium alginate solution without $CaCl_2$ was selected as coating material for future studies.

Experimental data presented in Table 3 are the inhibition of *E. coli* and *B. cinerea* by combined concentrations of C and MC in alginate edible coatings.

The highest value (as the average of the three replicates) for antimicrobial activity against *E. coli* and *B. cinerea* was obtained by the combination of 1.25% (w/w) C and MC. It was also observed that the inhibition of both pathogens was mainly dependent on carvacrol concentration. The statistical analysis results of the FFD (Table 4) showed that only C had a significant ($p \leq 0.1$) effect on both microorganisms. These results also suggested that the MC range from 0.25 to 1.25% (w/w) was probably too low to achieve significant antimicrobial activity. Therefore, in the following central composite design, higher concentrations of MC, ranging from 0.5 to 2.5% (w/w), were selected, whereas the concentrations of C remained the same in the range of 0.25−1.25% (w/w).

Table 2. Antifungal Activity of Alginate Coating Solutions Generated from the FFD with and without Calcium Chloride[a]

compound concn (% w/w)		inhibitory zone on *B. cinerea* (mm^2)	
carvacrol	methyl cinnamate	alginate coating with $CaCl_2$	alginate coating without $CaCl_2$
0.25	0.25	0.00 ± 0.00	0.00 ± 0.00
1.25	0.25	2.56 ± 0.56b	81.2 ± 13.5a
0.25	1.25	0.00 ± 0.00b	4.62 ± 0.85a
1.25	1.25	6.88 ± 1.33b	83.5 ± 14.1a
0.75	0.75	0.00 ± 0.00b	46.1 ± 10.6a

[a]Data shown are the means of three replicates ± standard deviation. Different letters within a row indicate significant differences among the two coating solution ($p < 0.05$).

Table 3. Experimental Design for Antimicrobial Alginate Edible Coating (FFD)

	variables (% w/w)		inhibitory zone (mm^2)	
run	carvacrol	methyl cinnamate	*B. cinerea*	*E. coli*
1	0.25	0.25	0.00	8.81
2	1.25	1.25	73.0	60.9
3	0.25	1.25	5.37	13.0
4	0.75	0.75	42.2	31.8
5	0.25	1.25	5.54	13.1
6	1.25	1.25	85.9	50.1
7	0.25	0.25	0.00	3.75
8	0.25	0.25	0.00	10.1
9	1.25	0.25	71.8	61.1
10	1.25	0.25	85.2	52.9
11	1.25	1.25	91.5	70.2
12	0.25	1.25	2.96	16.7
13	1.25	0.25	86.6	55.0
14	0.75	0.75	49.98	29.44
15	0.75	0.75	51.25	31.85

Table 4. Statistical Analysis and Estimated Effect of FFD

	variables			
	carvacrol		methyl cinnamate	
response	effect	p value[a]	effect	p value
E. coli	47.44	0.00a	5.39	0.105
B. cinerea	80.07	0.00a	3.43	0.349

[a]a, statistically significant at $p < 0.001$.

Antimicrobial Activity of Carvacrol and Methyl Cinnamate in Alginate-Based Edible Coating Evaluated by CCD. Table 5 shows the experimental design and the results obtained for the response variables. The ANOVA for coating

dx.doi.org/10.1021/jf4042886 | J. Agric. Food Chem. 2014, 62, 984−990

Table 5. Experimental Design[a] Used To Obtain Different Combinations of C and MC in Alginate-Based Edible Coating for Antimicrobial Activity and Experimental Results for Response Variables

	concentration (% w/w)		inhibitory zone[b] (mm^2)		responses[c]		
run	C	MC	*E. coli*	*B. cinerea*	turbidity	W_i	viscosity
1	0.25	0.50	0.00	4.40	1613	66.9	83.81
2	1.25	0.50	20.9	11.2	6670	75.0	74.45
3	0.25	2.50	0.00	1030	10380	71.6	50.64
4	1.25	2.50	21.5	1241	25583	74.4	80.77
5	0.04	1.50	0.00	253	2077	68.9	58.48
6	1.46	1.50	41.9	508	16600	78.2	76.79
7	0.75	0.09	8.69	70.5	490	69.8	71.87
8	0.75	2.91	9.22	1347	26489	81.2	77.97
9	0.75	1.50	10.8	480	10817	76.6	77.76
10	0.75	1.50	3.78	525	1257	76.2	77.92
11	0.75	1.50	18.9	617	9730	77.2	77.76

[a]Central composite design (CCD) with 11 experimental points (4 star points, 4 cube points, and 3 central points). [b]Inhibitory zone indicates the antimicrobial activity against *E. coli* and *B. cinerea*. [c]Turbidity, NTU; W_i, whitish index; viscosity, cP.

antimicrobial activity against *E. coli* (Table 6) indicated that the quadratic model was found to adequately describe the

Table 6. Analysis of Variance (ANOVA) for Regression Equation Fitted to Experimental Response Values Obtained from the Optimization of the Concentration of Carvacrol and Methyl Cinnamate into Alginate Coating Solution (p Value)[a]

	inhibitory zone[b] (mm^2)				
source[c]	*E. coli*	*B. cinerea*	turbidity[d]	W_i[e]	viscosity[f]
X_1 (C)	0.002*	0.037*	0.000**	0.000**	0.034*
X_2 (MC)	0.939	0.000**	0.000**	0.026*	
X_1^2	0.198	0.098	0.316	0.003*	0.102*
X_2^2	0.436	0.039*	0.090	0.001*	
X_1X_2	0.960	0.432	0.021*	0.011*	
regression	0.021*	0.000**	0.000**	0.000**	0.003*
R^2	0.886	0.985	0.985	0.990	0.859
R^2 (adjust)	0.771	0.970	0.970	0.977	0.812
lack of fit	0.756	0.412	0.153	0.367	0.750

[a]*, significant at $p < 0.05$; **, significant at $p < 0.001$. [b]Inhibitory zone indicates the antimicrobial activity against *E. coli* and *B. cinerea*, mm^2. [c]C: carvacrol; MC: methyl cinnamate. [d]Turbidity, NTU. [e]W_i, whitish index. [f]Viscosity, cP.

experimental result without any significant lack of fit ($p > 0.05$). The main effect of C was found to be significant ($p < 0.05$), and the positive regression coefficient (Table 7) indicated that the antimicrobial activity of the coating increased when C was added into the solution. On the other hand, as in previous results, MC did not show any significant activity on *E. coli*. However, it did have a strong linear effect against *B. cinerea* ($p < 0.001$) (Table 6). On the basis of the regression coefficient terms (Table 7), the linear (499.34) and quadratic (94.92) terms of MC showed the largest antimicrobial effect against *B. cinerea*, followed by the linear effect of C (80.56). These results indicated that the increased concentration of MC in the coating significantly increased the antimicrobial activity of this compound, although no significant interaction between the

Table 7. Regression Coefficients for the Model Fitted to the Experimental Response Values

	coefficients				
	inhibitory zone[a] (mm^2)				
model term[b]	*E. coli*	*B. cinerea*	turbidity[c]	W_i[d]	viscosity[e]
constant	11.14	540	1.0601	76.66	76.54
X_1 (C)	12.71	80.56	5099	3.006	6.201
X_2 (MC)	0.1747	499.34	8054	0.9249	
X_1^2	3.81	−69.20	−719	−1.62	−4.592
X_2^2	−2.14	94.92	1354	−2.92	
X_1X_2	0.16	34.54	2536	−1.325	

[a]Inhibitory zone indicates the antimicrobial activity against *E. coli* and *B. cinerea*: mm^2. [b]C, carvacrol; MC, methyl cinnamate. [c]Turbidity, NTU. [d]W_i, whitish index. [e]Viscosity, cP.

two variables was observed (Table 6). The positive quadratic term of MC indicated that the antimicrobial activity of the coating increased quadratically when this compound was incorporated. The significant p value of regression ($p < 0.001$) and the nonsignificant lack of fit ($p > 0.05$) in the ANOVA proved that the proposed second-order polynomial model was fitted to represent the relationship between the two variables and the experimental results on antimicrobial activity against *B. cinerea*. This relationship can be better understood by examining the surface plots depicted in Figure 1, in which the

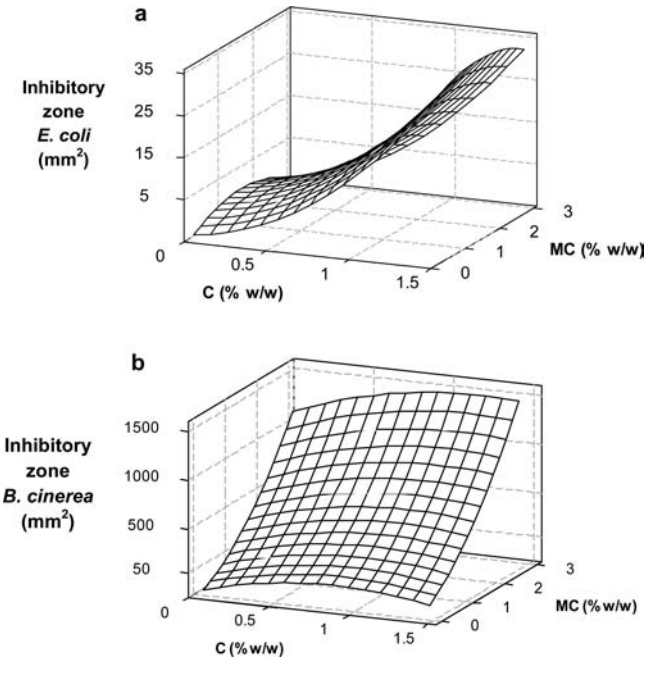

Figure 1. Response surface of antimicrobial activity against (a) *E. coli* and (b) *B. cinerea* as a function of carvacrol and methyl cinnamate (% w/w).

effects of the independent variables (C and MC) on the inactivation of selected microorganisms (*E. coli* and *B. cinerea*) were evaluated. Figure 1a shows that the inhibitory action of C on *E. coli* was very effective and directly proportional with its concentration, whereas MC did not exert a significant antimicrobial activity against this foodborne pathogen within the range of concentration studied. Conversely, in Figure 1b, we observe a highly linear increase in the inhibitory action of

dx.doi.org/10.1021/jf4042886 | J. Agric. Food Chem. 2014, 62, 984−990

MC on *B. cinerea* growth, with an increase in MC concentration in the coating, whereas C was not effective in deterring *B. cinerea* growth under the indicated concentrations range. The efficacy of C incorporated into edible films against *E. coli* O157:H7 was previously reported by Du[32] and Rojas-Grau.[33] They indicated that the addition of carvacrol into tomato-based edible films and apple puree edible films caused inactivation of *E. coli* and that the inactivation was directly related to the increase of C levels in the films. Carvacrol is considered a broad-spectrum antimicrobial, because it is effective against bacteria, yeasts, and fungi.[34] The biocidal mode of carvacrol on bacteria occurs via membrane damage resulting in an increase in membrane permeability to protons and potassium ions, depletion of the intracellular ATP pool, and disruption of the proton-motive force, ultimately leading to cell death.[35] The antifungal activity of C was reported in previous works[36,37] where spore germination and mycelium growth of *B. cinerea* were reduced when exposed to carvacrol's vapor, and the reduction was significantly greater as carvacrol concentration in the vapor increased, showing a high potential to improve the shelf life and safety of perishable foods. The antifungal properties of C against a wide range of foodborne fungi have been previously documented[38,39] and compared with those of other naturally occurring compounds, showing a high potential application against important phytopathogic fungi affecting food products.[40] The antifungal effectiveness of C could be further amplified by exploiting the high antifungal properties of MC. However, the combination of the two compounds did not show any synergistic effect on either foodborne pathogen (Table 6); the incorporation of C and MC exerted high antimicrobial activity. C (X_1) significantly ($p < 0.05$) inhibited *E. coli* and *B. cinerea*, whereas MC (X_2) significantly ($p < 0.001$) inhibited *B. cinerea*.

Effect of Carvacrol and Methyl Cinnamate on Turbidity. The results from ANOVA (Table 6) showed the significant fitting of the turbidity experimental data to the quadratic model presented a determination coefficient (R^2) of 0.985. This implied that 98.5% of the variations could be explained by the fitted model.[41] The turbidity of the coating solutions was negatively affected ($p < 0.05$) by the addition of the antimicrobial compounds. A strong linear effect ($p < 0.001$) was observed for both antimicrobial compounds and their interaction ($p < 0.05$). However, a higher positive regression coefficient was observed for MC, which suggested that it had a stronger effect on the turbidity of the coating compared to C. This fact is further supported by the response surface shown in Figure 2, where an upsurge in turbidity with an increase in MC concentration was observed but only a slight rising trend was observed as C concentration increased. Alginate coating without antimicrobial compounds served as control in the statistical comparison with the antimicrobial alginate solutions to determine if the addition of C and MC affected the turbidity of the coatings. The control alginate coating presented a significantly lower value ($p < 0.05$) of turbidity (144.3 ± 4.04) compared to all antimicrobial solutions containing C and/or MC. Turbidity is an optical property of liquids defined as the measurement of the scattered light that results from the interaction of incident light with suspended solids in the liquid.[42] The presence of particulate material in all antimicrobial solutions increased the turbidity values of the coating. Those particulates in the solutions were probably formed due to the water-insoluble property of MC. Moreover, the production of oil in water emulsions, due to the presence of C in water-based alginate solution, could have also increased the turbidity of the coating.[43]

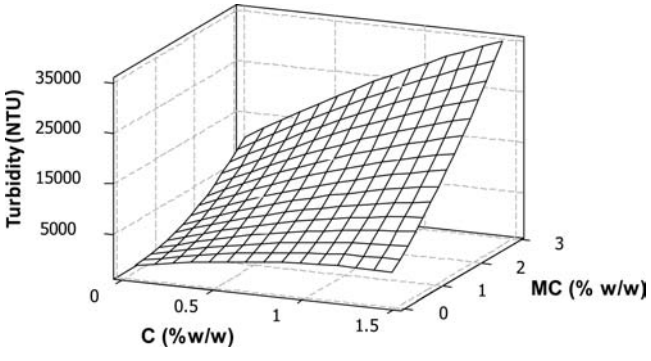

Figure 2. Response surface of turbidity (NTU) as a function of carvacrol and methyl cinnamate (% w/w).

Effect of Carvacrol and Methyl Cinnamate on W_i. With regard to visual characteristics, an edible coating for fruit applications should improve the appearance of the product and impart a natural aspect at the same time. Color is an important property to be considered when a new coating is developed. In this study, W_i was calculated because the incorporation of antimicrobial compounds led to a change of the color from transparent to white, compared to the control (Figure 3). Table 6 shows the results of ANOVA, in which carvacrol presented the highest significant effect ($p < 0.001$), achieving a negative impact on coating transparency. Additionally, the data show that the quadratic term of C, the linear and quadratic terms of MC, and the linear interaction between the two active compounds were also significant ($p < 0.05$), even when the quadratic and interaction terms of the regression coefficient of the variables were negative (Table 7). The regression model was highly significant with a determination coefficient (R^2) of 0.990, which indicated that almost the total variation was explained by the model. The value of the adjusted R^2 (0.977) confirmed that the model was highly significant on the W_i. The fitness of the quadratic model was further confirmed by the significant regression p value ($p < 0.05$) and no significant ($p > 0.05$) lack of fit (Table 6).

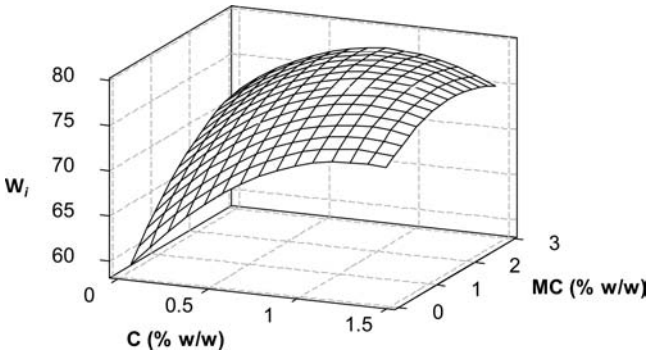

Figure 3. Response surface of whitish index (W_i) as a function of carvacrol and methyl cinnamate (% w/w).

Effect of Carvacrol and Methyl Cinnamate on Viscosity. Alginate was used as primary ingredient in edible coating solution due to its unique property of increased viscosity upon hydration. Aqueous solutions of alginate are considered non-Newtonian fluids, being characterized by shear-

dx.doi.org/10.1021/jf4042886 | J. Agric. Food Chem. 2014, 62, 984−990

thinning characteristic, meaning that the viscosity decreases as the shear rate increases.[44] Therefore, in this study the shear rate was maintained constant at 125 rpm. The effect of the addition of antimicrobial compounds was studied on the viscosity of the fluid to identify whether their incorporation would affect the fluid characteristic of the coating solution and eventually compromise further coating process application. Considering the coating and strawberry physical characteristics, preliminary studies indicated a decrease in coating performance at viscosity values above 83 cP. Hence, viscosity values lower than 83 cP were used as a target for the optimization of the solution. Table 7 shows the results of ANOVA for the fitting model of the viscosity experimental data to a second-order function, which was found to describe the experimental response influenced by the antimicrobial variables without any significant ($p > 0.05$) lack of fit (Table 6). Because the full model was not able to predict viscosity responses based on antimicrobial variables, the model was reduced by excluding the nonsignificant linear and quadratic terms of MC, as well as the interaction between C and MC, to adequately correlate the quadratic relationship between the concentrations of the antimicrobial compounds and viscosity of the fluid. The results showed that only the linear and quadratic effect of C significantly ($p < 0.05$) affected the viscosity of the coating solution (Table 6). However, the positive linear term (+6.20) and the negative quadratic term of the regression coefficient (−4.59) indicated that increasing C concentrations led to an increase in viscosity until a turning point was reached at 0.68% (w/w) C. Concentrations of C above this value tend to decrease the viscosity of the coating solution, probably due to the plasticizer action of C. It has been reported that C reduces the intermolecular forces in polymer chains, thus decreasing the viscosity of the coatings.[45] Similar results were observed when different concentrations of essential oils, above 1.5% (w/w), were added into apple and tomato edible films.[46,47]

Multiple Responses Optimization. On the basis of the findings of each response surface model, an overall optimization study was performed to obtain an antimicrobial coating with physical properties suitable for strawberry application. The optimum condition for alginate coatings with the most desirable characteristics, obtained by the overall desirability function, was at 0.98% (w/w) carvacrol and 1.45% (w/w) methyl cinnamate concentrations.

AUTHOR INFORMATION

Corresponding Author

*(G.P.) E-mail: greta.peretto@gmail.com. Fax: +39 049 8272839. Phone: +39 049 8272826.

Funding

This work was supported by the Department of Agronomy, Food, Natural Resources, Animals and Environment (DAFNAE) of the University of Padova (Italy).

Notes

The authors declare no competing financial interest.

ACKNOWLEDGMENTS

We are grateful for the assistance provided by the Western Regional Research Center, U.S. Department of Agriculture, Agricultural Research Service.

REFERENCES

(1) Lynch, M. F.; Tauxe, R. V.; Hedberg, C. W. The growing burden of foodborne outbreaks due to contaminated fresh produce: risks and opportunities. *Epidemiol. Infect.* **2009**, *137*, 307−315.

(2) Du, W.-X.; Avena-Bustillos, R. J.; Hua, S. S. T.; McHugh, T. H. Antimicrobial volatile essential oils in edible films for food safety. In *Science against Microbial Pathogens: Communicating Current Research and Technological Advances*; Mendez-Vilas, A., Ed.; Formatex Research Center: Badajoz, Spain, 2011; Vol. 2, pp 1124−1134.

(3) Hao, C.; Zhao, Y.; Leonard, S. W.; Traber, M. G. Edible coatings to improve storability and enhance nutritional value of fresh and frozen strawberries (*Fragaria x ananassa*) and raspberry (*Rubus ideaus*). *Postharvest Biol. Technol.* **2004**, *33*, 67−78.

(4) Kader, A. A. Postharvest biology and technology: an overview. In *Postharvest Technology of Horticultural Crops*; Kader, A. A., Ed.; University of California, Agriculture and Natural Resources: Davis, CA, USA, 2002; Chapter 4, pp 39−48.

(5) Krochta, J. M.; De-Mulder-Johnston, C. Edible and biodegradable polymer films: challenged and opportunities. *Food Technol.* **1997**, *51*, 61−74.

(6) Lacroix, M.; LeTien, C. Edible films and coatings from non-starch polysaccharides. In *Innovation in Food Packaging*; Han, J. H., Ed.; Elsevier Academic Press: New York, 2005; pp 338−361.

(7) Ribeiro, C.; Vicente, A. A.; Teixeira, J. A.; Miranda, C. Optimization of edible coating composition to retard strawberry fruit senescence. *Postharvest Biol. Technol.* **2007**, *44*, 63−70.

(8) García, M. A.; Martino, M. N.; Zaritzky, N. E. Plasticized starch-based coatings to improve strawberry (*Fragaria* × *Ananassa*) quality and stability. *J. Agric. Food Chem.* **1999**, *46*, 758−3767.

(9) Park, S. I.; Stan, S. D.; Daeschel, M. A.; Zhao, Y. Antifungal coatings on fresh strawberries (*Fragaria* × *ananassa*) to control mold growth during cold storage. *J. Food Sci.* **2005**, *70*, M202−M207.

(10) Roopa, B. S.; Bhattacharya, S. Alginate gels: characterization of textural attributes. *J. Food Eng.* **2008**, *85*, 123−131.

(11) Azarakhsh, N.; Osman, A.; Ghazali, H. M.; Tan, C. P; Mohd Adzahan, N. Optimization of alginate and gellan-based edible coating formulations for fresh-cut pineapples. *Int. Food Res. J.* **2012**, *19*, 279−285.

(12) Gombotz, W. R.; Wee, S. F. Protein release from alginate matrices. *Adv. Drug Delivery Rev.* **1998**, *31*, 267−285.

(13) Campos, A. C.; Gerschenson, L. N.; Flores, S. K. Development of edible films and coatings with antimicrobial activity. *Food Bioprocess Technol.* **2011**, *4*, 849−875.

(14) Oms-Oliu, G.; Soliva-Fortuny, R.; Martín-Belloso, O. Edible coatings with antibrowning agents to maintain sensory quality and antioxidant properties of fresh-cut pears. *Postharvest Biol. Technol.* **2008**, *50*, 97−84.

(15) Rojas-Graü, M. A.; Tapia, M. S.; Rodríguez, F. J.; Carmona, A. J.; Martin-Belloso, O. Alginate and gellan-based edible coatings as carriers of antibrowning agents applied on fresh-cut Fuji apples. *Food Hydrocolloids* **2007**, *21*, 118−127.

(16) Ponce, A. G.; Roura, S. I.; Del Valle, C. E.; Moreira, M. R. Antimicrobial and antioxidant activities of edible coatings enriched with natural plant extracts: *in vitro* and *in vivo* studies. *Postharvest Biol. Technol.* **2008**, *49*, 294−300.

(17) Raybaudi-Massilia, R. M.; Mosqueda-Melgar, J.; Martín-Belloso, O. Edible alginate-based coating as carrier of antimicrobials to improve shelf-life and safety of fresh-cut melon. *Int. J. Food Microbiol.* **2008**, *121*, 313−327.

(18) Rojas-Graü, M. A.; Soliva-Fortuny, R.; Martín-Belloso, O. Edible coatings to incorporate active ingredients to fresh-cut fruits: a review. *Trends Food Sci. Technol.* **2009**, *20*, 438−447.

(19) Burt, S. Essential oils: their antibacterial properties and potential applications in foods − a review. *Int. J. Food Microbiol.* **2004**, *94* (3), 223−253.

(20) López, P.; Sánchez, C.; Batlle, R.; Nerín, C. Development of flexible antimicrobial films using essential oils as active agents. *J. Agric. Food Chem.* **2007**, *55*, 8814−8824.

(21) Lunkenbein, S.; Bellido, M.; Aharoni, A.; Salentijin, E. M. J.; Kaldenhoff, R.; Coiner, H. A.; Munoz-Blanco, J.; Schwab, W. Cinnamate metabolism in ripening fruit. Characterization of a UDP-glucose; cinnamate glucosyltranferase from strawberry. *Plant Physiol.* **2006**, *140*, 1047−1058.
(22) Ali, N. A. M.; Rahmani, M.; Shaari, K.; Ali, A. M.; Cheng Lian, G. E. Antimicrobial activity of *Cinnamomum Impressicostatum* and *C. pubescens* and bioassay-guided isolation of bioactive (*E*)-methyl cinnamate. *J. Biol. Sci.* **2010**, *10*, 101−106.
(23) El-Shiekh, Y. W. A.; El-Din, N. H.; Shaymaa, M. A. A.; El-Din, K. A. Z. Antifungal activity of some naturally occurring compounds against economically important phytopathogenic fungi. *Nat. Sci.* **2012**, *10*, 114−123.
(24) Wannissorn, B.; Maneesin, B.; Tubtimted, S.; Wangchanachai, G. Antimicrobial activity of essential oils extracted from Thai herbs and spices. *Asian J. Food Ag-Ind.* **2009**, *2*, 677−689.
(25) Peretto, G.; Du, W. X.; Avena-Bustillos, R.; Sarreal, S. B. L.; Hua, S. S. T.; Sambo, P.; McHugh, T. H. Increasing strawberry shelf-life with caracrol and methyl cinnamate antimicrobial vapors released from edible films. *Postharvest Biol. Technol.* **2014**, *89*, 11−18.
(26) Du, W. X.; Olsen, C. W.; Avena-Bustillos, R. J.; McHugh, T. H.; Levin, C. E.; Friedman, M. Storage stability and antimicrobial activity against *Escherichia coli* O157:H7 of carvacrol in edible apple films prepared by two different casting methods. *J. Agric. Food Chem.* **2008**, *56*, 3082−3088.
(27) Avena-Bustillos, R. J.; Krochta, J. M. Optimization of edible coating formulation on zuvvhini to reduce weight loss. *J. Food Eng.* **1994**, *21*, 197−214.
(28) Derringer, G.; Suich, R. Simultaneous optimization of several response variables. *J. Quality Technol.* **1980**, *12* (4), 214−219.
(29) Murphy, T. E.; Tsui, K. L.; Allen, J. K. A review of robust design methods for multiple responses. *Res. Eng. Des.* **2005**, *15*, 201−205.
(30) Liu, X.; Lu, L.; Dai, L.; Tong, Z. Difference in concentration dependence of relaxation critical exponent n for alginate solutions at sol−gel transition induced by calcium cations. *Biomacromulecules* **2005**, *6*, 2150−2156.
(31) Seifert, D. B.; Phillips, J. A. Production of small, monodispersed alginate beads for cell immobilization. *Biotechnol. Prog.* **1997**, *13*, 562−568.
(32) Du, W. X.; Olsen, C. W.; Avena-Bustillos, R. J.; McHugh, T. H.; Levin, C. E.; Friedman, M. Antibacterial activity against *E. coli* O157:H7, physical properties, and storage stability of novel carvacrol-containing edible tomato films. *J. Food Sci.* **2008**, *73* (7), M378−M383.
(33) Rojas-Grau, M. A.; Avena-Bustillos, R. J.; Friedman, M.; Henika, P. R.; Martin-Belloso, O.; McHugh, T. H. Mechanical, barrier, and antimicrobial properties of apple puree edible films containing plant essential oils. *J. Agric. Food Chem.* **2006**, *54*, 9262−9267.
(34) Sivropoulou, A.; Papanikolaou, E.; Nikolaou, C.; Kokkini, S.; Lanaras, T.; Arsenakis, M. Antimicrobial and cytotoxic activities of origanum essential oils. *J. Agric. Food Chem.* **1996**, *44*, 1202−1205.
(35) Kiskó, G.; Roller, S. Carvacrol and *p*-cymene inactivate *Escherichia coli* O157:H7 in apple juice. *BMC Microbiol.* **2005**, 5−36.
(36) Martínez-Romero, D.; Guillén, F.; Valverde, J. M.; Bailén, G.; Zapata, P.; Serrano, M.; Castillo, S.; Valero, D. Influence of carvacrol on survival of *Botrytis cinerea* inoculated in table grapes. *Int. J. Food Microbiol.* **2007**, *115*, 144−148.
(37) Adam, K.; Sivropoulou, A.; Kokkini, S.; Lanaras, T.; Arsenakis, M. Antifungal activities of *Origanum vulgare* subsp. *hirtum*, *Mentha spicata*, *Lavandula angustifolia*, and *Salvia fruticosa* essential oils against human pathogenic fungi. *J. Agric. Food Chem.* **1998**, *46*, 1739−1745.
(38) Jantan, I. B.; Moharam, B. A. K.; Santhanam, J.; Jamal, J. A. Correlation between chemical composition and antifungal activity of the essential oils of eight *Cinnamomum* species. *Pharm. Biol.* **2008**, *46*, 406−412.
(39) Suppakul, P.; Miltz, J.; Sonneveld, K.; Bigger, S. W. Antimicrobial properties of basil and its possible application in food packaging. *J. Agric. Food Chem.* **2003**, *51*, 3197−3207.
(40) Karam El-Din, A. Z.; El-Shiekh, Y. W. A.; Nour El-Din, A. H.; Mohamed, A. A. S. Antifungal activity of some naturally occurring compounds against economically important phytopathogic fungi. *Nat. Sci.* **2012**, *10*, 114−123.
(41) Chen, W.; Wang, W. P.; Zhang, H. S.; Huang, Q. Optimization of ultrasonic-assisted extraction of water-soluble polysaccharides from *Boletus edulis* mycelia using response surface methodology. *J. Agric. Food Chem.* **2012**, *87*, 614−619.
(42) Gippel, C. J. Potential of turbidity monitoring for measuring the transport of suspended solids in streams. *Hydrol. Process.* **1995**, *9*, 83−97.
(43) Han, J. H.; Hwang, H. M.; Min, S.; Krochta, J. M. Coating of peanuts with edible whey protein film containing α-tocopherol and ascorbyl palmitate. *J. Food Sci.* **2008**, *8*, 349−355.
(44) Storz, H.; Zimmermann, U.; Zimmermann, H.; Kulicke, W. M. Viscoelastic properties of ultra-high viscosity alginates. *Rheol. Acta* **2010**, *49*, 155−167.
(45) Nostro, A.; Scaffaro, R.; D'Arrigo, M.; Botta, L.; Filocamo, A.; Marino, A.; Bisignano, G. Study on carvacrol and cinnamaldehyde polymeric films: mechanical properties, release kinetics and antibacterial and antibiofilm activities. *Appl. Microbiol. Biotechnol.* **2012**, *96*, 1029−1038.
(46) Du, W.-X.; Olsen, C. W.; Avena-Bustillos, R. J.; McHugh, T. H.; Levin, C. E.; Friedman, M. Effects of allspice, cinnamon and clove bud essential oils in apple films on antimicrobial activities against *Escherichia coli* O157:H7, *Salmonella enterica*, and *Listeria monocytogenes*. *J. Food Sci.* **2009**, *74* (7), 372−378.
(47) Du, W.-X.; Olsen, C. W.; Avena-Bustillos, R. J.; McHugh, T. H.; Levin, C. E.; Friedman, M.; Mandrell, R. E. Effects of oregano, allspice, and garlic essential oils in tomato films on antimicrobial activities against *Escherichia coli* O157:H7, *Salmonella enterica*, and *Listeria monocytogenes*. *J. Food Sci.* **2009**, *74* (7), 390−397.

electrophoresis was determined to further evaluate the effect of SSA on the plasmid DNA structure. Moreover, theoretical docking was carried out to visualize the position and preferential docking sites of SSA in ctDNA. This study may provide insight into the binding mechanism of SSA with ctDNA at the molecular level and potential hazards of the sweetener.

MATERIALS AND METHODS

Materials. The stock solution (4.87×10^{-3} mol L^{-1}) of SSA (Aladdin Chemical Co. Shanghai, China) was prepared in ultrapure water. A highly polymerized fibrous form of ctDNA was purchased from Sigma-Aldrich Co. (St. Louis, MO, USA), and its stock solution was prepared by dissolving the required amount of ctDNA in 0.1 mol L^{-1} NaCl solution and stored at 4 °C. The concentration of ctDNA in stock solution was 3.61×10^{-3} mol L^{-1} determined by UV−vis absorption at 260 nm using the molar absorption coefficient ε_{260} = 6600 L mol^{-1} cm^{-1}.[15] The purity of ctDNA was determined by the ratio of the absorbance at 260 nm to that at 280 nm. The ctDNA solution gave a ratio of $A_{260}/A_{280} > 1.8$, suggesting that the ctDNA was sufficiently free from proteins.[16,17] Supercoiled pUC18 plasmid DNA was obtained from Beijing Solarbio Science and Technology Ltd. (Beijing, China). All stock solutions were diluted to the required concentrations with 0.05 mol L^{-1} Tris-HCl buffer, pH 7.4. All chemicals were of analytical reagent grade, and ultrapure water (18.2 MΩ cm) was used throughout the experiment.

Fluorescence Measurements. The fluorescence spectral titrations were performed on a spectrofluorometer (model F-4500, Hitachi, Japan) with a DC-2006 thermostat bath (Ningbo Xinyi Ultrasonic Instrument Co., Ningbo, China). Three milliliters of SSA (8.12×10^{-5} mol L^{-1}) was first added to a 1.0 cm quartz cell, and various concentrations of ctDNA were then gradually titrated to the cell using a micropipet. The fluorescence emission spectra were measured at 292, 298, 304, and 310 K over a wavelength range of 340−540 nm with an exciting wavelength at 277 nm. All solutions were under conditions of stirring and allowed to equilibrate for 5 min before measurements were conducted. To eliminate the possible reabsorption and inner filter effect arising from UV−vis absorption of ctDNA, the fluorescence data of SSA were corrected for absorption of excitation and emitted light according to the relationship[18]

$$F_c = F_m\, e^{(A_1+A_2)/2} \quad (1)$$

where F_c and F_m are the corrected and measured fluorescence, respectively, and A_1 and A_2 are the absorbance of the ctDNA solutions at 277 and 430 nm, respectively.

Iodide quenching experiments were performed by adding different amounts of potassium iodide solution ($(0-1.09) \times 10^{-2}$ mol L^{-1}) to SSA and SSA−ctDNA complex solutions, respectively. The single-strand ctDNA (ss ctDNA) solution was prepared by heating native double-stranded ctDNA (ds ctDNA) solution in a boiling water bath for 10 min, followed by rapid cooling in an ice−water bath. When the temperature was gradually increased to 298 K, ds ctDNA became ss ctDNA.[19] A comparison of the quenching effects of ss ctDNA and ds ctDNA was carried out by progressively adding ss ctDNA or ds ctDNA solution to SSA solution at a constant concentration of 8.12×10^{-5} mol L^{-1}. The corresponding fluorescence intensity was recorded, and then the quenching constants were calculated.

The effect of NaCl on the fluorescence of the SSA−ctDNA system was determined by gradually adding various amounts of NaCl ($(0-2.67) \times 10^{-2}$ mol L^{-1}) to the fixed amount of SSA and SSA−DNA complex solutions to measure the changes in fluorescence intensity.

Deveplopment of the Expanded Data Matrix for MCR−ALS. The UV−vis absorption spectra were measured on a Shimadzu UV-2450 spectrophotometer equipped with a controlled cell holder matched with 1.0 cm quartz cells. To determine the interaction between SSA and ctDNA, two separate experiments were carried out by fluorescence and UV−vis absorption spectra titrations in Tris-HCl buffer (pH 7.4) at room temperature, following methods standardized in our laboratory to get the expanding data matrix for MCR−ALS.[20] For experiment 1, the concentration of SSA was kept constant at 8.12×10^{-5} mol L^{-1}, and different amounts of ctDNA were added progressively to the solution. For experiment 2, the concentration of ctDNA was fixed at 6.00×10^{-5} mol L^{-1}, and various amounts of SSA were added to the solution. All of the samples were allowed to stand for 5 min before the spectroscopic measurements. The UV−vis absorption spectra (220−320 nm) and fluorescence spectra (340−540 nm) were both collected every 1 nm. Therefore, four data matrices, $\boldsymbol{D}_F^{SSA}$ (31 × 201) and $\boldsymbol{D}_{UV}^{SSA}$ (31 × 101) from experiment 1 and $\boldsymbol{D}_F^{ctDNA}$ (31 × 201) and $\boldsymbol{D}_{UV}^{ctDNA}$ (31 × 101) from experiment 2, were obtained, and these data matrices for two different experiments were combined and an expanded data matrix was established.

DNA Melting Studies. In a typical DNA melting experiment, the absorbance change at 260 nm of ctDNA and SSA−ctDNA complex was investigated as a function of temperature ranging from 20 to 100 °C. The values of melting temperature (T_m) were obtained from the transition midpoint of the melting curves based on f_{ss} versus temperature (T), where $f_{ss} = (A - A_0)/(A_f - A_0)$, A_0, A, and A_f being the initial absorbance, the absorbance corresponding to different temperatures, and the final absorbance, respectively.[10]

Viscosity Measurements. The viscosity measurements were made on an Ubbelohde viscometer (Φ 0.7−0.8 mm, Shanghai Qianfeng Rubber and Glass Co., Shanghai, China) maintained at 25 ± 0.1 °C by an electronic thermostat water bath (Shanghai Yuejin Medical Instrument Co., Shanghai, China). The concentration of ctDNA was kept at 4.81×10^{-5} mol L^{-1}, and aliquots of SSA solution were added directly into the viscometer. The solutions were mixed thoroughly, and the flow times of ctDNA alone and its mixtures with different ratios of SSA to ctDNA ([SSA]/[ctDNA]) through the capillary were then measured in five replicates using a digital stopwatch with an accuracy of ±0.20 s. The data were presented as $(\eta/\eta_0)^{1/3}$ versus the molar ratios,[21] where η_0 and η are the specific viscosities of ctDNA alone and the SSA−ctDNA complex. Viscosity values were determined from the observed flow time of DNA-containing solutions (t) and corrected for buffer solution (t_0), $\eta = (t - t_0)/t_0$.[13]

CD Measurements. CD spectra of ctDNA in the absence and presence of different amounts of SSA were recorded at a wavelength range of 220−320 nm under constant nitrogen flush by a Bio-Logic MOS 450 CD spectrometer (Bio-Logic, Claix, France) equipped with a 1.0 mm path length quartz cuvette. The CD measurements were carried out in pH 7.4 Tris-HCl buffer at room temperature, and all observed CD profiles were corrected for the buffer signal.

FT-IR Analyses. A FT-IR spectrometer (Thermo Nicolet-5700) equipped with a germanium attenuated total reflection (ATR) accessory was used to measure infrared spectra as reported earlier.[10,20] All spectra were recorded on OMNIC software via the ATR method over the spectral range of 1800−800 cm^{-1} with a resolution of 4 cm^{-1} and 64 scans after 2 h of incubation of SSA with the ctDNA solution. Due to sugar C−C and C−O stretching vibrations, the band of DNA at 968 cm^{-1} exhibited no spectral change upon ligand−DNA complexation.[22] Thus, this band was generally used as an internal reference in the different spectra ([ctDNA solution + SSA solution] − [SSA solution]). The intensity ratios (R) of the bands due to several ctDNA in-plane vibrations related to base pairs and the PO_2 stretching vibrations versus the SSA concentrations were obtained after peak standardization using $R_i = I_i/I_{968}$, where I_i is the intensity of absorption peak at i cm^{-1} for free ctDNA and the SSA−ctDNA complex at different concentrations of SSA and I_{968} is the intensity of the 968 cm^{-1} peak (internal reference).[23]

Molecular Modeling. The following molecular docking studies were implemented with the software package AutoDock version 4.2. The crystal structure of the B-DNA with identifier 425D[24] was downloaded from the Protein Data Bank (http://www.rcsb.org/pdb). The 3D structure of the ligand SSA was constructed in Sybyl ×1.1 (Tripos Inc., St. Louis, MO, USA), and its energy-minimized conformation was obtained with the MMFF94 force field.[20] In the process of docking preparation, all of the water molecules were removed, whereas Gasteiger charges and essential hydrogen atoms were added with the aid of AutoDock tools. The grid spacing was set

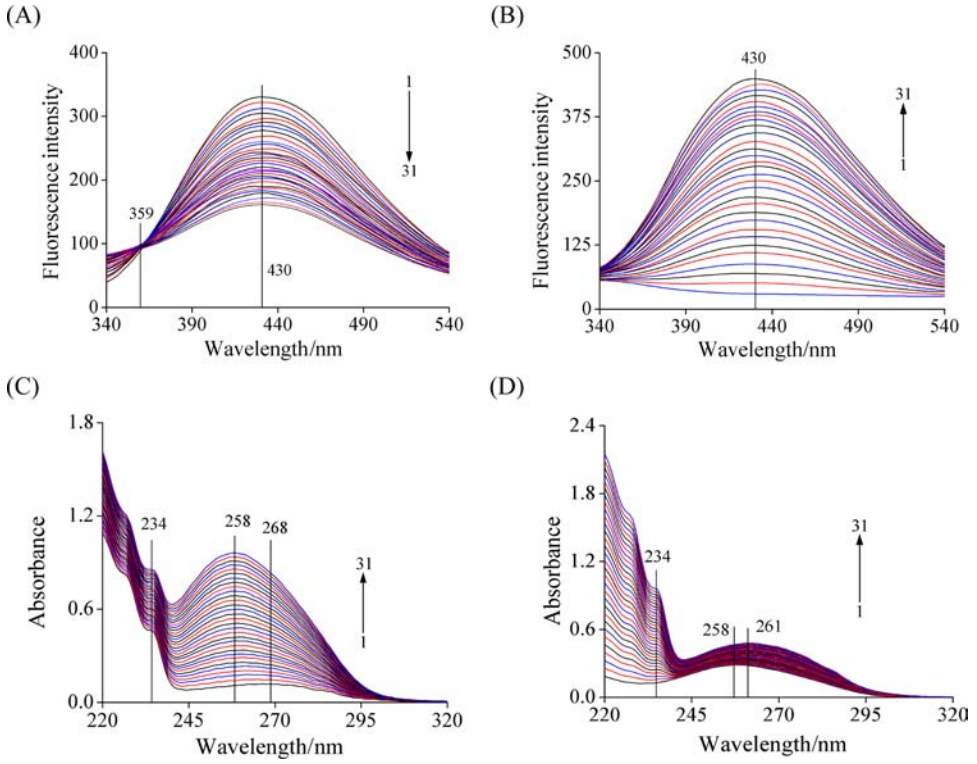

Figure 2. Spectra obtained from different experiments. Experiment 1: (A) fluorescence (D_F^{SSA}) and (C) UV−vis (D_{UV}^{SSA}), c(SSA) = 8.12 × 10^{-5} mol L^{-1}, and c(ctDNA) = 0, 0.60, 1.20, ..., 18.0 × 10^{-5} mol L^{-1} for curves 1−31, respectively. Experiment 2: (B) fluorescence (D_F^{ctDNA}) and (D) UV−vis (D_{UV}^{ctDNA}), c(ctDNA) = 6.0 × 10^{-5} mol L^{-1}, and c(SSA) = 0, 0.49, 0.98, ..., 14.70 × 10^{-5} mol L^{-1} for curves 1−31, respectively.

to be 0.375 Å with a dimension of 118 Å × 74 Å × 118 Å to encompass the whole DNA molecule. After the docking procedure was run successfully, the binding site and the possible conformation of the complex were generated from the reaction between SSA and DNA.

Gel Electrophoresis. Supercoiled pUC18 plasmid DNA (5 μL, 450 μg mL^{-1}) was treated with different concentrations of SSA followed by dilution with Tris-HCl buffer (0.05 mol L^{-1}) containing 0.05 mol L^{-1} NaCl (pH 7.4) to a total volume of 15 μL. The samples of DNA and SSA−DNA complex were incubated for 24 h at 37 °C. A loading buffer (5 μL) containing 0.03% bromophenol blue, 0.03% xylene cyanol, and 30% glycerol was added and electrophoresis performed at 80 V for 1.0 h in 1× Tris−acetate−EDTA (TAE) buffer using 1.0% agarose gel containing 1.0 μg mL^{-1} ethidium bromide. After the electrophoresis, the gel was visualized and photographed by a UV illuminator.

Chemometrics Methods. MCR−ALS has often been used to estimate an optimal concentration and spectra profiles of the species during the chemical reaction.[25,26] Resolution of these chemical species can be largely enhanced when several runs of different spectrophotometric titrations of the same chemical reaction system are resolved simultaneously.[27] Mathematically, the experimental data matrix, $\boldsymbol{D}$, was decomposed into the two smaller factor matrices, $\boldsymbol{C}$ and $\boldsymbol{S}^T$, according to the algebraic model

$$\mathbf{D}(m \times n) = \mathbf{C}(m \times f) \times \mathbf{S}^T(f \times n) + \mathbf{E}(m \times n) \quad (2)$$

where $\boldsymbol{D}$ is the experimental data matrix with dimensions m (spectral objects) × n (wavelengths); $\boldsymbol{C}$ ($m \times f$) is the concentration profile matrix of pure species in the samples; $\boldsymbol{S}^T$ ($f \times n$) is the transposed matrix consisting of, for example, the emission spectra; the f rows of this matrix contain the pure spectra associated with the f species in the samples; and $\boldsymbol{E}$ ($m \times n$) is the residuals matrix. The MCR−ALS algorithm was performed in the following several steps. First, the number of components, f, involved in the chemical reaction process was estimated. This determination was implemented by rank analysis, singular value decomposition (SVD),[28] based on the assumption that the singular values related to chemical components are larger than those associated with errors and noise in the experiment. Second, the constrained alternating least-squares (ALS) regression procedure was utilized to iteratively optimize the initial estimates of $\boldsymbol{S}^T$ or $\boldsymbol{C}$, which are created by evolving factor analysis (EFA).[29] Once the number of species, f, has been extracted, the initial concentration profiles and pure spectra of all the contributing species can be established by the MCR−ALS method.

In the study, two-way fluorescence and the UV−vis spectral expanded data matrix, $\boldsymbol{D}$, were built up by placing the individual data matrices corresponding to the two types of spectra side by side. The related bilinear model for MCR−ALS analysis could be expressed by the following equation:

$$[\mathbf{D}_{UV}\mathbf{D}_F] = \mathbf{C} \times [\mathbf{S}_{UV}^T\mathbf{S}_F^T] + [\mathbf{E}_{UV}\mathbf{E}_F] \quad (3)$$

$\boldsymbol{D}_{UV}$ and $\boldsymbol{D}_F$ are the measurements for the same experiment obtained with two different spectroscopic techniques. Thus, a single-concentration profile matrix, $\boldsymbol{C}$, and a row-wise augmented matrix of pure spectra, $\boldsymbol{S}^T$, can be resolved by the MCR−ALS algorithm.

RESULTS AND DISCUSSION

Fluorescence and Absorption Spectra of Interaction between SSA and ctDNA. Figure 2A shows the emission spectra of SSA in the presence of various concentrations of ctDNA. It was found that the fluorescence intensity of SSA at 430 nm decreased regularly without any significant shift of the peak with the increasing concentration of ctDNA (curves from 1 to 31). A weak fluorescence spectrum of ctDNA could be seen in Figure 2B;with the gradual addition of SSA solution, the fluorescence signal of ctDNA was enhanced (curves from 1 to 31), and a new peak at 430 nm was observed. The UV−vis absorption spectra of SSA exhibited two absorption bands at 234 and 268 nm, and upon the addition of ctDNA, the absorption intensity of SSA at 268 nm increased gradually with a significant blue shift (from 268 to 258 nm, corresponding to

dx.doi.org/10.1021/jf405085g | J. Agric. Food Chem. 2014, 62, 991−1000

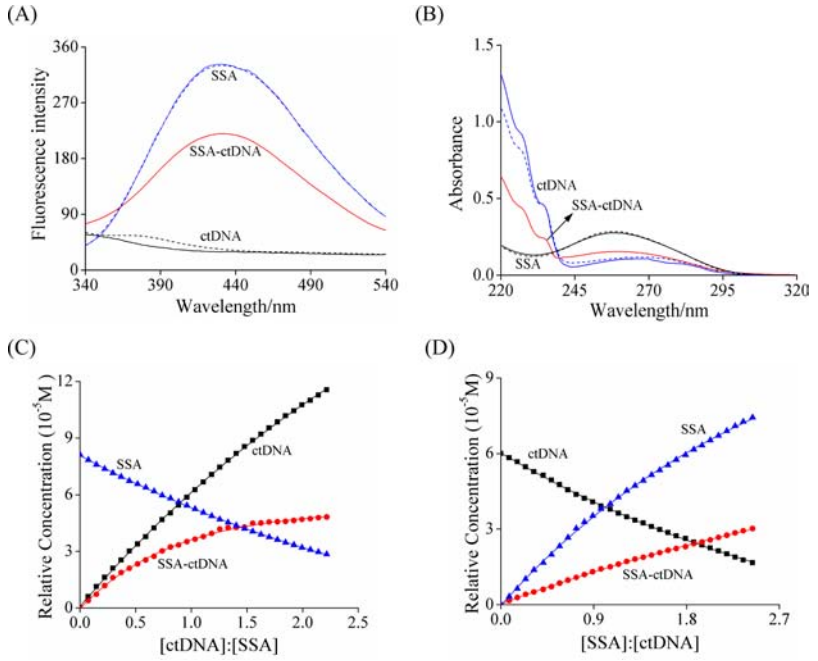

Figure 3. Results obtained from the simultaneous analysis of the UV−vis and fluorescence data of the two experiments by MCR−ALS: (A) recovered fluorescence spectra; (B) recovered UV−vis spectra (solid line, recovered spectra; dashed line, measured spectra); recovered concentration profiles for experiment 1 (C) and experiment 2 (D).

curves from 1 to 31, Figure 2C). On the other hand, with increasing amounts of SSA, the absorption peak of ctDNA at 258 nm, which resulted from the strong absorption of purine and pyrimidine bases in ctDNA, showed a gradual increase accompanied by a significant red shift (from 258 to 261 nm, corresponding to curves from 1 to 31, Figure 2D).

As the collected spectral profiles were highly spectrally overlapped and complicated, it was difficult to deduce the concentration changes of reaction components and gain the spectrum of the SSA−ctDNA complex by the conventional fluorescence and UV−vis absorption methods. Furthermore, no quantitative and qualitative information was available from these profiles.[25] Therefore, in the study, the expanded spectroscopic data matrix obtained from SSA−ctDNA mixtures was simultaneously resolved by the MCR−ALS to extract useful information of the SSA−ctDNA reaction system, such as the concentration profiles and the pure spectra for each species so as to determine the SSA−ctDNA interaction.

Decomposition of the Expanded Fluorescence and UV−Vis Data Matrix by MCR−ALS. The expanded fluorescence and UV−vis data matrix, $[\boldsymbol{D}_F, \boldsymbol{D}_{UV}]$ was analyzed using the SVD model, and the number of significant factors related to the chemical species was evaluated. The extracted first four eigenvalues were determined to be 102.32, 31.62, 10.23, and 1.99, indicating that three significant factors for the prediction of three separate chemical components existed in the system, namely, SSA, ctDNA, and SSA−ctDNA complex. As the spectra of these three components in the mixtures significantly overlapped, a powerful chemometics method, MCR−ALS, was applied to resolve the combined fluorescence and UV−vis absorption data matrix to obtain the concentrations and pure spectra of the three species. Panels A and B of Figure 3 display the pure fluorescence and UV−vis spectra recovered for different species, which correspond to $\boldsymbol{S}_F^T$ and $\boldsymbol{S}_{UV}^T$, respectively. The resolved spectra (solid line) of the free SSA and ctDNA kept good consistency and prediction with the measured counterparts (dashed line). The consistency between the predicted and measured spectral profiles of SSA and ctDNA suggested that the concentration profiles were correctly resolved. Moreover, the fluorescence and UV−vis spectra of the SSA−ctDNA complex (Figure 3A,B) were extracted with the aid of MCR−ALS, which were difficult to be observed by conventional methods. The obtained concentration profiles of SSA, ctDNA, and SSA−ctDNA complex by MCR−ALS analysis showed that the concentration of SSA−ctDNA complex increased gradually along with the decrease of the concentration of SSA upon the addition of ctDNA (Figure 3C), and some superfluous free ctDNA existed in the reaction system. A similar increasing tendency of the concentration of the SSA−ctDNA complex accompanied by a decreasing tendency of ctDNA concentration with increase in concentration of SSA was observed from Figure 3D. It was thus concluded that SSA bound to ctDNA, and a SSA−ctDNA complex was formed.

Fluorescence Quenching Assays. At the excitation wavelength of 277 nm, SSA exhibited a strong fluorescence emission peak at 430 nm (Figure 4A). When different amounts of ctDNA were titrated into a fixed concentration of SSA, the fluorescence intensity of SSA decreased regularly, indicating that an interaction between SSA and ctDNA existed.[30]

The possible quenching mechanism can be made clear by the well-known Stern−Volmer equation

$$\frac{F_0}{F} = 1 + K_{SV}[Q] = 1 + K_q\tau_0[Q] \quad (4)$$

where F_0 and F are the fluorescence intensities of SSA in the absence and in the presence of ctDNA, respectively. [Q] is the concentration of ctDNA. K_{SV} and K_q are the Stern−Volmer quenching constant and the bimolecular quenching constant, repectively, and K_q equals K_{SV}/τ_0. τ_0 denotes the average lifetime of the fluorophore in the absence of quencher, the value of τ_0 of the biopolymer is 10^{-8} s.[31]

dx.doi.org/10.1021/jf405085g | J. Agric. Food Chem. 2014, 62, 991−1000

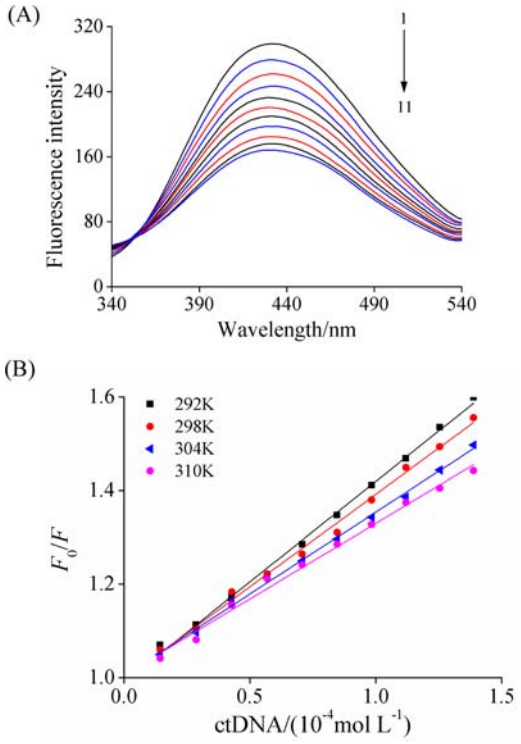

Figure 4. (A) Effect of ctDNA on fluorescence spectra of SSA (T = 298 K, pH 7.4, λ_{ex} = 277 nm, λ_{em} = 430 nm); c(SSA) = 8.12 × 10^{-5} mol L^{-1}; and c(ctDNA) = 0, 1.44, 2.87, 4.28, 5.69, 7.08, 8.46, 9.83, 11.19, 12.54, and 13.88 × 10^{-5} mol L^{-1}, for curves 1−11, respectively. (B) Stern−Volmer plots for the fluorescence quenching of SSA by ctDNA at different temperatures.

The fluorescence data at different temperatures (292, 298, 304, and 310 K) were fitted by Stern−Volmer plots (Figure 4B), and the corresponding K_{SV} values for the interaction between SSA and ctDNA are shown in Table 1. The results clearly showed that the K_{SV} was inversely correlated with temperature, and the calculated K_q values were 4.31 × 10^{11}, 3.96 × 10^{11}, 3.50 × 10^{11}, and 3.23 × 10^{11} L mol^{-1} s^{-1} at 292, 298, 304, and 310 K, respectively, which were higher than the maximum scatter collision quenching constant of various quenchers with biopolymers, 2.0 × 10^{10} L mol^{-1} s^{-1}.[31] These results suggested that the probable quenching mechanism of SSA by ctDNA was static quenching.[32]

The modified Stern−Volmer equation used in the static quenching to calculate the association constant of SSA−ctDNA interaction was[33]

$$\frac{F_0}{F_0 - F} = \frac{1}{f_a K_a}\frac{1}{[Q]} + \frac{1}{f_a} \quad (5)$$

where f_a is the fraction of accessible fluorescence, and K_a is the modified Stern−Volmer association constant for the accessible fluorophores, which equals the quotient of an ordinate $1/f_a$ and slope $1/f_aK_a$. The dependence of $F_0/(F_0 - F)$ on the reciprocal value of the quencher concentration $1/[Q]$ is linear. As shown in Table 1, the values of K_a tended to a decreased trend with increasing temperature. This observation could be because the stability of the SSA−ctDNA complex was reduced. It should be noted that the K_a value obtained here was lower than that reported for classical intercalators, such as ethidium bromide (2.6 × 10^6 L mol^{-1}) and acridine orange (4.0 × 10^5 L mol^{-1}),[34] but corresponded to the groove binders of DNA.[35,36]

Thermodynamic Parameters and Binding Forces. Essentially, interaction forces, including hydrogen bonds, van der Waals forces, electrostatic forces, and hydrophobic interaction forces, play major roles in the interaction between DNA and ligands.[37] The estimated thermodynamic parameters such as enthalpy change ($\Delta H°$) and entropy change ($\Delta S°$) for DNA reactions can determine the main factor contributing to binding affinity and specificity. Thus, to further characterize the interaction forces between SSA and ctDNA, the relevant thermodynamic parameters dependent on temperatures were analyzed by the van't Hoff equation

$$\log K_a = -\frac{\Delta H°}{2.303RT} + \frac{\Delta S°}{2.303R} \quad (6)$$

where R is the gas constant (8.314 J mol^{-1} K^{-1}). Four different temperatures of 292, 298, 304, and 310 K were used. The values of $\Delta H°$ and $\Delta S°$ were obtained from the slope and intercept of the linear van't Hoff plot based on log K_a versus $1/T$. The free energy change ($\Delta G°$) could be calculated from the following equation:

$$\Delta G° = \Delta H° - T\Delta S° \quad (7)$$

The negative $\Delta H°$ and $\Delta S°$ values (Table 1) showed that the binding of SSA to ctDNA was driven mainly by hydrogen bond and van der Waals forces,[38] and the negative $\Delta G°$ indicated that the interaction process was spontaneous. The formation of SSA−ctDNA complex, which was exothermic and enthalpy-favored according to obtained thermodynamic data, led to a more ordered state, possibly due to the freezing of the motional freedom of both SSA and ctDNA molecules.[35]

Melting Studies. The thermal behavior of DNA in the presence of small molecules could provide information about its interaction mode with ligands. Interaction of small molecules with DNA could influence the melting temperature (T_m), the temperature at which the double helix denatures into single-stranded nucleic acid.[39] It was reported that intercalative binding increased the stability of DNA helix, and the T_m was increased by about 5−8 °C, but nonintercalative binding, like groove binding mode or electrostatic, led to no obvious

Table 1. Quenching Constants (K_{SV}), Association Constants (K_a), and Thermodynamic Parameters for the Interaction of ctDNA with SSA at Four Temperatures

T (K)	K_{SV} (×10^3 L mol^{-1})	R^a	K_a (×10^3 L mol^{-1})	R^b	$\Delta H°$ (kJ mol^{-1})	$\Delta S°$ (J mol^{-1} K^{-1})	$\Delta G°$ (kJ mol^{-1})	R^c
292	4.31	0.9964	7.62	0.9928			−21.92	
298	3.96	0.9946	5.01	0.9941	−63.19	−141.73	−20.91	0.9914
304	3.50	0.9969	2.92	0.9975			−19.90	
310	3.23	0.9909	1.72	0.9949			−18.90	

[a] R is the correlation coefficient for K_{SV} values. [b] R is the correlation coefficient for K_a values. [c] R is the correlation coefficient for the thermodynamic parameters.

increase in the T_m.[13,40] Thus, melting measurement can be used as an approach to investigating the binding properties of SSA to ctDNA. As shown in Figure 5A, the T_m of ctDNA increased from 74.8 to 75.6 °C after binding with SSA. That is, SSA provides lower accessibility for DNA binding than the intercalating bound molecules.

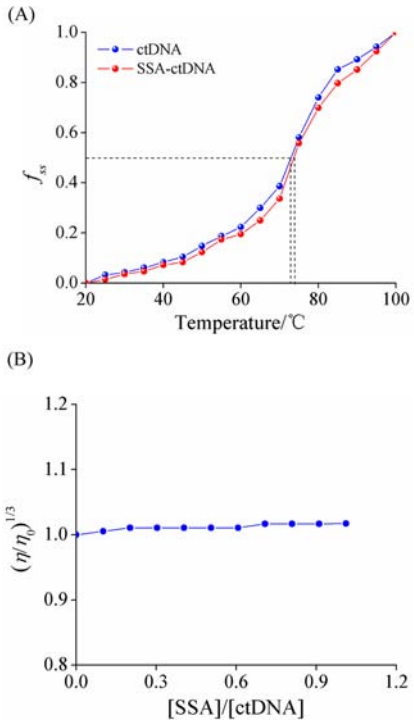

Figure 5. (A) Melting curves of ctDNA in the absence and presence of SSA at pH 7.4. c(SSA) = 8.12 × 10^{-5} mol L^{-1}, and c(ctDNA) = 1.17 × 10^{-4} mol L^{-1}. (B) Effect of increasing amounts of SSA on the relative viscosity of ctDNA at 298 K. c(ctDNA) = 4.81 × 10^{-5} mol L^{-1}.

Viscosity Investigation. An extraordinary feature of the classic intercalative binding mode first proposed by Lerman was the lengthening of the DNA helix as the base pairs were separated to bind the ligand, which resulted in a significant increment in DNA viscosity.[41] In contrast, there was little effect on the viscosity of DNA if groove or electrostatic binding occurred in the binding process.[42] As shown in Figure 5B, the relative viscosity of ctDNA showed no significant change with the continuous addition of SSA, indicating that the binding mode of SSA with ctDNA was not intercalation but groove or electrostatic binding.

Ionic Strength Effect. Probing the effect of the ionic strength on the interaction is an efficient way to investigate the electrostatic interaction of small molecules to DNA. Although NaCl is not an anionic quencher of DNA,[43] it could compete for phosphate anion. Addition of NaCl solution was reported to impair electrostatic interaction between DNA and small molecules.[44] The effect of the sodium ion strength on the interaction between SSA and ctDNA was investigated with different concentrations of NaCl in the absence and presence of ctDNA. The results (Figure 6A) showed that the addition of NaCl had no obvious effect on the fluorescence of SSA and SSA−ctDNA, suggesting that the electrostatic binding of SSA to ctDNA could be excluded.

Iodide Quenching Effect. Iodide quenching experiments could provide evidence for the groove binding of SSA to DNA.

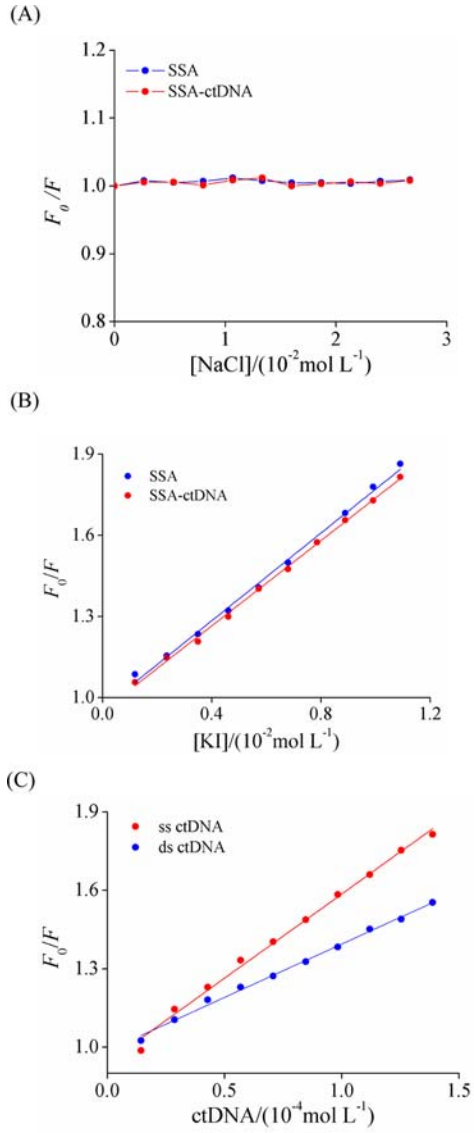

Figure 6. (A) Effect of ionic strength on the fluorescence of SSA and SSA−ctDNA system. c(SSA) = 8.12 × 10^{-5} mol L^{-1}, and c(ctDNA) = 1.17 × 10^{-4} mol L^{-1}. (B) Fluorescence quenching plots of SSA by KI in the absence and presence of ctDNA at pH 7.4. c(SSA) = 8.12 × 10^{-5} mol L^{-1}, and c(ctDNA) = 1.17 × 10^{-4} mol L^{-1}. (C) Fluorescence quenching plots of SSA by ds ctDNA and ss ctDNA at pH 7.4. c(SSA) = 8.12 × 10^{-5} mol L^{-1}.

Negatively charged I^- was chosen for the important purpose: a highly negatively charged quencher will be repelled by the negatively charged phosphate backbone of DNA, and an intercalator should be prevented from being quenched by anionic quencher.[45] However, the groove binders should be quenched easily by anionic quenchers. The quenching constants (K_{SV}) for SSA and SSA−ctDNA were determined from the Stern−Volmer equation. The K_{SV} values of free SSA and SSA−ctDNA by I^- ion were 81.1 and 78.8 L mol^{-1}, respectively (Figure 6B). There was only a small change in iodide quenching interactions after SSA−ctDNA interaction, which indicated that the bound SSA molecules did not intercalate into the base pairs of ctDNA. In other words, SSA molecules bound to ctDNA through groove binding.

Effects of SSA on ss ctDNA and ds ctDNA. Further support for the groove binding of SSA to DNA was obtained

dx.doi.org/10.1021/jf405085g | J. Agric. Food Chem. 2014, 62, 991−1000

through comparison of the effects of SSA on ss ctDNA and ds ctDNA because the groove mode may lead to a greater quenching effect of ss ctDNA than ds ctDNA. By contrast, intercalation mode should cause a weaker quenching effect of ss ctDNA than that of ds ctDNA.[42] As shown in Figure 6C, ss ctDNA exhibited a higher slope than ds ctDNA. The values of K_{SV} for ds ctDNA and ss ctDNA were calculated to be 4.09×10^3 and 6.45×10^3 L mol^{-1}, respectively. The results further confirmed that there was a groove binding mode between SSA and ctDNA.

CD Spectra. To explore the possible influence of SSA binding with ctDNA on the secondary structure of ctDNA, CD measurements were performed in the presence and absence of SSA at different concentrations. It was reported that the CD spectrum of ctDNA exhibited a positive band at 275 nm due to base stacking and a negative band at 245 nm caused by helicity, which are characteristics of DNA in right-handed B form.[46,47] If a small molecule binds to DNA through intercalation, the intensity of positive and negative bands will decrease significantly, whereas groove binders do not significantly unwind DNA base pairs.[48]

As shown in Figure 7, with increasing concentration of SSA, the negative band decreased and the positive band increased

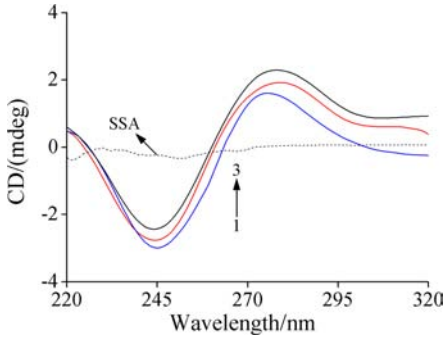

Figure 7. (A) Circular dichroism spectra of ctDNA in the presence of increasing amounts of SSA at pH 7.4. c(ctDNA) = 3.61×10^{-4} mol L^{-1}. The molar ratios of SSA to ctDNA were 0:1, 4:1, and 8:1 for curves 1−3, respectively. c(SSA) = 4.87×10^{-4} mol L^{-1} (dashed line).

remarkably. There was an inconspicuous wavelength shift detected in the negative band but a significant red shift was observed in the positive band. Similar results were reported,[49−51] and this type of change in the CD spectra was deemed as a transformation from B-like DNA structure to A-like conformation in groove binding mode.

FT-IR Studies. The FT-IR spectra of free ctDNA and SSA−ctDNA complex at different molar ratios are shown in Figure 8A. The characteristic spectrum of B-form DNA mainly consists of six peaks at 1717 cm^{-1} (guanine), 1667 cm^{-1} (thymine), 1610 cm^{-1} (adenine), 1490 cm^{-1} (cytosine), 1222 cm^{-1} (PO_2 asymmetric vibrations), and 1088 cm^{-1} (PO_2 symmetric vibrations).[20,52]

According to changes in the intensity and position of these peaks (Figure 8), some information about the interaction of SSA with the nitrogenous bases of ctDNA can be obtained. As shown in Figure 8A, the band of guanine at 1717 cm^{-1} shifted toward a higher frequency at 1727 cm^{-1} (by 10 cm^{-1}) for SSA−ctDNA complex, whereas the effects on the cytosine band at 1490 cm^{-1}, the thymine band at 1667 cm^{-1}, the adenine band at 1610 cm^{-1}, and the $-PO_2$ bands at 1222 and 1088 cm^{-1} were mild (shifted by 2−3 cm^{-1}). These observations

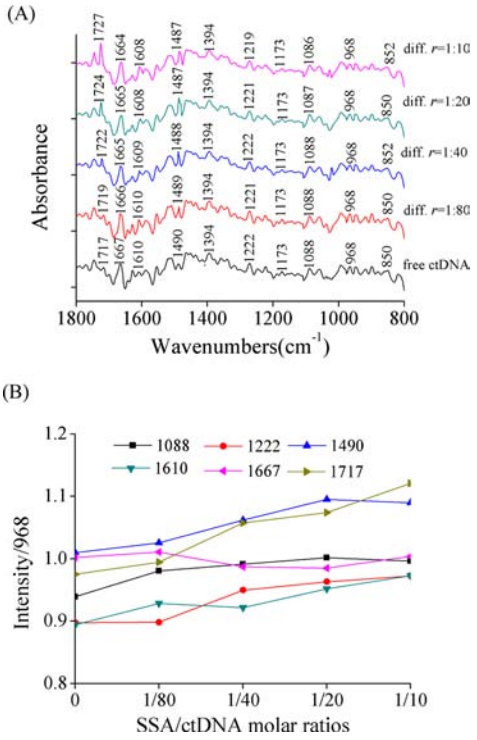

Figure 8. (A) FT-IR spectra and difference spectra [(ctDNA + SSA) solution − SSA solution] in the region of 1800−800 cm^{-1} for free ctDNA and SSA−ctDNA complex in an aqueous solution. (B) Intensity ratio variations of several ctDNA vibrations as a function of different SSA/ctDNA molar ratios. c(ctDNA) = 3.61×10^{-3} mol L^{-1}.

could be because the SSA bound to guanine bases of ctDNA directly.[53] Moreover, a significant increase in the intensity of the band at 1717 cm^{-1} was also observed when the SSA concentration was increased (Figure 8B). Compared with the former, the intensity change at 1667 cm^{-1} and those at 1610, 1490, 1222, and 1088 cm^{-1} were weaker. Small changes in peak position and intensity of the $-PO_2$ bands and cytosine, thymine, and adenine bands indicated that SSA affected their stability to some degree. The results suggested that SSA preferentially bound to guanine, and the binding caused a slight perturbation to the ctDNA molecule.

Computational Docking Simulation of SSA Binding to ctDNA. The molecular modeling method can offer the visual representation of the binding characteristics of small ligands to DNA, which is helpful to complement and substantiate the experimental results.[47]

After the 100 docking runs were successfully performed, a total of 19 multimember conformational clusters were formed. Cluster analysis was carried out using a rmsd tolerance of 2.0 Å, and the binding energy of the distributed conformations is shown in Figure 9A. The highest populated cluster contained 17 of the 100 analyzed conformations and possessed an estimated binding energy of −4.99 kcal mol^{-1}. However, the most populated cluster was not the most energetically favorable cluster. Thus, the predicted binding model with the lowest docking energy was then selected for binding orientation analysis.[54]

As exhibited in Figure 9B, the SSA molecule bound to the DNA minor groove with the lowest binding energy (−6.78 kcal mol^{-1}). Moreover, two hydrogen bonds were formed between SSA and guanine. One hydrogen bond was built by the oxygen atom O-5 linked S-4 of SSA with the H-22 hydrogen atom

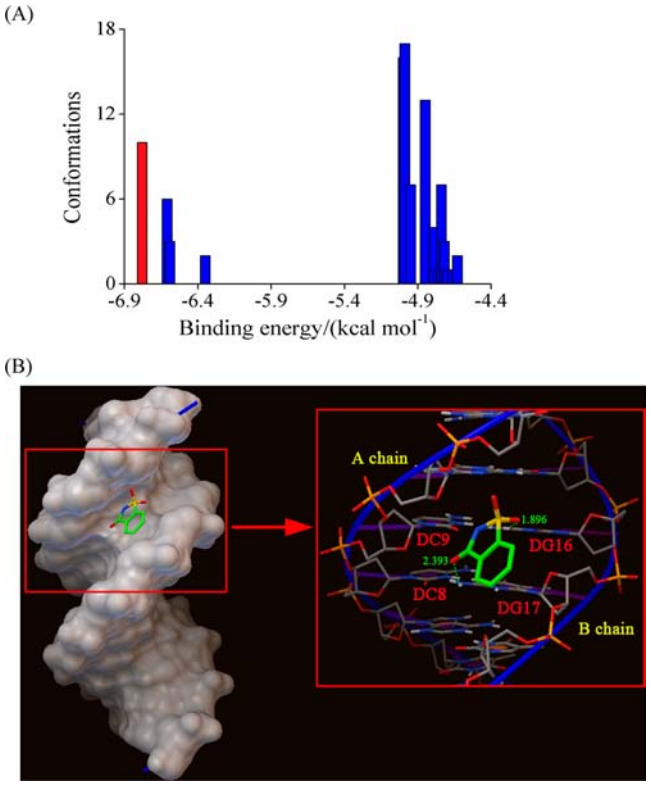

Figure 9. (A) Cluster analyses of the AutoDock docking runs of SSA with DNA. (B) Molecular modeling results of the energy-minimized structure of the SSA−DNA system. The green dashed lines stand for hydrogen bonds.

associated with N-2 of guanine (DG16 of the B chain). The other one was formed between the oxygen atom O-2 linked C-1 of SSA and the H-22 hydrogen atom associated with N-2 of guanine (DG17 of the B chain); their lengths were 1.896 and 2.393 Å, respectively. These docking results have shown that SSA was prone to bind to the guanine base of ctDNA and implied that hydrogen bond forces played an important role in SSA interaction with ctDNA. The docking results were consistent with the experimental results shown above.

DNA Cleavage Activity of SSA. DNA cleavage activity of SSA was analyzed by agarose gel electrophoresis using supercoiled pUC18 plasmid DNA. When circular plasmid DNA is run on electrophoresis, three forms of plasmid DNA may be observed: form I, an intact supercoiled form; form II, an open circular form or nicking form; and form III, a linear form. Their migration speeds were expected to be in the order form I > form III > form II.[55] As shown in Figure 10, the migration of form I was unchanged with increasing concentration of SSA, and both forms II and III cannot be observed. These results indicated that SSA did not have any significant cleavage activity of plasmid DNA.[56,57] These findings along with CD and FT-IR results support the assumption that SSA does not damage but perturbs the DNA structure.

In summary, the binding interaction of SSA with ctDNA in physiological buffer was investigated by multispectroscopic techniques, as well as viscosity measurements, DNA melting analysis, and molecular modeling studies. The mode of binding interaction of SSA with ctDNA has been found to be principally groove binding, and hydrogen bonds and van der Waals forces played major roles in the binding process. The FT-IR analysis implied that SSA was prone to bind to guanine of ctDNA,

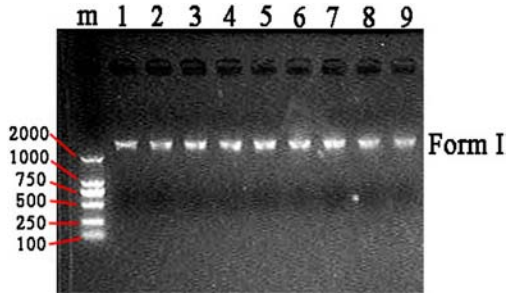

Figure 10. Gel electrophoresis of plasmid pUC18 supercoiled DNA (112.5 μg mL^{-1}) in the presence of increasing amounts of SSA after 24 h of incubation at 37 °C. Lanes: M, DNA marker; 1, supercoiled plasmid DNA; 2−9, SSA + plasmid DNA, and c(SSA) = 2.44, 4.87, 7.31, 9.74, 12.18, 14.61, 17.05, and 19.48 × 10^{-4} mol L^{-1}, respectively.

which was consistent with modeling studies. The results of CD spectra revealed that the binding of SSA to ctDNA resulted in a slight perturbation in ctDNA double-helix conformation. Gel electrophoresis studies showed that this binding did not induce significant DNA cleavage. Moreover, MCR−ALS was applied to resolve the combined fluorescence and UV−vis data matrix to evaluate the progress of SSA interaction with ctDNA. Significantly, the spectra of pure SSA, ctDNA, and especially the SSA−ctDNA complex along with their concentration profiles were successfully obtained.

This study presented binding characteristics of the minor groove interaction of SSA with ctDNA, which further advanced our knowledge of the interaction of small molecules with ctDNA and could be useful in assessing the toxicologic effects of this food sweetener. It should be noted that the maximum residue level (MRL) of SSA in different foods was set from 80 to 2500 mg L^{-1}.[2] The SSA concentration used in this study (8.12 × 10^{-5} mol L^{-1}, i.e., 16.41 mg L^{-1}) is comparable to the amount currently used as a food additive.

AUTHOR INFORMATION

Corresponding Author

*(G.Z.) Phone: +86 791 88305234. Fax: +86 791 88304347. E-mail: gwzhang@ncu.edu.cn.

Funding

We are grateful for financial support provided by the National Natural Science Foundation of China (21167013 and 31060210), the Program of Jiangxi Provincial Department of Science and Technology (20112BBF60010), and the Research Program of State Key Laboratory of Food Science and Technology of Nanchang University (SKLF-ZZB-201305, SKLF-ZZA-201302, and SKLF-KF-201203).

Notes

The authors declare no competing financial interest.

REFERENCES

(1) U.S. FDA. Artificial sweeteners: no calories... sweet. *FDA Consum.* **2006**, *40*, 27−28.

(2) Wang, Y.; Xu, Z. L.; Xie, Y. Y.; Tian, Y. X.; Shen, Y. D.; Young, G. M.; Wang, H.; Lei, H. T.; Sun, Y. M. Development of polyclonal antibody-based indirect competitive enzyme-linked immunosorbent assay for sodium saccharin residue in food samples. *Food Chem.* **2011**, *126*, 815−820.

(3) Weihrauch, M. R.; Diehl, V. Artificial sweeteners—do they bear a carcinogenic risk? *Ann. Oncol.* **2004**, *15*, 1460−1465.

(4) Andreatta, M. M; Munoz, S. E; Lantieri, M. J; Eynard, A. R; Navarro, A. Artificial sweetener consumption and urinary tract tumors in Cordoba, Argentina. *Prev. Med.* **2008**, *47*, 136−139.
(5) Whitehouse, C. R.; Boullata, J.; McCauley, L. A. The potential toxicity of artificial sweeteners. *AAOHN J.* **2008**, *56*, 251−259.
(6) Bosetti, C.; Gallus, S.; Talamini, R.; Montella, M.; Franceschi, S.; Negri, E.; La Vecchia, C. Artificial sweeteners and the risk of gastric, pancreatic, and endometrial cancers in Italy. *Cancer Epidemiol. Biomarkers Prev.* **2009**, *18*, 2235−2238.
(7) Shen, H. Y.; Zhang, Y.; Lin, F.; Xu, N. Y.; Zheng, H. M. In vitro study on the interactions between native herring sperm DNA and melamine in the presence of Ca^{2+} by spectroscopic and voltammetric techniques. *Int. J. Electrochem. Sci.* **2012**, *7*, 3817−3834.
(8) Sarkar, D.; Das, P.; Basak, S.; Chattopadhyay, N. Binding interaction of cationic phenazinium dyes with calf thymus DNA: a comparative study. *J. Phys. Chem. B* **2008**, *112*, 9243−9249.
(9) Dolatabadi, J. E. N.; Kashanian, S. A review on DNA interaction with synthetic phenolic food additives. *Food Res. Int.* **2010**, *43*, 1223−1230.
(10) Ma, Y. D.; Pan, J. H.; Zhang, G. W.; Zhang, Y. Binding properties of butylated hydroxytoluene with calf thymus DNA in vitro. *J. Photochem. Photobiol., B* **2013**, *126*, 112−118.
(11) Arvin, M.; Dehghan, G.; Hosseinpourfeizi, M. A.; Moosavi-Movahedi, A. A. Spectroscopic and electrochemical studies on the interaction of carmoisine food additive with native calf thymus DNA. *Spectrosc. Lett.* **2013**, *46*, 250−256.
(12) Kashanian, S.; Zeidali, S. H. DNA binding studies of tartrazine food additive. *DNA Cell. Biol.* **2011**, *30*, 499−505.
(13) Ma, Y. D.; Zhang, G. W.; Pan, J. H. Spectroscopic studies of DNA interactions with food colorant indigo carmine with the use of ethidium bromide as a fluorescence probe. *J. Agric. Food. Chem.* **2012**, *60*, 10867−10875.
(14) Kashanian, S.; Khodaei, M. M.; Kheirdoosh, F. In vitro DNA binding studies of Aspartame, an artificial sweetener. *J. Photochem. Photobiol., B* **2013**, *120*, 104−110.
(15) Hegde, A. H.; Prashanth, S. N.; Seetharamappa, J. Interaction of antioxidant flavonoids with calf thymus DNA analyzed by spectroscopic and electrochemical methods. *J. Pharm. Biomed. Anal.* **2012**, *63*, 40−46.
(16) Raman, N.; Pothiraj, K.; Baskaran, T. DNA interaction, antimicrobial, electrochemical and spectroscopic studies of metal(II) complexes with tridentate heterocyclic Schiff base derived from 2′-methylacetoacetanilide. *J. Mol. Struct.* **2011**, *1000*, 135−144.
(17) Santhiya, D.; Dias, R. S.; Dutta, S.; Das, P. K.; Miguel, M. G.; Lindman, B.; Maiti, S.. Kinetic studies of amino acid-based surfactant binding to DNA. *J. Phys. Chem. B* **2012**, *116*, 5831−5837.
(18) Steiner, R. F.; Weinryb, I. *Excited States of Protein and Nucleic Acid*; Plenum Press: New York, 1971; p 40.
(19) Ye, B.; Ju, H. Determination of yeast DNA based on its quenching the fluorescence emission of norfloxacin. *Anal. Lett.* **2003**, *36*, 1351−1364.
(20) Zhang, Y.; Zhang, G. W.; Li, Y.; Hu, Y. T. Probing the binding of insecticide permethrin to calf thymus DNA by spectroscopic techniques merging with chemometrics method. *J. Agric. Food Chem.* **2013**, *61*, 2638−2647.
(21) Xu, M.; Ma, Z. R.; Huang, L.; Chen, F. J.; Zeng, Z. Z. Spectroscopic studies on the interaction between Pr(III) complex of an ofloxacin derivative and bovine serum albumin or DNA. *Spectrochim. Acta, Part A* **2011**, *78*, 503−511.
(22) Nafisi, S.; Bonsaii, M.; Manouchehri, F.; Abdi, K. Interaction of glycyrrhizin and glycyrrhetinic acid with DNA. *DNA Cell. Biol.* **2012**, *31*, 114−121.
(23) Froehlich, E.; Mandeville, J. S.; Weinert, C. M.; Kreplak, L.; Tajmir-Riahi, H. A. Bundling and aggregation of DNA by cationic dendrimers. *Biomacromolecules* **2010**, *12*, 511−517.
(24) Wang, G.; Wang, D.; Lu, Y. Exploring the binding mechanism of phosphoramidate derivative with DNA: spectroscopy, calorimetry and modeling. *Spectrochim. Acta, Part A* **2012**, *104*, 492−496.
(25) Ni, Y.; Wei, M.; Kokot, S. Electrochemical and spectroscopic study on the interaction between isoprenaline and DNA using multivariate curve resolution-alternating least squares. *Int. J. Biol. Macromol.* **2011**, *49*, 622−628.
(26) Martí-Aluja, I.; Ruisánchez, I.; Larrechi, M. S. Quantitative analysis of the effect of zidovudine, efavirenz, and ritonavir on insulin aggregation by multivariate curve resolution alternating least squares of infrared spectra. *Anal. Chim. Acta* **2013**, *760*, 16−24.
(27) Mirzaei, M.; Khayat, M.; Saeidi, A. Determination of para-aminobenzoic acid (PABA) in B-complex tablets using the multivariate curve resolution-alternating least squares (MCR−ALS) method. *Sci. Iran.* **2012**, *19*, 561−564.
(28) Maeder, M. Evolving factor analysis for the resolution of overpalling chromatographic peaks. *Anal. Chem.* **1987**, *59*, 527−530.
(29) Vives, M.; Gargallo, R.; Tauler, R. Multivariate extension of the continuous variation and mole-ratio methods for the study of the interaction of intercalators with polynucleotides. *Anal. Chim. Acta* **2000**, *424*, 105−114.
(30) Saha, I.; Kumar, G. S. Phenazinium dyes methylene violet 3RAX and indoine blue bind to DNA by intercalation: evidence from structural and thermodynamic studies. *Dyes Pigm.* **2013**, *96*, 81−91.
(31) Lakowicz, J. R. *Principles of Fluorescence Spectroscopy*, 3rd ed.; Plenum Press: New York, 2006.
(32) Feroz, S. R.; Mohamad, S. B.; Bujang, N.; Malek, S. N. A.; Tayyab, S. Multispectroscopic and molecular modeling approach to investigate the interaction of flavokawain B with human serum albumin. *J. Agric. Food Chem.* **2012**, *60*, 5899−5908.
(33) Kumaraswamy, P.; Sethuraman, S.; Krishnan, U. M. Mechanistic insights of curcumin interactions with the core-recognition motif of β-amyloid peptide. *J. Agric. Food Chem.* **2013**, *61*, 3278−3285.
(34) Cao, Y.; He, X. W. Studies of interaction between safranine T and double helix DNA by spectral methods. *Spectrochim. Acta Part A* **1998**, *54*, 883−892.
(35) Shahabadi, N.; Fili, S. M.; Kheirdoosh, F. Study on the interaction of the drug mesalamine with calf thymus DNA using molecular docking and spectroscopic techniques. *J. Photochem. Photobiol., B* **2013**, *128*, 20−26.
(36) Ahmadi, F.; Alizadeh, A. A.; Bakhshandeh-Saraskanrood, F.; Jafari, B.; Khodadadian, M. Experimental and computational approach to the rational monitoring of hydrogen-bonding interaction of 2-imidazolidinethione with DNA and guanine. *Food Chem. Toxicol.* **2010**, *48*, 29−30.
(37) Liu, Z.; Xiang, Q.; Du, L.; Song, G.; Wang, Y.; Liu, X. The interaction of sesamol with DNA and cytotoxicity, apoptosis, and localization in HepG2 cells. *Food Chem.* **2013**, *141*, 289−296.
(38) Ross, P. D.; Subramanian, S. Thermodynamics of protein association reactions: forces contributing to stability. *Biochemistry* **1981**, *20*, 3096−3102.
(39) Cui, F.; Huo, R.; Hui, G.; Lv, X.; Jin, J.; Zhang, G.; Xing, W. Study on the interaction between aglycon of daunorubicin and calf thymus DNA by spectroscopy. *J. Mol. Struct.* **2011**, *1001*, 104−110.
(40) Jana, B.; Senapati, S.; Ghosh, D.; Bose, D.; Chattopadhyay, N. Spectroscopic exploration of mode of binding of ctDNA with 3-hydroxyflavone: a contrast to the mode of binding with flavonoids having additional hydroxyl groups. *J. Phys. Chem. B* **2011**, *116*, 639−645.
(41) Lerman, L. Structural considerations in the interaction of DNA and acridines. *J. Mol. Biol.* **1961**, *3*, 18−30.
(42) Kashanian, S.; Khodaei, M. M.; Roshanfekr, H.; Shahabadi, N.; Mansouri, Gh. DNA binding, DNA cleavage and cytotoxicity studies of a new water soluble copper(II) complex: the effect of ligand shape on the mode of binding. *Spectrochim. Acta, Part A* **2012**, *86*, 351−359.
(43) Pratviel, G.; Bernadou, J.; Meunier, B. Carbon−hydrogen bonds of DNA sugar units as targets for chemical nucleases and drugs. *Angew. Chem., Int. Ed. Engl.* **1995**, *34*, 746−769.
(44) Wu, F. Y.; Xie, F. Y.; Wu, Y. M.; Hong, J. I. Interaction of a new fluorescent probe with DNA and its use in determination of DNA. *J. Fluoresc.* **2008**, *18*, 175−181.

(45) Ling, X.; Zhong, W.; Huang, Q.; Ni, K. Spectroscopic studies on the interaction of pazufloxacin with calf thymus DNA. *J. Photochem. Photobiol., B* **2008**, *93*, 172−176.
(46) Ahmadi, S. M.; Dehghan, G.; Hosseinpourfeizi, M. A.; Dolatabadi, J. E. N.; Kashanian, S. Preparation, characterization, and DNA binding studies of water-soluble quercetin−molybdenum(VI) complex. *DNA Cell. Biol.* **2011**, *30*, 517−523.
(47) Lin, J.; Gao, C.; Liu, R. Interaction mechanism of Trp−Arg dipeptide with calf thymus DNA. *J. Fluoresc.* **2013**, *23*, 921−927.
(48) Sahoo, B. K.; Ghosh, K. S.; Bera, R.; Dasgupta, S. Studies on the interaction of diacetylcurcumin with calf thymus-DNA. *Chem. Phys.* **2008**, *351*, 163−169.
(49) Jalali, F.; Dorraji, P. S. Electrochemical and spectroscopic studies of the interaction between the neuroleptic drug, gabapentin, and DNA. *J. Pharm. Biomed. Anal.* **2012**, *70*, 598−601.
(50) Shahabadi, N.; Hadidi, S. Spectroscopic studies on the interaction of calf thymus DNA with the drug levetiracetam. *Spectrochim. Acta, Part A* **2012**, *96*, 278−283.
(51) Yasrebi, S. A.; Mobasheri, H.; Sheikhshoaie, I.; Rahban, M. DNA-binding studies of two dioxomolybdenum(VI) complexes of salicylaldehyde benzoylhydrazone ligands. *Inorg. Chim. Acta* **2013**, *400*, 222−227.
(52) Jangir, D. K.; Charak, S.; Mehrotra, R.; Kundu, S. FTIR and circular dichroism spectroscopic study of interaction of 5-fluorouracil with DNA. *J. Photochem. Photobiol., B* **2011**, *105*, 143−148.
(53) Dorraji, P. S.; Jalali, F. Investigation of the interaction of sertraline with calf thymus DNA by spectroscopic methods. *J. Braz. Chem. Soc.* **2013**, *24*, 939−945.
(54) Zhang, Y.; Zhang, G. W.; Zhou, X. Y.; Yu, L. Determination of acetamiprid partial-intercalative binding to DNA by use of spectroscopic, chemometrics, and molecular docking techniques. *Anal. Bioanal.Chem.* **2013**, *405*, 8871−8883.
(55) Leelavathy, L.; Anbu, S.; Kandaswamy, M.; Karthikeyan, N.; Mohan, N. Synthesis and characterization of a new series of unsymmetrical macrocyclic binuclear vanadyl(IV) complexes: electrochemical, antimicrobial, DNA binding and cleavage studies. *Polyhedron* **2009**, *28*, 903−910.
(56) Du, Y. F.; Lu, J. Z.; Guo, H. W.; Jiang, J.; Chao, P.; Chen, F.; Pan, J. M. DNA binding and photocleavage properties of two mixed-ligand oxovanadium complexes. *Transition Met. Chem.* **2010**, *35*, 859−864.
(57) Shahabadi, N.; Maghsudi, M. Gel electrophresis and DNA interaction studies of the food colorant quinoline yellow. *Dyes Pigm.* **2012**, *96*, 377−382.

amounts of such enzymes,[14] and their ability to perform aryl hydroxylation has been shown.[15] Furthermore, horseradish is a root vegetable. If cultivated in contaminated soil, its edible parts are in direct and permanent contact with environmental contaminants and are likely to incorporate them to a certain extent as was shown for the edible root parts of carrot plants.[4] This makes horseradish suitable for studies on the uptake of environmental contaminants and on metabolite elucidation in the context of agricultural and environmental research.

UPLC high-resolution mass spectrometry using MS^E was proven to be an outstanding method for the analysis of metabolites enabling both their sensitive detection and deducing their elemental composition from their exact masses.[16] Due to interfering matrix compounds, coextracted from the plant tissue, the visual discovery of metabolites in total ion current chromatograms will be restricted to very abundant signals. Common strategies to search for metabolites are neutral loss scans and precursor ion scans using a QqQ mass spectrometer. However, these approaches can be too selective as they exclude unexpected metabolites. In general, methods of multivariate data analysis are promising to investigate the metabolism of xenobiotics in plant cells to handle the large quantities of obtained chromatographic and mass spectrometric data and to evaluate them in an unbiased and comprehensive manner. Principal component analysis (PCA) in combination with orthogonal projection to latent structures discriminant analysis (OPLS-DA) is increasingly applied to handle the large amount of data in metabolomics studies, whereas their application in environmental or contaminant metabolism research is rarely reported. In the following study the advantages of the above-mentioned method for the elucidation of metabolites of xenobiotica in plants are presented using the example of triclosan applied to a hairy root culture of horseradish (*Armoracia rusticana*).

EXPERIMENTAL PROCEDURES

Chemicals. Triclosan (5-chloro-2-(2,4-dichlorophenoxy)phenol, >97.0%) was provided by Fluka (Buchs, Switzerland) and methanol (Hypergrade) by Merck (Darmstadt, Germany). Acetonitrile, ammonium acetate, and acetic acid (all of ULC/MS grade) were provided by Biosolve (Valkenswaard, The Netherlands).

Root Culture Treatment and Sample Processing. A hairy root culture of horseradish (*A. rusticana*) was cultivated in 100 mL of MS culture medium in Erlenmeyer flasks as described elsewhere.[17] Ten days after subcultivation, triclosan was dissolved in methanol and applied to the culture medium to a concentration of 0.6 μg mL^{-1} (2 μM). The incubation was terminated at day 1, 2, or 5 of exposure to detect and identify triclosan metabolites in plant material.

The plant material was separated from the culture medium by suction filtration, immediately frozen in liquid nitrogen, and stored at −20 °C prior to further sample processing. The plant material was ground under liquid nitrogen using a mortar and pestle and transferred to 45 mL glass centrifuge tubes with a magnetic stir bar. The plant material was extracted three times with 8 mL of water/acetonitrile 1:1 (v/v) with 5 mM ammonium acetate and 0.5% glacial acetic acid by stirring at room temperature and centrifuged for 5 min at 4500 rpm. The three biological replicates of each sampling day were combined to obtain a higher concentration of metabolites in the extract. The supernatants were collected and concentrated to a volume of 1 mL by removing acetonitrile using a rotary evaporator followed by water removal employing lyophilization. The samples were filtered through syringe filters (0.45 μm) prior to liquid chromatographic−mass spectrometric analysis.

UPLC-QToF-MS Analysis. The analysis was performed on a Waters Acquity UPLC system connected to Synapt G2S QToF mass spectrometer equipped with an electrospray ionization source (Waters, Milford, MA, USA). An aliquot of 10 μL of each sample was injected onto the column. UPLC separation was achieved using an Acquity UPLC HSS-T3 column (100 × 2.1 mm, 1.7 μm particle size) at a flow rate of 0.6 mL min^{-1} and a column temperature of 60 °C. The mobile phase consisted of (A) water and (B) ACN, both with 5 mM NH_4OAc and 0.05% acetic acid. The gradient applied was as follows: 0 min, 5% B; 7 min, 95% B; 8 min, 95% B; 8.1 min, 5% B; 10 min, 5% B. Electrospray ionization was carried out in separate analyses under negative and positive polarity by applying capillary voltages of −0.7 and +0.7 kV, respectively. The source temperature was set to 140 °C and the desolvation temperature to 550 °C. The sampling cone voltage was set to 35 V and source offset at 50 V. Nitrogen and argon were used as cone and collision gases, respectively. The desolvation gas flow was 950 L h^{-1}.

The mass spectrometric data were collected from m/z 50 to 1200 in centroid mode with a 0.15 s scan time. To ensure m/z accuracy, leucine enkephaline was infused via the reference probe as lockspray and a two-point calibration was applied. Two sets of data were collected in parallel using MS^E acquisition. One data set contains low collision energy data (4 eV, MS, effectively the accurate mass of molecular ions) and the second data set the elevated collision energy data (15−35 eV, MS^E, all of the fragment ions).

Each sample was measured three times in a randomized order.

Data Processing. Centroid raw mass spectrometric data obtained under low collision energy were processed using MarkerLynx application manager for MassLynx 4.1 software (Waters). The parameters used were as follows: retention time ranging from 0 to 8 min, m/z ranging from 50 to 1200, retention time tolerance 0.05 min, a m/z tolerance of 0.01 Da, and a marker intensity threshold of 500.

The intensity of each ion was normalized with respect to the total ion count to generate a data matrix that consisted of the retention time, m/z value, and normalized peak area using MarkerLynx software. The data matrix was reduced by applying a mass defect filtering of ±0.150 u of triclosan and processed by EZinfo software (Waters). The unsupervised segregation of control and exposed cell extract was checked by PCA using pareto-scaled data. The S-plot of the supervised partial least-squares-discriminant analysis (PLS-DA) and orthogonal projection to latent structures (OPLS) enabled the selection of analytes that are responsible for the distinction of control and exposed cell extract ($|p(corr)| > 0.5$ on S-plot). These analytes are subsequently analyzed for chlorine pattern, that is, two signals with a m/z difference of 1.9970 u (±0.0030 u), by applying an isotopic pattern filter (Macro for Microsoft Excel). The m/z values of potential candidates were arranged according to their retention time and peak profile to align the signals of molecular ions, adducts, and fragment ions.

The assignment of the chemical formula was accomplished according to the following criteria: The deviation for ion mass was set to ≤5 ppm and the following element limits: C (0−100), H (0−100), O (0−30), N (0−4), S (0−4), Cl (0−6), and P (0−2). The chlorine number was restricted further according to the observed isotopic pattern.

RESULTS AND DISCUSSION

To overcome the limitations of a targeted analysis, in which a limited set of probable and predictable metabolites has to be defined before analysis, a more unbiased approach was chosen. A screening by recording high-resolution full scan mass spectra combined with their treatment by multivariate statistics and data filter techniques was performed to include possible unexpected and minor abundant metabolites in this study, as well. Therefore, the extracts of control and triclosan-exposed horseradish hairy root tissues were analyzed by UPLC−high-resolution mass spectrometry applying the MS^E mode. Abundant triclosan metabolites with high signal intensities became apparent by comparing base peak chromatograms of extracts of control and exposed root tissues (Figure 1). In contrast, less abundant metabolites are difficult to discover in

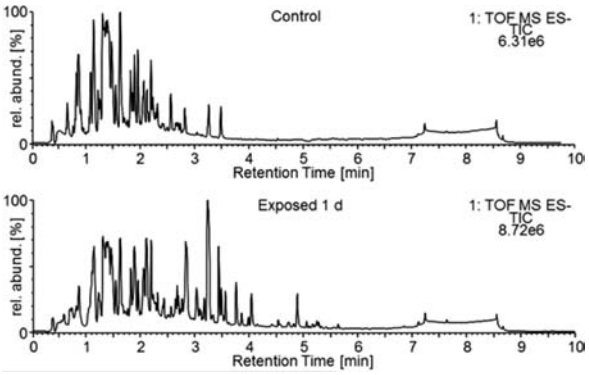

Figure 1. Low collision energy total ion current chromatograms (ESI neg) of extracts of control (top) and triclosan-exposed (bottom) horseradish root tissues.

the presence of intense signals of the biogenic plant matrix. This requires the use of multivariate data analysis.

In addition, two filter techniques were applied, which consider likely mass spectrometric features of the triclosan metabolites and discriminate them from matrix compounds. The application of the mass defect filter results from the knowledge that mass defect values of a parent compound and its metabolites are quite similar and enable the discrimination of matrix ions that arise from endogenous compounds. Compared to others,[18−20] we applied a rather broad filter of ±0.150 u for mass defect filtering to account for extensively conjugated metabolites. The mass defect filter was applied to the raw data set and reduced the number of candidate signals from 6939 to 3867.

These signals were further processed via PCA. PCA provided a clear separation of the extracts of control and treated hairy root tissues (Figure 2a). By using OPLS-DA of the untreated horseradish sample and the triclosan-treated horseradish samples (different treatment periods (1, 2, and 5 days) now considered as replicates), the number of signals representing potential metabolites was further reduced to 572 ($|p(\mathrm{corr})| > 0.5$ on S-plot, Figure 2b). Differentiation within the S-plot occurs because of concentration differences, and metabolites with a higher intensity yield a better separation from the background ions.

The reduced data matrix was treated with a second filter method, with the assumption that metabolites contain at least one chlorine atom of the three originally present in the triclosan molecule. This isotopic pattern filter utilizes the isotopic pattern of chlorinated organic compounds, that is, two signals with $\Delta m/z$ of 1.9970 u (±0.0030 u) and a relative intensity of $m + 2/m$ of at least 32%. Dehalogenation might occur during the plant metabolism of organic contaminants,[21−23] but it is unlikely that all three chlorine atoms are removed at once. It was essential to reduce the data matrix by mass defect filter and multivariate statistics prior to the application of the isotopic pattern filter. Otherwise, due to the complex mixture of coeluting matrix compounds, the sole application of the isotopic filter would have led to a large number of false positives because molecular ions of coeluting compounds appear as an isotopic pattern of chlorinated compounds.

The final step of the data processing was to arrange the m/z values according to their retention time and peak shape. This led to a further reduction of the number of potential triclosan metabolites, because several m/z values could be assigned as

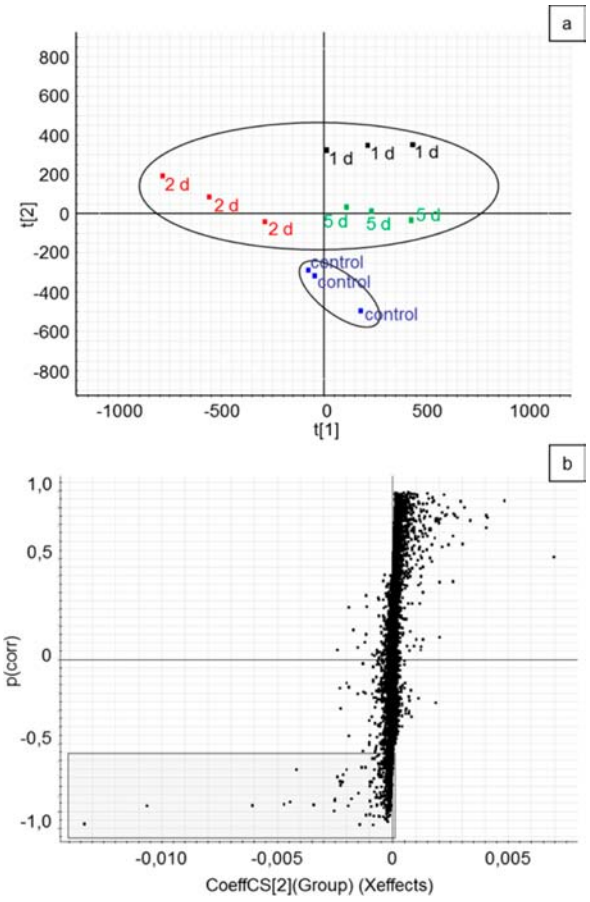

Figure 2. Score plot (a) of the principal component analysis of the acquired data set and S-plot (b) comparing the data from control and exposed (1, 2, and 5 days) horseradish cultures via orthogonal projection to latent structures discriminant analysis. The rectangle includes data that contribute significantly ($|p(\mathrm{corr})| > 0.5$) to the differentiation between extracts of control and treated cultures.

molecular ion, fragment ions, and adduct ions of one compound. Thirty-three potential triclosan metabolites were considered for structure elucidation. The same procedure was applied to the mass spectrometric data generated by positive ionization. However, the ion intensities of the triclosan metabolites obtained in positive mode were generally low, so that only abundant metabolites were visible and no additional metabolites were detected. Therefore, only data generated in negative mode are considered here.

Structure Elucidation. According to the fragmentation behavior of their molecular anions, these 33 metabolites were categorized into four groups.

Triclosan Sulfosaccharides (Group 1). The signal that contributes most to the differentiation between the extracts of exposed and control tissue cultures was detected at a retention time of 3.22 min (M9). The low collision energy mass spectrum of this compound shows a signal at m/z 694.9100 (Figure 3a) with the characteristic isotopic pattern of a trichlorinated compound and a mass 407.6967 u heavier than the parent triclosan. For this m/z a sum formula of $C_{21}H_{18}Cl_3O_{16}S_2$ was derived. The intensity of the molecular anion is very low, whereas the fragment ion at m/z 614.9544 is far more abundant. This fragment ion ($C_{21}H_{18}Cl_3O_{13}S$) arises from a neutral loss of 79.9556 u, corresponding to the loss of

dx.doi.org/10.1021/jf404784q | J. Agric. Food Chem. 2014, 62, 1001−1009

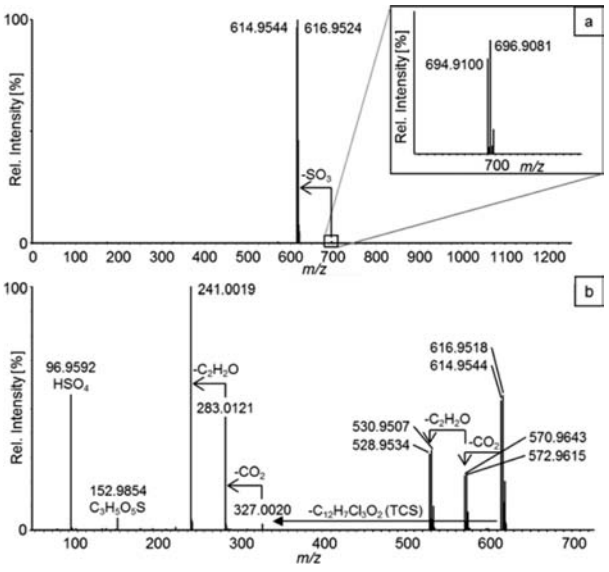

Figure 3. Low (a) and high (b) collision energy mass spectra (ESI neg) of metabolite M9 tentatively identified as triclosan (malonyl disulfo) hexopyranoside.

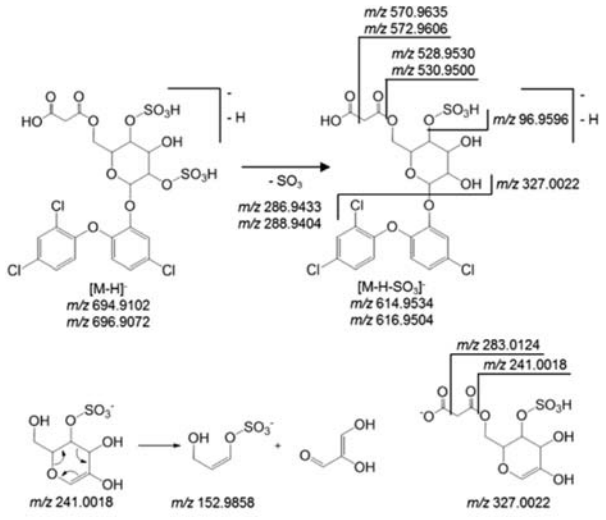

Figure 4. Proposed fragmentation pathway of metabolite M19 and structures of the fragment ions (spectrum shown in Figure 3).

SO_3 from a sulfate moiety of $[M - H]^-$. This is confirmed by a product ion at m/z of 96.9592 (HSO_4^-).

As visible from the high collision energy mass spectrum (Figure 3b), collision-induced fragmentation gave rise to a number of further fragment ions, of which some showed the trichloro isotopic pattern. The most intense fragment ion without chlorine substituent (m/z 327.0020; $C_9H_{11}O_{11}S$) arises from the neutral loss of triclosan (287.9524 u) from the $[M - HSO_3]^-$ ion. The corresponding triclosan fragment ion (m/z 286.9426) was also recorded, although with a very low relative intensity. This suggests that this metabolite was transformed solely at the phenolic moiety of triclosan. Further ions detected at m/z 283.0121 ($C_8H_{11}O_9S$) and 241.0019 ($C_6H_9O_8S$) are formed by the successive neutral losses of 43.9901 u ($-CO_2$) and 42.0109 u (− ketene, C_2H_2O). They point to a malonyl moiety. The remaining $C_6H_9O_8S$ fragment ion was assumed to be a sulfohexopyranose. The formation of a fragment ion of m/z 152.9854 via a retro-Diels−Alder cleavage suggests that C5 of the hexopyranose is sulfated. Therefore, this metabolite was tentatively identified as triclosan (malonylhexopyranosyl) disulfate, the suggested fragmentation pathway of which is given in Figure 4. Additionally, trichlorinated fragment ions were detected at m/z 570.9643 ($C_{20}H_{18}Cl_3O_{11}S$) and 528.9534 ($C_{18}H_{16}Cl_3O_{10}S$). These are formed by losses of 43.9901 and 42.0109 u from $[M - HSO_3]^-$, respectively, as has been analogously observed for the $C_9H_{11}O_{11}S$ fragment ion. Besides the very low abundant $[M - H]^-$ at m/z 694.9100, no further hints for the presence of two sulfate groups were detected. For comparison, the fragmentation behavior of the reference compound D-glucosamine 3,6-disulfate was studied. In agreement with the fragmentation pathway of M9, a very facile loss of SO_3 was observed already in the low collision energy mass spectrum of D-glucosamine 3,6-disulfate. This led to a molecular anion of low abundance but a rather prominent $[M - H - SO_3]^-$.

Analogous to this example, a total four sulfo- and disulfosaccharide conjugates of triclosan were tentatively identified by their mass spectra (Table 1). Among the most intensive ones was the triclosan hexopyranosyl sulfate (M18) as another example of a sulfated monosaccharide, eluting at 3.76 min.

Conjugation of organic contaminants with sulfate is very important for the animal xenobiotic metabolism. For plants, only a few studies exist on the formation of 2-*O*-sulfate glucosides and 6-*O*-sulfate glucosides.[24,25] Disulfated carbohydrate conjugates, however, have not been described so far. This may partly be due to their lability, which leads to the facile loss of one of the sulfate groups upon ionization.

Triclosan Saccharide and Sulfate Conjugates (Group 2). Besides the triclosan sulfosaccharide conjugates, which formed predominately fragment ions of the glycon moiety, an additional group of metabolites has been detected. Contrary to the sulfosaccharides, the collision-induced dissociation of their molecular anions gave rise almost exclusively to the triclosan fragment ion at m/z 286.9433 (calcd). One of these seven metabolites is M19, which eluted after 3.98 min and gave rise to a series of trichlorinated ions in its low collision energy mass spectrum (Figure 5a). Whereas the signal m/z 448.9952 ($C_{18}H_{16}Cl_3O_7$) was assigned to the molecular ion, m/z 484.9724, 495.0013, and 509.0170 were assigned to its chloride, formate, and acetate adducts, respectively. The molecular formula and mass gain of 162.0519 u compared to triclosan suggest that an anhydrohexose moiety was added, and M19 therefore is the triclosan hexoside. The preferred loss of the anhydrohexose moiety and formation of the aglycon (triclosan) anion is typical for glycoside conjugates.[26] In comparison to the metabolites of group 1, the hexoside lacks a sulfate group to stabilize the negative charge at the glycon moiety. The conjugation with hexose plays a central role in the proposed pathway of triclosan metabolism in the hairy root culture of horseradish and is crucial for the formation of almost all further metabolites (Figure 6).

By analogy, the molecular anions of the metabolites M10 and M14 were detected at m/z 611.0493 ($C_{24}H_{26}Cl_3O_{12}$) and m/z 595.0547 ($C_{24}H_{26}Cl_3O_{11}$), respectively. These point to additional hexose and desoxyhexose moieties and thus to the metabolites triclosan hexosyl hexoside (M10) and triclosan desoxyhexosyl hexoside (M14), respectively.

The molecular anion of M13 was detected at 3.44 min in the low collision energy mass spectrum at m/z 534.9968 ($C_{21}H_{18}Cl_3O_{10}$). This is 86.0016 u higher than that of the

dx.doi.org/10.1021/jf404784q | J. Agric. Food Chem. 2014, 62, 1001−1009

Table 1. LC-MS Data of the Triclosan Metabolites Detected in the Horseradish Cell Extract

metabolite[a]	RT (min)	molecular anion $[M-H]^-$ m/z (deviation (ppm))	sum formula of molecular anion $[M-H]^-$	fragments m/z (deviation (ppm))	sum formula of fragment anions[b]	structure proposal
Group 1: Metabolites Showing a Neutral Loss of Triclosan						
M5	2.98	761.0100 (3) 763.0081 (3)	$C_{27}H_{28}{}^{35}Cl_3O_{17}S$ $C_{27}H_{28}{}^{35}Cl_2{}^{37}ClO_{17}S$	96.9595 (1) 283.0109 (5) 614.9527 (1) 616.9506 (0)	HSO_4 $C_8H_{11}O_9S$ $C_{21}H_{18}{}^{35}Cl_3O_{13}S$ $C_{21}H_{18}{}^{35}Cl_2{}^{37}ClO_{13}S$	triclosan (desoxyhexosyl malonyl hexosyl) sulfate
M6a	3.13	675.0099 (1) 677.0068 (−1)	$C_{24}H_{26}{}^{35}Cl_3O_{14}S$ $C_{24}H_{26}{}^{35}Cl_2{}^{37}ClO_{14}S$	387.0587 (3)	$C_{12}H_{19}O_{12}S$	triclosan desoxyhexosyl hexoside sulfate
M9	3.22	694.9100 (0) 696.9081 (−1)	$C_{21}H_{18}{}^{35}Cl_3O_{16}S_2$ $C_{21}H_{18}{}^{35}Cl_2{}^{37}ClO_{16}S_2$	96.9592 (4) 152.9854 (3) 241.0019 (0) 283.0121 (1) 327.0020 (1) 286.9426 (2) 288.9398 (2) 528.9534 (−1) 530.9507 (−1) 570.9643 (−1) 572.9615 (−2) 614.9544 (−2) 616.9518 (−2)	HSO_4 $C_3H_5O_5S$ $C_6H_9O_8S$ $C_8H_{11}O_9S$ $C_9H_{11}O_{11}S$ $C_{12}H_6{}^{35}Cl_3O_2$ $C_{12}H_6{}^{35}Cl_2{}^{37}ClO_2$ $C_{18}H_{16}{}^{35}Cl_3O_{10}S$ $C_{18}H_{16}{}^{35}Cl_2{}^{37}ClO_{10}S$ $C_{20}H_{18}{}^{35}Cl_3O_{11}S$ $C_{20}H_{18}{}^{35}Cl_2{}^{37}ClO_{11}S$ $C_{21}H_{18}{}^{35}Cl_3O_{13}S$ $C_{21}H_{18}{}^{35}Cl_2{}^{37}ClO_{13}S$	triclosan malonyl hexosyl disulfate
M6b	3.38	675.0119 (−1) 677.0088 (−1)	$C_{24}H_{26}{}^{35}Cl_3O_{14}S$ $C_{24}H_{26}{}^{35}Cl_2{}^{37}ClO_{14}S$	387.0594 (1)	$C_{12}H_{19}O_{12}S$	triclosan desoxyhexosyl hexoside sulfate
M12	3.43	614.9528 (1) 616.9495 (1)	$C_{21}H_{18}{}^{35}Cl_3\ O_{13}S$ $C_{21}H_{18}{}^{35}Cl_2{}^{37}ClO_{13}S$	96.9592 (4) 241.0019 (0) 286.9446 (−5) 288.9413 (−3) 528.9527 (1) 530.9504 (−1)	HSO_4 $C_6H_9O_8S$ $C_{12}H_6{}^{35}Cl_3O_2$ $C_{12}H_6{}^{35}Cl_2{}^{37}ClO_2$ $C_{18}H_{16}{}^{35}Cl_3O_{10}S$ $C_{18}H_{16}{}^{35}Cl_2{}^{37}ClO_{10}S$	triclosan malonyl hexosyl sulfate
M18	3.76	528.9544 (−3) 530.9515 (−3)	$C_{18}H_{16}{}^{35}Cl_3O_{10}S$ $C_{18}H_{16}{}^{35}Cl_2{}^{37}ClO_{10}S$	96.9594 (2) 152.9857 (1) 241.0024 (−2) 286.9435 (−1) 288.9404 (0)	HSO_4 $C_3H_5O_5S$ $C_6H_9O_8S$ $C_{12}H_6{}^{35}Cl_3O_2$ $C_{12}H_6{}^{35}Cl_2{}^{37}ClO_2$	triclosan hexosyl sulfate
Group 2: Metabolites Showing Triclosan Anion as Fragment Ion						
M7	3.16	637.0631 (2) 639.0598 (3)	$C_{26}H_{28}{}^{35}Cl_3O_{12}$ $C_{26}H_{28}{}^{35}Cl_2{}^{37}ClO_{12}$	153.0545 (5) 286.9432 (0) 288.9400 (1)	$C_8H_9O_3$ $C_{12}H_6{}^{35}Cl_3O_2$ $C_{12}H_6{}^{35}Cl_2{}^{37}ClO_2$	triclosan acetyl desoxyhexosyl hexoside
M10	3.32	611.0493 (0) 613.0474 (−2)	$C_{24}H_{26}{}^{35}Cl_3O_{12}$ $C_{24}H_{26}{}^{35}Cl_2{}^{37}ClO_{12}$	286.9432 (0) 288.9406 (−1)	$C_{12}H_6{}^{35}Cl_3O_2$ $C_{12}H_6{}^{35}Cl_2{}^{37}ClO_2$	triclosan hexosyl hexoside
M13	3.44	534.9968 (0) 536.9944 (−2) 1071.0035 (−2) 1073.0010 (−3)	$C_{21}H_{18}{}^{35}Cl_3O_{10}$ $C_{21}H_{18}{}^{35}Cl_2{}^{37}ClO_{10}$ $C_{42}H_{37}{}^{35}Cl_6O_{20}$ $C_{42}H_{37}{}^{35}Cl_5{}^{37}ClO_{20}$	491.0063 (1) 493.0041 (−1) 286.9432 (0) 288.9403 (0)	$C_{20}H_{18}{}^{35}Cl_3O_8$ $C_{20}H_{18}{}^{35}Cl_2{}^{37}ClO_8$ $C_{12}H_6{}^{35}Cl_3O_2$ $C_{12}H_6{}^{35}Cl_2{}^{37}ClO_2$	triclosan malonyl hexoside
M14	3.56	595.0536 (1) 597.0510 (0)	$C_{24}H_{26}{}^{35}Cl_3O_{11}$ $C_{24}H_{26}{}^{35}Cl_2{}^{37}ClO_{11}$	286.9432 (0) 288.9406 (−1)	$C_{12}H_6{}^{35}Cl_3O_2$ $C_{12}H_6{}^{35}Cl_2{}^{37}ClO_2$	triclosan desoxyhexosyl hexoside
M15	3.59	491.0062 (1) 493.0042 (−1)	$C_{20}H_{18}{}^{35}Cl_3O_8$ $C_{20}H_{18}{}^{35}Cl_2{}^{37}ClO_8$	286.9432 (0) 288.9402 (1)	$C_{12}H_6{}^{35}Cl_3O_2$ $C_{12}H_6{}^{35}Cl_2{}^{37}ClO_2$	triclosan acetyl hexoside
M19	3.98	448.9952 (2) 450.9926 (1)	$C_{18}H_{16}{}^{35}Cl_3O_7$ $C_{18}H_{16}{}^{35}Cl_2{}^{37}ClO_7$	286.9428 (2) 288.9399 (2)	$C_{12}H_6{}^{35}Cl_3O_2$ $C_{12}H_6{}^{35}Cl_2{}^{37}ClO_2$	triclosan hexoside

dx.doi.org/10.1021/jf404784q | J. Agric. Food Chem. 2014, 62, 1001−1009

Table 1. continued

metabolite[a]	RT (min)	molecular anion $[M - H]^-$ m/z (deviation (ppm))	sum formula of molecular anion $[M - H]^-$	fragments m/z (deviation (ppm))	sum formula of fragment anions[b]	structure proposal
Group 2: Metabolites Showing Triclosan Anion as Fragment Ion						
M20	4.04	366.9006 (−1) 368.8976 (−1)	$C_{12}H_6{}^{35}Cl_3O_5S$ $C_{12}H_6{}^{35}Cl_2{}^{37}ClO_5S$	286.9429 (1) 288.9397 (2)	$C_{12}H_6{}^{35}Cl_3O_2$ $C_{12}H_6{}^{35}Cl_2{}^{37}ClO_2$	triclosan sulfate
Group 3: OH-Triclosan Conjugates						
M1a	2.02	630.9478 (1) 632.9444 (1)	$C_{21}H_{18}{}^{35}Cl_3O_{14}S$ $C_{21}H_{18}{}^{35}Cl_2{}^{37}ClO_{14}S$	266.9600 (6) 268.9557 (11)	$C_{12}H_5{}^{35}Cl_2O_3$ $C_{12}H_5{}^{35}Cl^{37}ClO_3$	OH-triclosan malonyl hexosyl sulfate
M2a	2.23	544.9466 (2) 546.9440 (2)	$C_{18}H_{16}{}^{35}Cl_3O_{11}S$ $C_{18}H_{16}{}^{35}Cl_2{}^{37}ClO_{11}S$	301.9298 (2) 303.9284 (−3)	$C_{12}H_5{}^{35}Cl_3O_3$ $C_{12}H_5{}^{35}Cl_2{}^{37}ClO_3$	OH-triclosan hexosyl sulfate
M1b	2.50	630.9472 (2) 632.9419 (1)	$C_{21}H_{18}{}^{35}Cl_3O_{14}S$ $C_{21}H_{18}{}^{35}Cl_2{}^{37}ClO_{14}S$	544.9462 (3) 546.9452 (−1)	$C_{18}H_{16}{}^{35}Cl_3O_{11}S$ $C_{18}H_{16}{}^{35}Cl_2{}^{37}ClO_{11}S$	OH-triclosan malonyl hexosyl sulfate
M3a	2.64	507.0026 (−2) 508.9989 (0)	$C_{20}H_{18}{}^{35}Cl_3O_9$ $C_{20}H_{18}{}^{35}Cl_2{}^{37}ClO_9$	266.9624 (−3) 268.9585 (0) 301.9303 (0) 303.9288 (−4)	$C_{12}H_5{}^{35}Cl_2O_3$ $C_{12}H_5{}^{35}Cl^{37}ClO_3$ $C_{12}H_5{}^{35}Cl_3O_3$ $C_{12}H_5{}^{35}Cl_2{}^{37}ClO_3$	OH-triclosan acetyl hexoside
M1c	2.68	630.9500 (−3) 632.9467 (−2)	$C_{21}H_{18}{}^{35}Cl_3O_{14}S$ $C_{21}H_{18}{}^{35}Cl_2{}^{37}ClO_{14}S$			OH-triclosan malonyl hexosyl sulfate
M2b	2.81	544.9449 (6) 546.9443 (1)	$C_{18}H_{16}{}^{35}Cl_3O_{11}S$ $C_{18}H_{16}{}^{35}Cl_2{}^{37}ClO_{11}S$			OH-triclosan hexosyl sulfate
M1d	3.33	630.9484 (0) 632.9457 (−1)	$C_{21}H_{18}{}^{35}Cl_3O_{14}S$ $C_{21}H_{18}{}^{35}Cl_2{}^{37}ClO_{14}S$	266.9608 (3) 268.9579 (3)	$C_{12}H_5{}^{35}Cl_2O_3$ $C_{12}H_5{}^{35}Cl^{37}ClO_3$	OH-triclosan malonyl hexosyl sulfate
M3b	3.51	507.0008 (2) 508.9984 (1)	$C_{20}H_{18}{}^{35}Cl_3O_9$ $C_{20}H_{18}{}^{35}Cl_2{}^{37}ClO_9$	266.9611 (2) 268.9578 (3)	$C_{12}H_5{}^{35}Cl_2O_3$ $C_{12}H_5{}^{35}Cl^{37}ClO_3$	OH-triclosan acetyl hexoside
M2c	3.84	544.9478 (0) 546.9453 (−1)	$C_{18}H_{16}{}^{35}Cl_3O_{11}S$ $C_{18}H_{16}{}^{35}Cl_2{}^{37}ClO_{11}S$	96.9596 (0) 241.0021 (−1) 266.9612 (1) 268.9585 (0)	HSO_4 $C_6H_9O_8S$ $C_{12}H_5{}^{35}Cl_2O_3$ $C_{12}H_5{}^{35}Cl^{37}ClO_3$	OH-triclosan hexosyl sulfate
M22	4.26	382.8949 (1) 384.8923 (−1)	$C_{12}H_6{}^{35}Cl_3O_6S$ $C_{12}H_6{}^{35}Cl_2{}^{37}ClO_6S$	266.9609 (3) 268.9579 (3) 302.9386 (−1) 304.9365 (−4)	$C_{12}H_5{}^{35}Cl_2O_3$ $C_{12}H_5{}^{35}Cl^{37}ClO_3$ $C_{12}H_6{}^{35}Cl_3O_3$ $C_{12}H_6{}^{35}Cl_2{}^{37}ClO_3$	OH-triclosan sulfate
Group 4: Unidentified Triclosan Metabolites						
M4a	2.96	967.0676 969.0654				unidentified
M4b	3.08	967.0675 969.0636		544.9455 (4) 546.9433 (3) 266.9606 (4) 268.9576 (4)	$C_{18}H_{16}{}^{35}Cl_3O_{11}S$ $C_{18}H_{16}{}^{35}Cl_2{}^{37}ClO_{11}S$ $C_{12}H_5{}^{35}Cl_2O_3$ $C_{12}H_5{}^{35}Cl^{37}ClO_3$	unidentified (contains OH-TCS)
M8	3.18	663.0542 665.0524				unidentified
M11	3.38	683.0328 685.0312				unidentified
M16a	3.63	640.0208 (1) 642.0184 (0)	$C_{24}H_{25}{}^{35}Cl_3NO_{11}S$ $C_{24}H_{25}{}^{35}Cl_2{}^{37}ClNO_{11}S$	352.0693		unidentified (triclosan as neutral loss)

dx.doi.org/10.1021/jf404784q | J. Agric. Food Chem. 2014, 62, 1001−1009

Table 1. continued

metabolite[a]	RT (min)	molecular anion $[M-H]^-$ m/z (deviation (ppm))	sum formula of molecular anion $[M-H]^-$	fragments m/z (deviation (ppm))	sum formula of fragment anions[b]	structure proposal
			Group 4: Unidentified Triclosan Metabolites			
M17	3.69	805.0363 (1) 807.0333 (1)	$C_{29}H_{32}{}^{35}Cl_3O_{18}S$ $C_{29}H_{32}{}^{35}Cl_2{}^{37}ClO_{18}S$			unidentified
M19	3.72	593.0387 (−1) 595.0369 (−2)	$C_{24}H_{24}{}^{35}Cl_3O_{11}$ $C_{24}H_{24}{}^{35}Cl_2{}^{37}ClO_{11}$	286.9432 (0) 288.9408 (−1)	$C_{12}H_6{}^{35}Cl_3O_2$ $C_{12}H_6{}^{35}Cl_2{}^{37}ClO_2$	unidentified
M16b	3.88	640.0209 (1) 642.0187 (0)	$C_{24}H_{25}{}^{35}Cl_3NO_{11}S$ $C_{24}H_{25}{}^{35}Cl_2{}^{37}ClNO_{11}S$	352.0701		unidentified (triclosan as neutral loss)
M16c	3.96	640.0215 (0) 642.0188 (−1)	$C_{24}H_{25}{}^{35}Cl_3NO_{11}S$ $C_{24}H_{25}{}^{35}Cl_2{}^{37}ClNO_{11}S$	352.0698		unidentified (triclosan as neutral loss)
M21	4.22	628.9709 630.9671		341.0210		unidentified (triclosan as neutral loss)

[a]Metabolites are numbered according to their elution order. Metabolites that are supposed to be isomers are labeled with the adjuncts a–d. [b]Molecular anions and fragment ions whose detected m/z values led to no or more than one possible sum formula could not assigned.

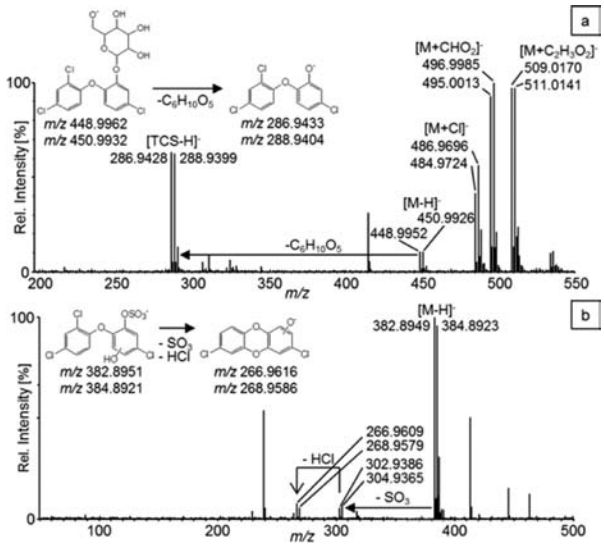

Figure 5. Low collision energy mass spectra (ESI neg) and proposed structure of (a) metabolite M19 tentatively identified as triclosan hexopyranoside and of (b) metabolite M22 tentatively identified as OH-triclosan sulfate.

triclosan hexoside. Additionally, an abundant signal of its dimeric anion $[2M-H]^-$ at m/z 1071.0035 was observed. The $[M-H]^-$ ion underwent a neutral loss of 43.9905 u (CO_2) to a fragment ion m/z 491.0063 ($C_{20}H_{18}Cl_3O_8$). Metabolite M13 was therefore tentatively identified as triclosan malonylhexoside. One metabolite that does not contain a carbohydrate moiety was M20 and eluted after 4.04 min. Its molecular anion at m/z 366.9006 corresponds to a sum formula of $C_{12}H_6Cl_3O_5S$ and gave rise also to the triclosan fragment ion. M20 was therefore assigned as triclosan sulfate and is one of two detected metabolites that are not conjugated with a hexose (Figure 6).

Hydroxytriclosan Conjugates (Group 3). In contrast to the previous two groups of metabolites, the mass spectra of a number of additional transformation products showed neither the triclosan fragment ion nor the neutral loss of triclosan. Rather, the fragmentation of most of these metabolites gave rise to only one fragment ion at m/z 266.9609 ($C_{12}H_5Cl_2O_3$) with the corresponding Cl_2 isotopic pattern. Because the molecular formulas and isotopic patterns of all corresponding molecular anions indicated trichlorinated metabolites, the fragment ion at m/z 266.9609 ($C_{12}H_5Cl_2O_3$) was interpreted as the dichlorodibenzodioxinol fragment ion, which was, likely, formed from

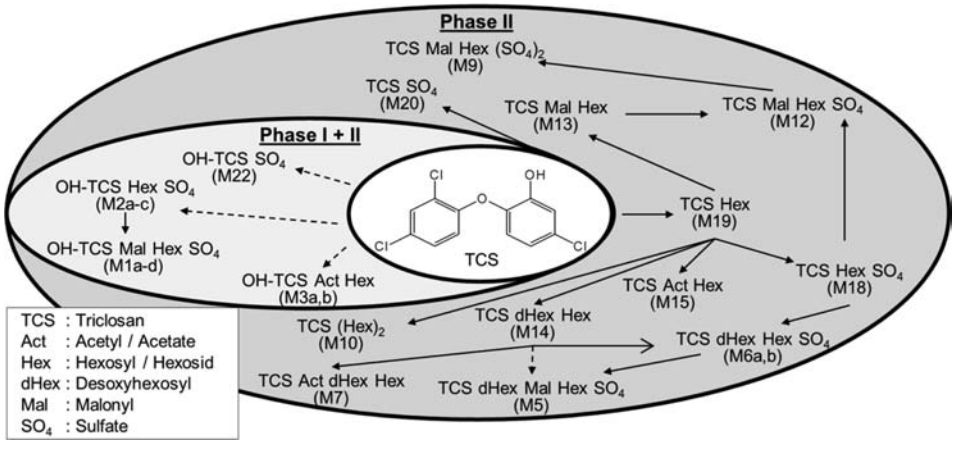

Figure 6. Proposed pathway of triclosan metabolization in hairy root cultures of horseradish. Dashed arrows represent multistep processes.

dx.doi.org/10.1021/jf404784q | J. Agric. Food Chem. 2014, 62, 1001–1009

the conjugates of hydroxylated triclosan (OH-triclosan) (Figure 5b). The likely precursor of this fragment ion, that is, the hydroxytriclosan fragment ion itself, was detected at m/z 302.9386 only for hydroxytriclosan sulfate (M22). Whereas the triclosan conjugates would also allow for ring closure upon HCl elimination, they would lack the additional hydroxy moiety to stabilize the negative charge of the anion.

Another fragmentation behavior of hydroxylated metabolites is observed for the metabolites M2 and M4, which form m/z 301.9306 ($C_{12}H_5Cl_3O_3$). This formula is consistent with a resonance-stabilized triclosan quinone radical anion. This nicely illustrates the diversity in mass spectrometric fragmentation behavior, which would have impeded the detection of all hydroxylated metabolites by a precursor ion scan. In sum, 11 hydroxylated triclosan metabolites with four different elemental compositions were detected and tentatively identified. Because their mass spectra show only a few diagnostic ions, the support for the proposed structures is low and no additional structural information can be obtained by formed fragment ions for more complex metabolites such as the OH-triclosan malonyl hexosyl sulfate M1. The introduction of an additional hydroxy group is expected to increase the polarity and, hence, to decrease the retention time during reversed phase chromatography of metabolites in comparison to nonhydroxylated ones. In contrast, the OH-triclosan sulfate eluted later than its nonhydroxylated equivalent.

The comparison of the peak intensities of hydroxylated and nonhydroxylated metabolites suggests that only a small portion of triclosan was subjected to phase I metabolism prior to conjugation. The ability of the horseradish culture to form hydroxylated species was already observed recently and can be ascribed to the existence of P450 monooxygenase in plant cells.[15] Except for the hydroxylated sulfate metabolite, several isomers (up to four) were formed for saccharide conjugates of OH-triclosan. However, with the fragment ions observed it was not possible to assign the sites of hydroxylation.

Despite this intensive study of the mass spectra generated at low and high collision energies, a total of 10 of the compounds recognized as triclosan metabolites could not be identified (Table 1, *group 4*). According to the m/z values and sum formula, respectively, three of these compounds contained nitrogen. As cysteine and glutathione conjugates might be formed during the plant metabolism, the sum formulas were examined to match respective structures, but no proper structure could be derived. For five of these unidentified compounds no sum formulas were determined from the exact m/z values of the molecular anions, because more than one probable sum formula was derived by the MassLynx 4.1 software.

Proposed Pathway of Triclosan Metabolism in Horseradish Hairy Root Cultures. A possible metabolic pathway for the formation of these 23 metabolites is provided in Figure 6. The detected metabolites are mainly pure phase II metabolites, that is, conjugates with endogenous compounds at the phenolic OH-group of triclosan. The conjugation of this OH-group with a hexose, probably β-D-glucose,[27] plays a central role, because the resulting triclosan hexoside (M19) is an intermediate for the formation of a number of further metabolites. The malonylation, acetylation, and sulfation of one OH-group of the glycon part gave rise to the malonylhexoside (M13), acetylhexoside (M15), and sulfohexoside (M18), respectively. Disaccharide conjugates such as M10 and M14 are formed by the glycosylation with one further hexose or desoxyhexose, respectively. Furthermore, products formed by combinations of these reactions were observed, such as the triclosan malonylsulfohexoside (M12), which upon further sulfation gives rise to triclosan malonyldisulfohexoside (M9). Even though the formation of sulfohexosides of contaminants was reported before, disulfation of hexose conjugates has not been observed, so far. Besides these metabolites, the triclosan sulfate (M20) is formed by the direct sulfation of the phenolic OH-group of triclosan and is one of the few metabolites that does not require the previous glycosylation. Besides this large number of metabolites, which are formed exclusively by a combination of phase II reactions, four conjugates of the phase I metabolite OH-triclosan were detected. Three of the OH-triclosan conjugates form two to four structural isomers as the detection of identical m/z values at several retention times indicates. In sum, the OH-triclosan conjugates had comparatively low signal intensities, and the phase I metabolite OH-triclosan itself was not detected. The phase I reactions seem to play a minor role in the entire metabolism of triclosan by the hairy root culture of horseradish. This may indicate that the conjugation reactions of triclosan with sulfate or a hexose are faster than the hydroxylation in the phase I metabolism. Nevertheless, this is the first report on the phase I metabolism of triclosan in plants.

The combination of phase I and II metabolism in plants may give rise to a complex mixture of structurally diverse metabolites of environmental contaminants of high and very low signal intensities. This emphasizes the need and usefulness of the reported strategy of an unbiased and comprehensive approach for sample analysis using UPLC-QToF-MS^E and data processing using statistical means. It reduces the risk of overlooking a part of the metabolites formed in a plant. Even though structure proposals could be derived for 23 of the 33 detected triclosan metabolites, about one-third remained unidentified. Further analytical effort would be required for their identification. The inclusion of this and similar analytical approaches to detect and identify metabolites into uptake studies of environmental contaminants into plants would provide a more comprehensive view on this issue. An important next challenge poses the quantification of these metabolites, as reference compounds are usually not available.

AUTHOR INFORMATION

Corresponding Author

*(T.R.) E-mail: thorsten.reemtsma@ufz.de, Phone: +49 (0341) 235 1261. Fax: +49 (0341) 235 450822.

Funding

A.M. thanks the Helmholtz Impulse and Networking Fund through the Helmholtz Interdisciplinary Graduate School for Environmental Research (HIGRADE) for the kind support.

Notes

The authors declare no competing financial interest.

ACKNOWLEDGMENTS

We thank Rudolf Harpaintner (Helmholtz Centre München), Steffi Schrader, and Ursula Winkler (both UFZ) for extensive technical assistance with the horseradish tissue cultivation and sample preparation.

REFERENCES

(1) Herklotz, P. A.; Gurung, P.; Vanden Heuvel, B.; Kinney, C. A. Uptake of human pharmaceuticals by plants grown under hydroponic conditions. *Chemosphere* **2010**, *78*, 1416−1421.

(2) Shenker, M.; Harush, D.; Ben-Ari, J.; Chefetz, B. Uptake of carbamazepine by cucumber plants − a case study related to irrigation with reclaimed wastewater. *Chemosphere* **2011**, *82*, 905−910.

(3) Eggen, T.; Asp, T. N.; Grave, K.; Hormazabal, V. Uptake and translocation of metformin, ciprofloxacin and narasin in forage- and crop plants. *Chemosphere* **2011**, *85*, 26−33.

(4) Macherius, A.; Eggen, T.; Lorenz, W. G.; Reemtsma, T.; Winkler, U.; Moeder, M. Uptake of galaxolide, tonalide, and triclosan by carrot, barley, and meadow fescue plants. *J. Agric. Food Chem.* **2012**, *60*, 7785−7791.

(5) Litz, N. T.; Müller, J.; Böhmer, W. Occurrence of polycyclic musks in sewage sludge and their behaviour in soils and plants. Part 2: Investigation of polycyclic musks in soils and plants. *J. Soil Sediment* **2007**, *7*, 36−44.

(6) Boxall, A. B. A.; Johnson, P.; Smith, E. J.; Sinclair, C. J.; Stutt, E.; Levy, L. S. Uptake of veterinary medicines from soils into plants. *J. Agric. Food Chem.* **2006**, *54*, 2288−2297.

(7) Sabourin, L.; Duenk, P.; Bonte-Gelok, S.; Payne, M.; Lapen, D. R.; Topp, E. Uptake of pharmaceuticals, hormones and parabens into vegetables grown in soil fertilized with municipal biosolids. *Sci. Total Environ.* **2012**, *431*, 233−236.

(8) Gottschall, N.; Topp, E.; Metcalfe, C.; Edwards, M.; Payne, M.; Kleywegt, S.; Russell, P.; Lapen, D. R. Pharmaceutical and personal care products in groundwater, subsurface drainage, soil, and wheat grain, following a high single application of municipal biosolids to a field. *Chemosphere* **2012**, *87*, 194−203.

(9) Aryal, N.; Reinhold, D. M. Phytoaccumulation of antimicrobials from biosolids: impacts on environmental fate and relevance to human exposure. *Water Res.* **2011**, *45*, 5545−5552.

(10) Wu, C.; Spongberg, A. L.; Witter, J. D.; Fang, M.; Czajkowski, K. P. Uptake of pharmaceutical and personal care products by soybean plants from soils applied with biosolids and irrigated with contaminated water. *Environ. Sci. Technol.* **2010**, *44*, 6157−6161.

(11) Komoßa, D.; Langebartels, C.; Sandermann Jr., H. Metabolic processes for organic chemicals in plants. In *Plant Contamination: Modeling and Simulation of Organic Chemical Processes*; Trapp, S., McFarlane, C., Eds.; Lewis Publishers: Boca Raton, FL, USA, 1995; pp 69−103.

(12) Cole, D. J. Detoxification and activation of agrochemicals in plants. *Pestic. Sci.* **1994**, *42*, 209−222.

(13) Macherius, A.; Eggen, T.; Lorenz, W.; Moeder, M.; Ondruschka, J.; Reemtsma, T. Metabolization of the bacteriostatic agent triclosan in edible plants and its consequences for plant uptake assessment. *Environ. Sci. Technol.* **2012**, *46*, 10797−10804.

(14) Van Eerd, L. L.; Hoagland, R. E.; Zablotowicz, R. M.; Hall, J. C. Pesticide metabolism in plants and microorganisms. *Weed Sci.* **2003**, *51*, 472−495.

(15) Huber, C.; Bartha, B.; Schröder, P. Metabolism of diclofenac in plants − hydroxylation is followed by glucose conjugation. *J. Hazard. Mater.* **2012**, *243*, 250−256.

(16) Bonn, B.; Leandersson, C.; Fontaine, F.; Zamora, I. Enhanced metabolite identification with MS^E and a semi-automated software for structural elucidation. *Rapid Commun. Mass Spectrom.* **2010**, *24*, 3127−3138.

(17) Huber, C.; Bartha, B.; Harpaintner, R.; Schröder, P. Metabolism of acetaminophen (paracetamol) in plants − two independent pathways result in the formation of a glutathione and a glucose conjugate. *Environ. Sci. Pollut. Res.* **2009**, *16*, 206−213.

(18) Bateman, K. P.; Castro-Perez, J.; Wrona, M.; Shockcor, J. P.; Yu, K.; Oballa, R.; Nicoll-Griffith, D. A. MS^E with mass defect filtering for in vitro and in vivo metabolite identification. *Rapid Commun. Mass Spectrom.* **2007**, *21*, 1485−1496.

(19) Zhu, M.; Ma, L.; Zhang, D.; Ray, K.; Zhao, W.; Humphreys, W. G.; Skiles, G.; Sanders, M.; Zhang, H. Detection and characterization of metabolites in biological matrices using mass defect filtering of liquid chromatography/high resolution mass spectrometry data. *Drug Metab. Dispos.* **2006**, *34*, 1722−1733.

(20) Zhang, H.; Zhang, D.; Ray, K.; Zhu, M. Mass defect filter technique and its applications to drug metabolite identification by high-resolution mass spectrometry. *J. Mass Spectrom.* **2009**, *44*, 999−1016.

(21) Bode, M.; Stöbe, P.; Thiede, B.; Schuphan, I.; Schmidt, B. Biotransformation of atrazine in transgenic tobacco cell culture expressing human P450. *Pest Manag. Sci.* **2004**, *60*, 49−58.

(22) Chu, W. K.; Wong, M. H.; Zhang, J. Accumulation, distribution and transformation of DDT and PCBs by *Phragmites australis* and *Oryza sativa* L.: I. Whole plant study. *Environ. Geochem. Health* **2006**, *28*, 159−168.

(23) Ferrari, R. P.; Laurenti, E.; Trotta, F. Oxidative 4-dechlorination of 2,4,6-trichlorophenol catalyzed by horseradish peroxidase. *J. Biol. Inorg. Chem.* **1999**, *4*, 232−237.

(24) Laurent, F.; Debrauwer, L.; Rathahao, E.; Scalla, R. 2,4-Dichlorophenoxyacetic acid metabolism in transgenic tolerant cotton (*Gossypium hirsutum*). *J. Agric. Food Chem.* **2000**, *48*, 5307−5311.

(25) Capps, T. M.; Barringer, V. M.; Eberle, W. J.; Brown, D. R.; Sanson, D. R. Identification of a unique glucosylsulfate conjugate metabolite of profenofos in cotton. *J. Agric. Food Chem.* **1996**, *44*, 2408−2411.

(26) Levsen, K.; Schiebel, H.-M.; Behnke, B.; Dötzer, R.; Dreher, W.; Elend, M.; Thiele, H. Structure elucidation of phase II metabolites by tandem mass spectrometry: an overview. *J. Chromatogr., A* **2005**, *1067*, 55−72.

(27) Laurent, F.; Canlet, C.; Debrauwer, L.; Pascal-Lorber, S. Metabolic fate of [^{14}C]-2,4-dichlorophenol in tobacco cell suspension cultures. *Environ. Toxicol. Chem.* **2007**, *26*, 2299−2307.

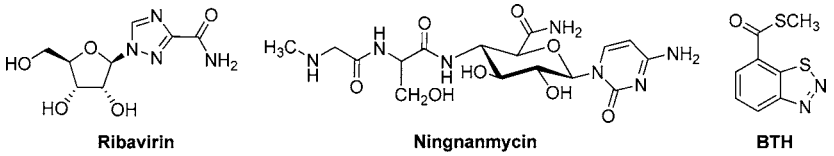

Figure 2. Virus inhibitors.

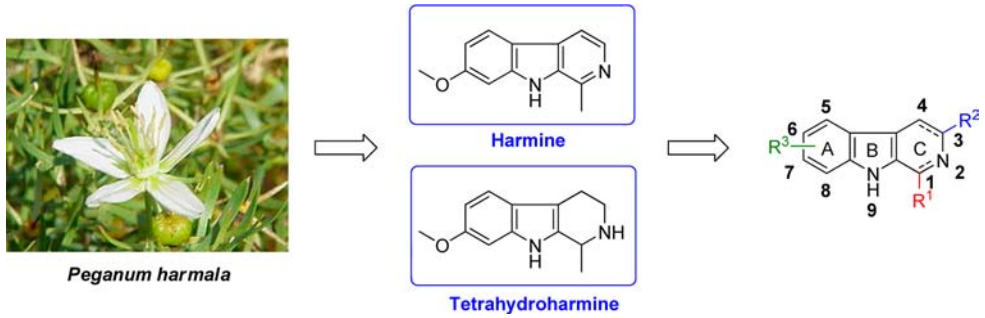

Figure 3. Design of target compounds.

Scheme 1. Synthesis of Harmalan, Tetrahydroharmane, and Harmane

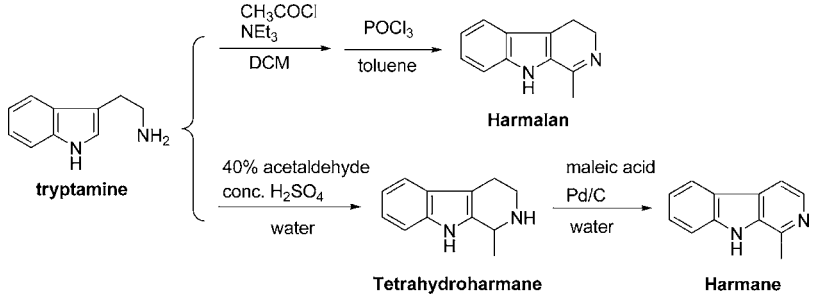

for 5 h. Then the mixture was washed with a saturated aqueous solution of $NaHCO_3$, dried over anhydrous Na_2SO_4, and filtered, and the solvent was removed under reduced pressure. The crude was dissolved in toluene (20 mL) and chloroform (20 mL), phosphorus oxychloride (3 mL) was added dropwise to the above solution, and then the mixture was heated at reflux for 7 h. The mixture was adjusted to pH 9 with a saturated aqueous solution of Na_2CO_3 after it was cooled to room temperature. The resulting solution was extracted with dichloromethane (3 × 20 mL), the combined organic phases were washed with brine (50 mL), dried over anhydrous Na_2SO_4, filtered, and concentrated in vacuo and purified by flash chromatography on silica gel using dichloromethane and methanol (v/v = 10:1) as eluent to give harmalan as a brown solid (0.35 g, 60%): mp = 180−183 °C (lit.[17] mp = 182−183 °C); ^{1}H NMR (400 MHz, $CDCl_3$) δ 9.47 (s, 1H, NH), 7.60 (d, $^3J_{HH}$ = 8.0 Hz, 1H, Ar−H), 7.48 (d, $^3J_{HH}$ = 8.4 Hz, 1H, Ar−H), 7.31 (t, $^3J_{HH}$ = 8.0 Hz, 1H, Ar−H), 7.16 (t, $^3J_{HH}$ = 8.0 Hz, 1H, Ar−H), 3.88 (t, $^3J_{HH}$ = 8.4 Hz, 2H, CH_2), 2.95 (t, $^3J_{HH}$ = 8.8 Hz, 2H, CH_2), 2.53 (s, 3H, CH_3); HRMS (ESI) calcd for $C_{12}H_{13}N_2$ $(M + H)^+$ 185.1073, found 185.1077.

Synthesis of Tetrahydroharmane (1-Methyl-2,3,4,9-tetrahydro-1*H*-pyrido[3,4-*b*]indole).[18] To a solution of 40% aqueous solution of acetaldehyde (8.1 mL, 43.75 mmol) in water (250 mL) was added concentrated H_2SO_4 (5 drops), the mixture was stirred at room temperature for 0.5 h. Then tryptamine (3.50 g, 21.88 mmol) was added, and the mixture was heated at reflux for 7 h. The mixture was adjusted to pH 10 with an aqueous solution of NaOH after it was cooled to room temperature. The resulting solution was extracted with dichloromethane (3 × 100 mL), and the combined organic phase was washed with brine (200 mL), dried over anhydrous Na_2SO_4, filtered, concentrated in vacuo, and then purified by flash chromatography on silica gel using dichloromethane and methanol (v/v = 5:1) as eluent to give tetrahydroharmane as a brown solid (2.53 g, 62%): mp = 173−175 °C (lit.[19] mp = 177−178 °C); ^{1}H NMR (400 MHz, DMSO-d_6) δ 10.68 (s, 1H, NH), 7.35 (d, $^3J_{HH}$ = 8.0 Hz, 1H, Ar−H), 7.27 (d, $^3J_{HH}$ = 8.0 Hz, 1H, Ar−H), 6.98−7.02 (m, 1H, Ar−H), 6.91−6.95 (m, 1H, Ar−H), 3.99−4.04 (m, 1H, CHNH), 3.33 (s, 1H, CHNH), 3.14−3.19 (m, 1H, CH_2NH), 2.81−2.87 (m, 1H, CH_2NH), 2.51−2.62 (m, 2H, CH_2CH_2), 1.36 (d, $^3J_{HH}$ = 6.8 Hz, 3H, CH_3CH); HRMS (ESI) calcd for $C_{12}H_{15}N_2$ $(M + H)^+$ 187.1230, found 187.1231.

Synthesis of Harmane (1-Methyl-9*H*-pyrido[3,4-*b*]indole).[20] To a stirred solution of maleic acid (0.53 g, 4.57 mmol) in water at room temperature was added 1-methyl-2,3,4,9-tetrahydro-1*H*-pyrido-[3,4-*b*]indole (0.85 g, 4.57 mmol), and the mixture was stirred until the solid dissolved in water (120 mL); then Pd/C (0.85 g) was added, and the mixture was heated at reflux for 8 h. Then the mixture was cooled and filtered, and the filtered solid was washed carefully with water. The combined filtrates were adjusted to pH 9 with aqueous NaOH and then extracted with dichloromethane (3 × 50 mL), and the combined organic phases were washed with brine (100 mL), dried over anhydrous Na_2SO_4, filtered, and concentrated in vacuo to give harmane as a white solid (0.50 g, 60%): mp = 244−245 °C (lit.[21] mp = 235−238 °C); ^{1}H NMR (400 MHz, $CDCl_3$) δ 8.41 (s, 1H, NH), 8.37 (d, $^3J_{HH}$ = 5.2 Hz, 1H, Ar−H), 8.12 (d, $^3J_{HH}$ = 8.0 Hz, 1H, Ar−H), 7.83 (d, $^3J_{HH}$ = 5.2 Hz, 1H, Ar−H), 7.52−7.57 (m, 2H, Ar−H), 7.26−7.32 (m, 1H, Ar−H), 2.84 (s, 3H, CH_3); HRMS (ESI) calcd for $C_{12}H_{11}N_2$ $(M + H)^+$ 183.0917, found 183.0915.

Synthesis of Quaternary Ammonium Salts 1. To a solution of harmine (0.50 g, 2.36 mmol) in ethyl acetate (120 mL) was added benzyl bromide (0.48 g, 2.83 mmol), and the mixture was heated at reflux for 12 h. Then the mixture was cooled and filtered, and the filter cake was washed with ethyl acetate and dried to give **1** as a white solid (0.67 g, 74%): mp = 276−277 °C; ^{1}H NMR (400 MHz, DMSO-d_6) δ 12.78 (s, 1H, NH), 8.74 (d, $^3J_{HH}$ = 6.4 Hz, 1H, Ar−H), 8.58 (d, $^3J_{HH}$ = 6.8 Hz, 1H, Ar−H), 8.37 (d, $^3J_{HH}$ = 8.8 Hz, 1H, Ar−H), 7.35−7.44

dx.doi.org/10.1021/jf404840x | J. Agric. Food Chem. 2014, 62, 1010−1018

(m, 3H, Ar−H), 7.23 (d, $^3J_{HH}$ = 7.2 Hz, 2H, Ar−H), 7.12 (d, $^4J_{HH}$ = 1.0 Hz, 1H, Ar−H), 7.08 (dd, $^3J_{HH}$ = 8.8 Hz, $^4J_{HH}$ = 1.0 Hz, 1H, Ar−H), 5.98 (s, 2H, CH_2), 3.95 (s, 3H, OCH_3), 2.98 (s, 3H, CH_3).

Synthesis of 2-Benzyl-7-methoxy-1-methyl-2,3,4,9-tetrahydro-1*H*-pyrido[3,4-*b*]indole (2). To a solution of **1** (0.67 g, 1.75 mmol) in methanol (150 mL) was added dropwise sodium borohydride (0.53 g, 14.00 mmol) in methanol (30 mL), and then the mixture was heated at reflux for 15 h. The solvent was distilled off, and the residue was diluted with dichloromethane (2 × 50 mL) and water (50 mL); the combined organic phase was washed with brine (50 mL), dried over anhydrous Na_2SO_4, filtered, concentrated in vacuo, and purified by flash chromatography on silica gel using dichloromethane and methanol (v/v = 5:1) as eluent to give **2** as a brown oil (0.47 g, 88%): ^{1}H NMR (400 MHz, $CDCl_3$) δ 7.68 (s, 1H, NH), 7.50−7.52 (m, 2H, Ar−H), 7.43−7.47 (m, 3H, Ar−H), 7.36−7.40 (m, 1H, Ar−H), 6.90 (dd, $^3J_{HH}$ = 8.8 Hz, $^4J_{HH}$ = 2.4 Hz, 1H, Ar−H), 6.83 (d, $^4J_{HH}$ = 2.4 Hz, 1H, Ar−H), 3.97 (d, $^2J_{HH}$ = 13.6 Hz, 1H, $CH_2C_6H_5$), 3.81 (q, $^3J_{HH}$ = 6.8 Hz, 1H, $CHCH_3$), 3.77 (d, $^2J_{HH}$ = 13.6 Hz, 1H, $CH_2C_6H_5$), 3.22−3.29 (m, 1H, CH_2CH_2), 2.85−2.95 (m, 2H, CH_2CH_2), 2.68−2.74 (m, 1H, CH_2CH_2), 1.61 (d, $^3J_{HH}$ = 6.8 Hz, 1H, $CHCH_3$).

Synthesis of 7-Methoxy-1-methyl-2,3,4,4a,9,9a-hexahydro-1*H*-pyrido[3,4-*b*]indole (3).[22] To a solution of **2** (0.70 g, 2.29 mmol) in 2,2,2-trifluoroethanol (120 mL) was added Pd/C (0.70 g), and then the reaction system was evacuated and purged with hydrogen three times; the mixture was stirred in a hydrogen atmosphere overnight at room temperature. The mixture was concentrated in vacuo and purified by flash chromatography on silica gel using dichloromethane and methanol (v/v = 10:1) as eluent to give **3** as a pale yellow solid (0.37 g, 74%): mp = 158−160 °C; ^{1}H NMR (400 MHz, $CDCl_3$) δ 6.93 (d, $^3J_{HH}$ = 8.0 Hz, 1H, Ar−H), 6.31 (dd, $^3J_{HH}$ = 8.0 Hz, $^4J_{HH}$ = 2.0 Hz, 1H, Ar−H), 6.26 (d, $^4J_{HH}$ = 2.0 Hz, 1H, Ar−H), 3.76 (s, 3H, OCH_3), 3.49 (s, 1H, NH), 3.39−3.45 (m, 1H, $CHCH_3$), 3.35 (t, $^3J_{HH}$ = 8.4 Hz, 1H, CH), 2.97−3.02 (m, 1H, CH), 2.69−2.72 (m, 1H, CH_2), 2.53−2.60 (m, 1H, CH_2), 2.08−2.20 (m, 2H, CH_2NH), 1.26 (s, 1H, NH), 1.23 (d, $^3J_{HH}$ = 6.4 Hz, 3H, CH_3); HRMS (ESI) calcd for $C_{13}H_{19}N_2O$ $(M + H)^+$ 219.1492, found 219.1494.

Data for 7-Methoxy-1-methyl-2,3,4,9-tetrahydro-1H-pyrido[3,4-b]indole (Tetrahydroharmine). The compound was synthesized using a similar procedure as for compound **3**; the mixture was stirred for 3 h to give tetrahydroharmine as a white solid (0.56 g, 80%): mp = 195−197 °C (lit.[23] mp = 198−200 °C); ^{1}H NMR (400 MHz, $CDCl_3$) δ 7.64 (s, 1H, NH), 7.35 (d, $^3J_{HH}$ = 8.8 Hz, 1H, Ar−H), 6.85 (d, $^4J_{HH}$ = 2.0 Hz, 1H, Ar−H), 6.77 (dd, $^3J_{HH}$ = 8.4 Hz, $^4J_{HH}$ = 2.4 Hz, 1H, Ar−H), 4.14−4.19 (m, 1H, $CHCH_3$), 3.84 (s, 3H, OCH_3), 3.33−3.39 (m, 1H, CH_2CH_2), 3.01−3.07 (m, 1H, CH_2CH_2), 2.66−2.78 (m, 2H, CH_2CH_2), 1.65 (s, 1H, NH), 1.44 (d, $^3J_{HH}$ = 6.8 Hz, 3H, CH_3); HRMS (ESI) calcd for $C_{13}H_{17}N_2O$ $(M + H)^+$ 217.1335, found 217.1337.

Synthesis of Compounds 4 and 5.[24] To a solution of harmane (0.20 g, 1.10 mmol) in glacial acetic acid (10 mL) was added NBS (0.20 g, 1.10 mmol) at room temperature, and the mixture was stirred at room temperature for 6 h. Then the mixture was concentrated under reduced pressure and adjusted to pH 10 with an aqueous solution of $NaHCO_3$, and the aqueous solution was extracted with dichloromethane (20 mL × 4). The combined organic layer was dried over anhydrous Na_2SO_4 and then was concentrated in vacuo and purified by flash chromatography on silica gel using dichloromethane and methanol (v/v = 40:1→20:1) as eluent to give **4** (0.24 g) and **5** (0.05 g).

6-Bromo-1-methyl-9H-pyrido[3,4-b]indole (4). This compound was obtained as a white solid in 83% yield: mp = 256−257 °C; ^{1}H NMR (400 MHz, $CDCl_3$) δ 8.44 (s, 1H, NH), 8.39 (d, $^3J_{HH}$ = 5.6 Hz, 1H, Ar−H), 8.24 (d, $^4J_{HH}$ = 2.0 Hz, 1H, Ar−H), 7.78 (d, $^3J_{HH}$ = 5.6 Hz, 1H, Ar−H), 7.63 (dd, $^3J_{HH}$ = 8.4 Hz, $^4J_{HH}$ = 2.0 Hz, 1H, Ar−H), 7.42 (d, $^3J_{HH}$ = 8.8 Hz, 1H, Ar−H), 2.83 (s, 3H, CH_3); HRMS (ESI) calcd for $C_{12}H_{10}BrN_2$ $(M + H)^+$ 261.0022, found 261.0026.

8-Bromo-1-methyl-9H-pyrido[3,4-b]indole (5). This compound was obtained as a yellow solid in 17% yield: mp = 201−204 °C; ^{1}H NMR (400 MHz, $CDCl_3$) δ 8.36−8.49 (m, 2H, NH and Ar−H), 8.05 (d, $^3J_{HH}$ = 6.4 Hz, 1H, Ar−H), 7.80 (s, 1H, Ar−H), 7.70 (d, $^3J_{HH}$ = 6.4 Hz, 1H, Ar−H), 7.18 (t, $^3J_{HH}$ = 6.4 Hz, 1H, Ar−H), 2.88 (s, 3H, CH_3); HRMS (ESI) calcd for $C_{12}H_{10}BrN_2$ $(M + H)^+$ 261.0022, found 261.0025.

Synthesis of Compounds 6 and 7.[25] To a mixture of harmane (0.40 g, 2.20 mmol) and sodium nitrate (0.93 g, 10.99 mmol) was added dropwise trifluoroacetic acid (20 mmol) at 0 °C, and then the mixture was stirred overnight at room temperature. The mixture was adjusted to pH 10−11 with an aqueous solution of $NaHCO_3$ in an ice bath and then was extracted by dichloromethane (20 mL × 3). The combined organic phase was concentrated in vacuo and purified by flash chromatography on silica gel using dichloromethane and methanol (v/v = 20:1) as eluent to give **6** (0.24 g) and **7** (0.06 g) .

1-Methyl-6-nitro-9H-pyrido[3,4-b]indole (6). This compound was obtained as a pale yellow solid in 72% yield: mp > 300 °C; ^{1}H NMR (400 MHz, DMSO-d_6) δ 12.36 (s, 1H, NH), 9.30 (d, $^4J_{HH}$ = 2.0 Hz, 1H, Ar−H), 8.41 (dd, $^3J_{HH}$ = 8.8 Hz, $^4J_{HH}$ = 3.0 Hz, 1H, Ar−H), 8.33 (d, $^3J_{HH}$ = 5.6 Hz, 1H, Ar−H), 8.20 (d, $^3J_{HH}$ = 5.2 Hz, 1H, Ar−H), 7.73 (d, $^3J_{HH}$ = 8.4 Hz, 1H, Ar−H), 2.79 (s, 3H, CH_3); HRMS (ESI) calcd for $C_{12}H_{10}N_3O_2$ $(M + H)^+$ 228.0768, found 228.0767.

1-Methyl-8-nitro-9H-pyrido[3,4-b]indole (7). This compound was obtained as a yellow solid in 12% yield: mp = 207−210 °C; ^{1}H NMR (400 MHz, DMSO-d_6) δ 11.77 (s, 1H, NH), 8.77 (d, $^3J_{HH}$ = 7.6 Hz, 1H, Ar−H), 8.50 (d, $^3J_{HH}$ = 8.0 Hz, 1H, Ar−H), 8.38 (d, $^3J_{HH}$ = 5.2 Hz, 1H, Ar−H), 8.11 (d, $^3J_{HH}$ = 5.2 Hz, 1H, Ar−H), 7.48 (t, $^3J_{HH}$ = 7.6 Hz, 1H, Ar−H), 2.92 (s, 3H, CH_3); HRMS (ESI) calcd for $C_{12}H_{10}N_3O_2$ $(M + H)^+$ 228.0768, found 228.0772.

Synthesis of Harmol (1-Methyl-9*H*-pyrido[3,4-*b*]indol-7-ol). A solution of harmine (0.50 g, 2.36 mmol) in glacial acetic acid (18 mL) and 40% hydrobromic acid solution (18 mL) was stirred at room temperature for 1 h, and then the mixture was heated at reflux for 10 h. After cooling to room temperature, the mixture was adjusted to pH 8 with a saturated aqueous solution of $NaHCO_3$. The yellow slurry was filtered, and the cake was washed with water to afford harmol as a yellow solid (0.46 g, 98%): mp > 300 °C (lit.[26] mp = 304−307 °C); ^{1}H NMR (400 MHz, DMSO-d_6) δ 11.24 (s, 1H, NH), 9.72 (s, 1H, OH), 8.11 (d, $^3J_{HH}$ = 5.2 Hz, 1H, Ar−H), 7.94 (d, $^3J_{HH}$ = 8.0 Hz, 1H, Ar−H), 7.75 (d, $^3J_{HH}$ = 5.2 Hz, 1H, Ar−H), 6.90 (d, $^4J_{HH}$ = 1.2 Hz, 1H, Ar−H), 6.69 (dd, $^3J_{HH}$ = 8.4 Hz, $^4J_{HH}$ = 1.6 Hz, 1H, Ar−H), 2.69 (s, 3H, CH_3); HRMS (ESI) calcd for $C_{12}H_{11}N_2O$ $(M + H)^+$ 199.0866, found 199.0867.

Synthesis of 1-Methyl-9*H*-pyrido[3,4-*b*]indol-7-yl isopropylcarbamate (8).[27] To a solution of harmol (0.50 g, 2.53 mmol) in DMF (50 mL) was added isopropyl isocyanate via syringe over 5 min, the mixture was stirred at room temperature for 2 h, then triethylamine (0.08 g, 0.758 mmol) was added, and the mixture was stirred overnight at room temperature. Then brine (100 mL) was added, the aqueous solution was extracted with ethyl acetate (20 mL × 4), and the combined organic layer was dried over anhydrous Na_2SO_4, concentrated in vacuo, and purified by flash chromatography on silica gel using dichloromethane and methanol (v/v = 20:1) as eluent to give **8** as a pale white solid (0.50 g, 70%): mp > 300 °C; ^{1}H NMR (400 MHz, DMSO-d_6) δ 11.58 (s, 1H, NH), 8.20 (d, $^3J_{HH}$ = 5.2 Hz, 1H, Ar−H), 8.16 (d, $^3J_{HH}$ = 8.8 Hz, 1H, Ar−H), 7.90 (d, $^3J_{HH}$ = 5.2 Hz, 1H, Ar−H), 7.76 (d, $^3J_{HH}$ = 8.0 Hz, 1H, NHCO), 7.27 (d, $^4J_{HH}$ = 1.6 Hz, 1H, Ar−H), 6.95 (dd, $^3J_{HH}$ = 8.4 Hz, $^4J_{HH}$ = 2.0 Hz, 1H, Ar−H), 3.65−3.73 (m, 1H, CH), 2.75 (s, 3H, CH_3), 1.16 (d, $^3J_{HH}$ = 6.4 Hz, 6H, $(CH_3)_2CH$); HRMS (ESI) calcd for $C_{16}H_{18}N_3O_2$ $(M + H)^+$ 284.1394, found 284.1399.

Synthesis of 1-Methyl-9*H*-pyrido[3,4-*b*]indol-7-yl dimethylcarbamate (9). To a solution of harmol (0.40 g, 2.02 mmol) in THF (150 mL) was added triethylamine (0.31 g, 3.03 mmol), and the mixture was stirred for 0.5 h. Then dimethylcarbamic chloride was added dropwise, and the mixture was stirred overnight at room temperature. Then water (20 mL) and dichloromethane (20 mL) were added. The separated organic layer was dried over anhydrous Na_2SO_4, filtered, concentrated in vacuo, and then purified by flash chromatography on silica gel using dichloromethane and methanol (v/v = 10:1) as eluent to give **9** as a pale white solid (0.48 g, 89%): mp = 225−227 °C; ^{1}H NMR (400 MHz, DMSO-d_6) δ 11.63 (s, 1H, NH),

8.20 (d, $^3J_{HH}$ = 5.2 Hz, 1H, Ar−H), 8.17 (d, $^3J_{HH}$ = 8.4 Hz, 1H, Ar−H), 7.91 (d, $^3J_{HH}$ = 5.2 Hz, 1H, Ar−H), 7.30 (d, $^4J_{HH}$ = 2.0 Hz, 1H, Ar−H), 6.97 (dd, $^3J_{HH}$ = 8.4 Hz, $^4J_{HH}$ = 2.0 Hz, 1H, Ar−H), 3.10 (s, 3H, CH_3), 2.94 (s, 3H, CH_3), 2.75 (s, 3H, CH_3); HRMS (ESI) calcd for $C_{15}H_{16}N_3O_2$ (M + H)$^+$ 270.1237, found 270.1240.

Compounds **10** and **11** were synthesized using a procedure similar to that used for compound **9**.

Data for 1-Methyl-9H-pyrido[3,4-b]indol-7-yl acetate (10). This compound was obtained as a white solid in 50% yield: mp = 237−240 °C; ^{1}H NMR (400 MHz, $CDCl_3$) δ 8.90 (s, 1H, NH), 8.23 (d, $^3J_{HH}$ = 2.4 Hz, 1H, Ar−H), 7.78 (d, $^3J_{HH}$ = 8.4 Hz, 1H, Ar−H), 7.70 (d, $^3J_{HH}$ = 2.0 Hz, 1H, Ar−H), 7.16 (s, 1H, Ar−H), 6.93 (d, $^3J_{HH}$ = 8.4 Hz, 1H, Ar−H), 2.76 (s, 3H, CH_3), 2.42 (s, 3H, CH_3CO); HRMS (ESI) calcd for $C_{14}H_{13}N_2O_2$ (M + H)$^+$ 241.2647, found 241.2650.

Data for Synthesis of 1-Methyl-9H-pyrido[3,4-b]indol-7-yl pivalate (11). This compound was obtained as a white solid in 85% yield: mp = 221−222 °C; ^{1}H NMR (400 MHz, $CDCl_3$) δ 8.68 (s, 1H, NH), 8.30 (d, $^3J_{HH}$ = 5.2 Hz, 1H, Ar−H), 7.75 (d, $^3J_{HH}$ = 8.4 Hz, 1H, Ar−H), 7.54 (d, $^3J_{HH}$ = 4.8 Hz, 1H, Ar−H), 7.09 (s, 1H, Ar−H), 6.86 (d, $^3J_{HH}$ = 8.0 Hz, 1H, Ar−H), 2.73 (s, 3H, CH_3), 1.45 (s, 9H, $C(CH_3)_3$); HRMS (ESI) calcd for $C_{17}H_{19}N_2O_2$ (M + H)$^+$ 283.1441, found 283.1446.

Synthesis of (*S*)-1-Methyl-9*H*-pyrido[3,4-*b*]indol-7-yl-2-(benzyloxycarbonylamino)-3-methylbutanoate (12). To a solution of amino acid (0.80 g, 3.03 mmol) in dichloromethane (150 mL) was added triethylamine (0.41 g, 4.04 mmol), 1-ethyl-3-(3-dimethylaminopropyl)carbodiimide (EDCI) (0.76 g, 4.04 mmol), and DMAP (0.50 g, 4.04 mmol), and then the mixture was stirred overnight at room temperature. The mixture was washed with a saturated aqueous solution of NH_4Cl (50 mL × 2) and a saturated aqueous solution of $NaHCO_3$ (50 mL) successively, dried over anhydrous Na_2SO_4, filtered, concentrated in vacuo, and then purified by flash chromatography on silica gel using dichloromethane and methanol (v/v = 20:1) as eluent to give **12** as a pale white solid (0.80 g, 90%): mp = 69−71 °C; ^{1}H NMR (400 MHz, $CDCl_3$) δ 8.54 (s, 1H, NH), 8.34 (d, $^3J_{HH}$ = 5.2 Hz, 1H, Ar−H), 7.92 (d, $^3J_{HH}$ = 8.4 Hz, 1H, Ar−H), 7.66 (d, $^3J_{HH}$ = 4.8 Hz, 1H, Ar−H), 7.35−7.38 (m, 5H, Ar−H), 7.19 (s, 1H, Ar−H), 6.94 (d, $^3J_{HH}$ = 8.4 Hz, 1H, Ar−H), 5.39 (d, $^3J_{HH}$ = 8.4 Hz, 1H, NHCO), 5.17 (s, 2H, CH_2), 4.54−4.66 (m, 1H, CHNH), 2.77 (s, 3H, CH_3), 2.38−2.50 (m, 1H, $CH(CH_3)_2$), 1.14 (d, $^3J_{HH}$ = 6.8 Hz, 3H, $CH(CH_3)_2$), 1.09 (d, $^3J_{HH}$ = 6.8 Hz, 3H, $CH(CH_3)_2$); HRMS (ESI) calcd for $C_{25}H_{26}N_3O_4$ (M + H)$^+$ 432.1918, found 432.1920.

Synthesis of (1*S*,3*S*)-1-Methyl-2,3,4,9-tetrahydro-1*H*-pyrido-[3,4-*b*]indole-3-carboxylic acid (13).[28] To a solution of L-tryptophan (20.00 g, 98.0 mmol) in water (500 mL) were added concentrated H_2SO_4 (2 mL) and a 40% aqueous solution of acetaldehyde (20 mL) successively, and the mixture was stirred overnight at room temperature. Then the mixture was adjusted to pH 6−7 with ammonia solution (25−28%, w/w), and a white solid precipitated. The white slurry was filtered, and the cake was washed with water to afford **13** as a white solid (16.7 g, 74%): mp = 278−280 °C; ^{1}H NMR (400 MHz, DMSO-d_6) δ 11.11 (s, 1H, COOH), 7.45 (d, $^3J_{HH}$ = 7.8 Hz, 1H, Ar−H), 7.34 (d, $^3J_{HH}$ = 8.0 Hz, 1H, Ar−H), 7.09 (t, $^3J_{HH}$ = 7.6 Hz, 1H, Ar−H), 7.00 (t, $^3J_{HH}$ = 7.2 Hz, 1H, Ar−H), 4.52 (q, $^3J_{HH}$ = 6.4 Hz, 1H, CH), 3.61 (dd, $^3J_{HH}$ = 11.6 Hz, $^3J_{HH}$ = 4.4 Hz, 1H, CH), 3.16 (dd, $^2J_{HH}$ = 16.0 Hz, $^3J_{HH}$ = 4.0 Hz, 1H, CH_2), 2.74−2.81 (m, 1H, CH_2), 1.62 (d, $^3J_{HH}$ = 6.4 Hz, 3H, CH_3); (dr = 11.7:1); HRMS (ESI) calcd for $C_{13}H_{15}N_2O_2$ (M + H)$^+$ 231.1128, found 231.1132.

Synthesis of Ethyl (1*S*,3*S*)-1-Methyl-2,3,4,9-tetrahydro-1*H*-pyrido[3,4-*b*]indole-3-carboxylate (14). To a solution of acid **13** (16.0 g, 69.0 mmol) in ethanol (500 mL) was added dropwise thionyl chloride in an ice bath, and then the mixture was heated at reflux for 5 h. The solvent was distilled off, the residue was dissolved in water (250 mL), and then the mixture was adjusted to pH 9 with an aqueous solution of $NaHCO_3$. The aqueous was extracted by ethyl acetate (150 mL × 3), the combined organic phase was washed with brine and dried over anhydrous Na_2SO_4, and then the mixture was concentrated in vacuo to give **14** as a light yellow solid (16.40 g, 92%): mp = 136−137 °C; ^{1}H NMR (400 MHz, $CDCl_3$) δ 7.86 (s, 1H, NH), 7.49 (d, $^3J_{HH}$ = 8.0 Hz, 1H, Ar−H), 7.33 (d, $^3J_{HH}$ = 8.0 Hz, 1H, Ar−H), 7.17 (t, $^3J_{HH}$ = 7.2 Hz, 1H, Ar−H), 7.11 (t, $^3J_{HH}$ = 7.2 Hz, 1H, Ar−H), 4.26−4.31 (m, 3H, CH and OCH_2), 3.81 (dd, $^3J_{HH}$ = 11.2 Hz, $^3J_{HH}$ = 4.4 Hz, 1H, CH), 3.13 (dd, $^2J_{HH}$ = 15.2 Hz, $^3J_{HH}$ = 4.0 Hz, 1H, CH_2), 2.79−2.86 (m, 1H, CH_2), 1.52 (d, $^3J_{HH}$ = 6.4 Hz, 3H, CH_3), 1.35 (t, $^3J_{HH}$ = 7.2 Hz, 3H, OCH_2CH_3); HRMS (ESI) calcd for $C_{15}H_{19}N_2O_2$ (M + H)$^+$ 259.1441, found 259.1443.

Synthesis of Ethyl 1-Methyl-9*H*-pyrido[3,4-*b*]indole-3-carboxylate (15).[29] A mixture of **14** (12.4 g, 47.7 mmol) and sulfur (3.10 g, 95.4 mmol) in xylene (150 mL) was heated at reflux for 12 h. Then the mixture was cooled to 0 °C and kept for 1 h, dichloromethane (10 mL) was added to the mixture, and pink solid was precipitated. The mixture was filtered, and the cake was washed with toluene to afford **15** as a brown solid (8.40 g, 69%): mp = 217−219 °C; ^{1}H NMR (400 MHz, $CDCl_3$) δ 9.60 (s, 1H, NH), 8.79 (s, 1H, Ar−H), 8.18(d, $^3J_{HH}$ = 8.0 Hz, 1H, Ar−H), 7.54−7.60 (m, 2H, Ar−H), 7.32−7.36 (m, 1H, Ar−H), 4.50 (d, $^3J_{HH}$ = 6.8 Hz, 2H, OCH_2), 2.79 (s, 3H, CH_3), 1.41 (t, $^3J_{HH}$ = 7.2 Hz, 3H, OCH_2CH_3); HRMS (ESI) calcd for $C_{15}H_{15}N_2O_2$ (M + H)$^+$ 255.1128, found 255.1131.

Synthesis of 1-Methyl-9*H*-pyrido[3,4-*b*]indole-3-carboxylic acid (16). To a solution of ester **15** (2.00 g, 7.87 mmol) in alcohol (60 mL) was added NaOH (0.47 g, 11.81 mmol) in portions, and then the mixture was heated at reflux for 6 h. Then the mixture was concentrated under reduced pressure, the residue was dissolved in water (50 mL), and the aqueous solution was extracted by diethyl ether (50 mL × 2). Then the solution was adjusted to pH 5−6 with an aqueous solution of diluted hydrochloric acid (3 M), the slight yellow slurry was filtered, and the cake was washed with water to afford **16** as a yellow solid (1.46 g, 82%): mp > 300 °C; ^{1}H NMR (400 MHz, DMSO-d_6) δ 12.04 (s, 1H, COOH), 8.77 (s, 1H, Ar−H), 8.36 (d, $^3J_{HH}$ = 8.0 Hz, 1H, Ar−H), 7.66 (d, $^3J_{HH}$ = 8.0 Hz, 1H, Ar−H), 7.60 (t, $^3J_{HH}$ = 7.2 Hz, 1H, Ar−H), 7.30 (d, $^3J_{HH}$ = 7.2 Hz, 1H, Ar−H), 7.31 (d, $^3J_{HH}$ = 7.2 Hz, 1H, Ar−H), 2.82 (s, 3H, CH_3); HRMS (ESI) calcd for $C_{13}H_{11}N_2O_2$ (M + H)$^+$ 227.0815, found 227.0811.

Synthesis of (1-Methyl-9*H*-pyrido[3,4-*b*]indol-3-yl)methanol (17). To a solution of ester **15** (2.00 g, 7.40 mmol) in THF (300 mL) was added $LiAlH_4$ (0.60 g, 15.7 mmol) in portions at 0 °C, and then the mixture was stirred overnight at room temperature. Then the reaction was quenched by water, and methanol (100 mL) was added. After the mixture had been stirred at room temperature for 2 h, the slurry was filtered, the cake was washed with dichloromethane, the filtrate was concentrated to afford **17** as a yellow solid (1.58 g, 95%): mp = 195−197 °C; ^{1}H NMR (400 MHz, DMSO-d_6) δ 11.46 (s, 1H, NH), 8.19 (d, $^3J_{HH}$ = 8.0 Hz, 1H, Ar−H), 7.95 (s, 1H, Ar−H), 7.56 (d, $^3J_{HH}$ = 8.0 Hz, 1H, Ar−H), 7.49−7.53 (m, 1H, Ar−H), 7.18−7.22 (m, 1H, Ar−H), 5.30 (t, $^3J_{HH}$ = 6.0 Hz, 1H, OH), 4.67 (d, $^3J_{HH}$ = 6.0 Hz, 2H, CH_2OH), 2.73 (s, 3H, CH_3).

Synthesis of 1-Methyl-9*H*-pyrido[3,4-*b*]indole-3-carbaldehyde (18). The mixture of alcohol **17** (1.16 g, 5.47 mmol) and IBX (3.04 g, 10.93 mmol) in DMSO (60 mL) was stirred overnight at room temperature. After water (200 mL) and dichloromethane (50 mL × 3) were added, the separated organic layer was dried over anhydrous Na_2SO_4, filtered, concentrated in vacuo, and purified by flash chromatography on silica gel using dichloromethane and methanol (v/v = 10:1) as eluent to give **18** as a white solid (0.46 g, 40%): mp = 194−196 °C; ^{1}H NMR (400 MHz, DMSO-d_6) δ 12.17 (s, 1H, NH), 10.07 (s, 1H, CHO), 8.68 (s, 1H, Ar−H), 8.38 (d, $^3J_{HH}$ = 7.6 Hz, 1H, Ar−H), 7.68 (d, $^3J_{HH}$ = 8.0 Hz, 1H, Ar−H), 7.61 (t, $^3J_{HH}$ = 7.6 Hz, 1H, Ar−H), 7.33 (t, $^3J_{HH}$ = 7.6 Hz, 1H, Ar−H), 2.87 (s, 3H, CH_3).

Synthesis of (*E*)-3-(1-Methyl-9*H*-pyrido[3,4-*b*]indol-3-yl)-acrylic acid (19). To a solution of aldehyde **18** (0.45 g, 2.14 mmol) and piperidine (3 drops) in pyridine was added malonic acid (0.33 g, 3.21 mmol), and the reaction mixture was heated at 120 °C for 4 h. Then the mixture was concentrated in vacuo, water was added (50 mL), the pH was adjusted to 11−12 with an aqueous solution of NaOH, and then the mixture was extracted with diethyl ether. The aqueous phase was adjusted to pH 5−6 with dilute hydrochloric acid (3 M), the yellow slurry was filtered, and the cake was washed with water to afford **19** as a yellow solid (0.51 g, 94%): mp = 220−223 °C; ^{1}H NMR (400 MHz, DMSO-d_6) δ 12.22 (s, 1H, NH), 11.85 (s, 1H, COOH), 8.31 (s, 1H,

Scheme 2. Synthesis of Tetrahydroharmine and 3

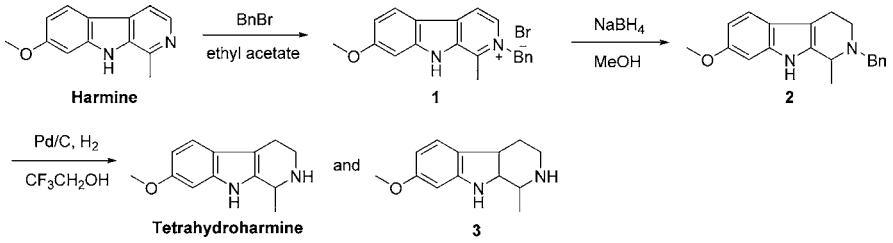

Scheme 3. Synthesis of Compounds 4−7

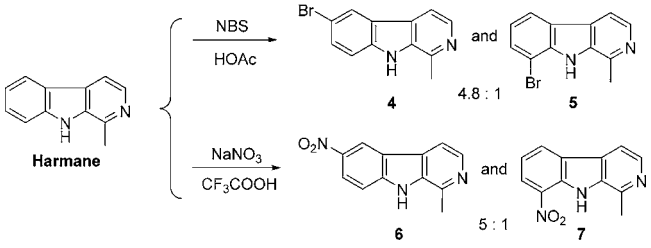

Ar−H), 8.21 (d, $^3J_{HH}$ = 7.6 Hz, 1H, Ar−H), 7.72 (d, $^3J_{HH}$ = 15.2 Hz, 1H, CHCH), 7.62 (d, $^3J_{HH}$ = 7.6 Hz, 1H, Ar−H), 7.56 (t, $^3J_{HH}$ = 7.6 Hz, 1H, Ar−H), 7.28 (t, $^3J_{HH}$ = 7.6 Hz, 1H, Ar−H), 6.78 (d, $^3J_{HH}$ = 15.6 Hz, 1H, CHCH), 2.80 (s, 3H, CH_3); HRMS (ESI) calcd for $C_{15}H_{13}N_2O_2$ $(M + H)^+$ 253.0972, found 253.0975.

Compounds **20** and **21** were synthesized using a procedure similar to that used for compound **19**.

*Data for (E)-3-(1-(Thiophen-2-yl)-9H-pyrido[3,4-b]indol-3-yl)-acrylic acid (**20**).* This compound was obtained as a yellow solid in 85% yield: mp = 248−250 °C; ^{1}H NMR (400 MHz, DMSO-d_6) δ 12.43 (s, 1H, NH), 12.10 (s, 1H, COOH), 8.47 (s, 1H, Ar−H), 8.28 (d, $^3J_{HH}$ = 8.0 Hz, 1H, Ar−H), 8.17 (d, $^3J_{HH}$ = 3.2 Hz, 1H, Ar−H), 7.80 (d, $^3J_{HH}$ = 4.8 Hz, 1H, Ar−H), 7.77−7.80 (m, 2H, Ar−H), 7.62 (t, $^3J_{HH}$ = 7.2 Hz, 1H, Ar−H), 7.33−7.38 (m, 2H, Ar−H and CHCH), 6.88 (d, $^3J_{HH}$ = 15.6 Hz, 1H, CHCH), 6.93 (d, $^3J_{HH}$ = 15.6 Hz, 1H, CHCH); HRMS (ESI) calcd for $C_{18}H_{13}N_2O_2S$ $(M + H)^+$ 321.0692, found 321.0694.

*Data for (E)-3-(1-(Pyridin-3-yl)-9H-pyrido[3,4-b]indol-3-yl)acrylic acid (**21**).* This compound was obtained as a yellow solid in 50% yield: mp > 300 °C; ^{1}H NMR (400 MHz, DMSO-d_6) δ 12.43 (s, 1H, NH), 12.10 (s, 1H, COOH), 9.31 (d, $^4J_{HH}$ = 1.6 Hz, 1H, Ar−H), 8.81 (dd, $^3J_{HH}$ = 4.8 Hz, $^4J_{HH}$ = 1.2 Hz, 1H, Ar−H), 8.61 (s, 1H, Ar−H), 8.56−8.59 (m, 1H, Ar−H), 8.31 (d, $^3J_{HH}$ = 7.6 Hz, 1H, Ar−H), 7.84 (d, $^3J_{HH}$ = 15.6 Hz, 1H, CHCH), 7.76 (dd, $^3J_{HH}$ = 7.6 Hz, $^4J_{HH}$ = 4.8 Hz, 1H, Ar−H), 7.70 (d, $^3J_{HH}$ = 8.0 Hz, 1H, Ar−H), 7.62 (t, $^3J_{HH}$ = 7.2 Hz, 1H, Ar−H), 7.35 (t, $^3J_{HH}$ = 7.2 Hz, 1H, Ar−H), 6.93 (d, $^3J_{HH}$ = 15.6 Hz, 1H, CHCH); HRMS (ESI) calcd for $C_{19}H_{14}N_3O_2$ $(M + H)^+$ 316.1081, found 316.1079.

Biological Assay. The anti-TMV and fungicidal activities of the synthesized compounds were tested using our previously reported methods.[30,31]

RESULTS AND DISCUSSION

Synthesis. Harmalan and tetrahydroharmane were obtained from tryptamine by Bischler−Napieralski and Pictet−Spengler reaction, respectively. Tetrahydroharmane was oxidized using the Pd/C−maleic acid system in water to give harmane in 60% yield (Scheme 1).

In the synthesis of Tetrahydroharmine, harmine was used as starting material. First, harmine was reacted with benzyl bromide to give a quaternary ammonium salt **1** in 74% yield, then it was reduced by sodium borohydride to give tetrahydrocarboline **2** in 88% yield, and finally tetrahydroharmine was obtained from **2** by debenzylation using palladium−carbon and hydrogen. The reaction time of debenzylation should be controlled at <3 h. Otherwise, the product will be over-reduced to give hexahydro-1*H*-pyridoindole **3**. When the reaction time was extended to 12 h, the product was converted into **3** completely (Scheme 2). In Scheme 3, the bromination and nitration products were synthesized from harmane using the reported methods.[22−24]

Harmol can be obtained from harmnine by a demethylation reaction (Scheme 4). It was reported that the demethylation reaction of harmine could be processed by BBr_3 in chloroform, but the reaction yield was low (<30%).[32] This was because of the poor solubility of harmine in conventional demethylation solvent (dichloromethane, chlorobenzene, etc.); thus, the demethylation reaction was very slow and incomplete. Therefore, in our trial on the demethylation of harmine, glacial acetic acid and 40% (m/m) aqueous hydrobromic acid (v/v = 1:1) were used instead of chloroform, and harmol was obtained in 98% yield, which was used in the synthesis of *O*-substituent derivatives **8**−**12** at the 7-position.

To investigate the influence of the degree of unsaturation of the C ring and the substituents at 3-position on the anti-TMV

Scheme 4. Synthesis of Harmol and Compounds 8−12

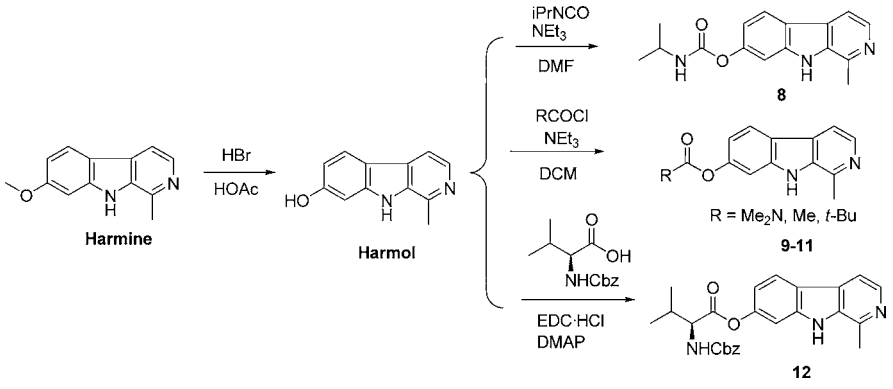

dx.doi.org/10.1021/jf404840x | J. Agric. Food Chem. 2014, 62, 1010−1018

Scheme 5. Synthesis of Compounds13−16 and 19−21

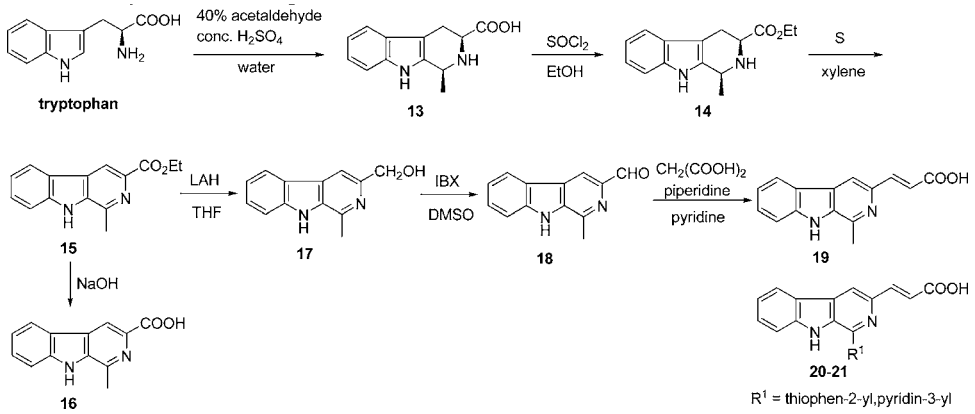

Table 1. In Vitro Antiviral Activity of Harmine, Harmane, Harmol, Harmalan, Tetrahydroharmane, Tetrahydroharmine, and Compounds 3, 4, 6−16, and 19−21 against TMV

compd	concn (μg/mL)	inhibition rate (%)	compd	concn (μg/mL)	inhibition rate (%)
Ribavirin	500	40	**9**	500	12.6
	100	12.9		100	0
harmine	**500**	**44.6**	**10**	500	30
	100	20		100	0
harmane	**500**	**54.5**	**11**	500	0
	100	16.4		100	0
harmol	500	32.6	**12**	500	20.7
	100	0		100	0
harmalan	**500**	**58.6**	**13**	500	28.6
	100	30		100	0
tetrahydroharmane	**500**	**63.7**	**14**	**500**	**46.5**
	100	28.4		100	21.8
tetrahydroharmine	**500**	**58.2**	**15**	500	33.3
	100	28.7		100	0
3	500	41.9	**16**	500	32.5
	100	12.4		100	0
4	500	44.5	**19**	500	25.8
	100	18.2		100	0
6	500	15.7	**20**	500	40.2
	100	0		100	0
7	500	30	**21**	500	17.8
	100	0		100	0
8	500	31.3			
	100	0			

activities, compounds **13−16** and **19−21** were synthesized using the method showed in Scheme 5.

Antiviral Activities. Most of the tested compounds displayed good antiviral activity in vitro, of which harmane, harmalan, tetrahydroharmane, tetrahydroharmine, and **14** exhibited higher inhibition than Ribavirin (Table 1). When the C ring (Figure 3) was dihydropyridine or tetrahydropyridine, the activities of these compounds were obviously higher than that of the compounds containing a pyridine moiety. For instance, the activities of harmalan, tetrahydroharmane, and tetrahydroharmine were 58.6, 63.7, and 58.2%, respectively, at 500 μg/mL, which were much higher than that of Ribavirin (40% at 500 μg/mL), whereas the activity of harmine was 44.6% at 500 μg/mL. The activity of tetrahydro-β-carboline **14** was 46.5%

dx.doi.org/10.1021/jf404840x | J. Agric. Food Chem. 2014, 62, 1010−1018

Table 2. In Vivo Antiviral Activity of Harmine, Harmane, Harmol, Harmalan, Tetrahydroharmane, Tetrahydroharmine, and Compounds 3, 4, 6−16, and 19−21 against TMV

compd	concn (μg/mL)	inactivation effect (%)	curative effect (%)	protection effect (%)
Ribavirin	500	37.4	36.2	38.5
	100	13.7	16.9	16.2
harmine	500	40.5	38.6	42.4
	100	11.4	15.8	16.3
harmane	**500**	**50.6**	**50**	**57.8**
	100	17.7	23.7	26.9
harmol	500	35.1	30	36.7
	100	0	0	9.5
harmalan	**500**	**62.3**	**55.1**	**60.3**
	100	32.7	34.8	35.6
tetrahydroharmane	**500**	**64.2**	**57.2**	**59.5**
	100	23.5	20.4	24.6
tetrahydroharmine	**500**	**59.8**	**55.5**	**54.6**
	100	26.4	27.3	24.2
3	500	44.1	45.2	37.7
	100	17.1	14.2	14.9
4	500	46.3	47.4	51.2
	100	14.9	19.3	20.4
6	500	21.5	18.5	26.1
	100	0	0	0
7	500	36.4	33.3	30.1
	100	10.5	0	5.8
8	500	29.5	32.7	40.3
	100	0	0	5.8
9	500	12	15.6	18.7
	100	0	0	0
10	500	20.3	24.1	27.2
	100	0	0	0
11	500	15.3	0	14.4
	100	0	0	0
12	500	13.6	12.5	19.6
	100	0	0	0
13	500	30.5	31.4	27.8
	100	0	0	0
14	**500**	**50.4**	**43.9**	**47.9**
	100	25.7	17.5	18.6
15	500	26.3	28.8	23.7
	100	0	0	0
16	500	27.3	29.6	21.4
	100	0	0	0
19	500	18.4	21.5	28.4
	100	0	0	0
20	500	39.6	36.2	35.1
	100	13.5	10	10.2
21	500	26.5	20.2	21.3
	100	0	0	0

at 500 μg/mL, whereas the activity of the corresponding β-carboline compound **15** was 33.3% at the same concentration. When tetrahydroharmine was further reduced to hexahydroharmine (**3**), the activity (41.9%, 500 μg/mL) was also reduced.

When the skeleton was β-carboline (C ring was pyridine) (Figure 3), it was detrimental to anti-TMV activity when a substituent was introduced to the benzene ring (A ring). For example, the in vitro activity of compound with no substituent on the benzene ring (harmane) was 54.5% at 500 μg/mL, whereas the activity was reduced to 44.6 and 32.6% when a methoxy (harmine) or a hydroxy (harmol) group was introduced to the 7-position. The derivatives of harmol (**8**−**11**) exhibited the same or lower activities against TMV compared with harmol. For the compound containing a carbamate moiety, the substituents on the nitrogen of amide had an obvious effect on the activity; the activity of a compound containing isopropylamino (**8**) (31.3%, 500 μg/mL) was better than that of a compound containing dimethylamino (**9**) (12.6%, 500 μg/mL). For the compounds containing an ester structure, the spatial arrangement of the substituents might have an impact on anti-TMV activity of the compounds, as the activity of compound containing acetyl (**10**) was 30% at 500 μg/mL, whereas when the substituent was changed to pivaloyl (**11**), the compound exhibited no activity against TMV. The activity of compound containing a bromo at 6-position (**4**) was equivalent to that of Ribavirin (40% at 500 μg/mL); when the substituent was changed to nitro at 6- or 8-position (**6** and **7**), the activities were reduced to 15.7 and 30% at 500 μg/mL, respectively.

The substituents on the 3-position of the β-carbolines or tetrahydro-β-carbolines played an important role in the activities. The activities of compounds containing ethyl formate (**14**) at the 3-position were better than that of compounds containing carboxylic acid (**13** and **16**) and acroleic acid (**19**−**21**). Among **19**−**21**, the substituents on the 1-position also had different effects on the antiviral activity; the 2-thienyl compound (**20**) was better than the methyl (**19**) and 3-pyridyl (**21**) compounds.

Further bioassay was conducted to investigate their inactivation, curative, and protection effects in vivo (Table 2). The result showed that most of the compounds exhibited good to excellent antiviral activity and similar structure−activity relationships to the activity in vitro. Harmane, harmalan, tetrahydroharmane, tetrahydroharmine, **3**, **4**, and **14** exhibited higher activities than Ribavirin; especially the activities of compounds harmalan (62.3, 55.1, and 60.3% at 500 μg/mL) and tetrahydroharmane (64.2, 57.2, and 59.5% at 500 μg/mL)

Table 3. Fungicidal Activity of Harmine, Harmane, Harmol, Harmalan, Tetrahydroharmane, Tetrahydroharmine, and Compounds 3, 4, 6−16, and 19−21 against 14 Kinds of Fungus

	fungicidal activity (%)/50 mg/kg													
compd	*F.C*[a]	*C.H*	*P.P*	*A.S*	*F.G*	*F.M*	*S.S*	*P.C*	*R.C*	*B.M*	*W.A*	*P.I*	*R.S*	*B.C*
harmine	19.2	69.2	11.9	15.8	26.2	42.9	9.8	12.5	44.7	22.7	35.7	22.7	36.8	21.2
harmane	19.2	92.3	61.9	68.4	23.8	35.7	33.3	15.6	42.1	36.4	46.4	9.1	26.3	12.1
harmol	26.9	46.2	23.8	26.3	23.8	28.6	5.9	25.0	42.1	31.8	46.4	22.7	50.0	9.1
harmalan	23.1	76.9	2.4	26.3	21.4	28.6	19.6	0.0	55.3	27.3	25.0	31.8	19.7	15.2
tetrahydro-harmane	19.2	61.5	26.2	26.3	14.3	14.3	9.8	0.0	42.1	18.2	32.1	18.2	52.6	12.1
tetrahydro-harmine	19.2	76.9	14.3	21.1	11.9	14.3	19.6	9.4	34.2	27.3	25.0	22.7	26.3	27.3
3	19.0	28.6	94.1	50.0	57.1	35.7	56.0	36.4	56.3	21.1	33.3	25.0	39.3	36.4
4	**65.4**	**84.6**	**61.9**	**73.7**	**76.2**	**64.3**	**41.2**	**93.8**	**68.4**	**86.4**	**92.9**	**45.5**	**96.1**	**45.5**
6	23.8	7.1	35.3	33.3	50.0	42.9	56.0	36.4	59.4	31.6	23.8	25.0	10.7	54.5
7	**61.9**	**71.4**	**88.2**	**88.9**	**64.3**	**71.4**	**76.0**	**90.9**	**71.9**	**94.7**	**85.7**	**70.0**	**71.4**	**59.1**
8	34.6	53.8	2.4	21.1	23.8	14.3	9.8	25.0	36.8	22.7	39.3	18.2	6.6	0.0
9	23.1	53.8	26.2	15.8	38.1	21.4	7.8	9.4	36.8	27.3	35.7	9.1	46.1	12.1
10	14.3	35.7	5.9	33.3	35.7	35.7	76.0	18.2	62.5	21.1	33.3	20.0	0.0	36.4
11	**52.4**	**71.4**	**76.5**	**66.7**	**78.6**	**50.0**	**80.0**	**93.9**	**90.6**	**78.9**	**71.4**	**50.0**	**42.9**	**54.5**
12	38.5	61.5	78.6	36.8	35.7	21.4	13.7	50.0	84.2	36.4	50.0	45.5	52.6	51.5
13	19.2	30.8	23.8	21.1	26.2	21.4	7.8	18.8	42.1	22.7	35.7	27.3	26.3	21.2
14	28.6	50.0	29.4	55.6	21.4	42.9	68.0	60.6	59.4	26.3	38.1	30.0	33.9	68.2
15	23.8	35.7	52.9	61.1	71.4	35.7	68.0	51.5	78.1	36.8	47.6	35.0	39.3	13.6
16	19.0	50.0	82.4	33.3	35.7	35.7	72.0	60.6	53.1	21.1	38.1	25.0	42.9	63.6
19	23.1	84.6	47.6	10.5	14.3	28.6	9.8	18.8	63.2	22.7	25.0	22.7	39.5	12.1
20	33.3	21.4	58.8	22.2	78.6	64.3	76.0	66.7	81.3	73.7	66.7	55.0	17.9	68.2
21	4.8	0.0	23.5	22.2	42.9	28.6	76.0	9.1	53.1	15.8	23.8	15.0	0.0	4.5
carbendazim	<50	<50	<50	<50	100	<50	100	<50	100	100	100	100	100	<50
chlorothalonil	100	73.3	100	73.3	<50	100	<50	100	100	91.3	91.3	86.4	100	100

[a]*F.C, Fusarium oxysporium* f. sp.*cucumeris*; *C.H, Cercospora arachidicola* Hori; *P.P, Physalospora piricola*; *A.S, Alternaria solani*; *F.G, Fusarium graminearum*; *F.M, Fusarium moniliforme*; *S.S, Sclerotinia sclerotiorum*; *P.C, Phytophthora capsici*; *R.C, Rhizoctonia cerealis*; *B.M, Bipolaris maydis*; *W.A,* watermelon anthracnose; P.I, *Phytophthora infestans*; *R.S, Rhizoctonia solani*; *B.C, Botrytis cinerea*.

were much higher than that of Ribavirin (37.4, 36.2, and 38.5% at 500 μg/mL); harmine, harmol, **7**, and **20** showed activities comparable to that of Ribavirin. It was interesting that the compound containing an ester on the 3-position (**14**) exhibited obviously higher activities (50.4, 43.9, and 47.9% at 500 μg/mL) than compounds having other substituents on the 3-position. In consideration of the better solubility and stability of compound **14**, it can be used as a new lead structure for further development of anti-TMV reagents.

Fungicidal Activities. These alkaloids and their derivatives also exhibited good fungicidal activities against 14 kinds of plant fungi (Table 3). When the C ring was pyridine, the compounds exhibited higher activities than those with dihydropyridine or tetrahydropyridine as the C ring. When the skeleton was β-carboline (C ring was pyridine), the types and positions of the substituents on the benzene ring (A ring) had a significant influence on the fungicidal activities. For instance, compound **7** (1-methyl-8-nitro-9*H*-pyrido[3,4-*b*]indole) exhibited excellent fungicidal activity against most of the tested fungi, whereas compound **6** (1-methyl-6-nitro-9*H*-pyrido[3,4-*b*]indole) exhibited only moderate activity; compound **11**, containing a pivaloyloxy group, exhibited higher fungicidal activity than the compound containing acetoxy (**10**). Some of these compounds selectively exhibited fungicidal activities to certain fungi. For example, the activities of harmane (against *Cercospora arachidicola* Hori) and compound **3** (against *Physalospora piricola*) were >90%, which was much higher than that against other fungi.

In summary, 6 known β-carboline, dihydro-β-carboline, or tetrahydro-β-carboline alkaloids and a series of their derivatives were designed, synthesized, and first assayed for their anti-TMV activities both in vitro and in vivo and for their fungicidal activity against 14 fungi. All of the compounds exhibited good to excellent anti-TMV activities. Especially, the inactivation, curative, and protection activities of compounds harmalan (62.3, 55.1, and 60.3%, respectively, at 500 μg/mL) and tetrahydroharmane (64.2, 57.2, and 59.5% at 500 μg/mL) in vivo were much higher than those of Ribavirin (37.4, 36.2, and 38.5% at 500 μg/mL). Compound **14** also exhibited obviously higher activities in vivo (50.4, 50.0, and 57.8% at 500 μg/mL) than Ribavirin and other derivatives, and its solubility and stability were better than those of the natural products, so it can be used as a lead structure for the development of anti-TMV drugs. Moreover, some of these compounds, especially compounds **4**, **7**, and **11**, exhibited good fungicidal activity against 14 kinds of fungi. Further studies on structural optimization are in progress in our laboratory.

AUTHOR INFORMATION

Corresponding Author

*(Q.W.) Phone: +86-(0)22-23503952. Fax: +86-(0)22-23503952. E-mail: wang98h@263.netm wangqm@nankai.edu.cn.

Funding

This work was supported by the National Key Project for Basic Research (2010CB126106), the National Natural Science Foundation of China (21132003, 21121002, 21372131), and the Specialized Research Fund for the Doctoral Program of Higher Education (20130031110017).

Notes

The authors declare no competing financial interest.

REFERENCES

(1) Ritzenthaler, C. Resistance to plant viruses: old issue, new answer. *Curr. Opin. Biotechnol.* **2005**, *16* (2), 118−122.

(2) Edwankar, C. R.; Edwankar, R. V.; Namjoshi, O. A.; Rallapappi, S. K.; Yang, J.; Cook, J. M. Recent progress in the total synthesis of indole alkaloids. *Curr. Opin. Drug Discovery Dev.* **2009**, *12* (6), 752−771.

(3) De Meester, C. Genotoxic potential of β-carbolines: a review. *Mutat. Res.* **1995**, *339* (3), 139−153.

(4) Jahaniani, F.; Ebrahimi, S. A.; Rahbar-Roshandel, N.; Mahmoudian, M. Xanthomicrol is the main cytotoxic component of *Dracocephalum kotschyii* and a potential anti-cancer agent. *Phytochemistry* **2005**, *66* (13), 1581−1592.

(5) Callaway, J. C. Various alkaloid profiles in decoctions of *Banisteriopsis caapi*. *J. Psychoactive Drugs* **2005**, *37* (2), 151−155.

(6) Callaway, J. C.; McKenna, D. J.; Grob, C. S.; Brito, G. S.; Raymon, L. P.; Poland, R. E.; Andrade, E. N.; Andrade, E. O.; Mash, D. C. Pharmacokinetics of *Hoasca* alkaloids in healthy humans. *J. Ethnopharmacol.* **1999**, *65* (3), 243−256.

(7) Massaro, E. J. *Handbook of Neurotoxicology*; Humana Press: Totowa, NJ, USA, 2002; p 237.

(8) Chen, Z. Y.; Cao, R. H.; Shi, B. X.; Guo, L.; Sun, J.; Ma, Q.; Fan, W. X.; Song, H. C. Synthesis and biological evaluation of 1,9-disubstituted β-carbolines as potent DNA intercalating and cytotoxic agents. *Eur. J. Med. Chem.* **2011**, *46* (10), 5127−5137.

(9) Barsanti, P. A.; Wang, W. B.; Ni, Z. J.; Duhl, D.; Brammeier, N.; Martin, E.; Bussiere, D.; Walter, A. O. The discovery of tetrahydro-β-carbolines as inhibitors of the kinesin Eg5. *Bioorg. Med. Chem. Lett.* **2010**, *20* (1), 157−160.

(10) Reniers, J.; Robert, S.; Frederick, R.; Masereel, B.; Vincent, S.; Wouters, J. Synthesis and evaluation of β-carboline derivatives as potential monoamine oxidase inhibitors. *Bioorg. Med. Chem.* **2011**, *19* (1), 134−144.

(11) Srivastava, S. K.; Agarwal, A.; Chauhan, P. M. S.; Agarwal, S. K.; Bhaduri, A. P.; Singh, S. N.; Fatima, N.; Chatterjee, R. K. Potent 1,3-disubstituted-9*H*-pyrido[3,4-*b*]indoles as new lead compounds in antifilarial chemotherapy. *J. Med. Chem.* **1999**, *42* (9), 1667−1672.

(12) Gohil, V. M.; Brahmbhatt, K. G.; Loiseau, P. M.; Bhutani, K. K. Synthesis and anti-leishmanial activity of 1-aryl-β-carboline derivatives against *Leishmania donovani*. *Bioorg. Med. Chem. Lett.* **2012**, *22* (12), 3905−3907.

(13) Tang, J. G.; Wang, Y. H.; Wang, R. R.; Dong, Z. J.; Yang, L. M.; Zheng, Y. T.; Liu, J. K. Synthesis of analogues of Flazin, in particular, Flazinamide, as promising anti-HIV agents. *Chem. Biodiver.* **2008**, *5* (3), 447−460.

(14) Formagio, A. S. N.; Santos, P. R.; Zanoli, K.; Ueda-Nakamura, T.; Tonin, D. L. T.; Nakamura, C. V.; Sarragiotto, M. H. Synthesis and antiviral activity of β-carboline derivatives bearing a substituted carbohydrazide at C-3 against poliovirus and herpes simplex virus (HSV-1). *Eur. J. Med. Chem.* **2009**, *44* (11), 4695−4701.

(15) Miller, J. F.; Turner, E. M.; Sherrill, R. G.; Gudmundsson, K.; Sethna, A. S. P.; Brown, K. W.; Harvey, R.; Romines, K. R.; Golden, P. Substituted tetrahydro-β-carbolines as potential agents for the treatment of human papillomavirus infection. *Bioorg. Med. Chem. Lett.* **2010**, *20* (1), 256−259.

(16) Wu, J. S.; Wang, F.; Ma, Y. P.; Cui, X.; Cun, L. F.; Zhu, J.; Deng, J. G.; Yu, B. L. Asymmetric transfer hydrogenation of imines and iminiums catalyzed by a water-soluble catalyst in water. *Chem. Commun.* **2006**, *42* (16), 1766−1768.

(17) Bobowski, G.; Shavel, J., Jr. 1,1-Disubstituted-2,3,4,9-tetrahydro-1*H*-pyrido[3,4-*b*]indolecarboxylic acid esters and ketones. The base catalyzed transformation of 1-(2′,3′,4′,9′-tetrahydrospiro [cyclohexane-1,1′-[1*H*] pyrido[3,4-*b*]indol]-2-yl) alkanones into 2-(4,9-dihydro-3*H*-pyrido[3,4-*b*]indol-1-yl)-1-alkylcyclohexanols. *J. Heterocycl. Chem.* **1985**, *22* (6), 1679−1688.

(18) Borisovich, S. B.; Aleksandrovich, N. K.; Vadimovich. K. V. Method of production of 1- and 1,1-disubstituted-4-phenyl-2,3,4,9-tetrahydro-1*H*-β-carboline. R.U. Patent 2004137708, 2004.

(19) Milen, M.; Hazai, L.; Kolonits, P.; Kalaus, G.; Szabó, L.; Gömöry, Á.; Szántay, C. Studies on stereoselective approaches to β-carboline derivatives. *Cent. Eur. J. Chem.* **2005**, *3* (1), 118−136.

(20) Akabori, S.; Saito, K. Synthetische versuche in der indol-gruppe, VIII: synthese von harman und harmin. *Ber. Dtsch. Chem. Ges. (A B Ser.)* **1930**, *63* (8), 2245−2248.

(21) Kusurkar, R. S.; Goswami, S. K. Efficient one-pot synthesis of anti-HIV and anti-tumour β-carbolines. *Tetrahedron* **2004**, *60* (25), 5315−5318.

(22) Bailey, P. D.; Beard, M. A.; Dang, H. P. T.; Phillips, T. R.; Price, R. A.; Whittaker, J. H. Debenzylation using catalytic hydrogenolysis in trifluoroethanol, and the total synthesis of (−)-raumacline. *Tetrahedron Lett.* **2008**, *49* (13), 2150−2153.

(23) Hochstein, F. A.; Paradies, A. M. Alkaloids of *Banisteria caapi* and *Prestonia amazonicum*. *J. Am. Chem. Soc.* **1957**, *79* (21), 5735−5736.

(24) Hino, T.; Lai, Z. P.; Seki, H.; Hara, R.; Kuramochi, T.; Nakagawa, M. 1-(1-Pyrrolin-2-yl)-β-carboline. Synthesis of Eudistomins H, I and P. *Chem. Pharm. Bull.* **1989**, *37* (10), 2596−2600.

(25) Ikeda, R.; Kimura, T.; Tsutsumi, T.; Tamura, S.; Sakai, N.; Konakahara, T. Structure−activity relationship in the antitumor activity of 6-, 8- or 6,8-substituted 3-benzylamino-β-carboline derivatives. *Bioorg. Med. Chem. Lett.* **2012**, *22* (10), 3506−3515.

(26) Lutomski, J. Isolation der Wichtigsten Alkaloide aus dem Kranz der Passionsblume (*P. incarnata*). *Biul. Instytut. Roslin Leczniczych* **1960**, *6*, 209−219.

(27) Im, G.-Y. J.; Bronner, S. M.; Goetz, A. E.; Paton, R. S.; Cheong, P. H.-Y.; Houk, K. N.; Garg, N. K. Indolyne experimental and computational studies: synthetic applications and origins of selectivities of nucleophilic additions. *J. Am. Chem. Soc.* **2010**, *132* (50), 17933−17944.

(28) Li, C. Y.; Zhang, X. Y.; Zhao, M.; Wang, Y. J.; Wu, J. H.; Liu, J. W.; Zheng, M. Q.; Peng, S. Q. A class of novel *N*-(1-methyl-β-carboline-3-carbonyl)-*N*′-(aminoacid-acyl)-hydrazines: aromatization leaded design, synthesis, in *vitro* anti-platelet aggregation/in *vivo* anti-thrombotic evaluation and 3D QSAR analysis. *Eur. J. Med. Chem.* **2011**, *46* (11), 5598−5608.

(29) Panarese, J. D.; Waters, S. P. Room-temperature aromatization of tetrahydro-β-carbolines by 2-iodoxybenzoic acid: utility in a total synthesis of Eudistomin U. *Org. Lett.* **2010**, *12* (18), 4086−4089.

(30) Wang, K. L.; Su, B.; Wang, Z. W.; Wu, M.; Li, Z.; Hu, Y. N.; Fan, Z. J.; Mi, N.; Wang, Q. M. Synthesis and antiviral activities of phenanthroindolizidine alkaloids and their derivatives. *J. Agric. Food Chem.* **2010**, *58* (5), 2703−2709.

(31) Zhao, H. P.; Liu, Y. X.; Cui, Z. P.; Beattie, D.; Gu, Y. C.; Wang, Q. M. Design, synthesis, and biological activities of arylmethylamine substituted chlorotriazine and methylthiotriazine compounds. *J. Agric. Food Chem.* **2011**, *59* (21), 11711−11717.

(32) Ishida, J.; Wang, H. K.; Bastow, K. F.; Hu, C. Q.; Lee, K. H. Antitumor agents 201. Cytotoxicity of harmine and β-carboline analogs. *Bioorg. Med. Chem. Lett.* **1999**, *9* (23), 3319−3324.

The goals of this study were first to directly compare the isoxazoline toxicological profiles of the [^{3}H]fluralaner binding site with that of [^{3}H]EBOB and [^{3}H]AVE in the *Musca* receptor and second to examine the relationship in *Musca* and honeybee (*Apis mellifera*) between binding site specificity and pest toxicity. The action of fluralaner in mammalian brain was also considered.

MATERIALS AND METHODS

Chemicals and Radioligands. Three radioligands were used: [^{3}H]fluralaner (14 Ci/mmol),[19] [^{3}H]EBOB (26 Ci/mmol),[10] and [^{3}H]AVE (11 Ci/mmol).[17] Fluralaner (**1**) was prepared as described,[19] and isoxazolines **2**–**15** (Figure 2) were provided by DuPont Crop Protection (Newark, DE). Other compounds were obtained from commercial sources.

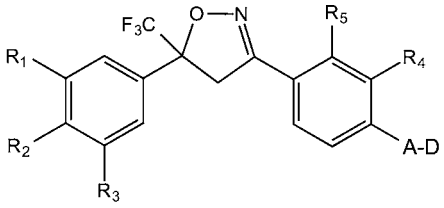

No.	R_1	R_2	R_3	R_4	R_5	A - D
1	Cl	H	Cl	Me	H	A
2	Cl	H	Cl	CN	H	B
3	Br	H	Br	CN	H	B
4	OMe	OMe	H	H	H	B
5	Cl	H	Cl	Cl	H	B
6	Cl	H	Cl	OMe	H	B
7	Cl	H	Cl	Me	H	B
8	Cl	H	Cl	H	H	B
9	Cl	H	Cl	H	H	C
10	Cl	H	Cl	CN	H	D
11	Cl	H	Cl	H	H	E
12	Cl	H	Cl	H	Cl	C
13	Cl	H	Cl	H	H	F
14	Cl	H	Cl	H	CF_3	B
15	H	MeCONH	H	CN	H	B

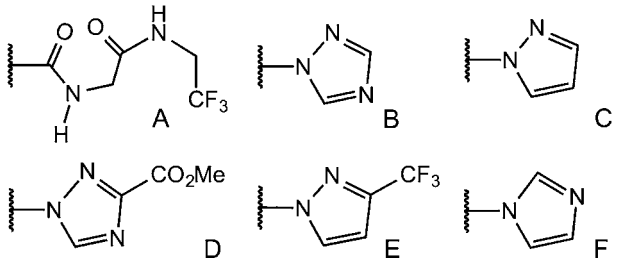

Figure 2. Structures of isoxazolines studied. Insecticidal activities are reported by Lahm et al.[6] for all compounds except **1**, **4**, **10**, **11**, and **12**.

Toxicity to Insects. Adult *Musca* (about 25 mg each) 3–5 days after emergence from the pupae (obtained from Benzon Research Inc., Carlisle, PA) were treated by intrathoracic injection with 0.03 μg of isoxazoline in 0.2 μL of DMSO–water (1:3), and the toxicity was determined at 24 h. Poisoning signs of this 1.2 μg/g isoxazoline dose were rated for each fly in groups of 40 as 0 (no effect), 1 (unable to walk or fly), and 2 (no response to prodding) following the reported method.[20,21] The assay was repeated two more times and averaged on a percentage basis. The values were calculated as follows: number of impaired flies (score 1) plus twice the number of dead flies (score 2); i.e., all impaired was scored 50, and complete mortality was scored 100.

The insecticidal activity of nine isoxazolines studied here was previously reported as ppm LC_{50} with four pest species, i.e., fall armyworm (*Spodoptera frugiperda*), corn earworm (*Helicoverpa zea*), potato leafhopper (*Empoasca fabae*), and western flower thrips (*Frankliniella occidentalis*).[6] Potency values for these pests were expressed as $1/LC_{50}$.

Membrane Receptor Preparation. *Musca* adults were frozen in liquid nitrogen and the heads recovered by shaking and sieving with a yield of about 1.0 g of heads per 1000 flies. The heads (1.0 g) were homogenized in 10 mL of ice-cold buffer A (250 mM sucrose, 10 mM Tris–HCl, pH 7.5) containing Haltphosphatase inhibitor cocktail (Thermo Scientific, Rockford, MA) (1%, v/v). The homogenate was filtered through four layers of nylon mesh (64 μm) and centrifuged at 700*g* for 30 min and the supernatant filtered again through four layers of nylon mesh. The membranes were then recovered by centrifugation at 25000*g* for 30 min. The pellet was resuspended in buffer A, kept on ice for 10 min, and then centrifuged again at 25000*g* for 30 min. The final membrane pellet was resuspended in buffer B [300 mM NaCl and 10 mM phosphate-buffered pH 7.5 saline (PBS)], filtered through four layers of nylon screen to remove particles, and employed for the binding assay after protein determination.[22] The same procedure was used to prepare *Apis* brain membranes from bees obtained at a local apiary.

Binding Assays. The receptor binding assays were based on our original studies with *Musca* for three radioligands, [^{3}H]fluralaner,[19] [^{3}H]EBOB,[10] and [^{3}H]AVE.[17] The binding assays consisted of sequential addition to incubation tubes (13 × 100 mm) of candidate inhibitor in DMSO (0.5 μL) and membrane preparation (200 μg of *Musca* or *Apis* protein) in PBS (1.0 mL). The radioligand [final concentration 0.1 nM [^{3}H]fluralaner, 0.5 nM [^{3}H]EBOB, or 0.5 nM [^{3}H]AVE] was introduced into 10 μL of buffer B with mixing. Incubations were for 70 min at 22 °C followed by addition of ice-cold PBS (5 mL) and filtration with GF/B glass-fiber filters and then two 5 mL rinse washes of cold PBS. Radioactivity on the filters was counted with 10 mL of scintillation fluid Safety-Solve cocktail (Research Products International Corp., Elk Grove, IL) after the filters were allowed to stand in the dark overnight. Nonspecific binding was determined with 5 μM fluralaner for [^{3}H]fluralaner, 5 μM fipronil for [^{3}H]EBOB, and 5 μM AVM for [^{3}H]AVE. Each experiment was repeated 3–5 times, and the results reported are the means with standard errors.

Mammalian GABA-R preparations and assays were as previously reported for rat brain membranes[23] and recombinant β_3 homopentamer.[24,25]

RESULTS

***Musca* and *Apis* [^{3}H]Fluralaner Binding Assays.** Optimization of the [^{3}H]fluralaner binding assay proved to be a challenge because of relatively high levels of nonspecific binding and possibly multiple binding sites.[8,19] The method described is acceptable but still far from ideal using 0.1 nM [^{3}H]fluralaner to give an adequate level of specific binding. Total and specific binding and percent specific binding for *Musca* averaged 2000 ± 100 dpm, 600 ± 100 dpm, and about 30%, respectively. The corresponding values for *Apis* averaged 1650 ± 100 dpm, 800 ± 50 dpm, and about 45%, respectively. [^{3}H]EBOB and [^{3}H]AVE were assayed with the same *Musca* preparation and method as for [^{3}H]fluralaner except with 0.5 nM radioligand. Total, nonspecific, and specific binding for *Musca* with [^{3}H]EBOB were 1200 ± 100 dpm, 600 ± 50 dpm, and about 50%, respectively, and with [^{3}H]AVE they were 2700 ± 100 dpm, 2100 ± 100 dpm, and about 75%, respectively.

Binding Site Profiles. *Musca [^{3}H]Fluralaner, [^{3}H]EBOB, and [^{3}H]AVE Binding Sites. Four Insecticide Chemotypes (Figure 3).* The four representative inhibitors used were isoxazoline (fluralaner), phenylpyrazole (fipronil), organochlorine (α-endosulfan), and macrocyclic lactone (AVE) tested at 0.1, 1, 10, 100, and 5000 nM (final concentration). The *Musca* [^{3}H]fluralaner site is highly sensitive to fluralaner and AVE with IC_{50} values of about 0.4 and 3 nM, respectively, but not to fipronil or α-endosulfan.[19] The [^{3}H]EBOB site is sensitive to fluralaner, fipronil, and α-endosulfan (IC_{50} values of

dx.doi.org/10.1021/jf4050809 | J. Agric. Food Chem. 2014, 62, 1019–1024

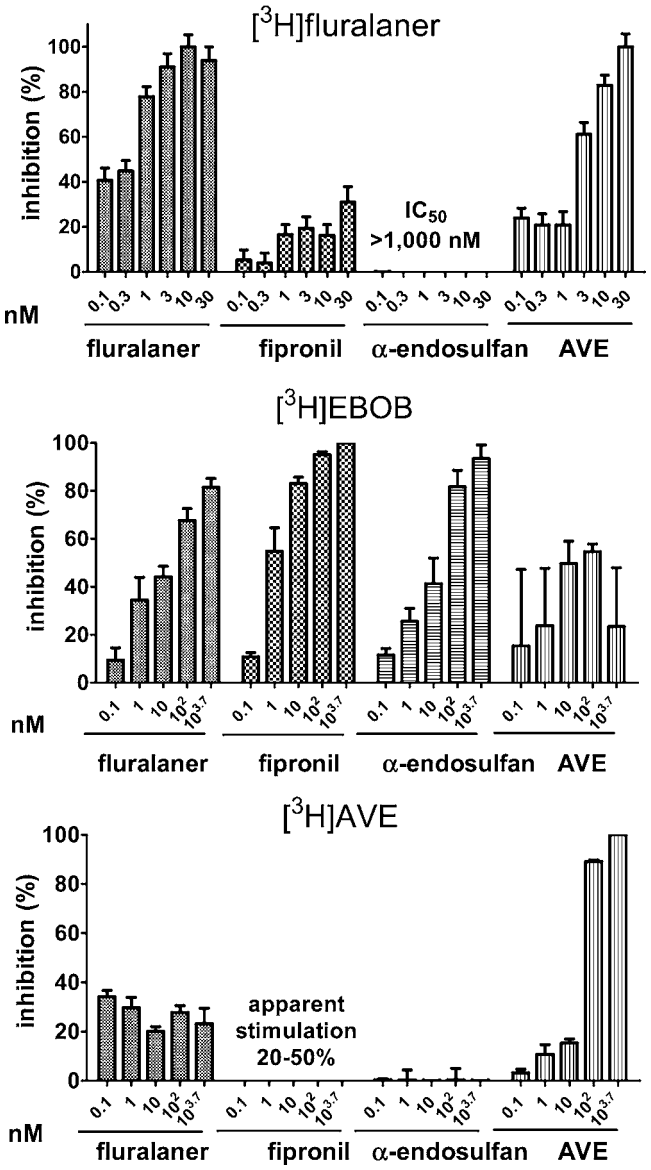

Figure 3. Effect in *Musca* of fluralaner, fipronil, α-endosulfan, and AVE on binding of [^{3}H]fluralaner, [^{3}H]EBOB, and [^{3}H]AVE. A concentration of 5000 nM is shown as $10^{3.7}$.

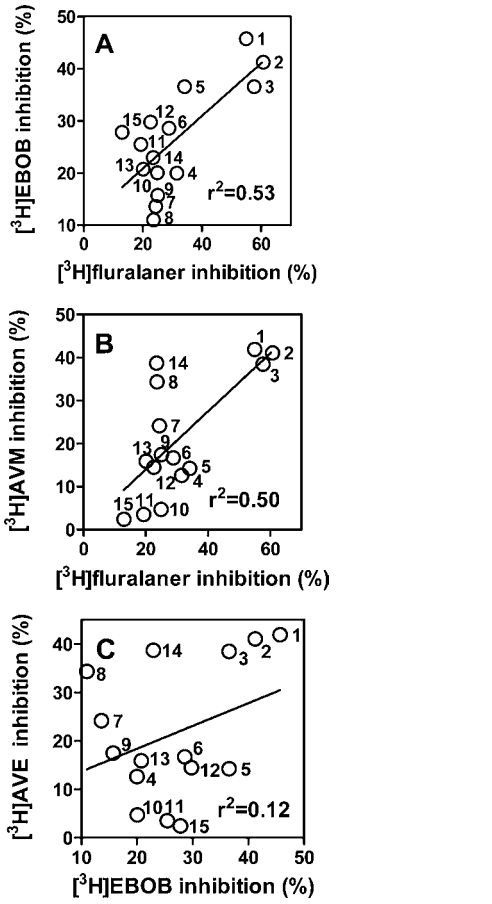

Figure 4. Potency relationships in *Musca* of 15 isoxazolines at 10 nM as inhibitors of [^{3}H]fluralaner versus [^{3}H]EBOB (A), [^{3}H]fluralaner versus [^{3}H]AVE (B), and [^{3}H]EBOB versus [^{3}H]AVE (C) binding.

39−41 nM) but much less so to AVE. The [^{3}H]AVE site is poorly sensitive to fluralaner, apparently stimulated to a small degree (20−50%) by fipronil, insensitive to α-endosulfan, and highly sensitive to AVE ($IC_{50} \approx 20$ nM).

Fifteen Isoxazolines (Figure 4). Fifteen isoxazolines were examined for their inhibitory activity to [^{3}H]fluralaner, [^{3}H]EBOB, and [^{3}H]AVE binding. The most active compounds were isoxazolines **1** (fluralaner), **2**, and **3**. The others were much weaker inhibitors. The binding site profiles for [^{3}H]fluralaner relative to [^{3}H]EBOB give a correlation coefficient of 0.53, about the same as that for [^{3}H]fluralaner versus [^{3}H]AVE (r^2 = 0.50) and much better than that for [^{3}H]EBOB versus [^{3}H]AVE (r^2 = 0.12). There are clearly common features of the target or coupled binding sites but not identity for isoxazolines interacting in the three radioligand assays.

Apis [^{3}H]Fluralaner Binding Site with 15 Isoxazolines (Figure 5A). The specificity of 15 isoxazolines for inhibition of [^{3}H]fluralaner binding was similar (r^2 = 0.55) for *Apis* and *Musca*.

Toxicity to Musca and Four Pest Species Relative to Musca and Apis [^{3}H]Fluralaner Binding Affinity. Musca (Figure 6). The set of 15 isoxazolines was assayed for toxicity to *Musca* adults by intrathoracic injection of a standard 1.2 μg/g dose. Only three of the isoxazolines (**1**−**3**) showed high toxicity, and they were the same ones most effective as inhibitors of [^{3}H]fluralaner binding and among the better inhibitors of [^{3}H]EBOB and [^{3}H]AVE binding.

Pest Species. The findings on toxicity to *Musca* and four pest species were compared with each other (Figure 7) and with the structure−activity relationships for inhibition in *Apis* of [^{3}H]fluralaner binding (Figure 5B−E). Isoxazoline poisoning of *Musca* was at best a moderate predictor of toxicity to *Spodoptera* and *Helicoverpa* and even poorer with *Frankliniella* and *Empoasca*. Compounds **2**, **3**, **7**, and **8** were highly active on all species, whereas **5** and **14** were intermediate in toxicity and **6**, **9**, and **13** had the lowest activity. The correlation of receptor binding with toxicity was always better for *Apis* (Figure 5 B−E) (r^2 = 0.75−0.84) than for *Musca* (r^2 = 0.30−0.68) (Supporting Information). The best correlation was for *Apis* [^{3}H]fluralaner binding inhibition with *Empoasca* toxicity (r^2 = 0.84).

Mammalian $GABA_A$-R (Figure 8). Fluralaner, fipronil, and heptachlor epoxide were compared for potency in the [^{3}H]EBOB binding assay with rat brain membranes and recombinant human β_3 homopentamer. Fluralaner gave 37% inhibition at 10^4 nM with rat brain membrane, consistent with

dx.doi.org/10.1021/jf4050809 | J. Agric. Food Chem. 2014, 62, 1019−1024

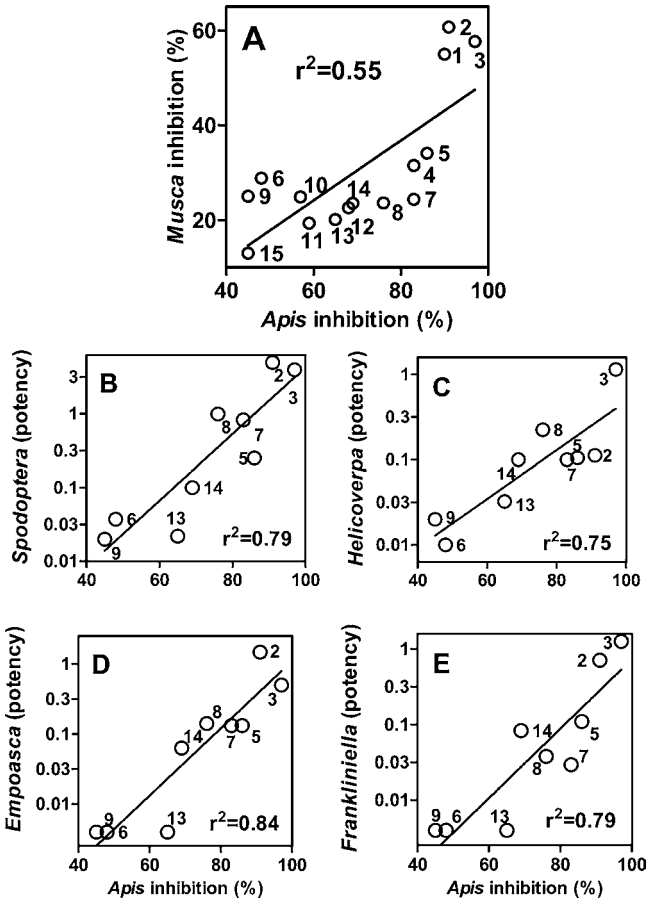

Figure 5. Potency relationships in *Apis* and *Musca* of 15 isoxazolines at 10 nM as inhibitors of [^{3}H]fluralaner binding (A) and for 9 isoxazolines relative to toxicity in four pest insects (B–E). The corresponding r^2 values for *Musca* were 0.56 for *Spodoptera*, 0.30 for *Helicoverpa*, 0.52 for *Empoasca*, and 0.68 for *Frankliniella* (see the Supporting Information).

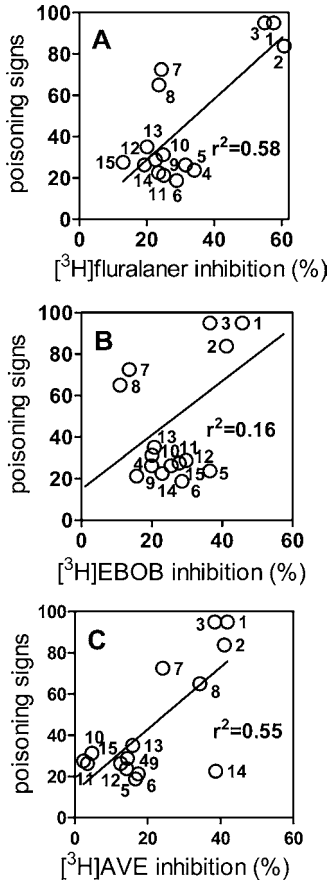

Figure 6. Potency in *Musca* of 15 isoxazolines at 10 nM as inhibitors of [^{3}H]fluralaner (A), [^{3}H]EBOB (B), and [^{3}H]AVE (C) binding relative to their toxicity.

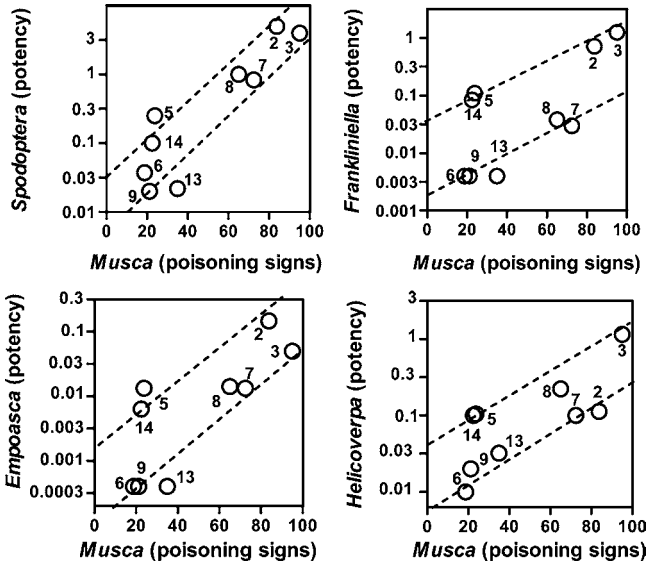

Figure 7. Toxicity of nine isoxazolines to *Musca* relative to four pest species.

an earlier report, [8] but it had almost no effect on the recombinant β_3 homopentamer. Heptachlor epoxide and fipronil showed high affinity for rat brain membranes with IC_{50} values of 200 and 800 nM, respectively, and even higher affinity for the recombinant human β_3 subunit with IC_{50} values of 5.4 and 3.4 nM, respectively.

DISCUSSION

The GABA receptor is the target for the isoxazoline insecticides based on several types of evidence. The most complete studies were for fluralaner acting on insect ligand-gated ion channels using MdGBCl and MdGluCl cDNAs, which encode the subunits of *Musca* GABA- and glutamate-gated chloride channels, respectively.[8] Two-electrode voltage clamp electrophysiology was used to confirm that fluralaner blocks GABA- and glutamate-induced chloride currents in *Xenopus* oocytes expressing MdGBCl or MdGluCl channels, with IC_{50} values of 5.3 and 80 nM, respectively. Blockade by fluralaner was observed in A2′S-MdGBCl and S2′A-MdGluCl mutant channels at levels similar to those of the respective wild types, and *Musca* expressing A2′S-MdGBCl channels were as susceptible to fluralaner as standard house flies. These findings indicated that fluralaner is a novel and specific blocker of insect ligand-gated chloride channels.[8]

The present study confirms the potency of fluralaner as a high-affinity inhibitor of the *Musca* [^{3}H]EBOB site[8] and shows directly the subnanomolar affinity of [^{3}H]fluralaner for *Musca*[19] and *Apis* GABA-R. The ecological impact of the isoxazoline-sensitive GABA-R site not only in target pests but also in *Apis* remains to be determined. The *Apis* GABA-R assay is better

dx.doi.org/10.1021/jf4050809 | J. Agric. Food Chem. 2014, 62, 1019–1024

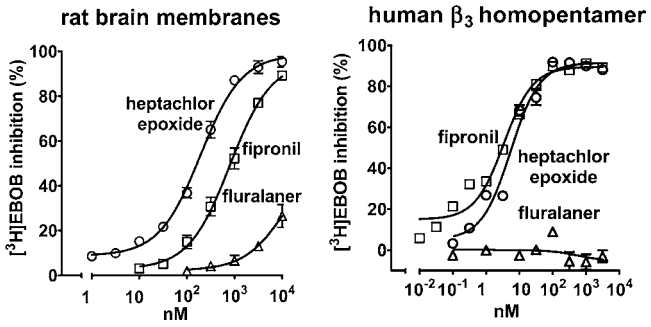

Figure 8. Potency in rat brain membranes and the recombinant human GABA-R β_3 homopentamer of fluralaner, fipronil, and heptachlor epoxide as inhibitors of [^{3}H]EBOB binding.

than the *Musca* GABA-R assay as a predictor of insecticidal activity, a finding rationalized as a higher ratio of the most relevant isoxazoline high-affinity binding site in the *Apis* assay. A marked difference is observed in the inhibitor specificity of the *Musca* [^{3}H]fluralaner and [^{3}H]EBOB sites, establishing that they are distinct but coupled. The AVE agonist site is coupled to both the fluralaner and EBOB sites but each in a unique way. The three distinct and coupled sites are all targets for insecticide action, but the isoxazoline site provides two unique features. It is much more important in insects than mammals, providing a high level of selective toxicity. The sites have no features in common that confer cross-resistance. This is an exciting observation stimulating interest in isoxazolines as possibly the next generation of GABAergic insecticides.

■ ASSOCIATED CONTENT

Supporting Information

Figure S1 showing the relation for nine isoxazolines between [^{3}H]fluralaner binding data in *Musca* and toxicity to four pest species. This material is available free of charge via the Internet at http://pubs.acs.org.

■ AUTHOR INFORMATION

Corresponding Author

*Phone: 510-642-5424. Fax: 510-642-6497. E-mail: ectl@berkeley.edu.

Present Address

†C.Z.: College of Science, China Agricultural University, Beijing, China 100193.

Funding

C.Z. was supported in part by State Scholarship Fund No. 2011635139 provided by the China Scholarship Council.

Notes

The authors declare no competing financial interest.

■ ACKNOWLEDGMENTS

We are greatly indebted to George P. Lahm, James D. Barry, and Thomas F. Pahutski of DuPont Crop Protection Stine Haskell Research Center (Newark, DE) for providing a set of 14 isoxazolines critical for the validating experiments on in vitro structure–activity relationships relative to insecticidal activity. C.Z. thanks Professor Lihong Qiu of the China Agricultural University for academic counsel and Berkeley laboratory colleagues Amanda Ly, Breanna Ford-Morris, Madhur Garg, and Stephen Lantz for assistance and advice. We thank Vincent Salgado and Brecht London of BASF Corp. (Research Triangle Park, NC) for helpful suggestions on preparing *Musca* membranes for [^{3}H]EBOB binding assays.

■ ABBREVIATIONS USED

AVE, avermectin B_{1a}; [^{3}H]EBOB, the radioligand 4′-ethynyl-4-*n*-propylbicycloorthobenzoate; fluralaner or A1443, 4-[5-(3,5-dichlorophenyl)-4,5-dihydro-5-(trifluoromethyl)-3-isoxazolyl]-2-methyl-*N*-[2-oxo-2-(phenylamino)ethyl]benzamide; GABA-R, γ-aminobutyric acid receptor; PBS, phosphate-buffered saline; [^{3}H]TBOB, the radioligand *tert*-butylbicycloorthobenzoate; [^{35}S]TBPS, the radioligand *tert*-butylbicyclophosphorothionate

■ REFERENCES

(1) Casida, J. E. Insecticide action at the GABA-gated chloride channel: Recognition, progress, and prospects. *Arch. Insect Biochem. Physiol.* **1993**, *22*, 13–23.

(2) Buckingham, S. D.; Sattelle, D. B. GABA receptor in insects. In *Comprehensive Molecular Insect Science*; Gilbert, L. K., Gill, S. S., Eds.; Elsevier: Amsterdam, 2005; Vol. 5, pp 107–142.

(3) Ozoe, Y.; Takeda, M.; Matsuda, K. γ-Aminobutyric acid receptors: A rationale for developing selective insect pest control chemicals. In *Biorational Control of Arthropod Pests*; Ishaaya, S., Horowitz, A. R., Eds.; Springer: New York, 2009; pp 131–162.

(4) Ozoe, Y. γ-Aminobutyrate- and glutamate-gated chloride channels as targets of insecticides. *Adv. Insect Physiol.* **2013**, *44*, 211–286.

(5) Lahm, G. P.; Shoop, W. L; Xu, M. Isoxazolines for controlling invertebrate pests. U.S. Patent 8231888, 2012.

(6) Lahm, G. P.; Cordova, D.; Barry, J. D.; Pahutski, T. F.; Smith, B. K.; Long, J. K.; Benner, E. A.; Holyoke, C. W.; Joraski, K.; Xu, M.; Schroeder, M. E.; Wagerle, T.; Mahaffey, M. J.; Smith, R. M.; Tong, M.-H. 4-Azolylphenyl isoxazoline insecticides acting at the GABA gated chloride channel. *Bioorg. Med. Chem. Lett.* **2013**, *23*, 3001–3006.

(7) Mita, T.; Kikuchi, T.; Mizukoshi, T.; Yaosaka, M.; Komoda, M. Isoxazoline-substituted benzamide compound and noxious organism control agent. WO 2005-085126; JP 2007-308471.

(8) Ozoe, Y.; Asahi, M.; Ozoe, F.; Nakahira, K.; Mita, T. The antiparasitic isoxazoline A1443 is a potent blocker of insect ligand-gated chloride channels. *Biochem. Biophys. Res. Commun.* **2010**, *391*, 744–749.

(9) Gassel, M.; Wolf, C.; Noack, S.; Williams, H.; Ilg, T. The novel isoxazoline ectoparasiticide fluralaner: Selective inhibition of arthropod γ-aminobutyric acid- and L-glutamate-gated chloride channels and insecticidal/acaricidal activity. *Insect Biochem. Mol. Biol.* **2014**, in press.

(10) Deng, Y.; Palmer, C. J.; Casida, J. E. House fly brain γ-aminobutyric acid-gated chloride channel: Target for multiple classes of insecticides. *Pestic. Biochem. Physiol.* **1991**, *41*, 60–65.

(11) Matsumura, F.; Ghiasuddin, S. M. Evidence for similarities between cyclodiene type insecticides and picrotoxinin in their action mechanisms. *J. Environ. Sci. Health* **1983**, *B18*, 1–14.

(12) Cohen, E.; Casida, J. E. Effects of insecticides and GABAergic agents on a house fly [^{35}S]*t*-butylbicyclophosphorothionate binding site. *Pestic. Biochem. Physiol.* **1986**, *25*, 63–72.

(13) Lawrence, L. J.; Palmer, C. J.; Gee, K. W.; Wang, X.; Yamamura, H. I.; Casida, J. E. *t*-[^{3}H]Butylbicycloorthobenzoate: New radioligand probe for the γ-aminobutyric acid-regulated chloride ionophore. *J. Neurochem.* **1985**, *45*, 798–804.

(14) Cole, L. M.; Nicholson, R. A.; Casida, J. E. Action of phenylpyrazole insecticides at the GABA-gated chloride channel. *Pestic. Biochem. Physiol.* **1993**, *46*, 47–54.

(15) Cole, L. M.; Saleh, M. A.; Casida, J. E. House fly head GABA-gated chloride channel: [^{3}H]α-Endosulfan binding in relation to polychlorocycloalkane insecticide action. *Pestic. Sci.* **1994**, *42*, 59–63.

(16) Rauh, J. J.; Benner, E.; Schnee, M. E.; Cordova, D.; Holyoke, C. W.; Howard, M. H.; Bai, D.; Buckingham, S. D.; Hutton, M. L.; Hamon, A.; Roush, R. T.; Sattelle, D. B. Effects of [^{3}H]-BIDN, a novel

bicyclic dinitrile radioligand for GABA-gated chloride channels of insects and vertebrates. *Br. J. Pharmacol.* **1997**, *121*, 1496−1505.
(17) Deng, Y.; Casida, J. E. House fly head GABA-gated chloride channel: Toxicologically relevant binding site for avermectins coupled to site for ethynylbicycloorthobenzoate. *Pestic. Biochem. Physiol.* **1992**, *43*, 116−122.
(18) Orr, N.; Shaffner, A. J.; Richey, K.; Crouse, G. D. Novel mode of action of spinosad: Receptor binding studies demonstrating lack of interaction with known insecticidal target sites. *Pestic. Biochem. Physiol.* **2009**, *95*, 1−5.
(19) García-Reynaga, P.; Zhao, C.; Sarpong, R.; Casida, J. E. New GABA/glutamate receptor target for [^{3}H]isoxazoline insecticide. *Chem. Res. Toxicol.* **2013**, *26*, 514−516.
(20) Shao, X.; Swenson, T. L.; Casida, J. E. Cycloxaprid insecticide: Nicotinic acetylcholine receptor binding site and metabolism. *J. Agric. Food Chem.* **2013**, *61*, 7883−7888.
(21) Shao, X.; Xia, S.; Durkin, K. A.; Casida, J. E. Insect nicotinic receptor interactions *in vivo* with neonicotinoid, organophosphorus, and methylcarbamate insecticides and a synergist. *Proc. Natl. Acad. Sci. U.S.A.* **2013**, *110*, 17273−17277.
(22) Bradford, M. M. Rapid and sensitive method for quantitation of microgram quantities of protein utilizing principle of protein-dye binding. *Anal. Biochem.* **1976**, *72*, 248−254.
(23) Cole, L. M.; Casida, J. E. GABA-gated chloride channel: Binding site for 4′-ethynyl-4-*n*-[2,3-$^3H_2$]propylbicycloorthobenzoate ([^{3}H]EBOB) in vertebrate brain and insect head. *Pestic. Biochem. Physiol.* **1992**, *44*, 1−8.
(24) Ratra, G. S.; Kamita, S. G.; Casida, J. E. Role of human $GABA_A$ receptor β_3 subunit in insecticide toxicity. *Toxicol. Appl. Pharmacol.* **2001**, *172*, 233−240.
(25) Chen, L.; Durkin, K. A.; Casida, J. E. Structural model for γ-aminobutyric acid receptor noncompetitive antagonist binding: Widely diverse structures fit the same site. *Proc. Natl. Acad. Sci. U.S.A.* **2006**, *103*, 5185−5190.

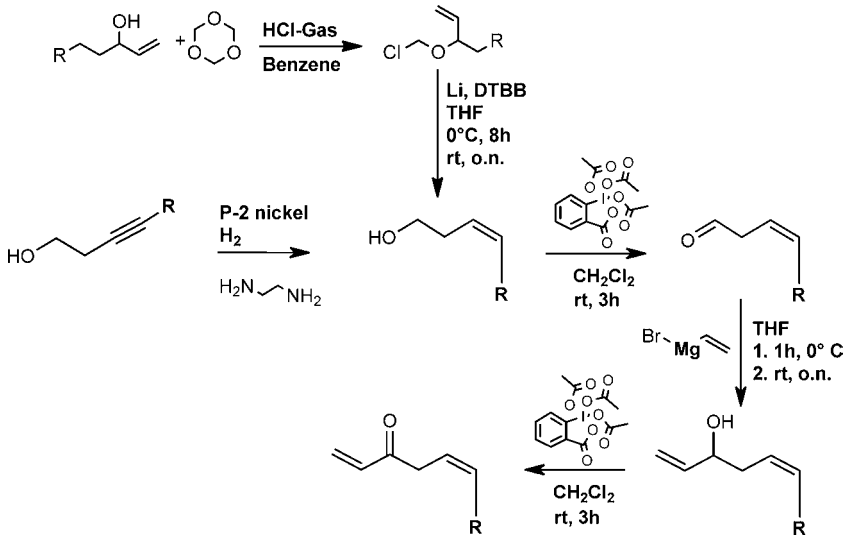

Figure 1. Synthetic routes leading to the (*Z*)-alka-1,5-dien-3-oxo compounds.

determination. A way to avoid such bias is to apply determination by gas chromatography−olfactometry, thereby involving an additional separation step so that odor threshold determination can be focused solely on the substance of interest. This methodology has been used for odor threshold determination in a series of studies in conjunction with[20,21] or without[22] an internal odorous standard, for example, (*E*)-dec-2-enal,[20,21] to correct for potential interindividual variations in sensitivity or odorant delivery. The latter has been used in a series of determinations until today and, accordingly, serves as a reference technique that allows for comparison of odor properties between substances and also between determinations in different laboratories.[23−25]

Accordingly, the following study has been based on this approach for elaborating the respective odor properties of the compounds investigated within this study.

MATERIALS AND METHODS

Chemicals. The following chemicals were purchased from the suppliers given in parentheses: octanal, nonanal, decanal, undecanal, undec-1-en-3-ol, dodec-1-en-3-ol, but-1-en-3-one, hex-1-en-3-ol, hept-1-en-3-ol, oct-1-en-3-ol, pent-1-en-3-one, hexa-1,5-dien-3-ol, (*Z*)-hex-3-en-1-ol, (*E*)-hex-3-en-1-ol, (*Z*)-non-3-en-1-ol, (*E*)-pent-3-enoic acid, (*E*)-hept-3-enoic acid, (*E*)-oct-3-enoic acid, (*E*)-non-3-enoic acid, (*E*)-dec-3-enoic acid, pent-3-in-1-ol, dec-3-in-1-ol, Dess−Martin periodinane, malonic acid, s-trioxane, vinylic magnesiumbromide (Aldrich, Steinheim, Germany); pent-1-en-3-ol, non-1-en-3-ol, oct-1-en-3-one, (*Z*)-oct-3-en-1-ol, hept-3-yn-1-ol (Lancaster, Mühlheim, Germany).

Syntheses. The identity of all intermediates and synthetic products was determined by MS/EI, as well as their retention indices on at least two capillary columns of different polarities (FFAP, SE-54 (DB5), and OV-1701) (data available in Supporting Information Tables S1−S6). Linear retention indices (RI) of the compounds were calculated as previously described.[26] Purity and concentration of all synthetic products were determined according to the method described by Milo,[27] using methyl octanoate or any other ester of high GC purity and a compound with the same effective carbon number as the substance to be determined.[28−30]

Hex-1-en-3-one and (*Z*)-octa-1,5-dien-3-one were synthesized according to the literature: Blank et al.,[23] Ullrich and Grosch.[9]

Hexa-1,5-dien-3-one, Hept-1-en-3-one, Non-1-en-3-one. Hexa-1,5-dien-3-one (Figure 1), hept-1-en-3-one, and non-1-en-3-one (Figure 2) were synthesized by a Dess−Martin oxidation of the corresponding alcohols using Dess−Martin periodinane.[31,32]

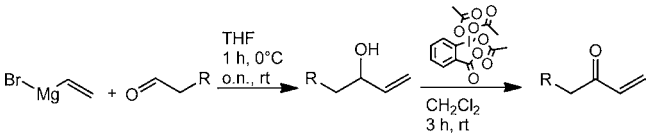

Figure 2. Synthetic route leading to the alk-1-en-3-oxo compounds.

(*Z*)-Hepta-1,5-dien-3-ol, (*Z*)-Nona-1,5-dien-3-ol, (*Z*)-Dodeca-1,5-dien-3-ol, (*Z*)-Hepta-1,5-dien-3-one, (*Z*)-Nona-1,5-dien-3-one, (*Z*)-Dodeca-1,5-dien-3-one. The target compounds were synthesized by stereospecific reduction of pent-3-yn-1-ol, hept-3-yn-1-ol, or dec-3-yn-1-ol, respectively, as described previously for the synthesis of (*Z*)-hex-3-en-1-ol,[33,34] followed by oxidation of the resulting (*Z*)-alk-3-en-1-ols to the corresponding (*Z*)-alk-3-enals using Dess−Martin periodinane.[31,32] A subsequent Grignard-type reaction of the aldehydes with vinylmagnesium bromide gave the (*Z*)-alka-1,5-dien-3-ols; their oxidation using Dess−Martin periodinane revealed the corresponding dienone (Figure 1).

(*Z*)-Deca-1,5-dien-3-ol, (*Z*)-Undeca-1,5-dien-3-ol, (*Z*)-Deca-1,5-dien-3-one, (*Z*)-Undeca-1,5-dien-3-one. (*Z*)-Deca-1,5-dien-3-one and (*Z*)-undeca-1,5-dien-3-one were synthesized by oxidation of (*Z*)-oct-3-en-1-ol or (*Z*)-non-3-en-1-ol using Dess−Martin periodinane[31,32] followed by a Grignard-type reaction of the obtained aldehydes with vinylmagnesium bromide to yield (*Z*)-deca-1,5-dien-3-ol or (*Z*)-undeca-1,5-dien-3-ol. Subsequent oxidation with Dess−Martin periodinane gave the corresponding ketones (Figure 1).

(*Z*)-Trideca-1,5-dien-3-ol, (*Z*)-Tetradeca-1,5-dien-3-ol, (*Z*)-Trideca-1,5-dien-3-one, (*Z*)-Tetradeca-1,5-dien-3-one. (*Z*)-Trideca-1,5-dien-3-ol and (*Z*)-tetradeca-1,5-dien-3-ol were synthesized by reaction of s-trioxane with undec-1-en-3-ol or dodec-1-en-3-ol[35] followed by a Wittig rearrangement[36] to form the (*Z*)-undec-3-en-1-ol or (*Z*)-dodec-3-en-1-ol. The latter compounds were oxidized using Dess−Martin periodinane[31,32] followed by a Grignard-type reaction of the obtained aldehydes with vinylmagnesium bromide to yield (*Z*)-trideca-1,5-dien-3-ol or (*Z*)-tetradeca-1,5-dien-3-ol. Dess−Martin periodinane gave the corresponding ketones (Figure 1).

Dec-1-en-3-ol, Undec-1-en-3-ol, Dodec-1-en-3-ol, Tridec-1-en-3-ol, Tetradec-1-en-3-ol, Dec-1-en-3-one, Undec-1-en-3-one, Dodec-1-en-3-one, Tridec-1-en-3-one, Tetradec-1-en-3-one. A Grignard-type reaction of octanal, nonanal, decanal, undecanal, or dodecanal, respectively, with vinylmagnesium bromide gave the alk-1-en-3-ols, and subsequent oxidation using Dess−Martin periodinane yielded the corresponding alk-1-en-3-ones (Figure 2).

(*E*)-Hepta-1,5-dien-3-ol, (*E*)-Octa-1,5-dien-3-ol, (*E*)-Nona-1,5-dien-3-ol, (*E*)-Deca-1,5-dien-3-ol, (*E*)-Undeca-1,5-dien-3-ol, (*E*)-Dodeca-1,5-dien-3-ol, (*E*)-Hepta-1,5-dien-3-one, (*E*)-Octa-1,5-dien-3-one, (*E*)-Nona-1,5-dien-3-one, (*E*)-Deca-1,5-dien-3-one,

dx.doi.org/10.1021/jf404885j | J. Agric. Food Chem. 2014, 62, 1025−1031

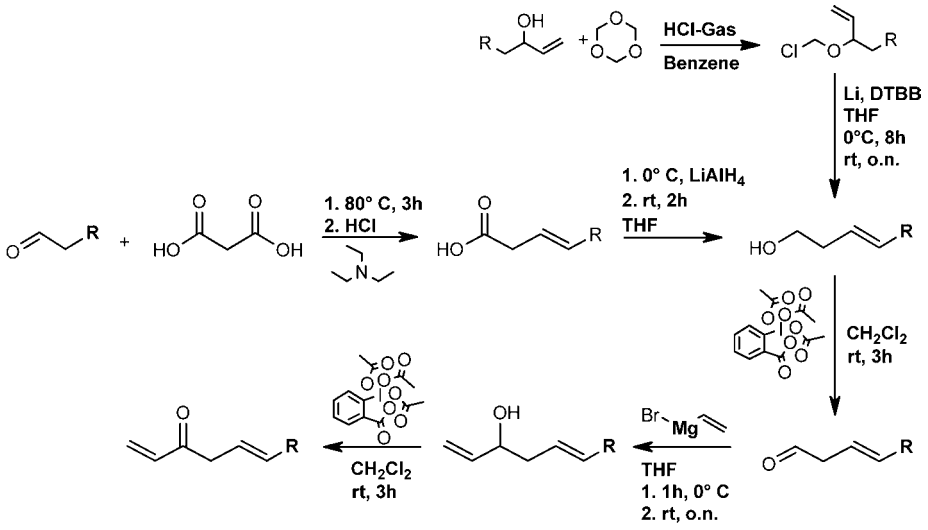

Figure 3. Synthetic routes leading to the (*E*)-alka-1,5-dien-3-oxo compounds.

Table 1. Odor Qualities and Odor Thresholds of Homologous (*Z*)-Alka-1,5-dien-3-ones

		threshold in air[a] (ng/L)		
odorant	odor quality[b]	by GC-O	data from lit.[c]	previously identified in food[c]
hexa-1,5-dien-3-one	geranium-, vegetable-like, metallic	0.01	nr	nr
(*Z*)-hepta-1,5-dien-3-one	geranium-like, metallic	0.0006	nr	nr
(*Z*)-octa-1,5-dien-3-one	geranium-like, metallic	0.003	0.003−0.006[3]	mushrooms,[3] soybean oil,[24] olive oil[40]
(*Z*)-nona-1,5-dien-3-one	herb-, mushroom-like	0.06	nr	nr
(*Z*)-deca-1,5-dien-3-one	herb-, mushroom-like	0.12	nr	nr
(*Z*)-undeca-1,5-dien-3-one	herb-, mushroom-like	0.18	nr	nr
(*Z*)-dodeca-1,5-dien-3-one	herb-, mushroom-like	1.1	nr	nr
(*Z*)-trideca-1,5-dien-3-one	herb-like, fresh	126	nr	nr
(*Z*)-tetradeca-1,5-dien-3-one	fresh, green, sweet	353	nr	nr

[a]Odor thresholds in air were determined as described by Ullrich and Grosch.[20] [b]Odor quality as perceived at the sniffing port. [c]nr, compound or odor threshold was not reported previously.

(*E*)-Undeca-1,5-dien-3-one, (*E*)-Dodeca-1,5-dien-3-one. (*E*)-Pent-3-enoic, (*E*)-hept-3-enoic, (*E*)-oct-3-enoic, (*E*)-non-3-enoic, and (*E*)-dec-3-enoic acid were reduced to the corresponding (*E*)-alk-3-en-1-ols[37] (Figure 3). Those and (*E*)-hex-3-en-1-ol were oxidized using Dess−Martin periodinane[31,32] followed by a Grignard-type reaction of the obtained aldehydes with vinylmagnesium bromide to yield (*E*)-hepta-1,5-dien-3-ol, (*E*)-octa-1,5-dien-3-ol, (*E*)-nona-1,5-dien-3-ol, (*E*)-deca-1,5-dien-3-ol, (*E*)-undeca-1,5-dien-3-ol, and (*E*)-dodeca-1,5-dien-3-ol. Dess−Martin periodinane gave the corresponding ketones.

(*E*)-Trideca-1,5-dien-3-ol, (*E*)-Tetradeca-1,5-dien-3-ol, (*E*)-Trideca-1,5-dien-3-one, (*E*)-Tetradeca-1,5-dien-3-one. (*E*)-Trideca-1,5-dien-3-ol, (*E*)-tetradeca-1,5-dien-3-ol, (*E*)-trideca-1,5-dien-3-one, and (*E*)-tetradeca-1,5-dien-3-one were synthesized following two different routes (Figure 3): The first route is identical with synthesis of the corresponding (*Z*)-compounds. (*E*)-Trideca-1,5-dien-3-ol and (*E*)-tetradeca-1,5-dien-3-ol were synthesized by reaction of s-trioxane with undec-1-en-3-ol or dodec-1-en-3-ol[35] followed by a Wittig rearrangement[36] to form the (*E*)-undec-3-en-1-ol or (*E*)-dodec-3-en-1-ol. The obtained compounds were oxidized using Dess−Martin periodinane[31,32] followed by a Grignard-type reaction of the obtained aldehydes with vinylmagnesium bromide to yield (*E*)-trideca-1,5-dien-3-ol or (*E*)-tetradeca-1,5-dien-3-ol. Dess−Martin periodinane gave the corresponding ketones. The second route starts with a Knoevenagel condensation of malonic acid with nonanal or decanal to form (*E*)-undec-3-enoic acid or (*E*)-dodec-3-enoic acid.[38] After reduction of the (*E*)-alk-3-enoic acid to the corresponding (*E*)-alk-3-en-1-ol, route 2 follows the same path as route 1.

High-Resolution Gas Chromatography−Olfactometry (HRGC-O) and HRGC−Mass Spectrometry (HRGC-MS). HRGC analyses were performed with a type 8000 gas chromatograph (Fisons Instruments, Mainz, Germany) and a Trace GC Ultra (Thermo Fisher Scientific GmbH, Dreieich, Germany) by using the following capillaries: FFAP (30 m × 0.32 mm fused silica capillary, free fatty acid phase FFAP, 0.25 μm; Chrompack, Mühlheim, Germany), SE-54 (DB5) (30 m × 0.32 mm fused silica capillary DB-5, 0.25 μm; J&W Scientific, Fisons Instruments), and OV-1701 (30 m × 0.32 mm fused silica capillary, DB-1701, 0.25 μm; Chrompack). The (*Z*)-alka-1,5-dien-3-oxo and alk-1-en-3-oxo samples were applied by the on-column injection technique at 35 °C (Supporting Information Tables S1, S3, S4, and S6). After 2 min, the temperature of the oven was raised at 40 °C/min to 50 °C (SE-54, OV-1701) or 60 °C (FFAP), respectively, held for 2 min isothermally, then raised at 6 °C/min to 180 °C, and finally raised at 10 °C/min to 230 °C and held for 10 min. The flow rate of the carrier gas helium was 2.5 mL/min. The (*E*)-alka-1,5-dien-3-oxo compounds were applied by the column injection technique at 40 °C (Supporting Information Tables S2 and S5). After 2 min, the temperature of the oven was raised at 10 °C/min to 240 °C, then raised at 40 °C/min to 280 °C (SE-54 (DB5)) or at 10 °C/min to 240 °C (FFAP), respectively, and held for 5 min. The flow rate of the carrier gas helium was 2.5 mL/min (DB5) or 1.3 mL/min (FFAP). At the end of the capillary, the effluent was split in a ratio 1:1 (by vol) into an FID and a sniffing port using two deactivated but uncoated fused silica capillaries (50 cm × 0.32 mm). The FID and the sniffing port were held at 220 and 240 °C, respectively. S analyses were performed with an MS-95 S (Finnigan, Bremen, Germany) in tandem, an Agilent MSD 5975C (Agilent Technologies, Waldbronn,

Table 2. Odor Qualities and Odor Thresholds of Homologous (*E*)-Alka-1,5-dien-3-ones

odorant	odor quality[b]	threshold in air[a] (ng/L) by GC-O	threshold in air[a] (ng/L) data from lit.[c]	previously identified in food[c]
hexa-1,5-dien-3-one	geranium-, vegetable-like, metallic	0.01	nr	nr
(*E*)-hepta-1,5-dien-3-one	geranium-like, metallic	0.9	nr	nr
(*E*)-octa-1,5-dien-3-one	geranium-like	1.4	nr	nr
(*E*)-nona-1,5-dien-3-one	geranium-like, flowery	2.8	nr	nr
(*E*)-deca-1,5-dien-3-one	geranium-like	18	nr	nr
(*E*)-undeca-1,5-dien-3-one	geranium-like, flowery	7.9	nr	nr
(*E*)-dodeca-1,5-dien-3-one	citrus-like	36	nr	nr
(*E*)-trideca-1,5-dien-3-one	citrus-like, green	92	nr	nr
(*E*)-tetradeca-1,5-dien-3-one	citrus-, plastic-like	192	nr	nr

[a]Odor thresholds in air were determined as described by Ullrich and Grosch.[20] [b]Odor quality as perceived at the sniffing port. [c]nr, compound or odor threshold was not reported previously.

Table 3. Odor Qualities and Odor Thresholds of Homologous Alk-1-en-3-ones

odorant	odor quality[b]	threshold in air[a] (ng/L) by GC-O	threshold in air[a] (ng/L) data from lit.[c]	previously identified in food[c]
pent-1-en-3-one	pungent, fish-like	0.17	20[22]	banana,[10,41] black tea,[42] tomato,[43] olive oil[40]
hex-1-en-3-one	metallic	0.02	0.02−0.04,[23] 0.7[22]	artichoke,[11] honey,[23] dill,[44] butter oil[45]
hept-1-en-3-one	vegetable-like, metallic	0.08	0.7[22]	grapefruit juice[12]
oct-1-en-3-one	mushroom-like, metallic	0.04	0.03−1.12,[24,25] 0.1[22]	artichoke,[11] mushrooms,[41] soybean oil,[44] olive oil[40]
non-1-en-3-one	mushroom-like	0.008	0.008,[40] 0.02[22]	raspberry,[42] yogurt,[46] sheep meat[40]
dec-1-en-2-one	mushroom-, geranium-, herb-like	0.08	1[22]	nr
undec-1-en-3-one	herb-, citrus-like, soapy	0.15	1[22]	nr
dodec-1-en-3-one	herb-, citrus-like, soapy	33	180[22]	white bread[47]
tridec-1-en-3-one	citrus-like, soapy	166	nr	nr
tetradec-1-en-3-one	soapy, plastic-like	771	nr	nr

[a]Odor thresholds in air were determined as described by Ullrich and Grosch.[20] [b]Odor quality as perceived at the sniffing port. [c]nr, compound or odor threshold was not reported previously.

Table 4. Odor Qualities and Odor Thresholds of Homologous Alka-1,5-dien-3-ols

odorant	odor quality[b]	threshold in air[a] (ng/L) by GC-O	threshold in air[a] (ng/L) data from lit.[c]	previously identified in food[c]
hexa-1,5-dien-3-ol	geranium-, vegetable-like, metallic	37.4	nr	nr
(*Z*)-hepta-1,5-dien-3-ol	geranium-like	4.7	nr	nr
(*Z*)-octa-1,5-dien-3-ol	geranium-like	1.3	nr	mushroom,[3,48] fish[14,49]
(*Z*)-nona-1,5-dien-3-ol	herb-, geranium-, mushroom-like	4.2	nr	nr
(*Z*)-deca-1,5-dien-3-ol	herb-, geranium-, mushroom-like	7.1	nr	nr
(*Z*)-undeca-1,5-dien-3-ol	herb-, geranium-, mushroom-like	20.7	nr	fish[14,49]
(*Z*)-dodeca-1,5-dien-3-ol	herb-, geranium-, mushroom-like	143	nr	nr
(*Z*)-trideca-1,5-dien-3-ol	geranium-like, fresh	173	nr	nr
(*Z*)-tetradeca-1,5-dien-3-ol	fresh, green	284	nr	nr

[a]Odor thresholds in air were determined as described by Ullrich and Grosch.[20] [b]Odor quality as perceived at the sniffing port. [c]nr, compound or odor threshold was not reported previously.

Germany), and a Thermo ITQ 900 (Thermo Fisher Scientific, Dreieich, Germany) with the capillaries described above. Mass spectra in the electron impact mode (MS/EI) were generated at 70 eV. Panelists were trained volunteers from the University of Erlangen (Erlangen, Germany), exhibiting no known illness at the time of examination and with audited olfactory function. In preceding weekly training sessions the assessors were trained for at least half a year in recognizing orthonasally about 90 selected known odorants at different concentrations according to their odor qualities and in naming these according to an in-house developed flavor language.

Odor Threshold Values. Thresholds in air were determined by GC-O with (*E*)-2-decenal as internal standard[20] (Tables 1−6). The thresholds were determined by two panelists. HRGC was performed on capillary SE-54 (DB5) and capillary FFAP as already described.

Odor Quality Determination. The odor qualities were determined during GC-O evaluation and were related to odor qualities of commercially available reference compounds, such as *Z*-octa-1,5-dien-3-one (geranium like) or pent-1-en-3-ol (pungent) and pent-1-en-3-one (pungent, fish-like).

RESULTS AND DISCUSSION

The odor threshold values in air and the odor qualities of the homologous (*Z*)-alka-1,5-dien-3-ones, (*E*)-alka-1,5-dien-3-ones, and alk-1-en-3-ones are given in Tables 1, 2, and 3. The data of the corresponding alcohols are given in Tables 4, 5, and 6. With regard to the bis-unsaturated compounds, we found a very low odor threshold minimum with 0.6 mg/L air for the seven-carbon compound of the (*Z*)-alka-1,5-dien-3-ones, thus being

Table 5. Odor Qualities and Odor Thresholds of Homologous (*E*)-Alka-1,5-dien-3-ols

odorant	odor quality[b]	threshold in air[a] (ng/L) by GC-O	threshold in air[a] (ng/L) data from lit.[c]	previously identified in food[c]
hexa-1,5-dien-3-ol	geranium-, vegetable-like, metallic	37.4	nr	nr
(*E*)-hepta-1,5-dien-3-ol	geranium-like	4.9	nr	nr
(*E*)-octa-1,5-dien-3-ol	geranium-like, green	36.2	nr	nr
(*E*)-nona-1,5-dien-3-ol	geranium-like	13	nr	nr
(*E*)-deca-1,5-dien-3-ol	geranium-like, green	4.1	nr	nr
(*E*)-undeca-1,5-dien-3-ol	green, geranium-like	133.6	nr	nr
(*E*)-dodeca-1,5-dien-3-ol	green, geranium-like	165	nr	nr
(*E*)-trideca-1,5-dien-3-ol	sweet, fresh, citrus-like	191.1	nr	nr
(*E*)-tetradeca-1,5-dien-3-ol	fresh, flowery, green	310.6	nr	nr

[a]Odor thresholds in air were determined as described by Ullrich and Grosch.[20] [b]Odor quality as perceived at the sniffing port. [c]nr, compound or odor threshold was not reported previously.

Table 6. Odor Qualities and Odor Thresholds of Homologous Alk-1-en-3-ols

odorant	odor quality[b]	threshold in air[a] (ng/L) by GC-O	threshold in air[a] (ng/L) data from lit.[c]	previously identified in food[c]
pent-1-en-3-ol	pungent	46	4300,[50] 660[22]	banana,[10,41] dill herb,[51] chicken fat,[52] fish,[14,49] black tea[53,54]
hex-1-en-3-ol	pungent, glue-like	2.3	70[22]	banana,[41] dill herb,[51] black tea[42]
hept-1-en-3-ol	vegetable-like, metallic	40.4	70[22]	banana,[10,41] dill herb[51]
oct-1-en-3-ol	mushroom-like	1.4	110,[22] 48[41]	banana,[10,41] fish[14,49]
non-1-en-3-ol	mushroom-like	2.7	40[22]	banana[10,41]
dec-1-en-3-ol	herb-, citrus-like	20.3	370[22]	nr
undec-1-en-3-ol	herb-, citrus-like	22.9	370[22]	nr
dodec-1-en-3-ol	herb-, citrus-like	285	3700[22]	nr
tridec-1-en-3-ol	citrus-like	1616	nr	nr
tetradec-1-en-3-ol	citrus-, plastic-like	4381	nr	nr

[a]Odor thresholds in air were determined as described by Ullrich and Grosch.[20] [b]Odor quality as perceived at the sniffing port. [c]nr, compound or odor threshold was not reported previously.

the most odor-active compound of all odorants under investigation. All (*Z*)-alka-1,5-dien-3-ones elicited a geranium-like odor quality, with the short-chain compounds possessing a merely metallic odor note, whereas an increase of the chain length results in a more herb- and mushroom-like odor quality. This change in odor qualities went along with an increase in the odor thresholds up to a factor of about 10^3. The same change in odor quality was observed for the homologous (*Z*)-alka-1,5-dien-3-ols. However, the minimum in the odor thresholds was not so pronounced for the seven-carbon compound. Generally, the most odor-active alkadienols in this series were the odorants with 7−10 carbon atoms with odor thresholds from 1 to 10 ng/L air. The odor thresholds then increased by a factor of about 10^2 from (*Z*)-deca-1,5-dien-3-ol to (*Z*)-dodeca-1,5-dien-3-ol.

Also, all (*E*)-alka-1,5-dien-3-ones elicited a geranium leaf-like odor quality. The short-chain compounds possessed a pungent and green odor note. An increase in the chain length resulted in a more citrus- and plastic-like odor. As in the case of the (*Z*)-compounds, this change was accompanied with an increase in the odor thresholds. The same changes in odor quality were observed for the homologous (*E*)-alka-1,5-dien-3-ols.

Whereas the overall geranium-like odor of the (*Z*)- and (*E*)-alka-1,5-dien-3-oxo compounds varied only slightly between homologues, the odor qualities of the alk-1-en-3-oxo compounds changed significantly with increasing chain length. The five- and six-carbon compounds were mainly described as pungent and glue-like but not mushroom-like. An increase of the chain length first led to a change to a metallic odor quality and then to the characteristic mushroom-like smells for the odorants with eight and nine carbon atoms. This change went along with two minima in the odor thresholds. The first one was observed for the pungent six-carbon compounds, followed by an increase in the odor threshold for hept-1-ene- odorants, and then a second minimum for the mushroom-like smelling eight- and nine-carbon compounds, respectively. A further increase of the chain length resulted in an increasing citrus-like, soapy, and herb-like odor quality as well as a significant increase in their odor thresholds by a factor of about 10^3 in both homologous series. Generally, the odor thresholds in air of the alk-1-ene and alka-1,5-diene carbonyl compounds were significantly lower than those of their corresponding alcohols.

Overall, most of the odor thresholds determined within the present study are in very close agreement with others previously reported for compounds that had been already investigated, for example, oct-1-en-3-one (Table 3). However, we observed a notable deviation from some reported values, for example, pent-1-en-3-one and oct-1-en-3-ol (Tables 3 and 6). In the case of these substances, odor thresholds provided by Koszinowski and Piringer[39] were higher by a factor of about 100−120, which may arise from the fact that in the previous study another approach of odor threshold determination was used based on GC-O but not utilizing an internal referencing substance such as (*E*)-2-decenal.

Overall, the results show that most of the investigated compounds in the homologous series of the (*Z*)-alka-1,5-dien-3-ones, (*E*)-alka-1,5-dien-3-ones, and alk-1-en-3-ones as well as their corresponding alcohols exhibit very low odor thresholds or very high odor potencies, respectively. Therefore, some of these compounds are possibly naturally occurring odorants but

were not yet identified in food materials perhaps due to their low concentrations. Our investigations now provide analytical data on these compounds such as retention indices as well as an evaluation of their odor qualities and odor thresholds, which can aid at their future analysis.

■ ASSOCIATED CONTENT

Supporting Information

Mass spectroscopic data for all investigated compounds. This material is available free of charge via the Internet at http://pubs.acs.org.

■ AUTHOR INFORMATION

Corresponding Author

*(A.B.) Phone: +49-9131-85 22739. E-mail: andrea.buettner@fau.de.

Notes

The authors declare no competing financial interest.

■ ABBREVIATIONS USED

FID, flame ionization detector; GC-O, gas chromatography−olfactometry; HRGC-MS, high-resolution gas chromatography−mass spectrometry; HRGC-O, high-resolution gas chromatography−olfactometry; MS/EI, mass spectrometry/electron ionization; o.n, overnight; RI, retention index; rt, Room temperature

■ REFERENCES

(1) Stark, W.; Forss, D. A. A compound responsible for metallic flavor in dairy products. I. Isolation and identification. *J. Dairy Res.* **1962**, *29*, 173−180.

(2) Swoboda, P. A. T.; Peers, K. E. Metallic odor caused by vinyl ketones formed in the oxidation of butterfat. The identification of octa-1,cis-5-dien-3-one. *J. Sci. Food Agric.* **1977**, *28*, 1019−1024.

(3) Tressl, R.; Bahri, D.; Engel, K. H. Formation of eight-carbon and ten-carbon components in mushrooms (*Agaricus campestris*). *J. Agric. Food Chem.* **1982**, *30*, 89−93.

(4) Nijssen, L. M.; Visscher, C. A.; Maarse, H.; Willemsen, L. *Volatile Compounds in Foods*; TNO Nutrition and Food Research Institute: Zeist, The Netherlands, 1996.

(5) Ullrich, F.; Grosch, W. Flavor deterioration of soya-bean oil: identification of intense odor compounds formed during flavor reversion. *Fat Sci. Technol.* **1988**, *90*, 332−336.

(6) Spitzer, J.; Buettner, A. Characterization of aroma changes in human milk during storage at −19°C. *Food Chem.* **2010**, *120*, 240−246.

(7) De Lumen, B. O.; Stone, E. J.; Kazeniac, S. J.; Forsythe, R. H. Formation of volatile flavor compounds in green beans from linoleic and linolenic acids. *J. Food Sci.* **1978**, *43*, 698−702, 708.

(8) Grosch, W. In *Reactions of Hydroperoxides. Products of Low Molecular Weight*; Academic: New York, 1987; pp 95−139.

(9) Ullrich, F.; Grosch, W. Identification of the most intense odor compounds formed during autoxidation of methyl linolenate at room temperature. *JAOCS, J. Am. Oil Chem. Soc.* **1988**, *65*, 1313−1317.

(10) Tressl, R.; Drawert, F.; Heimann, W.; Emberger, R. Gas chromatographic survey of aromatic materials of bananas. *Z. Naturforsch. B* **1969**, *24*, 781−783.

(11) Buttery, R. G.; Guadagni, D. G.; Ling, L. C. Volatile aroma components of cooked artichoke. *J. Agric. Food Chem.* **1978**, *26*, 791−793.

(12) Buettner, A.; Schieberle, P. Characterization of the most odor-active volatiles in fresh, hand-squeezed juice of grapefruit (*Citrus paradisi* Macfayden). *J. Agric. Food Chem.* **1999**, *47*, 5189−5193.

(13) Roberts, D. D.; Acree, T. E. Effects of heating and cream addition on fresh raspberry aroma using a retronasal aroma simulator and gas chromatography olfactometry. *J. Agric. Food Chem.* **1996**, *44*, 3919−3925.

(14) Yajima, I.; Nakamura, M.; Sakakibara, H.; Ide, J.; Yanai, T.; Hayashi, K. Volatile flavor components of dried bonito (Katsuobushi). II. From the neutral fraction. *Agric. Biol. Chem.* **1983**, *47*, 1755−1760.

(15) Bodyak, N.; Slotnick, B. Performance of mice in an automated olfactometer: odor detection, discrimination and odor memory. *Chem. Senses* **1999**, *24*, 637−645.

(16) Dravnieks, A.; Schmidtsdorff, W.; Meilgaard, M. Odor thresholds by forced-choice dynamic triangle olfactometry: reproducibility and methods of calculation. *J. Air Pollut. Control Assoc.* **1986**, *36*, 900−905.

(17) Encen, T. The sense of smell. *Annu. Rev. Psychol.* **1973**, *24*, 187−206.

(18) Leonardos, G.; Kendall, D.; Barnard, N. Odor threshold determinations of 53 odorant chemicals. *J. Air Pollut. Control Assoc.* **1969**, *19*, 91−95.

(19) Beauchamp, J.; Frasnelli, J.; Buettner, A.; Scheibe, M.; Hansel, A.; Hummel, T. Characterization of an olfactometer by proton-transfer-reaction mass spectrometry. *Meas. Sci. Technol.* **2010**, *21*, 025801/1−025801/9.

(20) Ullrich, F.; Grosch, W. Identification of the most intense volatile flavor compounds formed during autoxidation of linoleic acid. *Z. Lebensm.-Unters. Forsch.* **1987**, *184*, 277−282.

(21) Buettner, A.; Schieberle, P. Aroma properties of a homologous series of 2,3-epoxyalkanals and trans-4,5-epoxyalk-2-enals. *J. Agric. Food Chem.* **2001**, *49*, 3881−3884.

(22) Koszinowski, J.; Piringer, O. Importance of oxidation products of unsaturated hydrocarbons in the sensorial properties of food packing. Part 1: Oxygen derivates of 1-alkenes. *Dtsch. Lebensm.-Rundsch.* **1983**, *79*, 179−183.

(23) Blank, I.; Fischer, K. H.; Grosch, W. Intensive neutral odorants of linden honey. Differences from honeys of other botanical origin. *Z. Lebensm.-Unters. Forsch.* **1989**, *189*, 426−433.

(24) Guth, H.; Grosch, W. Comparison of stored soya-bean and rapeseed oils by aroma extract dilution analysis. *Lebensm.-Wiss. Technol.* **1990**, *23*, 59−65.

(25) Boerger, D.; Buettner, A.; Schieberle, P. *State-of-the-Art in Flavour Chemistry and Biology*; Deutsche Forschungsanstalt für Lebensmittelchemie: Eisenach, Germany, 2005.

(26) Halang, W. A.; Langlais, R.; Kugler, E. Cubic spline interpolation for the calculation of retention indices in temperature-programmed gas-liquid chromatography. *Anal. Chem.* **1978**, *50*, 1829−1832.

(27) Milo, C. Identification and quantification of aroma compounds. *Curr. Protoc. Food Anal. Chem.* **2001**, G1.3.1−G1.3.12.

(28) Jones, F. W. Estimation of flame-ionization detector relative response factors for oligomers of alkyl and aryl ether polyethoxylates using the effective carbon number concept. *J. Chromatogr. Sci.* **1998**, *36*, 223−226.

(29) Morvai, M.; Palyka, I.; Molnar-Perl, I. Flame ionization detector response factors using the effective carbon number concept in the quantitative analysis of esters. *J. Chromatogr. Sci.* **1992**, *30*, 448−452.

(30) Scanlon, J. T.; Willis, D. E. Calculation of flame ionization detector relative response factors using the effective carbon number concept. *J. Chromatogr. Sci.* **1985**, *23*, 333−340.

(31) Fielder, S.; Rowan, D. D. The synthesis of 3,4-2H2-3Z-hexenal and 6,6,6-2H3-3Z-hexenal. *J. Labelled Compds. Radiopharm.* **1995**, *36*, 465−470.

(32) van den Nieuwendijk, A. M. C. H.; Kriek, N. M. A. J.; Brussee, J.; van Boom, J. H.; van der Gen, A. Stereoselective synthesis of (2R,5R)- and (2S,5R)-5-hydroxylysine. *Eur. J. Org. Chem.* **2000**, *2000*, 3683−3691.

(33) Brown, H. C.; Brown, C. A. Reaction of sodium borohydride with nickel acetate in ethanol solution; a highly selective nickel hydrogenation catalyst. *J. Am. Chem. Soc.* **1963**, *85*, 1005−1006.

(34) Brown, C. A.; Ahuja, V. K. P-2 nickel catalyst with ethylenediamine, a novel system for highly stereospecific reduction of alkynes to cis-olefins. *J. Chem. Soc., Chem. Commun.* **1973**, 553−554.

(35) Bedford, C. D.; Harris, R. N., III; Howd, R. A.; Goff, D. A.; Koolpe, G. A.; Petesch, M.; Koplovitz, I.; Sultan, W. E.; Musallam, H. A. Quaternary salts of 2-[(hydroxyimino)methyl]imidazole. 3. Synthesis and evaluation of (alkenyloxy)-, (alkynyloxy)-, and (aralykyloxy)methyl quaternized 2-[(hydroxyimino)methyl]-1-alkylimidazolium halides as reactivators and therapy for soman intoxication. *J. Med. Chem.* **1989**, *32*, 504−516.
(36) Macia, B.; Gomez, C.; Yus, M. [2,3]-Wittig rearrangement by a chlorine-lithium exchange. *Tetrahedron Lett.* **2005**, *46*, 6101−6104.
(37) Donde, Y.; Nguyen, J. H.; Burk, R. M. Preparation of substituted cyclopentanes having prostaglandin activity for the treatment of glaucoma. WO2009061811A1, 2009.
(38) Rao, B.; Vijayalakshmi, P.; Subbarao, R. Synthesis of long-chain (E)-3-alkenoic acids by the Knoevenagel condensation of aliphatic aldehydes with malonic acid. *J. Am. Oil Chem. Soc.* **1993**, *70*, 297−299.
(39) Koszinowski, J.; Piringer, O. Evaluation of off-odors in food packaging − the role of conjugated unsaturated carbonyl compounds. *J. Plast. Film Sheeting* **1986**, *2*, 40−50.
(40) Reiners, J.; Grosch, W. Odorants of virgin olive oils with different flavor profiles. *J. Agric. Food Chem.* **1998**, *46*, 2754−2763.
(41) Tressl, R.; Drawert, F.; Heimann, W.; Emberger, R. Biogenesis of aroma substances in plants and fruits. VI. Esters, alcohols, carbonyl compounds, and pheno ether as constituents of banana aroma. *Z. Lebensm.-Unters. Forsch.* **1970**, *142*, 313−321.
(42) Mick, W.; Schreier, P. Additional volatiles of black tea aroma. *J. Agric. Food Chem.* **1984**, *32*, 924−929.
(43) Buttery, R. G.; Teranishi, R.; Ling, L. C. Fresh tomato aroma volatiles: a quantitative study. *J. Agric. Food Chem.* **1987**, *35*, 540−544.
(44) Blank, I.; Grosch, W. Evaluation of potent odorants in dill seed and dill herb (*Anethum graveolens* L.) by aroma extract dilution analysis. *J. Food Sci.* **1991**, *56*, 63−67.
(45) Widder, S.; Sen, A.; Grosch, W. Changes in the flavor of butter oil during storage. Identification of potent odorants. *Z. Lebensm.-Unters. Forsch.* **1991**, *193*, 32−35.
(46) Ott, A.; Fay, L. B.; Chaintreau, A. Determination and origin of the aroma impact compounds of yogurt flavor. *J. Agric. Food Chem.* **1997**, *45*, 850−858.
(47) Obretenov, T.; Khadzhieva, P. Gas chromatographic-mass spectral analysis of aroma compounds of bread. *Z. Lebensm.-Unters. Forsch.* **1977**, *165*, 195−199.
(48) Vanhaelen, M.; Vanhaelen-Fastre, R.; Geeraerts, J. Occurrence in mushrooms (Homobasidiomycetes) of cis- and trans-octa-1,5-dien-3-ol, attractants to the cheese mite *Tyrophagus putrescentiae* (Schrank) (Acarina, Acaridae). *Experientia* **1980**, *36*, 406−407.
(49) Sakakibara, H.; Ide, J.; Yanai, T.; Yajima, I.; Hayashi, K. Volatile flavor compounds of some kinds of dried and smoked fish. *Agric. Biol. Chem.* **1990**, *54*, 9−16.
(50) Hall, G.; Andersson, J. Volatile fat oxidation products. I. Determination of odor thresholds and odor intensity functions by dynamic olfactometry. *Lebensm.-Wiss. Technol.* **1983**, *16*, 354−361.
(51) Schreier, P.; Drawert, F.; Heindze, I. The quantitative composition of natural and technologically changed aromas of plants. VIII. Volatile constituents of fresh dill herb, *Anethum graveolens*, L. (Umbelliferae). *Lebensm.-Wiss. Technol.* **1981**, *14*, 150−152.
(52) Noleau, I.; Toulemonde, B. Volatile components of roasted chicken fat. *Lebensm.-Wiss. Technol.* **1987**, *20*, 37−41.
(53) Fischer, N.; Nitz, S.; Drawert, F. Bound flavor compounds in plants. Part 2. Free and bound flavor compounds in green and black tea (*Camellia sinensis*). *Z. Lebensm.-Unters. Forsch.* **1987**, *185*, 195−201.
(54) Owuor, P. O. Comparison of gas chromatographic volatile profiling methods for assessing the flavor quality of Kenyan black teas. *J. Sci. Food Agric.* **1992**, *59*, 189−197.

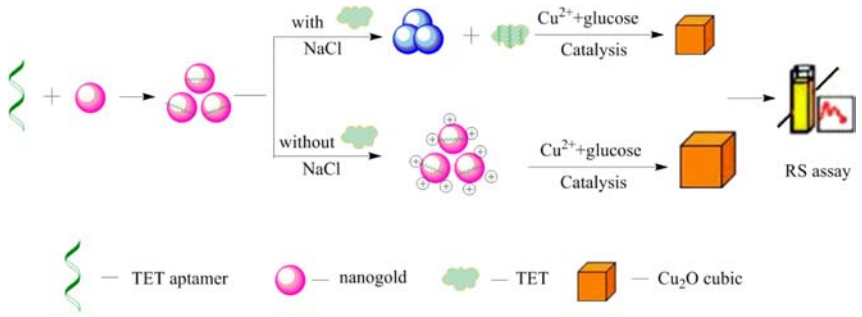

Figure 1. Principle of the ACNG catalytic RS assay for TET.

their high affinity to target substances and low cost of *in vitro* synthesis, aptamers have been increasingly applied in biochemical analysis and environmental monitoring.[22,30] In 2008, Niazi et al.[31] successfully selected the TET aptamer using the *in vitro* method. This TET aptamer has high affinity to the target TET and has already been used to analyze TET in real samples with satisfactory results. For example, Zhou and his coworkers developed an electrochemical aptasensor to detect TET with a limit of detection of 5 nM.[32] However, reports involving the catalytic activity of nanogold and RS method to detect TET are still limited.

MATERIALS AND METHODS

Chemicals. Standard TET, thiamphenine, kanamycin, aztreonam, glucose, L-tyrosine, L-valine, and L-lysine were obtained from Sigma-Aldrich (St. Louis, MO). NaCl, NaOH, $CuSO_4$, sodium potassium tartrate tetrahydrate, trisodium citrate, trichloroacetic acid, chloroauric acid ($HAuCl_4$), and *N*-(2-hydroxyethyl)piperazine-*N*-2-ethanesulfonic acid (HEPES) were obtained from Shanghai Chemical Reagent Company (Shanghai, China). The aptamer sequence of tetracycline is 5′-CGTACGGAATTCGCTAGCCCCCCGGCAGGCCACGGCTTGGGTTGGTCCCACTGCGCGTGGATCCGAGCTCCACGTG-3′,[31] and it was synthesized by Invitrogen Co., Ltd. (Shanghai, China). The tetracycline aptamer sample was dissolved in a 50 mM HEPES buffer solution and stored at 4 °C for use. Ultrapure water (Milli-Q, Millipore system) was used for the preparation of all aqueous solutions. Unless otherwise stated, all chemicals are of analytical reagent grade and were used without further purification.

Apparatus. A model F-4500 fluorescence spectrophotometer (Hitachi, Japan) was used to record the RS intensity. A nanoparticle size analyzer (NANOS, Nanos/ZS90, Malvern, U.K.) was used to obtain the Cu_2O cubic size in the system. Scanning electron microscopy (SEM, Siron 200, U.S.A.) was used to observe the Cu_2O shape. X-ray diffraction (XRD, D8 ADVANCE, Bruker, Germany) was used to confirm the catalytic products.

Preparation of Nanogold Particles. The method of nanogold particle preparation via sodium citrate reduction of $HAuCl_4$ was followed by a literature procedure.[33] All glassware used in this procedure were cleaned in a bath of freshly prepared 3:1 (v/v) HNO_3/HCl, then rinsed thoroughly in ultrapure water, and air-dried. Nanogold particles were prepared by adding 3.5 mL of 1% (w/v) trisodium citrate to a boiling solution of $HAuCl_4$ (100 mL, 0.01%, w/w) and stirred for 30 min. Within that time, the color of the solution changed from light gray, blue, purple, to wine red. After that, the mixture was stirred for an additional 15 min after removal from the heater. Finally, the cooled solution was filtrated in a 0.2 μm ultrafiltration membrane [polyvinylidene fluoride (PVDF)] to remove aggregated particles and then stored in dark glass bottles at 4 °C for further use.

Pretreatment of the Milk Sample. All of the milk sampsles were purchased from a local supermarket. They were pretreated with trichloroacetic acid to remove the proteins according to the procedure described by Tan and Chen,[34] with a slight modification. A 2% trichloroacetic acid solution and milk sample were added together into a centrifuge tube, mixed well, and ultrasonicated for 30 min.[35,36] The mixture was centrifuged at 10 000 rpm for 8 min, and the supernatant was filtered through a 0.2 μm ultrafiltration membrane (PVDF) to remove lipids. After the pH was adjusted to neutral with NaOH, the filtrate was stored at 4 °C for further detection.

Procedure for TET Determination. A total of 6 μL of 5 μM TET aptamer and 5 μL of TET solution with varying concentration were added to a plastic tube, mixed well, and then incubated in a 25 °C thermostatic incubator. The blank sample was added to 5 μL of ultrapure water instead of TET solution. After 15 min, 100 μL of nanogold solution was added to it, mixed thoroughly, and incubated for another 15 min under the same conditions. After the first two steps were finished, 7 μL of 500 mmol/L NaCl solution was added to it and diluted to 500 μL with ultrapure water.

A total of 100 μL of 6.25 mol/L NaOH solution, 10 μL of 0.028 mol/L $CuSO_4$ solution, 200 μL of 1.23 mol/L $KNaC_4H_4O_6$ solution, 50 μL of 10 mg/mL glucose solution, and 500 μL of the aptamer mixture were successively added to a centrifuge tube, diluted to 1000 μL with ultrapure water, and mixed well. Then, the tube was placed in a 60 °C thermostatic incubator for 6 min. The reaction was stopped by the tap water cooling.

A total of 500 μL of the catalytic reaction solution was transferred to a quartz cell. The RS intensity was recorded using a F-4500 fluorescence spectrophotometer with settings as follows: volt, 700 V; excited slit, 5 nm; emission slit, 2.5 nm; and synchronous scanning wavelength range, from 500 to 700 nm. The RS spectrum, the RS intensity at 620 nm ($I_{620\ nm}$), and the $(I_{620\ nm})_b$ of blank solutions without TET were recorded. The values for $\Delta I_{620\ nm} = (I_{620\ nm})_b - I_{620\ nm}$ were calculated.

RESULTS AND DISCUSSION

Principle of the ACNG Catalytic RS Assay. Single-stranded oligonucleotide (ssDNA) can coat on the surface of nanogold particles through van der Waals and intermolecular forces in proper conditions. This keeps nanogold against aggregation when the salt concentration is proper.[37] In addition, Fehling reactions barely happened at room temperature and happened indeed at 60 °C. Upon the addition of a nanocatalyst, such as ACNG, the reaction occurred apparently and Cu_2O cubic was produced quickly. In this paper, the aptamer was used to modify nanogold to obtain the catalytic ACNG, which could catalyze the Fehling reaction, yielding Cu_2O cubic at 60 °C. In the absence of TET, the aptamer absorbed on the surface of the nanogold and kept the nanogold distributing evenly in solution. Under this condition, enough ACNG could catalyze the Fehling reaction to yield a bigger Cu_2O cubic and obtain a higher RS signal. In the presence of TET, owing to the high affinities between TET and aptamers, the nanogold surface became naked and aggregated under proper NaCl concentration existence. At this time, less ACNG

dx.doi.org/10.1021/jf403566e | J. Agric. Food Chem. 2014, 62, 1032−1037

catalyzes the Fehling reaction, yielding a smaller Cu_2O cubic and obtaining a lower RS signal. Therefore, the amount of TET was negatively proportional to the amount of ACNG and, in turn, was negative to the RS signal intensity. As a results, by measuring the RS signal intensity, it is possible to determine the amount of TET. The schematic diagram is shown in Figure 1.

Aggregation of Nanogold Particles by NaCl. According to the study by Brook et al., the mechanisms of nanogold aggregations caused by salts is called the non-cross-linking pattern. The aggregation is induced by electrostatic and electrostatic stabilization without any interparticle bonds. Under this mechanism, nanogold aggregated rapidly and kept steady in appropriate conditions.[38] NaCl was chosen as an efficient cation to disturb the electronic equilibrium of nanogold surface charges to obtain aggregation in most cases.[39−41] The aggregated nanogolds induced a significant RS signal change, and the intensities were linear to the diameter of particles.[39,41−43] According to our previous reports,[42,43] aggregated nanogold has a strong RS peak at 550 nm wavelength and was chosen for use. For the nanogold aggregation reaction, the volume of aptamer, TET, NaCl, and nanogold on $I_{550\ nm}$ through RS detection was considered. In the aggregation experiments, the $\Delta I_{550\ nm}$ increased as the NaCl concentration changed from 0 to 8 mM (see Figure S1 of the Supporting Information). Moreover, when the NaCl concentrations surpassed 8 mM, the $\Delta I_{550\ nm}$ was nearly unchanged. This meant that NaCl in this system was saturated. Thus, 8 mM NaCl and 30 nM aptamer were chosen for the optimal nanogold aggregation concentration. When the volume of aptamer was 6 μL, the volume of TET was 5 μL, the volume of nanogold was 100 μL and the volume of NaCl was 8 μL, the $\Delta I_{550\ nm}$ values were the largest. The effects of the reaction time and the order of adding solutions were also investigated. The results demonstrated that $\Delta I_{550\ nm}$ attained maximum values when the reaction time was 15 min and the solution addition order was aptamer, TET, nanogold, and NaCl.

Catalytic Reaction between the Fehling Reagent and Glucose. The Fehling reaction is wildly used in the determination of reducing sugar. However, the reaction only occurs at 100 °C in a water bath for minutes when there are no catalysts. In 2010, Tao and his co-workers[19] found that 10 nm nanogold particles have a strong catalytic activity on the Fehling reaction and can reduce the Cu^{2+}−glucose system to yield Cu_2O cubic, which makes the RS intensity at 620 nm increase with an increasing nanocatalytic concentration. Here, we control the concentration of nanogold catalyst through TET dosage, which means that the catalytic capability of the nanogold has a negative correlation with the concentration of TET. The catalytic reaction conditions, such as reagent concentration, reaction time, and temperature, were optimized. The results showed the largest $\Delta I_{620\ nm}$ value when 28 nM $CuSO_4$, 625 mM NaOH, 246 nM $KNaC_4H_4O_6$, and 0.5 μg/L glucose were added, then incubated at 60 °C using a thermostatic incubator for 6 min, and chosen for use. The products of the ACNG catalytic system were obtained and used for XRD with a scanning range of 10.0−80.0° (2θ), a step size of 0.02° (2θ), a scanning step time of 0.6 s, an anode material of Cu, a current of 40 mA, and a voltage of 40 kV. According to the standard XRD spectrum of Cu_2O (see Figure S9b of the Supporting Information), the characteristic peaks are at 29.51°, 36.36°, 42.24°, 61.30°, 73.42°, and 77.27°. Our catalytic product pattern (Figure S9a of the Supporting Information) indicated that there was only Cu_2O cubic in the products. The products were also analyzed by SEM (Figure S10 of the Supporting Information). SEM showed that Cu_2O particles were cubic with a side length of about 0.5 μm, which was in agreement with the results of XRD and laser scattering image (LSI) (discussed later).

Transformation of RS Spectra. The study demonstrated that diameters of particles were the crucial factors for the RS values, but the site of the RS peak was determined by three factors: the light source of the apparatus, the absorption of the free molecule, and the RS effect of particles.[23] Results showed that the scattering peak at 620 nm was only characteristic to Cu_2O particles and chosen for analysis. Figure S12 of the Supporting Information shows that the RS values increased as the TET concentrations in solution decrease, which means that some large particles formed during catalytic reaction. From the LSI obtained by NaNo-ZS90 particle size and ζ potentiometer analyzer, the particle size distribution was in agreement with the RS value and SEM observation between the different TET concentrations. The results (see Figure S11 of the Supporting Information) show the LSI of the blank and 0.2 μM TET in solution. The average sizes were 294 and 451 nm, respectively. Therefore, the larger Cu_2O particle products were the reason for the change of the RS value.

Sensitivity of the Biosensor for TET Detection. Different concentrations of TET from 0 to 2500 nM were added to evaluate the sensitivity of the present biosensor, and the signals of RS intensity at 620 nm were recorded. As shown in Figure S12 of the Supporting Information, RS values gradually decreased with an increasing concentration of TET. To quantify the detection limit of the present biosensor, the variations of RS intensity (ΔI) at 620 nm were plotted and the calibration curve (Figure 2) looked like a sigmoid shape. It can

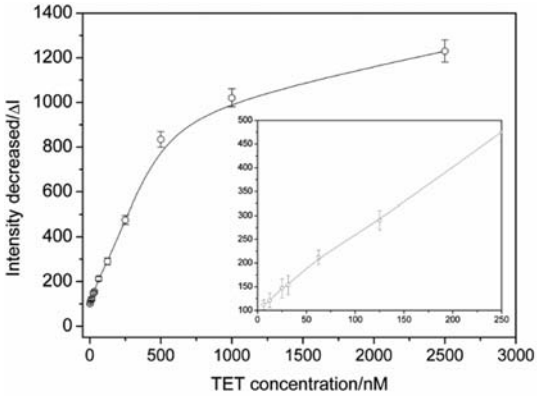

Figure 2. Calibration curve of the ACNG catalytic RS assay. The curve was fitted to a sigmoid shape with a correlation coefficient of 0.998. (Inset) RS intensity increased values at low TET concentration.

be observed that the RS intensity changed slightly when the concentrations of TET were over 625 nM in detection solutions, which indicated that the binding interaction between the aptamer and TET had reached balance and saturation. The $\Delta I_{620\ nm}$ at low TET concentrations was fitted to a linear expression with the equation of $\Delta I_{620\ nm} = 1.4793C_{TET} + 107.69$ ($R^2 = 0.998$). According to our previous research,[13,20] 3σ/slope was used to determine the detection limit of the biosensor and calculated as 11.6 nM, which is much lower than the EU-defined MRL (225 nM) and the MRL in U.S. animal products. The present biosensor is more sensitive than the detection methods reported before (Table 1), and the advantage was

Table 1. Comparison of TET Detection Analytic Methods

analyte	method	LOD	matrix	reference
TET	CE	1.8 μM	milk	45
TET	electrochemical biosensor	200 nM	water	46
TET	HPLC	99 nM	milk	9
TET	colorimetric biosensor	45.8 nM	milk	47
TET	RS	11.6 nM	milk	this paper

applying the catalytic activity of nanogold. This difference in sensitivity may be ascribed to the strong catalytic activity of nanogold to catalyze the Fehling reaction to produce a bigger Cu_2O cubic, which would lead to a high RS signal in the detection of TET. The assay could be used to detect trace levels of TET in milk samples with a comparable sensitivity. In comparison to the detection methods of TET reported before, the experimental results shown here offer the possibility of a rapid and high sensitive monitoring method for TET.

Selectivity of the Biosensor for TET Detection. The selectivity of the biosensor for TET detection was also investigated. A variety of foreign substances, such as antibiotics and organic molecules, including thiamphenine, kanamycin, aztreonam, L-tyrosine, L-valine, and L-lysine, were individually added to the reaction solutions, and the $\Delta I_{620\ nm}$ was calculated. Figure 3 showed that the RS assay had a slight change to these substances, which demonstrated that this method had high selectivity to TET detection.

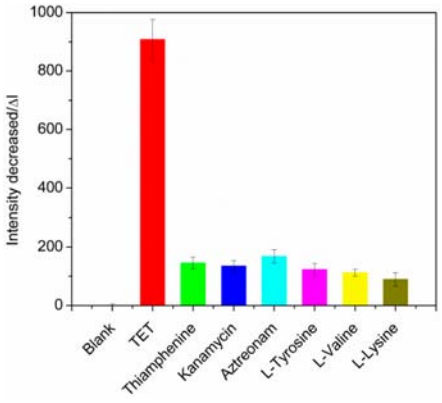

Figure 3. Specificity of the ACNG catalitc RS assay for TET detection. The concentrations of foreign substances were all 0.5 μM.

Application in the Milk Sample. At first, four analyzed milk samples with different concentrations of TET were made by adding different amounts of standard TET.[5,44] Then, they were treated and detected according to the method and procedure described before and repeated 5 times. The results are shown in Table 2. The recoveries were in the range of 105−109%, and the relative standard deviation was in the range of 1.9−4.2%. These indicated that this method had a relatively stable precision and satisfactory reproducibility.

■ ASSOCIATED CONTENT

Ⓢ Supporting Information

Effect of the NaCl concentration on the nanogold aggregation system (Figure S1), effect of the aptamer concentration on the nanogold aggregation system (Figure S2), effect of the NaOH concentration on the catalytic RS assay (Figure S3), effect of the $KNaC_4H_4O_6$ concentration on the catalytic RS assay (Figure S4), effect of the reaction temperature on the catalytic RS assay (Figure S5), effect of the reaction time on the catalytic RS assay (Figure S6), effect of the $CuSO_4$ concentration on the catalytic RS assay (Figure S7), effect of the glucose concentration on the catalytic RS assay (Figure S8), (a) XRD pattern for the products of the ACNG catalytic reaction, with 0.20 μM TET and (b) standard Cu_2O pattern (Figure S9), SEM of the ACNG catalytic reaction product Cu_2O cubic (Figure S10), diameter distribution of ACNG catalytic reaction products (Figure S11), and RS spectra of the ACNG catalytic assay for TET detection (Figure S12). This material is available free of charge via the Internet at http://pubs.acs.org.

■ AUTHOR INFORMATION

Corresponding Author

*Telephone: +86-021-34205762. E-mail: zhoupei@sjtu.edu.cn.

Funding

This work was supported by the National High-Tech Research and Development Plan (2012AA101405), the Special Fund for Agro-scientific Research in the Public Interest of China (200903056), the Shanghai Natural Science Foundation (13ZR1421700), the Shanghai Science and Technology Commission, China (11DZ2210800), and the Special Funds for Shanghai Zhangjiang National Independent Innovation Demonstration Area (201209-SJ-A0-001).

Notes

The authors declare no competing financial interest.

■ REFERENCES

(1) Chopra, I.; Roberts, M. Tetracycline antibiotics: Mode of action, applications, molecular biology, and epidemiology of bacterial resistance. *Microbiol. Mol. Biol. Rev.* **2001**, *65*, 232−260.

(2) Nicolaou, K. C.; Chen, J. S.; Edmonds, D. J.; Estrada, A. A. Recent advances in the chemistry and biology of naturally occurring antibiotics. *Angew. Chem., Int. Ed.* **2009**, *48*, 660−719.

(3) De Wasch, K.; Okerman, L.; De Brabander, H.; Van Hoof, J.; Croubels, S.; De Backer, P. Detection of residues of tetracycline antibiotics in pork and chicken meat: Correlation between results of screening and confirmatory tests. *Analyst* **1998**, *123*, 2737−2741.

(4) Croubels, S.; Van Peteghem, C.; Baeyens, W. Sensitive spectrofluorimetric determination of tetracycline residues in bovine milk. *Analyst* **1994**, *119*, 2713−2716.

(5) Tan, H.; Ma, C.; Song, Y.; Xu, F.; Chen, S.; Wang, L. Determination of tetracycline in milk by using nucleotide/lanthanide coordination polymer-based ternary complex. *Biosens. Bioelectron.* **2013**, *50*, 447−452.

(6) Tan, H.; Ma, C.; Song, Y.; Xu, F.; Chen, S.; Wang, L. Determination of tetracycline in milk by using nucleotide/lanthanide

Table 2. Within-Batch Recovery and Repeatability (RSD) for TET in Milk Samples Spiked at Different Levels

milk samples	spiked level (nM)	found (nM)					recovery (%)	RSD (%)
1	50	51.45	53.34	51.68	51.32	54.12	105	2.4
2	80	85.23	83.12	81.31	84.89	83.98	105	1.9
3	100	108.97	106.53	102.43	103.21	105.32	105	2.5
4	120	138.45	130.52	123.8	134.56	128.5	109	4.2

coordination polymer-based ternary complex. *Biosens. Bioelectron.* **2013**, *50*, 447−452.
(7) Moats, W. A. Determination of tetracycline antibiotics in beef and pork tissues using ion-paired liquid chromatography. *J. Agric. Food Chem.* **2000**, *48*, 2244−2248.
(8) Kowalski, P. Capillary electrophoretic method for the simultaneous determination of tetracycline residues in fish samples. *J. Pharm. Biomed. Anal.* **2008**, *47*, 487−493.
(9) Fritz, J. W.; Zuo, Y. Simultaneous determination of tetracycline, oxytetracycline, and 4-epitetracycline in milk by high-performance liquid chromatography. *Food Chem.* **2007**, *105*, 1297−1301.
(10) Zhang, Y.; Lu, S.; Liu, W.; Zhao, C.; Xi, R. Preparation of anti-tetracycline antibodies and development of an indirect heterologous competitive enzyme-linked immunosorbent assay to detect residues of tetracycline in milk. *J. Agric. Food Chem.* **2006**, *55*, 211−218.
(11) Okerman, L.; Croubels, S.; De Baere, S.; Hoof, J. V.; De Backer, P.; De Brabander, H. Inhibition tests for detection and presumptive identification of tetracyclines, β-lactam antibiotics and quinolones in poultry meat. *Food Addit. Contam.* **2001**, *18*, 385−393.
(12) Aga, D. S.; O'Connor, S.; Ensley, S.; Payero, J. O.; Snow, D.; Tarkalson, D. Determination of the persistence of tetracycline antibiotics and their degradates in manure-amended soil using enzyme-linked immunosorbent assay and liquid chromatography−mass spectrometry. *J. Agric. Food Chem.* **2005**, *53*, 7165−7171.
(13) Wu, Y.; Zhan, S.; Xu, L.; Shi, W.; Xi, T.; Zhan, X.; Zhou, P. A simple and label-free sensor for mercury(II) detection in aqueous solution by malachite green based on a resonance scattering spectral assay. *Chem. Commun.* **2011**, *47*, 6027−6029.
(14) Long, Y. F.; Huang, C. Z.; Li, Y. F. Hybridization detection of DNA by measuring organic small molecule amplified resonance light scattering signals. *J. Phys. Chem. B* **2007**, *111*, 4535−4538.
(15) Jiang, Z.; Zhang, S.; Liang, A.; Huang, S. Resonance scattering spectral detection of ultratrace IgG using immunonanogold−$HAuCl_4$−NH_2OH catalytic reaction. *Sci. China, Ser. B: Chem.* **2008**, *51*, 440−446.
(16) Li, J.-F.; Jiang, Z.-L.; Deng, A.-P. A rapid and highly selective resonance scattering spectral assay for trace carcinoembryonic antigen. *Chin. J. Chem.* **2008**, *26*, 2297−2301.
(17) Liang, A.; Zhou, L.; Qin, H.; Zhang, Y.; Ouyang, H.; Jiang, Z. A highly sensitive aptamer-nanogold catalytic resonance scattering spectral assay for melamine. *J. Fluoresc.* **2011**, *21*, 1907−1912.
(18) Liu, S.; Luo, H.; Li, N.; Liu, Z.; Zheng, W. Resonance Rayleigh scattering study of the interaction of heparin with some basic diphenyl naphthylmethane dyes. *Anal. Chem.* **2001**, *73*, 3907−3914.
(19) Tao, H.; Wei, L.; Liang, A.; Li, J.; Jiang, Z.; Jiang, H. Highly sensitive resonance scattering detection of DNA hybridization using aptamer-modified gold nanopaticle as catalyst. *Plasmonics* **2010**, *5*, 189−198.
(20) Wu, Y.; Zhan, S.; Wang, F.; He, L.; Zhi, W.; Zhou, P. Cationic polymers and aptamers mediated aggregation of gold nanoparticles for the colorimetric detection of arsenic(III) in aqueous solution. *Chem. Commun.* **2012**, *48*, 4459−4461.
(21) Jiang, Z.; G., W.; Fan, Y.; Jiang, C.; Liu, Q.; Huang, Z.; Liang, A. A highly selective nanogold−aptamer catalytic resonance scattering spectral assay for trace Hg^{2+} using $HAuCl_4$−ascorbic acid as indicator reaction. *Talanta* **2010**, *80*, 1287−1291.
(22) Wu, Y.; Liu, L.; Zhan, S.; Wang, F.; Zhou, P. Ultrasensitive aptamer biosensor for arsenic(III) detection in aqueous solution based on surfactant-induced aggregation of gold nanoparticles. *Analyst* **2012**, *137*, 4171−4178.
(23) Jiang, Z.; Fan, Y.; Chen, M.; Liang, A.; Liao, X.; Wen, G.; Shen, X.; He, X.; Pan, H.; Jiang, H. Resonance scattering spectral detection of trace Hg^{2+} using aptamer-modified nanogold as probe and nanocatalyst. *Anal. Chem.* **2009**, *81*, 5439−5445.
(24) Cao; Jin, R.; Mirkin, C. A. DNA-modified core−shell Ag/Au nanoparticles. *J. Am. Chem. Soc.* **2001**, *123*, 7961−7962.
(25) Ellington, A. D.; Szostak, J. W. In vitro selection of RNA molecules that bind specific ligands. *Nature* **1990**, *346*, 818−822.
(26) Robertson, D. L.; Joyce, G. F. Selection in vitro of an RNA enzyme that specifically cleaves single-stranded DNA. *Nature* **1990**, *344*, 467−468.
(27) Freeman, R.; Liu, X.; Willner, I. Chemiluminescent and chemiluminescence resonance energy transfer (CRET) detection of DNA, metal ions, and aptamer−substrate complexes using hemin/G-quadruplexes and CdSe/ZnS quantum dots. *J. Am. Chem. Soc.* **2011**, *133*, 11597−11604.
(28) Rodriguez, M. C.; Kawde, A.-N.; Wang, J. Aptamer biosensor for label-free impedance spectroscopy detection of proteins based on recognition-induced switching of the surface charge. *Chem. Commun.* **2005**, *0*, 4267−4269.
(29) Strehlitz, B.; Stoltenburg, R. Selex and its recent optimizations. *Aptamers in Bioanalysis*; John Wiley and Sons, Inc.: Hoboken, NJ, 2008; pp 31−59.
(30) Liu, J.; Cao, Z.; Lu, Y. Functional nucleic acid sensors. *Chem. Rev.* **2009**, *109*, 1948−1998.
(31) Niazi, J. H.; Lee, S. J.; Gu, M. B. Single-stranded DNA aptamers specific for antibiotics tetracyclines. *Bioorg. Med. Chem.* **2008**, *16*, 7245−7253.
(32) Zhou, L.; Li, D. J.; Gai, L.; Wang, J. P.; Li, Y. B. Electrochemical aptasensor for the detection of tetracycline with multi-walled carbon nanotubes amplification. *Sens. Actuators, B* **2012**, *162*, 201−208.
(33) Wang, Y.; Yang, F.; Yang, X. Colorimetric biosensing of mercury(II) ion using unmodified gold nanoparticle probes and thrombin-binding aptamer. *Biosens. Bioelectron.* **2010**, *25*, 1994−1998.
(34) Tan, H.; Chen, Y. Silver nanoparticle enhanced fluorescence of europium (III) for detection of tetracycline in milk. *Sens. Actuators, B* **2012**, *173*, 262−267.
(35) Jiao, Y.; Zuo, Y. Ultrasonic extraction and HPLC determination of anthraquinones, aloe-emodine, emodine, rheine, chrysophanol and physcione, in roots of *Polygoni multiflori*. *Phytochem. Anal.* **2009**, *20*, 272−278.
(36) Zuo, Y.; Zhang, L.; Wu, J.; Fritz, J. W.; Medeiros, S.; Rego, C. Ultrasonic extraction and capillary gas chromatography determination of nicotine in pharmaceutical formulations. *Anal. Chim. Acta* **2004**, *526*, 35−39.
(37) Li, D.; Wieckowska, A.; Willner, I. Optical analysis of Hg^{2+} ions by oligonucleotide−gold−nanoparticle hybrids and DNA-based machines. *Angew. Chem., Int. Ed.* **2008**, *47*, 3927−3931.
(38) Brook, M. A.; Zhao, W.; Li, Y. F. Design of gold nanoparticle-based colorimetric biosensing assays. *ChemBioChem* **2008**, *9*, 2363−2371.
(39) Chen, C.; G., T. S.; Ren, J. S.; Qu, X. G. A simple and sensitive colorimetric pH meter based on DNA conformational switch and gold nanoparticle aggregation. *Chem. Commun.* **2008**, *46*, 6149−6151.
(40) Su, X.; Kanjanawarut, R. Control of metal nanoparticles aggregation and dispersion by PNA and PNA−DNA complexes, and its application for colorimetric DNA detection. *ACS Nano* **2009**, *3*, 2751−2759.
(41) Doria, G.; Larguinho, M.; Dias, J. T.; Pereira, E.; Franco, R.; Baptista, P. V. Gold−silver-alloy nanoprobes for one-pot multiplex DNA detection. *Nanotechnology* **2010**, *21*, 1−5.
(42) Zhan, S.; Wu, Y.; He, L.; Wang, F.; Zhan, X.; Zhou, P.; Qiu, S. A silver-specific DNA-based bio-assay for Ag(I) detection via the aggregation of unmodified gold nanoparticles in aqueous solution coupled with resonance Rayleigh scattering. *Anal. Methods* **2012**, *4*, 3997−4002.
(43) He, L.; Zhi, W.; Wu, Y.; Zhan, S.; Wang, F.; Xing, H.; Zhou, P. A highly sensitive resonance scattering based sensor using unmodified gold nanoparticles for daunomycin detection in aqueous solution. *Anal. Methods* **2012**, *4*, 2266−2271.
(44) Nebot, C.; Regal, P.; Miranda, J. M.; Fente, C.; Cepeda, A. Rapid method for quantification of nine sulfonamides in bovine milk using HPLC/MS/MS and without using SPE. *Food Chem.* **2013**, *3*, 2294−2299.
(45) Santos, S. M.; Henriques, M.; Duarte, A. C.; Esteves, V. I. Development and application of a capillary electrophoresis based

method for the simultaneous screening of six antibiotics in spiked milk samples. *Talanta* **2007**, *71*, 731−737.
(46) Wang, H.; Zhao, H.; Quan, X. Gold modified microelectrode for direct tetracycline detection. *Front. Environ. Sci. Eng.* **2012**, *6*, 313−319.
(47) He, L.; Luo, Y.; Zhi, W.; Zhou, P. Colorimetric sensing of tetracyclines in milk based on the assembly of cationic conjugated polymer-aggregated gold nanoparticles. *Food Anal. Methods* **2013**, *26*, 1−8.

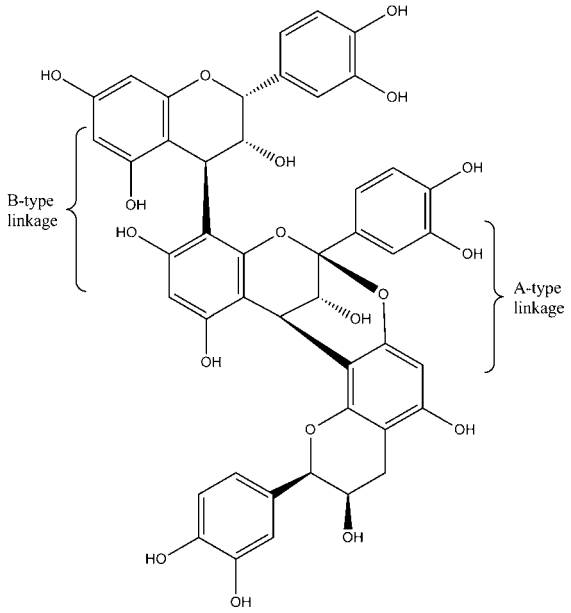

Figure 1. Representative structure of a trimeric proantocyanidin with both A-type and B-type linkages.

phase separation conditions using water and methanol[9,19,21,22] or acetonitrile[3,12,18,23] as mobile phases were used. Regarding quantitative aspects, HPLC proved to be useful for the determination of B-type proanthocyanidins in several food products. However, the red-berry product analyses were less effective due to the presence of both A-type and B-type proanthocyanidins and the lack of adequate standards.[24] The structural diversity of proanthocyanidins in red berry products led to complex profiles with poor chromatographic resolution. Furthermore, their analysis resulted in a great challenge due to the variety and quantity of proanthocyanidin-polymerized compounds.[9,21] High resolution mass spectrometry (HRMS) has also been proposed for the characterization of polyphenols in fruit products. Rockenbach et al.[18] used Fourier-transform ion cyclotron resonance mass spectrometry (FTICR-MS) to characterize and assign the elemental composition of 251 different flavan-3-ol compounds in grapes. Regarding cranberry-based products, Iswaldi et al.[12] proposed the use of time-of-flight mass spectrometry (TOF-MS) for the characterization of the phenolic fraction in cranberry syrup.

Capillary electrophoresis (CE) also appeared as an alternative technique for the analysis and characterization of polyphenolic compounds in fruit-based products.[25−29] There are, however, only a few studies that apply these techniques to the analysis of red berry fruits.[14,15] Because of the strong absorption of proanthocyanidins at 545 nm, simple colorimetric assays are still employed for the quantitative analysis of proanthocyanidins in cranberry-based products. The assay relying on the reaction of proanthocyanidins with 4-dimethylaminocinnamaldehyde is one of the most popular.[21,24]

Characterization and classification of fruit-based products can be tackled from compositional profiles as a source of analytical information. Polyphenols, as well as other low molecular weight organic acids, alcohols, esters, etc., have been found to be efficient descriptors of some climatic, agricultural, and technological features. It has also been found that the variability of compounds will depend strongly on the fruit of origin. Therefore, polyphenolic profile can be a useful platform for reliable discrimination between fruit-based products via chemometric methods such as principal component analysis (PCA). Information recovered mathematically may be essential in order to prevent misuses in the production of commercial fruit-based extracts with health-promoting properties.

The aim of this work was the development of straightforward methods for the characterization of fruit products based on polyphenolic composition. The resulting instrumental profiles were exploited to carry out the authentication of natural extracts according to the fruit of origin. For that purpose, the potentiality of capillary zone electrophoresis (CZE) and HPLC, combined with several sample extraction and treatment procedures, was evaluated in order to obtain compositional data with high discriminant ability. Different kinds of samples were analyzed including fruits (cranberry, blueberry, grapes, and raisins), fruit-based products such as grape-juice and cranberry-juice, as well as commercial cranberry-based products such as pharmaceutical natural extracts, powder capsules, syrup, and sachets. CZE and HPLC data from each method were considered as a source of potential descriptors for the authentication of fruit-based products.

MATERIALS AND METHODS

Reagents and Solutions. Unless otherwise stated, all reagents were of analytical grade. Acetic acid, formic acid, sodium tetraborate, Sephadex LH-20 and HPLC gradient grade acetone were obtained from Sigma-Aldrich (Steinhein, Germany). HPLC gradient grade acetonitrile and methanol were purchased from Panreac (Barcelona, Spain). Hydrochloric acid was from Merck (Darmstadt, Germany) and sodium hydroxide from Fluka (Steinhein, Germany).

Background electrolyte (BGE) for CE was prepared daily by diluting a 100 mM sodium tetraborate aqueous solution and by adding a 5% (v/v) of methanol. BGE solutions were filtered through 0.45 μm nylon filters (Whatman, Clifton, NJ) and sonicated before being used. Mobile phases for LC were prepared daily by adding 1% (v/v) acetic acid or 0.1% (v/v) formic acid to water, methanol, or acetonitrile.

Water was purified using an Elix 3 coupled to a Mili-Q system (Millipore, Bedford, MA) and filtered through a 0.22 μm nylon filter integrated into the Milli-Q system.

Fruit Products. Different kinds of fruits (cranberries, blueberries, grapes, and raisins) and 6 juices (3 based on cranberry and 3 based on grapes) were purchased from Barcelona markets. In addition, a total of 10 raw extract materials and commercial cranberry products, presented as powder capsules, syrup, sachets, and natural extracts were provided by Deiters, S.L. Company (Badalona, Spain). Prior to sample treatment, fruits and liquid samples (juices and cranberry pharmaceutical syrup) were freeze-dried to achieve a fully lyophilized product with a texture similar to that of natural extracts and commercial pharmaceutical samples (powder samples). So, samples remained 24 h inside a lyophilizer from −80 °C to room temperature, and then were kept for 6.5 h at 40 °C.

Sample Treatment. In order to extract phenolic compounds from fruit products different sample extraction procedures were evaluated as follows:

Sample Extraction Method 1.1: A 0.5-g portion of sample was dispersed in 10 mL of MeOH:H_2O (10:90 v/v) with 0.2% HCl. Then, the mixture was sonicated for 30 min and centrifuged for 15 min at 3500 rpm.[3]

Sample Extraction Method 1.2: Same as sample extraction method 1.1 with an additional SPE step after centrifugation. SPE was carried out using two g-bed C18 cartridges (Scharlab, Barcelona, Spain) previously conditioned with 10 mL of methanol and 10 mL of water. After loading the extract, the cartridge was washed with 10 mL of water and, finally, phenolic compounds were eluted with 10 mL of methanol.[30]

Sample Extraction Method 2.1: A 0.5-g portion of sample were dispersed in 10 mL of MeOH/H_2O (85:15 v/v). Then, the mixture was sonicated for 30 min and centrifuged for 15 min at 3500 rpm.[31]

dx.doi.org/10.1021/jf404776d | J. Agric. Food Chem. 2014, 62, 1038−1046

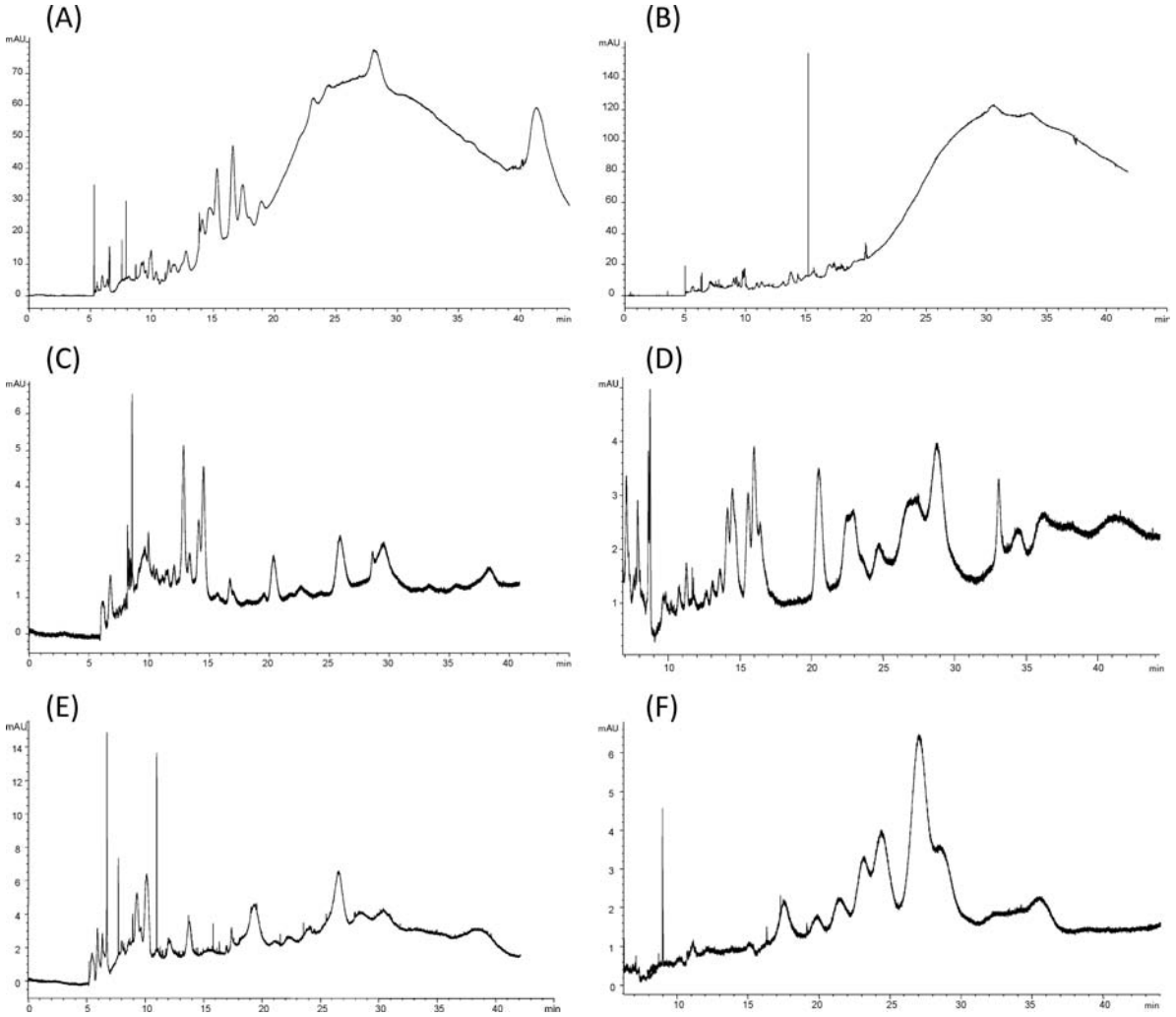

Figure 2. Electrophoretic polyphenolic profiles of a natural cranberry extract obtained after applying sample extraction methods 1.1 (A), 1.2 (B), 2.1 (C), 2.2 (D), 2.3 (E), and 3 (F). Electropherograms registered at 280 nm.

Sample Extraction Method 2.2: Same as sample extraction method 2.1, except from the extraction solvent, which in this case was acetone/MeOH/H_2O (40:40:20 v/v/v).[31]

Sample Extraction Method 2.3: Same as sample extraction method 2.1, except from the extraction solvent, which in this case was MeOH/H_2O/acetic acid (85:14.5:0.5 v/v/v).[31]

Sample Extraction Method 3: A 0.1-g portion of sample were dispersed in 10 mL of acetone/H_2O/HCl (70:29.9:0.1 v/v/v) and sonicated for 30 min. After that, the mixture was centrifugated for 15 min at 3500 rpm. The supernatant was then concentrated and semipurified using a 3 g Sephadex LH-20 cartridge (Sigma-Aldrich) preconditioned overnight in 30% methanol solution. After sample loading, the cartridge was washed with 10 mL of the 30% methanol solution and eluted with 10 mL of acetone/H_2O/HCl (70:29.9:0.1 v/v/v).[9,13]

All of the extracts were stored at −4 °C until analyzed. Before injection extracts were filtered through 0.45 μm nylon filters (Whatman).

Apparatus. *Capillary Zone Electrophoresis.* CZE experiments were performed in an Agilent HP 3D-CE system (Santa Clara, CA) equipped with a diode-array detector. The electrophoretic separation was carried out using fused-silica capillaries with a total length of 60 cm (effective length of 50 cm), and a 75 μm i.d. Background electrolyte (BGE) consisted of a 35-mM sodium tetraborate aqueous solution (pH 9.4) containing 5% (v/v) methanol. Capillary temperature was held at 25 °C. The BGE was degassed by sonication before use. Samples were loaded by pressure-assisted hydrodynamic injection (10 s, 3.5 kPa). Electrophoretic separations were performed by applying a capillary voltage of +25 kV. Analyses were carried out for 40 min and direct UV absorption was recorded from 190 to 310 nm. Electrophoretic data were processed at 280 nm.

New capillaries for CE were pretreated with 0.1 M hydrochloric acid for 60 min, water for 60 min, 0.1 M sodium hydroxide for 60 min, and finally they were washed with water for 60 min. At the beginning of each working session, the capillary was rinsed with 0.1 M sodium hydroxide for 30 min, water for 30 min, and with the BGE for 60 min. The capillary was rinsed with BGE for 5 min between runs. At the end of each session, the capillary was stored after rinsing with water.

Liquid Chromatography. LC experiments were performed on an Agilent LC 1100 System (Santa Clara, CA) equipped with a diode array detection system. Separation was carried out on a 100 × 4.6 mm^2 i.d., 2.6 μm, Kinetex C18 reversed-phase column, with a 4.0 × 3.0 mm^2 i.d. guard column of the same material (Phenomenex, Torrance, CA). The injection volume was 10 μL and UV absorption was recorded from 191 to 780 nm. Chromatographic data were processed at 280 nm. Three different gradient profiles were considered for the separation of polyphenolic fractions as follows:

Gradient Method A. Gradient method A was created from solvent A (H_2O with 0.1% formic acid) and solvent B (MeOH) as follows: 0−3 min, linear gradient from 5 to 25% B; 3−6 min isocratic step at 25% B; 6−9 min linear gradient from 25 to 37% B; 9−13 min isocratic step at 37% B; 13−18 min linear gradient from 37 to 54% B; 18−22 min isocratic step at 54% B; 22−26 min linear gradient from 54 to 95% B; 26−29 min isocratic step at 95% B; 29−29.15 min back to initial

conditions at 5% B; and from 29.15 to 36 min isocratic step at 5% B. The flow rate was 1 mL/min.

Gradient Method B. Gradient method B was created from solvent A (H_2O with 1% acetic acid) and solvent B (acetonitrile with 1% acetic acid) as follows: 0−2 min linear gradient from 0 to 5% B; 2−4 min isocratic step at 5% B; 4−30 min linear gradient from 5 to 100% B; 30−35 min isocratic step at 100% B; and from 35 to 40 min back to initial conditions at 0% B. The flow rate was 1 mL/min.

Gradient Method C. Gradient method C created from solvent A (H_2O with 1% acetic acid) and solvent B (acetonitrile with 1% acetic acid) as follows: 0−20 min linear gradient from 0 to 8% B; 20−24 min linear gradient from 8 to 15% B; 24−44 min linear gradient from 15 to 40% B; 44−45 min linear gradient from 40 to 100% B; and from 45 to 46 min back to initial conditions at 0% B. The flow rate was 1 mL/min.

Data Analysis. MATLAB (Version 6.5) was used for calculations. Principal component analysis (PCA) was from the PLS-Toolbox.[32] A detailed description of this method is given elsewhere.[33]

The plot of scores showing the distribution of the samples on the principal components (PCs) revealed patterns that may be correlated to sample characteristics, which in this case, was the fruit of origin. The study of the distribution of variables from the so-called loading plot provided information dealing with their correlations as well as dependences of proanthocyanidins and polyphenolic compounds on fruit product properties.

Data matrices to be treated were generated as a function of the separation technique, separation method and sample treatment procedure. Separation techniques were coded by CE for the CZE method, and by A, B, C for the three HPLC methods. Extraction procedures were coded numerically as 1.1, 1.2, etc. in the same way as described in the sample treatment section. As a result, data matrices were referred to as CE.1.1, CE.1.2, ..., A.1.1, ..., B.1.1, C.1.1, and so on. Dimensions of these matrices were number of samples × number of time (or area) points.

HRMS (Orbitrap) Analysis. In order to identify and confirm the presence of proanthocyanidins in commercial natural extracts accurate mass measurements were carried out with an LTQ Orbitrap Velos mass spectrometer (Thermo Scientific, Hemel Hempstead, UK) equipped with an ESI source in negative mode. Mass spectra were acquired in profile mode with a setting resolution of 30 000 at m/z 400. Operation parameters were as follows: source voltage, 3.5 kV; sheath gas flow rate, 40 arbitrary units (a.u.); auxiliary gas flow rate, 10 au; sweep gas flow rate, 10 au; and capillary temperature, 320 °C. Default values were used for other acquisition parameters [Fourier transform (FT) Automatic gain control (AGC) target 10^6 for MS mode]. Maximum injection time was set to 100 ms with two microscans for MS analysis. Full scan mass range was from m/z 100 to 2000. XCalibur software was used for data acquisition and analysis.

HPLC method A was employed for LC-ESI-LTQ-Orbitrap-MS analysis by using an Accela chromatograph (Thermo Scientific) equipped with a quaternary pump, a photodiode-array detector and a thermostatted autosampler. Commercial natural extracts analyzed by LC-ESI-LTQ-Orbitrap-MS were treated with sample extraction method 3. MS data were processed by ExactFinder 2.0 software (ThermoFisher) by applying a user target database list of polyphenolic compounds including proanthocyanidins. Several parameters such as retention time, accurate mass errors, and isotopic pattern matches were used to confirm the identity of compounds.

RESULTS AND DISCUSSION

Capillary Zone Electrophoresis. In this study, both methanol and isopropanol were evaluated as organic modifiers to obtain better electrophoretic separations of polyphenolic profiles of cranberries products. For preliminary assays, a natural cranberry extract sample was homogenized and extracted according to method 1.1. The extract was then analyzed by CZE using a 35 mM sodium tetraborate solution containing 5% of each organic solvent. Electropherograms obtained using methanol provided more peak signals, with better resolution and peak efficiency than those obtained with isopropanol. As a result, 35 mM sodium tetraborate buffer with 5% methanol was selected as the optimum BGE, and it was used in further CZE studies.

The sample treatment procedures were investigated in term of capacity of classification/discrimination of fruit samples considering the polyphenolic profiles as the analytical information. Figure 2 shows, as an example, the electropherograms corresponding to each extraction procedure. Methods 1.1 and 1.2 were focused on obtaining a general polyphenolic profile with data of various families of compounds and they were adapted from refs 3, 20, and 30 dealing with the analysis of phenolic compounds in berries. In sample extraction method 1.2 an additional SPE cleanup and preconcentration step using C18 cartridges was added. As it can be seen in electropherograms 2A and 2B, a high absorption pattern was observed from 20 to 45 min, which was attributed to the presence of some plant pigments such as anthocyanins.

Sample treatments 2.1, 2.2, and 2.3 differed in the polarity of solvents that were used. These procedures were adapted from those previously described in the literature.[31,34] Sample extraction method 2.1 employed a methanol/water 85:15 v/v solution, and it was focused on the recovery of the most polar fractions of compounds. Extraction method 2.2 used acetone/methanol/water 40:40:20 v/v/v solution for the extraction of less polar compounds occurring in cranberries. Additionally, methanol/water/acetic acid 85:14.5:0.5 v/v/v solution was used in method 2.3 to obtain the anthocyanin fraction of fruits. The corresponding electropherograms (Figures 2C−E) showed complex profiles with multiple peaks throughout the migration time.

Finally, sample extraction method 3 was developed for a more specific recovery of proanthocyanidins from cranberry products.[9,13,21,35] For that purpose, after an extraction using acetone:water:hydrochloric acid 70:29.9:0.1 v/v/v solution, sonication and centrifugation, the supernatant was concentrated and purified using a lipophilic inorganic resin (Sephadex LH-20 cartridges). Electrophoretic profiles (Figure 2F) contained more characteristic information concerning proanthocyanidins as various broad peaks corresponding to these compounds were obtained.

Principal Component Analysis of Electrophoretic Data. Sample extracts resulting from the 6 treatment procedures were analyzed by the proposed CZE-UV method. The resulting electrophoretic profiles were used as a source of information for tackling characterization and classification of fruit products. An important issue in this study was finding which procedure was able to provide the most discriminant profiles for sample featuring.

In preliminary studies, analytical data to be treated consisted of the raw electrophoretic profiles at 280 nm recorded for the set of samples. In all of the cases, electropherograms showed noticeable differences depending on the sample type. For instance, pharmaceutical products (syrup, capsules, and sachets) displayed more intense signals than those of fruit and juice samples. This finding was attributed to the high contents of polyphenols in the pharmaceuticals.

Raw electropherograms displayed some imperfections such as baseline drifts and peak shifts that may hinder the interpretation of PCA results. When raw data were analyzed PCA models were highly complex. Furthermore, the first PCs were focused on modeling the electrophoretic variability while

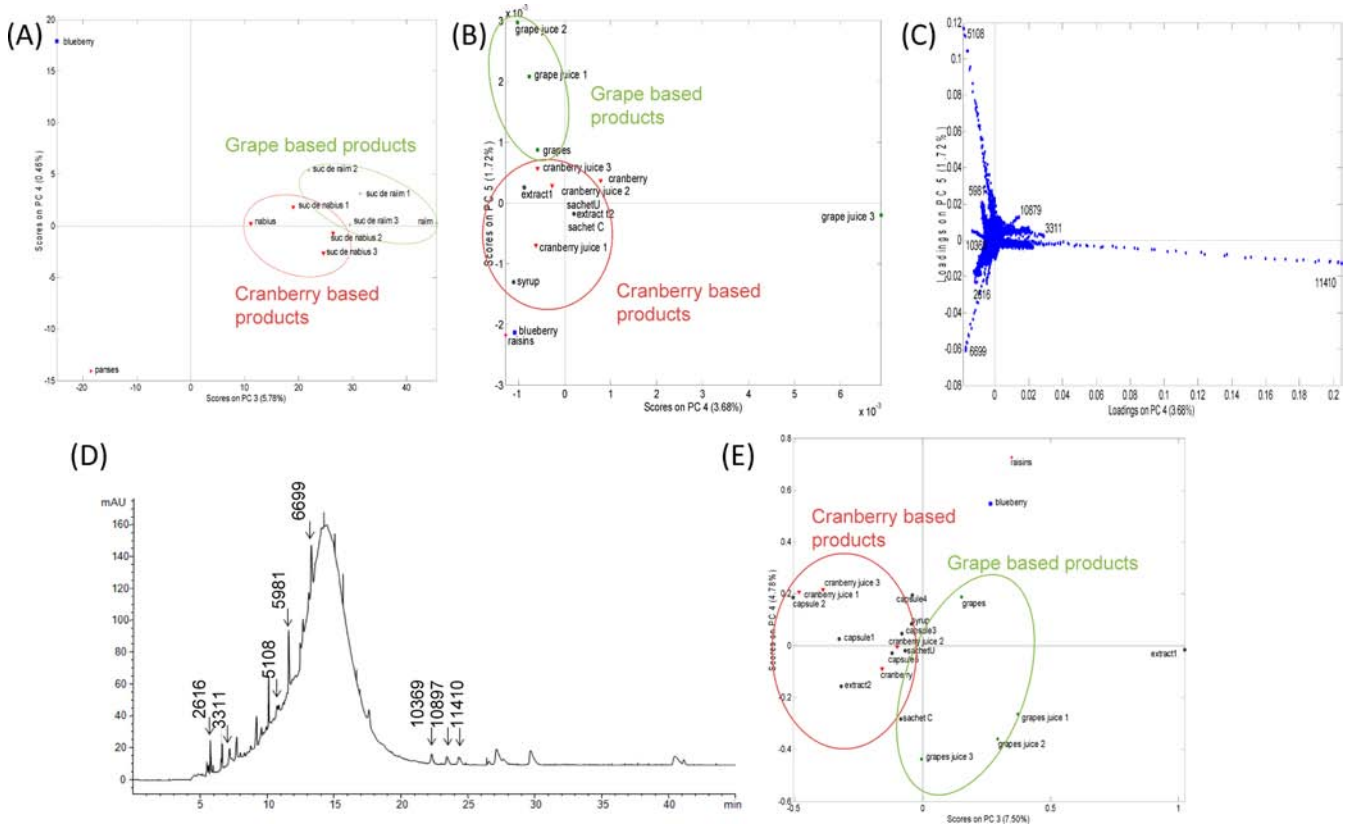

Figure 3. (A) PCA result (PC3 vs PC4 score plot) using electrophoretic polyphenolic profiles obtained with sample extraction method 1.2 for fruits and juice samples; (B) PCA results (PC4 vs PC5 score plot) using electrophoretic polyphenolic profiles obtained with sample extraction method 2.1 for all samples except pharmaceutical capsules. (C) Loading plot using peak signal areas and sample extraction method 2.1. (D) Electropherogram obtained for a cranberry commercial capsule using sample extraction method 2.1. Discriminant peak signals are indicated with an arrow. (E) PCA result (PC3 vs PC4 score plot) using eight discriminant peak signal areas and sample extraction method 2.1.

descriptive information regarding samples was hidden in further PCs. In these circumstances, the assessment of solid conclusions on the sample characteristics and classifications was hindered.

PCA was preliminarily applied to electropherogram profiles of fruits and juice samples. As an example, results showed that PC1 and PC2 for data matrix CE.1.2. were mainly focused on the description of the type of product (juice or fruit), and variance dealing with fruit of origin (cranberry or grapes) was captured by PC3 and PC4 (Figure 3A). As a result, fruits and juices were classified according to the kind of fruit that they contained. Similar results were obtained when using the other sample extraction methods.

For the simultaneous evaluation of pharmaceutical and fruit products, it was found that electrophoretic profiles of pharmaceuticals were much more intense that those obtained for fruits and juices, so data normalization was needed. Only the scatter plot of scores of PC4 versus PC5 generated with data from sample extraction method 2.1 (see Figure 3B) showed the same groups of samples than the ones achieved with the model built only with fruits and juices when considering also data related to cranberry syrup, sachets, and natural extract, whereas the model completely changed when the electropherograms of cranberry commercial capsules were considered and then no groups were observed.

Up to this point, the results obtained by PCA using raw electrophoretic polyphenolic profiles indicated that none of the data sets was capable of characterizing all of the targeted samples according to their fruit of origin. This drawback was solved using the peak areas of the most relevant peaks as a source of analytical information, thus avoiding variability of migration times and baseline drifts. For that purpose, loading plots were evaluated for choosing the most discriminant peak signals as shown in Figure 3C regarding CE.2.1 data set. After analyzing these results, eight peaks were selected as relevant ones. As an example, Figure 3D depicts the electropherogram of a cranberry commercial capsule where the eight discriminant peak signals selected are marked with an arrow. It should be mentioned that again normalization was applied to compensate differences in intensities between fruit or juice samples and commercial products.

Characterization models using the selected peaks indicated that information of the fruit of origin was captured by PC3 and PC4. The best descriptive models were obtained from the treatment of data set CE.2.1 (see the corresponding scatter plot in Figure 3E). As can be seen, grape-based products were located on the right part, whereas cranberry-based products appeared on the left side, grouped independently of the kind of product (fruit, juice, syrup, natural extract, capsules, or sachets). Sample products belonging to other fruits, such as blueberry and raisins, were plotted far away from the two main groups corresponding to grape- or cranberry-based products.

After analyzing these results, it was observed that cranberry extract 1 was not located in the area corresponding to cranberry-based products. This natural extract, used on the production of pharmaceutical products to reduce urinary tract

dx.doi.org/10.1021/jf404776d | J. Agric. Food Chem. 2014, 62, 1038−1046

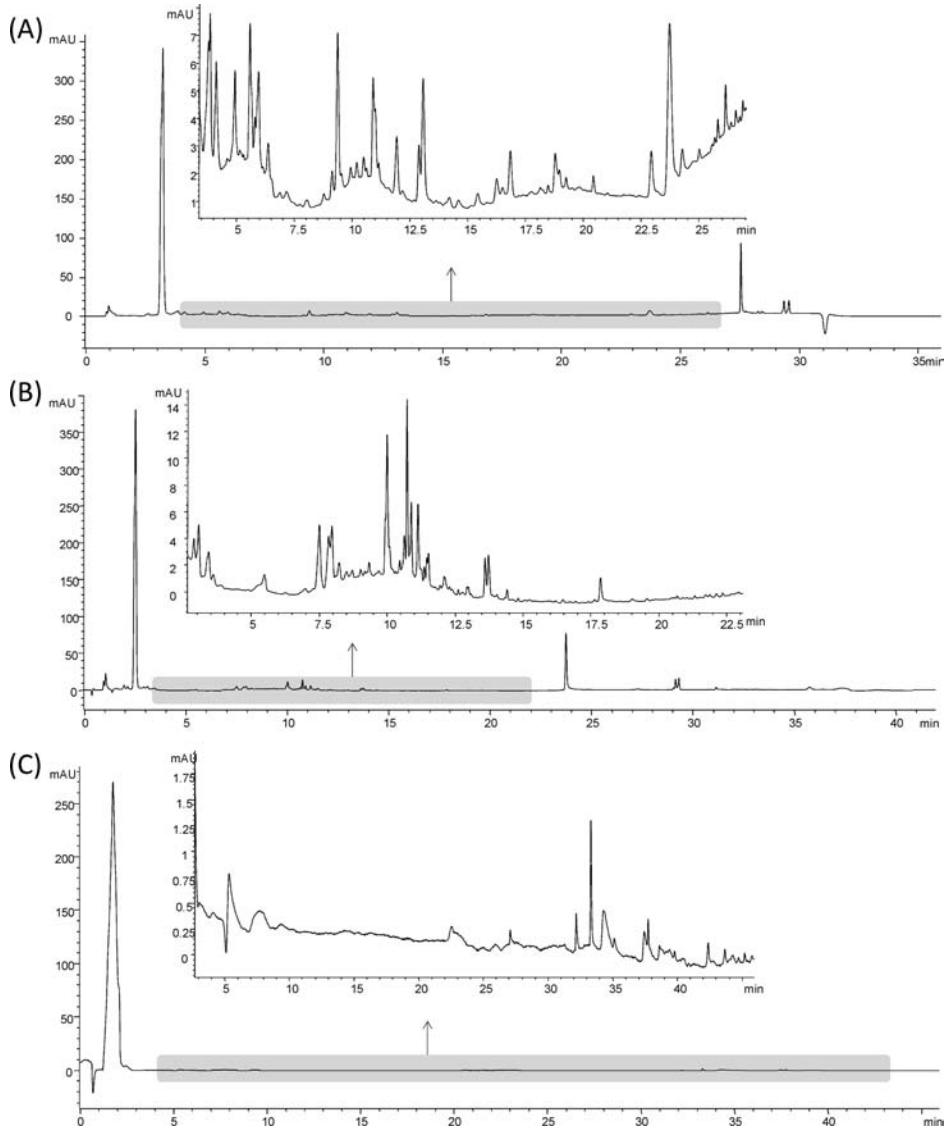

Figure 4. Chromatographic polyphenolic profiles of a natural cranberry extract obtained with (A) HPLC method A, (B) HPLC method B, and (C) HPLC method C, after applying sample extraction method 1.1. Chromatograms registered at 280 nm.

infections, was supposed to be elaborated from cranberries. However, our results suggested that the fruit of origin could be suspicious and, in general, it was more similar to grape products. This assumption was studied thoroughly to try to confirm the authenticity of this natural extract by high resolution mass spectrometry (HRMS).

These results show that the combination of CZE with sample extraction method 2.1 and PCA analysis using eight discriminant peak signal areas is a good strategy for the characterization of food products based on their fruit of origin and could be proposed for the authentication of commercial natural and pharmaceutical products.

Liquid Chromatography. Chromatograms corresponding to polyphenolic fractions were exploited in order to tackle the classification and authentication of cranberry-based natural extracts. For that purpose, three reversed-phase HPLC methods, which differed in the elution gradient program, were applied to obtain the compositional profiles. As an example, Figure 4 shows the chromatograms of a cranberry natural extract analyzed with each HPLC method. For HPLC method A (Figure 4A), previously developed in our research group for the characterization of wines and fruits, the chromatographic profile was complex. In the time range from 4 to 28 min, the elution of most of phenolic acids and flavonoids was produced so this data could be useful for the fruit product characterization. HPLC method B provided also complex chromatograms with a high number of peak signals that could be useful for characterization purposes (Figure 4B). In contrast, chromatograms from HPLC method C (Figure 4C) were simpler, at least in terms of peak signals, but it provided important information of proanthocyanidins composition.

Sample extracts of a cranberry juice according to the six sample treatment procedures are compared in Figure 5. As can be seen, very different chromatographic profiles were obtained depending on the sample extraction. However, in general, more peak signals were here observed than in the case of CZE. Chromatograms (A), (C), and (E) were similar in shape and corresponded to methods focused on the overall recovery of polyphenols of different families. In general, it was found that the extraction of polyphenols was better in the case (E). Conversely, chromatograms (B), (D), and (F) concerned the

dx.doi.org/10.1021/jf404776d | J. Agric. Food Chem. 2014, 62, 1038−1046

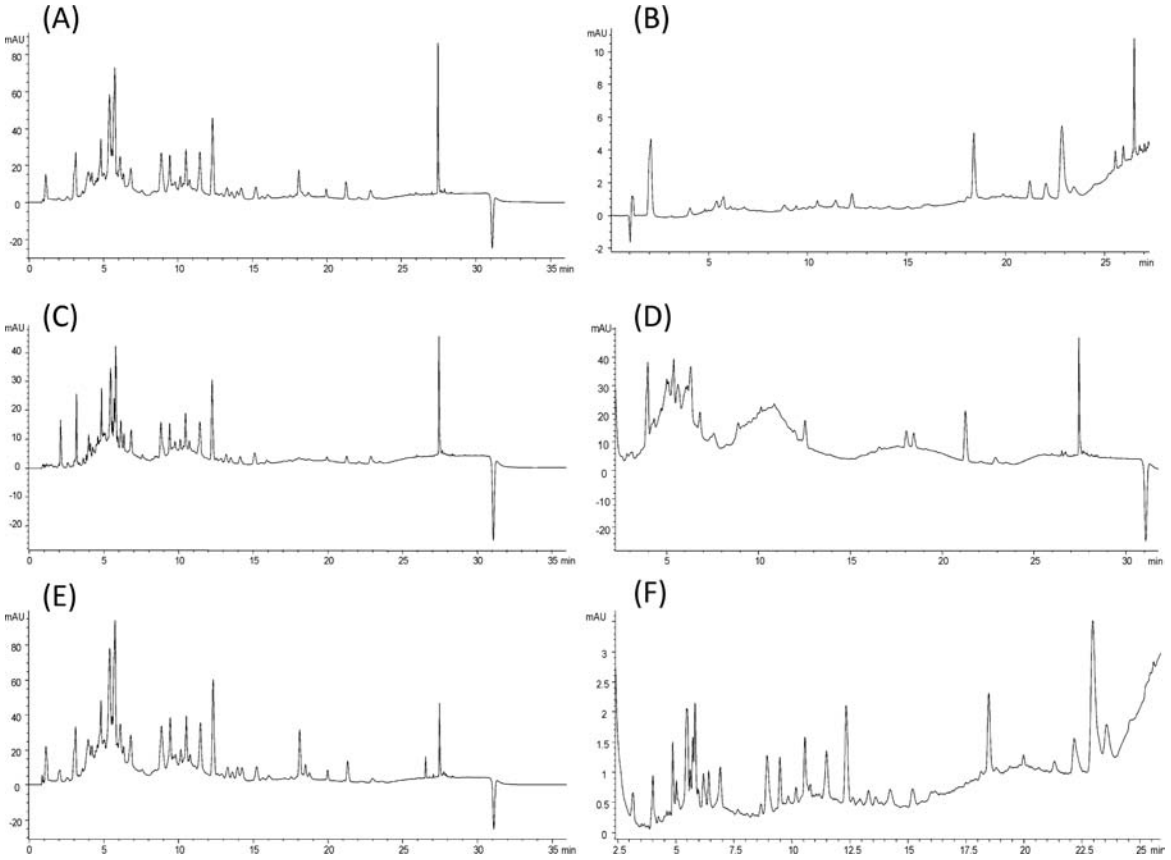

Figure 5. Chromatographic polyphenolic profiles of a cranberry juice sample obtained using HPLC method A after applying sample extraction methods 1.1 (A), 1.2 (B), 2.1 (C), 2.2 (D), 2.3 (E), and 3 (F). Chromatograms registered at 280 nm.

most extraction of polyphenols of some families. Amounts recovered from simple phenolic acids and flavonoids were lower so that more characteristic peaks related to complex polyphenols such as proanthocyanidins were observed.

Principal Component Analysis of Chromatographic Data. Analytical data to be treated by PCA consisted of raw chromatograms recorded at 280 nm. Data sets were arranged in matrix structures corresponding to each HPLC method/sample extraction combination. For more efficient modeling, specific time ranges were selected to work with the most discriminant zones of chromatograms, while avoiding disturbing variance from nonretained components and cleaning steps. In particular, time ranges dealing with high influence of proanthocyanidins were chosen. Here, these chromatographic zones were established from the injection of cranberry-based pharmaceutical products, which reasonably contained high concentrations of proanthocyanidins. Since proanthocyanidin absorption was almost selective at 520 nm,[19,21] corresponding to the detection of colored components, the elution range of the proanthocyanidins fraction was deduced from chromatograms recorded at this specific wavelength. As a result, time ranges chosen were as follows: HPLC Method A from 7 to 15 min, HPLC Method B from 6 to 15 min, and HPLC Method C from 12 to 20 min. Another drawback to be considered was that chromatograms showed noticeable differences on signal intensities depending on the sample type. In this study, data were preprocessed by normalization to equalize the influence of each sample in the PCA model for a more effective comparison of product features.

The results obtained by PCA for all data matrices indicated that PC1, PC2, and PC3 were mainly focused on the description of the type of product regardless the nature of the fruit of origin (i.e., fruit, juice, natural extract, sachet, capsule, and syrup) since this was a main contribution to the variance. In contrast, information dealing with the fruit of origin, if existent, was captured by further PCs. In particular, for matrices A.1.1, A.1.2, A.2.1, A.2.3, B.1.1, B.3, C.2.1, and C.2.3, PC4 and PC5 showed a noticeable sample organization as a function of the fruit of origin. Such a correlation was not observed for the rest of the matrices. The most favorable data set to tackle the description and classification of fruit product was achieved with HPLC method A and sample extraction procedure 3 which combined a high chromatographic resolution with a more specific recovery of proanthocyanidins. In the PCA results corresponding to matrix A.1.1. (Figure 6), grape-based products were located on the top, whereas cranberry-based products appeared below. In addition, sample products belonging to raisins and blueberry were plotted far from grape- and cranberry-based products areas.

One cranberry natural extract (referred to as extract 1), was classified as a grape-based product. In order to confirm the authenticity of this extract, HRMS experiments were carried out comparing the supposedly wrong with genuine samples.

High Resolution Mass Spectrometry (Orbitrap) Study. As described in the Introduction section, cranberries are characterized for their high content of A-type proanthocyanidins. Sample extract 1 was analyzed by UHPLC-HRMS using an LTQ-Orbitrap mass analyzer. For comparison purposes, commercial sample extract 2, which was correctly assigned as a

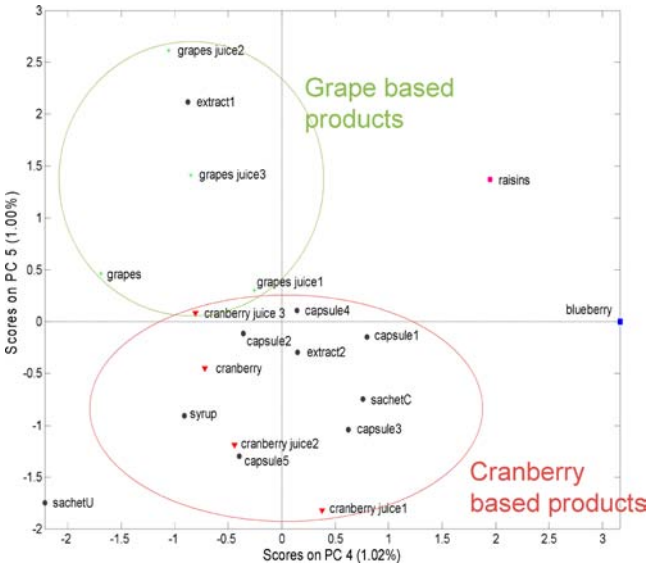

Figure 6. PCA results (PC4 vs PC5 score plot) using chromatographic polyphenolic profiles obtained using HPLC method C and sample extraction 3.

cranberry-based product with both CZE and HPLC methodologies, was also analyzed by UHPLC-HRMS as a reference of genuine products. Results obtained regarding the presence of procyanidins and proanthocyanidins are shown in Table 1. It should be pointed out that many other polyphenolic compounds such as catechin, epicatechin, protocatechuic acid, 2,5-dihydroxybenzoic acid, 4-hydroxybenzoic acid, caffeic acid, coumaric acid, cinnamic acid, vanillic acid, and quercetin, among others, were confirmed by HRMS in this kind of samples.

Table 1 shows the list of procyanidin and proanthocyanidin compounds detected and identified by HRMS Orbitrap MS analyzer. Experimental m/z values and mass errors observed (always lower than 3.4 ppm) are also indicated. A- and B-type procyanidins were found in both commercial extracts whereas C-type procyanidins were only detected and confirmed in commercial extract sample 2. Regarding proanthocyanidins, only trimer BA was detected in both samples, while the presence of higher polymeric proanthocyanidin compounds with A-type bonds, such as trimer AA and tetramer BAA, were only detected and confirmed in commercial extract sample 2. The HRMS analysis reporting the lack of presence of A-type proanthocyanidin compounds in commercial sample extract 1 allowed us to confirm that this sample was not mainly cranberry-based extract, as suspected.

The results obtained in this work proved that both CZE and HPLC combined with PCA analysis (selecting the most relevant peak signals in CZE, and using the polyphenolic chromatographic data within a delimited time range in HPLC) resulted in cheap, straightforward, and useful strategies for authentication of natural extracts according to the food of origin. PCA results from both CZE and HPLC showed that sample extract 1 was not a cranberry-based product, which was confirmed by HRMS analysis. By means of these results, the suitability of the proposed methods for the characterization of fruit-based products has been validated and demonstrated. So the information recovered with the proposed methods could be used to easily detect adulterations and prevent misuse.

AUTHOR INFORMATION

Corresponding Author

*Tel: +34-93-4033706; fax: +34-93-4021233; e-mail: oscar.nunez@ub.edu.

Notes

The authors declare no competing financial interest.

ACKNOWLEDGMENTS

Authors wished to thank Deiters S.L. Company for providing some cranberry-based raw material extracts and commercial cranberry-based products.

REFERENCES

(1) Basu, A.; Rhone, M.; Lyons, T. J. Berries: Emerging Impact on Cardiovascular Health. *Nutr. Rev.* **2010**, *68*, 168−177.

(2) Wojdyio, A.; Oszmianski, J.; Bober, I. The Effect of Chokeberry, Flowering Quince Fruits and Rhubarb Juice to Strawberry Jams on Their Polyphenol Content, Antioxidant Activity and Colour. *Eur. Food Res. Technol.* **2008**, *227*, 1043−1051.

(3) Sanchez-Patan, F.; Bartolome, B.; Martin-Alvarez, P. J.; Anderson, M.; Howell, A.; Monagas, M. Comprehensive Assessment of the Quality of Commercial Cranberry Products. Phenolic Characterization and in Vitro Bioactivity. *J. Agric. Food Chem.* **2012**, *60*, 3396−3408.

(4) Foo, L. Y.; Lu, Y.; Howell, A. B.; Vorsa, N. The Structure of Cranberry Proanthocyanidins Which Inhibit Adherence of Uropathogenic P-Fimbriated *Escherichia coli* in Vitro. *Phytochemistry* **2000**, *54*, 173−181.

(5) Howell, A. B.; Reed, J. D.; Krueger, C. G.; Winterbottom, R.; Cunningham, D. G.; Leahy, M. A-type Cranberry Proanthocyanidins and Uropathogenic Bacterial Anti-Adhesion Activity. *Phytochemistry* **2005**, *66*, 2281−2291.

(6) Weiss, E. I.; Kozlovsky, A.; Steinberg, D.; Lev-Dor, R.; Bar Ness Greenstein, R.; Feldman, M.; Sharon, N.; Ofek, I. A High Molecular Mass Cranberry Constituent Reduces Mutants Streptococci Level in Saliva and Inhibits in Vitro Adhesion to Hydroxyapatite. *FEMS Microbiol. Lett.* **2004**, *232*, 89−92.

(7) Borges, G.; Degeneve, A.; Mullen, W.; Crozier, A. Identification of Flavonoid and Phenolic Antioxidants in Black Currants, Blueberries, Raspberries, Red Currants, And Cranberries. *J. Agric. Food Chem.* **2010**, *58*, 3901−3909.

Table 1. Proanthocyanidin Detection and Confirmation in Commercial Extract Samples by LC-HRMS

compound	formula	exact m/z	commercial extract sample 1		commercial extract sample 2	
			experimental m/z	mass error (ppm)	experimental m/z	mass error (ppm)
A-type procyanidins	$C_{30}H_{24}O_{12}$	575.1195	575.1179	−2.85	575.1183	−2.00
B-type procyanidins	$C_{30}H_{26}O_{12}$	577.1351	575.1341	−1.83	577.1343	−1.41
C-type procyanidins	$C_{45}H_{18}O_{18}$	868.1935	n.d.	n.d.	865.1956	−3.37
proanthocyanidin trimer AA	$C_{45}H_{34}O_{18}$	861.1672	n.d.	n.d.	861.1669	−0.43
proanthocyanidin trimer BA	$C_{45}H_{36}O_{18}$	863.1829	863.1812	−2.01	863.1814	−1.73
proanthocyanidin tetramer BAA	$C_{60}H_{46}O_{24}$	1149.2306	n.d.	n.d.	1149.2290	−1.41

(8) Gu, L.; Kelm, M. A.; Hammerstone, J. F.; Beecher, G.; Holden, J.; Haytowitz, D.; Prior, R. L. Screening of Foods Containing Proanthocyanidins and Their Structural Characterization Using LC-MS/MS and Thiolytic Degradation. *J. Agric. Food Chem.* **2003**, *51*, 7513−7521.
(9) Patel, K. D.; Scarano, F. J.; Kondo, M.; Hurta, R. A. R.; Neto, C. C. Proanthocyanidin-Rich Extracts from Cranberry Fruit (*Vaccinium macrocarpon* Ait.) Selectively Inhibit the Growth of Human Pathogenic Fungi *Candida* spp. and *Cryptococcus neoformans*. *J. Agric. Food Chem.* **2011**, *59*, 12864−12873.
(10) Motilva, M. J.; Serra, A.; Macia, A. Analysis of Food Polyphenols by Ultra High-Performance Liquid Chromatography Coupled to Mass Spectrometry: An Overview. *J. Chromatogr. A* **2013**, *1292*, 66−82.
(11) Appeldoorn, M. M.; Vincken, J. P.; Sanders, M.; Hollman, P. C. H.; Gruppen, H. Combined Normal-Phase and Reversed-Phase Liquid Chromatography/ESI-MS as a Tool To Determine the Molecular Diversity of A-type Procyanidins in Peanut Skins. *J. Agric. Food Chem.* **2009**, *57*, 6007−6013.
(12) Iswaldi, I.; Gomez-Caravaca, A. M.; Arraez-Roman, D.; Uberos, J.; Lardon, M.; Segura-Carretero, A.; Fernandez-Gutierrez, A. Characterization by High-Performance Liquid Chromatography with Diode-Array Detection Coupled to Time-of-Flight Mass Spectrometry of the Phenolic Fraction in a Cranberry Syrup Used to Prevent Urinary Tract Diseases, Together with a Study of Its Antibacterial Activity. *J. Pharm. Biomed. Anal.* **2012**, *58*, 34−41.
(13) Wallace, T. C.; Giusti, M. M. Extraction and Normal-Phase HPLC-Fluorescence-Electrospray MS Characterization and Quantification of Procyanidins in Cranberry Extracts. *J. Food Sci.* **2010**, *75*, C690−C696.
(14) Vallverdu-Queralt, A.; Jauregui, O.; Medina-Remon, A.; Andres-Lacueva, C.; Lamuela-Raventos, R. M. Improved Characterization of Tomato Polyphenols Using Liquid Chromatography/Electrospray Ionization Tandem Mass Spectrometry. *Rapid Commun. Mass Spectrom.* **2010**, *24*, 2986−2992.
(15) Ajila, C. M.; Brar, S. K.; Verma, M.; Tyagi, R. D.; Godbout, S.; Valero, J. R. Extraction and Analysis of Polyphenols: Recent Trends. *Crit. Rev. Biotechnol.* **2011**, *31*, 227−249.
(16) Ignat, I.; Volf, I.; Popa, V. I. A Critical Review of Methods for Characterisation of Polyphenolic Compounds in Fruits and Vegetables. *Food Chem.* **2011**, *126*, 1821−1835.
(17) Del Bubba, M.; Checchini, L.; Chiuminatto, U.; Doumett, S.; Fibbi, D.; Giordani, E. Liquid Chromatography/Electrospray Ionization Tandem Mass Spectrometric Study of Polyphenolic Composition of Four Cultivars of *Fragaria vesca* L. Berries and Their Comparative Evaluation. *J. Mass Spectrom.* **2012**, *47*, 1207−1220.
(18) Rockenbach, I. I.; Jungfer, E.; Ritter, C.; Santiago-Schuebel, B.; Thiele, B.; Fett, R.; Galensa, R. Characterization of Flavan-3-ols in Seeds of Grape Pomace by CE, HPLC-DAD-MSn, and LC-ESI-FTICR-MS. *Food Res. Int.* **2012**, *48*, 848−855.
(19) Seeram, N. P.; Adams, L. S.; Hardy, M. L.; Heber, D. Total Cranberry Extract versus Its Phytochemical Constituents: Antiproliferative and Synergistic Effects against Human Tumor Cell Lines. *J. Agric. Food Chem.* **2004**, *52*, 2512−2517.
(20) Seeram, N. P.; Adams, L. S.; Zhang, Y.; Lee, R.; Sand, D.; Scheuller, H. S.; Heber, D. Blackberry, Black Raspberry, Blueberry, Cranberry, Red Raspberry, and Strawberry Extracts Inhibit Growth and Stimulate Apoptosis of Human Cancer Cells in Vitro. *J. Agric. Food Chem.* **2006**, *54*, 9329−9339.
(21) Feliciano, R. P.; Shea, M. P.; Shanmuganayagam, D.; Krueger, C. G.; Howell, A. B.; Reed, J. D. Comparison of Isolated Cranberry (*Vaccinium macrocarpon* ait.) Proanthocyanidins to Catechin and Procyanidins A2 and B2 for Use As Standards in the 4-(Dimethylamino)cinnamaldehyde Assay. *J. Agric. Food Chem.* **2012**, *60*, 4578−4585.
(22) Wang, W.; Yagiz, Y.; Buran, T. J.; Nunes, C.d.N; Gu, L. Phytochemicals from Berries and Grapes Inhibited the Formation of Advanced Glycation End-Products by Scavenging Reactive Carbonyls. *Food Res. Int.* **2011**, *44*, 2666−2673.
(23) Riihinen, K. R.; Goedecke, T.; Pauli, G. F. Purification of Berry Flavonol Glycosides by Long-Bed Gel Permeation Chromatography. *J. Chromatogr. A* **2012**, *1244*, 20−27.
(24) Prior, R. L.; Fan, E.; Ji, H.; Howell, A.; Nio, C.; Payne, M. J.; Reed, J. Multi-Laboratory Validation of a Standard Method for Quantifying Proanthocyanidins in Cranberry Powders. *J. Sci. Food Agric.* **2010**, *90*, 1473−1478.
(25) Sawalha, S. M. S.; Arraez-Roman, D.; Segura-Carretero, A.; Fernandez-Gutierrez, A. Quantification of Main Phenolic Compounds in Sweet and Bitter Orange Peel Using CE-MS/MS. *Food Chem.* **2009**, *116*, 567−574.
(26) Helmja, K.; Vaher, M.; Puessa, T.; Kaljurand, M. Analysis of the Stable Free Radical Scavenging Capability of Artificial Polyphenol Mixtures and Plant Extracts by Capillary Electrophoresis and Liquid Chromatography-Diode Array Detection-Tandem Mass Spectrometry. *J. Chromatogr. A* **2009**, *1216*, 2417−2423.
(27) Peres, R. G.; Micke, G. A.; Tavares, M. F. M.; Rodriguez-Amaya, D. B. Multivariant Optimization, Validation, And Application of Capillary Electrophoresis for Simultaneous Determination of Polyphenols and Phenolic Acids in Brazilian Wines. *J. Sep. Sci.* **2009**, *32*, 3822−3828.
(28) Franquet-Griell, H.; Checa, A.; Núñez, O.; Saurina, J.; Hernandez-Cassou, S.; Puignou, L. Determination of Polyphenols in Spanish Wines by Capillary Zone Electrophoresis. Application to Wine Characterization by Using Chemometrics. *J. Agric. Food Chem.* **2012**, *60*, 8340−8349.
(29) Carrasco-Pancorbo, A.; Gomez-Caravaca, A. M.; Segura-Carretero, A.; Cerretani, L.; Bendini, A.; Fernandez-Gutierrez, A. Use of Capillary Electrophoresis with UV Detection to Compare the Phenolic Profiles of Extra-Virgin Olive Oils Belonging to Spanish and Italian PDOs and Their Relation to Sensorial Properties. *J. Sci. Food Agric.* **2009**, *89*, 2144−2155.
(30) Ehala, S.; Vaher, M.; Kaljurand, M. Characterization of Phenolic Profiles of Northern European Berries by Capillary Electrophoresis and Determination of Their Antioxidant Activity. *J. Agric. Food Chem.* **2005**, *53*, 6484−6490.
(31) Cote, J.; Caillet, S.; Dussault, D.; Sylvain, J. F.; Lacroix, M. Effect of Juice Processing on Cranberry Antibacterial Properties. *Food Res. Int.* **2011**, *44*, 2922−2929.
(32) Wise, B.; Gallager, N. B. *PLS_Toolbox for use with MATLAB*, version 2.0; Eigenvector Research Inc.; Mason, WA, 1992.
(33) Massart, D. L.; Vandeginste, B. G. M.; Buydens, L. M. C.; de Jong, S.; Lewi, P. J.; Smeyers-Verbeke, J. *Handbook of Chemometrics and Qualimetrics*; Elsevier: Amsterdam, 1997.
(34) Caillet, S.; Lorenzo, G.; Cote, J.; Doyon, G.; Sylvain, J. F.; Lacroix, M. Cancer Chemopreventive Effect of Fractions from Cranberry Products. *Food Res. Int.* **2012**, *45*, 320−330.
(35) Duarte, S.; Gregoire, S.; Singh, A. P.; Vorsa, N.; Schaich, K.; Bowen, W. H.; Koo, H. Inhibitory Effects of Cranberry Polyphenols on Formation and Acidogenicity of *Streptococcus mutans* Biofilms. *FEMS Microbiol. Lett.* **2006**, *257*, 50−56.

Table 1. 88 Apple Varieties under Study Including 27 Apple Varieties, Which Were Grafted between the Years 2003 and 2008 on Two Individual Trees Termed "F" and "L"

1	Alkmene	23	Hauxapfel	45	Roter Griesapfel	L224	London Pepping
2	Ananasrenette	24	Herrenapfel	46	Roter James Grieve	L220	Magna Super
3	Berneder	25	Jonathan	47	Roter Passamaner	L203	Mostzigeuner
4	Bismarck	26	Kammerapfel	48	Roter Stettinger	L209	Rajka
5	Boikenapfel	27	Kanada Renette	49	Samareiner Rosmarien	L200	Rheinischer Winterrambour
6	Carpetin	28	Kleiner Feiner	50	Schieblers Taubenapfel	L226	Ribston Pepping
7	Champagner Renette	29	Lesans Kalvill	51	Schmidberger Renette	L217	Roter Herbstkalvill
8	Damason Renette	30	Liberty	52	Schöner von Wiltshire	L207	Seeländer Reinette
9	Deans Küchenapfel	31	Maschanzker	53	Sommerrambour	L202	Zuccalmanglios Renette
10	Dülmäner Rosenapfel	32	Odenwälder	54	Spitzapfel	F213	Christkindler
11	Fasslapfel	33	Pilot	55	Spitzling	F221	Discovery
12	Florianer Rosmarin	34	Pinova	56	Steirischer Maschanzker	F218	Florina
13	Geheimrat Oldenburg	35	Piros	57	Weißer Passamaner	F215	Freyperg
14	Gelber Bellefleur	36	Plankenapfel	58	Weißer Winter-Taffetapfel	F225	Grüter Edelapfel
15	Gelber Edelapfel	37	Pom. Kongress	59	Winter-Goldparmäne	F223	Roter von Siemonffi
16	Glasapfel	38	Prinzenapfel	60	Zabergau Renette	F204	Royal Gala
17	Glockenapfel	39	Relinda	61	Zuccalmaglios Renette	F222	Sponheimer Flurapfel
18	Goldrenette Freiherr von Berlepsch	40	Retina	L214	Berlepsch	F212	Stäubli 2
19	Graue Herbstrenette	41	Rewena	L205	Blenheim	F216	Topaz
20	Grüner Boskoop	42	Rheinischer Krummstiel	L201	Dr. Seeligs Orangenpepping	F219	Wachsrenette
21	Harberts Renette	43	Riesenboikenapfel	L211	Gewürzluiken	F210	Weißer Winterkalvill
22	Hausapfel	44	Roter Boskoop	L206	Hallauer Maienapfel	F208	Winterzitrone

This holds true especially for noncommercial, old varieties that are only grown in restricted geographic regions.

In this study the phytochemical composition of apple juices derived from 88 mostly noncommercial old varieties of apples cultivated in Upper Austria was determined. Information on the vast majority of the analyzed juices, especially concerning the polyphenolic content, is still lacking. The results of our study will help to identify available local apple varieties that are of particular interest for the development of apple-based food with a strong focus on health beneficial effects.

MATERIALS AND METHODS

Materials and Reagents. (+)-Catechin, α-amylase from porcine pancreas, AAPH (2,2′-azobis(amidinopropane) dihydrochloride), ABTS (2,2′-azinobis(3-ethylbenzthiazoline-6-sulfonic acid), acetonitrile, AG1478, bovine catalase, epidermal growth factor (EGF), fluorescein sodium salt, Folin−Ciocalteu reagent, in vitro toxicology assay kit, methanosulfonic acid, phenolphthalein, potassium persulfate, potassium phosphate, nitric acid, rosmarinic acid, sodium bicarbonate, sodium hydroxide, trifluoroacetic acid (TFA), and Trolox [(±)-6-hydroxy-2,5,7,8-tetramethylchromane-2-carboxylic acid] were purchased from Sigma Aldrich (Taufkirchen, Germany). Standards for K^+, Mg^{2+}, and Ca^{2+} (Certipur, cation multielement standard III) and antimony tartrate solution were from Merck-Millipore (Vienna, Austria). Potassium dihydrogen orthophosphate, ascorbic acid, methanol, and ammonium molybdate were purchased from VWR (Vienna, Austria). Sulfuric acid was obtained from Fisher Scientific (Vienna, Austria). Chlorogenic acid, epicatechin, epigallocatechin, epigallocatechin gallate, epicatechin gallate, procyanidin B1, procyanidin B2, and phloridzin were purchased from Extrasynthese (Genay, France). 96-Well plates were from Greiner Bio-One (Kremsmünster, Austria). Fetal calf serum, penicillin/streptomycin, and DMEM high glucose medium were purchased from PAA (Pasching, Austria). A protein phosphorylation analysis kit termed "cell-based Delfia assay" including a europium-labeled anti-phosphotyrosine-antibody was obtained from Perkin-Elmer (Rodgau, Germany). The Syto62 cell stain reagent was from Life Technologies (Darmstadt, Germany).

Apple Variety Selection and Preparation. All apple varieties were grown under organic conditions in the Eferding region of Upper Austria. This region termed Eferdinger Becken is a plain landscape area near the Danube river and has the most moderate climate in Upper Austria. The soil in this region consists mainly of loose or clayey sediments and is low or free of lime. The apples were collected in September and October 2010 and immediately processed to apple juice. Apples were washed and the juice was pressed out using a conventional juice maker (Kenwood JE 850 XXL). At least 10 apples harvested from three to five individual trees were processed to generate a combined juice for each variety to account for differences within apples from the same variety. The samples were stored at <−60 °C without addition of ascorbic acid. Analyzed apple varieties are shown in Table 1.

Total Phenolic Content (TPC). Total phenolic content was determined using Folin−Ciocalteu reagent as described previously[13] with small modifications. In short, apple juice was centrifuged at 10,000 rpm for 10 min and only the supernatant was used for total phenolic quantitation, since the cloudiness of apple juice has been reported to influence the obtained TPC values.[14] Deionized water (1.4 mL) was mixed with 16.7 μL of apple juice supernatant and 83.3 μL of Folin−Ciocalteu reagent. The mixture was allowed to stand for 3−6 min at room temperature followed by addition of 167 μL of sodium bicarbonate solution (200 g/L). After 70−75 min incubation at room temperature in the dark absorbance was measured at 750 nm. Total phenolic content was expressed as (+)-catechin equivalents in mg/L apple juice. Each juice was measured in triplicate.

Trolox Equivalent Antioxidant Capacity (TEAC). Total antioxidant capacity of different apple juices was measured using the ABTS decolorization assay.[15] Apple juices were diluted 1:10 with deionized water and analyzed by mixing 500 μL of diluted ABTS radical solution with 10 μL of diluted juice. After 5 min incubation at 30 °C the absorbance was measured at 734 nm. Results were quantitated based on a dilution series of Trolox ranging from 6.25 μM to 1 mM. Each juice was measured in triplicate.

Oxygen Radical Absorbance Capacity (ORAC) Measurements. The ORAC assay was performed as described previously with slight modifications.[16] Apple juices were centrifuged (5 min; 10,000 rpm) prior to measurement. Supernatant was further diluted (1:200) with phosphate buffer (10 mM, pH 7.4). In short, 150 μL of fluorescein (10 nM) was pipetted into each well and 25 μL of the standard (Trolox) or diluted apple juice was added. The plate was incubated at 37 °C for 30 min in the dark followed by addition of 25 μL of AAPH solution (240 mM) per well. The decrease in fluorescence of fluorescein was determined by collecting readings at

excitation of 485 nm and emission of 520 nm every minute for 90 min on a plate reader (POLARstar omega, BMG LABTECH, Ortenberg, Germany). The ORAC value was calculated using the ORAC plugin of the Omega MARS plate reader software. Each juice was measured in triplicate.

Mineral Nutrients, Phosphate, and Trace Elements. The minerals K^+, Mg^{2+}, and Ca^{2+} were quantitated by ion chromatography (Dionex ICS1000, Thermo Fisher Scientific, Vienna, Austria). An Ionpac CS 12A 4 mm column was used for the separation of the different cations. The mobile phase consisted of 20 mM methanosulfonic acid, the flow rate was 1 mL/min, and sample injection volume was 25 μL.

Phosphate concentrations were measured using a phosphomolybdate method.[17] The apple juices were passed through a 0.45 μm filter. 500 μL of apple juice, 2 mL of ddH_2O water, 100 μL of ascorbic acid solution (10 g of ascorbic acid in 100 mL of ddH_2O), and 200 μL of ammonium molybdate solution were mixed and filled up to 5 mL with ddH_2O. As a phosphate standard, potassium dihydrogen orthophosphate was used. Absorbance was measured at 880 nm.

The trace elements Mn^{2+}, Cu^{2+}, and Fe^{2+} were quantitated by inductively coupled plasma mass spectrometry (ICP-MS). Prior to measurement 1 mL of apple juice was mixed with 3 mL of HNO_3 and microwave-digested using the MLS Ultraclave-IV. The resulting clear solution was diluted 1:10 with ddH_2O. ICP-MS measurements were performed using an Agilent ICP-MS 7500 cx spectrometer (Agilent Technologies, Santa Clara, CA, USA) operated in He mode (Mn^{2+} and Cu^{2+}) or H_2 mode (Fe^{2+}). Each juice was measured in triplicate.

Identification and Quantitation of Polyphenols by HPLC. RPC-MS analysis was performed on an Agilent 1100 HPLC system equipped with a vacuum degasser, a quaternary pump, an autosampler, and a UV−vis diode array detector (all from Agilent Technologies, Santa Clara, CA, USA). Separations were carried out using an ODS Hypersil column (250 mm × 4.6 mm inner diameter; 1.8 μm particle size; Thermo Fisher Scientific, Austria). Analytes were separated by gradient elution with 0.1% (v/v) formic acid (A) and acetonitrile containing 0.1% (v/v) formic acid (B) at a flow rate of 1 mL/min. The linear gradient elution program was as follows: starting conditions 97.5% A and 2.5% B; the proportion of B was increased to 10% at 20 min, 20% at 32 min, 50% at 45 min, and 80% at 50 min. The column was thermostatted at 40 °C, and the injection volume was 20 μL.

MS measurements were done on a 6520 quadrupole/time-of-flight (Q-TOF) instrument equipped with an electrospray ionization source (Agilent Technologies, Santa Clara, CA, USA). Results were obtained using the following settings: MS capillary voltage 3750 V, fragmentor voltage 180 V, drying-gas (nitrogen) flow rate 12 L/min, drying-gas temperature 350 °C, and nebulizer pressure 60 psi. Scanning mass range was from m/z 70 to 3200 with an acquisition rate of 1.0 spectra/s in the negative MS mode.

Quantitation of identified polyphenols was done using UV absorption by reference substances of known concentrations prepared in deionized water. For reversed phase chromatography (RPC) analysis a Jasco LC-2000 Plus Series system comprising a quaternary pump with build-in degasser, an autosampler, a temperature controlled column compartment, and a diode array detector (DAD) equipped with Chrompass software (all from Jasco Corporation, Tokyo, Japan) was used. Separation was performed on a Hypersil ODS C18 column (250 mm × 4.6 mm inner diameter, 5 μm particle size; Thermo Fisher Scientific, Vienna, Austria). Column temperature was set to 40 °C, and elution was carried out at 1 mL/min. The injection volume for all samples was 20 μL, and eluted substances were detected using multiple UV wavelengths from 200 to 350 nm. The following conditions were used for RPC analysis: Mobile phase A contained 0.1% TFA in water. Mobile phase B contained acetonitrile, water, and TFA in the ratio 50:50:0.1 (%). Mobile phase C contained 0.1% TFA in acetonitrile. The starting conditions were 95% A and 5% B. Elution was performed with a linear gradient: The proportion of B was increased to 20% at 20 min, 40% at 32 min, and 100% at 45 min. Limit of detection (LOD) was defined as signal-to-noise ratio of 2:1 and limit of quantitation (LOQ) as 4:1. For flavan-3-ols LOD of 0.1 mg/L and LOQ of 0.4 mg/L were defined with a linear range of 1−500 mg/L. For hydroxycinnamic acids LOD of 0.05 mg/L and LOQ of 0.2 mg/L were defined with a linear range of 1−1,000 mg/L. For quercetin derivates LOD of 0.1 mg/L and LOQ of 0.3 mg/L were defined with a linear range of 0.1−100 mg/L. Apple juice samples were centrifuged for 10 min at 15,000 rpm followed by 0.1 μm filtration to remove any remaining solids before analysis.

Quantitation of Acid Content by HPLC. Malic and citric acid content was quantitated for each sample using a RPC method described previously.[18] Quantitation was done using purified malic and citric acid dissolved in deionized water. For RPC analysis a Jasco LC-2000 Plus Series system was used as described above. Separation was performed on a Sorbax SB-C18 column (75 mm × 4.6 mm inner diameter, 3.5 μm particle size; Agilent Technologies, Santa Clara, CA, USA). Column temperature was set to 35 °C, and isocratic elution was carried out at 0.5 mL/min. A 50 mM potassium phosphate buffer adjusted to pH 2.8 was used as mobile phase. Apple juice samples were centrifuged for 10 min at 15,000 rpm followed by 0.1 μm filtration to remove any remaining solids before analysis. The injection volume for all samples was 2 μL, and eluted substances were detected at 215 nm. Limit of detection (LOD) was defined as signal-to-noise ratio of 2:1 and limit of quantification (LOQ) as 4:1. For citric acid a LOD of 20 mg/L and LOQ of 50 mg/L were defined with a linear range of 20−1,000 mg/L. For malic acid the LOD was defined at 50 mg/L and the LOQ at 100 mg/L with a linear range of 0.1−20 g/L.

Quantitation of Fruit Acids by Titration. Total acid content was determined using the acidic titration method described in an OECD guideline for food production, which can be found on the OECD Web site (www.oecd.org/agriculture). In short, apple juice was diluted 1:10 with deionized water, mixed with 3 μL of phenolphthalein, and titrated with 0.1 M sodium hydroxide until the point of neutrality was reached (indicator changes from colorless to pink). Results were expressed as g/L of malic acid.

Quantitation of Anthocyanin Pigment Content. The anthocyanin content of apple juices was determined using a pH differential method.[19] In brief, apple juices were diluted 1:5 either in pH = 1.0 buffer (0.025 M potassium chloride) or in pH = 4.5 buffer (0.4 M sodium acetate) adjusted with HCl and transferred to 10 mm cuvettes. Absorbance (A) of each diluted sample was determined at 520 and 700 nm within 15 min after preparation for both pH values. The anthocyanin pigment concentration was calculated as cyanidin-3-glucoside equivalent. The quantitation limit for this method was determined to be 0.1 mg/L. Each juice was measured in triplicate.

Sugar Content Measurements. The sugar content of analyzed apple juice samples was measured using a RHB-55 refractometer (PCE-group, Meschede, Germany). In short, a single drop of undiluted apple juice was loaded onto the prism and the °Brix value was read from the graduation.

Amylase Activity. Inhibition of amylase activity by various apple juices was analyzed using a modified commercial amylase assay (Abcam, Cambridge, U.K.). The nitrophenol included in the assay was used to generate a standard curve. The apple juice samples were incubated with 1 mg/mL α-amylase for varying time periods in 96-well plates. For α-amylase activity measurements, double distilled water was used as a reagent blank, and rosmarinic acid (1.5 mg/mL), a known α-amylase inhibitor,[20] served as a positive control. 50 μL of the individual samples (apple juice diluted 1:10 in ddH_2O) was mixed with 100 μL of reaction reagent composed of 50 μL of assay buffer and 50 μL of substrate mix (containing substrate and α-glucosidase). Absorption was measured using a plate reader (POLARstar omega, BMG LABTECH, Ortenberg, Germany) at 405 nm (absorption mode) at 1 min timed intervals. Each juice was measured in triplicate.

Cytotoxicity. Cytotoxicity was analyzed using a resazurin-based assay. Human adenocarcinoma HeLa (DSMZ, Braunschweig, Germany) and human hepatocarcinoma HuH-7 cells (kind gift from John McLauchlan, University of Glasgow) were seeded in 96-well plates (30,000 cells/well) in 200 μL of DMEM high glucose medium supplemented with 10% fetal calf serum and 100 μg/mL penicillin/streptomycin. Cells were grown to 90% confluency in a humidified atmosphere at 37 °C and 5% CO_2. Test substances were added at varying concentration followed by incubation at 37 °C for different

Table 2. Ripeness Parameters (°Brix, Titratable Acidity, Malic Acid, Citric Acid) of Apple Juice Prepared from 88 Apple Varieties

	units	mean	SD	% CV	min	max	range
°Brix		12.9	2.0	15.2	8.0	18.9	10.9
TA	(% as malic)	0.80	0.31	36.90	0.27	1.95	1.68
malic acid	(mg/L)	7175.4	4261.4	59.4	127.5	17245.1	17117.6
citric acid	(mg/L)	115.9	91.6	79.0	28.4	522.6	494.2

Table 3. Total Phenolic Content (TPC) and Antioxidant Capacities of Apple Juices under Study

	units	mean	SD	% CV	min	max	range
TPC	(mg/L)	777.7	447.2	57.5	103.2	2275.6	2172.4
TEAC	(mmol/L)	3.3	1.6	48.3	0.8	7.8	6.9
ORAC	(mmol/L)	18.8	9.5	50.5	3.0	58.9	55.9

time periods. Catalase was added for some experiments. The cells were washed once with medium and incubated with 10% resazurin solution in cell culture medium for two hours at 37 °C and 5% CO_2. Finally, fluorescence intensity (544 nm excitation, 590 nm emission) was measured using a plate reader (POLARstar omega, BMG LABTECH, Ortenberg, Germany). Data analysis was done using the OmegaMARS Data analysis software package (BMG Labtech, Ortenberg, Germany). Each juice was measured in triplicate.

EGFR Activity. The epidermoid carcinoma cell line A431 (DSMZ, Braunschweig, Germany) was grown in DMEM high glucose culture medium in 96-well plates for 16 h (50,000 cells/well). Complete cell culture medium was removed, and cells were starved (DMEM + 0.1% BSA without FBS) for 3 h followed by incubation with different apple juices or a known inhibitor of EGFR phosphorylation (AG1478) for 6 h. Cells were then washed once with PBS and treated with EGF (170 nM) for 5 min. Immediately afterward cells were fixed and permeabilized by addition of 100 μL of −20 °C cold methanol for 10 min. After an additional PBS washing step 100 μL of Delfia-Eu-anti-phosphotyrosine-antibody was added at a concentration of 300 ng/mL (diluted in Delfia Assay Buffer supplemented with 0.5% BSA). The plate was incubated for 2 h at room temperature and then washed four times with Delfia Wash Solution. 200 μL/well Delfia Enhancement solution was added for 5 min, and the fluorescence intensity was measured using the time-resolved fluorescence protocol on a POLARstar Omega plate reader (BMG Labtech, Ortenberg, Germany) with the following settings: start time 400 μs, cycle time 1 ms, excitation 355 nm, and emission 620 nm. Results were normalized to the total cell number per well using Syto62 cell staining. Each juice was measured in triplicate.

RESULTS AND DISCUSSION

Physicochemical Properties of Investigated Apple Varieties. It is a common sense that different maturity of fruits affects the accumulation of phytochemicals.[8] Thus the ripeness of the investigated apple varieties by quantitation of the sugar content (°Brix value) and the sample acidity (titratable acidity (TA), malic and citric acid) was determined. As shown in Table 2 a mean °Brix value of 12.9 ranging from 8.0 to 18.9, and a mean titratable acidity of 0.8 (% as malic acid) ranging from 0.27 to 1.95 was found. These results indicate a high sugar:acid ratio being consistent with a ripe state as specified by the FAO. The values for the analyzed apple juices can be found in Supplementary Table 1 in the Supporting Information. All samples are characterized by high sugar levels, and the vast majority have been found to have low acidity. Some apple juice varieties, e.g., Zuccalmaglios Renette or Geheimrat Oldenburg, have been demonstrated to have rather high, variety-specific acidity levels. Nevertheless, those samples were included in our study since the obtained °Brix values are within an acceptable range. Taken together, collected data confirm a sufficient maturity of the apples at the time of harvesting.

Quantitation of Polyphenols. A high variability for TPC was found ranging from only 103.2 mg/L up to 2.3 g/L in some varieties (Table 3). For the full list see Supplementary Table 1 in the Supporting Information. The mean TPC of all 88 analyzed varieties was determined to be 777.7 mg/L. A large standard deviation of 447.2 mg/L emphasizes the significant differences of the polyphenol content among the apple varieties. Our results clearly showed that the TPC levels of certain, popular apple varieties are relatively low: For example, the TPC content of juice prepared from Royal Gala (F204) or Topaz (F216) apples grown in the Eferding region was found to be only 185.8 and 257.4 mg/L, respectively. Gala apples are among the most common sold apple varieties worldwide (number 2 on the US market), and Topaz apples are highly popular especially in Central Europe. The great majority of the apple varieties (~60%) that were investigated within this study are used as dessert apples, 25% for the production of nonalcoholic or alcoholic beverages, and 15% as industrial apples that can be, e.g., utilized for food production. However, the economic significance of most of these apple varieties is rather low and limited to the region of Eferding in Upper Austria. Thus, attempts for a broader distribution of selected dessert apple varieties with high TPC levels as characterized in this study (e.g., Harberts Renette, Odenwälder, and Zuccalmaglios Renette) should be made to tap the full potential of these varieties.

A drawback of the FC method is that other reducing reagents present in the apple juice supernatant, such as ascorbic acid, might lead to an overestimation of obtained TPC values.[21] In addition, being a major feature of this study, the assay is not sufficient to predict the antioxidant effect of apple juice, since biological effects are to be expected from different polyphenols. To address this question, the exact composition of the polyphenol components has to be unraveled. Importantly, using the Phenol-Explorer,[22] information on the polyphenolic content could only be extracted for two apple varieties that are included in this study, namely *Royal Gala* and *Grüner Boskoop*. However, a direct comparison to our results appears difficult due to application of juice extracts for these studies rather than analyzing untreated apple juice.[23,24]

Fifteen polyphenolic compounds belonging to four different major polyphenolic groups were identified in the apple juices prepared from each variety: chlorogenic, caffeic, and 4-*p*-coumaroylquinic acid (hydroxycinnamic acids), phloretin-2′-*O*-xyloglucoside and phloridzin (dihydrochalcone derivates),

Table 4. Single Polyphenol Content (mg/L) of Apple Juices under Study

	mean	SD	% CV	min	max	range
Hydroxycinnamic Acids						
chlorogenic acid	216.3	223.8	103.5	+[a]	1209.2	1209.2
caffeic acid	3.8	4.4	116.4	+	32.5	32.5
4-*p*-coumaroylquinic acid	11.7	13.3	114.7	+	55.5	55.5
∑ hydroxycinnamic acids	231.8					
Dihydrochalcone Derivates						
phloretin-2′-*O*-xyloglucoside	12.8	10.1	78.8	+	54.3	54.3
thloridzin	6.8	5.9	85.6	+	29.5	29.5
∑ dihydrochalcone derivates	19.6					
Flavan-3-ols						
procyanidin B1	3.5	5.2	147.6	+	23.0	23.0
procyanidin B2	40.1	48.3	120.4	+	338.1	338.1
(−)-epicatechin	13.3	17.5	131.8	+	104.7	104.7
epigallocatechin	3.3	6.6	200.8	+	38.2	38.2
epichatechingallate	11.3	10.4	91.9	+	51.0	51.0
∑ flavan-3-ols	71.5					
Flavonols						
quercetin-3-*O*-galactoside	0.7	2.9	396.7	+	26.4	26.4
quercetin-3-*O*-xyloside	2.5	4.9	194.8	+	41.1	41.1
quercetin-3-*O*-rhamnoside	2.4	3.3	137.2	+	25.2	25.2
quercetin	3.0	5.9	196.0	+	49.2	49.2
quercetin-3-*O*-rutinoside	0.3	1.8	580.6	+	15.7	15.7
∑ flavonols	8.9					
∑ anthocyanins	1.01	1.41	139.41	0.13	6.79	6.66
total polyphenol amount (HPLC)	331.8					

[a] +, < limit of quantitation.

procyanidin B1 and B2, (−)-epicatechin, epigallocatechin, and epicatechingallate (flavan-3-ols), and five quercetin derivates (flavonols). A representative HPLC-DAD diagram, indicating retention times and maximal wavelengths of each compound, is shown in Supplementary Figure 1 in the Supporting Information. Table 4 summarizes the content of selected polyphenolics of all 88 apple juice samples. In addition, obtained values for each variety can be found in Supplementary Table 2 in the Supporting Information. Among the five investigated polyphenolic groups, the hydroxycinnamic acid group was found to be the most abundant one, with chlorogenic acid being the main compound in this polyphenol group. The ratio between chlorogenic acid and *p*-coumaroylquinic acid content in different varieties has been reported to vary between 1.2 and 37.1.[25] Those ratio limits are in good agreement with the mean ratio of 20.3 of the apple juice samples presented in this study. However, for some samples much higher ratios up to 104.1 (L203) or 181.5 (L214) were found, which was mainly caused by high levels of chlorogenic acid and at the same time a very low concentration of *p*-coumaroylquinic acid being detected in these varieties. The low amounts of caffeic acid found in most samples are in good agreement with other studies.[26]

Flavan-3-ols represent the second largest group of polyphenols detected in the investigated apple juices. Procyanidin B2 and epicatechin were the most abundant polyphenolic substances in this group with a mean concentration of 40.1 and 13.3 mg/L, respectively. Similar amounts were reported in a previous study analyzing untreated apple juices.[9] Two dihydrochalcone derivates were found in most apple juices: With a mean content of 6.8 mg/L phloridzin and 12.8 mg/L phloretin-2′-*O*-xyloglucoside, our results are within the range of a previous study (∼1−25 mg/L each).[27] Our measurements also confirmed the presence of flavonols. However, this polyphenol group was found in very low concentrations (∼2% of total polyphenol amount). Anthocyanin pigments were found only in a few juice samples at low concentrations ranging from 0.13 to 6.79 mg/L. This is in line with the presence of these phytochemicals exclusively in apples characterized by a red skin.[28]

In agreement with the results from TPC measurements, RPC analysis unraveled great differences in the polyphenol content and composition of apple juices from different apple varieties. For example, the amount of chlorogenic acid for some varieties ranged from 1.79 mg/L (Royal Gala, F204) up to 1209.7 mg/L (Harberts Renette). In general, the estimated TPC values correlate with the concentration of polyphenols found by HPLC measurements. However, a high TPC level does not necessarily correlate with the detected amounts of the analyzed single polyphenols. For example, the varieties F213, L202, and L203 are all characterized by a similar TPC value of about 1.000 mg/L. However, the concentration of chlorogenic acid was found to vary between 76.4, 149.73, and 145.89 mg/L, respectively. Thus, our results clearly showed that juices prepared from various apple varieties are highly diverse in their content of total polyphenols and show great variations in their individual polyphenol composition. Furthermore, when comparing different apple varieties grafted on the same tree (F and L series, respectively), it could be observed that these varieties retain their individual polyphenolic profile. The described differences are likely to depend mainly on genetic factors, which is consistent with a study analyzing the genetic variability of apples.[29] In conclusion, grafting proves to be a superior tool for a fast growth of selected apple varieties with varying phytochemical concentration, without the need for the time-consuming cultivation of the whole tree.

dx.doi.org/10.1021/jf4051232 | J. Agric. Food Chem. 2014, 62, 1047−1056

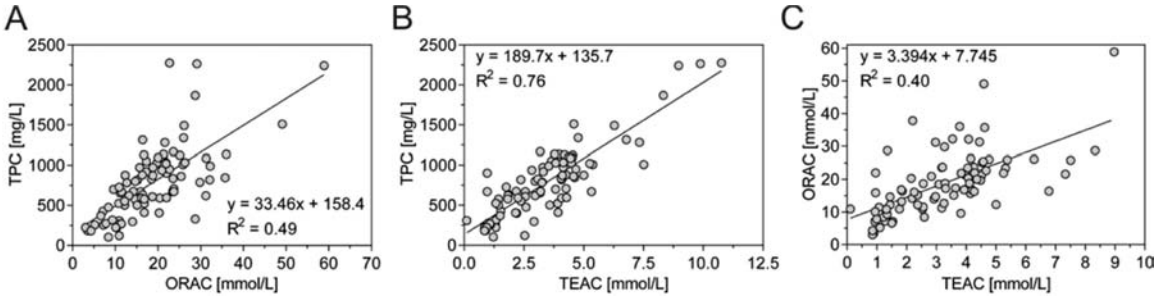

Figure 1. Linear correlation regression analysis. Correlations between (A) TPC and ORAC; (B) TPC and TEAC; (C) ORAC and TEAC. TPC: total phenolic content. ORAC: oxygen radical absorbance capacity. TEAC: Trolox equivalent antioxidant capacity.

Table 5. Mineral Content of Apple Juices under Study

	units	mean	SD	% CV	min	max	range
K^+	(mg/L)	1082.7	23.5	23.5	620.4	2064.0	1443.6
Mg^{2+}	(mg/L)	30.7	1.2	45.0	8.4	64.4	56.1
Ca^{2+}	(mg/L)	23.7	0.8	41.8	6.7	57.5	50.9
Cu^{2+}	(μg/L)	320.3	9.7	35.9	109.8	572.2	462.5
Mn^{2+}	(μg/L)	307.9	18.4	70.8	59.5	688.5	629.0
Fe^{2+}	(μg/L)	268.3	10.5	46.5	130.0	670.0	540.0
PO_4^{3-}	(mg/L)	209.7	5.3	33.9	90.0	420.3	330.3

Quantitation of Total Antioxidant Capacity. Several studies have shown that apples possess a strong antioxidant capacity.[6,30] Here two different methods (TEAC and ORAC) were used to measure the total antioxidant capacity of the different apple juices. Table 3 summarizes the TEAC and ORAC values derived from all samples. The antioxidant capacity of these juices ranged from 0.8 to 7.8 mM (TEAC) and 3.0 to 58.9 mM (ORAC), which is in good agreement with similar studies.[31] The full list of TEAC and ORAC values from all apple juice samples can be found in Supplementary Table 1 in the Supporting Information. Our results indicate the general dependence of the antioxidant capacity on the total polyphenolic concentration as can be seen by the linear regression and correlation analysis. The coefficients of determination (R^2) are given in Figure 1. All R values (correlation coefficients) were positive at the $P < 0.0001$ significance level, indicating that the values of antioxidant capacities, assayed by the two different methods, were highly correlated (R values for TPC/ORAC, 0.69; TPC/TEAC, 0.87; ORAC/TEAC, 0.63). The regression coefficient value obtained for TPC and ORAC assay was lower compared with TEAC assay, but significant in both systems. These results indicated that the two assays were suitable and reliable for assessing total antioxidant capacities. Thus, despite the aforementioned limitations of the FC method to determine the TPC, it can possibly be considered as a first indicator of antioxidant capacity of apple juice.

It was observed that some varieties contained equal (TPC of Lesans Kalvill similar to Samareiner Rosmarien) or even more total polyphenols than others (TPC Riesenboikenapfel > Glasapfel), but lower antioxidant capacity as determined by both TEAC and ORAC measurements. This effect can be explained by the different antioxidant activity of individual polyphenols as reported in previous studies.[32] Consequently, the antioxidant capacity is dependent on the phenolic composition of an individual juice.

The low TEAC and ORAC values of juice prepared from certain apple varieties, including Topaz, is consistent with other studies analyzing the antioxidant capacity of a number of old and new apple varieties in Poland.[33] The Topaz apple is a good example of a new apple variety (introduced in the 1980s), which offers several advantages for agriculture including resistance to apple scab, high yields, and good storage properties. It is also a common apple variety for organic farming. However, the low level of phenolic substances in these varieties has not been taken into consideration so far. Consequently, the distribution of apple varieties with a higher content of polyphenols should be supported to promote their positive effects on human health.

Analysis of Minerals, Phosphate, and Trace Elements. The mean and range values of the major minerals K^+, Mg^{2+}, and Ca^{2+} are indicated in Table 5, and results for individual varieties can be found in Supplementary Table 1 in the Supporting Information. The potassium concentration ranged from 620.4 (Retina) to 2064.0 mg/L (Grüner Boskoop) with large variations between individual varieties. Compared to potassium, the concentration of magnesium and calcium was significantly lower, ranging from 8.4 to 64.4 (Mg^{2+}) and 6.7 to 57.5 (Ca^{2+}) mg/L, respectively. Similar to the potassium concentration, remarkable variations for calcium and magnesium between the different varieties could be observed. Collected data, especially for potassium and copper, are in good agreement with other studies analyzing minerals and trace elements of different apple varieties.[26,34]

The PO_4^{3-} concentration of juice prepared from 56 apple varieties was found to range between 90.0 and 420.0 mg/L (Table 5), which is consistent with the work of Eisele et al., who reported PO_4^{3-} values ranging from 86.0 to 459.0 mg/L.[26] The variation between individual apple varieties was found to be in a similar range as observed for potassium.

Finally, 52 apple juice samples were analyzed for their copper and manganese content and 27 (F and L series) for iron, respectively. The observed variations between individual samples, especially those for Mn^{2+} and Fe^{2+}, were highly pronounced for these elements. The mean and range values for the Cu^{2+}, Mn^{2+}, and Fe^{2+} content are summarized in Table 5.

dx.doi.org/10.1021/jf4051232 | J. Agric. Food Chem. 2014, 62, 1047−1056

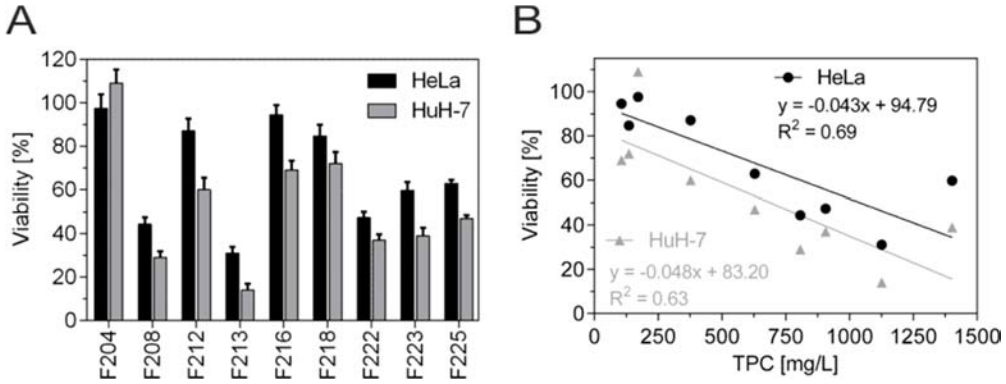

Figure 2. Cytotoxicity of selected apple juice varieties. (A) Resazurin based cytotoxicity test. HeLa or HuH-7 cells were grown to 90% confluency in 96-well plates and incubated with apple juice diluted in cell culture medium (1:5 dilution) for 6 h. Cell viability is normalized to a nontreated sample. Error bars are based on the standard error of the mean (n = 4). (B) Linear correlation regression analysis between TPC and viability. Correlation analysis reveals a significant interrelation of the total phenolic content (TPC) and the cell viability.

Taken together, our results show large variations between the different apple varieties, which is in good agreement with a previous study analyzing the concentration of various minerals in juice prepared from 175 apple varieties.[26] These variations can also be observed for various apple varieties grafted on a single tree (F and L series). Thus, apples harvested from grafted trees retain not only their polyphenolic profiles but also their characteristic mineral, trace element, and phosphate concentrations. From this point of view an intensified cultivation of selected apple varieties identified in this work should be considered. However, the availability of many of the varieties that possess these positive compositions for large scale cultivation remains a limiting factor. Engrafting turned out to be an excellent way to enhance growth rates and provide resistance to bacterial or fungal infections. By engrafting 27 different apple varieties on two trees grown close to each other, it could be shown that the apple fruits in fact remain their primary ingredient characteristics. This fact is clearly of key importance for the promotion of selected apple varieties.

Biological Effects of Selected Apple Juice Varieties. Different assays were used to determine several biological effects of apple juice varieties that were preselected by a pronounced variation of different ingredients including polyphenolics, minerals, and trace elements. Juices from nine apple varieties grafted on a single tree (F series) were used for these analyses. First, the cytotoxic effects of apple juice were determined on two different human cancer cell lines using a resazurin based assay. Apple juice has been reported to be a strong cancer chemopreventive.[35] Several studies have already shown the inhibitory effect on cell proliferation of cultured cancer cell lines.[36] Two human cell lines were used for investigation of the growth inhibition of selected apple juices. As shown in Figure 2A a strong reduction of cell viability could be observed in both cell lines for several apple juices at a 1:5 dilution. The observed inhibitory effect was clearly dependent on the apple juice concentration: no reduction in cell viability could be observed at higher dilution rates >1:50 (Supplementary Figure 1 in the Supporting Information). Using apple juice in cell culture medium might lead to H_2O_2 formation and pronounced cytotoxic effects.[37] Addition of catalase (100 U/mL) to prevent the formation of H_2O_2 further slightly reduced these cytotoxic effects (data not shown). Interestingly, a clear correlation between TPC levels and the described cytotoxic effects was found (Figure 2B). Our results show that certain apple juices reduce the viability of the analyzed human cancer cell lines in a TPC dependent manner. Interestingly, Veeriah et al. showed that native apple extracts were about twice as potent as a composed mixture of low molecular weight apple polyphenols in inhibiting cancer cell growth.[36] This indicates that other constituents, such as oligomeric procyanidines, substantially contribute to the potent antiproliferative properties of polyphenol-rich apple juices. Thus, the usage of apple juices instead of extract appears straightforward.

In a second experiment a putative apple juice dependent inhibition of human α-amylase, a major digestive enzyme that breaks down long-chain carbohydrates, was evaluated. Salivary and pancreatic α-amylases lead to the formation of maltose and other related oligomers by catalyzing the hydrolysis of α-1,4-linked glucose chains.[38] Several studies indicated a beneficial health effect of bioactive substances from apples, e.g., a reduced risk of chronic diseases including type 2 diabetes. In this regard the inhibition of α-amylase activity by these substances is of particular importance.[39] As shown in Figure 3 a 30−40% inhibition of α-amylase activity was observed when rosmarinic acid (1.5 mg/mL) was added, confirming the inhibitory potential of this substance. All tested apple juices of the F series also showed an incubation-time-dependent inhibition of α-amylase activity between ∼80% (24 h incubation) and ∼50%

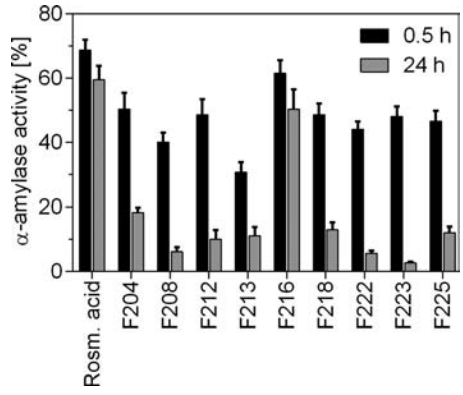

Figure 3. Inhibition of α-amylase activity by selected apple juice varieties. Rosmarinic acid (Rosm. acid; 1.5 mg/mL) or different apple juice samples diluted 1:10 were incubated with 1 mg/mL α-amylase for 30 min or 24 h, respectively. Inhibition was measured by the use of a commercial amylase activity assay containing α-glucosidase. Error bars are based on the standard error of the mean (n = 3).

dx.doi.org/10.1021/jf4051232 | J. Agric. Food Chem. 2014, 62, 1047−1056

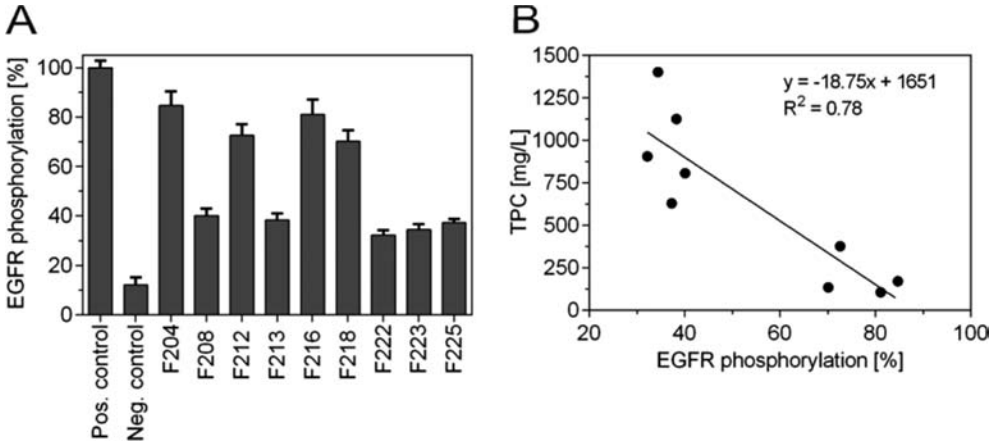

Figure 4. Epidermal growth factor receptor (EGFR) activity test. (A) HeLa cells endogenously expressing high levels of EGFR were grown to 90% confluency in 96-well plates and starved in cell culture medium without serum for 3 h, followed by incubation with the EGFR inhibitor AG1478 or selected apple juice varieties (diluted 1:20 in starving medium) for a further 6 h. After addition of 170 nM EGF, receptor phosphorylation was measured by the use of a fluorescent antibody in combination with time-resolved fluorescence. Results were normalized to EGF treated cells (positive control). AG1478 served as a negative control. Error bars are based on the standard error of the mean (n = 3). (B) Linear correlation regression analysis reveals a significant interrelation of the total phenolic content (TPC) and the EGFR phosphorylation level.

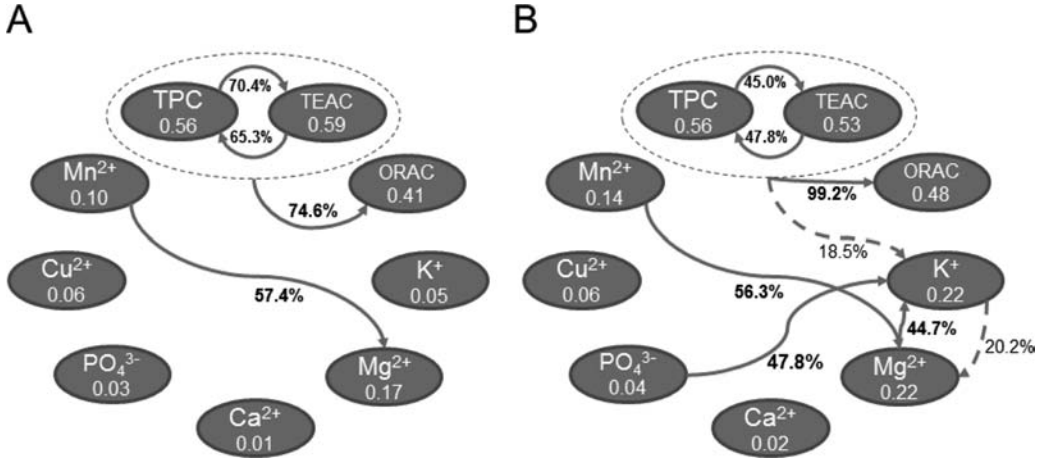

Figure 5. Graphical representation of modeling results and variable interactions using linear regression and random forests. All variables were modeled using linear regression (LR) and random forest regression (RF, 50 trees). Each node represents a variable, and the number given below a variable indicates the average quality (R^2) of the models. In order to estimate the influence of the variables on each other, all variables are mutually excluded from the modeling process, and the resulting modeling quality decrease is calculated. If the exclusion of a variable a leads to a significant decrease of the modeling quality for variable b, then a directed edge is shown; continuous lines indicate modeling influences of at least 40%, dashed lines indicate modeling influences of at least 15%, and weaker influences are not shown. As TPC and TEAC are very strongly correlated (correlation R^2 0.7125), these two variables are always excluded from the modeling process in combination, which is indicated by the dashed circles around these two variables.

(30 min incubation). In these experiments differences between individual varieties ranging from 40 to 70% (30 min) and 50 to 98% (24 h) inhibition of α-amylase activity could be observed. In contrast to the antioxidant capacity, the observed inhibitory effect was not dependent on the TPC levels of the apple juice varieties as statistical analysis determining Kendall's and Spearman's rank correlation coefficient did not reveal any significant correlation (data not shown). These results are in good agreement with a recent study excluding a positive correlation between α-amylase inhibitory activity and total phenolic content.[39] However, single polyphenols that have been shown to inhibit this enzyme (e.g., chlorogenic acid)[40] are found at high concentrations in our apple varieties.

Finally, the effects of different apple juice varieties on the activity of the epidermal growth factor receptor (EGFR) were analyzed. The EGFR plays a major role in cellular signaling: insufficient signaling may lead to the development of neurodegenerative diseases,[41] while excessive EGFR signaling is associated with the development of a wide variety of tumors. Highly elevated EGFR signaling seems to be a critical factor in the development and malignancy of these tumors.[42] Several studies have indicated that apple polyphenols inhibit EGFR activity in various cell lines.[43−45] Thus, apples rich in polyphenols are thought to prevent the formation of various cancer types in the human body. In total nine apple juice varieties of the F series were analyzed for a potential phosphorylation inhibition of the EGFR. As shown in Figure 4A the applied time-resolved-fluorescence based ELISA-assay is well-suited to detect phosphorylation of the EGFR upon stimulation. AG1478 pretreatment for 4 h clearly inhibited the phosphorylation upon EGF stimulation. When cells were incubated for 4 h with juice from different apple varieties (1:20;

dx.doi.org/10.1021/jf4051232 | J. Agric. Food Chem. 2014, 62, 1047−1056

in the presence of catalase), a pronounced inhibition of EGFR phosphorylation could be observed. Our experiments indicated remarkable differences in the degree of phosphorylation inhibition depending on the used apple varieties. Further analysis showed that the observed inhibitory effects significantly correlated with the respective TPC levels (Figure 4B), which is consistent with similar studies. Individual polyphenols such as the procyanidin dimers B1 and B2 or phloretin and phloretin-2′-*O*-xylogucoside have been found to specifically affect the EGFR activity.[43−45] Accordingly, apple juice varieties that inhibited the EGFR activity to the highest extent (F208, F213, and F223) were especially rich in these polyphenols.

In-Depth in Silico Analysis. The described dependence of the antioxidant capacity on the TPC levels is in agreement with previous studies.[6] This research was extended by the use of mathematical modeling that allowed us to identify variable interaction networks based on the analysis of apple component data. Regression models that approximate selected target variables using other available parameters in this data set have been identified. The relevance of a variable in this context can be defined via the frequency of its occurrence in models identified by evolutionary machine learning methods or via the decrease in modeling quality after removing it from the data set.[46] The following algorithms have been applied for the data set generated in this study including the results for TPC, TEAC, ORAC, Mn^{2+}, Mg^{2+}, Ca^{2+}, Cu^{2+}, K^+, and PO_4^{3-}: linear regression and random forests.[47] As shown in Figure 5A, linear regression confirms the relationship of the antioxidant capacity (TEAC and ORAC) and the TPC level. In addition, a significant interrelationship of Mg^{2+} and Mn^{2+} was found. These findings were confirmed when nonlinear modeling using random forest was applied (Figure 5B). The latter model also indicated a strong relevance of PO_4^{3-} and Mg^{2+} on the modeling of K^+. Even though importance in regression and correlation do not imply causality, this analysis implies that apples that are rich in Mg^{2+} by trend also contain higher levels of Mn^{2+}. The same assumption holds true for K^+ and PO_4^{3-}. Mn^{2+} and Mg^{2+} are abundant elements and essential to all living cells. For example Mg^{2+} plays a major role in manipulating biological compounds including DNA, RNA, and ATP. In addition, a great number of enzymes require Mg^{2+} for their function. The same is true for Mn^{2+} ions, which are essential cofactors for many enzymes. However, many of these enzymes can use Mg^{2+} as a replacement of Mn^{2+}.[48] Of special interest is the function of Mn^{2+} enzymes to detoxify superoxide free radicals in mitochondria.[49] In analogy copper and zinc bound enzymes are necessary for detoxification in the cytosol.[50] Thus, similar to polyphenols, Mn^{2+} and Cu^{2+} ions play a key role in preventing the human organism from oxidative damage.

■ ASSOCIATED CONTENT

Supporting Information

Figure depicting HPLC elution profile of a representative apple juice sample. Figure depicting influence of selected apple juice samples with varying total phenolic content on HuH-7 cell viability. Table presenting overview of the phytochemical composition of juice prepared from 88 apple cultivars. Table presenting overview of single polyphenol content of juice prepared from 88 apple cultivars. This material is available free of charge via the Internet at http://pubs.acs.org.

■ AUTHOR INFORMATION

Corresponding Author

*Phone: +43(0) 50804 44403. E-mail: julian.weghuber@fh-wels.at.

Author Contributions

‡P.L. and J.W. contributed equally to this work

Funding

This work was funded by the program "Regionale Wettbewerbsfähigkeit OÖ 2007−2013" with financial means of the European fund for regional development as well as the country of Upper Austria.

Notes

The authors declare no competing financial interest.

■ REFERENCES

(1) Bundesministerium für Ernährung und Landwirtschaft. In *Statistisches Jahrbuch über Ernährung, Landwirtschaft und Forsten*; Landwirtschaftsverlag Münster Hiltrup: Münster, 2011.

(2) Tomaschek, B. Konsumerhebung 2009/10: Ein Blick in die österreichische Speisekammer. In Statistik Austria; Vienna, 2011.

(3) Boyer, J.; Liu, R. H. Apple phytochemicals and their health benefits. *Nutr. J.* **2004**, *3*, 5.

(4) Le Marchand, L.; Murphy, S. P.; Hankin, J. H.; Wilkens, L. R.; Kolonel, L. N. Intake of flavonoids and lung cancer. *J. Natl. Cancer Inst.* **2000**, *92*, 154−60.

(5) Manach, C.; Mazur, A.; Scalbert, A. Polyphenols and prevention of cardiovascular diseases. *Curr. Opin. Lipidol.* **2005**, *16*, 77−84.

(6) Lee, K. W.; Kim, Y. J.; Kim, D. O.; Lee, H. J.; Lee, C. Y. Major phenolics in apple and their contribution to the total antioxidant capacity. *J. Agric. Food Chem.* **2003**, *51*, 6516−20.

(7) Scapagnini, G.; Vasto, S.; Abraham, N. G.; Caruso, C.; Zella, D.; Fabio, G. Modulation of Nrf2/ARE pathway by food polyphenols: a nutritional neuroprotective strategy for cognitive and neurodegenerative disorders. *Mol. Neurobiol.* **2011**, *44*, 192−201.

(8) Duda-Chodak, A.; Tarko, T.; Tuszynski, T. Antioxidant activity of apples–an impact of maturity stage and fruit part. *Acta Sci. Pol., Technol. Aliment.* **2011**, *10*, 443−54.

(9) Kahle, K.; Kraus, M.; Richling, E. Polyphenol profiles of apple juices. *Mol. Nutr. Food Res.* **2005**, *49*, 797−806.

(10) Panzella, L.; Petriccione, M.; Rega, P.; Scortichini, M.; Napolitano, A. A reappraisal of traditional apple cultivars from Southern Italy as a rich source of phenols with superior antioxidant activity. *Food Chem.* **2013**, *140*, 672−9.

(11) Hampson, C. R.; Kemp, H. Characteristics of Important Commercial Apple Cultivars. In *Apples. Botany, Production and Uses*; CABI Publishing: 2003; p 64.

(12) Muehl, F. In *Alte und neue Apfelsorten.* Obst- und Gartenbauverlag: Munich, 2007.

(13) Ainsworth, E. A.; Gillespie, K. M. Estimation of total phenolic content and other oxidation substrates in plant tissues using Folin-Ciocalteu reagent. *Nat. Protoc.* **2007**, *2*, 875−7.

(14) Huemmer, W.; Dietrich, H.; Will, F.; Schreier, P.; Richling, E. Content and mean polymerization degree of procyanidins in extracts obtained from clear and cloudy apple juices. *Biotechnol. J.* **2008**, *3*, 234−43.

(15) Re, R.; Pellegrini, N.; Proteggente, A.; Pannala, A.; Yang, M.; Rice-Evans, C. Antioxidant activity applying an improved ABTS radical cation decolorization assay. *Free Radical Biol. Med.* **1999**, *26*, 1231−7.

(16) Huang, D.; Ou, B.; Hampsch-Woodill, M.; Flanagan, J. A.; Prior, R. L. High-throughput assay of oxygen radical absorbance capacity (ORAC) using a multichannel liquid handling system coupled with a microplate fluorescence reader in 96-well format. *J. Agric. Food Chem.* **2002**, *50*, 4437−44.

(17) Shyla, B.; Mahadevaiah; Nagendrappa, G. A simple spectrophotometric method for the determination of phosphate in soil, detergents, water, bone and food samples through the formation

of phosphomolybdate complex followed by its reduction with thiourea. *Spectrochim. Acta, Part A* **2011**, *78*, 497−502.
(18) Weikle, K. Determination of citric acid in fruit juices using HPLC. *Concordia Coll. J. Anal. Chem.* **2012**, *57*−62.
(19) Lee, J.; Durst, R. W.; Wrolstad, R. E. Determination of Total Monomeric Anthocyanin Pigment Content of Fruit Juices, Beverages, Natural Colorants, and Wines by the pH Differential Method: Collaborative Study. *J. AOAC Int.* **2005**, *10*, 1269−1278.
(20) McCue, P. P.; Shetty, K. Inhibitory effects of rosmarinic acid extracts on porcine pancreatic amylase in vitro. *Asia Pac. J. Clin. Nutr.* **2004**, *13*, 101−6.
(21) Hollman, P. C.; Cassidy, A.; Comte, B.; Heinonen, M.; Richelle, M.; Richling, E.; Serafini, M.; Scalbert, A.; Sies, H.; Vidry, S. The biological relevance of direct antioxidant effects of polyphenols for cardiovascular health in humans is not established. *J. Nutr.* **2011**, *141*, 989S−1009S.
(22) Rothwell, J. A.; Perez-Jimenez, J.; Neveu, V.; Medina-Remon, A.; M'Hiri, N.; Garcia-Lobato, P.; Manach, C.; Knox, C.; Eisner, R.; Wishart, D. S.; Scalbert, A. Phenol-Explorer 3.0: a major update of the Phenol-Explorer database to incorporate data on the effects of food processing on polyphenol content. *Database (Oxford)* **2013**, *2013*, bat070.
(23) Podsedek, A.; Wilska-Jeszka, J.; Anders, B.; Markowski, J. Compositional characterisation of some apple varieties. *Eur. Food Res. Technol.* **2000**, *210*, 268−72.
(24) Vrhovsek, U.; Rigo, A.; Tonon, D.; Mattivi, F. Quantitation of polyphenols in different apple varieties. *J. Agric. Food Chem.* **2004**, *52*, 6532−8.
(25) Sanoner, P.; Guyot, S.; Marnet, N.; Molle, D.; Drilleau, J. P. Polyphenol profiles of French cider apple varieties (Malus domestica sp.). *J. Agric. Food Chem.* **1999**, *47*, 4847−53.
(26) Eisele, T. A.; Drake, S. R. The partial compositional characteristics of apple juice from 175 apple varieties. *J. Food Compos. Anal.* **2005**, *18*, 213−21.
(27) Gliszczynska-Swiglo, A.; Tyrakowska, B. Quality of Commercial Apple Juices Evaluated on the Basis of the Polyphenol Content and the TEAC Antioxidant Activity. *J. Food Sci.* **2003**, *68*, 1844−9.
(28) Lister, C. E.; Lancaster, J. E.; Sutton, K. H.; Walker, J. R. Developmental changes in the concentration and composition of flavonoids in skin of a red and a green apple cultivar. *Sci. Food Agric.* **1994**, *64*, 155−61.
(29) Volz, R. K.; McGhie, T. K. Genetic variability in apple fruit polyphenol composition in Malus x domestica and Malus sieversii germplasm grown in New Zealand. *J. Agric. Food Chem.* **2011**, *59*, 11509−21.
(30) Tsao, R.; Yang, R.; Xie, S.; Sockovie, E.; Khanizadeh, S. Which polyphenolic compounds contribute to the total antioxidant activities of apple? *J. Agric. Food Chem.* **2005**, *53*, 4989−95.
(31) Karaman, S.; Tutem, E.; Baskan, K. S.; Apak, R. Comparison of antioxidant capacity and phenolic composition of peel and flesh of some apple varieties. *J. Sci. Food Agric.* **2013**, *93*, 867−75.
(32) Sun, J.; Chu, Y. F.; Wu, X.; Liu, R. H. Antioxidant and antiproliferative activities of common fruits. *J. Agric. Food Chem.* **2002**, *50*, 7449−54.
(33) Wojdylo, A.; Oszmianski, J.; Laskowski, P. Polyphenolic compounds and antioxidant activity of new and old apple varieties. *J. Agric. Food Chem.* **2008**, *56*, 6520−30.
(34) Abid, M.; Jabbar, S.; Wu, T.; Hashim, M. M.; Hu, B.; Lei, S.; Zeng, X. Sonication enhances polyphenolic compounds, sugars, carotenoids and mineral elements of apple juice. *Ultrason. Sonochem.* **2014**, *21*, 93−7.
(35) Gerhauser, C. Cancer chemopreventive potential of apples, apple juice, and apple components. *Planta Med.* **2008**, *74*, 1608−24.
(36) Veeriah, S.; Kautenburger, T.; Habermann, N.; Sauer, J.; Dietrich, H.; Will, F.; Pool-Zobel, B. L. Apple flavonoids inhibit growth of HT29 human colon cancer cells and modulate expression of genes involved in the biotransformation of xenobiotics. *Mol. Carcinog.* **2006**, *45*, 164−74.
(37) Lapidot, T.; Walker, M. D.; Kanner, J. Can apple antioxidants inhibit tumor cell proliferation? Generation of H(2)O(2) during interaction of phenolic compounds with cell culture media. *J. Agric. Food Chem.* **2002**, *50*, 3156−60.
(38) Hanhineva, K.; Torronen, R.; Bondia-Pons, I.; Pekkinen, J.; Kolehmainen, M.; Mykkanen, H.; Poutanen, K. Impact of dietary polyphenols on carbohydrate metabolism. *Int. J. Mol. Sci.* **2010**, *11*, 1365−402.
(39) Barbosa, A. C.; Pinto Mda, S.; Sarkar, D.; Ankolekar, C.; Greene, D.; Shetty, K. Varietal influences on antihyperglycemia properties of freshly harvested apples using in vitro assay models. *J. Med. Food* **2010**, *13*, 1313−23.
(40) Sales, P. M.; Souza, P. M.; Simeoni, L. A.; Silveira, D. alpha-Amylase inhibitors: a review of raw material and isolated compounds from plant source. *J. Pharm. Pharm. Sci.* **2012**, *15*, 141−83.
(41) Bublil, E. M.; Yarden, Y. The EGF receptor family: spearheading a merger of signaling and therapeutics. *Curr. Opin. Cell Biol.* **2007**, *19*, 124−34.
(42) Cho, H. S.; Leahy, D. J. Structure of the extracellular region of HER3 reveals an interdomain tether. *Science* **2002**, *297*, 1330−3.
(43) Fridrich, D.; Kern, M.; Pahlke, G.; Volz, N.; Will, F.; Dietrich, H.; Marko, D. Apple polyphenols diminish the phosphorylation of the epidermal growth factor receptor in HT29 colon carcinoma cells. *Mol. Nutr. Food Res.* **2007**, *51*, 594−601.
(44) Kern, M.; Tjaden, Z.; Ngiewih, Y.; Puppel, N.; Will, F.; Dietrich, H.; Pahlke, G.; Marko, D. Inhibitors of the epidermal growth factor receptor in apple juice extract. *Mol. Nutr. Food Res.* **2005**, *49*, 317−28.
(45) Teller, N.; Roth, M.; Esselen, M.; Fridrich, D.; Boettler, U.; Blust, V.; Will, F.; Dietrich, H.; Raul, F.; Hummer, W.; Richling, E.; Schreier, P.; Marko, D. Apple procyanidins affect several members of the ErbB receptor tyrosine kinase family in vitro. *Food Funct.* **2013**, *4*, 689−97.
(46) Winkler, S.; Kronberger, G.; Affenzeller, M.; Stekel, H. Variable Interaction Networks in Medical Data. *Int. J. Privacy Health Inf. Manage.* **2013**.
(47) Breiman, L. Random Forests. *Mach. Learn.* **2001**, *45*, 5−32.
(48) Crowley, J. D.; Traynor, D. A.; Weatherburn, D. C. Enzymes and proteins containing manganese: an overview. *Met. Ions Biol. Syst.* **2000**, *37*, 209−78.
(49) Borgstahl, G. E.; Parge, H. E.; Hickey, M. J.; Beyer, W. F., Jr.; Hallewell, R. A.; Tainer, J. A. The structure of human mitochondrial manganese superoxide dismutase reveals a novel tetrameric interface of two 4-helix bundles. *Cell* **1992**, *71*, 107−18.
(50) Tainer, J. A.; Getzoff, E. D.; Richardson, J. S.; Richardson, D. C. Structure and mechanism of copper, zinc superoxide dismutase. *Nature* **1983**, *306*, 284−7.

necessary for tyrosinase to contain two copper ions in the active site, catalyzing colorful pigments or melanin by the above oxidations. One of the major protocols for treating these pigmentation-related dermatological disorders is to inhibit tyrosinase activity.

Human skin is under daily oxidative stress from both external and internal sources, such as free radicals, reactive oxygen species, or ultraviolet (UV) radiation.[6] It has been well reported that skin exposure to oxidative stress or UV radiation is the cause for skin aging or tumorigenesis. At present, the main lethal reason of ineffective treatment is tumor proliferation, which may lead to death. Within the past several decades, these are etiological factors responsible for producing melanoma, which is a form of malignant tumor of uncontrollable melanocytes and is among the most fatal of skin cancers.[7] Melanoma is one of the most aggressive cancers, resistant to medical treatments such as surgery, radiotherapy, or chemotherapy.[8] Treatments these days for melanoma are not effective enough to reduce mortalities and enhance survival rate of patients with melanoma because of a lack of therapeutic remedy. For this reason, to improve the efficacy of cancer treatment, it is essential to develop novel natural medicinal compounds for anticancer therapies. The purpose of biological aspects of this study was therefore to elucidate the antioxidative, tyrosinase-inhibitory, and anticancer properties of *C. philippinense* compounds. We further analyzed the cytotoxicity of isophilippinolide A in a human skin melanoma cancer cell line, A375.S2, to discuss the apoptotic genetic and molecular mechanisms.

MATERIALS AND METHODS

Plant Material. The roots of *C. philippinense* were collected from Taipei County, in May 2008. A voucher specimen was identified by Dr. Yen-Ray Hsui of the Chungpu Research Center, Taiwan Forestry Research Institute, and deposited in the Department of Medical Laboratory Science and Biotechnology, School of Medical and Health Sciences, Fooyin University, Kaohsiung, Taiwan.

Reagents. 2,2′-Azinobis(3-ethylbenzthiazoline-6-sulfonic acid) (ABTS), butylated hydroxyanisole (BHA), 2,2-diphenyl-1-(2,4,6-trinitrophenyl)hydrazyl (DPPH), dimethyl sulfoxide (DMSO), ethylenediaminetetraacetic acid (EDTA), ferrozine, $FeCl_3$, $FeCl_2{\cdot}4H_2O$, kojic acid, 3-(4,5-dimethylthiazol-2-yl)-2,5-diphenyl tetrazolium bromide (MTT), mushroom tyrosinase, vitamin C, peroxidase type I from horseradish (HRPase), potassium ferricyanide [$K_3Fe(CN)_6$], propidium iodide (PI), trichloroacetic acid, and L-tyrosine were purchased from Sigma-Aldrich Chemical Co. (St. Louis, MO, USA). Fetal bovine serum (FBS), minimum essential medium (MEM), and Dulbecco's modified Eagle's medium (DMEM) were obtained from GIBCO BRL (Gaithersburg, MD, USA). An Annexin V/Dead Cell Apoptosis Kit was purchased from Invitrogen (Carlsbad, CA, USA). All buffers and other reagents were of the highest purity commercially available.

Instruments. Melting points were determined using a Yanagimoto micromelting point apparatus and are uncorrected. Optical rotations were measured with a JASCO DIP-370 digital polarimeter. UV spectra were obtained on a JASCO V-530 spectrophotometer in MeCN. IR spectra were measured on a Hitachi 260-30 spectrophotometer (Hitachi, Tokyo, Japan). ^{1}H (400 MHz, using $CDCl_3$ as solvent for measurement), ^{13}C (100 MHz), DEPT, HETCOR, COSY, NOESY, and HMBC spectra were obtained on a Varian (Unity Plus) NMR spectrometer. Low-resolution FABMS and ESIMS spectra were obtained on an API 3000 (Applied Biosystems) and high-resolution FABMS and ESIMS spectra on a Bruker Daltonics APEX II 30e spectrometer (Bruker, Bremen, Germany). Silica gel 60 (Merck, 70–230 mesh, 230–400 mesh) was used for column chromatography. Precoated silica gel plates (Merck, Kieselgel 60 F-254), 0.20 and 0.50 mm, were used for analytical TLC and preparative TLC, respectively, and visualized with 50% H_2SO_4. Flow cytometry analysis was done by a Coulter Epics XL-MCL (Beckman Coulter, CA, USA) flow cytometer. Labeling dyes, such as PI, were used to investigate the events involved in apoptosis.

Extraction and Isolation. The roots (3.7 kg) of *C. philippinense* were air-dried and extracted repeatedly with MeOH (5 L × 6) at room temperature. The combined MeOH extracts (54.3 g) were obtained by concentration under reduced pressure and partitioned to yield $CHCl_3$ (34.4 g) and H_2O (8.8 g) extracts. The concentrated $CHCl_3$ extract (34.4 g) was chromatographed over silica gel using *n*-hexane–EtOAc–MeOH as eluent to produce six fractions. Fraction 1 (6.33 g) was separated by silica gel CC with increasingly polar mixtures of *n*-hexane–EtOAc to give 10 fractions (1-1 to 1-10). Fraction 1-1 (2.15 g) was resubjected to silica gel CC, eluting with *n*-hexane–EtOAc (60:1) and enriched gradually with EtOAc to obtain five fractions (1-1-1 to 1-1-5). Fraction 1-1-2 (0.85 g) was further purified by another silica gel CC using *n*-hexane–EtOAc to obtain philippinolide B (16 mg). Fraction 1–-2 (1.85 g) was further separated by silica gel CC (*n*-hexane–EtOAc (60:1)) and preparative TLC (*n*-hexane–EtOAc (100:1)), giving philippinolide A (24 mg) and isophilippinolide A (37 mg). Fraction 2 (4.93 g) was separated by silica gel CC with increasingly polar mixtures of *n*-hexane–EtOAc to give five fractions (2-1 to 2-5). Fraction 2-1 (2.52 g) was resubjected to silica gel CC, eluted with $CHCl_3$–MeOH (100:1), and gradually enriched with MeOH to obtain 10 fractions (2-1-1 to 2-1-10). Fraction 2-1-1 (0.11 g) was resubjected to silica gel CC and purified by preparative TLC to yield cinnaretamine (5 mg). Three new compound structures (see Figure 1) were identified as the following.

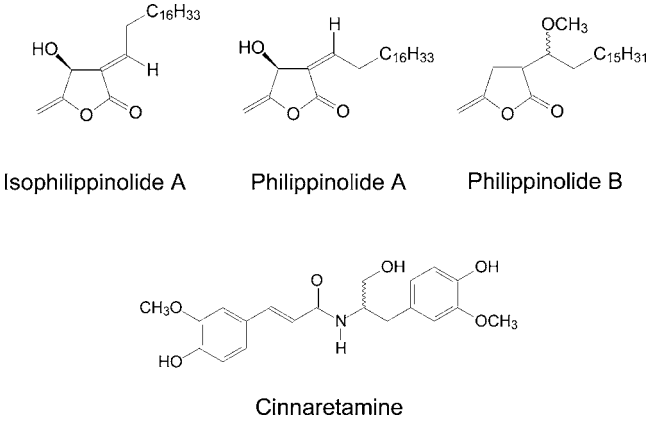

Figure 1. Chemical structures of four compounds from *C. philippinense*.

Isophilippinolide A: pale yellowish liquid; $[\alpha]^{25}_D$ −24.6 (*c* 0.05, $CHCl_3$); UV λ_{max} (MeCN) (log ε) 225 (4.12) nm; IR (neat) ν_{max} 3450 (br, OH), 1770, 1670 (α,β-unsaturated γ-lactone), 1465, 1360, 1090 cm^{-1}; ^{1}H NMR (400 MHz, $CDCl_3$) δ 0.88 (3H, t, J = 6.8 Hz, H-18′), 1.25 (28H, br s, H-4′–17′), 1.52 (2H, m, H-3′), 2.45 (2H, m, H-2′), 4.72 (1H, dd, J = 2.8, 1.2 Hz, H-6a), 4.94, (1H, dd, J = 2.8, 1.2 Hz, H-6b), 5.24 (1H, br s, H-4), 7.07 (1H, td, J = 7.6, 2.4 Hz, H-1′); ^{13}C NMR (100 MHz, $CDCl_3$) δ 14.0 (C-18′), 22.8 (C-17′), 28.2–29.7 (C-2′–15′), 32.0 (C-16′), 66.6 (C-4), 91.5 (C-6), 127.2 (C-3), 150.2 (C-1′), 157.7 (C-5), 165.5 (C-2); FABMS m/z 365 [M + H]$^+$, 211 (15), 167, 149 (16), 139 (14), 125 (33), 111 (100), 97 (70), 83 (81), 69 (90); HRFABMS m/z 365.3055 [M + H]$^+$ (calcd for $C_{23}H_{41}O_3$, 365.3056).

Philippinolide A: pale yellowish liquid; $[\alpha]^{25}_D$ −22.3 (*c* 0.05, $CHCl_3$); UV λ_{max} (MeCN) (log ε) 225 (4.11) nm; IR (neat) ν_{max} 3450 (br, OH), 1770, 1670 (α,β-unsaturated γ-lactone), 1465, 1365, 1090 cm^{-1}; ^{1}H NMR (400 MHz, $CDCl_3$) δ 0.88 (3H, t, J = 7.2 Hz, H-18′), 1.25 (28H, br s, H-4′–17′), 1.48 (2H, m, H-3′), 2.77 (2H, m, H-2′), 4.67 (1H, dd, J = 2.8, 1.6 Hz, H-6a), 4.89, (1H, dd, J = 2.8, 1.6 Hz, H-6b), 5.11 (1H, br s, H-4), 6.68 (1H, td, J = 7.6, 2.0 Hz, H-1′); ^{13}C NMR (100 MHz, $CDCl_3$) δ 14.0 (C-18′), 22.6 (C-17′), 28.3–29.8

(C-2′−15′), 31.9 (C-16′), 68.8 (C-4), 90.4 (C-6), 126.7 (C-3), 151.3 (C-1′), 157.5 (C-5), 165.5 (C-2); FABMS m/z 365 $[M + H]^+$ (5), 211 (21), 149 (11), 139 (13), 125 (46), 111 (100), 97 (75), 83 (80), 69 (92); HRFABMS m/z 365.3053 $[M + H]^+$ (calcd for $C_{23}H_{41}O_3$, 365.3056).

Philippinolide B: colorless oil; $[\alpha]^{25}_D$ −21.8 (c 0.05, $CHCl_3$); UV λ_{max} (MeCN) (log ε) 265 (4.05) nm; IR (neat) ν_{max} 3500 (br, OH), 1780, 1680 (α,β-unsaturated γ-lactone), 1290 cm^{-1}; ^1H NMR (400 MHz, $CDCl_3$) δ 0.87 (3H, t, J = 6.8 Hz, H-17′), 1.25 (26H, br s, H-4′−16′), 1.60−1.77 (4H, m, H-2′, 3′), 3.34 (3H, s, OMe-1′), 4.11 (1H, dd, J = 7.4, 4.8 Hz, H-1′), 4.87, 5.19 (each 1H, d, J = 2.4 Hz, H-6a, b), 7.21 (1H, br s, H-4); ^{13}C NMR (100 MHz, $CDCl_3$) δ 14.2 (C-17′), 22.6 (C-16′), 25.5 (C-3′), 29.1−30.3 (C-4′−14′), 31.6 (C-15′), 35.1 (C-2′), 57.5 (OMe-1′), 77.4 (C-1′), 98.0 (C-6), 137.7 (C-4), 137.7 (C-3), 155.0 (C-5), 169.8 (C-2); HRESIMS m/z 387.2877 $[M + Na]^+$ (calcd for $C_{23}H_{40}O_3Na$, 387.2875).

DPPH• Radical Scavenging Capacity Assay. The antioxidant activity of the tested compounds was determined as their ability to donate hydrogen or remove radicals by utilizing the stable DPPH• method.[9] Briefly, various concentrations of *C. philippinense* compounds were added to 0.1 mL of aqueous stable DPPH• (60 μM) solution. When DPPH• reacts with an antioxidant compound that can donate hydrogen, it is reduced, resulting in a decrease in the absorbance at 517 nm. The analyzed time interval was 10 min per point, totaling up to 30 min, using a UV−vis spectrophotometer (BioTek Co., Winooski, VT, USA). Vitamin C acted as a positive control. According to the preliminary investigations, the antioxidative results of using four compounds failed to reach high inhibitions toward the values of IC_{50}. We presented the inhibitory data at suitable concentrations in all of the antioxidative assays. The DPPH• radical scavenging activity (%) was determined as

$$\text{scavenging activity (\%)} = \frac{(A_{\text{control}} - A_{\text{sample}})}{A_{\text{control}}} \times 100\% \quad (1)$$

Metal-Chelating Activity. The ferrous ion chelating potentials of all compounds were probed according to the method described previously.[10] In short, various tested concentrations of samples dissolved in DMSO were added to a solution of 2 mM $FeCl_2 \cdot 4H_2O$ (0.01 mL). Ferrozine (5 mM; 0.02 mL) was added to the reaction, and the mixture was strongly shaken and left standing at room temperature for 10 min. The absorbance of the mixture was read at 562 nm against a blank. EDTA was used as a positive control, and the formula for calculation of the chelating activity was similar to eq 1.

Reducing Power Assay. The reducing power of the four compounds was measured on the basis of the previous method.[10] Briefly, different concentrations of each test sample were mixed with 0.085 mL of 67 mM phosphate buffer (pH 6.8) and 2.5 μL of 20% potassium ferricyanide ($K_3Fe(CN)_6$). The mixture was incubated at 50 °C for 20 min, and 0.16 mL of trichloroacetic acid (10%) was then added to the mixture, which was then centrifuged for 10 min at 3000g. The upper layer of the solution (75 μL) was mixed with 2% $FeCl_3$ (25 μL), and the absorbance was measured at 700 nm. BHA was used as a positive control. In this assay, a higher absorbance demonstrated a higher reductive capability.

Inhibition of Mushroom Tyrosinase Activity. Tyrosinase activity inhibition was determined spectrophotometrically according to the previously described method, with minor modifications.[10] Assays were carried out with an optics plate reader used to determine the absorbance at 475 nm. Kojic acid was used as a positive control for the tyrosinase inhibitory assay. The substances tested were dissolved in aqueous DMSO and incubated with L-tyrosine (2.5 mg/mL) in a 50 mM phosphate buffer (pH 6.8). All samples were dissolved in DMSO, because DMSO did not affect tyrosinase activity when <1% of the total volume. Then, 25 U/mL of mushroom tyrosinase in the same buffer was added, and the mixture was incubated at 37 °C for 30 min. Tyrosinase inhibitory activity was measured by the following equation:

$$\text{tyrosinase inhibition activity (\%)} = \frac{[(A - B) - (C - D)]}{(A - B)} \times 100\% \quad (2)$$

In this equation, A is the optical density (OD_{475}) without the tested substance, B is the OD_{475} without the tested substance, but with tyrosinase, C is the OD_{475} with the tested substance, and D is the OD_{475} with the tested substance, but without tyrosinase.

Cell Cultures. The A375.S2 (Bioresource Collection and Research Center, BCRC no. 60039, ROC) human melanoma cell line was maintained in monolayer culture within MEM supplemented with 10% fetal bovine serum and 100 U/mL penicillin, 100 mg/mL streptomycin, and 0.25 μg/mL amphotericin B. Neonatal foreskin primary human epidermal melanocytes were bought from Cascade Biologics and cultured in Medium 254 (Cascade Biologics, Life Technologies, Portland, OR, USA) supplemented with human melanocyte growth supplement. Human skin fibroblasts were grown from foreskin primary culture that was obtained from Chung-Ho Memorial Hospital, Kaohsiung Medical University. All of the cell types were incubated at 37 °C under a humidified atmosphere of 5% CO_2 in air and routine passage by trypsinization.[11,12]

Cell Cytotoxicity Assays. The effects of compounds on cell growth were evaluated using a MTT assay.[13] In short, cells were seeded in 96-well plates at a density of 7×10^3 cells/well. The medium was changed, and cells were maintained either in medium by themselves (control cells) or in the presence of the indicated drug concentrations in a final volume of 100 μL in 10% FBS culture medium. The testing samples were dissolved in sterile DMSO to create a working concentration of 1, 10, 25, 50, 100, or 200 μM. After 24 h of incubation, the medium was substituted with 100 μL of fresh medium including 0.5 mg/mL MTT. The plate was then cultured in a 37 °C incubator filled with 5% CO_2 for 2 h. Each precipitate in a specific well was treated with 100 μL of DMSO to dissolve the purple formazan crystals. After the dishes were gently shaken for 10 min in the dark to ensure maximal dissolution of the formazan crystals, the absorbance (A) values of the supernatant were measured at 595 nm. Cell viability was calculated as

$$\text{cell viabilty (\%)} = \frac{(A_{\text{sample}} - A_{\text{blank}})}{(A_{\text{control}} - A_{\text{blank}})} \times 100\% \quad (3)$$

Cell Cycle Analysis by Flow Cytometry. To determine phase distribution of DNA content in A375.S2 cells, PI staining was performed as previously described.[14,15] In short, cells were treated with vehicle (medium containing 0.05% DMSO, as the control) or eq 2 at desired final concentrations for 24 h. After treatments, the floating and trypsin-detached A375.S2 cells were collected and washed twice with ice-cold PBS and then fixed in 70% cold ethanol. The cells were stained in PBS containing 10 μL/ml PI, 10 μg/mL RNase A, and 0.05% Triton X-100 for 15 min at room temperature in the dark. The DNA content of A375.S2 cells was analyzed with a FACScan flow cytometer (Becton-Dickinson, Mansfield, MA, USA). At least 10000 events were analyzed for each test sample. Data analyses were performed with Cell-Quest and Modfit software (Becton-Dickinson).

Annexin V and PI Double Staining. We followed published protocols with minor modifications,[16] In brief, 1.3×10^5 A375.S2 cells in a 6-well microplate (at 70−80% confluency) were treated with vehicle or component for 24 h, subsequently trypsinized and washed with PBS, and then marked with annexin V−FITC (10 μg/mL)/PI (10 μg/mL); the percentage of four quadrants on treated cells was analyzed by flow cytometry. The left lower quadrant means normal cells, the lower and upper right quadrants refer to the early and late apoptotic cells, and the left upper quadrant means necrotic cells, respectively.

Western Blot Analysis. A total of 1×10^6 cells were treated with isophilippinolide A or vehicle control for 24 h. The cells were washed two times with ice-cold phosphate-buffered saline, harvested, and disrupted in lysis buffer (50 mM Tris-HCl, pH 7.5, 137 mM sodium chloride, 1 mM EDTA, 1% Nonidet P-40, 10% glycerol, 0.1 mM sodium orthovanadate, 10 mM sodium pyrophosphate, 20 mM β-

Table 1. Antioxidant Activity and Mushroom Tyrosinase Inhibition of Four Compounds at 100 and 200 μM, Respectively[a]

	DPPH inhibition (%)		chelating inhibition (%)		reducing power (OD_{700})		tyrosinase inhibition (%)	
sample	100 μM	200 μM	100 μM	200 μM	100 μM	200 μM	100 μM	200 μM
isophilippinolide A	ns	ns	15.1 ± 0.3	22.1 ± 1.5	0.113 ± 0.00	0.112 ± 0.01	ns	25.3 ± 1.9
philippinolide A	ns	ns	14.3 ± 1.2	21.2 ± 3.1	0.112 ± 0.01	0.109 ± 0.01	ns	21.3 ± 2.0
philippinolide B	ns	ns	10.8 ± 1.1	18.9 ± 0.8	0.098 ± 0.02	0.109 ± 0.02	ns	22.8 ± 0.7
cinnaphitamine	43.7 ± 1.2	66.5 ± 3.4	ns	19.0 ± 1.4	0.287 ± 0.01	0.438 ± 0.01	ns	16.4 ± 1.6
vitamin C[b]	75.5 ± 5.3	–	–	–	–	–	–	–
EDTA[c]	–	–	62.3 ± 3.8	–	–	–	–	–
BHA[d]	–	–	–	–	0.489 ± 0.01	0.589 ± 0.02	–	–
kojic acid[e]	–	–	–	–	–	–	65.0 ± 4.1	86.0 ± 2.5

[a]Data are expressed as means ± SD of three independent experiments. ns, not significant; –, not tested. [b]Vitamin C was used as a positive control on DPPH assay at 100 μM. [c]EDTA was used as a positive control on metal chelating ability at 100 μM. [d]BHA was used as a positive control on reducing power at 100 μM. [e]Kojic acid was used as a positive control of mushroom tyrosinase assay at 100 μM.

glycerophosphate, 50 mM sodium fluoride, 1 mM phenylmethanesulfonyl fluoride, 2 μM leupeptin, and 2 μg/mL aprotinin).[6,12] The cell lysate was centrifuged at 10000*g* for 30 min at 4 °C, and the protein concentration in the supernatant was determined with the bicinchoninic acid protein assay kit (Pierce, Rockford, IL, USA). In short, equal amounts of protein were separated by sodium dodecyl sulfate–polyacrylamide gel electrophoresis (SDS-PAGE) and then electrotransferred onto polyvinylidene fluoride (PVDF, PALL Life Science, Ann Arbor, MI, USA). The membrane was clogged for 1 h with 5% nonfat milk in PBS-T buffer (phosphate-buffered saline containing 0.1% Tween 20). The membranes were incubated with corresponding primary antibodies, washed two times with PBS, and incubated with secondary antibodies against the corresponding primary antibodies. The signals were visualized utilizing enhanced chemiluminescence substrate (PerkinElmer, Boston, MA, USA). The signal intensities of proteins were analyzed by the software Gel-Pro v 3.0 (Media Cybernetics, Carlsbad, CA, USA).

Statistical Analysis. All data values are presented as the mean values (±SD) of at least three independent experiments. When appropriate, data were analyzed by Student's *t* test. Statistical significance was assumed of a p value of <0.05.

RESULTS AND DISCUSSION

Structure Elucidation of the New Butanolides. Isophilippinolide A, a pale yellowish liquid, also had the molecular formula $C_{23}H_{40}O_3$, as deduced from HRFABMS, and its spectroscopic data (IR, UV, and ^1H and ^{13}C NMR) were similar to those of philippinolide A. However, differences in chemical shift of H-1′ and its coupling constant supported an *E* configuration for $\Delta^{3(1')}$ in philippinolide A. The ^1H NMR spectrum of philippinolide A was similar to that of isotenuifolide A,[17] indicating that it has the same β-hydroxy-γ-methylene-α,β-unsaturated γ-lactone skeleton and the same *E* geometry of the trisubstituted double bond. The structure of isotenuifolide A is similar to that of philippinolide A, just different in the lipid long chain.[17] A broad singlet at δ 1.25 was again attributed to the 28 protons in the aliphatic chain in philippinolide A. The exocyclic olefinic protons appeared at δ 4.72 and 4.94, and a hydroxymethine proton resonated at δ 5.24. Philippinolide A was shown to be levorotatory, indicating the configuration at C-4 to be *S* by comparison with reported compounds.[18] Thus, the structure of isophilippinolide A was elucidated as (4*S*,3*E*)-4-hydroxy-5-methylene-3-octadecylidene-dihydrofuran-2-one.

Philippinolide A was isolated as a pale yellowish liquid and its molecular formula, $C_{23}H_{40}O_3$, was established by HRFABMS. The UV absorption at 225 nm was similar to that of tenuifolide A, consistent with the presence of an α,β-conjugated γ-lactone moiety.[17] The IR spectrum showed absorption bands for a hydroxy group at 3440 cm^{-1} and an α,β-unsaturated γ-lactone moiety at 1770 and 1670 cm^{-1}. The ^1H NMR spectrum of isophilippinolide A was similar to that of tenuifolide A,[17] indicating that philippinolide A has the same β-hydroxy-γ-methylene-α,β-unsaturated γ-lactone skeleton and the same *Z* geometry of the trisubstituted double bond. The structure of tenuifolide A is similar to that of isophilippinolide A, just different in the lipid long chain.[17] The presence of a broad singlet at δ 1.25 was attributed to protons in an aliphatic chain in isophilippinolide A. The exocyclic olefinic protons appeared at δ 4.67 and 4.89, and one hydroxymethine proton was located at δ 5.11. Isophilippinolide A was found to be levorotatory, which indicated an *S* configuration at C-4.[19] Thus, the structure assigned for philippinolide A was (4*S*,3*Z*)-4-hydroxy-5-methylene-3-octadecylidene-dihydrofuran-2-one.

Philippinolide B was isolated as a colorless oil, and the molecular formula was determined to be $C_{23}H_{40}O_3$ by ESIMS ($[M + Na]^+$, m/z 387) and HRESIMS. The presence of an α,β-unsaturated γ-lactone moiety was apparent from a UV absorption maximum at 265 nm.[20] The IR peaks at 1780 and 1680 cm^{-1} supported the presence of an α,β-unsaturated γ-lactone moiety. The ^1H NMR spectrum of philippinolide B indicated the presence of an exomethylene group and an alkene proton, which was located on the β-carbon of the unsaturated lactone, as deduced from its downfield chemical shift. In addition, signals corresponding to a methoxy functionality at δ 3.34, an oxymethine proton at δ 4.11, and long-chain aliphatic protons at δ 1.25 (26H, br s) and 1.60–1.77 (4H, m) were evident. Furthermore, the data of philippinolide B were found to be similar to those of the known butanolide, 3-(1-methoxyeicosyl)-5-methylene-5*H*-furan-2-one.[17] Thus, the structure of philippinolide B was elucidated as 3-(1-methoxyheptadecyl)-5-methylene-5*H*-furan-2-one. The configuration at C-1′ remains undefined, because the specific rotation could not be correlated to any known compound.

Free Radical Scavenging Activities of *C. philippinense* Compounds. It is well-known that the accumulation of free radicals can result in the growth of tumor or cancer cells and speed the oxidation of lipids in cosmetics and manufactured foods. Natural antioxidants, particularly free radical removing properties, are therefore necessary in skin care products and functional foods.[21,22] The inhibitory data for four compounds to 1,1-diphenyl-2-picrylhydrazyl (DPPH) at 100 and 200 μM are listed in Table 1. In this assay, antioxidants lessen the stable DPPH radicals to diphenylpicrylhydrazine, which is yellow. On the basis of this information, cinnaretamine might function as a chain-breaking agent or radical ion neutralizer inhibiting the

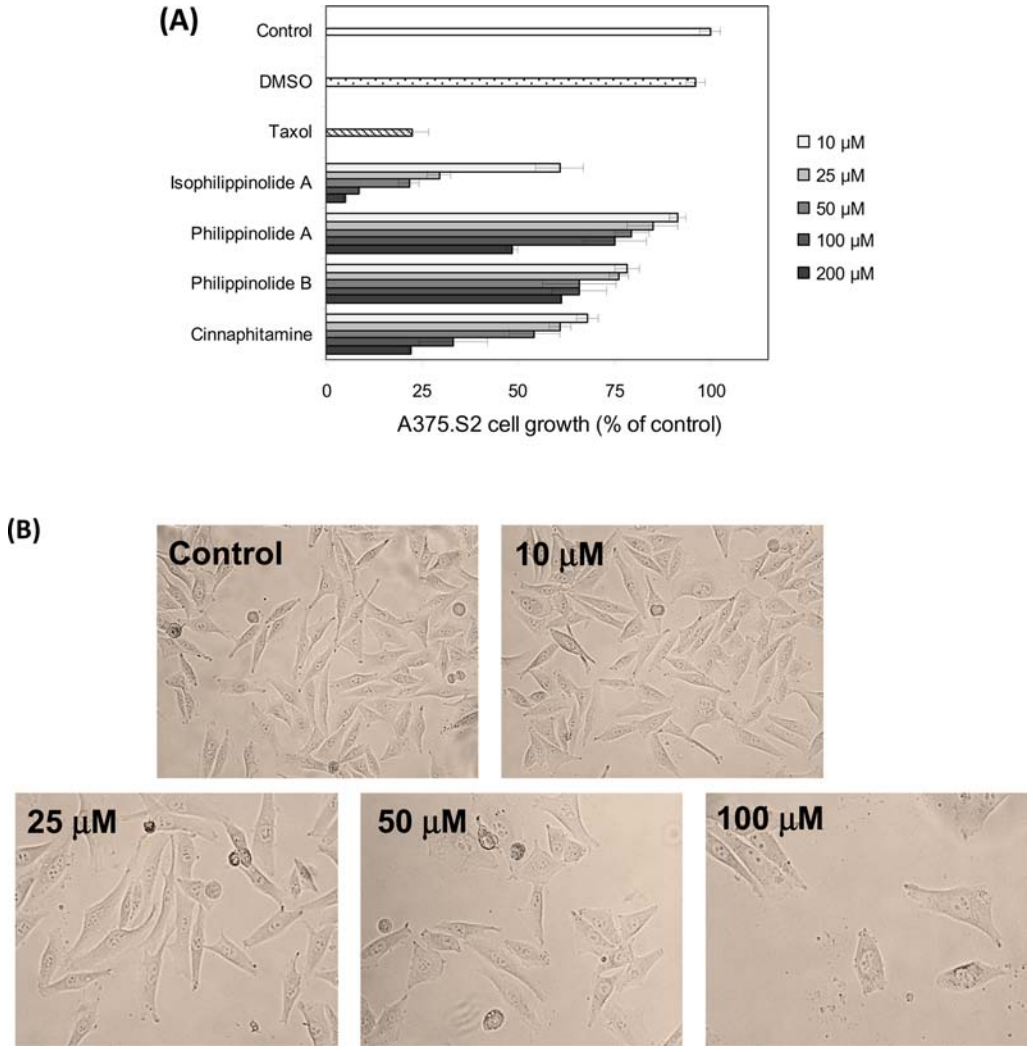

Figure 2. Antiproliferative effects of four compounds after 24 h. Data are expressed as means ± SD of three independent experiments. (A) Control, no treatment; DMSO, 0.5%; taxol, 1.0 μM. Tested compounds: from top to bottom, 10, 25, 50, 100, and 200 μM, respectively. Control had no testing sample. Bars, SD; *, $p < 0.05$. (B) Isophilippinolide A suppressed cellular proliferation and induced cytotoxicity in A375.S2 cells. Cell images were captured using a FLoid Cell Imaging Station REF: 4471136 microscope at 100×.

accumulation of harmful free radicals compared to vitamin C at the same concentration (100 μM).

Studies in the past have declared the reducing power and the chelating ability to metal ions by a biochemical agent might be major signs of its possible antioxidative aptitude. The ferrous ion chelating data for four compounds are presented in Table 1, where 100 μM EDTA was utilized as a positive control. The reagent used is ferrozine, which is capable of forming complexes with Fe(II) that are dark red in color. When this reaction is disrupted, the degree of disruption can be quantified spectrophotometrically. It was observed that all tested compounds, at doses of 100 and 200 μM, exhibited minor Fe(II) chelating properties.

The reducing power examination is an uncomplicated, fast, and dependable assay to measure reducing power with a Fe(III)−ferricyanide complex reaction. The color of the solution changes from light yellow to various shades ranging from dark green to blue, depending on tested antioxidant qualities. As reported in Table 1, cinnaretamine's reducing power was similar to the antioxidative power of BHA at the same doses.

Mushroom Tyrosinase Inhibitory Properties of *C. philippinense* Compounds. Our previous studies showed that the oxidative stress accumulation with UV exposure might induce skin darkening and the increase in reactive oxygen species in carcinogenesis.[4−7,14,21,22] For skin whitening and hyperpigmentation prevention, we examined the inhibitory properties of *C. philippinense* compounds on in vitro mushroom tyrosinase inhibition. The inhibitory effects of four compounds show only minor inhibitions to mushroom tyrosinase activity at 200 μM (Table 1). It was possible that these compounds might be useful in an assisting role and were still prime candidate factors for use in cosmetics and pharmaceuticals because of their other beneficial properties.

Antiproliferative Properties of *C. philippinense* Compounds on A375.S2 Cell. The cytotoxic properties of four compounds from *C. philippinense* were examined. The MTT assay is used to determine the cytotoxicities of *C. philippinense* compounds against human skin cancer melanoma cell line, A375.S2. Melanoma cells were incubated in the company of different concentrations of tested compounds (10, 25, 50, 100, and 200 μM), and cell growth was measured in every concentration (Figure 2A). The anticancer drug Taxol

dx.doi.org/10.1021/jf403730z | J. Agric. Food Chem. 2014, 62, 1057−1065

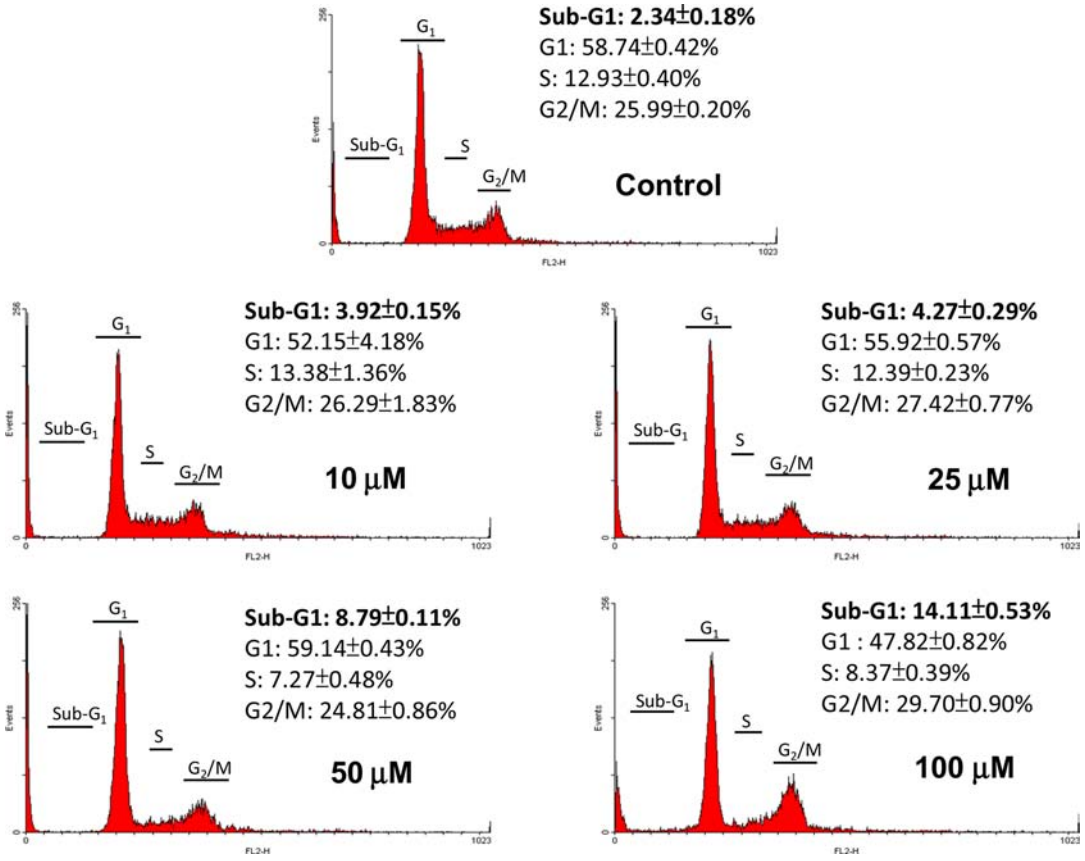

Figure 3. Isophilippinolide A induced sub-G1 cell apoptosis of A375.S2 cells. A375.S2 cells were treated at 0, 10, 25, 50, and 100 μM for 24 h, respectively. Values were obtained from three independent experiments, and representative histograms are shown. Data analyses and quantification were performed with Cell-Quest and Modfit software.

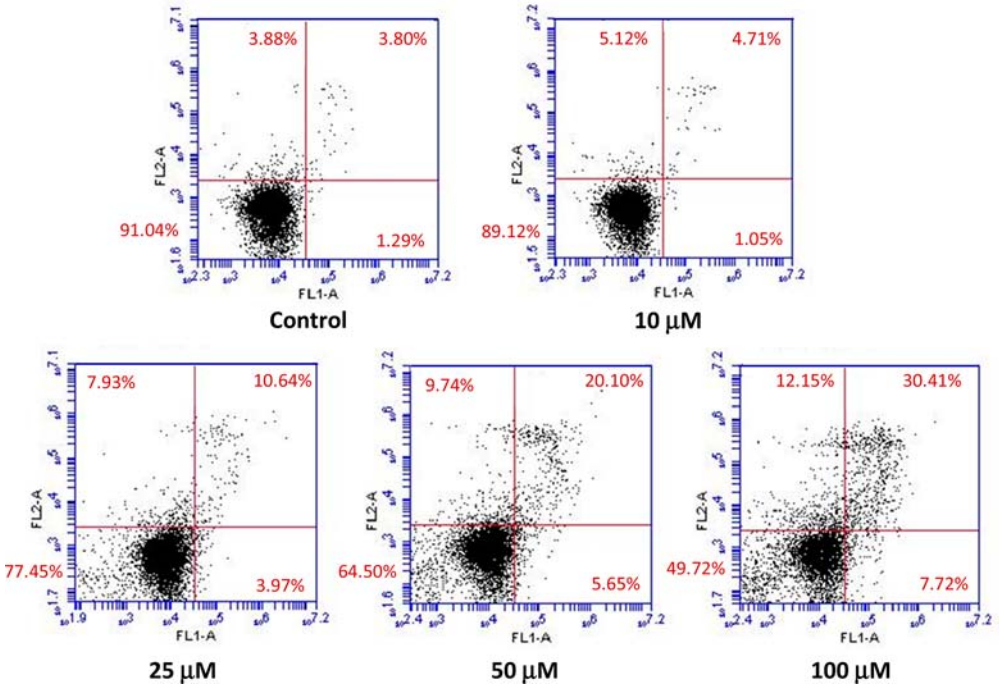

Figure 4. Isophilippinolide A induced A375.S2 cell apoptotic responses. Apoptosis was analyzed by flow cytometry after exposure to isophilippinolide A from 0 to 100 μM at 24 h and staining with annexin-V/PI.

(Paclitaxel) has been shown to cause defects in chromosome segregation, mitotic spindle assembly, and cell division to stabilize the microtubule polymer and keep it from disassembly within cells. It obstructs the progression of mitosis to prolong

dx.doi.org/10.1021/jf403730z | J. Agric. Food Chem. 2014, 62, 1057−1065

the activation of the mitotic checkpoint and to induce cell cycle arrest in various human cancer cell lines.[6] Consequently, we applied Taxol as a positive control in this study. Multiplication of A375.S2 cells was found to be suppressed by the four compounds in a dose-dependent manner from 10 to 200 μM. Isophilippinolide A exhibited an influential mean IC_{50} value of 26.7 μM after a 24 h treatment, and the other three compounds showed moderate antiproliferative activities. Morphological changes of treated isophilippinolide A were surveyed with a bright field microscope, and the magnification was 200× without staining (Figure 2B). We further investigated the detailed cellular proliferative suppression and cytotoxic mechanisms of isophilippinolide A in human melanoma.

Evaluations of Cell Cycle Arrest and Sub-G1 Accumulation of Isophilippinolide A. One parameter for assessing responsible degrees of DNA damage and consequences of cell cycle arrest distribution of treated A375.S2 cells, flow cytometry, was analyzed. Cells were processed with isophilippinolide A at 0, 10, 25, 50, and 100 μM for 24 h, respectively, followed by PI staining prior to being subjected into flow cytometric analysis (Figure 3). In cell cycle analysis, the pronounced sub-G1 population represented an indicative sign for apoptotic cells due to treatments with agents. Compared to the vehicle control group, the target compound induced apoptosis in sub-G1 phase at 2.34, 3.92, 4.27, 8.79, and 14.11% in a dose-liable way from 0 to 100 μM. It had a noticeable variation over 6-fold at 100 μM compared to the vehicle control group on sub-G1 phase, which meant the cells carried through apoptosis and that the DNA was split into bits. DNA impairment is a potential mechanism for antiproliferation effectivenesses of this agent, and more studies are required to examine the antimelanoma mechanism. Moreover, possible clinical use of isophilippinolide A shall not begin before it is proved safe to normal human cells.

Annexin V/PI Staining To Uncover Apoptotic Mechanism of Isophilippinolide A in A375.S2 Cells. A375.S2 cell pellets were mixed well with annexin V−FITC/PI (annexin V was applied as a probe to identify the event of apoptosis cells, which expressed phosphatidylserine (PS) on the cellular membrane surface with calcium buffer; PI is a cellular membrane fluorescent impermeant dye that binds with nucleic acids and is normally excluded from healthy cells) and incubated for 15 min at 25 °C and gently shaken every 30 s (as stated by the manufacturer's protocols). Unattached annexin V−FITC and PI dyes were gotten rid of by rinsing the cells with complete medium. Single-layer fluorescent marked cells were replanted into the slide and then fluorescent images were taken, respectively. A375.S2 cells were exposed to isophilippinolide A for 24 h, and there was an obvious apoptotic performance between cells treated with experimental groups and the vehicle control group (Figure 4). An augmentative increase to 30.41% at the stage of late apoptosis was found in the indicated group treated with 100 μM, compared with 3.80% of the control one. Isophilippinolide A triggered apoptosis on A375.S2 cells in dose-dependent apoptotic features from 0 to 100 μM. A375.S2 cells were all gradually withered under the existence of isophilippinolide A, which was verified to benefit the anticancer cellular proliferation that was acknowledged earlier.

Effects of Apoptotic Related Proteins in Isophilippinolide A Treated A375.S2 Cells. The activations of caspase associate proteins are indispensable to carry out apoptosis by various apoptotic stimuli. As a result, to understand the roles played by caspases in apoptotic effects caused by isophilippinolide A in human melanoma A375.S2 cells, Western blots were inspected after 24 h (Figure 5). These molecular proteins

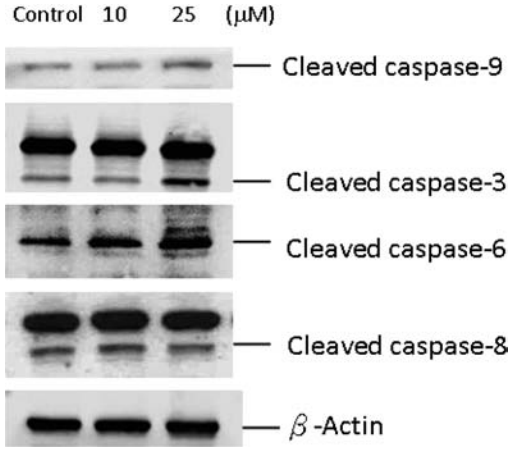

Figure 5. Western blotting was performed to compare caspase expressions in A375.S2 with and without addition of isophilippinolide A at concentrations of 10 and 25 μM for 24 h.

associated with apoptosis presented alterations, including enhanced proteolytically activated forms of caspase-9, caspase-3, and caspase-6. These cellular proteins were known to respond to apoptotic nuclear DNA damage/repair or assist organelle decomposition. We inferred that isophilippinolide A could bring about the proteolytic activations of various caspase proteins to obstruct the physiological behavior of A375.S2 cells. Additionally, to examine whether the extrinsic apoptotic pathway was activated by isophilippinolide A, the Western blot for caspase-8, the hallmark of extrinsic apoptotic pathway, was carried out. As presented in Figure 5, the cleaved form of caspase-8 was not detected as significantly changed. These results were confirmed by the cell cycle arrest in sub-G1 accumulation (Figure 3) and annexin V/PI staining in apoptotic phase (Figure 4). Accordingly, the above results suggested that isophilippinolide A induced a mitochondria-mediated apoptosis and caused sub-G1 cell cycle accumulation. However, we cannot rule out the possibility for the involvement of autophagy or necrosis, and it needs to be further investigated in the future.

The biological activities of pure chemical compounds are hugely influenced by functional groups of the compound's geometric structures. On the basis of our previous studies, it was discovered that the antiproliferation of isokotomolide A was more potent than the antiproliferation of kotomolide A.[23,24] In this study, we discovered that isophilippinolide A inhibited cellular proliferation compared to philippinolide A. We believe that the alkylidene side chain of isokotomolide A and isophilippinolide A were *trans* to the carbonyl groups, which was the key point of anticancer proliferation.

Cellular Cytotoxicities of *C. philippinense* Compounds of Normal Human Skin Cells. As natural compounds are being developed for cosmetic or therapeutic applications, safety measures, such as tests for allergies, sensitivities, or toxicities, are needed to be implemented.[13,25] We illustrated the cellular viabilities of human normal skin melanocytes (epidermal, Figure 6A) and fibroblasts (dermal, Figure 6B) after being treated for 24 h with various concentrations of *C. philippinense* compounds. Considering DMSO's likely antiproliferative

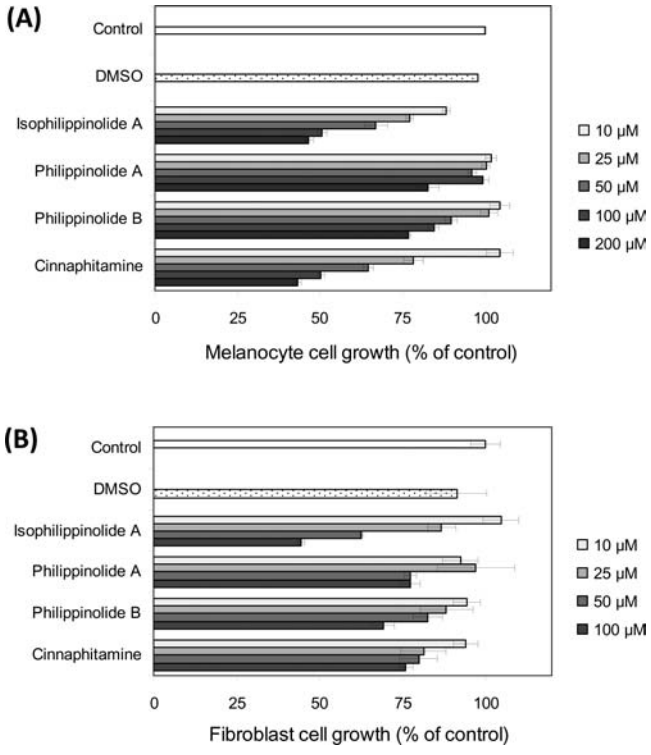

Figure 6. Human melanocyte (A) and fibroblast (B) cell growth with four compounds at various concentrations after 24 h treatments. Data are expressed as means ± SD of three independent experiments. Symbols are similar to those in Figure 2.

effects, we added a maximal amount (0.5%) of DMSO to cultures and took them as positive controls. DMSO with this maximal dose was observed not to affect the growth of human epidermal and dermal cells. These data indicated isophilippinolide A and cinnaretamine had reductions in two cell growths to illustrate cytotoxicities. Philippinolide A and philippinolide B had very little discernible toxicities toward normal human skin cells, suggesting that they will not produce cytotoxic side effects in cells.

Taken together, our present work demonstrated the potential anticancer compound, isophilippinolide A, on human melanoma A375.S2 cells via regulating DNA cell cycle arrest in sub-G1 phase and triggering apoptotic caspase protein expressions with less cytotoxicity to human normal skin cells (Figure 7). Accordingly, isophilippinolide A could inhibit human skin cancer cellular growth, bringing hope to melanoma treatment at the level of a better understanding of the molecular mechanism.

AUTHOR INFORMATION

Corresponding Author

*(H.-M.D.W.) Mailing address: 100 Shih-Chuan First Road, San-Ming District, Department of Fragrance and Cosmetic Science, Kaohsiung Medical University, Kaohsiung City 807, Taiwan, ROC. Phone: +(886)-7-312-1101, ext. 2804. Fax: +(886)-7-3136059. E-mail: davidw@kmu.edu.tw.

Funding

This work was financially supported by the National Science Council of the Republic of China under Grants NSC-97-2320-B-242-002-MY3, NSC-99-2221-E-037-006-MY3, NSC 102-2622-E-037-002, and NSC 102-2221-E-037-005.

Notes

The authors declare no competing financial interest.

ACKNOWLEDGMENTS

We thank His-An Chen for his assistance and Katherine Chang and Ching-chun Chen for English editing.

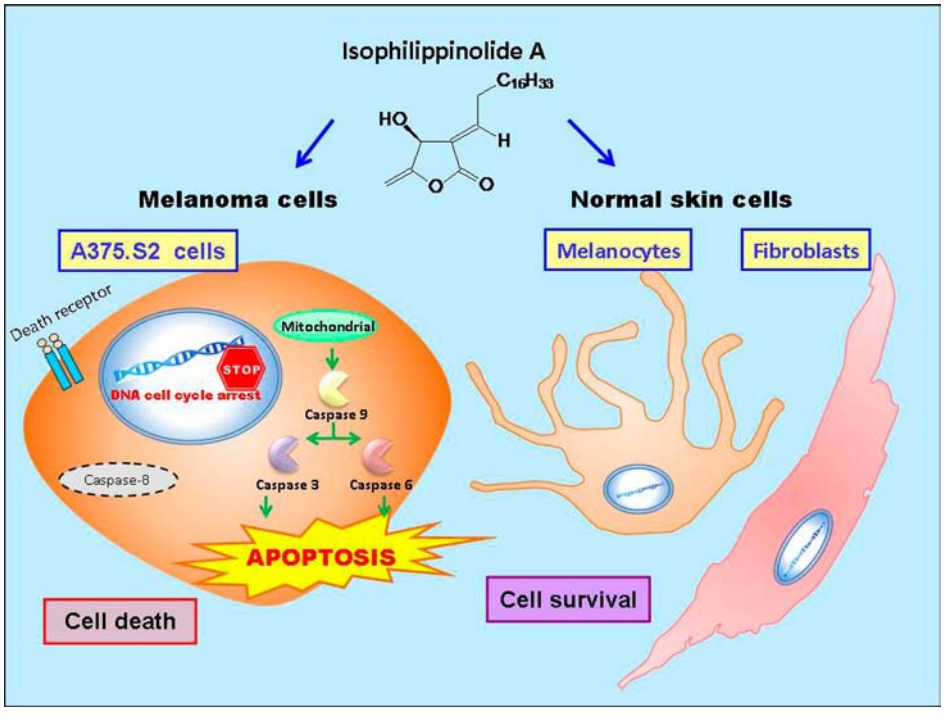

Figure 7. Proposed schematic diagram of isophilippinolide A biofunctions.

REFERENCES

(1) Wu, T. S.; Leu, Y. L.; Chan, Y. Y.; Yu, S. M.; Teng, C. M.; Su, J. D. Lignans and an aromatic acid from *Cinnamomum philippinense*. *Phytochemistry* **1994**, *36*, 785−788.

(2) Scalbert, A.; Johnson, I. T.; Saltmarsh, M. Polyphenols: antioxidants and beyond. *Am. J. Clin. Nutr.* **2005**, *81*, 215S−217S.

(3) Kim, J. H.; Baek, S. H.; Kim, D. H.; Choi, T. Y.; Yoon, T. J.; Hwang, J. S.; Kim, M. R.; Kwon, H. J.; Lee, C. H. Downregulation of melanin synthesis by haginin A and its application to *in vivo* lightening model. *J. Invest. Dermatol.* **2008**, *128*, 1227−1235.

(4) Wang, H. M.; Cheng, K. C.; Lin, C. J.; Hsu, S. W.; Fang, W. C.; Hsu, T. F.; Chiu, C. C.; Chang, H. W.; Hsu, C. H.; Lee, A. Y. Obtusilactone A and (−)-sesamin induce apoptosis in human lung cancer cells via inhibiting mitochondrial Lon protease and activating DNA damage checkpoints. *Cancer Sci.* **2010**, *101*, 2612−2620.

(5) Wang, H. M.; Pan, J. L.; Chiu, C. C.; Chen, C. Y.; Yang, M. H.; Chang, J. S. Identification of anti-lung cancer extract from *Chlorella vulgaris* C-C by antioxidant property using supercritical carbon dioxide extraction. *Process Biochem.* **2010**, *45*, 1865−1872.

(6) Wang, H. M.; Chiu, C. C.; Wu, P. F.; Chen, C. Y. Subamolide E from *Cinnamomum subavenium* induces sub G1 cell cycle arrest, caspase-dependent apoptosis, and reduces migration ability of human melanoma cells. *J. Agric. Food Chem.* **2011**, *59*, 8187−8192.

(7) Chen, C. Y.; Kuo, P. L.; Chen, Y. H.; Huang, J. C.; Ho, M. L.; Lin, R. J.; Chang, J. S.; Wang, H. M. Tyrosinase inhibition, free radical scavenging, antimicrobial and anticancer proliferation activities of *Sapindus mukorossi* extracts. *J. Taiwan Inst. Chem. Eng.* **2010**, *41*, 129−135.

(8) Baldea, I.; Mocan, T.; Cosgarea, R. The role of ultraviolet radiation and tyrosine stimulated melanogenesis in the induction of oxidative stress alterations in fair skin melanocytes. *Exp. Oncol.* **2009**, *31*, 200−208.

(9) Wang, H. M.; Chen, C. Y.; Chen, H. A.; Huang, W. C.; Lin, W. R.; Chen, T. C.; Lin, C. Y.; Chien, H. J.; Lu, P. L.; Lin, C. M.; Chen, Y. H. *Zingiber officinale* (ginger) compounds have tetracycline-resistance modifying effects against clinical extensively drug-resistant *Acinetobacter baumannii*. *Phytother. Res.* **2010**, *24*, 1825−1830.

(10) Wang, H. M.; Chen, C. Y.; Chen, C. Y.; Ho, M. L.; Chou, Y. T.; Chang, H. C.; Lee, C. H.; Wang, C. Z.; Chu, I. M. (−)-*N*-Formylanonaine from *Michelia alba* as a human tyrosinase inhibitor and antioxidant. *Bioorg. Med. Chem.* **2010**, *18*, 5241−5247.

(11) Wang, H. M.; Chou, Y. T.; Wen, Z. H.; Wang, Z. R.; Chen, C. H.; Ho, M .L. Novel biodegradable porous scaffold applied to skin regeneration. *PLoS One* **2013**, *8* (6), e56330.

(12) Chen, C. Y.; Chiu, C. C.; Wu, C. P.; Chou, Y. T.; Wang, H. M. Enhancements on skin cell proliferations and migrations via 6-dehydrogingerdione. *J. Agric. Food Chem.* **2012**, *61*, 1349−1356.

(13) Wang, H. M.; Chen, C. Y.; Wen, Z. H. Identifying melanogenesis inhibitors from *Cinnamomum subavenium* with *in vitro* and *in vivo* screening systems by targeting the human tyrosinase. *Exp. Dermatol.* **2011**, *20*, 242−248.

(14) Chen, B. H.; Chang, H. W.; Huang, H. M.; Chong, I. W.; Chen, J. S.; Chen, C. Y.; Wang, H. M. (−)-Anonaine induces DNA damage and inhibits growth and migration of human lung carcinoma h1299 cells. *J. Agric. Food Chem.* **2011**, *59*, 2284−2290.

(15) Chen, C. Y.; Chen, C. H.; Lo, Y. C.; Wu, B. N.; Wang, H. M.; Lo, W. L.; Yen, C. M.; Lin, R. J. Anticancer activity of isoobtusilactone A from *Cinnamomum kotoense*: involvement of apoptosis, cell-cycle dysregulation, mitochondria regulation, and reactive oxygen species. *J. Nat. Prod.* **2008**, *71*, 933−940.

(16) Lee, Y. J.; Won, A. J.; Lee, J.; Jung, J. H.; Yoon, S.; Lee, B. M.; Kim, H. S. Molecular mechanism of SAHA on regulation of autophagic cell death in tamoxifen-resistant MCF-7 breast cancer cells. *Int. J. Med. Sci.* **2012**, *9*, 881−893.

(17) Lin, R. J.; Cheng, M. J.; Huang, J. C.; Lo, W. L.; Yeh, Y. T.; Yen, C. M.; Lu, C. M.; Chen, C. Y. J. Cytotoxic compounds from the stems of *Cinnamomum tenuifolium*. *Nat. Prod.* **2009**, *72*, 1816−1824.

(18) Anderson, J. E.; Ma, W.; Smith, D. L.; Chang, C. J.; Mclaughlin, J. L. Biologically active gamma-lactones and methylketoalkenes from Lindera benzoin. *J. Nat. Prod.* **1992**, *55*, 71−83.

(19) Martinez, J. C.; Yoshida, M.; Gottlieb, O. R. ω-Ethyl, ω-ethenyl and ω-ethynyl-α-alkylidene-γ-lactones from Clinostemon mahuba. *Phytochemistry* **1981**, *20*, 459−464.

(20) Tanaka, H.; Nakamura, T.; Ichino, K.; Ito, K. Secoisolancifolide and secoisoobtusilactone in *Actinodaphne longifolia*. *Phytochemistry* **1989**, *28*, 1905−1907.

(21) Wang, H. M.; Chou, Y. T.; Hong, Z. L.; Chen, H. A.; Chang, Y. C.; Yang, W. L.; Chang, H. C.; Mai, C. T.; Chen, C. Y. Bioconstituents from stems of *Synsepalum dulcificum Daniell* (Sapotaceae) inhibit human melanoma proliferation, reduce mushroom tyrosinase activity and have antioxidant properties. *J. Taiwan Inst. Chem. Eng.* **2011**, *42*, 204−211.

(22) Chen, C. T.; Kuo, P. L.; Chen, Y. H.; Huang, J. C.; Ho, M. L.; Lin, R. J.; Chang, J. S.; Wang, H. M. Tyrosinase inhibition, free radical scavenging, antimicrobial and anticancer proliferation activities of *Sapindus mukorossi* extracts. *J. Taiwan Inst. Chem. Eng.* **2010**, *41*, 129−135.

(23) Chen, C. Y.; Hsu, Y. L.; Chen, Y. Y.; Hung, J. Y.; Huang, M. S.; Kuo, P. L. Isokotomolide A, a new butanolide extracted from the leaves of *Cinnamomum kotoense*, arrests cell cycle progression and induces apoptosis through the induction of p53/p21 and the initiation of mitochondrial system in human non-small cell lung cancer A549 cells. *Eur. J. Pharmacol.* **2007**, *574*, 94−102.

(24) Chen, C. Y.; Hsu, Y. L.; Tsai, Y. C.; Kuo, P. L. Kotomolide A arrests cell cycle progression and induces apoptosis through the induction of ATM/p53 and the initiation of mitochondrial system in human non-small cell lung cancer A549 cells. *Food Chem. Toxicol.* **2008**, *46*, 2476−2484.

(25) Lee, C. C.; Chiu, C. C.; Liao, W. T.; Wu, P. F.; Chou, Y. T.; Huang, K. C.; Chen, Y. T.; Wen, Z. H.; Wang, H. M. *Alpinia oxyphylla* Miq. bioactive extracts from supercritical fluid carbon dioxide extraction. *Biochem. Eng. J.* **2013**, *78*, 101−107.

At the eighth week of treatment, the rats were fasted overnight and an oral glucose tolerance test (OGTT) was performed. Briefly, 2 g of glucose/kg of bw was dissolved in water and administered by oral gavage, and tail blood samples were taken at 0, 15, 30, and 120 min after the administration of the glucose load. The plasma glucose and insulin levels were measured.

At the ninth week of treatment, the rats were fasted overnight, tail blood samples were taken, and insulin levels were measured.

After 12 weeks of GSPE treatment, the overnight fasted animals were anesthetized with 50 mg of pentobarbital/kg of bw and sacrificed by bleeding. The blood was collected and treated with a commercial DPP4 inhibitor (Millipore, Madrid, Spain) and a serine protease inhibitor, Pefabloc SC (Roche, Barcelona, Spain), to prevent the inactivation of active GLP-1 and ghrelin, respectively. The animal tissue specimens were immediately frozen in liquid nitrogen and stored at −80 °C until further analysis.

All of the procedures were approved by the Experimental Animal Ethics Committee of the Universitat Rovira i Virgili (permission number 4250).

Intestinal GLP-1 Extraction. Active GLP-1 was extracted from the colon as previously described.[17] Briefly, colon samples were homogenized using an ethanol/acid solution (100% ethanol/sterile water/12 M HCl, 74:25:1), placed for 24 h at 4 °C, and centrifuged at 2000*g* for 20 min at 4 °C. Supernatants were collected, diluted in 1× PBS, and stored at −80 °C until further analysis. Active GLP-1 was measured following the instructions of the manufacturer.

Measurement of DPP4 Activity. DPP4 was extracted from rat intestine as previously described.[6] Briefly, intestine samples were homogenized using lysis buffer [phosphate-buffered saline (PBS) containing 100 Kallikrein inhibitor units (KIU)/mL aprotinin and 1% Triton X-100], centrifuged at 1000*g* at 4 °C for 10 min to eliminate the cellular debris, and centrifuged twice at 20000*g* at 4 °C for 10 min. The supernatants were stored at −80 °C until further analysis.

To determine the activity of DPP4 in the intestinal lysates and the rat plasma samples, the specimens were incubated with 0.2 mM *H*-glycylprolyl-pnitroanilide *p*-tosyalte in Tris−HCl buffer at 37 °C and the release of *p*-nitroanilide absorbance was measured every minute at 405 nm for 30 min.

Western Blot. Protein was extracted from the intestine using radioimmunoprecipitation assay (RIPA) lysis buffer [15 mM Tris−HCl, 1% Triton X-100, 0,1% sodium dodecyl sulfate (SDS), 167 mM NaCl, and 0.5% Na−deoxycholate] with a protease inhibitor cocktail (diluted 1:1000, Sigma-Aldrich) and 1 mM phenylmethanesulfonyl fluoride (PMSF). The total protein levels of the lysates were determined using the Bradford method.[18] The proteins were loaded and run on 10% SDS−polyacrylamide gels. The samples were transferred onto polyvinylidene difluoride (PVDF) membranes (Bio-Rad Laboratories, Hercules, CA), blocked at room temperature using 5% (w/v) non-fat milk in Tris-buffered saline with 0.2% (v/v) Tween-20 (TBST) buffer, and incubated overnight at 4 °C with rabbit anti-*β*-actin antibody (Sigma-Aldrich) or anti-CD26 (Abcam, Cambridge, U.K.). After washing with TBST, the blots were incubated at room temperature with peroxidase-conjugated anti-rabbit secondary antibody (GE Healthcare, Buckinghamshire, U.K.). The blots were washed thoroughly in TBST, followed by Tris-buffered saline (TBS) after immunoblotting, and the immunoreactive proteins were visualized using the ECL Plus western blotting detection system (GE Healthcare). Densitometric analysis of the immunoblots was performed using ImageJ 1.44p software; all proteins were quantified relative to the loading control.

Quantitative Reverse Transcription Polymerase Chain Reaction (RT-PCR). The total RNA from the hypothalamus was extracted using a RNAeasy kit (Qiagen, Hilden, Germany), and the total RNA from the duodenum and colon was extracted using the TRIzol reagent following the protocols of the manufacturers. cDNA was generated using a high-capacity cDNA reverse transcription kit (Applied Biosystems, Madrid, Spain). Quantitative PCR amplification and detection were performed using the following TaqMan assay-on-demand probes (Applied Biosystems): Rn00562910_m1 for DPP4, Rn00571500_m1 for GIP, Rn00562293_m1 for proglucagon, Rn01460420_g1 for PYY, Rn00572200_m1 for chromogranin A (CgA), and Rn00562406_m1 for GLP-1 receptor (GLP-1R). *β*-Actin was used as the reference gene (Rn00667869_m1). The relative mRNA expression levels were calculated using the $\Delta\Delta C_t$ method.

Data Analyses. The area under the curve (AUC) and homeostatic model assessment-estimated insulin resistance (HOMA-IR) were calculated as previously described by Ou et al. and Matthews et al., respectively.[19,20]

The results are expressed as the mean values ± standard error of the mean (SEM). The effects were assessed by analysis of variation (ANOVA) and Student's *t* test. All calculations were performed using SPSS software (SPSS, Chicago, IL).

RESULTS

GSPE Limits the Cafeteria-Diet-Induced Decrease in Intestinal GLP-1 Biosynthesis. To analyze whether a preventive treatment with procyanidins modulates the incretin levels in cafeteria-diet-fed rats, basal GIP and GLP-1 levels in plasma were assessed in rats fed a cafeteria diet for 12 weeks simultaneously with 25 mg of GSPE/kg of bw. As shown in Figure 1A, cafeteria-fed rats exhibited reduced plasma levels of active GLP-1. GSPE did not alter the active GLP-1 levels compared to the vehicle-treated cafeteria-fed rats. Total GIP levels were modified by neither the cafeteria diet nor the GSPE treatment (Figure 1B).

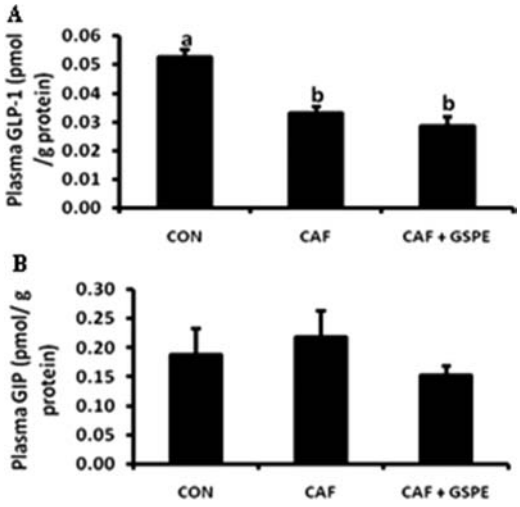

Figure 1. Effect of the cafeteria diet and GSPE on incretin plasma levels. Effects on (A) plasma-active GLP-1 levels and (B) total GIP levels were assayed after 12 weeks of cafeteria diet and preventive treatment with 25 mg of GSPE/kg of bw. The data are displayed as the mean ± SEM, with a and b as statistically significant differences at $p < 0.05$.

To assess the effect of the cafeteria diet and GSPE treatment on incretin biosynthesis, we measured the GLP-1 levels and proglucagon gene expression in the colon as well as GIP gene expression in the duodenum. As shown in Figure 2, the colon levels of GLP-1 were decreased by the cafeteria diet by approximately 30% compared to the control diet (Figure 2A), a reduction that was accompanied by a significant down-regulation of the proglucagon gene expression (Figure 2B). The GSPE treatment prevented the decrease in colon levels of GLP-1 produced by the cafeteria diet, although it did not reach control levels (Figure 2A). This effect was also observed for the expression of the proglucagon gene, as shown in Figure 2B. GIP gene expression in the duodenum was unaffected by either the cafeteria diet or the GSPE treatment [0.93 ± 0.17 and 0.89

dx.doi.org/10.1021/jf405239p | J. Agric. Food Chem. 2014, 62, 1066−1072

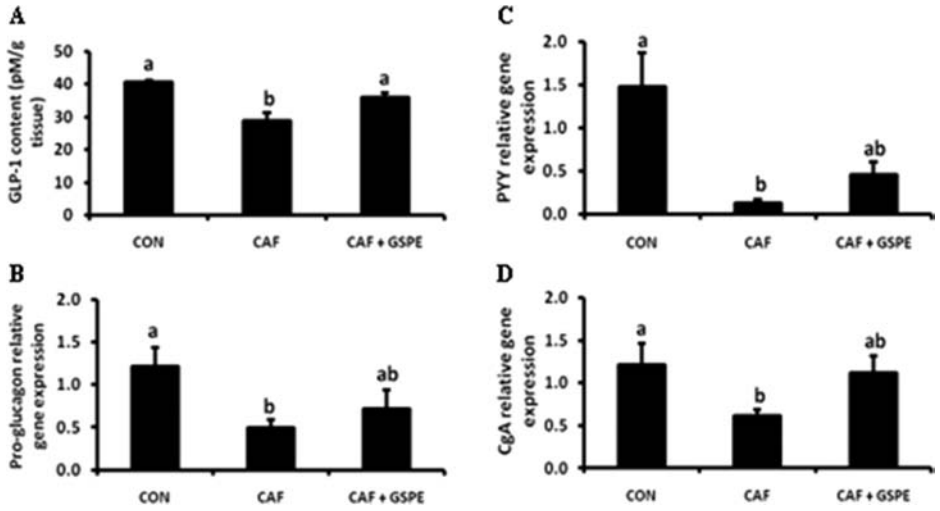

Figure 2. Effect of the cafeteria diet and GSPE on hormone production and CgA gene expression in the colon. Effects on (A) colon-active GLP-1 content and gene expression of (B) proglucagon, (C) PYY, and (D) CgA were determined after 12 weeks of cafeteria diet and simultaneous treatment with 25 mg of GSPE/kg of bw. The data are displayed as the mean ± SEM, with a, b and c as statistically significant differences at $p < 0.05$.

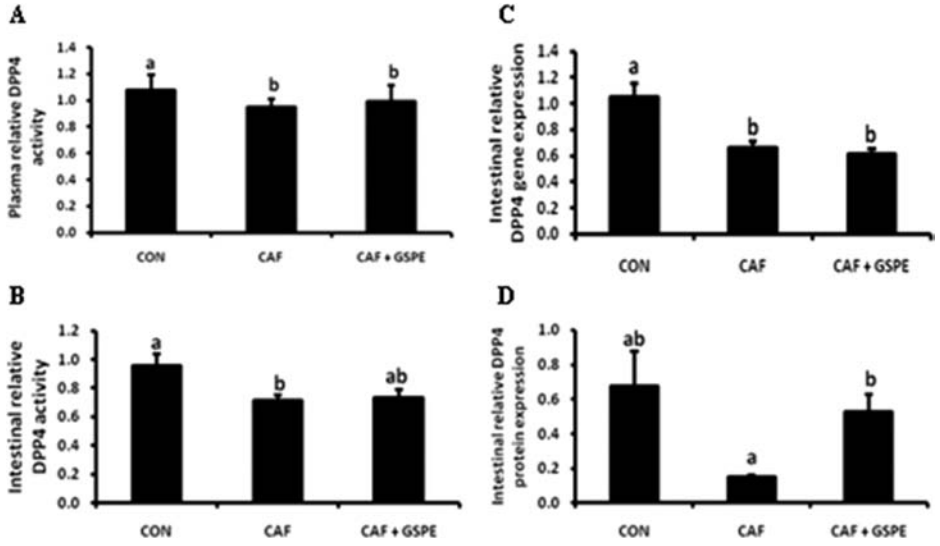

Figure 3. Effect of the cafeteria diet and GSPE on DPP4. After 12 weeks of cafeteria diet and simultaneous treatment with 25 mg of GSPE/kg of bw, DPP4 activity was determined in (A) plasma and (B) intestine. Intestinal DPP4 (C) gene expression and (D) protein expression were also assessed by RT-PCR and western blot, respectively. The data are displayed as the mean ± SEM, with a, b and c as statistically significant differences at $p < 0.05$.

± 0.10, respectively, versus the control (1.03 ± 0.09) ($p > 0.05$)].

GSPE Prevents the Cafeteria-Diet-Induced Decrease of Enteroendocrine Cells in the Colon. To determine whether the reduction in GLP-1 is due to a modulation of GLP-1 gene expression or a general effect on GLP-1-producing cells, we tested the effects of the cafeteria diet and GSPE on PYY, another hormone that is also secreted by intestinal L cells. We evaluated PYY gene expression, and as shown in Figure 2C, it was significantly downregulated as a result of the cafeteria diet, whereas GSPE treatment partially blocked this effect.

Next, we analyzed the gene expression of CgA, a marker of endocrine differentiation. Figure 2D shows that the expression of the CgA gene in the colon was significantly decreased in the CAF group, whereas GSPE treatment prevented the effect of the cafeteria diet, similar to the effect observed for GLP-1 and PYY. The expression of the CgA gene in the duodenum was also assessed, but it was unaffected by the cafeteria diet or the GSPE treatment [0.88 ± 0.11 and 1.13 ± 0.27, respectively, versus the control (1.16 ± 0.22) ($p > 0.05$)].

GSPE Modulates Intestinal DPP4. To assess whether the cafeteria diet and the GSPE treatment could also modify the enzyme responsible for incretin degradation, DPP4, the plasma and intestinal levels of DPP4 activity were measured at the end of the treatment. As shown in Figure 3A, plasma DPP4 activity was slightly but significantly decreased by the cafeteria diet, whereas it was unaffected by the GSPE treatment. Intestinal DPP4 activity was also reduced by the cafeteria diet, whereas in contrast to the effects in plasma, the simultaneous GSPE treatment prevented this decrease (Figure 3B). To analyze whether the preventive effect elicited by GSPE was due to a modulation of DPP4 production, its gene and protein expression were also evaluated in the intestine. As shown in panels C and D of Figure 3, DPP4 gene expression and protein

levels were reduced by the cafeteria diet, which is consistent with what was observed in terms of its activity. GSPE prevented the cafeteria-induced decrease in DPP4 protein expression but elicited no effect at the gene expression level.

GSPE Treatment Modulates the Expression of GLP-1 and GLP-1 Receptor Genes in the Hypothalamus. To evaluate the systemic preventive effects of GSPE on GLP-1 production, proglucagon gene expression was also assessed in the hypothalamus. As shown in Figure 4A, the cafeteria diet

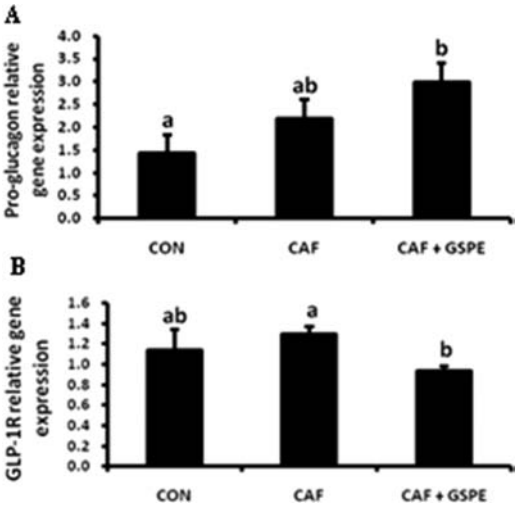

Figure 4. Effect of the cafeteria diet and GSPE on hypothalamic GLP-1 and GLP-1R. Effects on hypothalamic gene expression of (A) proglucagon and (B) GLP-1R were assessed after 12 weeks of cafeteria diet and preventive treatment with 25 mg of GSPE/kg of bw. The data are displayed as the mean ± SEM, with a and b as statistically significant differences at $p < 0.05$.

tended to upregulate proglucagon expression and GSPE treatment further enhanced this effect. We also evaluated the sensitivity to GLP-1 by assaying GLP-1R gene expression and found that its expression was unaffected by the cafeteria diet, whereas it was downregulated by the GSPE treatment compared to cafeteria-fed rats treated with the vehicle (Figure 4B).

GSPE Modulates Insulinemia after 9 Weeks of Treatment. To assess whether a preventive GSPE treatment can modulate insulinemia, an OGTT of 2 h was performed at the eighth week of treatment. As shown in Figure 5, insulin AUC was increased in cafeteria-diet-fed rats, whereas a preventive GSPE treatment prevented this effect.

Moreover, fasting plasma insulin and glucose levels were measured after 9 and 12 weeks, to test whether preventive GSPE treatment affects insulin resistance induced by the cafeteria diet. As shown in Figure 6A, HOMA-IR was significantly increased after 9 weeks of cafeteria diet, whereas a simultaneous treatment with 25 mg of GSPE/kg of bw prevented this effect, resulting in a healthier HOMA-IR. However, after 12 weeks, GSPE treatment was unable to prevent the increase in HOMA-IR induced by the cafeteria diet (Figure 6B).

DISCUSSION

Procyanidins from grape seed have been shown to improve insulin resistance, eliciting a corrective effect when the glucose homeostasis of the animal has been slightly disturbed by a

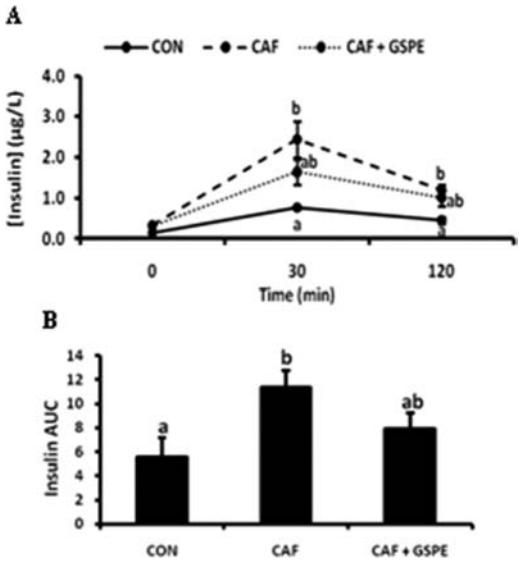

Figure 5. Effect of the cafeteria diet and GSPE on insulinemia. After 8 weeks of cafeteria diet and a preventive treatment with 25 mg of GSPE/kg of bw, a 2 h OGTT was performed, (A) insulin was analyzed at time 0, 30, and 120 min, and (B) AUC was calculated. The data are displayed as the mean ± SEM, with a and b as statistically significant differences at $p < 0.05$.

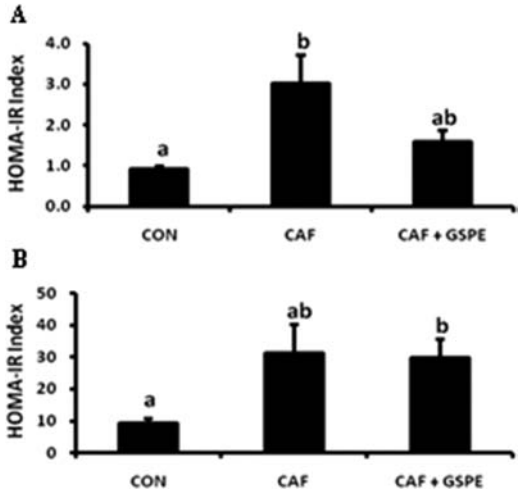

Figure 6. Effect of the cafeteria diet and GSPE on insulin resistance. Plasma glucose and insulin levels were measured, and HOMA-IR was calculated after (A) 9 weeks and (B) 12 weeks of cafeteria diet and preventive treatment with 25 mg of GSPE/kg of bw. The data are displayed as the mean ± SEM, with a and b as statistically significant differences at $p < 0.05$.

cafeteria diet.[1,2,5,21] However, whether GSPE can act in a preventive way has not yet been described. Moreover, GSPE has been shown to elicit an incretin-like effect in healthy rats.[6] However, our understanding of the effects of GSPE on the incretin system in animals with disturbed glucose homeostasis remains limited. In this study, we developed a 12-week cafeteria diet-fed model that caused a decrease in GLP-1 plasma levels and production in the intestine, with no effects on GLP-1 production and detection in the hypothalamus. The cafeteria diet also caused a decrease in the amount of DPP4 enzyme at the plasma level and in the intestine, and the HOMA-IR clearly revealed the induction of insulin resistance. We found that

dx.doi.org/10.1021/jf405239p | J. Agric. Food Chem. 2014, 62, 1066−1072

procyanidins were able to counteract several of these effects, which were predominantly found in the intestine.

With regard to GLP-1 production, the CAF + GSPE animals exhibited an increased amount of GLP-1 in colonic cells, with a simultaneous increase in GLP-1 mRNA. Similarly, Dao et al. reported that resveratrol increased the colon levels of active GLP-1, together with an increase in proglucagon gene expression, in mice fed with a HFD.[10] Dao et al. also suggested that the increase in GLP-1 production by resveratrol might explain its preventive effects on plasma levels of GLP-1, which are reduced in the vehicle-treated HFD-fed mice after the administration of an oral glucose load but are increased in the resveratrol-treated HFD-fed animals.[10] Actually, an acute dose of GSPE has also been found to effectively improve glucose-stimulated GLP-1 secretion in healthy rats (submitted results). Besides, some other proanthocyanidins (i.e., berry purees[22] and the tetrameric procyanidin cinnamtannin A2[23]) have been shown to elicit this effect.

Our results showed that treatment with GSPE also upregulated the colon expression of the PYY gene, a hormone that has been reported to be co-expressed with GLP-1 in enteroendocrine L cells.[24] Enteroendocrine cells actively self-renew and differentiate throughout the life of an animal,[25] and procyanidins are known to modify cell proliferation.[21,26,27] Therefore, we assessed whether GSPE modulated CgA levels, a marker of endocrine cells.[28,29] We found that GSPE again counteracted the effects of the cafeteria diet. Our results suggest that the modulation on GLP-1 production is due to not only a direct modulation of its gene expression but also changes in the amount of enteroendocrine cells, which were reduced by the cafeteria diet. There are no previous studies that have analyzed the effects of a cafeteria diet on the number of enteroendocrine cells. A HFD was suggested to increase the proliferation of L cells, causing a dysfunction and reducing GLP-1 secretion.[30] The different results might be attributed to differences in experimental conditions (type of diet, animal gender, and length of the study) between studies. Moreover, that study analyzed the effects within the duodenum, whereas we found effects that were limited to the colon, the predominant location for GLP-1 production.[31] In contrast, we found that the expression of CgA and GIP genes in the duodenum, where GIP-producing cells are predominantly found,[32] was unchanged in our experiment, which is consistent with the unaltered plasma levels of GIP.

The effects of GSPE on DPP4 are consistent with our previous results, which demonstrated the sensitivity of intestinal DPP4 to GSPE and a lack of GSPE effects on plasma DPP4.[6] In this study, we found that GSPE prevents the decrease in intestinal DPP4 activity and protein caused by a cafeteria diet. These results differ from previous observations because we had shown an inhibitory effect of 25 mg of GSPE/kg of bw after 45 days of treatment in healthy animals or after 30 days in animals with cafeteria-diet-induced insulin resistance.[6] The effect that a cafeteria diet elicited on DPP4 is unclear. Several authors have reported an increase in circulating DPP4 activity in humans with obesity or type 2 diabetes[33−35] and in rats with type 1 diabetes or impaired glucose tolerance.[36,37] However, limited studies in humans have shown decreased plasma DPP4 activity in diabetic subjects[38] and unchanged activity in obese, diabetic, and impaired-glucose tolerance subjects.[34,39] Taken together, these data indicate that a severe degree of hyperglycemia is required to induce an increase on circulating DPP4 activity, whereas mild hyperglycemia is insufficient to induce its increase.[34,39] Our model supports this conclusion because the cafeteria diet did not affect glycemia, which is consistent with the lack of increased DPP4. In contrast, we found a decrease that is partially prevented by GSPE. In a completely different context, the flavonoid apigenin has been reported to counteract the decrease in DPP4 activity caused by cancer in a colorectal carcinoma cell line, an observation that is in line with the effects on DPP4 observed in our study.[40] However, there is limited information regarding DPP4 activity in the intestine. Thus, it is difficult to make further conclusions. Considering that this is the first preventive study on GSPE effects, further studies are warranted to fully assess the implications of the DPP4 inhibition in the cafeteria-diet-fed model and the opposing effects elicited by GSPE.

To evaluate the systemic preventive effects of GSPE on GLP-1, we analyzed GLP-1 and its receptor in the hypothalamus, where they are also expressed.[41,42] Previous studies have shown that brain proglucagon gene expression is upregulated by a HFD.[43,44] We observed a tendency to increase hypothalamic proglucagon gene expression. However, we found that GLP-1 expression was stimulated in CAF + GSPE rats. This stimulation is consistent with the reduced expression of the GLP-1R gene. Knauf et al. found that blockade of brain GLP-1R in HF-fed mice improves insulin resistance and enhances glucose use by muscles.[43] The available evidence suggests that enteric glucose absorption activates GLP-1R-sensitive central nervous system (CNS) networks that promote enhanced glucose disposal. Furthermore, brain GLP-1R signaling controls peripheral blood flow and insulin sensitivity predominantly under hyperinsulinemic/hyperglycemic conditions. The relative importance of central versus peripheral GLP-1 action for the control of glucose homeostasis remains unclear.[42]

All of these results demonstrate that GSPE interacts with the GLP-1 system, predominantly preventing the negative effects induced by a cafeteria diet. Therefore, the CAF + GSPE animals were expected to show an improved glucose metabolism compared to the CAF group. At the eighth week, we performed an OGTT and found that the GSPE treatment corrected the glucose-induced increase in insulin AUC as expected. Indeed, these results are consistent with the action of a GSPE corrective treatment of 4 weeks, which was previously shown to improve peripheral insulin resistance at the same dose.[2] This effect was maintained at 9 weeks, when we observed an improved HOMA-IR as a result of GSPE pretreatment. However, surprisingly, after 12 weeks, our results do not show a clear improvement in HOMA-IR by the GSPE treatment. This might be due to the dose of GSPE, because we previously described high variability on the insulin levels after different GSPE doses. Working with healthy animals, we have previously shown that this variability is not dose-dependent.[45] In fact, higher GSPE doses for a longer time showed an improved insulinemia and glycemia in type 2 diabetic rats.[46,47] This was accompanied by an improved functionality of β cells related to the GSPE treatment, as we have previously found with lower doses.[5,27]

In conclusion, we have found that a cafeteria diet induces a decrease in active GLP-1 levels by decreasing GLP-1 production in the colon, which might be attributed to a loss of enteroendocrine cells, an effect that is prevented by simultaneous treatment with GPSE. GSPE treatment also increased hypothalamic GLP-1 production and downregulated GLP-1R, opposing the effects of the cafeteria diet. This

preventive action also impacts intestinal DPP4, predominantly by preventing the decrease in its activity and protein levels.

AUTHOR INFORMATION

Corresponding Author

*Telephone: 34-977-559566. Fax: 34-977-558232. E-mail: anna.ardevol@urv.cat.

Funding

This study was supported by a grant (AGL2011-23879) from the Spanish government. Noemí González-Abuín is a recipient of a Formación de Personal Investigador (FPI) fellowship from the Spanish Ministry of Science and Innovation (MICINN), and Neus Martínez-Micaelo is recipient of a fellowship from Universitat Rovira i Virgili.

Notes

The authors declare no competing financial interest.

ACKNOWLEDGMENTS

The authors acknowledge the technical support of Niurka Llopiz from Universitat Rovira i Virgili. The authors thank members of the Nutrigenomics group that have collaborated with caring for and sampling the animals.

ABBREVIATIONS USED

DPP4, dipeptidyl-peptidase 4; GSPE, grape-seed procyanidin extract; bw, body weight; OGTT, oral glucose tolerance test; GIP, glucose-dependent insulinotropic peptide; GLP-1, glucagon-like peptide-1; GLP-1R, glucagon-like peptide-1 receptor; CgA, chromogranin A

REFERENCES

(1) Pinent, M.; Cedó, L.; Montagut, G.; Blay, M.; Ardévol, A. Procyanidins improve some disrupted glucose homoeostatic situations: An analysis of doses and treatments according to different animal models. *Crit. Rev. Food Sci. Nutr.* **2012**, *52*, 569−584.

(2) Montagut, G.; Bladé, C.; Blay, M.; Fernández-Larrea, J.; Pujadas, G.; Salvadó, M. J.; Arola, L.; Pinent, M.; Ardévol, A. Effects of a grapeseed procyanidin extract (GSPE) on insulin resistance. *J. Nutr. Biochem.* **2009**, *21*, 961−967.

(3) Pinent, M.; Blay, M.; Blade, M.; Salvado, M.; Arola, L.; Ardevol, A. Grape seed-derived procyanidins have an antihyperglycemic effect in streptozotocin-induced diabetic rats and insulinomimetic activity in insulin-sensitive cell lines. *Endocrinology* **2004**, *145*, 4985−4990.

(4) Montagut, G.; Onnockx, S.; Vaqué, M.; Bladé, C.; Blay, M.; Fernández-Larrea, J.; Pujadas, G.; Salvadó, M. J.; Arola, L.; Pirson, I. Oligomers of grape-seed procyanidin extract activate the insulin receptor and key targets of the insulin signaling pathway differently from insulin. *J. Nutr. Biochem.* **2010**, *21*, 476−481.

(5) Castell-Auví, A.; Cedó, L.; Pallarès, V.; Blay, M.; Pinent, M.; Ardévol, A. Grape seed procyanidins improve β-cell functionality under lipotoxic conditions due to their lipid-lowering effect. *J. Nutr. Biochem.* **2012**, *24*, 948−953.

(6) Gonzalez-Abuin, N.; Martínez-Micaelo, N.; Blay, M.; Pujadas, G.; Garcia-Vallvé, S.; Pinent, M.; Ardévol, A. Grape seed-derived procyanidins decrease dipeptidyl-peptidase 4 activity and expression. *J. Agric. Food Chem.* **2012**, *60*, 9055−9061.

(7) Gautier, J.; Fetita, S.; Sobngwi, E.; Salaün-Martin, C. Biological actions of the incretins GIP and GLP-1 and therapeutic perspectives in patients with type 2 diabetes. *Diabetes Metab.* **2005**, *31*, 233−242.

(8) Vilsbøll, T.; Krarup, T.; Deacon, C. F.; Madsbad, S.; Holst, J. J. Reduced postprandial concentrations of intact biologically active glucagon-like peptide 1 in type 2 diabetic patients. *Diabetes* **2001**, *50*, 609−613.

(9) Toft-Nielsen, M.; Damholt, M. B.; Madsbad, S.; Hilsted, L. M.; Hughes, T. E.; Michelsen, B. K.; Holst, J. J. Determinants of the impaired secretion of glucagon-like peptide-1 in type 2 diabetic patients. *J. Clin. Endocrinol. Metab.* **2001**, *86*, 3717−3723.

(10) Dao, T. M. A.; Waget, A.; Klopp, P.; Serino, M.; Vachoux, C.; Pechere, L.; Drucker, D. J.; Champion, S.; Barthélemy, S.; Barra, Y. Resveratrol increases glucose induced GLP-1 secretion in mice: A mechanism which contributes to the glycemic control. *PloS One* **2011**, *6*, No. e20700.

(11) Nauck, M.; Weber, I.; Bach, I.; Richter, S.; Ørskov, C.; Holst, J.; Schmiegel, W. Normalization of fasting glycaemia by intravenous GLP-1 ([7-36 amide] or [7-37]) in type 2 diabetic patients. *Diabetic Med.* **1998**, *15*, 937−945.

(12) Meier, J. J.; Gallwitz, B.; Salmen, S.; Goetze, O.; Holst, J. J.; Schmidt, W. E.; Nauck, M. A. Normalization of glucose concentrations and deceleration of gastric emptying after solid meals during intravenous glucagon-like peptide 1 in patients with type 2 diabetes. *J. Clin. Endocrinol. Metab.* **2003**, *88*, 2719−2725.

(13) Parlevliet, E. T.; de Leeuw van Weenen, J. E.; Romijn, J. A.; Pijl, H. GLP-1 treatment reduces endogenous insulin resistance via activation of central GLP-1 receptors in mice fed a high-fat diet. *Am. J. Physiol. Endocrinol. Metab.* **2010**, *299*, E318−E324.

(14) Hussein, G. M. E.; Matsuda, H.; Nakamura, S.; Akiyama, T.; Tamura, K.; Yoshikawa, M. Protective and ameliorative effects of maté (*Ilex paraguariensis*) on metabolic syndrome in TSOD mice. *Phytomedicine* **2011**, *19*, 88−97.

(15) Hussein, G. M. E.; Matsuda, H.; Nakamura, S.; Hamao, M.; Akiyama, T.; Tamura, K.; Yoshikawa, M. Mate tea (*Ilex paraguariensis*) promotes satiety and body weight lowering in mice: Involvement of glucagon-like peptide-1. *Biol. Pharm. Bull.* **2011**, *34*, 1849−1855.

(16) Quiñones, M.; Guerrero, L.; Suarez, M.; Pons, Z.; Aleixandre, A.; Arola, L.; Muguerza, B. Low-molecular procyanidin rich grape seed extract exerts antihypertensive effect in males spontaneously hypertensive rats. *Food Res. Int.* **2013**, *51*, 587−595.

(17) Cani, P. D.; Hoste, S.; Guiot, Y.; Delzenne, N. M. Dietary non-digestible carbohydrates promote L-cell differentiation in the proximal colon of rats. *Br. J. Nutr.* **2007**, *98*, 32−37.

(18) Bradford, M. M. A rapid and sensitive method for the quantitation of microgram quantities of protein utilizing the principle of protein−dye binding. *Anal. Biochem.* **1976**, *72*, 248−254.

(19) Matthews, D.; Hosker, J.; Rudenski, A.; Naylor, B.; Treacher, D.; Turner, R. Homeostasis model assessment: Insulin resistance and β-cell function from fasting plasma glucose and insulin concentrations in man. *Diabetologia* **1985**, *28*, 412−419.

(20) Ou, B.; Hampsch-Woodill, M.; Prior, R. L. Development and validation of an improved oxygen radical absorbance capacity assay using fluorescein as the fluorescent probe. *J. Agric. Food Chem.* **2001**, *49*, 4619−4626.

(21) Cedó, L.; Castell-Auví, A.; Pallarès, V.; Blay, M.; Ardévol, A.; Pinent, M. Grape seed procyanidin extract improves insulin production but enhances bax protein expression in cafeteria-treated male rats. *Int. J. Food Sci.* **2013**, *2013*, No. 875314.

(22) Torronen, R.; Sarkkinen, E.; Niskanen, T.; Tapola, N.; Kilpi, K.; Niskanen, L. Postprandial glucose, insulin and glucagon-like peptide 1 responses to sucrose ingested with berries in healthy subjects. *Br. J. Nutr.* **2012**, *107*, 1445−1451.

(23) Yamashita, Y.; Okabe, M.; Natsume, M.; Ashida, H. Cinnamtannin A2, a tetrameric procyanidin, increases GLP-1 and insulin secretion in mice. *Biosci., Biotechnol., Biochem.* **2013**, *77*, 888−891.

(24) Bohórquez, D. V.; Chandra, R.; Samsa, L. A.; Vigna, S. R.; Liddle, R. A. Characterization of basal pseudopod-like processes in ileal and colonic PYY cells. *J. Mol. Histol.* **2011**, *42*, 3−13.

(25) Schonhoff, S. E.; Giel-Moloney, M.; Leiter, A. B. Minireview: Development and differentiation of gut endocrine cells. *Endocrinology* **2004**, *145*, 2639−2644.

(26) Pinent, M.; Castell, A.; Baiges, I.; Montagut, G.; Arola, L.; Ardévol, A. Bioactivity of flavonoids on insulin-secreting cells. *Compr. Rev. Food Sci. Food Saf.* **2008**, *7*, 299−308.

(27) Cedó, L.; Castell-Auví, A.; Pallarès, V.; Blay, M.; Ardévol, A.; Arola, L.; Pinent, M. Grape seed procyanidin extract modulates

proliferation and apoptosis of pancreatic β-cells. *Food Chem.* **2012**, *138*, 524−530.
(28) Portela-Gomes, G. M.; Stridsberg, M.; Johansson, H.; Grimelius, L. Complex co-localization of chromogranins and neurohormones in the human gastrointestinal tract. *J. Histochem. Cytochem.* **1997**, *45*, 815−822.
(29) Jenny, M.; Uhl, C.; Roche, C.; Duluc, I.; Guillermin, V.; Guillemot, F.; Jensen, J.; Kedinger, M.; Gradwohl, G. Neurogenin3 is differentially required for endocrine cell fate specification in the intestinal and gastric epithelium. *EMBO J.* **2002**, *21*, 6338−6347.
(30) Gniuli, D.; Calcagno, A.; Dalla Libera, L.; Calvani, R.; Leccesi, L.; Caristo, M.; Vettor, R.; Castagneto, M.; Ghirlanda, G.; Mingrone, G. High-fat feeding stimulates endocrine, glucose-dependent insulinotropic polypeptide (GIP)-expressing cell hyperplasia in the duodenum of Wistar rats. *Diabetologia* **2010**, *53*, 2233−2240.
(31) Moran-Ramos, S.; Tovar, A. R.; Torres, N. Diet: Friend or foe of enteroendocrine cells—How it interacts with enteroendocrine cells. *Adv. Nutr.* **2012**, *3*, 8−20.
(32) Yip, R. G.; Wolfe, M. M. GIF biology and fat metabolism. *Life Sci.* **1999**, *66*, 91−103.
(33) Ryskjaer, J.; Deacon, C. F.; Carr, R. D.; Krarup, T.; Madsbad, S.; Holst, J.; Vilsboll, T. Plasma dipeptidyl peptidase-IV activity in patients with type-2 diabetes mellitus correlates positively with HbAlc levels, but is not acutely affected by food intake. *Eur. J. Endocrinol.* **2006**, *155*, 485−493.
(34) Mannucci, E.; Pala, L.; Ciani, S.; Bardini, G.; Pezzatini, A.; Sposato, I.; Cremasco, F.; Ognibene, A.; Rotella, C. Hyperglycaemia increases dipeptidyl peptidase IV activity in diabetes mellitus. *Diabetologia* **2005**, *48*, 1168−1172.
(35) Carr, R. D.; Larsen, M. O.; Jelic, K.; Lindgren, O.; Vikman, J.; Holst, J. J.; Deacon, C. F.; Ahren, B. Secretion and dipeptidyl peptidase-4-mediated metabolism of incretin hormones after a mixed meal or glucose ingestion in obese compared to lean, nondiabetic men. *J. Clin. Endocrinol. Metab.* **2010**, *95*, 872−878.
(36) Kirino, Y.; Sato, Y.; Kamimoto, T.; Kawazoe, K.; Minakuchi, K.; Nakahori, Y. Interrelationship of dipeptidyl peptidase IV (DPP4) with the development of diabetes, dyslipidaemia and nephropathy: A streptozotocin-induced model using wild-type and DPP4-deficient rats. *J. Endocrinol.* **2009**, *200*, 53−61.
(37) Kirino, Y.; Kamimoto, T.; Sato, Y.; Kawazoe, K.; Minakuchi, K.; Nakahori, Y. Increased plasma dipeptidyl peptidase IV (DPP IV) activity and decreased DPP IV activity of visceral but not subcutaneous adipose tissue in impaired glucose tolerance rats induced by high-fat or high-sucrose diet. *Biol. Pharm. Bull.* **2009**, *32*, 463−467.
(38) Meneilly, G.; Demuth, H.; McIntosh, C.; Pederson, R. Effect of ageing and diabetes on glucose-dependent insulinotropic polypeptide and dipeptidyl peptidase IV responses to oral glucose. *Diabetic Med.* **2000**, *17*, 346−350.
(39) Pala, L.; Ciani, S.; Dicembrini, I.; Bardini, G.; Cresci, B.; Pezzatini, A.; Giannini, S.; Mannucci, E.; Rotella, C. Relationship between GLP-1 levels and dipeptidyl peptidase-4 activity in different glucose tolerance conditions. *Diabetic Med.* **2010**, *27*, 691−695.
(40) Lefort, É.C.; Blay, J. The dietary flavonoid apigenin enhances the activities of the anti-metastatic protein CD26 on human colon carcinoma cells. *Clin. Exp. Metastasis* **2011**, *28*, 337−349.
(41) Cabou, C.; Burcelin, R. GLP-1, the gut−brain, and brain−periphery axes. *Rev. Diabetic Stud.* **2011**, *8*, 418−431.
(42) Campbell, J. E.; Drucker, D. J. Pharmacology, physiology, and mechanisms of incretin hormone action. *Cell Metab.* **2013**, *17*, 819−837.
(43) Knauf, C.; Cani, P. D.; Ait-Belgnaoui, A.; Benani, A.; Dray, C.; Cabou, C.; Colom, A.; Uldry, M.; Rastrelli, S.; Sabatier, E. Brain glucagon-like peptide 1 signaling controls the onset of high-fat diet-induced insulin resistance and reduces energy expenditure. *Endocrinology* **2008**, *149*, 4768−4777.
(44) Burmeister, M. A.; Ferre, T.; Ayala, J. E.; King, E. M.; Holt, R. M.; Ayala, J. E. Acute activation of central GLP-1 receptors enhances hepatic insulin action and insulin secretion in high-fat-fed, insulin resistant mice. *Am. J. Physiol. Endocrinol. Metab.* **2012**, *302*, E334−E343.
(45) Castell-Auví, A.; Cedó, L.; Pallarès, V.; Blay, M. T.; Pinent, M.; Motilva, M. J.; Garcia-Vallvé, S.; Pujadas, G.; Maechler, P.; Ardévol, A. Procyanidins modify insulinemia by affecting insulin production and degradation. *J. Nutr. Biochem.* **2012**, *23*, 1565−1572.
(46) Ding, Y.; Dai, X.; Jiang, Y.; Zhang, Z.; Bao, L.; Li, Y.; Zhang, F.; Ma, X.; Cai, X.; Jing, L. Grape seed proanthocyanidin extracts alleviate oxidative stress and ER stress in skeletal muscle of low-dose streptozotocin- and high-carbohydrate/high-fat diet-induced diabetic rats. *Mol. Nutr. Food Res.* **2013**, *57*, 365−369.
(47) Ding, Y.; Zhang, Z.; Dai, X.; Jiang, Y.; Bao, L.; Li, Y.; Li, Y. Grape seed proanthocyanidins ameliorate pancreatic β-cell dysfunction and death in low-dose streptozotocin- and high-carbohydrate/high-fat diet-induced diabetic rats partially by regulating endoplasmic reticulum stress. *Nutr. Metab.* **2013**, *10*, 51.

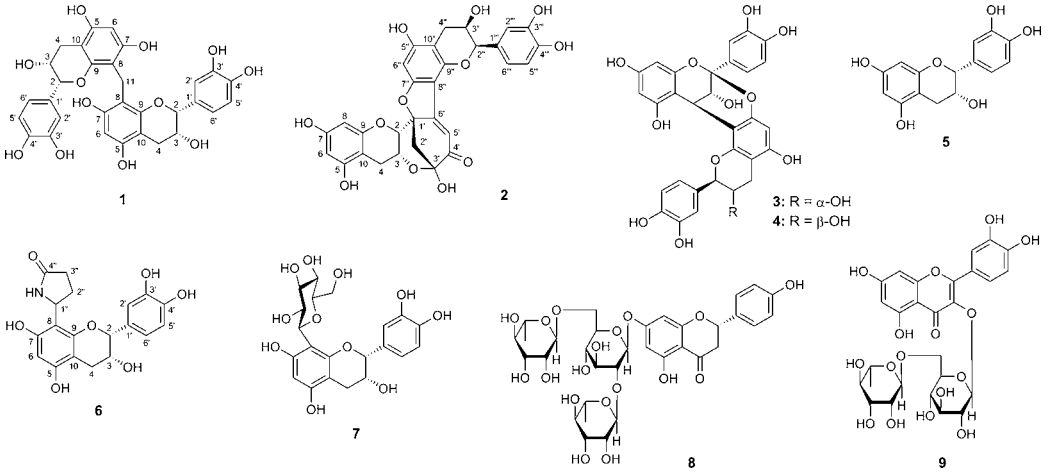

Figure 1. Structures of compounds **1**–**9** from the pericarps of *L. chinensis*.

Table 1. ^{1}H and ^{13}C NMR Data of Compounds 1 and 6 in CD_3OD

	1		6	
C/H	δ_H (multiplet, *J* in Hz)	δ_C (DEPT)	δ_H (multiplet, *J* in Hz)	δ_C
2	4.76 (2H, br s)	80.4 (CH)	4.84 (br s)	80.1
3	4.10 (2H, br dd, 4.7, 3.7)	67.2 (CH)	4.17 (ddd, 4.5, 3.0, 1.0)	66.9
4	2.83 (2H, dd, 16.6, 4.7)	29.0 (CH_2)	2.87 (dd, 16.7, 4.5)	29.4
	2.69 (2H, dd, 16.6, 3.7)		2.77 (ddd, 16.7, 3.0, 1.0)	
5		155.8 (C)		157.2
6	5.96 (2H, s)	96.8 (CH)	6.00 (s)	96.4
7		155.2 (C)		156.3
8		106.7 (C)		107.7
9		153.6 (C)		155.5
10		100.5 (C)		100.0
11	3.88 (2H, s)	16.8 (CH_2)		
1′		131.7 (C)		132.2
2′	6.96 (2H, br s)	115.4 (CH)	6.98 (d, 2.0)	115.3
3′		145.9 (C)		145.9
4′		145.9 (C)		146.0
5′	6.73 (2H, br s)	116.0 (CH)	6.76 (d, 8.2)	115.9
6′	6.73 (2H, br s)	119.7 (CH)	6.80 (dd, 8.2, 2.0)	119.5
1″			5.42 (dd, 9.2, 5.3)	50.3
2″			2.45 (m)	26.7
			2.38 (m)	
3″			2.53 (m)	32.2
			2.30 (m)	
4″				181.3

Daltonics Inc., Bremen, Germany). Optical rotation was acquired on a Perkin-Elmer (Waltham, MA) 343 polarimeter. Ultraviolet (UV) radiation was recorded on a Perkin-Elmer Lambda 650 UV–vis spectrophotometer (Perkin-Elmer). Infrared (IR) radiation was obtained on a WQF-520 FT-IR spectrometer (Beijing Rayleigh Analytic Instrument Co., Beijing, China).

Plant Material. Fresh ripe litchi fruits, cv. 'Heiye', were collected from the Fruit Tree Research Institute, Guangdong Academy of Agricultural Sciences (Guangzhou, China) in June 2012, and the pericarps were manually separated from the fruits.

Extraction and Isolation. The fresh pericarps (5.0 kg) were immersed in 85% aqueous ethanol, chopped with a multifood processor, transferred to flasks, and then heated at 50 °C for 2 h. Twenty liters of 85% aqueous ethanol was used each time, and the extraction was repeated three times. The solution was filtered and evaporated under vacuum to give an ethanolic extract (320 g). The extract (315 g) was dissolved in 2.0 L of water and then sequentially fractionated with ethyl acetate (1.5 L × 5) and *n*-butanol (1.2 L × 7) to afford ethyl acetate-soluble (109.35 g) and *n*-butanol-soluble (79.30 g) fractions after being taken to dryness under reduced pressure. The ethyl acetate-soluble fraction (107.35 g) was subjected to silica gel (2330 g, 100–200 mesh) column [545 mm × 120 mm (inside diameter)] chromatography and eluted with a chloroform ($CHCl_3$)/methanol (MeOH) mixture (v/v, 10:0, 38 L → 98:2, 24 L → 95:5, 19 L → 9:1, 33 L → 85:15, 38 L → 8:2, 25 L → 7:3, 25 L → 6:4, 9 L → 0:10, 9 L) to furnish fractions E1–E15 after they had been pooled according to their TLC profiles. Fraction E10 (10.7 g) was further subjected to silica gel (440 g, 200–300 mesh) column [720 mm × 44 mm (inside diameter)] chromatography and eluted with a $CHCl_3$/MeOH mixture (v/v, 95:5, 2.75 L → 9:1, 8.75 L → 85:15, 6.25 L) to yield fractions E10-1–E10-4. Fraction E10-4 was separated by MPLC and eluted with a MeOH/H_2O mixture (v/v, 2:8, 3:7, 4:6, 5:5, 6:4, and 7:3, each 2.4 L) at a flow rate of 10 mL/min to produce fractions E10-4-1–10-4-4. Fractions E10-4-1 and E10-4-2 were individually separated by silica gel (200–300 mesh) column chromatography to afford compounds **1** (15 mg) and **5** (11 mg), respectively. Fraction

dx.doi.org/10.1021/jf405750p | J. Agric. Food Chem. 2014, 62, 1073–1078

Table 2. ^{1}H and ^{13}C NMR Data of Compound 2 in CD_3OD

C/H	δ_H (multiplet, J in Hz)	δ_C	C/H	δ_H (multiplet, J in Hz)	δ_C
2	3.82 (br s)	72.9	2″	5.03 (br s)	80.8
3	4.45 (br d, 4.8)	65.1	3″	4.30 (br d, 3.9)	66.4
4	2.83 (br d, 16.5)	25.0	4″	2.89 (dd, 16.5, 3.9)	29.5
	2.65 (dd, 16.5, 4.8)			2.83 (br d, 16.5)	
5		157.5	5″		166.5
6	5.92 (d, 2.0)	96.6	6″	6.17 (s)	91.7
7		157.7	7″		167.0
8	5.94 (d, 2.0)	95.5	8″		104.7
9		155.6	9″		156.2
10		98.9	10″		103.6
1′		91.8	1‴		131.2
2′	2.94 (d, 15.3)	40.5	2‴	7.04 (br s)	115.1
	2.83 (d, 15.3)				
3′		95.5	3‴		146.1
4′		193.8	4‴		146.2
5′	6.55 (s)	113.6	5‴	6.81 (d, 8.0)	116.1
6′		164.7	6‴	6.86 (br d, 8.0)	119.2

E10-4-3 was purified by preparative HPLC using a MeOH/H_2O mixture (46:54, v/v) as the mobile phase at a flow rate of 5 mL/min to give compound **2** [retention time (t_R) of 53.4 min, 25 mg]. Fraction E11 (13.88 g) was passed through a MCI gel column [259 mm × 26 mm (inside diameter)] for depigmentation, and the obtained MeOH eluate (7.20 g) was separated by MPLC and purified by preparative HPLC using an acetonitrile/H_2O/acetic acid (AcOH) mixture (15:85:0.1, v/v/v) as the mobile phase at a flow rate of 5 mL/min to yield compounds **3** (t_R of 60.7 min, 32 mg) and **4** (t_R of 90.5 min, 30 mg). The *n*-butanol-soluble fraction (79.3 g) was subjected to silica gel (1310 g, 100−200 mesh) column [800 mm × 75 mm (inside diameter)] chromatography and eluted with a $CHCl_3$/MeOH mixture (v/v, 9:1, 5.6 L → 85:15, 18.2 L → 8:2, 14.7 L → 7:3, 10.5 L → 0:10, 5.3 L) to furnish fractions B1−B7. Fraction B4 (12.4 g) was separated by silica gel (200−300 mesh) column chromatography, MPLC, and Sephadex LH-20 column [1215 mm × 14 mm (inside diameter)] chromatography that was eluted with MeOH to afford compound **6** (8 mg). Fraction B6 (2.8 g) was separated by MPLC to give fractions B6-1−B6-7. Fraction B6-1 was further separated by Sephadex LH-20 column chromatography and purified by preparative HPLC using a MeOH/H_2O mixture (13:87, v/v) as the mobile phase at a flow rate of 5 mL/min to yield compound **7** (t_R of 95.4 min, 4 mg). Fraction B6-6 was separated by Sephadex LH-20 column chromatography and purified by preparative HPLC using a MeOH/H_2O/AcOH mixture (42:58:0.1, v/v/v) as the mobile phase at a flow rate of 5 mL/min to obtain compounds **8** (t_R of 46.2 min, 15 mg) and **9** (t_R of 44.5 min, 22 mg).

Bis(8-epicatechinyl)methane (1). Off-white amorphous powder: $[\alpha]_D^{20}$ −103.7 (*c* 0.138, MeOH); UV (MeOH) λ_{max} (nm) (log ε) 281 (3.65); IR (KBr) ν_{max} 3377, 1618, 1524, 1454, 1284, 1113 cm^{-1}; HR-ESI-MS positive *m/z* 593.1651 $[M + H]^+$ (calcd for $C_{31}H_{29}O_{12}^+$, 593.1654, error of 0.5 ppm), 615.1474 $[M + Na]^+$ (calcd for $C_{31}H_{28}O_{12}Na^+$, 615.1473, error of −0.1 ppm); ESI-MS positive *m/z* 593 $[M + H]^+$, 615 $[M + Na]^+$, negative *m/z* 591 $[M - H]^-$; ^1H NMR (400 MHz, CD_3OD) and ^{13}C NMR (100 MHz, CD_3OD) data in Table 1.

Dehydrodiepicatechin A (2). Yellowish amorphous powder: $[\alpha]_D^{20}$ 373.8 (*c* 0.064, MeOH); ESI-MS positive *m/z* 577 $[M + H]^+$, 599 $[M + Na]^+$, negative *m/z* 575 $[M - H]^-$; ^1H NMR (400 MHz, CD_3OD) and ^{13}C NMR (100 MHz, CD_3OD) data in Table 2.

8-(2-Pyrrolidinone-5-yl)-(−)-epicatechin (6). White amorphous powder: $[\alpha]_D^{20}$ −14.5 (*c* 0.345, MeOH); ESI-MS positive *m/z* 374 $[M + H]^+$, 396 $[M + Na]^+$, negative *m/z* 372 $[M - H]^-$, 408 $[M + Cl]^-$; ^1H NMR (400 MHz, CD_3OD) and ^{13}C NMR (100 MHz, CD_3OD) data in Table 1.

FRAP Assay. Ferric reducing ability of the compounds was determined following the procedures as previously described.[5] FRAP reagent was made freshly by mixing 300 mM acetate buffer (pH 3.6), a 10 mM TPTZ solution in 40 mM hydrochloric acid, and a 20 mM aqueous ferric chloride ($FeCl_3$) solution in a 10:1:1 (v/v/v) ratio. The TPTZ solution was prepared on the same day. Test compounds were dissolved in methanol and diluted 2-fold to six concentrations. Twenty microliters of the compound solution and 180 μL of FRAP reagent were mixed in 96-well plates. L-Ascorbic acid was dissolved in methanol and used as a positive reference. Each treatment was conducted in quadruplicate. The plates were incubated at 37 °C for 30 min in the dark. The absorbance of the product (ferrous TPTZ complex) in each well was read at 595 nm using a Genios microplate reader (Tecan Group, Männedorf, Switzerland). One milliliter of ferrous sulfate ($FeSO_4$) at six different concentrations and 1 mL of 10 mM TPTZ and 10 mL of 300 mM acetate buffer (pH 3.6) were used for a calibration curve. FRAP values were calculated and expressed as means ± the standard deviation (SD) in millimoles of Fe(II) per gram.

DPPH Radical Scavenging Assay. The DPPH radical scavenging ability of the compounds was evaluated according to the method as previously described.[5] DPPH was freshly prepared in methanol at a concentration of 0.1 mM. Test compounds were dissolved in methanol and diluted 2-fold to six concentrations. Twenty microliters of the compound solution and 180 μL of the DPPH solution were mixed in 96-well plates. L-Ascorbic acid was dissolved in methanol and used as a positive reference. The control contained methanol instead of the compound solution, and the blank contained methanol in place of the DPPH solution. Each treatment was conducted in quadruplicate. The plates were incubated at 37 °C for 30 min in the dark. The absorbance (OD) in each well was read at 515 nm on a Genios microplate reader (Tecan). The inhibitory rates of DPPH radicals were calculated according to the formula

$$\text{inhibition}\,(\%) = [1 - (OD_{treated} - OD_{blank})/OD_{control}] \times 100$$

SC_{50} values (the concentrations required to scavenge 50% DPPH radicals present in the test solution) were calculated and expressed as means ± SD in micromolar.

ABTS Radical Cation Decolorization Assay. The ABTS radical cation ($ABTS^{\bullet+}$) scavenging activity of the compounds was determined according to the method described previously.[6,7] ABTS was dissolved in deionized water to a concentration of 7 mM. $ABTS^{\bullet+}$ was produced by reacting the ABTS solution with 2.45 mM (final concentration) potassium persulfate, and the mixture was kept at room temperature for 12−16 h in the dark before being used. The $ABTS^{\bullet+}$ solution was diluted with phosphate-buffered saline (PBS, pH 7.4) to an absorbance of 0.70 ± 0.02 at 734 nm. Test compounds were dissolved in dimethyl sulfoxide (DMSO) and diluted to 400, 200, 100, 50, 25, and 12.5 μg/mL. Ten microliters of the compound solution and 200 μL of the diluted $ABTS^{\bullet+}$ solution were mixed in 96-well

plates. L-Ascorbic acid was used as a positive reference. The control contained DMSO instead of the compound solution. Each treatment was conducted in triplicate. After a mixing time of 10 s and an incubation period of 6 min at 37 °C in the dark, the absorbance (OD) in each well was read at 415 nm on a Varioskan Flash microplate reader (Thermo Scientific). The inhibitory rates of $ABTS^{\bullet+}$ were calculated according to the formula

$$\text{inhibition}\,(\%) = (1 - OD_{treated}/OD_{control}) \times 100$$

IC_{50} values were calculated and expressed as means ± SD in micromolar.

RESULTS AND DISCUSSION

Compound **1** was obtained as an off-white amorphous powder and deduced to have the molecular formula $C_{31}H_{28}O_{12}$ from the positive ESI-MS ion peaks at m/z 593 $[M + H]^+$ and 615 $[M + Na]^+$ as well as their HR-ESI-MS data. The IR spectrum displayed absorptions of the hydroxyl group at 3377 cm^{-1} and the phenyl moiety at 1618, 1523, and 1454 cm^{-1}. The ^1H NMR (Table 1) spectrum demonstrated eight aromatic protons at δ 6.73 (4H, br s), 6.96 (2H, br s), and 5.96 (2H, s), four protons at δ 4.76 (2H, br s, H-2) and 4.10 (2H, br dd, J = 4.7, 3.7 Hz, H-3) connected to oxygenated carbons, and four aliphatic protons at δ 2.83 (2H, dd, J = 16.6, 4.7 Hz, H-4) and 2.69 (2H, dd, J = 16.6, 3.7 Hz, H-4) that can be attributed to two methylenes. These signals suggested the presence of two epicatechinyl moieties in a symmetric state.[5] Moreover, the ^1H NMR spectrum exhibited a signal of two protons at δ 3.88 (s, H_2-11) that were readily recognized for an additional methylene. The ^{13}C NMR and DEPT (Table 1) spectra showed signals of 31 carbons, including a methylene carbon at δ 16.8 (C-11), among which the carbons at the same positions of two symmetric epicatechinyl moieties were overlapped. With the aid of the HSQC spectrum, all the protons were assigned to their corresponding carbons. In the HMBC spectrum (Figure 2), the correlations from H_2-11 to δ 155.2 (C-7), 106.7 (C-8), and 153.6 (C-9), δ 4.76 (H-2) to C-9 and C-4 (δ 29.0), and δ 2.83 and 2.69 (H_2-4) to C-9 and C-5 (δ 155.8) ascertained the connection of the methylene to C-8 of two epicatechinyl moieties. Consequently, compound **1** was determined to be bis(8-epicatechinyl)methane. Bis(8-catechinyl)methane was previously obtained from several plants such as *Rhopalocnemis phalloides* (Balanophoraceae)[8] and *Baccaurea ramiflora* (Euphorbiaceae)[9] and synthesized by hydrogenation of substituted aromatic aldehyde.[10] The differences between these two compounds were shown by coupling constants $J_{2,3}$ and $J_{4,3}$, which were 7.5 Hz and 8.8 or 5.4 Hz, respectively,[8,10] rather different from those of compound **1**.

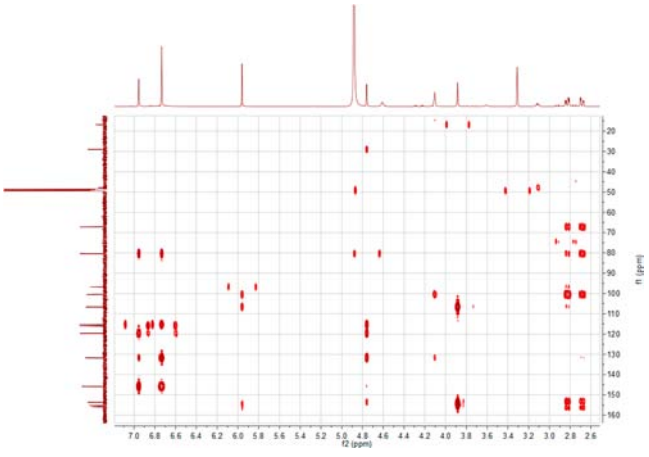

Figure 2. HMBC spectrum of compound **1**.

Compound **2** was deduced to have a molecular weight of 576 from the ESI-MS positive and negative ion peaks at m/z 577 $[M + H]^+$, 599 $[M + Na]^+$, and 575 $[M - H]^-$. The ^1H NMR (Table 2) spectrum exhibited three ABX-type aromatic protons at δ 7.04 (1H, br s, H-2‴), 6.81 (1H, d, J = 8.0 Hz, H-5‴), and 6.86 (1H, br d, J = 8.0 Hz, H-6‴), two *meta*-coupled aromatic protons at δ 5.92 (1H, d, J = 2.0 Hz, H-6) and 5.94 (1H, d, J = 2.0 Hz, H-8), two singlet aromatic protons at δ 6.55 (1H, H-5′) and 6.17 (1H, H-6″), four protons at δ 5.03 (1H, br s, H-2″), 4.45 (1H, br d, J = 4.8 Hz, H-3), 4.30 (1H, br d, J = 3.9 Hz, H-3″), and 3.82 (1H, br s, H-2) connected to oxygenated carbons, and six aliphatic protons from δ 2.65 to 2.94. The ^{13}C NMR (Table 2) spectrum displayed signals of a total of 30 carbons, including a carboxyl carbon at δ 193.8 (C-4′), four oxygenated carbons at δ 80.8 (C-2″), 72.9 (C-2), 66.4 (C-3″), and 65.1 (C-3), and three aliphatic carbons at δ 40.5 (C-2′), 29.5 (C-4″), and 25.0 (C-4). Careful analysis of the HMBC spectrum (Figure 3) such as the correlations from H-2 to C-2′ and C-6′ (δ 164.7), H-3 to C-3′ (δ 95.5), H-5′ to C-1′ (δ 91.8), C-3′, and C-8″ (δ 104.7), and H-6″ to C-8″ led us to elucidate it as dehydrodiepicatechin A. This compound was originally obtained from (−)-epicatechin by biotransformation with crude extracellular enzymes of wood rotting fungi, *Coriolus versicolor* and *Pycnoporus coccineus*,[11] and later from tea epicatechin by oxidation with peroxyl radicals generated by thermolysis of the initiator azo-bisisobutyrylnitrile.[12] This was the first report of it as a natural product.

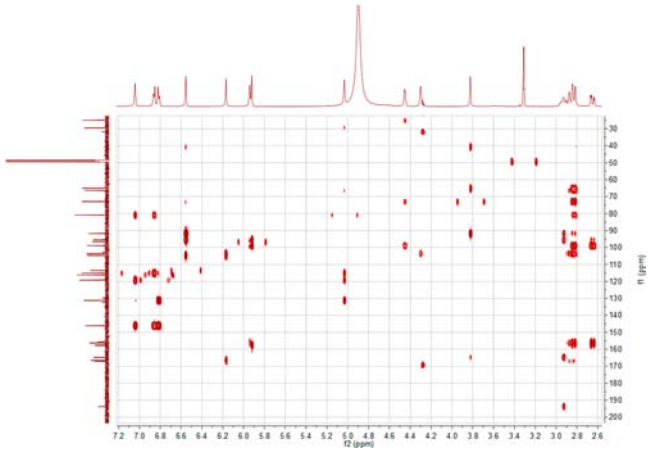

Figure 3. HMBC spectrum of compound **2**.

Compound **6** was deduced to have a molecular weight of 373 from the ESI-MS ion peaks of m/z 374 $[M + H]^+$, 396 $[M + Na]^+$, 372 $[M - H]^-$, and 408 $[M + Cl]^-$, which indicated the presence of an odd-numbered nitrogen atom. The ^1H and ^{13}C NMR spectra showed signals readily assigned for an epicatechinyl moiety as compound **1** (Table 1). In the HMBC spectrum, the correlations from δ 5.42 (1H, dd, J = 9.2, 5.3 Hz, H-1″) to δ 156.3 (C-7), 107.7 (C-8), 155.5 (C-9), and 181.3 (C-4″), δ 2.45 and 2.38 (each 1H, m, H_2-2″) to C-8 and C-4″, and δ 4.84 (1H, br s, H-2) to C-9 were observed, which suggested the presence of a pyrrolidin-2-one moiety[13] and its connection to C-8. Hence, compound **6** was identified as 8-(2-pyrrolidinone-5-yl)-(−)-epicatechin. Jang et al.[14] obtained a 2:1 mixture of two diastereomers of this compound

dx.doi.org/10.1021/jf405750p | J. Agric. Food Chem. 2014, 62, 1073−1078

from the roots of *Actinidia arguta* for the first time, which showed two sets of ^{1}H and ^{13}C NMR data. However, compound **6** exhibited only one set of ^{1}H and ^{13}C NMR data, which were in good agreement with those of the major isomer. It was the first report of this compound as a single stereoisomer.

The other known compounds were identified as proanthocyanidin A1 (**3**),[15] proanthocyanidin A2 (**4**),[15] (−)-epicatechin (**5**),[16] (−)-epicatechin 8-*C*-*β*-D-glucopyranoside (**7**),[17] naringenin 7-*O*-(2,6-di-*O*-*α*-L-rhamnopyranosyl)-*β*-D-glucopyranoside (**8**),[18] and rutin (**9**)[19] by analyses of their ^{1}H and ^{13}C NMR and ESI-MS data in combination with the comparison of their data with the reported values. Among them, compounds **2** and **6**−**8** were reported from this species for the first time.

Compounds **1**, **2**, and **6**−**8** were evaluated for antioxidant activity by FRAP, DPPH radical, and ABTS$^{\bullet+}$ scavenging assays. As shown in Table 3, the FRAP values of compounds **1** and **6** were 10.6 ± 0.3 and 8.3 ± 0.1 mmol of Fe(II)/g, respectively, which were comparable to that of the positive reference, L-ascorbic acid (11.6 ± 0.5), and their IC_{50} values toward DPPH radicals and ABTS$^{\bullet+}$ were lower than those of three other test compounds and L-ascorbic acid. Compounds **2** and **7** exhibited potent DPPH radical and ABTS$^{\bullet+}$ scavenging activity and moderate FRAP values, while compound **8** was very weak in FRAP and DPPH radical scavenging assays. It was noteworthy that we reported the potent antioxidant activity of proanthocyanidin A1 (**3**), proanthocyanidin A2 (**4**), and (−)-epicatechin (**5**) from the seeds of *L. chinensis* by FRAP and DPPH radical scavenging assays in a previous report.[5] In addition, the *in vitro* antioxidant properties of rutin (**9**), including strong DPPH radical scavenging activity and effective inhibition of lipid oxidation, were also reported previously.[20]

Table 3. Antioxidant Activities of Compounds 1, 2, and 6−8[a]

compd	FRAP (mmol/g)	DPPH (SC_{50}, μM)	ABTS (IC_{50}, μM)
1	10.6 ± 0.3	10.0 ± 0.4	9.7 ± 0.1
2	3.1 ± 0.1	16.4 ± 0.9	12.4 ± 0.4
6	8.3 ± 0.1	11.7 ± 0.1	9.1 ± 0.2
7	4.5 ± 0.1	28.0 ± 0.9	27.6 ± 0.4
8	0.5 ± 0.0	>100	20.3 ± 0.6
L-ascorbic acid	11.6 ± 0.5	35.6 ± 0.3	36.8 ± 0.2

[a]Values represent means ± SD.

This study reveals the structures of nine flavonoids; five of them were reported from litchi for the first time. Bioassay results in this study and previous reports revealed that these flavonoids were important antioxidants present in litchi pericarps.

■ ASSOCIATED CONTENT

Supporting Information

ESI-MS and NMR spectra of compounds **1**, **2**, and **6**. This material is available free of charge via the Internet at http://pubs.acs.org.

■ AUTHOR INFORMATION

Corresponding Author

*Telephone: +86-20-37080950. Fax: +86-20-37252537. E-mail: xiehaih@scbg.ac.cn.

Funding

The research was financially supported by the National Nature Science Foundation of China (31171680), the National Basic Research Program of China (2013CB127106), and the Knowledge Innovation Program of the Chinese Academy of Sciences (KSCX2-EW-J-28).

Notes

The authors declare no competing financial interest.

■ REFERENCES

(1) Liu, L.; Xie, B. J.; Cao, S. Q.; Yang, E. N.; Xu, X. Y.; Guo, S. S. A-type procyanidins from *Litchi chinensis* pericarp with antioxidant activity. *Food Chem.* **2007**, *105*, 1446−1451.

(2) State Administration of Traditional Chinese Medicine. *Chinese Materia Medica*; Shanghai Science & Technology Press: Shanghai, 1999; Vol. *13*, pp 119.

(3) Zhao, M. M.; Yang, B.; Wang, J. S.; Li, B. Z.; Jiang, Y. M. Identification of the major flavonoids from pericarp tissues of lychee fruit in relation to their antioxidant activities. *Food Chem.* **2006**, *98*, 539−544.

(4) Sarni-Manchado, P.; Le Roux, E.; Le Guernevé, C.; Lozano, Y.; Cheynier, V. Phenolic composition of litchi fruit pericarp. *J. Agric. Food Chem.* **2000**, *48*, 5995−6002.

(5) Xu, X. Y.; Xie, H. H.; Wang, Y. F.; Wei, X. Y. A-type proanthocyanidins from lychee seeds and their antioxidant and antiviral activities. *J. Agric. Food Chem.* **2010**, *58*, 11667−11672.

(6) Re, R.; Pellegrini, N.; Proteggente, A.; Pannala, A.; Yang, M.; Rice-Evans, C. Antioxidant activity applying an improved ABTS radical cation decolorization assay. *Free Radical Biol. Med.* **1999**, *26*, 1231−1237.

(7) Dudonné, S.; Vitrac, X.; Coutière, P.; Woillez, M.; Mérillon, J. M. Comparative study of antioxidant properties and total phenolic content of 30 plant extracts of industrial interest using DPPH, ABTS, FRAP, SOD, and ORAC assays. *J. Agric. Food Chem.* **2009**, *57*, 1768−1774.

(8) She, G. M.; Hu, J. B.; Zhang, Y. J.; Yang, C. R. Phenolic constituents from *Rhopalocnemis phalloides* with DPPH radical scavenging activity. *Pharm. Biol.* **2010**, *48*, 116−119.

(9) Yang, X. W.; Wang, J. S.; Ma, Y. L.; Xiao, H. T.; Zuo, Y. Q.; Lin, H.; He, H. P.; Li, L.; Hao, X. J. Bioactive phenols from the leaves of *Baccaurea ramiflora*. *Planta Med.* **2007**, *73*, 1415−1417.

(10) Boyer, F. D.; Ducrot, P. H. Hydrogenation of substituted aromatic aldehydes: Nucleophilic trapping of the reaction intermediate, application to the efficient synthesis of methylene linked flavanol dimers. *Tetrahedron Lett.* **2005**, *46*, 5177−5180.

(11) Nishida, Y.; Mitsunaga, T. Chemical structures and GTase inhibitory effects of converted compounds from catechins by the extracellular enzymes of wood rotting fungi. *Tennen Yuki Kagobutsu Toronkai Youshishu* **1998**, *40*, 643−648.

(12) Sang, S. M.; Tian, S. Y.; Wang, H.; Stark, R. E.; Rosen, R. T.; Yang, C. S.; Ho, C. T. Chemical studies of the antioxidant mechanism of tea catechins: Radical reaction products of epicatechin with peroxyl radicals. *Bioorg. Med. Chem.* **2003**, *11*, 3371−3378.

(13) Staubmann, R.; Schubert-Zsilavecz, M.; Hiermann, A.; Kartnig, T. A complex of 5-hydroxypyrrolidin-2-one and pyrimidine-2,4-dione isolated from *Jatropha curcas*. *Phytochemistry* **1999**, *50*, 337−338.

(14) Jang, D. S.; Lee, G. Y.; Lee, Y. M.; Kim, Y. S.; Sun, H.; Kim, D. H.; Kim, J. S. Flavan-3-ols having a *γ*-lactam from the roots of *Actinidia arguta* inhibit the formation of advanced glycation end products *in vitro*. *Chem. Pharm. Bull.* **2009**, *57*, 397−400.

(15) Lou, H. X.; Yamazaki, Y.; Sasaki, T.; Uchida, M.; Tanaka, H.; Oka, S. A-type proanthocyanidins from peanut skins. *Phytochemistry* **1999**, *51*, 297−308.

(16) Shi, J. Y.; Sun, J.; Wei, X. Y.; Shi, J.; Cheng, G. P.; Zhao, M. M.; Wang, J. S.; Yang, B.; Jiang, Y. M. Identificaion of (−)-epicatechin as the direct substrate for polyphenol oxidase from longan fruit pericarp. *LWT—Food Sci. Technol.* **2008**, *41*, 1742−1747.

(17) Stark, T.; Hofmann, T. Application of a molecular sensory science approach to alkalized cocoa (*Theobroma cacao*): Structure determination and sensory activity of nonenzymatically *C*-glycosylated flavan-3-ols. *J. Agric. Food Chem.* **2006**, *54*, 9510−9521.
(18) Kim, H. K.; Jeon, W. K.; Ko, B. S. Flavanone glycosides from *Citrus junos* and their anti-influenza virus activity. *Planta Med.* **2001**, *67*, 548−549.
(19) Markham, K. R.; Ternai, B. ^{13}C NMR of flavonoids. II: Flavonoids other than flavone and flavonol aglycones. *Tetrahedron* **1976**, *32*, 2607−2612.
(20) Yang, J. X.; Guo, J.; Yuan, J. F. *In vitro* antioxidant properties of rutin. *LWT—Food Sci. Technol.* **2008**, *41*, 1060−1066.

monosaccharides, would greatly increase the biorefinery opportunities for sugar beet pulp. Thus far, little has been reported on the prebiotic potential and fermentation characteristics of the complex mixture of oligosaccharides, which is obtained after enzymatic saccharification of sugar beet pulp.

Therefore, the aim of this work was to study the *in vitro* fermentation characteristics of the oligosaccharides obtained after enzymatic saccharification of sugar beet pulp using fecal inocula from humans and pigs. Moreover, the fate of the different types of oligosaccharides and the changes in human fecal bacterial populations during *in vitro* fermentation were studied. Fructo-oligosaccharides (FOS) were selected as a reference substrate for the *in vitro* fermentation experiments, because these are one of the most frequently described prebiotic oligosaccharides and much is already known about their *in vitro* fermentation behavior.

MATERIALS AND METHODS

Chemicals. All chemicals used in this study were at least of analytical grade.

Substrates. FOS (Frutalose OFP) were obtained from Sensus (Roosendaal, Netherlands), and sugar beet pectic oligosaccharides (SBPOS) were obtained from Cosun Biobased Products (Breda, Netherlands).

Culture Medium. The culture medium was based on the modified standard ileal efflux medium (SIEM) as described before.[15] All medium components were obtained from Tritium Microbiology (Veldhoven, Netherlands). The pH of the medium was adjusted to 6.0 using 2-(*N*-morpholino)ethanesulfonic acid (MES) buffer.

Fecal Inoculum. *Human Fecal Inoculum.* A standardized pool of adult fecal inoculum was prepared as described and validated before.[15,16] The fecal samples used to produce the standardized inoculum were pooled and obtained from 10 healthy European adults, who did not receive antibiotics in the 2 months before donation. The ratio of males to females in the human subject pool was 4:1. Their mean age was 44.7 years, with a standard error of the mean of 3.54 years. Their mean body mass index (BMI) was 23.3 kg/m^2, with a standard error of the mean of 0.85 kg/m^2.

Pig Fecal Inoculum. Three multiparous non-lactating sows (Dutch Landrace, aged 4 years) were used in this study. Their mean body weight was 233.0 kg, with a standard error of the mean of 10.02 kg. The sows did not receive any antibiotics for at least 2 months prior to feces collection. The sows were individually housed in pens at the experimental facilities of Wageningen University. The sows were fed twice daily a commercial pelleted maize- and wheat-based maintenance diet (AgruniekRijnvallei, Lienden, Netherlands). Immediately after defecation, feces were collected in a plastic container prefilled with CO_2. Extra CO_2 was decanted into the container with feces to ensure anaerobic storage conditions. The container with feces was closed and immediately placed in an insulated box containing crushed ice. After pooling, the feces were diluted 6 times (w/v) with sterilized 0.9% (w/v) NaCl solution and, subsequently, homogenized and filtered using a filter bag (type BA6041/STR, Seward, Worthing, U.K.) and a stomacher (model Classic 400, Seward). The filtered fecal solution was subsequently added to the culture medium with a ratio of 5:82 (v/v) to obtain the final inoculum. All liquids were kept at 39 °C under anaerobic conditions. Inoculum was prepared within 60 min after feces collection. All experimental procedures were performed in compliance with the appropriate rules and institutional guidelines and were approved by Wageningen University.

***In Vitro* Fermentations.** Substrates (100 mg) were weighed into 20 mL flasks. Next, 9 mL of prewarmed culture medium and 1 mL of inoculum was added to the flasks. Control samples without added substrate were used to monitor the background fermentation. All handling was performed in an anaerobic cabinet (gas phase: 96% N_2 and 4% H_2) to maintain anaerobic conditions. Flasks were closed with rubber stoppers and aluminum caps and were put in an incubator shaker (Innova 4000, New Brunswick Scientific, Enfield, CT) at 100 rpm and 37 °C (human inoculum) or 39 °C (pig inoculum). After different time points of incubation, the flasks were opened and the liquid was divided over two test tubes. One of these tubes was immediately frozen in liquid nitrogen and stored at −80 °C to preserve the sample for microbiological analysis (only for samples with human inoculum). The other tube was put into a boiling water bath for 5−10 min. This sample was used for analysis of pH, SCFA, lactate, and oligosaccharide degradation. The experiments with human inoculum and pig inoculum were performed on separate days. Both *in vitro* fermentations were run in duplicate.

Analytical Methods. *Constituent Monosaccharide Composition.* The constituent monosaccharide composition of the carbohydrates present in the substrates was analyzed as described previously.[10]

SCFA and Lactate. Acetate, propionate, butyrate, and lactate were measured in triplicate using a high-performance liquid chromatography (HPLC) system with conductivity detection equipped with an Aminex HPX-87H analytical column (7.8 × 300 mm; Bio-Rad Laboratories, Hercules, CA). An anion micromembrane suppressor (AMMS-ICE300, Thermo Scientific, Waltham, MA; 10 mM NH_4OH) was used to reduce the background conductivity. The column temperature was maintained at 45 °C, and the flow rate was 0.6 mL/min. The injection volume was 50 μL. The mobile phase was composed of 1.6 mM heptafluorobutyric acid, and elution was performed isocratically. An electrochemical detector (ED40, Thermo Scientific) was used in conductivity mode and set at a range of 200 μS. The data were processed using Empower software (Waters Corporation, Milford, MA).

Oligosaccharide Characterization. Hydrophilic interaction chromatography with mass spectrometry detection (HILIC−MS) was used to obtain information on the amount and type of oligosaccharides that were present at different time points during the *in vitro* fermentations. Chromatographic separation was performed on an Acquity UPLC BEH Amide column (1.7 μm, 2.1 × 150 mm; Waters Corporation) in combination with an Acquity UPLC BEH Amide VanGuard precolumn (1.7 μm, 2.1 × 5 mm; Waters Corporation). Analysis was performed as described previously,[17] using adapted gradient and MS settings. The mobile phase was composed of (A) H_2O, (B) acetonitrile, and (C) 200 mM ammonium formate with 2% (v/v) formic acid. The eluent profile was as follows: 0−30 min, linear from 15% A, 80% B, and 5% C to 45% A, 50% B, and 5% C; 30−32 min, linear to 75% A, 20% B, and 5% C; 32−37 min, isocratic 75% A, 20% B, and 5% C; 37−39 min, linear to 15% A, 80% B, and 5% C; and 39−45 min, isocratic 15% A, 80% B, and 5% C. A Velos Pro ion trap MS was used (Thermo Scientific). MS detection was performed in negative mode, with the ion source voltage set to −4.5 kV, the capillary voltage set to −5 V, a capillary temperature of 350 °C, a heated electrospray ionization (ESI) source temperature of 225 °C, a sheath gas flow rate of 40 (arbitrary units), an auxiliary gas flow rate of 12 (arbitrary units), and a sweep gas flow rate of 2 (arbitrary units).

Molecular Techniques. DNA from the *in vitro* fermentation samples was isolated using the AGOWA mag mini DNA isolation kit (AGOWA, Berlin, Germany), according to the instructions of the manufacturer. Approximately 100 pg of DNA template was used for polymerase chain reaction (PCR). Generation of the PCR amplicon library was performed by amplification of V5−V7 hypervariable region of the small subunit rDNA gene (16S rDNA). Amplification was performed using the forward primer 785F (5′-GGATTAGATACCCBRGTAGTC-3′) and reverse primer 1175R (5′-ACGTCRTCCCCDCCTTCCTC-3′). The primers were fitted with the 454 Life Sciences Adapter A (forward primer) and B (reverse primer), fused to the 5′ end of the 16S rDNA bacterial primer sequences. The forward primer also included a unique barcode. The amplification mix contained 2 units of Pfu Ultra II Fusion HS DNA polymerase (Stratagene, La Jolla, CA) and 1× PfuUltra II reaction buffer (Stratagene), 200 μM dNTP PurePeak DNA polymerase mix (Pierce Nucleic Acid Technologies, Milwaukee, WI), and 0.2 μM of each primer. After an initial denaturation (94 °C for 2 min), 30 PCR cycles were performed that consisted of denaturation (94 °C for 30 s), annealing (50 °C for 40 s), and extension (72 °C for 80 s). Samples with DNA recovery of equal or less than 10 pg/μL DNA were cycled

Table 1. Constituent Monosaccharide Composition and Total Sugar Levels of Substrates Used for *in Vitro* Fermentations[a]

substrate	glc	fru	ara	gal	rha	xyl	man	fuc	galA	glcA	total
SBPOS	5	0	16	17	12	1	1	1	43	4	90
FOS	10	90	0	0	0	0	0	0	0	0	95

[a]Sugar annotation: glc, glucose; fru, fructose; ara, arabinose; gal, galactose; rha, rhamnose; xyl, xylose; man, mannose; fuc, fucose; galA, galacturonic acid; and glcA, glucuronic acid. Values are expressed as mol % of the total sugar content of substrate samples. The total sugar content is expressed as w/w % of substrate samples.

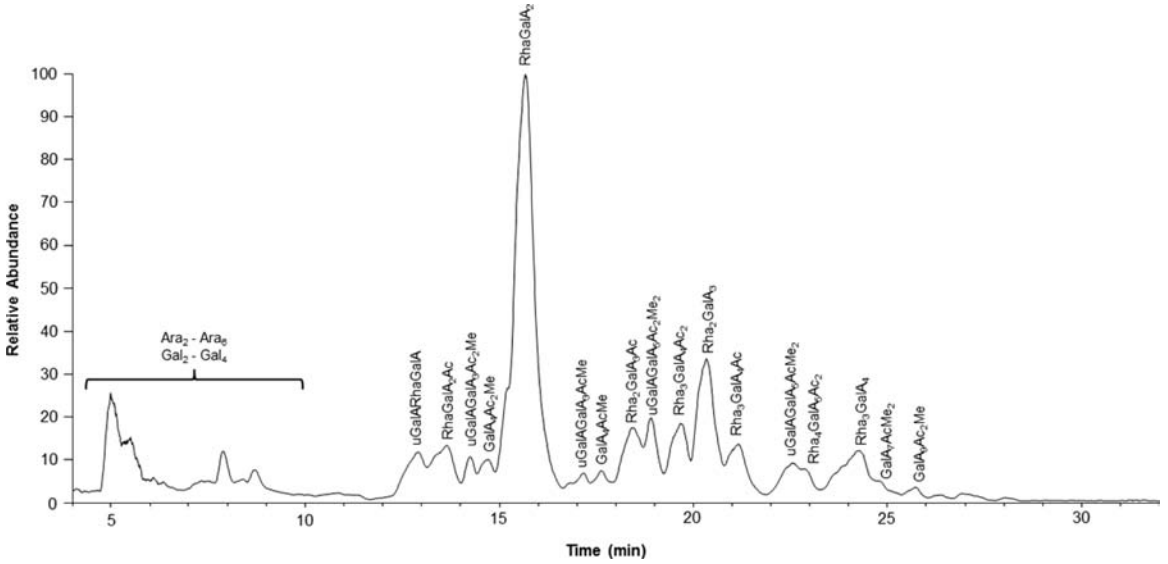

Figure 1. HILIC elution pattern of SBPOS. Peak annotation: Ara, arabinose; Gal, galactose; GalA, galacturonic acid; uGalA, unsaturated galacturonic acid; Rha, rhamnose; Ac, acetyl group; and Me, methyl ester.

35 times using the same protocol. Amplicons were size-checked and quantified by gel electrophoresis and Quant-iT Picogreen dsDNA assay (Invitrogen, Carlsbad, CA) on an Infinite M200 (Tecan, Männedorf, Switzerland). Amplicons of the individual samples were pooled equimolar and purified from agarose gel by means of QIAquick Gel Extraction Kit Protocol (Qiagen, Hilden, Germany). The library was sequenced unidirectionally in the forward direction (A adapter) in one run in the 454 GS-FLX titanium sequencer (Roche, Branford, CT) by Keygene (Wageningen, Netherlands).

Sequence Processing and Analyses. FASTA-formatted sequences and corresponding quality scores were extracted from the .sff data file generated by the GS-FLX titanium sequencer using the GS Amplicon software package (Roche, Branford, CT). GS-FLX titanium sequencing data were processed using modules implemented in the Mothur version 1.20.0 software platform module.[18] Because of the unique barcodes, sequences were initially binned by sample of origin. For further downstream analyses, sequences were trimmed. In brief, barcodes, primer sequences, and low-quality data [containing ambiguous base calls (N) in the sequence, more than eight homopolymers anywhere in the sequence, shorter than 50 nucleotides (nt) after trimming with a window average below 35 or a length of >500 or <200 base pairs (bp)] were removed. The data set was simplified using the "unique.seqs" command to generate a non-redundant (unique) set of sequences. Unique sequences were aligned using the "align.seqs" command and an adaptation of the Bacterial SILVA SEED database as a template (http://www.mothur.org/wiki/Alignment_database). Alignment was performed using the RDP template. To ensure that comparable regions of the 16S rDNA gene were analyzed across all reads, sequences that started before the 2.5 percentile or ended after the 97.5 percentile in the alignment were filtered. Sequences were denoised using the "pre.cluster" command. This command applies a pseudo-single linkage algorithm with the goal of removing sequences that are likely due to pyrosequencing errors.[19] A total of 16 814 potentially chimeric sequences were detected and removed using the "chimera.uchime" command.[20] High-quality aligned sequences were classified using the RDP-II naïve Bayesian Classifier database. Aligned sequences were clustered into operation taxonomic units (OTUs; defined by 97% similarity) and were calculated by the average linkage clustering commando method. Unclassified sequences were also grouped in OTUs and were represented with a random number to distinguish them from the different OTUs found within the same phyla.

RESULTS AND DISCUSSION

Constituent Monosaccharide Composition and Structure of SBPOS and FOS. To characterize the substrates used in this study, their constituent monosaccharide composition was analyzed and oligosaccharide structures were identified. The constituent monosaccharide composition of SBPOS and FOS is given in Table 1. SBPOS were mainly composed of uronic acids (galacturonic and glucuronic acid in a ratio of 10:1), galactose, arabinose, rhamnose, and to a lesser extent, glucose, xylose, mannose, and fucose. Approximately 15% (w/w) of these saccharides were present as mono- or disaccharides (results not shown). The different oligosaccharide structures that were present in the SBPOS mixture were identified using HILIC−MS (Figure 1). It was revealed that SBPOS were composed of several classes of oligosaccharides, which mainly consisted of rhamnogalacturonan oligosaccharides, mostly containing a terminal galacturonic acid residue at both reducing and non-reducing ends (Rha_nGalA_{n+1}), acetylated rhamnogalacturonan oligosaccharides ($Rha_nGalA_{n+1}Ac_x$), partially methyl-esterified and/or acetylated homogalacturonan oligosaccharides ($GalA_nAc_xMe_y$), and partially methyl-esterified and/or acetylated homogalacturonan oligosaccharides containing an unsaturated galacturonic acid residue at the non-reducing end ($uGalAGalA_nAc_xMe_y$). Precise structural details of these classes

dx.doi.org/10.1021/jf4049676 | J. Agric. Food Chem. 2014, 62, 1079−1087

Table 2. pH and SCFA and Lactate Formation during *in Vitro* Fermentation of SBPOS and FOS Using Human and Pig Fecal Inocula[a]

		human fecal inoculum						pig fecal inoculum					
substrate	time (h)	pH	acetate (mmol/g)	propionate (mmol/g)	butyrate (mmol/g)	total SCFA (mmol/g)	lactate (mmol/g)	pH	acetate (mmol/g)	propionate (mmol/g)	butyrate (mmol/g)	total SCFA (mmol/g)	lactate (mmol/g)
SBPOS	0	6.05 (0.00)	0.23 (0.05)	0.05 (0.01)	0.05 (0.01)	0.33 (0.05)	0.03 (0.01)	5.97 (0.02)	0.16 (0.01)	<0.01	<0.01	0.16 (0.01)	0.06 (0.01)
	3	6.12 (0.01)	1.34 (0.03)	0.34 (0.02)	0.24 (0.01)	1.92 (0.04)	0.12 (0.01)	5.87 (0.00)	0.63 (0.02)	0.13 (0.01)	0.03 (0.01)	0.79 (0.03)	0.47 (0.04)
	6	6.11 (0.01)	3.70 (0.19)	1.04 (0.02)	0.53 (0.02)	5.28 (0.22)	0.08 (0.01)	5.82 (0.03)	1.36 (0.08)	0.30 (0.03)	0.03 (0.03)	1.69 (0.13)	0.57 (0.07)
	9	5.93 (0.01)	6.60 (0.11)	2.20 (0.09)	0.86 (0.03)	9.66 (0.11)	0.02 (0.01)	5.98 (0.01)	1.97 (0.11)	0.70 (0.04)	0.19 (0.01)	2.86 (0.06)	0.35 (0.04)
	12	5.90 (0.01)	8.08 (0.11)	2.90 (0.09)	1.03 (0.03)	12.01 (0.18)	0.02 (0.01)	6.10 (0.01)	2.90 (0.21)	0.96 (0.03)	0.50 (0.02)	4.36 (0.21)	<0.01
	24	5.94 (0.01)	9.81 (0.19)	4.00 (0.28)	1.81 (0.07)	15.61 (0.30)	0.02 (0.01)	6.14 (0.01)	5.30 (0.11)	2.40 (0.15)	2.23 (0.07)	9.93 (0.32)	<0.01
	48	6.16 (0.01)	11.60 (0.11)	4.95 (0.15)	3.11 (0.07)	19.66 (0.24)	0.02 (0.01)	6.34 (0.01)	8.14 (0.56)	3.70 (0.23)	3.24 (0.19)	15.08 (0.97)	<0.01
FOS	0	6.16 (0.01)	0.25 (0.05)	0.05 (0.01)	0.04 (0.01)	0.34 (0.06)	0.04 (0.01)	6.19 (0.02)	0.13 (0.01)	<0.01	<0.01	0.13 (0.01)	0.05 (0.01)
	3	6.13 (0.00)	1.17 (0.02)	0.21 (0.01)	0.22 (0.01)	1.60 (0.03)	0.22 (0.01)	5.99 (0.02)	0.48 (0.03)	0.15 (0.02)	<0.01	0.63 (0.05)	0.96 (0.03)
	6	5.14 (0.01)	4.21 (1.15)	0.47 (0.09)	0.70 (0.20)	5.38 (1.44)	1.91 (0.55)	5.66 (0.01)	1.38 (0.02)	0.35 (0.02)	<0.10	1.73 (0.01)	2.53 (0.07)
	9	4.91 (0.01)	6.78 (0.27)	0.64 (0.08)	1.15 (0.07)	8.58 (0.34)	3.39 (0.12)	4.59 (0.02)	2.98 (0.18)	0.69 (0.07)	0.08 (0.01)	3.74 (0.25)	7.52 (0.59)
	12	4.95 (0.03)	7.25 (0.20)	0.79 (0.07)	1.20 (0.11)	9.23 (0.36)	3.41 (0.30)	4.75 (0.02)	4.15 (0.27)	1.89 (0.08)	0.34 (0.02)	6.38 (0.35)	5.69 (0.18)
	24	5.06 (0.02)	7.42 (0.10)	0.83 (0.03)	1.23 (0.07)	9.49 (0.09)	3.51 (0.12)	5.67 (0.00)	2.05 (0.10)	1.47 (0.08)	3.15 (0.14)	6.66 (0.20)	<0.01
	48	5.54 (0.01)	4.56 (0.18)	0.87 (0.05)	4.86 (0.07)	10.29 (0.18)	0.04 (0.01)	6.22 (0.01)	3.62 (0.10)	2.18 (0.16)	3.90 (0.14)	9.70 (0.09)	<0.01
control	0	6.15 (0.00)	0.19 (0.03)	0.04 (0.01)	0.03 (0.01)	0.26 (0.02)	0.03 (0.01)	6.20 (0.01)	0.19 (0.02)	<0.01	<0.01	0.19 (0.02)	0.03 (0.01)
	9	6.47 (0.01)	2.28 (0.25)	0.62 (0.03)	0.64 (0.07)	3.54 (0.35)	0.06 (0.01)	6.32 (0.01)	1.09 (0.01)	0.53 (0.02)	0.12 (0.01)	1.74 (0.03)	<0.01
	24	6.61 (0.01)	4.25 (0.08)	1.44 (0.08)	1.25 (0.11)	6.94 (0.11)	0.01 (0.01)	6.68 (0.02)	3.66 (0.17)	1.18 (0.01)	1.44 (0.07)	6.28 (0.12)	<0.01

[a]Values are means of triplicate measurements, with standard deviation in parentheses. SCFA and lactate results are expressed as mmol/g organic matter.

dx.doi.org/10.1021/jf4049676 | J. Agric. Food Chem. 2014, 62, 1079−1087

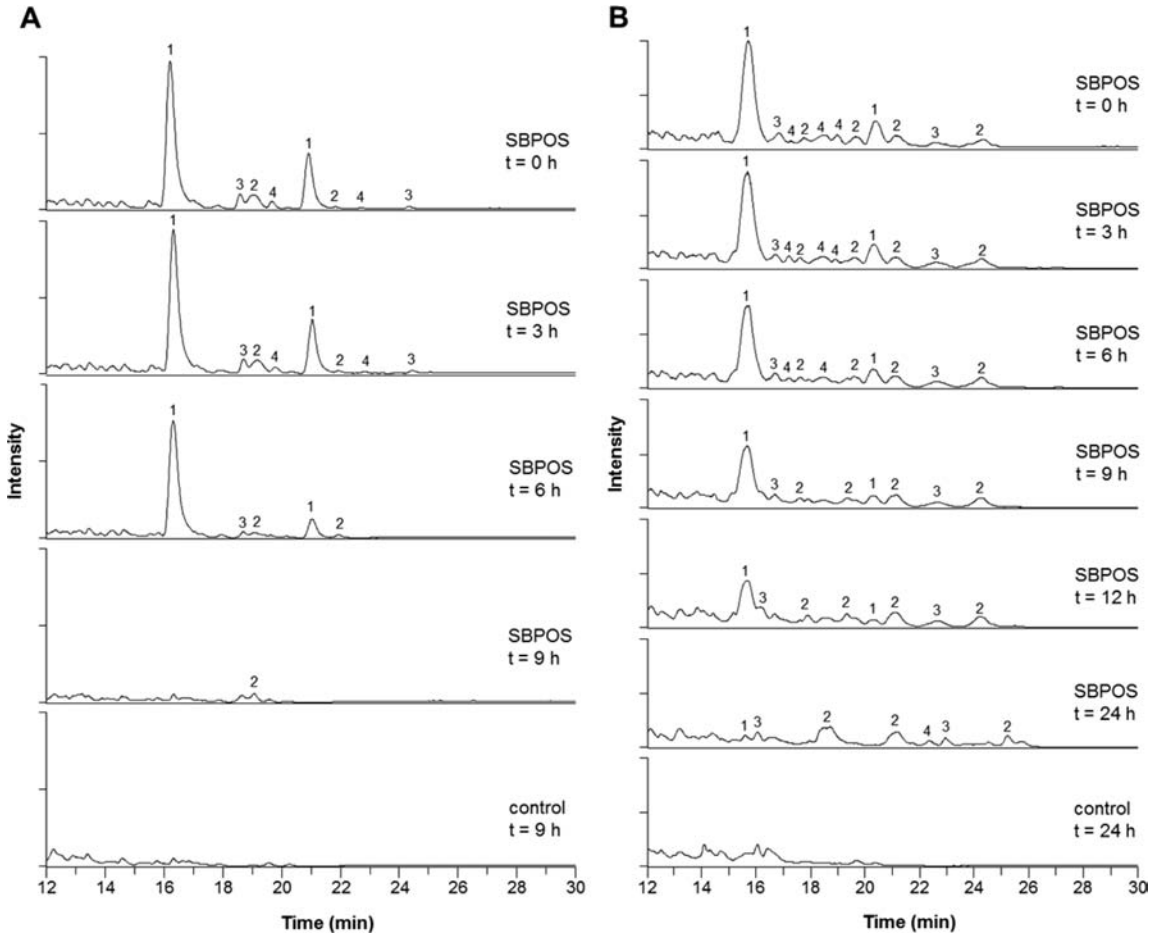

Figure 2. HILIC elution patterns obtained after several time points during *in vitro* fermentation of SBPOS using (A) human or (B) pig fecal inoculum. HILIC elution patterns obtained after 9 h (human fecal inoculum) and 24 h (pig fecal inoculum) of *in vitro* fermentation of the control sample are presented to show which peaks correspond to the medium components. Peak annotation: 1, Rha_nGalA_{n+1}; 2, $Rha_nGalA_{n+1}Ac_x$; 3, $GalA_nAc_xMe_y$; and 4, $uGalAGalA_nAc_xMe_y$.

of pectic oligosaccharides have been described elsewhere.[10] These special classes of oligosaccharides are distinct from the classes of SBPOS that have been used for *in vitro* fermentation studies previously.[4−6] Besides these classes of oligosaccharides, smaller amounts of arabinan and galactan oligosaccharides were present. The average degree of polymerization of the SBPOS was around 5.

FOS were composed of fructose and glucose residues in a ratio of 9:1. Approximately 8% (w/w) of the fructose and glucose in FOS was present as mono- or disaccharides (results not shown). FOS are obtained by partial enzymatic hydrolysis of inulin and are composed of a mixture of linear oligofructose chains, which can be terminated by a glucose residue. The fructose molecules are linked to each other by β-(2,1)-glycosidic bonds. The average degree of polymerization of FOS was 4−5 (according to the specification of the supplier).

Changes in pH. The pH was measured to monitor the course of the *in vitro* fermentations. Table 2 shows the pH after 0, 3, 6, 9, 12, 24, and 48 h of *in vitro* fermentation. For both SBPOS and FOS, the pH initially decreased. For SBPOS, the pH increased again after 12 h (human fecal inoculum) and 6 h (pig fecal inoculum). For FOS, the pH increased again after 9 h (in the case of both human and pig fecal inoculum). The decrease in pH is the result of the initially high carbohydrate availability, which results in saccharolytic fermentation and subsequent formation of SCFA and lactate, thereby lowering the pH. The decrease in pH was largest for FOS. It is likely that this was caused by the formation of lactic acid, which has a lower pK_a (3.73) compared to acetic, propionic, and butyric acid (4.76, 4.87, and 4.82, respectively). The observed increase in pH after a certain time point may be partly due to a shift to a more proteolytic fermentation.[21] The protein degradation products (e.g., ammonia) will increase the pH. For FOS, the decrease in lactate concentration (e.g., after 12−24 h) will also have contributed to the observed pH increase during the end of the *in vitro* fermentations. The gradual increase of the pH of the control samples (medium without added substrate) is most likely caused by early protein degradation because of the lack of available carbohydrates.[21] For SBPOS, the pH at t = 0 was lower compared to FOS and the control, because of the acidic nature of SBPOS.

Formation of SCFA and Lactate. The SCFA and lactate formation during *in vitro* fermentation is often used as an indicator of fiber fermentability. In our study, an increase in acetate, propionate, butyrate, and lactate was measured (Table 2). Other metabolites, such as valerate and succinate, were also analyzed and were present only in minor amounts (results not shown). The total SCFA content at the end of the fermentation was higher for SBPOS than for FOS, both when human and pig fecal inocula were used (Table 2). Substantial amounts of lactate were produced during the first stage of fermentation of FOS, by both human and pig fecal microbiota. The ratios

dx.doi.org/10.1021/jf4049676 | J. Agric. Food Chem. 2014, 62, 1079−1087

acetate/propionate/butyrate/lactate for SBPOS were generally different compared to the ratios for FOS. Acetate and propionate were mainly produced during *in vitro* fermentation of SBPOS, while for FOS, lactate and acetate were the most dominant SCFA. Total SCFA concentrations were higher when using human fecal inoculum compared to pig fecal inoculum, for both SBPOS and FOS, which is in accordance with previous work.[12]

However, more lactate was produced by pig fecal microbiota. This was especially the case for FOS but also for SBPOS. The proportion of butyrate considerably increased after 24−48 h of fermentation using human fecal inoculum and after 12−24 h using pig fecal inoculum. An increased butyrate production and, subsequently, higher butyrate proportion during the second stage of *in vitro* fermentation of pectic oligosaccharides and FOS were reported previously.[22,23]

For pig fecal microbiota, lactate was the major metabolite during the first 12 h of fermentation of FOS. The formation of lactate during *in vitro* fermentation of FOS is in accordance with previous studies.[12,24] Lactate is an intermediary product of carbohydrate fermentation and can be converted into acetate, propionate, and butyrate by common intestinal bacteria.[25] This explains the decrease of lactate and the large increase of butyrate during the second stage of fermentation of FOS (i.e., between 24 and 48 h for human fecal inoculum and between 12 and 24 h for pig fecal inoculum). Part of the butyrate may also have been formed from acetate because butyrate producing bacteria can be net utilizers of acetate.[26]

Oligosaccharide Degradation. The degradation of SBPOS during *in vitro* fermentations was monitored by HILIC−MS and is shown in Figure 2. The SBPOS were used after 9 h of *in vitro* fermentation by human fecal microbiota (Figure 2A). The increase in pH after this time corroborates that the microbiota switched to proteolytic fermentation, because all available carbohydrates were used up. Figure 2B illustrates that the degradation pattern of SBPOS during *in vitro* fermentation using pig fecal inoculum is quite different compared to the human fecal inoculum. Using pig fecal inoculum, most of the SBPOS were still clearly detectable after 12 h and some of the SBPOS were even detectable after 24 h of *in vitro* fermentation. Previously, it was demonstrated that pig fecal microbiota had limited ability to ferment citrus and soy pectin compared to human fecal microbiota.[12] Therefore, it can be expected that SBPOS are also degraded slower by pig fecal microbiota compared to human fecal microbiota.

HILIC−MS analysis also enabled us to plot the degradation rate of the different classes of oligosaccharides that were present after different fermentation times. Figure 3 shows the results for the first 24 h of *in vitro* fermentation. Using human fecal inoculum, the degradation rate of the rhamnogalacturonan oligosaccharides (Rha_nGalA_{n+1} and $Rha_nGalA_{n+1}Ac_x$) and partially methyl-esterified and/or acetylated homogalacturonan oligosaccharides ($GalA_nAc_xMe_y$) tended to be a bit slower during the first 6 h of *in vitro* fermentation compared to the other classes of oligosaccharides (Figure 3A). Nevertheless, most of the oligosaccharides were fermented after 9 h of fermentation. For comparison, the degradation of FOS during the first 6 h of *in vitro* fermentation appeared to be faster than most of the SBPOS classes (Figure 3A).

Figure 3B illustrates that the class $Rha_nGalA_{n+1}Ac_x$ was degraded slower by pig fecal microbiota than the other three SBPOS classes. The degradation rate of all classes of SBPOS by

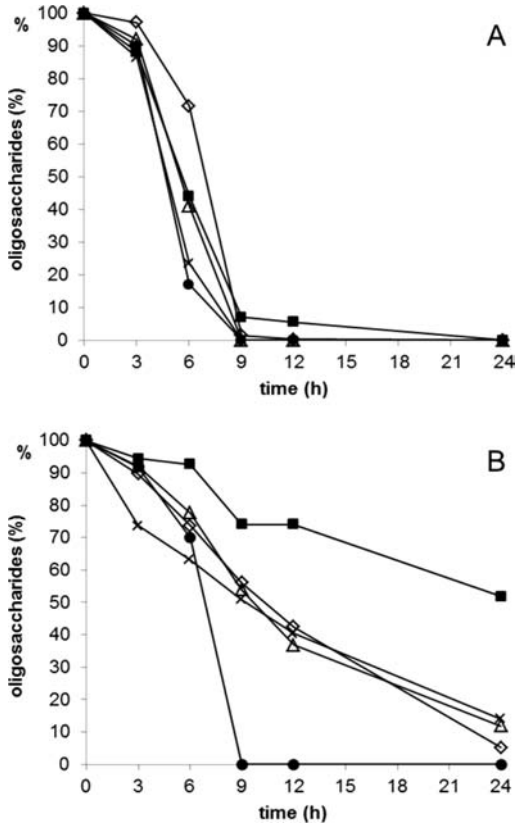

Figure 3. Degradation rate, expressed as a decrease in the percentage of the initial content of different classes of oligosaccharides during 24 h of *in vitro* fermentation by (A) human or (B) pig fecal inoculum. Legend: ◇, Rha_nGalA_{n+1}; ■, $Rha_nGalA_{n+1}Ac_x$; △, $GalA_nAc_xMe_y$; ×, $uGalAGalA_nAc_xMe_y$; and ●, FOS.

pig fecal microbiota was lower compared to human fecal microbiota. $Rha_nGalA_{n+1}Ac_x$ was shown to be the most recalcitrant class of oligosaccharides, because approximately half of the initial amount was still detectable after 24 h. For comparison, FOS were completely used up after 9 h of *in vitro* fermentation. Nevertheless, FOS was fermented slower by pig fecal microbiota compared to human fecal microbiota.

It was demonstrated previously that the degree of methyl esterification of pectic oligosaccharides influences the degradation rate *in vitro*.[11] Our study shows that acetylation of rhamnogalacturonan oligosaccharides also hinders the degradation by pig fecal microbiota but not by human fecal microbiota. The latter differs from results on xylooligosaccharides,[27] where acetylated xylooligosaccharides were degraded more slowly by human fecal microbiota compared to non-substituted xylooligosaccharides.

All classes of SBPOS were used up after 48 h (data not shown), thereby showing that both human and pig fecal microbiota possess the appropriate enzymes to fully degrade the SBPOS. The slower degradation of pectin compared to FOS by pig fecal microbiota is in accordance with previous findings.[12] Most likely, pig fecal microbiota were not very well adapted to the use of pectic oligosaccharides, because the diet of the pigs used in our study was mainly maize- and wheat-based, therefore containing low amounts of pectin.[28] Human fecal microbiota are much more adapted to pectic oligosaccharides because the human diet usually contains pectin-rich fruits or vegetables.[29]

Changes in Microbiota Composition. Figure 4 shows the human fecal microbiota composition on the genus level at

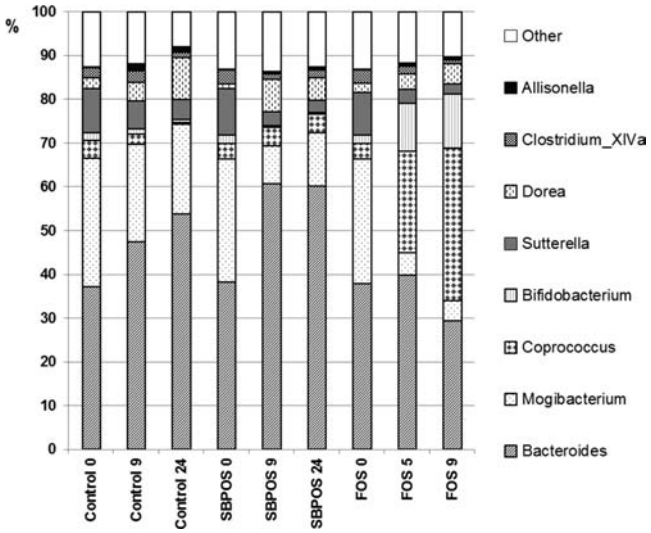

Figure 4. Human fecal microbiota composition (genus level) during *in vitro* fermentations of SBPOS and FOS.

different time points of *in vitro* fermentation of SBPOS compared to FOS and the control. The initial microbiota composition was rather similar for the different fermentations, as expected.

Bacteroides were mainly stimulated during *in vitro* fermentation of SBPOS (Figure 4). No bifidogenic effect was noticed for SBPOS, because no increase in the population of *Bifidobacterium* was observed during *in vitro* fermentation of SBPOS. By contrast, a considerable increase in the population of *Bifidobacterium* was observed after 5 and 9 h of *in vitro* fermentation of FOS. Our findings are in agreement with previous studies,[13,30] showing the limited bifidogenic effect of pectic oligosaccharides compared to FOS. It was also described previously that *Bacteroides* spp. were able to metabolize rhamnogalacturonan oligosaccharides, whereas *Bifidobacterium* strains were not able to metabolize galacturonan oligosaccharides.[31]

To highlight other interesting changes in bacterial populations, the changes in microbial genera composition were calculated after 9 and 24 h of *in vitro* fermentation compared to the control incubation (Table 3). It is shown that *Bifidobacterium* spp. were relatively decreased when SBPOS was added as a substrate. The growth of several other groups of bacteria was increased during *in vitro* fermentation of SBPOS. *Blautia* spp. increased after 9 and 24 h of *in vitro* fermentation (6- and 33-fold, respectively). These bacteria were found to be reduced in patients with colorectal cancer.[32] Some species, such as *Blautia hydrogenotrophica*, have been shown to boost the efficiency of the fermentation of dietary carbohydrates.[33] A 10-fold increase in *Coprococcus* spp. was also noticed after 24 h of *in vitro* fermentation of SBPOS. As a comparison, the increase in *Coprococcus* spp. was even higher for FOS (i.e., 18-fold increase after 9 h of *in vitro* fermentation). *Coprococcus* spp. have been recognized previously to produce high amounts of butyrate *in vitro*.[34] Furthermore, it has been hypothesized that when the growth of this group of bacteria together with *Dorea* spp. is suppressed, it may lead to the flourishing of other groups, such as clostridia, which are linked to inflammation.[35]

Table 3. Fold Changes in Microbiotal Genera after 9 and 24 h of *in Vitro* Fermentation of SBPOS and 9 h of *in Vitro* Fermentation of FOS Using Human Fecal Inoculum[a]

	SBPOS		FOS
genus	t = 9 h	t = 24 h	t = 9 h
Bifidobacterium	0.17	0.30	8.17
Slackia	0.12	0.76	0.51
Parabacteroides	1.06	2.36	0.85
Paraprevotella	1.47	2.15	0.57
Prevotella	0.51	0.45	0.44
Alistipes	0.24	0.37	0.21
Bacteroides	1.24	1.09	0.61
Sutterella	0.41	0.65	0.37
Bilophila	0.11	0.06	0.35
Escherichia_Shigella	0.39	0.33	0.66
Clostridium_sensu_stricto	0.55	0.29	0.06
Mogibacterium	0.41	0.62	0.21
Blautia	6.89	33.99	3.09
Clostridium_XlVa	0.36	1.06	0.32
Coprococcus	2.22	10.56	18.40
Dorea	2.25	0.70	1.28
Lachnospiracea_incertae_sedis	7.52	12.04	6.29
Butyricicoccus	2.67	7.11	6.68
Faecalibacterium	11.47	14.89	1.58
Oscillibacter	0.81	0.55	0.81
Catenibacterium	0.63	3.54	12.99
Erysipelotrichaceae_incertae_sedis	1.66	1.90	5.44
Phascolarctobacterium	4.20	1.13	0.47
Allisonella	0.24	0.41	0.39
Dialister	1.94	4.96	3.64

[a]For each substrate, the ratio between a sampling time point and t = 0 was calculated (e.g., $t9/t0$ and $t24/t0$). The ratio for this value and the corresponding control was then determined to obtain fold changes. A value equal to 1 indicates no change; a value of >1 indicates an increase; and a value of <1 indicates a decrease of the respective microbiotal genera.

In addition, an increase in *Butyricicoccus* spp. was observed. It has been described previously that patients with inflammatory bowel disease had lower numbers of *Butyricicoccus* spp. in their stools than healthy subjects and oral administration of *Butyricicoccus pullicecorum* improved the epithelial barrier function.[36] *Faecalibacterium* spp. also increased, and members of this group are known by their anti-inflammatory properties. Their decrease is associated with ulcerative colitis.[37]

Besides the stimulation of certain groups of bacteria that can be associated with host health, a decrease of several groups of bacteria that may have adverse effects on host health and well-being was also noticeable. *Sutterella* spp. decreased after 9 and 24 h of *in vitro* fermentation of SBPOS. Members of this group have been isolated from individuals suffering from ulcerative colitis and Crohn's disease and are abundant in children with gastrointestinal dysfunction and autism.[38] *Alistipes* spp. and *Allisonella* spp. also decreased after 9 and 24 h of *in vitro* fermentation of SBPOS. Several species of *Alistipes* are mostly correlated with the frequency of abdominal pain in patients with irritable bowel syndrome.[39] Proportions of *Allisonella* spp. are high in patients with irritable bowel syndrome with diarrhea−constipation episodes.[40]

In conclusion, this study provides new information on the *in vitro* fermentation characteristics of SBPOS. It was shown that SBPOS can be completely fermented by human and pig fecal

dx.doi.org/10.1021/jf4049676 | J. Agric. Food Chem. 2014, 62, 1079−1087

microbiota, thereby producing butyrate yet mainly acetate and propionate. The degradation rate of SBPOS by pig fecal microbiota was lower compared to human fecal microbiota. In general, rhamnogalacturonan oligosaccharides were more slowly degraded than homogalacturonan oligosaccharides. Acetylation of rhamnogalacturonan oligosaccharides lowered the degradation rate by pig fecal microbiota but not by human fecal microbiota. A classic prebiotic effect could not be demonstrated for SBPOS, because no increase in bifidobacteria or lactobacilli was observed. However, several other potentially beneficial modifications in the microbiota composition were observed during *in vitro* fermentation of SBPOS using human fecal inoculum. Further *in vivo* work is needed to ultimately confirm these specific prebiotic properties of SBPOS. Because SBPOS are produced as a sidestream of the production of monosaccharides from sugar beet pulp, they are available in large quantities. This makes it feasible to conduct future *in vivo* experiments with SBPOS.

AUTHOR INFORMATION

Corresponding Author

*Telephone: +31-317-482239. Fax: +31-317-484893. E-mail: henk.schols@wur.nl.

Funding

Koen Venema acknowledges the support of the European Science Foundation (ESF), in the framework of the Research Networking Programme, the European Network for Gastrointestinal Health Research.

Notes

The authors declare no competing financial interest.

ACKNOWLEDGMENTS

The authors thank Uttara Ramasamy and Christiane Rösch for their help with *in vitro* fermentations and Sebastiaan van Berchum for his support with analysis of SCFA and lactate.

ABBREVIATIONS USED

FOS, fructo-oligosaccharides; HILIC−MS, hydrophilic interaction chromatography with mass spectrometry detection; MES, 2-(*N*-morpholino)ethanesulfonic acid; SBPOS, sugar beet pectic oligosaccharides; SCFA, short-chain fatty acids; SIEM, standard ileal efflux medium

REFERENCES

(1) Rastall, R. A. Functional oligosaccharides: Application and manufacture. *Annu. Rev. Food Sci. Technol.* **2010**, *1*, 305−339.

(2) Patel, S.; Goyal, A. The current trends and future perspectives of prebiotics research: A review. *3 Biotech* **2012**, *2*, 115−125.

(3) Saad, N.; Delattre, C.; Urdaci, M.; Schmitter, J. M.; Bressollier, P. An overview of the last advances in probiotic and prebiotic field. *LWT—Food Sci. Technol.* **2013**, *50*, 1−16.

(4) Al-Tamimi, M. A. H. M.; Palframan, R. J.; Cooper, J. M.; Gibson, G. R.; Rastall, R. A. *In vitro* fermentation of sugar beet arabinan and arabino-oligosaccharides by the human gut microflora. *J. Appl. Microbiol.* **2006**, *100*, 407−414.

(5) Holck, J.; Hjernø, K.; Lorentzen, A.; Vigsnæs, L. K.; Hemmingsen, L.; Licht, T. R.; Mikkelsen, J. D.; Meyer, A. S. Tailored enzymatic production of oligosaccharides from sugar beet pectin and evidence of differential effects of a single DP chain length difference on human faecal microbiota composition after *in vitro* fermentation. *Process Biochem.* **2011**, *46*, 1039−1049.

(6) Vigsnæs, L. K.; Holck, J.; Meyer, A. S.; Licht, T. R. *In vitro* fermentation of sugar beet arabino-oligosaccharides by fecal microbiota obtained from patients with ulcerative colitis to selectively stimulate the growth of *Bifidobacterium* spp. and *Lactobacillus* spp. *Appl. Environ. Microbiol.* **2011**, *77*, 8336−8344.

(7) Scheppach, W.; Luehrs, H.; Menzel, T. Beneficial health effects of low-digestible carbohydrate consumption. *Br. J. Nutr.* **2001**, *85*, S23−S30.

(8) Wächtershäuser, A.; Stein, J. Rationale for the luminal provision of butyrate in intestinal diseases. *Eur. J. Nutr.* **2000**, *39*, 164−171.

(9) Hu, S.; Dong, T. S.; Dalal, S. R.; Wu, F.; Bissonnette, M.; Kwon, J. H.; Chang, E. B. The microbe-derived short chain fatty acid butyrate targets miRNA-dependent p21 gene expression in human colon cancer. *PLoS One* **2011**, *6*, No. e16221.

(10) Leijdekkers, A. G. M.; Bink, J. P. M.; Geutjes, S.; Schols, H. A.; Gruppen, H. Enzymatic saccharification of sugar beet pulp for the production of galacturonic acid and arabinose; a study on the impact of the formation of recalcitrant oligosaccharides. *Bioresour. Technol.* **2013**, *128*, 518−525.

(11) Dongowski, G.; Lorenz, A.; Proll, J. The degree of methylation influences the degradation of pectin in the intestinal tract of rats and *in vitro*. *J. Nutr.* **2002**, *132*, 1935−1944.

(12) Jonathan, M. C.; van den Borne, J. J. G. C.; van Wiechen, P.; Souza da Silva, C.; Schols, H. A.; Gruppen, H. *In vitro* fermentation of 12 dietary fibres by faecal inoculum from pigs and humans. *Food Chem.* **2012**, *133*, 889−897.

(13) Van Laere, K. M. J.; Hartemink, R.; Bosveld, M.; Schols, H. A.; Voragen, A. G. J. Fermentation of plant cell wall derived polysaccharides and their corresponding oligosaccharides by intestinal bacteria. *J. Agric. Food. Chem.* **2000**, *48*, 1644−1652.

(14) Grootaert, C.; Delcour, J. A.; Courtin, C. M.; Broekaert, W. F.; Verstraete, W.; Van de Wiele, T. Microbial metabolism and prebiotic potency of arabinoxylan oligosaccharides in the human intestine. *Trends Food Sci. Technol.* **2007**, *18*, 64−71.

(15) Ladirat, S. E.; Schols, H. A.; Nauta, A.; Schoterman, M. H. C.; Keijser, B. J. F.; Montijn, R. C.; Gruppen, H.; Schuren, F. H. J. High-throughput analysis of the impact of antibiotics on the human intestinal microbiota composition. *J. Microbiol. Methods* **2013**, *92*, 387−397.

(16) Maathuis, A.; Hoffman, A.; Evans, A.; Sanders, L.; Venema, K. The effect of the undigested fraction of maize products on the activity and composition of the microbiota determined in a dynamic *in vitro* model of the human proximal large intestine. *J. Am. Coll. Nutr.* **2009**, *28*, 657−666.

(17) Leijdekkers, A. G. M.; Sanders, M. G.; Schols, H. A.; Gruppen, H. Characterizing plant cell wall derived oligosaccharides using hydrophilic interaction chromatography with mass spectrometry detection. *J. Chromatogr., A* **2011**, *1218*, 9227−9235.

(18) Schloss, P. D.; Westcott, S. L.; Ryabin, T.; Hall, J. R.; Hartmann, M.; Hollister, E. B.; Lesniewski, R. A.; Oakley, B. B.; Parks, D. H.; Robinson, C. J.; Sahl, J. W.; Stres, B.; Thallinger, G. G.; Van Horn, D. J.; Weber, C. F. Introducing mothur: Open-source, platform-independent, community-supported software for describing and comparing microbial communities. *Appl. Environ. Microbiol.* **2009**, *75*, 7537−7541.

(19) Huse, S. M.; Welch, D. M.; Morrison, H. G.; Sogin, M. L. Ironing out the wrinkles in the rare biosphere through improved OTU clustering. *Environ. Microbiol.* **2010**, *12*, 1889−1898.

(20) Edgar, R. C.; Haas, B. J.; Clemente, J. C.; Quince, C.; Knight, R. UCHIME improves sensitivity and speed of chimera detection. *Bioinformatics* **2011**, *27*, 2194−2200.

(21) Cone, J. W.; van Gelder, A. H.; Driehuis, F. Description of gas production profiles with a three-phasic model. *Anim. Feed Sci. Technol.* **1997**, *66*, 31−45.

(22) Manderson, K.; Pinart, M.; Tuohy, K. M.; Grace, W. E.; Hotchkiss, A. T.; Widmer, W.; Yadhav, M. P.; Gibson, G. R.; Rastall, R. A. *In vitro* determination of prebiotic properties of oligosaccharides derived from an orange juice manufacturing by-product stream. *Appl. Environ. Microbiol.* **2005**, *71*, 8383−8389.

(23) Chen, J.; Liang, R.-h.; Liu, W.; Li, T.; Liu, C.-m.; Wu, S.-s.; Wang, Z.-j. Pectic-oligosaccharides prepared by dynamic high-pressure

microfluidization and their *in vitro* fermentation properties. *Carbohydr. Polym.* **2013**, *91*, 175−182.
(24) Hernot, D. C.; Boileau, T. W.; Bauer, L. L.; Middelbos, I. S.; Murphy, M. R.; Swanson, K. S.; Fahey, G. C. *In vitro* fermentation profiles, gas production rates, and microbiota modulation as affected by certain fructans, galactooligosaccharides, and Polydextrose. *J. Agric. Food. Chem.* **2009**, *57*, 1354−1361.
(25) Macfarlane, S.; Macfarlane, G. T. Regulation of short-chain fatty acid production. *Proc. Nutr. Soc.* **2003**, *62*, 67−72.
(26) Duncan, S. H.; Holtrop, G.; Lobley, G. E.; Calder, A. G.; Stewart, C. S.; Flint, H. J. Contribution of acetate to butyrate formation by human faecal bacteria. *Br. J. Nutr.* **2004**, *91*, 915−923.
(27) Kabel, M. A.; Kortenoeven, L.; Schols, H. A.; Voragen, A. G. J. *In vitro* fermentability of differently substituted xylo-oligosaccharides. *J. Agric. Food. Chem.* **2002**, *50*, 6205−6210.
(28) McNab, J. M.; Shannon, D. W. F. The nutritive value of barley, maize, oats and wheat for poultry. *Br. Poult. Sci.* **1974**, *15*, 561−567.
(29) Marlett, J. A. Content and composition of dietary fiber in 117 frequently consumed foods. *J. Am. Diet. Assoc.* **1992**, *92*, 175−186.
(30) Olano-Martin, E.; Gibson, G. R.; Rastall, R. A. Comparison of the *in vitro* bifidogenic properties of pectins and pectic-oligosaccharides. *J. Appl. Microbiol.* **2002**, *93*, 505−511.
(31) Gullón, B.; Gullón, P.; Sanz, Y.; Alonso, J. L.; Parajó, J. C. Prebiotic potential of a refined product containing pectic oligosaccharides. *LWT—Food Sci. Technol.* **2011**, *44*, 1687−1696.
(32) Chen, W.; Liu, F.; Ling, Z.; Tong, X.; Xiang, C. Human intestinal lumen and mucosa-associated microbiota in patients with colorectal cancer. *PLoS One* **2012**, *7*, No. e39743.
(33) Rey, F. E.; Faith, J. J.; Bain, J.; Muehlbauer, M. J.; Stevens, R. D.; Newgard, C. B.; Gordon, J. I. Dissecting the *in vivo* metabolic potential of two human gut acetogens. *J. Biol. Chem.* **2010**, *285*, 22082−22090.
(34) Duncan, S. H.; Barcenilla, A.; Stewart, C. S.; Pryde, S. E.; Flint, H. J. Acetate utilization and butyryl coenzyme A (CoA): Acetate-CoA transferase in butyrate-producing bacteria from the human large intestine. *Appl. Environ. Microbiol.* **2002**, *68*, 5186−5190.
(35) Bailey, M. T.; Dowd, S. E.; Galley, J. D.; Hufnagle, A. R.; Allen, R. G.; Lyte, M. Exposure to a social stressor alters the structure of the intestinal microbiota: Implications for stressor-induced immunomodulation. *Brain, Behav., Immun.* **2011**, *25*, 397−407.
(36) Eeckhaut, V.; Machiels, K.; Perrier, C.; Romero, C.; Maes, S.; Flahou, B.; Steppe, M.; Haesebrouck, F.; Sas, B.; Ducatelle, R.; Vermeire, S.; Van Immerseel, F. *Butyricicoccus pullicaecorum* in inflammatory bowel disease. *Gut* **2012**, *0*, 1−8.
(37) Varela, E.; Manichanh, C.; Gallart, M.; Torrejón, A.; Borruel, N.; Casellas, F.; Guarner, F.; Antolin, M. Colonisation by *Faecalibacterium prausnitzii* and maintenance of clinical remission in patients with ulcerative colitis. *Aliment. Pharmacol. Ther.* **2013**, *38*, 151−161.
(38) Williams, B. L.; Hornig, M.; Parekh, T.; Lipkin, W. I. Application of novel PCR-based methods for detection, quantitation, and phylogenetic characterization of *Sutterella* species in intestinal biopsy samples from children with autism and gastrointestinal disturbances. *mBio* **2012**, *3*, No. e00261-11.
(39) Saulnier, D. M.; Riehle, K.; Mistretta, T. A.; Diaz, M. A.; Mandal, D.; Raza, S.; Weidler, E. M.; Qin, X.; Coarfa, C.; Milosavljevic, A.; Petrosino, J. F.; Highlander, S.; Gibbs, R.; Lynch, S. V.; Shulman, R. J.; Versalovic, J. Gastrointestinal microbiome signatures of pediatric patients with irritable bowel syndrome. *Gastroenterology* **2011**, *141*, 1782−1791.
(40) Kassinen, A.; Krogius-Kurikka, L.; Mäkivuokko, H.; Rinttilä, T.; Paulin, L.; Corander, J.; Malinen, E.; Apajalahti, J.; Palva, A. The fecal microbiota of irritable bowel syndrome patients differs significantly from that of healthy subjects. *Gastroenterology* **2007**, *133*, 24−33.

pressures of ~1000 atm, and heating and cooling rates above 10^{10} K/s.[14] The acoustic cavitations could generate a mechanical effect from shear force caused by rapid collapsing of the cavitation bubbles and free radicals from dissociation of the water. These two effects would degrade the huge polysaccharides into small particals.[14−16]

However, most of the research about ultrasonic degradation of sulfated polysaccharides has focused on heterostructural polysaccharides from sea algae, which induced difficulties in investigating the structural changes such as chain linkage and sulfation pattern during the degradation reaction, thus cause difficulty in eliciting the degradation mechanism of the ultrasonic degradation. To our best knowledge, there have been only a few reports on ultrasonic degradation of marine sulfated polysaccharides with well-repeated units, and investigations on the structural and bioactivity changes during the ultrasonication of the polysaccharides are even fewer. In the present study, we applied ultrasound to control degradation of the previously reported fucoidan from the sea cucumber, which was a linear sulfated polysaccharide with well-repeating tetrasaccharide units.[7] Changes in the structures and antioxidant activities of the degraded products were also examined to investigate the degradation mechanism.

MATERIALS AND METHODS

Materials and Chemicals. Standard monosaccharides, dextran, and Trolox were purchased from Sigma Chemical Co. (St. Louis, MO, USA). 1-Phenyl-3-methyl-5-pyrazolone (PMP), 1,1-diphenyl-2-picrylhydrazyl (DPPH), fluorescein (FL) sodium salt, azodiisobutyramidine dihydrochloride (AAPH), sodium chloride, and HPLC-grade potassium bromide were obtained from Sinopharm Chemical Reagent Co., Ltd. (Shanghai, China). A TSK-G4000 PWxl column (30 cm × 7.8 mm, i.d. 13 μm, 500A, optimum separation range of polysaccharides is 1−700 kDa) was acquired from TOSOH Biosep (Tokyo, Japan). A Compact IC 761 (Metrohm, Herisau, Switzerland) was equipped with a separation column (Shodex IC SI-90E, 250 mm × 4.6 mm). Fucoidan was extracted from *I. badionotus* after papain digestion as we previously described.[7]

Ultrasonic Treatment. Ultrasound process was administered with an ultrasonic processor (Scientz-IID, Ningbo Scientz Biotechnology Co., Ningbo, Zhejiang, China) equipped with a 10 mm horn microtip. The ultrasonic processor had a maximum power of 950 W and operated at the frequency of 21−25 kHz. The sample was dissolved in 20 mL of nanopure water in a glass tube (diameter = 3 cm, height = 10 cm), which was immersed into a water bath (DC-1006, Safe Corp., Ningbo, Zhejiang, China) to maintain a stable temperature. The ultrasonic probe was submerged into the solution 1 cm from the top surface of the suspension.

The effects of the following ultrasonic parameters were investigated: duration (0−220 min), temperature (5, 15, 25, 35, and 45 °C), sample concentration (0.1, 1, 5, and 10 mg/mL), and input power level (5, 15, 25, 35, and 45% of the total input power). The general ultrasound conditions of all treatments were as follows: extraction temperature at 5 °C, input power level of 35%, extraction time of 20 min, and pulse mode (2 s on and 2 s off).

The intensity of the ultrasonic power that dissipated from the microtip with a radius of 10 mm was calculated according to the formula $I = P/(\pi r^2)$, where I is the ultrasound intensity, P is the input power, and r is the radius of the ultrasound probe.[17] The input power levels were set at 5, 15, 25, 35, and 45% of the total input power, which corresponded to ultrasonic powers of 61, 182, 303, 424, and 545 W/cm^2, respectively.

Degradation Kinetics Models. The kinetic models of degradation under ultrasound with different temperatures were obtained by graphical analysis. A trial-and-error procedure was applied to find the best fit reaction order. The zero-order, first-order, second-order models are as follows:

$$M_{wt} - M_{w0} = kt \quad (0)$$

$$\mathrm{Ln}(M_{wt}/M_{w0}) = kt \quad (1)$$

$$1/M_{wt} - 1/M_{w0} = kt \quad (2)$$

k is the rate constant (mol/g min) of M_w degradation during sonolysis; t is the sonolysis time (min); M_{wt} and M_{w0} are the weight-average molar mass at time t and at time 0 (Da), respectively. The model with the best correlation coefficient (R^2) was selected to predict the ultrasonic degradation.

Optimization by Response Surface Methodology (RSM). The three-level−two-factor central composite design (CCD) was employed to optimize the ultrasonic degradation conditions. Temperature (X) and ultrasonic intensity (Y) were studied at three levels (−1, 0, +1). The complete experimental plan with respect to each value in actual and coded forms is shown in the Supporting Information (Supplementary Table 1). A set of 13 experiments was carried out. The response variable was fitted into a quadratic model as follows: $Z = a + Bx + cY + dX^2 + eY^2 + fXY$, where Z is the response calculated by the model, X represents temperature (°C), Y represents ultrasonic intensity (W/cm^2), a is the intercept, b and c are linear coefficients, d and e are squared coefficients,and f is the interaction coefficient. The coefficients of the full regression model and their statistical significance were determined and evaluated using Minitab software. Statistical analysis of the model was performed to evaluate the analysis of variance (ANOVA).

Determination of the Average Molecular Weight and Molecular Weight Distribution. The average molecular weight (average M_w) and polydispersity index were determined by GPC according to the method described by Houben[18] with some modifications. The average M_w determination was carried out on a Waters 1525 HPLC system (Waters, Milford, MA, USA) with a TSK-GEL 4000 column (Tosoh Bioscience, Tokyo, Japan). Twenty microliters of the sample solution was injected and eluted with 0.2 M NaCl at 40 °C for 25 min at a flow rate of 0.5 mL/min. The eluent was monitored with a Waters 2414 refractive index detector. The results were analyzed by the GPC software. The standard dextran (Sigma) with different molecular weights was used to obtain the calibration curves each time.

Determination of Monosaccharide Composition. Monosaccharide compositions were determined using the PMP-HPLC method as described previously.[19] In brief, 2 mg of fucoidan was hydrolyzed with 2 M trifluoroacetic acid at 110 °C for 8 h. The hydrolyzed samples were dissolved into 0.3 M NaOH (450 μL) and 0.5 M methanol solution of PMP (450 μL) at 70 °C for 30 min. Lactose was added as an internal standard to each sample before derivatization. The mixture was neutralized with 450 μL of HCl (0.3 M) after cooling to room temperature and extracted with 1 mL of chloroform three times. HPLC analyses were performed on an Agilent ZORBAX Eclipse XDB-C18 column (Agilent, Santa Clara, CA, USA; 5 μm, 4.6 mm × 150 mm) at 25 °C with UV detection at 250 nm. The mobile phase was aqueous 0.05 M KH_2PO_4 (pH 6.9) with 15% (solvent A) and 40% (solvent B) acetonitrile, respectively. A gradient of B (8−19%) within a period of 25 min was applied.

Determination of Sulfate Content. Sulfate content was determined by ion chromatography.[20] Two milligrams of fucoidan fraction was hydrolyzed with 2 M TFA at 110 °C under nitrogen for 8 h. The hydrolysate was dried under vacuum before dissolving in water prior to ion chromatography. The chromatographic system used was a Compact IC 761 (Metrohm) equipped with a separation column (Shodex IC SI-90E, 250 mm × 4.6 mm) and a suppressor system. The eluent for the ion chromatographic determination was 1 mM Na_2CO_3 + 4 mM $NaHCO_3$ with 2.5% acetone at the flow rate of 1.2 mL min^{-1}. The standard curve was obtained according to the peak area and known concentration of the standard sulfate. The sulfate contents of the samples were determined from the conductivity signal after the injection of 20 μL of sample.

FTIR and NMR. Fucoidan samples (0.5 mg) were mixed with KBr (50 mg) and pressed into KBr pellets. FTIR spectra were collected by a Nicolet 5700 (Thermo Fisher Scientific, USA) at the absorbance

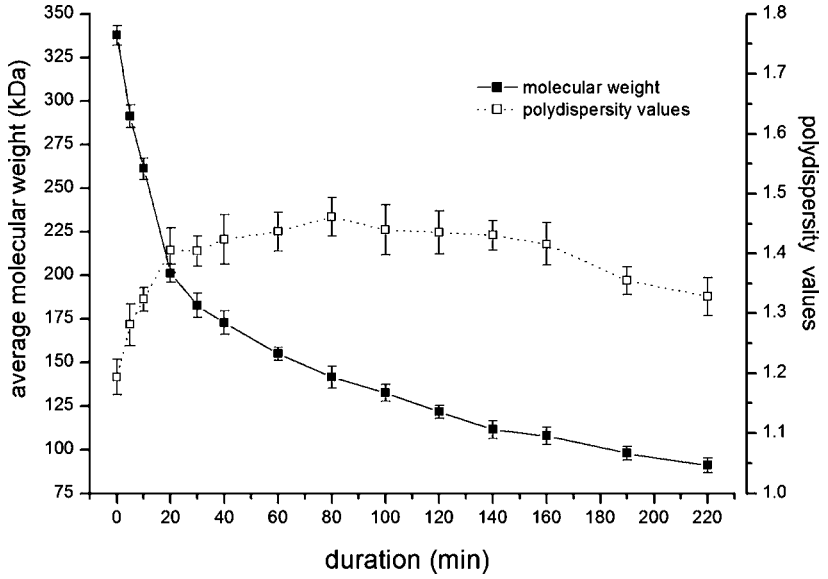

Figure 1. Effects of ultrasonic duration on the average M_w and polydispersity values of fucoidan. Ultrasound treatment conditions: temperature, 5 °C; ultrasonic intensity, 424 W/cm^2; concentration, 1 mg/mL.

mode in the frequency range of 4000−400 cm^{-1}, with a resolution of 4 cm^{-1}.

For NMR analysis, fucoidan fractions (50 mg) were coevaporated with 500 μL of D_2O (99.8%) twice via lyophilization before final dissolution in 500 μL of high-quality D_2O (99.96%) containing 0.1 μL of acetone. Both ^{13}C NMR and ^{1}H NMR spectra were obtained by a Bruker AVIII 600 M (Switzerland) at room temperature. The observed ^{1}H and ^{13}C chemical shifts were corrected by internal acetone standard (2.23 and 33.1 ppm, respectively). The number of scans (ns) in each experiment was dependent on the sample concentration.

DPPH Radical Scavenging Activity Assay. Three milliliters of sample solution (1 mg/mL), 0.6 mL of DPPH solution (0.4 mM prepared in ethanol), and 6 mL of deionized water were mixed in test tube. The absorbance was determined at 515 nm after 30 min at room temperature. All samples were run in triplicate. A standard curve was prepared using different concentrations of Trolox. The DPPH scavenging effect was calculated as

$$\text{scavenging effect } (\%) = [A_0 - (A - A_b)/A_0] \times 100\%$$

where A_0 is the absorbance of DPPH without sample, A is the absorbance of sample and DPPH, and A_b is the absorbance of sample without DPPH.

The inhibition percentage of absorbance was plotted versus the amount of fucoidan sample to obtain a regression line. The Trolox equivalent antioxidant activity (TEAC) was calculated by the ratio between the slopes of the sample and Trolox.

Oxygen Radical Absorbance Capacity (ORAC) Assay. ORAC analyses were carried out in a Fluoroskan Ascent microplate reader (Thermo Electron Corp., Vantaa, Finland) using 96-well plates. The ORAC value was determined as previously described.[21] The reaction was carried out in 75 mM phosphate buffer (pH 7.4). Twenty-five microliters of FL (504 nmol/L) and 25 μL of sample solution placed in the microplate were preincubated for 15 min at 37 °C, and then 150 μL of AAPH solution (17.07 mmol/L) was rapidly added. The fluorescence was recorded every 2 min for 180 min, with an excitation wavelength of 485 nm and an emission filter of 538 nm. The final results were calculated using the differences in areas under the FL decay curves between the blank and the sample. The results were expressed as TEAC values.

Statistical Analysis. Each treatment was repeated three times. All data were expressed as the mean ± SD and statistically evaluated with SPSS/16.00 software. Duncan's multiple-range tests were used to evaluate differences among groups.

RESULTS AND DISCUSSION

Effects of Different Ultrasonic Factors on the Molecular Properties of Fucoidan. *Duration.* The duration-dependent effects of ultrasound on changes in average M_w of the degraded fucoidan fractions are shown in Figure 1. No foam was formatted during the ultrasonic process. The average M_w decreased rapidly in the initial 30 min from 338 to 182 kDa and then gradually tended to a constant value of 91 kDa after 220 min. The polydispersity values, which indicate M_w distribution, increased quickly from 1.193 to 1.461 during the first 80 min of treatments and dropped gradually to 1.328 by the end of 220 min.

It has been reported that fracture of the polysaccharide molecule by ultrasound was mainly caused by shear force produced from the rapid collapse of cavitation bubbles.[22,23] Large polymers with longer chains are preferentially broken by shear force, whereas small molecules with shorter chains are not sensitive to it.[11] Thus, the average M_w of the sample decreased obviously in the first 30 min, and then the rate slowed as most of the fucoidans fractured into small particles. The increase of PDI values in the first 80 min was because both native and fractured fucoidan molecules were present in the solution, which led to the solution changing from a homogeneous to an inhomogeneous state. After further ultrasonic treatment, more native fucoidans were fractured and shifted to the lower molecular weight region, thus leading to a narrow M_w distribution.

Ultrasonic Intensity. Ultrasonic intensity is one of the most important factors affecting the distinct stages of acoustic cavitations, namely, nucleation, bubble growth, and collapse. The effect of ultrasound intensity on the average M_w of degraded fucoidan fractions is shown in Figure 2a. The average M_w decreased from 338 to 166, 142, 130, 124, and 122 kDa under ultrasonic intensities of 61, 182, 303, 424, and 545 W/cm^2, respectively, in 100 min. A significant increase in degradation efficiency was observed with the increase of ultrasonic intensity, indicating the importance of ultrasonic intensity on fucoidan sonolysis ($P < 0.05$).

dx.doi.org/10.1021/jf404717y | J. Agric. Food Chem. 2014, 62, 1088−1095

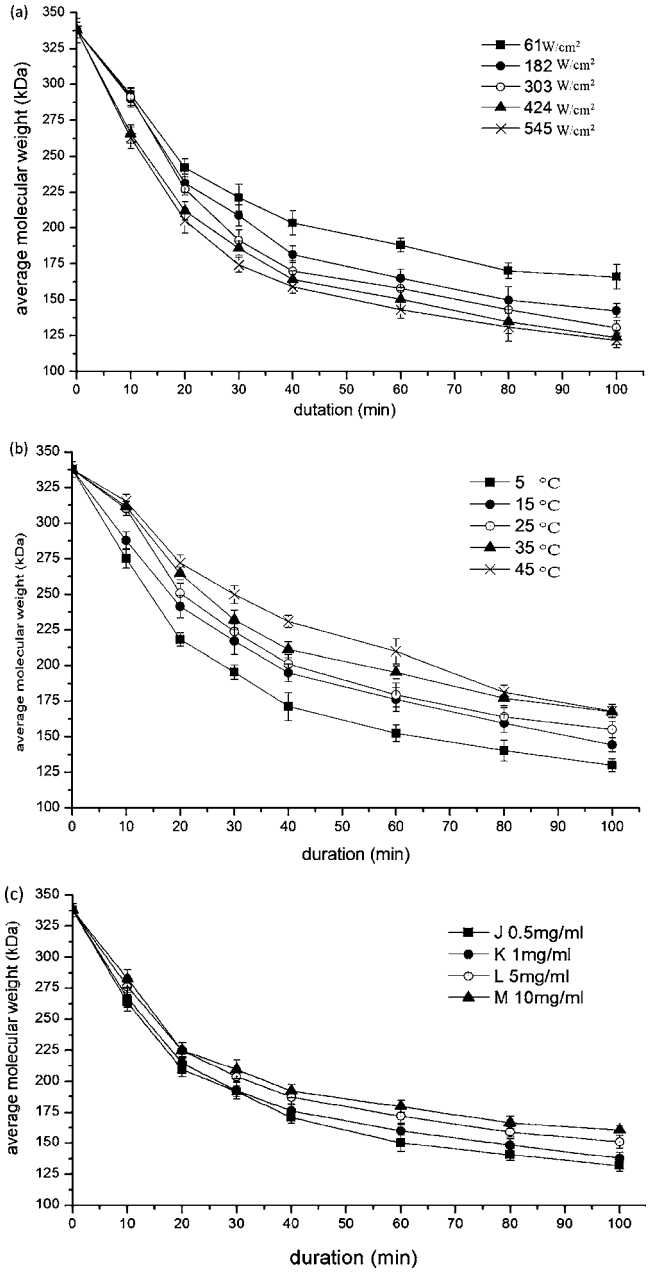

Figure 2. Effects of ultrasound factors on the average M_w of fucoidan: (a) ultrasonic intensity (ultrasonic intensity, 61, 182, 303, 424, or 545 W/cm^2; temperature, 5 °C; concentration, 1 mg/mL; and duration, 20 min); (b) temperature (temperature, 5, 15, 25, 35, or 45 °C; amplitude, 35%; concentration, 1 mg/mL; and duration, 20 min); (c) solution concentration (concentration, 0.1, 1, 5, or 10 mg/mL; amplitude, 35%; temperature, 5 °C; and duration, 20 min).

Table 1. Correlation Coefficients (R^2) from Plots of Zero-, First-, and Second-Order Reactions

temperature (°C)	zero order (M_t/M_0) vs time	first order (ln M_t/M_0) vs time	second order ($1/M_t - 1/M_0$) vs time
5	0.521	0.758	0.913
15	0.668	0.846	0.955
25	0.734	0.860	0.945
35	0.760	0.869	0.943
45	0.877	0.954	0.991

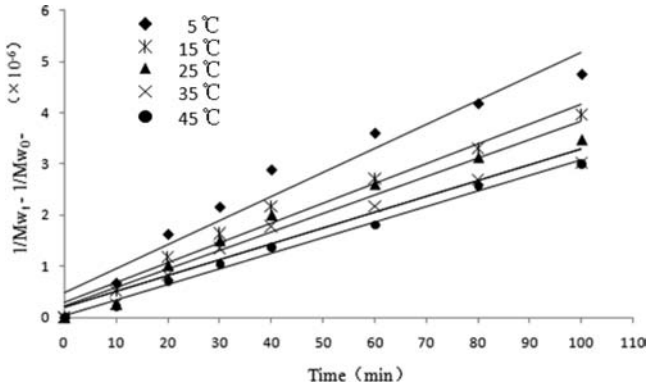

Figure 3. Degradation kinetics curves of fucoidan under ultrasonic treatment in different temperatures obtained by plotting ($1/M_{wt} - 1/M_{w0}$) of each sample versus time of ultrasonication (t).

Table 2. Reaction Rate Constants k and Half-Life Periods ($t_{1/2}$) of Fucoidan under Ultrasonic Treatment

temperature (°C)	k (mol/g min) × 10^{-8}	$t1/2$ (min)
5	5.400	54.83
15	4.299	66.84
25	3.932	75.30
35	3.372	87.80
45	3.104	95.39

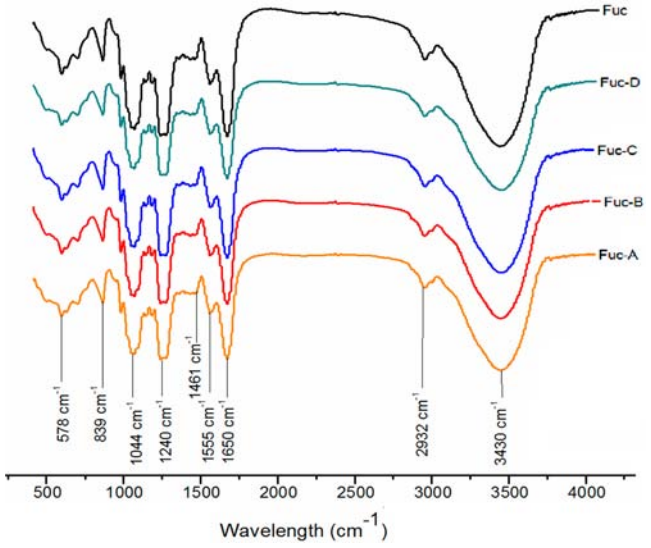

Figure 4. FTIR spectra of native fucoidan and ultrasonic degraded fucoidan fractions. Fuc-A, Fuc-B, Fuc-C, and Fuc-D were assigned to degraded fucoidan fractions prepared by ultrasonication for 30, 60, 120, and 200 min, respectively.

In a certain range, higher ultrasonic intensity could increase the energy of cavitation, lower the threshold of cavitation, and enhance the quantity of the cavitation bubbles.[24] This can explain the sharp decrease of average M_w from 166 to 124 kDa as the ultrasonic intensity increased from 61 to 424 W/cm^2. However, as the ultrasonic intensity continued to rise, more cavitation bubbles were produced around the acoustic source, which dampened the efficiency of energy transmission into the reaction medium and hampered the propagation of the ultrasound wave.[8,25] Thus, no obvious change of average M_w was observed when the ultrasonic intensity increased from 424 to 545 W/cm^2.

dx.doi.org/10.1021/jf404717y | J. Agric. Food Chem. 2014, 62, 1088−1095

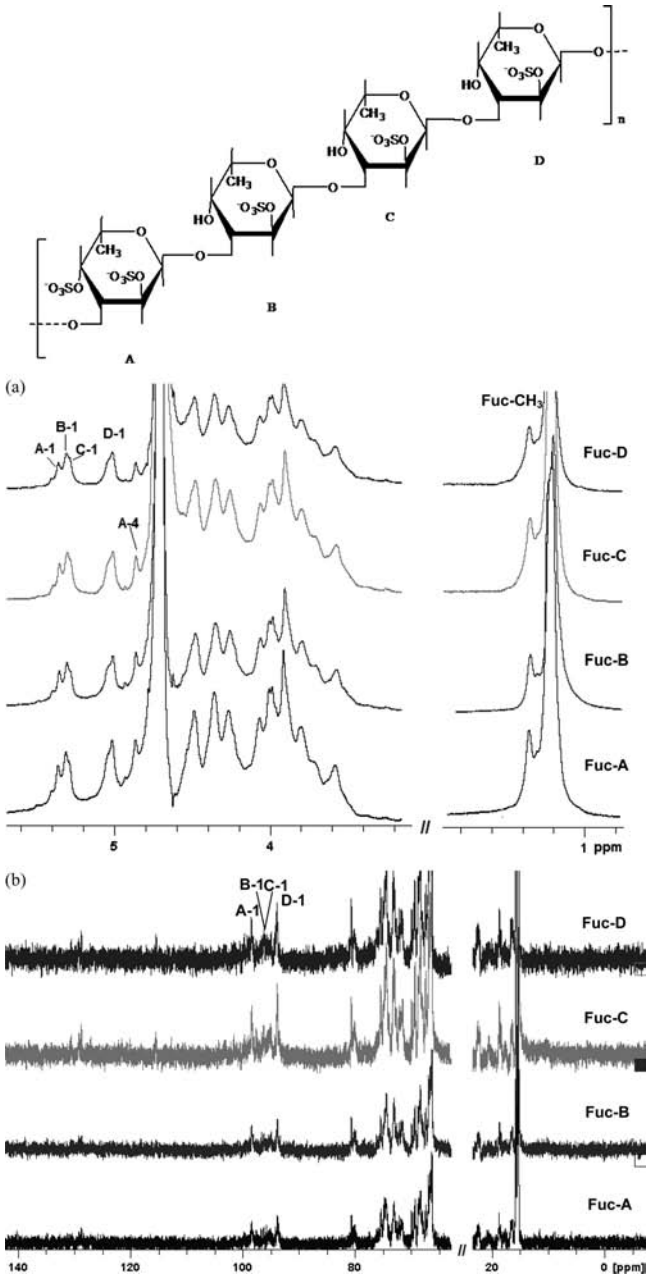

Figure 5. NMR spectra of ultrasonic degraded fucoidan fractions: (a) ^{1}H NMR; (b) ^{13}C NMR. Fuc-A, Fuc-B, Fuc-Cm and Fuc-D were assigned to degraded fucoidan fractions prepared by ultrasonication for 30, 60, 120, and 200 min, respectively.

Temperature. Figure 2b shows the effect of temperature on ultrasonic degradation efficiency. The result indicated higher temperature would lead to a lower degradation efficiency. The average M_w of the sample treated under 5, 15, 25, 35, and 45 °C was decreased from the initial 338 kDa to 130, 144, 155, 167, and 168 kDa after 100 min of treatment, respectively. This trend was due to the increasing reaction temperature allowing cavitation to be achieved with lower acoustic intensity, which was a direct consequence of the rising vapor pressure associated with the heated liquid.[26]

Initial Solution Concentration. The effect of concentration on degradation efficiency was investigated as shown in Figure 2c. The average M_w values of fucoidan after the ultrasonic processes were 131, 138, 151, and 160 kDa as the

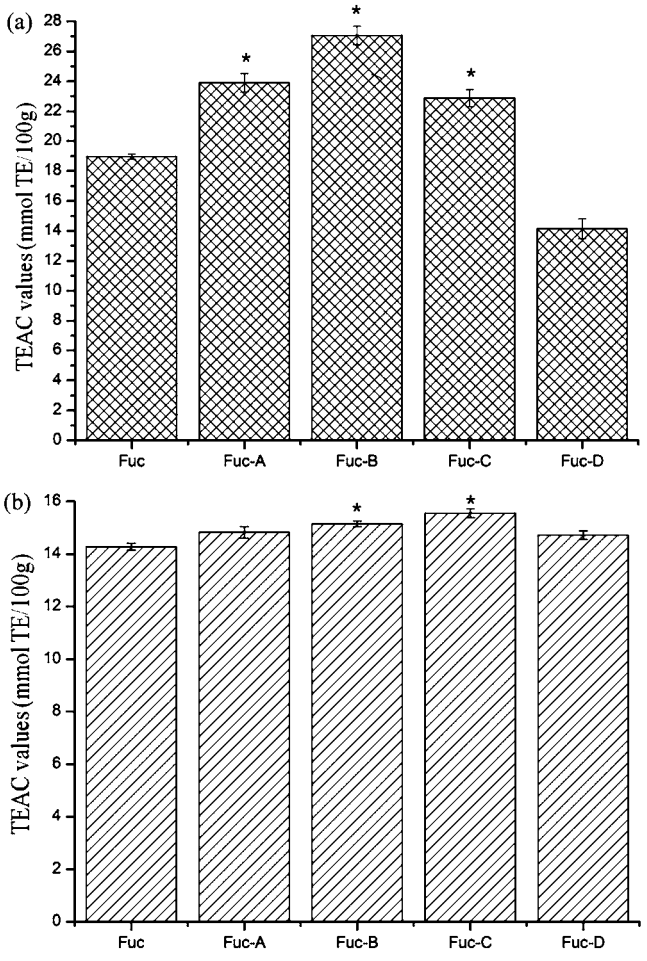

Figure 6. Antioxidant activities of native fucoidan and degraded fucoidian fractions: (a) DPPH radical scavenging activity; (b) oxygen radical absorbance capacity. The results were expressed by TEAC (Trolox equivalent antioxidant activity) values. Fuc-A, Fuc-B, Fuc-C, and Fuc-D were assigned to degraded fucoidan fractions prepared by ultrasonication for 30, 60, 120, and 200 min, respectively. An asterisk (*) indicates significant differences ($p < 0.05$).

concentration rose from 0.1 to 10 mg/mL. This trend could be explained by more diluted concentration leading to less intense entanglement between the polysaccharide chains in solution. Thus, the random coiled structure of the molecule extended more freely and became more vulnerable to the attack of shear force.[27] Moreover, the velocity gradients around the collapsing bubbles are higher in more diluted solutions, which would also benefit the ultrasonic degradation.[28]

Degradation Kinetics of Fucoidan under Ultrasound Treatment. To further predict the degradation efficiency of ultrasonic treatment on fucoidan from the sea cucumber, the correlation coefficients (R^2) among ($M_{wt} - M_{w0}$), ($\ln M_{wt}/M_{w0}$), ($1/M_{wt} - 1/M_{w0}$), and time at different temperatures are summarized in Table 1. The degradation kinetics model of fucoidan under ultrasonic treatments was best fitted to a second-order kinetic equation: $1/M_{wt} - 1/M_{w0} = kt$. Similar results can be found in ultrasound degradation on pectin,[13] dextran,[29] agarose, and carrageenans.[12]

The kinetic curves under different temperatures are presented in Figure 3 by plotting ($1/M_{wt} - 1/M_{w0}$) of each sample versus time of ultrasonication (t). The reaction rate constants (k) and half-life periods ($t_{1/2}$) were calculated

dx.doi.org/10.1021/jf404717y | J. Agric. Food Chem. 2014, 62, 1088−1095

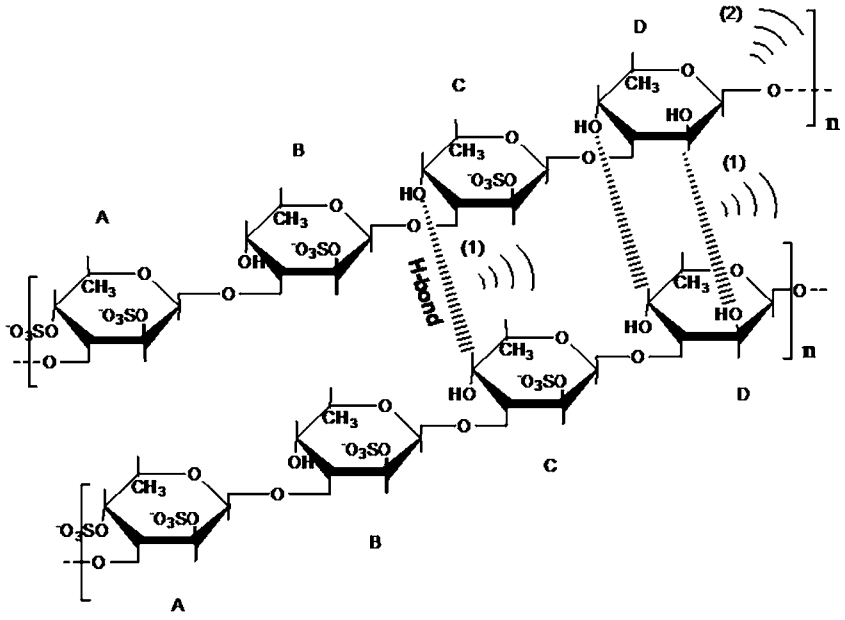

Figure 7. Possible mechanism of ultrasonic action on the fucoidan: (1) mechanical effect broke the hydrogen bonds among the fucoidan molecules; (2) free radicals produced by ultrasonic treatment acted on the nonsulfated fucose in the backbone.

according to the second-order reaction model (Table 2). The k value was much higher at lower temperatures. As the temperature increased from 5 to 45 °C, the k value dropped from 5.4×10^{-8} to 3.104×10^{-8} mol/g min while $t_{1/2}$ increased from 54.83 to 95.39 min. The retarded depolymerization effect was attributed to the loss of cavitation energy, because the energy escaped more easily from the cavitation bubbles at a higher temperature. As a consequence, the degradation efficiency dropped continuously as the temperature increased from 5 to 45 °C.

Optimization by Response Surface Methodology (RSM). On the basis of single-factor analysis, the relationship between response (average M_w) and variables (temperature and ultrasonic intensity) was further optimized by RSM. The results at each design point are shown in Supplementary Table 1 in the Supporting Information. The regression equation in terms of the coded value of the variables was calculated as $Z = 243.12 + 2.954X - 17.785Y + 1.164X^2 - 3.532Y^2 - 5.135XY$, which represents the average M_w of the degradation products (Z) as a function of temperature (X) and ultrasonic intensity (Y). The determination coefficient R^2 of 0.9411 for average M_w of the degradation products suggested that the fitted model could explain 94.11% of the total variation, indicating that the regression model was reliable in predicting the average M_w changes of fucoidan during ultrasonic process by the model.

ANOVA was conducted to assess the significance and adequacy of the model. As shown in Supplementary Table 2, the ANOVA of the quadratic regression model showed the model F value was 22.38, and a low value of "probability >F" ($P < 0.001$) demonstrated that the model was highly significant. XY is a significant model term ($P < 0.05$); the intercept and Y are highly significant model terms ($P < 0.01$). The "lack of fit F value" of 0.335 implied the lack of fit is significant.

On the basis of the regression equation, the optimum temperature and ultrasonic intensity were calculated to be 12 °C and 508 W/cm^2, respectively. The minimum average M_w of fucoidan was predicted to be 207 kDa under the optimized condition. To confirm the prediction, ultrasound degradation was performed under optimum conditions, and the average M_w of the degradation product was tested to be 208 kDa, which was quite close to the predicted value.

Structure Analysis of Degraded Fucoidan Fractions. The structure of the fucoidan from the sea cucumber *I. badionotus* has been identified as a simple linear backbone with well-repeated units of tetrasaccharides (Figure 5). These features facilitated our investigation on the structural changes of the sample during ultrasonication treatments and the possible mechanism of degradation.

Low M_w fucoidan fractions were prepared for further analyses of structure and antioxidant activity. The fractions treated under the optimum ultrasonic conditions for 30, 60, 120, and 200 min were named Fuc-A, Fuc-B, Fuc-C, and Fuc-D, respectively.

Monosaccharide Composition and Sulfate Content. Monosaccharide composition analysis showed that fucose was the only monosaccharide detected in all fucoidan fractions. The sulfate contents of the native fucoidan and the degraded fucoidan fractions (Fuc-A, Fuc-B, Fuc-C, Fuc-D) were 31.22, 32.08, 33.42, 34.11, and 34.74%, respectively. The sulfate content was slightly increased with prolonged ultrasonic duration. This trend indicated that, on the one hand, the polysaccharide chain might have suffered minor destruction; on the other hand, the sulfate group, which was critical to the bioactivity, was not severely damaged throughout the ultrasound process.

FTIR Spectra. The structures of the ultrasonic-treated fucoidan fractions were investigated by FTIR spectra, and the results are shown in Figure 4. The characteristic absorption peaks of the samples are assigned as follows:[30,31] major absorption bands around 3430 cm^{-1} were attributed to O—H stretching; the signal at 2932 cm^{-1} was due to C—H stretching of CH_2 groups; an absorption at 1650 arose from stretching vibration of C═O, C═N; the feature at 1555 cm^{-1} was due to the bending vibration of −NH; an absorption at 1461 cm^{-1} was the stretching vibration of C═O from carboxyl group and the bending vibration of −OH; the signal at 1240 cm^{-1} was caused

by S═O stretching; bands around 1044 cm^{-1} were assigned to C−O stretching vibrations (C—O—H, C—O—C); absorption at 839 cm^{-1} was attributed to COS bending vibration; and the feature at 578 cm^{-1} was assigned to the asymmetric and symmetric O═S═O deformation of sulfates.

The similarity of the IR spectra between degraded and native focuidan indicated the main repeated units of the fucoidan chain were not destroyed by ultrasonication. Moreover, there was no obvious changing in the characteristic peaks at 1240 and 839 cm^{-1} caused by S═O stretching and C—O—S bending vibration,[7] indicating that there was no obvious desulfation during the ultrasonic treatment.

NMR Spectroscopy. The detailed structure, especially the chain linkage and sulfation pattern change, was further investigated by 1D NMR, and the results are shown in Figure 5. The assignment of the proton signals was based on our previous research, which gave in detail assignments of the signals based on mass spectra and 2D NMR.[7] In the ^{1}H NMR spectra (Figure 5a), all four samples showed very similar spectra: anomeric signals at 5.22 ppm (J = 3.92, A-α), 5.26 ppm (J = 3.60, B-α), 5.20 ppm (J = 3.81, C-α), and 5.00 ppm (J = 3.22, D-α) all appeared, and they were attributed to the anomeric proton of fucose residues A, B, C, and D, respectively, in Figure 5. The signals among 3.5−4.5 ppm were attributed to the cross-ring protons; those at 1.23 ppm were attributed to the methyl of the fucose units. No signal was obviously changed during the ultrasonic prosess, indicating that the unique repeated units of tetrasaccharides of the fucoidan remained.

However, there were some minor changes after ultrasonic treatment. The strength of the anomeric signals at 5.00 ppm (unit D, the nonsulfated fucose in the tetrasaccharide repeat) of the ultrasonic-treated samples decreased slightly as the time increased. The proportions of D-1 at 5.00 ppm to the total anomeric proton (A1 to D-1), in Fuc-A, Fuc-B, Fuc-C, and Fuc-D, are 0.315, 0.306, 0.298, and 0.278, respectively. The slight decrease in proton of unit D indicated the nonsulfated fucose might be liable to destruction during ultrasonic treatment, which was a coincidence with the slight increase in the sulfate content. As the mechanical effect of the ultrasonic was usually acted on the hydrogen bond of the polysaccharides molecules, the destruction of unit D may have caused the free radicals produced during the ultrasonic treatment. A similar trend was identified during the acid hydrolysis of this fucodian in our previous research;[7] the acid was also more likely to act on the middle nonsulfated fucose (unit D).

^{13}C NMR (Figure 5b) showed similar spectra for the four fractions. Although limited by the low resolution of the signals in the experimental conditions, we can still observe there were no obvious differences in the nonsulfated fucose anomeric carbon signals. Thus, we further confirmed the main backbone structure was not changed.

Antioxidant Activities Change. The antioxidant activities of the degraded fucoidan fractions were evaluated by DPPH and ORAC assays, and the data are shown in Figure 6. Both of the experiments indicated that the antioxidant activity of the degraded sample increased rapidly during the first period of the ultrasonication and then showed a decreasing trend as the ultrasonication continued. The increase in the antioxidant activity in the first stage may due to the following reasons: First, lower M_w polysaccharides with a mild effect of intramolecular hydrogen bonds would have more free hydroxyl and amino groups.[32] Second, lower M_w polysaccharides have higher contents of reducing sugars at the same mass concentration level.[33]

However, in the second stage, the reduction of the average M_w became slower, and the destruction of the polysaccharide structure was more severe as more free radicals were produced, which resulted in the reduction of the antioxidant activity. Thus, it is important to control the ultrasonic time to control the molecular size as well as to improve its antioxidant activity.

Mechanism of Ultrasonic Degradation of Fucoidan. The ultrasonic process is a mild, effective, and environmentally friendly method to degrade polysaccharides. It is widely acknowledged that the ultrasonic wave could yield the shear force and $H^•$ and $HO^•$ radicals.[15] The current opinion on the mechanism in the ultrasonic degradation of polysaccharides, for example, the sulfated polysaccharide from a red algae, may be explained more by mechanical and less by radical effects.[34] On the basis of the results of the structure analysis and the antioxidant activity, we speculated the possible ultrasonic mechanism acting on the fucoidan may be a combination a mechanical and free radical degradation (Figure 7).

During the initial stage, the average M_w of fucodian decreased sharply and no obvious structure change was observed. Meanwhile, the antioxidant activities of the degraded fractions were significantly improved. Thus, we speculated that the degradation was mainly due to the mechanical effect on dissociated aggregate polymer rather than the chemical reaction. The active groups for the antioxidant activity were not damaged. Therefore, the broken hydrogen bonds among the fucoidan molecules was the main reason causing the average M_w to decrease during this stage. As the ultrasonication continues, the M_w could hardly decrease anymore because the polysaccharide chains have been broken to be a single chain and become harder and harder to fracture. At the same time, the decreasing antioxidant activity is an indication of the destruction of some chemical groups. Thus, it is difficult for the mechanical effect to act on the chain, and the degradation might be due to the free radicals that attacked the nonsulfated fucose in the backbone. However, the specific degradation bonds should be further confirmed by other analysis tools.

Our research was based on a homogeneous fucoidan from the sea cucumber *I. badionotus* with well-defined tetrasaccharide repeating units, which showed excellent anticoagulant, antithrombotic, and antioxidant activities. Applying the ultrasonic process to obtain low molecular fuodian will not only improve its oral absorption and utilization rate but also help to understand the mechanism of ultrasonication on marine polysaccharides and further optimize the processing condition. The low M_w fucoidans prepared deserve further development as a marine antithrombotic drug.

■ ASSOCIATED CONTENT

Supporting Information

Additional tables. This material is available free of charge via the Internet at http://pubs.acs.org.

■ AUTHOR INFORMATION

Corresponding Author

*(S.C.) E-mail: chenshiguo210@163.com. Phone: 86-571-88982151.

Author Contributions

‖X.G. and X.Y. contributed equally to this work.

Notes

The authors declare no competing financial interest.

REFERENCES

(1) Mulloy, B.; Avles, A.; Ana-Paula, R.; Vieira, R. P.; Mourao, P. A. S. Sulfated fucans from echinoderms have a regular tetrasaccharide repeating unit defined by specific patterns of sulfation at the 0−2 and 0−4 positions. *J. Biol. Chem.* **1994**, *269*, 22113−22123.

(2) Mulloy, B.; Ribeiro, A. C.; Vieira, R. P.; Mourao, P. A. Structural analysis ofsulfated fucans by high-field NMR. *Braz. J. Med. Biol. Res.* **1994**, *27*, 515−521.

(3) Chen, S.; Li, G.; Wu, N.; Guo, X.; Liao, N.; Ye, X.; Liu, D.; Xue, C.; Chai, W. Sulfation pattern of the fucose branch is important for the anticoagulant and antithrombotic activities of fucosylated chondroitin sulfates. *Biochim. Biophys. Acta−Gen. Subj.* **2013**, *1830*, 3054−3066.

(4) Zhang, Y. J.; Song, S. L.; Song, D.; Liang, H.; Wang, W. L.; Ji, A. G. Proliferative effects on neural stem/progenitor cells of a sulfated polysaccharide purified from the sea cucumber *Stichopus japonicas*. *J. Biosci. Bioeng.* **2010**, *109*, 67−72.

(5) Wang, Y.; Su, W.; Zhang, C. Y.; Xue, C.; Chang, Y.; Wu, X.; Tang, Q.; Wang, J. Protective effect of sea cucumber (*Acaudina molpadioides*) fucoidan against ethanol-induced gastric damage. *Food Chem.* **2012**, *133*, 1414−1419.

(6) Kariya, Y.; Mulloy, B.; Imai, K.; Tominaga, A.; Kaneko, T.; Asari, A.; Suzuki, K.; Masuda, H.; Kyogashima, M.; Ishii, T. Isolation and partial characterization of fucan sulfates from the body wall of sea cucumber *Stichopus japonicas* and their ability to inhibit osteoclastogenesis. *Carbohydr. Res.* **2004**, *339*, 1339−1346.

(7) Chen, S.; Hu, Y.; Ye, X.; Li, G.; Yu, G.; Xue, C.; Chai, W. Sequence determination and anticoagulant and antithrombotic activities of a novel sulfated fucan isolated from the sea cucumber *Isostichopus badionotus*. *Biochim. Biophys. Acta−Gen. Subj.* **2012**, *1820*, 989−1000.

(8) Iida, Y.; Tuziuti, T.; Yasui, K.; Towata, A.; Kozuka, T. Control of viscosity in starch and polysaccharide solutions with ultrasound after gelatinization. *Innovative Food Sci. Emerging Technol.* **2008**, *9*, 140−146.

(9) Liu, H.; Bao, J.; Du, Y.; Zhou, X.; Kennedy, J. F. Effect of ultrasonic treatment on the biochemphysical properties of chitosan. *Carbohydr. Polym.* **2006**, *64*, 553−559.

(10) Jeon, Y. J.; Park, P. J.; Kim, S. K. Antimicrobial effect of chitooligo-saccharides produced by bioreactor. *Carbohydr. Polym.* **2001**, *44*, 71−76.

(11) Czechowska, R.; Rokita, B.; Lotfy, S.; Ulanski, P.; Rosiak, J. M. Degradation of chitosan and starch by 360-kHz ultrasound. *Carbohydr. Polym.* **2005**, *60*, 175−184.

(12) Lii, C. Y.; Chen, C. H.; Yeh, A. I.; Lai, V. M. F. Preliminary study on the degradation kinetics of agarose and carrageenans by ultrasound. *Food Hydrocolloids* **1999**, *13*, 477−481.

(13) Zhang, L.; Ye, X.; Ding, T.; Sun, X.; Xu, Y.; Liu, D. Ultrasound effects on the degradation kinetics, structure and rheological properties of apple pectin. *Ultrason. Sonochem.* **2013**, *20*, 222−231.

(14) Suslick, K. S.; Price, G. J. Applications of ultrasound to materials chemistry. *Annu. Rev. Mater. Sci.* **1999**, *29*, 295−326.

(15) Makino, K.; Mossoba, M. M.; Riesz, P. Chemical effects of ultrasound on aqueous solutions. Formation of hydroxyl radicals and hydrogen atoms. *J. Phys. Chem.* **1983**, *87* (8), 1369−1377.

(16) Riesz, P.; Kondo, T. Free radical formation induced by ultrasound and its biological implications (review). *Free Radical Biol. Med.* **1992**, *13* (3), 247−270.

(17) Li, H. Z.; Pordesimo, L.; Weiss, J. High intensity ultrasound-assisted extraction of oil from soybeans. *Food Res. Int.* **2004**, *37*, 731−738.

(18) Houben, K.; Jolie, R. P.; Fraeye, I.; Loey, A. M. V.; Hendrickx, M. E. Comparative study of the cell wall composition of broccoli, carrot, and tomato: structural characterization of the extractable pectins and hemicelluloses. *Carbohydr. Res.* **2011**, *346*, 1105−1111.

(19) Strydom, D. Chromatographic separation of 1-phenyl-3-methyl-5-pyrazolone derivatized neutral, acidic and basic aldoses. *J. Chromatogr., A* **1994**, *678*, 17−23.

(20) Ohira, S.; Toda, K. Ion chromatographic measurement of sulfide, methanethiolate, sulfite and sulfate in aqueous and air samples. *J. Chromatogr., A* **2006**, *1121*, 280−284.

(21) Ou, B.; Hampsch-Woodill, M.; Prior, R. L. Development and validation of an improved oxygen radical absorbance capacity assay using fluorescein as the fluorescent probe. *J. Agric. Food Chem.* **2001**, *49*, 4619−4626.

(22) Grönroos, A.; Pentti, P.; Kyllönen, H. Ultrasonic degradation of aqueous carboxymethylcellulose: effect of viscosity, molecular mass, and concentration. *Ultrason. Sonochem.* **2008**, *15*, 644−648.

(23) Wu, T.; Zivanovic, S.; Hayes, D. G.; Weiss, J. Efficient reduction of chitosan molecular weight by high-intensity ultrasound: underlying mechanism and effect of process parameters. *J. Agric. Food Chem.* **2008**, *56*, 5112−5119.

(24) Jiang, Y.; Pétrier, C.; David Waite, T. Kinetics and mechanisms of ultrasonic degradation of volatile chlorinated aromatics in aqueous solutions. *Ultrason. Sonochem.* **2002**, *9*, 317−323.

(25) Sun, Y.; Ma, G.; Ye, X.; Kakuda, Y.; Meng, R. Stability of all-trans-β-carotene under ultrasound treatment in a model system: effects of different factors, kinetics and newly formed compounds. *Ultrason. Sonochem.* **2010**, *17*, 654−661.

(26) Sivakumar, M.; Tatake, P. A.; Pandit, A. B. Kinetics of p-nitrophenol degradation: effect of reaction conditions and cavitational parameters for a multiple frequency system. *Chem. Eng. J.* **2002**, *85*, 327−338.

(27) Tsaih, M. L.; Tseng, L. Z.; Chen, R. H. Effects of removing small fragments with ultrafiltration treatment and ultrasonic conditions on the degradation kinetics of chitosan. *Polym. Degrad. Stab.* **2004**, *86*, 25−32.

(28) Zou, Q.; Pu, Y.; Han, Z.; Fu, N.; Li, S.; Liu, M.; Huang, L.; Lu, A.; Mo, J.; Chen, S. Ultrasonic degradation of aqueous dextran: effect of initial molecular weight and concentration. *Carbohydr. Polym.* **2012**, *90*, 447−451.

(29) Lorimer, J. P.; Cuthbert, T. C.; Brookfield, E. A. Effect of ultrasound on the degradation of aqueous native dextran. *Ultrason. Sonochem.* **1995**, *2*, 55−57.

(30) Gomez-Ordonez, E.; Ruperez, P. FTIR-ATR spectroscopy as a tool for polysaccharide identification in edible brown and red seaweeds. *Food Hydrocolloids* **2011**, *25*, 1514−1520.

(31) Sekkal, M.; Legrand, P. A. Spectroscopic investigation of the carrageenans and agar in the 1500−100 cm^{-1} spectral range. *Spectrochim. Acta A* **1993**, *49*, 209−221.

(32) Xing, R.; Liu, S.; Yu, H.; Zhang, Q.; Li, Z.; Li, P. Preparation of low-molecular-weight and high-sulfate-content chitosans under microwave radiation and their potential antioxidant activity in vitro. *Carbohydr. Res.* **2004**, *339*, 2515−2519.

(33) Qi, H.; Zhao, T.; Zhang, Q.; Li, Z.; Zhao, Z.; Xing, R. Antioxidant activity of different molecular weight sulfated polysaccharides from *Ulva pertusa* Kjellm (*Chlorophyta*). *J. Appl. Phycol.* **2005**, *17*, 527−534.

(34) Zhou, C.; Ma, H. Ultrasonic degradation of polysaccharide from a red algae (*Porphyra yezoensis*). *J. Agric. Food Chem* **2006**, *54* (6), 2223−2228.

24 kDa. Caseinates are flexible proteins that readily adsorb to lipid surfaces with coverage of 1 mg protein/m^2. β-Lactoglobulin, the major protein component of WPI, has a molecular weight of about 18 kDa. Although β-lactoglobulin and caseinates have similar interfacial energy lowering properties,[14] globulins are more compact and slower to reorganize upon adsorption resulting in a higher amount for surface coverage, 2−3 mg/m^2. SPI is also a globulin but much larger, 200−350 kDa. The surface charge upon adsorption is highly dependent on pH. At acidic and neutral pH encountered in the digestive system, dairy and SPI proteins are highly cationic or anionic, respectively. The release of protein encapsulated lipids may also be assisted by digestive enzymes. *In vitro* digestion by gastric pepsin did not significantly increase release of lipids encapsulated by SPI, WPI, or β-lactoferrin, but intestinal pancreatin significantly accelerated release of emulsion stabilized by β-lactoglobulin and WPI.[15] Differences in size, conformation, hydrophobic amino acid content, and ionic amino content contribute to different emulsion size, protein layer thickness, stability to aggregation, and stabilization of the lipid core to oxidation. Proteins (like SC, WPI, and SPI) are thought to be able to better protect BC and lipids against oxidation and degradation in encapsulated systems[3,16] compared to small molecule surfactants (like Tween 20), because of the free radical scavenging and metal chelating properties of cysteine, tyrosine, tryptophan, phenylalanine, and histidine.[17]

Although protein emulsifiers are GRAS, there are concerns regarding the safety and potential cytotoxicity of nanosystems because they may be inhaled or absorbed via pinocytosis by the intestinal epithelial cells.[18] Hu et al. investigated the cytotoxicity of chitosan−caseinophosphopeptide nanocomplexes by MTT assay and found no significant toxicity.[19] He et al. showed that the viability of cells exposed to food protein stabilized nanoemulsions was greater than 85% at 3 mg/mL concentration, while other traditional emulsifiers (like Tween 80) caused a significant decrease in cell viability.[15] To date, there have been no reports about the cellular cytotoxicity and *in vitro* uptake of BC loaded nanoparticles with Caco-2 cells.

In the present study, SC, WPI, and SPI were used as emulsifiers to develop food-grade, relatively stable nano- and microparticles for oral delivery of BC. The effects of emulsifiers and the concentrations on physicochemical stability of BC loaded nanoparticles during storage were evaluated. We hypothesize that although the residual BC of the nanoparticles prepared by the solvent evaporation is likely to be a solid, uptake by Caco-2 cells will still occur because of the high surface area. The cytotoxicity and cellular uptake of prepared BC loaded nanoparticles in an *in vitro* digestive system were also investigated.

MATERIALS AND METHODS

Materials. BC (≥97.0%, UV) was purchased from Sigma-Aldrich (St. Louis, MO). Sodium caseinate (SC) powder (protein content >95% and 1.0% fat on dry basis by manufacturer) was obtained from Fonterra Co-operative Group (Auckland, New Zealand). Whey protein isolate (WPI; Hilmar 9410, 93.0% protein, 0.2% lactose, 1.0% fat, and 2.0% ash, on a dry basis, and 4.5% water) was obtained from Hilmar Food International, Inc., Livingston, CA). SPI was extracted in our laboratory from dehulled and defatted soybean meal by the alkali-solution and acid-isolation method (protein content >93% and 0.96% fat content on dry basis by measurement).[20] Dulbecco's modified Eagle's medium (DMEM) (containing 4.5 g/L D-glucose and GlutaMAX), penicillin and streptomycin (100×), fetal bovine serum (FBS), TrypLE Select, Hanks' balanced salt solution (HBSS), and phosphate buffer solution (PBS) (10×) were purchased from GIBCO (Grand Island, NY). The human colon carcinoma cell lines (Caco-2 cells, ATCC, Manassas, VA) were grown in DMEM. Cells after 25−40 passages were used in the uptake study. All other chemicals and reagents used were HPLC-grade and obtained from Sigma-Aldrich (St. Louis, MO).

Methods. *BC Loaded Nanoparticle Preparation.* SC, WPI, and SPI were dispersed (0.10−1.50%, w/w) separately in 5 mM phosphate buffer pH 7.0 containing 0.02 wt % sodium azide antimicrobial agent. The dispersions were stirred for 2 h and refrigerated overnight to maximize dissolution. Then, 0.1% β-carotene (BC) (w/w) solutions were prepared in ethyl acetate. BC loaded nanoparticles were prepared according to the method described by Tan and Nakajima[10] with minor changes. Water, 100 mL, was saturated with 8.3 g of ethyl acetate[21] prior to formulating the protein solution in order to prevent precipitation of BC during homogenization. The BC in ethyl acetate solution was combined with the ethyl acetate saturated protein solution at a ratio of 1:9. The mixtures were homogenized for 10 min at 8000 rpm using an Ultra-Turrax homogenizer (T25, Ika-Werke, Staufen, Germany) to form a coarse emulsion before additional homogenization using a two-stage valve homogenizer (APV-1000 high-pressure homogenizer, Wilmington, MA) for one cycle at 70 MPa. After the homogenization, ethyl acetate was removed from the emulsions on a rotary evaporator at 40 °C. The residual ethyl acetate was determined by headspace gas chromatography and found to be less than 0.001% (data not shown), less than that reported by other investigators.[22] Samples of 5 mL of each nanoparticles were stored in 10 mL amber glass vials flushed with nitrogen at 4 and 25 °C for analysis of BC retention during 30 d storage.

Measurement of Surface Tension and CMC. Surface tension was measured using the pendant plate method with the DataPhysics DCAT21 dynamic contact angle meter and tensiometer (DataPhysics Instruments, Germany) according to the method described by Mao et al.[16] The critical micelle concentration (CMC) of SC in this study was determined by using DataPhysics DCAT21 similar to the method previously described.[23] Briefly, several concentrations of protein nanoparticles were prepared by dilution of the protein stock solution (20 mg mL^{-1}) with sterile ultrapure water. The CMC is the point at which the surface tension no longer increases with increasing protein concentration. Temperature was kept constant at 25.0 ± 0.2 °C with a circulating water bath system.

Particle Diameter and ζ-Potential Analysis. The characteristics of BC loaded nanoparticle solutions were determined by measuring the mean particle diameter, diameter distribution, and ζ-potential of nanoparticles by dynamic light scattering technique using a Malvern Zetasizer (Nano-ZS; Malvern Instruments, Worcestershire, U.K.). Refractive indices of 1.47 for BC and 1.33 for phosphate buffers were used. To reduce multiple scattering effects, the nanoparticles dispersions were diluted 100 times with 5 mM phosphate buffer pH 7.0 prior to the measurements that were performed in triplicate.

Particle diameter measurements to determine the effect of storage on BC loaded nanoparticle solutions stabilized by the three proteins were conducted at 0, 16, and 30 d at 4 and 25 °C.

Color Evaluation. The color of nanoparticles of BC and its isomers depends on their concentration, stability, and particle diameter. The color parameters (L^*, a^*, b^*) were determined using a tristimulus colorimeter Ultra Scan PRO (Hunterlab, Japan). L^* values are a measure of lightness, a^* indicates degree of greenness (for negative a^* values) and degree of redness (for positive a^* values), and b^* also ranges from negative to positive values indicating degree of blueness to yellowness, respectively. The color of the nanoparticle samples all prepared with 1.0% (w/w) proteins was determined by measuring the reflectance from the surface of a transparent flat-faced quartz cuvette. All measurements were repeated three times. Color changes (color differences) were calculated using the following formula:

$$\Delta E^* = [(L^* - L_0)^2 + (a^* - a_0)^2 + (b^* - b_0)^2]^{1/2} \quad (2)$$

Here, subscript 0 indicates color at start of storage period.

dx.doi.org/10.1021/jf404073c | J. Agric. Food Chem. 2014, 62, 1096−1104

Transmission Electron Microscopy (TEM) Analysis. TEM was used to observe differences in internal structure of the nanoparticles and to confirm diameter by dynamic light scattering. Samples were prepared by the conventional negative-staining method. Nanoparticles were placed on copper grids and negatively stained with 2% (w/v) phosphotungstic acid for several minutes at room temperature. Grids bearing nanoparticles were analyzed with a Hitachi H-700 transmission electron microscope (Hitachi, Tokyo, Japan).

Cytotoxicity of BC Loaded Nanoparticles on Caco-2 Cells. Cell viability, a commonly used indicator of *in vitro* cytotoxicity, was evaluated by the 3-(4,5-dimethylthiazol-2-yl)-2,5-diphenyltetrazolium bromide (MTT) assay. The colorimetric MTT assay measures the activity of cellular enzymes that reduce MTT to its insoluble purple formazan form.[24] Caco-2 cells were incubated in DMEM containing 10% FBS, 1× nonessential amino acid (NAA), and 1× penicillin and streptomycin. Caco-2 cells in DMEM were seeded at a density of 1.2×10^5 cells/well onto 96-well plates and incubated (Sanyo, Osaka, Japan) at 37 °C in 90% humidity and 5% CO_2. After 48 h incubation, the media was discharged, and BC loaded nanoparticles diluted with DMEM were added to the wells. After 24 h incubation at 37 °C the nanoparticles containing media were replaced with 100 μL of DMEM containing MTT (10 μL, 5 mg/mL in 1× PBS, pH 7.2) and incubated for 2 h at 37 °C. Finally, the supernatant was removed and 100 μL of dimethyl sulfoxide (DMSO) added. The 96-well plates were analyzed with a Multilabel microplate counter (Victor,[3] PerkinElmer, Waltham, MA) at 570 nm. Cell viability was calculated by the percentage of absorbance relative to control (treated with DMEM only).

Cellular Uptake of BC Loaded Nanoparticles. Caco-2 cells were incubated in DMEM containing 10% FBS, 1× nonessential amino acid (NAA), and 1× penicillin and streptomycin at 37 °C in a 90% humidity and 5% CO_2 incubator (Sanyo, Osaka, Japan) onto 12-well plates.[25] Caco-2 cells were seeded at a density of 1.2×10^5 cells/well. The media was changed every two days. After five days, the cell monolayers were observed by optical microscopy (Leica, IL) to ensure that the cells reached about 90% confluence. Caco-2 cell monolayers were washed with DMEM three times. Both protein encapsulated BC loaded nanoparticles and BC in THF/DMSO (1:1, v/v) solution (as control) were diluted in DMEM to a final BC concentration of 5 μg/mL. A 1 mL portion of the BC encapsulated nanoparticle and control in THF/DMSO were added to separate wells containing washed Caco-2 cells. The final concentration of THF was less than 0.1%. Following 24 h incubation at 37 °C in a CO_2 incubator, the supernatants were removed, and the cell monolayers were washed three times with precooled PBS solution to stop uptake and wash the surface of cell monolayers. After that, 0.5 mL of 10% ethanolic PBS solution was added to dissociate cell monolayers. Cell suspensions were obtained with cell scrapers. A 0.4 mL portion of cell suspension was extracted with solvent and analyzed for BC content by HPLC (procedure given below), and the remaining 0.1 mL was used for protein content determination.

Protein Content Analysis. Caco-2 cell protein content was determined using the bicinchoninic acid (BCA) assay at 560 nm with bovine serum albumin as the standard.[26]

Extraction and Quantification of BC from Nanoparticles and Caco-2 Cells. The BC in nanoparticles was extracted with 3 mL of ethanol/*n*-hexane (1:2, v/v) three times. The hexane fractions were combined and brought up to 10 mL for HPLC analysis. The effect of storage on BC loaded nanoparticle dispersion stabilized by the three proteins was conducted at 0, 2, 9, 16, 23, and 30 days at both temperature conditions.

A 25 μL portion of 5 μg/mL trans-β-Apo-8′-carotenal in ethanol was added to 0.4 mL Caco-2 cell suspension as an internal standard. The cell suspensions (0.4 mL) were extracted three times with 3 mL of ethanol/*n*-hexane (1:2, v/v). Organic fractions were removed and combined with transfer pipets, and the extract was dried under a stream of nitrogen gas at 40 °C. The BC extract was dissolved in 0.1 mL of methanol/dichloromethane (1:1, v/v) containing 0.1% BHT for HPLC analysis. The recovery of trans-β-Apo-8′-carotenal from Caco-2 cells was greater than 94%.

HPLC quantification of BC was performed using an Agilent 1100 HPLC system with DAD UV−vis absorption detector (Agilent, Santa Clara, CA), according to the published method.[27] BC quantitation range (0.1 μg/mL to 100 ug/mL) was established for HPLC analysis of BC in nanoparticles and Caco-2 cells. A polymeric carotene C_{30} reverse-phase analytical column (250 mm × 4.6 mm i.d., 5 μm, YMC, Inc., Wilmington, NC) was used to separate BC with a flow rate of 1 mL/min at room temperature. The guard column was a reverse-phase C_{18} column (50 mm × 3.0 mm i.d., 5 μm, YMC, Inc.). The injection volume was 20 μL, and the detection wavelength was 450 nm. The chromatography conditions were as follows: solvent A, methanol/acetonitrile/H_2O (84:14:2, v/v/v); solvent B, dichloromethane. The solvent gradient program was 80% A/20% B at 0 min and was changed linearly to 45% A/55% B in 15 min, and maintained for 5 min, and followed by a linear return to 80% A/20% B at 25 min.

Statistics. All measurements were performed at least three times and were reported as mean ± standard deviation. The data were analyzed by the analysis of variance (ANOVA) using the SPSS 17.0 package (IBM, New York). Duncan's multiple range test was used to determine the significant differences of the mean values ($P < 0.05$).

RESULTS AND DISCUSSION

Particle Diameter. The particle diameter distributions of solid BC nanoparticles encapsulated by SC, WPI, and SPI at the concentrations resulting in the smallest mean particle diameter are shown in Figure 1, and the mean diameter and

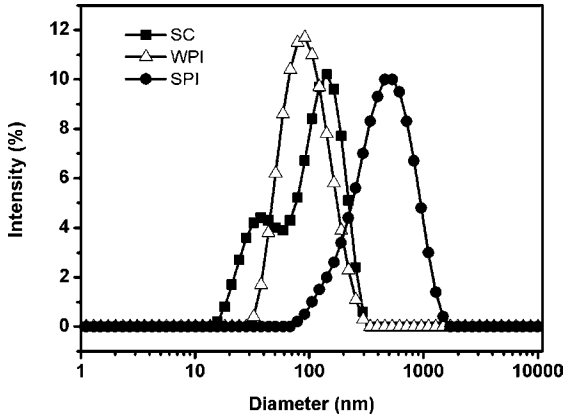

Figure 1. Particle diameter distributions of SC (1.0%, w/w), WPI (1.0%, w/w), and SPI (1.0%, w/w) encapsulated BC loaded nanoparticles.

polydispersity index determined by dynamic light scattering (DLS) are shown in Table 1. The loading capacity of BC in nanoparticles was 1.07%, 1.05%, and 1.06% for SC, WPI, and SPI, respectively. For all three different protein solid lipid nanoparticles, the efficiencies of encapsulation of BC are 99.1%, 98.8%, and 98.7%, respectively, for SC, WPI, and SPI at 1.0% (w/w), respectively, indicating BC was fully encapsulated by three proteins. Although evaporation of the solvent resulted in solid lipid nanoparticles, DSC and X-ray diffraction did not show crystalline cores (results not shown). The SC, WPI, and SPI used contained 1% residual lipids (Materials and Methods section). The ethyl acetate used to solubilize BC and saturate the protein solution most likely also extracted the residual lipids from the protein emulsifying agents. We speculate that the extracted lipids and BC formed a mixture that was not crystalline.

Lipid soluble nutrients including triglycerides and BC are reduced to nanosized mixed micelles of phospholipids and bile acids *in vivo*[28] suggesting that small diameter may be necessary

Table 1. Effect of Different Concentrations of Emulsifiers on the Particle Diameter of BC Loaded Nanoparticles (Mean ± STD, $n = 3$)[α]

	SC		WPI		SPI	
conc (%)	D (nm)	PDI	D (nm)	PDI	D (nm)	PDI
0.10	162.4 ± 3.7e	0.098 ± 0.008a	190.9 ± 3.5e	0.165 ± 0.010a	493.4 ± 10.4e	0.315 ± 0.001b
0.25	125.8 ± 2.0d	0.206 ± 0.016b	131.1 ± 2.8d	0.218 ± 0.012b	450.6 ± 6.5d	0.297 ± 0.031ab
0.50	121.7 ± 2.9c	0.310 ± 0.008c	125.1 ± 2.8c	0.156 ± 0.023a	421.8 ± 2.9c	0.356 ± 0.020c
0.75	75.0 ± 1.5a	0.305 ± 0.124c	113.6 ± 3.2b	0.231 ± 0.006bc	402.3 ± 7.4b	0.360 ± 0.010c
1.00	77.8 ± 0.2a	0.386 ± 0.003d	89.7 ± 1.7a	0.245 ± 0.002c	371.8 ± 6.8a	0.286 ± 0.003a
1.25	103.1 ± 2.6b	0.449 ± 0.152e	90.1 ± 1.5a	0.351 ± 0.007d	397.5 ± 5.0b	0.471 ± 0.004e
1.50	121.3 ± 2.0c	0.357 ± 0.026d	88.5 ± 2.5a	0.340 ± 0.020d	400.1 ± 3.2b	0.416 ± 0.006d

[α]Values are the mean and standard deviation of triplicates. Values in the same column with different letters (a−e) are significantly different ($p \leq 0.05$).

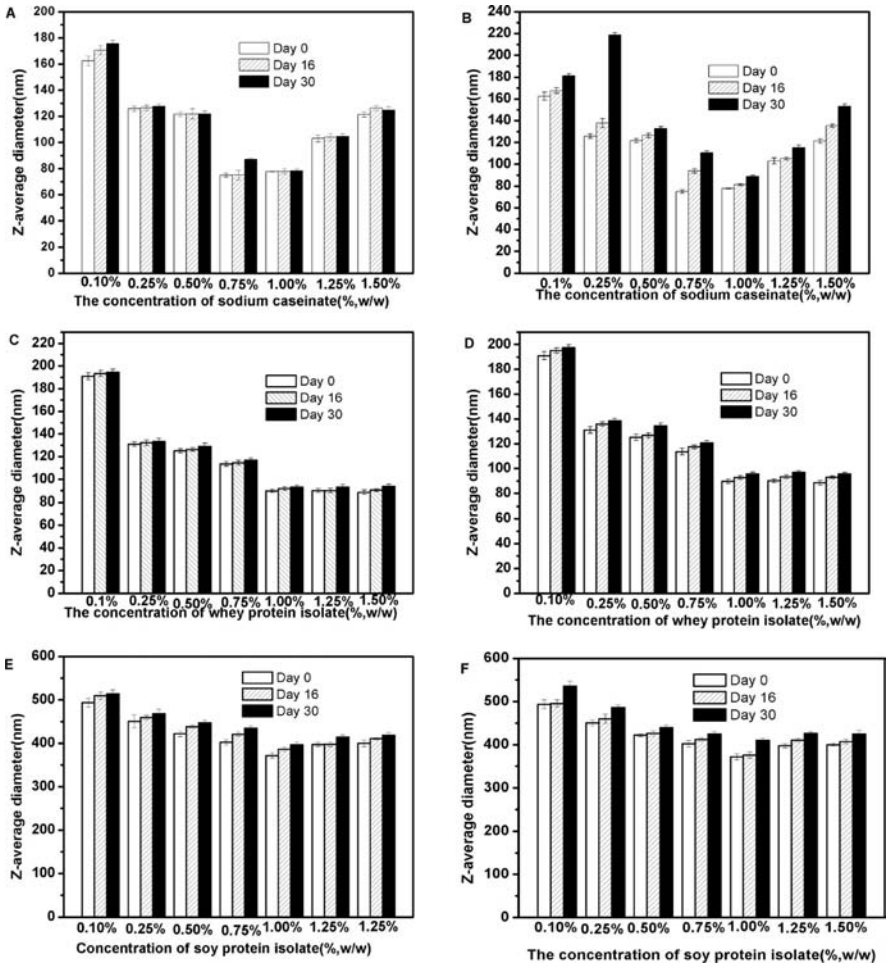

Figure 2. Change of Z-average diameters of three protein encapsulated BC loaded nanoparticles over time (30 days) under storage at 4 °C (A, C, E) and 25 °C (B, D, F). A and B refer to SC, C and D refer to WPI, and E and F refer to SPI. Data are represented as the mean ± STD ($n = 3$).

or simply facilitates uptake. Increasing the emulsifier concentration of SC, WPI, and SPI from 0.10% to 1.00% generally resulted in a significant ($P < 0.05$) decrease in particle diameter (Table 1). The Z-average particle diameter of 0.1% (w/w) SC stabilized nanoparticles was 162.4 nm (Table 1), and some unemulsified BC-lipid solids could be observed after evaporation, illustrating that BC was not fully emulsified. When SC was increased to 0.25% (w/w), the mean diameter decreased drastically ($P < 0.05$) to 125.8 nm. However, the particle distribution was now bimodal with peaks at about 100 and 30 nm. Increasing concentrations of SC increased the relative amounts of the 30 nm peak at the expense of the 100 nm. This suggests that the amount of SC limits the formation of the smaller particles due to their higher surface area. At 0.75% (w/w) SC, the particle diameter reached its minimum (75.0 nm). The critical micelle concentration (CMC) of SC in this study was determined to be 0.688%. When the concentration of SC exceeded the CMC, SC self-associated to form micelles leading to a slight ($P > 0.05$) increase in diameter of BC loaded nanoparticles to 77.8 nm at 1.0% (w/w). Continuing to increase the SC concentration to 1.5% (w/w) resulted in a significant increase of particle diameter to 121.3 nm ($P < 0.05$),

dx.doi.org/10.1021/jf404073c | J. Agric. Food Chem. 2014, 62, 1096−1104

Table 2. Slopes of the Linear Plots Describing BC Loss (w/w/day) with Changing Formulation[a]

	SC		WPI		SPI	
protein [(w/w)]	4 °C	25 °C	4 °C	25 °C	4 °C	25 °C
0.10	4.23×10^{-3}	2.04×10^{-2}	4.15×10^{-3}	2.11×10^{-2}	1.44×10^{-2}	2.60×10^{-2}
0.25	3.77×10^{-3}	1.83×10^{-2}	6.03×10^{-3}	1.89×10^{-2}	1.01×10^{-2}	2.33×10^{-2}
0.50	3.38×10^{-3}	1.54×10^{-2}	3.73×10^{-3}	1.61×10^{-2}	1.01×10^{-2}	1.96×10^{-2}
0.75	2.89×10^{-3}	1.33×10^{-2}	3.34×10^{-3}	1.42×10^{-2}	7.08×10^{-3}	2.25×10^{-2}
1.00	2.18×10^{-3}	1.24×10^{-2}	2.42×10^{-3}	1.30×10^{-2}	6.16×10^{-3}	1.90×10^{-2}
1.25	2.53×10^{-3}	1.14×10^{-2}	2.46×10^{-3}	1.22×10^{-2}	6.69×10^{-3}	1.79×10^{-2}
1.50	2.14×10^{-3}	1.12×10^{-2}	2.13×10^{-3}	1.19×10^{-2}	5.36×10^{-3}	1.80×10^{-2}

[a]Storage condition: no light, full of nitrogen.

indicating that some SC aggregated and associated into submicelles or aggregates as reported during high pressure homogenization.[29] Dickinson has also suggested that at the molecular level pressure-induced disintegration of casein micelles arises from the disruption of internal hydrophobic interactions and dissociation of colloidal calcium phosphate resulting in interparticle bridges leading to aggregation and association.[30]

The mean particle diameter of WPI nanoparticles gradually decreased from 190.9 to 89.7 nm when the concentration of WPI increased from 0.10% to 1.0% (w/w). The particle diameter of the nanoparticles did not change with increasing WPI concentration from 1.0% to 1.5% (w/w). These results suggest that the surplus WPI in solution did not form multiple adsorption layers or aggregate at the surface of droplets due to net negative charges on the free protein and adsorbed proteins.

SPI is composed of the following two major proteins: 7S and 11S with molecular weights of approximately 200 000 and 350 000 Da, respectively. When SPI was used as an emulsifier, the particle diameter of the nanoparticles was approximately two times larger than when using SC or WPI. This could be attributed to the poor emulsifying ability of SPI, and fewer hydrophobic amino acids on the surface to bind to the lipid core in comparison with milk proteins. Because SPI does not efficiently stabilize the newly formed droplets, coalescence occurs and results in larger particle diameter.

The PDI value is a measure of the variability in the distribution of particle diameter. All samples had a relatively narrow distribution with a PDI value less than 0.471. As protein concentration increased, the SC and WPI stabilized nanoparticles exhibited an increased PDI, possibly due to the formation of an increasing population of smaller particles. The PDI of the SPI encapsulated nanoparticles did not change with increasing protein concentration, and the particle size did not decrease as much as the milk proteins.

Particle Diameter of BC Loaded Nanoparticles During Storage. The diameter stability of nanoparticles is important for their utilization in foods because texture and appearance depend on structural stability. The particle diameters increased less than 10% at 4 °C, and in general, there was a greater increase in particle diameter at 25 °C (10−76%) during the 30 day storage period (Figure 2). The stability to storage is probably due to the repulsive forces due to the negative surface charges at pH 7 (ζ-potential Table 3). Yang et al.[5] also noted that the diameter increments of nanoparticles were greater at higher temperatures and attributed the temperature effect to more rapid movement at higher temperature that increased gravitational flocculation. Although the initial diameters of the particles encapsulated by SC were smaller at the start of storage, the diameter increase was greater than those

Table 3. Droplet ζ-Potential (Mean ± STD, $n = 3$)[a] of BC Loaded Nanoparticles at pH 7.0 Stabilized by SC, WPI, and SPI at 1.0%

emulsifiers	SC	WPI	SPI
ζ-potential (mV)	−35.7 ± 0.4b	−29.9 ± 0.5a	−37.8 ± 0.4c

[a]Values are the mean ± STD of triplicates. Values in the same column with different letters (a−c) are significantly different ($p \leq 0.05$).

encapsulated by the globuler proteins WPI and SPI at all concentrations after 30 days. The larger WPI and SPI particles are expected to increase in diameter with storage due to their more rapid rise to the surface and subsequent aggregation or flocculation. While flocculation due to gravitational separation probably occurs, it is slow compared to other mechanisms. In the case of SC emulsions, increasing protein concentration allows for intermolecular bridging of adsorbed proteins by proteins not adsorbed to the lipid surface. In conclusion, storage temperature may be an important factor to determine nanoparticles' physical stability. There were no obvious BC lipid solids or sediments in the stored BC nanoemulsion samples indicating that they were fairly stable.

Effect of Emulsifier Type and Concentrations on BC Chemical Stability. Samples of BC dissolved in ethyl acetate were used as the control. Compared to the control samples, BC in nanoparticles showed significantly improved chemical stability and higher retentions at both temperatures (4 and 25 °C) (Figure 3), indicating nanoparticles were a good delivery system in enhancing stability of encapsulated lipophilic molecules. The order of chemical stability of BC loaded nanoparticles was the following: SC > WPI > SPI (Table 2). The chemical stability of corn oil, containing 70% polyunsaturated linoleic acid, emulsions was in the following order: SC > WPI > SPI.[13] The decrease in BC concentration was fit to a zero-order kinetic reaction model (Figure 3) as suggested by Cornacchia and Roos.[31] The rate of loss was greater at 25 °C than that at 4 °C (Table 2). The regression coefficients (R^2) are from 0.896 to 0.998 and the intercepts are from 0.919 to 1.00 (Supporting Information, Table 1S).

The oxidative stability of the BC core is affected by two predominant properties of the encapsulating protein: the binding of metal ions and the thickness of the encapsulating layer. Binding of transition metal ions by cysteine, tyrosine, tryptophan, phenylalanine, and histidine from the aqueous phase can reduce free radical oxidation; however, if the binding site is at the interfacial layer, proximity of transition metals may increase oxidation. The phosphoserine residues in casein increased stability by binding pro-oxidative iron and copper ions.[32] WPI also has about 8 mol binding sites for iron per mol of protein.[33] Hwang et al.[34] reported that there was a positive

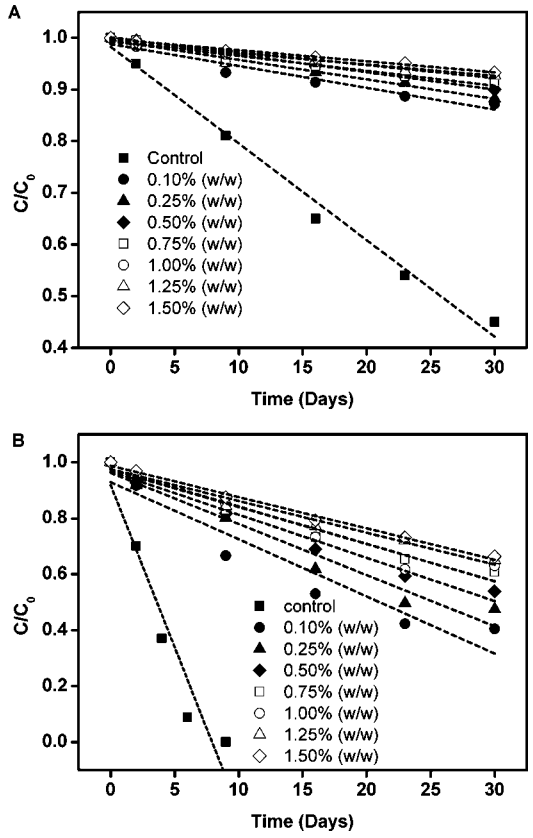

Figure 3. Kinetics of degradation of pure BC in ethyl acetate (as control) and BC loaded nanoparticles prepared with different concentrations of SC under 30 days storage at 4 °C (A) and 25 °C (B).

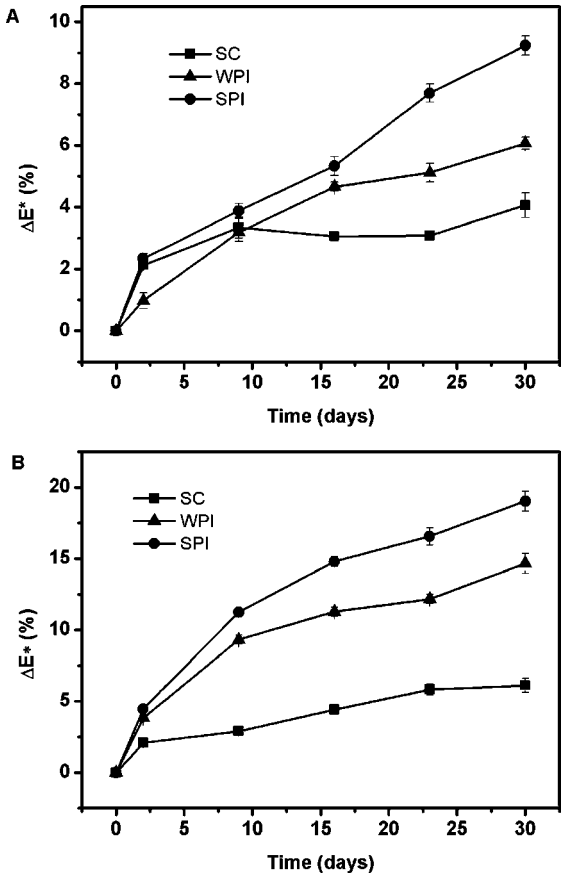

Figure 4. Influence of emulsifiers on total color evolutions (ΔE^*) during 30 days of storage of BC loaded nanoparticles under 4 °C (A) and 25 °C (B) (1.0% SC; 1.0% WPI; 1.0% SPI).

relationship between the carboxyl group content of ethylenediaminetetraacetic dianhydride (EDTAD)-modified SPI and metal-binding ability.

Casein, in excess, can form a thick interfacial layer around carrier oil droplets extending from 10 to 15 nm compared to 2−3 nm for whey proteins.[35] The greater thickness may reduce the interaction between BC and pro-oxidants in aqueous phase.

At low protein concentrations (0.1−1.0%, w/w), the BC lipid surface may not be fully covered by the emulsifier, and direct contact with metal ions, pro-oxidants, and dissolved oxygen may increase BC oxidation. Increasing the protein content (SC, WPI, SPI) in solution resulted in a decrease in the loss rate of BC (Table 2). Most likely, oxidation was initiated by dissolved oxygen during the high speed mixing step.

Impact of Emulsifiers on Total Color Change (ΔE^*). The color and appearance are important visual factors for food choice by consumers.[36] The apparent color of carotenoids varies (red/orange/yellow) with concentration, oxidation, and particle diameter. The lightness (L) of three BC nanoparticles increased during storage, an indicating the color fading and BC loss. The decrease of a value suggested the decrease of redness of BC nanoparticles, while the yellowness (b) increased with increasing storage (Supporting Information, Table 2S). The degree of total color change, as expressed by ΔE^*, with storage temperature was consistent with the decrease of BC. The color changes at 25 °C were greater than at 4 °C (Figure 4), and the order was SC < WPI < SPI at both temperatures. The BC loaded nanoparticles produced in this study had better physicochemical stability than those previously reported by Qian et al.[3] perhaps due to solid lipid cores which have been reported to have lower susceptibility to degradation than BC in solution.[37]

TEM of BC Loaded Nanoparticles. The shape of the BC nanoparticles stabilized by three proteins (SC, WPI, and SPI) was observed by transmission electron microscope (TEM). As shown in Figure 5, the three nanoparticles were spherically shaped and uniformly dispersed, suggesting BC was fully encapsulated by proteins. The TEM images of BC loaded nanoparticles prepared by the solvent displacement technique emulsified by gelatin and Tween 20[38] were also spherical.

Cell Toxicity of BC Loaded Nanoparticles. BC loaded nanoparticle toxicity was evaluated by the MTT assay which is a commonly used, sensitive colorimetric method to determine cell viability.[39] The cell viability was determined at different dilution times (DT) by the MTT assay (Figure 6). Pure β-carotene was used as a control. Pure β-carotene is insoluble in water, so β-carotene dissolved in THF/DMSO (1:1) was diluted in DMEM as control to study the toxicity of β-carotene. No cytoxicity was observed with Caco-2 cells treated with pure β-carotene at the same concentrations in nanoparticles. At DT = 0 (initial protein concentration = C_o =10 mg/mL), the cell viabilities treated with the three BC loaded nanoparticles were 84 ± 8% for SC, 80 ± 7% for WPI, and 83 ± 7% for SPI, respectively. The viabilities of Caco-2 cells when exposed to food protein (WPI and SPI) stabilized nanoemulsions at 3 mg/mL were about 85%,[15] which was similar to our finding. He et al.[15] also reported that the food proteins had a better biocompatibility, compared to egg phosphatidylcholine (EPC)

dx.doi.org/10.1021/jf404073c | J. Agric. Food Chem. 2014, 62, 1096−1104

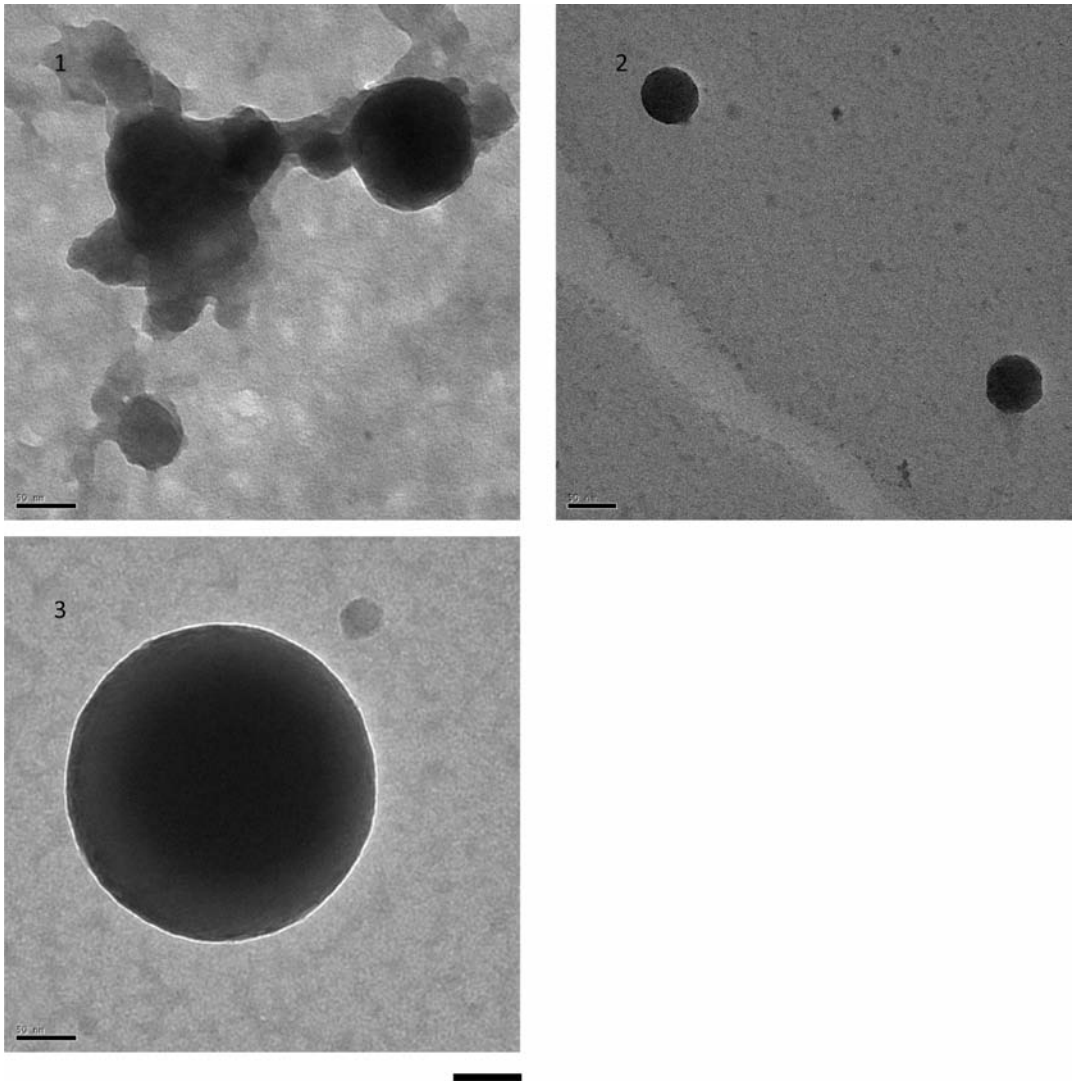

Figure 5. Transmission electron micrographs of BC loaded nanoparticles prepared with SC (1), WPI (2), and SPI (3), respectively, at a final concentration of 1% (w/w). Scale bar indicates 50 nm.

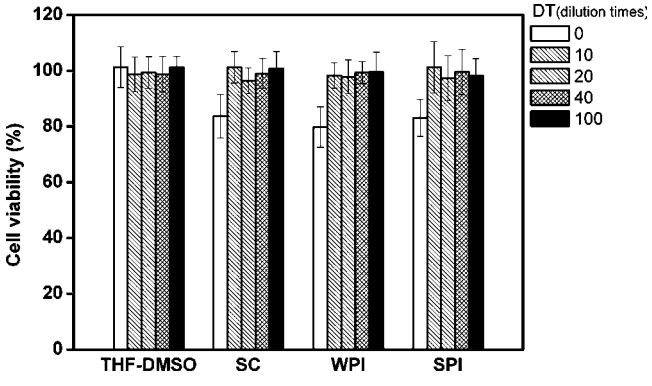

Figure 6. *In vitro* cytotoxicity of pure BC (as control) and three BC loaded nanoparticles at different dilution times (DT) on Caco-2 cells measured by MTT assay. Cell viability was expressed as mean ± STD (n = 3).

and other surfactants. In addition, at DT = 10 ($0.1 \times C_o$) or greater, all the cell viabilities were above 95% indicating that the BC loaded nanoparticles were nontoxic when the concentrations of protein emulsifiers were below 1 mg/mL. The results suggest that protein-based nanoparticles are biocompatible.

BC Loaded Nanoparticle Uptake *in Vitro*. Cellular accumulation of micellar BC was found to be proportional to up to 30 h of incubation time. A 24 h period was chosen for the uptake of BC nanoparticles with Caco-2 cells.[40] The rate and extent of nanoparticle uptake is determined by the properties of the particle, like, diameter, shape, charge, and interfacial characteristics. The uptake of BC loaded nanoparticles prepared by homogenization−solvent evaporation was greater than BC in THF/DMSO suspension (Figure 7). This was surprising since in both cases, BC nanoparticles versus BC suspension THF/DMSO at 5 μg/mL, BC was in solid form. However, BC in THF/DMSO may have precipitated in the crystalline form whereas BC in the nanoparticles, by X-ray diffraction, appears to be in an amorphous solid. We hypothesize that a mixture composed of residual lipids extracted by ethyl acetate from SC, WPI, and SPI prevented crystallization. The nanoparticles were also smaller in diameter. The cellular uptake of BC in THF/DMSO suspension was 264 ± 37 pmol/mg protein (Figure 7). While the uptake values of SC, WPI, and SPI BC loaded nanoparticles were 687 ± 69, 891 ± 142, and 452 ± 48 pmol/

dx.doi.org/10.1021/jf404073c | J. Agric. Food Chem. 2014, 62, 1096−1104

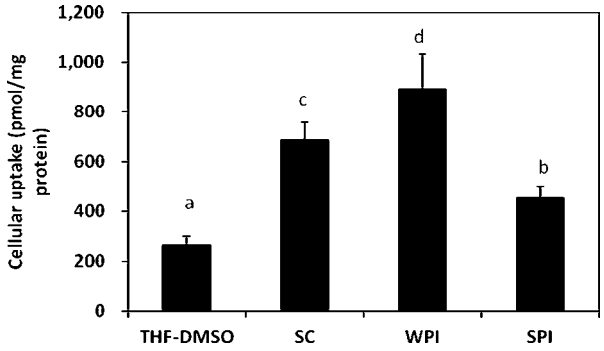

Figure 7. Uptake of BC by Caco-2 cells monolayers incubated with BC THF/DMSO suspension SC stabilized BC loaded nanoparticles, WPI stabilized BC loaded nanoparticles, and SPI stabilized BC loaded nanoparticles at BC concentration of 5 μg/mL. Values were expressed as mean ± STD (n = 3). Values with different letters (a–d) are significantly different ($p \leq 0.05$).

mg protein, respectively, which was a 2.6-, 3.4-, and 1.7-fold increase, respectively. The cellular uptake values among the three nanoparticles were significantly different ($P < 0.05$) and increased in the following order: SPI < SC < WPI. Differences in particle diameter of the BC core may be the main reason for differences in uptake. The BC core diameter is probably related to encapsulated nanoparticle diameter although there will be differences in the thickness of the adsorbed protein layers. However, the mean diameter of SPI encapsulated BC loaded nanoparticle was 372 ± 7 nm, and much larger than SC stabilized (77.8 ± 0.2 nm) or WPI stabilized BC loaded nanoparticles (89.7 ± 1.7 nm). Besides the increased surface area of smaller particles nanosized objects, the release properties of the lipid may be affected by its crystallinity and distribution within the particle.

Although transport by scavenger receptor SR-BI is believed to be the conventional means of BC absorption,[41] the literature also reports that nanosize droplets (d < 200 nm) may be directly transported across the epithelium cell layer by paracellular mechanism, passive diffusion or an "endocytosis" mechanism.[41,42] There was a significant negative correlation between BC uptake and the nanoparticles' negative surface charge (ζ-potential) ($P < 0.05$). ζ-Potential is influenced by ionic strength, and the measurements were made in 5 mM (pH 7.0) phosphate buffer while the concentration of the main sources of ions in cell culture media was about 150 mM. Therefore, our ζ-potential measurements may not be reliable although Dagliesh et al.[43] found that the ζ-potential for casein became more negative by only 1.5 mV going from 100 mM to 20 mM NaCl. Previous research has indicated that surface charge is an important factor in permeation of nanoparticles.[44] The surface of enterocytes (Caco-2 monolayers) is coated with a negatively charged mucin layer. The negative electrical charge of the surface of three protein encapsulated BC loaded nanoparticles may interact with the mucin layer through electrostatic repulsion, restricting the uptake of BC. The largest ζ-potential value of SPI nanoparticles also had the least BC uptake content. These results indicated that changing surface charge may be an effective method to improve cellular uptake.

In summary, our study shows that BC loaded nanoparticles can be prepared and stabilized by food grade proteins. The toxicity of nanoparticles appears to be low at about 10 mg BC/100 mL and insignificant when diluted 10 times or more. The evaporation method produced spherical solid BC cores probably mixed with residual protein lipids. The protein encapsulated nanoparticles had increased uptake of BC compared to BC in THF/DMSO suspension. Oxidative stability was highest in BC loaded nanoparticles stabilized by SC proteins due to the different interfacial characteristics at the droplet surface and the amino acid compositions. The intrinsic antioxidative capacity of proteins contributed to oxidative stability. This study contributes to interest in designing new delivery systems to increase stability and uptake of lipophilic nutrients in the food industry.

■ ASSOCIATED CONTENT

Supporting Information

Additional tables. This material is available free of charge via the Internet at http://pubs.acs.org.

■ AUTHOR INFORMATION

Corresponding Author

*Phone: +86-510-85197876. Fax: +86-510-85197876. E-mail: fzhong@jiangnan.edu.cn.

Funding

This work was financially supported by National 125 Program 2011BAD23B02, 2013AA1022207; NSFC 31171686; NSF-Jiangsu-BK2012556; 111 Project B07029 and PCSIRT0627.

Notes

The authors declare no competing financial interest.

■ ABBREVIATIONS USED

BC, β-carotene; SC, sodium caseinate; WPI, whey protein isolate; SPI, soy protein isolate; PDI, polydispersity index; MTT, 3-(4,5-dimethylthiazol-2-yl)-2,5-diphenyltetrazolium bromide; DMEM, the dulbecco's modified eagle medium; DMSO, dimethyl sulfoxide

■ REFERENCES

(1) Ziouzenkova, O.; Plutzky, J. Retinoid metabolism and nuclear receptor responses: New insights into coordinated regulation of the PPAR–RXR complex. *FEBS Lett.* **2008**, *582*, 32–38.

(2) Ono, K.; Yamada, M. Vitamin A and Alzheimer's disease. *Geriatr. Gerontol. Int.* **2012**, *12*, 180–188.

(3) Qian, C.; Decker, E. A.; Xiao, H.; McClements, D. J. Physical and chemical stability of β-carotene-enriched nanoemulsions: Influence of pH, ionic strength, temperature, and emulsifier type. *Food Chem.* **2012**, *132*, 1221–1229.

(4) McClements, D. J.; Decker, E. A.; Park, Y.; Weiss, J. Structural design principles for delivery of bioactive components in nutraceuticals and functional foods. *Crit. Rev. Food Sci. Nutr.* **2009**, *49*, 577–606.

(5) Yang, X.; Tian, H.; Ho, C.-T.; Huang, Q. Inhibition of citral degradation by oil-in-water nanoemulsions combined with antioxidants. *J. Agric. Food Chem.* **2011**, *59*, 6113–6119.

(6) Huang, Q.; Yu, H.; Ru, Q. Bioavailability and delivery of nutraceuticals using nanotechnology. *J. Food Sci.* **2010**, *75*, R50–R57.

(7) McClements, D. J. Edible nanoemulsions: Fabrication, properties, and functional performance. *Soft Matter* **2011**, *7*, 2297–2316.

(8) Liang, R.; Shoemaker, C. F.; Yang, X.; Zhong, F.; Huang, Q. Stability and bioaccessibility of β-carotene in nanoemulsions stabilized by modified starches. *J. Agric. Food Chem.* **2013**, *61*, 1249–1257.

(9) Boon, C. S.; McClements, D. J.; Weiss, J.; Decker, E. A. Factors influencing the chemical stability of carotenoids in foods. *Crit. Rev. Food. Sci. Nutr.* **2010**, *50*, 515–32.

(10) Tan, C.; Nakajima, M. [beta]-Carotene nanodispersions: preparation, characterization and stability evaluation. *Food Chem.* **2005**, *92*, 661–671.

(11) Yuan, Y.; Gao, Y.; Mao, L.; Zhao, J. Optimisation of conditions for the preparation of [beta]-carotene nanoemulsions using response surface methodology. *Food Chem.* **2008**, *107*, 1300−1306.
(12) Silva, H. D.; Cerqueira, M. A.; Souza, B. W. S.; Ribeiro, C.; Avides, M. C.; Quintas, M. A. C.; Coimbra, J. S. R.; Carneiro-da-Cunha, M. G.; Vicente, A. A. Nanoemulsions of beta-carotene using a high-energy emulsification-evaporation technique. *J. Food Eng.* **2011**, *102*, 130−135.
(13) Hu, M.; McClements, D. J.; Decker, E. A. Lipid oxidation in corn oil-in-water emulsions stabilized by casein, whey protein isolate, and soy protein isolate. *J. Agric. Food Chem.* **2003**, *51*, 1696−1700.
(14) Dickinson, E. Properties of emulsions stabilized with milk proteins: Overview of some recent developments. *J. Dairy Sci.* **1997**, *80*, 2607−2619.
(15) He, W.; Tan, Y.; Tian, Z.; Chen, L.; Hu, F.; Wu, W. Food protein-stabilized nanoemulsions as potential delivery systems for poorly water-soluble drugs: Preparation, in vitro characterization, and pharmacokinetics in rats. *Int. J. Nanomed.* **2011**, *6*, 521−533.
(16) Mao, L.; Xu, D.; Yang, J.; Yuan, F.; Gao, Y.; Zhao, J. Effects of small and large molecule emulsifiers on the characteristics of β-carotene nanoemulsions prepared by high pressure homogenization. *Food Technol. Biotechnol.* **2009**, *47*, 336−342.
(17) Singh, H. Aspects of milk-protein-stabilised emulsions. *Food Hydrocolloids* **2011**, *25*, 1938−1944.
(18) Conner, S. D.; Schmid, S. L. Regulated portals of entry into the cell. *Nature* **2003**, *422*, 37−44.
(19) Hu, B.; Ting, Y.; Zeng, X.; Huang, Q. Cellular uptake and cytotoxicity of chitosan−caseinophosphopeptides nanocomplexes loaded with epigallocatechin gallate. *Carbohydr. Polym.* **2012**, *89*, 362−370.
(20) Wu, W.; Zhang, C.; Kong, X.; Hua, Y. Oxidative modification of soy protein by peroxyl radicals. *Food Chem.* **2009**, *116*, 295−301.
(21) Altshuller, A. P.; Everson, H. E. The solubility of ethyl acetate in water. *J. Am. Chem. Soc.* **1953**, *75*, 1727−1727.
(22) Lee, S. J.; Choi, S. J.; Li, Y.; Decker, E. A.; McClements, D. J. Protein-stabilized nanoemulsions and emulsions: Comparison of physicochemical stability, lipid oxidation, and lipase digestibility. *J. Agric. Food Chem.* **2011**, *59*, 415−427.
(23) Chu, B. S.; Ichikawa, S.; Kanafusa, S.; Nakajima, M. Preparation and characterization of beta-carotene nanodispersions prepared by solvent displacement technique. *J. Agric. Food Chem.* **2007**, *55*, 6754−6760.
(24) Berridge, M. V.; Herst, P. M.; Tan, A. S., Tetrazolium dyes as tools in cell biology: New insights into their cellular reduction. In *Biotechnology Annual Review*; El-Gewely, M. R., Ed.; Elsevier: New York, 2005; Vol. *11*, pp 127−152.
(25) Sy, C.; Gleize, B.; Dangles, O.; Landrier, J.-F.; Veyrat, C. C.; Borel, P. Effects of physicochemical properties of carotenoids on their bioaccessibility, intestinal cell uptake, and blood and tissue concentrations. *Mol. Nutr. Food Res.* **2012**, *56*, 1385−1397.
(26) Walker, J. The bicinchoninic acid (BCA) assay for protein quantitation. In *The Protein Protocols Handbook*; Walker, J., Ed.; Humana Press: Totowa, NJ, 2009; pp 11−15.
(27) Yi, J.; Li, Y.; Zhong, F.; Yokoyama, W. The physicochemical stability and in vitro bioaccessibility of beta-carotene in oil-in-water sodium caseinate emulsions. *Food Hydrocolloids* **2014**, *35*, 19−27.
(28) Harrison, E. H. Mechanisms involved in the intestinal absorption of dietary vitamin A and provitamin A carotenoids. *Biochim. Biophys. Acta, Mol. Cell Biol. Lipids* **2012**, *1821*, 70−77.
(29) Lee, L.; Norton, I. T. Comparing droplet breakup for a high-pressure valve homogeniser and a microfluidizer for the potential production of food-grade nanoemulsions. *J. Food Eng.* **2013**, *114*, 158−163.
(30) Dickinson, E. Structure formation in casein-based gels, foams, and emulsions. *Colloids Surf., A* **2006**, *288*, 3−11.
(31) Cornacchia, L.; Roos, Y. H. Stability of β-carotene in protein-stabilized oil-in-water delivery systems. *J. Agric. Food Chem.* **2011**, *59*, 7013−7020.
(32) Gaucheron, F.; Famelart, M.-H.; Graët, Y. L. Iron-supplemented caseins: preparation, physicochemical characterization and stability. *J. Dairy Res.* **1996**, *63*, 233−243.
(33) Sugiarto, M.; Ye, A.; Singh, H. Characterisation of binding of iron to sodium caseinate and whey protein isolate. *Food Chem.* **2009**, *114*, 1007−1013.
(34) Hwang, D.-C.; Damodaran, S. Metal-chelating properties and biodegradability of an ethylenediaminetetraacetic acid dianhydride modified soy protein hydrogel. *J. Appl. Polym. Sci.* **1997**, *64*, 891−901.
(35) Dickinson, E. Proteins at interfaces and in emulsions stability, rheology and interactions. *J. Chem. Soc., Faraday Trans.* **1998**, *94*, 1657−1669.
(36) Barbut, S. Effect of retail lights on acceptability of salami. *Meat Sci.* **2004**, *66*, 219−223.
(37) Vásquez-Caicedo, A. L.; Heller, A.; Neidhart, S.; Carle, R. Chromoplast morphology and β-carotene accumulation during postharvest ripening of mango Cv. 'Tommy Atkins'. *J. Agric. Food Chem.* **2006**, *54*, 5769−5776.
(38) Ribeiro, H. S.; Chu, B. S.; Ichikawa, S.; Nakajima, M. Preparation of nanodispersions containing [beta]-carotene by solvent displacement method. *Food Hydrocolloids* **2008**, *22*, 12−17.
(39) Yu, H.; Huang, Q. Investigation of the cytotoxicity of food-grade nanoemulsions in Caco-2 cell monolayers and HepG2 cells. *Food Chem.* **2013**, *141*, 29−33.
(40) Garrett, D. A.; Failla, M. L.; Sarama, R. J.; Craft, N. Accumulation and retention of micellar β-carotene and lutein by Caco-2 human intestinal cells. *J. Nutr. Biochem.* **1999**, *10*, 573−581.
(41) Reboul, E.; Borel, P. Proteins involved in uptake, intracellular transport and basolateral secretion of fat-soluble vitamins and carotenoids by mammalian enterocytes. *Prog. Lipid Res.* **2011**, *50*, 388−402.
(42) McClements, D. J.; Xiao, H. Potential biological fate of ingested nanoemulsions: Influence of particle characteristics. *Food Funct.* **2012**, *3*, 202−220.
(43) Dalgleish, D. G. Measurement of electrophoretic mobilities and zeta-potentials of particles from milk using laser Doppler electrophoresis. *J. Dairy Res* **1984**, *51*, 425−438.
(44) Gåserød, O.; Jolliffe, I. G.; Hampson, F. C.; Dettmar, P. W.; Skjåk-Bræk, G. The enhancement of the bioadhesive properties of calcium alginate gel beads by coating with chitosan. *Int. J. Pharm.* **1998**, *175*, 237−246.

greater than 95%) and the rest of the reagents were provided by Sigma-Aldrich (St. Louis, MO).

Determination of the Fatty Acid Profile. *Sample Preparation.* The fatty acid profile was determinated by a gas chromatography procedure by methylation with cold methanolic solution of potassium hydroxide. In a 5 mL screw top test tube, 0.10 g of the HSO sample was weighed. A total of 3 mL of heptane and 500 μL of 2 N methanolic potassium hydroxide solution were added. The sample was shaken vigorously for 15 s, leaving it to stratify until the upper solution became clear. The upper layer containing the methyl esters was decanted.[23]

Chromatographic Conditions. The fatty acid methyl esters (FAMEs) were analyzed in a Hewlett-Packard 6890 gas chromatograph equipped with a flame ionization detector (FID), using a SP2380 silica capillary column (30 m × 0.32 mm internal diameter, 0.25 mm film). The initial column temperature was 165 °C, which was held for 10 min and programmed from 165 to 200 °C at 1.5 °C/min. The injector temperature was 210 °C, and the detector temperature was 250 °C. FAMEs were identified by retention time comparison to that of the corresponding standard peaks.

Unsaponifiable Extraction. The unsaponifiable matter of HSO was isolated following conventional procedures, and its components were analyzed following the International Union of Pure and Applied Chemistry (IUPAC) method.[24] A total of 5 g of HSO, 1 mL of internal standard (IS) solution (1 mg/mL α-colestanol and 0.5 mg/mL eicosanol in chroloform), and 50 mL of a 2 N potassium hydroxide solution in ethanol/water (80:20, v/v) were put into a 250 mL flask; saponification was carried out by boiling and stirring the sample for 1 h. After cooling, 100 mL of distilled water was added, and the sample was transferred to a separating funnel and extracted 3 times with 80 mL of ethyl ether. The ether extracts were pooled into a separating funnel (with 125 mL of distilled water) and washed with distilled water (125 mL each time), until the wash gave a neutral reaction. Then, the wash water was removed; the organic sample was dried with anhydrous sodium sulfate, filtered, and taken to dryness; and the residue was weighed.[25]

Separation of the Unsaponifiable Components. HSO unsaponifiable matter was by means of both flash and plate chromatography, providing fractions with superimposable profiles. Preparative thin-layer chromatography (TLC) was preferred over column chromatography because of its greater handiness and convenience of operation. The unsaponifiable fraction dissolved in chroloform was deposed on a 1 mm silica gel 60 F_{254} PLC plate, 20 × 20 (Merck, Darmstadt, Germany). The plate was placed into the developing chamber and eluted with hexane/diethyl ether (65:35, v/v). After development and solvent evaporation, the plate was developed with 2′,7′-dichlorofluorescein solution and important bands was evidenced.[25] The most important bands were scraped separately from the plate and extracted first with hot chloroform (10 mL) and then with ethyl ether (10 mL). The two solvent extracts were mixed and taken to dryness. The residue was finally dissolved and sylilated with 200 μL of a solution of pyridine−hexamethyldisilazane−trimethylchlorosilane to 15−30 mg of the insaponificables in glass-stoppered tubes.[20]

Chromatographic Conditions. Sterol and alcohol fractions were analyzed with a HP5890 Series II gas chromatograph (Boston, MA) equipped with a capillary column SPB5, 30 m length, 0.25 mm inner diameter, and 0.25 μm film thickness of poly(5% diphenyl/95% dimethyl siloxane) stationary phase. Carrier gas was hydrogen, with a head pressure of 110 kPa and 1:60 split ratio. The injector and detector temperature was 300 °C. The isotherm program to 255 °C was programmed to the sterol fraction for 30 min, and the oven temperature was programmed from 225 to 280 °C with a rate of 3 °C/min for the alcohol fraction for 50 min. The analysis was carried out following the amending Regulation (EC) 2568/91 on the characteristics of olive and the relevant method of analysis. The mass spectrometry (MS) analyses were performed using Kratos MS 80 mass spectrometer equipped with a NBSLIB2 data system. Scan time and mass range were 1 s and m/z 50−500, respectively. Fraction components were quantified by means of the ISs, and the total concentration in HSO was calculated as the sum of individual peak concentrations.

Determination of Hydrocarbon and Wax Contents. The wax esters, formed by the reaction of alcohols (aliphatic, triterpenic, methylsterols, and sterols) and free fatty acids, are present in seed and fruits. The usual procedure was followed by column chromatography. This method has been adopted by the European Union. A solution of lauryl arachinodate (0.1 mg/mL) and methyl heptadecanoate (0.1 mg/mL) in methanol was used as the IS. The wax esters eluted just before the triacylglycerols, thereby the addition of a colorant (Sudan I) with R_f similar to that of the triacylglycerols allows for visualization when the elution of wax esters ends. The fraction isolated contains also other minor components, such as the hydrocarbons. After isolation, this fraction was carried out by the gas chromatographic system (Agilent Technologies 6890N) equipped with an on-column injector and FID and using a short capillary-fused silica column (10 m) coated with 5% phenylmethylsilicone.[26]

Analysis of Tocopherols. The tocopherol content was analyzed by high-performance liquid chromatography (HPLC) in accordance with the IUPAC 2432 method.[27] A total of 1.5 g of HSO was dissolved in the solution (10 mL) of 0.5% isopropanol in *n*-hexane (mobile phase). The chromatographic separation was performed using a Perkin-Elmer liquid chromatograph equipped with an isocratic pump LC200 and an ultraviolet−visible (UV−vis) detector Lc295. A normal-phase column Lichrosphere Si60 (250 mm length, 4.6 mm inner diameter, and 5 μm particle size) was used with an injection volume of 20 μL and a flow rate of 1.0 mL/min. The absorbance was measured at 295 nm. The results were expressed as milligrams of tocopherol per 100 g of oil.

Statistical Analysis. All sample preparation and analyses of all of the classes of analytes (sterols, alcohols, hydrocarbons, waxes, fatty acids, phenols, and tocopherols) were performed in triplicate and were calculated with respect to respective ISs. Values are expressed as the mean, and standard error of the mean (SEM) is given. Each chromatogram is the most representative of three similar analyses.

RESULTS AND DISCUSSION

Industrial hemp is widely known to provide high-quality fibers and materials for textile, paper, or bio-building uses. Complementary products along with fibers should be taken into account in growing hemp because they might significantly enhance its competitiveness. The HSO and secondary metabolites, which can be found in the unsaponifiable fraction, are only some examples of potential complementary products that can be derived from industrial hemp.[28] The unsaponifiable fraction has received very little attention by researchers, despite the potential relevance that it may have in phytomedical technology, the discipline of studying the plant-derived pharmaceutical and nutraceutical compounds.[29]

In our analysis, the main fatty acids of HSO were linoleic acid (RT, 15.718), α- and γ-linolenic acids (RT, 18.223 and 18.323, respectively), and oleic acid (RT, 13.465), which together comprised 88% of the total fatty acids (Table 1). The fatty acid profile of HSO was similar to that reported in Canada[4,30] and for hemp cultivated in Europe with slightly higher linolenic acids.[31] The palmitic, stearic, and oleic acid contents of HSO were similar to those of evening primrose oil (EPO).[32] The PUFAs of the oil amounted to 76% of the total of fatty acids, while the monounsaturated and saturated fatty acids amounted to 12% each. The high amounts of α-linolenic acid (17%) may have favorable nutritional implications and beneficial physiological effects on the prevention of coronary heart disease and cancer.[33,34] The presence of γ-linolenic acid (3.4%) provides it with a high pharmaceutical value for degenerative chronic diseases.[35] The oil was characterized by a high polyunsaturated/saturated (P/S) ratio, which is regarded favorably for the

Table 1. Fatty Acid Profile (GC) in HSO

name	mean ± SEM (%)
palmitic acid (16:0)	5.62 ± 0.04
palmitoleic acid (16:1)	0.31 ± 0.02
estearic acid (18:0)	2.68 ± 0.12
oleic acid (18:1)	11.90 ± 0.35
linoleic acid (18:2, ω-6)	55.05 ± 0.47
eicosanoic acid (20:0)	2.50 ± 0.15
α-linolenic acid (18:3, ω-3)	16.70 ± 0.08
γ-linolenic acid (18:3, ω-6)	3.40 ± 0.12
eicosenoic acid (20:1)	1.44 ± 0.01
docosanoic acid (22:0)	0.40 ± 0.03
saturated fatty acids	11.20
monounsaturated fatty acids	13.34
polyunsaturated fatty acids	75.46
P/S ratio	6.7
ω-6/ω-3 ratio	3.5

Table 2. Amount of 4-Desmethylsterols (GC) in the Unsaponifiable Fraction from HSO

peak	retention time	name	mean ± SEM (mg/kg of oil)
1	7.824	colesterol	0.92 ± 0.03
2	8.362	α-colestanol (IS)	
3	9.298	24-methylene cholesterol	7.05 ± 0.14
4	10.310	campesterol	505.69 ± 32.04
5	10.811	estigmasterol	100.23 ± 7.47
6	11.499	clerosterol	58.39 ± 8.82
7	12.859	β-sitosterol	1905.07 ± 59.27
8	13.025	Δ_5-avenasterol	142.80 ± 7.68
9	13.384	Δ_5-24-estigmastadienol	31.97 ± 3.66
10	13.715	Δ_7-estigmasterol	21.74 ± 3.03
11	14.179	Δ_7-avenasterol	19.87 ± 2.18
total sterols			2793.73 ± 124.32

reduction of serum cholesterol and atherosclerosis and prevention of heart diseases.[36] Similarly, the ratio of ω-6/ω-3 fatty acids was 3.

On other hand, little effort has been expended to study other minor compounds present in HSO. The present work has isolated and characterized the different and interesting fractions from unsaponifiable HSO. A great amount of qualitative information was generated in every analysis. A yield (1.84−1.92%) of unsaponifiable matter was obtained.

Sterols were isolated from the HSO unsaponifiable matter and represented a 15.18% from this fraction. The identification of the different phytosterols has been made by gas chromatography (GC) and GC−MS comparing their relative retention time (RR_t) values and their MS fragments to literature values. Chromatographic analyses are shown in Figure 1 and Table 2. β-Sitosterol (1905.07 ± 59.27 mg/kg of oil) and campesterol (505.69 ± 32.04 mg/kg of oil) were predominant in the phytosterol fraction (2793.73 ± 124.32 mg/kg of oil). This proportion shows that EPO is twice as rich as olive oil in these natural products.[37] Plant sterols and stanols in fat matrices effectively lower low-density lipoprotein (LDL) cholesterol levels in hypercholesterolemic and diabetic patients and healthy human volunteers. Recent studies also show that dietary intake of plant sterols is related to a lower risk of myocardial infarction, lowering LDL cholesterol even when incorporated in non-fat matrices.[38] In addition, they may reduce biomarkers of oxidative stress and inflammation and modulate the atherosclerosis development.[20,39]

Another interesting fraction is the aliphatic alcohols.[40] Phytol (167.59 ± 1.81 mg/kg of oil) and geranylgeraniol (26.06 ± 0.08 mg/kg of oil) were predominant in the aliphatic alcohol fraction (226.94 ± 2.26 mg/kg of oil), and the abundant linear aliphatic alcohol was hexacosanol (16.17 ± 0.21 mg/kg of oil) (Figure 2 and Table 3). Chemical and nutritional studies have shown that mixtures of long-chain primary alcohols extracted from waxy materials from different sources, such as beeswax, rice bran, wheat germ, sugar cane, and grain sorghum, are able to exert several beneficial physiological effects, such as reducing platelet aggregation, endothelial damage, and cholesterol-lowering effects.[40,41] On the other hand, recent investigations

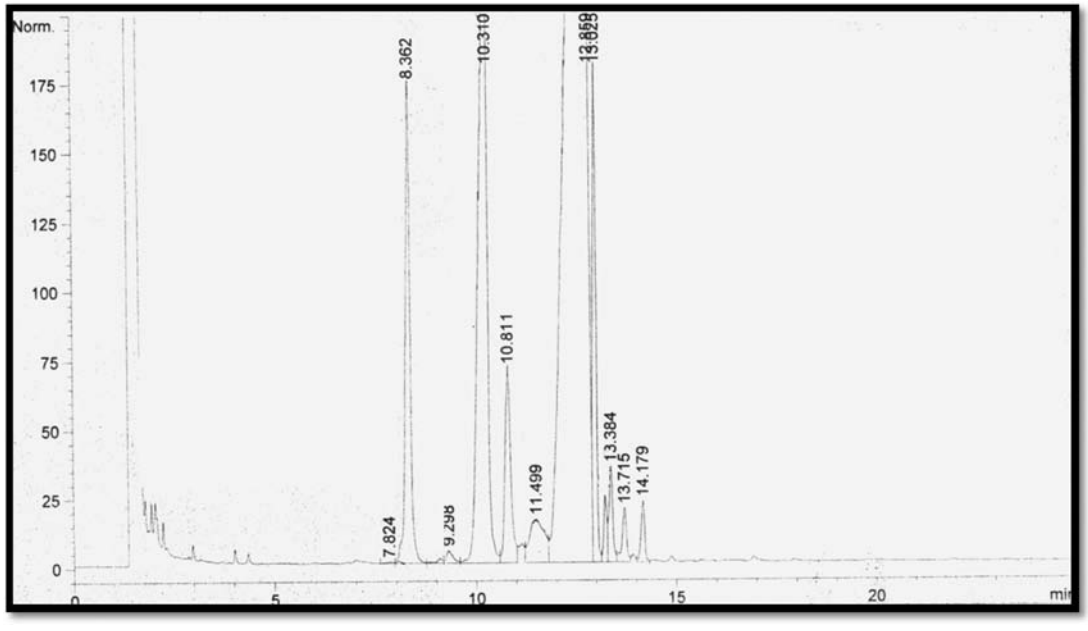

Figure 1. Gas chromatogram of the 4-desmethylsterol, erythrodiol, and uvaol fractions from unsaponifiable HSO.

dx.doi.org/10.1021/jf404278q | J. Agric. Food Chem. 2014, 62, 1105−1110

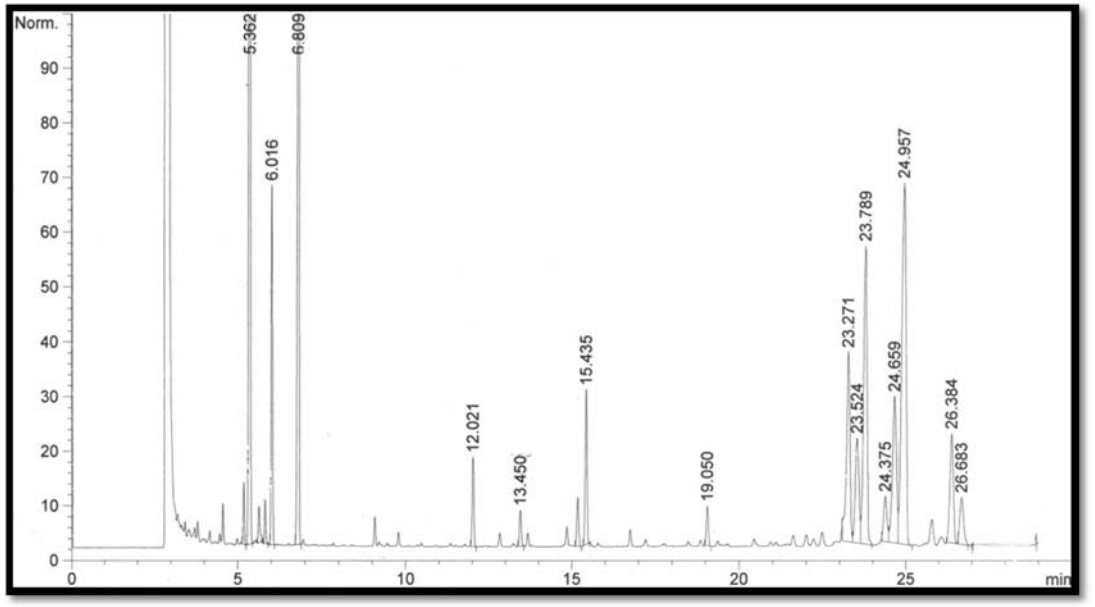

Figure 2. Gas chromatogram of linear aliphatic alcohol, triterpene alcohol, and 4-methylsterol fractions from unsaponifiable HSO.

Table 3. Amount of Linear Aliphatic Alcohols, Triterpene Alcohols, and 4-Methylsterols (GC) in the Unsaponifiable Fraction from HSO

peak	retention time	name	mean ± SEM (mg/kg of oil)
		Linear Aliphatic Alcohols	
1	5.362	phytol	167.59 ± 1.81
2	6.016	geranylgeraniol	26.06 ± 0.08
3	6.809	C_{20} (IS)	
4	12.021	C_{24}	8.78 ± 0.02
5	13.450	C_{25}	3.84 ± 0.06
6	15.435	C_{26}	16.17 ± 0.21
7	19.050	C_{28}	4.50 ± 0.08
total policosanols			226.94 ± 2.26
		Triterpene Alcohols	
8	23.271	dammaradienol	38.19 ± 1.07
9	23.524	taraxterol	22.18 ± 1.15
10	23.789	β-amirin	58.40 ± 2.03
11	24.375	butirospermol	8.97 ± 0.61
12	24.659	cycloeucalenol	34.03 ± 0.76
13	24.957	cycloartenol	90.55 ± 3.44
14	26.384	24-methylencycloartenol	21.75 ± 0.86
		4-Methylsterols	
15	26.683	citrostadienol	10.20 ± 0.42

performed by our group demonstrated that a similar linear alcohol fraction isolated from pomace olive oil (a byproduct of olive oil) has a protective effect on some mediators involved in the inflammatory damage development.[19] Phytol, a constituent of chlorophyll, is mainly found in human food, such as spinach, beans, raw vegetables, and asparagus, and has both anticancer and antioxidant actions.[42]

HSO did not prove be rich in squalene (Table 4), which had a presence of 80.52 mg/kg, if compared to other known plants rich in squalene (olive oil or *Amaranthus* oil).[43] The levels of saturated hydrocarbons were 451.77 ± 26.05 mg.

Tocopherols, another minor oil component, belong to a group of lipid-soluble compounds generally referred to as vitamin E, encompassing α-, β-, γ-, and δ-tocopherols. Because

Table 4. Amount of Squalene, Linear Hydrocarbons, and Waxes (GC) in the Unsaponifiable Fraction from HSO

name	mean ± SEM (mg/kg of oil)
squalene	80.52 ± 1.35
total linear hydrocarbons	451.77 ± 26.05
aliphatic waxes	0.98 ± 0.08
terpenic waxes	42.37 ± 0.61
total waxes	43.35 ± 0.69

of their ability to scavenge free radicals involving a tocopherol−tocopheryl semiquinone redox system, tocopherols are the most important natural antioxidants. Moreover, these compounds were shown to exhibit various beneficial effects on degenerative diseases, such as atherosclerosis, cardiovascular disease, Alzheimer's disease, or certain types of cancer.[44] The major tocopherol in HSO was the γ isomer at 91 ± 1.4% of the total tocopherol (Table 5). Similar results of γ-tocopherol,

Table 5. Tocopherol Contents in the Unsaponifiable Fraction from HSO (mg/100 g) by HPLC

name	mean ± SEM (mg/100 g of oil)
α-tocopherol	3.22 ± 0.65
β-tocopherol	0.81 ± 0.16
γ-tocopherol	73.38 ± 2.86
δ-tocopherol	2.87 ± 0.83
total tocopherols	80.28 ± 4.50

accounting for 90% of the total, have been reported for *C. ruderalis* L.[45] Concentrations of tocopherol isomers from HSO were in the range reported for hemp cultivars grown in Canada.[4] α-Tocopherol is considered to be the predominant antioxidant in olive oil, sunflower oil, and EPO, while γ-tocopherol prevails in rapeseed oil.[46−48]

This study is an important contribution for *C. sativa* L. valorization as a source of bioactive compounds. Finally, the extraction of high-value bioactive compounds can be perfectly integrated with the large-scale applications of hemp, contribu-

dx.doi.org/10.1021/jf404278q | J. Agric. Food Chem. 2014, 62, 1105−1110

ting to research novel applications in the food, pharmaceutical, cosmetic, and other non-food industries.

AUTHOR INFORMATION

Corresponding Author

*Telephone: +34659603457. E-mail: arche@us.es.

Notes

The authors declare no competing financial interest.

ACKNOWLEDGMENTS

We are grateful to Dr. Carmen Pérez-Camino (Department of Food Characterization and Analysis, Spanish National Research Council), who collaborated in the identified components in this study.

REFERENCES

(1) Pringle, H. Ice age community may be earliest known net hunters. *Science* **1997**, *277*, 1203−1204.

(2) Zias, J.; Stark, H.; Sellgman, J.; Levy, R.; Werker, E.; Breuer, A.; Mechoulam, R. Early medical use of cannabis. *Nature* **1993**, *363*, 215.

(3) Holler, J. M.; Bosy, T. Z.; Dunkley, C. S.; Levine, B.; Past, M. R.; Jacobs, A. Δ^9-tetrahydrocannabinol content of commercially available hemp products. *J. Anal. Toxicol.* **2008**, *32*, 428−432.

(4) Oomah, B. D.; Busson, M.; Godfrey, D. V.; Drover, J. C. G. Characteristics of hemp (*Cannabis sativa* L.) seed oil. *Food Chem.* **2002**, *76*, 33−43.

(5) Callaway, J. C. Hempseed as a nutritional resource: An overview. *Euphytica* **2004**, *140*, 65−72.

(6) de Padua, L. S.; Bunyaprafatsara, N.; Lemmens, R. H. M. J. *Plant Resources of South-East Asia: Medicinal and Poisonous Plants*; Backhuys Publishers: Leiden, Netherlands, 1999; Vol. *1*, No. 12, pp 167−175.

(7) Orhan, U. S.; kumenoglu, S.; Sener, B. GC−MS analysis of the seed oil of *Cannabis sativa* L. cultivated in Turkey. *J. Fac. Pharm. Gazi Univ.* **2000**, *17*, 79−81.

(8) Deferne, J. L.; Pate, D. W. Hemp seed oil: A source of valuable essential fatty acids. *J. Int. Hemp Assoc.* **1996**, *3*, 4−7.

(9) Yu, Y.; Cai, Z.; Zheng, J.; Chen, J.; Zhang, X.; Huang, X. F.; Li, D. Serum levels of polyunsaturated fatty acids are low in Chinese men with metabolic syndrome, whereas serum levels of saturated fatty acids, zinc, and magnesium are high. *Nutr. Res. (N. Y., NY, U. S.)* **2012**, *32*, 71−77.

(10) Scorletti, E.; Byrne, C. D. ω-3 fatty acids, hepatic lipid metabolism, and nonalcoholic fatty liver disease. *Annu. Rev. Nutr.* **2013**, *33*, 231−248.

(11) Prociuk, M. A.; Edel, A. L.; Richard, M. N.; Gavel, N. T.; Ander, B. P.; Dupasquier, C. M.; Pierce, G. N. Cholesterol-induced stimulation of platelet aggregation is prevented by a hempseed-enriched diet. *Can. J. Physiol. Pharmacol.* **2008**, *86*, 153−159.

(12) Schwab, U. S.; Callaway, J. C.; Erkkilä, A. T.; Gynther, J.; Uusitupa, M. I. J.; Järvinen, T. Effects of hempseed and flaxseed oil on the profile of serum lipids, serum total and lipoprotein lipid concentrations and haemostatic factors. *Eur. J. Nutr.* **2006**, *45*, 470−477.

(13) Kaul, N.; Kreml, R.; Austria, J. A.; Richard, M. N.; Edel, A. L.; Dibrov, E.; Hirono, S.; Zettler, M. E.; Pierce, G. N. A comparison of fish oil, flaxseed oil and hempseed oil supplementation on selected parameters of cardiovascular health in healthy volunteers. *J. Am. Coll. Nutr.* **2008**, *27*, 51−58.

(14) Al-Khalifa, A.; Maddaford, T. G.; Chahine, M. N.; Austria, J. A.; Edel, A. L.; Richard, M. N.; Ander, B. P.; Gavel, N.; Kopilas, M.; Ganguly, R.; Ganguly, P. K.; Pierce, G. N. Effect of dietary hempseed intake on cardiac ischemia-reperfusion injury. *Am. J. Physiol.: Regul., Integr. Comp. Physiol.* **2007**, *292*, R1198−R1203.

(15) Richard, M. N.; Ganguly, R.; Steigerwald, S. N.; Al-Khalifa, A.; Pierce, G. N. Dietary hempseed reduces platelet aggregation. *J. Thromb. Haemostasis* **2007**, *5*, 424−425.

(16) Li, Y.; Yang, R.; Hu, X.; Long, Z.; et al. Initial study of Hemp seeds protein on antifatigue and the immunomodulation effects in mice. *Wei Sheng Yan Jiu* **2008**, *37*, 175−178 (in Chinese).

(17) Callaway, J.; Schwab, U.; Harvima, I.; Halonen, P.; Mykkänen, O.; Hyvönen, P.; Järvinen, T. Efficacy of dietary hempseed oil in patients with atopic dermatitis. *J. Dermatol. Treat.* **2005**, *16*, 87−94.

(18) Anwar, F.; Latif, S.; Ashraf, M. Analytical characterization of Hemp (*Cannabis sativa*) seed oil from different agro-eocological zones of Pakistan. *J. Am. Oil Chem. Soc.* **2006**, *83*, 323−329.

(19) Fernandez-Arche, A.; Marquez-Martin, A.; De la Puerta-Vazquez, R.; Perona, J. S.; Terencio, C.; Perez-Camino, C.; Ruiz-Gutierrez, V. Long-chain fatty alcohols from pomace olive oil modulate the release of proinflammatory mediators. *J. Nutr. Biochem.* **2009**, *20*, 155−162.

(20) Montserrat-de la Paz, S.; Fernandez-Arche, M. A.; Angel-Martin, M.; Garcia-Gimenez, M. D. The sterols isolated from evening primrose oil modulate the release of proinflammatory mediators. *Phytomedicine* **2012**, *19*, 1072−1076.

(21) Ramos, P. A. B.; Guerra, A. R.; Guerreiro, O.; Freire, C. S. R.; Silva, A. M. S.; Duarte, M. F.; Silvestre, A. J. D. Lipophilic extracts of *Cynara cardunculus* L. var. *altilis* (DC): A source of valuable bioactive terpenic compounds. *J. Agric. Food Chem.* **2013**, *61*, 8420−8429.

(22) Montserrat-de la Paz, S.; Garcia-Gimenez, M. D.; Angel-Martin, M.; Pérez-Camino, M. C.; Fernandez-Arche, M. A. Long-chain fatty alcohols from evening primrose oil inhibit the inflammatory response in murine peritoneal macrophages. *J. Ethnopharm.* **2014**, *151*, 131−136.

(23) Cert, A.; Moreda, W.; Perez-Camino, M. C. Methods of preparation of fatty acid methyl esters (FAME). Statistical assessment of the precision characteristics from a collaborative trials. *Grasas Aceites (Sevilla, Spain)* **2000**, *6*, 447−456.

(24) International Union of Pure and Applied Chemistry (IUPAC). Determination of the unsaponifiable matter. Method 2401. In *Standard Methods for the Analysis of Oils, Fats and Derivatives*, 7th ed.; Paquot, C., Hautfenne, A., Eds.; Blackwell: Oxford, U.K., 1992.

(25) Caligiani, A.; Bonzanini, F.; Palla, G.; Cirlini, M.; Bruni, R. Characterization of a potential nutraceutical ingredient: Pomegranate (*Punica granatum* L.) seed oil unsaponifiable fraction. *Plant Foods Hum. Nutr.* **2010**, *65*, 277−283.

(26) Cert, A.; Moreda, W.; Perez-Camino, M. C. Chromatographic analysis of minor constituents in vegetable oils. *J. Chromatogr., A* **2000**, *881*, 131−148.

(27) International Union of Pure and Applied Chemistry (IUPAC). Determination of tocopherols and tocotrienols in vegetable oils and fats by HPLC. Method 2432. In *Standard Methods for the Analysis of Oils, Fats and Derivatives*, 7th ed.; Paquot, C., Hautfenne, A., Eds.; Blackwell: Oxford, U.K., 1992.

(28) Ranalli, P.; Venturi, G. Hemp as a raw material for industrial applications. *Euphytica* **2004**, *140*, 1−6.

(29) Nissen, L.; Zatta, A.; Stefanini, I.; Grandi, S.; Sgorbati, B.; Biavati, B.; Monti, A. Characterization and antimicrobial activity of essential oils of industrial hemp varieties (*Cannabis sativa* L.). *Fitoterapia* **2010**, *81*, 413−419.

(30) Blade, S. F. Industria hemp in Alberta. In *Alberta Hemp Symposia Proceedings*; Blade, S., Ed.; Alberta Agriculture, Food and Rural Development: Red Deer, Alberta, Canada, 1998; pp 2−11.

(31) Theimer, R. R.; Molleken, H. Analysis of the oils from different hemp (*Cannabis sativa* L.) cultivars—Perspective for economic utilization. In *Bioresource Hemp*, 2nd ed.; Nova Institute: Cologne, Germany, 1995; pp 536−545.

(32) Montserrat-de la Paz, S.; Fernández-Arche, M. A.; Ángel-Martín, M.; García-Giménez, M. D. Phytochemical characterization of potential nutraceutical ingredients from evening primrose oil (*Oenothera biennis* L.). *Phytochem. Lett.* **2014**, DOI: 10.1016/j.phytol.2013.08.008.

(33) Arshad, A.; Al-Leswas, D.; Stephenson, J.; Metcalfe, M.; Dennison, A. Potential applications of fish oils rich in ω-3 fatty acids in the palliative treatment of advanced pancreatic cáncer. *Br. J. Nutr.* **2011**, *106*, 795−800.

(34) Fretts, A. M.; Mozaffarian, D.; Siscovick, D. S.; Heckbert, S. R.; McKnight, B.; King, I. B.; Rimm, E. B.; Psaty, B. M.; Sacks, F. M.; Song, X.; Spiegelman, D.; Lemaitre, R. N. Associations of plasma phospholipid and dietary α-linolenic acid with incident atrial fibrillation in older adults: The cardiovascular health study. *J. Am. Heart Assoc.* **2013**, *2*, No. e003814.
(35) Montserrat-de la Paz, S.; García-Giménez, M. D.; Ángel-Martín, M.; Marin-Aguilar, F.; Fernández-Arche, M. A. Dietary supplementation evening primrose oil improve symptoms of fybromyalgia syndrome. *J. Funct. Foods* **2013**, *5*, 1279−1287.
(36) Reena, M. B.; Lokesh, B. R. Hypolipidemic effect of oils with balanced amounts of fatty acids obtained by blending and interesterification of coconut oil with rice bran oil or sesame oil. *J. Agric. Food Chem.* **2007**, *55*, 10461−10469.
(37) Weihrauch, J. L.; Gardner, J. M. Sterol content of foods of plant origin. *J. Am. Diet. Assoc.* **1978**, *73*, 39−47.
(38) Klingberg, S.; Ellegård, L.; Johansson, I.; Jansson, J. H.; Hallmans, G.; Winkvist, A. Dietary intake of naturally occurring plant sterols is related to a lower risk of a first myocardial infarction in men but not in women in northern Sweden. *J. Nutr.* **2013**, *143*, 1630−1635.
(39) Lou-Bonafonte, J. M.; Arnal, C.; Navarro, M. A.; Osada, J. Efficacy of bioactive compounds from extra virgin olive oil to modulate atherosclerosis development. *Mol. Nutr. Food Res.* **2012**, *56*, 1043−1057.
(40) Seo, W. D.; Yuk, H. J.; Curtis-Long, M. J.; Jang, K. C.; Lee, J. H.; Han, S. I.; Kang, H. W.; Nam, M. H.; Lee, S. J.; Lee, J. H.; Park, K. H. Effect of the growth stage and cultivar on policosanol profiles of barley sprouts and their adenosine 5′-monophosphate-activated protein kinase activation. *J. Agric. Food Chem.* **2013**, *61*, 1117−23.
(41) Martino, F.; Puddu, P. E.; Pannarale, G.; Colantoni, C.; Martino, E.; Niglio, T.; Zanoni, C.; Barillà, F. Low dose chromium-polynicotinate or policosanol is effective in hypercholesterolemic children only in combination with glucomannan. *Atherosclerosis* **2013**, *228*, 198−202.
(42) Vetter, W.; Schröder, M.; Lehnert, K. Differentiation of refined and virgin edible oils by means of the *trans*- and *cis*-phytol isomer distribution. *J. Agric. Food Chem.* **2012**, *60*, 6103−6107.
(43) Ostlund, R. E. M.; Racette, S. B.; Stenson, W. F. Effect of trace components of dietary fat on cholesterol metabolism: Phytosterols, oxysterols and squalene. *Nutr. Rev.* **2002**, *60*, 349−359.
(44) Fromm, M.; Bayha, S.; Kammerer, D. R.; Carle, R. Identification and quantitation of carotenoids and tocopherols in seed oils recovered from different Rosaceae species. *J. Agric. Food Chem.* **2012**, *60*, 10733−10742.
(45) Ivanov, S. A.; Aitzetmuller, K. Tocopherol and tocotrienol composition of the seed lipids of a number of species representing the Bulgarian flora. *Fett/Lipid* **1998**, *100*, 348−352.
(46) Velasco, J.; Andersen, M. L.; Skibsted, L. H. Electron spin resonance spin trapping for analysis of lipid oxidation in oils: Inhibiting effect of the spin trap α-phenyl-*N*-*tert*-butylnitrone on lipid oxidation. *J. Agric. Food Chem.* **2005**, *53*, 1328−1336.
(47) Blekas, G.; Tsimidou, M.; Boskou, D. Contribution of atocopherol to olive oil stability. *Food Chem.* **1995**, *52*, 289−294.
(48) Koski, A.; Psomiadou, E.; Tsimidou, M.; Hopia, A.; Kefalas, P.; Wahala, K.; Heinonen, M. Oxidative stability and minor constituents of virgin olive oil and cold-pressed rapeseed oil. *Eur. Food Res. Technol.* **2002**, *214*, 294−298.

Hydrolysis of methyl ester groups from the pectin backbone by PME can occur via three different mechanisms.[16,17] The first mechanism involves a multiple chain reaction, in which PME removes one methyl ester from the pectin chain and then dissociates from the substrate, resulting in random deesterification of the chain. This is typically the mode of action of acidic fungal PME.[16,18] The second mechanism is single chain, or linear, deesterification, where PME follows along one chain and cleaves all the methoxyl groups, which results in blocks of demethylated pectin. This is generally the mode of deesterification for higher plant PME.[16,18] This would suggest that carrot PME also employs linear deesterification, although no research to date has confirmed this. The third mechanism involves multiple attacks of the enzyme on methyl esters, where only a limited number of methyl groups are removed from each pectin substrate. The mechanism by which carrot PME catalyzes deesterification of carrot pectin has not yet been determined.

Carrot Juice Cloud Stability. The rate of juice clarification is governed by two mechanisms: flocculation and sedimentation. Flocculation is the phenomenon in which particles cluster together to form aggregates, increasing the effective particle size. Sedimentation is the settling out of flocculated particles from suspension to the bottom of the container. Typically, flocculation leads to faster sedimentation in accordance with Stokes' Law. Larger particles formed from flocculation increase the rate of sedimentation and, hence, cause more rapid loss of cloud stability.

If particle size influences the rate of cloud loss and clarification, then it is worthwhile exploring how particle size increases within juices over storage time. In a suspension, particles remain separate from one another due to the presence of an energy barrier between them, which reduces their rate of collision. The energy barrier is influenced by several different contributions, including attractive van der Waals interactions (which reduce the barrier) and repulsive electrostatic forces (which increases it).[19−22] Factors that lower the energy barrier make it more likely that cloud particles will closely approach one another, at which point they can "stick" to each other and floc as a result of short-range attraction.

In juices with active enzymes, PME cleaves methoxyl groups from the pectin backbone and additional negatively charged residues are exposed. These like-charged residues would normally enhance the repulsive interparticle energy barrier; however, naturally present divalent cations such as calcium may bind to these sites, creating electrostatic attractive interactions between particles. The calcium can then cross-link pectin chains on different particles together, thereby forming insoluble calcium pectate within aggregates that are large enough to sediment out according to Stokes' Law.[1,17,20,23]

Little research has been conducted regarding the effect that residual PME levels have on cloud stability of carrot juice, which is a low-acid juice product. Therefore, the goal of this study was to observe the effects of adding PME to pasteurized carrot juice and suggest a mechanism for cloud flocculation and sedimentation.

MATERIALS AND METHODS

Material Sourcing. Sugarsnax variety carrots (*Daucus carota* L. ssp. sativa cv. 'Sugarsnax') were used to make the PME extraction, and were sourced from Bolthouse Farms in Bakersfield, CA. The average PME activity in raw carrot juice made from these carrots was found to be 0.43 U/g (range: 0.218−0.806 U/g), as measured by individually juicing 30 Sugarsnax carrots on a benchtop juicer. Commercial pasteurized Bolthouse carrot juice (pH 6.20) was purchased from a local grocery store. All containers of purchased juice were mixed together to ensure a uniform starting material. The PME activity of the commercial juice was found to be less than 5% of the average carrot juice PME.

Reagents. Sodium chloride, monobasic monohydrate sodium phosphate, dibasic anhydrous sodium phosphate, citric acid monohydrate, sodium citrate, hydrochloric acid, sodium hydroxide, sulfamic acid, and ferric ammonium sulfate were obtained from Fisher Scientific (Fair Lawn, NJ). Trizma base, Trizma hydrochloride, citrus pectin, Bradford Reagent, lauryl sulfate, bovine serum albumin (BSA), Fluoral-P, alcohol oxidase, and 3-methyl-2-benzothiazolinone hydrazine hydrochloride hydrate were obtained from Sigma Aldrich Co. (St. Louis, MO). Micro Bio-Spin desalting columns were obtained from Bio Rad (Hercules, CA), and membrane tubing was sourced from Spectrum Medical Industries, Inc. (Houston, TX). Deionized distilled water was used in all experiments.

PME Preparation and Characterization. *PME Extraction.* PME added to commercial carrot juice was prepared from an extraction of raw carrots based on the method of Ly-Nguyen et al.[24] A sample of 600−700 g of washed carrots was homogenized with 600 mL deionized water in a Vita-Mix blender set on high for 2 min (Model VM0101D, Vita-Mix Co., Cleveland, OH). The homogenate was filtered through four layers of cheesecloth, and the filtrate was discarded. The pellet was washed four times with 1 L deionized water to ensure the removal of color and organic compounds. The pellet was then mixed with 1:4 (w/v) 0.2 M Tris and 1 M NaCl (pH 8.0) for 30 min to extract PME into the supernatant, and the carrot slurry was filtered through four layers of cheesecloth. The supernatant was collected and the pellet discarded.

The supernatant was stirred with 30% ammonium sulfate for 30 min as a purification step to precipitate large proteins that were not PME. This mixture was then centrifuged at 18 000*g* for 15 min at 20 °C in a Sorvall centrifuge (Model RC5C, DuPont, Wilmington, DE). After centrifugation, the pellet was discarded and the supernatant was vacuum filtered (Whatman #4) to remove any remaining large particles.

To precipitate the PME enzyme, 80% ammonium sulfate was slowly mixed into the supernatant. The mixture was stirred for 30 min, and then centrifuged at 18 000*g* for 15 min at 20 °C. The supernatant was discarded, and the PME precipitate that collected on the side of the centrifuge tubes was redissolved in 0.05 M citric acid/sodium citrate buffer (pH 6.5). The redissolved PME was then dialyzed in membrane tubing (MWCO 3500) in the citric acid/sodium citrate buffer in two stages. In the first stage, PME was dialyzed for 1 h at 4 °C, during which time highly concentrated molecules such as salts rapidly diffuse into the surrounding buffer and slow further diffusion. Therefore, for the second stage, fresh buffer solution was added to allow for continuous rapid diffusion, and the PME was dialyzed overnight at 4 °C. Once dialysis was complete, the PME, suspended in buffer, was stored in 1 mL aliquots at −20 °C.

The specific activity of three sample replicates from the extraction was measured by the PME assay and Bradford protein determination, and these three activity values were averaged to obtain the specific activity of that batch of PME extract. This concentrated PME preparation had an activity of 116 U/mL, and a specific activity of 123 U/mg protein.

Bradford Protein Determination. The Bradford protein assay was based on the method described in the Technical Bulletin of the Bradford Reagent by Sigma-Aldrich.[25] The procedure was modified so that only one-third of the assay volume was used, in order to cut down on hazardous waste. Therefore, 0.33 mL of samples and standards was added to 1 mL Bradford reagent, and the solution was incubated at room temperature (25 °C) for 5−10 min and then measured at 595 nm in a Shimadzu spectrophotometer (Columbia, MD).

PME Assay. PME activity was determined based on the assay developed by Anthon and Barrett (2004), in which a crude extract of PME from carrot juice was added to a standard amount of pectin.[26] The methanol produced in this reaction was used to quantify the

amount of enzyme activity and, hence, the amount of enzyme present in the sample. Pectin used in the assay was dialyzed overnight in water. Assays were started by adding 5 μL of a 10-fold dilution of the carrot juice to 95 mL of the assay medium, which contained 3 mg/mL pectin and had a pH of 7.5. All samples were placed into a 30 °C water bath, and at four time points (40, 70, 100, and 130 min) after the start of the assay, 0.1 mL aliquots were removed and added to 0.1 mL of a solution containing 5 mg/mL of each ferric ammonium sulfate and sulfamic acid. After 30 min at room temperature, 0.8 mL of water was added and absorbance at 620 nm was determined using a Shimadzu spectrophotometer (Columbia, MD). Methanol concentrations were determined from a separate methanol standard curve. The amount of methanol formed was plotted and the activity was calculated from the slope of the plot.

Cloud Stability during Juice Storage. *PME Addition.* The PME extract, made as described above, was added to commercial carrot juice in 5 quantities, 0, 0.15, 0.25, 0.5, and 1 U/g, where a unit of enzyme activity (U) is defined as the number of micromoles of methanol produced in 1 min, and grams refers to the mass of carrot juice. Since different volumes of PME extract (enzyme suspended in 0.05 M citric acid/sodium citrate buffer) were added to the juice to achieve different enzyme levels, it was necessary to compensate for the subsequent changes in juice volume. The largest volume of extract added (for addition of 1 U/g) was used as a baseline, and the other samples had a combination of enzyme extract and citric acid/sodium citrate buffer added so that all samples had the same final volume. This was done to ensure each juice was diluted the same small amount and any effects of the buffer were mitigated. Final juice pH after PME addition was 6.20. To prevent microbial growth during the storage study, 0.2% sodium azide was added to the juice. Juices were stored for up to 56 days at 5 °C.

Relative Sediment Height. Relative sediment height, also known as the sedimentation test, is a measure of the quantity of visible settling that occurs in the juice.[21,27] It is the height ($H_{sediment}$) of the cloud sediment divided by the total height (H_{total}) of the juice in a vial.

Samples used for measuring the relative sediment height of the sediment were placed in 7 mL glass vials with screw caps and allowed to remain undisturbed except for gentle transportation of the vials from the refrigerator to the laboratory bench for measurements. A caliper was used to make height measurements in triplicate.

Relative Turbidity. Relative turbidity is a spectrophotometric method to determine cloud stability by comparing the turbidity in a juice sample before and after centrifugation.[21,22,28−30] For the carrot juices examined here, absorbance at 660 nm was used as the measure of juice turbidity. At this wavelength, absorbance is predominantly determined by the scattering due to the particles, rather than specific chemical absorption.[31] Relative turbidities were determined by measuring the absorbance values for the whole juice and for the supernatants obtained after centrifugation (4200*g*, 15 min, 20 °C). When absorbance values measured in standard 1 cm cuvettes were unacceptably high, shorter path length cuvettes (0.5 mm for whole juice and 5.0 mm for juice supernatants) were used. Turbidity (τ) was calculated as the absorbance divided by the path length used for measurement. Relative turbidities (expressed as %) were calculated as $\tau_{serum}/\tau_{total} \times 100$.

Particle Size Determination. Static light scattering was used to measure average particle size.[21,28,30,32−34] A laser is passed through the sample and, upon hitting a particle, diffracts and creates a light pattern against the detector that depends on the particle size. Measurements were performed using a Microtrac S3500 (Montgomeryville, PA). Results were obtained as the volume fraction of particles contained within a discrete size range (bin). The mean diameter was determined as a volume average:

$$D_{4,3} = \frac{\sum (n_I d_I^4)}{\sum (n_I d_I^3)} \quad (1)$$

Here $D_{4,3}$ is the volume mean diameter, n_i is the number of particles in bin *i*, and d_i is their diameter. Carrot juice was inverted gently 10 times to ensure even distribution of particles and then added to the instrument sample port, which was operated at a flow rate of 15% of maximum. Particles were assumed to be irregular in shape and absorbing, and a refractive index value for water of 1.333 was used. Three replicates were measured for each sample.

RESULTS

Effect of Added PME on Cloud Stability. It is generally understood that PME impacts juice cloud stability, but the time frame over which destabilization occurs and the impact of the amount of active enzyme is not known, nor is the mechanism of cloud destabilization by PME well understood. Therefore, a storage study was conducted that examined the effects of different quantities of added enzyme on the cloud stability of commercial carrot juice. Commercial pasteurized carrot juice was preferred as the starting material for these studies, rather than raw unpasteurized juice made in the laboratory, because of the former's uniform particle content and minimal active PME (see Material Sourcing in Materials and Methods). Starting with juice that lacked any PME, then adding known amounts of a partially purified carrot PME, juices with different known levels of PME activity could be obtained. The levels of PME added (0.15, 0.25, 0.5, and 1.0 U/g) were based on the level of endogenous PME measured in raw Sugarsnax carrot juice made with a benchtop juicer. This level varied widely across the juice from individual carrots, even within carrots planted and harvested at the same time and grown in the same field. For 30 individually measured carrots, the PME activity of the juice ranged from 0.218 to 0.806 U/g, with an average of 0.43 U/g.

Cloud stability was measured via relative turbidity ($\tau_{serum}/\tau_{total}$), which has been used previously by others as a method sensitive to the extent of flocculation within the cloud.[21,28,29] Flocculation creates larger particles within the suspension, which are removed more effectively by centrifugation, and leave behind a serum with a lower particle concentration and lower turbidity. Thus, smaller values of $\tau_{serum}/\tau_{total}$ indicate that more flocculation has occurred. As shown in Figure 1, at all levels of

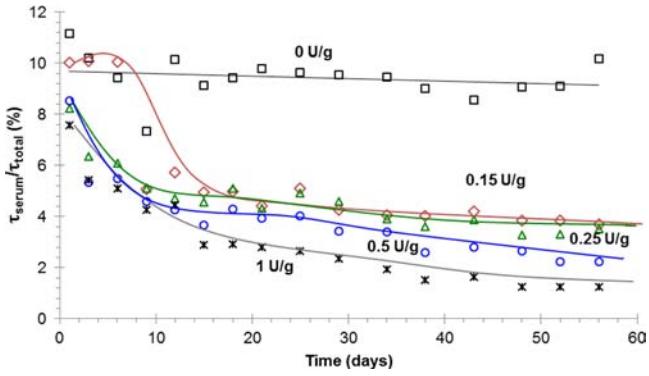

Figure 1. Relative turbidity ($\tau_{serum}/\tau_{total}$, %) of carrot samples with 0 (□), 0.15 (◇), 0.25 (△), 0.5 (○), and 1.0 (∗) U/g of added PME enzyme over the course of 56 days of storage.

added PME the cloud was less stable than in the control juice with no added enzyme. The relative turbidity of the control sample remained consistently high throughout storage, while those samples with added PME showed a large degree of clarification after centrifugation (Figure 1).When the amount of added PME was at or above 0.25 U/g, there was an inverse relationship at the 90% confidence level between the level of PME addition and the relative turbidity of the cloud at periods longer than 15 days.

dx.doi.org/10.1021/jf4043979 | J. Agric. Food Chem. 2014, 62, 1111−1118

Loss of cloud stability and juice clarification was also monitored by measuring relative sediment height ($H_{sediment}/H_{total}$). Consistent with the results for relative turbidity, much less clarification occurred in the control than in the enzyme-treated samples (Figure 2). However, the relative sediment height of the control juice increased slowly over the course of the storage period, indicating that there was natural settling occurring within the juice that is not attributable to PME activity.

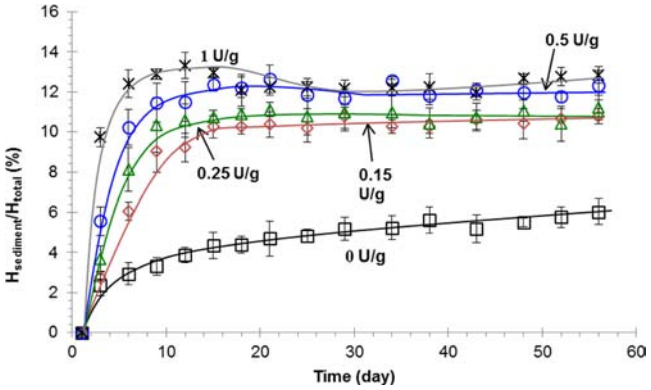

Figure 2. Relative sediment height ($H_{sediment}/H_{total}$, %) of carrot samples with 0 (□), 0.15 (◇), 0.25 (△), 0.5 (○) and 1.0 (∗) U/g of added PME over the course of 56 days of storage at 5 °C.

All samples containing active PME had an initial period (~10 d) of rapid sedimentation, after which the sediment height leveled off (Figure 2). The kinetics of this process can be represented using the empirical formula

$$\frac{H_{sediment}}{H_{total}} = \frac{t^2 H_\infty}{t^2 + T_o^2} \quad (2)$$

where t is time, H_∞ is the steady-state dimensionless plateau height, and T_o is a characteristic time of the initial, rapid sedimentation period. H_∞ and T_o could thus be obtained by a fit of eq 2 to the data in Figure 2; results for these two fit parameters are given in Table 1.

Table 1. Sediment Plateau Height and Time of Initial Height Increase From Eq 2, for the Four Levels of Added PME Enzyme

			quality of fit	
enzyme added (U/g)	H_∞ plateau height (%)	T_o (days)	R^2	χ^2
0	-	-	-	-
0.15	11	4.9	0.99	1.3
0.25	11	3.9	0.98	0.80
0.50	13	3.2	0.98	1.2
1.00	13	2.1	0.92	2.1

Carrot juice with greater amounts of added enzyme became unstable more quickly during storage, as shown by the number of days (T_o) it took for the initial rapid sedimentation period to occur (Table 1). With added enzyme, just a few days were needed for the cloud to separate visually into a sediment layer with approximately steady thickness. The thickness of that sediment layer increased slightly but significantly ($p \geq 0.05$) as more enzyme was added into individual samples.

Effects of Added PME on Particle Size. Measurements of relative turbidity and sedimentation indicated that PME addition increased both flocculation and clarification rates in the cloud. Rates of flocculation can be estimated more directly by analyzing changes in particle sizes. As discussed above, the particle size distribution of the entire juice sample was measured by gently inverting the juice samples, thus ensuring an even distribution of particle sizes throughout each sample, and then using static light scattering to determine particle diameters. Inspection of the particle size distribution profiles for each level of enzyme added showed that the carrot juice started with a trimodal distribution (Figure 3), i.e., three overlapping populations with different modes of approximately 0.7, 1.7, and 13 μm. In the absence of enzyme, this distribution did not change over time (Figure 3a). For the enzyme-containing systems, (Figure 3b–e), there was a rapid initial change occurring over the first ~9 days, during which the second modes shifted to larger diameters, leaving the size of the other two modes unaffected. As a result, the height of the first peak at smaller sizes shrank over time as that of the larger mode grew.

Examination of all enzyme levels (Figure 4a) indicated that the extent of this shift at earlier times did not strongly depend on the amount of enzyme; there was a similar increase in particle size for mode 2 at all levels of added enzyme. The first rapid shift was followed by a second, slower change in the distribution, as the second peak diameter gradually increased to merge with the third mode over ~30–40 days. This second growth process occurred more rapidly at higher enzyme concentrations at longer times. Consequently, data at day 5 exhibited little dependence on the amount of enzyme added, as long as some active enzyme was present (Figure 4a). Samples with 0.15, 0.25, and 0.5 U/g added PME also had very similar particle size distributions at 33 days of storage; it was only the sample with 1.0 U/g added PME that had a significantly greater particle size (Figure 4b). Finally, at day 43, the two highest enzyme concentrations both exhibited more significant particle growth than the other samples (Figure 4c).

The increase in particle size is an indication that flocculation was occurring within the cloud.[30,35] This is qualitatively visible in the light microscopy photos (Figure 5), as one can distinguish the individual particles that make up an aggregate. Clearly, the presence of active enzyme corresponded to the formation of flocs in the mixture, with the size of those flocs larger in the two samples with highest amounts of enzyme. Overall, the data in Figures 1–5 consistently indicates that as particles flocculated and grew in diameter, they began to settle out, causing clarification. Therefore, it can be concluded that the amount of enzyme present had a direct effect on the rate of flocculation and sedimentation. In addition, measurements of turbidity, sedimentation, and particle size distributions all indicate a process that occurred more rapidly over an initial period of ~5–10 days. This period is followed by a time of slower flocculation rates with little change in the observed sediment layer, although changes in the cloud structure were still occurring.

DISCUSSION

Adding PME to carrot juice caused juice clarification, as measured by sediment height and relative turbidity. With more added enzyme, the juice clarified more rapidly and to a greater extent. The clarification was accompanied by an increase in particle size. Although no previous research has been found on

dx.doi.org/10.1021/jf4043979 | J. Agric. Food Chem. 2014, 62, 1111–1118

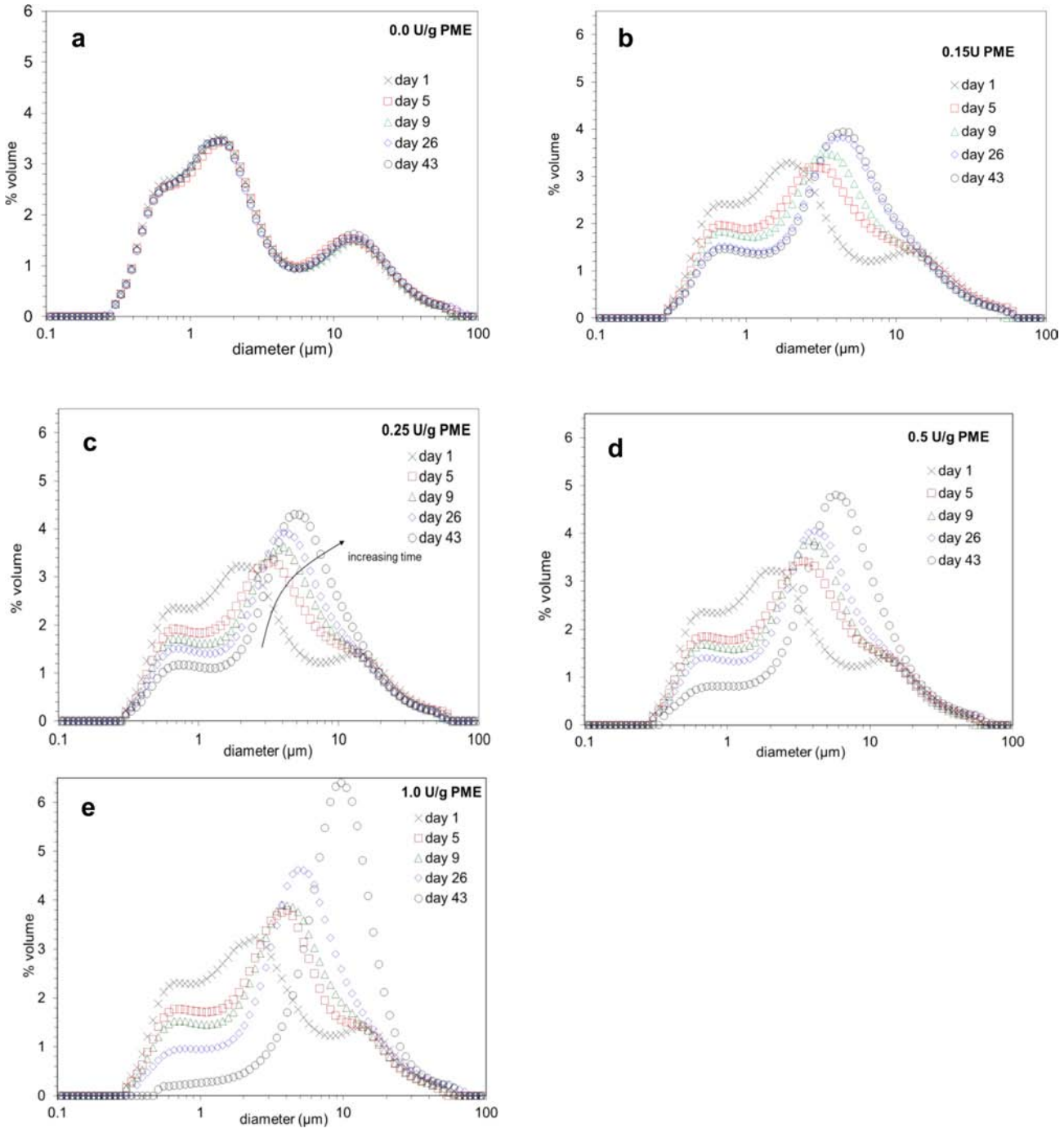

Figure 3. Particle size distribution curves for commercial carrot juice with no added PME (a) and with the following amounts of enzyme added: 0.15 (b), 0.25 (c), 0.5 (d), and 1.0 U/g (e). Though particle sizes were measured every three days for 56 days, data for only days 1, 5, 9, 26, and 43 were used to represent the size changes that occurred.

the addition of different enzyme levels back into juice, these results are consistent with those reported for native residual enzyme activity in commercial juices. In citrus and tomato juices, clarification occurred above a certain minimum threshold of PME activity.[7−9] In pineapple juice, residual PME activities of 4.1×10^{-4} U/mL did not cause complete clarification, whereas PME values 10 times greater resulted in complete clarification.[6]

Commercial juice was used instead of raw, unpasteurized juice for consistency and relevancy to the industry. However, there are important differences between commercial, pasteurized juice and raw juice that could affect the results. Preliminary work showed that juice made in the laboratory and filtered through cheesecloth had particle sizes 50 times greater than those of commercial carrot juice, with much greater variation in particle size. Additionally, our laboratory juice had 1.25 times more solid matter than commercial juice. Interestingly, when the carrots were blanched before juicing in the laboratory, the amount of solid matter became equal to that of the commercial juice, which would suggest that the heating of the carrot weakens the internal structure and allows particles to be broken down into smaller sizes and removed. This could account in

dx.doi.org/10.1021/jf4043979 | J. Agric. Food Chem. 2014, 62, 1111−1118

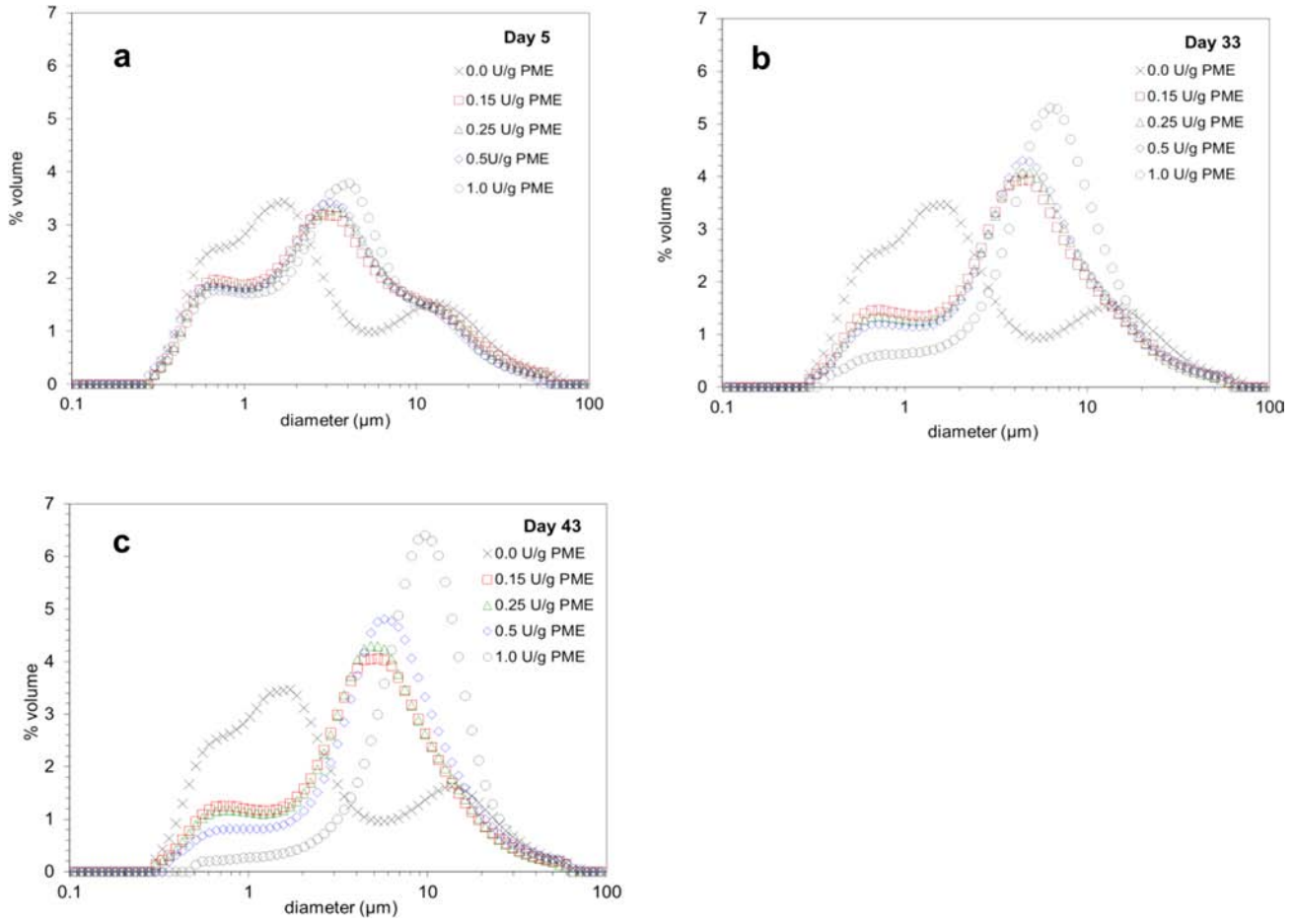

Figure 4. Comparison of particle size distribution of carrot juices with different amounts of added PME after 5 (a), 33 (b), and (c) 43 days.

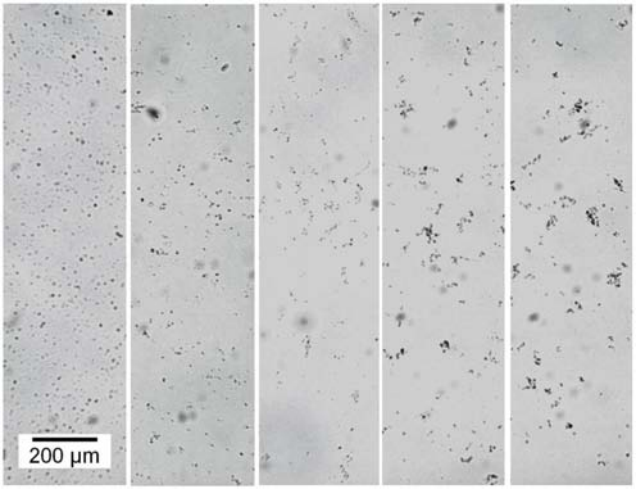

Figure 5. Commercial carrot juice with added enzyme viewed with 20× light microscopy at 56 days of storage at 5 °C. From left to right, enzyme levels are 0, 0.15, 0.25, 0.5, and 1.0 U/g.

part for the smaller particle sizes in pasteurized commercial carrot juice versus raw laboratory juice, and is supported by the work of Reiter et al. who found that pasteurized juice had smaller particle diameters than unpasteurized juice.[30] Processing techniques have a significant impact on cloud particle size; a study by Reiter et al.[30] showed the wide range of particle sizes (0.1−700 μm) for carrot juices produced with decanter technology from five different manufacturers. The commercial juice used in this study had <1% of particles >10 μm.[28] This indicates there is a wide range of processing techniques used in the juice industry that can result in different particle sizes.

The changes in sediment height and relative turbidity observed here were similar to one another in that both indicated an initially rapid destabilization process, followed by slower changes over time. Both also showed small but significant differences between juices with the three highest amounts of PME added at the later stages of the storage time course. Changes in particle size showed a similar trend. Over the first 5−10 days of storage, there was a relatively rapid increase in diameter of the population of smallest particles in the mixture. At longer times, sizes in the population of larger particles grew slowly, with the rate of this growth showing a modest dependence on enzyme concentration especially at the highest levels of added PME. By the end of the storage time course, all three measures of juice clarification, sediment height, relative turbidity, and particle size distribution, showed similar small differences between the juices with different levels of added PME. If PME induced clarification is due to enzymatic de-esterification of the juice pectins, then one might expect that clarification would occur more rapidly with more added enzyme but that all the juices would eventually reach the same end point.

Why the final states of the juices differed with differing amounts of added enzyme is not clear. One possibility is that the de-esterification of pectin by PME was only partial and that

dx.doi.org/10.1021/jf4043979 | J. Agric. Food Chem. 2014, 62, 1111−1118

the final degree of pectin esterification achieved depended on the amount of enzyme added. It is known that in the absence of high salt concentrations, PME binds strongly to de-esterified stretches of pectin, resulting in the formation of inactive PME−pectin complexes.[36] As a result, PME typically only partially de-esterifies a pectin chain before becoming inactive. It is possible that at higher levels of added PME, a higher final level of de-esterification is obtained because more pectin can be de-esterified before all the PME enzyme forms inactive PME−pectin complexes and de-esterification stops. The differences in particle size, aggregation, flocculation, and sedimentation between samples with different levels of added PME may all result from this difference in this final degree of esterification. It is even possible that all the PME catalyzed de-esterification in the juice occurred very rapidly, within the first day or two of the experiment. In that case, not only the different extents but also the different time courses for the particle sizes and sedimentation over the next 56 days could be due to the differences in final pectin esterification between the different levels of added PME, rather than being from different rates of de-esterification.

A second possibility is that particle aggregation and clarification is partially due to direct protein binding effects. Proteins (including PME) present in the high salt extract of cell wall material that was used as the source of the added PME may bind to the particulate matter in the juice, possibly affecting particle size aggregation. This is supported by the observations of Schmelter et al. who found that even thermally inactivated PME was able to cause pectin gelation in the presence of salts.[37] This ability of PME to create gels even when inactivated was taken as an indication that, in addition to its catalytic mechanism, the PME protein could participate in direct electrostatic and hydrophobic interactions with the pectin. Proteins also have the capability of interacting with each other in high acid environments (pH 4.4), and it has been argued that it is protein−protein interactions that influence cloud stability more than protein-pectin interactions.[30]

Our micrograph data and the overall kinetics in the system may indicate that particle growth is in the diffusion limited aggregation (DLA) regime. In such a regime, once a nucleation site is formed, additional particles may be added one at a time via the "hit and stick," describing a rapid, irreversible flocculation, without time for rearrangement.[38] Loose, fractal flocs are the result of such a mechanism,[35,39] consistent with what is observed in Figure 5. As more PME is added, flocculation occurs at a greater rate, creating even looser and therefore larger flocs. Such flocs have a greater effective diameter, and so sediment out more with centrifugation (Figure 1), yet they do not pack as tightly on the bottom because of their loose structure (Figure 2). Initially, in juice with a high level of added PME, it may be that particles do not have to diffuse far to encounter another particle with which they are able to flocculate. High amounts of PME create more particles of pectin that have a higher lower degree of esterification, and the PME itself can participate in flocculation. This would account for the relatively rapid increase in particle size at the beginning of storage.

AUTHOR INFORMATION

Corresponding Author

*Telephone, (530)752-4800; e-mail, dmbarrett@ucdavis.edu.

Present Address

[§]A.K.S.: 500 Linden Street, Fort Collins, CO, 80524.

Funding

The authors would like to thank the National Science Foundation Center for Advanced Processing and Packaging for their generous funding of this research.

Notes

The authors declare no competing financial interest.

ABBREVIATIONS

DLA, diffusion limited aggregation; PME, pectin methylesterase; U, unit of enzyme activity

REFERENCES

(1) Hirsch, A. R.; Foerch, K.; Neidhart, S.; Wolf, G.; Carle, R. Effects of thermal treatments and storage on pectin methylesterase and peroxidase activity in freshly squeezed orange juice. *J. Agric. Food Chem.* **2008**, *56* (14), 5691−5699.

(2) Anthon, G. E.; Barrett, D. M. Kinetic parameters for the thermal inactivation of quality-related enzymes in carrots and potatoes. *J. Agric. Food Chem.* **2002**, *50* (14), 4119−4125.

(3) Suzuki, Y.; Sugimoto, A.; Kakuda, T.; Ikegawa, Y. Manufacturing process of carrot juice. United States Patent US 6340489, Jan. 22, 2002.

(4) Sampedro, F.; Geveke, D. J.; Fan, X.; Zhang, H. Q. Effect of PEF, HHP and thermal treatment on PME inactivation and volatile compounds concentration of an orange juice-milk based beverage. *Innovative Food Sci. Emerging Technol.* **2009**, *10* (4), 463−469.

(5) Carbonell, J. V.; Contreras, P.; Carbonell, L.; Navarro, J. L. Pectin methylesterase activity in juices from mandarins, oranges and hybrids. *Eur. Food Res. Technol.* **2006**, *222* (1−2), 83−87.

(6) Castaldo, D.; Laratta, B.; Loiudice, R.; Giovane, A.; Quagliuolo, L.; Servillo, L. Presence of residual pectin methylesterase activity in thermally stabilized industrial fruit preparations. *LWT—Food Sci. Technol.* **1997**, *30* (5), 479−484.

(7) Rothschild, G.; Vliet, C.; Karsenty, A. Pasteurization conditions for juice and comminuted products of Isralie citrus fruits. *J. Food Sci. Technol.* **1975**, *10*, 29−38.

(8) Fachin, D.; Van Loey, A. M.; Nguyen, B. L.; Verlent, I.; Indrawati; Hendrickx, M. E. Comparative study of the inactivation kinetics of pectinmethylesterase in tomato juice and purified form. *Biotechnol. Prog.* **2002**, *18* (4), 739−744.

(9) De Sio, F.; Dipollina, G.; Villari, G.; Loiudice, R.; Laratta, B.; Castaldo, D. Thermal resistance of pectin methylesterase in tomato juice. *Food Chem.* **1995**, *52* (2), 135−138.

(10) Jolie, R. P.; Duvetter, T.; Houben, K.; Clynen, E.; Sila, D. N.; Van Loey, A. M.; Hendrickx, M. E. Carrot pectin methylesterase and its inhibitor from kiwi fruit: Study of activity, stability and inhibition. *Innovative Food Sci. Emerging Technol.* **2009**, *10* (4), 601−609.

(11) Walter, R. H. *The Chemistry and Technology of Pectin*; Academic Press: San Diego, CA, 1991; p 276.

(12) Brummell, D. A.; Harpster, M. H. Cell wall metabolism in fruit softening and quality and its manipulation in transgenic plants. *Plant Mol. Biol.* **2001**, *47* (1−2), 311−340.

(13) Anthon, G. E.; Sekine, Y.; Watanabe, N.; Barrett, D. M. Thermal inactivation of pectin methylesterase, polygalacturonase, and peroxidase in tomato juice. *J. Agric. Food Chem.* **2002**, *50* (21), 6153−6159.

(14) Duvetter, T.; Sila, D. N.; Van Buggenhout, S.; Jolie, R.; Van Loey, A.; Hendrickx, M. Pectins in processed fruit and vegetables: Part I—Stability and catalytic activity of pectinases. *Compr. Rev. Food Sci. Food Saf.* **2009**, *8* (2), 75−85.

(15) van Alebeek, G.-J. W. M.; van Scherpenzeel, K.; Beldman, G.; Schols, H. A.; Voragen, A. G. J. Partially esterified oligogalacturonides are the preferred substrates for pectin methylesterase of Aspergillus niger. *Biochem. J.* **2003**, *372* (1), 211−218.

(16) Catoire, L.; Pierron, M.; Morvan, C.; du Penhoat, C. H.; Goldberg, R. Investigation of the action patterns of pectinmethylesterase isoforms through kinetic analyses and NMR spectroscopy—

Implications in cell wall expansion. *J. Biol. Chem.* **1998**, *273* (50), 33150−33156.
(17) Wicker, L.; Ackerley, J. L.; Hunter, J. L. Modification of pectin by pectinmethylesterase and the role in stability of juice beverages. *Food Hydrocolloids* **2003**, *17* (6), 809−814.
(18) Benen, J. A. E.; Alebeek, H.-J. W. M. V.; Voragen, A. G. J.; Visser, J. *Handbook of Food Enzymology*; Marcel Dekker, Inc.: New York, NY, 2003; Vol. *122*.
(19) Benítez, E. I.; Genovese, D. B.; Lozano, J. E. Effect of pH and ionic strength on apple juice turbidity: Application of the extended DLVO theory. *Food Hydrocolloids* **2007**, *21* (1), 100−109.
(20) Castaldo, D.; Servillo, L.; Loiudice, R.; Balesterieri, C.; Laratta, B.; Quagliuolo, L.; Giovane, A. The detection of residual pectin methylesterase activity in pasteurized tomato juices. *Int. J. Food Sci. Technol.* **1996**, *31* (4), 313−318.
(21) Mensah-Wilson, M.; Reiter, M.; Bail, R.; Neidhart, S.; Carle, R. Cloud stabilizing potential of pectin on pulp-containing fruit beverages. *Fruit Process.* **2000**, *2*, 47−54.
(22) Mollov, P.; Mihalev, K.; Buleva, M.; Petkanchin, I. Cloud stability of apple juices in relation to their particle charge properties studied by electro-optics. *Food Res. Int.* **2006**, *39* (5), 519−524.
(23) Cameron, R. G.; Baker, R. A.; Grohmann, K. Multiple Forms of Pectinmethylesterase from Citrus Peel and Their Effects on Juice Cloud Stability. *J. Food Sci.* **1998**, *63* (2), 253−256.
(24) Ly-Nguyen, B.; Loey, A. M. V.; Fachin, D.; Verlent, I.; Indrawati; Hendrickx, M. E. Partial purification, characterization, and thermal and high-pressure inactivation of pectin methylesterase from carrots (Daucus carrota L.). *J. Agric. Food Chem.* **2002**, *50* (19), 5437−5444.
(25) RC; JDS; MAM. Bradford Reagent Technical Bulletin. Sigma-Aldrich, Ed., 2011.
(26) Anthon, G. E.; Barrett, D. M. Comparison of three colorimetric reagents in the determination of methanol with alcohol oxidase. Application to the assay of pectin methylesterase. *J. Agric. Food Chem.* **2004**, *52* (12), 3749−3753.
(27) Silva, V. M.; Kawazoe Sato, A. C.; Barbosa, G.; Dacanal, G.; Ciro-Velasquez, H. J.; Cunha, R. L. The effect of homogenisation on the stability of pineapple pulp. *Int. J. Food Sci. Technol.* **2010**, *45* (10), 2127−2133.
(28) Reiter, M.; Neidhart, S.; Carle, R. Sedimentation behaviour and turbidity of carrot juices in relation to the characteristics of their cloud particles. *J. Sci. Food Agric.* **2003**, *83* (8), 745−751.
(29) Ibrahim, G. E.; Hassan, I. M.; Abd-Elrashid, A. M.; El-Massry, K. F.; Eh-Ghorab, A. H.; Manal, M. R.; Osman, F. Effect of clouding agents on the quality of apple juice during storage. *Food Hydrocolloids* **2011**, *25* (1), 91−97.
(30) Reiter, M.; Stuparic, M.; Neidhart, S.; Carle, R. The role of process technology in carrot juice cloud stability. *Lebensm.-Wiss. Technol.* **2003**, *36* (2), 165−172.
(31) Harrison, D.; Fisch, M. *Turbidity Measurement* [Online]; CRC Press LLC: Boca Raton, FA, 2000. http://www.engnetbase.com.
(32) Croak, S.; Corredig, M. The role of pectin in orange juice stabilization: Effect of pectin methylesterase and pectinase activity on the size of cloud particles. *Food Hydrocolloids* **2006**, *20* (7), 961−965.
(33) Ellerbee, L.; Wicker, L. Calcium and pH influence on orange juice cloud stability. *J. Sci. Food .. Agric.* **2011**, *91* (1), 171−177.
(34) Wicker, L.; Ackerley, J. L.; Corredig, M. Clarification of juice by thermolabile valencia pectinmethylesterase is accelerated by cations. *J. Agric. Food Chem.* **2002**, *50* (14), 4091−4095.
(35) Benitez, E. I.; Lozano, J. E.; Genovese, D. B. Fractal dimension and mechanism of aggregation of apple juice particles. *Food Sci. Technol. Int.* **2010**, *16* (2), 179−186.
(36) Lineweaver, H.; Ballou, G. A. The effects of cations on the activity of alfalfa pectinesterase (pectase). *Arch. Biochem.* **1945**, *6*, 373−387.
(37) Schmelter, T.; Vreeker, R.; Klaffke, W. Characterisation of a novel gel system containing pectin, heat inactivated pectin methylesterase and NaCl. *Carbohydr. Polym.* **2001**, *45* (3), 277−284.
(38) Russel, W. B.; Saville, D. A.; Schowalter, W. R. *Colloidal Dispersions*; Cambridge University Press: Cambridge, MA, 1989.
(39) Beveridge, T. Letter to the Editor: Fractile images and apple juice haze. *Food Res. Int.* **1998**, *31* (5), 411−414.

MATERIALS AND METHODS

Plant Materials and Treatment. Fresh broccoli (*B. oleracea* var. *italica*) that was kindly supplied by the orchard of Anhui Academy of Agricultural Sciences, Anhui, China, and selected to avoid florets showing physical damage or microbial infection was used throughout this study. Solutions of sodium hydrosulfide ($NaHS{\cdot}3H_2O$, Sigma) were used as the hydrogen sulfide (H_2S) donor. Aqueous solutions (150 mL) of 0, 0.40, 0.80, 1.20, 1.60, 2.00, 2.40, 2.80, or 3.20 mM NaHS were prepared in sealed containers (volume 3 L). Six pieces of freshly cut broccoli florets (approximately 35 ± 2 g) from six different broccoli shoots were fumigated with H_2S in the sealed containers at 25 °C and 85−90% relative humidity. For dark-promoted senescence, the containers were stored in darkness. Treatment solutions were renewed daily and florets were observed every 24 h. Each experiment was repeated three times.

Visual Evaluation of Broccoli Senescence. The appearance of fresh-cut broccoli fumigated with H_2S gas was evaluated subjectively by 20 people using five indexes: freshness, rotting rate, yellowness, flavor, texture, and floret organization.[11] Each index was divided into four ranks and assigned scores of 2.0, 1.5, 1.0 and 0, with higher numbers assigned to better visual evaluation, and the sum of the five indexes is shown as a score from 0 to 10.

Determination of Functional Compounds in Broccoli. Chlorophyll content of broccoli florets was determined using the colorimetric method of Lichtenthaler and Wellburn with minor modifications.[12] About 0.50 ± 0.01 g of finely chopped broccoli floret samples was placed in an Erlenmeyer flask containing 5−10 mL of 80% acetone as extraction solvent. After extraction, the OD value of supernatant was recorded at 645 and 663 nm. Every analysis was repeated in triplicate, and the results were expressed as mg/g FW (fresh weight).

Carotenoid content of broccoli samples was determined by the method of Nath et al.[13] Fresh .50 ± 0.01 g sample was ground with 5−10 mL of acetone by adding 1.00 g of anhydrous Na_2SO_4. The supernatant was transferred to a beaker and the extraction step was repeated three times. The combined supernatants were transferred to a separating funnel, and 5−10 mL of petroleum ether was added and mixed thoroughly. The upper layer of petroleum ether was collected and absorbance recorded at 452 nm, and the amount of carotenoid was expressed as mg/g FW.

The following procedures were used for the assays of total phenols, flavonoids, and anthocyanin. Broccoli samples of 1.00 ± 0.01 g were homogenized with 10 mL of aqueous methanolic HCl (50% methanol, 0.05% concentrated HCl, pH 3.5), the brei was allowed to macerate for 24 h in the dark (0−4 °C), and the mixture was filtered for subsequent determination. Determination of total phenols was performed according to the method of Pirie and Mullins.[14] The content of total phenols was determined spectrophotometrically at 280 nm. A calibration curve was prepared for total phenols using gallic acid as the standard.

The determination of flavonoids was performed according to the work of Zhishen et al. with slight modification.[15] A 1.0 mL portion of filtrate was placed in a 10 mL volumetric flask, distilled water was added to make 5 mL, 0.3 mL of 5% $NaNO_2$ was added, and the solution was mixed thoroughly. After 5 min, 3 mL of 10% $Al(NO_3)_3$ was added, and the solution was mixed thoroughly. After 6 min, 2 mL of 1 M NaOH was added, the total was adjusted to 10 mL with distilled water, and the solution was mixed thoroughly again. The content of flavonoids was determined spectrophotometrically at 510 nm with rutin used as the standard for calibration.

The determination of anthocyanin was estimated according to the method of Lee and Wicker.[16] Absorption of the filtrate was recorded at 530, 620, and 650 nm. The content of anthocyanin was calculated using the formula below. One unit of anthocyanin content was expressed as a change of 0.1 OD value.

$$OD = (OD_{530} - OD_{620}) - 0.1 \times (OD_{650} - OD_{620})$$

Ascorbate was determined by the method described by Nath et al.[13] Floret samples of 2.00 ± 0.01 g were ground with 15 mL of 4% oxalic acid, and the homogenate was filtered through filter paper. The volume of filtrate was adjusted to 25 mL with 4% oxalic acid and titrated with 2,6-dichlorophenol-indophenol to a pink color.

Determination of the Contents of Reducing Sugar, Soluble Protein, Total Soluble Solids, and Free Amino Acids. For reducing sugars, broccoli samples (1.00 ± 0.01 g) were ground with 5 mL of sodium phosphate buffer (pH 7.0, 200 mM), the homogenate was centrifuged at 10 000 rpm for 30 min, and the supernatant was collected for subsequent analysis. The determination of reducing sugar was performed spectrophotometrically according to Miller's dinitrosalicylic acid method.[17] Each analysis was repeated in triplicate, and the results were expressed as mg/g FW.

Total soluble solid content was determined using a digital refractometer (Tongfang Inc., Shanghai, China) according to the method of Jiang et al.[18]

The content of soluble protein was determined by the method described by Bradford.[19] Supernatant (0.1 mL) was mixed with 0.9 mL of distilled water and 5 mL of 0.1 mg/mL Coomassie Brilliant Blue G-250. After 5 min, the OD value was recorded at 595 nm by spectrophotometer. Analyses were repeated in triplicate and the results expressed as mg/g FW.

Free amino acid content was measured according to the work of Hu et al. using an automatic amino acid analyzer (model S433D, Syknm, Germany).[8] Fresh-cut broccoli florets (0.50 ± 0.01 g) were ground with 5 mL of 80% ethanol, the homogenate was centrifuged at 10 000 rpm for 5 min, and the supernatant was heated at 80 °C to remove ethanol and to concentrate the sample to 1 mL.

Determination of Superoxide Anion ($\bullet O_2^-$), Hydrogen Peroxide (H_2O_2), and Malondialdehyde (MDA). Contents of $\bullet O_2^-$, H_2O_2, and MDA were determined according to the methods described by Hu et al.[8]

Determination of Enzyme Activities. Activities of guaiacol peroxidase (POD), ascorbate peroxidase (APX), catalase (CAT), glutathione reductase (GR), and lipoxidase (LOX) were determined by the procedures described by Hu et al.[8] Frozen broccoli floret samples (0.50 ± 0.01 g) were homogenized with 5 mL of ice-cold sodium phosphate buffer (200 mM, pH 7.8) containing 1.0 mM EDTA. The homogenate was centrifuged at 12 000 rpm (4 °C, 20 min), and the supernatant was used for activity measurement. Analysis of guaiacol POD activity was based on the oxidation of guaiacol by hydrogen peroxide. The reaction mixture contained 1.7−1.8 mL of sodium phosphate buffer (50 mM, pH 6.1), 0.1 mL of 3% H_2O_2, 1 mL of 1% guaiacol, and 100−200 μL of enzyme extract. The increase in absorbance at 420 nm was recorded. APX activity was determined in the presence of 0.5 mM ascorbate and 0.5 mM H_2O_2 by monitoring the decrease in absorbance at 290 nm. CAT activity was determined spectrophotometrically by monitoring the decrease in absorbance at 240 nm. The reaction mixture contained 2.8 mL of sodium phosphate buffer (50 mM, pH 7.0), 100 μL of 3% H_2O_2, and 100 μL of enzyme extract. The decrease of GR activity in absorbance at 340 nm was recorded. One unit of POD, APX, CAT, and GR activity was defined as an increase or decrease of 0.01 OD value per minute. The results were expressed as U/g FW.

The activity of LOX was determined in the presence of linoleic acid by monitoring the changes in absorbance at 234 nm. One unit of LOX activity was defined as a decrease of 0.01 OD value in absorbance per minute. The results were expressed as U/g FW.

The activity of polyphenol oxidase (PPO) was determined by procedures described by Benjamin and Montgomery.[20] Broccoli samples (2.00 ± 0.05 g) were homogenized with 5.0 mL of sodium phosphate buffer (50 mM, pH 6.8). After centrifugation, the supernatant was used for the activity assay using catechol as substrate. One unit of PPO activity was defined as an increase of 0.01 OD value in absorbance at 410 nm per minute. The results were expressed as U/g FW.

The activity of phenylalanine ammonia lyase (PAL) was determined by the procedures described by Beaudoin-Eagan and Thorpe.[21] One unit of PAL activity was defined as a change of 0.01 OD value in absorbance at 290 nm per minute. The results were expressed as U/g FW.

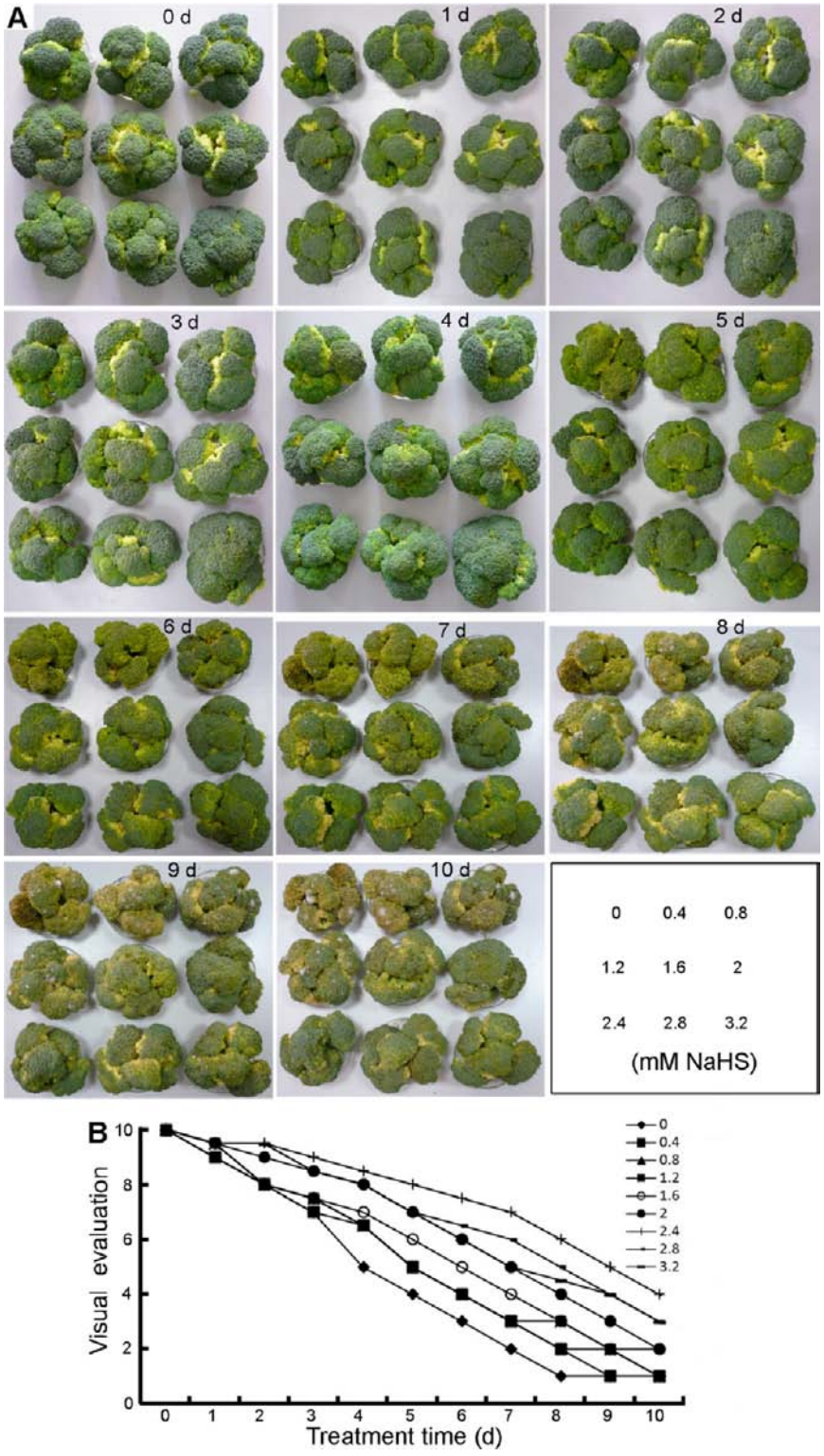

Figure 1. Effects of H_2S on the senescence and visual evaluation in postharvest broccoli. Broccoli florets were fumigated with different concentrations (0, 0.4, 0.8, 1.2, 1.6, 2.0, 2.4, 2.8, or 3.2 mM) of aqueous solutions of NaHS for 0−10 d, respectively, and the experimental treatments are shown in lower right of part A. Photographs (A) were taken from day 0 to 10, and visual evaluation (B) was recorded. The experiments and following ones were carried out at room temperature and 85−90% relative humidity.

The activity of protease was measured according to the method described by Reimerdes and Klostermeyer.[22] Broccoli florets (0.50 ± 0.01 g) were homogenized with 5 mL of ice-cold Tris-HCl buffer [50 mM, pH 7.5, included 1 mM ethylene diamine tetraacetic acid (EDTA), 15 mM β-mercaptoethanol, and 1% PVP]. The homogenate was centrifuged at 10 000 rpm (4 °C, 30 min), and the supernatant was used for activity determination. One unit of protease activity was defined as an increase of 0.01 OD value at 278 nm per hour, and the results were expressed as U/g FW.

RNA Extraction and Reversed Transcript Polymerase Chain Reaction (PCR). Fresh-cut broccoli florets were ground in liquid nitrogen, and RNA was extracted by the RNAiso Plus according to the

dx.doi.org/10.1021/jf4047122 | J. Agric. Food Chem. 2014, 62, 1119−1129

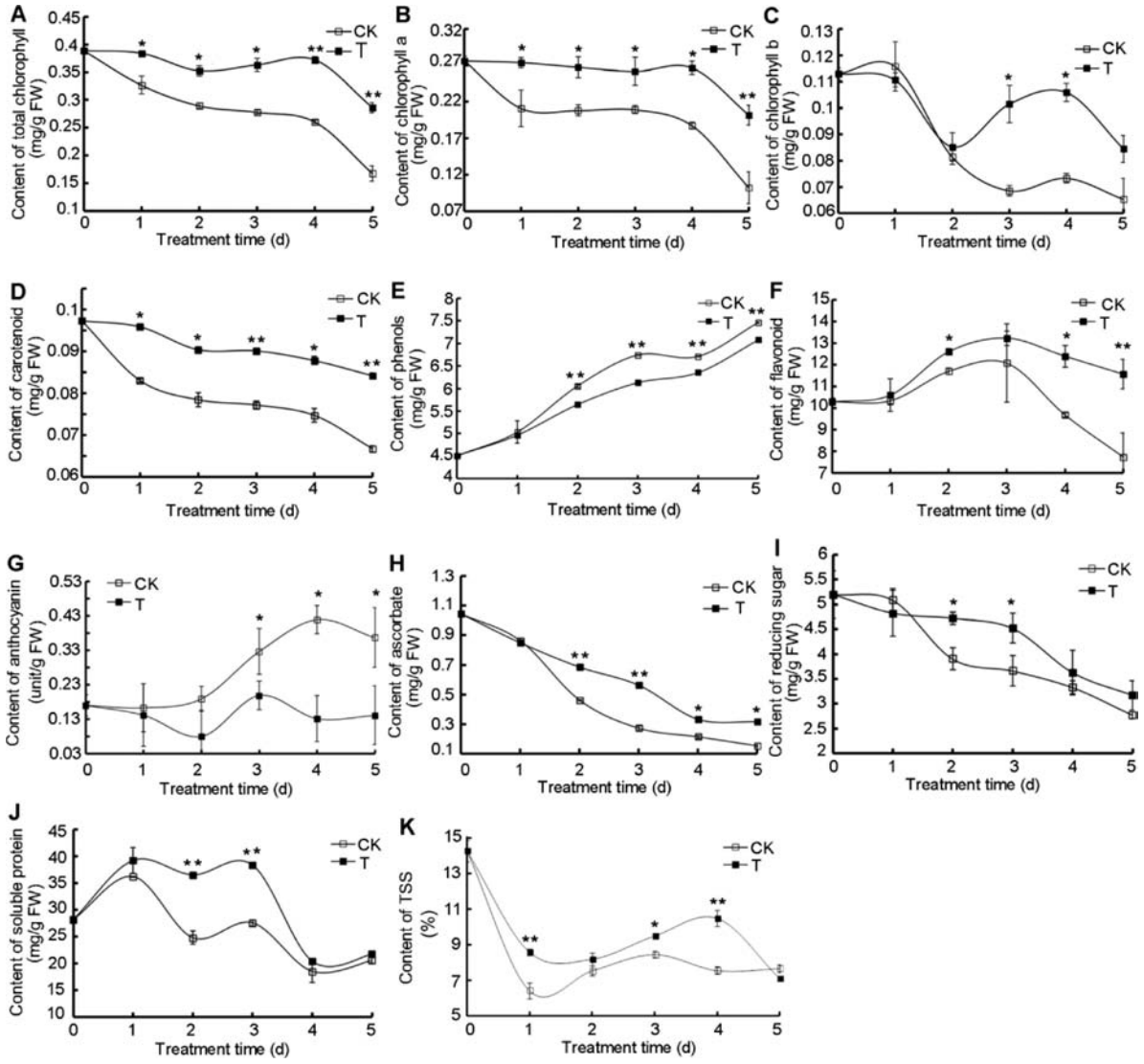

Figure 2. Effects of H_2S on the contents of total chlorophyll (A), chlorophyll *a* (B), chlorophyll *b* (C), carotenoid (D), total phenols (E), flavonoid (F), anthocyanin (G), ascorbate (H), reducing sugar (I), soluble protein (J), and total soluble solids (TSS) (K) in postharvest broccoli. Broccoli florets were fumigated with 2.4 mM H_2S donor NaHS aqueous solution (T) with water as the control groups (CK) for 0−5 d. Data are presented as means ± SD (n = 3). * and ** in this figure and following ones stand for a significant difference between CK and T at $P < 0.05$ and $P < 0.01$, respectively.

manufacturer's instructions (Takara, Kyoto, Japan), and total RNA was used for cDNA synthesis using a reverse transcription kit (Prime Script RT Master Mix, Takara, Kyoto, Japan). The resulting cDNA was applied as template for PCR using a PCR system with Easy Taq DNA Polymerase (TransGen, Beijing, China). The PCR primers used for detecting the genes *BoSGR* (stay-green protein), *BoNYC* (chlorophyll *b* reductase), *BoCLH1* (chlorophyllase 1), *BoCLH2* (chlorophyllase 2), *BoPaO* (pheophorbide *a* oxygenase), *BoPPH* (pheophytinase), *BoRCCR* (red catabolite chlorophyll reductase), and *BoACT* (actin) followed the methods of Hasperué et al.[23] The following primers were utilized to assess relative expression of *BoCP1* (cysteine protease) and *BoLOX1* (lipoxygenase 1) by PCR: *BoCP1*, 5′-CGCCGATCTG-ACCAACGAA-3′ and 5′-CCGCTCCAATCGCAGAAAA-3′; *BoLOX1*, 5′-TCTCCACGAATTTCTGGGAAACAAAG-3′ and 5′-AGTCCTCTGAGTGTGTAGCCTTTC-3′. Three independent extracts of RNA were done and similar results were obtained.

Analysis of Rubisco. Fresh-cut broccoli florets were homogenized using a chilled mortar and pestle in sodium phosphate buffer (50 mM, pH 7.5) containing 1 mM EDTA, 15 mM 2-mercaptoethanol, and 1% (v/v) PVP, and the homogenate was centrifuged at 15 000 rpm for 10 min at 4 °C. Then the supernatant was collected for Rubisco analysis. The Rubisco was visualized by nondenaturing PAGE with Coomassie Brilliant Blue R-250 staining according to the method of Ono et al.[24]

Other Vegetables and Fruits Fumigated with H_2S. Fresh-cut lotus root, potato, yams, lettuce, pumpkin, and peach, kindly supplied by the orchard of Anhui Academy of Agricultural Sciences, Anhui, China, were fumigated with different concentrations of H_2S donor NaHS and photographed.

Statistical Analysis. Statistical significance was tested by one-way analysis of variance (ANOVA), and the results are expressed as the mean values ± standard deviation (SD) of three independent experiments. Fisher's least significant differences (LSD) were calculated following a significant ($P < 0.01$ or $P < 0.05$) t test.

RESULTS

H_2S Alleviates the Senescence of Postharvest Broccoli. In our experiments, broccoli florets were fumigated with H_2S released by different concentrations of aqueous solutions of NaHS with water as the control. As shown in Figure 1A, H_2S fumigation alleviated postharvest senescence of broccoli in a dose-dependent manner. Water control broccoli

Table 1. Effects of H_2S Fumigation on the Content of the Free Amino Acids in Postharvest Broccoli Florets[a]

	Asp	Ser	Glu	Gly	Ala	Val	Ile
CK0	6728.88 ± 413.05 a	4416.75 ± 289.77 a	2403.05 ± 155.63 a	80.21 ± 10.67 a	1208.06 ± 83.21 a	431.72 ± 23.46 a	122.72 ± 10.83 a
CK1	5807.36 ± 39.95 b	5853.02 ± 31.23 b	3289.47 ± 5.78 b	360.45 ± 228.82 b	1892.4 ± 113.87 b	842.95 ± 3.39 b	348.61 ± 2.84 b
T1	4750.38 ± 118.91 c	5197.02 ± 150.02 c	2957.29 ± 102.78 c	531.91 ± 23.15 b	1940.39 ± 56.59 b	753.51 ± 16.28 c	308.27 ± 9.36 b
CK2	5772.42 ± 210.27 b	6518.72 ± 172.31 d	2795.89 ± 107.71 c	807.53 ± 24.1 c	1953 ± 55.1 b	1102.45 ± 26.81 d	485.03 ± 16.73 c
T2	4901.75 ± 32.34 c	5423.44 ± 60.63 c	2328.08 ± 34.78 a	748.96 ± 18.62 d	1906.37 ± 34.43 b	984.81 ± 15.53 e	402.74 ± 6.58 d
	Leu	Tyr	Phe	His	Lys	Arg	total AA
CK0	99.03 ± 7.67 a	23.35 ± 6.22 a	67.63 ± 8.03 a	186.03 ± 15.53 a	84.92 ± 7.15 a	424. ± 223.38 a	16276.31 ± 1254.58 a
CK1	304.86 ± 2.1 b	91.22 ± 0.79 b	198.99 ± 4.16 b	275.49 ± 0.1 b	229.79 ± 2.68 b	925.03 ± 4.96 b	20419.61 ± 244.69 b
T1	262.72 ± 6.98 c	86.68 ± 8.47 b	188.68 ± 7.07 b	273.92 ± 4.14 b	212.76 ± 6.69 b	877.08 ± 24.28 b	18340.6 ± 534.74 a
CK2	364.99 ± 14 d	137.59 ± 5.69 c	318.24 ± 10.25 c	350.64 ± 6.1 c	326.38 ± 8.81 c	1342.21 ± 36.36 c	22275.08 ± 694.25 b
T2	250.66 ± 4.4 c	104.24 ± 18.41 b	326.7 ± 0.91 c	311.98 ± 1.27 d	257.63 ± 2.81 d	1047. ± 16.46 d	18994.34 ± 247.16 a

[a]Postharvest broccoli were fumigated with 2.4 mM H_2S donor NaHS aqueous solution (T) with water as the control groups (CK) for 0−2 d (CK0, CK1, CK2, T1, and T2). Data are presented as means ± SD (n = 3). The contents of free amino acids were determined by automatic amino acid analyzer (model S433D, Sykmn). Different letters indicate significant differences ($p < 0.05$) between the treatments.

matured and yellowed quickly after 3 days of storage, while different NaHS treatment alleviated the postharvest yellowing of broccoli with an optimal concentration of 2.4 mM. Visual quality was evaluated according to the freshness, rotting rate, yellowness, flavor, texture, and organization. As shown in Figure 1B, 2.4 mM NaHS treatment showed the optimal effect on the visual quality of postharvest broccoli and thus was used in subsequent experiments.

Effect of H_2S on the Contents of Chlorophyll, Carotenoid, Total Phenols, Flavonoids, Anthocyanin, Ascorbate, Reducing Sugar, Soluble Proteins, and Total Soluble Solids. To further understand how H_2S alleviated yellowing and browning of fumigated broccoli, we determined the contents of chlorophyll, carotenoid, phenols, flavonoids, anthocyanin, and ascorbate in broccoli. Chlorophyll contents (Figure 2A) were expressed as the sum of chlorophyll *a* (Figure 2B) and chlorophyll *b* (Figure 2C). As shown in Figure 2A−C, total chlorophyll content as well as the amounts of chlorophylls *a* and *b* decreased gradually during storage in water controls, while H_2S fumigation maintained a relatively stable level of total chlorophyll and chlorophyll *a* until day 4, followed by a decrease on day 5, and also a higher level of chlorophyll *b* at the late stage of storage.

Carotenoid pigments protect cellular membranes by scavenging or quenching free radicals[25] acting as an essential lipid-soluble antioxidant in plants. Changes in carotenoid content, which consist of *β*-carotene and lutein, are shown in Figure 2D. The content of carotenoid decreased rapidly in the water control, whereas H_2S fumigation significantly prevented this decrease.

Regardless of treatment, total phenols increased steadily in broccoli florets with time (Figure 2E). However, broccoli fumigated with H_2S maintained lower levels of total phenols compared with water controls after 2 d of storage. As shown in Figure 2F, flavonoid content increased gradually in both treatments until 3 d followed by a rapid decrease in water controls, while H_2S fumigation alleviated the decrease and sustained a significantly higher level of flavonoids on days 4 and 5.

The content of anthocyanin in broccoli florets increased steadily in the water control until 5 d of storage, as shown in Figure 2G, but anthocyanin content in H_2S-fumigated broccoli was maintained at a significantly lower level compared with that of water controls. As shown in Figure 2H, the content of ascorbate in broccoli florets decreased during postharvest storage in both treatments; however, H_2S fumigation significantly alleviated the decrease after 2 d of storage.

The contents of reducing sugars and soluble proteins are shown in Figure 2I,J. The content of reducing sugar decreased gradually in both H_2S-fumigated and water control tissue throughout the storage time; however, the content of reducing sugar in postharvest broccoli fumigated with H_2S was higher than that of control on days 2 and 3 of storage. As shown in Figure 2J, soluble protein levels in H_2S-fumigated broccoli increased on day 1 and remained stable until day 3 followed by a drop on day 4. A similar pattern was observed in water control, except that the soluble protein level decreased sharply on day 2 and increased slightly on day 3. H_2S fumigation sustained significantly higher level of soluble protein on days 2 and 3 relative to that of water control.

The contents of soluble solids decreased sharply after 1 day of storage in H_2S treatment and water controls; thereafter, the contents varied slightly (Figure 2K). However, H_2S application

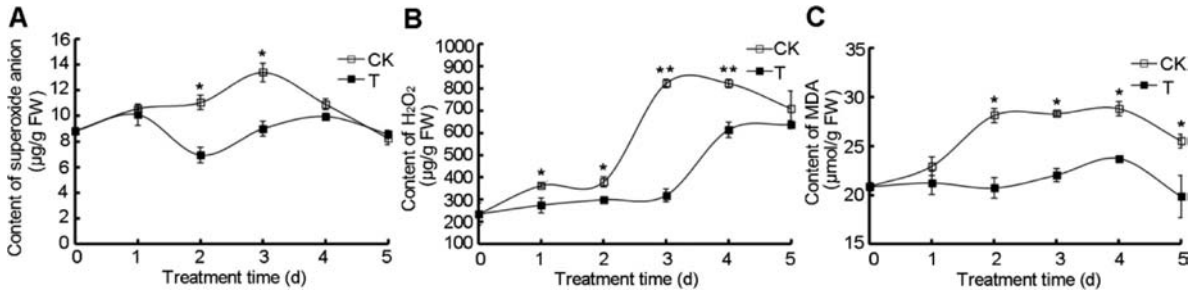

Figure 3. Effects of H_2S on the accumulation of superoxide anion ($\bullet O_2^-$) (A), hydrogen peroxide (H_2O_2) (B), and malonaldehyde (MDA) (C). Broccoli florets were fumigated with 2.4 mM H_2S donor NaHS aqueous solution (T) with water as the control groups (CK) for 0−5 d. Data are presented as means ± SD (n = 3).

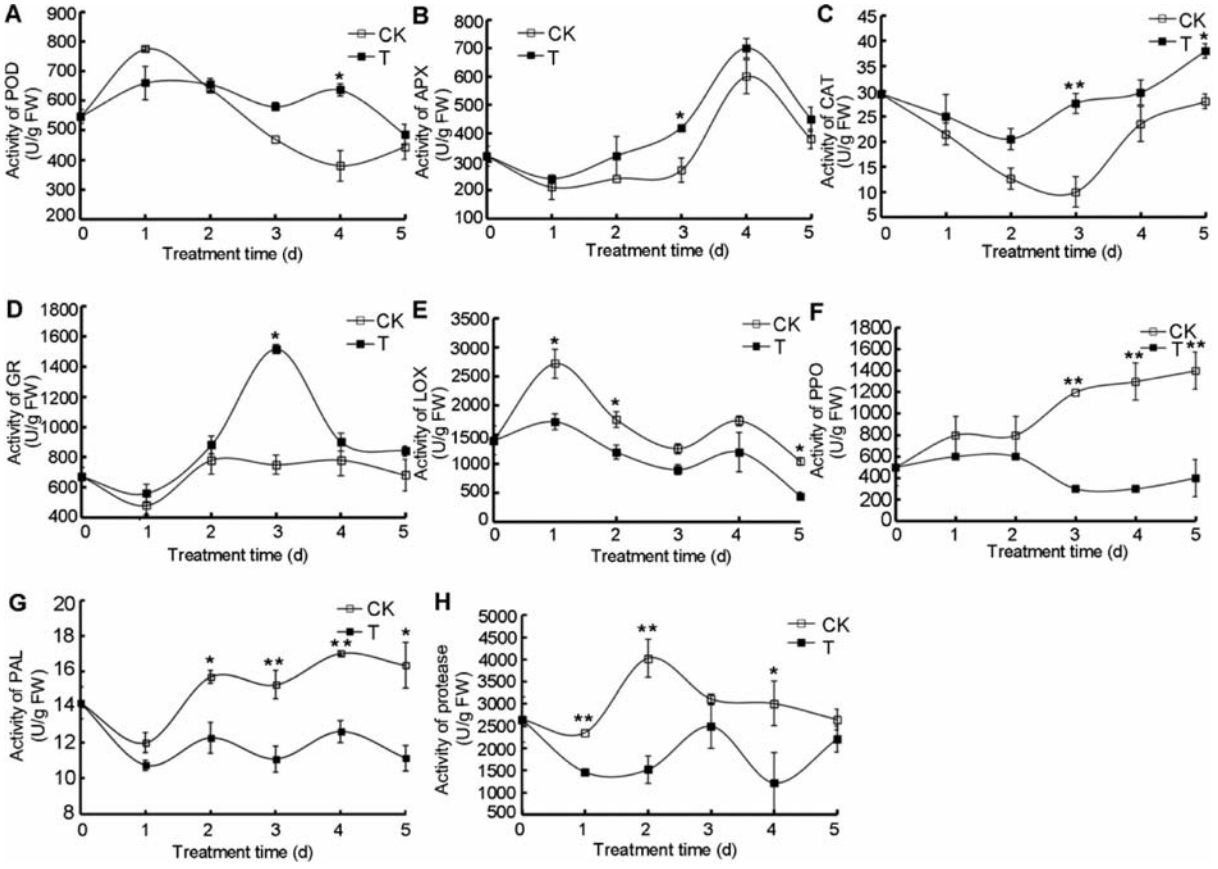

Figure 4. Role of H_2S in the regulation of the activities of guaiacol peroxidase (POD) (A), ascorbate peroxidase (APX) (B), catalase (CAT) (C), and glutathione reductase (GR) (D) and the down-regulation of lipoxygenase (LOX) (E), polyphenol oxidase (PPO) (F), phenylalanine ammonia lyase (PAL) (G), and protease (H) in postharvest broccoli florets. Postharvest broccoli florets were fumigated with 2.4 mM H_2S donor NaHS aqueous solution (T) with water as the control groups (CK) for 0−5 d. Data are presented as means ± SD (n = 3).

maintained significantly higher levels of soluble solids than water controls on days 1, 3 and 4.

Effect of H_2S on the Contents of Free Amino Acids in Postharvest Broccoli. H_2S fumigation sustained lower levels of free amino acids compared with water control (Table 1). Storage and senescence induced a rapid increase of total amino acid contents, regardless of treatment, although exposure to H_2S gas alleviated the increase. With the exception of Asp, the content of free amino acids in H_2S-fumigated and control broccoli was higher than that of freshly harvested broccoli. In addition, H_2S did not significantly affect the levels of Gly, Ala, and His on day 1, while a significant decrease of Gly and His appeared on day 2 compared with water control. Many amino acids, including Asn, Cys, Gln, Met, Pro, Thr, Trp, and Tyr, were not detected in broccoli during storage.

H_2S Decreases the Content of MDA and Reactive Oxygen Species, $\bullet O_2^-$ and H_2O_2. The contents of $\bullet O_2^-$, H_2O_2 and MDA in broccoli fumigated with H_2S and water are shown in Figure 3A−C. The overproduction of reactive oxygen species and the occurrence of oxidative damage are universal events during vegetable storage. $\bullet O_2^-$ accumulated steadily during the first 3 d of storage in water controls followed by a gradual decrease, whereas H_2S fumigation significantly alleviated $\bullet O_2^-$ accumulation at 2 and 3 d of storage (Figure 3A). H_2O_2 production in postharvest broccoli was rapidly enhanced on 3 d of storage and thereafter was maintained at a relatively higher level than that of H_2S-fumigated florets (Figure

dx.doi.org/10.1021/jf4047122 | J. Agric. Food Chem. 2014, 62, 1119−1129

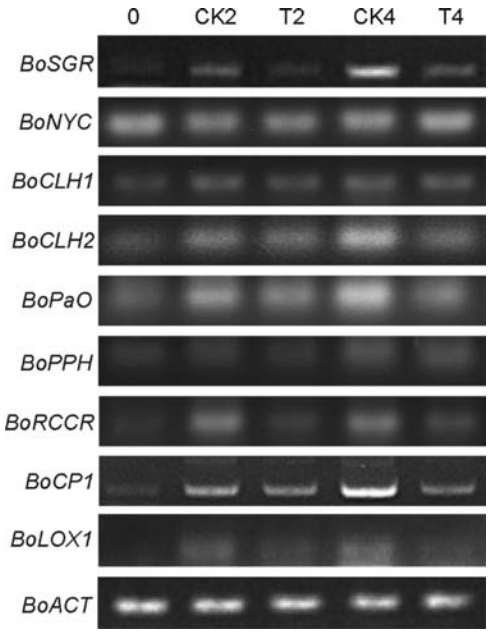

Figure 5. Effect of H_2S on the relative expression of *BoSGR* (stay-green protein), *BoNYC* (chlorophyll *b* reductase), *BoCLH1* (chlorophyllase 1), *BoCLH2* (chlorophyllase 2), *BoPaO* (pheophorbide *a* oxygenase), *BoPPH* (pheophytinase), *BoRCCR* (RCC reductase), *BoCP1* (cysteine protease), *BoLOX1* (lipoxygenase), and *BoACT* (actin, AF044573) in broccoli florets fumigated with 2.4 mM H_2S donor NaHS aqueous solution (T) and water as the control groups (CK) for 0, 2, and 4 d, respectively. *BoACT* was used as a control gene.

3B). In contrast, H_2O_2 content of H_2S-treated tissue was maintained at a low level for 3 d until a burst appeared on d 4.

As shown in Figure 3C, MDA accumulated steadily in control broccoli during the first 2 d of storage and then was maintained at a stable level until 4 d followed by a slight decline. In contrast, H_2S fumigation sustained a constant lower level of MDA during storage compared with water control (Figure 3C).

Changes in the Activities of Guaiacol Peroxidase, Ascorbate Peroxidase, Catalase, Glutathione Reductase, Lipoxygenase, Polyphenol Oxidase, and Phenylalanine Ammonia Lyase. The activities of enzymes involved in oxidative metabolism in plants, such as guaiacol peroxidase (POD), ascorbate peroxidase (APX), catalase (CAT), glutathione reductase (GR), lipoxygenase (LOX), polyphenol oxidase (PPO), and phenylalanine ammonia lyase (PAL) were measured in broccoli exposed to 2.4 mM NaHS and water (Figure 4). As shown in Figure 4A, POD activities in H_2S-treated broccoli were maintained at a higher level than those of controls after 4 d of storage and then decline. In control tissue, POD increased on day 1 and decreased steadily until 4 d of storage. Figure 4B illustrates similar changes in the activity of APX in broccoli exposed to H_2S or water. APX activity increased in both treatments after 1 d of storage and peaked on day 4 followed by a decline. The activity of APX in H_2S-fumigated broccoli was always higher than that of control during 5 d storage. The activities of CAT in postharvest broccoli under both treatments are described in Figure 4C. CAT activity in H_2S and water controls decreased gradually with the lowest level appearing on days 2 and 3, respectively. Thereafter, CAT activity increased steadily in both treatments, while H_2S fumigation always maintained higher CAT activity than water control. For instance, on day 3 of storage, H_2S fumigation induced a 3-fold increase of CAT activity compared with water control. Figure 4D showed similar variations in GR activities in both treatments, except that H_2S fumigation induced a burst of GR activity on 3 d of storage. GR activities decreased slightly during the first day of storage in both treatments, but H_2S fumigation induced a rapid increase of GR activity until day 3, followed by a sharp decline on day 4. In contrast, GR activity in water control was maintained at a relative lower and stable level compared with H_2S treatment.

LOXs belong to a large family of plant enzymes that catalyze the hydroperoxidation of polyunsaturated fatty acids. Figure 4E showed a similar change pattern in LOX activity between control and H_2S treatment, while H_2S fumigation sustained a lower level of LOX compared with water controls. LOX activity was induced greatly in the first day of storage and then fluctuated in water controls. However, LOX activity was maintained at a lower level in H_2S-treated tissue than in water controls.

Changes in the activities of PPO are illustrated in Figure 4F and show that H_2S fumigation maintained lower PPO activities compared with controls during the entire postharvest storage period. PPO activities increased gradually in control broccoli, while those of H_2S-treated florets were maintained at lower levels. Changes in PAL activity, an enzyme that catalyzes the first step in the phenylpropanoid pathway, are shown in Figure 4G. PAL activity declined during the first day of storage in both treatments. Thereafter, PAL activity increased gradually in water control broccoli, whereas the activity fluctuated at a lower level in H_2S treatment. Surface browning is frequently observed in fresh-cut vegetables and is highly related to the activities of PPO and PAL. We observed lower levels of phenols and lower PAL and PPO activities in H_2S-fumigated broccoli compared with water control, suggesting that H_2S postponed the browning process in postharvest broccoli.

The changes of protease activities are shown in Figure 4H. Consistent with the higher level of soluble protein in H_2S-fumigated broccoli (Figure 2J), the activity of protease in H_2S-fumigated broccoli was always lower than that of controls. On day 2 of storage, protease activity was enhanced greatly in water control broccoli. Consistent with the lower level of protease in H_2S-fumigated broccoli, the total free amino acids in H_2S-fumigated samples were lower than that of water controls (Table 1).

Effect of H_2S on the Relative Expressions of Senescence-Related Genes. Broccoli senescence is accompanied by chlorophyll degradation and protein degradation. Therefore, we examined the effects of H_2S fumigation on the expression of the chlorophyll degradation related genes *BoSGR*, *BoCLH2*, *BoPaO*, *BoRCCR*, cysteine protease gene *BoCP1*, and lipoxygenase gene *BoLOX1*. As shown in Figure 5, the expression of *BoSGR*, *BoCLH2*, *BoPaO*, *BoRCCR*, *BoCP1*, and *BoLOX1* were induced after 2 d of storage in water, suggesting that these genes were expressed along with senescence, while H_2S fumigation showed lower expression levels of these genes on days 2 and 4 of storage. In contrast, the expression levels of *BoNYC*, *BoCLH1*, and *BoPPH* were relatively stable during storage and H_2S fumigation showed marginal effects on the expression of these genes.

Effect of H_2S Fumigation on Dark-Promoted Senescence. Dark treatments have been used as a conventional method to induce plant senescence.[26] Thus, we examined whether H_2S fumigation could alleviate dark-promoted

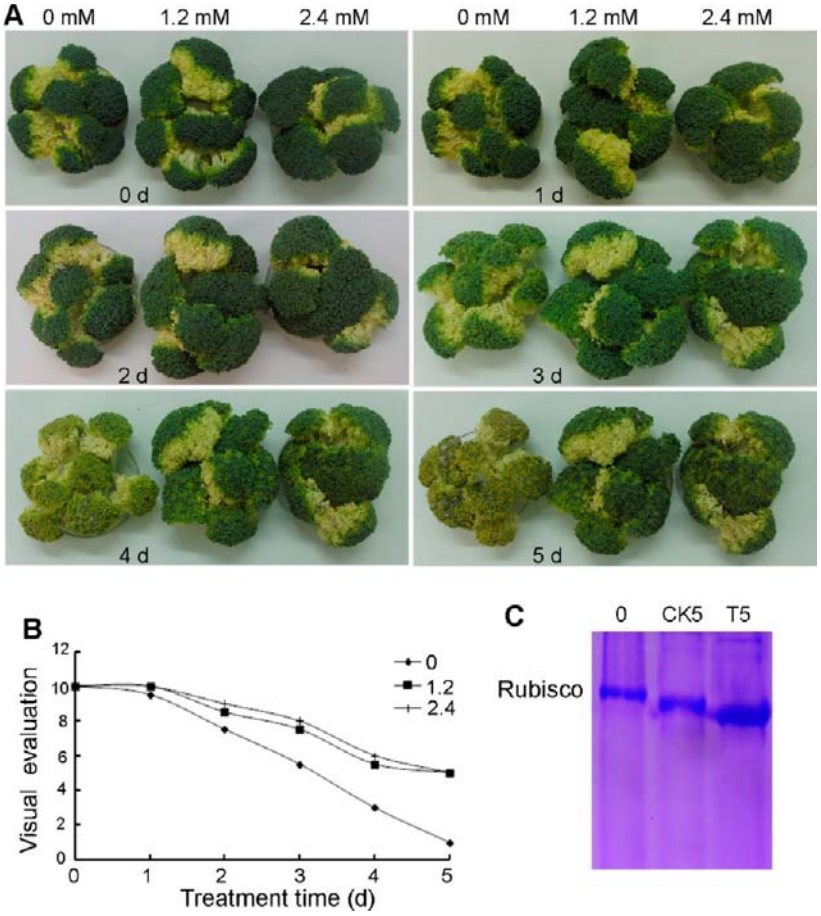

Figure 6. Effects of H_2S on dark-induced senescence, visual evaluation, and Rubisco degradation in postharvest broccoli. Broccoli florets were fumigated with different concentrations (0, 1.2, and 2.4 mM) of aqueous solutions of NaHS for 0−5 d, respectively. Photographs (A) were taken from day 0 to 5, and the visual evaluation (B) was recorded. Effect of H_2S on the degradation of Rubisco in darkness (C) in broccoli florets fumigated with 2.4 mM H_2S donor NaHS aqueous solution (T) and water as the control groups (CK) for 0−5 d. Lanes 1−3 from left to right in part B represent broccoli florets in dark-induced senescence for 0 d, 5 d (CK5), and 5 d (T5), respectively. The proteins of broccoli samples were separated by nondenaturing PAGE and then stained with Coomassie Brilliant Blue R-250.

senescence in broccoli. As shown in Figure 6A, 1.2 and 2.4 mM NaHS treatments effectively alleviated the dark-promoted senescence of postharvest broccoli. Visual evaluation showed that NaHS treatment maintained higher quality of postharvest broccoli than water controls (Figure 6B).

During leaf senescence, Rubisco is gradually degraded, and its components are recycled within the plant; therefore, we examined whether H_2S fumigation alleviated Rubisco degradation during broccoli senescence. As shown in Figure 6C, during dark-promoted senescence, H_2S fumigation maintained higher level of Rubisco compared with water treatment, suggesting the important role of H_2S in alleviating Rubisco degradation.

H_2S Alleviates the Senescence of Other Vegetables and Fruits. As shown in Figure 7, when postharvest lotus root, potato, yams, lettuce, pumpkin, and peach were fumigated with different concentrations of the H_2S donor NaHS, their shelf lives were prolonged. H_2S fumigation also prevented the surface browning of lotus root, potato, yams, lettuce, and peach. This survey of H_2S fumigation on the senescence of these postharvest vegetables and fruits also suggests that the role of H_2S in alleviating senescence might be universal in plants, probably by the activation of the antioxidant enzymes. H_2S also reduced the browning process in fumigated postharvest lotus root, potato, yam, and lettuce, further confirming a role for H_2S in regulating postharvest processes in these plants.

DISCUSSION

Due to the reduction in the content of carbohydrate, protein, vitamins, and antioxidants, broccoli florets are perishable and senescent after harvest.[1,25] As broccoli deteriorates, it undergoes chlorophyll degradation, lipid peroxidation, cell necrosis.[27] Our results show that H_2S can alleviate the senescence of postharvest broccoli under natural and dark-promoted senescence conditions (Figures 1 and 6) and maintain higher contents of nutrients (Figure 2). During postharvest storage, we observed a decrease of chlorophylls, carotenoids, flavonoids, and ascorbate, while H_2S application to postharvest broccoli can alleviate such decreases. The nonenzymatic antioxidant system in plants consists of ascorbate, carotenoids, and flavonoids and is capable of quenching ROS generated during postharvest storage.[28,29] The yellowing of plants is positively correlated to the degradation of chlorophyll.[30] The stable content of chlorophyll under H_2S fumigation, as observed in the present study (Figure 1A), strongly supports the role of H_2S in alleviating senescence. The content of anthocyanin accumulated highly in water control compared to H_2S-fumigated broccoli during storage. Anthocyanin accumulated in leaves during autumn senescence,[31] suggesting that in the present study H_2S fumigation postponed senescence in broccoli florets.

Figure 7. Effect of H_2S fumigation on the senescence of other vegetables and fruits. Fresh-cut vegetables and fruits of lotus root (A), potato (B), yams (C), lettuce (D), pumpkin (E), and peach (F) were fumigated with different concentrations of NaHS as shown in the lower part of every figure. Photographs were taken at different times, as shown in each single figure.

The reducing sugar, soluble protein, soluble solid, and free amino acids were also determined in broccoli during postharvest storage. H_2S sustained higher level of reducing sugar, soluble protein, and soluble solid than water control. In contrast, the total content of free amino acids accumulated more in water control than in H_2S-fumigated broccoli. Consistently, H_2S sustained lower level of protease activity, whose primary role in plant senescence is to remobilize the nutrients out of dying cells into actively growing tissues in the plant.[30]

Overproduction of reactive oxygen species and oxidative damage are universal events during vegetable storage. In the present study, H_2S significantly alleviated the accumulation of superoxide anion, hydrogen peroxide, and MDA. Plants have evolved the capacity to scavenge ROS by antioxidants, such as ascorbate and phenols, and antioxidative enzymes SOD, POD, APX, CAT, and GR.[32] The ascorbate−glutathione cycle maintains homeostasis of ascorbate and glutathione in plants, and consequently, we measured their levels during broccoli senescence.[28] In the present study, we observed decreased levels of H_2O_2, $\bullet O_2^-$, and MDA and enhanced activities of POD, CAT, APX, and GR, suggesting the signaling role of H_2S in activating the antioxidant enzymes.

The senescence of postharvest vegetables is accompanied with lipid peroxidation mediated mainly by LOXs (lipoxygenases). LOXs belong to a large family of plant enzymes that catalyze the hydroperoxidation of polyunsaturated fatty acids and lead to the production of MDA.[27] We found that H_2S sustained lower levels of LOX and lower expression level of *BoLOX1* compared with water control. Correspondingly, the accumulation of MDA was also reduced by H_2S, suggesting that oxidative stress in postharvest broccoli was alleviated by H_2S.

Surface browning is frequently observed in fresh-cut vegetables. Phenylalanine ammonia lyase (PAL) and polyphenol oxidase (PPO) are two key enzymes in the synthesis of free phenolics and the catalytic oxidation of phenolics to brown-colored pigments, respectively, and were found to have a strong relevance to surface browning.[33,34] We observed a lower level of phenols and lower levels of PAL and PPO activities in H_2S-fumigated broccoli compared with water control, implicating that H_2S postponed the browning process in fresh-cut broccoli. The study of H_2S on the senescence of other vegetables and fruits also suggested that the role of H_2S in alleviating senescence might be universal in plants. The reduced browning process observed in H_2S-fumigated fresh-cut lotus root, potato, yam, and lettuce further confirms a role of H_2S in browning inhibition.

H_2S can be produced endogenously in plants, and H_2S emission has been observed in plants attacked by pathogens or when under abiotic stresses as part of sulfur-induced resistance (SIR) response,[5] suggesting a signaling role of H_2S in plant growth and development. More recently, we found that

dx.doi.org/10.1021/jf4047122 | J. Agric. Food Chem. 2014, 62, 1119−1129

exogenous H_2S is involved in preventing senescence of cut flowers and strawberry.[7,8] Álvarez et al. found that the *DES1* mutation led to premature leaf senescence and induced autophagy phenotype in *Arabidopisis*, suggesting an important role of sulfide in senescence.[9,10] The underlying mechanism of hydrogen sulfide in senescence alleviation is not completely known. Here we found that the expression of chlorophyll degradation related genes *BoSGR*, *BoCLH2*, *BoPaO*, *BoRCCR*, cysteine protease gene *BoCP1*, and lipoxygenase gene *BoLOX1* was down-regulated in broccoli fumigated with H_2S during storage. During chlorophyll degradation, transformation from Chl *b* to Chl *a* is catalyzed by a Chl(ide) *b* reductase encoded by a gene named non-yellow coloring 1 (*NYC1*).[35] Dephytilation of chlorophyll by chlorophyllase (CHL) is required in chlorophyll degradation. Schelbert et al. proposed that a new enzyme, pheophytinase (PPH), is involved in dephytilation of pheophytine to generate pheophorbide.[36] Pheophorbide *a* oxygenase (PaO) catalyzes the opening of the porphyrin ring of pheophorbide and generates red chlorophyll catabolytes (RCC). This reaction is followed by the reduction of RCC by RCC reductase (RCCR). Since the photosynthetic competence of *sgr* leaves decreases normally during that period, it is classified as one of the nonfunctional type stay-green mutants. Then we tried to discover whether the delayed yellowing effect of H_2S on broccoli is a nonfunctional stay-green type. We detected the content of Rubisco in dark-promoted senescence and found that H_2S not only alleviated chlorophyll degradation but also prevented Rubisco degradation during senescence of broccoli.

In the present study, H_2S treatment maintained higher levels of metabolites and lower accumulation of ROS and MDA in broccoli compared with water control, suggesting that H_2S treatment provides a safe way to alleviate senescence during vegetable storage. Besides, H_2S could be produced endogenously in plants.[5] Our previous report showed that the levels of endogenous H_2S in fruits treated with exogenous H_2S gas are 10−20% higher than those of the water control, further suggesting its safe usage in postharvest storage.[8]

The ripening and senescence of postharvest vegetables are regulated by endogenous signaling molecules and hormones, including ethylene, jasmonic acid, ABA, H_2O_2, and NO.[8,37−40] In this work, we confirm the role of H_2S in prevention of the senescence of broccoli and other vegetables and fruits, implying that H_2S might be universal signal in endogenous maturation and senescence in plants. However, whether and how H_2S is involved in cross-talk with other hormones and signaling molecules, such as ethylene, jasmonic acid, and NO, requires further elucidation.

AUTHOR INFORMATION

Corresponding Author

*E-mail: hzhanglab@gmail.com. Phone: +86-18919661103. Fax: +86-551-62901043.

Author Contributions

§These authors contributed equally to this work.

Notes

The authors declare no competing financial interest.

ACKNOWLEDGMENTS

We acknowledge Russell Jones, University of California at Berkeley, for critical reading of the manuscript. This work was supported by Natural Science Foundation of China (31271803, 31301820, 31300133), the Scientific Research Foundation for Returned Overseas Chinese Scholars (SRF for ROCS, SEM), the Natural Science Foundations of Anhui Province (11040606M85), and the Anhui Provincial Education Department (2012AJZR0028, ZD200910).

ABBREVIATIONS USED

APX, ascorbate peroxidase; CAT, catalase; FW, fresh weight; GR, glutathione reductase; LOX, lipoxygenase; MDA, malondialdehyde; $\bullet O_2^-$, superoxide anion; PAL, phenylalanine ammonia lyase; POD, guaiacol peroxidase; PPO, polyphenol oxidase; ROS, reactive oxygen species.

REFERENCES

(1) Fernández-León, M. F.; Fernández-León, A. M.; Lozano, M.; Ayuso, M. C.; González-Gómez, D. Different postharvest strategies to preserve broccoli quality during storage and shelf life: Controlled atmosphere and 1-MCP. *Food Chem.* **2013**, *138*, 564−573.

(2) Page, T.; Griffiths, G.; Buchanan-Wollaston, V. Molecular and biochemical characterization of postharvest senescence in broccoli. *Plant Physiol.* **2001**, *125*, 718−727.

(3) Lisjak, M.; Teklic, T.; Wilson, I. D.; Whiteman, M.; Hancock, J. T. Hydrogen sulfide: Environmental factor or signalling molecule? *Plant Cell Environ.* **2013**, *36*, 1607−1616.

(4) Winner, W. E.; Smith, C. L.; Koch, G. W.; Mooney, H. A.; Bewley, J. D.; Krouse, H. R. Rates of emission of H_2S from plants and patterns of stable sulfur isotope fractionation. *Nature* **1981**, *289*, 672−673.

(5) Rausch, T.; Wachter, A. Sulfur metabolism: A versatile platform for launching defence operations. *Trends Plant Sci.* **2005**, *10*, 503−509.

(6) Zhang, H.; Hu, L. Y.; Hu, K. D.; He, Y. D.; Wang, S. H.; Luo, J. P. Hydrogen sulfide promotes wheat seed germination and alleviates oxidative damage against copper stress. *J. Integr. Plant Biol.* **2008**, *50*, 1518−1529.

(7) Zhang, H.; Hu, S. L.; Zhang, Z. J.; Hu, L. Y.; Jiang, C. X.; Wei, Z. J.; Liu, J.; Wang, H. L.; Jiang, S. T. Hydrogen sulfide acts as a regulator of flower senescence in plants. *Postharvest Biol. Technol.* **2011**, *60*, 251−257.

(8) Hu, L. Y.; Hu, S. L.; Wu, J.; Li, Y. H.; Zheng, J. L.; Wei, Z. J.; Liu, J.; Wang, H. L.; Liu, Y. S.; Zhang, H. Hydrogen sulfide prolongs postharvest shelf life of strawberry and plays an antioxidative role in fruits. *J. Agric. Food Chem.* **2012**, *60*, 8684−8693.

(9) Álvarez, C.; Calo, L.; Romero, L. C.; García, I.; Gotor, C. An *O*-acetylserine (thiol) lyase homolog with L-cysteine desulfhydrase activity regulates cysteine homeostasis in *Arabidopsis*. *Plant Physiol.* **2010**, *152*, 656−669.

(10) Álvarez, C.; García, I.; Moreno, I.; Pérez-Pérez, M. E.; Crespo, J. L.; Romero, L. C.; Gotor, C. Cysteine-generated sulfide in the cytosol negatively regulates autophagy and modulates the transcriptional profile in *Arabidopsis*. *Plant Cell* **2012**, *24*, 4621−4634.

(11) Alvarez, M. V.; Ponce, A. G.; Moreira, M. R. Antimicrobial efficiency of chitosan coating enriched with bioactive compounds to improve the safety of fresh cut broccoli. *LWT-Food Sci. Technol.* **2012**, *50*, 78−87.

(12) Lichtenthaler, H. K.; Wellburn, A. R. Determinations of total carotenoids and chlorophylls *a* and *b* of leaf extracts in different solvents. *Biochem. Soc. Trans.* **1983**, *11*, 591−592.

(13) Nath, A.; Bagchi, B.; Misra, L. K.; Deka, B. C. Changes in postharvest phytochemical qualities of broccoli florets during ambient and refrigerated storage. *Food Chem.* **2011**, *127*, 1510−1514.

(14) Pirie, A.; Mullins, M. G. Changes in anthocyanin and phenolics content of grapevine leaf and fruit tissues treated with sucrose, nitrate and abscisic acid. *Plant Physiol.* **1976**, *58*, 468−472.

(15) Zhishen, J.; Mengcheng, T.; Jianming, W. The determination of flavonoid contents in mulberry and their scavenging effects on superoxide radicals. *Food Chem.* **1999**, *64*, 555−559.

(16) Lee, H. S.; Wicker, L. Anthocyanin pigments in the skin of lychee fruit. *J. Food Sci.* **1991**, *56*, 466−468.
(17) Miller, G. L. Use of dinitrosalicylic acid reagent for determination of reducing sugar. *Anal. Chem.* **1959**, *31*, 426−428.
(18) Jiang, W.; Sheng, Q.; Jiang, Y.; Zhou, X. Effects of 1-methylcyclopropene and gibberellic acid on ripening of Chinese jujube (*Zizyphus jujuba* M) in relation to quality. *J. Food Agric.* **2003**, *84*, 31−35.
(19) Bradford, M. M. A rapid and sensitive method for the quantitation of microgram quantities of protein utilizing the principle of protein−dye binding. *Anal. Biochem.* **1976**, *72*, 248−254.
(20) Benjamin, N. D.; Montgomery, M. W. Polyphenol oxidase of Royal Ann cherries: Purification and characterization. *Food Sci.* **1973**, *38*, 799−806.
(21) Beaudoin-Eagan, L. D.; Thorpe, T. A. Tyrosine and phenylalanine ammonia lyase activities during shoot initiation in tobacco callus cultures. *Plant Physiol.* **1985**, *78*, 438−441.
(22) Reimerdes, E. H.; Klostermeyer, H. [3] Determination of proteolytic activities on casein substrates. *Methods Enzymol.* **1976**, *45*, 26−28.
(23) Hasperué, J. H.; Gómez-Lobato, M. E.; Chaves, A. R.; Civello, P. M.; Martínez, G. A. Time of day at harvest affects the expression of chlorophyll degrading genes during postharvest storage of broccoli. *Postharvest Biol. Technol.* **2013**, *82*, 22−27.
(24) Ono, Y.; Wada, S.; Izumi, M.; Makino, A.; Ishida, H. Evidence for contribution of autophagy to Rubisco degradation during leaf senescence in *Arabidopsis thaliana*. *Plant Cell Environ.* **2013**, *36*, 1147−1159.
(25) Singh, J.; Upadhyay, A. K.; Prasad, K.; Bahadur, A.; Rai, M. Variability of carotenes, vitamin C, E and phenolics in *Brassica* vegetables. *J. Food Compost. Anal.* **2007**, *20*, 106−112.
(26) Smart, C. M. Tansley review no. 64. Gene expression during leaf senescence. *New Phytol.* **1994**, *126*, 419−448.
(27) Gomez-Lobatoa, M. E.; Civello, P. M.; Martínez, G. A. Expression of a lipoxygenase encoding gene (*BoLOX1*) during postharvest senescence of broccoli. *Postharvest Biol. Technol.* **2012**, *64*, 146−153.
(28) Noctor, G.; Foyer, C. H. Ascorbate and glutathione: Keeping active oxygen under control. *Annu. Rev. Plant Physiol. Plant Mol. Biol.* **1998**, *49*, 249−279.
(29) Apel, K.; Hirt, H. Reactive oxygen species: Metabolism, oxidative stress, and signal transduction. *Annu. Rev. Plant Biol.* **2004**, *55*, 373−399.
(30) Eason, J. R.; Ryan, D. J.; Watson, L. M.; Hedderley, D.; Christey, M. C.; Braun, R. H.; Coupe, S. A. Suppression of the cysteine protease, aleurain, delays floret senescence in *Brassica oleracea*. *Plant Mol. Biol.* **2005**, *57*, 645−657.
(31) Keskitalo, J.; Bergquist, G.; Gardeström, P.; Jansson, S. A cellular timetable of autumn senescence. *Plant Physiol.* **2005**, *139*, 1635−1648.
(32) Mittler, R.; Vanderauwera, S.; Gollery, M.; Van Breusegem, F. Reactive oxygen gene network of plants. *Trends Plant Sci.* **2004**, *9*, 490−498.
(33) Nguyen, T. B. T.; Ketsa, S.; van Doorn, W. G. Relationship between browning and the activities of polyphenoloxidase and phenylalanine ammonia lyase in banana peel during low temperature storage. *Postharvest Biol. Technol.* **2003**, *30*, 187−193.
(34) Mishra, B. B.; Gautan, S.; Sharma, A. Free phenolics and polyphenol oxidase (PPO): The factors affecting post-cut browning in eggplant (*Solanum melongena*). *Food Chem.* **2013**, *139*, 105−114.
(35) Hörtensteiner, S.; Kräutler, B. Chlorophyll breakdown in higher plants. *Biochim. Biophys. Acta* **2011**, *1807*, 977−988.
(36) Schelbert, S.; Aubry, S.; Burla, B.; Agne, B.; Kessler, F.; Krupinska, K.; Hörtensteiner, S. Pheophytin pheophorbide hydrolase (pheophytinase) is involved in chlorophyll breakdown during leaf senescence in *Arabidopsis*. *Plant Cell* **2009**, *21*, 767−785.
(37) Leshem, Y. Y.; Wills, R. B.; Ku, V. V. V. Evidence for the function of the free radical gas—nitric oxide (NO•)—as an endogenous maturation and senescence regulating factor in higher plants. *Plant Physiol. Biochem.* **1998**, *36*, 825−833.
(38) Zhu, S. H.; Zhou, J. Effect of nitric oxide on ethylene production in strawberry fruit during storage. *Food Chem.* **2007**, *100*, 1517−1522.
(39) Jiang, Y.; Joyce, D. C. ABA effects on ethylene production, PAL activity, anthocyanin and phenolic contents of strawberry fruit. *Plant Growth Regul.* **2003**, *39*, 171−174.
(40) Manjunatha, G.; Lokesh, V.; Neelwarne, B. Nitric oxide in fruit ripening: Trends and opportunities. *Biotechnol. Adv.* **2010**, *28*, 489−499.

partitioning of skin tannin[19] compared extraction in buffered solution (pH 7.5) to tannin remaining bound to the residue following extraction, presumed to be cell wall fragments. Both the buffer-soluble extract, designated the vacuolar fraction, and the cell wall-bound fraction were further extracted using acidified methanol.[19] The experiment showed that the mean degree of polymerization (mDP) of tannin within the vacuole did not change during grape development, yet the mDP of tannins associated with the cell wall was higher and tended to increase at the end of maturation. However, in said study,[19] the mDP of tannins isolated from cell walls was markedly lower than observations from studies on the same cultivar using 70% v/v acetone extraction.[10,14,16] This may indicate that a greater fraction of tannin is desorbed from the grape cell wall using acetone. This phenomenon has been shown definitively for tannin extracted from apple using methanol or aqueous acetone, in which acetone extraction yielded tannin of higher mDP.[22] Furthermore, in that work, aqueous acetone was shown to completely desorb high mDP tannin bound to cell wall material, in a fashion similar to the application of urea. It is therefore evident that further research is needed to better understand the factors which influence partitioning of tannin to extractable and nonextractable fractions.

Recent work using model studies has demonstrated the high affinity of purified grape cell wall material for tannin and highlighted that these interactions may limit tannin extraction during vinification. This may explain some of the significant variability that is observed in wine-extractable tannin between grape cultivars and grape ripeness stages.[16,23−26] For grape skin tannin from red grapes, highly polymerized tannins had a low affinity for skin cell walls compared with tannin of intermediate molecular mass.[16] However, it was found that with the progression of ripening, changes in skin cell wall composition facilitated an enhanced adsorption of this high mDP tannin fraction.[25] Structural changes in skin cell wall polysaccharides were found to occur early in grape development, before or close to veraison, and as such the altered adsorption properties of cell wall material for tannin during late-stage ripening could not be directly linked to changes in polysaccharide composition. Rather, it was noted that the specific enhancement of high molecular mass tannin adsorption was consistent with increases in cell wall porosity. Theoretically, an enhanced porosity could enable penetration and encapsulation of high molecular mass tannins within the cell wall structure and has been observed to contribute to cell wall−tannin interactions in apple.[27−29] In ripening grapes, multiple factors may influence tannin extractability: interactions with cell walls, cell integrity, tannin concentration, tannin molecular mass, tannin structural modification, and interaction with other phenolics, including self-association.[30] As reviewed here, these factors can change simultaneously during grape ripening, rendering the system highly complex.

The work presented in the current study has sought to build on previous research using model experiments, to observe how differences at a cellular level might affect skin tannin extractability during ripening. Extraction of grape skins has been carried out in various concentrations of aqueous ethanol to determine whether differences in tannin extractability could be related to ripening stage. In certain samples, ethanolic extraction was compared to a harsh or "total" extraction in 70% v/v acetone. Whole extracts were subjected to gel permeation chromatography (GPC) to observe whether changes in tannin extractability were associated with differences in tannin molecular mass distribution. Tannin and anthocyanin solutions were combined with isolated cell walls to determine the effect of concentration on their respective adsorption affinities. In addition, scanning electron microscopy (SEM) and nitrogen adsorption isotherms were used to characterize changes in cell wall surface area (porosity) during ripening.

MATERIALS AND METHODS

Instrumentation. An Agilent model 1100 HPLC (Agilent Technologies Australia Pty Ltd., Melbourne, Australia) was used with Chemstation software for chromatographic analyses. For SEM, a Philips XL30 field emission scanning electron microscope (Philips, Eindhoven, The Netherlands) was used.

Grape Sample Preparation and Extraction. *Vitis vinifera* L. cv. Cabernet Sauvignon grape samples were obtained from a commercial vineyard in the Langhorne Creek growing region of South Australia (Pernod Ricard Australia, Orlando Wines) at different commercial ripeness stages in the 2010 season. Berry samples were collected from three rows distributed within the vineyard block to obtain a representative sample, pooled, and processed fresh. A 200 berry subsample was processed fresh, and the juice centrifuged at 1730g for 5 min and analyzed for total soluble solids (°Brix) using a digital refractometer. This data has been published previously.[3] Triplicate subsamples of 100 berries were prepared for cell wall isolation, and a further 36 subsamples of 10 berries each were prepared for phenolic extraction experiments.

The 100-berry samples were weighed, and skins were then separated from flesh and seed while kept on ice. Recovered skin material was weighed to determine the proportion of fresh skin material to total berry mass, frozen in liquid nitrogen, and stored at −80 °C until used for the isolation of cell wall material. Cell wall material was isolated from frozen grape skins as described previously.[25] For the purpose of comparing ripening-related changes in cell walls, two early-stage (preveraison and veraison) cell wall samples were retained from a previous study.[25]

The 10-berry samples were peeled, and the skins were rinsed with ice-cold 30 mM aqueous citric acid, gently blotted with a paper towel, weighed, and immediately transferred to 30 mL of extraction solvent. Four different extraction solvents were used, 10, 20, or 50% v/v ethanol and 70% v/v acetone, each containing aqueous 0.01% v/v trifluoroacetic acid (TFA). To minimize sample degradation and prevent any partial extraction during the rinsing step, a maximum number of 10 fresh berries could be processed per experiment. The ratio of solid material to solvent was 1:15, according to the optimal conditions described by Verries and co-workers,[21] to ensure that extraction efficiency was not influenced by saturation of the extraction medium, and the concentrations of tannin and anthocyanin within extracts did not exceed 1 and 0.6 g/L, respectively. Extractions were in triplicate, performed at 25 °C in the dark, under nitrogen in sealed 50 mL centrifuge tubes. To ensure continuous contact of skins and solvent, centrifuge tubes were placed flat and mixed gently using a platform shaker. All extractions were performed over 64 h to keep the conditions consistent between experiments. The extraction time was selected to optimize tannin extraction in dilute ethanol solutions (10 and 20% v/v), which was maximal at 64 h, whereas tannin extraction containing 50% v/v ethanol or 70% v/v acetone reached a plateau at 42 h (Supporting Information Figure S1). Following extraction, 50 mL tubes containing residual skin solids were centrifuged at 1730*g* for 5 min, and aliquots of the supernatant were directly analyzed as described below.

Analysis of Skin Tannin and Anthocyanin. A 500 μL aliquot of 70% v/v acetone extract was dried under a stream of nitrogen and reconstituted in the same volume of aqueous ethanol (20% v/v). Aqueous ethanol extracts were directly analyzed in duplicate. Tannin and anthocyanin concentrations in aqueous ethanolic extracts were determined in a 96-well plate format using the high-throughput method described previously.[31] Tannin concentration was expressed as (−)-epicatechin equivalents using an external standard curve (Sigma-Aldrich, St. Louis, MO, USA). To standardize tannin analysis across

Table 1. Tannin and Anthocyanin Content Per Berry at Different Total Soluble Solids Level Determined by Extraction in Aqueous Ethanol[a]

		tannin		anthocyanin	
extraction solvent	total soluble solids (°Brix)	mg/berry	mg/g skin FW	mg/berry	mg/g skin FW
10% ethanol	22	0.50 ± 0.10g	2.55 ± 0.52e	0.94 ± 0.04g	4.75 ± 0.19g
	23	0.70 ± 0.01fg	3.56 ± 0.03de	1.07 ± 0.02fg	5.47 ± 0.08fg
	24	0.81 ± 0.05f	4.07 ± 0.26d	1.17 ± 0.01fg	5.86 ± 0.04fg
	26	0.91 ± 0.05ef	4.36 ± 0.28d	1.25 ± 0.09ef	5.98 ± 0.45f
20% ethanol	22	0.74 ± 0.06f	3.72 ± 0.31d	1.09 ± 0.09fg	5.49 ± 0.46fg
	23	1.25 ± 0.06cd	6.38 ± 0.32c	1.58 ± 0.13d	8.06 ± 0.64de
	24	1.13 ± 0.04de	5.65 ± 0.18c	1.44 ± 0.02d	7.21 ± 0.08e
	26	1.38 ± 0.05c	6.59 ± 0.25c	1.66 ± 0.05cd	7.96 ± 0.26de
50% ethanol	22	1.29 ± 0.11cd	6.54 ± 0.55c	1.67 ± 0.13cd	8.42 ± 0.68cd
	23	2.01 ± 0.10b	10.27 ± 0.51b	1.93 ± 0.11b	9.86 ± 0.57b
	24	1.95 ± 0.07b	9.75 ± 0.35b	1.90 ± 0.06bc	9.51 ± 0.31bc
	26	2.64 ± 0.11a	12.63 ± 0.54a	2.39 ± 0.09a	11.45 ± 0.44a

[a]Data are the mean ± SE. Data compared by ANOVA, $n = 36$, $P < 0.001$, followed by post-hoc Student's t test; different letters indicate statistically significant differences between means. FW, fresh weight.

the staggered time points at which grape sampling and extraction took place, a purified commercial seed extract (Tarac Technologies, Nuriootpa, Australia) was included for each 96-well plate assayed. Data were expressed on a skin weight and per berry basis. Berry weight data have been previously published.[25]

Gel Permeation Chromatography. An aliquot of each skin extract was dried under a stream of nitrogen and recovered in *N*,*N*-dimethylformamide. Samples were centrifuged at 16000*g* for 5 min and directly analyzed by GPC as describedin ref 32. Preveraison skin tannin fractions of known molecular mass (by phloroglucinolysis) were used as standards for calibration.[23] For calibration, a second-order polynomial was fitted with the tannin elution time at 50% for each standard.

Cell Wall Surface Area. The cell wall material samples were mounted on specimen stubs with carbon tabs and coated with 5 nm of platinum in a Cressington 208HR sputter coater (Cressington Scientific Instruments Ltd., Watford, UK). Samples were examined in a Philips XL30 field emission scanning electron microscope operated at an accelerating voltage of 10 kV. Specific surface areas of dry cell wall isolates were determined using an automated manometric gas adsorption apparatus[33] providing data collection for samples at 77 K and subatmospheric pressures. An accurate liquid nitrogen level control of up to ±0.2 mm was achieved and maintained throughout each measurement by a custom-built liquid nitrogen delivery system.[34] Ultrahigh-purity grade gaseous helium (>99.9%) and ultrahigh-purity grade gaseous nitrogen (>99.9%) (both from BOC Gases, Australia) were used for dead-volume and nitrogen adsorption measurements at 77 K, respectively. Duplicate analyses were performed at staggered points in the construction of nitrogen adsorption isotherms to confirm the reproducibility of measurements.

Binding Reaction of Tannin and Cell Wall Material. Skins prepared fresh from commercially ripe Cabernet Sauvignon grape samples were extracted for 18 h in either 70% v/v acetone or 15% v/v ethanol containing 0.01% v/v TFA. Tannin was purified from extracts according to a published method.[24] Tannin isolates were characterized by phloroglucinolysis,[12] which yielded mDP values of 11 units for the 15% v/v ethanol extract and 33 units for the 70% v/v acetone extract. The absence of monomeric phenolics, in particular anthocyanin, from the tannin fractions was confirmed by GPC analysis[32] (negligible material eluting later than 16.3 min). Tannin solutions were prepared in 12% v/v ethanol containing 0.01% v/v TFA. Tannin concentrations were from a minimum of 0.25 g/L and up to a maximum of 10 g/L. These were combined in 1 mL aliquots with 10 mg of a skin cell wall preparation, which corresponded to the most ripe harvest date in the current study, in 1.5 mL centrifuge tubes. Cell wall solutions were vortexed and then incubated for 1 h at 27 °C with shaking and thereafter centrifuged at 16000*g* for 20 min. For each experiment a standard blank of the respective tannin solution without cell wall material was included. Supernatants were analyzed by GPC. The loss of tannin in supernatants through interaction with cell wall material was determined by difference in GPC peak area, calibrated for the respective tannin preparations used in the study, as described previously.[26] Adsorption isotherms were fitted using the Langmuir equation,[35] modeling the quantity of tannin bound (mg/g) as a function of the concentration of tannin remaining in solution, at theoretical equilibrium. Curve fit R^2 values of 0.99 were obtained for both tannin types tested, and these results were used to derive the apparent affinity constant (K_L) and the maximum adsorption capacity N_{max} of cell wall material for each tannin type, where N represents the mass of tannin bound (mg) per gram of cell wall material.

Binding Reaction of Monoglucoside Anthocyanins with Cell Wall Material. Shiraz grapes at commercial ripeness (24 °Brix) were partially homogenized with a blender. Crude methanolic extracts (50% v/v) were prepared from the grape slurry and then concentrated under reduced pressure at 30 °C. A Toyopearl (660 mL bed volume) column equilibrated with 0.1% v/v TFA was prepared, and aqueous extracts were loaded in 100 mL batches. Water-soluble nonadsorbent compounds were eluted in 2 L of the loading solvent. The monoglucoside anthocyanin fraction was eluted with 1.5 L of 30% v/v methanol containing 0.1% v/v TFA. The column was then washed with 2 L of 2:1 v/v acetone/water and re-equilibrated with 0.1% v/v TFA. The eluate was concentrated under reduced pressure at 30 °C, frozen at −80 °C, and then lyophilized, yielding ≅200 mg of dry material, which was stored under nitrogen at −80 °C until used. Extract purity was verified by HPLC,[31] and the sample was free of acetylated or coumaroylated anthocyanins, derived pigments, and polymeric material. The extract was found to have trace quantities of early-eluting material at 280 nm, but this was below the detection limit for quantification, indicating minimal contribution of non-anthocyanin phenolics. Anthocyanin concentration was determined as the sum of individual 3-*O*-monoglucoside anthocyanins, as malvidin-3-glucoside units using a commercial standard (Polyphenols Laboratories, Norway). Anthocyanin was added to a solution of 12% v/v ethanol containing 0.01% v/v TFA at increasing concentration from 0.1 and 2 g/L either alone or combined with a 1.25 g/L solution of the 33 mDP tannin. These were combined in 1 mL aliquots with 10 mg of a skin cell wall preparation that corresponded to the most ripe harvest date in the current study, in 1.5 mL centrifuge tubes. Cell wall solutions were vortexed and then incubated for 1 h at 27 °C with shaking and thereafter centrifuged at 16000*g* for 20 min. Methyl cellulose

dx.doi.org/10.1021/jf4050606 | J. Agric. Food Chem. 2014, 62, 1130−1141

precipitation[31] was selected to analyze tannin concentration in supernatants. This was due to the potential interference of a high anthocyanin concentration in the phloroglucinolysis and GPC methods, which would require an additional sample purification step. Anthocyanin was analyzed as the sum of individual 3-*O*-monoglucosides, quantified by HPLC.[31] Anthocyanin adsorption isotherms were fitted using the Langmuir equation as described for tannin adsorption experiments, above.

RESULTS AND DISCUSSION

Skin Tannin and Anthocyanin Extraction in Aqueous Ethanol. The extraction of both skin tannin and anthocyanin increased with the addition of ethanol to the solvent (Table 1). For extraction using dilute, 10% v/v ethanol, significant increases in both tannin and anthocyanin content were evident only between the first sampling point (22 °Brix) and the final sampling point (26 °Brix). When 20% v/v ethanol was used as the extraction solvent, extractable tannin and anthocyanin content increased from the first to the second sampling point and thereafter remained constant. When ethanol concentration was increased to 50% v/v, it was evident that there was an increase in the extraction of both skin tannin and anthocyanin with advancing ripeness. However, for the transition from 23 to 24 °Brix, there was no increase in either anthocyanin or tannin extracted in 50% v/v ethanol from the skin samples.

Partitioning of Tannin to a Nonextractable Fraction. In the previous experiment it was reported that no differences were found in the extraction of tannin in dilute ethanol (10 and 20% v/v) between the 23, 24, and 26 °Brix samples. Extraction in 70% v/v acetone was also performed on samples from these ripeness stages and is hereafter referred to as "total" tannin, because this acetone/water ratio presents a more exhaustive extraction for tannin than the ethanol-based solvents.[17] Nevertheless, we note that some residual high molecular mass tannin remains nonextractable in 70% v/v acetone,[24,25] which was not accounted for in the current sample set.

It was found that during late-stage ripening, there was a continuous increase in total skin tannin content (Figure 1). When the tannin content extracted at different ethanol concentrations was expressed as a percentage of total tannin,

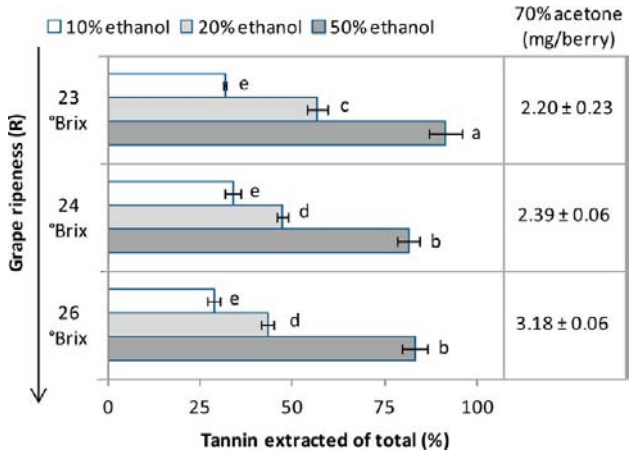

Figure 1. Ripening-related changes in tannin extracted using an increasing concentration of aqueous ethanol as a proportion (%) of total tannin extractable in aqueous acetone (data are the mean ± SE; data compared by ANOVA, $n = 27$, $P < 0.001$, followed by post-hoc Student's t test; different letters indicate statistically significant differences between means).

the proportion of tannin extractable in 10% v/v ethanol remained constant during ripening. However, at 20 and 50% v/v ethanol, it was evident that with the progression of ripening a fraction of skin tannin became nonextractable at 24 and 26 °Brix in comparison with the 23 °Brix sample. As a more hydrophobic solvent, ethanol disrupts hydrophobic interactions, potentially between tannin and cell walls, protein, or other skin phenolics,[36] thereby facilitating greater extraction. It is evident that a portion of grape skin tannin remained readily extractable in aqueous ethanol, independent of the total tannin concentration.

To characterize the size distribution of fractions extractable under the different solvent conditions, extracts were subjected to GPC analysis (Figure 2). The cumulative molecular mass distribution based on unpurified extracts represents both polymeric material and smaller molecular mass phenolics. For all of the GPC distribution data, quantitatively greater differences in molecular mass between treatments were evident at later elution by GPC (70% elution), which corresponds to the polymeric fraction (mDP ≅ 3−15). This is consistent with the observed increases in tannin concentration with increasing ethanol concentration in the solvent (Table 1). For all ethanolic extracts, the distribution was shifted toward a higher molecular mass average with advancing ripeness (Figure 2A−C). For 70% v/v acetone extracts, the curves were more closely overlaid (Figure 2D), indicating that higher total grape tannin content resulted in increases across the entire molecular mass distribution. Two effects are evident: first, that higher molecular mass tannins were increasingly extracted as solvent polarity decreased and, second, that at the latest grape sampling point, a fraction of intermediate molecular mass tannin was more extractable in ethanol. This finding points to greater complexity in the factors that drive tannin extractability of during ripening and raises questions as to whether there are (a) changes in the interaction of tannin with skin cell walls with advancing ripeness; (b) changes in tannin concentration that affect the selectivity of tannin adsorption by cell walls as a function of tannin molecular mass; and/or (c) changes in the composition of other phenolics, namely, anthocyanins, that affect the interaction of tannin with cell walls. These questions are further addressed below through cell wall characterization and model adsorption experiments.

Analysis of Grape Cell Wall Surface Characteristics with Advancing Ripeness. Previous research on the tannin adsorption properties of skin cell walls from the same grape sample series presented in the current study demonstrated that the selective adsorption of high molecular mass tannin increased in the late stages of ripening.[25] The analysis of cell wall polysaccharides indicated that major compositional changes occurred around veraison, with a preveraison loss of galacturonic acid (galacturonan) followed by losses in arabinogalactan I, consistent with published research.[37] However, compositional changes in cell wall polysaccharides in late-stage ripening were found to be minor and could not be used to qualify the changes in cell wall binding properties for tannin. These cell wall samples[25] were further characterized by SEM and for surface area using nitrogen adsorption isotherms. It is evident from scanning electron micrographs that preveraison grape cell walls display a regular, relatively smooth (Figure 3A) surface structure with defined pit fields (Figure 3B). The presence of defined pit fields was not detectable in cell walls imaged at veraison (Figure 3C), which is consistent with losses in homogalacturonan-rich regions of the cell wall,[38]

dx.doi.org/10.1021/jf4050606 | J. Agric. Food Chem. 2014, 62, 1130−1141

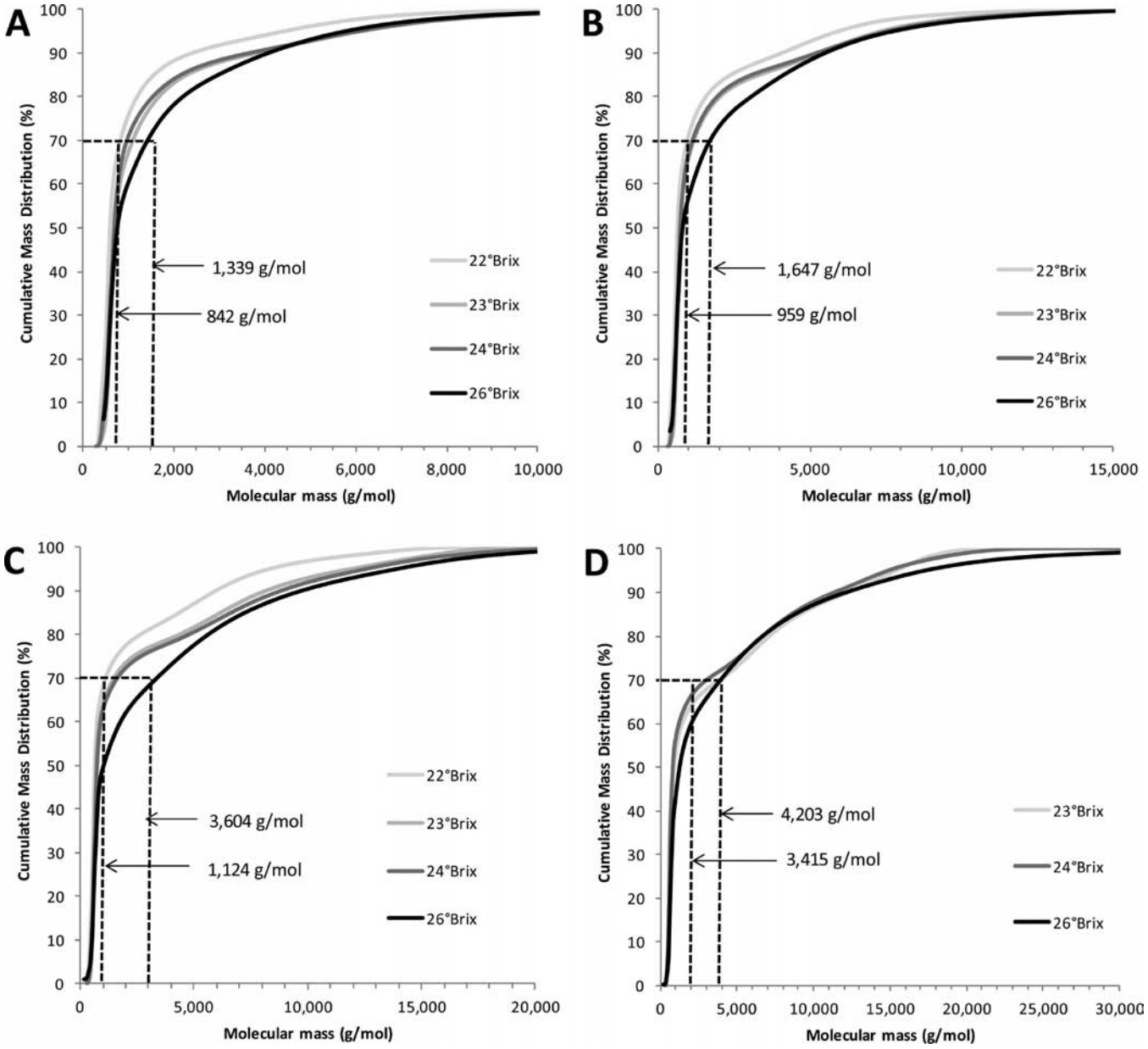

Figure 2. Cumulative molecular mass distribution of grape skin extracts at different ripeness levels according to their grape juice total soluble solids determined by gel permeation chromatography: (A) extracts in 10% v/v ethanol; (B) extracts in 20% v/v ethanol; (C) extracts in 50% v/v ethanol; (D) extracts in 70% v/v acetone.

which confirmed earlier cell wall analysis.[25] In the later stages of ripening, deepening of folds in the cell wall was evident, leading to a "wavy" appearance (Figure 3D–F). Initially, we considered that this might be a fault of the tissue preparation method, because lyophilization is noted to cause collapse of the cell wall structure and a reduction in macroporosity.[28] This effect is particularly evident in the case of harsher drying methods.[27] However, we note that this phenomenon has been documented previously in fixed tissue from ripening grape skins, using transmission electron microscopy.[39] The authors proposed that a "wavy" appearance resulted from localized swelling of the cell wall. However, it was noted that the appearance of an undulating cell wall was concomitant with degradation of the middle lamella. Therefore, it is possible that cell wall conformation was retained through the extraction and drying steps, and the SEM images may reflect true changes in cell wall structure with ripening. These observable changes in the surface structure of cell walls were of interest because previous observations related to enhanced adsorption of high molecular mass tannins at late-stage ripening were consistent with a greater cell wall porosity.[25] The working hypothesis is that a greater surface area over which tannin binds to cell walls can occur via hydrogen bonding and hydrophobic interactions within cell wall cavities. In the absence of pores, high molecular mass tannins may be excluded from the cell wall and have limited interaction.[24]

To quantify the SEM observations, and as a prerequisite for employing the unripe cell wall fraction as a reference material, specific surface areas were defined for cell wall preparation from the ripening series. Although the specific surface area of each sample was low, well-defined low-pressure isotherms were obtained with negligible uncertainty (values were approximately

dx.doi.org/10.1021/jf4050606 | J. Agric. Food Chem. 2014, 62, 1130–1141

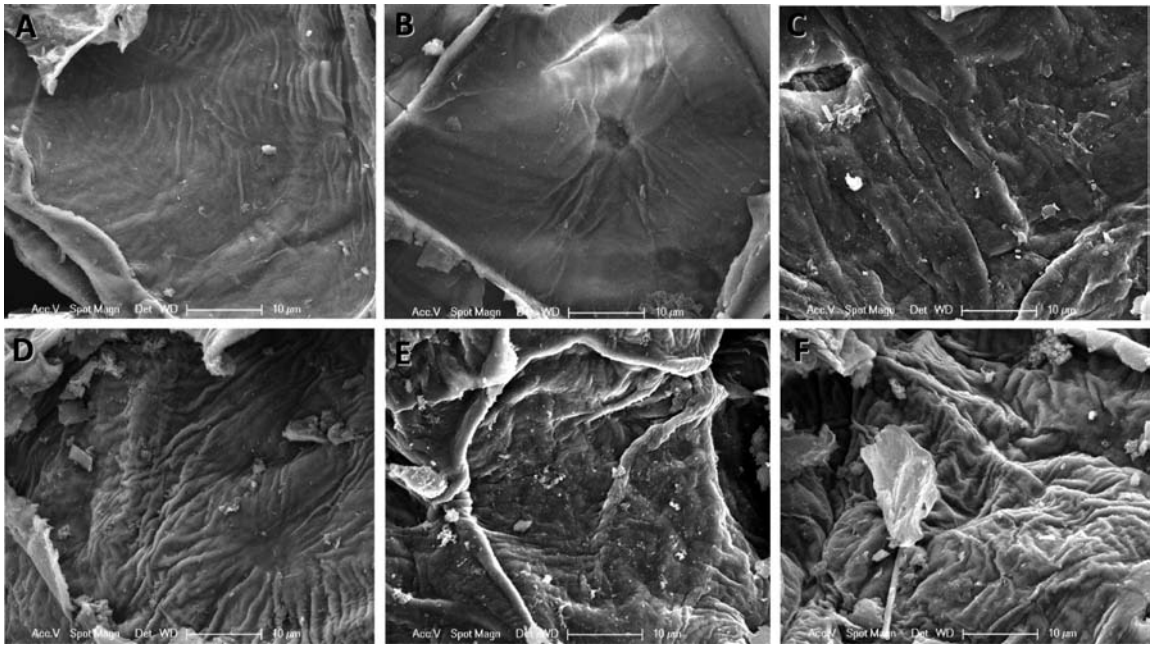

Figure 3. Scanning electron micrographs (5000× magnification) of isolated cell wall material from unripe and ripening Cabernet Sauvignon grape skins: (A, B) January 15, −11 DAV, preveraison; (C) January 26, DAV, veraison; (D) February 23, 28 DAV, 22 °Brix; (E) March 2, 35 DAV, 23 °Brix; (F) March 17, 50 DAV, 26 °Brix (DAV = days after veraison, bars = 10 μm).

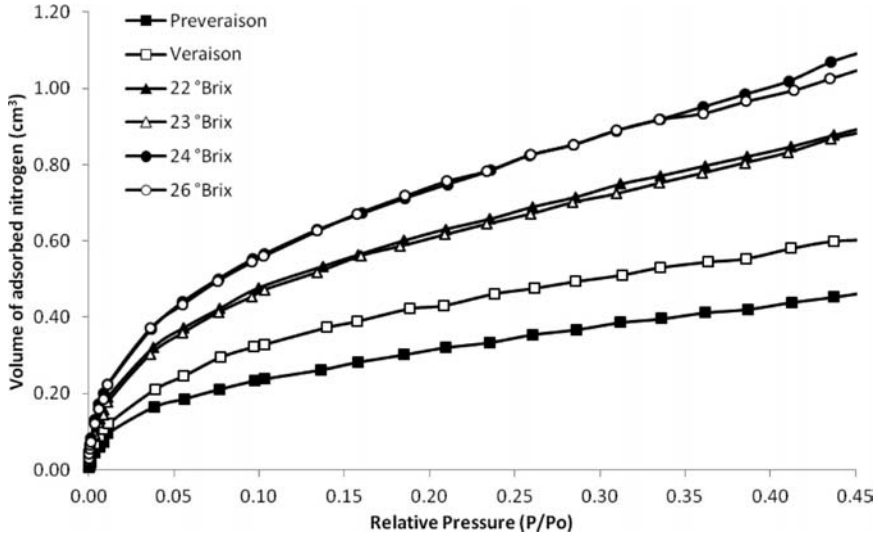

Figure 4. Nitrogen gas adsorption isotherms determined at standard temperature and pressure for isolated cell wall material from unripe and ripening Cabernet Sauvignon grape skins (P = sample cell pressure; Po = nitrogen vapour pressure at 77K; preveraison = January 15, 11 days before veraison; veraison = January 26).

the size of the symbols used) (Figure 4), leading to area values with precision suitable for three significant figures, and this data is presented in Table 2. As expected, the folds seen by SEM represent a roughened surface leading to an increased specific surface area susceptible to nitrogen gas analyses. For the sample series under investigation, two surface area categories were noted in ripening skin cell walls, corresponding to the ripeness grades 22 and 23 °Brix, as distinct from 24 and 26 °Brix, respectively. This conclusion is better defined by reference to the isotherms in Figure 4 than from the subtle, but real, differences in the specific surface areas extracted from these isotherms.

Enhancement of cell wall porosity with the progression of ripening lends support to the hypothesis that greater penetration of high molecular mass tannin within cell wall pores could occur.[25] This could result in a reduced extractability of this tannin fraction with ripening, due to greater encapsulation within pores and, therefore, adsorption by cell wall components. The measurable changes in ethanol-extractable tannin (Table 1) showed that no change in tannin extraction to dilute ethanol solution occurred, despite increases in cell wall porosity. However, when the partitioning of tannin extractable in aqueous ethanol was compared with that by 70% acetone extraction, a stronger relationship with cell wall porosity could be demonstrated (Figure 1). The highest cell wall porosity category was for samples collected at 24 and 26 °Brix (Figure 4; Table 2), and the corresponding samples demonstrated a reduction in ethanol-extractable tannin (in 20

dx.doi.org/10.1021/jf4050606 | J. Agric. Food Chem. 2014, 62, 1130−1141

Table 2. Cell Wall Surface Area Estimated by Nitrogen Adsorption Using the Brunauer–Emmet–Teller (BET) Isotherm Model

sample	surface area (m^2/g)
preripening (control)[a]	
preveraison	1.24
veraison	1.66
ripening[b]	
22 °Brix	2.42
23 °Brix	2.34
24 °Brix	2.87
26 °Brix	2.89

[a]Cell wall samples from unripe grape cell walls in the same developmental series were used as a control for comparison with ripening samples. [b]Cell wall samples isolated from grapes at different stages of commercial ripeness as measured by the juice total soluble solids level.

and 50% v/v ethanol) as a proportion of acetone-extracted tannin. A possible interpretation of this result is that increased porosity in skin cell walls during late-stage ripening may facilitate sequestering of tannins as an adsorbed fraction within the cell wall. On the basis of the published cell wall–tannin interaction data for these samples,[25] it would be expected that the adsorbed tannin fraction would consist primarily of high molecular mass tannin, which is nonextractable even at increased ethanol concentration. Despite this observation, it was evident that increased total acetone-extractable tannin concentration in the final sampling date (26 °Brix) (Figure 1) resulted in two measurable phenomena: (a) enhanced tannin extraction in 50% v/v ethanol (Table 1) and (b) increased tannin molecular mass in the extract (Figure 2C). These observations may be influenced by cell wall porosity but cannot be explained by this effect alone.

Effect of Tannin Concentration and Molecular Mass on the Interaction with a Porous Skin Cell Wall Material. Binding isotherms were constructed for two purified tannins of low and high average molecular mass (mDP 11 and 33). The tannins were prepared using different extraction methods to selectively extract molecular mass classes, 15% v/v ethanol and 70% v/v acetone, and were not subjected to further fractionation. Therefore, both tannin fractions were heterogeneous in terms of their molecular mass distribution (data not shown). In particular, the 70% v/v acetone extract had a distribution of high (>15000 g/mol), intermediate, and low molecular mass material, which reflects the broad spectrum present in grape skins in situ. The dilute ethanol extract reflected the distribution of wine-extractable skin tannin (<15000 g/mol).

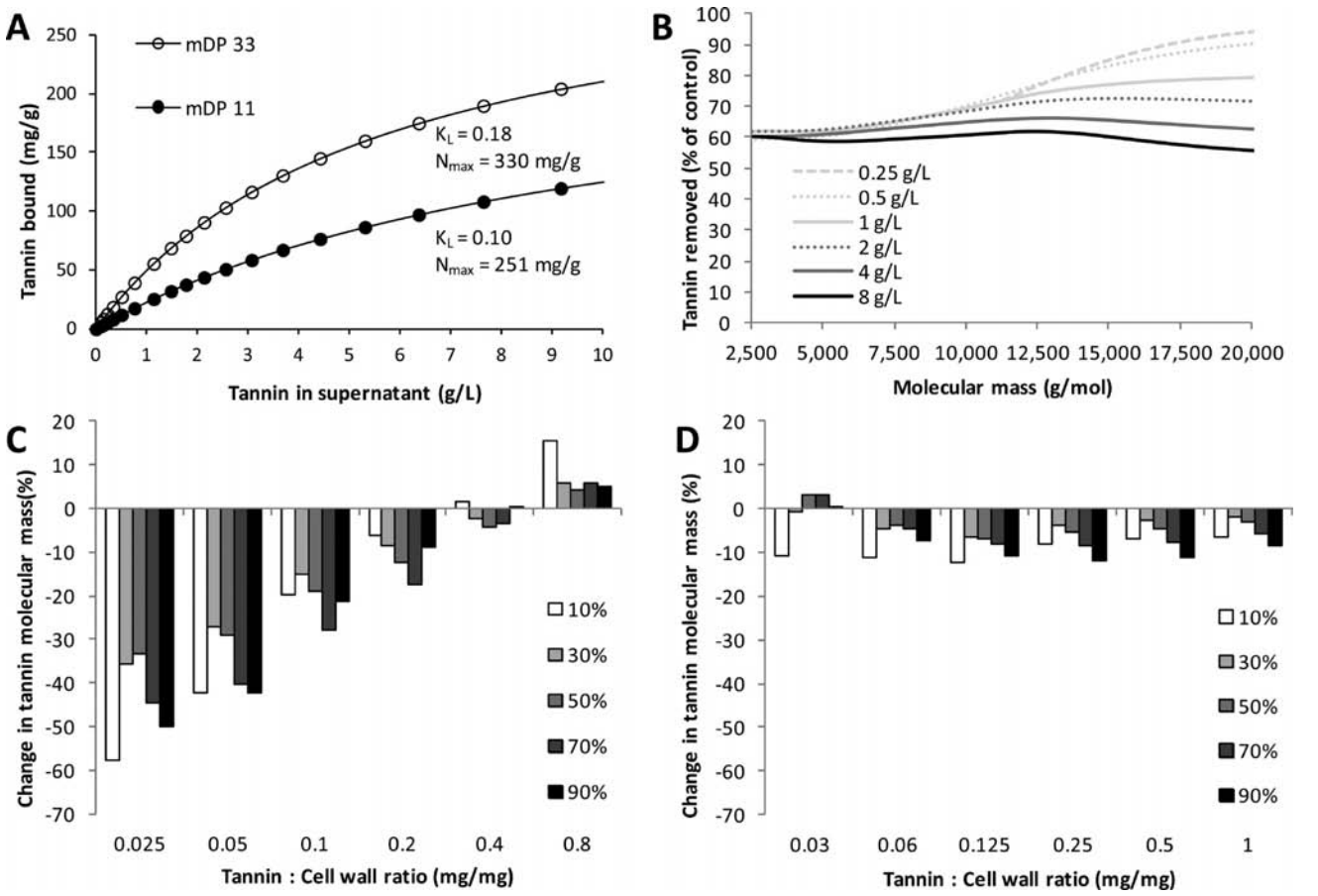

Figure 5. Effect of skin tannin concentration and mean degree of polymerization (mDP) on the binding reaction with 10 mg of porous, ripe skin cell wall material (26 °Brix), analyzed by gel permeation chromatography: (A) constructed adsorption isotherms for mDP 33 and mDP 11 tannins with estimated affinity constants (K_L) and maximum adsorption capacity (N_{max}); (B) percentage of mDP 33 tannin removed by adsorption to cell walls as a function of tannin molecular mass; (C) change in cumulative molecular mass (% elution) following adsorption of mDP 33 tannin; (D) change in cumulative molecular mass (% elution) following addition of mDP 11 tannin.

dx.doi.org/10.1021/jf4050606 | J. Agric. Food Chem. 2014, 62, 1130–1141

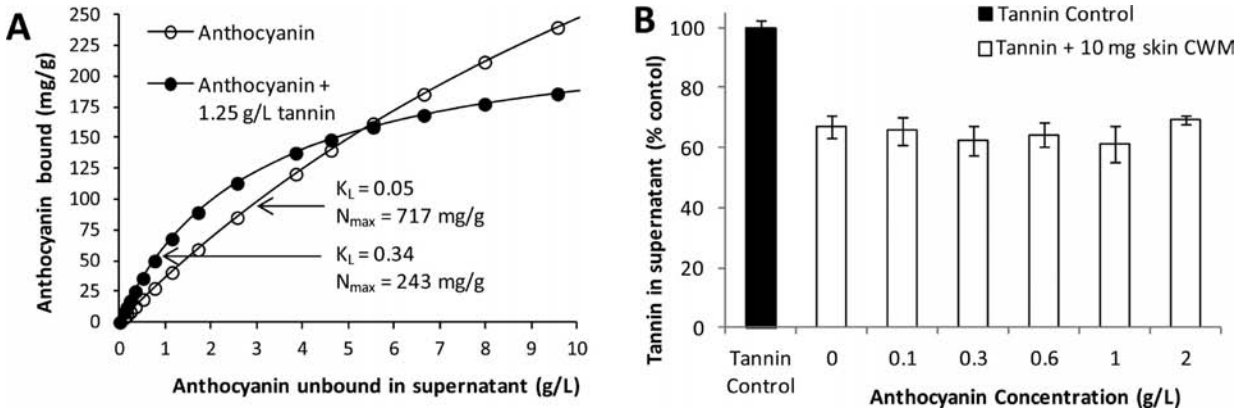

Figure 6. Binding reaction of a porous, ripe skin cell wall material (26 °Brix) with monoglucoside anthocyanin, alone or in combination with 1.25 g/L of a purified skin tannin extract (mDP 33.1): (A) adsorption isotherms showing estimated affinity constants (K_L) and maximum adsorption capacity (N_{max}) constructed using the Langmuir equation; (B) change in tannin concentration as a percentage of a 1.25 g/L control (100%) following addition of 10 mg of skin cell wall material with increasing concentration of anthocyanin (mean ± SE).

The affinity constant (K_L) and estimated saturation level (N_{max}) derived from Langmuir isotherms (Figure 5A) for tannin adsorption by skin cell walls differed as a function of tannin molecular mass. Adsorption of high molecular mass tannin by cell wall material gave higher K_L and N_{max} values by comparison with the lower molecular mass tannin sample. The binding constants calculated from the isotherms would suggest that for skin cell walls, higher molecular mass tannin was bound more effectively even at high concentrations. However, an analysis of the selectivity of binding showed that this was not the case. From the molecular mass distribution data obtained via GPC, for high molecular mass tannin applied at low concentration, adsorption in the highest molecular mass range approached 100% (Figure 5B). As the tannin concentration increased, the selective adsorption of this molecular mass fraction decreased significantly, whereas, the adsorption of the intermediate molecular mass tannins remained relatively constant at 60%. This result indicates a concentration-dependent effect, whereby the averages taken at different molecular mass cutoff points (% elution) shifted with increasing tannin concentration (Figure 5C): decreased molecular mass at low concentrations and increased molecular mass at the highest tannin concentration. Conversely, for the low molecular mass tannin fraction applied, there was less selectivity observed in binding events, and molecular mass decreased for all tannin molecular mass classes, independent of tannin concentration (Figure 5D). These results show that increases in tannin concentration may have resulted in a higher total amount of tannin adsorbed by cell walls, but also reduced adsorption of higher molecular mass tannins. For the current study, the tannin/cell wall ratio in situ would have been ≅0.2 (2 g/L tannin application) based on published data for cell wall yield.[25] This means that for even a small change in total skin tannin concentration, the molecular mass of the nonadsorbed tannin fraction could shift to a higher average as a result of a changing selectivity pattern by the cell walls.

Althought it cannot be conclusively shown from the current data, the loss of selectivity for higher molecular mass material even at low applied tannin concentrations suggests the early saturation of direct binding sites on the cell wall. The saturation constant calculated from the Langmuir equation, first, exceeds the solubility of tannin in aqueous ethanol (Figure 5A) and, second, fails to account for the selectivity of binding. Previous work[25] showed that more porous cell walls (later ripeness) more effectively adsorb higher molecular mass tannin (>15000 g/mol), and this can account in part for the observed sequestering of tannin to a nonextractable fraction in riper skins. Increased porosity may facilitate a greater surface area over which high molecular mass tannin can bind. Hence, it might be expected that the saturation of cell wall binding sites would be reduced in riper skins, concomitant with increased total tannin concentration.

Nevertheless, it is evident that the effect of ripening on tannin extraction is more complex. The ongoing binding of intermediate molecular mass tannins even at higher applied concentrations, together with the high estimated saturation constant, could indicate that secondary interactions occur between surface-bound tannin and tannin in solution. This effect has been demonstrated in studies on tannin−cell wall interactions in apple[22,27,28] with the strong emphasis made that the formation of tannin "multilayers" through noncovalent interactions is likely to account for high saturation constants in the binding reaction. In particular, it was noted that this effect may favor multilayer formation by tannins of intermediate molecular mass[27] (±2900 g/mol) due to their increased propensity to form aggregates, a phenomenon observed to be lower for high molecular mass tannin (±20000 g/mol). This observation may further explain the reduction in adsorption of high molecular mass tannin at higher applied tannin concentrations, whereas the adsorption of intermediate molecular mass tannins remained constant (Figure 5B,D).

From a reinterpretation of the tannin extraction data obtained using aqueous ethanol concentrations, it is evident from the GPC cumulative molecular mass distribution that the highest molecular mass tannins were poorly extracted in aqueous ethanol, even at 50% v/v (Figure 2A−C). Rather, they were extractable only in 70% acetone, as shown by the shift in the cumulative molecular mass distribution of the extract (Figure 2D), which approached a molecular mass of 30000 g/mol at 100% elution. Therefore, quantitatively, the greatest effect of increasing ethanol in the extraction solvent was found for tannins within the intermediate molecular mass range (Figure 2A−C). This suggests that ethanol may selectively extract tannins of intermediate molecular mass, which are potentially associated as multilayers with cell wall constituents. Our previous work using model experiments in grape[24] highlighted this effect, such that small changes in ethanol concentration (12−20% v/v) reduce the interaction of tannins

dx.doi.org/10.1021/jf4050606 | J. Agric. Food Chem. 2014, 62, 1130−1141

of intermediate molecular mass with cell wall material, whereas a negligible effect of ethanol is exerted on the adsorption of high molecular mass tannin. Quantitative data from this experiment is shown in the Supporting Information (Figure S2). The selective effect of ethanol in driving the tannin−cell wall interaction response may also indicate the contribution of hydrophobic interactions, as indicated by Le Bourvellec and co-workers.[28]

Interaction of Cell Walls with Tannin and Anthocyanin. It was noteworthy from the extraction experiments that anthocyanin extraction was limited by ethanol concentration in a similar manner to tannin (Table 1). It is known that anthocyanin can associate with plant cell walls,[40] although the interaction of monomeric flavan-3-ols is thought to be negligible.[22] We have shown previously, using a wine system containing both tannin and monomeric anthocyanin, that grape cell wall material can remove anthocyanin in the presence of tannin.[41] What was unknown at the outset of the study is whether the interaction of tannin and anthocyanin influences binding events with the cell wall. In a model experiment, the adsorption of anthocyanin by cell walls was significant (29% removed from a 1 g/L solution) and enhanced by the presence of tannin (45% removed from a 1 g/L solution). The binding isotherms for this experiment across a range of anthocyanin concentrations are shown in Figure 6A. As anthocyanin concentration increased, tannin adsorption by cell wall material was not affected (Figure 6B). The estimated saturation constant for anthocyanin using the Langmuir equation was lower in the presence of tannin, but at the concentration range present in grapes, the system would be well below saturation. It therefore appears that for the conditions of the current study, anthocyanin did not influence tannin adsorption by cell walls. At the same time, skin tannin present in grapes might limit the extraction of anthocyanin.

In general, 50% v/v ethanol is considered a good solvent for anthocyanin, correlating well with accepted methods for anthocyanin analysis, and is useful in the prediction of anthocyanin extractability during grape ripening.[42] Conversely, some degradation of anthocyanin was found in acetone extracts (data not shown). From the results of the extraction experiment, it would therefore be expected that the 50% v/v ethanol extraction reflects true differences in anthocyanin concentration between grape samples, although this is not the case for tannin. Furthermore, the results indicated that anthocyanin content increased in riper samples, but that these differences were not reflected in dilute ethanol extracts except for the least ripe (22 °Brix) sample, which had the lowest extractable anthocyanin (Table 1). On the basis of the data from the model binding experiment with anthocyanin and grape cell walls, we propose that the poor extraction of anthocyanin at low ethanol concentration may be due, in part, to a significant interaction with cell walls. Increased anthocyanin extraction at higher ethanol concentrations may be due to a loss of hydrophobic interactions between anthocyanin and cell walls or between anthocyanin and cell wall-bound tannin, but does not exclude the contribution of ionic interactions.[40] This result showed that in a like manner for skin tannin, anthocyanin extraction could potentially be restricted by multiple noncovalent interactions. Further to this, an important observation toward interpreting the tannin extraction data was that anthocyanin is unlikely to affect the adsorption of tannin by cell walls within the concentration range occurring in grapes.

As discussed, the effect of either ripeness stage or increasing ethanol in the solvent on tannin extraction was mirrored by changes in anthocyanin extraction. Therefore, a pertinent question was whether complexing between anthocyanin and tannin could enhance the 280 nm absorbance, leading to erroneous conclusions regarding changes in tannin concentration using the methyl cellulose precipitable tannin assay. We have noted in previous research using tannins purified from the same grape sample set presented in the current study that anthocyanin incorporation into the tannin polymer caused minor increases in tannin color in immature grapes,[16] but from 22 °Brix onward there was no further color change observed. In comparing the methyl cellulose precipitation results from the same purified tannins[16] at different ripeness stages (Supporting Information Figure S3), it was found that no change in the methyl cellulose precipitation result was detected for a fixed concentration of tannin. On the basis of these results, and our observations that the presence of tannin in combination with grape cell walls potentially restricts anthocyanin extraction, we conclude that the similarity in anthocyanin and tannin extraction data between the different grape samples was a true effect.

Potential Mechanisms That May Increase Skin Tannin Concentration and Facilitate Sequestering to Cell Walls. In grapes, research has shown that the biosynthetic pathway for the synthesis of flavan-3-ols (precursors to tannin) is active up until the onset of ripening (veraison), and thereafter gene expression is down-regulated by the hormone abscisic acid (ABA), which signals the onset of veraison.[43] Whereas the cessation of gene expression for flavan-3-ol biosynthetic enzymes prior to veraison may indicate that tannin should decline during ripening, a concurrent decrease in monomeric flavan-3-ols is also observed. The reason for this phenomenon has not been addressed in the literature and, speculatively, flavan-3-ols could become polymerized to tannin during the ripening period if they remain intact within a subcellular compartment. A recent paper has suggested that the site of tannin polymerization in the grape cell is within a chloroplast-derived structure, the "tannosome".[44] These organelles originate from thylakoids within the chloroplast and are transported within membrane-bound vesicles, which become incorporated to the vacuole by invagination of the tonoplast membrane. According to the preliminary work by Brillouet and co-workers,[44] polymerization could occur within these organelles at any point following formation of the tannosome because these remain separated from cytoplasmic or vacuolar contents by a membrane. An important consideration based on this work[44] is that tannin may remain sequestered by a membrane at all ripeness stages, meaning that interaction between tannin and cell walls in situ would be improbable and potentially occur only once grape cell compartments are disrupted during crushing and fermentation. Nevertheless, in other studies on grape, the partitioning of tannin has been observed between vacuolar and cell wall fractions in both grape skins and seeds, with higher levels of polymerization occurring in cell wall-associated fractions.[18,19] Some studies have demonstrated that a fraction of high molecular mass tannin is nonextractable in acetone (<5% of acetone-extractable tannin), and this may possibly be covalently bound to the cell wall.[24,25] Furthermore, ultrastructural studies of grape skin cells show aggregations of phenolic-rich inclusions in immature grape cell walls, which are no longer evident in late-stage ripening, concomitant with increased invagination of the cell wall.[39] If a

pathway for tannin transport to the cell wall exists, the mechanism is currently unknown. However, a recent review on tannin biosynthesis, drawn from work on various plant species, has suggested that sequestering of tannin at the cell wall could be mediated by vesicle trafficking, where following deposition at the cell wall, tannin may be further oxidized and potentially polymerized by apoplastic polyphenol oxidase.[45] Irrespective of whether cell wall−tannin interactions occur in situ in the grape berry or only following grape crushing as the result of cell disruption, it appears that this phenomenon plays a significant role in limiting tannin extraction.

Implications for Winemaking Practice. In commercial winemaking, a correlation has been observed between enhanced skin tannin concentration, tannin molecular mass, and allocation grading.[46] Furthermore, in a wine sensory "quality" study, grapes with enhanced skin tannin and anthocyanin were associated with increased wine tannin and color, resulting in an improvement in rating by wine judges.[47] On the basis of the current data set, it is evident that despite increases in grape tannin and anthocyanin content with the progression of ripening, delaying grape harvest may not necessarily facilitate a higher skin tannin extraction. This would appear to be due to the significant limitation in extractability exerted by the interaction of skin tannin and anthocyanin with cell walls and, secondarily, the possibility that further tannin increases were sequestered within cell wall pores and therefore not extractable. The hypothesis that ripening could facilitate an enhancement of tannin extractability under the conditions of ferment (similar to our experiments with dilute alcohol) was not strongly supported by our results. Nevertheless, the molecular mass of tannin extracted from riper grapes increased, even when the extractable tannin content was not significantly affected. Although an increased wine tannin molecular mass may be associated with higher wine quality,[46] this may also cause excessive astringency in the wine, introducing the requirement for fining.

In conclusion, the current study has shown that the factors which underpin skin tannin extractability are complex:

(a) Increases in total skin tannin content with the progression of ripening were not consistently reflected by increases in ethanol-extractable skin tannin.
(b) The observed increase in cell wall porosity with ripening may partly explain this, because the proportion of skin tannin bound by noncovalent interactions within cell wall pores appears to increase in a corresponding manner, rendering a fraction of tannin nonextractable.
(c) The molecular mass of the ethanol-extractable skin tannin fraction shifted to a higher molecular mass average as total skin tannin content increased. This may be due to a change in the selectivity of tannin adsorption by cell walls at higher tannin concentrations. This could occur without a change in extractable tannin content because the total amount of tannin adsorbed by cell walls increases with ripening.[25]
(d) A relatively high affinity of anthocyanin adsorption by skin cell walls was observed, meaning that the extraction of anthocyanin in dilute ethanol (10 and 20% v/v ethanol) may also be limited by the interaction with cell walls. However, at wine-like concentration (2 g/L), anthocyanin did not reduce the adsorption of tannin by cell walls.

These observations highlight that skin cell walls may play a significant role in introducing noncovalent interactions with tannin, which in turn limits its extractability. Further research is required to move away from a simplistic model of tannin extraction, as directly dependent upon tannin concentration, to one that builds upon the multiple levels at which noncovalent interactions between tannin and macromolecules can occur. Ongoing research is needed to better understand how tannin forms colloid complexes with insoluble cell walls, as well as soluble polysaccharide and protein, and how these might affect tannin extractability.

■ ASSOCIATED CONTENT

Ⓢ Supporting Information

S1, tannin extraction kinetics from grape skins in different extraction solvents; S2, effect of increasing ethanol concentration on the adsorption of high and low molecular mass tannin fractions by cell wall material; S3, comparison of results of the phloroglucinolysis and methyl cellulose precipitable tannin assays on purified grape skin tannins from different ripeness stages. This material is available free of charge via the Internet at http://pubs.acs.org.

■ AUTHOR INFORMATION

Corresponding Author

*(K.A.B.) Phone: +61-8-83136190. Fax: +61-8-83136601. E-mail: keren.bindon@awri.com.au.

Funding

The Australian Wine Research Institute, a member of the Wine Innovation Cluster in Adelaide, is supported by Australian grapegrowers and winemakers through their investment body, the Grape and Wine Research and Development Corporation, with matching funds from the Australian government.

Notes

The authors declare no competing financial interest.

■ ACKNOWLEDGMENTS

We thank Pernod Ricard Australia (Orlando Wines) and the University of Adelaide for the donation of grape samples. We gratefully acknowledge Lynette Waterhouse of Adelaide Microscopy, The University of Adelaide, for SEM imaging of cell wall samples. We also acknowledge Alex Shulkin at the Australian Wine Research Institute for the isolation of grape anthocyanins.

■ REFERENCES

(1) Busse-Valverde, N.; Bautista-Ortin, A. B.; Gomez-Plaza, E.; Fernandez-Fernandez, J. I.; Gil-Munoz, R. Influence of skin maceration time on the proanthocyanidin content of red wines. *Eur. Food Res. Technol.* **2012**, *235*, 1117−1123.

(2) Cerpa-Calderon, F. K.; Kennedy, J. A. Berry integrity and extraction of skin and seed proanthocyanidins during red wine fermentation. *J. Agric. Food Chem.* **2008**, *56*, 9006−9014.

(3) Bindon, K.; Varela, C.; Kennedy, J.; Holt, H.; Herderich, M. Relationships between harvest time and wine composition in *Vitis vinifera* L. cv. Cabernet Sauvignon 1. Grape and wine chemistry. *Food Chem.* **2013**, *138*, 1696−1705.

(4) Cadot, Y.; Caille, S.; Samson, A.; Barbeau, G.; Cheynier, V. Sensory representation of typicality of Cabernet franc wines related to phenolic composition: Impact of ripening stage and maceration time. *Anal. Chim. Acta* **2012**, *732*, 91−99.

(5) Canals, R.; Llaudy, M. C.; Valls, J.; Canals, J. M.; Zamora, F. Influence of ethanol concentration on the extraction of color and

phenolic compounds from the skin and seeds of Tempranillo grapes at different stages of ripening. *J. Agric. Food Chem.* **2005**, *53*, 4019−4025.
(6) Esteban, M. A.; Villanueva, M. J.; Lissarrague, J. R. Effect of irrigation on changes in the anthocyanin composition of the skin of cv Tempranillo (*Vitis vinifera* L) grape berries during ripening. *J. Sci. Food Agric.* **2001**, *81*, 409−420.
(7) Joutei, K. A.; Glories, Y. Étude en conditions modèles de l'extractibilité des composés phénoliques des pellicules et des pépins de raisins rouges. *J. Int. Sci. Vigne Vin.* **1994**, *28*, 303−317.
(8) Ojeda, H.; Andary, C.; Kraeva, E.; Carbonneau, A.; Deloire, A. Influence of pre- and postveraison water deficit on synthesis and concentration of skin phenolic compounds during berry growth of *Vitis vinifera* cv. Shiraz. *Am. J. Enol. Vitic.* **2002**, *53*, 261−267.
(9) Porter, L. J.; Hrstich, L. N.; Chan, B. G. The conversion of procyanidins and prodelphinidins to cyanidin and delphinidin. *Phytochemistry* **1986**, *25*, 223−230.
(10) Kennedy, J. A.; Matthews, M. A.; Waterhouse, A. L. Effect of maturity and vine water status on grape skin and wine flavonoids. *Am. J. Enol. Vitic.* **2002**, *53*, 268−274.
(11) Harbertson, J. F.; Kennedy, J. A.; Adams, D. O. Tannin in skins and seeds of Cabernet Sauvignon, Syrah, and Pinot noir berries during ripening. *Am. J. Enol. Vitic.* **2002**, *53*, 54−59.
(12) Kennedy, J. A.; Jones, G. P. Analysis of proanthocyanidin cleavage products following acid-catalysis in the presence of excess phloroglucinol. *J. Agric. Food Chem.* **2001**, *49*, 1740−1746.
(13) Fournand, D.; Vicens, A.; Sidhoum, L.; Souquet, J.-M.; Moutounet, M.; Cheynier, V. Accumulation and extractability of grape skin tannins and anthocyanins at different advanced physiological stages. *J. Agric. Food Chem.* **2006**, *54*, 7331−7338.
(14) Hanlin, R.; Downey, M. Condensed tannin accumulation and composition in skin of Shiraz and Cabernet Sauvignon grapes during berry development. *Am. J. Enol. Vitic.* **2009**, *60* (11), 13−23.
(15) Downey, M. O.; Harvey, J. S.; Robinson, S. P. Analysis of tannins in seeds and skins of Shiraz grapes throughout berry development. *Aust. J. Grape Wine Res.* **2003**, *9*, 15−27.
(16) Bindon, K. A.; Kennedy, J. A. Ripening-Induced changes in grape skin proanthocyanidins modify their interaction with cell walls. *J. Agric. Food Chem.* **2011**, *59*, 2696−2707.
(17) Downey, M. O.; Hanlin, R. L. Comparison of ethanol and acetone mixtures for extraction of condensed tannin from grape skin. *S. Afr. J. Enol. Vitic.* **2010**, *31*, 154−159.
(18) Geny, L.; Saucier, C.; Bracco, S.; Daviaud, F.; Glories, Y. Composition and cellular localization of tannins in grape seeds during maturation. *J. Agric. Food Chem.* **2003**, *51*, 8051−8054.
(19) Gagne, S.; Saucier, C.; Geny, L. Composition and cellular localization of tannins in Cabernet Sauvignon skins during growth. *J. Agric. Food Chem.* **2006**, *54*, 9465−9471.
(20) Obreque-Slier, E.; Pena-Neira, A.; Lopez-Solis, R.; Zamora-Marin, F.; Ricardo-da-Silva, J. M.; Laureano, O. Comparative study of the phenolic composition of seeds and skins from Carmenere and Cabernet Sauvignon grape varieties (*Vitis vinifera* L.) during ripening. *J. Agric. Food Chem.* **2010**, *58*, 3591−3599.
(21) Verries, C.; Guiraud, J. L.; Souquet, J. M.; Vialet, S.; Terrier, N.; Ollé, D. Validation of an extraction method on whole pericarp of grape berry (*Vitis vinifera* L. cv. Shiraz) to study biochemical and molecular aspects of flavan-3-ol synthesis during berry development. *J. Agric. Food Chem.* **2008**, *56*, 5896−5904.
(22) Renard, C. M. G. C.; Baron, A.; Guyot, S.; Drilleau, J. F. Interactions between apple cell walls and native apple polyphenols: quantification and some consequences. *Int. J. Biol. Macromol.* **2001**, *29*, 115−125.
(23) Bindon, K. A.; Smith, P. A.; Kennedy, J. A. Interaction between grape-derived proanthocyanidins and cell wall material. 1. Effect on proanthocyanidin composition and molecular mass. *J. Agric. Food Chem.* **2010**, *58*, 2520−2528.
(24) Bindon, K. A.; Smith, P. A.; Holt, H.; Kennedy, J. A. Interaction between grape-derived proanthocyanidins and cell wall material. 2. Implications for vinification. *J. Agric. Food Chem.* **2010**, *58*, 10736−10746.
(25) Bindon, K. A.; Bacic, A.; Kennedy, J. A. Tissue-specific and developmental modifications of grape cell walls influence the adsorption of proanthocyanidins. *J. Agric. Food Chem.* **2012**, *60*, 9249−9260.
(26) Bindon, K. A.; Smith, P. A. Comparison of the affinity and selectivity of insoluble fibres and commercial proteins for wine proanthocyanidins. *Food Chem.* **2013**, *136*, 917−928.
(27) Le Bourvellec, C.; Renard, C. M. G. C. Non-covalent interaction between procyanidins and apple cell wall material. Part II: Quantification and impact of cell wall drying. *Biochim. Biophys. Acta* **2005**, *1725*, 1−9.
(28) Le Bourvellec, C.; Watrelot, A. A.; Ginies, C.; Imberty, A.; Renard, C. M. G. C. Impact of processing on the noncovalent interactions between procyanidin and apple cell wall. *J. Agric. Food Chem.* **2012**, *60*, 9484−9494.
(29) Le Bourvellec, C.; Bouchet, B.; Renard, C. M. G. C. Non-covalent interaction between procyanidins and apple cell wall material. Part III: Study on model polysaccharides. *Biochim. Biophys. Acta* **2005**, *1725*, 10−18.
(30) Cheynier, V.; Duenas-Paton, M.; Salas, E.; Maury, C.; Souquet, J. M.; Sarni-Manchado, P.; Fulcrand, H. Structure and properties of wine pigments and tannins. *Am. J. Enol. Vitic.* **2006**, *57*, 298−305.
(31) Mercurio, M. D.; Dambergs, R. G.; Herderich, M. J.; Smith, P. A. High throughput analysis of red wine and grape phenolics − adaptation and validation of methyl cellulose precipitable tannin assay and modified Somers color assay to a rapid 96 well plate format. *J. Agric. Food Chem.* **2007**, *55*, 4651−4657.
(32) Kennedy, J. A.; Taylor, A. W. Analysis of proanthocyanidins by high-performance gel permeation chromatography. *J. Chromatogr., A* **2003**, *995*, 99−107.
(33) Badalyan, A.; Pendleton, P.; Wu, H. Development of an automated gas adsorption apparatus for the characterization of the surface area, pore size distribution, and density of powdered materials. *Rev. Sci. Instrum.* **2001**, *72*, 3038−3045.
(34) Badalyan, A.; Pendleton, P. Analysis of uncertainties in manometric gas-adsorption measurements. I: Propagation of uncertainties in BET analyses. *Langmuir* **2003**, *19*, 7919−7928.
(35) Langmuir, I. The adsorption of grases on plane surfaces of glass, mica and platinum. *J. Am. Chem. Soc.* **1918**, *40*, 1361−1403.
(36) Le Bourvellec, C.; Guyot, S.; Renard, C. M. G. C. Non-covalent interaction between procyanidins and apple cell wall material: Part I. Effect of some environmental parameters. *Biochim. Biophys. Acta* **2004**, *1672*, 192−202.
(37) Nunan, K. J.; Sims, I. M.; Bacic, A.; Robinson, S. P.; Fincher, G. B. Changes in cell wall composition during ripening of grape berries. *Plant Physiol.* **1998**, *118*, 783−792.
(38) Orfila, C.; Knox, J. P. Spatial regulation of pectic polysaccharides in relation to pit fields in cell walls of tomato fruit pericarp. *Plant Physiol.* **2000**, *122*, 775−781.
(39) Huang, X. M.; Huang, H. B.; Wang, H. C. Cell walls of loosening skin in post-veraison grape berries lose structural polysaccharides and calcium while accumulate structural proteins. *Sci. Hortic.* **2005**, *104*, 249−263.
(40) Padayachee, A.; Netzel, G.; Netzel, M.; Day, L.; Zabaras, D.; Mikkelsen, D.; Gidley, M. Binding of polyphenols to plant cell wall analogues − Part 1: Anthocyanins. *Food Chem.* **2012**, *134*, 155−161.
(41) Guerrero, R.; Smith, P.; Bindon, K. Application of insoluble fibers in the fining of wine phenolics. *J. Agric. Food Chem.* **2013**, *61*, 4424−4432.
(42) Fragoso, S.; Mestres, M.; Busto, O.; Guasch, J. Comparison of three extraction methods used to evaluate phenolic ripening in red grapes. *J. Agric. Food Chem.* **2010**, *58* (7), 4071−4076.
(43) Lacampagne, S.; Gagne, S.; Geny, L. Involvement of abscisic acid in controlling the proanthocyanidin biosynthesis pathway in grape skin: new elements regarding the regulation of tannin composition and leucoanthocyanidin reductase (LAR) and anthocyanidin reductase (ANR) activities and expression. *J. Plant Growth Regul.* **2010**, *29*, 81−90.

(44) Brillouet, J.-M.; Romieu, C.; Schoefs, B.; Solymosi, K.; Cheynier, V.; Fulcrand, H.; Verdeil, J.-L.; Conéjéro, G. The tannosome is an organelle forming condensed tannins in the chlorophyllous organs of Tracheophyta. *Ann. Bot.* **2013**, *112*, 1003−1014.
(45) Zhao, J.; Pang, Y. Z.; Dixon, R. A. The mysteries of proanthocyanidin transport and polymerization. *Plant Physiol.* **2010**, *153*, 437−443.
(46) Kassara, S.; Kennedy, J. A. Relationship between red wine grade and phenolics. 2. Tannin composition and size. *J. Agric. Food Chem.* **2011**, *59*, 8409−8412.
(47) Ristic, R.; Bindon, K.; Francis, L. I.; Herderich, M. J.; Iland, P. G. Flavonoids and C-13-norisoprenoids in *Vitis vinifera* L. cv. Shiraz: relationships between grape and wine composition, wine colour and wine sensory properties. *Aust. J. Grape Wine Res.* **2010**, *16*, 369−388.

physical stability.[21−23] However, apart from the studies of Horn et al.,[24,25] which evaluated protein-based emulsifiers (whey protein isolate and sodium caseinate) with phospholipid-based emulsifiers (with either 20 or 75% phospholipids), no previous studies have been reported on the physical and oxidative stabilization of fish oil-in-water emulsions with casein−phospholipid combinations. The results obtained by Horn et al.[24,25] demonstrated some advantages of using a combination of milk proteins and milk phospholipids, but it was not possible to assess the precise role of individual milk proteins or milk phospholipids on lipid oxidation.

Therefore, the objectives of this work were (i) to evaluate the antioxidant properties of three common phospholipids (soy lecithin, phosphatidylcholine, and phosphatidylethanolamine) to obtain a more comprehensive understanding of the antioxidant mechanisms of phospholipids and (ii) to investigate the additive effects of each of these three phospholipids and casein as emulsifiers on the physical and oxidative stabilities of fish oil-in-water emulsions at pH 7.

MATERIALS AND METHODS

Materials. Commercial cod liver oil was provided by Maritex A/S, a subsidiary of TINE, BA (Sortland, Norway), and stored at −40 °C until use. Sodium caseinate, CAS (Miprodan 30), was kindly donated by Arla Foods Ingredients amba (Viby J, Denmark). Arla reported a protein content of 93.5% in sodium caseinate for Miprodan 30. Fat-free soybean lecithin, LC (LIPOID P 20); phosphatidylcholine from soybean, PC (LIPOID S 100), and soy phosphatidylethanolamine, PE (LIPOID S PE), were kindly donated by Lipoid (Steinhausen, Switzerland). Data sheets from Lipoid reported the following compositions: for LIPOID P 20, 25% (w/w) phosphatidylcholine, 20% (w/w) phosphatidylethanolamine, 10% (w/w) phosphatidylinositol, 5% (w/w) phosphatidic acid and 40% (w/w) others (mostly glycolipids); a content of 97.3% (w/w) phosphatidylcholine for LIPOID S 100 and a concentration of 99.6% (w/w) phosphatidylethanolamine for LIPOID S PE. All other chemicals and solvents used were of analytical grade.

Characterization of the Fish Oil and the Phospholipids. Fatty acid compositions of the fish oil and the three phospholipids were determined by fatty acid methylation,[26] followed by separation through GC.[27] The quality of the three PL-based emulsifiers and the fish oil was determined by their peroxide value (PV), employing the colorimetric ferric−thiocyanate method at 500 nm as described by Shantha and Decker.[28] Furthermore, their content of tocopherol was also determined.[29]

Antioxidant Activity Assays. The methods for antioxidant activity assays were modified slightly from the original to adapt for microplate readings using a Synergy 2 Multi-Mode (BioTek Instruments, Inc., Winooski, VT, USA) microplate reader.

1,1-Diphenyl-2-picrylhydrazyl (DPPH) Radical Scavenging Activity. The scavenging effect on DPPH free radical was measured according to the method of Shimada et al.[30] with some modifications. One percent (w/w) solutions of the three phospholipids in ethanol were prepared and then diluted according to different dilution factors. In brief, 150 μL of each phospholipid solution was mixed with 150 μL of 0.1 mM ethanolic solution of DPPH. The mixture was then kept at room temperature in the dark for 30 min, and the absorbance was measured at 515 nm. For the blank, 150 μL of ethanol was used instead of the sample, and sample control was also made for each fraction by mixing 150 μL of sample with 150 μL of 95% ethanol. Triplicate measurements were performed. A BHT solution, 0.02% (w/w), was employed as positive control. Radical scavenging capacity was calculated as follows:

$$\text{DPPH inhibition (\%)} = \left(1 - \frac{(A_{\text{sample}} - A_{\text{sample.control}})}{A_{\text{blank}}}\right) \times 100 \quad (1)$$

Iron (Fe^{2+}) Chelating Activity. The iron chelating activity of the extracts was estimated according to the modified method of Dinis et al.[31] Phospholipids were dissolved in ethanol obtaining different solutions, 10% (w/w) for LC, 1% (w/w) for PC, and 5% (w/w) for PE, which were then diluted according to several dilution factors. First, 270 μL of distilled water was added to 200 μL of each phospholipid solution. Then, 10 μL of 2 mM ferrous chloride was added, and after 3 min, the reaction was inhibited by the addition of 20 μL of 5 mM ferrozine solution. The mixture was shaken vigorously and left at room temperature for 10 min; thereafter, the absorbance was measured at 562 nm. A blank was run in the same way by using ethanol instead of sample. Sample control was made for each sample without the addition of ferrozine. Triplicate measurements were carried out. An EDTA solution, 0.006% (w/w), was employed as positive control. The chelating capacity was calculated as follows:

$$\text{Fe}^{2+}\text{ chelating activity (\%)} = \left(1 - \frac{(A_{\text{sample}} - A_{\text{sample.control}})}{A_{\text{blank}}}\right) \times 100 \quad (2)$$

Reducing Power. The reducing power was measured according to the method of Oyaizu[32] with some modifications. Phospholipids were dissolved in ethanol, obtaining different solutions 1% (w/w), which were then diluted according to several dilution factors. To 200 μL of each phospholipid solution was added 200 μL of 0.2 M phosphate buffer (pH 6.6) and 200 μL of 1% (w/w) potassium ferricyanide. The mixture was incubated for 20 min at 50 °C. Then, 200 μL of 10% (w/w) trichloroacetic acid solution was added, and the mixture was shaken vigorously. Finally, 144 μL of this solution was mixed with 342 μL of distilled water and 46 μL of 0.1% (w/w) $FeCl_3$. After 10 min at room temperature, the absorbance was measured at 700 nm. Increased absorbance (A_{700}) of the reaction mixture indicated increased reducing power. Triplicate measurements were performed. An ascorbic acid solution, 0.009% (w/w), was employed as positive control.

Preparation of Emulsions and Sampling. Four emulsions were prepared with 10% (w/w) fish oil and emulsifier concentrations as follows: (i) emulsion 0.3CAS stabilized with 0.3% (w/w) of CAS, (ii) emulsion 0.3CAS+0.5LC stabilized with 0.3% (w/w) of CAS and 0.5% (w/w) of LC, (iii) emulsion 0.3CAS+0.5PC stabilized with 0.3% (w/w) of CAS and 0.5% (w/w) of PC, and (iv) emulsion 0.3CAS+0.5PE stabilized with 0.3% (w/w) of CAS and 0.5% (w/w) of PE. The buffer used was a 10 mM sodium acetate imidazole buffer (pH 7.0). CAS, LC, PC, and PE were dispersed in the buffer overnight at approximately 5 °C. Primary homogenization was done by adding the fish oil slowly to the buffer during mixing at 16000 rpm (Ystral mixer, Ballrechten-Dottingen, Germany). The fish oil was added during the first minute of mixing, and the total mixing time was 3 min. Secondary homogenization was done on a microfluidizer (M110L Microfluidics, Newton, MA, USA) equipped with a ceramic interaction chamber (CIXC, F20Y, internal dimension = 75 μm). Emulsions were homogenized at a pressure of 9000 psi, running three passes. To the emulsions were added 100 μM $FeSO_4$ to accelerate lipid oxidation and 0.05% (w/w) sodium azide to prevent microbial growth. Emulsions were stored in 100 mL closed bluecap bottles at room temperature (19−20 °C) in the dark for 14 days. Each bottle contained approximately 50 mL. Samples were taken at days 0, 4, 9, and 14 for lipid oxidation measurements. Measurements of pH, viscosity, and droplet size distributions were carried out at days 1 and 14, whereas zeta potential was determined at day 2. Samples for protein content in the aqueous phase were taken at day 3. A similar set of emulsions were also prepared at pH 3.5. However, as some of these emulsions were not physically stable, only data obtained at pH 7 will be shown and discussed in detail, but, when appropriate, reference to results obtained at pH 3.5 will be made.

Characterization of the Emulsions. *pH and Zeta Potential.* The pH values of emulsions were measured at room temperature directly in the sample during stirring (pH meter, 827 pH Lab, Methrom Nordic ApS, Glostrup, Denmark). Measurements were done in duplicate.

Table 1. Characterization of the Fish Oil and Phospholipids[a]

	fish oil	LC	PC	PE
PV, mequiv O_2/kg	0.28 ± 0.03	<5[b]	1.48 ± 0.07	4.01 ± 0.32
fatty acid, % (w/w)[c]				
C16:0	9.5	21.5	12.7	12.9
C16:1n-7	8.7	0.2	0.2	0.2
C18:0	2.0	3.6	3.7	3.6
C18:1n-9	16.3	13.6	10.1	8.6
C18:1n-7	4.8	1.5	1.6	1.6
C18:2n-6	1.8	53.3	64.9	65.9
C18:3n-3	2.6	4.7	5.9	6.4
C20:1n-11	12.6	nd	nd	nd
C20:5n-3	9.2	nd	nd	nd
C22:1n-11	6.0	0.5	0.2	0.1
C22:6n-3	11.4	0.3	nd	nd
others	15.1	0.8	0.7	0.7
total	100	100	100	100
tocopherol, μg/g				
α	200 ± 10.2	nd	1976 ± 166.2	1006 ± 15.6
β	5 ± 0.2	nd	nd	nd
γ	96 ± 2.6	37 ± 0.1	100 ± 7.5	nd
δ	42 ± 0.7	14 ± 0.2	40 ± 2.8	nd

[a]LC, lecithin; PC, phosphatidylcholine; PE, phosphatidylethanolamine; PV, peroxide value; nd, not detected. [b]As reported on the data sheet provided by the manufacturers. [c]Data are means of triplicate determinations. SD < 2%.

The zeta potential was measured in a Zetasizer (Zetasizer Nano ZS, Malvern Instruments Ltd., Worcestershire, UK) with a DTS-1060C cell at 25 °C. Before analysis, the emulsions were diluted 2:1000 in 10 mM sodium acetate imidazole buffer (pH 7). The zeta potential range was set to −100 to +50 mV, and the samples were analyzed with 100 runs. Measurements were done in triplicate.

Droplet Size. Droplet sizes were measured by laser diffraction using two different pieces of equipment: (i) With the Mastersizer 2000 (Malvern Instruments, Ltd.), emulsion was diluted in recirculating water (3000 rpm) until it reached an obscuration of 12−15%. Results are given in surface area mean diameter: $D_{3,2} = \sum d^3/\sum d^2$. Measurements were made in duplicate. (ii) A Zetasizer (Zetasizer Nano ZS, Malvern Instruments Ltd.) with a DTS-1060C cell was used at 25 °C. The samples were prepared as described for the zeta potential measurement. The results are given as *Z*-average diameter. For both types of equipment the refractive indices of sunflower oil (1.469) and water (1.330) were used as particle and dispersant, respectively. Measurements were made in duplicate.

Protein Concentration in the Aqueous Phase. Protein concentration in the aqueous phase was determined as previously described by Horn et al.[33] Samples (approximately 35 g) were centrifuged at 45000*g* for 50 min at 10 °C (Sorvall RC-6 PLUS, Thermo Fisher Scientific, Osterode, Germany). The lower aqueous phase was extracted with a syringe and needle and centrifuged once more at 70000*g* for 60 min at 15 °C (Beckman ultracentrifuge L8-60M, Fullerton, CA, USA). Once more, the lower aqueous phase was extracted and then filtered (Minisart NML 0.20 μm filter, Sartorius, Hannover, Germany). The protein content in the aqueous phase was determined with a BCA Protein Assay Reagent Kit (Pierce, Thermo Scientific, Rockford, IL, USA). Prior to analysis, samples were diluted 1:9 in 10 mM sodium acetate imidazole buffer (pH 7). Measurements were performed in duplicate.

Viscosity. Viscosities of the emulsions (15 mL) were measured using a stress-controlled rheometer (Stresstech, Reologica Instruments AB, Lund, Sweden) equipped with a CC25 standard bob cup system in a temperature vessel. Measurements were done at 20 °C over a shear stress range from 0.0125 to 1.64 Pa. Viscosities are given as the average viscosity of the linear part of the plot of shear stress versus viscosity expressed in centipoise (cP). Viscosities were measured twice on each emulsion.

Measurements of Lipid Oxidation. *Determination of Peroxide Value and Tocopherol Content.* Lipids were extracted from the dispersions according to the Bligh and Dyer method using a reduced amount of the chloroform/methanol (1:1 w/w) solvent.[34] Two extractions were made from each sample, and PV measurement was performed in duplicate. PV was measured according to the method described earlier.[28] For tocopherol determination, lipid extracts (1−2 g) were weighed off and evaporated under nitrogen and redissolved in hexane prior to analysis by using the same method as described previously.[29]

Secondary Oxidation Products, SPME GC-MS. Approximately 4 g of emulsion, 30 mg of internal standard (4-methyl-1-pentanol, 30 μg/g water), and 1 mL of antifoam (Synperonic 800 μL/L water) were weighed out in a 100 mL purge bottle. The bottle was heated in a water bath at 45 °C while purging with nitrogen (flow = 150 mL/min, 30 min). Volatile secondary oxidation products were trapped on Tenax GR tubes. The volatiles were desorbed again by heat (200 °C) in an Automatic Thermal Desorber (ATD-400, Perkin-Elmer, Norwalk, CT, USA), cryofocused on a cold trap (−30 °C), released again (220 °C), and led to a gas chromatograph (HP 5890IIA, Hewlett-Packard, Palo Alto, CA, USA; column, DB-1701, 30 m × 0.25 mm × 1.0 μm; J&W Scientific, Folsom, CA, USA). The oven program had an initial temperature of 45 °C for 5 min, increasing at 1.5 °C/min until 55 °C, at 2.5 °C/min until 90 °C, and at 12.0 °C/min until 220 °C, where the temperature was kept for 4 min. The individual compounds were analyzed by mass spectrometry (HP 5972 mass-selective detector, Agilent Technologies, USA; electron ionization mode, 70 eV; mass to charge ratio scan between 30 and 250). The individual compounds were identified both by MS library searches (Wiley 138 K, John Wiley and Sons, Hewlett-Packard) and by authentic external standards. The external standards employed were 1-penten-3-one, pentanal, 1-penten-3-ol, (*E*)-2-pentenal, 1-pentanol, hexanal, (*E*)-2-pentenol, (*E*)-2-hexenal, heptanal, (*E*)-4-heptenal, (*E*,*E*)-2,4-heptadienal, nonanal, (*E*,*Z*)-2,6-nonadienal, 2-ethylfuran, and 2-pentylfuran. These compounds were dissolved in 96% ethanol and diluted to concentrations of approximately 0.5, 1, 5, 10, 25, and 50 μg/g. Two calibration curves were made by injecting these solutions (30 mg) on 4 g of emulsion (0.3CAS and 0.3CAS+0.5LC emulsions). Measurements were made in triplicate in each sample.

Statistical Analysis. Statgraphics software (version 5.1) was used to carry out one-way analysis of variance (ANOVA) on the data.

Tukey's test was employed for that purpose, and differences between means were considered significant at $p \leq 0.05$. Furthermore, oxidation data were subjected to multivariate data analysis (The Unscrambler X, version 10.2, CAMO Software AS, Oslo, Norway). A principal component analysis (PCA) was carried out with the four different emulsions as objects and peroxide values and volatiles data as variables, with one variable representing the average of a given peroxide value or volatile at a specific sampling time point. Data were autoscaled to make the variables contribute equally to the model, and the PCA model was validated systematically segmented, according to replicates of the emulsions.

RESULTS AND DISCUSSION

Composition of Fish Oil and Phospholipids. The quality of the raw materials can have a great influence on the physical and oxidative stabilities of the final emulsions. For this reason, the fish oil and the three soybean phospholipids employed as emulsifiers were characterized in terms of peroxide value, fatty acid composition, and tocopherol content (Table 1). It was observed that the commercial cod liver oil utilized presented a very low PV (0.28 mequiv O_2/kg), a considerable content of monounsaturated fatty acids (16.3% of C18:1n-9 and 12.6% of C21:1n-9), and a percentage of omega-3 PUFA >20% (mainly EPA, C20:5n-3, and DHA, C22:6n-3). With regard to the tocopherol composition, it contained mainly α-tocopherol (200 μg/g) and γ-tocopherol (96 μg/g).

The three phospholipids had considerably higher PV than the fish oil, ranging from 1.48 for PC to 4.01 for PE. In terms of fatty acid composition, PC and PE presented almost the same content for each fatty acid, mainly C16:0 (~13%), C18:1n-9 (~9%), C18:2n-6 (~65%), and C18:3n-3 (~6%). This finding is explained by the fact that, according to the manufacturer, PE was produced from purified PC by conversion of the headgroup. Likewise, LC was composed by the same major fatty acids as PC and PE. However, it presented a higher content of saturated (21.5% of C16:0) and monounsaturated fatty acids (13.6% of C18:1n-9) and a lower percentage of polyunsaturated fatty acids (53.3% of C18:2n-6 and 4.7% of C18:3n-3) than the two other phospholipids. As far as their tocopherol composition is concerned (Table 1), PC contained almost twice as much α-tocopherol as PE, whereas α-tocopherol was not detected in LC. This may be due to the addition of α-tocopherol as antioxidant in the pr,oduction process of PC and PE. No other homologues of tocopherol were found in PE, and low percentages of γ- and δ-tocopherol were obtained for LC and PC.

Antioxidant Activity of Phospholipids. Phospholipids may act as antioxidants by different mechanisms. As a consequence, their antioxidant properties were evaluated by different methods such as DPPH, Fe^{2+} chelating and reducing power. To the best of the authors' knowledge, such a systematic study on the antioxidant properties of phospholipids has not previously been reported.

DPPH Radical Scavenging Activity. Figure 1a shows the DPPH radical scavenging activity of the three phospholipids assayed (LC, PC, and PE). Although they presented different α-tocopherol contents (Table 1), they exhibited similar DPPH inhibition, approximately 95% at a concentration of 1% (w/w). It was also observed that for LC, PC, and PE, the DPPH radical scavenging activity decreased with decreasing concentration until being practically constant at concentrations below 0.11% (w/w), equating to a dilution factor of 9. This radical scavenging activity may be related, similarly to the regeneration of α-tocopherol by phospholipids, to the proton-donating

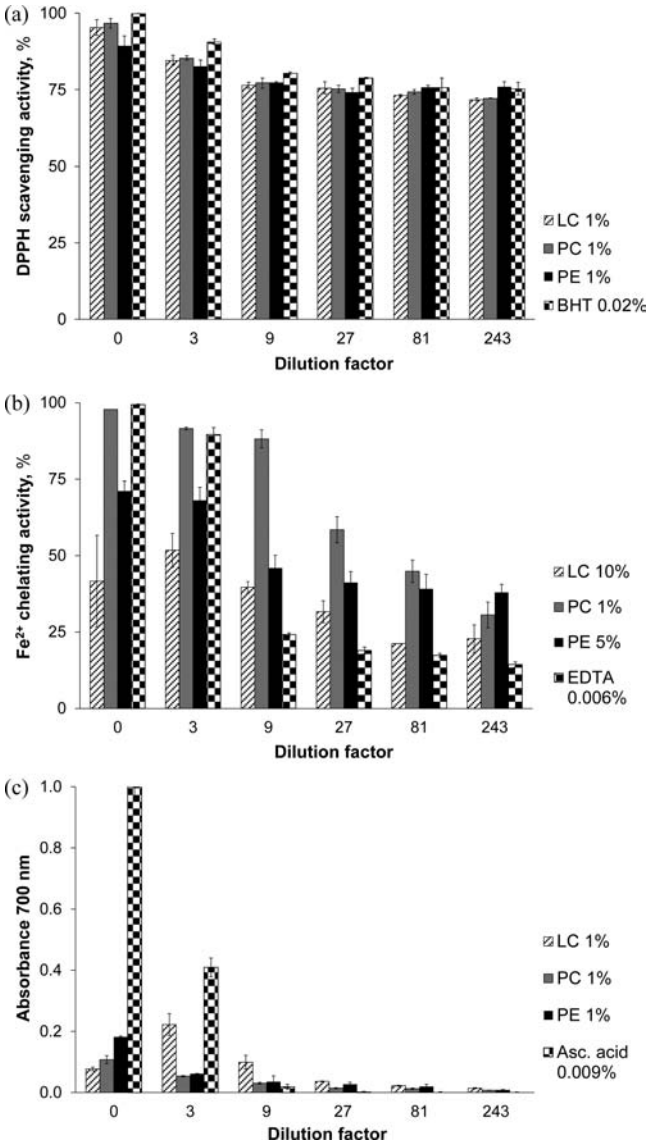

Figure 1. Antioxidant capacity of the phospholipids: (a) DPPH radical scavenging activity; (b) Fe^{2+} chelating activity; (c) reducing power. Results are the average of triplicate determinations ± standard deviation. Legends indicate the concentration of the raw solutions (dilution factor of 0). LC, lecithin; PC, phosphatidylcholine; PE, phosphatidylethanolamine; Asc. acid, ascorbic acid.

capacity of the amino group of phosphatidylcholine and phosphatidylethanolamine.[18] Nevertheless, it should be mentioned that the three phospholipids tested were found to be less effective DPPH scavengers than BHT. Espín et al.[35] reported DPPH radical scavenging activity for phospholipids presented in the lipid fraction of several vegetable oils, but it was considerably lower when compared with DPPH inhibition of α-tocopherol. On the other hand, Reiss et al.[36] reported a marked free radical scavenging activity for plasmalogen phospholipids (plasmenylethalomine and plasmenylcholine). The authors mainly attributed this fact to interactions of enol ether double bond with initiating peroxyl radical, which result in products of enol ether oxidation that apparently do not propagate the oxidation of polyunsaturated fatty acids. Furthermore, peroxyl radicals can also react with phosphatidylcholine to yield stable molecules such as trimethylammonium oxides.[37]

dx.doi.org/10.1021/jf405073x | J. Agric. Food Chem. 2014, 62, 1142−1152

Additionally, phospholipids have been proven to considerably enhance the antioxidant activity of chain-breaking antioxidants such as α-tocopherol, both in bulk oils[18,19] and in oil-in-water emulsions.[20] A synergistic effect of phospholipids with trolox, another phenolic antioxidant, was also described by Chen et al.[38]

Iron (Fe^{2+}) Chelating Activity. Transition metal ions, mainly Fe^{2+} and Cu^{2+}, highly contribute to lipid autoxidation in real food emulsions. Thus, antioxidants that behave as metal chelators are considered to play an important role in the improvement of the oxidative stability of emulsions.[39] Phospholipids have been reported to exhibit chelating activity, but contradictory results were described in the literature. Pokorný et al.[17] stated that phosphatidylinositol and other acidic phospholipids form inactive complexes with metal ions, whereas phosphatidylcholine and phosphatidylethanolamine do not possess such metal chelating properties. On the contrary, Yoon and Min[40] found that phospholipids, including phosphatidylcholine, improved the oxidative stability of purified soybean oil when iron was added. Zambiazi et al.[41] attributed the metal chelating properties to the amino group of phosphatidylcholine, phosphatidylethanolamine, and phosphatidylserine and to the sugar moiety of phosphatidylinositol.

In the present study, except for dilution factor 243, it was observed that PC presented the highest capacity to bind metal ions followed by PE, whereas LC exhibited the lowest metal chelating activity (Figure 1b). For all three phospholipids, Fe^{2+} chelating activity was concentration dependent, increasing with concentration. Although all of the phospholipids were considerably less effective than EDTA in binding metal ions, they may represent a unique type of chelator in case they can act in the lipid phase.[37] However, more studies are necessary to explain why PC had better metal chelating activity than PE and LC.

The superior Fe^{2+} chelating activity of PC may explain the results obtained by Cardenia et al.[37] These authors found that phosphatidylcholine with either oleic or palmitic acid aliphatic side chain was more effective than 1,2-dioleoyl-*sn*-glycero-3-phosphoethanolamine at inhibiting lipid oxidation in 1% (w/w) stripped soybean oil-in-water emulsions at pH 7. Bandarra et al.[18] also described that the addition of phosphatidylcholine to refined sardine oil resulted in a higher protection against lipid oxidation when compared to the addition of phosphoethanolamine, cardiolipin, and α-tocopherol.

Reducing Power. The reducing power of phospholipids was evaluated to determine their capacity to donate electrons. In that way, they may convert free radicals to more stable products and terminate the radical chain reactions.[42] However, compounds exhibiting reducing power may also have a prooxidative effect, especially when Fe^{3+} is reduced to Fe^{2+} in the presence of already existing hydroperoxides.[43]

Figure 1c shows the reducing power for LC, PC, and PE. It was observed that they exhibited an insignificant reducing power when compared with ascorbic acid. For the three cases, absorbances at 700 nm lower than 0.2 were obtained for 1% (w/w) solutions. The higher reducing power exhibited by PE at a dilution factor of 0 may be explained by the fact that ascorbyl palmitate was added during the manufacturing process for its stabilization. Ascorbyl palmitate was reported in previous studies to exhibit reducing power.[43,44]

Characterization of the Emulsions. *pH and Zeta Potential.* Table 2 shows that the actual pH of the emulsions was exactly the pH aimed at (pH 7). With regard to the surface

Table 2. Values of pH, Zeta Potential, Droplet Size, Concentration of Protein in the Aqueous Phase, and Viscosity of the Emulsions

			droplet size					
			$D_{3,2}$ (nm)		Z-average diameter (nm)			viscosity (cP)
emulsion[a]	pH	zeta potential[b] (mV)	day 1[b]	day 14[b,c]	day 1[b]	day 14[b,c]	protein[b] (mg/mL)	day 1[b]	day 14[b,c]
0.3CAS	7.1 ± 0.0	−29.5 ± 0.1w	255.5 ± 2.1w	307.5 ± 4.9w,*	330.3 ± 0.3w	352.1 ± 12.7w,*	0.69 ± 0.02w	1.61 ± 0.08w	1.81 ± 0.04w,*
0.3CAS+0.5LC	7.0 ± 0.0	−32.9 ± 0.2x	210.0 ± 5.6x	203.5 ± 3.5x,ns	270.5 ± 0.7x	266.9 ± 1.7x,*	1.62 ± 0.26x	1.45 ± 0.16wx	1.85 ± 0.08w,*
0.3CAS+0.5PC	7.0 ± 0.0	−22.8 ± 1.3y	212.0 ± 1.4x	195.0 ± 2.8x,*	265.9 ± 0.4y	262.7 ± 2.1x,*	1.90 ± 0.15x	1.43 ± 0.05x	2.04 ± 0.27w,*
0.3CAS+0.5PE	7.1 ± 0.0	−23.8 ± 0.4y	306.0 ± 1.4y	369.0 ± 8.5y,*	332.3 ± 0.8z	357.8 ± 4.5w,*	1.65 ± 0.20x	1.37 ± 0.01x	1.68 ± 0.01w,*

[a]0.3CAS, 0.3% (w/w) of casein; 0.3CAS+0.5LC, 0.3% (w/w) of casein and 0.5% (w/w) of lecithin; 0.3CAS+0.5PC, 0.3% (w/w) of casein and 0.5% (w/w) of phosphatidylcholine; 0.3CAS+0.5PE, 0.3% (w/w) of casein and 0.5% (w/w) of phosphatidylethanolamine. [b]For each column letters w−z indicate significant differences between samples ($p < 0.05$). [c]Significant differences between days 1 and 14 are indicated by either *, significantly different ($p < 0.05$), or ns, not significantly different.

dx.doi.org/10.1021/jf405073x | J. Agric. Food Chem. 2014, 62, 1142−1152

charge of the droplets, negative zeta potentials, ranging from −22.8 to −32.9 mV, were obtained for all of the emulsions (Table 2). This finding can be explained by the fact that casein is negatively charged at pH values above its isoelectric point (around pH 4.6).[45] In addition, phosphatidylcholine and phosphatidylethanolamine, which are zwitterionic ions, do not carry net charge at neutral conditions. Likewise, in the case of lecithin, which is a mixture of phospholipids, phosphatidylinositol (anionic ion) is also negatively charged at pH 7,[46] and this explains why the use of a combination of casein and LC made the zeta potential slightly more negative compared to the use of casein alone, whereas less negative zeta potential values were obtained for the combinations of casein with PC and PE.

On the contrary, emulsions (0.3CAS and 0.3CAS+0.5PC) prepared at similar conditions but at a lower pH (3.5) showed positive values of zeta potential, 22.4 and 20.5 mV, respectively (data not shown). As for the emulsions at high pH, these results also revealed that the addition of PC did not improve the zeta potential of the emulsion. Indeed, the difference between both values (22.4 ± 2.4 and 20.5 ± 1.8 mV) was not statistically significant.

Particle Size Distribution (PSD), Droplet Size, Casein Content in the Aqueous Phase, and Viscosity. As far as the PSD of the emulsions is concerned, the results obtained from the analysis with the Mastersizer 2000 revealed that the emulsion stabilized only with casein had a monomodal PSD with a peak at 450 nm (data not shown). In contrast, the three emulsions in which combinations of casein and phospholipids were employed presented bimodal distributions, with a larger population of smaller droplets (mean diameter at peak = 200−400 nm) and a smaller population of larger droplets (mean diameter at peak = 1000−1200 nm). Although large unilamellar vesicles could present diameters >100 nm,[47] the peak found between 200 and 400 nm may be more likely due to the existence of small droplets covered by a phospholipid monolayer, protein−phospholipid, or protein alone. Similar bimodal distributions were reported by Fang and Dagleish[48] for 20% soybean oil-in-water emulsion stabilized with 0.7% casein and 0.5% dioleoylphosphatidylcholine and by Lu et al.[47] for 9.5% fish oil-in-water emulsions stabilized with 0.5% lecithin obtained from fish byproducts.

Likewise, the Zetasizer analysis gave similar monomodal and biomodal PSD values for the emulsions stabilized with casein alone and with combinations of casein and phospholipids, respectively (data not shown). Due to the fact that the PSD of the emulsions with casein and phospholipids did not present any peak around 4 nm, it was assumed that micelles were not formed from monolayers of phospholipid molecules.[49]

With regard to the mean droplet sizes of the emulsions, the results given as surface are mean diameter ($D_{3,2}$) and as *Z*-average diameter followed the same rank order for the four emulsions evaluated (Table 2). At day 1, the mean droplet sizes of the four emulsions increased in the order 0.3CAS+0.5LC ≈ 0.3CAS+0.5PC < 0.3CAS < 0.3CAS+0.5PE. Smaller droplet sizes are preferred to increase the physical stability of the emulsions.[47] Fang and Dalgleish[48] also reported a reduction on the initial droplet size when incorporating dioleoylphosphatidylcholine to emulsions stabilized with casein. Table 2 also shows that the addition of phospholipids increased the protein concentration in the aqueous phase for the emulsions with LC, PC, and PE. This finding suggested that part of the casein at the interface was substituted by phospholipids. This was in agreement with the suggestion by Fang and Dalgleish.[21] Nevertheless, as the protein concentration in the aqueous phase is also dependent on the temperature employed for the separation,[50] it should be noted that the values shown in Table 2 were obtained at 10 °C.

Although emulsions with LC and PC exhibited good physical stability, emulsions with only casein and casein plus PE increased their mean droplet sizes, and their size distributions moved to larger sizes after 14 days of storage. This denotes that only 0.3% of casein was not a sufficient amount of emulsifier to stabilize 10% fish oil-in-water emulsions during 14 days. In the case of the emulsion 0.3CAS+0.5PE, the physical instability could be due to the lower hydrophilic−lipophilic balance (HLB) of PE at neutral pH, which makes it less appropriate to stabilize oil-in-water emulsions.[51] Despite the increase in droplet sizes observed for 0.3 CAS and 0.3 CAS+PE during storage, no creaming occurred in any of the emulsions during the 14 days. Considering the emulsions prepared at pH 3.5 (0.3CAS and 0.3CAS+0.5PC), larger mean droplet sizes at day 0 and more physically unstable emulsions were obtained (results not shown). Creaming was also observed during storage, particularly for the emulsion with PC. This behavior could perhaps be related to the swelling of PC, which becomes more hydratable at acidic pH, diminishing its capacity as emulsifier.[52]

The rheology of the emulsion can determine the diffusion of prooxidants in the system.[53] The viscosities at day 1 of the four emulsions ranged from 1.37 to 1.61 cP (Table 2). It was observed that the addition of phospholipids as secondary emulsifiers produced a significant and almost identical reduction in the viscosity of 0.3CAS+0.5LC, 0.3CAS+0.5PC, and 0.3CAS+0.5PE emulsions compared to the value obtained for the 0.3CAS emulsion. This decrease in viscosity is not explained by a reduction in the mean droplet size. Therefore, it may be related to other properties of the emulsions such as the composition of the interfacial layer and the concentration of protein in the aqueous phase.[54] As shown in Table 2, the viscosities of the four emulsions increased significantly after 14 days of storage. This may suggest that molecular interactions between casein and phospholipids took place, but this needs further investigation.

Tocopherol Concentration. The amount of α-tocopherol in the emulsions significantly decreased during storage (Table 3), whereas this was not the case for β-, γ-, and δ-tocopherol, which were maintained practically constant for all of the emulsions at 4, 90, and 37 μg/g lipid, respectively. The highest content of α-

Table 3. Tocopherol Content for the Emulsions

	α-tocopherol (μg/g lipid)	
emulsion[a]	day 0[b,c]	day 14[b,c]
0.3CAS	181.7 ± 6.1w,*	157.1 ± 2.4w,*
0.3CAS+0.5LC	195.1 ± 2.1x,*	158.8 ± 1.1w,*
0.3CAS+0.5PC	253.9 ± 9.6y,*	231.9 ± 0.9x,*
0.3CAS+0.5PE	226.5 ± 4.7z,*	197.8 ± 5.2y,*

[a]0.3CAS, 0.3% (w/w) of casein; 0.3CAS+0.5LC, 0.3% (w/w) of casein and 0.5% (w/w) of lecithin; 0.3CAS+0.5PC, 0.3% (w/w) of casein and 0.5% (w/w) of phosphatidylcholine; 0.3CAS+0.5PE, 0.3% (w/w) of casein and 0.5% (w/w) of phosphatidylethanolamine. [b]For each column letters w−z indicate significant differences between samples ($p < 0.05$). [c]Significant differences between days 0 and 14 are indicated by either *, significantly different, $p < 0.05$, or ns, not significantly different.

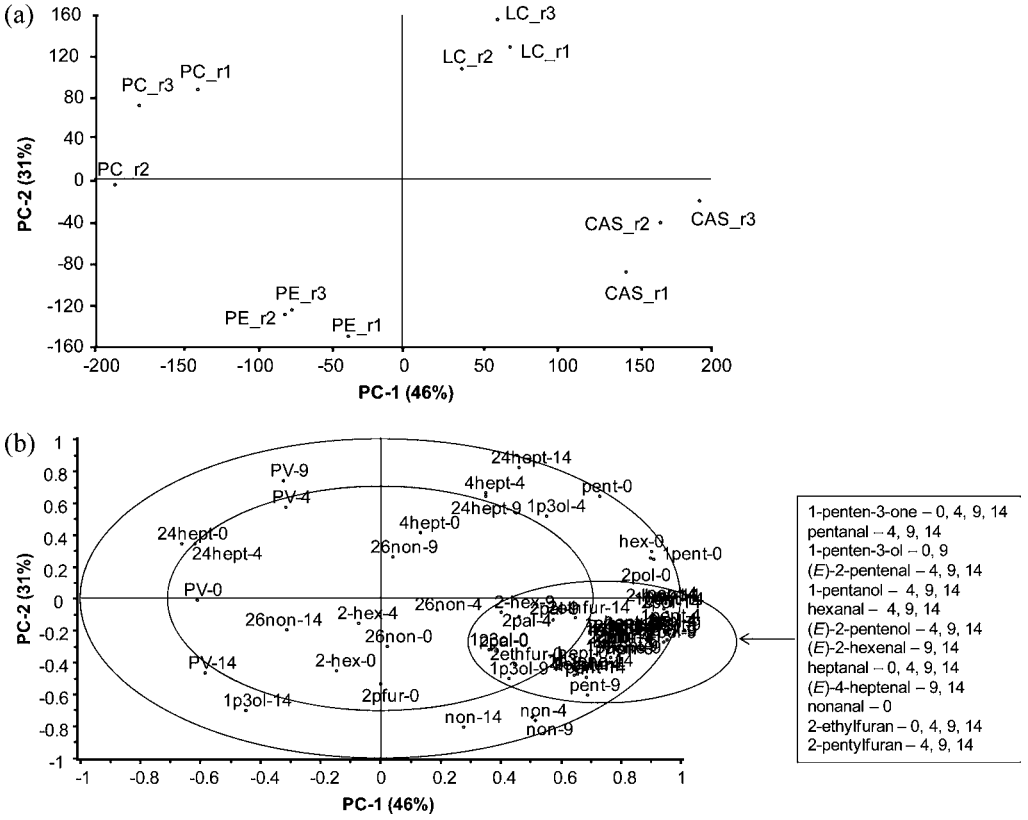

Figure 2. Principal component analysis (PCA) plots of lipid oxidation data: (a) scores plot with all sample replicates (r1, r2, and r3); (b) loadings plot (0–14 indicate sampling days 0–14). PV, peroxide value; LC, lecithin; PC, phosphatidylcholine; PE, phosphatidylethanolamine.

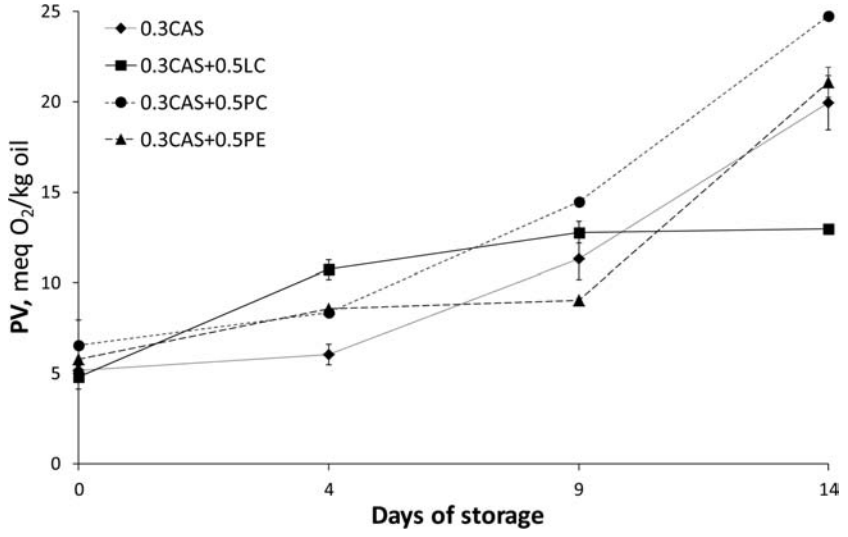

Figure 3. Peroxide value of the emulsions during storage at room temperature. Results are the average of duplicate determination ± standard deviation. 0.3CAS, 0.3% (w/w) of casein; 0.3CAS+0.5LC, 0.3% (w/w) of casein and 0.5% (w/w) of lecithin; 0.3CAS+0.5PC, 0.3% (w/w) of casein and 0.5% (w/w) of phosphatidylcholine; 0.3CAS+0.5PE, 0.3% (w/w) of casein and 0.5% (w/w) of phosphatidylethanolamine.

tocopherol was presented for the 0.3CAS+0.5PC emulsion followed by the 0.3CAS+0.5PE emulsion due to the higher α-tocopherol content of these two phospholipids. It was also observed that the consumption of α-tocopherol, calculated as α-tocopherol concentration at day 0 minus α-tocopherol concentration at day 14, followed the order 0.3CAS+0.5LC > 0.3CAS+0.5PE > 0.3CAS > 0.3CAS+0.5PC.

Lipid Oxidation in Emulsions. A PCA model was calculated to get a visual overview of all variables and to interpret correlations between the variables. In the PCA, the first principal component (PC1) explained 46% of the variance and the second principal component (PC2) explained 31% (Figure 2a). The scores plot showed that replicates for each type of emulsion were located together in the plot. Furthermore, the plot showed that the LC emulsion was located in the first quadrant, the PC emulsion in the second quadrant, the PE emulsion in the third quadrant, and the CAS emulsion in the fourth quadrant. Hence, the different emulsions

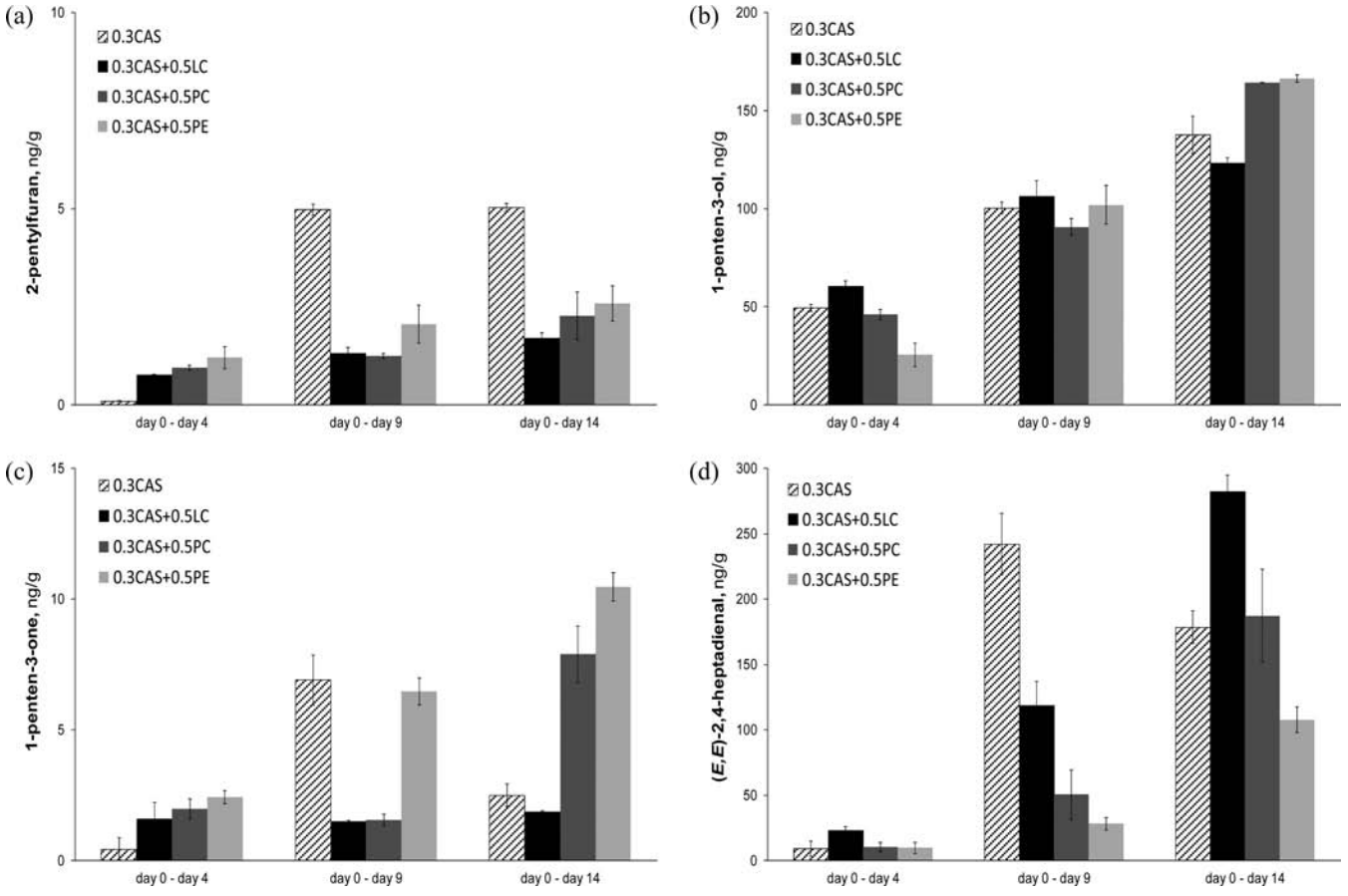

Figure 4. Increase of the concentration of secondary oxidation products in the emulsions (a) 2-pentylfuran, (b) 1-penten-3-ol, (c) 1-penten-3-one, and (d) (*E*,*E*)-2,4-heptadienal during storage at room temperature. Results are the average of triplicate determinations ± standard deviation. 0.3CAS, 0.3% (w/w) of casein; 0.3CAS+0.5LC, 0.3% (w/w) of casein and 0.5% (w/w) of lecithin; 0.3CAS+0.5PC, 0.3% (w/w) of casein and 0.5% (w/w) of phosphatidylcholine; and 0.3CAS+0.5PE: 0.3% (w/w) of casein and 0.5% (w/w) of phosphatidylethanolamine.

had different values on both the PC1 and PC2 axes, indicating that they behaved differently with respect to the parameters measured.

Peroxide Value. The PCA loadings plot showed that peroxide values were located to the left in the plot, in the second and third quadrants, indicating that PE and especially PC emulsions had higher PVs than the other two emulsions (Figure 2b). PV at initial time (PV-0) has a value of approximately 0 in PC2, indicating less contribution from this variable than the other PV variables. The raw data confirmed this interpretation of the model, as it was observed that all of the emulsions had a similar initial PV (~6 mequiv O_2/kg oil) and all of them suffered an increase in PV over time of storage. The emulsion with PC had the highest concentration of hydroperoxides after 14 days (24.7 mequiv O_2/kg oil), followed by the emulsion with PE (21.1 mequiv O_2/kg oil) and then the emulsion stabilized with only casein (19.9 mequiv O_2/kg oil) (Figure 3). Although PV increased rapidly between days 0 and 4 for the emulsion with LC, the scores for this emulsion correlated negatively with PV-14 in the PCA, and the raw data also indicated that it had the lowest PV at day 14 (12.9 mequiv O_2/kg oil).

Secondary Volatile Oxidation Products. The PCA loadings plot showed that the most volatiles were located in the fourth quadrant, indicating a higher concentration of volatiles in the CAS emulsion than the other emulsions (Figure 2b). This was confirmed by the raw data because CAS emulsion suffered a higher increase from day 0 to day 14 in the concentration of the following volatiles: 2-pentylfuran (Figure 4a), 2-ethylfuran, (*E*)-4-heptenal, heptanal, and (*E*)-2-hexenal (data not shown). This may be due to the physical instability, the second most negative zeta potential, and the lowest protein content in the aqueous phase shown by the emulsion stabilized with only 0.3% (w/w) of CAS (Table 2).

Figure 2b also suggests that the emulsion with PE presented the highest content of 1-penten-3-ol at day 14. It was confirmed by the raw data shown in Figure 4b, although a similar level of 1-penten-3-ol was found for the emulsion with PC. In addition, the emulsion with PE also had the largest increase in concentrations of other volatiles, namely, 1-pentanol, pentanal, hexanal, (*E*)-2-pentenol, and nonanal (data not shown). The emulsion with PC was the third most oxidized with high increases in the content of 1-penten-3-ol (Figure 4b), 1-penten-3-one (Figure 4c), (*E*,*E*)-2,4-heptadienal (Figure 4d), and (*E*,*Z*)-2,6-nonadienal (data not shown). This emulsion may present a lower concentration of volatiles than the emulsion with PE due to (i) the superior chelating properties shown by PC (Figure 1b) and (ii) its improved physical stability when compared with the emulsion stabilized with PE (Table 2).

The emulsion with LC presented the highest content of (*E*,*E*)-2,4-heptadienal at day 14 (Figure 4d), as was also indicated by the PCA. However, this emulsion showed the lowest increase from day 0 to day 14 for the following volatiles: 2-pentylfuran, 1.7 ng/g (Figure 4a); 1-penten-3-ol, 123.0 ng/g

dx.doi.org/10.1021/jf405073x | *J. Agric. Food Chem.* 2014, 62, 1142−1152

(Figure 4b); and 1-penten-3-one, 1.8 ng/g (Figure 4c). These findings, together with the lowest PV determined at day 14 (12.9 mequiv O_2/kg oil) and the maximum consumption of α-tocopherol during storage observed for this emulsion when compared with the others, indicated that the emulsion stabilized with the combination of casein and LC was the most oxidatively stable.

Nevertheless, this finding cannot be explained by the physical data obtained for this emulsion (Table 2). The emulsion with LC had the most negative zeta potential (−32.9 mV), which would increase the attraction of transition metal ions to the interface, and the lowest droplet size ($D_{3,2}$ = 210 nm), which implies larger surface for the contact between metal ions and hydroperoxides. Both facts could lead to less oxidatively stable emulsions[55,56] because metal ions catalyze the initiation of free radicals as well as the decomposition of hydroperoxides to secondary oxidation products. In addition, the protein content in the aqueous phase of this emulsion was practically identical to that of the other emulsions with phospholipids (Table 2), and LC also did not show better metal chelating activity than the other phospholipids (Figure 1b). Moreover, the DPPH scavenging activity of LC was not higher than the rest of phospholipids (Figure 1a), but it resulted in similar percentages of inhibition despite a lower α-tocopherol content than the other phospholipids (Table 1).

Therefore, these results suggested that the improved oxidative stability of the LC emulsion may be related to other factors such as the characteristics of the interface. In this regard, previous studies stated that a change in the thickness and structure of the interfacial layer was obtained when lecithin was added to emulsions stabilized with a low concentration of casein (0.3% w/w).[21,48] According to these authors, the surface concentration of casein is not the only important factor influencing the adsorbed casein layer thickness. They concluded that a thicker interfacial layer is produced due to the fact that the added phospholipids take up space at the interface, leading casein to adopt a conformation that projects farther into the aqueous phase. In this study, incorporation of phospholipids at the interface may have occurred as suggested by the increase of protein concentration in the aqueous phase for the emulsions with phospholipids when compared with the CAS emulsion (Table 2). Thus, it could lead to the previously commented modification of the interface. In the case of LC, its content in charged phospholipids such as phosphatidylinositol and phosphatidic acid, which are more soluble in water and are then more easily adsorbed at the oil−water interface,[57] may cause the suggested differences in the physical structure and thickness of the LC emulsion. However, this requires further research to be confirmed.

By comparison of the emulsions at pH 3.5 and 7, it was observed that emulsions at pH 3.5 presented a lower content of hydroperoxides but their volatiles content was considerably higher. Although the positive zeta potential of these emulsions may result in a repulsion of metal ions, causing a decrease of lipid oxidation, at low pH the solubility of iron increases, accelerating the decomposition of hydroperoxides to volatiles.[25]

In conclusion, it may be stated that employing a combination of soybean lecithin, 0.5% (w/w), and casein, 0.3% (w/w), as emulsifier improved the physical and oxidative stabilities of fish oil-in-water emulsions at pH 7, when compared to an emulsion stabilized only with casein, 0.3% (w/w). Soy LC is preferred instead of pure soy PC or PE due to its superior emulsifying properties as a consequence of the different phospholipids (phosphatidylcholine, phosphatidylethanolamine, phosphatidylinositol, and phosphatidic acid) present in its composition. Moreover, the addition of LC could result in a favorable structure and thickness of the interfacial layer, which may reduce lipid oxidation. Additionally, LC is a cheaper product and, thus, its application to food processing is more economically viable when compared to pure phospholipids.

AUTHOR INFORMATION

Corresponding Author

*(P.J.G.-M) Phone: +34958241329. Fax: +34958248992. E-mail: pjgarcia@ugr.es.

Funding

This work was supported by the Spanish National Plan I+D+i (Project CTQ2008-02978). P.J.G.-M. acknowledges an FPI grant from the Spanish Ministry of Science and Innovation. In addition, the work carried out was also partly funded by the project Omega-3 food emulsions: Control and investigation of molecular structure in relation to lipid oxidation. This project was financed by the Danish Food Ministry (FERV).

Notes

The authors declare no competing financial interest.

ACKNOWLEDGMENTS

We thank Lipoid for kindly providing the phospholipids tested in this work, ARLA Foods Ingredients amba for donating sodium caseinate, and Maritex A/S, Norway, subsidiary of TINE, BA for providing the fish oil. Furthermore, we acknowledge Marie-Louise Nouard for her contribution to some of the results presented. Finally, we are grateful to Lis Berner, Inge Holmberg, Victoria Rothman, and Trang Vu for their help in the laboratory work.

REFERENCES

(1) Uauy, R.; Valenzuela, A. Marine oils: the health benefits of n-3 fatty acids. *Nutrition* **2000**, *16*, 680−684.

(2) Ward, O. P.; Singh, A. Omega-3/6 fatty acids: alternative sources of production. *Process Biochem.* **2005**, *40*, 3627−3652.

(3) Sloan, E. Top 10 trends in functional food. *Food Technol.* **2006**, *60*, 22−40.

(4) Let, M. B.; Jacobsen, C.; Meyer, A. S. Lipid oxidation in milk, yoghurt, and salad dressing enriched with neat fish oil or pre-emulsified fish oil. *J. Agric. Food Chem.* **2007**, *55*, 7802−7809.

(5) Ye, A.; Cui, J.; Taneja, A.; Zhu, X.; Singh, H. Evaluation of processed cheese fortified with fish oil emulsion. *Food Res. Int.* **2009**, *42*, 1093−1098.

(6) Nielsen, N. S.; Jacobsen, C. Methods for reducing lipid oxidation in fish-oil-enriched energy bars. *Int. J. Food Sci. Technol.* **2009**, *44*, 1536−1546.

(7) McClements, D. J.; Decker, E. A. Lipid oxidation in oil-in-water emulsions: impact of molecular environment on chemical reactions in heterogeneous food systems. *J. Food Sci.* **2000**, *65*, 1270−1282.

(8) Hunt, J. A.; Dalgleish, D. G. Adsorption behaviour of whey protein isolate and caseinate in soya oil-in-water emulsions. *Food Hydrocolloids* **1994**, *8*, 175−187.

(9) Krog, N. Emulsifiers and emulsions in dairy foods. In *Encyclopedia of Dairy Sciences*; Roginski, H., Ed.; Elsevier: Oxford, UK, 2002; pp 891−900.

(10) Creamer, L. K. Milk proteins/casein nomenclature, structure and association properties. In *Encyclopedia of Dairy Sciences*; Roginski, H., Ed.; Elsevier: Oxford , UK, 2002; pp 1895−1902.

(11) Díaz, M.; Dunn, C. M.; McClements, D. J.; Decker, E. A. Use of caseinophosphopeptides as natural antioxidants in oil-in-water emulsions. *J. Agric. Food Chem.* **2003**, *51*, 2365−2370.

(12) Chen, Z. Y.; Nawar, W. W. Prooxidative and antioxidative effects of phospholipids on milk fat. *J. Am. Oil Chem. Soc.* **1991**, *68*, 938−940.
(13) Sugino, H.; Ishikawa, M.; Nitoda, T.; Koketsu, M.; Juneja, L. R.; Kim, M.; Yamamoto, T. Antioxidative activity of egg yolk phospholipids. *J. Agric. Food Chem.* **1997**, *45*, 551−554.
(14) Cho, S.-Y.; Joo, D.-S.; Choi, H.-G.; Nara, E.; Miyashita, K. Oxidative stability of lipids from squid tissues. *Fish. Sci.* **2001**, *67*, 738−743.
(15) Judde, A.; Villeneuve, P.; Rossignol-Castera, A.; Guillou, A. L. Antioxidant effect of soy lecithins on vegetable oil stability and their synergism with tocopherols. *J. Am. Oil Chem. Soc.* **2003**, *80*, 1209−1215.
(16) Saito, H.; Ishihara, K. Activity and active sites of phospholipids as antioxidants. *J. Am. Oil Chem. Soc.* **1997**, *74*, 1531−1536.
(17) Pokorný, J. Major factors affecting the autoxidation of lipids. In *Autoxidation of Unsaturated Lipids*; Chan, H. W. S., Ed.; Academic Press: London, UK, 1987; pp 141−206.
(18) Bandarra, N. M.; Campos, R. M.; Batista, I.; Nunes, M. L.; Empis, J. M. Antioxidant synergy of α-tocopherol and phospholipids. *J. Am. Oil Chem. Soc.* **1999**, *76*, 905−913.
(19) Lee, J.; Choe, E. Effects of phospholipids on the antioxidant activity of α-tocopherol in the singlet oxygen oxidation of canola oil. *New Biotechnol.* **2011**, *28*, 691−697.
(20) Lu, F. S. H.; Nielsen, N. S.; Baron, C. P.; Diehl, B. W. K.; Jacobsen, C. Oxidative stability of dispersions prepared from purified marine phospholipid and the role of α-tocopherol. *J. Agric. Food Chem.* **2012**, *60*, 12388−12396.
(21) Fang, Y.; Dalgleish, D. G. Casein adsorption on the surfaces of oil-in-water emulsions modified by lecithin. *Colloids Surf. B: Biointerfaces* **1993**, *1*, 357−364.
(22) Courthaudon, J. L.; Dickinson, E.; Christie, W. W. Competitive adsorption of lecithin and β-casein in oil-in-water emulsions. *J. Agric. Food Chem.* **1991**, *39*, 1365−1368.
(23) Dickinson, E.; Iveson, G. Adsorbed films of β-lactoglobulin + lecithin at the hydrocarbon−water and triglyceride−water interfaces. *Food Hydrocolloids* **1993**, 533−541.
(24) Horn, A. F.; Nielsen, N. S.; Andersen, U.; Søgaard, L. H.; Horsewell, A.; Jacobsen, C. Oxidative stability of 70% fish oil-in-water emulsions: impact of emulsifiers and pH. *Eur. J. Lipid Sci. Technol.* **2011**, *113*, 1243−1257.
(25) Horn, A. F.; Nielsen, N. S.; Jacobsen, C. Iron-mediated lipid oxidation in 70% fish oil-in-water emulsions: effect of emulsifier type and pH. *Int. J. Food Sci. Technol.* **2012**, *47*, 1097−1108.
(26) AOCS. *AOCS Official Method Ce 2-66. Preparation of Methyl Esters of Long Chain Fatty Acids*; AOCS: Champaign, IL, USA, 1998.
(27) AOCS. *AOCS Official Method Ce 1b-89. Fatty Acid Composition by GLC, Marine Oils*; AOCS: Champaign, IL, USA, 1998.
(28) Shantha, N. C.; Decker, E. A. Rapid, sensitive, iron-based spectrophotometric methods for determination of peroxide values of food lipids. *J. AOAC Int.* **1994**, *77*, 421−424.
(29) AOCS. *AOCS Official Method Ce 8-89. Determination of Tocopherols and Tocotrienols in Vegetable Oils and Fats by HPLC*; AOCS: Champaign, IL, USA, 1998.
(30) Shimada, K.; Fujikawa, K.; Yahara, K.; Nakamura, T. Antioxidative properties of xanthan on the autoxidation of soybean oil in cyclodextrin emulsion. *J. Agric. Food Chem.* **1992**, *40*, 945−948.
(31) Dinis, T. C.; Maderia, V. M.; Almeida, L. M. Action of phenolic derivatives (acetaminophen, salicylate, and 5-aminosalicylate) as inhibitors of membrane lipid peroxidation and as peroxyl radical scavengers. *Arch. Biochem. Biophys.* **1994**, *315*, 161−169.
(32) Oyaizu, M. Studies on products of browning reactions: antioxidative activities of browning products of browning reaction prepared from glucosamine. *Jpn. J. Nutr.* **1986**, *44*, 307−315.
(33) Horn, A. F.; Wulff, T.; Nielsen, N. S.; Jacobsen, C. Effect of α-lactalbumin and β-lactoglobulin on the oxidative stability of 10% fish oil-in-water emulsions depends on pH. *Food Chem.* **2013**, *141*, 574−581.
(34) Bligh, E. G.; Dyer, W. J. A rapid method of total lipid extraction and purification. *Can. J. Biochem. Physiol.* **1959**, *37*, 911−917.
(35) Espín, J. C.; Soler-Rivas, C.; Wichers, H. J. Characterization of the total free radical scavenger capacity of vegetable oils and oil fractions using 2,2-diphenyl-1-picrylhydrazyl radical. *J. Agric. Food Chem.* **2000**, *48*, 648−656.
(36) Reiss, D.; Beyer, K.; Engelmann, B. Delayed oxidative degradation of polyunsaturated diacyl phospholipids in the presence of plasmalogen phospholipids in vitro. *Biochem. J.* **1997**, *323*, 807−814.
(37) Cardenia, V.; Waraho, T.; Rodriguez-Estrada, M. T.; McClements, D. J.; Decker, E. A. Antioxidant and prooxidant activity behavior of phospholipids in stripped soybean oil-in-water emulsions. *J. Am. Oil Chem. Soc.* **2011**, *88*, 1409−1416.
(38) Chen, B.; Han, A.; Laguerre, M.; McClements, D. J.; Decker, E. A. Role of reverse micelles on lipid oxidation in bulk oils: impact of phospholipids on antioxidant activity of α-tocopherol and trolox. *Food Funct.* **2011**, *2*, 302−309.
(39) Mancuso, J. R.; McClements, D. J.; Decker, E. A. The effects of surfactant type, pH, and chelators on the oxidation of salmon oil-in-water emulsions. *J. Agric. Food Chem.* **1999**, *47*, 4112−4116.
(40) Yoon, S. H.; Min, D. B. Roles of phospholipids in flavor stability of soybean oil. *Korean J. Food Sci. Technol.* **1987**, *19*, 23−28.
(41) Zambiazi, R. C.; Przybylski, R. Effect of endogenous minor components on the oxidative stability of vegetable oils. *Lipid Technol.* **1998**, *10*, 58−62.
(42) Yen, G.-C.; Chen, H.-Y. Antioxidant activity of various tea extracts in relation to their antimutagenicity. *J. Agric. Food Chem.* **1995**, *43*, 27−32.
(43) Sørensen, A.-D. M.; Nielsen, N. S.; Decker, E. A.; Let, M. B.; Xu, X.; Jacobsen, C. The efficacy of compounds with different polarities as antioxidants in emulsions with omega-3 lipids. *J. Am. Oil Chem. Soc.* **2011**, *88*, 489−502.
(44) Mäkinen, M.; Kähkönen, M.; Hopia, A. Ascorbic acid and ascorbyl palmitate have only minor effect on the formation and decomposition of methyl linoleate hydroperoxides. *Eur. J. Lipid Sci. Technol.* **2001**, *103*, 683−687.
(45) Hu, M.; McClements, D. J.; Decker, E. A. Lipid oxidation in corn oil-in-water emulsions stabilized by casein, whey protein isolate, and soy protein isolate. *J. Agric. Food Chem.* **2003**, *51*, 1696−1700.
(46) Wang, G.; Wang, T. Oxidative stability of egg and soy lecithin as affected by transition metal ions and pH in emulsion. *J. Agric. Food Chem.* **2008**, *56*, 11424−11431.
(47) Lu, F. S. H.; Nielsen, N. S.; Baron, C. P.; Jensen, L. H. S.; Jacobsen, C. Physico-chemical properties of marine phospholipid emulsions. *J. Am. Oil Chem. Soc.* **2012**, *89*, 2011−2024.
(48) Fang, Y.; Dalgleish, D. G. Comparison of the effects of three different phosphatidylcholines on casein-stabilized oil-in-water emulsions. *J. Am. Oil Chem. Soc.* **1996**, *73*, 437−442.
(49) Thompson, A. K.; Hindmarsh, J. P.; Haisman, D.; Rades, T.; Singh, H. Comparison of the structure and properties of liposomes prepared from milk fat globule membrane and soy phospholipids. *J. Agric. Food Chem.* **2006**, *54*, 3704−3711.
(50) Dickinson, E.; Tanai, S. Temperature dependence of the competitive displacement of protein from the emulsion droplet surface by surfactants. *Food Hydrocolloids* **1992**, *6*, 163−171.
(51) Carlsson, A. Physical properties of phospholipids. In *Phospholipid Technology and Applications*; Oily Press: Bridgwater, UK, 2008; pp 95−137.
(52) Comas, D. I.; Wagner, J. R.; Tomás, M. C. Creaming stability of oil in water (O/W) emulsions: influence of pH on soybean protein−lecithin interaction. *Food Hydrocolloids* **2006**, *20*, 990−996.
(53) Waraho, T.; McClements, D. J.; Decker, E. A. Mechanisms of lipid oxidation in food dispersions. *Trends Food Sci. Technol.* **2011**, *22*, 3−13.
(54) Floury, J.; Desrumaux, A.; Lardières, J. Effect of high-pressure homogenization on droplet size distributions and rheological properties of model oil-in-water emulsions. *Innovative Food Sci. Emerging Technol.* **2000**, *1*, 127−134.
(55) Jacobsen, C.; Hartvigsen, K.; Lund, P.; Thomsen, M. K.; Skibsted, L. H.; Adler-Nissen, J.; Hølmer, G. K.; Meyer, A. S. Oxidation in fish oil-enriched mayonnaise 3: assessment of the

influence of the emulsion structure on oxidation by discriminant partial least squares regression analysis. *Eur. Food Res. Technol.* **2000**, *211*, 86−98.
(56) Lethuaut, L.; Métro, F.; Genot, C. Effect of droplet size on lipid oxidation rates of oil-in-water emulsions stabilized by protein. *J. Am. Oil Chem. Soc.* **2002**, *79*, 425−430.
(57) Rydhag, L.; Wilton, I. The function of phospholipids of soybean lecithin in emulsions. *J. Am. Oil Chem. Soc.* **1981**, *58*, 830−837.

from Luzchem (Ottawa, Canada) using the third harmonic (355 nm) of a pulsed Q-switched Nd:YAG laser (Brilliant B, Les Ulis, France) attenuated to 14 mJ·cm^{-2} as the excitation source with 8 ns of pulse duration. Appropriate UV cutoff filters were used to minimize the sample degradation by the monitoring light. The samples were excited in 1.0 cm ×1.0 cm fluorescence cuvettes from Hellma (Mulheim, Germany). The signal from the monochromator/photomultiplier detection system was captured by a Tektronix TDS 2012 digitizer (Beaverton, OR). The laser system and the digitizer were connected to a personal computer via General Purpose Instrumentation Bus (GPIB) and serial interfaces controlling all the experimental parameters and providing suitable processing and data storage capabilities. Each kinetic trace was averaged 16 times, and observed rate constants were determined by fitting the data with MatLab R2008 to exponential decay functions (Mathworks Inc., Natick, MA). All measurements were made with fresh solutions thermostatted at 25.0 ± 0.1 °C and purged with high-purity N_2 (White-Martins, Sertãozinho-SP, Brazil) for 60 min before the experiment.

Fluorescence Measurements. Fluorescence measurements were carried out using a Hitachi F-7000 fluorescence spectrometer (Hitachi High-Tech, Tokyo, Japan) at 25 °C using a thermostated cell holder. Samples were excited in 1.0 cm ×1.0 cm fluorescence cuvettes from Hellma (Mulheim, Germany), and the emission spectra were recorded for excitation at 445 nm. Fluorescence lifetime measurements were performed with an Optical Building Blocks Corp. Fluorometer (Birmingham, United Kingdom), using the time-resolved mode. The excitation and emission wavelengths were λ = 460 and 530 nm, respectively. Fluorescence decay times were fitted using a mono-exponential decay function, and the best fit was obtained by optimized Chi-square residuals and standard deviation parameters. All solutions were deaerated by purging the cuvette with high-purity N_2 (White-Martins, Sertãozinho-SP, Brazil).

Time Resolved Fluorescence Spectroscopy. Time-resolved fluorescence of the sample was measured by time-correlated single-photon counting using a picosecond spectrometer equipped with Glan-Laser polarizers (Newport, Irvine, CA), a Peltier-cooled PMTMCP from Hamamatsu model R3809U-50 (Hamamatsu, Japan) as the photon detector, and Tennelec-Oxford (Oxford, Abingdon, U.K.) counting electronics. The light pulse was provided by frequency doubling the 200 fs laser pulse of a Mira 900 Ti-sapphire laser pumped by a Verdi 5 W coherent laser (Santa Clara, CA), and the pulse frequency was reduced to 800 kHz using a pulse picker (Conoptics, Danbury, CT). The fluorescence decays were taken in magic angle (λ_{exc} = 400 nm) and analyzed by a reconvolution procedure with instrument response function (irf) with exponential decay models, and the goodness of the fit was evaluated by the Chi-square statistical parameters. Steady-state fluorescence was measured on a Hitachi F-7000 spectrofluorometer (Hitachi Hi-Tech, Mito, Japan) at 25 ± 0.1 °C. All solutions were deaerated by purging the cuvette with high-purity N_2 (White-Martins, Sertãozinho-SP, Brazil).

Steady State Photolysis. An aqueous solution (pH = 7.4, ionic strength 0.2 mol·L^{-1}, 25 ± 0.5 °C) with 40 × 10^{-6} mol·L^{-1} riboflavin and 8 × 10^{-6} mol·L^{-1} myoglobin was exposed to 436 nm monochromatic light generated by a mercury lamp (HBO 200 w/4 short arc, Osram, Augsburg, Germany) accommodated with a focusing quartz lens, a water-filled heat filter and an Oriel narrow-band interference filter (center wavelength, 436 nm; Oriel Corp., Irvine, CA). The intensity of light, I_o, was measured by ferrioxalate actinometry[19] and had the average value of 2 × 10^{-6} einstein·s^{-1}·cm^{-2}. The absorbance measurements were carried out employing a Hitachi U-3501 (Hitachi-Hitech, Japan) spectrophotometer. All solutions were deaerated by purging the cuvette with high-purity N_2 (White-Martins, Sertãozinho-SP, Brazil).

SDS–PAGE Electrophoresis. Protein containing samples were collected and diluted in SDS sample buffer to a protein concentration of 1 mg·mL^{-1} (106 mM Tris·HCl, 141 mM Tris·Base, 2% SDS, 10% glycerol, 0.51 mM EDTA, 0.22 mM SERVA Blue G250, 0.175 mM Phenol Red; pH 7.4) and boiled for 5 min. 15 μL was loaded onto Tris-acetate gels (10% polyacrylamide, Invitrogen, Carlsbad, CA) and run at 125 V for 45 min. Gels were stained with 0.1% Coomassie brilliant blue R-250 colorant. Following destaining, proteins were identified by comparing relative motilities to molecular weight standards (Precision Plus Protein ALL Blue Standards; Bio-Rad, Berkley, CA) run under the same experimental conditions.

Western Blotting. 25 μL of protein (1.0 mg·mL^{-1}) from samples added to 25 μL in 4× LDS sample buffer with 50 mM DTT was electrophoresed on 8–12% SDS–polyacrylamide gel under reducing conditions and transferred to polyvinylidene difluoride membranes (0.20 μm pore size; Invitrogen, Carlsbad, CA) using a Nu-PAGE Transfer Buffer (Invitrogen, Carlsbad, CA) with 10% methanol. The membranes were blocked in 5% nonfat dried milk in Tris-buffered saline/Tween-20 (TBS-T; 20 mM Tris, pH 7.5, 150 mM NaCl, 0.3% Tween-20) for 1 h at room temperature. Immunoblotting was performed using a mouse monoclonal affinity-purified antibody (1:1000) to myoglobin, for 24 h at 4 °C in 1% nonfat dried milk in TBS-T. The membrane was then washed three times in TBS-T and incubated with a 1:2000 horseradish peroxidase-conjugated mouse affinity-purified antibody to mouse IgG, (GE Healthcare, Litle Chalfont, U.K.), in TBS-T for 2 h at room temperature. After three washes in TBS-T, proteins were visualized using the enhanced chemiluminescent system model ECL-plus.

RESULTS AND DISCUSSION

Oxidation of meat and meat products involves lipids, proteins, and heme-pigments and leads to rancidity, loss of tenderness, and discoloration.[16,17] Oxidation processes in meat are initiated by exposure to light, by iron catalysis, and by enzymatic processes including pseudoperoxidase activity of heme-pigments.[20,21] Notably, oxidation of lipids, proteins, and pigments is coupled, and the relative importance of the various initiators under specific conditions still remains an open question.

Riboflavin shows strong absorption in the spectral region for which fluorescent light used for retail display has high intensity, see Figure 1. Oxymyoglobin, MbFe(II)O_2, and metmyoglobin,

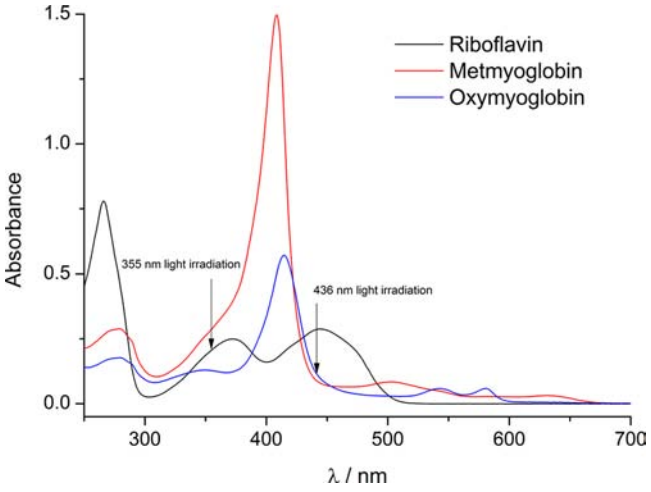

Figure 1. UV–vis absorption spectra for aqueous phosphate buffer pH 7.4 of riboflavin, 27 × 10^{-6} mol·L^{-1}, metmyoglobin, 8 × 10^{-6} mol·L^{-1}, and oxymyoglobin, 4.610^{-6} mol·L^{-1}. Arrows indicate the excitation wavelength for the steady-state photolysis (436 nm) and laser flash photolysis (355 nm).

MbFe(III), both absorb light in the visible region, but since the quantum yield for oxidation of MbFe(II)O_2 is very small for visible light and MbFe(III) is not photoreactive, direct photooxidation is of little importance.[22] None-heme meat proteins does not absorb visible light, and as for MbFe(II)O_2, riboflavin photosensitized processes should rather be considered.[2]

dx.doi.org/10.1021/jf405182f | J. Agric. Food Chem. 2014, 62, 1153–1158

Riboflavin is highly fluorescent as may be seen from the emission spectra shown in Figure 2A for aqueous solutions of

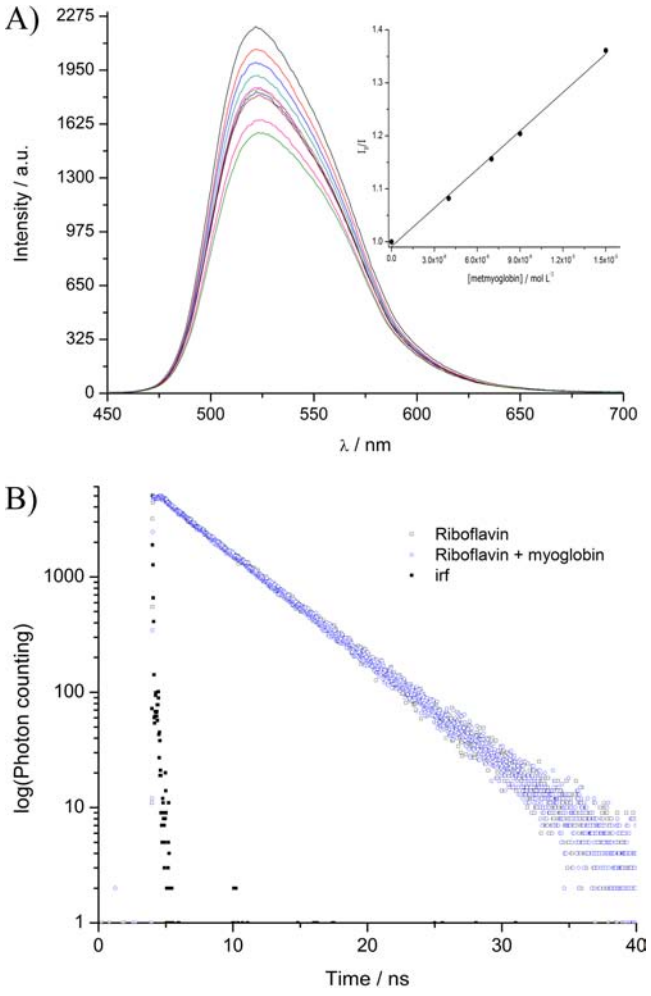

Figure 2. (A) Fluorescence emission spectra of riboflavin, 10×10^{-6} mol·L^{-1}, in aqueous solution pH 7.4 for increasing concentration of metmyoglobin ranging from 1 to 20×10^{-6} mol·L^{-1}. Inset: Stern–Volmer plot, see eq 1. (B) Fluorescence lifetime measurements by time-resolved single photon counting for riboflavin, 18×10^{-6} mol·L^{-1}, in the absence or presence of 7×10^{-6} mol·L^{-1} metmyoglobin in anaerobic aqueous phosphate buffer pH 7.4, irf = instrument response function.

riboflavin with increasing concentration of MbFe(III). Excitation at 436 nm was used in order to reduce inner-filter effects, compare with Figure 1, and the reduction in fluorescence intensity by the presence of MbFe(III) can rather be assigned to quenching by myoglobin. The fluorescent lifetime was found to have the value of $\tau = 4.8$ ns at 25 °C independent of the presence of MbFe(III) as seen from Figure 2B, in agreement with static rather than dynamic quenching of ^{1}Rib by MbFe(III). The fluorescence intensity was analyzed according to the Stern–Volmer equation,

$$\frac{I_o}{I} = 1 + k_q \times t \times [\text{MbFe(III)}] \quad (1)$$

in which I_o is the fluorescence intensity at 525 nm in the absence of MbFe(III), and I is the intensity for increasing concentration of MbFe(III), see inset in Figure 2A. The observed linearity of the Stern–Volmer plot provided an apparent value for k_q of 4.84×10^{12} L·mol^{-1}·s^{-1} and similar value for MbFe(II)O_2, see Table 1, which both are above the

Table 1. Second-Order Rate Constant of Singlet-Excited State Riboflavin Quenching, ^1k_q, and of Triplet-Excited State Riboflavin Reductive Quenching, k_2, by Myoglobins in Aqueous Phosphate Buffer pH 7.4 (0.2 mol L^{-1} NaCl) at 25 °C

species	^1k_q (L·mol^{-1}·s^{-1})[a]	k_2 (L·mol^{-1}·s^{-1})
metmyoglobin	6.4×10^{12}	$3.1 \pm 0.4 \times 10^9$
oxymyoglobin	4.8×10^{12}	$3.0 \pm 0.5 \times 10^9$

[a] from the Stern–Volmer treatment of the steady-state fluorescence data for dynamic quenching.

diffusion limit for a second-order process, further confirming that the quenching of ^{1}Rib is static rather than dynamic. The quenching was accordingly rather analyzed accordingly to[23]

$$\frac{\log I_o + I}{I} = \log K_a + n \times \log[\text{MbFe(III)}] \quad (2)$$

in which K_a is the equilibrium constant for

$$\text{Rib} + n\text{MbFe(III)} \leftrightharpoons \text{Rib(MbFe(III))}_n \quad (3)$$

and n is the number of quenchers binding to the emitting compound in the ground state. The values determined for K_a and n for the three temperatures, see Figure 3, is collected in Table 2 and provides the thermodynamic parameters $\Delta H° = -112 \pm 22$ kJ·mol^{-1} and $\Delta S° = -296 \pm 75$ J·mol^{-1}·K^{-1} for the reaction of eq 3 using the Van't Hoff equation. The binding of MbFe(III) to Rib is an exothermic process with a 1:1 stoichiometry, and the static quenching is highest at low temperatures as usually observed for hydrophobic interaction.

The good linearity seen for the plot according to eq 2 for each of the three temperatures indicates that the quenching is dominating by the ground state binding of the MbFe(III) to Rib rather than by a dynamic process, as is also in agreement with the values of K_a around 10^4 mol·L^{-1}. The decrease in entropy for binding of MbFe(III) to Rib could indicate a strong hydrophobic interaction without significant solvent involvement. The isoalloxazine ring of riboflavin is hydrophobic and has the possibility of binding to a hydrophobic surface region of myoglobin.

The singlet excited state of riboflavin is too short-lived for bimolecular reactions in contrast to the triplet excited state, ^{3}Rib, with a lifetime of 15 μs in aqueous solution. The reaction of ^{3}Rib as generated by laser flash photolysis with 355 nm excitation, see Figure 1, with MbFe(II)O_2 and MbFe(III) was followed using transient absorption spectroscopy. The decay of ^{3}Rib, absorbing in the near-infrared region, was increased in rate by the presence of myoglobins as seen from Figure 4 for MbFe(II)O_2 and MbFe(III). The rate of decay of ^{3}Rib followed first-order kinetics, and the observed pseudo-first-order rate constant was found to depend on the myoglobin concentration according to

$$k_{obs} = k_o + k_2[\text{myoglobin}] \quad (4)$$

both for MbFe(II)O_2 and for MbFe(III), as seen from the insets in Figure 4. The second-order rate constant for reaction of ^{3}Rib with MbFe(III) had the value of $k_2 = (3.1 \pm 0.4) \times 10^9$ L·mol^{-1}·s^{-1} and with MbFe(II)O_2 the value of $k_2 = (3.0 \pm 0.5) \times 10^9$ L·mol^{-1}·s^{-1}. ^{3}Rib is a strong oxidant, and the reaction

dx.doi.org/10.1021/jf405182f | J. Agric. Food Chem. 2014, 62, 1153–1158

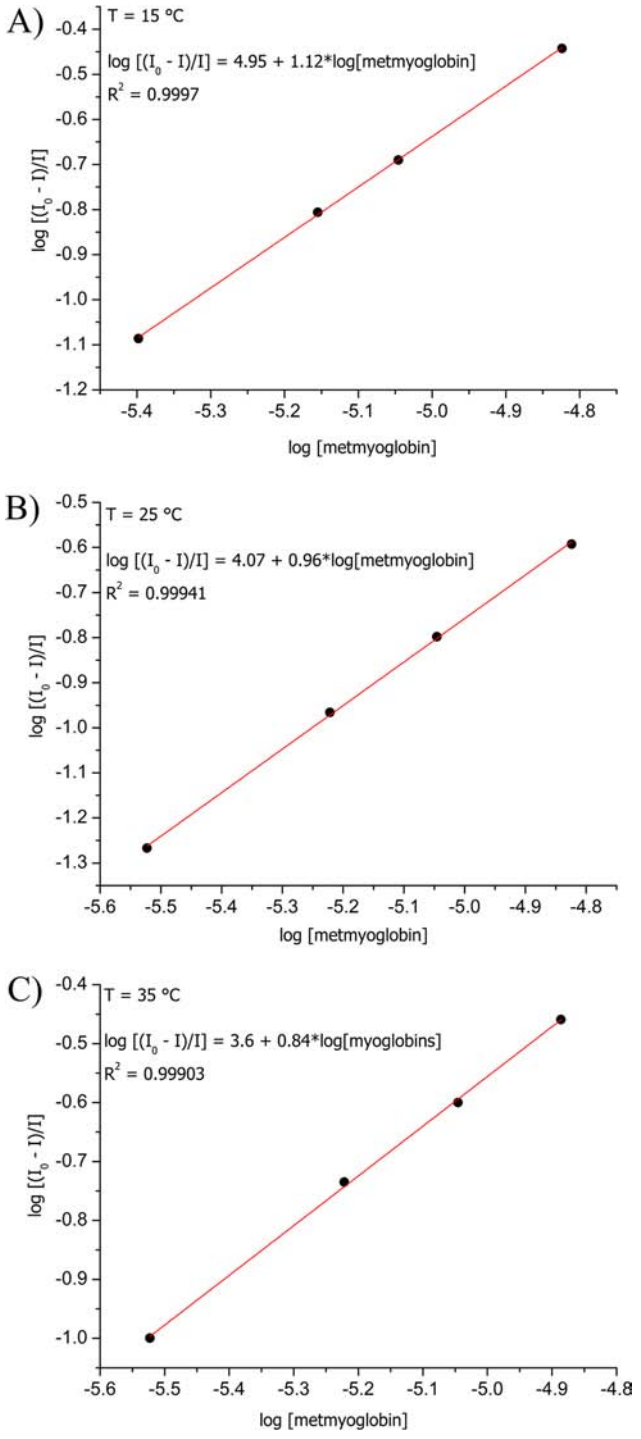

Figure 3. Quenching of ^{1}Rib fluorescence by metmyoglobin at different temperatures, (A) 15 °C, (B) 25 °C, and (C) 35 °C, plotted according to eq 2 for static quenching.[23]

Table 2. Association Constant and Binding Number for the Formation of the Metmyoglobin−Riboflavin Ground State Complex in Aqueous Phosphate Buffer pH 7.4 (0.2 mol L^{-1} NaCl) at Different Temperatures

temp (°C)	K_a (L·mol^{-1})	n
15 ± 0.1	9.1 ± 1 × 10^4	0.84 ± 0.01
25 ± 0.1	1.2 ± 0.1 × 10^4	0.97 ± 0.01
35 ± 0.1	4.5 ± 2 × 10^3	1.12 ± 0.01

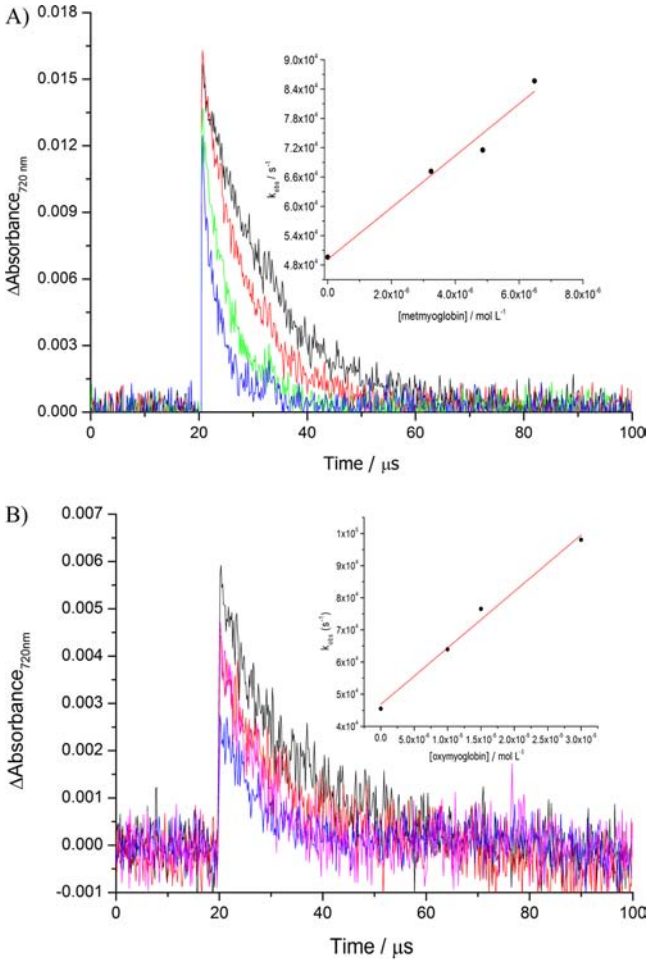

Figure 4. Triplet-excited riboflavin decay profile probed at 720 nm by transient absorption laser flash photolysis for anaerobic aqueous solution pH 7.4 of 30 × 10^{-6} mol·L^{-1} riboflavin with increasing concentration of (A) metmyoglobin and (B) oxymyoglobin. Insets: (A) k_{obs} from exponential fitting of absorption decay versus metmyoglobin concentration according to eq 4. (B) k_{obs} from exponential fitting of absorption decay versus oxymyoglobin concentration according to eq 4

with the myoglobins is an electron-transfer reaction from the protein backbone in myoglobin to ^{3}Rib in agreement with assignment of the reaction of ^{3}Rib with other water-soluble compounds as electron donors. Metmyoglobin was in agreement with this assignment found to be cross-linked using SDS−PAGE electrophoresis[24] and at the same time degrading into smaller protein units, see Figure 5. Western blotting confirmed the degradation of MbFe(III) by reaction with ^{3}Rib, see Figure 6. The involvement of radicals in the degradation of myoglobins upon reaction with ^{3}Rib is further confirmed by SDS−PAGE electrophoresis, as addition of DMPO, a nitrone spin-trap, yields significant protection of MbFe(III), indicating that quenching of ^{3}Rib by MbFe(III) involves electron transfer rather than energy transfer.

The rate of reaction between ^{3}Rib and each of the two myoglobins is faster by almost a factor of 10 when compared with other proteins like β-casein, β-lactoglobulin, and bovine serum albumin for which the same reaction with ^{3}Rib has been studied.[2] The facile reaction seems to be related to the hydrophobic interaction in the ground state between the two reactants as detected by fluorescence quenching of ^{1}Rib by

dx.doi.org/10.1021/jf405182f | J. Agric. Food Chem. 2014, 62, 1153−1158

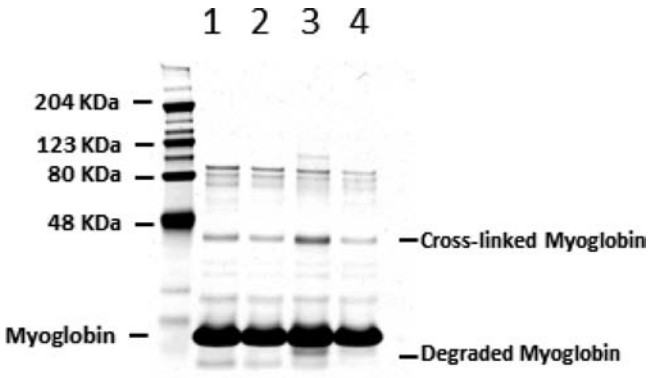

Figure 5. SDS–PAGE profile for aqueous phosphate buffer solution pH 7.4 containing (1) 8×10^{-6} mol·L^{-1} myoglobin and 30×10^{-6} mol·L^{-1} riboflavin kept in the dark; (2) 8×10^{-6} mol·L^{-1} metmyoglobin, 30×10^{-6} mol·L^{-1} riboflavin, and 30×10^{-3} mol·L^{-1} DMPO kept in the dark; (3) 8×10^{-6} mol·L^{-1} metmyoglobin and 30×10^{-6} mol·L^{-1} riboflavin exposed to 436 nm light for 1 h; (4) 8×10^{-6} mol·L^{-1} metmyoglobin, 30×10^{-6} mol·L^{-1} riboflavin, and 30×10^{-3} mol·L^{-1} DMPO exposed to 436 nm light for 1 h.

MbFe(III). The close interaction between ^{3}Rib and MbFe(III) or MbFe(II)O_2 will limit the diffusion distance or requirement of rearrangement prior to electron transfer resulting in the high effective rate approaching the diffusion limit. However, the observation of second-order kinetics for the electron transfer implies that the process is not intramolecular but rather a reaction between two molecules.

The heme iron was not affected by the reaction with ^{3}Rib in MbFe(III) or MbFe(II)O_2 as the visible spectrum of MbFe(II)O_2 did not change during reaction of MbFe(II)O_2 with ^{3}Rib. Neither was MbFe(III) oxidized to MbFe(IV)=O or reduced to MbFe(II) by ^{3}Rib (data not shown).

Oxymyoglobin is light sensitive, but only UV light is of importance for direct photooxidation to yield metmyoglobin, and UV absorbers in the food packing material protect meat color.[21] Riboflavin may, however, through photosensitized reactions, oxidize myoglobins, as shown by laser flash photolysis and transient absorption spectroscopy. The very efficient electron transfer between myoglobin and triplet-excited state riboflavin will, however, not affect the heme iron but only the myoglobin protein. For meat, riboflavin is accordingly concluded to be a photosensitizer for protein degradation but not for discoloration.

AUTHOR INFORMATION

Corresponding Author

*D.R.C.: e-mail, drcardoso@iqsc.usp.br; phone, +55 16 33 73 99 76. L.H.S.: e-mail, ls@food.ku.dk; phone, + 45 35 33 32 21.

Notes

The authors declare no competing financial interest.

This research is part of the bilateral Brazilian/Danish Food Science Research Program "BEAM - Bread and Meat for the Future" supported by FAPESP (Grant 2011/51555-7) to D.R.C. and by the Danish Research Council for Strategic Research (Grant 11-116064) to L.H.S. D.R.C. thanks CNPq for the research fellowship.

ACKNOWLEDGMENTS

Prof. Marcelo H. Gehlen (IQSC-USP) is acknowledged for the time-resolved single photon counting measurements (FAPESP Grant 2011/18215-8). The student Ceder Alloo is thanked for helping with the SDS–PAGE and Western-blotting experiments.

REFERENCES

(1) Massey, V. The chemical and biological versatility of riboflavin. *Biochem. Soc. Trans.* **2000**, *28*, 283–296.

(2) Cardoso, D. R.; Libardi, S. H.; Skibsted, L. H. Riboflavin as a photosensitizer. Effects on human health and food quality. *Food Funct.* **2012**, *3*, 487–502.

(3) Jung, M. Y.; Oh, Y. S.; Kim, D. K.; Kim, H. J.; Min, D. B. Photoinduced generation of 2,3-butanedione from riboflavin. *J. Agric. Food Chem.* **2007**, *55*, 170–174.

(4) Cardoso, D. R.; Scurachio, R. S.; Santos, W. G.; Homem-de-Mello, P.; Skibsted, L. H. Riboflavin-Photosensitized Oxidation Is Enhanced by Conjugation in Unsaturated Lipids. *J. Agric. Food Chem.* **2013**, *61*, 2268–2275.

(5) Diaz, M.; Luiz, M.; Alegretti, P.; Furlong, J.; Amat-Guerri, F.; Massad, W.; Criado, S.; Garcia, N. A. Visible-light-mediated photodegradation of 17 beta-estradiol: Kinetics, mechanism and photoproducts. *J. Photochem. Photobiol.* **2009**, *202*, 221–227.

(6) Burns, C. S.; Heyerick, A.; De Keukeleire, D.; Forbes, M. D. E. Mechanism for formation of the lightstruck flavor in beer revealed by time-resolved electron paramagnetic resonance. *Chem.—Eur. J.* **2001**, *7*, 4553–4561.

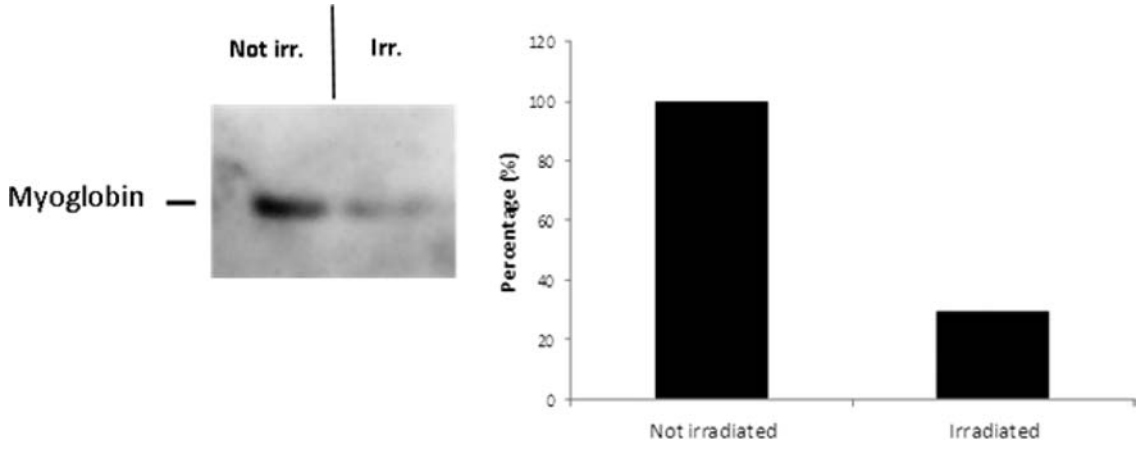

Figure 6. Western-blotting gel profile and band intensity for an aqueous solution pH 7.4 containing 8×10^{-6} mol·L^{-1} myoglobin and 30×10^{-6} mol·L^{-1} riboflavin. Left lane: sample was kept in the dark. Right lane: sample was exposed to 436 nm light for 1 h.

(7) Heelis, P. F. The photophysical and photochemical properties of flavins (isoalloxazines). *Chem. Soc. Rev.* **1982**, *11*, 15−39.
(8) Mortensen, G.; Sorensen, J.; Danielsen, B.; Stapelfeldt, H. Effect of specific wavelengths on light-induced quality changes in Havarti cheese. *J. Dairy Res.* **2003**, *70*, 413−421.
(9) Martin, C. B.; Shi, X. F.; Tsao, M. L.; Karweik, D.; Brooke, J.; Hadad, C. M.; Platz, M. S. The photochemistry of riboflavin tetraacetate and nucleosides. A study using density functional theory, laser flash photolysis, fluorescence, UV-Vis, and time resolved infrared spectroscopy. *J. Phys. Chem.* **2002**, *106*, 10263−10271.
(10) Megerle, U.; Wenninger, M.; Kutta, R.-J.; Lechner, R.; Koenig, B.; Dick, B.; Riedle, E. Unraveling the flavin-catalyzed photooxidation of benzylic alcohol with transient absorption spectroscopy from sub-pico- to microseconds. *Phys. Chem. Chem. Phys.* **2011**, *13*, 8869−8880.
(11) Choe, E.; Min, D. B. Chemistry and reactions of reactive oxygen species in foods. *Crit. Rev. Food Sci. Nutr.* **2006**, *46*, 1−22.
(12) Cardoso, D. R.; Franco, D. W.; Olsen, K.; Andersen, M. L.; Skibsted, L. H. Reactivity of bovine whey proteins, peptides, and amino acids toward triplet riboflavin as studied by laser flash photolysis. *J. Agric. Food Chem.* **2004**, *52*, 6602−6606.
(13) Huvaere, K.; Skibsted, L. H. Light-Induced Oxidation of Tryptophan and Histidine. Reactivity of Aromatic N-Heterocycles toward Triplet-Excited Flavins. *J. Am. Chem. Soc.* **2009**, *131*, 8049−8060.
(14) de la Rochette, A.; Silva, E.; Birlouez-Aragon, I.; Mancini, M.; Edwards, A. M.; Morliere, P. Riboflavin photodegradation and photosensitizing effects are highly dependent on oxygen and ascorbate concentrations. *Photochem. Photobiol.* **2000**, *72*, 815−820.
(15) Huvaere, K.; Cardoso, D. R.; Homem-de-Mello, P.; Westermann, S.; Skibsted, L. H. Light-Induced Oxidation of Unsaturated Lipids as Sensitized by Flavins. *J. Phys. Chem. B* **2010**, *114*, 5583−5593.
(16) Faustman, C.; Sun, Q.; Mancini, R.; Suman, S. P. Myoglobin and lipid oxidation interactions: Mechanistic bases and control. *Meat Sci.* **2010**, *86*, 86−94.
(17) Lund, M. N.; Heinonen, M.; Baron, C. P.; Estevez, M. Protein oxidation in muscle foods: A review. *Mol. Nutr. Food Res.* **2011**, *55*, 83−95.
(18) Libardi, S. H.; Borges, J. C.; Skibsted, L. H.; Cardoso, D. R. Deactivation of Ferrylmyoglobin by Vanillin as Affected by Vanillin Binding to beta-Lactoglobulin. *J. Agric. Food Chem.* **2011**, *59*, 6202−6208.
(19) Hatchard, C. G.; Parker, C. A. A new sensitive chemical actinometer 0.2. potassium ferrioxalate as a standard chemical actinometer. *Proc. R. Soc. London, Ser. A* **1956**, *235*, 518−536.
(20) Carlsen, C. U.; Moller, J. K. S.; Skibsted, L. H. Heme-iron in lipid oxidation. *Coord. Chem. Rev.* **2005**, *249*, 485−498.
(21) Park, E. Y.; Imazu, H.; Matsumura, Y.; Nakamura, Y.; Sato, K. Effects of Peptide Fractions with Different Isoelectric Points from Wheat Gluten Hydrolysates on Lipid Oxidation in Pork Meat Patties. *J. Agric. Food Chem.* **2012**, *60*, 7483−7488.
(22) Bertelsen, G.; Skibsted, L. H. Photooxidation of oxymyoglobin - wavelength dependence of quantum yields in relation to light discoloration of meat. *Meat Sci.* **1987**, *19*, 243−251.
(23) Alarcon, E.; Aspee, A.; Abuin, E. B.; Lissi, E. A. Evaluation of solute binding to proteins and intra-protein distances from steady state fluorescence measurements. *J. Photochem. Photobiol.* **2012**, *106*, 1−17.
(24) Nakhost, Z.; Karel, M. Measurement of oxidation-related changes in proteins of freeze-dried meats. *J. Food Sci.* **1984**, *49*, 1171−1173.

MATERIALS AND METHODS

Wines. We studied commercial sparkling wines that had been produced on an industrial scale at the Freixenet S.A. winery. The production process involved removing the lees and adding the appropriate amount of *liqueur d'expédition* that corresponded to the Brut category (sugar content < 12 g/L). The wines were produced from a blending of the grape varieties Macabeu, Xarel·lo, and Parellada. For over 2 years, six series of sparkling wine (coded A, B, C, D, E, and F) were kept under three temperatures: room (20 °C), cellar (16 °C), and fridge (4 °C). Production involved either the traditional (A, B, E, and F) or Charmat (C and D) methods. Wines E and F were Reserva category (>15 months of aging). Two bottles from each series of wine at each temperature were taken at 0, 4, 8, 12, and 20 months of storage for wines A–D and at 0, 4, 12, and 30 months for wines E and F. In total, we used 144 bottles of 75 cL from six series of commercial sparkling wines. Table 1 shows some of the enological parameters of each series at the initial sampling point (time zero). All bottles were opened in the dark, degassed, and stored at −20 °C until analysis.

Table 1. Commercial Sparkling Wine Characteristics at the Initial Sampling Point

sampling wine series	pH	free SO_2 (mg/L)	total SO_2 (mg/L)	total sugar content (g/L)	alcohol content (vol %)	CO_2 pressure (bar)
A	3.02	18	132	9.8	11.6	6.2
B	3.03	18	116	10.2	11.7	6.2
C	3.03	22	131	11	10.6	4.9
D	3.03	22	116	10.8	10.4	5.1
E	2.98	21	126	9.5	11.7	6.0
F	2.98	19	104	9.3	11.8	6.1

Chemicals. Deionized water was purified with a Milli-Q water system (Millipore, Bedford, MA). Acetonitrile [high-performance liquid chromatography (HPLC) grade] and acetic acid were purchased from Prolabo-VWR (Fontenays/Bois, France). Gallic acid (>98%), tyrosol (>98%), caftaric acid (>97%), caffeic acid (98%), catechin (>98%), *p*-coumaric acid (>98%), and 5-HMF (>99%) were supplied by Sigma-Aldrich (Saint Quentin Fallavier, France), while protocatechuic acid (>90%) and ferulic acid were acquired from Extrasynthese (Genay, France).

Enological Parameters. The total sugar content, alcohol content, pH, and free and total sulfur dioxide were measured using well-established standard methods[21] (Table 1).

Absorbance at 420 nm was considered as the browning index because it is a typical, fast, and easy parameter that is used by the producers of Spanish sparkling wines. It was measured using a 10 mm path length quartz cuvette. Values were multiplied 1000-fold and expressed as milli-absorbance units (mAU). A Shimadzu UV-3600 spectrophotometer (Duisburg, Germany) was used. All measurements were taken in duplicate.

Identification and Quantification of Phenolics. We used a Thermo Finnigan Surveyor HPLC system (Les Ulis, France) comprised of an autosampler (Surveyor Autosampler Plus), a quaternary pump (Surveyor LC Pump Plus), and an ultraviolet–visible (UV–vis) detector (Surveyor PDA Plus) hyphenated to a fluorescence detector (Finnigan FLD Plus) and a Thermo-Finnigan LCQ Advantage MS spectrometer equipped with an ion trap mass analyzer, all controlled by the Xcalibur data treatment system. Photodiode array (PDA) detection was configured to read from 200 to 600 nm, while for the fluorescence detection, λ_{ex} = 280 nm and λ_{em} = 320 nm [superhigh photomultiplier tube (PMT) voltage]. Electrospray ionization mass spectrometry was performed in negative and positive modes, reading m/z between 80.00 and 1200.00 with the following optimized parameters: capillary temperature, 300 °C; capillary voltage, −5 V; nebulizer gas flow, 1.75 L/min; desolvation gas flow, 1 L/min; and spray voltage, 5 kV.

The analyses were carried out in a Nucleosil 100-5 C_{18} column (250 × 4 mm, 5 μm, Agilent, France) at room temperature, and the samples were kept at 8 °C in the sample tray. The following eluents were used: solvent A, water/acetic acid (99:1, v/v); and solvent B, acetonitrile/acetic acid (99:1, v/v). The elution gradient was as follows: 0 min, 3% B; 24 min, 6% B; 30 min, 6% B; 38 min, 12% B; 46 min, 20% B; 50 min, 20%; 58 min, 60% B; 63 min, 80% B; and 68 min, 80% B. The system was re-equilibrated for 10 min before the next injection.

For identification proposes (Table 2), 5 mL of sparkling wine samples was evaporated under vacuum (below 30 °C) and the residue was redissolved in 500 μL of solvent A from the HPLC methodology (concentration of 10:1). The concentrated fraction was used for compound identification by high-performance liquid chromatography–photodiode array–fluorometric detection–mass spectrometry (HPLC–PDA–FLD–MS), by comparing the retention times to co-injected commercial standards (when available), UV spectra, and mass spectrometry (MS) spectra (in positive and negative modes).

Table 2. Identification and Quantification Parameters of the Phenolics in the Sparkling Wine Samples[a]

compound	Rt (min)	λ (nm)	std add	ESI–MS	% CV
gallic acid	6.6	272	+	(−) 169	5
protocatechuic acid	11.4	260	+	(−) 153	5
tyrosol	16.0	257	+	(+) 139	4
caftaric acid	18.1	328	+	(−) 311	5
caffeic acid	19.2	323	+	(−) 179	6
GRP	22.8	365		(−) 616	7
cis-coutaric acid	23.3	308		(−) 295	6
trans-coutaric acid	27.8	308		(−) 295	5
catechin	29.3	280/320[b]	+	(−) 289	6
fertaric acid	37.4	329		(−) 325	5
p-coumaric acid	43.9	308	+	nf	6
HMF	0.7	284	+	(+) 127	4

[a]The retention times, maximum wavelength, and m/z used for the identification as well as confirmation by a standard addition (std add) method, when available, and the coefficient of variation (% CV) of the method are shown. Rt, retention time; λ, wavelength; std add, standard addition; ESI–MS, positive or negative and its m/z; nf, not found. [b]Excitation and emission.

For the quantification, recently filtered (0.45 μm) wine samples, with no prior treatment, were injected directly (20 μL) into the system. Each sample was injected in duplicate. Each compound was quantified using an external calibration curve obtained from the corresponding standard measured at the maximum wavelength, except for caftaric, grape reaction product or 2-*S*-glutathyonilcaftaric (GRP), *cis*-/*trans*-coutaric, and fertaric acids, in which the respective free non-esterified standards (caffeic, *p*-coumaric, and ferulic acids) were used. Quantification was performed by PDA detection at the maximum wavelength of each compound, except for catechin, for which fluorometric detection (FLD) was used.

5-HMF Quantification. The method described by Serra-Cayuela et al.[18] was used for the determination of this compound. Briefly, an ultra-high-performance liquid chromatography (UHPLC) Acquity chromatographic system (Waters, Milford, MA) with a binary pump, an autosampler, and a photodiode array detector (DAD, Waters 2996) was employed. The system was controlled by Empower Pro 2 (Waters, Milford, MA). Chromatographic separation was carried out using a BEH C_{18} column (50 × 1.0 mm inner diameter) with a particle size of 1.7 μm (Waters, Milford, MA), kept at 40 °C. The mobile phase consisted of eluent A as a solution of acetonitrile/water/formic acid (2:97:1, v/v/v) and eluent B as a solution of acetonitrile/water/formic acid (80:19:1, v/v/v). The mobile phase was passed through a 0.22 μm polytetrafluoroethylene (Acrodisc, CR PTFE, Waters, Milford, MA) filter. Sample vials in the injector were maintained at 10 °C, and the injected volume was 5 μL. The linear gradient conditions were as follows: 0 min, 0% B, 3 min, 20% B; 3.5 min, 100% B; 4 min, 0% B; and 5 min, 0% B, at a flow rate of 0.800 mL/min. Data were acquired

dx.doi.org/10.1021/jf403281y | J. Agric. Food Chem. 2014, 62, 1159–1166

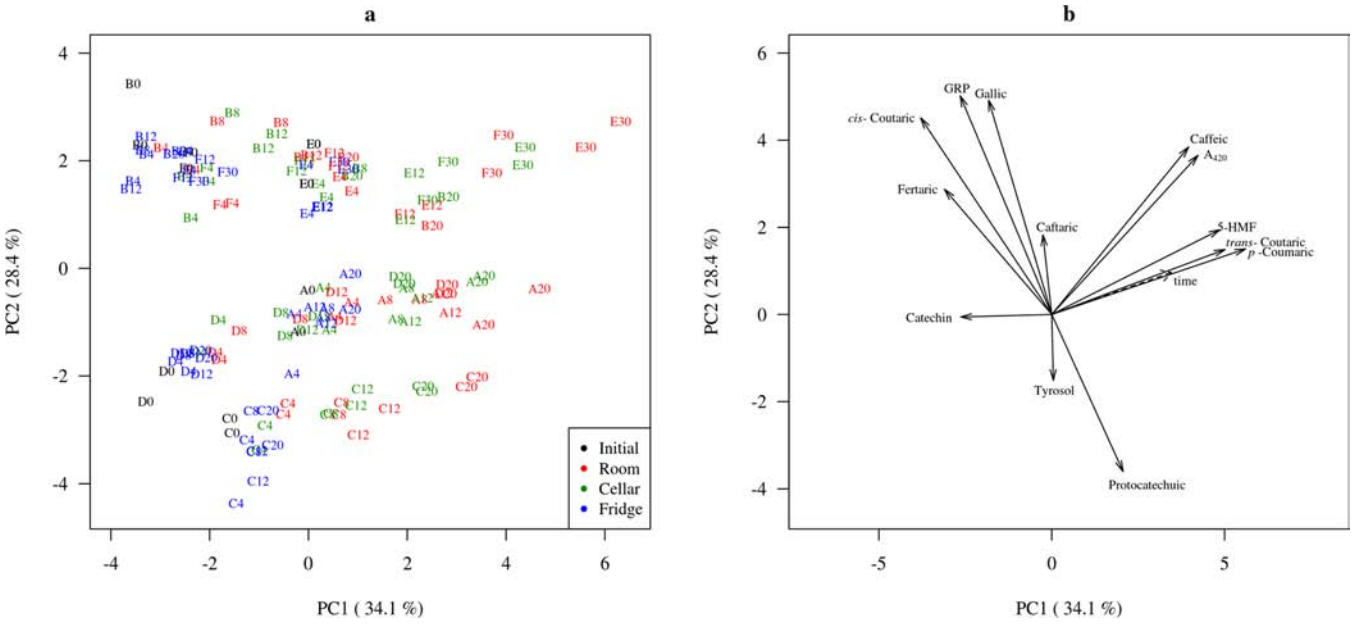

Figure 1. PCA: (a) scores and (b) loadings plot of the six series of sparkling wines (A, B, C, D, E, and F). Scores are coded by the series (letter) and length (number) and temperature (color) of storage.

with the Empower Pro 2 software. Chromatograms were monitored at 284 nm. Sparkling wine samples and the 5-HMF standard were passed through a Waters (Waters, Milford, MA) 13 mm polypropylene (PP) of 0.22 μm pore size filter before injection. All samples were analyzed in duplicate using external calibration curves.

Statistical Analysis. The analytical replicates were averaged to produce the sample (bottle) value and then the variance within the two bottles; finally, the variances within the wines series (A–F) were used to calculate the overall variance and 95% confidence limits.

Principal component analysis (PCA) was employed to observe trends in the data. The first two principal components were used to plot the scores and loadings separately.

Analysis of variance (ANOVA) was applied for the parameters analyzed (general parameters, phenolics, A_{420}, and 5-HMF) to observe whether the factors time and temperature were significant as well as their interaction with the series factor. To show the compound behaviors along shelf life, the coefficients of variation (% CV) between initial and final concentrations were calculated as well as the means and the 95% confidence intervals of each series and time–temperature points. When there was not interaction time series, all of the series were joined, at each temperature, and the statistical differences between time points were carried out.

Linear regression was used to determinate the relationships between the compounds with time at each temperature and also to calculate the velocity constants (k). To check whether there were differences between the slopes (velocity constants), we performed the Tukey honest significant difference (HSD) multi-range test.[22] To check the goodness of fit of the models, the observed values were plotted against the predicted values.

A box-and-whisker plot was performed as an exploratory data analysis to show the distribution of 5-HMF values and to establish the interval covered by the middle 50%, interquartile range, of the data (box Q_{25}–Q_{75}). Whiskers are drawn from the edges of the box to the largest and smallest values, unless there are concentrations unusually far away from the box (outliers). The outliers are considered when their values are higher than 1.5-fold the interquartile range (box height) above or below the box, and they are represented by circles. Only the threshold of outliers above the interquartile range (Q_{75}–Q_{25}) was considered (upper inner fence). With the difference between this upper limit and the median, the maximum variation that a wine can undergo before it has overbrowned was calculated.

Statistical significances were set at $p < 0.05$. Version 2.15 of the R (Foundation for Statistical Computing, Vienna, Austria), with the FactoMineR and Hmisc packages, was used for all statistical and graphical analyses.

RESULTS AND DISCUSSION

Six series of commercial sparkling wines were stored at three temperatures (fridge, 4 °C; cellar, 16 °C; and room, 20 °C) for over 2 years. Table 1 shows the main enological parameters of the series at the initial sampling point (time zero). All parameters remained constant during storage, except for free SO_2. For all series, the concentration of free SO_2 fell below the limit of quantification (LOQ; 6 mg/L) within the first 4 months and until the end of sampling (data not shown). In model wines, it has been observed that this compound can react with aldehydes, such as 5-HMF, and flavonoids, such as catechin.[23,24] However, the lowest concentration of free SO_2 (which is the reactive form) seems to not have a relevant impact on the compounds studied in comparison to the effect of the temperature and time factors throughout the study. Further work would be required to specifically assess the impact of SO_2 and catechin on the kinetics of 5-HMF accumulation in sparkling wines.

PCA was used to observe the trends of the compounds during storage (Figure 1). Scores were affected by the factors time, temperature, and sparkling wine series (Figure 1a). The first component showed that the scores for the sparkling wine samples tended to change positively with time. 5-HMF, *trans*-coutaric acid, *p*-coumaric acid, caffeic acid, catechin, and the A_{420} parameter were the variables that contributed greatly to this first component (Figure 1b) and went in the same direction as time, except catechin, which went in the opposite direction. Thus, the more aged wines have higher amounts of 5-HMF, *trans*-coutaric acid, and *p*-coumaric acid, while they have less catechin ($p < 0.05$). In contrast, the scores for the second component were mainly distributed by sparkling wine series, determining the gallic acid, GRP, *cis*-coutaric acid, and caffeic acid amounts.

dx.doi.org/10.1021/jf403281y | J. Agric. Food Chem. 2014, 62, 1159–1166

Table 3. Mean Content of Phenolics, 5-HMF, and Browning at the Three Temperatures[a]

		A		B		C		D		E		F	
compound	T (°C)	i (mg/L)	$((\Delta f - i)/i)$ (%)	i (mg/L)	$((\Delta f - i)/i)$ (%)	i (mg/L)	$((\Delta f - i)/i)$ (%)	i (mg/L)	$((\Delta f - i)/i)$ (%)	i (mg/L)	$((\Delta f - i)/i)$ (%)	i (mg/L)	$((\Delta f - i)/i)$ (%)
gallic acid	4	0.89	*b*	1.06	*b*	0.62	*b*	0.66	8	0.81	*b*	0.98	−5
	16		*b*		−16		*b*		*b*		*b*		−15
	20		−27		−28		*b*		*b*		*b*		−9
protocatechuic acid	4	4.54	9	1.51	*b*	3.97	*b*	1.17	12	1.38	*b*	1.68	*b*
	16		24		*b*		48		12		−8		*b*
	20		25		*b*		55		*b*		*b*		*b*
tyrosol	4	11.68	*b*	3.85	*b*	3.54	*b*	13.25	7	4.14	*b*	7.42	*b*
	16		*b*		*b*		*b*		*b*		*b*		*b*
	20		4		*b*		−18		*b*		*b*		*b*
caftaric acid[c]	4	4.98	*b*	4.73	*b*	3.82	*b*	4.04	*b*	5.19	*b*	3.95	*b*
	16		*b*		*b*		−10		−6		−20		−15
	20		−14		−23		−15		−15		−23		−23
caffeic acid	4	0.72	*b*	0.59	*b*	0.48	*b*	0.42	*b*	0.87	*b*	0.76	*b*
	16		26		*b*		40		77		21		16
	20		24		23		45		76		29		23
GRP	4	1.96	*b*	13.19	*b*	2.25	*b*	3.02	*b*	8.49	*b*	10.91	*b*
	16		*b*		−50		−27		−38		−39		−42
	20		−34		−36		−34		−44		−48		−48
cis-coutaric acid[d]	4	1.00	*b*	2.13	*b*	0.85	*b*	1.1	*b*	1.53	−6	1.83	−9
	16		−34		−51		−36		−30		−41		−50
	20		−43		−43		−42		−38		−48		−47
trans-coutaric acid[d]	4	1.31	13	1.12	*b*	1.08	*b*	1.01	*b*	1.47	*b*	1.14	*b*
	16		44		57		48		105		30		71
	20		44		35		43		91		40		60
catechin	4	0.44	−20	0.48	*b*	0.54	−19	0.49	−15	0.44	*b*	0.47	*b*
	16		*b*		−22		−22		−16		−7		−16
	20		*b*		−29		−29		−32		*b*		−17
fertaric acid[e]	4	0.94	*b*	1.22	*b*	0.82	*b*	1.12	*b*	1.00	*b*	1.21	*b*
	16		*b*		*b*		*b*		*b*		*b*		*b*
	20		*b*		−20		−9		*b*		−16		−15
p-coumaric	4	0.53	14	0.36	*b*	0.44	*b*	0.32	*b*	0.66	*b*	0.45	*b*
	16		51		97		47		141		44		68
	20		55		62		57		131		63		95
5-HMF	4	0.46	15	0.46	17	0.34	22	0.32	30	0.78	21	0.73	21
	16		289		279		393		410		208		212
	20		373		423		576		603		304		352
A_{420}[f]	4	72	*b*	77	*b*	58	*b*	51	*b*	79	*b*	69	*b*
	16		19		15		27		29		26		25
	20		26		17		37		46		35		32

[a]The percentage of variation $((\Delta f - i)/i)$ between the final and initial values within each series is also shown. [b]No differences were found by the ANOVA test ($p > 0.05$). [c]Using caffeic acid as the standard. [d]Using *p*-coumaric acid as the standard. [e]Using ferulic acid as the standard. [f]The mean is expressed as mAU.

dx.doi.org/10.1021/jf403281y | J. Agric. Food Chem. 2014, 62, 1159−1166

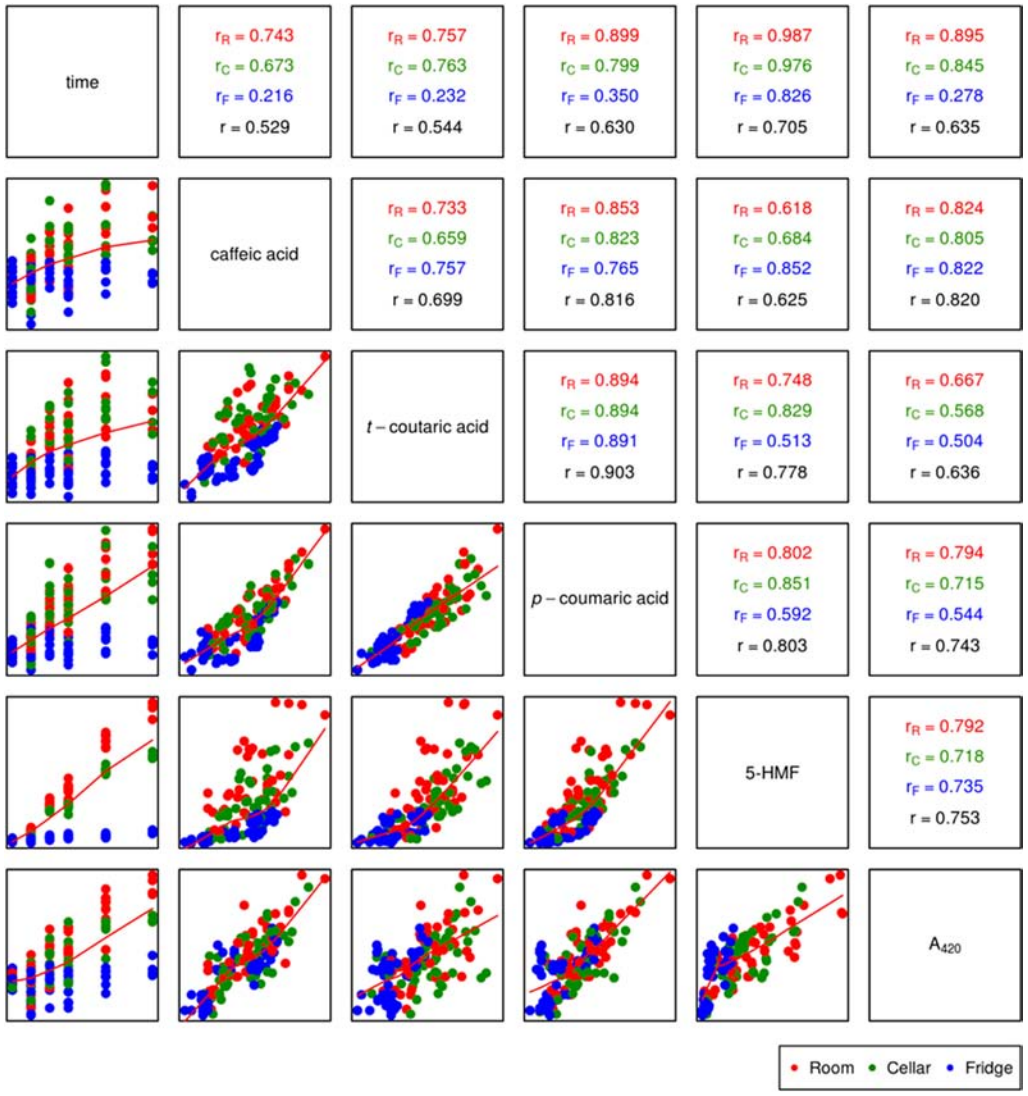

Figure 2. Pearson correlation between selected phenolics, 5-HMF, A_{420}, and time at each temperature and the overall value.

Table 3 shows the initial values of each compound and the A_{420} parameter. GRP, caftaric acid (both quantified as caffeic acid equivalent), tyrosol, and protocatechuic acid were the compounds with the highest concentration. In contrast, flavan-3-ol catechin and the hydroxycinnamic *p*-coumaric acid were the phenolics with the lowest content. Table 3 also shows the percentage of variation between the final and initial point for each wine series and each storage temperature. These percentages of variation are only shown when the difference was statistically significant by the ANOVA test. The compound 5-HMF had by far the greatest positive variation during shelf life. Thus, this compound underwent considerable changes during storage at the temperatures studied. To a lesser extent, caffeic acid, *trans*-coutaric acid, *p*-coumaric acid, and A_{420} also underwent positive variation during storage. A compound must meet a certain requirement to be used as a marker; it should behave in the same way in all series. Consequently, gallic acid, tyrosol, and fertaric acid were discarded as markers. These compounds, along with protocatechuic acid, were rejected because they increased or decreased depending upon the wine series. Finally, caftaric acid, GRP, *cis*-coutaric acid, and catechin were not further considered, because all of these compounds always decreased with time. A marker cannot disappear over the shelf life of a product, because this would make it difficult to determine the storage time.

Figure 2 shows the correlation of the compounds that had the highest coefficient of variation and always increased over time (5-HMF, caffeic acid, *trans*-coutaric acid, and *p*-coumaric acid), as well as the classic browning parameter (A_{420}). All compounds had a high correlation with A_{420}, with caffeic acid being the compound with highest correlation. The correlation with caffeic and *p*-coumaric acids could be due to the fact that both arise from the hydrolysis of their respective esters (caftatic and *cis*-coumaric acids). Caffeic, *trans*-coutaric, and *p*-coumaric acids did not change significantly at low temperatures (ANOVA test), and no difference was observed between 16 and 20 °C (Figure 2 and Table 3). Thus, only 5-HMF changed significantly ($p < 0.05$) at all temperatures and wine series. Therefore, this compound had the most suitable characteristics to be a time−temperature marker, which led us to study its kinetics. Moreover, 5-HMF was correlated ($p < 0.05$) with the A_{420} parameter, which is usually monitored in wineries by measuring browning[3,25] (Figures 1b and 2).

5-HMF and A_{420} Models. The kinetics of 5-HMF (Figure 3a) and A_{420} (Figure 3b) were studied and compared. To determinate the reaction order, the integrated kinetic equations

dx.doi.org/10.1021/jf403281y | J. Agric. Food Chem. 2014, 62, 1159−1166

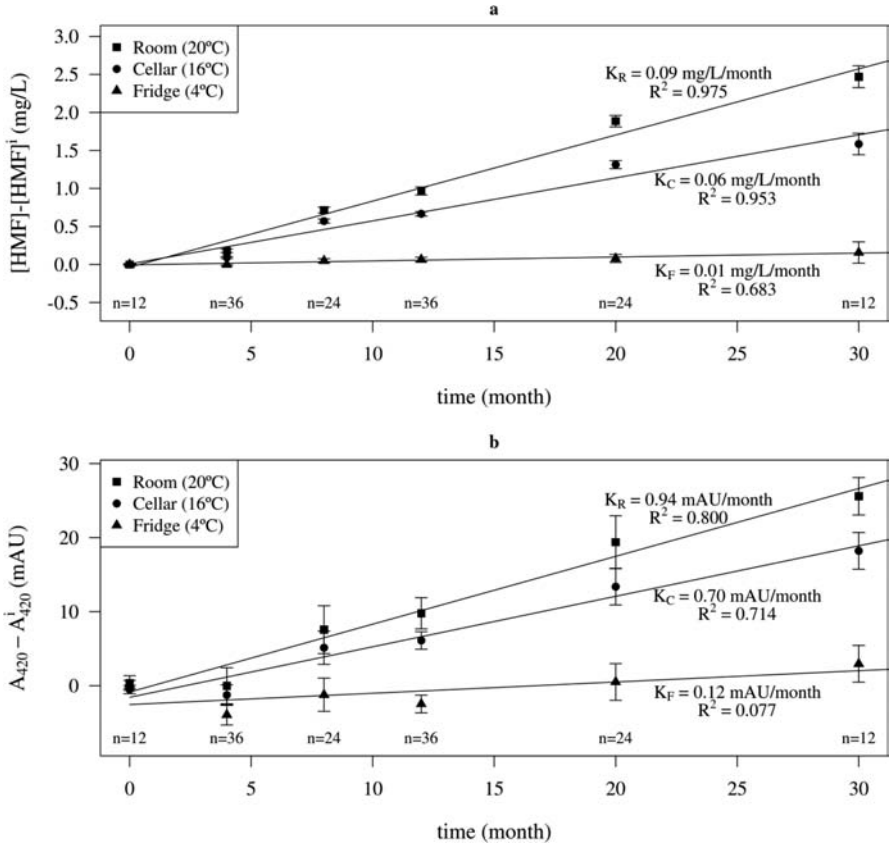

Figure 3. Kinetics of (a) 5-HMF and (b) A_{420} of commercial sparkling wines during storage at three temperatures (room, cellar, and fridge). The mean, the 95% confidence interval, and the number of samples (n) for the set of all series (A–F) at each time point are plotted. The velocity constant of formation (k) of the zero-order kinetics is also shown for each temperature.

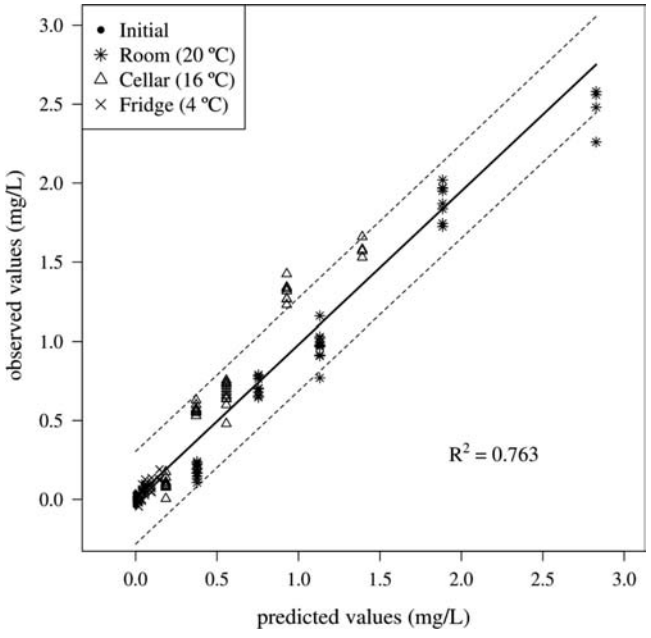

Figure 4. Correlation between observed versus predicted values to check the goodness of fit of the prediction model of 5-HMF, with dashed line representing the 95% prediction interval.

of zero, first, and second order were tested to find the reaction order that best fit the experimental data (data not shown). Both 5-HMF and A_{420} showed zero-order kinetics (eq 1), increasing linearly over time

$$Y = Y_i + kt \quad (1)$$

where Y is the 5-HMF content (mg/L) or absorbance at 420 nm (mAU), Y_i is the initial value of the 5-HMF content (mg/L) or initial absorbance (mAU), k is the velocity constant (expressed as mg L^{-1} $month^{-1}$ for 5-HMF or mAU/month for A_{420}), and t is time (in months).

The velocity constants (k) were calculated at each temperature (k_R, room; k_C, cellar; and k_F, fridge. 5-HMF (Figure 3a) showed higher differentiation than the A_{420} parameter between the velocity constants at various temperatures (Tukey HSD test) because 5-HMF has lower variability than A_{420} (Figure 3b). Moreover, the A_{420} parameter at the fridge temperature did not change significantly with time (Figure 3b and Table 3). According to the results indicated above, we will focus only on 5-HMF kinetics to construct a prediction model because this compound has less variability, is more sensitive, and can be used in a larger range of temperatures than the A_{420} parameter. We used the Arrhenius equation (eq 2) to predict k at any temperature

$$k = Ae^{\left(\frac{-E_a}{R(T+273.15)}\right)} \quad (2)$$

where k is the pseudo-zero-order rate constant (mg L^{-1} $month^{-1}$), A is the pre-exponential constant, T is the temperature (°C), E_a is the activation energy (kJ/mol), and R is the universal gas constant (8.314 J K^{-1} mol^{-1}). E_a and A are obtained from a representation of the natural logarithm of eq 2. The slope multiplied by R provided E_a, while A was obtained from the y intercept. For 5-HMF, the values were E_a =

dx.doi.org/10.1021/jf403281y | J. Agric. Food Chem. 2014, 62, 1159–1166

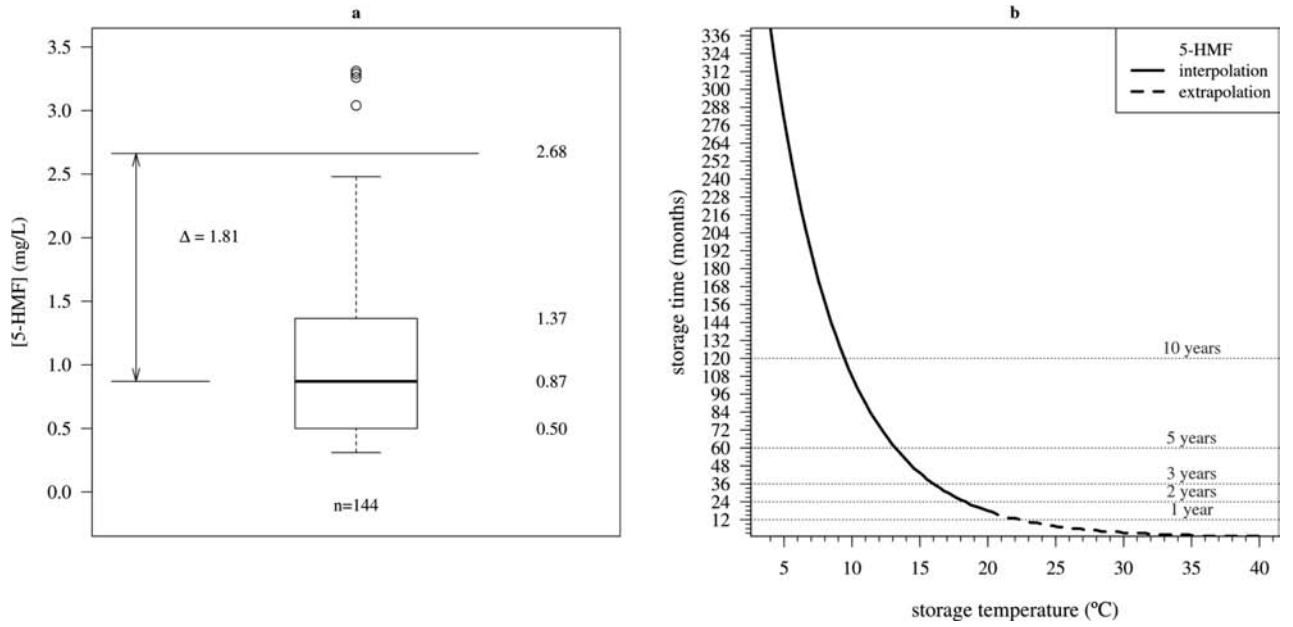

Figure 5. (a) Box-and-whisker plot of 5-HMF values for all of the series samples. The first, second, and third quartiles and the minimum and maximum values of each category are shown. The outlier limit, defined as 1.5-fold the interquartile difference, and its distance to the median are indicated. The outliers are represented by circles. (b) Time−temperature plot for predicting the shelf life of sparkling wines. The dashed lines indicate the extrapolation of the models.

125 kJ/mol and $A = 2 \times 10^{21}$ mg L^{-1} $month^{-1}$. These E_a and A values allowed us to establish eq 3, which was obtained by substituting eq 2 into eq 1. This equation can be used to predict the 5-HMF content, depending upon the length and temperature of storage

$$[\text{HMF}] = [\text{HMF}]_i + 1.7 \times 10^{21} e^{\left(\frac{-15014}{(T+273.15)}\right)} t \quad (3)$$

where [HMF] is the content of 5-HMF in mg/L, $[\text{HMF}]_i$ is the initial content (mg/L), T is the temperature (°C), and t is the time (months).

Sparkling Wine Shelf Life Prediction. Figure 4 shows the correlation between observed versus predicted values to show the goodness of the fitted model. The predicted model could be used to assess the length of storage depending upon the temperature conditions. At higher temperatures (outside the range studied) the behavior may be used by extrapolation. For instance, a sparkling wine stored at 25 °C for 15 months would increase its 5-HMF content by 4.05 mg/L.

The "best before" date of wine is regulatory not considered. However, it is of great interest for winemakers to know the shelf life of a wine. To determine whether a wine had anomalous data related to browning, we performed a box-and-whisker plot for 5-HMF (Figure 5a), which shows the median and upper inner fence for all of the samples. The latter parameter indicates the limit from which point the samples were considered overdeveloped (statistical outliers) and is defined as 1.5-fold the interquartile difference ($Q_{75}-Q_{25}$). Thus, the difference between the upper inner fence and median was considered the maximum variation that a wine can undergo before it has overdeveloped. This assessment is purely mathematical and does not take into account sensory aspects. The variation was 1.81 mg/L (Figure 5a); therefore, eq 4 is obtained substituting this value in eq 3. With this equation (eq 4), we can predict the maximum time of storage, depending upon the temperature

$$t = 9.9 \times 10^{-22} e^{\left(\frac{15014}{(T+273.15)}\right)} \quad (4)$$

where t is the time (months) and T is the temperature (°C).

Thus, this equation can be used to predict the maximum time before a wine overdevelops at a certain temperature or vice versa. Figure 5b graphically represents eq 4. The representation is also extrapolated outside the range of temperatures studied (dashed curve), thus showing the behavior in most common storage conditions. Thus, a sparkling wine stored at 20 °C would have overdeveloped after the first year and a half according to measurements of 5-HMF. At lower temperatures (4−16 °C), wines evolve slowly, with their life lengthening for many years. For instance, by extrapolation of the prediction model, at intermediate temperatures (16−24 °C), the shelf life of the sparkling wines would range from around 1 to several years. For storage at higher temperatures (above 27 °C), the prediction model indicates that sparkling wines should be consumed as soon as possible (within the first few months). Notwithstanding, because sparkling wines are produced from different grape varieties (blanc de blanc or blanc de noir) and blending, we believe that each winery could calculate the shelf life of their sparkling wine using their own initial value and the limit beyond which they consider the wine has overdeveloped. Once these values have been determined, the shelf life could be calculated by applying them to eq 3.

In summary, sparkling wines are stable at regular storage temperatures. Lower temperatures (fridge) can almost completely prevent browning and inhibit other reactions that involve phenolics. The hydroxycinnamic acids: caffeic, *trans*-coutaric, and *p*-coumaric, were the phenolics that have the highest correlation with browning and time, and their concentration increased over time. The compound 5-HMF proved to be a better time−temperature marker than A_{420} or any of the phenolics tested, because it increased linearly with time at all temperatures, was more sensitive, even at low temperatures, and more precise (with lower variability). The

dx.doi.org/10.1021/jf403281y | J. Agric. Food Chem. 2014, 62, 1159−1166

mathematical models allow us to determinate the concentration of 5-HMF, depending upon the length and temperature of storage. The model could be used by wineries to predict sparkling wine shelf life, that is, to determinate how long sparkling wines can be stored at a certain temperature before they overdevelop. Furthermore, in the case of complaint, the wineries can use 5-HMF as a reliable marker to reveal the conditions under which the sparkling wine had been stored.

AUTHOR INFORMATION

Corresponding Author

*Telephone: +34-934033795. Fax: +34-934035931. E-mail: montseriu@ub.edu.

Funding

This study was made possible by funding from the Spanish Comisión Interministerial de Ciencia y Tecnología (CICYT) Grant AGL2011-23872, the ACC1Ó EVALXARTA2010 (EX12) and the Generalitat de Catalunya (2009SGR-606). The Ph.D. student Arnau Serra-Cayuela was awarded a grant and scholarship from the Universitat de Barcelona (APIF-UB).

Notes

The authors declare no competing financial interest.

ACKNOWLEDGMENTS

The authors thank Freixenet S.A. wineries for providing the samples.

ABBREVIATIONS USED

LOQ, limit of quantification; GRP, grape reaction product (2-*S*-glutathyonilcaftaric); 5-HMF, 5-hydroxymethylfurfural; PCA, principal component analysis; *k*, velocity constant; *A*, pre-exponential constant; E_a, activation energy

REFERENCES

(1) Maury, C.; Clark, A. C.; Scollary, G. R. Determination of the impact of bottle colour and phenolic concentration on pigment development in white wine stored under external conditions. *Anal. Chim. Acta* **2010**, *660*, 81−86.

(2) Salacha, M.-I.; Kallithraka, S.; Tzourou, I. Browning of white wines: Correlation with antioxidant characteristics, total polyphenolic composition and flavanol content. *Int. J. Food Sci. Technol.* **2008**, *43*, 1073−1077.

(3) Singleton, V. L.; Kramlinga, T. E. Browning of white wines and an accelerated test for browning capacity. *Am. J. Enol. Vitic.* **1976**, *27*, 157−160.

(4) Bosch-Fusté, J.; Sartini, E.; Flores-Rubio, C.; Caixach, J.; López-Tamames, E.; Buxaderas, S. Viability of total phenol index value as quality marker of sparkling wines, "cavas". *Food Chem.* **2009**, *114*, 782−790.

(5) Ibern-Gómez, M.; Andrés-Lacueva, C.; Lamuela-Raventós, R. M.; Buxaderas, S.; Singleton, V. L.; de la Torre-Boronat, M. C. Browning of cava (sparkling wine) during aging in contact with lees due to the phenolic composition. *Am. J. Enol. Vitic.* **2000**, *51*, 29−36.

(6) Serra-Cayuela, A.; Aguilera-Curiel, M.; Riu-Aumatell, M.; Buxaderas, S.; López-Tamames, E. Browning during biological aging and commercial storage of cava sparkling wine and the use of 5-HMF as a quality marker. *Food Res. Int.* **2013**, *53*, 226−231.

(7) Li, H.; Guo, A.; Wang, H. Mechanisms of oxidative browning of wine. *Food Chem.* **2008**, *108*, 1−13.

(8) Oliveira, C. M.; Ferreira, A. C. S.; De Freitas, V.; Silva, A. M. S. Oxidation mechanisms occurring in wines. *Food. Res. Int.* **2011**, *44*, 1115−1126.

(9) Chamkha, M.; Cathala, B.; Cheynier, V.; Douillard, R. Phenolic composition of champagnes from Chardonnay and Pinot Noir vintages. *J. Agric. Food Chem.* **2003**, *51*, 3179−3184.

(10) Pozo-Bayón, M. A.; Hernández, M. T.; Martín-Álvarez, P. J.; Polo, M. C. Study of low molecular weight phenolic compounds during the aging of sparkling wines manufactured with red and white grape varieties. *J. Agric. Food Chem.* **2003**, *51*, 2089−2095.

(11) Hernanz, D.; Gallo, V.; Recamales, Á. F.; Meléndez-Martínez, A. J.; González-Miret, M. L.; Heredia, F. J. Effect of storage on the phenolic content, volatile composition and colour of white wines from the varieties Zalema and Colombard. *Food Chem.* **2009**, *113*, 530−537.

(12) Berg, H. W.; Akiyoshi, M. Some factors involved in browning of white wines. *Am. J. Enol. Vitic.* **1956**, *7*, 1−7.

(13) Kallithraka, S.; Salacha, M. I.; Tzourou, I. Changes in phenolic composition and antioxidant activity of white wine during bottle storage: Accelerated browning test versus bottle storage. *Food Chem.* **2009**, *113*, 500−505.

(14) Mayén, M.; Barón, R.; Mérida, J.; Medina, M. Changes in phenolic compounds during accelerated browning in white wines from cv. Pedro Ximenez and cv. Baladi grapes. *Food Chem.* **1997**, *58*, 89−95.

(15) Sioumis, N.; Kallithraka, S.; Makris, D. P.; Kefalas, P. Kinetics of browning onset in white wines: Influence of principal redox-active polyphenols and impact on the reducing capacity. *Food Chem.* **2006**, *94*, 98−104.

(16) Delgado-Andrade, C.; Seiquer, I.; Haro, A.; Castellano, R.; Navarro, M. P. Development of the Maillard reaction in foods cooked by different techniques. Intake of Maillard-derived compounds. *Food Chem.* **2010**, *122*, 145−153.

(17) Teixidó, E.; Núñez, O.; Santos, F. J.; Galceran, M. T. 5-Hydroxymethylfurfural content in foodstuffs determined by micellar electrokinetic chromatography. *Food Chem.* **2011**, *126*, 1902−1908.

(18) Serra-Cayuela, A.; Castellari, M.; Bosch-Fusté, J.; Riu-Aumatell, M.; Buxaderas, S.; López-Tamames, E. Identification of 5-hydroxymethyl-2-furfural (5-HMF) in cava sparkling wines by LC−DAD−MS/MS and NMR spectrometry. *Food Chem.* **2013**, *141*, 3373−3380.

(19) Pereira, V.; Albuquerque, F. M.; Ferreira, A. C.; Cacho, J.; Marques, J. C. Evolution of 5-hydroxymethylfurfural (HMF) and furfural (F) in fortified wines submitted to overheating conditions. *Food. Res. Int.* **2011**, *44*, 71−76.

(20) Chen, L.; Huang, H.; Liu, W.; Peng, N.; Huang, X. Kinetics of the 5-hydroxymethylfurfural formation reaction in Chinese rice wine. *J. Agric. Food Chem.* **2010**, *58*, 3507−3511.

(21) International Organisation of Vine and Wine (OIV). *Compendium of International Methods of Wine and Must Analysis*; OIV: Paris, France, 2004.

(22) Zar, J. H. *Biostatistical Analysis*, 5th ed.; Pearson: London, U.K., 2009.

(23) Es-Safi, N.-E.; Cheynier, V.; Moutounet, M. Study of the reactions between (+)-catechin and furfural derivatives in the presence or absence of anthocyanins and their implication in food color change. *J. Agric. Food Chem.* **2000**, *48*, 5946−5954.

(24) Nonier, M. F.; Vivas, N.; Gaulejac, N. V.; de Absalon, C.; Vitry, C. Study by LC/ESI/MS^n and ESI/HR/MS of SO_2 interactions in flavanols−aldehydes nucleophilic reactions. *Food Chem.* **2010**, *122*, 488−494.

(25) Zoecklein, B. W. *Wine Analysis and Production*; Chapman and Hall: London, U.K., 1995.

PFOS distribution and elimination in food animals is critical for assessing dietary exposures and predicting associated risks. Exposures to cattle grazing on PFOS-contaminated pastures in both Europe and the United States have heightened concerns over human contact with PFOS in meat products.[23,24] Considering the very high bioaccumulation factor (BAF) and bioconcentration factor (BAC) for PFOS, limiting human exposures to PFOS is important.[1] To this end, a study was conducted to determine the accumulation and depletion of PFOS in plasma, and the tissue distribution of PFOS in cattle administered a single oral bolus dose of PFOS at 8 mg/kg.

MATERIALS AND METHODS

Safety. The toxicity of PFOS is believed to be minimal at the concentrations utilized for the study; however, all treated animals and corresponding samples produced from the study were considered radioactive due to the coadministered PFOA and were handled and disposed of by proper laboratory methods.

Chemicals and Materials. Perfluorooctane sulfonate (purity ≥98%), tetrabutylammonium hydrogen sulfate (TBAHS), and ammonium acetate were purchased from Sigma-Aldrich (St. Louis, MO). Other reagents included sodium carbonate (Fisher, Pittsburgh, PA), methyl *tert*-butyl ether (MTBE, BDH, Radnor, PA), HPLC grade methanol (MeOH, Honeywell Burdick and Jackson, Morristown, NJ), and 1,1,1,3,3,3-hexafluoroisopropanol (HFP, TCI, Portland, OR).

Study Design and Sample Collection. Four Lowline steers (#179−182, *Bos taurus*) were purchased from Effertz EZ Ranch (Bismarck, ND). The steers were raised in 3.1 × 3.4 m concrete-floored pens at the Biosciences Research Laboratory in Fargo, ND, for 8 months prior to the study. The Institutional Animal Care and Use Committee (IACUC) and the USDA Radiation Safety Committee approved the animal protocol. Twenty-four hours prior to dosing, the steers (329 ± 36 kg) were acclimated to stainless steel metabolism crates, during which time jugular catheters were surgically inserted for blood collection. The steers were provided feed and water ad libitum. To determine background levels of PFOS in the steers and to have control samples, blood, urine, and feces were collected 24 h prior to dosing. After the 24 h acclimation period, three of the steers were administered a single, oral dose of PFOS in a gelatin capsule at approximately 8 mg/kg body weight (bw). A relatively high dose of PFOS was utilized in this preliminary study to ensure that PFOS residues would be readily detectable in the tissues. Steers were housed in stainless steel metabolism crates for the duration of the 28-day study. Since PFOS and PFOA are commonly detected in the same samples, all of the steers (#179−182) were also given a simultaneous oral dose of [1-^{14}C]-perfluorooctanoic acid (PFOA, 1 mg/kg bw, 0.6 mCi per steer) to assess the pharmacokinetics of PFOA (previously published work).[25]

Blood was collected at 1, 2, 4, 8, 12, 24, 36, 48, 72, and 96 h, and at 6, 8, 10, 13, 15, 17, 21, 24, and 28 days after dosing. Jugular catheters were used to collect whole blood via a syringe which contained heparin to prevent clotting. When jugular catheters lost patency (most often due to the action of neck rubbing against the headgate), heparinized polypropylene Vacutainer tubes (BD, Franklin Lakes, NJ), were used to collect whole blood through 21 gauge needles. Collected whole blood was centrifuged at 1160*g* for 15 min at 5 °C to separate the plasma from the corresponding red blood cell fraction, which were put into separate vials and then frozen at −20 °C until analysis.

Urine and feces were collected quantitatively in 24 h increments for all 28 days. Urine was collected as described by Paulson and Cottrell.[26] Briefly, modified incontinent bags were attached to the steers with Tygon tubing (Saint-Gobain Performance Plastics, Akron, OH) running into polypropylene buckets. Urine was weighed daily and thoroughly mixed, and an aliquot was removed for later analysis. Feces were collected in stainless steel trays in the bottom of the large metabolism crates. All feces within each steer's daily 24 h collection period were thoroughly mixed in a stainless steel mixing bowl using a Hobart mixer, weighed, and subsampled. All urine aliquots and feces subsamples were stored frozen at −20 °C until analysis.

The steers were euthanized, eviscerated, and deboned on day 28 of the study. Liver, kidney, spleen, lung, brain, pancreas, diaphragm, muscle, bile, and carcass remainder (trimmings) were quantitatively collected for analysis. Representative samples of back fat and intraperitoneal (IP) fat were subsampled for analysis. All other tissues collected were whole organs/tissues that were ground and homogenized before a subsample was removed. The masses of the skin and bone were taken, but these compartments were not analyzed. Blood volumes were estimated from the relationship of animal body weight and blood volume to calculate PFOS percent dose in blood,[27] but the whole volume or weight of the blood was not recorded at time of slaughter. All plasma and tissue subsamples were frozen at −20 °C until analysis.

Extraction Procedure and LC−MS/MS Analysis. Extraction of PFOS from plasma and urine was accomplished by the modified ion-pairing method described by Hansen et al.[28] Briefly, 0.5 mL of plasma or urine was added to 1 mL of 0.5 M TBAHS (pH 10), 2 mL of 0.25 M sodium carbonate, and 5 mL of MTBE, shaken using a Magni Whirl shaker (Blue M, Blue Island, IL) for 15 min, and subsequently centrifuged at 1160*g* for 15 min. The MTBE layer was pipetted into a second tube, and the extraction was repeated two more times. Combined MTBE layers were evaporated to dryness under nitrogen, reconstituted with 0.5 mL of MeOH, and filtered through a 0.2 μm nylon syringe filter prior LC−MS/MS analysis.

One to two grams of tissue or feces was also extracted using the above ion-pairing liquid−liquid extraction method, but with two additional steps described by previously.[28,29] Tissue or feces samples were homogenized in TBAHS (1 mL) and sodium carbonate (8 mL) using an Ultra-Turrax Tissumizer (Tekmar Company, Cincinnati, OH). After homogenization, the sample was extracted with MTBE as described above and evaporated under nitrogen to 0.5 mL, 0.5 mL of HFP was added, and extracts were vortexed for 30 s to precipitate proteins. Extracts were then centrifuged at 3210*g* for 25 min, and the supernatants were filtered through a 0.45 μm nylon syringe filter. Filtered extracts were evaporated to dryness under nitrogen, reconstituted with 0.5 mL of MeOH, and filtered again through a 0.2 μm nylon syringe filter prior to LC−MS/MS analysis.

A MeOH extraction method previously described was utilized to extract adipose tissue and carcass remainder.[30] Briefly, 1−2 g of tissue was weighed and homogenized in MeOH (8 mL) for 30−60 s with a Tissumizer. Samples were shaken for 20 min on a Magni Whirl shaker and centrifuged at 2060*g* for 15 min, and the MeOH was decanted. The process was repeated two more times. MeOH extracts were combined and evaporated to dryness under nitrogen and then reconstituted with 0.5 mL of MeOH. Each sample was then filtered through a 0.2 μm nylon syringe filter prior to LC−MS/MS analysis.

A sample set consisted of 10 vials including 8 samples (plasma, urine, feces, or tissue), 1 control matrix (blank tissue), and 1 recovery matrix (spiked at 0.3 μg/mL PFOS for plasma and urine and 0.1 μg/g PFOS for tissues or feces). Control and recovery matrices were used for quality assurance and control purposes. The control matrix allowed for detection of any laboratory or residual contamination, and the recovery matrix assured the extraction was working properly. The control and recovery matrices for plasma, urine, and feces were from the steers used in this study but were collected prior to dosing. The control and recovery matrices for tissues were from beef liver, swine muscle, and swine fat from previous, nonrelated studies conducted in our lab, as well as the control animal. Extraction recoveries for PFOS in plasma, urine, feces, liver, muscle, and fat were 86.7 ± 14% (n = 8), 95.5 ± 10% (n = 8), 64.8 ± 7% (n = 6), 96.9 ± 20% (n = 4), 101.9 ± 0.7% (n = 3), and 101.3 ± 23% (n = 4), respectively. Extraction recoveries and reproducibility in different matrices were within acceptable standards for LC−MS/MS analysis established by previous work from our lab.[25]

PFOS in sample extracts (10 μL) was quantified by LC−MS/MS on an Alliance HPLC (Waters, Milford, MA) coupled to a quadrupole time of flight mass analyzer (QTOF, Waters). A Waters C-18 Symmetry column (2.1 mm × 100 mm, 3.5 μm particle size) and

mobile phase (0.3 mL/min) consisting of 95/5 water/MeOH with 2 mM ammonium acetate (mobile phase A) and 100% MeOH with 2 mM ammonium acetate (mobile phase B) were used to separate PFOS from matrix interferences. The mobile phase was initially 70/30 A/B (held for 0.2 min), which was then linearly changed to 15/85 A/B during the next 21 min; the mobile phase composition was then constant for 5 min and then returned to starting conditions. Using these chromatographic conditions, PFOS eluted at 17.9 min. Ionization of the analyte was achieved by electrospray ionization in negative ion mode. The desolvation temperature was 350 °C, and source temperature was 120 °C. The desolvation gas flow was 500 L/h, the cone gas flow was 20 L/h, and the capillary, cone, and collision voltages were 3.4 kV, 20 V, and 5 V, respectively. Precursor and fragment ions of m/z 498.9, 229.9, 98.9, and 79.9 were monitored in MS/MS scan mode for PFOS. Every sample extract injection was scanned also in MS scan mode to monitor for metabolite formation.

An 8-point external standard curve ranging from 0.007 to 1 μg/mL was made fresh in MeOH on the day of analysis from a stock solution (10 μg/mL PFOS) in acetonitrile. The linear portion of the standard curve was used to quantify PFOS in the extracts; if PFOS concentrations were above the linear portion, extracts were diluted and reanalyzed. A blank injection was performed after 4 sample injections to ensure that there was no carry-over. A check standard injection was performed after 20 injections to confirm instrument performance. Check standards were required to be within ±20% of actual concentration over the entire course of a sample set to guarantee accuracy of the calculated PFOS concentrations in the extracts. A method limit of detection (LOD) and limit of quantitation (LOQ) were determined in plasma to be 0.014 μg/mL and 0.048 μg/mL, respectively. Concentrations of PFOS in other tissues such as muscle, kidney, and liver were well above the standard curve and needed dilution, therefore a method LOD and LOQ were not determined.

Kinetic Parameter Estimates. Parameters (A, E, α, and β) describing PFOS absorption and distribution were estimated on the mean concentrations from plasma vs time data (0−17 days) using noncompartmental methods (PK-Solutions software; Summit Research Services; Montrose, CO); the calculated concentration maximum (C_{max}) and time maximum (T_{max}) are reported for plasma. To describe the initial absorption and distribution phases, only data from 0 to 17 days was used. For predictive purposes, plasma concentrations at each time point were averaged across all animals and least-squares parameter estimates were calculated after curve-stripping. Predicted plasma PFOS concentrations (C) were calculated using

$$C = A\ e^{-\alpha t} + E\ e^{-\beta t}$$

where t is time (h); and A and E are Y intercepts of lines having slopes of α and β, respectively.

RESULTS

PFOS Concentrations in Plasma. Average concentrations of PFOS in steer plasma ranged from 0.016 ± 0.008 μg/mL to 52.6 ± 3.4 μg/mL over 28 days following a single oral dose of 8 mg/kg bw (Figure 1). The corresponding mean (±SD) plasma concentrations are presented in the Supporting Information for each time point (Table S1). A plasma elimination half-life was not calculated because PFOS concentrations increased during the last week of the 28-day study. However, using the data in Figure 1 from 0 to 17 days, a C_{max} of 36.3 μg/mL and T_{max} of 4.7 days were calculated. After an apparent plasma peak and depletion, PFOS levels increased to a mean concentration of 52.6 ± 3.4 μg/mL at day 28, which was approximately 35.8 ± 4.3% of the PFOS dose (Table 1).

PFOS Concentrations and Excretion in Urine and Feces. Urine concentrations increased during the first 6 days, after which concentrations stayed nearly steady (0.12−0.16 μg/mL) until day 25, when levels began to drop below 0.1 μg/mL

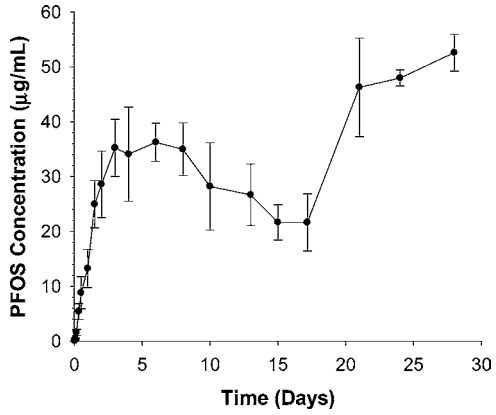

Figure 1. Mean plasma PFOS concentrations (μg/mL) and time data through 28 days after a single oral dose given to steers. Points represent mean concentrations of three animals from LC−MS/MS analysis ± one standard deviation.

Table 1. Mass Balance Mean (n = 3) Amounts and Percentages for PFOS in Steer Body Compartments at 28 Days Following Dosing

tissue	total amount[a] (mg)	% of dose
plasma	946.7 ± 113.2#	35.8 ± 4.3
feces (0−28 days)	291.1 ± 34.0*	11.0 ± 1.3
carcass remainder	149.6 ± 41.8#	5.7 ± 1.6
muscle	113.8 ± 15.9#	4.3 ± 0.6
liver	58.8 ± 5.5#	2.2 ± 0.2
bile	24.1 ± 13.6#	0.9 ± 0.5
urine (0−28 days)	14.5 ± 1.9*	0.5 ± 0.07
lung	12.8 ± 11.8#	0.5 ± 0.4
kidney	3.1 ± 0.9#	0.1 ± 0.03
spleen	1.4 ± 0.3#	0.05 ± 0.01

[a](*) Total sum for all days of study. (#) Total from slaughter.

(Figure 2a). Cumulatively, PFOS excretion in urine was linear over 28 days but is presented on a log scale because of the range of values. Overall only 0.5 ± 0.07% of the dose was excreted in urine over the course of the 28-day study (Table 1).

Fecal concentrations increased over the first 6 days of the study to an apparent maximum of 6.4 ± 4.4 μg/g dw (Figure 3a). Thereafter, mean concentrations in feces ranged between 1.6 and 5.1 μg/g dw with a general decline (Figure 3a). Cumulative fecal excretion of PFOS was linear over the 28 days but was presented on a log scale due to the range of values (Figure 3b). Feces was the major route of elimination of PFOS, and cumulatively 11.0 ± 1.3% of the PFOS dose was excreted in the feces over the 28-day study. Urine and fecal mean (±SD) PFOS concentrations for each day are presented in the Supporting Information (Table S2).

PFOS Concentrations in Tissues and Body Burden. Figure 4 presents the mean concentrations of PFOS in plasma, urine, feces, liver, bile, muscle, kidney, lung, spleen, back fat, IP fat, and carcass remainder at the termination of the study. The muscle, liver, and bile mean PFOS concentrations were 1.1 ± 0.1 μg/g wet weight (ww), 17.9 ± 2.3 μg/g ww, and 36.9 ± 13.2 μg/mL, respectively. Kidney, lung, and spleen mean PFOS concentrations were 3.7 ± 0.5, 2.9 ± 0.6, and 2.3 ± 0.4 μg/g ww, respectively. Carcass remainder, back fat, and IP fat mean PFOS concentrations were 3.8 ± 0.5 μg/g ww, 5.7 ± 2.1 μg/g ww, and 3.5 ± 0.5 μg/g ww, respectively. The overall percents of dose for tissues are presented in Table 1. After plasma, the

dx.doi.org/10.1021/jf404355b | J. Agric. Food Chem. 2014, 62, 1167−1173

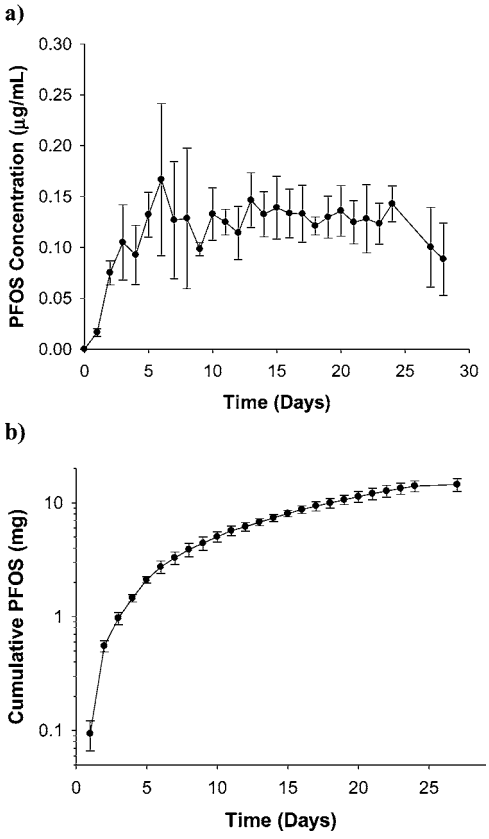

Figure 2. Mean urine PFOS concentrations (μg/mL) and time data through 28 days after a single oral dose given to steers (a). Cumulative urine PFOS amounts (mg) on a log scale excreted over time through 28 days after a single oral dose given to steers (b). Points represent mean concentrations (a) or cumulative PFOS amounts (b) of three animals from LC−MS/MS analysis ± one standard deviation.

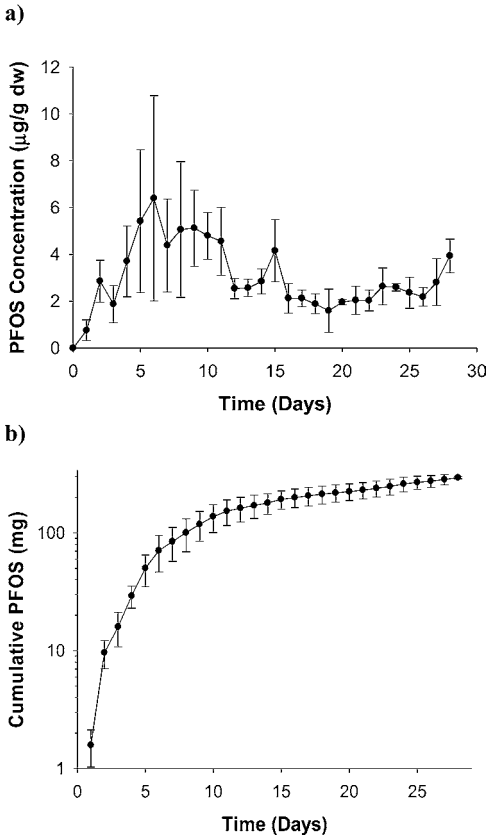

Figure 3. Mean fecal PFOS concentrations (μg/g dry weight) and time data through 28 days after a single oral dose given to steers (a). Cumulative fecal PFOS amounts (mg) on a log scale excreted over time through 28 days after a single oral dose given to steers (b). Points represent mean concentrations (a) or cumulative PFOS amounts (b) of three animals from LC−MS/MS analysis ± one standard deviation.

highest dose percents were in the carcass remainder at 5.7 ± 1.6% of administered dose, muscle at 4.3 ± 0.6%, and liver at 2.2 ± 0.2%. All other tissues were under 1% of the dose.

The mean overall body burden depletion from steers is linear with time (Figure 5). Each day of urine and feces PFOS amounts was cumulatively subtracted from the total dose. Using linear regression a body burden half-life can be calculated ($y = -11.532x + 2639.5$ and $r^2 = 0.9759$) to be 114.2 days.

DISCUSSION

This study was conducted to determine the tissue distribution and excretion of a single oral dose (~8 mg/kg bw) of PFOS in beef cattle. To date the only studies published on the fate of PFOS in ruminants are for sheep and dairy cattle.[12,20] Additional nonruminant models have been studied, including monkeys, rats, chickens, and mice.[6,21,31−36] In the U.S., the high rate of beef cattle production and the utilization of diverse feed sources including pasture, hay, and grain make them a logical and important food animal for investigations of persistent organic chemicals.[14,37,38] The major beef breed in production in the U.S. is Angus (full and crossbred);[39−41] therefore, Lowline Angus steers, an Angus breed of small stature, were used in this study to make dosing and handling easier.[42]

Plasma concentrations of PFOS were at or above the LOD (0.014 μg/mL) and LOQ (0.048 μg/mL) at all time points after 1 h. The calculated C_{max} and T_{max} were 36.3 μg/mL and 4.7 days, respectively, indicating the absorption of PFOS is

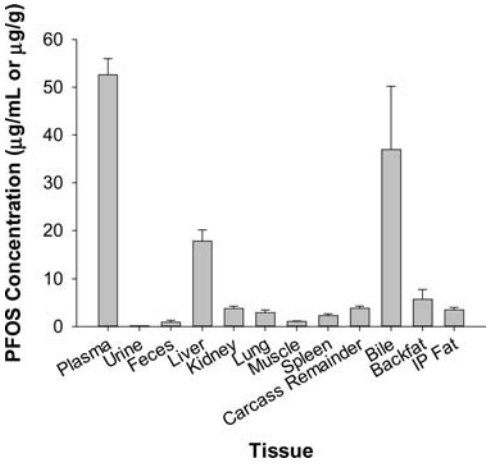

Figure 4. Mean tissue PFOS concentrations (μg/mL or μg/g) after 28 days following a single oral dose given to steers. Columns represent mean concentrations of three animals from LC−MS/MS analysis ± one standard deviation. Day 28 plasma, urine, and fecal concentrations are shown for comparison.

slower than that of PFOA, which had a T_{max} of 24 h.[25] Plasma concentrations increased until 6 days into the study (36.3 ± 3.5 μg/mL), when a distribution phase started. During the distribution phase, plasma concentrations slowly declined to 21.6 ± 5.2 μg/mL from days 6 to 17, but there were only small

dx.doi.org/10.1021/jf404355b | J. Agric. Food Chem. 2014, 62, 1167−1173

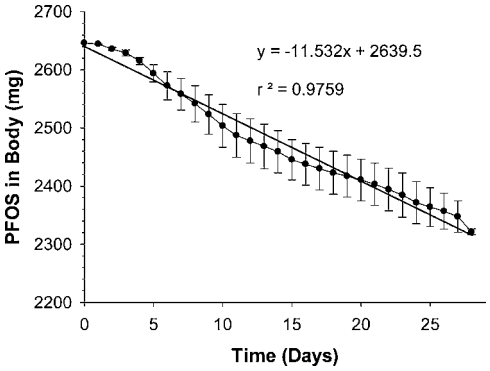

Figure 5. Mean PFOS remaining in the steer body (mg) with time through the 28 days after a single oral dose. Points represent mean amounts (mg) of PFOS remaining of three animals ± one standard deviation. Linear regression analysis provided a line equation of $y = -11.532x + 2639.5$ and an r^2 coefficient of 0.9759.

amounts of PFOS elimination in feces and urine, indicating PFOS was distributed to other parts of the steer. After day 17, plasma concentrations gradually increased to 52.6 ± 3.4 μg/mL at day 28, the last day of the study. A similar increase in PFOS concentration subsequent to an initial absorption and distribution phase has also been observed in an additional, longer duration study (Lupton et al., unpublished) in cattle. The secondary increase of PFOS plasma concentrations was possibly due to redistribution of PFOS from tissue. The continual high concentrations of PFOS in plasma could be the result of protein binding for transportation purposes throughout the body for distribution. At day 28 a large percentage of the dosed PFOS (~35%) was still circulating in the blood. A terminal plasma elimination half-life was not calculated due to the lack of an observable PFOS depletion phase. Extremely slow PFOS elimination contrasts with that of PFOA, which has a plasma elimination half-life of 19 h and is nearly quantitatively eliminated via the urine within two weeks of dosing.[25] PFOS serum depletion half-life estimates for monkeys and humans are on the order of hundreds of days to years.[43] Due to the approved study design, it was not feasible to continue this study for the period of time needed to determine the PFOS plasma half-life in steers. Even though we were not able to calculate a plasma elimination half-life, it was possible to calculate a body burden half-life of 114.2 days from the PFOS amounts remaining in the steers over time using the linear regression equation.

No metabolites of PFOS were observed in any of the compartments analyzed. The stability and chemical properties of PFOS would not likely allow for metabolite formation through defluorination or conjugation, and neither of these metabolic events were observed in other studies.[6,33,44] Since PFOS was not metabolized in steers, it must be excreted intact to reduce the body burden. In this study, the major route of excretion was through feces (11% of the PFOS dose); and elevated levels of PFOS were still being excreted in the feces at 28 days. The small amount of PFOS found in feces during the first few days of the study suggests that a majority of the PFOS was absorbed into the body and not excreted directly into feces. Higher amounts of PFOS excreted in the feces during later days of the study are most likely through contributions from the biliary elimination in feces.[6,12,44] At slaughter, biliary PFOS concentrations were second only to plasma at 36.9 μg/mL, which equates to approximately 0.9% of the dose in the bile volume collected at slaughter. There was minimal excretion of PFOS in the urine (0.5% of the PFOS dose), indicating urine was not a major route for PFOS clearance from steers. Similarly, urinary PFOS excretion was a minor route of elimination in rats, sheep, and dairy cows.[12,20,35] Considering that the small volume of bile (15−40 mL depending on steer) taken at slaughter contained almost double the amount of PFOS excreted in urine over the entire study (0.9% vs 0.5%), it is likely that the longer plasma half-life could be attributed to enterohepatic circulation, which is explained below. When the high rate of PFOS absorption, the rate of digesta passage, and the relatively low amount of PFOS elimination in urine and feces early in the study are collectively considered, probable involvement of enterohepatic circulation in PFOS distribution and elimination is logical.[27]

Taking into account the high concentrations of PFOS in the blood but minimal elimination through urine, it is likely that PFOS reaches the kidney through the blood but is either protein bound and unable to pass through the glomerulus or that PFOS circulates unbound and is filtered, but reabsorbed rather than excreted.[27] Obviously, the presence of PFOS in urine, even in small amounts, indicates that some unbound PFOS is filtered at the glomerulus and is moved through the tubules for urine excretion. Organic anion transporting polypeptides in the kidney can also bind to PFOS and prevent urinary excretion but allow passage to the liver and eventual secretion into bile and feces.[34,45] PFOS elimination differs markedly from the excretion of PFOA, which is quantitatively eliminated through the urine by steers, but reasons remain unclear as to why.[25] There are structural and chemical differences of PFOA and PFOS that could result in the differential elimination. For example, carboxylic vs sulfonic acid functional groups, water solubilities at 25 °C (9.5 g/L vs 680 mg/L, respectively), and pK_a (2.5 vs −3.3, respectively) differences.[6] Specifically, the pK_a can have an effect on protein binding. Once PFOS is in the liver, it is either transported to the bile and reabsorbed by the intestinal tract or eliminated in feces.

The highest concentrations of PFOS in the tissues, besides plasma and bile, were in liver (17.9 ± 2.3 μg/g). The high PFOS concentrations in liver and bile, and the prolonged presence of PFOS in plasma, collectively indicate the important role that enterohepatic circulation plays in PFOS fate and distribution. For steers, tissues ordered from highest concentration to lowest concentration were liver > back fat > kidney > intraperitoneal fat > lung > spleen > muscle. Fat samples were analyzed in this study to determine if any PFOS is distributed to those tissues. The fat samples (back fat and IP fat) have consistently higher concentrations than muscle samples, averaging 5.7 and 3.5 μg/g, respectively, vs 1.1 μg/g in muscle. These results are not typical where some studies observe low accumulation of PFOS in fat tissues,[31,34] however PFOS concentrations in fat samples from this study are lower than those concentrations observed in the liver and plasma, indicating that these tissues are still the primary accumulators of PFOS. Even though the muscle concentrations and carcass remainder (which consists of the remaining fat and tissues not collected separately) concentrations are lower than liver concentrations, muscle and carcass remainder still have the largest body burdens due to size of the tissue compartments compared to liver. For muscle (average mass 101 kg) and carcass remainder (average mass 46.4 kg), 4.3 ± 0.6% and 5.7 ± 1.6%, respectively, of the PFOS dose remained in these

compartments, compared to 2.2 ± 0.2% in the liver (average mass 3.8 kg). Higher liver and kidney concentrations of PFOS compared to muscle were also observed in sheep and dairy cows.[12,20] Unlike the observation of the high elimination of PFOA in steer urine,[25] PFOS circulated and was redistributed in the steer for a long period of time; this was confirmed by the large portion of the dose circulating in the bloodstream (~35%) at slaughter and the gradual decline then incline of PFOS concentrations in the plasma over the 28-day study. Approximately 39% of the dose was not accounted for in the mass balance, therefore, large compartments such as skin and bone, which were not in the carcass remainder, could be pools where PFOS is distributed in the steer. One other study that analyzed skin and bone observed concentrations similar to those observed in blood, indicating that distribution to these tissues is a likely source of the unaccounted PFOS.[34]

In this study an acute dose of PFOS was administered to steers. The elimination of PFOS was slow, and the study time of 28 days was not sufficient to allow us to calculate a plasma elimination half-life; however, a body burden half-life was calculated to be 114.2 days. An additional longer study is being conducted to determine the plasma elimination half-life in steers. To fully assess accumulation of PFOS in cattle and the possible human exposure to PFOS through beef consumption, studying the effects of chronic exposure would be necessary. Chronic exposure is an important aspect to consider because it will occur with beef cattle due to the continual application of biosolids to pastures.[8−10,24]

■ ASSOCIATED CONTENT

Supporting Information

The mean ± SD PFOS plasma concentrations (μg/mL, n = 3) for each time point (Table S1). The mean ± SD urine and fecal concentrations (μg/mL or μg/g dw, n = 3) for each day (Table S2). This material is available free of charge via the Internet at http://pubs.acs.org.

■ AUTHOR INFORMATION

Corresponding Author

*Tel: (701)239-1236. Fax: (701)239-1430. E-mail: Sara.Lupton@ars.usda.gov.

Funding

Partial funding for this study was provided via an FSIS-ARS Interagency Agreement FSIS-IA-9-102.

Notes

The authors declare no competing financial interest.

■ ACKNOWLEDGMENTS

The authors would like to acknowledge Dee Ellig, Theresa Wilson, Grant Herges, Santana Nez, Colleen Pfaff, Jason Holthusen, Grant Harrington, Margaret Lorentzsen, Michael Giddings, Kristin McDonald, Theresa Goering, Jean Picard, and Erin Loeb for their help with animal care and sample collection. We would also like to acknowledge Dr. Sarah Wagner, North Dakota State University, for her help with inserting jugular catheters. The use of trade, firm, or corporation names in this publication is for the information and convenience of the reader. Such use does not constitute an official endorsement or approval by the United States Department of Agriculture, the Agricultural Research Service, or the Food Safety and Inspection Service of any product or service to the exclusion of others that may be suitable. USDA is an equal opportunity provider and employer.

■ REFERENCES

(1) Conder, J. M.; Hoke, R. A.; de Wolf, W.; Russell, M. H.; Buck, R. C. Are PFCAs bioaccumulative? A critical review and comparison with regulatory criteria and persistent lipophilic compounds. *Environ. Sci. Technol.* **2008**, *42*, 995−1003.

(2) Noorlander, C. W.; van Leeuwen, S. P. J.; te Biesebeek, J. D.; Mengelers, M. J. B.; Zeilmaker, M. J. Levels of perfluorinated compounds in food and dietary intake of PFOS and PFOA in The Netherlands. *J. Agric. Food Chem.* **2011**, *59*, 7496−7505.

(3) Committee on Toxicity. COT statement on the tolerable daily intake for perfluorooctane sulfonate. *COT of Chemicals in Food, Consumer Products and the Environment*; 2006; pp 1−21.

(4) Beach, S. A.; Newsted, J. L.; Coady, K.; Giesy, J. P. Ecotoxicological evaluation of perfluorooctanesulfonate (PFOS). *Rev. Environ. Contam. Toxicol.* **2006**, *186*, 133−174.

(5) Lau, C.; Butenhoff, J. L.; Rogers, J. M. The developmental toxicity of perfluoroalkyl acids and their derivatives. *Toxicol. Appl. Pharmacol.* **2004**, *198*, 231−241.

(6) European Food Safety Authority (EFSA). Opinion of the scientific panel on contaminants in the food chain on perfluorooctane sulfonate (PFOS), perfluorooctanoic acid (PFOA) and their salts. *EFSA J.* **2008**, *653*, 1−131.

(7) Loganathan, B. G.; Sajwan, K. S.; Sinclair, E.; Kumar, K. S.; Kannan, K. Perfluoroalkyl sulfonates and perfluorocarboxylates in two wastewater treatment facilities in Kentucky and Georgia. *Water Res.* **2007**, *41*, 4611−4620.

(8) Clarke, B. O.; Smith, S. R. Review of 'emerging' organic contaminants in biosolids and assessment of international research priorities for the agricultural use of biosolids. *Environ. Int.* **2011**, *37*, 226−247.

(9) Sepulvado, J. G.; Blaine, A. C.; Hundal, L. S.; Higgins, C. P. Occurrence and fate of perfluorochemicals in soil following the land application of municipal biosolids. *Environ. Sci. Technol.* **2011**, DOI: 10.1021/es103903d.

(10) Washington, J. W.; Yoo, H.; Ellington, J. J.; Jenkins, T. M.; Libelo, E. L. Concentrations, distribution, and persistence of perfluoroalkylates in sludge-amended soils near Decatur, Alabama, USA. *Environ. Sci. Technol.* **2010**, *44*, 8390−8396.

(11) Stahl, T.; Heyn, J.; Thiele, H.; Huther, J.; Failing, K.; Georgii, S.; Brunn, H. Carryover of perfluorooctanoic acid (PFOA) and perfluorooctane sulfonate (PFOS) from soil to plants. *Arch. Environ. Contam. Toxicol.* **2009**, *57*, 289−298.

(12) Kowalczyk, J.; Ehlers, S.; Fürst, P.; Schafft, H.; Lahrssen-Wiederholt, M. Transfer of perfluorooctanoic Acid (PFOA) and perfluoroctane sulfonate (PFOS) from contaminated feed into milk and meat of sheep: Pilot study. *Arch. Environ. Contam. Toxicol.* **2012**, *63*, 288−298.

(13) Yoo, H.; Washington, J. W.; Jenkins, T. M.; Ellington, J. J. Quantitative determination of perfluorochemicals and fluorotelomer alcohols in plants from biosolid-amended fields using LC/MS/MS and GC/MS. *Environ. Sci. Technol.* **2011**, DOI: 10.1021/es102972m.

(14) Tittlemier, S. A.; Pepper, K.; Seymour, C.; Moisey, J.; Bronson, R.; Cao, X. L.; Dabeka, R. W. Dietary exposure of Canadians to perfluorinated carboxylates and perfluorooctane sulfonate via consumption of meat, fish, fast foods, and food items prepared in their packaging. *J. Agric. Food Chem.* **2007**, *55*, 3203−3210.

(15) Ericson, I.; Martí-Cid, R.; Nadal, M.; Van Bavel, B.; Linström, G.; Domingo, J. L. Human exposure to perfluorinated chemicals through the diet: Intake of perfluorinated compounds in food from the Catalan (Spain) market. *J. Agric. Food Chem.* **2008**, *56*, 1787−1794.

(16) Clarke, D. B.; Bailey, V. A.; Routledge, A.; Lloyd, A. S.; Hird, S.; Mortimer, D. N.; Gem, M. Dietary intake estimate for perfluorooctanesulphonic acid (PFOS) and other perfluorocompounds (PFCs) in UK retail foods following determination using standard addition LC-MS/MS. *Food Addit. Contam. A* **2010**, *27*, 530−545.

(17) Haug, L. S.; Salihovic, S.; Jogsten, I. E.; Thomsen, C.; Van Bavel, B.; Lindström, G.; Becher, G. Levels in food and beverages and daily intake of perfluorinated compounds in Norway. *Chemosphere* **2010**, *80*, 1137−1143.
(18) Zhang, T.; Sun, H. W.; Wu, Q.; Zhang, X. Z.; Yun, S. H.; Kannan, K. Perfluorochemicals in meat, eggs and indoor dust in China: Assessment of sources and pathways of human exposure to perfluorochemicals. *Environ. Sci. Technol.* **2010**, *44*, 3572−3579.
(19) Guruge, K. S.; Manage, P. M.; Yamanaka, N.; Miyazaki, S.; Taniyasu, S.; Yamashita, N. Species-specific concentrations of perfluoralkyl contaminants in farm and pet animals in Japan. *Chemosphere* **2008**, *73*, S210−S215.
(20) Kowalczyk, J.; Ehlers, S.; Oberhausen, A.; Tischer, M.; Fürst, P.; Schafft, H.; Lharssen-Wiederholt, M. Absorption, distribution, and milk secretion of perfluoroalkyl acids PFBS, PFHxS, PFOS, and PFOA by dairy cows fed naturally contaminated feed. *J. Agric. Food. Chem.* **2013**, *61*, 2903−2912.
(21) Seacat, A. M.; Thomford, P. J.; Hansen, K. J.; Olsen, G. W.; Case, M. T.; Butenhoff, J. L. Subchronic toxicity studies on perfluorooctanesulfonate potassium salt in Cynomolgus monkeys. *Toxicol. Sci.* **2002a**, *68*, 249−264.
(22) Luebker, D. J.; Case, M. T.; York, R. G.; Moore, J. A.; Hansen, K. J.; Butenhoff, J. L. Two-generation reproduction and cross-foster studies of perfluorooctanesulfonate (PFOS) in rats. *Toxicology* **2005**, *215*, 126.148.
(23) van Asselt, E. D.; Rietra, R. P. J. J.; Römkens, P. F. A. M.; van der Fels-Klerx, H. J. Perfluorooctane sulphonate (PFOS) throughout the food production chain. *Food Chem.* **2011**, *128*, 1−6.
(24) Renner, R. EPA finds record PFOS, PFOA levels in Alabama grazing fields. *Environ. Sci. Technol.* **2008**, *43*, 1245−1246.
(25) Lupton, S. J.; Huwe, J. K.; Smith, D. J.; Dearfield, K. L.; Johnston, J. J. Absorption and excretion of ^{14}C-perfluorooctanoic acid (PFOA) in Angus Cattle (*Bos Taurus*). *J. Agric. Food Chem.* **2012**, *60*, 1128−1134.
(26) Paulson, G. D.; Cottrell, D. An apparatus for quantitative collection of urine from male cattle. *Am. J. Vet. Res.* **1984**, *42*, 2150−2151.
(27) Reece, W. O. *Dukes' physiology of domestic animals*, 12th ed..; Reece, W. O., Erickson, H. H., Goff, J. P., Jennings, D. P., Eds.; Cornell University Press: Ithaca, NY, 2004; pp 73−93, 184, 416−417.
(28) Hanson, K. J.; Clemen, L. A.; Ellefson, M. E.; Johnson, H. O. Compound-specific, quantitative characterization of organic fluorochemicals in biological matrices. *Environ. Sci. Technol.* **2001**, *35*, 766−770.
(29) Furdui, V. I.; Stock, N. L.; Ellis, D. A.; Butt, C. M.; Whittle, D. M.; Crozier, P. W.; Reiner, E. J.; Muir, D. C. G.; Mabury, S. A. Spatial distribution of perfluoroalkyl contaminants in lake trout from the Great Lakes. *Environ. Sci. Technol.* **2007**, *41*, 1554−1559.
(30) D'eon, J. C.; Mabury, S. A. Production of perfluorinated carboxylic acids (PFCAs) from the biotransformation of polyfluoroalkyl phosphate surfactants (PAPS): Exploring routes of human contamination. *Environ. Sci. Technol.* **2007**, *41*, 4799−4805.
(31) Yoo, H.; Guruge, K. S.; Yamanaka, N.; Sato, C.; Mikami, O.; Miyazaki, S.; Yamashita, N.; Giesy, J. P. Depuration kinetics and tissue disposition of PFOA and PFOS in white leghorn chickens (*Gallus gallus*) administered by subcutaneous implantation. *Ecotoxicol. Environ. Saf.* **2009**, *72*, 26−36.
(32) Yeung, L. W. Y.; Loi, E. I. H.; Wong, V. Y. Y.; Guruge, K. S.; Yamanaka, N.; Tanimura, N.; Hasegawa, J.; Yamashita, N.; Miyazaki, S.; Lam, P. K. S. Biochemical responses and accumulation properties of long-chain perfluorinated compounds (PFOS/PFDA/PFOA) in juvenile chickens (*Gallus gallus*). *Arch. Environ. Contam. Toxicol.* **2009**, *57*, 377−386.
(33) Borg, D.; Bogdanska, J.; Sundström, M.; Nobel, S.; Håkansson, H.; Bergman, Å.; Depierre, J. W.; Halldin, K.; Bergström, U. Tissue distribution of ^{35}S-labelled perfluorooctane sulfonate (PFOS in C57Bl/6 mice following late gestational exposure. *Reprod. Toxicol.* **2010**, *30*, 558−565.
(34) Bogdanska, J.; Borg, D.; Sundström, M.; Bergström, U.; Halldin, K.; Abedi-Valugerdi, M.; Bergman, Å.; Nelson, B.; DePierre, J.; Nobel, S. Tissue distribution of ^{35}S-labelled perfluorooctane sulfonate in adult mice after oral exposure to a low environmentally relevant dose or a high experimental dose. *Toxicology* **2011**, *284*, 54−62.
(35) Cui, L.; Liao, C. Y.; Zhou, Q. F.; Xia, T. M.; Yun, Z. J.; Jiang, G. B. Excretion of PFOA and PFOS in male rats during a subchronic exposure. *Arch. Environ. Contam. Toxicol.* **2010**, *58*, 205−213.
(36) Seacat, A. M.; Thomford, P. J.; Hansen, K. J.; Clemen, L. A.; Eldridge, S. R.; Elcombe, C. R.; Butenhoff, J. L. Sub-chronic dietary toxicity of potassium perfluorooctanesulfonate in rats. *Toxicology* **2002**, *183*, 117−131.
(37) U.S. Department of Agriculture Economic Research Service. *Food availability (per capita) data system*. Available: http://www.ers.usda.gov/Data/FoodConsumption. Accessed August 30, 2013.
(38) U.S. Department of Agrigulture, Agriculture Research Service. *Retail food commodity intakes: Mean amounts of retail commodities per individual, 2001−2002*. 2011. Available: www.ars.usda.gov/Services/docs.htm?docid=21992. Accessed August 30, 2013.
(39) American Angus Association. *Frequently asked questions about the world's largest beef breed registry*. 2013. Available: http://www.angus.org/Pub/FAQs.aspx. Accessed August 30, 2013.
(40) *Cattle Today Inc. Breeds of Cattle; Angus*. 2011. Available: http://cattle-today.com/Angus.php. Accessed August 30, 2013.
(41) *The Cattle Site. Cattle Breeds; Aberdeen Angus*. 2011. Available: http://www.thecattlesite.com/breeds/beef/7/aberdeen-angus/overview. Accessed August 30, 2013.
(42) *American Lowline Registry. Lowline FAQ*. 2011. Available: http://www.usa-lowline.org/faq.html. Accessed August 30, 2013.
(43) Harada, K.; Inoue, K.; Morikawa, A.; Yoshinaga, T.; Saito, N.; Koizumi, A. Renal clearance of perfluoroctane sulfonate and perfluoroctanoate in humans and their species-specific excretion. *Environ. Res.* **2005**, *99*, 253−261.
(44) Johnson, J. D.; Gibson, S. J.; Ober, R. E. Cholestyramine-enhanced elimination of carbon-14 in rats after administration of ammonium [^{14}C]perfluorooctanoate or potassium [^{14}C]-perfluorooctanesulfonate. *Fundam. Appl. Toxicol.* **1984**, *4*, 972−976.
(45) Hagenbuch, B.; Meier, P. J. The superfamily of organic anion transporting polypeptides. *Biochim. Biophys. Acta* **2003**, *1609*, 1−18.

toxin.[13,14] Because deoxynivalenol-3-*O*-*β*-D-glucopyranoside inhibited protein synthesis of wheat ribosomes in vitro much more weakly than deoxynivalenol, it appeared that glycosylation of deoxynivalenol is a detoxification process in plants.[15]

The Joint FAO/WHO Expert Committee on Food Additives (JECFA) in 2010 evaluated the health risks of 3-acetyldeoxynivalenol, 15-acetyldeoxynivalenol, and deoxynivalenol-3-*O*-*β*-D-glucopyranoside as well as deoxynivalenol. The Committee decided to set a group provisional maximum tolerable daily intake (PMTDI) at 1.0 mg/kg of body weight per day for deoxynivalenol, 3-acetyldeoxynivalenol, and 15-acetyldeoxynivalenol, but deoxynivalenol-3-*O*-*β*-D-glucopyranoside was not included in the group because data on the toxicity and occurrence were insufficient at that time.[16] However, recently, the occurrence of deoxynivalenol-3-*O*-*β*-D-glucopyranoside in various foods has been reported since its analytical standard became commercially available.[17−19] In addition, deoxynivalenol can be released from deoxynivalenol-3-*O*-*β*-D-glucopyranoside by some human intestinal bacteria.[20,21] On the basis of these backgrounds, not only deoxynivalenol acetates but also deoxynivalenol-3-*O*-*β*-D-glucopyranoside are considered to pose potential risks to humans.

In addition to deoxynivalenol-3-*O*-*β*-D-glucopyranoside, some masked trichothecene mycotoxins, such as glucosides of nivalenol, T-2 toxin, and HT-2 toxin, were detected in artificially contaminated cereals by MS analysis.[22−24] Because there is a possibility that these compounds exert their toxic effects after the release of aglycone during digestion, information about the occurrence of the glucosides in food products is important for conducting risk assessment of the parent mycotoxins. However, the lack of commercially available standards prevents the quantitative analysis of the glucosides.

The aims of this study were two-fold. The first was to isolate a glucoside of nivalenol from naturally contaminated wheat and to determine the chemical structure by NMR analysis. Information about a glucoside of nivalenol is as important as that for deoxynivalenol-3-*O*-*β*-D-glucopyranoside because nivalenol is frequently detected in various cereals. Second, methods for the simultaneous determination of nivalenol, deoxynivalenol, and their glucosides in wheat were developed to verify their occurrence.

MATERIALS AND METHODS

Chemicals. Solid crystals of deoxynivalenol and nivalenol and a standard solution of deoxynivalenol-3-*O*-*β*-D-glucopyranoside (50 ng/mL in acetonitrile) were purchased from Sigma-Aldrich (St. Louis, MO, USA). Liquid chromatography grade acetonitrile and water and other chemicals were purchased from Wako Pure Chemicals (Osaka, Japan).

Q-TOF LC-MS Conditions. The LC system consisted of an Agilent 1200 series (Agilent Technologies, Palo Alto, CA, USA). The LC conditions were as follows: mobile phase, 10 mM ammonium acetate/acetonitrile; hold at 5% acetonitrile for 3 min, linear gradient of 5−90% acetonitrile for 10 min, hold at 90% acetonitrile for 6 min, linear gradient of 90−5% acetonitrile for 1 min, followed by equilibration at 5% acetonitrile for 20 min before the next injection. The flow rate was 0.2 mL/min, and the column used was a 150 mm × 2.1 mm i.d., 3 μm, InertSustain C18 (GL Sciences Inc., Tokyo, Japan). The column oven was held at 40 °C, and the autosampler tray was maintained at 4 °C. The HPLC system was connected to an Agilent 6530 Q-TOF mass spectrometer. An electrospray ionization (ESI) interface with Agilent Jet Stream Technology in the negative mode was used. The instrument was calibrated in the high-resolution mode (4 GHz) with a standard mass range (m/z < 3200). Reference masses at m/z 119.0363 and 980.0164 were continually introduced along with the LC stream for accurate mass calibration. The drying gas (nitrogen) temperature was set at 325 °C, drying gas flow at 10 L/min, nebulizer pressure at 30 psi, and capillary voltage (Vcap) at 3500 V. A centroid datum within the mass range m/z 100−1000 was acquired at a 1 spectrum/s rate with a MassHunter workstation (Agilent). Peak identification was performed using Qualitative Analysis software version B.04.00 (Agilent).

Purification of Nivalenol-3-*O*-*β*-D-glucopyranoside from Naturally Contaminated Wheat. Naturally contaminated ground wheat (12 kg) was extracted with 48 L of acetonitrile/water (85:15, v/v). Extraction was performed on a horizontal shaker for 120 min at 100 rpm. The filtrate was collected by vacuum filtration using an A-3S aspirator (Tokyo Rikakikai Co., Tokyo, Japan), 1.2 kg of silica gel 60 (63−200 mm particle size) (Merck KGaA, Darmstadt, Germany) was added to the filtrate, and the mixture was dried by removing the solvent on a rotary evaporator. Fifty grams of the dried silica gel was packed in a column (50 cm × 3 cm i.d.) and eluted with *n*-hexane (400 mL), ethyl acetate (400 mL), and ethyl acetate/methanol (80:20, v/v, 600 mL), successively. This process was repeated until all of the dried silica gel had been treated. The ethyl acetate/methanol fraction containing nivalenol-3-*O*-*β*-D-glucopyranoside was evaporated to dryness, and the residue was suspended in water. The suspension was extracted twice with ethyl acetate. The remaining water layer was evaporated to dryness, and the residue (40 g yield) was suspended in 400 mL of water. After centrifugation (3000*g*, 10 min), 2 mL of the supernatant was subjected to an HF Mega BE-C18 (5 mg) cartridge (Agilent), which was preequilibrated with 20 mL of water containing 10 mM ammonium acetate. The column was washed with 20 mL of water containing 10 mM ammonium acetate, and nivalenol-3-*O*-*β*-D-glucopyranoside was eluted from the cartridge with 20 mL of 10% acetonitrile in water containing 10 mM ammonium acetate. This process was repeated until all of the supernatant had been treated. The eluate was evaporated to dryness, and the residue (3.6 g yield) was subjected to an LC-20A series HPLC system (Shimadzu Corp., Kyoto, Japan). The column used was a 250 mm × 10 mm i.d., 5 μm, Inertsil ODS-3 (GL Sciences). Isocratic elution with 5% acetonitrile in water at a flow rate of 4.0 mL/min with detection at 220 nm was used to obtain fraction A (18.5−21 min retention time, 100 mg yield). Fraction A was purified by reverse-phase HPLC equipped with the same column. Isocratic elution with water containing 0.1% trifluoroacetic acid from 0 to 5 min and then gradient elution of 0−5% acetonitrile in 0.1% trifluoroacetic acid from 5 to 50 min at a flow rate of 4.0 mL/min with detection at 220 nm was used to obtain fraction B (45 min retention time, 16.9 mg yield). Fraction B was purified by reverse-phase HPLC equipped with the same column. Isocratic elution with water from 0 to 2 min and then gradient elution of 0−4% acetonitrile in water from 2 to 74 min at a flow rate of 4.0 mL/min with detection at 220 nm was used to obtain nivalenol-3-*O*-*β*-D-glucopyranoside (65 min retention time, 9.2 mg (19%) yield): $[\alpha]_D^{20}$ −5.5 (*c* 0.25, H_2O); HRESI-TOF/MS m/z 474.1743 (calcd for $C_{21}H_{30}O_{12}$, 474.1737); ^1H and ^{13}C NMR, see Table 1.

D-Glucose Oxidase Digestion. Five hundred micrograms of nivalenol-3-*O*-*β*-D-glucopyranoside was mixed with 4 M HCl (1 mL) and then hydrolyzed in a sealed test tube at 100 °C for 4 h. The reaction solution was dried on a rotary evaporator and lyophilized for 12 h. The resulting residue was dissolved in 400 μL of water and mixed with 50 μL of a 0.5 M potassium phosphate buffer (pH 6.0) and 100 U of D-glucose oxidase (Sigma-Aldrich) in 50 μL of water. The reaction solution was incubated at 35 °C for 1 h, and the solution was directly infused into the LC-MS. D-Glucose oxidase digestion resulted in the disappearance of the signal corresponding to glucose (m/z 179 $[M - H]^-$), which originated from nivalenol-3-*O*-*β*-D-glucopyranoside, and the appearance of a new signal corresponding to gluconolactone (m/z 177 $[M - H]^-$).

Analytical Method with the Multifunctional Column. Twenty-five grams of the wheat sample was extracted with 200 mL of acetonitrile/water (85:15, v/v). The extraction was performed on a horizontal shaker for 30 min at 180 rpm, and then the extract was filtered through a filter paper (Toyo Roshi Kaisha, Tokyo, Japan). A portion (10 mL) of the filtered extract was transferred into an InertSep VRA-3 multifunctional column (GL Sciences). The first 4 mL of eluate

Table 1. NMR Spectroscopic Data for Nivalenol-3-*O*-*β*-D-glucopyranoside

position	δ_C[a]	δ_H[a] (*J* in Hz)	HMBC[b]
2	80.2	3.94, d (4.4)	4, 5, 11, 12
3	86.7	4.33, dd (4.4, 3.7)	4, 1′
4	78.7	4.64, d (3.7)	3, 5, 6, 12
5	49.8		
6	54.5		
7	74.4	4.88, s	5, 6, 8, 11, 15
8	202.7		
9	138.5		
10	137.8	6.67, d (5.1)	6, 8, 11, 16
11	71.4	4.63, d (5.1)	7, 10, 12, 15
12	66.2		
13	47.0	3.15, d (5.0)	2, 5, 12
		3.19, d (5.0)	
14	8.2	1.05, s	4, 5, 6, 12
15	60.8	3.82, d (12.7)	5, 6, 7, 11
		3.85, d (12.7)	
16	15.4	1.82, s	8, 9, 10
1′	103.3	4.74, d (7.8)	3, 2′, 3′
2′	73.8	3.38, dd (9.3, 7.8)	1′, 3′
3′	76.7	3.53, dd (9.3, 8.0)	2′
4′	70.3	3.46	
5′	76.9	3.47	
6′	61.4	3.74, dd (12.0, 4.6)	
		3.89, d (12.0)	

[a]150 MHz (δ_C) and 500 MHz (δ_H) in D_2O. Dioxane δ_C 67.5 and DSS δ_H 0.00 were used as external standards. [b]From protons stated to the indicated carbon.

was discarded, and the next 4 mL of eluate was collected and evaporated to dryness. The residue was dissolved in 1 mL of 10% acetonitrile in water.

Analytical Method with the Immunoaffinity Column. Twenty-five grams of the wheat sample was extracted with 100 mL of distilled water and then shaken for 30 min. The extract was transferred to a 50 mL centrifuge tube and centrifuged at 1410*g* for 10 min. Aliquots of 10 mL of the supernatant were diluted with 50 mL of phosphate-buffered saline (PBS). After the diluted extract was filtered through a glass fiber filter GA-55 (Toyo Roshi Kaisha), 6 mL of the filtrate (equivalent to 0.25 g sample matrix) was applied to a DON-NIV WB immunoaffinity column (VICAM, Milford, MA, USA). The immunoaffinity column had a capacity of approximately 1 μg of nivalenol, deoxynivalenol, and their glucosides, respectively. When the toxins in the highly contaminated wheat samples (no. 1, 3, 4, and 5 in Table 3) were analyzed, the amount of the filtrate applied to the column was decreased to 1 mL (equivalent to 0.042 g of sample matrix). The column was washed with 10 mL of PBS followed by a wash with 10 mL of distilled water. Toxins were eluted using 0.5 mL of methanol followed by 1.5 mL of acetonitrile. The eluate was dried under nitrogen at 40 °C. The residue was dissolved in 0.25 mL of 10% acetonitrile in water.

LC-MS/MS Conditions. LC-MS/MS analyses were performed with a 3200 Q TRAP LC-MS/MS system (AB Sciex, Foster City, CA, USA) equipped with an ESI source and an LC-20A series high-performance LC system (Shimadzu Corp.). The column used was a 150 mm × 2.1 mm i.d., 3 μm, Inertsil ODS-3 (GL Sciences). Chromatographic separation was achieved at 40 °C, using a gradient elution of 5−73% acetonitrile in water from 0 to 8 min and then isocratic elution of 90% acetonitrile in water from 8 to 10 min at a flow rate of 0.2 mL/min. The sample was centrifuged at 10000*g* for 5 min before analysis. The injection volume was 10 μL. The ESI source was operated at 400 °C in the negative ionization mode. Other MS parameters were as follows: curtain gas at 10 psi, nebulizer gas (GS1) at 50 psi, turbo heater gas (GS2) at 50 psi, collision-activated dissociation gas at 5 (arbitrary units), multiple reaction monitoring, dwell time of 250 ms, and a 5 ms pause between mass ranges. The following multiple reaction monitoring transitions were used: nivalenol, 371 $[M + CH_3COO]^-$ to 281 (collision energy, −18 eV); nivalenol-3-*O*-*β*-D-glucopyranoside, 533 $[M + CH_3COO]^-$ to 263 (collision energy, −28 eV); deoxynivalenol, 295 $[M - H]^-$ to 265 (collision energy, −12 eV); deoxynivalenol-3-*O*-*β*-D-glucopyranoside, 517 $[M + CH_3COO]^-$ to 427 (collision energy, −24 eV).

Method Validation. The method was validated with deoxynivalenol-negative wheat (Trilogy Analytical Laboratory Inc., Washington, MO, USA) spiked at four concentrations, 10, 50, 250, and 1000 μg/kg, with six replicates for each analyte. When using the DON-NIV WB immunoaffinity column, the amount of the filtrate applied to the column was 6 mL for the samples spiked at 10, 50, and 250 μg/kg and 1 mL for the sample spiked at 1000 μg/kg. Detected concentrations were calculated on a peak area basis using Analyst version 1.5.1 software (AB Sciex). Limits of detection (LODs) and limits of quantification (LOQs) were calculated on the basis of signal-to-noise ratios of 3:1 and 10:1, respectively.

RESULTS AND DISCUSSION

Detection of a Nivalenol Glycoside in Naturally Contaminated Wheat. Naturally contaminated wheat was

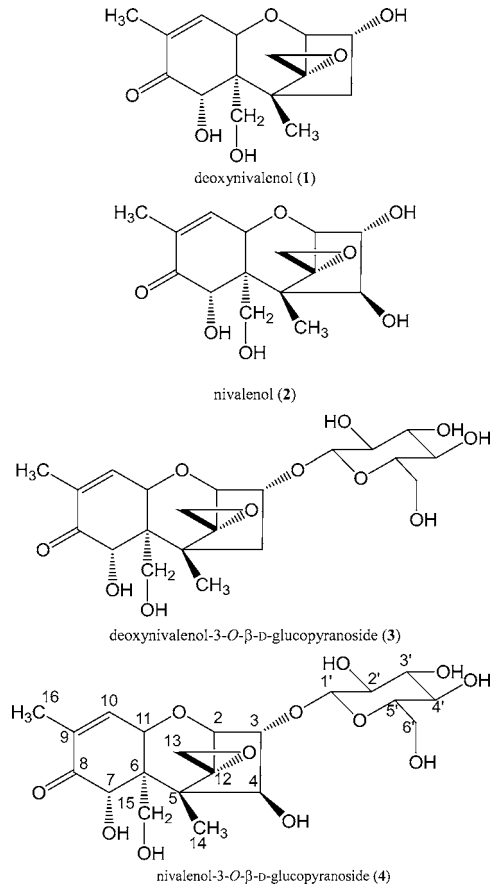

Figure 1. Structures of deoxynivalenol, nivalenol, and their glucosides.

extracted with 85% acetonitrile in water, and the extract was analyzed by Q-TOF LC-MS. Compounds having estimated molecular formulas of $C_{15}H_{20}O_7$ and $C_{21}H_{30}O_{12}$ (compound **4**) were observed at retention times of 7.5 and 8.0 min, respectively. The former compound was identified as nivalenol. The molecular formula of **4** was larger than that of nivalenol by $C_6H_{10}O_5$. As a result of MS/MS fragmentation analysis, common fragment ions (*m*/*z* 191, 217, 233, 281) were found

dx.doi.org/10.1021/jf4048644 | J. Agric. Food Chem. 2014, 62, 1174−1180

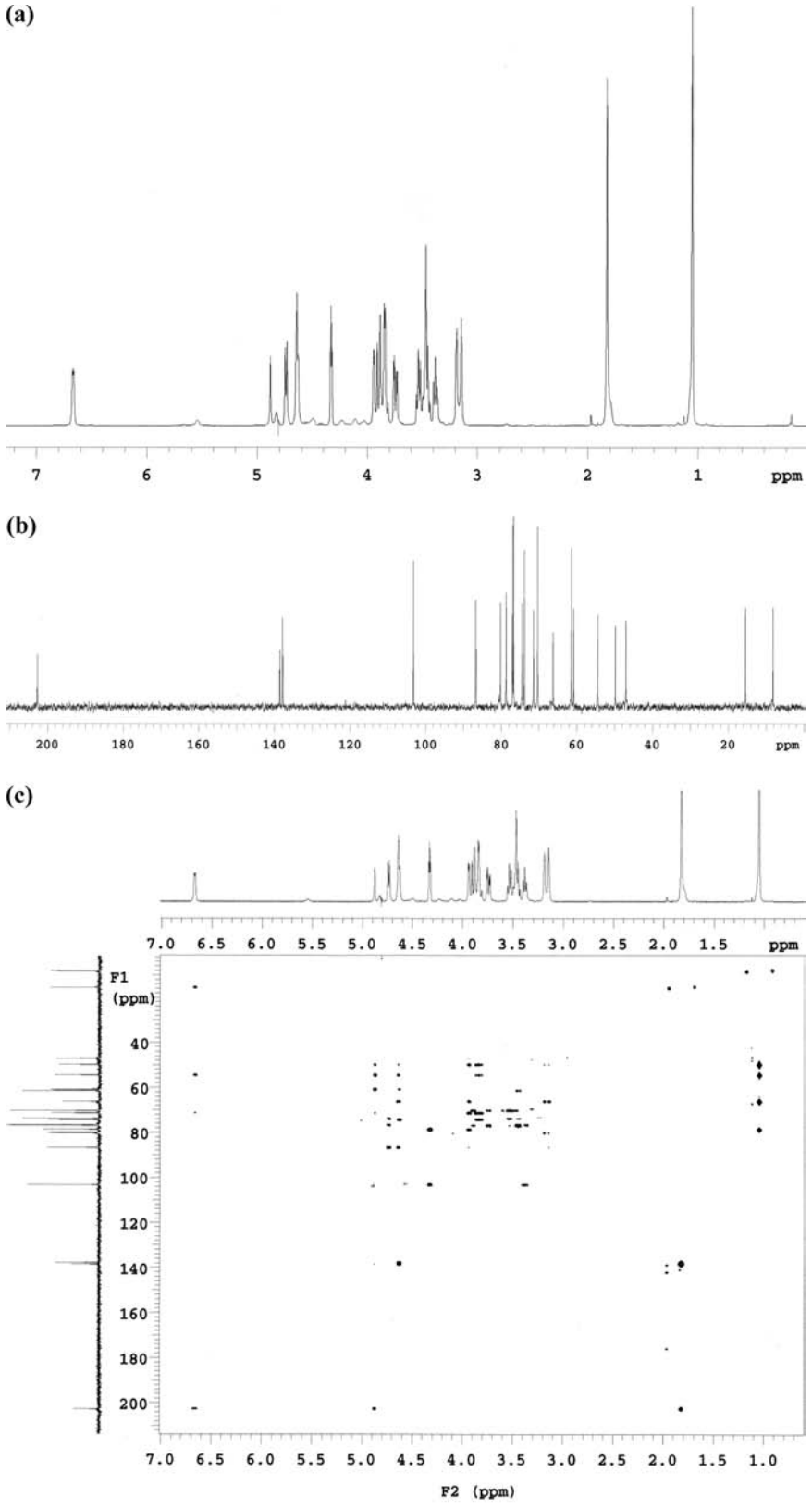

Figure 2. ^{1}H NMR spectrum (a), ^{13}C NMR spectrum (b), and HMBC spectrum (c) of nivalenol-3-*O*-*β*-D-glucopyranoside.

in nivalenol and **4** product ion spectra. From these results, **4** was suspected to be a nivalenol monoglycoside.

Isolation and Structure Determination of a Nivalenol Glycoside. Compound **4** was extracted from acetonitrile/water (85:15, v/v) from wheat. The extracts were fractionated by silica gel column chromatography, followed by liquid−liquid extraction. Further purification by C18 cartridges and reverse-phase HPLC afforded **4** in a yield of 9.2 mg from 12 kg of wheat. The ^{1}H and ^{13}C NMR spectra of **4** confirmed that it is a monoglycoside of nivalenol (Figure 2a,b). The sugar present in

dx.doi.org/10.1021/jf4048644 | J. Agric. Food Chem. 2014, 62, 1174−1180

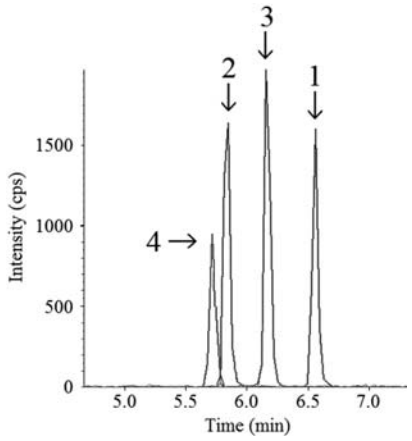

Figure 3. LC-MS/MS chromatogram of a standard solution (30 ng/mL concentrations of each analyte). Peaks: deoxynivalenol (**1**) (m/z 295 → 265); nivalenol (**2**) (m/z 371 → 281); deoxynivalenol-3-*O*-*β*-D-glucopyranoside (**3**) (m/z 517 → 427); nivalenol-3-*O*-*β*-D-glucopyranoside (**4**) (m/z 533 → 263).

4 was identified as glucose from NMR data, which are summarized in Table 1. A long-range coupling between C-3 of the nivalenol moiety and C-1′ of glucose observed in the HMBC spectrum of **4** showed that **4** was a nivalenol-3-*O*-glucopyranoside (Figure 2c). The $J_{H\text{-}1',H\text{-}2'}$ value (7.8 Hz) indicated a *β*-glycosidic linkage. Treating the acid hydrolysate of **4** with D-glucose oxidase showed the D configuration of the glucose residue of **4**. The structure of **4** was thus assigned as nivalenol-3-*O*-*β*-D-glucopyranoside (Figure 1).

Analytical Methods for Determination of Nivalenol, Deoxynivalenol, and Their Glucosides. Two purification methods were examined for the simultaneous determination of nivalenol, nivalenol-3-*O*-*β*-D-glucopyranoside, deoxynivalenol, and deoxynivalenol-3-*O*-*β*-D-glucopyranoside. The first is a method using a multifunctional column, InertSep VRA-3. The column, which contains ion exchange and reverse phase resins, is designed for purifying mycotoxins and agricultural chemicals from cereals. Previously, our group has reported a purification method using InertSep VRA-3 for the identification of deoxynivalenol, 3-acetyldeoxynivalenol, 15-acetyldeoxynivalenol, and deoxynivalenol-3-*O*-*β*-D-glucopyranoside in corn-based products.[25] The reported method was slightly modified to obtain good recoveries for nivalenol and nivalenol-3-*O*-*β*-D-glucopyranoside. The second is a method using a commercial immunoaffinity column. Some immunoaffinity columns that are designed for simultaneous purification of deoxynivalenol and nivalenol have recently been developed. In a preliminary study, deoxynivalenol, nivalenol, and their glucosides could be recovered from an immunoaffinity column, DON-NIV WB. Quantitation of the mycotoxins was performed by LC-MS/MS. A typical chromatogram is shown in Figure 3. To validate the two methods, they were applied to the analysis of spiked wheat samples containing nivalenol, nivalenol-3-*O*-*β*-D-glucopyranoside, deoxynivalenol, and deoxynivalenol-3-*O*-*β*-D-glucopyranoside at four levels in six replicates. Recoveries in the InertSep VRA-3 method were 81.5−91.3% for nivalenol, 69.8−75.3% for nivalenol-3-*O*-*β*-D-glucopyranoside, 65.8−71.7% for deoxynivalenol, and 68.3−85.3% for deoxynivalenol-3-*O*-*β*-D-glucopyranoside, whereas recoveries in the DON-NIV WB method were 87.1−93.3% for nivalenol, 94.1−103.5% for nivalenol-3-*O*-*β*-D-glucopyranoside, 86.4−96.5% for deoxynivalenol, and 95.0−100.1% for deoxynivalenol-3-*O*-*β*-D-glucopyranoside (Table 2). The LOQs for all analytes were within the range of 1−3 μg/kg. This result showed that both methods could be used to determine the four mycotoxins and that the recoveries obtained by the immunoaffinity column method were better than those obtained by the multifunctional column method.

The concentrations of nivalenol, nivalenol-3-*O*-*β*-D-glucopyranoside, deoxynivalenol, and deoxynivalenol-3-*O*-*β*-D-glucopyranoside in wheat samples were quantitated by the analytical method using an immunoaffinity column (Table 3). Nivalenol

Table 2. Limits of Quantitation (LOQ), Spiking Concentrations, and Recovery of Toxins for Validation of the Methods

			recovery (%)			
			InertSep VRA-3		DON-NIV WB	
analyte	LOQ (μg/kg)	spiking concn (μg/kg)	mean	RSD	mean	RSD
nivalenol	2	10	85.9	11.3	92.9	5.9
		50	85.3	3.1	93.3	3.2
		250	81.5	4.0	87.1	3.9
		1000	91.3	2.5	87.4	1.1
nivalenol-3-*O*-*β*-D-glucopyranoside	3	10	75.3	12.5	96.9	6.4
		50	73.6	4.9	103.1	5.5
		250	69.8	1.7	94.1	2.0
		1000	73.0	0.8	103.5	3.7
deoxynivalenol	2	10	71.1	9.0	94.8	12.0
		50	66.1	3.7	96.5	4.5
		250	65.8	3.0	86.4	1.0
		1000	71.7	1.2	88.6	4.4
deoxynivalenol-3-*O*-*β*-D-glucopyranoside	1	10	68.3	8.6	99.3	4.6
		50	77.2	5.8	100.1	4.3
		250	77.0	2.6	95.0	2.3
		1000	85.3	1.7	98.7	3.9

dx.doi.org/10.1021/jf4048644 | J. Agric. Food Chem. 2014, 62, 1174−1180

Table 3. Concentrations of Nivalenol, Nivalenol-3-*O*-*β*-D-glucopyranoside, Deoxynivalenol, and Deoxynivalenol-3-*O*-*β*-D-glucopyranoside in Wheat

wheat no.	nivalenol (mg/kg)	nivalenol-3-*O*-*β*-D-glucopyranoside (mg/kg)	nivalenol-3-*O*-*β*-D-glucopyranoside/nivalenol (mol %)	deoxynivalenol (mg/kg)	deoxynivalenol-3-*O*-*β*-D-glucopyranoside (mg/kg)	deoxynivalenol-3-*O*-*β*-D-glucopyranoside/deoxynivalenol (mol %)
1	0.37	0.15	27	10	1.5	10
2	0.54	0.22	27	0.67	0.15	14
3	1.5	0.54	24	3.6	0.27	5
4	1.7	0.30	12	5.6	0.62	7
5	15	4.0	18	0.23	0.05	14

and nivalenol-3-*O*-*β*-D-glucopyranoside were detected in all samples, and the percentages of nivalenol-3-*O*-*β*-D-glucopyranoside to nivalenol ranged from 12 to 27%. Deoxynivalenol and deoxynivalenol-3-*O*-*β*-D-glucopyranoside were also found in the samples, and the percentage of deoxynivalenol-3-*O*-*β*-D-glucopyranoside to deoxynivalenol was within the range of 5−14%.

In this study, a new derivative of nivalenol was isolated from nivalenol-contaminated wheat and was identified as nivalenol-3-*O*-*β*-D-glucopyranoside. Methods for the simultaneous determination of nivalenol, deoxynivalenol, and their glucosides in wheat were successfully developed and validated. Co-contamination of nivalenol-3-*O*-*β*-D-glucopyranoside with nivalenol, deoxynivalenol, and deoxynivalenol-3-*O*-*β*-D-glucopyranoside was observed in wheat, and the ratio of nivalenol-3-*O*-*β*-D-glucopyranoside to nivalenol was equivalent to that of deoxynivalenol-3-*O*-*β*-D-glucopyranoside to deoxynivalenol reported previously.[17] Because glycosylation is considered to be a detoxification process, it seems likely that nivalenol-3-*O*-*β*-D-glucopyranoside shows lower toxicity than nivalenol. However, as with deoxynivalenol-3-*O*-*β*-D-glucopyranoside, nivalenol-3-*O*-*β*-D-glucopyranoside may be hydrolyzed by intestinal bacteria and toxic nivalenol may be produced in the body. Therefore, nivalenol-3-*O*-*β*-D-glucopyranoside can be an important contributor to dietary exposure to trichothecene mycotoxins and should be monitored together with nivalenol, deoxynivalenol, and deoxynivalenol-3-*O*-*β*-D-glucopyranoside in foodstuffs.

■ ASSOCIATED CONTENT

Supporting Information

HPLC chromatograms of the three steps of purification of nivalenol-3-*O*-*β*-D-glucopyranoside. This material is available free of charge via the Internet at http://pubs.acs.org.

■ AUTHOR INFORMATION

Corresponding Author

*(T.Y.) Phone: +81-3-3700-1141. Fax: +81-3-3700-9852. E-mail: t-yoshinari@nihs.go.jp.

Funding

This study was funded by The Tojuro Iijima Foundation for Food Science and Technology.

Notes

The authors declare no competing financial interest.

■ ACKNOWLEDGMENTS

We thank Dr. T. Nakajima (Ministry of Agriculture, Forestry and Fisheries) for donating wheat samples.

■ REFERENCES

(1) McCormick, S. P.; Stanley, A. M.; Stover, N. A.; Alexander, N. J. Trichothecenes: from simple to complex mycotoxins. *Toxins* **2011**, *3*, 802−814.

(2) Tanaka, T.; Sugiura, Y. Levels and pattern of contamination with trichothecenes in cereal grains and their risk assessment. *JSM Mycotoxins* **2003**, *53*, 119−121.

(3) Schollenberger, M.; Müller, H. M.; Rüfle, M.; Suchy, S.; Plank, S.; Drochner, W. Natural occurrence of 16 *Fusarium* toxins in grains and feedstuffs of plant origin from Germany. *Mycopathologia* **2006**, *161*, 43−52.

(4) Scudamore, K. A.; Patel, S. Occurrence of *Fusarium* mycotoxins in maize imported into the UK, 2004−2007. *Food Addit. Contam. A* **2009**, *26*, 363−371.

(5) Kubosaki, A.; Aihara, M.; Park, B. J.; Sugiura, Y.; Shibutani, M.; Hirose, M.; Suzuki, Y.; Takatori, K.; Sugita-Konishi, Y. Immunotoxicity of nivalenol after subchronic dietary exposure to rats. *Food Chem. Toxicol.* **2008**, *46*, 253−258.

(6) Takahashi, M.; Shibutani, M.; Sugita-Konishi, Y.; Aihara, M.; Inoue, K.; Woo, G. H.; Fujimoto, H.; Hirose, M. A 90-day subchronic toxicity study of nivalenol, a trichothecene mycotoxin, in F344 rats. *Food Chem. Toxicol.* **2008**, *46*, 125−135.

(7) Sobrova, P.; Adam, V.; Vasatkova, A.; Beklova, M.; Zeman, L.; Kizek, R. Deoxynivalenol and its toxicity. *Interdiscip. Toxicol.* **2010**, *3*, 94−99.

(8) Peraica, M.; Radić, B.; Lucić, A.; Pavlović, M. Toxic effects of mycotoxins in humans. *Bull. WHO* **1999**, *77*, 754−766.

(9) Food Safety Commission of Japan. Risk assessment report deoxynivalenol and nivalenol (mycotoxin); available online at http://www.fsc.go.jp/english/evaluationreports/nm_toxins/rar_donniv_fs872_2010_nm.pdf (accessed Oct 1, 2013).

(10) European Food Safety Authority. Scientific opinion on risks for animal and public health related to the presence of nivalenol in food and feed. *EFSA J.* **2013**, *11*, 3262.

(11) Berthiller, F.; Crews, C.; Dall'Asta, C.; Saeger, S. D.; Haesaert, G.; Karlovsky, P.; Oswald, I. P.; Seefelder, W.; Speijers, G.; Stroka, J. Masked mycotoxins: a review. *Mol. Nutr. Food Res.* **2013**, *57*, 165−186.

(12) Berthiller, F.; Dall'Asta, C.; Schuhmacher, R.; Lemmens, M.; Adam, G.; Krska, R. Masked mycotoxins: determination of a deoxynivalenol glucoside in artificially and naturally contaminated wheat by liquid chromatography-tandem mass spectrometry. *J. Agric. Food Chem.* **2005**, *53*, 3421−3425.

(13) Miller, J. D.; Young, J. C. Deoxynivalenol in an experimental *Fusarium graminearum* infection of wheat. *Can. J. Plant Pathol.* **1985**, *7*, 132−134.

(14) Boutigny, A. L.; Richard, F. F.; Barreau, C. Natural mechanisms for cereal resistance to the accumulation of *Fusarium* trichothecenes. *Eur. J. Plant Pathol.* **2008**, *121*, 411−423.

(15) Poppenberger, B.; Berthiller, F.; Lucyshyn, D.; Sieberer, T.; Schuhmacher, R.; Krska, R.; Kuchler, K.; Glössl, J.; Luschnig, C.; Adam, G. Detoxification of the *Fusarium* mycotoxin deoxynivalenol by a UDP-glucosyltransferase from *Arabidopsis thaliana*. *J. Biol. Chem.* **2003**, *278*, 47905−47914.

(16) WHO. *Evaluation of Certain Contaminants in Food*; WHO Technical Report Series 959; WHO: Rome, Italy, 2010; pp 37−48.

(17) Berthiller, F.; Dall'Asta, C.; Corradini, R.; Marchelli, R.; Sulyok, M.; Krska, R.; Adam, G.; Schuhmacher, R. Occurrence of deoxynivalenol and its 3-β-D-glucoside in wheat and maize. *Food Addit. Contam. A* **2009**, *26*, 507−511.
(18) Rasmussen, P. H.; Nielsen, K. F.; Ghorbani, F.; Spliid, N. H.; Nielsen, G. C.; Jørgensen, L. N. Occurrence of different trichothecenes and deoxynivalenol-3-β-D-glucoside in naturally and artificially contaminated Danish cereal grains and whole maize plants. *Mycotoxin Res.* **2012**, *28*, 181−190.
(19) Varga, E.; Malachova, A.; Schwartz, H.; Krska, R.; Berthiller, F. Survey of deoxynivalenol and its conjugates deoxynivalenol-3-glucoside and 3-acetyl-deoxynivalenol in 374 beer samples. *Food Addit. Contam. A* **2013**, *30*, 137−146.
(20) Berthiller, F.; Krska, R.; Domig, K. J.; Kneifel, W.; Juge, N.; Schuhmacher, R.; Adam, G. Hydrolytic fate of deoxynivalenol-3-glucoside during digestion. *Toxicol. Lett.* **2011**, *206*, 264−267.
(21) Gratz, S. W.; Duncan, G.; Richardson, A. J. The human fecal microbiota metabolizes deoxynivalenol and deoxynivalenol-3-glucoside and may be responsible for urinary deepoxy-deoxynivalenol. *Appl. Environ. Microbiol.* **2013**, *79*, 1821−1825.
(22) Nakagawa, H.; Ohmichi, K.; Sakamoto, S.; Sago, Y.; Kushiro, M.; Nagashima, H.; Yoshida, M.; Nakajima, T. Detection of a new *Fusarium* masked mycotoxin in wheat grain by high-resolution LC-Orbitrap MS. *Food Addit. Contam. A* **2011**, *28*, 1447−1456.
(23) Busman, M.; Poling, S. M.; Maragos, C. M. Observation of T-2 toxin and HT-2 toxin glucosides from *Fusarium sporotrichioides* by liquid chromatography coupled to tandem mass spectrometry (LC-MS/MS). *Toxins* **2011**, *3*, 1554−1568.
(24) Lattanzio, V. M.; Visconti, A.; Haidukowski, M.; Pascale, M. Identification and characterization of new *Fusarium* masked mycotoxins, T2 and HT2 glycosyl derivatives, in naturally contaminated wheat and oats by liquid chromatography-high-resolution mass spectrometry. *J. Mass Spectrom.* **2012**, *47*, 466−475.
(25) Yoshinari, T.; Ohnishi, T.; Kadota, T.; Sugita-Konishi, Y. Development of a purification method for simultaneous determination of deoxynivalenol and its acetylated and glycosylated derivatives in corn grits and corn flour by liquid chromatography-tandem mass spectrometry. *J. Food Prot.* **2012**, *75*, 1355−1358.

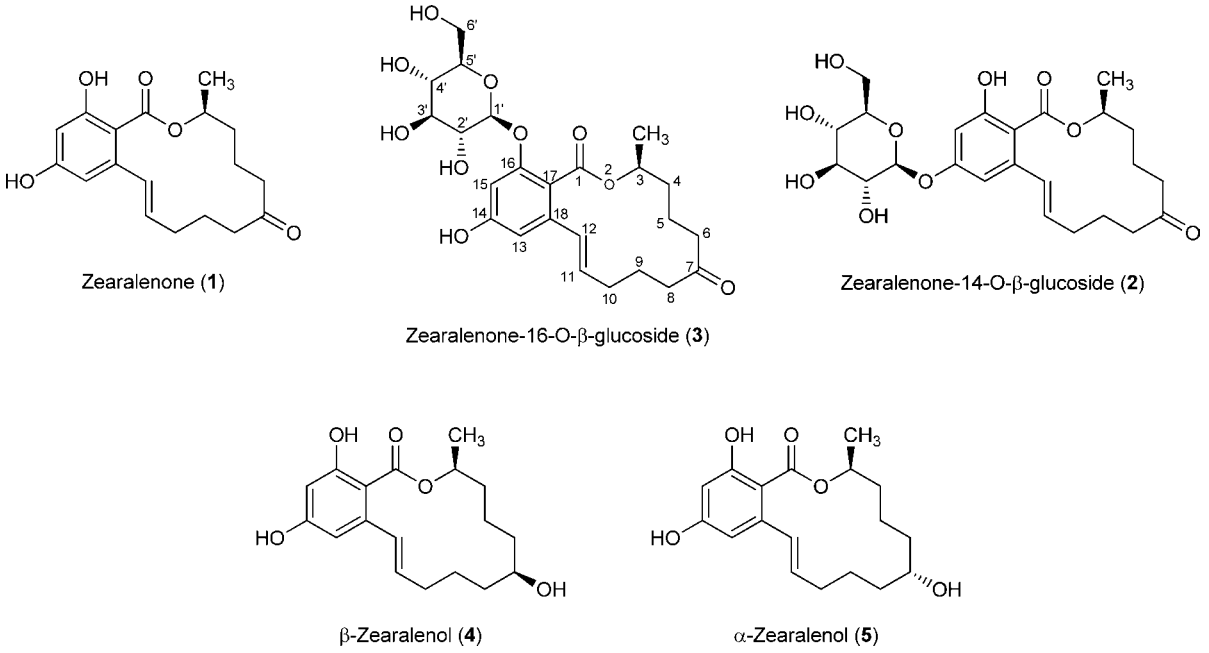

Figure 1. Chemical structures of zearalenone metabolites and numbering of atoms in zearalenone: zearalenone (**1**); zearalenone-14-*O*-*β*-glucoside (**2**); zearalenone-16-*O*-*β*-glucoside (**3**); *β*-zearalenol (**4**); *α*-zearalenol (**5**).

glucosides.[14] Analysis of the metabolization of zearalenone by *Arabidopsis* seedlings revealed that they very rapidly convert zearalenone to zearalenone-14-*O*-*β*-glucoside.[15] However, the accumulation is transient, and mass spectrometric analysis revealed that further derivatives were formed, such as zearalenone-malonyl-glucoside, zearalenone-dihexoside, and a zearalenone-pentosylhexoside. Also, the glucosides of the phase I metabolites (*β*-zearalenol (**4**) and *α*-zearalenol (**5**)) were observed.[15] The natural occurrence of a zearalenol-glucoside in maize was recently reported.[16] Zearalenone-14-*O*-*β*-glucoside does not interact with the human estrogen receptor in vitro,[13] but when fed to pigs it is rapidly converted back to zearalenone.[17] Thus, on a molar basis the estrogenicity of zearalenone-14-*O*-*β*-glucoside may be nearly equal to that of zearalenone in mammals (and humans), but no solid data are available.

Zearalenone co-occurs with other *Fusarium* toxins such as deoxynivalenol, but is typically formed rather late during the infection.[1,7] Previously, we reported several UDP-glucosyltransferases of barley, which were transcriptionally induced specifically by a deoxynivalenol-producing strain of *Fusarium graminearum*[18] and by deoxynivalenol application,[19] and characterized these genes by heterologous expression in yeast.[20] Because most of these genes did not confer increased resistance to deoxynivalenol, we tested for activity with zearalenone.

MATERIALS AND METHODS

Incubation of Toxin-Sensitive Yeast Expressing HvUGT14077 with Zearalenone. Three independent transformants of the toxin-sensitive *Saccharomyces cerevisiae* strain YZGA515 expressing the UDP-glucosyltransferase HvUGT14077 (GU170356.1),[20] or containing the empty vector, were propagated in liquid selective medium lacking leucine (SC-LEU) to an OD_{600} of 0.7 at 30 °C and 180 rpm. Fifty milliliters of the yeast suspensions was harvested by centrifugation, and the pellets were resuspended in 5 mL of SC-LEU, which contained 5 mg/L (=15.7 *μ*M) of zearalenone and was buffered with 50 mM sodium phosphate to pH 7.0. The zearalenone stock solution (5 mg/mL) was prepared in acetone. Zearalenone and zearalenone-14-*O*-*β*-glucoside were purified at the IFA-Tulln. Other chemicals, unless stated otherwise, were obtained from Sigma-Aldrich (Vienna, Austria). Cultures were incubated at 30 °C and 180 rpm, and samples were collected for HPLC-MS/MS analysis after 4, 8, 18, and 24 h.

HPLC-MS/MS Analysis. Zearalenone and its glucosylated derivatives were analyzed as described previously,[15] with slight modifications. Briefly, an 1100 HPLC system (Agilent Technologies, Waldbronn, Germany) was coupled to a QTrap LC-MS/MS system (AB Sciex, Foster City, CA, USA). Ionization was performed with an electrospray interface in negative ionization mode. Deviating from the original method, the column used was a 150 mm × 4.6 mm i.d., 5 *μ*m, Zorbax Eclipse C-8 (Agilent Technologies) for separation of the analytes by applying the same solvent gradient system (5 mM aqueous ammonium acetate/methanol). For zearalenone, the deprotonated precursor (m/z 317.1, declustering potential (DP) −51 V) was fragmented to m/z 130.9 (collision energy (CE) −38 V). The same selected reaction monitoring transition (m/z 479.1 → m/z 317.1, DP 31 V, CE 22 eV) was used for the detection and quantification of both zearalenone-14-*O*-*β*-glucoside and zearalenone-16-*O*-*β*-glucoside. To verify the apparent recovery of the method using complex fermentation media (with fecal bacteria), blanks were spiked at three concentration levels in triplicates.

LC-HR-MS spectra of the purified zearalenone-16-*O*-*β*-glucoside were acquired on a 6550 iFunnel QTOF coupled to a 1290 Infinity UHPLC system (Agilent Technologies). One microliter of a 1 mg/L solution of zearalenone-16-*O*-*β*-glucoside in MeOH/H_2O (30:70, v/v) was injected on a 150 mm × 2.1 mm i.d., 1.8 *μ*m, Zorbax SB-C18 rapid-resolution high-definition column (Agilent Technologies). A linear water/methanol gradient (both with 0.1% HCOOH) was applied. Full scan spectra over a range of m/z 50−1000 were acquired after positive and negative electrospray ionization. MassHunter B.05.01 was used for data acquisition, whereas MassHunter Qualitative Analysis B.06.00 was used for data evaluation.

Biocatalytical Production and Purification of Zearalenone-16-*O*-*β*-glucoside. Yeast strain YZGA515 expressing HvUGT14077 was cultivated in a 20 L single-wall glass autoclavable bioreactor (Applikon, Schiedeam, Netherlands) at 30 °C and 100 rpm. An overnight culture was added to 10 L of selective medium buffered with 50 mM sodium phosphate, resulting in an OD_{600} of 0.05. The cells were incubated overnight at 30 °C and 100 rpm, and the pH was kept

dx.doi.org/10.1021/jf405627d | J. Agric. Food Chem. 2014, 62, 1181−1189

constant during the fermentation at 7.0 by addition of 10 N NaOH. The zearalenone stock was added to reach 5 mg/L. After 4, 8, and 22 h, additional zearalenone was administered corresponding to further steps of 5 mg/L. After 24 h of incubation, the yeast supernatant was collected in 500 mL portions by centrifugation and 800 mL of methanol was added to the 8 L of supernatant. Zearalenone-14-*O*-*β*-glucoside and zearalenone-16-*O*-*β*-glucoside were purified from the supernatant as previously described.[14]

Structure Characterization by NMR. NMR spectra were measured in CD_3OD solution on an Avance DRX-400 FT-NMR spectrometer (Bruker BioSpin, Rheinstetten, Germany), operating at 400.13 MHz for ^1H and at 100.62 MHz for ^{13}C, at 300 K using a 5 mm inverse broadband Z-gradient probe head. Data were recorded and evaluated using TOPSPIN 1.3 (Bruker Biospin). All pulse programs were taken from the Bruker software library. Chemical shifts (established on the basis of the residual solvent resonances) are given in parts per million (ppm) relative to tetramethylsilane and coupling constants are in hertz (Hz).

Incubation of Barley, Wheat, and *Brachypodium distachyon* with Zearalenone. Barley seeds of the varieties 'Morex' (six-rowed spring malting, University of Minnesota) and 'Signora' (a two-rowed spring barley brewing variety dominant in Austria) were surface-sterilized by incubation with a solution containing 5% (v/v) sodium hypochlorite (14% active chlorine) and 0.1% (v/v) Triton X-100 for 7 min. The sterilization solution was removed completely, and seeds were incubated with 70% (v/v) ethanol for 1 min and washed three times with sterile distilled water. The seeds were placed on Murashige and Skoog basal medium containing 0.5% (w/v) sucrose and 2% (w/v) agar in magenta plant culture boxes with a cycle of 15 h of light at 20 °C and 9 h of darkness at 10 °C for 1 week.

Seedlings were transferred to liquid macronutrient salt medium (1650 mg/L ammonium nitrate, 1900 mg/L potassium nitrate, 370 mg/L ammonium sulfate, 50 mM phosphoric acid, buffered to pH 7.0 with 10 N NaOH) without sugar containing 5 mg/L zearalenone and 1 mg/L deoxynivalenol. The 5 mg/mL zearalenone stock was prepared in acetone, and the 1 mg/mL deoxynivalenol stock was prepared in water. Plants were incubated at 21 °C with constant light at 100 rpm. Metabolites were extracted from roots and leaves separately after 24 h of incubation by adding 1 mL of ethanol to 200 mg of plant material and wet grinding of the tissue with a Retsch Mixer Mill (Retsch, Haan, Germany) for 1 min at high speed.

The *Triticum aestivum* suspension culture (derived from wheat cultivar Heines Koga II, DSMZ PC-998) was obtained from the Plant Cell Culture Collection of the Leibniz Institute, DSMZ, German Collection of Microorganisms and Cell Cultures, Braunschweig, Germany) and weekly subcultured in Gamborg B5 medium (Duchefa Biochemie, Netherlands) in constant light at 21 °C and 100 rpm. The *B. distachyon* cell culture[21] derived from line Bd21 was kindly provided by Dr. Carl Ng (University College, Dublin, Ireland) and cultivated in SCM medium containing 4.4 g/L Linsmaier and Skoog medium basal salt mix including vitamins (Duchefa Biochemie, The Netherlands), 3% (w/v) maltose (Roth, Germany), 7.5 mg/L 2,4-dichlorophenoxyacetic acid (2,4-D), and 0.75 mg/L kinetin with pH set to 5.8 with 1 M KOH. Bd21 cells were propagated at 21 °C in darkness and also subcultured weekly by combining 50 mL of culture with 50 mL of fresh medium. About 200 mg of each cell culture was harvested by centrifugation and resuspended in 1 mL of the respective medium containing 2 mg/L of zearalenone and 1 mg/L deoxynivalenol. Samples were incubated at 21 °C and shaken for 4, 18, and 24 h. The cells were centrifuged, and the metabolites were extracted from the cell pellet as described for barley roots and leaves. All supernatants were analyzed by HPLC-MS/MS.

Incubation of Intestinal Bacteria with Zearalenone-16-*O*-*β*-glucoside. The in vitro fecal hydrolysis assay was conducted using samples collected from six healthy donors (four women and two men, ages 28−38 years) who had signed informed consent forms. Two incubation media were tested: (a) distilled water and (b) the complex fermentation medium as previously described by Dall'Erta et al.[22] For the fecal slurry, 4 mL of water was added to 1 g of fecal material and homogenized. Five hundred microliters of a 2 mg/L zearalenone-16-*O*-*β*-glucoside solution in the respective medium was added to 500 μL of fecal slurry, and samples were flushed with nitrogen for 10 s. Tubes were incubated at 37 °C, and the reaction was stopped after 0.5 and 2 h of incubation by adding 1 mL of ethanol. As a negative control, 500 μL of water was added to 500 μL of fecal slurry, and as a positive control 500 μL of water was added to the incubation medium containing 2 mg/L of zearalenone-16-*O*-*β*-glucoside. Supernatants were sterilized using Ultrafree-CL sterile filters with a pore size of 0.2 μm (Millipore, Schwalbach, Germany) prior to analysis by HPLC-MS/MS.

RESULTS

HvUGT14077 Expression in Yeast Interferes with Estrogen Receptor Activation. In a previous study, we reported the functional analysis of four barley UDP-glucosyltransferase genes,[20] which were highly induced by the application of the *Fusarium* mycotoxin deoxynivalenol.[19] Although recombinant HvUGT14077 protein was clearly detected in yeast, no deoxynivalenol resistance was observed. To test for activity with zearalenone, we transformed the expression vectors into the previously described yeast estrogen reporter strain YZCP908[13] and observed diminished activation.

Production of a New Glucoside by HvUGT14077 Expression in Yeast Transformants Treated with Zearalenone. To determine the mechanism in which HvUGT14077 metabolizes zearalenone and hence interferes with estrogen receptor activation, we incubated YZGA515 expressing HvUGT14077 and the empty vector control with 5 mg/L (15.7 μM) zearalenone. Analysis of the supernatant by LC-MS/MS revealed the production of zearalenone-14-*O*-*β*-glucoside[13] and a second compound with the same mass, however, with a different retention time (Figure 2). As shown later, the hypothesis that this new metabolite might be zearalenone-16-*O*-*β*-glucoside (**3**) was confirmed. In a small-scale experiment (50 mL shake culture), the transformed yeast strain was able to metabolize the administered zearalenone rapidly, most of it within 4 h (Figure 3). At time point 0 only about 50% of the input was detected in the supernatant. After

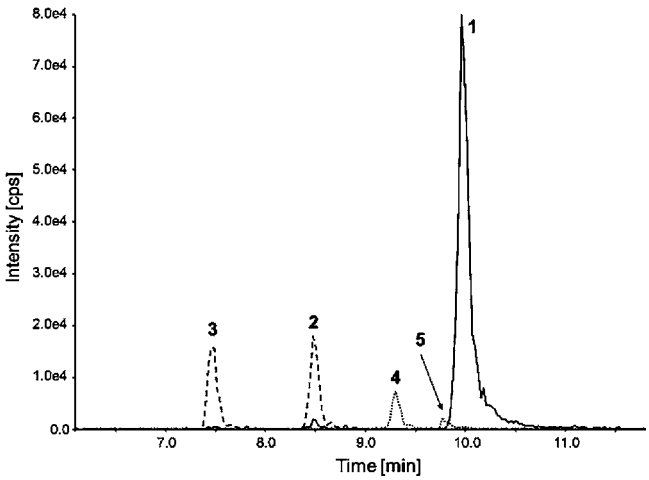

Figure 2. Chromatogram of metabolites produced by zearalenone-treated yeast strain YZGA515 expressing HvUGT14077. Each mass transition is displayed as a separate line. Zearalenone (**1**) has a retention time of 9.9 min; *α*-zearalenol (**5**), 9.8 min; *β*-zearalenol (**4**), 9.5 min; and zearalenone-14-*O*-*β*-glucoside (**2**), 8.5 min. The new compound, zearalenone-16-*O*-*β*-glucoside (**3**), with a retention time of 7.5 min, has the same mass-to-charge-ratio as compound **2**.

dx.doi.org/10.1021/jf405627d | J. Agric. Food Chem. 2014, 62, 1181−1189

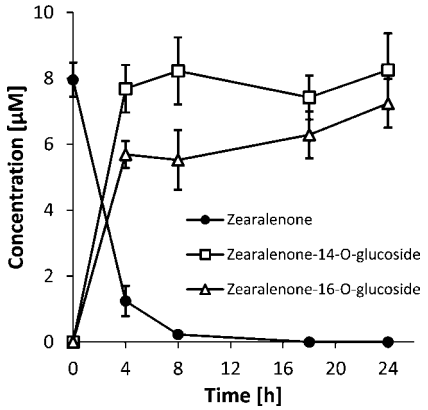

Figure 3. Time course of metabolization of zearalenone in a small-scale experiment.

24 h, a nearly complete conversion of the zearalenone input, to a mixture of both glucosides with roughly 1:1 ratio, was observed (about 44% zearalenone-16-*O*-*β*-glucoside, Figure 3).

Biocatalytic Production and Purification of the New Glucoside. To obtain enough of the new zearalenone-glucoside for structure elucidation, the strain YZGA515 expressing HvUGT14077 was cultivated in 10 L of medium at pH 7.0 in a 20 L bioreactor. Due to its limited solubility in aqueous medium and its toxicity for the yeast strain at higher concentrations, 5 mg/L zearalenone was added consecutively at the beginning and again after 4, 8, and 22 h of incubation. The pH levels remained stable between 6.7 and 7.0, and the yeast showed normal growth starting at an OD_{600} of 5.3 and reaching 10.7 after 24 h. In the fermentation supernatant with a zearalenone input of 200 mg after 24 h, 39 mg of zearalenone-14-*O*-*β*-glucoside and 38 mg of zearalenone-16-*O*-*β*-glucoside were obtained. As a first purification step, 500 mL portions of the fermentation supernatant containing 10% (v/v) methanol were loaded to equilibrated C18 solid phase extraction columns. None of the zearalenone metabolites were detected in the flow-through. Washing the column with 10 mL of 30% methanol resulted in some losses (1.9 mg of zearalenone-14-*O*-*β*-glucoside and 9.5 mg of zearalenone-16-*O*-*β*-glucoside). The glucosides were eluted from the columns with 60% (v/v) methanol, which resulted in a recovery of 34.4 mg of zearalenone-14-*O*-*β*-glucoside and 27.8 mg of zearalenone-16-*O*-*β*-glucoside. A second purification step was conducted using preparative HPLC. The retention time for zearalenone-14-*O*-*β*-glucoside was 5.0 and that for zearalenone-16-*O*-*β*-glucoside was 3.7 min. After evaporation of the solvent, totals of 24.3 mg of zearalenone-14-*O*-*β*-glucoside and 21.4 mg of zearalenone-16-*O*-*β*-glucoside were obtained.

Structural Characterization by HR-MS and NMR. HR-MS verified the isolated substance to be a $C_{24}H_{32}O_{10}$ compound, consistent with the hypothesis of a zearalenone-glucoside. In positive ion mode the $[M + H]^+$ ion showed an m/z value of 481.2064 (Δm = −0.81 ppm), whereas the $[M + Na]^+$ ion was measured at m/z 503.1887 (Δm = −0.23 ppm). After negative electrospray ionization, the $[M - H]^-$ ion showed an m/z value of 479.1929 (Δm = 1.37 ppm) and the $[M + HCOO]^-$ ion, m/z 525.1969 (Δm = −1.62 ppm). MS/MS spectra showed the cleavage of the glucose moiety. Further fragments from zearalenone could not be used to differentiate between zearalenone-16-*O*-*β*-glucoside and zearalenone-14-*O*-*β*-glucoside.

The ^1H and ^{13}C NMR data for zearalenone-16-*O*-*β*-glucoside are shown in Figure 4 and summarized in Table 1. For structure elucidation, HH-COSY, HC-HSQC, and HC-HMBC spectra were recorded. Using these two-dimensional methods, the structure of zearalenone-16-*O*-*β*-glucoside was confirmed, and complete signal assignments were established. In particular, the carbon signals of the benzene ring were assigned on the basis of direct and long-range correlations of the aromatic (H13, H15) and olefinic (H11, H12) protons. Then, the attachment position of the glucose moiety at the zearalenone skeleton could be determined by long-range coupling of the glucosyl-H1 to the C16 carbon.

Formation of Zearalenone-16-*O*-*β*-glucoside in Zearalenone-Treated Barley. To test whether zearalenone-16-*O*-*β*-glucoside is also formed in planta, we treated barley seedlings with an initial root length of about 1.5 cm with 5 mg/L zearalenone in liquid cultures. The average values of two biological replicates each containing pools of three seedlings are shown in Figure 5. In the control medium without added zearalenone, none was detected, whereas in the spiked control medium with a theoretical input of 78.5 nmol only 61.9 nmol was determined after 24 h. Zearalenone was not detected in the supernatants or in the roots of 'Morex' and 'Signora' seedlings incubated in medium lacking zearalenone. Approximately 1−7% of the added zearalenone was still present in the supernatants of both varieties, and only a small portion of the input (0.5−1%) was recovered as zearalenone-14-*O*-*β*-glucoside and zearalenone-16-*O*-*β*-glucoside in the supernatant. Although a significant amount of the added zearalenone was recovered in the root extracts, 66 and 87% of the input were converted to zearalenone-16-*O*-*β*-glucoside by 'Morex' and 'Signora' seedlings, respectively. The cotyledons were upright above the zearalenone-containing medium, without direct contact. They contained only minimal amounts of zearalenone and zearalenone metabolites. Only 3−5% of the administered zearalenone was metabolized to the previously described masked mycotoxin zearalenone-14-*O*-*β*-glucoside in barley; about 16−18-fold more zearalenone-16-*O*-*β*-glucoside than zearalenone-14-*O*-*β*-glucoside was detected in the barley root samples.

Zearalenone Glycosylation by Wheat and *Brachypodium* Suspension Cultures. Due to a higher sensitivity of suspension cultures, only 2 mg/L of zearalenone was added to the media instead of the 5 mg/L used in the barley seedling test. Panels a and b of Figure 6 show the results of a time course of treatment of the *Brachypodium* suspension culture with zearalenone as an average of three biological replicates. The input of 6.2 *μ*mol of zearalenone was metabolized by the approximately 200 mg of wet weight of cells, and within 18 h only 21% remained in the medium. A significant portion of zearalenone (50% after 4 h and 14% after 24 h) was found to be present in the extracted cell pellet. About 46% of the input was converted to zearalenone-16-*O*-*β*-glucoside within 4 h, which further increased to 76% after 18 h.

A very different situation was observed with a wheat suspension culture (Figure 6c,d). Again, zearalenone added to the medium rapidly became undetectable, but compared to *Brachypodium* the intracellular concentrations of zearalenone, zearalenone-14-*O*-*β*-glucoside, and zearalenone-16-*O*-*β*-glucoside remained low. After 24 h, only 13% of the input was converted to zearalenone-14-*O*-*β*-glucoside and zearalenone-16-*O*-*β*-glucoside, respectively, and detected in the cell extracts. Compared to *Brachypodium*, a larger portion of zearalenone-14-

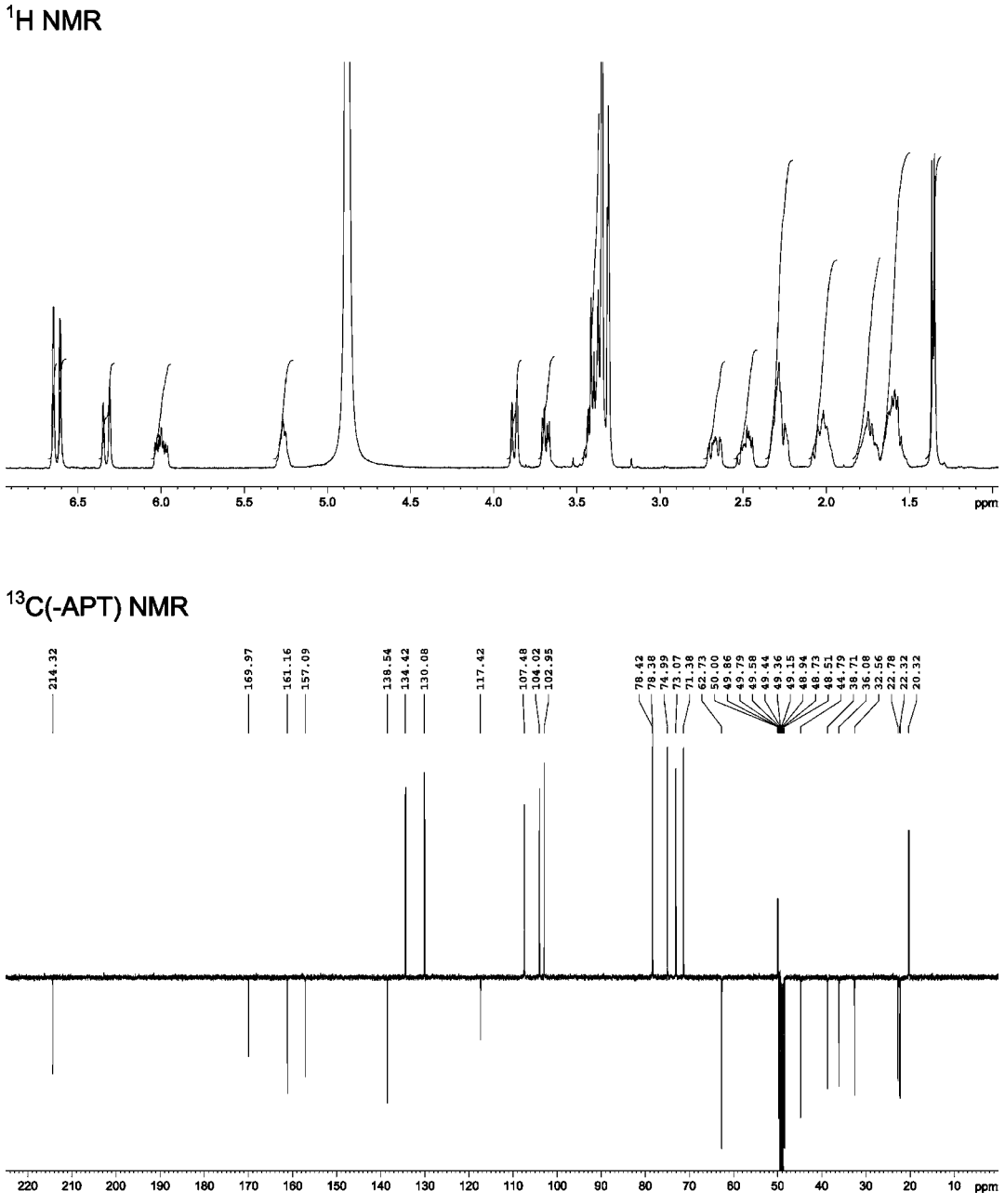

Figure 4. ^{1}H and ^{13}C(-APT) NMR spectra of zearalenone-16-*O*-*β*-glucoside.

O-*β*-glucoside also appeared in the supernatant of wheat cells, but practically no zearalenone-16-*O*-*β*-glucoside was detected. Zearalenone, zearalenols, and zearalenone-glucosides add up to only about 40%; a significant portion of the administered zearalenone is unaccounted for. A search for masses of other possible zearalenone metabolites revealed that a large portion of the input might be present in the cells as zearalenone-malonyl-glucoside, for which a reference substance is not yet available. The crude assumption that zearalenone-malonyl-glucoside shows the same response during ionization in the mass spectrometer leads to the estimate that potentially 30% of the added zearalenone may be converted to zearalenone-malonyl-glucoside in the wheat suspension culture.

Hydrolysis of Zearalenone-16-*O*-*β*-glucoside by Intestinal Bacteria. Dall'Erta et al.[22] showed a high conversion of zearalenone-14-*O*-*β*-glucoside by intestinal bacteria incubated in a complex medium containing starch, peptone, tryptone, yeast extract, pectin, mucin, casein, arabinogalactan, etc., in grams per liter amounts. In pilot experiments using 1 mg/L zearalenone-16-*O*-*β*-glucoside also an almost complete conversion to zearalenone was observed by intestinal bacteria incubated in water (data not shown). To test the differences between incubating fecal samples in the complex medium of Dall'Erta[22] and water, a concentration of 1 mg/L zearalenone-16-*O*-*β*-glucoside was selected. The fecal samples are a complex analytical matrix causing high variability. The recovery of zearalenone in the feces resuspended in the Dall'Erta fermentation mix was only 35%, with large variability (22% relative standard deviation), whereas the water-resuspended samples were rather unproblematic (on average 81% recovery with 11% relative standard deviation). Overall, due to the high relative standard deviation, the results are to be regarded as

dx.doi.org/10.1021/jf405627d | J. Agric. Food Chem. 2014, 62, 1181−1189

Table 1. ^{1}H and ^{13}C NMR Shifts of Zearalenone-16-*O*-*β*-glucoside

position	^{1}H (ppm)	mult	^{13}C (ppm)
1			170.0
3	5.27	m	73.1
3-CH_3	1.35	d, 6.3 Hz	20.3
4	1.75, 1.59	m	36.1
5	1.77, 1.58	m	22.3
6	2.48, 2.28	m	44.8
7			214.3
8	2.67, 2.26	m	38.7
9	2.00, 1.62	m	22.8
10	2.30, 2.04	m	32.6
11	6.00	ddd, 15.5, 9.7, 4.4 Hz	134.4
12	6.33	d, 15.5 Hz	130.1
13	6.65	d, 1.7 Hz	107.5
14			161.2
15	6.61	d, 1.7 Hz	104.0
16			157.1
17			117.4
18			138.5
1′	4.87	d	102.9
2′, 3′, 4′, 5′	3.37−3.41	m	78.4 (2), 75.0, 71.4
6′	3.88 3.69	dd, 12.0, 1.5 Hz dd, 12.0, 4.8 Hz	62.7

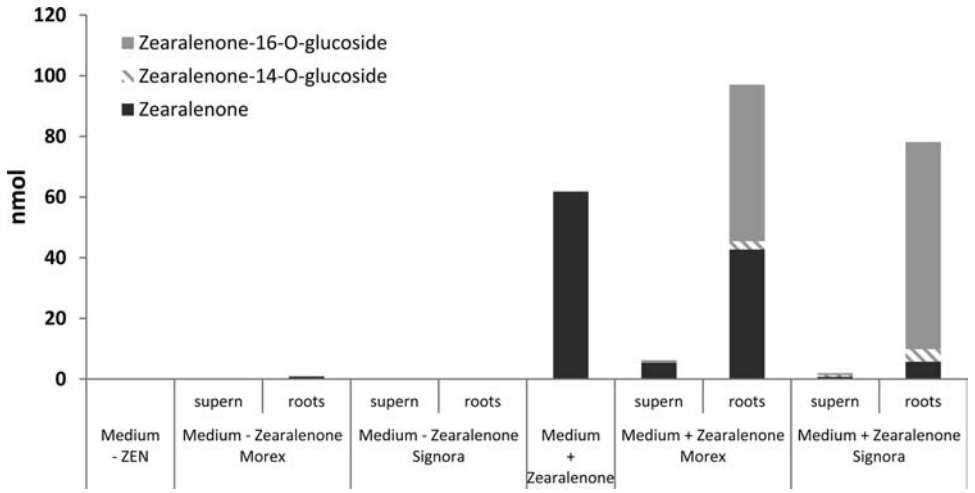

Figure 5. Distribution of zearalenone and its metabolites 24 h after incubation with 15.7 μM zearalenone with axenic cultures of seedlings of the barley cultivars 'Morex' and 'Signora'. Shown are zearalenone and detected metabolites remaining in the medium (supernatant, abbreviated supern.) and extracted from the roots.

semiquantitative. In both cases very rapid hydrolysis of zearalenone-16-*O*-*β*-glucoside was observed and nearly all of the input was recovered as zearalenone within 30 min of incubation, regardless of the suspension medium (Table 2). No remaining zearalenone-16-*O*-*β*-glucoside was found in the spiked fecal slurry of any of the volunteers after 2 h.

DISCUSSION

We elucidated that the UDP-glucosyltransferase HvUGT14077 can produce a mixture of the known masked mycotoxin zearalenone-14-*O*-*β*-glucoside (**2**) and the new zearalenone-16-*O*-*β*-glucoside (**3**) in roughly equimolar amounts. The diminished response to zearalenone in the engineered yeast strain YZCP908 expressing this gene is a first indication that zearalenone-16-*O*-*β*-glucoside, like zearalenone-14-*O*-*β*-glucoside,[13] no longer interacts with the estrogen receptor. This hypothesis will be tested with the new metabolite at hand in future in vitro interaction studies. Yeast expressing the *HvUGT14077* gene allowed straightforward production of zearalenone-16-*O*-*β*-glucoside. The use of an ABC transporter-deficient strain increases the uptake of zearalenone[23] but has the disadvantage of increasing sensitivity. Concentrations higher than 5 mg/L are toxic for the strain YZGA515. The conditions used for fermentation can still be optimized to increase the yield of glucosides, for example, by more sophisticated zearalenone administration regimes. The cleanup from large volumes of rather dilute fermentation broth is clearly a viable alternative to chemical synthesis. So far, we are only aware of one publication describing the chemical synthesis of zearalenone-16-*O*-*β*-glucoside, as a byproduct of synthesis of zearalenone-14-*O*-*β*-glucoside.[24] Presumably, only small amounts were obtained, which were insufficient for structural

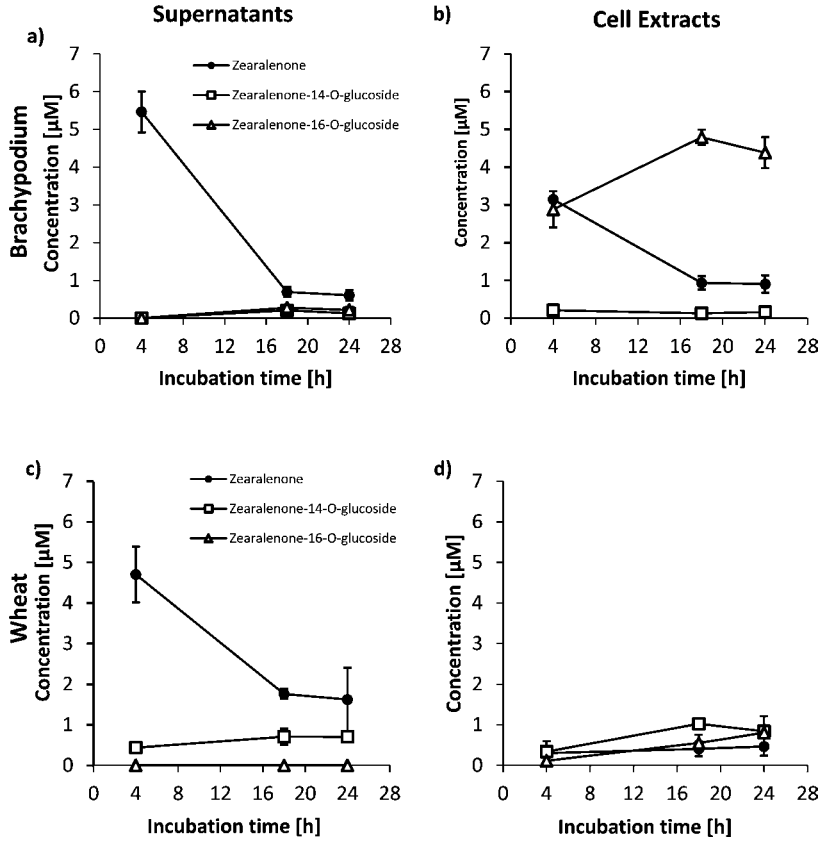

Figure 6. Time course of zearalenone metabolization by suspension cultures *Brachypodium distachyon* Bd21 (a, b) and wheat (PC-998) (c, d). Initial concentration was 6.2 μM zearalenone.

Table 2. Hydrolysis of Zearalenone-16-*O*-glucoside (3) to Zearalenone (1) by Intestinal Bacteria[a]

		t = 0.5 h			t = 2 h		
medium	sample	**3** (nmol)	**1** (nmol)	conversion (%)	**3** (nmol)	**1** (nmol)	conversion (%)
H_2O	A	0.02	2.34	113	0.00	2.29	110
	B	0.00	2.21	106	0.00	1.85	89
	C	0.11	1.90	92	0.00	2.38	115
	D	0.00	1.78	86	0.00	1.87	90
	E	0.00	1.86	90	0.00	2.01	97
	F	0.00	1.62	78	0.00	2.51	121
Dall'Erta mix	A	0.34	2.26	109	0.00	2.03	98
	B	0.00	2.14	103	0.00	2.17	105
	C	0.40	1.57	75	0.00	1.96	94
	D	0.00	1.69	81	0.00	2.26	109
	E	0.00	2.01	97	0.01	2.39	115
	F	0.09	2.26	109	0.05	2.57	124

[a]The input of 2.08 nmol of **3** was used as 100% to calculate conversion. Samples A–F represent the six feces donors. Values shown have a relative standard deviation of 11% for samples in water and 22% for the Dall'Erta fermentation mix,[22] respectively.

characterization. However, the authors did test three commercially available zearalenone immuno-affinity columns with the compound "tentatively identified as zearalenone-16-*O*-β-glucoside" and reported recoveries below 1%.[23] It is therefore highly likely that zearalenone-16-*O*-β-glucoside escapes widely used antibody-based detection methods, one of the criteria for a "masked" mycotoxin. The yeast biocatalytical production and cleanup described in this work are straightforward, and with this approach it should be possible to produce the worldwide need of an analytical reference substance. It would also be possible to produce larger amounts for future toxicological studies.

Using the yeast-produced reference substance, we investigated zearalenone metabolization in two barley cultivars ('Morex' and 'Signora') and found that both preferentially convert zearalenone into the new glucoside (16–18 times more zearalenone-16-*O*-β-glucoside than zearalenone-14-*O*-β-glucoside was observed in roots). Because HvUGT14077 produces a near 1:1 mixture, the preferential accumulation of zearalenone-16-*O*-β-glucoside in barley suggests that other UGTs exist in

the barley genome that can nearly exclusively generate zearalenone-16-*O*-*β*-glucoside. UDP-glycosyltransferases, most of which are expected to be glucosyltransferases, are encoded in plant genomes by an extremely large family. The model plants *A. thaliana* and *B. distachyon*[25,26] contain approximately 120 and 178 predicted UGTs, respectively.[27,28] An alternative hypothesis is that the zearalenone-glucosides transiently observed are the result of a dynamic equilibrium, as the glucosides are rapidly metabolized into further compounds such as malonyl-gucoside and diglucoside and other unknown forms. Potentially, the speed of downstream reactions could be largely different for the two zearalenone-glucosides and different in various plant species. In zearalenone-treated *Arabidopsis*, zearalenone-14-*O*-*β*-glucoside was found inside the plant transiently in high levels, but after 24 h, intracellular zearalenone-14-*O*-*β*-glucoside was decreased and much of the input was converted to unknown compounds.[15] Zill et al.[29] showed that in maize suspension cells treated with radiolabeled zearalenone 50% of the input was found in the nonextractable "insoluble residue".

In zearalenone-treated transgenic yeast, nearly all of the zearalenone-glucosides that are produced are efficiently transported across the plasma membrane by unknown transporters and released into the medium. In contrast, in the plant cell experiments only a small percentage of the zearalenone-glucosides was found in the medium; most of it is presumably stored in vacuoles. The soluble derivative is a "masked" mycotoxin if it is hydrolyzed by intestinal hydrolytic enzymes of the intestinal flora. In principle, two different types of hydrolytic enzymes could be relevant for reactivation of masked mycotoxins. Some bacteria contain either periplasmatic *β*-glucosidases (e.g., *Sphingomonas*[30]) or presumably cytosolic glycoside hydrolase family 1 members (e.g., the lactic acid bacterium *Oenococcus*[31]). Such enzymes can be easily expressed in *Escherichia coli* and are not sensitive to aerobic conditions or require cell integrity. The complex nutrient-rich incubation buffer used by Dall'Erta et al.[22] to generate the fecal slurry should be unnecessary, or in the worst case some ingredients may even be inhibitory (e.g., glucose released from starch due to end product inhibition). Alternatively bacteria have phosphoenolpyruvate-dependent phosphotransferase systems, where uptake of *β*-glucosides is coupled with phosphorylation of the incoming glucose. After translocation, intracellular 6-phospho-*β*-glucosidases[32] cleave the *β*-glycosidic bond, releasing 6-P-*β*-glucose, which is utilized by the bacteria. Avoiding oxidative damage of cells by maintaining strictly anaerobic conditions during resuspension and the incubation[22] may be relevant in this case to allow efficient uptake. Yet phosphoenolpyruvate-dependent phosphotransferase systems for *β*-glucosides are generally transcriptionally repressed by the presence of preferred nutrients (as present in the Dall'Erta mix), but this process is expected to become evident only after longer incubation. We have not found evidence that resuspending fecal samples in water instead of the complex mixture described by Dall'Erta reduces the ability of fecal bacteria to hydrolyze zearalenone-glucosides. An advantage of resuspending the samples in water is that matrix effects are lower and the recovery rates much higher. In pilot experiments, we furthermore found that fecal samples stored for 24 h under aerobic conditions at 4 °C have essentially unchanged ability to hydrolyze zearalenone-14-*O*-*β*-glucoside (data not shown). Maintaining strict anaerobic conditions does not seem to be critical. In conclusion, one can assume that ingested zearalenone-16-*O*-*β*-glucoside is cleaved in the intestines and therefore available for absorption. Zearalenone-16-*O*-*β*-glucoside fulfills the criteria of a masked mycotoxin. Studies on the natural occurrence and toxicological relevance are therefore warranted.

■ ASSOCIATED CONTENT

Ⓢ Supporting Information

Supplementary Figures S1 and S2. This material is available free of charge via the Internet at http://pubs.acs.org.

■ AUTHOR INFORMATION

Corresponding Author

*(G.A.) E-mail: gerhard.adam@boku.ac.at. Phone: +43 147654 6380. Fax: +43 147654 1186.

Present Addresses

△(M.P.K.P.) BIOMIN GmbH, Industriestraße 21, A-3130 Herzogenburg, Austria.

▽(W.S.) Institute for Biotechnology in Plant Production, Department for Agrobiotechnology (IFA-Tulln), University of Natural Resources and Life Sciences, Vienna, Konrad Lorenz Straße 20, A-3430 Tulln, Austria.

Funding

This work was funded by Austrian Science Fund (FWF) special research project F37 (F3706, F3708) and by funding from the U.S. Wheat and Barley Scab Initiative (U.S. Department of Agriculture, Agricultural Research Service) and the Minnesota Small Grains Initiative to G.J.M. Furthermore, we acknowledge the Federal Ministry of Economy, Family and Youth, the National Foundation for Research, Technology and Development, BIOMIN Holding GmbH. and Nestec Ltd. for funding the Christian Doppler Laboratory for Mycotoxin Metabolism.

Notes

The authors declare no competing financial interest.

■ ACKNOWLEDGMENTS

We thank Andreas Hartig and Fabian Istl (University of Vienna) for providing access to the fermentor and Carl Ng (University College, Dublin, Ireland) for generously providing the *Brachypodium* suspension culture. Franziska Löschenberger (Saatzucht Donau, Probstdorf, Austria) kindly provided barley seeds. We thank Johannes Leitner and Christoph Schüller for critically reading the manuscript.

■ ABBREVIATIONS USED

UGT, UDP-glucosyltransferase; TDI, tolerable daily intake; SC-LEU-HIS, synthetic complete lacking leucine and histidine; SCM, suspension culture medium; OD_{600}, optical density at 600 nm

■ REFERENCES

(1) Desjardins, A. E. Chapter 2. Zearalenone. In *Fusarium Mycotoxins: Chemistry, Genetics and Biology*; APS Press:: St. Paul, MN, USA, 2006; pp 65−78.

(2) Zinedine, A.; Soriano, J. M.; Moltó, J. C.; Mañes, J. Review on the toxicity, occurrence, metabolism, detoxification, regulations and intake of zearalenone: an oestrogenic mycotoxin. *Food Chem. Toxicol.* **2007**, *45*, 1−18.

(3) Kuiper-Goodman, T.; Scott, P. M.; Watanabe, H. Risk assessment of the mycotoxin zearalenone. *Regul. Toxicol. Pharmacol.* **1987**, *7*, 253−306.

(4) Kuiper, G. G. J. M.; Lemmen, J. G.; Carlsson, B.; Corton, J. C.; Safe, S. H.; van der Saag, P. T.; van der Burg, B.; Gustafsson, J.-Å.

Interaction of estrogenic chemicals and phytoestrogens with estrogen receptor β. *Endocrinology* **1998**, *139*, 4252−4263.
(5) EFSA Panel on Contaminants in the Food Chain (CONTAM). Scientific Opinion on the risks for public health related to the presence of zearalenone in food. *EFSA J.* **2011**, *9*, 2197 [124 pp].
(6) European legislation (EC 1881/2006). Commission Regulation (EC) No. 1881/2006 setting maximum levels for certain contaminants in foodstuff − consolidated version 03.12.2012. Brussels (Belgium): European Community (EC); http://eur-lex.europa.eu/LexUriServ/LexUriServ.do?uri=CONSLEG:2006R1881:20121203:EN:PDF (accessed Aug 23, 2013).
(7) Edwards, S. G. Zearalenone risk in European wheat. *World Mycotoxin J.* **2011**, *4*, 433−438.
(8) Zaied, C.; Zouaoui, N.; Bacha, H.; Abid, S. Natural occurrence of zearalenone in Tunisian wheat grains. *Food Control* **2012**, *25*, 773−777.
(9) Berthiller, F.; Crews, C.; Dall'Asta, C.; De Saeger, S.; Haesaert, G.; Karlovsky, P.; Oswald, I. P.; Seefelder, W.; Speijers, G.; Stroka, J. Masked mycotoxins: a review. *Mol. Nutr. Food Res.* **2013**, *57*, 165−186.
(10) Engelhardt, G.; Zill, G.; Wohner, B.; Wallnöfer, P. R. Transformation of the *Fusarium* mycotoxin zearalenone in maize cell suspension cultures. *Naturwissenschaften* **1988**, *75*, 309−310.
(11) Metzler, M. Proposal for a uniform designation of zearalenone and its metabolites. *Mycotoxin Res.* **2011**, *27*, 1−3.
(12) Schneweis, I.; Meyer, K.; Engelhardt, G.; Bauer, J. Occurrence of zearalenone-4-β-D-glucopyranoside in wheat. *J. Agric. Food Chem.* **2002**, *50*, 1736−1738.
(13) Poppenberger, B.; Berthiller, F.; Bachmann, H.; Lucyshyn, D.; Peterbauer, C.; Mitterbauer, R.; Schuhmacher, R.; Krska, R.; Glössl, J.; Adam, G. Heterologous expression of *Arabidopsis* UDP-glucosyltransferases in *Saccharomyces cerevisiae* for production of zearalenone-4-*O*-glucoside. *Appl. Environ. Microbiol.* **2006**, *72*, 4404−4410.
(14) Berthiller, F.; Hametner, C.; Krenn, P.; Schweiger, W.; Ludwig, R.; Adam, G.; Krska, R.; Schuhmacher, R. Preparation and characterization of the conjugated *Fusarium* mycotoxins zearalenone-4-*O*-β-D-glucopyranoside, α-zearalenol-4-*O*-β-D-glucopyranoside and β-zearalenol-4-*O*-β-D-glucopyranoside by MS/MS and two-dimensional NMR. *Food Addit. Contam.* **2009**, *26*, 207−213.
(15) Berthiller, F.; Werner, U.; Sulyok, M.; Krska, R.; Hauser, M.-T.; Schuhmacher, R. Liquid chromatography coupled to tandem mass spectrometry (LC-MS/MS) determination of phase II metabolites of the mycotoxin zearalenone in the model plant *Arabidopsis thaliana*. *Food Addit. Contam.* **2006**, *23*, 1194−1200.
(16) De Boevre, M.; Di Mavungu, J. D.; Maene, P.; Audenaert, K.; Deforce, D.; Haesaert, G.; Eeckhout, M.; Callebaut, A.; Berthiller, F.; Van Peteghem, C.; De Saeger, S. Development and validation of an LC-MS/MS method for the simultaneous determination of deoxynivalenol, zearalenone, T-2-toxin and some masked metabolites in different cereals and cereal-derived food. *Food Addit. Contam.* **2012**, *29*, 819−835.
(17) Gareis, M.; Bauer, J.; Thiem, J.; Plank, G.; Grabley, S.; Gedek, B. Cleavage of zearalenone-glycoside, a "masked" mycotoxin, during digestion in swine. *J. Vet. Med. B.* **1990**, *37*, 236−240.
(18) Boddu, J.; Cho, S.; Muehlbauer, G. J. Transcriptome analysis of trichothecene-induced gene expression in barley. *Mol. Plant−Microbe Interact.* **2007**, *20*, 1364−1375.
(19) Gardiner, S. A.; Boddu, J.; Berthiller, F.; Hametner, C.; Stupar, R. M.; Adam, G.; Muehlbauer, G. J. Transcriptome analysis of the barley-deoxynivalenol interaction: evidence for a role of glutathione in deoxynivalenol detoxification. *Mol. Plant−Microbe Interact.* **2010**, *23*, 962−976.
(20) Schweiger, W.; Boddu, J.; Shin, S.; Poppenberger, B.; Berthiller, F.; Lemmens, M.; Muehlbauer, G. J.; Adam, G. Validation of a candidate deoxynivalenol-inactivating UDP-glucosyltransferase from barley by heterologous expression in yeast. *Mol. Plant−Microbe Interact.* **2010**, *23*, 977−986.
(21) Islam, M. N.; Chambers, J. P.; Ng, C. K-Y. Lipid profiling of the model temperate grass, *Brachypodium distachyon*. *Metabolomics* **2012**, *8*, 598−613.
(22) Dall'Erta, A.; Cirlini, M.; Dall'Asta, M.; Del Rio, D.; Galaverna, G.; Dall'Asta, C. Masked mycotoxins are efficiently hydrolyzed by human colonic microbiota releasing their aglycones. *Chem. Res. Toxicol.* **2013**, *26*, 305−312.
(23) Mitterbauer, R.; Weindorfer, H.; Safaie, N.; Krska, R.; Lemmens, M.; Ruckenbauer, P.; Kuchler, K.; Adam, G. A sensitive and inexpensive yeast bioassay for the mycotoxin zearalenone and other compounds with estrogenic activity. *Appl. Environ. Microbiol.* **2003**, *69*, 805−811.
(24) Veršilovskis, A.; Huybrecht, B.; Tangni, E. K.; Pussemier, L.; De Saeger, S.; Callebaut, A. Cross-reactivity of some commercially available deoxynivalenol (DON) and zearalenone (ZEN) immunoaffinity columns to DON- and ZEN-conjugated forms and metabolites. *Food Addit. Contam. Part A* **2011**, *28*, 1687−1693.
(25) International *Brachypodium* Initiative. Genome sequencing and analysis of the model grass *Brachypodium distachyon*. *Nature* **2010**, *463*, 763−768.
(26) Caputi, L.; Malnoy, M.; Goremykin, V.; Nikiforova, S.; Martens, S. A genome-wide phylogenetic reconstruction of family 1 UDP-glycosyltransferases revealed the expansion of the family during the adaptation of plants to life on land. *Plant J.* **2012**, *69*, 1030−1042.
(27) Bowles, D.; Lim, E.-K.; Poppenberger, B.; Vaistij, F. E. Glycosyltransferases of lipophilic small molecules. *Annu. Rev. Plant Biol.* **2006**, *57*, 567−597.
(28) Schweiger, W.; Pasquet, J.-C.; Nussbaumer, T.; Kovalsky Paris, M. P.; Wiesenberger, G.; Macadré, C.; Ametz, C.; Berthiller, F.; Lemmens, M.; Saindrenan, P.; Mewes, H.-W.; Mayer, K. F. X.; Dufresne, M.; Adam, G. Functional characterization of two clusters of *Brachypodium distachyon* UDP-glycosyltransferases encoding putative deoxynivalenol detoxification genes. *Mol. Plant−Microbe Interact.* **2013**, *26*, 781−792.
(29) Zill, G.; Engelhardt, G.; Wohner, B.; Wallnöfer, P. The fate of the fusarium mycotoxin zearalenone in maize cell suspension cultures. *Mycotoxin Res.* **1990**, *6*, 31−40.
(30) Marques, A. R.; Coutinho, P. M.; Videira, P.; Fialho, A. M.; Sá-Correia, I. *Sphingomonas paucimobilis* β-glucosidase Bgl1: a member of a new bacterial subfamily in glycoside hydrolase family 1. *Biochem. J.* **2003**, *370*, 793−804.
(31) Michlmayr, H.; Schümann, C.; Wurbs, P.; Barreira Braz da Silva, N. M.; Rogl, V.; Kulbe, K. D.; Del Hierro, A. M. A β-glucosidase from *Oenococcus oeni* ATCC BAA-1163 with potential for aroma release in wine: cloning and expression in *E. coli*. *World J. Microbiol. Biotechnol.* **2010**, *26*, 1281−1289.
(32) Michalska, K.; Tan, K.; Li, H.; Hatzos-Skintges, C.; Bearden, J.; Babnigg, G.; Joachimiak, A. GH1-family 6-P-β-glucosidases from human microbiome lactic acid bacteria. *Acta Crystallogr. Sect. D* **2013**, *69*, 451−463.

^{13}C labeled (U-^{13}C) glucose, and the chemical shift reference compound [3-(trimethylsilyl)propionic-d_4 acid] sodium salt (TSP, δ = 0 ppm) were purchased from Cortecnet (Voisins-Le-Bretonneux, France). $CDCl_3$ (99.8% D) containing 0.03% TMS was purchased from Euriso-Top (Saint-Aubin, France). CD_3OD (99.8% D), 1,12-dibromododecane 98%, triethylamine, brucine sulfate salt hydrate, and benzoic acid were purchased from Sigma-Aldrich (Tres Cantos, Spain). Sulfo(4)calixarene was prepared as described previously.[32] Surfactant 1,12-bis(triethylammonium bromide) was prepared from 1,12-dibromododecane and ethanol using the method described by Lago et al.[33] The sample of [U-^{13}C]colanic acid was obtained by expression in *Escherichia coli* K92 using the protocol described by Gonzalez-Clemente et al.[34] and using U-^{13}C-labeled glucose as the source of carbon.

Sample Preparation. Samples were prepared in 5 mm NMR standard tubes. The sample of benzoic acid was prepared as 20 mM in 0.6 mL of D_2O/CD_3OD 1:1 v/v with 0.03% of TSP. The sample of wine was prepared by mixing 0.4 mL of wine of type Anciño-Ribeiro with 0.1 mL of a buffer of 1 M deuterated sodium acetate (pH 4.5) containing 0.5 mM TSP. The olive oil sample was prepared by mixing 0.5 mL of olive oil from Andalucía (Spain) in 0.1 mL of $CDCl_3$. A sample of brucine was prepared as 30 mM in 0.6 mL of $CDCl_3$. A sample of 10 mM sulfo(4)calixarene and 10 mM dodecane 1,12-bis(triethylammonium bromide) surfactant was prepared in 0.6 mL of a 1:1 v/v mixture of solvents D_2O/CD_3OD. A sample of the isolated U-^{13}C-labeled polysaccharide colanic acid was prepared by dissolving 15 mg of the dry polysaccharide in 0.6 mL of D_2O.

Nuclear Magnetic Resonance Measurements. The NMR spectra were acquired at 25 °C in an Agilent (Varian) Inova 17.6 T spectrometer (750 MHz proton resonance) equipped with an inverse detection triple resonance probe ^{1}H /^{13}C /^{31}P and triple axis shielded PFG gradients for use with conventional 5 mm NMR tubes. NMR data processing and analysis were performed with Mestrenova software (Mestrelab Research Inc.)

Theoretical Background. *Theory of 1D s-Filter Experiment.* The s-filter pulse sequence proposed for the editing of ^{1}H singlet peaks is shown in Figure 1a. The sequence incorporates two basic elements after the first excitation pulse: one is a spin−echo ($^{\Delta}/_2$−180°−$^{\Delta}/_2$) period for the evolution of single quantum coherences (SQC), and the second element is a zero-quantum coherence (ZQC) filter scheme [90°−(180°$_{SL}$ + G_{SL})−90°] originally proposed by Thrippleton and Keeler.[35] For a signal with a nominal value J of the proton−proton scalar coupling, the application of the s-filter sequence of Figure 1a with just one cycle (n = 1) generates the product operators at the selected points as shown in Scheme 1.

During the spin−echo element, a coupled signal evolves into a sum of SQC in-phase and antiphase terms. The SQC in-phase term generated at point 2 is stored as z-magnetization during the subsequent MQC/ZQC filter and is the only term that is finally detected in the experiment. The SQC antiphase term generated at point 2 is converted during the MQC/ZQC filter into a mixture of DQC/ZQC terms that are purged (dephased) at point 4 by the spatial encoding PFG gradient G_{SL} applied simultaneously with the π adiabatic inversion pulse.[35] Strong coupled multiplets (i.e., $|^nJ_{HaHb}| \leq |\nu_a - \nu_b|$) are also eliminated at point 4 when the second $^{\pi}/_2$ pulse is applied with phase $\phi_3 = x$ or $-x$, as they are efficiently transformed into a mixture of coherences of even order MQC and ZQC terms.[24] Neglecting relaxation effects, in one cycle of the s-filter experiment of Figure 1a the intensity of a signal, S, is given by eq 1

$$S \propto S_0 \cos(\pi J \Delta) \quad (1)$$

where S_0 is the original intensity of the signal and Δ the delay used in the spin−echo.

For our goal to eliminate coupled signals, the generation of SQC antiphase terms must be maximized at point 2, which occurs when the suppression condition $\Delta = 1/(2J)$ is matched. Nevertheless, for the general case of a NMR spectrum containing signals with different couplings, some of them will necessarily mismatch the suppression condition. Thus, the s-filter experiment of Figure 1a used with just a single cycle (n = 1) can only provide strong suppression in a small range of coupling constants that match the aforementioned condition. To better sculpt the suppression profile for an arbitrary set of coupling constants in the ^{1}H spectrum, the s-filter is cycled for a number of steps n that explore several values of the delay Δ (Figure 1a). For a generic signal, S, its intensity after n cycles of s-filter is given by eq 2. The incorporation of the relaxation effects during the s-filter experiment gives eq 3.

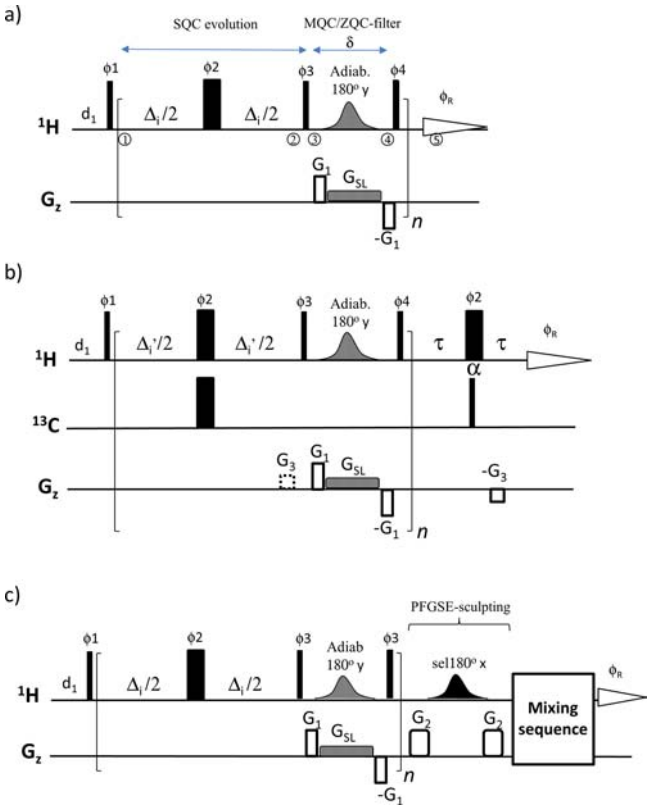

Figure 1. (a) Pulse sequence of 1D ^{1}H s-filter experiment. (b) Pulse sequence 1D ^{1}H s-filter experiment with suppression of proton signals attached to ^{13}C (e.g., ^{13}C satellites). (c) Generic scheme of 1D ^{1}H-selective s-filter experiments by combination of the s-filter and PFGSE-sculpting method. A mixing sequence such as ROESY, NOESY, DOSY, T_1, or T_2 is optionally introduced at the end of the experiment before the acquisition. In these experiments, narrow and wide lines correspond to hard pulses of 90° and 180°, respectively. The delays Δ_i are taken from Table 1 for the suppression of coupled protons. The delays Δ_i' are calculated as the closest value to the corresponding Δ_i of Table 1 that match the condition $\Delta_i' = k \times 1/(2J_{CH})$, where k is an integer number and J_{CH} is the one bond ^{1}H−^{13}C coupling constant. The shaped pulse (striped pulse) is an adiabatic inversion CHIRP pulse of 4 ms duration and 20 kHz bandwidth which is applied simultaneously with a slice-selection gradient G_{SL} with a nominal power ~3.38 G/cm. The power of G_{SL} is steadily increased between 5 and 10% for consecutive cycles to prevent accidental refocusing of coherences. G_1 is an optional purge gradient of power 15 G/cm and G_2 is 23 G/cm. G_3 and $-G_3$ are small gradients of 1 ms used for coherence selection with a power of 3.8 and −3.8 G/cm, respectively. G_3 is only applied during the first cycle of the series (n = 1). In sequence b, the ^{13}C pulse labeled with α is a hard pulse with a nominal flip angle of 90° or 270°, and the delay τ is set to $1/(2J_{CH})$. The phase cycling is $\phi_1 = \phi_R$ = 0, 0, 2, 2, 2, 2, 0, 0; ϕ_2 = 1, 1, 3, 3, 3, 3, 1, 1; and ϕ_3 = 0. Other phases are indicated. Compensation of T_1 relaxation occurring during the n cycles of MQC/ZQC filter can be obtained by setting ϕ_3 = 0 and the slice-selective gradient positive (+1 × G_{SL}) for cycles with odd number and by setting ϕ_3 = 2 and the slice-selective gradient negative (−1 × G_{SL}) for cycles with even number.

dx.doi.org/10.1021/jf4044869 | J. Agric. Food Chem. 2014, 62, 1190−1197

Scheme 1

① $I_{1z} \xrightarrow{90°_x} -I_{1y}$

② $\xrightarrow{\Delta/2\text{-}180°_y\text{-}\Delta/2} -I_{1y}\cos(\pi\cdot J\cdot\Delta) + 2I_{1x}I_{2z}\sin(\pi\cdot J\cdot\Delta)$

③ $\xrightarrow{90°_x} -I_{1z}\cos(\pi\cdot J\cdot\Delta) + 2I_{1x}I_{2y}\sin(\pi\cdot J\cdot\Delta)$

④ $\xrightarrow{[180°_y+G_{SL}]} +I_{1z}\cos(\pi\cdot J\cdot\Delta) + \sout{ZQ/DQ\ -2I_{1x}I_{2y}\sin(\pi\cdot J\cdot\Delta)}$

⑤ $\xrightarrow{90°_x} -I_{1y}\cos(\pi\cdot J\cdot\Delta)$

$$S \propto S_0 \prod_{i=1}^{n} \cos(\pi J_i \Delta_i) \tag{2}$$

$$S = S_0 \prod_{i=1}^{n} \cos(\pi J_i \Delta_i) \exp\left(-\frac{n\Delta_i}{T_2}\right)\left[1 - 2\exp\left(-\frac{n\delta}{T_1}\right)\right] \tag{3}$$

where n is the number of cycles, Δ_i the SQC evolution periods, δ the (constant) duration of the MQC/ZQC filter during each cycle, and T_2 and T_1 are the transversal and longitudinal relaxation times.

Neglecting relaxation effects, numerical analysis of eq 2 provided optimum values of the delays Δ_i for a given number of cycles n of the s-filter experiment (Figure 1a). These results are given in Table 1 and correspond to the best possible performance for the editing of singlets and small coupled signals in a convenient range that was fixed to ${}^nJ_{HH} \leq 3$ Hz. In Figure 2 are represented the signal intensity profiles using the optimized parameters of Table 1 for a number of cycles between 2 and 5. It can be seen in Figure 2a (or Figure 2b) that when the 1D s-filter experiment is used with a limited number of cycles, $n = 2$ (or $n = 3$), the experiment does not provide sufficiently strong attenuation (over 90%) for all possible couplings above 3 Hz. On the contrary, by using the optimized parameters for a number of cycles $n > 3$, strong attenuation over 90% is attained for signals with couplings above 3 Hz, while those signals with smaller couplings, and in particular singlets, have substantially stronger intensity, as can be seen in the profiles of Figure 2c,d.

It can be noticed in Table 1 that as the number of cycles n is increased, so is the required mixing time of the s-filter experiment, which introduces a certain penalty in the sensitivity of the detected signals due to relaxation effects (eq 3). In general, samples of small metabolites in solution often have sufficiently long relaxation times to accommodate the mixing times of Table 1 without compromising their sensitivity; otherwise, a compromise must be found to limit the number of cycles n.

The s-filter spectrum has a semiquantitative character. In principle, the integrals measured for a certain metabolite in samples of the same type could be directly analyzed with multivariate statistical analysis methods for metabolite profiling.[1−4] The expected differences of T_1's and T_2 among metabolites, in general, advise against the direct analysis of the integrals in the s-filter spectrum to determine relative or absolute concentrations of metabolites. However, the mentioned quantitative analysis could be feasible if signal correction factors are determined using the reference integrals of the ^{1}H spectrum.[36] In this way, the corrected quantitative integrals could be introduced into the statistical treatment of the integrals used for metabolomics studies.[1−4]

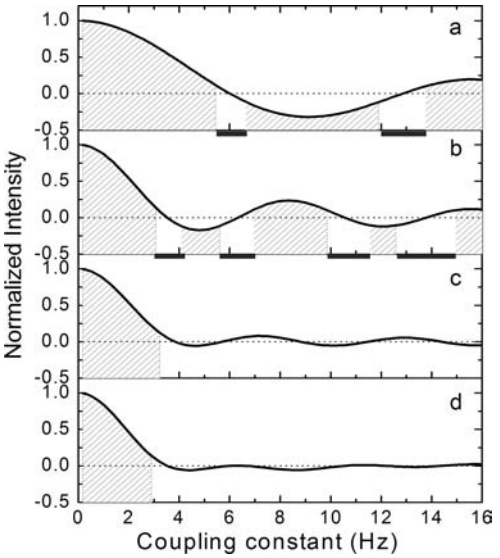

Figure 2. Signal intensity profile vs nominal value of the coupling constant in the 1D s-filter experiment. The curves are obtained by application of eq 2 to the optimized parameters of Table 1. (a) 1D s-filter[2] with two cycles ($n = 2$), (b) 1D s-filter[3] with three cycles, (c) 1D s-filter[4] with four cycles, and (d) 1D s-filter[5] with five cycles. The shaded areas under the curve represent signals with normalized absolute intensity above 10%.

A final point that was considered refers to the duration of the ZQC/MQC block in Figure 1a. The duration of this block introduces T_1 relaxation losses during the n cycles of the s-filtering sequence (eq 3). As deduced theoretically by Thrippleton and Keeler,[35] ZQC cancelation critically depends on the duration of the 180° adiabatic pulse. The attenuation can be approximated to $1/(\Omega_{ZQ}\tau_f)$, where Ω_{ZQ} is the difference of frequency (in rad s^{-1}) of two coupled signals, and τ_f is the duration of the adiabatic pulse.[35] As the s-filter experiment is normally employed with several cycles, a compromise was made here to set τ_f conveniently short. In the examples presented in this work a Chirp adiabatic inversion pulse of duration $\tau_f = 4$ ms and 40 kHz bandwidth were employed. Theoretically, under such conditions the intensity of ZQC terms of two coupled signals with Ω_{ZQ} of 500 Hz would be attenuated to 8% of its original size.

Theory of 1D s-Filter Experiment with Suppression of Protons Bound to ^{13}C. The removal of the ^{13}C satellites of all the proton signals is of interest for the identification of small signals of metabolites that could be hidden on the ^{13}C satellite peaks. On the basis of the same principles described above for the ^{1}H s-filter sequence of Figure 1a, the modified sequence of Figure 1b is proposed to obtain a ^{1}H s-filter experiment with suppression of the signals of protons directly attached to ^{13}C (e.g., ^{13}C satellites), either for singlet or multiplet peaks. The sequence incorporates one 180° ^{13}C pulse at the middle of each spin−echo. The delay Δ_i' of each cycle n has to be slightly

Table 1. Optimized Values of the Delays Δ_i in the 1D s-Filter Experiment for a Given Number of Cycles n[a]

selected couplings (Hz)	s-filter^n cycles, n	Δ_1 (ms)	Δ_2 (ms)	Δ_3 (ms)	Δ_4 (ms)	Δ_5 (ms)	Δ_6 (ms)	mixing time (ms)[b]	Q_f[c]
0.1, 3	2	39	83					139	0.747
0.1, 3	3	36	79	142				269	1.179
0.1, 3	4	35	57	88	131			327	2.847
0.1, 3	5	35	41	75	83	142		396	5.330
0.1, 3	6	33	38	55	75	88	131	444	13.31

[a]These parameters are the more favorable for the editing of singlets and signals with small couplings (${}^nJ_{HH} \leq 3$ Hz). [b]The calculated mixing time includes a period $\delta = 4$ ms for each cycle of the ZQC/MQC filter. [c]The quality factor (Q_f) is calculated as the signal intensity in the selected range of couplings divided by the signal intensity outside the selected range of couplings. The full range of couplings explored covers from 0.1 to 20 Hz.

dx.doi.org/10.1021/jf4044869 | J. Agric. Food Chem. 2014, 62, 1190−1197

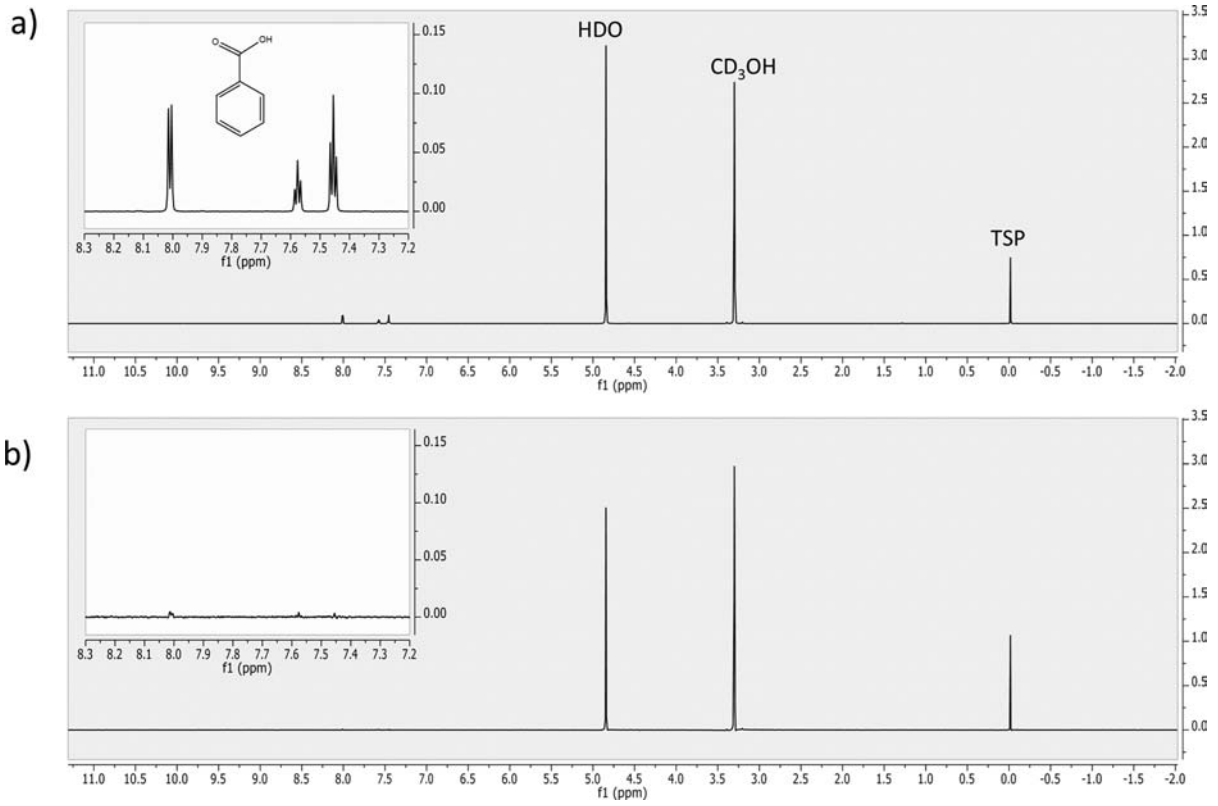

Figure 3. Spectra of a sample of benzoic acid in D_2O/CH_3OD and TSP. (a) 1D ^1H spectrum and (b) 1D ^1H s-filter[3] spectrum obtained with the experimental parameters simulated in Table 1 for three cycles (n = 3). The two spectra are normalized and represented at the same vertical scale. The inset shows the signals of benzoic acid.

modified from the correspondingly value Δ_i in Table 1 (as described in the caption of Figure 1b). The objective is to synchronize the total duration of each spin−echo so as to maximize the generation of $^1H-^{13}C$ terms of the form $2 \times H_xC_z$ exactly at the end of the spin−echo. This term is then converted into a ZQC term of the form $2 \times H_zC_z$ by effect of the second 90° proton pulse, and it is filtered out during the subsequent MQC/ZQC filter block. Thus, through the several cycles n of the sequence, the signals of all the protons bound to ^{13}C are efficiently suppressed.

Theory of 1D s-Filter Reverse Experiment (s-Filter^{rev}) for the Editing of Multiplets. The s-filter experiment in combination with difference spectroscopy is a straightforward possibility to obtain a 1D reverse s-filter spectrum (s-filter^{rev}), that is, a spectrum that shows only the signals of the multiplets but not the singlets (or small couplings).

For optimum results, the 1D s-filter^{rev} spectrum is obtained by subtraction in alternate scans of the FIDs of two subspectra: one is the T_1-filter spectrum based in the well-known inversion−recovery sequence (180°−τ_{rec}−90°−acq), and the other is the s-filter[1] experiment of Figure 1a (number of cycles n = 1). The total scan duration and other relevant parameters are made the same for the two subspectra, so as to minimize potential subtraction errors due to the relaxation effects during the two scans. In particular, the same mixing time is used in both subspectra by setting the delay τ_{rec} of the inversion−recovery spectrum equal to the duration $\Delta + \delta$ of the s-filter[1] experiment.

RESULTS AND DISCUSSION

As mentioned in the Introduction, discerning singlet peaks in areas of the NMR spectrum with overlapping metabolites is not always feasible with 1D or 2D proton homonuclear NMR spectra. The 1D s-filter experiment is proposed for the specific editing/filtering of singlets peaks and signals with small couplings.

As a proof of concept of the application of the 1D s-filter experiment to the selection of singlets, the experiment of Figure 1a was tested with a sample of benzoic acid dissolved in D_2O/CD_3OD and TSP. Figure 3 shows the excellent suppression of the aromatic multiplets in this sample while the signals of the singlets corresponding to HDO, CD_3OH, and TSP are cleanly edited in the s-filtered spectrum.

The excellent performance of the s-filter obtained in the previous example encouraged us to test the methodology with real cases of complex mixtures of foodstuffs that are of interest in the food industry. The first type of sample chosen for study is a wine sample. The spectra of parts a and b of Figure 4correspond to the 1D ^1H and the 1D s-filter spectra of the wine sample, respectively. Clearly, the 1D s-filter spectrum offers a remarkable simplification of the proton spectrum; singlets peaks of acetyl groups and other singlets or peaks with small couplings ($^nJ_{HH} \leq 3$ Hz) are clearly edited in the s-filter spectrum of Figure 4b, while the remaining signals (multiplets) are completely or significantly attenuated. The reverse s-filter experiment (1D s-filter^{rev}) obtained for this wine sample is shown in Figure 4c. It provided a clean editing of the multiplets with good phase properties and semiquantitative character. For this wine sample, the combination of s-filter and s-filter^{rev} spectra of Figure 4b,c improved the possibilities for signal assignment and quantification in those regions in which singlets and multiplets strongly overlap.

A second type of food sample tested with the s-filter methodology is olive oil. The typical proton spectrum of olive oil contains a number of strong signals of fatty acids that overlap with the signals of other less abundant metabolites. In addition, the ^{13}C satellites of such strong signals also have a

dx.doi.org/10.1021/jf4044869 | J. Agric. Food Chem. 2014, 62, 1190−1197

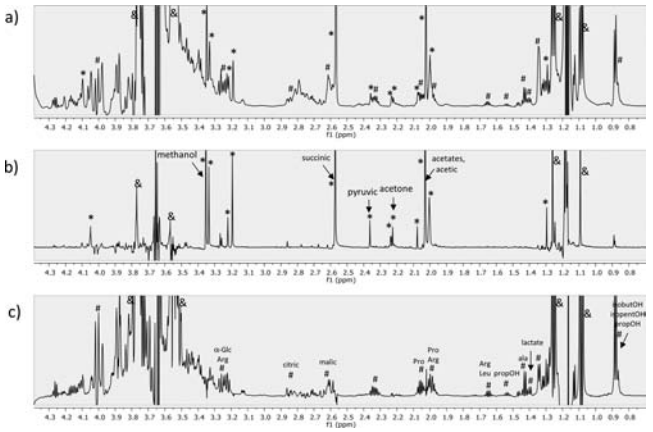

Figure 4. Region of the ^{1}H NMR spectra of a sample of wine. (a) 1D ^{1}H watergate spectrum, (b) 1D s-filter[4] watergate spectrum based on the sequence of Figure 1a. The delays were adjusted to the values reported in Table 1 for a number of cycles $n = 4$. (c) 1D ^{1}H s-filter^{rev} watergate spectrum based on the subtraction of the FIDs of a T_1-filter and s-filter (sequence of Figure 1a) in alternate scans with a mixing time of 75 ms (i.e., duration of the inversion−recovery and Δ delay is 75 ms). In the three spectra the strong water peak at 4.7 ppm was suppressed by watergate and the strong signals of ethanol at 1.17 and 3.65 ppm were partially suppressed by presaturation. Singlets and multiplets having very small couplings are labeled with asterisks. Multiplets with larger couplings are labeled with the hash symbol. The ^{13}C satellites signals of ethanol are labeled with the ampersand symbol.

relevant intensity, and unless the spectrum is obtained with ^{13}C decoupling, they contribute to the spectral overlapping. The application of the s-filter experiments to the olive oil sample is shown in Figure 5, where parts a and b compare the ^{1}H spectrum and the ^{1}H s-filter[4] spectrum with ^{13}C satellite suppression. There are a number of signals that can be identified as singlets in the second spectrum that are not evident in the former spectrum, in particular, the singlets in the region between 0.4 and 1.1 ppm. The s-filter^{rev} spectrum of this sample is given in Figure 5c and shows that all the singlet peaks are cleanly suppressed while the intensities of the multiplets are relatively well preserved, as compared with the proton spectrum of Figure 5a. Again, the combination of s-filter and s-filter^{rev} spectra of Figure 5b,c eased the task of signal assignment and quantification in those regions in which singlets and multiplets strongly overlap.

A different type of application of the ^{1}H s-filter^{rev} experiment is for the suppression of residual signals of certain solvent/s that generate singlets in the proton spectrum. Some typical cases are solvents such as D_2O or CD_3OD when they are not completely deuterated. An important advantage of the method is that, as the s-filter^{rev} experiment does not rely in selective pulses to accomplish the suppression, it potentially allows the observation of multiplet signals that could be hidden under a relative intense singlet solvent peak. An example of the use of the s-filter^{rev} for multiple solvent suppression is provided in Figure S1 (Supporting Information).

s-Filter Hybrid Experiments. The s-filter sequence of Figure 1a can be implemented as a building block for excitation in other types of NMR experiments. Thus, the resulting 1D or *n*D s-filter hybrid experiment should provide the editing of the responses of the signals of singlets and small couplings in the type of spectrum selected.

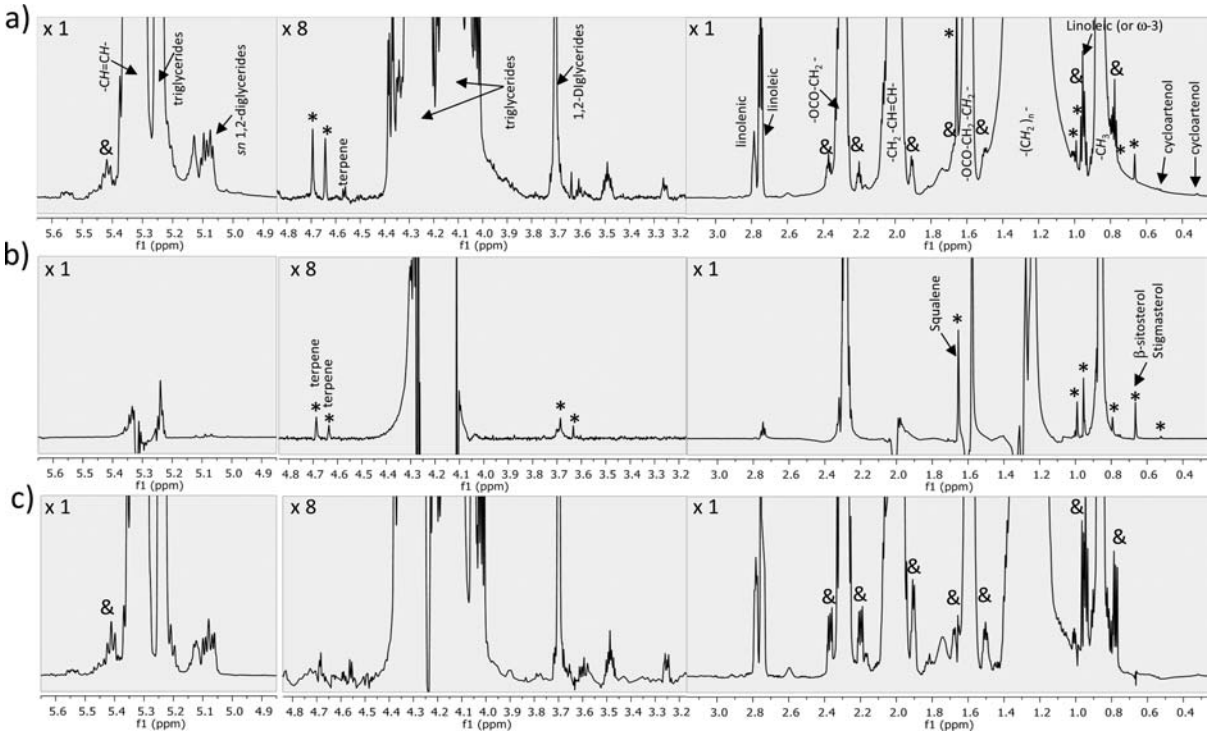

Figure 5. NMR spectra of a sample of olive oil dissolved in $CDCl_3$. (a) 1D ^{1}H spectrum, (b) 1D ^{1}H s-filter[4] spectrum with ^{13}C satellite suppression (sequence Figure 1b), and (c) 1D ^{1}H s-filter^{rev} spectrum based on the subtraction of the FIDs of a T_1-filter and s-filter (sequence Figure 1a) in alternate scans with a mixing time of 75 ms (i.e., duration of the inversion−recovery and Δ delay is 75 ms). The spectra show three regions represented at the relative vertical scale. Singlets peaks are indicated with an asterisk. In parts a and c, the ^{13}C satellites signals are labeled with the ampersand symbol. The assignment of signals is based on ref [12].

dx.doi.org/10.1021/jf4044869 | J. Agric. Food Chem. 2014, 62, 1190−1197

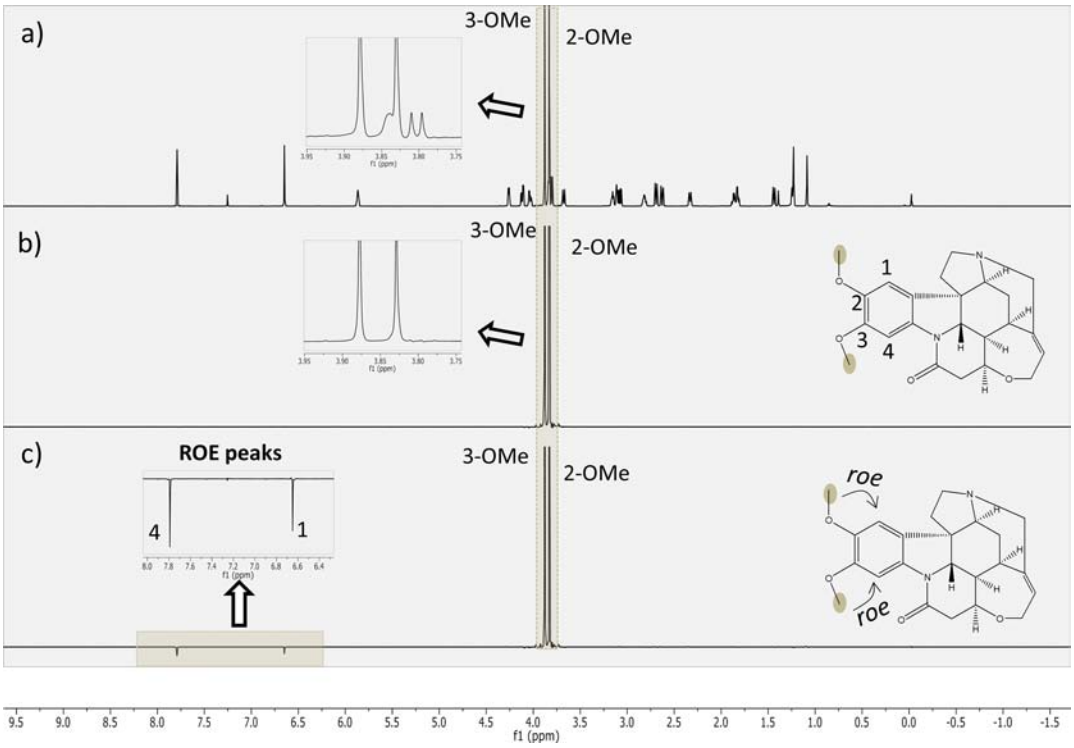

Figure 6. Spectra of a sample of brucine dissolved in $CDCl_3$. (a) ^1H spectrum, (b) selective 1D s-filter^3-PFGSE spectrum, and (c) selective 1D s-filter^3-PFGSE-ROESY spectrum with a ROESY mixing time of 400 ms. In spectra b and c the selective pulse was an r-snob pulse of 12 ms applied at 3.85 ppm and covering a bandwidth of 0.2 ppm.

One of the possibilities explored was the incorporation of s-filter into the well-known excitation sculpting scheme based on the sequence of PFGSE (pulse-field gradient spin−echo).[37] Such combination results in the 1D selective s-filter sequence (1D sel-s-filter) of Figure 1c. Additionally, a mixing sequence (e.g., ROESY, NOESY, DOSY, T_1, T_2, etc.) can be incorporated at the end of this sequence for the observation of a certain property of interest. The main advantage of the 1D sel-s-filter experiment proposed is that it permits one to isolate the response(s) of specific signal(s) of singlets that may overlap with multiplets in crowded spectra. As a proof of concept of the method, Figure 6 shows the results obtained for the molecule brucine. The 1D sel-sfilter spectrum of Figure 6b shows that the selective excitation of the two singlets of brucine at ∼3.85 ppm without the appearance of the signals of the multiplets that are in their proximities or partially overlap with them is possible. Figure 6c shows that a 1D sel-s-filter-ROESY spectrum permits the detection of the ROE responses exclusively from the two singlet peaks selected.

Other straightforward possibilities for hybrid experiments is the combination of s-filter with a conventional 2D NMR experiment such as HSQC, HMBC, ROESY, T_1, T_2, or DOSY. One example of a 2D s-filter HSQC hybrid spectrum is shown in Figure S2 (Supporting Information). The 2D s-filter-HSQC experiment can potentially be useful as a complement for assignment in combination with methyl-TROSY HSQC based NMR experiments,[38] as the former experiment will show exclusively the signals of isolated methyls. Methyl-TROSY experiments are usually performed with either fully or partially ^{13}C isotopically enriched samples, and there are situations in which the distinction between singlets protons bound to ^{13}C from singlets protons bound to other type of nuclei is relevant. For this reason, a version of the s-filter experiment is given in Figure S3 (Supporting Information), which edits the responses of the mentioned types of singlet protons with opposite phase. One example of the application of the s-filter experiments of Figures 1a,b and S3 (Supporting Information) for the editing or suppression of singlet protons bound to ^{13}C in a uniformly ^{13}C-labeled sample is provided in Figure S4 (Supporting Information).

Metabolomics Applications of s-Filter Experiments. The s-filtered experiments described above could find application to enable the detection, assignment, and/or quantification of target compounds in NMR-based chemometric applications of complex mixtures of metabolites. The type of sample that can be studied with this methodology includes those of agriculture origin, food, and biofluids. In this regard, the s-filter methodology permits the spectral editing of a number metabolites that generate singlet peaks, such as isolated methyls, methoxys, and acetyl groups that are present in metabolites such as glycine, creatine, *N*-acetyl aspartate, choline, and succinic acid. A list of compounds that can be edited with the s-filter experiment in wine and olive oil samples is provided in Tables S1 and S2 (Supporting Information), respectively. Software for automatic analysis and peak peaking algorithms could also benefit from the type of spectral simplification that the s-filter provides.

■ ASSOCIATED CONTENT

Ⓢ Supporting Information

A 1D NMR singlet filtered experiment (s-filter) is presented for the clean editing of singlets peaks in ^1H NMR spectra. The experiment provided a useful simplification of congested NMR spectra of foodstuffs and the signals retained most of the sensitivity and quantitativity of the unfiltered spectrum. This

dx.doi.org/10.1021/jf4044869 | J. Agric. Food Chem. 2014, 62, 1190−1197

material is available free of charge via the Internet at http://pubs.acs.org

AUTHOR INFORMATION

Corresponding Author

*E-mail: manuel.martin@usc.es. Phone: 00 (34) 881 816231.

Notes

The authors declare no competing financial interest.

ACKNOWLEDGMENTS

The author is grateful to prof. Miguel Ángel Ferrero García (Dept. Biología Molecular, Universidad de León, Spain) for providing the uniformly ^{13}C labeled sample of colanic acid polysaccharide.

ABBREVIATIONS USED

MQC, multiple quantum coherence; PFG, pulse field gradient; PFGSE, pulse-field gradient spin−echo; s-filter, singlet filter; s-filter^{rev}, reverse singlet filter; SQC, single quantum coherence; ZQC, zero quantum coherence.

REFERENCES

(1) Lindon, J. C.; Nicholson, J. K.; Holmes, E.; Everett, J. R. Metabonomics: Metabolic Processes Studied by NMR Spectroscopy of Biofluids. *Concepts Nucl. Magn. Reson.* **2000**, *12*, 289−320 1.

(2) Wishart, D. S. Quantitative Metabolomics Using NMR. *Trends Anal. Chem.* **2008**, *27*, 228−237.

(3) Hong, Y.-S. NMR-Based Metabolomics in Wine Science. *Magn. Reson. Chem.* **2011**, *49*, S13−S21.

(4) Anastasiadi, M.; Zira, A.; Magiati, P.; Haroutounian, S. A.; Skaltsounis, A. L.; Mikro, E. 1H NMR-Based Metabonomics for the Classification of Greek Wines According to Variety, Region, and Vintage. Comparison with HPLC Data. *J. Agric. Food. Chem.* **2009**, *57*, 11067−11074.

(5) Nilsson, N.; Duarte, I. F.; Almeida, C.; Delgadillo, I.; Goodfelow, B. J.; Gil, A. M.; Morris, G. A. High-Resolution NMR and Diffusion-Ordered Spectroscopy of Port Wine. *J. Agric. Food. Chem.* **2004**, *52*, 3736−3743.

(6) López-Rituerto, E.; Cabredo, S.; López, M.; Avenoza, A.; Busto, J. H.; Peregrina, J. M. A Thorough Study on the Use of Quantitative 1H NMR in Rioja Red Wine Fermentation Process. *J. Agric. Food Chem.* **2009**, *57*, 2112−2118.

(7) Godelman, R.; Fang, F.; Humpfer, E.; Schütz, B.; Bansbach, M.; Schäfer, H. Targeted and Nontargeted Wine Analysis by 1H NMR Spectroscopy Combined with Multivariate Statistical Analysis. Differentiation of Important Parameters: Grape Variety, Geographical Origin, Year of Vintage. *J. Agric. Food. Chem.* **2013**, *61*, 5610−5619.

(8) Hong, Y.-S.; Cilindre, C.; Liger-Belair, G.; Jeandet, P.; Hertkorn, N.; Schmitt-Kopplin, P. Metabolic Influence of *Botrytis cinerea* Infection in Champagne Base Wine. *J. Agric. Food. Chem.* **2011**, *59*, 7237−7345.

(9) Busto, J.; López-Rituerto, E.; Avenoza, A.; Peregrina, J. A NMR Study of Histidine Metabolism during Wine Fermentations and Their Influence on Production of Histamine. *J. Agric. Food Chem.* **2013**, *61*, 9464−9469.

(10) Godelmann, R.; Fang, F.; Humpfer, E.; Schütz, B.; Bansbach, M.; Schäfer, H.; Spraul, M. Targeted and Non-Targeted Wine Analysis by 1H NMR Spectroscopy Combined with Multivariate Statistical Analysis. Differentiation of Important Parameters: Grape Variety, Geographical Origin, Year of Vintage. *J. Agric. Food Chem.* **2013**, *61*, 5610−5619.

(11) Mannina, L.; Sobolev, A. P.; Segre, A. Olive Oil As Seen by NMR and Chemometrics. *Spectrosc. Eur.* **2003**, 6−14.

(12) Alonso-Salces, R. M.; Holland, M. V.; Guillou, C. 1H-NMR Fingerprinting To Evaluate the Stability of Olive Oil. *Food Control* **2011**, *22*, 2041−2046.

(13) Almeida, C.; Duarte, I. F.; Barros, A.; Rodrigues, J.; Spraul, M.; Gil, A. M. Composition of Beer by 1H NMR Spectroscopy: Effects of Brewing Site and Date of Production. *J. Agric. Food Chem.* **2006**, *54*, 700−706.

(14) Bertelli, D.; Lolli, M.; Papotti, G.; Bortolotti, L.; Serra, G.; Plessi, M. Detection of Honey Adulteration by Sugar Syrups Using One-Dimensional and Two-Dimensional High-Resolution Nuclear Magnetic Resonance. *J. Agric. Food Chem.* **2010**, *58*, 8495−8501.

(15) Spraul, M.; Schütz, B.; Humpfer, E.; Mörtter, M.; Schäfer, H.; Koswig, S.; Rinke, P. Mixture Analysis by NMR As Applied to Fruit Juice Quality Control. *Magn. Reson. Chem.* **2009**, *47*, 130−137.

(16) Chen, S.; Zeng, J.; Helms, G.; Gao, X. Quantification of Wheat Straw Lignin Structure by Comprehensive NMR Analysis. *J. Agric. Food Chem.* **2013**, *61*, 10848−10857.

(17) Gruppen, H.; Neumuller, K.; Carvalho de Souza, A.; van Rijn, J.; Appeldoorn, M.; Streekstra, H.; Schols, H. A Fast and Robust Method to Determine Phenoyl and Acetyl Esters of Polysaccharides by Quantitative 1H NMR. *J. Agric. Food Chem.* **2013**, *61*, 6282−6287.

(18) Mannina, L.; Capitani, D.; Sobolev, A.; Tomassini, A.; Sciubba, F.; De Salvador, R.; Delfini, M. Peach Fruit: A Metabolic Comparative Analysis of Two Varieties with Different Resistance to Insect Attacks by NMR Spectroscopy. *J. Agric. Food Chem.* **2013**, *61*, 1718−1726.

(19) Pacifico, D.; Casciani, L.; Ritota, M.; Mandolino, G.; Onofri, C.; Moschella, A.; Parisi, B.; Cafiero, C.; Valentini, M. NMR-Based Metabolomics for Organic Farming Traceability of Early Potatoes. *J. Agric. Food Chem.* **2013**, *61*, 11201−11211.

(20) Clausen, M. R.; Bach, V.; Edelenbos, M.; Bertram, H. C. Metabolomics Reveals Drastic Compositional Changes during Over-wintering of Jerusalem Artichoke (*Helianthus tuberosus L.*) Tubers. *J. Agric. Food Chem.* **2012**, *60*, 9495−9501.

(21) Cinel, B.; Prema, D.; Pilfold, J.; Krauchi, J.; Church, J.; Donkor, K. K. Rapid Determination of Total Conjugated Linoleic Acid Content in Select Canadian Cheeses by 1H NMR Spectroscopy. *J. Agric. Food Chem.* **2013**, *61*, 9915−9921.

(22) Claridge, T. D. W. *High-Resolution NMR Techniques in Organic Chemistry (Tetrahedron Organic Chemistry)*; Elsevier Ltd, Oxford, UK, 1999; Vol. *19*.

(23) Ludwig, C.; Viant, M. R. Two-Dimensional J-Resolved NMR Spectroscopy: Review of a Key Methodology in the Metabolomics Toolbox. *Phytochem. Anal.* **2010**, *21*, 22−32.

(24) Rastrelli, F.; Jha, S.; Mancin, F. Seeing through Macromolecules: T2-Filtered NMR for the Purity Assay of Functionalized Nanosystems and the Screening of Biofluids. *J. Am. Chem. Soc.* **2009**, *131*, 14222−14224.

(25) Antalek, B. Using Pulsed Gradient Spin Echo NMR for Chemical Mixture Analysis: How to Obtain Optimum Results. *Concepts Nucl. Magn. Reson.* **2002**, *1*, 225−258.

(26) Vega-Vázquez, M.; Cobas, J. C.; Oliveira de Sousa, F. F.; Martin-Pastor, M. A NMR Reverse Diffusion Filter for the Simplification of Spectra of Complex Mixtures and the Study of Drug Receptor Interactions. *Magn. Reson. Chem.* **2011**, *49*, 464−468.

(27) Kim, H.; Wild, J. M.; Allen, P. S. Strategy for the Spectral Filtering of Myo-Inositol and Other Strongly Coupled Spins. *Magn. Reson. Med.* **2004**, *51*, 263−272.

(28) Manjunatha-Reddy, G. N.; Guro-Row, T. N.; Suryaprakash, N. Discerning the Degenerate Transitions of Scalar Coupled 1H NMR Spectra: Correlation and Resolved Techniques at Higher Quantum. *J. Magn. Reson.* **2009**, *196*, 119−126.

(29) Manjunatha-Reddy, G. N.; Caldarelli, S. Improved Excitation Uniformity in Multiple Quantum NMR Experiments of Mixtures. *Magn. Reson. Chem.* **2013**, *51*, 240−244.

(30) Lack, J. S.; Spielman, D.; Adalsteinsson, E.; Kurhanewicz, J.; Terris, D. J.; Vigneron, D. B. In Vivo Lactate Editing with Simultaneous Detection of Choline, Creatine, NAA, and Lipid Singlets at 1.5 T Using PRESS Excitation with Applications to the Study of Brain and Head and Neck Tumors. *J. Magn. Reson.* **1998**, *133*, 243−254.

(31) Snyder, J.; Hanstock, C. C.; Wilman, A. H. Spectral Editing of Weakly Coupled Spins Using Variable Flip Angles in PRESS Constant

Echo Time Difference Spectroscopy: Application to GABA. *J. Magn. Reson.* **2009**, *200*, 245−250.
(32) Basilio, N.; García-Río, L.; Martín-Pastor, M. Counterion Binding in Solutions of *p*-Sulfonatocalix[4]arene. *J. Phys. Chem. B* **2010**, *114*, 7201−7206.
(33) Lago, C.; Nilsson, M.; Valente, A.; Bonini, M.; Soderman, O. NMR Diffusometry and Conductometry Study of the Host−guest Association between *β*-Cyclodextrin and Dodecane 1,12-Bis-(trimethylammonium bromide). *J Colloid Interface Sci.* **2006**, *300*, 782−787.
(34) Gonzalez-Clemente, C.; Luengo, J. M.; Rodríguez-Aparicio, L. B.; Ferrero, M. A.; Reglero, A. High Production of Polysialic Acid [Neu5Ac alpha(2,8)-Neu5Ac alpha(2−9)]n by *Escherichia coli* K92 Grown in a Chemically Defined Medium. Regulation of Temperature. *Biol. Chem. Hoppe Seyler.* **1990**, *371*, 1101−1106.
(35) Thrippleton, M. J.; Keeler, J. Elimination of Zero-Quantum Interference in Two-Dimensional NMR Spectra. *Angew. Chem., Int. Ed.* **2003**, *42*, 3938−3941.
(36) Lewis, I. A.; Schommer, S. C.; Hodis, B.; Robb, K. A.; Tonelli, M.; Westler, W. M.; Sussman, M. R.; Markley, J. L. Method for Determining Molar Concentrations of Metabolites in Complex Solutions from Two-Dimensional 1H−13C NMR Spectra. *Anal. Chem.* **2007**, *79*, 9385−9390.
(37) Stott, K.; Stonehouse, J.; Keeler, J.; Hwang, T.-L.; Shaka, A. J. Excitation Sculpting in High-Resolution Nuclear Magnetic Resonance Spectroscopy: Application to Selective NOE Experiments. *J. Am. Chem. Soc.* **1995**, *117*, 4199−4200.
(38) Sheppard, D.; Sprangers, R.; Tugarinov, V. Experimental Approaches for NMR Studies of Side-Chain Dynamics in High-Molecular-Weight Proteins. *Progr. Nucl. Magn. Spectrosc.* **2010**, *56*, 1−45.

that can be further taken up by the host and thus appear in plasma and urine.[30]

Despite the metabolism of main GTE components being fairly well understood, the in vivo bioactivity of specific GTE catechins (free and/or conjugated) are largely unknown.[26] A number of in vitro studies have related specific catechins and various metabolic effects relating to inflammation,[31] nitric oxide production,[32] adipocyte proliferation,[33,34] lipogenic activity,[35] altered nutrient absorption,[36,37] and thermogenic properties.[38] It has also already been shown that certain catechins may be more potent at inducing metabolic effects in vitro, specifically those catechins that possess a gallate ester.[31,39] It is important to highlight that the concentrations of catechins are approximately 5−50 times lower in human plasma than concentrations usually used in vitro.[39−42] In addition, in vitro studies predominantly have used the parent compounds found in GTE and free catechins, despite catechins predominantly being in the conjugated form in vivo.[26]

Exploring the bioactivity of GTE catechins in vivo may be an alternative approach to in vitro testing. With this in mind, we have previously shown using a metabolomics approach that 7 days of GTE supplementation intake is capable of inducing changes in a number of endogenous metabolites including but not limited to fat metabolism, TCA cycle intermediates, lipolysis, and phospholipids and sphingolipid at rest and during exercise.[43] However, although our data show that 7 days (chronic) of GTE supplementation is capable of targeting an array of biological processes, the acute effects on endogenous metabolites upon consumption of a single bolus dose of GTE remain unclear. Determining these effects at peak catechin concentrations in blood may give insight into specific potential bioactive catechin candidates, their biological targets, and the mechanisms underlying the acute effects that have been observed on vascular function[7,44] and fat oxidation.[10]

The primary aim of this placebo-controlled intervention study was therefore to assess the concentrations of seven total (conjugated + free) and free GTE catechins and some catechin metabolites (henceforth called catechin/metabolites) in human plasma after a single dose (acute) of GTE or placebo (PLA) and following 1 day (GTE1), 7 days (GTE7) GTE (2 × 559 mg catechins/day, 120 mg caffeine/day), or PLA supplementation using a targeted LC-MRM-MS-based method. This analytic approach ensured comprehensive insights into the plasma concentrations of free catechins in comparison to total catechin concentrations. Second, the study also aimed to assess the acute effects on a large number of endogenous metabolites 2 h after the intake of the single bolus drink of GTE or PLA. This approach allowed for gaining a greater understanding of the metabolic effects that are induced when catechin concentrations peak in the circulation. The endogenous metabolites were measured in plasma using 4-phase metabolite profiling and catecholamine profiling as previously outlined.[43] In addition, the current study also explored correlations between the concentrations of free and total conjugated catechin/metabolites and the most affected endogenous metabolites in order to identify potential bioactive catechins. The current investigation adds to previous published work reporting results on whole body fat oxidation[24] and on the metabolome at baseline and during exercise following GTE7.[43]

MATERIAL AND METHODS

Study Design. The study was designed as a placebo-controlled, double-blind, randomized, parallel study (Figure 1) and has been

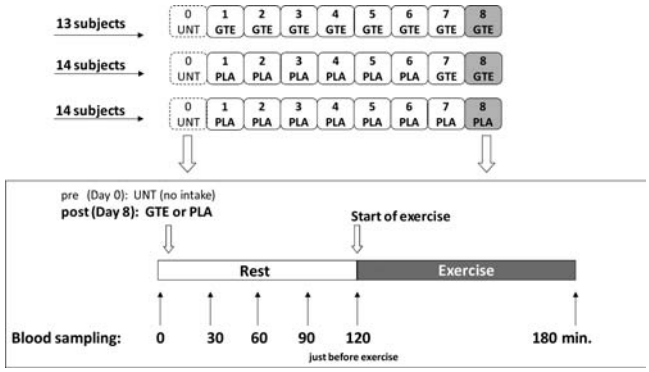

Figure 1. Study design.

described previously.[24,43] In brief, 39 healthy physically active male participants were recruited for the purposes of the study. Participants were randomly allocated into a group who received 7 days of GTE supplementation (GTE7) (n = 13, age 22 ± 5 y, weight 77.6 ± 12.0 kg, BMI 24.3 ± 3.0 kg/m^2), a group who received 6 days of PLA followed by 1 day GTE supplementation (GTE1) (n = 12, age 21 ± 2 y, weight 77.7 ± 9.6 kg, BMI 24.2 ± 1.9 kg/m^2), or a groups who received only PLA for 7 days (PLA) (n = 14, age 22 ± 8 y, weight 78.8 ± 10.2 kg, BMI 24.7 ± 2.7 kg/m^2). The study was approved by the University of Birmingham Ethics Committee. Subjects visited the Human Performance Lab on two separate occasions, namely, pre (Day 0, D0) and post (Day 8, D8) supplementation, following a 10 h overnight fast and having refrained from caffeine, alcohol, and physical activity for 24 h. Each participant received a controlled diet that was consumed 24 h prior to both visiting occasions. On D0 and D8, respectively, an initial 5-mL fasted blood sample was taken at t = 0 min (baseline). Participants then rested in a seated position for 2 h with a blood sample taken at t = 30, 60, 90, and 120 min. Following this, each participant performed a 1-h exercise session on a cycle ergometer at a moderate intensity (50% Wmax), with blood samples collected throughout (t = 140, 150, 160, 180 min). The D0 and D8 trials were identical apart from the ingestion of a single bolus of either GTE (559 mg catechins, 120 mg caffeine), for those who had received GTE7 or GTE1, or PLA following the fasted blood sample (t = 0 min) on D8. Subjects began consuming the supplements on the day following the D0 trial. The supplements were provided in the form of a 330-mL drink. Participants were instructed to consume two drinks per day, 1 h prior to breakfast and another 1 h prior to dinner. The GTE (Taiyo International, Japan) provided a total catechin concentration of 559 mg and 120 mg of caffeine per drink. A breakdown of the composition of GTE and PLA drinks is shown in Table 1.

The current investigation adds to previous published work reporting results on whole body fat oxidation[24] and on the metabolome.[24,43] It first assessed the concentrations of GTE catechin/metabolites across rest (t = 0−120 min) and exercise (t = 120−180 min) on D8 only, which was not established in our previous work.[43] Secondly, it assessed the acute effects of GTE on various metabolites at rest following the final single bolus of GTE or PLA on D8 (t = 0−120 min), as opposed to baseline (t = 0) and during exercise (t = 120−180 min) following GTE7 or PLA, as reported previously.[24,43]

Sample Collection. Each blood sample was collected in chilled EDTA-containing tubes (Becton Dickinson) and stored on ice. Subsequently, plasma was separated by centrifugation (1500g, 10 min, 4 °C), aliquoted in 1-mL samples, and stored at −80 °C for later analysis.

Plasma Analysis of Polyphenols. In the present study, the concentrations of catechin/metabolites collected through the 180-min experiment trial were measured with and without prior enzymatic deconjugation of glucuronides and suphates. This yielded the concentrations of total (free + glucuronides + sulphates) and free (polyphenols not conjugated to glucuronides and sulphates) catechin/metabolites. To determine the total concentrations of specific polyphenols, the polyphenols were deconjugated by β-D-glucuroni-

Table 1. Composition of GTE

	treatment[a]	GTE	PLA
mg/330-mL can	caffeine	120.4	10
	GC	55.1	0
	EGC	181.1	0
	C	11.9	0
	EC	47	0
	EGCG	207.5	0
	GCG	31	0
	ECG	25.6	0
	CG	0	0
total mg/330-mL can	catechins	559.2	0
	caffeine	120.4	10
total mg/day	catechins	1118.4	0
	caffeine	240.8	20

[a]GC, gallocatechin; EGC, epigallocatechin; C, catechin; EC, epicatechin; EGCG, epigallocatechin gallate; GCG, gallocatechingallate; ECG, epicatechingallate; CG, catechingallate.

dase. For this, 200 μL of EDTA plasma, 20 μL of stabilizer solution (10% ascorbic acid containing 0.1% EDTA), 20 μL of 1.5 mol L^{-1} sodium acetate (NaOAc, pH 4.8), and 10 μL of β-glucuronidase (50,000 U L^{-1} in acetate buffer) were mixed and incubated at 37 °C for 45 min. To measure the concentrations of nondeconjugated (free) polyphenols, only 200 μL EDTA plasma, 20 μL of stabilizer solution (10% ascorbic acid containing 0.1% EDTA) and 20 μL of 1.5 mol L^{-1} sodium acetate (NaOAc, pH 4.8) were mixed.

Then 40 μL of internal standard ((±)-taxifolin, TXF, 250 ng L^{-1} in methanol/water, 1:1), 300 μL of water, 10 μL of 2 M HCl, and 1 mL of ethyl acetate (EtOAc) were added, vortexed for 30 s, and centrifuged at 3000*g* for 10 min. The EtOAc top layer was transferred to a clean screw-capped glass tube. The extraction with EtOAc was repeated twice. Ten microliters of 0.4% ascorbic acid was added to the combined EtOAc fractions and dried under N_2 at room temperature. The residue was dissolved in 100 μL of methanol, vortexed, and sonicated for 10 min. Then 100 μL of Milli-Q water was added. The samples were vortexed, sonicated, and centrifuged at 17000*g* for 10 min. From the supernatant, 5 μL was injected into the high-performance liquid chromatography multiple-reaction monitoring mass spectrometer (HPLC-MRM-MS) system (Agilent 6410 mass spectrometer equipped with an Agilent 1200SL HPLC (Agilent Technologies, Amstelveen, The Netherlands) and an HTC PAL autosampler (CTC Analytics, Zwingen, Switzerland). The phenolic compounds were separated on a XBridge Phenyl plus guard column [2.1 mm × 150 mm, 3.5 μm] (Waters, Milford, US) at a flow rate of 0.2 mL/min and at a column temperature of 55 °C using solvent A (0.1% (v/v) acetic acid in water) and solvent B (0.1% (v/v) acetic acid in acetonitrile) programmed in the following gradient: 0−3 min 2% B, until 3 min 2% B, until 4 min 10% B, until 14 min 20% B, until 29 min 100% B, until 34 min 100% B, until 35 min 2% B, until 45 min 2% B.

The HPLC system was coupled to a triple-quadrupole mass spectrometer (Agilent 6410). The separated phenolic compounds were detected in the API negative multiple-reaction monitoring mode. The capillary voltage was 4 kV, the gas temperature was kept at 350 °C, the gas flow was 12 L/min and the nebulizer pressure was 30 psi. The MS settings of the phenolic compounds are shown in Supporting Information (Supplementary Table S1).

Samples were analyzed batch-wise and controlled by two quality control samples (QCs) per sample batch. The QCs were prepared by spiking commercial human plasma with 11 phenolic standards until a final concentration of 100 μg L^{-1}. The standards included (−)-catechin (C), (−)-epicatechin (EC), (−)-gallocatechin (GC), (−)-epigallocatechin (EGC), (−)-epicatechin gallate (ECG), (−)-epigallocatechin gallate (EGCG), 3/4-*O*-methylgallic acid (3/4-OMGA), 5-(3′,4′-dihydroxyphenyl)-γ-valerolactone (3,4-diOH-VL), and 5-(3′-methoxy-4′-hydroxyphenyl)-γ-valerolactone (3MeO-4-OH-VL). These phenolic compounds were quantified in plasma by means of 10-point calibration curves using external standards.

Under the currently described conditions, 3-*O*-methylgallic acid (3-OMGA) could not be fully separated from 4-*O*-methylgallic acid (4-OMGA). Therefore, combined values for 3/4-OMGA are reported. Similarly, combined ECG values are reported for ECG and CG. The peak areas of the internal standards as well as the target compounds were determined using Agilent's MassHunter Quantitative Analysis software (version B.03.02, Agilent Technologies, Santa Clara, CA).

Metabolite Profiling of Plasma. Four-phase metabolite profiling was performed at Metanomics Health GmbH, Berlin, Germany. Due to limited resources, only the plasma samples collected on Day 8 at t = 0 and 120 min from subjects following GTE7 and PLA supplementation were analyzed. This approach included the semi-quantitative broad metabolite profiling (GC−MS and LC−MS/MS) of the lipid and polar phases of plasma. In addition, 10 catecholamines and their related metabolites were measured by online SPE-LC−MS/MS. The methods have been published elsewhere.[43] In total, 238 mostly endogenous metabolites were detected including 163 known metabolites and 75 metabolites that were not chemically identified with sufficient certainty (i.e., thus excluded in the present study).

Data and Statistical Analysis. To assess the acute effect on the endogenous metabolites after a single bolus intake of GTE or PLA, the differences between the metabolite concentrations measured at t = 120 min and t = 0 min (Δ(T120−0)) on D8 were calculated for each of the 163 endogenous metabolites to exclude the baseline (chronic) effects due to 7-day GTE supplementation. Multivariate analysis including PCA [principal component analysis] and PLS-DA [partial least-squares/projection to latent structures-discriminant analysis] was performed using SIMCA P+ version 12 software (Umetrics, Umea, Sweden). Data were scaled to unit variance, which introduces a common scale for all metabolites independent of their absolute amount of variance. The unsupervised PCA was used to detect outliers, trends, patterns, and groupings among samples and variables. Two subjects were identified as outliers and thus excluded from further analysis. The supervised projection method PLS-DA was used to display the maximum covariance of data with a defined Y variable (class, categorical) in the data set. For this the data set was grouped in two classes (GTE and PLA). To ensure validation of the PLS-DA the cross-validated cumulative Q^2 value was used as a measure of the predictive value. A 7-fold cross-validation was performed by the leave-one-subject-out method to ensure that cross-validation was not inappropriately facilitated by the presence of related samples. A Q^2 value of 1 indicates maximum predictive power, whereas Q^2 values close to or below 0 indicate a lack of predictive power. In addition, 999 models with randomly permutated data were calculated to determine the significance of the model and to avoid overfitting. The significance was calculated by dividing the number of random models with Q^2 values larger than the actual model to the total number of random models. Metabolites that significantly contributed to the discrimination of the GTE and PLA groups were selected on the basis of their importance. Box plots and t tests of the most important metabolites were calculated for additional verification of the PLS-DA results.

To identify potential bioactive components of GTE catechins/metabolites, a correlation matrix (Pearson) was calculated correlating the $\Delta(t_{120} - t_0)$ values of the catechin/metabolties and those endogenous metabolites that were affected by GTE. To make sure that the dependency of the overall pattern was above noise level, the overall strength of the correlations was checked by permutation tests.

RESULTS

Catechin Kinetics in Plasma. The total (conjugated + free) and free concentrations of 7 catechins, 3/4-OMGA, and 2 valerolactones were measured in human plasma from subjects in the GTE7, GTE1, and PLA groups following ingestion of a single bolus drink of GTE or PLA on D8. Their average concentrations are plotted in Figure 2, and their maximum concentrations (c_{max}) as well as the area under the curve values

between t = 0 min and t = 180 min (AUC(t_0−t_{180})) are shown in Table 2.

Relative to the other catechins, EGCG was the most abundant catechin in the GTE supplement (37.1% of total catechins) and in plasma (35.0% of AUC(t_0−t_{180})$_{total}$ (GTE7), 36.1% (GTE1). In contrast, ECG (4.6%) and EC (8.4%) were low abundant in the GTE supplement but were present at relatively high concentrations in plasma, when compared to the other catechins (ECG/GC: 21.9% (GTE7) and 16.3% (GTE1); EC: 13.71% (GTE7) and 15.61% (GTE1)). In comparison, the concentration of C (2.1%) and GC (9.85%) were also at low concentrations in the GTE supplement, yet only 0.41% (GTE7) and 0.46% (GTE1) of C and 0.12% (GTE7) and 0.14 (GTE1) % of GC relative to total catechins were detected in plasma. Less pronounced differences between the relative concentrations in the GTE supplement and in plasma were found for GCG and EGC. The ratios of the concentrations in plasma to those in the GTE supplement relative to total catechins, respectively, followed the order ECG/CG > EC > GCG > EGCG > EGC > C > GC.

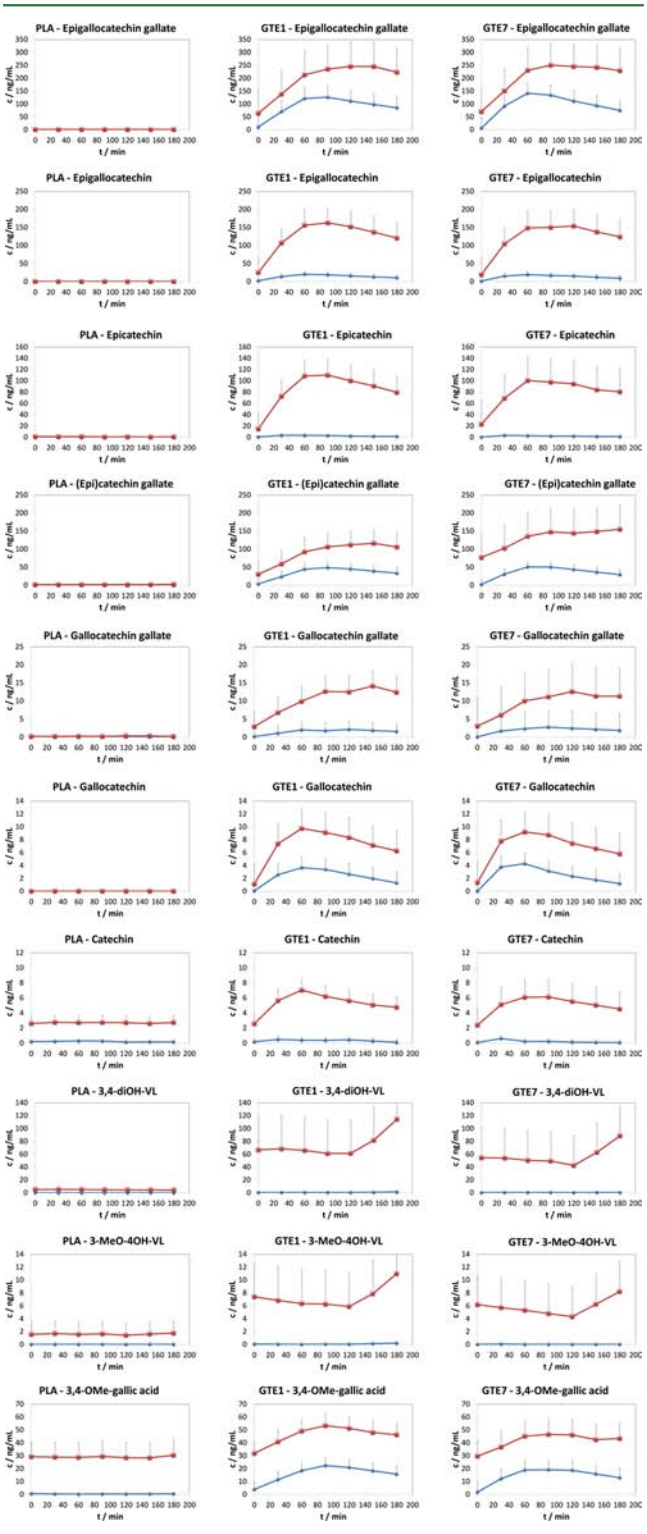

Figure 2. Individual catechin/metabolite concentrations and standard deviations in plasma at rest (0−120 min) and after exercise (180 min) following GTE7, GTE1, and PLA supplementation. The red and blue curves indicate the total (conjugated + free) and free concentrations, respectively.

In total 32% (GTE7) and 30% (GTE1) (based on c_{max}) of all catechins were present in the free form, meaning that the majority of catechins circulate in plasma as glucuronates and sulphates (Table 2, Figure 2). Free catechins were mostly found in those that possessed a gallic acid moiety, including EGCG, ECG/CG, as well as GC and GCG contributing 57%, 33%, 47%, and 22% to their total concentrations in GTE7, respectively. In comparison, EGC, EC, and C mainly appeared in the conjugated form contributing 88%, 97%, and 90% to their total concentrations in GTE7, respectively.

Although our data did not allow for determining the bioavailability because of incomplete kinetic curves (no return to baseline), we estimated the concentrations of total catechins with respect to their concentrations in the GTE. For this, we calculated the sum of the plasma concentrations of all catechins that were measured within 3 h excluding the baseline levels (t = 0 min). Assuming a total blood volume of 5 L for a typical male and no differences in catechin concentrations between plasma and blood, only 0.47 ± 0.2% (GTE7) and 0.49 ± 0.17% (GTE1) of the total amount of ingested catechins (559 mg) were on the average retrievable in plasma within 3 h after GTE consumption.

No significant differences in free or conjugated catechin concentrations were observed between GTE7 and GTE1 following the intake of the single bolus drink on D8. There was also no significant difference in baseline values between GTE7 and GTE1, except for the higher concentration of ECG after 7-day GTE consumption when compared to 1-day GTE consumption (GTE7: 77 ± 56 ng/mL; GTE1: 30 ± 19 ng/mL; p = 0.016) .

The average t_{max} for the catechins was 60−120 min following ingestion, which coincided with the beginning of the exercise bout (120 min). The exercise bout did not appear to alter the catechin kinetics in the plasma, as represented in the final 60 min of the trial (120−180 min) (Figure 2).

The two gut microbial-derived valerolactones, 3,4-diOH-VL and 3-MeO-4-OH-VL, were present at baseline and only increased after 120 min following GTE supplementation on D8. They were only present in the conjugated form. In general, higher concentrations were observed for 3,4-diOH-VL than for 3-MeO-4-OH-VL. We also observed a large increase in 3/4-OMGA over the course of the trial with t_{max} between 90 and 120 min. Those subjects who ingested PLA also had an elevated 3/4-OMGA concentration throughout the trial, despite the significantly lower total catechin concentrations (Figure 2). Marginally elevated concentrations of 3MeO-4-OH-VL, 3,4-diOH-VL, and C were also observed in those subjects receiving PLA. This may be explained by the consumption of

dx.doi.org/10.1021/jf404872y | J. Agric. Food Chem. 2014, 62, 1198−1208

Table 2. Plasma Kinetics of Catechin/Metabolites on D8 Following Ingestion of a Single Bolus Drink of PLA in the PLA Group and of GTE in the GTE7 and GTE1 Groups. Average Maximum Plasma Concentration (c_{max}, ng/mL) and Area under the Curve (AUC, min ng/mL) Values (t_0–t_{180})

	GTE7				GTE1				PLA			
	c_{max}		AUC		c_{max}		AUC		c_{max}		AUC	
	free	total	free	total	free	total	free	total	free	total	free	total
						EGCG						
mean	141	250	18368	38060	126	246	17241	36659	0.06	1.1	1.9	131
SD	45	68	951	1611	40	69	896	1684	0.02	0.2	0.5	2
CV%	31.8	27.0	5.2	4.2	31.6	27.9	5.2	4.6	37.8	14.0	25.8	1.8
						EGC						
mean	19	154	2499	22976	20	163	2604	23608	0.04	0.04	3.2	2.0
SD	6	48	117	1018	6	48	126	1032	0.02	0.02	0.5	0.4
CV%	32.0	30.9	4.7	4.4	30.3	29.2	4.8	4.4	46.8	41.5	14.1	21.6
						ECG/CG						
mean	51	155	6796	23845	49	116	6554	16618	0.0	2.2	0.0	310
SD	17	29	365	716	16	32	371	817	0.0	0.2	0.0	3
CV%	33.1	18.8	5.4	3.0	32.5	27.7	5. 7	4.9	0.0	9.2	0.0	0.9
						EC						
mean	3.2	100	346.	14925	3.4	110	424	15876	0.24	1.0	16	143
SD	1.0	27	17	574	1.1	33	22	709	0.07	0.2	2	5
CV%	30.7	26.6	5.0	3.8	33.1	30.0	5.1	4.5	30.8	20.6	9.8	3.3
						C						
mean	0.6	6.1	38	941	0.5	7.0	61	998	0.29	2.75	37	485
SD	0.2	1.3	4	26	0.1	1.4	2	28	0.06	0.07	2	1
CV%	31.9	21.0	10.4	2.8	27.7	20.0	4.0	2.8	20.8	2.5	4.6	0.2
						GC						
mean	4.3	9.2	474	1300	3.7	9.7	446	1362	0.01	0.0	0.17	0.0
SD	1.5	2.6	31	49	1.3	2.9	26	56	0.00	0.0	0.07	0.0
CV%	35.2	28.6	6.6	3.8	34.1	29.3	5.9	4.1	37.8	0.0	40.8	0.0
						GCG						
mean	2.8	12	1748	6796	2.1	14	1906	6554	0.19	0.32	38	0.0
SD	0.9	3	87	365	0.7	4	101	371	0.03	0.07	2	0.0
CV%	32.0	27.7	5.0	5.4	33.0	28	5.3	5. 7	16.8	21.8	4.5	0.0
						3,4-diOH-VL						
mean	0.58	89	70	9908	1.2	114	110	12867	0.02	5.1	1.3	820
SD	0.12	15	2	315	0.3	19	7	406	0.01	0.4	0.1	11
CV	20.2	17.0	3.4	3.2	23.6	16.7	5.9	3.2	29.5	7.8	10.1	1.4
						3MeO-4-OH-VL						
mean	0.21	11	2.5	1007	0.07	8.2	10.5	1271	0.01	1.7	0.20	287
SD	0.07	2	0.5	28	0.02	1.3	1.7	36	0.00	0.1	0.06	2
CV	34.1	15.8	18.7	2.8	36.7	15.4	16.0	2.9	39.3	6.3	30.3	0.7
						3/4-OMGA						
mean	19	47	2757	7606	22	53	3025	8449	0.5	30.3	61	5203
SD	6	6	135	146	6	7	153	175	0.1	0.7	2	10
CV	32.2	13.2	4.9	1.9	28.6	13.8	5.1	2.1	20.2	2.3	3.7	0.2

other polyphenol food sources during the 24 h prior to the trial.[45]

Effects on Endogenous Metabolites Following Acute GTE Intake. Using 4-phase metabolite profiling and targeted analysis of 10 catecholamines, the relative concentrations of a total of 163 known, mostly endogenous metabolites were measured in plasma at baseline (t = 0) and 2 h after the single bolus intake on Day 8 (t = 120 min) under resting conditions. Differences between the concentrations at t = 120 min and t = 0 ($\Delta(t_{120} - t_0)$) were calculated for each metabolite and for each subject in the GTE7 and PLA groups to assess the pure acute effects of the single bolus intake without taking into account any baseline (chronic) effects due to the 7 day GTE supplementation. The multivariate analysis (PLS-DA) identified a significant discrimination between metabolite changes induced by GTE7 and PLA (Q^2 = 0.492 with a significance of 2.2%) (Figure 3). On the basis of the PLS-DA, a total of 27 metabolites were found to be the most important in driving the significant discrimination between GTE7 and PLA (Figure 3, panel D). In addition, t tests were performed on each metabolite resulting in 16 significant ($p < 0.05$) metabolite changes between the GTE7 and PLA groups. They were also found using PLS-DA. The discrepancy in the number of significant metabolite changes between multivariate (27) and univariate (16) statistical analysis may be explained by combined effects only observed in multivariate analysis. The changes of the 16 altered metabolites are visualized using box plots (Figure 4). Significant reductions were observed for hippuric acid and cholesterylesters (C16:0, C18:1, C18:2), while the concentrations of caffeine, salicylic acid, taurine, 3,4-

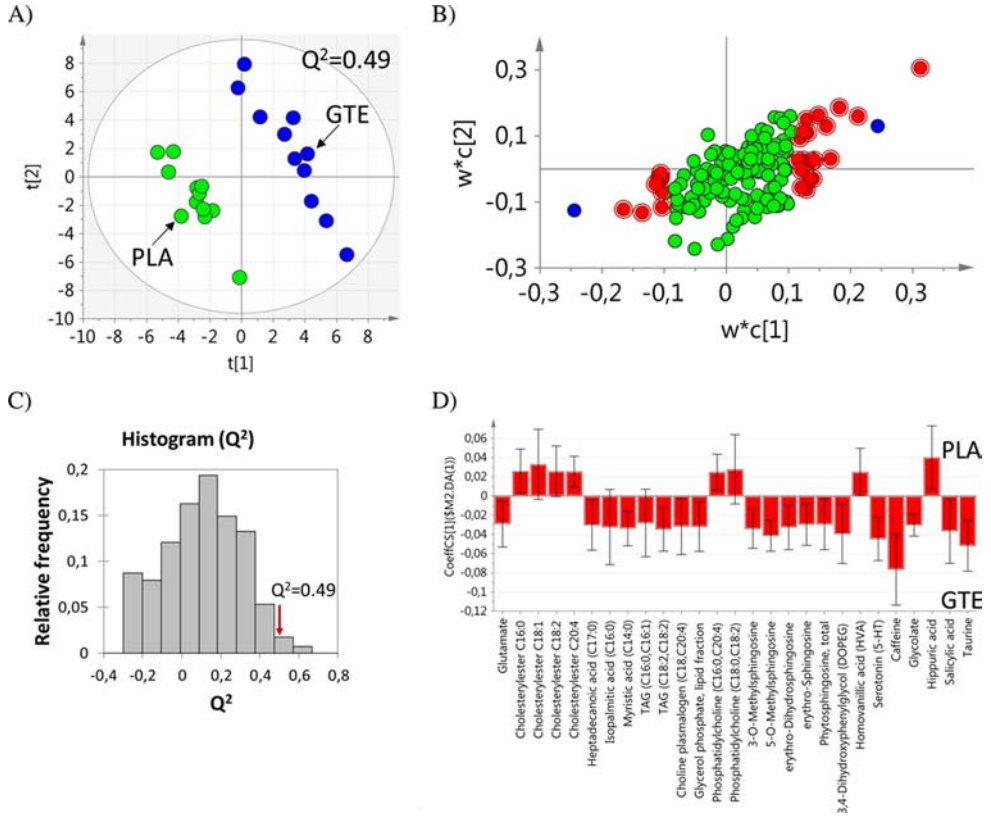

Figure 3. (A) PLS-DA score plot of PC-1PC-2 based on 163 metabolite concentrations and unit-variance scaling. The data represent differences between relative concentrations measured on D8 at time point t = 120 min and t = 0 min. The blue and green circles indicate the GTE7 and PLA treatment groups, respectively. R^2X = 0.184, R^2Y = 0.972, Q^2 = 0.492. (B) Loading plots (w*c) for PC1 and PC2; green/red and blue circles indicate the x- and y-loadings, respectively. (C) Histogram of Q^2-values of 999 models from randomly permuted data. (D) Coefficient plot of PC1 including only the most important variables as selected from loading plot (panel B, red circles).

dihydroxyphenylethylene glycol, serotonin, TAG (C16:0, C16:1), TAG (18:2, C18:2), sphingosines (3-*O*-methylsphingosine, 5-*O*-methylsphingosine, *erythro*-dihydrosphingosine), and fatty acids (C17:0, C14:0) were significantly increased 2 h after the single bolus intake of GTE when compared to PLA.

Correlation between Exogenous and Endogenous Metabolites. To investigate which catechin/metabolite potentially induced an effect on an endogenous metabolite, a Pearson correlation matrix was calculated based on the $\Delta(t_{120} - t_0)$ values of total, free, and conjugated (conj = total − free) catechin/metabolites and the endogenous metabolites that significantly changed after the single bolus GTE intake on D8. Several strong positive ($R > 0.72$, $p < 0.01$) and negative ($R < -0.72$, $p < 0.01$) correlations between the endogenous and exogenous metabolites were observed, which are shown in Figure 5.

DISCUSSION

In this study we found that the ratios of the maximum concentrations in plasma to the concentrations in the GTE supplement relative to the total catechins, respectively, followed the order: ECG/CG > EC > GCG > EGCG > EGC > C > GC. Another key outcome of the present analyses is that EGCG, CG/ECG, GC and GCG in their free form contributed 57%, 33%, 47% and 22% to their total plasma concentrations, respectively, while EGC, EC, and C mainly appeared in the conjugated form. We also observed significant effects on 16 mostly endogenous metabolites 2 h after the intake of a single bolus drink of GTE, when compared to PLA. These included reductions in hippuric acid and cholesterylesters (C16:0, C18:1, C18:2) and increases in caffeine, salicylic acid, taurine, 3,4-dihydroxyphenylethylene glycol, serotonin, TAG (C16:0, C16:1), TAG (18:2, C18:2) and sphingosines (3-*O*-methylsphingosine, 5-*O*-methylsphingosine, *erythro*-dihydrosphingosine) and fatty acids (C17:0, C14:0).

Catechin Kinetics in Plasma. Our results on the catechin/metabolite concentrations in plasma are in agreement with previous studies, while also extending the current literature on GTE bioavailability through the comprehensive investigation of seven catechins, 3/4-OMGA, and two gut microbial-derived metabolites. We showed that GTE7 and GTE1 resulted in similar transient increases in both total and free catechins when compared to PLA over the course of a 180-min trial (Figure 2). As previously shown,[15,25,46] t_{max} was observed between 60 and 120 min following a single bolus of GTE on the final day of supplementation (Day 8), which was similar for GTE7 and GTE1 (Figure 2). This illustrates that catechins in general did not accumulate in the circulation following GTE7, despite the longer supplementation duration. In agreement, Chow et al.[15] have shown that 4 weeks of 400 mg/day EGCG or polyphenol E did not alter the AUC for free or total EGCG, EGC, and EC. Also in this study, the ratio of free to conjugated catechins were virtually identical in the GTE1 and GTE7 groups, indicating that 7 days of supplementation did not affect the catechin metabolism by, for instance, inducing metabolizing enzymes that would result in a higher percentage of conjugated catechins with respect to free catechins. At baseline, only ECG was increased after 7-day GTE supplementation when compared to

dx.doi.org/10.1021/jf404872y | J. Agric. Food Chem. 2014, 62, 1198−1208

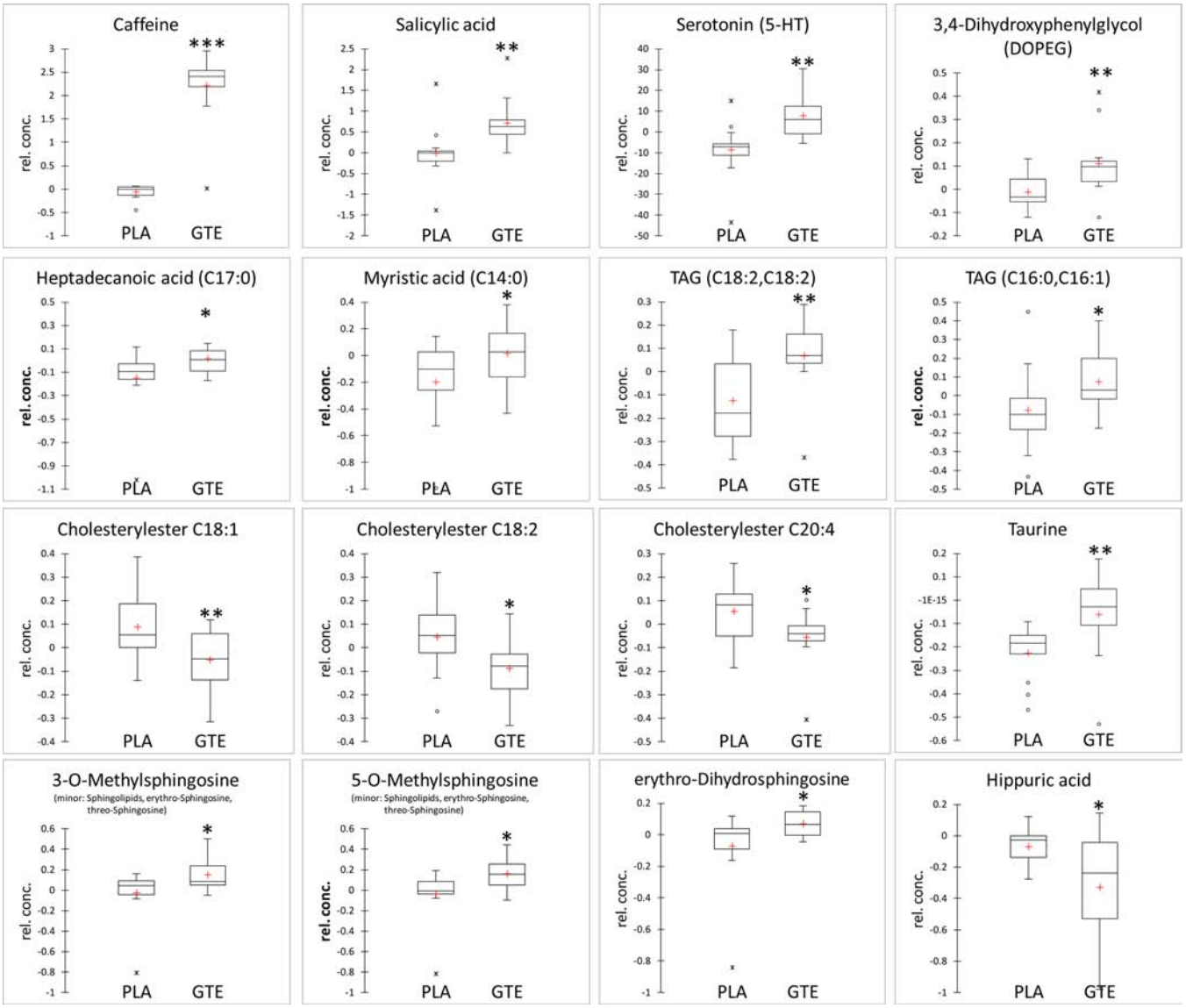

Figure 4. Box plots of the most important metabolites that contribute to the PLS-DA discrimination between the GTE7 and PLA supplementation. (* $p < 0.05$, ** $p < 0.01$, *** $p < 0.001$). The boxplots were calculated on the differences between relative concentrations measured on D8 at time point $t = 120$ min and $t = 0$ min.

1-day GTE supplementation, which is in line with a recent study also showing high levels of ECG in fasting plasma after chronic consumption.[16] We estimated that only 0.48% of total ingested catechins reached the circulation within 3 h after tea consumption suggesting poor bioavailability, which has also been proposed by others.[28] EGCG, as previously shown,[28] had the highest c_{max} when compared to the other catechins. Interestingly, C and GC were found at lower concentrations in the circulation, while ECG/CG and EC were present at higher concentrations in plasma when compared to their relative concentrations in the GTE supplement. The relatively better absorbance of ECG is in agreement with a recent study.[16] In contrast, a higher relative bioavailability of EGC compared with that of EGCG as shown in other studies[25,47,48] could not be confirmed in this study. However, it is well-known that variations in the plasma concentrations of the individual catechins depend on the dose, the composition of the green tea, the food format, and the study population.[14,48] Further, catechins were also converted by gut microbiota to 3,4-diOH-VL and 3MeO-4-OH-VL in the colon, with 3,4-diOH-VL being the more abundant metabolite. Both microbial metabolites appeared later in the plasma when compared to catechins with an onset at 120 min. These results are in agreement with the previous findings.[49,50]

While the bioconversion of catechins to their conjugated metabolites in vivo is well understood, fewer studies[15,16,25,51,52] have assessed the plasma concentrations of free catechins that may display different biological activity when compared to their glucuronides and sulphates.[53] The free catechins are those that escape phase II metabolism and appear in the circulation.[28] We found that 68−70% of all catechins appeared in the conjugated form. In agreement with other studies,[15,25,54,55] the catechins C, EGC, and EC were predominantly in the conjugated form, contributing 90%, 88%, and 97% to total catechin concentration, respectively. In contrast, the gallated catechins EGCG, ECG/CG, GC, and GCG underwent less conjugation, possibly because of their higher polarity and/or steric hindrance. Other studies[16,25,28] have found larger percentages of free catechins

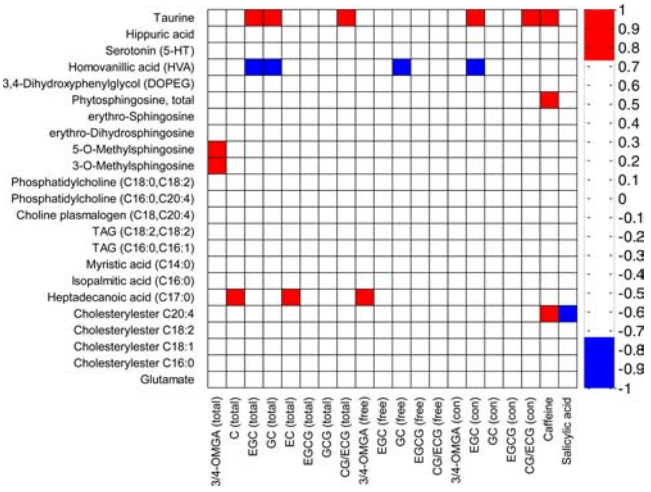

Figure 5. Pearson correlation matrix of total, free, and conjugated (conj = total − free) catechin/metabolites and endogenous metabolites that were most significantly affected by the consumption of a single bolus drink of GTE on D8. Only correlations $R > 0.72$ or $R < -0.72$ corresponding to $p < 0.01$ are displayed (red and blue colors for positive and negative values, respectively).

[ref 28: EGCG (100%); ref 16: EGCG (100%), EGC (30%), and ECG (75%); ref 25: EGCG (77%), EGC (31%), and EC (21%)] when compared to our study [EGCG (57%) ECG: (33%), EGC (12%), EC (3%)]. In contrast, Kotani et al.[51] have found GCG to be mostly (91%) present in the conjugated form, while we found GC and GCG to be present mostly in the free (53% and 78%, respectively) form. Further investigations are needed to explain these inconsistent results.

Metabolite Changes Following Acute GTE Intake. In addition to the metabolism of GTE catechins already being well understood, we explored the effects on the endogenous metabolism at a time point when the catechin/metabolites were at their maximum concentrations in plasma. Significant changes in 16 metabolites were found when comparing the concentrations of 163 metabolites 2 h after the intake of a single bolus of GTE or PLA (Figures 3 and 4).

As expected, caffeine was increased, because the GTE contained 120 mg of caffeine. Caffeine has been shown to peak 1 h following intake.[18] Furthermore, salicylic acid was found to be significantly increased in plasma following the single bolus intake of GTE, which has not been documented to date. Salicylic acid has been identified in green tea infusion[56] and thus may be considered as exogenous metabolite. Salicylic acid also is a hydrolysis product of acetyl salicylic acid (ASA), otherwise known as aspirin. The metabolic effects of salicylic acid in vivo are largely unknown. Salicylic acid is capable of yielding hydrogen peroxide, which in vitro has been shown to activate numerous signaling molecules that are associated with mitochondrial biogenesis, namely, sirtuin 1 (SIRT1) and proliferator-activated receptor-gamma coactivator-1-α (PGC1-α).[57] The up-regulation of these signaling pathways in the skeletal muscle over time (through pharmaceutical, exercise, and nutritional interventions[58,59]) causes mitochondrial biogenesis, fiber type transformation, and greater capacity to oxidize fat.[60] Similarly, chronic GTE has also been suggested to regulate the signaling pathways that regulate mitochondrial content and substrate metabolism in vitro[61] and in animals at rest[62] and in combination with endurance exercise training.[63] In contrast, Deschamps et al.[64] have shown that a single dose of salicylic acid fed to mice at high concentrations led to significant reductions in long chain fatty acid oxidation. The authors also showed that hepatic triglyceride concentrations was significantly increased following salicylic acid, which may provide indirect evidence for the elevated TAG concentration (TAG C16:0, C16:1; TAG C18:2, C18:2) observed in the current study (Figure 4).

Interestingly, we found significant reductions in several cholesterylesters (C16:0, C18:1, C18:2, 20:4) 2 h after the GTE intake, which is in line with the hypocholesterolemic effect of tea catechins suggested earlier based on a study in rats.[65] A more in-depth investigation has attributed the hypocholesterolemic effect to the inhibition of intestinal cholesterol absorption and specifically to gallated tea catechins.[39] Further evidence has been provided by an in vitro study showing that gallated catechins are potent and selective inhibitors of rat squalene epoxidase, a rate-limiting enzyme of cholesterol biogenesis.[66] It has also been shown that EGCG but no other green tea catechins reduced the activity of an ileal transporter, namely, apical sodium-dependent bile acid transporter (ASBT), which is responsible for reabsorption of bile acids.[67] Alternatively or in addition, a decrease in intestinal lipid absorption by GTE catchins, especially EGCG,[68] may be due to the inhibition of pancreatic phospholipase A_2, an important enzyme interfering with the intestinal hydrolysis of phosphaditylcholines, which has been demonstrated in an animal study.[69] Interestingly, two phosphatidylcholines (C16:0, C20:4; C18:2, C18:2) were also reduced in the current study upon the consumption of a single bolus GTE drink. The acute effects on the cholesterylesters and phosphaditylcholines found in the current study are most likely transient, because these effects were not retained after 7-day supplementation.[43] However, it remains unclear whether the cholesterol lowering effects observed after long-term supplementation of green tea[70] may at least partially be explained by reduced lipid absorption.

In the current study we also observed that the intake of a single bolus GTE induced a significant increase in taurine when compared to PLA. Taurine has important metabolic roles in health and disease, for example, leading to improved insulin sensitivity,[71] cholesterol metabolism,[72] and fat metabolism.[73] Yet, taurine adopts many diverse biological functions such as conjugation of bile acids, membrane stabilization, osmoregulation, and neurotransmission, and therefore the implication of our finding is unclear. Similarly, serotonin is a polyfunctional signaling molecule acting, inter alia, as neurotransmitter and vasoconstrictor. The increase in serotonin found in the current study may thus entail effects on blood pressure, mood, appetite, and sleep. Remarkably, several sphingosines were increased upon acute GTE intake. Sphingosine can be produced from ceramides and further phosphorylated to potent signaling lipids. Although the functions of individual spingosines are largely unknown, it has already been suggested that alterations in sphingolipid biology play a pivotal role in regulation of vascular function.[74]

Identification of Potential Bioactive GTE Catechin/Metabolites. To date the bioactivity of specific catechins in vivo has lacked research. Furthermore, while in vitro evidence provides insight into the bioactivity of specific catechins in various cell lines, many investigations have used supra-physiological concentrations of catechins in the free form (5−50 times greater than in human plasma). These studies therefore provide an unrealistic physiological environment to what would be seen in human plasma, let alone in human

dx.doi.org/10.1021/jf404872y | J. Agric. Food Chem. 2014, 62, 1198−1208

cells.[75] Therefore in an attempt to provide new insights into the bioactivity of specific catechins in humans, we examined the in vivo association between the transient increases in GTE catechins and those significant metabolite changes (Figure 5). Besides a few consistent correlations, namely, the correlations between total and conjugated EGC and ECG/CG and taurine, only scattered correlations and no clear patterns were observed, suggesting that there is no straightforward relation between exogenous and endogenous metabolites in plasma. Interestingly, a clear superiority of EGCG or gallated catechins did not become apparent, although EGCG has been identified as the most pharmacologically active catechin[76] and gallated catechins are considered to be more potent at inducing the metabolic effects in vitro.[31,39] Considering that metabolite concentrations in plasma represent the spillover of many effects occurring in diverse tissues and cells, clearer relationships may be found in specific cells and tissues where catechin/metabolites exert their bioactivity. Another limitation of the correlation analysis is that associations do not necessarily imply causations. Nevertheless, the current study highlights the need for future studies to examine the metabolic effects of specific catechins, especially in vivo or alternatively in vitro using physiological doses and forms of catechins found in vivo.

In conclusion, this study confirms and extends our current knowledge regarding the transient increases in 10 catechin/metabolites in plasma following acute GTE intake. In particular, the concentrations provided in both the free and total (conjugated and free) form delivered deeper insight into the different species circulating in blood. This information can still be refined by identifying the conjugation pattern of the catechin/metabolites similar to a study by Stalmach et al., who have already quantified 16 different methylated, sulphated, and glucuronidated conjugates of (epi)catechin and (epi)-gallocatechins.[52] This list still is incomplete, in particular with respect to gut microbial metabolites. This warrants further investigations including study designs with longer sampling periods and using sensitive high-resolution mass spectrometers that are capable of covering in an untargeted manner a wider range of the catechin/metabolites.

Furthermore, the current study demonstrates that a single bolus dose of GTE intake induced significant acute effects on diverse endogenous metabolites when compared to PLA. These acute effects differed from the metabolic effects observed after 7-day supplementation of GTE,[43] suggesting that the acute metabolic effects may be subject to different mechanisms or that long-term GTE supplementation is required for progressive regulation of various proteins and enzymes at certain sites in the body leading to systemic shifts on the endogenous metabolites. The diversity of these metabolites possibly indicates that GTE catechin/metabolites target different pathways. The changes in cholesterylesters and phosphatidylcholines may point toward changes in lipid metabolism. Other changes, such as those in sphingosines, sertonine, and salicylic acid may be related to vascular function. Overall, however, there is still too little known about the importance of specific metabolite changes in plasma to physiology. In addition, as many of the observed effects were subtle, the present results should be confirmed in further studies, as an initial step toward building systematic hypotheses on structure-physiology relationships.

■ ASSOCIATED CONTENT

Supporting Information

Supplementary table. This material is available free of charge via the Internet at http://pubs.acs.org.

■ AUTHOR INFORMATION

Corresponding Author

*Tel: +31 10 460 5987. Fax: +31 10 460 5310. E-mail: doris.jacobs@unilever.com.

Author Contributions

A.B.H., R.K.R., T.M., D.M.J., and A.E.J. conceived and designed experiments; A.B.H. and R.K.R. performed the experiments; D.M.J. and K.M.-J.-T analyzed the data; D.M.J. and A.H. wrote the paper; A.E.J., D.J.M., and S.L. provided significant advice.

Notes

The authors declare no competing financial interest.

■ ACKNOWLEDGMENTS

We thank Metanomics-Health GmbH for analyzing the samples. In addition, we thank Christian Grün for implementing the LC-MRM-MS method.

■ REFERENCES

(1) Rietveld, A.; Wiseman, S. Antioxidant effects of tea: evidence from human clinical trials. *J. Nutr.* **2003**, *133* (10), 3285S−3292S.

(2) Thielecke, F.; Boschmann, M. The potential role of green tea catechins in the prevention of the metabolic syndrome−a review. *Phytochemistry* **2009**, *70* (1), 11−24.

(3) Kovacs, E. M.; Mela, D. J. Metabolically active functional food ingredients for weight control. *Obes. Rev.* **2006**, *7* (1), 59−78.

(4) Westerterp-Plantenga, M. S. Green tea catechins, caffeine and body-weight regulation. *Physiol. Behav.* **2010**, *100* (1), 42−46.

(5) Sae-tan, S.; Grove, K. A.; Lambert, J. D. Weight control and prevention of metabolic syndrome by green tea. *Pharmacol. Res.* **2011**, *64* (2), 146−154.

(6) Bohn, S. K.; Ward, N. C.; Hodgson, J. M.; Croft, K. D. Effects of tea and coffee on cardiovascular disease risk. *Food Funct.* **2012**, *3* (6), 575−591.

(7) Moore, R. J.; Jackson, K. G.; Minihane, A. M. Green tea (*Camellia sinensis*) catechins and vascular function. *Br. J. Nutr.* **2009**, *102* (12), 1790−1802.

(8) Wang, H.; Wen, Y.; Du, Y.; Yan, X.; Guo, H.; Rycroft, J. A.; Boon, N.; Kovacs, E. M.; Mela, D. J. Effects of catechin enriched green tea on body composition. *Obesity* **2010**, *18* (4), 773−779.

(9) Hursel, R.; Viechtbauer, W.; Dulloo, A. G.; Tremblay, A.; Tappy, L.; Rumpler, W.; Westerterp-Plantenga, M. S. The effects of catechin rich teas and caffeine on energy expenditure and fat oxidation: a meta-analysis. *Obes. Rev.* **2011**, *12* (7), e573−e581.

(10) Dulloo, A. G.; Duret, C.; Rohrer, D.; Girardier, L.; Mensi, N.; Fathi, M.; Chantre, P.; Vandermander, J. Efficacy of a green tea extract rich in catechin polyphenols and caffeine in increasing 24-h energy expenditure and fat oxidation in humans. *Am. J. Clin. Nutr.* **1999**, *70* (6), 1040−1045.

(11) Venables, M. C.; Hulston, C. J.; Cox, H. R.; Jeukendrup, A. E. Green tea extract ingestion, fat oxidation, and glucose tolerance in healthy humans. *Am. J. Clin. Nutr.* **2008**, *87* (3), 778−784.

(12) Hodgson, A. B.; Randell, R. K.; Jeukendrup, A. E. The effect of green tea extract on fat oxidation at rest and during exercise: evidence of efficacy and proposed mechanisms. *Adv. Nutr.* **2013**, *4* (2), 129−140.

(13) Moon, H. S.; Lee, H. G.; Choi, Y. J.; Kim, T. G.; Cho, C. S. Proposed mechanisms of (−)-epigallocatechin-3-gallate for anti-obesity. *Chem. Biol. Interact.* **2007**, *167* (2), 85−98.

(14) Chow, H. H.; Cai, Y.; Alberts, D. S.; Hakim, I.; Dorr, R.; Shahi, F.; Crowell, J. A.; Yang, C. S.; Hara, Y. Phase I pharmacokinetic study of tea polyphenols following single-dose administration of epigalloca-

techin gallate and polyphenon E. *Cancer Epidemiol., Biomarkers Prev.* **2001**, *10* (1), 53−58.
(15) Chow, H. H.; Cai, Y.; Hakim, I. A.; Crowell, J. A.; Shahi, F.; Brooks, C. A.; Dorr, R. T.; Hara, Y.; Alberts, D. S. Pharmacokinetics and safety of green tea polyphenols after multiple-dose administration of epigallocatechin gallate and polyphenon E in healthy individuals. *Clin. Cancer Res.* **2003**, *9* (9), 3312−3319.
(16) Fung, S. T.; Ho, C. K.; Choi, S. W.; Chung, W. Y.; Benzie, I. F. Comparison of catechin profiles in human plasma and urine after single dosing and regular intake of green tea (*Camellia sinensis*). *Br. J. Nutr.* **2013**, *109* (12), 2199−2207.
(17) Nakagawa, K.; Okuda, S.; Miyazawa, T. Dose-dependent incorporation of tea catechins, (−)-epigallocatechin-3-gallate and (−)-epigallocatechin, into human plasma. *Biosci. Biotechnol. Biochem.* **1997**, *61* (12), 1981−1985.
(18) Nakagawa, K.; Nakayama, K.; Nakamura, M.; Sookwong, P.; Tsuduki, T.; Niino, H.; Kimura, F.; Miyazawa, T. Effects of co-administration of tea epigallocatechin-3-gallate (EGCG) and caffeine on absorption and metabolism of EGCG in humans. *Biosci. Biotechnol. Biochem.* **2009**, *73* (9), 2014−2017.
(19) Van Amelsvoort, J. M.; Van Hof, K. H.; Mathot, J. N.; Mulder, T. P.; Wiersma, A.; Tijburg, L. B. Plasma concentrations of individual tea catechins after a single oral dose in humans. *Xenobiotica* **2001**, *31* (12), 891−901.
(20) Yang, C. S.; Chen, L.; Lee, M. J.; Balentine, D.; Kuo, M. C.; Schantz, S. P. Blood and urine levels of tea catechins after ingestion of different amounts of green tea by human volunteers. *Cancer Epidemiol., Biomarkers Prev.* **1998**, *7* (4), 351−354.
(21) Grassi, D.; Mulder, T. P.; Draijer, R.; Desideri, G.; Molhuizen, H. O.; Ferri, C. Black tea consumption dose-dependently improves flow-mediated dilation in healthy males. *J. Hypertens.* **2009**, *27* (4), 774−781.
(22) Hodgson, J. M.; Puddey, I. B.; Burke, V.; Beilin, L. J.; Jordan, N. Effects on blood pressure of drinking green and black tea. *J. Hypertens.* **1999**, *17* (4), 457−463.
(23) Hodgson, J. M.; Puddey, I. B.; Croft, K. D.; Burke, V.; Mori, T. A.; Caccetta, R. A.; Beilin, L. J. Acute effects of ingestion of black and green tea on lipoprotein oxidation. *Am. J. Clin. Nutr.* **2000**, *71* (5), 1103−1107.
(24) Randell, R. K.; Hodgson, A. B.; Lotito, S. B.; Jacobs, D. M.; Boon, N.; Mela, D. J.; Jeukendrup, A. E. No effect of 1 or 7 d of green tea extract ingestion on fat oxidation during exercise. *Med. Sci. Sports Exercise* **2013**, *45* (5), 883−891.
(25) Lee, M. J.; Maliakal, P.; Chen, L.; Meng, X.; Bondoc, F. Y.; Prabhu, S.; Lambert, G.; Mohr, S.; Yang, C. S. Pharmacokinetics of tea catechins after ingestion of green tea and (−)-epigallocatechin-3-gallate by humans: formation of different metabolites and individual variability. *Cancer Epidemiol., Biomarkers Prev.* **2002**, *11* (10 Pt 1), 1025−1032.
(26) Kroon, P. A.; Clifford, M. N.; Crozier, A.; Day, A. J.; Donovan, J. L.; Manach, C.; Williamson, G. How should we assess the effects of exposure to dietary polyphenols in vitro? *Am. J. Clin. Nutr.* **2004**, *80* (1), 15−21.
(27) Crozier, A.; Del, R. D.; Clifford, M. N. Bioavailability of dietary flavonoids and phenolic compounds. *Mol. Aspects Med.* **2010**, *31* (6), 446−467.
(28) Chow, H. H.; Hakim, I. A. Pharmacokinetic and chemoprevention studies on tea in humans. *Pharmacol. Res.* **2011**, *64* (2), 105−112.
(29) Selma, M. V.; Espin, J. C.; Tomas-Barberan, F. A. Interaction between phenolics and gut microbiota: Role in human health. *J. Agric. Food Chem.* **2009**, *57* (15), 6485−6501.
(30) Roowi, S.; Stalmach, A.; Mullen, W.; Lean, M. E.; Edwards, C. A.; Crozier, A. Green tea flavan-3-ols: colonic degradation and urinary excretion of catabolites by humans. *J. Agric. Food Chem.* **2010**, *58* (2), 1296−1304.
(31) Ludwig, A.; Lorenz, M.; Grimbo, N.; Steinle, F.; Meiners, S.; Bartsch, C.; Stangl, K.; Baumann, G.; Stangl, V. The tea flavonoid epigallocatechin-3-gallate reduces cytokine-induced VCAM-1 expression and monocyte adhesion to endothelial cells. *Biochem. Biophys. Res. Commun.* **2004**, *316* (3), 659−665.
(32) Chan, M. M.; Fong, D.; Ho, C. T.; Huang, H. I. Inhibition of inducible nitric oxide synthase gene expression and enzyme activity by epigallocatechin gallate, a natural product from green tea. *Biochem. Pharmacol.* **1997**, *54* (12), 1281−1286.
(33) Ahmad, N.; Mukhtar, H. Green tea polyphenols and cancer: biologic mechanisms and practical implications. *Nutr. Rev.* **1999**, *57* (3), 78−83.
(34) Yang, C. S.; Wang, Z. Y. Tea and cancer. *J. Natl. Cancer Inst.* **1993**, *85* (13), 1038−1049.
(35) Kimura, Y.; Okuda, H.; Okuda, T.; Yoshida, T.; Hatano, T.; Arichi, S. Studies on the activities of tannins and related compounds of medicinal plants and drugs. III. Effects of various tannins and related compounds on adrenocorticotropic hormone-induced lipolysis and insulin-induced lipogenesis from glucose in fat cells. (2). *Chem. Pharm. Bull. (Tokyo)* **1983**, *31* (7), 2501−2506.
(36) Juhel, C.; Armand, M.; Pafumi, Y.; Rosier, C.; Vandermander, J.; Lairon, D. Green tea extract (AR25) inhibits lipolysis of triglycerides in gastric and duodenal medium in vitro. *J. Nutr. Biochem.* **2000**, *11* (1), 45−51.
(37) Kobayashi, Y.; Suzuki, M.; Satsu, H.; Arai, S.; Hara, Y.; Suzuki, K.; Miyamoto, Y.; Shimizu, M. Green tea polyphenols inhibit the sodium-dependent glucose transporter of intestinal epithelial cells by a competitive mechanism. *J. Agric. Food Chem.* **2000**, *48* (11), 5618−5623.
(38) Dulloo, A. G.; Seydoux, J.; Girardier, L.; Chantre, P.; Vandermander, J. Green tea and thermogenesis: interactions between catechin-polyphenols, caffeine and sympathetic activity. *Int. J. Obes. Relat. Metab. Disord.* **2000**, *24* (2), 252−258.
(39) Ikeda, I.; Imasato, Y.; Sasaki, E.; Nakayama, M.; Nagao, H.; Takeo, T.; Yayabe, F.; Sugano, M. Tea catechins decrease micellar solubility and intestinal absorption of cholesterol in rats. *Biochim. Biophys. Acta* **1992**, *1127* (2), 141−146.
(40) Barthelman, M.; Bair, W. B., III; Stickland, K. K.; Chen, W.; Timmermann, B. N.; Valcic, S.; Dong, Z.; Bowden, G. T. (−)-Epigallocatechin-3-gallate inhibition of ultraviolet B-induced AP-1 activity. *Carcinogenesis* **1998**, *19* (12), 2201−2204.
(41) Hong, J.; Smith, T. J.; Ho, C. T.; August, D. A.; Yang, C. S. Effects of purified green and black tea polyphenols on cyclooxygenase- and lipoxygenase-dependent metabolism of arachidonic acid in human colon mucosa and colon tumor tissues. *Biochem. Pharmacol.* **2001**, *62* (9), 1175−1183.
(42) Jung, Y. D.; Kim, M. S.; Shin, B. A.; Chay, K. O.; Ahn, B. W.; Liu, W.; Bucana, C. D.; Gallick, G. E.; Ellis, L. M. EGCG, a major component of green tea, inhibits tumour growth by inhibiting VEGF induction in human colon carcinoma cells. *Br. J. Cancer* **2001**, *84* (6), 844−850.
(43) Hodgson, A. B.; Randell, R. K.; Boon, N.; Garczarek, U.; Mela, D. J.; Jeukendrup, A. E.; Jacobs, D. M. Metabolic response to green tea extract during rest and moderate-intensity exercise. *J. Nutr. Biochem.* **2013**, *24* (1), 325−334.
(44) Miller, R. J.; Jackson, K. G.; Dadd, T.; Mayes, A. E.; Brown, A. L.; Lovegrove, J. A.; Minihane, A. M. The impact of the catechol-O-methyltransferase genotype on vascular function and blood pressure after acute green tea ingestion. *Mol. Nutr. Food Res.* **2012**, *56* (6), 966−975.
(45) Scalbert, A.; Williamson, G. Dietary intake and bioavailability of polyphenols. *J. Nutr.* **2000**, *130* (8S Suppl), 2073S−2085S.
(46) Chow, H. H.; Hakim, I. A.; Vining, D. R.; Crowell, J. A.; Ranger-Moore, J.; Chew, W. M.; Celaya, C. A.; Rodney, S. R.; Hara, Y.; Alberts, D. S. Effects of dosing condition on the oral bioavailability of green tea catechins after single-dose administration of Polyphenon E in healthy individuals. *Clin. Cancer Res.* **2005**, *11* (12), 4627−4633.
(47) Henning, S. M.; Niu, Y.; Lee, N. H.; Thames, G. D.; Minutti, R. R.; Wang, H.; Go, V. L.; Heber, D. Bioavailability and antioxidant activity of tea flavanols after consumption of green tea, black tea, or a green tea extract supplement. *Am. J. Clin. Nutr.* **2004**, *80* (6), 1558−1564.

(48) Renouf, M.; Marmet, C.; Guy, P. A.; Beaumont, M.; Lepage, M.; Williamson, G.; Dionisi, F. Dose-response plasma appearance of green tea catechins in adults. *Mol. Nutr. Food Res.* **2013**, *57* (5), 833−839.
(49) Li, C.; Lee, M. J.; Sheng, S.; Meng, X.; Prabhu, S.; Winnik, B.; Huang, B.; Chung, J. Y.; Yan, S.; Ho, C. T.; Yang, C. S. Structural identification of two metabolites of catechins and their kinetics in human urine and blood after tea ingestion. *Chem. Res. Toxicol.* **2000**, *13* (3), 177−184.
(50) Meng, X.; Sang, S.; Zhu, N.; Lu, H.; Sheng, S.; Lee, M. J.; Ho, C. T.; Yang, C. S. Identification and characterization of methylated and ring-fission metabolites of tea catechins formed in humans, mice, and rats. *Chem. Res. Toxicol.* **2002**, *15* (8), 1042−1050.
(51) Kotani, A.; Miyashita, N.; Kusu, F. Determination of catechins in human plasma after commercial canned green tea ingestion by high-performance liquid chromatography with electrochemical detection using a microbore column. *J. Chromatogr. B: Anal. Technol. Biomed. Life Sci.* **2003**, *788* (2), 269−275.
(52) Stalmach, A.; Mullen, W.; Steiling, H.; Williamson, G.; Lean, M. E.; Crozier, A. Absorption, metabolism, and excretion of green tea flavan-3-ols in humans with an ileostomy. *Mol. Nutr. Food Res.* **2010**, *54* (3), 323−334.
(53) Crozier, A.; Del, R. D.; Clifford, M. N. Bioavailability of dietary flavonoids and phenolic compounds. *Mol. Aspects Med.* **2010**, *31* (6), 445−467.
(54) Lee, M. J.; Wang, Z. Y.; Li, H.; Chen, L.; Sun, Y.; Gobbo, S.; Balentine, D. A.; Yang, C. S. Analysis of plasma and urinary tea polyphenols in human subjects. *Cancer Epidemiol., Biomarkers Prev.* **1995**, *4* (4), 393−399.
(55) Renouf, M.; Redeuil, K.; Longet, K.; Marmet, C.; Dionisi, F.; Kussmann, M.; Williamson, G.; Nagy, K. Plasma pharmacokinetics of catechin metabolite 4′-O-Me-EGC in healthy humans. *Eur. J. Nutr.* **2011**, *50*, 575−580.
(56) Gruz, J.; Novák, O.; Strnad, M. Rapid analysis of phenolic acids in beverages by UPLC-MS/MS. *Food Chem.* **2008**, *111* (3), 789−794.
(57) Kamble, P.; Selvarajan, K.; Aluganti, N. C.; Nandave, M.; Parthasarathy, S. Aspirin may promote mitochondrial biogenesis via the production of hydrogen peroxide and the induction of Sirtuin1/PGC-1alpha genes. *Eur. J. Pharmacol.* **2013**, *699* (1−3), 55−61.
(58) Coffey, V. G.; Hawley, J. A. The molecular bases of training adaptation. *Sports Med.* **2007**, *37* (9), 737−763.
(59) Hawley, J. A.; Burke, L. M.; Phillips, S. M.; Spriet, L. L. Nutritional modulation of training-induced skeletal muscle adaptations. *J. Appl. Physiol.* **2011**, *110* (3), 834−845.
(60) Wang, Y. X.; Zhang, C. L.; Yu, R. T.; Cho, H. K.; Nelson, M. C.; Bayuga-Ocampo, C. R.; Ham, J.; Kang, H.; Evans, R. M. Regulation of muscle fiber type and running endurance by PPARdelta. *PLoS Biol.* **2004**, *2* (10), e294.
(61) Danesi, F.; Di, N. M.; Boschetti, E.; Bordoni, A. Green tea extract selectively activates peroxisome proliferator-activated receptor beta/delta in cultured cardiomyocytes. *Br. J. Nutr.* **2009**, *101* (12), 1736−1739.
(62) Serisier, S.; Leray, V.; Poudroux, W.; Magot, T.; Ouguerram, K.; Nguyen, P. Effects of green tea on insulin sensitivity, lipid profile and expression of PPARalpha and PPARgamma and their target genes in obese dogs. *Br. J. Nutr.* **2008**, *99* (6), 1208−1216.
(63) Murase, T.; Haramizu, S.; Shimotoyodome, A.; Nagasawa, A.; Tokimitsu, I. Green tea extract improves endurance capacity and increases muscle lipid oxidation in mice. *Am. J. Physiol.: Regul., Integr. Comp. Physiol.* **2005**, *288* (3), R708−R715.
(64) Deschamps, D.; Fisch, C.; Fromenty, B.; Berson, A.; Degott, C.; Pessayre, D. Inhibition by salicylic acid of the activation and thus oxidation of long chain fatty acids. Possible role in the development of Reye's syndrome. *J. Pharmacol. Exp. Ther.* **1991**, *259* (2), 894−904.
(65) Muramatsu, K.; Fukuyo, M.; Hara, Y. Effect of green tea catechins on plasma cholesterol level in cholesterol-fed rats. *J. Nutr. Sci. Vitaminol. (Tokyo)* **1986**, *32* (6), 613−622.
(66) Abe, I.; Seki, T.; Umehara, K.; Miyase, T.; Noguchi, H.; Sakakibara, J.; Ono, T. Green tea polyphenols: novel and potent inhibitors of squalene epoxidase. *Biochem. Biophys. Res. Commun.* **2000**, *268* (3), 767−771.
(67) Annaba, F.; Kumar, P.; Dudeja, A. K.; Saksena, S.; Gill, R. K.; Alrefai, W. A. Green tea catechin EGCG inhibits ileal apical sodium bile acid transporter ASBT. *Am. J. Physiol Gastrointest. Liver Physiol.* **2010**, *298* (3), G467−G473.
(68) Ikeda, I.; Tsuda, K.; Suzuki, Y.; Kobayashi, M.; Unno, T.; Tomoyori, H.; Goto, H.; Kawata, Y.; Imaizumi, K.; Nozawa, A.; Kakuda, T. Tea catechins with a galloyl moiety suppress postprandial hypertriacylglycerolemia by delaying lymphatic transport of dietary fat in rats. *J. Nutr.* **2005**, *135* (2), 155−159.
(69) Wang, S.; Noh, S. K.; Koo, S. I. Green tea catechins inhibit pancreatic phospholipase A(2) and intestinal absorption of lipids in ovariectomized rats. *J. Nutr. Biochem.* **2006**, *17* (7), 492−498.
(70) Hartley, L.; Flowers, N.; Holmes, J.; Clarke, A.; Stranges, S.; Hooper, L.; Rees, K. Green and black tea for the primary prevention of cardiovascular disease. *Cochrane Database Syst. Rev.* **2013**, *6*, CD009934.
(71) Anuradha, C. V.; Balakrishnan, S. D. Taurine attenuates hypertension and improves insulin sensitivity in the fructose-fed rat, an animal model of insulin resistance. *Can. J. Physiol. Pharmacol.* **1999**, *77* (10), 749−754.
(72) Chen, W.; Guo, J. X.; Chang, P. The effect of taurine on cholesterol metabolism. *Mol. Nutr. Food Res.* **2012**, *56* (5), 681−690.
(73) Rutherford, J. A.; Spriet, L. L.; Stellingwerff, T. The effect of acute taurine ingestion on endurance performance and metabolism in well-trained cyclists. *Int. J. Sport Nutr. Exercise Metab.* **2010**, *20* (4), 322−329.
(74) Spijkers, L. J.; van den Akker, R. F.; Janssen, B. J.; Debets, J. J.; De Mey, J. G.; Stroes, E. S.; van den Born, B. J.; Wijesinghe, D. S.; Chalfant, C. E.; MacAleese, L.; Eijkel, G. B.; Heeren, R. M.; Alewijnse, A. E.; Peters, S. L. Hypertension is associated with marked alterations in sphingolipid biology: a potential role for ceramide. *PLoS One* **2011**, *6* (7), e21817.
(75) Williamson, G. The use of flavonoid aglycones in in vitro systems to test biological activities: Based on bioavailability data, is this a valid approach? *Phytochem. Rev.* **2002**, *1* (2), 215−222.
(76) Kao, Y. H.; Hiipakka, R. A.; Liao, S. Modulation of endocrine systems and food intake by green tea epigallocatechin gallate. *Endocrinology* **2000**, *141* (3), 980−987.

IMPLICATIONS

Applications for the future of food and agriculture are exciting to consider, but a look at the current literature reveals a precautionary note struck by researchers. Implications involve risks for both the environment and organisms within that environment (including humans). Researchers in this area are studying hazards by examining the harm done when nanomaterials reach the nanobio interface. They are also studying exposure by determining how ENMs transport in the environment, how ENMs might accumulate, the types and quantities of ENMs we are currently exposed to through products we already consume, and what the fate of those materials might be in our digestive tracts.

Researchers have asked the following questions: How do we measure the ecotoxicity of these emerging technologies? How do we make these technologies safe/ How do we make these technologies sustainable?

Reviews of econanotoxicology found in this ACS Select describe the challenge of quantifying the hazards of ENMs that vary in size, shape, surface area, and coating to a wide variety of organisms ranging over several trophic levels. The researchers' goal is to understand how to make these ENMs more sustainable before full-scale release to the environment. Zhu et al. summarize the current understanding of the cellular uptake, intracellular fate, and transformation as affected by the physicochemical properties of ENMs and suggest that the advancement of research in this field along with better analytical capabilities and in silico simulation may lead to safe-by-design ENMs.[7] Mauer-Jones et al. discuss three grand challenges for chemists involved in econanotoxicity work: functional level toxicity assessment; detecting ENMs and distinguishing them from the background particles; and particle characterization in complex environments.[8] In addition, Kahru et al. review the econanotoxicological research done on aquatic species concluding that although computational methods such as quantitative structure−activity relationships (QSARs) are attractive for solving the problem, too many material types and too many organism types make these relationships difficult to apply due to lack of quality experimental data.[9] As a new approach to this problem, in their review Holden et al. propose high-throughput screening integrated with dynamic energy budget models.[10]

Whether nanoparticles are intentionally applied during agricultural processes or they are present as contaminants, it is important to understand what effects they will have on plants and more specifically plants grown for food. To investigate this question, Dimpka et al. amended sand with silver nanoparticles and grew wheat plants, disrupting the growth of shoots and roots in a dose-dependent manner.[11]

Ma et al. performed a similar study utilizing *Arabidopsis thaliana* and either CeO_2 or In_2O_3 nanoparticles. The physiological and molecular responses were different between the two particles, with CeO_2 inhibiting root and shoot growth in a dose-dependent manner (concentrations ranged from 0 to 2000 ppm).[12] Reviewing the direct and indirect effects of many different types of ENMs on algae, a species at the bottom of the ocean food web, Quigg et al. noted that the presence of exopolymeric substances produced by the organisms play a major role in the toxicity demonstrated by the particles.[13] In addition, they discuss how little is known about the biological uptake mechanisms and toxicity of nanoparticles in general.

Nanomaterial fate in the environment is discussed by Bately et al., who suggest that currently there is low risk of exposure, that the concentrations reaching the nanobio interface will be very low, and that work needs to be continued on studying toxicity under real environmental conditions to define no-effect concentrations.[14]

Although environmental concentrations may be low, there is a risk that these materials will accumulate in certain receptors and compartments, resulting in much higher concentrations. Three studies found in this ACS Select examine the potential for bioaccumulation. Metallic and metal oxide ENMs can be measured in samples taken from plants using X-ray fluorescence; using this technique, Hernandez-Viezcas and coauthors examined whether soil contaminated with zinc oxide and cerium oxide ENMs results in a bioaccumulation of particles in soybean crops.[15] Their results indicate that changing particle types will alter how they interact with the plant and whether or not they will accumulate. Using a transmission electron microscopy approach, Wang et al. demonstrated that copper oxides will bioaccumulate in maize plants translocating from the roots to the shoots and back again.[16] Another important process that is just beginning to be studied is trophic transfer, the movement of pollutants up the food chain. A simulated transfer of soil contaminated with gold nanoparticles to earthworms and subsequently to bullfrogs undertaken by Unrine and coauthors showed that this transfer does occur, but concentrations decrease by 2 orders of magnitude with each step.[17]

Humans are exposed to ENMs through food consumption. What is the current level of exposure? How are we processing them once they enter our digestive systems? Two research papers highlighted in this ACS Select ask these questions by examining the titanium dioxide found in food products already on the market and performing an in vitro study designed to simulate digestion of products containing a silica nanoparticle additive. Analysis by Weir et al. showed that children may have the highest exposure level to titanium dioxide in food because candy products contain a relatively high concentration of the material.[18] When silica ENMs enter our digestive systems, Peters and coauthors showed nanoscale particles could appear in the gut epithelium after digestion in the stomach, cause for concern and further research.[19]

Scientists agree that although nanoscale technology is promising for food and agriculture, the development must be done in a sustainable manner. Governments, through existing regulations, will play a large part of this development. It was through this lens that Bergeson examined if existing laws are sufficient to govern ENM development in a sustainable manner; because the state of knowledge is still playing catchup, development entities involved in regulation must adapt new procedures to promote sustainability.[20]

Despite the fact that the environmental health and safety of some ENMs have been extensively studied in the past decade, as evident in this issue of ACS Select, knowledge gaps still widely exist in many aspects including

- measurement and metrology of ENMs in complex matrixes;
- environmental fates and transformation of currently known ENMs and ever-increasing number of new ENMs;
- nanobio interface between ENMs with human body and ecosystem species;

- exposure and full life cycle assessment;
- risk assessment and management of diverse uses of ENMs;
- safety by design; and
- sustainable nanomaterials and nanomanufacturing.

Predictive models for the effects of nanomaterials on cells/living tissues have shown promise but still have a long way to go to be fully useful. High-throughput and high-content screening approaches using model biological species may be used to more effectively reveal mechanisms of nanomaterials safety. Nanoinformatics for nanomaterials design, data integration, and communication is an emerging field of study. In addition, risk governance of nanotechnology for societal benefit is still in a formative stage.

CONCLUSION

Nanoscale science is an exciting scientific frontier focusing on the length scale of approximately 1−100 nm. Advancement of analytical instrumentation has tremendously enhanced our ability to observe physical and biological worlds at the nanoscale and lead to creation of numerous new materials and functions at this length scale. Emergence of novel concepts and discovery of unexpected properties stimulate new approaches in traditional scientific disciplines. Combining these developments with the need to feed a predicted 9 billion people by 2050 establishes the intersection of nanotechnology, food, and agriculture as a research priority in the coming years.

Many applications of nanotechnology have been explored across the whole spectrum of national economic sectors, including agriculture, food, forest, and the environment, with demonstrated societal benefits. In the vast literature of nanoscale science, engineering, and technology, the majority is of discovery and application nature, whereas a relatively small portion, one estimate at <15%, in implication. Nanotechnology has been an essential megatrend in science and engineering worldwide and will continue its exponential growth in R&D as the primary science and technology platform in the years ahead. Given that nanotechnology is still in its formative stage in many regards, it is anticipated that fundamental and application-related publications will dominate the literature, whereas implication-related papers will continue to grow to fill knowledge gaps and become more effective supports to regulation and policy development for the safety and health of consumers and ecosystem. We invite researchers to continue submitting their works to ACS journals and reading the excellent works of their colleagues. A bright future through exploration and exploitation of nanoscale science, engineering, and technology indeed lies ahead for the benefit of a sustainable society.

Hongda Chen[*,†]
James N. Seiber[§]
Matt Hotze[#]

[†]National Institute of Food and Agriculture, U.S. Department of Agriculture, 1400 Independence Avenue, S.W., Washington, D.C. 20250, United States

[§]Department of Environmental Toxicology, University of California, One Shields Avenue, Davis, California 95616, United States

[#]Managing Editor, *Journal of Agricultural and Food Chemistry*, American Chemical Society, 1155 Sixteenth Street, N.W., Washington, D.C. 20036, United States

AUTHOR INFORMATION

Corresponding Author

*(H.C.) E-mail: hchen@nifa.usda.gov.

Notes

Views expressed in this editorial are those of the authors and not necessarily the views of the ACS, the U.S. government, or the National Institute of Food and Agriculture (NIFA) of the U.S. Department of Agriculture (USDA).

ACKNOWLEDGMENTS

We thank the teams from *Accounts of Chemical Research*, *ACS Nano*, *Analytical Chemistry*, *ACS Sustainable Chemistry & Engineering*, *Environmental Science & Technology*, and *Journal of Agricultural and Food Chemistry* for helping support this ACS Select by identifying content for inclusion.

REFERENCES

(1) Kayaci, F.; Ertas, Y.; Uyar, T. Enhanced thermal stability of eugenol by cyclodextrin inclusion complex encapsulated in electrospun polymeric nanofibers. *J. Agric. Food Chem.* **2013**, *61*, 8156−8165.

(2) Li, Q.; McGinnis, S.; Sydnor, C.; Wong, A.; Renneckar, S. Nanocellulose life cycle assessment. *ACS Sustainable Chem. Eng.* **2013**, *1*, 919−928.

(3) Farahi, R. H.; Passian, A.; Tetard, L.; Thundat, T. Critical issues in sensor science to aid food and water safety. *ACS Nano* **2012**, *6*, 4548−4556.

(4) Zhang, B.; Hou, L.; Tang, D.; Liu, B.; Li, J.; Chen, G. Simultaneous multiplexed stripping voltammetric monitoring of marine toxins in seafood based on distinguishable metal nanocluster-labeled molecular tags. *J. Agric. Food Chem.* **2012**, *60*, 8974−8982.

(5) Apak, R.; Demirci Çekiç, S.; Çetinkaya, A.; Filik, H.; Hayvalı, M.; Kılıç, E. Selective determination of catechin among phenolic antioxidants with the use of a novel optical fiber reflectance sensor based on indophenol dye formation on nano-sized TiO_2. *J. Agric. Food Chem.* **2012**, *60*, 2769−2777.

(6) Zhang, C.; Yin, A.-X.; Jiang, R.; Rong, J.; Dong, L.; Zhao, T.; Sun, L.-D.; Wang, J.; Chen, X.; Yan, C.-H. Time−temperature indicator for perishable products based on kinetically programmable Ag overgrowth on Au nanorods. *ACS Nano* **2013**, *7*, 4561−4568.

(7) Zhu, M.; Nie, G.; Meng, H.; Xia, T.; Nel, A.; Zhao, Y. Physicochemical properties determine nanomaterial cellular uptake, transport, and fate. *Acc. Chem. Res.* **2012**, *46*, 622−631.

(8) Mauer, L. J.; Chernyshova, A. A.; Hiatt, A.; Deering, A.; Davis, R. Melamine detection in infant formula powder using near- and mid-infrared spectroscopy. *J. Agric. Food Chem.* **2009**, *57*, 3974−3980.

(9) Kahru, A.; Ivask, A. Mapping the dawn of nanoecotoxicological research. *Acc. Chem. Res.* **2012**, *46*, 823−833.

(10) Holden, P. A.; Nisbet, R. M.; Lenihan, H. S.; Miller, R. J.; Cherr, G. N.; Schimel, J. P.; Gardea-Torresdey, J. L. Ecological nanotoxicology: integrating nanomaterial hazard considerations across the subcellular, population, community, and ecosystems levels. *Acc. Chem. Res.* **2012**, *46*, 813−822.

(11) Dimkpa, C. O.; McLean, J. E.; Martineau, N.; Britt, D. W.; Haverkamp, R.; Anderson, A. J. Silver nanoparticles disrupt wheat (*Triticum aestivum* L.) growth in a sand matrix. *Environ. Sci. Technol.* **2012**, *47*, 1082−1090.

(12) Ma, C.; Chhikara, S.; Xing, B.; Musante, C.; White, J. C.; Dhankher, O. P. Physiological and molecular response of *Arabidopsis thaliana* (L.) to nanoparticle cerium and indium oxide exposure. *ACS Sustainable Chem. Eng.* **2013**, *1*, 768−778.

(13) Quigg, A.; Chin, W.-C.; Chen, C.-S.; Zhang, S.; Jiang, Y.; Miao, A.-J.; Schwehr, K. A.; Xu, C.; Santschi, P. H. Direct and indirect toxic effects of engineered nanoparticles on algae: role of natural organic matter. *ACS Sustainable Chem. Eng.* **2013**, *1*, 686−702.

(14) Batley, G. E.; Kirby, J. K.; McLaughlin, M. J. Fate and risks of nanomaterials in aquatic and terrestrial environments. *Acc. Chem. Res.* **2012**, *46*, 854−862.

(15) Hernandez-Viezcas, J. A.; Castillo-Michel, H.; Andrews, J. C.; Cotte, M.; Rico, C.; Peralta-Videa, J. R.; Ge, Y.; Priester, J. H.; Holden, P. A.; Gardea-Torresdey, J. L. *In situ* synchrotron X-ray fluorescence mapping and speciation of CeO_2 and ZnO nanoparticles in soil cultivated soybean (*Glycine max*). *ACS Nano* **2013**, *7*, 1415−1423.
(16) Wang, Z.; Xie, X.; Zhao, J.; Liu, X.; Feng, W.; White, J. C.; Xing, B. Xylem- and phloem-based transport of CuO nanoparticles in maize (*Zea mays* L.). *Environ. Sci. Technol.* **2012**, *46*, 4434−4441.
(17) Unrine, J. M.; Shoults-Wilson, W. A.; Zhurbich, O.; Bertsch, P. M.; Tsyusko, O. V. Trophic transfer of Au nanoparticles from soil along a simulated terrestrial food chain. *Environ. Sci. Technol.* **2012**, *46*, 9753−9760.
(18) Weir, A.; Westerhoff, P.; Fabricius, L.; Hristovski, K.; Von Goetz, N. Titanium dioxide nanoparticles in food and personal care products. *Environ. Sci. Technol.* **2012**, *46*, 2242−2250.
(19) Peters, R.; Kramer, E.; Oomen, A. G.; Herrera Rivera, Z. E.; Oegema, G.; Tromp, P. C.; Fokkink, R.; Rietveld, A.; Marvin, H. J. P.; Weigel, S.; Peijnenburg, A. A. C. M.; Bouwmeester, H. Presence of nano-sized silica during *in vitro* digestion of foods containing silica as a food additive. *ACS Nano* **2012**, *6*, 2441−2451.
(20) Bergeson, L. L. Sustainable nanomaterials: emerging governance systems. *ACS Sustainable Chem. Eng.* **2013**, *1*, 724−730.

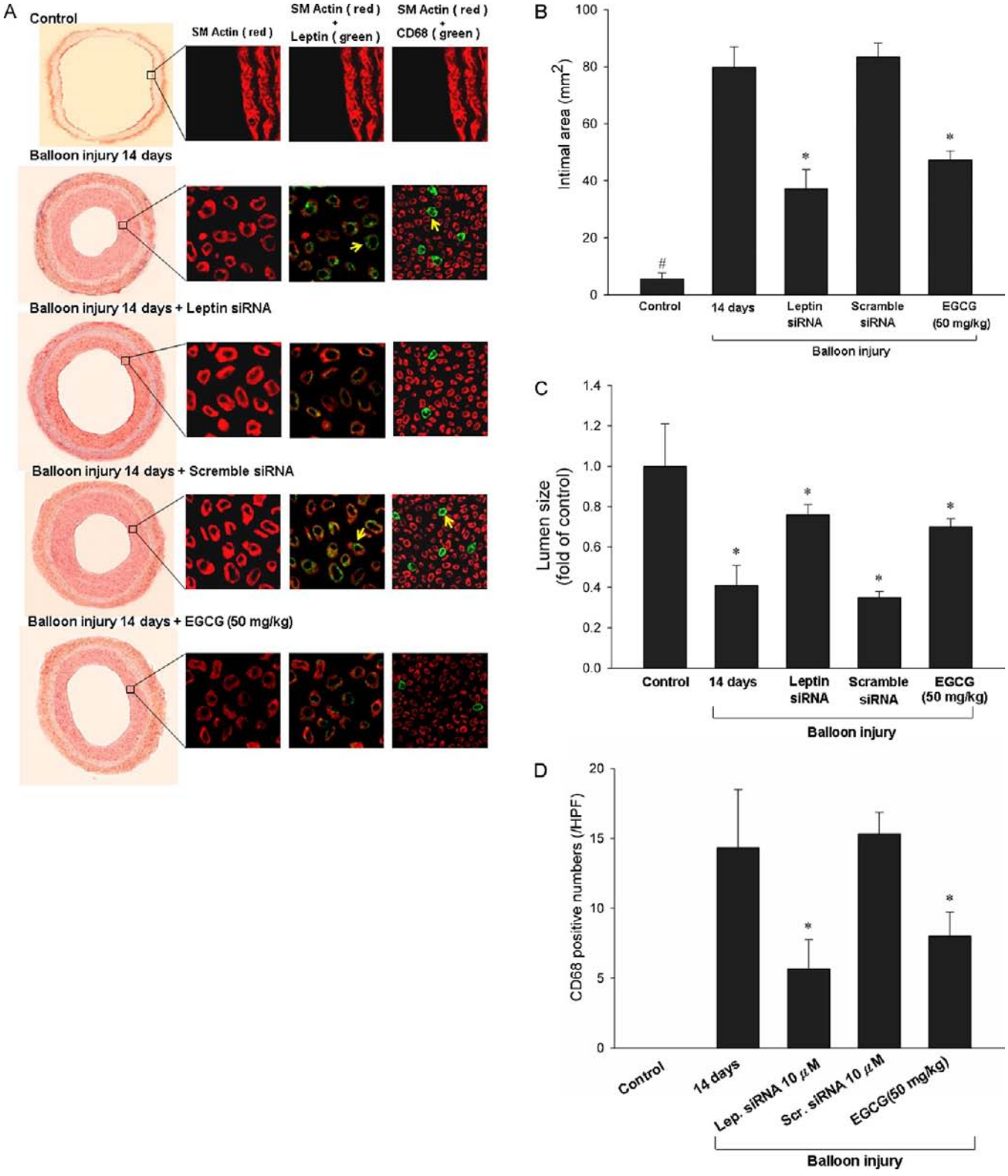

Figure 2. Attenuating effect of EGCG and leptin siRNA on balloon injury-induced neointimal formation. (A) The left panel showed a representative cross-section of carotid artery stained with hematoxylin and treated with EGCG (50 mg/kg) or leptin siRNA after carotid balloon injury for 14 days. The three panels on the right showed double staining for leptin siRNA (green color) or CD68 for macrophages (green color) by smooth muscle actin labeling (red color), respectively. (B) Quantitative analysis of a cross-sectional area of intima measured 14 days after carotid balloon injury. (C) Quantitative analysis of cross-sectional lumen size measured 14 days after carotid balloon injury. (D) Quantitative analysis of CD68 numbers measured 14 days after carotid balloon injury ($n = 4$ per group). *, $P < 0.05$ when compared to the balloon injury induced group. #, $P < 0.05$ when comparing the control group to the balloon injury induced group (Wilcoxon rank sum test). SM, smooth muscle.

dx.doi.org/10.1021/jf404479x | J. Agric. Food Chem. 2014, 62, 1213−1220

tion,[16] the molecular mechanism of atherosclerotic modulation in balloon injury is unclear. The first aim of this study is that we will elucidate the effect of EGCG on balloon injuries and angiotensin II-induced aortic VSMCs and also investigate the aortic lumen, neointimal formation, and molecular modulation.

The therapeutic approach for controlling atherosclerotic formation, compared with conventional angioplasty or agents, is adjunctive intervention using natural phytochemicals. The second aim of this study is that we investigate the effects of EGCG potential phytochemicals on attenuation of the atheroma progression. Results from the molecular mechanisms of EGCG identified in the aortic neointimal formations of rats, and VSMC culture studies, strongly support our findings regarding the control of human cardiovascular diseases.

MATERIALS AND METHODS

Chemical Reagents. (−)-Epigallocatechin gallate (EGCG) with high purity (>98%) was purchased from Wako Pure Chemical Industry (Osaka, Japan). Dulbecco's modified Eagle's medium (DMEM) was purchased from GIBCO (Invitrogen Co., Grand Island, NY, USA). Angiotensin II (Ang II) was obtained from CytoLab Ltd. (Rehovot, Israel), and trysolol (aprotinin) was purchased from Bayer CropScience Co. Ltd. (Leverkusen, Germany). Dimethyl sulfoxide (DMSO), penicillin, and streptomycin were obtained from Sigma-Aldrich Chemical Co. (St. Louis, MO, USA). Matrigel basement membrane matrix was acquired from Becton Dickinson (Bedford, MA, USA). Antibodies were purchased from R&D Systems (Minneapolis, MN, USA), Cell Signaling Technology, Inc. (Beverly, MA, USA), or Santa Cruz Biotechnology, Inc. (CA, USA). SP600125 (a potent, cell-permeant, selective and reversible inhibitor of JNK, 25 μmol/L), SB203580 (a highly specific cell-permeant inhibitor of p38 MAPK, 3 μmol/L), and PD98059 (extracellular-signal-regulated kinase, ERK, 50 μmol/L) were purchased from Calbiochem (Merck, Darmstadt, Germany). EGCG was dissolved with DMSO, and the DMSO concentration was below one thousand.

Small Interfering RNA (siRNA) Design. The rat leptin mRNA was designed by siRNA duplexes targeting (GenBank accession no. NM144741). The most effective siRNA duplexes were initially screened, and then the 25-nucleotide RNAs were synthesized by in vitro transcription (Invitrogen). Further experiments were evaluated with the most efficient siRNA duplex. No significant similarities to any genes other than leptin were found using BLAST against the rat reference sequence database.

Vascular Smooth Muscle Cell (VSMC) Culture. Primary cultures of VSMCs were incubated by the explant technique from the thoracic aorta of 220−260 g male Wistar rats, as documented previously.[13] The animal experiments approved and carried out in accordance with the Guide for the Care and Use of Laboratory Animals published by the U.S. National Institute of Health (NIH Publication no. 85-23, revised 1996). Adult Wistar rats were anaesthetized with isoflurane (3%) and subjected to a balloon catheter injury of the right carotid artery as described previously.[17] To test the effect of (−)-epigallocatechin gallate (EGCG) on vessel remodeling after balloon injury, EGCG at 50 mg/kg of body weight was given by oral gavage for 2 weeks after balloon injury.

Immunohistochemical Analysis. The carotid artery was harvested, and fixed in 10% formaldehyde and sliced into 5-μm-thick paraffin sections. Immunohistochemical staining analysis was performed as previously described. [18]

Migration Assay. The migration assay was performed as previously described.[19] Briefly, 250 μL of Matrigel was coated onto each well of a 24-well multiple-plate Boyden chamber (BW 200s; Neuroprobe, Cain John, MD, USA) with polycarbonate filters (pore size, 8 μm) and then incubated at 37 °C for 30 min. Then, 5×10^4 VSMCs were implanted onto each of the upper Boyden chamber's wells, and EGCG-, leptin siRNA-, SP600125-, SB203580-, and PD98059-treated medium was filled in the lower chamber to a total volume of 1 mL. After 18 h of incubation at 37 °C and 5% CO_2, the Matrigel was removed. Then, cells that had migrated to the reverse side of the filter (upper chamber) were stained with Liu's stain solution (Handsel Technologies, Inc., Taipei, Taiwan). Following a photograph of four randomized visual fields, the percentage of cell migration was measured by counting the number of VSMCs that had migrated through the membrane. The data is presented as percentages of control.

Proliferation Assay. The VSMCs proliferation was determined using the [^{3}H]-thymidine incorporation assay. Vascular smooth muscle cells were seeded on a ViewPlate (Packard Instrument) for 60 min at a density of 5×10^3 cells per well in serum-free medium and incubated overnight. Angiotensin II (Ang II), EGCG, leptin siRNA, SP600125, SB203580, PD98059, and DMSO were then added to the plates. Thymidine uptake was measured by the addition of 500 nCi/ml [^{3}H]-thymidine (Perkin-Elmer, Boston, MA). The detailed procedure was performed as previously described. [18]

Electrophoretic Mobility Shift Assay (EMSA). Oligonucleotide sequences included the AP-1 (activating factor 1) consensus binding region (5′-CGCTTGATGACTCAGCCGGAA-3′) and the AP-1 mutant oligonucleotide sequence (5′-CGCTTGATGACTTGGCCG-GAA-3′). After annealing, these double-stranded oligonucleotides were labeled with (γ-^{32}P)-ATP probes by T4 polynucleotide kinase (Mission Biotech Company, Taipei, Taiwan). In each case, controls were performed in which mutant oligonucleotides competed with the labeled sequence. The detailed procedure was performed as described previously.[19]

Quantification of Leptin Protein. Leptin antibodies were purchased from Oncogene (San Diego, CA, USA). VSMCs were grown to confluence and subsequently stimulated with or without Ang II. Western blot analyses were performed as previously documented.[18]

RNA Isolation and Reverse Transcription. RNA was isolated from cells using the single-step acid guanidinium thiocyanate/phenol/chloroform extraction method. RNA isolation and reverse transcription were performed as previously described.[18]

Statistical Analysis. The data were expressed as the mean ± SD of three replicates from four separate experiments. Statistical significance was determined by analysis of variance (GraphPad Software Inc., San Diego, CA, USA). The Dunnett's test was used to compare multiple groups to a single control group. The Tukey−Kramer comparison test was used for pairwise comparisons between multiple groups after the ANOVA. A value of $P < 0.05$ was considered to be statistically significant.

RESULTS

EGCG and Leptin siRNA Attenuates Intimal Thickening and Increases Lumen Size after Carotid Artery Balloon Injury. Carotid artery balloon injury sustained for 14 days significantly increased the thickness of the intimal area and narrowed the vascular lumen, compared with the uninjured control group (Figure 2A, left panel). Leptin siRNA and (−)-epigallocatechin gallate (EGCG) treatment significantly attenuated the thickness of the intimal area after balloon injury. The thickness of the intimal area decreased 53.4% with leptin siRNA delivery and 40.7% with administering EGCG treatment (Figure 2B). The control siRNA (scrambled siRNA) did not reduce the thickness of intimal area induced by balloon injury. Leptin siRNA delivery and EGCG treatment similarly and both significantly increased the vessel lumen size after balloon injury. The lumen size increased 85.4% after delivering leptin siRNA, and 70.7% after administrating EGCG treatment (Figure 2C). The control siRNA did not change the lumen size after balloon injury. Immunohistochemical double staining demonstrated strongly leptin-positive labeled cells 14 days after carotid injury, whereas the intimal layer in the sham group did not express leptin (Figure 2A, right panel). Leptin siRNA and EGCG diminished the leptin and CD68 labeling signal intensity after carotid artery balloon injury (Figure 2D). Scrambled siRNA did

not alter the expression of leptin labeling after carotid artery injury.

Inhibitory Effect of Leptin siRNA, EGCG, and the JNK Inhibitor on VSMC Migration Induced by Ang II. We performed a cell migration assay to evaluate the effects of leptin siRNA, EGCG, and the JNK inhibitor on phenotypic alterations of VSMCs induced by Ang II. Ang II (10 ng/mL) treatment significantly augmented the migratory activity of the VSMCs. However, pretreatment with leptin siRNA, EGCG (100 μM), or SP600125 (JNK inhibitor) diminished the migratory activity of VSMCs induced by Ang II (Figure 3A,B).

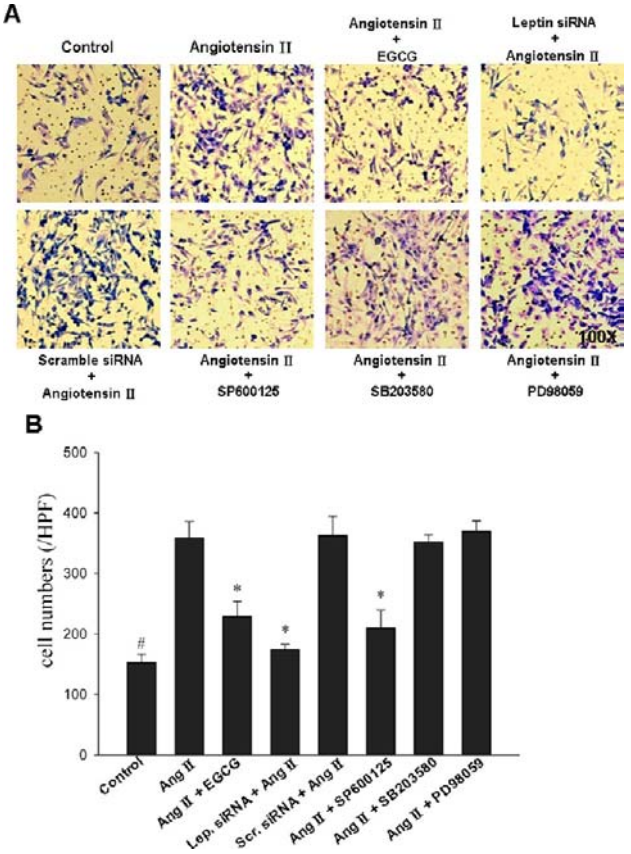

Figure 3. Effects of EGCG and leptin siRNA on migration activity of Ang II-induced vascular smooth muscle cells (VSMCs). Panel A: VSMCs migrated through Boyden chamber filters were stained. Panel B: Quantitative analysis of migration of VSMCs. VSMCs were treated with different agents for 18 h, and the migrating cells were then quantified (n = 4 per group). The assay was performed in triplicate. *, $P < 0.05$ when compared to the Ang II induced group. #, $P < 0.05$ when comparing the control group to the Ang II-induced VSMC (Wilcoxon rank sum test).

Attenuated Proliferation Effects of Leptin siRNA, EGCG, and SP600125 on VSMCs. We performed a [^{3}H]-thymidine incorporation assay to investigate the effects of leptin siRNA and EGCG on the Ang II-induced proliferation of VSMCs. Figure 4 presented that Ang II (10 ng/mL) treatment significantly increased the VSMCs proliferation. Pretreatment with leptin siRNA, EGCG (100 μM), or SP600125 attenuated the of VSMC proliferation induced by Ang II (Figure 4).

Suppressive Effects of EGCG on Balloon-Injury-Induced AP-1 Binding Activity, and the c-Jun Mediated Leptin-JNK Pathway. As shown in Figure 5, the EMSA indicted that balloon injury increased AP-1 DNA−protein

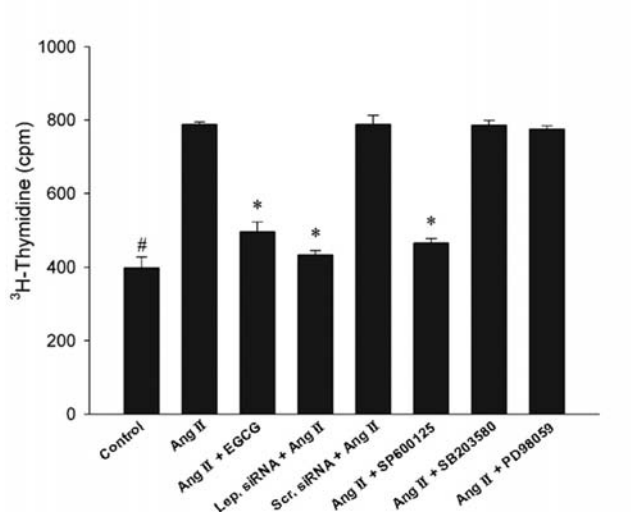

Figure 4. Attenuated proliferation of EGCG-treated VSMCs after Ang II induction. Representative [^{3}H]-thymidine incorporation assays showing the proliferation of VSMCs after Ang II (10 ng/mL) induction in the presence or absence of EGCG (100 μM), leptin siRNA, or JNK inhibitor SP600125 (n = 5 per group). The assay was performed in triplicate. *, $P < 0.05$ when compared to the Ang II induced group. #, $P < 0.05$ when comparing the control group to the Ang II-induced VSMC (Wilcoxon rank sum test).

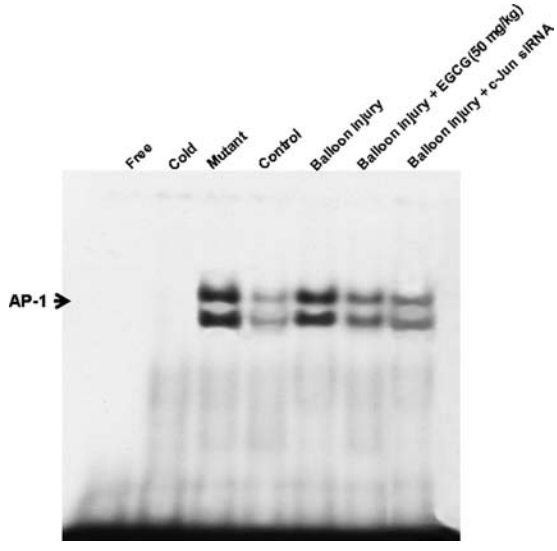

Figure 5. Balloon injury enhanced the AP-1-binding activity, and EGCG inhibited the AP-1-binding activity through JNK. Representative EMSA showing protein binding to the AP-1 oligonucleotide in nuclear extracts of VSMCs after carotid balloon injury sustained for 14 days. The assay was performed in triplicate.

binding activity, which reached its peak after 1 h. When an excess amount of the unlabeled probe with the AP-1 binding site competed with the isotope labeled probe, the binding activity decreased. An excess of the labeled probe with a 2-bp substitution at the AP-1 binding site did not reduce the AP-1 binding when competing with a nonmutated probe. The addition of EGCG (50 mg/kg) abolished the DNA−protein binding activity induced by balloon injury. The production of DNA-binding complexes induced by balloon injury can be supershifted by a monoclonal AP-1 antibody, indicating the presence of this protein in these complexes. These results

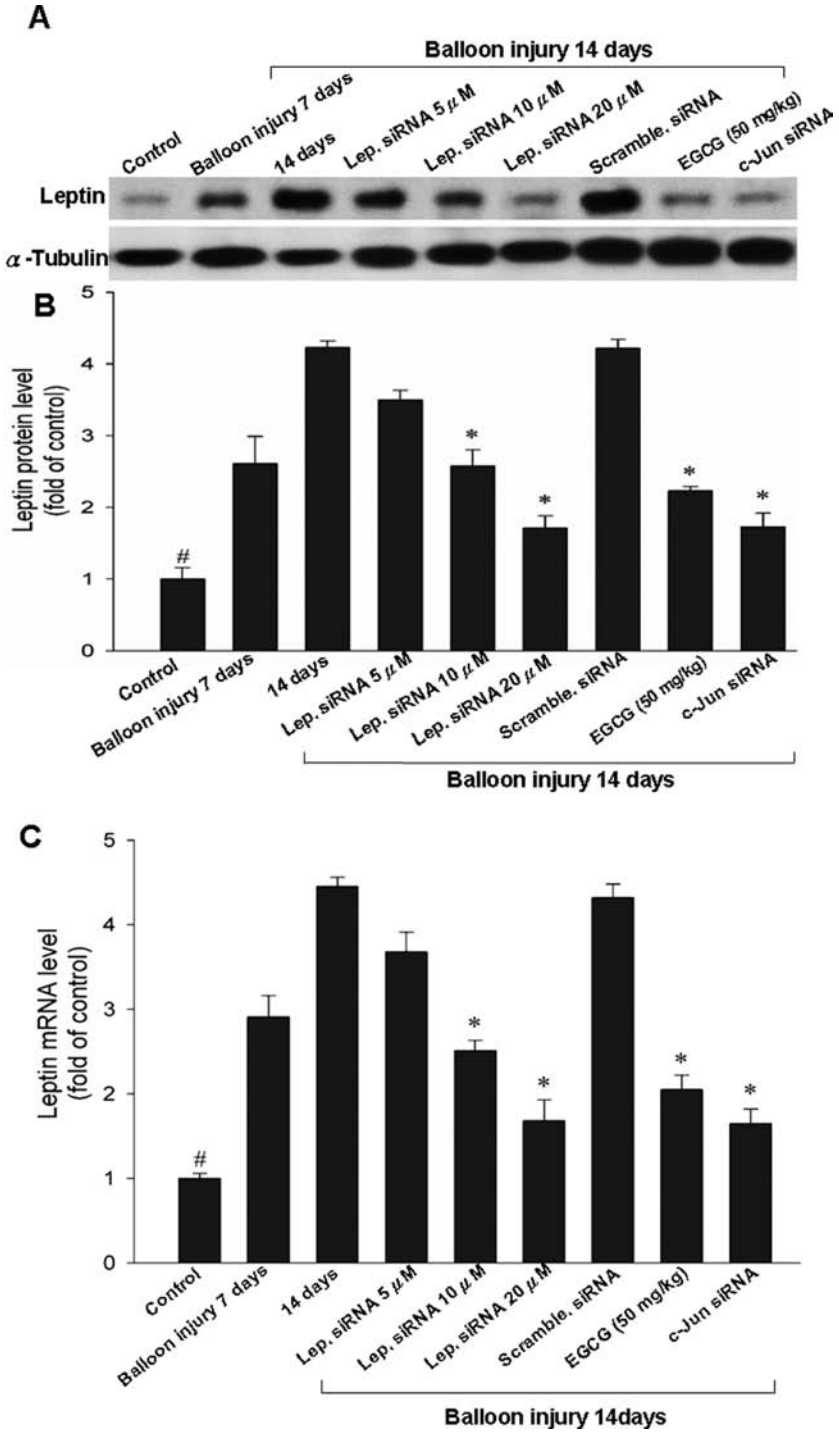

Figure 6. Effects of EGCG, leptin siRNA, and c-Jun siRNA on carotid artery leptin protein expression. Panel A: Representative Western blot for leptin in the injured carotid artery for 14 days with different doses of leptin siRNA. Panel B: Quantitative analysis of leptin protein levels. Panel C: Quantitative analysis of leptin mRNA by real-time PCR. The assay was performed in triplicate. *, $P < 0.05$ when compared to the balloon injury induced group. #, $P < 0.05$ when comparing the control group to the balloon injury group (Wilcoxon rank sum test; $n = 5$ per group).

suggested that the AP-1 binding site in the c-Jun is critical for transcriptional regulation by balloon injury and that EGCG regulates c-Jun activity through the JNK/AP-1 pathway.

EGCG-Induced Leptin Reduction through JNK. To demonstrate the efficiency of siRNA delivery into the carotid artery through electric pulses, control siRNA was labeled with Cy3 (cyanine 3) at the 5′-side (Invitrogen). The carotid artery was transfected with siRNA by using electric pulses, and successful transfection was evidenced by green staining observed under the fluorescence microscope at the area of intimal thickening 14 days after balloon injury (data not shown). After 7 and 14 days of balloon injury, leptin protein expression was significantly induced compared with the control group (Figure 6). Delivering leptin siRNA into the carotid artery after balloon injury reduced leptin protein expression in a dose-dependent manner. The most potent dose of leptin siRNA that reduced leptin protein expression after balloon injury was 20 μM (Figure 6A). No inhibitory effect of

dx.doi.org/10.1021/jf404479x | J. Agric. Food Chem. 2014, 62, 1213−1220

scrambled leptin siRNA on leptin protein expression was observed in the concentration-dependent manners. Daily EGCG treatment with 50 mg/kg of body weight significantly inhibited the leptin protein expression induced by carotid artery injury. Leptin mRNA expression was similar to leptin protein expression. Leptin siRNA and EGCG significantly reduced the leptin mRNA expression induced by balloon injury (Figure 6B).

DISCUSSION

EGCG was isolated from green tea, of which is the main polyphenolic constituent of green tea. Green tea has been used as a health-promoting remedy for thousands of years in China, and has rarely exhibited adverse effects during administration in both animals and humans. Recent studies have suggested that EGCG produces nutraceutical and medicinal benefits.[20,21] Increasing evidence from these investigations supports that EGCG has an antiatherosclerosis through the modulation of inflammatory pathways in various cells, such as EGCG supplemented olive oil improved endothelial dysfunction in early atherosclerosis and reduced leukocytes,[22] and the effect of EGCG on reduction of plasma IL-6 level, and NF-kappaB/AP-1 pathway in myocardial ischemia reperfusion injury in rats.[23] Compared with the model of EGCG-treated cardiovascular diseases, our balloon injury-induced model was used to mimic the pathphysiologic condition in the percutaneous angioplasty of vascular atherosclerosis. These studies have proved that EGCG inhibited neointimal formation through leptin modulation in cell cultures. However, the influence of EGCG on the expression of leptin and the molecular pathway is still unclear. Our study is the first to examine the effect of EGCG on intimal thickening and its molecular mechanism. Trovati et al. reported that leptin promotes atherogenesis through intracellular signaling molecules including JAK/STAT, PI3K/Akt, ERK 1/2, and p38 MAPK.[24] Tao et al. documented that perivisceral aortic leptin in ApoE(−/−) mice induced local aortic medial degeneration and augmented angiotensin II-induced aneurysm.[25] Our in vitro model is consistent with the existence of angiotensin II/leptin modulation in aorta or vascular smooth muscle cells.

EGCG has been reported to attenuate atherogenic regulation in both human aortic smooth muscle cells and macrophages through IL-6/MCP-1 and anti-inflammatory ROS systems.[26,27] Comparison with Won's study, pretreatment with EGCG inhibited the Ang II-induced phosphorylation of ERK 1/2, JNK 1/2, or p38 MAPK, and the presentation of c-jun or c-fos mRNA.[28] We investigated the effect of EGCG on attenuating rat aortic leptin expression, neointimal formation, Ang II-induced VSMCs and the molecular modulation of cell proliferation and migration. In our study, treatment with EGCG inhibited the selective JNK/AP-1 pathway (Figure 4A) but did not inhibit the MAPK, P38, or PI3K pathways. The novel presentation revealed that EGCG exhibited antiatherosclerosis in the carotid balloon injury model, the modulating mechanism suggested through the attenuation of inflammation. Furthermore, polyphenol resveratrol and quercetin interacted to inhibit neointimal hyperplasia in mice with carotid injury as well as VSMC proliferation and macrophage chemotaxis.[29] Polyphenol EGCG was reported to reduce evolving atherosclerotic lesions in apolipoprotein E−null mice.[30] When compared with these previous studies, our data displayed that EGCG attenuated significantly the neointimal formation and reduced aortic lumen narrowing after carotid balloon injury in rats.

A significant relationship between leptin and atherosclerosis has been reported, whereby modulated signaling is involved in endothelial function and smooth muscle cells, regulating numerous pathological processes, including vascular calcification and Ang II-induced VSMC activation and vasoconstriction.[13,31,32] Rapidly accumulating evidence has also revealed that leptin acts as a key cytokine in processing atherosclerosis in various cells. In previous studies, the daily administration of leptin to ob/ob mice after carotid artery injury with ferric chloride markedly increased neointimal thickness and the severity of luminal stenosis.[33] EGCG was used to treat atherosclerosis, whereas aortic leptin attenuation was not documented. We used EMSA to determine that EGCG inhibited the expression of leptin after balloon injury in a concentration-dependent manner (Figure 5). Additionally, in the cell migration/thymidine incorporation assay and molecular signaling analysis, the addition of EGCG, leptin siRNA, and the SB600125 inhibitor in Ang II-induced VSMCs showed that leptin contributed to the atherogenic process. The results of antimigration and signaling studies indicated that EGCG might particulate in crucial anti-inflammatory activity through the Ang II/leptin/JNK pathway.

Obesity accelerates vascular diseases; thus, the regulation of Ang II-induced leptin expression has been studied to focus on cellular molecular modulation.[34,35] Herbs, such as extracts of Chinese herb "Danshen" and Ginkgo biloba, have been shown to prevent atherosclerosis and restenosis in altering aortic lumen phenotypes after balloon injury.[36,37] In a previous plant study, the habitual consumption of green tea beverages reduced the incidences of cardiovascular events and reduced surrogate markers of atherosclerosis and lipid peroxidation.[38] Regarding dose, Chyu et al. reported that daily treatment with intraperitoneal injections of EGCG (10 mg/kg) reduced evolving atherosclerotic lesions without affecting the size of aortic sinus plaque or the aortic plaque size in apolipoprotein E−null mice.[30] In our study, EGCG (50 mg/kg) treatment eliminated atheroma formation, caused the experimental group to exhibit a similar aortic lumen size with the control group, and attenuated neointimal formation after carotid balloon injury in rats. The neointimal formation discrepancy between our data and previous studies on EGCG-treated aortic balloon injuries assumed to result from a concentration-dependent effect.

The data demonstrated that EGCG attenuated vascular smooth muscle cell (VSMC) migration and proliferation through the Ang II/leptin/JNK pathway by regulating the activation of transcription factor AP-1, thereby suppressing neointimal formation. Our study adds evidence to the claim that EGCG has therapeutic potential for preventing and controlling of atherosclerosis in future clinical applications.

AUTHOR INFORMATION

Corresponding Author

*E-mail: shyukg@ms12.hinet.net. Phone: 886-2-28332211, ext 2094. Fax: 886-2-28365775.

Author Contributions

#Equal contributor to corresponding author.

Funding

This work was supported in part of grants from the Shin Kong Wu Ho-Su Memorial Hospital, Taipei, Taiwan (Grant Nos. SKH-8302-102-0501 and SKH-8302-102-0502).

Notes

The authors declare no competing financial interest.

■ ABBREVIATIONS

EGCG, (−)-epigallocatechin-3-gallate; Ang II, angiotensin II; AP-1, activator protein-1

■ REFERENCES

(1) Misra, A.; Garg, A. Leptin: its receptor and obesity. *J. Invest. Med.*. **1996**, *44*, 540−548.

(2) Flanagan, D. E.; Vaile, J. C.; Petley, G. W.; Phillips, D. I.; Godsland, I. F.; Owens, P.; Moore, V. M.; Cockington, R. A.; Robinson, J. S. Gender differences in the relationship between leptin, insulin resistance and the autonomic nervous system. *Regul. Pept.* **2007**, *140*, 37−42.

(3) Beltowski, J.; Wojcicka, G.; Gorny, D.; Marciniak, A. Human leptin administered intraperitoneally stimulates natriuresis and decreases renal medullary Na+, K+-ATPase activity in the rat − impaired effect in dietary-induced obesity. *Med. Sci. Monit.* **2002**, *8*, BR221−229.

(4) Bodary, P. F.; Westrick, R. J.; Wickenheiser, K. J.; Shen, Y.; Eitzman, D. T. Effect of leptin on arterial thrombosis following vascular injury in mice. *J. Am. Med. Assoc.* **2002**, *287*, 1706−1709.

(5) Chaldakov, G. N.; Fiore, M.; Stankulov, I. S.; Hristova, M.; Antonelli, A.; Manni, L.; Ghenev, P. I.; Angelucci, F.; Aloe, L. NGF, BDNF, leptin, and mast cells in human coronary atherosclerosis and metabolic syndrome. *Arch. Physiol. Biochem.* **2001**, *109*, 357−360.

(6) Singh, M.; Bedi, U. S.; Singh, P. P.; Arora, R.; Khosla, S. Leptin and the clinical cardiovascular risk. *Int. J. Cardiol.* **2010**, *140*, 266−271.

(7) Wallace, A. M.; McMahon, A. D.; Packard, C. J.; Kelly, A.; Shepherd, J.; Gaw, A.; Sattar, N. Plasma leptin and the risk of cardiovascular disease in the west of Scotland coronary prevention study (WOSCOPS). *Circulation* **2001**, *104*, 3052−3056.

(8) Beyar, R. Novel approaches to reduce restenosis. *Ann. NY Acad. Sc.* **2004**, *1015*, 367−378.

(9) Ross, R. Atherosclerosis is an inflammatory disease. *Am. Heart J.* **1999**, *138*, S419−420.

(10) Inoue, T.; Croce, K.; Morooka, T.; Sakuma, M.; Node, K.; Simon, D. I. Vascular inflammation and repair: implications for re-endothelialization, restenosis, and stent thrombosis. *JACC Cardiovasc. Interv.* **2011**, *4*, 1057−1066.

(11) Fogelstrand, P.; Mellander, S.; Mattsson, E. Increased vascular injury reduces the degree of intimal hyperplasia following angioplasty in rabbits. *J. Vasc. Res.* **2011**, *48*, 307−315.

(12) Zargham, R. Preventing restenosis after angioplasty: a multistage approach. *Clin. Sci. (London)* **2008**, *114*, 257−264.

(13) Shyu, K. G.; Chen, S. C.; Wang, B. W.; Cheng, W. P.; Hung, H. F. Mechanism of the inhibitory effect of atorvastatin on leptin expression induced by angiotensin II in cultured human coronary artery smooth muscle cells. *Clin. Sci. (London)* **2012**, *122*, 33−42.

(14) Wolfram, S. Effects of green tea and EGCG on cardiovascular and metabolic health. *J. Am. Nutr.* **2007**, *26*, 373S−388S.

(15) Bettuzzi, S.; Brausi, M.; Rizzi, F.; Castagnetti, G.; Peracchia, G. Corti, A: Chemoprevention of human prostate cancer by oral administration of green tea catechins in volunteers with high-grade prostate intraepithelial neoplasia: a preliminary report from a one-year proof-of-principle study. *Cancer Res.* **2006**, *66*, 1234−1240.

(16) Cai, Y.; Kurita-Ochiai, T.; Hashizume, T.; Yamamoto, M. Green tea epigallocatechin-3-gallate attenuates Porphyromonas gingivalis −induced atherosclerosis. *Pathog. Dis.* **2013**, *67*, 76−83.

(17) Liu, G. N.; Teng, Y. X.; Yan, W. Transfected synthetic DNA enzyme gene specifically inhibits Egr-1 gene expression and reduces neointimal hyperplasia following balloon injury in rats. *Int. J. Cardiol.* **2008**, *129*, 118−124.

(18) Shyu, K. G.; Lien, L. M.; Wang, B. W.; Kuan, P.; Chang, H. Resistin contributes to neointimal formation via oxidative stress after vascular injury. *Clin. Sci. (London)* **2011**, *120*, 121−129.

(19) Lin, C. M.; Chen, Y. H.; Ma, H. P.; Wang, B. W.; Chiu, J. H.; Chua, S. K.; Ong, J. R.; Shyu, K. G. Silibinin inhibits the invasion of IL-6-stimulated colon cancer cells via selective JNK/AP-1/MMP-2 modulation in vitro. *J. Agric. Food Chem.* **2012**, *60*, 12451−12457.

(20) Suzuki, Y.; Miyoshi, N.; Isemura, M. Health-promoting effects of green tea. *Proc. Jpn. Acad. Ser. B Phys. Biol. Sci.* **2012**, *88*, 88−101.

(21) Cooper, R.; Morré, D. J.; Morré, D. M. Medicinal benefits of green tea: Part I. Review of noncancer health benefits. *J. Altern. Complement. Med.* **2005**, *11*, 521−528.

(22) Widmer, R. J.; Freund, M. A.; Flammer, A. J.; Sexton, J.; Lennon, R.; Romani, A.; Mulinacci, N.; Vinceri, F. F.; Lerman, L. O.; Lerman, A. Beneficial effects of polyphenol-rich olive oil in patients with early atherosclerosis. *Eur. J. Nutr.* **2013**, *52*, 1223−1231.

(23) Aneja, R.; Hake, P. W.; Burroughs, T. J.; Denenberg, A. G.; Wong, H. R.; Zingarelli, B. Epigallocatechin, a green tea polyphenol, attenuates myocardial ischemia reperfusion injury in rats. *Mol. Med.* **2004**, *10*, 55−62.

(24) Trovati, M.; Doronzo, G.; Barale, C.; Vaccheris, C.; Russo, I.; Cavalot, F. Leptin and Vascular Smooth Muscle Cells. *Curr. Pharm. Des.* **2013**.

(25) Tao, M.; Yu, P.; Nguyen, B. T.; Mizrahi, B.; Savion, N.; Kolodgie, F. D.; Virmani, R.; Hao, S.; Ozaki, C. K.; Schneiderman, J. Locally applied leptin induces regional aortic wall degeneration preceding aneurysm formation in apolipoprotein E-deficient mice. *Arterioscler. Thromb. Vasc. Biol* **2013**, *33*, 311−320.

(26) Ivanov, V.; Roomi, M. W.; Kalinovsky, T.; Niedzwiecki, A.; Rath, M. Anti-atherogenic effects of a mixture of ascorbic acid, lysine, proline, arginine, cysteine, and green tea phenolics in human aortic smooth muscle cells. *J. Cardiovasc. Pharmacol.* **2007**, *49*, 140−145.

(27) Li, M.; Liu, J. T.; Pang, X. M.; Han, C. J.; Mao, J. J. Epigallocatechin-3-gallate inhibits angiotensin II and interleukin-6-induced C-reactive protein production in macrophages. *Pharmacol. Rep.* **2012**, *64*, 912−918.

(28) Won, S. M.; Park, Y. H.; Kim, H. J.; Park, K. M.; Lee, W. J. Catechins inhibit angiotensin II-induced vascular smooth muscle cell proliferation via mitogen-activated protein kinase pathway. *Exp. Mol. Med.* **2006**, *38*, 525−534.

(29) Khandelwal, A..R.; Hebert, V. Y.; Kleinedler, J. J.; Rogers, L. K.; Ullevig, S. L.; Asmis, R.; Shi, R.; Dugas, T. R. Resveratrol and quercetin interact to inhibit neointimal hyperplasia in mice with a carotid injury. *J. Nutr.* **2012**, *142*, 1487−1494.

(30) Chyu, K. Y.; Babbidge, S. M.; Zhao, X.; Dandillaya, R.; Rietveld, A. G.; Yano, J.; Dimayuga, P.; Cercek, B.; Shah, P. K. Differential effects of green tea-derived catechin on developing versus established atherosclerosis in apolipoprotein E-null mice. *Circulation* **2004**, *109*, 2448−2453.

(31) Penumetcha, M.; Merchant, N.; Parthasarathy, S. Modulation of leptin levels by oxidized linoleic acid: a connection to atherosclerosis? *J. Med. Food* **2011**, *14*, 441−443.

(32) Gonzalez, M.; Lind, L.; Söderberg, S. Leptin and endothelial function in the elderly: The Prospective Investigation of the Vasculature in Uppsala Seniors (PIVUS) study. *Atherosclerosis* **2013**, *228*, 485−490.

(33) Schäfer, K.; Halle, M.; Goeschen, C.; Dellas, C.; Pynn, M.; Loskutoff, D. J.; Konstantinides, S. Leptin promotes vascular remodeling and neointimal growth in mice. *Arterioscler. Thromb. Vasc. Biol.* **2004**, *24*, 112−117.

(34) Al-Daghri, N. M.; Bindahman, L. S.; Al-Attas, O. S.; Saleem, T. H.; Alokail, M. S.; Alkharfy, K. M.; Draz, H. M.; Yakout, S.; Mohamed, A. O.; Harte, A. L.; McTernan, P. G. Increased circulating ANG II and TNF-α represents important risk factors in obese saudi adults with hypertension irrespective of diabetic status and BMI. *PLoS One* **2012**, *7*, e51255.

(35) Rodríguez, A.; Gómez-Ambrosi, J.; Catalán, V.; Fortuño, A.; Frühbeck, G. Leptin inhibits the proliferation of vascular smooth muscle cells induced by angiotensin II through nitric oxide-dependent mechanisms. *Mediators Inflamm.* **2010**, *2010*, 105489.
(36) Hur, K. Y.; Seo, H. J.; Kang, E. S.; Kim, S. H.; Song, S.; Kim, E. H.; Lim, S.; Choi, C.; Heo, J. H.; Hwang, K. C.; Ahn, C. W.; Cha, B. S.; Jung, M.; Lee, H. C. Therapeutic effect of magnesium lithospermate B on neointimal formation after balloon-induced vascular injury. *Eur. J. Pharmacol.* **2008**, *586*, 226−233.
(37) Liu, F.; Zhang, J.; Yu, S.; Wang, R.; Wang, B.; Lai, L.; Yin, H.; Liu, G. Inhibitory effect of Ginkgo biloba extract on hyperhomocysteinemia-induced intimal thickening in rabbit abdominal aorta after balloon injury. *Phytother. Res.* **2008**, *22*, 506−510.
(38) Basu, A.; Lucas, E. A. Mechanisms and effects of green tea on cardiovascular health. *Nutr. Rev.* **2007**, *65*, 361−375.

(Millipore, Bedford, MA) water purification system. All other solvents and reagents used in the present study were of HPLC grade or analytical grade.

Preparation of Standard Solutions. A stock standard solution containing thiabendazole was prepared by weighing the analytical standard and dissolving it in methanol. One set of working standard solutions (0.01, 0.02, 0.1, 1, 2, and 5 mg/L) were prepared by diluting the stock solution or a working solution using methanol. All standard solutions were maintained in amber bottles at 4 °C.

Trials for Uptake Study. The application of thiabendazole was carried out by either spraying the pesticide directly on substrates (spraying treatment) or premixing thiabendazole with the substrates (premixing treatment). The substrates for shimeji and king oyster mushrooms consisted of cotton seed hulls (50%), corn cob (30%), rice bran (10%), and wheat bran (10%), and the amount of water was approximately 65%. The substrate for oyster mushroom consisted of cotton seed hulls (50%), corn cob (30%), rice bran (10%), and sawdust (10%), and the amount of water was approximately 70%.[17] Both nonsterilized and sterilized substrates were used in the study. The sterilization was carried out at 120 °C and 0.1 MPa for 2 h. Five substrates, i.e., one nonsterilized substrate and the four sterilized substrates, were treated with thiabendazole by either premixing or spraying treatment. In the spraying treatment, the suspension concentrate formulation containing 50% (w/v) of thiabendazole was sprayed on the substrates at the rate of 0.75 g a.i./m^2 using the JACTO-HD sprayer. In the premixing treatment, thiabendazole was premixed with the substrate at the ratio of 1:2500 (active ingredient:substrate, w/w). Then three edible fungi of mycelia were inoculated to the sterilized substrates which were treated with thiabendazole. Each experiment was carried out in a plot of 10 m^2.

The treated substrate samples were collected from each plot on days 0, 1, 3, 5, 7, 10, 14, 21, 28, 35, and 42 days after the application. The edible fungi were collected from each plot on days 3, 5, and 7 after producing mushroom. Based on the OCED guidelines,[18] the substrate sample was randomly collected from a minimum of 12 separate spots and the collected samples (total approximately 0.5 kg) were composted. In the mature stage, edible fungi samples (including pileus, stipe, and volva) were collected. Then, each of the three treated edible fungi samples (approximately 0.5 kg each) were separated into pileus, stipe, and volva, respectively. All samples were stored in individual polyethylene bags and stored a refrigerator at −20 °C until being analyzed.

Extraction and Cleanup. The analytical method for determination of the thiabendazole residues in the edible fungi parts and substrates was derived from the reference methods using the QuEChERS technique,[19−21] followed by LC−MS/MS analysis.

Extraction. Samples including fungus parts and the substrates were ground with dry ice before extraction. After the dry ice was sublimated, the ground sample (5.00 g) was weighted into an Erlenmeyer flask. Forty-five (45.0) mL of acetonitrile was added. The sample mixture was macerated using the homogenizer for 1 min. The probe of the homogenizer was rinsed with a portion of 5.0 mL of the extraction solvent (acetonitrile), and the rinsate was added to the extraction flask. The sample was transferred into a centrifuge tube containing anhydrous magnesium sulfate and mixed. The mixture was centrifuged at 10000*g* for 5 min. Then, a portion (5 mL) of the supernatant was transferred to a 15 mL plastic centrifuge tube for cleanup.

Cleanup. A QuEChERS packet containing 100 mg of PSA and 100 mg of ODS-C18 was added to the sample extract (5 mL of the supernatant). The sample mixture was vortexed for 2 min. After centrifugation (5 min, 10000*g*), a portion of the supernatant (1 mL) was transferred to another centrifuge tube and dried at 40 °C on the N-EVAP under a stream of nitrogen. The thiabendazole residues were dissolved in 1 mL of methanol. The extract was filtered through a 0.22 μm nylon filter into an autosampler vial. The sample was analyzed using LC−MS/MS.

LC−MS/MS Analysis. The LC−MS/MS analysis was carried out using the Agilent LC−MS/MS. The parameters used were as follows: mobile phase A, water containing 0.1% of formic acid (v/v); mobile phase B, methanol containing 0.1% of formic acid (v/v); injection volume 5 μL; flow rate 1.0 mL/min; mobile phase gradients of binary pump, 20% B (0−0.50 min), 50%-95% B (ramp, 0.51−2.00 min), 95% B (2.01−6.00 min), and 10% B (6.01−7.00 min); electrospray positive ionization (ESI+); gas flow 10 L/min; gas temperature 350 °C; nebulizer pressure 40 psi; capillary voltage 2800 V. The multiple reaction monitoring (MRM) transitions were 202 > 175 (collision energy, CE = 27) and 202 > 131 (CE = 35 V). Transition 202 > 131 was for quantitation. The retention time was 2.3 min.

Per the SANCO/10684/2009 Guideline,[22] calibration curves were obtained by plotting the concentrations of thiabendazole standards injected versus peak areas. The concentrations of thiabendazole in the samples were calculated using the peak areas obtained against the calibration curves.

RESULTS AND DISCUSSION

Method Validation. *Calibration, LOD, and LOQ.* The 6-point calibration curves were obtained ranging from 0.01 mg/L to 5 mg/L. The calibration curves showed good linearity with a typical correlation coefficient (R^2 > 0.990). These were used to calculate the concentrations of thiabendazole residues in edible fungi and substrates. The limit of quantitation (LOQ) was set to be the lowest fortification level at which acceptable recovery data (between 70% and 120%) were obtained.[23] Three fortification levels (0.01, 0.1, and 1.0 mg/kg) were analyzed for thiabendazole, and LOQ was set to 0.01 mg/kg for all matrices. The limit of detection (LOD) is defined as the lowest calibration standard used whose signal−noise ratio is found to be greater than 3.[23] In this work, the lowest calibration standard used was 0.01 mg/L and injection volume of 10 μL. Thus, LOD = 0.01 mg/L × 5 μL = 0.05 ng.

Table 1. Recoveries of Thiabendazole (n = 3)

matrix	spike level (mg/kg)	recovery (%)	RSD (%)
shimeji mushroom (*H. marmoreus*)	0.01	104.3	4.4
	0.1	87.9	13.1
	1.0	96.9	3.4
king oyster mushroom (*P. eryngii*)	0.01	84.8	4.9
	0.1	92.4	9.7
	1.0	78.6	8.5
oyster mushroom (*P. ostreatus*)	0.01	91.3	10.9
	0.1	86.2	4.1
	1.0	105.7	7.8
substrate	0.01	82.5	8.9
	0.1	76.2	11.1
	1.0	93.7	7.1

Accuracy and Precision. The accuracy was evaluated by determining the spike recoveries at various levels in a complex matrix. The precision of the method can be evaluated in terms of the relative standard deviation (RSD) of the spike recoveries. In this study, samples were prepared with a modified QuEChERS method. Acetonitrile was selected as the extraction solvent and then cleaned up with PSA and ODS-C18 sorbents. A total of three replicate measurements were performed for each fortification level and for each matrix. The data of spike recoveries are given in Table 1. The average recoveries ranged from 76.2% to 105.7% for thiabendazole in four different matrices, and the relative standard deviations (RSD) ranged from 3.4% to 13.1%. The recovery and precision results are acceptable according to China's National Standard.[23]

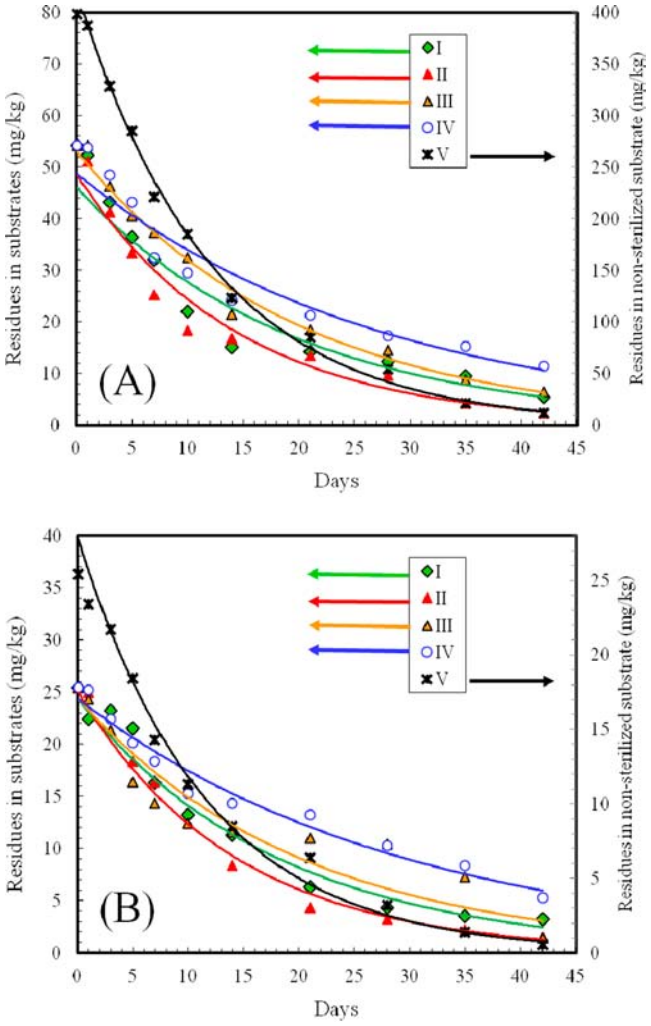

Figure 1. Degradation trends of thiabendazole in 5 different substrates for (A) premixing treatment and (B) spraying treatment. The substrates are as follows: (I) substrates with shimeji mushroom (*H. marmoreus*); (II) substrates with king oyster mushroom (*P. eryngii*); (III) substrates with oyster mushroom (*P. ostreatus*); (IV) sterilized substrates without mycelium; and (V) nonsterilized substrates. Left vertical axis for curves I, II, III, and IV; right vertical axis for curves V.

Degradation of Thiabendazole in Substrates. The degradation of thiabendazole in different substrates is modeled by a first-order equation,

$$C_t = C_0\, e^{-rt}$$

where C_t is the thiabendazole concentration at time t (days) after treatment, C_0 the initial concentration, and r the first-order rate constant (1/day). The degradation half-life ($t_{1/2}$) of thiabendazole is calculated by $t_{1/2} = \ln(2)/r$ in each experiment.[24−26] The degradation trends of thiabendazole in different substrates are shown in Figure 1. The data of half-lives and first-order equations are given in Table 2.

Premixing and Spraying Treatments. For premixing, the trends of degradation of thiabendazole in different substrates are shown in Figure 1A. In the five substrates, half-lives of thiabendazole were found to be 13.6 days for shimeji mushroom (*H. marmoreus*), 10.0 days for king oyster mushroom (*P. eryngii*), 13.7 days for oyster mushroom (*P. ostreatus*), 19.1 days for sterilized substrate, and 8.4 days for nonsterilized substrate, respectively, Table 2. The data indicate that sterilization at high temperature (120 °C) and high pressure (0.1 MPa) kill most of the microbials and thus a longer half-life for sterilized substrate was observed. However, the half-lives were 10−13.7 days in the substrates with the three fungi, indicating that the decrease in thiabendazole residue was due to either degradation resulting from the enzymes generated by the mushrooms or uptake by the edible fungi. The order of the half-lives is king oyster < shimeji mushroom ≈ oyster mushroom, suggesting that king oyster has the most effect on thiabendazole residues on the substrates.

For spraying, the half-lives and the trends of degradation are shown in Table 2 and Figure 1B, respectively. As can be seen in Table 2, the half-life data are consistent with those in the premixing treatment. Thus, the longest and shortest half-lives were found to be 19.5 and 8.1 days for the nonsterilized and sterilized substrates, respectively. Also, the order of the half-lives is nonsterilized < king oyster < shimeji mushroom ≈ oyster mushroom < sterilized.

The spraying treatment leads to higher residue concentration on the surfaces of the substrates while premixing is expected to generate homogeneous concentrations of thiabendazole in the substrates. The data suggest that the degradation of thiabendazole in substrates is not affected significantly by the means of pesticide treatments. It was reported that microorganism in mushroom substrates influenced the degradation of pesticide in the substrates.[27,28] Thus, spent mushroom substrates have been used as biofuel, for animal feeding, mushroom recultivation, soil bioremediation, and biodegradation of organic pollutants, as a soil conditioner, amendment, and fertilizer, for remediation of acidic mine wastewater, and as a sorbent for various heavy metals and organic pollutants.[27,28]

Thiabendazole Residues in Edible Fungi Parts. The thiabendazole residues in three edible fungi's parts (pileus, stipe, and volva) are listed in Table 3. For both spraying and premixing treatments, the highest residues of thiabendazole were found in volva and the lowest in stipe for all three mushrooms. This can probably be ascribed to the fact that the volva is a cuplike structure at the base of the mushroom and is often partially buried in the substrate, and therefore, more

Table 2. First-Order Kinetic Equations and Half-Lives of Thiabendazole

substrate	premixing treatment			spraying treatment		
	1st-order eq	half-life (day)	R^{2a}	1st-order eq	half-life (day)	R^2
substrates with shimeji mushroom (*H. marmoreus*)	$C_t = 46.141\, e^{-0.0508t}$	13.6	0.9390	$C_t = 24.393\, e^{-0.0546t}$	12.7	0.9692
substrates with king oyster mushroom (*P. eryngii*)	$C_t = 48.717\, e^{-0.069t}$	10.0	0.9704	$C_t = 25.126\, e^{-0.0709t}$	9.8	0.9874
substrates with oyster mushroom (*P. ostreatus*)	$C_t = 53.200\, e^{-0.0505t}$	13.7	0.9883	$C_t = 24.455\, e^{-0.0493t}$	14.1	0.7931
sterilized substrates	$C_t = 48.802\, e^{-0.0362t}$	19.1	0.9497	$C_t = 24.402\, e^{-0.0335t}$	19.5	0.9708
nonsterilized substrates	$C_t = 421.29\, e^{-0.0824t}$	8.4	0.9914	$C_t = 27.953\, e^{-0.086t}$	8.1	0.9814

[a]Correlation coefficient.

dx.doi.org/10.1021/jf405208h | J. Agric. Food Chem. 2014, 62, 1221−1226

Table 3. Thiabendazole Residues (mg/kg) in Edible Fungus Parts (Mean ± SD, n = 3)

	thiabendazole residues (mg/kg)											
	shimeji mushroom (*H. marmoreus*)				king oyster mushroom (*P. eryngii*)				oyster mushroom (*P. ostreatus*)			
days[a]	pileus	stipe	volva	P + S[b]	pileus	stipe	volva	P + S[b]	pileus	stipe	volva	P + S[b]
Spraying Treatment												
3	0.33 ± 0.07	0.14 ± 0.02	1.88 ± 0.12	0.18	0.46 ± 0.08	1.27 ± 0.22	2.88 ± 0.42	1.23	0.23 ± 0.04	0.14 ± 0.04	1.54 ± 0.14	0.19
5	0.36 ± 0.02	0.19 ± 0.05	1.98 ± 0.11	0.22	0.57 ± 0.11	1.69 ± 0.31	3.33 ± 0.37	1.63	0.25 ± 0.06	0.15 ± 0.08	1.86 ± 0.14	0.20
7	0.41 ± 0.02	0.22 ± 0.03	2.75 ± 0.17	0.26	0.46 ± 0.04	1.27 ± 0.19	2.88 ± 0.25	1.23	0.33 ± 0.02	0.18 ± 0.07	2.34 ± 0.23	0.26
Premixing Treatment												
3	0.23 ± 0.04	0.07 ± 0.06	1.44 ± 0.11	0.10	0.31 ± 0.02	0.58 ± 0.11	2.13 ± 0.42	0.57	0.14 ± 0.03	0.08 ± 0.03	1.43 ± 0.17	0.11
5	0.24 ± 0.06	0.11 ± 0.08	1.65 ± 0.18	0.14	0.34 ± 0.03	0.84 ± 0.14	2.43 ± 0.22	0.82	0.22 ± 0.05	0.12 ± 0.06	2.33 ± 0.22	0.17
7	0.25 ± 0.01	0.14 ± 0.01	1.17 ± 0.24	0.16	0.45 ± 0.01	1.22 ± 0.05	2.73 ± 0.51	1.18	0.24 ± 0.02	0.17 ± 0.08	2.53 ± 0.19	0.21

[a]Days are the number of days after producing of mushroom. [b]P + S = residues (pileus) × weight percent (pileus) + residues (stipe) × weight percent (stipe). The weight ratios (P:S, pileus to stipe) for *H. marmoreus*, *P. eryngii*, and *P. ostreatus* were 25:75, 5:95, and 50:50, respectively.

pesticide residues are taken by the volva part.[29,30] The spraying treatment results in higher residues of thiabendazole in three fungi (and their mushrooms' parts) than premixing treatment. The residues increase with increasing the number of growing days, except king oyster mushroom (*P. eryngii*) by spraying treatment. This can be understood as, when the fungi are cultivated longer, more thiabendazole residues are taken up from the substrate by the fungi. The highest residue was found in the oyster mushroom (*P. eryngii*) and day 5, however, the residue data of the oyster mushroom of days 3, 5, and 7 were identical within the experimental errors. The results indicate that the king oyster mushroom (*P. eryngii*) has the greater uptake ability of thiabendazole from substrates.

Typically, pileus and stipe are the edible parts of the mushrooms. The total residues (P + S) in the edible mushrooms are calculated by combining pesticide residues in the edible parts (pileus and stipe). Thus,

$$\mathrm{P + S} = \sum [(\text{residue}) \times (\text{weight percent})]$$

$$= (\text{residue in pileus}) \times (\%\text{pileus}) + (\text{residue in stipe}) \times (\%\text{stipe})$$

where the weight ratios (pileus to stipe) in the three different fungi (i.e., *H. marmoreus*, *P. eryngii*, and *P. ostreatus*) are 25:75, 5:95, and 50:50, respectively. Based on the mass balance, the total mass of extractable thiabendazole in the system decreased with the incubation time extended, since the residues in mushroom parts are increased slightly while those in the substrates decreased more rapidly. This indicates that the loss of thiabendazole in the substrates is due to the uptake by the mushrooms, degradation, and volatilization. The change in thiabendazole residues in the mushrooms may be caused by combined effects of mushrooms' uptake (increase residues), degradation by metabolism (decreasing residues), and dilution (growth, decreasing residues).[27,28,30]

The residues in edible fungi are important to human health and the environment. Compared with the existing maximum residue limits (MRLs) on mushroom in different countries and organizations, i.e., 5 mg/kg in China (preharvest interval is 14 days),[31] 40 mg/kg in the USA,[32] 60 mg/kg in Codex Alimentarius Commission,[33] and 10 mg/kg in the EU,[34] the thiabendazole residues in three mushrooms were found to be below 5 mg/kg, which is less than these established MRLs.

Plant uptake and distribution have been shown to be dependent on the physicochemical properties of the chemicals, the characteristics of the cultivation, and the plant species and physiology, including properties, such as lipid, enzymes, or water contents and transpiration rates.[30,35,36] It has been demonstrated that an aqueous extract of *P. pulmonarius* carpophores is able to reduce 89.8% of chlorothalonil concentration in a 1 h reaction. The fact is that this degradation rate was lower than the one observed with the spent mushroom substrates (100% in 45 min), indicating that microorganisms and enzymes other than *P. pulmonarius* were present in the spent substrate and contributed to degrade the insecticide faster.[37] Spent compost of oyster mushroom (*P. pulmonarius*) provides an integrated system of biosorption and biodegradation to remove pentachlorophenol. Spent mushroom substrates offer a nutrient source and an attachment substratum for a consortium of micro-organisms. In addition, it offers a solid support to the immobilized enzymes secreted by the mushroom during growth and fruiting.[38]

The study demonstrates that the thiabendazole residues in mushroom media (substrates) by spraying and premixing are readily taken up by three selected edible fungi and subsequently translocated as a function of time. The degradation rate of thiabendazole in nonsterilized substrates was the fastest and in sterilized substrates was the slowest, respectively, without mycelia present in the substrates. The thiabendazole residues in substrates show different degradation rates with edible fungus mycelia. These results also suggest that the thiabendazole uptake ability by *P. eryngii* is stronger than that of the other two fungi. Further research is needed to characterize the ability of the enzymatic system and the mycelia of edible fungi involved in the degradation of thiabendazole and other pesticides.

AUTHOR INFORMATION

Corresponding Author

*Tel: 86-25-84391116. Fax: 86-25-84390401. E-mail: yzuzzy@163.com.

Funding

This work was financially supported by the Natural Science Foundation of China (Grant No. 31000869). The authors wish to thank Michigan State University for the support.

Notes

The authors declare no competing financial interest.

REFERENCES

(1) Sadler, M. Nutritional properties of edible fungi. *Nutr. Bull.* **2003**, *28*, 305−308.

(2) Norikura, T.; Fujiwara, K.; Yanai, T.; Sano, Y.; Sato, T.; Tsunoda, T.; Kushibe, K.; Todate, A.; Morinaga, Y.; Iwai, K.; Matsue, H. *β*−Terphenyl derivatives from the mushroom *Thelephora aurantiotincta* suppress the proliferation of human hepatocellular carcinoma cells via iron chelation. *J. Agric. Food Chem.* **2013**, *61*, 1258−1264.

(3) Yang, T. K.; Lee, Y. H.; Paudel, U.; Bhattarai, G.; Yun, B. S.; Hwang, P. H.; Yi, H. K. Davallialactone from mushroom reduced premature senescence and inflammation on glucose oxidative stress in human diploid fibroblast cells. *J. Agric. Food Chem.* **2013**, *61*, 7089−7095.

(4) Wu, X. Q; Ge, X. S.; Liang, S. X.; Sun, H. W. A Highly Sensitive method for the determination of thiophanate methyl, cyromazine, and their metabolites in edible fungi by ultra-performance liquid chromatography using accelerated solvent extraction and cleanup with solid-phase extraction. *Food Anal. Methods* **2013**, DOI: 10.1007/s12161-013-9680-y.

(5) Llorent-Martínez, E. J.; Fernández-de Córdova, M. L.; Ruiz-Medina, A.; Ortega-Barrales, P. Fluorimetric determina tion of thiabendazole residues in mushrooms using sequential injection analysis. *Talanta* **2012**, *96*, 190−194.

(6) Environmental Protection Agency, EPA-738-F-02-002, 2002.

(7) Cacho, C.; Schweitz, L.; Turiel, E.; Pérez-Conde, C. Molecularly imprinted capillary electrochromatography for selective determination of thiabendazole in citrus samples. *J. Chromatogr., A* **2008**, *1179*, 216−223.

(8) Blažková, M.; Rauch, P.; Fukal, L. Strip-based immunoassay for rapid detection of thiabendazole. *Biosens. Bioelectron.* **2010**, *25*, 2122−2128.

(9) Jamieson, J. A.; Duncan, J. Determination of thiabendazole residues in potatoes using high pressure liquid chromatography. *Potato Res.* **1989**, *32*, 123−126.

(10) Schirra, M.; D'hallewin, G.; Cabras, P.; Angioni, A.; Ben-Yehoshua, S.; Lurie, S. Chilling injury and residue uptake in cold-stored 'Star Ruby' grapefruit following thiabendazole and imazalil dip treatments at 20 and 50°C. *Postharvest Biol. Technol.* **2000**, *20*, 91−98.

(11) Waite, D. T.; Cessna, A. J.; Grover, R.; Kerr, L. A.; Snihura, A. D. Environmental concentrations of agricultural herbicides: 2,4-D and triallate. *J. Environ. Qual.* **2002**, *31*, 129−144.

(12) Duttweiler, D. W.; Malakhov, S. G. USA-USSR Symposium on environmental transport and transformation of pesticides. *J. Agric. Food Chem.* **1977**, *25*, 975−978.

(13) Travis, C. C.; Arms, A. D. Bioconcentration of organics in beef, milk, and vegetation. *Environ. Sci. Technol.* **1988**, *22*, 271−274.

(14) Jones, K. C.; Keating, T.; Diage, P.; Chang, A. C. Transport and food chain modeling and its role in assessing human exposure to organic chemicals. *J. Environ. Qual.* **1991**, *20*, 317−329.

(15) Dowdy, D. L.; McKone, T. E. Predicting plant uptake of organic chemicals from soil or air using octanol/water and octanol/air partition ratios and a molecular connectivity index. *Environ. Toxicol. Chem.* **1997**, *16*, 2448−2456.

(16) Thomas, G. O.; Sweetman, A. J.; Jones, K. C. Input−output balance of polychlorinated biphenyls in a long-term study of lactating dairy cows. *Environ. Sci. Technol.* **1999**, *33*, 104−112.

(17) Qu, M. Q. Study on residue and bioaccumuiation of pesticides in three edible fungi. Master degree Thesis. Jilin Agricultural University. May 2006.

(18) OECD guideline for the testing of chemicals-Crop field trial. Available online: http://www.oecd-ilibrary.org/docserver/download/fulltext/9770901e.pdf?expires=1343889849&id=id&accname=freeContent&checksum=762477549C26EA9C6DAD0719C7130351. Accessed: September 2009.

(19) Lehotay, S. J. Validation of a fast and easy method for the determination of residues from 229 pesticides in fruits and vegetables using gas and liquid chromatography and mass spectrometric detection. *J. AOAC Int.* **2005**, *88*, 595−614.

(20) Norman, S. M.; Fouse, D. C.; Craft, C. C. Thiabendazole residues on and in citrus. *J. Agric. Food Chem.* **1972**, *20*, 1227−1230.

(21) Lafuente, M. T.; Tadeo, J. T.; Tuset, J. J. GLC analysis of thiabendazole residues in citrus fruit. *J. Chromatogr. Sci.* **1987**, *25*, 84−87.

(22) SANCO/10684/2009. Method validation and quality control procedures for pesticide residue analysis in food and feed. Document No. SANCO/10684/2009 Supersedes Document No. SANCO/3131/2007. Implemented by 01/01/2010.

(23) NY/T 788-2004. *Guideline on pesticide residue trials*; China agriculture press: Beijing, China, 2004.

(24) Ma, Q.; Rahman, A.; Holland, P. T.; James, T. K.; McNaughton, D. E. Field dissipation of acetochlor in two New Zealand soils at two application rates. *J. Environ. Qual.* **2004**, *33*, 930−938.

(25) Zhang, X.; Shen, Y.; Yu, X. Y.; Liu, X. J. Dissipation of chlorpyrifos and residue analysis in rice, soil and water under paddy field conditions. *Ecotoxicol. Environ. Saf.* **2012**, *78*, 276−280.

(26) Zhang, Z. Y.; Shan, W. L.; Song, W. C.; Gong, Y.; Liu, X. J. Phytotoxicity and uptake of chlorpyrifos in cabbage. *Environ. Chem. Lett.* **2011**, *9*, 547−552.

(27) Chiu, S. W.; Law, S. C.; Ching, M. L.; Cheung, K. W.; Chen, M. J. Themes for mushroom exploitation in the 21st century: Sustainability waste management, and conservation. *J. Gen. Appl. Microbiol.* **2000**, *46*, 269−282.

(28) Paredes, C.; Medina, E.; Moral, R.; Pérez-Murcia, M. D.; Moreno-Caselles, J.; Bustamante, M. A.; Cecilia, J. A. Characterization of the different organic matter fractions of spent mushroom substrate. *Commun. Soil Sci. Plant Anal.* **2009**, *40*, 150−161.

(29) Kirk, P. M.; Cannon, P. F.; Minter, D. W.; Stalpers, J. A. *Dictionary of the Fungi*, 10th ed.; CAB International: Wallingford, U.K., 2008; p 727.

(30) Karanasios, E.; Tsiropoulos, N. G.; Karpouzas, D. G.; Ehaliotis, C. Degradation and Adsorption of Pesticides in Compost-Based Biomixtures as Potential Substrates for Biobeds in Southern Europe. *J. Agric. Food Chem.* **2010**, *58*, 9147−9156.

(31) GB 2763-2012 (National Food Safety Standards of China). *National food safety standard maximum residue limits for pesticides in food*; Standards Press of China: Beijing, 2012.

(32) The USA's Tolerances and exemptions for pesticide chemical residues in food. Available online at: http://www.ecfr.gov/cgi-bin/text-idx?SID=15c783413ee662fc2f05b76e6ffb2bfb&node=40:25.0.1.1.27.3.19.65&rgn=div8.

(33) CAC's maximum residue limits (MRLs) for pesticides. Available online at: http://www.codexalimentarius.org/standards/list-of-standards/en/?provide=standards&orderField=fullReference&sort=asc&num1=CAC/MRL.
(34) European pesticide residues and maximum residue levels database, Regulation (EC) No. 396/2005. Available online at: http://ec.europa.eu/sanco_pesticides/public/index.cfm?event=substance.resultat&s=1.
(35) Paterson, S.; Mackay, D.; McFarlane, C. A model of organic chemical uptake by plants from soil and the atmosphere. *Environ. Sci. Technol.* **1994**, *28*, 2256−2259.
(36) Ling, W. T.; Zhu, L. Z.; Gao, Y. Z.; Xiong, W. Root uptake and its prediction model of PAHs from soils. *Acta Ecol. Sin.* **2005**, *25*, 2320−2325.
(37) Juárez, R. A.; Dorry, L. L.; Bello-Mendoza, R.; Sánchez, J. E. Use of spent substrate after *Pleurotus pulmonarius* cultivation for the treatment of chlorothalonil containing wastewater. *J. Environ. Manage.* **2011**, *92*, 948−952.
(38) Law, W. M.; Lau, W. N.; Lo, K. L.; Wai, L. M.; Chiu, S. W. Removal of biocide pentachlorophenol in water system by the spent mushroom compost of *Pleurotus pulmonarius*. *Chemosphere* **2003**, *52*, 1531−1537.

transplanted to the field. Plants were visually screened for red coloration phenotype. Target *RG* mutant had the inflorescence bagged upon emergence for self-pollination. *RG* M_{1-3} lines were bagged and followed by single-seed descent and progeny phenotypically scored for leaf coloration.

Morphological Characterization of *RG*. Phenotype was examined over the course of three generations. Three discrete zones are defined in the *RG* leaf, the green zone (no red), the transition zone where green and red tissues are present, and the red zone, which comprises the red area of the leaf (no green, phase 3). Chlorophyll content was measured[12] (n = 4 leaf disks per leaf from n = 10 plants).

Spectrophotometric Analyses. Extraction and pigment quantification were carried out on fully expanded *RG* and wild type leaves (dried for 2 days at 37 °C). Each biological sample comprised the same physiological and ontological leaf type from multiple plants (n = 10), and four biological pool replicates were used. For the analysis of total pigments, sample (10 mg) was extracted in acidified methanol (1 mL HCl/100 mL) and centrifuged, and supernatant absorbance measured at 480 nm as previously described.[7] 3-Deoxyanthocyanin content was estimated as luteolinidin equivalents (ε = 31000), because it was the dominant pigment in the samples. Total phenolic were measured as ferulic acid equivalents as previously described.[13] Condensed tannins were estimated using the vanillin−HCl method described by Butler et al.[14] Chlorogenic acid was determined as described.[15]

HPLC and LC-MS Analysis. Analysis of 3-deoxyanthocyanidin composition in sorghum leaf tissue was performed using a HPLC-DAD (Agilent 1200 system) as previously described.[8] A Kinetex C18 75 × 4.6 mm i.d. column (Phenomenex, Torrance, CA, USA) thermostated at 40 °C was used; UV−vis spectra were collected between 200 and 700 nm. LC-MS analysis was performed by a reverse phase quadrupole time-of-flight (Q-TOF) mass spectrometer equipped with an Agilent Jet Stream electrospray ionization (ESI) ion source with continuous introduction of reference mass compounds: 121.050873, 922.009798 (positive ion mode) (QTOF MS/MS) on an Agilent 1200 LC stack interfaced with an Agilent 6530A (Agilent Technologies, Santa Clara, CA, USA). Samples (5 μL) were separated using an Acquity BEH Shield RP-18 analytical column (1.7 μm 2.1 × 150 mm, Waters Corp., Milford, MA, USA) maintained at 40 °C. Sample analysis was triplicated. The MS/MS data were used to infer the anthocyanidin species. Quantification of the 3-deoxyanthocyanins was achieved by comparing HPLC peak areas at 480 nm to those obtained using pure standards (apigeninidin, luteolinidin, 7-*O*-methylluteolinidin, 7-*O*-methylapigeninidin, 5-*O*-methylapigeninidin, 5,7-*O*-dimethylluteolinidin, and 5,7-*O*-dimethylapigeninidin). The 3-deoxyanthocyanin standards were purchased from AlsaChim (Strasbourg, France); all standards were at least 97% pure.

Dihydroflavonolreductase (DFR) Activity. Plant samples were homogenized in liquid N_2 and total protein extracted.[16] Protein concentration was measured and standardized between samples using the Bradford method; the DFR activity was measured according to the method in ref 17. The absorbance due to cyanidin in the butanol solvent at 550 nm (absorption coefficient = 34.7)[18] was normalized for the 550 nm absorbance due to chlorophyll at 600 nm (absorbance at 550 nm − absorbance at 600 nm). Control used heat-inactivated enzyme. (n = 3 biological pooled samples each comprising five leaves.)

Statistical Analysis. Statistical analyses consisted of Student's t test or one-way ANOVA with a post hoc Tukey test and performed using PRISM4 (Graphpad, La Jolla, CA, USA) (significance established at $P < 0.05$).

RESULTS

Identification of *REDforGREEN* (*RG*). Within an M_1 generation of chemically mutagenized *S. bicolor* L. var. Della, the *RG* mutant was identified from approximately 12000 M_1 individuals on the basis of distinct red coloration of lamina tissue throughout development, which carried through to subsequent M_2 and M_3 generations. Self-pollination of the M_1 *RG* selection resulted in 761 M_2 generation individuals. These inherited the trait in a nearly 3:1 ratio of red coloration of lamina (*RG*) to wild type (green lamina) (567:194, χ^2 = 0.05573, df = 1, P = 0.4067), which would be expected for a dominant allele. Furthermore, the single wild type segregant failed to inherit the trait in subsequent generations. Two subsequent backcrosses were made between the red coloration mutant *RG* and wild type *S. bicolor* L. var. Della (referred to throughout as wild type). Each backcross was carried through to the M_2 generation and the inheritance examined. Interestingly, the heterozygous individuals failed to carry lighter lamina pigmentation than homozygous *RG*, suggesting the *RG* allele in the heterozygote was fully penetrant. The progeny of the M_2 were examined to determine homozygosity of the allele and the homozygote used in the third backcross. Both rounds of backcrossing resulted in 3:1 red versus green lamina coloration, consistent with single gene dominant inheritance of the target allele. The third backcross *RG* line was used during mutant characterization.

Between 3 and 5 days post-germination *RG* displayed no distinguishable difference from the sorghum wild type seedling. Onset of pigmentation was evident from the cotyledon and each true leaf lamina thereafter (Figure 1). Upon the leaf completing expansion, light-driven pigment accumulation initiated at the leaf apex and progressed to the base, termed basipetal accumulation (Figure 1A−N). Subsequent basipetal progression of red coloration occurred in all lamina during the plant life cycle (Figure 1). Visual examination indicated that coloration was predominantly interveinal (Figure 1B,C). As a general trend, basipetal red/purple coloration of lamina began after cellular expansion had plateaued. The red/purple coloration therefore progressed in a hierarchical manner (with the earliest emerged leaves being fully red, and newly emerged and expanding leaves being green). This phenotype led to a continuum of green terminal leaves and red fully expanded leaves. Red/purple leaf coloration extended partially into the leaf sheath (shown in Figure 1L−N). The process of complete red/purple coloration of the lamina took progressively longer (2 days for leaves 1−3 to 21 days for leaves subtending the inflorescence).

Spectrophotometric Determination of Pigment and Related Polyphenols. To estimate the pigment accumulation, we spectrophotometrically quantified (as luteolinidin equivalents, LUTe)[7] pigments in whole lamina at various temporal points during leaf development (leaves 1−2, 3, 5, and 7; Figure 2A). Fully pigmented *RG* leaves were compared with leaves from a wild type plant at the identical spatial and temporal ontology. Results demonstrated (1) that pigments accumulated until reaching a plateau level (Figure 2A) and (2) a >20-fold LUTe increase in the *RG* leaf material compared with wild type, with a maximum value of 10.05 mg g^{-1} db LUTe in *RG* (Figure 2A). The LUTe levels observed in the *RG* leaves were much higher than those reported for high-pigment black sorghum grains[7] and are economically relevant when current anthocyanin pigment yield from commercial sources, such as red cabbage, are considered.[19]

Measurements of total phenolics, condensed tannins, and chlorogenic acid content were also completed in *RG* and wild type leaves (Figure 2B−D). Results showed that the *RG* accumulated between 2- and 6-fold greater total phenolics than wild type ($P < 0.05$; Figure 2B). Condensed tannins also were up to 4-fold higher in the *RG* leaf material when compared with wild type leaf ($P < 0.05$; Figure 2C). As a general trend, total phenolics and tannins positively correlated with the LUTe

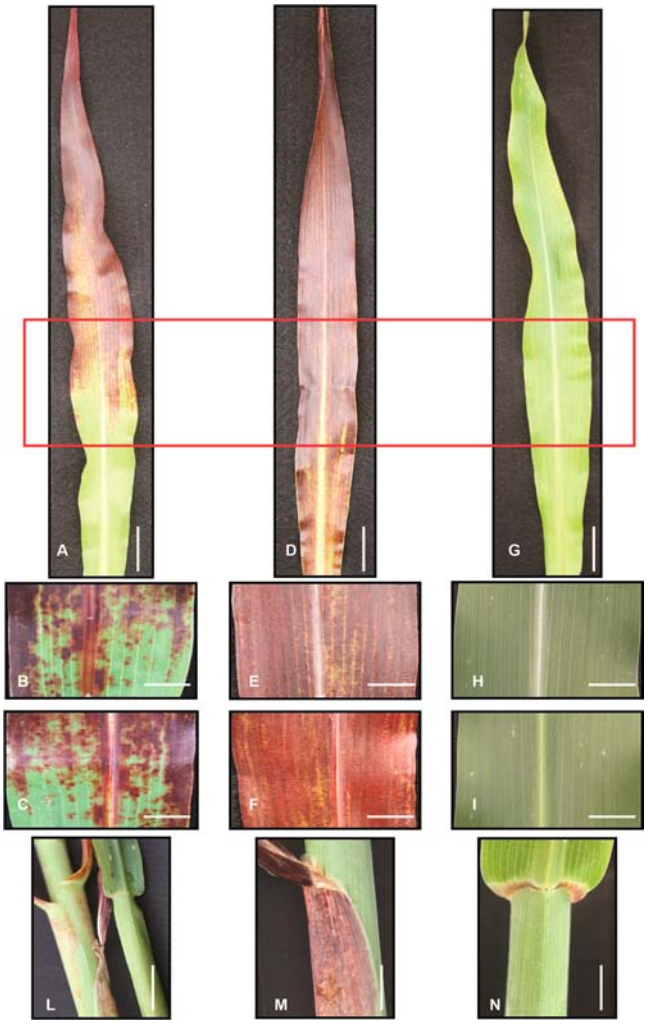

Figure 1. *RG* phenotype development (basipetal progression of pigment accumulation in *RG* leaves): (A, D) full-length leaves of *RG* partially and fully pigmented; (G) wild type leaf with no pigment (scale bar = 2 cm); (B, E, H) detailed image of the abaxial leaf surface with evidence of transition from red to green (B), completed accumulation and no green tissue (E), and all green tissue in WT (H); (C, F, I) detailed view of the adaxial leaf surface; (L, M, N) leaf sheath displaying pigment accumulation for *RG* but not for the wild type (scale bar = 1 cm); (A) 2-week-old plantlet with evidence of pigment accumulation (scale bar = 1 cm); (B) comparison and progression of pigment accumulation on cotyledon, first and second leaf of *RG*, and WT (scale bar = 1 cm).

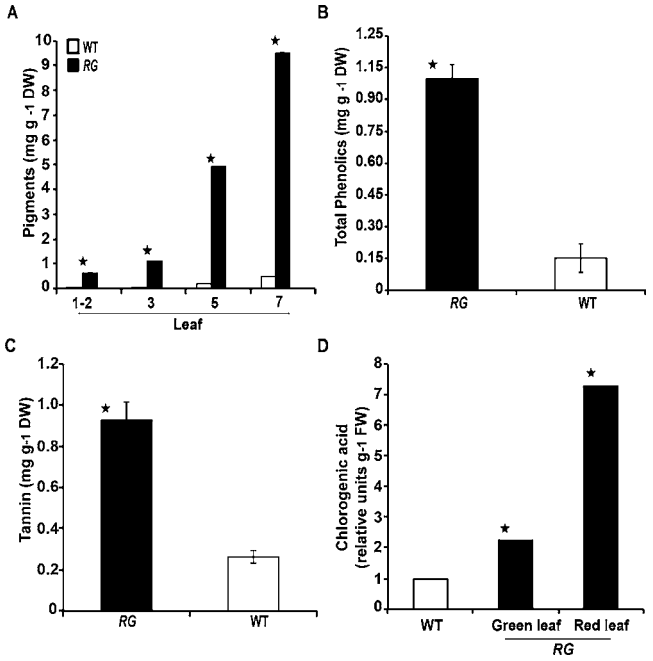

Figure 2. Metabolite analyses for the *RG* and WT leaf tissues: (A) pigment evaluation across a developmental gradient (leaves 1−7); (B) total phenolics estimation; (C) soluble tannin quantification; (D) chlorogenic acid evaluation on wild type (WT) and *RG* green and red leaf tissue (expressed as a relative unit per gram of fresh weight (FW)). (n = 4 biological pooled sample each containing 10 leaves.) Significance ($P < 0.05$) is indicated by a star (★). DW, dry weight.

pigments, thus suggesting a coordinated metabolic response in the *RG* mutant leaves. In agreement with this trend, chlorogenic acid content was also higher in the *RG* mutant versus the wild type, with the red leaf being up to 7-fold greater and the *RG*-green being up to 2-fold greater than the wild type (Figure 2D). The presence of other polyphenols generally helps to stabilize the pigments via condensation reactions or copigmentation;[20,21] thus, the coaccumulation of the non-pigmented polyphenols may improve functionality of the 3-deoxyanthocyanins from the leaf tissue. Additionally, there is a potential for the *RG* leaves to serve as a source of bioactive dietary polyphenols.

Chemical Characterization of Pigment Composition. The specific composition of accumulated pigments was investigated using HPLC and LC-MS. We identified LUT as the dominant 3-deoxyanthocyanidin compound in the *RG* leaf, accounting for 68% of resolved 3-deoxyanthocyanin peaks, followed by apigeninidin (APG) (16%), and 7-*O*-methyl-luteolinidin (13%) (Table 1; Figure 3). Results demonstrated 1768 μg g^{-1} db LUT was present in RG leaves compared to trace amounts in wild type (Table 1). Low levels of 7-*O*- and 5-*O*-glucosides and diglycosides of LUT and APG, as well as 7-*O*- and 5-*O*-glucosides and diglycosides of *O*-methyl derivatives of LUT and APG, were also detected (Figure 3). In addition, dimers of LUT and its 7-*O*-methyl derivative were also detected at low levels (Figure 3); such dimers (apigenin- or luteolin-flavene dimer) were recently reported as highly stable compared to the monomeric 3-deoxyanthocyanins.[8] In general, LUT and its derivatives accounted for >80% of total 3-deoxyanthocyanins, whereas APG and its derivatives accounted for the rest (Table 1). The 3-deoxyanthocyanin composition of the *RG* was generally comparable to the typical composition observed in sorghum grains derived from purple plant phenotypes.[22] Thus, the potential performance of these pigments as natural food colorants should be equivalent to those previously reported.[7−23]

LC-MS data revealed the presence of significant quantities of various mono- and diglycosides of the flavones luteolin and apigenin (Table 2). These flavones are common components of sorghum grain and tissue;[24] however, the extensive degree of glycosylation with glucose, galactose, and rhamnose observed in this study is not typically reported for sorghum. Interestingly, the relative proportions of the glycosides of luteolin and apigenin seemed to match the relative proportions of LUT and APG pigments, yet the luteolin glycosides were much more predominant. The higher proportion of LUT family pigments and corresponding luteolin-based flavones compared to APG/

dx.doi.org/10.1021/jf405324j | J. Agric. Food Chem. 2014, 62, 1227−1232

Table 1. Composition of the Major 3-Deoxyanthocyanidins from Sorghum Leaves of the *RG* and Wild Type (WT) (Micrograms per Gram, Dry Weight)

RT[a] (min)	6.7	10.7	11.7	14.7	17.4	19.0	19.7	
compound[b]	**LUT**	**APG**	**7MeOH LUT**	**5MeOH**	**7MeOH APG**	**DiMeOH LUT**	**DiMeOH APG**	**total**
RG	1768	421	336	31.2	38.8	trace	16.5	2612
WT	trace	trace	trace	0	0	0	0	

[a]RT, HPLC retention time. [b]LUT, luteolidin; APG, apigeninidin; 7MeO,: 7-*O*-methyl; 5MeOH, 5-*O*-methyl; DiMeOH, 5,7-dimethyl.

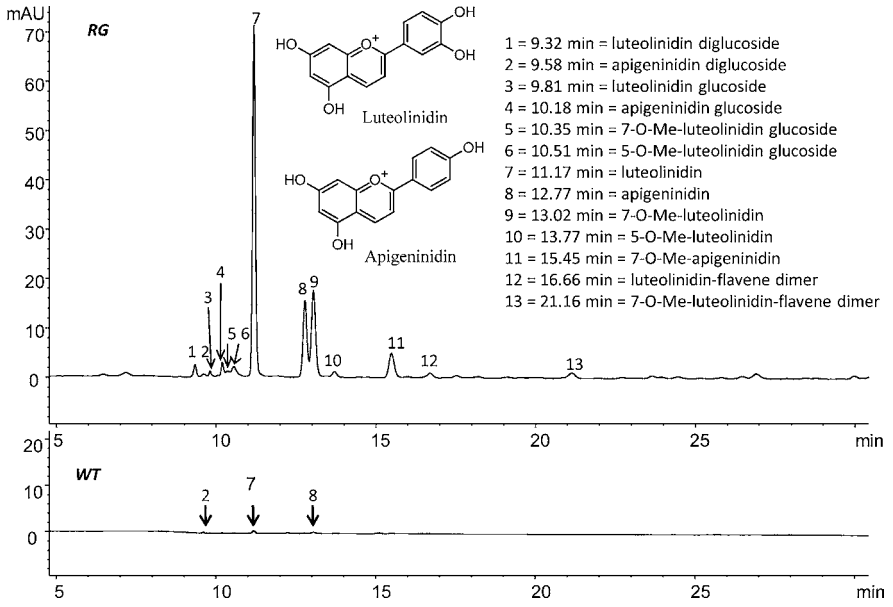

Figure 3. HPLC analysis of 3-deoxyanthocyanidins in *RG* and WT leaves: HPLC chromatograms of *RG*-3-deoxyanthocyanidins extracted from *RG* and WT sorghum. The 3-deoxyanthocyanidins peaks are numbered, and the corresponding names are reported in the top right corner. The chromatogram was recorded at the wavelength of 480 nm.

Table 2. Mass Spectrometric Data Obtained for Luteolin-Based Flavone Glycoside Peaks as They Appeared in Chromatograms from both Wild Type (WT) and *RG* Sorghum Samples

	m/z			
retention time	aglycon	parent ion, other diagnosticions	flavone glycoside	biomass, relative abundance[a]
6.54	271	595, 433, 397	luteolinidin-diglucoside	WT, *RG*
7.38	271	595, 433	luteolinidin-diglycoside	*RG* > WT
7.39	287	611, 449	luteolin diglucoside	*RG* > WT
7.47	287	449, 329, 299	luteolin 7-*O*-glucoside	*RG* > WT
7.82	287	449	luteolin 5-*O*-glucoside	*RG* > WT
8.06	287	449	luteolin 7-*O*-galactoside	WT, *RG*
8.34	287	595, 449	luteolin-*O*-glucoside-*O*-rhamnoside	WT, *RG*
8.64	287	449	luteolin-5-*O*-galactoside	*RG* > WT
9.10	287	595, 449	luteolin-*O*-galactoside-*O*-rhamnoside	*RG* > WT

[a]">" indicates peak area for extracted ions in the chromatograms was greater in one pooled sample over another. Not all peaks in the chromatograms were identified.

apigenin family of compounds has been reported for purple sorghum plant phenotype.[22] Red plant sorghum phenotypes, on the other hand, express the opposite effect, with the APG/apigenin compounds dominating.[22,24] In general, accumulations of most of these compounds were much higher in the *RG* compared to wild type, following the overall trend observed for the other phenolics.

Quantification of Seed Bran Pigments. The sorghum seed bran accumulates 3-deoxyanthocyanidins in the red, brown, and black varieties.[7−25] *S. bicolor* Della is a "brown" variety displaying accumulation of 3-deoxyanthocyanidin. However, no increase in the pigment content or in total phenolics was observed between the seed bran of *RG* and wild type (pigments: *RG*, 48 ± 8.6 μg g^{-1} seed; WT, 51 ± 6.2 μg g^{-1} seed), consistent with visual observations and the *RG* leaf specific accumulation of anthocyanins in the broad sense.

DFR Activity Supports Accumulation of 3-Deoxyanthocyanidins in *RG*. DFR catalyzes the reduction of dihydroflavonols to leucoanthocyanidins[26] and the conversion of naringenin to apiferol.[27] The DFR products are substrates for downstream steps in both branches of the PPP that lead to 3-deoxyanthocyanidins and 3-hydroxyflavonoids. Consistent with greater LUT and APG accumulations in *RG* (Tables 1 and 2), DFR activity (Figure 4) was significantly higher in the

dx.doi.org/10.1021/jf405324j | J. Agric. Food Chem. 2014, 62, 1227−1232

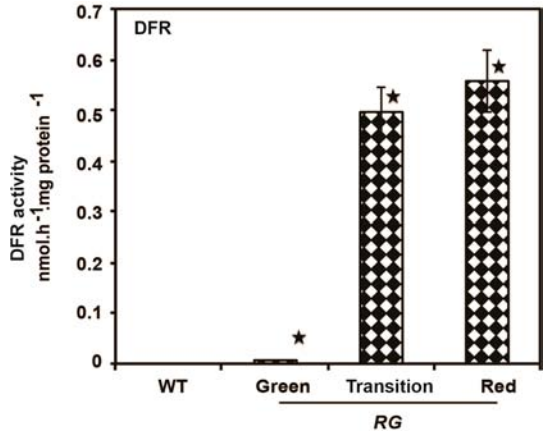

Figure 4. Estimation of the dihydroflavonolreductase (DFR) activity in *RG* leaves. The DFR activity was determined in green and red leaf tissues and compared to the wild type (WT) green tissues. (n = 3 biological pooled sample each containing 5 leaves.) Significance (P < 0.05) is indicated by a star (★).

RG red leaf tissue than in wild type (0.36 nmol h^{-1} mg $protein^{-1}$). Notably, despite a lack of anthocyanin in the green zone of *RG*, detectable DFR activity was observed, which was not the case for wild type leaves, suggesting early onset of precursor accumulation (Figure 4).

Pigment Progression Is Paralleled by Total Chlorophyll Reduction. The large and progressive increase in 3-deoxyanthocyanidins in the *RG* mutant led us to ask if in parallel there was an alteration in the chlorophyll content. It was found that no significant changes in total chlorophyll occurred in the green and transition zone, but a significant reduction in total chlorophyll was evident in the red zone (Figure 5A). A lower proportion of chlorophyll *a* versus chlorophyll *b* was observed (Figure 5B,C). Thus, total chlorophyll levels were not impeded in *RG* until the fully red leaf stage.

DISCUSSION

The suitability of sorghum 3-deoxyanthocyanin pigments as potential natural food colorants has been established in prior studies (pH stability and antioxidant).[23,28] Prior work has identified dark bran sorghum lines as possible sources for natural food colorants,[9] but the bran yield remains low relative to other parts of the plant. In this work we have sought to identify a sorghum plant (via mutagenesis-assisted breeding) with increased concentration of 3-deoxyanthocyanin in leaf tissue. Leaves are vastly more abundant than bran and can be easily stored and harvested using existing technology. *RG* displayed intense red/purple coloration of the normally green lamina tissue (Figure 1). The *RG* mutant accumulated a >1000-fold increase in 3-deoxyanthocyanidin structures LUT and AP (and variants thereof, Figure 3) in leaves. In addition, we identified by LC-MS/MS a range of glycosylated flavones, which also contribute to the complex phenolic fingerprint of the sorghum *RG* leaf. The *RG* mutant also caused an antithetic leaf-stem accumulation−depletion of lignin.[29] Increased aglycosylated flavones, 3-deoxyanthocyanin, and lignin suggest that the *RG* locus simultaneously influenced multiple branches in the phenylpropanoid pathway.

In our measurements, *RG* leaf material contained up to 10.1 mg of pigment per gram of dry leaf tissue. This concentration compares favorably to popular commercial sources of anthocyanin pigments, such as red cabbage, on a dry weight basis.[19] Because most commercial sources of anthocyanin colorants are succulent tissues high in moisture and enzyme activity, and thus having poor storability (e.g., purple carrots, sweet potatoes, and red cabbage), the opportunity to add sorghum leaf tissue to the mix seems interesting. Moreover, sorghum leaves are very thin and easy to dehydrate for transportation and/or long-term storage.

Many variables would influence the production of pigment from the *RG* mutant, and the agronomic appropriateness of the crop was not part of the current work scope. However, drawing rough estimates from agronomic data such as density of planting (typically, between 20000 nonirrigated and 60000 irrigated plants per acre), leaf yield (approximately 70:30 to 50:50 ratio of stem to leaf), and biomass per acre (between 6 and 13 tons per acre), the yield of pigment would be approximately between 27 and 45 kg/acre (or 67−111 kg/ha). This again compares favorably to pigment yield from, for example, red cabbage, of 17−98 kg/ha.[19] Additional advantages of using a high pigment accumulating sorghum variety (*RG*) to obtain 3-deoxyanthocyanins are that it displays C4 photosynthesis, which confers drought tolerance. A row crop alternative may also offer cost-effective planting and harvesting compared with below-ground crops (purple-fleshed sweet potato and carrots, which are limited to water and soil type constraints). However, it is important to note that the 3-deoxyanthocyanins are not replacements for anthocyanins, but are complementary to them, because each class of pigments displays distinctly

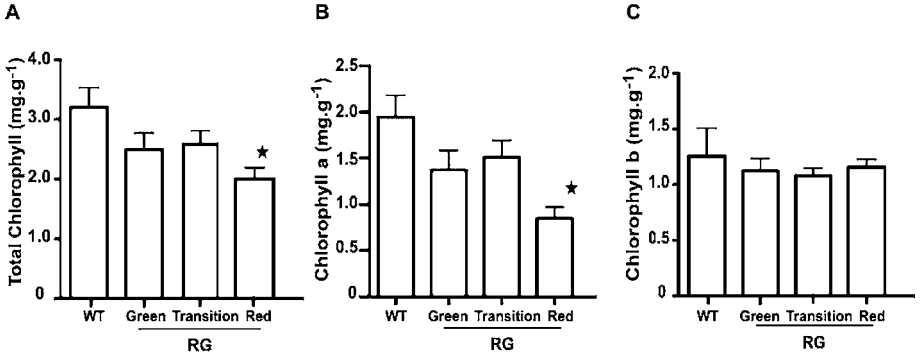

Figure 5. Chlorophyll estimation in *RG* and WT leaves: (A) total chlorophyll content for the *RG*, measurements made on red, green, and transition zone and compared to WT leaves at an equal developmental stage; (B, C) chlorophylls *a* and *b* were estimated as in (A). A star (★) indicates significant difference between the columns (four leaf disks for each leaf, leaf number = 6). (P < 0.05, ANOVA with a post hoc Tukey test.)

dx.doi.org/10.1021/jf405324j | J. Agric. Food Chem. 2014, 62, 1227−1232

different hues and would thus work in different applications or as blends to achieve expanded hues for water-soluble plant-based food colorants.

AUTHOR INFORMATION

Corresponding Author

*(S.D.) Phone: (859) 257 8654. Fax: (859) 257 2934. E-mail: sdebo2@uky.edu.

Funding

This work was supported by Grant NSF EFRI-0937657) (S.D., M.C.) and by the U.S. Department of Energy (DOE) under Award DE-FG36-O8GO88043. We gratefully acknowledge the financial support of the U.S. Department of Agriculture National Institute for Food and Agriculture, Biomass Research and Development Initiative Grant 2011-10006-30363 (M.T., S.D.) and Hatch KAES13-17.

Notes

The authors declare no competing financial interest.

REFERENCES

(1) Koukal, J.; Conn, E. E. The metabolism of aromatic compounds in higher plants. IV. Purification and properties of the phenylalanine deaminase of *Hordeum vulgare*. *J. Biol. Chem.* **1961**, *236*, 2692−2698.

(2) Kähkönen, M. P.; Heinämäki, J.; Ollilainen, V.; Heinonen, M. Berry anthocyanins: isolation, identification and antioxidant activities. *J. Sci. Food Agric.* **2003**, *83* (14), 1403−1411.

(3) Treutter, D. Significance of flavonoids in plant resistance: a review. *Environ. Chem. Lett.* **2006**, *4* (3), 147−157.

(4) Naoumkina, M. A.; Zhao, Q.; Gallego-Giraldo, L.; Dai, X.; Zhao, P. X.; Dixon, R. A. Genome-wide analysis of phenylpropanoid defence pathways. *Mol. Plant Pathol.* **2010**, *11* (6), 829−846.

(5) Das, P. K.; Shin, D. H.; Choi, S.-B.; Park, Y.-I. Sugar-hormone cross-talk in anthocyanin biosynthesis. *Mol. Cells* **2012**, *34* (6), 501−507.

(6) Lan, J. X.; Li, A. L.; Chen, C. X. Effect of transient accumulation of anthocyanin on leaf development and photoprotection of *Fagopyrum dibotrys* mutant. *Biol. Planta.* **2011**, *55* (4), 766−770.

(7) Awika, J. M.; Rooney, L. W.; Waniska, R. D. Properties of 3-deoxyanthocyanins from sorghum. *J. Agric. Food Chem.* **2004**, *52* (14), 4388−4394.

(8) Geera, B.; Ojwang, L. O.; Awika, J. M. New highly stable dimeric 3-deoxyanthocyanidin pigments from *Sorghum bicolor* leaf sheath. *J. Food Sci.* **2012**, *77*, C566−C572.

(9) Awika, J. M.; McDonough, C. M.; Rooney, L. W. Decorticating sorghum to concentrate healthy phytochemicals. *J. Agric. Food Chem.* **2005**, *53* (16), 6230−6234.

(10) Kayodé, A. P. P.; Nout, M. J. R.; Linnemann, A. R.; Hounhouigan, J. D.; Berghofer, E.; Siebenhandl-Ehn, S. Uncommonly high levels of 3-deoxyanthocyanidins and antioxidant capacity in the leaf sheaths of dye sorghum. *J. Agric. Food Chem.* **2011**, *59* (4), 1178−1184.

(11) Hipskind, J. D.; Hanau, R.; Leite, B.; Nicholson, R. L. Phytoalexin accumulation in sorghum − identification of an apigeninidin acyl ester. *Physiol. Mol. Plant Pathol.* **1990**, *36* (5), 381−396.

(12) Sims, D. A.; Gamon, J. A. Relationships between leaf pigment content and spectral reflectance across a wide range of species, leaf structures and developmental stages. *Remote Sensing Environ.* **2002**, *81* (2−3), 337−354.

(13) Singleton, V. L.; Orthofer, R.; Lamuela-Raventós, R. M. Analysis of total phenols and other oxidation substrates and antioxidants by means of Folin-Ciocalteu reagent. *Methods Enzymol.* **1999**, *299*, 152−178.

(14) Butler, L. G.; Price, M. L.; Li, C.; Hu, Q. Vanillin assay for proanthocyanidins (condensed tannins): modification of the solvent for estimation of the degree of polymerization. *J. Agric. Food Chem.* **1982**, *30* (6), 1087−1089.

(15) De Menezes, H. C. The relationship between the state of maturity of raw coffee beans and the isomers of caffeoylquinic acid. *Food Chem.* **1994**, *50* (3), 293−296.

(16) Aksamit-Stachurska, A.; Korobczak-Sosna, A.; Kulma, A.; Szopa, J. Glycosyltransferase efficiently controls phenylpropanoid pathway. *BMC Biotechnol.* **2008**, 8−25.

(17) Murray, J. R.; Hackett, W. P. Dihydroflavonol reductase activity in relation to differential anthocyanin accumulation in juvenile and mature phase *Hedera helix* L. *Plant Physiol.* **1991**, *97*, 343−351.

(18) Stafford, H. A.; Lester, H. H. Flavan-3-ol biosynthesis. The conversion of (+)-dihydroquercetin and flavan-3,4-diol (leucocyanidin) to (+)-catechin by reductases from cell suspension cultures of Douglas fir. *Plant Physiol.* **1984**, *76*, 184−186.

(19) Piccaglia, R.; Marotti, M.; Baldoni, G. Factors influencing anthocyanin content in red cabbage (*Brassica oleracea* var. *capitata* L. f. rubra (L) Thell). *J. Sci. Food Agric.* **2002**, *82* (13), 1504−1509.

(20) González-Paramás, A. M.; Lopes da Silva, F.; Martín-López, P.; Macz-Pop, G.; González-Manzano, S.; Alcalde-Eon, C.; Pérez-Alonso, J. J.; Escribano-Bailón, M. T.; Rivas-Gonzalo, J. C.; Santos-Buelga, C. Flavanol−anthocyanin condensed pigments in plant extracts. *Food Chem.* **2006**, *94* (3), 428−436.

(21) Awika, J. M. Behavior of 3-deoxyanthocyanidins in the presence of phenolic copigments. *Food Res. Int.* **2008**, *41* (5), 532−538.

(22) Dykes, L.; Rooney, L. W.; Waniska, R. D.; Rooney, W. L. Phenolic compounds and antioxidant activity of sorghum grains of varying genotypes. *J. Agric. Food Chem.* **2005**, *53* (17), 6813−6818.

(23) Ojwang, L.; Awika, J. M. Effect of pyruvic acid and ascorbic acid on stability of 3-deoxyanthocyanidins. *J. Sci. Food Agric.* **2008**, *88* (11), 1987−1996.

(24) Dykes, L.; Seitz, L. M.; Rooney, W. L.; Rooney, L. W. Flavonoid composition of red sorghum genotypes. *Food Chem.* **2009**, *116* (1), 313−317.

(25) Awika, J. M.; Rooney, L. W.; Waniska, R. D. Anthocyanins from black sorghum and their antioxidant properties. *Food Chem.* **2005**, *90* (1−2), 293−301.

(26) Gollop, R.; Even, S.; Colova-Tsolova, V.; Perl, A. Expression of the grape dihydroflavonol reductase gene and analysis of its promoter region. *J. Exp. Bot.* **2002**, *53* (373), 1397−1409.

(27) Lo, S.-C. C.; Nicholson, R. L. Reduction of light-induced anthocyanin accumulation in inoculated sorghum mesocotyls: implications for a compensatory role in the defense response. *Plant Physiol.* **1998**, *116* (3), 979−989.

(28) Ojwang, L. O.; Awika, J. M. Stability of apigeninidin and its methoxylated derivatives in the presence of sulfites. *J. Agric. Food Chem.* **2010**, *58* (16), 9077−9082.

(29) Petti, C.; Harman-Ware, A. E.; Tateno, M.; Kushwaha, R.; Shearer, A.; Downie, A. B.; Crocker, M.; DeBolt, S. Sorghum mutant *RG* displays antithetic leaf shoot lignin accumulation resulting in improved stem saccharification properties. *Biotechnol. Biofuels* **2013**, *6*, 146.

interaction with the origin of TMV RNA (oriRNA), exhibiting its virus inhibition by binding to oriRNA and interfering with virus assembly initiation.[19] Moreover, structure−activity relationship (SAR) studies showed that most compounds of the phenanthroindolizidine-based library with structural diversity exhibited antiviral effect against TMV.

In previous work, the SAR studies mainly focused on (1) substituted patterns of methoxyl group on the phenanthrene ring, (2) the number of methoxyl groups on the phenanthrene ring, (3) derivatation at the C-14 position, and (4) D ring opened derivatives.[20,21] However, there is no investigation on the variation of basic skeletons of phenanthroindo/quinolizines, which will largely change the conformation of the molecules. To study the influence of the variation of basic skeletons and conformations of these phenanthroindo/quinolizidine alkaloids, two types of structurally novel phenanthroindo/quinolizidine alkaloid analogues were designed, synthesized, and evaluated for their antiviral activity against TMV. The SAR study of these compounds against TMV is also discussed.

MATERIALS AND METHODS

Instruments. ^{1}H NMR spectra were obtained at 400 MHz using a Bruker AC-P 400. Chemical shift values (δ) were given in parts per million and were downfield from internal tetramethylsilane. High-resolution mass spectra (HRMS) were recorded on an FT-ICR MS (Ionspec, 7.0 T). Melting points were determined on an X-4 binocular microscope melting point apparatus (Beijing Tech Instruments Co., Beijing, China) and were uncorrected. Reagents were purchased from commercial sources and were used as received. All anhydrous solvents were dried and purified according to standard techniques just before use.

1-(2,3,6,7-Tetramethoxyphenanthren-9-yl)ethanone 3. To a solution of phenanthryl carboxylic acid (6.84 g, 20 mmol) in THF (100 mL) was added MeLi (28.8 mL, 1.6 M, 46 mmol) dropwise via a syringe at −78 °C under an atmosphere of nitrogen. The reaction mixture was stirred at this temperature for 30 min and then warmed to room temperature. Two hours later, saturated aqueous NH_4Cl (10 mL) was added to quench the reaction. After evaporation of THF, the aqueous layer was extracted with CH_2Cl_2 (80 mL × 3). The combined organic phase was washed sequentially with diluted aqueous HCl, water, and brine, dried over $MgSO_4$, filtered, and concentrated under reduced pressure. Crude product was recrystallized from MeOH to give compound **3** (5.2 g, 77%) as a white solid: mp 214−215 °C; ^{1}H NMR (400 MHz, DMSO) δ 8.44 (s, 1H), 8.41 (s, 1H), 7.98 (s, 1H), 7.95 (s, 1H), 7.53 (s, 1H), 4.07 (s, 3H), 4.04 (s, 3H), 3.94 (s, 3H), 3.89 (s, 3H), 2.77 (s, 3H); ^{13}C NMR (100 MHz, DMSO) δ 201.0, 151.2, 148.9, 148.8, 148.8, 130.3, 129.5, 126.5, 124.9, 124.0, 122.4, 109.6, 106.8, 103.7, 103.3, 55.9, 55.7, 55.4, 55.1, 29.5; HRMS (ESI) calcd for $C_{20}H_{20}NO_5Na$ $(M + H)^+$ 363.1203, found 263.1205.

***tert*-Butyl 2-(2-Oxo-2-(2,3,6,7-tetramethoxyphenanthren-9-yl)ethyl)pyrrolidine-1-carboxylate 5a.** To a solution of compound **3** (0.68 g, 2.0 mmol) and i-Pr_2NEt (0.38 g, 3.0 mmol) in CH_2Cl_2 (50 mL) was added TMSOTf (0.53 g, 2.4 mmol) in CH_2Cl_2 (10 mL) dropwise. The reaction mixture was stirred at room temperature for 4 h and then quenched with water (30 mL). After separation, the organic phase was washed sequentially with water and brine, dried over $MgSO_4$, filtered, and concentrated under reduced pressure. Crude product **4** was dissolved in CH_2Cl_2 (50 mL) without further purification, and then compound **2** (0.44 g, 2.18 mmol) was added. $BF_3{\cdot}Et_2O$ (3.0 mL, 30%) in CH_2Cl_2 (10 mL) was added dropwise at −78 °C. The reaction mixture was stirred at this temperature for 1 h, warmed to room temperature, and then quenched with diluted aqueous NaOH. After separation, the organic phase was washed with water and brine, dried over $MgSO_4$, filtered, and concentrated under reduced pressure. The residue was purified by column chromatography on silica gel to give compound **5a** (0.73 g, 72%) as a light yellow solid: mp 147−149 °C; ^{1}H NMR (400 MHz, $CDCl_3$) δ 8.51 (s, 1H), 8.33 (s, 1H), 7.80 (s, 1H), 7.77 (s, 1H), 7.32 (s, 1H), 4.44 (br, 1H), 4.15 (s, 3H), 4.13(s, 3H), 4.06 (s, 6H), 3.86 (d, J = 14.8 Hz, 1H), 3.40 (br, 2H), 3.10−2.98 (m, 1H), 2.13 (br, 1H), 1.89 (br, 3H), 1.48 (s, 9H); ^{13}C NMR (100 MHz) δ 199.2, 156.7, 152.2, 151.0, 150.4, 149.0, 130.3, 130.14 126.0, 125.1, 124.9, 123.5, 109.5, 107.2, 105.9, 102.6, 81.2, 56.1, 56.0, 55.9, 55.8, 46.0, 44.3, 33.1, 28.6, 24.9; HRMS (ESI) calcd for $C_{29}H_{36}NO_7$ $(M + H)^+$ 510.2486, found 510.2490.

2-(2-(2,3,6,7-Tetramethoxyphenanthren-9-yl)ethyl)-pyrrolidine 6a. To a solution of compound **5a** (0.37 g, 0.73 mmol) in EtOH (50 mL) was added $NaBH_4$ (0.1 g, 2.6 mmol). The reaction mixture was stirred at room temperature for 2 h and then quenched with water. After evaporation, the aqueous layer was extracted with CH_2Cl_2 (30 mL × 3). The combined organic phase was washed with brine, dried over Na_2SO_4, and concentrated under reduced pressure. Crude product was dissolved in CH_2Cl_2 (50 mL) without further purification, and then Et_3SiH (0.18 mL, 1.13 mmol) and CF_3COOH (0.33 mL, 4.4 mmol) were added. The reaction mixture was stirred at room temperature overnight and then quenched with diluted aqueous NaOH. After separation, the organic layer was washed with brine, dried over Na_2SO_4, and concentrated under reduced pressure. The residue was purified by column chromatography on silica gel to give compound **6a** (0.27 g, 93%) as a white solid: mp 224−226 °C; ^{1}H NMR (400 MHz, $CDCl_3$) δ 7.63 (s, 1H), 7.56 (s, 1H), 7.30 (s, 1H), 7.23 (s, 1H), 7.04 (s, 1H), 4.08 (s, 6H), 4.02 (s, 3H), 3.97 (s, 3H), 3.40−3.30 (m, 1H), 3.28−3.22 (m, 1H), 3.19−3.05 (m, 2H), 2.99−2.88 (m, 1H), 2.22−2.17 (m, 1H), 2.11−1.90 (m, 3H), 1.89−1.76 (m, 1H), 1.57−1.52 (m, 1H); ^{13}C NMR (100 MHz, $CDCl_3$) δ 148.4, 148.4, 148.3, 130.9, 125.9, 124.7, 124.5, 123.2, 122.9, 107.9, 104.1, 102.9, 102.2, 60.6, 56.2, 55.8, 55.8, 44.5, 31.9, 30.8, 30.3, 23.6; HRMS (ESI) calcd for $C_{24}H_{30}NO_4$ $(M + H)^+$ 396.2169, found 396.2168.

2,3,6,7-Tetramethoxy-11,12,13,13a,14,15-hexahydro-9*H*-phenanthro[9,10-e]pyrrolo[1,2-*a*]azepine 7a. To a solution of compound **6a** (0.2 g, 0.51 mmol) in toluene (20 mL) were added formaldehyde (1.0 mL, 30%) and CF_3COOH (0.5 mL, 6.7 mmol). A Dean−Stark trap topped with a reflux condenser was attached to the reaction vessel, and the reaction mixture was heated at reflux. Seven hours later, the solvent was evaporated under reduced pressure, and then aqueous NaOH was added to the residue. The aqueous solution was extracted with CH_2Cl_2 (30 mL × 3), and the combined organic phase was washed with brine, dried over Na_2SO_4, and concentrated under reduced pressure. The residue was purified by column chromatography on silica gel to give compound **7a** (0.18 g, 87%) as a light yellow solid: mp 178−180 °C; ^{1}H NMR (400 MHz, $CDCl_3$) δ 7.84 (s, 2H), 7.53 (s, 2H), 4.69 (s, 1H), 4.12 (s, 3H), 4.11 (s, 3H), 4.06 (s, 3H), 4.05(s, 3H), 3.88−3.83 (m, 1H), 3.65 (dd, J = 15.0, 7.5 Hz, 1H), 3.21 (s, 1H), 3.09 (t, J = 12.0 Hz, 1H), 2.69 (s, 2H), 2.22−2.10 (m, 1H), 2.00 (s, 1H), 1.78 (s, 2H), 1.57−1.40 (m, 2H); ^{13}C NMR (100 MHz, $CDCl_3$) δ 148.0, 147.8, 147.7, 147.5, 133.9, 127.4, 124.3, 123.8, 123.7, 122.9, 103.5, 103.2, 102.4, 102.3, 76.3, 76.0, 75.7, 55.0, 54.9, 54.8, 49.3, 30.2, 29.8, 28.7, 25.4, 19.9; HRMS (ESI) calcd for $C_{29}H_{30}NO_4$ $(M + H)^+$ 408.2169, found 408.2169.

2-(2,3,6,7-Tetramethoxyphenanthren-9-yl)acetonitrile 9. To a solution of compound **8** (7.2 g, 18.4 mmol) in DMF (150 mL) was added NaCN (1.0 g, 20.4 mmol). The reaction was stirred at room temperature for 5 h, and then solvent was evaporated under reduced pressure. Water and CH_2Cl_2 were added to the residue, and, after separation, the aqueous layer was extracted with CH_2Cl_2. The combined organic phase was washed with brine, dried over Na_2SO_4, filtered, and concentrated in vacuo. The residue was purified by column chromatography on silica gel to give compound **9** (4.2 g, 68%) as a white solid: mp 198−200 °C; ^{1}H NMR (400 MHz, $CDCl_3$) δ 7.86 (s, 1H), 7.77 (s, 1H), 7.70 (s, 1H), 7.23 (s, 1H), 7.14 (s, 1H), 4.14 (s, 3H), 4.13 (s, 3H), 4.12 (s, 2H), 4.07 (s, 3H), 4.05 (s, 3H); ^{13}C NMR (100 MHz, $CDCl_3$) δ 148.7, 148.3, 148.1, 148.0, 124.6, 123.9, 123.6, 123.4, 122.7, 120.3, 116.7, 107.2, 102.6, 102.3, 101.6, 55.1, 55.0, 54.9, 21.3; HRMS (ESI) calcd for $C_{20}H_{23}N_2O_4$ $(M + NH_4)^+$ 499.2551, found499.2552.

2-(2,3,6,7-Tetramethoxyphenanthren-9-yl)ethanamine 10. To a solution of compound **9** (0.3 g, 0.89 mmol) in THF (30 mL) was added BH_3 (2.7 mL, 1 M in THF) at 0 °C under an atmosphere of

nitrogen. Then, the reaction was heated at reflux for 3 h. After the mixture had cooled to room temperature, diluted aqueous HCl was added to quench the reaction. The mixture was heated at reflux for an additional 0.5 h and then was cooled to room temperature. The mixture was extracted with EtOAc, and the aqueous layer was basified by aqueous NaOH to pH >7. The aqueous layer was extracted with EtOAc and then washed with brine, dried over Na_2SO_4, filtered, and concentrated under reduced pressure to give compound **10** (0.25 g, 67%) as a white solid: mp 148−149 °C; ^{1}H NMR (400 MHz, $CDCl_3$) δ 7.82 (s, 1H), 7.75 (s, 1H), 7.44 (s, 1H), 7.38 (s, 1H), 7.17 (s, 1H), 4.11 (s, 3H), 4.09 (s, 3H), 4.05 (s, 3H), 4.02 (s, 3H), 3.21 (m, 4H), 2.2 (br, 1H); ^{13}C NMR (100 MHz, $CDCl_3$) δ 148.9, 148.8, 148.6, 130.8, 126.2, 125.3, 125.0, 124.6, 123.7, 107.9, 104.6, 103.4, 102.7, 56.1, 56.0, 55.9, 55.8, 41.8, 37.1; HRMS (ESI) calcd for $C_{20}H_{24}NO_4$ $(M + H)^+$ 342.1700, found 342.1702.

4-Oxo-4-((2-(2,3,6,7-tetramethoxyphenanthren-9-yl)ethyl)-amino)butanoic Acid 12a. To a solution of amine **10** (0.4 g, 1.17 mmol) in $CHCl_3$ (30 mL) was added dihydrofuran-2,5-dione (0.23 g, 2.34 mmol). The reaction was stirred at room temperature for 2 h, and then water (30 mL) was added and stirred for an additional 1 h. After separation, the aqueous layer was extracted with $CHCl_3$ (30 mL × 3). The combined organic phase was dried over Na_2SO_4, filtered, and concentrated under reduced pressure. The residue was purified by column chromatography on silica gel to give compound **12a** (0.46 g, 89%) as a white solid: mp 203−204 °C; ^{1}H NMR (400 MHz, DMSO) δ 8.16 (t, J = 5.2 Hz, 1H), 8.03 (s, 1H), 7.97 (s, 1H), 7.65 (s, 1H), 7.47 (s, 1H), 7.33 (s, 1H), 4.03 (s, 3H), 4.01 (s, 3H), 3.98 (s, 3H), 3.89 (s, 3H), 3.42−3.36 (m, 2H), 3.13 (t, J = 8 Hz, 2H), 2.46 (d, J = 6.4 Hz, 2H), 2.35 (t, J = 6.8 Hz, 2H); ^{13}C NMR (100 MHz, DMSO) δ 173.6, 171.1, 148.8, 148.7, 148.6, 148.5, 130.6, 125.8, 124.9, 124.5, 124.1, 123.3, 108.1, 105.0, 104.3, 103.7, 55.9, 55.8, 55.5, 55.3, 33.5, 30.1, 29.2; HRMS (ESI) calcd for $C_{24}H_{28}NO_7$ $(M + H)^+$ 442.1860, found 442.1866.

1-(2-(2,3,6,7-Tetramethoxyphenanthren-9-yl)ethyl)-pyrrolidine-2,5-dione 13a. To a solution of compound **12a** (0.46 g, 1.04 mmol) in Ac_2O (20 mL) was added AcONa (0.1 g). The reaction was stirred at 70 °C for 2 h and then cooled to room temperature. The reaction was quenched with water and stirred for an additional 1 h. After separation, the aqueous phase was extracted with CH_2Cl_2 (3 × 30 mL). The combined organic phase was dried over Na_2SO_4, filtered, and concentrated under reduced pressure. The residue was purified by column chromatography on silica gel to give compound **13a** (0.43 g, 98%) as a white solid: mp 262−263 °C; ^{1}H NMR (400 MHz, $CDCl_3$) δ 7.82 (s, 1H), 7.76 (s, 1H), 7.75 (s, 1H), 7.50 (s, 1H), 7.17 (s, 1H), 4.18 (s, 3H), 4.13 (s, 3H), 4.11 (s, 3H), 4.02 (s, 3H), 3.83 (t, J = 8.6 Hz, 2H), 3.25 (t, J = 8.6 Hz, 2H), 2.74 (s, 4H); ^{13}C NMR (100 MHz, $CDCl_3$) δ 177.2, 149.02, 148.9, 129.4, 126.21, 125.2, 124.8, 124.0, 107.9, 104.7, 103.3, 102.8, 77.3, 77.0, 76.7, 56.2, 56.1, 56.0, 55.9, 39.2, 32.1, 28.2; HRMS (ESI) calcd for $C_{24}H_{26}NO_6$ $(M + H)^+$ 424.1755, found 424.1754.

5-Hydroxy-1-(2-(2,3,6,7-tetramethoxyphenanthren-9-yl)-ethyl)pyrrolidin-2-one 14a. To a solution of compound **13a** (0.48 g, 1.13 mmol) in CH_2Cl_2 (20 mL) was added $LiEt_3BH$ (1 M, 2.2 mL) at −60 °C. The reaction mixture was stirred for 2 h and then quenched with water. After separation, the aqueous layer was extracted with CH_2Cl_2 (3 × 30 mL). The combined organic phase was dried over Na_2SO_4, filtered, and concentrated under reduced pressure. The residue was purified by column chromatography on silica gel to give compound **14a** (0.44 g, 92%) as a white solid: mp 187−188 °C; ^{1}H NMR (400 MHz, $CDCl_3$) δ 7.81 (s, 1H), 7.75 (s, 1H), 7.68 (s, 1H), 7.44 (s, 1H), 7.13 (s, 1H), 4.99 (s, 1H), 4.12 (s, 3H), 4.11(s, 3H), 4.10 (s, 3H), 4.06−4.02 (m, 1H), 4.00 (s, 3H), 3.82−3.72 (m, 1H), 3.67−3.63 (m, 1H), 3.39−3.29 (m, 2H), 2.63−2.52 (m, 1H), 2.37−2.19 (m, 2H), 1.82−1.77 (m, 1H); ^{13}C NMR (100 MHz, $CDCl_3$) δ 173.6, 148.1, 148.0, 147.9, 129.7, 125.2, 123.7, 122.9, 106.8, 103.9, 102.1, 101.8, 83.2, 55.2, 55.1, 55.0, 54.9, 40.7, 31.4, 27.9, 27.8; HRMS (ESI) calcd for $C_{24}H_{28}NO_6$ $(M + H)^+$ 426.1911, found 426.1913.

2,3,12,13-Tetramethoxy-5,6,10,10a-tetrahydrodibenzo[*f*,*h*]-pyrrolo[2,1-*a*]isoquinolin-8(9*H*)-one 15a. To a solution of compound **14a** (0.4 g, 0.94 mmol) in CH_2Cl_2 (20 mL) was added TMSI (0.44 g, 2.1 mmol) at −55 °C. The reaction was stirred for 1 h and then quenched with diluted aqueous NaOH. After separation, the aqueous layer was extracted with CH_2Cl_2 (3 × 30 mL). The combined organic phase was dried over Na_2SO_4, filtered, and concentrated under reduced pressure. The residue was purified by column chromatography on silica gel to give compound **15a** (0.3 g, 80%) as a light yellow solid: mp 222−224 °C; ^{1}H NMR (400 MHz, $CDCl_3$) δ 7.86 (s, 1H), 7.83 (s, 1H), 7.29 (s, 1H), 7.25 (s, 1H), 5.45 (br, 1H), 4.66 (d, J = 11.7 Hz, 1H), 4.13 (s, 6H), 4.06 (s, 3H), 4.05 (s, 3H), 3.18 (br, 2H), 3.14−2.98 (m, 2H), 2.71 (br, 1H), 2.48 (br, 1H), 1.80 (br, 1H); ^{13}C NMR (100 MHz, $CDCl_3$) δ 149.1, 148.7, 148.6, 128.9, 125.9, 125.5, 124.3, 123.7, 123.2, 123.1, 104.6, 104.2, 103.7, 103.3, 56.2, 56.1, 56.0, 36.6, 29.7, 29.1, 26.6; HRMS (ESI) calcd for $C_{24}H_{26}NO_5$ $(M + H)^+$ 408.1805, found 408.1805.

2,3,12,13-Tetramethoxy-5,6,8,9,10,10a-hexahydrodibenzo-[*f*,*h*]pyrrolo[2,1-*a*]isoquinoline 16a. To a solution of compound **15a** (0.29 g, 0.71 mmol) in THF (30 mL) was added $LiAlH_4$ (50.0 mg, 1.3 mmol). The reaction mixture was heated at reflux for 2 h and then quenched with diluted aqueous NaOH after cooling to room temperature. After separation, the aqueous layer was extracted with CH_2Cl_2 (3 × 30 mL). The combined organic phase was dried over Na_2SO_4, filtered, and concentrated under reduced pressure. The residue was purified by column chromatography on silica gel to give compound **16a** (0.23 g, 82%) as a light yellow solid: mp 155−158 °C; ^{1}H NMR (400 MHz, $CDCl_3$) δ 7.83 (s, 1H), 7.83 (s, 1H), 7.35 (s, 1H), 7.30 (s, 1H), 4.66 (t, J = 8.1 Hz, 1H), 4.12 (s, 6H), 4.05 (s, 6H), 3.25−3.16 (m, 2H), 3.15−3.04 (m, 4H), 2.73−2.69 (m, 1H), 2.04−1.92 (m, 2H), 1.84−1.72 (m, 1H); ^{13}C NMR (100 MHz, $CDCl_3$) δ 147.8, 147.5, 147.3, 147.2, 129.3, 124.5, 124.2, 123.5, 122.9, 122.4, 104.1, 103.2, 102.4, 102.3, 58.8, 55.1, 55.0, 54.9, 54.8, 51.9, 44.2, 31.2, 23.4, 22.4; HRMS (ESI) calcd for $C_{24}H_{28}NO_4$ $(M + H)^+$ 394.2013, found 394.2018.

2-(Piperidin-2-yl)-1-(2,3,6,7-tetramethoxyphenanthren-9-yl)ethanone 5b. The synthetic procedure was similar to that of compound **5a**, and compound **5b** was obtained as a light yellow solid (73%): mp 203−205 °C; ^{1}H NMR (400 MHz, DMSO) δ 8.55 (s, 1H), 8.45 (s, 1H), 8.07 (s, 1H), 8.03 (s, 1H), 7.64 (s, 1H), 4.09 (s, 3H), 4.06 (s, 3H), 3.95 (s, 3H), 3.90 (s, 3H), 3.85−3.77 (m, 1H), 3.69 (s, 1H), 3.57−3.55 (m, 1H), 3.26 (s, 2H), 2.97 (s, 1H), 1.94−1.91 (m, 1H), 1.77−1.75 (m, 4H); ^{13}C NMR (100 MHz, DMSO) δ 200.1, 151.5, 149.1, 149.0, 148.8, 130.0, 128.9, 126.7, 125.0, 123.9, 122.3, 109.7, 106.7, 103.8, 103.4, 56.0, 55.8, 55.5, 55.2, 52.6, 44.3, 28.9, 22.6, 22.2, 14.0; HRMS (ESI) calcd for $C_{25}H_{30}NO_5$ $(M + H)^+$ 424.2118, found 424.2123.

2-(2-(2,3,6,7-Tetramethoxyphenanthren-9-yl)ethyl)-piperidine 6b. The synthetic procedure was similar to that of compound **6a**, and compound **6b** was obtained as a white solid (88%): mp 175−176 °C; ^{1}H NMR (400 MHz, $CDCl_3$) δ 7.83 (s, 1H), 7.76 (s, 1H), 7.41 (s, 1H), 7.40 (s, 1H), 7.16 (s, 1H), 4.11 (s, 6H), 4.05 (s, 3H), 4.03 (s, 3H), 3.09 (t, J = 8.0 Hz, 3H), 2.71−2.59 (m, 2H), 1.89−1.82 (m, 4H), 1.64−1.61 (m, 2H), 1.52−1.32 (m, 2H); ^{13}C NMR (100 MHz, $CDCl_3$) δ 148.7, 148.5, 134.0, 126.4, 125.4, 124.9, 123.5, 107.9, 104.8, 103.4, 102.8, 77.3, 77.0, 76.7, 56.9, 56.1, 56.0, 55.9, 55.8, 47.2, 37.8, 33.0, 29.8, 26.7, 24.8; HRMS (ESI) calcd for $C_{25}H_{32}NO_4$ $(M + H)^+$ 410.2326, found 410.2331.

2,3,6,7-Tetramethoxy-9,11,12,13,14,14a,15,16-octahydrophenanthro[9,10-*e*]pyrido[1,2-*a*]azepine 7b. The synthetic procedure was similar to that of compound **7a**, and compound **7b** was obtained as a white solid (68%): mp 216−218 °C; ^{1}H NMR (400 MHz, $CDCl_3$) δ 7.83 (s, 2H), 7.50 (s, 1H), 7.45 (s, 1H), 4.37 (d, J = 14.9 Hz, 1H), 4.16−4.02 (m, 13H), 3.56−3.53 (m, 1H), 3.30−3.19 (m, 1H), 3.06−3.04 (m, 1H), 2.60−2.41 (m, 2H), 2.01 (s, 1H), 1.68−1.60 (m, 5H), 1.49 (s, 1H), 1.34−1.31 (m, 1H); ^{13}C NMR (100 MHz, $CDCl_3$) δ 148.7, 148.6, 148.5, 148.3, 125.7, 124.2, 123.7, 104.6, 104.3, 103.4, 103.3, 94.5, 77.3, 77.0, 76.7, 56.8, 56.0, 55.9, 55.8, 55.7, 33.9, 33.5, 26.8, 26.5, 23.8; HRMS (ESI) calcd for $C_{26}H_{32}NO_4$ $(M + H)^+$ 422.2326, found 422.2332.

5-Oxo-5-((2-(2,3,6,7-tetramethoxyphenanthren-9-yl)ethyl)-amino)pentanoic acid 12b. The synthetic procedure was similar to that of compound **12a**, and compound **12b** was obtained as a white

Scheme 1. Synthetic Route for Compounds 7a and 7b

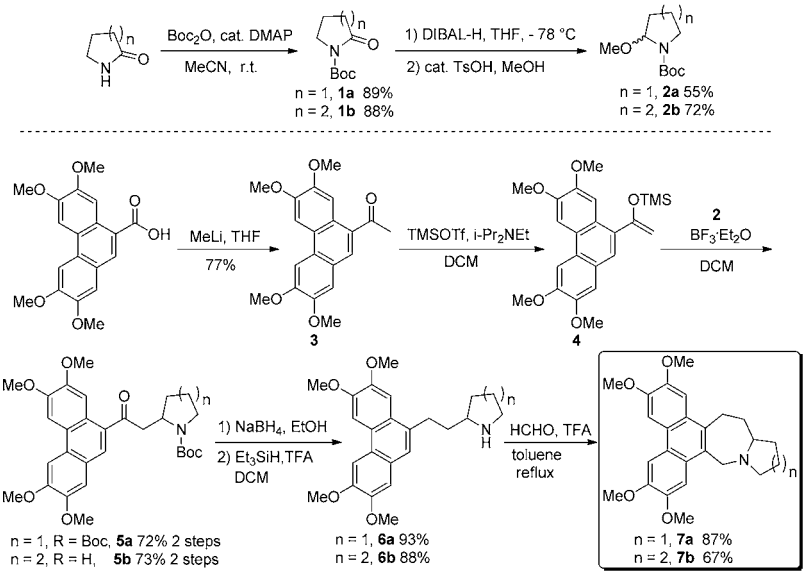

Scheme 2. Synthetic Route for Compounds 16a and 16b

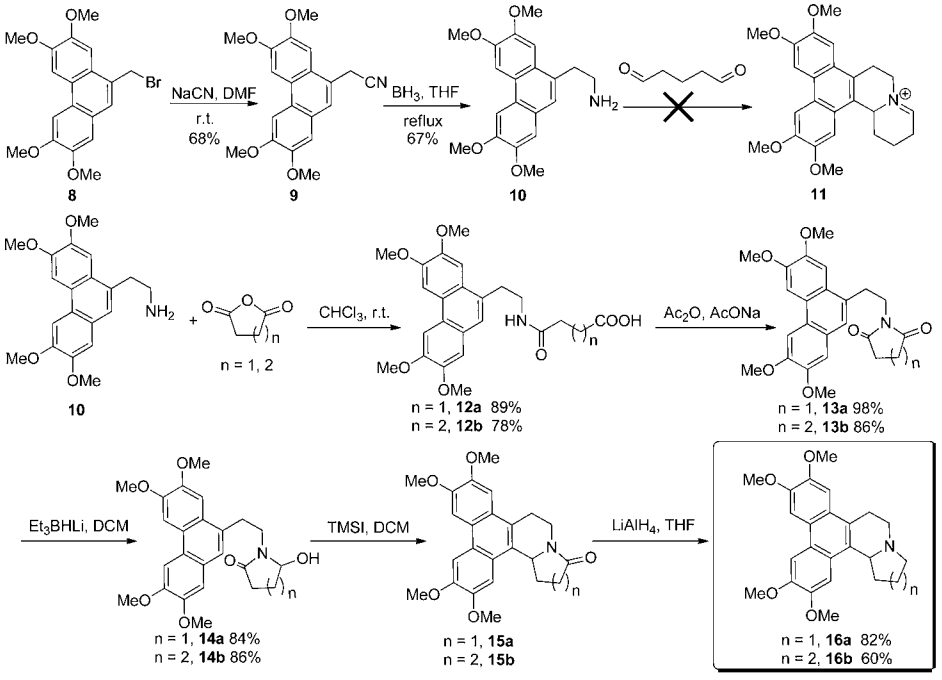

solid (78%): mp 158−160 °C; ^{1}H NMR (400 MHz, $CDCl_3$) δ 7.80 (s, 1H), 7.74 (s, 1H), 7.54 (s, 1H), 7.37 (s, 1H), 7.14 (s, 1H), 5.92 (s, 1H), 4.10 (s, 3H), 4.09 (s, 3H), 4.08 (s, 3H), 4.01 (s, 3H), 3.67 (d, J = 6.8 Hz, 2H), 3.25 (t, J = 6.8 Hz, 2H), 2.39 (t, J = 6.8 Hz, 2H), 2.25 (t, J = 7.2 Hz, 2H), 1.98−1.90 (m, 2H); ^{13}C NMR (100 MHz, $CDCl_3$) δ 176.0, 171.7, 147.9, 129.3, 123.5, 106.9, 103.8, 102.4, 101.8, 55.2, 55.1, 55.0, 54.9, 38.9, 34.3, 32.5, 28.9, 19.7, 15.3; HRMS (ESI) calcd for $C_{25}H_{30}NO_4(M + H)^+$ 456.2017, found 456.2018.

1-(2-(2,3,6,7-Tetramethoxyphenanthren-9-yl)ethyl)-piperidine-2,6-dione 13b. The synthetic procedure was similar to that of compound **13a**, and compound **13b** was obtained as a white solid (86%): mp 261−263 °C; ^{1}H NMR (400 MHz, $CDCl_3$) δ 7.89 (s, 1H), 7.83 (s, 1H), 7.78 (s, 1H), 7.54 (s, 1H), 7.19 (s, 1H), 4.21 (s, 3H), 4.13−4.08 (m, 8H), 4.03 (s, 3H), 3.28−3.16 (m, 2H), 2.71 (t, J = 8.4 Hz, 4H), 2.04−1.93 (m, 2H); ^{13}C NMR (100 MHz, $CDCl_3$) δ 171.5, 148.0, 147.9, 147.8, 147.7, 129.4, 125.3, 124.6, 124.2, 123.7, 122.9, 106.9, 104.3, 102.1, 101.7, 55.3, 55.1, 55.0, 54.9, 39.5, 31.8, 31.5, 16.2; HRMS (ESI) calcd for calcd for $C_{25}H_{27}NO_6Na^+$ $(M + Na)^+$ 460.1731, found 460.1735.

6-Hydroxy-1-(2-(2,3,6,7-tetramethoxyphenanthren-9-yl)-ethyl)piperidin-2-one 14b. The synthetic procedure was similar to that of compound **14a**, and compound **14b** was obtained as a white solid (86%): mp 202−204 °C; ^{1}H NMR (400 MHz, $CDCl_3$) δ 7.81 (s, 1H), 7.80 (s, 1H), 7.76 (s, 1H), 7.45 (s, 1H), 7.14 (s, 1H), 4.74 (s, 1H), 4.18−4.09 (m, 9H), 4.01 (s, 3H), 3.91−3.81 (m, 1H), 3.71−3.64 (m, 1H), 3.41−3.35 (m, 2H), 2.56−2.46 (m, 1H), 2.40−2.27 (m, 2H), 1.99−1.89 (m, 1H), 1.82−1.73 (m, 1H), 1.73−1.65 (m, 2H); ^{13}C NMR (100 MHz, $CDCl_3$) δ 170.4, 148.9, 148.9, 148.8, 148.8, 131.7, 126.3, 125.7, 124.8, 123.8, 107.8, 105.4, 103.2, 102.8, 81.1, 56.3, 56.1, 56.0, 55.9, 47.5, 32.6, 31.1, 15.9; HRMS (ESI) calcd for $C_{25}H_{30}NO_6^+$ $(M + H)^+$ 440.2068, found 440.2064.

2,3,13,14-Tetramethoxy-9,10,11,11a-tetrahydro-5*H*-dibenzo[*f*,*h*]pyrido[2,1-*a*]isoquinolin-8(6*H*)-one 15b. The synthetic procedure was similar to that of compound **15a**, and compound

dx.doi.org/10.1021/jf405562r | J. Agric. Food Chem. 2014, 62, 1233−1239

15b was obtained as a white solid (80%): mp 153−155 °C; ^{1}H NMR (400 MHz, $CDCl_3$) δ 7.85 (s, 1H), 7.82 (s, 1H), 7.32 (s, 1H), 7.21 (s, 1H), 5.35 (d, J = 10.8 Hz, 1H), 5.18 (dd, J = 12.4, 3.2 Hz, 1H), 4.13 (s, 6H), 4.05 (s, 3H), 4.04 (s, 3H), 3.19 (t, J = 16.0 Hz, 1H), 3.14−3.03 (m, 1H), 2.85−2.75 (m, 1H), 2.76−2.66 (m, 2H), 2.60−2.48 (m, 1H), 2.09−1.93 (m, 2H), 1.40−1.35 (m, 1H); ^{13}C NMR (100 MHz, $CDCl_3$) δ 169.8, 149.2, 148.6, 148.53, 128.2, 127.6, 125.5, 124.5, 123.5, 123.3, 104.2, 104.1, 103.8, 103.3, 56.2, 56.1, 56.1, 56.0, 56.9, 38.0, 32.1, 31.6, 26.8, 20.0, 14.2; HRMS (ESI) calcd for $C_{25}H_{27}NO_5$ $(M + H)^+$ 422.1962, found 422.1959.

2,3,13,14-Tetramethoxy-6,8,9,10,11,11a-hexahydro-5*H*-dibenzo[*f*,*h*]pyrido[2,1-*a*]isoquinoline 16b. The synthetic procedure was similar to that of compound **16a**, and compound **16b** was obtained as a white solid (60%): mp 89−92 °C; ^{1}H NMR (300 MHz, $CDCl_3$) δ 7.83 (s, 1H), 7.82 (s, 1H),7.32 (s, 1H), 7.25 (s, 1H), 4.26 (d, J = 9.7 Hz, 1H), 4.11 (s, 6H), 4.04 (s, 3H), 4.03 (s, 3H), 3.47−3.39 (m, 1H), 3.28−3.25 (m, 1H), 3.21−3.13 (m, 2H), 2.93−2.87 (m, 1H), 2.21 (d, J = 11.9 Hz, 1H), 1.96−1.63 (m, 6H); ^{13}C NMR (100 MHz, $CDCl_3$) δ 149.5, 149.3, 148.8, 131.1, 126.6, 126.5, 124.7, 124.5, 124.2, 105.4, 104.8, 104.3, 103.9, 60.5, 56.8, 56.7, 56.6, 56.5, 46.3, 29.2, 28.5, 26.6, 22.5; HRMS (ESI) calcd for $C_{25}H_{30}NO_4$ $(M + H)^+$ 408.2169, found 408.2170.

Antiviral Biological Assay. The procedure of purifying TMV and the method to test the anti-TMV activity of the synthesized compounds were the same with those reported previously in the literature.[22]

RESULTS AND DISCUSSION

Chemistry. The synthesis of D-ring expanded phenanthroindo/quinolizidine alkaloid analogues **7a** and **7b** is shown in Scheme 1, which features a Mukaiyama−Aldol reaction and a Pictet−Spengler cyclization. The precursors **2** of the Mukaiyama−Aldol reaction were prepared from commercially available lactams through literature protocols.[23] Silylenol ether **4** was synthesized from acetophenanthrone **3**, which was obtained from readily available phenanthryl acid.[24] After extensive reaction screening, it was found that boron trifluoride was the optimal Lewis acid for the desired Mukaiyama−Aldol reactions, giving compounds **5** in good yields. Ketones **5** were reduced to alcohols by sodium borohydride, followed by deprotection and further reduction of the benzylic hydroxyl by triethylsilicane under acidic conditions, furnishing amines **6** efficiently. It is worth noting that the following Pictet−Spengler cyclization did not occur when concentrated hydrochloric acid was used as catalyst in ethanol, which may be due to the energy of the seven-membered ring transition state being too high. When the reaction was performed in a high boiling point solvent (toluene) using much stronger acid CF_3COOH as catalyst, the desired cyclized products **7** were obtained in good yields.

The synthesis of the isomerized phenanthroindo/quinolizidine analogues **16a** and **16b** is shown in Scheme 2, featuring a Bischler−Napieralski cyclization. Using readily available phenanthryl bromide **8** as starting material,[25] intermediate **10** could be easily be prepared via sequential nucleophilic substitution and reduction. With the phenanthrylethylamine **10** in hand, we initially attempted to construct the pentacyclic skeleton through Pictet−Spengler cyclization/condensation sequence. Unfortunately, although much effort was devoted to the screening of reaction conditions, including catalysts, solvents, and reaction temperature, all attempts to perform the desired Pictet−Spengler cyclization failed. The main difficulty was proposed to be the Pictet−Spengler cyclization, presumably because reactivity of the key intermediate formed through condensation of amine and aldehyde was so slow that self-condensation of the aldehyde occurred quickly. To improve the reactivity of the intermediate of the cyclization, we turned to an alternative Bischler−Napieralski cyclization approach, which employed highly reactive acyl iminium as key intermediate. Imides **13** prepared from amine **10** and corresponding anhydride were subjected to partial reduction, affording compounds **14**. The subsequent Bischler−Napieralski cyclization went smoothly when trimethyliodosilane was employed. After reduction, isomerized phenanthroindo/quinolizidine alkaloid analogues **16** were obtained in good yields.

Antiviral Activity. To make a judgment of the designed structurally novel phenanthroindo/quinolizidine alkaloid analogues **7a**, **7b**, **16a**, and **16b**, two commercially available antiviral agents were used as control. To further investigate the influence of the variation of the basic skeletons of the natural alkaloids on the antiviral effects, corresponding tylophorine **I** and phenanthroquinolizidine **II** (Figure 1) were also used for comparison, which were synthesized using methods reported previously by our group.[24] The in vitro and in vivo (protection, inactivation, and curative effect) antiviral results against TMV of phenanthroindo/quinolizidine alkaloids **I** and **II**, analogues **7a**, **7b**, **16a**, and **16b**, ribavirin, and ningnanmycin are listed in Table 1. All of the compounds were tested at both 500 and 100 μg/mL.

Table 1. In Vitro and in Vivo Antiviral Activity of Compounds 7a, 7b, 16a, and 16b against TMV

		inhibition rate (%)			
compd	concn (μg/mL)	in vitro effect	protection effect	inactivation effect	curative effect
I	500	38.5	40.4	45.2	42.6
	100	15.3	18.2	17.5	13.1
7a	500	43.8	46.5	47.3	42.5
	100	20	21.6	20.3	10.6
16a	500	60	54.1	55.8	58.6
	100	30.6	24.1	26.7	30
II	500	67.5	65.8	64.2	68.9
	100	32.4	32.1	30	34.7
7b	500	54.7	48.3	52.6	50.7
	100	27.6	26.9	28.9	21.7
16b	500	37.7	42.9	41.7	39.5
	100	10	17.5	18.3	12.4
ribavirin	500	41.3	38.9	37.2	39.4
	100	18.5	15.6	11.9	14.7
ningnanmycin	500	69.3	57.9	54.2	58.7
	100	26.8	38.4	20.0	23.1

The first in vitro anti-TMV bioassay demonstrated that all of the synthesized sturcturally novel analogues except for **16b** exhibted higher activity than ribavirin at both high (500 μg/mL) and low (100 μg/mL) concentrations. Especially, although compounds **16a** and **7b** showed only comparable inhibitory effect with that of ningnanmycin at 500 μg/mL, they exhibited higher antiviral activity at 100 μg/mL. Further in vivo anti-

dx.doi.org/10.1021/jf405562r | J. Agric. Food Chem. 2014, 62, 1233−1239

TMV bioassay indicated that all of the newly designed analogues displayed protection and inactivation effects superior to those of ribavirin at both concentrations, and all of them also showed preferable curative effects except for **7a** and **16b** at 100 μg/mL. Compared with ningnanmycin, perhaps the most effective commercial plant virucide, analogue **16a** can also exhibit higher inactivation effect at both concentrations, and **7b** and **16a** showed inactivation and curative effects superior to those of ningnanmycin at 100 μg/mL.

The SARs demonstrated that phenanthroindolizidine analogue **7a** with the six-membered D-ring of natural alkaloid expanded to seven-membered ring that showed higher in vitro, protection, and inactivation effects than tylophorine **I** at both concentrations. The isomerized analogue **16a** also displayed preferable antiviral effects both in vitro and in vivo relative to its precursor **I** at both high and low concentrations. Then, we can conclude that for natural phenanthroindolizidine alkaloid **I**, no matter how the six-membered D-ring was expanded to seven-membered or the fused pattern of D/E rings was changed, analogues **7a** and **16a** showed superior antiviral activity to that of the precursor **I**, which indicated that the original conformation of the phenanthroindolizidine was not optimal and deserved further optimization. However, no matter how the D-ring was expanded from six-membered to seven-membered or the fused pattern of D/E rings was changed, both phenanthroquinolizidine analogues **7b** and **16b** exhibited inferior inhibitory effects against TMV, indicating that the original conformation of the phenanthroquinolizidine was a relatively preferential conformation. Another interesting result was that although six-membered E ring compound **7b** showed higher activity than five-membered E ring compound **7a**, their corresponding counterparts **16b** and **16a** displayed reverse bioactive results, which suggested that the fused pattern of D/E rings of phenanthroquinolizidine alkaloid also has a great effect on its activity, and the original fused pattern is relatively optimal.

In summary, two types of structurally totally novel analogues of phenanthroindo/quinolizidines were synthesized and evaluated for their antiviral activities aganist TMV for the first time. The bioassay results indicated that most of the four designed structural analogues showed good to excellent in vivo anti-TMV activity, among which analogue **16a** dispalyed comparable activity with that of one of the most successful commercial antiviral agents, ningnanmycin, thus emerging as a potential inhibitor of plant virus. Further structure−activity relationships demonstrated for the first time that the original skeleton of the pentacyclic structure of phenanthroindolizidine is not optimal, and further optimization for preferential conformation is needed, whereas changes of the original skeleton of the phenanthroquinolizidine descreased its antiviral activity, indicating that the original conformation is a relative preferential conformation. Further investigations on structual optimization and mode of action are currently underway in our laboratories.

■ ASSOCIATED CONTENT

Supporting Information

^{1}H and ^{13}C NMR spectra of compounds **3**−**7**, **9**, **10**, and **12**−**16**. This material is available free of charge via the Internet at http://pubs.acs.org.

■ AUTHOR INFORMATION

Corresponding Author

*(Q.W.) Phone: +86-022-23503952. Fax: +86-022-23503952. E-mail: wangqm@nankai.edu.cn.

Author Contributions

‖B.S. and F.C. contributed equally to this work.

Funding

We are grateful to the National Key Project for Basic Research (2010CB126100), the National Natural Science Foundation of China (21132003, 21121002, 21372131, 21002053), Tianjin Natural Science Foundation (11JCZDJC20500), and Specialized Research Fund for the Doctoral Program of Higher Education (20130031110017).

Notes

The authors declare no competing financial interest.

■ REFERENCES

(1) Hari, V.; Das, P. Ultra microscopic detection of plant viruses and their gene products. In *Plant Disease Virus Control*; Hadidi, A., Khetarpal, R. K., Koganezawa, H., Eds.; APS Press: St. Paul, MN, USA, 1998; pp 417−427.

(2) Bos, L. 100 years of virology: from vitalism via molecular biology to genetic engineering. *Trends Microbiol.* **2000**, *8*, 82−87.

(3) Ouyang, G. P.; Cai, X. J.; Chen, Z.; Song, B. A.; Bhadury, P. S.; Yang, S.; Jin, L. H.; Xue, W.; Hu, D. Y.; Zeng, S. Synthesis and antiviral activities of pyrazole derivatives containing an oxime moiety. *J. Agric. Food Chem.* **2008**, *56*, 10160−10167.

(4) Reichman, M.; Devash, Y.; Suhadolnik, R. J.; Sela, I. Human leukocyte interferon and the antiviral factor (AVF) from virus-infected plants stimulate plant tissues to produce nucleotides with antiviral activity. *Virology* **1983**, *128*, 240−244.

(5) Chen, M. H.; Chen, Z.; Song, B. A.; Bhadury, P. S.; Yang, S.; Cai, X. J.; Hu, D. Y.; Xue, W.; Zeng, S. Synthesis and antiviral activities of chiral thiourea derivatives containing an α-aminophosphonate moiety. *J. Agric. Food Chem.* **2009**, *57*, 1383−1388.

(6) Li, Y. M.; Zhang, Z. K.; Jia, Y. T.; Shen, Y. M.; He, H. P.; Fang, R. X.; Chen, X. Y.; Hao, X. J. 3-Acetonyl-3-hydroxyoxindole: a new inducer of systemic acquired resistance in plants. *Plant Biotechnol. J.* **2008**, *6*, 301−308.

(7) Sidwell, R. W.; Huffman, J. H.; Khare, G. P.; Allen, L. B.; Witkowski, J. T.; Robins, R. K. Broad-spectrum antiviral activity of virazole: 1-β-D-ribofuranosyl-1,2,4-triazole-3-carboxamide. *Science* **1972**, *177*, 705−706.

(8) Bachrach, U. Antiviral activity of oxidized polyamines. *Amino Acids* **2007**, *33*, 267−272.

(9) De Meester, C. Genotoxic potential of β-carbolines: a review. *Mutat. Res.* **1995**, *339*, 139−153.

(10) Qian, X. H.; Lee, P. W.; Cao, S. China: forward to the green pesticides via a basic research program. *J. Agric. Food Chem.* **2010**, *58*, 2613−2623.

(11) Seiber, J. N. Sustainability and agricultural and food chemistry. *J. Agric. Food Chem.* **2011**, *59*, 1−2.

(12) Gellert, E. The indolizidine alkaloids. *J. Nat. Prod.* **1982**, *45*, 50−73.

(13) Gellert, E.; Rudzats, R. The antileukemia activity of tylocrebrine. *J. Med. Chem.* **1964**, *7*, 361−362.

(14) Damu, A. G.; Kuo, P. C.; Shi, L. S.; Li, C. Y.; Kuoh, C. S.; Wu, P. L.; Wu, T. S. Phenanthroindolizidine alkaloids from the stems of *Ficus septica*. *J. Nat. Prod.* **2005**, *68*, 1071−1075.

(15) Yang, C. W.; Chen, W. L.; Wu, P. L.; Tseng, H. Y.; Lee, S. J. Antiinflammatory mechanisms of phenanthroindolizidine alkaloids. *Mol. Pharmacol.* **2006**, *69*, 749−758.

(16) Baumgartner, B.; Erdelmeier, C. A. J.; Wright, A. D.; Rali, T.; Sticher, O. An antimicrobial alkaloid from *Ficus septica*. *Phytochemistry* **1990**, *29*, 3327−3330.

(17) Choi, J. Y.; Gao, W.; Odegard, J.; Shiah, H. S.; Kashgarian, M.; McNiff, J. M.; Baker, D. C.; Cheng, Y. C.; Craft, J. Abrogation of skin disease in LUPUS-prone MRL/FASIpr mice by means of a novel tylophorine analog. *Arthritis Rheum.* **2006**, *54*, 3277−3283.
(18) An, T. Y.; Huang, R. Q.; Yang, Z.; Zhang, D. K.; Li, G. R.; Yao, Y. C.; Gao, J. Alkaloids from *Cyanachum komarovii* with inhibitory activity against the tobacco mosaic virus. *Phytochemistry* **2001**, *58*, 1267−1269.
(19) Xi, Z.; Zhang, R. Y.; Yu, Z. H.; Ouyang, D. The interaction between tylophorine B and TMV RNA. *Bioorg. Med. Chem. Lett.* **2006**, *16*, 4300−4304.
(20) Wang, Z.; Wei, P.; Xizhi, X.; Liu, Y.; Wang, L.; Wang, Q. Design, synthesis, and antiviral activity evaluation of phenanthrene-based antofine derivatives. *J. Agric. Food Chem.* **2012**, *60*, 8544−8551.
(21) Wang, K.; Su, B.; Wang, Z.; Wu, M.; Li, Z.; Hu, Y.; Fan, Z.; Mi, N.; Wang, Q. Synthesis and antiviral activities of phenanthroindolizidine alkaloids and their derivatives. *J. Agric. Food Chem.* **2009**, *58*, 2703−2709.
(22) Wang, Z.; Wang, L.; Ma, S.; Liu, Y.; Wang, L.; Wang, Q. Design, synthesis, antiviral activity, and SARs of 14-aminophenanthroindolizidines. *J. Agric. Food Chem.* **2012**, *60*, 5825−5831.
(23) Pichon, M.; Figadère, B.; Cavé, A. C-Glycosylation of cyclic *N*-acyliminium ions with trimethylsilyloxyfuran. *Tetrahedron Lett.* **1996**, *37*, 7963−7966.
(24) Wang, K.; Lv, M.; Wang, Q.; Huang, R. Iron(III) chloride-based mild synthesis of phenanthrene and its application to total synthesis of phenanthroindolizidine alkaloids. *Tetrahedron* **2008**, *64*, 7504−7510.
(25) Su, B.; Cai, C.; Wang, Q. Enantioselective approach to 13*a*-methylphenanthroindolizidine alkaloids. *J. Org. Chem.* **2012**, *77*, 7981−7987.

and silica, were of interest as a sorbent trap to extract nitrosamines from the liquid extract of frankfurter sausage after SWE. Because PS−DVB and P-DVB possess high hydrophobicity and thermal stability, they are likely to absorb fat and nonpolar matrix. Silica was chosen because it was successfully used as a fat retainer[20] and also provides a high thermal stability.

EXPERIMENTAL SECTION

Chemicals and Sample. For polymer-based monolith capillary synthesis, γ-(trimethoxysilyl)propyl methacrylate (98.0%) obtained from Acros (Morris Plains, NJ) and glacial acetic acid from BDH (Poole, U.K.) were used as silanization solutions. Styrene monomer (99.0%) was purchased from Fluka (Buchs, Switzerland), and divinylbenzene monomer (80.0%) was from Sigma-Aldrich (Steinheim, Germany). Decanol (99.0%) from Acros (Morris Plains, NJ), tetrahydrofuran (99.9%) from Fisher (Loughborough, U.K.), and dodecanol (>99.5%) from Fluka (Buchs, Switzerland) were used as porogenic agents. Dibenzoyl peroxide (75%) from Acros (Morris Plains, NJ) was employed as an initiator. For silica-based monolith capillary synthesis, polyethylene glycol [MW of 10 000 g/mol; analytical reagent (AR) grade] was bought from Sigma-Aldrich (Steinheim, Germany), while urea of analytical grade and tetramethoxysilane (98.0%) were obtained from Merck (Darmstadt, Germany). Both polymeric and silica-based monoliths were synthesized inside a 0.32 mm inner diameter × 10 m bare fused silica capillary tubing with polyimide coating purchased from SGE (SGE Analytical Science, Melbourne, Victoria, Australia).

Standard nitrosamines, namely, *N*-nitrosodiethylamine or NDEA (99.0%) from Fluka (Buchs, Switzerland), *N*-nitrosopiperidine or NPIP (99.0%) and *N*-nitrosopyrrolidine or NPYR (99.0%) from Sigma-Aldrich (Milwaukee, WI), and *N*-nitrosomorpholine or NMOR (5.0 mg/mL in methanol) from Supelco (Bellafonte, PA) were used in this study. Each 1.0 mg/mL standard stock solution was prepared in methanol. *N*-Nitroso-di-*n*-propylamine or NDPA from Supelco (Bellafonte, PA) was used as an internal standard for quantification. Other chemicals were of analytical grade.

Frankfurter sausages from a local supermarket in Bangkok were chopped and homogenized. A 1.0 g sample was fortified with 100 μg of each nitrosamine, rehomogenized, and left at room temperature for 10 min.

Monolith Capillary Preparation. *Silanization of the Inner Wall of the Capillary.* The silanization method described by Coufal et al. was used. In brief, silanization solution was prepared from 1.817 g of glacial acetic acid mixed with 20 μL of γ-(trimethoxysilyl)propyl methacrylate in a 5.00 mL volumetric flask and adjusted to the volume by decanol. The solution was filled into a 0.32-mm inner diameter × 100 cm bare fused silica capillary, where both ends of the capillary were subsequently sealed with a septum. The sealed capillary was then incubated in an oven at 60 °C for 20 h. After cooling to room temperature, it was rinsed with acetone to remove the silanizing solution, dried with a gentle flow of nitrogen gas for 1 h, and finally cut into 10.0 cm pieces.

PS−DVB and P-DVB Monolith Capillary. A PS−DVB polymerization mixture consisted of 200 μL of styrene monomer, 200 μL of divinylbenzene, 520 μL of decanol, 80 μL of tetrahydrofuran porogen, and 10 mg/mL dibenzoyl peroxide initiator. The formulation of the PS−DVB polymerization solution used the method by Premstaller et al.[21,22] The P-DVB polymerization solution was a mixture of 400 μL of divinylbenzene monomer, 520 μL of dodecanol, 80 μL of toluene, and 10 mg/mL dibenzoyl peroxide, and its formulation was from the method by Svec and Kurganov.[18] Either polymerization solution was filled in the 10 cm silanized capillary for about 5 cm. The capillary was sealed at both ends and kept at 70 °C for 24 and 20 h for PS−DVB and P-DVB synthesis, respectively. To remove the porogen and monomeric residues, the fabricated monolith in capillary was flushed with either acetonitrile or methanol at a flow rate of 10 μL/min for 3 h and then dried with nitrogen gas flow.

Silica Monolith Capillary. A fabrication method for silica monolith capillary was adapted from one previously reported by Tanaka et al.[9] In brief, a 0.32 mm. inner diameter × 100 cm bare fused silica capillary was pretreated with 1 M NaOH, and both ends were tightly sealed with a septum. The filled tubing was kept at 40 °C for 6 h, rinsed with deionized water, and dried with nitrogen gas. The sol−gel solution for silica monolith synthesis was a mixture of 400 μL of tetramethoxysilane, 0.088 g of polyethylene glycol, and 0.09 g of urea in 0.01 M acetic acid. The solution was stirred in an ice bath for 45 min and then filled into the pretreated capillary that was subsequently heated at 40 °C for 24 h. The temperature was then raised to 120 °C for 6 h. After cooling, the monolith in capillary was washed with methanol and then dried with nitrogen gas. The fabricated PS−DVB, P-DVB, and silica monolith capillaries were cut perpendicular to the cross-section into 0.50 cm long pieces, and the specimens were subjected to scanning electron microscopy (SEM) using a JSM-5600 SEM microscope (JEOL, Japan) at 20 kV.

SWE. The SWE system was similar to the one described previously.[6,23] In brief, degassed double-deionized water was delivered by a ConstraMetric 3200 HPLC pump (LDC Analytical, Riviera Beach, FL) passing through a 1 m × 0.51 mm inner diameter stainless-steel preheating coil (Alltech Chromatography, Columbia, MD) to a 15 cm × 4.6 mm inner diameter stainless-steel extraction cell containing 1.0 g of fortified frankfurter sausage sample. Glass wool was put at both ends of the cell, where 2 μm stainless-steel frits and screw caps were subsequently mounted. Both the preheating coil and extraction cell were heated in an oven at 140 °C for 5 min of static time. The end of the outlet tubing was crimped to control pressure to more than 300 psi. After that, the water was reflowed and the aqueous extract was cooled using a stainless-steel cooling coil wrapped with aluminum fins. The aqueous extract was collected for 10 mL in a vial containing 2 g of NaCl and 2 mL of dichloromethane (DCM). The cloudy mixture in the vial was transferred to centrifuge at 1100 rpm for 7 min, and the DCM layer was filtered and dried with anhydrous Na_2SO_4. To preconcentrate, the organic phase was purged with nitrogen gas and then adjusted to 100 μL with the solvent.

Monolith Capillary GC Setup. A 1 μL sample of the organic extract was subjected to extraction, separation, and quantification by coupling a fabricated monolith sorbent with GC. To set up the connection, a 0.32 mm inner diameter × 5.0 cm bare fused silica tubing was connected with an injection port of a HP5890 series II gas chromatograph (Hewlett-Packard, Palo Alto, CA) at one end and the other end was connected with a fabricated monolith capillary, where a glass connector led to a 0.32 mm inner diameter × 0.52 μm film thickness × 25 m HP-5 column (Hewlett-Packard, Polo Alto, CA). The temperature program was started by ramping from 40 to 80 °C at 7 °C/min, held for 8 min, then increased to 200 °C at 15 °C/min, and maintained for 5 min. Either a flame ionization detector (FID) or HP 5989B mass spectrometer (MS, Hewlett-Packard, Polo Alto, CA) in an electron impact mode was employed as a detector. The injector and FID temperatures were maintained at 250 and 280 °C, respectively. The temperatures of the ion source and quadrupole mass analyzer were 200 and 100 °C, respectively. During optimization of the monolith sorbent capillary, the FID was operated with nitrogen carrier gas and the split ratio at the injection port was 1:15. For quantification by using GC−MS, the operation was in splitless mode and nitrogen was replaced with helium carrier gas.

RESULTS AND DISCUSSION

Optimization of Monolith. The types of primarily studied monolith for fat adsorbent were chosen from two individual properties, namely, polarity and thermal stability. The monolith should be adequately nonpolar to retain fat while releasing the polar analytes. It must also have sufficiently high thermal stability to tolerate heat in the oven during the desorption step. When the monolith capillary was connected to the analytical column, the column head pressure increased, particularly for the polymeric monolith. The pressure was measured from the

column head pressure gauge in the front panel of the GC instrument. The maximum scale of the gauge corresponded to 40 psi. Although a high surface area was obtained with a long monolith capillary, the longer the monolith, the higher the column head pressure, and the gas flow stopped at the maximum allowed length for different types of monoliths. At high carrier gas flow through the column, increased resistance occurred, and as a consequence, a higher pressure was needed to drive gas through both the monolith capillary and analytical column to obtain the required column flow rate. The maximum pressure was restricted to 40 psi because of a limitation of the GC instrument. Figure 1 shows the average column head

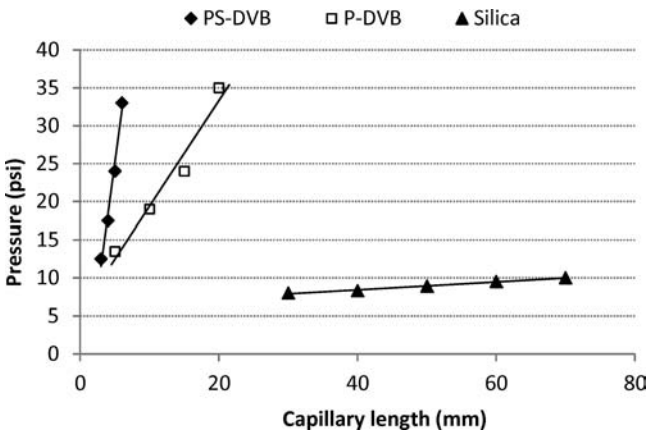

Figure 1. Average column head pressure for the GC column connected with different types of synthesized monolith capillary.

pressure when connected with each type of monolith with the flow of 1.4 mL/min. No flow occurred for PS−DVB and P-DVB monoliths of more than 6 and 20 mm, respectively.

With the coupling of the PS−DVB monolith to the analytical column, nitrosamines did not separate well. For the 5−6 mm long monoliths, baseline drift occurred and all compounds gave broad and tailing peaks, presumably as a result of their strong interaction with the polymeric phase. Besides, NDPA and NPYR peaks were completely overlapped. For 4.0 and 3.0 mm monoliths, a better peak shape was obtained but NDPA and NPYR peaks remained completely overlapped (Figure 2). Because of thermal stability and hydrophobic properties similar to those of PS−DVB, P-DVB was investigated as a nonpolar monolith sorbent trap. After varying the length of polymer monolith from 5 to 20 mm, the best separation in this experiment occurred using a 5 mm P-DVB monolith. Despite the higher column permeability and effective surface area than those of PS−DVB, an improved peak shape was obtained but the separation of NPYR and NDPA was still not possible. It was then concluded that both polymer monoliths gave rather poor performance in retaining fat. According to our previous study[6] in which silica sorbent was primarily used as a lipid retainer, a silica monolith was then synthesized and studied, despite the fact that it has rather high polarity. A scanning electron micrograph of the silica monolith in the capillary showed a skeleton with large through pores, and the microglobule diameter was on average 1 μm. The specific surface area was 32−43 m^2/g determined by inverse size-exclusion chromatography.[24] Because of large macropores, silica monoliths provide several times higher column permeability than the two polymer monoliths and permeability of silica monolith was not affected by the capillary length. The flow was almost constant when

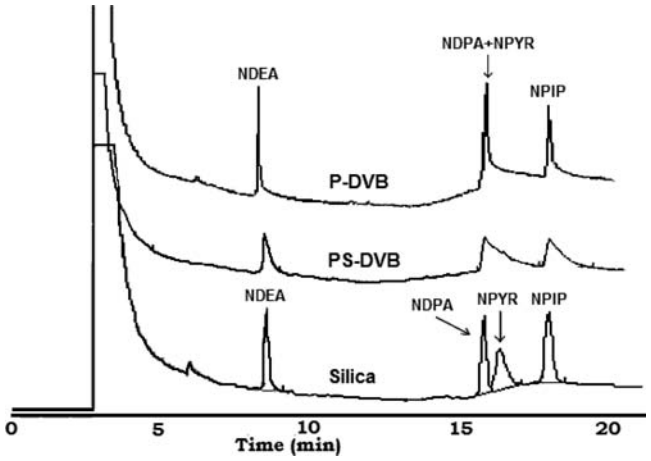

Figure 2. Separation of nitrosamines on a HP-5 column coupled with online sorbent of 5 mm P-DVB and 3 mm PS−DVB and 30 mm silica monolith sorbent. Temperature program: 60−100 °C at 7 °C/min, maintained for 8 min, then raised to 120 °C at 7 °C/min, and maintained for 5 min.

increasing the capillary length. This led to the feasibility of using a very long silica capillary. Better separation of nitrosamines was obtained with a short silica monolith, owing to the lower interaction of nitrosamines with silica sorbent. Separation of all nitrosamines was achieved for the silica monolith, although the NPYR peak was rather broad. Gradually reducing the monolith length from 70 to 60, 50, and 40 mm improved both the peak shape and separation. A 30 mm long monolith gave the most favorable separation, and the chromatogram is shown in Figure 2. Further reducing sorbent capillary length likely caused poor nonpolar matrix trapping, thus affecting the separation efficiency of nitrosamines.

Capability and reusability of a silica monolith capillary as a nonpolar sorbent trap was studied to investigate the feasibility of multiple use before disposal. Figure 3 shows the chromato-

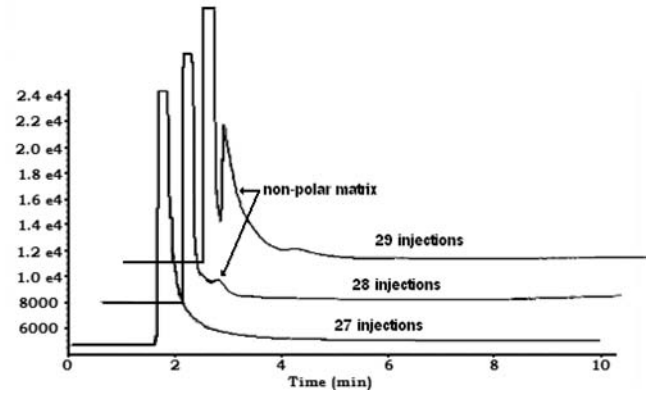

Figure 3. GC chromatograms obtained from different numbers of repeated injections of unfortified frankfurter extract on 30 mm silica monolith connected with a HP-5 column.

gram of the nonpolar matrix of frankfurter sausage. The extract was repeatedly injected onto the monolith coupled with the HP-5 column, the peak area of the nonpolar matrix was observed after 27 injections for a 30 mm long silica monolith (Figure 3). The number of repeated injections was also dependent upon the amount of contaminating fat, and for our sample, the fat content from the frankfurter sausage package

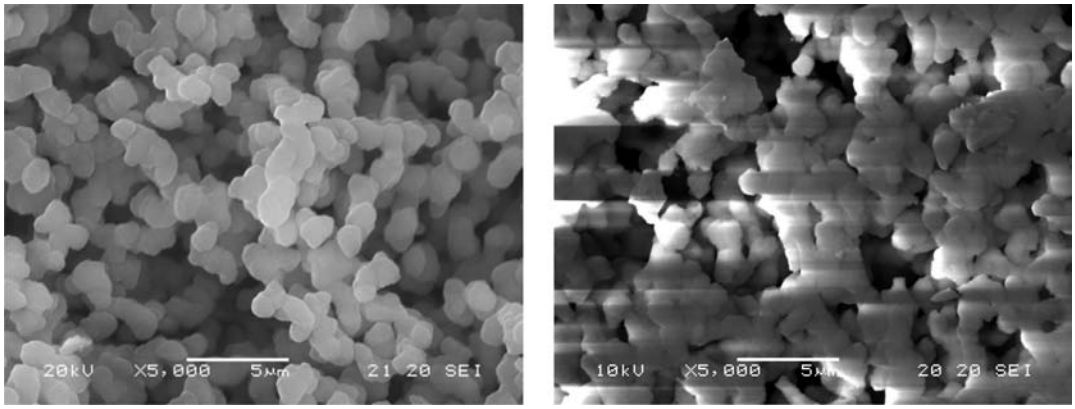

Figure 4. Scanning electron micrograph of silica monolith (a) before and (b) after use as a sorbent trap for frankfurter extract.

label was 30% by weight. The sample of absorbed fat on the monolith after 30 injections was also subjected to SEM (Figure 4), confirming that the deposit of fat and other nonpolar matrix covered the monolithic skeleton. The deposition might occur from both condensation and adsorption of the volatile fat and other nonpolar components onto the silica surface, because the operating temperature was lower than the smoke point of lard (188 °C). It was then concluded that the reusability of a 30 mm fabricated silica monolith capillary as a sorbent trap for a fat matrix was up to 27 times. In practice, for prevention of fat leachate reaching an analytical column, the number of reuses should be reduced by a quarter or to about 20.

Application to Real Samples. When the silica monolith trap was connected to the HP-5 analytical column, the elution order of NPYR and NPDA was obviously swapped, in comparison to the one without the silica monolith. NPYR changed the retention with the silica trap, and its peak shape was quite broad. The phenomenon possibly occurred from an increased dipole−(induced) dipole interaction of NPYR to the silica surface, because NPYR is more polar than the other chosen nitrosamines. However, the interaction that caused the broad peak was traded off by better separation between the NPYR and NDPA peaks, giving benefits to the overall nitrosamine separation.

A two-tailed *t*-test also revealed no significant difference in the average peak area of each nitrosamine obtained from its separation on the analytical column with and without the silica monolith trap. The $|t|$ values of NDEA, NPYR, NPIP, and NDPA were 0.1532, 0.5815, 0.6317, and 0.2820, respectively, lower than the *t*-critical value of 4.30 at the 95% confidence limit. A 20 μg/g fortified sausage extract was repeatedly injected onto the same capillary and different capillaries to show the reliability of the method for each nitrosamine. The percent relative standard deviations (%RSDs) of an average area ratio of each analyte to the internal standard showed very good precision for injection−injection (0.79−1.46%) and reasonably good precision for capillary−capillary (2.4−6.0%) experiments, and %RSDs of average retention time of both comparison tests were very good (0.09−0.22%). Such results confirm that fat adsorption on the silica monolith did not significantly affect either the quantification or retention of nitrosamines.

Efficiency of the extraction and determination method was assessed by an investigation of detection limits and percent recovery of all analytes. The detection limits of nitrosamine were found to lie in a range of 2.1−5.4 ng injected for all components. The detection limits of all analytes obtained was not as low as expected, probably because of the small amount of sausage packed in the extraction cell and an insufficiently high sensitivity of the HP 5989B mass spectrometric detector used in the work. It was then postulated that the detection limits could be reduced using more sensitive and selective detectors, such as a tandem mass spectrometric detector (tandem MS) and thermal energy analyzer (TEA).

The recoveries of nitrosamine extraction from frankfurter sausage using SWE coupled with monolith sorbent capillary were compared to SWE−conventional SPE in our previous study[6] and determined by GC−MS analysis. The recovery of nitrosamines was in a range of 74.7−88.4%, which lies within the acceptable range, and precision of the coupling method was satisfactory, varying between 2.09 and 3.85%. Although the results showed the same trend for both methods, the recovery obtained from SWE−conventional SPE was slightly higher than those from SWE−silica monolith: about 7% for NPYR, 10% for NDEA, and 18% for NPIP. Silica monolith has obviously proven to be the most optimal monolith absorbent for our purpose. No additional ions of significant relative abundance were detected in those spectra measured with the silica monolith capillary coupled to the HP-5, indicating that the method was very clean with no interference with similar retention and fragmented mass.

The coupling method of SWE with a silica monolith capillary for nitrosamine determination from frankfurter sausage in our present work was compared to other extraction methods and our previous work for several meat products, as shown in Table 1. Although the extraction efficiency, represented by percent recovery, of the proposed method was close to those of other methods,[2,25,26] this method gave more advantages by reducing solvent consumption, amount of sample, and analysis time. For example, in the method by Byun et al.,[3] up to 600 mL of DCM was consumed per sample for additional extraction after distillation. The necessary organic solvent volume for the methods by Yurchenko et al.[25,26] and our previous classical SPE[6] were 52, 72, and 30 mL, respectively. The total volume of extracting organic solvent used in this work was significantly reduced at less than 3 mL, related to a fast preconcentration step, compared to those methods. The required amount of sample was also significantly reduced in this work. Only 1 g of food sample was subjected to the overall preconcentration and cleanup process, while the amount was 2−200-fold larger for the other techniques.[2,27−35]

Some reference methods require several steps of sample preparation and are therefore time-consuming. For example,

Table 1. Method Comparison for Determination of Nitrosamine from Different Meat Matrices (Adapted from Ref 6)

sample matrix	preparation method	analytical method	sample mass (g)	percent recovery (%)	detection limit	reference
pork luncheon meat, pig liver	steam distillation (alkali and acid), electrochemical reduction, and amine derivative method	HPLC	200	42−77 yield of derivative	1−10 μg/kg	27
frankfurter sausage	supercritical CO_2 coupled with SPE (Florisil)	GC−TEA	2.5	84.3−104.8		30
sausages	two-step SPE with Extrelut and Florisil	GC−TEA	6.0	40−100	0.3 ppb	31
fresh and preserved food	liquid−liquid extraction with DCM and SPE with basic alumina	GC−TEA	10.0	60−90	0.1−0.5 μg/kg	32
cured ham, bacon, and sausage	flow-injection method (on the basis of photochemical cleavage of the N−NO bond) and then nitrite was detected	DAD	2.0	91.6−105.8	6.0 ng/mL	28
meat products	steam distillation, extraction with DCM, and denitrosation	HPLC with fluorescence	80−100	72−76	0.7−2.2 ng	2
canned sausage	steam distillation (rotary vacuum evaporator) and SPE with active carbon	MEKC	150	38.2−55.0		29
dried seafood	steam distillation and extraction with DCM	GC−TEA	25	83.2−102.2	0.1 μg/kg	38
fermented sausage	steam distillation on a steam generator and extraction with DCM	GC−TEA	20	87−93	0.1 μg/kg	3
sausage	headspace solid-phase microextraction	GC−TEA	2.5	105−110	3 μg/kg	33
fish sample	two-step SPE with Extrelut and Florisil	GC−MS	6.0	79−88	0.10 μg/kg	25
sausage	supercritical fluid CO_2 coupled with SPE (Florisil)	MEKC	0.2	21−82		39
meats	two-step SPE with Extrelut and Florisil	GC−MS	6.0	79−88	0.09 μg/g	26
meat products	two-step SPE with Extrelut and Florisil	GC × GC−NCD	6.0		1.66−3.86 μg/g	34
meat sample	two-step SPE with Extrelut and Florisil	GC × GC−NCD	6.0	83.1−89.8	1.54−1.86 pg	35
meat products	microwave-assisted extraction (MAE) and dispersive liquid−liquid microextraction (DLLME)	GC−MS	0.25	36−74	0.003−0.014 ng/mL for NPIP and NMEA	40
frankfurter	SWE and LLE couple with SPE (Florisil)	GC−MS	1.0	81−106	0.47−1.48 ng	6
frankfurter	SWE and LLE couple with silica monolith capillary	GC−MS	1.0	74.7−88.4	2.10−5.40 ng injected/g	proposed method

dx.doi.org/10.1021/jf4036645 | J. Agric. Food Chem. 2014, 62, 1240−1246

the AOAC reference method using vacuum distillation takes about 75 min per sample followed by a second step of DCM extraction of the distillate.[36] The total sample preparation time is approximately 2 h. A cleaning and preconcentration process using a conventional SPE took about 1 h in the work by Yurchenko et al.,[26] but it was reduced to less than 10 min for separation of those components using a coupling technique of monolith capillary with GC after 20 min of extraction with superheated water. In addition, one monolith capillary could be reused with the liquid extract more than 20 times (corresponding to 20 samples).

Many significant benefits were obtained for the determination of nitrosamines in sausage by coupling of SWE with a silica monolith capillary and GC. The detection limits results were, however, not as low as expected. To improve the sensitivity, additional steps, such as denitrosation,[37] could be introduced prior to detection. Specific detectors, namely, a TEA or highly sensitive tandem MS, can enhance the detection efficiency. Furthermore, the monolith capillary can also be adapted to couple with other methods of extraction for further preconcentration and purification of a wide range of analytes prior to chromatographic analysis. This method investigated here has also been proven to be a green technique with environmental advantages, because it greatly reduced solvent consumption and minimized analysis time and costs associated with obtaining reproducible results.

AUTHOR INFORMATION

Corresponding Author

*Telephone: 662-562-5555, ext. 2136. Fax: 662-579-3955. E-mail: fsciopc@ku.ac.th.

Funding

Financial support from the Kasetsart University Research and Development Institute (KURDI) and the Thailand Research Fund (TRF) (Project RSA5580019) is gratefully acknowledged. The authors thank the Center of Excellence for Innovation in Chemistry (PERCH-CIC), Office of the Higher Education Commission, Ministry of Education, for the studentships of Panee Subprasert, Anupop Sasook, and Narumol Ramnut, and the Department of Chemistry, Faculty of Science, Kasetsart University, for instruments and facilities support.

Notes

The authors declare no competing financial interest.

ABBREVIATIONS USED

DCM, dichloromethane; FID, flame ionization detector; GC, gas chromatography; HPLC, high-performance liquid chromatography; LLE, liquid−liquid extraction; MS, mass spectrometer; NDEA, *N*-nitrosodiethylamine; NPIP, *N*-nitrosopiperidine; NPYR, *N*-nitrosopyrrolidine; NMOR, *N*-nitrosomorpholine; P-DVB, polydivinylbenzene; PS−DVB, polystyrene−divinylbenzene; RSD, relative standard deviation; SPE, solid-phase extraction; SWE, superheated water extraction; TEA, thermal energy analyzer

REFERENCES

(1) Kimoto, W. I.; Pensabene, J. W.; Fiddler, W. Isolation and identification of *N*-nitrosothiazolidine in fried bacon. *J. Agric. Food Chem.* **1982**, *30*, 757−760.

(2) Komarova, N. V.; Velikanov, A. A. Determination of volatile nitrosamines in food by high-performance liquid chromatography with fluorescence detection. *J. Anal. Chem.* **2001**, *56*, 359−363.

(3) Byun, M. W.; Ahn, H. J.; Kim, J. H.; Lee, J. W.; Yook, H. S.; Han, S. B. Determination of volatile *N*-nitrosamines in irradiated fermented sausage by gas chromatography coupled to a thermal energy analyzer. *J. Chromatogr. A* **2004**, *1054*, 403−407.

(4) Filho, S.; Rios, P. J.; Valcárcel, A.; Zanin, M.; Caramão, K. D. B. Determination of nitrosamines in preserved sausages by solid-phase extraction−micellar electrokinetic chromatography. *J. Chromatogr. A* **2003**, *985*, 503−512.

(5) Huang, Z.; Lee, H. K. Materials-based approaches to minimizing solvent usage in analytical sample preparation. *Trends Anal. Chem.* **2012**, *39*, 228−244.

(6) Chienthavorn, O.; Subprasert, P.; Insuan, W. Nitrosamines extraction from frankfurter sausage by using superheated water. *Sep. Sci. Technol.* **2014**, DOI: 10.1080/01496395.2013.863338.

(7) Ishizuka, N.; Kobayashi, H.; Minakuchi, H.; Nakanishi, K.; Hiraoa, K.; Hosoyab, K.; Ikegamib, T.; Tanaka, N. Monolithic silica columns for high-efficiency separations by high-performance liquid chromatography. *J. Chromatogr. A* **2002**, *960*, 85−96.

(8) Kobayashi, H.; Ikegami, T.; Kimura, H.; Hara, T.; Tokuda, D.; Tanaka, N. Properties of monolithic silica columns for HPLC. *Anal. Sci.* **2006**, *22*, 491−501.

(9) Tanaka, N.; Kobayashi, H.; Ishizuka, N.; Minakuchi, H.; Nakanishi, K.; Hosoy, K.; Ikegami, T. Monolithic silica columns for high-efficiency chromatographic separations. *J. Chromatogr. A* **2002**, *965*, 35−49.

(10) Zhu, G.; Zhang, L.; Yuan, H.; Liang, Z.; Zhang, W.; Zhang, Y. Recent development of monolithic materials as matrices in micro-column separation systems. *J. Sep. Sci.* **2007**, *30*, 792−803.

(11) Rodŕiguez, S. A.; Colón, L. A. Investigations of a sol−gel derived stationary phase for open tubular capillary electrochromatography. *Anal. Chim. Acta* **1999**, *397*, 207−215.

(12) Ming-Ming, Z.; Ge-Deng, R.; Yu-Qi, F. Hybrid organic−inorganic silica monolith with hydrophobic/strong cation-exchange functional groups as a sorbent for micro-solid phase extraction. *J. Chromatogr. A* **2009**, *1216*, 7739−7746.

(13) Ghanem, A.; Ikegami, T. Recent advances in silica-based monoliths: Preparations, characterizations and applications. *J. Sep. Sci.* **2011**, *34*, 1−13.

(14) Chirita, R.-I.; Finaru, A.-L.; Elfakir, C. Evaluation of fused-core and monolithic versus porous silica-based C18 columns and porous graphitic carbon for ion-pairing liquid chromatography analysis of catecholamines and related compounds. *J. Chromatogr. B: Anal. Technol. Biomed. Life Sci.* **2011**, *879*, 633−640.

(15) Minakuchi, H.; Nakanishi, K.; Soga, N.; Ishizuka, N.; Tanaka, N. Octadecylsilylated porous silica rods as separation media for reversed-phase liquid chromatography. *Anal. Chem.* **1996**, *68*, 3498−3501.

(16) Li, W.; Fries, D. P.; Malik, A. Sol−gel stationary phases for capillary electrochromatography. *J. Chromatogr. A* **2004**, *1044*, 23−53.

(17) Ming-Luan, C.; Ming-Ming, Z.; Yu-Qi, F. Preparation of organic−inorganic hybrid silica monolith with octyl and sulfonic acid groups for capillary electrochromatograhpy and application in determination of theophylline and caffeine in beverage. *J. Chromatogr. A* **2010**, *1217*, 3547−356.

(18) Svec, F.; Kurganov, A. A. Less common applications of monoliths III. Gas chromatography. *J. Chromatogr. A* **2008**, *1184*, 281−295.

(19) Chienthavorn, O.; Dararuang, K.; Sasook, A.; Ramnut, N. Purge and trap with monolithic sorbent for gas chromatographic analysis of pesticides in honey. *Anal. Bioanal. Chem.* **2012**, *402*, 955−964.

(20) Björklund, E.; Christoph, v. H.; Anklam, E. Fast extraction, clean-up and detection methods for the rapid analysis and screening of seven indicator PCBs in food matrices. *Trends Anal. Chem.* **2002**, *21*, 40−53.

(21) Premstaller, A.; Oberacher, H.; Huber, C. G. High-performance liquid chromatography−electrospray ionization mass spectrometry of single- and double-stranded nucleic acids using monolithic capillary columns. *Anal. Chem.* **2000**, *72*, 4386−4393.

(22) Coufal, P.; Cihák, M.; Suchánková, J.; Tesarová, E.; Bosáková, Z.; Stulík, K. Methacrylate monolithic columns of 320 μm I.D. for capillary liquid chromatography. *J. Chromatogr. A.* **2002**, *946*, 99−106.
(23) Chienthavorn, O.; Pengpumkiat, S.; Noomhorm, A.; Smith, R. M. Superheated water extraction and phase transfer methylation of phenoxy acid herbicides from solid matrices. *J. Chromatogr. A* **2007**, *1152*, 268−273.
(24) Sasook, A. Characterization of silica monolithic column by inverse gas chromatography. M.S. Thesis, Kasetsart University, Bangkok, Thailand, 2008.
(25) Yurchenko, S.; Mölder, U. Volatile *N*-nitrosamines in various fish products. *Food Chem.* **2006**, *96*, 325−333.
(26) Yurchenko, S.; Mölder, U. The occurrence of volatile *N*-nitrosamines in Estonian meat products. *Food Chem.* **2007**, *100*, 1713−1721.
(27) Cox, G. B. Estimation of volatile *N*-nitrosamines by high-performance liquid chromatography. *J. Chromatogr.* **1973**, *83*, 471−481.
(28) Encarnación, L. P.; Ríos, A.; Valcárcel, M. Automated flow-injection spectrophotometric determination of nitrosamines in solid food samples. *Fresenius' J. Anal Chem.* **2001**, *371*, 891−895.
(29) Filho, P. J. S.; Rios, A.; Valcárcel, M.; Caramao, E. B. Development of a new method for the determination of nitrosamines by micellar electrokinetic capillary chromatography. *Water Res.* **2003**, *37*, 3837−3842.
(30) Maxwell, R. J.; Pensabene, J. W.; Fiddler, W. Multiresidue recovery at PPB levels of 10 nitrosamines from frankfurters by supercritical fluid extraction. *J. Chromatogr. Sci.* **1993**, *31*, 212−215.
(31) Raoul, S.; Gremaud, E.; Biaudet, H.; Turesky, R. J. Rapid solid-phase extraction method for the detection of volatile nitrosamines in food. *J. Agric. Food Chem.* **1997**, *45*, 4706−4713.
(32) Mitacek, E. J.; Brunnemann, K. D.; Suttajit, M.; Martin, N.; Limsila, T.; Ohshima, H.; Caplan, L. S. Exposure to *N*-nitroso compounds in a population of high liver cancer regions in Thailand: Volatile nitrosamine (VNA) levels in Thai food. *Food Chem. Toxicol.* **1999**, *37*, 297−305.
(33) Andrade, R.; Reyes, F. G. R.; Rath, S. A method for the determination of volatile *N*-nitrosamines in food by HS−SPME−GC−TEA. *Food Chem.* **2005**, *91*, 173−179.
(34) Ozel, M. Z.; Gogus, F.; Yagci, S.; Hamilton, J. F.; Lewis, A. C. Determination of volatile nitrosamines in various meat products using comprehensive gas chromatography−nitrogen chemiluminescence detection. *Food Chem. Toxicol.* **2010**, *48*, 3268−3273.
(35) Kocak, D.; Ozel, M. Z.; Gogus, F.; Hamilton, J. F.; Lewis, A. C. Determination of volatile nitrosamines in grilled lamb and vegetables using comprehensive gas chromatography−nitrogen chemiluminescence detection. *Food Chem.* **2012**, *135*, 2215−2220.
(36) AOAC International. Method 982.22. *AOAC Official Methods of Analysis of the Association of Official Analytical Chemists*; AOAC International: Gaithersburg, MD, 1995.
(37) Cárdenes, L.; Ayala, J. H.; González, V.; Afonso, A. M. Fast microwave-assisted dansylation of *N*-nitrosamines: Analysis by high-performance liquid chromatography with fluorescence detection. *J. Chromatogr. A* **2002**, *946*, 133−140.
(38) Lee, S. J.; Shin, J. H.; Sung, N. J.; King, J. G.; Hotchkiss, J. H. Effect of cooking on the formation of *N*-nitrosodimethylamine in Korean dried seafood products. *Food Addit. Contam.* **2003**, *20*, 31−36.
(39) Filho, P. S.; Rios, A.; Valcarcel, M.; Zanin, K. D.; Caramao, E. B. Method of determination of nitrosamines in sausage by CO_2 supercritical fluid extraction (SFE) and micellar electrokinetic chromatography (MEKC). *J. Agric. Food Chem.* **2007**, *55*, 603−607.
(40) Campillo, N.; Viñas, P.; Martínez-Castillo, N.; Hernández-Córdoba, M. Determination of volatile nitrosamines in meat products by microwave-assisted extraction and dispersive liquid−liquid microextraction coupled to gas chromatography−mass spectrometry. *J. Chromatogr. A* **2011**, *1218*, 1815−1821.

and randomly chosen. A portion of each item was minced three times with a meat grinder, packed into polyethylene bags, frozen, and stored at −20 °C until it was submitted to the specific sample preparation procedure preceding the assay. All commercial food labels were maintained and their data collected; food labeling in Italy is enforced by Council Directive 2000/13/EC on labeling: in the European Union the list of ingredients is compulsory on the labeling of food products, where under the term "Ingredient" there should be the list of any substance, including additives, used in the manufacture or preparation of a food and present in the final product, even in altered form. In this investigation, after examining the label information, we divided cooked ham items into three different groups that were characterized by a different use of P-containing ingredients and additives during the production processes. We classified them as follows: "regular", when no evidence of P-containing ingredients and additives was present on the package label (n = 8); "enhanced with P-containing additives" (EWP), when the words "containing polyphosphates" or the coding "E338−E341, E450−452" was used on the package labelling (n = 8); "enhanced with P-containing ingredients and additives" (EWPIA), when the words "containing polyphosphates" or the coding "E338−E341, E450−452" together with the key words "milk proteins", "plant protein extracts", "soy protein isolates", "wine" were mentioned on the package labeling (n = 8).

Chemicals, Reagents, and Certified Reference Materials. Potassium dihydrogen phosphate (KH_2PO_4), sodium hydroxide (NaOH), sulfuric acid 96% (H_2SO_4), sodium sulfate (Na_2SO_4), trichloroacetic acid 99%, chloroform, and methanol were used as analytical grade and provided by Sigma-Aldrich (St. Louis, MO, USA). Ammonium heptamolybdate tetrahydrate ($(NH_4)_6Mo_7O_{24}{\cdot}4H_2O$), hydrogen peroxide solution 30% (H_2O_2), and L-ascorbic acid were purchased from Carlo Erba (Milano, Italy). KH_2PO_4 and Na_2SO_4 were dried in an oven (110 °C for 2 h) and cooled in a desiccator overnight before use. Meat reference material, lyophilized pork muscle powder (ERM-BB384), was supplied by LGC Standards (Teddington, UK), whereas a 1 g/L phosphorus standard solution (Certified Reference Material, CRM) was supplied by Carlo Erba. Calibrated class A glassware and bidistilled water (specific conductivity < 18 mS) were used in the preparation of all solutions. In particular, the following solutions were prepared: 4 M sulfuric acid, 100 g/L trichloroacetic acid solution, P working standard solution at a concentration of 5 mg/L by using the 1 g/L P standard solution, 18 g/L ammonium molibdate solution by dissolving ammonium heptamolybdate tetrahydrate and 25 g/L ascorbic acid, these latter freshly prepared.

Instrumentation. Absorbance was measured by a UV−visible spectrophotometer (CP/2300, CGA Strumenti Scientifici, Firenze, Italy) in a 1 cm quartz cell, against reagent blank. Mineralization of samples and solutions was performed using a heating digester with programmable temperature controller (DK 20/26, Velp Scientifica Ertec, Poland). Samples were centrifuged by a laboratory centrifuge (4235A, ALC, Milano, Italy) with an angle rotor (maximum speed 6000 rpm, RCF 4800g, angle 45°, Falcon tubes 50 mL). Minced samples were obtained by using a manual meat grinder having a plate with 3 mm diameter holes. Homogenization of samples and solutions was performed using an Ultra-Turrax T 25 homogenizer with an S25N-18G dispersing tool (IKA-Werke GmbH, Staufen, Germany). For solvent evaporation a Rotavapor R-114 (Büchi Labortechnik AG, Flawil, Switzerland) with a water bath B-480 (Büchi Labortechnik AG) was used.

Total and Different Subtypes of Phosphorus. Total P, inorganic P, P from phospholipids, and P from phosphoproteins were detected by molybdenum blue method on wet ashing samples, preceded by a specific sample preparation.

Total Phosphorus (TP): Sample Preparation Method and Wet Ashing Procedure. Total P was determined as previously described.[11] In brief, the sample (0.4 g fresh mass, fm) was wet mineralized with 96% sulfuric acid and 30% hydrogen peroxide by using the temperature digestion program shown in Table 1. The cool digest was then transferred to a 100 mL volumetric flask and made up to the mark with bidistilled water, and it underwent a final measurement of P by using the P quantification procedure.

Table 1. Wet Digestion Program for TP, IP, PL, and PP Measurement Analyses

step	temperature (°C)	digestion time (min)
1	120	45
2	260	60
3	320	90
4[a]	420	180

[a]PP and PL sometimes needed an extra 60 min at step 4.

Inorganic Phosphorus (IP): Sample Preparation Method and Wet Ashing Procedure. Soluble phosphate ions, which usually include either natural or, to a greater extent, added inorganic P, were extracted according to the method described by Jastrzębska et al. modified in our laboratory: the samples (5 g fm) were extracted with 10 mL of 1 mM NaOH, using an orbital shaker for 60 min.[6,12] The extracts were separated by centrifugation at 6000 rpm (RCF 4800g) for 30 min, and supernatant was filtered under vacuum with a Whatman no. 1 filter paper. Filtrate was transferred to a 50 mL volumetric flask, where it was made up to the mark with bidistilled water. Afterward, a 5 mL aliquot of the sample solution was moved to a 125 mL digestion flask where, after the addition of 5 mL of 96% sulfuric acid and 5 mL of 30% H_2O_2, it was digested until the mixture was clear, by using the temperature program reported in Table 1. The so-obtained cool digest was transferred to a 100 mL volumetric flask and made up to the mark with bidistilled water, and it underwent a final measurement of P by using the P quantification procedure.

Phosphorus from Phospholipids (PL): Sample Preparation Method and Wet Ashing Procedure. P derived from phospholipid content was determined in the polar lipid extract of samples. On the basis of the results reported by Pérez-Palacios et al., lipid extraction was performed according to the method of Folch.[13,14] In practice, the samples (2 g fm) were mixed with 20 mL of a chloroform/methanol (2:1, v/v) mixture and immediately homogenized for 2 min at medium speed (motor speed set to 13500 rpm) in an Ultra-Turrax homogenizer. The apparatus was rinsed twice with 5 mL of the above-mentioned chloroform/methanol mixture, and the extracts were then combined. The pooled extract was centrifuged (10 min, 4000 rpm, RCF 2000g) and filtered through Whatman no. 1 filter paper. The residue in the filter paper was washed with 5 mL of chloroform/methanol (2:1, v/v), and all of the filtrates were then combined. Subsequently, 4 mL of bidistilled water was added, and the new mixture was shaken vigorously. The final biphasic system was separated by centrifugation (10 min, 4000 rpm, RCF 2000g). The upper aqueous layer was eliminated, 1 g of anhydrous sodium sulfate was added to the organic phase, and the mixture was shaken vigorously. The chloroform phase was filtered by Whatman no. 1 filter paper and collected. The residue in the filter paper was washed with 5 mL of chloroform, and the filtrates were then combined. The solvent was further evaporated with a rotary evaporator under vacuum and, finally, the glass vessels with the residue, which contained the lipids, were dried in an oven (100 °C for 30 min). Cool lipid extract content was then weighed, and half of it (from 40 to 80 mg) was then placed into a 125 mL digestion flask, to which 5 mL of 96% sulfuric acid and 5 mL of 30% H_2O_2 were added, and digested until the mixture was clear by using the temperature program reported in Table 1. The cool digest was transferred to a 100 mL volumetric flask and made up to the mark with bidistilled water, and it underwent a final measurement of phosphorus by using the phosphorus quantification procedure.

Phosphorus from Phosphoprotein (PP): Sample Preparation Method and Wet Ashing Procedure. The quantification method for P from phosphoprotein was strictly derived from that published by Dušek et al.:[9] samples (1.5 g fm) were homogenized in 36.5 mL of bidistilled water for 2 min at medium speed (motor speed set to 13500 rpm) by an Ultra-Turrax homogenizer. The apparatus was rinsed with 1 mL of bidistilled water, and the solutions were then combined. The so-obtained mixture was boiled for 30 min on a hot plate. After cooling, 10 mL of a 100 g/L trichloroacetic acid solution was added. The precipitate was filtered through Whatman no. 1 filter paper and

dried in an oven (100 °C for 30 min). After cooling, the filter was weighed, and about 50% of it (equivalent to 0.75 g fm) was placed in a 125 mL digestion flask and digested as described above. The cool digest was transferred to a 100 mL volumetric flask and made up to the mark with bidistilled water, and it underwent a final measurement of phosphorus by using the P quantification procedure.

Phosphorus Quantification Procedure: Molybdenum Blue Method on Wet Ashing Sample. Orthophosphate ions contained in wet mineralized sample solutions from TP, IP, PP, and PL were determined by using the Molybdenum Blue method according to Soderberg[15] and Italian Dairy Product Official Methods of Analysis. In brief, the mineralized sample solutions (800 μL) were transferred to a 10 mL volumetric flask and then were added the following reagents: 7 mL of bidistilled water, 390 μL of 4 M sulfuric acid solution, 400 μL of an 18 g/L ammonium molibdate solution, and 400 μL of a 25 g/L ascorbic acid solution. Each flask was gently swirled and finally placed in boiling water for 30 min to form characteristic molybdenum blue species. The solutions were then cooled to room temperature and made up to the mark with bidistilled water, and absorbance was measured by spectrophotometry at 650 nm against a blank.

Reference Samples. The TP method was tested by the ERM-BB384 Certified Reference Material (lyophilized pork muscle), the mean value and expanded uncertainty of which were provided by the certificate of analysis.

For IP analysis, one of the regular samples was spiked at two different levels: 100 mg P/100 g fresh sample or 150 mg P/100 g fresh sample. Because hydrolysis of polyphosphates leads to orthophosphate anions,[12] 443.8 and 665.7 mg of KH_2PO_4 were respectively added to 100 g of minced cooked ham, which was then passed twice through a meat grinder. Spiked samples were stored at −20 °C until assayed. The measurement uncertainty in spiked samples was calculated by type B evaluation of uncertainty. For PP and PL methods suitable meat certified reference materials were not available on the market; hence, in-house reference samples were prepared from "regular" cooked ham samples as reported below.

The PP in-house reference sample was obtained using the following procedure. Bidistilled water was added to a cooked ham sample and homogenized. The mixture thus obtained was boiled on a hot plate and, after cooling, trichloracetic acid was added. The precipitate was filtered and then was dried in a laboratory oven and allowed to cool in a desiccator overnight. Amounts of this dried filtrate were used as reference samples for PP analysis.

The PL in-house reference sample was prepared using the method developed by Folch.[14] In brief, the sample of cooked ham was mixed with a solution of chloroform/methanol (2:1, v/v) and homogenized. The extract was centrifuged and filtered. Bidistilled water was added to the filtrate and was shaken vigorously. The final biphasic system was allowed to separate by centrifugation. The upper aqueous phase was discharged, and anhydrous sodium sulfate (about 2 g) was added to the mixture to dry the organic phase. Then the chloroformic phase was filtered, the solvent was further evaporated under vacuum, and, finally, the glass vessel with the residue, which contained phospholipids, was dried in a laboratory oven. Cool lipid extract content was stored at −20 °C until assayed.

Reference values of P in-house reference samples of PP and PL were determined by the TP method as the averages of 10 measurements spread over three weeks. The standard deviations of average divided by the square root of the number of measurements were used as estimation of uncertainty of measurements. Coverage factors k, accordingly based on Student's test to a level of confidence of 95%, were applied to calculate the expanded uncertainties from the uncertainties of in-house reference samples used in PP and PL methods and of two spiked levels in IP method.

Calibration Curve. The linearity of the calibration curve was established for the concentration range of 0.1−1.2 mg P/L. The calibration curve was built using nine calibrators obtained by appropriate dilution of the 5 mg P/L working standard solution by bidistilled water. Their concentration values were 0.10−0.20−0.30−0.40−0.65−0.90−1.00−1.10−1.20 mg P/L. Calibration solutions underwent a P quantification procedure, after adjustment of the H_2SO_4 concentration by adding 190 μL of 4 M H_2SO_4, as required by the Molybdenum Blue quantitation method.[16,17] Notably, the amount of H_2SO_4 added to the calibrators was for matching its concentration in the samples from wet ashing. The instrumental limit of detection (LOD) and limit of quantification (LOQ) were calculated by the formulas $(y + 3s_{y/x})/b$ and $(10s_{y/x})/b$, respectively, where y is the intercept of the calibration line, $s_{y/x}$ is the standard deviation in the y-direction of the calibration line, and b is the slope of the calibration line.[18] Both values were expressed as mg P/L.

Analytical Performances of TP, IP, PP, and PL Measurement Methods. Precision and bias of TP, PP, and PL methods were estimated by using both Certified Reference Material ERM-BB384 and in-house reference standards. Sample spiking at two P addition levels, as previously described, was used for the IP method. Results were calculated as an average of five measurements spread over three weeks. All data were expressed as a mean value ± μ (confidence interval, p = 95%). Intermediate precisions were evaluated as the between-day coefficient of variation (CV) and the standard error of the mean (M). Measurement bias of each TP, IP, PP, and PL analytical procedure was determined by evaluating the deviation between the average value obtained from a series of measurements and the theoretical reference value. It includes the percent method recovery (REC), calculated as 100(obtained concentration/theoretical concentration).[19] Each method's LOD and LOQ, expressed as mg P/100 g fm, were calculated from instrumental LOD and LOQ values taking into account weights, dilutions, and percent method recovery.

Assay Quality Control in Cooked Ham Analysis. Each sample batch of cooked ham samples for the quantification of TP, PP, or PL included two reference (certified or in-house) samples, whereas two spiked and two unspiked samples were used for the IP determinations. Set measurements were rejected and repeated when the absolute difference between measured average values and reference (certified, in-house, or spiked) values were outside the range ± expanded uncertainty reported in the certificate of analysis for CRM and ± estimation of expanded uncertainty for in-house or spiked values. All sample analyses were performed in duplicate. Notably, food label nutritional content was blinded to all laboratory technicians to have no influence on the final results.

Statistical Analysis. Two relationships, the first between the concentration of P and absorbance at 650 nm in the calibration curve and the second between TP and the total differential P (DfP), which was the sum of the subtypes of sample P in form of IP plus PP and PL (DfP = IP + PP + PL) in cooked ham samples, were evaluated by paired t test for the significance of the Pearson product−moment correlation coefficient. The experimental t test value (t_{exp}) was compared to its tabulated value (t_{crit}). A linear relationship between variables was accepted at a significance level of $p < 0.001$. The unbiased measurement of any TP, IP, PL, and PP methods was verified with Student's paired test, when REC was not significantly different from 100 at a significance level of $p < 0.01$. Differences in P values from TP, IP, PL, and PP in each group of cooked ham were compared by one-way ANOVA post hoc tests. The null hypothesis was rejected at a significance level of $p < 0.05$. When a significant effect was detected, the comparison of means was done using Fisher's least significant difference (LSD) test.

RESULTS AND DISCUSSION

Calibration Curve of TP, IP, PP, and PL. The regression parameters of the calibration curve are shown in Table 2. The calibration line exhibits both a coefficient of determination close to 1 and a nearly 0 intercept, which suggests a satisfactory linearity. The calculated experimental t test value (t_{exp}) was higher than the theoretical values (t_{crit}), indicating that there was a significant linear relationship ($p < 0.001$) between the concentration of P and absorbance at 650 nm in the selected calibration solution range. The standard deviations (SD) of either slope and intercept were 1.3×10^{-3} and 9×10^{-4}, respectively. Instrumental LOD and LOQ values were 41 and

dx.doi.org/10.1021/jf404187n | J. Agric. Food Chem. 2014, 62, 1247−1253

Table 2. Analytical Parameters of Calibration Curves

parameter	value
slope	0.2841
standard deviation of slope	±0.0013
intercept	0.0016
standard deviation of intercept	±0.0009
coefficient of determination, R^2	0.9991
LOD[a] (μg P/L)	41
LOQ[b] (μg P/L)	118
molar absorptivity, ε/(L mol^{-1} cm^{-1})	8.80×10^3

[a]LOD, instrumental limit of detection. [b]LOQ, instrumental limit of quantification.

118 μg P/mL, respectively. In our study instrumental LOQ value was a few units higher than the lowest concentration of standard solutions. These data were in agreement with the data in the literature for P determination by phosphomolybdic acid with different reducing agents methods.[20−22]

Analytical Performances of the Proposed Procedures for TP, IP, PP, and PL. The amounts of TP, PL, and PP, as an average of the five replicates above-mentioned (certificate and in-house references), are reported in Table 3. The estimated amounts of IP in two spiked samples, in five replicates, are reported in Table 4. In the TP analysis, REC, between-day CV, and *M* were 100.7%, 1.3%, and 5.1, respectively. For the assessment of the TP method performance, the measured value of CRM lyophilized pork muscle was compared to the certified value, confirming that no significant difference ($p < 0.05$) was present and REC was not significantly different from 100 at a significance level of $p < 0.01$. Therefore, the TP method showed a satisfactory precision and was unbiased. A previous study comparing several spectrophotometric procedures for total P determination in meat samples reported between-day CV from 0.34 to 1.48%, *M* from 0.11 to 0.66, and REC in the range of 99.6−101.5% by using Standard Meat Reference Material.[22] Indeed, the present study provides analytical performances for TP method in agreement with those reported in the paper by Jastrzębska.[22] In addition, LOD and LOQ values were 13 and 37 mg P/100 g fm, respectively.

For the assessment of the IP method performance, the measured REC values for the two spiked levels were compared by using Student's paired test, and no significant difference ($p < 0.01$) was present, thus indicating that REC was stable in the range of 100−150 mg P added to 100 g of cooked ham samples (Table 4). Lower between-day CV and *M* in the 100 mg P spiking level with respect to those measured in the 150 mg P spiking level showed that the IP method precision worsens when the inorganic phosphate content is increased. The measured values of IP spiked samples were compared to the reference values, and significant differences ($p > 0.05$) were present. Values of between-day CV and *M* ranged from 0.4 to 2.6% and from 0.2 to 1.6, respectively, and thus indicate satisfactory precision; data from REC showed an acceptable method bias. Therefore, these results are in agreement with data present in the literature. In particular, Lee et al.[23] reported within-day relative standard error (RSD) values of 2.39 and 9.49% in raw and cooked beef meats, respectively, and Jastrzębska et al.[12] a within-day RSD of 9.9% in fresh pork meat and a within-day RSD ranging form 6.01 to 11.7% in polyphosphate-spiked fresh pork meat, whereas Jastrzębska et al.[24] reported between-day CV and REC ranging from 2.22 to 4.25% and from 95 to 97%, respectively, in polyphosphate-spiked pork meat. LOD and LOQ values for IP were 11 and 33 mg P/100 g fm, respectively.

Table 4. Results of Phosphorus Determination in Spiked Sample IP Methods (Number of Samples = 5)

		level 1	level 2
spiked sample	av (mg P/100 g sample)	100	150
	uncertainty[a] (mg P/100 g sample)	1	2
$(w \pm \mu)^b$ (mg P/100 g sample)		90 ± 1	135 ± 4
standard error of mean, *M*		0.2	1.6
coefficient of variation, CV%		0.4	2.6
recovery %[c] ($w \pm \sigma$)		90 ± 1	90 ± 2
LOD[d] (mg P/100 g sample)		11	
LOQ[d] (mg P/100 g sample)		33	

[a]Expanded uncertainty reference value. [b]Measured average phosphorus content with the confidence limits for $p = 95\%$. [c]Average % recoveries with standard deviations. [d]LOD, LOQ from calibration curve.

In the PP analysis, REC, between-day CV, and *M* were 97.5%, 1.2%, and 0.7, respectively. For the assessment of the PP method performance, the measured value of PP in-house reference samples was compared to the reference values, and a significant difference ($p > 0.05$) was present. Therefore, the PP method showed a satisfactory precision and an acceptable method bias. In addition, LOD and LOQ values were 2 and 20 mg P/100 g fm, respectively. To the best of the authors' knowledge, no data about the analytical performance of the PP method are present in the literature.

In the PL analysis, REC, between-day CV, and *M* were 93.1%, 1.2%, and 2.1, respectively. For the assessment of the PL

Table 3. Results of Phosphorus Determination in Reference Materials by TP, PP, and PL Methods (Number of Samples = 5)

		methods		
parameter		TP	PP	PL
reference	av (mg P/100 g sample)	870	131	433
sample	uncertainty[a] (mg P/100 g sample)	50	2	4
$(w \pm \mu)^b$ (mg/100 g)		876 ± 14	128 ± 2	404 ± 6
standard error of mean, *M*		5.1	0.7	2.1
coefficient of variation, CV%		1.3	1.2	1.2
recovery %[c]		100.7 ± 1.3	97.5 ± 0.1	93.1 ± 1.1
LOD[d](mg P/100 g sample)		13	2	6
LOQ[d](mg P/100 g sample)		37	20	16

[a]Expanded uncertainty certified value for TP, reference value for PP and PL. [b]Measured average phosphorus content with the confidence limits for $p = 95\%$. [c]Average % recoveries with standard deviations. [d]LOD − LOQ from calibration curve.

Table 5. Results of Phosphorus Determination in Cooked Ham Samples (mg/100 g Fresh Samples; Number of Samples = 24)

	TP	IP	PP	PL	DfP
$(w \pm \sigma)^a$ (mg P/100 g sample)	251 ± 59	154 ± 50	39 ± 14	37 ± 16	229 ± 57
w %[b]	100	61	16	14	91
RSD%[c]	24	33	35	43	25
range min−max[d] (mg P/100 g sample)	174−331	87−238	22−67	16−60	155−311

[a]Average phosphorus content with standard deviations. [b]% average phosphorus content. [c]Relative standard deviation of average phosphorus content. [d]Values range min−max.

method performance, the measured value of PL in-house reference samples was compared to the reference values, and a significant difference ($p < 0.05$) was present. Therefore, the PL method showed a satisfactory precision and an acceptable method bias. In addition, LOD and LOQ values were 6 and 16 mg P/100 g fm, respectively. Quantification of phospholipids by using total P content in lipid extracts from biological samples is currently used, but only a few data regarding the validation of these procedures are reported in the literature.[25−29] In particular, Kirkpatrick et al.[17] reported a recovery range from 95 to 101% and a relative standard deviation of 1.7% by using organophosphate and phosphonate pure standards, and Xi et al.[30] found recoveries within 93−103% and CV from 0.6 to 6.1% by using phospholipid pure standards. The present study provides analytical performances for the PL method in agreement with those published in the literature.

In conclusion, the analytical performances of the proposed procedures for differential measurement of TP, IP, PP, and PL prove their suitability for routine analyses. Whereas our innovative measurements are derived from well-known methods and make use of instrumentations present in routine analytical laboratories, our novel combinations and refinements of these techniques enable accurate and differential quantification of the different types of P more practical and hence more attractive.

Determinations of Phosphorus Type and Content in Different Brands of Cooked Ham Samples. The proposed analytical methods were applied to cooked ham samples of 24 different brands. Table 5 shows the results obtained for TP, IP, PP, and PL, as well as DfP.

TP average content and value range were 251 and 174−331 mg P/100 g fm, respectively. These results are in agreement with data present in the literature. In particular, Dušek et al.[9] reported values from cooked hams with listed phosphorus-containing additives ranging in the interval 204−366 mg P/100 g fm and Hrynczyszyn et al.[31] values between 141 and 197 mg P/100 g fm from tinned pork foods, between 106 and 111 mg P/100 g fm from luncheon pork meats, and 100 mg P/100 g fm from a single smoked pork ham sample, whereas Jastrzębska[7] reported values of 222 and 286 mg P/100 g fm, respectively, from single samples of cooked ham and smoked ham with a reported content of orthophosphate additives. Moreover, the obtained values for TP content in cooked ham samples were in close agreement with both previously published results[6] and data reported in the Food Composition Table of the National Research Institute for Food and Nutrition, Italy.[32]

IP average content and value ranges were 154 and 87−238 mg P/100 g fm, respectively. These results are in agreement with data present in the literature. In particular, Dušek et al.[9] reported an average content of 212 mg P/100 g fm and values ranging in the interval of 136−292 mg P/100 g fm from cooked hams with listed phosphorus-containing additives and Hrynczyszyn et al.[31] values between 124 and 173 mg P/100 g fm from tinned pork foods, between 73 and 88 mg P/100 g fm from luncheon pork meats, and 75 mg P/100 g fm from a single smoked pork ham sample.

PP average content and value ranges were 39 and 22−67 mg P/100 g fm, respectively. To the best of our knowledge, no data about PP contents in meat products were present in the literature. Only Dušek et al.[9] reported values ranging in the interval of 22−43 mg P/100 g fm in fresh meat from different species.

DfP average content and value ranges were 229 and 155−311 mg P/100 g fm, respectively. In our series of experiments the average DfP value was slightly lower than the measured average TP (229 vs 251 mg/100 g), indicating that we succeeded in measuring 91% of the constituents of the TP accurately. This gap of approximately 9%, by TP with respect to DfP, may be due to the technical difficulties of completely extracting the inorganic P from the food matrix, as reported by Jastrzębska et al.,[12] or due to yet other unmeasured types of P present in cooked ham items. Figure 1 shows the scatter plot of

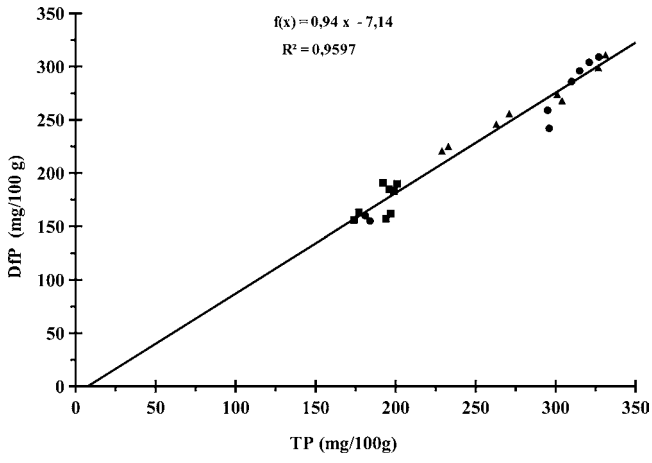

Figure 1. Scatter plot of the correlation between the sum of the subtypes of sample P and the measured total P: EWPIA (▲), EWP (●), and regular (■).

the correlation between the measured TP (X axis) and DfP (Y axis). The relationship between DfP and TP was evaluated by t test for the significance of the Pearson product−moment correlation coefficient. The calculated experimental t test value (t_{exp}) was higher than the theoretical values (t_{crit}), indicating that there was a significant linear relationship (Figure 1) for all intervals of TP measured (174−331 mg P/100 g) that include both EWPIA and EWP regular cooked ham items. Large RSD values in TP as well as in IP, PL, and PP content in cooked ham (ranged from 23 to 43%) demonstrate a wide variability in P contents. To explain this, we classified TP, IP, PL, and PP contents into three different groups of cooked ham items: EWPIA, EWP, and regular. Table 6 shows the results of TP as

dx.doi.org/10.1021/jf404187n | J. Agric. Food Chem. 2014, 62, 1247−1253

Table 6. Results of Phosphorus Determination into Three Different Groups of Cooked Ham Brands (mg P/100 g Fresh Samples; Number of Samples = 8)

group	TP	IP	PP	PL	DfP
EWPIA $(w \pm \sigma)^a$	282 ± 40	159 ± 18	55 ± 7	48 ± 11	263 ± 32
EWP $(w \pm \sigma)^a$	279 ± 60	199 ± 50	27 ± 4	25 ± 14	251 ± 62
regular $(w \pm \sigma)^a$	191 ± 10	103 ± 12	35 ± 8	36 ± 13	173 ± 15

[a]Average phosphorus content with standard deviations.

well as IP, PP, and PL contents classified into the three groups of cooked ham items. As expected, TP content was significantly higher in EWPIA and EWP than regular but no significant difference was observed for EWPIA with respect to EWP. Differences in inorganic phosphorus content were found not only between the regular group as compared to both EWPIA and EWP, but also in IP content, being higher in the EWP group than in regular products. Therefore, obtained results of TP and IP contents showed that the addition of P-containing ingredients, such as milk proteins and plant protein extracts or isolates, decreased the amount of functional additives, such as polyphosphates and phosphate salts, used in the production processes of EWPIA with respect to EWP.

PP content was higher in EWPIA than in EWP and regular samples, and no significant difference was observed for EWP with respect to regular, although the average value of PP content of EWP was lower with respect to those of regular. The key reason for higher measured PP contents in EWPIA with respect to EWP and regular was the addition of ingredients, such as milk proteins and plant protein extracts or isolates, in which there was a large increase of P from phosphoprotein with respect to total phosphorus content.

PL content was higher in EWPIA than EWP, and no significant difference was observed from EWP with respect to regular, although the average value of PL content of EWP was lower with respect to those of regular items. The dilution effect due to inclusion of water in ingredients (reported on the package label) of each EWPIA and EWP with respect to regular (in which water was not listed on the product label) may explain even lower PL and PP values measured in EWP with respect to those of regular items.

AUTHOR INFORMATION

Notes

The authors declare no competing financial interest.

ABBREVIATIONS USED

CRM, Certified Reference Material; CV, coefficient of variation; DfP, differential P; EWP, enhanced with phosphorus-containing additives; EWPIA, enhanced with phosphorus-containing ingredients and additives; IP, inorganic phosphorus; LOD, limit of detection; LOQ, limit of quantification; *M*, standard error of mean; P, phosphorus; PL, phosphorus from phospholipids; PP, phosphorus from phosphoprotein; RCF, relative centrifugal force; REC, recovery; RPM, rounds per minute; RSD, relative standard deviation; TP, total phosphorus

REFERENCES

(1) Cupisti, A.; Kalantar-Zadeh, K. Management of natural and added dietary phosphorus burden in kidney disease. *Semin. Nephrol.* **2013**, *33*, 180−190.

(2) Boaz, M.; Smetana, S. Regression equation predicts dietary phosphorus intake from estimate of dietary protein intake. *J. Am. Diet. Assoc.* **1996**, *96*, 1268−1270.

(3) Kalantar-Zadeh, K.; Gutekunst, L.; Mehrotra, R. Understanding sources of dietary phosphorus in the treatment of patients with chronic kidney disease. *Clin. J. Am. Soc. Nephrol.* **2010**, *5*, 519−530.

(4) Sherman, R. A.; Mehta, O. Dietary phosphorus in dialysis patients: potential impact of processed meat, poultry, and fish products as protein sources. *Am. J. Kidney Dis.* **2009**, *54*, 18−23.

(5) León, J. B.; Sullivan, C. M.; Sehgal, A. R. The prevalence of phosphorus-containing food additives in top-selling foods in grocery stores. *J. Ren. Nutr.* **2013**, *23*, 265−270.

(6) Benini, O.; D'Alessandro, C.; Gianfaldoni, D.; Cupisti, A. Extra phosphate load from food additives in commonly eaten foods: a real and insidious danger for renal patients. *J. Ren. Nutr.* **2011**, *21*, 303−308.

(7) Jastrzębska, A. Determination of sodium tripolyphosphate in meat samples by capillary zone electrophoresis with on-line isotachophoretic sample pre-treatment. *Talanta* **2006**, *69*, 1018−1024.

(8) Baldini, M.; Fabietti, F.; Giammarioli, S.; Onori, R.; Orefice, L.; Stacchini, A. Metodi di analisi utilizzati per il controllo chimico degli alimenti. *Rapporti ISTISAN* **1996**, *34*, 179−183 (in Italian).

(9) Dušek, M.; Kvasnika, F.; Lukášková, L.; Krátká, J. Isotachophoretic determination of added phosphate in meat products. *Meat Sci.* **2003**, *65*, 765−769.

(10) Cupisti, A.; Benini, O.; Ferretti, V.; Gianfaldoni, D.; Kalantar-Zadeh, K. Novel differential measurement of natural and added phosphorus in cooked ham with or without preservatives. *J. Ren. Nutr.* **2012**, *22*, 533−540.

(11) Cupisti, A.; Comar, F.; Benini, O.; Lupetti, S.; D'Alessandro, C.; Barsotti, G.; Gianfaldoni, D. Effect of boiling on dietary phosphate and nitrogen intake. *J. Ren. Nutr.* **2006**, *16*, 36−40.

(12) Jastrzębska, A.; Hol, A.; Szłyk, E. Simultaneous and rapid determination of added phosphorus(V) compounds in meat samples by capillary isotachophoresis. *LWT−Food Sci. Technol.* **2008**, *41*, 2097−2103.

(13) Pérez-Palacios, T.; Ruiz, J.; Martín, D.; Muriel, E.; Antequera, T. Comparison of different methods for total lipid quantification in meat and meat products. *Food Chem.* **2008**, *110*, 1025−1029.

(14) Folch, J.; Lees, M.; Stanley, G. H. S. A simple method for the isolation and purification of total lipids from animal tissues. *J. Biol. Chem.* **1957**, *226*, 497−509.

(15) Soderberg, D. L. Meat and meat products. In *Official Methods of Analysis of AOAC International*, 16th ed.; Horowitz, W., Ed.; AOAC International: Gaithersburg, MD, USA, 1995; pp 4−5.

(16) Crouch, S. R.; Malmstadt, H. V. A mechanistic investigation of molybdenum blue method for determination of phosphate. *Anal. Chem.* **1967**, *39*, 1084−1089.

(17) Kirkpatrick, D. S.; Bishop, S. H. Simplified wet procedure for total phosphorus analysis of organophosphonates in biological samples. *Anal. Chem.* **1971**, *43*, 1707−1709.

(18) Miller, J. N.; Miller, J. C. Calibration methods in instrumental analysis: regression and correlation. In *Statistics and Chemometrics for Analytical Chemistry*, 6th ed.; Pearson Education: Harlow, UK, 2010; pp 110−153.

(19) Thompson, M.; Ellison, S. L. R.; Fajgelj, A.; Willetts, P.; Wood, R. Harmonised guidelines for the use of recovery information in analytical measurement. *Pure Appl. Chem.* **1999**, *71*, 337−348.

(20) Li, C. B.; Zhou, G. H.; Xu, X. L.; Huang, M.; Li, M. Y. The mineral composition and microscopic changes in thoracic buttons of Chinese Yellow steer with age. *Meat Sci.* **2005**, *69*, 101−106.

(21) O'Toole, M.; Lau, K. T.; Shepherd, R.; Slater, C.; Diamond, D. Determination of phosphate using a highly sensitive paired emitter-detector diode photometric flow detector. *Anal. Chim. Acta* **2007**, *597*, 290−294.
(22) Jastrzębska, A. Modifications of spectrophotometric methods for total phosphorus determination in meat samples. *Chem. Pap.* **2009**, *63*, 47−54.
(23) Lee, B. J.; Hendricks, D. G.; Cornforth, D. P. Effect of sodium phytate, sodium pyrophosphate and sodium tripolyphosphate on physico-chemical characteristics of restructured beef. *Meat Sci.* **1998**, *50*, 273−283.
(24) Jastrzębska, A.; Szlyk, E. Application of ^{31}P NMR for added polyphosphate determination in pork meat. *Chem. Pap.* **2009**, *63*, 414−419.
(25) Lazaryan, D. S.; Sotnikova, E. M. Determination of the content of lipid phosphorus and phospholipids in bee brood. *Pharm. Chem. J.* **2004**, *38*, 517−519.
(26) Suzumura, M. Phospholipids in marine environments: a review. *Talanta* **2005**, *66*, 422−434.
(27) Morcuende, D.; Estevez, M.; Ramirez, R.; Cava, R. Effect of the Iberian Duroc reciprocal cross on productive parameters, meat quality and lipogenic enzyme activities. *Meat Sci.* **2007**, *76*, 86−94.
(28) Hernandez, P.; Cesari, V.; Blasco, A. Effect of genetic rabbit lines on lipid content, lipolytic activities and fatty acid composition of hind leg meat and perirenal fat. *Meat Sci.* **2008**, *78*, 485−491.
(29) Rakhuba, D.; Novika, G.; Dey, E. S. Application of supercritical carbon dioxide ($scCO_2$) for the extraction of glycolipids from *Lactobacillus plantarum* B-01. *J. Supercrit. Fluids* **2007**, *49*, 45−51.
(30) Xi, Z.; Gilbert, A. Improved procedures for the determination of lipid phosphorus by malachite green. *J. Lipid Res.* **1992**, *33*, 1233−1236.
(31) Hrynczyszyn, P.; Jastrzębska, A.; Szłyk, E. Determination of phosphate compounds in meat products by 31-phosphorus nuclear magnetic resonance spectroscopy with methylenediphosphonic acid after alkaline extraction. *Anal. Chim. Acta* **2010**, *673*, 73−78.
(32) INRAN, National Research Institute for Food and Nutrition. Tabelle di composizione degli alimenti, http://www.inran.it/646/tabelle_di_composizione_degli_alimenti.html (accessed Sept 15, 2013).

contamination have been reported in shellfish samples collected from different regions,[28−30] an effective method for on-site detecting OA in shellfishes is required. Therefore, this study produced a mAb against OA and successfully applied it to an ultrasensitive ELISA and gold nanoparticle immunochromatographic strip for detecting OA in shellfish samples.

MATERIALS AND METHODS

Materials. Okadaic acid (OA) and dinophysistoxin-1 (Figure 1) were obtained from Taiwan Algal Science Co. (Taiwan). An analytical

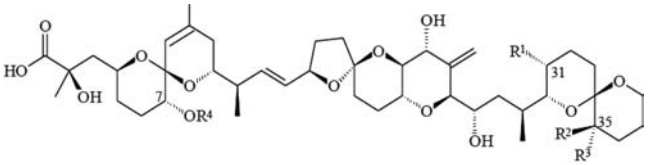

	R^1	R^2	R^3	R^4
OA	CH_3	H	H	H
DTX-1	CH_3	CH_3	H	H

Figure 1. Structures of okadaic acid (OA) and dinophysistoxin-1 (DTX-1).

standard solution of OA at 20 μg/mL was a product from Calbiochem (San Diego, CA). Bovine serum albumin (BSA), γ-globulin, gelatin, ovalbumin (OVA), ammonium biocarbonate, Tween 20, dimethyl sulfoxide (DMSO), 1,1′-carbonyldiimidazole (CDI), 1-ethyl-3-[3-dimethylaminopropyl]-carbodimide (EDC), and *N*-hydroxysuccinimide (NHS) were purchased from Sigma (MO, USA). Keyhole limpet hemocyanin (KLH) and antimouse−peroxidase conjugate from goat were purchased from Pierce (IL, USA). Horseradish peroxidase (HRP), BM Condimed H1 Hybridoma Cloning Supplement (BMH1), and the mouse mAb isotyping kit were from Roche (Mannheim, Germany). TMB (3,3′,5,5′-tetramethylbenzidine) is a substrate solution of HRP from Neogen Corp (KY, USA). Acetonitrile (HPLC grade), methanol (HPLC grade), ammonium sulfate, and absolute ethanol were obtained from Merck (Darmstadt, Germany). Polyethylene glycol (PEG 1500), hypoxanthine (H), aminopterin (A), and thymidine (T) were purchased from Boehringer Mannheim Biochemicals (IN, USA). Microtiter plates and strips with various protein binding abilities were obtained from Nunc (Roskilde, Demark). The fetal calf serum and penicillin−streptomycin were obtained from GIBCO Laboratories (Grand Island, NY). Gold nanoparticles with diameters of 20 and 40 nm were obtained from BB International (Cardiff, United Kingdom). The murine myeloma cell line P3/NS-1/1-AG4-1 (NS-1) was obtained from Bioresources Collection and Research Center in Taiwan, and virus-free BALB/c mice (9 to 10-week-old, female) were ordered from National Animal Research Center (Taipei, Taiwan).

Preparation of Different OA Conjugates. *Conjugation of OA to γ-Globulin.* OA was conjugated to γ-globulin in the presence of EDC.[31] The EDC and NHS solutions (1.0 mg of EDC and 1.0 mg of NHS in 0.04 mL of DMSO) were freshly prepared and then mixed with an OA solution containing 1.0 mg of OA in 0.2 mL of DMSO. The mixture (0.24 mL) was added slowly into 0.4 mL of γ-globulin solution (2.0 mg in 0.1 M carbonate buffer, pH 9.6), and then the reaction was conducted at room temperature for 2 h. Continuously, the mixture was dialyzed against 0.01 M phosphate buffer containing 0.15 M NaCl (PBS, pH 7.5) for three constitutive days with two exchanges of PBS. Final products were lyophilized for storage at −20 °C.

OA-KLH/OVA Conjugation. As a solid-phase antigen for indirect competitive ELISA, OA was conjugated to KLH or OVA by the EDC and NHS method.[31] Generally, 0.5 mg of OA in 0.1 mL of DMSO was added with 0.5 mL mg of KLH or OVA (2.5 mg in 0.1 M carbonate buffer, pH 9.6) first, and then EDC and NHS solutions (1.0 mg of EDC and 0.75 mg of NHS in 0.04 mL of DMSO) were added to the mixed solution at room temperature with a constant stirring for 2 h. The final product was dialyzed against PBS for three days and then lyophilized for storage.

Preparation of OA−Peroxidase. Conjugation of OA to HRP was achieved by the EDC and NHS method.[26,31] Briefly, 0.2 mg of OA in 0.1 mL of DMSO was mixed with 0.6 mg of EDC and 0.4 mg of NHS, and then an HRP solution (0.8 mg of HRP in 0.3 mL of 0.1 M carbonate buffer, pH 9.6) was added. After being stirred at room temperature for 2 h, the mixture was dialyzed against PBS for 72 h and then lyophilized.

Monoclonal Antibody (mAb) Production. *Immunization.* Female BALB/c mice (9−10 weeks of age) were intraperitoneally (ip) injected with 40 μg of OA-γ-globulin in 0.1 mL of PBS solution, which had been emulsified with 0.1 mL of Freund's complete adjuvant. Four weeks after the first injection, sequential boosters were conducted weekly with 40 μg of immunogen in 0.1 mL of PBS without adjuvant. After each booster, blood samples were collected from the tail vein of each mouse, and serum was isolated by centrifugation. The antibody specificity was determined by a competitive indirect ELISA (ciELISA) as described below.

Fusion and Cloning. The mouse showing the highest antibody specificity, 9 weeks after the initial immunization, was chosen for further fusion reaction. The selected mouse was primed with a total of 50 μg of OA-γ-globulin four days before fusion, and then the mouse was euthanized on the fusion day. The entire spleen was removed aseptically, mashed with a glass pestle, and then passed through a sieve-tissue grinder kit equipped with mesh 80 (CD-1, Sigma). Spleen cell suspension at a single-cell stage was mixed with 1×10^7 of myeloma cells. The cells were centrifuged and suspended in 0.2 mL of HT medium, and then 1 mL of PEG 1500 was dropped into the cell pellet within one minute. To dilute the PEG1500, 15 mL of HT medium was added gradually within 10 min. After centrifugation at 300*g* for 5 min, the pelleted cells were resuspended in the HAT medium containing hypoxanthine, aminopterin, and thymidine plus BMH1 (final concentration 10%) and plated into 96-well tissue culture plates. The plates were fed with freshly prepared HAT medium every five days. When the cell colonies reached at least half-confluence in the well, ciELISA was applied to screen hybridomas secreting specific antibodies against OA. Finally, hybridoma cells from three wells were found to be positive and were further cloned by the limiting dilution method.[32]

Ascites Fluid Generation. Female BALB/c mice, 10 weeks old, were injected with pristine (0.5 mL, ip); seven days later, 2×10^6 hybridoma cells suspended in DMEM were injected (ip). Three weeks after the injection, ascites were collected every other day and centrifuged at room temperature for 5 min. IgG antibodies in the supernatant fluid were precipitated with 50% of ammonium sulfate solution twice. Purified antibodies were stored at −70 °C for future usage.

Characterization of Monoclonal Antibodies. *Determination of the mAb Isotype.* Identification of specific immunoglobulin was carried out by a mouse mAb isotyping kit (Roche, Germany) according to the manufacturer's protocol.

Competitive Indirect ELISA (ciELISA). The process of ciELISA was conducted primarily according to Yu et al.[31] with a slight modification. OA−OVA (0.1 mL) was coated on each well of a microtiter plate which then was kept at 4 °C overnight. After the plate had been washed four times with Tween−PBS, 0.17 mL of gelatin−PBS (0.17 mL per well; 0.1% gelatin in PBS) was poured into the wells and incubated at 37 °C for 30 min. The plate was washed again, and 0.05 mL of OA standard with concentrations from 0.01 to 100 ng/mL in PBS or extracted sample solutions were added to each well. Then the anti-OA mAb (25 ng/mL in PBS, 0.05 mL per well) was added to all wells and incubated at 37 °C for 50 min. The plate was washed again, and 0.1 mL of goat antimouse IgG−HRP conjugate (1:20 000 dilution) was added and incubated at 37 °C for 45 min. The plate was washed, and 0.1 mL of TMB substrate solution (Neogen Corp) was added and waited the color development for 10 min. Then hydrochloric acid (0.1 mL, 1 N) was added to stop the reaction. A

Vmax ELISA reader (Molecular Devices Co.; Menlo Park, CA) was used to determine the absorbance value at 450 nm.

cdELISA. The process of cdELISA was conducted primarily according to Liu et al.[26] with a slight modification. The anti-OA mAb from ascites in PBS (1:10 000 dilution; 1 μg/mL) was used to coat the plate (0.1 mL/well). After a series of washing and blocking steps, OA standards (concentrations from 0.01 to 100 ng/mL) or samples together with the OA-HRP conjugate (10 ng/mL in PBSl) were added and incubated at 37 °C for 50 min. The plate was washed with PBS−Tween and incubated with TMB solution (Neogen Corp) at room temperature in the dark for 10 min. The absorbance at 450 nm was determined in the Vmax automatic ELISA reader

cdELISA of Shellfish Samples Contaminated with OA. Twenty shellfish samples, including clam, scallop, mussel, and oyster, were obtained from local stores for OA level determination. Briefly, 5 g of each sample (whole body) was homogenized with 20 mL of extraction solvent (methanol/water, 80/20, v/v) for 5 min[24,33] and then centrifuged at 14 000*g* for 10 min. An amount of 1 mL of supernatant fluid was mixed with 1 mL of hexane by vortex for 1 min, and then 3 mL of chloroform was added. After centrifugation for 5 min, the lower chloroform layer was aspirated and dried under a rotary vacuum evaporator. The dried sample was reconstituted with 1 mL of PBS buffer for cdELISA analysis or for the immunostrip assay.

Preparation of the Antibody-Gold Nanoparticle Probe. For conjugation, OA mAbs were dialyzed in boric acid−borax buffer (pH 8) for 24 h at 4 °C, and the gold nanoparticle solution was adjusted to pH 9.0 with 0.1 M K_2CO_3 (pH 11.5).[27,28] An amount of 5 μL of anti-OA mAb (1 μg/μL) was added dropwise to 2 mL of gold nanoparticle solution with gentle stirring. After 1 h reaction at room temperature, 10% (w/v) filtered BSA was added to block the reaction for 30 min and then centrifuged at 19 000*g* for 30 min at 4 °C. The pellets containing an OA mAb−gold nanoparticle conjugate were resuspended in 450 μL of 20 mM Tris-buffered saline (pH 8.0) containing 1% BSA and 0.1% sodium azide and stored at 4 °C for further usage.

Preparation of Immunochromatographic Strip. An Easypack Developer's Kit composed of three pads (sample, conjugate release, and absorbent pads), glass fiber, cover tape, and nitrocellulose (NC) membrane plates (pore sizes of 5 and 15 μM) are purchased from Advanced Microdevices P. Ltd. (Ambala Cantt, India). With the aid of a Double Axes Programmable Control Printer (model P-602 from Troy Technology, Taiwan), the test and control zones of the NC membrane were drawn with 0.5 μL of OA−KLH (0.8 mg/mL) conjugate and 0.5 μL of rabbit−antimouse IgG antibody (1 mg/mL), respectively, and then dried for 10 min at room temperature. Subsequently, the OA mAb−gold nanoparticle conjugate (5 μL/strip) was added to the conjugate release pad and dried at 37 °C for 5−10 min. The release pad was first pasted on the plate by overcrossing 4 mm with the NC membrane. Then, the sample pad was further pasted on the plate by overcrossing 6 mm with the release pad. Finally, the top of the membrane sheet was pasted on an absorbent pad. The whole assembled sheet was cut lengthways with an automatic cutter and divided into strips (5 mm × 75 mm).[27,28]

Assay of OA in Shellfish Samples with an Immunochromatographic Strip. Three hundred microliters of sample extract solutions as mentioned above or various concentrations of OA analytical standard (0−50 ng/mL) were poured into the wells of a microtiter plate. Subsequently, one immunochromatographic strip was dipped per well vertically. The extracted samples or OA standard solution migrated upward the membrane by capillary action. Ten minutes after color development, test results on the strip were determined visually.

RESULTS

Monoclonal Antibody Production. Mice were injected with OA-γ-globulin and boosted 4 times with the same antigen, and the mouse with serum that had the highest affinity for OA was sacrificed for a hybridoma screening. Following the NS-1/spleen cell fusion and growing, the ciELISA with OA−OVA as a coated reagent was used for screening the hybridoma cells, which secreted mAbs specific to OA. In the about 500 examined wells, three clones displayed strong positive color results in the ciELISA; of these, the clone 6B1 had the highest affinity for OA. Therefore, the clone 6B1 culture was aspirated from the fusion well and subjected to limiting dilution for a single hybridoma selection. After limiting dilution and ciELISA screening, clone 6B1A3, which showed the highest affinity for OA, was used to generate culture supernatant and ascites fluid.

Antibody Characterization. *Isotype Determination.* The isotype of the mAb, secreted from the hybridoma cell line 6B1A3, was identified as immunoglobulin G1, κ-light chain.

Competitive Direct and Indirect ELISA. The specificity of 6B1A3 mAb was measured by both cdELISA and ciELISA. As shown in Figure 2A, the concentrations causing 50% inhibition

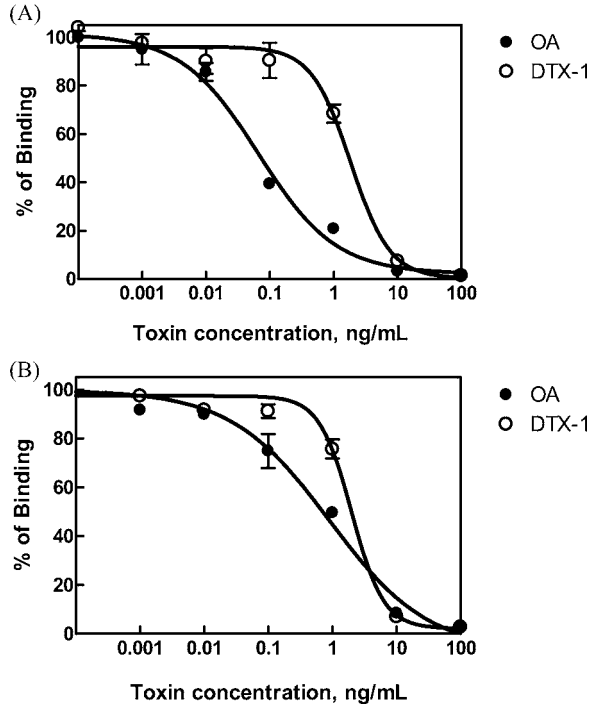

Figure 2. (A) Cross-reactivity of anti-OA antibodies with OA (●) and DTX-1 (○) in a cdELISA. (B) Cross-reactivity of anti-OTA antibodies with OA (●) and DTX-1 (○) as determined by a ciELISA. All data were obtained based on the average of three sets of experiments. The absorbance of the control, A0, with no toxin present, was 2.0.

(IC_{50}) of binding of OA−HRP to the mAb by OA and DTX-1 were calculated to be 0.077 and 1.870 ng/mL, respectively, in cdELISA. The ciELISA revealed similar results for OA−OVA coated onto the microplate wells to serve as a solid-phase antigen. The IC_{50} values for mAb binding to OA−OVA by free OA and DTX-1 were 0.58 and 2.0 ng/mL, respectively (Figure 2B). However, other phycotoxins such as domoic acid and saxitoxin, even at concentrations as high as 10 μg/mL, did not inhibit the mAb binding to the OA-enzyme/protein conjugates (OA−HRP or OA−OVA) in either ELISA system.

Assay of OA in Shellfishes with mAb-Based cdELISA. Twenty shellfish samples were purchased from local supermarkets and subjected to cdELISA to measure OA contamination; Table 1 presents the measurement results. The proposed detection system revealed that ten of the twenty examined samples were OA-positive. Sample 7 showed the highest OA levels (0.517 ng/mL; 2.068 ng/g). The OA levels

Table 1. ELISA and Immunochromatographic Strip Analysis of OA in Shellfish Samples

		ELISA[a]		
no.		(ng/mL ± SD)	(ng/g ± SD)[b]	immunochromatographic strip[a]
1.	clam	0.051 ± 0.008	0.204 ± 0.032	−
2.	clam	0.143 ± 0.005	0.572 ± 0.020	−
3.	mussel	0.106 ± 0.004	0.424 ± 0.016	−
4.	clam	ND[c]	ND	
5.	oyster	ND	ND	
6.	scallop	0.196 ± 0.018	0.784 ± 0.072	−
7.	clam	0.517 ± 0.004	2.068 ± 0.016	−
8.	clam	0.195 ± 0.012	0.780 ± 0.048	−
9.	clam	0.307 ± 0.012	1.228 ± 0.048	−
10.	oyster	ND	ND	
11.	scallop	ND	ND	
12.	scallop	ND	ND	
13.	clam	0.388 ± 0.005	1.552 ± 0.020	−
14.	mussel	ND	ND	
15.	clam	ND	ND	
16.	scallop	0.216 ± 0.026	0.864 ± 0.104	−
17.	crab	ND	ND	
18.	clam	0.112 ± 0.023	0.448 ± 0.092	−
19.	oyster	ND	ND	
20.	oyster	ND	ND	

[a]Each sample was extracted twice, and each extract was analyzed in triplicate. [b]1 mL of extract solution contains 0.25 g of shellfish samples. [c]ND, not detectable.

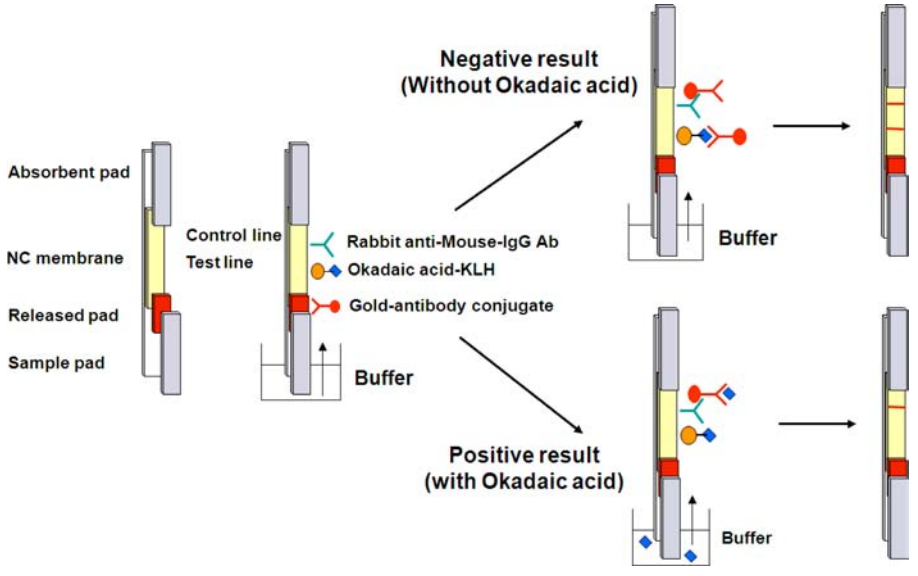

Figure 3. Schematic illustration of the immunochromatographic strip for OA. C, control zone (rabbit antimouse IgG); T, test zone (OA−KLH).

of samples 9 and 13 are also higher than 1.0 ng/g. The OA levels in the other seven positive samples were lower than 1.0 ng/g. However, all the oyster samples are free of OA contamination.

Assembly of the Immunochromatographic Strip. The mAb−gold nanoparticle conjugates were used to fabricate an immunochromatographic strip, in which OA in the sample solution competes with the OA−KLH conjugate on the membrane for the antibody−gold nanoparticle label. Figure 3 is a schematic description of the immunochromatographic strip test format. A sufficient OA level in the sample solution occupied all the antibody binding sites of the antibody−gold nanoparticle conjugates, which prevented the limited antibody−gold nanoparticle conjugates from binding with the OA−KLH conjugate in the test zone. The absence of the red line in the test zone indicated a positive result (Figure 3). In contrast, when OA is absent in sample solution, the antibody−gold nanoparticle conjugate trapped and bound by the OA−KLH conjugate to form a red line in the test zone indicated a negative result (Figure 3). The control zone was designed with rabbit-antimouse secondary antibody to confirm that the assay had been performed properly; regardless of the presence of OA, the control zone on the membrane will show one red line (Figure 3).

Characterizaion of Immunochromatographic Strip for OA. Different concentrations of OA analytical standard solution (0−50 ng/mL) were subjected to an immunochromatographic strip test. This assay required no more than 10

dx.doi.org/10.1021/jf404827s | J. Agric. Food Chem. 2014, 62, 1254−1260

min, and the detection limit of the strip test for OA approached 5 ng/mL (Figure 4). At least five measurements were examined

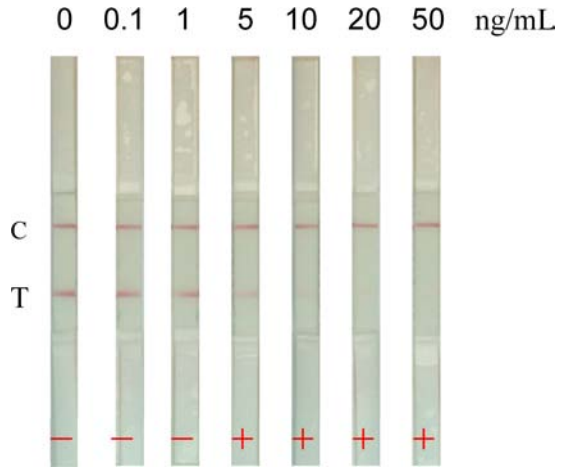

Figure 4. Detection limit of OA with immunochromatographic strip. A series of dilutions (0−50 ng/mL) of certificated standard OA was dissolved in PBS. A concentration higher than 5 ng/mL of OA caused a disappearance of a red line at the test zone.

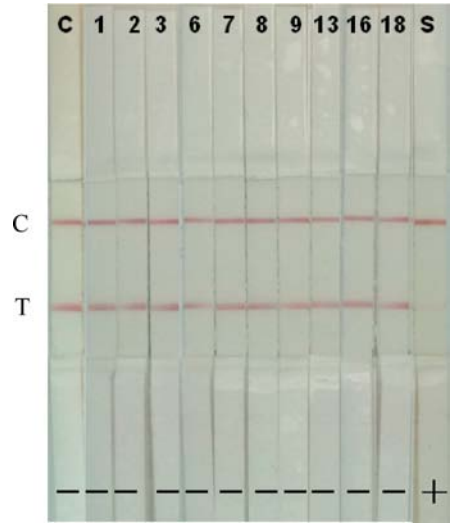

Figure 5. Detection of OA with immunochromatographic strip in control (C), spiked (S), and 10 shellfish samples. A spiked strip containing 5 ng/mL of OA in shellfish extract indicates that a red line disappeared in the test zone, verifying that it is OA positive. All samples containing OA lower than 5 ng/mL showed two red lines on the membrane indicating that they are OA negative.

by the strip detection system to define the cutoff level for each selected concentration. When OA levels are higher than 5 ng/mL, all antibody−gold nanoparticle conjugates were bound by free OA, which restricted the antibody−gold nanoparticle conjugates to bind with the OA−KLH in the test zone of the membrane. Finally, rabbit antimouse secondary antibody captured antibody−gold nanoparticle conjugates in the control zone which resulted in only one red line on the membrane.

Analysis of OA in Shellfish Samples by Immunochromatographic Strip Assay. The strip was further applied to examine OA contamination shellfishes. Table 1 shows the analytical results. Ten contaminated shellfish samples with OA levels ranging from 0.051 to 0.517 ng/mL, according to cdELISA results (Table 1), had two red lines on the immunostrip membranes, which indicated a negative outcome (Figure 5). However, in one spiked sample (S) containing 5.0 ng/mL of OA in shellfish extract, one red line disappeared in the test zone, which indicated that the sample was OA-positive (Figure 5).

DISCUSSION

Since OA is a nonimmunogenic phycotoxin with low molecular weight, conjugating OA to a protein carrier is needed to contribute to its immunogenicity. Our laboratory has successfully produced a polyclonal antibody for OA using the OA−γ-globulin conjugate as an antigen and established a sensitive ELISA for detecting OA. Since this study obtained a hybridoma clone secreting mAb specific to OA, the supply of mAb for OA is theoretically unlimited. Both mAbs produced from culture supernatant and mouse ascites could be adopted in the cdELISA. However, the rabbit-antimouse Fc secondary antibody must be coated onto the microplate before adding the supernatant. In contrast, cdELISA can be run by directly coating the microplate with mAb purified from ascites.

The mAb obtained from 6B1A3 showed a better affinity (IC50 value) for OA compared to DTX-1 in both cd- and ciELISA systems. The IC50 value of the mAb-based cdELISA for OA was 0.077 ng/mL, and the detection limit of OA in PBS solution in the cdELISA approximated 0.004 ng/mL based on a 90% confidence interval at 10% of inhibition of binding of the OA−HRP conjugate. Therefore, the proposed ELISA method is about 2 orders of magnitude higher than that of the mAb-based ELISA reported by Lu et al.[16] (IC50 and detection limits of 4.4 and 0.45 ng/mL, respectively) and that of Kreuzer et al.[14] with an IC50 of 100 ng/mL.

After using a combination of water/methanol (20:80, v/v) to extract OA from shellfishes, 1 mL of clear supernatant solution was diluted with 9 mL before cdELISA analysis. The analytical results showed that all examined samples were slightly OA positive because the matrix components caused interference in the cdELISA. Therefore, a cleanup procedure was incorporated into the sample preparation procedure. Washing the methanolic sample extracts with hexane effectively eliminated the lipid in the extract solution to avoid the matrix interference.[24] The cdELISA analysis of shellfishes demonstrated that 10 of the 20 shellfish samples had a low-level contamination with OA (Table 1). In all samples, OA was lower than 2.068 ng/g, which was approximately 80-fold below the regulatory limit of EU which is 160 ng/g of OA in shellfish samples.[7] This concentration is consistent with a previous report by Lee et al.[29] that gastropod samples collected in Korea had OA concentrations up to 21.5 ng/g but is lower than that reported by Ciminiello et al.[28] with OA concentrations of 100−200 ng/g.

To establish an assay that could be broadly used for field detection of OA-contaminated shellfish samples, this study further developed an mAb-based rapid immunochromatographic strip for faster and simpler screening compared to cdELISA. The mAb-based immunochromatographic strip established in this study for on-site OA determination had a limit of detection of about 5.0 ng/mL. In Lu et al.,[17] a lateral flow assay developed for OA analysis had a detection limit of 30−50 ng/mL, which may not be sensitive enough for a practical sample test. Several factors also correlated with the effectiveness of an immunochromatographic strip include the size of the gold nanoparticles, the membrane pore size, and the test line of OA−protein conjugates. Therefore, both 20 and 40

nm gold particles were adopted to prepare mAb−gold particle conjugates. On the nitrocellulose membrane, the 40 nm particles provided better visibility compared to the 20 nm gold particles, probably due to their optimal size and their lower steric hindrance between conjugation of 40 nm gold particles and antibody. To test the effectiveness of 5 and 15 μm membrane pore size, in the membrane pore size of 15 μm, the red gold nanoparticles provided a more obvious visual effect and also a faster migration during the process. Finally, 15 μm membrane pore size and 40 nm gold particles were selected for all immunochromatographic strips. Either OA−KLH or OA−OVA is drawn onto the membrane test zone to compare their effectiveness in binding OA in the sample with the antibody−gold nanoparticle conjugate. Compared to OA−OVA, the OA−KLH proved to be a suitable protein conjugate because coating OA−KLH onto the test zone of a strip obtained a stronger red color line in the strips and also had a lower detection limit of 5 ng/mL compared with 20 ng/mL in which it was coated with OA−OVA onto the test line (data not shown).

Results of sample analysis acquired by the immunochromatographic strip were in good agreement with those acquired by ELISA (Table 1). The test strip can be directly immersed into 300 μL of sample extraction solution, and the test can be performed in 10 min. Therefore, the strip test is effective for on-site OA detection not only in terms of accuracy and sensitivity but also in terms of labor and speed. This study obtained a novel hybridoma cell line for secreting mAb against OA and successfully applied it to an ultrasensitive ELISA and gold nanoparticle immunostrip for detecting OA in shellfish. The IC_{50} value of ELISA was 0.077 ng/mL, and the gold nanoparticle immunostrip had a visual detection limit of 5.0 ng/mL. The OA immunostrip is a semiquantitative, rapid, and visual assay that uses gold nanoparticles as a color tracer to provide visual indication to examine OA in shellfish samples within 10 min. This strip will be conceivably applicable for on-site detection of OA in the seafood industry.

AUTHOR INFORMATION

Corresponding Author

*Tel.: 886-4-24730022 ext 11816. Fax: 886-4-23758184. E-mail: fengyu@csmu.edu.tw.

Author Contributions

⊥Equal contribution to first author.

Funding

This work was supported by grants NSC 100-2923-B-040-001-MY2 and 101-2313-B-040-005 from the National Science Council of the Taiwan.

Notes

The authors declare no competing financial interest.

ACKNOWLEDGMENTS

Ted Knoy is appreciated for his editorial assistance.

ABBREVIATIONS USED

A, aminopterin; BMH1, BM Condimed H1 Hybridoma Cloning Supplement (BMH1); BSA, bovine serum albumin; CDI, 1,1′-carbonyldiimidazole; DMEM, Dulbeco Modified Eagle's Medium; DMSO, dimethyl sulfoxide; EDC, 1-ethyl-3-[3-dimethylaminopropyl] carbodimide; ELISA, enzyme-linked immunosorbent assay; cdELISA, competitive direct ELISA; ciELISA, competitive indirect ELISA; H, hypoxanthine; iELISA, indirect ELISA; HRP, horseradish peroxidase; KLH, keyhole limpet hemocyanin; mAb, monoclonal antibody; MES, 2-*N*-morpholinoethane-sulfonic acid; NHS, *N*-hydroxysuccinimide; NS-1, P3/NS-1/1-AG4-1; PBS, phosphate buffer containing 0.15 M NaCl; PEG 1500, polyethylene glycol; OVA, ovalbumin; T, thymidine; TMB, 3,3′,5,5′-tetramethylbenzidine

REFERENCES

(1) Codd, G. A.; Ward, C. J.; Bell, S. G. Cyanobacterial toxins:occurrence, mode of action, health effects and exposure routes. *Arch. Toxicol. Suppl.* **1997**, *19*, 399−410.

(2) Scoging, A.; Bahl, M. Diarrhetic shellfish poisoning in the UK. *Lancet* **1998**, *352*, 117.

(3) Armi, Z.; Turki, S.; Trabelsi, E.; Ceredi, A.; Riccardi, E.; Milandri, A. Occurrence of diarrhetic shellfish poisoning (DSP) toxins in clams (*Ruditapes decussatus*) from Tunis north lagoon. *Environ. Monit. Assess.* **2012**, *184*, 5085−5095.

(4) Hossen, V.; Jourdan-da Silva, N.; Guillois-Becel, Y.; Marchal, J.; Krys, S. Food poisoning outbreaks linked to mussels contaminated with okadaic acid and ester dinophysistoxin-3 in France, June 2009. *Euro. Surveill.* **2011**, *16*, Article3.

(5) Li, A.; Ma, J.; Cao, J.; McCarron, P. Toxins in mussels (*Mytilus galloprovincialis*) associated with diarrhetic shellfish poisoning episodes in China. *Toxicon* **2012**, *60*, 420−425.

(6) Carvalho, P. S.; Catian, R.; Moukha, S.; Matias, W. G.; Creppy, E. E. Comparative study of Domoic Acid and Okadaic Acid induced-chromosomal abnormalities in the Caco-2 cell line. *Int. J. Environ. Res. Public Health* **2006**, *3*, 4−10.

(7) European Commission. Commission Regulation (EU) amending Regulation (EC) No 2074/2005 as regards recognized testing methods for detecting marine biotoxins in live bivalve molluscs. *Off. J. Eur. Union* **2011**, *15*, 3−6.

(8) Gerssen, A.; Mulder, P. P.; McElhinney, M. A.; de Boer, J. Liquid chromatography-tandem mass spectrometry method for the detection of marine lipophilic toxins under alkaline conditions. *J. Chromatogr. A.* **2009**, *1216*, 1421−1430.

(9) Louppis, A. P.; Badeka, A. V.; Katikou, P.; Paleologos, E. K.; Kontominas, M. G. Determination of okadaic acid, dinophysistoxin-1 and related esters in Greek mussels using HPLC with fluorometric detection, LC-MS/MS and mouse bioassay. *Toxicon* **2010**, *55*, 724−733.

(10) Suzuki, T.; Quilliam, M. A. LC-MS/MS analysis of diarrhetic shellfish poisoning (DSP) toxins, okadaic acid and dinophysistoxin analogues, and other lipophilic toxins. *Anal. Sci.* **2011**, *27*, 571−584.

(11) Stobo, L. A.; Lacaze, J. P.; Scott, A. C.; Gallacher, S.; Smith, E. A.; Quilliam, M. A. Liquid chromatography with mass spectrometry–detection of lipophilic shellfish toxins. *J. AOAC Int.* **2005**, *88*, 1371−82.

(12) Draisci, R.; Croci, L.; Giannetti, L.; Cozzi, L.; Lucentini, L.; De Medici, D.; Stacchini, A. Comparison of mouse bioassay, HPLC and enzyme immunoassay methods for determining diarrhetic shellfish poisoning toxins in mussels. *Toxicon* **1994**, *32*, 1379−1384.

(13) Hokama, Y. Recent methods for detection of seafood toxins: recent immunological methods for ciguatoxin and related polyethers. *Food Addit. Contam.* **1993**, *10*, 71−82.

(14) Kreuzer, M. P.; O'Sullivan, C. K.; Guilbault, G. G. Development of an ultrasensitive immunoassay for rapid measurement of okadaic acid and its isomers. *Anal. Chem.* **1999**, *71*, 4198−4202.

(15) Lamas, N. M.; Stewart, L.; Fodey, T.; Higgins, H. C.; Velasco, M. L.; Botana, L. M.; Elliott, C. T. Development of a novel immunobiosensor method for the rapid detection of okadaic acid contamination in shellfish extracts. *Anal. Bioanal. Chem.* **2007**, *389*, 581−587.

(16) Lu, S. Y.; Zhou, Y.; Li, Y. S.; Lin, C.; Meng, X. M.; Yan, D. M.; Li, Z. H.; Yu, S. Y.; Liu, Z. S.; Ren, H. L. Production of monoclonal antibody and application in indirect competitive ELISA for detecting okadaic acid and dinophytoxin-1 in seafood. *Environ. Sci. Pollut. Res. Int.* **2011**, *19*, 2619−2626.

(17) Lu, S. Y.; Lin, C.; Li, Y. S.; Zhou, Y.; Meng, X. M.; Yu, S. Y.; Li, Z. H.; Li, L.; Ren, H. L.; Liu, Z. S. A screening lateral flow immunochromatographic assay for on-site detection of okadaic acid in shellfish products. *Anal. Biochem.* **2012**, *422*, 59−65.
(18) Matsuura, S.; Hamano, Y.; Kita, H.; Takagaki, Y. Preparation of mouse monoclonal antibodies to okadaic acid and their binding activity in organic solvents. *J. Biochem.* **1993**, *114*, 273−278.
(19) Mountfort, D. O.; Kennedy, G.; Garthwaite, I.; Quilliam, M.; Truman, P.; Hannah, D. J. Evaluation of the fluorometric protein phosphatase inhibition assay in the determination of okadaic acid in mussels. *Toxicon* **1999**, *37*, 909−922.
(20) Stewart, L. D.; Hess, P.; Connolly, L.; Elliott, C. T. Development and single-laboratory validation of a pseudofunctional biosensor immunoassay for the detection of the okadaic acid group of toxins. *Anal. Chem.* **2009**, *81*, 10208−10214.
(21) Stewart, L. D.; Elliott, C. T.; Walker, A. D.; Curran, R. M.; Connolly, L. Development of a monoclonal antibody binding okadaic acid and dinophysistoxins-1, −2 in proportion to their toxicity equivalence factors. *Toxicon* **2009**, *54*, 491−498.
(22) Tsumuraya, T.; Fujii, I.; Hirama, M. Production of monoclonal antibodies for sandwich immunoassay detection of Pacific ciguatoxins. *Toxicon* **2010**, *56*, 797−803.
(23) Vale, P.; Sampayo, M. A. Comparison between HPLC and a commercial immunoassay kit for detection of okadaic acid and esters in Portuguese bivalves. *Toxicon* **1999**, *37*, 1565−1577.
(24) Wang, L.; Sang, Y. X.; Wang, X. H. Enzyme-linked immunosorbent assay for okadaic acid: investigation of analytical conditions and sample matrix on assay performance. *J. AOAC Int.* **2011**, *94*, 1531−1539.
(25) Paek, S. H.; Lee, S. H.; Cho, J. H.; Kim, Y. S. Development of rapid one-step immunochromatographic assay. *Methods* **2000**, *22*, 53−60.
(26) Liu, B. H.; Tsao, Z. J.; Wang, J. J.; Yu, F. Y. Development of a monoclonal antibody against ochratoxin A and its application in enzyme-linked immunosorbent assay and gold nanoparticle immunchromatographic strip. *Anal. Chem.* **2008**, *80*, 7029−7035.
(27) Tsao, Z. J.; Liao, Y. C.; Liu, B. H.; Su, C. C.; Yu, F. Y. Development of a monoclonal antibody against domoic acid and its application in enzyme-linked immunosorbent assay and colloidal gold immunostrip. *J. Agric. Food Chem.* **2007**, *55*, 4921−4927.
(28) Ciminielo, P.; Dellaversano, C.; Fattorusso, E.; Forino, M.; Magno, S.; Santelia, F.; Tsoukatou, M. Investigation of the toxin profile of Greek mussels Mytilus galloprovincialis by liquid chromatography-mass spectrometry. *Toxicon* **2006**, *47*, 174−181.
(29) Lee, K. J.; Mok, J. S.; Song, K. C.; Yu, H.; Lee, D. S.; Jung, J. H.; Kim, J. H. First detection and seasonal variation of lipophilic toxins okadaic acid, dinophysistoxin-1, and yessotoxin in Korean gastropods. *J. Food Prot.* **2012**, *75*, 2000−2006.
(30) Vale, P.; Veloso, V.; Amorim, A. Toxin composition of a *Prorocentrum lima* strain isolated from the Portuguese coast. *Toxicon* **2009**, *54*, 145−152.
(31) Yu, F. Y.; Liu, B. H.; Chou, H. R.; Chu, F. S. Development of a sensitive ELISA for the determination of microcystins in algae. *J. Agric. Food Chem.* **2002**, *50*, 4176−4182.
(32) Oi, V. T.; Herzenberg, L. A. In *Selected Methods in Cellular Immunlogy*; Mishell, B. B., Shiigi, S. M., Eds.; Freeman: San Francisco, CA, 1980; pp 351−371.
(33) Kelly, S. S.; Bishop, A. G.; Carmody, E. P.; James, K. J. Isolation of dinophysistoxin-2 and the high-performance liquid chromatographic analysis of diarrhetic shellfish toxins using derivatisation with 1-bromoacetylpyrene. *J. Chromatogr. A* **1996**, *749*, 33−40.

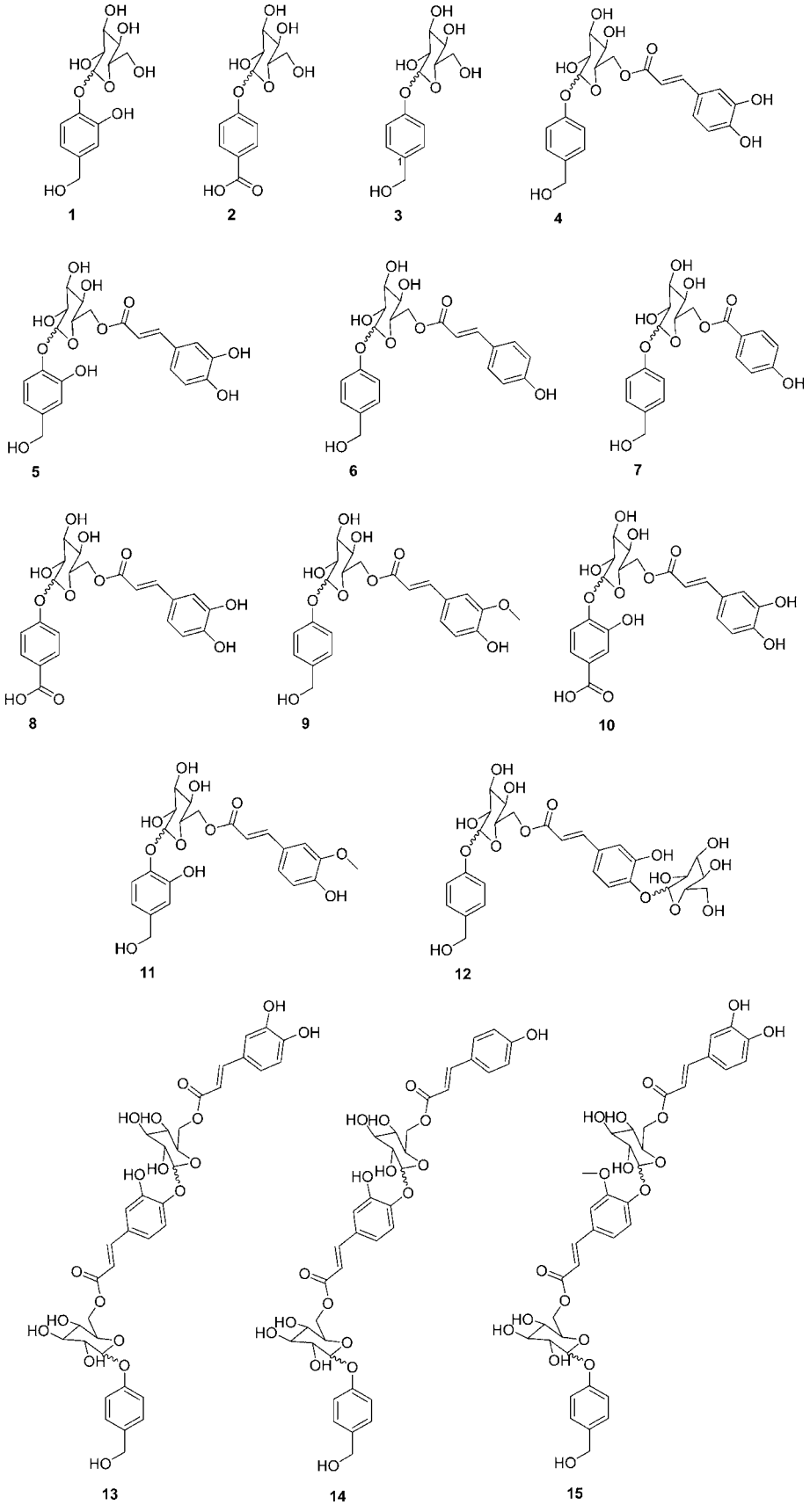

Figure 1. continued

dx.doi.org/10.1021/jf4053989 | J. Agric. Food Chem. 2014, 62, 1261−1271

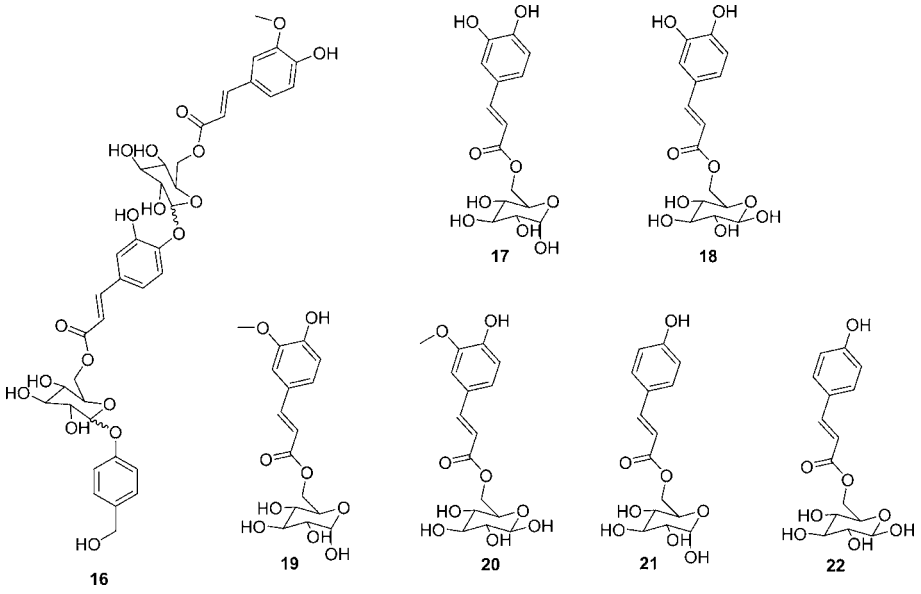

Figure 1. Representative structures of *Lagenaria siceraria* Stand. phenolic glycosides.

loop, and a DAD detector with a light-pipe flow cell (recording at 254, 280, and 320 nm and scanning from 200 to 600 nm). This was interfaced with an ion-trap mass spectrometer fitted with an ESI source (Bruker Daltonics HCT Ultra, Bremen, Germany) operating in full-scan, auto-MS^n mode to obtain fragment ion m/z. Tandem mass spectra were acquired in auto-MS^n mode (smart fragmentation) using a ramping of the collision energy. The maximum fragmentation amplitude was set to 1 V, starting at 30% and ending at 200%. MS operating conditions (negative mode) had been optimized using 5-*O*-caffeoylquinic acid with a capillary temperature of 365 °C, a dry gas flow rate of 10 L/min, and a nebulizer pressure of 10 psi. High-resolution LC−MS was performed using the same HPLC instrument equipped with a MicrOTOF mass spectrometer (Bruker Daltonics, Bremen, Germany) fitted with an ESI source, and internal calibration was achieved with 10 mL of 0.1 M sodium formate solution injected through a six-port valve prior to each chromatographic run. Calibration was done using the enhanced quadratic mode.

HPLC Coupled to MS. Separation was achieved on a 250 × 3 mm i.d. column containing diphenyl 5 μm, with a 5 mm × 3 mm i.d. guard column (Varian, Darmstadt, Germany). Solvent A was water/formic acid (1000:0.05, v/v), and solvent B was methanol. Solvents were delivered at a total flow rate of 500 μL/min. The gradient profile was from 10% B to 70% B linearly in 70 min followed by isocratic conditions for 10 min and a return to 10% B at 90 and isocratic conditions for 10 min to re-equilibrate.

Base Hydrolysis. A 10 mg sample of plant extract was dissolved in 2 mL of 0.5 M NaOH solution and the resulting solution stirred at room temperature for 2 h. The reaction mixture was neutralized by adding 1 g of acidic resin (Amberlite IR-120, H^+). The reaction mixture was filtered, washed with water (2 mL), and directly used for HPLC−MS^n.

NMR. ^{1}H and ^{13}C NMR spectra were recorded on a JEOL-ECX 400 spectrometer operating at 400 MHz for ^{1}H NMR and 100 MHz for ^{13}C NMR at room temperature in acetone-d_6 or methanol-d_4 using a 5 mm probe. The chemical shifts (δ) are reported in parts per million and were referenced to the residual solvent peak. The coupling constants (J) are quoted in hertz.

Synthesis of 6-*O*-Caffeoylglucoses 17 and 18. To a solution of 1,2-*O*-isopropylidene-α-D-glucofuranose (1.00 g, 4.54 mmol) and DMAP (200 mg, 1.63 mmol) in DCM (50 mL) were added pyridine (5 mL, 62 mmol) and 3,4-di-*O*-allylcaffeoyl chloride (1.58 g, 5.70 mmol)[22] at room temperature. The reaction mixture was stirred for 24 h at room temperature and acidified (pH ≈ 3) with 2 M HCl. The layers were separated, and the aqueous phase was extracted with DCM (3 × 50 mL). The combined organic layers were dried over sodium sulfate and filtered, and the solvent was removed in vacuo. The crude product was purified by column chromatography on silica gel (ethyl acetate−petroleum ether, 30−50%) to give 6-*O*-(3,4-di-*O*-allylcaffeoyl)-1,2-*O*-isopropylidene-α-D-glucofuranose (80%): δ_H (acetone-d_6) 7.62 (1H, d, J = 15.6, $C_{Ar}CH$), 7.32 (1H, dd, J = 1.8, $C_{Ar}H$), 7.17 (1H, dd, J = 8.7, 2.3 $C_{Ar}H$), 6.99 (1H, d, J = 8.2, $C_{Ar}H$), 6.41 (1H, d, J = 16.0, $C_{Ar}CH$═CH), 6.08 (2H, m, CH_2═CH), 5.85 (1H, d, J = 3.6, *H*-3), 5.43 (2H, m, CHH═CH), 5.23 (2H, m, CH*H*═CH), 4.65 (4H, m, $C_{Ar}OCH_2$), 4.49 (1H, d, J = 3.7, *H*-2), 4.31 (2H, m, *H*-6a, *H*-6b), 4.12 (2H, m, *H*-4, *H*-5), 1.39 (3H, s, OCH_3), 1.24 (3H, s, OCH_3); δ_C (acetone-d_6) 166.6 (−COOC), 150.9 ($C_{Ar}OCH_2$), 148.9 ($C_{Ar}OCH_2$), 144.5 ($C_{Ar}CH$), 133.9 (CH_2═CH), 133.5 (CH_2═CH), 127.7 ($C_{Ar}CH$), 122.9 (C_{Ar}), 116.9 (CH_2═CH), 116.5 (CHCOO), 115.7 (C_{Ar}), 113.7 (C_{Ar}), 112.6 ($H_3COCOCH_3$), 111.2 ($H_3COCOCH_3$), 105.0 (*C*-3), 85.3 (*C*-6), 80.4 (*C*-1), 74.4 (*C*-2), 69.4 (*C*-4), 69.2 ($C_{Ar}OCH_2$), 67.1 ($C_{Ar}OCH_2$), 66.8 (*C*-5), 26.4 (OCH_3), 25.6 (OCH_3).

To a solution of 6-*O*-(3,4-di-*O*-allylcaffeoyl)-1,2-*O*-isopropylidene-α-D-glucofuranose (1.00 g, 2.23 mmol) and *p*-TsOH (50 mg) in methanol−water (9:1, 50 mL) was added 10% Pd/C (350 mg) at room temperature. The reaction mixture was heated at 70 °C for 48 h, cooled to room temperature, and filtered, and methanol was removed in vacuo. The aqueous reaction mixture was extracted with ethyl acetate (3 × 50 mL). The combined organic layers were dried over sodium sulfate and filtered, and the solvent was removed in vacuo. The crude product was purified by column chromatography on silica gel (ethyl acetate−petroleum ether, 50−95%) to give 6-*O*-caffeoyl-1,2-*O*-isopropylidene-α-D-glucofuranose (62%). The resulting ester 6-*O*-caffeoyl-1,2-*O*-isopropylidene-α-D-glucofuranose (400 mg, 1.10 mmol) was dissolved in a mixture of 20 mL of TFA and water (8:2) at room temperature and the resulting solution stirred for 1 h. The solvents were removed in vacuo to obtain the resulting esters 6-*O*-caffeoylglucoses **17** and **18** in quantitative yield: δ_H (methanol-d_3) 7.54 (1H, d, J = 16.0, $C_{Ar}CH$), 7.02 (1H, d, J = 2.2, $C_{Ar}H$), 6.92 (1H, dd, J = 8.2, 1.4, $C_{Ar}H$), 6.75 (1H, d, J = 8.2, $C_{Ar}H$), 6.25 (1H, J = 16.5, $C_{Ar}CH$═CH), 5.10 (1H, d, J = 3.7, gluc *H*-1), 4.45 (1H, m, gluc *H*-6a), 4.30 (1H, m, gluc *H*-6b), 4.05 (1H, m, gluc *H*-4), 3.28−3.37 (2H, m, gluc *H*-2, gluc *H*-5); δ_C (methanol-d_3) 167.9 (COOC), 148.3 (C_{Ar}), 145.8 ($C_{Ar}CH$), 145.5 (C_{Ar}), 126.4 (C_{Ar}), 123.6 (C_{Ar}), 121.6 (C_{Ar}), 115.2 (CH_2═CH), 113.7 (CHCOO), 113.6 (CH_2═CH), 96.8 (β-gluc *C*-1), 92.6 (α-gluc *C*-1), 76.7 (β-gluc *C*-3), 74.9 (β-gluc *C*-2), 74.1 (β-gluc *C*-5), 73.5 (α-gluc *C*-3), 72.2 (α-gluc *C*-2), 71.6 (α-gluc *C*-5), 70.4 (α-gluc *C*-4), 69.6 (β-gluc *C*-4), 63.6 (β-gluc *C*-6), 63.5 (α-gluc *C*-6).

RESULTS AND DISCUSSION

For all the compounds the high-resolution mass data were in good agreement with the theoretical molecular formulas, all displaying a mass error of below 5 ppm, thus confirming their elemental composition. In general, peak identities were consistent both within and between analyses. However, when the mass spectrum for a particular substance included two ions of similar mean intensities, within-analysis experimental error dictated that in some individual MS scans one would be more intense while for other scans the reverse would be true. This phenomenon was encountered primarily when the signal intensity was lower, that is, with quantitatively minor components and/or higher order spectra. For example, one of the phenolics (**21**) produces MS^2 ions at m/z 235 and 265 which were essentially coequal in some spectra. However, in this particular case the higher mass ion was assigned consistently as the base peak. Fragment ions with intensities <5% of that of the base peak were reported only when they were needed for comparison. The phenolic glycosides were positively identified by their typical UV absorptions at 254, 280, and 320 nm. From the literature[37,38] it is known that bottle gourd fruit contains 3,4-dihydroxybenzyl alcohol and 4-hydroxybenzyl alcohol glucosides. In these glucosides the glucosyl unit (C-1′ of glucosyl) is connected with the C-4 of the phenolic hydroxyl of 3,4-dihydroxybenzyl alcohol and 4-hydroxybenzyl alcohol by an ether linkage while the cinnamic acids are connected with the glucosyl hydroxyl (C-6′) by an ester linkage (Figure 1). In this study we also observed 6-*O*-caffeoyl-, 6-*O*-feruloyl-, and 6-*O*-*p*-coumaroylglucoses in bottle gourd fruit. For the confirmation of ester linkages we used base hydrolysis, which gave the hydrolysis products 4-hydroxybenzyl alcohol−glucose, 3,4-dihydroxybenzyl alcohol−glucose, caffeic acid, ferulic acid, and *p*-coumaric acid. To confirm the *cis*−*trans* isomers of the caffeoyl residue in a molecule, we performed a photochemical experiment as reported previously.[21,33,34]

Characterization of 4-*O*-Glucosyl-3,4-dihydroxybenzyl Alcohol (M_r = 302), 4-*O*-Glucosyl-4-hydroxybenzoic Acid (M_r = 300), and 4-*O*-Glucosyl-4-hydroxybenzyl Alcohol (M_r = 286). One peak was detected at m/z 301 which produced the MS^2 base peak at m/z 139 ([3,4-dihydroxybenzyl alcohol − H^+]$^-$) by the loss of a glucosyl residue (162 Da) (Figure 2 and Table 1). It produced the MS^3 base peak at m/z 121 ([3,4-dihydroxybenzyl alcohol − H_2O − H^+]$^-$) by the loss of H_2O and a secondary peak at m/z 93 ([3,4-dihydroxybenzyl alcohol − CO − H_2O − H^+]$^-$) by the loss of CO and H_2O (Figure 2 and Table 1). In MS^3 it is possible to lose a CO molecule from a 1,2-benzoquinone moiety (Figure 2). On the basis of the fragmentation pattern and the HRMS data, this isomer was assigned as calleryanin, 4-*O*-glucosyl-3,4-dihydroxybenzyl alcohol (**1**). Calleryanin was previously reported in *Prunus lusitanica* (Rosaceae).[39]

One peak was detected at m/z 299 which produced the MS^2 base peak at m/z 137 ([4-hydroxybenzoic acid − H^+]$^-$) by the loss of a glucosyl residue (162 Da) (Figure 2 and Table 1). It produced the MS^3 base peak at m/z 93 ([4-hydroxybenzoic acid − CO_2 − H^+]$^-$) by the loss of CO_2 (Figure 2 and Table 1). From this it was clear that the loss of CO_2 was only possible from an acid. On the basis of the fragmentation pattern and the HRMS data, this isomer was assigned as 4-*O*-glucosyl-4-hydroxybenzoic acid (**2**).

One peak was detected at m/z 285 which produced the MS^2 base peak at m/z 123 ([4-hydroxybenzyl alcohol − H^+]$^-$) by the loss of a glucosyl residue (162 Da) and secondary peaks at m/z 161 ([glucose − H_2O − H^+]$^-$) by the loss of the 4-hydroxybenzyl alcohol moiety and at m/z 207 ([M − 78 Da − H^+]$^-$) (Figure 2 and Table 1). It produced the MS^3 base peak at m/z 105 ([4-hydroxybenzyl alcohol − H_2O − H^+]$^-$) by the loss of H_2O (Figure 2 and Table 1). On the basis of the fragmentation pattern and the HRMS data, this isomer was assigned as 4-*O*-glucosyl-4-hydroxybenzyl alcohol (**3**).

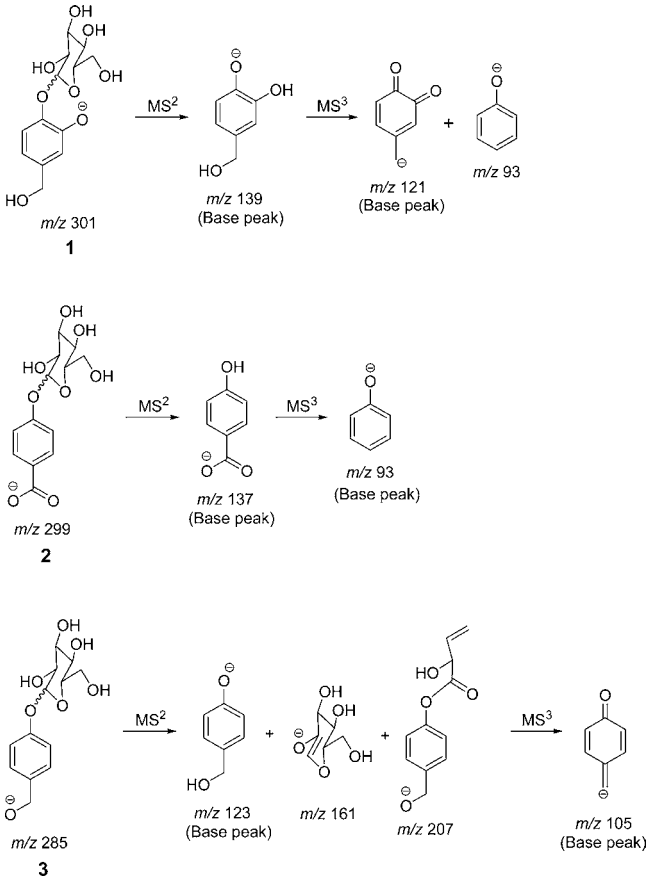

Figure 2. Fragmentation pathway of 4-*O*-glucosyl-3,4-dihydroxybenzyl alcohol (**1**), 4-*O*-glucosyl-4-hydroxybenzoic acid (**2**), and 4-*O*-glucosyl-4-hydroxybenzyl alcohol (**3**) in negative ion mode.

Characterization of 4-*O*-(6′-*O*-Glucosylcaffeoyl)-4-hydroxybenzyl Alcohol (M_r = 448). One peak was detected at m/z 447 which produced the MS^2 base peak at m/z 323 ([caffeoylglucose − H_2O − H^+]$^-$) by the loss of the 4-hydroxybenzyl alcohol moiety (124 Da). It produced secondary peaks at m/z 179 ([caffeic acid − H^+]$^-$) by the loss of the 4-*O*-glucosyl-4-hydroxybenzyl alcohol residue (268 Da), at m/z 161 ([caffeic acid − H_2O − H^+]$^-$) by the loss of the 4-*O*-glucosyl-4-hydroxybenzyl alcohol moiety (286 Da), at m/z 221 ([caffeoylglucose − hydroxybenzyl alcohol − 120 Da − H^+]$^-$), at m/z 251 ([caffeoylglucose − hydroxybenzyl alcohol − 90 Da − H^+]$^-$), and at m/z 263 ([caffeoylglucose − hydroxybenzyl alcohol − 78 Da − H^+]$^-$) by the loss of the 4-hydroxybenzyl residue (106 Da) and 78 Da (Figure 3 and Table 1). It produced the MS^3 base peak at m/z 179 ([caffeic acid − H^+]$^-$) by the loss of the glucosyl residue. It produced secondary peaks at m/z 161 ([caffeic acid − H_2O − H^+]$^-$) by the loss of the glucosyl residue (162 Da), at m/z 221 ([caffeoylglucose − 120 Da − H^+]$^-$), at m/z 251 ([caffeoylglucose − 90 Da − H^+]$^-$), and at m/z 263

dx.doi.org/10.1021/jf4053989 | J. Agric. Food Chem. 2014, 62, 1261−1271

Table 1. Retention Times and MS^4 Fragmentation (Negative Ion Mode) of Bottle Gourd Phenolics

compd no.	compd	retention time (min)	parent ion (M − H)	characteristic *m/z* of ions in negative ion mode
1	4-*O*-glucosyl-3,4-dihydroxybenzyl alcohol	6.9	301	MS^2 → 139 (100); MS^3 → 121 (100), 93 (8)
2	4-*O*-glucosyl-4-hydroxybenzoic acid	10.9	299	MS^2 → 137 (100)
3	4-*O*-glucosyl-4-hydroxybenzyl alcohol	6.3	285	MS^2 → 123 (100), 161 (41), 207 (11); MS^3 → 105 (100)
4	4-*O*-(6′-*O*-glucosylcaffeoyl)-4-hydroxybenzyl alcohol	34.8	447	MS^2 → 323 (100), 280 (7), 263 (39), 251 (16), 221 (85), 203 (19), 161 (27), 135 (20); MS^3 → 179 (100), 280 (7), 263 (42), 251 (9), 221 (95), 203 (25), 161 (23), 135 (20); MS^4 → 135 (100), 149 (34)
5	4-*O*-(6′-*O*-glucosylcaffeoyl)-3,4-dihydroxybenzyl alcohol	34.5	463	MS^2 → 323 (100), 301 (5), 221 (9), 179 (6), 161 (16), 135 (20); MS^3 → 179 (100), 263 (29), 251 (12), 221 (90), 203 (32), 161 (25), 135 (19)
6	4-*O*-(6′-*O*-glucosyl-*p*-coumaroyl)-4-hydroxybenzyl alcohol	39.7	431	MS^2 → 307 (100), 163 (5), 145 (16); MS^3 → 145 (100), 247 (44), 219 (10), 205 (36), 187 (55), 163 (60), 119 (12)
7	4-*O*-(6′-*O*-glucosyl-4″-hydroxybenzoyl)-4-hydroxybenzyl alcohol	34.2	405	MS^2 → 281 (100), 137 (14); MS^3 → 137 (100), 93 (5); MS^4 → 93 (100)
8	4-*O*-(6′-*O*-glucosylcaffeoyl)-4-hydroxybenzoic acid	38.7	461	MS^2 → 323 (100), 403 (7), 221 (8), 179 (7); MS^3 → 221 (100), 263 (37), 251 (12), 233 (12), 203 (30), 161 (24), 135 (21)
9	4-*O*-(6′-*O*-glucosylferuloyl)-4-hydroxybenzyl alcohol	39.4	461	MS^2 → 337 (100), 193 (9), 175 (16); MS^3 → 175 (100), 277 (17), 245 (14), 235 (9), 217 (32), 193 (92), 160 (12), 134 (12)
10	4-*O*-(6′-*O*-glucosylcaffeoyl)-3,4-dihydroxybenzoic acid	35.9	477	MS^2 → 323 (100), 221 (9), 179 (9), 161 (7); MS^3 → 178 (100), 263 (32), 221 (72), 203 (28), 161 (21), 135 (20)
11	4-*O*-(6′-*O*-glucosylferuloyl)-3,4-dihydroxybenzyl alcohol	39.0	477	MS^2 → 337 (100), 193 (5), 175 (5); MS^3 → 175 (100), 217 (42), 193 (40), 149 (8), 134 (11)
12	4-*O*-(6′-*O*-glucosylcaffeoylglucosyl)-4-hydroxybenzyl alcohol	8.0	609	MS^2 → 447 (100), 323 (5); MS^3 → 323 (100), 221 (11), 179 (9), 161 (15); MS^4 → 221 (100), 263 (48), 251 (12), 203 (34), 179 (99), 161 (31), 135 (27)
13	4-*O*-(6′-*O*-glucosylcaffeoylglucosyl-caffeoyl)-4-hydroxybenzyl alcohol	41.9	771	MS^2 → 447 (100), 647 (12), 609 (13); MS^3 → 323 (100), 221 (11), 179 (15), 161 (22); MS^4 → 179 (100), 263 (52), 221 (76), 203 (23), 161 (54), 135 (11)
14	4-*O*-(6′-*O*-glucosylcaffeoylglucosyl-*p*-coumaroyl)-4-hydroxybenzyl alcohol	42.9	755	MS^2 → 447 (100), 631 (10), 323 (15); MS^3 → 323 (100), 221 (16), 179 (15), 161 (18); MS^4 → 221 (100), 263 (40), 251 (5), 203 (15), 179 (80), 161 (16)
15	4-*O*-(6′-*O*-glucosylferuloylglucosyl-caffeoyl)-4-hydroxybenzyl alcohol	45.0	785	MS^2 → 323 (100), 661 (50), 623 (4), 599 (4), 517 (25), 499 (95), 461 (12); MS^4 → 221 (100), 263 (60), 251 (10), 203 (40), 179 (95), 161 (25)
16	4-*O*-(6′-*O*-glucosylcaffeoylglucosyl-feruloyl)-4-hydroxybenzyl alcohol	46.2	785	MS^2 → 447 (100), 323 (16); MS^3 → 323 (100), 263 (5), 221 (12), 179 (10), 161 (30); MS^4 → 179 (100), 263 (30), 251 (15), 221 (60), 203 (15), 161 (40)
17	6-*O*-caffeoyl-*α*-glucose	19.5	341	MS^2 → 281 (100), 323 (12), 251 (65), 221 (25), 179 (56), 135 (5); MS^3 → 179 (100), 221 (42), 135 (9)
18	6-*O*-caffeoyl-*β*-glucose	17.1	341	MS^2 → 281 (100), 323 (10), 251 (66), 221 (24), 179 (50), 135 (4); MS^3 → 179 (100), 221 (38), 135 (11)
19	6-*O*-feruloyl-*α*-glucose	26.3	355	MS^2 → 265 (100), 337 (5), 295 (96), 247 (7), 235 (73), 217 (7), 193 (30); MS^3 → 193 (100), 217 (6)
20	6-*O*-feruloyl-*β*-glucose	23.9	355	MS^2 → 265 (100), 337 (5), 295 (99), 247 (7), 235 (72), 217 (5), 193 (31); MS^3 → 193 (100), 217 (5)
21	6-*O*-*p*-coumaroyl-*α*-glucose	25.1	325	MS^2 → 265 (100), 307 (6), 235 (99), 205 (12), 163 (14); MS^3 → 205 (100), 247 (6), 187 (13), 163 (56), 145 (11), 119 (13); MS^4 → 161 (100), 133 (5)
22	6-*O*-*p*-coumaroyl-*β*-glucose	22.5	325	MS^2 → 265 (100), 307 (5), 235 (99), 205 (10), 163 (17); MS^3 → 205 (100), 247 (5), 187 (11), 163 (56), 145 (7), 119 (11); MS^4 → 161 (100), 133 (6)

([caffeoylglucose − 78 Da − H^+]$^-$) (Figure 3 and Table 1). The MS^2 secondary peaks at *m/z* 323, 221, 203, 251, and 263 suggested that caffeic acid (C-9″) was connected with the glucosyl residue by an ester linkage (C-6′). In a recent study Mohan et al.[17] isolated 4-*O*-(6′-*O*-glucosylcaffeoyl)-4-hydroxybenzyl alcohol (**4**) from bottle gourd fruit. On the basis of the above points, this compound was tentatively assigned as 4-*O*-(6′-*O*-glucosylcaffeoyl)-4-hydroxybenzyl alcohol (**4**).

Characterization of 4-*O*-(6′-*O*-Glucosylcaffeoyl)-3,4-dihydroxybenzyl Alcohol (M_r = 464). One peak was detected at *m/z* 463 and produced the MS^2 base peak at *m/z* 323 ([caffeoylglucose − H_2O − H^+]$^-$) by the loss of the 3,4-dihydroxybenzyl alcohol moiety (140 Da). It produced secondary peaks at *m/z* 179 ([caffeic acid − H^+]$^-$) by the loss of the 4-*O*-glucosyl-3,4-dihydroxybenzyl alcohol residue (284 Da), at *m/z* 161 ([caffeic acid − H_2O − H^+]$^-$) by the loss of the 4-*O*-glucosyl benzyl alcohol moiety (302 Da), at *m/z* 221 ([caffeoylglucose − dihydroxybenzyl alcohol − 120 Da − H^+]$^-$), at *m/z* 301 ([M − caffeoyl − H^+]$^-$), and at *m/z* 135 ([caffeic acid − CO_2 − H^+]$^-$) by the loss of the 4-*O*-glucosyl-3,4-dihydroxybenzyl alcohol residue (284 Da) and CO_2 (Figure 4 and Table 1). It produced the MS^3 base peak at *m/z* 179 ([caffeic acid − H^+]$^-$) by the loss of the glucosyl residue. It produced secondary peaks at *m/z* 161 ([caffeic acid − H_2O − H^+]$^-$) by the loss of the glucosyl residue (162 Da), at *m/z* 221 ([caffeoyl glucose − 120 Da − H^+]$^-$), at *m/z* 251 ([caffeoyl glucose − 90 Da − H^+]$^-$), and at *m/z* 263 ([caffeoyl glucose − 78 Da − H^+]$^-$) (Figure 4 and Table 1). The MS^2 secondary peaks at *m/z* 323, 221, 203, 251, and 263 suggested that caffeic acid (C-9″) was connected with the glucosyl residue by an ester linkage (C-6′).

An MRM (multi-reaction monitoring) of *m/z* 301 produced ions at *m/z* 139 by the loss of the glucosyl residue and *m/z* 121 by the loss of the glucosyl residue and H_2O. The absence of the MRM ions generated by the caffeoyl moiety at *m/z* 179, 161, and 135 suggested that the glucosyl residue (C-1′) was connected at C-4 by an ether linkage. In a recent study Mohan et al. [17] also isolated 4-*O*-(6′-*O*-glucosylcaffeoyl)-3,4-dihydroxybenzyl alcohol (**5**) from bottle gourd fruit. On the basis of the

dx.doi.org/10.1021/jf4053989 | J. Agric. Food Chem. 2014, 62, 1261−1271

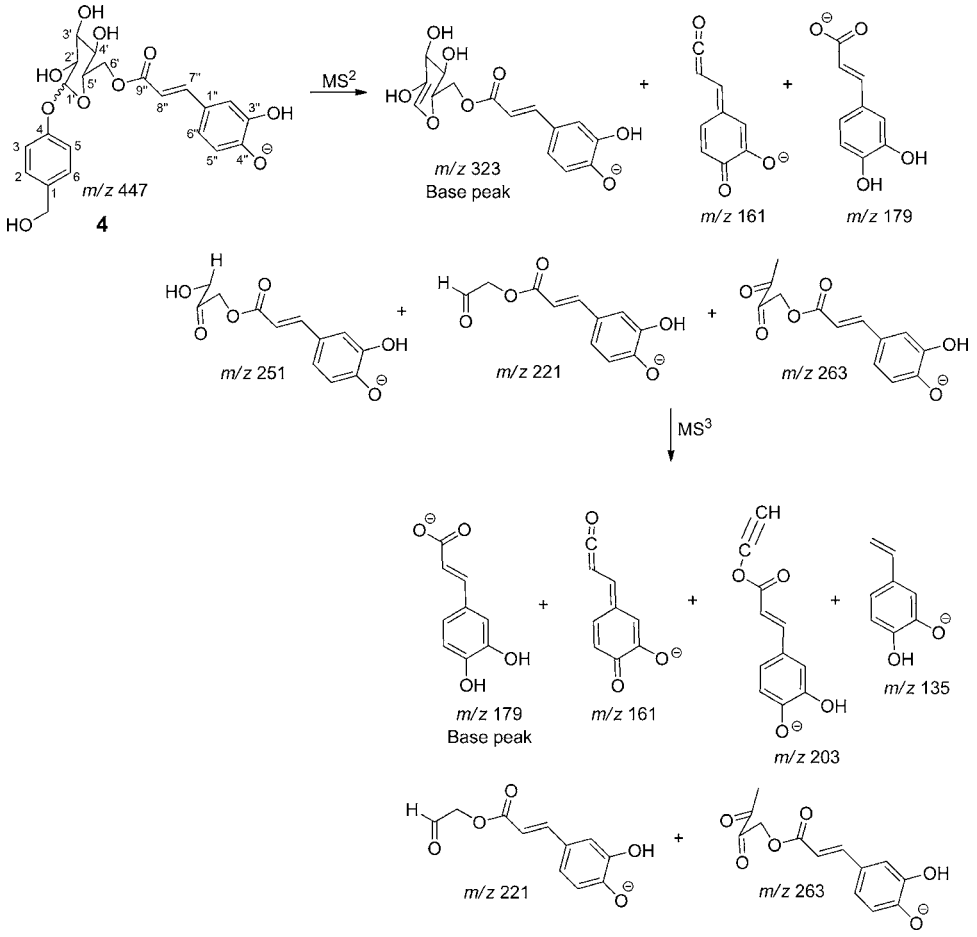

Figure 3. Fragmentation pathway of 4-*O*-(6′-*O*-glucosylcaffeoyl)-4-hydroxybenzyl alcohol (**4**) at *m*/*z* 447 in negative ion mode.

above points, this compound was tentatively assigned as 4-*O*-(6′-*O*-glucosylcaffeoyl)-3,4-dihydroxybenzyl alcohol (**5**).

Characterization of 4-*O*-(6′-*O*-Glucosyl-*p*-coumaroyl)-4-hydroxybenzyl Alcohol (M_r = 432). One peak was detected at *m*/*z* 431 which produced the MS^2 base peak at *m*/*z* 307 ([*p*-coumarylglucose − H_2O − H^+]$^-$) by the loss of the 4-hydroxybenzyl alcohol moiety (124 Da) and a secondary peak at *m*/*z* 145 ([*p*-coumaric acid − H_2O − H^+]$^-$) by the loss of the 4-*O*-glucosyl-4-hydroxybenzyl alcohol residue (268 Da) and H_2O (Figure 5 and Table 1). It produced the MS^3 base peak at *m*/*z* 145 ([*p*-coumaric acid − H_2O − H^+]$^-$) by the loss of the glucosyl residue. It produced secondary peaks at *m*/*z* 163 ([*p*-coumaric acid − H^+]$^-$) by the loss of the glucosyl residue (162 Da), at *m*/*z* 187 ([*p*-coumaroylglucose − 138 Da − H^+]$^-$) by the loss of $C_4H_{10}O_5$, at *m*/*z* 205 ([*p*-coumaroylglucose − 120 Da − H^+]$^-$) by the loss of $C_4H_8O_4$, and at *m*/*z* 247 ([*p*-coumaroylglucose − 78 Da − H^+]$^-$) by the loss of $C_2H_6O_3$ (Figure 5 and Table 1). The MS^2 and MS^3 peaks at *m*/*z* 305, 187, 205, and 247 suggested that *p*-coumaric acid (C-9″) was connected with the glucosyl residue by an ester linkage (C-6′). This compound showed an MS fragmentation analogy with compound **4** and was tentatively assigned as 4-*O*-(6′-*O*-glucosyl-*p*-coumaroyl)-4-hydroxybenzyl alcohol (**6**) (Figures 3 and 5 and Table 1).

Characterization of 4-*O*-(6′-*O*-Glucosyl-4″-hydroxybenzoyl)-4-hydroxybenzyl Alcohol (M_r = 406). One peak was detected at *m*/*z* 405 which produced the MS^2 base peak at *m*/*z* 281 ([(hydroxybenzoyl)glucose − H_2O − H^+]$^-$) by the loss of the 4-hydroxybenzyl alcohol moiety (124 Da) and a secondary peak at *m*/*z* 137 ([hydroxybenzoic acid − H^+]$^-$) by the loss of the 4-*O*-glucosyl-4-hydroxybenzyl alcohol residue (268 Da) (Figure 5 and Table 1). It produced the MS^3 base peak at *m*/*z* 137 ([hydroxybenzoic acid − H^+]$^-$) by the loss of the glucosyl residue and a secondary peak at *m*/*z* 93 ([hydroxybenzoic acid − CO_2 − H^+]) by the loss of glucosyl residue and CO_2 (Figure 5 and Table 1). The MS^2 and MS^3 peaks at *m*/*z* 281, 137, and 93 suggested that 4-hydroxybenzoic acid (C-7″) was connected with the glucosyl residue by an ester linkage (C-6′). This compound showed an MS fragmentation analogy with compounds **4** and **6** and was tentatively assigned as 4-*O*-(6′-*O*-glucosyl-4″-hydroxybenzoyl)-4-hydroxybenzyl alcohol (**7**) (Figures 4 and 5 and Table 1).

Characterization of 4-*O*-(6′-*O*-Glucosylcaffeoyl)-4-hydroxybenzoic Acid and 4-*O*-(6′-*O*-Glucosylferuloyl)-4-hydroxybenzyl Alcohol (M_r = 462). Two peaks were detected at *m*/*z* 461 and were tentatively assigned as 4-*O*-(6′-*O*-glucosylcaffeoyl)-4-hydroxybenzoic acid (**8**) and 4-*O*-(6′-*O*-glucosylferuloyl)-4-hydroxybenzyl alcohol (**9**). Isomer **8** produced the MS^2 base peak at *m*/*z* 323 ([caffeoylglucose − H_2O − H^+]$^-$) by the loss of the 4-hydroxybenzoic acid moiety (138 Da). It produced secondary peaks at *m*/*z* 179 ([caffeic acid − H^+]$^-$) by the loss of the 4-*O*-glucosyl-4-hydroxybenzoic acid residue (282 Da), at *m*/*z* 221 ([caffeoylglucose − 120 Da − H^+]$^-$) by the loss of $C_4H_8O_4$, and at *m*/*z* 403 ([M − 58 Da − H^+]$^-$) by the loss of $C_2H_2O_2$ (Figure 5 and Table 1). It produced the MS^3 base peak at *m*/*z* 221 ([caffeoylglucose −

dx.doi.org/10.1021/jf4053989 | J. Agric. Food Chem. 2014, 62, 1261−1271

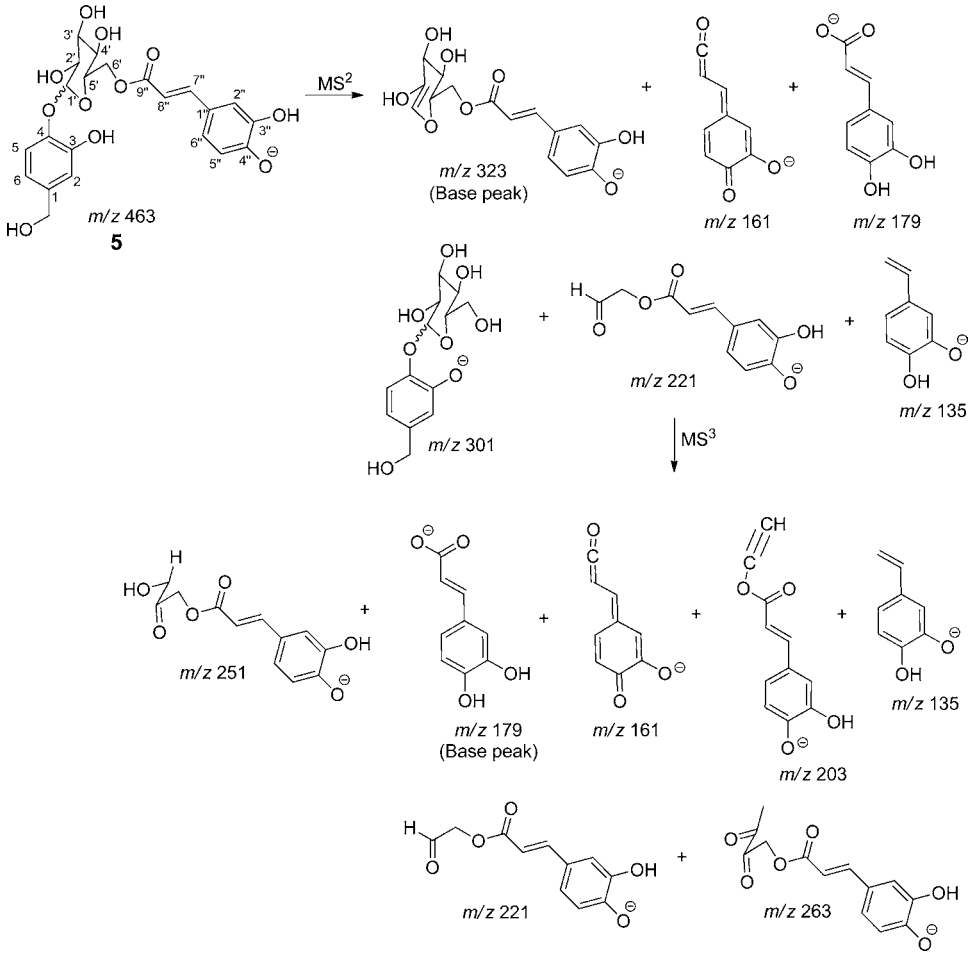

Figure 4. Fragmentation pathway of 4-*O*-(6′-*O*-glucosylcaffeoyl)-3,4-dihydroxybenzyl alcohol (**5**) at *m*/*z* 463 in negative ion mode.

120 Da − H^+]$^-$) by the loss of $C_4H_8O_4$. It produced secondary peaks at *m*/*z* 179 ([caffeic acid − H^+]$^-$) by the loss of the glucosyl residue (144 Da), at *m*/*z* 161 ([caffeic acid − H_2O − H^+]$^-$) by the loss of the glucosyl residue (162 Da), at *m*/*z* 203 ([caffeoylglucose − 120 Da − H_2O − H^+]$^-$) by the loss of $C_4H_8O_4$, and at *m*/*z* 263 ([caffeoylglucose − 60 Da − H_2O − H^+]$^-$) by the loss of $C_2H_4O_2$ (Figure 5 and Table 1). The MS^2 and MS^3 secondary peaks at *m*/*z* 323, 221, 203, and 263 suggested that caffeic acid (C-9″) was connected with the glucosyl residue by an ester linkage (C-6′). Hydrolysis experiments confirmed the presence of 4-hydroxybenzoic acid, which is connected with C-1′ of the glucose moiety by an ether linkage (C-4). On the basis of the above points, isomer **8** was assigned as 4-*O*-(6′-*O*-glucosylcaffeoyl)-4-hydroxybenzoic acid.

Isomer **9** produced the MS^2 base peak at *m*/*z* 337 ([feruloylglucose − H_2O − H^+]$^-$) by the loss of the 4-hydroxybenzyl alcohol moiety (124 Da). It produced secondary peaks at *m*/*z* 193 ([ferulic acid − H^+]$^-$) by the loss of the 4-*O*-glucosyl-4-hydroxybenzyl alcohol residue (268 Da) and at *m*/*z* 175 ([ferulic acid − H_2O − H^+]$^-$) by the loss of 4-*O*-glucosyl-4-hydroxybenzyl alcohol (Figure 5 and Table 1). It produced the MS^3 base peak at *m*/*z* 175 ([ferulic acid − H_2O − H^+]$^-$) by the loss of the glucosyl residue (162 Da). It produced secondary peaks at *m*/*z* 193 ([ferulic acid − H^+]$^-$) by the loss of the glucosyl residue (144 Da), at *m*/*z* 235 ([feruloylglucose − 120 Da − H^+]$^-$) by the loss of $C_4H_6O_3$, at *m*/*z* 134 ([ferulic acid − CO_2 − CH_3 − H^+]$^-$) by the loss of the glucosyl residue (144 Da), CO_2, and a CH_3 residue, at *m*/*z* 217 ([feruloylglucose − 120 Da − H_2O − H^+]$^-$) by the loss of $C_4H_8O_4$, and at *m*/*z* 277 ([caffeoylglucose − 60 Da − H_2O − H^+]$^-$) by the loss of $C_2H_4O_2$ (Figure 5 and Table 1). The MS^2 and MS^3 peaks at *m*/*z* 337, 217, 235, and 277 suggested that ferulic acid (C-9″) was connected with the glucosyl residue by an ester linkage (C-6′). Isomer **9** showed a fragmentation analogy with compounds **4**−**7** (Figures 3−5 and Table 1) and was assigned as 4-*O*-(6′-*O*-glucosylferuloyl)-4-hydroxybenzyl alcohol.

Characterization of 4-*O*-(6′-*O*-Glucosylcaffeoyl)-3,4-dihydroxybenzoic Acid and 4-*O*-(6′-*O*-Glucosylferuloyl)-3,4-dihydroxybenzyl alcohol (M_r = 478). Two peaks were detected at *m*/*z* 477 and were tentatively assigned as 4-*O*-(6′-*O*-glucosylcaffeoyl)-3,4-dihydroxybenzoic acid (**10**) and 4-*O*-(6′-*O*-glucosylferuloyl)-3,4-dihydroxybenzyl alcohol (**11**). These isomers showed a fragmentation analogy with compounds **8** and **9**, respectively (Figures 5 and 6 and Table 1).

Characterization of 4-*O*-(6′-*O*-Glucosylcaffeoylglucosyl)-4-hydroxybenzyl Alcohol (M_r = 610) and 4-*O*-(6′-*O*-Glucosylcaffeoylglucosylcaffeoyl)-4-hydroxybenzyl Alcohol (M_r = 772). One peak was detected at *m*/*z* 609 and was tentatively assigned as 4-*O*-(6′-*O*-glucosylcaffeoylglucosyl)-4-hydroxybenzyl alcohol (**12**). It produced MS^n spectra identical to MS^{n-1} spectra of compound **4** (Figures 3 and 6 and Table 1).

One peak was detected at *m*/*z* 771 and was tentatively assigned as 4-*O*-(6′-*O*-glucosylcaffeoylglucosylcaffeoyl)-4-hy-

dx.doi.org/10.1021/jf4053989 | J. Agric. Food Chem. 2014, 62, 1261−1271

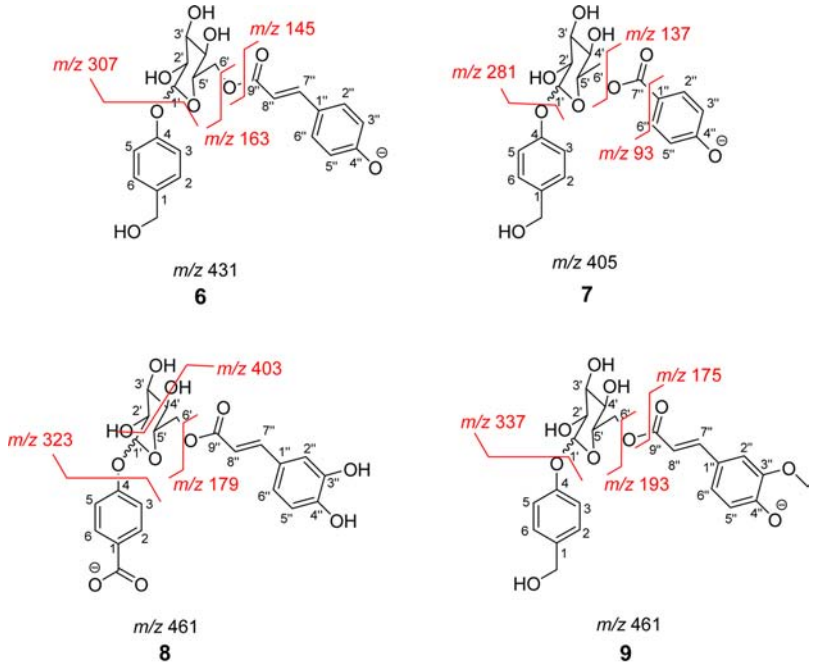

Figure 5. Fragmentation pathways of 4-*O*-(6′-*O*-glucosyl-*p*-coumaroyl)-4-hydroxybenzyl alcohol (**6**), 4-*O*-(6′-*O*-glucosyl-4″-hydroxybenzoyl)-4-hydroxybenzyl alcohol (**7**), 4-*O*-(6′-*O*-glucosylcaffeoyl)-4-hydroxybenzoic acid (**8**), and 4-*O*-(6′-*O*-glucosylferuloyl)-4-hydroxybenzyl alcohol (**9**) in negative ion mode.

droxybenzyl alcohol (**13**). It produced MS^n spectra identical to MS^{n-1} spectra of compound **12** (Figure 6 and Table 1). MRM of the MS^2 ion at m/z 771 produced ions similar to those of compound **12** (Figure 6 and Table 1).

Characterization of 4-*O*-(6′-*O*-Glucosylcaffeoylglucosyl-*p*-coumaroyl)-4-hydroxybenzyl Alcohol (M_r = 756), 4-*O*-(6′-*O*-Glucosylferuloylglucosylcaffeoyl)-4-hydroxybenzyl Alcohol, and 4-*O*-(6′-*O*-Glucosylcaffeoylglucosylferuloyl)-4-hydroxybenzyl Alcohol (M_r = 786). One peak was detected at m/z 755 and was tentatively assigned as 4-*O*-(6′-*O*-glucosylcaffeoylglucosyl-*p*-coumaroyl)-4-hydroxybenzoic acid (**14**). This isomer showed a fragmentation analogy with compound **13** (Figures 6 and 7 and Table 1).

Two peaks were detected at m/z 785 and were tentatively assigned as 4-*O*-(6′-*O*-glucosylferuloylglucosylcaffeoyl)-4-hydroxybenzyl alcohol (**15**) and 4-*O*-(6′-*O*-glucosylcaffeoylglucosylferuloyl)-4-hydroxybenzyl alcohol (**16**). These isomers showed a fragmentation analogy with compounds **13** and **14** (Figures 6 and 7 and Table 1).

Characterization of 6-*O*-Caffeoylglucoses (M_r = 342), 6-*O*-Feruloylglucoses (M_r = 356), and 6-*O*-*p*-Coumaroylglucoses (M_r = 326). Two peaks were detected at m/z 341 in the extracted ion chromatogram (λ_{max} = 320 nm) and were tentatively assigned as caffeoyl glucoses (**17** and **18**). They produced the MS^2 base peak at m/z 281 ($[M - H^+ - 60\ Da]^-$) by the loss of $C_2H_4O_2$ and secondary peaks at m/z 251 ($[M - H^+ - 90\ Da]^-$) by the loss of $C_3H_6O_3$, at m/z 221 ($[M - H^+ - 120\ Da]^-$) by the loss of $C_4H_8O_4$, and at m/z 179 ([caffeic acid $- H^+]^-$) by the loss of a glucosyl residue ($C_6H_{10}O_5$) (Figure 8 and Table 1). Isomers **17** and **18** produced the ions $[M - H^+ - 60\ Da]^-$, $[M - H^+ - 90\ Da]^-$, and $[M - H^+ - 120\ Da]^-$, which are characteristic of glycosides.

Further evidence for the assignment of the caffeoylglucoses came from an independent synthesis of 6-*O*-caffeoyl-α-glucose (**17**) and 6-*O*-caffeoyl-β-glucose (**18**). A β stereochemistry was assigned on the basis of the characteristic $^3J_{HCCH}$ coupling constant between the anomeric hydrogen and the hydrogen at C-2 of glucose, with 6-*O*-caffeoyl-α-glucose (**17**) showing values between 3 and 4 Hz and 6-*O*-caffeoyl-β-glucose (**18**) showing values between 7 and 8 Hz. On standing in methanol-d_3, the mixture of 6-*O*-caffeoylglucoses equilibrated to yield after one day exclusively the β-anomers. The retention times and fragmentation patterns of synthetic 6-*O*-caffeoylglucoses **17** and **18** were identical to those of isomers **17** and **18** present in *L. siceraria*. On the basis of these arguments, the first eluting isomer was assigned as 6-*O*-caffeoyl-β-glucose (**18**) and the later eluting isomer as 6-*O*-caffeoyl-α-glucose (**17**).

Two peaks were detected at m/z 355 in the extracted ion chromatogram (λ_{max} = 320 nm) and were tentatively assigned as feruloylglucoses **19** and **20**. They produced the MS^2 base peak at m/z 295 ($[M - H^+ - 60\ Da]^-$) by the loss of $C_2H_4O_2$ and secondary peaks at m/z 265 ($[M - H^+ - 90\ Da]^-$) by the loss of $C_3H_6O_3$, at m/z 235 ($[M - H^+ - 120\ Da]^-$) by the loss of $C_4H_8O_4$, and at m/z 193 ([ferulic acid $- H^+]^-$) by the loss of a glucosyl residue ($C_6H_{10}O_5$) (Figure 8 and Table 1). Compounds **19** and **20** showed a fragmentation analogy to compounds **17** and **18** (Figure 8 and Table 1). On the basis of these arguments, isomer **20** was assigned as 6-*O*-feruloyl-β-glucose and isomer **19** as 6-*O*-feruloyl-α-glucose.

Two peaks were detected at m/z 325 in the extracted ion chromatogram (λ_{max} = 320 nm) and were tentatively assigned as *p*-coumaroylglucoses **21** and **22**. They produced the MS^2 base peak at m/z 265 ($[M - H^+ - 60\ Da]^-$) by the loss of $C_2H_4O_2$ and secondary peaks at m/z 235 ($[M - H^+ - 90\ Da]^-$) by the loss of $C_3H_6O_3$, at m/z 205 ($[M - H^+ - 120\ Da]^-$) by the loss of $C_4H_8O_4$, and at m/z 163 ([*p*-coumaric acid $- H^+]^-$) by the loss of a glucosyl residue ($C_6H_{10}O_5$) (Figure 8 and Table 1). Compounds **21** and **22** showed a fragmentation

dx.doi.org/10.1021/jf4053989 | J. Agric. Food Chem. 2014, 62, 1261−1271

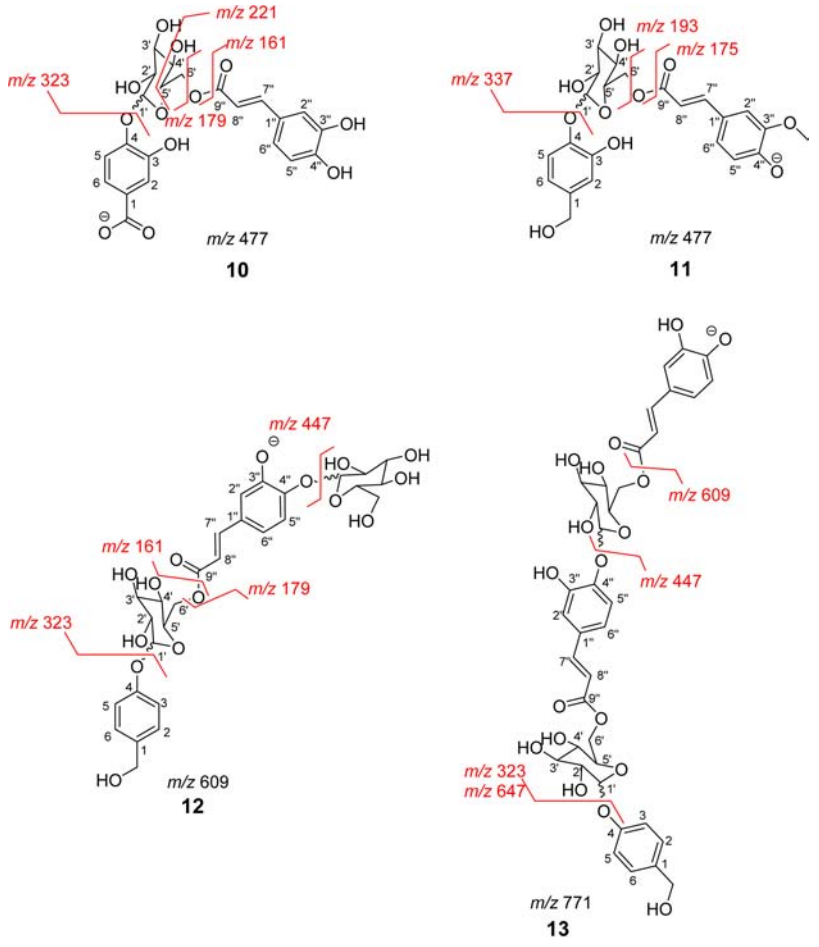

36

Figure 6. Fragmentation pathways of 4-*O*-(6′-*O*-glucosylcaffeoyl)-3,4-dihydroxybenzoic acid (**10**), 4-*O*-(6′-*O*-glucosylferuloyl)-3,4-dihydroxybenzyl alcohol (**11**), 4-*O*-(6′-*O*-glucosylcaffeoylglucosyl)-4-hydroxybenzyl alcohol (**12**), and 4-*O*-(6′-*O*-glucosylcaffeoylglucosylcaffeoyl)-4-hydroxybenzyl alcohol (**13**) in negative ion mode.

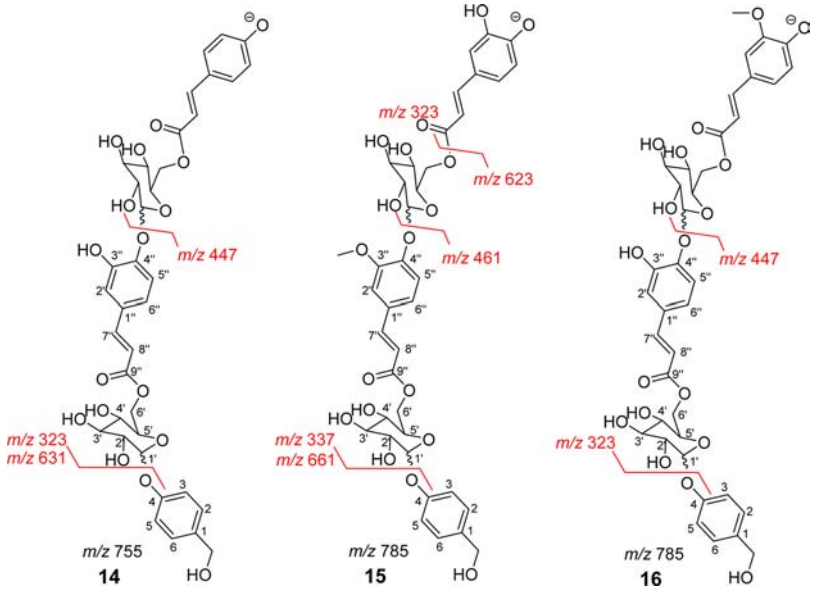

Figure 7. Fragmentation pathway and MS^4 spectra of 4-*O*-(6′-*O*-glucosylcaffeoylglucosyl-*p*-coumaroyl)-4-hydroxybenzyl alcohol (**14**), 4-*O*-(6′-*O*-glucosylferuloylglucosylcaffeoyl)-4-hydroxybenzyl alcohol (**15**), and 4-*O*-(6′-*O*-glucosylcaffeoylglucosylferuloyl)-4-hydroxybenzyl alcohol (**16**) in negative ion mode.

dx.doi.org/10.1021/jf4053989 | *J. Agric. Food Chem.* 2014, 62, 1261−1271

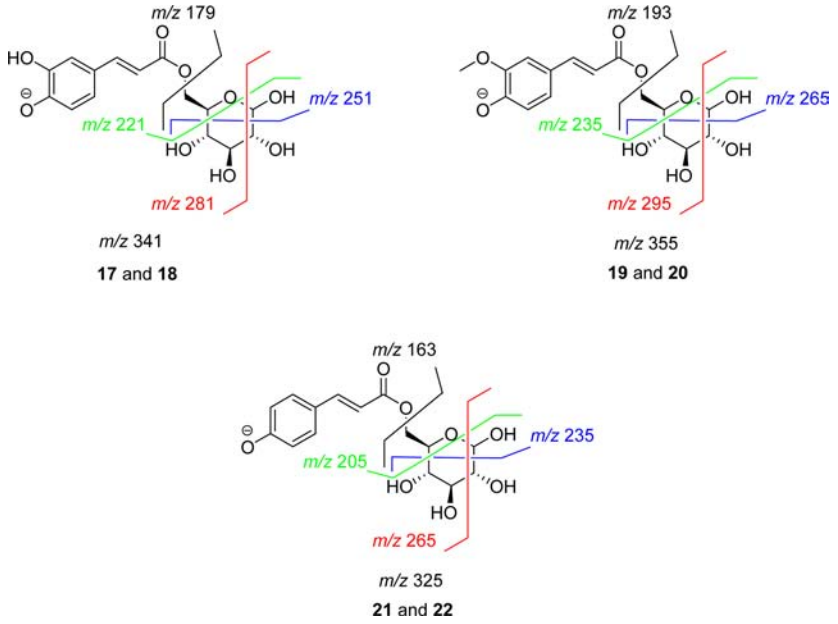

Figure 8. Fragmentation pathways of 6-*O*-caffeoylglucoses **17** and **18**, 6-*O*-feruloylglucoses **19** and **20**, and 6-*O*-*p*-coumaroylglucoses **21** and **22** in negative ion mode.

analogy to compounds **17**−**20** (Figure 8 and Table 1). On the basis of these arguments, isomer **22** was assigned as 6-*O*-*p*-coumaroyl-*β*-glucose and isomer **21** as 6-*O*-*p*-coumaroyl-*α*-glucose.

In this study we showed that bottle gourd is a rich source of phenolic glucosides which are not commonly present in fruits and vegetables. During this study we were able to identify and characterize the phenolics of bottle gourd (*L. siceraria*). We also developed a tandem mass spectrometric method for the positive identification of the phenolic glucosides. This tandem MS method can be applied for the rapid identification and characterization of new analogous compounds and their derivatives. The phenolic acids caffeic acid, dimethoxycinnamic acid, 3,4-dihydroxybenzoic acid, and gallic acid have been reported in bottle gourd,[17] but in the present study we did not observe them.

■ ASSOCIATED CONTENT

Supporting Information

High-resolution MS data (Table S1) and MS^4 spectra (Figures S1−S16) of bottle gourd phenolics in negative ion mode. This material is available free of charge via the Internet at http://pubs.acs.org.

■ AUTHOR INFORMATION

Corresponding Authors

*Phone: 49 421 200 3680. Fax: 49 421 200 3229. E-mail: r.jaiswal@jacobs-university.de.

*Phone: 49 421 200 3120. Fax: 49 421 200 3229. E-mail: n.kuhnert@jacobs-university.de.

Funding

This work was supported by Jacobs University Bremen, Germany.

Notes

The authors declare no competing financial interest.

■ ACKNOWLEDGMENTS

Excellent technical support by Anja Müller is acknowledged.

■ REFERENCES

(1) Idowu, T. O.; Ogundaini, A. O.; Salau, A. O.; Obuotor, E. M.; Bezabih, M.; Abegaz, B. M. Doubly linked, A-type proanthocyanidin turner and other constituents of *Ixora coccinea* leaves and their antioxidant and antibacterial properties. *Phytochemistry* **2010**, *71*, 2092−2098.

(2) Joshi, S. S.; Kuszynski, C. A.; Bagchi, M.; Bagchi, D. Chemopreventive effects of grape seed proanthocyanidin extract on Chang liver cells. *Toxicology* **2000**, *155*, 83−90.

(3) Rajavelu, A.; Tulyasheva, Z.; Jaiswal, R.; Jeltsch, A.; Kuhnert, N. The inhibition of the mammalian DNA methyltransferase 3a (Dnmt3a) by dietary black tea and coffee polyphenols. *BMC Biochem.* **2011**, *12*, 1−8.

(4) Bomser, J. A.; Singletary, K. W.; Wallig, M. A.; Smith, M. A. L. Inhibition of TPA-induced tumor promotion in CD-1 mouse epidermis by a polyphenolic fraction from grape seeds. *Cancer Lett.* **1999**, *135*, 151−157.

(5) Preuss, H. G.; Montamarry, S.; Echard, B.; Scheckenbach, R.; Bagchi, D. Long-term effects of chromium, grape seed extract, and zinc on various metabolic parameters of rats. *Mol. Cell. Biochem.* **2001**, *223*, 95−102.

(6) Bayeta, E.; Lau, B. H. S. Pycnogenol inhibits generation of inflammatory mediators in macrophages. *Nutr. Res. (N. Y., NY, U. S.)* **2000**, *20*, 249−259.

(7) He, J. L.; Chen, Y. Z.; Farzan, M.; Choe, H. Y.; Ohagen, A.; Gartner, S.; Busciglio, J.; Yang, X. Y.; Hofmann, W.; Newman, W.; Mackay, C. R.; Sodroski, J.; Gabuzda, D. CCR3 and CCR5 are co-receptors for HIV-1 infection of microglia. *Nature* **1997**, *385*, 645−649.

(8) Witte, M. B.; Thornton, F. J.; Efron, D. T.; Barbul, A. Enhancement of fibroblast collagen synthesis by nitric oxide. *Nitric Oxide: Biol. Chem.* **2000**, *4*, 572−582.

(9) Ni, Z.; Mu, Y.; Gulati, O. Treatment of melasma with Pycnogenol®. *Phytother. Res.* **2002**, *16*, 567−571.

(10) Das, D. K.; Sato, M.; Ray, P. S.; Maulik, G.; Engelman, R. M.; Bertelli, A. A. E.; Bertelli, A. Cardioprotection of red wine: Role of polyphenolic antioxidants. *Drugs Exp. Clin. Res.* **1999**, *25*, 115−120.

(11) Bagchi, D.; Ray, S. D.; Patel, D.; Bagchi, M. Protection against drug- and chemical-induced multiorgan toxicity by a novel IH636 grape seed proanthocyanidin extract. *Drugs Exp. Clin. Res.* **2001**, *27*, 3−15.

(12) Shah, B. N.; Seth, A. K.; Desai, R. V. Phytopharmacological profile of *Lagenaria siceraria*: A review. *Asian J. Plant Sci.* **2010**, *9*, 152−157.
(13) Prajapati, R. P.; Kalariya, M.; Parmar, S. K.; Sheth, N. R. Phytochemical and pharmacological review of *Lagenaria sicereria*. *J. Ayurveda Integr. Med.* **2010**, *1*, 266−272.
(14) Jasani, N.; Kapoor, M.; Tripathi, N.; Acharya, N.; Acharya, S.; Kumar, V. Anti-asthmatic & anti-allergic activity of *Lagenaria siceraria* Mol. Standley. *J. Nat. Rem.* **2012**, *12*, 72−76.
(15) Mali, V. R.; Mohan, V.; Bodhankar, S. L. Antihypertensive and cardioprotective effects of the *Lagenaria siceraria* fruit in N^G-nitro-L-arginine methyl ester (L-NAME) induced hypertensive rats. *Pharm. Biol.* **2012**, *50*, 1428−1435.
(16) Mayakrishnan, V.; Veluswamy, S.; Sundaram, K. S.; Kannappan, P.; Abdullah, N. Free radical scavenging potential of *Lagenaria siceraria* (Molina) Standl fruits extract. *Asian Pac. J. Trop. Med.* **2013**, *6*, 20−26.
(17) Mohan, R.; Birari, R.; Karmase, A.; Jagtap, S.; Bhutani, K. K. Antioxidant activity of a new phenolic glycoside from *Lagenaria siceraria* Stand. fruits. *Food Chem.* **2012**, *132*, 244−251.
(18) Chen, C. R.; Chen, H. W.; Chang, C. I. D:C-friedooleanane-type triterpenoids from *Lagenaria siceraria* and their cytotoxic activity. *Chem. Pharm. Bull.* **2008**, *56*, 385−388.
(19) Krauzebaranowska, M.; Cisowski, W. High-performance liquid-chromatographic determination of flavone C-glycosides in some species of the Cucurbitaceae family. *J. Chromatogr., A* **1994**, *675*, 240−243.
(20) Karakoese, H.; Jaiswal, R.; Kuhnert, N. Characterization and quantification of hydroxycinnamate derivatives in *Stevia rebaudiana* leaves by LC-MS^n. *J. Agric. Food Chem.* **2011**, *59*, 10143−10150.
(21) Jaiswal, R.; Kiprotich, J.; Kuhnert, N. Determination of the hydroxycinnamate profile of 12 members of the Asteraceae family. *Phytochemistry* **2011**, *72*, 781−790.
(22) Jaiswal, R.; Dickman, M. H.; Kuhnert, N. First diastereoselective synthesis of methyl caffeoyl- and feruloyl-*muco*-quinates. *Org. Biomol. Chem.* **2012**, *10*, 5266−5277.
(23) Jaiswal, R.; Kuhnert, N. Hierarchical scheme for liquid chromatography/multi-stage spectrometric identification of 3,4,5-triacyl chlorogenic acids in green Robusta coffee beans. *Rapid Commun. Mass Spectrom.* **2010**, *24*, 2283−2294.
(24) Jaiswal, R.; Matei, M. F.; Ullrich, F.; Kuhnert, N. How to distinguish between cinnamoylshikimate esters and chlorogenic acid lactones by liquid chromatography-tandem mass spectrometry. *J. Mass Spectrom.* **2011**, *46*, 933−942.
(25) Kuhnert, N.; Jaiswal, R.; Matei, M. F.; Sovdat, T.; Deshpande, S. How to distinguish between feruloyl quinic acids and isoferuloyl quinic acids by liquid chromatography/tandem mass spectrometry. *Rapid Commun. Mass Spectrom.* **2010**, *24*, 1575−1582.
(26) Jaiswal, R.; Kuhnert, N. How to identify and discriminate between the methyl quinates of chlorogenic acids by liquid chromatography-tandem mass spectrometry. *J. Mass Spectrom.* **2011**, *46*, 269−281.
(27) Jaiswal, R.; Kuhnert, N. Identification and characterization of five new classes of chlorogenic acids in burdock (*Arctium lappa* L.) roots by liquid chromatography. *Food Funct.* **2011**, *2*, 63−71.
(28) Jaiswal, R.; Jayasinghe, L.; Kuhnert, N. Identification and characterization of proanthocyanidins of 16 members of the *Rhododendron* genus (Ericaceae) by tandem LC-MS. *J. Mass Spectrom.* **2012**, *47*, 502−515.
(29) Jaiswal, R.; Kuhnert, N. Identification and characterization of two new derivatives of chlorogenic acids in Arnica (*Arnica montana* L.) flowers by high-performance liquid chromatography/tandem mass spectrometry. *J. Agric. Food Chem.* **2011**, *59*, 4033−4039.
(30) Matei, M. F.; Jaiswal, R.; Kuhnert, N. Investigating the chemical changes of chlorogenic acids during coffee brewing: Conjugate addition of water to the olefinic moiety of chlorogenic acids and their quinides. *J. Agric. Food Chem.* **2012**, *60*, 12105−12115.
(31) Jaiswal, R.; Patras, M. A.; Eravuchira, P. J.; Kuhnert, N. Profile and characterization of the chlorogenic acids in green Robusta coffee beans by LC−MS^n: Identification of seven new classes of compounds. *J. Agric. Food Chem.* **2010**, *58*, 8722−8737.
(32) Clifford, M. N.; Wu, W.; Kirkpatrick, J.; Jaiswal, R.; Kuhnert, N. Profiling and characterisation by liquid chromatography/multi-stage mass spectrometry of the chlorogenic acids in Gardeniae Fructus. *Rapid Commun. Mass Spectrom.* **2010**, *24*, 3109−3120.
(33) Jaiswal, R.; Sovdat, T.; Vivan, F.; Kuhnert, N. Profiling and characterization by LC-MS^n of the chlorogenic acids and hydroxycinnamoylshikimate esters in mate (*Ilex paraguariensis*). *J. Agric. Food Chem.* **2010**, *58*, 5471−5484.
(34) Jaiswal, R.; Deshpande, S.; Kuhnert, N. Profiling the chlorogenic acids of *Rudbeckia hirta*, *Helianthus tuberosus*, *Carlina acaulis* and *Symphyotrichum novae-angliae* leaves by LC-MS^n. *Phytochem. Anal.* **2011**, *22*, 432−441.
(35) Jaiswal, R.; Matei, M. F.; Golon, A.; Witt, M.; Kuhnert, N. Understanding the fate of chlorogenic acids in coffee roasting using mass spectrometry based targeted and non-targeted analytical strategies. *Food Funct.* **2012**, *3*, 976−984.
(36) Jaiswal, R.; Matei, M. F.; Golon, A.; Witt, M.; Kuhnert, N. Understanding the fate of chlorogenic acids in coffee roasting using mass spectrometry based targeted and non-targeted analytical strategies. *Food Funct.* **2012**, *3*, 976−984.
(37) Wu, Z.; Chen, X.; Fang, D.; Qi, H.; Ren, W.; Zhang, G. Analysis of phenolic glycosides from *Ilex litseaefolia* using electrospray ionization quadrupole time-of-flight mass spectrometry. *Rapid Commun. Mass Spectrom.* **2009**, *23*, 3881−3885.
(38) Zhang, A.; Ye, Q.; Li, B.; Qi, H.; Zhang, G. Phenolic and triterpene glycosides from the stems of *Ilex litseaefolia*. *J. Nat. Prod.* **2005**, *68*, 1531−1535.
(39) Challice, J. S.; Loeffler, R. S. T.; Williams, A. H. Structure of calleryanin and its benzylic esters from *Pyrus* and *Prunus*. *Phytochemistry* **1980**, *19*, 2435−2437.

the analysis of food-borne toxicants such as acrolein,[9] acrylamide,[39] furan,[40] or glycidamide.[41] However, to the best of my knowledge, no further method for the quantitation of crotonaldehyde using a stable isotopically labeled internal standard has been reported yet (after submission of this paper, I became aware of a similar approach of a Belgian group, which is not yet published), except our recently presented preliminary studies using synthesized deuterium or ^{13}C-labeled crotonaldehyde.[42,43]

Because it is a common trend in high-temperature cooking to use vegetable oils with a high degree of unsaturation, the aims of the present study were (i) to develop a stable isotope dilution analysis using a ^{13}C-labeled internal standard for the quantitation of crotonaldehyde, which also enables the simultaneous determination of acrolein using [$^{13}C_3$]-acrolein, (ii) to compare the data obtained by three different techniques, namely, a direct headspace GC−MS analysis (method I) and two indirect analyses using liquid−liquid extraction combined with a high-vacuum distillation after derivatization by means of GC−MS (with pentafluorophenylhydrazine, method II) and LC−MS/MS (with 2,4-dinitrophenylhydrazine, method III), and (iii) to apply these methods on thermally treated oils differing in their fatty acid composition as well as on fried foods.

MATERIALS AND METHODS

Safety. Acrolein, [$^{13}C_3$]-acrolein, crotonaldehyde, and [$^{13}C_4$]-crotonaldehyde are hazardous and must be handled carefully.

Food Samples. Potatoes, wheat flour, eggs, whole milk, sugar, and vegetable fats and oils (coconut oil, extra virgin olive oil, rapeseed oil, safflower oil, and linseed oil) were purchased at local supermarkets.

Chemicals. [$^{13}C_2$]-Acetaldehyde (99%), crotonaldehyde, 2,4-DNPH (99% purity, stabilized with 50% water), and PFPH (97%) were obtained from Sigma-Aldrich (Steinheim, Germany). Acrolein and sodium methylate were from Fluka (Steinheim). [$^{13}C_3$]-Acrolein (99%) was obtained from Isotec (Ohio, IL). All other reagents were of analytical grade.

Synthesis of the Stable Isotopically Labeled Standard [$^{13}C_4$]-Crotonaldehyde. To a solution (8 mL) of [$^{13}C_2$]-acetaldehyde in dichloromethane (500 mg in 8 mL) were added, first, a solution (8 mL) of pyrrolidine in dichloromethane (48.3 mg in 10 mL) under stirring at 4 °C and, second, a solution (8 mL) of pure acetic acid in dichloromethane (81.5 mg in 10 mL) using a dropping funnel. After a reaction time of 30 min, the mixture was extracted with a solution (2 × 15 mL) of saturated sodium hydrogen carbonate, and the organic phase was dried over anhydrous sodium sulfate. For purification, the solution was first subjected to high-vacuum distillation, and then the solvent was distilled off using a Vigreux column (60 cm × 1 cm i.d.). The residue was dissolved in pentane (1.5 mL), and the obtained solution was applied onto a silica gel column (water-cooled, 45 g of silica gel 60 (0.040−0.063 mm) containing 7% water) using the following elution: pentane (P)/diethyl ether (E) = 100/0 (v/v; 100 mL, fraction 1), P/E = 90/10 (v/v; 100 mL, fraction 2), P/E = 80/20 (v/v; 100 mL, fraction 3), and P/E = 70/30 (v/v; 100 mL, fraction 4). The target compound [$^{13}C_4$]-crotonaldehyde (isotopic purity >97%) was obtained in fraction 4. The concentration of [$^{13}C_4$]-crotonaldehyde was determined using methyl octanoate as the internal standard using a response factor of 0.90 calculated from data obtained by GC-FID analysis of a mixture of unlabeled crotonaldehyde and methyl octanoate.

Fatty Acid Composition Analysis. The fatty acid composition was determined by GC-FID after transesterification with methanol/sodium methylate to obtain the corresponding fatty acid methyl esters closely following the IUPAC standard method.[44]

Aliquots of the oil (100 mg) were accurately weighed into screw-capped centrifuge tubes, and tetrahydrofuran (1 mL) was added. After the oil was dissolved by shaking, sodium methylate (2 mL, 0.5 mol/L) was added, and the solution was heated for 1 h at 50 °C. Then, water (5 mL) and hexane (5 mL) were added, the suspension was mixed using a vortexer (1 min), and the organic layer was separated and, finally, dried over anhydrous sodium sulfate. Aliquots (2 μL) of the solutions were analyzed by means of a Thermo Quest gas chromatograph (Thermo Finnigan, Egelsbach, Germany), equipped with a fused silica DB-5 column (30 m × 0.25 mm i.d., 0.25 μm film thickness) (J&W Scientific, Agilent Technologies, Köln, Germany) using the cold-on-column technique at 60 °C. After 2 min, the temperature was raised at 10 °C/min to 240 °C and, finally, held for 10 min isothermally. The flow of the carrier gas helium was 2.5 mL/min. A flame ionization detector was used at 250 °C. Identification was carried out using a reference mixture of fatty acid methyl esters.

Sample Preparation. To check possible matrix effects during the quantitation of crotonaldehyde by headspace analysis of fats and oils, first, either crotonaldehyde or [$^{13}C_4$]-crotonaldehyde (100 ng each, dissolved in pentane/diethyl ether (70/30, v/v)) was added to unheated extra virgin olive oil (1 g in 20 mL vials), which did not contain crotonaldehyde above the detection limit. After 20 min of continuous stirring at room temperature, the samples were subjected to mass spectrometric analysis as described below.

Oil Heating Process. Oil samples (5 g) were weighed into glass tubes (200 mm × 15 mm i.d.) covered with aluminum foil and were heated in a metal block. Heating was controlled by a thermocouple placed inside the oil. Samples were singly heated at 100, 140, 180 (regular deep-frying temperature), and 220 °C for 24 h each. In a further series of experiments, the samples were heated at 180 °C for 2, 4, 8, 16, 24, and 55 h. Immediately after the samples were cooled to room temperature, [$^{13}C_4$]-crotonaldehyde (0.5−150 μg, dissolved in pentane/diethyl ether (70/30, v/v), depending on the amounts determined in preliminary experiments) and [$^{13}C_3$]-acrolein (0.5−250 μg) were added, the glass tubes were closed and kept at −20 °C prior to analysis.

Preparation of Deep-Fried Food. *Dough Recipe for Donuts.* After the yeast (42 g) was dissolved in warm water, wheat flour (500 g), whole milk (150 mL), sugar (50 g), eggs (100 g), and water (25 mL) were mixed until a homogeneous dough was obtained. The dough was then divided into pieces of about 50 g and incubated at 30 °C for 2 h. Deep-frying (4 min at 180 °C) was performed as mentioned below for potatoes.

Deep-Frying of Potatoes. Thin slices (peeled, 1.5 mm cross section) were fried for 2.5 min at 180 °C in an electrical deep-fryer (Kenwood DF320, Heusenstamm, Germany) containing 2.3 L of oil, which was preheated for 10 min prior to frying. The potato-to-oil mass ratio was about 1:7. After the potatoes were cooled to room temperature, an aliquot (10 g) of the chips was weighed into a headspace vial (20 mL), [$^{13}C_4$]-crotonaldehyde and [$^{13}C_3$]-acrolein (each 150 ng) were added, and the mixture was stirred for equilibration (15 min). To provide the most similar conditions, the first five batches of the respective fried food were rejected, and only the sixth batch was used for analysis.

Quantitation of Crotonaldehyde by Headspace High-Resolution Gas Chromatography−Mass Spectrometry (HRGC−MS) (Method I). Aliquots (250−2000 μL) of the headspace volume were injected into the hot PPKD injector (Thermo Finnigan) of a Trace 2000 series gas chromatograph (Thermo Finnigan) using a Combi Pal autosampler (CTC Analytics, Zwingen, Switzerland) held at 20 °C and equipped with a 2 mL gastight syringe (SGE Analytic Science, Darmstadt, Germany). After each injection, a possible carry-over into the syringe was eliminated by an automatic syringe flush (helium). The headspace autosampler conditions were set as follows: incubation temperature, 30 °C; syringe temperature, 35 °C; syringe injection volume, 2 mL; syringe injection speed, 0.1 mL/s. The effluent was quantitatively transferred into a cold trap (initial temperature, −150 °C for 0.1 min; heating rate, 15 °C/s; final temperature, 240 °C for 3 min) (SGE Analytic Science) using a moving column stream switching system (Thermo Finnigan). After the cooling was turned off, the trapped compounds were transferred onto a fused silica DB-5 MS column (30 m × 0.25 mm i.d., 1.0 μm film thickness) (J&W Scientific). The oven was heated from 10 °C to 60 °C at 6 °C/min and then to 220 °C at 10 °C/min. The effluent was monitored by an ion trap mass spectrometer, Saturn 2000 (Varian, Darmstadt), running in the chemical ionization mode (70 eV ionization energy) with methanol as the reagent gas. Crotonaldehyde and [$^{13}C_4$]-crotonaldehyde were

located by means of their molecular masses obtained in the full scan mode (the mass range from m/z 50 to m/z 250 was recorded; m/z 71 for the analyte and m/z 75 for the labeled standard were used for determination) and by means of their retention indices. Crotonaldehyde concentrations were calculated from the area counts obtained from the mass chromatograms using the following equation:

$$m(\text{crotonaldehyde}) = R_f \times \frac{A(\text{crotonaldehyde}) \times m([^{13}C_4]\text{-crotonaldehyde})}{A([^{13}C_4]\text{-crotonaldehyde})}$$

where A(crotonaldehyde) is the area of unlabeled crotonaldehyde, $A([^{13}C_4]$-crotonaldehyde) is the area of $[^{13}C_4]$-crotonaldehyde, and $m([^{13}C_4]$-crotonaldehyde) is the amount of added $[^{13}C_4]$-crotonaldehyde. The response factor (R_f) was determined by analysis of defined mixtures of crotonaldehyde and $[^{13}C_4]$-crotonaldehyde (10:1, 5:1, 3:1, 1:1, 1:3, 1:5, and 1:10, w/w) as described below using the resulting response curve showing a very good linearity (coefficient of determination (R^2) of 0.99). Applied concentration ranges varied from 0.2 to 200 μg of crotonaldehyde depending on the amounts determined in preliminary experiments.

Quantitation of Acrolein by Headspace HRGC−MS. Quantitation of acrolein was performed by headspace high-resolution gas chromatography−mass spectrometry using $[^{13}C_3]$-acrolein as the internal standard as previously described.[9]

Quantitation of Crotonaldehyde by HRGC−MS after Derivatization with PFPH (Method II) or by High-Performance Liquid Chromatography−Tandem Mass Spectrometry (HPLC−MS/MS) after Derivatization with 2,4-DNPH (Method III). *Preparation of Reference Substances.* First, the reference derivatives of both crotonaldehyde and labeled crotonaldehyde were made up by adding these aldehydes into olive oil to consider possible matrix interferences, which might also occur during the analysis of real samples. Therefore, unheated extra virgin olive oil (10 g) was spiked singly either with crotonaldehyde or with $[^{13}C_4]$-crotonaldehyde (5 μg each, dissolved in pentane/diethyl ether (70/30, v/v)). After the addition of PFPH solution (0.5 mL; 2 mg of PFPH were dissolved in 1 mL of 0.1 mol/L HCl, method II) or 2,4-DNPH solution (1 mL; first, 100 mg of 2,4-DNPH were dissolved in 10 mL of 2.0 mol/L HCl using an ultrasonic bath and, then, diluted with 90 mL of methanol, method III), the mixture was stirred for 60 min (PFPH) or for 180 min (2,4-DNPH) at room temperature using a magnetic stirrer. In the same way, acrolein and $[^{13}C_3]$-acrolein were derivatized with PFPH[9] or 2,4-DNPH.

Then, the water-in-oil emulsion was extracted with dichloromethane (50 mL) by continuous liquid−liquid extraction. The PFPH derivatives as well as the 2,4-DNPH derivatives of crotonaldehyde and $[^{13}C_4]$-crotonaldehyde were separated from the bulk of the fat by the solvent-assisted flavor evaporation (SAFE) technique[45] at 48 °C under vacuum (5×10^{-3} Pa). The distillate was dried over anhydrous sodium sulfate and concentrated to a final volume of ∼1 mL using a Vigreux column (100 cm × 3 cm i.d.) at 48 °C. Aliquots (2 μL) of the solution were analyzed by GC−MS or LC−MS/MS as described below.

Analyses of Oil Samples. Oil samples were prepared as described above for the oil-heating process. To aliquots (approximately 5 g) was added PFPH (method II) or 2,4-DNPH (method III) solution, and the mixture was stirred for 20 min at room temperature. Further workup was done as described above for the reference substances.

Instrumental Conditions for HRGC−MS (Method II). Using a Combi Pal autosampler (CTC Analytics), an aliquot (2 μL) of the sample was injected into the hot PPKD injector of a Trace 2000 series gas chromatograph and transferred onto a DB-1701 column (30 m × 0.25 mm i.d., 0.25 μm film thickness) (J&W Scientific). The following temperature program was used: 40 °C for 2 min and then at 8 °C/min to 230 °C for 10 min. The effluent was monitored using an ion trap mass spectrometer Saturn 2000 running in the chemical ionization mode (70 eV ionization energy) with methanol as the reagent gas.

The derivatives of crotonaldehyde and $[^{13}C_4]$-crotonaldehyde were characterized by means of their molecular masses obtained in the full scan mode (the mass range from m/z 50 to m/z 300 was recorded; m/z 251 (analyte) and m/z 255 (labeled standard) for the PFPH derivatives were used for determination) and by means of their retention indices.

Instrumental Conditions for HPLC−MS/MS (Method III). Mass spectra were recorded by means of a triple-quadrupole tandem mass spectrometer (TSQ Quantum Discovery) (Thermo Electron, Dreieich, Germany) coupled to a Surveyor high-performance liquid chromatography system (Thermo Finnigan) equipped with a thermostated (20 °C) autosampler and an 120 mm × 2.0 mm i.d., 3 μm Nucleosil C18 120 Å HPLC column (Macherey-Nagel, Düren, Germany) kept at 30 °C connected to a 4 mm × 2.0 mm i.d. C18 precolumn (Phenomenex, Aschaffenburg, Germany). The solvent system was composed of formic acid in water (0.1% by weight; solvent A) and formic acid in acetonitrile (0.1% by weight; solvent B). A linear gradient was applied by increasing the concentration of solvent B from 30% to 100% within 15 min. Separation was performed at a flow rate of 0.2 mL/min. For quantitation, mass spectrometry was performed with positive electrospray ionization (ESI^+) in multiple reaction monitoring (MRM) mode with a spray needle voltage of 3.3 kV. The temperature of the capillary was 300 °C. The sheath gas and auxiliary gas (nitrogen) were adjusted to 35 and 10 arbitrary units, respectively. The collision cell was operated at a collision gas (argon) pressure of 0.20 Pa.

First, the derivatives of crotonaldehyde and $[^{13}C_4]$-crotonaldehyde were characterized by means of their molecular masses obtained in the full-scan mode. Clear molecular ions were obtained $[M + H]^+$: m/z 251 for derivatized crotonaldehyde and m/z 255 for derivatized $[^{13}C_4]$-crotonaldehyde. These were then subjected to MS/MS (collision energy 20 V). First, the most intense transitions of the precursor ions were determined, and second, the yields of the product ions were optimized by performing a series of runs with different collision energies and flow rates of the sheath gas and auxiliary gas. Finally, the mass transitions m/z 251 to m/z 234 and m/z 251 to m/z 157 for crotonaldehyde as well as m/z 255 to m/z 238 and m/z 255 to m/z 161 for $[^{13}C_4]$-crotonaldehyde were selected for quantitation, including the signal-to-noise ratio in oil samples as criteria.

Next, the 2,4-DNPH derivatives of acrolein and $[^{13}C_3]$-acrolein were characterized by means of their molecular masses obtained in the full-scan mode. Again, clear molecular ions were obtained $[M + H]^+$: m/z 237 for derivatized acrolein and m/z 240 for derivatized $[^{13}C_3]$-acrolein. These were then subjected to MS/MS (collision energy 20 V). First, the most intense transitions of the precursor ions were determined, and second, the yields of the product ions were optimized by performing a series of runs with different collision energies and flow rates of the sheath gas and auxiliary gas. Finally, the mass transitions m/z 237 to m/z 220 and m/z 237 to m/z 143 for acrolein as well as m/z 240 to m/z 223 and m/z 240 to m/z 146 for $[^{13}C_3]$-acrolein were selected for quantitation, including the signal-to-noise ratio in oil samples as criteria.

On both mass filter quadrupoles, the resolution setting was 0.8 full width at half-maximum, the scan time for each transition and single reaction monitoring (SRM) was 0.20 s, the scan width was 0.8 amu, and the source collision-induced dissociation (CID) voltage was 12 V.

Quantitation of Acrolein by HRGC−MS after Derivatization with PFPH. Quantitation of acrolein after derivatization with PFPH was performed by high-resolution gas chromatography−mass spectrometry using $[^{13}C_3]$-acrolein as the internal standard as previously described.[9]

Calibration Curves. For calibration, seven mixtures of crotonaldehyde and $[^{13}C_4]$-crotonaldehyde as well as of acrolein and $[^{13}C_3]$-acrolein in defined concentrations (molar ratios 10:1 to 1:10) were analyzed for all methods as described above, and the response factors were calculated from the results as previously described.[41] Calibration was always performed prior to sample measurement.

Limit of Detection (LoD) and Limit of Quantitation (LoQ). Calculation of the LoD and LoQ was carried out on the basis of a correlation between the intensity of the respective ions and the background noise with a minimum ratio of 3:1. Unheated oil samples were spiked with known amounts of crotonaldehyde (or acrolein for method III) in decreasing concentrations (100, 50, 25, 20, 15, 10, 5, 2.5, 1.25, and 0.5 μg/kg) and were analyzed in triplicate using all three methods. A control run without addition of crotonaldehyde and $[^{13}C_4]$-

crotonaldehyde (or acrolein and [$^{13}C_3$]-acrolein) was performed to ensure the absence of the respective mass signals in the oil samples.

HRGC−Sector Field Mass Spectrometry. To obtain mass spectra in electron impact (EI) as well as in chemical ionization (CI) mode for the PFPH derivatives of crotonaldehyde and [$^{13}C_4$]-crotonaldehyde, HRGC−MS analyses were performed by means of a Hewlett-Packard gas chromatograph, type 5890 series II (Hewlett-Packard, Waldbronn, Germany), coupled to a sector field mass spectrometer, type MAT 95 S (Finnigan MAT, Bremen, Germany), running either in EI mode (70 eV ionization energy) or in CI mode using isobutane as the reagent gas (115 eV ionization energy). The samples were injected by the cold on-column technique at 40 °C onto a DB-FFAP fused silica capillary column (30 m × 0.25 mm i.d., 0.25 μm film thickness) (J&W Scientific). The oven temperature was held for 2 min isothermally and then raised by 8 °C/min to 230 °C for 10 min.

RESULTS AND DISCUSSION

Synthesis of the Stable Isotopically Labeled Internal Standard [$^{13}C_4$]-Crotonaldehyde. Due to the fact that the deuterated labeled standard, which was used in preliminary trials,[42] showed a heterogeneous labeling pattern ([$^2H_{3-4}$]-crotonaldehyde), first, a new ^{13}C-labeled standard was synthesized using [$^{13}C_2$]-acetaldehyde. By Aldol condensation, 4-fold-labeled [$^{13}C_4$]-crotonaldehyde was obtained (Figure 1),

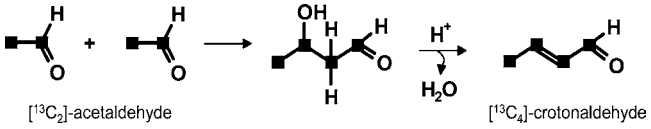

Figure 1. Reaction scheme for the synthesis of the internal standard [$^{13}C_4$]-crotonaldehyde. The symbol "■" indicates ^{13}C-labeling.

revealing a ratio between [$^{13}C_4$]-(*E*)-2-butenal (=[$^{13}C_4$]-crotonaldehyde) and [$^{13}C_4$]-(*Z*)-2-butenal of 95:5. Stereochemistry was confirmed by comparison of the retention index using commercially available (*E*)-2-butenal. Mass spectrometry experiments in the EI and CI modes have proven the successful incorporation of the labeling into the internal standard [$^{13}C_4$]-crotonaldehyde. The isotopic purity of [$^{13}C_4$]-crotonaldehyde was >97% (data not shown).

Development of the Analytical Procedure. *Method I (Headspace GC−MS).* In the first experiment, crotonaldehyde and [$^{13}C_4$]-crotonaldehyde (2 μg, dissolved in pentane/diethyl ether (70/30, v/v)) were singly placed into two 20 mL headspace vials, and after 20 min of equilibration, the solutions were analyzed by headspace GC−MS. The mass chromatogram of crotonaldehyde obtained by chemical ionization showed a clear peak at *m/z* 71. At the same retention index, the labeled isotopologue revealed a peak at *m/z* 75. Next, either crotonaldehyde or [$^{13}C_4$]-crotonaldehyde (100 ng each, dissolved in pentane/diethyl ether (70/30, v/v)) was singly added to unheated extra virgin olive oil (1 g in 20 mL vials). The analyte and the labeled analogue were characterized by selected ion monitoring at *m/z* 71 (for crotonaldehyde) and *m/z* 75 (for [$^{13}C_4$]-crotonaldehyde) as well as by their retention indices. The results showed that the fatty matrix neither contained coeluting compounds showing a signal either at *m/z* 71 or at *m/z* 75 at the respective retention index nor contained crotonaldehyde above the detection limit.

Method II (GC-MS after Derivatization) and Method III (LC−MS/MS after Derivatization). The crucial factor in headspace analysis of low molecular weight compounds such as crotonaldehyde is, however, the low specificity of the mass traces. This prompted us to develop two additional methods to confirm the reliability of the results obtained by the headspace method similar to the development of a derivatization method using 2-mercaptobenzoic acid for the quantitation of acrylamide,[39] also having an *m/z* signal of 72 (MS-CI) with a low specificity, or using pentafluorophenylhydrazine (PFPH) for the quantitation of acrolein (*m/z* 57, MS-CI).[9]

Preliminary trials showed a good conversion of crotonaldehyde by derivatization with the nucleophiles PFPH or 2,4-DNPH, and the respective adducts were analyzed. Both hydrazines were found to convert crotonaldehyde within 60 min (PFPH) or 180 min (2,4-DNPH) (120 min for acrolein using 2,4-DNPH) with high yields into stable hydrazones, which were detected either by GC−MS (PFPH) or by LC−MS/MS (2,4-DNPH).

For method development, first, the derivatives were synthesized by reacting crotonaldehyde as well as [$^{13}C_4$]-crotonaldehyde singly with either PFPH (Figure 2A) or 2,4-DNPH (Figure 2B) to obtain stable derivatives. Samples were analyzed by GC−MS (CI mode) or by LC−MS/MS (ESI$^+$ mode).

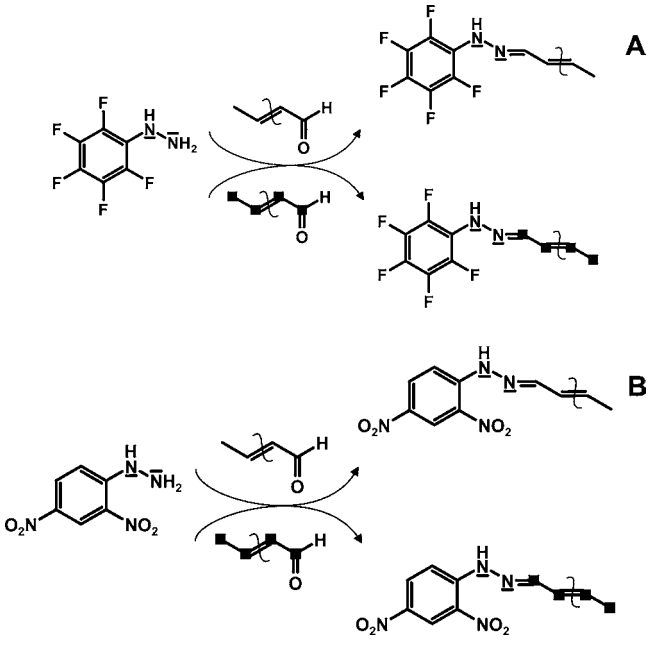

Figure 2. Derivatization scheme used for the conversion of crotonaldehyde (analyte) and [$^{13}C_4$]-crotonaldehyde (internal standard) into stable pentafluorophenylhydrazones (method II, A) or 2,4-dinitrophenylhydrazones (method III, B) prior to analysis. The symbol "■" indicates ^{13}C-labeling.

PFPH Derivatives of Crotonaldehyde and [$^{13}C_4$]-Crotonaldehyde (Method II, GC−MS). As PFPH itself has a lower retention time compared to the crotonaldehyde derivatives, the MS detector was switched off during its elution to avoid any contamination of the ion trap. The mass spectra (EI mode) of the PFPH derivatives of crotonaldehyde and [$^{13}C_4$]-crotonaldehyde are given in Figure 3A and 3B. Various ions were obtained, which are postulated to be [C_5F_3]$^+$, [C_5F_4]$^+$, [C_5F_5]$^+$, and [$C_6F_5NH_2$]$^+$.[9] The fragment *m/z* 183 in the spectrum is attributable to the cleavage of the hydrazone bond between both nitrogen atoms, whereas the fragments *m/z* 155, 136, and 117 may be formed by rearrangement of the aromatic ring. Intense [M]$^+$ ions of the unlabeled (*m/z* 250) and the labeled (*m/z* 254)

dx.doi.org/10.1021/jf404902m | J. Agric. Food Chem. 2014, 62, 1272−1282

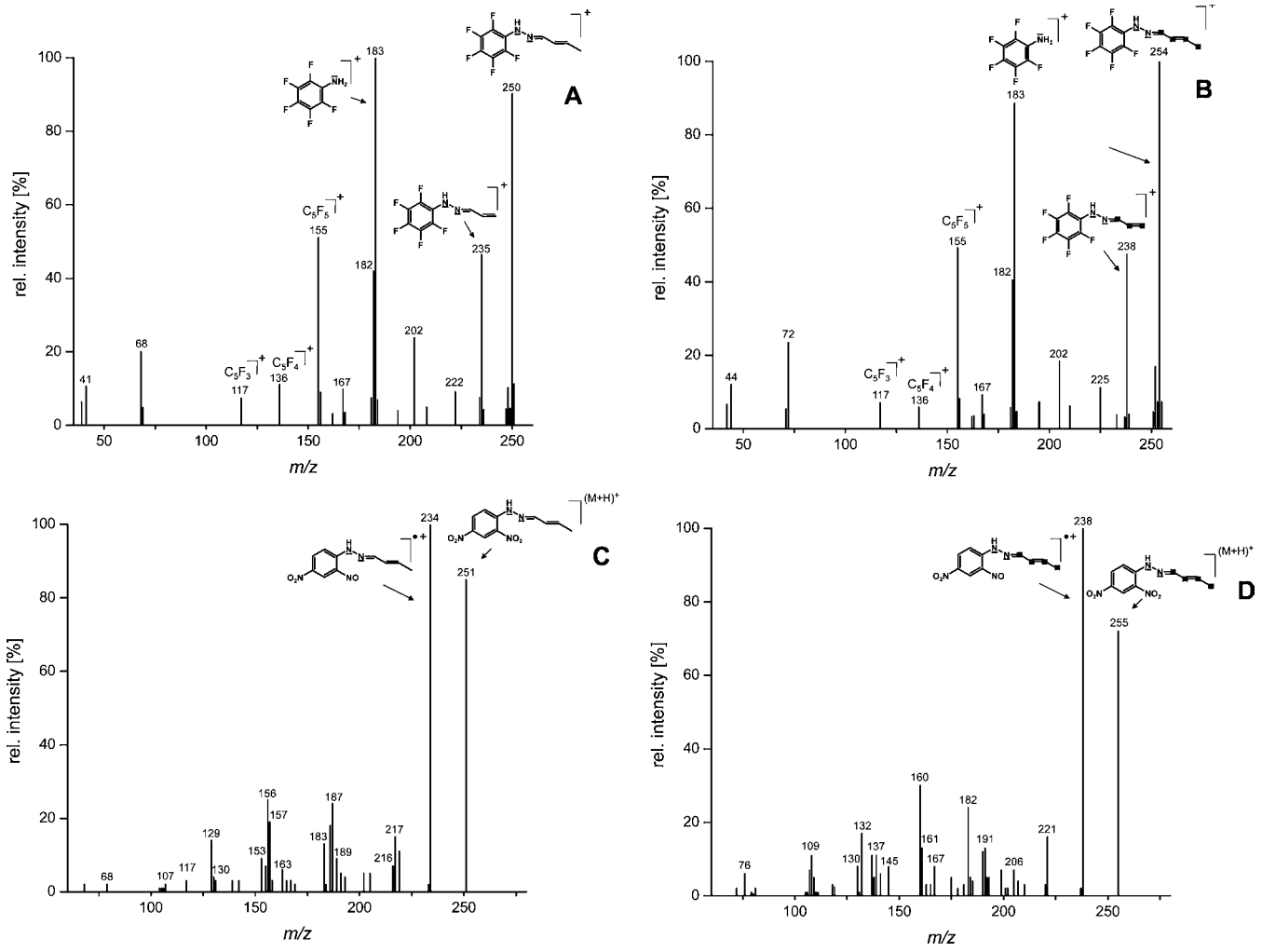

Figure 3. Mass spectra (GC−MS, EI) of the PFPH derivatives of crotonaldehyde (A) and [$^{13}C_4$]-crotonaldehyde (B) as well as mass spectra (LC−MS/MS, ESI$^+$) of the 2,4-DNPH derivatives of crotonaldehyde (C) and [$^{13}C_4$]-crotonaldehyde (D). The symbol "■" indicates ^{13}C-labeling.

crotonaldehyde derivatives confirmed the successful derivatization reactions of crotonaldehyde and its isotopologue using PFPH. In contrast to the assumption that two peaks (syn and anti forms of the enamine) might be generated, double peaks were not detected in the chromatogram, probably because the two isomers did not separate on the stationary phase used (Figure 4).

Next, unheated oil samples (10 g) were spiked with crotonaldehyde and [$^{13}C_4$]-crotonaldehyde (each 5 μg, dissolved in pentane/diethyl ether (70/30, v/v)), and the solutions were derivatized with PFPH. The best results to remove interfering compounds from the derivatives were obtained by high-vacuum distillation, the so-called SAFE technique.[45] Thus, mass spectra were obtained for the oil extracts identical to those shown in Figure 3A and 3B obtained from the model solutions, proving the workup procedure to be suitable for the quantitation of crotonaldehyde. Last, similar to the development of method I, unheated extra virgin olive oil was analyzed without addition of either crotonaldehyde or [$^{13}C_4$]-crotonaldehyde. Again, no signals for m/z 251 and m/z 255 (both MS-CI) were detected in the respective unspiked samples, revealing again that crotonaldehyde is, if at all, only present below its detection limit and that [$^{13}C_4$]-crotonaldehyde is an appropriate internal standard.

2,4-DNPH Derivatives of Crotonaldehyde and [$^{13}C_4$]-Crotonaldehyde (Method III, LC−MS/MS). The mass spectra (ESI$^+$, full scan mode) of the 2,4-DNPH derivatives of crotonaldehyde and [$^{13}C_4$]-crotonaldehyde are shown in Figure 3C and 3D. The following molecular ions were obtained [M + H]$^+$: m/z 251 for derivatized crotonaldehyde and m/z 255 for derivatized [$^{13}C_4$]-crotonaldehyde. Subjection to MS/MS revealed the following mass transitions, which were used for quantitation: m/z 251 to m/z 234 and m/z 251 to m/z 157 (crotonaldehyde) as well as m/z 255 to m/z 238 and m/z 255 to m/z 161 ([$^{13}C_4$]-crotonaldehyde). Even if m/z 157 and m/z 161 did not reveal the highest intensities, they showed the best signal-to-noise ratios in real samples besides m/z 234 and m/z 238.

2,4-DNPH Derivatives of Acrolein and [$^{13}C_3$]-Acrolein (Method III, LC−MS/MS). Next, the 2,4-DNPH derivatives of acrolein and [$^{13}C_3$]-acrolein were characterized by means of their molecular masses obtained in the full scan mode, revealing the following molecular ions [M + H]$^+$: m/z 237 for derivatized acrolein and m/z 240 for derivatized [$^{13}C_3$]-acrolein (data not shown). Subjection to MS/MS resulted in the following mass transitions for quantitation: m/z 237 to m/z 220 and m/z 237 to m/z 143 (acrolein) as well as m/z 240 to m/z 223 and m/z 240 to m/z 146 ([$^{13}C_3$]-acrolein).

dx.doi.org/10.1021/jf404902m | J. Agric. Food Chem. 2014, 62, 1272−1282

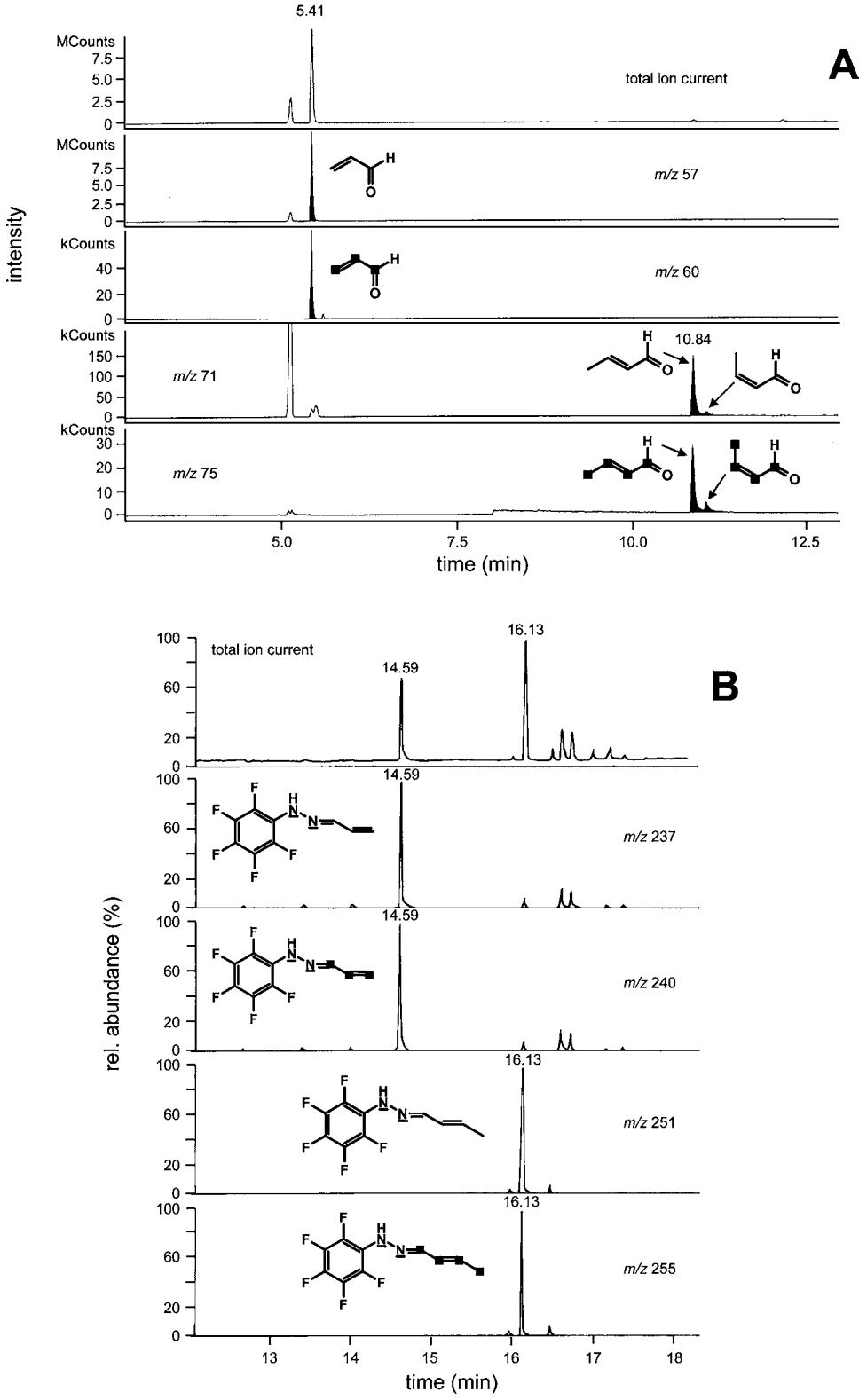

Figure 4. Extracts of GC−mass chromatograms (MS-CI) obtained for the analysis of crotonaldehyde (about 0.1 mg/kg) and acrolein (about 0.3 mg/kg) in a heat-processed olive oil sample using method I (without derivatization, A) and method II (derivatization with PFPH, B), respectively. The symbol "■" indicates ^{13}C-labeling.

Again, unheated oil samples (10 g) were spiked with crotonaldehyde and [$^{13}C_4$]-crotonaldehyde (each 5 μg, dissolved in pentane/diethyl ether (70/30, v/v)) as well as with acrolein and [$^{13}C_3$]-acrolein (each 5 μg, dissolved in methanol/dichloromethane (50/50, v/v)). Then, the solutions were derivatized with 2,4-DNPH and subjected to SAFE distillation.[45] In this way, mass spectra were obtained for the oil extracts identical to those of the reference compounds from the model solutions, proving the workup procedure to be suitable for the quantitation of crotonaldehyde and acrolein.

dx.doi.org/10.1021/jf404902m | J. Agric. Food Chem. 2014, 62, 1272−1282

Last, similar to the development of methods I and II, unheated extra virgin olive oil was analyzed without addition of crotonaldehyde, [$^{13}C_4$]-crotonaldehyde, acrolein, or [$^{13}C_3$]-acrolein. Again, no signals for m/z 251, 255, 237, or 240 were detected in the respective unspiked samples, revealing again that crotonaldehyde and acrolein are, if at all, only present below their detection limits and that [$^{13}C_4$]-crotonaldehyde and [$^{13}C_3$]-acrolein are appropriate internal standards.

Calibration Curves, LoDs, and LoQs. A calibration curve was generated for each method by analyzing seven model mixtures in unheated extra virgin olive oil containing defined amounts of labeled and unlabeled crotonaldehyde in different molar ratios (10:1 to 1:10). The mixtures were worked up for each method as described above and were analyzed by headspace GC−MS (method I), GC−MS (method II), or LC−MS/MS (method III). The $[M + H]^+$ mass ratios of the area counts of the analyte (m/z 71 for method I and m/z 251 for methods II and III) and the labeled standard (m/z 75 for method I and m/z 255 for methods II and III) were plotted against the concentration ratios. From these data, three response curves were obtained showing a good linearity ($R^2 > 0.99$).

For all three methods, limits of detection were calculated on the basis of a signal-to-noise ratio of 3:1. For this purpose, unheated extra virgin olive oil samples were spiked with different amounts of crotonaldehyde and acrolein (each 0.5−100 μg/kg, methods I−III), worked up, and measured by headspace GC−MS, GC−MS, or LC−MS/MS. The results allowed the calculation of LoDs for crotonaldehyde of 3 μg/kg for method I, 2 μg/kg for method II, and 1.5 μg/kg for method III as well as LoQs of 9 μg/kg for method I, 6 μg/kg for method II, and 4.5 μg/kg for method III. Interestingly, all three methods revealed nearly the same LoDs, pointing out method III as the most sensitive one due to MS/MS detection. For acrolein, LoDs were determined to be 3 μg/kg for method I and 2 μg/kg for methods II and III and LoQs to be 9 μg/kg for method I and 6 μg/kg for methods II and III. Thus, the main goal of this method development, using selective quantifier fragments of m/z 251 (analyte) and m/z 255 (internal standard) to check the correctness of the results obtained by the headspace GC−MS method (method I) using less selective quantifier signals of m/z 71 (analyte) and m/z 75 (internal standard), was achieved.

Generation of Acrolein and Crotonaldehyde during Thermal Processing of Oils. To estimate the influence of the fatty acid composition on the amounts of crotonaldehyde formed after heating, five different oil samples varying in their fatty acid compositions were heated at 180 °C for 24 h, and analyses were carried out using all three methods. First, the fatty acid composition of the fat and oil samples was determined (Table 1). In agreement with the literature, coconut oil was dominated by lauric and myristic acid, while olive oil mainly consisted of oleic acid. Also in rapeseed oil, oleic acid was the most prominent fatty acid, while safflower oil showed the highest amount of linoleic acid, and linseed oil was highest in linolenic acid. To check the influence of heat-processing on the fatty acid composition, the five fats were heated for various times (up to 96 h) at 180 °C and were analyzed again, revealing only marginal decreases, particularly for the unsaturated fatty acids (data not shown).

Typical chromatograms of heated oil samples obtained by method I (Figure 4A), method II (Figure 4B), and method III (Figure 5) are exemplarily shown for a thermally processed olive oil sample, showing clear peaks for acrolein and crotonaldehyde and their respective internal standards, [$^{13}C_3$]-acrolein and

Table 1. Fatty Acid Composition of the Unheated Fat and Oil Samples

	concn[a] (g/100 g of fat)					
sample	C12:0[b]	C14:0[c]	C16:0[d]	C18:1[e]	C18:2[f]	C18:3[g]
coconut oil	50	18	9	7	<1	<1
olive oil	<1	<1	11	79	7	<1
rapeseed oil	<1	<1	4.6	63	19.4	8.6
safflower oil	<1	<1	6.3	12.8	73	<1
linseed oil	<1	<1	5.4	20.4	14.9	55.3
frying fat	48	<1	12	25	14	<1

[a]Data are mean values of triplicate measurements. [b]C12:0 = lauric acid. [c]C14:0 = myristic acid. [d]C16:0 = palmitic acid. [e]C18:1 = oleic acid. [f]C18:2 = linoleic acid. [g]C18:3 = linolenic acid.

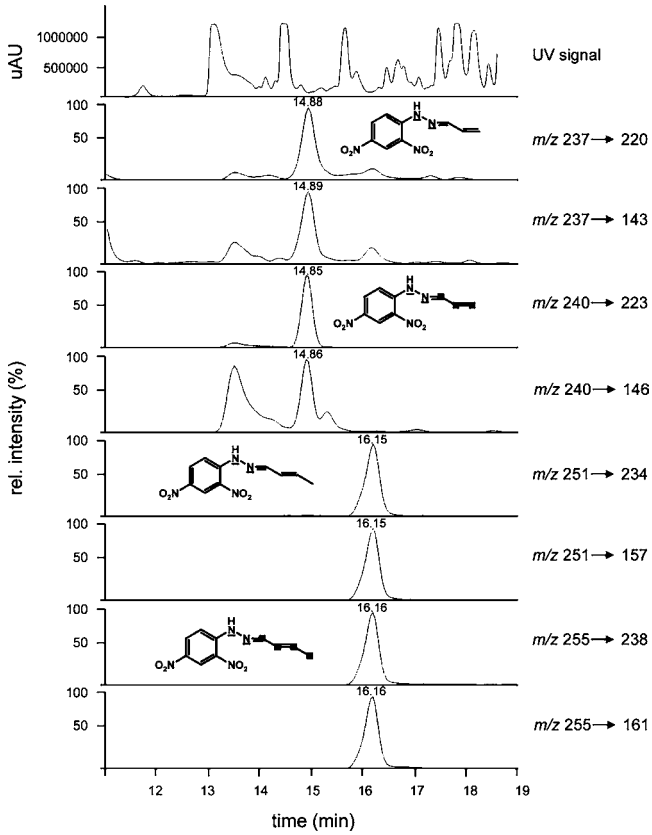

Figure 5. Extract of an LC−MS/MS chromatogram (ESI^+) obtained for the analysis of crotonaldehyde (about 0.1 mg/kg) and acrolein (about 0.3 mg/kg) in a heat-processed olive oil sample using method III (derivatization with 2,4-DNPH). The symbol "■" indicates ^{13}C-labeling.

[$^{13}C_4$]-crotonaldehyde. Interestingly, the separation of crotonaldehyde ((*E*)-2-butenal) from its stereo isomer (*Z*)-2-butenal was only achieved using method I, which can be explained by the use of a thick film capillary (Figure 4A).

The quantitative results obtained for the five different oils by all three methods are summarized in Table 2. A first observation was that all three methods resulted in very similar data, proving that the quick direct headspace GC−MS measurement, which does not require any time-consuming workup steps, can be used without any interference of coeluting compounds (m/z 71 for crotonaldehyde and m/z 75 for [$^{13}C_4$]-crotonaldehyde, MS-CI). Thereby, both derivatization methods using the same type of conversion by forming stable hydrazones, but different

dx.doi.org/10.1021/jf404902m | J. Agric. Food Chem. 2014, 62, 1272−1282

Table 2. Comparison of the Concentration of Crotonaldehyde Formed in Five Oil Samples after the Samples were Heated at 180 °C for 24 h

	concn[a] (mg/kg)		
sample	method I[b]	method II[c]	method III[d]
coconut oil	0.30 (0.27/0.32)	0.32 (0.30/0.34)	0.29 (0.27/0.31)
olive oil	1.32 (1.26/1.37)	1.42 (1.34/1.50)	1.30 (1.26/1.33)
rapeseed oil	11.6 (11.2/12.0)	12.3 (11.8/12.8)	11.7 (11.2/12.2)
safflower oil	0.63 (0.60/0.65)	0.68 (0.64/0.72)	0.64 (0.61/0.67)
linseed oil	33.9 (33.4/34.4)	34.4 (33.3/35.5)	34.1 (33.7/34.4)

[a]Mean values (concentration ranges) on the basis of two independent heat-processings. [b]Headspace GC−MS. [c]GC−MS after derivatization with PFPH. [d]LC−MS/MS after derivatization with 2,4-DNPH.

separation (GC, method II; LC, method III) and detection (MS-CI, method II; MS/MS-ESI$^+$, method III) techniques, revealed nearly the same results in comparison to headspace GC−MS-CI (method I). Thus, the small amount of (*Z*)-2-butenal (not separated by methods II and III) present in the [$^{13}C_4$]-crotonaldehyde standard solution (cf. Figure 4A) did not significantly influence the quantitative data of crotonaldehyde.

At first glance, it seems that heat-processing of oils with higher amounts of unsaturated fatty acids, in particular linolenic acid, generated higher amounts of crotonaldehyde: linseed oil revealed about 34 mg/kg and rapeseed oil about 12 mg/kg in comparison to coconut oil with only 0.3 mg/kg (cf. Tables 1 and 2). This result is in good accordance with previous studies about the formation of acrolein upon heat-processing of oils depending on the fatty acid composition.[9]

To have the possibility of a direct comparison of the formation of crotonaldehyde and acrolein, the amounts of acrolein were determined in parallel in this study, especially due to the fact that a different model system was used for heat-processing compared to the method of Ewert et al.[9] Although another model was applied in the present study and, therefore, different concentrations of acrolein were generated, the tendency was clearly the same. Again, safflower oil, containing by far more linoleic acid compared to, e.g., rapeseed oil, showed remarkably lower contents of both crotonaldehyde and acrolein. Although its mean fatty acid is linoleic acid, safflower oil commonly contains a high level of antioxidants, e.g., tocopherols, which might explain its higher stability and, thus, the lowered formation of 2-alkenals. Since saturated or monounsaturated fatty acids are more stable during thermal oxidation, this may be the reason for the significantly lower generation of crotonaldehyde and acrolein from coconut and olive oil, respectively (Tables 2 and 3).

To study the influence of the temperature on crotonaldehyde formation, the five oil samples were analyzed after being heated at four different temperatures using headspace GC−MS (method I). With the exception of coconut oil and safflower oil, an increase of the temperature from 100 to 180 °C led first to a clear increase in crotonaldehyde formation, followed by a decrease from 180 to 220 °C after 24 h of heating (Table 3). Probably, at this quite high temperature, crotonaldehyde already undergoes reactions with other degradation products of these oils. In contrast, coconut oil and safflower oil did not show a maximum of crotonaldehyde formation up to 220 °C, and the amounts were much lower as compared to those of linseed oil and rapeseed oil. Exactly the same tendency, but in much higher concentrations compared to that of crotonaldehyde, was obtained for the formation of acrolein, with the only exception that safflower oil showed the same decrease in acrolein content from 180 to 220 °C as linseed oil, rapeseed oil, and olive oil (Table 3). These results confirmed that obviously the content of linolenic acid is crucial for the formation of both crotonaldehyde and acrolein during heating of oils. Furthermore, the data confirmed the findings of previous studies on acrolein formation[9] and acrolein release into the air[46,47] during frying of foods in different oils.

In a further series of experiments, the influence of the heating time on crotonaldehyde and acrolein formation was studied using again the headspace GC−MS method. For this purpose, the oil samples were heated at 180 °C, applying different heating times from 2 to 55 h. Thereby, linseed oil and rapeseed oil showed quite high amounts of crotonaldehyde and acrolein already after 2 h (Table 4). With increasing heating time, all analyzed oil samples revealed increasing amounts of both crotonaldehyde and acrolein, whereat normally the acrolein concentration dominates, except for olive oil, for which the formed amounts of both 2-alkenals are very similar after a heating time of >4 h. For coconut oil and rapeseed oil, crotonaldehyde concentrations increase until 16 h, followed by a decrease from 16 to 24 h and, finally, a further increase from 24 to 55 h. In contrast, olive oil and safflower oil had their maxima already after 8 h of heating, and linseed oil showed no maximum at all, still showing an increase of crotonaldehyde up to 55 h. Interestingly, the highest amounts of formed acrolein were determined already after 4 or 8 h for all oils. Thus, the results indicated the presence of different precursors, of different amounts of precursors, or at least of different conversion rates into crotonaldehyde or acrolein in the analyzed oils (Table 4).

Due to the fact that most of the available quantitative data for crotonaldehyde in different foods are more than 20 years old,[13−18] finally, the three newly developed quantitation methods for crotonaldehyde and acrolein were applied on self-prepared potato chips as well as on donuts. Therefore, thin slices of potatoes and donut dough were deep-fried in rapeseed oil and

Table 3. Influence of the Temperature on the Amounts of Crotonaldehyde (C) and Acrolein (A) Formed from the Five Oils after the Oils were Heated for 24 h

	concn[a] (mg/kg)									
	coconut oil		olive oil		rapeseed oil		safflower oil		linseed oil	
temp (°C)	C	A	C	A	C	A	C	A	C	A
100	<LoQ	0.02[b]	0.04[b]	0.12[b]	4.78[d]	11.2[d]	0.06[b]	0.67[b]	6.30[d]	12.6[d]
140	<LoQ	0.04[b]	1.40[c]	2.88[d]	8.57[d]	14.1[d]	0.37[c]	2.73[c]	22.2[d]	26.8[d]
180	0.32[c]	0.62[c]	1.52[c]	3.74[d]	12.0[d]	23.4[d]	0.64[d]	8.97[d]	34.2[d]	51.7[d]
220	0.55[c]	3.12[d]	1.07[c]	2.66[c]	9.02[d]	17.0[d]	0.83[d]	4.22[d]	22.3[d]	32.2[d]

[a]Headspace GC−MS (method I) was used. Data are mean values of triplicate measurements. [b]Relative standard deviation amounted to not more than 15%. [c]Relative standard deviation amounted to not more than 10%. [d]Relative standard deviation amounted to not more than 5%.

Table 4. Influence of Heating Time on the Amounts of Crotonaldehyde (C) and Acrolein (A) Formed from the Five Oils at 180 °C

	concn[a] (mg/kg)									
	coconut oil		olive oil		rapeseed oil		safflower oil		linseed oil	
time (h)	C	A	C	A	C	A	C	A	C	A
2	0.03[b]	2.14[c]	4.22[c]	10.0[c]	3.44[c]	40.5[d]	1.87[d]	11.1[d]	12.4[d]	76.3[d]
4	0.11[b]	2.40[d]	10.9[d]	17.7[d]	5.20[d]	63.2[d]	3.12[d]	16.1[d]	19.5[d]	92.2[d]
8	0.29[c]	2.82[c]	14.2[d]	12.4[d]	13.0[d]	50.8[d]	4.22[d]	14.6[d]	24.7[d]	97.5[d]
16	0.56[c]	0.74[b]	6.18[d]	6.46[c]	27.5[d]	34.7[d]	2.52[d]	10.0[d]	28.4[d]	76.5[d]
24	0.32[c]	0.62[c]	1.52[c]	3.74[d]	12.0[d]	23.4[d]	0.64[d]	8.97[d]	34.2[d]	51.7[d]
55	0.83[d]	1.01[b]	3.29[d]	4.64[c]	13.5[d]	28.2[d]	1.30[d]	6.81[d]	40.8[d]	53.4[d]

[a]Headspace GC−MS (method I) was used. Data are mean values of triplicate measurements. [b]Relative standard deviation amounted to not more than 15%. [c]Relative standard deviation amounted to not more than 10%. [d]Relative standard deviation amounted to not more than 5%.

in olive oil at 180 °C for 2.5 and 4 min, respectively. As shown in Table 5, crotonaldehyde and acrolein were detected in all samples, but in order of magnitude lower concentrations compared to those in the heated oils. Similar results were obtained for all three methods, again proving the possible use of the quick headspace GC−MS method for both matrixes.

Table 5. Concentrations of Crotonaldehyde (C) and Acrolein (A) in Fried Foods

	concn[a] (μg/kg)					
	method I[b]		method II[c]		method III[d]	
sample	C	A	C	A	C	A
potato chips, prepared in olive oil	12.6[e]	23.1[e]	11.9[e]	22.8[f]	11.5[e]	23.7[f]
potato chips, prepared in rapeseed oil	24.8[f]	26.3[f]	23.8[f]	25.4[e]	23.9[e]	26.2[g]
donuts, prepared in olive oil	<LoQ	14.2[e]	8.15[e]	14.0[e]	8.02[e]	14.4[e]
donuts, prepared in rapeseed oil	18.2[e]	15.4[e]	18.8[g]	14.4[e]	17.7[g]	14.9[e]

[a]Mean values of triplicate measurements. [b]Headspace GC−MS. [c]GC−MS after derivatization with PFPH. [d]LC−MS/MS after derivatization with 2,4-DNPH. [e]Relative standard deviation amounted to not more than 20%. [f]Relative standard deviation amounted to not more than 15%. [g]Relative standard deviation amounted to not more than 10%.

Interestingly, crotonaldehyde concentrations differed both in the heat-processed oils and in the final food (potato chips and donuts) depending on the oil used (e.g., olive oil and rapeseed oil). In contrast, acrolein concentrations were very similar in both potato chips and donuts without reflecting the different oils used for processing (cf. Tables 2−5). A possible explanation for these results might be the higher reactivity of acrolein, reported to be 150-fold higher with the thiol group in glutathione using in vitro systems compared to that of crotonaldehyde.[48] Thus, the differences in acrolein concentrations originally occurring in the various frying media and, consequently, being transferred into the food during the frying process cannot be found in the final products due to a quick formation of acrolein adducts with different food constituents. These data may confirm recent findings by Watzek et al., who recovered higher amounts of acrolein mercapturic acids in human urine after consumption of potato crisps than expected compared to the before analyzed amounts of free acrolein in the crisps.[49] In contrast, for crotonaldehyde, showing less reactivity, these differences seem still to be analyzable in the respective foods (Table 5). In addition, also the generally higher amounts of acrolein formed in all types of frying media in comparison to those of crotonaldehyde were not reflected in the final products.

In summary, the results showed that all three newly developed methods on the basis of stable isotope dilution assays can be used for a simultaneous quantitation of crotonaldehyde and acrolein in frying oils as well as in food. Furthermore, the data suggested that linolenic acid might be an important precursor not only for acrolein but also for crotonaldehyde formation during heat-processing of oils. Thus, oils containing higher amounts of linolenic acid should be more carefully recommended for, e.g., frying purposes. Further studies on the formation pathway of crotonaldehyde are under way.

AUTHOR INFORMATION

Corresponding Author

*Phone: +49-8161-712987. Fax: +49-8161-712970. E-mail: michael.granvogl@ch.tum.de.

Notes

The authors declare no competing financial interest.

ACKNOWLEDGMENTS

I acknowledge the skillful assistance of Jörg Stein. I also thank Ines Otte for performing the LC−MS/MS measurements.

REFERENCES

(1) Chang, S.; Peterson, R.; Ho, C. Chemical reactions involved in deep-fat-frying of foods. *J. Am. Oil Chem. Soc.* **1978**, *55*, 718−727.

(2) Doberganes, M.; Marquez-Ruiz, G. Formation and analysis of oxidized monomeric, dimeric and higher oligomeric triglycerides. In *Deep Frying: Chemistry, Nutrition and Practical Applications*, 2nd ed.; Perkins, E., Erickson, M., Eds.; AOCS Press: Urbana, IL, 1997; pp 89−111.

(3) Frankel, E. Frying fats. In *Lipid Oxidation*; Christie, W., Ed.; The Oily Press: Dundee, Scotland, 1998; pp 227−248.

(4) Buttery, R. G.; Ling, L. C. Characterization of nonbasic steam volatile components of potato chips. *J. Agric. Food Chem.* **1972**, *20*, 698−700.

(5) Gassenmeier, K.; Schieberle, P. Comparison of important odorants in puff-pastries prepared with butter or margarine. *Lebensm.-Wiss. Technol.* **1994**, *27*, 282−288.

(6) Chetschik, I.; Granvogl, M.; Schieberle, P. Quantitation of key peanut aroma compounds in raw peanuts and pan-roasted peanut meal. Aroma reconstitution and comparison with commercial peanut products. *J. Agric. Food Chem.* **2010**, *58*, 11018−11026.

(7) Umano, K.; Shibamoto, T. Analysis of acrolein from heated cooking oils and beef fat. *J. Agric. Food Chem.* **1987**, *35*, 14−18.

(8) Casella, I. G.; Contursi, M. Quantitative analysis of acrolein in heated vegetable oils by liquid chromatography with pulsed electrochemical detection. *J. Agric. Food Chem.* **2004**, *52*, 5816−5821.

(9) Ewert, A.; Granvogl, M.; Schieberle, P. Development of two stable isotope dilution assays for the quantitation of acrolein in heat-processed fats. *J. Agric. Food Chem.* **2011**, *59*, 3582−3589.
(10) Moldoveanu, S.; Coleman, W., III; Wilkins, J. Determination of carbonyl compounds in exhaled cigarette smoke. *Beitr. Tabakforsch. Int.* **2007**, *22*, 346−357.
(11) Lipari, F.; Dasch, J. M.; Scruggs, W. F. Aldehyde emissions from wood-burning fireplaces. *Environ. Sci. Technol.* **1984**, *18*, 326−330.
(12) Schauer, J. J.; Kleeman, M. J.; Cass, G. R.; Simoneit, B. R. T. Measurement of emissions from air pollution sources. 5. C_1−C_{32} organic compounds from gasoline-powered motor vehicles. *Environ. Sci. Technol.* **2002**, *36*, 1169−1180.
(13) Linko, R. R.; Kallio, H.; Pyysalo, T.; Raimo, K. Volatile monocarbonyl compounds of carrot roots at various stages of maturity. *Z. Lebensm.-Unters. Forsch.* **1978**, *166*, 208−211.
(14) Douillard, C.; Guichard, E. The aroma of strawberry (*Fragaria ananassa*): characterisation of some cultivars and influence of freezing. *J. Sci. Food Agric.* **1990**, *50*, 517−531.
(15) Yasuhara, A.; Morita, M. Identification of volatile organic components in mussel. *Chemosphere* **1987**, *16*, 2559−2565.
(16) Seaman, V. Y.; Bennett, D. H.; Cahill, T. M. Indoor acrolein emission and decay rates resulting from domestic cooking events. *Atmos. Environ.* **2009**, *43*, 6199−6204.
(17) Sponholz, W. R. Analysis and occurrence of aldehydes in wines (in German). *Z. Lebensm.-Unters. Forsch.* **1982**, *174*, 458−462.
(18) Miller, B. E.; Danielson, N. D. Derivatization of vinyl aldehydes with anthrone prior to high-performance liquid chromatography with fluorimetric detection. *Anal. Chem.* **1988**, *60*, 622−626.
(19) Neudecker, T.; Lutz, D.; Eder, E.; Henschler, D. Crotonaldehyde is mutagenic in a modified *Salmonella typhimurium* mutagenicity testing system. *Mutat. Res.* **1981**, *91*, 27−31.
(20) Eder, E.; Henschler, D.; Neudecker, T. Mutagenic properties of allylic and α,β-unsaturated compounds: consideration of alkylating mechanisms. *Xenobiotica* **1982**, *12*, 831−848.
(21) Woodruff, R. C.; Mason, J. M.; Valencia, R.; Zimmering, S. Chemical mutagenesis testing in *Drosophila*. V. Results of 53 coded compounds tested for the National Toxicology Program. *Environ. Mutagen.* **1985**, *7*, 677−702.
(22) Kawanishi, M.; Matsuda, T.; Sasaki, G.; Yagi, T.; Matsui, S.; Takebe, H. A spectrum of mutations induced by crotonaldehyde in shuttle vector plasmids propagated in human cells. *Carcinogenesis* **1998**, *19*, 69−72.
(23) Steinhagen, W. H.; Barrow, C. S. Sensory irritation structure-activity study of inhaled aldehydes in B6C3F1 and Swiss-Webster mice. *Toxicol. Appl. Pharmacol.* **1984**, *72*, 495−503.
(24) Chung, F.-L.; Tanaka, T.; Hecht, S. S. Induction of liver tumors in F344 rats by crotonaldehyde. *Cancer Res.* **1986**, *46*, 1285−1289.
(25) Chen, H.-J. C.; Chung, F.-L. Formation of etheno adducts in reactions of enals via autoxidation. *Chem. Res. Toxicol.* **1994**, *7*, 857−860.
(26) Chung, F.-L.; Young, R.; Hecht, S. S. Formation of cyclic 1,N^2-propanodeoxyguanosine adducts in DNA upon reaction with acrolein or crotonaldehyde. *Cancer Res.* **1984**, *44*, 990−995.
(27) Foiles, P. G.; Akerkar, S. A.; Miglietta, L. M.; Chung, F. L. Formation of cyclic deoxyguanosine adducts in Chinese hamster ovary cells by acrolein and crotonaldehyde. *Carcinogenesis* **1990**, *11*, 2059−2061.
(28) Marnett, L. J. DNA adducts of α,β-unsaturated aldehydes and dicarbonyl compounds. In *DNA Adducts: Identification and Biological Significance*; Hemminki, K., Dipple, A., Shuker, D. E. G., Kadlubar, F. F., Segerbäck, D., Bartsch, H., Eds.; International Agency for Research and Cancer (WHO): Lyon, France, 1994; pp 151−163.
(29) Esterbauer, H.; Shaur, R.; Zollner, H. Chemistry and biochemistry of 4-hydroxynonenal, malonaldehyde and related aldehydes. *Free Radical Biol. Med.* **1991**, *11*, 81−128.
(30) Wang, M.; Nishikawa, A.; Chung, F.-L. Differential effects of thiols on DNA modifications via alkylation and Michael addition by α-acetoxy-*N*-nitrosopyrrolidine. *Chem. Res. Toxicol.* **1992**, *5*, 528−531.
(31) Colombo, G.; Aldini, G.; Orioli, M.; Giustarini, D.; Gornati, R.; Rossi, R.; Colombo, R.; Carini, M.; Milzani, A.; Dalle-Donne, I. Water-soluble α,β-unsaturated aldehydes of cigarette smoke induce carbonylation of human serum albumin. *Antioxid. Redox Signaling* **2010**, *12*, 349−364.
(32) *Integrated Risk Information System*; US Environmental Protection Agency: Chicago, IL, 1991; Crotonaldehyde, CASRN 123-73. http://www.epa.gov/iris/subst/0464.htm (accessed October 29, 2013).
(33) International Agency for Research on Cancer. Crotonaldehyde. *IARC Monogr. Eval. Carcinog. Risks Hum.* **1995**, *63*, 373−391.
(34) Fujisaki, M.; Endo, Y.; Fujimoto, K. Retardation of volatile aldehyde formation in the exhaust of frying oil by heating under low oxygen atmospheres. *J. Am. Oil Chem. Soc.* **2002**, *79*, 909−914.
(35) Lin, Y.-L.; Wang, P.-Y.; Hsieh, L.-L.; Ku, K.-H.; Yeh, Y.-T.; Wu, C.-H. Determination of linear aliphatic aldehydes in heavy metal containing waters by high-performance liquid chromatography using 2,4-dinitrophenylhydrazine derivatization. *J. Chromatogr., A* **2009**, *1216*, 6377−6381.
(36) Wang, Q.; O'Reilly, J.; Pawliszyn, J. Determination of low-molecular mass aldehydes by automated headspace solid-phase microextraction with in-fibre derivatisation. *J. Chromatogr., A* **2005**, *1071*, 147−154.
(37) Steinhaus, M.; Fritsch, H.; Schieberle, P. Quantitation of (*R*)- and (*S*)-linalool in beer using solid phase microextraction (SPME) in combination with a stable isotope dilution assay (SIDA). *J. Agric. Food Chem.* **2003**, *51*, 7100−7105.
(38) Schieberle, P.; Grosch, W. Quantitative analysis of aroma compounds in wheat and rye bread crusts using a stable isotope dilution assay. *J. Agric. Food Chem.* **1987**, *35*, 252−257.
(39) Jezussek, M.; Schieberle, P. A new LC/MS-method for the quantitation of acrylamide based on a stable isotope dilution assay and derivatization with 2-mercaptobenzoic acid. Comparison with two GC/MS methods. *J. Agric. Food Chem.* **2003**, *51*, 7866−7871.
(40) Goldmann, T.; Perisset, A.; Scanlan, F.; Stadler, R. H. Rapid determination of furan in heated foodstuffs by isotope dilution solid phase micro-extraction-gas chromatography - mass spectrometry (SPME-GC-MS). *Analyst* **2005**, *130*, 878−883.
(41) Granvogl, M.; Koehler, P.; Latzer, L.; Schieberle, P. Development of a stable isotope dilution assay for the quantitation of glycidamide and its application to foods and model systems. *J. Agric. Food Chem.* **2008**, *56*, 6087−6092.
(42) Granvogl, M.; Ahlig, S.; Ewert, A.; Schieberle, P. Development of a stable isotope dilution analysis for the quantification of crotonaldehyde in fried foods (in German). In *41. Deutscher Lebensmittelchemikertag*; Gesellschaft Deutscher Chemiker e.V., Seltersdruck & Verlag Lehn: Niederselters, Germany, 2012; p 84.
(43) Granvogl, M.; Schieberle, P. Desirable (aroma-active) and undesirable (food-borne toxicants) bio-actives in foods: formation and analysis. *Abstracts of Papers*, 246th ACS National Meeting & Exposition, Indianapolis, IN, Sept 8−12, 2013; American Chemical Society: Washington, DC, 2013; AGFD-4.
(44) International Union of Pure and Applied Chemistry (IUPAC). *Standard Methods for the Analysis of Oils, Fats and Derivatives*, 7th revised and enlarged ed.; Paquot, C., Hautfenne, A., Eds.; Blackwell Scientific Publications: London, U.K., 1987.
(45) Engel, W.; Bahr, W.; Schieberle, P. Solvent assisted flavour evaporation—a new and versatile technique for the careful and direct isolation of aroma compounds from complex food matrices. *Eur. Food Res. Technol.* **1999**, *209*, 237−241.
(46) Da Silva, T.; Pereira, P. Influence of time, surface-to-volume ratio, and heating process (continuous or intermittent) on the emission rates of selected carbonyl compounds during thermal oxidation of palm and soybean oils. *J. Agric. Food Chem.* **2008**, *56*, 3129−3135.
(47) Fullana, A.; Carbonell-Barrachina, A.; Sidhu, S. Comparison of volatile aldehydes present in the cooking fumes of extra virgin olive, olive, and canola oils. *J. Agric. Food Chem.* **2004**, *52*, 5207−5214.
(48) Witz, G. Biological interactions of α,β-unsaturated aldehydes. *Free Radical Biol. Med.* **1989**, *7*, 333−349.

(49) Watzek, N.; Scherbl, D.; Feld, J.; Berger, F.; Doroshyenko, O.; Fuhr, U.; Tomalik-Scharte, D.; Baum, M.; Eisenbrand, G.; Richling, E. Profiling of mercapturic acids of acrolein and acrylamide in human urine after consumption of potato crisps. *Mol. Nutr. Food Res.* **2012**, *56*, 1825−1837.

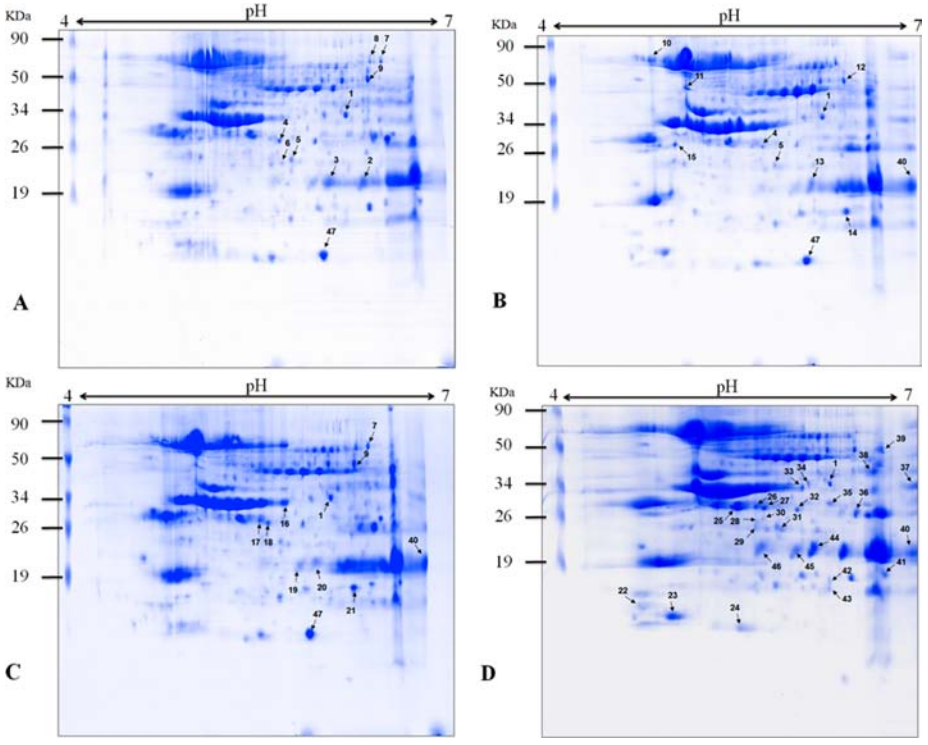

Figure 1. Two-dimensional electrophoresis was carried out using a narrow-range 18 cm IPG strip of pH 4−7: analyses of the proteins extracted using a thiourea/urea protocol from *Glycine max* cultivars (A) BRS 257, (B) BRS 258, (C) Embrapa 48, and (D) BRS 267. Identical numbers refer to the same spots, and distinct numbers correspond to differential spots present in each cultivar. The sizes of the protein markers in kilodaltons (kDa) are shown at the left of the images.

administration of these proteins in hypercholesterolemic rats.[18] Zhang et al.[19] demonstrated that hydrolyzed soybean proteins reduced the plasma level of very low-density lipoproteins cholesterol and triglycerides in mice. Additionally, the 11S globulin has hypotensive effects that are attributed to its ability to inhibit the angiotensin I-converting enzyme.[20] Peptides derived from the 7S globulin can act as blockers of fatty acid synthase, an enzyme present in large quantities in diseases such as cancer, obesity, and other metabolic disorders.[21]

Because of their health benefits, especially in the prevention and treatment of noncommunicable diseases, soybean proteins are the only proteins to offer benefits for cardiovascular disease that are certified by the American Dietetic Association (ADA).[22] According to the ADA, soybean products that provide 6.25 g of soy protein per serving are allowed to state on the label that "25 g of soy protein a day as part of a diet low in saturated fat and cholesterol may reduce the risk of coronary heart disease". The consumption of 3−4 tablespoons of soybeans (56−67 g of grains) each day meets the FDA requirements regarding the ingestion of 25 g of protein.

Despite the nutritional and functional properties mentioned above, the consumption of soybeans in Brazil is limited due to the characteristic flavor caused by lipoxygenases, which oxidize lipids and cause a beany flavor. In addition, gastrointestinal distress may be caused by the presence of oligosaccharides, raffinose, stachyose, phytic acid, and protease inhibitors.[23] *Embrapa-Soja*, *Empresa Brasileira de Pesquisa Agropecuária*, developed conventional cultivars in 2008 to stimulate consumption.[24] These cultivars were obtained by crossing different varieties to mitigate flavor and improve nutritional value. This process resulted in lipoxygenase-free grains with higher levels of carbohydrates and improved protein content.

The use of proteomics in nutrition is diverse and offers different possibilities for nutritional interventions of great value. The proteome study represents an important tool when associated with nutrigenomics as it provides insights into promises of future dietary approaches.[25] One proteomic strategy is the separation of proteins by polyacrylamide gel electrophoresis (in one or two dimensions), followed by the analysis and identification of proteins by mass spectrometry.[26] Another approach is a combination of liquid chromatography and mass spectrometry, which has become a powerful approach for the identification of proteins and peptides occurring in complex mixtures.[27]

The production of conventional plants with improved sensory qualities and nutritional characteristics is an important strategy to increase soybean consumption. However, the impact of these changes and the soybean improvements should be investigated by methods such as comparative analysis of protein expression profiles. This analysis will allow for the determination of the legume proteins that interfere with the nutritional and functional properties. We analyzed the protein profiles of four conventional soybean seeds (BRS 257, BRS 258, Embrapa 48, and BRS 267) using proteomic tools.

MATERIALS AND METHODS

Plant Materials. *G. max* seeds were kindly donated by the *Empresa Brasileira de Pesquisa Agropecuária* (EMBRAPA - Soja, Londrina, PR, Brazil). The cultivars used in this study were the following: BRS 257, BRS 258, EMBRAPA 48, and BRS 267. The grains of these four cultivars were ground in a mechanical mill (Retsch ZM 1) using a metallic sieve with a pore size of 0.5 mm until a fine powder was obtained. The samples were stored at −20 °C until analysis.

Extraction of Proteins from Seeds. The samples were delipidated with hexane until a colorless supernatant was obtained and then

Table 1. Soybean Seed Proteins Identified by MALDI-TOF-TOF

SID[a]	protein[b]	NCBI accession no.	MW/p*I*[c]	BRS 257	BRS 258	EMBRAPA 48	BRS 267
1	35 kDa seed maturation protein	gil351726750	35.320/5.96	+[d]	+	+	+
2	glycinin G1/A1aBx	gil225651	56.284/5.78	+	−	−	−
3	glycinin G1/A1aBx	gil225651	56.284/5.78	+	−	−	−
	glycinin G2/A2B1 precursor	gil351725363	54.927/5.46				
	glycinin G4/A5A4B3 subunit	gil126144648	64.196/5.17				
4	lectin (soybean agglutinin)	gil6729836	27.555/5.15	+	+	−	−
5	allergen Gly m Bd 28K	gil12697782	52.780/5.73	+	+	−	−
6	allergen Gly m Bd 28K	gil12697782	52.780/5.73	+	−	−	−
7	seed biotinylated protein 68 kDa isoform	gil240254706	67.963/6.18	+	−	+	−
8	seed biotinylated protein 68 kDa isoform	gil240254706	67.963/6.18	+	−	−	−
9	embryonic protein DC-8-like	gil356533407	48.766/6.12	+	−	+	−
10	α-subunit of β-conglycinin	gil9967361	65.160/5.23	−	+	−	−
11	glycinin G4/A5A4B3 subunit	gil121279	64.005/5.29	−	+	−	−
12	sucrose binding protein homologue S-64	gil6179947	56.142/6.32	−	+	−	−
13	glycinin G1/A1aBx	gil225651	56.284/5.78	−	+	−	−
	glycinin G2/A2B1 precursor	gil351725363	54.927/5.46				
14	seed maturation protein PM31	gil351722245	17.907/6.10	−	+	−	−
15	seed maturation protein PM25	gil6648966	25.827/4.99	−	+	−	−
	seed maturation protein PM26	gil351721132	26.201/4.83				
16	alcohol dehydrogenase	gil4039115	37.042/6.13	−	−	+	−
17	glycinin G2/A2B1 precursor	gil351725363	54.927/5.46	−	−	+	−
18	lectin (soybean agglutinin)	gil6729836	27.555/5.15	−	−	+	−
19	lectin (soybean agglutinin)	gil6729836	27.555/5.15	−	−	+	−
20	glycinin G1/A1aBx	gil225651	56.284/5.78	−	−	+	−
21	glycinin G1/A1aBx	gil225651	56.284/5.78	−	−	+	−
	glycinin G2/A2B1 precursor	gil351725363	54.927/5.46				
22	Kunitz trypsin inhibitor subtype B	gil125023	20.256/4.66	−	−	−	+
	Kunitz-type trypsin inhibitor KTI1	gil125722	22.817/4.97				
23	Kunitz trypsin inhibitor subtype B	gil125023	20.256/4.66	−	−	−	+
24	2S albumin precursor	gil351727517	19.018/5.20	−	−	−	+
25	lectin (soybean agglutinin)	gil6729836	27.555/5.15	−	−	−	+
26	lectin (soybean agglutinin)	gil6729836	27.555/5.15	−	−	−	+
27	glycinin G1/A1aBx	gil225651	56.284/5.78	−	−	−	+
	lectin (soybean agglutinin)	gil6729836	27.555/5.15				
28	lectin (soybean agglutinin)	gil6729836	27.555/5.15	−	−	−	+
29	allergen Gly m Bd 28K	gil12697782	52.780/5.73	−	−	−	+
30	allergen Gly m Bd 28K	gil12697782	52.780/5.73	−	−	−	+
31	allergen Ara h 1, clone P41B-like	gil356538162	82.003/5.32	−	−	−	+
32	allergen Gly m Bd 28K	gil12697782	52.780/5,73	−	−	−	+
33	uncharacterized protein LOC100305847	gil351724719	27.847/5.72	−	−	−	+
34	glycinin G1/A1aBx	gil225651	56.284/5.78	−	−	−	+
	glycinin G2 precursor	gil351725363	54.927/5.46				
35	isoflavone reductase homologue 2	gil351726399	33.919/5.60	−	−	−	+
36	glucose and ribitol dehydrogenase homologue 1	gil356505868	32.147/5.34	−	−	−	+
37	7S seed globulin precursor	gil1401240	47.006/8.68	−	−	−	+
38	glycinin G2 precursor	gil351725363	54.927/5.46	−	−	−	+
39	glyceraldehyde-3-dehydrogenase C subunit	gil351723699	36.815/6.72	−	−	−	+
40	elongation factor 1-α-like isoform 1	gil356558807	49.717/9.14	−	+	−	+

Table 1. continued

SID[a]	protein[b]	NCBI accession no.	MW/p*I*[c]	BRS 257	BRS 258	EMBRAPA 48	BRS 267
41	glycinin G1/A1aBx	gil225651	56.284/5.78	−	−	−	+
	glycinin G2 precursor	gil351725363	54.927/5.46				
42	glycinin G1/A1aBx	gil225651	55.657/5.78	−	−	−	+
43	18.2 kDa class I heat shock protein	gil356501111	17.283/6.75	−	−	−	+
44	glycinin G2 precursor	gil351725363	54.927/5.46	−	−	−	+
	glycinin G1/A1aBx	gil225651	56.284/5.78				
45	glycinin G2 precursor	gil351725363	54.927/5.46	−	−	−	+
46	glycinin G1/A1aBx	gil225651	56.284/5.78	−	−	−	+
47	glycinin	gil18641	64.35/5.21	+	+	+	−

[a]Number of spot identified. [b]Proteins identified by MALDI-TOF-TOF. [c]Molecular weight (MW) and isoelectric point (p*I*). [d]"+" indicates the presence of a spot and "−" the absence of a spot in the soybean cultivar. Protein spot data for this analysis were recorded (Supporting Information).

lyophilized. A 50 mg lyophilized sample was added to 495 μL of buffer containing 5 M urea, 2 M thiourea, 4% CHAPS, 65 mM DTT, 0.8% ampholytes at either pH 3−10 or pH 4−7, and 0.002% bromophenol blue. A 5 μL aliquot of a protease inhibitor cocktail (made up of 104 mM benzenesulfonyl fluoride hydrochloride, 80 μM aprotinin, 4 mM bestatin hydrochloride, 1.4 mM E-64, 2 mM leupeptin, and 1.5 mM pepstatin A) was added. After sonication for 20 min, the samples were centrifuged at 13000*g* for 15 min at room temperature, and supernatants were stored at −80 °C according to the methodology described by Herman et al.[28] with modifications. The protein content was determined using the protocol described by Peterson.[29]

One-Dimensional Gel Electrophoresis (1D SDS-PAGE). For 1D analysis, 90 μg of protein from each cultivar that had been previously extracted using a thiourea/urea method was applied to three lanes (30 μg in each lane) of a 12% SDS-PAGE gel (8.3 × 7.3 cm dimensions). The gels were fixed and stained with CBB G-250. One-dimensional separation was performed following the method described by Laemmli.[30] The experiments were performed with biological triplicates. After the image analysis, each lane was arbitrarily divided into approximately 2.5 mm slices and subjected to in-gel proteolysis with trypsin.

Two-Dimensional Gel Electrophoresis (2D SDS-PAGE). One milligram of soybean protein that had been extracted using a thiourea/urea method was applied to 18 cm IPG strips. The first dimension (isoelectric focusing) was performed using linear IPG strips that covered a pH range of 4.0−7.0 in an Ettan IPGphor (Amersham Biosciences) with the following program: 12 V for 12 h (rehydration), 200 V for 1 h, 500 V for 1 h, 1000 V for 1 h, 4000 V for 0.5 h, and 75067 V for 9.38 h. For the second dimension, the IPG strips were incubated with 50 mM Tris-HCl (pH 8.8), 6 M urea, 30% glycerol, 2% SDS, 0.002% bromophenol blue, and 65 mM DTT for 15 min. The strips were alkylated with iodoacetamide (25 mg/mL) and subsequently placed onto 15% polyacrylamide gels. The gels were run in a DALTsix system (GE Healthcare) at 2.5 W/gel for 30 min followed by 100 W for six gels until the end of the run. The reference gel was obtained after the analysis of biological triplicates. The experiments were performed in technical triplicates.

Gel Staining, Scanning, and Image Analysis. After 2D gel electrophoresis, gels were kept for 20 min in a fixation solution (2% orthophosphoric acid and 30% ethanol), washed with 2% orthophosphoric acid, and stained with a solution containing 2% orthophosphoric acid, 15% ammonium sulfate, 18% ethanol, and 0.002% CBB G-250. Direct scanning and image analysis were performed using an ImageScanner with ImageMaster 2D Platinum software (GE Healthcare). For MALDI-TOF/TOF mass spectrometry analysis, the presence or absence of spots in each cultivar was considered.

In-Gel Digestion. Each 1D gel band or 2D gel spot was excised, cut into smaller pieces, and destained overnight with a solution of 25 mM NH_4HCO_3 and 50% acetonitrile (ACN) at pH 8.0. For 1D gels, protein

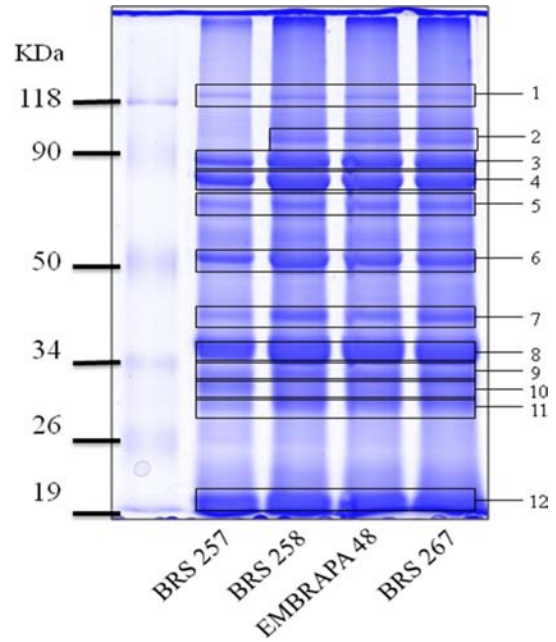

Figure 2. 1D SDS-PAGE analysis of protein extracts suitable for 2D SDS-PAGE from BRS 257, BRS 258, Embrapa 48, and BRS 267. Excised bands are identified at the right of the gel (numbered 1−12). The sizes of the protein markers in kilodaltons (kDa) are shown at the left of the figure.

disulfide bonds were reduced with 10 mM DTT in 25 mM NH_4HCO_3 at 56 °C for 1 h. The supernatant was then removed, and the gel pieces were incubated with 55 mM iodoacetamide for 30 min at room temperature in the dark. The pieces were washed with 25 mM NH_4HCO_3 to remove excess reagent. Finally, the 1D and 2D gel pieces were dehydrated with 100% ACN for 5 min and dried completely using a Speed-Vac system. The excised spots and bands were then rehydrated in 15 μL of digestion buffer containing 10 ng/μL of trypsin (Promega, modified sequencing grade) in 25 mM NH_4HCO_3 in an ice-cold bath for 10 min. The digestion was performed at 37 °C for 20 h. Following the incubation, the microcentrifuge tubes containing the samples were centrifuged, and 4 μL of 1% formic acid was added. The liquid from each gel piece was transferred into a clean microcentrifuge tube. The peptides were extracted from the gel pieces twice by incubation with 50% ACN in 5% trifluoroacetic acid (TFA) for 30 min. The resulting solutions from the two extractions were pooled together and concentrated to near dryness using a Speed-Vac system. Each sample was then solubilized in 20 μL of deionized water. Prior to mass spectrometry, peptides were

Table 2. Soybean Seed Proteins Identified by ESI-Q-TOF Mass Spectrometry

band[a]	protein[b]	NCBI accession no.	MM/pI[c]	BRS 257	BRS 258	EMBRAPA 48	BRS 267
1	α-subunit of β-conglycinin	gil9967357	63.184/4.92	+[d]	+	+	+
	uncharacterized protein LOC100780139	gil356515096	117.977/8.55	+	+	−	+
	uncharacterized protein LOC100801440	gil356561627	96.970/5.94	+	+	−	+
	β-subunit of β-conglycinin	gil356575855	50.468/5.88	+	+	−	+
	glycinin G1/A1aBx	gil225651	56.284/5.78	+	−	−	+
	glycinin G2 precursor	gil351725363	54.927/5.46	+	+	−	−
	P24 oleosin isoform B	gil351722277	23.378/8.89	+	−	−	+
	sucrose-binding protein-like	gil356536206	58.353/6.08	+	+	-	+
	P24 oleosin isoform A	gil356571311	23.575/8.89	+	-	-	+
	seed maturation protein PM39	gil5802248	46.665/5.69	+	+	−	+
	lipoxygenase 2	gil126404	97.370/6.27	−	−	−	+
	lipoxygenase 3	gil126406	97.970/5.94	−	−	−	+
	glycinin G5/A3B4 subunit	gil126144646	58.120/5.78	−	−	−	+
	lipoxygenase 1	gil351727907	94.580/5.91	−	−	−	+
2	lipoxygenase 3	gil161318157	97.107/6.12	−	+	+	+
	lipoxygenase 2	gil295388395	97.472/6.15	−	+	+	+
	chain a lipoxygenase-1 (soybean) i553l mutant	gil171849009	94.580/5.91	−	+	+	+
	seed linoleate 9S-lipoxygenase-2	gil356525977	97.082/6.70	−	+	−	−
	α-subunit of β-conglycinin	gil9967357	63.184/4.92	−	+	−	−
	α-subunit of β-conglycinin	gil9967357	63.184/4.92	−	−	−	+
	lipoxygenase 5	gil161318161	91.337/6.08	−	+	−	−
	glycinin G1/A1aBx	gil225651	56.284/5.78	−	+	−	−
	lipoxygenase 9	gil351724717	96.637/6.54	−	+	+	+
	β-subunit of β-conglycinin	gil356575855	50.468/5.88	−	−	+	−
	lipoxygenase 10	gil351725145	97.419/5.99	−	+	−	−
3	α-subunit of β-conglycinin	gil9967361	65.161/5.23	+	+	+	+
	β-subunit of β-conglycinin	gil356575855	50.468/5.88	+	+	+	+
	heat shock protein 90-1	gil351726363	80.700/4.94	+	+	+	+
	methionine synthase	gil351724907	84.401/5.93	+	−	+	+
	glycinin G1/A1aBx	gil225651	56.284/5.78	+	+	+	−
	5-methyltetrahydropteroyltriglutamate-homocysteine methyltransferase-like	gil356508448	89.065/6.41	−	−	+	+
	heat shock protein 83-like	gil356530818	80.624/4.96	+	−	+	−
	24 kDa oleosin isoform	gil18720	15.801/8.23	+	−	−	−
	sucrose-binding protein-like	gil356536206	58.353/6.08	+	+	+	+
	glycinin G4/A5A4B3 subunit	gil255224	64.097/5.38	+	−	−	−
	glycinin G5/A3B4 subunit	gil126144646	58.120/5.78	−	+	+	+
	uncharacterized protein LOC100527853	gil351720923	16.490/9.78	−	+	−	−
	lipoxygenase 3	gil161318157	97.107/6.12	−	−	−	+
	lipoxygenase 2	gil126404	97.370/6.27	−	−	−	+
	lipoxygenase 1	gil351727907	94.538/5.95	−	−	−	+
4	α-subunit of β-conglycinin	gil9967357	63.184/4.92	+	+	+	+
	β-subunit of β-conglycinin	gil356575855	50.468/5.88	+	+	+	+
	seed biotinylated protein 68 kDa isoform	gil240254706	67.963/6.18	−	+	+	+
	heat shock 70 kDa protein-like	gil356500683	71.981/5.20	+	−	+	+
	endoplasmic reticulum HSC70-cognate binding protein precursor	gil2642238	73.822/5.15	+	+	+	+
	sucrose-binding protein-like	gil356536206	58.353/6.08	+	+	+	+
	glycinin G2 precursor	gil351725363	54.927/5.46	+	−	+	+
	glycinin G1/A1aBx	gil225651	56.284/5.78	+	+	+	+
	glycinin G4/A5A4B3 subunit	gil255224	64.097/5.38	+	+	+	−
	glycinin G3/A1ab1B subunit	gil121278	54.835/5.73	−	−	+	−
	glycinin G5/A3B4 subunit	gil126144646	58.120/5.78	−	−	−	+
	glycyl-tRNA synthetase 1 mitochondrial-like	gil356527475	81.691/7.03	−	−	+	+
5	sucrose-binding protein-like	gil356536206	58.353/6.08	+	+	+	+
	α-subunit of β-conglycinin	gil9967357	63.184/4.92	+	+	+	+
	β-subunit of β-conglycinin	gil341603993	50.044/6.14	−	+	−	−

dx.doi.org/10.1021/jf404351g | J. Agric. Food Chem. 2014, 62, 1283−1293

Table 2. continued

band[a]	protein[b]	NCBI accession no.	MM/pI[c]	BRS 257	BRS 258	EMBRAPA 48	BRS 267
	protein disulfide isomerase	gil171854980	58.953/5.13	−	−	+	+
	glycinin G1/A1aBx	gil225651	56.284/5.78	−	−	−	+
	lipoxygenase 3	gil161318157	97.107/6.12	−	−	−	+
6	β-subunit of β-conglycinin	gil341603993	50.044/6.14	+	+	+	+
	α-subunit of β-conglycinin	gil9967361	65.160/5.23	+	+	+	+
	unknown	gil255636348	50.590/5.81	−	+	−	−
	elongation factor 1-α	gil1352345	49.689/9.14	−	+	+	−
	uncharacterized protein LOC100794313	gil359807071	43.082/6.28	−	−	+	+
	glycinin	gil18641	64.351/5.21	−	−	+	−
	pea protein precursor	gil351727923	49.484/7.08	−	−	+	−
	uncharacterized protein LOC100797606	gil359807483	42.140/6.90	−	−	−	+
7	glyceraldehyde-3-dehydrogenase C subunit	gil351723699	36.815/6.72	+	+	+	+
	glycinin G5/A3B4 subunit	gil126144646	58.120/5.78	−	+	+	+
	glycinin G1/A1aBx	gil225651	56.284/5.78	−	+	+	+
	fructose-bisphosphate aldolase. cytoplasmic isozyme-like	gil356500825	38.469/7.12	−	−	+	+
	α-subunit of β-conglycinin	gil9967357	63.184/4.92	−	−	−	+
	glycinin G2 precursor	gil351725363	54.927/5.46	−	−	−	+
	hydroxysteroid 11-β-dehydrogenase 1-like protein-like	gil356539128	40.972/5.89	−	−	−	+
	β-subunit of β-conglycinin	gil356575855	50.468/5.88	−	−	−	+
	P24 oleosin isoform A	gil356571311	23.575/8.89	−	−	−	+
	seed maturation protein PM34	gil351722943	32.032/6.60	−	−	−	+
	cytosolic malate dehydrogenase	gil351727793	35.846/6.32	−	−	−	+
	P24 oleosin isoform B	gil351722277	23.378/8.89	−	−	−	+
	Kunitz trypsin inhibitor subtype B	gil125023	20.256/4.66	−	−	−	+
8	glycinin G1/a1ab1b	gil356505023	56.299/5.89	+	+	+	+
	glycinin G2 precursor	gil351725363	54.927/5.46	+	+	+	+
	glycinin G4/A5A4B3 subunit	gil255224	64.351/5.21	+	−	+	−
	seed maturation protein PM34	gil351722943	32.032/6.60	−	+	−	−
9	lectin (soybean agglutinin)	gil6729836	27.555/5.15	+	+	+	+
	glycinin G2 precursor	gil351725363	54.927/5.46	−	+	−	+
	uncharacterized protein LOC100806472	gil363807732	36.000/7.72	−	+	+	−
	glycinin G1/A1aBx	gil225651	56.284/5.78	−	+	+	+
	uncharacterized protein LOC100809384	gil359807588	32.097/6.38	−	+	−	−
	P24 oleosin isoform A	gil1709459	23.487/8.01	−	+	−	−
	seed maturation protein PM34	gil351722943	32.032/6.60	−	+	−	−
	P24 oleosin isoform B	gil351722277	23.378/8.89	−	+	−	−
	dehydrin	gil119709430	25.370/6.10	−	+	−	−
	seed maturation protein PM34	gil351722943	32.032/6.60	−	−	+	−
10	lectin (soybean agglutinin)	gil6729836	27.555/5.15	+	−	+	+
	glycinin G1/A1aBx	gil225651	56.284/5.78	+	−	−	−
	uncharacterized protein LOC100809384	gil359807588	32.097/6.38	−	+	−	+
	glycinin G2 precursor	gil351725363	54.927/5.46	−	+	−	−
	seed maturation protein PM26	gil351721132	26.201/4.83	−	−	+	−
	ribosomal protein L2	gil351723983	28.224/10.45	−	−	−	+
	7S seed globulin precursor	gil1401240	47.006/8.68	−	−	−	+
11	7S seed globulin precursor	gil1401240	47.006/8.68	−	+	−	−
	dehydrin	gil37495451	23.774/5.97	−	+	+	+
	7S seed globulin precursor	gil1401240	47.006/8.68	−	−	+	−
	glycinin G2 precursor	gil351725363	54.927/5.46	−	−	−	+
	glycinin G1/A1aBx	gil225651	56.284/5.78	−	−	−	+
12	glycinin G1/A1aBx	gil225651	56.284/5.78	+	−	+	+
	glycinin G4 subunit	gil255224	64.097/5.38	+	−	+	+
	glycinin G5/A3B4 subunit	gil126144646	58.120/5.78	+	−	+	+

Table 2. continued

band[a]	protein[b]	NCBI accession no.	MM/pI[c]	BRS 257	BRS 258	EMBRAPA 48	BRS 267
	glycinin G2 precursor	gil351725363	54.927/5.46	+	−	+	+
	Kunitz trypsin inhibitor subtype B	gil125023	20.256/4.66	−	−	−	+
	Kunitz trypsin inhibitor subtype A precursor	gil351724949	24.275/4.99	+	−	−	−
	Kunitz-type trypsin inhibitor KTI1	gil125722	22.817/4.97	−	−	+	+
	Kunitz-type trypsin inhibitor KTI2	gil125723	23.071/6.14	−	−	−	+
	7S seed globulin precursor	gil1401240	47.006/8.68	+	−	+	+
	glycinin G3 precursor	gil99909	54.953/5.28	+	−	+	−
	soybean trypsin inhibitor	gil3318877	20.310/4.61	−	−	+	−
	2S albumin precursor	gil351727517	19.018/5.20	−	−	−	+

[a]Number of band identified. [b]Proteins identified by ESI-Q-TOF mass spectrometry. [c]Molecular weight (MW) and isoelectric point (p*I*). [d]"+" indicates the presence of a protein and "−" the absence of a protein in the soybean cultivar band. Protein band data for this analysis were recorded (Supporting Information).

desalted using a mini-reverse phase column PerfectPure C-18 Tip (Eppendorf). The tips were conditioned in 100% acetonitrile and washed three times with water. The peptide solution was aspirated and expelled from the tips 10 times. After three washings of the tip with water, the peptides were eluted with 50% ACN. The samples were dried using a Speed-Vac system and resuspended in solution of 0.1% formic acid and 3% ACN.

MALDI-TOF/TOF Mass Spectrometry Analysis. The mass spectrometry (MS) and tandem mass spectrometry (MS/MS) experiments were performed using a 5800 Proteomics Analyzer (Applied Biosystems, Foster City, CA). Approximately 0.6 μL of the extracted peptide solution was mixed with an equal volume of α-cyano-4-hydroxycinnamic acid matrix solution (Aldrich, Milwaukee, WI, USA) at 10 mg/mL in 50% ACN/0.1% TFA. Samples were placed on the target plate and allowed to dry at room temperature. Both MS and MS/MS data were acquired with a neodymium-doped yttrium aluminum garnet (Nd:YAG) laser with a 200 Hz repetition rate. Typically, 1600 shots were accumulated for spectra in the MS mode and 2400 shots were accumulated for spectra in the MS/MS mode. MS and MS/MS spectra were acquired in reflector mode. Up to eight of the most intense ion signals with signal-to-noise ratios above 30 were selected as precursors for MS/MS acquisition. The external calibration in MS mode was performed using a mixture of the following four peptides: des-Arg1-bradykinin (m/z 904.468), angiotensin I (m/z 1296.685), Glu1-fibrinopeptide B (m/z 1570.677), and adrenocorticotropic hormone (18−39) (m/z 2465.199). MS/MS spectra were externally calibrated using known fragment ion masses observed in the MS/MS spectrum of angiotensin I.

ESI-Q-TOF Mass Spectrometry Analysis. The peptides extracted from the 1D gel slices were desalted and fractionated by liquid chromatography (LC) coupled online with an electrospray ionization quadrupole time-of-flight mass spectrometer (ESI-Q-TOF). A 7.5 μL aliquot of the sample was loaded on a Waters nanoACQUITY UPLC System (Waters, Milford, MA, USA) with a Waters symmetry C18 trap column coupled to a Q-Tof MicroMass spectrometer. Afterward, the peptides were fractioned by a nanoEase BEH 130 C18 100 mm × 100 μm column (Waters) at a flow rate of 0.5 μL/min and eluted with a linear acetonitrile gradient (from 10 to 40%) of 0.1% formic acid. The ESI voltage was set at 3.5 kV using a metal needle. The source temperature was 80 °C, and the cone voltage was 40 V. Instrument control and data acquisition were conducted using a MassLynx data system (version 4.1, Waters). The experiments were performed by scanning a mass-to-charge ratio (m/z) of 300−2000 using a scan time of 1 s during the entire chromatographic process. A maximum of three ions with charge states of 2, 3, or 4 were selected for MS/MS from a single MS survey. Collision-induced dissociation (CID) MS/MS spectra were obtained using argon as the collision gas at a pressure of 1 bar. The collision voltage varied between 22 and 60 eV depending on the mass and charge of the precursor. The reference ion used was the monocharged ion m/z 588.8692 of phosphoric acid. Mass spectra corresponding to each signal from the total ion current (TIC) chromatogram were averaged, allowing for an accurate molecular mass determination. Exact mass MS/MS was automatically determined using the LockSpray source (Waters).

The acquired peak lists were analyzed by searching the National Center for Biotechnology Information (NCBI) database using the MASCOT search engine (www.matrixscience.com) for identification based on the MS/MS ions. Under standard thresholds (mass error tolerance, ±50 ppm for MALDI-TOF-MS and 0.2 Da for ESI-Q-TOF mass spectrometry analysis; MS/MS tolerance, ±0.2 Da for MALDI-TOF-MS and ESI-Q-TOF mass spectrometry analysis; fixed modifications, Cys-carbamidomethylation; variable modifications, methionine oxidation; one tolerated missed cleavage), proteins with a MOWSE score of at least 54 were considered as significantly identified. The functional classification of the identified proteins was performed by searching the http://www.ncbi.nlm.nih.gov, http://www.uniprot.org, and www.genome.jp/kegg databases.

Statistical Analysis. The statistical analysis was performed using the program GraphPad Prism 5.0 for Windows. A one-way ANOVA was applied followed by Tukey's test ($p \leq 0.05$).

RESULTS AND DISCUSSION

Plant breeding is one of the strategies used to enhance the sensory characteristics and increase the nutritional properties of foods. However, the impact of this technique on both environmental and human health should be monitored. In this study, we investigated the proteome profiles of four new soybean varieties (BRS 257, BRS 258, Embrapa 48, and BRS 267) and the relationships between the protein expression profiles and the nutritional properties of these cultivars.

Alves et al.[31] showed that BRS 258 has higher protein content than BRS 257, Embrapa 48, and BRS 267. Such a finding is in accordance with our results. The thiourea/urea method of protein extraction provided the following amounts of protein (μg/g dry matter ± SD): BRS 257 had a protein content of 144000 ± 10324, BRS 258 had a protein content of 168700 ± 12587, Embrapa 48 had a protein content of 153400 ± 46528, and BRS 267 had a protein content of 138450 ± 46315.

Comparative Analysis of Soybean Seed Proteomes by 2D SDS-PAGE. Proteins from four soybean cultivars were extracted using a urea/thiourea protocol. These proteins were then separated by 2D SDS-PAGE (Figure 1), followed by protein identification using mass spectrometry (Table 1).

The image data from the triplicate 2D gel experiment were analyzed for each cultivar. The numbers of proteins spots (±SD) detected for BRS 257, BRS 258, Embrapa 48, and BRS 267 were 102 ± 22, 124 ± 5, 113 ± 32, and 99 ± 23, respectively. After this analysis, the differentially expressed protein spots were identified using MALDI-TOF-TOF mass spectrometry (Figure 1). A total of 47 protein spots were identified (Table 1).

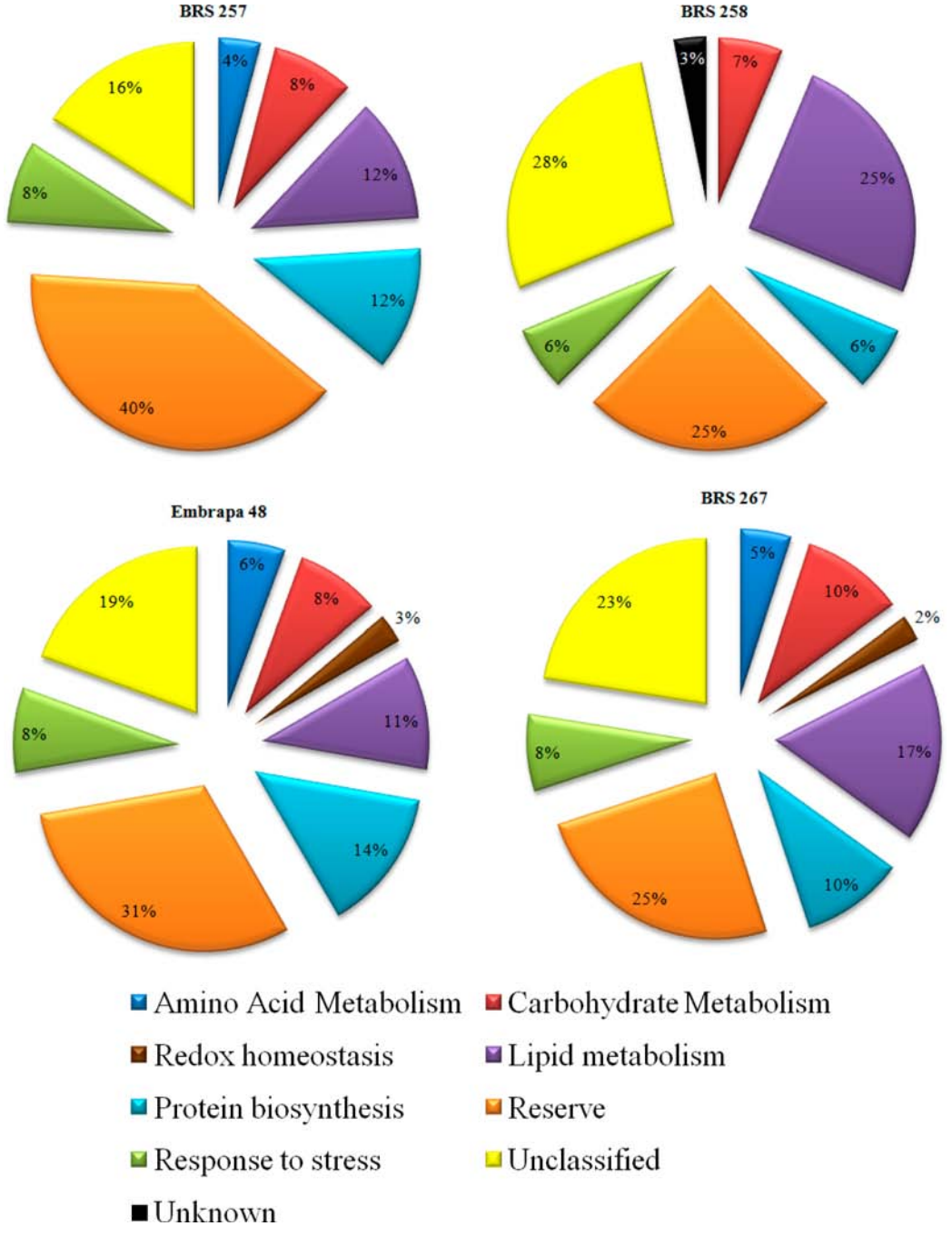

Figure 3. Functional classification of the soybean proteins isolated from BRS 257, BRS 258, Embrapa 48, and BRS 267 identified by 1D gel electrophoresis followed by ESI-Q-TOF mass spectrometry.

It has been reported that various soybean seeds may have different protein profiles due to genetic variability.[32,33] Among the analyzed spots, we found storage, allergenic, maturation, and agglutinin proteins as well as trypsin inhibitors. The comparative study of the 2D gels showed that the cultivar BRS 267 had the highest diversity for the identified spots (approximately 53%); this cultivar also had a greater number of spots corresponding to allergenic proteins and antinutrients, such as lectin and Kunitz inhibitor.

Eighteen glycinin and β-conglycinin spots were detected in the four soybean seeds. As the data show, these protein spots are distributed over a wide p*I* range in the same MW region. This pattern suggests the presence of isoforms or post-translational modifications of glycinin that occur during seed development, such as dissociation and reassembly.[12] Conversely, some authors attribute the occurrence of different spots for the same protein to the natural variation among different cultivars.[34]

Comparative Analysis of the Soybean Seed Proteomes by 1D SDS-PAGE. A 1D SDS-PAGE (Figure 2) analysis was performed using a protein extract suitable for 2D separation. The gels were stained with CBB, and proteins were identified by ESI-Q-TOF mass spectrometry. After image analysis, each intense Coomassie staining lane of the gel was divided into approximately 2.5 mm slices; the slices were then subjected to in-gel proteolysis with trypsin. A total of 117 proteins were identified from 12 bands in the 1D SDS-PAGE gel of soybean seed proteins.

dx.doi.org/10.1021/jf404351g | *J. Agric. Food Chem.* 2014, 62, 1283−1293

Distinct differences between the cultivars were found. Table 2 shows a comparative scheme indicating the presence or absence of the proteins identified in each cultivar.

Band 1 is the result of proteolysis. Lipoxygenase was detected in this band only in the BRS 267 cultivar. BRS 257 contains the lipid storage P24 oleosin isoforms A and B in this band, whereas only the α-subunit of β-conglycinin was identified in Embrapa 48.

These data confirm that BRS 257 is a cultivar without lipoxygenase, which is in accordance with information from Embrapa-soja.[24] Scientists have recently verified that a soybean seed lacking lipoxygenase had higher contents of calcium, magnesium, glucosides, and the aglycone forms of isoflavones and phytate compared to cultivars containing lipoxygenase.[35]

Other proteins were found only in the BRS 267 cultivar, including the following: 2S albumin precursor (band 12 and spot 24), cytosolic malate dehydrogenase (band 7), and hydroxysteroid 11-β-dehydrogenase 1-like protein-like (band 7). A 24 kDa oleosin isoform was found in BRS 257. The antinutrients lectin and Kunitz trypsin inhibitor were present in all soybean seeds.

The analyses of band 11 of BRS 257 and band 12 of BRS 258 were not reliable in any replicate. It is possible that some form of contamination occurred.

Functional Classification of the Identified Soybean Proteins. Classification according to the biological function of the proteins identified for each cultivar is illustrated in Figure 3. The proteins identified by ESI-Q-TOF-MS from the 1D SDS-PAGE analysis were grouped into nine categories according to their possible biological functions, based on molecular function, using the Universal Protein Knowledgebase (UniprotKB) and NCBI databases.

Comparison of the four soybean cultivars revealed similar protein function profiles. The distribution of proteins from the cultivars BRS 257 and BRS 258 had greater differentiation between categories than was observed in BRS 267 and Embrapa 48. Cultivars BRS 267 and Embrapa 48 had similar distributions of proteins between the categories; among the four cultivars, BRS 267 and Embrapa 48 had the greatest amounts of total sugar. These cultivars are described in the literature as having similar characteristics and as containing more sucrose.[36]

The highest percentage of storage proteins was found in BRS 257 (40%), followed by Embrapa 48 (31%), BRS 258 (25%), and BRS 267 (25%). The second largest protein group was unclassified proteins, which ranged from 16 to 28% of the total protein content.

The third major group of proteins observed was related to lipid metabolism (11−25%). Although BRS 257 does not possess lipoxygenases, lipid metabolism proteins represented 12% of the total protein content. Other observed protein categories were protein biosynthesis (6−14%) and stress response proteins (6−8%). Protein disulfide isomerase, a redox homeostasis enzyme, was observed only in the cultivars Embrapa 48 and BRS 267. Amino acid metabolism proteins were not observed in BRS 258.

According to the literature, BRS 258 is a soybean cultivar with a milder flavor and high protein content,[31] which is in agreement with our finding of a higher extraction yield of protein, although the values found were similar to those of other cultivars. Another distinctive feature of this cultivar is the significant percentage of proteins related to lipid metabolism.

An investigation of the proteomics of seed filling in soybean was reported by Hajduch et al.[37] The authors demonstrated that the largest functional class was unclassified proteins (28%), followed by metabolic proteins (22%; mainly lipid and sterol metabolism) and protein destination and storage proteins (10%). We noted that the maximal percentages in our study were similar for unclassified proteins and those associated with lipid metabolism. It must be noted that the protein profile is changed during seed filling; there is a decrease in lipid and sterol metabolism proteins and an increase in storage proteins.

Asakura et al.[38] characterized the gene expression patterns of developing soybeans. This group demonstrated that gene expression changes according to the stages of seed development. These changes could contribute to the differences in protein content. Kottapalli et al.[39] identified variations between four peanut cultivars. Proteins such as storage proteins, antinutritive proteins, and allergens were present in some peanut cultivars and absent in others. According to their study, the expression of some identified protein spots was cultivar specific.

According to Embrapa-soja,[24] BRS 257, BRS 258, Embrapa 48, and BRS 267, are promising options for human nutrition due to their elevated levels of carbohydrates and the high quality of the proteins. The diversity of proteins among the four soybean seeds in this study suggests that there are significant differences in the functional and nutritional properties of these seeds. Nevertheless, little is known about the protein composition of new conventional soybean varieties. The results obtained in this study indicate which cultivars are most suitable for human consumption and can direct the development of new cultivars with consideration of the protein composition.

■ ASSOCIATED CONTENT

Supporting Information

Spreadsheets containing molecular weight, isoelectric point, matched peptides, percent sequence coverage, and MOWSE scores of protein for identified proteins in the spots and bands from 2D SDS-PAGE and 1D SDS-PAGE, respectively, of soybean cultivars BRS 257, BRS 258, Embrapa 48, and BRS 267. This material is available free of charge via the Internet at http://pubs.acs.org.

■ AUTHOR INFORMATION

Corresponding Author

*(E.F.) Mailing address: Departamento de Nutrição Básica e Experimental, Instituto de Nutrição Josué de Castro, Centro de Ciências da Saúde, Universidade Federal do Rio de Janeiro, UFRJ, Caixa Postal 68041, Cidade Universitária, Ilha do Fundão, Rio de Janeiro, CEP 21941-590, Brazil. E-mail: fialho@nutricao.ufrj.br. Fax: + 55 21 2280 8343. Phone: + 55 21 2562 6599.

Funding

This work was supported by Coordenação de Aperfeiçoamento de Pessoal de Nível Superior (CAPES) and Fundação de Amparo à Pesquisa Carlos Chagas Filho do Estado do Rio de Janeiro (FAPERJ).

Notes

The authors declare no competing financial interest.

■ ACKNOWLEDGMENTS

We thank Ana Lúcia O. Carvalho and Augusto Vieira Magalhães (IBqM-UFRJ) for their helpful assistance. We also thank *Embrapa-soja* for the kind donation of soybean seeds.

■ ABBREVIATIONS USED

ACN, acetonitrile; CBB, Coomassie brilliant blue; DTT, dithiothreitol; EMBRAPA, Empresa Brasileira de Pesquisa Agropecuária; ESI-Q-TOF, electrospray ionization-quadrupole-time of flight; FDA, U.S. Food and Drug Administration; HDL-c,

high-density lipoprotein cholesterol; IPG, immobilized pH gradient; kDa, kilodalton; KTI, Kunitz trypsin inhibitor; LDL-c, low-density lipoprotein cholesterol; MALDI-TOF, matrix-assisted laser desorption ionization−time of flight; MOWSE, molecular weight search; MS, mass spectrometry; NCBI, National Center for Biotechnology Information; PAGE, polyacrylamide gel electrophoresis; SDS, sodium dodecyl sulfate; TFA, trifluoroacetic acid

REFERENCES

(1) Paucar-Menacho, L. M.; Amaya-Farfán, J.; Berhow, M. A.; Mandarino, J. M. G.; Mejia, E. G.; Chang, Y. K. A high-protein soybean cultivar contains lower isoflavones and saponins but higher minerals and bioactive peptides than a low-protein cultivar. *Food Chem.* **2010**, *120*, 15−21.

(2) Hughes, G. J.; Ryan, D. J.; Mukherjea, R.; Schasteen, C. S. Protein digestibility-corrected amino acid scores (PDCAAS) for soy protein isolates and concentrate: criteria for evaluation. *J. Agric. Food Chem.* **2011**, *59*, 12707−12712.

(3) Anvisa - Agência Nacional de Vigilância Sanitária. Alimentos com Alegações de Propriedades Funcionais e ou de Saúde, Novos Alimentos/Ingredientes, Substâncias Bioativas e Probióticos; http://www.anvisa.gov.br/alimentos/comissoes/tecno_lista_alega.htm) (accessed April 27, 2013).

(4) Xu, Z.; Li, Y.; Wang, J.; Wu, B.; Li, J. Effect of omega-3 polyunsaturated fatty acids to reverse biopsy-proven parenteral nutrition-associated liver disease in adults. *Clin. Nutr.* **2011**, *31*, 1−7.

(5) Li, Y.; Kong, D.; Bao, B.; Ahmad, A.; Sarkar, F. H. Induction of cancer cell death by isoflavone: the role of multiple signaling pathways. *Nutrients* **2011**, *3*, 877−896.

(6) Kurimoto, Y.; Shibayama, Y.; Inoue, S.; Soga, M.; Takikawa, M.; Ito, C.; Nanba, F.; Yoshida, T.; Yamashita, Y.; Ashida, H.; Tsuda, T. Black soybean seed coat extract ameliorates hyperglycemia and insulin sensitivity via the activation of AMP-activated protein kinase in diabetic mice. *J. Agric. Food Chem.* **2013**, *61*, 5558−5564.

(7) Hsieh, C. C.; Hernández-Ledesma, B.; Lumen, B. O. Soybean peptide lunasin suppresses in vitro and in vivo 7,12-dimethylbenz[a]-anthracene-induced tumorigenesis. *J. Food Sci.* **2010**, *75*, H311−H316.

(8) González-Espinosa de los Monteros, L.; Ramón-Gallegos, E.; Torres-Torres, N.; Mora-Escobedo, R. Effect of germinated soybean protein hydrolysates on adipogenesis and adipolysis in 3T3-L1 cells. *Plant Foods Hum. Nutr.* **2011**, *66*, 355−362.

(9) Silva, J. B.; Carrão-Panizzi, M. C.; Prudêncio, S. H. Chemical and physical composition of grain-type and food-type soybean for food processing. *Pesq. Agropec. Bras.* **2009**, *44*, 777−784.

(10) Hill, J. E.; Breidenbach, R. W. Proteins of soybean seeds. *Plant Physiol.* **1974**, *53*, 742−746.

(11) Žilić, S. M.; Barać, M. B.; Pešic, M. B.; Drinić, S. D. M.; Ignjatović-Micić; Srebrić, M. B. Characterization of proteins from kernel of different soybean varieties. *J. Sci. Food Agric.* **2011**, *91*, 60−67.

(12) Nielsen, N. C.; Dickinson, C. D.; Cho, T. J.; Thanh, V. H.; Scallon, B. J.; Fischer, R. L.; Sims, T. L.; Drews, G. N.; Goldberg, R. B. Characterization of the glycinin gene family in soybean. *Plant Cell* **1989**, *1*, 313−328.

(13) Carrão-Panizzi, M. C.; Kwanyuen, P.; Erhan, S. Z.; Lopes, I. O. N. Genetic variation and environmental effects on beta-conglycinin and glycinin content in Brazilian soybean cultivars. *Pesq. Agropec. Bras.* **2008**, *43*, 1105−1114.

(14) Clemente, A.; Moreno, F. J.; Marín-Manzano, M. C.; Jiménez, E.; Domoney, C. The cytotoxic effect of Bowman−Birk isoinhibitors, IBB1 and IBBD2, from soybean (*Glycine max*) on HT29 human colorectal cancer cells is related to their intrinsic ability to inhibit serine proteases. *Mol. Nutr. Food Res.* **2010**, *54*, 396−405.

(15) Ribeiro, J. K. C.; Cunha, D. D. S.; Fook, J. M. S. L. L.; Sales, M. P. New properties of the soybean trypsin inhibitor: inhibition of human neutrophil elastase and its effect on acute pulmonary injury. *Eur. J. Pharmacol.* **2010**, *644*, 238−244.

(16) Ye, X. J.; Ng, T. B. Antitumor and HIV-1 reverse transcriptase inhibitory activities of a hemagglutinin and a protease inhibitor from mini-black soybean. *Evidence-Based Complement. Alternat. Med.* **2011**, *2011*, 1−12.

(17) Ferreira, E. S.; Silva, M. A.; Demonte, A.; Neves, V. A. β-Conglycinin (7S) and glycinin (11S) exert a hypocholesterolemic effect comparable to that of fenofibrate in rats fed a high-cholesterol diet. *J. Funct. Foods* **2010**, *2*, 275−283.

(18) Fassini, P. G.; Noda, R. W.; Ferreira, E. S.; Silva, M. A.; Neves, V. A.; Demonte, A. Soybean glycinin improves HDL-C and suppresses the effects of rosuvastatin on hypercholesterolemic rats. *Lipids Health Dis.* **2011**, *10*, 165−171.

(19) Zhang, H.; Bartley, G. E.; Zhang, H.; Jing, W.; Fagerquist, C. K.; Zhong, F.; Yokoyama, W. Peptides identified in soybean protein increase plasma cholesterol in mice on hypercholesterolemic diets. *J. Agric. Food Chem.* **2013**, *61*, 8389−8395.

(20) Gouda, K. G. M.; Gowda, L. R.; Rao, A. G. A.; Prakash, V. Angiotensin I-converting enzyme inhibitory peptide derived from glycinin, the 11S globulin of soybean (*Glycine max*). *J. Agric. Food Chem.* **2006**, *54*, 4568−4573.

(21) Martinez-Villaluenga, C.; Rupasinghe, S. G.; Schuler, M. A.; Mejia, E. G. Peptides from purified soybean β-conglycinin inhibit fatty acid synthase by interaction with the thioesterase catalytic domain. *FEBS J.* **2010**, *277*, 1481−1493.

(22) American Dietetic Association (ADA). Position of the American Dietetic Association: functional foods. *J. Am. Diet. Assoc.* **2009**, *109*, 735−746.

(23) Mussatto, S. I.; Mancillha, I. M. Non-digestible oligosaccharides: a review. *Carbohydr. Polym.* **2007**, *68*, 587−597.

(24) Amorim, A.; Freitas, A. L.; Mallassa, M. R.; Passos, S. P. Paraná − Destaques econômicos. Embrapa apresenta cultivares de soja. *Analise Conjuntural* **2008**, *30*, 19−29; http://www.ipardes.gov.br/webisis.docs/bol_30_1i.pdf (accessed Sept 24, 2013).

(25) Trujillo, E.; Davis, C.; Milner, J. Nutrigenomics, proteomics, metabolomics, and the practice of dietetics. *J. Am. Diet. Assoc.* **2006**, *106*, 403−413.

(26) Ferguson, P. L.; Smith, R. D. Proteome analysis by mass spectrometry. *Annu. Rev. Biophys. Biomol. Struct.* **2003**, *32*, 399−424.

(27) Guijarro-Díez, M.; García, M. C.; Marina, M. L.; Crego, A. L. LC-ESI-TOF MS method for the evaluation of the immunostimulating activity of soybeans via the determination of the functional peptide soymetide. *J. Agric. Food Chem.* **2013**, *61*, 3611−3618.

(28) Herman, E. M.; Helm, R. M.; Jung, R.; Kinney, A. J. Genetic modification removes an immunodominant allergen from soybean. *Plant Physiol.* **2003**, *132*, 36−43.

(29) Peterson, G. L. Determination of total protein. *Methods Enzymol.* **1983**, *91*, 95−121.

(30) Laemmli, U. K. Cleavage of structural proteins during the assembly of the head of bacteriophage T4. *Nature* **1970**, *227*, 680−685.

(31) Alves, F. P.; Oliveira, M. A.; Mandarino, J. M. G.; Benassi, V.; Leite, R. S.; Seibel, N. F. Composição centesimal de grãos de soja de oito diferentes cultivares. Resumos expandidos. VI Jornada Acadêmica da Embrapa Soja, 2011; ISSN 0021-8561; http://www.cnpso.embrapa.br/download/Jornada2011.pdf (accessed April 26, 2013).

(32) Zarkadas, C. G.; Gagnon, C.; Gleddie, S.; Khanizadeh, S.; Cober, E. R.; Guillemette, R. J. D. Assessment of the protein quality of fourteen soybean [*Glycine max* (L.) Merr.] cultivars using amino acid analysis and two-dimensional electrophoresis. *Food Res. Int.* **2007**, *40*, 129−146.

(33) Natajaran, S. S.; Xu, C.; Bae, H.; Caperna, T. J.; Garrett, W. M. Characterization of storage proteins in wild (*Glycine soja*) and cultivated (*Glycine max*) soybean seeds using proteomic analysis. *J. Agric. Food Chem.* **2006**, *54*, 3114−3120.

(34) Natarajan, S. S. Natural variability in abundance of prevalent soybean proteins. *Regul. Toxicol. Pharmacol.* **2010**, *58*, S26−S29.

(35) Esteves, E. A.; Martino, H. S. D.; Oliveira, F. C. E.; Bressan, J.; Costa, N. M. B. Chemical composition of a soybean cultivar lacking lipoxygenases (LOX2 and LOX3). *Food Chem.* **2010**, *122*, 238−242.

(36) Oliveira, M. A.; Carrão-Panizzi, M. C.; Mandarino, J. M. G.; Leite, R. S.; Filho, P. J. C.; Vicentini, M. B. Quantification of the sugars,

oligosaccharides and starch in special soybean genotypes/cultivars (*Glycine max* (L) Merril) for human consumption. *Braz. J. Food Technol.* **2010**, *13*, 23−29.

(37) Hajduch, M.; Ganapathy, A.; Stein, J. W.; Thelen, J. J. A systematic proteomic study of seed filling in soybean. Establishment of high-resolution two-dimensional reference maps, expression profiles, and an interactive proteome database. *Plant Physiol.* **2005**, *137*, 1397−1419.

(38) Asakura, T.; Tamura, T.; Terauchi, K.; Narikawa, T.; Yagasaki, K.; Ishimaru, Y.; Abe, K. Global gene expression profiles in developing soybean seeds. *Plant Physiol. Biochem.* **2012**, *52*, 147−153.

(39) Kottapalli, K. R.; Payton, P.; Rakwal, R.; Agrawal, G. K.; Shibato, J.; Burow, M.; Puppala, N. Proteomics analysis of mature seed of four peanut cultivars using two-dimensional gel electrophoresis reveals distinct differential expression of storage, anti-nutritional, and allergenic proteins. *Plant Sci.* **2008**, *175*, 321−329.

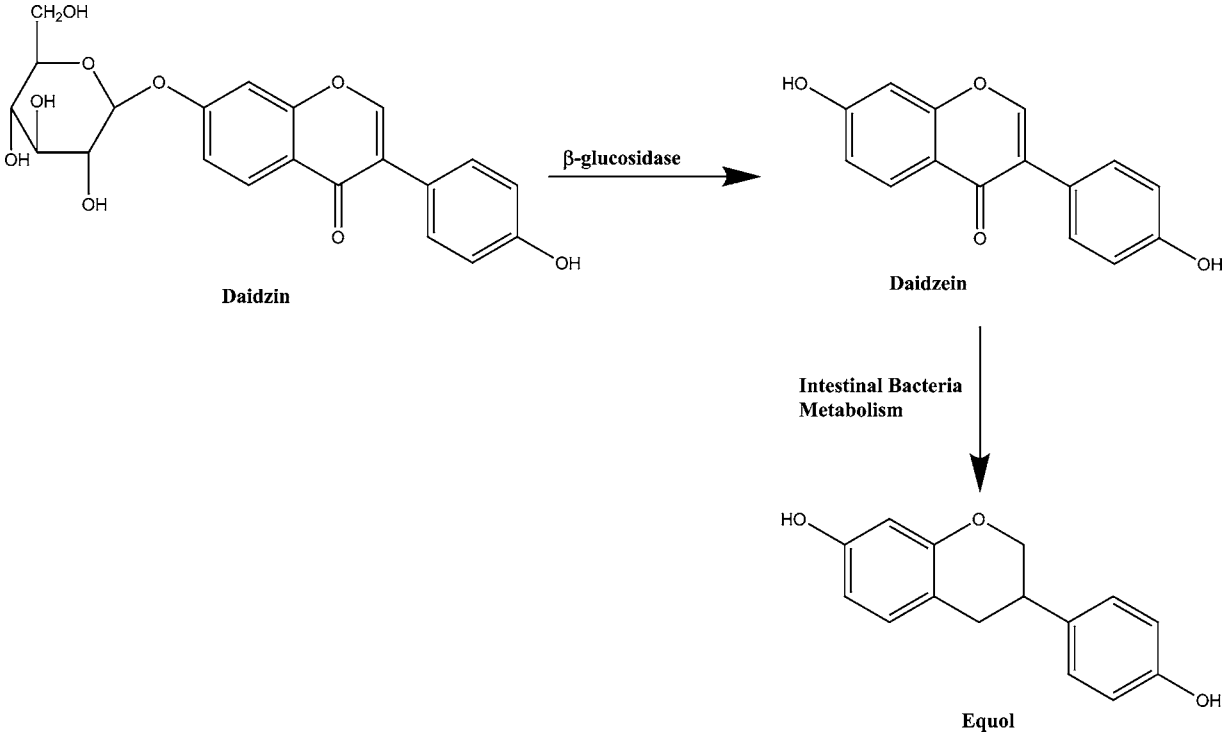

Figure 1. Schematic of equol production from intestinal bacteria metabolism of daidzein.

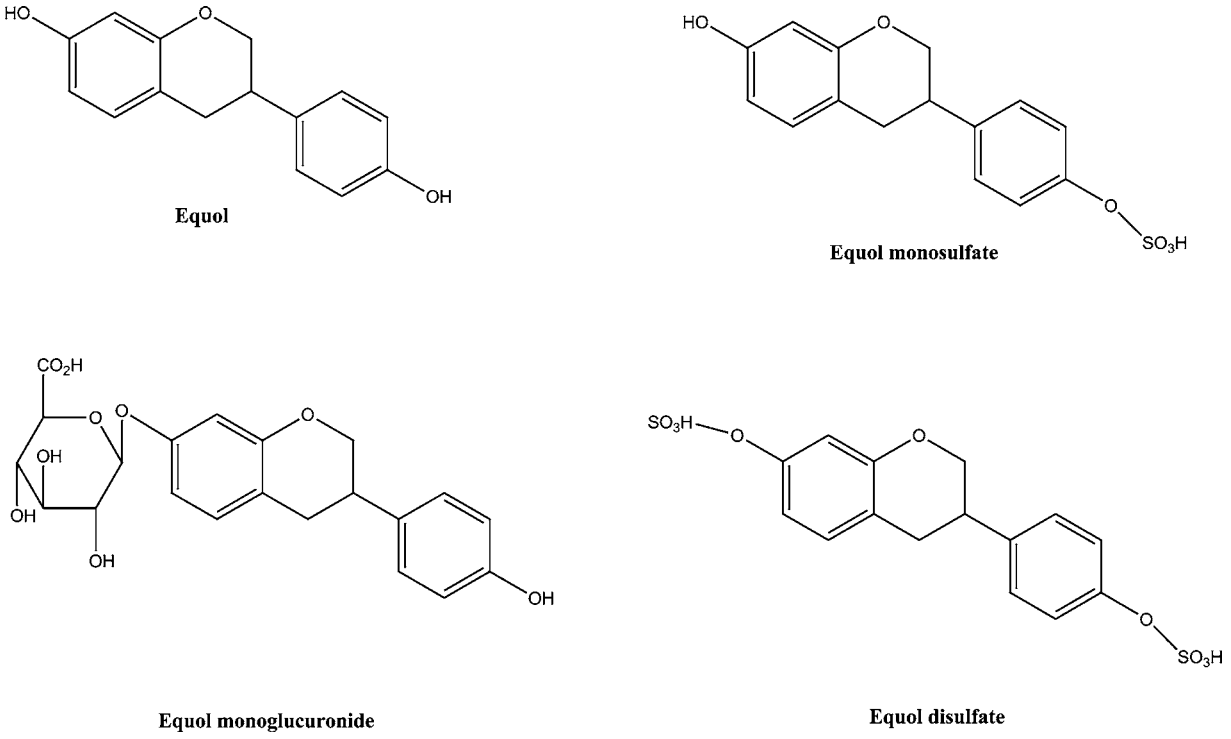

Figure 2. Chemical structures of equol and its conjugates.

MATERIALS AND METHODS

Animal Procedures. Three-month-old female Sprague−Dawley rats were purchased from Harlan (Indianapolis, IN, USA) and underwent ovariectomy (OVX) surgery. Rats were maintained on an AIN-93 M diet[32] with corn oil replacing soybean oil (to eliminate the potential presence of phytoestrogens in diet) for 1 week before undergoing pharmacokinetics. Animals were housed in individual cages in temperature- and humidity-controlled rooms with a 12 h−12 h on−off light cycle. After a 2 day acclimation period, animals were grouped into pairs and divided into two treatment groups: dietary daidzein (n = 6 pairs) and dietary equol (n = 6 pairs). Animals were matched on the basis of body weight, and pairs were selected to ensure similar body weight average across treatment groups.

Chemicals. Daidzein was obtained from a commercial source (Indofine Chemical Co., Hillsborough, NJ, USA). Racemic equol (50% *R*-equol, 50% *S*-equol) as well as equol sulfate conjugates (equol monosulfate and disulfate) were generously provided by the Helferich

dx.doi.org/10.1021/jf400097m | *J. Agric. Food Chem.* 2014, 62, 1294−1300

Table 1. Equol Metabolites Detected in Plasma of Ovarectiomized Rats Fed a Single Oral Dose of Dietary Daidzein (n = 4 Pairs, 10 mg/mL) or Equol (n = 5 Pairs, 2 mg/mL)

metabolite	retention time (min)	m/z transition
equol	10.8	241/119
equol disulfate	8.83	401/321
equol glucuronide	8.72	417/241
equol monosulfate	9.76	321/121

(Division of Nutritional Sciences, University of Illinois, Urbana, IL, USA) and Botting laboratories (Department of Chemistry, St. Andrew's University, Fife, UK), respectively. Synthesis details including purity for racemic equol[33] and equol conjugates[34] are described in earlier work. All other reagents were obtained from Sigma-Aldrich (St. Louis, MO, USA).

Materials. For formulation of oral gavage solutions, both daidzein and equol were suspended in 4.5% starch solution for single oral doses of 10 and 2 mg/mL, respectively. The oral equol dose represents a daily intake of 200 mg racemic equol/kg diet based on a physiologically relevant level for dietary racemic equol seen in earlier research in our laboratory.[35] The oral daidzein dose (1000 mg daidzein/kg diet) was selected due to the fact it produced similar circulating equol levels as seen with the dietary dose of 200 mg racemic equol/kg diet.

Pharmacokinetics. Animals were implanted with jugular catheters for blood collection 2 days before pharmacokinetics. Animals received a single oral gavage solution (2 mL) of dietary daidzein (10 mg/mL) or dietary equol (2 mg/mL). Blood (0.2 mL) was drawn via jugular catheter from each rat at the following time points: 0, 0.5, 1, 2, 3, 4, 6, 8, 12, 16, 20, and 24 h. For each pair of animals, blood was pooled at each time point (total of 0.4 mL). Animals weighed between 200 and 250 g. To replenish animals from blood loss, fluids (50:50, saline/5% dextrose, 2 mL) were given after the 3 h time point. After the last blood collection, animals were euthanized by CO_2 inhalation. All procedures were approved by the Purdue University Animal Care and Use Committee (Protocol 08-112).

Sample Preparation, Extraction and Analysis. Plasma samples were processed through two separate sample preparations to determine total aglycone and equol conjugate concentrations. To determine total plasma aglycone equol, samples underwent enzymatic hydrolysis as described previously.[36] In brief, two conjugates, phenolphthalein β-glucuronide (PHG) and 4-methylumbelliferone sulfate (4-MUS), were added to all samples as markers of effective hydrolysis along with an internal standard, chrysin (CHYS). Isoflavones were recovered by diethyl ether extraction. The ether extracts were evaporated under a stream of nitrogen and reconstituted with 100 μL of an 80% aqueous methanol solution for analysis.

To determine circulating levels of free equol and equol sulfate conjugates, plasma samples (200 μL) underwent protein precipitation. Methanol containing 1% acetic acid solution and a mixed set of internal standards (10 μM 4-MUS−PHG−CHYS) were added to each sample in a ratio of 4:1. Samples were centrifuged for 10 min at 3000g and 4 °C. The supernatants were used for analysis.

Total unconjugated equol, free equol, equol monosulfate, and equol disulfate concentrations were identified and quantified using a highly sensitive and specific electrospray ionization liquid chromatography−multiple reaction ion monitoring (MRM) mass spectrometry method

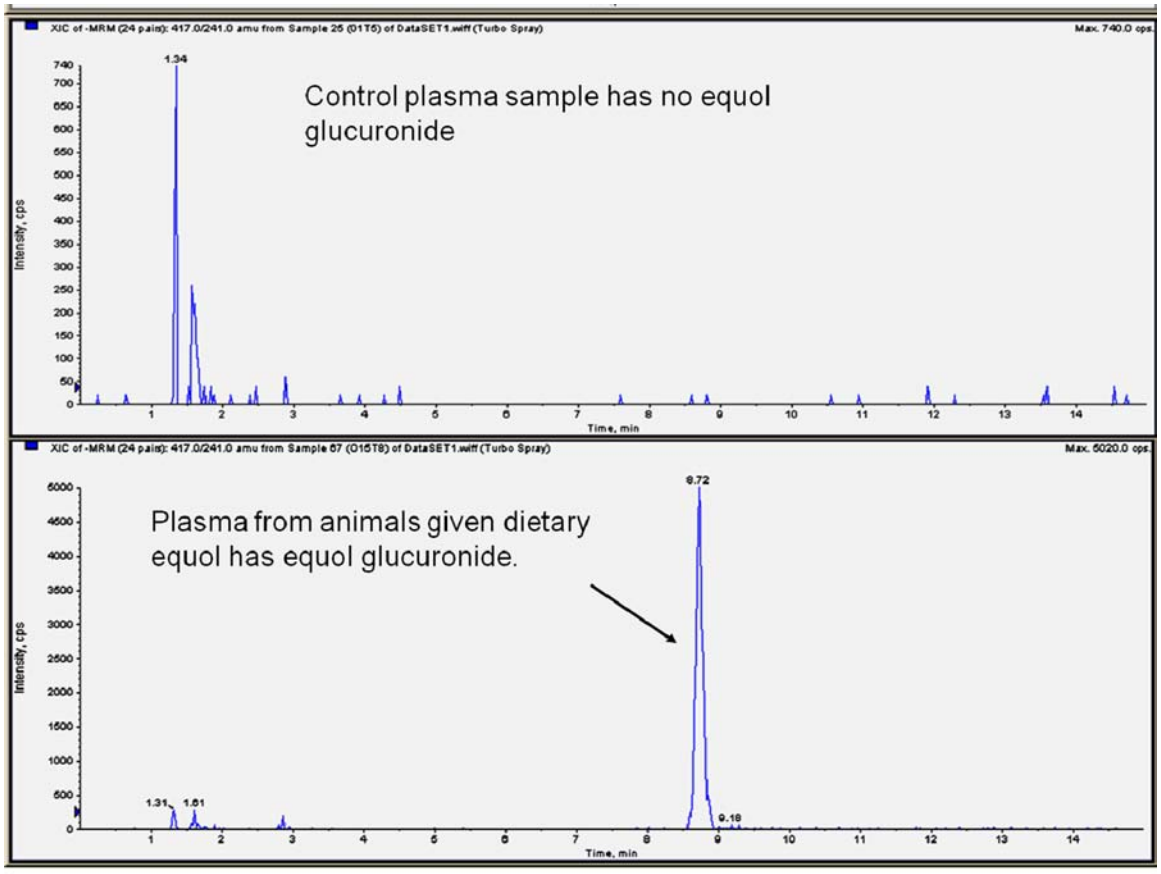

Figure 3. MS/MS chromatogram of control sample and product ion mass spectra of plasma samples from rats fed dietary equol (2 mg/mL). The presence of equol glucuronides was determined by monitoring the m/z 417/241 transition using a triple-quadrupole mass spectrometer (4000 QTRAP, ABSCIEX, Framingham, MA, USA) with chromatography details described previously.[35]

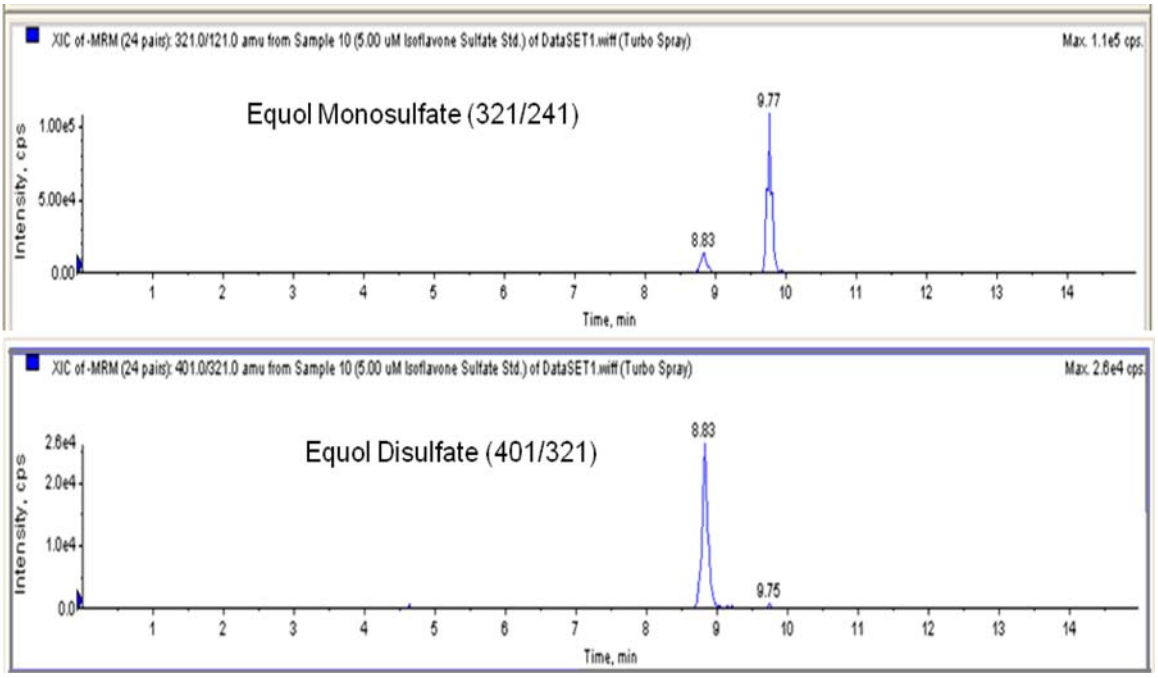

Figure 4. Representative MS/MS chromatogram of a 5 μM isoflavone sulfate standard containing equol monosulfate and disulfate.

as previously described[37] with chromatography conditions detailed in earlier work[35] and with the following modifications: equol monosulfate and disulfate were detected using their precursor to product ion transitions of m/z 321/121 and m/z 401/321, respectively. Identification and quantitation of equol and its sulfate conjugates were determined on the basis of comparison of MS/MS fragmentation pattern and retention time to reference material. LC-MS/MS method did not distinguish between *R*- and *S*-equol enantiomers. Due to limited availability of known standard for equol glucuronide, it was identified by its m/z 417/241 transition, and concentrations were determined using the following equation, which assumes that only equol sulfate and glucuronide conjugates are present:

$$\begin{aligned}&\text{equol glucuronide conjugates (nM)}\\&\quad = \text{total aglycone equol (nM)} - \text{free equol (nM)}\\&\qquad - \text{equol sulfate conjugates (nM)}\end{aligned} \quad (1)$$

The limit of detection for all analytes of interest was 5 nM. All parameters for metabolite identification including retention times and m/z transitions are listed in Table 1. To validate calculation for equol glucuronide conjugates and ensure no other metabolites were present, a control plasma sample was analyzed along with a sample from the dietary equol group. All pertinent m/z transitions were monitored. Representative chromatograms of equol glucuronide and equol sulfates are shown in Figures 3 and 4.

Pharmacokinetic Parameters. The following pharmacokinetic parameters were determined using noncompartmental methods (WinNonlin Pro version 4.01, Pharsight Corp., Mountain View, CA, USA): C_{max} (maximum concentration), HL (elimination half-life), t_{max} (time of maximum concentration), AUC_{0-24} (area under plasma concentration time curve from 0 to 24h), CL/F (clearance rate), and V/F (volume of distribution).

RESULTS AND DISCUSSION

Pharmacokinetic parameters for equol metabolites from dietary daidzein and racemic equol are detailed in Tables 2 and 3. There were higher levels of equol glucuronides than equol monosulfate for both dietary daidzein and racemic equol groups. There were no detectable levels of equol disulfate.

Table 2. Pharmacokinetic Parameters of Equol Metabolites from a Single Oral Gavage of Dietary Daidzein Administered to Ovariectomized Rats (n = 4−6 Pairs)[a]

metabolite	t_{max} (h)	C_{max} (nM)	AUC_{0-24} (nM·h)
total equol	20.67 ± 4.67	3682 ± 2675	24346 ± 8778
unconjugated equol	20.00 ± 4.90	1.21 ± 0.64	9.34 ± 8.43
equol monosulfate	20.00 ± 3.27	3.15 ± 3.04	19.16 ± 17.76
equol glucuronides	20.67 ± 4.67	3349 ± 2799	22438 ± 9907

[a]Values are means ± SD. Pharmacokinetic parameters: t_{max} (time of maximum concentration), C_{max} (maximum concentration), AUC_{0-24} (area under plasma concentration time curve from 0 to 24 h).

There were significantly higher maximum concentrations of all equol metabolites from dietary racemic equol compared to *S*-equol produced from dietary daidzein. Plasma concentrations of equol metabolites peaked around 2−3 h for dietary racemic equol and appeared in large levels at 8−13 h for dietary daidzein. The late appearance of equol metabolites with dietary daidzein was expected due to time required for bacterial conversion of daidzein to equol in the large intestine and therefore is a measure of intestinal transit.

Dietary equol led to rises in circulating equol and equol conjugates at 1, 4−5, and 8−9 h (Figure 5). The initial rise at 1 h is attributed to its rapid absorption in the small intestine, which is also seen in both in vitro[27] and in vivo[30] studies of equol metabolism. The second and third peaks at 4−5 and 8−9 h may be indicators of enterohepatic recycling and additional absorption occurring in the large intestine, respectively. Increases in equol metabolite levels during 16−24 h could also reflect enterohepatic recirculation, as previously reported with other isoflavones.[18] Small rises in equol metabolite levels could also be due to high biological variation. Additional studies with greater animals are needed to confirm if plasma increases are significant. Equol conjugates had lower clearance rates (CL/F) than unconjugated equol, which is unexpected due to polarity of conjugates, and warrants further investigation.

Table 3. Pharmacokinetic Parameters of Equol Metabolites from a Single Oral Gavage of Dietary Equol Administered to Ovariectomized Rats (n = 5−6 Pairs)[a]

metabolite	HL (h)	t_{max} (h)	C_{max} (nmol/L)	AUC_{0-24} (nmol/L·*h)	CL/F (L/h)	V/F (L)
total equol	21.9 ± 8.02	2.17 ± 2.91	8815 ± 2988	104337 ± 20531	0.08 ± 0.03	2.32 ± 0.26
unconjugated equol	9.41 ± 3.93	4.42 ± 4.50	9.46 ± 3.56	96.0 ± 41.9	179 ± 138	1,937 ± 692
equol monosulfate	14.4 ± 9.26	3.20 ± 2.95	23.9 ± 8.54	234 ± 97	43.7 ± 11.7	912 ± 703
equol glucuronides	23.0 ± 2.91	2.17 ± 2.91	8775 ± 2976	104082 ± 20516	0.08 ± 0.03	2.38 ± 0.50

[a]Values are means ± SD. Pharmacokinetic parameters: HL (elimination half-life), t_{max} (time of maximum concentration), C_{max} (maximum concentration), AUC_{0-24} (area under plasma concentration time curve from 0 to 24 h), CL/F (clearance rate) = D/AUC_{0-24}, V/F (volume of distribution)

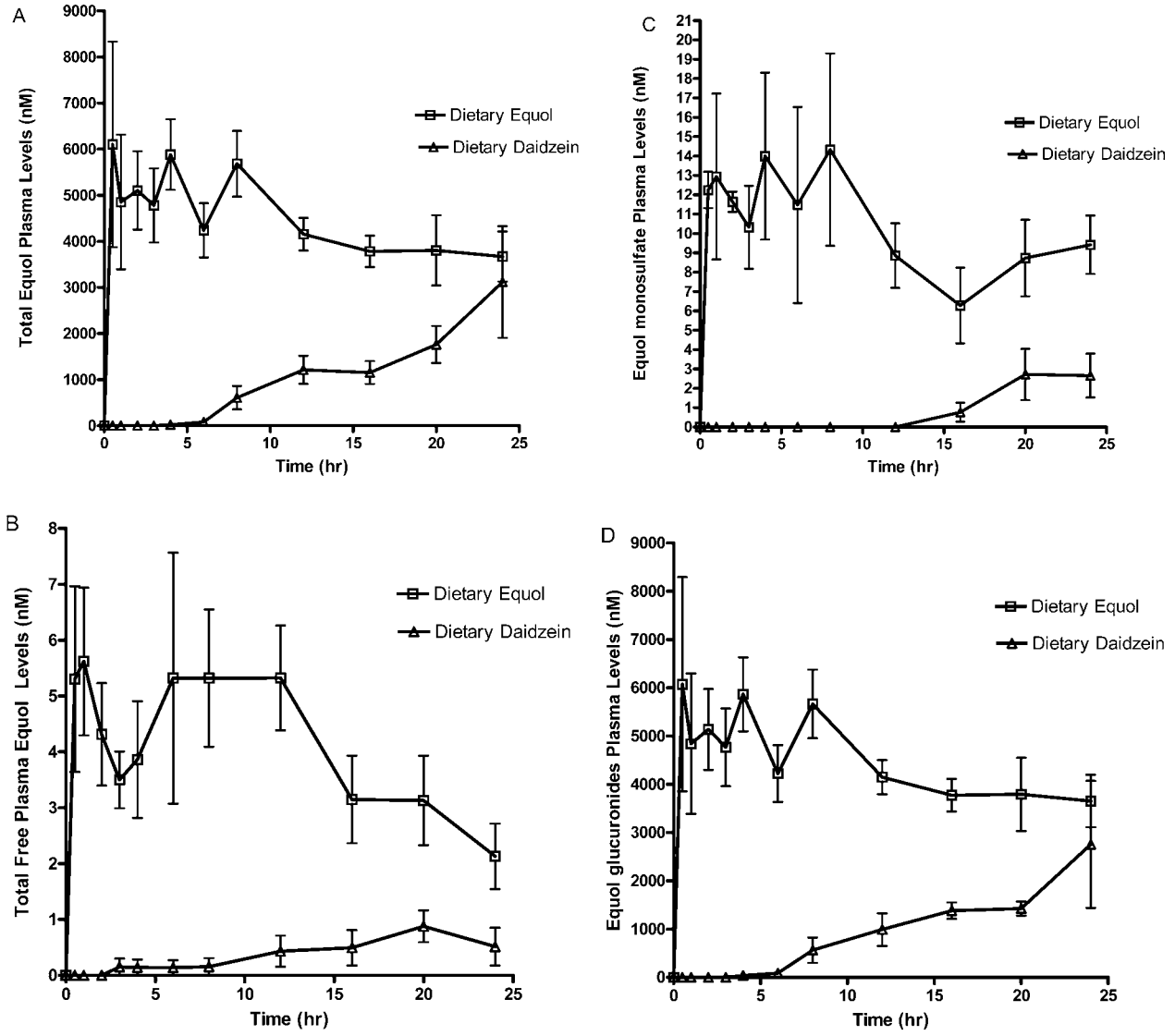

Figure 5. Pharmacokinetic curves over a 24 h period in ovarectiomized rats after a single oral dose of dietary daidzein (n = 6 pairs) (10 mg/mL) or equol (n = 6 pairs) (2 mg/mL) for plasma (A) total aglycone equol, (B) unconjugated or free equol, (C) equol monosulfate, and (D) equol glucuronides. The equol glucuronide was calculated as the difference between the total plasma equol concentration and the sum of the plasma unconjugated and sulfated equol.

The first appearance of equol metabolites (total equol and equol glucuronides) after administration of dietary daidzein occurred around 7−8 h (Figure 5A,D). This corresponds to findings from previous studies.[15,17,38] In the dietary daidzein treatment group, total equol, unconjugated equol, and equol glucuronide levels from dietary daidzein rose between 8 and 13 h and all metabolites peaked between 20 and 24 h, consistent with earlier work assessing the bioavailability of daidzein and genistein conjugates in rats.[15] None of the equol metabolites reached a plateau after 24 h (Figure 5). There were few data to accurately assess HL, CL/F, and V/F of equol metabolite produced from dietary daidzein. Both findings suggest that a longer time frame is needed to adequately assess the pharmacokinetic profile of equol metabolites from daidzein consumption.

Our results indicate there were higher levels of circulating equol metabolites with dietary racemic equol compared to equol produced from dietary daidzein in ovariectomized rats. We also observed poor clearance of equol metabolites as well as high enterohepatic recirculation as seen previously with other soy isoflavones.[18] Most of the circulating equol was conjugated equol, specifically equol glucuronides, which agrees with findings from other in vivo studies. Pharmacokinetics studies of *S*-equol in various species (rat, monkey, human) show similar metabolism including rapid absorption.[12,29,30] Future studies could utilize animal models to determine mechanisms of action for various forms of equol. More elucidation on the impact of the forms of equol (various enantiomers, dietary vs intestinal production) as well as the effect of equol conjugates on health benefits of equol is needed.

AUTHOR INFORMATION

Corresponding Author

*(C.M.W.) Phone: (765) 494-8237. Fax: (765) 494-0674. E-mail: weavercm@purdue.edu.

Funding

This study was funded by the National Institutes of Health Purdue−UAB Botanical Center for Age-Related Diseases (NIH Grants P50 AT00477, P50 AT00477-07S1). Funds for the mass spectrometer used in the study were provided by a NIH Shared Instrumentation Grant to S.B. (S10 RR19261).

Notes

The authors declare the following competing financial interest(s): Stephen Barnes has a U.S. patent on the use of conjugated isoflavones and prevention of osteoporosis. Connie Weaver serves as an advisory board member of Pharmavite.

ACKNOWLEDGMENTS

We thank Pamela Lachcik and Emily Hohman for their assistance with the study as well as William Helferich and the Helferich Laboratory for providing racemic equol and Nigel Botting and the Botting Laboratory for providing equol sulfate standards.

REFERENCES

(1) Tezval, M.; Sehmisch, S.; Seidlova-Wuttke, D.; Rack, T.; Kolios, L.; Wuttke, W.; Stuermer, K. M.; Stuermer, E. K. Changes in the histomorphometric and biomechanical properties of the proximal femur of ovariectomized rat after treatment with the phytoestrogens genistein and equol. *Planta Med.* **2010**, *76* (3), 235−240.

(2) Rachon, D.; Seidlova-Wuttke, D.; Vortherms, T.; Wuttke, W. Effects of dietary equol administration on ovariectomy induced bone loss in Sprague-Dawley rats. *Maturitas* **2007**, *58* (3), 308−315.

(3) Kolios, L.; Sehmisch, S.; Daub, F.; Rack, T.; Tezval, M.; Stuermer, K. M.; Stuermer, E. K. Equol but not genistein improves early metaphyseal fracture healing in osteoporotic rats. *Planta Med.* **2009**, *75* (5), 459−465.

(4) Setchell, K. D.; Brown, N. M.; Lydeking-Olsen, E. The clinical importance of the metabolite equol-a clue to the effectiveness of soy and its isoflavones. *J. Nutr.* **2002**, *132* (12), 3577−3584.

(5) Setchell, K. D.; Lydeking-Olsen, E. Dietary phytoestrogens and their effect on bone: evidence from in vitro and in vivo, human observational, and dietary intervention studies. *Am. J. Clin. Nutr.* **2003**, *78* (3 Suppl.), 593S−609S.

(6) Xu, X.; Harris, K. S.; Wang, H. J.; Murphy, P. A.; Hendrich, S. Bioavailability of soybean isoflavones depends upon gut microflora in women. *J. Nutr.* **1995**, *125* (9), 2307−2315.

(7) Adlercreutz, H.; van der Wildt, J.; Kinzel, J.; Attalla, H.; Wahala, K.; Makela, T.; Hase, T.; Fotsis, T. Lignan and isoflavonoid conjugates in human urine. *J. Steroid Biochem. Mol. Biol.* **1995**, *52* (1), 97−103.

(8) Shelnutt, S. R.; Cimino, C. O.; Wiggins, P. A.; Badger, T. M. Urinary pharmacokinetics of the glucuronide and sulfate conjugates of genistein and daidzein. *Cancer Epidemiol. Biomarkers Prev.* **2000**, *9* (4), 413−419.

(9) Thomas, B. F.; Zeisel, S. H.; Busby, M. G.; Hill, J. M.; Mitchell, R. A.; Scheffler, N. M.; Brown, S. S.; Bloeden, L. T.; Dix, K. J.; Jeffcoat, A. R. Quantitative analysis of the principle soy isoflavones genistein, daidzein and glycitein, and their primary conjugated metabolites in human plasma and urine using reversed-phase high-performance liquid chromatography with ultraviolet detection. *J. Chromatogr., B: Biomed. Sci. Appl.* **2001**, *760* (2), 191−205.

(10) Wong, C. K.; Keung, W. M. Daidzein sulfoconjugates are potent inhibitors of sterol sulfatase (EC 3.1.6.2). *Biochem. Biophys. Res. Commun.* **1997**, *233* (3), 579−583.

(11) Zhang, Y.; Song, T. T.; Cunnick, J. E.; Murphy, P. A.; Hendrich, S. Daidzein and genistein glucuronides in vitro are weakly estrogenic and activate human natural killer cells at nutritionally relevant concentrations. *J. Nutr.* **1999**, *129* (2), 399−405.

(12) Schwen, R. J.; Nguyen, L.; Jackson, R. L. Elucidation of the metabolic pathway of S-equol in rat, monkey and man. *Food Chem. Toxicol.* **2012**, *50* (6), 2074−2083.

(13) Fang, N.; Yu, S.; Badger, T. M. Characterization of isoflavones and their conjugates in female rat urine using LC/MS/MS. *J. Agric. Food Chem.* **2002**, *50* (9), 2700−2707.

(14) Holder, C. L.; Churchwell, M. I.; Doerge, D. R. Quantification of soy isoflavones, genistein and daidzein, and conjugates in rat blood using LC/ES-MS. *J. Agric. Food Chem.* **1999**, *47* (9), 3764−3770.

(15) King, R. A. Daidzein conjugates are more bioavailable than genistein conjugates in rats. *Am. J. Clin. Nutr.* **1998**, *68* (6 Suppl.), 1496S−1499S.

(16) King, R. A.; Broadbent, J. L.; Head, R. J. Absorption and excretion of the soy isoflavone genistein in rats. *J. Nutr.* **1996**, *126* (1), 176−182.

(17) Sepehr, E.; Cooke, G. M.; Robertson, P.; Gilani, G. S. Effect of glycosidation of isoflavones on their bioavailability and pharmacokinetics in aged male rats. *Mol. Nutr. Food Res.* **2009**, *53* (Suppl. 1), S16−S26.

(18) Sfakianos, J.; Coward, L.; Kirk, M.; Barnes, S. Intestinal uptake and biliary excretion of the isoflavone genistein in rats. *J. Nutr.* **1997**, *127* (7), 1260−1268.

(19) Soucy, N. V.; Parkinson, H. D.; Sochaski, M. A.; Borghoff, S. J. Kinetics of genistein and its conjugated metabolites in pregnant Sprague-Dawley rats following single and repeated genistein administration. *Toxicol. Sci.* **2006**, *90* (1), 230−240.

(20) Anupongsanugool, E.; Teekachunhatean, S.; Rojanasthien, N.; Pongsatha, S.; Sangdee, C. Pharmacokinetics of isoflavones, daidzein and genistein, after ingestion of soy beverage compared with soy extract capsules in postmenopausal Thai women. *BMC Clin. Pharmacol.* **2005**, *5*, 2.

(21) Doerge, D. R.; Chang, H. C.; Churchwell, M. I.; Holder, C. L. Analysis of soy isoflavone conjugation in vitro and in human blood using liquid chromatography-mass spectrometry. *Drug Metab. Dispos.* **2000**, *28* (3), 298−307.

(22) Hosoda, K.; Furuta, T.; Yokokawa, A.; Ogura, K.; Hiratsuka, A.; Ishii, K. Plasma profiling of intact isoflavone metabolites by high-performance liquid chromatography and mass spectrometric identification of flavone glycosides daidzin and genistin in human plasma after administration of kinako. *Drug Metab. Dispos.* **2008**, *36* (8), 1485−1495.

(23) Rufer, C. E.; Bub, A.; Moseneder, J.; Winterhalter, P.; Sturtz, M.; Kulling, S. E. Pharmacokinetics of the soybean isoflavone daidzein in its aglycone and glucoside form: a randomized, double-blind, crossover study. *Am. J. Clin. Nutr.* **2008**, *87* (5), 1314−1323.

(24) Setchell, K. D.; Brown, N. M.; Desai, P.; Zimmer-Nechemias, L.; Wolfe, B. E.; Brashear, W. T.; Kirschner, A. S.; Cassidy, A.; Heubi, J. E. Bioavailability of pure isoflavones in healthy humans and analysis of

commercial soy isoflavone supplements. *J. Nutr.* **2001**, *131* (4 Suppl.), 1362S−1375S.
(25) Shelnutt, S. R.; Cimino, C. O.; Wiggins, P. A.; Ronis, M. J.; Badger, T. M. Pharmacokinetics of the glucuronide and sulfate conjugates of genistein and daidzein in men and women after consumption of a soy beverage. *Am. J. Clin. Nutr.* **2002**, *76* (3), 588−594.
(26) Zhang, Y.; Wang, G. J.; Song, T. T.; Murphy, P. A.; Hendrich, S. Urinary disposition of the soybean isoflavones daidzein, genistein and glycitein differs among humans with moderate fecal isoflavone degradation activity. *J. Nutr.* **1999**, *129* (5), 957−962.
(27) Walsh, K. R.; Failla, M. L. Transport and metabolism of equol by Caco-2 human intestinal cells. *J. Agric. Food Chem.* **2009**, *57* (18), 8297−8302.
(28) Setchell, K. D.; Clerici, C.; Lephart, E. D.; Cole, S. J.; Heenan, C.; Castellani, D.; Wolfe, B. E.; Nechemias-Zimmer, L.; Brown, N. M.; Lund, T. D.; Handa, R. J.; Heubi, J. E. S-equol, a potent ligand for estrogen receptor beta, is the exclusive enantiomeric form of the soy isoflavone metabolite produced by human intestinal bacterial flora. *Am. J. Clin. Nutr.* **2005**, *81* (5), 1072−1079.
(29) Setchell, K. D.; Zhao, X.; Jha, P.; Heubi, J. E.; Brown, N. M. The pharmacokinetic behavior of the soy isoflavone metabolite S-(−)equol and its diastereoisomer R-(+)equol in healthy adults determined by using stable-isotope-labeled tracers. *Am. J. Clin. Nutr.* **2009**, *90* (4), 1029−1037.
(30) Setchell, K. D.; Zhao, X.; Shoaf, S. E.; Ragland, K. The pharmacokinetics of S-(−)equol administered as SE5-OH tablets to healthy postmenopausal women. *J. Nutr.* **2009**, *139* (11), 2037−2043.
(31) Jackson, R. L.; Greiwe, J. S.; Desai, P. B.; Schwen, R. J. Single-dose and steady-state pharmacokinetic studies of S-equol, a potent nonhormonal, estrogen receptor beta-agonist being developed for the treatment of menopausal symptoms. *Menopause* **2011**, *18* (2), 185−193.
(32) Reeves, P. G.; Nielsen, F. H.; Fahey, G. C., Jr. AIN-93 purified diets for laboratory rodents: final report of the American Institute of Nutrition ad hoc writing committee on the reformulation of the AIN-76A rodent diet. *J. Nutr.* **1993**, *123* (11), 1939−1951.
(33) Muthyala, R. S.; Ju, Y. H.; Sheng, S.; Williams, L. D.; Doerge, D. R.; Katzenellenbogen, B. S.; Helferich, W. G.; Katzenellenbogen, J. A. Equol, a natural estrogenic metabolite from soy isoflavones: convenient preparation and resolution of R- and S-equols and their differing binding and biological activity through estrogen receptors alpha and beta. *Bioorg. Med. Chem.* **2004**, *12* (6), 1559−1567.
(34) Clarke, D. B.; Lloyd, A. S.; Botting, N. P.; Oldfield, M. F.; Needs, P. W.; Wiseman, H. Measurement of intact sulfate and glucuronide phytoestrogen conjugates in human urine using isotope dilution liquid chromatography-tandem mass spectrometry with [^{13}C(3)]isoflavone internal standards. *Anal. Biochem.* **2002**, *309* (1), 158−172.
(35) Legette, L. L.; Martin, B. R.; Shahnazari, M.; Lee, W. H.; Helferich, W. G.; Qian, J.; Waters, D. J.; Arabshahi, A.; Barnes, S.; Welch, J.; Bostwick, D. G.; Weaver, C. M. Supplemental dietary racemic equol has modest benefits to bone but has mild uterotropic activity in ovariectomized rats. *J. Nutr.* **2009**, *139* (10), 1908−1913.
(36) Hedlund, T. E.; Maroni, P. D.; Ferucci, P. G.; Dayton, R.; Barnes, S.; Jones, K.; Moore, R.; Ogden, L. G.; Wahala, K.; Sackett, H. M.; Gray, K. J. Long-term dietary habits affect soy isoflavone metabolism and accumulation in prostatic fluid in Caucasian men. *J. Nutr.* **2005**, *135* (6), 1400−1406.
(37) Sites, C. K.; Cooper, B. C.; Toth, M. J.; Gastaldelli, A.; Arabshahi, A.; Barnes, S. Effect of a daily supplement of soy protein on body composition and insulin secretion in postmenopausal women. *Fertil. Steril.* **2007**, *88* (6), 1609−1617.
(38) Allred, C. D.; Twaddle, N. C.; Allred, K. F.; Goeppinger, T. S.; Churchwell, M. I.; Ju, Y. H.; Helferich, W. G.; Doerge, D. R. Soy processing affects metabolism and disposition of dietary isoflavones in ovariectomized BALB/c mice. *J. Agric. Food Chem.* **2005**, *53* (22), 8542−8550.

Preparations of Ovalbumin−Dextran (O−D) Conjugates. Ovalbumin (250 mg) and an equal amount of dextran were mixed and dissolved in 100 mL of water. The pH of the solution was adjusted to pH 8.0 using a 0.1 N NaOH. Afterward, this solution was lyophilized to form a fine powder. The dry powder was heated at 60 °C with 79% relative humidity in a desiccator containing saturated KBr solution for 2 days to form the O−D conjugates. The conjugates were stored at −20 °C and used without any further purification.

Sodium Dodecyl Sulfate−Polyacrylamide Gel Electrophoresis (SDS-PAGE) Analysis of O−D Conjugates. The formation of O−D conjugates was confirmed using SDS-PAGE on a gel electrophoresis apparatus to detect the molecular weight distributions of ovalbumin and the O−D conjugates. Proteins were separated on gels made of 10% acrylamide and 0.1% SDS. Stacking gel made of 5% acrylamide and 0.1% SDS was used to load the samples. Samples were treated with 100 mM dithiothreitol and boiled for 5 min before loading. After electrophoresis, the gel was stained for protein and carbohydrate using Coomassie Blue R-250 and Fuchsin solution, respectively. The protein and carbohydrate stain were destained with 10% acetic acid (v/v) containing 10% methanol (v/v) and 7.5% acetic acid (v/v) water solution, respectively. The ovalbumin content reacted with dextran was analyzed using UN-SCAN-IT gel analysis software (version 6.1, Silk Scientific, Inc., Orem, UT, USA).

Preparations of EGCG O−D Conjugate Nanoparticles and Cross-Linked EGCG O−D Conjugate Nanoparticles. Briefly, 50 mg of O−D conjugate and 25 mg of EGCG were dissolved in 10 mL of deionized water (mass ratio of ovalbumin to EGCG was 1:1). After adjustment of the pH to 5.2, the solution was incubated at 80 °C for 60 min to form EGCG O−D conjugate nanoparticles. The resulting nanoparticle suspension was stored at 4 °C before analysis.

Cross-linked EGCG O−D conjugate nanoparticles were prepared by adding 5 μL of glutaraldehyde to 1 mL of nanoparticle suspension. The cross-linking process was carried out at room temperature for 24 h under a stirring speed of 750 rpm.

Particle Size and Particle Morphology. Particle size was measured in aqueous suspension. One milliliter of EGCG O−D conjugate nanoparticles or cross-linked nanoparticles was centrifuged at 13300 rpm for 5 min, and the sediments were resuspended in 5 mL of deionized water. Mean particle size (number-weighted distribution) was measured using dynamic light scattering (DLS) on Zetatrac (Microtrac Inc., Largo, FL, USA). Samples were measured in four replicates at 25 °C to calculate the average particle size.

The morphology of dry EGCG O−D conjugate nanoparticles and cross-linked nanoparticles was measured using a field emission scanning electron microscope (model JSM-633OF, JEOL Ltd., Tokyo, Japan).

Loading Efficiency and Loading Capacity Assessments. The nanoparticle suspensions were centrifuged at 13300 rpm for 5 min to collect the supernatant. The supernatant was analyzed using HPLC for EGCG content. The loading efficiency and the loading capacity were calculated using the following equations:

$$\text{loading efficiency} = (\text{EGCG amount used for nanoparticle fabrication} - \text{EGCG amount in supernatant}) / \text{EGCG amount used for nanoparticle fabrication} \times 100\%$$

$$\text{loading capacity} = (\text{EGCG amount used for nanoparticle fabrication} - \text{EGCG amount in supernatant}) / \text{dry nanoparticle amount} \times 100\%$$

Nanoparticle Characterization under Different pH Conditions. Briefly, 1 mL of EGCG O−D conjugate nanoparticles or cross-linked EGCG O−D conjugate nanoparticles was centrifuged at 13300 rpm for 5 min, and the sediments were resuspended in 5 mL of deionized water. The pH of the suspension was adjusted to 2.5, 3.0, 4.0, 5.0, 6.0, 7.0, and 7.5 using a diluted HCl or NaOH solution. Mean particle size (number-weighted distribution) and zeta-potential were immediately measured on Zetatrac (Microtrac Inc.). Samples were measured in duplicates at 25 °C to calculate the average particle size and zeta-potential.

Nanoparticle Stability in Simulated Gastric or Intestinal Fluid. One milliliter of EGCG O−D conjugate or cross-linked EGCG O−D conjugate nanoparticles was centrifuged at 13300 rpm for 5 min, and the sediments were resuspended in 5 mL of SGF (pH 4.0, fed state) or SIF (pH 6.0) at 37 °C for 0.5, 1, 1.5, and 2 h. At each time point, particle size (number-weighted distribution) was measured on Zetatrac (Microtrac Inc.). Samples were measured in duplicates to calculate the average particle size.

Release of EGCG in Simulated Digestive Fluids. The cumulative release of EGCG in the nanoparticles was measured in SGF without or with pepsin and in SIF without or with pancreatin.[19] Briefly, after centrifugation, nanoparticles were resuspended in deionized water and then lyophilized. The dry nanoparticles were suspended in 5 mL of SGF (pH 4.0) with or without 0.1% pepsin (w/v) and incubated at 37 °C for 0.5 h. Subsequently, 1 mL of the sample was centrifuged at 13300 rpm for 5 min. Supernatant was measured on HPLC for EGCG content. The nanoparticles were suspended in 5 mL of SIF (pH 6.0) with or without 1.0% pancreatin (w/v) and incubated at 37 °C for 2 h. Then, 1 mL of sample was centrifuged at 13300 rpm for 5 min. The supernatant obtained was measured by HPLC analysis. Samples were measured in four replicates. An Agilent Zorbax SB C18 column (4.6 mm × 250 mm) was used to analyze EGCG. The binary mobile phase consisted of 0.04% acetic acid/water (A) and acetonitrile (B). A 22 min gradient was used as follows: 0−20 min, 10−30% B linear; 20−22 min, 30−10% B linear; followed by 2 min of re-equilibration of the column before the next run. The detection wavelength on the diode array detector was 280 nm. The injection volume was 5 μL with a flow rate at 1 mL/min. The cumulative EGCG release was calculated using the following equation:

$$\text{cumulative EGCG release (\%)} = (\text{EGCG amount in supernatant}/\text{EGCG amount in dry nanoparticles}) \times 100\%$$

EGCG Absorption on Caco-2 Cell Monolayers. Caco-2 cells were seeded in 6-well transwell plates with an internal diameter of 24 mm and a membrane growth area of 4.67 cm^2 (Corning Inc., Lowell, MA, USA). The cells were cultured using Dulbecco's modified Eagle media containing 20% fetal bovine serum, 1% penicillin−streptomycin, and 1% nonessential amino acids. The cells were grown to confluence and allowed to mature for 17 days at 37 °C and 5% CO_2. The cell culture media were changed every 1−2 days. The permeability study was carried out in triplicate after the transepithelial electrical resistance (TEER) was 500−600 Ω × cm^2, measured using an epithelial volt-ohm meter (Millicell ERS-2, Millipore Corp., Billerica, MA, USA). The permeability study followed a published paper with minor modifications.[29] EGCG or EGCG O−D conjugate nanoparticles were added into Hank's balanced salt solution (HBSS, pH adjusted to 6.0) to control EGCG concentration at 0.025 mg/mL. HBSS buffer was used as a blank. One and a half milliliters of each sample was transferred to the apical chamber of the transwells, and 2.6 mL of the fresh buffer was added to the basolateral chamber. After incubation at 37 °C for 30, 60, 90, and 120 min, the TEER was measured. Subsequently, 0.5 mL of the samples was taken from the basolateral chamber, acidified with ascorbic acid solution to adjust the pH to 2.5 and stored in −80 °C until analyses. The fresh buffer (0.5 mL) was refilled in the basolateral chamber. The samples were analyzed by HPLC-ESI-MS^n using a published method with minor modifications.[29] An Agilent Zorbax SB C18 column (4.6 mm × 250 mm) was used for compound separation. The binary mobile phase consisted of 0.04% acetic acid/water (A) and acetonitrile (B). A 22 min gradient was as follows: 0−20 min, 10−30% B linear; 20−22 min, 30−10% B linear; followed by 2 min of re-equilibration of the column before the next run. The injection volume was 20 μL with a flow rate at 1 mL/min. Electrospray ionization in negative mode was performed using a nebulizer at 65 psi, drying gas at 11 L/min, drying temperature of 350

°C, and capillary at 4000 V. The MRM was used to monitor the transition of deprotonated EGCG m/z 457 $[M - H]^-$ to the product ion m/z 169. EGCG was used as an external standard. Quantification was conducted using QuantAnalysis (version 2.0, Bruker Daltonics Inc., Billerica, MA, USA). The apparent permeability coefficient (P_{app}) of EGCG was calculated using the equation

$$P_{app} = (dQ/dt) \times (1/AC_0)$$

where dQ/dt is the permeability rate (μg/s), C_0 is the initial concentration in the apical chamber (μg/mL), and A is the surface area of the filter (cm^2), which was 4.67 cm^2 in this study.

Statistical Analyses. Data were expressed as the mean ± standard deviation. Student's t test was used to compare mean values between two groups using JMP software (version 8.0, SAS Institute Inc., Cary, NC, USA). A difference with $p \leq 0.05$ was considered significant.

RESULTS

Synthesis and Characterization of O−D Conjugates. Natural ovalbumin showed a single band (45 kDa), whereas dextran did not show any bands on electrophoresis gel (Figure 1A). The ovalbumin/dextran physical mixture showed the same band as the ovalbumin sample, indicating that no reaction took place between ovalbumin and dextran. After the ovalbumin and dextran mixture was incubated at 60 °C under a relative humidity of 79% for 2 days, a new smear band (80−230 kDa) appeared, and the ovalbumin single band became smaller. In Figure 1B, the ovalbumin and ovalbumin/dextran physical mixture showed a single band in carbohydrate stained gel. This was because ovalbumin itself is a glycoprotein. No band appeared on dextran samples because dextran could not enter the gel. However, O−D conjugate samples showed a smear band and the ovalbumin band was weaker, which further confirmed that dextran was covalently conjugated with ovalbumin. Gel analysis using UN-SCAN-IT software showed that about 27% of ovalbumin reacted with dextran to form conjugates.

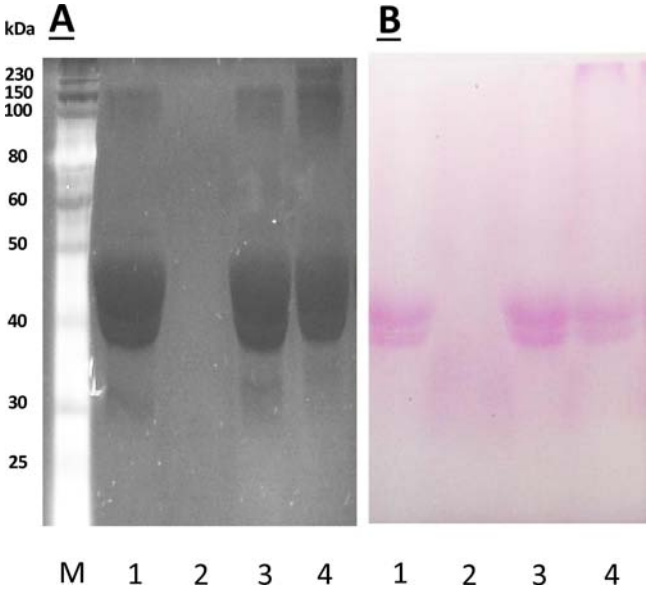

Figure 1. SDS-PAGE analysis of ovalbumin, dextran, ovalbumin/dextran physical mixture, and O−D conjugates: (A) protein stain; (B) carbohydrate stain. Lanes: M, molecular weight marker; 1, 2, 3, and 4, ovalbumin, dextran, ovalbumin/dextran physical mixture, and O−D conjugates, respectively. The amount of ovalbumin in each lane was 22 μg. The amount of dextran was 22 μg.

Particle Size, Morphology, EGCG Loading Efficiency, and Loading Capacity. After nanoparticles were resuspended in water, EGCG O−D conjugate nanoparticles and cross-linked EGCG O−D conjugate nanoparticles showed average particle sizes of 285 and 339 nm, respectively (Figure 2A1,A2). Both dry EGCG O−D conjugate nanoparticles and cross-linked nanoparticles showed spherical morphology, visualized by SEM (Figure 2B1,B2).The sizes measured by Zetatrac were larger than those measured by SEM because dry particles were used in the SEM assessment.[13] The loading efficiencies of EGCG in EGCG O−D conjugate nanoparticles and cross-linked nanoparticles were 23.4 and 30.0%, respectively (Table 1). The loading capacities of EGCG in the nanoparticles were 19.6 and 20.9%, respectively. No significant differences were observed in either loading efficiency or loading capacity between EGCG O−D conjugate nanoparticles and cross-linked nanoparticles.

Nanoparticle Characterization under Different pH Conditions. EGCG O−D conjugate nanoparticles showed a particle size of 210 nm in aqueous suspension at pH 2.5, and size remained at 323 and 308 nm when the pH was adjusted to 3.0 and 4.0, respectively (Figure 3A). Particle size increased to 634 nm when the pH of EGCG O−D conjugate nanoparticle suspension was 5.0 and then decreased to between 168 and 211 nm in the pH range from 6.0 to 7.5. Cross-linked EGCG O−D conjugate nanoparticles showed particle sizes of 173, 336, and 347 nm at pH 2.5, 3.0, and 4.0, respectively. When the pH of the nanoparticle suspension was adjusted to 5.0, cross-linked EGCG O−D conjugate nanoparticles had a size of 325 nm, and particle sizes remained between 244 and 340 nm in a pH range of 6.0−7.5.

EGCG O−D conjugate nanoparticles and cross-linked nanoparticles had comparable zeta-potentials in a pH range from 2.5 to 7.5 (Figure 3B). Both EGCG O−D conjugate nanoparticles and cross-linked nanoparticles showed a zeta-potential of around 10 mV at pH 2.5 and 3.0. Decreased zeta-potentials were observed in EGCG O−D conjugate nanoparticles (between 6.71 and −1.37 mV) and cross-linked nanoparticles (between 1.45 and −6.07 mV) in a pH range of 4.0−6.0. This was because such a pH range was close to the isoelectric point of ovalbumin (around 4.5−4.8). When the pH was above 7, both of the nanoparticles had a zeta-potential around −10 mV.

Stability of Nanoparticles in Simulated Digestive Fluids. The initial particle sizes of EGCG O−D conjugate nanoparticles and cross-linked nanoparticles resuspended in SGF were 261 and 380 nm, respectively (Figure 4A). Incubating these two types of nanoparticles in SGF at 37 °C for 2 h did not cause a significant change in particle size. The particle sizes of EGCG O−D conjugate nanoparticles were 183, 349, 294, and 299 nm at 0.5, 1, 1.5, and 2 h, respectively. Similarly, cross-linked EGCG O−D conjugate nanoparticles showed average particles sizes of 478, 294, 527, and 439 nm after 0.5, 1, 1.5, and 2 h of incubation, respectively.

Both EGCG O−D conjugate nanoparticles and cross-linked nanoparticles appeared stable in the SIF at 37 °C for 2 h (Figure 4B). After EGCG O−D conjugate nanoparticles and cross-linked nanoparticles were resuspended in SIF, particle sizes were 232 and 206 nm, respectively. After 0.5 h of incubation, the particle sizes of these two nanoparticles were 217 and 280 nm, and the size remained at 291 and 265 nm for 2 h.

EGCG Release from Nanoparticles in Simulated Digestive Fluids. After incubation of the nanoparticles in

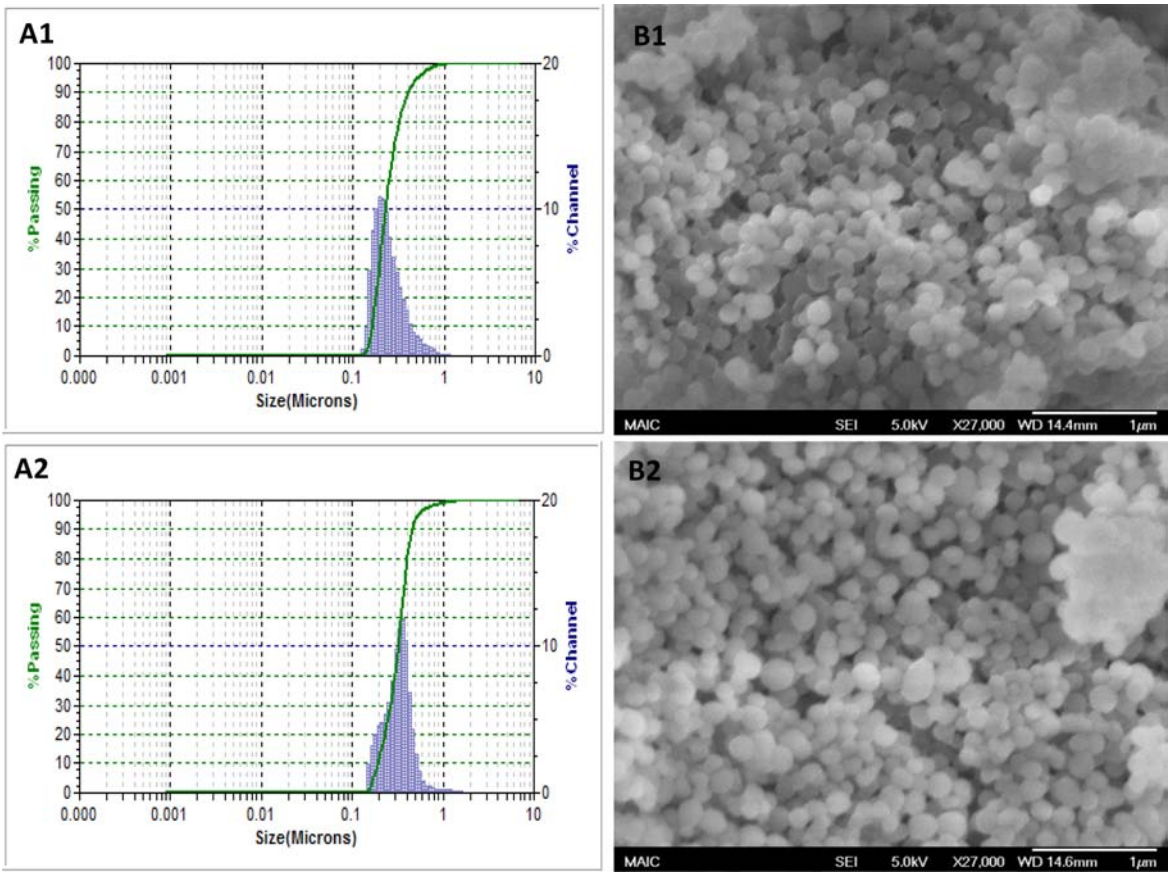

Figure 2. Particle size of (A1) EGCG O−D conjugate nanoparticles and (A2) cross-linked EGCG O−D conjugate nanoparticles measured in aqueous suspension and morphology of (B1) EGCG O−D conjugate nanoparticles and (B2) cross-linked EGCG O−D conjugate nanoparticles measured by scanning electron microscopy (SEM), respectively.

Table 1. Loading Efficiency and Loading Capacity of EGCG in EGCG O−D Conjugate Nanoparticles and Cross-Linked EGCG O−D Conjugate Nanoparticles[a]

nanoparticles	loading efficiency (%)	loading capacity (w/w %)
EGCG O−D conjugate	23.4 ± 2.9	19.6 ± 3.2
cross-linked EGCG O−D conjugate	30.0 ± 4.9	20.9 ± 3.8

[a]Data are the mean ± standard deviation of four replicates. No significant differences are observed between samples using Student's t test at $p \leq 0.05$.

SGF for 0.5 h, 12.3 and 8.3% of EGCG was released from EGCG O−D conjugate nanoparticles and cross-linked nanoparticles, respectively (Figure 5A). Introducing pepsin into the SGF significantly increased release of EGCG to 17.2 and 14.9%, respectively. Similarly, 27.1 and 21.9% of EGCG was released from EGCG O−D conjugate nanoparticles and cross-linked nanoparticles in SIF at 2 h, respectively (Figure 5B). Adding pancreatin in SIF significantly increased EGCG release to 37.9 and 32.5% of EGCG, respectively. Cross-linking of ovalbumin in the nanoparticles retarded the EGCG release in SIF with or without pancreatin.

EGCG Transport on Caco-2 Monolayers. Cross-linking using glutaraldehyde did not show significant advantages compared with non-cross-linked ones, except for a slight reduction of accumulated release in simulated intestinal fluids. Such minor benefit did not warrant the cross-linking step using toxic glutaraldehyde. Therefore, EGCG O−D conjugate nanoparticles were used on a permeability study. The TEER percentage of Caco-2 monolayers treated by HBSS buffer (blank) dropped to 100.6, 95.6, 94.1, and 89.9% of initial value at 30, 60, 90, and 120 min, respectively (Figure 6A). TEER percentages of Caco-2 monolayers treated by EGCG were 98.1, 95.1, 91.7, and 85.0% of the initial value at different incubation periods. EGCG O−D conjugate nanoparticles caused theTEER to decrease to 95.2, 90.9, 89.3, and 79.8% of the initial value at 30, 60, 90, and 120 min, respectively. However, there were no significant differences of TEER percentage among Caco-2 monolayers treated by the nanoparticles, EGCG, or buffer.

The apparent permeability coefficient (P_{app}) of EGCG from the apical to the basolateral side on Caco-2 monolayers was investigated after incubation of EGCG solution or EGCG O−D conjugate nanoparticles with Caco-2 monolayers for up to 120 min (Figure 6B). The P_{app} of EGCG in EGCG solution was between 0.28 and 0.42 × 10^{-6} cm/s during the incubation period. However, the P_{app} of EGCG in the nanoparticles was between 0.52 and 0.78 × 10^{-6} cm/s, and significantly higher than those of EGCG solution.

DISCUSSION

The Maillard reaction forms covalent bonds between carbonyl groups and amino groups.[26] The O−D conjugates were generated by controlling the Maillard reaction at an early stage, the Amadori rearrangements.[27,28,30]

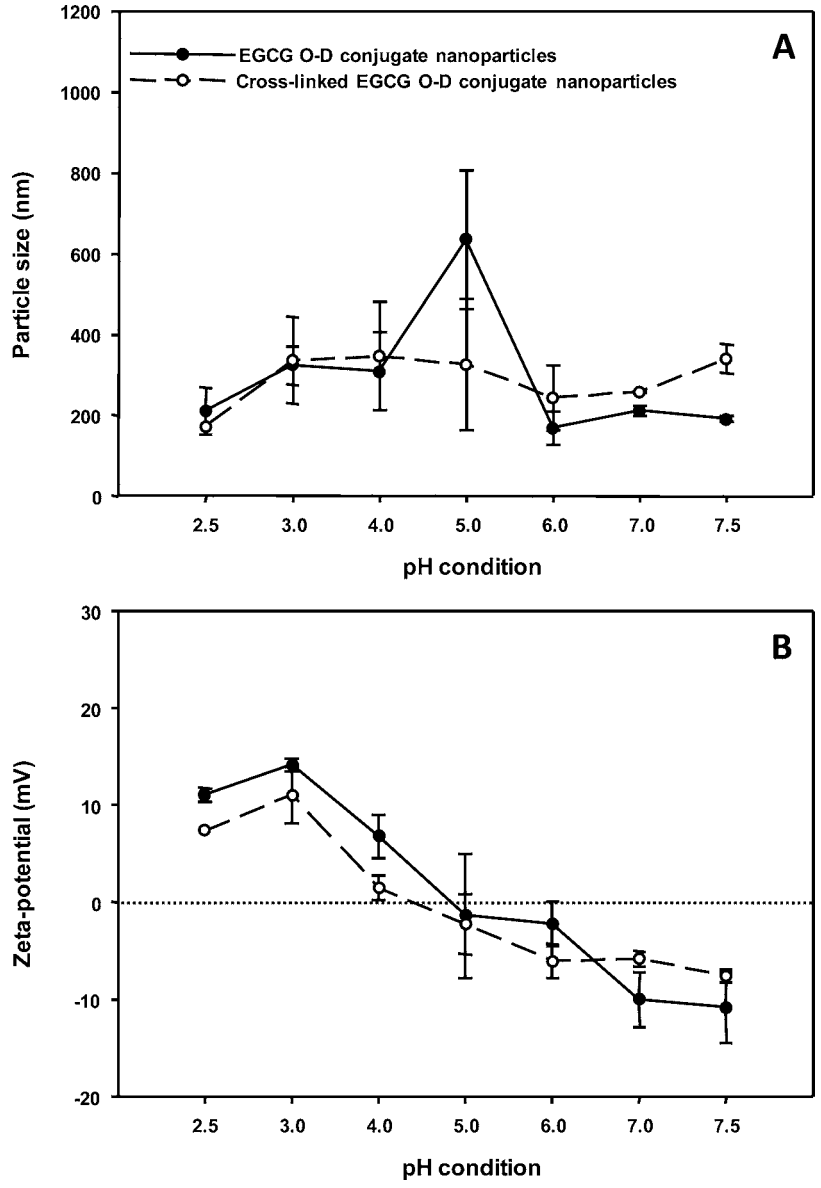

Figure 3. (A) Particle size and (B) zeta-potential of EGCG O−D conjugate nanoparticles and cross-linked EGCG O−D conjugate nanoparticles in the pH range from 2.5 to 7.5.

After the O−D conjugates had been mixed with EGCG and the pH of the solution had been adjusted to 5.2, heating the mixture at 80 °C for 60 min caused the formation of a white milky suspension. The heating step induced the gelation of ovalbumin, which led to the heat-induced unfolding of ovalbumin.[31] The protein−protein interactions (hydrogen bonding, electrostatic and hydrophobic interactions, and disulfide−sulfhydryl interchange) and protein−EGCG interactions (hydrogen bonding and hydrophobic interactions) caused the self-assembly of EGCG and O−D conjugates. This resulted in encapsulation of EGCG in the nanoparticles.[13,15,31] Conjugation of ovalbumin with dextran increased the hydrophilic property of O−D conjugates, which helped to stabilize the nanoparticles in aqueous suspension. Glutaraldehyde was added to the nanoparticle suspension to cross-link the ovalbumin proteins, which further stabilized the structure of EGCG O−D conjugate nanoparticles. The loading efficiency and the loading capacity of EGCG in EGCG O−D conjugate nanoparticles and cross-linked EGCG O−D conjugate nanoparticles were not affected by additional cross-linking because glutaraldehyde was used after the heating step (Table 1). The formation of EGCG O−D conjugate nanoparticles is illustrated in Figure 7. We hypothesized that the core of the nanoparticles was formed by the hydrophobic peptides of ovalbumin and that the hydrophilic dextran was on the surface of the nanoparticles as the shell. Our data showed that the heating process degraded about 2.4% EGCG. Therefore, the degradation of EGCG was not a concern.

The pH in the human gastrointestinal tract varies drastically in different segments, such as pH 6.5−7.0 in the mouth, 1.5 (fast state)−5.0 (fed state) in the stomach, 5.0−7.0 in the small intestine, and 7.0−7.4 in the large intestine.[10,11] The size and surface charge of protein-based nanoparticles depend on pH conditions. Weakened repulsion among the nanoparticles caused particle precipitation when the pH was around the isoelectric point of the selected proteins.[16] Therefore, it is important to understand the change of particle size and zeta-potential under different pH conditions. In the present study,

dx.doi.org/10.1021/jf404621f | J. Agric. Food Chem. 2014, 62, 1301−1309

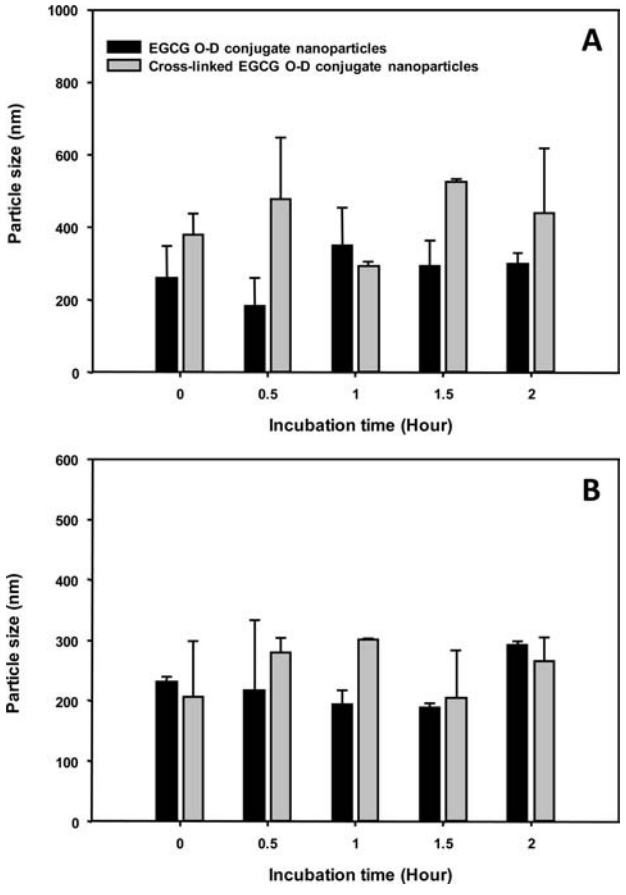

Figure 4. Particle size of EGCG O−D conjugate nanoparticles and cross-linked EGCG O−D conjugate nanoparticles in (A) simulated gastric fluid (SGF, pH 4.0) and (B) simulated intestinal fluid (SIF, pH 6.0) at 37 °C for 0, 0.5, 1, 1.5, and 2 h.

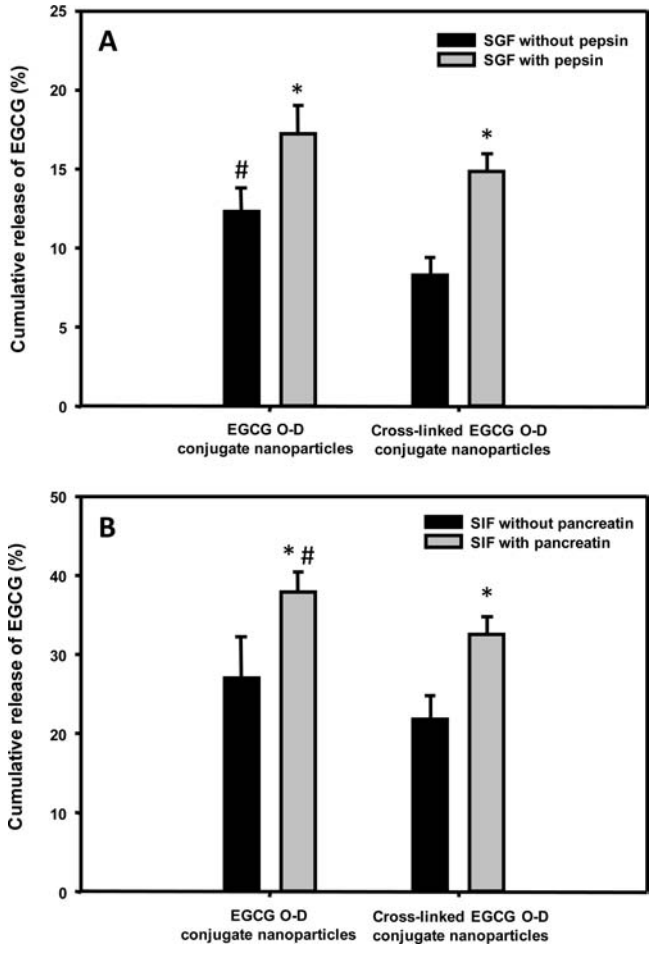

Figure 5. Cumulative release of EGCG from EGCG O−D conjugate nanoparticles and cross-linked EGCG O−D conjugate nanoparticles in (A) simulated gastric fluid (SGF, pH 4.0) without or with pepsin for 0.5 h and (B) simulated intestinal fluid (SIF, pH 6.0) without or with pancreatin for 2 h at 37 °C. ∗ indicates significant differences between simulated fluid without enzyme and fluid with enzyme. # indicates significant differences between EGCG O−D conjugate nanoparticles and cross-linked nanoparticles.

both EGCG O−D conjugate nanoparticles and cross-linked EGCG O−D conjugate nanoparticles remained nanosized in a pH range from 2.5 to 7.5 (Figure 3). Dextran has been reported to enhance colloidal stability.[23,32,33] Thus, hydrophilic dextran on the surface of the nanoparticles may retard the aggregation of ovalbumin proteins. The zeta-potential of nanoparticles is primarily determined by protein, and zeta-potential varies according to pH conditions. Both EGCG O−D conjugate and cross-linked nanoparticles showed positive zeta-potentials in a pH range from 2.5 to 3.0, whereas negative charges were observed when the pH was adjusted above 7.0. Both types of nanoparticles showed weakened zeta-potentials (−6.07 to 6.76 mV) at pH 4.0−6.0. Mucus layers in the small intestine possess negative charges and serve as a barrier between drugs and intestinal epithelia.[34] Thus, nanoparticles with strong negative or positive charges may be repulsed or adsorbed by mucus layers to hinder contact with epithelial cells, whereas weakly charged nanoparticles may readily penetrate the mucus layers.[34,35] EGCG O−D conjugate nanoparticles and cross-linked EGCG O−D conjugate nanoparticles had weak zeta-potentials at pH 5.0−6.0, which may enhance the penetration of nanoparticles through the mucus layers to reach epithelial cells in the upper portion of the small intestine.

It takes about 0.5−2 and 2−4 h for ingested food to pass through the stomach and small intestine, respectively.[10,11] Thus, the stability of nanoparticles in the stomach and small intestine is critical. The majority of ingested nanoparticles should maintain nanosize to enhance the absorption of loaded drugs. In SGF (pH 4.0, fed state) for 2 h, EGCG O−D conjugate nanoparticles showed an average particle size between 183 and 349 nm, whereas the sizes of cross-linked EGCG O−D conjugate nanoparticles were between 294 and 527 nm. More importantly, both types of nanoparticles showed particle sizes of below 300 nm in SIF (pH 6.0, upper portion of the small intestine) for up to 2 h. This was explained by the capacity of dextran to stabilize nanoparticles in the gastrointestinal tract with high salt concentration and pH conditions.[33] Nanoparticles with better stability in the gastrointestinal tract may increase permeation of EGCG in the small intestine.

Release of bioactive compounds from nanoparticles in the gastrointestinal tract is attributed to the diffusion of bioactive compounds in gastrointestinal fluid. More importantly, degradation of nanoparticles by digestive enzymes in the gastrointestinal tract may cause the burst release of bioactive compounds.[19,36] For example, pepsin in the stomach and trypsin, chymotrypsin, elastase, and carboxypeptidases A and B in the small intestine can hydrolyze protein to amino acids, whereas α-amylase can hydrolyze 1,4-α-D-glucosidic linkages in

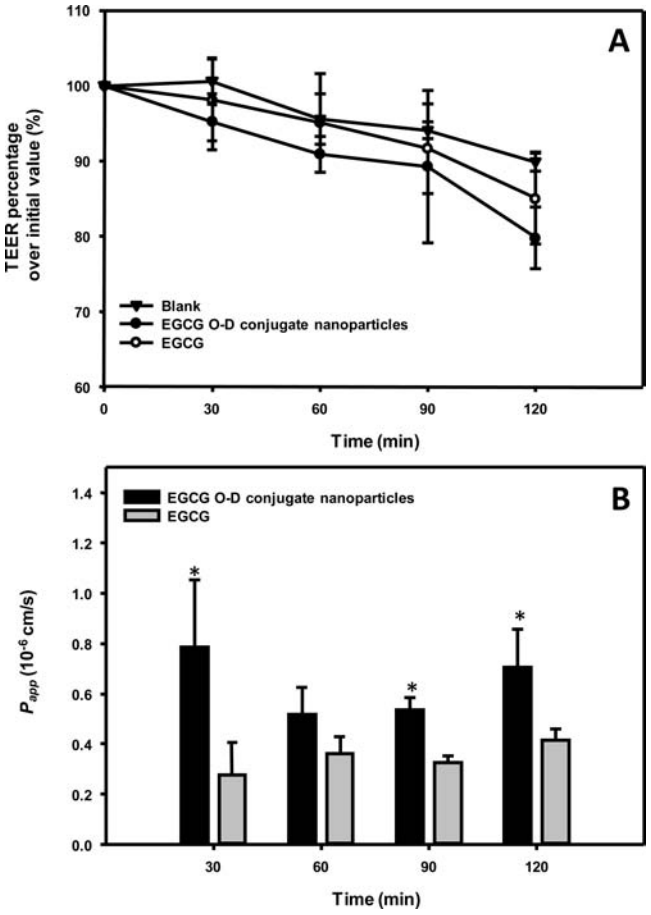

Figure 6. (A) Transepithelial electric resistance (TEER) and (B) apparent permeability coefficient (P_{app}) of EGCG in solution and EGCG O−D conjugate nanoparticles at 37 °C for 30, 60, 90, and 120 min. ∗ indicates significant differences between nanoparticles and solutions at $p \leq 0.05$.

polysaccharides. Dextran consists of the straight chains with α-1,6 glycosidic linkages between glucoses and branches with α-1,3 linkage. This structure makes dextran resistant to hydrolysis by amylase in the gastrointestinal tract.[25] In the present study, the release of EGCG from both types of nanoparticles in simulated fluids with digestive enzymes was higher than that without digestive enzymes. This suggests that ovalbumin was hydrolyzed by proteinases in both SGF and SIF. It should be noted that EGCG O−D conjugate nanoparticles and cross-linked EGCG O−D conjugate nanoparticles showed similar EGCG release percentages in the simulated fluid with digestive enzymes. This may be explained by dextran on the surface of the nanoparticles, which protected the proteins from digestion by hindering contact between ovalbumin and proteinase. Also, ovalbumin was reported to be resistant to pepsin digestion in the stomach at fed state, and the conformational change of ovalbumin after thermal process provided resistance against trypsin, chymotrypsin, and elastase in the small intestine.[20,21,37] Furthermore, cross-linking ovalbumin in nanoparticles decreased EGCG release in simulated fluids with or without digestive enzymes, which suggested that protein cross-linking further improved the stability of nanoparticles in the presence of proteinases.

Caco-2 cell monolayers have been widely used to estimate the permeability of phenolic compounds in vitro.[38,39] Monolayers were formed after the TEER value of Caco-2 cells was between 150 and 1600 Ω × cm^2.[40] The TEER value of Caco-2 monolayers in the present study was 500−600 Ω × cm^2. A significant decrease of TEER indicated that the tight junctions of the monolayers were disrupted or monolayer integrity was compromised. Nanoparticles with a size <20 nm have the capacity to reversibly open tight junctions among cells and facilitate the permeation of loaded drugs via the paracellular pathway.[10] In this study, TEER values of Caco-2 monolayers were similar among the blank, EGCG solution, and EGCG O−D conjugate nanoparticles. This suggested that the concentration of EGCG had little adverse effect on the integrity of the monolayer, and nanoparticles did not open tight junctions of the monolayers to facilitate the permeation of EGCG by the paracellular pathway.

The main mechanism for nanoparticles to enhance the permeability of bioactive compounds was the cellular uptake of the nanoparticles via endocytosis, including clathrin- and/or caveolae-mediated endocytosis.[10,11,41] It has been proposed that clathrin-mediated endocytosis allowed nanoparticles with an average size below 300 nm to penetrate the cell membrane, whereas nanoparticles with a size below 500 nm could be internalized into cells by caveolae-mediated endocytosis.[42] Upon internalization, nanoparticles can either be delivered into endo/lysosome for release of bioactive compounds by

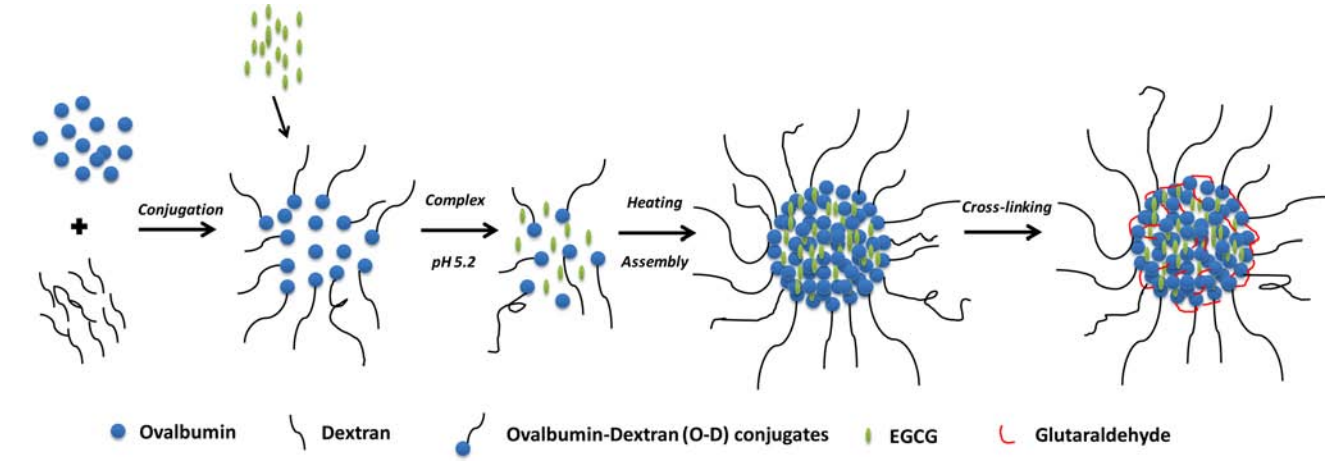

Figure 7. Hypothetical illustration of formation of EGCG O−D conjugate nanoparticles and cross-linked EGCG O−D conjugate nanoparticles.

degradation or escape the endo/lysosome to arrive at the basolateral side by exocytosis.[10,11] In the present study, the P_{app} of EGCG in EGCG solution was (0.28−0.42) × 10^{-6} cm/s, which was in accordance with previous studies.[29,43] EGCG O−D conjugate nanoparticles significantly increased the P_{app} of EGCG to (0.54−0.78) × 10^{-6} cm/s. We hypothesized that the P_{app} increase of EGCG using EGCG O−D conjugate nanoparticles was mainly attributed to the cellular uptake of nanoparticles by Caco-2 cells.

In conclusion, ovalbumin and dextran were conjugated using the Maillard reaction. EGCG O−D conjugate nanoparticles and cross-linked EGCG O−D conjugate nanoparticles were formed using a heat-induced self-assembly. These particles showed a spherical morphology and had sizes of 285 and 339 nm in aqueous suspension. The loading efficiencies of EGCG in these conjugate nanoparticles were 23.4 and 30.0%, whereas the loading capacities were 19.6 and 20.9%, respectively. EGCG O−D conjugate nanoparticles and cross-linked nanoparticles remained nanosized in a pH range from 2.5 to 7.5, and the size remained stable in SGF and SIF. EGCG in EGCG O−D conjugate nanoparticles showed higher apparent permeability coefficient (P_{app}) on Caco-2 monolayers compared to EGCG solution.

AUTHOR INFORMATION

Corresponding Author

*(L.G.) Phone: (352) 392-1991, ext. 210. Fax: (352) 392-9467. E-mail: LGu@ufl.edu.

Notes

The authors declare no competing financial interest.

ACKNOWLEDGMENTS

We sincerely acknowledge Dr. Paul L. Carpinone for technical assistance with the operation of SEM and data interpretation. We thank Jung-Heun Ha and Dr. Sukru Gulec for their help in SDS-PAGE analyses and operation of UN-SCAN-IT gel analysis.

ABBREVIATIONS USED

EGCG, (−)-epigallocatechin gallate; O−D, ovalbumin−dextran; P_{app}, apparent permeability coefficients; SEM, scanning electron microscopy; SGF, simulated gastric fluid; SIF, Simulated intestinal fluid; SDS-PAGE, sodium dodecyl sulfate−polyacrylamide gel electrophoresis; TEER, transepithelial electric resistance

REFERENCES

(1) Jung, Y. D.; Kim, M. S.; Chay, K. O.; Ahn, B. W.; Liu, W.; Bucana, C. D.; Gallick, G. E.; Ellis, L. M. EGCG, a major component of gree tea, inhibits tumour growth by inhibiting VEGF induction in human colon carcinoma cells. *Br. J. Cancer* **2001**, *84*, 844−850.

(2) Annabi, B.; Bouzeghrane, M.; Moumdjian, R.; Moghrabi, A.; Béliveau, R. Probing the infiltrating character of brain tumors: inhibition of RhoA/ROK-mediated CD44 cell surface shedding from glioma cells by the green tea catechin EGCg. *J. Neurochem.* **2005**, *94*, 906−916.

(3) Chung, L. Y.; Cheung, T. C.; Kong, S. K.; Fung, K. P.; Choy, Y. M.; Chan, Z. Y.; Kwok, T. T. Induction of apoptosis by green tea catechins in human prostate cancer DU145 cells. *Life Sci.* **2001**, *68*, 1207−1214.

(4) Ahn, W. S.; Huh, S. W.; Bae, S.-M.; Lee, I. P.; Lee, J. M.; Namkoong, S. E.; Kim, C. K.; Sin, J.-I. A major constituent of green tea, EGCG, inhibits the growth of a human cervical cancer cell line, CaSki cells, through apoptosis, G1 arrest, and regulation of gene expression. *DNA Cell Biol.* **2003**, *22*, 217−224.

(5) Kemberling, J. K.; Hampton, J. A.; Keck, R. W.; Gomez, M. A.; Selman, S. H. Inhibition of bladder tumor growth by the green tea derivative epigallocatechin-3-gallate. *J. Urol.* **2003**, *170*, 773−776.

(6) Nagle, D. G.; Ferreira, D.; Zhou, Y.-D. Epigallocatechin-3-gallate (EGCG): chemical and biomedical perspectives. *Phytochemistry* **2006**, *67*, 1849−1855.

(7) Zhu, M.; Chen, Y.; Li, R. C. Oral absorption and bioavailability of tea catechins. *Planta Med.* **2000**, *66*, 444−447.

(8) Nakagawa, K.; Miyazawa, T. Absorption and distribution of tea catechin, (−)-epigallocatechin-3-gallate, in the rat. *J. Nutr. Sci. Vitaminol.* **1997**, *43*, 679−684.

(9) Yang, C. S.; Chen, L.; Lee, M. J.; Balentine, D.; Kuo, M. C.; Schantz, S. P. Blood and urine levels of tea catechins after ingestion of different amounts of green tea by human volunteers. *Cancer Epidemiol. Biomarkers Prev.* **1998**, *7*, 351−354.

(10) Acosta, E. Bioavailability of nanoparticles in nutrient and nutraceutical delivery. *Curr. Opin. Colloid Interface Sci.* **2009**, *14*, 3−15.

(11) Roger, E.; Lagarce, F.; Garcion, E.; Benoit, J.-P. Biopharmaceutical parameters to consider in order to alter the fate of nanocarriers after oral delivery. *Nanomedicine* **2010**, *5*, 287−306.

(12) des Rieux, A.; Fievez, V.; Garinot, M.; Schneider, Y.-J.; Préat, V. Nanoparticles as potential oral delivery systems of proteins and vaccines: a mechanistic approach. *J. Controlled Release* **2006**, *116*, 1−27.

(13) Li, Z.; Percival, S. S.; Bonard, S.; Gu, L. Fabrication of nanoparticles using partially purified pomegranate ellagitannins and gelatin and their apoptotic effects. *Mol. Nutr. Food Res.* **2011**, *55*, 1096−1103.

(14) Zhao, D.; Zhao, X.; Zu, Y.; Li, J.; Zhang, Y.; Jiang, R.; Zhang, Z. Preparation, characterization, and *in vitro* targeted delivery of folate-decorated paclitaxel-loaded bovine serum albumin nanoparticles. *Int. J. Nanomed.* **2010**, *5*, 669−677.

(15) Zou, T.; Li, Z.; Percival, S. S.; Bonard, S.; Gu, L. Fabrication, characterization, and cytotoxicity evaluation of cranberry procyanidins-zein nanoparticles. *Food Hydrocolloids* **2012**, *27*, 293−300.

(16) Li, Z.; Gu, L. Effects of mass ratio, pH, temperature, and reaction time on fabrication of partially purified pomegranate ellagitannin−gelatin nanoparticles. *J. Agric. Food Chem.* **2011**, *59*, 4225−4231.

(17) Yi, K.; Cheng, G.; Xing, F. Gelatin/tannin complex nanospheres via molecular assembly. *J. Appl. Polym. Sci.* **2006**, *101*, 3125−3130.

(18) Capanni, C.; Taddei, N.; Gabrielli, S.; Messori, L.; Orioli, P.; Chiti, F.; Stefani, M.; Ramponi, G. Investigation of the effects of copper ions on protein aggregation using a model system. *Cell. Mol. Life Sci.* **2004**, *61*, 982−991.

(19) Luo, Y.; Zhang, B.; Whent, M.; Yu, L.; Wang, Q. Preparation and characterization of zein/chitosan complex for encapsulation of α-tocopherol, and its in vitro controlled release study. *Colloids Surf. B: Biointerfaces* **2011**, *85*, 145−152.

(20) Cuccioloni, M.; Sparapani, L.; Amici, M.; Lupidi, G.; Eleuteri, A. M.; Angeletti, M. Kinetic and equilibrium characterization of the interaction between bovine trypsin and I-ovalbumin. *Biochim. Biophys. Acta−Proteins Proteomics* **2004**, *1702*, 199−207.

(21) Martos, G.; Contreras, P.; Molina, E.; López-Fandiño, R. Egg white ovalbumin digestion mimicking physiological conditions. *J. Agric. Food Chem.* **2010**, *58*, 5640−5648.

(22) Moncrief, J. A.; Darin, J. C.; Canizaro, P. C.; Sawyer, R. B. Use of dextran to prevent arterial and venous thrombosis. *Ann. Surg.* **1963**, *158*, 553−559.

(23) de Raucourt, E.; Mauray, S.; Chaubet, F.; Maiga-Revel, O.; Jozefowicz, M.; Fischer, A. M. Anticoagulant activity of dextran derivatives. *J. Biomed. Mater. Res.* **1998**, *41*, 49−57.

(24) Varga, R.; Török, L.; Szabó, A.; Kovács, F.; Keresztes, M.; Varga, G.; Kaszaki, J.; Boros, M. Effects of colloid solutions on ischemia-reperfusion-induced periosteal microcirculatory and inflammatory reactions: comparison of dextran, gelatin, and hydroxyethyl starch. *Crit. Care Med.* **2008**, *36*, 2828−2837.

(25) Sery, T. W.; Hehre, E. J. Degradation of dextrans by enzymes of intestinal bacteria. *J. Bacteriol.* **1956**, *71*, 373−380.
(26) Jaeger, H.; Janositz, A.; Knorr, D. The Maillard reaction and its control during food processing. The potential of emerging technologies. *Pathol. Biol.* **2010**, *58*, 207−213.
(27) Kato, A.; Sasaki, Y.; Furuta, R.; Kobayashi, K. Functional protein-polysaccharide conjugate prepared by controlled dry-heating of ovalbumin-dextran mixtures. *Agric. Biol. Chem.* **1990**, *54*, 107−112.
(28) Choi, S. J.; Kim, H. J.; Park, K. H.; Moon, T. W. Molecular characteristics of ovalbumin−dextran conjugates formed through the Maillard reaction. *Food Chem.* **2005**, *92*, 93−99.
(29) Zhang, L.; Zheng, Y.; Chow, M. S. S.; Zuo, Z. Investigation of intestinal absorption and disposition of green tea catechins by Caco-2 monolayer model. *Int. J. Pharm.* **2004**, *287*, 1−12.
(30) Zhou, H.; Sun, X.; Zhang, L.; Zhang, P.; Li, J.; Liu, Y.-N. Fabrication of biopolymeric complex coacervation core micelles for efficient tea polyphenol delivery via a green process. *Langmuir* **2012**, *28*, 14553−14561.
(31) Deng, W.; Li, J.; Yao, P.; He, F.; Huang, C. Green preparation process, characterization and antitumor effects of doxorubicin−BSA−dextran nanoparticles. *Macromol. Biosci.* **2010**, *10*, 1224−1234.
(32) Sun, G.; Shen, Y.-I.; Ho, C. C.; Kusuma, S.; Gerecht, S. Functional groups affect physical and biological properties of dextran-based hydrogels. *J. Biomed. Mater. Res. Part A* **2010**, *93A*, 1080−1090.
(33) Jang, H.; Ryoo, S.-R.; Kostarelos, K.; Han, S. W.; Min, D.-H. The effective nuclear delivery of doxorubicin from dextran-coated gold nanoparticles larger than nuclear pores. *Biomaterials* **2013**, *34*, 3503−3510.
(34) Ensign, L. M.; Cone, R.; Hanes, J. Oral drug delivery with polymeric nanoparticles: the gastrointestinal mucus barriers. *Adv. Drug Delivery Rev.* **2012**, *64*, 557−570.
(35) Norris, D. A.; Puri, N.; Sinko, P. J. The effect of physical barriers and properties on the oral absorption of particulates. *Adv. Drug Delivery Rev.* **1998**, *34*, 135−154.
(36) Shutava, T. G.; Balkundi, S. S.; Vangala, P.; Steffan, J. J.; Bigelow, R. L.; Cardelli, J. A.; O'Neal, D. P.; Lvov, Y. M. Layer-by-layer-coated gelatin nanoparticles as a vehicle for delivery of natural polyphenols. *ACS Nano* **2009**, *3*, 1877−1885.
(37) Mellet, P.; Michels, B.; Bieth, J. G. Heat-induced conversion of ovalbumin into a proteinase inhibitor. *J. Biol. Chem.* **1996**, *271*, 30311−30314.
(38) Gao, S.; Hu, M. Bioavailability challenges associated with development of anti-cancer phenolics. *Mini Rev. Med. Chem.* **2010**, *10*, 550−567.
(39) Walgren, R. A.; Walle, U. K.; Walle, T. Transport of quercetin and its glucosides across human intestinal epithelial Caco-2 cells. *Biochem. Pharmacol.* **1998**, *55*, 1721−1727.
(40) Shah, P.; Jogani, V.; Bagchi, T.; Misra, A. Role of Caco-2 cell monolayers in prediction of intestinal drug absorption. *Biotechnol. Prog.* **2006**, *22*, 186−198.
(41) Wang, J.; Byrne, J. D.; Napier, M. E.; DeSimone, J. M. More effective nanomedicines through particle design. *Small* **2011**, *7*, 1919−1931.
(42) Rejman, J.; Oberle, V.; Zuhorn, I. S.; Hoekstra, D. Size-dependent internalization of particles via the pathways of clathrin- and caveolae-mediated endocytosis. *Biochem. J.* **2004**, *377*, 159−169.
(43) Hu, B.; Ting, Y.; Yang, X.; Tang, W.; Zeng, X.; Huang, Q. Nanochemoprevention by encapsulation of (−)-epigallocatechin-3-gallate with bioactive peptides/chitosan nanoparticles for enhancement of its bioavailability. *Chem. Commun.* **2012**, *48*, 2421−2423.

oxidative stress-induced cell death *in vitro* by using RGC-5 cells, a transformed retinal ganglion cell line. We also report neuroprotective properties *in vivo* against retinal damage following optic nerve crush (ONC) in mice.

MATERIALS AND METHODS

Chemicals. First grade solvents were used for extraction fractionation, and column chromatography. Kiesel gel 60 (70−230 mesh, Art, 7734 Merck) was used as the column packing material. Kiesel 60 F_{254} (precoated plate, Art. 5559, Merck) was used for thin layer chromatography (TLC). Iodine vapor and 10% H_2SO_4 were used for TLC detection. Hoechst 33342 and propidium iodide (PI) were from Molecular Probes (Eugene, OR). Antipoly (ADP-ribose) polymerase (PARP) and anticleaved caspase-3 were purchased from Cell Signaling Technology (Beverly, MA). All other chemicals and reagents were purchased from Sigma-Aldrich (St Louis, MO).

Animals. All animal studies were carried out in a pathogen-free barrier zone at the KIST Gangneung Institute and were done in accordance with the procedure outlined in the Association for Research in Vision and Ophthalmology (ARVO) Statement for the Use of Animals in Ophthalmic and Vision Research. Procedures used in this study were approved by the Animal Care and Use Committee of KIST.

In the present study, male adult Sprague−Dawley rats weighing between 250 and 300 g (8 weeks of age) and male ICR mice weighing between 30 and 35 g (8 weeks of age) were used for the protective effects on NMDA and ONC induced retinal damage, and were acclimated for one week, caged in groups of five for mice and two for rat, and were fed with a diet of animal chow and water *ad lib.* They were housed at 23 ± 0.5 °C and 10% humidity with a 12 h light−dark cycle.

Plant Material and Isolation of Compounds. The *C. denticulatum* samples were collected in the vicinity of Gangneung, Korea, and the voucher specimen (Voucher No. D-043) was deposited at the Herbarium of Functional Food Center, KIST Gangneung Institute, Korea. The dried aerial section of deposited sample (10.0 kg) was extracted three times with hot 94% EtOH (57.0 L) for 4 h. This residue was evaporated *in vacuo* to yield the total extract (1.4 kg).

Dried plants (1.0 kg) were extracted three times by sonication with 94% ethanol for 4 h at room temperature. The residue was evaporated to yield ethanol extract of *C. denticulatum* (EECD, 70 g) under reduced pressure. High-performance liquid chromatography (HPLC)−ultraviolet chromatograms of EECD were obtained as follows. The HPLC system was equipped with an Agilent (Palo Alto, CA) series 1200 liquid chromatograph and a Shiseido MG II C_{18} column packed with 5 μm particles (4.6 mm × 250 mm, film thickness 4 μm) (Shiseido Inc., Japan). The temperature of the column oven was 35 °C, and the injection volume was 10 μL. Separations and simultaneous determination were performed using a mixture of acetonitrile and 0.3% formic acid in water (18:82) as a mobile phase. The flow rate was 1.0 mL/min, and UV detection was performed at 330 nm.

EECD (2.0 g) was chromatographed on a Sephadex LH-20 column (2.5 cm × 65 cm, 100% methanol) to yield fractions 1−9. Chicoric acid was isolated by semipreparative HPLC using the YMC Hydrosphere C_{18} column (20 mm × 250 mm, film thickness 5 μm) with acetonitrile containing 0.1% trifluoroacetic acid in an aqueous gradient (20−30% acetonitrile for 40 min, 10 mL/min) from fraction 4. 3,5-Dicaffeoylquinic acid (3,5-DCQA) was purified using semi-preparative HPLC (acetonitrile containing 0.1% trifluoroacetic acid in aqueous isocratic 25% acetonitrile for 40 min at a flow rate of 2 mL/min, using the YMC Hydrosphere C_{18} column [10 mm × 250 mm, film thickness 5 μm]) from fraction 5. Chemical structures were confirmed by ^1H and ^{13}C nuclear magnetic resonance spectroscopy and compared with the literature.[22−24]

The contents of chicoric acid and 3,5-DCQA in 1 g of EECD were found to be 12.44 mg/g ± 0.25 and 3.80 mg/g ± 0.10, respectively.

Culture of RGC-5 Cells and Cell Viability. RGC-5 cells were used in this study, which have been previously shown to express ganglion cell markers and exhibit ganglion cell-like behavior in culture.[25] In previous report, RGC-5 cells have been proven to be mice origin.[26]

There were 5.0 × 10^3 cells seeded in 96 well plates for 24 h for incubation, and they were then exposed to DMEM containing 1% FBS plus samples or plus vehicle. After 1 h pretreatment with samples, 1-buthionine-(*S*,*R*)-sulfoximine (BSO) (0.5 mM) plus glutamate (10 mM) (glutamate/BSO) was added to cultures. To test cell viability, MTT was added to the cells in 96-well plates at a final concentration of 0.5 mg/mL for 1 h at 37 °C. Optical density of the solubilized formazan product in each well was measured using a spectrophotometer (BioTek Instruments, VT) with a 570 nm test wavelength and a 690 nm reference wavelength.[27]

Microscopic Analysis of Cell Viability by PI and Hoechst 33342 Double Staining. The cells were stained with 8 μM of Hoechst 33342 with or without 1.5 μM of PI for 30 min at 37 °C in order to determine apoptotic or necrotic cell death caused by glutamate/BSO.[13] After being washed twice with serum free media, the cells were imaged using a fluorescence microscope (Olympus, Tokyo, Japan).

Assessment of ROS. Intracellular ROS was quantified using the dye, dichlorodihydrofluorescein diacetate (DCFH-DA), as a radical probe.[28,29] The RGC-5 cells were seeded at a density of 5.0 × 10^3 cells per well into 96-well plates, and 24 h later, the cell-culture medium was replaced with DMEM containing 1% FBS. The cells were loaded with the radical probe DCFH-DA (10 μM) through incubation for 20 min at 37 °C. Then, the cell-culture medium was replaced to remove the extra probe. To generate the radical species, we added H_2O_2 at 1 mM (H_2O_2 radical), H_2O_2 at 1 mM plus 100 μM of iron(II) perchlorate hexahydrate ($^{\bullet}OH$) or KO_2 at 1 mM ($O_2^{\bullet-}$), to the radical probe loading-medium. Fluorescence was then measured after ROS-generating compounds had been present for various time-periods, using excitation/emission wavelengths of 485/535 nm (luminescence spectrometer LS50B, Perkin-Elmer Ltd., England).

Superoxide radicals were assessed using the dye dihydroethidium (DHE) according to previous methods.[30,31] Red fluorescence was detected using a laser scanning confocal microscope (model Leica TCS SP5; Leica, Germany). Excitation wavelength was set at 514 nm and emissions filters at 590 nm. Quantifying of images was analyzed with Leica Application Suite 2.02 software using four representative fields from each well, and images of four wells were sampled per group (n = 16 in each group).

Protein Extraction and Western Blot Analysis. After the pretreatment with different concentrations of EECD for 1 h in RGC-5 cells, the cells were treated with glutamate/BSO for 24 h. For Western blot analysis using retina in rat or mice, four animals (4 retinas) were used from three independent experiments. After cells were washed with cold D-PBS, the cells were scraped using a cell scraper and centrifuged at 14 000 × *g* for 10 min. The cell pellets were resuspended in cell lysis buffer (1 M Tris pH 7.4, 2 M NaCl, 1 M EDTA, 10% NP40, 1 × protease inhibitors, 1 mM PMSF) and then incubated on ice for 10 min. After centrifuging at 14 000 × *g* for 30 min at 4 °C, the supernatant was sonicated, and the total protein concentration was determined using a Bio-Rad Protein Assay kit (Bio-Rad Laboratories, Hercules, CA). A 10 μg sample of protein from the retina homogenates was loaded per lane on a 10% polyacrylamide gel and then transferred to a polyvinylidenedifluoride (PVDF) membrane (Hybond-P; Amersham Biosciences, GE Healthcare, U.K.).

Western blot analysis was performed with the primary antibodies including anti-PARP, anticleaved caspase-3 (1:1000, Cell Signaling Technology, Beverly, MA), and secondary antibodies (1:3000, Santa Cruz Biotechnology, CA). Immunoreactive bands were detected using the enhanced chemiluminescence reagents (Amersham Bioscience, GE Healthcare, U.K.) and were measured *via* densitometry using a LAS-4000 image reader and Multi Gauge 3.1 software (Fuji Photo Film, Japan)

Quantification of mRNA Using Real-Time RT-PCR. Total RNA was extracted from RGC-5 cells using the RNeasy minikit (Qiagen, Valencia, CA) according to the manufacturer's protocol. After quantification, total RNA (1 μg) was used to synthesize cDNA by

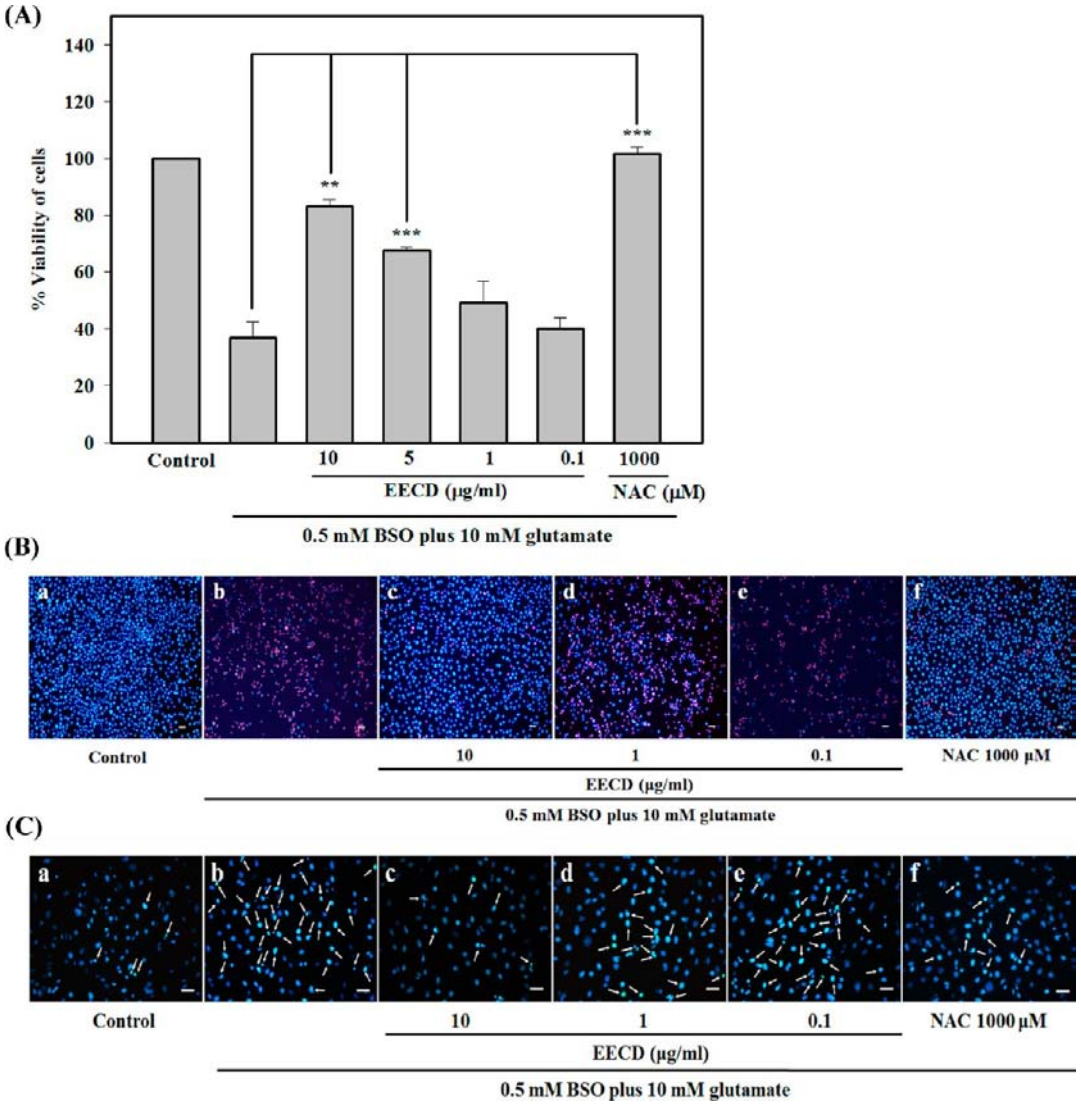

Figure 1. (A) Effect of EECD on the viability of RGC-5 cells exposed to 10 mM glutamate plus 0.5 mM BSO for 24 h as measured by the MTT assay. 1 mM *N*-acetyl-L-cysteine (NAC) was used as a positive control. The results are mean values with error bars indicating ± SEM where $n = 6$ independent experiment (** $p < 0.01$, *** $p < 0.001$). (B) Representative fluorescence microscopy of PI (red) and Hoechst 33342 (blue) staining. (a) Control RGC-5 cells in culture. (b) 10 mM glutamate plus 0.5 mM BSO treated RGC-5 cells in culture. (c−e) Pretreatment with EECD (0.1−10 μg/mL concentration) followed by 10 mM glutamate plus 0.5 mM BSO. (f) Pretreatment with NAC (1 mM concentration) followed by 10 mM glutamate plus 0.5 mM BSO. Scale bar = 50 μm. (C) Representative fluorescence microscopy of Hoechst 33342 stained RGC-5 cells. (a) Control RGC-5 cells in culture. (b) 10 mM glutamate plus 0.5 mM BSO treated RGC-5 cells in culture. (c−e) Pretreatment with EECD (0.1−10 μg/mL concentration) followed by 10 mM glutamate plus 0.5 mM BSO. (f) Pretreatment with NAC (1 mM concentration) followed by 10 mM glutamate plus 0.5 mM BSO. Scale bar = 50 μm.

reverse transcription with the Omniscript reverse transcription kit and the T7-$(dT)_{24}$ primer (Qiagen). Quantitative real-time RT-PCR was performed to evaluate mRNA expression for PARP and caspase-3 with the Light-Cycler Real-Time PCR System (Roche, Manheim, Germany). The primers for PARP were 5′-AGGCCGCCT-ACTCTATCCTC-3′ (sense) and 5′-GATTCACTG-CTGCCTTGAGA-3′ (antisense). The primers for caspase-3 were 5′-GAGGCTGACTTCCTGTATGCTT-3′ (sense) and 5′-AACCACGACCCGTCCTTT-3′ (antisense). The primers for GAPDH as control were 5′-AGGCAAAAGACACCGTCAAG-3′ (sense) and 5′-CACAAGAAGATGCGGCTGT-3′ (antisense). Analysis was based on the results of three independent experiments.

Lipid Peroxidation Assay. Lipid peroxidation was tested for the amount of formation for thiobarbituric acid reactive species (TBARS) as described in previous studies.[13,32] The rat brain was homogenized in ice-cold 0.9% saline, centrifuged at 1000 × *g* for 10 min at 4 °C, and the supernatant was used for the lipid peroxidation assays. The lipid peroxidation in rat homogenate was evaluated using the TBARS method as described previously.[33] Absorbance of the samples was measured at 532 nm, and the amount of TBARS was determined using a standard curve of the malondialdehyde (MDA) derivative 1,1,3,3-tetraethoxypropane (0.63−100 μM). Protein concentration was determined using a Bio-Rad protein assay kit (Bio-Rad, Richmond, CA) using bovine serum albumin as the standard.

NMDA-Induced Retinal Damage and Histological Analysis. Retinal damage caused by NMDA was determined according to previous methods.[14] Rats ($n = 7$) were put under anesthesia with a Zoletil (1.6 μg/g, Verbac Laboratories 06515, France) and Rompun (0.05 μL/g, Bayer) mixture, and retinal damage was induced using an injection (2 μL/eye) of NMDA (2.5 mM dissolved in 0.01 M PBS) to the left eye using a 30 gauge Hamilton syringe (final concentration 5 nmol/eye).[34] Seven days after the injection, the eyeballs were enucleated for histological analysis. Previous study has shown that 18 h after an NMDA injection into a rabbit retina, typical apoptotic

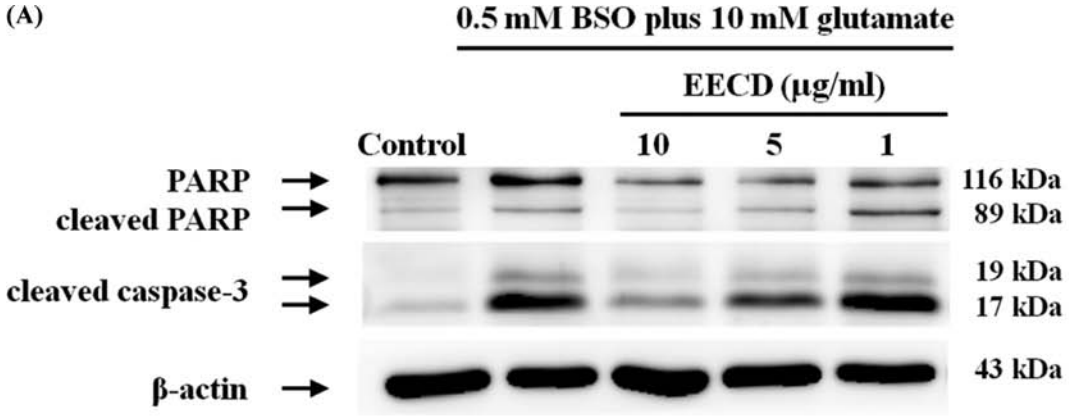

	Concentration (μg/ml)	cleaved PARP/β-actin	cleaved caspase-3/β-actin
Control	-	1.00 ± 1.53	1.00 ± 0.55
0.5 mM BSO plus 10 mM glutamate	-	11.47 ± 0.15	33.81 ± 6.10
EECD (μg/ml)	10	1.80 ± 0.05	6.10 ± 0.25
	5	6.47 ± 0.10	10.20 ± 0.44
	1	15.78 ± 0.33	36.91 ± 0.81

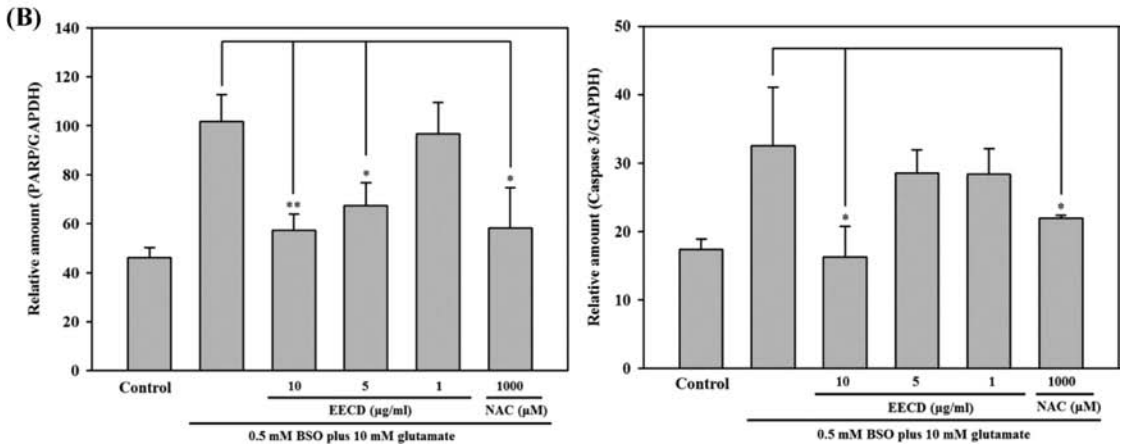

Figure 2. (A) Expression of apoptotic protein levels (PARP, cleaved caspase-3) in RGC-5 cells subjected to 10 mM glutamate plus 0.5 mM BSO with or without EECD treatment. Protein level values are expressed as mean ± SEM from three independent experiments. (B) Expression of mRNA level (PARP and caspase-3) in RGC-5 cells subjected to 10 mM glutamate plus 0.5 mM BSO with or without EECD treatment. Values are expressed as mean ± SEM from three independent experiments.

features in degenerative cells in the retinal ganglion cell layer (GCL) and the inner nuclear layer (INL) were noted by electron microscopy. TUNEL positive nuclei were detected in these layers as early as 4 h showing maximal numbers at 18 h.[35,36] For this reason, the animals were killed 18 h after the NMDA injection and fixed for the TUNEL assay, and 7 days after the NMDA injection they were fixed for histological analysis.

The enucleated eyes were fixed in 10% formalin for 24 h, embedded in paraffin, and sectioned through an equatorial plane at 4 μm thickness using a HM340E microtome (Walldof, Germany). Four sections (n = 4) were used for analysis.

Hematoxylin solution was added to the retina section (0.1% hematoxylin, 10% ammonium) for 8 min. The sections were then washed three times with distilled water. Bluing reagent (0.2% lithium carbonate solution) was added to the section for 1 min. The sections were quickly rinsed in 95% alcohol, and 1% Eosin Y solution was added to the sections for 1 min. Eosin Y was washed off with 95% alcohol three times, and the sections were coverslipped with a mounting medium and observed under a light-microscope (Olympus, Tokyo, Japan).

TUNEL Staining. To analyze TUNEL-positive cells, the sections were submitted to enzymatic digested with 20 μg/mL of proteinase K for 15 min, then washed with PBS and incubated with 3% hydrogen peroxide in PBS for 5 min at room temperature, and twice rinsed in PBS. They were then immersed, incubated with a stock solution of terminal deoxynucleotidyl transferase (TdT) reaction enzyme in a humidified chamber at 37 °C for 1 h, and then washed three times in PBS for 1 min. The sections were subsequently incubated with antidigoxygenin peroxidase conjugate and peroxidase substrate to detect signs of apoptosis, which appear brown.

The histological aspect of apoptosis was observed using a light microscope (Olympus, Tokyo, Japan).

Optic Nerve Crush (ONC) and Quantification of Retinal Ganglion Cells. Mice (n = 8) were put under anesthesia by

dx.doi.org/10.1021/jf4046232 | J. Agric. Food Chem. 2014, 62, 1310−1323

intraperitoneal injection of Zoletil (1.6 μg/g, Verbac Laboratories 06515, France) and Rompun (0.05 μL/g, Bayer) mixture, and retinal damage was induced using optic nerve crush.[37] The optic nerve of the left eye was exposed by opening the meninges of the optic nerve with the sharp tips of a forceps, followed by blunt dissection. ONC was crushed 2 mm behind the globe for 7 s with a cross-action calibrated forceps. The samples were injected intravitreally 1 h before ONC, and the animals were killed 7 days after the ONC and the eyeballs enucleated immediately after sacrifice. The eyeballs were fixed for retrograde label of RGCs.

RGC Labeling and Retinal Flat Mount Preparation. Mice were anesthetized by intraperitoneal administration of a mixture of Zoletil (1.6 μg/g, Verbac Laboratories 06515, France) and Rompun (0.05 μL/g, Bayer), and to the superior colliculi in mice was applied 5% solution of the neurotracer dye Fluorogold (Invitrogen, NY) by a piece of soaked gelfoam. Skull openings were then sealed with a petrolatum based antibiotic ointment. The overlying skin was sutured and antibiotic ointment applied externally.

Seven days after the application of Fluorogold, eyes were enucleated, and the retinas were detached at the ora serrata and cut with a trephine around the optic nerve head. Four radial relaxing incisions were made and the retinas prepared as flattened whole mounts on silane-coated microscope slides.[38]

Statistical Analysis. The data are expressed as a mean percentage of the control value plus standard error of the mean (SEM). Statistical comparisons were made using a one-way ANOVA followed by a Dunnett's test. Statistical analyses were conducted using GraphPad Prism (version 4.0) (GraphPad, San Diego, CA). $p < 0.05$ was considered significant.

RESULTS

Effect of EECD on the Apoptotic Cell Death Caused by an Insult of Glutamate/BSO. Figure 1 shows the protective effects of EECD against oxidative stress-induced RGC-5 cell death (Figure 1). When glutamate/BSO was added to RGC-5 cells for 24 h, cell viability was significantly decreased by 36.7%. However, this decrease in cell viability was significantly attenuated by EECD in a concentration-dependent manner (Figure 1A).

The protective effect of EECD caused by oxidative stress was confirmed by microscopic analysis using a Hoechst 33342/PI double staining method for DNA (Figure 1B).

Hoechst 33342 is a blue fluorescent dye that is permeable to live or fixed cells, while PI is a red membrane-impermeant dye and is, therefore, commonly used to identify dead cells.[13]

As shown in Figure 1B, there were few red-stained nuclei in cells under basal conditions. However, cells treated with glutamate/BSO showed numerous red-stained nuclei. Pretreatment with EECD attenuated red-stained nuclei and chromatin condensation in a concentration-dependent manner (Figure 1B,C).

To determine whether EECD's protective effects on oxidative stress-induced RGC-5 cell death were due to antiapoptotic activities, Western blot analysis was performed to evaluate the change in apoptotic protein levels for cleaved PARP and cleaved caspase-3 (Figure 2). Exposure to glutamate/BSO resulted in the up-regulation of protein levels for cleaved PARP and cleaved caspase-3; however, EECD significantly reduced this up-regulation in a concentration-dependent manner (Figure 2A). Moreover, EECD significantly reduced the mRNA expression of PARP and caspase-3 caused by glutamate/BSO in a concentration-dependent manner (Figure 2B).

Effect of EECD on the Intracellular Levels of ROS. Inhibitory effects of EECD on ROS production were determined by DCFH-DA as a ROS fluorescence probe. ROS was induced by different oxidative insults including H_2O_2, $O_2^{\bullet-}$, and $^{\bullet}OH$.

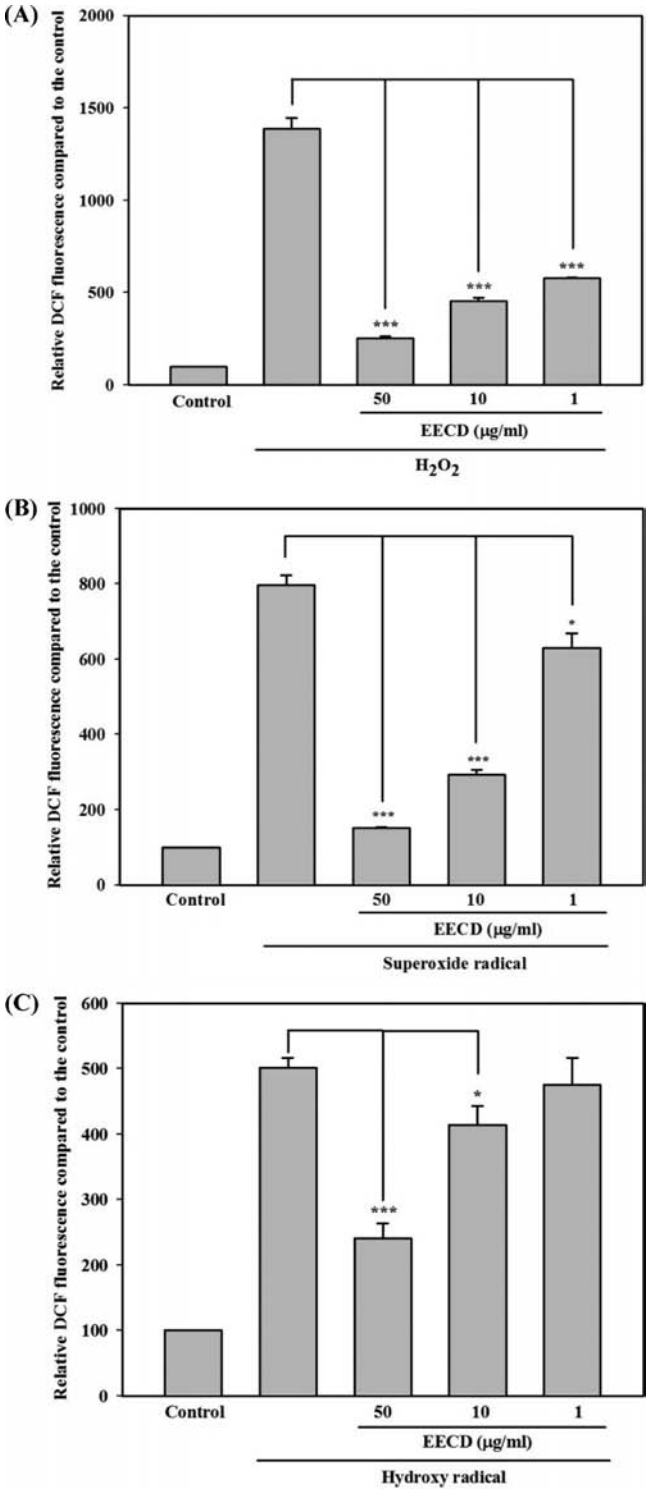

Figure 3. Radical scavenging capacities of EECD against the production of three radical species (H_2O_2, $O_2^{\bullet-}$, and $^{\bullet}OH$) in RGC-5. ROS production was stimulated with H_2O_2 at 1 mM, or with KO_2 at 1 mM, or with H_2O_2 at 1 mM plus ferrous perchlorate(II) at 100 μM. (A) H_2O_2-induced oxidation of DCFH in RGC-5, (B) $O_2^{\bullet-}$-induced oxidation of DCFH in RGC-5, and (C) $^{\bullet}OH$-induced oxidation of DCFH in RGC-5. Results are mean values with error bars indicating ± SEM where $n = 3$ (* $p < 0.05$, *** $p < 0.001$).

dx.doi.org/10.1021/jf4046232 | J. Agric. Food Chem. 2014, 62, 1310−1323

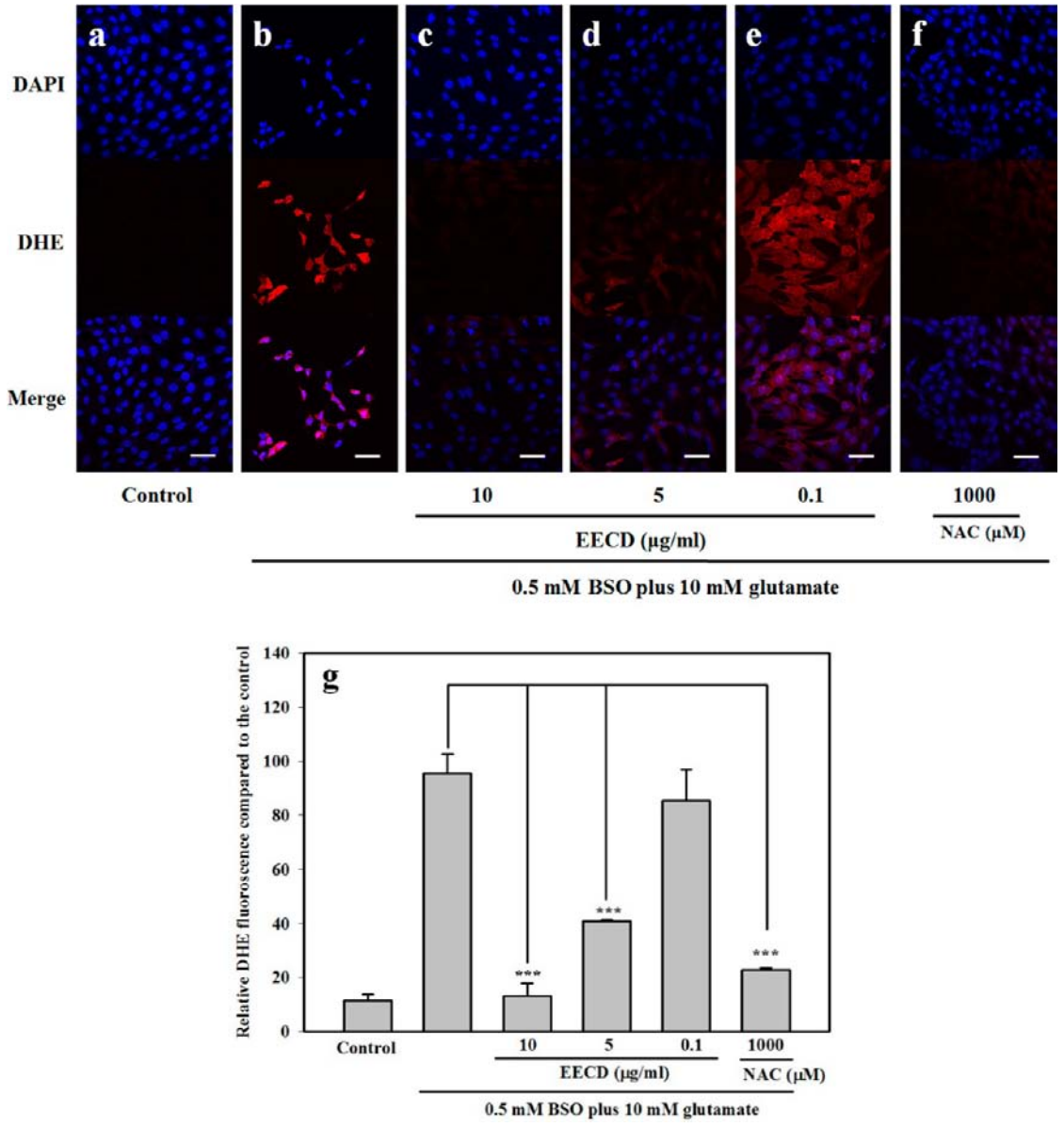

Figure 4. Effect of EECD on ROS levels in RGC-5 cells subjected to oxidative stress induced by 10 mM glutamate plus 0.5 mM BSO for 24 h. DHE assay was used to demonstrate the intensity of intracellular ROS generated by oxidative stress. Images were obtained by confocal microscopy (400×). DAPI was used to demonstrate live cells. (a) Control RGC-5 cells in culture. (b) 10 mM glutamate plus 0.5 mM BSO treated RGC-5 cells in culture. (c–e) Pretreatment of EECD (0.1–10 μg/mL concentration) with 10 mM glutamate plus 0.5 mM BSO. (f) Pretreatment of NAC (1 mM concentration) with 10 mM glutamate plus 0.5 mM BSO. (g) Quantification of DHE fluorescence was analyzed with Leica Application Suite 2.02 software (Leica, Germany) using four representative fields from each well, and images of four wells were sampled per group (n = 16 in each group). Scale bar = 50 μm. The results are mean values with error bars indicating ± SEM (*** $p < 0.001$).

ROS activity was increased more than 13 times when the RGC-5 cells were exposed to H_2O_2 at 1 mM, from the basal level of 100.63 ± 27.36 to 1343.13 ± 103.27 (Figure 3A). However, pretreatment with EECD markedly inhibited ROS production in a concentration-dependent manner (Figure 3A). Moreover, EECD also scavenged $O_2^{\bullet-}$ and $^{\bullet}OH$ radicals in a similar manner (Figure 3B,C).

To test the ability of EECD to inhibit the superoxide production caused by glutamate/BSO, DHE staining was used, and the results are shown in Figure 4. DHE fluorescence is blue in the cell cytoplasm, but is converted to red fluorescence by ROS production upon DNA intercalation. DAPI staining was used to verify the DHE staining of live cells because DAPI is able to penetrate live cell membranes and to bind double-stranded DNA in the nucleus, and to dye live cells (Figure 4).

When the cells were exposed to glutamate/BSO, the number of live cells decreased while red fluorescence increased by approximately 9-fold (relative DHE fluorescence 97.3 ± 8.2) compared to control. However, enhancement of this red fluorescence was clearly attenuated in a concentration-dependent manner by pretreatment of EECD, with 10 μg/mL showing the highest potency (DHE fluorescence 10.8 ± 5.2 relative to control) (Figure 4).

EECD Inhibition of Sodium Nitropruside (SNP)-Induced Lipid Peroxidation in Rat Forebrain Homogenates. Malondialdehyde (MDA) is the final product of lipid peroxidation and a marker for oxidative stress-induced injury.

dx.doi.org/10.1021/jf4046232 | J. Agric. Food Chem. 2014, 62, 1310–1323

Table 1. Effect of EECD on Inhibition of Lipid Peroxidation Induced by Sodium Nitroprusside (SNP) in Rat Forebrain Homogenates[a]

	lipid peroxidation		
sample	conc (μg mL)	inhibition (%)	IC_{50} (μg mL)
EECD	2.5	57.78 ± 16.41	1.72
EECD	1.25	42.93 ± 13.84	1.72
EECD	0.625	33.19 ± 10.59	1.72
EECD	0.3125	27.22 ± 11.20	1.72
EGCG	0.23	63.06 ± 7.48	0.12
EGCG	0.115	48.72 ± 7.66	0.12
EGCG	0.0575	38.16 ± 12.40	0.12
EGCG	0.028 75	27.53 ± 12.67	0.12

[a]SNP at a concentration of 20 μM caused a submaximum stimulation of TBARS in a previous study; therefore, this SNP concentration was used to determine the inhibitory effects in the samples. Different concentrations of EECD were preincubated with brain homogenates at 37 °C for 5 min. SNP was then added at the concentrations indicated, and the homogenates were incubated for a further 10 min. Results are means values ± SEM of three independent experiments.

The TBARS method was used to assess the production of MDA in rat brains. As shown in Table 1, MDA levels were increased following SNP (20 μM) stimulation in rat forebrain homogenates as compared to the control group. However, pretreatment with EECD inhibited the production of MDA in a concentration-dependent manner, with an IC_{50} value of 1.72 μg/mL (Table 1). EGCG as a positive control inhibited the stimulation of TBARS induced by SNP, with an IC_{50} value of 0.12 μg/mL (Table 1).

Effect of EECD on NMDA-Induced Retinal Damage. To determine whether EECD had neuroprotective effects *in vivo*, the changes in ganglion cell numbers and IPL thickness caused by the intravitreal injection of NMDA into rat retinas were determined. After intravitreal injection of NMDA, significant thinning of the IPL was observed (compare Figure 5b to Figure 5a). However, this IPL thinning was attenuated by treatment with EECD (2 μg/mL, intravitreal injection) (Figure 5c,e).

The antiapoptotic properties of EECD against NMDA-induced damage to ganglion cells were tested using TUNEL staining (Figure 6). There were few TUNEL-positive cells in the normal control (Figure 6a,e). At 24 h after the intravitreal injection of NMDA, prominent TUNEL-positive cells were found in the GCL as shown in Figure 6b,e. After pretreatment with 2 μg/mL of EECD, the number of TUNEL-positive cells was decreased as shown in Figure 6c–e.

Effect of EECD on Optic Nerve Crush (ONC)-Induced Retinal Damage. The neuroprotective effect of EECD was tested following ONC in mice by injecting the fluorescent retrograde tracer Fluorogold into the superior colliculus.

RGC death was observed in mice after ONC by the loss of fluorescent Fluorogold-labeled RGCs (Figure 7b,e,h), as compared with the normal control (Figure 7a,d,g). However, the degeneration of RGCs caused by ONC was significantly attenuated by pretreatment with EECD (Figure 7c,f,i).

Major Compounds in EECD and Their Protective Effects on Oxidative Stress-Induced RGC-5 Cells and

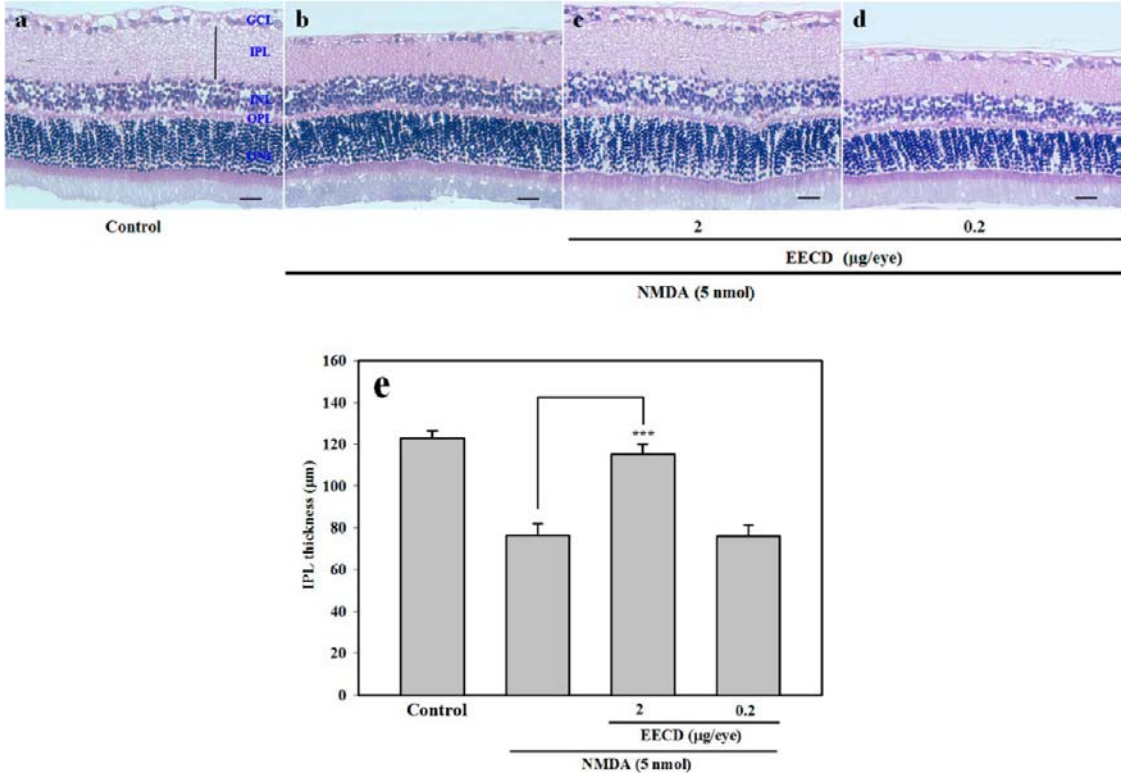

Figure 5. Effect of EECD on retinal damage induced by intravitreous injection of *N*-methyl-D-aspartate (NMDA) in rats. Representative photomicrographs showing the histologic appearance of retinal cross sections with hematoxylin and eosin staining at 7 days after treatment with or without NMDA. (a) Nontreated, (b) NMDA (5 nmol), (c) NMDA (5 nmol) plus EECD (2 μg/mL), (d) NMDA (5 nmol) plus EECD (0.2 μg/mL). Quantification of the thickness of the IPL is shown in part e. The scale bar represents 50 μm. Results are the mean values with error bars indicating ± SEM from six independent experiments (*** $p < 0.001$).

dx.doi.org/10.1021/jf4046232 | J. Agric. Food Chem. 2014, 62, 1310–1323

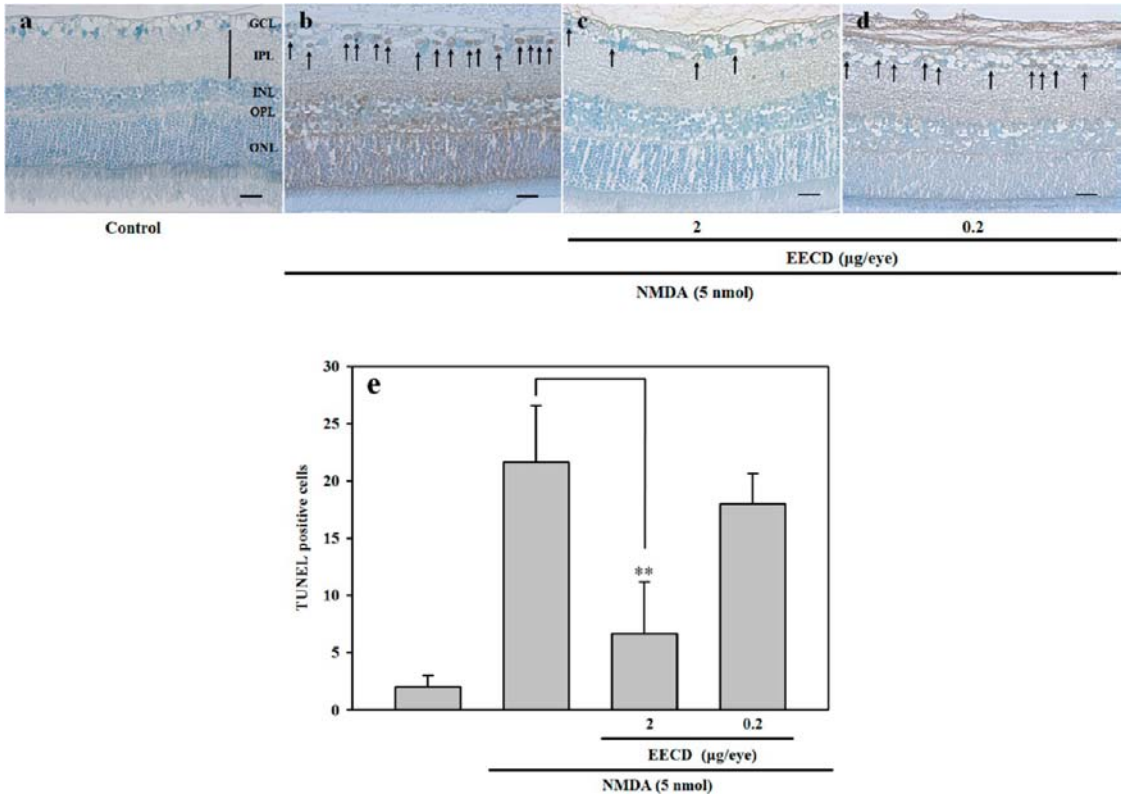

Figure 6. Antiapoptotic effect of EECD demonstrated by a TUNEL assay. Representative photomicrographs showing the histologic appearance of retinal cross sections with TUNEL stain after 18 h with or without NMDA. Retinal damage was induced by an intravitreous injection of NMDA. (a) Nontreated, (b) NMDA (5 nmol), (c) NMDA (5 nmol) plus EECD (2 μg/mL), (d) NMDA (5 nmol) plus EECD (0.2 μg/mL). The arrows indicate TUNEL-positive cells (brown stain). Quantification of the TUNEL positive cells is shown in part e. The scale bar represents 50 μm.

Optic Nerve Crush (ONC)-Induced Retinal Damage. As shown in Figure 8, the HPLC profile of EECD was recorded at 330 nm. Matching the compounds isolated from EECD with HPLC data indicated that the major constituents of EECD were chicoric acid and 3,5-DCQA.

It has also reported from our laboratory that 3,5-DCQA isolated from *Gymnaster koraiensis* can protect RGCs *in vitro* and *in vivo*;[14] thus, we have focused on the effects of chicoric acid in this study.

Chicoric acid showed protective effects against glutamate/BSO-induced RGC-5 cell death in a concentration-dependent manner (Figure 9A). This was confirmed by the Western blot analysis, and chicoric acid significantly reduced this up-regulation of protein levels for cleaved PARP and cleaved caspase-3 in a concentration-dependent manner (Figure 9B). Moreover, chicoric acid significantly reduced the mRNA expression of PARP and caspase-3 caused by glutamate/BSO (Figure 9C).

From the ONC model, RGCs death caused by ONC was also significantly attenuated by pretreatment with 5 nmol/eye (Figure 9Dc,g,E) and 25 nmol/eye chicoric acid (Figure 9Cd,h), as compared with vehicle group (Figure 9Db,f,E), although the attenuation by 5 nmol/eye chicoric acid-treated group was not statistically significant (Figure 9E).

■ DISCUSSION

In this study, we presented *in vitro* and *in vivo* evidence that EECD and its isolated compounds protects against retinal degeneration.

Using quantitative analysis of cell death, our *in vitro* studies showed a concentration-dependent effect of EECD to protect against the retinal degeneration caused by glutamate/BSO-induced oxidative stress (Figure 1).

It has been shown that glutamate/BSO can induce apoptosis in RGC-5 cells and up-regulate cleaved caspase-3 and cleaved PARP proteins.[39] We confirmed these observations in our study and also found that pretreatment with EECD inhibited in a concentration-dependent manner this up-regulation of apoptotic proteins and mRNA level (Figure 2). This suggests that EECD protects against the retinal degeneration from antiapoptotic effects by inhibiting the activation of apoptotic proteins.

Retinal degeneration may occur by various mechanisms including neurotrophic factor deprivation, ischemia, glial cell activation, glutamate excitotoxicity, and abnormal immune response.[40]

These mechanisms can induce oxidative stress caused by imbalance the production of ROS and have been recognized as critical mediators in RGC death.[41]

Increased levels of ROS cause significant molecular damage within cells, which can lead to neuronal death by several mechanisms including protein modification and DNA damage.[42] In addition, accumulating evidence from experimental models indicates that oxidative stress, including oxidative damage in the trabecular meshwork and retina, is implicated in glaucoma.[43,44]

It is therefore proposed that antioxidants that regulate oxidative imbalance may be therapeutic strategies for retinal degeneration. Furthermore, natural antioxidants may be

dx.doi.org/10.1021/jf4046232 | J. Agric. Food Chem. 2014, 62, 1310−1323

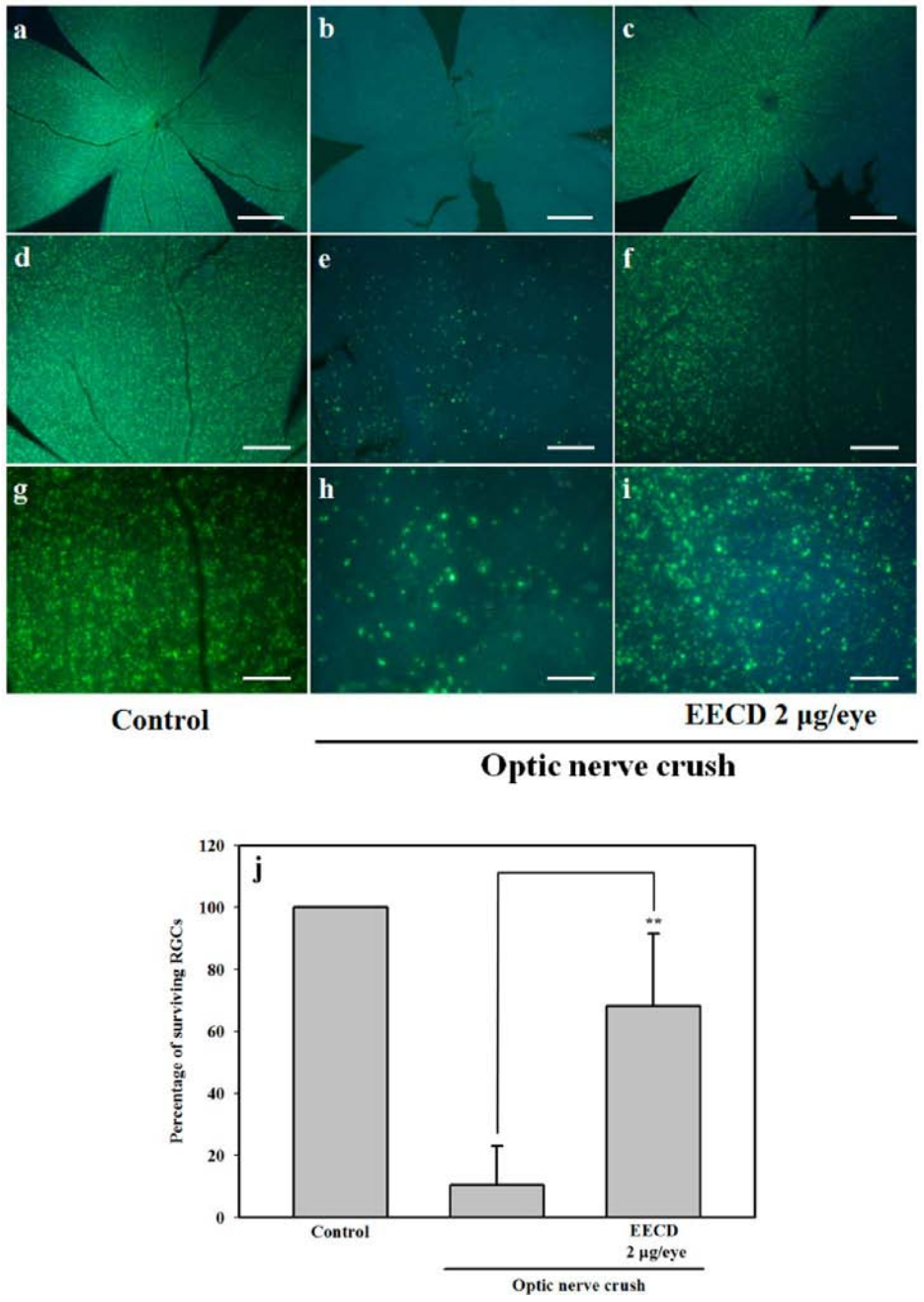

Figure 7. Fluorogold labeled RGCs in the mouse 1 week after optic nerve crush (ONC). Retrogradely labeled RGCs of mice with uninjured and injured optic nerves. RGCs were labeled by injecting 3% Fluorogold into the superior colliculi of the brain. The figure shows representative micrographs of normal retina (a) and damaged retina 1 week after ONC with (c) or without EECD (b). Scale bars in parts a–c represent 500 μm. Low-magnification (×100) images of labeled RGCs in a–c are shown in d–f. Scale bars in d–f represent 100 μm. High magnification (×200) images of a–c are shown in g–i. Scale bars in g–i represent 50 μm. The results showed a significant increase in RGC survival after EECD treatment compared with vehicle treatment (j). Experimental values are expressed as percentage of surviving RGCs with error bars indicating ± SEM from three independent experiments (** $p < 0.01$).

putative agents for treating or preventing retinal degeneration such as in glaucoma.[45] In view of the roles of oxidative stress in the retinal degeneration, we have shown that in RGC-5 cells EECD ameliorates the effects of the ROS production induced by H_2O_2, $O_2^{\bullet-}$, or $^{\bullet}OH$ by scavenging radicals (Figure 3). Moreover, the inhibitory effects of EECD on ROS were clearly confirmed by using the DHE assay, which directly measures intracellular $O_2^{\bullet-}$ (Figure 4).[46]

Lipid peroxidation can be referred to as oxidative degeneration of lipids, and it has been shown that lipid peroxidation is implicated in glaucoma.[47] In a study using UV-spectrophotometry and fluorescent analysis of lipid extracts from lenses, aqueous humor, and blocks containing trabecular and Schlemms canal tissues in primary open-angle glaucoma (POAG), significant changes of lipid peroxidation in comparison with the control were observed.[48]

MDA is final product of lipid peroxidation, and MDA levels were estimated in rat brain homogenates after induction by SNP using a TBARS assay.[13] In our hands, treatment with EECD clearly inhibited lipid peroxidation in a concentration-

dx.doi.org/10.1021/jf4046232 | J. Agric. Food Chem. 2014, 62, 1310–1323

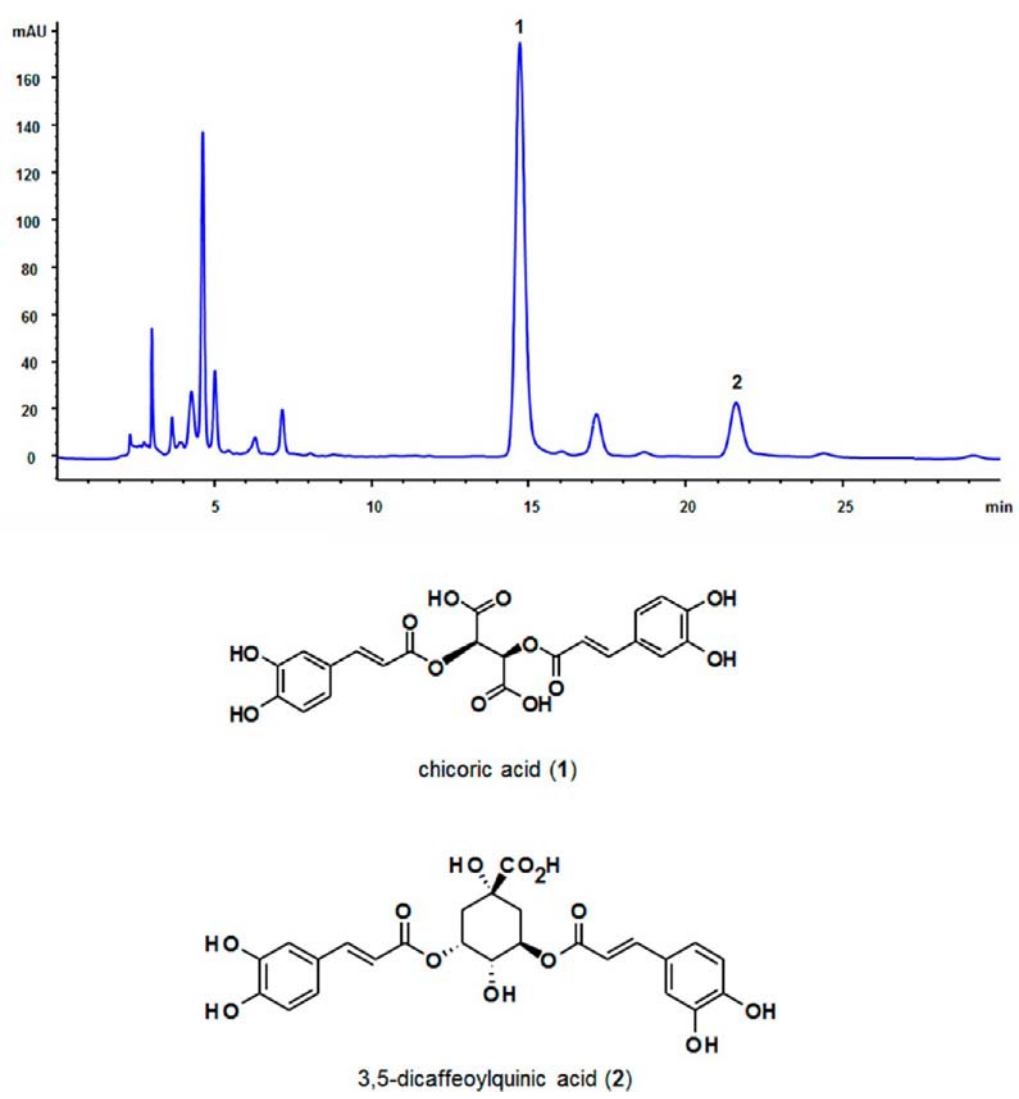

Figure 8. Chromatogram of the HPLC profile for EECD at 330 nm. Peaks: (1) chicoric acid, (2) 3,5-dicaffeoylquinic acid.

dependent manner (Table 1). Thus, taken together, our results suggest that the neuroprotective effects of EECD *in vitro* occur through antiapoptotic and antioxidative mechanisms.

In order to confirm the neuroprotective effects of EECD, we examined the number of TUNEL-positive cells in the GCL and the thickness of IPL following a single intravitreal injection of NMDA because excessive activation of the excitatory amino acid glutamate has been implicated in retinal neuronal cell death and in the pathogenesis of glaucoma.[49] NMDA receptors have been identified on RGC and amacrine cells, and NMDA-receptor activation causes apoptosis *via* ROS production through intracellular Ca^{2+} influx.[50] It was previously reported that NMDA administered in rat eye caused cell death in the GCL and reduction of IPL thickness, and that the blockade of excessive glutamate could be a possible strategy for development of neuroprotective agents.[51−53] Moreover, IPL thicknesses are well correlated with retinal nerve fiber layer thickness and visual field sensitivity, and the IPL thickness can provide the index of INL damage after retinal injury.[54] The present study showed that EECD attenuated the detrimental effects caused by NMDA (Figures 5 and 6).

These results indicate that, in addition to its direct inhibition of oxidative stress, EECD protection of RGC may be due to blockade of the downstream signaling pathways involved in NMDA-induced excitotoxicity.

We also determined whether EECD was effective in optic nerves to protect RGC following optic nerve crush (ONC) (Figure 7).

ONC is a common experimental model of chronic glaucoma in which the optic nerve is surgically exposed and clamped for several seconds.[55] There are several possible mechanisms for the degeneration of RGCs by ONC, including blockade of axonal transport resulting in inadequate supply of neurotrophic factors, disturbances of intracellular calcium homeostasis, activation of cell death genes, and local excitotoxicity due to uncontrolled activation of NMDA receptors.[56,57] Another mechanism of degeneration may be through ROS production, which causes the slow, chronic, and synchronous death of RGCs.[58] In our study the density of RGCs was decreased by ONC; however, pretreatment with EECD significantly reduced the loss of RGCs (Figure 7).

Our HPLC results identified the major components in EECD as chicoric acid and 3,5-DCQA (Figure 8).

Previous studies have shown that 3,5-DCQA from propolis extracts have neuroprotective effects on oxidative stress induced retinal damage.[8] It was also reported that 3,5-DCQA isolated

dx.doi.org/10.1021/jf4046232 | J. Agric. Food Chem. 2014, 62, 1310−1323

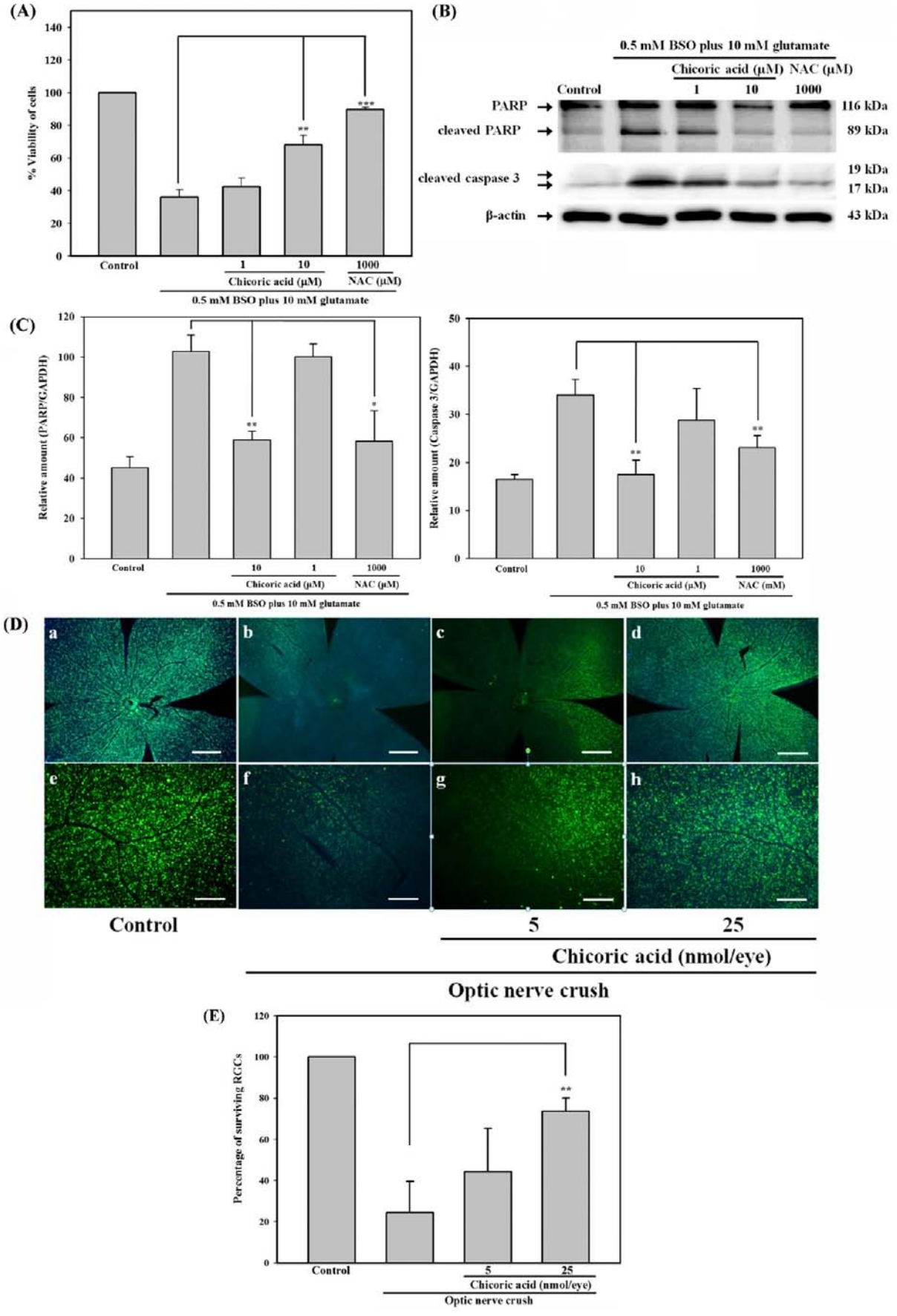

Figure 9. (A) Effect of chicoric acid on the viability of RGC-5 cells exposed to 10 mM glutamate plus 0.5 mM BSO for 24 h as measured by the MTT assay. 1 mM *N*-acetyl-L-cysteine (NAC) was used as a positive control. The results are mean values with error bars indicating ± SEM where *n*

dx.doi.org/10.1021/jf4046232 | *J. Agric. Food Chem.* 2014, 62, 1310−1323

Figure 9. continued

= 5 independent experiment (** $p < 0.01$, *** $p < 0.001$). (B) Expression of apoptotic protein levels (PARP, cleaved caspase-3) in RGC-5 cells subjected to 10 mM glutamate plus 0.5 mM BSO with or without chicoric acid treatment. Protein level values are expressed as mean ± SEM from three independent experiments. (C) Expression of mRNA level (PARP and caspase-3) in RGC-5 cells subjected to 10 mM glutamate plus 0.5 mM BSO with or without chicoric acid treatment. Values are expressed as mean ± SEM from three independent experiments. (D) Fluorogold labeled RGCs in the mouse 1 week after optic nerve crush (ONC). Retrogradely labeled RGCs of mice with uninjured and injured optic nerves. RGCs were labeled by injecting 3% Fluorogold into the superior colliculi of the brain. The figure shows representative micrographs of normal retina (a) and damaged retina 1 week after ONC with 5 nmol (c) and 25 nmol chicoric acid (d), or without chicoric acid (b). Scale bars in parts a–d represent 500 μm. High magnification (×100) images of parts a–d are shown in parts e–h. Scale bars in parts e–h represent 100 μm. (E) The results showed a significant increase in RGC survival after chicoric acid treatment compared with vehicle treatment. Experimental values are expressed as percentage of surviving RGCs with error bars indicating ± SEM from three independent experiments (** $p < 0.01$).

from *Gymnaster koraiensis* can protect RGCs from oxidative stress *in vitro* and from NMDA-induced excitotoxicity *in vivo*.[14]

We have proven that 3,5-DCQA has protective effects on retinal degeneration in previous research, thus focused on the effects of chicoric acid in this study.

Our present study supported that chicoric acid, the major phenolic compound of EECD, has protective effects both *in vitro* and *in vivo* (Figure 9), which could be postulated that chicoric acid and 3,5-DCQA are active compounds for the RGCs protective effects of EECD.

This is the first report of the presence of chicoric acid in *C. denticulatum* and the potential value in retinal degeneration.

Variations in food matrices and/or phenolic composition can contribute to having a major influence on intestinal bioavailability, since there are controversial results by observing the oral bioavailability of hydroxycinnamic acids intake.[59] Thus, further study will be needed for the bioavailability of chicoric acid and 3,5-DCQA with the *C. denticulatum* as food matrices. This is supported by another report that chicoric acid strengthens the anti-inflammatory activity of luteolin through NF-κB attenuation.[60]

In conclusion, the present study demonstrated that EECD and its isolated compound of chicoric acid can ameliorate RGC degeneration caused by oxidative stress both *in vitro* and *in vivo*, and that this protective effect may be mediated by its antioxidative and antiapoptotic effects.

Taken together, these findings support EECD as a potential bioactive wild vegetable that could be used as functional food for the prevention of neurodegenerative diseases such as glaucoma and age-related macular degeneration. Moreover, chicoric acid and 3,5-DCQA isolated from *C. denticulatum* are suggested to be offered as mark compounds for the standardization in the development of functional food.

AUTHOR INFORMATION

Corresponding Author

*E-mail: shjung507@gmail.com. Phone: +82-33-650-3653. Fax: +82-33-650-3679.

Notes

The authors declare no financial conflict of interest.

The authors declare no competing financial interest.

ACKNOWLEDGMENTS

The RGC-5 cells were a generous gift from Alcon Research, Ltd. This work was financially supported by an intramural grant (2Z03850) from the Korea Institute of Science and Technology (KIST), Republic of Korea.

ABBREVIATIONS USED

EECD, ethanol extract of *Crepidiastrum denticulatum*; ONC, optic nerve crush; RGC, retinal ganglion cell; IOP, intraocular pressure; NMDA, *N*-methyl-D-aspartate; TLC, thin layer chromatography; PI, propidium iodide; ARVO, Association for Research in Vision and Ophthalmology; HPLC, high-performance liquid chromatography; 3,5-DCQA, 3,5-dicaffeoylquinic acid; DMEM, Dulbecco's modified Eagle's medium; FBS, fetal bovine serum; BSO, 1-buthionine-(*S*,*R*)-sulfoximine plus glutamate; NAC, *N*-acetyl-L-cysteine; MTT, (3-(4,5-dimethylthiazol-2-yl)-2,5-diphenyltetrazolium bromide; DMSO, dimethyl sulfoxide; ROS, reactive oxygen species; DCFH-DA, dichlorodihydrofluorescein diacetate; DHE, dihydroethidium; PMSF, phenylmethylsulfonyl fluoride; PVDF, polyvinylidene difluoride; TBARS, thiobarbituric acid reactive species; MDA, malondialdehyde; PBS, phosphate-buffered saline; TdT, terminal deoxynucleotidyl transferase; TUNEL, terminal deoxynucleotidyl transferase dUTP nick end labeling; SEM, standard error of the mean; SNP, sodium nitroprusside; GCL, ganglion cell layer; POAG, primary open-angle glaucoma; RT-PCR, reverse transcription-polymerase chain reaction

REFERENCES

(1) Akihisa, T.; Franzblau, S. G.; Ukiya, M.; Okuda, H.; Zhang, F.; Yasukawa, K.; Suzuki, T.; Kimura, Y. Antitubercular activity of triterpenoids from Asteraceae flowers. *Biol. Pharm. Bull.* **2005**, *28*, 158–160.

(2) Yun, J. H.; Lee, S. B.; Lee, H. J.; Kim, C. Y.; Kim, M. A.; Sohn, Y. C.; Nho, C. W. Bi-functional induction of the quinone reductase and cytochrome P450 1A1 by youngiasides via Nrf2-ARE and AhR-XRE pathways. *Biol. Pharm. Bull.* **2010**, *33*, 1650–1657.

(3) Kang, K.; Jho, E. H.; Lee, H. J.; Oidovsambuu, S.; Yun, J. H.; Kim, C. Y.; Yoo, J. H.; Kim, Y. J.; Kim, J. H.; Ahn, S. Y.; Nho, C. W. *Youngia denticulata* protects against oxidative damage induced by tert-butylhydroperoxide in HepG2 cells. *J. Med. Food* **2011**, *14*, 1198–1207.

(4) Maeda, G.; Takara, K.; Wada, K.; Oki, T.; Masuda, M.; Ichiba, T.; Chuda, Y.; Ono, H.; Suda, I. Evaluation of antioxidant activity of vegetables from *Okinawa prefecture* and determination of some antioxidative compound. *Food Sci. Technol. Res.* **2006**, *12*, 8–14.

(5) Meyer, A. S.; Frankel, E. N. Antioxidant activity of hydroxycinnamic acids on human low-density lipoprotein oxidation. *Methods Enzymol.* **2001**, *335*, 256–265.

(6) Tousch, D.; Lajoix, A. D.; Hosy, E.; Azay-Milhau, J.; Ferrare, K.; Jahannault, C.; Cros, G.; Petit, P. Chicoric acid, a new compound able to enhance insulin release and glucose uptake. *Biochem. Biophys. Res. Commun.* **2008**, *377*, 131–135.

(7) Kim, H. G.; Oh, M. S. Natural products as potential anticonvulsants: caffeoylquinic acids. *Arch. Pharm. Res.* **2012**, *35*, 389–392.

(8) Nakajima, Y.; Shimazawa, M.; Mishima, S.; Hara, H. Water extract of propolis and its main constituents, caffeoylquinic acid

derivatives, exert neuroprotective effects via antioxidant actions. *Life Sci.* **2007**, *80*, 370−377.
(9) Chu, K. O.; Chan, K. P.; Wang, C. C.; Chu, C. Y.; Li, W. Y.; Choy, K. W.; Rogers, M. S.; Pang, C. P. Green tea catechins and their oxidative protection in the rat eye. *J. Agric. Food Chem.* **2010**, *58*, 1523−1534.
(10) Sacca, S. C.; Izzotti, A.; Rossi, P.; Traverso, C. Glaucomatous outflow pathway and oxidative stress. *Exp. Eye Res.* **2007**, *84*, 389−399.
(11) Tanaka, J.; Nakanishi, T.; Ogawa, K.; Tsuruma, K.; Shimazawa, M.; Shimoda, H.; Hara, H. Purple rice extract and anthocyanidins of the constituents protect against light-induced retinal damage in vitro and in vivo. *J. Agric. Food Chem.* **2011**, *59*, 528−536.
(12) Kumar, D. M.; Agarwal, N. Oxidative stress in glaucoma: A burden of evidence. *J. Glaucoma* **2007**, *16*, 334−343.
(13) Jung, S. H.; Kim, B. J.; Lee, E. H.; Osborne, N. N. Isoquercitrin is the most effective antioxidant in the plant *Thuja orientalis* and able to counteract oxidative-induced damage to a transformed cell line (RGC-5 cells). *Neurochem. Int.* **2010**, *57*, 713−721.
(14) Kim, K. A.; Kang, K. D.; Lee, E. H.; Nho, C. W.; Jung, S. H. Edible wild vegetable, *Gymnaster koraiensis* protects retinal ganglion cells against oxidative stress. *Food Chem. Toxicol.* **2011**, *49*, 2131−2143.
(15) Kalt, W.; Hanneken, A.; Milbury, P.; Tremblay, F. Recent research on polyphenolics in vision and eye health. *J. Agric. Food Chem.* **2010**, *58*, 4001−4007.
(16) Quigley, H. A. Number of people with glaucoma worldwide. *Br. J. Ophthalmol.* **1996**, *80*, 389−393.
(17) Nucci, C.; Tartaglione, R.; Rombola, L.; Morrone, L. A.; Fazzi, E.; Bagetta, G. Neurochemical evidence to implicate elevated glutamate in the mechanisms of high intraocular pressure (IOP)-induced retinal ganglion cell death in rat. *Neurotoxicology* **2005**, *26*, 935−941.
(18) Levin, L. A.; Peeples, P. History of neuroprotection and rationale as a therapy for glaucoma. *Am. J. Manag. Care* **2008**, *14*, S11−14.
(19) Leske, M. C.; Heijl, A.; Hussein, M.; Bengtsson, B.; Hyman, L.; Komaroff, E. Factors for glaucoma progression and the effect of treatment: the early manifest glaucoma trial. *Arch. Ophthalmol.* **2003**, *121*, 48−56.
(20) Baltmr, A.; Duggan, J.; Nizari, S.; Salt, T. E.; Cordeiro, M. F. Neuroprotection in glaucoma—Is there a future role? *Exp. Eye Res.* **2010**, *91*, 554−566.
(21) Marcic, T. S.; Belyea, D. A.; Katz, B. Neuroprotection in glaucoma: A model for neuroprotection in optic neuropathies. *Curr. Opin. Ophthalmol.* **2003**, *14*, 353−356.
(22) Adegawa, S.; Miyase, T.; Fukushima, S. Sesquiterpene glycosides from *Youngia denticulata* (Houtt) Kitam. *Chem. Pharm. Bull.* **1986**, *34*, 3769−3773.
(23) Carnat, A.; Heitz, A.; Fraisse, D.; Carnat, A. P.; Lamaison, J. L. Major dicaffeoylquinic acids from *Artemisia vulgaris*. *Fitoterapia* **2000**, *71*, 587−589.
(24) Wang, T.; Jiang, X.; Yang, L.; Wu, S. pH-gradient counter-current chromatography isolation of natural antioxidant chlorogenic acid from *Lonicera japonica* Thumb. using an upright coil planet centrifuge with three multi-layer coils connected in series. *J. Chromatogr. A* **2008**, *1180*, 53−58.
(25) Krishnamoorthy, R. R.; Agarwal, P.; Prasanna, G.; Vopat, K.; Lambert, W.; Sheedlo, H. J.; Pang, I. H.; Shade, D.; Wordinger, R. J.; Yorio, T.; Clark, A. F.; Agarwal, N. Characterization of a transformed rat retinal ganglion cell line. *Brain Res. Mol. Brain Res.* **2001**, *86*, 1−12.
(26) Van Bergen, N. J.; Wood, J. P. M.; Chidlow, G.; Trounce, I. A.; Casson, R. J.; Ju, W. K.; Weinreb, R. N.; Crowston, J. G. Recharacterization of the RGC-5 retinal ganglion cell line. *Invest. Ophthalmol. Vis. Sci.* **2009**, *50*, 4267−4272.
(27) Mosmann, T. Rapid colorimetric assay for cellular growth and survival: application to proliferation and cytotoxicity assays. *J. Immunol. Methods* **1983**, *65*, 55−63.
(28) Shimazawa, M.; Nakajima, Y.; Mashima, Y.; Hara, H. Docosahexaenoic acid (DHA) has neuroprotective effects against oxidative stress in retinal ganglion cells. *Brain Res.* **2009**, *1251*, 269−275.
(29) Kim, K. A.; Kim, S. M.; Kang, S. W.; Il Jeon, S.; Um, B. H.; Jung, S. H. Edible seaweed, *Eisenia bicyclis*, protects retinal ganglion cells death caused by oxidative stress. *Mar. Biotechnol.* **2012**, *14*, 383−395.
(30) Kang, K. D.; Majid, A. S. A.; Kim, K. A.; Kang, K.; Ahn, H. R.; Nho, C. W.; Jung, S. H. Sulbutiamine counteracts trophic factor deprivation induced apoptotic cell death in transformed retinal ganglion cells. *Neurochem. Res.* **2010**, *35*, 1828−1839.
(31) Huang, H.-L.; Wu, S.-L.; Liao, H.-F.; Jiang, C.-M.; Huang, R.-L.; Chen, Y.-Y.; Yang, Y.-C.; Chen, Y.-J. Induction of apoptosis by three marine algae through generation of reactive oxygen species in human leukemic cell lines. *J. Agric. Food Chem.* **2005**, *53*, 1776−1781.
(32) Zhang, B.; Osborne, N. N. Oxidative-induced retinal degeneration is attenuated by epigallocatechin gallate. *Brain Res.* **2006**, *1124*, 176−187.
(33) Jung, S. H.; Kang, K. D.; Ji, D.; Fawcett, R. J.; Safa, R.; Kamalden, T. A.; Osborne, N. N. The flavonoid baicalin counteracts ischemic and oxidative insults to retinal cells and lipid peroxidation to brain membranes. *Neurochem. Int.* **2008**, *53*, 325−337.
(34) Inokuchi, Y.; Shimazawa, M.; Nakajima, Y.; Suemori, S.; Mishima, S.; Hara, H. Brazilian green propolis protects against retinal damage in vitro and in vivo. *J. Evidence-Based Complementary Altern. Med.* **2006**, *3*, 71−77.
(35) Kwong, J. M.; Lam, T. T. *N*-Methyl-D-aspartate (NMDA) induced apoptosis in adult rabbit retinas. *Exp. Eye Res.* **2000**, *71*, 437−444.
(36) Park, Y. W.; Chae, S. H.; Lee, J.; Kwon, O. J.; Shin, J. P.; Jeon, C. J.; Kim, S. Y. *N*-Methyl-D-aspartate (NMDA)-induced apoptosis in rabbit retina. *J. Korean Ophthalmol. Soc.* **2008**, *49*, 1146−1153.
(37) Li, Y.; Schlamp, C. L.; Nickells, R. W. Experimental induction of retinal ganglion cell death in adult mice. *Invest. Ophthalmol. Vis. Sci.* **1999**, *40*, 1004−1008.
(38) Danias, J.; Lee, K. C.; Zamora, M. F.; Chen, B.; Shen, F.; Filippopoulos, T.; Su, Y. L.; Goldblum, D.; Podos, S. M.; Mittag, T. Quantitative analysis of retinal ganglion cell (RGC) loss in aging DBA/2NNia glaucomatous mice: comparison with RGC loss in aging C57/BL6 mice. *Invest. Ophthalmol. Vis. Sci.* **2003**, *44*, 5151−5162.
(39) Kim, K. A.; Shim, S. H.; Ahn, H. R.; Jung, S. H. Protective effects of the compounds isolated from the seed of *Psoralea corylifolia* on oxidative stress-induced retinal damage. *Toxicol. Appl. Pharmacol.* **2013**, *269*, 109−120.
(40) Kuehn, M. H.; Fingert, J. H.; Kwon, Y. H. Retinal ganglion cell death in glaucoma: mechanisms and neuroprotective strategies. *Ophthalmol. Clin. North Am.* **2005**, *18* (vi), 383−395.
(41) Galaris, D.; Pantopoulos, K. Oxidative stress and iron homeostasis: mechanistic and health aspects. *Crit. Rev. Clin. Lab. Sci.* **2008**, *45*, 1−23.
(42) Andersen, J. K. Oxidative stress in neurodegeneration: cause or consequence? *Nat. Med.* **2004**, *10* (Suppl), S18−25.
(43) Ko, M. L.; Peng, P. H.; Ma, M. C.; Ritch, R.; Chen, C. F. Dynamic changes in reactive oxygen species and antioxidant levels in retinas in experimental glaucoma. *Free Radical Biol. Med.* **2005**, *39*, 365−373.
(44) Izzotti, A.; Bagnis, A.; Sacca, S. C. The role of oxidative stress in glaucoma. *Mutat. Res.* **2006**, *612*, 105−114.
(45) Mozaffarieh, M.; Grieshaber, M. C.; Orgul, S.; Flammer, J. The potential value of natural antioxidative treatment in glaucoma. *Surv. Ophthalmol.* **2008**, *53*, 479−505.
(46) Kang, K. D.; Majid, A. S.; Kim, K. A.; Kang, K.; Ahn, H. R.; Nho, C. W.; Jung, S. H. Sulbutiamine counteracts trophic factor deprivation induced apoptotic cell death in transformed retinal ganglion cells. *Neurochem. Res.* **2010**, *35*, 1828−1839.
(47) Aslan, M.; Cort, A.; Yucel, I. Oxidative and nitrative stress markers in glaucoma. *Free Radical Biol. Med.* **2008**, *45*, 367−376.
(48) Babizhayev, M. A.; Bunin, A. Lipid peroxidation in open-angle glaucoma. *Acta Ophthalmol.* **1989**, *67*, 371−377.

(49) Lam, T. T.; Abler, A. S.; Kwong, J. M.; Tso, M. O. *N*-methyl-D-aspartate (NMDA)-induced apoptosis in rat retina. *Invest. Ophthalmol. Vis. Sci.* **1999**, *40*, 2391−2397.
(50) Ng, Y. K.; Zeng, X. X.; Ling, E. A. Expression of glutamate receptors and calcium-binding proteins in the retina of streptozotocin-induced diabetic rats. *Brain Res.* **2004**, *1018*, 66−72.
(51) Joo, C. K.; Choi, J. S.; Ko, H. W.; Park, K. Y.; Sohn, S.; Chun, M. H.; Oh, Y. J.; Gwag, B. J. Necrosis and apoptosis after retinal ischemia: involvement of NMDA-mediated excitotoxicity and p53. *Invest. Ophthalmol. Vis. Sci.* **1999**, *40*, 713−720.
(52) Brandstatter, J. H.; Hartveit, E.; Sassoe-Pognetto, M.; Wassle, H. Expression of NMDA and high-affinity kainate receptor subunit mRNAs in the adult rat retina. *Eur. J. Neurosci.* **1994**, *6*, 1100−1112.
(53) Mizuno, K.; Koide, T.; Yoshimura, M.; Araie, M. Neuroprotective effect and intraocular penetration of nipradilol, a beta-blocker with nitric oxide donative action. *Invest. Ophthalmol. Vis. Sci.* **2001**, *42*, 688−694.
(54) Hughes, W. F. Quantitation of ischemic damage in the rat retina. *Exp. Eye Res.* **1991**, *53*, 573−582.
(55) Leung, C. K.; Lindsey, J. D.; Crowston, J. G.; Lijia, C.; Chiang, S.; Weinreb, R. N. Longitudinal profile of retinal ganglion cell damage after optic nerve crush with blue-light confocal scanning laser ophthalmoscopy. *Invest. Ophthalmol. Vis. Sci.* **2008**, *49*, 4898−4902.
(56) Kreutz, M. R.; Seidenbecher, C. I.; Sabel, B. A. Molecular plasticity of retinal ganglion cells after partial optic nerve injury. *Restor. Neurol. Neurosci.* **1999**, *14*, 127−134.
(57) Schuettauf, F.; Rejdak, R.; Thaler, S.; Bolz, S.; Lehaci, C.; Mankowska, A.; Zarnowski, T.; Junemann, A.; Zagorski, Z.; Zrenner, E.; Grieb, P. Citicoline and lithium rescue retinal ganglion cells following partial optic nerve crush in the rat. *Exp. Eye Res.* **2006**, *83*, 1128−1134.
(58) Steinsapir, K. D.; Goldberg, R. A. Traumatic optic neuropathy. *Surv. Ophthalmol.* **1994**, *38*, 487−518.
(59) Erk, T.; Renouf, M.; Williamson, G.; Melcher, R.; Steiling, H.; Richling, E. Absorption and isomerization of caffeoylquinic acids from different foods using ileostomist volunteers. *Eur. J. Nutr.* **2013**, DOI: 10.1007/s00394-013-0512-z.
(60) Park, C. M.; Jin, K. S.; Lee, Y. W.; Song, Y. S. Luteolin and chicoric acid synergistically inhibited inflammatory responses via inactivation of PI3K-Akt pathway and impairment of NF-κB translocation in LPS stimulated RAW 264.7 cells. *Eur. J. Pharmacol.* **2011**, *660*, 454−459.

peroxidation and tumor cell proliferation.[12] Betalains are more effective than tea catechins in protecting against the oxidation of human low-density lipoprotein and metmyoglobin.[13] Beetroot extracts showed a significant inhibitory effect against skin and lung cancer in mice.[14] An investigation into the differences between the chemical structures and activity of various betaxanthins and betacyanins with respect to their free radical-scavenging capacities was also suggested.[15]

Betaine is a modified amino acid commonly known as trimethylglycine or glycinebetaine. It is distributed widely in animals, plants, and microorganisms, and the rich dietary sources of betaine include many foods such as wheat germ or bran (≈1% or 1339 mg), spinach (≈0.7% or 600−645 mg), and sugar beets (0.2−0.3% or 117−297 mg/100 g fresh weight).[16,17]

Betaine was first discovered in the juice of sugar beets (*B. vulgaris*) in the 19th century and subsequently found in several other organisms.[16] It is naturally found in the body due to the breakdown of choline. The principal role of betaine in plants is thought to be the protection of cells against osmotic inactivation by adjusting the osmotic balance inside the plant cells and tissues.[18] By this natural defense mechanism, betaine helps the plants to overcome the environmental stress caused by salinity,[19,20] water stress,[21,22] and cold stress.[23] For example, the betaine content increased significantly in spinach grown in saline soil, up to 3% of the fresh weight.[20] Red beetroot grown under saline conditions also showed an increase in betaine in the tissue, indicating its ability to synthesize and regulate betaine production.[18]

In addition to the osmotic functions resulting from environmental stress, betaine has been used as a dietary supplement in animal nutrition for the purpose of promoting overall health.[16] Red beetroot is a rich source of betaine, although it is often overlooked as a food source.[24] Betaine has the biological properties of lowering blood homocysteine levels,[25,26] regulating osmolyte function in the kidney,[27] and protecting the liver from toxins such as chloroform.[28] Betaine is believed to be the most active naturally occurring osmoprotectant molecule for bacteria, and dimethylthetin has been suggested as a useful model for the development of antibacterial agents.[29] The betaine content of foods has been found to vary greatly when different individual food sources were analyzed and different cooking methods were used; for example, boiling led to the greatest loss of betaine.[24]

In this study, we investigated the distribution of betalains and betaine in various beetroot cultivars grown in a greenhouse or in the field, and we also evaluated the cytotoxic activities of betanin and betaine in human cancer cells. The objectives of this study were (1) to separate and quantify the individual betalains and betaine from beetroots, (2) to compare the contents of betalains and betaine among nine beetroot cultivars, (3) to test the environmental effects on the composition of both compounds between the greenhouse and field, and (4) to examine the cytotoxicity of betanin and betaine to HepG2 cells to promote the health benefits of beetroots.

MATERIALS AND METHODS

Chemical Reagents and Plant Materials. All chemicals and solvents were purchased from Sigma-Aldrich (St. Louis, MO, USA) or Fisher Scientific (Pittsburgh, PA, USA). All other chemicals used were of analytical grade. Authentic betanin (red beetroot extract diluted with dextrin) was purchased from TCI (Tokyo Chemical Industry Co., Tokyo, Japan), and betaine was obtained from Sigma-Aldrich. The seeds of beetroot cultivars were obtained from Burpee (Warminster, PA, USA) (Table 1). Yellow-red Swiss chard, red-violet portulaca, and red cactus pear fruit were purchased from local markets.

Table 1. Cultivars, Root Colors, and Sample Identification Codes of Beetroots (*Beta vulgaris* L.)

cultivar	root color	identification code
Little Chicago hybrid	red	I
Detroit King	red	II
Red Heart hybrid	red	III
Red Cloud hybrid	red	IV
Scarlet Prince	red	V
Bull's Blood	red	VI
Burpee's Red Ball	red	VII
Detroit Supreme	red	VIII
Burpee's Golden Globe	yellow-gold	IX

Production of Beetroots. Beetroots were cultivated in a field in Weslaco (26° 15′ N, 97° 98′ W) in the Rio Grande Valley of southern Texas and in the greenhouse at College Station (30° 36′ N, 96° 18′W) at Texas A&M University. The soils were clay or loam types, with a pH ranging from 7.4 to 8.2. Average soil sulfur levels were 120−150 ppm. In the greenhouse, beetroots were planted in a 7- L pot filled with Sunshine mix 1 (Sun Grow Horticulture, Agwam, MA, USA), and the plants were watered with a modified fertilizer solution,[30] as necessary. The plants were managed by commercial standard cultural practices.

Beetroots were harvested at a stage of commercial harvest maturity from each location and transported to the labortory. Harvested beetroots were washed, and approximately 100 g was cut from the midsection of the root. The root sample was chopped into small pieces, placed into a plastic bag, and stored at −20 °C until analysis.

Preparation of Crude Betalain Extracts. Approximately 50 g of the frozen tissue was pulverized with a rubber mallet and mixed thoroughly while the tissue remained frozen. Five grams of tissues was homogenized with 30 mL of 80% aqueous methanol and 0.1% ascorbic acid using a homogenizer (model PT 10-35, Brinkmann, Westbury, NY, USA). The homogenates were centrifuged at 10000*g* for 20 min, and the supernatants were filtered. All extracts were stored at 4 °C until HPLC analysis.

In addition to beetroot extracts, we analyzed and compared betalains extracted from different plant sources for use as references to identify betalains because betalains are abundant in cactus fruit (*Opuntia* spp.),[9,31] portulaca flowers,[32] and Swiss chard.[4] They were processed as mentioned above.

Analysis of Betalains. Betalains were separated and quantified using a Perkin-Elmer HPLC system (Shelton, CT, USA) equipped with a series 200 pump, autosampler, and diode array detector (DAD). An analytical column (Spherisorb ODS2, Waters, 4.6 × 250 mm, 5 μm) was used with a guard cartridge. Solvents A and B were water and methanol, both containing 0.01% acetic acid, respectively. The solvent gradient was programmed as follows: from 0 to 60% solvent B over 45 min at a flow rate of 1.0 mL/min, then changed to 100% solvent B (0% A) for 5 min to flush the column. The calibration standards and sample extracts were injected via a 20 μL sample loop. Chromatographic detection was set at 480 nm for betaxanthins and at 540 nm for betacyanins. Spectral data were simultaneously collected between 200 and 700 nm.

Purification of Betalains. Betalains were purified by a semipreparative HPLC method. A semipreparative column (Waters Spherisorb ODS2, 20 × 250 mm) was used, and 1 mL of crude betalain extracts was injected using a manual injector. The solvents were water and methanol (40:60, v/v) at a flow rate of 4 mL/min. Peak fractions of column eluates were repeatedly collected, combined, and lyophilized for use as betalain standard compounds. The purity of the compounds was tested on the basis of the peak areas detected by the analytical HPLC method.

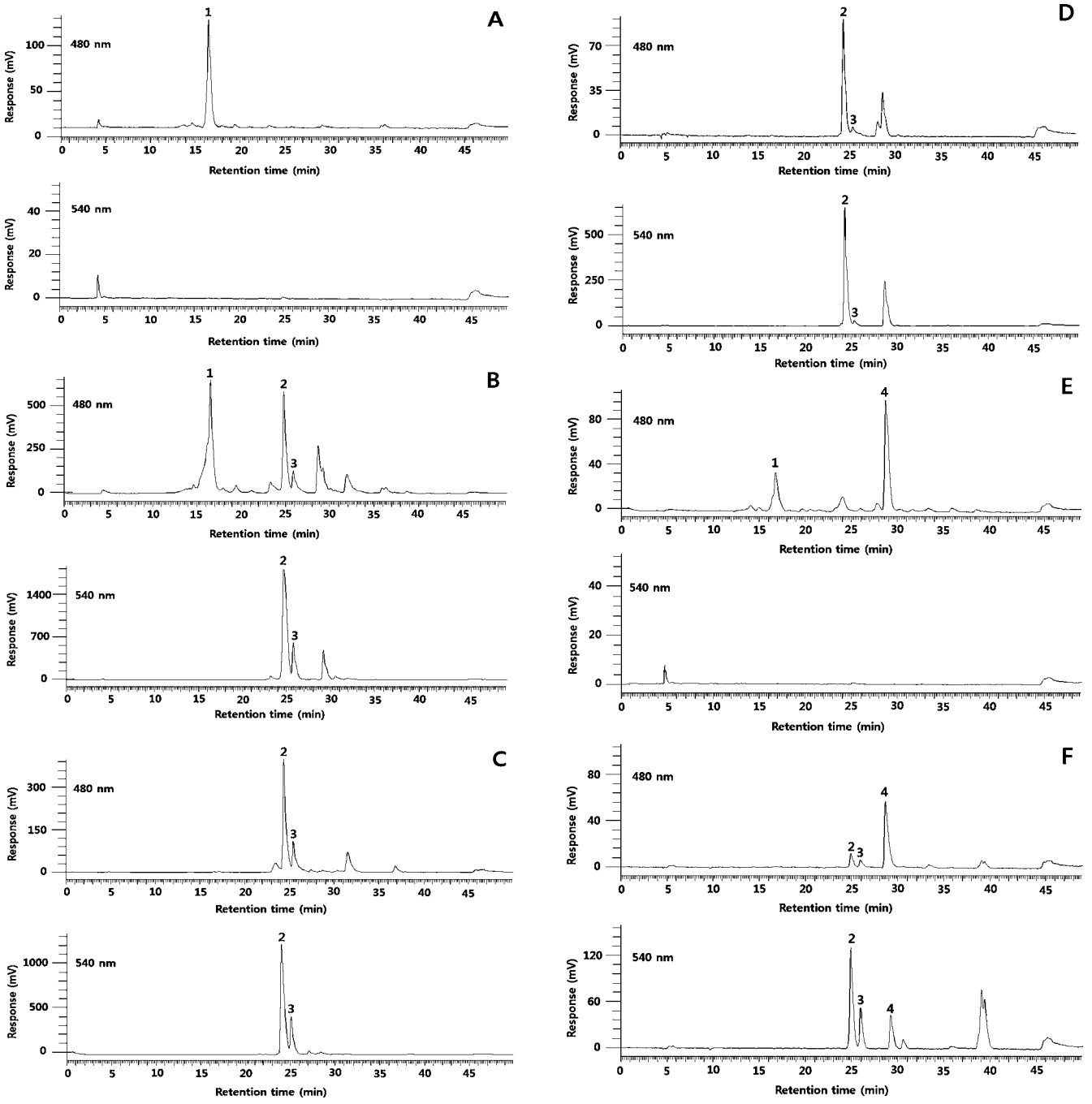

Figure 1. HPLC chromatograms of betalains extracted from different plants: yellow beetroot (A); red beetroot (B); red cactus pear (C); petals of red-violet portulaca (D); petioles of yellow Swiss chard (E); petioles of red Swiss chard (F). Elution was monitored at 480 nm for betaxanthin (A) and at 540 nm for betacyanin (B). The numbers on the peaks refer to the betalains listed in Table 1.

Identification of Betalains. Electrospray ionization in positive ion mode was carried out by applying 4.5 kV at the spray needle to create positive ions. Sheath gas and auxiliary gas flow rates were 50 and 10 arbitrary units, respectively. The transfer capillary temperature was maintained at 250 °C. The Xcalibur 2.0 software package (ThermoFinnigan) was used to control the LC-MS system and for data acquisition and processing. Identities were also determined by comparing the experimental data with previously reported HPLC-MS data from a betanin standard using the analytical HPLC method, as described above, and by spectral analysis.[4,31−34]

Quantification of Betalains. The concentrations of individual betacyanins (betanin and isobetanin) and betaxanthins (vulgaxanthin I and miraxanthin V) were calculated using extinction coefficient values ($E^{1cm}_{1\%}$) of 1120 at 537 nm and 750 at 480 nm with their respective absorption maxima, respectively.[35,36] The total betacyanins and betaxanthins of beetroots were expressed as betanin equivalents or vulgaxanthin equivalents, respectively, because they were the predominant compounds in beetroots. The total betalain content was calculated by summing the total betacyanin and betaxanthin contents.

Extraction and Analysis of Betaine. Three grams of tissues obtained from the pulverized sample was homogenized in 30 mL of 80% ethanol. Homogenates were filtered and 20 μL samples were injected into an HPLC system with a refractive index detector and a 700 CH carbohydrate column (Alltech, Deerfield, IL, USA) with a guard cartridge. A betaine standard was dissolved in 80% ethanol, and the concentrations were calculated using standard curves between 0 and 10 mg/mL.

dx.doi.org/10.1021/jf404648u | J. Agric. Food Chem. 2014, 62, 1324−1331

Table 2. HPLC, HPLC-MS, and Purity of Isolated Betalains from Beetroots and Petioles of Swiss Chard

peak	retention time (min)	λ_{max} (nm)	m/z $[M + H]^+$	purity (%)	name	source
1	16.8	470	340	97	vulgaxanthin I	yellow beetroot
2	24.8	534	551	92	betanin	red beetroot
3	25.3	534	551	76	isobetanin	red beetroot
4	29.1	461	347	95	miraxanthin V	yellow Swiss chard

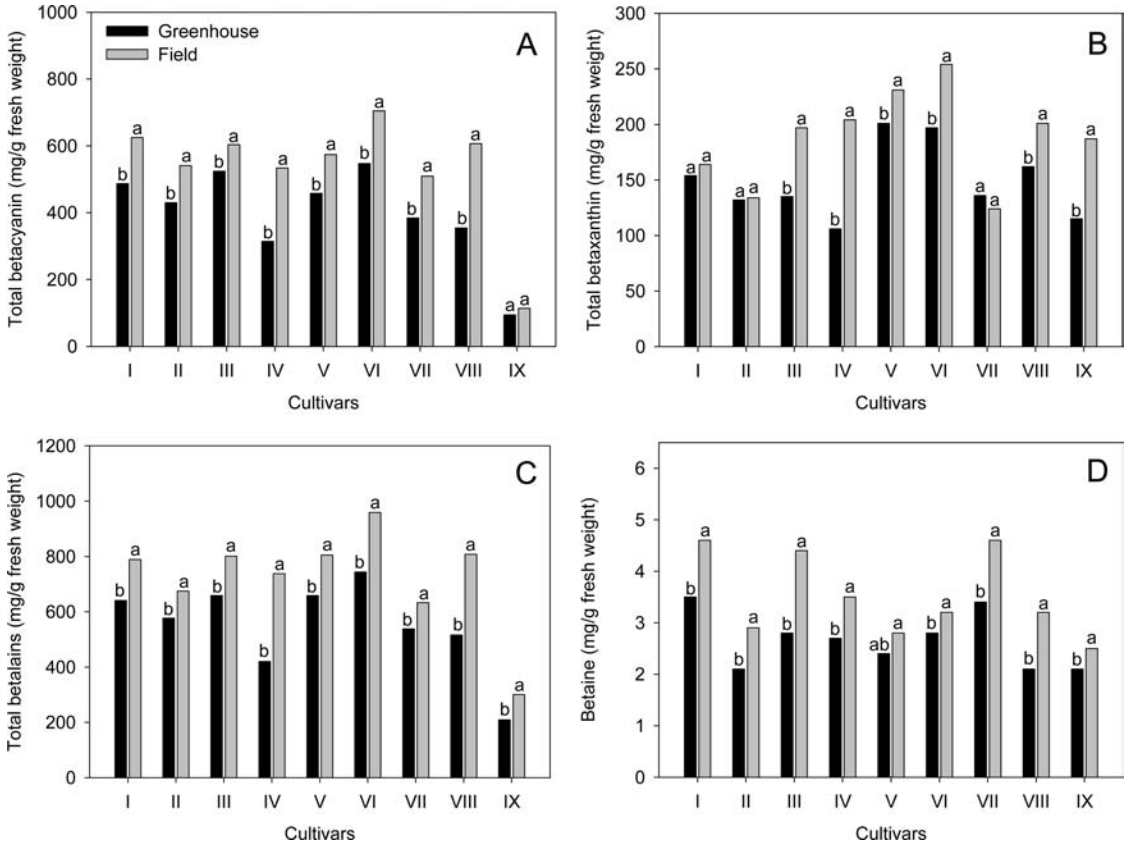

Figure 2. Total betacyanins (A), betaxanthin (B), betalains (C), and betaine (D) contents of various beetroot cultivars grown in a greenhouse or in the field. Beetroot cultivars are listed in Table 1. Means in each cultivar with different letters are significantly different according to Duncan's multiple-range test at $P < 0.05$.

Cell Culture and MTT Assay. HepG2 cells (ATCC) were cultured in Dulbecco's modified Eagle medium (DMEM) containing 10% fetal bovine serum at 37 °C in a 5% CO_2 incubator. Betanin isolated from beetroot extracts and standard betaine were used for cytotoxicity assay. The cancer cell proliferation inhibitory activity of betanin and betaine was determined using the 3-(4,5-dimethylthiazol-2-yl)-2,5-diphenyl tetrazolium bromide (MTT) staining method.[37] A total of 0.8×10^4 HepG2 cells in DMEM was placed in each well of a 96-well plate and incubated to stabilize for 12 h. The growth medium was removed, and media containing increasing concentrations of betanin (0, 25, 50, 100, 200, and 400 μg/mL) and betaine (0, 25, 50, 100, 200, 400, and 800 μg/mL) were added to the cells for 48 h, with media being refreshed every 12 h. The cell proliferation was determined using the colorimetric MTT assay. After 4 h of incubation with a thiazolyl blu,e tetrazolium bromide dissolved in sodium perborate at 5 mg/mL, the media, MTT reagents, and dead cells were aspirated. Dimethyl sulfoxide (100 μL) was added to all wells and mixed thoroughly for 2 h to dissolve the purple formazan crystals. After verification that all crystals were dissolved, the MTT absorbance was measured at 570 nm using a multidetection microplate reader (SpectraMax M2e, Molecular Devices, Sunnyvale, CA, USA).

Data Analysis. Experiments were conducted using a randomized block design with three replicates and determined using SAS 9.0 for Windows (SAS Institute, Cary, NC, USA). Each replicate included five beetroots. The means were separated using Duncan's multiple-range test at $P < 0.05$.

RESULTS AND DISCUSSION

HPLC Chromatograms and Identification of Betalains. The HPLC chromatograms of betalains from the extracts of different plant sources, monitored at 480 nm (betaxanthins) and 540 nm (betacyanins), are shown in Figure 1. Information regarding the identified individual betalains is presented in Table 2.

Figure 1 shows the different betalain patterns of differently colored plants. Betanin (peak 2) was a major compound in red cactus pear (C), petals of red-violet portulaca (D), and petioles of red Swiss chard (F); however, miraxanthin V (peak 4), known as dopamine-betaxanthin, was the major betaxanthin in the petioles of yellow Swiss chard (E). It was eluted at 29.1 min and showed its maximum absorbance at 461 nm. We could obtain the compound at a high purity of 95% from the yellow petioles of Swiss chard (Table 2). It was reported that miraxanthin V and vulgaxanthin I accounted for 37 and 34% of the whole peak area of all identified betaxanthins at 470 nm in yellow-colored Swiss chard petioles, and they also accounted

dx.doi.org/10.1021/jf404648u | J. Agric. Food Chem. 2014, 62, 1324−1331

for up to 55 and 25% in red-purple petioles, respectively.[4] As shown in Figure 1, however, vulgaxanthin I (peak 1) was not detected in the red petioles of Swiss chard (F) and miraxanthin V (peak 4) was identified in extracts of both the yellow (E) and red (F) petioles of Swiss chard.

In this study, we identified and isolated only four predominant betalains, which were two betacyanins (betanin and isobetanin) and two betaxanthins (vulgaxanthin I and miraxanthin V), because they comprised >90% of betalains detected in our samples and analysis system. Individual betalains identified and listed according to their retention times during analysis are vulgaxanthin I (peak 1), betanin (peak 2), isobetanin (peak 3), and miraxanthin V (peak 4) (Table 2). Vulgaxanthin I was isolated from yellow beetroot extracts with a purity of 97% and showed a retention time of 16.8 min and a maximum absorbance at 470 nm (Table 2). As shown in Figure 1A, vulgaxanthin I (peak 1) is only one major betaxanthin identified in yellow beetroot extract, along with other trace compounds that were not identified. Other betaxanthins, such as indicaxanthin, vulgaxanthin IV, and miraxanthin V, were analyzed in yellow beetroot, but they have been detected only in suspension cultures of yellow beetroot due to their low concentrations.[8] Betacyanins were completely absent in extracts from yellow beetroot in our study. The two main betacyanin peaks in red beetroot extract were identified as betanin (peak 2) and isobetanin (peak 3) (Figure 1B), according to their absorption maxima and protonated molecular ions (m/z 551) (Table 2). Both molecules differ only in the absolute configuration of their C15 chiral center[38] and were eluted at very close retention times, 24.8 and 25.3 min, respectively. Due to this difficulty, we were able to obtain purities of 92 and 76% for betanin and isobetanin from red beetroot extract, respectively (Table 2). Vulgaxanthin I (peak 1) is the third major compound, together with betanin and isobetanin. Trace amounts of other unknown compounds were also detected at 480 and 540 nm, although we did not identify them.

Quantification of Betalains. To compare the betalain contents of various beetroot cultivars produced in the field or a greenhouse, we cultivated a total of nine beetroot cultivars, consisting of eight red-colored (I–VIII) and one yellow-colored (IX) beetroot (Table 1). The total betacyanins and betaxanthins were calculated by the spectrophotometric method and are shown in Figure 2. Additionally, the analysis of individual betalains of the two cultivars, 'Bull's Blood' (A) and 'Burpee's Golden Globe' (B), which were obtained from the field, was performed by DAD-HPLC, and the concentrations of individual betalains are presented in Figure 3.

Figure 2A shows the results obtained for the total betacyanin contents, expressed as betanin equivalents, in beetroots grown in the greenhouse or in the field. All beetroot cultivars (Table 1) grown in field conditions showed higher contents of total betacyanins compared with those from the greenhouse, except for the 'Burpee's Golden Globe' cultivar (IX), which was yellow in color. The total betaxanthins of each cultivar from the field were relatively higher or similar to the total betaxanthin contents of beetroots from the greenhouse (Figure 2B). Consequently, the total betalains of beetroots produced in the field were between 650 and 800 μg/g fresh weight, showing >25% higher total betalain content than those from the greenhouse (Figure 2C). The total betalains of the 'Burpee's Golden Globe' cultivar (IX) were 301 μg/g fresh weight, the sum of 114 μg/g for betacyanins and 187 μg/g for betaxanthins.

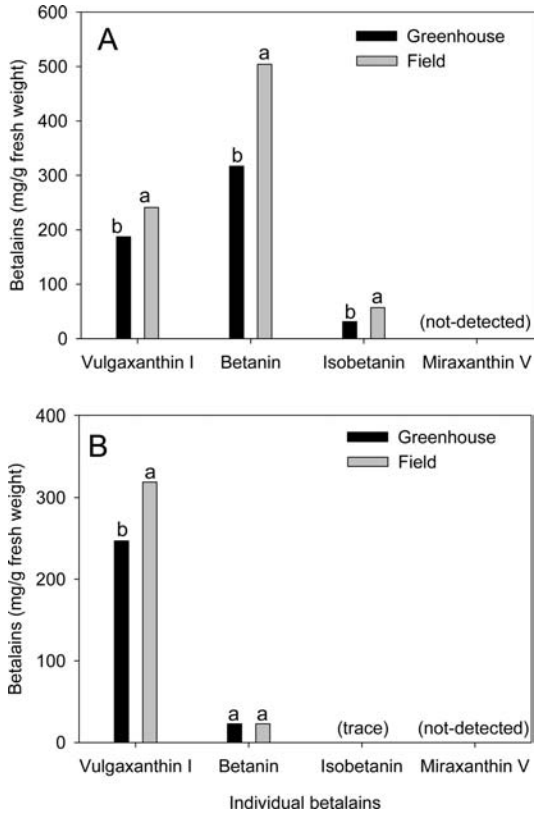

Figure 3. Individual betalains content of beetroot 'Bull's Blood' (A) and 'Burpee's Golden Globe' (B) cultivars grown in a greenhouse or in the field. Means in each cultivar with different letters are significantly different according to Duncan's multiple-range test at $P < 0.05$.

The content of betalains differed greatly among cultivars as well as growing conditions.

The compositions of the four individual betalains for the 'Bull's Blood' (A) and 'Burpee's Golden Globe' cultivars (B) are presented in Figure 3. Betanin is one of the major betacyanins of red beetroots, comprising >60% of the total pigments, followed by vulgaxanthin I and isobetanin. Miraxanthin V was not detected in our analysis due to its low concentration in red and yellow beetroots. However, vulgaxanthin I was the most abundant betaxanthins in the yellow 'Burpee's Golden Globe' cultivar, whereas betanin was a minor compound and isobetanin was detected in trace amounts. Similar results were reported in other previous studies.[9,39]

It has been well-known that light is a physical factor that can affect metabolite production. A positive correlation between increasing light intensity and levels of betalains has been reported.[40,41] Light enhances betalain production in red beetroots[42,43] and portulaca[40,44] by increasing tyrosinase activity, catalyzing the formation of both L-(3,4-dihydroxyphenyl)alanine (DOPA) and *cyclo*-DOPA, which are precursors in betalain biosynthesis in higher plant.[45] In addition, blue light was more effective for the production of betalains than other lights.[40]

The signal transduction pathway of light-induced betacyanin and anthocyanin synthesis may be similar to the light quality- and quantity-influenced betacyanin synthesis of *Suaeda salsa* calli.[46] Most studies of light-induced betalain biosynthesis have been focused and conducted on cultured cells. Little is known about the mechanism of light-induced betalain biosynthesis of beetroots grown under field or greenhouse conditions.

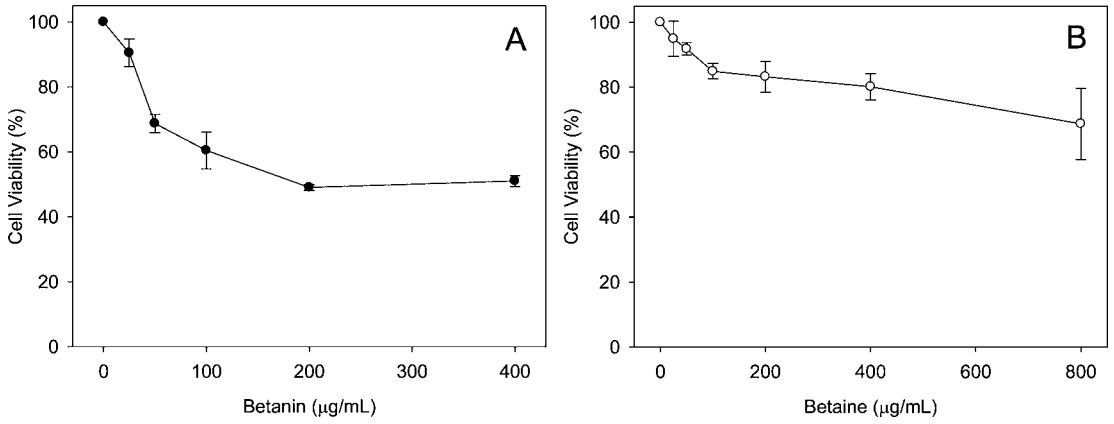

Figure 4. Cytotoxicity on HepG2 cells after their exposure to betanin (A) and betaine (B) for 48 h at 37 °C. Vertical bars represent the standard errors.

However, we could assume that sufficient or high light intensity from natural sunlight promoted betalain biosynthesis, resulting in high levels of betalain accumulation in beetroots grown in the field. In greenhouse studies, the light quantity was deficient and/or the quality of light was insufficient, probably due to the significantly reduced levels of UV light passing through the cover plastic, resulting in betalain contents lower than in the field.

In addition to stimulus by light, plants might be exposed to other environmental factors that aid in the accumulation of betalain pigments in cells. Thus, it is of interest to explore whether betalain biosynthesis can be induced by common stimuli, such as soil conditions, high temperatures, or growing practices from conventional, organic, or integrated farming systems, as aspects of promoting the health benefits of beetroots.

Quantification of Betaine. Figure 2D shows that beetroots grown under field conditions accumulated more betaine, regardless of the cultivar. There was also great variation in betaine concentrations among cultivars. It has been reported that betaine is synthesized in response to abiotic stress, especially to water or salt stress.[19−21] Under our growing conditions, the water capacities of soil in the field and the greenhouse were completely different. The plants had different water supplies in the greenhouse (automatic irrigation to obtain ∼60% water capacity) and in the field (automatic irrigation to obtain ∼30% water capacity). Thus, we could assume that betaine was increased significantly in beetroots grown in the field as a consequence of a long-term or frequent drought in Texas. In addition, soil sulfur levels of >100 ppm in Texas fields[47−49] and high temperature extremes might influence betaine biosynthesis in beetroots during field cultivation as sources of abiotic stress, but it has not yet been scientifically reported in beetroots.

In Vitro Inhibition of HepG2 Cell Proliferation. The MTT test was carried out to evaluate the effect of betanin and betaine, which are major dietary compounds for human health in beetroots, on HepG2 cell inhibition after 48 h of incubation. As shown in Figure 4A, treatment with betanin exhibited dose-dependent inhibition of HepG2 cell proliferation at concentrations between 0 and 200 μg/mL. However, the HepG2 cells were inhibited by 25% when treated with a betaine concentration of 800 μg/mL (Figure 4B). The addition of betaine at a concentration of 1600 μg/mL showed a similar level of cell cytotoxicity (data not shown). Although betanin was more effective in reducing cell viability than betaine in this study, an overall reduction of cell viability was observed in the MTT assay.

The free radical-scavenging and biological activities of betanin or betalains as extracts of beetroots against human cancer as well as some other diseases have been reported.[12,50,51] In vitro HepG2 cell cytotoxicity by betalains extracted from *Rivina humilis* berries[50] and *Tamarindus indica* fruit pulp[52] was also confirmed. Similarly, our results showed that betanin obtained from beetroots has anticancer activity (49% proliferation inhibition) especially against HepG2 cells at relatively high concentration of betanin (200 μg/mL). Although betaine has been shown to protect the liver in animals[16,53] and act as an antimicrobial agent,[29] there was a slight effect with respect to HepG2 cell cytotoxicity in our study.

AUTHOR INFORMATION

Corresponding Authors

*(J.K.) E-mail: jeongyunkim@dankook.ac.kr. Phone: +82-41-550-1255. Fax: +82-41-561-1256.

*(K.S.Y.) E-mail: ksyoo@yu.ac.kr. Phone: +82-53-810-2947. Fax: +82-53-810-4659.

Funding

This material was supported by the Cooperative State Research, Education, and Extension Service, U.S. Department of Agricultural, under Agreement 2009-34402-19831, "Designing Foods for Health" through the Vegetable and Fruit Improvement Center, Texas AgriLife Research. This work was also supported by the Basic Science Research Program through the National Research Foundation of Korea funded by the Ministry of Education, Science and Technology (NRF-116436).

Notes

The authors declare no competing financial interest.

REFERENCES

(1) Liu, X.; Gao, Y.; Xu, H.; Wang, Q.; Yang, B. Impact of high-pressure carbon dioxide combined with thermal treatment on degradation of red beet (*Beta vulgaris* L.) pigments. *J. Agric. Food Chem.* **2008**, *56*, 6480−6487.

(2) Vinson, J. A.; Hao, Y.; Su, X.; Zubik, L. Phenol antioxidant quantity and quality in foods: vegetable. *J. Agric. Food Chem.* **1998**, *46*, 3630−3634.

(3) Jackman, R. L.; Smith, J. I. Anthocyanin and betalains. In *Natural Food Colourants*, 2nd ed.; Hendry, G. A. F., Houghton, J. D., Eds.; Chapman & Hall; London, UK, 1996; pp 244−309.
(4) Kugler, F.; Stintzing, F. C.; Carle, R. Identification of betalains from petioles of differently colored Swiss (*Beta vulgaris* L. spp. *cicla* [L.] Alef. Cv. Bright Lights) by high-performance liquid chromatography-electrospray ionization mass spectrometry. *J. Agric. Food Chem.* **2004**, *52*, 2975−2981.
(5) Stintzing, F. C.; Carle, R. Functional properties of anthocyanins and betalains in plants, food, and in human nutrition. *Trends Food Sci. Technol.* **2004**, *15*, 19−38.
(6) Stafford, H. A. Anthocyanins and betalains: evolution of the mutually exclusive pathway. *Plant Sci.* **1994**, *101*, 91−98.
(7) Steglich, W.; Strack, D. Betalains. In *The Alkaloids − Chemistry and Pharmacology*; Brossi, A., Ed.; Academic Press: San Diego, CA, USA, 1990; pp 1−62.
(8) Delgado-Vargas, F.; Jiménez, A. R.; Paredes-López, O. Natural pigments: carotenoids, anthocyanins, and betalains − characteristics, biosynthesis, processing, and stability. *Crit. Rev. Food Sci. Nutr.* **2000**, *40*, 173−289.
(9) Stintzing, F. C.; Schieber, A.; Carle, R. Identification of betalains from yellow beet (*Beta vulgaris* L.) and cactus pear [*Opuntia ficus-indica* (L.) Mill.] by high-performance liquid chromatography-electrospray ionization mass spectrometry. *J. Agric. Food Chem.* **2002**, *50*, 2302−2307.
(10) Nemzer, B.; Pietrzkowski, Z.; Spórma, A.; Stalica, P.; Thresher, W.; Michalowski, T.; Wybraniec, S. Betalainic and nutritional profiles of pigment-enriched red beet root (*Beta vulgaris* L.) dried extracts. *Food Chem.* **2011**, *127*, 42−53.
(11) Marmion, D. M. *Handbook of US Colorants: Food, Drugs, Cosmetics, and Medicinal Devices*; Wiley-Interscience: New York, 1991.
(12) Reddy, M. K.; Alexander-Lindo, R. L.; Nair, M. G. Relative inhibition of lipid peroxidation, cyclooxygenase enzyme, and human tumor cell proliferation by natural food colors. *J. Agric. Food Chem.* **2005**, *53*, 9268−9273.
(13) Palumbo, B.; Efthimiou, Y.; Stamatopoulos, J.; Oguogho, A.; Budinsky, A.; Palumbo, R.; Sinzinger, H. Prickly pear induces upregulation of liver LDL binding in familial heterozygous hypercholesterolemia. *Nucl. Med. Rev.* **2003**, *6*, 35−39.
(14) Kapadia, G. J.; Tokuda, H.; Konoshima, T.; Nishino, H. Chemopreventive of lung and skin cancer by *Beta vulgaris* (beet) root extract. *Cancer Lett.* **1996**, *100*, 211−214.
(15) Cai, Y.; Sun, M.; Corke, H. Antioxidant activity of betalains from plants of the Amaranthaceae. *J. Agric. Food Chem.* **2003**, *51*, 2288−2294.
(16) Craig, S. A. S. Betaine in human nutrition. *Am. J. Clin. Nutr.* **2004**, *80*, 539−549.
(17) Zeisel, S. H.; Mar, M. H.; Howe, J. C.; Holden, J. M. Concentrations of choline-containing compounds and betaine in common foods. *J. Nutr.* **2003**, *133*, 1302−1307.
(18) Subbarao, G. V.; Wheeler, R. M.; Levine, L. H.; Stuttle, G. W. Glycine betaine accumulation, ionic and water relations of red-beet at contrasting levels of sodium supply. *J. Plant Physiol.* **2001**, *158*, 767−776.
(19) Yamada, N.; Promden, W.; Yamane, K.; Tamagake, H.; Hibino, T.; Tanaka, Y.; Takabe, T. Preferential accumulation of betaine uncoupled to choline monooxygenase in young leaves of sugar beet − importance of long-distance translocation of betaine under normal and salt-stressed conditions. *J. Plant Physiol.* **2009**, *166*, 2058−2070.
(20) Martino, C. D.; Delfine, S.; Pizzuto, R.; Loreto, F.; Fuggi, A. Free amino acids and glycine betaine in leaf osmoregulation of spinach responding to increasing salt stress. *New Phytol.* **2003**, *158*, 455−463.
(21) Yancey, P. H.; Clark, M. E.; Hand, S. C.; Bowlus, R. D.; Somero, G. N. Living with water stress: evolution of osmolyte systems. *Science* **1982**, *217*, 1214−1222.
(22) Choluj, D.; Karwowska, R.; Jasinska, M.; Harber, G. Growth and dry matter partitioning in sugar beet plants (*Beta vulgaris* L.) under moderate drought. *Plant Soil Environ.* **2004**, *50*, 265−272.
(23) Zhang, X. Y.; Liang, C.; Wang, G. P.; Luo, Y.; Wang, W. The protection of wheat plasma membrane under cold stress by glycine betaine overproduction. *Biol. Plant.* **2010**, *54*, 83−88.
(24) De Zwart, F. J.; Slow, S.; Payne, R. J.; Lever, M.; George, P. M.; Gerrard, J. A.; Chambers, S. T. Glycine betaine and glycine betaine analogues in common foods. *Food Chem.* **2003**, *83*, 197−204.
(25) Breksa, A. P., III; Garrow, T. A. Recombinant human liver betaine-homocysteine *S*-methyltransferase: identification of three cysteine residues critical for zinc binding. *Biochemistry* **1999**, *38*, 13991−13998.
(26) Schwab, U.; Törrönen, A.; Toppinen, L.; Alfthan, G.; Saarinen, M.; Aro, A.; Uusitupa, M. Betaine supplementation decreases plasma homocysteine concentrations but does not affect body weight, body composition, or resting energy expenditure in human subjects. *Am. J. Clin. Nutr.* **2002**, *76*, 961−967.
(27) Pummer, S.; Dantzler, W. H.; Lien, Y. H.; Moeckel, G. W.; Völker, K.; Silbernagl, S. Reabsorption of betaine in Henle's loops of rat kidney in vivo. *Am. J. Physiol.* **2000**, *278*, F434−F439.
(28) Kim, S. K.; Kim, Y. C.; Kim, Y. C. Effects of singly administered betaine on hepatotoxicity of chloroform in mice. *Food Chem. Toxicol.* **1998**, *36*, 655−661.
(29) Chambers, S. T.; Kunin, C. M.; Miller, D.; Hamada, A. Dimethylthetin can substitute for glycine betaine as an osmoprotectant molecules for *Escherichia coli*. *J. Bacteriol.* **1987**, *169*, 4845−4847.
(30) Steiner, A. A. A universal method for preparing nutrient solutions of a certain desired composition. *Plant Soil* **1961**, *15*, 134−154.
(31) Castellanos-Santiago, E.; Yahia, E. M. Identification and quantification of betalains from the fruits of 10 Mexican prickly pear cultivars by high-performance liquid chromatography and electrospray ionization mass spectrometry. *J. Agric. Food Chem.* **2008**, *56*, 5758−5764.
(32) Gandía-Hirrero, F.; Escribano, J.; García-Carmona, F. Betaxanthin as pigments responsible for visible fluorescence in flower. *Planta* **2005**, *222*, 586−593.
(33) Chethaha, S.; Nayak, C. A.; Raghavarao, K. S. M. S. Aqueous two phase extraction for purification and concentration of betalains. *J. Food Eng.* **2007**, *81*, 679−687.
(34) Chauhan, S. P.; Sheth, N. R.; Rathod, I. S.; Suhagia, B. N.; Maradia, R. B. Analysis of betalains from fruits of *Opuntia* species. *Phytochem. Rev.* **2013**, *12*, 35−45.
(35) Chethana, S.; Nayak, C. A.; Raghavarao, K. S. M. S. Aqueous two phase extraction for purification and concentration of betalains. *J. Food Eng.* **2007**, *81*, 679−687.
(36) Nilsson, T. Studies into the pigments in beetroot (*Beta vulgaris* L. ssp. *vulgaris* var. *rubra* L.). *Lantbrukshoegsk. Ann.* **1970**, *36*, 179−219.
(37) Mosmann, T. Rapid colorimetric assay for cellular growth and survival: application to proliferation and cytoxocity assays. *J. Immunol. Methods* **1983**, *65*, 55−63.
(38) Wilcox, M. E.; Wyler, H.; Dreiding, A. S. Streochemie von betanidin und isobetanidin. 8. Mitteilung. Zur Konstitution des Randenfarbstoffes Betanin. *Helv. Chim. Acta* **1965**, *48*, 1134−1147.
(39) Kujala, T. S.; Vienola, M. S.; Klika, K. D.; Loponen, J. M.; Pihlaja, K. Betalain and phenolic compositions of four beetroot (*Beta vulgaris*) cultivars. *Eur. Food Res. Technol.* **2002**, *214*, 505−510.
(40) Kishima, Y.; Shimaya, A.; Adachi, T. Evidence that blue light induces betalain pigmentation in *Portulaca callus*. *Plant Cell, Tiss. Org. Cult.* **1995**, *43*, 67−70.
(41) Chappell, J.; Hahlbrock, K. Transcription of plant defence genes in responses to UV light or fungal elicitor. *Nature* **1984**, *311*, 76−78.
(42) Girod, P. A.; Zryd, J. P. Secondary metabolism in cultured red beet (*Beta vulgaris* L.) cells: differential regulation of betaxanthin and betacyanin biosynthesis. *Plant Cell, Tiss. Org. Cult.* **1991**, *25*, 1−12.
(43) Shin, K. S.; Murthy, H. N.; Heo, J. W.; Paek, K. Y. Induction of betalain pigmentation in hairy roots of red beet under different radiation sources. *Biol. Plant.* **2003**, *47*, 149−152.

(44) Bhuiyan, N. H.; Murakami, K.; Adachi, T. Variation in betalain content and factors affecting the biosynthesis in *Portulaca* sp. 'Jewel' cell cultures. *Plant Biotechnol.* **2002**, *19*, 369−376.
(45) Steiner, U.; Schliemann, W.; Böhm, H.; Strack, D. Tyrosinase involved in betalain biosynthesis of higher plants. *Planta* **1999**, *208*, 114−124.
(46) Zhao, S. Z.; Sun, H. Z.; Chen, M.; Wang, B. W. Light-regulated betacyanin accumulation in euhalophyte *Suaeda salsa* calli. *Plant Cell, Tiss. Org. Cult.* **2010**, *102*, 99−107.
(47) Hamilton, B. K.; Yoo, K. S.; Pike, L. M. Changes in pungency of onions by soil type, sulphur nutrition and bulb maturity. *Sci. Hortic.* **1998**, *74*, 249−256.
(48) Yoo, K. S.; Pike, L.; Crosby, K.; Jones, R.; Leskovar, D. Differences in onion pungency due to cultivars, growth environment, and bulb sizes. *Sci. Hortic.* **2006**, *110*, 144−149.
(49) Lee, E. J.; Yoo, K. S.; Jifon, J.; Patil, B. S. Application of extra sulfur to high soils does not increase pungency and related compounds in shortday onions. *Sci. Hortic.* **2009**, *123*, 178−183.
(50) Khan, M. I.; Sri Harsha, P. S. C.; Giridhar, P.; Ravishankar, G. A. Pigment identification, nutritional composition, bioactivity, and in vitro cancer cell cytotoxicity of *Rivina humilis* L. berries, potential source of betalains. *LWT−Food Sci. Technol.* **2012**, *47*, 315−323.
(51) Givind, J. K.; Tokuda, H.; Konoshima, T.; Nishino, H. Chemopreventive of lung and skin cancer by *Beta vulgaris* (beet) root extract. *Cancer Lett.* **1996**, *100*, 211−214.
(52) Razali, N.; Aziz, A. A.; Junit, S. M. Gene expression profiles in human HepG2 cells treated with extracts of the *Tamarindus indica* fruit pulp. *Genes Nutr.* **2010**, *5*, 331−341.
(53) Gansen, B.; Buddhan, S.; Anandan, R.; Sivakumar, R.; AnbinEzhilan, R. Antioxidant defense of betaine against isoprenaline-induced myocardial infarction in rats. *Mol. Biol. Rep.* **2010**, *37*, 1319−1327.

METHODS AND MATERIALS

***In Vitro* Fermentation Using Human Fecal Inoculums.** Potential human fecal sample donors were recruited on the University of Minnesota campus. Subjects were screened using a questionnaire. Inclusion criteria were self-reported absence of disease ("healthy"), consumption of a nonspecific western diet, and no antibiotic use for three months prior to the study. Fecal samples were collected using a Commode Specimen Collection System (Sage, IL) lined with a 2 mm thickness plastic bag. Samples were immediately placed into an anaerobic bag (Remel, Lenexa, KS) containing an AnaeroPouch anaerobic sachet (Mitsubishi Gas Company, Tokyo Japan), sealed with a Pouch Clip (Remel, Lenexa, KS) and placed on ice in an insulated container to maintain microbial viability and ensure standardized sample preparation. Fecal samples were delivered to the laboratory and processed within 2 h.

Fiber samples were provided by Nestle Health Science S.A. (Lutry, Switzerland) in coded pouches, and investigators were blinded to the treatments. The fibers tested were fructo-oligosaccharides (FOS, Beneo, Morris Plains NJ), inulin (Beneo, Morris Plains NJ), gum acacia (Nexira, Somerville NJ), outer pea fiber (Nutri-Pea Limited, Manitoba Canada), and a 50:50 soluble/insoluble blend of FOS, inulin, gum acacia, and outer pea fiber. Half a gram (0.5 g) of each fiber or blend was weighed and placed into sterilized 100 mL serum bottles. Forty milliliters of sterile trypticase peptone fermentation media was added to each bottle and fibers were allowed to hydrate for 12 h at 4 °C.[18] The fiber/media slurry was heated to 37 °C and 10 mL of fecal inoculum was added to each bottle along with 0.8 mL of oxyrase (Oxyrase Inc., Mansfield, OH) to remove oxygen from the environment. Fecal inoculum was prepared by pooling three fecal samples with phosphate buffer solution (1:6 w/v) and then mixing two parts reducing solution (950 mL of distilled water, 6.25 g of cysteine hydrochloride, 40 mL 1 M sodium hydroxide, 6.25 g of sodium sulfide nonahydrate) to 15 parts diluted fecal inoculum (v/v).[19] Bottles were flushed with carbon dioxide and sealed. Sealed bottles were placed in a 37 °C shaking water bath and allowed to ferment for 0, 4, 8, 12, and 24 h (triplicate bottles for each time point).

***In Vitro* pH, Gas Volume, and SCFA.** At each time point, aliquots were taken for measurement of pH, gas volume, and SCFAs. Gas volume was measured by piercing the rubber cap of the sealed fermentation bottle with a 50 or 100 mL glass syringe fitted with a stainless steel needle and allowing the gas to fill the syringe.[20] The pH of the fermented treatments was measured with a calibrated pH probe, and following pH measurement, 1 mL of copper sulfate (200 g/L) was added into the serum bottles to inhibit further fermentation. A 2-mL aliquot was removed from each triplicate for SCFA measurement and frozen at −20 °C until subsequent analysis.

Enteral Nutrition Human Feeding Study. *Subjects and Subject Protocol.* For a full description of the subject inclusion/exclusion criteria and the subject protocol, please refer to ref 21. Briefly, healthy adult men and women were recruited on the University of Minnesota campus. Written informed consent was obtained from each subject and the study was approved by the University of Minnesota Institutional Review Board for Human Research Protection Program (IRB Number 1103M96878). Each subject completed the randomized, double-blind, crossover protocol. Subjects consecutively consumed habitual diet for 14 days, enteral diet 1 for 14 days, habitual diet for 28 days, and enteral diet 2 for 14 days. During each period, subjects recorded diet records, and anaerobically collected a fecal sample on day 14 (as described in the *in vitro* section). Subjects exclusively consumed (orally) formula during the enteral periods and were provided with formula in excess of their total energy needs as calculated by the Harris-Benedict equation and adjusting with physical activity factors.[22] Subjects were withdrawn from the study if their intake was below 75% of the target volume for two consecutive days. Formula was provided in 250 mL cans that were identically labeled with the exception of four different product codes (to ensure blinding).

Enteral Formula and Diet Measurements. Enteral formulas were nutritionally complete and identical in composition except for fiber content. Base formula contained 1500 kcal/L, 67.6 g protein/L, 64.8 g fat/L, and 168 g carbohydrate/L. The formula contained casein as the sole protein source. Fiber containing formula was base supplemented with 15 g/L of fiber blend. The fiber blend was composed of a 50:50 insoluble/soluble mixture of FOS, pea hull fiber, gum acacia, and inulin.

Enteral formula energy and protein intake was calculated from 14 day diet records during the formula periods. Enteral formula fiber intake was calculated from 14 day diet records during the fiber formula period. Habitual diet reports were generated by entering the diet records into Nutrition Data System for Research (University of Minnesota, Version 2011). Habitual diet energy, fiber, and protein intake values were averaged from the 2-day diet records recorded during the run-in and washout phases.

Human Subject Fecal Sample Preparation. Anaerobically packaged fecal samples were kneaded for 2 min to homogenize. A 10 g aliquot of fecal sample was diluted 1:10 (w/w) in phosphate buffered saline (PBS, 0.1 M, pH 7.2). The fecal/PBS mixture was homogenized in a stomacher for 2 min and the slurry was aliquoted for SCFA. The remaining sample was used for pH measurement via calibrated pH probe.

***In Vitro* and Human Subject Short Chain Fatty Acid Measurement.** SCFA were completed in triplicate using a modified Schneider method.[23] *In vitro* fermentation liquid aliquots were thawed at 4 °C. To the fermentation liquid, 1.6 mL of distilled water and 0.4 mL 50% sulfuric acid were added and vortex mixed. Two milliliters of diethyl ether and 2 μL of 2-ethylbutyric acid (99%, internal standard) were added to each tube. Tubes were sealed, vortex mixed and orbitally shaken at 300 rpm for 45 min. Samples were centrifuged at 2060*g* for 5 min and the supernatant was transferred to a test tube containing solid calcium chloride to remove residual water. The final sample was filtered through a 0.2 μm nylon filter, placed into a 2 mL glass gas chromatography vial and sealed.

For the human subjects samples, approximately 2 mL of PBS/stool slurry was centrifuged at 9300*g* for 10 min. To 1 mL of fecal supernatant were added 0.4 mL of 50% sulfuric acid and 2 mL of ether containing 1 μL/mL of 2-ethyl butyric acid (99%, internal standard). The sample was sealed, vortex mixed for 10 s and shaken at 300 rpm for 45 min. The ether was retained, excess water removed with calcium chloride, and the final sample placed into a 2 mL glass gas chromatography vial and sealed.

All SCFA samples were analyzed using a HP 5890 gas chromatograph (in split mode) equipped with a 30 m × 0.53 mm × 1 μm film thickness Stabilwax-DA (Restek Corporation, Bellefonte PA) column. The injection port temperature was 220 °C, the detector 240 °C, and oven program 110 °C for 0.5 min followed by 10 °C/min to 180 °C and then 50 °C/min to 240 °C, hold 3 min. Acetate, propionate, and butyrate were quantified for *in vitro* samples. Acetate, propionate, isobutyrate, butyrate, isovalerate, and valerate were quantified for *in vivo* samples. All quantification was performed using standard curves generated from known amounts of acids and internal standard.

Statistical Analysis. All data analysis was performed in SAS (Version 9.2). *In vitro* longitudinal repeated measurements were compared between fibers using a mixed-effects linear model, with a random intercept to model within-fiber correlation. Gas volume was log transformed before analysis. To adjust for multiple comparisons, Bonferroni correction for multiple comparisons was used: differences were considered significant at the $P < 0.05/10 = P < 0.005$ since there were 10 comparisons among treatments.

Baseline characteristics of human subject data were compared using a *t* test. All other human subject data was compared using longitudinal regression models with random subject effect to model the within-subject correlation. For each outcome, period, gender and unequal carryover effects were tested for. Data collected during the initial habitual diet and washout periods were combined and adjusted for period effects. Differences were considered significant at $P < 0.05$.

Table 1. Gas Volume Produced during 24 h Batch *in Vitro* Fermentation of Fibers[a]

	gas volume (mL)			
fiber	4 h	8 h	12 h	24 h
Inulin	22.6 (6.5, 78.4) bc	62.2 (40.1, 96.6) c	76.3 (66.8, 87.2) d	100.3 (90.0, 111.8) d
FOS[b]	1.8 (0.5, 6.1) ac	55.2 (35.6, 85.7) c	68.7 (60.1, 78.4) d	83.7 (75.1, 93.2) ad
Gum acacia	1.6 (0.5, 5.6) ab	0.5 (0.3, 0.8) a	26.9 (23.5, 30.7) a	73.5 (66.0, 81.9) a
Fiber blend	0.5 (0.1, 1.7) a	2.5 (1.6, 3.9) b	12.6 (11.0, 14.4) b	24.6 (22.1, 27.4) b
Outer Pea	0.5 (0.1, 1.7) a	0.5 (0.3, 0.8) a	0.5 (0.5, 0.5) c	2.3 (2.1, 2.6) e
Control	0.9 (0.4, 2.2) a	0.5 (0.4, 0.7) a	0.5 (0.5, 0.6) c	0.5 (0.5, 0.5) c

[a]Geometric mean (95% CI). Means with no letters in common were significantly different at the 0.05 level after Bonferroni correction within each time point. [b]FOS: Fructo-oligosaccharides.

Table 2. pH of Fecal Slurry during 24 h Batch *in Vitro* Fermentation of Fibers[a]

	pH				
fiber	0 h	4 h	8 h	12 h	24 h
FOS[b]	9.09 (0.26) a	5.82 (0.10) c	5.62 (0.09) d	5.86 (0.08) c	6.04 (0.08) d
Inulin	9.01 (0.26) a	5.81 (0.10) c	5.81 (0.09) d	5.93 (0.08) c	5.88 (0.08) a
Gum acacia	9.02 (0.26) a	7.12 (0.10) a	6.79 (0.09) a	6.54 (0.08) a	5.87 (0.08) a
Outer pea	9.13 (0.26) a	6.98 (0.10) a	6.99 (0.09) c	6.85 (0.08) b	6.76 (0.08) e
Fiber blend	8.98 (0.26) a	6.5 (0.10) b	6.48 (0.09) b	6.43 (0.08) a	6.37 (0.08) b
Control	9.05 (0.26) a	7.07 (0.09) a	6.99 (0.08) c	6.91 (0.08) b	6.86 (0.07) c

[a]Values are means (SEM). Means with no letters in common were significantly different at the 0.05 level after Bonferroni correction within each outcome. [b]FOS: fructo-oligosaccharides.

Table 3. Total SCFA during 24 h Batch *in Vitro* Fermentation of Fibers[a]

	Total SCFA (mmol/L)				
fiber	0 h	4 h	8 h	12 h	24 h
FOS[b]	115 (4) a	238 (28) a	322 (23) a	487 (34) ac	531 (59) acd
Inulin	115 (4) a	244 (28) a	431 (23) c	598 (59) c	643 (59) c
Gum acacia	116 (4) a	214 (29) ac	255 (23) ab	356 (34) abd	513 (59) ad
Outer pea	112 (4) ab	189 (29) cd	256 (23) a	215 (34) d	316 (70) d
Fiber blend	105 (4) b	131 (28) b	267 (23) ab	309 (34) bd	214 (59) bd
Control	112 (3) a	154 (27) bd	215 (18) b	220 (24) bd	230 (54) bd

[a]Values are means (SEM). Total SCFA reflects the sum of acetate, propionate, and butyrate. Means with no letters in common were significantly different at the 0.05 level after Bonferroni correction within each time point. [b]FOS: Fructo-oligosaccharides.

RESULTS

***In Vitro* Fermentation Study.** Three volunteers (aged 24–32; one male, two female) provided fecal samples for the fermentation. Samples were pooled and used in the fermentation.

All fiber/fecal slurries produced more than 3 mL of gas during the 24 h fermentation except the negative control and pea fiber (Table 1). At 4 h, gas production was the highest for inulin followed by 10 times less gas for FOS and gum acacia and essentially no gas from the fiber blend. By 8 h, inulin and FOS produced approximately 20 times more gas than the fiber blend. At 12 h, inulin and FOS continued to have the highest gas production (and statistically similar) that was three times higher than the gum acacia and five times more than the fiber blend. At the final 24 h time point, FOS and inulin produced the most (and statistically similar) amount of gas, followed by gum acacia (which was similar to FOS levels). The blend produced intermediate amounts at approximately a quarter of that produced by inulin and FOS.

Due to the fermentation media used, the initial pH of the system was approximately 9, and no statistical differences were found between any fibers at time 0 (Table 2). At 4 h, the FOS and inulin both had dropped approximately 3 pH units from baseline (time 0) and were significantly lower than all other fibers. Statistically different, but somewhat higher than FOS and inulin was the fiber blend (pH 6.5), followed by approximately pH neutral values for the outer pea, gum acacia and control. At 8 h, the inulin and FOS continued to have the lowest (and statistically similar) pH, followed by (in increasing pH) fiber blend and gum acacia. Outer pea and control remained approximately pH neutral. By 12 h, FOS and inulin had the lowest (and statistically similar) pH at approximately 5.9 with increased and similar values for the fiber blend and gum acacia (~pH 6.5), followed by the pH neutral outer pea and control. At the end of the 24 h fermentation, the control continued to remain approximately neutral followed by (highest to lowest) outer pea, fiber blend, inulin and gum acacia and FOS.

Total SCFA production (sum of acetate, propionate, and butyrate) from the *in vitro* fermentation is shown in Table 3. At baseline, all fiber samples had similar SCFA values except fiber blend that was 7–10 mmol/L lower than the rest. At 4 h, FOS and inulin had the highest (and similar) SCFA values, whereas gum acacia and outer pea had intermediate concentrations and the control and outer pea fiber had the lowest values. By 8 h, inulin had the highest production that was statistically different from all other fibers. FOS, fiber blend, gum acacia and outer pea had intermediate values with the control the lowest. At 12 h

inulin continued to have the highest SCFA followed by (in decreasing concentration) FOS, gum acacia, fiber blend, control and outer pea. At the conclusion of the fermentation, inulin produced the highest SCFA, but was statistically similar to FOS. Gum acacia produced similar amounts of SCFA as FOS and these were not statistically distinguishable from fiber blend, pea fiber or control.

Proportions of the short chain fatty acids from the *in vitro* fermentation of the fiber blend are presented in Table 4.

Table 4. 24 h Batch *in Vitro* Fermentation of a Blend of Inulin, FOS, gum Acacia, and Pea Fiber: Proportions of Acetate, Propionate, and Butyrate[a,b]

	fiber blend		
time	acetate %	propionate %	butyrate %
0 h	36.2 (0.4) a	32.8 (0.5) a	30.9 (0.4) a
4 h	41.1 (0.4) b	34.9 (0.5) ad	24.0 (0.4) bd
8 h	33.5 (0.4) c	47.1 (0.5) b	19.4 (0.4) c
12 h	33.9 (0.4) ace	42.5 (0.5) c	23.6 (0.4) d
24 h	31.9 (0.4) de	37.4 (0.5) d	30.7 (0.4) a

[a]Values are means (SEM). Acid proportions were compared between time points (within column comparison). Means with no letters in common were significantly different at the 0.05 level after Bonferroni correction. [b]FOS: Fructo-oligosaccharides.

Acetate increased approximately 5% by 4 h but decreased to significantly lower than initial concentrations by 24 h. Propionate increased significantly by almost 15% by 8 h, steadily decreased until 24 h, but still remained above initial values. Butyrate significantly decreased by 10% from 0 to 8 h but increased to levels similar to the initial value by 24 h.

Enteral Nutrition Human Feeding Study. Twenty-four subjects were enrolled, and 20 subjects (10 men, 10 women) completed the study. The mean age, BMI, and habitual diet energy and fiber intake of the women and men did not statistically differ. Overall mean subject age was 25.8 (±9.9 SD) with a BMI of 25.8 (±2.5 SD). Age, BMI and habitual diet energy and fiber intake of the two sequence groups (fiber blend-fiber free vs fiber free-fiber blend) were also compared, and no statistical differences were found. Subject dietary intake is listed in Table 5.

Fecal Acids. Human samples were analyzed for both SCFA and BCFA. Total SCFA refers to total amounts of acetate, propionate, and butyrate. Total BCFA refers to amounts of isobutyrate, isovalerate and valerate. SCFA and BCFA are reported per milliliter of fecal water. Human subject fecal acid content is reported in Table 6.

Total SCFA were approximately 2 times higher during the habitual diet phase than during the formula phases ($p < 0.0001$). Between the formula periods, SCFA on the fiber blend was 1.1% higher than the fiber free formula ($p = 0.029$). Individual SCFA also differed; butyrate proportion was approximately 1.6 times higher in the habitual diet compared to both formulas (both $p < 0.0001$), and 1% higher in the fiber free formula compared to the fiber formula ($p = 0.041$). Propionate was in a lower proportion in habitual diet than both formula diets (both $p < 0.03$), but did not differ between formulas. Acetate was also in a lower proportion during habitual diet than both formulas (both $p < 0.0001$) and did not differ between formulas. Total BCFA were 1% higher in habitual diet compared to the fiber blend formula ($p = 0.046$), but fiber free did not statistically differ from habitual diet or fiber blend formula.

Table 6. Fecal SCFA and BCFA of Human Subjects Consuming Formula and Habitual Diets[a]

	habitual diet	fiber free formula	fiber blend formula
Total SCFA (mmol/L)	80.9 (2.7) a	39.7 (2.3) b	43.5 (2.3) c
Acetate %	39.5 (0.6) a	49.2 (1.0) b	50.2 (0.9) b
Propionate %	29.7 (1.1) a	31.6 (1.3) b	31.5 (1.3) b
Butyrate %	30.7 (1.1) a	19.2 (0.8) b	18.3 (0.8) c
Total BCFA (mmol/L)	11.5 (1.2) a	10.5 (1.1) ab	10.1 (1.1) b

[a]Values are means (SEM). Means with no letters in common were significantly different at $P < 0.05$ within each outcome.

DISCUSSION

Fiber source and structure, as well as the bacterial populations present, affect fiber fermentation patterns in both *in vitro* and *in vivo* models.[2,24] Fermentation leads to the production of acids, which are considered to be a beneficial product of fermentation, but also gas that can lead to reduced tolerance of fiber *in vivo*. Greater gas volume is perceived more in the proximal bowel compared to the distal colon, so rapidly fermented fibers would be expected to cause more gastrointestinal intolerance than those that are more slowly fermented.[25] Human studies have found that dietary supplementation with short chain fibers such as FOS and inulin lead to increased side effects.[26−28] In contrast, complex molecules, such as gum acacia are tolerated at doses up to 40 g/day, and a 1:1 combination of gum acacia and FOS fed to humans led to reduced gastrointestinal side effects than FOS alone.[29,30] Others have reported the use of fiber blends of varying chain length to attenuate gas production *in vitro*.[5,31]

Our results demonstrate similar trends in gas production. Fermentation of soluble shorter chain, single fibers (FOS and inulin) typically led to higher gas production at earlier time points (4 and 8 h). In contrast, gas production was almost

Table 5. Human Subject Diet Characteristics[a]

	fiber (g/day)		protein (g/day)		
	habitual diet[b]	fiber blend formula[c]	habitual diet[b]	fiber blend formula[d]	no fiber formula[d]
Women	16.8 (4.2)	16.2 (1.9)	71.5 (21.4)	73.2 (9.1)	72.4 (9.7)
Men	15.1 (6.5)[e]	21.6 (3.8)[e]	102.4 (27.9)	98.1 (16.3)	102.5 (15.5)
Total	16.0 (5.3)	18.9 (4.0)	89.6 (29.2)	85.6 (18.1)	87.4 (19.9)

[a]Values are means (SD). [b]Habitual diet values were averaged from the 2-day diet records recorded during the run-in and washout periods. Values were generated by entering the diet records into Nutrition Data System for Research (University of Minnesota, Version 2011). [c]Enteral formula fiber intake was calculated from 14-day diet records during the fiber formula period. [d]Enteral formula protein intake was calculated from 14-day diet records during each of the formula periods. [e]In men, fiber intake on habitual diet is different from formula diet ($p = 0.0153$).

undetectable at these time points for the larger and more complex soluble gum acacia, insoluble pea fiber and fiber blend. Pea fiber has been shown to be poorly fermented and would be expected to contribute minimally to gas production.[32] While the fiber blend contains inulin, FOS, and gum acacia that are known to be fermentable, it also contains pea fiber that changed the fermentation pattern as a whole and resulted in delayed gas production until 12 and 24 h. The slower fermentation could lead to improved tolerance *in vivo*, as gas is perceived more in the proximal bowel.[25] The results of the human feeding study were parallel to the *in vitro* gas production from the fiber blend. As published in our previous article,[21] no differences in gas and bloating were detected between any diets. This result suggests that the fiber blend did not induce symptoms beyond subject's normal levels and was well tolerated at the dose delivered.

In general, *in vitro* pH changes were consistent with changes in gas production. pH values were lower at earlier time points for substrates comprised entirely of rapidly fermented, short chain fructans (FOS, inulin). A similar *in vitro* study found the greatest decrease in pH for FOS and inulin after 8 h fermentation, which is consistent with our results.[31] In agreement with a more gradual fermentation, the addition of higher molecular weight molecules resulted in a delayed decrease in pH. As a single source, gum acacia maintained a relatively high pH until 24 h, after which it decreased to values lower than other single fiber treatments. Similarly, the blend had a significantly lower pH than the control and pea fiber that can be attributed to delayed fermentation of the gum acacia fraction of the blend. For reference, fecal pH of the human samples was statistically lower during habitual diet period (pH 6.5) than both formula periods (pH 7.5).[21]

In vitro total SCFA production followed a similar pattern as gas and pH, although significant differences between treatments were more difficult to detect due to high standard errors. Among the single fiber treatments, total SCFA levels were higher at early time points for inulin and FOS compared to gum acacia and pea fiber. Later in the fermentation, total levels were difficult to statistically distinguish, but inulin produced the greatest SCFA levels overall. Since SCFAs are a product of fermentation, these results are consistent with rapid fermentation of short chain molecules, and more gradual fermentation of fibers with higher molecule weight.[32] More gradual fermentation may translate into increased SCFA production throughout the entire colon, which may have additional health benefits.[33]

In vivo SCFA are more complex. Absorption of SCFA is thought to occur via ionic exchange and nonionic diffusion and in human rectal studies, absorption rates can be manipulated by changing electrolyte composition.[34] Furthermore, in an animal model, acetate absorption rates increased with increasing concentration.[35] Fecal SCFA, then, reflect residual SCFA after both production and absorption with potentially differing rates depending on concentration. Fecal SCFA of the subjects on habitual diet was approximately 2 times higher than both of the formulas, although it should be noted that the whole gut transit times were approximately 1.5 times longer on the formula diet versus the habitual diet (data not shown). Longer transit times may influence SCFA and water absorption.[36] Furthermore, the types of fiber from habitual diet likely differed from the fiber blend. Between formulas, the fiber blend formula may have had increased SCFA concentration compared to the fiber free formula due to more substrate present, but because concentration may influence absorption, it is difficult to make a conclusion. Similarly, it is difficult to draw conclusions regarding the proportions of SCFA measured in the fecal samples since differences may be due to production or absorption.

Differences also existed between the *in vitro* and *in vivo* SCFA proportions for the fiber blend. *In vivo* proportions of SCFA on the fiber blend formula yielded much higher concentrations of acetate (50%) and low butyrate (18%), whereas after a 24 h fermentation of the fiber blend in the *in vitro* system, propionate was the highest (37%) with other acid concentrations in similar concentrations (varying from propionate by approximately 6%). Differences may be due to different *in vitro* vs *in vivo* fecal donors as well as the absorption in the *in vivo* study. A more clear comparison would have been possible with the same donors for both portions, although varying absorption and transit times would confound the comparison.

BCFA, although not directly detrimental, reflect a process that also produces undesirable metabolites. Measured levels of BCFA were the highest on habitual diet despite similar protein intakes between the habitual and formula diets. Between the two formulas, it was surprising that the fiber free formula diet did not have higher BCFA since the diet was devoid of fiber and the only substrates reaching the colon would be undigested formula, endogenous mucus, sloughed off cells, and digestive secretions.[2] Although these substances would also be present during the fiber containing formula, carbohydrate fermentation is preferred over protein and it was hypothesized that BCFA would be found in lower amounts.[3] A possible explanation is that the SCFA and BCFA produced were almost completely absorbed and the residual amounts reflected equilibrium concentrations. Whether residual values are useful in evaluating *in vivo* fermentation is unclear.

Overall, the fermentation of fibers with a range of physicochemical properties yielded differing profiles of pH, gas and SCFA. By blending insoluble and soluble fibers, an intermediate fermentation profile was observed when fed to healthy human subjects. During the human intervention study, fecal SCFA was increased on the fiber containing formula compared to the fiber free that may have indicated increased fermentation in the gut. Although not directly comparable, *in vitro* and *in vivo* models provide complementary information on fermentation in the gut.

AUTHOR INFORMATION

Corresponding Author

*Address: 1334 Eckles Ave., St. Paul, MN 55108. E-mail, jslavin@umn.edu; phone, (612) 624-7234; fax, (612) 625-5272.

Author Contributions

J.L.S., W.T., D.A.T., A.S.K., J.A.N. and K.J.K. designed the research. D.A.T., A.S.K., J.A.N. and K.J.K. conducted the research. Nestle Health Science S.A. provided essential reagents and materials. W.T., D.A.T., A.S.K., J.A.N. and K.J.K. analyzed data and performed statistical analysis. K.J.K., J.A.N., A.S.K., W.T. and D.A.T. wrote the paper. J.L.S. had final responsibility for final content. All authors have read and approved the final manuscript.

Funding

Experimental fibers, liquid diets and research support were provided by Nestle Health Science S.A. (Lutry, Switzerland).

Notes

The authors declare no competing financial interest.

■ ACKNOWLEDGMENTS

The authors wish to thank Nestle Health Science S.A. (Lutry, Switzerland) for providing the isolated fibers, the liquid diets in the human study and the financial support.

■ REFERENCES

(1) Guarner, F.; Malagelada, J. Gut flora in health and disease. *Lancet* **2003**, *361*, 512−9.
(2) Cummings, J.; Macfarlane, G. The control and consequences of bacterial fermentation in the human colon. *J. Appl. Bacteriol.* **1991**, *70*, 443−59.
(3) Macfarlane, G. T.; Gibson, G. R.; Cummings, J. H. Comparison of fermentation reactions in different regions of the human colon. *J. Appl. Bacteriol.* **1992**, *72*, 57−64.
(4) Macfarlane, G. T.; Gibson, G. R.; Beatty, E.; Cummings, J. H. Estimation of short-chain fatty acids production from protein by human intestinal bacteria based on branched-chain fatty acid measurements. *FEMS Microbiol. Ecol.* **1992**, *101*, 81−8.
(5) Vester Boler, B.; Hernot, D.; Boileau, T.; Bauer, L.; Middelbos, I.; Murphy, M.; et al. Carbohydrates blended with Polydextrose lower gas production and short-chain fatty acid production in an in vitro system. *Nutr. Res. (N.Y.)* **2009**, *29*, 631−9.
(6) Demigne, C.; Remesy, C.; Morand, C. Short chain fatty acids. In *Colonic Microbiota, Nutrition and Health*, 1st ed,; Gibson, G, Roberfroid, M, Eds.; Kluwer Academic Publishers: Boston, MA, 1999; pp 55−70.
(7) Binder, H. Role of colonic short-chain fatty acid transport in diarrhea. *Annu. Rev. Physiol.* **2010**, *72*, 297−313.
(8) Wong, J.; de Souza, R.; Kendall, C.; Emam, A.; Jenkins, D. Colonic health: Fermentation and short chain fatty acids. *J. Clin. Gastroenterol.* **2006**, *40*, 235−43.
(9) Binder, H.; Mahta, P. Short-chain fatty acids stimulate active na and cl absorption in vitro in the rat distal colon. *Gastroenterology* **1989**, *96*, 989−96.
(10) Roediger, W. E. Utilization of nutrients by isolated epithelial cells of the rat colon. *Gastroenterology* **1982**, *83*, 424−9.
(11) Peters, S. G.; Pomare, E. W.; Fisher, C. A. Portal and peripheral blood short chain fatty acid concentrations after caecal lactulose instillation at surgery. *Gut* **1993**, *33*, 1249−52.
(12) Chaia, A. P.; Oliver, G. Intestinal microflora and metabolic activity. In *Gut Flora, Nutrition, Immunity and Health*; 1st ed.; Fuller, R, Perdigon, G, Eds.; Blackwell Publishing: Oxford, U.K., 2003; pp 77−98.
(13) Wisker, E.; Daniel, M.; Rave, G.; Feldheim, W. Fermentation of non-starch polysaccharides in mixed diets and single fibre sources: Comparative studies in human subjects and in vitro. *Br. J. Nutr.* **1998**, *80*, 253−61.
(14) Millet, S.; van Oeckel, M.; Aluwe, M.; Delezie, E.; de Brabander, D. Prediction of in vivo short-chain fatty acid production in hindgut fermenting mammals: Problems and pitfalls. *Crit. Rev. Food Sci. Nutr.* **2010**, *50*, 605−19.
(15) Stroud, M.; Duncan, H.; Nightingale, J. Guidelines for enteral feeding in adult hospital patients. *Gut* **2003**, *52* (Suppl VII), 1−12.
(16) Elia, M.; Engfer, M.; Green, C.; Silk, D. Systematic review and meta-analysis: The clinical and physiological effects of fibre-containing enteral formulae. *Aliment. Pharmacol. Ther.* **2008**, *27*, 120−45.
(17) Klosterbuer, A.; Roughead, Z. F.; Slavin, J. Benefits of dietary fiber in clinical nutrition. *Nutr. Clin. Pract.* **2011**, *26*, 625−35.
(18) McBurney, M. I.; Thompson, L. U. Effect of human faecal inoculum on in vitro fermentation variables. *Br. J. Nutr.* **1987**, *58*, 233−43.
(19) Goering, H. K.; Van Soest, P. J. *Forage Fiber Analysis: Apparatus, Reagents, Procedures and Some Applications*; Department of Agriculture, Agriculture Handbook No. 379; US Government Printing Office: Washington, D.C., 1970; pp 1−20.
(20) Timm, D. A.; Stewart, M. L.; Hospattankar, A.; Slavin, J. L. Wheat dextrin, psyllium, and inulin produce distinct fermentation patterns, gas volumes, and short-chain fatty acid profiles in vitro. *J. Med. Food.* **2010**, *13*, 961−6.
(21) Koecher, K.; Thomas, W.; Slavin, J. Healthy subjects experience bowel changes on enteral diets; addition of a fiber blend attenuates stool weight and gut bacteria decreases without changes in gas. *J. Parenter. Enteral Nutr.* **2014**, DOI: 10.1177/0148607113510523.
(22) Frary, C. D.; Johnson, R. Energy. In *Krause's Food and Nutrition Therapy*, 12th ed.; Mahan, L. K., Escott-Stump, S, Eds; Saunders Elsevier: Philadelphia, PA, 2008; pp 22−38.
(23) Schneider, S.; Girard-Pipau, F.; Anty, R.; van der Linde, E.; Philipsen-Geerling, B.; Knol, J.; et al. Effects of total enteral nutrition supplemented with a multi-fibre mix on faecal short-chain fatty acids and microbiota. *Clin. Nutr.* **2006**, *25*, 82−90.
(24) Eastwood, M.; Morris, E. Physical properties of dietary fiber that influence physiological function: A model for polymers along the gastrointestinal tract. *Am. J. Clin. Nutr.* **1992**, *55*, 436−42.
(25) Harder, H.; Serra, J.; Azpiroz, F.; Passos, M.; Aquade, S.; Malagelada, J. R. Intestinal gas distribution determines abdominal symptoms. *Gut* **2003**, *52*, 1708−13.
(26) Ripoll, C.; Flourie, B.; Megnien, S.; Hermand, O.; Janssens, M. Gastrointestinal tolerance to an inulin-rich soluble roasted chicory extract after consumption in healthy subjects. *Nutrition* **2010**, *26*, 799−803.
(27) Slavin, J.; Feirtag, J. Chicory inulin does not increase stool weight or speed up intestinal transit time in healthy male subjects. *Food Funct.* **2011**, *2*, 72−7.
(28) Gibson, G. R.; Probert, H. M.; Van Loo, J.; Rastall, R. A.; Roberfroid, M. B. Dietary modulation of the human colonic microbiota: Updating the concept of prebiotics. *Nutr. Res. Rev.* **2004**, *17*, 259−75.
(29) Goetze, O.; Fruehauf, H.; Pohl, D.; Giarre, M.; Rochat, F.; Ornstein, K.; et al. Effect of a prebiotic mixture on intestinal comfort and general wellbeing in health. *Br. J. Nutr.* **2008**, *100*, 1077−85.
(30) Cherbut, C.; Michel, C.; Raison, V.; Kravtchenko, T.; Severine, M. Acacia gum is a bifidogenic dietary fibre with high digestive tolerance in healthy humans. *Microb. Ecol. Health Dis.* **2003**, *15*, 43−50.
(31) Hernot, D.; Boileau, T. W.; Bauer, L.; Middelbos, I.; Murphy, M.; Swanson, K.; et al. In vitro fermentation profiles, gas production rates and microbiota modulation as affected by certain fructans, galactooligosaccharides and Polydextrose. *J. Agric. Food Chem.* **2009**, *57*, 1354−61.
(32) Titgemeyer, E.; Bourquin, L.; Fahey, G.; Garleb, K. Fermentability of various fiber sources by human fecal bacteria in vitro. *Am. J. Clin. Nutr.* **1991**, *53*, 1418−24.
(33) Stewart, M.; Timm, D.; Slavin, J. Fructooligosaccharides exhibit more rapid fermentation than long-chain inulin in an in vitro fermentation system. *Nutr. Res. (N.Y.)* **2008**, *28*, 329−34.
(34) Holtug, K.; Hove, H.; Mortensen, P. B. Stimulation of butyrate absorption in the human rectum in vivo. *Scand. J. Gastroenterol.* **1995**, *30*, 982−8.
(35) Rechkemmer, G.; von Engelhardt, W. Concentration and pH dependence of short-chain fatty acid absorption in the proximal and distal colon of guinea pig (cavia porcellus). *Comp. Biochem. Physiol., Part A* **1988**, *91*, 659−63.
(36) Billich, C.; Levitan, R. Effects of sodium concentration and osmolality on water and electrolyte absorption from the intact human colon. *J. Clin. Invest.* **1969**, *48*, 1336−47.

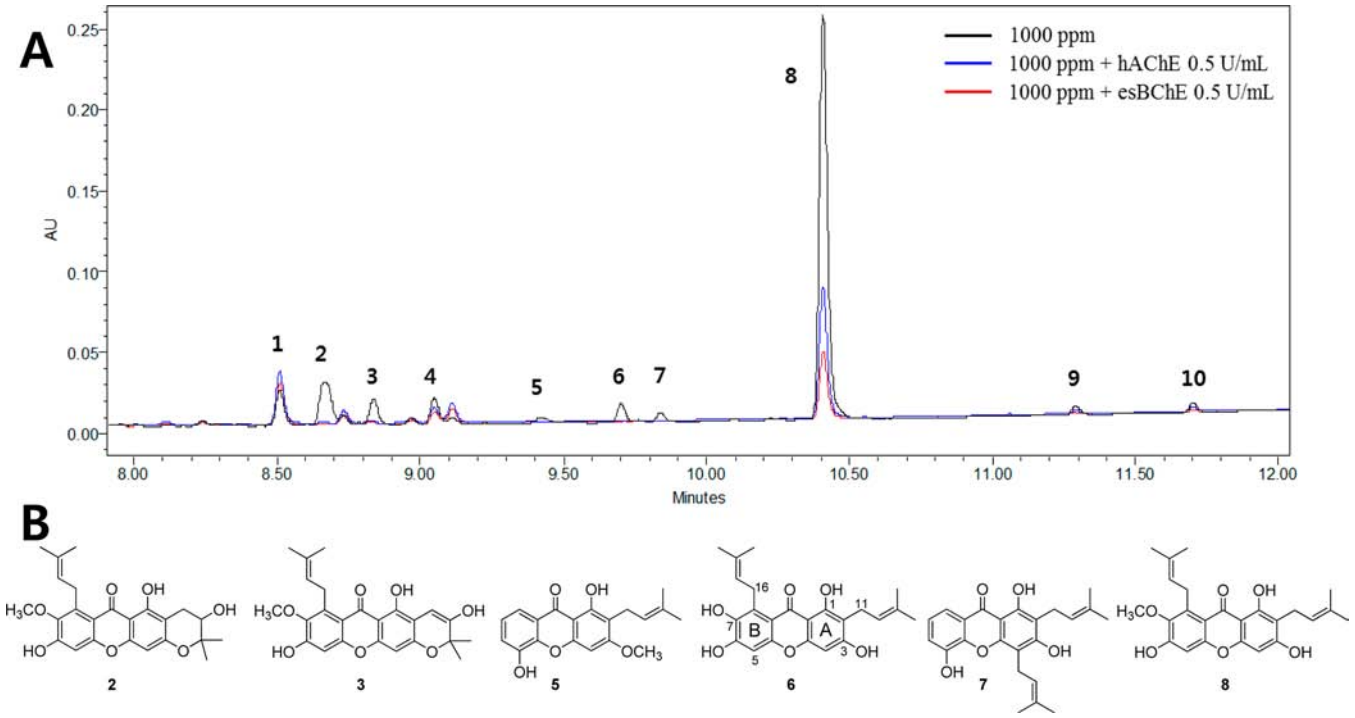

Figure 1. (A) UPLC-PDA chromatograms of the chloroform extract of *G. mangostana* seedcases: (black) not exposed to enzyme, (blue) after the incubation with hAChE, (red) after incubation with esBChE. Peaks numbered as **1**−**10** were isolated from *G. mangostana* seedcases in our study. (B) Chemical structures of isolated xanthonoids (**2**, **3**, and **5**−**8**) from the *G. mangostana*.

MATERIALS AND METHODS

General Apparatus and Chemicals. NMR spectra were recorded on a Bruker AM500 instrument (^{1}H NMR at 500 MHz, ^{13}C NMR at 125 MHz, Billerica, Massachusetts, U.S.A.). Electron ionization (EI) and EI-high resolution (HR) mass spectra were obtained on a JEOL JMS-700 instrument (JEOL Ltd., Tokyo, Japan). Optical rotations were measured on a Perkin-Elmer 343 polarimeter (Perkin-Elmer, Bridgeport, U.S.A.). Melting points were measured on a Thomas Scientific Capillary Melting Point Apparatus and are uncorrected. Column chromatography was performed on RP-18 (ODS-AQ, 25 and 10 μm, YMC, Kyoto, Japan). Thin layer chromatography (TLC) was done on precoated TLC plates with silica gel 60 F_{254} (0.25 mm, normal phase, Darmstadt, Merck). These were visualized using a UVGL-58 254 nm Hand-held UV lamp (UVP, Cambridge, U.K.) or by spraying with 10% H_2SO_4 in ethanol followed by heating. CD_3OD, acetone-d_6, and $CDCl_3$ were purchased from Cambridge Isotope Lab. Inc., (MA, U.S.A.). CH_3CN (HPLC grade) and water were purchased from J.T. Baker (U.S.A.). Equine serum BChE (esBChE), *Electrophorus electricus* AChE (eeAChE), human erythrocyte AChE (hAChE), acetylthiocholine iodide (AtCh), butyrylthiocholine iodide (BtCh), 5-5′-dithiobis(2-nitrobenzoic acid) (DTNB), NaH_2PO_4, Na_2HPO_4, and DMSO were purchased from Sigma-Aldrich Co., U.S.A. All solvents were distilled before use.

Plant Materials. *G. mangostana* (Clusiaceae) [imported from Vietnam, as permitted by Korea Food and Drug Administration (KFDA)] was purchased from LanSea Food Co., Ltd. (www.lansea.co.kr, Seoul, Korea).

UPLC-PDA-QTOF-MS Analysis. The chloroform extracts were analyzed by UPLC PDA QTOF-MS. Chromatographic separations were performed on a 2.1 × 100 mm, 1.7 μm ACQUITY BEH C18 chromatography column. The column temperature was maintained at 35 °C, and the mobile phases A and B were water with 0.1% formic acid and acetonitrile with 0.1% formic acid, respectively. The gradient duration program was as follows: 0−1 min, 10% B; 1−12 min, 10−98% B; wash to 13.5 min with 98% B; and a 1.5 min recycle time. The flow rate was 0.4 mL/min.

The mass spectrometer was operated in positive ion mode. N_2 was used as the desolvation gas. The desolvation temperature was set to 350 °C at a flow rate of 500 L/h and source temperature of 100 °C. The capillary and cone voltages were set to 2300 and 35 V, respectively. The Q-TOF premier was operated in the more sensitive "V" mode with 9000 mass resolving power. The data were collected for each test sample from 100 to 1500 Da with a 0.25 s scan time and a 0.01 s interscan delay over a 15 min analysis time. Leucine-enkephalin was used as the reference compound (m/z 554.2615 in the negative mode) and an infusion flow rate of 1 μL/min.

Enzyme Binding Affinity of Cholinesterase. To 75 μL of 100 mM sodium phosphate buffer was added 5 μL cholinesterase (100 U/mL in 100 mM sodium phosphate buffer) and 20 μL of 5 mg/mL $CHCl_3$ extract in MeOH subsequently. The final concentration of extract was adjusted to 1000 ppm. The mixture was incubated for 30 min at 37 °C on a plate shaker. Then, the sample was centrifuged at 12 000 rpm for 10 min and the supernatant was collected for analysis. The supernatant solution was filtered through a membrane (PTFE 0.2 μm, hydrophobic, Advantec, Japan), and 2 μL solutions were injected for UPLC-PDA-QTOF-MS analysis. Control experiment was carried out with the same procedure without enzyme.[16,18]

Cholinesterase Inhibitory Activity. The *in vitro* inhibition assays of BChE (EC 3.1.1.8, 0.05 U/mL) from equine serum, AChE (EC 3.1.1.7, 0.05 U/mL) from electric eel, and human AChE (0.25 U/mL) were run in sodium phosphate buffer 100 mM, pH 8.0 (reaction buffer). AtCh and BtCh were used, respectively, as substrates, and DTNB was used as the chromophoric reagent.[19] Inhibition assays were carried out on a SpectraMax M2Multi-Mode Microplate Reader (Molecular Devices, CA, U.S.A.) equipped with a 10.0 mm quartz cell (or plate) and a thermostatted bath. Solutions of tested compounds were prepared starting from 10 mM stock solutions in DMSO, which were diluted into aqueous assay medium to give a final content of organic solvent lower than 1%. hAChE inhibitory activity was determined in a reaction mixture containing 2 μL of a solution of hAChE (0.25 U/mL in 100 mM sodium phosphate buffer, pH 8.0), 30 μL of a 3.3 mM solution of DTNB in 100 mM sodium phosphate buffer (pH 8.0), 10 μL of a solution of the inhibitor (5−10 concentrations ranging from 0.1 to 200 μM), and 138 μL of reaction buffer. After incubation for 10 min at 37 °C, ACh (20 μL of 1 mM aqueous solution) was added as the substrate, and hAChE-catalyzed hydrolysis was followed by measuring the increase of

dx.doi.org/10.1021/jf405072e | J. Agric. Food Chem. 2014, 62, 1338−1343

Table 1. Peak Numbers, Name, Analytical Parameters, and Xanthonoids Identified in *G. mangostana* Seedcases

peak	UPLC t_R (min)	HRESIMS $[M+H]^+$	ppm	molecular fomular	UV−vis maxima (nm)	control (area)	after AChE (area)	after BChE	xanthonoids assignation
1	8.62	425.1594	−2.7	$C_{24}H_{24}O_7$	219, 316	37053	58700	49789	mangostingone
2	8.77	427.1758	1.4	$C_{24}H_{26}O_7$	219, 321	67077	2057	1125	mangostanol
3	8.94	425.1590	−1.6	$C_{24}H_{24}O_7$	221, 319	24780	3574	2698	allanxanthone E
4	9.16	409.1657	1.5	$C_{24}H_{24}O_6$	221, 317	26375	12553	9534	mangostenone F
5	9.53	327.1221	−4.3	$C_{19}H_{18}O_5$	221, 320	7885	trace	trace	gudraxanthone
6	9.79	397.1637	1.3	$C_{23}H_{24}O_7$	221, 317	20732	trace	trace	γ-mangostin
7	9.93	381.1729	7.1	$C_{23}H_{24}O_5$	221, 319	10124	trace	trace	8-deoxygartanin
8	10.51	411.1791	−7.1	$C_{24}H_{26}O_6$	242, 317	500597	158012	80803	α-mangostin
9	11.40	409.1676	6.1	$C_{24}H_{24}O_6$	222, 289	9617	2377	1631	9-hydroxycalabaxanthone
10	11.81	425.1971	1.6	$C_{25}H_{28}O_6$	222, 316	11640	2057	1975	β-mangostin

Table 2. Inhibitory Effects of Extracts and Xanthonoids (2, 3, and 5−9) on Cholinesterase Activities

	cholinesterase					
compound	IC_{50}[a] (μM) human erythrocytes AChE	type of inhibition K_i (μM)[b]	IC_{50}[a] (μM) electrophor s electricus AChE	type of inhibition K_i (μM)[b]	IC_{50}[a] (μM) equine serum BChE	type of inhibition K_i (μM)[b]
$CHCl_3$	2.7 μg/mL	NT[d]	4.8 μg/mL	NT	6.5 μg/mL	NT
EtOH	7.9 μg/mL	NT	45.6 μg/mL	NT	31.8 μg/mL	NT
50% EtOH	34.2 μg/mL	NT	ND	NT	ND	NT
water	ND[c]	NT	ND	NT	ND	NT
2	14.6 ± 0.7	mixed (6.4 ± 0.2)	6.3 ± 5.4	mixed (4.3 ± 0.6)	6.0 ± 0.2	mixed(12.8 ± 0.4)
3	15.0 ± 1.2	mixed (11.5 ± 0.9)	67.4 ± 0.3	mixed (75.7 ± 0.9)	11.0 ± 0.4	mixed (12.4 ± 0.2)
5	11.7 ± 0.7	mixed (7.7 ± 0.5)	18.9 ± 1.7	mixed (12.6 ± 1.2)	9.0 ± 1.2	mixed (6.5 ± 1.3)
6	5.4 ± 0.3	mixed (5.1 ± 0.4)	2.5 ± 3.3	mixed (2.8 ± 0.2)	0.7 ± 0.03	mixed (0.4 ± 1.3)
7	6.2 ± 0.3	mixed (4.8 ± 0.3)	11.0 ± 0.6	mixed (10.9 ± 0.2)	9.2 ± 0.5	mixed (12.0 ± 0.1)
8	8.0 ± 0.5	mixed (3.7 ± 0.2)	6.3 ± 0.6	mixed (8.0 ± 0.5)	2.9 ± 0.7	mixed (3.0 ± 0.5)
9	>100	NT	>100	NT	86.3 ± 2.4	NT
eserine	0.043 ± 0.002	NT	0.049 ± 0.003	NT	0.073 ± 0.006	NT

[a]All compounds were examined in a set of experiments repeated five times; IC_{50} values of compounds represent the concentration that caused 50% enzyme activity loss. [b]Values of inhibition constant. [c]ND is not detected. [d]NT is not tested.

absorbance at 412 nm for 5.0 min at 37 °C. The concentration of compound that caused 50% inhibition of the hAChE activity (IC_{50}) was calculated by nonlinear regression of the response/log (concentration) curve, using Sigma Plot, version 10.0 (SPCC Inc., Chicago, IL). eeAChE and esBChE inhibitory activities were assessed similarly using acetylthiocholine iodide as the substrate. Kinetic parameters were determined using the Lineweaver−Burk double-reciprocal-plot method at increasing concentrations of substrates and inhibitors.[20] The inhibitor, eserine (Sigma-Aldrich, St. Louis, MO), was used in the assays for comparison.

Fluorescence Quenching Measurements. All fluorescence spectra were measured on a SpectraMax M2Multi-Mode Microplate Reader (Molecular Devices, CA, U.S.A.) equipped with a 10.0 mm quartz cell and a thermostatted bath. In a typical fluorescence measurement, 2 μL of hAChE solution (100 mM sodium phosphate buffer, pH 8.0), 0.25 U/mL, was added to the quartz cell and addition of inhibitor solution (10 μL) to attain final concentrations. Fluorescence spectra of hAChE-xanthone mixture were recorded in the range from 300 to 400 nm. Both slits of excitation and emission were 2 nm with an excitation wavelength at 276 nm.[21−23]

Extraction and Isolation of the Inhibitors from *G. mangostana*. The seedcases of *G. mangostana* (1 kg) were extracted by chloroform for 3 days at room temperature to give crude extract (40 g). Crude extract (10 g) was submitted to MPLC (LC-Forte/R, YMC Korea Co. LTD) reversed phase silica gel (YMC ODS-AQ, 25 μm, 120 g) using a stepwise MeOH−H_2O gradient (10−100% methanol, 10 mL/min, 120 min) to give 60 fractions. This MPLC procedure was repeated four times using the same conditions before further isolation. The bioactive constituents from each MPLC column were eluted as a single, UV-absorbing band and pooled. Fractions 18−25 (8.0 g) were chromatographed on a Sephadex LH-20 column eluted with MeOH and isolated by preparative (prep)-HPLC using a reversed-phase column (1.9 × 25 cm, YMC ODS-AQ, 10 μm particle size), eluted with ACN−H_2O gradient (5−70% ACN, 14 mL/min, 60 min) by repeated injection of 10 mg/mL MeOH dilutions to yield pure **2** (82 mg) and **3** (65 mg). Fractions 26−37 (980 mg) were chromatographed on a Sephadex LH-20 column eluted with MeOH and isolated by prep-HPLC using a reversed-phase column (2.0 × 25 cm, YMC ODS-AQ, 10 μm, 120 g), eluted with MeOH−H_2O gradient (10−80% methanol, 10 mL/min, 60 min) by repeated injection of 10 mg/mL MeOH dilutions to yield pure **5** (11 mg) and a mixture of **6** and **7** (Fr. 26−37-B). Fractions 26−37-B (118 mg) were chromatographed by prep-HPLC using a reversed-phase column [Waters Atlantis T3 column (1.9 × 25 cm, 5 μm particle size), eluted with MeOH−H_2O gradient (5−70% methanol, 60 min) by repeated injection of 10 mg/mL MeOH dilutions to yield pure **6** (48 mg) and **7** (38 mg). Fractions 39−49 (8.7 g), enriched with compound **8**, were purified over a silica gel (10 × 50 cm, 230−400 mesh, 300 g) column using the solvent system hexane−acetone (10−90% acetone, 10 mL/min, 60 min) to afford **8** (1730 mg). All isolated compounds were identified on the basis of the following spectroscopic data (Supporting Information).

Statistical Analysis. All the measurements were made in triplicate. The results were subject to variance analysis using Sigma plot. Differences were considered significant at $p < 0.05$.

RESULTS AND DISCUSSION

The extracts from different polar solvents ($CHCl_3$, EtOH, and H_2O) were tested for enzymatic inhibitory activities against ChEs. The high potency of the chloroform extract (IC_{50} = 2.7 μg/μL, hAChE) encouraged us to identify the compounds responsible for its ChEs inhibition. Protein binding affinity can be used to identify inhibitors of a particular enzyme. This is because, for inhibition to occur, an enzyme inhibitor complex

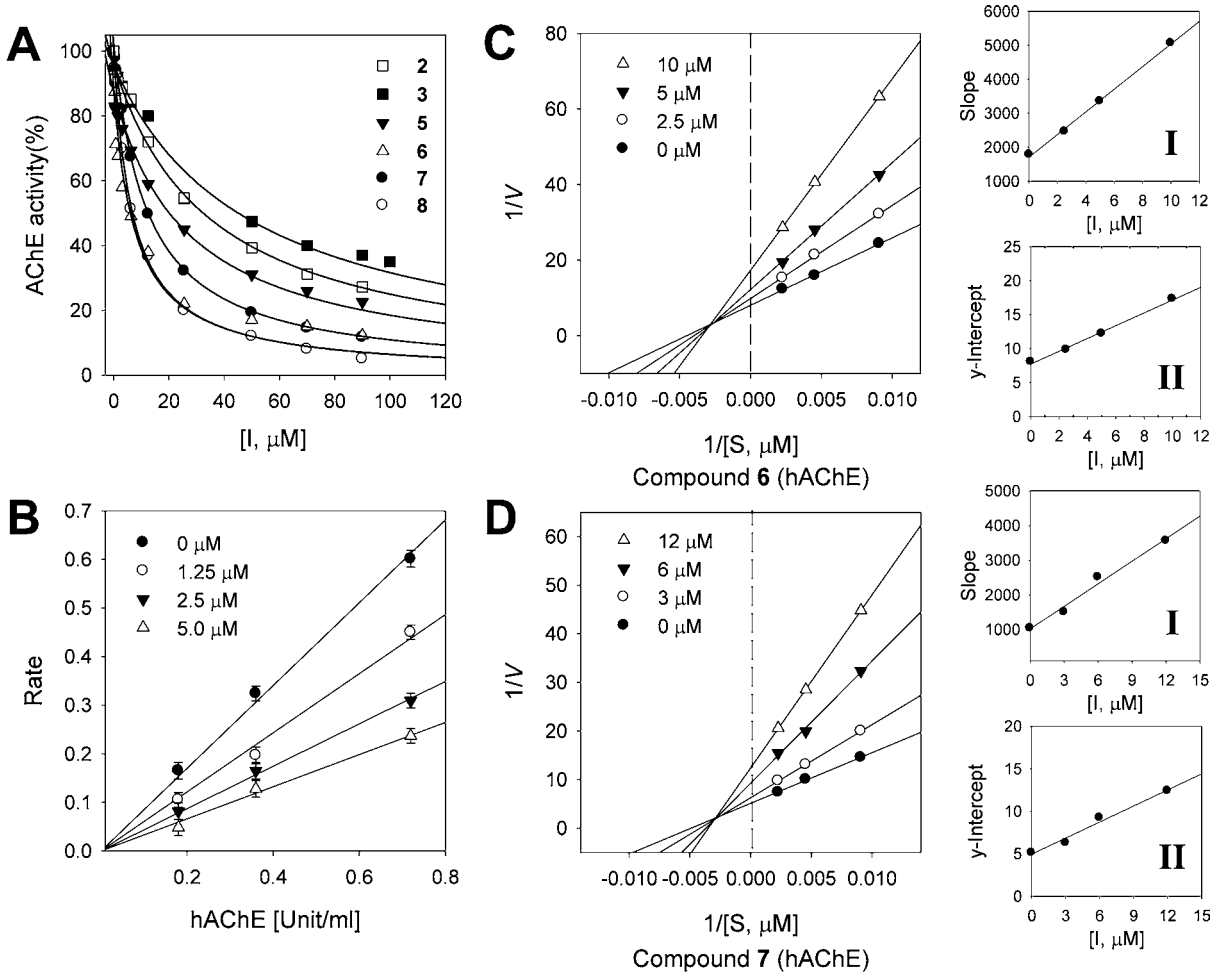

Figure 2. (A) Effect of xanthonoids (**2**, **3**, and **5**−**8**) on the hAChE catalyzed hydrolysis of acetylthiocholine iodide. (B) Hydrolytic activity of hAChE as a function of enzyme concentration at different concentrations of compound **6**. Concentrations of compound **6** for curves from top to bottom were 0, 1.25, 2.5, and 5.0 μM, respectively. (C, D) Lineweaver−Burk plot showing inhibition of compounds **6** and 7 on the hydrolytic activity of hAChE. The plot is expressed as 1/velocity versus 1/thiocholine (mM^{-1}) without or with inhibitor. (Inset) Insets I and II represent the secondary plot of the slope and the intercept of the straight lines versus concentration of compounds (**6** and 7), respectively.

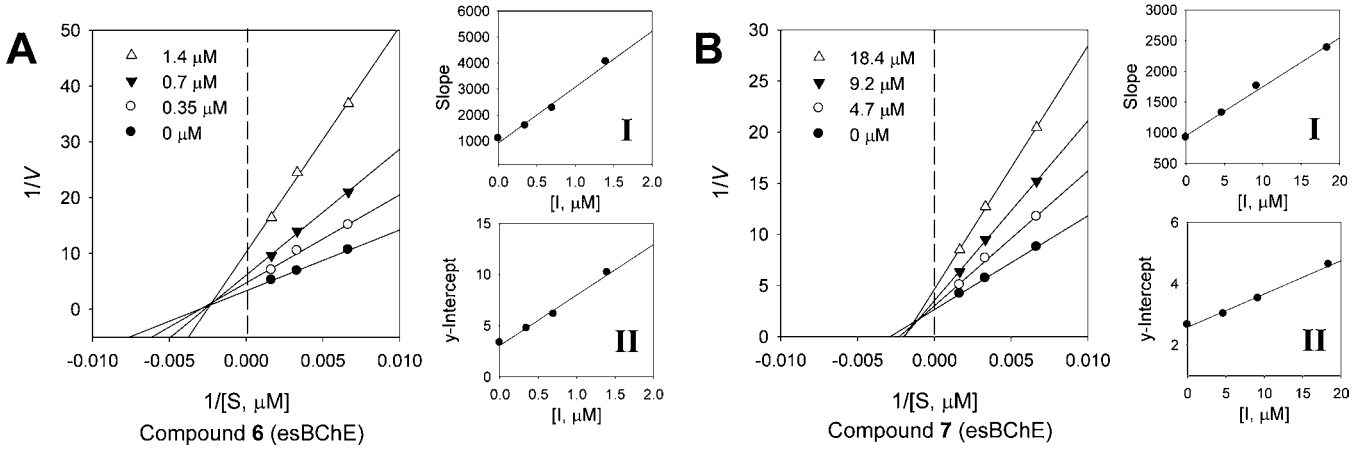

Figure 3. (A, B) Lineweaver−Burk plot for the inhibition of esBChE by compounds **6** and **7**. The plot is expressed as 1/velocity versus 1/thiocholine (mM^{-1}) with or without inhibitor. (Inset) Insets I and II represent the secondary plot of the slope and the intercept of the straight lines versus concentration of compounds (**6** and 7), respectively.

must form. Herein small molecules within the extracts of mangosteen seedcases that bind to cholinesterase were identified by assessing which compounds were lost from the crude extract upon incubation with the enzyme. The binding event was assessed using an experimental set up involving an initial incubation step (1000 ppm extracts with 0.5 U enzyme), followed by centrifugation, and finally analysis of the flow through (i.e., fraction not bound by the enzyme) using UPLC-

dx.doi.org/10.1021/jf405072e | J. Agric. Food Chem. 2014, 62, 1338−1343

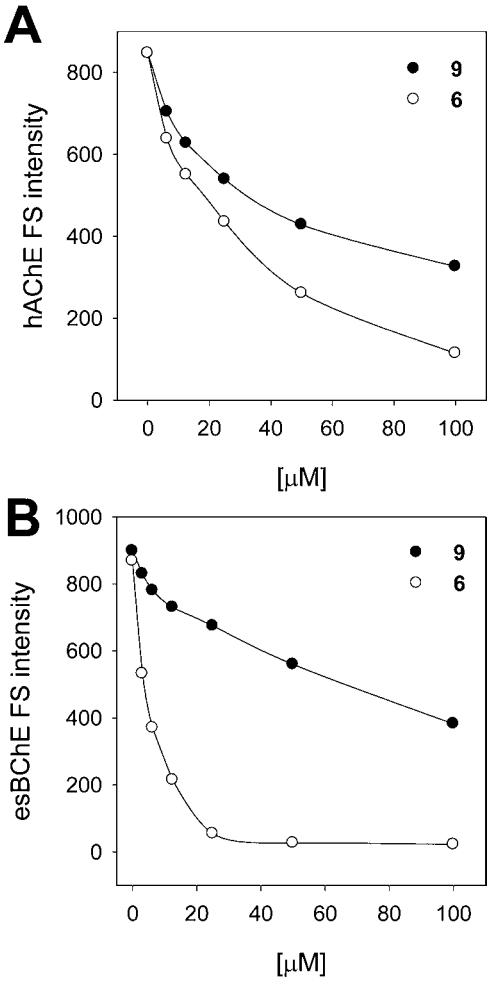

Figure 4. (A, B) Effect of compounds **6** and **9** on intrinsic fluorescence of hAChE. Measurement conditions: xanthonoids (**6** and **9**) concentrations were at 0, 6.25, 12.5, 25, 50, and 100 μM, respectively. [hAChE] = 0.25 units, [esBChE] = 0.05 units, pH 8.0, at 37 °C, λ_{ex} = 276 nm, λ_{em} = 305 nm.

PDA-QTOF-MS. By comparing the UPLC traces from experiments carried out in the presence and absence of enzyme, peaks that were reduced when the enzyme was present were correlated with compounds that bind the enzyme. Representative UPLC-PDA chromatograms of extracts are shown in Figure 1A. The peak areas of six compounds (**2**, **3**, and **5**−**8**) within the chloroform extract of mangosteen were significantly reduced upon treatment with hAChE (blue) and esBChE (red). This result indicates that six compounds, corresponding to peaks (**2**, **3**, and **5**−**8**) have significant interaction with both ChEs. Importantly, the extent to which the peak areas were reduced did not correlate with peak size (for instance **1** and **2** have similar sizes but **2** was reduced by approximately 100% whereas **1** had a very small depletion). This indicates binding is dictated by affinity rather than bulk concentration.

UPLC-PDA-QTOF-MS analyses were carried out using a C18 column with a linear gradient of acetonitile/water. As presented in Figure 1A, complete chromatographic separation of xanthonoids (**1**−**10**) was achieved within 15 min. Each peak was characterized using MS. The exact molecular ions $[M+H]^+$ of peaks (**1**−**10**) were 425, 427, 425, 409, 327, 397, 381, 411, 409, and 425. Table 1 shows UV−vis absorption maxima, retention times, and mass spectral data of molecular ions of xanthonoids in comparison with previously published data.[11,12,24] Thus, peaks (**1**−**10**) were identified as mangostingone (**1**, peak 1), mangostanol (**2**, peak 2), allznxanthone E (**3**, peak 3), mangostenone F (**4**, peak 4), gudraxanthone (**5**, peak 5), γ-mangostin (**6**, peak 6), 8-deoxygartanin (**7**, peak 7), α-mangostin (**8**, peak 8), 9-hydroxycalabaxanthone (**9**, peak 9), and β-mangostin (**10**, peak 10). We next isolated the six active compounds using chromatography over octadecyl-functionalized silica gel. The isolated compounds were fully characterized with spectroscopic data including 2D-NMR. The representative xanthone **6** was obtained as a yellowish powder having molecular formula $C_{23}H_{24}O_7$ and 12 degrees of unsaturation, as established by high-resolution electrospray ionization mass spectrometry (HRESIMS) (m/z 397.1637 $[M+H]^+$, calcd for $C_{23}H_{25}O_6$, 397.1573). ^{1}H and ^{13}C NMR data in combination with molecular formula indicated a tricyclic skeleton with two aromatic rings, corresponding to a xanthone. Two prenyl appendages were identified by successive connectivities in the COSY spectrum. HMBC correlations of H-11 (δ_H 3.21) with C-2 (δ_C 112.6) and of H-16 (δ_H 4.03) with C-8 (δ_C 129.5) unveiled that these prenyl chemotypes were situated on C-2 and C-8 (Supporting Information). Thus, compound **6** was confirmed to be γ-mangostin (Figure 1B).

The purified compounds were next assayed for inhibition of hAChE. Eserine, a known ChE inhibitor, was used as a positive control.[25] Xanthonoids (**2**, **3**, and **5**−**8**) showed dose-dependent inhibitory effects against hAChE, with IC_{50} values ranging between 5.4 and 15.0 μM (Table 2). Consistent with the amount of reduction of intensity in the UPLC assay, there was a significant difference in inhibitory potencies of the strong binding compound set (**2**, **3**, and **5**−**8**, IC_{50}s = 5.4−15.0 μM) and the weaker binding compound **9** (peak 9, IC_{50} > 100). This indicates that hAChE binding affinity facilitates ranking of inhibitors of hAChE in a complex mixture. Our compounds feature at least one prenyl group. According to a previous study, parent compound, 1,3,5,6-tetrahydroxyxanthone, showed very low efficacy (IC_{50} > 200 μM) toward AChE.[26] Thus, prenyl appendages within the isolated active compounds appear to play a pivotal role in the inhibition of cholinesterase. All inhibitors showed a similar relationship between enzyme activity and concentration. The inhibition of hAChE (K_m = 0.1 mM) by compound **6**, the most potent inhibitor (K_i = 5.1 μM) is illustrated in Figure 2, representatively. Increasing the inhibitor concentration resulted in lowering of the slope of the line (Figure 2A). The plots of residual enzyme activity versus enzyme concentration at different concentrations of compound **6** gave a family of straight lines with a y-axis intercept indicating that **6** is a reversible inhibitor (Figure 2B). The enzyme inhibitory properties of target compound **6** were modeled using double reciprocal plots (Lineweaver−Burk and Dixon analysis). The results show a family of lines with common intercept on the left of the vertical axis and above the horizontal axis (Figure 2C and D). This implies that increasing inhibitor concentration leads to a decrease in V_{max} and an increase in K_m, indicating that compound **6** was a mixed-type inhibitor.[20] The K_i values of all compounds were measured by Dixon plot (Table 2). On the other hand, as illustrated in Table 2, the isolated six xanthones (**2**, **3**, and **5**−**8**) were found to exhibit a significant degree of esBChE inhibition with IC_{50} values ranging between 0.7−11.0 μM. These compounds were also mixed inhibitors of this enzyme (Figure 2C and D, and Figure 3).

The binding affinities of the purified inhibitors to ChEs were measured by monitoring quenching of intrinsic protein

fluorescence. hAChE has high intrinsic fluorescence arising from 14 Trp, 17 Tyr, and 30 Phe.[21] The quenching of the intrinsic fluorescence of hAChE by compounds **6** and **9** is displayed in Figure 4. A dramatic difference in fluorescence quenching was observed between **6** and **9**: hAChE **6** (IC_{50} = 5.4 μM) versus **9** (IC_{50} > 100 μM); esBChE **6** (IC_{50} = 0.7 μM) versus **9** (IC_{50} = 86.3 μM). This is in agreement with the affinity difference between both compounds observed in the UPLC-PDA chromatogram (Figure 1, peaks 6 and 9).

■ ASSOCIATED CONTENT

Supporting Information

Characterization data. This material is available free of charge via the Internet at http://pubs.acs.org.

■ AUTHOR INFORMATION

Corresponding Author

*Tel.: +82-55-772-1965. Fax +82-55-772-1969. E-mail khpark@gnu.ac.kr.

Author Contributions

‖H.W.R. and S.-R.O. equally contributed this work.

Notes

The authors declare no competing financial interest.

■ ACKNOWLEDGMENTS

This research was supported by National Research Foundation Grant founded by Korea government (MEST) (2013M3A9A6003180), Rural Development Administration, Republic of Korea, and a grant from the Next-Generation BioGreen 21 Program (SSAC, PJ009571), Rural Development Administration, Republic of Korea.

■ ABBREVIATIONS:

AD, Alzheimer's disease; IC50, The inhibitor concentration leading to 50% activity loss; AChE, acetylcholinesterase; BChE, butyrylcholinesterase; ACh, acetylcholine; HRESIMS, High-resolution electrospray ionization mass spectrometry

■ REFERENCES

(1) Gabrovska, K.; Marinov, I.; Godjevargova, T.; Portaccio, M.; Lepore, M.; Grano, V.; Diano, N.; Mita, D. G. The influence of the support nature on the kinetics parameters, inhibition constants, and reactivation of immobilized acetylcholinesterase. *Int. J. Biol. Macromol.* **2008**, *43*, 339−345.

(2) Bartus, R. T.; Dean, R. L., 3rd; Beer, B.; Lippa, A. S. The cholinergic hypothesis of geriatric memory dysfunction. *Science* **1982**, *217*, 408−414.

(3) Wollen, K. A. Alzheimer's disease: The pros and cons of pharmaceutical, nutritional, botanical, and stimulatory therapies, with a discussion of treatment strategies from the perspective of patients and practitioners. *Altern. Med. Rev.* **2010**, *15*, 223−244.

(4) Yu, Q. S.; Holloway, H. W.; Utsuki, T.; Brossi, A.; Greig, N. H. Synthesis of novel phenserine-based-selective inhibitors of butyrylcholinesterase for Alzheimer's disease. *J. Med. Chem.* **1999**, *42*, 1855−1861.

(5) Fallarero, A.; Oinonen, P.; Gupta, S.; Blom, P.; Galkin, A.; Mohan, C. G.; Vuorela, P. M. Inhibition of acetylcholinesterase by coumarins: The case of coumarin 106. *Pharmacol. Res.* **2008**, *58*, 215−221.

(6) Greig, N. H.; Utsuki, T.; Ingram, D. K.; Wang, Y.; Pepeu, G.; Scali, C.; Yu, Q. S.; Mamczarz, J.; Holloway, H. W.; Giordano, T.; Chen, D.; Furukawa, K.; Sambamurti, K.; Brossi, A.; Lahiri, D. K. Selective butyrylcholinesterase inhibition elevates brain acetylcholine, augments learning and lowers Alzheimer beta-amyloid peptide in rodent. *Proc. Natl. Acad. Sci. U.S.A* **2005**, *102*, 17213−17218.

(7) Jung, H. A.; Su, B. N.; Keller, W. J.; Mehta, R. G.; Kinghorn, A. D. Antioxidant xanthones from the pericarp of *Garcinia mangostana* (Mangosteen). *J. Agric. Food Chem.* **2006**, *54*, 2077−2082.

(8) Naczk, M.; Towsend, M.; Zadernowski, R.; Shahidi, F. Protein-binding and antioxidant potential of phenolics of mangosteen fruit (*Garcinia mangostana*). *Food Chem.* **2011**, *128*, 292−298.

(9) Chomnawang, M. T.; Surassmo, S.; Wongsariya, K.; Bunyapraphatsara, N. Antibaceterial activity of Thai medicinal plants against Methicillin-resistant *Staphylococcus aureus*. *Fitoterapia* **2009**, *80*, 102−104.

(10) Chen, L. G.; Yang, L. L.; Wang, C. C. Anti-inflammatory activity of mangostins from *Garcinia mangostana*. *Food Chem. Toxicol.* **2008**, *46*, 688−693.

(11) Ryu, H. W.; Cho, J. K.; Curtis-Long, M. J.; Yuk, H. J.; Kim, Y. S.; Jung, S. I.; Kim, Y. S.; Lee, B. W.; Park, K. H. α-Glucosidase inhibition and antihyperglycemic activity of prenylated xanthones from *Garcinia mangostana*. *Phytochemistry* **2011**, *72*, 2148−2154.

(12) Ryu, H. W.; Curtis-Long, M. J.; Jung, S. I.; Jin, Y. M.; Cho, J. K.; Ryu, Y. B.; Lee, W. S.; Park, K. H. Xanthones with neuraminidase inhibitory activity from the seedcases of *Garcinia mangostana*. *Bioorg. Med. Chem.* **2010**, *18*, 6258−6264.

(13) Shan, T.; Ma, Q.; Guo, K.; Liu, J.; Li, W.; Wang, F.; Wu, E. Xanthones from mangosteen extracts as natural chemopreventive agents: Potential anticancer drugs. *Curr. Mol. Med.* **2011**, *12*, 666−677.

(14) Pedraza-Chaverri, J.; Cárdenas-Rodríguez, N.; Orozco-Ibarra, M.; Pérez-Rojas, J. M. Medicinal properties of mangosteen (*Garcinia mangostana*). *Food Chem. Toxicol.* **2008**, *46*, 3227−3239.

(15) Chin, Y. W.; Kinghorn, A. D. Structural characterization, biological effects, and synthetic studies on xanthones from Mangosteen (*Garcinia mangostana*), a popular botanical dietary supplement. *Mini-Rev. Org. Chem.* **2008**, *5*, 355−364.

(16) Luo, L.; Shen, L.; Sun, F.; Ma, Z. Immunoprecipitation coupled with HPLC−MS/MS to discover the aromatase ligands from *Glycyrrhiza uralensis*. *Food Chem.* **2013**, *138*, 315−320.

(17) Zhang, Y.; Peng, M.; Liu, L.; Shi, S.; Peng, S. Screening, identification, and potential interaction of active compounds from *Eucommia ulmodies* leaves binding with bovine serum albumin. *J. Agric. Food Chem.* **2012**, *60*, 3119−3125.

(18) Sun, F.; Shen, L.; Ma, Z. Screening for ligands of human aromatase from mulberry (*Mori alba* L.) leaf by using high-performance liquid chromatography/tandem mass spectrometry. *Food Chem.* **2011**, *126*, 1337−1343.

(19) Ellman, G. L.; Courtney, K. D.; Andres, V.; Featherstone, R. M. A new and rapid colorimetric determination of acetylcholinesterase activity. *Biochem. Pharmacol.* **1961**, *7*, 88−95.

(20) Bowden, A. C. A simple graphical method for determining the inhibition constants of mixed, uncompetitive and non-competitive inhibitors. *Biochem. J.* **1974**, *137*, 143−144.

(21) Ryu, H. W.; Curtis-Long, M. J.; Jung, S. I.; Jeong, I. Y.; Kim, D. S.; Kang, K. Y.; Park, K. H. Anticholinesterase potential of flavonols from paper mulberry (*Broussonetia papyrifera*) and their kinetic studies. *Food Chem.* **2012**, *132*, 1244−1250.

(22) Radic, Z.; Kalisiak, J.; Fokin, V. V.; Sharpless, K. B.; Taylor, P. Interaction kinetics of oximes with native, phosphylated, and aged human acetylcholinesterase. *Chemico-Biol. Interact.* **2010**, *187*, 163−166.

(23) Radic, Z.; Taylor, P. Interaction kinetics of reversible inhibitors and substrates with acetylcholinesterase and its fasciculin 2 complex. *J. Biol. Chem.* **2001**, *276*, 4622−4633.

(24) Nilar, L. J. H. Xanthones from the heartwood of *Garcinia mangostana*. *Phytochemistry* **2002**, *60*, 541−548.

(25) Chemnitius, J. M.; Haselmeyer, K. H.; Gonska, B. D.; Kreuzer, H.; Aech, R. Mipafox differential inhibition assay for heart muscle cholinesterases: Substrate specificity and inhibition of three isoenzymes by physostigmine and quinidine. *Gen. Pharmac.* **1977**, *28*, 567−575.

(26) Sabphon, C.; Sermboonpaisarn, T.; Sawasdee, P. Cholinesterase inhibitory activities of xanthones from *Anaxagorea luzonensis* A. Gray. *J. Med. Plants Res.* **2012**, *6*, 3781−3785.

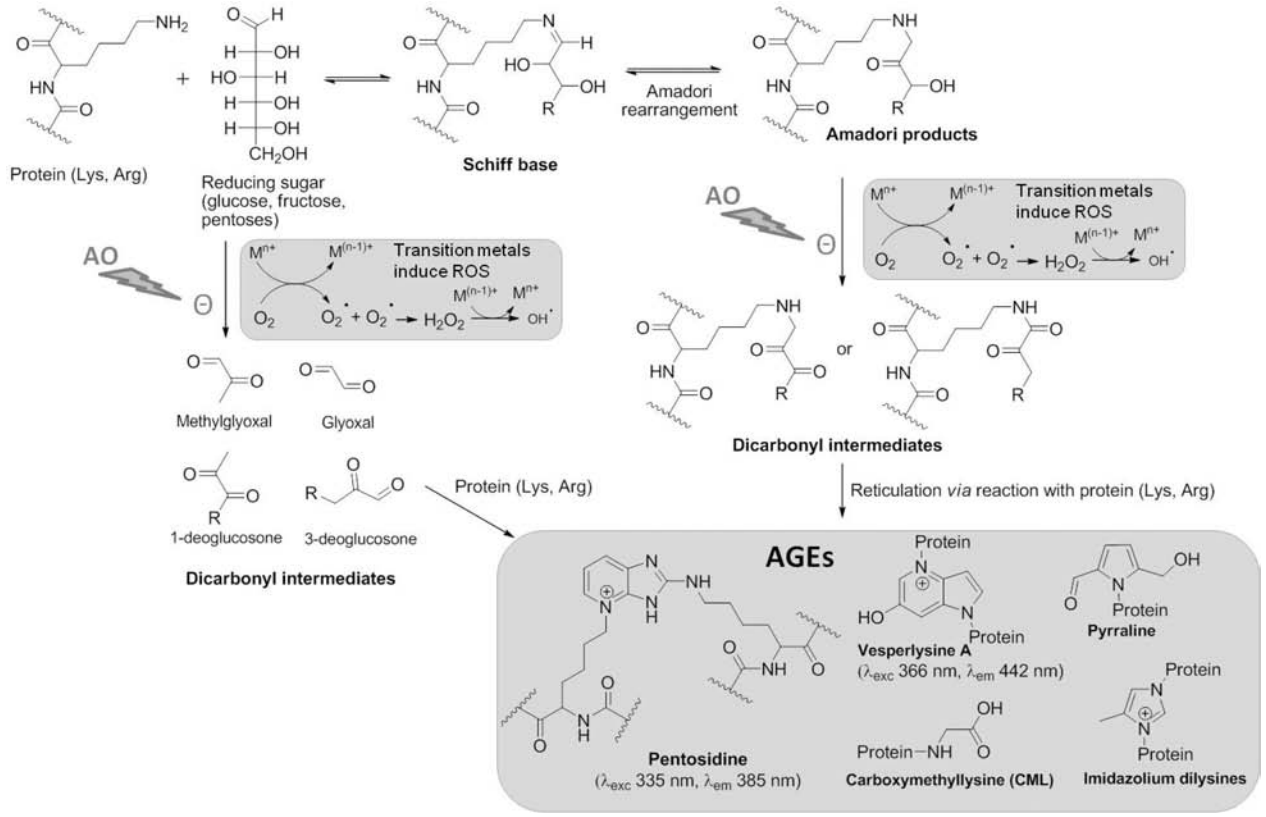

Figure 1. Schematic formation of AGEs. AGEs inhibitors may follow different inhibition pathways in order to prevent AGEs formation. For exemple, they can prevent glycation via reaction with free amino groups in proteins or carbonyl groups on reducing sugars. In addition, compounds with antioxidant (AO) properties (free radical scavengers or transition metal chelators) may reduce reactive oxygen species (ROS). Finally, they can also scavenge α,β-dicarbonyl intermediates or break them (AGEs breakers) [adapted from Ahmed, 2005[8]].

from different places in France (Figure 2) were homogeneously mixed to undergo this study. For the same reason, various

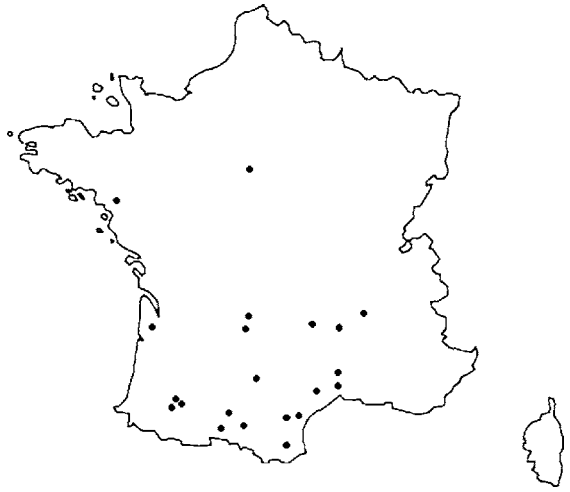

Figure 2. Collection sites of French propolis samples.

extracts using different solvents or mixtures of solvents were prepared in order to find the more appropriate extraction conditions.

MATERIALS AND METHODS

Chemicals. 1,1-Diphenyl-2-picrylhydrazyl (DPPH), aluminum chloride hexahydrate, Folin−Ciocalteu reagent, potassium acetate, 2,4-dinitrophenylhydrazine, formic acid, gallic acid, quercetin, naringenin, *p*-coumaric acid, ferulic acid, isoferulic acid, 3,4-dimethoxycinnamic acid, prenyl caffeate, bovine serum albumin (BSA, fraction V), potassium phosphate monobasic, potassium phosphate dibasic trihydrate, sodium azide, aminoguanidine hydrochloride, all of analytical grade, were purchased from Sigma-Aldrich (St Quentin Fallavier, France). 2,2′-Azobis (2-methylpropionamidine) dihydrochloride (AAPH), fluorescein (FL), 6-hydroxy-2,5,7,8-tetramethylchroman-2-carboxylic acid (Trolox), 5′-caffeoylquinic acid (chlorogenic acid), caffeic acid, and chrysin were obtained from Acros Organics (Geel, Belgium). Ribose was from Alfa Aesar (Schiltigheim, France). Galangin was purchased from Extrasynthese (Genay, France), and caffeic acid phenylethyl ester was purchased from Tocris biosciences (Bristol, United Kingdom). Pinocembrin, pinobanksin-3-acetate, and pinostrobin were isolated from the DCM extract of propolis.

Propolis Batch. A batch (240 g) corresponding to 24 propolis samples (10 g of each), collected in 2010 and 2011 in apiaries originating from different regions of France was used for this study. This batch was provided by the "Ballot-Flurin Apiculteurs" company, specialized in organic beekeeping. The different collection sites of propolis samples are given in Figure 2.

Instrumentation. NMR spectra (1D and 2D) were recorded on a Bruker (Wissembourg France) Avance spectrometer at 500 MHz for ^{1}H and 125 MHz for ^{13}C. Absorbances were obtained from a Tecan (Lyon, France) Infinite M200 microplate spectrophotometer.

dx.doi.org/10.1021/jf4053397 | J. Agric. Food Chem. 2014, 62, 1344−1351

Extractions. The propolis batch was homogeneously pulverized in the presence of liquid nitrogen and divided into 1 g samples. Four different extractions were then carried out on 1 g samples with water (E1), 95% EtOH (E2), 70% EtOH (E3), and MeOH (E4). Then, two extractions, preceded by a cyclohexane wax elimination, were independently performed on 1 g samples with DCM (E5) and a mixture of DCM, MeOH, and H_2O (31/19/4) (E6). For E1, a decoction of 1 g of propolis powder was boiled in 20 mL H_2O at 100 °C for 15 min. After the samples were cooled, the solidified wax and the residue were removed by filtration, and the filtrate was concentrated. For other solvents, 1 g of propolis powder (or of residue issued from a previous extraction) was macerated in 3 × 20 mL of solvent. After stirring for 3 × 2 h at room temperature, the mixture was filtered. The filtrates were gathered and evaporated under vacuum.

Total Polyphenol Content. Total polyphenol content was determined according to the Folin−Ciocalteu colorimetric method.[15] Briefly, 20 μL of extract solution (2.5 mg/mL in MeOH) were mixed with 280 μL of distilled water and 100 μL of Folin−Ciocalteu's phenol reagent. After 3 min, 1200 μL of distilled water and 400 μL of 20% aqueous sodium carbonate solution were added. Aliquots (200 μL) of each solution were distributed in a 96-well microtiter plate. The absorbance was measured at 760 nm after 30 min in the dark at room temperature. A blank was prepared in the same way by using MeOH instead of the extract solution. Gallic acid was used to calculate the calibration curve (0.4−1.2 mg/mL; $y = 0.5800x$; $r^2 = 0.9941$), and total polyphenol contents were expressed in terms of gallic acid equivalent (mg) per gram of extract (mg GAE/g). All measurements were performed in triplicate.

Flavone and Flavonol Content. Flavone and flavonol content was determined according to the aluminum chloride colorimetric method described by Woisky and Salantino.[16] Three hundred microliters of 95% EtOH was mixed with 100 μL of extract solution (1.5 mg/mL in EtOH 80%), 20 μL of 10% aqueous aluminum chloride solution, 20 μL of 1 M potassium acetate aqueous solution, and 560 μL of distilled water. Two hundred microliters of each solution was put into the 96-well microtiter plate. After the samples were incubated at room temperature for 30 min, the absorbance was measured at 415 nm. The amount of 10% aqueous aluminum chloride solution was replaced by the same amount of distilled water in blank for each extract solution. Quercetin, used as standard, was prepared at concentrations of 25−200 μg/mL to build the calibration curve ($y = 2.7677x$; $r^2 = 0.9988$). Flavone and flavonol content were expressed as mg QE/g (quercetin equivalent per gram of extract). All assays were performed in triplicate.

Flavanone and Dihydroflavonol Content. The modified method described by Nagy and Grancai[17] was used to determine flavanone and dihydroflavonol content. Briefly, 500 μL of extract solution (2.5 mg/mL in MeOH) was reacted with 250 μL of MeOH and 500 μL of 1% 2,4-dinitrophenylhydrazine (DNP) solution (500 mg of DNP mixed with 1 mL of 96% sulfuric acid and diluted to 50 mL with MeOH) at 50 °C for 50 min. After the solution was cooled, 500 μL of the solution were mixed with 500 μL of 20% potassium hydroxide in 70% EtOH and then centrifuged at 4000 rpm for 10 min to remove the precipitate. Twenty microliters of the supernatant was collected, put into the 96-well microtiter plate, and mixed with 180 μL of 1% potassium hydroxide methanolic solution. Absorbance was measured at 495 nm. A blank was prepared using the same amount of MeOH instead of the extract solution. Standard solutions of (+)-naringenin (0.25−2.00 mg/mL in MeOH) were used to build the calibration curve ($y = 0.2053x$; $r^2 = 0.9945$). Flavanone and dihydroflavonol content was calculated as mg NE/g (naringenin equivalent per gram of extract). All measurements were performed in triplicate.

HPLC-DAD and HPLC-MS Procedures. Five milligrams of propolis extracts dissolved in 1 mL of MeOH were centrifuged at 13000 rpm for 10 min and filtered through a 0.2 μm nylon-membrane syringe filter prior to injection (10 μL). Analytical HPLC was run on a 2695 Waters (Guyancourt, France) separation module equipped with a diode array detector 2996 Waters. Separation was achieved on a Phenomenex (Le Pecq, France) Luna column 3 μm C18 100A (150 × 4.6 mm i.d., 3 μm) protected with a Phenomenex SecurityGuard cartridge C18 (4 × 3 mm i.d.) at a flow rate of 0.4 mL/min. The mobile phase consisted of 0.1% formic acid in water (solvent A) and 0.1% formic acid in MeOH (solvent B). The separation was performed using the following gradient: 40% B (0−10 min), 40−50% B (10−25 min), 50−60% B (25−55 min), 60−90% B (55−70 min), 90% B (70−80 min). UV detection and quantification were achieved at two wavelengths: 254 and 280 nm. The mass analyses were performed on a Bruker (Bremen, Germany) ESI/APCI Ion Trap Esquire 3000+ in both, positive and negative modes, with the conditions as follows: collision gas, He; collision energy amplitude, 1.3 V; nebulizer and drying gas, N2, 7 L/min; pressure of nebulizer gas, 30 psi; dry temperature, 340 °C; flow rate, 1.0 mL/min; solvent split ratio 1:9; scan range, m/z 100−1000.

Quantification of 12 Compounds by HPLC/DAD. MeOH stock solutions of 12 major compounds chosen as markers for this quantification analysis were prepared as follows: caffeic acid (0.5 mg/mL), *p*-coumaric acid (0.5 mg/mL), ferulic acid (0.3 mg/mL), isoferulic acid (0.3 mg/mL), 3,4-dimethoxycinnamic acid (0.3 mg/mL), pinocembrin (0.8 mg/mL), pinobanksin-3-acetate (1.0 mg/mL), prenyl caffeate (0.4 mg/mL), chrysin (0.8 mg/mL), caffeic acid phenylethyl ester (CAPE) (0.3 mg/mL), galangin (0.6 mg/mL) and pinostrobin (0.2 mg/mL). Stock solutions were diluted (3/4, 1/2, 1/4, 1/8, 1/16) and used to determine the calibration curves of the 12 markers ($n = 2$): caffeic acid ($y = 78{,}027x$; $r^2 = 0.9999$), *p*-coumaric acid ($y = 113{,}20x$; $r^2 = 0.9999$), ferulic acid ($y = 78{,}364x$; $r^2 = 0.9999$), isoferulic acid ($y = 103{,}68x$; $r^2 = 0.9998$), 3,4-dimethoxycinnamic acid ($y = 77{,}748x$; $r^2 = 0.9998$), pinocembrin ($y = 54{,}982x$; $r^2 = 0.9998$), pinobanksin-3-acetate ($y = 49{,}022x$; $r^2 = 0.9994$), prenyl caffeate ($y = 60{,}462x$; $r^2 = 0.9987$), chrysin ($y = 100{,}4x$; $r^2 = 0.9998$), CAPE ($y = 43{,}434x$; $r^2 = 0.9996$), galangin ($y = 48{,}653x$; $r^2 = 0.9984$) and pinostrobin ($y = 93{,}633x$; $r^2 = 0.9995$). All propolis extracts (E1 to E6) were analyzed in triplicate.

Fractionation by Flash Chromatography. Fifty grams of the propolis mixture was extracted with cyclohexane (3 × 200 mL, 2 h, room temperature) to remove beewax. Then, the residue was extracted with DCM (5 × 200 mL, 2 h, room temperature), filtered, and concentrated to give 25.0 g of DCM extract (50% yield). Twenty-one grams of DCM extract was dissolved in 200 mL of DCM, mixed with 42 g of silica gel (extract/silica gel: 1/2), and concentrated to obtain a dry thin powder. Fractionation was performed using a CombiFlash Teledyne ISCO (Lincoln, NE, U.S.A.) apparatus, on a prepacked silica gel column (Interchim PF-50SI HC/300g, 50 μm, 20 bar) at a flow rate of 100 mL/min with the following gradient: 100% C_6H_{12} (2.0 L), C_6H_{12}:EtOAc 90:10 (1.7 L),

Table 1. Extraction Yield, Total Polyphenol (TP), Flavone/Flavonol (FF), and Flavanone/Dihydroflavonol (FD) Contents of French Propolis Extracts (E1−E6)

extract	solvent	extraction yield (%)	TP[a] (mg GAE/g)	FF[b] (mg QE/g)	FD[c] (mg NE/g)
E1	H_2O	6.9 ± 0.4	292.1 ± 13.1	20.5 ± 1.2	76.6 ± 7.7
E2	EtOH	68.4 ± 0.8	253.6 ± 5.1	67.0 ± 2.6	153.1 ± 2.5
E3	70% EtOH	65.3 ± 1.5	246.3 ± 10.6	69.3 ± 3.7	158.6 ± 8.5
E4	MeOH	67.3 ± 0.4	238.6 ± 13.3	66.4 ± 4.9	156.8 ± 3.1
E5	DCM	50.3 ± 0.5	273.5 ± 6.8	78.6 ± 2.7	176.0 ± 9.9
E6	mixed solvents	58.6 ± 0.7	281.0 ± 7.1	80.0 ± 1.2	156.0 ± 10.2

[a]Total polyphenol contents were determined by the Folin−Ciocalteu method. The results are expressed as milligram of gallic acid equivalent per gram of extract. [b]Flavone/flavonol contents were determined by $AlCl_3$ coloration. The results are expressed as milligram of quercetin equivalent per gram of extract. [c]Flavanone/dihydroflavonol contents were determined by the DNP method. The results are expressed as milligram of naringenin equivalent per gram of extract. For all, each value is the mean ± standard deviation (n = 3).

C_6H_{12}:EtOAc 90:10 to 80:20 (2.2 L), C_6H_{12}:EtOAc 80:20 to 70:30 (2.5 L), C_6H_{12}:EtOAc 70:30 to 60:40 (2.2 L), C_6H_{12}:EtOAc 60:40 to 50:50 (3.0 L), and at last DCM:MeOH 96:4 (2.2 L). UV detection, achieved at 254 and 280 nm, allowed us to separate 21 fractions.

Scavenging of DPPH Radicals. The diphenyl-picrylhydrazyl (DPPH) radical scavenging evaluations of propolis extracts were carried out using a modified previously established methodology.[18] Tested compounds and standards were diluted in absolute EtOH at 0.02 mg/mL from stock solutions at 1 mg/mL in DMSO. Aliquots (100 μL) of these diluted solutions were placed in 96-well plates in triplicates. The reaction was initiated by adding 25 μL of freshly prepared DPPH solution (1 mM) and 75 μL of absolute EtOH using the microplate reader's injector (Infinite 200, Tecan, France) to obtain a final volume of 200 μL per well. After 30 min in the dark and at room temperature, the absorbance was determined at 517 nm. EtOH was used as a blank, whereas 10, 25, 50, and 75 μM solutions of Trolox (hydrophilic α-tocopherol analog) were used for the calibration curve. A sample of chlorogenic acid ethanolic solution (0.02 mg/mL) was used as the quality control standard. Results were expressed in terms of Trolox equivalents (micromoles of TE per gram of extract).

Measurement of Oxygen Radical Absorbance Capacity (ORAC). ORAC assays were carried out according to the method described by Huang et al.[19] with some modifications. The assay was performed in a 96-well plate. The reaction mixture contained 100 μL of 75 mM phosphate buffer (pH 7.4), 100 μL of freshly prepared fluorescein (FL) solution (0.1 μM in phosphate buffer), 50 μL of freshly prepared 2,2′-azobis(2-methylpropionamidine) dihydrochloride (AAPH) solution (51.6 mg/mL in phosphate buffer), and 20 μL of sample per well. Samples were analyzed in triplicate and diluted in phosphate buffer at different concentrations (25, 12.5, 6.25, and 3.12 μg/mL) from stock solutions at 1 mg/mL in DMSO. FL, phosphate buffer, and samples were preincubated at 37 °C for 10 min. The reaction was started by the addition of AAPH using the microplate reader's injector (Infinite 200, Tecan, France). Fluorescence was then measured and recorded during 40 min (λ_{exc} 485 nm, λ_{em} 520 nm). The 75 mM phosphate buffer was used as a blank, and 12.5, 25, 50, and 75 μM solutions of Trolox were used as calibration solutions. A chlorogenic acid solution in phosphate buffer (8.8 μM) was used as quality control standard. The final ORAC values were calculated using a regression equation between the Trolox concentration, and the net area under the FL decay curve and were expressed as micromole of Trolox equivalents per gram of dry matter. Areas under curves were calculated using Magellan data analysis software (Tecan, France).

Determination of Sample Concentrations Inhibiting 50% of AGEs Formation. IC_{50} values were determined using a previously described method[20] with slight modifications. Briefly, BSA (10 mg/mL) was incubated with D-ribose (0.5 M) together with the tested compound (3 μM to 3 mM) or extract (1 μg to 1 mg) in 50 mM phosphate buffer at pH 7.4 (NaN_3, 0.02%). Solutions were incubated in 96-well microtiter plates at 37 °C for 24 h in a closed system before AGE fluorescence measurement. Fluorescence resulting from the incubation, under the same BSA (10 mg/mL) and tested compound (3 μM to 3 mM) or extract (1 μg to 1 mg) conditions, was subtracted for each measurement. A control (i.e., no inhibition of AGEs formation) consisted of wells with BSA (10 mg/mL) and D-ribose (0.5 M). A blank control (i.e., 100% inhibition of AGEs formation) consisted of wells with only BSA. The final assay volume was 100 μL. Pentosidine-like (λ_{exc} 335 nm, λ_{em} 385 nm) AGEs fluorescence was measured using a microplate spectrofluorometer. In this type of automation, a single analysis is sufficient for an accurate IC_{50} determination.[20,21] The percentage of AGEs formation was calculated as follows for each compound/extract concentration:

$$\text{AGEs}(\%) = \frac{\text{fluorescence intensity(sample)} - \text{fluorescence intensity(blank of sample)}}{\text{fluorescence intensity(control)} - \text{fluorescence intensity(blank of control)}} 100$$

Dose−effect curves were best fitted with a sigmoidal dose−response equation using Sigma Plot 12.0 software, which enabled calculation of the IC_{50} values.

RESULTS AND DISCUSSION

Extraction Yield. As shown in Table 1, the extraction yield of E1 was very low (6.9%), whereas those of the alcoholic extracts E2−E4 were much higher (65−69%). Those of E5 and E6 were, respectively, 50.3 and 58.6% after a prior cyclohexanic extraction, to remove waxes, which exhibited a 33.0% yield. Thus, yields of E2−E4 were higher than those of EtOH extracts of propolis (EEP) collected in Greece and Cyprus (23.9 to 61.2%).[22] These yields were also higher than those observed for 70% EtOH propolis extracts from Bulgaria (58%), Albania (41%), Egypt (18%), Brazil (12−55%)[5], and a MeOH propolis extract from Mexico (40%).[23]

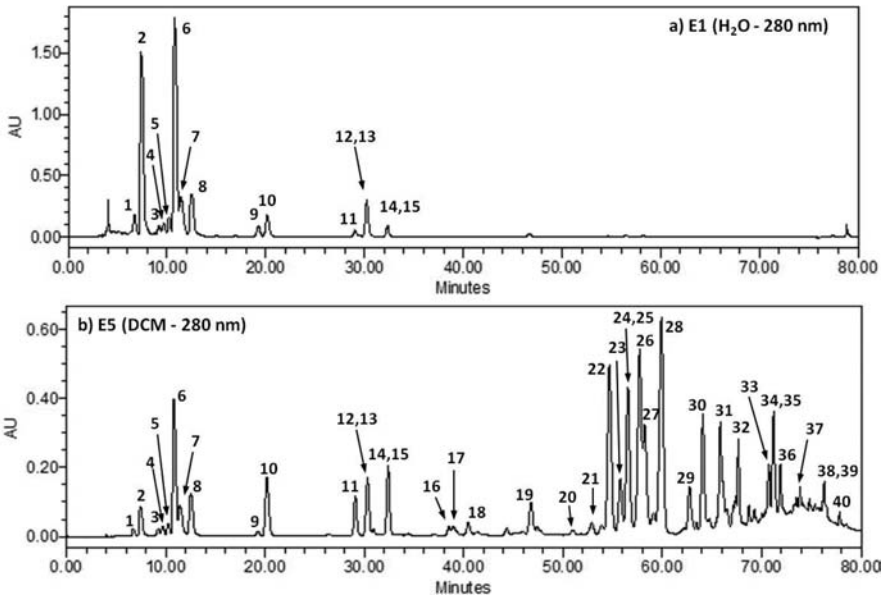

Figure 3. HPLC chromatograms of E1 (a) and E5 (b): **1** 3,4-dihydroxybenzaldehyde, **2** caffeic acid, **3** 4-hydroxybenzaldehyde, **4** vanilline, **5** 4-hydroxyacetophenone, **6** *p*-coumaric acid, **7** ferulic acid, **8** isoferulic acid, **9** benzoic acid, **10** 3,4-dimethoxycinnamic acid, **11** pinobanksin-5-methyl ether, **12** cinnamic acid, **13** 4-methoxycinnamic acid, **14** pinobanksin, **15** naringenin, **16** 1,3-dicoumaroylglycerol, **17** kaempferol, **18** apigenin, **19** cinnamylidene acetic acid, **20** rhamnetin, **21** pinocembrin-5-methyl ether, **22** pinocembrin, **23** isopent-3-enyl caffeate, **24** benzyl caffeate, **25** 2-acetyl-1,3-dicoumaroylglycerol, **26** pinobanksin-3-acetate, **27** prenyl caffeate, **28** chrysin, **29** caffeic acid phenylethyl ester (CAPE), **30** galangin, **31** benzyl *p*-coumarate, **32** cinnamyl caffeate, **33** pinostrobin, **34** cinnamyl isoferulate, **35** cinnamyl *p*-coumarate, **36** tectochrysin, **37** alpinone-3-acetate, **38** benzyl cinnamate, **39** cinnamyl cinnamate, **40** cinnamyl cinnamylidene acetate.

Table 2. Contents of the 12 Markers in Propolis Extracts (E1−E6)

	content[a] (mg/g of extract)					
	E1: H_2O	E2: 95% EtOH	E3: 70% EtOH	E4: MeOH	E5: DCM	E6: mixed solvents
caffeic acid (**2**)	76.9 ± 0.6	6.9 ± 0.1	6.0 ± 0.1	6.6 ± 0.1	5.0 ± 0.1	8.0 ± 0.1
p-coumaric acid (**6**)	61.4 ± 0.3	10.7 ± 0.1	11.1 ± 0.1	10.2 ± 0.1	15.4 ± 0.1	12.0 ± 0.1
ferulic acid (**7**)	20.8 ± 0.4	4.1 ± 0.1	4.4 ± 0.1	3.9 ± 0.1	6.2 ± 0.1	4.2 ± 0.1
isoferulic acid (**8**)	16.2 ± 0.2	4.5 ± 0.1	4.4 ± 0.1	4.1 ± 0.1	6.5 ± 0.1	4.6 ± 0.1
3,4-dimethoxy-cinnamic acid (**10**)	9.9 ± 0.1	7.7 ± 0.1	7.7 ± 0.1	7.1 ± 0.1	10.8 ± 0.1	7.7 ± 0.1
pinocembrin (**22**)	N.D.	35.2 ± 0.2	33.4 ± 0.2	33.0 ± 0.2	49.6 ± 0.4	36.8 ± 0.3
pinobanksin-3-acetate (**26**)	N.D.	40.2 ± 0.3	38.7 ± 0.5	38.1 ± 0.2	59.1 ± 0.5	42.8 ± 0.4
prenyl caffeate (**27**)	N.D.	20.2 ± 0.5	20.2 ± 0.3	19.5 ± 0.2	27.4 ± 0.3	22.0 ± 0.4
chrysin (**28**)	N.D.	24.7 ± 0.1	23.5 ± 0.2	23.1 ± 0.2	36.5 ± 0.4	27.6 ± 0.2
CAPE (**29**)	N.D.	11.2 ± 0.2	10.6 ± 0.2	10.4 ± 0.4	15.8 ± 0.7	11.8 ± 0.2
galangin (**30**)	N.D.	21.9 ± 0.2	20.7 ± 0.3	20.4 ± 0.5	31.1 ± 0.8	23.5 ± 0.4
pinostrobin (**33**)	N.D.	10.7 ± 0.1	12.9 ± 0.3	10.0 ± 0.2	8.1 ± 0.4	7.8 ± 0.3
total	185.3 ± 1.5	195.3 ± 1.1	193.7 ± 1.8	186.5 ± 1.8	271.6 ± 3.5	208.9 ± 2.4

[a]Each value is the mean of triplicate analyses ± standard deviation. N.D. = not detected.

Total Polyphenol Content. Total polyphenol (TP) contents (Table 1) were high for E1−E6, in a range of 238.6 to 292.1 mg GAE/g. This is in accordance with values observed for European and Asian poplar-type propolis (≈200−300 mg GAE/g).[1] Best TP contents were observed for E1, E5, and E6. E2 (253.6 mg GAE/g) had a similar value to EEP from Ukraine (255 mg GAE/g) and United States (256 mg GAE/g) but higher than the ones found in Hungary (242 mg GAE/g), Bulgaria (220 mg GAE/g), Argentina (212 mg GAE/g), Uzbekistan (174 mg GAE/g), Brazil (120 mg GAE/g), South Africa (100 mg GAE/g), and Thailand (31 mg GAE/g).[1]

Flavone/Flavonol and Flavanone/Dihydroflavonol Contents. As indicated in Table 1, E1 showed the lowest flavone/flavonol (FF) and flavanone/dihydroflavonol (FD) contents (respectively, 21 mg QE/g and 77 mg NE/g), whereas FF contents of the other extracts were in a range of 66−80 mg QE/g and FD contents in a range of 153−176 mg NE/g, E5 and E6 showing the best values. For all extracts, FD was superior to FF contents. Alcoholic extracts E2−E4 had similar values (66−69 mg QE/g for FF and 153−159 mg NE/g for FD contents), which appeared superior to those of propolis from Northeastern Spain (≈48.2 mg/g for FF and 78.8 mg/g for FD).[2] They seem closer to those of EEP from Pueblo de Alamos in Northwestern Mexico (57.8 mg/g for FF and 150.6 mg/g for FD content.[24] Nevertheless, FF and FD contents of E2−E4 differed from those of Italian and Swiss 70% EtOH propolis extracts where FF > FD.[25]

Identification of Components by HPLC Analysis with DAD and MS Detection. Figure 3 shows the HPLC chromatograms of E1 and E5, the profiles of E2−E4 and E6

Table 3. Antioxidant and Anti-AGEs Activities of Propolis Extracts (E1−E6)

extract/compd	solvent	DPPH[a] (μmol TE/g)	ORAC[a] (μmol TE/g)	anti-AGEs[b] IC_{50} (mg/mL)
E1	H_2O	1731 ± 28	9722 ± 273	0.34
E2	EtOH	1605 ± 26	8155 ± 114	0.05
E3	70% EtOH	1650 ± 149	9890 ± 480	0.03
E4	MeOH	1386 ± 171	7769 ± 360	0.03
E5	DCM	1437 ± 105	9242 ± 739	0.03
E6	mixed solvents	1964 ± 124	11278 ± 11	0.04
propolis (Greece)[c]	EtOH	1110 ± 70	N.D.	N.D.
propolis (Colombia)[d]	EtOH	190	1965	N.D.
E392[e]	EtOH	591 ± 20	2433 ± 88	0.60
S. japonicum[f]	EtOH	1714 ± 68	7896 ± 711	0.09
chlorogenic acid		2740 ± 64	11289 ± 531	0.04
quercetin		6723 ± 66	13907 ± 662	0.06

[a]DPPH and ORAC results are expressed as micromoles of Trolox equivalent per gram of extract. For both, each value is the mean ± standard deviation ($n = 3$). [b]Anti-AGEs activity is evaluated by the half maximal inhibitory concentration (IC_{50}) expressed as milligram per milliliter (mg/mL) ($n = 1$). [c](Kalogeropoulos et al., 2009). [d](Rodríguez et al., 2012). [e]*Rosmarinus officinalis*. [f]*Styphnolobium japonicum*. N.D. = not determined.

(not shown) being very similar to E5. As expected with differences in solvent polarities, we observed two profile types: the aqueous type with retention times ranging from 6 to 33 min and the organic one, with retention times of most compounds ranging from 10 to 72 min. Chemical profiling was achieved by comparison with literature data (UV/MS), using pure standards or, when needed, after isolation through ^1H and ^{13}C (1D and 2D) NMR analysis. These studies allowed us to identify 40 compounds as benzaldehyde, benzoic, and cinnamic acid derivatives and their ester, glycerols, and different classes of flavonoids (flavones, flavonols, flavanones, and dihydroflavonols). E1 contained benzaldehyde and benzoic acid derivatives (**1**, **3**−**5**, **9**), cinnamic acid derivatives (**2**, **6**−**8**, **10**, **12**, **13**) and some flavanones/dihydroflavonols (**11**, **14**, **15**). E5 exhibited the same compounds, in less quantities, added with cinnamylidene acetic acid **19**, cinnamic ester derivatives (**23**, **24**, **27**, **29**, **31**, **32**, **34**, **35**, **38**−**40**), glycerol derivatives (**16**, **25**), and other flavonoids, as flavanones/dihydroflavonols (**21**, **22**, **26**, **33**, **36**), flavones/flavonols (**17**, **18**, **20**, **28**, **30**, **37**). So, mainly exhibiting cinnamic acid derivatives (caffeic and *p*-coumaric acids...) and their esters (prenyl caffeate, CAPE...), and flavonoids (pinocembrin, pinobanksin-3-acetate, chrysin, galangin...), this French propolis clearly belongs to the poplar type with polyphenols originating from *Populus* spp. of section *Aigeiros* and especially *P. nigra* L.[7,26]

Quantification of 12 Major Compounds. Results of the quantitative analysis of E1−E6 are given in Table 2. As already outlined in Figure 2a, E1 contained mainly phenolic acids with a majority of caffeic **2** and *p*-coumaric **6** acids with 76.9 ± 0.6 and 61.4 ± 0.3 mg/g, respectively. In E2−E6, pinobanksin-3-acetate **28** appeared as the major component, followed by pinocembrin **25**, chrysin **32**, galangin **34**, and prenyl caffeate **29**. Taken as a whole, the higher cumulative amount of these 12 components was observed for E5 with 271.6 ± 3.5 mg/g, whereas the lowest indexes were associated with E4 and E1 (186 and 185.3 mg/g, respectively). For the aqueous extract (E1), it can be noticed that this amount corresponded to only five detectable markers (phenolic acids). Therefore, the quantification results were in accordance with our total polyphenol and flavonoid contents (Table 1). The same three major compounds were also observed in different proportions with poplar type propolis from China (chrysin ≫ pinocembrin > pinobanksin-3-acetate), Hungary (chrysin ≫ pinobanksin-3-acetate > pinocembrin), and Uruguay (pinobanksin-3-acetate > chrysin > pinocembrin).[1]

Antioxidant and Anti-AGEs Activities. AO and anti-AGEs activities observed for E1−E6 are shown in Table 3. E1−E6 are compared with specific references (extract or pure compounds) on the one hand and literature data on the other hand. E392 is an ethanolic rosemary extract used as an AO food additive in Europe (Official Journal of European Union, Directive 2010/67/UE, L 277/17). It should be noticed that, at least in our survey, E392 only showed very weak activities. As expected, E1 exhibited good AO activities but, lacking flavonoids, no real antiglycation potential. At the opposite, E6 showed very good overall activities due to a comprehensive polyphenol extraction. However, as far as anti-AGEs activity was concerned, similar results were obtained with E3−E5. Therefore, from a food additive point of view, a mother tincture such as E3, exhibiting fair AO activities associated with a true anti-AGEs potential, appears as quite interesting. According to its very good anti-AGEs activity (IC_{50} = 0.03 mg/mL), combined with the best cumulative content of the 12 quantified markers (272 mg/g), E5 was chosen for a bioguided fractionation by Flash chromatography.

Anti-AGEs Guided Fractionation of E5. Among 21 fractions (F) issued from the flash chromatography, F1−F5 did not exhibit any activity (IC_{50} > 1 mg/mL), whereas the IC_{50} values for F6−21 were in a range of 0.01 to 0.13 mg/mL. Eight fractions showing $IC_{50} \leq 0.04$ mg/mL (namely, F8−F12 and F16−F18, i.e., F8:0.02; F9:0.04; F10:0.01; F11:0.03; F12:0.03; F16:0.03; F17:0.03 and F18:0.04 mg/mL) were then selected for a chemical profiling, and the anti-AGEs activities of purified components were finally achieved (Table 4). The 16 analyzed compounds can be divided into three groups. The first one contained the most active components in our assay, with $IC_{50} \leq$ 0.10 mM (i.e., in decreasing order, pinobanksin-3-acetate **26**, 2-acetyl-1,3-dicoumaroylglycerol **25**, pinobanksin **14**, prenyl caffeate **27** and pinobanksin-5-methyl ether **11**) The second group was composed of moderately anti-AGEs compounds ($0.2 \leq IC_{50} \leq 1.6$ mM) like naringenin **15**, caffeates **24**, **38** and **29**, ferulic and isoferulic acids **7** and **8**, and ester **34**. The last group exibited non active molecules (IC_{50} > 3 mM) like *p*-coumaric and cinnamic acids **6** and **12** as well as chrysin **28**. Thus, among the most active components, three of them were pinobanksin derivatives (flavanones **26**, **14**, and **11**). Besides, a trisubstituted

dx.doi.org/10.1021/jf4053397 | J. Agric. Food Chem. 2014, 62, 1344−1351

Table 4. Anti-AGEs Activities of Compounds Present in the Eight Selected Fractions (with $IC_{50} \leq 0.04$ mg/mL)

compd (no.)	anti-AGEs[a] IC_{50} (mM)	fraction
pinobanksin-3-acetate (**26**)	0.06	F8
2-acetyl-1,3-dicoumaroylglycerol (**25**)	0.07	F17
pinobanksin (**14**)	0.08	F9
prenyl caffeate (**27**)	0.09	F10
pinobanksin-5-methyl ether (**11**)	0.10	F18
naringenin (**15**)	0.2	F11−F12
benzyl caffeate (**24**)	0.4	F11
cinnamyl caffeate (**38**)	0.5	F11
cinnamyl isoferulate (**34**)	0.6	F8
ferulic acid (**7**)	0.7	F16
isoferulic acid (**8**)	0.9	F18
CAPE (**29**)	1.6	F11
p-coumaric acid (**6**)	>3	F16
cinnamic acid (**12**)	>3	F9
chrysin (**28**)	>3	F9

[a]The anti-AGEs activity was evaluated by the means of the half maximal inhibitory concentration (IC_{50}) expressed as millimole of compound per liter (mM) (n = 1). Reference: quercetin IC_{50} = 0.2 mM.

glycerol (**25**) and a prenylated caffeate (**27**) also appeared as good glycation inhibitors.

There is nowadays a growing interest in compounds exhibiting antiglycation combined with antioxidant properties. However, if a fair anti-AGEs activity is expected from any AO compound (Figure 1), the measured effect may be deceptive, at least because glycation spontaneously occurs so that AO must exhibit long lifetimes. Indeed, whereas coincubation of methylglyoxal (MGO) and reduced glutathione or Trolox totally prevents ROS production, it only partially prevents the MGO-induced decrease of brain cell viability.[27] A contrario, an AO synthetic compound such as aminosalicylic acid proved in vitro more effective than aminoguanidine in reducing the antiproliferative effects of both high glucose and BSA-issued AGEs.[28] One may then turn to natural AO, especially in the search for compounds exhibiting low toxicities. As a food ingredient used from ancient times with very high AO activity, it was therefore of great interest to evaluate the antiglycation potential of our propolis batch. Our study actually demonstrates that a mother tincture of propolis such as E3 represents a very good candidate for further food development.

Bioactive compound may also act by blocking the interaction between AGEs and their specific receptors (i.e., RAGEs). As far as neurodegeneration is concerned, it was recently demonstrated that inhibiting the upregulation of RAGEs transcripts, pinocembrin (**22**), a major component in E2−E6 extracts, truly improved cognitive function, preserved the ultrastructural neuropil, and decreased the neurodegeneration of the cerebral cortex in amyloid-β-peptide-treated mice.[29] All in all, a poplar type propolis like this French batch have therefore great potential to be used as food additive to prevent glycoxidation.

■ ASSOCIATED CONTENT

Supporting Information

Chemical structures of the identified compounds with their UV/MS data and the anti-AGEs guided fractionation of E5. This material is available free of charge via the Internet at http://pubs.acs.org.

■ AUTHOR INFORMATION

Corresponding Author

*E-mail: pascal.richomme@univ-angers.fr. Fax: +33 241226634. Tel.: +33 241226667.

Funding

This study was financed by Ballot-Flurin Apiculteurs Cie. There is no other competing interest.

Notes

The authors declare no competing financial interest.

■ ACKNOWLEDGMENTS

We thank Mrs. Isabelle Péruchès, from Ballot-Flurin Apiculteurs who provided propolis samples and Dr. Ingrid Freuze from the "Plateforme d'Ingénierie et Analyses Moléculaires" (PIAM), University of Angers, for MS analyses.

■ ABBREVIATION USED

AGEs: advanced glycation end-products; AO: antioxidant; APCI: atmospheric pressure chemical ionization; BSA: bovin serum albumin; DCM: dichloromethane; DPPH: diphenylpicrylhydrazyl; DNP: 2,4-dinitrophenylhydrazine; ESI: electrospray ionization; FD: flavanone/dihydroflavonol; FF: flavone/flavonol; HPLC/DAD: high-performance liquid chromatography coupled with diode array detector; MGO: methylglyoxal; NMR: nuclear magnetic resonance; ORAC: oxygen radical absorbance capacity; RAGEs: receptor for advanced glycation end-products; ROS: reactive oxygen species; TP: total polyphenol

■ REFERENCES

(1) Ahn, M.-R.; Kumazawa, S.; Bang, K.-S.; Hamasaka, T.; Nakayama, T. Antioxidant Activity of Propolis of Various Geographic Origins. *J. Agric. Food Chem.* **2004**, *52*, 7286−7292.

(2) Bonvehí, J.; Gutiérrez, A. Antioxidant Activity and Total Phenolics of Propolis from the Basque Country (Northeastern Spain). *J. Am. Oil Chem. Soc.* **2011**, *88*, 1387−1395.

(3) Castaldo, S.; Capasso, F. Propolis, an Old Remedy Used in Modern Medicine. *Fitoterapia* **2002**, *73* (Supplement 1), S1−S6.

(4) Popova, M.; Silici, S.; Kaftanoglu, O.; Bankova, V. Antibacterial Activity of Turkish Propolis and Its Qualitative and Quantitative Chemical Composition. *Phytomedicine* **2005**, *12*, 221−228.

(5) Kujumgiev, A.; Tsvetkova, I.; Serkedjieva, Y.; Bankova, V.; Christov, R.; Popov, S. Antibacterial, Antifungal, and Antiviral Activity of Propolis of Different Geographic Origin. *J. Ethnopharmacol.* **1999**, *64*, 235−240.

(6) Bankova, V.; De Castro, S. L.; Marcucci, M. C. Propolis: Recent Advances in Chemistry and Plant Origin. *Apidologie* **2000**, *31*, 3−15.

(7) Bankova, V. Chemical Diversity of Propolis and the Problem of Standardization. *J. Ethnopharmacol.* **2005**, *100*, 114−117.

(8) Ahmed, N. Advanced Glycation Endproducts—Role in Pathology of Diabetic Complications. *Diabetes Res. Clin. Pract.* **2005**, *67*, 3−21.

(9) Takeuchi, M.; Yamagishi, S. Possible Involvement of Advanced Glycation End-Products (AGEs) in the Pathogenesis of Alzheimers Disease. *Curr. Pharm. Des* **2008**, *14*, 973−978.

(10) Jandeleit-Dahm, K.; Cooper, M. E. The Role of AGEs in Cardiovascular Disease. *Curr. Pharm. Des.* **2008**, *14*, 979−986.

(11) Miyata, T.; Iida, Y.; Horie, K.; Cai, Z.; Sugiyama, S.; Maeda, K. Pathophysiology of Advanced Glycation End-Products in Renal Failure. *Nephrol,. Dial., Transplant.* **1996**, *11*, 27−30.

(12) Yoo, N. H.; Jang, D. S.; Yoo, J. L.; Lee, Y. M.; Kim, Y. S.; Cho, J.-H.; Kim, J. S. Erigeroflavanone, a Flavanone Derivative from the Flowers of Erigeron Annuus with Protein Glycation and Aldose Reductase Inhibitory Activity. *J. Nat. Prod.* **2008**, *71*, 713−715.

(13) Hegazi, A. G.; Abd El Hady, F. K.; Abd Allah, F. A. M. Chemical Composition and Antimicrobial Activity of European Propolis. *Z. Naturforsch.* **2000**, *55c*, 70−75.
(14) De Castro Ishida, V. F.; Negri, G.; Salatino, A.; Bandeira, M. F. C. L. A New Type of Brazilian Propolis: Prenylated Benzophenones in Propolis from Amazon and Effects against Cariogenic Bacteria. *Food Chem.* **2011**, *125*, 966−972.
(15) Rebiai, A.; Lanez, T.; Belfar, M. L. In Vitro Evaluation of Antioxidant Capacity of Algerian Propolis by Spectrophotometrical and Electrochemical Assays. *Int. J. Pharmacol.* **2011**, *7*, 113−118.
(16) Woisky, R. G.; Salatino, A. Analysis of Propolis: Some Parameters and Procedures for Chemical Quality Control. *J. Agric. Res.* **1998**, *37*, 99−105.
(17) Nagy, M.; Grancai, D. Colorimetric Determination of Flavanones in Propolis. *Pharmazie* **1996**, *51*, 100−101.
(18) Abdel-Lateff, A.; König, G. M.; Fisch, K. M.; Höller, U.; Jones, P. G.; Wright, A. D. New Antioxidant Hydroquinone Derivatives from the Algicolous Marine Fungus Acremonium Sp. *J. Nat. Prod.* **2002**, *65*, 1605−1611.
(19) Huang, D.; Ou, B.; Hampsch-Woodill, M.; Flanagan, J. A.; Prior, R. L. High-Throughput Assay of Oxygen Radical Absorbance Capacity (ORAC) Using a Multichannel Liquid Handling System Coupled with a Microplate Fluorescence Reader in 96-Well Format. *J. Agric. Food Chem.* **2002**, *50*, 4437−4444.
(20) Séro, L.; Sanguinet, L.; Blanchard, P.; Dang, B. T.; Morel, S.; Richomme, P.; Séraphin, D.; Derbré, S. Tuning a 96-Well Microtiter Plate Fluorescence-Based Assay to Identify AGE Inhibitors in Crude Vegetal Extracts. *Molecules* in press.
(21) Derbré, S.; Gatto, J.; Pelleray, A.; Coulon, L.; Séraphin, D.; Richomme, P. Automating a 96-Well Microtiter Plate Assay for Identification of AGEs Inhibitors or Inducers: Application to the Screening of a Small Natural Compounds Library. *Anal. Bioanal. Chem.* **2010**, *398*, 1747−1758.
(22) Kalogeropoulos, N.; Konteles, S. J.; Troullidou, E.; Mourtzinos, I.; Karathanos, V. T. Chemical Composition, Antioxidant Activity and Antimicrobial Properties of Propolis Extracts from Greece and Cyprus. *Food Chem.* **2009**, *116*, 452−461.
(23) Li, F.; Awale, S.; Tezuka, Y.; Esumi, H.; Kadota, S. Study on the Constituents of Mexican Propolis and Their Cytotoxic Activity against PANC-1 Human Pancreatic Cancer Cells. *J. Nat. Prod.* **2010**, *73*, 623−627.
(24) Velazquez, C.; Navarro, M.; Acosta, A.; Angulo, A.; Dominguez, Z.; Robles, R.; Robles-Zepeda, R.; Lugo, E.; Goycoolea, F. M.; Velazquez, E. F.; Astiazaran, H.; Hernandez, J. Antibacterial and Free-Radical Scavenging Activities of Sonoran Propolis. *J. Appl. Microbiol.* **2007**, *103*, 1747−1756.
(25) Popova, M.; Bankova, V.; Butovska, D.; Petkov, V.; Nikolova-Damyanova, B.; Sabatini, A. G.; Marcazzan, G. L.; Bogdanov, S. Validated Methods for the Quantification of Biologically Active Constituents of Poplar-type Propolis. *Phytochem. Anal.* **2004**, *15*, 235−240.
(26) Rubiolo, P.; Casetta, C.; Cagliero, C.; Brevard, H.; Sgorbini, B.; Bicchi, C.; Populus Nigra, L. Bud Absolute: A Case Study for a Strategy of Analysis of Natural Complex Substances. *Anal. Bioanal. Chem.* **2013**, *405*, 1223−1235.
(27) Heimfarth, L.; Loureiro, S. O.; Pierozan, P.; Lima, B. O.; de Reis, K. P.; Torres, E. B.; Pessoa-Pureur, R. Methylglyoxal-Induced Cytotoxicity in Neonatal Rat Brain: A Role for Oxidative Stress and MAP Kinases. *Metab. Brain. Dis.* **2013**, *28*, 429−438.
(28) Duraisamy, Y.; Gaffney, J.; Slevin, M.; Smith, C. A.; Williamson, K.; Ahmed, N. Aminosalicylic Acid Reduces the Antiproliferative Effect of Hyperglycaemia, Advanced Glycation Endproducts and Glycated Basic Fibroblast Growth Factor in Cultured Bovine Aortic Endothelial Cells: Comparison with Aminoguanidine. *Mol. Cell. Biochem.* **2003**, *246*, 143−153.
(29) Liu, R.; Wu, C.; Zhou, D.; Yang, F.; Tian, S.; Zhang, L.; Zhang, T.; Du, G. Pinocembrin Protects against B-Amyloid-Induced Toxicity in Neurons through Inhibiting Receptor for Advanced Glycation End Products (RAGE)-Independent Signaling Pathways and Regulating Mitochondrion-Mediated Apoptosis. *BMC Medicine* **2012**, *10*, 105.

aggressive type of lung cancer, and it is unclear whether these properties are conserved in more aggressive lung cancers such as small lung cancer cell types. Additionally, while several mechanisms of action of 6S have been identified, no study has considered the contribution of M2 to the mechanisms of action of 6S in cancer cells. Also, the mechanism of action of 6S *in vivo* remains largely unexplained, especially in light of its quick metabolism. In the present study, we test the hypothesis that the M2 metabolite can account for all or most of 6S bioactivity by activating similar molecular pathways in a determined sequence. We further correlate our findings on both compounds *in vivo* using a mouse xenograft model. Overall, this work describes for the first time that 6S and M2 can activate a similar cascade of pathways, ultimately leading to cancer cell apoptosis. It also demonstrates that the cysteine-conjugated metabolite has a superior *in vivo* cancer chemopreventive potential, in addition to its ability to discriminate between cancer and normal cells.

MATERIALS AND METHODS

Cell Culture and Reagents. A549 cells were cultured in F12K medium (Corning, NY) supplemented with 10% fetal bovine serum and 1% penicillin/streptomycin (Gemini Bio-Products, West Sacramento, CA). Protease and phosphatase inhibitor mix was from Thermo Scientific (Waltham, MA). Antibodies for Western blotting were from Cell Signaling (Danvers, MA). Protein concentrations were determined from cell lysates using a Pierce BCA kit (Thermo Fisher Scientific, Rockford, IL). BrdU (5-bromo-2-deoxyuridine) was from Sigma-Aldrich (St. Louis, MO). Apoptag plus Peroxydase In Situ Apoptosis Detection Kit was from Millipore (Billerica, MA), and the BrdU Immunohistochemistry Kit was from Chemicon International (Temecula, CA).

6S was purified from ginger extract in our laboratory.[12] M2 was synthesized in our laboratory, as previously reported.[29] HPLC-grade solvents and other reagents were obtained from VWR International (South Plainfield, NJ). LC/MS (liquid chromatography/mass spectrometry) grade solvents and other reagents were obtained from Thermo Fisher Scientific (Rockford, IL). Glutathione, sulfatase from *Aerobacter aerogenes*, and β-glucuronidase from *Helix aspersa* were obtained from Sigma Aldrich (St. Louis, MO).

Metabolism of 6S and M2 in A549 and IMR90 Cells. A549 or IMR90 cells (1.0×10^6) were plated in 6-well culture plates and allowed to attach for 24 h at 37 °C in 5% CO_2 incubator. 6S or M2 (in DMSO) was then added to culture media to reach a final concentration of 10 or 20 μM, respectively. At different time points (0, 30, 1, 2, 4, 8 min, and 24 h), 190 μL samples of supernatant were taken and transferred to vials containing 10 μL of 0.2% acetic acid to stabilize 6S, M2, and their respective metabolites. To extract compounds from the culture media, an equal volume of acetonitrile was added to the supernatant samples and these mixtures were centrifuged. The supernatant was harvested and the samples were analyzed by HPLC-ECD as described by us previously.[14]

Determination of Cell Viability. A549 cell viability was determined by a 3-(4,5-dimethylthiazol-2-yl)-2,5-diphenyltetrazolium bromide (MTT) colorimetric assay.[30] A549 cells (6000 cells/well) were plated in 96-well microtiter plates and allowed to attach for 24 h at 37 °C and 5% CO_2. 6S or M2 (in DMSO) were added to cell culture medium to desired final concentrations (0−80 μM; final DMSO concentrations for control and treatments were 0.1%). After the cells were cultured for 24 h, the medium was aspirated and the cells were treated with 2.41 mM MTT in fresh media. After incubation for 3 h at 37 °C, the medium containing MTT was removed, 100 μL of DMSO was added to the wells, and the plates were shaken gently for an hour at room temperature. Absorbance values were derived from the plate reading at 550 nm on a Biotek Synergy 2 plate reader (Winooski, VT). The experiment was repeated independently to confirm the results.

Determination of Apoptosis. We used the Cell Death Detection ELISA (Enzyme-linked immunoabsorbant assay) Plus kit from Roche (Mannheim, Germany). A549 cells (10 000 cells/well) were plated in 96-well microtiter plates and allowed to attach for 24 h at 37 °C and 5% CO_2. 6S or M2 (in DMSO) was added to cell culture medium to desired final concentrations (10 or 20 μM; final DMSO concentration for control and treatments was 0.1%). After 24 h, the microplate was centrifuged for 10 min at 1200 rpm, and the supernatant was removed. Then, 200 μL of the lysis buffer was added in each well and the microplate was incubated for 30 min at room temperature. The plate was then centrifuged for 10 min at 1200 rpm and 20 μL of the supernatant was transferred to streptavidin-coated microwells. ELISA assay was performed according to manufacturer's instruction. Absorbance in each well was measured at 405 nm in absorbance units (AU), and the enrichment factor (EF) in small nucleosomes was calculated with the formula $EF = AU_{(treated)}/AU_{(DMSO)}$. The experiment was repeated independently to confirm the results.

Intracellular Glutathione (GSH) Measurement. The total GSH content was measured using a HT Glutathione Assay kit (Trevigen, Galthersburg, MD). Briefly, A549 cells were plated in 60 × 15 mm culture plates and were allowed to attach overnight at 37 °C. Cells were treated with 10 μM M2 and incubated for 0, 2, 4, 8, or 24 h. Cells were harvested and proteins were precipitated with 5% (w/v) metaphosphoric acid. Samples were then processed following the manufacturer's instructions. The measurement of the absorbance of 5-thio-2-nitrobenzoic acid (TNB) at 405 nm was used to quantify glutathione levels in each sample, which was then compared to the standard curve and corrected for protein concentration. The experiment was repeated independently to confirm the results.

For measurement of oxidized glutathione (Glutathione Disulfide or GSSG), samples and GSSG standards were treated with 2 M 4-vinylpyridine (1 μL/50 μL sample) at room temperature for 1 h. 4-Vinylpyridine (Sigma Aldrich, St. Louis, MO) blocks free thiols present in the reaction, consequentially blocking the formation of new GSSG by GSH. The 2 M solution was freshly prepared by diluting 4-vinylpyridine in ethanol in a ratio of approximately 1:3:6. After incubation, samples were processed using the Trevigen kit's protocol and absorbance was measured at 405 nm as described above.

The quantity of reduced cellular glutathione (or GSH) is obtained by subtracting the oxidized samples values from the total glutathione values or: $GSH_{(reduced)} = GSH_{(total)} - GSSG_{(oxidized)}$. Ratios of reduced to oxidized glutathione are shown to further represent cellular redox status after treatment with 6S or M2. The experiment was repeated independently to confirm the results.

Western Blotting. Cell extracts were prepared by incubating cells for 5 min on ice with RIPA (Radio-Immunoprecipitation Assay) buffer (Thermo Fisher Scientific, Rockford, IL) supplemented with a protease and phosphatase inhibitor mix. Cell lysate was then centrifuged at 13 000 rpm at 4 °C for 20 min, and supernatant was harvested for Western blot analysis. Briefly, 30−60 μg of protein extract was separated on a 10−16% polyacrylamide gel and transferred on PVDF (polyvinylidene difluoride) membrane (Biorad, Hercules, CA). Membrane was blocked using a 1% casein solution in Tris-buffered saline-Tween 20 (TBS-T). Primary rabbit antibodies were diluted in blocking solution and incubated with the membrane overnight at 4 °C. After the membrane was washed with 3 changes of TBS-T, secondary Horse Radish Peroxydase (HRP)-conjugated anti-rabbit antibody was diluted 1:3000 in blocking solution and incubated with PVDF membrane for 1 h at room temperature. Signal was then revealed using FEMTO chemoluminescent substrate (Thermo Scientific, Waltham, MA) and by exposing the membrane to photosensitive photographic films for various times. Films were developed using a SRX-101A Konica Minolta developer (Tokyo, Japan).The experiment was repeated independently twice to confirm the results. Fold-induction of proteins was calculated by normalizing the band of interest to the loading control (β-actin), and this adjusted intensity was compared to the control (DMSO) sample.

GSH Rescue Assay. A549 cells were plated on 60 mm culture dishes, at 0.5×10^6 density. After 24 h, DMSO, 6S or M2 (10, 20, 40, 80, 120 μM) were added to the cells and incubated with or without the

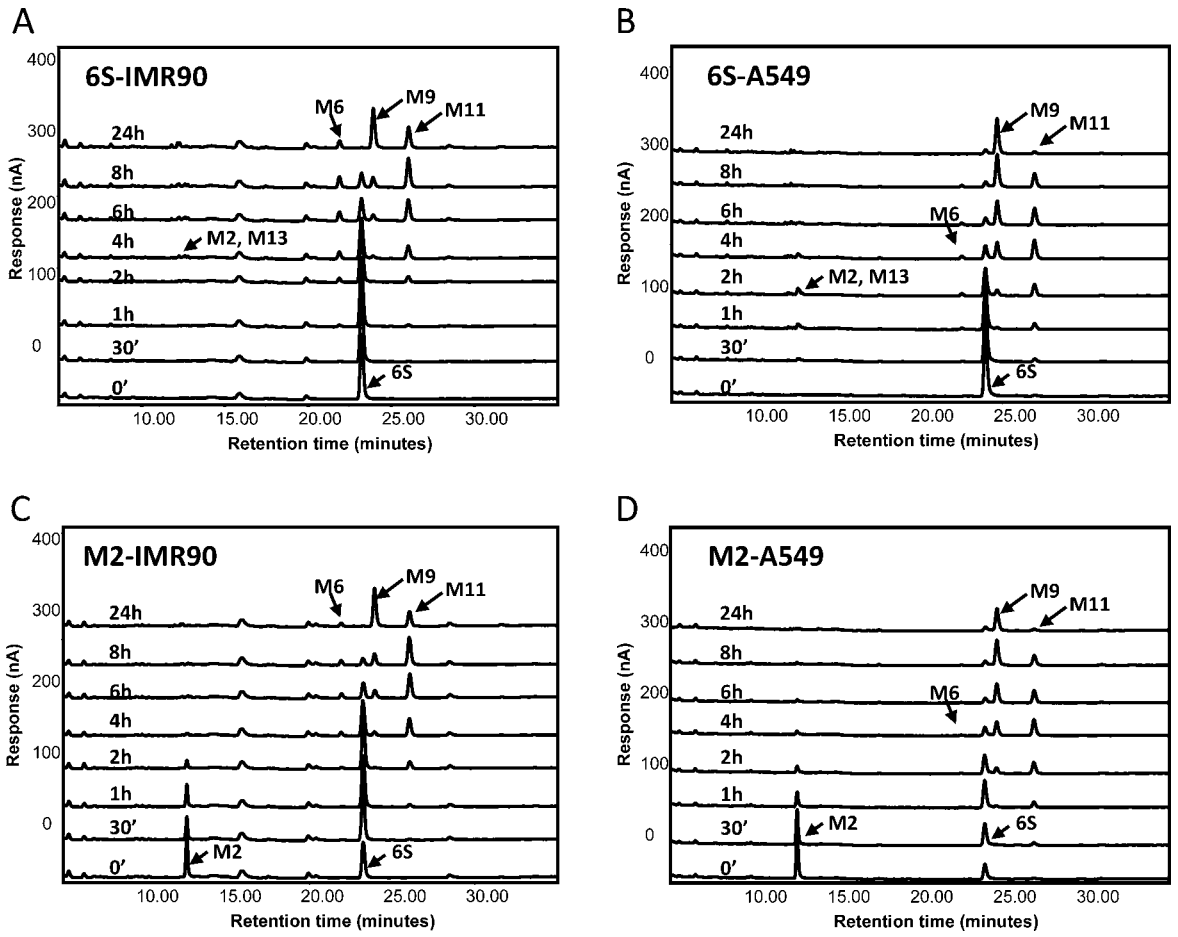

Figure 1. HPLC metabolic profile of IMR90 (A and C) or A549 (B and D) cells exposed to 10 μM of 6S (A and B) or M2 (C and D) after 0, 0.5, 1, 2, 4, 6, 8, and 24 h.

addition of 5 mM GSH in the culture media. After 24 h, toxicity was assessed using the MTT assay and using the method described above. The experiment was repeated independently to confirm the results.

Animal Experiments. Experiments with mice were carried out according to protocol approved by the Institutional Review Board for the Animal Care and Facilities Committee at North Carolina Research Campus and North Carolina Agricultural and Technical State University. Nu/J nude mice were obtained from Jackson Laboratories (Bar Harbor, ME). Animals were randomized into 4 groups. A549 cells (5×10^6 cells) were implanted in both flanks of 8-weeks old Nu/J mice. One week after implantation, animals were given 100 μL of the following treatments through oral gavage 5 times/week: DMSO 0.25 mL/kg (control; $n = 4$); 6S 10 mg/kg ($n = 4$); 6S 30 mg/kg ($n = 4$) or M2 30 mg/kg ($n = 5$). Compounds were diluted in a solution of 5% DMSO in corn oil. Animal body weight and tumor volume were recorded for the duration of the experiment. Tumor volume was calculated by measuring the length and width of the tumors using a digital caliper and using the formula (Length × Width^2)/2. One hour before sacrifice, mice were given one last treatment dose as well as one intraperitoneal injection of BrdU (7.5 mg/kg in 100 μL PBS). After 7 weeks, tumor tissues were harvested and weighed. A portion of the tumors was snap frozen in liquid nitrogen and another portion was placed in a histology cassette and immersed in formalin solution.

Immunohistochemistry. Formalin-fixed tissues were sent to Precision Histology Lab (Oklahoma City, OK) for embedding in paraffin blocks. Paraffin blocks were then processed into 3–4 μm sections that were then put on microscope slides. Sections were then deparaffinized by using a succession of 3 baths of xylene (5 min each), 2 baths of absolute ethanol (5 min each), 95% ethanol for 3 min, 70% ethanol for 3 min, and rinsed in PBS. Immunostaining with TUNEL (terminal deoxynucleotidyl transferase dUTP nick end labeling) and BrdU staining kits was performed following manufacturer's recommendation. For staining quantification, sequential high-power field pictures of tumors were taken (10 pictures per tumor) using an A1 Zeiss microscope (Oberkochen, Germany). Images were processed using the Image J software,[31,32] which was used to count positive, brown-colored cells in each field. Average number per tumor was calculated by averaging the number obtained for each field, and the average number of positive cells per group was obtained by averaging the values of each tumor belonging to the experimental group.

Statistics. Statistics were calculated using either a two-tailed Student t test, or ANOVA followed by Bonferroni's post-test. Results were considered significant when $p < 0.05$.

RESULTS

6S and M2 Are Similarly Metabolized by IMR90 and A549 Cells. We recently published that 6S is metabolized in cancer cells and that its bioactivity -i.e. selective toxicity- can be attributed to some of its metabolites, notably M2.[28,29] For this study, we first needed to determine if 6S or M2 are similarly metabolized in our model of small cell lung cancer A549 human cells as well as in IMR90 human normal lung cells. After exposing A549 or IMR90 cells to 10 μM of 6S or M2, we analyzed the metabolic profiles obtained from the culture supernatants at different time points using HPLC-ECD. We confirmed that 6S is metabolized by IMR90 or A549 cells (Figure 1, panel A or B, respectively), with an initial conversion into mostly the metabolites named M2, M13 and M11, while in later time points, most of 6S has been metabolized into M9.[29] The structures of all metabolites were confirmed using LC/MS

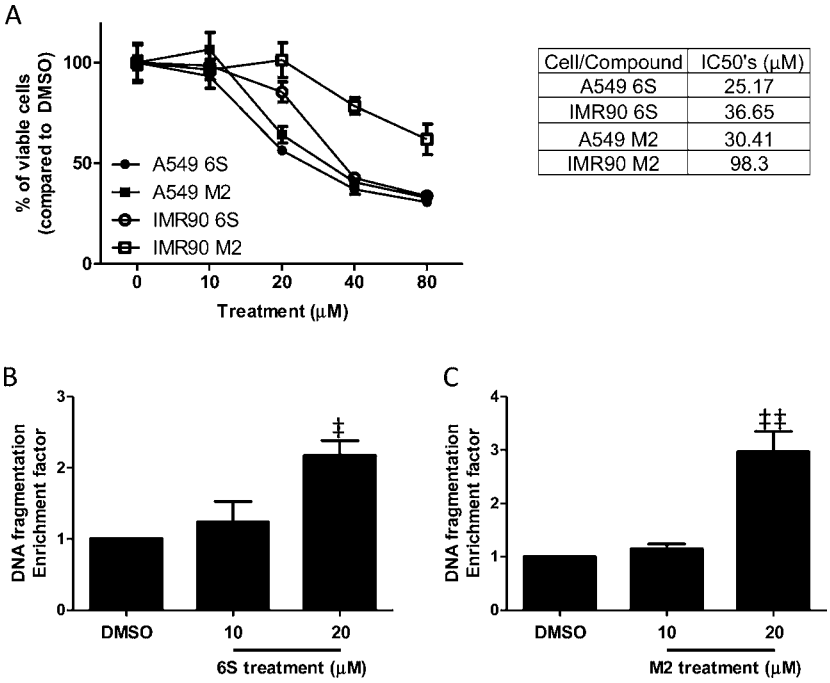

Cell/Compound	IC50's (μM)
A549 6S	25.17
IMR90 6S	36.65
A549 M2	30.41
IMR90 M2	98.3

Figure 2. (A) 6S and M2 toxicity in A549 cancer cells and IMR90 normal lung cells using MTT assay, with the corresponding IC_{50} values on the right side table. (B) Apoptosis measured by ELISA assay in A549 cells after 24 h treatment with 10 or 20 μM of 6S. (C) Apoptosis measured by ELISA assay in A549 cells after 24 h treatment with 10 or 20 μM of M2. *Bars*, SEM; ‡, $p < 0.05$; ‡‡, $p < 0.01$ using one-way ANOVA followed by Bonferroni's post-test.

analysis (data not shown). As initially reported in HCT-116 and H-1299 cells,[28] M2 metabolism in IMR90 (Figure 1C) or A549 cells (Figure 1D) was also characterized by an initial conversion of this cysteine-conjugated metabolite back into 6S, which is then metabolized in a similar pattern than described above for 6S. These results show that normal lung IMR90 and lung cancer A549 cells can quickly metabolize 6S and M2 in a similar pattern, which correlates with the observations in other cell models.[28]

M2 Toxicity Can Selectively Target Cancer Cells Compared to 6S. Our results show that M2 can quickly revert back to 6S native form when metabolized by A549 cells. We wanted to determine if that reversion led to a distinct bioactivity or if the parent compound and M2 shared the same bioactivity. We used an MTT assay to compare the bioactivity of 6S and M2 in A549 cells as well as in IMR90 human, noncancerous lung cells. The results are summarized in Figure 2A. When treated with increased concentration of 6S or M2, we detected an increase in toxicity in A549 cells with IC_{50}'s of 25.2 and 30.4 μM, respectively. In IMR90 cells, the IC_{50} was 36.6 and 98.3 μM for 6S and M2, respectively. In other words, in normal cells the IC_{50} value was 45.6% higher for 6S and 223.2% higher for M2 when compared to A549 cells. These results show that 6S and M2 exert similar toxicity toward A549 cells. However, M2 toxicity is greatly diminished against non-cancerous cells compared to that of 6S.

6S and M2 Activate the Apoptosis and p53 Pathways. Since our results show that 6S and M2 are bioactive against A549 cancer cells, we tried to determine the potential mechanisms of activation by looking at apoptosis, since it is one of the major pathways that can be specifically activated by the exposure to environmental stressors, and that ultimately leads to cell death. We used an ELISA assay that quantified the release of cytoplasmic histone-associated DNA fragments in A549 cells exposed to 6S or M2 for 24 h. Figure 2B shows that after 24 h these apoptotic markers were significantly higher (enrichment factor of 2.2) for cells treated with 20 μM of 6S. We also detected a significant increase in apoptotic markers (about 3-fold enrichment) after treatment with 20 μM M2 (Figure 2C).

To confirm these results, we performed Western blot analysis on extracts of A549 cells treated with 20 or 40 μM of 6S or M2 for 2 or 24 h. The results are summarized in Figure 3. For both concentrations of 6S or M2, we found that the pro-apoptotic markers cytochrome C, cleaved caspases 3 and 9 were markedly elevated after 2 h. Only cleaved caspases 3 and 9 levels remained elevated after 24 h, especially at the 40 μM concentration. Consistently, we could detect a small increase of caspases 3 and 9 after 2 h of exposure, and these levels were lower after 24 h. Markers of the mitochondrial apoptotic pathway Bax, Bak and Bcl-2 were all slightly elevated after 2 h of exposure to the test compound, but their levels were close to that of DMSO-treated cells after 24 h.

Since we could not detect any meaningful changes in the mitochondrial apoptotic pathway associated with the release of cytochrome C and subsequent caspase cascade activation,[33] we looked into the p53 pathway since it is responsive to oxidative stress and capable of triggering apoptosis.[34] Indeed, our results showed an increase in p53 levels after 2 and 24 h treatment with 6S or M2. It correlated with an increase of one of its downstream targets PUMA (p53 upregulated modulator of apoptosis), which was most evident after 24 h (Figure 3, top lines). These results show that both 6S and M2 can activate the p53 and the apoptosis pathways.

Excess GSH Can Rescue A549 Cells from 6S and M2 Toxicity and Suppress p53 Activation. Recent studies in our group showed that 6S can modulate GSH levels in HCT-116 colon cancer cells,[14] and we wanted to determine if that

dx.doi.org/10.1021/jf405573e | J. Agric. Food Chem. 2014, 62, 1352−1362

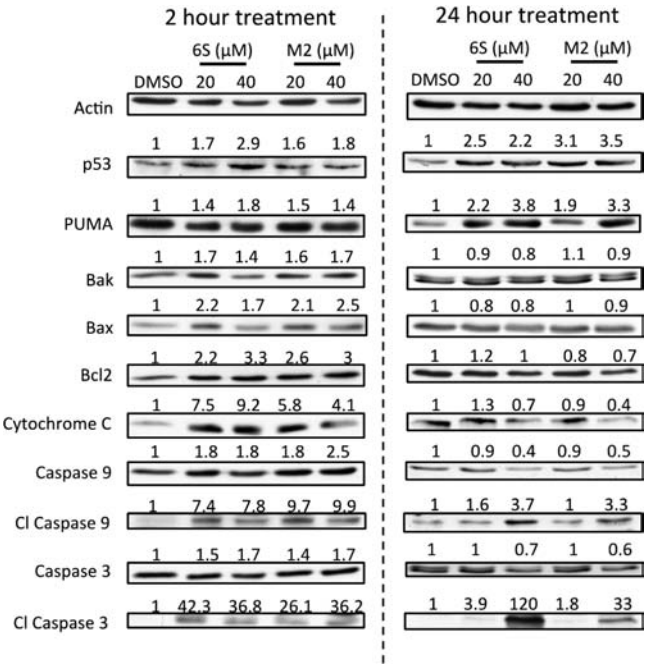

Figure 3. Western blot analysis of cell extracts after treatment with DMSO (control), 20 or 40 μM of 6S or M2 for 2 and 24 h. Markers are indicated on the left. Fold induction for each marker compared to DMSO is indicated over the corresponding line and was calculated as indicated in Material and Methods section.

effect was also present in the A549 small lung cancer cells model using 6S and M2. Figure 4A,B shows that GSH levels are significantly depleted as early as 2 h after exposure to 10 μM of 6S or M2. This depletion further continues after 4 h. After 8 h, GSH levels were still significantly lower in 6S treated cells, and significantly higher in M2 treated cells. After 24 h, GSH levels were significantly increased after exposure to both compounds compared to baseline. While changes of GSH levels are not as large as those of 6S in the case of M2, it is nonetheless significant for all tested time points.

When cells are exposed to increased levels of oxidative stress, GSSG will accumulate and the ratio of GSH to GSSG will decrease.[35] The results of a GSH/GSSG assay are presented in Figures 4C (for 6S) and 4D (for M2). This experiment shows that after 2 h the GSH/GSSG ratio is significantly lower for 6S-treated (10 μM) cells but not for M2-treated (10 μM) cells. After 4 h of exposure to 6S or M2, the GSH/GSSG ratio is significantly lower and after 24 h of exposure it is significantly higher. Collectively, these results show that both 6S and M2 can deplete GSH levels and induce oxidative stress in A549 cells in a similar fashion.

We demonstrated that 6S and M2 can modify GSH levels, but it is unclear whether this effect can be directly linked to their apoptotic activity. We wanted to verify the link between GSH modulation and apoptosis by conducting a GSH rescue assay in which excess GSH in the culture medium essentially prevented any fluctuation in GSH level after treatment with the test compounds. Excess GSH in the culture media completely rescued A549 cells from both 6S and M2 toxicity, with modified IC_{50}'s over 80 μM (Figure 5A). Western blot analysis showed that in the presence of excess GSH, there was no change in p53 expression in the 24 h extracts of cells treated with 40 μM 6S or M2 (Figure 5B). These results show that the changes in GSH levels induced by both 6S and M2 in A549 cells are necessary to induce toxicity and the p53 pathway.

The p53 Pathway Is Involved in 6S and M2-induced Toxicity and Apoptosis. We further investigated the involvement of p53 pathway in 6S or M2-induced toxicity and apoptosis by using the p53-specific inhibitor pifithrin μ

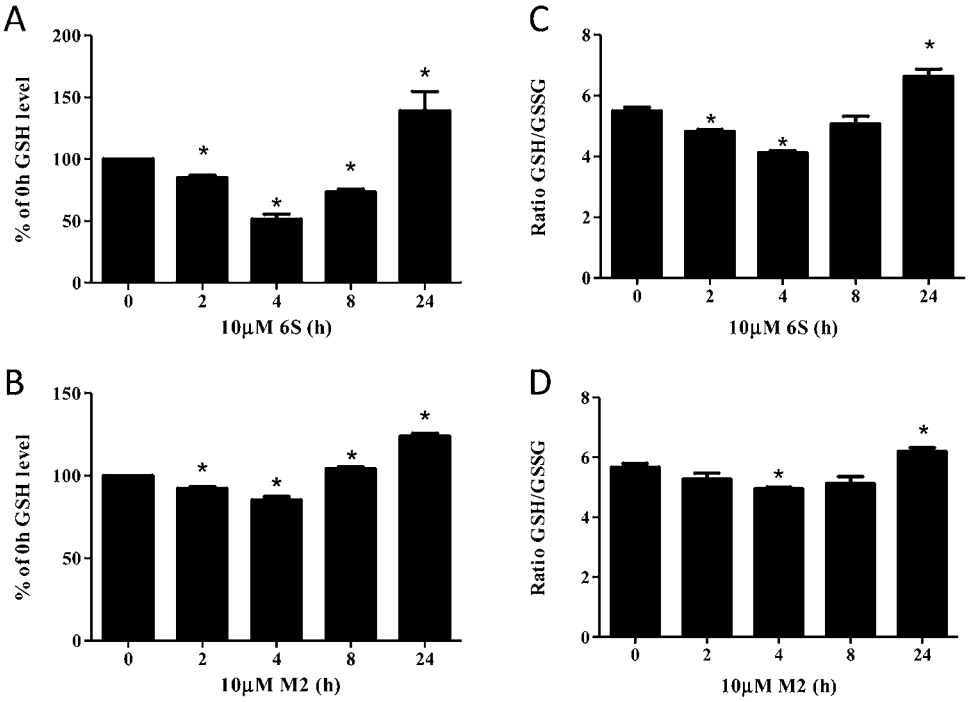

Figure 4. (A) Intracellular total GSH levels and (C) GSH/GSSG ratio in A549 cells treated with 10 μM of 6S for 0, 2, 4, 8, and 24 h. $[GSH]_{DMSO\ 0h}$ = 43.37 ± 5.85 nmol/mg. (B) Intracellular total GSH levels and (D) GSH/GSSG ratio in A549 treated with 10 μM of M2 for 0, 2, 4, 8, and 24 h. $[GSH]_{DMSO\ 0h}$ = 44.46 ± 5.16 nmol/mg. *Bars*, SEM *, $p < 0.05$ by Student t test.

dx.doi.org/10.1021/jf405573e | J. Agric. Food Chem. 2014, 62, 1352−1362

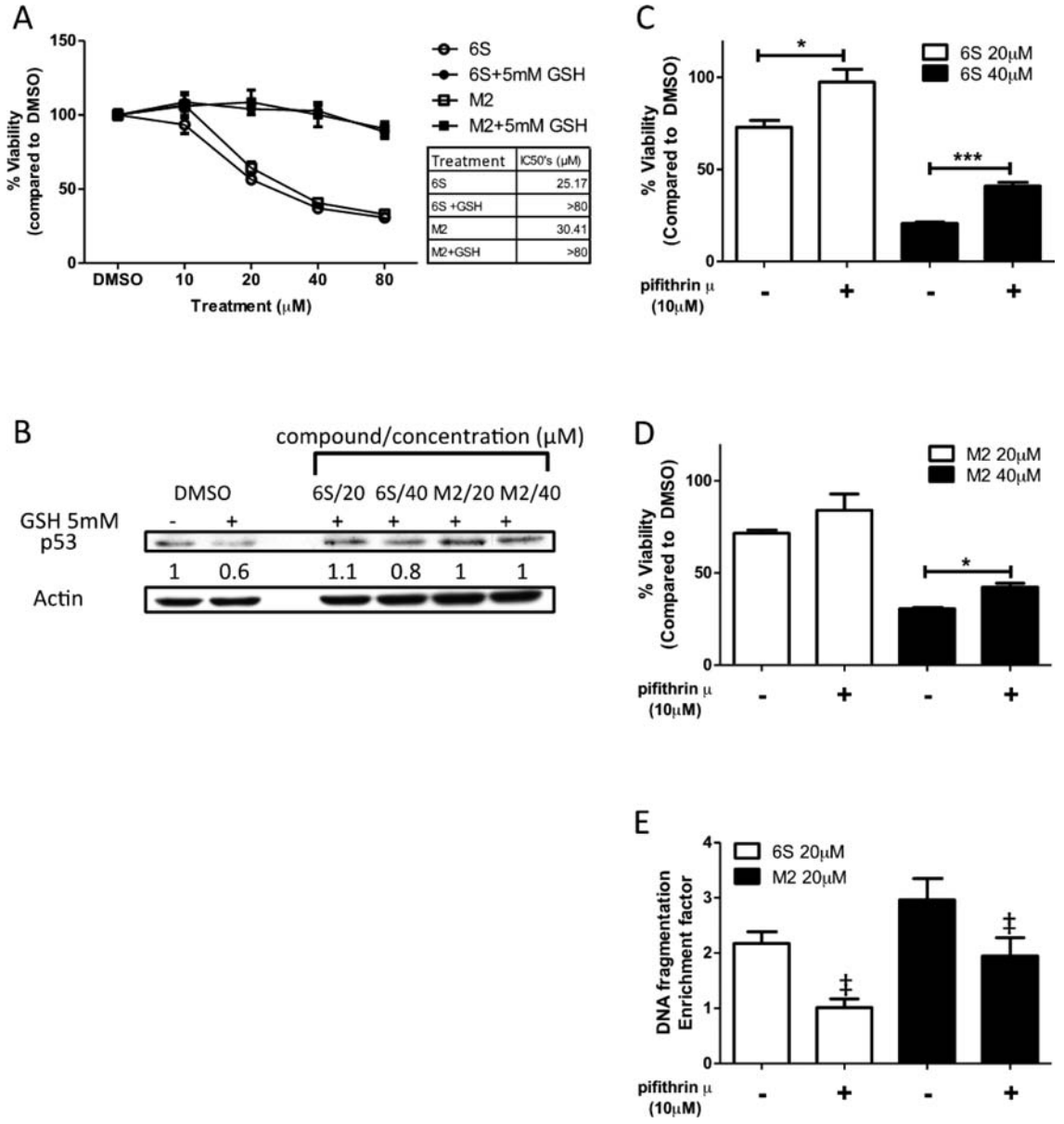

Figure 5. (A) GSH rescue assay in A549 cells. Cells were treated for 24 h with 0, 10, 20, 40, or 80 μM of 6S or M2 in the presence or absence of 5 mM GSH. The associated table indicates the IC_{50} values for each treatment. (B) Western blotting analysis of cell extracts treated with DMSO, 20 or 40 μM of 6S or M2 for 24 h with or without 5 mM of GSH. Fold induction for each marker compared to DMSO is indicated under the corresponding line and was calculated as indicated in Material and Methods section. (C) Effect of pft treatment on A549 cell death after treatment with 20 or 40 μM of 6S for 24 h. (D) Effect of pft treatment on A549 cell death after treatment with 20 or 40 μM of M2 for 24 h. (E) Effect of pft treatment on A549 cell apoptosis after treatment with 20 μM of 6S or M2 for 24 h. *Bars*, SEM *, $p < 0.05$; ***, $p < 0.001$ using a paired Student's *t* test; ‡, $p < 0.05$ using one-way ANOVA followed by Bonferroni's post-test.

(pft). This inhibitor can block the direct interaction and mitochondrial relocation of p53 with members of the Bcl-2 family.[37]

Treatment of A549 cells with pft in addition to 6S was very effective in reducing the toxic effect of both 6S (Figure 5C) and M2 (Figure 5D). When treated with 20 μM of 6S or M2 for 24 h, the percentage of viable cells was close to 100% for 6S and 84.2% for M2. Without pft to block p53 interaction with Bcl-2 family members, the percentage of viable cells was only around 72% in both cases. This effect was also observed at a higher dose of compound (40 μM). In the case of 6S, the percentage of viable cells was significantly higher (20.6% of viable cells without pft and 41% of viable cells with pft). For 40 μM M2, the effect was similar, with 30.6% of viable cells without pft and 42.4% of viable cells with pft. These results show that interfering with p53 signaling can at least partially rescue cells from 6S and M2-induced toxicity.

Since pft directly interferes with p53 signaling toward the mitochondria, we also tried to determine the effect of pft on apoptosis induction in A549 cells. For this experiment, a 20 μM dose was used since we established it to be the most effective dose for this assay (Figure 3B,C). The treatment with pft reduces the enrichment factor in small nucleosomes by a factor of 1 for both 6S and M2 (Figure 5E): in the case of 6S, the presence of pft significantly returned the enrichment factor to baseline (about 1), while in the case of M2, the enrichment factor is significantly down to 2 with pft from 3 without pft. Altogether these results show that 6S and M2 induce cell

dx.doi.org/10.1021/jf405573e | J. Agric. Food Chem. 2014, 62, 1352−1362

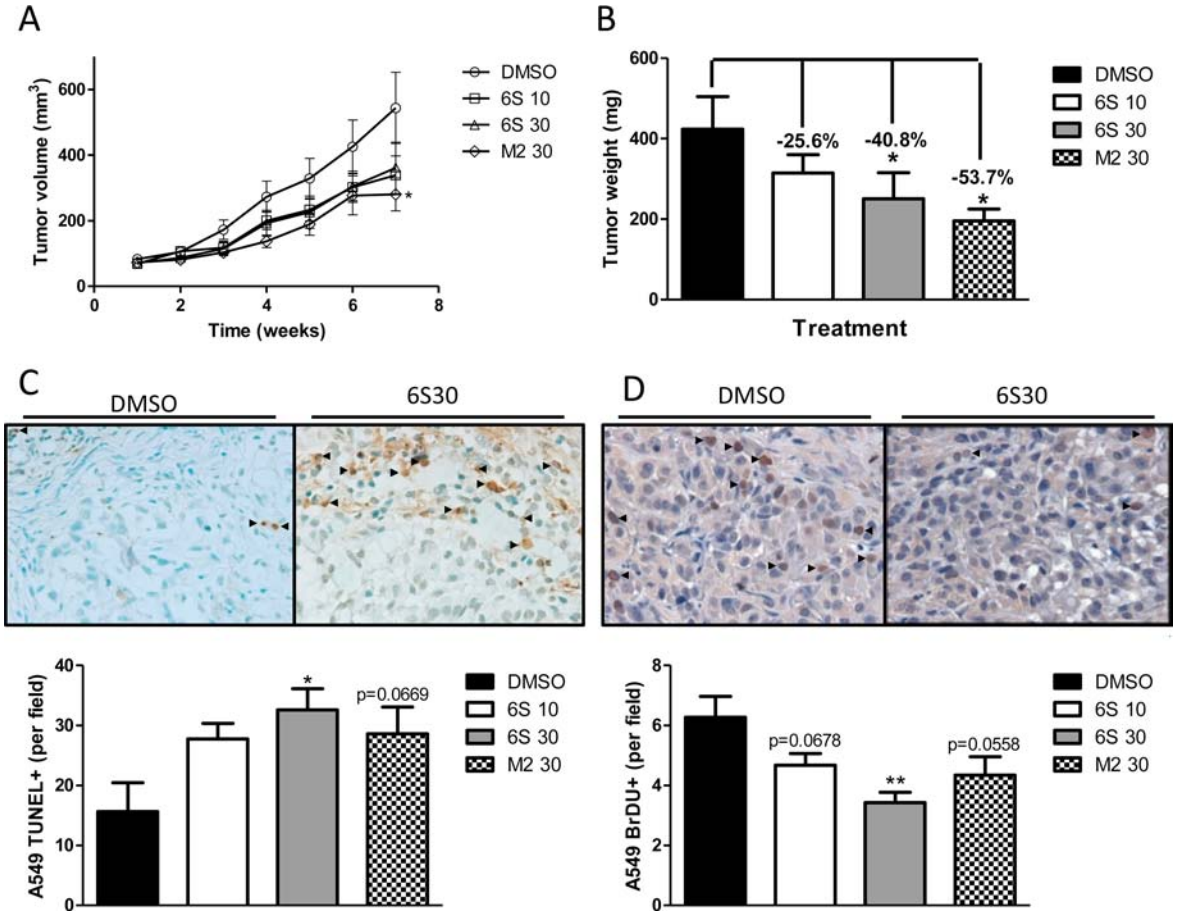

Figure 6. Xenograft experiment using A549 cells in nude mice. Animals were oral-gavaged 5×/week for 7 weeks with DMSO (control), 10 mg 6S/kg body wt (6S 10), 30 mg 6S/kg body wt (6S 30), or 30 mg M2/kg body wt (M2 30). (A) Changes in tumor volume (in mm^3) after 1-, 2-, 3-, 4-, 5-, 6-, and 7-week treatment with test compounds. (B) Wet tumor weight after 7-week treatment. (C) TUNEL immunostaining of 3−4 μm sections of tumor tissue. Representative picture from the DMSO and the 30 mg 6S/kg body wt (6S30) groups are showed on the top, and TUNEL-positive apoptotic cell quantification is presented at the bottom. (D) BrdU immunostaining of 3−4 μm sections of tumor tissue. Representative picture from the DMSO and the 30 mg 6S/kg body wt (6S 30) group are showed on the top, and BrdU-positive cell quantification is presented at the bottom. *Bars*, SEM *, $p < 0.05$; **, $p < 0.01$ using unpaired Student's *t* test.

apoptosis through the modulation of GSH levels and the activation of a p53 pathway.

6S and M2 Can Reduce Tumor Burden in Nu/J Mice. It is always uncertain how an observed anticancer bioactivity of a given natural compound translates *in vivo*, mainly due to the fast turnover and degradation of the compounds.[16,27] To ascertain the bioactivity of 6S and M2 *in vivo*, we studied their effect on the development of A549 tumors in a mouse xenograft model.

Exposure of animals to a daily oral gavage for up to 7 weeks did not induce any significant changes in body weight between groups (data not shown). Tumor volume in the control group grew exponentially, tumors from the groups receiving 6S 10 mg/kg, 6S 30 mg/kg or M2 30 mg/kg grew markedly slower, with tumors from the M2 group being significantly different by week 7 (Figure 6A). After 7 weeks, tumor weight was significantly lower in both 6S 30 mg/kg (minus 40.8% compared to DMSO-treated control) and M2 30 mg/kg (minus 53.7% compared to DMSO-treated control). Tumor weight was also markedly lower in the 6S 10 mg/kg group (minus 25.6%), albeit not significantly (Figure 6B). Taken altogether, both treatments were sufficient to lower the tumor burden of A549 engrafted cells at a 30 mg/kg body weight. Interestingly M2 appeared to be the most active compound *in vivo*, albeit not significantly when compared to the 6S 30 mg/kg treatment.

6S and M2 Induce Apoptosis and Reduce Cell Proliferation in A549 Xenografts. Next we sought to investigate the mechanisms by which 6S and M2 can reduce tumor burden in A549 xenografts tissues. TUNEL staining of tumor tissues (Figure 6C) showed a marked increase of apoptotic bodies in the animals treated with 6S 10 mg/kg body wt (27.8 TUNEL+ cells/field) compared to control (about 15.5 TUNEL+ cells/field). This trend became significant in the tumors from animals treated with 6S 30 mg/kg, with an average of 32.6 TUNEL+ cells/field. In the case of the animals treated with M2 30 mg/kg, we also observed the same trend (28.6 TUNEL+ cells/field) that was very close to being significant ($p = 0.0669$). BrdU staining of tumor tissues (Figure 6D) showed a significant reduction of cell proliferation in the animals treated with 6S 30 mg/kg body wt (3.4 BrdU+ cells/field) compared to control (about 6.3 BrdU+ cells/field). We also detected a marked reduction of cell proliferation in the 6S 10 mg/kg group (4.7 BrdU+ cells/field) that was very close to significance ($p = 0.0678$ by unpaired *t* test compared to control). While there was also a slight decrease in the M2 30 mg/kg group (4.3 BrdU+ cells/field), it was also very close to significance ($p = 0.0558$ by unpaired *t* test compared to control). These results

dx.doi.org/10.1021/jf405573e | J. Agric. Food Chem. 2014, 62, 1352−1362

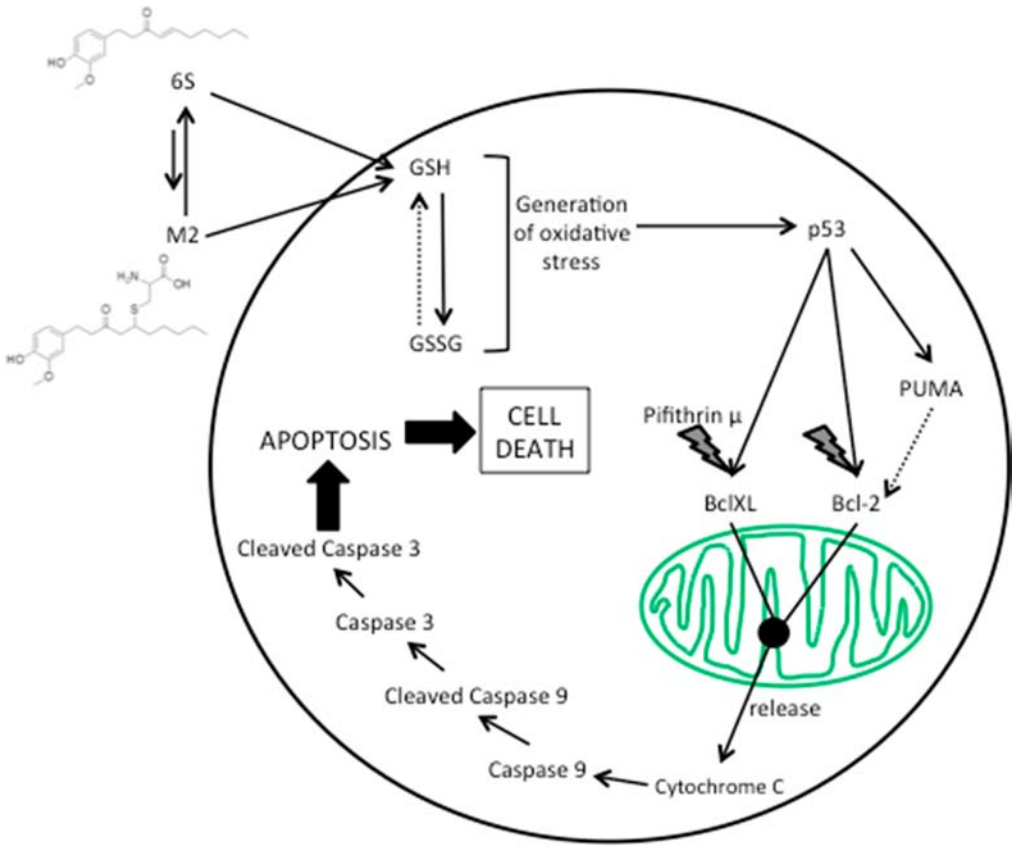

Figure 7. Schematic representation of the proposed mechanism of apoptosis activation in A549 cells by 6S and its cysteine-conjugated metabolite M2. Dotted arrows: possible interactions. Plain arrows: proposed interactions.

show that the reduction in tumor burden *in vivo* can be correlated to the induction of apoptosis for 6S and M2. In the case of 6S, it can also be associated to others molecular mechanisms such as cell proliferation.

■ DISCUSSION

Dietary intervention is a well-accepted mean of reducing cancer events. Cohort studies show that increased intake of fruits, vegetables and spices are indeed inversely correlated with the risk of various cancers.[3,4] While a full explanation for these observations is still heavily investigated, there is no doubt that dietary compounds can have long-term health benefits in terms of cancer prevention despite their fast metabolisms. Our lab showed that 6S, the major component of dried ginger, can be rapidly metabolized in colon and nonsmall cell lung cancer cells.[28] This proved to be also true in the human lung cancer cell model A549 (Figure 1), which is of the more aggressive type of lung cancer.

We initially assessed the bioactivity of 6S and M2 in A549 using an MTT assay. While both compounds displayed a significant toxicity toward cancer cells, it was remarkable that M2 was significantly less toxic toward noncancerous cells. 6S did not possess this property, suggesting that the cysteine-conjugation of 6S allowed discrimination between cancerous and normal human lung cells. This result validated its usefulness as a superior anticancer compound compared to 6S, and justified further investigation of M2. While the noncancerous lung cell line IMR-90 is from a different embryonic origin than A549, there is no perfect normal cell line that is currently available *in vitro*. In consequence, further *in vivo* toxicity study of 6S and M2 is warranted.

We then tried to gain insight into the mechanism of action of both compounds. Our laboratory previously demonstrated in others models that 6S and several other metabolites were able to trigger apoptosis,[16,29] a mechanism of programmed cell death that is often impaired in cancer cells. We determined that 6S and its metabolite M2 could also activate the apoptosis pathway in A549 cells. This was demonstrated by the detection of cytoplasmic histone-associated-DNA-fragments in A549 cells upon treatment with 6S or M2 for 24 h. Notably, we demonstrated that while the IC_{50} of M2 is higher than 6S, its capacity to specifically induce apoptosis was superior (as shown in Figure 2). Additionally, we showed the activation of the apoptosis pathway by demonstrating the modulation of final apoptotic markers such as cytochrome C, capases 3 and 9 and their cleaved isoforms. Caspase 9 was also slightly elevated after 2 h of exposure, but it could be the result of newly synthesized protein to reinforce the already activated apoptotic pathway. These markers are part of the mitochondrial apoptotic pathways, but interestingly the traditionally associated markers of the Bcl-2 family (Bak, Bax) were not affected. Bcl-2 showed a small increase after 2 h, but the increase did not appear to be concentration-dependent and was very modest compared to the others markers, which suggest a very limited influence. On the other hand, we were able to detect a very early increase in p53 and PUMA, two major actors in the transmission of cellular changes such as (but not limited to) oxidative stress. Indeed, as was previously described in other cell lines, treatment of A549 cells with 6S and M2 led to a clear disturbance in GSH

dx.doi.org/10.1021/jf405573e | J. Agric. Food Chem. 2014, 62, 1352−1362

homeostasis, which would explain the generation of oxidative stress. This disturbance has been observed before and can be explained by the property of dietary electrophiles to activate the transcription factor Nrf2:[38] after the initial depletion of GSH to detoxify electrophiles compounds, the cellular GSH levels can be restored and even enhanced by the subsequent Nrf2-mediated signal and GSSG recycling. This mechanism exists in order to maintain cell equilibrium, and rescuing it from oxidative damage or others carcinogens. However, GSH variation, if too great, can also be interpreted by cellular components as irreparable damage, which requires the cell to engage into the apoptotic pathway.

The next question was to determine the mechanism of transition from oxidative stress to apoptosis. p53 is known to be able to trigger apoptosis through interaction with members of the Bcl-2 family such as Bax, Bcl-2 or Bcl-XL to trigger apoptosis without modifying their level of transcription.[39,40] Using the chemical inhibitor pft, we show here that the interaction between Bcl-2 or Bcl-XL and p53 might be disrupted, as evidenced by a reduced toxicity of both 6S and M2 (Figure 5C,D), as well as the induction of apoptosis (Figure 5E). It has been reported that pft is also a known inhibitor of hsp70.[36] Whether hsp70 is also a target of 6S or M2 is a topic for future study. Nevertheless, our results suggest a direct relationship between the propagation of a mitochondrial apoptotic signal and an induction of p53 expression, which could explain the lack of variation in the Bcl-2 family markers expression. The proposed pathway of cancer cell apoptosis induction is summarized in Figure 7. It is interesting to note, however, that while apoptosis could be almost completely abolished by pft in lower doses of compounds, the cell viability could never be completely rescued. We also observed a marked increase in PUMA expression, especially after 24 h of exposure to both 6S and M2 (Figure 3). PUMA is another molecule that can mediate the p53 apoptotic message through its interaction with members of the Bcl-2 family.[41] This suggests that apoptosis is in part accountable for the death of A549 cells, and that multiple mechanisms inducing apoptosis and/or toxicity in cancer cell might be acting together.

While we determined that both 6S and its metabolite M2 can trigger similar biological responses and mechanisms in A549 cells, it was unclear if this would still be true *in vivo*. This was a concern especially when taking into account the short half-life of these compounds due to their quick metabolisms, as our previous studies reported.[14] To this end, we carried out a xenograft experiment where A549 tumor growth was significantly delayed by both 6S and M2. Additionally, M2-treated animals showed a further reduction in tumor burden compared to the animals treated with 6S at an equivalent dose of 30 mg/kg body wt (Figure 6B). As demonstrated by TUNEL staining of tumor tissues, 6S could significantly induce apoptosis *in vivo*, while M2 was very close to also having a significant effect. However, there was still a clear trend and it is probable that the number of animals used was not sufficient and that an increased number would allow for the detection of a significant induction of apoptosis even by M2 (Figure 6C). We also demonstrated that both 6S and M2 can decrease cell proliferation (Figure 6D). Similarly to what we observed by TUNEL staining, only 6S at the higher dose was shown to have a significant effect, while M2 was close to having a significant effect. As described above, this is expected since we showed that blocking of the apoptotic pathway through chemical methods *in vitro* could only partially rescue cells from the toxicity of 6S and M2. Similarly, the percentage of apoptotic cells detected by ELISA could not be entirely restored to DMSO (control)-treated levels, especially at the higher concentration (40 μM) of the compounds, when treated with pft. The fact that the exposure to our compounds results in an increase of the multiacting molecule p53 can also explain the activation of multiples pathways. The p53 pathway has been demonstrated to have multiple effects, and is a major regulator of the cell cycle.[42] In this light, it is not surprising that cell proliferation would be affected by the exposure to compounds that can increase p53 expression. It is particularly interesting in terms of cancer prevention since p53 expression is lost in most late-stage cancers but can still be active in early stage cancers or even aggressive cancers, such as in A549 cells. 6S and its metabolites could exert their activity in an optimal manner in these conditions, while M2 could also exert this activity and being harmless against normal cells.

Altogether, this study shows that the traditional model of bioactivity by natural compounds can be challenged and that the products of degradation of the parent compound can be responsible for the observed bioactivity. This would also explain how dietary compounds can exert a long-term effect despite being quickly metabolized. Finally, there is evidence that drug conjugation using cysteine can be an effective tool to deliver drugs to its target, as in the case of antibody-drug conjugates.[43,44] Our lab previously suggested that M2 could act as a carrier for 6S to prolong or enhance its activity,[28] and the current study clearly reinforces this hypothesis. The cysteine group can be hydrolyzed out of M2 to form 6S in both A549 human lung cancer cells and IMR90 human normal lung cells. It appears that natural modifications of dietary compounds through metabolism, such as cysteine addition, can be a fertile source for the discovery of novel bioactive molecules and the identification of novel targets and strategies for cancer prevention and treatment.

AUTHOR INFORMATION

Corresponding Author

*Address: Center for Excellence in Post-Harvest Technologies, North Carolina Agricultural and Technical State University, North Carolina Research Campus, 500 Laureate Way, Kannapolis, NC 28081, USA. Tel: +1 704-250-5710. Fax: +1 704-250-5709. E-mail: ssang@ncat.edu.

Funding

Funding for this investigation was partially provided by grants CA138277 (S. Sang) from the National Cancer Institute and CA138277S1 (S. Sang) from National Cancer Institute and Office of Dietary Supplement of National Institutes of Health.

Notes

The authors declare no competing financial interest.

REFERENCES

(1) Greenwald, P.; Nixon, D. W.; Malone, W. F.; Kelloff, G. J.; Stern, H. R.; Witkin, K. M. Concepts in cancer chemoprevention research. *Cancer* **1990**, *65*, 1483−1490.

(2) American Cancer Society *Cancer Facts and Figures 2013*; ACS Annual Reports; American Cancer Society: Atlanta, GA, 2013.

(3) Verhoeven, D. T.; Goldbohm, R. A.; van Poppel, G.; Verhagen, H.; van den Brandt, P. A. Epidemiological studies on brassica vegetables and cancer risk. *Cancer Epidemiol., Biomarkers Prev.* **1996**, *5*, 733−748.

(4) Kolonel, L. N.; Hankin, J. H.; Whittemore, A. S.; Wu, A. H.; Gallagher, R. P.; Wilkens, L. R.; John, E. M.; Howe, G. R.; Dreon, D.

M.; West, D. W.; Paffenbarger, R. S., Jr. Vegetables, fruits, legumes and prostate cancer: a multiethnic case-control study. *Cancer Epidemiol., Biomarkers Prev.* **2000**, *9*, 795−804.
(5) Mannisto, S.; Smith-Warner, S. A.; Spiegelman, D.; Albanes, D.; Anderson, K.; van den Brandt, P. A.; Cerhan, J. R.; Colditz, G.; Feskanich, D.; Freudenheim, J. L.; Giovannucci, E.; Goldbohm, R. A.; Graham, S.; Miller, A. B.; Rohan, T. E.; Virtamo, J.; Willett, W. C.; Hunter, D. J. Dietary carotenoids and risk of lung cancer in a pooled analysis of seven cohort studies. *Cancer Epidemiol., Biomarkers Prev.* **2004**, *13*, 40−48.
(6) Ruano-Ravina, A.; Figueiras, A.; Freire-Garabal, M.; Barros-Dios, J. M. Antioxidant vitamins and risk of lung cancer. *Curr. Pharm. Des.* **2006**, *12*, 599−613.
(7) Shukla, Y.; Singh, M. Cancer preventive properties of ginger: a brief review. *Food Chem. Toxicol.* **2007**, *45*, 683−690.
(8) Surh, Y. J.; Lee, E.; Lee, J. M. Chemoprotective properties of some pungent ingredients present in red pepper and ginger. *Mutat. Res.* **1998**, *402*, 259−267.
(9) Baliga, M. S.; Haniadka, R.; Pereira, M. M.; D'Souza, J. J.; Pallaty, P. L.; Bhat, H. P.; Popuri, S. Update on the chemopreventive effects of ginger and its phytochemicals. *Critical Rev. Food Sci. Nutr.* **2011**, *51*, 499−523.
(10) Citronberg, J.; Bostick, R.; Ahearn, T.; Turgeon, D. K.; Ruffin, M. T.; Djuric, Z.; Sen, A.; Brenner, D. E.; Zick, S. M. Effects of ginger supplementation on cell-cycle biomarkers in the normal-appearing colonic mucosa of patients at increased risk for colorectal cancer: results from a pilot, randomized, and controlled trial. *Cancer Prev. Res.* **2013**, *6*, 271−281.
(11) Jolad, S. D.; Lantz, R. C.; Solyom, A. M.; Chen, G. J.; Bates, R. B.; Timmermann, B. N. Fresh organically grown ginger (Zingiber officinale): composition and effects on LPS-induced PGE2 production. *Phytochemistry* **2004**, *65*, 1937−1954.
(12) Sang, S.; Hong, J.; Wu, H.; Liu, J.; Yang, C. S.; Pan, M. H.; Badmaev, V.; Ho, C. T. Increased growth inhibitory effects on human cancer cells and anti-inflammatory potency of shogaols from Zingiber officinale relative to gingerols. *J. Agric. Food Chem.* **2009**, *57*, 10645−10650.
(13) Chen, C. Y.; Liu, T. Z.; Liu, Y. W.; Tseng, W. C.; Liu, R. H.; Lu, F. J.; Lin, Y. S.; Kuo, S. H.; Chen, C. H. 6-shogaol (alkanone from ginger) induces apoptotic cell death of human hepatoma p53 mutant Mahlavu subline via an oxidative stress-mediated caspase-dependent mechanism. *J. Agric. Food Chem.* **2007**, *55*, 948−954.
(14) Chen, H.; Soroka, D. N.; Hu, Y.; Chen, X.; Sang, S. Characterization of thiol-conjugated metabolites of ginger components shogaols in mouse and human urine and modulation of the glutathione levels in cancer cells by [6]-shogaol. *Mol. Nutr. Food Res.* **2013**, *57*, 447−458.
(15) Pan, M. H.; Hsieh, M. C.; Kuo, J. M.; Lai, C. S.; Wu, H.; Sang, S.; Ho, C. T. 6-Shogaol induces apoptosis in human colorectal carcinoma cells via ROS production, caspase activation, and GADD 153 expression. *Mol. Nutr. Food Res.* **2008**, *52*, 527−537.
(16) Chen, H.; Lv, L.; Soroka, D.; Warin, R. F.; Parks, T. A.; Hu, Y.; Zhu, Y.; Chen, X.; Sang, S. Metabolism of [6]-shogaol in mice and in cancer cells. *Drug Metab. Dispos.* **2012**, *40*, 742−753.
(17) Hung, J. Y.; Hsu, Y. L.; Li, C. T.; Ko, Y. C.; Ni, W. C.; Huang, M. S.; Kuo, P. L. 6-Shogaol, an active constituent of dietary ginger, induces autophagy by inhibiting the AKT/mTOR pathway in human non-small cell lung cancer A549 cells. *J. Agric. Food Chem.* **2009**, *57*, 9809−9816.
(18) Ishiguro, K.; Ando, T.; Maeda, O.; Ohmiya, N.; Niwa, Y.; Kadomatsu, K.; Goto, H. Ginger ingredients reduce viability of gastric cancer cells via distinct mechanisms. *Biochem. Biophys. Res. Commun.* **2007**, *362*, 218−223.
(19) Gan, F. F.; Nagle, A. A.; Ang, X.; Ho, O. H.; Tan, S. H.; Yang, H.; Chui, W. K.; Chew, E. H. Shogaols at proapoptotic concentrations induce G(2)/M arrest and aberrant mitotic cell death associated with tubulin aggregation. *Apoptosis* **2011**, *16*, 856−867.
(20) Weng, C. J.; Wu, C. F.; Huang, H. W.; Ho, C. T.; Yen, G. C. Anti-invasion effects of 6-shogaol and 6-gingerol, two active components in ginger, on human hepatocarcinoma cells. *Mol. Nutr. Food Res.* **2010**, *54*, 1618−1627.
(21) Ling, H.; Yang, H.; Tan, S. H.; Chui, W. K.; Chew, E. H. 6-Shogaol, an active constituent of ginger, inhibits breast cancer cell invasion by reducing matrix metalloproteinase-9 expression via blockade of nuclear factor-kappaB activation. *Br. J. Pharmacol.* **2010**, *161*, 1763−1777.
(22) Kim, E. C.; Min, J. K.; Kim, T. Y.; Lee, S. J.; Yang, H. O.; Han, S.; Kim, Y. M.; Kwon, Y. G. [6]-Gingerol, a pungent ingredient of ginger, inhibits angiogenesis in vitro and in vivo. *Biochem. Biophys. Res. Commun.* **2005**, *335*, 300−308.
(23) Hessien, M.; El-Gendy, S.; Donia, T.; Sikkena, M. A. Growth inhibition of human non-small lung cancer cells h460 by green tea and ginger polyphenols. *Anti-Cancer Agents Med. Chem.* **2012**, *12*, 383−390.
(24) Chen, C. Y.; Yang, Y. H.; Kuo, S. Y. Effect of [6]-shogaol on cytosolic Ca^{2+} levels and proliferation in human oral cancer cells (OC2). *J. Nat. Prod.* **2010**, *73*, 1370−1374.
(25) Tan, B. S.; Kang, O.; Mai, C. W.; Tiong, K. H.; Khoo, A. S.; Pichika, M. R.; Bradshaw, T. D.; Leong, C. O. 6-Shogaol inhibits breast and colon cancer cell proliferation through activation of peroxisomal proliferator activated receptor gamma (PPARgamma). *Cancer Lett.* **2013**, *336*, 127−139.
(26) Hu, R.; Zhou, P.; Peng, Y. B.; Xu, X.; Ma, J.; Liu, Q.; Zhang, L.; Wen, X. D.; Qi, L. W.; Gao, N.; Li, P. 6-Shogaol induces apoptosis in human hepatocellular carcinoma cells and exhibits anti-tumor activity in vivo through endoplasmic reticulum stress. *PloS one* **2012**, *7*, e39664.
(27) Zick, S. M.; Djuric, Z.; Ruffin, M. T.; Litzinger, A. J.; Normolle, D. P.; Alrawi, S.; Feng, M. R.; Brenner, D. E. Pharmacokinetics of 6-gingerol, 8-gingerol, 10-gingerol, and 6-shogaol and conjugate metabolites in healthy human subjects. *Cancer Epidemiol., Biomarkers Prev.* **2008**, *17*, 1930−1936.
(28) Chen, H.; Soroka, D. N.; Zhu, Y.; Hu, Y.; Chen, X.; Sang, S. Cysteine-conjugated metabolite of ginger component [6]-shogaol serves as a carrier of [6]-shogaol in cancer cells and in mice. *Chem. Res. Toxicol.* **2013**, *26*, 976−985.
(29) Zhu, Y.; Warin, R. F.; Soroka, D. N.; Chen, H.; Sang, S. Metabolites of ginger component [6]-shogaol remain bioactive in cancer cells and have low toxicity in normal cells: chemical synthesis and biological evaluation. *PLoS One* **2013**, *8*, e54677.
(30) Mosmann, T. Rapid colorimetric assay for cellular growth and survival: application to proliferation and cytotoxicity assays. *J. Immunol. Methods* **1983**, *65*, 55−63.
(31) Schneider, C. A.; Rasband, W. S.; Eliceiri, K. W. NIH Image to ImageJ: 25 years of image analysis. *Nat. Methods* **2012**, *9*, 671−675.
(32) Collins, T. J. ImageJ for microscopy. *BioTechniques* **2007**, *43*, 25−30.
(33) Ow, Y. P.; Green, D. R.; Hao, Z.; Mak, T. W. Cytochrome c: functions beyond respiration. *Nat. Rev. Mol. Cell Biol.* **2008**, *9*, 532−542.
(34) Walia, V.; Kakar, S.; Elble, R. Micromanagement of the mitochondrial apoptotic pathway by p53. *Front. Biosci.* **2011**, *16*, 749−758.
(35) Guntherberg, H.; Rost, J. The true oxidized glutathione content of red blood cells obtained by new enzymic and paper chromatographic methods. *Anal. Biochem.* **1966**, *15*, 205−210.
(36) Leu, J. I.; Pimkina, J.; Frank, A.; Murphy, M. E.; George, D. L. A small molecule inhibitor of inducible heat shock protein 70. *Mol. Cell* **2009**, *36*, 15−27.
(37) Strom, E.; Sathe, S.; Komarov, P. G.; Chernova, O. B.; Pavlovska, I.; Shyshynova, I.; Bosykh, D. A.; Burdelya, L. G.; Macklis, R. M.; Skaliter, R.; Komarova, E. A.; Gudkov, A. V. Small-molecule inhibitor of p53 binding to mitochondria protects mice from gamma radiation. *Nat. Chem. Biol.* **2006**, *2*, 474−479.
(38) Nakamura, Y.; Miyoshi, N. Electrophiles in foods: the current status of isothiocyanates and their chemical biology. *Biosci., Biotechnol., Biochem.* **2010**, *74*, 242−255.

(39) Chipuk, J. E.; Maurer, U.; Green, D. R.; Schuler, M. Pharmacologic activation of p53 elicits Bax-dependent apoptosis in the absence of transcription. *Cancer Cell* **2003**, *4*, 371−381.
(40) Vaseva, A. V.; Marchenko, N. D.; Moll, U. M. The transcription-independent mitochondrial p53 program is a major contributor to nutlin-induced apoptosis in tumor cells. *Cell Cycle* **2009**, *8*, 1711−1719.
(41) Nakano, K.; Vousden, K. H. PUMA, a novel proapoptotic gene, is induced by p53. *Mol. Cell* **2001**, *7*, 683−694.
(42) Blagosklonny, M. V. P53: an ubiquitous target of anticancer drugs. *International journal of cancer. J. Int. Cancer* **2002**, *98*, 161−166.
(43) Saito, G.; Swanson, J. A.; Lee, K. D. Drug delivery strategy utilizing conjugation via reversible disulfide linkages: role and site of cellular reducing activities. *Advanced Drug Delivery Rev.* **2003**, *55*, 199−215.
(44) Lyon, R. P.; Meyer, D. L.; Setter, J. R.; Senter, P. D. Conjugation of anticancer drugs through endogenous monoclonal antibody cysteine residues. *Methods Enzymol.* **2012**, *502*, 123−138.

pid–protein monolayers by phospholipase A_2 using similar model systems and simple intestinal conditions.[20]

In this study, we aimed at elucidating the interactions between bile salts and milk phospholipids occurring at the oil–water interface of milk fat globules and liposomes during the early stages of digestion in the small intestine using a simplified model system (not including free fatty acids from lipolysis and pancreatic lipases). We extracted phospholipids from whey buttermilk, a rich source of MFGM. As others have shown that the composition of the interface has an impact on digestion[2,21] and mostly adsorption of bile salts onto the interface at the early stages of digestion,[22] and that MFGM contains proteins, we also aimed to characterize the impact of the presence of proteins at the interface. Due to the lack of commercially available MFGM proteins and the difficulty in purifying them, we used two widely studied milk proteins known to interact with the MFGM during milk processing and commonly used as emulsifiers but with different conformation at the interface.[18] To investigate the effect of bile composition on milk phospholipid layer systems, a mixture of bile salts and a crude bile extract were used.

MATERIALS AND METHODS

Samples and Reagents. The phospholipid extract was obtained from whey buttermilk processed as described by Costa et al.[23] Total lipids were extracted using the modified Mojonnier ether extraction method,[24] and the phospholipids were recovered by solid-phase extraction according to the method of Bitman et al.[25] The phospholipid extract was analyzed by HPLC according to the method of Rombaut et al.[26] and contained 57.1 ± 12.4% of phosphatidylethanolamine (PE), 22.0 ± 3.7% of phosphatidylcholine (PC), 11.0 ± 1.7% of phosphatidylserine (PS), 6.2 ± 1.2% of sphingomyelin (SM), and 3.7 ± 2.0% of phosphatidylinositol (PI). Bovine milk β-casein (*Bio*Ultra, ≥98% from PAGE analysis) and bovine milk β-lactoglobulin (≥90% from PAGE analysis) were purchased from Sigma-Aldrich Corp. (St. Louis, MO, USA) and stored at −20 °C. A mixture of negatively charged bile salts (Fluka, 50% sodium cholate (430.55 Da) and 50% sodium deoxycholate (414.55 Da)) and a crude bovine bile extract from ox gall (including glycocholic acid, glycodeoxycholic acid, taurocholic acid, taurodeoxycholic acid, and cholic acid (60% w/w) from TLC analysis) were purchased from Sigma-Aldrich Corp. and stored at 4 °C. A detailed composition of the bile extract is given elsewhere.[27] As a crude bile extract, it is likely to also contain phospholipids, cholesterol, bilirubin, and electrolytes.[3] All solvents (Fisher Scientific, Pittsburgh, PA, USA) were of HPLC grade. The fluorescent headgroup-labeled phospholipid analogue Texas Red 1,2-dihexadecanoyl-*sn*-glycero-3-phosphoethanolamine, triethylammonium salt (Tx-Red-DHPE, 0.1 mL/mL in chloroform, Invitrogen, Molecular Probes (Carlsbad, CA, USA)) allows the detection of phase coexistence within phospholipid monolayers under an epifluorescence microscope. Milli-Q water (18 MΩ cm, pH 5.5–6.5) was used to prepare buffers and was purified by means of a Millipore filtration device (Millipore Corp., Bedford, MA, USA). For AFM imaging, AC 240 TS cantilevers (Asylum Research, Santa Barbara, CA, USA) were used for alternating current (AC) mode imaging.

Langmuir Isotherms. A Minitrough Langmuir film balance (KSV Instruments, Helsinki, Finland) with a platinum Wilhelmy plate and mounted on an Olympus BX60 microscope, equipped with an Olympus QColorA mercury lamp, was used to acquire Langmuir isotherms and fluorescent images of phospholipid and phospholipid–protein monolayers before and after addition of bile salts or extract. All glassware was thoroughly cleaned with detergent, rinsed with Milli-Q water and then with ethanol, and dried in a 100 °C oven. Tx-Red-DHPE was added to the phospholipid extract at a concentration of 2% by mass, which is low enough to avoid introducing significant perturbations to the membrane system.[28] The phospholipid extract was dissolved in chloroform to a concentration of 1 mg mL^{-1}, β-casein and β-lactoglobulin were prepared fresh daily and diluted to 1 mg mL^{-1} in PBS buffer (pH 7.45), and stock solutions (120 or 60 mM) of bile salts and bile extract were prepared with simulated intestinal fluid (SIF, 150 mM NaCl, 10 mM $CaCl_2$, pH 7.0). SIF was used as the subphase simulating the ionic strength and the pH found in the small intestine. At pH 7, both proteins carry a negative net charge.[13,17] The aqueous surface was cleaned before and between experiments until a surface pressure of <0.1 mN m^{-1} was reached after full compression of the symmetric barriers.

Forty microliters of phospholipid extract was carefully spread onto the surface with a gastight microsyringe, and the solvent was allowed to evaporate over 5 min. The phospholipid monolayer was then compressed to 15 or 25 mN m^{-1} or to 6 mN m^{-1} if β-casein or β-lactoglobulin was added to the subphase with a gastight microsyringe. If not specified, the phospholipid/protein ratio was 1:1 (w/w). The surface pressure stabilized after 30 min of addition of the protein, and the phospholipid–protein monolayer was then compressed to 15 or 25 mN m^{-1}. A surface pressure of 15 mN m^{-1} was chosen as it is lower than the collapse pressure of the proteins but high enough so that phase coexistence occurred. A surface pressure of 25 mN m^{-1} was found at the oil–water interface of emulsions.[16] Bile salts or bile extract were then added gently in a single injection to the subphase with a gastight syringe from the stock solution, to a final subphase concentration of 0.22 or 4.4 mM. A concentration of 4.4 mM is physiologically relevant.[27] The surface pressure was recorded at constant area, and fluorescence images were acquired every 5 min. Different ratios of phospholipid/protein (1:2 and 2:1, w/w) were also used. All isotherm experiments were conducted in duplicate at 20.0 ± 0.5 and 37.0 ± 0.5 °C, and all imaging experiments were performed at 20.0 ± 0.5 °C. The experiments were carried out at least in duplicates to confirm the reproducibility of the experiment.

As a control, bile salts and bile extract were added to the subphase on a clean air–water interface at 20 and 37 °C and the surface pressure was recorded at constant area.

Langmuir–Blodgett Films and Atomic Force Microscopy. Imaging on the trough was not possible at 37 °C due to condensation on the objective lens; thus, the preparation of the Langmuir–Blodgett films to be imaged with an atomic force microscope (AFM) was performed at 20 °C. All LB films were prepared by equilibrating the phospholipid and phospholipid–protein monolayers at a surface pressure of 25 mN m^{-1} for 5 min before addition of bile salts or bile extract. The phospholipid and phospholipid–protein monolayer films spread at 20 °C on Milli-Q water at pH 7 before and 5 min after addition of bile salts or bile extract were transferred to a clean glass microscope slide, as described previously,[12,13] forming LB films. The addition of salt in the subphase can lead to the formation of salt crystals on the glass slide, making the imaging with an AFM difficult.

To obtain higher resolution images of the monolayers, an MFP-3D AFM (Asylum Research) was used to image the LB films in air and with tapping mode as described elsewhere.[13]

RESULTS AND DISCUSSION

Effect of Temperature and Ionic Strength. Figure 1 presents the compression isotherms of milk phospholipids spread at 20 or 37 °C on Milli-Q water or SIF. All three isotherms showed similar features. The lift-off of the isotherm represents the transition from a gas phase to a liquid-ordered/liquid-disordered coexisting phases, as observed in our previous work.[12] This phase coexistence exists during the monotonous increase in surface pressure, which plateaus at the collapse of the monolayer, denoting the transition to a solid-like phase. Milli-Q water is slightly acidic, and SIF has a pH of 7.0 and contains sodium, calcium, and chloride ions. The slight difference in pH and ionic strength did not affect the compression isotherms of phospholipids. Phospholipid monolayers spread at 20 °C on Milli-Q water or SIF collapsed at about 45 mN m^{-1}. However, the increase in temperature led to an earlier liftup (end of the gas phase) of the compression

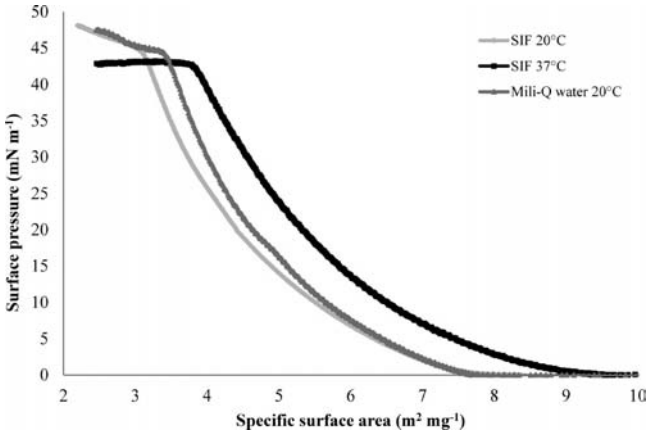

Figure 1. Lateral compression surface pressure−area isotherms of milk phospholipids at 20 °C spread on Milli-Q water (dark gray) or SIF (light gray) and at 37 °C spread on SIF (black).

isotherm. The effects of temperature, pH, and ionic strength on phospholipid−β-casein (1:1, w/w) and phospholipid−β-lactoglobulin (1:1, w/w) monolayers were similar.

Interfacial Properties of Bile Salts and Bile Extract. The addition of bile salts (Figure 2) and bile extract (results not shown) to a clean air−water interface gave similar final surface pressures at 20 and 37 °C. Upon injection of 0.22 mM bile salts (Figure 2), the surface pressure increased rapidly to about 27 mN m^{-1} and equilibrated after 5−10 min at 22−23 mN m^{-1}, whereas upon addition of a physiologically relevant concentration of bile salts, 4.4 mM, the surface pressure equilibrated within <1 min at 30 mN m^{-1}. For comparison with data reported in the literature and with the available equipment, it was not possible to stir the subphase. However, Brownian motion is quite effective in distributing salts in solution, as observed with the rapid increase in surface pressure after injection of bile salts or bile extract.

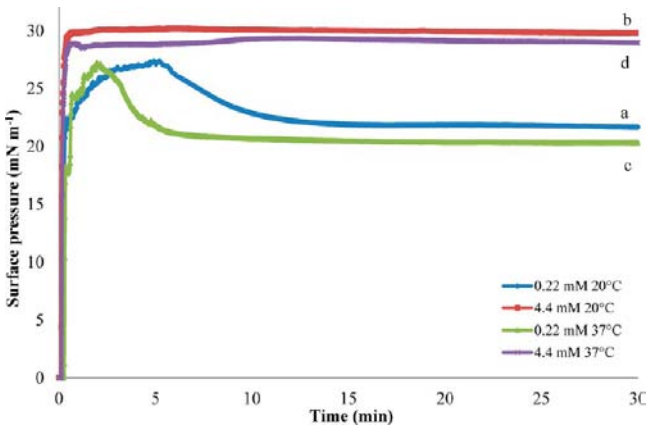

Figure 2. Surface pressure change of the clean air−water interface upon single addition of 0.22 mM (blue (a) and green (c)) or 4.4 mM (red (b) and purple (d)) bile salts at 20 °C (blue (a) and red (b)) or 37 °C (green (c) and purple (d)) to the SIF subphase.

The contrast between the monotonous increase in surface pressure to a plateau at a bile salt concentration of 4.4 mM and the increase in surface pressure followed by a decrease at a concentration of 0.22 mM may suggest a rearrangement or solubilization of bile salts at lower concentrations and a rapid saturation of the interface at higher concentrations. Bile salts adsorb rapidly due to a strong affinity for oil−water and air−water interfaces.[4] Their behavior at both surfaces is similar,[29] and they decrease the interfacial tension or increase the surface pressure with increasing concentration up to a limiting value.[22] Similar values of maximal surface pressure reached by physiological concentrations of bile salts have been reported in the literature; Maldonado-Valderrama et al.[30] reported a surface pressure value of <30 mN m^{-1}, even at concentration above the critical micellar concentration, and Chu et al.[16] found a surface pressure of 25 mN m^{-1} reached by 9.7 mM of a mixture of two conjugated bile salts. The final surface pressure is not the result of a synergism between two bile salts but the ratio of the surface pressure reached by each pure bile salt.[17]

Upon injection of 0.22 or 4.4 mM bile extract to a clean air−water interface, the final surface pressure equilibrated at 40 mN m^{-1} within 5 min (results not shown). As a crude product, bile extract is likely to contain negatively charged (at physiological pH) conjugated bile salts, phospholipids (mostly PC), and cholesterol.[3] Thus, the higher surface pressure found for bile extract is likely due to the presence of the other molecules, such as cholesterol.

Interactions of Bile Salts and Bile Extract with Phospholipid and Phospholipid−Protein Monolayers. The effect of a single injection of 0.22 mM bile salts on the surface pressure of a monolayer of phospholipids and β-lactoglobulin at different ratios, spread at 20 or 37 °C and after 5 min of equilibration at either 15 or 25 mN m^{-1}, is reported in Figure 3. The addition of bile salts to a phospholipid−β-lactoglobulin (1:1, w/w) monolayer stabilized at 15 mN m^{-1} at 37 °C led to an increase in surface pressure up to 20 mN m^{-1} within 5 min (Figure 3). Similar results were obtained with phospholipid and phospholipid−β-casein monolayers (Table 1). The surface pressure increase found by Chu et al.[16] after addition of a 0.144 mM bile salt mixture at 37 °C was higher for dipalmitoylphosphatidylcholine (DPPC) monolayers but lower for digalactosyldiacylglycerol (DGDG) monolayers. Welzel and Cammenga[5] added 0.47 mM sodium cholate to a dimyristoylphosphatidylcholine monolayer stabilized at 20 °C at 15

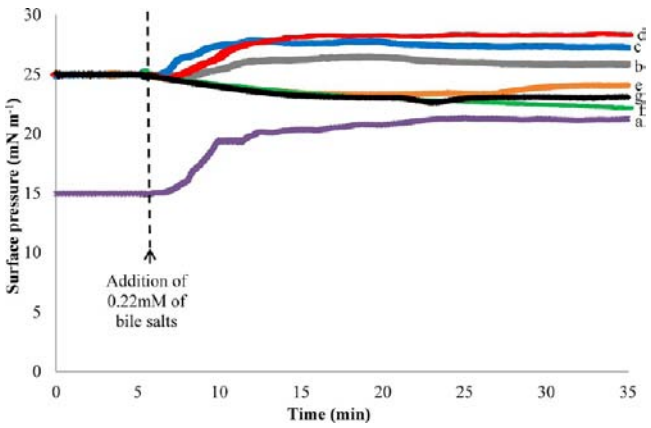

Figure 3. Surface pressure change upon single addition of 0.22 mM bile salts to phospholipid−β-lactoglobulin monolayers on SIF subphase at 20 °C (orange (e), green (f), and black (g)) or 37 °C (purple (a), gray (b), blue (c), and red (d)). The phospholipid/β-lactoglobulin ratios (w/w) are 1:1 (purple (a), gray (b), and orange (e)), 2:1 (blue (c) and green (f)), and 1:2 (red (d) and black (g)). The initial surface pressures of the monolayers before addition of bile salts are 15 mN m^{-1} (purple (a)) and 25 mN m^{-1} (all others).

dx.doi.org/10.1021/jf404448d | J. Agric. Food Chem. 2014, 62, 1363−1372

Table 1. Surface Pressure Change (mN m^{-1}) upon Single Addition of 0.22 mM Bile Salts to Phospholipid, Phospholipid−β-Casein, and Phospholipid−β-Lactoglobulin Monolayers on SIF Subphase at 20 or 37 °C[a]

	phospholipid	phospholipid−β-casein	phospholipid−β-lactoglobulin
37 °C native surface pressure = 15 mN m^{-1}	22.5	21.4 (1:1)	21.2 (1:1)
20 °C native surface pressure = 15 mN m^{-1}	19.4	20.2 (1:1)	20.9 (1:1)
37 °C native surface pressure = 25 mN m^{-1}	27.1	26.2 (1:1)	25.8 (1:1)
		28.2 (1:2)	28.3 (1:2)
		28.5 (2:1)	27.6 (2:1)
20 °C native surface pressure = 25 mN m^{-1}	24.5	22.8 (1:1)	24.1 (1:1)
		24.2 (1:2)	23.1 (1:2)
		23.9 (2:1)	22.2 (2:1)

[a]The phospholipid/protein ratios (w/w) are indicated in parentheses. The initial surface pressures of the monolayers before addition of bile salts are 15 or 25 mN m^{-1}.

mN m^{-1}, which led to an increase in surface pressure to 35 mN m^{-1}, and addition at 25 mN m^{-1} led to an increase to 39 mN m^{-1}. Thus, bile salts adsorbed less onto milk phospholipid monolayers than onto pure phospholipid monolayers but more than onto DGDG monolayers.

The addition of bile salts to a phospholipid−β-lactoglobulin (1:1, 1:2, or 2:1, w/w) monolayer previously stabilized at 25 mN m^{-1} at 20 °C led to a decrease in surface pressure to 21−23 mN m^{-1} (Figure 3), which is similar to the surface pressure reached by a bile salt system only (Figure 2) but different from the increase found by Welzel and Cammenga,[5] whereas at 37 °C it led to an increase in surface pressure to 26−28 mN m^{-1} (Figure 3), which is higher than the surface pressure reached by a bile salt system only (Figure 2). Similar results were observed for phospholipid and phospholipid−β-casein monolayers (Table 1). When 4.4 mM bile salts were added to a phospholipid monolayer stabilized at 25 mN m^{-1} at 37 °C, the surface pressure increased and stabilized at 27.5 mN m^{-1} (results not shown).

When 0.22 mM bile extract was added to phospholipid and phospholipid−protein monolayers stabilized at 15 or 25 mN m^{-1} at 20 °C (results not shown), the surface pressure reached the same values as those after addition of 0.22 mM bile salts (Figure 3). When bile extract was added at a concentration of 0.22 or 4.4 mM to a phospholipid, phospholipid−β-casein or phospholipid−β-lactoglobulin monolayer stabilized at 15 or 25 mN m^{-1} at 37 °C, the surface pressure increased to 40 mN m^{-1} (results not shown), which is the surface pressure reached when bile extract was added to a clean interface (Figure 2). This suggests that displacement by bile extract may be more efficient than that by bile salts. As the lipid packing, and thus the phase coexistence, of milk phospholipids is affected by temperature,[12] the interaction of bile salts with the monolayer molecules is likely to be affected by the temperature of the system.

Bile salts are known to lie parallel, thus flat, onto phospholipid membranes.[31] The hydrophilic part faces the water side, and the hydrophobic part interacts with the phospholipid polar head groups and condenses the hydrocarbon chains of phospholipids.[4] The adsorption of bile salts improves the stability of phospholipid monolayers,[32] as observed in Figure 3 where the surface pressure of the phospholipid−bile salt monolayers stabilize rapidly at constant area. As negatively charged molecules at physiological pH, bile salts bring a negative charge to the surface, whereas calcium ions decrease the electrostatic repulsions between phospholipid headgroups. Steric and electrostatic effects govern the adsorption of phospholipids and bile salts at the oil−water interface.[33] Bile salt adsorption is affected by micellar state;[31] thus, the increase in surface pressure at 37 °C and decrease in surface pressure at 20 °C after injection of bile salts may be due to different micellar state, but also different lipid packing, at different temperatures. Indeed, the critical micellar concentration of bile salts increases with increasing temperature,[34] and phospholipid monolayers are less fluid at 20 °C than at 37 °C and thus likely more resistant to penetration by bile salts. The increase in surface pressure at 37 °C is likely due to a synergism between bile salts and phospholipids and possible remaining proteins. The decrease in surface pressure at 20 °C indicates a solubilization of phospholipids (and proteins) with the possible formation of mixed bile salt−phospholipid vesicles and micelles in the subphase. Unlike here, the displacement of protein monolayers by bile salts was reported to be similar at 37 °C and at room temperature and the adsorption of bile salts into protein monolayers was slower, on the order of 20 min.[17]

Microstructural Changes upon Addition of Bile Salts or Bile Extract. Morphological insights into the formation of domains upon compression of monolayers and phase coexistence changes upon addition of surfactants can be obtained using epifluorescence microscopy and appropriate fluorescent probe. The microstructure of the phospholipid, phospholipid−β-casein, or phospholipid−β-lactoglobulin monolayers stabilized at 20 °C at 15 or 25 mN m^{-1} and 30 min after the addition of 0.22 mM bile salts or bile extract was investigated with an epifluorescence microscope (Figure 4). In our previous study,[12] the fluorescent phospholipid analogue, Tx-Red-DHPE, was shown to be located preferentially in the liquid-disordered phase, leaving the tightly packed liquid-ordered phase, likely rich in SM, dark. The native phospholipid, phospholipid−β-casein, or phospholipid−β-lactoglobulin monolayers presented "snowflake"-shaped liquid-ordered domains; the largest ones were observed in phospholipid−β-casein monolayers, and the domains increased in size and number from 15 to 25 mN m^{-1} (Figure 4). As proteins were not labeled, it was not possible to locate them.

The addition of bile salts and bile extract to all monolayers led to microstructural changes within a few minutes and the

dx.doi.org/10.1021/jf404448d | J. Agric. Food Chem. 2014, 62, 1363−1372

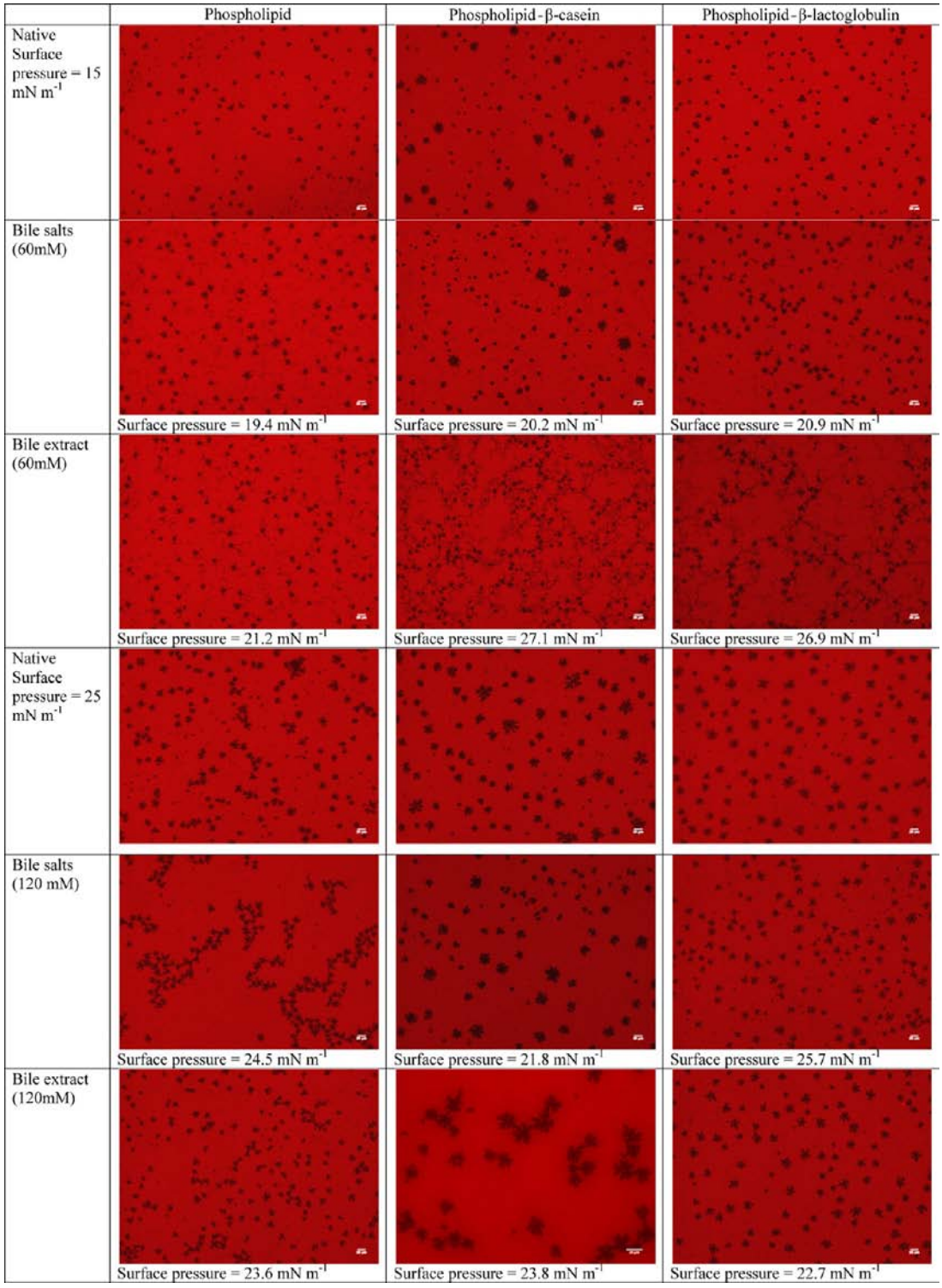

Figure 4. Epifluorescence microscopic images of phospholipid, phospholipid–β-casein (1:1, w/w), and phospholipid–β-lactoglobulin (1:1, w/w) monolayers spread on SIF at 20 °C before (native) and after the addition (30 min) of 0.22 mM bile salts or bile extract from a 60 or 120 mM stock solution. The bile salts or bile extract was added after the monolayers had been stabilized for 5 min at either 15 or 25 mN m^{-1}. Scale bar = 20 μm.

formation of mixed bile salt–phospholipid films. It was not possible to conclude whether or not the addition of bile salts caused the displacement of proteins. The main changes were seen when bile salts and bile extract were added from a 60 mM stock solution to a monolayer previously stabilized at 15 mN m^{-1} (Figure 4). Some gray thin linear network, another phase domain where a small amount of fluorescent phospholipid analogue is dissolved, was observed within the liquid-disordered phase 30 min after the addition of bile salts. The network was more evident after the addition of bile extract, and the network was stretching out from the branches of the "snowflake"-shaped domains. The network formed very quickly, within 5 min in phospholipid monolayers and within 7–10 min for phospholipid–protein monolayers (results not shown). Similar

dx.doi.org/10.1021/jf404448d | J. Agric. Food Chem. 2014, 62, 1363–1372

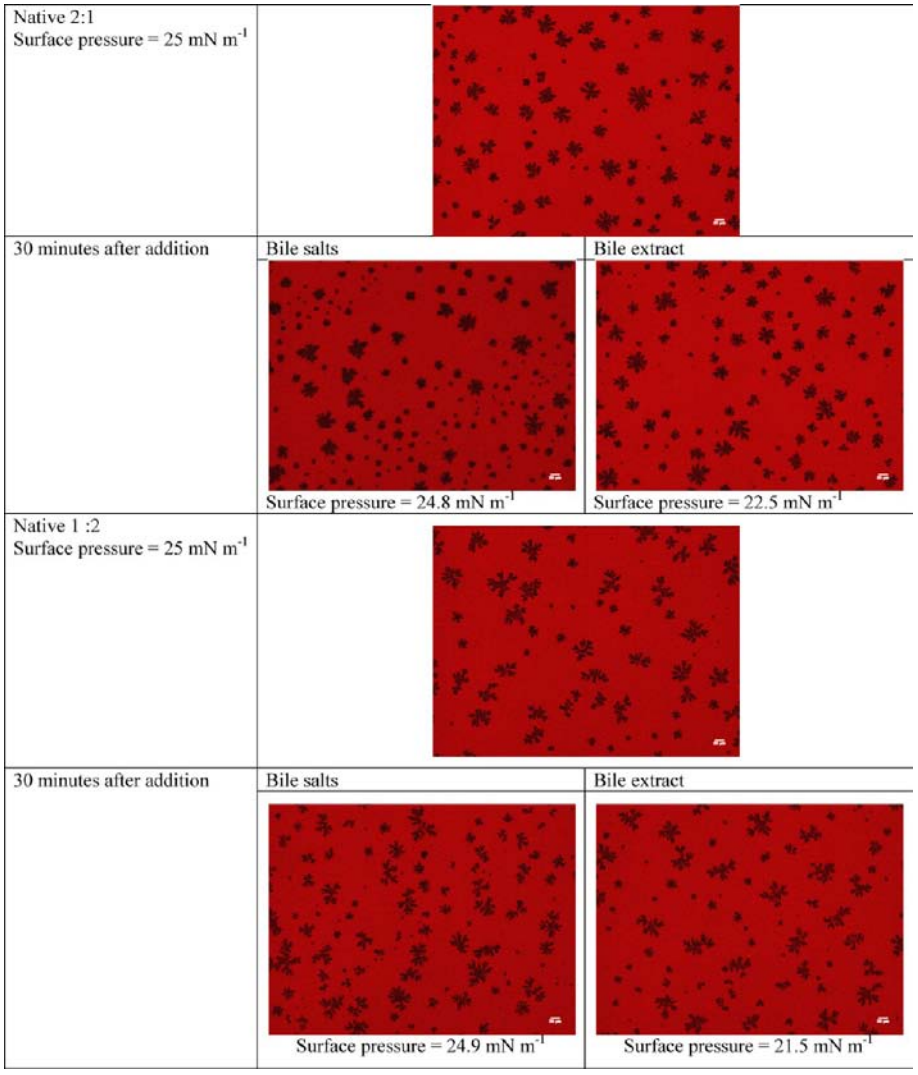

Figure 5. Epifluorescence microscopic images of phospholipid–β-lactoglobulin (2:1 or 1:2, w/w) monolayers spread on SIF at 20 °C before (native) and after the addition (30 min) of 0.22 mM bile salts or bile extract from a 120 mM stock solution. The bile salts or bile extract was added after the monolayers had been stabilized for 5 min at 25 mN m^{-1}. Scale bar = 20 μm.

branching was observed by Nagadome et al.[35] studying a system of cholesterol and bile acids at the air–water interface. The branching segments were identified as bile acids and were more pronounced in the presence of cholesterol. Thus, here, bile salts were likely responsible for the network (Figure 4) within the liquid-disordered phase, which could be accentuated in the presence of cholesterol from the bile extract. The cholesterol molecules were likely to interact with the liquid-ordered domains because of the preference of cholesterol for saturated SM.[12] The "thinning" of the branches of the "snowflake"-shaped domains was probably due to cholesterol molecules reducing the line tension at the liquid-ordered–liquid-disordered interface.[36]

When bile salts and bile extract were added from a 120 mM solution to a phospholipid, phospholipid–β-casein, or phospholipid–β-lactoglobulin monolayer stabilized at 15 mN m^{-1}, the network was less distinct but the liquid-ordered domains were clustered linearly, and additional small round black domains were seen within the liquid-disordered phase 30 min after the addition of bile salts (results not shown). The rate of addition of bile salts to phospholipid membranes affects the bile salt/phospholipid molar ratio related to the micellar state.[37] A slow rate of addition will allow time for structural reorganization of the bile salt/phospholipid membranes. When bile salts are added rapidly, an inhomogeneous or micellar morphological rearrangement takes place. This could explain the difference in partitioning of bile salts in phospholipid and phospholipid–protein monolayers when added from a 60 or 120 mM stock solution. The clustering of liquid-ordered domains is likely due to a reduction of the electrostatic forces between domains in the presence of bile components.[38]

When bile salts were added from a 120 mM stock solution after stabilization of the monolayers at 25 mN m^{-1}, lateral microstructural changes were observed only in phospholipid monolayers with linear clustering of a few liquid-ordered domains, whereas when bile extract was added, linear clustering of liquid-ordered domains was also observed in phospholipid–β-casein monolayers (Figure 4). It is possible that bile salts penetrate the monolayers more easily when the latter are compressed at 15 mN m^{-1} than at 25 mN m^{-1}, as phase separation (presence of liquid-ordered domains) was more pronounced at 25 mN m^{-1}, as seen in Figure 4.

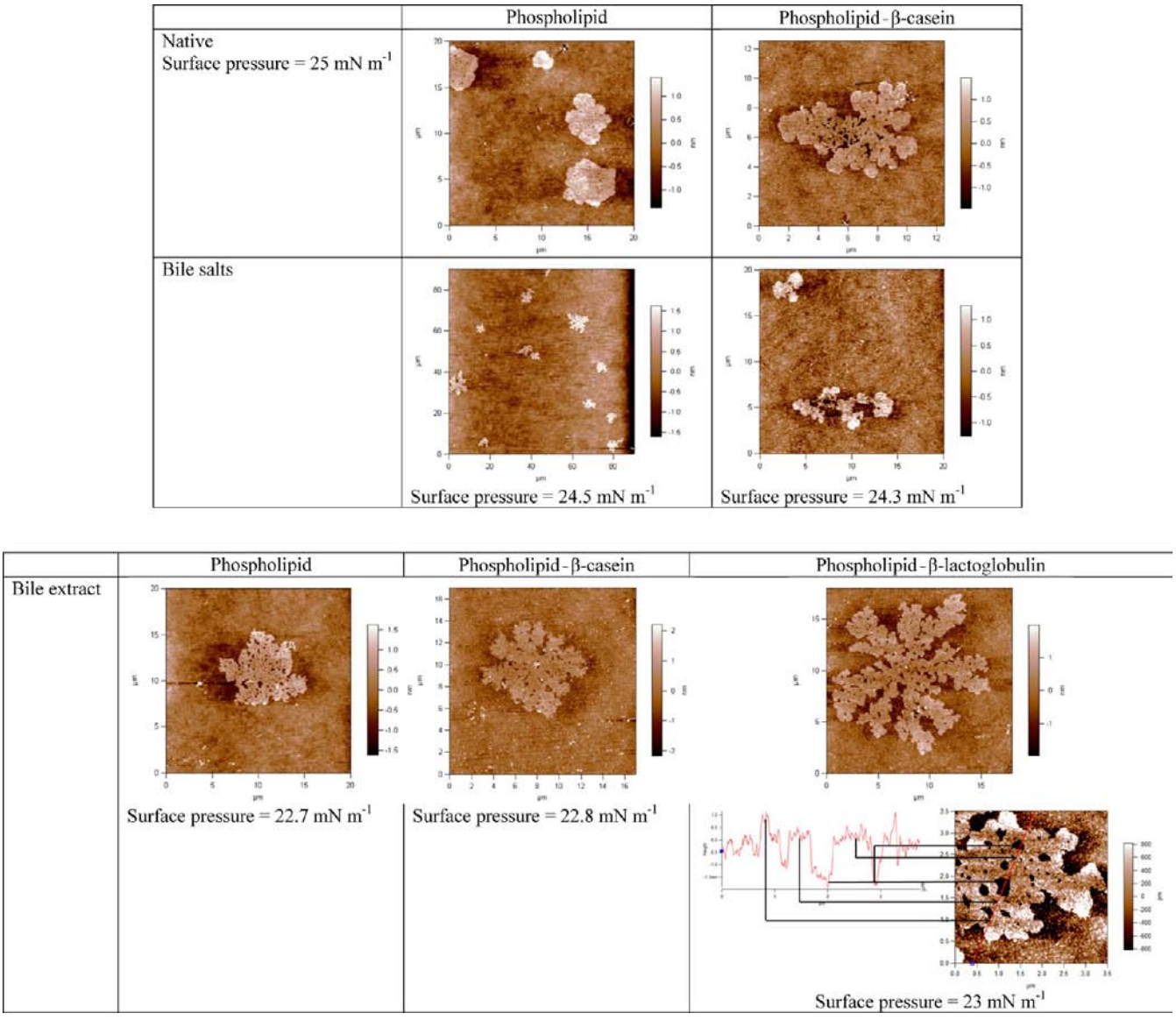

Figure 6. Atomic force microscopic height images of phospholipid, phospholipid−*β*-casein (1:1, w/w), and phospholipid−*β*-lactoglobulin (1:1, w/w) monolayers spread on SIF at 20 °C before (native) and after the addition (5 min) of 0.22 mM bile salts or bile extract from a 120 mM stock solution. The bile salts or bile extract was added after the monolayers had been stabilized for 5 min at 25 mN m^{-1}. The height measurement corresponds to the red line on the zoomed height image.

Figure 5 presents the effect of adding 0.22 mM bile salts or bile extract on the lateral microstructure of a phospholipid−*β*-lactoglobulin (2:1 or 1:2, w/w) monolayer previously stabilized at 25 mN m^{-1} and observed with an epifluorescence microscope. No change in microstructure of the native monolayers was observed using either phospholipid/*β*-lactoglobulin ratio, suggesting that under these conditions (surface pressure higher than the equilibrium surface pressure of the protein) phospholipids dominated the interface. The addition of bile salts or bile extract to phospholipid−*β*-lactoglobulin (2:1 or 1:2, w/w) monolayers did not induce any microstructural changes (Figure 5). The displacement of proteins by bile salts depends on the native structure of the proteins and the concentration of the bile salts.[31] *β*-Lactoglobulin is a compact globular protein, and its displacement may be incomplete due to the presence of intramolecular disulfide bonds. This may explain the absence of branching and clustering of the liquid-ordered domains. In addition, the surface pressure may also play a role as, at 25 mN m^{-1}, which is higher than the collapse pressure of *β*-lactoglobulin, no change in the morphology of the phospholipid−*β*-lactoglobulin monolayers was observed after addition of bile salts or bile extract (Figures 4 and 5).

The interactions between phospholipids and *β*-casein are weak at neutral pH at the air−water interface, allowing for the displacement of the protein by the phospholipids.[39] In addition, phospholipids dominate the air−water interface at high phospholipid/protein ratios. At surface pressures higher than the collapse pressure of *β*-casein, in this study 25 mN m^{-1}, *β*-casein and phospholipids interact to some extent. Thus, the displacement of the remaining proteins or weakly associated proteins by bile salts and cholesterol may be facilitated in the presence of phospholipids and at 25 mN m^{-1}.

The effect of the addition of bile salts and bile extract to phospholipid, phospholipid−*β*-casein, or phospholipid−*β*-lactoglobulin monolayers previously stabilized at 25 mN m^{-1}

dx.doi.org/10.1021/jf404448d | J. Agric. Food Chem. 2014, 62, 1363−1372

at 20 °C was studied with an atomic force microscope (Figure 6). Five minutes was sufficient to reach the final surface pressure after the addition of bile salts (Figure 3) or bile extract (results not shown). The native monolayers presented liquid-ordered domains with round edges (Figure 6). As seen in Figures 4 and 5, the addition of bile salts and bile extract led to a stretching of the branches of the "snowflake"-shaped domains (Figure 6). The shape of fractal-like or "snowflake"-like domains is governed by electrostatic repulsive forces, which maximize the intermolecular distance within a domain.[40] Thus, the increase of negative charges at the surface from the adsorbed bile salts is likely responsible for the change of the domain shape. The use of AFM revealed extra features within the liquid-ordered domains. The interactions of the bile salts and bile extract with the monolayers led to the formation of small platforms within the "snowflake"-shaped domains (Figure 6). As seen from the height measurement on the zoomed height image, the liquid-ordered domains were 1 nm higher than the liquid-disordered phase and the platforms were between 1.5 and 2 nm lower than the liquid-ordered domains (Figure 6).

Bile salts tend to form clusters at the oil−water interface.[31] The platforms within the liquid-ordered domains (Figure 6) are thus likely to be bile salt-rich areas. Bile salts may be able to disturb the order of the hydrocarbons chains of SM and insert themselves into defects present in the liquid-ordered domains or at the borders between the liquid-disordered and liquid-ordered phases. At the domain boundaries, the line tensions are lower, facilitating the insertion of bile salts into the monolayers. This could explain the clustering of liquid-ordered domains upon adsorption of bile salts seen in Figures 4 and 5. In DPPC monolayers, the liquid-condensed phase was solubilized into a liquid-expended phase upon association of bile salts with DPPC head groups.[30] However, SM and cholesterol molecules are solubilized at higher concentration of bile salts;[41] thus, liquid-ordered domains are still present here after the addition of 0.22 mM bile salts and bile extract.

The MFGM acts as a barrier against lipolysis by inhibiting the access of the triglyceride core to the pancreatic lipase.[14] Chu et al.[16] found that the pancreatic colipase−lipase complex adsorbed preferentially onto the mixed bile salt−DPPC regions rather than onto the liquid-condensed phase of monolayers. As the liquid-ordered domains are tightly packed, the colipase−lipase complex is likely to adsorb onto the bile salt-rich platforms within the liquid-ordered domains and in the liquid-disordered phase, where there is more space between molecules allowing the adsorption of the colipase−lipase complex.

Most often, studies are carried out at 20−27 °C,[5,29,37] which is not physiologically relevant, but there are some technical difficulties associated with working at 37 °C such as evaporation of the aqueous subphase and condensation on the optical lens. However, some AFM work was performed at 37 °C[16] or the adsorption experiment was performed at 37 °C but the LB films were prepared at 20 °C.[18] It is important to keep in mind that lipid packing is affected by temperature.[12,42] Thus, performing the adsorption experiment at 37 °C and then decreasing the temperature to 20 °C before the preparation of LB films was not possible in this study.

Using a physiological concentration of conjugated bile salts, Patton et al.[43] investigated the release of MFGM to understand the intestinal lipolysis of fat globules from different species. After addition of up to 1 mM bile salts to washed milk fat globules, MFGM fragments were recovered as a pellet after centrifugation. Above a bile salt concentration of 1 mM, most phospholipids were recovered in the subnatant, likely associated with bile salts. Thus, depending on the temperature and concentration of bile salts, either a solubilization or an interaction phenomenon takes place between bile salts and phospholipids. It is likely that, at a physiological concentration of 4.4 mM bile salts, phospholipids are solubilized.

This study showed that the adsorption of bile salts to phospholipid and phospholipid−protein monolayers was affected by the temperature, the surface pressure, and the addition rate, concentration, and composition of bile. The presence of β-casein did not seem to affect the adsorption of bile salts, whereas β-lactoglobulin seemed to play a role in maintaining some of the microstructural features of native phospholipid−β-lactoglobulin monolayer films. The surface pressure of the phospholipid and phospholipid−protein monolayers before the addition of bile salts and bile extract was also a determining factor of resistance to penetration by bile components. The formation of bile salt-rich platforms within the liquid-ordered domains might play a role in the adsorption of pancreatic lipase and colipase at the surface of the milk fat globules and milk phospholipid liposomes in the duodenum.

AUTHOR INFORMATION

Corresponding Author

*(S.G.) Mail: Danone Nutricia Research, Uppsalalaan 12, 3584 CT Utrecht (or P.O. Box 80141, 3508 TC Utrecht), The Netherlands. E-mail: Sophie.Gallier@danone.com. Phone: +31 611568079.

Funding

The work was supported by a Centre of Research Excellence fund from the Tertiary Education Commission, Ministry of Education, New Zealand, and by the California State University Agricultural Research Initiative.

Notes

The authors declare no competing financial interest.

ACKNOWLEDGMENTS

We thank Julia Cuthbert for her help in the AFM imaging and Tracey Nguyen for HPLC analysis.

ABBREVIATIONS USED

MFGM, milk fat globule membrane; DPPC, dipalmitoylphosphatidylcholine; DGDG, digalactosyldiacylglycerol; LB, Langmuir−Blodgett; AFM, atomic force microscopy; SIF, simulated intestinal fluid; Tx-Red-DHPE, Texas Red 1,2-dihexadecanoyl-*sn*-glycero-3-phosphoethanolamine; SM, sphingomyelin; PC, phosphatidylcholine

REFERENCES

(1) Gallier, S.; Singh, H. The physical and chemical structure of lipids in relation to digestion and absorption. *Lipid Technol.* **2012**, *24*, 271−273.

(2) Armand, M. Lipases and lipolysis in the human digestive tract: where do we stand? *Curr. Opin. Clin. Nutr.* **2007**, *10*, 156−164.

(3) Staggers, J. E.; Hernell, O.; Stafford, R. J.; Carey, M. C. Physical-chemical behavior of dietary and biliary lipids during intestinal digestion and absorption. 1. Phase behavior and aggregation states of model lipid systems patterned after aqueous duodenal contents of healthy adult human-beings. *Biochemistry* **1990**, *29*, 2028−2040.

(4) Leonard, M. R.; Bogle, M. A.; Carey, M. C.; Donovan, J. M. Spread monomolecular films of monohydroxy bile acids and their

salts: influence of hydroxyl position, bulk pH, and association with phosphatidylcholine. *Biochemistry* **2000**, *39*, 16064−16074.
(5) Welzel, P. B.; Cammenga, H. K. Equilibrium penetration of DMPC monolayers by sodium cholate. *J. Colloid Interface Sci.* **1998**, *207*, 70−77.
(6) Gallier, S.; Gragson, D.; Jimenez-Flores, R.; Everett, D. Using confocal laser scanning microscopy to probe the milk fat globule membrane and associated proteins. *J. Agric. Food Chem.* **2010**, *58*, 4250−4257.
(7) Zou, X.-Q.; Guo, Z.; Huang, J.-H.; Jin, Q.-Z.; Cheong, L.-Z.; Wang, X.-G.; Xu, X.-B. Human milk fat globules from different stages of lactation: a lipid composition analysis and microstructure characterization. *J. Agric. Food Chem.* **2012**, *60*, 7158−7167.
(8) Hamosh, M.; Peterson, J. A.; Henderson, T. R.; Scallan, C. D.; Kiwan, R.; Ceriani, R. L.; Armand, M.; Mehta, N. R.; Hamosh, P. Protective function of human milk: the milk fat globule. *Semin. Perinatol.* **1999**, *23*, 242−249.
(9) Thompson, A. K.; Haisman, D.; Singh, H. Physical stability of liposomes prepared from milk fat globule membrane and soya phospholipids. *J. Agric. Food Chem.* **2006**, *54*, 6390−6397.
(10) Gulseren, I.; Corredig, M. Storage stability and physical characteristics of tea polyphenol bearing nanoliposomes prepared with milk fat globule membrane phospholipids. *J. Agric. Food Chem.* **2013**, *61*, 3242−3251.
(11) Gulseren, I.; Guri, A.; Corredig, M. Encapsulation of tea polyphenols in nanoliposomes prepared with milk phospholipids and their effect on the viability of HT-29 human carcinoma cells. *Food Dig.* **2012**, *3*, 36−45.
(12) Gallier, S.; Gragson, D.; Jimenez-Flores, R.; Everett, D. W. Surface characterization of bovine milk phospholipid monolayers by Langmuir isotherms and microscopic techniques. *J. Agric. Food Chem.* **2010**, *58*, 12275−12285.
(13) Gallier, S.; Gragson, D.; Jiménez-Flores, R.; Everett, D. W. β-Casein−phospholipid monolayers as model systems to understand lipid−protein interactions in the milk fat globule membrane. *Int. Dairy J.* **2012**, *22*, 58−65.
(14) Gallier, S.; Ye, A.; Singh, H. Structural changes of bovine milk fat globules during in vitro digestion. *J. Dairy Sci.* **2012**, *95*, 3579−3592.
(15) Gallier, S.; Zhu, X. Q.; Rutherfurd, S. M.; Ye, A.; Moughan, P. J.; Singh, H. In vivo digestion of bovine milk fat globules: effect of processing and interfacial structural changes. II. Upper digestive tract digestion. *Food Chem.* **2013**, *141*, 3215−3223.
(16) Chu, B. S.; Gunning, A. P.; Rich, G. T.; Ridout, M. J.; Faulks, R. M.; Wickham, M. S. J.; Morris, V. J.; Wilde, P. J. Adsorption of bile salts and pancreatic colipase and lipase onto digalactosyldiacylglycerol and dipalmitoylphosphatidylcholine monolayers. *Langmuir* **2010**, *26*, 9782−9793.
(17) Maldonado-Valderrama, J.; Woodward, N. C.; Gunning, A. P.; Ridout, M. J.; Husband, F. A.; Mackie, A. R.; Morris, V. J.; Wilde, P. J. Interfacial characterization of β-lactoglobulin networks: displacement by bile salts. *Langmuir* **2008**, *24*, 6759−6767.
(18) Maldonado-Valderrama, J.; Gunning, A. P.; Wilde, P. J.; Morris, V. J. In vitro gastric digestion of interfacial protein structures: visualisation by AFM. *Soft Matter* **2010**, *6*, 4908−4915.
(19) Maldonado-Valderrama, J.; Gunning, A. P.; Ridout, M. J.; Wilde, P. J.; Morris, V. J. The effect of physiological conditions on the surface structure of proteins: setting the scene for human digestion of emulsions. *Eur. Phys. J. E* **2009**, *30*, 165−174.
(20) Gallier, S.; Shaw, E.; Cuthbert, J.; Gragson, D.; Singh, H.; Jiménez-Flores, R. Hydrolysis of milk phospholipid and phospholipid-protein monolayers by pancreatic phospholipase A2. *Food Res. Int.* **2013**, *54*, 718−725.
(21) Torcello-Gomez, A.; Maldonado-Valderrama, J.; Martin-Rodriguez, A.; McClements, D. J. Physicochemical properties and digestibility of emulsified lipids in simulated intestinal fluids: influence of interfacial characteristics. *Soft Matter* **2011**, *7*, 6167−6177.
(22) Torcello-Gomez, A.; Jodar-Reyes, A. B.; Maldonado-Valderrama, J.; Martin-Rodriguez, A. Effect of emulsifier type against the action of bile salts at oil-water interfaces. *Food Res. Int.* **2012**, *48*, 140−147.
(23) Costa, M. R.; Elias-Argote, X. E.; Jimenez-Flores, R.; Gigante, M. L. Use of ultrafiltration and supercritical fluid extraction to obtain a whey buttermilk powder enriched in milk fat globule membrane phospholipids. *Int. Dairy J.* **2010**, *20*, 598−602.
(24) IDF-ISO-AOAC, AOAC Official Method 989.05 Fat in Milk, Modified Mojonnier Ether Extraction Method, 1992.
(25) Bitman, J.; Wood, D. L.; Mehta, N. R.; Hamosh, P.; Hamosh, M. Comparison of the phospholipid-composition of breast-milk from mothers of term and preterm infants during lactation. *Am. J. Clin. Nutr.* **1984**, *40*, 1103−1119.
(26) Rombaut, R.; Camp, J. V.; Dewettinck, K. Analysis of phospho- and sphingolipids in dairy products by a new HPLC method. *J. Dairy Sci.* **2005**, *88*, 482−488.
(27) Capolino, P.; Guerin, C.; Paume, J.; Giallo, J.; Ballester, J. M.; Cavalier, J. F.; Carriere, F. In vitro gastrointestinal lipolysis: replacement of human digestive lipases by a combination of rabbit gastric and porcine pancreatic extracts. *Food Dig.* **2011**, *2*, 43−51.
(28) Möhwald, H. Phospholipid and phospholipid-protein monolayers at the air/water interface. *Annu. Rev. Phys. Chem.* **1990**, *41*, 441−476.
(29) Tiss, A.; Ransac, S.; Lengsfeld, H.; Hadvary, P.; Cagna, A.; Verger, R. Surface behaviour of bile salts and tetrahydrolipstatin at air/water and oil/water interfaces. *Chem. Phys. Lipids* **2001**, *111*, 73−85.
(30) Maldonado-Valderrama, J.; Wilde, P.; Macierzanka, A.; Mackie, A. The role of bile salts in digestion. *Adv. Colloid Interface Sci.* **2011**, *165*, 36−46.
(31) Euston, S. R.; Bellstedt, U.; Schillbach, K.; Hughes, P. S. The adsorption and competitive adsorption of bile salts and whey protein at the oil-water interface. *Soft Matter* **2011**, *7*, 8942−8951.
(32) Wickham, M.; Garrood, M.; Leney, J.; Wilson, P. D. G.; Fillery-Travis, A. Modification of a phospholipid stabilized emulsion interface by bile salt: effect on pancreatic lipase activity. *J. Lipid Res.* **1998**, *39*, 623−632.
(33) Wickham, M.; Wilde, P.; Fillery-Travis, A. A physicochemical investigation of two phosphatidylcholine/bile salt interfaces: implications for lipase activation. *Biochim. Biophys. Acta−Mol. Cell. Biol. Lipids* **2002**, *1580*, 110−122.
(34) Subuddhi, U.; Mishra, A. K. Micellization of bile salts in aqueous medium: a fluorescence study. *Colloid. Surf. B−Biointerfaces* **2007**, *57*, 102−107.
(35) Nagadome, S.; Suzuki, N. S.; Mine, Y.; Yamaguchi, T.; Nakahara, H.; Shibata, O.; Chang, C.-H.; Sugihara, G. Monolayers (Langmuir films) behavior of multi-component systems composed of a bile acid with different sterols and with their 1:1 mixtures. *Colloid. Surf. B−Biointerfaces* **2007**, *58*, 121−136.
(36) McConnell, H. M. Structures and transitions in lipid monolayers at the air-water interface. *Annu. Rev. Phys. Chem.* **1991**, *42*, 171−195.
(37) Andrieux, K.; Forte, L.; Lesieur, S.; Paternostre, M.; Ollivon, M.; Grabielle-Madelmont, C. Insertion and partition of sodium taurocholate into egg phosphatidylcholine vesicles. *Pharm. Res.* **2004**, *21*, 1505−1516.
(38) McConnell, H. M.; Tamm, L. K.; Weis, R. M. Periodic structures in lipid monolayer phase transitions. *Proc. Natl. Acad. Sci. U.S.A.* **1984**, *81*, 3249−3253.
(39) Maldonado-Valderrama, J.; Rodriguez Patino, J. M. Interfacial rheology of protein-surfactant mixtures. *Curr. Opin. Colloid Interface Sci.* **2010**, *15*, 271−282.
(40) Staneva, G.; Momchilova, A.; Wolf, C.; Quinn, P. J.; Kouman, K. Membrane microdomains: role of ceramides in the maintenance of their structure and functions. *Biochim. Biophys. Acta−Biomembranes* **2009**, *1788*, 666−675.
(41) Barenholz, Y.; Gatt, S. Chapter 4. Sphingomyelin: metabolism, chemical synthesis, chemical and physical properties. In *New Comprehensive Biochemistry*; Hawthorne, J. N., Ansell, G. B., Eds.; Elsevier: Amsterdam, The Netherlands, 1982; Vol. 4, pp 129−177.
(42) Bagatolli, L. A.; Ipsen, J. H.; Simonsen, A. C.; Mouritsen, O. G. An outlook on organization of lipids in membranes: searching for a

realistic connection with the organization of biological membranes. *Prog. Lipid Res.* **2010**, *49*, 378−389.
(43) Patton, S.; Borgstrom, B.; Stemberger, B. H.; Welsch, U. Release of membrane from milk-fat globules by conjugated bile-salts. *J. Pediactr. Gastroenterol. Nutr.* **1986**, *5*, 262−267.

applications in winemaking. Among them, as a consequence of its high content in GSH, g-IDYs have been claimed to preserve wine aroma and color during wine storage. Although, as has been recently stated,[17] no literature could be found on the industrial preparation of g-IDYs[15] and it is still not clear whether exogenous GSH enrichment is allowed during the manufacturing process, the release of reduced GSH (the form active against oxidation) into the wines has been recently proven.[18,19] However, the effectiveness of the GSH released by these preparations on wine oxidation inhibition has not yet been investigated. Andujar-Ortíz and collaborators[20] recently revealed significant differences between rosé Grenache wines produced by using a g-IDY preparation and nontreated wines in some sensory aroma attributes but only after 9 months of wine aging. This effect could be attributable to the GSH released from IDY or the stimulating effect of amino acids and other peptides from the IDY on GSH synthesis by yeast under winemaking conditions.[18,19]

Considering the current interest of the wine industry in the use of g-IDY preparations to preserve the aroma of wines and the lack of published literature on this topic, the aim of this work was to evaluate the effect of a g-IDY preparation on some typical and desirable wine aroma compounds (linalool, α-terpineol, β-citronellol, and nerol) by using model wines submitted to accelerated oxidative conditions. The effect of a second type of IDY preparation with a different claim (fermentative nutrient) and the effect of commercial GSH were also evaluated. To further understand the role of GSH from the IDY formulations, the wines were spiked with the low molecular weight fraction (<3 kDa) obtained by cold ultracentrifugation, avoiding the interaction of other yeast components (glycoproteins) with the aroma compounds.[21,22] To conclude, chemical characterization of both IDY permeates (<3 kDa fraction) was carried out by using targeted and nontargeted metabolomic approaches using Fourier transform ion cyclotron resonance mass spectrometry (FT-ICR-MS) and capillary electrophoresis−mass spectrometry (CE-MS) analytical platforms.

MATERIALS AND METHODS

IDY Samples. Two types of enological IDY preparations were selected for being representative of the current preparations in the enological market and because they are widely used in winemaking: a GSH-enriched IDY (g-IDY) recommended to reduce the oxidation of wine aroma compounds because of the presence of higher amounts of GSH, and an IDY preparation commonly used as fermentation nutrient (n-IDY). The comparison between both types of IDYs (with and without GSH in their composition) should better provide evidence about the role of GSH released by IDY in wine aroma oxidation.

Isolation of <3 kDa Fraction from the IDY Preparations by Ultrafiltration. Four grams of each IDY powder was weighed into 50 mL centrifuge tubes. Samples were extracted with 50 mL of water/ethanol solution (87:13, v/v) in an ultrasonic bath (3 cycles, 5 min each) at 4 °C. The mixture was then centrifuged (15 min at 5000*g* and 10 °C), and the supernatant was ultrafiltered using a Centricon device (Amicon Inc., Beverly, MA, USA) with a 10 kDa cutoff membrane. The obtained permeates were submitted to a second ultrafiltration step through a 3 kDa cutoff membrane Centricon (Amicon Inc.). Both ultrafiltration steps were carried out at cold temperature (below 10 °C). The obtained <3 kDa permeates from each IDY preparation were freeze-dried and kept at −20 °C until use. Prior to chemical characterization, permeates were reconstituted with water to 100 mg/mL dry residue. Only for FT-ICR-MS analysis were reconstituted samples dialyzed by using a Float-a-Lyzer G2 device with a 0.1−0.5 kDa cutoff membrane from Spectrum (Breda, The Netherlands) to remove salts.

Model Wine Solutions under Accelerated Aging Conditions. Model wine solutions (50 mL) were prepared in 100 mL vials by adding ethanol (VWR, Leuven, Belgium) at 120 mL/L and 4 g/L tartaric acid (Panreac, Barcelona, Spain). The pH was adjusted at 3.5 using a 5 M NaOH solution (Panreac). Model wines were spiked with single terpene compounds (nerol, β-citronellol, α-terpineol, and linalool) from Sigma (Stenheim, Germany) at a final concentration of 25 mg/L each. Finally, 100 μL of the reconstituted <3 kDa fractions isolated from g-IDY or n-IDY at 100 mg/mL was added. In addition, another set of model wines were individually aromatized with the four aroma compounds and spiked with commercial GSH (Sigma) to a final concentration of 10 mg/L. Finally, four control model wines, one with each aroma compound but without addition of the IDY fractions or commercial GSH, were also prepared. Two vials of the model wines containing each terpene compound were analyzed at the beginning of the experiment (t = 0 days). The different model wine mixtures were submitted to an accelerated oxidation process during 3 weeks at 25 °C, saturating the headspace of the vials with oxygen (t = 21 daus). All of the preparations were carried out in duplicate.

HS-SPME-GC/MS Analysis. Model wine aroma analysis was performed before (t = 0 days) and after (t = 21 days) model wine oxidation process. It was carried out by headspace solid-phase microextraction coupled to gas chromatography−mass spectrometry (HS-SPME-GC-MS). Model wine samples (8 mL), 2.3 g of NaCl, and 40 μL of an internal standards solution (400 mg/L 3,4-dimethylphenol and 2.5 mg/L methyl nonanoate) were added to a 20 mL SPME vial. The SPME procedure and chromatographic conditions were detailed in a previous work.[23] Briefly, the extraction procedure was automatically performed using a CombiPal system (CTC Analytics AG, Zwingen, Switzerland) with a 50/30 μm DVB/CAR/PDMS fiber of 2 cm length from Supelco (Bellefonte, PA, USA). Samples were preincubated for 10 min at 50 °C, and extraction was performed in the headspace of each vial for 30 min at 50 °C. Desorption was performed in the injector of the GC system in splitless mode for 1.5 min at 270 °C. After each injection, the fiber was cleaned for 20 min to avoid any memory effect. The chromatographic separation was performed in a GC-MS instrument (Agilent 6890GC, Agilent 5973 N MS) equipped with a Supra-Wax fused silica capillary column (60 m × 0.25 mm i.d. × 0.50 μm film thickness) from Konik (Barcelona, Spain). Helium was used as the carrier gas at a flow rate of 1 mL/min. The oven temperature was initially held at 40 °C for 5 min, then increased at 4 °C/min to 240 °C, and held at 240 °C for 20 min. The acquisitions were performed in scan (from 35 to 350 amu) and electronic impact mode (70 eV). Other MS conditions were 270, 150, and 230 °C for the transfer line, quadrupole, and ion source, respectively. The signal corresponding to a specific ion of quantification (m/z 93, 59, 69, and 69 for linalool, α-terpineol, β-citronellol, and nerol, respectively) was calculated by the data system. Compound identification was carried out by comparison of retention times and mass spectra of the reference compounds with those reported in the mass spectrum library NIST 2.0. Data were obtained by calculating the relative peak area (RPA) in relation to that of the corresponding internal standard (3,4-dimethylphenol, for all of the aroma compounds except for nerol, which was methyl nonanoate).

Analysis of Reduced Glutathione (GSH), Total Glutathione, and γ-Glutamylcysteine (γ-glu-cys) by RP-HPLC-FL. Reversed-phase HPLC using a liquid chromatograph consisting of a Waters 600 Controller programmable solvent module (Waters, Milford, MA, USA), a WISP 710B autosampler (Waters), and a HP 104-A fluorescence detector (Hewlett-Packard, Palo Alto, CA, USA) was used following the procedure previously optimized and validated.[18] The mobile phase was composed of methanol (Lab-Scan, Sowinskiego, Poland) and an aqueous solution of phosphate buffer (10 mM $NaH_2PO_4 \cdot 12H_2O$ at pH 8.5) with a ratio of 15:85 (v/v). The sample (30 μL) was placed in a 1 mL vial (by using an insert), and the precolumn derivatization was automatically made in the autosampler at 12 °C as follows: to a sample vial were added 105 μL from the dithiotreitol (Sigma-Aldrich) solution vial [5 mM and 0.5 mM in

borate buffer (0.2 M H_3BO_4, pH 9.2) to determine total GSH or reduced GSH, respectively] and 15 μL of 2,3-naphthalenedialdehyde (NDA) (Sigma-Aldrich) solution (5 mg mL^{-1} in ethanol); then, two mixture cycles of the total content of the insert were carried out, and 100 μL was injected in the chromatographic system. Separation was carried out on a Nova Pack C18 (150 mm × 3.9 mm i.d., 60 A, 4 μm) column (Waters) in isocratic mode (flow at 1 mL min^{-1}), and detection was performed by fluorescence ($\lambda_{excitation}$ = 467 nm, $\lambda_{emission}$ = 525 nm). The derivatization conditions for the determination of γ-glu-cys were the same as previously described. Calibrations were carried out by using pure standard compound solutions of GSH and γ-glu-cys. The analysis of the samples was made in duplicate.

ORAC-Fluorescein (ORAC-FL) Assay. The antioxidant capacity of IDY permeates and GSH was measured by ORAC-FL assay based on that proposed previously.[24] Briefly, the reaction was carried out at 37 °C in 75 mM phosphate buffer (pH 7.4), and the final assay mixture (200 μL) contained FL (70 nM), AAPH (12 mM), and antioxidant [Trolox (1−8 μM) or sample at different concentration]. The plate was automatically shaken before the first reading, and the fluorescence was recorded every minute for 80 min. A polestar Galaxy plate reader (BMG Labtechnologies GmbH, Offemburg, Germany) with 485-P excitation and 520-P emission filters was used. The equipment was controlled by Fluostar Galaxy software (version 4.11-0) for fluorescence measurement. Black 96-microwell microplates (96F untreated, Nunc, Denmark) were used. AAPH and Trolox solutions were prepared daily, and FL was diluted from a stock solution (1.17 mM in 75 mM phosphate at pH 7.4). Fluorescence measurements were normalized to the curve of the blank (no antioxidant). From the normalized curves, the area under the fluorescence decay curve (AUC) was calculated. The regression equation between net AUC and antioxidant concentration was calculated, and the slope of the equation was used to calculate the ORAC-FL value by using the Trolox curve obtained for each assay. Final ORAC-FL values were expressed as micromoles of Trolox equivalent per milligram of dry permeate (for the <3 kDa permeates from g-IDY and n-IDY) and in micromoles of Trolox equivalent per milligram of pure compound for commercial GSH.

Total Free Amino Acids and Peptides. Free amino acids and peptides in model wine were determined according to the protocols proposed by Doi and co-workers.[25] Free amino acids were determined by the reaction of ninhydrin/Cd with the free amino group by measuring the absorbance at 507 nm (method 5).[25] On the other hand, free amino acids plus peptides were determined by the reaction of the amino group with ninhydrin/Sn by measuring the absorbance at 570 nm (method 1).[25] A DU 70 spectrophotometer from Beckman Coulter (Fullerton, CA, USA) was used. Quantification was carried out on the basis of the standard curve of leucine, and results were expressed as milligrams N/L. All of the model wine samples were analyzed in duplicate.

Analysis of Amino Acids by RP-HPLC-FL. Amino acids were analyzed in duplicate by reversed-phase HPLC using a liquid chromatograph as described under Analysis of Reduced Glutathione (GSH), Total Glutathione, and γ-Glutamylcysteine (γ-glu-cys) by RP-HPLC-FL. Samples were submitted to automatic precolumn derivatization with *o*-phthaldehyde (OPA) in the presence of 2-mercaptoethanol following the method described by Moreno-Arribas and collaborators.[26] Separation was carried out on a Waters Nova Pack C18 (150 × 3.9 mm i.d., 60 A, 4 μm) column and the same type of precolumn. Detection was performed by fluorescence ($\lambda_{excitation}$ = 340 nm, $\lambda_{emission}$ = 425 nm).

Analysis of Sulfur-Containing Metabolites by CE-MS. CE analyses were carried out in a P/ACE 5500 CE apparatus from Beckman Coulter. The CE system was coupled to a TOF MS instrument from Bruker Daltonics (Bremen, Germany) through an orthogonal ESI interface model G1607A from Agilent Technologies (Palo Alto, CA, USA). Electrical contact at the ESI needle tip was established via a sheath liquid delivered by a 74900-00-05 Cole Palmer syringe pump (Vernon Hills, IL, USA). The electrophoretic separation was carried out using an uncoated fused-silica capillary (50 μm internal diameter, 363 μm outside diameter, and 80 cm total length) from Composite Metal Services (Worcester, UK). Before first use, the separation capillary was conditioned by rinsing with 1 M NaOH for 10 min, followed by 20 min with water, both using pressurized N_2 at 20 psi (1380 mbar). After each run, the capillary was conditioned with water during 2 min, followed by BGE during 4 min. Injections were made at the anodic end using N_2 pressure at 0.5 psi (34.5 mbar) for 80 s. Electrophoretic separation was achieved by applying +25 kV at room temperature in a BGE composed of 3 M formic acid. Electrical contact at the ESI needle tip was established via a sheath liquid based on isopropanol/water (50:50, v/v) and delivered at a flow rate of 0.24 mL/min. The mass spectrometer operated in the positive ion mode. The nebulizer and drying gas conditions were 0.4 bar N_2 and 4 L/min N_2, respectively, and the ESI chamber temperature was maintained at 250 °C. Spectra were acquired in the m/z 50−700 range every 90 ms. External and internal calibration of the TOF MS instrument was performed by introducing a 10 mM sodium formate solution through the separation capillary. The ions used for the calibration of the TOF MS instrument were next: m/z 90.9766, 158.9641, 226.9515, 294.9389, 362.9263, 430.9138, 498.9012, and 566.8886. TOF MS provided a high mass resolution and high mass accuracy with errors usually below 10 ppm. Selected mass spectra were processed through the software DataAnalysis (Bruker Daltonics), which provided a list of possible elemental formulas by using the Generate-Molecular Formula Editor (Bruker Daltonics), which provided standard functionalities such as minimum/maximum elemental range, electron configuration, and ring-plus double bond equivalents, as well as a comparison between the theoretical and experimental isotopic pattern (Sigma-Value) for increased confidence in the theoretical molecular formula assignment.

Nontargeted Metabolomic Analysis by FT-ICR MS. FT-ICR MS was used to obtain ultrahigh-resolution (>100,000) mass spectra. Separation and identification of the metabolites were possible without the need of chromatography or derivatization due to the ultrahigh mass accuracy. Commercial beer maltooligosaccharides were used as mass calibrants and tuning standards in both the positive and negative ion modes.[27] The maximum mass error achieved was below 2 ppm.

Experiments were performed on a hybrid triple-quadruple-FT-ICR instrument Varian 920 MS provided with a 7.0 T actively shielded superconducting magnet and equipped with an electrospray ionization (ESI) source. The conditions in the electrospray were as follows: In positive mode the potential in the needle was set at 4.5 kV and 600 V in the shield. The capillary potential to pass the ions from the source to the skimmer was set in a range between 40 and 60 V. Nitrogen was employed as nebulizer gas, and its pressure was 50 psi. The pressure for drying gas was set at 18 psi and the temperature at 300 °C. The flow rate of the sample was kept at 15 μL/min and injected by direct infusion. In negative mode MS parameters were as follows: −3.5 kV, 600 V, from −70 to −90 V in the capillary, 18 psi, and 300 °C. Sample flow rate was 15 μL/min. Air was used instead of nitrogen as nebulizer gas. The spectra were acquired in full scan mode, defining a mass range from m/z 100 to 1000. The internal detection signal in the cell detector of the FT-ICR was optimized for a mass of m/z 500.

Monoisotopic mass and isotope cluster profiles were extracted from the raw data by using Varian MS Peak Hunter software version 4.1.89. These two parameters were used by the same software to get the elemental composition following the next criteria: error was set at 2 ppm, and only chemical formulas containing C, H, N, O, P, and S were allowed. The spectra were exported to mzXML format and applied against XCMS[28] online METLIN database. When the results from the METLIN database were in good agreement in accordance with the chemical formula found in Varian MS Peak Hunter, the metabolite was given as a good result.

Statistical Analysis. Data from the analysis of aroma compounds (RPAs) from the model wine experiments were submitted to one-way ANOVA and LSD to test the effect of wine treatment.

RESULTS AND DISCUSSION

Effect of the Addition of GSH and the <3 kDa Permeates Isolated from IDYs on Specific Wine

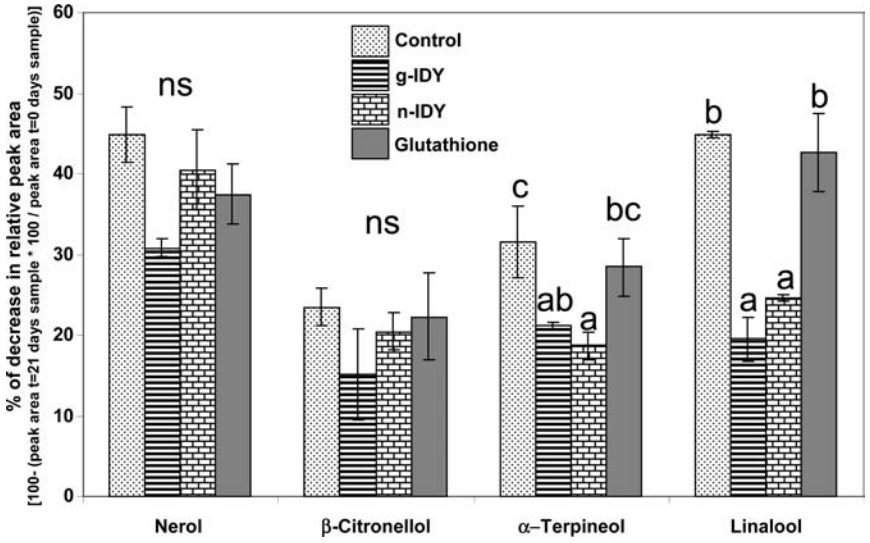

Figure 1. Percentage of decrease in the relative peak area of the aroma compounds in the model wines submitted to accelerated aging conditions (wines supplemented with the <3 kDa permeates isolated from g-IDY and n-IDY, wines with added 10 mg/L of commercial glutathione, and control wines without any treatment) compared to the original model wines (0 days). Results of ANOVA and LSD test are indicated with different letters (a–c). ns: no significant differences.

Terpenes in Model Wines under Accelerated Aging Conditions. To determine the effect of GSH-enriched IDY preparations on the evolution of aroma compounds during aging and whether the GSH released from IDYs into the wines might have a role in the behavior of aroma compounds during aging, the <3 kDa permeate from a g-IDY preparation was isolated by ultracentrifugation and spiked into model wines, as described under IDY Samples. Model wines spiked with this permeate were coded g-IDY-W. Ultrafiltration ensured the removal of glycoproteins (with molecular masses >3 kDa) from the IDY preparations that might interact with volatiles,[21,22] masking the potential action of GSH on the aroma compounds, which was the main objective of this study. In addition, to compare the effect of a different type of IDY preparation currently commercialized as a fermentation nutrient (without any claim on wine aroma protection), the <3 kDa permeate was also isolated and added to model wines (n-IDY-W). In addition, two other types of model wines with added commercial GSH (10 mg/L) referred to as glut-W and control model wines, without any addition (cont-W), were also prepared. To avoid chemical transformations due to the high reactivity of terpene compounds,[3] each model wine solution was individually aromatized with a single aroma compound (nerol, β-citronellol, α-terpineol, and linalool). These aromas were selected because they are characteristic of young wines providing pleasant floral-fruity nuances and are very sensitive to the oxidation phenomena.[3,29,30] The behavior of the four terpene compounds was evaluated in all of the model wines at the beginning of the experiment (t = 0 days), corresponding to nonoxidized model wines, and after 3 weeks of accelerated aging conditions (t = 21 days). Figure 1 shows the percentage of decrease in relative peak area (RPA) between the initial wine sample (nonoxidized) and the wines after 21 days of aging for each aroma compound and wine type. As can be seen, there was a general decrease in RPAs for all of the aromas during aging, which ranged from 24 to 45%, therefore confirming the outstanding effect of aging on the loss produced in these types of aroma compounds,[2,3,14] which can be attributable to oxidation phenomena.[3,29,30] Interestingly, compared to the control wine solution, α-terpineol and linalool showed a lower reduction in RPAs in the model wines supplemented with the <3k Da permeate isolated from either of both preparations (g-IDY or n-IDY). In the case of nerol, a slightly lower reduction in RPAs was also observed in the g-IDY model wine, although this effect was not statistically significant. β-Citronellol did not show a significant effect either. These results seemed to indicate a protective effect of these preparations on some specific aroma compounds, which is in agreement with the aroma sensory differences recently found between control rosé wines (without IDY added) and rosé wines produced in cellar conditions with the same type of g-IDY after 9 months of aging.[20]

However, the addition of commercial GSH to the model wine solutions did not have a significant effect under the essayed conditions. Different published works have shown an inhibition of the decline of certain aroma compounds when using GSH at a similar or even lower dosage in wines or model wine systems.[4,6−9] Nonetheless, it is well-known that the main effect of GSH in wines is its ability to react with *o*-quinones produced by oxidation of caftaric acid (and other polyphenols) to give grape reaction product (GRP) by the action of polyphenol oxidases blocking the subsequent steps in which polyphenols are involved (polymerization) and responsible for browning.[4,6,17] Moreover, *o*-diphenols can be directly oxidized in the presence of oxygen and some cations (iron, copper) to *o*-quinones and hydrogen peroxide, which might be involved in subsequent aroma oxidation.[4] In our experimental conditions this action mechanism was limited because of the absence of polyphenols to react with GSH in the model wine, which seems to explain the absence of a noticeable effect of GSH on aroma protection in the model wines supplemented with commercial GSH. However, GSH presents scavenging hydroperoxide and hydroxyl radical properties, which might have allowed it to act as an antioxidant by other mechanisms different from its capacity to interact with *o*-quinones in polyphenol-free systems.[10,11] Nonetheless, on the basis of our results, this mechanism did not seem as significant in our experimental conditions. Despite this, it is important to highlight that this model system allowed us to uncover the potential role of other

yeast components, different from GSH and contained in the <3 kDa fraction, which seemed to be related to the protection of some terpenes in model wines submitted to accelerated aging conditions.

Following this rationale, to find out if the observed reduction in peak areas for some of the terpenes employed in our study was effectively related to an antioxidant effect exerted by the IDY permeates, the radical scavenging activity of both of them was calculated by using the ORAC-FL method. The ORAC values were 0.33 and 0.22 μmol TE/mg dry permeate for g-IDY and n-IDY permeates, respectively, showing that the two permeates had a positive and similar antioxidant capacity. These results are in agreement with the previous experiment, in which g-IDY-W and n-IDY-W wines showed a similar reduction in the corresponding peak areas for the same aroma compounds (linalool and α-terpineol). In addition, to confirm the antioxidant activity of the commercial GSH employed in this experiment, the ORAC value for the pure compound was also calculated; this is 10.7 μmol TE/mg pure compound, thus corroborating its high antioxidant capacity, comparable to other important wine antioxidants such as polyphenols. As an example, for a representative set of pure polyphenolic compounds, the calculated ORAC values ranged between 2.35 and 18.16 μmol TE/mg pure compound determined for myricetin and caffeic acid, respectively.[31] Nevertheless, and as previously stated, despite the high antioxidant activity determined for GSH, this compound did not exert a noticeable effect in preventing aroma oxidation in a model wine in the absence of polyphenols, as used in the present work. However, these results confirmed the antioxidant properties of both IDY permeates in agreement with the better preservation of some terpenes observed in the model wines supplemented with them. However, this effect, at least in the g-IDY wines, might have been a consequence of the higher amount of GSH contained in the g-IDY permeate compared to that added into the wines by using commercial GSH (10 mg/L), which on the basis of its radical scavenging properties might be responsible for the lower aroma loss in g-IDY wines. Therefore, a quantitative determination of GSH, total GSH, and the precursor γ-glutamylcysteine, was carried out.

Determination of GSH, Total GSH, and γ-Glutamylcysteine. Reduced GSH, total GSH, and the precursor γ-glutamylcysteine were analyzed by using a previously optimized RP-HPLC-FL method.[18] These results are shown in Table 1. As can be seen, only the g-IDY permeate presented detectable levels of GSH (1293 mg/L) and γ-glutamyl-cysteine (873 mg/L). The amount of total GSH was higher (3147 mg/L), meaning that only 41% of glutathione was in its reduced form (GSH) and available to act as a potential antioxidant. However, in the n-IDY permeate, there were traces of GSH or GSH-related compounds. This is in agreement with some previously published works in which in a screening of commercial enological IDY preparations, only those claimed to be GSH-enriched IDY preparations released reduced GSH into synthetic wines.[18] With the amount of each permeate added into the model wines (100 μL) taken into consideration, the final amounts of reduced and total GSH in g-IDY-W model wines were 2.6 and 6.3 mg/L, respectively, which are very close to the amounts determined in model wines when using IDYs at the recommended wine dosage (0.3 g IDYs/L), which has been established to be between 1 and 2.5 mg/L.[18,19] Considering that no GSH (or other GSH-related compounds) was detected in n-IDY-W model wine and that the amount of GSH determined in g-IDY-W was lower than the amount of commercial GSH employed in the GSH-W model wine (10 mg/L), it could be concluded that the observed antioxidant effect of these preparations on the reduction of aroma loss during wine aging did not seem to be linked to the sole antioxidant action of GSH but could be due to other compounds or to the combined action of GSH and other antioxidant compounds from yeast origin present in the permeates (at least in n-IDY-W model wine). In the attempt to elucidate these compounds, a comprehensive chemical characterization of both g-IDY and n-IDY permeates was carried out.

Table 1. Concentration of Total GSH, Reduced GSH, and γ-Glutamyl-cysteine Determined in the <3 kDa Permeates Isolated from g-IDY and n-IDY Preparations

IDY preparation	total GSH (mg/L)	reduced GSH (mg/L)	γ-glutamyl-cysteine (mg/L)
g-IDY	3147 ± 118	1293 ± 76	873 ± 63
n-IDY	nd[a]	nd	nd

[a]nd, not detected.

Analysis of Other Sulfur-Containing Compounds by CE-MS. In addition to GSH, other biological sulfur-containing compounds have been said to present antioxidant properties.[32] Thus, the analysis of other low molecular weight sulfur-containing compounds in the <3 kDa permeates from both g-IDY and n-IDY samples was performed by using CE-MS. This targeted analysis was carried out on the basis of the presence of at least one S atom in the molecular structure. The existence of sulfur in the molecule requires the presence in the mass spectra of an isotopic peak 2 Da higher than the molecular ion and at least 4% in intensity per sulfur. After further inspection of n-IDY and g-IDY CE-MS profiles, besides the 2 sulfur-containing amino acids methionine and cysteine, another 14 highly abundant sulfur-containing compounds were found in the permeate from the g-IDY sample. In Figure 2, extracted ion electropherograms (EIEs) from these two amino acids and the most abundant sulfur-containing compounds are represented (continuous and dotted lines for g-IDY and n-IDY samples, respectively). The electropherogram from n-IDY showed, however, only three major peaks (compounds **1**, **3**, and **5**), and methionine and cysteine were not detected either. Detailed information about the identity of these compounds is shown in Table 2. As can be seen in this table, 8 of 14 compounds could be tentatively identified. Most of them corresponded to glutathione derivatives (compounds **7**, **8**, **10**, **11**, and **14**) and, in general, the rest of the identified compounds were compounds related to the amino acids cysteine and methionine. Many sulfur compounds, including the sulfur-containing amino acids, have been shown to exhibit antioxidant properties in vivo and in vitro,[32,33] and all of them are synthesized from methionine.[29,33] Therefore, the absence of this amino acid in the n-IDY permeate is in agreement with the lack of sulfur-containing compounds in this sample. In synthetic wines, Papadopoulou and Roussis[8] showed that some sulfur-containing compounds, such as *N*-acetylcysteine, are effective at decreasing the rate of reduction of some aroma compounds (including terpenes) during wine aging. On the basis of existent literature and the chemical structure of the sulfur-containing compounds identified in g-IDY, the involvement of these compounds in the antioxidant activity determined in the model

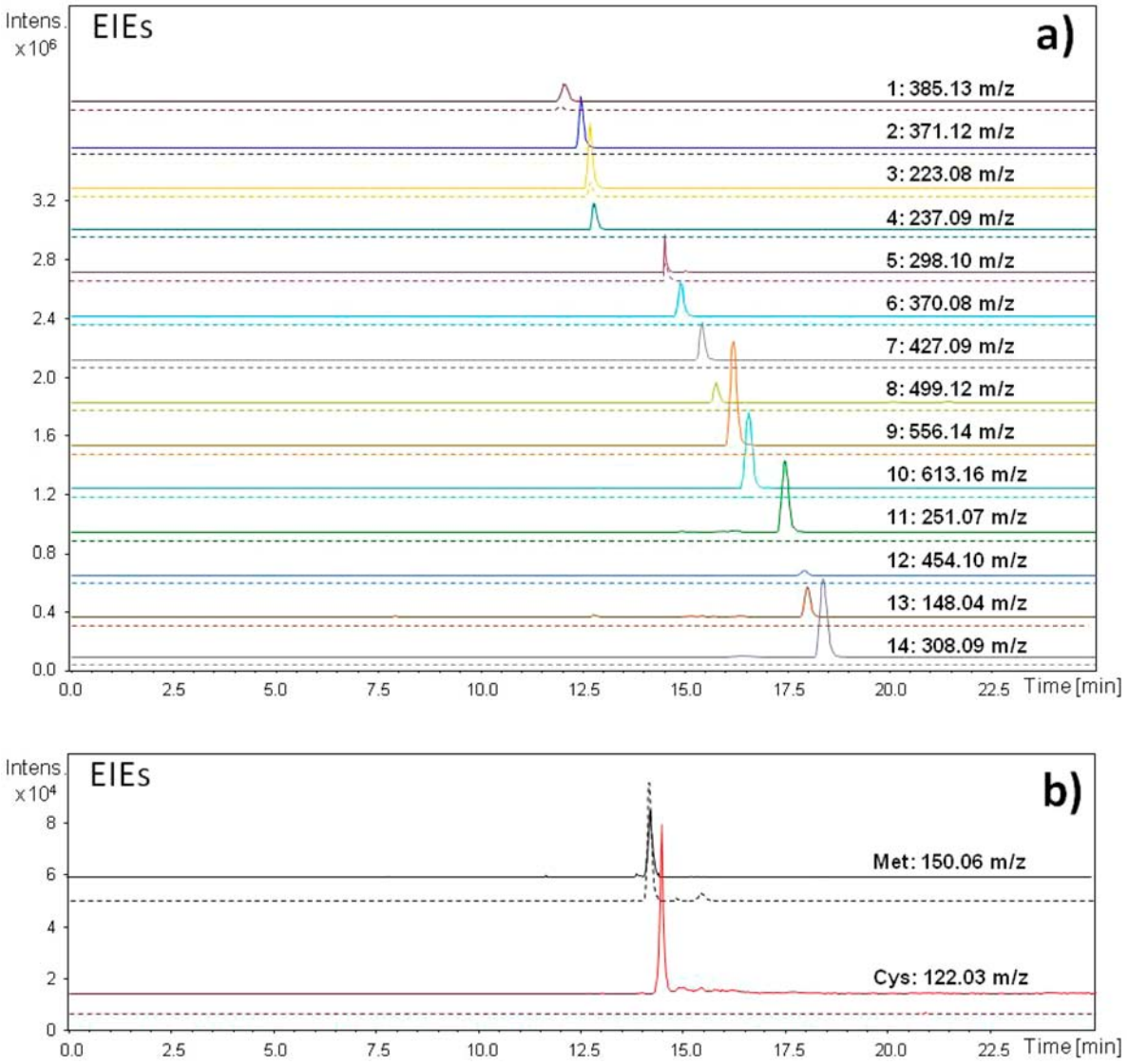

Figure 2. CE-TOF-MS extracted ion electropherograms (EIEs) of (a) the 14 most abundant sulfur-containing compounds and (b) methionine and cysteine from g-IDY and n-IDY samples. A continuous line for g-IDY permeate and a dotted line for n-IDY permeate are used. See Analysis of Sulfur-Containing Metabolites by CE-MS for experimental conditions.

wines spiked with the g-IDY permeate seems plausible. However, the absence of sulfur-containing compounds in the n-IDY permeate might indicate that the antioxidant effect determined in n-IDY-W model wines should be due to compounds from a different nature.

Analysis of Nitrogen-Containing Compounds. Previous works have already shown that free amino acids represent the greatest nitrogen fraction released by IDYs into model wines, the specific composition of which depends on the type of IDYs.[22] In addition, the antioxidant effect exerted by different types of nitrogen compounds such as peptides and amino acids (other than sulfur-containing amino acids) has also been described.[34,35] Therefore, to determine which other chemicals might be responsible for the antioxidant effect found in both permeates, their nitrogen composition was determined. Table 3 shows the content of total free amino acids, free amino acids and peptides, and individual amino acids determined by RP-HPLC-FL. As can be seen, both permeates exhibited important qualitative and quantitative differences. First, the content of free amino acids was clearly higher in the g-IDY permeate (2964 mg N/L) than in the n-IDY permeate (1248 mg N/L). However, the n-IDY permeate was richer in N from peptides. Besides, the amino acid profile showed important differences between IDYs. For instance, the major amino acids in g-IDY permeate were glutamic acid (62.2 mg/L), threonine (56.27 mg/L), and β-alanine (45.82 mg/L), whereas histidine (56.39 mg/L), glycine (33.15 mg/L), and lysine (21.99 mg/L) were most abundant in the permeate from n-IDY. Some amino acids have been associated with relatively important radical scavenging activities in the order tryptophan > tyrosine > methionine > cysteine > phenylalanine.[34] In this sense, only tyrosine was detected in the free form in both permeates, although in relatively low concentrations (5.6 and 1.05 mg/L for g-IDY and n-IDY permeates, respectively), whereas phenylalanine and tryptophan were not detected in any of the samples. Corroborating the previous results obtained by CE-MS, methionine was identified only in the g-IDY permeate (1.55 mg/L). However, the analytical method employed did not allow the detection of cysteine, although its sole presence in the g-IDY permeate was previously confirmed by CE-MS analysis. Therefore, consider-

Table 2. Tentative Identification of Sulfur-Containing Compounds Found in the <3 kDa Permeates Isolated from g-IDY and n-IDY Preparations after CE-MS Analysis

				m/z					
compd	time (min)	peak area (g-IDY)	peak area (n-IDY)	exptl	theor	error (ppm)	formula	tentative ID	HMDB[a] code
1	12.03	1489462	204104	385.1318	385.1289	7.6	$C_{14}H_{20}N_6O_5S$	*S*-adenosylhomocysteine	HMDB00939
2	12.45	2807046	ND[b]	371.1182				NF[c]	
3	12.68	3650062	782426	223.0792				NF	
4	12.75	1427597	ND	237.091	237.09034	−2.7	$C_8H_{16}N_2O_4S$	methionyl-serine, serinyl-methionine, *S*-aminomethyldihydrolipoamide	HMDB29045, HMDB29045, HMDB06239
5	14.49	891150	740927	298.1011	298.0968	−14.3	$C_{11}H_{15}N_5O_3S$	5′-methylthioadenosine	HMDB01173
6	14.87	2142027	ND	370.0768				NF	
7	15.41	2245896	ND	427.0974	427.0952	−5.2	$C_{13}H_{22}N_4O_8S_2$	*S*-glutathionyl-L-cysteine	HMDB00656
8	15.74	3898205	ND	499.1182	499.116311	−3.8	$C_{16}H_{26}N_4O_{10}S_2$	*N*,*N*′-bis(γ-glutamyl)-cystine	HMDB38458
9	16.18	7992966	ND	556.1404	278.5817			NF	
10	16.55	6240395	ND	613.16, 307.0921	613.1592	−2.5	$C_{20}H_{32}N_6O_{12}S_2$	oxidized glutathione	HMDB03337
11	17.43	5710438	ND	251.0716	251.0696	−7.9	$C_8H_{14}N_2O_5S$	γ-glutamyl-cysteine	HMDB01049
12	17.9	369996	ND	454.096				NF	
13	17.98	2125131	ND	148.0446				NF	
14	18.37	6861257	ND	308.0952	308.0911	−13.4	$C_{10}H_{17}N_3O_6S$	glutathione	HMDB00125

[a]HMDB, Human Metabolome Database (http://www.hmdb.ca). [b]ND, not detected. [c]NF, not found.

Table 3. Amino Acid Composition (Milligrams per Liter) of the <3 kDa Permeates Isolated from g-IDY and n-IDY Preparations

	g-IDY		n-IDY	
amino acid	mean	±SD	mean	±SD
free amino acids	2964	342	1248	22
free amino acids and peptides	2865	29	1604	74
aspartic acid	19.56	0.51	18.66	0.48
glutamic acid	62.21	2.31	nd[a]	
asparragine	7.88	0.17	5.17	0.11
serine	15.75	0.53	6.60	0.22
glutamine	21.57	0.37	10.62	0.18
histidine	24.53	0.65	56.40	1.50
glycine	nd		33.15	1.08
threonine	56.43	1.51	12.77	0.34
arginine	8.79	0.22	6.95	0.17
β-alanine	45.82	0.32	4.43	0.03
α-alanine	nd		3.41	0.10
γ-aminobutyric acid	4.01	0.14	4.05	0.14
tyrosine	5.70	0.08	1.05	0.01
α-aminobutyric acid	2.61	0.02	2.51	0.02
methionine	1.59	0.01	nd	
valine	2.32	0.05	1.76	0.04
phenylalanine	nd		nd	
tryptophan	nd		nd	
isoleucine	4.38	0.11	4.67	0.11
leucine	nd		nd	
ornithine	27.75	0.48	5.43	0.09
lysine	31.47	0.54	22.00	0.37

[a]nd, not detected.

ing the amino acidic profile, the contribution of free amino acids to the total antioxidant activity of g-IDY and n-IDY permeates did not seem very relevant, meaning that there were still other compounds which should be more related to this activity.

Nontargeted Metabolomic ESI FT-ICR MS Analysis. Direct infusion ESI-FT-ICR-MS was further employed to gain insight into the chemical metabolites responsible for the antioxidant effect exerted by the two permeates. This technique has been proposed as one of the best techniques to directly investigate complex natural mixtures[36] due to the high mass resolving power and mass accuracy. It has also been recently applied to food materials such as coffee[37] and other metabolomic studies of natural products.[38]

Panels a and b of Figure 3 show the ESI-FT-ICR-MS spectra from g-IDY and n-IDY permeates, respectively. Although they were acquired in the positive and negative ion mode, Figure 3 depicts only the MS from the positive mode. Visually, it is possible to see that both MS profiles were substantially different. This is in good agreement with the more thorough ion identification study that was performed and summarized in Table 4. Using positive and negative ionization modes, it was possible to tentatively identify a total of 10 compounds, 8 of which were detected in the g-IDY permeate and only 4 in the n-IDY permeate. Some of the identified compounds were sulfur-containing compounds, such as *S*-glutathionyl-L-cyteine, γ-glutamyl-cystine, and oxidized glutathione, which were already identified by CE-MS in the g-IDY sample. In addition, the ion *m/z* 556.1379 was identified as a biotinil-5-AMP, an intermediary in the synthesis of biotin.[39] This compound was already detected but not identified by CE-MS in the g-IDY permeate. In any case, in agreement with the results obtained from other analytical techniques (HPLC-FL, CE-MS), there were non-sulfur-containing compounds in the n-IDY permeate. However, a very interesting finding was the detection in both samples of some small peptides, specifically tripeptides. Two of them were found in both permeates and were tentatively identified as histidine/cysteine/lysine- and methionine/lysine/histidine-containing peptides. Their MS and chemical structures are shown in Figure 4. Because of their low concentration in the sample, it was not possible to confirm their sequence. Even more interestingly was the finding of another two peptides only in the n-IDY permeate containing methionine/aspartic/tryptophane and tyrosine/histidine/methionine (Figure 4). It is worth mentioning that the antioxidant properties of small peptides, mainly contained in fermented food, have been

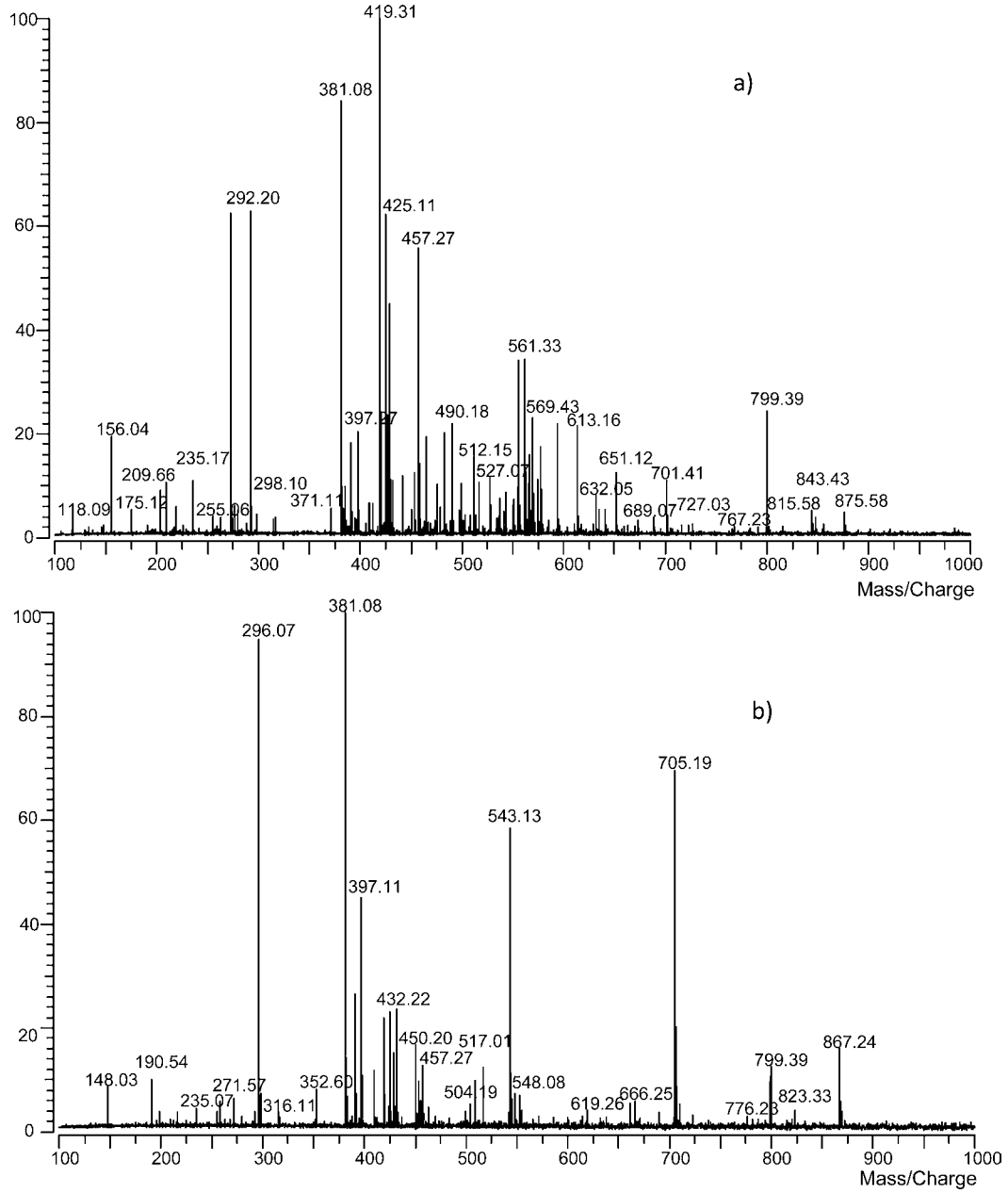

Figure 3. ESI (+) FT-ICR MS of the <3 kDa permeate from g-IDY (a) and n-IDY (b) samples.

Table 4. Tentative Identification of the Compounds Found in the <3 kDa Permeates Isolated from g-IDY and n-IDY Preparations after FT-ICR-MS Analysis

m/z								
exptl	theor	error (ppm)	formula	g-IDY	n-IDY	tentative ID	METLIN ID	HMDB code
399.1447	399.1451	1.0	$C_{15}H_{22}N_6O_5S + H$			*S*-adenosylmethionine	6064	HMDB01185
425.1137	425.1131	1.4	$C_{17}H_{22}N_4O_8S + H - H_2O$	*		*S*-(4-nitrobenzyl)glutathione	4098	
425.1364	425.1368	0.9	$C_{15}H_{26}N_6O_4S + K$	*	*	His, Cys, Lys	21589	
427.0949	427.0952	0.7	$C_{13}H_{22}N_4O_8S_2 + H$	*		*S*-glutathionyl-L-cysteine	63433	
431.1416	431.1394	5.1	$C_{20}H_{26}N_4O_6S - H_2O - H$		*	Met, Asp, Trp	18421	
453.1675	453.1681	1.3	$C_{17}H_{30}N_6O_4S + K$	*	*	Met Lys His	21819	
470.1526	470.1479	10.0	$C_{20}H_{27}N_5O_5S + Na - 2H$		*	Tyr, His, Met	18106	
499.1173	499.1163	2.0	$C_{16}H_{26}N_4O_{10}S_2 + H$	*		*N*,*N*′-bis(γ-glutamylcystine)	63634	
556.1371	556.1379	1.4	$C_{20}H_{28}N_7O_9PS + H - H_2O$	*		biotinyl-5′-AMP	58228	HMDB04220
561.3273	561.3235	6.8	$C_{28}H_{50}N_4O_3S + K$	*		oleic acid-biotin	45287	
613.1599	613.1598	0.2	$C_{20}H_{32}N_6O_{12}S_2 + H$	*		oxidized glutathione	45	

dx.doi.org/10.1021/jf402866q | *J. Agric. Food Chem.* 2014, 62, 1373−1383

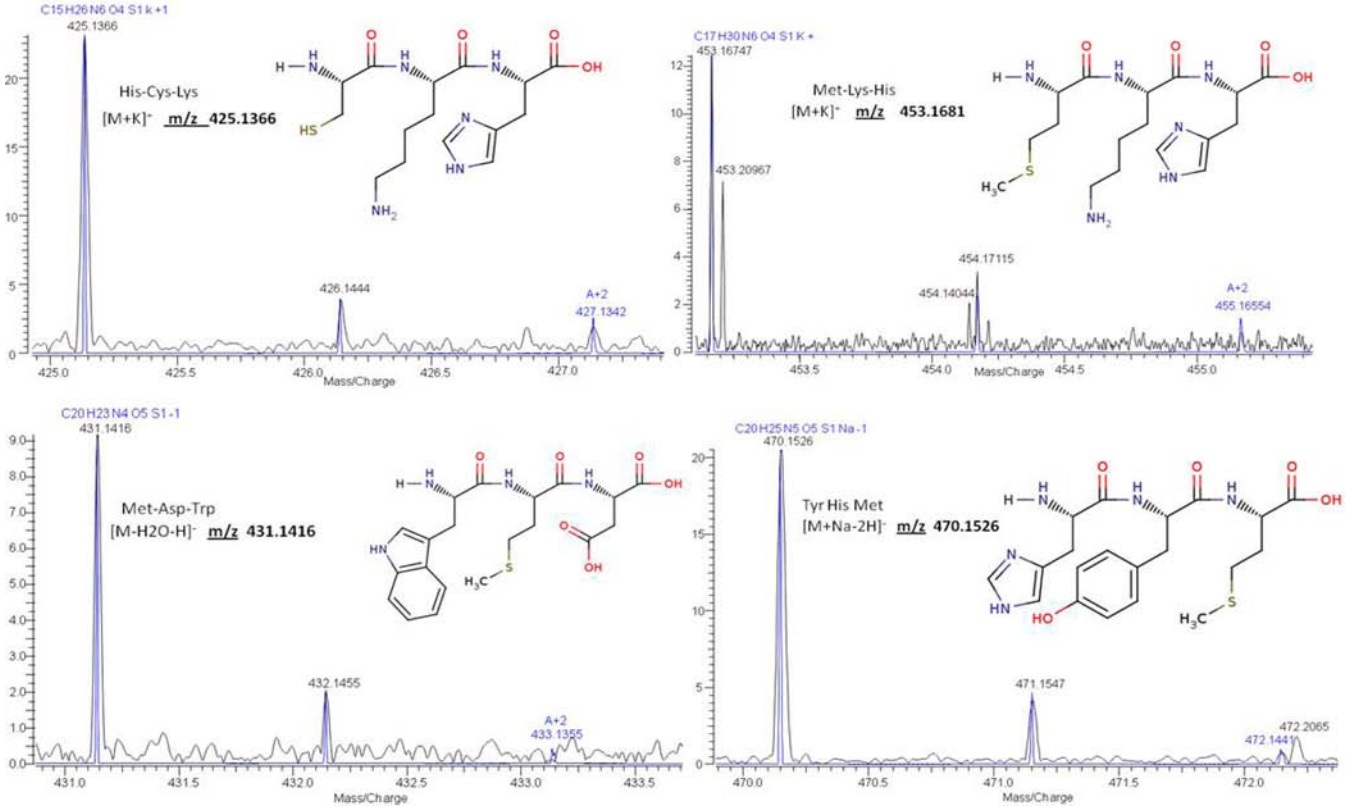

Figure 4. Chemical structures and EI-FT-ICR MS corresponding to the peptides identified in the <3 kDa permeates from g-IDY and n-IDY. Met/Asp/Trp and Tyr/His/Met were identified only in the permeate from n-IDY.

extensively documented.[35] As was previously commented, small peptides containing tryptophan, tyrosine, methionine, cysteine, and phenylalanine have been described to exhibit a high antioxidant activity.[34] In the present study, from the two peptides detected in the permeates from g-IDY and n-IDY, only one (histidine/cysteine/lysine) had an amino acid (cysteine) that could be involved in the antioxidant properties. However, the two peptides exclusively identified in the n-IDY permeate (methionine/aspartic acid/tryptophan and tyrosine/histidine/methionine) contained two of these amino acids each. In addition, both peptides contained tryptophan and tyrosine, the two most highly antioxidant amino acids. Previously published works have already described the biological activities (antioxidant, antihypertensive) of peptides from yeast origin found in synthetic wines submitted to autolytic conditions[40] and in red wines,[41,42] although their chemical structures remained unresolved. Moreover, considering these results, the preservation of aroma and reduction of aroma loss in wines aged on lees that has been linked to the GSH released by yeast autolysis[6] might also be attributable to other types of small peptides, which could have even greater antioxidant properties than GSH.

In conclusion, it has been proven that the use of IDY preparations (with or without GSH) reduces the loss of certain terpenes during the accelerated aging of model wines. It has also been shown that g-IDY preparations do in fact contain GSH in their reduced state, which can contribute to the aroma preservation in model wines, but they also contain other sulfur compounds of yeast origin that might also act as antioxidants. In addition, both g-IDY and n-IDY contained small peptides (tripeptides) with methionine, tryptophan, and tyrosine, which seem to be involved in the antioxidant properties determined in the permeates isolated from both IDYs, also being effective in the preservation of some terpenes during model wine aging. Because of the instability of GSH in wines (easily oxidized, fast combination with polyphenols, etc.), this finding could be of technological interest, assuming the higher stability of these antioxidant peptides when used, for example, after wine bottling. Subsequent work will be directed to unequivocally identify the sequence of these compounds, and further studies are needed to confirm the antioxidant effect of these peptides in closer winemaking conditions. Undoubtedly, this will be interesting for the wine and biotechnological industry to redirect the formulation of IDY preparations to achieve specific and effective winemaking applications.

AUTHOR INFORMATION

Corresponding Author

*(M.A.P.B.) Phone: +34 910 017 961. Fax:+34 910 017 905. E-mail: m.delpozo@csic.es.

Funding

This work was funded by the MINECO (AGL2012-04172-C02-01) and CONSOLIDER INGENIO 2010 (FUN-C-FOOD, CSD2007-063, Projects) and by Agrovín, S.A. (I+D 20132446 Contract). J.J.R.B. thanks CSIC for the JAE-doc contract.

Notes

The authors declare no competing financial interest.

ACKNOWLEDGMENTS

We thank Dr. Hernández-Ledesma for her valuable assistance during the ORAC-FL analysis.

REFERENCES

(1) Escudero, A.; Asensio, E.; Cacho, J.; Ferreira, V. Sensory and chemical changes of young white wines stored under oxygen. An assessment of the role played by aldehydes and some other important odorants. *Food Chem.* **2002**, *77*, 325−331.

(2) Ferreira, V.; Escudero, A.; Fernandez, P.; Cacho, J. F. Changes in the profile of volatile compounds in wines stored under oxygen and their relationship with the browning process. *Z. Lebensm. Unters. Forsch. A* **1997**, *205*, 392−396.

(3) Marais, J. Terpenes in the aroma of grapes and wines: a review. *S. Afr. J. Enol. Vitic.* **1983**, *4*, 49−58.

(4) Ugliano, M.; Kwiatkowski, M.; Vidal, S.; Capone, D.; Siebert, T.; Dieval, J.-B.; Aagaard, O.; Waters, E. J. Evolution of 3-mercaptohexanol, hydrogen sulfide, and methyl mercaptan during bottle storage of Sauvignon blanc wines. Effect of glutathione, copper, oxygen exposure, and closure-derived oxygen. *J. Agric. Food Chem.* **2011**, *59*, 2564−2572.

(5) Pozo-Bayon, M. A.; Monagas, M.; Bartolome, B.; Moreno-Arribas, M. A. Wine features related to safety and consumer health: an integrated perspective. *Crit. Rev. Food Sci.* **2012**, *52*, 31−54.

(6) Dubourdieu, D.; Lavigne-Cruège, V. The role of glutathione on the aromatic evolution of dry white wine. *Vinidea.net* **2004**, *02*.

(7) Papadopoulou, D.; Roussis, I. G. Inhibition of the decline of linalool and α-terpineol in muscat wines by glutathione and *N*-acetylcysteine. *Ital. J. Food Sci.* **2001**, *13*, 413−419.

(8) Papadopoulou, D.; Roussis, I. G. Inhibition of the decrease of volatile esters and terpenes during storage of a white wine and a model wine medium by glutathione and *N*-acetylcysteine. *Int. J. Food Sci.* **2008**, *43*, 1053−1057.

(9) Roussis, I. G.; Lambropoulus, I. G.; Tzimas, P. Protection of volatiles in a wine with low sulfur dioxide by caffeic acid or glutathione. *Am. J. Enol. Vitic.* **2007**, *58*, 274−278.

(10) Fahey, R. C.; Sundquist, A. R. Evolution of glutathione metabolism. *Adv. Enzymol. Relat. Areas Mol. Biol.* **1991**, *64*, 1−53.

(11) Field, J. A.; Thurman, E. M. Glutathione conjugation and contaminant transformation. *Environ. Sci. Technol.* **1996**, *30*, 1413−1418.

(12) Penninckx, M. A short review on the role of glutathione in the response of yeasts to nutritional, environmental, and oxidative stresses. *Enzyme Microb. Technol.* **2000**, *26*, 737−742.

(13) Penninckx, M. J. An overview on glutathione in *Saccharomyces* versus non-conventional yeasts. *FEMS Yeast Res.* **2002**, *2*, 295−305.

(14) Roussis, I. G.; Lambropoulos, I.; Papadopoulou, D. Inhibition of the decline of volatile esters and terpenols during oxidative storage of Muscat-white and Xinomavro-red wine by caffeic acid and *N*-acetylcysteine. *Food Chem.* **2005**, *93*, 485−492.

(15) Roussis, I. G.; Sergianitis, S. Protection of some aroma volatiles in a model wine medium by sulphur dioxide and mixtures of glutathione with caffeic acid or gallic acid. *Flavour Fragrance J.* **2008**, *23*, 35−39.

(16) Pozo-Bayon, M. A.; Andujar-Ortiz, I.; Moreno-Arribas, M. A. Scientific evidences beyond the application of inactive dry yeast preparations in winemaking. *Food Res. Int.* **2009**, *42*, 754−761.

(17) Kritzinger, E. C.; Bauer, F. F.; du Toit, W. J. Role of glutathione in winemaking: a review. *J. Agric. Food Chem.* **2013**, *61*, 269−277.

(18) Andujar-Ortiz, I.; Pozo-Bayon, M. A.; Moreno-Arribas, M. V.; Martin-Alvarez, P. J.; Rodriguez-Bencomo, J. J. Reversed-phase high-performance liquid chromatography-fluorescence detection for the analysis of glutathione and its precursor γ-glutamyl cysteine in wines and model wines supplemented with oenological inactive dry yeast preparations. *Food Anal. Methods* **2012**, *5*, 154−161.

(19) Kritzinger, E. C.; Stander, M. A.; Du Toit, W. J. Assessment of glutathione levels in model solution and grape ferments supplemented with glutathione-enriched inactive dry yeast preparations using a novel UPLC-MS/MS method. *Food Addit. Contam. A* **2013**, *30*, 80−92.

(20) Andújar-Ortiz, I.; C., C.; Martín-Álvarez, P. J.; Moreno-Arribas, M. A.; Pozo-Bayón, M. A. Impact of using new commercial gluthatione enriched inactive dry yeast oenological preparations on the aroma and sensory properties of wines. *Int. J. Food Prop.* **2013**, DOI: 10.1080/10942912.2012.685682.

(21) Comuzzo, P.; Tat, L.; Tonizzo, A.; Battistutta, F. Yeast derivatives (extracts and autolysates) in winemaking: release of volatile compounds and effects on wine aroma volatility. *Food Chem.* **2006**, *99*, 217−230.

(22) Pozo-Bayon, M. A.; Andujar-Ortiz, I.; Alcaide-Hidalgo, J. M.; Martin-Alvarez, P. J.; Moreno-Arribas, M. V. Characterization of commercial inactive dry yeast preparations for enological use based on their ability to release soluble compounds and their behavior toward aroma compounds in model wines. *J. Agric. Food Chem.* **2009**, *57*, 10784−10792.

(23) Rodríguez-Bencomo, J. J.; Muñoz-Gonzalez, C.; Andujar-Ortiz, I.; Martin-Alvarez, P. J.; Moreno-Arribas, M. V.; Pozo-Bayon, M. A. Assessment of the effect of the non-volatile wine matrix on the volatility of typical wine aroma compounds by headspace solid phase microextraction/gas chromatography analysis. *J. Sci. Food Agric.* **2011**, *91*, 2484−2494.

(24) Davalos, A.; Gomez-Cordoves, C.; Bartolome, B. Extending applicability of the oxygen radical absorbance capacity (ORAC-fluorescein) assay. *J. Agric. Food Chem.* **2004**, *52*, 48−54.

(25) Doi, E.; Shibata, D.; Matoba, T. Modified colorimetric ninhydrin methods for peptidase assay. *Anal. Biochem.* **1981**, *118*, 173−184.

(26) Moreno-Arribas, M. V.; Bartolome, B.; Pueyo, E.; Polo, M. C. Isolation and characterization of individual peptides from wine. *J. Agric. Food Chem.* **1998**, *46*, 3422−3425.

(27) Clowers, B. H.; Dodds, E. D.; Seipert, R. R.; Lebrilla, C. B. Dual polarity accurate mass calibration for electrospray ionization and matrix-assisted laser desorption/ionization mass spectrometry using maltooligosaccharides. *Anal. Biochem.* **2008**, *381*, 205−213.

(28) Tautenhahn, R.; Patti, G. J.; Rinehart, D.; Siuzdak, G. XCMS Online: a Web-based platform to process untargeted metabolomic data. *Anal. Chem.* **2012**, *84*, 5035−5039.

(29) Batiashvili, T. A.; Bezzubov, A. A.; Chichashvili, N. D.; Rodopulo, A. K. Changes in essential-oil composition of grapes during their processing. *Appl. Biochem. Microbiol.* **1981**, *16*, 450−452.

(30) Neuenschwander, U.; Guignard, F.; Hermans, I. Mechanism of the aerobic oxidation of α-pinene. *ChemSusChem* **2010**, *3*, 75−84.

(31) Villano, D.; Fernandez-Pachon, M. S.; Troncoso, A. M.; Garcia-Parrilla, M. C. Comparison of antioxidant activity of wine phenolic compounds and metabolites in vitro. *Anal. Chim. Acta* **2005**, *538*, 391−398.

(32) Battin, E. E.; Brumaghim, J. L. Antioxidant activity of sulfur and selenium: a review of reactive oxygen species scavenging, glutathione peroxidase, and metal-binding antioxidant mechanisms. *Cell Biochem. Biophys.* **2009**, *55*, 1−23.

(33) Parcell, S. Sulfur in human nutrition and applications in medicine. *Altern. Med. Rev.* **2002**, *7*, 22−44.

(34) Hernandez-Ledesma, B.; Davalos, A.; Bartolome, B.; Amigo, L. Preparation of antioxidant enzymatic hydrolysates from α-lactalbumin and β-lactoglobulin. Identification of active peptides by HPLC-MS/MS. *J. Agric. Food Chem.* **2005**, *53*, 588−593.

(35) Samaranayaka, A. G. P.; Li-Chan, E. C. Y. Food-derived peptidic antioxidants: a review of their production, assessment, and potential applications. *J. Funct. Food* **2011**, *3*, 229−254.

(36) Brown, S. C.; Kruppa, G.; Dasseux, J. L. Metabolomics applications of FT-ICR mass spectrometry. *Mass Spectrom. Rev.* **2005**, *24*, 223−231.

(37) Garrett, R.; Vaz, B. G.; Hovell, A. M. C.; Eberlin, M. N.; Rezende, C. M. Arabica and Robusta coffees: identification of major polar compounds and quantification of blends by direct-infusion electrospray ionization-mass spectrometry. *J. Agric. Food Chem.* **2012**, *60*, 4253−4258.

(38) Feng, X.; Siegel, M. M. FTICR-MS applications for the structure determination of natural products. *Anal. Bioanal. Chem.* **2007**, *389*, 1341−1363.

(39) Rodríguez-Melendez, R. Importancia del metabolismo de la biotina. *Rev. Invest. Clin.* **2000**, *52*, 194−199.

(40) Alcaide-Hidalgo, J. M.; Pueyo, E.; Polo, M. C.; Martinez-Rodriguez, A. J. Bioactive peptides released from *Saccharomyces*

cerevisiae under accelerated autolysis in a wine model system. *J. Food Sci.* **2007**, *72*, M276−M279.
(41) Pozo-Bayon, M. A.; Alcaide, J. M.; Polo, M. C.; Pueyo, E. Angiotensin I-converting enzyme inhibitory compounds in white and red wines. *Food Chem.* **2007**, *100*, 43−47.
(42) Takayanagi, T.; Yokotsuka, K. Angiotensin I converting enzyme-inhibitory peptides from wine. *Am. J. Enol. Vitic.* **1999**, *50*, 65−68.

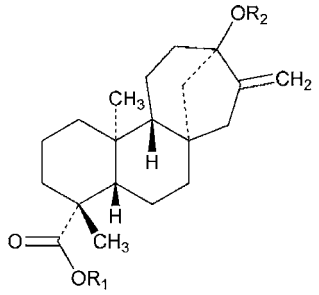

Compound name	R_1	R_2
Stevioside	β-Glc	β-Glc-β-Glc(2→1)
Rebaudioside A	β-Glc	β-Glc-β-Glc(2→1) | β-Glc(3→1)
Rebaudioside B	H	β-Glc-β-Glc(2→1) | β-Glc(3→1)
Rebaudioside C	β-Glc	β-Glc-α-Rha(2→1) | β-Glc(3→1)
Rebaudioside D	β-Glc-β-Glc(2→1)	β-Glc-β-Glc(2→1) | β-Glc(3→1)
Rebaudioside F	β-Glc	β-Glc-β-Xyl(2→1) | β-Glc(3→1)
Dulcoside A	β-Glc	β-Glc-α-Rha(2→1)
Rubusoside	β-Glc	β-Glc
Steviolbioside	H	β-Glc-β-Glc(2→1)

Glc = glucose **Rha** = rhamnose **Xyl** = xylose

Figure 1. Structures of the nine components of JECFA's steviol glycoside food ingredient.

comprehensive quality assessments of commercial products. Potential new HPLC−UV conditions for improving the chromatography of steviol glycosides have been reported, including the use of gradient elution with C18 columns or the use of HILIC columns with isocratic elution, but none have been sufficiently evaluated or validated for use as standardized methods.[2,10]

The new chromatographic method presented here not only shows an improved and acceptable chromatographic performance but also features significant improvements of three other analytical elements of current HPLC analysis standards for steviol glycosides. Included are the addition of system suitability tests, the HPLC peak identification approach, and the use of modern and efficient quantitation approaches for measuring individual glycosides. System suitability tests are used to verify whether a chromatography system is fit for the analysis it will undertake on the day of analysis for critical parameters such as precision and resolution.[11] Such tests are missing in current standardized methods of analysis for steviol glycosides and are critical and essential to ensure their reliable use in quality control laboratories. Peak identification in the current HPLC method established by JECFA uses a mixed standard solution prepared with nine individual standards.[1] This approach is not practical for routine analysis, given the current cost of purchasing high-purity reference materials. Quantitation of individual steviol glycosides in the current JECFA methods is conducted using a quantitative stevioside reference standard and molecular weight correction factors.[1] This approach assumes that all nine measured steviol glycosides have equal molar UV absorptivities. Reports supporting the validity of this assumption are lacking and are necessary to ensure the accuracy of the approach. The relative response factor approach is a well-established quantitative approach and was established for this method.[12]

In this work, a reversed-phase HPLC−UV method with acceptable selectivity for typical steviol glycoside products was developed and validated, and optimal separation of the critical pair rebaudioside A and stevioside was established. The versatility of the method was demonstrated by evaluating forced degradation samples of rebaudioside A, a primary component in commercial samples. Additionally, reference standards and criterion-based system suitability tests were developed for the HPLC method to ensure efficient and reliable performance for quantitative measurements. Finally, the research provides validation data for establishing the linearity, accuracy, precision, and ruggedness of the developed HPLC method.

MATERIALS AND METHODS

Reagents and Chemicals. Reagent-grade potassium dihydrogen phosphate (KH_2PO_4), 85% phosphoric acid (H_3PO_4), concentrated hydrochloric acid (HCl, 12.1 M), a sodium hydroxide (NaOH) solution [50% (w/w) in water], and pH 2.00 and 4.00 buffer solutions were purchased from Fisher-Scientific (Pittsburgh, PA). A pH 4.01 buffer solution was also obtained from Thermo-Scientific (Waltham, MA). HPLC-grade acetonitrile (ACN) was obtained from Merck KGaA (Darmstadt, Germany) and Fisher Scientific. Water (H_2O) was purified using the Millipore (Billerica, MA) Advantage A10 system. A peroxide (H_2O_2) solution (30% in H_2O) was purchased from Sigma-Aldrich (St. Louis, MO). Karl Fisher reagents Hydranol solvent and Titrant 5 were purchased from Fluka (Trademark of Sigma-Aldrich). United States Pharmacopeia (USP, Rockville, MD) primary reference standards were used for rebaudioside A, B, and D, rubusoside, stevioside, and steviolbioside. Reference standards for rebaudioside C and F, dulcoside A, isosteviolmonoside, steviol, and isosteviol were purchased from ChromaDex (Irvine, CA). A USP system suitability reference standard containing the nine steviol glycosides (Figure 1) to be measured with this method was used for performing system suitability checks. Four commercial samples of high-purity steviol glycoside ingredients used in this study were generous donations from three different suppliers.

Standard and Sample Solutions. Potassium phosphate buffer (5 mM, pH 3.0) was prepared by dissolving KH_2PO_4 in H_2O, and the pH was adjusted to 3.0 using H_3PO_4 on a Thermo-Scientific Orion 3 Star benchtop pH meter. The buffer solution was vacuum filtered by being passed through a filter membrane with a 0.45 μm pore size. The diluent solution was prepared by mixing 5 mM potassium phosphate buffer (pH 3.0) with ACN in a 65:35 (v/v) ratio. For quantitative measurements, standard and sample materials were equilibrated at ambient temperature for ≥24 h because of their hygroscopic nature. The moisture (H_2O) content was determined by Karl Fisher titration using a Mettler-Toledo (Columbus, OH) DL38 titrator. Materials were accurately weighed on a Mettler-Toledo analytical balance (AT201), and solutions were routinely prepared in volumetric flasks. A brief sonication step (2−5 min) was used to dissolve materials.

Rebaudioside A Forced Degradation Studies. Sample solutions of rebaudioside A (5 mM) were tested following several different types of degrading paradigms to test system stability and specificity. A 5.0 mL aliquot of a rebaudioside A solution (10 mM in diluent) was mixed with 5.0 mL of NaOH in one experiment, and HCl solutions (500 mM in H_2O) in a separate experiment, both conducted at ambient temperature. The monitored reaction times were 2, 7, and 24 h. The reaction mixtures were neutralized with an equal molar ratio of acid or base and diluted 10-fold for analysis (0.5 mM rebaudioside

dx.doi.org/10.1021/jf4047557 | J. Agric. Food Chem. 2014, 62, 1384−1389

A). A 5.0 mL aliquot of a rebaudioside A solution (10 mM in diluent) was incubated with 5.0 mL of 30% H_2O_2 at ambient temperature. After incubation for 2 h, 1 day, and 5 days, 1.0 mL aliquots of the reaction mixture were removed and diluted as described above for analysis. Control reaction mixtures containing all components except degradant were analyzed, along with chromatographic controls containing all components except rebaudioside A. Rebaudioside A powder was exposed to UV (total of 1958 W h^{-1} m^{-2}) and white light (total of 2302 klx/h) using a Caron (Marietta, OH) photostability chamber (model 6545-2). Light stability studies were conducted for up to 72 h, and samples were removed at 24, 48, and 72 h for analysis at a concentration of 1.2 mg/mL. Similarly, rebaudioside A powder was incubated at 60 °C in a Yamato (Santa Clara, CA) vacuum oven for up to 8 days. Customarily, photodiode array (PDA) peak purity analysis of rebaudioside A was attempted to provide evidence of the spectral purity of the main peak after forced degradation. Because of a lack of a unique UV spectrum for the main component (λ_{max} = 210 nm), peak purity analysis could not be applied to identify a co-elution. However, mass balance to control reactions was evaluated to determine the amount or lack of significant degradation.

Chromatographic Conditions. Agilent (Wilmington, DE) 1200 and Waters (Milford, MA) Alliance 2965 HPLC systems consisting of a degasser, a quaternary pump, an autosampler, a column compartment, and a PDA detector were used for analysis. Both of the HPLC systems were controlled using Waters Empower 2 software. The method used a YMC (Kyoto, Japan) ODS-AQ column (250 mm × 4.6 mm, 5 μm) and mobile phase consisting of solvent A [5 mM potassium dihydrogen phosphate buffer (pH 3.0)] and solvent B (ACN). Two step gradients with ACN were used to elute analytes of interest as follows: 10 to 35% solvent B over 10 min, held for 15 min at 35% solvent B, 35 to 75% solvent B over 10 min, and held for 15 min at 75% solvent B. The column was re-equilibrated to the starting condition of 10% solvent B and 90% solvent A for 15 min. The column was maintained at 32 °C with a flow rate of 0.5 mL/min. The injection volume was 15 μL for both sample and standard solutions, which were kept under ambient conditions in the autosampler. UV detection at 210 nm with a 4 nm bandwidth was used for analysis. Other tested columns for method development purposes included Shiseido (Tokyo, Japan) Capcell Pak C18 MGII (250 mm × 4.6 mm, 5 μm, JECFA, 2010) and Imtakt USA (Philadelphia, PA) Scherzo SM-C18 (250 mm × 4.6 mm, 3 μm) columns.

System Suitability Tests. A solution of the *USP* system suitability reference standard was prepared at a concentration of 1.2 mg/mL, and five replicate injections of the solution were performed to assess the HPLC system performance in terms of critical pair separation, system precision, and detector sensitivity. The following acceptance criteria were defined per *USP* general chapter ⟨621⟩[11] and intended use of method: a resolution of rebaudioside A and stevioside of ≥1.5, a percent relative standard deviation (%RSD) of the rebaudioside A peak area responses for the five injections of ≤1.5%, and %RSD of the rubusoside peak responses of ≤2.5%.

Total Assay Determination. Standard solutions of rebaudioside A were prepared at concentrations of 0.5 mg/mL (S1) and 0.03 mg/mL (S2) to quantify major and minor analyte peaks in samples. The standard solutions were prepared in duplicate and confirmed to have weight-corrected UV responses (response factors) within 2.5% of each other. The nominal concentration for sample solutions was established at 1.2 mg/mL, which provided adequate detection of major and minor peaks. Separately, equal volumes of sample solutions at the nominal concentration were injected. The chromatograms from the system suitability solutions were used to identify the nine steviol glycosides in the samples. The percentages of each component in the sample were calculated as follows:

$$\%\ \text{assay} = (r_U/r_S) \times (C_S/C_U) \times (1/F) \times 100$$

where r_U is the peak area for the analyte in the sample, r_S is the peak area for rebaudioside A in S1 or S2, C_S is the concentration of USP rebaudioside A RS in S1 or S2 corrected for water and purity, C_U is the concentration in the sample solution corrected for water content, and F is the relative response factor (RRF) (see Table 2).

Note solution S1 was used to quantify rebaudioside A and stevioside, which were the two major components, and solution S2 was used to quantify all other minor components. It is noteworthy that if r_U for rebaudioside A or stevioside was less than 12% of r_S in solution S1, then solution S2 was used for a more accurate quantification. The sum of percentages of the nine measured steviol glycosides was determined as the total assay.

Method Validation. The *USP* general chapter ⟨1225⟩ validation of compendial procedures was used to design validation experiments.[13] The validation was limited to the nine named steviol glycosides in the JECFA monograph because of their established significance as components of the food ingredient.[1] The linearity range for the procedure was evaluated at a concentration level of 0.01−1.2 mg/mL for the two major components, rebaudioside A and stevioside. The range for the seven minor components was 0.01−0.06 mg/mL, except for rebaudioside C, which was evaluated up to 0.25 mg/mL because of its higher natural abundance in evaluated commercial samples. Linear regression analysis was performed to determine the correlation coefficient. The RRF values for each of the eight steviol glycosides with reference to rebaudioside A were determined at a single concentration (0.05−0.08 mg/mL) with duplicate preparations.

The accuracy of the method was assessed by conducting the total assay determinations at the 80, 100, and 120% levels of the nominal assay concentration using a commercial product with an established assay value determined using an alternative procedure. Triplicate samples at each level were prepared and analyzed (n = 9). The precision of the method was determined by evaluating the %RSD of assay measurements with six sample preparations (n = 6) at the nominal concentration. The intermediate precision (ruggedness) was examined by performing assay determinations with six sample preparations by a different analyst using a different column and HPLC system, on a different day. The difference of the means was determined at the 90% confidence interval. The robustness of the method was evaluated by introducing small deliberate changes to key chromatographic conditions and assessing the effect upon critical pair separation and system precision. The modifications included the monitored wavelength at ±3 nm, a column temperature of ±2 °C, and a relative change of ±10% of the initial ACN content and flow rate.

RESULTS AND DISCUSSION

Method Development. A reversed-phase HPLC−UV method with acceptable selectivity for typical steviol glycoside products was developed for its ease and widespread use of methodology. The method was also capable of the separation and identification of steviol and isosteviol, the 2-unglycosylated aromatic aglycons, and a rarely occurring monoglycosylated structure known as isosteviolmonoside. Figure 2 shows a chromatogram of a solution composed of individual reference standards for each analyte combined at the concentration listed in Table 1. The analytes were eluted with an ACN gradient that was the key parameter affecting the selectivity of the method

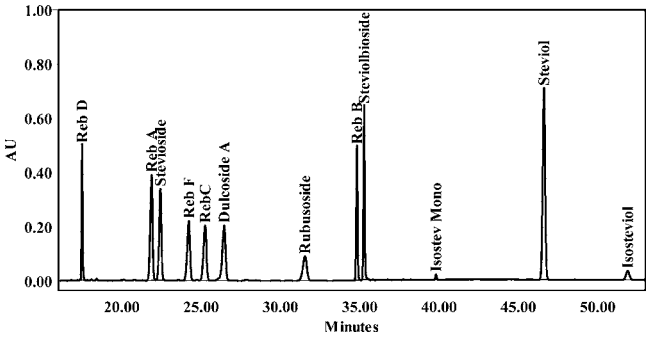

Figure 2. Representative chromatogram of a mixture of several reference standards of steviol glycosides in solution.

Table 1. Elution Profile of Steviol Glycosides[a]

peak name	concn (mg/mL)	RT (min)	RT (% RSD)	resolution (*R*)
rebaudioside D	0.6	17.5	0.1	–
rebaudioside A	0.9	21.9	0.2	20.3
stevioside	0.6	22.4	0.2	2.0
rebaudioside F	0.7	24.2	0.2	5.9
rebaudioside C	0.6	25.2	0.2	3.0
dulcoside A	0.6	26.4	0.2	3.3
rubusoside	0.8	31.5	0.2	11.9
rebaudioside B	0.6	34.8	0.1	10.4
steviolbioside	0.6	35.3	0.0	3.0
isosteviolmonoside	0.2	39.8	0.0	28.2
steviol	0.6	46.6	0.0	29.4
isosteviol	0.6	51.9	0.0	15.0

[a]Individual characteristics of reference standards in solution tested in Figure 2.

under reversed-phase conditions. Two step gradients were introduced; the first served to resolve the hydrophilic components at an acceptable resolution [*R* of ≥2.0 (Table 1)], and the second one allowed for efficient elution of the hydrophobic diterpenoids. The %RSD for retention time [RT (Table 1)] was obtained from five replicate injections of the mixture solution from three independent experiments on different days, which showed minimal shifts in retention time (%RSD, ≤0.2%), and well-resolved peaks ($R \geq 2.0$) were consistently achieved.

The optimal separation of the critical pair rebaudioside A and stevioside was also established by evaluating up to 10 commercial samples with various ratios of the critical pair that demonstrated *R* values in the range of 1.7−2.2. The worst-case scenario (*R* of 1.7) was observed for a commercial product containing 95% rebaudioside A and 1% stevioside. In addition, aside from the primary column, C18 columns from two other manufacturers with slight differences in particle packing and size were tested that provided *R* of ≥1.9 for the critical pair.

The stability-indicating capability of the newly developed method was determined by conducting forced degradation studies of rebaudioside A. As shown in Figure 3, a sample solution of rebaudioside A (5 mM) was tested following several different types of degrading paradigms to test system stability and specificity. Solutions depicted were subjected to degradation in the following conditions: base (250 mM NaOH, 2 h), peroxide (15% in H_2O_2, 5 days), acid (250 mM HCl, 7 h), heat (60 °C, 8 days), and UV and white light (1958 W h^{-1} m^{-2} and 2302 klx/h, 72 h). Heat exposure and UV and white light exposure were used for rebaudiside A powder, while base, peroxide, and acid incubations were used in solution.

Hydrolysis of the ester-linked sugar leading to rebaudioside B was observed within 2 h of incubation in a strong base [RT = 34.8 min (Figure 3)]. In addition, an unknown peak at a RT of 20.3 min appeared to be well-resolved (*R* = 5.9) from rebaudioside A and rebaudioside D. An acid-induced degradant eluted near rebaudioside A within 7 h of incubation (RT = 22.7; *R* = 3.3). As shown in Figure 3, several minor unknown peaks that eluted close to rebaudioside D were also observed during the prolonged oxidative condition (5 days). Rebaudioside D, however, was resolved from the degradation peaks at *R* values of ≥1.7. Rebaudioside A powder exposed to UV and white light for up to 72 h and incubation at 60 °C for up to 8 days did not lead to known or unknown structures as compared to an unexposed sample. Stability-indicating HPLC methods provided the ability to discover compromises to product quality more efficiently.

System Suitability Tests. Validation of the system suitability criteria was obtained via five independent experiments conducted on different days, by two different analysts, and on two different HPLC instrument setups. The assessments established that the resolution of the critical pair, rebaudioside A and stevioside, was observed at 1.8−2.1 with a criterion of ≥1.5. The system precision was monitored by evaluating the %RSD of the rebaudioside A peak area response from five replicate injections, which was determined at 0.12−0.46% with a criterion of ≤1.5%. The %RSD of the rubusoside peak response was used to evaluate detector sensitivity as the smallest peak (0.004 AU) in the mixture. The variation in peak area response was detected at a %RSD of 1.3−1.8% with a criterion of ≤2.5%. The acceptable performance of the HPLC method against the evaluated system suitability criteria

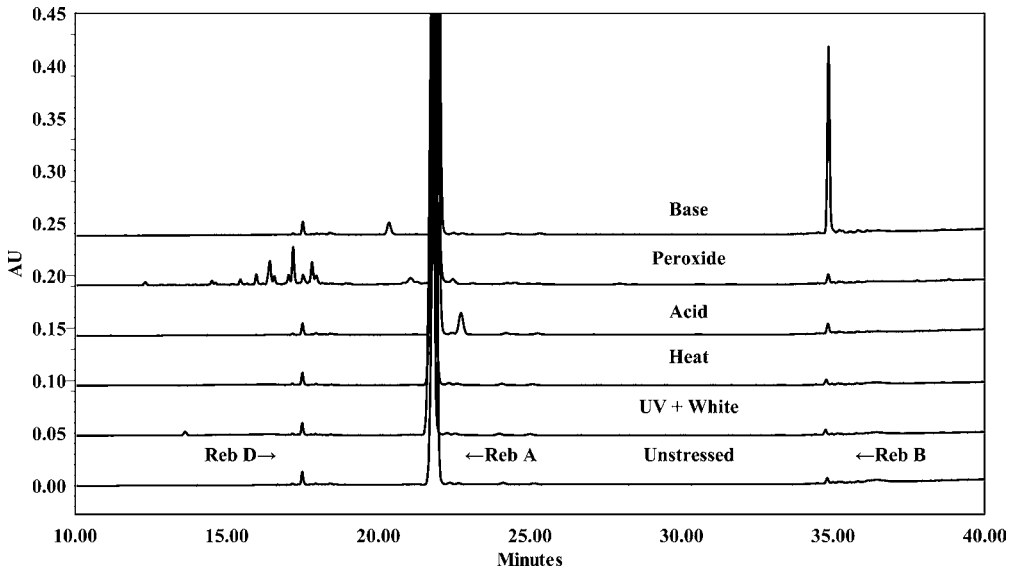

Figure 3. Overlaid chromatograms of degraded sample solutions of rebaudiside A (Reb A).

dx.doi.org/10.1021/jf4047557 | J. Agric. Food Chem. 2014, 62, 1384−1389

established that the method was suitable for quantitative measurements.

Method Validation. The linearity of the UV response for each of the analytes of interest was evaluated independently at concentration ranges commonly observed in commercial samples. Results of the study established the linearity of the method at a correlation coefficient of 1.000 with a negligible intercept (≤2%). The limit of quantification was determined to be 1% of the nominal concentration of 1.2 mg/mL (~0.01 mg/mL) established as the lowest concentration point of the linearity curve for each of the glycosides. RRF values were determined at a single concentration level with duplicate preparations within the linear range for all analytes. In addition, the ratio of the slopes from the linear regression studies provided equivalent values. Table 2 lists the RRF values and relative retention times (RRTs) determined for the eight other steviol glycosides with reference to rebaudioside A in the USP system suitability reference standard solution. The RRF values were intended to correct for intrinsic differences in the UV response among steviol glycosides.[12] This was especially important for assay determinations, where rebaudioside A was used for quantification of all other related analytes in uncharacterized samples. Similarly, the RRT values served to easily identify analytes in uncharacterized samples. *USP* resolution values are defined in *USP* General Chapter ⟨621⟩[11] and are used to demonstrate the acceptable separation of neighboring peaks.

Table 2. Chromatographic Profile of Steviol Glycosides with Respect to Rebaudioside A

name	relative retention time (RRT)	USP resolution	relative response factor (RRF)
rebaudioside D	0.80	not available	0.83
rebaudioside A	1.00	21.3	1.00
stevioside	1.03	2.1	1.22
rebaudioside F	1.10	5.6	1.02
rebaudioside C	1.15	3.1	0.98
dulcoside A	1.21	3.5	1.16
rubusoside	1.44	8.6	1.06
rebaudioside B	1.59	12.2	1.07
steviolbioside	1.61	3.0	1.38

Average method accuracy values were 99.1, 99.9, and 100.9% at 80, 100, and 120%, respectively, of the nominal concentration of 1.2 mg/mL. The %RSD for six independent assay determinations at the nominal concentration was 1.0%. A second analyst repeated the precision experiment with a different HPLC system and column, on a different day. The difference of means at the 90% confidence interval was within 2.0%, which was deemed an acceptable equivalence for the intended purpose.

The method was determined to be robust for minor changes in column temperature, initial ACN content, and flow rate. A significant difference in the peak area response was observed when the detection wavelength changed ±3 nm. Specifically, a 40% decline in the peak area response was measured at 213 nm for rebaudioside A and rubusoside during system suitability evaluations. However, the %RSD for the two affected analyte peaks and the resolution of the critical pair met the established acceptance criteria, indicating a negligible impact on analysis.

The validation results met the established acceptance criteria for linearity, accuracy, precision, and ruggedness. The acceptance criteria for the validation experiments were developed using industry-accepted guidance[14,15] and were based on the intended use of the method for quantification of steviol glycosides within JECFA's monograph specification of ≥95.0%.

Total Assay Determinations. Standard solutions of rebaudioside A were prepared at concentrations of 0.5 mg/mL (S1) and 0.03 mg/mL (S2) to generate a two-point calibration curve. Duplicate preparations of standard solutions showed response factors in the range of −0.1 to 2.2% throughout the validation experiments. Figure 4 illustrates profiles of select commercial samples, which showed the major components to be rebaudioside A and stevioside, with rebaudioside C observed at 3−8%. The other minor components were observed at 0.8−1.8% of the total assay. Assay determinations of individual and total steviol glycosides for commercial purposes were in close agreement with the manufacturer's certificate of analysis (data available in Table S1 of the Supporting Information) and within the JECFA Steviol Glycosides monograph specification of ≥95.0% (JECFA, 2010). The acceptable results of the analysis added further evidence to

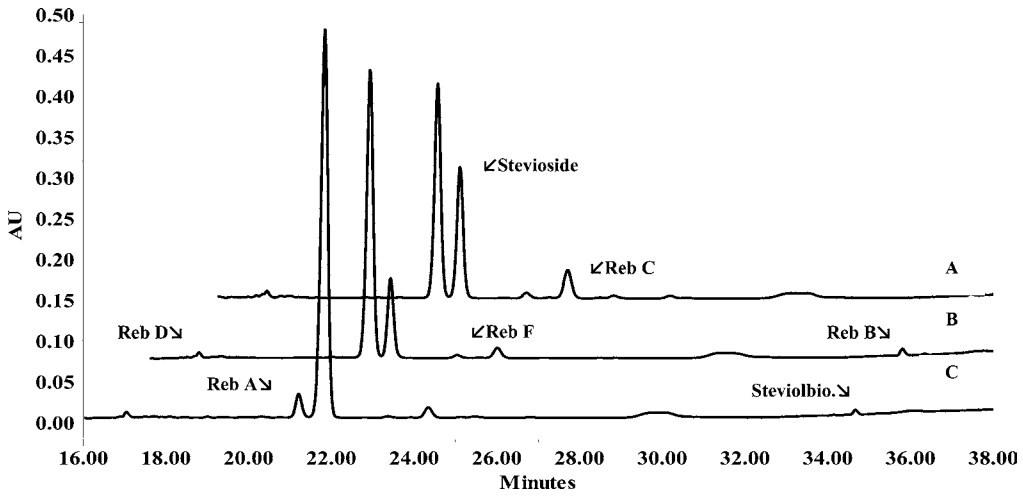

Figure 4. Overlaid chromatograms of sample analysis that illustrate the varying ratios of the critical pair rebaudioside A and stevioside in commercial samples. Traces are offset to illustrate peak differences.

the utility of the method for quality and strength determinations of commercial steviol glycoside products.

Advantages. Steviol glycoside products are known to contain a mixture of highly hydrophilic analytes carrying multiple sugar moieties, whereas other compounds in the mixture exhibit the hydrophobic nature of the diterpenoid backbone common to all of the glycosides. The developed reversed-phase HPLC method was capable of separating the nine related structures known to be components of steviol glycoside products with exceptional reproducibility. In addition, the method was able to identify the 2-diterpenoid backbones found in the glycosylated structures and a rarely occurring glycoside. Moreover, the rebaudioside A forced degradation studies provided solid evidence that the developed reversed-phase HPLC method could resolve known and unknown structures that may arise from extreme stress conditions of these products. The method validation results met the established acceptance criteria for linearity, accuracy, precision, and ruggedness. The method was also found to be robust for minor changes to LC parameters that may arise during routine analysis. The validated HPLC method was found to be suitable for quality and strength assessments and is to be included by USP in the *Food Chemicals Codex* compendial standard for steviol glycosides.

■ ASSOCIATED CONTENT

Ⓢ Supporting Information

Commercial sample assay results. This material is available free of charge via the Internet at http://pubs.acs.org.

■ AUTHOR INFORMATION

Corresponding Author

*E-mail: jm@usp.org. Phone: (301) 816-8288. Fax: (301) 816-8157.

Notes

The authors declare no competing financial interest.

■ ABBREVIATIONS

%RSD, percent relative standard deviation; ACN, acetonitrile; CoA, certificate of analysis; FCC, Food Chemicals Codex; GB, Chinese Guobiao; JECFA, Joint FAO/WHO Expert Committee on Fodd Additives; PDA, photodiode array; RT, retention time; RRT, relative retention time; RRF, relative response factor; USP, United States Pharmacopeia

■ REFERENCES

(1) JECFA. Steviol glycosides, monograph 10. In Food and Agricultural Organization of the United Nations. Combined Compendium of Food Additive Specifications; 2010 (http://www.fao.org/food/food-safety-quality/scientific-advice/jecfa/jecfa-additives/en/) (accessed July 17, 2013).

(2) Zimmermann, B. F.; Woelwer-Reick, U.; Papagiannopoulos, M. Separation of steviol glycosides by hydrophilic liquid interaction chromatography. *Food Anal. Methods* **2011**, *5*, 266−271.

(3) Woelwer-Rieck, U.; Lankes, C.; Wawrzum, A.; Wust, M. Improved HPLC method for the evaluation of the major steviol glycosides in leaves of *Stevia rebaudiana*. *Eur. Food Res. Technol.* **2010**, *231*, 581−588.

(4) Pol, J.; Hohnova, B.; Hyotylainen, T. Characterization of *Stevia rebaudiana* by comprehensive two-dimensional liquid chromatography time-of-flight mass spectrometry. *J. Chromatogr., A* **2007**, *1150*, 85−92.

(5) Pieri, V.; Belancic, A.; Morales, S.; Stuppner, H. Identification and quantification of major steviol glycosides in *Stevia rebaudiana* purified extracts by ^{1}H NMR spectroscopy. *J. Agric. Food Chem.* **2011**, *59*, 4378−4384.

(6) People [sic] Republic of China. GB 8270. Food additive−steviosides. 1999 (http://www.freestd.us/soft/173907.htm) (accessed July 17, 2013).

(7) JECFA. Steviol glycosides, monograph 5. In Food and Agricultural Organization of the United Nations, Combined Compendium of Food Additive Specifications; 2008 (http://www.fao.org/food/food-safety-quality/scientific-advice/jecfa/jecfa-additives/en/) (accessed July 17, 2013).

(8) USP. *Food Chemicals Codex. FCC Second Supplement to the Eighth edition*; The United States Pharmacopeial Convention: Rockville, MD, 2009.

(9) Markosyan, A. A. Stevia analysis: Current status overview and development outlook. Institute of Food Technologists Annual Meeting, New Orleans, LA, June 2011.

(10) Hutapea, A. M.; Toskulkao, C.; Wilairat, P.; Buddhasukh, D. High-performance liquid chromatographic separation and quantitation of stevioside and its metabolites. *J. Liq. Chromatogr. Relat. Technol.* **1999**, *22*, 1161−1170.

(11) *United States Pharmacopeia and National Formulary (USP 36-NF 31)*; The United States Pharmacopeial Convention: Rockville, MD, 2012; pp 268−275.

(12) Elmer, J.; Curgess, C.; Kleinschmidt, G.; Miller, J. H. M. Performance Parameters, Calculations and Tests. In *Method Validation in Pharmaceutical Analysis: A Guide to Best Practice*; Ermer, J., Miller, J. H. M., Eds.; Wiley-VCH,: Weinheim, Germany, 2005; pp 72−74.

(13) USP. USP general Chapter ⟨1225⟩. In *USP 36-NF 31*; The United States Pharmacopeial Convention: Rockville, MD, 2012; pp 983−988.

(14) Thompson, M.; Ellison, S. L. R.; Wood, R. Harmonized guidelines for single-laboratory validation of methods of analysis. *Pure Appl. Chem.* **2002**, *74*, 835−855.

(15) *Guidelines for Single Laboratory Validation of Chemical Methods for Dietary Supplements and Botanicals*; Association of Official Analytical Chemists: Gaithersburg, MD, 2002.

induced resistance responses using NO donor sodium nitroprusside (SNP) and SNP plus U0126.

MATERIALS AND METHODS

Fruit Materials and Treatments. Cherry tomato (*Lycopersicon esculentum* Mill. cv. Qian-xi) fruits were harvested at the mature green stage in Guangxi, China, and immediately transported to the laboratory. The fruits were selected based on the uniform size and shape without physical injuries or infections. The fruits were then surface-disinfected with 2% (v/v) sodium hypochlorite for 2 min, washed with distilled water, and air-dried at room temperature. The fruits were infiltrated in either (1) water (the control), (2) 10 μM U0126 (LC Laboratories, Woburn, MA, USA), (3) 0.2 mM NO donor sodium nitroprusside (SNP, Sigma-Aldrich, St Louis, MO, USA), or (4) 0.2 mM SNP plus 10 μM U0126 solutions under a pressure of −35 kPa for 0.5 min, then kept in the solution under air pressure for 2 min and then air-dried. All fruits were stored at 25 ± 1 °C with 85−90% relative humidity (RH). The fruits were divided into four treatment groups of 265 fruits each. Then, each treatment group of fruits was divided into two further categories. One category was used in the inoculation experiment (45 fruits); the other category was sampled at 0 h, 0.5 h, 1 h, 4 h, 8 h, 16 h, 24 h, 2 d, 4 d, 6 d, and 8 d for measurements of *LeMAPK1/2/3* gene expression, NO content, nitric oxide synthase (NOS) activity, and defense enzyme activities. Pericarp tissues from the fruits equatorial region were cut into small pieces, frozen in liquid nitrogen and stored at −80 °C until analysis.

Pathogen Inoculation and Disease Symptom Measurement. *B. cinerea* (ACCC 36028) was purchased from Agricultural Culture Collection of China (Haidian, Beijing). *B. cinerea* was incubated on potato dextrose agar medium, at 25 °C for 7−10 d. Spore suspensions (2×10^6 conidia mL^{-1}) were prepared by brushing the surface of the plates and suspending them in sterile distilled water containing 0.01% Tween-80. After being treated for 24 h, the inoculations were carried out. Forty-five fruits were sterilized with 75% ethanol before inoculation. A 2 mm wide × 4 mm deep wound was cut with a sterile nail on the equator of the fruits. Then 10 μL of spore suspension of *B. cinerea* was injected into the wound with a pipet and the fruits were stored at 25 ± 1 °C and 90−95% relative humidity (RH).

Decay development was monitored daily after inoculation. Disease incidence was expressed as the percentage of fruits showing disease symptoms. Lesion area = 3.14 × (lesion diameter/2)^2.

Measurement of NO Accumulation and NOS Activity. Frozen fruit samples (3 g) were ground with a mortar and pestle in a 3-mL ice-cold extraction buffer [50 mM phosphate buffer saline (PBS, pH 7.4) containing 1 mM dithiothreitol, 1 mM $MgCl_2$].[23] After centrifugation at 12 000*g* for 20 min at 4 °C, supernatant was collected and used for NO determination. NO content was determined according to the instruction of the nitric oxide assay kit (Nanjing Jiancheng Bioengineering Institute, Jiangsu, China). Briefly, NO reacts with oxygen to form a variety of end products, including nitrite (NO_2^-) and nitrate (NO_3^-). The reduction of NO_3^- to NO_2^- was then achieved using nitrate reductase. The determination of NO_2^- was based on the Griess reaction. NO content was expressed as $\mu M \cdot g^{-1}$ fresh weight (FW).

Frozen fruit samples (3 g) were homogenized in a 3-mL extraction buffer (50 mM HEPES, pH 7.4, containing 0.1 mM NADPH, 10 nM CaM, 30 μL BH_4, 1.25 mM $CaCl_2$, and 1 mM EGTA). After centrifugation at 12 000*g* for 15 min, the supernatant was collected and recentrifuged at 12 000*g* for 15 min at 4 °C. The supernatant was then used for NOS determination. We used the conversion of L-arginine to NO to determine NOS activity as described.[24]

Determination of Defense Enzyme Activities. To determine activities of defense enzymes, 1 g of frozen fruit sample was extracted with a 5-mL extraction buffer (100 mM PBS (pH 6.8) for PPO; 0.2 mM boric acid buffer pH 8.8, containing 10% (w/v) polyvinyl pyrrolidone and 1 mM EDTA for PAL; 100 mM acetic acid buffer (pH 5.2) for CHI and GLU) and centrifuged at 12 000*g* for 15 min at 4 °C. The supernatant was collected and used for defense enzyme determination.

CHI (EC 3.2.1.14) (Chitinase) activity was measured according to the method of Boller, et al.[25] with some modifications. The reaction mixture contained 0.5 mL of crude enzyme extract and 0.5 mL of colloidal chitin. It was incubated at 37 °C for 1 h. After the addition of 0.1 mL of 3% desalted snailase, the mixture was incubated at 37 °C for 1 h. The reaction was stopped by the addition of 0.3 mL of 0.6 M potassium tetraborate and was boiled at 100 °C for 5 min. After the samples were cooled immediately in ice, 2 mL of 20 $g \cdot L^{-1}$ 4-(dimethylamino) benzaldehyde reagent diluted with glacial acetic acid:HCl (39:1 v/v) was added and the mixture was incubated at 37 °C for 40 min. The absorbance was measured at 585 nm. A control was also included by measuring the fluorescence of the reaction mixture without the enzyme extract. CHI activity was expressed as $U \cdot g^{-1}$ FW, and one unit of CHI activity was defined as the amount of 10^{-9} mol *N*-acetyl-D-glucosamine being produced per hour.

GLU (EC 3.2.1.39) (β-1,3-glucanase) activity was measured according to the methods of Boller et al.[26] and Hinton and Pressey[27] with some modifications. The reaction mixture contained 100 μL of crude enzyme extract and 50 μL of 0.4% laminarin. Incubation was carried out at 37 °C for 40 min with shaking. The reaction was stopped by the addition of 1.8 mL of H_2O and 1.5 mL of 3.5-dinitrosalicylic and was boiled at 100 °C for 3 min. The mixture was then cooled immediately in ice and added to 25 mL of distilled water. The absorbance was measured at 540 nm. Quantification was carried out with a standard curve using the solutions of glucose with different concentrations. GLU activity was expressed as $U \cdot g^{-1}$ FW, based on glucose reducing equivalents from laminarin, and one unit of GLU activity was defined as the formation of 1 μmol of glucose per hour.

PPO (EC 1.10.3.2) (polyphenol oxidase) activity was measured according to the method of Liu et al.[28] with some modifications. The enzyme solution (0.5 mL) was rapidly reacted with 2 mL of PBS buffer (100 mM, pH 6.8) and 1 mL of 100 mM catechol. The change in absorbance at 420 nm was recorded over 2 min. PPO activity was expressed as $U \cdot g^{-1}$ FW, and one unit of PPO activity was defined as the amount of enzyme that caused a change of 1 in absorbance per minute.

PAL (EC 4.3.1.5) (phenylalanine ammonia-lyase) activity was measured according to the method of Koukol and Conn[29] with some modifications. The reaction mixture contained 0.5 mL of crude enzyme extract, 1 mL of 20 mM L-phenylalanine, and 2 mL of boric acid buffer (200 mM, pH 8.8). Incubation was carried out at 37 °C for 1 h. PAL activity was expressed as $U \cdot g^{-1}$ FW, and one unit of PAL activity was defined as the amount of enzyme that caused an increase in absorbance of 1 at 290 nm per hour.

Quantitative Real-Time PCR. Trizol reagent (Invitrogen, Carlsbad, CA, USA) was used to extract total RNA from 2 g of frozen fruit samples. Any remaining genomic DNA was removed by digestion with RNase-free DNase I (Promega, Madison, WI, USA), according to the manufacturer's instructions. Reverse transcription was completed to synthesize the first-strand of cDNA with 2 g of total RNA according to the manufacturer's protocol from Promega. The oligo $(dT)_{18}$ was used as a primer and the reverse transcription reaction was incubated at 42 °C for 60 min in a total volume of 25 μL.

Real-time PCR was performed using the Chromo4 Real-Time PCR Detection System (Biorad, Hercules, CA, USA). Specific primers used for PCR were designed, including *LeMAPK1* (GenBank accession AJ535702), 5′-CTTTACCGTCGACAATCATTTACTG-3′ and 5′-TGGTATTCAGGATTAAATGCAATCG-3′; *LeMAPK2* (GenBank accession AY261513), 5′-CTTTACCGTCGACAATCATTTGTC-3′, and 5′-TGGTATTCGGGATTAAATGCAAGAC-3′; *LeMAPK3* (GenBank accession AY261514), 5′-AGCATTAGCTCATCCCTACCTC-3′ and 5′-GCTCTTCTCCTATCCCTTGTTG-3′. The PCR reaction contained a total volume of 25 μL, containing 1 μL of cDNA template, 1 μL of specific primer, and 12.5 μL of 2 × SYBR GREEN I MasterMix (Toyobo, Osaka, Japan). PCR was performed with an initial step of 2 min at 94 °C followed by 40 cycles of 15 s at 94 °C, 20 s at 60 °C, and 45 s at 72 °C. The gene transcript levels for

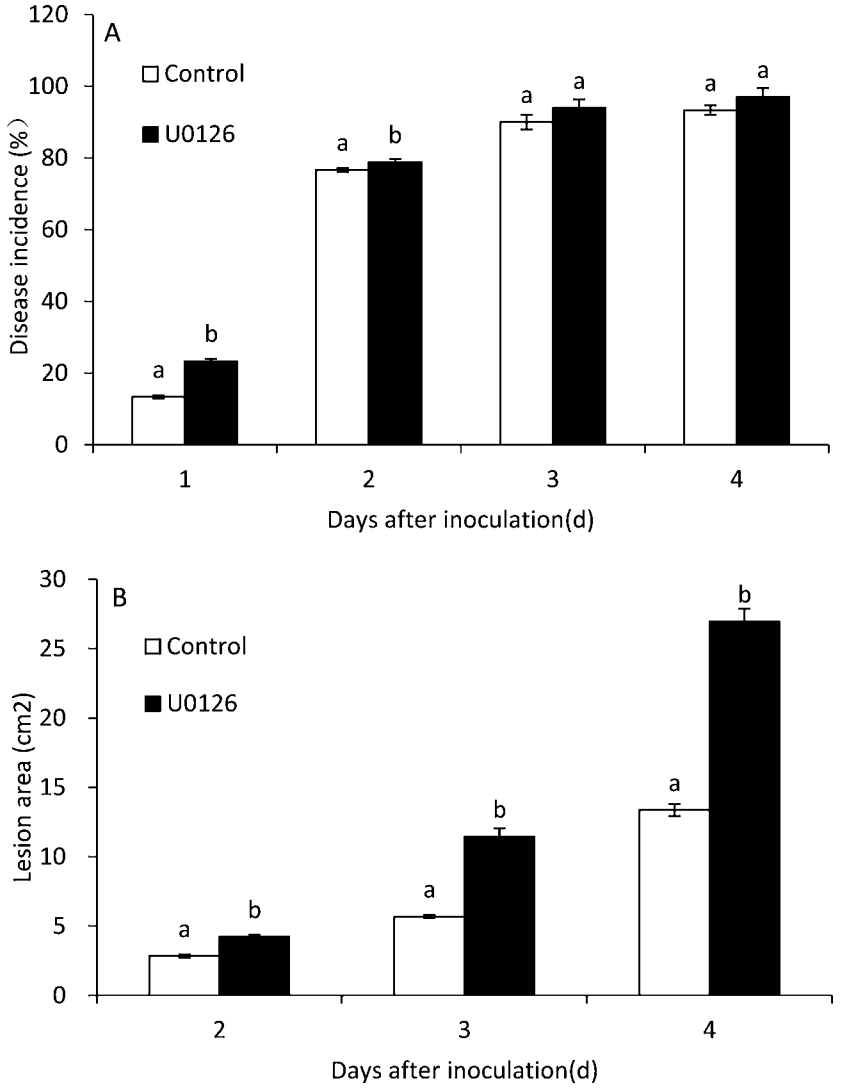

Figure 1. Effects of 10 μM U0126 on disease incidence (A) and lesion area (B) in 'Qian-xi' cherry tomato fruit inoculated with *Botrytis cinerea*. Tomato fruits were inoculated with *Botrytis cinerea* (2×10^6 conidia mL^{-1}) 1 d after treatment and incubated at 25 ± 1 °C and relative humidity (RH) of 90–95%. Disease symptoms on each fruit were recorded on days 1, 2, 3, and 4 after inoculation. Data with different lowercase letters in each column are significantly different at $P < 0.05$. Data are expressed as mean ± SD of triplicate assays.

each sample were normalized to Ubi3 Ct value and calculated using the formula $2^{-\Delta\Delta Ct}$.

Statistical Analysis. All data were presented as the mean ± standard deviation (SD). One-way analysis of variance (ANOVA) and Duncan's multiple range tests were carried out to determine significant differences ($p < 0.05$) between the means by the statistical software SPSS 18.0 (IBM Corp., Armonk, NY).

RESULTS

Effects of U0126 on Disease Incidence and Lesion Area. Treatment with U0126 increased the disease symptoms to different degrees (Figure 1). This observation suggests that the existence of MAPKs is important for the tomato fruit to resist pathogen infection in common physiological processes. Disease incidence in the U0126-treated fruits was increased by 75.0%, 2.8%, 4.4%, and 3.9% on day 1, 2, 3, and 4 after inoculation, respectively (Figure 1A). The lesion areas in the U0126-treated fruits increased by 48.6%, 103.0%, and 101.7% with respect to those of control fruits, respectively (Figure 1B, $P < 0.01$). After inoculation with *B. cinerea*, significant differences of disease incidence were only observed on day 1 and 2. However, lesion areas increased significantly as days go on after inoculation. It may be owing to that MAPKs mainly role in postinfection than in preinfection in tomato fruits. The results support the idea that MAPKs are necessary for the defense response against the invasion and expansion of *B. cinerea*.

Effects of SNP and SNP+U0126 on Disease Incidence and Lesion Area. Disease symptoms appeared on the third day after inoculation and increased with storage time (Figure 2). Treatment with SNP reduced disease symptoms in the tomato fruits after inoculation with *B. cinerea*. Disease incidence in the SNP-treated fruits was inhibited by 11.5%, 15.4%, 4.1%, and 1.5% on day 3, 4, 5, and 6 after inoculation, respectively. In contrast, SNP + U0126 treatment accelerated the increase in the incidence of disease compared to the control fruits ($P < 0.01$). Lesion areas were significantly smaller in SNP-treated fruits than those of the control fruits on day 4, 5, and 6 ($P < 0.01$). However, treatment with the MAPK pathway inhibitor U0126 weakened the effect of NO. Fruits treated with SNP showed smaller lesion areas than control fruits. In contrast, the lesion areas in (SNP + U0126)-treated fruits were 1.9, 1.6, and

dx.doi.org/10.1021/jf404870d | J. Agric. Food Chem. 2014, 62, 1390–1396

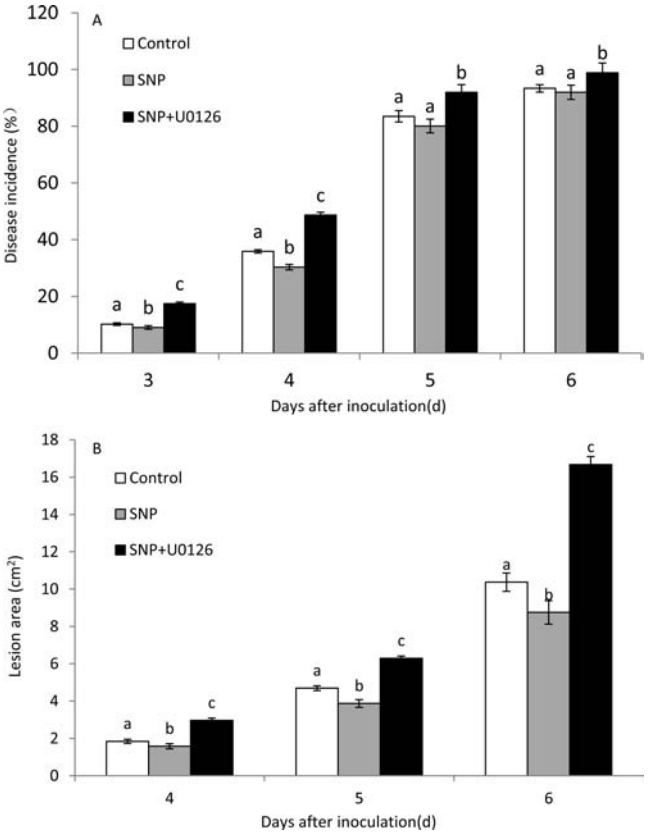

Figure 2. Effects of SNP and SNP+U0126 treatments on disease incidence (A) and lesion area (B) in 'Qian-xi' cherry tomato fruit inoculated with *Botrytis cinerea*. Tomato fruits were inoculated with *Botrytis cinerea* (2×10^6 conidia mL^{-1}) 1 d after treatment and incubated at 25 ± 1 °C and relative humidity (RH) of 90−95%. Disease symptoms on each fruit were recorded on days 3, 4, 5, and 6 after inoculation. Data with different lowercase letters in each column are significantly different at $P < 0.05$. Data are expressed as mean ± SD of triplicate assays.

1.9 times higher than those in SNP-treated fruits. The results commit to the idea that MAPKs are necessary for the NO-induced defense response against invasion and expansion of *B. cinerea*.

Effects of SNP and SNP+U0126 on NO Content and NOS Activity. NOS activity is significantly increased in SNP-treated fruits than in control fruits during the whole storage period except for the fourth hour ($P < 0.01$, Figure 3A). However, treatment with a MAPK pathway inhibitor U0126 weakened the effect of NO treatment on NOS activity. NOS activities in (SNP + U0126)-treated fruits were lower than those in SNP-treated fruits during storage. NO content in SNP-treated fruits was higher than in the control fruits (Figure 3B). NO content in SNP-treated fruits increased rapidly and reached a maximum of 14.66 $\mu M \cdot g^{-1}$ FW at 8 h, and then slowly fell after this rise, but still remained higher than that in the control. (SNP + U0126)-treated fruits shared a trend similar to the SNP-treated fruits. However, the NO content of (SNP + U0126)-treated fruits remained at a higher level throughout the storage period than that of the control fruits; the peak value was 1.36-fold higher compared to the control fruits.

Effects of SNP and SNP+U0126 on CHI, GLU, PPO, and PAL Activities. CHI activity showed a fluctuating increase in SNP treatment (Figure 4A). During the whole storage period, CHI activity in SNP-treated fruits was significantly higher ($P <$

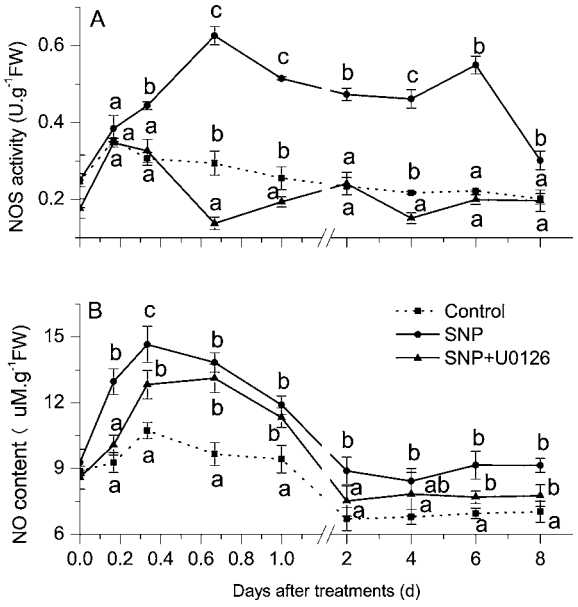

Figure 3. Effects of SNP and SNP+U0126 treatments on NOS activity (A) and NO concentration (B). The sampling time courses of treated tomato fruits are 0, 4, 8, 16, and 24 h, and 2, 4, 6, and 8 days. Values followed by different letters are significantly different according to Duncan's multiple range test at $P < 0.05$. Data are expressed as mean ± SD of triplicate assays.

0.05) than that in the control fruits. Treatment with a MAPK pathway inhibitor U0126 influenced the effect of NO-improved accumulation of defense enzymes. CHI activity in the (SNP + U0126)-treated fruits was significantly lower ($P < 0.05$) than in the SNP-treated fruits except for the fourth hour, but SNP + U0126 treatment had less effect on CHI activity than in the control during most of the storage period.

SNP treatment increased the activity of GLU. Two peaks of GLU activity in SNP-treated fruits were observed at 16 h and 6 d (Figure 4B) during the whole storage period. However, the GLU activity in (SNP+U0126)-treated fruits remained at a low level throughout the storage period.

SNP-treated tomato fruits exhibited a marked increase in PPO activity and reached a maximum of 1.03 $U \cdot g^{-1}$ FW at 8 h (Figure 4C). SNP treatment maintained a higher PPO activity compared with the control during the storage period. However, (SNP + U0126)-treated fruits showed significantly lower ($P <$ 0.05) PPO activity than the control during storage except for days 4 and 6.

PAL activity was induced rapidly by NO during the early stages of storage and peaked at the eighth hour of 4.33 $U \cdot g^{-1}$ FW (Figure 4D), then declined with some fluctuation. Treatment with U0126 inhibited the effect of NO on PAL activity. A significant decrease was found in (SNP + U0126)-treated fruits ($P < 0.05$) compared with SNP-treated fruits.

LeMAPK1/2/3 Relative Expression Analysis with Real-Time PCR. NO significantly enhanced the expression levels of *LeMAPK1*, *LeMAPK2* and *LeMAPK3* genes in the tomato fruits ($P < 0.05$). The expression patterns of *LeMAPK1* and *LeMAPK2* were similar in the SNP-treated fruits. NO-induced expression of *LeMAPK1* and *LeMAPK2* reached a peak at 8 h, then declined (Figure 5A and B). The expression of *LeMAPK3* was induced rapidly by NO and reached the maximum expression at 1 h (Figure 5C). However, treatment with U0126 weakened the effect of NO. The expression of

dx.doi.org/10.1021/jf404870d | J. Agric. Food Chem. 2014, 62, 1390−1396

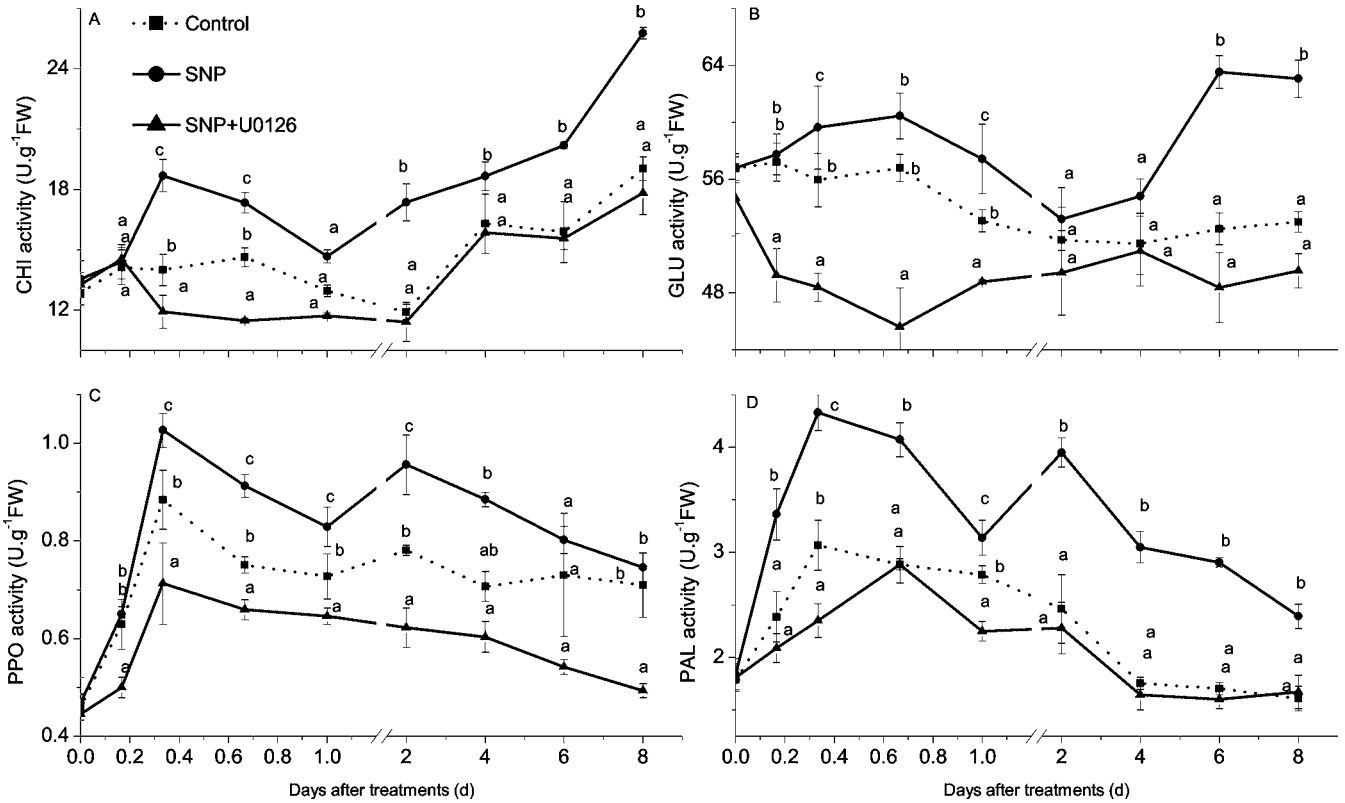

Figure 4. Effects of SNP and SNP+U0126 treatments on the activities of defense enzymes: (A) chitinase; (B) β-1,3-glucanase; (C) polyphenol oxidase; and (D) phenylalanine ammonia-lyase. The sampling time courses of treated tomato fruits are 0, 4, 8, 16, and 24 h, and 2, 4, 6, and 8 days. Values followed by different letters are significantly different according to Duncan's multiple range test at $P < 0.05$. Data are expressed as mean ± SD of triplicate assays.

LeMAPK1, *LeMAPK2*, and *LeMAPK3* in (SNP + U0126)-treated fruits was significantly lower than that in the SNP-treated fruits ($P < 0.05$).

■ DISCUSSION

NO is known to have a critical role in both regulating defense responses and inducing resistance to fungal pathogens. Exogenous NO treatment has been shown to result in lower decay incidence and improved disease resistance in several fruits.[30,31] No generation was induced by conditional activation of MAPK cascades in *Nicotiana benthamiana* leaves.[32] Plant MAPK cascades play pivotal roles in signaling plant defense against pathogen attack.[14,15,18,33] However, most of the supporting experimental data focuses on the level of disease prevention by NO, while little is known about how durable the disease prevention is and how it interacts with other signaling molecules.[34] This study investigated the interaction between NO and *LeMAPK1/2/3* in the defense response to the pathogen *B. cinerea* in postharvest tomato fruits. These findings further extend our understanding on the functions of *LeMAPK1/2/3* in defense response. We found that U0126 could significantly increase the disease symptoms caused by *B. cinerea* in the tomato fruits (Figure 1), while exogenous SNP treatment could reduce the disease incidence and lesion area. The MAPKs inhibitor weakened NO-induced resistance to pathogen invasion and development (Figure 2). This indicated that MAPKs play a crucial role in the postharvest tomato fruits defense response induced by NO.

Previous studies indicate that NOS is closely related to NO production in plants.[35] Recently, Zheng et al.[36] also found that NOS is a key enzyme regulating NO production in induced resistance in tomatoes. In adipose tissue, MAPKs are implicated in the regulation of NOS activity. Catherine et al.[37] reported that MAPKs inhibitor (U0126) could abolish NOS activity stimulated by insulin. In the present investigation, NO treatment resulted in an increase in NOS activity, but the MAPKs inhibitor (U0126) abolished NOS activity resulted by NO (Figure 3A). These results in part suggest that the MAPKs participated in the action of NO. NO burst is considered an early event during resistance response.[38] This conclusion is also supported by our results from the SNP and SNP + U0126 treatment. However, effects of the MAPKs inhibitor on NO content were not obvious, possibly owing to the fact that NO rapid bursts and MAPK cascades are the downstream signal molecule of NO.[39]

GLU, CHI, PPO, and PAL have been categorized as primary defense systems against fungal pathogens. Both GLU and CHI are well-known as pathogenesis-related (PR) proteins, belonging to the PR-2 and PR-3 families, respectively. These enzymes are involved in plant defense mechanisms against fungal infection and are currently used as markers for innate immunity.[40] PPO, which catalyzes the O_2-dependent oxidation of phenolic compounds to form quinines, has been proposed as a component of plant defense mechanisms, and is associated with induced defense responses in plants.[41] PAL is a key, rate-limiting enzyme in plant secondary metabolism, especially in the phenylpropanoid pathway and is established as an enzyme downstream of NO action.[42] Thus, the variation of these enzyme activities can indirectly reflect plant disease resistance. There is a close relationship between the change of disease

dx.doi.org/10.1021/jf404870d | J. Agric. Food Chem. 2014, 62, 1390−1396

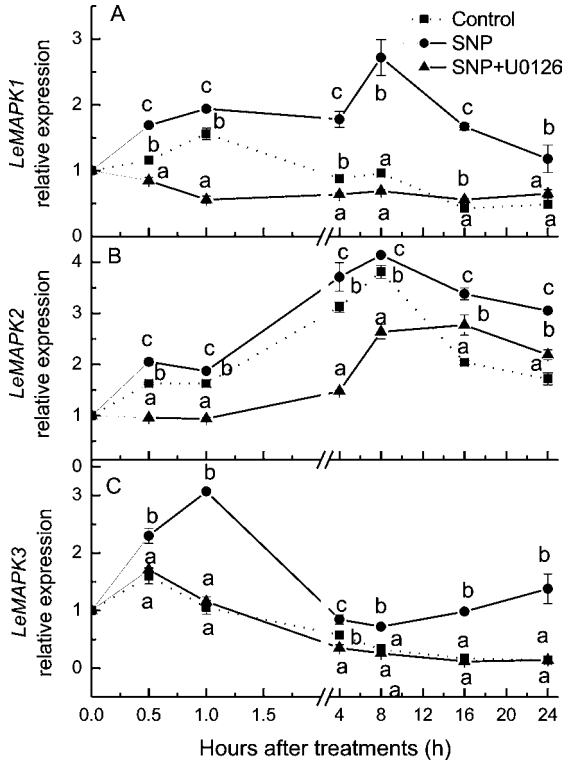

Figure 5. Effects of SNP and SNP+U0126 treatments on the relative expression of *LeMAPK1/2/3* in tomato fruits. The sampling time courses of treated-tomato fruits are 0, 0.5, 1, 4, 8, 16, and 24 h. The expression levels of *LeMAPK1/2/3* were evaluated by quantitative real-time PCR, normalized to the host *Ubis3* gene, and set relative to control sample from day 0 according to the $2^{-\Delta\Delta Ct}$ method. Values followed by different letters are significantly different according to Duncan's multiple range test at $P < 0.05$. Data are expressed as mean ± SD of triplicate assays.

incidence and the activities of defense enzymes (Figures 2A and 4).The present results showed NO induces higher activities of GLU, CHI, PPO, and PAL in tomato fruits compared with the control. Meanwhile, NO inhibits disease incidence after inoculation with *B. cinerea*. However, the MAPKs inhibitor weakened the effects of NO on defense enzymes (Figure 4) which further supposed the participation of MAPKs in the action of NO. These results suggest an intermediate role of MAPKs in NO-induced disease resistance in harvested tomato fruits.

Specific virus-induced gene silencing (VIGS) of *LeMAPK1*, *LeMAPK2* and *LeMAPK3* resulted in the reduction of defense gene expression and defense response against herbivorous insects.[15,22] In our study, the levels of *LeMAPK1* and *LeMAPK2* expression increased rapidly in response to SNP vapor treatment and peaked at 8 h. Besides, a quick increase in the expression of *LeMAPK1*, *LeMAPK2*, and *LeMAPK3* was seen in the control fruits, which may be attributable to the wound response caused by the vacuum infiltration method adopted in our study.[43] Meanwhile, NO content (Figure 3B), PPO activity, and PAL activity (Figure 4C and D) reached a peak value at 8 h. These results suggest that the expression of *LeMAPK1*, *LeMAPK2*, and *LeMAPK3* was positively correlated with NO content, PPO activity, and PAL activity. The expression of *LeMAPK3* induced by NO seemed to be somewhat different from *LeMAPK1* and *LeMAPK2*. The expression of *LeMAPK3* reached a maximum value at 1 h and a minimum value at 8 h. However, the expression levels of *LeMAPK1*, *LeMAPK2*, and *LeMAPK3* in SNP-treated fruits were all higher than that in the control fruits. The MAPKs inhibitor significantly decreased the expression of *LeMAPK1*, *LeMAPK2*, and *LeMAPK3*. These were accompanied by an obvious decrease in defense enzymes in fruits treated with SNP + U0126 throughout the storage period. These data indicated that (i) *LeMAPK1*, *LeMAPK2*, and *LeMAPK3* played a critical role in tomato disease resistance, and (ii) *LeMAPK1*, *LeMAPK2*, and *LeMAPK3* mediated the NO-induced defense response against *B. cinerea*. These results should be useful in the integrated control of postharvest diseases of fruit. Recently, Zheng et al.[44] indicated that preharvest L-arginine (the precursor of NO) treatment may be a promising measure for controlling postharvest decays on a commercial scale.

AUTHOR INFORMATION

Corresponding Author

*E-mail: shen5000@cau.edu.cn; Phone: +86-10-62738456; Fax: +86-10-62737620.

Funding

This work was supported by the National Natural Science Foundation of China (31371847).

Notes

The authors declare no competing financial interest.

ABBREVIATIONS USED

NO, Nitric oxide; MAPKs, mitogen-activated protein kinases; U0126, 1,4-diamino-2,3-dicyano-1,4-bis(o-amino-phenylmercapto) butadiene; SNP, sodium nitroprusside; CHI, Chitinase; GLU, β-1,3-glucanase; PPO, polyphenol oxidase; PAL, phenylalanine ammonia-lyase; *B. cinerea*, *Botrytis cinerea*; NOS, nitric oxide synthase; RH, relative humidity; PBS, phosphate buffer saline; FW, fresh weight; VIGS, virus-induced gene silencing

REFERENCES

(1) Kombrink, E.; Somssich, I. E. Defense responses of plants to pathogens. *Adv. Bot. Res.* **1995**, *21*, 1−34.

(2) Fan, B.; Shen, L.; Liu, K. L.; Zhao, D. Y.; Yu, M. M.; Sheng, J. P. Interaction between nitric oxide and hydrogen peroxide in postharvest tomato resistance response to *Rhizopus nigricans*. *J. Sci. Food Agric.* **2008**, *88*, 1238−1244.

(3) Qiao, W. H.; Fan, L. M. Nitric oxide signaling in plant responses to abiotic stresses. *J. Integr. Plant Biol.* **2008**, *50*, 1238−1246.

(4) Besson-Bard, A.; Pugin, A.; Wendehenne, D. New insights into nitric oxide signaling in plants. *Annu. Rev. Plant Biol.* **2008**, *59*, 21−39.

(5) Noritake, T.; Kawakita, K.; Doke, N. Nitric oxide induces phytoalexin accumulation in potato tuber tissues. *Plant Cell Physiol.* **1996**, *37*, 113−116.

(6) Clarke, A.; Desikan, R.; Hurst, R. D.; Hancock, J. T.; Neill, S. J. NO way back: Nitric oxide and programmed cell death in *Arabidopsis thaliana* suspension cultures. *Plant J.* **2000**, *24*, 667−677.

(7) Bellin, D.; Asai, S.; Delledonne, M.; Yoshioka, H. Nitric oxide as a mediator for defense responses. *Mol. Plant−Microbe Interact.* **2013**, *26*, 271−277.

(8) Asai, S.; Yoshioka, H. Nitric oxide as a partner of reactive oxygen species participates in disease resistance to necrotrophic pathogen *Botrytis cinerea* in *Nicotiana benthamiana*. *Mol. Plant-Microbe Interact.* **2009**, *22*, 619−629.

(9) Yamamoto, A.; Katou, S.; Yoshioka, H.; Doke, N.; Kawakita, K. Involvement of nitric oxide generation in hypersensitive cell death induced by elicitin in tobacco cell suspension culture. *J. Gen. Plant Pathol.* **2004**, *70*, 85−92.

(10) Yang, S.-H.; Sharrocks, A. D.; Whitmarsh, A. MAP kinase signalling cascades and transcriptional regulation. *Gene* **2013**, *513*, 1−13.
(11) Asai, T.; Tena, G.; Plotnikova, J.; Willmann, M. R.; Chiu, W.-L.; Gomez-Gomez, L.; Boller, T.; Ausubel, F. M.; Sheen, J. MAP kinase signalling cascade in *Arabidopsis* innate immunity. *Nature* **2002**, *415*, 977−983.
(12) Meng, X.; Zhang, S. MAPK Cascades in Plant Disease Resistance Signaling. *Annu. Rev. Phytopathol.* **2013**, *51*, 245−266.
(13) Liu, Y. D.; Jin, H. L.; Yang, K. Y.; Kim, C. Y.; Baker, B.; Zhang, S. Q. Interaction between two mitogen-activated protein kinases during tobacco defense signaling. *Plant J.* **2003**, *34*, 149−160.
(14) Meng, X. Z.; Xu, J.; He, Y. X.; Yang, K.-Y.; Mordorski, B.; Liu, Y. D.; Zhang, S. Q. Phosphorylation of an ERF transcription factor by *Arabidopsis* MPK3/MPK6 regulates plant defense gene induction and fungal resistance. *Plant Cell* **2013**, *25*, 1126−1142.
(15) Kandoth, P. K.; Ranf, S.; Pancholi, S. S.; Jayanty, S.; Walla, M. D.; Miller, W.; Howe, G. A.; Lincoln, D. E.; Stratmann, J. W. Tomato MAPKs LeMPK1, LeMPK2, and LeMPK3 function in the systemin-mediated defense response against herbivorous insects. *Proc. Natl. Acad. Sci., U. S. A.* **2007**, *104*, 12205−10.
(16) Romeis, T.; Piedras, P.; Zhang, S. Q.; Klessig, D. F.; Hirt, H.; Jones, J. D. Rapid Avr9-and Cf-9-dependent activation of MAP kinases in tobacco cell cultures and leaves: Convergence of resistance gene, elicitor, wound, and salicylate responses. *Plant Cell* **1999**, *11*, 273−287.
(17) Zhang, X. T.; Cheng, T. C.; Wang, G. H.; Yan, Y. F.; Xia, Q. Y. Cloning and evolutionary analysis of tobacco MAPK gene family. *Mol. Biol. Rep.* **2013**, *40*, 1407−1415.
(18) Galletti, R.; Ferrari, S.; De Lorenzo, G. Arabidopsis MPK3 and MPK6 play different roles in basal and oligogalacturonide- or flagellin-induced resistance against *Botrytis cinerea*. *Plant Physiol.* **2011**, *157*, 804−814.
(19) Berriri, S.; Garcia, A. V.; dit Frey, N. F.; Rozhon, W.; Pateyron, S.; Leonhardt, N.; Montillet, J.-L.; Leung, J.; Hirt, H.; Colcombet, J. Constitutively active mitogen-activated protein kinase versions reveal functions of *Arabidopsis* MPK4 in pathogen defense signaling. *Plant Cell* **2012**, *24*, 4281−4293.
(20) Holley, S. R.; Yalamanchili, R. D.; Moura, D. S.; Ryan, C. A.; Stratmann, J. W. Convergence of signaling pathways induced by systemin, oligosaccharide elicitors, and ultraviolet-B radiation at the level of mitogen-activated protein kinases in *Lycopersicon peruvianum* suspension-cultured cells. *Plant Physiol.* **2003**, *132*, 1728−1738.
(21) Stulemeijer, I. J.; Stratmann, J. W.; Joosten, M. H. Tomato mitogen-activated protein kinases LeMPK1, LeMPK2, and LeMPK3 are activated during the Cf-4/Avr4-induced hypersensitive response and have distinct phosphorylation specificities. *Plant Physiol.* **2007**, *144*, 1481−1494.
(22) Chen, Y. Y.; Lin, Y. M.; Chao, T. C.; Wang, J. F.; Liu, A. C.; Ho, F. I.; Cheng, C. P. Virus-induced gene silencing reveals the involvement of ethylene-, salicylic acid- and mitogen-activated protein kinase-related defense pathways in the resistance of tomato to bacterial wilt. *Physiol. Plant.* **2009**, *136*, 324−335.
(23) Hao, G. P.; Xing, Y.; Zhang, J. H. Role of nitric oxide dependence on nitric oxide synthase-like activity in the water stress signaling of maize seedling. *J. Integr. Plant Biol.* **2008**, *50*, 435−442.
(24) Zhang, X.; Shen, L.; Li, F.; Meng, D.; Sheng, J. Methyl salicylate-induced arginine catabolism is associated with up-regulation of polyamine and nitric oxide levels and improves chilling tolerance in cherry tomato fruit. *J. Agric. Food Chem.* **2011**, *59*, 9351−9357.
(25) Boller, T.; Gehri, A.; Mauch, F.; Vögeli, U. Chitinase in bean leaves: Induction by ethylene, purification, properties, and possible function. *Planta* **1983**, *157*, 22−31.
(26) Siefert, F.; Langebartels, C.; Boller, T.; Grossmann, K. Are ethylene and 1-aminocyclopropane-1-carboxylic acid involved in the induction of Chitinase and β-1, 3-glucanase activity in sunflower cell-suspension cultures? *Planta* **1994**, *192*, 431−440.
(27) Hinton, D. M.; Pressey, R. Glucanases in fruits and vegetables. *J. Am. Soc. Hortic. Sci.* **1980**, *105*, 499−502.
(28) Liu, J.; Tian, S. P.; Meng, X. H.; Xu, Y. Effects of chitosan on control of postharvest diseases and physiological responses of tomato fruit. *Postharvest Biol. Technol.* **2007**, *44*, 300−306.
(29) Koukol, J.; Conn, E. E. The metabolism of aromatic compounds in higher plants IV. Purification and properties of the phenylalanine deaminase of *Hordeum vulgare*. *J. Biol. Chem.* **1961**, *236*, 2692−2698.
(30) Ferreira, P. G.; Lima, M. A. S. S.; Bernedo-Navarro, R. A.; Conceicao, R. A.; Linhares, E.; Sawaya, A. C. H. F.; Yano, T.; Salgado, I. Stimulation of acidic reduction of nitrite to nitric oxide by soybean phenolics: possible relevance to gastrointestinal host defense. *J. Agric. Food Chem.* **2011**, *59*, 5609−5616.
(31) Yu, Q.; Chen, Q.; Chen, Z. W.; Xu, H. K.; Fu, M. N.; Li, S.; Wang, H. Z.; Xu, M. J. Activating defense responses and reducing postharvest blue mold decay caused by *Penicillium expansum* in peach fruit by yeast saccharide. *Postharvest Biol. Technol.* **2012**, *74*, 100−107.
(32) Asai, S.; Ohta, K.; Yoshioka, H. MAPK signaling regulates nitric oxide and NADPH oxidase-dependent oxidative bursts in *Nicotiana benthamiana*. *Plant Cell* **2008**, *20*, 1390−1406.
(33) Meldau, S.; Wu, J. Q.; Baldwin, I. T. Silencing two herbivory-activated MAP kinases, SIPK and WIPK, does not increase *Nicotiana attenuata*'s susceptibility to herbivores in the glasshouse and in nature. *New Phytol.* **2009**, *181*, 161−73.
(34) Lai, T. F.; Wang, Y. Y.; Li, B. Q.; Qin, G. Z.; Tian, S. P. Defense responses of tomato fruit to exogenous nitric oxide during postharvest storage. *Postharvest Biol. Technol.* **2011**, *62*, 127−132.
(35) Chandok, M. R.; Ytterberg, A. J.; van Wijk, K. J.; Klessig, D. F. The pathogen-inducible nitric oxide synthase (iNOS) in plants is a variant of the P protein of the glycine decarboxylase complex. *Cell* **2003**, *113*, 469−482.
(36) Zheng, Y.; Shen, L.; Yu, M. M.; Fan, B.; Zhao, D. Y.; Liu, L. Y.; Sheng, J. P. Nitric oxide synthase as a postharvest response in pathogen resistance of tomato fruit. *Postharvest Biol. Technol.* **2011**, *60*, 38−46.
(37) Ribière, C.; Jaubert, A.-M.; Sabourault, D.; Lacasa, D.; Giudicelli, Y. Insulin stimulates nitric oxide production in rat adipocytes. *Biochem. Biophys. Res. Commun.* **2002**, *291*, 394−399.
(38) Foissner, I.; Wendehenne, D.; Langebartels, C.; Durner, J. In vivo imaging of an elicitor-induced nitric oxide burst in tobacco. *Plant J.* **2000**, *23*, 817−824.
(39) Klessig, D. F.; Durner, J.; Noad, R.; Navarre, D. A.; Wendehenne, D.; Kumar, D.; Zhou, J. M.; Shah, J.; Zhang, S. Q.; Kachroo, P. Nitric oxide and salicylic acid signaling in plant defense. *Proc. Natl. Acad. Sci., U. S. A.* **2000**, *97*, 8849−8855.
(40) Van Loon, L. C.; Van Strien, E. A. The families of pathogenesis-related proteins, their activities, and comparative analysis of PR-1 type proteins. *Physiol. Mol. Plant Pathol.* **1999**, *55*, 85−97.
(41) Ramiro, D. A.; Guerreiro-Filho, O.; Mazzafera, P. Phenol contents, oxidase activities, and the resistance of coffee to the leaf miner *Leucoptera coffeella*. *J. Chem. Ecol.* **2006**, *32*, 1977−1988.
(42) Durner, J.; Wendehenne, D.; Klessig, D. F. Defense gene induction in tobacco by nitric oxide, cyclic GMP, and cyclic ADP-ribose. *Proc. Natl. Acad. Sci., U. S. A.* **1998**, *95*, 10328−10333.
(43) Barkai-Golan, R.; Lavy-Meir, G.; Kopeliovitch, E. Stimulation of fruit ethylene production by wounding and by *Botrytis cinerea* and *Geotrichum candidum* infection in normal and non-ripening tomatoes. *J. Phytopathol.* **1989**, *125*, 148−156.
(44) Zheng, Y.; Sheng, J.; Zhao, R.; Zhang, J.; Lv, S.; Liu, L.; Shen, L. Preharvest L-arginine treatment induced postharvest disease resistance to *Botrysis cinerea* in tomato fruits. *J. Agric. Food Chem.* **2011**, *59*, 6543−6549.

Another area of controversy is the acceptability of hard cheeses in the diet management of galactosemia. Bacterial fermentation and aging of some cheeses substantially reduces the galactose content.[16] Negligible amounts of lactose and galactose were found in European sources of Gruyere, Emmentaler, Jarlsberg, grated and block Italian Parmesan (Parmigiano Reggiano, Grana Padona), and Cheddar cheese aged for >1 year produced by the UK West Country Farmhouse Cheese Makers Association in England.[16] Minibel Emmental (Laughing Cow), a mild processed Emmentaler cheese produced in France, did contain various amounts of residual lactose, with an average of 6 mg galactose/100 g.[17] A study of 30 8−12-month-aged Cheddar cheeses reported undetectable concentrations of lactose and galactose using HPLC with refractive index detection,[18] whereas others have reported variable amounts of galactose in hard cheeses.[19−22] Analysis of additional sources of these cheeses has not been completed in recent years; thus, it is not known whether these aged cheeses can be universally recommended for those with galactosemia. In addition, caseinates may contain negligible galactose and need to be further evaluated.[23] Understandably, addition of milk-based products has been especially difficult to accept by families who are hesitant to include these foods without adequate assurance regarding their safety. Thus, a second aim of this current study is to determine the galactose content of these same hard cheeses produced in the United States and Canada and to analyze sources of food-grade caseinates to provide additional data to help establish dietary recommendations for classic galactosemia.

MATERIALS AND METHODS

Various types of cheeses (n = 19) and sodium and calcium caseinate (n = 6) were purchased between June and August 2011 in different locations in North America. These products were analyzed at a commercial food analysis laboratory (Covance, Inc., Madison, WI, USA). Each sample was ground to ensure consistent composition, and a 2 g aliquot was extracted with room temperature water. The sample was shaken for ∼1 min with 10 volumes of chloroform to remove lipids and then centrifuged for 5 min. The aqueous fraction was filtered through a 0.45 μm filter. The quality control sample used for the analysis was a cereal product that had ranges determined on 60 replicates of the material.

Total galactose content was determined from both lactose and galactose quantitated by a high-performance anion exchange chromatograph equipped with a pulsed amperometric detector (HPAEC-PAD).[24] Each standard curve had an r^2 > 0.995. The individual standard concentrations for each analyte were within 10% of the theoretical concentrations. For any sample containing lactose, 53% of total lactose was considered galactose, on the basis of the molecular weights of 342 for lactose and 180 for galactose. All galactose concentrations are expressed as milligrams per 100 g product. For dairy products, a galactose content <5.1 mg/100 g product was considered below quantitation limits. The published method reported carbohydrate recoveries of 94.9−105% and a coefficient of variation of 3.3%.[24]

For legume analysis, commercially canned garbanzo beans (kabuli chickpeas), black beans, red kidney beans, and pinto beans were selected. One can of three national brands of each product were purchased in Madison, WI, USA, in December 2012. From each sample can, liquid was drained and weighed, and beans were briefly rinsed with distilled water to ensure that all canning liquid was collected. Whole beans were macerated in a food processor, and both the liquid (38−51 g sample) and beans (61−82 g sample) were freeze-dried separately. Sugar extraction and analysis were completed in Food, Nutrition and Health at the University of British Columbia in Vancouver using the method of Sanchez-Mata et al.[25] with an extraction temperature of 60 °C. Duplicates of each freeze-dried bean and liquid sample were extracted in 80% ethanol before analysis of galactose and galacto-oligosaccharides using an Agilent 1100 series HPLC system with an aminopropyl Zorbax carbohydrate column (4.6 × 250 mm, 5 μm particle size, 30 °C). Sugars were detected using an Agilent 1200 series refractive index detector (Agilent Technologies, Canada, Inc., Mississauga, ON, Canada) regulated at 35 °C. The isocratic mobile phase was premixed 75:25 acetonitrile/water, at 2.0 mL/min. Sample aliquots of 100 μL were injected. Total galactose, free galactose, melibiose, raffinose, ciceritol, and stachyose were quantitated and expressed in milligrams sugar per 100 g product. Commercial standards for all compounds except ciceritol were used to construct standard curves for quantitation (r^2 > 0.99). The galactose, melibiose, and stachyose standards were purchased from Sigma-Aldrich Canada (Oakville, ON, Canada), and raffinose was purchased from Fisher Scientific Canada (Ottawa, ON, Canada). All sugar standards were of 98% purity or higher. Ciceritol concentrations were estimated using the raffinose standard curve with a correction for the molecular weight.

RESULTS AND DISCUSSION

Addressing the galactose content of caseinates, hard cheeses, and legumes will provide further data to address the inclusion or restriction of these foods and ingredients in the diet for classic galactosemia.

Caseins, a complex group of proteins comprising α_{s1}, α_{s2}, β, and κ gene products, are present in milk in the range of 2.4−2.9 g/100 mL.[27] The isolated proteins, termed caseinates, are used as food ingredients in a wide range of products for emulsification, stabilizing, water binding, film formation, and nutritional purposes. Therefore, restricting caseinate in the galactosemia diet eliminates many foods that could add dietary and nutritional variety.

Caseinates can be manufactured via acid precipitation or enzymatic (chymosin) precipitation. After precipitation, the caseinate is washed and dewatered. The isolated caseinate is subsequently solubilized by the addition of an alkali or polyphosphates and dried.[26] Because of the removal of whey via precipitation and extensive washing of the precipitated protein, the concentration of lactose, and therefore galactose, remaining in the final caseinate is expected to be low. Analysis of food grade caseinates in this study confirmed this observation. Residual lactose was detected in three of six caseinate samples with equivalent galactose contents ranging from 40 to 96 mg/100 g powder (Table 1). Typically, the amount of caseinates added to various foods ranges from 1 to

Table 1. Galactose Content of Sodium and Calcium Caseinate[a]

	country of origin	galactose (mg/100 g)
sodium caseinate	USA (Wisconsin)	95.5
	New Zealand	62.0
	The Netherlands	<5.1
	mean ± SD	54.2 ± 45.7
calcium caseinate	USA (Wisconsin)	<5.1
	New Zealand	40.3
	The Netherlands	<5.1
	mean ± SD	16.8 ± 20.4
	total mean ± SD	35.5 ± 37.7

[a]Values reported are from a single analysis.

25% by weight,[27] which suggests that foods containing caseinates are an insignificant dietary source of galactose.

Cheesemaking is a complex process, and there are multiple factors that may affect the residual galactose concentration in the final product. Reports of residual galactose in cheese vary within the same type of cheese and can be attributed to minor variations in the milk itself[28] but, more importantly, to the specific starter and the nonstarter (secondary) cultures, the processing steps used to separate the curd from the lactose-rich whey, and the conditions used for cheese aging.[29] Hard cheeses that are aged for extended periods of time may be expected to have lower residual galactose content due to the metabolic activity of the secondary cultures[30,31] and, in some cases, persistence of the starter culture.[32]

For all analyzed cheese samples, only one sample contained both residual lactose and galactose. For all other cheeses, lactose was below quantitation limits and only galactose was measurable. The data confirm that Gruyere, Emmentaler, and brick Parmesan cheeses produced in U.S. dairies contain negligible lactose or galactose, similar to results reported for these cheese varieties produced in Europe.[16] The galactose content was below quantitation limits in Emmentaler and Gruyere cheeses produced in Switzerland and Wisconsin (Table 2). In North America, Emmentaler cheese may be called "Swiss" cheese; one sample of Swiss cheese contained 7.4 mg galactose/100 g. Another study also reported the absence of lactose and galactose, determined enzymatically, for Swiss cheese manufactured in the United States.[33] The specific bacterial starter culture used may contribute to differences in the residual galactose in Emmentaler cheese. For example, *Streptococcus salivarius* subsp. *thermophilus* and *Lactobacillus helveticus* are thermophilic starter species typically used for Emmentaler or Swiss cheese production. The presence of *L. helveticus* is essential to produce a low-galactose cheese, as only a fraction of *S. thermophilus* strains are able to metabolize galactose;[34] however, *L. helveticus* strains vary in their ability to deplete galactose during the initial stages of cheesemaking.[35]

One sample of block Parmesan cheese aged for >10 months contained galactose below quantitation limits (Table 2). Unlike grated Parmesan cheese from Italy found to contain negligible galactose by enzymatic analysis,[16,36] a commercial brand of grated cheese from the United States contained 23.6 mg galactose/100 g. Similarly, using HPLC-PAD, eight New Zealand-produced Parmesan cheese samples varying in age from 6 to 19 months were found to contain an average of 38 ± 21 mg galactose/100 g, whereas two samples aged for 7 and 20 months contained 378 and 156 mg galactose/100 g, respectively[22] As with Emmentaler cheese, the growth and metabolic activity of the specific *Lactobacillus* species in the starter culture and during aging may affect residual galactose. Together, the data suggest that Parmesan cheese produced using traditional methods and aging are likely to have the lowest free galactose content.

Cheddar cheese is classified by the length of aging; mild Cheddar is aged for 2−3 months, medium Cheddar for 4−6 months, and sharp Cheddar, for >9 months. Nine samples of sharp Cheddar cheese were analyzed, averaging 28.9 mg galactose/100 g. One sample of medium Cheddar cheese and two samples of mild Cheddar cheese contained negligible galactose. Interestingly, sharp Cheddar cheeses produced in smaller regional dairies contained 7.8 ± 4.0 mg/100 g compared to 55.4 ± 37.2 mg/100g found in sharp Cheeses produced by a larger multinational producer (Kraft Foods Global, Northfield, IL, USA). This suggests that a more consistent product may be produced in smaller dairies. A similar conclusion was reached in analysis of sharp cheeses produced in England; cheeses produced at the UK West Country Farmhouse Cheese Makers Association contained negligible amounts of galactose determined enzymatically, whereas less consistency was found from other manufacturers.[16,17] It may be speculated that smaller producers are more consistent in the use of a traditional Cheddar process, whereas larger plants may adapt various modifications to reduce costs and/or increase efficiency of the operation. For example, high residual galactose concentrations were reported in a Cheddar cheese made using a 42 °C cook temperature to decrease production time.[30] Cheddar cheese is usually made with mesophilic *Lactococcus lactis* subsp. *cremoris* and/or *lactis* starter culture and a cook temperature of 38 °C. However, at the higher temperature, *L. lactis* was not effective in metabolizing galactose and was not active during cheese ripening due to a high salt sensitivity and extensive autolysis. In these experimental Cheddar cheeses, lactose was undetectable after 3−5 months of aging, but galactose was slower to decrease and was present in some samples at approximately 170 mg/100 g cheese after 6 months.[30]

Table 2. Galactose Content of Various Types of Cheese[a]

type	brand/manufacturer	galactose (mg/100 g)
Cheddar, sharp		
sharp, aged 1 year	Brennan's Cellars/Brennan's, New Glarus, WI	6.6
seriously sharp	Cabot Vermont/Creamery Cooperative, VT	<5.1
naturally sharp	Cracker Barrel/Kraft Foods Global, IL	60.4
extra sharp white	Cracker Barrel/Kraft Foods North America, IL	16.5
sharp	Tillamook/Tillamook County Creamery Association, OR	14.7
sharp	Kraft/Kraft Foods Global, IL	104.3
sharp	JS Brands/JS Brands of Wisconsin, WI	7.4
old Cheddar	Cracker Barrel/Kraft Canada, ON	40.3
old Cheddar	Best Buy/Lucerne Foods, AB	<5.1
	mean ± SD	28.93 ± 34
Cheddar, mild and medium		
medium, aged 6 months	Brennan's Cellars/Brennan's, New Glarus, WI	<5.1
mild, aged 3 months	Brennan's Cellars/Brennan's, New Glarus, WI	5.6
mild, yogurt base	Cabot Vermont/Cabot Creamery Cooperative, VT	<5.1
Emmentaler	Whole Foods Market/Emmi Ltd., Switzerland	<5.1
	Brennan's Cellars/Brennan's, New Glarus, WI	<5.1
Swiss	Crystal Farms/Crystal Farm, WI	7.4
Gruyere	Whole Foods Market/Emmi Ltd., Switzerland	<5.1
	Brennan's Cellars/Brennan's, New Glarus, WI	<5.1
Parmesan		
powder	Kraft/Kraft Foods Global, IL	23.6
block, aged 10 months	Brennan's Cellars/Brennan's, New Glarus; WI	<5.1

[a]Values reported are from a single analysis.

dx.doi.org/10.1021/jf404995a | J. Agric. Food Chem. 2014, 62, 1397−1402

Table 3. Free Galactose, Bound Galactose in Four Oligosaccharides, and Total Galactose in Commercially Canned Legumes and Canning Liquid[a]

legume	mass ratio beans/liquid	free galactose	melibose	raffinose	ciceritol	stachyose	total
garbanzo beans	1.1	24.6	ND[b]	49.3	248.5	185.6	507.9
	1.0–1.3	0.0–52.5		29.1–64.6	167.9–295.2	102.3–236.7	320.5–636.0
canning liquid		39.5	2.0	113.7	539.3	474.8	1169.2
		9.0–56.3	0.0–5.9	106.4–125.9	463.9–653.1	427.2–519.1	1090.9–1307.0
kidney beans	2.7	ND	ND	47.0	4.2	391.8	443.0
	2.0–4.1			39.1–52.9	0.0–12.5	367.5–404.4	406.6–469.4
canning liquid		17.7	11.7	42.4	ND	506.0	577.9
		0.0–28.9	5.4–17.0	41.3–43.6		380.8–572.1	427.4–660.4
black beans	2.7	5.3	ND	66.7	ND	428.3	500.3, 453.4–529.0
	1.8–3.7	0.0–15.9		51.8–77.3		401.7–451.7	
canning liquid		ND	48.3	105.6	15.7	932.3	1101.8
			38.5–57.9	90.6–119.7	5.9–26.3	848.5–1091.4	1012.5–1274.3
pinto beans	2.7	ND	ND	40.4	ND	253.2	293.6
	1.4–3.7			36.8–43.7		181.4–349.1	222.1–392.8
canning liquid		ND	23.4	48.1	ND	411.8	483.3
			16.3–34.7	28.1–81.7		250.7–622.5	304.6–738.8

[a]Values are the average and range of three analyses. Carbohydrate values are in milligrams per 100 g beans or 100 mL liquid. [b]ND, not detected.

Free galactose is toxic to plant cells and is highly regulated, so it is a very minor component of most plants and often not reported.[37] Instead, the major source of galactose in legumes is galacto-oligosaccharides, which are thought to aid in seed tolerance to desiccation and to serve as an energy reserve for germination.[38,39] The most common linear oligosaccharides include raffinose, stachyose, and verbascose, with one, two, or three galactosyl residues, respectively, linked α-1−6 to the glucose residue of sucrose and α-1−6 to each other. Galactose can also be linked to inositols; for example, ciceritol, found in garbanzo beans, is the α-digalactoside of pinitol (α-D-galactopyranosyl-(1→6)-α-D-galactopyranosyl-(1→2)-4-*O*-methyl-*chiro*-inositol).

The effect of various legume preparation methods on galacto-oligosaccharides has been reported;[15,40−43] however, there is almost no information on the effect of these treatments on free galactose concentrations. Although soaking and cooking reduce the oligosaccharide content, it is not clear whether these compounds are simply lost from the tissue or whether they are subject to enzymatic or thermal degradation, which may release free galactose.

The galactose content of various commercially canned legumes and canning liquid is shown in Table 3 Free galactose was highest in garbanzo beans (24.6 ± 26.4 mg/100 g whole beans and 39.5 ± 26.5 mg/100 mL canning liquid) compared to the other varieties examined. Free galactose was also found in black beans (5.3 ± 9.2 mg/100 g) but was not detected in whole red kidney beans or pinto beans; however, free galactose was detected in the canning liquid of kidney beans (17.7 ± 15.5 mg/100 mL). Stachyose contributed the greatest amount of bound galactose in pinto, black, and kidney beans, whereas ciceritol was the highest source of bound galactose in garbanzo beans.

Free galactose found in the canned garbanzo beans and the canning liquid is equivalent to approximately 180 mg/100 g bean dry weight (calculated accounting for the weight of each portion). This value is substantially lower than the 444 mg/100 g reported by Acosta and Gross,[7] but similar to concentrations of 184, 110, and 80 mg/100 g reported by others.[44−46] The high concentration reported by Acosta and Gross may be due in part to a different variety of garbanzo bean or the different analytical technique used for quantitation. Although similar extraction methods were used in all studies, Acosta and Gross reduced and derivatized the sugars to alditol acetates for analysis by gas chromatography, which would exaggerate the galactitol peak with any galactitol naturally present in the beans. As well, the difference may be related to the bean preparation method. Soaking beans at room temperature prior to cooking as done by Acosta and Gross would initiate germination, which, in turn, initiates hydrolysis of galacto-oligosaccharides by α-galactosidase with possible liberation of free galactose.[47]

In addition, the higher free galactose concentration found in the canning liquid indicates that the free galactose content associated with the consumption of canned legumes can be significantly reduced if the canning or cooking liquid is discarded and any residual liquid on the legumes is removed by rinsing.

Although the maximum amount of dietary galactose safely tolerated by those with classic galactosemia remains unknown,[3,48] results from this study find that the galactose content of specific cheeses, caseinates, and legumes are within those found in currently allowed foods and ingredients and are low enough to be acceptable in the diet for classic galactosemia. Allowing some previously restricted foods in the diet could improve both adherence and nutrient intake of individuals who require chronic galactose restriction. These analytical findings may have important implications for patients with galactosemia and support a review of current dietary recommendations for classic galactosemia.

AUTHOR INFORMATION

Corresponding Author

*(C.H.S.) Phone: 1 (604) 822-1804. Fax: 1 (604) 822-5143. E-mail: christine.scaman@ubc.ca.

Funding

This work was supported by the Galactosemia Foundation, Mandeville, LA 70470-2401.

Notes

The authors declare no competing financial interest.

■ ACKNOWLEDGMENTS

We thank Benny Chan for technical assistance in the analysis of legume samples.

■ REFERENCES

(1) Friedovich-Keil, J. L.; Walter, J. H. Galactosemia. In *The Online Metabolic and Molecular Basis of Inherited Disease*; Beaudet, A. L., Vogelstein, B., Kinzler, K. W., Antonarakis, S. E., Ballabio, A., Eds.; McGraw-Hill: New York, 2008; Vol. 7, Chapter 72, http://www.ommbid.com.

(2) Bosch, A. Classical galactosemia revisited. *J. Inherit. Metab. Dis.* **2006**, *29*, 516−525.

(3) Berry, G.; Elsas, L. Introduction to the Maastricht workshop: lessons from the past and new directions in galactosemia. *J. Inherit. Metab. Dis.* **2011**, *34*, 249−255.

(4) Berry, G. T.; Nissim, I.; Zhiping, L.; Mazur, A. T.; Gibson, J. B.; Segal, S. Endogenous synthesis of galactose in normal men and patients with hereditary galactosaemia. *Lancet* **1995**, *346*, 1073−1074.

(5) Berry, G. T.; Reynolds, R. A.; Yager, C. T.; Segal, S. Extended ^{13}C-galactose oxidation studies in patients with galactosemia. *Mol. Genet. Metab.* **2004**, *82*, 130−136.

(6) Gross, K. C.; Acosta, P. Fruits and vegetables are a source of galactose: implications in planning the diets of patients with galactosemia. *J. Inherit. Metab. Dis.* **1991**, *14*, 253−258.

(7) Acosta, P.; Gross, K. C. Hidden sources of galactose in the environment. *Eur. J. Pediatr.* **1995**, *154*, S87−S92.

(8) Wiesmann, U. N.; Rosé-Beutler, B.; Schlüchter, R. Leguminosae in the diet: the raffinose-stachyose question. *Eur. J. Pediatr.* **1995**, *154*, S93−S96.

(9) Gropper, S.; Weese, J. O.; West, P. A.; Gross, K. C. Free galactose content of fresh fruits and strained fruit and vegetable baby foods: more foods to consider for the galactose-restricted diet. *J. Am. Diet. Assoc.* **2000**, *100*, 573−575.

(10) Kim, H.; Hartnett, C.; Scaman, C. H. Free galactose content in selected fresh fruits and vegetables and soy beverages. *J. Agric. Food Chem.* **2007**, *55*, 8133−8137.

(11) Hartnett, C.; Kim, H.; Scaman, C. H. Effect of processing on galactose in selected fruits. *Can. J. Diet. Pract. Res.* **2007**, *68*, 46−50.

(12) Scaman, C. H.; Jim, V.; Hartnett, C. Free galactose concentrations in fresh and stored apples (*Malus domestica*) and processed apple products. *J. Agric. Food Chem.* **2004**, *52*, 511−517.

(13) Gitzelman, R.; Auricchio, S. The handling of soya α-galactosides by a normal and a galactosemic child. *Pediatrics* **1965**, *36*, 231−235.

(14) Van Calcar, S. C.; Bernstein, L. E. Nutrition management of classical and Duarte galactosemia: results from an international survey (abstract). *J. Inherit. Metab. Dis.* **2011**, *102*, 262.

(15) Queiroz, K.; Oliveira, A.; Helbig, E. Soaking the common bean in a domestic preparation reduced the contents of raffinose-type oligosaccharides but did not interfere with nutritive value. *J. Nutr. Sci. Vitaminol.* **2002**, *44*, 283−289.

(16) Portnoi, P. A.; MacDonald, A. Determination of the lactose and galactose content of cheese for use in the galactosemia diet. *J. Hum. Nutr. Diet.* **2009**, *22*, 400−408.

(17) Portnoi, P. A.; MacDonald, A. The lactose content of Mini Babybel and suitability for galactosaemia. *J. Hum. Diet. Nutr.* **2011**, *24*, 620−621.

(18) Lues, J. F. R. Organic acid and residual sugar variation in a South African Cheddar cheese and possible relationships with uniformity. *J. Food Compos. Anal.* **2000**, *13*, 819−825.

(19) Bouzas, J.; Kantt, C. A.; Bodyfelt, F. W.; Torres, J. A. Simultaneous determination of sugars and organic acids in Cheddar cheese by high-performance liquid chromatography. *J. Food Sci.* **1991**, *56*, 276−278.

(20) Bouzas, J.; Kantt, C. A.; Bodyfelt, F. W.; Torres, J. A. Time and temperature influence on chemical aging indicators for a commercial Cheddar cheese. *J. Food Sci.* **1993**, *58*, 1307−1313.

(21) Harvey, C. D.; Jenness, R.; Morris, H. A. Gas chromatographic quantitation of sugars and nonvolatile water-soluble organic acids in commercial Cheddar cheese. *J. Dairy Sci.* **1981**, *64*, 1648−1654.

(22) Gopal, P.; Richardson, R. K. A rapid and sensitive method for estimation of galactose in Parmesan cheese. *Int. Dairy J.* **1996**, *6*, 399−406.

(23) Broderick, G. Department of Dairy Science, College of Agriculture and Life Sciences, University of Wisconsin—Madison, 2011; personal communication.

(24) Lilla, Z.; Sullivan, D.; Ellefson, W.; Welton, K.; Crowley, R. Determination of "net carbohydrates" using high-performance anion exchange chromatography. *J. AOAC Int.* **2005**, *88*, 714−719.

(25) Sanchez-Mata, M. C.; Penuela-Teruel, M. J.; Camara-Hurtado, M.; Diez-Marques, C.; Torija-Isasa, M. E. Determination of mono-, di-, and oligosaccharides in legumes by high-performance liquid chromatography using an amino-bonded silica column. *J. Agric. Food Chem.* **1998**, *46*, 3648−3652.

(26) O'Kennedy, B. T. Dairy ingredients in non-dairy food systems. In *Dairy Derived Ingredients − Food and Nutraceutical Uses*; Corredig, M., Ed.; CRC Press: Boca Raton, FL, USA, 2009; pp 482−506.

(27) Southward, C. R. Casein products. Chemical processes in New Zealand, New Zealand Dairy Research Institute, http://nzic.org.nz/ChemProcesses/dairy/3E.pdf (accessed Nov 5, 2013).

(28) Fox, P. F.; Guinee, T. O.; Cogan, T. M.; McSweeney, P. L. H. Chemistry of milk constituents, In *Fundamentals of Cheese Science*; Aspen Publishers: Gaithersburg, MD, USA, 2000; pp 19−44.

(29) Fox, P. F.; Guinee, T. O.; Cogan, T. M.; McSweeney, P. L. H. Biochemistry of cheese ripening. In *Fundamentals of Cheese Science*; Aspen Publishers: Gaithersburg, MD, USA, 2000; pp 236−281.

(30) Michel, V.; Martley, F. G. *Streptococcus thermophilus* in Cheddar cheese − production and fate of galactose. *J. Dairy Res.* **2001**, *68*, 317−325.

(31) Adamberg, K.; Antonsson, M.; Vogensen, F. K.; Nielsen, E. W.; Kask, S.; Møller, P. L.; Ardö, Y. Fermentation of carbohydrates from cheese sources by non-starter lactic acid bacteria isolated from semi-hard Danish cheese. *Int. Dairy J.* **2005**, *15*, 873−882.

(32) Falentin, H.; Henaff, N.; Le Bivic, P.; Deutsch, S.-M.; Parayre, S.; Richoux, R.; Sohier, D.; Thierry, A.; Lortal, S.; Postollec, F. Reverse transcription quantitative PCR revealed persistency of thermophilic lactic acid bacteria metabolic activity until the end of the ripening of Emmental cheese. *Food Microbiol.* **2012**, *29*, 132−140.

(33) Govindasamy-Lucey, S.; Jaeggi, J. J.; Martinelli, C.; Johnson, M. E.; Lucey, J. A. Standardization of milk using cold ultrafiltration retentates for the manufacture of Swiss cheese: effect of altering coagulation conditions on yield and cheese quality. *J. Dairy Sci.* **2011**, *94*, 2719−2730.

(34) Mora, D.; Fortina, M. G.; Parini, C.; Ricii, G.; Gatti, M.; Giraffa, G.; Manachini, P. L. Genetic diversity and technological properties of *Streptococcus thermophilus* strains isolated from dairy products. *J. Appl. Microbiol.* **2002**, *93*, 278−287.

(35) Deutsch, S.; Ferain, T.; Delcour, J.; Lortal, S. Lysis of lysogenic strains of *Lactobacillus helveticus* in Swiss cheeses and first evidence of concomitant *Streptococcus thermophilus* lysis. *Int. Dairy J.* **2002**, *12*, 591−600.

(36) Pecorari, M.; Gambini, G.; Reverberi, P.; Caroli, A.; Panari, G. Andamento della glicolisi nelle prime fasi di maturazione del Parmigiano-Reggiano. *Sci. Tecn. Lattiero−Casearia* **2003**, *54*, 149−162.

(37) Joersbo, M.; Jørgensen, K.; Brunstedt, J. A selection system for transgenic plants based on galactose as selective agent and a UDP-glucose:galactose-1-phosphate uridyltransferase gene as selective gene. *Mol. Breed.* **2003**, *11*, 315−323.

(38) Horbowicz, M.; Obendorf, R. L. Seed desiccation tolerance and storability: dependence on flatulence-producing oligosaccharides and cyclitols − review and survey. *Seed Sci.* **1994**, *4*, 385−405.

(39) French, D. The raffinose family of oligosaccharides. In *Advances in Carbohydrate Chemistry*; Wolfrom, M. L., Tipson, R. S., Pigman, W., Eds.; Academic Press: New York, 1954; Vol. 9, pp 149−185.
(40) Frias, J.; Vidal-Valverde, C.; Sotomayor, C.; Diaz-Pollan, C.; Urbano, G. Influence of processing on available carbohydrate content and antinutritional factors of chickpeas. *Eur. Food Res. Technol.* **2000**, *210*, 340−345.
(41) Han, I. H.; Baik, B. K. Oligosaccharide content and composition of legumes and their reduction by soaking, cooking, ultrasound, and high hydrostatic pressure. *Cereal Chem. J.* **2006**, *83*, 428−433.
(42) Vidal-Valverde, C.; Sierra, I.; Frias, J.; Prodanov, M.; Sotomayor, C.; Hedley, C. L.; Urbano, G. Nutritional evaluation of lentil flours obtained after short-time soaking processes. *Eur. Food Res. Technol.* **2002**, *215*, 138−144.
(43) Pugalenthi, M.; Siddhuraju, P.; Vadivel, V. Effect of soaking followed by cooking and the addition of α-galactosidase on oligosaccharides levels in different Canavalia accessions. *J. Food Compos. Anal.* **2006**, *19*, 512−517.
(44) Berrios, J. D. J.; Morales, P.; Cámara, M.; Sánchez-Mata, M. C. Carbohydrate composition of raw and extruded pulse flours. *Food Res. Int.* **2010**, *43*, 531−536.
(45) Aguilera, Y.; Martín-Cabrejas, M. A.; Benítez, V.; Mollá, E.; López-Andréu, F. J.; Esteban, R. M. Changes in carbohydrate fraction during dehydration process of common legumes. *J. Food Compos. Anal.* **2009**, *22*, 678−683.
(46) Lineback, D. R.; Ke, C. H. Starches and low-molecular-weight carbohydrates from chick pea and horse bean flours. *Cereal Chem.* **1975**, *52*, 334−347.
(47) Mittal, Y.; Sharma, C. B. Development of α-galactosidase isoenzymes in chickpea seeds. *Plant Sci.* **1991**, *77*, 185−190.
(48) Coss, K. P.; Byrne, J. C.; Coman, D. J.; Adamczyk, B.; Abrahams, J. L.; Saldova, R.; Brown, A. Y.; Walsh, O.; Hendroff, U.; Carolan, C.; Rudd, P. M.; Treacy, E. P. IgG N-glycans as potential biomarkers for determining galactose tolerance in classical galactosaemia. *Mol. Genet. Metab.* **2012**, *105*, 212−220.

intended use as possible, i.e., in contact with the food that they are intended to be used with, while maintaining storage times and temperatures consistent with consumer practices. Alternatively, exaggerated conditions can be used to assess a worst-case scenario, so that measures can be taken to protect even the most careless consumer. Where possible, the food that the intended food packaging material is to be used with should be used in the migration tests because the nexus of interrelationships, such as water availability and viscosity, is not accounted for when using food simulants.

Simulation models can be a valuable resource in risk assessment, particularly in migration[9] and exposure assessments.[10] Simulation models can be used as an initial screening tool to provide a range of values likely to result from a given scenario, reducing the need for expensive, time-consuming migration tests. Simulation models can also provide guidance on expected migration ranges, hence guiding the selection of sensitive analytical techniques. Model design inherently involves the incorporation of multiple factors that affect the overall system and the collation of variability and uncertainty of all known factors that contribute to the models output. For example, a migration model requires inputs; these inputs should account for all of the attributes that affect migration in a packaging−food system. Often existing interrelations between input factors can be found in the literature,[11] and these can be useful as a starting framework. By reviewing the literature on existing knowledge regarding mass-transfer phenomena, these systems can be mathematically simulated to calculate potential nanoparticle migration for a particular scenario. When the necessary data are available, exposure assessments are a logical progression from migration testing, particularly when dealing with migration into real foodstuffs. Exposure assessments can improve our understanding of the risks associated with migration. They can make migration results more tangible as the migration figures are combined with likely consumption levels of the particular food in question while also considering the relative body weight of an individual. Hence, the objective of this study was to analytically assess the migration of silver and copper nanoparticles from polyethylene (PE) matrices into a food matrix and to use known interrelationships reported in the literature to create a simulation model to predict likely migration levels. The migration results were also used for an exposure assessment, focusing on the oral route of exposure, following the ingestion of chicken meat packaged with a nanopolymer.

MATERIALS AND METHODS

Experimental Procedure. *Nanoparticle Synthesis.* To make the silver nanoparticles, an $AgNO_3$ solution (0.1 M) was prepared in ethanol at 45 °C to make 10 nm nanoparticles. An equal amount of 0.1 M polyvinylpyrrolidone (PVP) solution in ethanol was then added to this at a rate of 0.667 mL min^{-1}. The solution was stirred for 2 h (800 rpm), until the solution had turned a stable orange−brown color. Silver nanoparticles were separated from solution by the addition of acetone at a volume ratio of approximately 1:4. The solution was sonicated for 10 min and centrifuged at 6000 rpm for 15 min. The supernatant was discarded; the pellet was redispersed in ethanol; and the separation step was repeated. The pellet was dried in an oven overnight at 60 °C and crushed to a powder; this procedure was adapted from Chen et al.[12] Scanning electron microscopy (SEM) images were taken of the particles (Figure 1)

To make the copper nanoparticles, CuCl (99% minimum), sodium formaldehyde sulfoxylate (SFS), and sodium citrate were purchased from Sigma-Aldrich. The concentration of all solutions was 0.5 M, and they were prepared in deionized water. Sodium citrate solution was added dropwise to CuCl solution under stirring at a 2:1 volume ratio, at 60 °C. The mixture was stirred for 30 min, before SFS solution was added dropwise. The mixture was stirred for a further 60 min. A brown precipitate was formed. The supernatant was discarded, and the precipitate was washed. The supernatant was again discarded, and the brown precipitate was dried at 60 °C. This procedure was adapted from Khanna et al.[13]

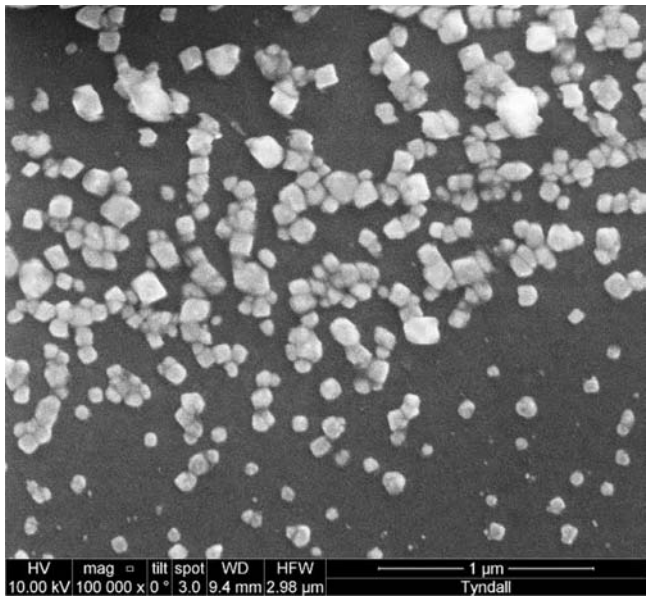

Figure 1. SEM images of silver nanoparticles that were incorporated into PE.

Composite Manufacture. PE-based composites were manufactured via extrusion in a micro 27 lab-scale twin screw extruder (Leistritz, Nuernberg, Germany) with a 27 mm screw diameter and a 38:1 length/diameter ratio, using the screw geometry as outlined by Gunning et al.[14] PE pellets (melt flow rate of 0.33 g/10 min and density of 921 kg/m^3) were supplied by Boxmore Plastics Co., Cavan, Ireland. In the compounding process, the temperature profile was increased from 160 °C at the hopper to 200 °C at the die with a screw speed of 120 rpm. Two PE nanocomposites were designed containing 0.5% (w/w) of the nanocomponent (properties of the PE used can be found in Table 1). The silver nanocomposite incorporated nanosilver with a logistic size distribution with a mean of 1.01×10^{-8} m and a standard deviation of 6.4×10^{-10} m (Figure 1). The copper nanocomposite incorporated nanocopper with a logistic size distribution with a mean of 1.14×10^{-8} and a standard deviation of 6.8×10^{-10} m. Skinless, boneless chicken breasts (samples) were sourced from an Irish supplier, and 32 samples were wrapped in 120 cm^2 of one of the prepared nanocomposites ($n = 16$ for both silver and copper). The packaging did not overlap. Aluminum foil was wrapped around these to eliminate any possible variation that light may impart.[15] Oxidation of silver nanoparticles because of ultraviolet (UV) radiation is known to facilitate silver dissolution.[16]

Each sample (nanocomposite and foiled unit) was then vacuum-packed in standard, heat-sealable, clear, PE vacuum packing bags to ensure maximum, consistent contact between the active nanocomposite and the samples. For such active packaging materials, sharing a common interface or physical contact with the food surface is essential for the desired effect to be observed.[17] Each unit was performed in quadruplicate. Also, eight control units were prepared, where samples were in contact with a PE packaging that did not contain added nanosilver or nanocopper.

Units were kept in constant temperature rooms for the duration of the experiment (t): either 1.1 or 3.1 days. The time periods chosen for the migration tests were thought to represent likely and unfavorable (however, possible) storage periods for chicken.

Table 1. Inputs, Constants, and Outputs of the Simulation Model

	name	subdivision	value	unit	symbol	equation	reference
			Inputs				
PE	dynamic viscosity	viscosity[a]	uniform (200,[b] 2300)	Pa s	$\eta(p)$		29
		temperature	uniform (473, 487.87[b])	K	x		29
	glass transition temperature		logistic (−120.565, 1.5667)	K	T_g		measured values (mv)
	density		921	kg/m^3	$\rho(p)_s$		product specification
nanoparticle	density	nanosilver	10490	kg/m^3	$\rho(n)_c$		
		nanocopper	8940	kg/m^3	$\rho(n)$		30
	diameter	nanosilver	logistic (1.14×10^{-8}, 6.8×10^{-10})	m	$2r$		mv
		nanocopper	uniform with a mean of 1.009×10^{-8} and σ^c of 1.145×10^{-9}	m	$2r$		mv
storage	time (there were two levels of this factor)	1.1 days	95040	s	t		mv
		3.1 days	267840	s	t		mv
	temperature (there were two levels of this factor)	T1	lognormal [0.306, 0.385, shift (7.8)] + 273	K	T		mv
		T2	logistic (21.86, 0.31) + 273	K	T		mv
system	surface area		uniform (0.0099, 0.0101)	m^2	a		mv
	concentration of nanoparticles in PE	nanosilver	d	kg/m^3	c		mv
		nanocopper	d	kg/m^3	c		mv
			Constants				
	pi		22/7		π		
	Boltzmann constant		1.3087×10^{-23}	J K^{-1}	k_B		11
	empirical parameter		17.44	K	C_1		11
	empirical parameter		51.6	K	C_2		11
			Outputs				
	viscosity at the glass transition temperature		distribution with a mean of 4.3×10^9 and σ^c of 2.13×10^9	Pa s	$\eta(T_g)$	1	
	temperature dependence of viscosity		distribution with a mean of 1.7×10^4 and σ^c of 8.4×10^4	dη/dT	$\eta(T)$	2	
	migratability	nanosilver	specific to the levels of the factors: t and T	m	M	3	
		nanocopper	specific to the levels of the factors: t and T	m	M	3	
	migratables		specific to the value of M and c and, thus, the factor $\rho(n)$	mg	N_{mg}	4	
	migration level			mg/dm^2	Q	5	

[a]Negatively correlated with the dynamic viscosity temperature, with a value of −0.8. [b]Calculated from extrapolation of values.[29] [c]Standard deviation of the distribution. [d]See Table 3.

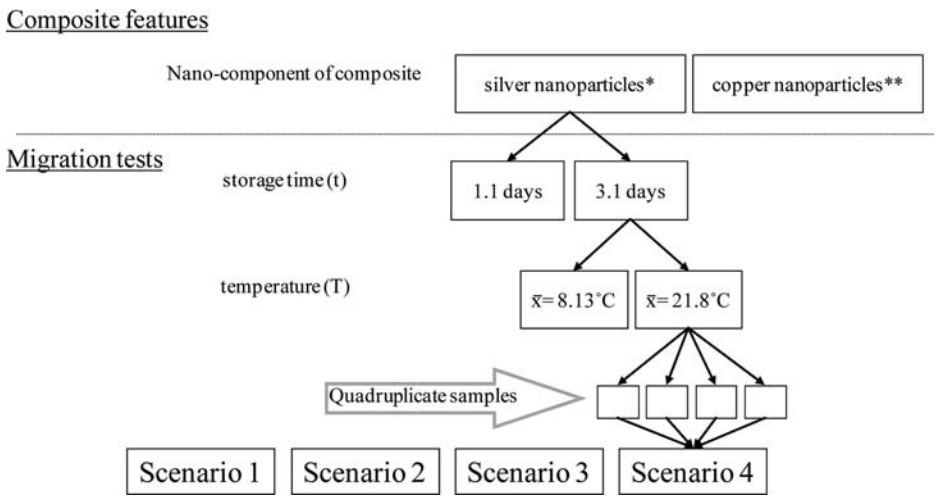

Figure 2. Experimental design, where composites containing either silver or copper nanoparticles undergo migration tests (into chicken breast samples) and are held for 1.1 or 3.1 days at an average temperature of 8.13 or 21.8 °C according to their respective scenario profile.

Temperature probes were used to log the internal temperatures of the samples at the various temperature levels (Figure 2). The effect of the temperature was determined by subjecting samples to different temperatures during the migration test time periods. The temperatures

dx.doi.org/10.1021/jf404038y | J. Agric. Food Chem. 2014, 62, 1403−1411

Table 2. Scenarios Showing Experimental Conditions with Corresponding Laboratory, Migration Modeling, and Exposure Results

migrant	scenario	time	temperature	mean migrant (mg/kg) (n = 4)	mean migrant (mg/dm^2) (n = 4)	mean predicted level (Q) (mg/dm^2) (n = 4) (5th−95th percentile)	95th percentile of exposure (e) (mg kg$_{bw}^{-1}$ day^{-1})
silver	1	T1	t1	0.026	0.003	0.003 (0.002−0.004)	5.89×10^{-5}
silver	2	T1	t2	0.031	0.004	0.003 (0.002−0.005)	7.06×10^{-5}
silver	3	T2	t1	0.042	0.005	0.004 (0.003−0.007)	8.9×10^{-5}
silver	4	T2	t2	0.039	0.004	0.005 (0.003−0.009)	7.97×10^{-5}
copper	1	T1	t1	0.265	0.032	0.038 (0.013−0.038)	2.26×10^{-5}
copper	2	T1	t2	0.351	0.044	0.040 (0.014−0.040)	5.67×10^{-5}
copper	3	T2	t1	0.207	0.024	0.044 (0.017−0.044)	4.24×10^{-5}
copper	4	T2	t2	0.382	0.049	0.047 (0.019−0.047)	1.17×10^{-4}

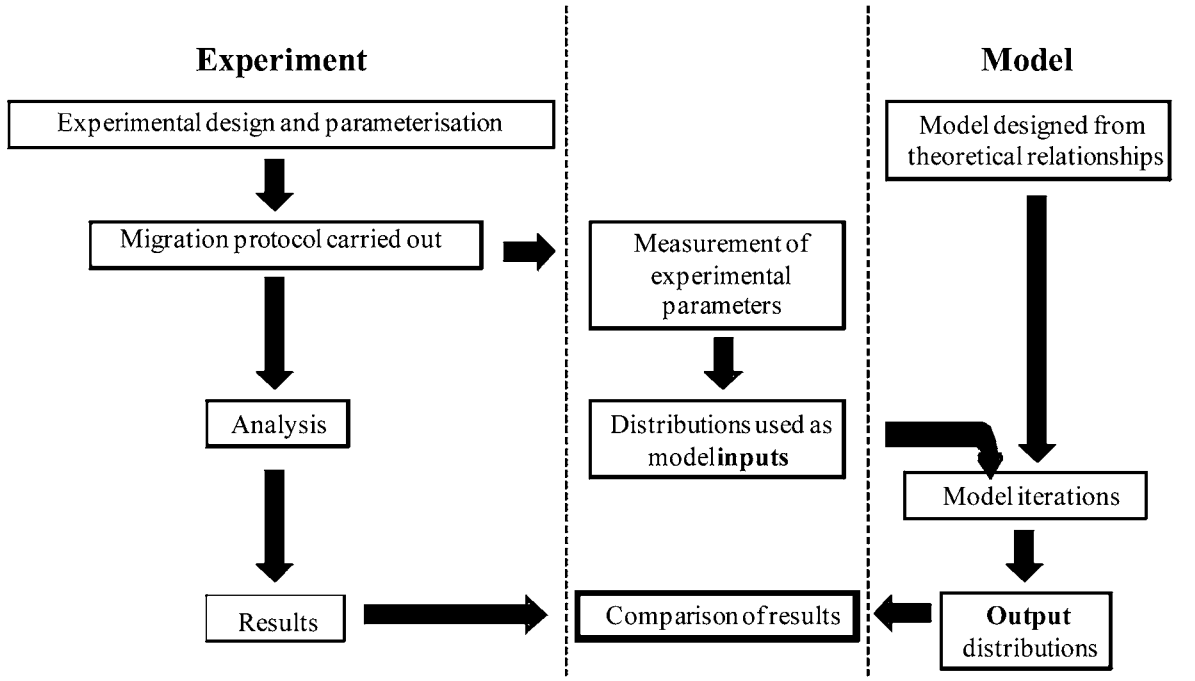

Figure 3. Study framework showing experimental procedures, modeling tasks, and their interrelationships culminating in the comparison of the two results to assess the performance of the migration model.

chosen to represent the conditions of a poorly performing/overcrowded refrigerator and ambient storage. The two levels of temperatures were set and then logged during the migration tests. The means ± standard deviations of the distributions T1 and T2 were 8.13 ± 0.48 and 21.80 ± 0.64 °C, respectively.

Following the migration tests, all packaging was removed from the samples. Each chicken breast sample was homogenized, and 2 g of it was added to a Teflon microwave vessel. A total of 10 mL of concentrated nitric acid (Fisher Scientific) was added to the vessel. The sample was digested using microwave-assisted acid dissolution at 200 °C (microwave unit from Mars Xpress supplied by CEM). The extract produced was diluted to 50 mL with deionized water. Digests were analyzed using inductively coupled plasma−mass spectrometry (ICP−MS, Agilent 7500 ICP−MS) according to the protocol assigned the ISO number DIN EN ISO 17294-2-E29. Standards were derived from stock solutions from Spectrosol.

Mathematical Model. A migration model was designed, and its validity was assessed by comparing migration predictions to the results of the laboratory migration tests, given the same set of conditions (time and temperature). Migratability and subsequent migratables were intermediate outputs that were also generated by the mathematical model. The equations to follow are applicable to polyolefins and not to non-amorphous polymers. The Williams−Landel−Ferry equation for time−temperature superposition was used with the dynamic viscosity of the polymer to obtain the viscosity at the glass transition temperature of the polymer, as used by Šimon et al.[11] and defined as

$$\eta(T_g) = \frac{\eta(T)}{\left(\exp\left(\frac{-1(C_1(T-T_g))}{C_2+T-T_g}\right)\right)} \quad (1)$$

where η is the viscosity, T_g is the glass transition temperature, T is the experimental temperature (as mentioned above; in this case, the dynamic viscosity information of the polymer was used), and C_1 and C_2 are constants with values of 17.44 and 51.6 K, respectively.

As seen from eq 2, the Williams−Landel−Ferry equation is also used for the subsequent calculation of the viscosity at a particular temperature. During validation, experimental temperatures were used as inputs.

$$\eta(T) = \eta(T_g)\exp\left(\frac{-1(C_1(T-T_g))}{C_2+T-T_g}\right) \quad (2)$$

Migratability (M) is a value of the likelihood of particles migrating from a given system and is defined as

Table 3. Inputs and Outputs of the Model of Nanosilver and Nanocopper Concentrations in the Nanocomposites

	value	symbol	unit	equation
	Inputs			
quantity of PE in the nanocomposite	triangular (99.48, 99.5, 99.52)	b	%, w/w	
quantity of silver in the nanocomposite	triangular (0.48, 0.5, 0.52)	d	%, w/w	
PE density	921	$\rho(p)$	kg/m^3	
silver density	10490	$\rho(n)_s$	kg/m^3	
copper density	8940	$\rho(n)_c$	kg/m^3	
	Outputs for Nanosilver Nanocomposite			
volume of PE	distribution with a mean of 1.08×10^{-3} and σ of 8.86×10^{-8}	f	m^3	$b/\rho(p)$
volume of silver	distribution with a mean of 4.76×10^{-7} and σ of 7.78×10^{-9}	g	m^3	$d/\rho(n)$
volume of 1 kg of nanocomposite	distribution with a mean of 1.08×10^{-3} and σ of 8.09×10^{-8}	h	m^3	$f + g$
weight of 1 m^3 of nanocomposite	distribution with a mean of 925 and σ of 0.07	j	kg/m^3	$1/h$
weight of nanosilver in 1 m^3 of nanocomposite	distribution with a mean of 1.53×10^{-5} and σ of 1.45×10^{-6}	c	kg/m^3	$j \times d$
	Outputs for Nanocopper Nanocomposite			
volume of PE	distribution with a mean of 1.08×10^{-3} and σ of 8.86×10^{-8}	f	m^3	$b/\rho(p)$
volume of copper	distribution with a mean of 4.76×10^{-7} and σ of 7.78×10^{-9}	g	m^3	$d/\rho(n)$
volume of 1 kg of nanocomposite	distribution with a mean of 1.08×10^{-3} and σ of 8.09×10^{-8}	h	m^3	$f + g$
weight of 1 m^3 of nanocomposite	distribution with a mean of 925 and σ of 0.07	j	kg/m^3	$1/h$
weight of nanocopper in 1 m^3 of nanocomposite	distribution with a mean of 1.53×10^{-5} and σ of 1.45×10^{-6}	c	mg/m^3	$j \times d \times 10^6$

$$M = \sqrt{\left(\frac{k_B T t}{24(\pi^2)\eta r}\right)} \quad (3)$$

where k_B is the Boltzmann constant ($k_B = 1.3807 \times 10^{-23}$ J K^{-1}), t is the time in seconds, and r is the radius of the particles. Migratables (N_{mg}) is the quantity of nanoparticles migrating from the polymer matrix[11] and is calculated as given in eq 4

$$N_{mg} = Mac \quad (4)$$

where a is the area of the nanocomposite−food interface and c is the initial concentration of nanoparticles in the nanocomposite assuming homogeneous distribution. The final migration level (Q) must consider background levels of the metal (eq 5). In this study, the background level of each metal was estimated using measurements taken from the control samples. This was particularly important in the case of the samples in contact with the copper nanocomposites because chicken breasts have naturally occurring background levels of copper (BL), which are highly variable relative to likely copper migration levels. A dimensionless uncertainty factor (e) is also included in the migration model to take into account the model uncertainty (eq 5). It was calculated by optimizing the representations of the experimental data of the models.

$$Q = (N_{mg} + \mathrm{BL})e \quad (5)$$

A Monte Carlo simulation was used so that inherent variability of the input parameters can be considered. The inputs, constants, and outputs of the model are given in Table 1. The @RISK 5.5 software (Palisade, Middlesex, U.K.), a package specifically used for risk assessment, was used as an add in in Microsoft Excel (Microsoft Office 2007). The model was run for 10 000 iterations, giving a final simulated output probability density distribution for the level of nanosilver and nanocopper likely to migrate into the food matrix.

Model−Experimental Synchronization. The conditions of the experiments were used as inputs in the model (Table 2). Scenario 1 used a time (t) of 1.1 days and a temperature (T) of 8.13 ± 0.48 °C. Scenario 2 used a time of 1.1 days and a temperature of 21.80 ± 0.64 °C. Scenario 3 was for a time of 3.1 days and a temperature of 8.13 ± 0.48 °C. Scenario 4 was for a time of 3.1 days and a temperature of 21.80 ± 0.64 °C. This allowed for the direct comparison of the model outputs to the experimental results. This framework is explained diagrammatically in Figure 3. The input variable of the concentration was converted from %, w/w (given in the Experimental Procedure above) to kg/m^3 to allow for comparison to model outputs (Table 3).

Exposure Model. If migration occurs, likely exposure arising from the migration can be calculated by an exposure assessment. In doing so, it was assumed that all silver was in its most harmful form, i.e., unagglomerated nanoparticles, because it is not known how readily silver nanoparticles produce silver ions or in what ratios they coexist. In addition, both processes are likely to vary according to pH, temperature, and/or time.[10] Any agglomeration of the nanoparticles is likely to reduce the active particle surface area and, hence, reduce toxicity, and therefore, the model assumed no agglomeration throughout the process. A mathematical model were created to generate probability distributions of human exposure to silver and copper nanoparticles as a result of the consumption of chicken after contact with the nanosilver PE nanocomposite and the nanocopper PE nanocomposite used in the migration tests. The results of the migration experiments fed into the exposure assessment as an input variable.[10] Monte Carlo simulation (10 000 iterations) was used so that the inherent uncertainty and variability of input parameters were considered. Risk analysis software (@Risk 5.5, Palisade, Middlesex, U.K.) was used to generate a predicted exposure estimate from the series of input distributions using eq 6

$$E_x = (y_x z)/\mathrm{bw} \quad (6)$$

where E is exposure in mg kg$_{bw}^{-1}$ day^{-1} and x is the particular migrant particle (in this case, nanosilver or nanocopper). The term y is migration in mg/kg into the particular food, chicken breast meat in this case. The term z is the consumption of that food in kg/day in a given population. The term bw refers to the body weight of an individual in kilograms in the given population. Chicken consumption data for Ireland,[18] for those who consumed chicken (67%; n = 1500), took account of "... all chicken eaten as meat only, chicken on the bone, chicken skin and chicken meat extracted from composite meals by way of an arbitrary percentage of 66.7%." The data provided was fit to a log-normal distribution (with a mean of 62.01 g/day and a standard deviation of 43.84 g/day) using @Risk 5.5 software to represent consumption (z). Irish adult body weight data[18] (bw) was fit to a normal distribution (with a mean of 77.48 kg and a standard deviation of 16.18 kg) using @Risk 5.5 software.

RESULTS AND DISCUSSION

Experimental Migration. The results of the experiments are presented in Table 2. All four scenarios were conducted at temperatures above the recommended storage temperature of a perishable food product (>5 °C); this is an important consideration when comparing the migration of nanosilver in this study to other studies or ingestion limits.

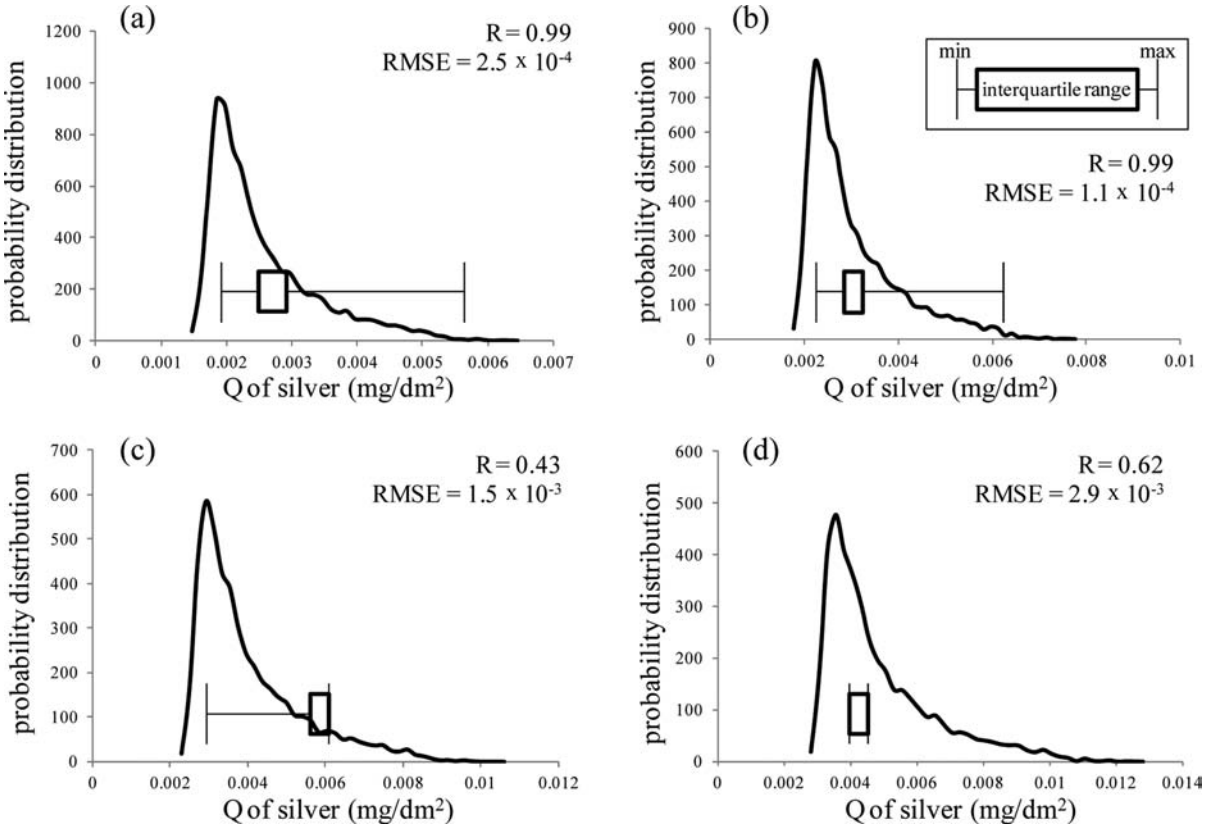

Figure 4. Probability density distribution of the final migration level (Q) of silver in chicken and the minimum, maximum, and interquartile range of the corresponding experimental values, following simulations and migration tests of the following conditions: (a) scenario 1, (b) scenario 2, (c) scenario 3, and (d) scenario 4.

SAS 9.1 was used to establish if there were any effects of time and temperature on the migration of silver or copper from the nanocomposites. No significant effects of time or temperature were observed in the samples analyzed for copper or silver ($p > 0.1$). In the case of both time and temperature, it is suggested that migration levels may have already plateaued over the time period studied, and hence, no significant effect in the migration results was observed. This is supported by the fact that recent research, which focused on a shorter time period, reported a reduction in the migration rate within the first day of contact.[19] It is likely that both of these time periods used in the migration tests of this study are beyond the point of the migration−time relationship, where an increase in time brings about an increase in silver levels. Silver ion release from a polyester matrix into liquid simulant reached a maximum in less than 5 min in another study,[20] but corresponding SEM imagery seemed to confirm that this was due to the dissolution of particles on the surface or very near the surface of the polyester matrix in which they were bound.

The quantities of silver in samples that had been in contact with the nanosilver PE composite (with a mean of 0.0041 mg/dm^2; $n = 16$) were significantly different from the control samples (with a mean of 0.001 mg/dm^2; $n = 8$) ($p < 0.001$). The samples in contact with the nanocopper PE composite had significantly higher copper levels (with a mean of 0.037 mg/dm^2; $n = 16$) than the control samples (with a mean of 0.0157 mg/dm^2; $n = 8$) ($p < 0.05$) but to a different level of significance than the silver experiments. This may be explained by the presence of copper in chicken meat as a naturally occurring biological mineral.

It should be noted that the levels of migration observed in this study are from a pilot bench-scale nanocomposite developed in a laboratory for experimental uses only. Commercially, it would be unlikely that nanocomposites containing 0.5% (w/w) fill of nanosilver or nanocopper would be produced because novel effects are observed at much lower levels.[19] This is particularly important because the level of nanoparticulate fill was identified as the most significant parameter in a recent study[10] influencing migration compared to other parameters of time, temperature, and nanoparticle size. Hence, it is feasible to engineer a functional antimicrobial nanocomposite, with a lower nanofiller percentage and which will potentially result in less migration.

Model Validation. It is shown in Figure 4 that the model proved to be reliable in predicting the migration results for nanosilver over a range of storage conditions with coefficients of correlation (R) of 0.99, 0.99, 0.943, and 0.62 and root-mean-square error (RMSE) values of 2.5×10^{-4}, 1.1×10^{-4}, 1.5×10^{-3}, and 2.9×10^{-3} for scenarios 1, 2, 3, and 4, respectively. In general, the model was slightly less accurate in predicting the levels of copper in the chicken samples, with R values of 0.65, 0.97, 0.99, and 0.66 and RMSE values of 9.6×10^{-3}, 3.4×10^{-2}, 1.4×10^{-2}, and 2.1×10^{-2} for scenarios 1, 2, 3, and 4, respectively, as shown in Figure 5. This suggests that the model may be a useful tool in the design and engineering of new nanopackaging materials that are likely to come on stream in the coming years as the fruits of the recent surge of nanotechnological research mature. The main appeal of this model to industry is that it reduces the need for expensive and time-consuming migration tests, thus also reducing costs.

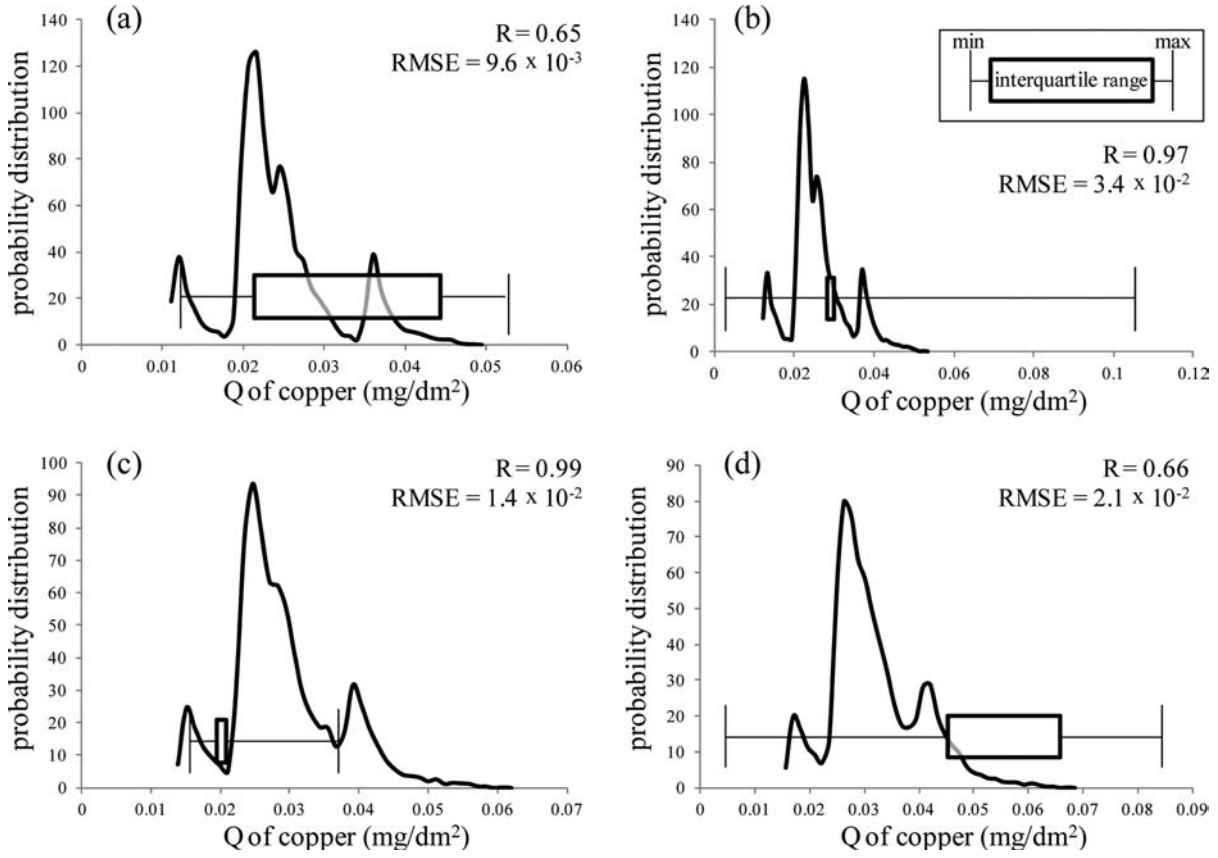

Figure 5. Probability density distribution of the final migration level (Q) of copper in chicken and the minimum, maximum, and interquartile range of the corresponding experimental values, following simulations and migration tests of the following conditions: (a) scenario 1, (b) scenario 2, (c) scenario 3, and (d) scenario 4.

The model, which took into account background levels (BL) in the food material in mg/dm^2, generated from control values, and a model error (e) of 0.32, had mean predicted migration levels (Q) ranging from 2.61×10^{-3} to 5.01×10^{-3} mg/dm^2 for silver (Table 2). The model for copper migration, which also included BL and an e of 1.1, had Q values ranging from 3.82×10^{-2} to 4.75×10^{-2} mg/dm^2 (Table 2). It can be seen from the R and RMSE values (Figures 4 and 5) that the model more accurately predicted the levels of silver in the samples than the levels of copper in the samples. It is likely that the highly variable BL for copper with a mean of 12.6×10^{-2} mg/kg and a standard deviation of 4.76×10^{-2} mg/kg (n = 8) makes it difficult to capture the true treatment effect. Therefore, the use of a food simulant rather than a real food may be more suited to studying nanoparticles that share a common element with food substances.

This study assesses the migration in a nanocomposite−food system not only from nanocomposites with a high nanoparticle fill level but at relatively high temperatures for the storage of perishable goods. An additive to the extreme conditions is the vacuum packaging procedure applied to the individual units. This maximized the contact surface area in the experiments. Hence, the study represents a pessimistic evaluation of potential commercial use and poor storage practices. The predicted migration values increased with time and temperature; this trend corresponds to results where a broader temperature range and longer time periods were studied.[11]

Exposure Assessment. The exposure model generated probability distributions describing the likely human exposure to nanoparticles, following the consumption of chicken wrapped in nancomposites based on the laboratory migration results and current population data. Because of the extreme nature of the migration testing conditions, the exposure must also be viewed as extreme. The 95th percentiles of human exposure to silver (as shown in Table 2) were 5.89×10^{-5}, 7.06×10^{-5}, 8.9×10^{-5}, and 7.97×10^{-5} mg kg_{bw}^{-1} day^{-1}, for scenarios 1, 2, 3, and 4, respectively. The 95th percentiles of human exposure to copper (as shown in Table 2) were 2.26×10^{-5}, 5.67×10^{-5}, 4.24×10^{-5}, and 1.17×10^{-4} mg kg_{bw}^{-1} day^{-1} for scenarios 1, 2, 3, and 4, respectively. Putting these values into context in terms of their potential to cause adverse effects is difficult because research on toxicity is sparse. However, a provisional ingestion limit (PIL) for silver nanoparticles of 0.084 mg kg_{bw}^{-1} day^{-1} was calculated for silver nanoparticles with a diameter of 10 nm[10] based on principles outlined by O'Brien and Cummins,[21] which, in turn, were derived from a nanosilver exposure study.[22] The exposure to silver nanoparticles calculated in this study ranged from 7.01×10^{-4} to 1.06×10^{-3}% of that PIL. In the study by Cushen et al. for similar sized silver nanoparticles migrating from a polyvinyl chloride (PVC) composite into chicken breasts stored at 5 °C for 4 days, 16.02% of the same PIL was reached. A crucial factor in the migration levels seen in the PVC study and the subsequent exposure values was the fill level. The fill level in this current study at 0.5% is 10 times less than that of the comparable study,[10] and migration and subsequent exposure levels are far lower because of this.

dx.doi.org/10.1021/jf404038y | J. Agric. Food Chem. 2014, 62, 1403−1411

No such nanocopper exposure studies exist, and therefore, a PIL cannot be calculated. However, the levels of migration measured in this study are not likely to lead to adverse effects because the simulated exposure levels in this experiment (with approximately half attributed to BL of copper in chicken), with the highest being 1.37×10^{-4} mg kg_{bw}^{-1} day^{-1}, are very low compared to the average dietary intake of copper. These were found to have averages of 1.42×10^{-2} and 1.9×10^{-2} mg kg_{bw}^{-1} day^{-1} for women and men, respectively [calculated using the Irish Universities Nutrition Alliance (IUNA) adult body weight distribution[18] and U.S.A. population values expressed in mg/day[23,24]].

It can be concluded that, if the effect of silver or copper nanoparticles incorporated into PE is optimally effective against the microbial spoilage profile of a particular food (and in line with properties and conditions investigated in this study), then their use may be recommended, because the migration and subsequent exposure (resulting for materials investigated in this study and representing pessimistic scenarios) did not exceed the safety limitation sourced from scientific literature. Having said this, the limits used to assess the safety of silver migration vary hugely,[2,10] and safety assessments are highly dependent upon the levels to which they are compared. The limit of 0.01 mg/kg (unauthorized substances) from European legislation that was used to assess the migration from the nanosilver−PE composites and Agion−PE composites to food simulants by Cushen et al.[2] is very restrictive. This precautionary approach is due to the lack of appropriate toxicity research available, and it is understandable that the European Commission cannot base permissible migration levels on the results of an insufficient number of toxicity studies. Until more research in this area becomes available, a ban has been imposed on nanomaterials being used in food contact materials,[9] unless specifically listed in the Union List of EU 10/2011.[9] Neither nanosilver nor nanocopper is mentioned on this list.

It is likely that the full antimicrobial potential (by ion release or the particles in nanoform) of nanosilver and nanocopper is excessive for delaying food spoilage at the fill rates tested in this study. The antimicrobial profile (including intensity and longevity) that is required to offset food spoilage should be defined and an antimicrobial system should be designed accordingly, including percentage fill rate, antimicrobial release mechanism, and recommended storage conditions. Such a development could see antimicrobial packaging systems becoming more food-specific, which is justifiable given the effect of food pH observed.[2] Because of the association between silver release, antimicrobial potential, and toxicity,[25−28] it can be deduced that composites that are excessively antimicrobial are more likely to lead to high exposure levels. Although the effect of both silver nanoparticles and silver ions on humans is largely unknown, recent initial studies into their effects on model organisms suggest that nanoparticles are more toxic than ions.[26−28] Considering this, antimicrobial potential and, therefore, fill rate should be minimized within the limits that allow for an acceptable antimicrobial effect.

The widespread use of antimicrobials in food packaging depends upon their active behavior, but any commercial success relies on how they perform in migration tests. It can be concluded that this study demonstrates the potential for nanosilver and nanocopper for use in food contact materials, with low migration levels observed in all scenarios tested. The migration and exposure models can be used by industry to study the migration behavior of nanosilver and nanocopper composites under varying conditions. It is acknowledged that there is still considerable uncertainty regarding the toxicity of materials at the nanoscale; hence, exposure estimates should be re-evaluated when more toxicity data become available.

AUTHOR INFORMATION

Corresponding Author

*Telephone: 00353-1-716-7476. E-mail: enda.cummins@ucd.ie.

Funding

This work was financially supported by Food Institutional Research Measure (FIRM) as part of the Strategy for Science, Technology and Innovation in the Department of Agriculture, Food and the Marine.

Notes

The authors declare no competing financial interest.

REFERENCES

(1) Cushen, M.; Kerry, J.; Morris, M.; Cruz-Romero, M.; Cummins, E. Nanotechnologies in the food industry—Recent developments, risks and regulation. *Trends Food Sci. Technol.* **2012**, *24* (1), 30−46.

(2) Cushen, M.; Kerry, J.; Morris, M.; Cruz-Romero, M.; Cummins, E. Silver migration to food simulants from nanosilver and Agion polyethylene composites. *Food Addit. Contam., Part A* **2014**, manuscript under review.

(3) Schrand, A. M.; Rahman, M. F.; Hussain, S. M.; Schlager, J. J.; Smith, D. A.; Syed, A. F. Metal-based nanoparticles and their toxicity assessment. *Wiley Interdiscip. Rev.: Nanomed. Nanobiotechnol.* **2010**, *2* (5), 544−568.

(4) Cioffi, N.; Ditaranto, N.; Torsi, L.; Picca, R. A.; Sabbatini, L.; Valentini, A.; Novello, L.; Tantillo, G.; Bleve-Zacheo, T.; Zambonin, P. G. Analytical characterization of bioactive fluoropolymer ultra-thin coatings modified by copper nanoparticles. *Anal. Bioanal. Chem.* **2005**, *381* (3), 607−616.

(5) O'Brien, N. J.; Cummins, E. J. A risk assessment framework for assessing metallic nanomaterials of environmental concern: Aquatic exposure and behavior. *Risk Anal.* **2011**, *31* (5), 706−726.

(6) Sherman, L. M. Chasing nanocomposites. *Plast. Technol.* 2004; http://www.ptonline.com/articles/chasing-nanocomposites (accessed Jan 2013).

(7) EFSA Panel on Food Contact Materials, Enzymes, Flavourings and Processing Aids (CEF).. Scientific opinion on the safety evaluation of the substance, titanium nitride, nanoparticles, for use in food contact materials. *EFSA J.* **2012**, *10* (3), 2641−2649.

(8) Magnuson, B. A.; Jonaitis, T. S.; Card, J. W. A brief review of the occurrence, use, and safety of food-related nanomaterials. *J Food Sci.* **2011**, *76* (6), 126−133.

(9) European Union (EU).. Commission Regulation (EU) No. 10/2011 of 14 January 2011 on plastic materials intended to come into contact with food. *Off. J. Eur. Union* **2011**, 1−132.

(10) Cushen, M.; Kerry, J.; Morris, M.; Cruz-Romero, M.; Cummins, E. Migration and exposure assessment of silver from a PVC nanocomposite. *Food Chem.* **2013**, *139*, 389−397.

(11) Šimon, P.; Chaudhry, Q.; Bakos, D. Migration of engineered nanoparticles from polymer packaging to food—A physicochemical view. *J. Food Nutr. Res.* **2008**, *47* (3), 105−113.

(12) Chen, D.; Qiao, X.; Qiu, X.; Chen, J. Synthesis and electrical properties of uniform silver nanoparticles for electronic applications. *J. Mater. Sci.* **2009**, *44* (4), 1076−1081.

(13) Khanna, P. K.; Gaikwad, S.; Adhyapak, P. V.; Singh, N.; Marimuthu, R. Synthesis and characterization of copper nanoparticles. *Mater. Lett.* **2007**, *61* (25), 4711−4714.

(14) Gunning, M. A.; Istrate, O. M.; Geever, L. M.; Lyons, J. G.; Blackie, P.; Chen, B.; Higginbotham, C. L. The effect of maleic anhydride grafting efficiency on the flexural properties of polyethylene composites. *J. Appl. Polym. Sci.* **2012**, *124*, 4799−4808.

(15) Cruz, J. M.; Sanches Silva, A.; Sendón García, R.; Franz, R.; Paseiro Losada, P. Studies of mass transport of model chemicals from packaging into and within cheeses. *J. Food Eng.* **2008**, *87* (1), 107−115.
(16) Gorham, J.; MacCuspie, R.; Klein, K.; Fairbrother, D. H.; Holbrook, R. D. UV-induced photochemical transformations of citrate-capped silver nanoparticle suspensions. *J. Nanopart. Res.* **2013**, *14* (10), 1−16.
(17) Vermeiren, L.; Devlieghere, F.; Debevere, J. Effectiveness of some recent antimicrobial packaging concepts. *Food Addit. Contam., Part A* **2002**, *19* (4, Supplement1), 163−171.
(18) Personal communication with Dr. Janette Walton based on information collected for the National Adult Nutrition Survey by Irish Universities Nutrition Alliance (IUNA), Dublin, Ireland, 2011.
(19) Song, H.; Li, B.; Lin, Q. B.; Wu, H. J.; Chen, Y. Migration of silver from nanosilver−polyethylene composite packaging into food simulants. *Food Addit. Contam., Part A* **2011**, *28* (12), 1758−1762.
(20) Quadros, M. E.; Pierson, R.; Tulve, N. S.; Willis, R.; Rogers, K.; Thomas, T. A.; Marr, L. C. Release of silver from nanotechnology-based consumer products for children. *Environ. Sci. Technol.* **2013**, *47* (15), 8894−8901.
(21) O'Brien, N.; Cummins, E. Ranking initial environmental and human health risk resulting from environmentally relevant nanomaterials. *J. Environ. Sci. Health, Part A: Toxic/Hazard. Subst. Environ. Eng.* **2010**, *45* (8), 992−1007.
(22) Kim, Y. S.; Kim, J. S.; Cho, H. S.; Rha, D. S.; Kim, J. M.; Park, J. D.; Choi, B. S.; Lim, R.; Chang, H. K.; Chung, Y. H.; Kwon, I. H.; Jeong, J.; Han, B. S.; Yu, I. J. Twenty-eight-day oral toxicity, genotoxicity, and gender-related tissue distribution of silver nanoparticles in Sprague-Dawley rats. *Inhalation Toxicol.* **2008**, *20* (6), 575−583.
(23) Tokman, N. The use of slurry sampling for the determination of manganese and copper in various samples by electrothermal atomic absorption spectrometry. *J. Hazard. Mater.* **2007**, *143*, 87−94.
(24) Shrivas, K.; Jaiswal, N. K. Dispersive liquid−liquid microextraction for the determination of copper in cereals and vegetable food samples using flame atomic absorption spectrometry. *Food Chem.* **2013**, *141* (3), 2263−2268.
(25) Xiu, Z.-m.; Zhang, Q.-b.; Puppala, H. L.; Colvin, V. L.; Alvarez, P. J. J. Negligible particle-specific antibacterial activity of silver nanoparticles. *Nan. Lett.* **2012**, *12* (8), 4271−4275.
(26) Asharani, P. V.; Wu, Y. L.; Gong, Z.; Valiyaveettil, S. Toxicity of silver nanoparticles in zebrafish models. *Nanotechnology* **2008**, *19* (25), 1−8.
(27) Olasagasti, M.; Gatti, A. M.; Capitani, F.; Barranco, A.; Pardo, M. A.; Escuredo, K.; Rainieri, S. Toxic effects of colloidal nanosilver in zebrafish embryos. *J. Appl. Toxicol.* **2014**, DOI: 10.1002/jat.2975.
(28) van Aerle, R.; Lange, A.; Moorhouse, A.; Paszkiewicz, K.; Ball, K.; Johnston, B. D.; de-Bastos, E.; Booth, T.; Tyler, C. R.; Santos, E. M. Molecular mechanisms of toxicity of silver nanoparticles in zebrafish embryos. *Environ. Sci. Technol.* **2013**, *47* (14), 8005−8014.
(29) Liu, C.; Wang, J.; He, J. Rheological and thermal properties of m-LLDPE blends with m-HDPE and LDPE. *Polymer* **2002**, *43* (13), 3811−3818.
(30) Illes, B.; Horvath, B.; Shinohara, T.; Harsanyi, G. Tin whisker growth from Sn−Cu (0−5 wt %) surface finishes. *Proceedings of the 17th International Symposium for Design and Technology in Electronic Packaging (SIITME)*; Timisoara, Romania, Oct 20−23, 2011.

MATERIALS AND METHODS

Chemicals. Acetonitrile was purchased from Fisher Scientific (Fair Lawn, NJ, USA). Water was purified to 18.1 MΩ·cm using a Barnstead E-Pure System (Barnstead International, Dubuque, IA, USA). Methanol was purchased from EMD Millipore Corporation (Billerica, MA, USA). Formic acid (98−100% purity) was purchased from EMD Chemicals (Gibbstown, NJ, USA). Met-Arg-Phe-Ala (MRFA) was purchased from Research Plus, Inc. (Barnegat, NJ, USA) and taurocholic acid sodium salt hydrate from Sigma-Aldrich (St. Louis, MO, USA) were used as internal standards.

Plant Material. Fifty genetically diverse non-GM commercial maize hybrids from DuPont Pioneer were planted at six different locations. Five of the locations were in the U.S. (Illinois, Kansas, Minnesota, Nebraska, and Texas) and the sixth location was in Ontario, Canada. Planting locations for the hybrids were selected based on days to maturity such that each location had 20 unique genotypes. At every location, each genotype was planted in three randomized blocks (three blocks and two replicate plots per block). Each block was separated by an alley at least 36 in. wide and surrounded on each end by two-row borders. Details and a pictorial representation are shown elsewhere.[10] Agronomic practices such as irrigation, fertilization, and herbicide and pesticide applications were applied uniformly across locations and were consistent with the normally acceptable practices for maize production. From the 50 genotypes, a core subset of five that were grown at all six locations were used for LC/MS analysis.

Two forage samples were collected from three plants after flowering for each genotype and block and placed immediately on dry ice. Each forage sample represented the pooled aerial portions of three entire plants. Collected frozen samples were stored temporally at less than or equal to −10 °C for less than 10 min. Each grain sample was collected at maturity from five hand pollinated ears from each genotype and block. For each sample, the resulting grain from five shelled ears were pooled and immediately placed on dry ice until transferred to a less than or equal to −10 °C freezer for temporary storage. The same harvesting protocol was adopted in all locations. Samples were shipped frozen to the DuPont Pioneer Regulatory Science processing laboratory in Ankeny, Iowa, where they were lyophilized and ground. Lyophilized forage and grain samples were then shipped on dry ice to the DuPont Pioneer metabolomics laboratory in Johnston, Iowa, where they were stored at −80 °C until analyzed.

Sample Preparation. For forage samples, metabolites were extracted from lyophilized tissue with a mean dry weight of 6.7 mg. Metabolites were extracted from grain samples with a mean dry weight of 29.9 mg. Five hundred microliters of cold extraction solvent (80% methanol/20% water) containing 10 mg/mL Met-Arg-Phe-Ala (MRFA) and 5 mg/mL taurocholate as internal standards for positive and negative electrospray, respectively, were added to each sample and reference sample in a 1.1 mL polypropylene microtube containing two 5/32 in. stainless steel ball bearings. Samples were homogenized in a 2000 Geno/Grinder ball mill (SPEX CertiPrep, Inc., Metuchen, NJ) at a setting of 1650 rpm for 1 min and then rotated on an end-over-end mixer (Glas-Col, LLC, Terre Haute, IN) at 4 °C for 30 min. Samples were then centrifuged at 1454*g* at 4 °C for 15 min. The supernatant of each sample was transferred to 0.2 μM (VWR International LLC, Radnor, PA) spin filter and centrifuged at 800*g*. Solution was transferred to a limited volume autosampler vial.

Forage and grain samples were rearranged into 10 analytical batches separately. Each batch contained samples from every genotype and location to minimize analytical errors and system bias in the acquired data. We prepared four quality control (QC) samples for each batch by pooling extract aliquots from each individual sample within the batch. In addition, we ran three reference samples in each batch that were prepared from pooled grain or forage material. The reference samples were sourced from grain or forage originating from all locations and containing all genotypes. Both QC and reference samples were placed at regular intervals within each batch.

Liquid Chromatography−Mass Spectrometry. Analyses were performed on an Accela ultra high pressure liquid chromatograph (uHPLC) system coupled to a LTQ-FT hybrid mass spectrometer (Thermo Scientific, West Palm Beach, FL, USA) via an electrospray ionization (ESI) interface. Sample extracts were separated via reversed phase on a Thermo Scientific Hypersil Gold C18 column (2.1 × 200 mm × 1.9 μm). The mobile phase consisted of water/0.1% formic acid (A) and acetonitrile/0.1% formic acid (B) and flow rate was set to 0.5 mL/min. A linear gradient was used beginning with 10% B at 0.98 min, reaching 100% B at 18 min, 100% B at 35 min, then recovered to initial condition within 30 s where it was held for 4.5 min. Injection volume and column temperature were 25 μL and 40 °C, respectively. The optimized parameters for positive and negative ion electrospray were set as follows: capillary temperature 250 °C; sheath gas flow rate 70 arbitrary units, sweep gas flow rate 5 arbitrary units. The instrument was tuned prior to each batch run. Metabolites were detected using the linear ion trap detector collecting full-scan data from 150 to 975 m/z. Automatic gain control were set at 30 000 for both positive and negative ionization modes. The source voltage was set at 2.5 kV for positive mode and 4 kV for negative mode. Xcalibur version 2.1.0 SP1 software (Thermo Scientific) was used for data acquisition.

Data Pretreatment. Xcalibur raw files were imported to Genedata Expressionist Refiner MS version 6.1 (Basel, Switzerland) for chromatogram gridding, aligning, chemical noise subtraction, peak detection, isotope clustering, adduct detection, and signal clustering. Preprocessed data consisted of intensities for each m/z value and retention time combination or peak. For a peak to be valid and retained, it had to be present in at least 50% of the samples in addition to being detected in all QC samples. The data matrix was exported to Genedata Expressionist Analyst version 2.2 for normalization by both internal standard signal and the sample dry weight. To further minimize unwanted variation in our data set due to within batch run order drift or across batch variability, we performed QC and reference sample normalizations in addition to internal standard and weight normalizations. QC samples normalization was used to minimize and correct for within batch variation. QC sample normalization was performed by dividing the relative abundance of each sample peak by the mean of that for the two bracketing QC samples within a batch. Reference sample normalization was used to correct for and minimize variability across batches. Reference sample normalization was performed after QC normalization by dividing the relative abundance of each sample peak by the mean of that peak in all reference samples within a batch. Fully normalized data were exported to Matlab or Excel 2007 for further data analysis. We used the LC/MS data individually and in combination with GC/MS data for statistical analyses. GC/MS data were obtained from the same samples and were processed in the same way as described elsewhere[10] prior to combining the two data sets.

Data Analysis. *Univariate Analysis.* To measure of the variance in metabolomics data due to different genotypes and environments, we calculated the coefficient of variation (CV) for each metabolite. The mean CV for all metabolites grown in all location was used to quantify the effect of the environment. The mean CV for all metabolites from each genotype using samples grown in each location was used to evaluate the effect of genotype. To investigate the effects of both environment and genotype, a paired student's t test for each metabolite was applied. The p-value was calculated for each metabolite and used to determine those metabolites that were significantly altered (p-value < 0.01). To determine effect of environment, the p-values of each metabolite from one location were compared to metabolites in other locations. To evaluate effect of genotype, p-values of every metabolite for a given genotype were compared to those from the other genotypes at the same location.

To further determine the consistency of those metabolites that were altered due to environment or genotype, we first identified those metabolites that were statistically significant from one location compared to the other five (total of 15 comparisons were made). We then calculated the number of paired comparisons (locations) in which the abundances of each of those metabolites were significantly altered (p-value < 0.01), for example, if a metabolite was altered between Kansas and Illinois, was it also altered in Kansas vs Texas, etc. A similar exercise was performed to identify those metabolites that

Table 1. Mean Percent CV of Metabolomics Data from Different Locations in (a) Forage and (b) Grain Samples Using LC/MS Data Set Alone and in Combination with GC/MS Data Set

locations	# of samples	LC/+ESI/MS	LC/−ESI/MS	LC/±ESI/MS	GC/MS and LC/MS
			(a)		
Illinois	30	41.63	38.11	41.48	41.46
Kansas	30	43.86	37.25	43.49	43.49
Minnesota	29	37.74	34.13	37.31	36.60
Nebraska	30	42.48	37.56	42.40	44.73
Ontario	23	43.48	35.96	43.02	42.87
Texas	30	48.73	45.55	48.39	50.97
			(b)		
Illinois	28	47.59	57.16	49.83	52.95
Kansas	27	45.9	62.79	49.86	55.7
Minnesota	29	44.85	61.22	48.69	52.51
Nebraska	30	47.95	56.94	50.05	59.42
Ontario	29	46.71	65.61	51.14	54.41
Texas	29	43.77	53.11	45.95	49.37

were altered due to genotype. For each location, we first determined the number of genotype paired comparisons in which a particular metabolite exhibited a significantly altered abundance (a total of 10 comparisons were made for every location). Comparisons across different locations asked the same question, for example, if metabolite X was altered between entries 1 vs 2 in Kansas was it also altered in other locations? Finally, those metabolites that were altered by both the environment and genotype were identified.

Multivariate Analysis. Principal component analysis (PCA) was performed by using Matlab version R2010b (Mathworks) installed with the PLS toolbox version 6.0.1 (eigenvector Research Inc., Wenatchee, WA). All data sets were normalized and autoscaled prior to modeling. R statistical package (version 2.12.1) was used for hierarchical cluster analysis (HCA) to generate dendrograms and heat maps and calculate correlations between metabolites.

RESULTS AND DISCUSSION

Data Variability in Grain and Forage (Coefficient of Variance Analysis). To evaluate the effect of the environment, we compared the mean percent CV of all metabolites detected using samples grown at different locations (Table 1). The mean percent CV for all metabolites in forage samples was lower than for grain samples grown at the same locations, with the exception of Texas. Similar trends were observed in the mean percent CV using LC/MS data acquired in positive or negative ionization mode analyzed independently, although more metabolites were detected in the positive mode (866 metabolites) compared to the negative mode (277 metabolites) as shown in Supporting Information Table S1. This result was also consistent with what we observed using GC/MS data, in which grain samples had the higher mean percent CV compared to forage samples originating from the same location.

To investigate the effect of different genotypes on data variability, we compared mean percent CV of all metabolites from different genotypes grown at different locations, as shown in Table 2. The number of samples per genotype and location is shown in Supporting Information Table S2. These results allowed for the comparison of the mean percent CV of one genotype to another within and across different environments. We did not observe any differences in mean percent CV across different locations for any genotype, indicative of good reproducibility across different locations. In addition, mean percent CV values for different genotypes at the same location were very similar to those for the same genotype at different locations with the exception of few cases. For example, grain samples from Minnesota had higher mean percent CV values compared to forage samples.

Table 2. Mean Percent CV of Metabolomics Data from Different Genotypes in Different Locations in (a) Forage and (b) Grain Samples Using LC/MS Data Set

genotype	Illinois	Kansas	Minnesota	Nebraska	Ontario	Texas
			(a)			
1	36.36	32.58	31.79	37.59	39.54	42.36
2	36.44	39.59	30.71	37.34	35	32.75
3	31.14	30.28	30.24	39.54	32.91	45.52
4	41.28	37.56	28.56	33.8	35.68	49.09
5	34.88	34.74	35.96	34.36	38.06	40.44
			(b)			
1	38.96	44.23	39.1	38.94	34.89	32.53
2	37.02	38.15	36.22	31.19	36.63	38.29
3	37.53	42.01	40.52	47.03	34	39.46
4	38.77	35.81	35.32	35.69	37.12	35.17
5	33.4	36.1	36.12	30.62	33.5	35.17

Univariate Analysis, Effect of Environment. To determine the number of metabolites detected by LC/MS that were affected by the environment (location), we calculated and compared *p*-values for the relative amount of each metabolite from one location to another in both grain and forage samples. Unless stated otherwise, herein and hereafter, LC/MS data sets were comprised of combined positive and negative ionization mode data. Table 3a,b shows the percentage of metabolites with statistically significant altered levels (*p*-values <0.01) between different locations in forage and grain samples, respectively. A total of 15 paired comparisons were made for each of 1143 metabolites. For forage, samples from Kansas versus Ontario had the highest percentage (47.17%) of metabolites altered between the two locations, while Nebraska versus Texas show the lowest percentage (21.49%) of metabolites altered. In general, more metabolites were altered in forage samples compared to grain samples for the same location to location comparisons. For example, only 8% of the metabolites detected in grain were altered between Illinois and Nebraska compared to 31.45% in forage samples. More metabolites were detected in forage samples than in grain samples. Similar results were obtained using LC/MS positive and negative ionization mode data analyzed independently (Supplemental Table S3, Supporting Information). The LC/

dx.doi.org/10.1021/jf404702g | J. Agric. Food Chem. 2014, 62, 1412−1422

Table 3. Percentage of Metabolites with Relative Abundances That Were Statistically Significant (p-value < 0.01) between Locations in (a) Forage and (b) Grain Samples Using LC/MS Data Set

	Illinois	Kansas	Minnesota	Nebraska	Ontario	Texas
			(a)			
Illinois	0					
Kansas	29.52	0				
Minnesota	42.31	46.72	0			
Nebraska	31.45	40.38	30.20	0		
Ontario	41.18	47.17	26.92	31.11	0	
Texas	33.60	43.55	31.45	21.49	31.33	0
			(b)			
Illinois	0					
Kansas	29.02	0				
Minnesota	28.32	19.93	0			
Nebraska	8.04	30.77	29.72	0		
Ontario	32.17	33.22	27.97	35.31	0	
Texas	11.19	28.32	29.37	9.79	37.76	0

MS results for forage agree very well with our previous findings with the same samples using metabolites detected by GC/MS where on average about 50% of the metabolites altered from one location to another.

Univariate Analysis, Effect of Genotype. To evaluate the effect of genotype on the metabolome, we eliminated the influence of the environment by comparing only samples grown at the same location. Table 4a,b shows the percentage of metabolites with statistically significant altered levels (p-values <0.01) between genotypes using LC/MS data sets from Illinois's forage and grain samples, respectively, as an example. In total, 10 paired comparison were done for each of the six locations and each of the 1143 metabolites. The percentage of metabolites that were altered between genotypes was very low compared to those that were altered due to the environment. In some cases, less than 1% of the metabolites were altered from one genotype to another. For example, only 0.45% of all metabolites detected in forage samples were altered between genotype 3 and 4. Similar results were obtained using samples from other locations as shown in Supplemental Tables S4 and S5, Supporting Information. With forage samples, the percentage number of metabolites altered between different genotypes was very similar across different locations. However, for grain samples, a higher percentage of metabolites were altered between genotype 5 and any of the other genotypes at all locations.

Multivariate Analysis, Effect of Environment. To evaluate the effect of the environment, visualization of the metabolomic profiles of forage samples from all locations was done using unsupervised PCA. Figure 1a,b shows PCA scores plots from forage samples using LC/MS data set and the combined LC/MS and GC/MS data sets, respectively. Forage samples from Illinois and Kansas were separated completely from samples from other locations along PC1 that accounted for about 17% of the total variance in the both the LC/MS data set (Figure 1a) and combined LC/MS and GC/MS data set (Figure 1b). The same pattern was observed using data sets of positive and negative ionization mode of LC/MS separately as shown in Supplemental Figure S1, Supporting Information. PCA scores plots show a strong environment effect in that samples are clustered based on where they were grown. The circles in the PCA score plots represent 95% confidence level. Quality control samples and reference samples were tightly clustered in the middle of the PCA score plot indicative of very good reproducibility and stability of our instrument during the run. This result also indicates that technical error is lower than environmental variability.

To further evaluate the effect of the environment on the plants' metabolomes, the same data were subjected to unsupervised HCA. Figure 1c,d shows heat maps and dendrograms obtained using LC/MS data sets and combined LC/MS and GC/MS data sets, respectively. HCA allowed for visualization of sample similarity across different locations. HCA results were also consistent with our PCA results where by samples from Kansas and Illinois clustered together, indicating that their metabolomes were very similar Figure 1c,d. In addition, samples from Minnesota and Ontario clustered together, indicative of substantial similarity of their metabolome profiles.

Unsupervised PCA was used to visualize the metabolomic profiles of grain samples from all locations. Figure 2a,b shows PCA scores plots for grain samples using LC/MS and the combined LC/MS and GC/MS data sets, respectively. Separation was observed based on where the samples were grown. For example, samples from Ontario and Minnesota separated along PC2 with LC/MS the only data set (Figure 2a) and along PC1 for LC/MS and GC/MS combined data sets (Figure 2b). The first two principle components accounted for 30.8% and 26.9% of total variance in grain using LC/MS only

Table 4. Percentage of Metabolites with Relative Abundances That Were Statistically Significant (p-value <0.01) between Genotypes in (a) Forage and (b) Grain Samples from Illinois Using LC/MS Data Set

	genotype 1	genotype 2	genotype 3	genotype 4	genotype 5
			(a)		
genotype 1	0				
genotype 2	1.13	0			
genotype 3	3.28	2.38	0		
genotype 4	2.04	1.92	0.45	0	
genotype 5	1.02	1.70	2.83	1.24	0
			(b)		
genotype 1	0				
genotype 2	3.50	0			
genotype 3	8.04	4.90	0		
genotype 4	9.44	7.69	5.59	0	
genotype 5	10.49	15.73	17.48	14.69	0

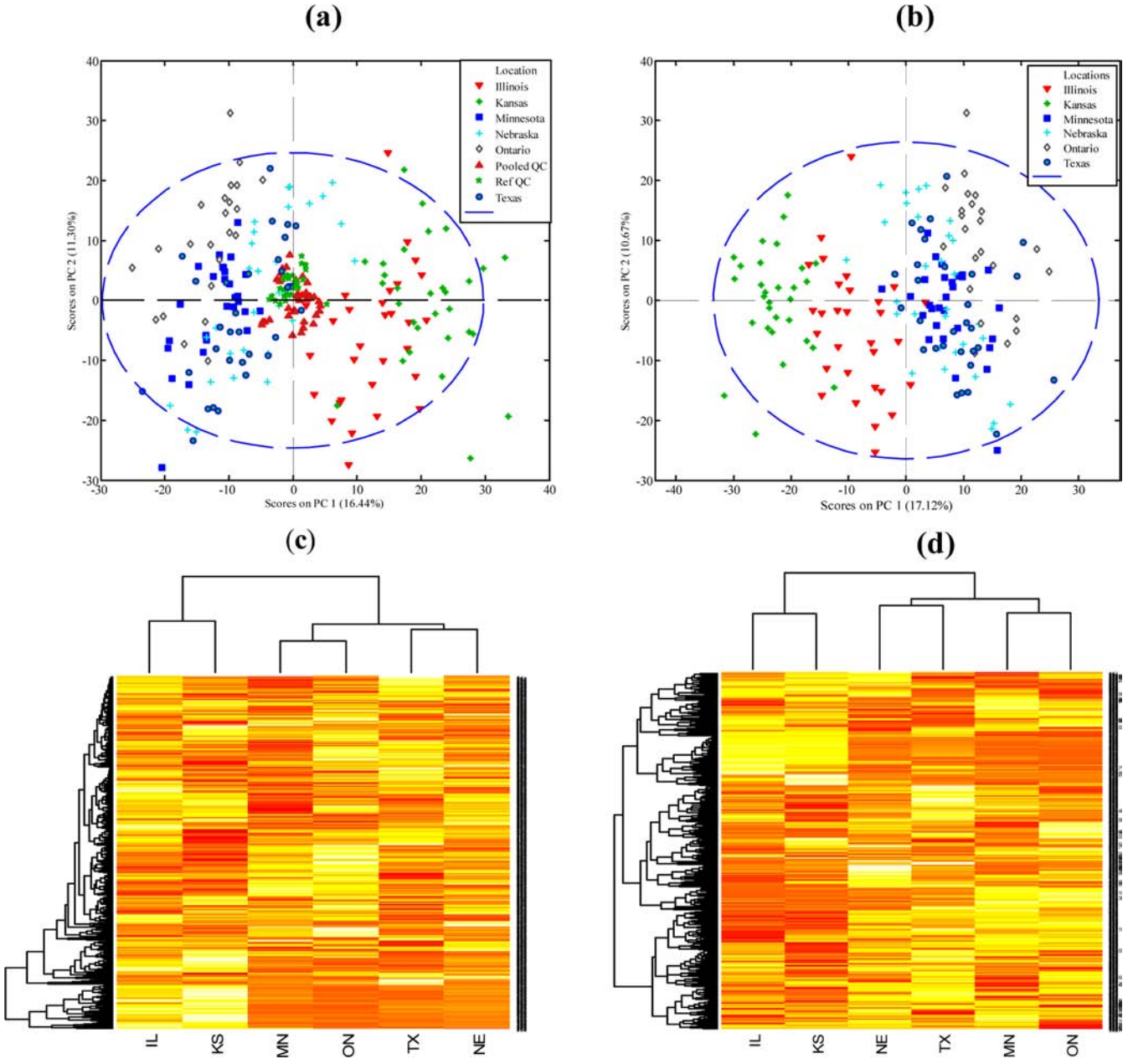

Figure 1. PCA scores plots showing the effect of environment on the metabolome in forage samples using (a) LC/MS data set and (b) combined LC/MS and GC/MS data sets. HCA and heat maps showing effect of environment using (c) LC/MS and (d) combined LC/MS and GC/MS data sets.

and LC/MS plus GC/MS data sets, respectively. Figure 2c,d shows HCA from grain samples collected from LC/MS data set and the combined LC/MS and GC/MS data sets, respectively. Grain samples from Minnesota and Kansas were clustered together as were those from Nebraska and Illinois. Therefore, we expect coclustered metabolomes to be very similar.

Multivariate Analysis: Effect of Genotype. To investigate the effect of genotype, metabolomics data derived from grain and forage samples collected from each location were subjected to unsupervised PCA separately. Figure 3a,b shows PCA scores plots using LC/MS and LC/MS plus GC/MS data sets from forage. No genotype could be classified separately; that is, samples from different genotypes were all clustered together. The same pattern was observed for grain samples with different genotypes as shown in Figure 3c,d, again from LC/MS and combined LC/MS and GC/MS data sets. In both cases (panels c and d), the total variance explained by PC1 and PC2 was about 30%. LC/MS positive and negative ionization mode data sets were subjected independently to unsupervised PCA as shown in Supplemental Figure S2, Supporting Information. Similar results were obtained, whereby no separation was observed among different genotypes.

Effect of Genotype × Environment Interaction (G × E). To investigate the genotype by environment interaction and understand the contribution of each to the measured metabolome, we first calculated the mean of each metabolite for each genotype from every location. The resulting data matrices were represented by 30 hybrids × 286 metabolites and 30 hybrids × 857 metabolites for grain and forage samples, respectively. These data sets were subjected to HCA separately.

dx.doi.org/10.1021/jf404702g | J. Agric. Food Chem. 2014, 62, 1412−1422

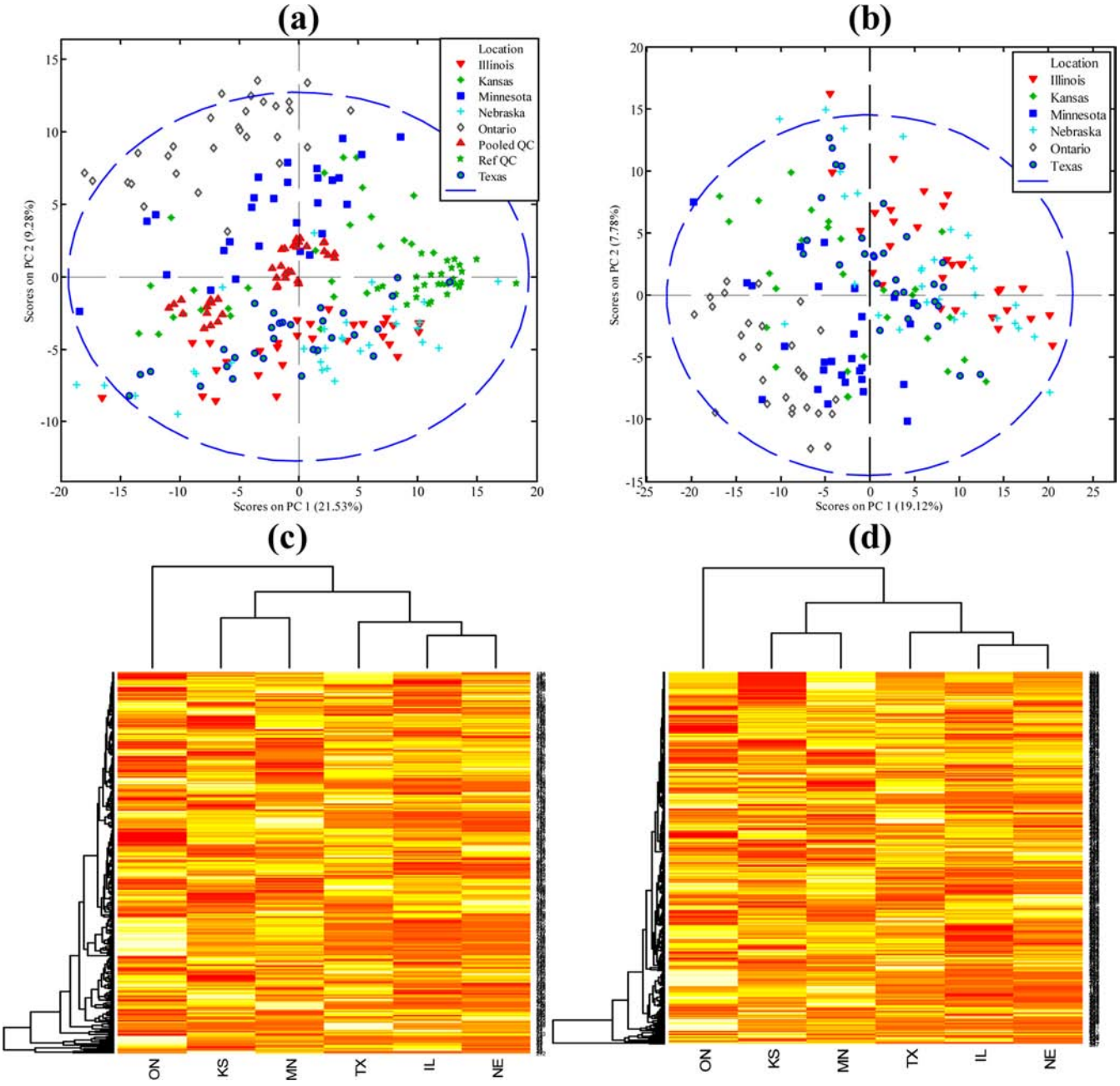

Figure 2. PCA scores plots showing the effect of environment on the metabolome in grain samples using (a) LC/MS data set and (b) combined LC/MS and GC/MS data sets. HCA and heat maps showing effect of environment using (c) LC/MS and (d) combined LC/MS and GC/MS data sets.

We reasoned that if the environment had a strong effect, we would expect to see samples from the same location clustered together regardless of genotype, and if the genotype had a strong effect, we would expect samples from the same genetic background cluster together regardless of where they were grown. Figure 4a,b shows dendrograms using the LC/MS data set and a combination of LC/MS and GC/MS data sets, respectively, from forage samples. The HCA from forage samples revealed a strong environmental effect, especially for samples from Illinois and Kansas. Figure 4c,d shows the analogous dendrograms from grain samples. These HCA did not show any strong clustering of samples based on the where they were grown or their genotype, except for samples from Ontario (Figure 4d). This finding is consistent with the results we obtained from the PCA analysis (see Figure 2a) with which samples originating from Ontario were slightly separated from the rest of the samples. Grain samples from genotype 5 were clustered together regardless of where the samples were grown. However, this finding was not the case for forage samples where the environment effect was very strong.

Figure 5a,b shows the percentage of metabolites that were significantly altered due to environment or genotype based on the number of paired comparisons in forage and grain samples. Those metabolites that were not altered at any location are represented by zero percent. From Figure 5a, it is evident that the relative amounts of approximately 40% of all metabolites detected in forage samples were not altered at all due to genotype, compared to only 20% not altered due to

dx.doi.org/10.1021/jf404702g | J. Agric. Food Chem. 2014, 62, 1412−1422

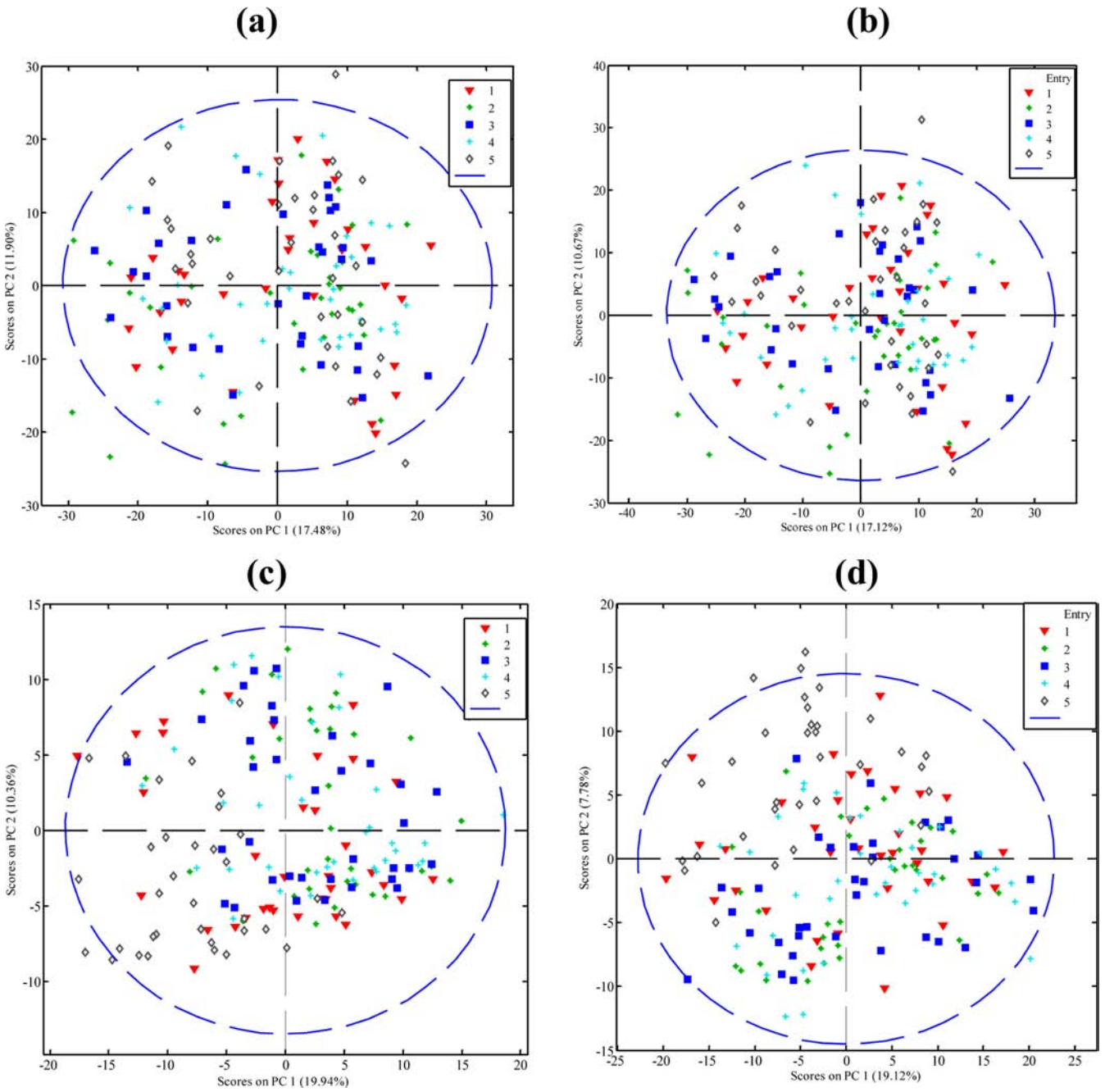

Figure 3. PCA scores plots showing the effect of genotype in forage using (a) LC/MS data set, (b) combined LC/MS and GC/MS and grain using (c) LC/MS and (d) combined LC/MS and GC/MS data sets.

environment. In grain samples, approximately 30% of the metabolites detected were not altered due to environment or genotype, as shown in Figure 5b. Figure 5c,d shows the cumulative percentage of metabolites that were altered based on paired comparisons due to environment and genotype, respectively. The percentage of metabolites altered due to environment or genotype in grain or forage decreased significantly as the number of paired comparisons increased. More metabolites were altered due to environment in forage samples compared to grain samples as shown in Figure 5c. For example, approximately 57% of the metabolites were significantly altered in five paired comparisons with forage compared to only 37% with grain. These results are consistent with what we present in Table 3. However, more metabolites were altered in grain samples due to genotype compared to forage samples, as shown in Figure 5d. For example, less than 2% of all metabolites detected in forage samples were altered in five paired comparisons compared to about 28% in grain samples. We determined those metabolites that were altered by both the environment and genotype based on the number of paired comparisons, as shown in Supporting Information Table S6a,b. Initially, a higher number of metabolites were altered by both the environment and genotype in less than five paired comparisons with both grain and forage; however, as the number of paired comparisons increased, very few metabolites were significantly altered.

In this study, LC/MS metabolomics method was applied to investigate the effect of environment, genotype, or both on

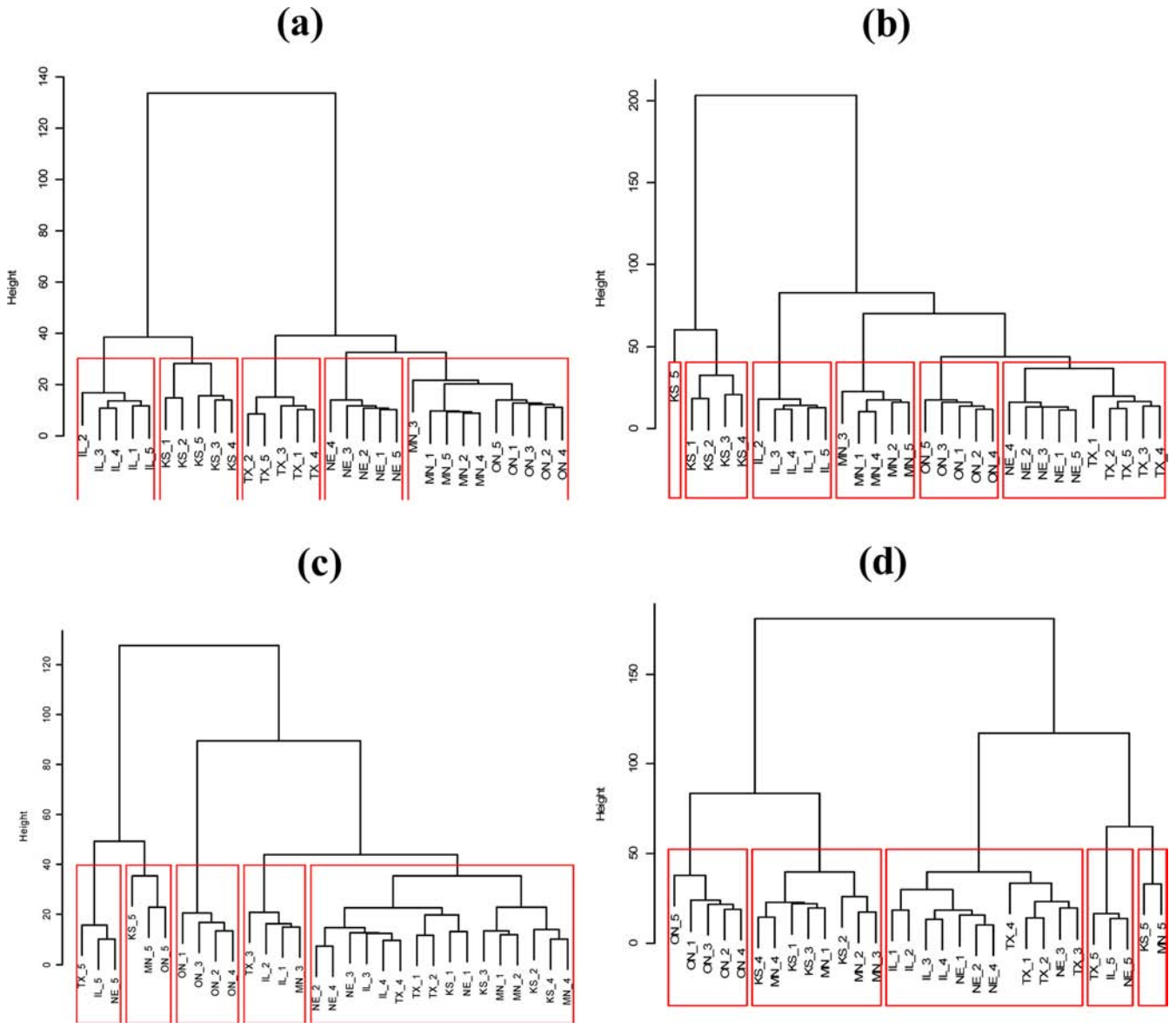

Figure 4. HCA showing effect of G × E in forage samples using (a) LC/MS data set, (b) combined LC/MS and GC/MS and grain samples using (c) LC/MS and (d) combined LC/MS and GCMS data sets.

variation of many metabolites in commercial maize. The effect of environment and genotype on forage and grain metabolomes was investigated individually using samples collected from five genetically diverse non-GMO DuPont Pioneer commercial hybrids grown at six North American locations. HCA was employed to visualize metabolic differences associated with genotype and environment in both tissue types. Our results obtained from either LC/MS, or a combination of LC/MS and GC/MS, show that the environment or growing location had the highest impact on the relative amounts of metabolites in both grain and forage. These finding are in an agreement with Frank et al. who reported that environment had a greater effect on the metabolite profiles in maize than either Bt or Roundup Ready genetic modifications.[18] Our LC/MS results showed more variability in grain compared to forage regardless of where the samples were grown or their genetics. These results are in agreement with our previous report using GC/MS for the same sample set that exhibited more variability in grain compared to forage.[10] Higher variability of grain metabolites has been reported previously.[38−41]

Our current research using LC/MS shows that the environment exerts a greater effect on the metabolomes of both grain and forage samples than genotype, consistent with previous research on other crops such as wheat, rice, and maize.[11,16,42] Previous research reported that amounts of macromolecule nutrients such as protein, fiber, and fat are very variable in grain samples.[39,40,43] Although we did not measure these constituents per se, we found that the concentrations of metabolites in grain samples were lower compared to those in forage samples. This finding is also consistent with the number of metabolites that we detected in our forage and grain samples. We detected generally more metabolites in forage than in grain.

This study not only confirmed our previous finding and what others have reported in the literature but also allowed us to probe other classes of metabolites that are not detected by GC/MS alone. By running LC/MS in the positive ionization mode,

dx.doi.org/10.1021/jf404702g | J. Agric. Food Chem. 2014, 62, 1412−1422

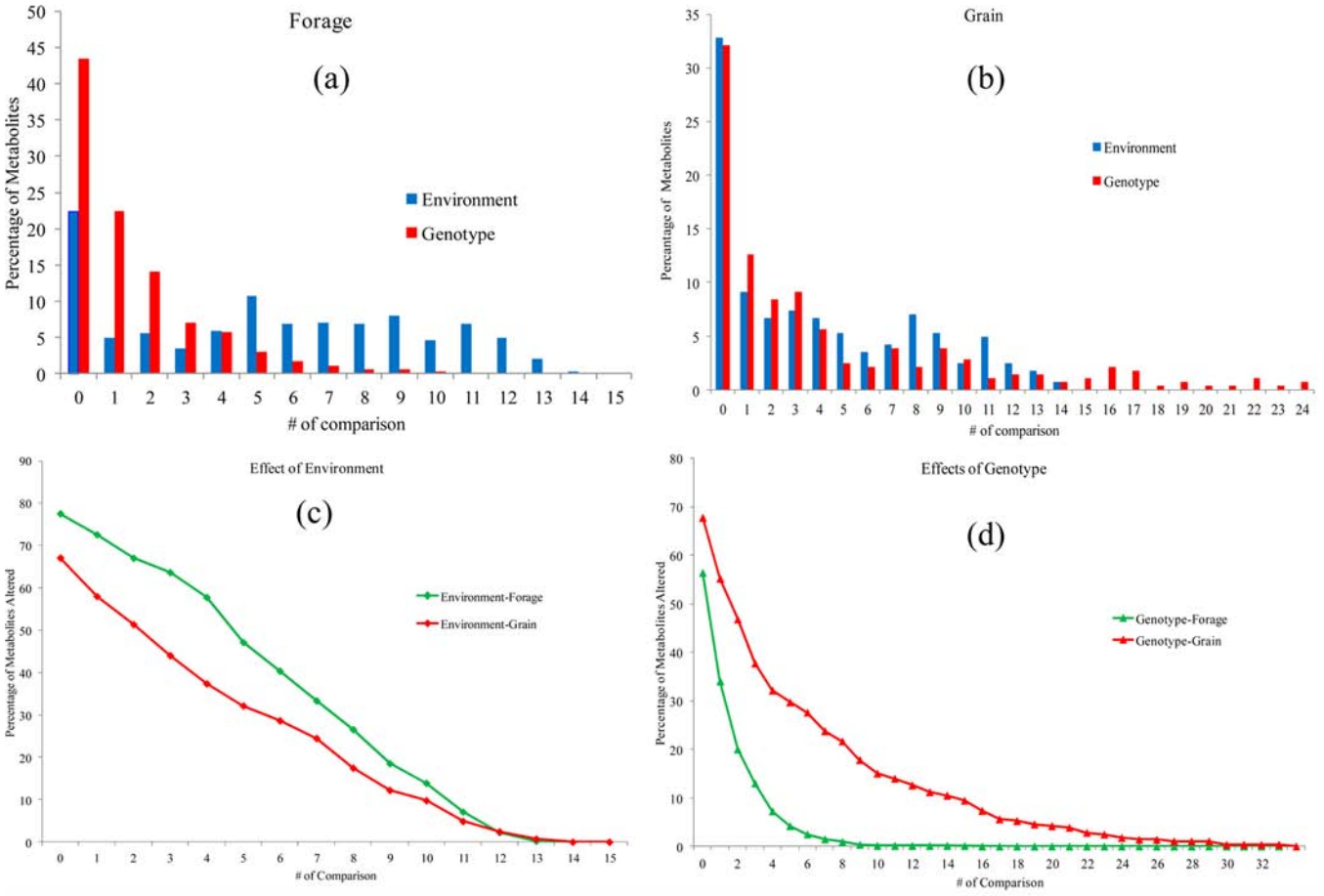

Figure 5. Percentage of metabolites that were significantly altered based on the number of paired comparisons done in (a) forage (b) grain samples and cumulative percentage of metabolites that were altered based on paired comparisons due to (c) environment and (d) genotype using LC/MS data sets.

we were able to detect 647 and 219 metabolites consistently in forage and grain, respectively, while the negative ionization mode presented 210 and 67 metabolites consistently in forage and grain, respectively. There were undoubtedly a number of metabolites detected in both positive and negative modes. In this study, those metabolites associated with differences due to genotype, environment, or both were not identified. Using untargeted metabolomics that generates a large number of variables and thus is especially susceptible to false discoveries, the emphasis should be on differences among samples rather than individual metabolites.

Although GM varieties were not included in this study, there is need to have a clear understanding of the biological variability of many metabolites in non-GMO crops before comparisons can be made with GM counterparts. We show clearly that although a metabolite can be significantly altered between two locations, it is very important to consider several locations before drawing broad conclusions. The same consideration should be made for differences due to genotype, since it is very important to determine if metabolome differences between two genotypes occur at more than one location. This approach helps eliminate any bias that might occur at a particular location that is unrelated to the genotype. There is also the need to consider more geographical locations, multiple years, and different growing environments before concluding if particular metabolites are altered by environment, genotype, or both.

In conclusion, LC/MS metabolomics was used to investigate the effect of environment, genotype, or both on the variation of many metabolites in commercial maize. Data reproducibility was satisfactory and metabolic differences caused by the environment and genotype were investigated using positive and/or negative ESI LC/MS data alone or in combination with previously acquired GC/MS data acquired from the same samples. Multivariate statistical analysis was used to determine the degree of metabolic difference caused by genotype and environment. Our results obtained from LC/MS or the combination of LC/MS and GC/MS show that environment had a greater impact on forage metabolites than those in grain. However, in both tissues, the metabolomic changes caused by genotype were minor.

■ ASSOCIATED CONTENT

Ⓢ Supporting Information

A summary of metabolites detected by LC/MS positive ESI mode, negative ESI mode, and GC/MS in forage and grain samples is presented. In addition, analysis using positive and negative ionization modes separately is shown. This material is available free of charge via the Internet at http://pubs.acs.org.

■ AUTHOR INFORMATION

Corresponding Author

*E-mail: Vincent.asiago@pioneer.com. Tel: (515) 535 7068. Fax: (515) 535 3367.

Notes

The authors declare no competing financial interest.

■ ACKNOWLEDGMENTS

The authors would like to thank Mary Locke, Bonnie Hong, Carl Maxwell, Ian Lamb, Lee Prochaska, John Duesing, and Deanne Vespestad for their help and discussion in designing the experiment and reviewing the study design. We wish to thank James Mickelson for managing all the field experiments, Jon Artist for handling sample shipments, and Brain Baumbover for managing the study records. We also wish to thank Ellen Royce for help in sample weighing.

■ REFERENCES

(1) Carpenter, J. E. Peer-reviewed surveys indicate positive impact of commercialized GM crops. *Nat. Biotechnol.* **2010**, *28*, 319−321.
(2) DeFrancesco, L. How safe does transgenic food need to be? *Nat. Biotechnol.* **2013**, *31*, 794−802.
(3) Herman, R. A.; Price, W. D. Unintended Compositional Changes in Genetically Modified (GM) Crops: 20 Years of Research. *J. Agric. Food Chem.* **2013**, *61*, 11695−11701.
(4) Kuiper, H. A.; Kleter, G. A.; Noteborn, H. P. J. M.; Kok, E. J. Assessment of the food safety issues related to genetically modified foods. *Plant J.* **2001**, *27*, 503−528.
(5) Rogers, R. A. How composition method are developed and validated. *J. Agric. Food Chem.* **2013**, *61*, 8312−8316.
(6) Ruebelt, M. C.; Leimgruber, N. K.; Lipp, M.; Reynolds, T. L.; Nemeth, M. A.; Astwood, J. D.; Engel, K. H.; Jany, K. D. Application of two-dimensional gel electrophoresis to interrogate alterations in the proteome of genetically modified crops. 1. Assessing analytical validation. *J. Agric. Food Chem.* **2006**, *54*, 2154−2161.
(7) Zolla, L.; Rinalducci, S.; Antonioli, P.; Righetti, P. G. Proteomics as a complementary tool for identifying unintended side effects occurring in transgenic maize seeds as a result of genetic modifications. *J. Proteome Res.* **2008**, *7*, 1850−1861.
(8) Cheng, K. C.; Beaulieu, J.; Iquira, E.; Belzile, F. J.; Fortin, M. G.; Stromvik, M. V. Effect of transgenes on global gene expression in soybean is within the natural range of variation of conventional cultivars. *J. Agric. Food Chem.* **2008**, *56*, 3057−3067.
(9) Parrott, W.; Chassy, B.; Ligon, J.; Meyer, L.; Patrick, J.; Zhou, J.; Herman, R.; Delaney, B.; Levine, M. Application of food and feed safety assessment principles to evaluate transgenic approaches to gene modulation in crops. *Food Chem. Toxicol.* **2010**, *48*, 1773−1790.
(10) Asiago, V. M.; Hazebroek, J.; Harp, T.; Zhong, C. Effects of genetics and environment on the metabolome of commercial maize hybrids: a multisite study. *J. Agric. Food Chem.* **2012**, *60*, 11498−11508.
(11) Chang, Y. W.; Zhao, C. X.; Zhu, Z.; Wu, Z. M.; Zhou, J.; Zhao, Y. N.; Lu, X.; Xu, G. W. Metabolic profiling based on LC/MS to evaluate unintended effects of transgenic rice with cry1Ac and sck genes. *Plant Mol. Biol.* **2012**, *78*, 477−487.
(12) Davies, H. V.; Shepherd, L. V.; Steward, D.; Frank, T.; Röhlig, R. M.; Engel, K. H. Metabolome variability in crop plant species−when, where, how much and so what? *Regul. Toxicol. Pharmacol.* **2010**, *58*, S54−S61.
(13) Kusano, M.; Redestig, H.; Hirai, T.; Oikawa, A.; Matsuda, F.; Fukushima, A.; Arita, M.; Watanabe, S.; Yano, M.; Hiwasa-Tanase, K.; Ezura, H.; Saito, K. Covering Chemical Diversity of Genetically-Modified Tomatoes Using Metabolomics for Objective Substantial Equivalence Assessment. *PloS One* **2011**, *6*, e16989.
(14) Catchpole, G. S.; Beckmann, M.; Enot, D. P.; Mondhe, M.; Zywicki, B.; Taylor, J.; Hardy, N.; Smith, A.; King, R. D.; Kell, D. B.; Fiehn, O.; Draper, J. Hierarchical metabolomics demonstrates substantial compositional similarity between genetically modified and conventional potato crops. *Proc. Natl. Acad. Sci. U.S.A.* **2005**, *102*, 14458−14462.
(15) Beleggia, R.; Platani, C.; Nigro, F.; De Vita, P.; Cattivelli, L.; Papa, P. Effect of genotype, environment and genotype-by-environment interaction on metabolite profiling in durum wheat (Triticum durumDesf.) grain. *J. Cereal Sci.* **2013**, *57*, 183−192.
(16) Baker, J. M.; Hawkins, N. D.; Ward, J. L.; Lovegrove, A.; Napier, J. A.; Shewry, P. R.; Beale, M. H. A metabolomic study of substantial equivalence of field-grown genetically modified wheat. *Plant Biotechnol. J.* **2006**, *4*, 381−392.
(17) Defernez, M.; Gunning, Y. M.; Parr, A. J.; Shepherd, L. V. T.; Davies, H. V.; Colquhoun, I. J. NMR and HPLC-UV profiling of potatoes with genetic modifications to metabolic pathways. *J. Agric. Food Chem.* **2004**, *52*, 6075−6085.
(18) Frank, T.; Röhlig, R. M.; Davies, H. V.; Barros, E.; Engel, K. H. Metabolite profiling of maize kernels: Genetic modification versus environmental influence. *J. Agric. Food Chem.* **2012**, *60*, 3005−3012.
(19) Heuberger, A. L.; Broeckling, C. D.; Kirkpatrick, K. R.; Prenni, J. E. Application of nontargeted metabolite profiling to discover novel markers of quality traits in an advanced population of malting barley. *Plant Biotechnol. J.* **2013**, DOI: 10.1111/pbi.12122.
(20) Le Gall, G.; Colquhoun, I. J.; Davis, A. L.; Collins, G. J.; Verhoeyen, M. E. Metabolite profiling of tomato (Lycopersicon esculentum) using H-1 NMR spectroscopy as a tool to detect potential unintended effects following a genetic modification. *J. Agric. Food Chem.* **2003**, *51*, 2447−2456.
(21) Roessner, U.; Wagner, C.; Kopka, J.; Trethewey, R. N.; Willmitzer, L. Technical advance: simultaneous analysis of metabolites in potato tuber by gas chromatography-mass spectrometry. *Plant J.* **2000**, *23*, 131−142.
(22) Shewry, P. R.; Hawkesford, M. J.; Piironen, V.; Lampi, A. M.; Gebruers, K.; Boros, D.; Andersson, A. A.; Aman, P.; Rakszegi, M.; Bedo, Z.; Ward, J. L. Natural variation in grain composition of what and related cereals. *J. Agric. Food Chem.* **2013**, *61*, 8295−8303.
(23) Wakasa, K.; Hasegawa, H.; Nemoto, H.; Matsuda, F.; Miyazawa, H.; Tozawa, Y.; Morino, K.; Komatsu, A.; Yamada, T.; Terakawa, T.; Miyagawa, H. High-level tryptophan accumulation in seeds of transgenic rice and its limited effects on agronomic traits and seed metabolite profile. *J. Exp. Bot.* **2006**, *57*, 3069−3078.
(24) Beale, M. H.; Ward, J. L.; Baker, J. M. Establishing substantial equivalence: metabolomics. *Methods Mol. Biol.* **2009**, *478*, 289−303.
(25) Ricroch, A. E. Assessment of GE food safety using "-omics" techniques and long-term animal feeding studies. *Nat. Biotechnol.* **2013**, *30*, 349−354.
(26) Chassy, B. M. Can -omics inform a food safety assessment? *Regul. Toxicol .Pharm.* **2010**, *58*, S62−S70.
(27) Frenzel, T.; Miller, A.; Engel, K. H. Metabolite profiling - A Fractionation method for analysis of major and minor compounds in rice grains. *Cereal Chem.* **2002**, *79*, 215−221.
(28) Tarpley, L.; Duran, A. L.; Kebrom, T. H.; Sumner, L. W. Biomarker metabolites capturing the metabolite variance present in a rice plant developmental period. *BMC Plant Biol.* **2005**, *5*.
(29) Metz, T. O.; Zhang, Q.; Page, J. S.; Shen, Y.; Callister, S. J.; Jacobs, J. M.; Smith, R. D. The future of liquid chromatography-mass spectrometry (LC-MS) in metabolic profiling and metabolomic studies for biomarker discovery. *Biomarkers Med.* **2007**, *1*, 159−185.
(30) De Vos, R. C.; Moco, S.; Lommen, A.; Keurentjes, J. J.; Bino, R. J.; Hall, R. D. Untargeted large-scale plant metabolomics using liquid chromatography coupled to mass spectrometry. *Nat. Protoc.* **2007**, *2*, 778−791.
(31) Morino, K.; Matsuda, F.; Miyazawa, H.; Sukegawa, A.; Miyagawa, H.; Wakasa, K. Metabolic profiling of tryptophan-overproducing rice calli that express a feedback-insensitive alpha subunit of anthranilate synthase. *Plant Cell Physiol.* **2005**, *46*, 514−521.
(32) Yoshida, H.; Mizukoshi, T.; Hirayama, K.; Miyano, H. Comprehensive analytical method for the determination of hydrophilic metabolites by high-performance liquid chromatography and mass spectrometry. *J. Agric. Food Chem.* **2007**, *55*, 551−560.
(33) Zhou, J.; Ma, C.; Xu, H.; Yuan, K.; Lu, X.; Zhu, Z.; Wu, Y.; Xu, G. Metabolic profiling of transgenic rice with cryIAc and sck genes: an evaluation of unintended effects at metabolic level by using GC-FID

and GC-MS. *J. Chromatogr. B: Anal. Technol. Biomed. Life Sci.* **2009**, *877*, 725−732.
(34) Want, E. J.; Cravatt, B. F.; Siuzdak, G. The expanding role of mass spectrometry in metabolite profiling and characterization. *ChemBiochem* **2005**, *6*, 1941−1951.
(35) Kim, H. K.; Choi, Y. H.; Verpoorte, R. NMR-based metabolomics analysis of plant. *Nat. Protoc.* **2010**, *5*, 536−549.
(36) Krishnan, P.; Kruger, N. J.; Ratcliffe, R. G. Metabolite fingerprinting and profiling in plants using NMR. *J. Exp. Bot.* **2005**, *56*, 255−265.
(37) Doerfler, H.; Lyon, D.; Nägele, T.; Sun, X.; Fragner, L.; Hadeck, F.; Egelhofer, V.; Weckwerth, W. Granger causality in intergrated GC-MS and LC-MS metabolomics data reveals the interface of primary and secondary metabolism. *Metabolomics* **2013**, *9*, 564−574.
(38) Reynolds, T. L.; Nemeth, M. A.; Glenn, K. C.; Ridley, W. P.; Astwood, J. D. Natural variability of metabolites in maize grain: differences due to genetic background. *J. Agric. Food Chem.* **2005**, *53*, 10061−10067.
(39) Harrigan, G. G.; Stork, L. G.; Riordan, S. G.; Reynolds, T. L.; Ridley, W. P.; Masucci, J. D.; Macisaac, S.; Halls, S. C.; Orth, R.; Smith, R. G.; Wen, L.; Brown, W. E.; Welsch, M.; Riley, R.; McFarland, D.; Pandravada, A.; Glenn, K. C. Impact of genetics and environment on nutritional and metabolite components of maize grain. *J. Agric. Food Chem.* **2007**, *55*, 6177−6185.
(40) Rohlig, R. M.; Eder, J.; Engel, K. H. Metabolite profiling of maize grain: differentiation due to genetics and environment. *Metabolomics* **2009**, *5*, 459−477.
(41) Skogerson, K.; Harrigan, G. G.; Reynolds, T. L.; Halls, S. C.; Ruebelt, M.; Iandolino, A.; Pandravada, A.; Glenn, K. C.; Fiehn, O. Impact of Genetics and Environment on the Metabolite Composition of Maize Grain. *J. Agric. Food Chem.* **2010**, *58*, 3600−3610.
(42) Barros, E.; Lezar, S.; Anttonen, M. J.; van Dijk, J. P.; Rohlig, R. M.; Kok, E. J.; Engel, K. H. Comparison of two GM maize varieties with a near-isogenic non-GM variety using transcriptomics, proteomics and metabolomics. *Plant Biotechnol. J.* **2010**, *8*, 436−451.
(43) Harrigan, G. G.; Chassy, B. Challenges for Metabolomics as Tool in Safety Assessments. In *Metabolomics*; Roessner, U., Ed.; InTech: New York, 2012; pp 331−348.

elaborated by Moncrief in 1961; he worked on material coatings that would enable discrimination between simple and complex aromas such as polychloride vinyl, gelatin, and plant fat. Moncrief proved that the electronic system containing an array of six sensors with different coatings is capable of detecting a large number of odors.[13,14] In 1964, Wilkens and Hartman developed another system for artificial smell detection, which was based on electrochemical reactions taking place on the electrodes as a result of stimulation with odorants. Wilkens and Hartman concluded that transformation of the sensor output in response to the chemical reaction is possible; in other words, the transformation of a chemical signal into an electrical signal is possible.[7,11] In the following 20 years, new sensors were designed, including MOSFET (metal oxide semiconductor field-effect transistor), BAW (bulk acoustic wave), ion exchange membrane, potentiometric biosensor, ISFET (ion sensitive field-effect transistor), PdMOS (palladium metal oxide semicoductor), and SAW (surface acoustic wave). In 1982, at the University of Manchester, Persaud and Dodd constructed the first electronic nose, which consisted of three metal oxide sensors and was capable of identifying 20 odorants. A detailed definition of an electronic nose was introduced by Gardner in 1988.[15] In 1985, Otto and Thomas presented the first system for liquid phase analysis by using a multisensor array.[16] Seven years later, at the University of Kyusho, the taste sensor was constructed by Toko; it consisted of ion-selective lipid membranes immobilized in PCV polymer.[17,18] In 1995, as a result of cooperation between Russia and Italy, the concept of an electronic tongue was presented; it was based on an inorganic chalgogenide glass sensor, which enables both qualitative and quantitative analysis.[19]

The history of the computer system for image analysis started in the 1960s. In 1964, Minsky began to realize the project that involved coupling a camera to a computer as well as the interpretation of the obtained image.[20] Five years later, Boyle and Smith received the Noble Prize for developing the CCD (charge coupled device) array used to register images in a videophone.[21] In 1970, attempts to better understand the methods for image edge extraction were made, which has resulted in the construction of 3D images.[22] At the same time, such algorithms as line labeling, articulated body model, and optical flow became popular. In 1982, David Marr proposed three levels of information (image) processing, that is, computational theory, representations and algorithms, and hardware implementation.[23] Since 1980 the research has focused on sophisticated mathematical techniques for the segmentation and modeling of shapes and contours. This phenomenon has given rise to the analysis of moving objects, the so-called tracking, which is presently applied on production lines. In 1989, the CMOS (complementary metal oxide semiconductor) array was developed, having principles of operation that are similar to those of the CCD array.[24,25]

Structure and the Principles of Operation of an Electronic Nose. An electronic nose is the analytical device used for the fast detection and identification of mixtures of odorants, which mimics the principles of operation of human smell. Specific chemical sensors are used in the device, which generates a characteristic odor profile, a so-called fingerprint, in response to the interaction with a gaseous mixture; identification of the mixture components is made by comparing the obtained odor profile with odor standards.[26] The electronic nose is similar to the human nose because it is based on the same principles of operation. The volatile components in the investigated sample are analyzed by chemical sensors that mimic olfactory cells present in the nose. Then the signal is sent to the data recognition system, which simulates brain functions.[17,27]

Usually, an electronic nose is composed of a set of sensors, electronic components, pumps, a flowmeter, and software, which is necessary for data processing and statistical analysis.[7] A sample dispensing system is the first element of the device. Sampling can be conducted in different ways, for example, by collecting a headspace sample, by using diffusion methods, and via prior sample enrichment. Commercially available electronic noses have two or more separate chambers, that is, a sample dispensing chamber and a sensor chamber. Temperature and humidity are measured in each chamber to determine the influence of these two factors on the conducted analysis. The sample dispensing chamber should be made of nonflammable and nonreactive materials to avoid the effect of "wall memory"; it should also be adjusted to the sample size.[28] Moreover, a thermostat is required to increase the amount of volatile components in the headspace for the volatile fraction analysis. Air or an inert gas in introduced into the sample chamber. A special system of pumps and tubes made of plastic or stainless steel delivers the gas together with the volatile sample components to the chamber where the second element of the electronic nose, that is, a set of sensors is located.[29] The sample injection step should be preceded by passing the clean and dry air through both chambers. Such a procedure should stabilize the signal at the baseline level and purge the remnants of sample that had been analyzed earlier.[30,31] Due to the contact between odorants and the active material, the electric properties of sensors change; for example, the conductivity changes, which results in an electric signal.[32] The strength of the response signal depends on the type and concentration of odorant. It is important to stabilize the sensors by heating them for two or three days prior to measurement. The time required to receive a sensor output is called a response time, whereas the time required for a sensor to return to baseline after a response is defined as a recovery time[33] (Figure 1). Depending on the application of an electronic nose, different numbers and types of sensors are used.

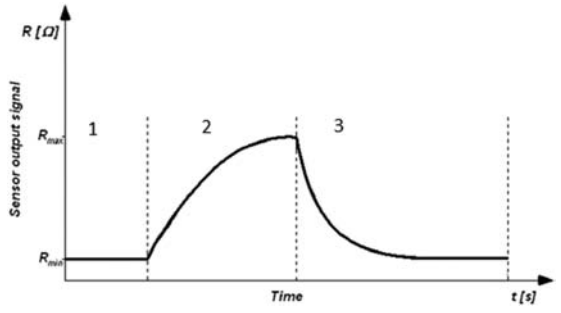

Figure 1. Response characteristics of a semiconductor-based electronic nose: R_{min}, baseline; R_{max}, resistance; 1, gas flow; 2, response time; 3, recovery time.

Structure and Principles of Operation of an Electronic Tongue. An electronic tongue, also known as an artificial tongue, or taste sensor, is the analytical device mainly used to classify the tastes of various chemical substances in liquid phase samples. Its mode of operation is based on the human sense of taste (Figure 2). An electronic tongue can be used to identify, classify, and analyze in a qualitative and quantitative way the

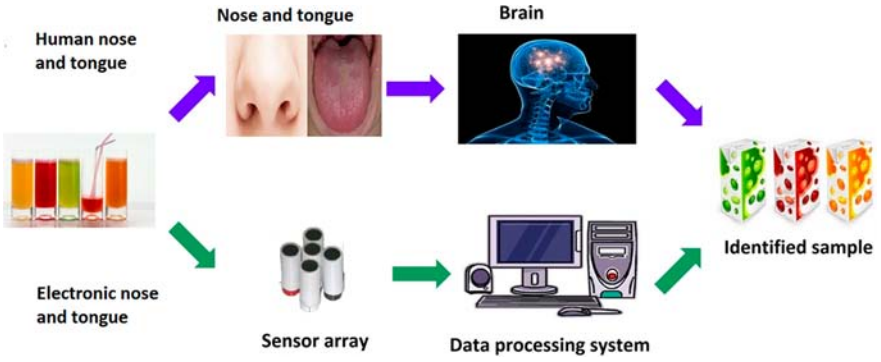

Figure 2. Comparison of the principles of operation of the senses of taste and smell and electronic tongue and electronic nose.

multicomponent mixtures by applying a fingerprint method, that is, by comparing the mixture profiles with those of standards.[31,32] An electronic tongue consists of three elements, that is, the sample-dispensing chamber or automatic sample dispenser (it is not necessary), an array of sensors of different selectivities, and software for data processing (image recognition system, which mimics brain functions).[34] The analysis of liquid phase samples is performed directly; solid phase samples have to be dissolved prior to analysis. An artificial tongue is most commonly used to evaluate food and pharmaceutical products.[35]

An electronic tongue consists of two chambers; the first chamber is used to analyze the sample, whereas the second one cleans the array of sensors after each analysis. A thermostat enables continuous monitoring of the sample temperature during analysis, which results in the repeatability of measurements. Two mechanized flow analysis techniques are used in artificial tongues, that is, flow injection analysis (FIA) and sequential injection analysis (SIA). The first-generation equipment (FIA), designed by Ruzik and Hanser in 1975, consists of a pump, injection valve, solenoid, and detector. In 1995, Ruzick and Marshal elaborated the second-generation apparatus (SIA) consisting of a single-channel duct, two-way pump, solenoid, multiposition valve, and flow sensor. Both techniques are commonly used; however, SIA has more advantages, including the capability to perform a larger number of analyses and a significantly lower use of reagents. The mechanized sample injection allows for decreasing analysis time and improving repeatability. The injected sample reaches the array of chemical sensors.[34] These sensors are characterized by low selectivity and generate information about a wide concentration range of different substances present in the mixture. The sensor response, which is a function of the concentration of components in the liquid, is presented via image recognition module. The signal from the chemical sensors is transformed into a data matrix. The identification and classification are based on a comparison of standard images and the image of the analyzed sample.[36] Depending on the application of an electronic tongue, sensors with different modes of operation are used.

Structure and Principles of Operation of Computer Image Processing. Computer image analysis system, called, "computer vision", includes subjects such as acquisition, processing, and analysis of images.[37] The main reason for creating the system was to understand the mode of operation of human vision. In general, the computer system consists of five elements, that is, lighting, a camera (in the case of an analog camera, a frame grabber is necessary, which allows for analog-to-digital signal conversion), a computer with software, and a high-resolution monitor[38,39] (Figure 3). The application of an

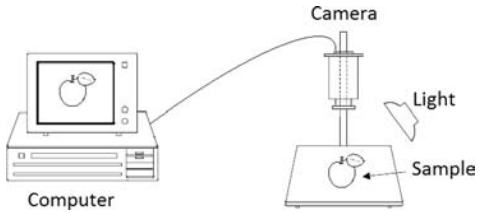

Figure 3. Schematic structure of an image analysis system.

image analysis system is very broad, particularly in the food industry. It is a fast, precise, and noninvasive way of evaluating the product quality already at the production step. Moreover, the system enables detection of imperfections, for example, in meat structure, and the onset of food deterioration, which are both invisible to the human eye.[40]

As in the case of the human eye, the operation of vision systems depends on the intensity of lighting. Properly designed lighting can improve the precision of analysis and decrease analysis time. Fluorescent and incandescent bulbs are the most frequently used light sources. Luminescent electric diodes (LED), quartz halogen lamps, metal halide lamps (applied in microscopy), and high-pressure sodium lamps (best suited for lighting large industrial buildings) are also used. However, due to more uniform and intensive light at specific wavelengths, fluorescent lamps are the most popular. There are two types of lamp arrangements, that is, a circular system used with flat samples and a scattered system for lighting ball-shaped samples. An X-ray tube is used to perform a detailed evaluation of the quality and ripeness of food products; the penetration of X-rays depends on the emitted energy, absorption coefficient, and density and thickness of the analyzed objects.[41] On the other hand, fluorescent spectroscopy is applied to monitor stress in plants.[42] Another part of the image analysis system is a still camera, movie camera, or scanner; its purpose is to record a photograph of a given object. There are two types of cameras, that is, analog and digital cameras, which are equipped with CCD or CMOS sensor arrays.[43] In an analog camera, the recorded image is transformed into the analog signal and then transferred to a frame grabber (in the form of a card), which transforms the analog signal into a digital data stream and sends it to the computer memory. In digital cameras, a frame grabber is not needed because the analog signal is sent directly to the computer via a USB or FireWire adapter.[38,41]

dx.doi.org/10.1021/jf403215y | J. Agric. Food Chem. 2014, 62, 1423−1448

SENSORS USED IN ELECTRONIC SENSES

Sensors are the most important element of electronic senses; their task is to collect information about the parameters measured.[27,29,43] During this process, the input signal, which occurs as some form of energy, is transformed into the output signal in a different energy form, for example, electric, magnetic, chemical, thermal, or radiation energy.[44] Sensors are divided into five groups: piezoelectric; electrochemical (potentiometric, voltammetric, amperometric, conductometric, and impedimetric) and colorimetric sensors; biosensors; and sensors based on gas chromatography and mass spectrometry.[7,34,36,45]

Conductometric Sensors. The mode of operation of a conductometric sensor is based on the changes in conductivity. These changes result from the interactions with the volatile odorants, which leads to the changes in the sensor's electrical resistance; the underlying mechanism differs depending on the material used. Despite the fact that various materials are used, the construction and distribution of specific elements in conductometric sensors are, in principle, the same. There are three types of conductometric sensors that are most commonly used in electronic noses; they are conductive polymer (CP) sensors, metal oxide semiconductors (MOS), and metal oxide semiconductor field-effect transistors (MOSFET). In addition, the conductometric sensors are divided into cold and hot sensors, the latter being capable of performing at higher temperatures.[7,30] Publications on the use of conductometric sensors in an electronic tongue are very scarce.[46]

The advantages of CP sensors are a low price and fast response, whereas susceptibility to humidity is the main disadvantage.[32] These sensors have been used in an electronic nose to, among others, identify stages of wine fermentation,[47] monitor decomposition in Atlantic salmon during its storage at different temperatures,[48,49] and detect spoiled vacuum-packed beef.[50] Cyranose 320, Aroma Scan A32/50S, and Bloodhound BH114 are commercially available electronic noses that employ CP sensors. MOS sensors are also inexpensive, stable, easy to use, and highly sensitive.[7,48] They require a high working temperature, which is a disadvantage.[51] These sensors are used in electronic noses to monitor red wine spoilage[52] and the dehydration process in tomatoes;[53] for the quality control of Atlantic salmon;[54] to determine the freshness of meat;[55] to classify fruits on the basis of their ripeness;[56,57] and to detect aflatoxins in corn.[58] The commercially available electronic noses that employ MOS type sensors are, among others, i-PEN, i-PEN3, PEN-2, PEN3, FOX 2000, 3000, 4000, 5000, FishNose (GEMINI), KAMINA, EOS^{835}, and FF-2A. Compared to the above-mentioned, the MOSET sensors are small and inexpensive; however, their main disadvantage is low sensitivity to ammonia and carbon dioxide and drifting baseline.[13] These sensors have been employed in electronic noses that are used to evaluate the oxidation level of olive oil stored under various conditions;[59] to detect the presence of fungi, bacteria, and ergosterol in grain samples;[60] to monitor fermentation in sausages;[61] and to determine the freshness of shrimp and cod roe.[62] NST 3210, NST 3220, and NST 3320 are the commercial electronic noses that employ MOSET type sensors.

Amperometric/Voltammetric Sensors. Measurements by means of these sensors are based on the electric current reading between the working and reference electrode in an electrochemical cell as a function of analyte concentration.[63] The main disadvantage of such sensors is the lack of selectivity. This type of sensor in electronic noses is used to assign the correct class to wheat samples in accordance with the quality classification,[64] whereas in the electronic tongue it is used to evaluate different conditions under which olive oil is stored,[59] to identify white wines with regard to the type of grape and geographical origin,[65] and to discriminate among various blends of fruit juices.[66] Additionally, similarly to potentiometric sensors, these sensors are used to monitor the aging phase of wine,[67] to monitor beer fermentation,[68] to control the freshness of milk stored at room temperature,[69] to detect chemically adulterated red wine,[70] and to identify rice wine with regard to its age.[71]

Potentiometric Sensors. Potentiometric sensors are based on the voltage measurement at null current, which is usually needed to retain the balance of electrochemical process.[7] Potentiometric sensors have the following positive properties: well-known principles of operation, low cost, ease of commercial production, the possibility of obtaining selective sensors, and the highest degree of similarity with the mechanism of molecular recognition. Their disadvantages are the dependence of the measured value on temperature and adsorption of the solution components onto the electrodes, which influences the changes in potential.[32,34,36] Potentiometric sensors are most frequently found in electronic tongues, which are used to monitor cheese fermentation;[72] to evaluate the impact of micro-oxygenation and oak chip maceration on wine composition, in particular, on the presence of phenol compounds;[73] to monitor changes during beer brewing;[74] and to identify the botanical origin of honey.[75]

Impedimetric Sensors. The principle of operation of impedimetric sensors is based on measuring the impedance at one constant frequency or for a frequency spectrum by means of impedance spectroscopy.[34] They could be employed in an electronic tongue; however, in practice, this happens only sporadically. This sensor was used, for example, to discriminate brands in red wines in an electronic tongue.[76]

Piezoelectric Sensors. The operation of piezoelectric sensors is based on a piezoelectric phenomenon. As a result of sensor exposure to odorants, a change in mass occurs due to the adsorption or absorption of odorants by the sensor, which, in turn, causes changes in the sensor resonance. Consequently, the electric current also changes, which is the output signal. The main advantages of piezoelectric sensors are high sensitivity, real-time measurements, small size, durability, low cost, and the principle of detecting analytes on the basis of the universal change in mass.[77] A quartz crystal microbalance (QMB) is an example of the application of a piezoelectric sensor.[7,29] Piezoelectric sensors are more commonly used in electronic noses (e.g., to determine the optimal time for harvesting apples[78] and to evaluate the quality of tomatoes[79]) than in electronic tongues. It seems, however, that their wider use in electronic tongues is just a question of time.[32]

Colorimetric Sensors. Colorimetric sensors are devices mostly based on the interaction of electromagnetic radiation with matter. Colorimetric sensors can be based on different phenomena such as fluorescence, reflection, and absorbance. These sensors consist of an indicator, detector, and light source, the latter set at a specific wavelength to maximize selectivity. Due to the interaction with an analyte, the properties of an indicator change, which influences the membrane absorbance or fluorescence. The changes are monitored via a detector, which converts the signal from optical into electric form.[32] There is a great variety of colorimetric sensors; therefore, they are characterized by low cost, simple procedure, and high

selectivity.[7] Thanks to the use of colorimetric sensors, it is possible to detect substances that are not electrochemically active and therefore cannot be detected by an electrochemical sensor. Colorimetric sensors have some disadvantages that significantly limit their application, for example, sensor durability and output signal distortion.[32] These sensors have been employed in electronic noses to discriminate commercial drinks[80] and in electronic tongues to evaluate the quality of beer brands[81] and discriminate wines with regard to wine age and grape variety.[82]

Electronic Noses Based on Gas Chromatography and Mass Spectrometry. In the electronic nose technology, it is possible to use the technique of fast gas chromatography. A fast gas chromatograph is a stationary device that requires a short time for analyzing samples; it simulates the work of a system consisting of hundreds of orthogonal sensors, which allows for precise separation of volatile components in the investigated sample. There are also electronic noses employing a mass spectrometer;[52,83−85] the mass spectra of particular substances are then used as the output signal from the sensor. However, due to the high cost of such devices, their application is relatively rare.[7,51] A mass spectrometer was used, for example, to predict the shelf life of pasteurized and homogenized low-fat milk in an electronic nose[86,87] and to discriminate bacterial strains and monitor the smell intensity during fermentation of milk and cheeses.[83]

Biosensors. A biosensor consists of a biological measuring element, which is located close to the transducer to achieve high sensitivity to the target analytes (Figure 4).[31] A biosensor-based electronic tongue is often called a bioelectronic tongue. Such a device can be described as an analytical system made of a number of biosensors that are sensitive to particular compounds present in a solution; the system is connected to the properly selected chemometric tool for data processing.[88] Until now, different principles of operation of bioelectonic tongues have been proposed, including voltammetric, amperometric, and potentiometric principle. Biosensor arrays display high selectivity due to enzyme−substrate interactions. Moreover, the biosensor efficiency can be improved by the introduction of electron mediators, which facilitate the transfer of electrons from the enzyme to the electrode.[89] Such sensors have been used to, among others, monitor changes occurring during the aging process in beer.[90]

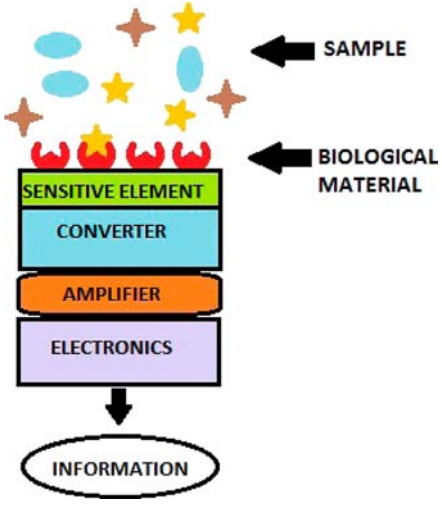

Figure 4. Exemplary structure of a biosensor.

Arrays in Still Cameras. *CCD Array.* A charge coupled device (CCD) array consists of hundreds of thousands of light-sensitive elements, or semiconductor sensors, which are called pixels. The creation and storage of the electric charge originating in the presence of light is one of the sensor's functions. The task of the whole array is to sample the image, be light-sensitive, and store and transport the created charges. CCD sensors are made of light and fragile materials; they can be in the form of diodes and a MOS capacitor stacked in rows. Light, upon reaching the array covered with a crystal silicon plate, ejects electrons from particular pixels. The number of ejected electrons is proportional to light intensity at a given pixel. A CCD array has two working modes, that is, passive and active. In passive mode, different numbers of electrons are gathered depending on light intensity, whereas in active mode the pixel readout takes place, where charges from higher levels are transferred one pixel lower. This process is repeated until all pixels have been read. Next, the content of consecutive rows ends up in the shift register, a so-called output register, where a conversion of charge into a voltage occurs at the output (Figure 5).[41]

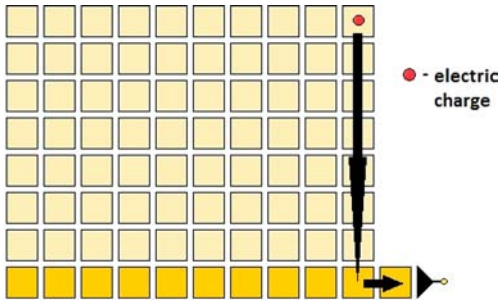

Figure 5. Simplified schematic representation of a CCD array.

Color Sensors. The most commonly used color sensors are a Bayer sensor and a device called 3CCD. The Bayer sensor is employed as an RGB (red, green, blue) filter in CCD sensors of digital cameras. It is a chess board-like grid having a filter pattern that is 50% green, 25% red, and 25% blue. Such an arrangement of colors results from the fact that a human eye is most sensitive to green color. Unfortunately, the filter transmits only a part of the spectrum; therefore, some information does not reach the sensor. Additional information is created by using a demosaicing algorithm. The 3CCD sensor has better color resolution because it contains three independent image sensors and dichroic prisms, which split light into red, green, and blue beams. This sensor is characterized by better light sensitivity as it absorbs the whole beam of light, whereas sensors covered with a Bayer filter absorb only 33%.[41]

CMOS Array. A complementary metal oxide semiconductor (CMOS) array is based on the same principle as a CCD array. Light absorbed by silicon crystals generates electric charges. The CMOS sensors differ from the CCD sensors with regard to distribution and structure (Figure 6). The basic difference is that each so-called active pixel has its own voltage transducer. As a result, the coefficient of a transformation of electric charge to voltage is almost the same for each pixel. Consequently, it is necessary to calibrate the CMOS array with regard to differences between pixels by using digital camera software. Contrary to the CCD array, the CMOS pixels can be read in

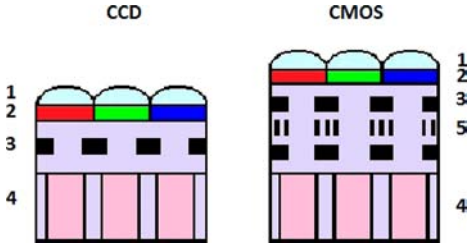

Figure 6. Comparison of the CMOS and CCD arrays: 1, microlenses; 2, color filter; 3, signal transmission path; 4, photodiodes; 5, transistors and amplifiers.

any order. The main advantages of the CMOS array are low energy use and the possibility to miniaturize the camera.[41,91,92]

METHODS OF SIGNAL ANALYSIS USED IN ELECTRONIC SENSES

A measurement performed by means of electronic senses generates a vast volume of data; therefore, it is necessary to apply methods of data analysis which allow for data classification. The simplest method is the graphical representation of data in the form of a histogram or circle diagram. Both of these graph types are used to determine the sample components that significantly differ from the others. Another method of signal analysis is based on statistical analysis or multidimensional data analysis. Besides the aforementioned methods, artificial neural networks can also be applied.

Artificial Neural Networks (ANN). An artificial neural network mimics a biological neural network, which collects and transfers signals to the central nervous system, processes the data, and makes specific decisions depending on the identified objects. The basic elements of ANN are artificial neurons. The most important parts of a neuron are the nucleus, dendrites, synapses, axon hillock, and axon. The nucleus is the computing center of the neuron. Dendrites are entrance gates of the neuron through which the input signals enter, whereas a synapse is the end part of dendrites and a so-called exit gate of the neuron. The input signal at a synapse undergoes a preliminary modification; that is, it is either amplified or attenuated. As in a dendrite, the axon is the exit gate from the neuron, whereas the axon hillock is the so-called neuron's exit.

In an axon, the neuron's exit is intertwined with the dendrites of other neurons (i.e., entrances), which enables further transfer of the signal. An artificial neuron has been designed to simulate its biological counterpart. The entrances, or more specifically the signals passing through them, correspond to dendrites. Weights are digital analogues of changes made in the signals at a synapse. The summation function block corresponds to a nucleus, the activation function block corresponds to the axon hillock, and the exit is analogous to the axon. Signal processing by an artificial neuron can be presented in a generalized way as follows. Signals delivered by the entrance gates are multiplied by weights. The multiplied signals are then summed using a summation function block, which results in the signal called a membrane potential. This signal is passed through an activation block, which can be described by different activation functions depending on the requirements. The value of a activation function is the neuron's output signal, which is transferred to the neurons in the next layer. The activation function can have one of three forms: step function (a so-called threshold function), linear function, and nonlinear function. Neurons are usually distributed in layers. The first neuron layer is called an input layer and is responsible for inputting data into the network. The number of neurons in this layer equals the number of values that are concurrently being fed into the network. The last neuron layer, a so-called output layer, is used to generate the output values. Hidden layers can be present between the input and output layers. Neurons assigned to specific hidden layers process the input information into the output information. Neurons in adjacent layers are connected, which results in a system of paths used for information transfer; these connections can be of a one-way or two-way type. One of the main advantages of neural networks compared to other methods of data processing is the learning process, which enables the proper reaction to signals that have not been foreseen by the constructor. Contrary to mathematical methods and algorithms, a neural network can be used for many different models without significant alterations. The aforementioned advantages are available only when a proper learning algorithm is employed. The most commonly used methods of training ANN include error back-propagation (BPNN) and its modified versions.[93−95] We can identify different types of ANN used in the analysis of data obtained through electronic senses: radial basis function (RBF), counterpropagation−artificial neural network (CP-ANN), generalized regression neural network (GRNN), time delay neural networks (TDNN), probabilistic neural networks (PNN), self-organizing maps (SOM), and neural networks of learning vector quantization (LVQ) type.

***k*-Nearest Neighbor (kNN) Algorithm.** The kNN algorithm belongs to the group of algorithms in which the description of the classifier's target function is not performed during the classifier's training, but at the stage of assigning an object to the specific classes. The underlying principle of the classifier's operation is that the object belonging to a specific class has in its close proximity other objects belonging to the same class. Classification is performed by comparing the fitted object to all objects stored in the training set and then choosing from among them k objects that are most alike. To estimate how similar the two feature vectors are, the Euclidean distance is commonly used; the objects that are separated by the shortest Euclidean distance are considered similar. The object is assigned to the class represented by the highest number of objects from among k selected neighbors. When more than one class is represented by the same number of neighbors, the class consisting of the closest neighbors is chosen. Parameter k is selected experimentally to obtain the best classification for a given data set.[96,97]

Hierarchical Cluster Analysis (HCA): Czekanowski's Method. Czekanowski's method/diagram is mainly used to cluster territorial units into homogeneous regions. The starting point of Czekanowski's method is the matrix of distances between the objects, $D[dii']$, which are defined on the basis of any distance type. The distance measures in the D matrix are divided into similarity classes of objects, and the appropriate graphical symbols are assigned to these classes. In this way, an unorganized Czekanowski's diagram is created, which allows for a visual evaluation of the object classification. Object sorting is performed by organizing the diagram, that is, by rearranging its rows and the corresponding columns to align the graphical symbols that code the shortest possible distances along the main diagonal. As the distance from the main diagonal increases, the symbols corresponding to larger distances appear. The sequence in which objects are organized is defined by the sequence of the corresponding rows (columns).[98]

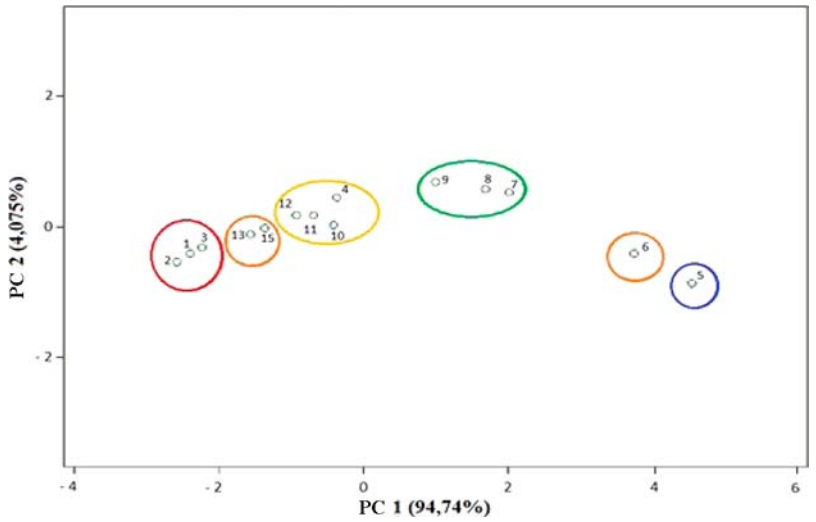

Figure 7. Example of a PCA plot for the varieties of Polish honey.

Cluster Analysis (CA). CA is a method that allows for grouping elements described by more than one feature into relatively homogeneous classes. The most important part of CA is the formation of clusters, that is, the sets of objects for which the similarity between any two objects from the same set is higher than that between any object from the same set and any object not belonging to the set. The clusters do not overlap; that is, none of the objects can belong to more than one class. The clusters are separated by a precisely determined distance, which can be defined in a number of ways. There are two types of clustering methods, that is, hierarchical methods that allow for generating a hierarchy of clusters depending on the distance between the clusters and nonhierarchical methods based on relocating objects from one cluster to another in the search for the most suitable scheme according to the desired criterion. Agglomeration and *k*-means clustering are considered hierarchical and nonhierarchical methods, respectively.[99,100]

Discriminant Function Analysis (DFA). DFA is used when the assumptions of a linear regression are met. The cases are classified into groups using a discriminant prediction equation to examine differences between or among groups. It allows for the rejection of variables that are little related to group distinctions and to determine the fastest way to distinguish groups of elements. Discriminant analysis is carried out in two stages. The first stage, the *F* test, is used to check whether the discriminant model as a whole is significant. The second step is carried out when the *F* test shows significance. The individual independent variables are evaluated to see which differ significantly in mean by the group, and they are used to classify the dependent variable.[101]

Principal Component Analysis (PCA). PCA is mainly used to model, compress, and visualize multivariate data (Figure 7). The aim of PCA is to present the data set *X*, with *m* objects and *n* variables, in the form of a product of two new matrices T $(m \times f)$ and P $(n \times f)$, where $f \ll n$; matrices T and P contain the object coordinates and parameters that lie on the first new coordinate (first principal component), which is the direction of maximum variance. The PCA model can be described by the equation

$$X_{[m,n]} = T_{[m,f]}P_{[f,n]}{}^{T} + E_{[m,n]}$$

where E is the matrix of residues for the PCA model with f principal components. The columns of matrices T and P contain the object coordinates and parameters that are assigned to new variables called principal components. The principal components are derived by iteration in such a way as to maximize the data variance. Each consecutive principal component explains the variance that has not been accounted for by the earlier principal components; therefore, the variance assigned to it decreases. Each principal component has an associated value, a so-called eigenvalue, v_i, which is computed by summing the squares of results for a specific principal component. Eigenvalues quantitatively describe the variance associated with the consecutive principal components. Principal components form a new coordinate system in which the Euclidean distances between the objects remain the same; that is, new distances are identical with the original distances in the data space. Each object has coordinates defined by specific results.[102]

Support Vector Machine (SVM). SVM is a mathematical model described by the supervised learning algorithm that is capable of making predictions. Similarly to ANN, the assignment of objects to specific classes by the SVM method is realized with the use of a training set. SVM is a great alternative to ANN because of better classification compared to the latter, for example. The underlying principle of SVM is the creation of an optimal hyperplane that would separate the data belonging to the opposite classes, with the highest possible confident margin. The SVM algorithm assumes that a maximum-margin hyperplane separates the two classes of data sets in the best way. The margin is a distance between the hyperplane and the support vectors. The support vectors are hyperplanes that separate two classes of data points and are supported by these data sets. Besides the standard support vector machine, different modifications of this method exist such as support vector regression (SVR) and least-squares support vector regression (LSSVR).[103]

Partial Least Squares (PLS). Partial least squares regression (PLSR) is a technique commonly used in data analysis. PLSR is a variant of PCA; a number of linear combinations of the predictors, which predict the response variable in a satisfactory way and are orthogonal, is sought. In the case of the PLSR method, the new explanatory variables should not only explain the variability of the original data but

also be correlated with the response variable. This method is used when one analyzes a relationship between one response variable and many explanatory variables. PLSR is particularly useful when the number of variables is larger than the number of data points. For these reasons, the method is frequently applied in chemometry. The multiple-regression methods, for example, PLS, can also be used to construct discriminant analysis models (PLSDA).[104]

Principal Component Regression (PCR). In PCR the model is composed of principal components instead of the original variables. The principal components are derived via iteration by decomposing the original data matrix X into the result matrix T and the weight matrix P. The role of principal components is to maximize the data variance. In general, a PCR model with f factors that allows for the prediction of dependent variables can be described by the following set of equations:

$$X_{[m,n]} = T_{[m,f]}P^{T}_{[f,n]} + E_{[m,n]}$$

$$Y_{[m,k]} = T_{[m,f]}Q^{T}_{[f,k]} + G_{[m,k]}$$

The coefficients of the regression model Q are estimated by the least-squares method, as follows:

$$Q_{[f,k]} = (T^{T}_{[f,m]}T_{[m,f]})^{-1}T^{T}_{[f,m]}Y_{[m,k]}$$

The principal components used for the construction of the PCR model are orthogonal. This property allows for the calculation of regression coefficients by applying the least-squares method. Moreover, a part of the experimental error of data set X is reduced after a couple of principal components have been chosen. The number of columns in matrix T, that is, the number of principal components used in the constructed model, defines the model's complexity. Matrices E and G contain this part of variance of X and Y, which has not been accounted for by the fitted model.[104]

Soft Independent Modeling of Class Analogies (SIMCA) Classifier. In the SIMCA method, a separate model is constructed for each class, which is based on the principal component approach. Next, a so-called confidence envelope (i.e., a certain volume or hypervolume) is created around the model, which should contain all elements belonging to the specific class with a given probability. For each class, the number of significant principal components in the model is individually chosen in accordance with the commonly used methods. In the case when only one principal component is significant for a given class, the component mean and the vector associated with this component become the model of the class. For two significant components, the model is defined by the location of class center and the plane determined by the component vectors. The remaining models are constructed in a similar way.[97]

Analysis of Variance (ANOVA). ANOVA is a parametric tool that allows for comparing more than two groups that had been categorized on the basis of one variable (one-way ANOVA). The underlying idea is to compare the variance of dependent variables within the groups that had been created on the basis of the values of independent variables. To apply ANOVA, the following assumptions must be fulfilled: the dependent variable is normally distributed; between-group variance is homogeneous; the dependent variable must be measured at least on an interval scale; and the analyzed groups should contain equal numbers of objects.[105,106]

Linear Discriminant Analysis (LDA). The aim of LDA is to construct linear discriminant functions for the samples in the model set that belong to specific groups. The constructed discriminant functions are used to classify new samples. The underlying idea of the method is to reduce the dimension of the data set and, at the same time, retain the value of the T^2 statistic, which is used to evaluate the hypothesis about the equality of means in a multidimensional space. As a result of LDA, a space is created having a dimension that had been reduced to $k - 1$ at best (k is the number of classes). For normal multidimensional distributions of the analyzed data in such a space, the discriminatory features remain intact. To properly apply LDA, a number of assumptions has to be fulfilled, that is, the distribution of objects in each group should be approximately normal; the groups should be linearly separable; variance−covariance matrices of each group should be linearly separable; and the total number of objects has to be at least 3 times larger than the number of variables. There are three variants of LDA, stepwise linear discriminant analysis (SLDA) being an example of one of them.[104,107]

Fisher Discriminant Analysis (FDA). FDA assumes that data vectors occupy p-dimensional space $X \times {}^{1}/_{2}R^{p}$, whereas its aim is to obtain a discrimination rule based on a linear function. For $g = 2$ (g is the number of classes), the rule determines the direction a in X that separates the two training sets in the best possible way and, at the same time, creates a distance measure between the classes that includes a within-group variability. A within-group dispersion should be characterized by appropriate covariance matrices that are based on suitable data. FDA requires that the information about classes, to which new observations are assigned, should be categorized by using the indicators of location and dispersion of g subsets in the training set.[108]

Quadratic Discriminant Analysis (QDA). QDA is also considered a statistical method however, of a more sophisticated type than LDA. In QDA, the data set is subdivided by using quadratic curves. This method is applied when variance−covariance matrices significantly differ. In the case of QDA, the boundaries between the groups are nonlinear.[107,108]

Multiple Linear Regression (MLR). The aim of MLR is to determine the relationships between many independent (explanatory) variables and the dependent (response) variable. In the regression analysis, the parameters of a theoretical model are estimated to reflect the true relationship in the best possible way, as illustrated by the plot of real and theoretical values of the response variable.

The basic regression models assume the existence of linear relationships between the response variable and the explanatory variables.[104]

Complex Data Analysis (CDA). CDA is based on the assumption that data consist of x vectors containing non-negative elements x_1, ..., x_D, which form a specific unity:

$$x_1 + ... + x_D = 1$$

The variables in the aforementioned equation are not independent because they sum to 1; such data are called closed data.

Information contained in the vectors is connected to the relative content of a component. Therefore, the relationships between the components can be expressed in the form of proportions. A transformation of the component vector spaces (simplex) into a Euclidean space can be performed by applying

logarithmic transformations. The characteristic feature of a complex data set is that each row in the data matrix corresponds to only one sample, whereas each matrix column corresponds to one component. Moreover, each matrix element is non-negative, and all matrix rows sum to 1 (e.g., proportions) or 100 (e.g., percentage shares).[108]

Canonical Correlation Analysis (CCA). CCA allows one to find points (variables) in the new coordinate system and points (objects) in the same coordinate system.

In this way, a relationship between the variables and objects under observation can be defined. The analysis of relationships between the variables and objects is conducted directly, which is contrary to the indirect analysis via relationships among the variables and factors, as in other factor-based methods. The rows of matrix X, that is, the input data matrix, can be interpreted geometrically as the coordinates of data points of the variables in n-dimensional object space R_n, whereas the matrix columns as the coordinates of points (objects) in m-dimensional variable space R_m. The input variables are made uniform by applying a canonical transformation. The standardization process in CCA aims at homogenizing the columns and rows of the relative frequency matrix. This type of standardization is performed by scaling the coordinates after matrix columns and matrix rows had been standardized.[109]

Color Image Analysis. *RGB Model.* The most popular method of color image analysis is the RGB model based on three components, that is, red (R), green (G), and blue (B). The RGB color space can be depicted in the form of a cube with three perpendicular axes R, G, and B, each with the axis range from 0 to 255,[25,110] as presented in Figure 8.

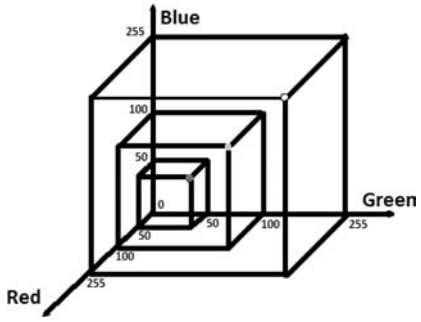

Figure 8. 3D volume of RGB model in a Cartesian coordinate system.

For $R = G = B = 0$, no light is present; therefore, such assignment indicates the color black. In the case when all components assume maximum values, white color is the outcome. Points with different hues of gray color, which lie along the achromatic axis of the RGB cube, are also shown in the figure. The achromatic axis has been defined as a set of points lying on the main diagonal of RGB cube between the points $[R_{min}\ G_{min}\ B_{min}] = [0,0,0]$ and $[R_{max}\ G_{max}\ B_{max}] = [255,255,255]$. The RGB model is called an additive color model because a broad spectrum of colors is obtained by adding beams of primary colors in space.[25,110]

CIE XYZ Model. The CIE XYZ, or CIE 1931 color space, is the first mathematically defined color space model. It is considered a standard and reference point for CIE $L^*a^*b^*$ and CIE $L^*u^*v^*$ color spaces. The abbreviation CIE stands for the International Commission on Illumination (Comission Internationale de I'Eclairage). The tristimulus values XYZ correspond to the percentage shares of primary colors in the RGB model.[111]

*CIE L*a*b* and CIE L*u*v**. Unfortunately, the CIE XYZ model has numerous flaws, for example, the lack of uniform color perception; that is, similar differences among colors are not separated by the same Euclidean distances in the color space. As a result of mathematical transformation of the CIE XYZ model, two models are produced: CIE $L^*a^*b^*$ and CIE $L^*u^*v^*$.[25,112] Colors in the CIE $L^*a^*b^*$ model are defined by three components: L^*, which is luminance, an achromatic property in the range between black and white; a^*, which is a chromatic component in the range between green and magenta; and b^*, another chromatic component in the range between blue and yellow.[111,112]

Contrary to the CIE L^*a^*b model, the CIE $L^*u^*v^*$ model is characterized by a simpler calculation required to transform the CIE XYZ model, which does not involve so many cube root operations. However, the transformation requires intermediate parameters, u^* and v^*. As in the previous model, the symbol L^* stands for luminance, whereas u^* is a chromatic component in the range between green and red and v^* is a chromatic component in the range between blue and yellow.[111,112]

HSV, HSL, and HSI Models. HSV, HSL, and HSI are other color space models; each letter codes a specific model component, that is, hue, saturation, value, lightness, and intensity. These models are modified versions of the RGB space that more precisely reflect the perception of a human eye and, at the same time, retain the simplicity of calculation.[41,113−115] Figure 9 shows a comparison of the three aforementioned models.

The HSV model has the shape of a pyramid, whereas the HSL and HSI models are a double pyramid and a cylinder, respectively. The HSV model is based on the cube that has resulted from the RGB model. The analogy is also visible in the HSL model. The HSI model has a different shape; saturation is expressed as a distance from the cylinder center, and intensity is defined as the axis height. As all color models, the HSV, HSL, and HSI models have certain flaws, for example, unspecified H value for $S = 0$. In the HSI model, intensity contains information that is tightly connected to the other system components. In the case when intensity is close to 0, the analysis of hue and saturation is pointless because of the possible occurrence of large errors.[113]

Analysis of Image Properties. An image has basic properties such as resolution, dimension, the number of discrete intensity levels for each pixel, color space, and the signal-to-noise ratio.[38,116] The processing of a raw image consists of many graphical operations, which enable the improvement of image quality by removing specific flaws, for example, geometric distortions, inappropriate sharpness, uneven lighting, and camera movement. Image analysis is mostly based on the discrimination between a given object and its background. There are three levels of image processing: low, medium, and high.[38,110] In low-level image processing, simple corrections can be introduced to the image by using geometrical operations such as moving, rotating, and scaling to correlate the image with the coordinate system. The consecutive processes that improve image quality are arithmetic operations; they allow for increasing the contrast and adjusting the brightness to increase the differences between the object and the background.[117] Image filtering is one of the possible operations where the intensity at pixel location is recalculated on the basis of the pixel intensity and the intensity of

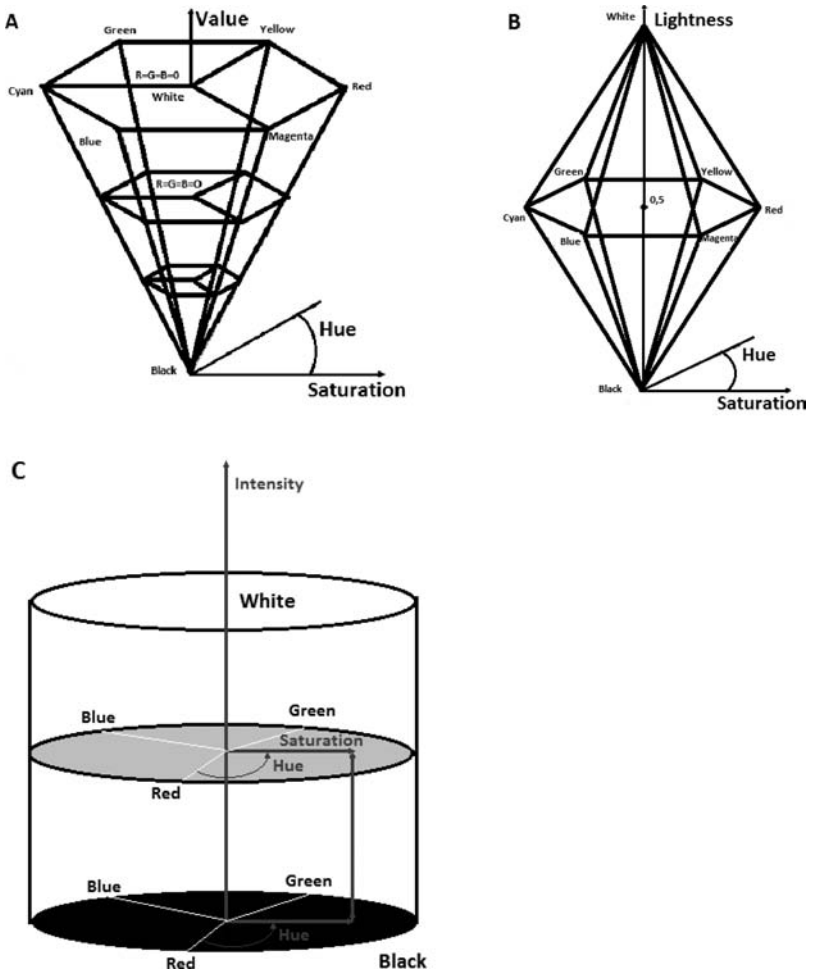

Figure 9. Three color models: (A) HSV; (B) HSL; (C) HSI.

neighboring pixels. Due to the use of filters, it is possible to improve image quality by removing the sensor noise or by correcting the nonuniformly lit image. Moreover, filtering enables the sharpness correction of edges and boundaries between the objects. Segmentation, which is considered a medium-level image processing, is one of the most important methods of image analysis. In this method, the previously filtered image is partitioned into fragments that correspond to specific objects. This allows delineation of image areas that fulfill the homogeneity criterion with regard to color, brightness, and texture.[38,118] A high-level image processing is based on image recognition and interpretation by using statistical classification, neural networks, and fuzzy logic. This stage of image processing supplies information that is necessary for quality control, sorting operations, and object classification on the production lines in food-processing plants.[38,119]

APPLICATION OF ARTIFICIAL SENSES TO FOOD ANALYSIS

At first, an electronic nose was used only to analyze the mixtures of volatile air contaminants that had already been detected by olfaction. At present, the application of this device is much broader and includes the analysis of liquids and oxygen-free gas mixtures. The use of electronic nose encompasses environmental monitoring (detection of air pollution, tracking of pollution pathways, and efficiency assessment of wastewater and waste gas treatment), medical sciences (identification of selected diseases, including tumors, based on odorants excreted by the infected cells and organs), the perfume industry (authentication of perfumes), the pharmaceutical industry (production control of medicines), forensic operations, and the food-processing industry.[7]

An electronic tongue is used to analyze liquid samples. This device enables a parallel analysis of multiple components present in the investigated liquid. The artificial tongue is applied in environmental monitoring (detection of contaminants in samples of water and wastewater), medical sciences (detection of pathogens in liquid samples), and the food-processing industry.[120]

On the other hand, computer vision is used in the food-processing industry for quality control. The system is commonly employed on the production lines for sorting and discriminating specific products.

Milk and Dairy Products. Dairy products are a very diverse group due to the fact that they comprise many types of yogurt, cheese, and milk, each of these foods being broadly diversified as well. Dairy products are made in various ways by using a wide spectrum of fermentation techniques, microorganisms, and food additives. This scenario stimulates the search for analytical tools that would allow for the discrimination of products and their quality evaluation. The electronic nose and tongue are used to monitor food processing, evaluate food freshness, authenticate products, and determine the shelf life of foods. This allows for reducing

the number of poisonings and allergic reactions in human. The electronic eye is employed to monitor visual changes in cheese during the pizza-baking process.[121]

In the case of food process monitoring, the electronic nose and tongue have been used to monitor fermentation in milk and cheese.[72,83] The application of artificial senses assures product quality at the very start of the food production line.

The monitoring of food freshness and product quality during storage is the foremost application of the electronic nose and tongue.[69,87,122−126] This allows the exclusion of spoiled products from the market as well as the determination of appropriate shelf times and storage conditions for milk and cheese to avoid financial losses by the dairy industry.

Another important application of electronic senses is product authentication. Thanks to this procedure, falsified products are excluded from the market; therefore, consumers can purchase merchandise of quality precisely specified by the manufacturer. In the case of dairy products, the conducted studies were aimed at discriminating the brands of milk and yogurt[127−130] and identifying hydrogen peroxide in cow's milk.[131] The determination of age, geographical origin, type, and maturation level in cheeses is also very important; such studies were conducted on a broad variety of cheeses by means of an electronic nose.[132−139] It is necessary to perform this type of research because the investigated parameters influence the cheese quality and therefore the price of specific cheese varieties.

Meat Products. Chemical analyses of meat products are mainly performed via an electronic nose; the use of an electronic tongue in this case is less suitable because it requires a more complex preparation of samples. On the other hand, an electronic eye can be employed to evaluate the freshness of different meat types,[140−145] the medical condition of meat,[146] and the influence of storage conditions on meat quality to determine an expiration date[147,148] based on color and shape. Computer image analysis was used to evaluate the freshness of beef,[140,142] pork,[141,144,147] and poultry.[144,146] The electronic tongue was applied to analyze ground meat to predict the level of chlorides, nitrates, and nitrites.[149] Actually, it is the electronic nose that has found a broader application in the field of meat product analysis. This device is used to, among others, monitor the curing process in Iberian ham to detect spoilage;[150] this allows exclusion of a production batch that could possibly pose a health risk to consumers. Moreover, the electronic nose is frequently used to detect spoilage, evaluate freshness,[55] and determine the storage time of meat. Until now, the conducted studies were aimed at discriminating between fresh and spoiled meat in samples of beef,[50,151,152] turkey meat,[153] sheep meat,[151] and sausages.[61] Another field of application of electronic senses is the freshness evaluation in meat during storage, which is aimed at determining the optimal storage time and conditions to avoid meat spoilage.[154] On the basis of freshness evaluation studies, different freshness categories of meat products can be defined. Research on the influence of storage time on meat quality was conducted on samples of veal,[155] beef,[156] lamb,[157] and meat products used in pizza production.[158] The meat price depends on the animal species from which meat is produced. Therefore, it is specifically important to avoid falsified or misidentified meat. The electronic nose was used to discriminate llama meat from alpaca meat,[159] identify the meat of Iberian pigs among other pork meat,[160] discriminate among hams and sausages on the basis of their type and quality,[161,162] and discriminate meats on the basis of the meat preparation.[163]

Fish and Shellfish. The electronic senses are employed in the fish-processing industry to mainly evaluate the freshness of fish and shellfish. The electronic nose has been used to perform such analysis in sardines,[164−166] shrimp and cod roe,[62] and Atlantic salmon,[54] whereas the electronic tongue has been used on samples of bream.[167] The electronic eye was employed to analyze the freshness of shrimp,[145,168] sturgeon fillets,[148] and salmon fillets.[143] The duration and conditions of storage have a great influence on the freshness of fish and shellfish. To protect consumers from the purchase of old fish, studies on the relationship between the duration and conditions of storage and product freshness were conducted by means of an electronic nose on cod fillets,[169] fresh and frozen Atlantic salmon,[48,49] tilapia,[170] Argentine hake,[171] and oysters.[172,173] Similar investigations were performed on gilt-head bream[174,175] and tench fillets[176] by employing an electronic tongue; in the case of gilt-head bream, the analysis aimed at predicting the biochemical and chemical parameters of spoilage.[175] Another aspect of the application of artificial senses is discrimination between fish species. The electronic tongue was used to discriminate between freshwater and marine fish species.[177] Similar studies were conducted by using an electronic eye.[176] Moreover, the electronic nose was applied to discriminate shrimp on the basis of the presence of phosphates, sulfates, and bleaching agents due to processing.[178]

Fruits and Vegetables. An electronic nose is mainly used to analyze fruits and vegetables. The application of this device is related to the monitoring of food processing and the evaluation of freshness, shelf life, and authenticity of food. On the other hand, the electronic tongue has been mostly used to classify cultivars (e.g., discrimination between onion and shallot),[179] tomatoes on the basis of various parameters,[180,181] apples,[182] and apricots, the latter being also discriminated on the basis of storage duration.[183] The electronic eye is employed to determine the quality of product by using shape and size parameters;[38,119,184−187] to identify the presence of unwanted objects, for example, twigs and leaves;[119,188] to establish the relationship between storage time and product condition on the basis of color analysis;[189−192] and to identify bruising.[191,193] The following fruits and vegetables have been investigated so far: bananas, apples, pears, oranges, strawberries, broccoli, potatoes, and carrots. The electronic nose was used to monitor dehydration in tomatoes[53] and grapes[194,195] to determine the optimal storage time. Studies aimed at evaluating the freshness of fruits and vegetables were conducted to determine the optimal harvest time (apples[78]), the ripeness level (bananas[56] and mandarins[57]), and quality (tomatoes,[79] tomato puree,[155] peaches,[196,197] and apricots[198]). Some products were analyzed to determine their shelf life and classify the ripeness levels (apples,[199−202] tomatoes,[203−205] peaches,[202,206] mandarins,[207] and pears[202]). The electronic nose has also become a useful tool for discriminating among the varieties of, among others, apricots,[208] mangoes,[209] and apples.[210,211] Yet another application of this device was the determination of selected parameters that influence the quality of fruits and vegetables such as oranges, apples,[212] peaches, nectarines,[213] pears,[214,215] and onions.[216] It has also been confirmed that the e-nose can be used for monitoring diseases in cucumbers, paprika, and tomatoes.[167]

Oils, Sauces, Vinegars, and Spices. Among this group of products, olive oil is most frequently analyzed because attempts to adulterate more expensive olive oil with its cheaper alternative are very common.[217] Therefore, the electronic

Table 1. Examples of the Application of an Electronic Nose to Food Analysis

application	sample	object of investigation	type of e-nose	method of data analysis	ref
food process monitoring	grape wine	discrimination of the sequential stages of fermentation	AromaScan A32S: 32 CP	PCA	47
	Australian red wine	monitoring of wine spoilage caused by yeasts	HP 4440 FOX 3000	PCA, PLS	52, 84
	Iberian ham	determination of the degree of spoilage in ham	tin oxide sensors	PCA, PNN	150
	milk, cheeses	monitoring of the smell intensity during fermentation	SMart Nose: MS	PCA	139, 140
	Cencara tomatoes	monitoring of the dehydration process	Air Sense: 10 MOS	PCA	53
	grapes	monitoring of the dehydration process in postharvest grapes	8 QMB	PCA, ANOVA	194
				CA, DA	195
	black tea	determination of the optimal duration of fermentation	8 MOS	TDNN, SOM,	255
evaluation of food freshness	cod fillets	discrimination of samples based on different storage times	LibraNose FreshSense	PLS	169
	smoked Atlantic salmon (fresh, frozen)	classification of spoilage in samples at different temperatures	FishNose: 6 MOS	PLS, PLSR	49, 54
	fresh tilapia fillets	discrimination of fillets based on storage times	eNose 4000: 12 CP	DFA	170
	Argentine hake	freshness evaluation in samples	MOS	PCA	171
	shrimp, cod roe		MOSFET	PCR, ANN	62
	oysters	predictive modeling of smell changes in shells	EEV model 4000: 12 CP	FDA DFA	172, 173
	sardines	freshness evaluation in sardines	6 MOS	PCA, SVM DFA	164−166
	fat-free milk	predicting the shelf life of different milk	MS	PCA	86, 87
		detection of bacteria and yeasts causing spoilage	BH-114: 14 CP	DFA, PCA	123
	veal, cod	discrimination of samples based on storage time	8 QMB	PCA, SOM	155
	ground beef/beef/sheep meat	detection of spoilage and rancidification	FOX 3000: 12 MOS	PCA, SVM,	151
		determination of changes in lipid ground beef	6 tin oxide sensors	PLS	152
	meat	freshness evaluation in meat in relation to storage time and storage conditions	KAMINA PEN2 FOX 4000	PCA, LDA, BPNN, CDA	55, 156, 157
	turkey meat	detection of rancidification in frozen turkey meat during storage	12 MOS, 10 MOSFET, IR sensor	PLSR, PCA	153
	vacuum-packed beef	detection of spoiled meat	4 MOS, 10 MOSFET	PLSR	50
	meat products used in pizza preparation	evaluation of product quality in relation to storage time	e-nose based on ion mobility	PLSR	158
	sausages	monitoring of the sausage fermentation process	4 MOS, 10 MOSFET	ANN	61
	eggs	determination of egg freshness based on storage time at room temperature	PEN3 4 tin oxide sensors	PCA, BPNN, SOM, ANN	301, 302
	apple juice	quality evaluation of juices	Prometheus: MS-nose	QDA	85
	apples	determination of the optimal harvest time	Libra Nose: QMBs	PCA, PLS, PCR	78
	bananas, mandarin oranges	discrimination of bananas as dependent on ripeness level	MOS, PEN2	PCA, LDA	56, 57
	apricots	use of an e-nose to sort apricots	8 QMB	PLS	198
	peaches	detection of ripeness level in peaches	8 MOS	PCA, LDA	196, 197
	tomato puree, tomatoes	monitoring of the puree spoilage and quality evaluation of tomatoes	8 QMB	PCA, SOM	79, 155
	corn	determination of aflatoxins in corn	PEN2: 10 MOS	PCA, LDA	58
	oats, rye, barley	discrimination of samples in relation to the presence of fungi and bacteria	NST 3210	ANN	60
	bread	discrimination of bread spoilage	Bloodhound BH-114	PCA, DFA, CA	236
	olive oil	detection of rancidification	32 CP	PCA	224
testing the shelf life of food	Pink Lady and Jonagold apples	discrimination of varieties ripeness level, shelf life and storage conditions	21 MOS, 12 QMB, MS LibraNose	PCA, ANN, PLS,	199−201
	tomatoes (*Lycopersicon esculentum* Mill.)	discrimination of ripeness level, shelf life, varieties, prediction of quality characteristics of fruit	LibraNose: 5 QMB, MS, PEN-2: 10 MOS	PCA, LDA, PLS	203−205
	peaches, pears, apples	classification of fruit samples at ripeness levels and varieties	PEN-2, tin oxide sensor	PCA, LDA,	202, 206
	mandarin oranges	testing shelf life during storage	PEN-2: 10 MOS	PCA, LDA	207
	Crescenza cheese	determination of maximum shelf life at different temperatures	NST 3320	PCA, CA, LDA	122
	milk	determining the influence of storage time on milk	FOX 4000	PCA	124, 125
	meat	determination of shelf life	NST 3210	LDA	154

Table 1. continued

application	sample	object of investigation	type of e-nose	method of data analysis	ref
	extra-virgin olive oil	evaluation of oxidation status under different storage conditions	NST 3320	PCA, LDA	59
authentication of food	tequila, whiskey, vodka	discrimination of four types of beverages	FOX 4000	PCA, DFA	268, 269
	Chinese spirits	discrimination of eight types of spirits	PEN3	PCA, CA, LDA	270
	Italian wines	detection of falsification	4 thin-film MOS	PCA, BP/ANN	282
	wines	classification of wine in relation to the botanical and geographical origin, aging process, and method	MOS, SAW MS	PCA, PNN SIMCA, PLS, LDA	273−281
	wines	detection of the falsification	FOX 4000	PCA	283
	beer	identification of beer brand	lab-made: 12 CP	PCA	271
	olive oil	detection of falsification	FOX 3000: 12 MOS	LDA, QDA, ANN	217
	extra-virgin olive oil	discrimination of geographical varieties	NST 3320	PCA, CP-ANN	219,
	plant oils	classification of plant oils	6 MOS	LDA	225
		quality discrimination	zNose	PCA	226
	balsamic vinegar of Modena	authentication	MS	PCA, SIMCA	230
	soy sauce	discrimination between soy sauces	31 CP	CA	227
	sesame seed oil	detection of corn oil in adulterated sesame seed oil	10 MOS	PCA, LDA, PNN	231
	Chinese vinegar	identification of some commercial vinegars	9 MOS	BPANN, kNN, PCA	228
	spices	discrimination of different spices	9 MOS	PCA, ANN	229
	orange juices	discrimination of geographical varieties	FOX 3000	PCA, FDA	264
			FOX 4000	PCA, DFA	265
	citrus juices	discrimination of citrus juices	FOX 3000: 12 MOS	LDA	266
	cola drinks	comparison of different brands	FOX 2000: 6 MOS	CA	256
	commercial beverages	discrimination of beverages	colorimetric sensors	HCA, PCA	80
	cheese	discrimination of geographical varieties and age in cheese	MGD-1 eNose 5000 MS, FOX 2000, CP	ANOVA, PCA, CA	132−136, 138, 139
	Pecorino cheese	discrimination of cheese at different maturation stages	AromaScan: 32 PC	PCA	137
	milk	discrimination between milk brands	7 MOS	PCA	127
			18 MOS		128
	dried sausages, cured ham	discrimination of dried sausages in relation to their origin	FOX 2000: 6 MOS	FDA	162
	ham	discrimination of different types of ham	tin oxide sensors	PCA, PNN	161
	products made of Iberian pigs	discrimination between products made from Iberian pigs and from other pigs	QCM, MOS	LDA	160
	llama and alpaca meat	discrimination of meat from llama and alpaca	BH114	LDA	159
	apricots	discrimination of varieties	FOX 4000	PCA	269
	mango	discrimination of fruit varieties and ripeness	FOX 4000	DFA	209
	apples	discrimination of apple varieties and types	tin oxide gas sensors	PCA, PLS, BP-ANN	211
			8 SAW		210
	honey	discrimination of honey in relation to its geographical and botanical origin	MOS-AOS system, SMart Nose	PCA, DFA	305, 307
	mushrooms	discrimination of lyophilized mushroom	AromaScan A20S	PCA	306
	coffee	discrimination of coffee brands, different quality criteria, and bean ripening time	FOX 4000 lab-made FOX 3000, EOS835	PCA, ANN	45, 220, 240, 241, 243
	green tea	discrimination of the quality classes in Longjing tea	PEN-2: 10 MOS	LDA, PCA,	245
				ANOVA, ANN	244
		identification of coumarin-enriched green tea	FF-2A: 10 MOS	PCA, CA	253
		discrimination of the green tea brands	8 MOS	PCA, ANN	316
	tea	classification of teas characterized by varying quality, regions, and brands	MOS	PCA, SOM, RBF, LDA, PNN	246, 248, 251
	rice	identification of rice varieties	Cyranose-320	PCA, CDA	235
	grains	discrimination of different samples and smell-based classification of grains	NST 3210 FOX 3000	ANN	233, 234
other applications	olive oil	discrimination of quality classes based on qualitative and quantitative information	8 CP	SOM,	221,
			MS	SIMCA, PLS	222,
			FOX 3000	PCA	223
	Cabernet red wine	monitoring of changes in wine aroma after bottle opening	8 QMB	PCA, SOM	154

Table 1. continued

application	sample	object of investigation	type of e-nose	method of data analysis	ref
	oranges, apples, peaches	postharvest quality evaluation	LibraNose: 7 TSM	PCA, PLS, ANN	212, 213
	pears	indicators for predicting quality	8 MOS	MLR, ANN, PLS	214, 215
	onions	determining the influence of edaphic factors on bulb quality	AromaScan A32S	PCA	216
	shrimp	discrimination of shrimp	12 CP	DFA	178

tongue and nose were both used to discriminate among olive oils on the basis of oil geographic origin[218−220] and type and quality.[59,221−223] In the case of olive oil, the conducted studies were also aimed at determining rancidity[224] and the relationship between storage time and oil quality.[59] Also, other plant oils were analyzed via an electronic tongue[89,219] and an electronic nose,[225,226] whereas soy sauces,[227] Chinese vinegars,[228] and selected spices[229] were analyzed by using an e-nose. As mentioned before, in the case of luxury and traditional products, it is of utmost importance to authenticate such merchandise to protect the consumer from purchasing substandard goods. The electronic nose was used to authenticate the balsamic vinegar of Modena[230] and sesame seed oil.[231]

Grains and Grain Products. In the case of grains and grain products, quality evaluation and authentication are important (wheat,[64,232−234] rice,[235] barley and oats,[233,234] and corn[186]); however, the critical issue for consumers is the evaluation of possible health risks of such products by means of electronic senses. Possible health risks are related to grain diseases, which often go unnoticed due to the fact that they are not visible to the naked eye. Mycotoxin contamination of grain, which also includes contamination with aflatoxins, and various diseases caused by fungi and bacteria are such risks. Studies on the subject of disease detection were performed on samples of corn[58] and oats, rye, and barley.[60] The electronic nose was used on samples of bread,[236] whereas an electronic eye was used on samples of rice[237] and corn.[238,239] The artificial senses allowed exclusion of samples that could have caused the development of a disease in consumers.

Teas, Coffees, and Herbal Infusions. Coffees, teas, and herbal infusions are mainly analyzed to distinguish among specific types, quality levels, and brands. This is due to the fact that these products are highly variable. Products of low and high quality are frequently mixed together to lower the overall production costs and then sold as top-quality merchandise. Coffees were discriminated on the basis of the quality,[220] brand,[45,177,240−242] and ripening period,[243] whereas teas were evaluated in relation to quality,[244−247] brand,[248−250] geographical origin,[251,252] and content of flavoring substances such as coumarin[253] and theaflavin.[254] Moreover, the electronic nose was used to monitor the fermentation process in black tea and to determine the optimal time for producing tea with the best flavor.[255]

Nonalcoholic Beverages. The analysis of alcohol-free beverages is among many applications of electronic senses. Until now, studies aimed at identifying brands and quality of such beverages were conducted in, for example, cola type drinks,[256] other commercial beverages,[80] mineral water,[257−260] and fruit juices and fruit juice-based drinks.[66,130,240,257,261,262] The beverages were analyzed by means of an electronic eye to determine the quality of orange juice on the basis of its color and color saturation.[263] Another example of the application of electronic senses is the identification of geographical origin in juices[263−265] as well as discrimination of juices on the basis of fruit type.[266]

Alcoholic Beverages. Alcoholic beverages are among the products that have been most frequently analyzed by means of electronic senses. Process monitoring in alcohol production requires fast analytical tools that can detect substandard products, discriminate among products, and authenticate products in real time. Wine and beer are mostly subjected to such type of monitoring because both beverages undergo fermentation that results in a release of specific compounds influencing the taste and aroma of the final product. The artificial senses monitored the processes of fermentation,[68] brewing,[74] and aging[90] in beer. In the case of wine, these devices were employed to control the aging process, to determine the influence of wooden barrels on aging and maceration,[67,73,267] and to monitor grape fermentation.[47] Authentication of alcohols is aimed not only at detecting adulterated products with substandard characteristics but also at identifying falsified products that can be potentially harmful to the consumer's health. Until now, the electronic nose was used to, among others, discriminate among vodkas,[268,269] spirits,[270] whiskeys,[268,269] wines,[268,269] tequilas,[268,269] beers,[269,271] and sorghum-based drinks.[272] The most widely researched group of alcoholic beverages is wines, which have been discriminated on the basis of geographical origin,[273,274] grape variety,[275] and type of maturation and aging process[276−281] as well as analyzed to detect cases of product adulteration.[282,283] The electronic tongue was applied to detect falsified vodkas,[284] whiskeys,[285] and wines; to determine the amount of ethanol in alcohols;[286] and to discriminate among beers on the basis of beer type[287−290] and quality.[81] Similarly to the electronic nose, the electronic tongue was used to analyze wines in relation to their geographical[65,259,291−294] and botanical origin,[65,71,82,294,295] brand,[293] and product adulteration,[70] as well as discrimination based on flavor, for example, bitterness level[296−298] and age.[82,295,299] The electronic eye was employed to monitor aging in wine on the basis of the color analysis.[300]

Others. Besides the aforementioned applications, the electronic nose has been used to, amont others, evaluate egg freshness,[301,302] discriminate honey on the basis of botanical[303,304] and geographical origin,[305] discriminate lyophilized mushroom species,[306] and detect pathogens in food.[307] The electronic tongue has been applied to discriminate honey on the basis of geographical[308] and botanical origin.[75,308−311] On the other hand, the electronic eye has been used to evaluate the quality of pizza,[312] corn tortillas,[313] potato fries,[314] and popular potato chips[315] on the basis of food appearance.

Examples of the application of e-nose, e-tongue, and computer image processing in food analysis are presented in Tables 1, 2, and 3, respectively.

SUMMARY

Due to growing consumer awareness, the need for safe and high-quality food increases. At present, consumers are willing to

Table 2. Examples of the Application of an Electronic Tongue to Food Analysis

application	sample	object of investigation	type of e-tongue	method of data analysis	ref
food process monitoring	bacterial cultures used in cheese production	monitoring of the fermentation process	30 potentiometric sensors	PLS	72
	milk	monitoring the origin of raw milk	voltammetric sensors	PCA	317
	red wines	monitoring of wine aging	13 voltammetric sensors	PCA, SIMCA	67
		evaluating the influence of micro-oxygenation and oak chip maceration on wine composition	potentiometric sensors	PCA, PLS, ANOVA	73, 267
	beer	variability monitoring of the brewing process	7 potentiometric sensors	PCA, PLS	74
		monitoring of changes during the aging process in beer	3 biosensors	PCA, LDA, RBF, PNN BP-NN	90
		monitoring of the fermentation process	potentiometric and voltammetric sensors	PLS	68
evaluation of food quality and freshness	fillets of farmed gilt-head seabream (*Sparus aurata*)	discrimination of storage time; predicting parameters of spoilage	potentiometric sensors	PCA, ANN, PLS MLR	174, 175
	tench (*Tinca tinca*)	discrimination of storage time	voltammetric sensors	PCA	176
	apricots	discrimination based on postharvest storage time and apricot varieties	7 potentiometric sensors	CDA, PLS	183
	nonalcoholic beverages	quality evaluation of high-fructose corn syrup	7 potentiometric sensors	SIMCA	74
	rice	quality evaluation of milling	potentiometric sensors	PCA	318
	milk	monitoring freshness of milk stored at room temperature	boltammetric sensors	PCA, ANN, CA, PLSR, LS-SVM	69, 126
stability testing of food	extra-virgin olive oil	evaluation of different storage conditions	2 amperometric sensors	LDA	59
authentication	honey	discrimination based on botanical origin	potentiometric sensors	PCA, PLS, ANN, LDA	75, 309
		discrimination based on botanical and geographical origin	6 voltametric sensors, Alpha-Astree	PCA, CA, CCA, ANN	308, 311
	yogurt	discrimination and evaluation of yogurt types	4 voltammetric sensors	PCA, DFA PLSR	129
	fermented milk	discrimination of different types	conductometric, potentiometric, and voltammetric sensors	PCA, ANN	46
	milk	discrimination of milk samples pasteurized in different ways	voltammetric sensors	PCA	130, 131
	alcoholic beverages	fast quality evaluation of alcoholic drinks and identification of brands	20 potentiometric sensors	PLS, LDA, PCA	284
		determination of ethanol content in alcohols from different sources	potentiometric sensors	PCA, SIMCA, PLS, PCR	286
		discrimination between cheap and expensive whiskies	voltammetric sensors	PCA	285
	beer	discrimination of beer based on type and manner of production	voltammetric sensors, potentiometric sensors	PCA, LDA	287
		discrimination of beers based on beer type and bitterness level	18 potentiometric sensors	PCA, CCA	288
			6 voltammetric sensors	CCA	289
		discrimination between alcoholic and nonalcoholic beers and between dark and light beers	potentiometric sensors	PCA, PLS, HCA	81, 319
	red wines	detection of chemical adulteration	voltammetric sensors	PLS, PCA	70
		discrimination of wines based on geographical origin	voltammetric sensors	PCA	291
				ANN, PCA	292
		discrimination of brands in red wines	impedimetric sensors	PCA, ANN	233
	white wines	discrimination based on grape variety and geographical origin	voltammetric sensors	PCA	294

dx.doi.org/10.1021/jf403215y | J. Agric. Food Chem. 2014, 62, 1423−1448

Table 2. continued

application	sample	object of investigation	type of e-tongue	method of data analysis	ref
			amperometric sensors	PCA	65
	wines	discrimination of wines based on geographical origin; discrimination of wines based on vintage, vineyard, and age	potentiometric sensors	PCA, ANN, PLS, SIMCA	293, 295, 299, 320
		discrimination of wines based on aging method and content of polyphenols	voltammetric sensors	PCA, CA, PLS, BP-ANN	71, 296, 297
		discrimination of wines based on age and grape species	colorimetric system and 6 potentiometric sensors	PCA, PLS	82
	beverages	discrimination between beverages of the same type and monitoring of aging in juice	potentiometric sensors	PCA, SOM, LDA, ANN	177, 242, 257
	mineral water	discrimination between high mineralized and low mineralized waters	potentiometric sensors	PCA, PLS, ANN, SOM	259
		discrimination of 13 brands of mineral water	ASTREE 2	PCA, HCA, SIMCA	260
	orange, pear, peach, apricot juices	discrimination of orange juice brands	potentiometric sensors	PLS, PCA, ANN	258, 261, 262
		discrimination of fruit juice brands	voltammetric sensors	PCA	130
	green tea	quality discrimination	7 potentiometric sensors	PCA, ANN	247
	tea, herbal infusions	discrimination of infusions	potentiometric sensors	PCA, PCR	154
		discrimination of green and black teas based on geographical origin	potentiometric sensors	PCA	321
			3 voltammetric sensors	PCA	322
		discrimination of black teas based on tea type and brand	5 voltammetric sensors	PCA, ANN	249
			potentiometric sensors	PCA, CA, LDA	250
		discrimination of black teas based on geographical origin	Alpha Astree II	PCA, PLS, LDA, ANOVA	252
	plant oils	discrimination of edible oils based on oil type and geographical origin	voltammetric sensors	PCA	323
	olive oil	discrimination of extra-virgin olive oil based on geographical origin and bitterness level	amperometric sensors	PCA, ANN	219
			voltammetric sensors	PCA	89
	apples	discrimination between apple varieties	potentiometric sensors	PCA, PLS	66, 182
	tomatoes	discrimination of varieties; determination of savory compounds	2 e-tongues: Alpha Astree and e-tongue with potentiometric	PCA, CDA, PLS, CCA	180, 181
	onions, shallots	discrimination between onion and shallot	21 potentiometric sensors	PCA	179
	fishes	discrimination between freshwater and marine fishes	30 potentiometric sensors	PCA	177
other applications	extra-virgin olive oil	discrimination of samples based on phenolic compunds content	voltammetric sensors	PCA, PLS, PLS-DA	324
	black tea	determination of theaflavin level	5 voltammetric sensors	PCA, ANN	254
	ground meat	prediction of the level of chlorides, nitrates, nitrites	voltammetric sensors	PLS	149

dx.doi.org/10.1021/jf403215y | J. Agric. Food Chem. 2014, 62, 1423−1448

Table 3. Examples of Computer Image Processing in Food Analysis

application	sample	object of investigation	method of data analysis	ref
monitoring of raw food	grain	analysis of morphological features in different grain varieties	DA	325
	wheat grain	analysis of physical properties and identification of varieties		232
	rice	verification of spoiled grains	ANN	237
	bananas	monitoring of changes during the aging process in bananas	*L,a,b*	192
	Golden Delicious apples	defect detection based on color	image segmentation algorithms	190
	Haunghau pears	identification of pear and pear peduncle shapes	ANN	119
	Iyokan oranges	analysis of shape, structure, and surface roughness	ANN	184
	oranges	identification of twigs and leaves	thinning algorithms	188
	strawberries	shape and size analysis	CIELAB	38
	broccoli	evaluation of ripeness level in broccoli flowers	DFT algorithms	189
	potatoes	discrimination between good and bad potatoes by color	HSI	193
	carrots	classification based on structure	ANN	187
	corncob	shape analysis	DA	186
	mushrooms	identification of discoloration caused by aging and damages		191
	pistachio nuts	classification of pistachio nuts based on the shape and shell opening		326
	pork tenderloin	quality analysis based on color identification	ANN, PLS	141
	poultry fillet	identification of tumors and bruised skin	ANN	146
	beef	detection of color changes in beef samples	CIELAB	142
	shrimp	visual measurement of shape, color, and size		145
monitoring of processed food	corn grain	quality control of spoiled grains		238
		mold identification		239
	raisins	classification of raisins based on the analysis of shape and surface	image analysis algorithms	280
	orange juice	color analysis, i.e., brightness, color saturation		263
	red wine	evaluation of color		327
		measurement of changes during wine aging process by means of e-nose, e-tongue, and e-eye	CIELAB	300
	potato chips	evaluation of color during frying		315
	French-fried potatoes	evaluation of color and texture	algorithms for statistical analysis	314
	pork	analysis of changes in color of freezer-stored meat packed in plastic bags	CIELAB *L,a,b*	147
	beef steak	color, shape, and structure analysis	ANN	140
	meat	evaluation of color and surface in pork and poultry slices	CIELAB	144
	sturgeon fillets	analysis of changes in color during storage	*L,a,b* CIELAB	148
	salmon fillets	color classification of salmon based on comparison with SalmonFAN color palette	*L,a,b*	143
	shrimp	evaluation of color to determine the water content in dehydrated shrimp	*L,a,b* ANN	168
	corn tortillas	color and shape analysis	*L,a,b*	313
	pizza	quality control based on color and size	image segmentation algorithms	312
	Cheddar and mozzarella cheese	comparison of cheese properties during cooking and baking	image processing algorithms	39

pay more for products that, beyond any doubt, have better quality and are naturally processed. Therefore, the companies that specialize in the processing, transport, and sale of food are put under increasing pressure to find new solutions that would parallel a sensory evaluation of food products. Sensory analysis is performed by testers; therefore, it is a subjective method that does not always reflects the true condition of a given product. Chromatographic techniques such as comprehensive two-dimensional chromatography coupled with detection by olfactometry require a long analysis time, and they often yield unreliable results mainly due to the complexity of the sample matrix. In the case of companies that process and sort food, time and reliability are the most significant and most valued parameters in relation to food quality evaluation. The equipment used until now is frequently being replaced with electronic senses, which, despite their many faults (e.g., complicated calibration, poor selectivity of sensors, and complicated data analysis), are promising alternatives. At present, electronic noses are widely applied to food evaluation with regard to both liquid and solid phase samples. Sample preparation is simple, and the analysis is noninvasive; therefore, different types of meat (e.g., veal, beef, and poultry) as well as different fruits and vegetables, alcoholic and nonalcoholic beverages, dairy products, etc., can be evaluated by means of an electronic nose. The conducted evaluations are also aimed at authenticating luxury products such as traditional balsamic vinegar of Modena and extra-virgin olive oil, detecting falsified wines, and determining the quality, freshness, and shelf life of food products. An electronic tongue has been used for similar purposes, although this device is mainly applied to evaluate liquid samples, for example, alcoholic and nonalcoholic beverages, oils, vinegars, and milk. It has been mostly used for product authentication and freshness evaluation. A computer image analysis system has found wide application

in production plants for sorting foods such as fruits, vegetables, meat, and fish and to discriminate packaging in which food is packed. The evaluated features are color, shape, size, morphology, discoloration, and color intensity. These parameters allow for excluding faulty or substandard products. It is an increasing trend to combine all artificial senses into a quality evaluation system that encompasses the evaluation of appearance, taste, and smell and most closely simulates the sensory analysis by testers. At the same time, such a system is much more sensitive, precise, and reliable. Projects dealing with the improvement of electronic senses via the search for better sensors create the opportunity to widen the range of applications of these devices in food analysis.

AUTHOR INFORMATION

Corresponding Author

*(M.Ś.) E-mail: m.e.sliwinska@gmail.com.

Notes

The authors declare no competing financial interest.

REFERENCES

(1) Orriss, G. D.; Whitehead, A. J. Hazard analysis and critical control point (HACCP) as a part of an overall quality assurance system in international food trade. *Food Control* **2000**, *11*, 345−351.

(2) Peri, C. The universe of food quality. *Food Qual. Pref.* **2006**, *17*, 3−8.

(3) Ehiri, J. E.; Morris, G. P.; McEwen, J. Implementation of HACCP in food businesses: the way ahead. *Food Control* **1995**, *6*, 341−345.

(4) Ropkins, K.; Beck, A. J. Evaluation of worldwide approaches to the use of HACCP to control food safety. *Trends Food Sci. Technol.* **2000**, *11*, 10−21.

(5) Boudouropoulos, I. D.; Arvanitoyannis, I. S. Current state and advances in the implementation of ISO 14000 by the food industry. Comparison of ISO 14000 to ISO 9000 to other environmental programs. *Trends Food Sci. Technol.* **1998**, *9*, 395−408.

(6) Wardencki, W.; Chmiel, T.; Dymerski, T.; Biernacka, P.; Plutowska, B. Application of gas chromatography, mass spectrometry and olfactometry for quality assessment of selected food products. *Ecol. Chem. Eng.* **2009**, *16*, 287−300.

(7) Dymerski, T. M.; Chmiel, T. M.; Wardencki, W. Invited Review Article: An odor-sensing system − powerful technique for foodstuff studies. *Rev. Sci. Instrum.* **2011**, *82*, 111101−111132.

(8) Huang, Y.; Lan, Y.; Lacey, R. E. Artificial senses for characterization of food quality. *J. Bionic Eng.* **2004**, *1*, 159−173.

(9) Vlasov, Y.; Legin, A. Non-selective chemical sensors in analytical chemistry: from "electronic nose" to "electronic tongue". *Fresenius' J. Anal. Chem.* **1998**, *361*, 255−260.

(10) Mauldin, C. E.; Puntambekar, K.; Murphy, A. R.; Liao, F.; Subramanian, V.; Fréchet, J. M. J.; DeLongchamp, D. M.; Fischer, D. A.; Toney, M. F. Solution-processable α,ω-distyryl oligothiophene semiconductors with enhanced environmental stability. *Chem. Mater.* **2009**, *21*, 1927−1938.

(11) Wilson, A. D.; Baietto, M. Applications and advances in electronic-nose technologies. *Sensors* **2009**, *9*, 5099−5148.

(12) Trinchi, A.; Li, Y. X.; Wlodarski, W.; Kaciulis, S.; Pandolfi, L.; Russo, S. P.; Duplessis, J.; Viticoli, S. Investigation of sol−gel prepared Ga−Zn oxide thin films for oxygen gas sensing. *Sens. Actuators, B* **2003**, *108*, 263−270.

(13) Sujatha, G.; Dhivya, N.; Ayyadurai, K.; Thyagarajan, D. Advances in electronic-nose technologies. *IJERA* **2012**, *4*, 2248−9622.

(14) Moncrieff, R. W. An instrument for measuring and classifying odors. *J. Appl. Physiol.* **1961**, *16*, 742−749.

(15) Gardner, J. W.; Bartlett, P. N. A brief history of electronic noses. *Sens. Actuators, B* **1994**, *211*, 18−19.

(16) Otto, M.; Thomas, J. D. R. Model studies on multiple channel analysis of free magnesium, calcium, sodium, and potassium at physiological concentration levels with ion-selective electrodes. *Anal. Chem.* **1985**, *57*, 2647−2651.

(17) Toko, T.; Murata, T.; Matsuno, T.; Kikkawa, Y.; Yamafuji, K. Taste map of beer by a multichannel taste sensor. *Sensor Mater.* **1992**, *4*, 145−151.

(18) Hayashi, K.; Toko, K.; Yamanaka, M.; Yoshihara, H.; Yamafuji, K.; Ikezaki, H.; Toykubo, R.; Satj, K. Electric characteristics of lipid-modified monolayer membranes for taste sensors. *Sens. Actuators, B* **1995**, *23*, 55−61.

(19) Di Natale, C.; D'Amico, A.; Vlasov, Y. G.; Legin, A. V.; Rudnitskaya, A. M. *Proceedings of the International Conference, EUROSENSORS IX*; Foundation for Sensor and Actuator Technology: Stockholm, Sweden, 1995; p 512.

(20) Boden, M. A. Setting a scene. In *Mind As Machine: A History of Cognitive Science*; Oxford University Press: Oxford, UK, 2006; p 1 −50.

(21) Smith, G. E. The invention and early history of the CCD. *Nucl. Instrum. Methods A* **2009**, *607*, 1−6.

(22) Roberts, L. G. Machine perception of three-dimensional solids. In *Optical and Electro-Optical Information Processing*; Tippett, J. T., Borkowitz, D. A., Clapp, L. C., Koester, C. J., Vanderburgh, A., Jr., Eds.; MIT Press: Cambridge, MA, USA, 1965; pp 159−197.

(23) Marr, D. *Vision: A Computational Investigation into the Human Representation and Processing of Visual Information*; Freeman: San Francisco, CA, USA, 1982; pp 23−24.

(24) Renshaw, D. R.; Denyer, P. B.; Wang, G.; Lu, M. *IEEE International Symposium on Date of Conference*, New Orleans, LA; IEEE: Piscataway, NJ, USA, 1990; Vol. 4, pp 3038−3041.

(25) Shih, T. Y. The reversibility of six geometric color spaces. *PE&RS* **1995**, *61*, 1223−1232.

(26) Shiers, V. P. *Proceedings of the Food Ingredients Europe Conference*; Maarssen, Ed.; Miller Freeman: San Franciso, CA, USA, 1995; pp 198−200.

(27) Deisingh, A. K. In *Sensors for Chemical and Biological Applications*; Ram, M. K., Bhethanabotla, V. R., Eds.; Taylor & Francis: Boca Raton, FL, USA, 2010; pp 173−194.

(28) Korel, F.; Balaban, M. Ö. In *Handbook of Food Analysis Instruments*; Ötles, S., Ed.; CRC: Boca Raton, FL, USA, 2009; pp 365−378.

(29) Nagle, H. T.; Schiffman, S. S.; Gutierrez-Osuna, R. The how and why of electronic noses. *IEEE Spectrum* **1998**, *35*, 22−34.

(30) Arshak, K.; Moore, E.; Lyons, G. M.; Harris, J.; Clifford, S. A review of gas sensors employed in electronic nose applications. *Sens. Rev.* **2004**, *24*, 181−198.

(31) Deisingh, A. K.; Stone, D. C.; Thompson, M. Applications of electronic noses and tongues in food analysis. *Int. J. Food Sci. Technol.* **2004**, *39*, 587−604.

(32) Ciosek, P.; Wróblewski, W. Sensor arrays for liquid sensing − electronic tongue systems. *Analyst* **2007**, *132*, 963−978.

(33) Patla, A. E. Understanding the roles of vision in the control of human locomotion. *Gait Posture* **1997**, *5*, 54−69.

(34) Escuder-Gilabert, L.; Peris, M. Review: highlights in recent applications of electronic tongues in food analysis. *Anal. Chim. Acta* **2010**, *665*, 15−25.

(35) Leake, L. L. Electronic noses and tongues. *Food Technol.* **2006**, *6*, 96−102.

(36) Ciosek, P.; Wróblewski, W. Elektroniczny język. *Analityka: Nauka Praktyka* **2004**, *2*, 14−17.

(37) Timmermans, A. J. M. Computer vision system for on-line sorting of pot plants based on learning techniques. *Acta Hortic.* **1998**, *421*, 91−98.

(38) Brosnan, T.; Sun, D.-W. Improving quality inspection of food products by computer vision. *J. Food Eng.* **2004**, *61*, 3−16.

(39) Wang, H.-H.; Sun, D.-W. Evaluation of the functional properties of cheddar cheese using a computer vision method. *J. Food Eng.* **2001**, *49*, 47−51.

(40) Du, C.-J.; Sun, D.-W. Learning techniques used in computer vision for food quality evaluation: a review. *J. Food Eng.* **2006**, *72*, 39−55.

(41) Wu, D.; Sun, D.-W. Colour measurements by computer vision for food quality control − a review. *Trends Food Sci. Technol.* **2013**, *29*, 5−20.
(42) Ruiz-Altisent, M.; Ruiz-Garcia, L.; Moreda, G. P.; Lu, R.; Hernandez-Sanchez, N.; Correa, E. C.; Diezma, B.; Nicolai, B.; Garcia-Ramos, J. Sensors for product characterization and quality of specialty crops − a review. *Comput. Electron. Agric.* **2010**, *74*, 176−194.
(43) Corcoran, P. Electronic odour sensing systems. *J. Inst. Electron. Commun. Eng. Jpn.* **1993**, *5*, 303−308.
(44) Wilson, A. D.; Baietto, M. Applications and advances in electronic-nose technologies. *Sensors* **2009**, *9*, 5099−5148.
(45) Schaller, E.; Bosset, J. O.; Escher, F. Electronic noses and their application to food. *Food Sci. Technol.* **1998**, *31*, 305−316.
(46) Winquist, F.; Holmin, S.; Krantz-Rückler, C.; Wide, P.; Lündström, I. A hybrid electronic tongue. *Anal. Chim. Acta* **2000**, *406*, 147−157.
(47) Pinheiro, C.; Rodrigues, C. M.; Schäfer, T.; Crespo, J. G. Monitoring the aroma production during wine-must fermentation with an electronic nose. *Biotechnol. Bioeng.* **2002**, *77*, 632−640.
(48) Du, W.-X.; Lin, C.-M.; Huang, T.; Kim, J.; Marshall, M.; Wei, C.-I. Potential application of the electronic nose for quality assessment of salmon fillets under various storage conditions. *J. Food Sci.* **2002**, *67*, 307−313.
(49) Olafsdottir, G.; Chanie, E.; Westad, F.; Jonsdottir, R.; Thalmann, C. R.; Bazzo, S.; Labreche, S.; Marcq, P.; Lundby, F.; Haugen, J. E. Prediction of microbial and sensory quality of cold smoked Atlantic salmon (*Salmo salar*) by electronic nose. *J. Food Sci.* **2005**, *70*, 563−574.
(50) Blixt, Y.; Borch, E. Using an electronic nose for determining the spoilage of vacuum-packaged beef. *Int. J. Food Microbiol.* **1999**, *46*, 123−134.
(51) Oh, S. Y.; Shin, H. D.; Kim, S. J.; Hong, J. Rapid determination of floral aroma compounds of lilac blossom by fast gas chromatography combined with surface acoustic wave sensor. *J. Chromatogr., A* **2008**, *1183*, 170−178.
(52) Cynkar, W.; Cozzolino, D.; Dambergs, B.; Janik, L.; Gishen, M. Feasibility study on the use of a head space mass spectrometry electronic nose (MS e-nose) to monitor red wine spoilage induced by *Brettanomyces* yeast. *Sens. Actuators, B* **2007**, *124*, 167−171.
(53) Pani, P.; Leva, A. A.; Riva, M.; Maestrelli, A.; Torreggiani, D. Influence of an osmotic pretreatment on structure-property relationships of air-dehydrated tomato slices. *J. Food Eng.* **2008**, *86*, 105−112.
(54) Haugen, J. E.; Chanie, E.; Westad, F.; Jonsdottir, R.; Bazzo, S.; Labreche, S.; Marcq, P.; Lundby, F.; Olafsdottir, G. Rapid control of smoked Atlantic salmon (*Salmo salar*) quality by electronic nose: correlation with classical evaluation methods. *Sens. Actuators, B* **2006**, *116*, 72−77.
(55) Musatov, V. Y.; Sysoev, V. V.; Sommer, M.; Kiselev, I. Assessment of meat freshness with metal oxide sensor microarray electronic nose: a practical approach. *Sens. Actuators, B* **2010**, *144*, 99−103.
(56) Llobet, E.; Hines, E. L.; Gardner, J. W.; Franco, S. Non-destructive banana ripeness determination using a neural network-based electronic nose. *Meas. Sci. Technol.* **1999**, *10*, 538−548.
(57) Gómez, A. H.; Wang, J.; Hu, G.; Pereira, A. G. Electronic nose technique potential monitoring mandarin maturity. *Sens. Actuators, B* **2006**, *113*, 347−353.
(58) Cheli, F.; Campagnoli, A.; Pinotti, L.; Savoini, G.; Dell'Orto, V. Electronic nose for determination of aflatoxins in maize. *Biotechnol. Agron. Soc. Environ.* **2009**, *13*, 39−43.
(59) Cosio, M. S.; Ballabio, D.; Benedetti, S.; Gigliotti, C. Evaluation of different storage conditions of extra virgin olive oils with a innovative recognition tool built by means of electronic nose and electronic tongue. *Food Chem.* **2007**, *101*, 485−491.
(60) Jonsson, A.; Winquist, F.; Schnürer, J.; Sundgren, H.; Lundström, I. Electronic nose for microbial quality classification of grains. *Int. J. Food Microbiol.* **1997**, *35*, 187−193.
(61) Eklov, T.; Johansson, G.; Winquist, F.; Lundstrom, I. Monitoring sausage fermentation using an electronic nose. In *Methods to Improve the Selectivity of Gas Sensors*; Eklov, T., Ed.; Licentiate thesis 565; Department of Physics and Measurement Technology, University of Linkoping, Sweden, 1997; pp 4−50.
(62) Winquist, F.; Sundgren, H.; Lundstrom, I. Electronic noses for food control. In *Biosensors for Food Analysis*; Scott, A. O., Ed.; Royal Society of Chemistry: Cambridge, UK, 1998; pp 170−179.
(63) Scampicchio, M.; Ballabio, D.; Arecchi, A.; Cosio, S. M.; Mannino, S. Amperometric electronic tongue for food analysis. *Microchim. Acta* **2008**, *163*, 11−21.
(64) Stetter, J. R.; Findlay, M. W.; Schroeder, K. M., Jr.; Yue, C.; Penrose, W. R. Quality classification of grain using a sensor array and pattern recognition. *Anal. Chim. Acta* **1993**, *284*, 1−11.
(65) Pigani, L.; Foca, G.; Ionescu, K.; Martina, V.; Ulrici, A.; Terzi, F.; Vignali, M.; Zanardi, C.; Seeber, R. Amperometric sensors based on poly(3,4-ethylenedioxythiophene)-modified electrodes: discrimination of white wines. *Anal. Chim. Acta* **2008**, *614*, 213−222.
(66) Martina, V.; Ionescu, K.; Pigani, L.; Terzi, F.; Ulrici, A.; Zanardi, C.; Seeber, R. Development of an electronic tongue based on a PEDOT-modified voltammetric sensor. *Anal. Bional. Chem.* **2007**, *387*, 2011−2110.
(67) Parra, V.; Arrieta, A. A.; Fernández-Escudero, J. A.; Iniguez, M.; de Saja, J. A.; Rodríguez-Méndez, M. L. Characterization of wines through the biogenic amine contents using chromatographic techniques and chemometric data analysis. *Anal. Chim. Acta* **2006**, *563*, 229−237.
(68) Kutyła-Olesiuk, A.; Zaborowski, M.; Prokaryn, P.; Ciosek, P. Monitoring of beer fermentation based on hybrid electronic tongue. *Bioelectrochemistry* **2012**, *87*, 104−113.
(69) Winquist, F.; Krantz-Rulcker, C.; Wide, P.; Lundström, I. Monitoring of freshness of milk by an electronic tongue on the basis of voltammetry. *Meas. Sci. Technol.* **1998**, *9*, 1937−1946.
(70) Parra, V.; Arrieta, A. A.; Fernández-Escudero, J. A.; Rodríguez-Méndez, M. L.; De Saja, J. A. Electronic tongue based on chemically modified electrodes and voltammetry for the detection of adulterations in wines. *Sens. Actuators, B* **2006**, *118*, 448−453.
(71) Wei, Z.; Wang, J.; Ye, L. Classification and prediction of rice wines with different marked ages by using a voltammetric electronic tongue. *Biosens. Bioelectron.* **2011**, *26*, 4767−4773.
(72) Esbensen, K.; Kirsanov, D.; Legin, A.; Rudnitskaya, A.; Mortensen, J.; Pedersen, J.; Vognsen, L.; Makarychev-Mikhailov, S.; Vlasov, Y. Fermentation monitoring using multisensor systems: feasibility study of the electronic tongue. *Anal. Bioanal. Chem.* **2004**, *378*, 391−395.
(73) Rudnitskaya, A.; Schmidtke, L. M.; Delgadillo, I.; Legin, A.; Scollaryd, G. Study of the influence of micro-oxygenation and oak chip maceration on wine composition using an electronic tongue and chemical analysis. *Anal. Chim. Acta* **2009**, *642*, 235−245.
(74) Tan, T.; Schmitt, V.; Isz, S. Electronic tongue: a new dimension in sensory. *Anal. Food Technol.* **2001**, *55*, 44−50.
(75) Dias, L. A.; Peres, A. M.; Vilas-Boas, M.; Rocha, M. A.; Estevinho, L.; Machado, A. A. S. C. An electronic tongue for honey classification. *Microchim. Acta* **2008**, *163*, 97−102.
(76) Riul, A.; de Sousa, H. C.; Malmegrim, R. R.; dos Santos, D. S.; Carvalho, A. C. P. L. F.; Fonseca, F. J.; Oliveira, O. N.; Mattoso, L. H. C. Wine classification by taste sensors made from ultra-thin films and using neural networks. *Sens. Actuators, B* **2004**, *98*, 77−82.
(77) Sun, H.; Mo, Z. H.; Choy, J. T. S.; Zhu, D. R.; Fung, Y. S. Piezoelectric quartz crystal sensor for sensing taste-causing compounds in food. *Sens. Actuators, B* **2008**, *131*, 148−158.
(78) Saevels, S.; Lammertyn, J.; Berna, A. Z.; Veraverbeke, E. A.; Di Natale, C.; Nicolaï, B. M. Electronic nose as a non-destructive tool to evaluate the optimal harvest date of apples. *Postharvest Biol. Technol.* **2003**, *30*, 3−14.
(79) Sinesio, F.; Di Natale, C.; Quaglia, G. B.; Bucarelli, F. M.; Moneta, E.; Macagnano, A.; Paolesse, R.; D'Amico, A. Use of electronic nose and trained sensory panel in the evaluation of tomato quality. *J. Sci. Food Agric.* **2000**, *80*, 63−71.
(80) Zhang, C.; Suslick, K. S. Colorimetric sensor arrays for soft drink analysis. *J. Agric. Food Chem.* **2007**, *55*, 237−242.

(81) Zhang, C.; Bailey, D. P.; Suslick, K. S. Colorimetric sensor arrays for the analysis of beers: a feasibility study. *J. Agric. Food Chem.* **2006**, *54*, 4925−4931.
(82) Gutiérrez, M.; Llobera, A.; Vila-Planas, J.; Capdevila, F.; Demming, S.; Büttgenbach, S.; Mínguez, S.; Jiménez-Jorquera, C. Hybrid electronic tongue based on optical and electrochemical microsensors for quality control of wine. *Analyst* **2010**, *135*, 1718−1725.
(83) Marilley, L.; Ampuero, S.; Zesiger, T.; Casey, M. G. Screening of aroma-producing lactic acid bacteria with an electronic nose. *Int. Dairy J.* **2004**, *14*, 849−856.
(84) Berna, A. Z.; Trowell, S.; Cynkar, W.; Cozzolino, D. Comparison of metal oxide-based electronic nose and mass spectrometry-based electronic nose for the prediction of red wine spoilage. *J. Agric. Food Chem.* **2008**, *56*, 3238−3244.
(85) Bleibaum, R. N.; Stone, H.; Tan, T.; Labreche, S.; Saint-Martin, E.; Isz, S. Comparison of sensory and consumer results with electronic nose and tongue sensors for apple juices. *Food Qual. Pref.* **2002**, *13*, 409−422.
(86) Marsili, R. T. Shelf-life prediction of processed milk by solid-phase microextraction, mass spectrometry, and multivariate analysis. *J. Agric. Food Chem.* **2000**, *48*, 3470−3475.
(87) Marsili, R. T. SPME−MS−MVA as an electronic nose for the study of off-flavors in milk. *J. Agric. Food Chem.* **1999**, *47*, 648−654.
(88) Holmberg, M.; Eriksson, M.; Krantz- Rülcker, C.; Artursson, T.; Winquist, F.; Lloyd-Spetz, A.; Lundström, I. 2nd Workshop of the Second Network on Artificial Olfactory Sensing (NOSE II). *Sens. Actuators, B* **2004**, *101*, 213−223.
(89) Apetrei, C.; Apetrei, I. M.; Villanueva, S.; de Saja, J. A.; Gutierrez-Rosales, F.; Rodriguez-Mendez, M. L. Combination of an e-nose, an e-tongue and an e-eye for the characterisation of olive oils with different degree of bitterness. *Anal. Chim. Acta* **2010**, *663*, 91−97.
(90) Ghasemi-Varnamkhasti, M.; Rodríguez-Méndez, M. L.; Mohtasebi, S. S.; Apetrei, C.; Lozano, J.; Ahmadi, H.; Razavi, S. H.; de Saja, J. A. Monitoring the aging of beers using a bioelectronic tongue. *Food Control* **2012**, *25*, 216−224.
(91) Litwiller, D. CMOs vs. CCD: maturing technologies, maturing markets. *Photonics Spectra* **2005**, *39*, 54−58.
(92) Qin, J. W. Hyperspectral imaging instruments. In *Hyperspectral Imaging for Food Quality Analysis and Control*; Sun, D.-W., Ed.; Academic Press/Elsevier: San Diego, CA, USA, 2010; pp 159−172.
(93) Silipo, R. Neural networks. In *Intelligent Data Analysis*; Bertold, M., Hand, D. J., Eds.; Springer: Berlin, Germany, 1999; pp 217−268.
(94) Hertz, J.; Krogh, A.; Palmer, R. G. *Wstęp do teorii obliczeń neuronowych*; WNT: Warszawa, Poland, 1993; pp 50−63.
(95) Staniec, I. http://oizet.p.lodz.pl/istan/pdf/rozIV.pdf (accessed May 15, 2013).
(96) Praczyk, T. Using a probabilistic neural network and the nearest neighbour method to identify ship radiostations. *Logistyka* **2011**, *3*, 2235−2242.
(97) Mazerski, J. Chemometria. Podstawy chemometrii, http://student.agh.edu.pl/~fraugi/Chemometria/podstawy_chemometrii/ (accessed May 16, 2013).
(98) Górka, J.; Chmurska, M. The use of a selected taxonomic method in the classification of districts of the Wielkopolskie province on the basis of selected tourism and recreation features, http://www.wbc.poznan.pl/Content/9676/XSL+Output.html (accessed May 16, 2013).
(99) Gatnar, E.; Walesiak, M. In *Metody statystycznej analizy wielowymiarowej w badaniach marketingowych*; Wydawnictwo Akademii Ekonomicznej: Wrocław, Poland, 2004; pp 195 − 215.
(100) Grabiński, T. In *Metody taksonometrii*; Wyd AE: Kraków, Poland, 1988; pp 10−15.
(101) http://seoul-humanlab.com/web/bbs/board.php?bo_table=83&wr_id=31 (accessed Oct 18, 2013).
(102) Daszykowski, M.; Walczak, B. Analiza czynników głównych i inne metody eksploracji danych, http://chemometria.us.edu.pl/AnalizaCzynnikowGlownych.pdf (accessed May 17, 2013).
(103) Goszczyński, J. Klasyfikacja tekstur za pomocą SVM − Maszyny wektorów wspierających. *Inżynieria Rolnicza* **2006**, *13*, 119−125.
(104) Stanimirova, I.; Daszykowski, M.; Walczak, B. Metody uczenia z nadzorem − kalibracja, dyskryminacja i klasyfikacja, http://chemometria.us.edu.pl/MetodyUczeniaZNadzorem.pdf (accessed May 17, 2013).
(105) Gamst, G.; Meyers, L. S.; Guariono, A. J. ANOVA and research design. In *Analysis of Variance Designs: A Conceptual and Computational Approach with SPSS and SAS*; Cambridge University Press: Cambrige, UK, 2008; pp 3−8.
(106) Jóźwiak, J.; Podgórski, J. Analiza wariancji. In *Statystyka od Podstaw*; PWE: Warszawa, Poland, 2006; pp 299−326.
(107) Koronacki, J.; Ćwik, J. Liniowe metody klasyfikacji. In *Statystyczne systemy uczące się*, 2nd ed.; Exit: Warsaw, Poland, 2008; pp 4−12
(108) Labus, K.; Labus, M. Zastosowanie analizy danych złożonych (CDA) w geologii. *Gospodarka Surowcami Mineralnymi* **2006**, *22*, 39−52.
(109) ter Braak, C. J. E.; Verdonschot, P. E. M. Canonical correspondence analysis and related multivariate methods in aquatic ecology. *Aquatic Sci.* **1995**, *57*, 255−289.
(110) Gunasekaran, S.; Ding, K. Using computer vision for food quality evaluation. *Food Technol.* **1994**, *6*, 151−154.
(111) Mendoza, F.; Dejmek, P.; Aguilera, J. M. Calibrated color measurements of agricultural foods using image analysis. *Postharvest Biol. Technol.* **2006**, *41*, 285−295.
(112) Fairchild, M. D.; Berns, R. S. Image color-appearance specification through extension of CIELAB. *Color Res. Appl.* **1993**, *18*, 178−190.
(113) Cheng, H. D.; Jiang, X. H.; Sun, Y.; Wang, J. Color image segmentation: advances and prospects. *Pattern Recognit.* **2001**, *34*, 2259−2281.
(114) Harrison, C. J.; Miller, R. L.; Bernstein, D. I. Reduction of recurrent HSV disease using imiquimod alone or combined with a glycoprotein vaccine. *Vaccine* **2001**, *19*, 1820−1826.
(115) Wang, F.; Manb, L.; Wang, B.; Xiao, Y.; Pan, W.; Lu, X. Fuzzy-based algorithm for color recognition of license plates. *Pattern Recognit. Lett.* **2008**, *29*, 1007−1020.
(116) Haralick, R. M.; Shanmugam, K.; Its'Hak, D. Textural features for image classification. *IEEE Trans. Syst., Man Cybernetics* **1973**, *3*, 610−621.
(117) Shirai, Y. Introduction. In *Three Dimensional Computer Vision*; Springer Verlag: Berlin, Germany, 1987; pp 1 −5.
(118) Haralick, R. M.; Shapiro, L. G. Image segmentation techniques. *Comput. Vis. Graph. Image Process.* **1985**, *29*, 100−132.
(119) Ying, Y.; Jing, H.; Tao, Y.; Zhang, N. Detecting stem and shape of pears using fourier transformation and an artificial neural network. *Trans. ASAE* **2003**, *46*, 157−162.
(120) Vlasov, Y.; Legin, A.; Rudnitskaya, A. Electronic tongues and their analytical application. *Anal. Bioanal. Chem.* **2002**, *373*, 136−146.
(121) Wang, H.-H.; Sun, D.-W. Melting characteristics of cheese: analysis of effects of cooking conditions using computer vision techniques. *J. Food Eng.* **2002**, *52*, 279−284.
(122) Benedetti, S.; Sinelli, N.; Buratti, S.; Riva, M. Shelf life of Crescenza cheese as measured by electronic nose. *J. Dairy Sci.* **2005**, *88*, 3044−3051.
(123) Magan, N.; Pavlou, A.; Chrysanthakis, I. Milk-sense: a volatile sensing system recognises spoilage bacteria and yeasts in milk. *Sens. Actuators, B* **2001**, *72*, 28−34.
(124) Capone, S.; Epifani, M.; Quaranta, F.; Siciliano, P.; Taurino, A.; Vasanelli, L. Monitoring of rancidity of milk by means of an electronic nose and a dynamic PCA analysis. *Sens. Actuators, B* **2001**, *78*, 174−179.
(125) Capone, S.; Siciliano, P.; Quaranta, F.; Rella, R.; Epifani, M.; Vasanelli, L. Analysis of vapours and foods by means of an electronic nose based on a sol-gel metal oxide sensors array. *Sens. Actuators, B* **2000**, *69*, 230−235.

(126) Wei, Z.; Wang, J.; Zhang, X. Monitoring of quality and storage time of unsealed pasteurized milk by voltammetric electronic tongue. *Electrochim. Acta* **2013**, *88*, 231−239.
(127) Brudzewski, K.; Osowski, S.; Markiewicz, T. Classification of milk by means of an electronic nose and SVM neural network. *Sens. Actuators, B* **2004**, *98*, 291−298.
(128) Wang, B.; Xu, S.; Sun, D.-W. Application of the electronic nose to the identification of different milk flavorings. *Food Res. Int.* **2010**, *43*, 255−262.
(129) Wei, Z.; Wang, J.; Jin, W. Evaluation of varieties of set yogurts and their physical properties using a voltammetric electronic tongue based on various potential waveforms. *Sens. Actuators, B* **2013**, *177*, 684−694.
(130) Winquist, F.; Wide, P.; Lundström, I. An electronic tongue based on voltammetry. *Anal. Chim. Acta* **1997**, *357*, 21−31.
(131) Paixão, T. R. L. C.; Bertotti, M. Fabrication of disposable voltammetric electronic tongues by using Prussian Blue films electrodeposited onto CD-R gold surfaces and recognition of milk adulteration. *Sens. Actuators, B* **2009**, *137*, 266−273.
(132) Pillonel, L.; Ampuero, S.; Tabacchi, R.; Bosset, J. O. Analytical methods for the determination of the geographic origin of Emmental cheese: volatile compounds by GC/MS-FID and electronic nose. *Eur. Food Res. Technol.* **2003**, *216*, 179−183.
(133) Gursoy, O.; Somervuo, P.; Alatossava, T. Preliminary study of ion mobility based electronic nose MGD-1 for discrimination of hard cheeses. *J. Food Eng.* **2009**, *92*, 202−207.
(134) O'Riordan, P. J.; Delahunty, C. M. Characterisation of commercial Cheddar cheese flavour. 1: Traditional and electronic nose approach to quality assessment and market classification. *Int. Dairy J.* **2003**, *13*, 355−370.
(135) Jou, K. D.; Harper, W. J. Pattern recognition of Swiss cheese aroma compounds by SPME/GC and an electronic nose. *Milchwissenschaft* **1998**, *53*, 259−263.
(136) Trihaas, J.; Vognsen, L.; Nielsen, P. V. Electronic nose: new tool in modeling the ripening of danish blue cheese. *Int. Dairy J.* **2005**, *15*, 679−691.
(137) Contarini, G.; Povolo, M.; Toppino, P. M.; Radovic, B.; Lipp, M.; Anklam, E. Comparison of three different techniques for the discrimination of cheese: application to the ewe's cheese. *Milchwissenschaft* **2001**, *56*, 136−140.
(138) Zannoni, M. Preliminary results of employ of an artificial nose for the evaluation of cheese. *Sci. Tecn. Lattiero−Casearia* **1995**, *46*, 277−289.
(139) Drake, M. A.; Gerard, P. D.; Kleinhenz, J. P.; Harper, W. J. Application of an electronic nose to correlate with descriptive sensory analysis of aged Cheddar cheese. *LWT−Food Sci. Technol.* **2003**, *36*, 13−20.
(140) Li, J.; Tan, J.; Martz, F. A. Predicting beef tenderness from image texture features. *ASAE Annual International Meeting Technical Papers*, St. Joseph, MI, USA, 1997; Paper 973124
(141) Lu, J.; Tan, J.; Shatadal, P.; Gerrard, D. E. Evaluation of pork color by using computer vision. *Meat Sci.* **2000**, *56*, 57−60.
(142) Larraín, R. E.; Schaefer, D. M.; Reed, J. D. Use of digital images to estimate CIE color coordinates of beef. *Food Res. Int.* **2008**, *41*, 380−385.
(143) Quevedo, R. A.; Aguilera, J. M.; Pedreschi, F. Color of salmon fillets by computer vision and sensory panel. *Food Bioprocess Technol.* **2010**, *3*, 637−643.
(144) Valous, N. A.; Mendoza, F.; Sun, D.-W.; Allen, P. Colour calibration of a laboratory computer vision system for quality evaluation of pre-sliced hams. *Meat Sci.* **2009**, *81*, 132−141.
(145) Luzuriaga, D. A.; Balaban, M.; Yeralan, S. Analysis of visual quality attributes of white shrimp by machine vision. *J. Food Sci.* **1997**, *62*, 113−130.
(146) Park, B.; Chen, Y. R.; Nguyen, M.; Hwang, H. Characterising multispectral images of tumorous, bruised, skin-torn, and wholesome poultry carcasses. *Trans. ASAE* **1996**, *39*, 1933−1941.
(147) O'Sullivan, M. G.; Byrne, D. V.; Martens, H.; Gidskehaug, L. H.; Andersen, H. J.; Martens, M. Evaluation of pork colour: prediction of visual sensory quality of meat from instrumental and computer vision methods of colour analysis. *Meat Sci.* **2003**, *65*, 909−918.
(148) Oliveira, A. C. M.; Balaban, M. O. Comparison of a colorimeter with a machine vision system in measuring color of Gulf of Mexico sturgeon fillets. *Appl. Eng. Agric.* **2006**, *22*, 583−587.
(149) Camposa, I.; Masota, R.; Alcañiza, M.; Gila, L.; Soto, J.; Vivancosa, J. L.; García-Breijo, E.; Labradora, R. H.; Barate, J. M.; Martínez-Mañez, R. Accurate concentration determination of anions nitrate, nitrite and chloride in minced meat using a voltammetric electronic tongue. *Sens. Actuators, B* **2010**, *149*, 71−78.
(150) García, M.; Aleixandre, M.; Horrillo, M. C. Electronic nose for the identification of spoiled Iberian hams. *Spanish Conference on Electron Devices*, Tarragona, Spain; IEEE: New York, 2005; pp 537−540.
(151) El Barbri, N.; Llobet, E.; El Bari, N.; Correig, X.; Bouchikhi, B. Electronic nose based on metal oxide semiconductor sensors as an alternative technique for the spoilage classification of red meat. *Sensors* **2008**, *8*, 142−156.
(152) McElyea, K. S.; Pohlman, F. W.; Meullenet, J. F.; Suwansri, S. Evaluation of the electronic nose for rapid determination of meat freshness. *AAES Res. Ser.* **2003**, *509*, 32−35.
(153) Haugen, J. E.; Lundby, F.; Wold, J. P.; Veberg, A. Detection of rancidity in freeze stored turkey meat using a commercial gas-sensor array system. *Sens. Actuators, B* **2006**, *116*, 78−84.
(154) Winquist, F.; Hörnsten, E. G.; Sundgren, H.; Lundström, I. Performance of an electronic nose for quality estimation of ground meat. *Meat Sci. Technol.* **1993**, *4*, 1493−1500.
(155) Di Natale, C.; Macagnano, A.; Davide, F.; D'Amico, A.; Paolesse, R.; Boschi, T.; Faccio, M.; Ferri, G. An electronic nose for food analysis. *Sens. Actuators, B* **1997**, *44*, 521−526.
(156) Hong, X.; Wang, J.; Hai, Z. Discrimination and prediction of multiple beef freshness indexes based on electronic nose. *Sens. Actuators, B* **2012**, *161*, 381−389.
(157) Braggins, T. J.; Frost, D. A. The effect of extended chilled storage in CO_2 atmosphere on the odour and flavour of sheepmeat as assessed by sensory panel and an electronic nose. *Proceedings of the 43rd ICoMST*; s.n.: Auckland, New Zealand, 1997; pp 198−199.
(158) Vestergaarda, J. S.; Martens, M.; Turkkia, P. Application of an electronic nose system for prediction of sensory quality changes of a meat product (pizza topping) during storage. *LWT−Food Sci. Technol.* **2007**, *40*, 1095−1101.
(159) Neely, K.; Taylor, C.; Prosser, O.; Hamlyn, P. F. Assessment of cooked alpaca and llama meats from the statistical analysis of data collected using an 'electronic nose'. *Meat Sci.* **2001**, *58*, 53−58.
(160) Gonzalez-Martin, I.; Perez-Pavon, J. L.; Gonzalez-Perez, C.; Hernandez-Mendez, J.; Alvarez-Garcia, N. Differentiation of products derived from Iberian breed swine by electronic olfactometry (electronic nose). *Anal. Chim. Acta* **2000**, *424*, 279−287.
(161) García, M.; Aleixandre, M.; Gutiérrez, J.; Horrillo, M. C. Electronic nose for ham discrimination. *Sens. Actuators, B* **2006**, *114*, 418−422.
(162) Vernat-Rossi, V.; Garcia, C.; Talon, R.; Denoyer, C.; Berdagué, J.-L. Rapid discrimination of meat products and bacterial strains using semiconductor gas sensors. *Sens. Actuators, B* **1996**, *37*, 43−48.
(163) Spanier, A. M.; Flores, M.; Toldra, F. Flavour differences due to processing in dry-cured and other ham products using conducting polymers (electronic nose). In *Flavour and Chemistry of Ethnic Foods*; Kluwer/Plenum: New York, 1997; pp 169−183.
(164) El Barbri, N.; Mirhisse, J.; Ionescu, R.; El Bari, N.; Correig, X.; Bouchikhi, B.; Llobet, E. An electronic nose system based on a micro-machined gas sensor array to assess the freshness of sardines. *Sens. Actuators, B* **2009**, *141*, 538−543.
(165) El Barbri, N.; Llobet, E.; El Bari, N.; Correig, X.; Bouchikhi, B. Application of a portable electronic nose system to assess the freshness of Moroccan sardines. *Mater. Sci. Eng., C* **2008**, *28*, 666−670.
(166) El Barbri, N.; Amari, A.; Vinaixa, M.; Bouchikhi, B.; Correig, X.; Llobet, E. Building of a metal oxide gas sensor-based electronic nose to assess the freshness of sardines under cold storage. *Sens. Actuators, B* **2007**, *128*, 235−244.

(167) Laothawornkitkul, J.; Moore, J. P.; Taylor, J. E.; Possell, M.; Gibson, T. D.; Hewitt, C. N.; Paul, N. D. Discrimination of plant volatile signatures by an electronic nose: a potential technology for plant pest and disease monitoring. *Environ. Sci. Technol.* **2008**, *42*, 8433−8439.
(168) Mohebbi, M.; Akbarzadeh-T, M.-R.; Shahidi, F.; Moussavi, M.; Ghoddusi, H. Computer vision systems (CVS) for moisture content estimation in dehydrated shrimp. *Comput. Electron. Agric.* **2009**, *69*, 128−134.
(169) Di Natale, C.; Olafsdottir, G.; Einarsson, S.; Martinelli, E.; Paolesse, R.; D'Amico, A. Comparison and integration of different electronic noses for freshness evaluation of cold-fish fillets. *Sens. Actuators, B* **2001**, *77*, 572−578.
(170) Korel, F.; Luzuriaga, D. A.; Balaban, M. Ö. Objective quality assessment of raw tilapia (*Oreochromis niloticus*) fillets using electronic nose and machine vision. *J. Food Sci.* **2001**, *66*, 1018−1024.
(171) O'Connell, M.; Valdora, G.; Peltzer, G.; Negri, R. M. A practical approach for fish freshness determinations using a portable electronic nose. *Sens. Actuators, B* **2001**, *80*, 149−154.
(172) Hu, X.; Mallikarjunan, P. K.; Vaughan, D. Development of non-destructive methods to evaluate oyster quality by electronic nose technology. *Sens. Instrum. Food Qual.* **2008**, *2*, 51−57.
(173) Tokusoglu, O.; Balaban, M. Correlation of odor and color profiles of oysters (*Crassostrea virginica*) with electronic nose and color machine vision. *J. Shellfish Res.* **2004**, *23*, 143−148.
(174) Gil, L.; Barat, J. M.; Escriche, I.; Garcia-Breijo, E.; Martínez-Mánez, R.; Soto, J. An electronic tongue for fish freshness analysis using a thick-film array of electrodes. *Microchim. Acta* **2008**, *163*, 121−129.
(175) Gil, L.; Barat, J. M.; Garcia-Breijo, E.; Ibañez, J.; Martínez-Máñez, R.; Soto, J.; Llobet, E.; Brezemes, J.; Aristoy, J. C.; Toldrá, F. Fish freshness analysis using metallic potentiometric electrodes. *Sens. Actuators, B* **2008**, *131*, 362−370.
(176) Rodríguez-Méndez, M. L.; Gay, M.; Apetrei, C.; De Saja, J. A. Biogenic amines and fish freshness assessment using a multisensor system based on voltammetric electrodes. Comparison between CPE and screen-printed electrodes. *Electrochim. Acta* **2009**, *54*, 7033−7041.
(177) Legin, A.; Rudnitskaya, A.; Seleznev, B.; Vlasov, Y. Recognition of liquid and flesh food using an 'electronic tongue'. *Int. J. Food Sci. Technol.* **2002**, *37*, 375−385.
(178) Gobbi, E.; Falasconi, M.; Concina, I.; Mantero, G.; Bianchi, F.; Mattarozzi, M.; Musci, M.; Sberveglieri, G. Electronic nose and *Alicyclobacillus* spoilage of fruit juices: an emerging diagnostic tool. *Food Control* **2010**, *21*, 1374−1382.
(179) Legin, A.; Rudnitskaya, A.; Seleznev, B.; Sparfel, G.; Doré, C. Electronic tongue distinguishes onions and shallots. *ISHS Acta Horticulturae 634: XXVI International Horticultural Congress: IV International Symposium on Taxonomy of Cultivated Plants*, Toronto, Canada; ISHS: Leuven, The Netherlands, 2004.
(180) Beullens, K.; Mészarós, P.; Vermeir, S.; Kirsanov, D.; Legin, A.; Buysens, S.; Cap, N.; Nicolai, B. M.; Larnmertyn, J. Analysis of tomato taste using two types of electronic tongues. *Sens. Actuators, B* **2008**, *131*, 10−17.
(181) Beullens, K.; Kirsanov, D.; Irudayaraj, J.; Rudnitskaya, A.; Legin, A.; Nicolaï, B. M.; Lammertyn, J. The electronic tongue and ATR−FTIR for rapid detection of sugars and acids in tomatoes. *Sens. Actuators, B* **2006**, *116*, 107−115.
(182) Rudnitskaya, A.; Kirsanov, D.; Legin, A.; Beullens, K.; Lammertyn, J.; Nicolaï, B. M.; Irudayaraj, J. Analysis of apples varieties − comparison of electronic tongue with different analytical techniques. *Sens. Actuators, B* **2006**, *116*, 23−28.
(183) Kantor, D. B.; Hitka, G.; Fekete, A.; Balla, C. Electronic tongue for sensing taste changes with apricots during storage. *Sens. Actuators, B* **2008**, *131*, 43−47.
(184) Kondo, N.; Ahmad, U.; Monta, M.; Murase, H. Machine vision based quality evaluation of Iyokan orange fruit using neural networks. *Comput. Electron. Agric.* **2000**, *29*, 135−147.
(185) Okamura, N. K.; Dewiche, M. J.; Thompson, J. F. Raisin grading by machine vision. *Trans. ASAE* **1993**, *36*, 485−491.
(186) Panigrahi, S.; Misra, M. K.; Willson, S. Evaluations of fractal geometry and invariant moments for shape classification of corn germplasm. *Comput. Electron. Agric.* **1998**, *20* (1), 1−20.
(187) Brandon, J. R.; Howarth, M. S.; Searcy, S. W.; Kehtarnavaz, N. *A Neural Network for Carrot Tip Classification*; ASAE: St. Joseph, MI, USA, 1990; p 13.
(188) Ruiz, L. A.; Moltó, E.; Juste, F.; Plá, F.; Valiente, R. Location and characterization of the stem−calyx area on oranges by computer vision. *J . Agric. Eng. Res.* **1996**, *64*, 165−172.
(189) Qui, W.; Shearer, S. A. Maturity assessment of broccoli using the discrete Fourier transform. *Trans. ASAE* **1992**, *35*, 2057−2062.
(190) Leemans, V.; Magein, H.; Destain, M.-F. Defects segmentation on 'Golden Delicious' apples by using colour machine vision. *Comput. Electron. Agric.* **1998**, *20*, 117−130.
(191) Vızhanyo, T.; Felfoldi, J. Enhancing colour differences in images of diseased mushrooms. *Comput. Electron. Agric.* **2000**, *26*, 187−198.
(192) Mendoza, F.; Aguilera, J. M. Application of image analysis for classification of ripening bananas. *J. Food Sci.* **2004**, *69*, 473 −477.
(193) Tao, Y.; Heinemann, P. H.; Varghese, Z.; Morrow, C. T.; Sommer, H. J. Machine vision for colour inspection of potatoes and apples. *Trans. ASAE* **1995**, *38*, 1555−1561.
(194) Santonico, M.; Bellincontro, A.; De Santis, D.; Di Natale, C.; Mencarelli, F. Electronic nose to study postharvest dehydration of wine grapes. *Food Chem.* **2010**, *121*, 789−796.
(195) Lopez de Lerma, N.; Bellincontro, A.; Mencarelli, F.; Moreno, J.; Peinado, R. A. Use of electronic nose, validated by GC−MS, to establish the optimum off-vine dehydration time of wine grapes. *Food Chem.* **2012**, *130*, 447−452.
(196) Zhang, H.; Chang, M.; Wang, J.; Ye, S. Evaluation of peach quality indices using an electronic nose by MLR, QPST and BP network. *Sens. Actuators, B* **2008**, *134*, 332−338.
(197) Guohua, H.; Yuling, W.; Dandan, Y.; Wenwen, D.; Linshan, Z.; Lvye, W. Study of peach freshness predictive method based on electronic nose. *Food Control* **2012**, *28*, 25−32.
(198) Di Natale, C.; Filippini, D.; Pennazza, G.; Santonico, M.; Paolesse, R.; Bellincontro, A.; Mencarelli, F.; D'Amico, A.; Lundström, I. Sorting of apricots with computer screen photoassisted spectral reflectance analysis and electronic nose. *Sens. Actuators, B* **2006**, *119*, 70−77.
(199) Brezmes, J.; Llobet, E.; Vilanova, X.; Orts, J.; Saiz, G.; Correig, X. Correlation between electronic nose signals and fruit quality indicators on shelf-life measurements with Pink Lady apples. *Sens. Actuators, B* **2001**, *80*, 41−50.
(200) Saevels, S.; Lammertyn, J.; Berna, A. Z.; Veraverbeke, E. A.; Di Natale, C.; Nicolaï, B. M. An electronic nose and a mass spectrometric based electronic nose for assessing apple quality during shelf life. *Postharvest Biol. Technol.* **2004**, *31*, 9−19.
(201) Herrmann, U.; Jonischkeit, T.; Bargon, J.; Hahn, U.; Li, Q.-Y.; Schalley, C. A.; Vogel, E.; Vögtle, F. Monitoring apple flavor by use of quartz microbalances. *Anal. Bioanal. Chem.* **2002**, *372*, 611−614.
(202) Brezmes, J.; Llobet, E.; Vilanova, X.; Saiz, G.; Correig, X. Fruit ripeness monitoring using an electronic nose. *Sens. Actuators, B* **2000**, *69*, 223−229.
(203) Berna, A. Z.; Lammertyn, J.; Saevels, S.; Di Natale, C.; Nicolaï, B. M. Electronic nose systems to study shelf life and cultivar effect on tomato aroma profile. *Sens. Actuators, B* **2004**, *97*, 324.
(204) Gómez, A. H.; Hu, G.; Wang, J.; Pereira, A. G. Evaluation of tomato maturity by electronic nose. *Comput. Electron. Agric.* **2006**, *54*, 44−52.
(205) Gómez, A. H.; Wang, J.; Hu, G.; Pereira, A. G. Monitoring storage shelf-life of tomato using electronic nose technique. *J. Food Eng.* **2008**, *85*, 625−631.
(206) Benedetti, S.; Buratti, S.; Spinardi, A.; Mannino, S.; Mignani, I. Electronic nose as a non-destructive tool to characterise peach cultivars and to monitor their ripening stage during shelf-life. *Postharvest Biol. Technol.* **2008**, *47*, 181−188.

(207) Gomez, A. H.; Wang, J.; Hu, G.; Pereira, A. G. Discrimination of storage shelf-life for mandarin by electronic nose technique. *LWT—Food Sci. Technol.* **2007**, *40*, 681−689.
(208) Solis-Solis, H. M.; Calderon-Santoyo, M.; Gutierrez-Martinez, P.; Schorr- Galindo, S.; Ragazzo-Sanchez, J. A. Discrimination of eight varieties of apricot (*Prunus armeniaca*) by electronic nose, LLE and SPME using GC−MS and multivariate analysis. *Sens. Actuators, B* **2007**, *125*, 415−421.
(209) Lebrun, M.; Plotto, A.; Goodner, K.; Ducamp, M.-N.; Baldwin, E. Discrimination of mango fruit maturity by volatiles using the electronic nose and gas chromatography. *Postharvest Biol. Technol.* **2008**, *48*, 122−131.
(210) Barié, N.; Bücking, M.; Rapp, M. A novel electronic noise based on miniaturized SAW sensor arrays coupled with SPME enhanced headspace-analysis and its use for rapid determination of volatile organic compounds in food quality monitoring. *Sens. Actuators, B* **2006**, *114*, 482−488.
(211) Xiaobo, Z.; Jiewen, Z. Comparative analyses of apple aroma by a tin-oxide gas sensor array device and GC/MS. *Food Chem.* **2008**, *107*, 120−128.
(212) Di Natale, C.; Macagnano, A.; Martinelli, E.; Paolesse, R.; Proietti, E.; D'Amico, A. The evaluation of quality of post-harvest oranges and apples by means of an electronic nose. *Sens. Actuators, B* **2001**, *78*, 26−31.
(213) Di Natale, C.; Macagnano, A.; Martinelli, E.; Proietti, E.; Paolesse, R.; Castellari, L.; Campani, S.; D'Amico, A. Electronic nose based investigation of the sensorial properties of peaches and nectarines. *Sens. Actuators, B* **2001**, *77*, 561−566.
(214) Zhang, H.; Wang, J.; Ye, S. Prediction of soluble solids content, firmness and pH of pear by signals of electronic nose sensors. *Anal. Chim. Acta* **2008**, *606*, 112−118.
(215) Zhang, H.; Wang, J.; Ye, S. Predictions of acidity, soluble solids and firmness of pear using electronic nose technique. *J. Food Eng.* **2008**, *86*, 370−378.
(216) Abbey, L.; Joyce, D. C.; Aked, J.; Smith, B.; Marshall, C. Electronic nose evaluation of onion headspace volatiles and bulb quality as affected by nitrogen, sulphur and soil type. *Ann. Appl. Biol.* **2004**, *145*, 41−50.
(217) Cerrato Oliveros, M. C.; Pérez Pavón, J. L.; García Pinto, C.; Fernández Laespada, M. E.; Moreno Cordero, B.; Forina, M. Electronic nose based on metal oxide semiconductor sensors as a fast alternative for the detection of adulteration of virgin olive oils. *Anal. Chim. Acta* **2002**, *459*, 219−228.
(218) Oliveros, C.; Boggia, R.; Casale, M.; Armanino, C.; Forina, M. Optimisation of a new headspace mass spectrometry instrument. *J. Chromatogr., A* **2005**, *1076*, 7−15.
(219) Cosio, M. S.; Ballabio, D.; Benedetti, S.; Gigliotti, C. Geographical origin and authentication of extra virgin olive oils by an electronic nose in combination with artificial neural networks. *Anal. Chim. Acta* **2006**, *567*, 202−210.
(220) Gardner, J. W.; Shurmer, H. V.; Tan, T. T. Application of an electronic nose to the discrimination of coffees. *Sens. Actuators, B* **1992**, *6*, 71−75.
(221) Pioggia, G.; Ferro, M.; Di Francesco, F. Towards a real-time transduction and classification of chemoresistive sensor array signals. *IEEE Sens. J.* **2007**, *7*, 227−241.
(222) López-Feria, S.; Cárdenas, S.; García-Mesa, J. A.; Valcárcel, M. Simple and rapid instrumental characterization of sensory attributes of virgin olive oil based on the direct coupling headspace-mass spectrometry. *J. Chromatogr., A* **2008**, *1188*, 308−313.
(223) Lacoste, F.; Bosque, F.; Raoux, R. Is it possible to use an "electronic nose" for the detection of sensorial defects in virgin olive oil? *Ol., Corps Gras, Lipides* **2001**, *8*, 78−81.
(224) Aparicio, R.; Rocha, S. M.; Delgadillo, I.; Morales, M. T. Detection of rancid defect in virgin olive oil by the electronic nose. *J. Agric. Food Chem.* **2000**, *48*, 853−860.
(225) Gonzalez-Martin, I.; Perez-Pavon, J.; Corder, B. M.; Pinto, C. G. Classification of vegetable oils by linear discriminant analysis of electronic nose data. *Anal. Chim. Acta* **1999**, *384*, 83−94.
(226) Gan, H. L.; Che Man, Y. B.; Tan, C. P.; NorAini, I.; Nazimah, S. A. H. Characterisation of vegetable oils by surface acoustic wave sensing electronic nose. *Food Chem.* **2005**, *89*, 507−518.
(227) Oshita, S.; Arase, H.; Seo, Y.; Kawagoe, Y.; Haruta, K.; Amitani, H.; Kawana, S.; Makino, Y. Odor recognition of soy sauce by semiconducting polymer sensors. *Trans. ASABE* **2006**, *49*, 1839−1844.
(228) Zhang, Q.; Zhang, S.; Xie, C.; Fan, C.; Bai, Z. Sensory analysis of Chinese vinegars using an electronic nose. *Sens. Actuators, B* **2008**, *128*, 586−593.
(229) Brezmes, J.; Ferreras, B.; Llobet, E.; Vilanova, X.; Correig, X. Neural network based electronic nose for the classification of aromatic species. *Anal. Chim. Acta* **1997**, *348*, 503−509.
(230) Cocchi, M.; Durante, C.; Marchetti, A.; Armanino, C.; Casale, M. Characterization and discrimination of different aged 'Aceto Balsamico Tradizionale di Modena' products by head space mass spectrometry and chemometrics. *Anal. Chim. Acta* **2007**, *589*, 96−104.
(231) Hai, Z.; Wang, J. Electronic nose and data analysis for detection of maize oil adulteration in sesame oil. *Sens. Actuators, B* **2006**, *119*, 449−455.
(232) Zayas, I. Y.; Martin, C. R.; Steele, J. L.; Katsevich, A. Wheat classification using image analysis and crush-force parameters. *Trans. ASAE* **1996**, *39*, 2199−2204.
(233) Borjesson, T. Detection of off-odours in grains using an electronic nose. *Olfaction and Electronic Nose, 3rd International Symposium*; s.n.: Toulouse, France, 1996.
(234) Börjesson, T.; Eklöv, T.; Jonsson, A.; Sundgren, H.; Schnürer, J. Electronic nose for odor classification of grains. *Cereal Chem.* **1996**, *73*, 457−461.
(235) Zheng, X.; Lan, Y.; Zhu, J.; Westbrook, J.; Hoffmann, W. C.; Lacey, R. E. Rapid identification of rice samples using an electronic nose. *J. Bionic Eng.* **2009**, *6*, 290−297.
(236) Needham, R.; Williams, J.; Beales, N.; Voysey, P.; Magan, N. Early detection and differentiation of spoilage of bakery products. *Sens. Actuators, B* **2005**, *106*, 20−23.
(237) Wan, Y. N.; Lin, C. M.; Chiou, J. F. Adaptive classification method for an automatic grain quality inspection system using machine vision and neural network. *Conference Paper 2000 ASAE Annual International Meeting*, Milwaukee, WI, USA, 2000; pp 1−19.
(238) Ni, B.; Paulsen, M. R.; Liao, K.; Reid, J. F. Design of an automated corn kernel inspection system for machine vision. *Trans. ASAE* **1997**, *40*, 491−497.
(239) Liu, V. J.; Paulsen, M. R. Corn whiteness measurement and classification using machine. *Trans. ASABE* **2000**, *43*, 757−763.
(240) Bartlett, P. N.; Blair, N.; Gardner, J. W. Electronic nose. Principles, applications and outlook. *ASIC*, 15th colloque, Montpellier, France; ASIC: Paris, France, 1993; pp 478−486.
(241) Fukunaga, T.; Mori, S.; Nakabayashi, Y.; Kanda, M.; Ehara, K. Application of flavor sensor to coffee. *ASIC, 16th International Scientific Collopuium on Coffee*, Kyoto, Japan; ASIC: Paris, France, 1995; pp 478−486
(242) Legin, A.; Rudnitskaya, A.; Vlasov, Y.; Di Natale, C.; Davide, F.; D'Amico, A. Tasting of beverages using an electronic tongue. *Sens. Actuators, B* **1997**, *44*, 291−296.
(243) Falasconi, M.; Pardo, M.; Sberveglieri, G.; Riccò, I.; Bresciani, A. The novel EOS835 electronic nose and data analysis for evaluating coffee ripening. *Sens. Actuators, B* **2005**, *110*, 73−80.
(244) Yu, H.; Wang, J. Discrimination of LongJing green-tea grade by electronic nose. *Sens. Actuators, B* **2007**, *122*, 134−140.
(245) Yu, H.; Wang, J.; Zhang, H.; Yu, Y.; Yao, C. Identification of green tea grade using different feature of response signal from E-nose sensors. *Sens. Actuators, B* **2008**, *128*, 455−461.
(246) Dutta, R.; Kashwan, K. R.; Bhuyan, M.; Hines, E. L.; Gardner, J. W. Electronic nose based tea quality standardization. *Neural Networks* **2003**, *16*, 847−853.
(247) Chen, Q.; Zhao, J.; Vittayapadung, S. Identification of green tea grade level using electronic tongue and pattern recognition. *Food Res. Int.* **2008**, *41*, 500−504.

(248) Tudu, B.; Jana, A.; Metla, A.; Ghosh, D.; Bhattacharyya, N.; Bandyopadhyay, R. Electronic nose for black tea quality evaluation by an incremental RBF network. *Sens. Actuators, B* **2009**, *138*, 90−95.
(249) Palit, M.; Tudu, B.; Bhattacharyya, N.; Dutta, A.; Dutta, P. K.; Jana, A.; Bandyopadhyay, R.; Chatterjee, A. Comparison of multivariate preprocessing techniques as applied to electronic tongue based pattern classification for black tea. *Anal. Chim. Acta* **2010**, *675*, 8−15.
(250) Palit, M.; Tudu, B.; Dutta, P. K.; Dutta, A.; Jana, A.; Roy, J. K.; Bhattacharyya, N.; Bandyopadhyay, R.; Chatterjee, A. Classification of black tea taste and correlation with tea taster's mark using voltammetric electronic tongue. *IEEE Trans. Instrum. Meas.* **2010**, *59*, 2230−2239.
(251) Roy, R. B.; Tudu, B.; Shaw, L.; Jana, A.; Bhattacharyya, N.; Bandyopadhyay, R. Instrumental testing of tea by combining the responses of electronic nose and tongue. *J. Food Eng.* **2012**, *110*, 356−363.
(252) Kovács, Z.; Dalmadi, I.; Lukács, L.; Sipos, L.; Szántai-Kőhegyi, K.; Kókai, Z.; Fekete, A. Geographical origin identification of pure Sri Lanka tea infusions with electronic nose, electronic tongue and sensory profile analysis. *J. Chemom.* **2009**, *24*, 121−130.
(253) Yanga, Z.; Dong, F.; Shimizu, K.; Kinoshita, T.; Kanamori, M.; Morita, A.; Watanabe, N. Identification of coumarin-enriched Japanese green teas and their particular flavor using electronic nose. *J. Food Eng.* **2009**, *92*, 312−316.
(254) Ghosh, A.; Tamuly, P.; Bhattacharyya, N.; Tudu, B.; Gogoi, N.; Bandyopadhyay, R. Estimation of theaflavin content in black tea using electronic tongue. *J. Food Eng.* **2012**, *110*, 71−79.
(255) Bhattacharya, N.; Tudu, B.; Jana, A.; Ghosh, D.; Bandhopadhyaya, R.; Bhuyan, M. Preemptive identification of optimum fermentation time for black tea using electronic nose. *Sens. Actuators, B* **2008**, *131*, 110−116.
(256) Tan, T. T.; Lucas, Q.; Moy, L.; Gardner, J. W.; Bartlett, P. N. The electronic nose − a new instrument for sensing vapours. *LC−GC Int.* **1995**, *8*, 218−225.
(257) Ciosek, P.; Brzózka, Z.; Wróblewski, W. Classification of beverages using a reduced sensor array. *Sens. Actuators, B* **2004**, *103*, 76−83.
(258) Gallardo, J.; Alegret, S.; del Valle, M. Application of a potentiometric electronic tongue as a classification tool in food analysis. *Talanta* **2005**, *66*, 1303−1309.
(259) Legin, A.; Rudnitskaya, A.; Vlasov, Y.; Di Natale, C.; Mazzone, E.; D'Amico, A. Application of electronic tongue for quantitative analysis of mineral water and wine. *Electroanalysis* **1999**, *11*, 814−820.
(260) Moreno, L.; Merlos, A.; Abramova, N.; Jiménez, C.; Bratov, A. Multi-sensor array used as an "electronic tongue" for mineral water analysis. *Sens. Actuators, B* **2006**, *116*, 130−134.
(261) Ciosek, P.; Augustyniak, E.; Wróblewski, W. Polymeric membrane ion-selective and cross-sensitive electrodes-based electronic tongue for qualitative analysis of beverages. *Analyst* **2004**, *129*, 639−644.
(262) Ciosek, P.; Mamińska, R.; Dybko, A.; Wróblewski, W. Potentiometric electronic tongue based on integrated array of microelectrodes. *Sens. Actuators, B* **2007**, *127*, 8−14.
(263) Fernandez-Vazquez, R.; Stinco, C. M.; Melendez-Martinez, A. J.; Heredia, F. J.; Vicario, I. M. Visual and instrumental evaluation of orange juice color: a consumers' preference study. *J. Sens. Stud.* **2011**, *26*, 436−444.
(264) Steine, C.; Beaucousin, F.; Siv, C.; Peiffer, G. Potential of semiconductor sensor arrays for the origin authentication of pure Valencia orange juices. *J. Agric. Food Chem.* **2001**, *49*, 3151−3160.
(265) Goodner, K. L.; Baldwin, E. A.; Jordan, M. J.; Shaw, P. E. The comparison of an electronic nose and gas chromatograph for differentiating NFC orange juices. *Proc. Fla. State Hortic. Soc.* **2001**, *114*, 158−160.
(266) Reinhard, H.; Sager, F.; Zoller, O. Citrus juice classification by SPME-GC-MS and electronic nose measurements. *Food Sci. Technol.* **2008**, *41*, 1906−1912.
(267) Gay, M.; Apetrei, C.; Nevares, I.; del Alamo, M.; Zurro, J.; Prieto, N.; De Saja, J. A.; Rodríguez-Méndez, M. L. Application of an electronic tongue to study the effect of the use of pieces of wood and micro-oxygenation in the aging of red wine. *Electrochim. Acta* **2010**, *55*, 6782−6788.
(268) Ragazzo, J. A.; Chalier, P.; Crouzet, J.; Ghommidh, C. In *Food Flavours and Chemistry: Advances of the New Millennium*; Spanier, A. H., Shahidi, F., Parliment, T. H., Mussinan, C., Ho, C.-T., Contis, E. T., Eds.; RSC: Cambridge, UK, 2001; pp 404−411.
(269) Ragazzo-Sanchez, J. A.; Chalier, P.; Chevalier, D.; Calderon-Santoyo, M.; Ghommidh, C. Identification of different alcoholic beverages by electronic nose coupled to GC. *Sens. Actuators, B* **2008**, *134*, 43−48.
(270) Liu, M.; Han, X.; Tu, K.; Pan, L.; Tud, J.; Tang, L.; Liu, P.; Zhan, G.; Zhong, Q.; Xiong, Z. Application of electronic nose in Chinese spirits quality control and flavour assessment. *Food Control* **2012**, *26*, 564−570.
(271) Pearce, T. C.; Gardner, J. W.; Friel, S.; Bartlett, P. N.; Blair, N. Electronic nose for monitoring the flavor of beers. *Analyst* **1993**, *118*, 371−377.
(272) Wang, H.-H. Assessment of solid state fermentation by a bioelectronic artificial nose. *Biotechnol. Adv.* **1993**, *11*, 701−710.
(273) Di Natale, C.; Davide, F. A. M.; D'Amico, A.; Nelli, P.; Groppelli, S.; Sberveglieri, G. An electronic nose for the recognition of the vineyard of a red wine. *Sens. Actuators, B* **1996**, *33*, 83−88.
(274) Cynkar, W.; Dambergs, R.; Smith, P.; Cozzolino, D. Classification of Tempranillo wines according to geographic origin: combination of mass spectrometry based electronic nose and chemometrics. *Anal. Chim. Acta* **2010**, *660*, 227−231.
(275) Cozzolino, D.; Smyth, H. E.; Cynkar, W.; Dambergs, R. G.; Gishen, M. Usefulness of chemometrics and mass spectrometry-based electronic nose to classify Australian white wines by their varietal origin. *Talanta* **2005**, *68*, 382−387.
(276) Lozano, J.; Fernández, M. J.; Fontecha, J.; Aleixandre, M.; Santos, J. P.; Sayago, I.; Arroyo, T.; Cabellos, J. M.; Gutiérrez, F. J.; Horrillo, M. C. Wine classification with a zinc oxide SAW sensor array. *Sens. Actuators, B* **2006**, *120*, 166−171.
(277) Aleixandre, M.; Lozano, J.; Gutiérrez, J.; Sayago, I.; Fernández, M. J.; Horrillo, M. C. Portable e-nose to classify different kinds of wine. *Sens. Actuators, B* **2008**, *131*, 71−76.
(278) Lozano, J.; Santos, J. P.; Gutiérrez, J.; Horrillo, M. C. Comparative study of sampling systems combined with gas sensors for wine discrimination. *Sens. Actuators, B* **2007**, *126*, 616−623.
(279) Martí, M. P.; Busto, O.; Guasch, J. Application of a headspace mass spectrometry system to the differentiation and classification of wines according to their origin, variety and ageing. *J. Chromatogr., A* **2004**, *1057*, 211−217.
(280) García, M.; Aleixandre, M.; Gutiérrez, J.; Horrillo, M. Electronic nose for wine discrimination. *Sens. Actuators, B* **2006**, *113*, 911−916.
(281) Lozano, J.; Arroyo, T.; Santos, J. P.; Cabellos, J. M.; Horrillo, M. C. Electronic nose for wine ageing detection. *Sens. Actuators, B* **2008**, *133*, 180−186.
(282) Penza, M.; Cassano, G. Recognition of adulteration of Italian wines by thin-film multisensor array and artificial neural networks. *Anal. Chim. Acta* **2004**, *509*, 159−177.
(283) Ragazzo-Sanchez, J. A.; Chalier, P.; Ghommidh, C. Coupling gas chromatography and electronic nose for dehydration and desalcoholization of alcoholized beverages. *Sens. Actuators, B* **2005**, *106*, 253−257.
(284) Legin, A.; Rudnitskaya, A.; Seleznev, B.; Vlasov, Y. Electronic tongue for quality assessment of ethanol, vodka and eau-de-vie. *Anal. Chim. Acta* **2005**, *534*, 129−135.
(285) Novakowski, W.; Bertotti, M.; Paixão, T. R. L. C. Use of copper and gold electrodes as sensitive elements for fabrication of an electronic tongue: discrimination of wines and whiskies. *Microchem. J.* **2011**, *99*, 145−151.
(286) Lvova, L.; Paolesse, R.; Di Natale, C.; D'Amico, A. Detection of alcohols in beverages: an application of porphyrin-based electronic tongue. *Sens. Actuators, B* **2006**, *118*, 439−447.

(287) Gutiérrez, J. M.; Haddi, Z.; Amari, A.; Bouchikhi, B.; Mimendia, A.; Cetó, X.; del Valle, M. Hybrid electronic tongue based on multisensor data fusion for discrimination of beers. *Sens. Actuators, B* **2013**, *177*, 989−996.
(288) Rudnitskaya, A.; Polshin, E.; Kirsanov, D.; Lammertyn, J.; Nicolai, B.; Saison, D.; Delvaux, F. R.; Delvaux, F.; Legin, A. Instrumental measurement of beer taste attributes using an electronic tongue. *Anal. Chim. Acta* **2009**, *646*, 111−118.
(289) Polshin, E.; Rudnitskaya, A.; Kirsanov, D.; Legin, A.; Saison, D.; Delvaux, F.; Delvaux, F. R.; Nicolaï, B. M.; Lammertyn, J. Electronic tongue as a screening tool for rapid analysis of beer. *Talanta* **2010**, *81*, 88−94.
(290) Arrieta, Á. A.; Rodríguez-Méndez, M. L.; de Saja, J. A.; Blanco, C. A.; Nimubona, D. Prediction of bitterness and alcoholic degree in beer using an electronic tongue. *Food Chem.* **2010**, *123*, 642−646.
(291) Parra, V.; Hernando, T.; Rodríguez-Méndez, M. L.; de Saja, J. A. Electrochemical sensor array made from bisphthalocyanine modified carbon paste electrodes for discrimination of red wines. *Electrochim. Acta* **2004**, *49*, 5177−5185.
(292) Di Natale, C.; Paolesse, R.; Macagnano, A.; Mantini, A.; D'Amico, A.; Ubigli, M.; Legin, A.; Lvova, L.; Rudnitskaya, A.; Vlasov, Y. Application of a combined artificial olfaction and taste system to the quantification of relevant compounds in red wine. *Sens. Actuators, B* **2000**, *69*, 342−347.
(293) Kirsanov, D.; Mednova, O.; Vietoris, V.; Kilmartin, P. A.; Legin, A. Towards reliable estimation of an "electronic tongue" predictive ability from PLS regression models in wine analysis. *Talanta* **2012**, *90*, 109−116.
(294) Rodríguez-Méndez, M. L.; Parra, V.; Apetrei, C.; Villanueva, S.; Gay, M.; Prieto, N.; Martínez, J.; de Saja, J. A. Electronic tongue based on voltammetric electrodes modified with materials showing complementary electroactive properties. *Appl. Microchim. Acta* **2008**, *163*, 23−31.
(295) Moreno-Codinachs, L.; Kloock, J. P.; Schöning, M. J.; Baldi, A.; Ipatov, A.; Bratov, A.; Jiménez-Jorquera, C. Electronic integrated multisensor tongue applied to grape juice and wine analysis. *Analyst* **2008**, *133*, 1440−1448.
(296) Apetrei, C.; Apetrei, I. M.; Nevares, I.; del Alamo, M.; Parra, V.; Rodríguez-Méndez, M. L.; De Saja, J. A. Using an etongue based on voltammetric electrodes to discriminate among red wines aged in oak barrels or aged using alternative methods. Correlation between electrochemical signals and analytical parameters. *Electrochim. Acta* **2007**, *52*, 2588−2594.
(297) Cetó, X.; Gutiérrez, J. M.; Gutiérrez, M.; Céspedes, F.; Capdevila, J.; Mínguez, S.; Jiménez-Jorquera, C.; del Valle, M. Determination of total polyphenol index in wines employing a voltammetric electronic tongue. *Anal. Chim. Acta* **2012**, *732*, 172−179.
(298) Rudnitskaya, A.; Nieuwoudt, H. H.; Muller, N.; Legin, A.; du Toit, M.; Bauer, F. F. Instrumental measurement of bitter taste in red wine using an electronic tongue. *Anal. Bioanal. Chem.* **2010**, *397*, 3051−3060.
(299) Rudnitskaya, A.; Delgadillo, I.; Legin, A.; Rocha, S. M.; Costa, A. M.; Simoes, T. Prediction of the Port wine age using an electronic tongue. *Chemom. Intell. Lab. Syst.* **2007**, *88*, 125−131.
(300) Apetrei, I. M.; Rodríguez-Méndez, M. L.; Apetrei, C.; Nevares, I.; del Alamo, M.; de Saja, J. A. Monitoring of evolution during red wine aging in oak barrels and alternative method by means of an electronic panel test. *Food Res. Int.* **2012**, *45*, 244−249.
(301) Dutta, R.; Hines, E. L.; Gardner, J. W.; Udrea, D. D.; Boilot, P. Nondestructive egg freshness determination: an electronic nose based approach. *Meas. Sci. Technol.* **2003**, *14*, 190−198.
(302) Liu, P.; Tu, K. Prediction of TVB-N content in eggs based on electronic nose. *Food Control* **2012**, *23*, 177−183.
(303) Ghidini, S.; Mercanti, C.; Dalcanale, E.; Pinalli, R.; Bracchi, P. G. Italian honey authentication. *Ann. Fac. Med. Vet. Parma* **2008**, *28*, 113−120.
(304) Benedetti, S.; Mannino, S.; Sabatini, A. G.; Marcazzan, G. L. *Apidologie* **2004**, *35*, 397−402.
(305) Ampuero, S.; Bogdanov, S.; Bosset, J. O. Classification of unifloral honeys with an MS-based electronic nose using different sampling modes: SHS, SPME, and INDEX. *Eur. Food Res. Technol.* **2004**, *218*, 198−207.
(306) Breheret, S.; Talou, T.; Bourrounet, B.; Gaset, A. In *Proceedings of Bioflavour*; Etiévant, P., Schreier, P., Eds.; INRA: Dijon, France, 1995; pp 103−107.
(307) Siripatrawan, U. Self-organizing algorithm for classification of packaged fresh vegetable potentially contaminated with foodborne pathogens. *Sens. Actuators, B* **2008**, *128*, 435−441.
(308) Wei, Z.; Wang, J.; Liao, W. Technique potential for classification of honey by electronic tongue. *J. Food Eng.* **2009**, *94*, 260−266.
(309) Escriche, I.; Kadar, M.; Domenech, E.; Gil-Sánchez, L. A potentiometric electronic tongue for the discrimination of honey according to the botanical origin. Comparison with traditional methodologies: physicochemical parameters and volatile profile. *J. Food Eng.* **2012**, *109*, 449−456.
(310) Wei, Z.; Wang, J. Separation of tryptophan enantiomers with polypyrrole electrode column by potential-induced technique. *Electrochim. Acta* **2011**, *56*, 4907−4915.
(311) Major, N.; Marković, K.; Krpan, M.; Šarić, G.; Hruškar, M.; Vahčić, N. Rapid honey characterization and botanical classification by an electronic tongue. *Talanta* **2011**, *85*, 569−574.
(312) Sun, D.-W. Inspecting pizza topping percentage and distribution by a computer vision method. *J. Food Eng.* **2000**, *44*, 245−249.
(313) Mery, D.; Chanona-Pérez, J. J.; Soto, A.; Aguilera, J. M.; Cipriano, A.; Veléz-Rivera, N.; Arzate-Vázquez, I.; Gutiérrez-López, G. F. Quality classification of corn tortillas using computer vision. *J. Food Eng.* **2010**, *101*, 357−364.
(314) Yin, H.; Panigrahi, S. Image processing techniques for internal texture evaluation of French fries. *ASAE Annual International Meeting Technical Papers*, St. Joseph, MI, USA, 1997; Paper 973127
(315) Scanlon, M. G.; Roller, R.; Mazza, G.; Pritchard, M. K. Computerized video image-analysis to quantify color of potato chips. *Am. Potato J.* **1994**, *71*, 717−733.
(316) Chen, Q.; Zhao, J.; Chen, Z.; Lin, H.; Zhao, D.-A. Discrimination of green tea quality using the electronic nose technique and the human panel test, comparison of linear and nonlinear classification tools. *Sens. Actuators, B* **2011**, *159*, 294−300.
(317) Winquist, F.; Bjorklund, R.; Krantz-Rückler, C.; Lundström, I.; Östergren, K.; Skoglund, T. An electronic tongue in the dairy industry. *Sens. Actuators, B* **2005**, *111*, 299 −304.
(318) Tran, T. U.; Suzuki, K.; Okadome, H.; Homma, S.; Ohtsubo, K. Analysis of the tastes of brown rice and milled rice with different milling yields using a taste sensing system. *Food Chem.* **2004**, *88*, 557−566.
(319) Arrieta, A. A.; Rodríguez-Méndez, M. L.; de Saja, J. A.; Blanco, C. A.; Nimubona, D. Prediction of bitterness and alcoholic strength in beer using an electronic tongue. *Food Chem.* **2010**, *123*, 642−646.
(320) Legin, A.; Rudniskaya, A.; Lvova, L.; Vlasov, Y.; Di Natale, C.; D'Amico, A. Evaluation of Italian wine by the electronic tongue: recognition, quantitative analysis and correlation with human sensory perception. *Anal. Chim. Acta* **2003**, *484*, 33−44.
(321) He, W.; Hua, X.; Zhao, L.; Liao, X.; Zhang, Y.; Zhang, M.; Wua, J. Evaluation of Chinese tea by the electronic tongue: correlation with sensory properties and classification according to geographical origin and grade level. *Food Res. Int.* **2009**, *42*, 1462−1467.
(322) Ivarsson, P.; Holmin, S.; Höjer, N.-E.; Krantz-Rülcker, C.; Winquist, F. Discrimination of tea by means of a voltammetric electronic tongue and different applied waveforms. *Sens. Actuators, B* **2001**, *76*, 449−454.
(323) Apetrei, C.; Rodríguez-Méndez, M. L.; de Saja, J. A. Modified carbon paste electrodes for discrimination of vegetable oils. *Sens. Actuators, B* **2005**, *111*, 403−409.
(324) Rodríguez-Méndez, M. L.; Apetrei, C.; de Saja, J. A. Evaluation of the polyphenolic content of extra virgin olive oils using an array of voltammetric sensors. *Electrochim. Acta* **2008**, *53*, 5867−5872.

(325) Majumdar, S.; Jayas, D. S. Classification of cereal grains using machine vision: IV. Combined morphology, colour, and texture models. *Trans. ASAE* **2000**, *43*, 1689−1694.
(326) Pearson, T.; Toyofuku, N. Automated sorting of pistachio nuts with closed shells. *Appl. Eng. Agric.* **2000**, *16*, 91−94.
(327) Martin, M. L. G. M.; Ji, W.; Luo, R.; Hutchings, J.; Heredia, F. J. Measuring colour appearance of red wines. *Food Qual. Prefer.* **2007**, *18*, 862−871.

current evidence strongly supports that hydroxytyrosol may also provide an indirect protection on the body through increasing the endogenous defense systems.[9] It was reported that the antioxidants of an extra virgin olive oil rich in phenolics concentrated on pancreatic islets and liver in the mice fed with a nonpurified diet.[10] The concentration of plasma hydroxytyrosol was greater in the mice fed with olive oil than in the control mice. The oxidized glutathione and the antioxidant capacity in plasma of the former were higher than those of the latter, and the glucose-stimulated insulin secretion became greater in the olive oil mice. It is concluded that the protective effects of extra virgin olive oil against oxidative stress occur mainly through a direct antioxidant action and an indirect mechanism involved in higher expressions of certain enzymes with antioxidant activities.

Anticancer Potential. Several epidemiological and animal research studies suggested that polyphenols might have a protective effect against some chronic degenerative diseases such as cancer. Dietary hydroxytyrosol has recently received particular attention because of its antioxidant, antiproliferative, proapoptotic, and anti-inflammatory activities, which can specifically counteract all cancer hallmarks.[11]

Investigations have shown that the incidence of various cancers is much lower in the Mediterranean area compared to other countries. Besides the chemopreventive ability, the antitumor effects of olive oil phenols with high antioxidant activity have been in-depth studied because of their capacities of inhibiting proliferation and promoting apoptosis.[12,13]

Growing experimental evidence has suggested that, in addition to antioxidant and anti-inflammatory abilities, hydroxytyrosol and other olive oil phenols exert anticancer effects through the activation of molecular signaling pathways, leading to cell apoptosis and growth arrest in several tumor cell lines in vitro.[14,15]

Cardioprotective Capacity. Hydroxytyrosol would be an effective dietary supplement for preventive therapy of cardiovascular diseases related to insulin decrease, and the reduction of hypertension risk. Among other healthy properties promoted by hydroxytyrosol, olive oil has beneficial effects on cardiovascular risk for its ability to reduce blood pressure and improve lipid profile.[16]

Health efficacy of olive oil intake on cardiovascular disease is greatly attributed to phenolic compounds such as hydroxytyrosol. A study involving 200 healthy male volunteers indicated that the intake of different kinds of virgin olive oil with various phenolic contents reduced lipid oxidative damage and increased HDL-cholesterol.[17]

EFSA endorsed the health claim that the consumption of olive oil polyphenols contributes to the protection of blood lipids on oxidative damage. Besides the ability to prevent LDL oxidation, hydroxytyrosol shows a beneficial effect on platelet function. Hydroxytyrosol derived from olive oil can inhibit platelet aggregation and production of eicosanoids in vitro, and olive derivatives share the same biological activities.[18,19]

A study involving the hyperlipidemic rabbits fed with hydroxytyrosol suggested an improvement of the antioxidant status and the reduction of the size of atherosclerotic lesions.[20] In order to examine the effect of extra virgin olive oil phenolic compounds on homocysteine-induced endothelial dysfunction, the structurally related compounds had been assayed for their ability to reduce homocysteine-induced monocyte adhesion as well as the expression of intercellular adhesion molecule-1 (ICAM-1) in EA.hy.926 cells.[21] All of the tested compounds, including hydroxytyrosol, significantly reduce the expression homocysteine-induced cell adhesion and ICAM-1. In addition, synergy of olive oil phenolic compounds in the modulation of the Hcy-induced ICAM-1 expression was investigated, and no synergistic effect has been observed when hydroxytyrosol and tyrosol are tested for their protective effects on ICAM-1 expression induced by TNFα.

Diabetes Treatment. *Olea europaea* leaves have been used in folk medicine to treat diabetes for many years. Supplementation with phenolic compounds of olive leaf, containing 51.1 mg of oleuropein and 9.7 mg of hydroxytyrosol per day for 12 weeks, improved the glucose regulation of insulin action and secretion in middle-aged overweight men. Insulin sensitivity and pancreatic β-cell secretory capacity were significantly improved in the people at risk of developing the metabolic syndrome.[22]

It was hypothesized that dietary antioxidants could reduce the risk of diabetes since oxidative stress plays a role in the pathogenesis of insulin resistance. Specific dietary strategies may be helpful in the prevention of this disease by improving glucose homeostasis.

Hydroxytyrosol supplementation to surviving diabetic rats greatly decreased the activities of intestinal lactase, lipase, maltase, and sucrose and enhanced the activities of superoxide dismutase, catalase, and glutathione peroxidase.[23] Moreover, significant decreases were observed in the level of thiobarbituric acid reactive substances and the activity of lactate dehydrogenase in diabetic rat pancreas after hydroxytyrosol administration. In addition, hydroxytyrosol increased lipid profile in diabetic rats through lowering the content of LDL-cholesterol and triglycerides and increasing HDL-cholesterol content. These properties of hydroxytyrosol are valuable when it is used as a therapeutic agent, especially as anti-hypocholesterolemic and diabetic drugs in biotechnological applications.

A long period of oxidative stress and inflammatory responses will cause many diseases. A proinflammatory cytokine plays an important role in the pathogenesis of chronic and autoimmune diseases. Some data shows that the intake of polyphenols such as oleuropein and hydroxytyrosol can affect the formation of advanced glycation end products and their interaction with respective receptors, and modulate chronic inflammatory diseases, for example, type II diabetes, rheumatoid arthritis, and inflammatory bowel disease.[24]

Neuroprotective Activity. As a major component of the Mediterranean diet, olive oil is very important to counteract neurodegenerative diseases such as Alzheimer's and Parkinson's diseases. Dietary hydroxytyrosol intake may have beneficial effects on neuroprotection.

Elevated oxidative and nitrosative stress can impair the integrity and function of brain tissue. The efficacy of a hydroxytyrosol-rich extract in diminishing NO-induced cytotoxicity in murine-dissociated brain cells was investigated. The addition of either Fe^{2+} or SNP (an NO donor) could cause a marked depolarization in mitochondrial membrane and a severe loss of cellular ATP, confirming the promising cytoprotection on brain cells by hydroxytyrosol-rich olive mill wastewater extract in different stressor paradigms.[25] Furthermore, correlation analyses revealed that the observed cytoprotective effects on PC-12 cells were likely due to the presence of hydroxytyrosol in the extract. Additionally, some evidence suggesting a physiological function of hydroxytyrosol, which is affected by ethanol consumption, warrants further investigation into the potential of intake of hydroxytyrosol extracts to exert a

Table 1. Potential Therapeutic Effects of Hydroxytyrosol

type of activity	protective effects and mechanisms	conditions	levels	ref
antioxidant activity	increasing CAT and SOD activities	in rats fed a cholesterol-rich diet	in vivo	36
	inhibiting the activities of 12-lipoxygenase and 5-lipoxygenase; reducing leukotriene B4 production	in rat platelets and rat polymorphonuclear leukocytes	in vitro	37
antiatherosclerosis and cardioprotection activity	preventing platelet aggregation and eicosanoid formation; inhibiting thromboxane B2 production	in platelet rich plasma	in vitro	19
	inhibiting thromboxane B2 production	in patients with uncomplicated type I diabetes	in vivo	38
	inhibiting leukotriene B4 generation; inhibiting 5-lipoxygenase	in rat peritoneal leukocytes	in vitro	39
	reducing monocytoid cell adhesion to stimulated endothelium; decreasing VCAM-1 mRNA and protein	in human umbilical vein endothelial cells	in vitro	40
	lowering serum TC and LDL-C; slowing the lipid peroxidation process	in rats fed a cholesterol-rich diet	in vivo	36
neuroprotective effect	attenuating Fe^{2+} and NO-induced cytotoxicity; increasing cellular ATP; reducing lipid peroxidation; hyperpolarizing basal mitochondrial membrane	in murine-dissociated brain cells and mice	in vitro ex vivo	25
	inhibiting lactate dehydrogenase (LDH) efflux in a concentration-dependent manner	in a model of hypoxia−reoxygenation in rat brain slices	in vivo	28
anticarcinogenic activity	inhibiting cell proliferation; inducing apoptosis by arresting the cells in the G0/G1 phase with a concomitant decrease in the cell percentage in the S and G2/M phases	in human promyelocytic leukemia cells HL60	in vitro	15
	a dose dependent growth inhibition of MCF-7 cells; inducing apoptosis by arresting the cells in the G0/G1 phase	in MCF-7 breast cancer cells	in vitro	12
	inhibiting cell proliferation through the inhibition of estrogen-dependent rapid signals involved in uncontrolled tumor cell growth; not be involved in estrogen receptor alpha-mediated regulation of gene expression	in MCF-7 breast cancer cells	in vitro	13
antibacterial activity	antimycoplasmal activity against *M. pneumoniae*, *M. hominis*, and *M. fermentans*	in mycoplasma	in vitro	34
diabetes treatment	decreasing considerably intestinal maltase, lactase, sucrose, and lipase activities and enhancing the superoxide dismutase, catalase, and glutathione peroxidase activities; decrease in the level of thiobarbituric acid reactive substances and lactate dehydrogenase activity; improving lipid profile by lowering LDL-cholesterol and triglycerides and increasing HDL-cholesterol content	in diabetic rats	in vivo	23

dx.doi.org/10.1021/jf405820v | J. Agric. Food Chem. 2014, 62, 1449−1455

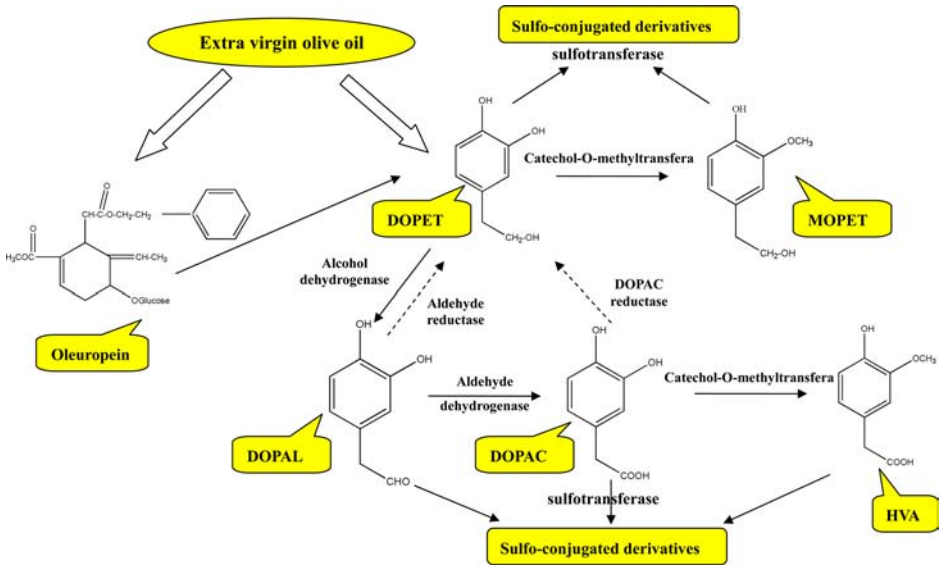

Figure 1. Pharmacokinetic analysis and metabolism pathways of exogenously administered hydroxytyparosol in rats. DOPET is hydroxytyparosol; MOPET is 4-hydroxy-3-methoxy-phenylethanol; DOPAL is 3,4-dihydroxy-phenylacetaldeyde; DOPAC is 3,4-dihydroxy-phenylacetic acid; HVA is 4-hydroxy-3-methoxy-phenylacetic acid.

beneficial effect on the body.[26] Hydroxytyrosol significantly attenuated the cytotoxic effect of stressors. In vivo data have provided evidence of neuroprotective effects of oral hydroxytyrosol intake. Both in vivo and in vitro data have identified that the mitochondria are among the preventive targets of hydroxytyrosol in the brain.

Oleuropein had shown neuroprotective activity by forming noncovalent complexes with the beta amyloid peptide, which is the major protein component of senile plaques formed in several neurodegenerative diseases such as Alzheimer's and Parkinson's diseases. Therefore, as the primary degradation product of oleuropein, hydroxytyrosol has been speculated to be a potential neuroprotective compound.[27]

The possible neuroprotective effect of hydroxytyrosol was tested using a model of hypoxia−reoxygenation in rat brain slices. Lactate dehydrogenase (LDH) was measured as a marker of brain cell death. Hydroxytyrosol significantly inhibited LDH efflux, providing an initial basis for further study of hydroxytyrosol as a potential neuroprotective compound.[28]

Modulation of Enzymes. The activities of enzymes potentially sensitive to phenolic compounds were tested in a variety of cellular models, such as platelets, leukocytes, and macrophages. Hydroxytyrosol was tested for enzyme-modulating activities, such as in vitro effects on the platelet function, where hydroxytyrosol inhibited chemically induced aggregation, the accumulation of proaggregant thromboxane in human serum, and the production of proinflammatory leukotrienes by activated human leukocytes.[29]

Hydroxytyrosol is able to regulate several enzymatic activities associated with cardiovascular disease. Its inhibitions on the inducible form of nitric oxide synthase, platelet aggregation, and proinflammatory enzymes such as 5-lipoxygenase have been demonstrated in vitro. The vasomodulating effects of olive leaf extracts have been demonstrated in a rabbit model, although the human relevance of these findings needs further investigation.[30]

Other Effects. Hydroxytyrosol also has many other significant activities. It could control and prevent various pathological changes caused by smoking. A low dose of hydroxytyrosol, administered through olive mill wastewater, reduced the consequences of sidestream smoke-induced oxidative stress in rats.[31] Data indicate that hydroxytyrosol is able to completely prevent artery and renal oxidative stress induced by cyclosporine A, and it has only a minor effect on the associated tubular injury and interstitial fibrosis without affecting the arteriolopathy.[32] Hydroxytyrosol significantly reduced the DNA strand breaks caused by *o*-phenylphenol (OPP) and effectively suppressed the formation of OPP-induced reactive oxygen species. The antioxidant activity of hydroxytyrosol may play an important role in attenuating the DNA damage of OPP.[33] In addition, growing experimental evidence suggested that hydroxytyrosol exerts antibacterial effects.[34] Moreover, hydroxytyrosol is a potent genotoxic compound and used as fungicides and antibacterial agents for pest control in agriculture.[35] Table 1 shows the main biological activities and potential therapeutic effects of hydroxytyrosol.

IN VIVO ABSORPTION AND METABOLIZATION

Bioavailability studies have demonstrated that hydroxytyrosol is dose dependently absorbed in animals and humans after olive oil ingestion, and systemically exerts biological effects.[41,42]

Absorption studies with olive oil and phenolic extracts derived from olive oil indicated that hydroxytyrosol is absorbed, while other phenolic components undergo metabolism in the small and large intestine.[43,44] Especially, oleuropein is not absorbed in the small intestine, and undergoes rapid degradation in the large intestine to yield hydroxytyrosol (Figure 1).

D'Angelo et al.[45] evaluated the toxicity of hydroxytyrosol and investigated its molecular pharmacokinetics. When orally administered to rats, hydroxytyrosol does not show appreciable toxicity up to 2 g/kg BW. To identify and quantify its metabolites, ^{14}C-hydroxytyrosol was synthesized and intravenously injected into rats. The pharmacokinetic analysis indicated a fast and extensive uptake of hydroxytyrosol by the organs and tissues with a preferential renal uptake. Moreover, 90% of the administered radioactivity was excreted in urine collected up to 5 h after injection, and about 5% was detectable

in feces and gastrointestinal content. The characterization of the labeled metabolites, extracted from the organs and urine, was performed by HPLC analysis, which showed that hydroxytyrosol was enzymatically converted in four oxidized and/or methylated derivatives. Moreover, a significant fraction of total radioactivity is associated with the sulfoconjugated forms, which also represent the major urinary excretion products.

Corona et al.[46] conducted an investigation into the absorption, metabolism, and microflora-dependent transformation of hydroxytyrosol, tyrosol, and their conjugated forms, which underwent rapid hydrolysis under gastric conditions, leading to significant increases of free hydroxytyrosol and tyrosol entering the small intestine. Both hydroxytyrosol and tyrosol transferred across rat segments of jejunum and ileum and human Caco-2 cell monolayers, and were subject to classic phase I/II biotransformation. The major metabolites identified were glucuronides of hydroxytyrosol, O-methylated derivative of hydroxytyrosol and tyrosol, and a novel glutathionylated conjugate of hydroxytyrosol. In contrast, there was no absorption of oleuropein in both models. However, oleuropein was rapidly degraded by the colonic microflora resulting in the formation of hydroxytyrosol. This study provided additional information regarding the breakdown of complex olive oil polyphenols in the GI tract, in particular the stomach and the large intestine.

Visioli et al. were the first to elucidate the metabolism of hydroxytyrosol.[47] Soon afterward they further studied the difference of metabolism and urinary excretion of hydroxytyrosol between rats and humans by evaluating excretion of hydroxytyrosol and its major metabolite. The results showed that the urinary excretion of hydroxytyrosol was greater in humans than in rats, suggesting that the rat is not the appropriate model for the study of hydroxytyrosol metabolism and that hydroxytyrosol-containing functional foods should be carefully formulated.[48] To date, the only study on human was conducted by González-Santiago et al., in which the absorption of high amounts of purified hydroxytyrosol administered as an aqueous solution is very low and produces a large number of metabolites.[49] The transient association with low-density lipoproteins observed in plasma may have physiological implications, but further research is needed using larger intervention trials with different hydroxytyrosol and formulations that render hydroxytyrosol more bioavailable before any conclusion can be made.

Administration of hydroxytyrosol in animal studies has been carried out as part of an extra virgin olive oil, using an olive oil mill wastewater extract or an aqueous solution as a drug for daily animal consumption. A study on the stability of hydroxytyrosol in aqueous solutions by varying its concentration, the temperature, and the ionic content showed that the storage of hydroxytyrosol is best at −20 °C where no significant degradation occurred for one week.[50] Hydroxytyrosol in lower concentrations was more prone to degrade than the higher ones. The results were of high relevance for future studies to predict the stability of potential liquid food samples containing hydroxytyrosol and perform quantitative determinations of hydroxytyrosol in biological fluids.

There may be some synergy effects between natural antioxidants. Evidence indicated that the cancer-preventive activity of olive oil could be mediated by the presence of minor components, such as antioxidant phenolic compounds. Hydroxytyrosol is one of the main olive oil phenols with a very strong antioxidant activity. Although it has not been reported yet, we believe that there will be a certain synergistic effect between hydroxytyrosol and other olive oil phenols or natural antioxidants, such as oleuropein, tyrosol, tea polyphenol, Vc, lycopene, and so on, when they act together. Zhang et al. studied the antagonistic effect of hydroxytyrosol on male reproductive toxicity induced by perfluorooctane sulfonate (PFOS).[51] Male mice were randomly divided into five groups: control group, PFOS group, PFOS plus low-dose hydroxytyrosol, PFOS plus midium-dose hydroxytyrosol, and PFOS plus high-dose hydroxytyrosol groups. After animals were fed with deionized water supplemented with PFOS and/or hydroxytyrosol for a month, the number of sperm in the rat groups with low, medium, and high dose of hydroxytyrosol increased significantly compared with that of PFOS exposure groups. At present, there is little research on the synergetic effects, which is worth being further researched.

SAFETY

The safety profile of hydroxytyrosol appears to be excellent; no untoward effects have been demonstrated even at very high doses.[52−54] An olive mill wastewater nutraceutical, i.e., Hidrox, containing 6% of hydroxytyrosol has been granted the GRAS status. In terms of safety profile, hydroxytyrosol has been investigated as the predominant part of raw olive mill wastewater extracts due to the previous unavailability of appropriate quantities of the pure compound. A toxicological evaluation on hydroxytyrosol was reported by Auñon-Calles et al., and they finally proposed a No Observed Adverse Effects Level (NOAEL) of 500 mg/kg/d based on the results.[55] In addition, their other research indicated that hydroxytyrosol is non-genotoxic and non-mutagenic at concentrations that far exceed those attainable after intake.[56]

Due to its variety of biological activities, hydroxytyrosol is currently one of the most actively investigated natural phenols in synthesis. Given its excellent safety profile, future availability as a health food supplement might be conceivable. Moreover, EFSA has endorsed the health claim that "on the basis of the data presented, the Panel concludes that a cause and effect relationship has been established between the consumption of olive oil polyphenols (standardized by the content of hydroxytyrosol and its derivatives) and protection of LDL particles from oxidative damage. The Panel considers that in order to bear the claim, 5 mg of hydroxytyrosol and its derivatives (e.g., oleuropein complex and tyrosol) in olive oil should be consumed daily."

In conclusion, hydroxytyrosol is being exploited as a potential peculiar supplement in the nutraceutical and food industry. It is noteworthy that there are a large number of patents on hydroxytyrosol and other olive phenols, and the number is in continuous increase.[30] Several industrial applications of hydroxytyrosol are being envisioned. In addition, hydroxytyrosol has been heavily exploited for the treatment and the prevention of heart disease, carcinogenesis, cerebral hemorrhage, atherosclerosis, and many other traditional therapeutic uses. It can be expected that, with the continuous accumulation of data in various areas of human health, other products in the fields of cosmetology or food science might be launched in the near future. Furthermore, new derivatives of hydroxytyrosol can be tested and developed for the purpose of potential applications.

With the demand for healthy organic food, the nutrition market exploring the potential health benefits of products from

olive and extra virgin olive oil is expanding. It is obvious that hydroxytyrosol from olive oil has significant bioactivity, which suggests its good potentiality for the development of dietary supplements. Further studies are needed to elaborate its physiological and pharmacological mechanisms to provide the theoretical basis for its use as health supplements.

AUTHOR INFORMATION

Corresponding Author

*J.-G.J.: e-mail, jgjiang@scut.edu.cn; phone, +86-20-87113849; fax, +86-20-87113843). X.-L.X.: e-mail, xuxilin@scut.edu.cn; phone, +86-20-38675626; fax, +86-20-38675626).

Notes

The authors declare no competing financial interest.

REFERENCES

(1) Han, X. Z.; Shen, T.; Lou, H. X. Dietary polyphenols and their biological significance. *Int. J. Mol. Sci.* **2007**, *8*, 950−988.

(2) Bach-Faig, A.; Berry, E. M.; Lairon, D.; Reguant, J.; Trichopoulou, A.; Dernini, S.; Medina, F. X.; Battino, M.; Belahsen, R.; Miranda, G.; Serra-Majem, L. Mediterranean diet pyramid today. Science and cultural updates. *Public Health Nutr.* **2011**, *14*, 2274−2284.

(3) The Local-Food Nutraceuticals Consortium. Understanding local Mediterranean diets: a multidisciplinary pharmacological and ethnobotanical approach . *Pharmacol. Res.* **2005**, *52*, 353-366.

(4) Santos, M. M.; Piccirillo, C.; Castro, P. M. L.; Kalogerakis, N.; Pintado, M. E. Bioconversion of oleuropein to hydroxytyrosol by lactic acid bacteria. *World J. Microbiol. Biotechnol.* **2012**, *28*, 2435−2440.

(5) Burattini, S.; Salucci, S.; Baldassarri, V.; Accorsi, A.; Piatti, E.; Madrona, A.; Espartero, J. L.; Candiracci, M.; Zappia, G.; Falcieri, E. Anti-apoptotic activity of hydroxytyrosol and hydroxytyrosyl laurate. *Food Chem. Toxicol.* **2013**, *55*, 248−256.

(6) Rodriguez-Gutierrez, G.; Duthie, G. G.; Wood, S.; Morrice, P.; Nicol, F.; Reid, M.; Cantlay, L. L.; Kelder, T.; Horgan, G. W.; Guzman, J. F. B.; de Roos, B. Alperujo extract, hydroxytyrosol, and 3,4-dihydroxyphenylglycol are bioavailable and have antioxidant properties in vitamin E-deficient ratsua proteomics and network analysis approach. *Mol. Nutr. Food Res.* **2012**, *56*, 1131−1147.

(7) Visioli, F.; Bellomo, G.; Galli, C. Free radical-scavenging properties of olive oil polyphenols. *Biochem. Biophys. Res. Commun.* **1998**, *247*, 60−64.

(8) Bernini, R.; Crisante, F.; Barontini, M.; Tofani, D.; Balducci, V.; Gambacorta, A. Synthesis and structure/antioxidant activity relationship of novel catecholic antioxidant structural analogues to hydroxytyrosol and its lipophilic esters. *J. Agric. Food Chem.* **2012**, *60*, 7408−7416.

(9) Jemai, H.; Bouaziz, M.; Fki, I.; El Feki, A.; Sayadi, S. Hypolipidimic and antioxidant activities of oleuropein and its hydrolysis derivative-rich extracts from Chemlali olive leaves. *Chem.-Biol. Interact.* **2008**, *176*, 88−98.

(10) Oliveras-López, M. J.; Berná, G.; Carneiro, E. M.; López-García de la Serrana, H.; Martín, F.; López, M. C. An extra-virgin olive oil rich in polyphenolic compounds has antioxidant effects in OF1 mice. *J. Nutr.* **2008**, *138*, 1074−1078.

(11) Casaburi, I.; Puoci, F.; Chimento, A.; Sirianni, R.; Ruggiero, C.; Avena, P.; Pezzi, V. Potential of olive oil phenols as chemopreventive and therapeutic agents against cancer: A review of in vitro studies. *Mol. Nutr. Food Res.* **2013**, *57*, 71−83.

(12) Bouallagui, Z.; Han, J.; Isoda, H.; Sayadi, S. Hydroxytyrosol rich extract from olive leaves modulates cell cycle progression in MCF-7 human breast cancer cells. *Food Chem. Toxicol.* **2011**, *49*, 179−184.

(13) Sirianni, R.; Chimento, A.; De Luca, A.; Casaburi, I.; Rizza, P.; Onofrio, A.; Iacopetta, D.; Puoci, F.; Ando, S.; Maggiolini, M.; Pezzi, V. Oleuropein and hydroxytyrosol inhibit MCF-7 breast cancer cell proliferation interfering with ERK1/2 activation. *Mol. Nutr. Food Res.* **2010**, *54*, 833−840.

(14) Han, J.; Talorete, T. P.; Yamada, P.; Isoda, H. Anti-proliferative and apoptotic effects of oleuropein and hydroxytyrosol on human breast cancer MCF-7 cells. *Cytotechnology* **2009**, *59*, 45−53.

(15) Fabiani, R.; De Bartolomeo, A.; Rosignoli, P.; Servili, M.; Montedoro, G. F.; Morozzi, G. Cancer chemoprevention by hydroxytyrosol isolated from virgin olive oil through G(1) cell cycle arrest and apoptosis. *Eur. J. Cancer Prev.* **2002**, *11*, 351−358.

(16) Fernández-Mar, M. I.; Mateos, R.; García-Parrilla, M. C.; Puertas, B.; Cantos-Villar, E. Bioactive compounds in wine: resveratrol, hydroxytyrosol and melatonin: A review. *Food Chem.* **2012**, *130*, 797−813.

(17) Covas, M. I.; Nyyssonen, K.; Poulsen, H. E.; Kaikkonen, J.; Zunft, H. J.; Kiesewetter, H.; Gaddi, A.; de la Torre, R.; Mursu, J.; Baumler, H.; Nascetti, S.; Salonen, J. T.; Fito, M.; Virtanen, J.; Marrugat, J. The effect of polyphenols in olive oil on heart disease risk factors: A randomized trial. *Ann. Intern. Med.* **2006**, *145*, 333−341.

(18) Dell'Agli, M.; Maschi, O.; Galli, G. V.; Fagnani, R.; Dal Cero, E.; Caruso, D.; Bosisio, E. Inhibition of platelet aggregation by olive oil phenols via cAMP-phosphodiesterase. *Br. J. Nutr.* **2008**, *99*, 945−951.

(19) Petroni, A.; Blasevich, M.; Salami, M.; Papini, N.; Montedoro, G. F.; Galli, C. Inhibition of platelet aggregation and eicosanoid production by phenolic components of olive oil. *Thromb. Res.* **1995**, *78*, 151−160.

(20) González-Santiago, M.; Martín-Bautista, E.; Carrero, J. J.; Fonollá, J.; Baró, L.; Bartolomé, M. V.; Gil-Loyzaga, P.; Lopez-Huertas, E. One-month administration of hydroxytyrosol, a phenolic antioxidant present in olive oil, to hyperlipemic rabbits improves blood lipid profile, antioxidant status and reduces atherosclerosis development. *Atherosclerosis* **2006**, *188*, 35−42.

(21) Manna, C.; Napoli, D.; Cacciapuoti, G.; Porcelli, M.; Zappia, V. Olive oil phenolic compounds inhibit homocysteine-induced endothelial cell adhesion regardless of their different antioxidant activity. *J. Agric. Food Chem.* **2009**, *57*, 3478−3482.

(22) de Bock, M.; Derraik, J. G. B.; Brennan, C. M.; Biggs, J. B.; Morgan, P. E.; Hodgkinson, S. C.; Hofman, P. L.; Cutfield, W. S. Olive (*Olea europaea L.*) leaf polyphenols improve insulin sensitivity in middle-aged overweight men: a randomized, placebo-controlled, crossover trial. *PLOS One* **2013**, *8*, e57622−e57630.

(23) Hamden, K.; Allouche, N.; Jouadi, B.; El-Fazaa, S.; Gharbi, N.; Carreau, S.; Damak, M.; Elfeki, A. Inhibitory action of purified hydroxytyrosol from stored olive mill waste on intestinal disaccharidases and lipase activities and pancreatic toxicity in diabetic rats. *Food Sci. Biotechnol.* **2010**, *19*, 439−447.

(24) Kawaguchi, K.; Matsumoto, T.; Kumazawa, Y. Effects of antioxidant polyphenols on TNF-alpha-related diseases. *Curr. Top. Med. Chem.* **2011**, *11*, 1767−1779.

(25) Schaffer, S.; Podstawa, M.; Visioli, F.; Bogani, P.; Muller, W. E.; Eckert, G. P. Hydroxytyrosol-rich olive mill wastewater extract protects brain cells in vitro and ex vivo. *J. Agric. Food Chem.* **2007**, *55*, 5043−5049.

(26) Schaffer, S.; Müller, W. E.; Eckert, G. P. Cytoprotective effects of olive mill wastewater extract and its main constituent hydroxytyrosol in PC12 cells. *Pharmacol. Res.* **2010**, *62*, 322−327.

(27) Bazoti, F. N.; Bergquist, J.; Markides, K.; Tsarbopoulos, A. Noncovalent interaction between amyloid-beta-peptide (1−40) and oleuropein studied by electrospray ionization mass spectrometry. *J. Am. Soc. Mass Spectrom.* **2006**, *17*, 568−575.

(28) González-Correa, J. A.; Navas, M. D.; Lopez-Villodres, J. A.; Trujillo, M.; Espartero, J. L.; de La Cruz, J. P. Neuroprotective effect of hydroxytyrosol and hydroxytyrosol acetate in rat brain slices subjected to hypoxia-reoxygenation. *Neurosci. Lett.* **2008**, *446*, 143−146.

(29) Visioli, F.; Galli, C.; Galli, G.; Caruso, D. Biological activities and metabolic fate of olive oil phenols. *Eur. J. Lipid Sci. Technol.* **2002**, *104*, 677−684.

(30) Visioli, F.; Bernardini, E. Extra virgin olive oil's polyphenols: biological activities. *Curr. Pharm. Des.* **2011**, *17*, 786−804.

(31) Visioli, F.; Galli, C.; Plasmati, E.; Viappiani, S.; Hernandez, A.; Colombo, C.; Sala, A. Olive phenol hydroxytyrosol prevents passive smoking-induced oxidative stress. *Circulation* **2000**, *102*, 2169−2171.

(32) Capasso, G.; Di Gennaro, C. I.; Della Ragione, F.; Manna, C.; Ciarcia, R.; Florio, S.; Perna, A.; Pollastro, R. M.; Damiano, S.; Mazzoni, O.; Galletti, P.; Zappia, V. In vivo effect of the natural antioxidant hydroxytyrosol on cyclosporine nephrotoxicity in rats. *Nephrol., Dial., Transplant.* **2008**, *23*, 1186−1195.
(33) Li, J. Q.; Yang, G.; Wang, S. P.; Jiang, L. P.; Liu, X. F.; Geng, C. Y.; Zhong, L. F.; Chen, M. The protective effects of hydroxytyrosol against ortho-phenylphenol-induced DNA damage in HepG2 cells. *Toxicol. Mech. Methods* **2012**, *22*, 432−437.
(34) Furneri, P. M.; Piperno, A.; Sajia, A.; Bisignano, G. Antimycoplasmal activity of hydroxytyrosol. *Antimicrob. Agents Chemother.* **2004**, *48*, 4892−4894.
(35) Yangui, T.; Sayadi, S.; Rhouma, A.; Dhouib, A. Potential use of hydroxytyrosol-rich extract from olive mill wastewater as a biological fungicide against Botrytis cinerea in tomato. *J. Pestic. Sci.* **2010**, *83*, 437−445.
(36) Fki, I.; Sahnoun, Z.; Sayadi, S. Hypocholesterolemic effects of phenolic extracts and purified hydroxytyrosol recovered from olive mill wastewater in rats fed a cholesterol-rich diet. *J. Agric. Food Chem.* **2007**, *55*, 624−631.
(37) Kohyama, N.; Nagata, T.; Fujimoto, S.; Sekiya, K. Inhibition of arachidonate lipoxygenase activities by 2-(3, 4-dihydroxyphenyl) ethanol, a phenolic compound from olives. *Biosci., Biotechnol., Biochem.* **1997**, *61*, 347−350.
(38) Léger, C. L.; Carbonneau, M. A.; Michel, F.; Mas, E.; Monnier, L.; Cristol, J. P.; Descomps, B. A thromboxane effect of a hydroxytyrosol-rich olive oil wastewater extract in patients with uncomplicated type I diabetes. *Eur. J. Clin. Nutr.* **2005**, *59*, 727−730.
(39) de la Puerta, R.; Gutierrez, V. R.; Hoult, J. R. S. Inhibition of leukocyte 5-lipoxygenase by phenolics from virgin olive oil. *Biochem. Pharmacol.* **1999**, *57*, 445−449.
(40) Carluccio, M. A.; Siculella, L.; Ancora, M. A.; Massaro, M.; Scoditti, E.; Storelli, C.; Visioli, F.; Distante, A.; De Caterina, R. Olive oil and red wine antioxidant polyphenols inhibit endothelial activation: antiatherogenic properties of Mediterranean diet phytochemicals. *Arterioscler. Thromb. Vasc. Biol.* **2003**, *23*, 622−629.
(41) Visioli, F.; Galli, C.; Bornet, F.; Mattei, A. Olive oil phenolics are dose-dependently absorbed in humans. *FEBS Lett.* **2000**, *468*, 159−160.
(42) Weinbrenner, T.; Fito, M.; de la Torre, R.; Saez, G. T. Olive oils high in phenolic compounds modulate oxidative/antioxidative status in men. *J. Nutr.* **2004**, *134*, 2314−2321.
(43) Pinto, J.; Paiva-Martins, F.; Corona, G.; Debnam, E. S.; Oruna-Concha, M. J.; Vauzour, D.; Gordon, M. H.; Spencer, J. P. E. Absorption and metabolism of olive oil secoiridoids in the small intestine. *Br. J. Nutr.* **2011**, *105*, 1607−1618.
(44) Miro-Casas, E.; Covas, M. I.; Farre, M.; Fito, M.; Ortuno, J.; Weinbrenner, T.; Roset, P.; de la Torre, R. Hydroxytyrosol disposition in humans. *Clin. Chem.* **2003**, *49*, 945−952.
(45) D'Angelo, S.; Manna, C.; Migliardi, V.; Mazzoni, O.; Morrica, P.; Capasso, G.; Pontoni, G.; Galletti, P.; Zappia, V. Pharmacokinetics and metabolism of hydroxytyrosol, a natural antioxidant from olive oil. *Drug Metab. Dispos.* **2001**, *29*, 1492−1498.
(46) Corona, G.; Tzounis, X.; Dessi, M. A.; Deiana, M.; Debnam, E. S.; Visioli, F.; Spencer, J. P. E. The fate of olive oil polyphenols in the gastrointestinal tract: implications of gastric and colonic microflora-dependent biotransformation. *Free Radical Res.* **2006**, *40*, 647−658.
(47) Caruso, D.; Visioli, F.; Patelli, R.; Galli, C.; Galli, G. Urinary excretion of olive oil phenols and their metabolites in humans. *Metabolism* **2001**, *50*, 1426−1428.
(48) Visioli, F.; Galli, C.; Grande, S.; Colonnelli, K.; Patelli, C.; Galli, G.; Caruso, D. Hydroxytyrosol excretion differs between rats and humans and depends on the vehicle of administration. *J. Nutr.* **2003**, *133*, 2612−2615.
(49) González-Santiagoa, M.; Fonolláa, J.; Lopez-Huertas, E. Human absorption of a supplement containing purified hydroxytyrosol, a natural antioxidant from olive oil, and evidence for its transient association with low-density lipoproteins. *Pharmacol. Res.* **2010**, *61*, 364−370.
(50) Zafra-Gómez, A.; Luzón-Toro, B.; Capel-Cuevas, S.; Morales, J. C. Stability of hydroxytyrosol in aqueous solutions at different concentration, temperature and with different ionic content: a study using UPLC-MS. *Food Nutr. Sci.* **2011**, *2*, 1114−1120.
(51) Zhang, X. M.; Liu, C.; Zhao, C. H. Antagonism of hydroxytyrosol on male reproductive toxicity of PFOS. *Chin. J. Public Health* **2013**, *29*, 699−701.
(52) D'Angelo, S.; Manna, C.; Migliardi, V. Pharmacokinetics and metabolism of hydroxytyrosol, a natural antioxidant from olive oil. *Drug Metab. Dispos.* **2001**, *29*, 1492−1498.
(53) Christian, M. S.; Sharper, V. A.; Hoberman, A. M. The toxicity profile of hydrolyzed aqueous olive pulp extract. *Drug Chem. Toxicol.* **2004**, *27*, 309−330.
(54) Soni, M. G.; Burdock, G. A.; Christian, M. S.; Bitler, C. M.; Crea, R. Safety assessment of aqueous olive pulp extract as an antioxidant or antimicrobial agent in foods. *Food Chem. Toxicol.* **2006**, *44*, 903−915.
(55) Auñon-Calles, D.; Canut, L.; Visioli, F. Toxicological evaluation of pure hydroxytyrosol. *Food Chem. Toxicol.* **2013**, *55*, 498−504.
(56) Auñon-Calles, D.; Giordano, E.; Bohnenberger, S.; Visioli, F. Hydroxytyrosol is not genotoxic in vitro. *Pharmacol. Res.* **2013**, *74*, 87−93.

bioindicators because <1% of microorganisms can be isolated from soil.[12]

Among soil enzymes, phosphatase is one of the most important enzymes. It is involved in nutrient cycling, mineralization, and plant nutrition and provides soil organic phosphorus (P).[13] The description of the action of these enzymes on P cycling is fully described in the literature.[14−17] Both acid and alkaline phosphomonoesterases can be found in soils according to the pH medium. Because phosphatases are involved in P cycling, which is essential for plant nutrition and soil fertility, the maintenance, preservation, and understanding of the behavior and the factors affecting these enzymes on soil are very important to ensure soil quality, plant growth, and agricultural productivity.

The aim of this study was to evaluate the effect of OM and CM on acid phosphomonoesterase (AcP) and alkaline phosphomonoesterase (AkP) and which factors within these soils would contribute the most with the variation on this enzyme activity on soil. For that, AcP and AkP activities were measured in soils under OM and CM, and the results were compared with those found for the native soil (NS), without any agricultural practices. The main physicochemical characteristics of soils that may affect AcP activity were also assayed.

MATERIALS AND METHODS

Materials. *p*-Nitrophenyl disodium phosphate was purchased from Sigma-Aldrich Co. (St. Louis, MO, USA). All other reagents were of analytical reagent grade and were used without further purification unless otherwise specified. Solutions were prepared with distilled deionized water.

Site Description and Soil Sampling. Soil samples were collected from areas under OM and CM sugar cane crop and NS field in Goiás, Brazil. Samples of up to 15 cm of soil were collected on December 13, 2011. This region is under tropical climate. For the season of November 2011, the rainfall precipitation was 279.4 mm; on average, the temperature was minimum 20 °C and maximum 30.8 °C.

There were three replications per land use type, and each replication was composed of three soil sample cores. Fresh samples were sieved (<2 mm) after removal of debris and stored at −8 °C for AcP assay. The geographical coordinates for CM replications were as follows: CM 1, 18.06806° S and 49.71139° W; CM 2, 18.06383° S and 49.71093° W; CM 3, 18.06384° S and 49.70392° W. For OM, the coordinates were as follows: OM 1, 18.07656° S and 49.67653° W; OM 2, 18.07394° S and 49.67653° W; OM 3, 18.07455° S and 49.68620° W. The coordinates for NS were as follows: NS 1, 18.07710° S and 49.67603° W; NS 2, 18.07912° S and 49.68508° W; NS 3, 18.08009° S and 49.68508° W.

To standardize the amount of soil weighed in each test, moisture was determined from weight loss after the samples had been dried at 105 °C for 48 h.

The area under OM has been treated with this management for 10 years. The cultivated area was fertigated with vinasse (average of 436 m^3/ha per year) and received 29.1 ton/ha of an organic compound that includes sugar cane bagasse and filter cake.

The area under CM has been treated with this management for more than 10 years. This area was fertigated with vinasse (average 306 m^3/ha per year). In addition, this area was also treated with commercial pesticides and fertilizers. In the past three years, the chemical compounds used in CM were amonium nitrate, amonium phosphate, (*RS*)-5-amino-1-(2,6-dichloro-α,α,α-trifluoro-*p*-tolyl)-4-trifluoromethylsulfinylpyrazole-3-carbonitrile, 3-(3,4-dichlorophenyl)-1,1-dimethylurea, 3-cyclohexyl-6-dimethylamino-1-methyl-1,3,5-triazine-2,4(1*H*,3*H*)-2′,4′-dichloro-5-(4-difluoromethyl-4,5-dihydro-3-methyl-5-oxo-1*H*-1,2,4-triazol-1-yl)methanesulfonanilide, limestone, gypsum, and a herbicide of the organoarsenic family.

The area under NS is a preserved Cerrado area in the sugar cane mill property, presenting the features of the vegetation of this biome, and has not been explored for any agriculture or livestock.

All of the managements in the study area were under rotation with *Crotalaria juncea* every 5 years.

Physicochemical Analyses. Physicochemical analyses were performed at the Laboratory of Soil Analysis of the School of Agronomy at Universidade Federal de Goiás according to methodology described by EMBRAPA.[18]

The analyses included the determination of clay, silt, and sand percentage (soil granulometry), soil organic matter (SOM), pH using $CaCl_2$ determined by potenciometer, saturation of acids (M %), saturation of alkalis (V %), potential acidity total (H^++Al^{3+} $cmol_c/dm^3$) determined by Schoemaker, McLean, and Pratt buffer (SMP),[19] aluminum (Al^{3+} $cmol_c/dm^3$) extracted with 1 mol/L KCl and determined by volumetric titration, inorganic phosphorus (P^+ $cmol_c/dm^3$, extracted by Mehlich 1 and determined by colorimetry), potassium (K^+ $cmol_c/dm^3$) extracted by a Mehlich 1 extractor and determined by flame photometry, magnesium (Mg^{2+} $cmol_c/dm^3$) and calcium (Ca^{2+} $cmol_c/dm^3$) extracted with 1 mol/L KCl and determined by atomic absorption spectrophotometry, and cation exchangeable capacity (CEC), Ca/K, Ca/Mg, Mg/K, Ca/CEC, K/CEC, and Mg/CEC.

All tests were carried out in triplicates and are shown as the mean ± standard deviation.

Optimum pH and Enzyme Assay. To determine the optimum pH for the measurement of enzyme activity, the reaction was performed at pH 2.0, 3.0, and 4.0 (0.1 M glycin buffer), pH 5.0 and 5.5 (0.1 M acetate buffer), pH 6.0 (0.1 M sodium citrate buffer), pH 7.0 and 8.0 (0.1 M TRIS buffer), and pH 9.0 and 11.0 (0.1 M glycin buffer) using samples from NS because it presents the natural conditions for native phosphatases from Cerrado.

The assay was performed following the standard methodology for phosphatase measurement described by Eivazi and Tabatabai[15] with modifications. The reaction was conducted using 16 mg of soil, 0.4 mL of the respective buffer, and 0.1 mL of 2.5 mM *p*-nitrophenyl disodium phosphate. The mixture reacted at 55 °C for 1 h. Then, 0.1 mL of 0.5 M Na_2CO_3 was added followed by the addition of 0.4 mL of 0.1 M NaOH to stop the reaction. The mixture was centrifuged and the supernatant measured at 400 nm using a UV−vis spectrophotometer. A control was performed by adding NaOH followed by Na_2CO_3 to stop the reaction immediately after addition of the substrate. One enzyme unit (U) was defined as the amount of enzyme that released 1 mg of *p*-nitrophenol (pNP) after 1 h of reaction per gram of soil.

After determination of the optimum pH for acid (AcP) and alkaline (AkP) phosphomonoesterase, the enzyme activity was tested in the different soil samples according to the description above. AcP was measured using 0.1 M acetate buffer, pH 5.0, for all samples or with 0.1 M citrate buffer, pH 5.6 for CM and pH 5.7 for OM. AkP was measured in pH 8.0 using 0.1 M TRIS buffer, pH 8.0.

Statistical Analyses. All experiments were conducted at least in triplicate, and the results were processed by central tendency (mean) and dispersion (standard deviation) measurements. Statistica software 7.0 (StatSoft Inc., Tulsa, OK, USA) was used to perform multivariate analysis (ANOVA) followed by correlation, as well as Tukey's test, to determine the significant differences among the means. The *p* level of significance used was 0.05.

Principal component analysis (PCA) was performed to evaluate the variables that would interfere in AcP activity according to soil management. Only principal components with eigen values that explain 10% of the total variance were retained. A Varimax rotation was performed to enhance the interpretability of the unrelated components.[20]

RESULTS

Physicochemical Characteristics. In regard to clay, silt, and sand, there were differences in the particle size distribution in the soils (Table 1). Even though Cerrado soils present a high percentage of sand (CM 37%; OM 54%; NS 44%), they are

Table 1. Amounts of Clay, Silt, Sand, and SOM and pH in the Cropped and Native Soils[a]

	management		
	conventional	organic	native soil
clay %	39a ± 1.4	34b ± 2.8	35ab ± 2.8
silt %	25a ± 0.9	16b ± 1.4	17b ± 1.1
sand %	37b ± 1.2	54a ± 1.1	44b ± 7.6
SOM %	2.9a ± 0.5	2.9a ± 0.6	3.0a ± 0.5
pH	5.6a ± 0.1	5.7a ± 0.2	4.9b ± 0.1

[a]Results are means ± standard deviation of three determinations. Data followed by the same letters in the same rwo are not significantly different ($p > 0.05$).

considered loamy.[18] The amounts of clay in the soils tested were CM 39%, OM 34%, and NS 35%.

Physicochemical analysis showed that there were no statistical differences in the SOM content among the samples tested ($p > 0.05$) (CM 2.9%; OM 2.9%; NS 3.0%).

Except for Mg^{2+}, there was significant difference of K^+ and inorganic P^+ contents (Table 2). The results showed higher K^+ and inorganic P^+ in OM (K^+ 0.25 $cmol_c/dm^3$; P^+ 11.3×10^{-3} $cmol_c/dm^3$) than in CM (K^+ 0.13 $cmol_c/dm^3$, P^+ 1.2×10^{-3} $cmol_c/dm^3$) and NS (K^+ 0.17 $cmol_c/dm^3$; P^+ 3×10^{-3} $cmol_c/dm^3$). The amount of Ca^{2+} was also different in all tested soils, with higher values in OM (2.6 $cmol_c/dm^3$).

The saturation of alkaline ions (V %) represents the capacity of a soil to exchange alkaline cations such as K^+, Mg^{2+}, and Ca^{2+}. The amounts of K^+, Mg^{2+}, and Ca^{2+} adsorbed on clay were higher in OM (71%) and CM (54%) (Table 2). This means that soils used in agriculture present more cations with exchangeable capacity than NS (35%), which is a consequence of management practices such as fertilizer addition in OM and CM.

The results showed that soil pH values in the cultivated areas (5.6 in CM and 5.7 in OM) were higher than in the NS (4.9). This pH variation among the studied soils occurred as a consequence of liming, which is also the reason for the higher amount of Ca^{2+} in cultivated soils.

Cerrado soils are known for presenting a high amount of aluminum, which is toxic for many plants by causing plasmolysis on plant roots. This problem is overcome by the precipitation of Al^{3+} by addition of limestone, which is converted in the soil into $Ca(OH)_2$, causing the precipitation of Al^{3+} by the formation of $Al(OH)_3$. The results showed the presence of Al^{3+} in NS (0.7 $cmol_c/dm^3$) and its absence in the cultivated soils.

Optimum pH. Figure 1 depicts the activity of phosphomonoesterases in NS expressed as U (mg^{-1} g^{-1} h^{-1}). The figure

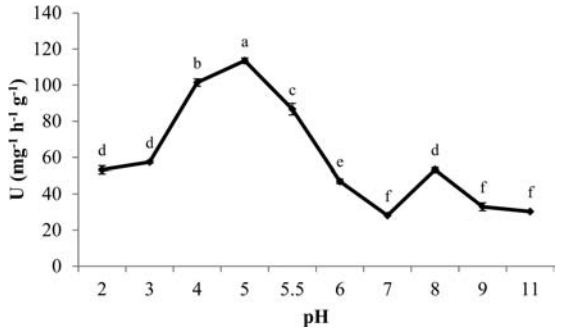

Figure 1. Effect of pH on the activity of phosphomonoesterase from native soil.

shows AcP presented a considerably higher activity than AkP and that the optimum pH values for AcP and AkP activity were pH 5 (113.5 U) and pH 8 (53.3 U), respectively.

Acid and Alkaline Phosphomonoesterase Activity in NS, OM, and CM. There was no difference in the AkP activity between the cultivated areas and NS, considering most of the samples (average of activity in CM 33.5 U, OM 31.5 U, and NS 39 U) (Figure 2). This result implies that sugar cane

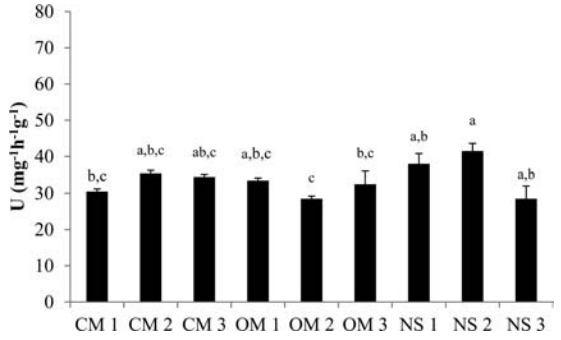

Figure 2. Alkaline phosphomonoesterase activity in cropped (organic and conventional management) and native soils.

management did not affect AkP activity. On the other hand, AcP activity is quite different among cultivated areas and NS (Figure 3). The activity observed in the NS (average of 96 U) was considerably higher than in the soils with sugar cane agriculture (average of CM 47.3 U and OM 45.6 U). In the original pH of soil, CM presented an average enzyme activity of 61.6 U and OM, 49 U.

Effects of Soil Physicochemical Characteristics on Acid Phosphomonoesterase Activity. An additional approach to estimate the relationship among physicochemical

Table 2. Values of Ions and Alkali Saturation (V %) on Cropped and Native Soils[a]

	management		
	conventional	organic	native soil
extractable P ($cmol_c/dm^3$)	1.2×10^{-3}b ± 0.0005	11.3×10^{-3}a ± 0.008	2×10^{-3}b ± 0.0007
extractable K ($cmol_c/dm^3$)	0.13b ± 0.02	0.25a ± 0.02	0.17b ± 0.05
extractable Ca ($cmol_c/dm^3$)	1.5b ± 0.3	2.6a ± 0.4	0.5c ± 0.2
extractable Mg ($cmol_c/dm^3$)	0.4a ± 0.1	0.6a ± 0.1	0.5a ± 0.2
V %	54a ± 8.2	71a ± 9.2	35b ± 10.2
CEC ($cmol_c/dm^3$)	4.6a ± 0.3	3.4b ± 0.7	3.3b ± 0.5

[a]Results are means ± standard deviation of three determinations. Data followed by the same letters in the same row are not significantly different ($p > 0.05$).

dx.doi.org/10.1021/jf403141w | J. Agric. Food Chem. 2014, 62, 1456−1463

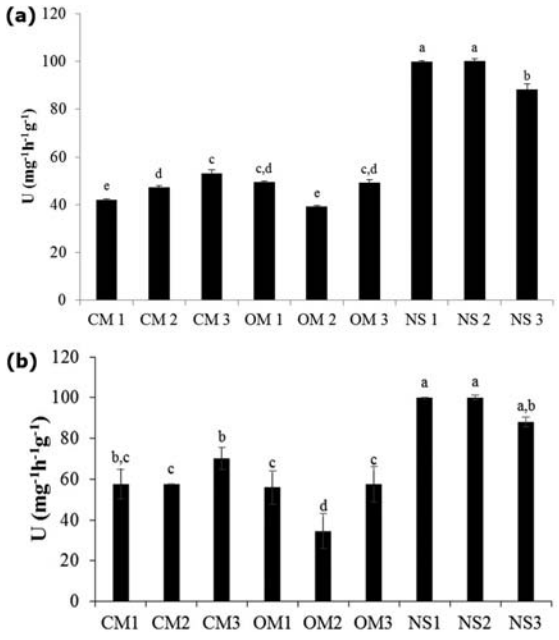

Figure 3. Acid phosphomonoesterase activity in cropped (organic and conventional management) and native soils in pH 5.0 (a) and in the natural pH for OM (5.7), CM (5.6), and NS (5.0) (b).

factors and AcP activity and to allow the distinction concerning these data, PCA was carried (Figure 4). PCA often reveals previously unexpected associations among variables and thereby allows interpretation that would not be possible otherwise.[21]

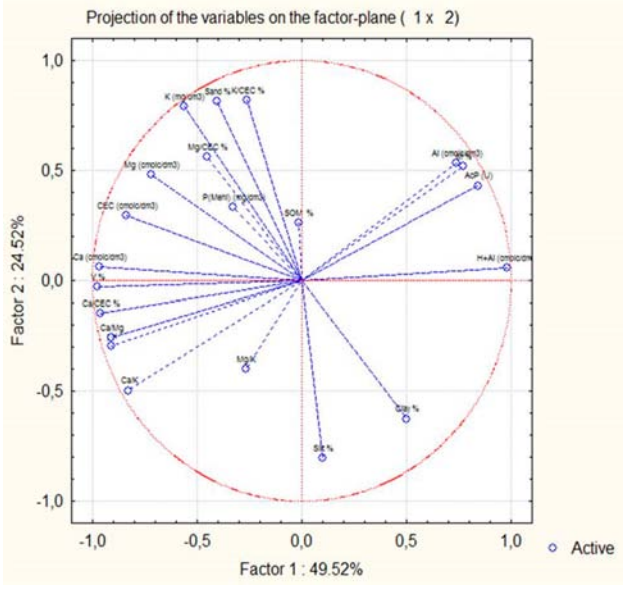

Figure 4. Principal component analysis of the soil physicochemical characteristics and acid phosphomonoesterase activity from organic and conventional management and native soils.

PCA (Table 3) showed that there were two factors explaining the variance of the data. Factor 1 explained 49.5% of the total of variance. The total of variance of this factor is defined by AcP, pH, Ca^{2+} ($cmol_c/dm^3$), Mg^{2+} ($cmol_c/dm^3$), H+Al, Al^{3+} ($cmol_c/dm^3$), CEC ($cmol_c/dm^3$), M %, and V %. Factor 2 explained 24.5% and is defined by silt %, sand %, and

Table 3. Principal Component Loadings after Varimax Rotation[a]

measurement	principal components[b] PC 1	PC 2
eigen values	10.4	5.1
explained variance %	49.5	24.5
rotated loading on two retained components[c]		
AcP	**0.8**	0.4
clay	0.5	−0.6
silt	0.1	**−0.8**
sand	−0.4	**0.8**
SOM	−0.01	0.26
pH	**−0.9**	−0.3
extractable P^+	−0.3	0.3
extractable K	−0.5	**0.7**
extractable Ca	**-0.9**	0.06
extractable Mg	**−0.7**	0.4
H+Al	**0.9**	0.05
extractable Al	**0.7**	0.5
CEC	**−0.8**	0.2
M	**0.7**	0.5
V	**−0.9**	−0.02
Ca/Mg	**−0.9**	−0.2
Mg/K	−0.2	−0.4
Ca/K	**−0.8**	−0.4
Ca/CEC	**−0.9**	−0.1
Mg/CEC	0.1	0.4
K/CEC	−0.2	**0.8**

[a]The soil parameters are grouped according to the maximum fittings to principal components (correlation coefficients > 0.50; n = 21). [b]Only principal components with eigen values >1 and those explaining >10% of the total variance were retained. [c]Correlations with absolute values >0.50 are in bold.

K^+ (mg/dm^3). Factor 1 is related to pH and CEC, and factor 2 is related to the soil's granulometry.

From the results of PCA (Figure 4), for AcP activity, it can be seen that this enzyme presentd a greater relationship with NS than with OM and CM and that the main factors related to AcP were those influencing soil pH, which is demonstrated by the high values and proximity of the loadings of aluminum and H^++Al^{3+}.

The correlation matrix showed positive correlations between AcP and H+Al (r = 0.8), Al^{3+} (r = 0.9), and M % (r = 0.9). However, negative correlations with AcP were found for pH (r = −0.8), Ca^{2+} (r = −0.8), and V % (r = −0.8).

According to PCA, granulometry also seems to be related to AcP activity. In fact, Table 1 shows a higher amount of sand in OM than in CM and NS and clay appears to be more related to AcP.

DISCUSSION

Soil Physicochemical Characteristics and Acid Phosphomonoesterase Activity. Cerrado soils present color variations from red to yellow and are classified as haplustox dystrophic.[18] They are deep and well-drained during the major part of the year, making them vulnerable to leaching, contributing to their low CEC (Table 1). This characteristic is related to the granulometry of soil particles, especially the sand content (Table 1). Even though Cerrado soils present a high percentage of sand, they are considered loamy because clay appears in a percentage >20% (Table 1). Loamy soils are

dx.doi.org/10.1021/jf403141w | J. Agric. Food Chem. 2014, 62, 1456−1463

generally considered fertile; however, Cerrado soils present low active clay, 1:1 of minerals proportion, making them less fertile soils.

It is important to consider a soil's granulometry when soil enzymes are studied, because they are often immobilized onto these particles. Several authors reported that enzyme immobilization on soil particles provides stability to this biocatalyst against unfavorable soil environment.[22,23] Then, the smaller the particle size, the higher the area available for enzyme immobilization. Indeed, considering that Cerrado soils present a high amount of clay, it is possible to assume that these soils constitute a favorable environment for soil enzymes. AcP produced by *Heloma cylindrosporum* and *Suillus collinitus* strains presented more affinity for clay than the other soil size fractions.[24] In addition, it has also been reported that clay with 1:1 minerals was able to retain more enzymes catalytically active.[25]

In fact, results from PCA showed a relationship between AcP activity and soil granulometry. Sand and silt are explained by factor 2 and are more related with OM and CM. Indeed, Table 1 shows a higher amount of sand on OM and a higher amount of silt on CM.

This result means that, apparently, the reduction of AcP activity on these soils is also affected by the size of the soil's granulometry because the support for enzyme immobilization is responsible for protecting enzymes against denaturation factors and conditions.[26−28] Several authors reported the influence of soil granulometry on enzyme activity. They report that soil granulometry can affect enzymes in distinct ways.[10,25,29,30]

This finding is important because knowledge of how managements affect biochemical characteristics on soil may allow agricultural techniques that reduce management impact on soil quality. In fact, the amount of sand and silt in agricultural soil is indicative of the possible reduction of AcP activity.

Not only clay but also the SOM content is important to soil quality, because it also acts as a support for enzyme immobilization and can influence enzyme activity and stability.

However, there was no statistical difference ($p > 0.05$) of SOM content in the studied soils, suggesting that this parameter is not the most relevant factor affecting AcP activity. This is an interesting result considering that the quality of the organic matter is expected to change according to organic and conventional managements.[31,32] In this sense, despite the probable difference in the quality of SOM in the studied soils, this parameter did not significantly affect AcP activity. Different amounts of SOM were reported by several authors according to different locations, management, cover, and soil type.

It is well-known that soils from Cerrado are acid, present aluminum toxicity, and are poor in essential nutrients such as calcium, magnesium, potassium, and some micronutrients. In this sense, these soils require amendments to allow sugar cane agriculture. The quantification of K^+ and inorganic P^+ among the tested soils showed that OM presented higher amounts of these cations (Table 2).

This result indicates one of the effects of the application of vinasse, a residue from the fractional distillation of sugar cane, in OM and CM because this residue is rich in organic matter and nutrients, especially K^+.[33] The application of vinasse was more frequent in OM than in CM, because there were applications in 2008 (572 m^3/ha) and 2010 (300 m^3/ha), whereas in CM there was application only in 2010 (306 m^3/ha).

The higher amount of vinasse applied in OM might be due to OM requirements, because only the addition of organic fertilizers is allowed, and it would also be an attempt to overcome the lower productivity of OM due to the presence of high amounts of nutrients in this residue. In addition, filter cake, another organic residue from the industrial processing of sugar cane, is also added to OM soil as fertilizer. This residue is rich in P^+, which contributes to its higher amount in OM. Then, the residual effect of vinasse and filter cake application over the years explains the high amount of some nutrients in soil, mainly K^+ and P^+.

Potassium is a very important macronutrient for sugar cane and is the most required nutrient by this culture. Among the functions of K^+ in sugar cane is the productivity effect. An adequate amount of K^+ is important to the conversion of sugars in sucrose,[34] to increase the amount of carbohydrates, oils, and proteins, and to promote sugar and starch storage. It also regulates water use in plants and increases resistance during dry periods. Additionally, an abundant amount of K^+ may interfere in the absorption of Ca^{2+} and Mg^{2+} by the plant.[35] The correlation matrix showed a positive correlation between K^+ and Ca^{2+} ($r = 0.6$) and between K^+ and Mg^{2+} ($r = 0.7$).

As can be observed in Table 2, the amount of potassium was higher in OM, and there was no statistical difference in the amount of K^+ between CM and NS ($p > 0.05$). Cerrado soil is poor in macronutrients such as potassium, and its vegetation is adapted to this condition. Haridasan[36] observed a low amount of potassium content in the biomass of Cerrado vegetal species, corroborating this adaptive mechanism. On the other hand, sugar cane presents a high demand for potassium, and it is added to the soil by different fertilization strategies used in OM and CM.

Shaviv et al.[37] reported that continuous addition of fertilizers in cultivated soils may cause a saturation effect, which may reduce its ability to fix the potassium added by fertilization. Therefore, the addition of fertilizers does not solve the problem of low nutrient content in soils because other factors in the composition must be considered.

In this scenario, the importance of soil particles is demonstrated by PCA. There was a positive correlation between K^+ and sand ($r = 0.9$) and a negative correlation between K^+ and clay ($r = -0.7$) and between K^+ and silt ($r = -0.7$). Murashkina et al.[38] studied the fixation of potassium in different soil size particles and reported that in soils with a predominant proportion of sand, this is the most important particle in the fixation of potassium. Because Cerrado soils present a high proportion of sand, especially in OM, this may be the explanation for the higher amount of potassium in this soil management.

This result indicates that the presence of nutrients in soils depends on the characteristics of the cover, management, biochemical factors, and proportion of soil size particles.

In regard to the amount of Ca^{2+}, liming is the main factor that contributes to the increased amount of this ion in the managed soils. OM presented the higher values among the tested soils. The effect of liming is also observed in the values of soil pH, which were higher in the cultivated areas (5.6 in CM and 5.7 in OM) than in the NS (4.9). This result explains part of the reduction on AcP activity in the cultivated soil (Figure 3). Liming is the agricultural practice responsible for increasing soil pH, and it explains the negative correlation between AcP activity and Ca^{2+}.

The saturation of alkaline ions (V %) represents the capacity of a soil to exchange alkaline cations such as K^+, Mg^{2+}, and Ca^{2+}. Soil with V % >50% is considered rich in nutrients or eutrophic, whereas V % <50% is poor in nutrients.[39] The amounts of K^+, Mg^{2+}, and Ca^{2+} adsorbed on clay were higher in OM and CM (Table 2). This means that managed soils present greater capacity of exchanging cations than NS.

However, it is important to point out that the value of V % alone does not guarantee soil quality, as it does not reflect the biochemical conditions of soil. Indeed, this result indicates that even though there are nutrients in soil, they may not be absorbed by plant nor perform their functions, because nutrient availability in soils depends not only on the presence of such nutrients but also on other soil conditions such as enzyme activities.

Moreover, these applications include nutrients ready for plant absorption. Then, if they do not aggregate with other soil fractions, they only attenuate the problem of nutrient losses by the agriculture practices and do not contribute to the maintenance and preservations of soil structure, biological, and biochemical characteristics that are important to preserve soil fertility.

Considering NS, the low value of V % is a consequence of the higher amount of H^+ and Al^{3+} sorbed on clay than the alkaline cations, which is characteristic of acid soils.

The acidity of soils influences the amount of Al^{3+} in it and affects its availability because an acid environment allows dissolution of Al^{3+} present in the clay structure. This process occurs especially in clay type 1:1 of minerals and the Al^{3+} released is toxic to plants, mainly to the Poaceae family. The addition of limestone to these soils decreases the Al^{3+} availability by the formation and precipitation of $Al(OH)_3$, which is not soluble in pH >5.5.[40,41]

Optimum pH. The optimum pH of a soil enzyme is not necessarily the same as the soil's. Nevertheless, enzyme activity is dependent on soil pH, because it affects the proper ionization, expression, enzyme stability, and release by soil microorganisms.[13] In this sense, it is important to assay the optimum pH for enzyme activity to establish the best catalysis conditions and to identify if the soil offers proper conditions for enzymatic catalysis.

Aiming to evaluate the effect of pH on phosphomonoesterase activity, tests were conducted on NS with pH ranging from 2 to 11 (Figure 1).

The presence of phosphatase activity is observed in both acid and alkaline ranges, with optimum at pH 5.0 and 8.0 for AcP and AkP, respectively. Despite the acid character of Cerrado soil, AkP were found in these samples. However, the AkP activity is remarkably lower (53.3 U) than that in AcP (113.5 U).

It is important to note that although most reports in the literature affirm that the optimum pH for assaying AcPs from soils is 6.5 or close to neutral[15,42] acid phosphatases from Cerrado soil did not follow the same profile. The optimum pH for AcP found in this study was 5.0, which is almost the same pH of the NS (pH 4.9).

Acid and Alkaline Phosphomonoesterase Activity in NS, OM, and CM. Another important result is that there was no difference of AkP activity between the cultivated areas and NS. This result implies that management does not affect AkP activity. The presence of AkP in acid soils such as soils from Cerrado is mainly from cell lyses of microorganisms and small animals and was adsorbed on clay or other solid component of soil that preserved its activity.

The lower activity of AkP is also explained because the expression of acid and alkaline phophomonoesterases is influenced by pH. Considering the acid pH of the soil samples, the microbial expression of AcP was induced in the tested soils, contributing to the higher amount of this enzyme compared to AkP. Therefore, AkP is not an effective enzyme to be used as a bioindicator of soil quality in acid soils.

Samples from the NS showed markedly higher AcP activity when compared to OM and CM. Moreover, it is noticeable that there was no difference between the two management practices, demonstrating that whatever the management is chosen, the enzyme activity is considerably affected.

Previous studies showed that agricultural practices affected biomass composition, enzyme activities, and organic and biomass C and that phosphatase activity was significantly greater in undisturbed soils compared to conventional agriculture.[43,44] Previous studies stated that a decrease in organic soil disturbance could improve microbial activity and it, consequently, would increase the synthesis and secretion of enzymes and that there were variations on enzyme activity due to different groundcover crops and soil tillage, demonstrating that enzymes are sensitive to soil disturbance.[41,45]

The activity found for AcP in NS from Cerrado (average of 96 U g^{-1}) was considerabley higher than that reported in the literature. In the best conditions for AcP catalysis, the maximum activity was 249 U kg^{-1} in a Kenyon loam soil (fine-loamy, mixed, mesic Typic Hapludoll) from Iowa,[46] USA. In a study about the effect of permanent cover crop from sandy Ultisol soil (Paraná, Brazil), the activity of AcP varied from 87 to 176 U kg^{-1}.[41] AcP had its activity affected in different management practices with activity varying from 200 to 300 U kg^{-1}; in addition, in this study organic C also influenced AcP with a maximum activity of 600 U^1 kg^{-1} in the presence of 3% of organic C.[43] Note that in these data, enzyme activity is given in U kg^{-1} and in this study AcP activity is expressed in U g^{-1} because of the high amount of this enzyme in Cerrado soils (NS).

The most important finding of this study is that OM affected AcP activity as well as CM. Some reports in the literature showed that OM presented better chemical, biochemical, and biological parameters compared to CM. Other studies have already observed that organic C was higher in OM than in CM. They also showed that OM presented higher mineralized C, potentially mineralized C, and basal respiration than CM.[1] However, soil microbial biomass and mineralized C per microorganism biomass unity showed no difference between OM and CM. Moreover, biological parameters such as the presence of arthropods sensitive to agriculture process was higher in CM than in OM.[45]

Another important observation is that the managed soils OM and CM did not favor any of the phosphatase forms (AcP and AkP) because the soil pH of OM and CM is higher than the optimum pH for AcP and lower than the optimum pH for AkP, compromising enzyme synthesis in these soils.

Conclusions. All of the results presented showed the importance of the identification of the physicochemical characteristic changes by the sugar cane management affecting soil enzymes. Reduction of AcP activity in both management practices, OM and CM, was observed. However, AkP activity was not affected by management.

Our results demonstrated that AcP is affected by soil pH and soil particle size. This enzyme showed higher activity in lower pH with optimum pH 5.0. Despite the acid characteristic of Cerrado soils, AkP was also found in the tested soil and presented optimum pH 8.0. This finding highlights the importance of research in soils because this ecosystem is still not well studied, especially with regard to the biological and biochemical characteristics, which are highly influenced and have particular characteristics according to the region, agricultural practice, and cultivated crop.

The presence of AkP in the tested soils demonstrated also the importance of the soil particle size for AcP and AkP, because according to PCA clay size particles are closely related with the enzyme activity because these particles support enzyme immobilization, contributing to the maintenance and protection of enzyme structure and activity, which also explains the presence of AkP on these soils becausse they do not offer favorable pH conditions for its secretion and hydrolysis.

AUTHOR INFORMATION

Corresponding Author

*(L.L.A.P.) E-mail: luizaluanna@gmail.com. Phone: +5562-35211492.

Funding

L. L. A. Purcena thanks FAPEGO and M. C. B. Di Medeiros thanks CAPES for fellowship support.

Notes

The authors declare no competing financial interest.

REFERENCES

(1) Mazzoncini, M.; Canali, S.; Giovannetti, M.; Castagnolli, M.; Tittarelli, F.; Antichi, D.; Nannelli, R.; Cristani, C.; Bàrberi, P. Comparison of organic and conventional stockless arable systems: a multidisciplinary approach to soil quality evaluation. *Appl. Soil Ecol.* **2010**, *44*, 124−134.

(2) Lopes, A. S. Soils under Cerrado: a success story in soil management. *Better Crops Int.* **1996**, *10*, 9−15.

(3) Lopes, A. S.; Guilherme, L. R. G. *Solos sob Cerrado: Manejo da Fertilidade para Produção Agropecuária*; ANDA: São Paulo, Brazil, 1994.

(4) Furtado, A. T.; Scandiffio, M. I. G.; Cortez, L. A. B. The Brazilian sugarcane innovation system. *Energy Policy* **2011**, *39*, 156−166.

(5) Klink, C. A.; Machado, R. B. Conservation of the Brazilian Cerrado. *Conservation Biol.* **2005**, *19*, 707−713.

(6) Ritz, K.; Black, H. I. J.; Campbell, C. D.; Harris, J. A.; Wood, C. Selecting biological indicators for monitoring soils: a framework for balancing scientific and technical opinion to assist policy development. *Ecol. Indicators* **2009**, *9*, 1212−1213.

(7) Martinez, C.; Hancock, G. R.; Kalma, J. D. Relationships between ^{137}Cs and soil organic carbon (SOC) in cultivated and never-cultivated soils: an Australian example. *Geoderma* **2010**, *158*, 137−147.

(8) Snapp, S. S.; Gentry, L. E.; Harwood, R. Management intensity − not biodiversity − the driver of ecosystem services in a long-term row crop experiment. *Agric., Ecosyst. Environ.* **2010**, *158*, 242−248.

(9) Dick, R. P.; Kandeler, E. Enzymes in soils. In *Encyclopedia of Soils in the Environment*; Hillel, D., Ed.; Elsevier: Oxford, UK, 2005; pp 448−455.

(10) Sarkar, J. M.; Leonovicz, A. Immobilization of enzymes on clays and soils. *Soil Biol. Biochem.* **1989**, *21*, 223−230.

(11) Gianfreda, L.; Rao, M. A.; Sannino, F.; Saccomandi, F.; Violante, A. Enzymes in soil: properties, behavior and potential applications. *Dev. Soil Sci.* **2002**, *28 B*, 301−327.

(12) Torsvik, V.; Ovreas, L. Microbial diversity and function in soil: from genes to ecosystems. *Curr. Opin. Microbiol.* **2002**, *5*, 240−245.

(13) Tabatabai, M. A. Soil enzymes. In *Methods of Soil Analysis: Microbiological and Biochemical Properties. Part 2 − Microbiological and Biochemical Properties*; Weaver, R. W., Angle, J. S., Bottomley, P. S., Eds.; Soil Science Society of America: Madison, WI, USA, 1994; pp 775−833.

(14) Zohar, I.; Shaviv, A.; Klass, T.; Roberts, K.; Paytan, A. A. Method for the analysis of oxygen isotopic composition of soil phosphate fractions. *Environ. Sci. Technol.* **2010**, *44*, 7583−7588.

(15) Eivazi, F.; Tabatabai, M. A. Phosphatases in soils. *Soil Biol. Biochem.* **1977**, *9*, 167−172.

(16) Liu, L.; Gundersen, P.; Zhang, T.; Mo, J. Effects of phosphorus addition on soil microbial biomass and community composition in three forest types in tropical China. *Soil Biol. Biochem.* **2012**, *44*, 31−38.

(17) Malcolm, R. E. Assessment of phosphatase activity in soils. *Soil Biol. Biochem.* **1983**, *15*, 403−408.

(18) Agropecuária-EMBRAPA, E. E. B. d. P. *Sistema Brasileiro de Classificação de Solos*, 2nd ed.; Serviço de Produção de Informação: Brasília, DF, Brazil, 1999; p 306.

(19) Shoemaker, H. E.; McLean, E. O.; Pratt, P. F. Buffer methods for determining lime requirements of soils with appreciable amounts of extractable aluminum. *Soil Sci. Soc.* **1961**, *25*, 274−277.

(20) Flury, B.; Riedwyl, H. *Multivariate Statistics. A Practical Approach*; Chapman and Hall: London, UK, 1988.

(21) Dinesh, R.; Srinivasan, V.; Hamza, S.; Parthasarathy, V. A.; Aipe, K. C. Physico-chemical, biochemical and microbial properties of the rhizospheric soils of tree species used as supports for black pepper cultivation in the humid tropics. *Geoderma* **2010**, *158*, 252−258.

(22) Yan, J.; Pan, G.; Ding, C.; Quan, G. Kinetic and thermodynamic parameters of -glucosidase immobilized on various colloidal particles from a paddy soil. *Colloids Surf., B* **2010**, *79*, 298−303.

(23) Huang, Q.; Zhu, J.; Qiao, X.; Cai, P.; Rong, X.; Liang, W.; Chen, W. Conformation, activity and proteolytic stability of acid phosphatase on clay minerals and soil colloids from an Alfisol. *Colloids Surf., B* **2009**, *74*, 279−283.

(24) Kedi, B.; Abadie, J.; Sei, J.; Quiquampoix, H.; Staunton, S. Diversity of adsorption affinity and catalytic activity of fungal phosphatases adsorbed on some tropical soils. *Soil Biol. Biochem.* **2012**, 1−8.

(25) Nannipieri, P.; Sequi, P.; Fusi, P. Humus and enzyme activity. In *Humic Substances in Terrestrial Ecosystems*; Piccolo, A., Ed.; Elsevier Science: Amsterdam, The Netherlands, 1996.

(26) Purcena, L. L. A.; Caramori, S. S.; Mitidieri, S.; Fernandes, K. F. The immobilization of trypsin onto polyaniline for protein digestion. *Mater. Sci. Eng. C* **2009**, *29*, 1077−1081.

(27) Caramori, S. S.; Fernandes, K. F. The use of poly(ethylene terephthalate)-poly(aniline) composite for trypsin immobilisation. *Mater. Sci. Eng. C* **2008**, *28*, 1159−1163.

(28) Silva, R. N.; Asquien, E. R.; Fernandes, K. F. Immobilization of *Aspergillus niger* glucoamylase onto a polyaniline polymer. *Process Biochem.* **2005**, *40*, 1155−1159.

(29) Carlo Lammirato, A. M.; Wick, L. Y.; Kästner, M. Hydrolysis of cellobiose by β-glucosidase in the presence of soil minerals e Interactions at solideliquid interfaces and effects on enzyme activity levels. *Soil Biol. Biochem.* **2010**, *42*, 2203−2210.

(30) Nannipieri, P. Characterization of humus-phosphatase complexes extracted from soil. *Soil Biol. Biochem.* **1988**, *20*, 683−691.

(31) Niemi, R. M.; Vepsäläinen, M.; Wallenius, K.; Erkomaa, K.; Kukkonen, S.; Palojärvi, A.; Vestberg, M. Conventional versus organic cropping and peat amendment: impacts on soil microbiota and their activities. *Eur. J. Soils Biol.* **2008**, *44*, 419−428.

(32) Garnier-Sillam, E.; Harry, M. Distribution of humic compounds in mounds of some soil-feeding termite species of tropical rain forests: its influence on soil structure stability. *Insectes Sociaux* **1995**, *42*, 167−185.

(33) Gonçalves, H. M.; Borges, J. D.; Silva, M. A. S. d. Heavy metals and sulphur acumulation on soil in areas of influence of vinasse channels of fertigation. *Biosci. J.* **2009**, *25*, 66−74.

(34) Suzuki, J. Biossíntese e acúmulo de sacarose em cana-de-açúcar (*Saccharum* spp); influência do íon potássio durante diferentes estádios de crescimento em solução nutritiva. Universidade de São Paulo, Piracicaba, Brazil, 1982.
(35) Marscher, H. *Mineral Nutrition of Higher Plants*, 2nd ed.; Elsevier: London, UK, 1995.
(36) Haridasan, M. Nutrição mineral de plantas nativas do Cerrado. *Rev. Bras. Fisiol. Vegetal* **2000**, *12*, 54−64.
(37) Shaviv, A.; Mattigod, S. V.; Pratt, P. F.; Joseph, M. Potassium exchange in five southern California soils with high K fixation capacity. *Soil Sci. Soc. Am. J.* **1985**, *49*, 1128−1133.
(38) Murashkina, M. A.; Southard, R. J.; Pettygrove, G. S. Silt and fine sand fractions dominate K fixation in soils derived from granitic alluvium of the San Joaquin Valley, California. *Geoderma* **2007**, *141*, 283−293.
(39) Sousa, D. M. G.; Lobato, E. *Cerrado: Correção do solo e Adubação*; Embrapa Cerrados: Planaltina, Brazil, 2002; p 416.
(40) Chepkwony, C. K.; Haynes, R. J.; Swift, R. S.; Harrison, R. Mineralization of soil organic P induced by drying and rewetting as a source of plant-available P in limed and unlimed samples of an acid soil. *Plant Soil* **2001**, *124*, 83−90.
(41) Balota, E. L.; Machineski, O.; Truber, P. V.; Auler, P. A. M. Effect of tillage systems and permanent groundcover intercropped with orange trees on soil enzyme activities. *Braz. Arch. Biol. Technol.* **2011**, *54*, 221−228.
(42) Tabatabai, M. A.; Bremner, J. M. Use of *p*-nitrophenylphosphate for assay of soil phosphatase activity. *Soil Biol. Biochem.* **1969**, *1*, 301−307.
(43) Deng, S. P.; Tabatabai, M. A. Effect of tillage and residue management on enzyme activities in soils: III. Phosphatases and arylsulfatase. *Biol. Fertil. Soils* **1997**, *24*, 141−146.
(44) Qin, S.; Hu, C.; He, X.; Dong, W.; Cui, J.; Wang, Y. Soil organic carbon, nutrients and relevant enzyme activities in particle-size fractions under conservational versus traditional agricultural management. *Appl. Soil Ecol.* **2010**, *45*, 152−159.
(45) Moscatelli, M. C.; Lagomarsino, A.; Garzillo, A. M. V.; Pignataro, A.; Grego, S. *β*-Glucosidase kinetic parameters as indicators of soil quality under conventional and organic cropping systems applying two analytical approaches. *Ecol. Indicators* **2012**, *13*, 322−327.
(46) Acosta-Martínez, V.; Tabatabai, M. A. Enzyme activities in a limed agricultural soil. *Biol. Fertil. Soils* **2000**, *31*, 85−91.

Table 1. Summary Statistics of Seed Isoflavone Concentrations (Values in μg/g) of MD96-5722 by Spencer RIL Population

	daidzein	glycitein	genistein	total isoflavones
		RIL Values (n = 92)		
range	323−474	417−693	499−671	1,266−1,776
mean	381.40	547.69	592.37	1,521.45
SD	24.84	58.47	36.76	104.68
skewness	0.44	0.11	−0.23	−0.03
kurtosis	0.65	−0.50	−0.20	−0.34
variance	616.83	3418.85	1351.60	10958.23
CV	6.51	10.68	6.21	6.88
		Parents Mean Values (n = 4)		
MD 96-5722	376.75	641.5	555.5	1573.75
SD	13.45	9.61	13.82	21.17
Spencer	388.75	676.75	585	1650.5
SD	42.93	51.08	26.65	44.86

Table 2. SNP Markers and Intervals Most Likely To Be Associated with the Isoflavone QTL for Mean Seed Daidzein and Glycitein Values across Two Environments[a]

trait	QTL	Chr/LG	position	marker interval	LOD	additive	R^2
daidzein	*qDaid001*	5/A1	11.70	ss245748832−ss245762437	4.55	1.92	0.023
glycitein	*qGly001*	9/K	0.60	ss24687662−ss246876937	2.66	9.76	0.002
glycitein	*qGly002*	14/B2	20.20	ss248275008−ss248278947	2.97	22.11	0.099

[a]The chromosome numbers assignments to linkage group based on SoyBase and the Soybean Breeder's Toolbox (http://soybase.org/LG2Xsome.php.

Soybean breeders need more QTL from different mapping populations with different genetic backgrounds and from multiple environments. Thus, the objective of this study was to identify additional QTL associated with daidzein, genistein, glycitein, and total isoflavone concentrations in a population of RILs of MD 96-5722 by Spencer. A genome-wide genetic map in a single population was used in identifying QTL associated with isoflavone content.

MATERIALS AND METHODS

Plant Material and Seed Analysis of Isoflavones. In this study, 92 $F_{5:8}$ RIL lines developed by crossing line MD 96-5722 with line Spencer were used for QTL analysis. The population was grown at Fayettvile State University campus, Fayetteville, in 2012. Plant to plant distance was 25 cm, and no additional fertilizer or insecticide was used. Seeds were harvested from the mature plants and were analyzed for isoflavone concentrations using a near-infrared reflectance (NIR) diode array feed analyzer (Perten, Springfield, IL, USA) following methodology previously reported.[25−27] Calibration equations were initially developed by the University of Minnesota using Thermo Galactic Grams PLS IQ from Perten. Twenty-five grams of seed from each line was ground using a Laboratory Mill 3600 (Perten), and the analysis was performed on a dry matter basis. Total isoflavones were calculated by adding the concentration of the three main isoflavones, daidzein, genistein, and glycitein.[25,28]

Genetic Map and QTL Detection. The MD 96-5722 by Spencer genetic linkage map[29] was constructed using JoinMap 4 (Kyazma BV, Wageningen, The Netherlands)[30] using 5376 SNPs from SoySNP6K BeadChip. Composite interval mapping (CIM) was used to detect QTL associated seed isoflavones using phenotypic data by running WinQTLCart 2.5 software (http://statgen.ncsu.edu/qtlcart/WQTLCart.htm).[31] Model 6 of WinQTLCart with four parameters for forward and backward stepwise regression, 10 cM window size, 1 cM step size, and five control markers was chosen.[30] The threshold was determined by permutations of 1000 times.

RESULTS

Phenotypic analysis shows the wide variation of seed daidzein, genistein, glycitein, and total isoflavone concentrations among the 92 RILs (Table 1). Variations among RIL lines were 6.51, 10.68, 6.21, and 6.88% for daidzein, glycitein, genistein, and total isoflavones, respectively. Among the two parents, the mean values of genistein, glycitein, and total isoflavones were higher for Spencer than for MD 96-5722; however, the mean values were lower for daidzein. Individual or total isoflavone means of RILs suggested that the segregation of these traits fits a normal distribution model as both the skewness and kurtosis values for these traits were <1.0 (Table 1). Mean values of daidzein were higher in RILs than in the parent MD 96-5722. However, glycitein content was lower than the parental means, genistein content was higher than the parental means, and total isoflavone content was lower than parental means.

A total of three QTL for seed isoflavone concentrations were identified on three different linkage groups (LGs) (Table 2; Figure 1). One QTL for seed daidzein concentration (*qDaid001*) was identified on LG A1 or chromosome (Chr) 5 at 11.70 cM position with a LOD score of 4.55. Two other QTL were identified for glycitein, *qGly001* and *qGly002* located on LG K (Chr 9) and LG B2 (Chr 14), respectively. LOD scores of these two QTL were 2.66 (*qGly001*) and 2.97 (*qGly002*).

DISCUSSION

Soybean isoflavone has been increasingly demanded by consumers because of its several beneficial health effects in humans as food ingredients, medicines, and cosmetics.[32] Therefore, breeders are interested in improving seed isoflavone concentration in soybean cultivars. The range of total isoflavones in these RIL populations was 1266−1776 μg g^{-1}. Wang and Murphy[33] also found a similar range for total isoflavone concentration in a cultivar from 1176 to 1749 μg g^{-1} among locations within the same year. Choi et al.[34] reported that total isoflavone concentration ranged from 458 to 2317 μg g^{-1} among cultivars in a single year. The variability observed in our recent study in 'PI438489B' by 'Hamilton' RIL population

dx.doi.org/10.1021/jf4040173 | J. Agric. Food Chem. 2014, 62, 1464−1468

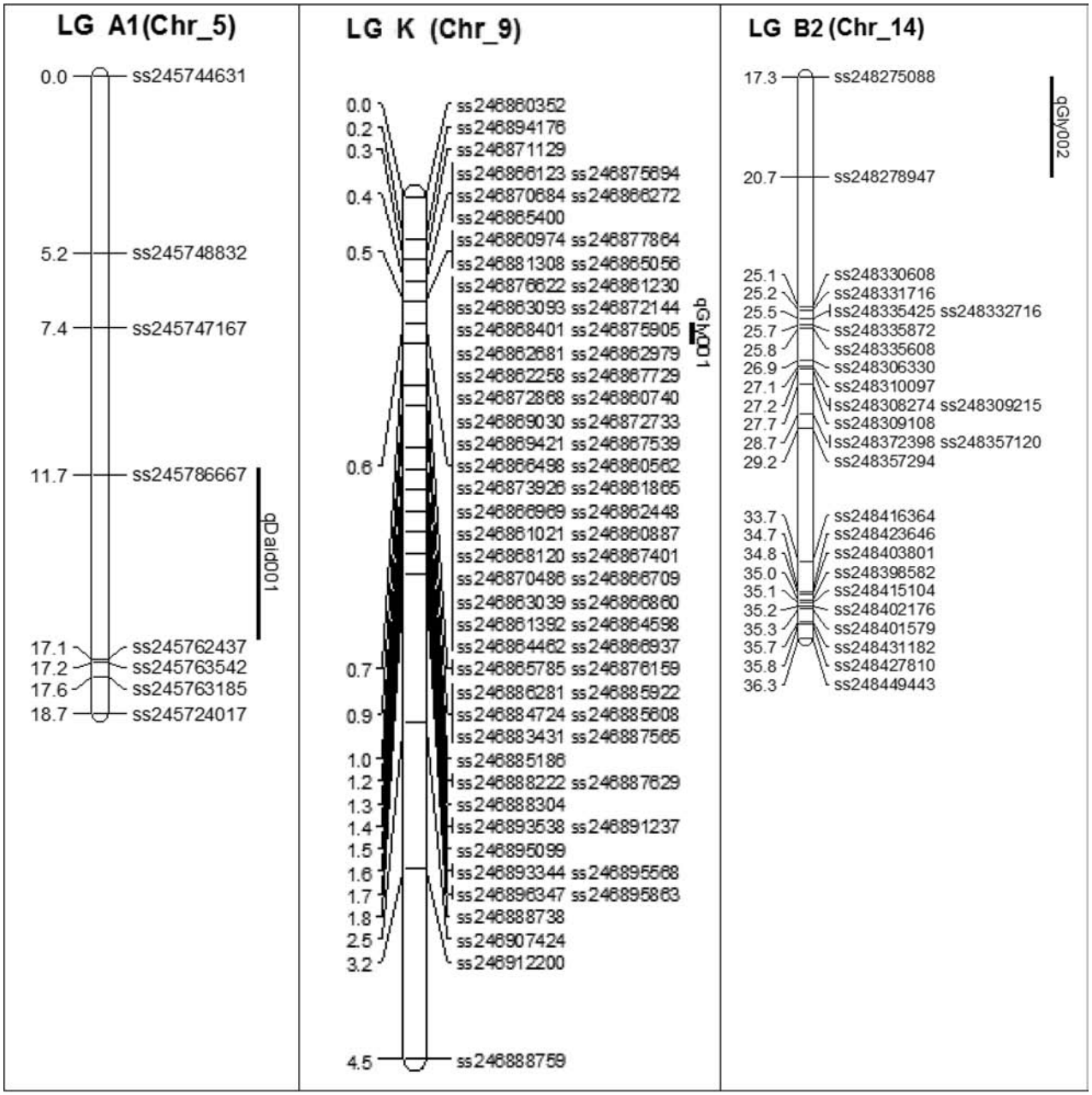

Figure 1. Locations of SNP markers and the QTL that underlie soybean seed daidzein (*qDaid001*) and glycitein (*qGly001* and *qGly002*) concentrations in the MD 96-5722 by Spencer RIL populations. LGs/Chr were drawn using MapChart[41] according to the 'Maryland' by 'Spencer' genetic linkage map.

for seed isoflavone concentration suggested that the control or accumulation of individual isoflavones was influenced by genotype, growing season/growing site, and their interactions. However, previous studies[10,34−36] showed that the main genotypic effects of total and individual isoflavones were effective in cultivar improvement.

A total of three QTL for seed isoflavone concentration have been identified in three different LGs or Chr. A QTL that controls daidzein (*qDaid001*) has been identified on LG A1 (Chr 5). Several other studies used different mapping populations and identified QTLs for daidzein concentrations in the same or different LGs. Smallwood[37] identified five QTL for daidzein in an 'Essex' × 'Williams 82' population; among those QTL was one on Chr 5 and the rest were on Chr 6, 9, 13, and 19. Gutierrez-Gonzalez et al.[37] identified six QTL for daidzein in Chr 5 (dai-A1), 8 (dai-A2), 2 (dai-D1b), 7 (dai-M), 12 (dai-H), and 19 (dai-L), although the QTL they identified for daidzein on Chr 5 (dai-A1) was located in a different position. Very recently, we identified four QTL for daidzein in the 'PI438489B' by 'Hamilton' RIL population on Chr 6, 7, 13m and 17 (unpublished data). Several other QTL were identified in different genetic regions on Chr 6, 9, and 13.[9,22,24,39]

Glycitein is the most variable individual isoflavone concentration among RILs of soybean MD 96-5722 by Spencer (Table 1). Two QTL have been identified for glycetein; *qGly001* and *qGly002* were identified on LG K (Chr 9) and LG B2 (Chr 14), respectively. Gutierrez-Gonzalez et al.[38] found a QTL for glycitein on LG K (Chr 9), and the QTL they reported for glycitein (*q*gly-K) is very apart from the QTL we

dx.doi.org/10.1021/jf4040173 | J. Agric. Food Chem. 2014, 62, 1464−1468

identified in this study. They also reported another five QTL for glycitein concentration on LG C2 (gly-C2), LG E (*q*gly-E), LG C2 (gly-C2), LG D2 (gly-D2_1 and gly-D2_2), and LG G (gly-G). Later, Gutierrez-Gonzalez et al.[40] also reported QTL for the glycitein QTL on LG C2 (Chr 6). Smallwood[37] identified three QTL for glycitein in an 'Essex' × 'Williams 82' population on LG C2 (Chr 6), LG K (Chr 9), and LG I (Chr 20). Interestingly, both of the above-mentioned studies[36,37] identified QTL for glycitein on LG K (Chr 9). Primomo et al.[9] identified QTL for daidzein and glycitein on LG M (Chr 7) using an 'AC756' by 'RCAT Angora' RIL population. However, previous studies have reported QTL for genistein, glycitein, daidzein, and total isoflavones on LG C2 (Chr 6) and LG L (Chr 19).[9,24,38−40] Very recently, we identified four QTL for glycitein in the 'PI438489B' by 'Hamilton' RIL population (unpublished data), and neither of those identified QTL were on LG K (Chr 9) or LG B2 (Chr 14). However, so far no study has yet identified the QTL for glycitein on LG B2 (Chr 14) that we identified in this study.

The additional three new QTL for daidzein and glycitein added to the existing QTL for isoflavones may increase the understanding of the genetic regions controlling isoflavone accumulation. Therefore, the QTL identified in this study represent a valuable resource for studying the genetic basis underlying isoflavone biosynthesis in soybean.

AUTHOR INFORMATION

Corresponding Author

*(M.A.K.) Phone: (910) 672-1692. Fax: (910) 672-1159. E-mail: mkassem@uncfsu.edu.

Funding

This work was supported by the Department of Defense (DOD) through Grant W911NF-11-1-0178 to M.A.K and S.K. This research was partially funded by the U.S. Department of Agriculture, Agricultural Research Service Project 6402-21220-012-00D. Mention of trade names or commercial products in this publication is solely for the purpose of providing specific information and does not imply recommendation or endorsement by the U.S. Department of Agriculture.

Notes

The authors declare no competing financial interest.

ACKNOWLEDGMENTS

We thank Pam Ratcliff and the rest of the undergraduate student crew at FSU for taking care of the plants in the greenhouse and field and Sandra Mosley at USDA-ARS, Stoneville, MS, for lab assistance on isoflavone analysis.

REFERENCES

(1) Wahajuddin; Taneja, I.; Arora, S.; Raju, K. S.; Siddiqui, N. Disposition of pharmacologically active dietary isoflavones in biological systems. *Curr. Drug Metab.* **2013**, *14* (4), 369−80.

(2) Miyazawa, M.; Sakoano, K.; Nakamura, S. I.; Kosaka, H. Antimutagenic activity of isoflavones from soybean seeds (*Glycine max* (L.) Merr. *J. Agric. Food Chem.* **1999**, *47*, 1346−1349.

(3) Wang, B. F.; Wang, J. S.; Lu, J. F.; Kao, T. H.; Chen, B. H. Antiproliferation effect and mechanism of prostate cancer cell lines as affected by isoflavones from soybean cake. *J. Agric. Food Chem.* **2009**, *57*, 2221−2232.

(4) Jiang, Q.; Payton-Stewart, F.; Elliott, S.; Driver, J.; Rhodes, L. V.; Zhang, Q.; Zheng, S.; Bhatnagar, D.; Boue, S. M.; Collins-Burow, B. M.; Sridhar, J.; Stevens, C.; McLachlan, J. A.; Wiese, T. E.; Burow, M. E.; Wang, G. Effects of 7-O substitutions on estrogenic and anti-estrogenic activities of daidzein analogues in MCF-breast cancer cells. *J. Med. Chem.* **2010**, *53*, 6153−6163.

(5) Regal, J. F.; Frazer, D. G.; Weeks, C. E.; Greenberg, N. A. Dietary phytoestrogens have anti-inflammatory activity in a guinea pig model of asthma. *Exp. Biol. Med.* **2000**, *223*, 372−378.

(6) Hedlund, T. E.; Johannes, W. U.; Miller, G. J. Soy isoflavonoid equol modulates the growth of benign and malignant prostatic epithelial cells in vitro. *Prostate* **2003**, *54*, 68−78.

(7) Mabrouk, Y.; Zourgui, L.; Delavault, P.; Simier, P.; Belhadj, O. Some compatible *Rhizobium leguminosrum* strains in peas decrease infections when parasitized by *Orobanche crenata*. *Weed Res.* **2007**, *47*, 44−53.

(8) Knight, D. C.; Eden, J. A. A review of the clinical effects of phytoestrogens. *Obstet. Gynecol.* **1996**, *7*, 897−904.

(9) Primomo, V. S.; Poysa, V.; Ablett, G. R.; Jackson, C. J.; Rajcan, I. Agronomic performance of recombinant inbred line populations segregating for isoflavone content in soybean seeds. *Crop Sci.* **2005**, *45*, 2203−2211.

(10) Hoeck, J. A.; Fehr, W. R.; Murphy, P. A.; Welke, G. A. Influence of genotype and environment on isoflavone contents of soybean. *Crop Sci.* **2000**, *40*, 48−51.

(11) Lark, K. G.; Chase, K.; Adler, F.; Mansur, L. M.; Orf, J. H. Interactions between quantitative trait loci in soybean in which trait variation at one locus is conditional upon a specific allele at another. *Proc. Natl. Acad. Sci. U.S.A.* **1995**, *92*, 4656−4660.

(12) Song, Q. J.; Marek, L. F.; Shoemaker, R. C.; Lark, K. G.; Concibido, V. C.; Delannay, X.; Specht, J. E.; Cregan, P. B. A new integrated genetic linkage map of the soybean. *Theor. Appl. Genet.* **2004**, *109*, 122−128.

(13) Cregan, P. B.; Jarvik, T.; Bush, A. L.; Shoemaker, R. C.; Lark, K. G.; Kahler, A. L.; Kaya, N.; VanToai, T. T.; Lohnes, D. G.; Chung, J.; Specht, J. E. An integrated genetic linkage map of the soybean genome. *Crop Sci.* **1999**, *39*, 1464−1490.

(14) Kassem, M. A.; Shultz, J.; Meksem, K.; Cho, Y.; Wood, A. J.; Iqbal, M. J.; Lightfoot, D. A. An updated 'Essex' by 'Forrest' linkage map and first composite map of QTL underlying six soybean traits. *Theor. Appl. Genet.* **2006**, *113*, 1015−1026.

(15) Kassem, M. A.; Ramos, L.; Leandro, L.; Mbofung, G.; Hyten, D.; Kantartzi, S.; Grier, R. L., IV; Cianzio, S.; Meksem, K. The first 'PI438489b' by 'Hamilton' SNP-based genetic linkage map of soybean [*Glycine max* (L.) Merr.] and quantitative trait loci (QTL) that underlie SDS resistance. *J. Plant Genome Sci.* **2012**, *1*, 18−30.

(16) Choi, I. Y.; Hyten, D. L.; Matukumalli, L. K.; Song, Q.; Chaky, J. M.; Quigley, C. V.; Chase, K.; Lark, K. G.; Reiter, R. S.; Yoon, M. S.; Hwang, E. Y.; Yi, S. I.; Young, N. D.; Shoemaker, R. C.; Van Tassel, C. P.; Specht, J. E.; Cregan, P. B. A soybean transcript map: gene distribution, haplotype and singlenucleotide polymorphism analysis. *Genetics* **2007**, *176*, 685−696.

(17) Hyten, D. L.; Choi, I. Y.; Song, Q. J.; Specht, J. E.; Carter, T. E.; Shoemaker, R. C.; Hwang, E. Y.; Matukumalli, L. K.; Cregan, P. B. A high density integrated genetic linkage map of soybean and the development of a 1536 universal soy linkage panel for quantitative trait locus mapping. *Crop Sci.* **2010**, *50*, 960−968.

(18) Ganal, M. W.; Durstewitz, G.; Polley, A.; Bérard, A.; Buckler, E. S.; Charcosset, A.; Clarke, J. D.; Graner, E.-M.; Hansen, M.; Joets, J.; Le Paslier, M.-C.; McMullen, M. D.; Montalent, P.; Rose, M.; Schön, C.-C.; Sun, Q.; Walter, H.; Martin, O. C.; Falque, M. A large maize (*Zea mays* L.) SNP genotyping array: development and germplasm genotyping, and genetic mapping to compare with the B73 reference genome. *PLoS One* **2011**, *6*, e28334.

(19) Song, Q.; Hyten, D. L.; Jia, G.; Quigley, C. V.; Fickus, E. W.; Nelson, R. L.; Cregan, P. B. Development and evaluation of SoySNP50K, a high-density genotyping array for soybean. *PLoS One* **2013**, *8* (1), e54985.

(20) Yan, J.; Yang, X.; Shah, T.; Sanchez-Viellda, H.; Li, J.; Warburton, M. L.; Zhou, Y.; Jonathan, J.; Xu, Y. High-throughput SNP genotyping with the GoldenGate assay in maize. *Mol. Breed.* **2010**, *25*, 441−451.

(21) Njiti, V. N.; Meksem, K.; Yuan, J.; Lightfoot, D. A.; Banz, W. J.; Winters, T. A. DNA markers associated with loci underlying seed phytoestrogen content in soybean. *J. Med. Food* **1999**, *2*, 185−187.
(22) Kassem, M. A.; Meksem, K.; Iqbal, M. J.; Wood, A. J.; Lightfoot, D. A. Definition of soybean genomic regions that control seed phytoestrogen amounts. *J. Biomed. Biotechnol.* **2004**, *1*, 52−60.
(23) Meksem, K.; Njiti, V. N.; Banz, W. J.; Iqbal, M. J.; Kassem, M. A.; Hyten, D. L.; Yuang, J.; Winters, T. A.; Lightfoot, D. A. Genomic regions that underlie soybean seed isoflavone content. *J. Biomed. Biotechnol.* **2001**, *1*, 38−45.
(24) Zeng, G.; Li, D.; Han, Y.; Teng, W.; Wang, J.; Qiu, L.; Li, W. Identification of QTL underlying isoflavone contents in soybean seeds among multiple environments. *Theor. Appl. Genet.* **2009**, *118*, 1455−1463.
(25) Bellaloui, N.; Mengistu, A. L.; Zobiole, H. S.; Shier, W. T. Resistance to toxin-mediated fungal infection: role of lignins, isoflavones, other seed phenolics, sugars, and boron in the mechanism of resistance to charcoal rot disease in soybean. *Toxin Rev.* **2012**, *31* (1−2), 16−26.
(26) Morrison, J.; Cober, E. R.; Saleem, M. F.; McLaughlin, N. B.; Fregeau-Reid, J.; Ma, B. L.; Yan, W.; Woodrow, L. Changes in isoflavone concentration with 58 years of genetic improvement of short-season soybean cultivars in Canada. *Crop Sci.* **2008**, *48* (6), 2201−2208.
(27) Sato, T.; Eguchi, K.; Hatano, T.; Nishiba, Y. Use of near-infra red reflectance spectroscopy for the estimation of isoflavone contents of soybean seeds. *Plant Prod. Sci.* **2008**, *11* (4), 481−486.
(28) Wang, C.; Sherrard, M.; Pagadala, S.; Wixon, R.; Scott, R. A. Isoflavone content among maturity group 0 to II soybeans. *J. Am. Oil Chem. Soc.* **2000**, *77* (5), 483−487.
(29) Akond, M.; Kantartzi, S. K.; Meksem, K.; Song, Q.; Wang, D.; Wen, Z.; Lightfoot, D. A.; Kassem, M. A. A SNP-based genetic linkage map of soybean using the SoySNP6K Illumina Infinium BeadChip genotyping array. *J. Plant Genom. Sci.* **2013**, *2* (3), DOI: 10.5147/jpgs.2013.0090.
(30) Van Ooijen, J. W. *JoinMap 4: Software for the Calculation of Genetic Linkage Maps in Experimental Populations*; Kyazma BV: Wageningen, The Netherlands, 2006.
(31) Wang, S.; Basten, C.; Zeng, Z. *Windows QTL Cartographer 2.5*; Department of Statistics, North Carolina State University: Raleigh, NC, USA, 2007
(32) Brouns, F. Soya isoflavones: a new and promising ingredient for the health food sector. *Food Res. Int.* **2002**, *35* (2−3), 187−193.
(33) Wang, H.; Murphy, P. Isoflavone composition of American and Japanese soybeans in Iowa: effects of variety, crop year, and location. *J. Agric. Food Chem.* **1994**, *42*, 1674−1677.
(34) Choi, J. S.; Kwon, T. W.; Kim, J. S. Isoflavone contents in some varieties of soybean. *Kor. Food Biotechnol.* **1996**, *5*, 167−169.
(35) Tsukamoto, C.; Shinji, S.; Kazunori, I.; Shigemitsu, K.; Makie, K. M.; Kazuyoshi, O.; Keisuke, K. Factors affecting isoflavone content in soybean seeds: changes in isoflavones, saponins and composition of fatty acids at different temperatures during seed development. *J. Agric. Food Chem.* **1995**, *43*, 1184−1192.
(36) Lee, S. J.; Yan, W.; Ahn, J. K.; Chung, I. M. Effects of year, site, genotype and their interactions on various soybean isoflavones. *Field Crops Res.* **2003**, *81*, 181−192.
(37) Smallwood, C. J. *Detection of Quantitative Trait Loci for Marker-Assisted Selection of Soybean Isoflavone Genistein*. Master's thesis, University of Tennessee, 2012 (http://trace.tennessee.edu/utk_gradthes/1208, 8/23/2013).
(38) Gutierrez-Gonzalez, J. J.; Wu, X. L.; Zhang, J.; Lee, J. D.; Ellersieck, M.; Shannon, J. G.; Yu, O.; Nguyen, H. T.; Sleper, D. A. Genetic control of soybean seed isoflavone content: Importance of statistical model and epistasis in complex traits. *Theor. Appl. Genet.* **2009**, *119*, 1069−1083.
(39) Gutierrez-Gonzalez, J. J.; Vuong, T. D.; Zhong, R.; Yu, O.; Lee, J. D.; Shannon, G.; Ellersieck, M.; Nguyen, H. T.; Sleper, D. A. Major locus and other novel additive and epistatic loci involved in modulation of isoflavone concentration in soybean seeds. *Theor. Appl. Genet.* **2011**, *123*, 1375−1385.
(40) Gutierrez-Gonzalez, J. J.; Wu, X. L.; Gillman, J. D.; Lee, J. D.; Zhong, R.; Yu, O.; Shannon, G.; Ellersieck, M.; Nguyen, H. T.; Sleper, D. A. Intricate environment-modulated genetic networks control isoflavone accumulation in soybean seeds. *BMC Plant Biol.* **2010**, *10*, 105.
(41) Voorrips, R. E. MapChart: software for the graphical presentation of linkage maps and QTLs. *J. Heredity* **2002**, *93* (1), 77−78.

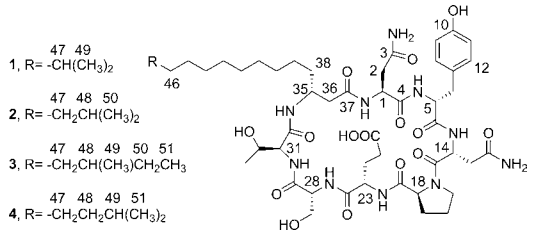

Figure 1. Structures of compounds **1**−**4**.

Bruker Avance II 800US2, Bruker Avance II 600, and Bruker DRX500 systems (Bruker Daltonics, Billerica, MA, USA). The spectra for compounds **1**−**4** were acquired in pyridine-d_5 (δ_H 7.19; δ_C 123.5) at room temperature. HR-ESI-MS spectra were obtained with a Waters Micromass LCT Premier XE (Waters, Milford, MA, USA), and HR-FAB-MS spectra were obtained with a JEOL JMS-700 spectrometer (JEOL, Tokyo, Japan). Preparative HPLC and HPLC analyses were performed with a Waters Alliance system.

Microorganisms. Soil samples collected in Ibaraki prefecture, Japan, were suspended in sterilized water and vortexed. The supernatants were serially diluted with sterilized water and spread on nutrient agar plates (15 × 90 mm). The plates were incubated at 30 °C for 48 h in darkness, and 500 colonies were transferred to other nutrient agar plates. Bacteria thus isolated were tested for their antifungal activity against a phytopathogenic fungus, *Botrytis cinerea* Persoon MAFF 744071. PCR amplification of the 16S rRNA gene of strain SD-32 with universal forward (5′-AGAGTTTGATCCTGG-CTCAG-3′) and reverse (5′-GGCTACCTTGTTACGACTT-3′) primers was carried out. The 16S sequence for SD-32 was deposited in GenBank (accession no. AB853319).

Isolation of Compounds 1−4. Strain SD-32 was grown at 30 °C with 150 rpm shaking for 64 h in 500 mL flasks containing liquid medium (50 mL/flask, total 800 mL) composed of maltose (80 g/L), soybean powder (80 g/L; J-OIL Mills, Tokyo, Japan), yeast extract (10 g/L; Becton, Dickinson and Co., Franklin Lakes, NJ, USA), $MgSO_4·7H_2O$ (2 g/L), $CaCl_2$ (2 g/L), K_2HPO_4 (1 g/L), $FeSO_4·7H_2O$ (0.1 g/L), $MnSO_4·5H_2O$ (0.1 g/L), and H_2O adjusted to pH 7.0 by Na_2CO_3. Antifungal metabolites were extracted from the culture filtrate (750 mL) with 1 L of EtOAc three times after adjustment of the pH to 4.0 with HCl. The EtOAc solution was dehydrated over anhydrous Na_2SO_4 and concentrated to dryness to afford an extract (3.8 g). The extract was dissolved in H_2O, and the pH of the solution was adjusted to 7.0. The solution was purified with solid-phase extraction (Oasis HLB 35 cc LP extraction cartridge, Waters) eluted stepwise with 50 mL each of 0, 20, 40, 60, 80, and 100% (v/v) MeOH in H_2O. The antifungal activity of each fraction was determined by the paper-disk method using *B. cinerea* as the test organism on a potato dextrose agar (PDA, Becton, Dickinson and Co.) plate at 20 °C for 3 days. The active fractions eluted with 60−80% MeOH in H_2O were combined and concentrated to dryness. The concentrate was subjected to Sephadex LH-20 column chromatography with MeOH. The active fractions were pooled and evaporated to dryness to afford a residue (0.80 g). The residue was further purified by preparative HPLC (XBridge C18, 250 × 10 mm) and eluted with 45% (v/v) CH_3CN−H_2O containing 0.1% TFA at a flow rate of 4.7 mL/min at 40 °C, and absorbance at 205 nm was measured to afford the active compounds **1** (23 mg), **2** (92 mg), **3** (120 mg), and **4** (56 mg).

Amino Acid Analysis. Compound **3** (1 mg) was hydrolyzed with 6 N HCl at 110 °C for 18 h, and the hydrolysate was dried with N_2. The amino acids were analyzed using the Shimadzu Prominence Amino Acid Analysis System (Shimadzu Corp., Tokyo, Japan) by postcolumn fluorescence derivatization with *o*-phthalaldehyde (OPA)/*N*-acetylcysteine as the reaction reagent.

***N*-Bromosuccinimide Cleavage and Edman Degradation.** Compound **3** (2.5 mg) was dissolved in 0.5 mL of 70% aqueous AcOH. *N*-Bromosuccinimide[19] (2.5 mg) was added, and the solution was allowed to stand for 1 h at room temperature. Three drops of formic acid were added to the solution to terminate the reaction. The open-up fragment of compound **3** was purified by preparative HPLC (XBridge C18, 250 × 4.6 mm) and eluted with 50% (v/v) CH_3CN−H_2O containing 0.1% TFA at a flow rate of 1.0 mL/min at 40 °C, and absorbance at 205 nm was measured. The N-terminal amino acid sequence of the fragment was determined by Edman degradation using Shimadzu Protein Sequencer PPSQ-23A.

Matrix-Associated Laser Desorption Ionization Time of Flight (MALDI-TOF) MS/MS Analysis. MALDI-TOF MS/MS was recorded by the Shimadzu AXIMA Resonance using a 337.1 nm nitrogen laser for desorption and ionization. 2,5-Dihydroxybenzoic acid (10 mg/mL) in 50% (v/v) CH_3CN−H_2O containing 0.1% TFA was used as the matrix solution. Positive-ion detection and reflectron mode were used.

Absolute Configuration of α-Amino Acid. Compound **3** (1 mg) was hydrolyzed with 0.5 mL of 6 N HCl at 110 °C for 18 h and dried with N_2. To the hydrolysate was added 100 μL of H_2O, 200 μL of 1% FDAA (Marfey's reagent)[20] in acetone, and 40 μL of 1 M $NaHCO_3$. The mixture was kept at 40 °C for 1 h, and 20 μL of 2 M HCl was added to terminate the reaction. The reaction mixture was analyzed by HPLC equipped with a reverse-phase column (XBridge C18, 250 × 4.6 mm) and eluted with a linear gradient of 10−50% (v/v) CH_3CN−H_2O containing 0.1% TFA in 45 min at a flow rate of 1.0 mL/min, 40 °C, and absorbance at 340 nm was measured. Derivatives of standard L- and D-amino acids were co-injected. To determine the absolute configuration of Asn1 and Asn2, two tripeptides, NH_2-L-Asp-D-Tyr-D-Asp and NH_2-D-Asp-D-Tyr-L-Asp, were used as standard peptides (Sigma-Aldrich). Compound **3** (3 mg) was hydrolyzed in 0.5 mL of 3 N HCl at 105 °C for 1 h and dried with N_2. To the hydrolysate was added 100 μL of H_2O, and the hydrolysate solution was analyzed by HPLC equipped with a phenyl column (XBridge Phenyl, 250 × 4.6 mm) and eluted with 5% (v/v) CH_3CN−H_2O containing 0.1% TFA at a flow rate of 1.0 mL/min, 40 °C, and absorbance at 280 nm was measured. Two standard tripeptides, NH_2-L-Asp-D-Tyr-D-Asp and NH_2-D-Asp-D-Tyr-L-Asp, were eluted at 8.2 and 7.3 min, respectively.

Absolute Configuration of β-Amino Fatty Acid. A β-amino fatty acid of compound **3** was produced by the hydrolysis (1 mL of 6 N HCl, 110 °C, 24 h) of compound **3** (10 mg) and extraction with chloroform. Dinitrophenylation of the β-amino fatty acid was carried out according to Sanger's procedure.[21] The Dnp derivative thus obtained was treated with *p*-methoxyaniline, 1-ethyl-3-(3-dimethylaminopropyl)carbodiimide, and 1-hydroxybenzotriazole in methylene chloride. The reaction products were purified by preparative HPLC using a column (XBridge C18, 250 × 4.6 mm) eluted with 90% (v/v) CH_3CN−H_2O containing 0.1% TFA at a flow rate of 1.0 mL/min at 40 °C, and absorbance at 340 nm was measured to yield the dinitrophenyl-*p*-methoxyaniline derivative (<1.0 mg). The structure was confirmed by mass ($[M + H]^+$, 557.4) and ^1H NMR ($CDCl_3$) spectra. The amount of the derivative was determined to be 0.41 mg by a calculation based on ε value at A_{347} in the literature.[22] The CD spectrum of the derivative was compared to that in the literature.[22] CD (c 8.4 × 10^{-5} M, MeOH) λ_{max} (Δ ε) 262 (+4.29), 300 (+0.54), 330 (+0.77), 400 (−1.82) nm.

In Vitro Assay against Plant Pathogens. We obtained the following from the National Institute of Agrobiological Science, Tsukuba, Japan: *Botrytis cinerea* Persoon MAFF 744071, *Rhizoctonia solani* J. G. Kuehn MAFF 305219, *Fusarium oxysporum* Schlechtendahl MAFF 410171, *Pyricularia grisea* (Cooke) Saccardo MAFF 101583, *Alternaria alternata* (Fries) Keissler MAFF 731001, *Botryosphaeria berengeriana* De Notaris f. sp. *pyricola* Koganezawa et Sakuma MAFF 645002, *Didymella bryoniae* (Fuckel) Rehm MAFF 235932, and *Pythium aphanidermatum* (Edson) Fitzpatrick MAFF 239200. The following strains were obtained from Biological Resource Center (NBRC), National Institute of Technology and Evaluation, Chiba, Japan: *Colletotrichum acutatum* Simmonds NBRC 32849, *Monilinia fructicola* (Winter) Honey NBRC 30451, *Penicillium expansum* Link ex S.F. Gray NBRC 5453, and *Sclerotinia sclerotiorum* (Libert) de Bary NBRC 4876. *Fusarium graminearum* Schwabe ARC 2075-1 was supplied from NARO Agricultural Research Center, Tsukuba, Japan. The DMSO solution (60 μL) of the each compound was added to

6 mL of PDA held at 50 °C. The agar medium was poured onto a 60 mm plate. Each compound was tested at concentrations of 2.5, 5.0, 10, 20, 40, and 80 μg/mL. A PDA disk (5 mm in diameter) with mycelia of each test pathogen was placed on each plate containing a compound. The pathogens were incubated at 22 °C for 1.5 days (*B. cinerea*, *D. bryoniae*, and *S. sclerotiorum*), 2 days (*R. solani*, *P. aphanidermatum*, *F. graminearum*, *B. berengeriana*, and *M. fructicola*), 2.5 days (*F. oxysporum*), 3 days (*P. expansum* and *C. acutatum*), 4 days (*A. alternata*), and 5 days (*P. grisea*). The pathogens growing on PDA (6 mL) containing 60 μL of DMSO were used as controls. All experiments were performed in triplicate. IC_{50} values (median inhibitory concentrations) were calculated using the inhibition rate of mycelial growth. That rate was calculated as

$$\text{inhibition rate of mycelial growth (\%)} = (1 - D_a/D_b) \times 100$$

where D_a is the diameter of the pathogen colony in the plate containing a test compound and D_b is the diameter of the colony in the control plate. The results were expressed as IC_{50} (mean ± SD, μM).

Leaf Disk Assay Using Cucumber Cotyledon and *Botrytis cinerea*. Cucumber seeds (*Cucumis stativus* L., Sagami-Hanjiro) were planted in 12 cm pots containing artificial soil and grown in the greenhouse at 16−23 °C without supplemental lighting. The cotyledons were collected from 3-week-old plants. The test compound was dissolved in an appropriate amount of phosphate buffer (40 mM, pH 7.2), and 50 μL of the solution was applied to a paper disk (8 mm in diameter, thick type, Advantec Toyo Kaisha, Ltd., Tokyo, Japan) on the cucumber cotyledon. For the control, only phosphate buffer was applied. Then the paper disks on the leaves were inoculated with 50 μL of *B. cinerea* spore suspension (2×10^4/mL) containing 0.2% (w/v) yeast extract and 2% (w/v) sucrose. Each compound was tested at final concentrations of 10, 20, 30, 40, 60, and 80 μM. The leaves were kept in a humidity chamber (relative humidity > 95%) at 20 °C for 4 days in darkness. The experiment was repeated four times. The inhibition rate of *B. cinerea* infection was calculated as

$$\text{inhibition rate of infection (\%)} = (1 - D_c/D_d) \times 100$$

where D_c is the diameter of the infection zone in the leaf with a test compound and D_d is the diameter of the infection zone in the control leaf. The results were expressed as inhibition rate (mean % ± SD).

RESULTS AND DISCUSSION

Isolation of Compounds 1−4 from *Bacillus amyloliquefaciens* SD-32. In our screening search, SD-32, a bacterium isolated from soil, was found to have strong antifungal activity against plant pathogen *Botrytis cinerea*. The PCR product of its 16S rRNA gene was sequenced to give a 1472 bp sequence followed by a BLAST similarity search; it was identified as *Bacillus amyloliquefaciens*. SD-32 was cultured in a medium (800 mL) composed of maltose, soybean powder, yeast extract, and some minerals at 30 °C for 64 h. Antifungal activity-guided purification of the EtOAc extract of the culture filtrate with solid-phase extraction, gel filtration, and preparative HPLC afforded compounds **1** (23 mg), **2** (92 mg), **3** (120 mg), and **4** (56 mg) as white amorphous powders. The HPLC profile at the final step of purification is shown in Figure 2.

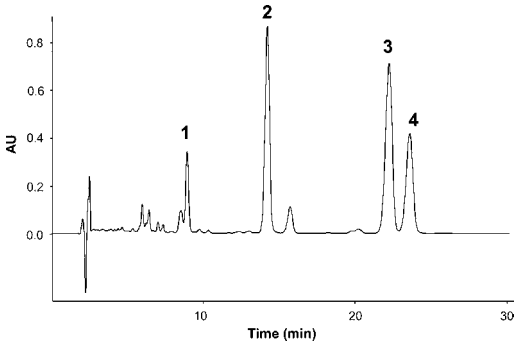

Figure 2. Preparative HPLC of compounds **1**−**4** in the active fractions after Sephadex LH-20 column chromatography.

Structures of Compounds 1−4. Compound **3** was most abundant in the culture broth, so we elucidated its structure first. Compound **3** gave an $[M + H]^+$ peak at m/z 1073.5902 (calcd for $C_{51}H_{81}N_{10}O_{15}$, 1073.5883) in HR-ESI-MS. Six α-amino acids, Asp, Tyr, Glu, Pro, Ser, and Thr, were found in a 2:1:1:1:1:1 ratio in an amino acid analysis of the hydrolysate. Because the ^{1}H NMR spectrum of compound **3** in DMSO-d_6 showed peaks due to a couple of conformers in the solution, pyridine-d_5 was used as NMR solvent. The ^{1}H NMR data for compound **3** (Table 1) indicated the presence of 11 amide protons (δ_H 9.66−7.80) and 7 α-protons (δ_H 5.39−4.72, partially overlapped) of amino acid residues of a peptide, a *p*-substituted benzene ring (δ_H 7.47 d, 7.06 d, 2H each), a long methylene chain (δ_H 1.20−1.15), and three terminal methyl groups (δ_H 1.34 d, 0.82 t, and 0.82 d, each 3H). The ^{13}C NMR data for compound **3** (Table 2) exhibited 49 signals, including 11 carbonyl groups (δ_C 175.5−171.1), a *p*-substituted benzene (δ_C 157.5, 1C; 131.3, 2C; 128.6, 1C; 116.1, 2C), methylene carbons (δ_C 63.5−26.1), and three methyl carbons (δ_C 20.8, 19.3, and 11.5). We deduced that compound **3** was *anteiso*-C_{17} bacillomycin D, a cyclic lipopeptide consisting of two Asn, one Tyr, one Pro, one Glu, one Ser, and one Thr residues and a β-amino acid with a $-(CH_2)_{10}CH(CH_3)CH_2CH_3$ group as a side chain from the ^{1}H−^{1}H COSY, HMBC, and NOESY data shown in Figure 3 and also by considering the molecular formula. To confirm this, we conducted chemical analysis and MALDI-TOF MS/MS analysis as follows. Compound **3** was cleaved at the C-terminus of the Tyr residue by *N*-bromosuccinimide,[19] and the cleaved product (oxidized form of Tyr with 2 mol of Br, molecular mass 1246) was purified by preparative HPLC. The fragment was analyzed by Edman degradation and yielded the following sequence: NH_2-Asn-Pro-Glu-Ser-Thr-X (Figure 4A). Compound **3** was also analyzed by MALDI-TOF MS/MS to afford the sequence information as shown in Figure 4B. These results confirmed that the structure of compound **3** was *anteiso*-C_{17} bacillomycin D.

The absolute configurations of α-amino acids in compound **3** were determined by treatment of the hydrolysate with Marfey's reagent[20] and HPLC analysis of the derivatives. The hydrolysates were shown to contain L-Asp, D-Tyr, D-Asp, L-Pro, L-Glu, D-Ser, and L-Thr. There is no ambiguity in the absolute configuration of the five amino acids other than Asn (in the form of the corresponding Asp). The absolute configurations of the two Asn were determined by HPLC comparison of the tripeptide in the partial hydrolysate of compound **3** with two synthesized tripeptides, NH_2-L-Asp-D-Tyr-D-Asp and NH_2-D-Asp-D-Tyr-L-Asp. The existence of NH_2-L-Asp-D-Tyr-D-Asp in the hydrolysate finally allowed us to establish the amino acid sequence, NH_2-L-Asn-D-Tyr-D-Asn-L-Pro-L-Glu-D-Ser-L-Thr of compound **3**.

To determine the absolute configuration of C3 in the β-amino fatty acid, the β-amino fatty acid was isolated from the hydrolysate of compound **3** and modified with dinitrofluorobenzene and *p*-methoxyaniline (Figure 4C). The CD spectrum of the dinitrophenyl-*p*-methoxyaniline derivative was similar to that of the derivative of iturinic acid,[22] indicating apparently that the β-amino fatty acid of compound **3** had an *R*-configuration, the same as iturinic acid.

The HRMS of compounds **1**, **2**, and **4** showed their $[M + H]^+$ ion peaks at m/z 1045.5552 (HR-FAB-MS; calcd for

Table 1. ^{1}H NMR Data for Compounds 1−4 in Pyridine-d_5[a]

moiety	position	δ_H (J in Hz)			
		1	2	3	4
L-Asn1	1	5.31m	5.27m	5.27m	5.27m
	2	3.08m,	3.08dd (15.3, 5.4),	3.08dd (15.4, 5.6),	3.07dd (15.4, 5.5),
		3.03m[b]	3.02m[b]	3.02m[b]	3.01m[b]
	1-NH	9.17brs	9.04brs	9.03brs	9.02brs
	3-NH_2	8.45brs[c], 7.89brs	8.38brs[c], 7.81brs	8.37brs[c], 7.80brs	8.37brs[c], 7.80brs
D-Tyr	5	5.40m	5.32m	5.32m	5.32m
	6	3.72dd (13.6, 4,6),	3.72m,	3.72dd (13.8, 4.7),	3.72dd (13.7, 4.6),
		3.41dd (13.6, 10.0)	3.40m	3.40dd (13.8, 9.8)	3.39dd (13.7, 10.0)
	8, 12	7.47d (8.1)	7.47d (8.2)	7.47d (8.3)	7.47d (8.1)
	9, 11	7.06d (8.1)	7.06d (8.2)	7.06d (8.3)	7.06d (8.1)
	5-NH	9.68brs	9.66brs	9.66brs	9.66brs
D-Asn2	14	5.55m	5.38m	5.39m	5.39m
	15	3.58dd (15.7, 8.6)	3.57dd (15.5, 9.1)	3.57dd (15.6, 9.2)	3.57dd (15.6, 9.3)
		3.18dd (15.7, 4.8)	3.18dd (15.5, 4.8)	3.18dd (15.6, 5.1)	3.18dd (15.6, 5.0)
	14-NH	9.00brs	8.96brs	8.95brs	8.94brs
	16-NH_2	8.62brs, 7.97brs	8.56brs, 7.90brs	8.55brs, 7.89brs	8.55brs, 7.88brs
L-Pro	18	4.73m	4.73dd (8.0, 5.3)	4.72dd (8.2, 5.4)	4.72dd (7.9, 5.6)
	19	2.10m, 2.08m	2.10m, 2.08m	2.11m, 2.08m	2.10m, 2.07m
	20	1.84m, 1.61m	1.86m, 1.65m	1.86m, 1.65m	1.86m, 1.65m
	21	4.22m, 4.00m	4.27m, 4.04m	4.26m, 4.03m	4.26m, 4.03m
L-Glu	23	4.87m[d]	4.87m[d]	4.87m[d]	4.87m[d]
	24	2.78m, 2.61m[e]	2.79m, 2.62m[e]	2.79m, 2.62m[e]	2.79m, 2.62m[e]
	25	3.03m[b], 2.94m	3.03m[b], 2.95m	3.03m[b], 2.95m	3.03m[b], 2.95m
	23-NH	8.45brs[c]	8.38brs[c]	8.36brs[c]	8.36brs[c]
D-Ser	28	4.92m[d]	4.89m[d]	4.89m[d]	4.89m[d]
	29	4.40m,	4.38dd (11.4, 3.3),	4.38dd (11.3, 3.2),	4.38dd (11.4, 3.0),
		4.33m	4.33dd (11.4, 3.5)	4.33dd (11.3, 3.5)	4.33dd (11.4, 3.2)
	28-NH	8.84brs	8.74brs	8.74brs	8.75brs
L-Thr	31	4.92m[d]	4.89m[d]	4.89m[d]	4.89m[d]
	32	4.94m[d]	4.95m	4.95m	4.95m
	33	1.34d (6.0)	1.34d (6.3)	1.34d (6.4)	1.34d (6.2)
	31-NH	8.23brs	8.16brs	8.15brs	8.14brs
D-β-AA	35	4.62m	4.62m	4.61m	4.61m
	36	2.64m[e], 2.45m	2.62m[e], 2.43m	2.62m[e], 2.43m	2.63m[e], 2.43m
	38	1.57m, 1.43m[f]	1.55m, 1.45m[f]	1.56m, 1.45m	1.56m, 1.45m[f]
	39	1.30m	1.30m	1.28m	1.30m
	40	1.18-1.12[g]	1.19-1.14[g]	1.20-1.15[g]	1.21-1.15[g]
	41	1.18-1.12[g]	1.19-1.14[g]	1.20-1.15[g]	1.21-1.15[g]
	42	1.18-1.12[g]	1.19-1.14[g]	1.20-1.15[g]	1.21-1.15[g]
	43	1.18-1.12[g]	1.19-1.14[g]	1.20-1.15[g]	1.21-1.15[g]
	44	1.18-1.12[g]	1.19-1.14[g]	1.20-1.15[g]	1.21-1.15[g]
	45	1.18-1.12[g]	1.19-1.14[g]	1.20-1.15[g]	1.21-1.15[g]
	46	1.08m	1.19-1.14[g]	1.20-1.15[g]	1.21-1.15[g]
	47	1.43m[f]	1.11m	1.24m[f], 1.08m	1.21-1.15[g]
	48	0.82d (6.6)	1.45m[f]	1.24m[f]	1.11m
	49	0.82d (6.6)	0.83d (6.7)	0.82d (6.3)	1.45m[f]
	50		0.83d (6.7)	1.24m[f]	0.83d (6.6)
	51			0.82t (7.4)	0.83d (6.6)
	35-NH	8.20brs	8.12brs	8.11brs	8.11brs

[a]Compound **1**, 500 MHz; **2**, 600 MHz; **3** and **4**, 800 MHz. [b,c,d,e,f,g]Overlapped in each column.

$C_{49}H_{77}N_{10}O_{15}$, 1045.5570), 1059.5756 (HR-ESI-MS; calcd for $C_{50}H_{79}N_{10}O_{15}$, 1059.5726), and 1073.5876 (HR-ESI-MS; calcd for $C_{51}H_{81}N_{10}O_{15}$, 1073.5883), respectively. A series of NMR spectral analyses revealed that compounds **1**, **2**, and **4** had the same amino acid sequence as compound **3**, except for the side-chain structures of the β-amino fatty acids. The ^{1}H NMR and ^{13}C NMR spectra of compounds **1**, **2**, and **4** showed the presence of the $-(CH_2)_9CH(CH_3)_2$, $-(CH_2)_{10}CH(CH_3)_2$, and $-(CH_2)_{11}CH(CH_3)_2$ groups, respectively. Thus, we concluded that compounds **1**, **2**, and **4** were *iso*-C_{15}, *iso*-C_{16}, and *iso*-C_{17} bacillomycin D, respectively.

dx.doi.org/10.1021/jf404531t | J. Agric. Food Chem. 2014, 62, 1469−1476

Table 2. ^{13}C NMR Chemical Shifts of Compounds 1−4 in Pyridine-d_5[a]

moiety	position	δ_C 1	2	3	4
L-Asn1	1	52.8	52.9	52.9	52.9
	2	37.1	37.1	37.1	37.1
	3	172.7[b]	172.7[b]	172.7[b]	172.7[b]
	4	173.0[b]	172.9[b]	172.9[b]	172.9[b]
D-Tyr	5	55.9	55.9	55.9	55.9
	6	36.4	36.5	36.5	36.4
	7	128.7	128.6	128.6	128.7
	8, 12	131.3	131.3	131.3	131.3
	9, 11	116.1	116.1	116.1	116.1
	10	157.4	157.5	157.5	157.5
	13	173.6[c]	173.7[c]	173.7[c]	173.7[c]
D-Asn2	14	50.2	50.3	50.3	50.3
	15	37.8	37.8	37.8	37.8
	16	172.5[b]	172.5[b]	172.6[b]	172.6[b]
	17	172.9[b]	172.7[b]	172.7[b]	172.7[b]
L-Pro	18	62.0	62.2	62.1	62.1
	19	29.6[d]	29.8[d]	29.7[d]	29.6[d]
	20	25.0	25.0	25.0	25.0
	21	48.5	48.6	48.6	48.5
	22	172.5[b]	172.4[b]	172.4[b]	172.4[b]
L-Glu	23	55.3	55.4	55.4	55.4
	24	27.7	27.7	27.7	27.7
	25	31.7	31.7	31.7	31.7
	26	175.6	175.5	175.5	175.5
	27	173.6[c]	173.8[c]	173.8[c]	173.7[c]
D-Ser	28	59.4	59.3	59.3	59.3
	29	63.4	63.6	63.5	63.5
	30	171.7	171.7	171.7	171.7
L-Thr	31	57.8	57.9	57.9	57.9
	32	66.4	66.2	66.2	66.2
	33	20.7	20.8	20.8	20.8
	34	171.1	171.1	171.1	171.1
D-β-AA	35	47.5	47.4	47.4	47.4
	36	41.9	42.0	42.0	42.0
	37	173.2[b]	173.2[b]	173.2[b]	173.2[b]
	38	35.7	35.7	35.7	35.7
	39	26.1	26.1	26.1	26.1
	40	29.6[d]	29.6[d]	29.6[d]	29.6[d]
	41	29.7[d]	29.9[d]	29.7[d]	29.7[d]
	42	29.8[d]	29.9[d]	29.9[d]	29.9[d]
	43	29.9[d]	29.9[d]	29.9[d]	29.9[d]
	44	29.9[d]	30.0[d]	30.0[d]	30.0[d]
	45	30.2[d]	30.2[d]	30.0[d]	30.0[d]
	46	39.2	30.5[d]	30.3[d]	30.0[d]
	47	28.1	39.2	36.8	30.2[d]
	48	22.7	28.2	34.6	39.2
	49	22.7	22.7	19.3	28.1
	50		22.7	27.4	22.7
	51			11.5	22.7

[a]Compound **1**, 125 MHz; **2**, 150 MHz; **3** and **4**, 200 MHz. [b,c,d]Assignments may be interchanged in each column.

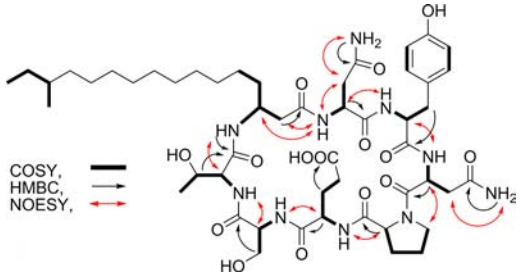

Figure 3. Key COSY, HMBC, and NOESY correlations detected for compound **3**.

Compounds **1** and **2** are known,[7] and compounds **3** and **4** are new. Compounds **3** and **4** have *anteiso*- and *iso*-C_{17} β-amino fatty acids and seven α-amino acids with the same chiral sequence, LDDLLDL, as the iturin family. This is the first study to establish the absolute structure of bacillomycin D. The metabolites assumed to be *anteiso*-C_{17} and *iso*-C_{17} bacillomycin D (**3** and **4**) were previously detected in mass spectrometric analyses of extracts from *Bacillus* species by Koumoutsi et al.,[23] Ramarathnam et al.,[24] Athukorala et al.,[25] and Liu et al.,[26] although their chemical structures were not determined. The lipid moieties of compounds **3** (*anteiso*-C_{17}) and **4** (*iso*-C_{17}) were previously reported in iturin A,[27,28] bacillomycin F,[8] and mycosubtilin,[11] and the reported contents of C_{17} homologues in iturin A, bacillomycin F, and mycosubtilin were 3, 39, and 61%, respectively. In the case of bacillomycin D, Peypoux et al.[7] reported percentages of each homologue (C_{14}, C_{15}, and C_{16}) in bacillomycin D were 48, 35, and 12%, respectively, and did not mention C_{17} homologues. Hourdou et al.[29] showed contents of each homologue (C_{14}, C_{15}, C_{16}, and C_{17}) in bacillomycin D were 48, 30, 22, and 0%, respectively. It is noteworthy that the content of the C_{17} bacillomycin D homologues was very high (60%) in the present study.

Activities of Compounds 1−4 against Plant Pathogens. The activities of compounds **1**−**4** were evaluated against 13 plant pathogens in PDA medium, and the results are shown in Table 3. The table reveals that the activities of compounds **3** and **4** (*anteiso*- and *iso*-C_{17}) were almost the same against all fungi tested and were stronger than those of compounds **1** and **2**; compound **1** was the weakest. Compounds **2**−**4** inhibited the growth of all fungi tested, and *B. berengeriana*, *B. cinerea*, *P. grisea*, *D. bryoniae*, *S. sclerotiorum*, and *M. fructicola* were the most sensitive to the compounds. By contrast, the oomycete *P. aphanidermatum* was not inhibited at all by any of the compounds. The activity of iturin family lipopeptides is attributed to their membrane-disruptive property through a direct lipopeptide−sterols interaction.[30] However, oomycetes do not synthesize sterols[31] and thus are assumed to be insensitive to bacillomycin D homologues.

The structure−antifungal activity relationships of iturin A,[32] bacillomycin Lc,[9] and bacillopeptins[10] have been studied. The activity of iturin A is directly related to the lipophilic side chain of its β-amino fatty acid; the activity increased with the number of carbon atoms in the β-amino fatty acid (C_{16} > C_{15} > C_{14}).

dx.doi.org/10.1021/jf404531t | J. Agric. Food Chem. 2014, 62, 1469−1476

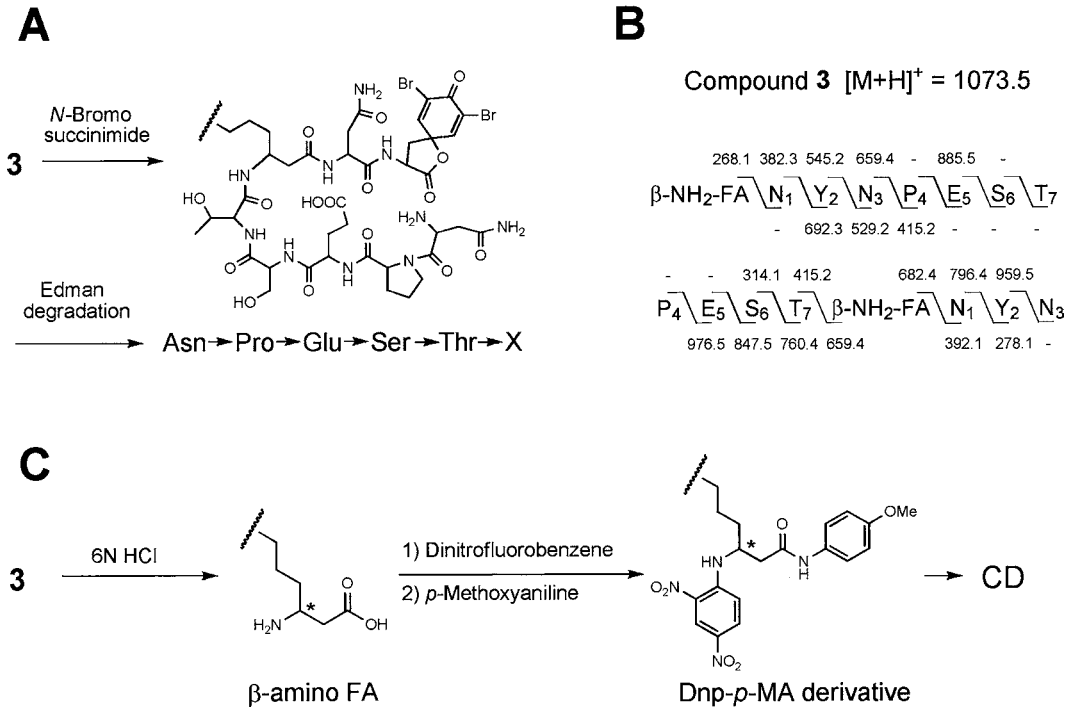

Figure 4. Reaction schemes for chemical analyses and MALDI-TOF MS/MS analysis: (A) *N*-bromosuccinimide cleavage of compound **3** followed by Edman degradation; (B) MALDI-TOF MS/MS analysis of compound **3**; (C) preparation of Dnp-*p*-MA derivative of *β*-amino fatty acid from compound **3** to determine the absolute configuration of *β*-amino fatty acid.

Table 3. Activities of Compounds 1−4 against Plant Pathogens

plant pathogen	IC_{50} (mean ± SD, μM)			
	1	**2**	**3**	**4**
Botryosphaeria berengeriana MAFF 645002	–[a]	5.0 ± 1.8	3.7 ± 1.8	4.0 ± 2.0
Botrytis cinerea MAFF 744071	28.2 ± 1.3	8.6 ± 1.5	4.2 ± 1.4	4.1 ± 1.5
Pyricularia grisea MAFF 101583	–	6.6 ± 1.8	4.3 ± 1.9	4.5 ± 1.7
Didymella bryoniae MAFF 235932	–	7.6 ± 2.2	4.7 ± 2.1	4.6 ± 2.2
Sclerotinia sclerotiorum NBRC 4876	–	6.9 ± 1.9	4.9 ± 2.0	4.6 ± 2.1
Monilinia fructicola NBRC 30451	–	7.3 ± 2.1	5.0 ± 2.8	4.8 ± 2.9
Rhizoctonia solani MAFF 305219	59.0 ± 2.1	12.8 ± 1.5	6.5 ± 2.0	7.9 ± 1.9
Colletotrichum acutatum NBRC 32849	30.5 ± 3.5	14.6 ± 3.7	10.6 ± 3.1	10.4 ± 3.2
Penicillium expansum NBRC 5453	29.0 ± 4.4	13.0 ± 4.2	10.9 ± 5.4	10.9 ± 4.0
Fusarium oxysporum MAFF 410171	43.9 ± 2.3	18.9 ± 2.9	14.1 ± 2.9	12.2 ± 2.3
Fusarium graminearum ARC 2075-1	–	17.4 ± 2.5	11.2 ± 2.8	12.8 ± 2.9
Alternaria alternata MAFF 731001	–	20.0 ± 3.2	14.6 ± 2.9	15.3 ± 2.0
Pythium aphanidermatum MAFF 239200	>40	>40	>40	>40

[a]Not tested.

Table 4. Leaf-Disk Assay Using Cucumber Cotyledon and *Botrytis cinerea*

compd	inhibition rate (%) ± SD (n = 4)					
	10 μM	20 μM	30 μM	40 μM	60 μM	80 μM
1	3.8 ± 9.0	15.9 ± 12.5	7.5 ± 26.6	−14.2 ± 11.0	19.5 ± 19.6	100
2	18.3 ± 12.3	29.1 ± 25.8	77.2 ± 22.9	100	100	100
3	3.8 ± 15.2	19.5 ± 21.3	100	100	100	100
4	21.9 ± 28.9	20.7 ± 5.4	100	100	100	100

The same results were obtained for bacillomycin Lc and bacillopeptins. Recently, Tabbene et al.[33] investigated bacillomycin D-like compounds and showed that their anti-*Candida* activity increased in the order of the side-chain length: C_{16} > C_{15} > C_{14}. Our result for bacillomycin D showed that the order of activity against plant pathogens was C_{17} > C_{16} > C_{15}; the activity of bacillomycin D increased with side-chain length until C_{17}. Recently, it was reported that mycosubtilin interacts preferentially with ergosterol compared to the other classes of lipids and that the presence of ergosterol makes it easier to insert the lipopeptide into the membrane.[34] The *β*-amino fatty acid with 17 carbon atoms in bacillomycin D is assumed to be the best-fitting molecule for hydrophobic interactions with the sterols in the membrane.

dx.doi.org/10.1021/jf404531t | J. Agric. Food Chem. 2014, 62, 1469−1476

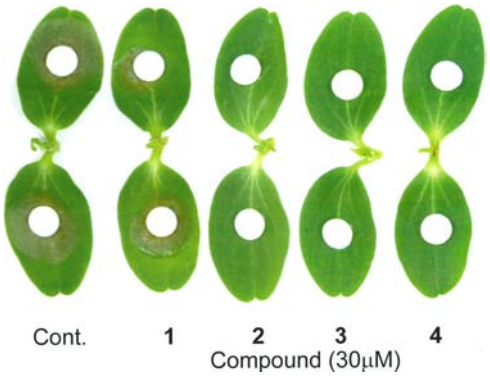

Figure 5. Leaf-disk assay using cucumber cotyledon and *Botrytis cinerea*.

Finally, to clarify the potential effect of bacillomycin D against gray mold disease, we conducted a leaf-disk assay using cucumber cotyledon and *B. cinerea*. The result is shown in Table 4 and Figure 5. Compounds **1**−**4** at concentrations of 80, 40, 30, and 30 μM, respectively, inhibited completely the *B. cinerea* infection in the cucumber leaf.

The present study demonstrates that strain SD-32 is unique because it produced higher contents of the C_{17} bacillomycin D homologues than other strains reported previously. Our result also showed that the activities of C_{17} bacillomycin D homologues are much stronger than the known C_{15} and C_{16} homologues, and from the cucumber leaf-disk assay the C_{17} bacillomycin D homologues can control gray mold disease. These indicate that this unique strain, SD-32, must be a potential promising resource for the biological control of plant disease, and experiments to assess its effect in fields are now being arranged.

■ ASSOCIATED CONTENT

Supporting Information

^{1}H NMR, ^{13}C NMR, COSY, HSQC, HMBC, and NOESY spectra of new compounds **3** and **4**; ^{1}H and ^{13}C NMR spectra of compounds **1** and **2**. This material is available free of charge via the Internet at http://pubs.acs.org.

■ AUTHOR INFORMATION

Corresponding Author

*(K.T.) Phone: +81-29-847-0989. Fax: +81-29-847-0346. E-mail: keijitsu_tanaka@sdsbio.co.jp.

Notes

The authors declare no competing financial interest.

■ ACKNOWLEDGMENTS

We thank Yusuke Amaki for his assistance with the isolation of the strain and Dr. Motoki Tanaka for his help in the identification of the strain.

■ REFERENCES

(1) Williamson, B.; Tudzynski, B.; Tudzynski, P.; van Kan, J. A. L. *Botrytis cinerea*: the cause of grey mould disease. *Mol. Plant Pathol.* **2007**, *8*, 561−580.

(2) Rosslenbroich, H. J.; Stuebler, D. *Botrytis cinerea* − history of chemical control and novel fungicide for its management. *Crop Prot.* **2000**, *19*, 557−561.

(3) Fravel, D. R. Commercialization and implementation of biocontrol. *Annu. Rev. Phytopathol.* **2005**, *43*, 337−359.

(4) Stein, T. *Bacillus subtilis* antibiotics: structures, syntheses and specific functions. *Mol. Microbiol.* **2005**, *56*, 845−857.

(5) Ongena, M.; Jacques, P. *Bacillus* lipopeptides: versatile weapons for plant disease biocontrol. *Trends Microbiol.* **2008**, *16*, 115−125.

(6) Peypoux, F.; Guinand, M.; Michel, G.; Delcambe, L.; Das, B. C.; Lederer, E. Structure of iturin A, a peptidolipid antibiotic from *Bacillus subtilis*. *Biochemistry* **1978**, *17*, 3992−3996.

(7) Peypoux, F.; Pommier, M. T.; Das, B. C.; Besson, F.; Delcambe, L.; Michel, G. Structures of bacillomycin D and bacillomycin L peptidolipid antibiotics from *Bacillus subtilis*. *J. Antibiot.* **1984**, *37*, 1600−1604.

(8) Peypoux, F.; Marion, D.; Maget-Dana, R.; Ptak, M.; Das, B. C.; Michel, G. Structure of bacillomycin F, a new peptidolipid antibiotic of the iturin group. *Eur. J. Biochem.* **1985**, *153*, 335−340.

(9) Eshita, S. M.; Roberto, N. H.; Beale, J. M.; Mamiya, B. M.; Workman, R. F. Bacillomycin Lc, a new antibiotic of the iturin group: isolation, structures, and antifungal activities of the congeners. *J. Antibiot.* **1995**, *48*, 1240−1247.

(10) Kajimura, Y.; Sugiyama, M.; Kaneda, M. Bacillopeptins, new cyclic lipopeptide antibiotics from *Bacillus subtilis* FR-2. *J. Antibiot.* **1995**, *48*, 1095−1103.

(11) Peypoux, F.; Pommier, M. T.; Marion, D.; Ptak, M.; Das, B. C.; Michel, G. Revised structure of mycosubtilin, a peptidolipid antibiotic from *Bacillus subtilis*. *J. Antibiot.* **1986**, *39*, 636−641.

(12) Moyne, A. L.; Shelby, R.; Cleveland, T. E.; Tuzun, S. Bacillomycin D: an iturin with antifungal activity against *Aspergillus flavus*. *J. Appl. Microbiol.* **2001**, *90*, 622−629.

(13) Oleinikova, G. K.; Kuznetsova, T. A.; Huth, F.; Laatsch, H.; Isakov, V. V.; Shevchenko, L. S.; Elyakov, G. B. Cyclic lipopeptides with fungicidal activity from the sea isolate of the bacterium *Bacillus subtilis*. *Russ. Chem. Bull., Int. Ed.* **2001**, *50*, 2231−2235.

(14) Oleinikova, G. K.; Dmitrenok, A. S.; Voinov, V. G.; Chaikina, E. L.; Shevchenko, L. S.; Kuznetsova, T. A. Bacillomycin D from the marine isolate of the bacterium *Bacillus subtilis* KMM 1922. *Chem. Nat. Compd.* **2005**, *41*, 240−242.

(15) Zhao, Z.; Wang, Q.; Wang, K.; Brian, K.; Liu, C.; Gu, Y. Study of the antifungal activity of *Bacillus vallismortis* ZZ185 *in vitro* and identification of its antifungal components. *Bioresour. Technol.* **2010**, *101*, 292−297.

(16) Yuan, J.; Li, B.; Zhang, N.; Waseem, R.; Shen, Q.; Huang, Q. Production of bacillomycin- and macrolactin-type antibiotics by *Bacillus amyloliquefaciens* NJN-6 for suppressing soilborne plant pathogens. *J. Agric. Food Chem.* **2012**, *60*, 2976−2981.

(17) Kumar, A.; Saini, S.; Wray, V.; Nimtz, M.; Prakash, A.; Johri, B. N. Characterization of an antifungal compound produced by *Bacillus* sp. A_5F that inhibits *Sclerotinia sclerotiorum*. *J. Basic Microbiol.* **2012**, *52*, 670−678.

(18) Cao, Y.; Xu, Z.; Ling, N.; Yuan, Y.; Yang, X.; Chen, L.; Shen, B.; Shen, Q. Isolation and identification of lipopeptides produced by *B. subtilis* SQR 9 for suppressing Fusarium wilt of cucumber. *Sci. Hortic.* **2012**, *135*, 32−39.

(19) Ramachandran, L. K.; Witkop, B. *N*-Bromosuccinimide cleavage of peptides. *Methods Enzymol.* **1967**, *11*, 283−299.

(20) Marfey, P. Determination of D-amino acids. II. Use of a bifunctional reagent, 1,5-difluoro-2,4-dinitrobenzene. *Carlsberg Res. Commun.* **1984**, *49*, 591−596.

(21) Sanger, F. The free amino groups of insulin. *Biochem. J.* **1945**, *39*, 507−515.

(22) Nagai, U.; Besson, F.; Peypoux, F. Absolute configuration of an iturinic acid as determined by CD spectrum of its DNP-p-methoxyanilide. *Tetrahedron Lett.* **1979**, *25*, 2359−2360.

(23) Koumoutsi, A.; Chen, X. H.; Henne, A.; Liesegang, H.; Hitzeroth, G.; Franke, P.; Vater, J.; Borriss, R. Structural and functional characterization of gene clusters directing nonribosomal synthesis of bioactive cyclic lipopeptides in *Bacillus amyloliquefaciens* strain FZB42. *J. Bacteriol.* **2004**, *186*, 1084−1096.

(24) Ramarathnam, R.; Bo, S.; Chen, Y.; Fernando, W. G. D.; Xuewen, G.; Kievit, T. Molecular and biochemical detection of fengycin- and bacillomycin D-producing *Bacillus* spp., antagonistic to fungal pathogens of canola and wheat. *Can. J. Microbiol.* **2007**, *53*, 901−911.

(25) Athukorala, S. N. P.; Fernando, W. G. D.; Rashid, K. Y. Identification of antifungal antibiotics of *Bacillus* species isolated from different microhabitats using polymerase chain reaction and MALDI-TOF mass spectrometry. *Can. J. Microbiol.* **2009**, *55*, 1021−1032.
(26) Liu, J.; Zhou, T.; He, D.; Li, X. Z.; Wu, H.; Liu, W.; Gao, X. Functions of lipopeptides bacillomycin D and fengycin in antagonism of *Bacillus amyloliquefaciens* C06 towards *Monilinia fructicola*. *J. Mol. Microbiol. Biotechnol.* **2011**, *20*, 43−52.
(27) Isogai, A.; Takayama, S.; Murakoshi, S.; Suzuki, A. Structures of β-amino acids in antibiotics iturin A. *Tetrahedron Lett.* **1982**, *23*, 3065−3068.
(28) Hiradate, S.; Yoshida, S.; Sugie, H.; Yada, H.; Fujii, Y. Mulberry anthracnose antagonists (iturins) produced by *Bacillus amyloliquefaciens* RC-2. *Phytochemistry* **2002**, *61*, 693−698.
(29) Hourdou, M. L.; Besson, F.; Tenoux, I.; Michel, G. Fatty acid and β-amino acid syntheses in strains of *Bacillus subtilis* producing iturinic antibiotics. *Lipids* **1989**, *24*, 940−944.
(30) Bonmatin, J. M.; Laprevote, O.; Peypoux, F. Diversity among microbial cyclic lipopeptides: iturins and surfactins. Activity-structure relationships to design new bioactive agents. *Comb. Chem. High Throughput Screen.* **2003**, *6*, 541−556.
(31) Latijnhouwers, M.; Wit, P. J. G. M.; Govers, F. Oomycetes and fungi: similar weaponry to attack plants. *Trends Microbiol.* **2003**, *11*, 462−469.
(32) Bland, J. M.; Lax, A. R.; Klich, M. A. HPLC separation and antifungal activity of the naturally occurring iturin-A homologs. *Peptides 1992: Proceedings of the Twenty-Second European Peptide Symposium*; Schneider, C. H., Eberle, A. N., Eds.; ESCOM: Leiden, The Netherlands, 1993; pp 332−333.
(33) Tabbene, O.; Kalai, L.; Slimene, I. B.; Karkouch, I.; Elkahoui, S.; Gharbi, A.; Cosette, P.; Mangoni, M. L.; Jouenne, T.; Limam, F. Anti-*Candida* effect of bacillomycin D-like lipopeptides from *Bacillus subtilis* B38. *FEMS Microbiol. Lett.* **2011**, *316*, 108−114.
(34) Nasir, M. N.; Besson, F. Interactions of the antifungal mycosubtilin with ergosterol-containing interfacial monolayers. *Biochim. Biophys. Acta* **2012**, *1818*, 1302−1308.

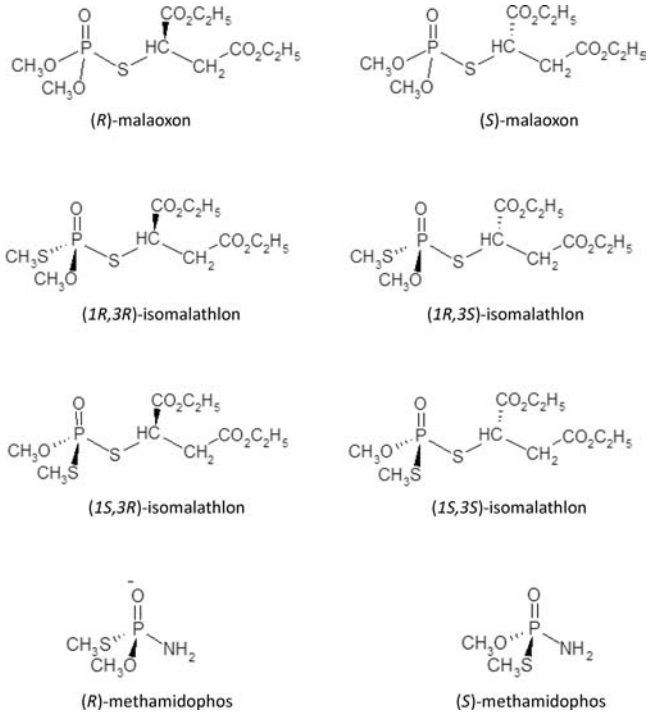

Figure 1. Enantiomers of malaoxon, isomalathion, and methamidophos. *, chiral center. Asymmetric phosphorus and carbon atoms of isomalathion were designated at positions 1 and 3, respectively.

13−29-fold.[15,16] Methamidophos (*O*,*S*-dimethyl phosphoramidothioate) is a highly toxic and widely used OP, which has an asymmetric center at the phosphorus atom and hence contains one pair of enantiomers (Figure 1).[17] The inhibitory potency of (*S*)-methamidophos was approximately 8.0−12.4 times stronger than that of (*R*)-methamidophos for AChE. It was noted that many studies had been conducted on postinhibitory reactions of AChE inactivated by enantiomers of isoparathion-methyl, malaoxon, and stereoisomers of isomalathion, and the results indicated that AChE inhibited by isomalathion stereoisomers with (1*S*)-configuration could not undergo a reactivation. The structural difference of inhibited AChE was thought to be responsible for the observation, that is, *S*-diethyl thiosuccinyl-*O*-methyl phosphorylated AChE incapable of reactivation was formed in the inhibition processes by (1*S*)-isomalathions due to the loss of thiomethyl as the primary leaving group, whereas inhibition of AChE by (1*R*)-isomalathions and enantiomers of isoparathion and malaoxon produced *O*,*O*-methyl or *O*,*S*-methyl phosphorylated AChEs, which were readily reactivated.[18]

The toxic effect of OPs has been observed for broad-spectrum plants and crops.[19−21] Previous studies showed that a variety of OPs could inhibit the activity of acid α-naphthyl acetate esterase, which is present in extracts from wheat.[22] The enantioselectivity in the inhibition was observed for malaoxon and isomalathion. The half-inhibition concentration (IC_{50}) values indicated (*R*)-malaoxon was 1.3 times stronger than its (*S*)-configuration, and the decreasing order of potency against ANAE was (1*R*,3*R*) > (1*R*,3*S*) > (1*S*,3*R*) > (1*S*,3*S*), with a 4.7-fold difference between (1*R*,3*R*) and (1*S*,3*S*).[9] However, selective inhibition kinetics and postinhibitory reactions, which were intensively studied in the inhibition of AChE by chiral OPs, were not included in those studies.

In an attempt to get the more detailed information on enantioselective reaction of ANAE with chiral OPs, we investigated enantioselective inhibition kinetics and post-inhibitory reactions of ANAE by chiral OPs and the difference in mechanism of ANAE inactivation between enantiomers of OPs.

EXPERIMENTAL PROCEDURES

Chemicals. Racemic isomalathion and malaoxon (purity > 99.5%) were obtained from Sigma Chemical Co. (St. Louis, MO, USA). Analytical standard of racemic methamidophos (purity > 99.0%) was purchased from Kefa New Technology Development Co. (Shengyang, China).The four resolved stereoisomers of isomalathion, two enantiomers of malaoxon, and two enantiomers of methamidophos were collected at the outlet of a high-performance liquid chromatograph (HPLC) with chiral columns and circular dichroism detectors during the observed responses.[17] The absolute configuration was determined according to the elution order of enantiomers on chiral columns described in a previous study.[23] Fast Blue B, α-naphthyl acetate, and α-naphthol were purchased from National Physic Chemical Co. (Shanghai, China). Other solvents or chemicals were of HPLC or analytical grade.

Preparation of ANAE. ANAE was extracted from wheat flour by using the process employed in our previous study.[9] Briefly, homogenized wheat flour and deionized water were gently mixed for 15 h at 4 °C and then centrifuged for 20 min at 5000 rpm. The supernatant containing ANAE was obtained and stored at 4 °C until use. Working solutions of the enzymes were prepared in 0.2 M potassium phosphate buffer (pH 6.38), in which the hydrolysis rates of plant enzyme were approximately 0.05−0.10 absorbance unit/min.

Assay for ANAE Inhibition. The extent of ANAE inhibition was evaluated by the bimolecular reaction constant (k_i), dissociation constant (K_d), and phosphorylation constant (k_p), which were determined according to the method from inhibition of AChE by OPs.[10,11,24] All kinetic assays depend on the ANAE-catalyzed hydrolysis of α-naphthyl acetate and the estimation of diazonium dye produced.[22] The remaining ANAE activity after incubation of the enzyme with a progression of inhibitor concentrations was measured to calculate the kinetic components K_d and k_p.[11] Briefly, ANAE solution (180 μL) was treated with 20 μL each of a progression of inhibitor concentrations. At predetermined time intervals, 20 μL of the enzyme-inhibitor solution was taken to measure the residual activity of enzyme. The line regression between ($-\ln(E_t/E_0)$) and t will give k_{app}, where E_0 is the initial activity of AChE, E_t is the remaining activity at the time of measurement, and t is the reaction time.

$$k_{app} = -\ln(E_t/E_0)/t \quad (1)$$

The kinetic parameters were then obtained by plots of 1/[I] versus 1/k_{app} (at the individual inhibitor concentration) using the following equation.

$$1/k_{app} = 1/k_p + K_d/(k_p[I]) \quad (2)$$

[I] is the concentration of inhibitor.

k_i is calculated by the following equation:

$$k_i = k_p/K_d \quad (3)$$

Spontaneous Reactivation of ANAE Inhibited. ANAE solution (180 μL) was added to vessels A and B, and then 20 μL of phosphate buffer (pH 6.38) and 20 μL of an inhibitor solution that caused 90% inhibition were added to vessel A as a control and B as a test, respectively. Following a 30 min incubation at 35 °C, an aliquot of 100 μL of ANAE inhibitor (or phosphate buffer) solution was drawn and diluted in vessel C, which contained 1.9 mL of phosphate buffer to halt further inhibition, and the enzyme activity was determined following a brief temperature equilibration. At predetermined time intervals, including a time point immediately following dilution (t = 0), 20 μL aliquots from vessel C were transferred to a well containing α-naphthyl acetate solution (100 mg/80 mL, 23 μL) and Fast Blue B solution

(125 mg/80 mL, 207 μL). Returned enzyme activity was followed for 50 min by measuring the increase in absorbance at 550 nm. The rate constants of spontaneous reactivation (k_3) were calculated from the linear portion of the slopes according to eq 4

$$\ln[100(A_0 - A_t')/(A_0 - A_0')] = -k_3 t \quad (4)$$

where A_0 is the ANAE activity without inhibitor at time = 0, A_t' is the ANAE activity of inhibited ANAE at time = t, and A_0' is the ANAE activity of inhibited ANAE at time = 0.

Statistical Analysis. At least four separate experiments were used to calculate all values, and the results were expressed as the mean ± standard deviation (SD). Significance of differences between means was determined by one-way ANOVA ($\alpha = 0.05$) or t tests ($p < 0.05$). All statistics and regressions were performed using Origin version 8.0 for Windows. An F test was employed to determine whether slopes of regression lines of reactivation plots were significantly different from zero ($p < 0.05$).

RESULTS AND DISCUSSION

The line regressions between $(-\ln(E_t/E_0))$ and t and between $1/[I]$ and $1/k_{app}$ for (R)-malaoxon are shown in Figure 2, and those for other compounds can be found in Figures SI1−7 in the Supporting Information; the kinetic parameters are given in Table 1.

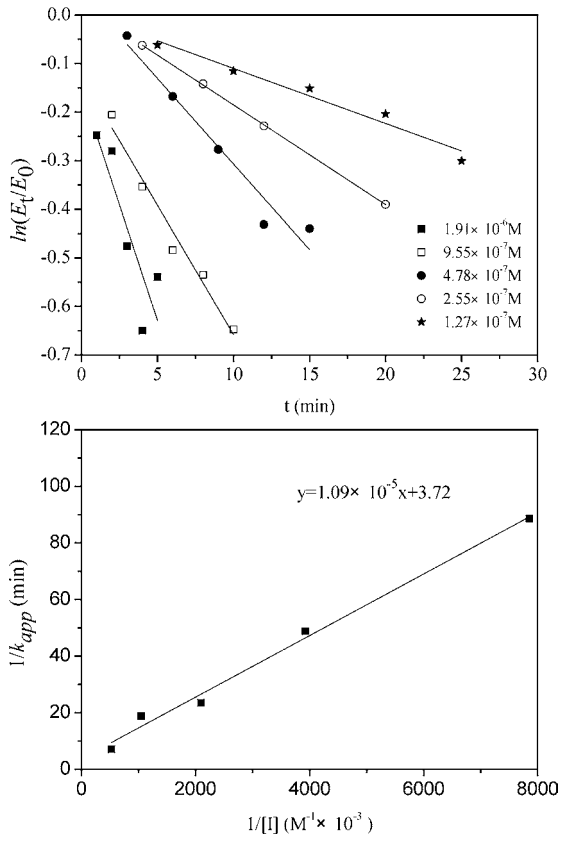

Figure 2. Typical plots for the determination of k_{app} and k_i for (R)-malaoxon.

Enantioselective Inhibition of ANAE by Malaoxon. The enantioselectivity of malaoxon in inhibition of AChE has been demonstrated by the difference for k_i values between (R)- and (S)-malaoxon. (R)-Malaoxon was always a more potent inhibitor of AChE than (S)-malaoxon with R/S ratios of 4.4−22.5. Similar to the enantioselective inhibition order of malaoxon to AChE, (R)-malaoxon was also a more potent inhibitor of ANAE than (S)-malaoxon as shown in Table 1. However, the difference of k_i values between (R)- and (S)-malaoxon for ANAE was less than that for AChE, indicating that ANAE was less preferential in enantioeselective recognition toward enantiomers of malaoxon than AChE. A further study was carried out to compare K_d and k_p values for ANAE with those for AChE, indicating that K_d and k_p values of enantiomers of malaoxon for ANAE were in the same order as those for AChE. Namely, (S)-malaoxon had higher K_d values for both ANAE and AChE than (R)-malaoxon, whereas k_p values of R-malaoxon were always higher than those of (S)-malaoxon for both ANAE and AChE. These results suggested that enantioselective interactions between the enzyme and malaoxon were similar for ANAE and AChE.

Table 1. Kinetic Constants for Enantiomers of Malaoxon, Isomalathion and Methamidophos against ANAE

	k_i	k_p	K_d
Malaoxon			
(R)-malaoxon	4.83 ± 0.10	0.27 ± 0.01	0.06 ± 0.00
(S)-malaoxon	3.78 ± 0.10	1.31 ± 0.03	0.08 ± 0.01
Isomalathion			
(1R,3R)-isomalathion	31.90 ± 1.01	0.55 ± 0.02	0.02 ± 0.00
(1R,3S)-isomalathion	20.42 ± 0.87	0.58 ± 0.01	0.03 ± 0.00
(1S,3R)-isomalathion	13.71 ± 0.55	0.15 ± 0.01	0.01 ± 0.00
(1S,3S)-isomalathion	8.49 ± 0.33	0.69 ± 0.02	0.08 ± 0.01
Methamidophos			
(R)-methamidophos	0.27 ± 0.01	0.20 ± 0.01	0.75 ± 0.02
(S)-methamidophos	1.18 ± 0.02	0.06 ± 0.00	0.05 ± 0.00

Enantioselective Inhibition of ANAE by Isomalathion. Previous studies found that the inactivation of AChE by isomalathion stereoisomers was in the order (1R,3R) > (1R,3S) > (1S,3R) >(1S,3S) according to k_i values, and chirality at both the phosphorus and carbon atoms influenced the rate of the inhibitory reaction of isomalathion with AChE.[15,16] The same order of k_i values and effect of chiral center on the rate of the inhibitory reaction were observed in the inhibition of ANAE by isomalathion stereoisomers as shown in Table 1. Additionally, changing the stereochemistry at the phosphorus atom could result in bigger k_i ratios than changing the stereochemistry at the carbon atom in the inhibition of AChE by isomalathion;[25] such results were also observed in the inhibition of ANAE by isomalathion. The observations indicated that stereoselective interactions between ANAE and isomalathion were similar to that between AChE and isomalathion.

Enantioselective Inhibition of ANAE by Methamidophos. Methamidophos exhibited significant enantioselectivity on the inhibition of AChE with the S/R ratios of 8.0−12.4.[17] The inhibitory potency of (S)-methamidophos was 4.4 times stronger than that of (R)-methamidophos for ANAE, indicating the active site of ANAE was less discriminatory toward enantiomers of methamidophos than that of AChE. However, the enantiomers of methamidophos were in the same order of potency in inhibiting ANAE as observed for AChE. This showed ANAE and AChE were similar in enantioselective interactions with methamidophos.

Although the enantioselectivity of ANAE is less potent toward malaoxon, isomalathion, and methamidophos than that of AChE, the orders of k_i values of malaoxon, isomalathion, and methamidophos enantiomers for ANAE are exactly the same as those for AChE.

dx.doi.org/10.1021/jf404959v | J. Agric. Food Chem. 2014, 62, 1477−1481

Postinhibitory Reactions of ANAE Inhibited by Chiral OPs. The spontaneous reactivation of ANAE inhibited by chiral OPs is shown in Figure 3. The rate constants of spontaneous reactivation (k_3) were calculated from the linear portion of the slopes in Figure 3 and are given in Table 2. The measured k_3 values indicated that spontaneous reactivation of ANAE inhibited by (*R*)-malaoxon was not different from that of ANAE inhibited by (*S*)-malaoxon (Table 2), implying that the two enantiomers generated the same organophosphorylated enzyme with identical stereochemistry in the malaoxon moiety that is covalently bonded to the active site. ANAE inhibited by (1*R*)-isomalathion can readily undergo a reactivation, whereas the enzyme inactivated by the (1*S*)-isomers was refractory toward reactivation. A >3-fold difference was observed in k_3 values for ANAE modified by (1*R*)- versus (1*S*)-isomalathion (Table 2). The results were very similar to those observed in spontaneous reactivation of inhibited AChE by isomalathions.[26] A pronounced difference in spontaneous reactivation was observed for ANAE inactivated by enantiomers of methamidophos; namely, ANAE inhibited by (*S*)-methamidophos spontaneously reactivated at a remarkable k_3 value, whereas spontaneous reactivation could not be detected for ANAE modified by (*R*)-methamidophos, which is indicated by a nearly zero value of k_3 (Table 2), suggesting the mechanism of ANAE inactivation was different between (*S*)- and (*R*)-methamidophos. The spontaneous reactivation of AChE inhibited by enantiomers of methamidophos has not received examination to date. Thus, the comparison of enantioselectivity in spontaneous reactivation between ANAE and AChE cannot be made. However, the primary leaving group in the inhibition of ANAE by methamidophos can be predicted as methoxy for (*S*)-methamidophos and as thiomethyl for (*R*)-methamidophos according to the similarity of spontaneous reactivation of ANAE inhibited by isomalathion stereoisomers and methamidophos enantiomers.

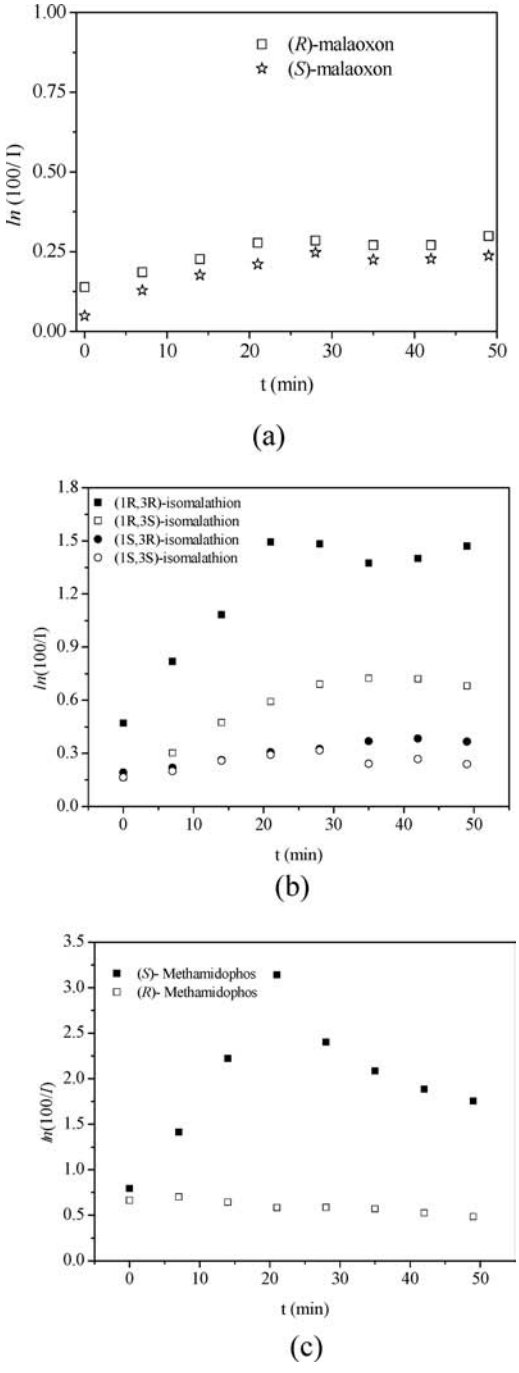

Figure 3. Representative plots of reactivation for ANAE inhibited by chiral organophosphorus insecticide enantiomers (a, malaoxon; b, isomalathion; c, methamidophos). The slopes of the initial linear portion of each serial represent k_3 (min^{-1}).

Table 2. Rate Constants of Spontaneous Reactivation (k_3) of ANAE Inhibited by the Enantiomers of Chiral Organophosphorus Insecticides

compound	$k_3 \times 10^3$ (min^{-1})
Malaoxon	
(*R*)-malaoxon	6.5 ± 0.33
(*S*)-malaoxon	5.6 ± 0.31
Isomalathion	
(1*R*,3*R*)-isomalathion	47.5 ± 1.8
(1*S*,3*R*)-isomalathion	5.1 ± 0.27
(1*S*,3*S*)-isomalathion	5.7 ± 0.23
(1*R*,3*S*)-isomalathion	19.1 ± 0.61
Methamidophos	
(*R*)-methamidophos	0 ± 0.01
(*S*)-methamidophos	112.0 ± 5.2

Overall, cholinesterase and ANAE are identified as the only enzymes that can be inhibited by OPs at the present. Furthermore, the enantioselectivity demonstrated to occur for inhibition of AChE by malaoxon, isomalathion, and methamidophos is conserved for ANAE. Thus, it can be concluded that ANAE and AChE had similar selective inhibition kinetics and postinhibitory reactions in reaction with chiral OPs. The results extend the knowledge on the enantioselective toxicity of chiral OPs.

■ ASSOCIATED CONTENT

Supporting Information

Figures SI1−7 for the deductions of k_i, K_d, and k_p. This material is available free of charge via the Internet at http://pubs.acs.org.

■ AUTHOR INFORMATION

Corresponding Author

*(W.L.) Phone: 86-571-8898-2341. Fax: 86-571-8898-2341. E-mail: wliu@zju.edu.cn.

Funding

This work was funded by the National Natural Science Foundation of China (Grants 41073090 and 20707022) and the Scientific Research Foundation of Zhejiang University of Technology (No. 20080116).

Notes

The authors declare no competing financial interest.

REFERENCES

(1) Demmer, C. S.; Krogsgaard-Larsen, N.; Bunch, L. Review on modern advances of chemical methods for the introduction of a phosphonic acid group. *Chem. Rev.* **2011**, *111*, 7981−8006.

(2) Merino, P.; Marqués-López, E.; Herrera, R. P. Catalytic enantioselective hydrophosphonylation of aldehydes and imine. *Adv. Synth. Catal.* **2008**, *350*, 1195−1208.

(3) Ordóñez, M.; Sayago, F. J.; Cativiela, C. Synthesis of quaternary α-aminophosphonic acids. *Tetrahedron* **2012**, *68*, 6369−6412.

(4) Boduszek, B.; Olszewski, T. K.; Goldeman, W.; Grzegolec, K.; Blazejewska, P. Preparation of new imidazol-2-yl-(amino)-methylphosphonates, phosphinates and phosphine oxides and their unexpected cleavage under acidic conditions. *Tetrahedron* **2012**, *68*, 1223−1229.

(5) Olszewski, T. K.; Boduszek, B. Synthesis of new thiazole-2, -4, and -5-yl-(amino)methylphosphonates and phosphinates: unprecedented cleavage of thiazole-2 derivatives under acidic conditions. *Tetrahedron* **2010**, *66*, 8661−8666.

(6) Olszewski, T. K.; Gałezowska, J.; Boduszek, B.; Kozłowski, H. New heterocyclic mono- and bis(α-hydroxymethyl)phosphinic acids: synthesis and Cu^{II} binding abilities. *Eur. J. Org. Chem.* **2007**, *21*, 3539−3546.

(7) Olszewski, T. K.; Boduszek, B. Application of bis(trimethylsilyl) phosphonite in the efficient preparation of new heterocyclic a-aminomethyl-*H*-phosphinic acids. *Synthesis* **2011**, *3*, 437−442.

(8) Michalska, J.; Boduszek, B.; Olszewski, T. K. New quinoline-2, -3, and 4-yl-(amino)methylphosphonates: synthesis and study on the C−P bond cleavage in quinoline-2 and -4 derivatives under acidic conditions. *Heteroat. Chem.* **2011**, *22*, 617−624.

(9) Zhang, A. P.; Xie, X. M.; Ye, J.; Lin, C. M.; Hu, X. Y. Stereoselective toxicity of malathion and its metabolites, malaoxon and isomalathion. *Environ. Chem. Lett.* **2011**, *9*, 369−373.

(10) Thompson, C. M.; Ryu, S.; Berkman, C. E. Consequence of phosphorus stereochemistry upon the postinhibitory reaction kinetics of acetylcholinesterase poisoned by phosphorothiolates. *J. Am. Chem. Soc.* **1992**, *114*, 10710−10715.

(11) Ryu, S.; Lin, J.; Thompson, C. M. Comparative anticholinesterase potency of chiral isoparathionmethyl. *Chem. Res. Toxicol.* **1991**, *4*, 517−520.

(12) George, K. M.; Schule, T.; Sandoval, L. E.; Jennings, L. L.; Taylor, P.; Thompson, C. M. Differentiation between acetylcholinesterase and the organophosphate-inhibited form using antibodies and the correlation of antibody recognition with reactivation mechanism and rate. *J. Biol. Chem.* **2003**, *278*, 45512−45518.

(13) Hassan, A.; Dauterman, W. C. Studies on the optically active isomers of *O*,*O*-diethyl malathion and *O*,*O*-diethyl malaoxon. *Biochem. Pharmacol.* **1968**, *17*, 1431−1439.

(14) Rodriguez, O. P.; Muth, G. W.; Berkman, C. E.; Kim, K.; Thompson, C. M. Inhibition of various cholinesterases with the enantiomers of malaoxon. *Bull. Environ. Contam. Toxicol.* **1997**, *58*, 171−176.

(15) Berkman, C. E.; Quinn, D. A.; Thompson, C. M. Interaction of acetylcholinesterase with the enantiomers of malaoxon and isomalathion. *Chem. Res. Toxicol.* **1993**, *6*, 724−730.

(16) Jianmongkol, S.; Berkman, C. E.; Thompson, C. M.; Richardson, R. J. Relative potencies of the four stereoisomers of isomalathion for inhibition of hen brain acetylcholinesterase and neurotoxic esterase *in vitro*. *Toxicol. Appl. Pharmacol.* **1996**, *139*, 342−348.

(17) Lin, K. D.; Zhou, S. S.; Xu, C.; Liu, W. P. Enantiomeric resolution and biotoxicity of methamidophos. *J. Agric. Food Chem.* **2006**, *54*, 8134−8138.

(18) Jianmongkol, S.; Marable, B. R.; Berkman, C. E.; Talley, T. T.; Thompson, C. M.; Richardson, R. J. Kinetic evidence for different mechanisms of acetylcholinesterase inhibition by (1*R*)- and (1*S*)-stereoisomers of isomalathion. *Toxicol. Appl. Pharmacol.* **1999**, *155*, 43−53.

(19) Howells, D. J.; Hambrook, J. L. The phytotoxicity of some methylphosphonofluoridates. *Pestic. Sci.* **1972**, *3*, 351−356.

(20) McKinlay, R. G. The phytotoxicity of insecticidal seed coatings and granular and spray soil treatments to grain yields in field experiments on the control of larvae of wheat bulb fly (*Delia coarctata* Fall.). *Crop Prot.* **1982**, *1*, 83−90.

(21) Zhang, Z. Y.; Shan, W. L.; Song, W. C.; Gong, Y.; Liu, X. J. Phytotoxicity and uptake of chlorpyrifos in cabbage. *Environ. Chem. Lett.* **2011**, *9*, 547−552.

(22) Wang, J. L.; Xia, Q.; Zhang, A. P.; Hu, X. Y.; Lin, C. M. Determination of organophosphorus pesticide residues in vegetables by an enzyme inhibition method using α-naphthyl acetate esterase extracted from wheat flour. *J. Zhejiang. Univ. Sci. B* **2012**, *13*, 267−273.

(23) Zhang, A. P.; Lai, W. F.; Sun, J. Q.; Hu, G. X.; Liu, W. P. Probing the chiral separation mechanism and the absolute configuration of malathion, malaoxon and isomalathion enantiomers by chiral high performance liquid chromatography coupled with chiral detector−binding energy computations. *J. Chromatogr., A* **2013**, *1281*, 26−31.

(24) Thompson, C. M.; Frick, J. A.; Natke, B. E.; Hansen, L. K. Preparation, analysis and anti-cholinesterase properties of *O*,*O*-dimethylphosphorothioate isomerides. *Chem. Res. Toxicol.* **1989**, *2*, 386−391.

(25) Doorn, J. A.; Talley, T. T.; Thompson, C. M.; Richardson, R. J. Probing the active sites of butyrylcholinesterase and cholesterol esterase with isomalathion: conserved stereoselective inactivation of serine hydrolases structurally related to acetylcholinesterase. *Chem. Res. Toxicol.* **2001**, *14*, 807−813.

(26) Doorn, J. A.; Gage, D. A.; Schall, M.; Talley, T. T.; Thompson, C. M.; Richardson, R. J. Inhibition of acetylcholinesterase by (1*S*,3*S*)-isomalathion proceeds with loss of thiomethyl: kinetic and mass spectral evidence for an unexpected primary leaving group. *Chem. Res. Toxicol.* **2000**, *13*, 1313−1320.

different drying methods. The use of both mature and immature maize kernels was to identify the effects of kernel drying in the field.

EXPERIMENTAL SECTION

Materials. Maize cobs from different maturity stages of plants were selected from a local farm (Warwick, QLD, Australia) by visual observation (late R4 and early R6 plants, as described by WeedSOFT decision support system, available at http://weedsoft.unl.edu/documents/growthstagesmodule/corn/corn. htm) and designated as immature maize (IM) and mature maize (MM), respectively. The kernels were manually scraped from the cobs using a knife for determination of moisture content and isolation of starch granules. The moisture contents of IM and MM kernels averaged from six cobs were 66.8% and 37.6%, respectively, with standard deviations of 4.1% and 2.5%, respectively. Potato tubers (PTs) of similar sizes (70 ± 6 g) were also collected from a local farm (Killarney, QLD, Australia). Canna tubers (CTs) were collected from a local garden in St. Lucia, QLD, Australia. Gelose 50 (G50) and Gelose 80 (G80) starches were obtained from Penford Australia Ltd. (now Ingredion Pty. Ltd., Lane Cove, NSW, Australia), and both are high-amylose maize starches.

Porcine pancreatin and fluorescein isothiocyanate conjugate tagged dextran (FITC-dextran, molar mass 20 kDa) were obtained from Sigma-Aldrich Pty. Ltd. (Castle Hill, NSW, Australia), and amyloglucosidase from *Aspergillus niger* (EC 3.2.1.3, 3260 U/mL) was obtained from Megazyme International Ltd. (Bray, Co., Wicklow, Ireland). The pancreatin had 4 times the activity specified by United States Pharmacopeia (USP), that is, at least 100 USP units of amylase and protease and at least 8 USP units of lipase per milligram of product.

Starch Isolation and Drying Processes. Brushed and washed PTs were peeled manually, diced, and stored in 0.1 M NaCl solution before starch isolation. Similarly, maize kernels were stored in 0.1 M NaCl solution. Starch granules were isolated from the maize kernels and PTs using the method of Whistler et al.,[8] and the purified starch granules were kept in 0.025% sodium azide solution until being used for further analyses or subjected to various drying methods. The apparent amylose contents of IM, MM, and PT starches, determined by an iodine colorimetric method,[9] were 20.2%, 25.3%, and 30.3%, respectively. The purified starches from IM, MM, and PT were dehydrated using three methods: oven, freeze, and ethanol drying. For oven drying (OD), wet starch granules were dried in an oven at 40 °C for 48 h, manually ground, and passed through a sieve with openings of 125 μm. For freeze-drying (FD), wet starch granules were frozen in a liquid nitrogen bath (from −210 to −196 °C) and dried using a freeze-dryer (VirTis Benchtop 4K, SP Industries, Inc., Warminster, PA), ground, and sieved in the same way as the OD starch samples. For ethanol drying (ED), wet starch granules were washed using absolute ethanol, centrifuged, and dried in a fume hood at ambient temperature under a flow of N_2. To separate the effects of freezing and drying steps during FD, starch granules were also frozen in a liquid nitrogen bath and then thawed at room temperature (frozen−thawed, FT). The wet (W) controls were starch granules that had never been dried.

CT starch granules were isolated in a same way as the PT starch granules and subjected to ED and FD processes. The G50 and G80 starch granules were dried commercially by the manufacturer and were dispersed in water before being subjected to ED and FD processes.

In Vitro Starch Digestion. Starch was digested following the method of Dhital et al.[10] with slight modifications. Starch granules (~50 mg, dry basis) were suspended in 15 mL of sodium acetate buffer (0.2 M, pH 6.0). Freshly prepared enzyme solution (500 μL) containing pancreatin (2 mg/mL) and amyloglucosidase (28 U/mL) was added to the starch suspension, and the mixture was incubated in a water bath at 37 °C with shaking. Aliquots (0.3 mL) were removed at specific time intervals, mixed with absolute ethanol (0.9 mL), and centrifuged at 4000*g* for 10 min. The undigested starch residues collected as precipitates after centrifugation were freeze-dried for further microscopic analysis. The concentration of glucose in the supernatant was determined using an enzymatic glucose reagent (TR 15104, Thermo Scientific, Noble Park, VIC, Australia), and the absorbance was measured at 505 nm. The glucose release (%) was calculated as

$$\text{glucose release (\%)} = \frac{\text{total weight of glucose in supernatant} \times 0.9}{\text{dry weight of starch}} \times 100 \quad (1)$$

where 0.9 is the molar mass conversion from glucose to anhydroglucose (the starch monomer unit). The glucose profile or digestogram was then fitted to a first-order equation[11] for the kinetics of starch digestion as follows

$$C = 1 - e^{-kt} \quad (2)$$

where t is the digestion time (min), C is the fraction of digested starch at digestion time t, and k is the digestion rate constant (min^{-1}). The value of k can be obtained from the slope of a linear-least-squares fit of a plot of $\ln(1 - C)$ against t.

Scanning Electron Microscopy. Starch granules were thinly spread onto a circular metal stub covered with a double-sided adhesive carbon tape. The starch granules were then coated with platinum to approximately 10-nm thickness using a sputter coater (Eiko IB3, Mito, Japan) for 3 min at 15 mA in an argon-gas environment. Images of the starch granules were acquired using a Philips XL30 scanning electron microscope (SEM, Philips, Eindhoven, The Netherlands) under an accelerating voltage of 5 kV and at several magnifications; 4000× and 1500× magnifications were used to obtain representative images for maize (IM and MM) and PT starches, respectively.

Confocal Laser Scanning Microscopy. Starch granules (~1 mg) were dispersed in 500 μL of FITC-dextran solution (2 mg/mL) in a microcentrifuge tube and mixed at 300 rpm overnight at room temperature in a thermomixer (Eppendorf, Hamburg, Germany).[12] The mixture was spread onto a glass slide and covered with a glass slip and observed using an LSM 700 confocal laser scanning microscope (CLSM, Zeiss, Oberkochen, Germany). The excitation wavelength of the argon-ion laser was set at 488 nm and was operating at 2% of capacity power, and the emission light was detected at 492−600 nm. The images of optical sections of granules were recorded with ZEN 2011 software (Zeiss, Oberkochen, Germany).

Differential Scanning Calorimetry. A differential scanning calorimeter (DSC, DSC 1, Mettler Toledo, Schwerzenbach, Switzerland) with an intracooler was used to analyze the gelatinization properties of starch, following the method of Zhang et al.[13] Starch granules (~5 mg) were mixed with deionized water (~12 mL) by a needle and hermetically sealed in an aluminum pan. The pan was held at 10 °C for 1 min and then heated to 95 °C at 10 °C/min. The enthalpy change (ΔH) and the onset (T_o), peak (T_p), and conclusion (T_c) temperature of starch gelatinization were calculated from the DSC endotherm using STARe software (Mettler Toledo, Schwerzenbach, Switzerland).

Wide-Angle X-ray Diffractometry. Starch granules were equilibrated in a chamber with 44% relative humidity at 20 °C for 48 h, to give a moisture content of ~11% w/w. X-ray diffraction analysis was performed with an X'Pert Pro powder X-ray diffractometer (PANalytical, Almelo, The Netherlands) operating at 40 kV and 30 mA with Cu Kα radiation (λ) at 0.15405 nm. The scanning region was set from 3° to 40° of the diffraction angle 2θ, which covers all of the significant diffraction peaks of starch crystallites. A step interval of 0.02° and a scan rate of 0.5°/min were employed for all samples. The percentages of crystalline and amorphous starch from the total scattering and the relative degree of crystallinity were determined following the fitting method of Dhital et al.[14]

Fourier Transform Infrared Spectroscopy. Fourier transform infrared (FTIR) spectra of starch granules were obtained using a Spectrum 100 FTIR spectrometer (Perkin-Elmer, Norwalk, CT) with an attenuated-total-reflectance (ATR) single-reflectance cell with a diamond crystal. For each spectrum, 32 scans were recorded over the range of 1200−800 cm^{-1} at a resolution of 4 cm^{-1}. A single-beam

dx.doi.org/10.1021/jf405196m | J. Agric. Food Chem. 2014, 62, 1482−1491

spectrum of the clean crystal was obtained as the background. The ratio of absorbance at 1045 cm^{-1} to that at 1022 cm^{-1} was calculated to represent the short-range ordered structure of starch.[15]

Solid-State Nuclear Magnetic Resonance Spectroscopy. Starch samples were analyzed by solid-state ^{13}C cross-polarized magic-angle-spinning (CP/MAS) nuclear magnetic resonance (NMR) spectroscopy using a Bruker MSL-300 spectrometer (Bruker, Billerica, MA) at a frequency of 75.46 MHz. Approximately 200 mg of starch was packed in a 4-mm-diameter, cylindrical PSZ (partially stabilized zirconium oxide) rotor with a Kel-F end cap. The rotor was spun at 5 kHz at the magic angle (54.7°). The 90° pulse width at 5 μs and a contact time of 1 ms were used for all starches with a recycle delay of 3 s. The spectral width was 38 kHz, the acquisition time was 50 ms, the number of time domain points was 2 k, the transform size was 4 k, and the line broadening was 20 Hz. At least 1000 scans were accumulated for each spectrum. The spectral acquisition and interpretation methodologies as described by Tan et al.[16] were used to quantify the double helices, single helices, and amorphous conformational features.

Statistical Analysis. Results are expressed as means with standard deviations of at least duplicate measurements. In the case of XRD and NMR spectroscopy, only one measurement was performed. The standard deviations of XRD and NMR measurements are typically within 2%.[17] Analysis of variance (ANOVA) was used to determine the least significance at $p < 0.05$ using Minitab 16 (Minitab Inc., State College, PA), and correlation coefficients were determined using Microsoft Office Excel 2011.

RESULTS AND DISCUSSION

Dehydration Effects on Starch Digestion Kinetics. Although in vitro methods oversimplify the digestion mechanisms in human and animal digestive tracts, such studies are still useful for comparing the digestion rates/extents among starches with different structures. Granular starches follow a "side-by-side" digestion process involving the apparently simultaneous digestion of crystalline and amorphous regions. As model studies consistently report that amorphous starch is digested more rapidly than crystalline starch, this suggests that the digestions of the molecular and crystalline structures are not the rate-limiting steps for either in vitro or in vivo digestion.[18−20] The digestograms of PT, MM, and IM starch granules subjected to different drying methods are shown in Figure 1. All samples show increasing trends of glucose release within 6 h of digestion time without reaching a plateau. All digestograms follow first-order behavior with R^2 values above 0.99, and the digestion rate coefficients (k) are summarized in Table 1. The k values of MM and IM starches were ca. 2 times higher than those of PT starch, which agrees with the results reported by others.[10,21]

There are no significant differences among the k values of OD, ED, and W samples of each type of starch (PT, MM, and IM) (Table 1), and they show similar digestograms (Figure 1). Therefore, the OD and ED methods do not seem to influence the digestion properties of PT, MM, and IM starches.

The PT-FD starch, on the other hand, shows greater glucose release under the same in vitro digestion method with a significantly higher k value than the other PT samples (Figure 1A and Table 1). The FD (or lyophilization) process consists of two steps: the formation of ice (freezing) and the sublimation of the ice as water molecules under vacuum (drying). To identify which step, freezing or sublimation, is critical for the increased starch digestion rate, the digestion kinetics of PT-FT (i.e., PT sample with the freezing step only) was determined. There are no significant differences between the k values of the PT-FT and PT-W samples (Table 1), suggesting that the rapid

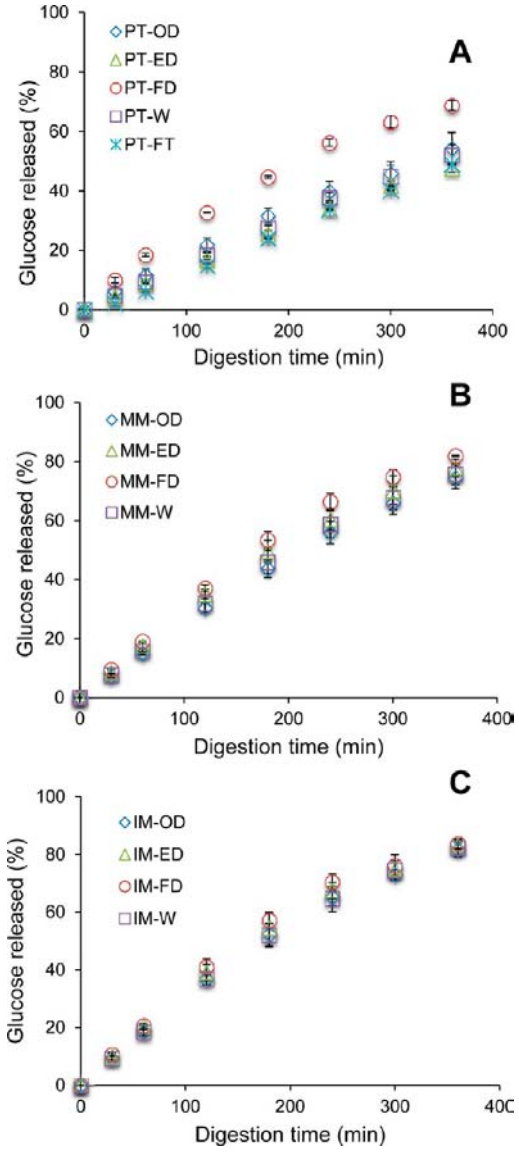

Figure 1. Digestion kinetic profiles of potato tuber (PT), mature maize (MM), and immature maize (IM) starch granules subjected to oven drying (OD), ethanol drying (ED), and freeze-drying (FD), as well as PT starch granules after freezing and immediate thawing (FT), compared with wet/never dried controls (W).

formation of ice crystals in the liquid nitrogen bath does not alter the digestion properties of PT starch granules. This is consistent with the observation of Waigh et al.[22] that some structural disorder of starch granules occurring at subzero temperatures is reversible. Therefore, the differences between the k values of the PT-FD and PT-W samples are likely caused by the sublimation step, including the external mass transfer of water vapor near the surface and the internal mass transfer from the inside of the PT starch granules.[23] This phenomenon, however, was not observed with MM and IM starches, where FD treatment does not significantly increase the k values of the starch granules compared with the W control counterparts and those from other drying methods (OD and ED). Thus, at least two hypotheses can be raised for the increased digestion rate of PT-FD starch: (1) FD breaks the smooth surface organization of potato starch granules that otherwise act as a barrier preventing the diffusion of enzymes into the inside or hilum of

Table 1. Digestion Rate Coefficients (k, min^{-1}) of Starch Samples[a,b]

treatment	PT	MM	IM	CT	G50
OD	$(2.15 \pm 0.27) \times 10^{-3}$ b	$(3.81 \pm 0.43) \times 10^{-3}$ c	$(4.69 \pm 0.33) \times 10^{-3}$ c	ND	ND
ED	$(1.83 \pm 0.02) \times 10^{-3}$ b	$(4.21 \pm 0.45) \times 10^{-3}$ c	$(4.94 \pm 0.29) \times 10^{-3}$ c	$(5.50 \pm 0.01) \times 10^{-4}$ d	$(6.16 \pm 0.63) \times 10^{-4}$ d
FD	$(3.29 \pm 0.19) \times 10^{-3}$ a	$(4.81 \pm 0.19) \times 10^{-3}$ c	$(5.11 \pm 0.39) \times 10^{-3}$ c	$(7.68 \pm 0.89) \times 10^{-4}$ d	$(7.30 \pm 0.22) \times 10^{-4}$ d
W	$(2.06 \pm 0.20) \times 10^{-3}$ b	$(3.97 \pm 0.44) \times 10^{-3}$ c	$(4.81 \pm 0.50) \times 10^{-3}$ c	ND	ND
FT	$(1.89 \pm 0.00) \times 10^{-3}$ b	ND	ND	ND	ND

[a]Means ± standard deviations from two measurements. Values in the same column with different letters are significantly different at $p < 0.05$. [b]PT, potato tuber; MM, mature maize; IM, immature maize; CT, canna tuber; G50, Gelose 50; OD, oven-dried; ED, ethanol-dried; FD, freeze-dried; W, wet/not dried; FT, frozen−thawed; ND, not determined.

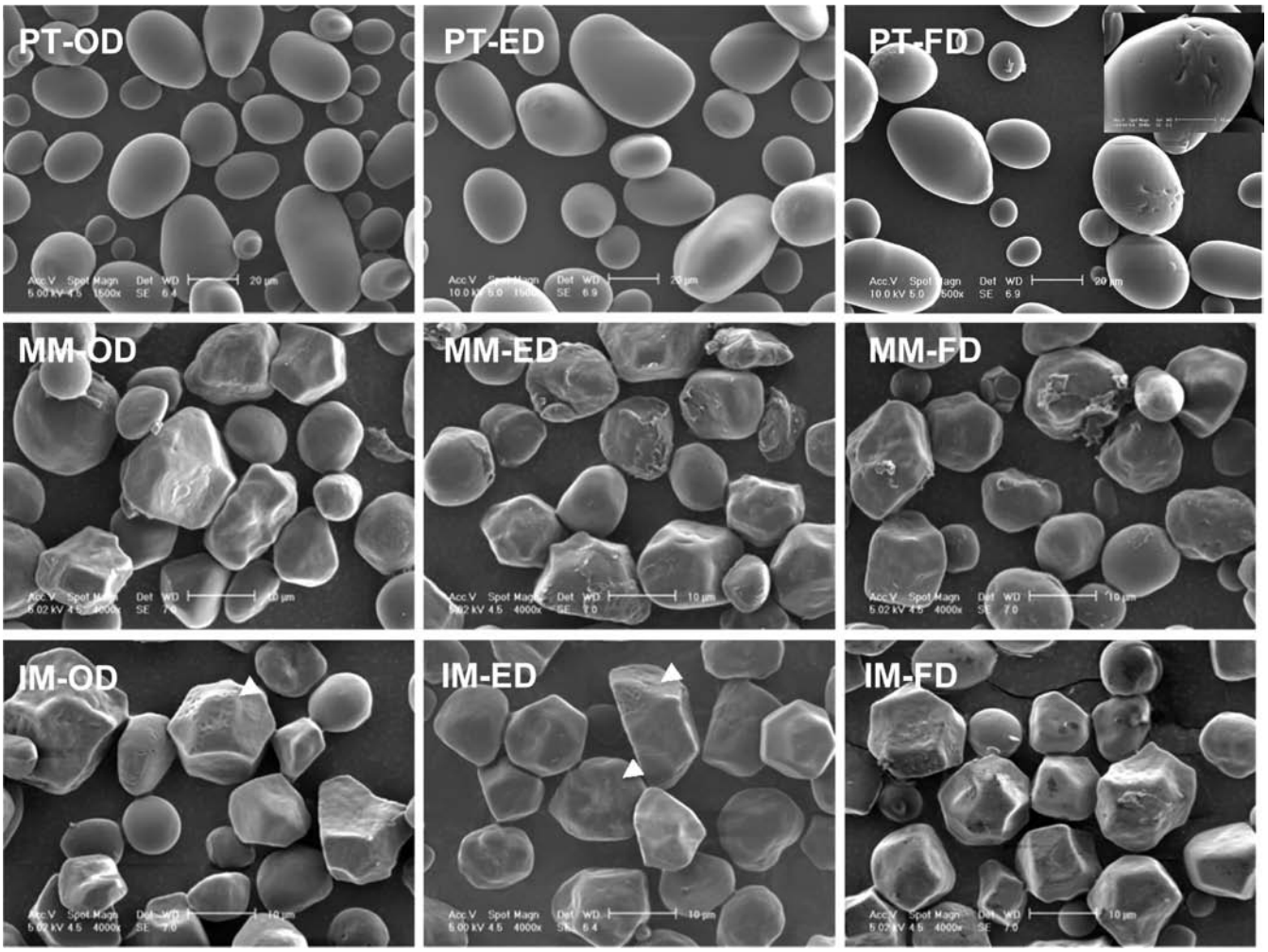

Figure 2. Morphologies of potato tuber (PT), mature maize (MM), and immature maize (IM) starch granules subjected to oven drying (OD), ethanol drying (ED), and freeze-drying (FD), compared with wet/never dried controls (W).

the granules and/or (2) starch molecular features, namely, starch crystallinity and molecular order, are disrupted during FD, leading to higher accessibility of enzymes to bind with starch molecules.

Surface Architecture of Granular and Partly Digested Starches. Electron micrographs of PT, MM, and IM starch granules subjected to various drying methods are shown in Figure 2. MM and IM starch granules have either round or irregular shapes with diameters of 5−30 μm, whereas PT starch granules have either ellipsoidal or round shapes with a wide range of granule sizes (5−100 μm). The variations in granule shape and size within each starch sample are likely due to the termination of starch granule synthesis at different growth stages and/or the synthesis of starch granules at different grain developmental stages. In general, maize starch granules show the presence of pores on the granule surface, whereas potato starch granules have smooth surfaces lacking pores.[24] The high k values of MM and IM starch granules compared with those of PT starch granules can be related to the surface pores linking the hilum and surface through interior channels, facilitating "inside-out" digestion from the hilum to the surface of the granules.[25,26] On the other hand, the smooth surface structure of PT starch granules limits the enzyme diffusion, and hence, the digestion takes place from the surface (exocorrosion).

PT-FD starch granules exhibit relatively more wrinkles or scratches on their surface than PT-OD and PT-ED starch

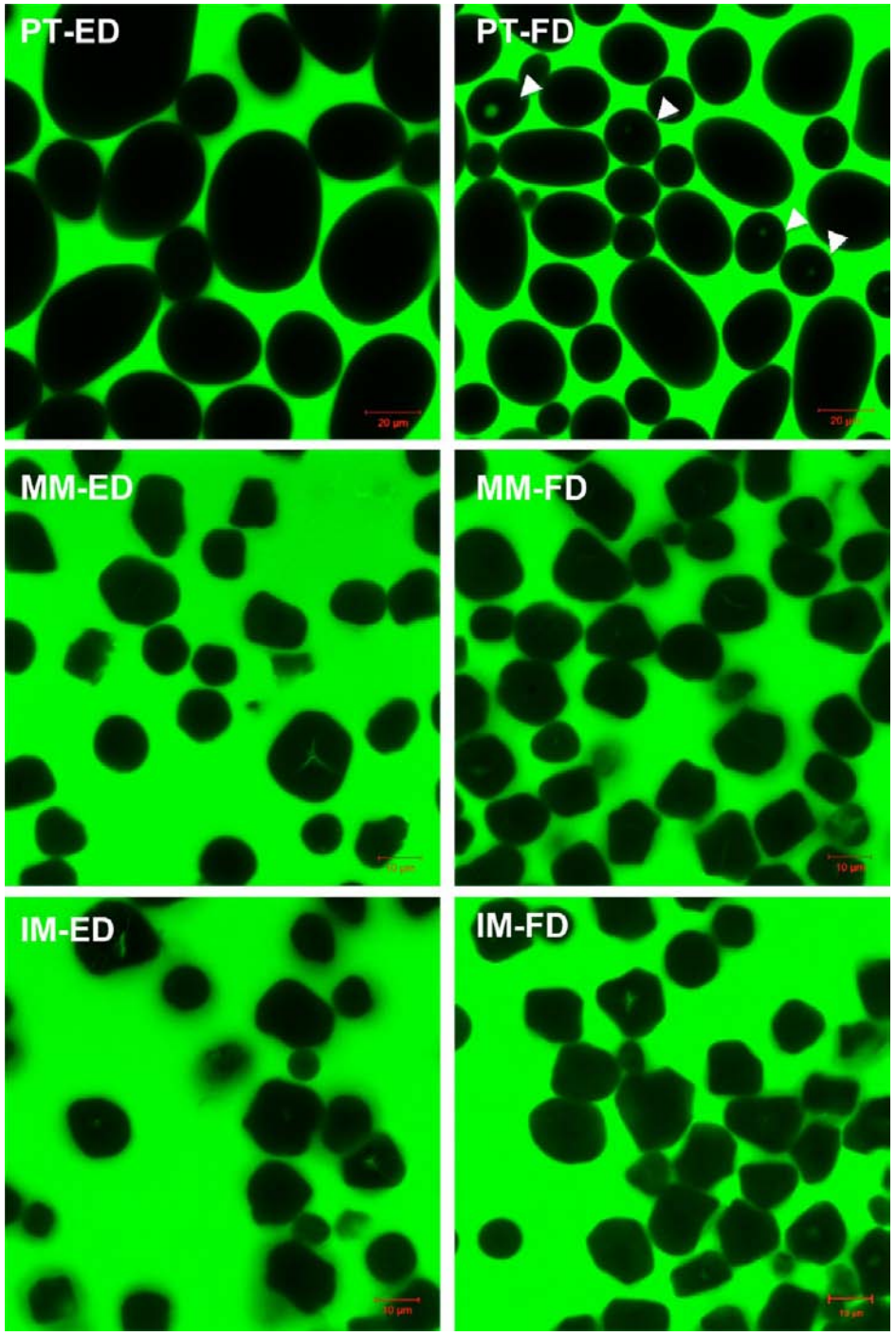

Figure 3. CLSM micrographs of ethanol- and freeze-dried starch granules suspended overnight in FITC-dextran solution (PT, potato tuber; MM, mature maize; IM, immature maize; ED, ethanol-dried; FD, freeze-dried).

granules, which show similar smooth surface structures (Figure 2). The scratches and roughness are likely caused by the forced distortion of starch granules due to local explosive release of water vapor from the builtup pressure inside the rigid granules, as the water molecules try to escape through the solid internal structure and smooth surface structure under the vacuum conditions. The presence of pores and channels on the surface and inside the MM and IM starch granules, respectively, facilitates the escape of water molecules during FD, resulting in no apparent changes to the granular structure when compared with the W controls and those after OD and ED processes.

Some micropores might be generated during FD but would not be easily observed by SEM, because the pores could be covered by the platinum sputter coating (at least 10-nm thickness) used in the sample preparation. To assess the possible generation of micropores, a fluorescent FITC-dextran probe (molar mass 20 kDa, $R_h \approx 3.3$ nm) was used, and its diffusion into starch granules was observed using CLSM.[12] The size of the FITC-dextran probe is similar to that of α-amylase, the rate-determining enzyme during granular starch digestion;[21] therefore, the diffusion of this probe can be used to identify the ability of α-amylase to diffuse into starch granules. CLSM

dx.doi.org/10.1021/jf405196m | J. Agric. Food Chem. 2014, 62, 1482−1491

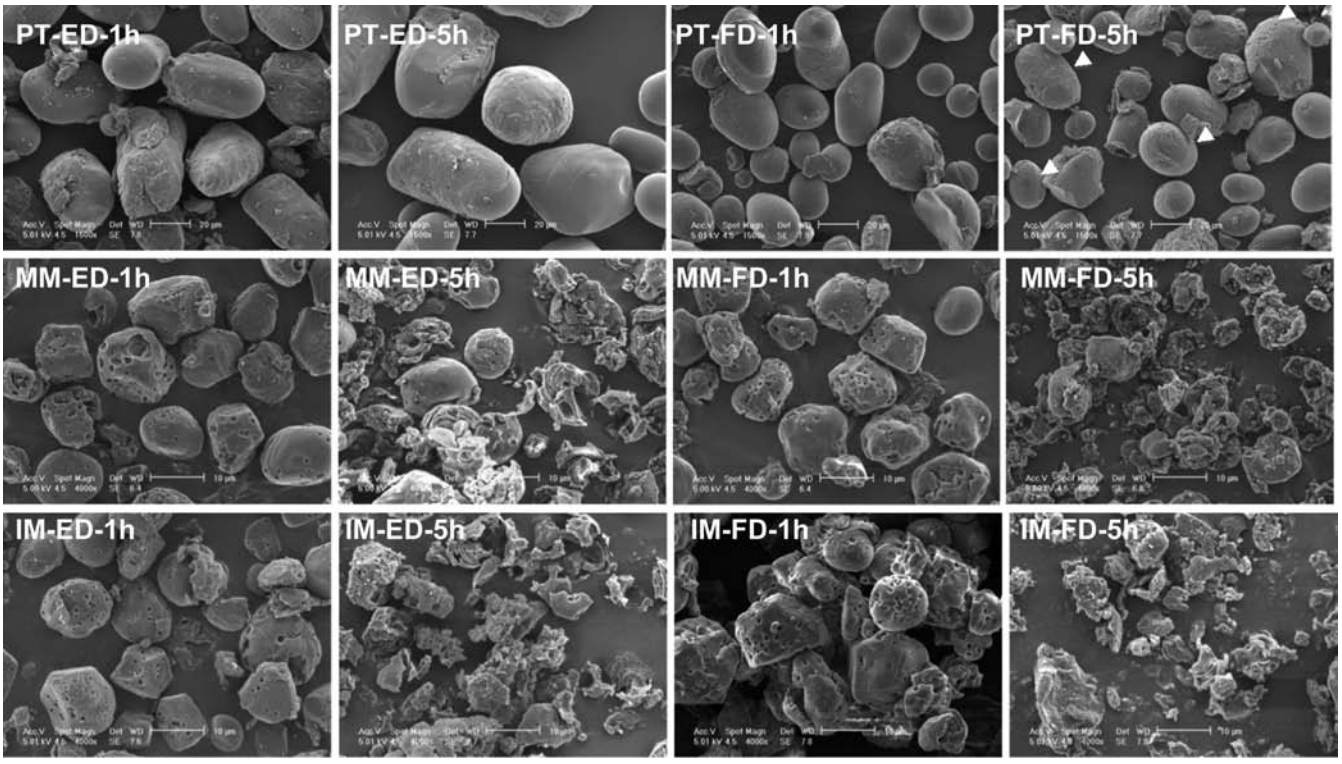

Figure 4. Morphologies of ethanol- and freeze-dried starch granules/fragments after 1- and 5-h in vitro digestion (PT, potato tuber; MM, mature maize; IM, immature maize; ED, ethanol-dried; FD, freeze-dried).

micrographs of PT, MM, and IM starch granules in the FITC-dextran solution are presented in Figure 3. No qualitative differences are observed in the internal structures of MM-ED, MM-FD, IM-ED, and IM-FD starch granules, which show the characteristic central cavity and extended channels of various sizes. There are, however, apparent differences between the internal structures of PT-ED and PT-FD starch granules. No internal fluorescence can be detected within PT-ED starch granules, especially at the hilum, after they had been exposed to the FITC-dextran probe, suggesting that the surface of PT starch granules was not greatly damaged by the ED process and that it was impermeable to the enzyme-sized FITC-dextran because of the effective barrier of tightly packed starch molecules.[27] The FITC-dextran probe, on the other hand, can diffuse into the hilum of the PT-FD starch granules under the same diffusion conditions as for the PT-ED starch granules. This clear distinction suggests that the surface of the PT-FD starch granules is more porous than those of the PT-OD and PT-ED starch granules.

After 1 h of in vitro digestion, the surface pores of maize starch granules (MM-ED, MM-FD, IM-ED, and IM-FD) became larger (Figure 4). The maize starch granules were broken into smaller fragments and debris, sometimes with visible growth rings after 5 h of in vitro digestion. The hydrolytic pattern of the amylolytic enzymes on starch granules is not random, with the surface pores and internal channels being rapidly attacked in the beginning of the digestion. The apparent diameter of these internal channels ranges from 0.007 to 0.1 μm, whereas that of the surface pores is larger, varying between 0.1 and 0.3 μm.[24,28,29] The presence of surface pores and internal channels in maize starch granules enables the diffusion of enzymes, namely, α-amylase (3−4 nm diameter) and amyloglucosidase (8−10 nm diameter), into the hilum of starch granules during digestion,[25,29,30] allowing the internal corrosion or inside-out digestion pattern.[18] After prolonged digestion, the internal structure of starch granules becomes hollow, which can then be easily broken into smaller fragments or debris. There are no qualitative differences among MM-ED, MM-FD, IM-ED, and IM-FD starch granules, consistent with their insignificantly different k values.

On the other hand, the granule surfaces of PT-ED and PT-FD starch granules were roughened, sometimes with visible scratches, after 1 h of in vitro digestion (Figure 4). A further increase in surface roughness, sometimes with deep cracks, is observed on some granules after 5 h of in vitro digestion. Potato starch granules lack surface pores and internal channels, and thus, they are slowly digested because the enzymes have to break through the dense molecular packing at the surface of starch granules to diffuse into the hilum ("exocorrosion" digestion pattern).[10] Furthermore, some pinholes can be observed on the surface of the PT-FD starch granules, but not the PT-ED starch granules, after 5 h of in vitro digestion. The SEM images of digested PT-FD starch granules are consistent with the higher porosity of undigested PT-FD starch granules deduced from CLSM micrographs (Figure 3). However, the drying process does not change the overall starch digestion pattern: inside-out pattern for maize starch granules and exocorrosion pattern for potato starch granules.

Gelatinization Properties. Starch gelatinization is an endothermic transition corresponding to the dissociation of amylopectin double helices from a semicrystalline structure to an amorphous conformation.[31] The gelatinization properties of starch granules dried using different methods are summarized in Table 2. The gelatinization temperatures of maize (IM and MM) and PT starch granules, except PT-FD starch granules, range from 64 to 78 °C, which are within the range reported by

Table 2. Gelatinization Properties (Measured by DSC) of Potato and Maize Starches under Different Drying Conditions[a]

starch sample[b]	T_o (°C)	T_p (°C)	T_c (°C)	ΔH (J/g)
PT-OD	63.3 ± 0.5 cd	66.2 ± 0.6ef	71.5 ± 0.7fg	19.7 ± 0.8ab
PT-ED	63.6 ± 0.3ef	66.4 ± 0.4g	71.7 ± 0.5g	19.3 ± 0.3b
PT-FD	49.7 ± 0.2h	56.0 ± 0.4h	63.7 ± 1.2h	11.8 ± 0.3gh
PT-W	63.9 ± 0.1de	66.7 ± 0.1fg	72.0 ± 0.4fg	20.1 ± 0.1a
MM-OD	65.3 ± 0.1b	70.2 ± 0.0b	75.5 ± 0.0b	13.1 ± 0.1de
MM-ED	64.5 ± 0.0 cd	69.4 ± 0.1c	75.1 ± 0.1b	12.5 ± 0.2efg
MM-FD	63.3 ± 0.1f	68.2 ± 0.1d	74.0 ± 0.1 cd	12.1 ± 0.1fgh
MM-W	67.9 ± 0.3a	72.7 ± 0.1a	78.1 ± 0.1a	14.5 ± 0.4c
IM-OD	64.7 ± 0.2c	68.7 ± 0.1d	73.6 ± 0.5de	12.7 ± 0.5def
IM-ED	63.3 ± 0.5f	68.2 ± 0.1d	74.0 ± 0.2 cd	13.3 ± 0.1d
IM-FD	62.7 ± 0.2g	67.4 ± 0.2e	73.6 ± 0.2ef	11.4 ± 0.4h
IM-W	64.8 ± 0.1bc	69.5 ± 0.0c	74.6 ± 0.0bc	13.5 ± 0.1d

[a]Means ± standard deviations from two measurements. Values in the same column with different letters are significantly different at $p < 0.05$. T_o, T_p, T_c, and ΔH are the onset temperature, peak temperature, conclusion temperature, and enthalpy change, respectively. [b]PT, potato tuber; MM, mature maize; IM, immature maize; OD, oven-dried; ED, ethanol-dried; FD, freeze-dried; W, wet/not dried.

others.[32] The gelatinization temperatures and ΔH values of MM starch granules are slightly higher than those of IM starch granules, which is likely due to the annealing of starch granules during field drying of MM.[33] All dehydrated starch granule samples show lower gelatinization temperatures and ΔH values than their W control counterparts. The FD process significantly decreases ($p < 0.05$) both the gelatinization temperatures and ΔH values of all starch granule samples, especially the PT starch granules. Other drying methods (OD and ED), in comparison, result in only slightly lower gelatinization temperatures and ΔH values, suggesting that OD and ED induce fewer structural changes than FD and/or the W controls are annealed during storage in the solution. The gelatinization temperature reflects the heat stability of the crystallites, whereas the ΔH value is associated with the amount of molecular order and crystallinity.[31] Therefore, the disruption of the crystalline arrangement (long-range ordered structures) and/or the reduction in the amount of double helices (short-range ordered structures) might have occurred during the FD process. To further understand the differences in the starch gelatinization properties after drying processes, the crystallinity and molecular conformation of starch after drying were analyzed and compared.

Starch Crystallinity and Molecular Order. XRD was used to study the type and level of starch crystallinity or long-range order. X-ray diffractograms of PT, MM, and IM starch granule samples are shown in Figure 5A. Maize starch granules, irrespective of the drying method or stage of maturity, exhibit the A-type polymorph (major peaks at ~15°, 17°, 18°, and 23° 2θ) with similar peak heights and widths. The percentages of crystallinity, calculated from the ratio of the total peak area to the total diffraction area, are similar for all maize starch granules (Table 3). On the other hand, PT starch granules show the B-type polymorphic pattern (major peaks at ~5°, 17°, 22°, and 24° 2θ) with marked differences observed in the type and level of crystallinity between the PT-OD/ED and PT-FD starch granules, where the peaks in the diffractogram of the PT-FD starch granules are lower and broader (less sharp) than those in the diffractogram of their OD/ED counterparts. Furthermore,

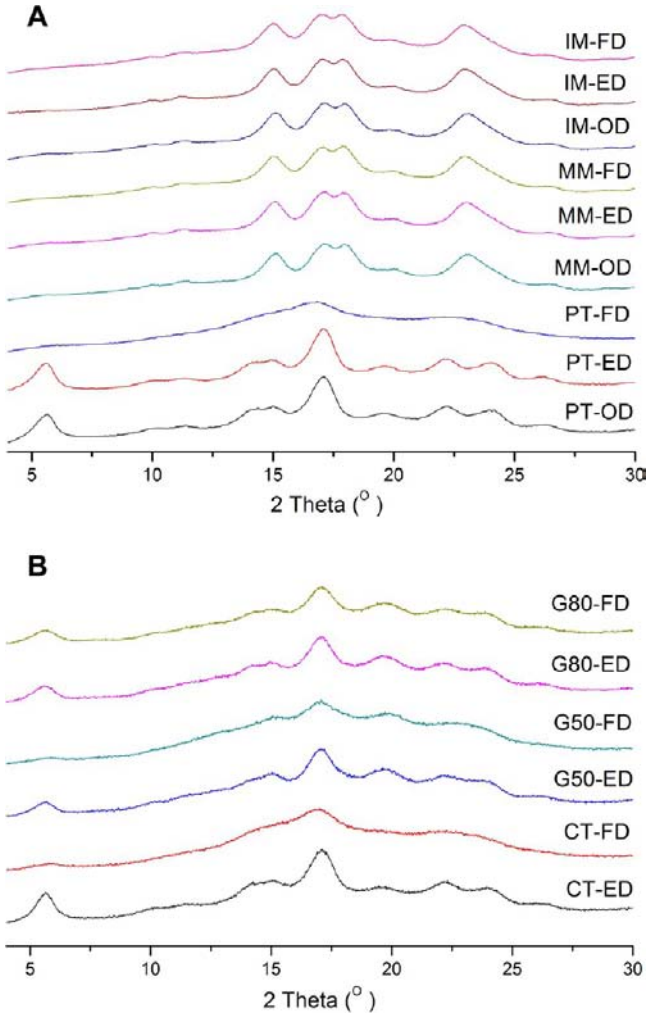

Figure 5. X-ray diffractograms of oven-, ethanol-, and freeze-dried starch granules (PT, potato tuber; MM, mature maize; IM, immature maize; CT, canna tuber; G50, Gelose 50; G80, Gelose 80; OD, oven-dried; ED, ethanol-dried; FD, freeze-dried).

the percentage crystallinity of the PT-FD starch granules is about 50% of that for those of the PT-OD and PT-ED starch granules. The results indicate that FD significantly alters the crystalline structure of the PT starch granules.

Solid-state NMR spectroscopy was used to determine whether the changes observed in long-range crystalline order are consistent with the changes in short-range molecular order; NMR spectra are shown in Figure 6. All maize starch granules, irrespective of drying method and stage of maturity, display similar spectra with a triplet in the C1 region at 101.6, 100.4, and 99.3 ppm, typical of the A-type double-helical conformation.[34] The PT-OD and PT-ED starch granule samples display a doublet in the C1 region with distinctive signals at 110.79 and 99.72 ppm, expected for the B-type polymorphic starch.[35−37] However, the intensity of this doublet is greatly reduced in PT-FD starch granules, where it is no longer visible in the NMR spectrum. To calculate the degree of molecular order in the starch granule samples, gelatinized maize starch was used as an amorphous standard, and its intensity at 84 ppm was matched to those in the NMR spectra of the starch granule samples.[16] Subtraction of the sample NMR spectrum from the amorphous standard spectrum reveals a doublet or a triplet in the C1 region for the double helix and a smaller peak around

Table 3. Crystallinity (Quantified by XRD) and Molecular Order (Measured by ^{13}C CP/MAS NMR Spectroscopy) of Potato and Maize Starches under Different Drying Conditions[a]

			^{13}C CP/MAS NMR spectroscopy		
starch sample[b]	XRD crystallinity (%)	FTIR 1045/1022 ratio[c]	double helix (%)	single helix (%)	amorphous (%)
PT-OD	36.1	0.705 ± 0.002 a	44	2	54
PT-ED	37.1	0.703 ± 0.002 a	44	5	51
PT-FD	18.8	0.653 ± 0.005 b	30	0	70
MM-OD	31.9	0.659 ± 0.008 b	36	3	61
MM-ED	32.0	0.655 ± 0.003 b	41	4	55
MM-FD	29.9	0.641 ± 0.002 b	43	4	53
IM-OD	31.6	0.654 ± 0.003 b	35	3	62
IM-ED	32.1	0.650 ± 0.005 b	41	4	55
IM-FD	29.5	0.651 ± 0.003 b	39	4	57

[a]XRD and NMR calculations are within standard deviations of 2%. Means ± standard deviations from two FTIR measurements. [b]PT, potato tuber; MM, mature maize; IM, immature maize; OD, oven-dried; ED, ethanol-dried; FD, freeze-dried. [c]Means ± standard deviations from two measurements. Values in the same column with different letters are significantly different at $p < 0.05$.

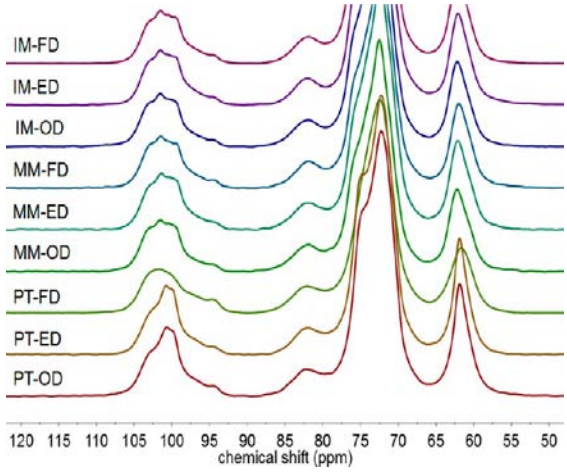

Figure 6. ^{13}C CP/MAS NMR spectra of oven-, ethanol-, and freeze-dried starch granules (PT, potato tuber; MM, mature maize; IM, immature maize; OD, oven-dried; ED, ethanol-dried; FD, freeze-dried).

103 ppm for the V-type single helix.[36] Calculating the areas of these peaks gives the percentages of double-helical, single-helical, and amorphous starch shown in Table 3. The results of molecular order from NMR analysis are similar for all maize starch granule samples, in a good agreement with the degree of crystallinity from XRD, indicating that both the long-range crystallinity and the short-range molecular order are conserved under the three drying methods. A similar phenomenon was observed for the PT-OD and PT-ED starch granule samples; however, a notable difference of a ~40% reduction in double-helical order was observed for the PT-FD starch granule sample, which is slightly lower than the loss of crystalline order (~50%) analyzed by XRD. It was reported in a previous study[31] that the amount of double helices is higher than the degree of crystallinity and, thus, not all double helices participate in the crystalline structure in native starch granules. The results suggest that FD causes slightly greater disruption to the long-range crystalline packing of PT starch granules than the short-range molecular order, that is, the misalignment or disruption of crystallites with less unwinding of the double helices.

The ratios of absorbance at 1045 and 1022 cm^{-1} from the FTIR spectra have been associated with ordered (organized) and amorphous (less organized) structures of starch, and their absorbance ratio can be used as an index to characterize the short-range alignment of double helices.[15] The absorbance ratios for all maize starch granule samples are similar (Table 3), irrespective of their drying method and stage of maturity, whereas that of the PT-FD starch granule sample is significantly lower than those of the PT-OD and PT-ED starch granule samples. The FTIR results are in good agreement with the XRD and NMR results, indicating that a decrease in the molecular order of PT starch granules by FD, which is likely to be associated with the disruption of double helices. As observed from the gelatinization properties of PT starch granule samples (Table 2), the PT-FD starch granules have considerably lower T_o and ΔH values, whereas these values are almost conserved for other drying methods compared with the PT-W control. The current results corroborate previous reports that showed a reduction in the ΔH and gelatinization temperatures of potato starch granules but not wheat starch granules after freeze-drying.[38−40]

From previous reports and the current findings, it is evident that freeze-drying has less of an effect on the structure and molecular packing of A-type polymorphic cereal starches (wheat and maize) than those of potato starch granules. This raises an interesting question as to the effects of drying methods on other B-type polymorphic starches from both cereals and tubers, which have not yet been reported but which would be useful for understanding the mechanism behind the alteration of molecular packing of freeze-dried starches. In a recent report, Zhang et al.[41] reported an increase in the crystallinity of starch granules isolated from freeze-dried Chinese yam; however, this does not represent the freeze-dried isolated starch granules.

The X-ray diffractograms of additional B-type polymorphic starches (CT, G50, and G80) after being subjected to ED and FD processes are presented in Figure 5B. Similarly to the PT starch granules, the diffraction peaks of CT and G50 starch granules are shorter and broader after the FD process than after the ED process, confirming the ability of FD to alter the molecular packing of B-type polymorphic starches. The decrease in crystallinity or increase in amorphous character results in an increase in the enzymatic hydrolysis rate of CT and G50 starches after FD (Table 1). However, the effects of FD are less apparent for G80 starch granules, probably because of the high amylose content and/or very small granular size of G80, which needs further investigation.

Apart from changes in surface morphology, the increased digestion rate of FD starches could be due to differences of molecular order in starch granules, related to the starch polymorphism rather than the botanical sources, for example, cereal grains versus tubers. At least two molecular-level hypotheses can be proposed to explain the alteration of short- and long-range molecular order after FD (but not FT treatment) in B-polymorphic starches. First, the higher amount of intracrystalline water in B-type polymorphic starch might distort the helical organization of amylopectin molecules by sublimation. However, this hypothesis should also apply to OD

samples, which do not show the effect. Alternatively, B-polymorphic starches with more stable intermolecular structures compared to A-polymorphic starches, due to more longer branch chains, might hinder the passage of subliming water, ultimately increasing internal pressure and destabilizing the helical structure and molecular order under high vacuum. In contrast, because of the lower and more scattered intercrystalline water and loosely packed internal structure caused by a larger population of short amylopectin branches, the subliming water molecules can escape A-polymorphic starch granules more easily, exerting lesser internal pressure. A key difference between the OD and FD methods is the effect of temperature on starch chain mobility. The greater rigidity of starch chains during FD compared with OD means that, although both processes involve removal of vapor-phase water, the lower temperature involved in freeze-drying is more likely to result in local fracture and structure disorganization events as a result of water removal. We therefore propose that the effect of freeze-drying on B-type polymorphic starches is due to a combination of local (crystalline packing, long branches) and larger-scale (lack of pores and channels) effects, resulting in structural disorganization from nanometer to micrometer length scales.

In summary, oven and ethanol drying are mild dehydration methods that do not significantly affect the digestion, thermal, or structural properties of starches compared with their counterparts that have never been dried. However, freeze-drying can result in a marked increase in the digestion rate of B-type polymorphic starches, but not that of A-type polymorphic starches. Freeze-drying not only generates some micropores on the surface of potato starch granules, but also disrupts both crystallinity and molecular order, each of which can cause an increase in the digestion rate.

AUTHOR INFORMATION

Corresponding Author

*Phone: +61 7 3346 7373. Fax: +61 7 3365 1177. E-mail: s.dhital@uq.edu.au.

Notes

The authors declare no competing financial interest.

ACKNOWLEDGMENTS

The authors acknowledge the facilities and scientific and technical assistance of Dr. Kim Sewell and Dr. Ying Yu of the Australian Microscopy & Microanalysis Research Facility at the Centre for Microscopy and Microanalysis, The University of Queensland.

ABBREVIATIONS USED

ANOVA, analysis of variance; CT, canna tuber; CLSM, confocal laser scanning microscopy/microscope; IM, immature maize; DSC, differential scanning calorimetry/calorimeter; ED, ethanol drying/ethanol-dried; FD, freeze-drying/freeze-dried; FT, frozen−thawed; FTIR, Fourier transform infrared; G50, Gelose 50; G80, Gelose 80; MM, mature maize; NMR, nuclear magnetic resonance; OD, oven drying/oven-dried; PT, potato tuber; SEM, scanning electron microscopy/microscope; W, wet/not dried; XRD, X-ray diffractometry/diffractometer

REFERENCES

(1) Zobel, H. F. Molecules to granules: A comprehensive starch review. *Starch/Stärke* **1988**, *40*, 44−50.

(2) Grant, L. A. Effects of starch isolation, drying, and grinding techniques on its gelatinization and retrogradation properties. *Cereal Chem.* **1998**, *75*, 590−594.

(3) Kayisu, K.; Hood, L. F. Effects of dehydration and storage conditions on the pancreatic alpha-amylase susceptibility of various starches. *J. Food Sci.* **1979**, *44*, 1728−1731.

(4) Malumba, P.; Massaux, C.; Deroanne, C.; Masimango, T.; Bera, F. Influence of drying temperature on functional properties of wet-milled starch granules. *Carbohydr. Polym.* **2009**, *75*, 299−306.

(5) Setiawan, S.; Widjaja, H.; Rakphongphairoj, V.; Jane, J. L. Effects of drying conditions of corn kernels and storage at an elevated humidity on starch structures and properties. *J. Agric. Food Chem.* **2010**, *58*, 12260−12267.

(6) Whistler, R. L.; Goatley, J. L.; Spencer, W. W. Effect of drying on the physical properties and chemical reactivity of corn starch granules. *Cereal Chem.* **1959**, *36*, 84−90.

(7) Apinan, S.; Yujiro, I.; Hidefumi, Y.; Takeshi, F.; Myllarinen, P.; Forssell, P.; Poutanen, K. Visual observation of hydrolyzed potato starch granules by α-amylase with confocal laser scanning microscopy. *Starch/Stärke* **2007**, *59*, 543−548.

(8) Whistler, R. L.; Spencer, W. W.; Goatley, J. L.; Nikuni, Z. Effect of drying on the presence of cavities in corn starch granules. *Cereal Chem.* **1958**, *35*, 331−336.

(9) Vilaplana, F.; Hasjim, J.; Gilbert, R. G. Amylose content in starches: Toward optimal definition and validating experimental methods. *Carbohydr. Polym.* **2012**, *88*, 103−111.

(10) Dhital, S.; Shrestha, A. K.; Gidley, M. J. Relationship between granule size and in vitro digestibility of maize and potato starches. *Carbohydr. Polym.* **2010**, *82*, 480−488.

(11) Goni, I.; Garcia-Alonso, A.; Saura-Calixto, F. A starch hydrolysis procedure to estimate glycemic index. *Nutr. Res. (N. Y., NY, U. S.)* **1997**, *17*, 427−437.

(12) Dhital, S.; Shelat, K. J.; Shrestha, A. K.; Gidley, M. J. Heterogeneity in maize starch granule internal architecture deduced from diffusion of fluorescent dextran probes. *Carbohydr. Polym.* **2013**, *93*, 365−373.

(13) Zhang, B.; Huang, Q.; Luo, F. X.; Fu, X. Structural characterizations and digestibility of debranched high-amylose maize starch complexed with lauric acid. *Food Hydrocolloids* **2012**, *28*, 174−181.

(14) Dhital, S.; Shrestha, A. K.; Hasjim, J.; Gidley, M. J. Physicochemical and structural properties of maize and potato starches as a function of granule size. *J. Agric. Food Chem.* **2011**, *59*, 10151−10161.

(15) vanSoest, J. J. G.; Tournois, H.; deWit, D.; Vliegenthart, J. F. G. Short-range structure in (partially) crystalline potato starch determined with attenuated total reflectance Fourier-transform IR spectroscopy. *Carbohydr. Res.* **1995**, *279*, 201−214.

(16) Tan, I.; Flanagan, B. M.; Halley, P. J.; Whittaker, A. K.; Gidley, M. J. A method for estimating the nature and relative proportions of amorphous, single, and double-helical components in starch granules by ^{13}C CP/MAS NMR. *Biomacromolecules* **2007**, *8*, 885−891.

(17) Lopez-Rubio, A.; Flanagan, B. M.; Gilbert, E. P.; Gidley, M. J. A novel approach for calculating starch crystallinity and its correlation with double helix content: A combined XRD and NMR study. *Biopolymers* **2008**, *89*, 761−768.

(18) Zhang, G. Y.; Ao, Z.; Hamaker, B. R. Slow digestion property of native cereal starches. *Biomacromolecules* **2006**, *7*, 3252−3258.

(19) Hasjim, J.; Lavau, G. C.; Gidley, M. J.; Gilbert, R. G. In vivo and in vitro starch digestion: Are current in vitro techniques adequate? *Biomacromolecules* **2010**, *11*, 3600−3608.

(20) Shrestha, A. K.; Blazek, J.; Flanagan, B. M.; Dhital, S.; Larroque, O.; Morell, M.; Gilbert, E. P.; Gidley, M. J. Molecular, mesoscopic and microscopic structure evolution during amylase digestion of maize starch granules. *Carbohydr. Polym.* **2012**, *90*, 23−33.

(21) Zhang, B.; Dhital, S.; Gidley, M. J. Synergistic and antagonistic effects of α-amylase and amyloglucosidase on starch digestion. *Biomacromolecules* **2013**, *12*, 1945−1954.

(22) Waigh, T. A.; Perry, P.; Riekel, C.; Gidley, M. J.; Donald, A. M. Chiral side-chain liquid-crystalline polymeric properties of starch. *Macromolecules* **1998**, *31*, 7980−7984.
(23) Cohen, J. S.; Yang, T. C. S. Progress in food dehydration. *Trends Food Sci. Technol.* **1995**, *6*, 20−25.
(24) Huber, K. C.; BeMiller, J. N. Channels of maize and sorghum starch granules. *Carbohydr. Polym.* **2000**, *41*, 269−276.
(25) Fannon, J. E.; Gray, J. A.; Gunawan, N.; Huber, K. C.; BeMiller, J. N. The channels of starch granules. *Food Sci. Biotechnol.* **2003**, *12*, 700−704.
(26) Dhital, S.; Shrestha, A. K.; Gidley, M. J. Effect of cryo-milling on starches: Functionality and digestibility. *Food Hydrocolloids* **2010**, *24*, 152−163.
(27) Oates, C. G. Towards an understanding of starch granule structure and hydrolysis. *Trends Food Sci. Technol* **1997**, *8*, 375−382.
(28) Huber, K. C.; BeMiller, J. N. Visualization of channels and cavities of corn and sorghum starch granules. *Cereal Chem.* **1997**, *74*, 537−541.
(29) Fannon, J. E.; Hauber, R. J.; BeMiller, J. N. Surface pores of starch granules. *Cereal Chem.* **1992**, *69*, 284−288.
(30) Payan, F.; Haser, R.; Pierrot, M.; Frey, M.; Astier, J. P.; Abadie, B.; Duée, E.; Buisson, G. The three-dimensional structure of α-amylase from porcine pancreas at 5 Å resolution—The active-site location. *Acta Crystallogr. B: Struct. Sci.* **1980**, *36*, 416−421.
(31) Cooke, D.; Gidley, M. J. Loss of crystalline and molecular order during starch gelatinization: Origin of the enthalpic transition. *Carbohydr. Res.* **1992**, *227*, 103−112.
(32) Jane, J. L.; Chen, Y. Y.; Lee, L. F.; McPherson, A. E.; Wong, K. S.; Radosavljevic, M.; Kasemsuwan, T. Effects of amylopectin branch chain length and amylose content on the gelatinization and pasting properties of starch. *Cereal Chem.* **1999**, *76*, 629−637.
(33) Liu, H. S.; Yu, L.; Simon, G.; Dean, K.; Chen, L. Effects of annealing on gelatinization and microstructures of corn starches with different amylose/amylopectin ratios. *Carbohydr. Polym.* **2009**, *77*, 662−669.
(34) Gidley, M. J.; Bociek, S. M. Molecular organization in starches: A ^{13}C CP/MAS NMR study. *J. Am. Chem. Soc.* **1985**, *107*, 7040−7044.
(35) Gidley, M. J. Quantification of the structual features of starch polysaccharides by NMR spectroscopy. *Carbohydr. Res.* **1985**, *139*, 85−93.
(36) Gidley, M. J.; Bociek, S. M. ^{13}C CP/MAS NMR studies of amylose inclusion complexes, cyclodextrins, and the amorphous phase of starch granules: Relationships between glycosidic linkage conformation and solid-state ^{13}C chemical shifts. *J. Am. Chem. Soc.* **1988**, *110*, 3820−3829.
(37) Veregin, R. P.; Fyfe, C. A.; Marchessault, R. H. ^{13}C CP/MAS NMR study of the polypivalolactone polymorphs. *Macromolecules* **1986**, *19*, 2379−2383.
(38) Ahmed, M.; Lelievre, J. Effect of various drying procedures on the crystallinity of starch isolated from wheat grains. *Starch/Stärke* **1978**, *30*, 78−79.
(39) Muhr, A.; Blanshard, J.; Bates, D. The effect of lintnerisation on wheat and potato starch granules. *Carbohydr. Polym.* **1984**, *4*, 399−425.
(40) Eliasson, A. C.; Larsson, K.; Miezis, Y. On the possibility of modifying the gelatinization properties of starch by lipid surface coating. *Starch/Stärke* **1981**, *33*, 231−235.
(41) Zhang, Z. D.; Gao, W. Y.; Li, X.; Jiang, Q. Q.; Xia, Y. Z.; Wang, H. Y.; Huang, L. Q.; Guo, L. P. Effect of different drying methods on the physicochemical and functional properties of *Dioscorea opposita* Thunb. starch. *Starch/Stärke* **2013**, *65*, 219−226.

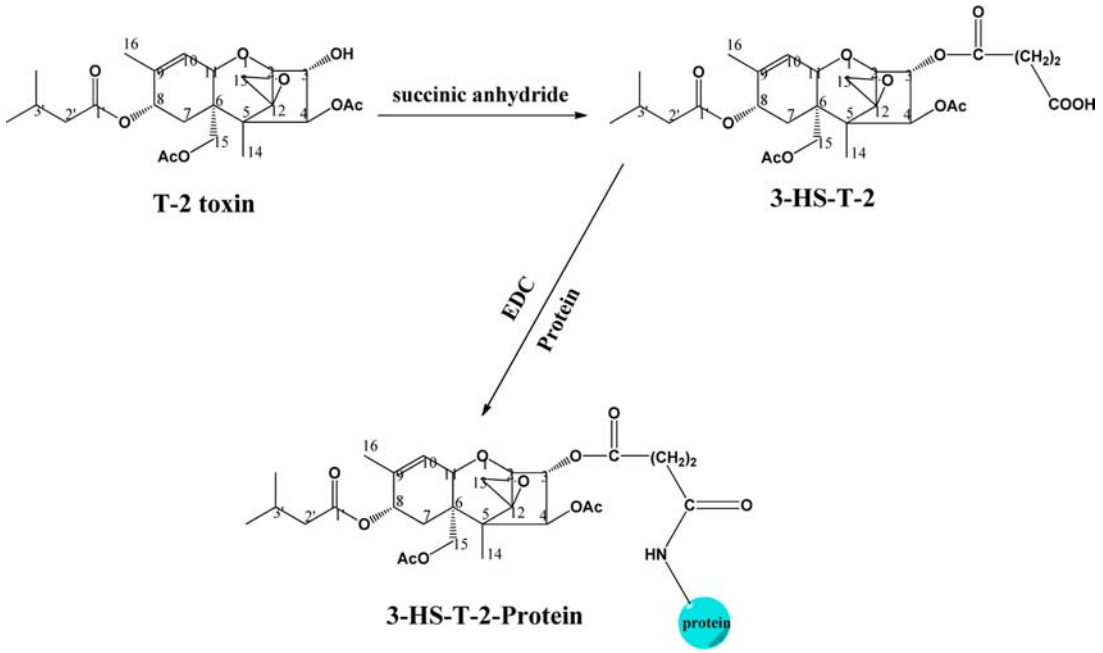

Figure 1. Synthesis of T-2 toxin immunogen and coating antigen.

assay (ELISA) is a very mature and well-applied technology for T-2 toxin monitoring.[29] For the screening of T-2 toxin, the ELISA method generally based on a competitive assay format by using a specific anti-T-2 toxin antibody. Moreover, compared with instrumental analytical methods, ELISA method does not need complicated sample preparation, and could be applied for T-2 toxin screening.[31]

Most antibodies used in the previously reported immunoassays cannot distinguish T-2 toxin and HT-2 toxin (a metabolite of T-2 toxin) in the ELISA method due to their similar structure (Supporting Information, SI, Figure S1).[31−33] When an ELISA method gave a positive result, it was difficult to make sure whether the contaminants were T-2 toxin, HT-2 toxin, or both. For this reason, a specific anti-T-2 toxin monoclonal antibody (mAb) was produced and characterized, which could only bind to T-2 toxin with negligible CR value to most mycotoxins, including HT-2 toxin. Using this specific antibody, an ELISA method for the determination of T-2 toxin in rice was developed. And this developed protocol was confirmed by UPLC-MS/MS (ultrahigh performance liquid chromatography-tandem mass spectrometry). To the best of our knowledge, this is the first time that T-2 toxin specific antibody was produced, and this developed ELISA method could specially recognize T-2 toxin rather than the combination of T-2 toxin and HT-2 toxin.

MATERIALS AND METHODS

Chemicals and Reagents. T-2 toxin, HT-2 toxin, 3-acetyl-deoxynivalenol (3-AcDON), 15-acetyl-deoxynivalenol (15-AcDON), deoxynivalenol (DON), neosolaniol (NEO), and nivalenol (NIV) standard were obtained from Fermentek biotechnology, Israel. BSA (bovine serum albumin), DOM-1 (SI Figure S1), OVA (ovalbumin), T-2-triol, and T-2-tetraol were obtained from Sigma-Aldrich (St. Louis. MO, U.S.). Peroxidase-conjugated goat antimouse IgG was obtained from Jackson ImmunoResearch Laboratories, Inc. (West Grove, Pa, U.S.). Water was purified using a Milli-Q Synthesis system from Millipore (Bedford, MA, U.S.). HPLC grade acetonitrile was purchased from Dima Technology (Muskegon, MI, U.S.). Other reagents were analytical grade obtained from Beijing Reagent Corp. (Beijing, China)

Apparatus. 96-Well polystyrene microtiter wells were purchased from Costar (Costar Inc., Milpitas, CA, U.S.). Waters Acquity UPLC system, Acquity BEH C18 column (50 × 2.1 mm^2 I.D., 1.7 μm particle size), and Micromass Quattro Premier XE triple quadrupole mass spectrometer were from Waters (MA, U.S.). Spectra Max M5 microplate reader (Molecular Devices, Sunnyvale, CA, U.S.) was obtained for this study.

Monoclonal Antibody (mAb) Production. The structure of T-2 toxin is shown in Figure 1. Hapten (3-HS-T-2) was prepared by esterification at the C3 position. Briefly, 10 mg of T-2 toxin was dissolved in 0.4 mL pyridine. Then 210 mg of succinic anhydride was added and stirred for 4 h in a boiling water bath. Dry pyridine and the residues were redissolved using 5 mL of chloroform. Five mL of deionized water was added for washing, and then the water was removed with centrifugation at 3000*g* for 5 min. The washing step was repeated 4 times. Then the chloroform was dried to obtain hapten 3-HS-T-2 under a gentle stream of nitrogen at 60 °C.

This hapten was used to prepare the immunogen (3-HS-T-2-BSA) and coating antigen (3-HS-T-2-OVA). Briefly, solution A was prepared by dissolving the hapten in 1 mL of DMF, while Solution B was prepared by adding 25 mg BSA (OVA) and 15 mg EDC in 5 mL PBS (0.1 M, pH 8.0). Then,solutions A and B were mixed and stirred for 24 h at room temperature. After that, the mixture was dialyzed in PBS (pH7.4, 0.01 M) for 3 d to obtain immunogen and coating antigen (the synthesis protocol shown in Figure 1).

The preparation procedure for anti-T-2 toxin mAb and immunoglobulin were performed as previously described.[34] Briefly, immunize ten female BALB/c mice subcutaneously with immunogen emulsified in Freund's complete adjuvant (FCA). For booster immunization, each mouse was immunized subcutaneously with immunogen in Freund's incomplete adjuvant (FICA) every four weeks for four times (immune procedure was shown in SI Table S1). In order to select the optimum mouse for the subsequent fusion, the serum of each mouse was collected and the titer was monitored by the ELISA method ten days after the last injection. The mouse was boost immunized with immnogen without adjuvants four days before fusion. The splenocytes were fused SP2/0 myelome cells with the help of PEG 1500, and the hybridomas were cultured in 96-well plates. Select and screen the culture supernatant to make sure the hybridomas which excreted the highest affinity anti-T-2 toxin mAb. The cultured

dx.doi.org/10.1021/jf404818r | J. Agric. Food Chem. 2014, 62, 1492−1497

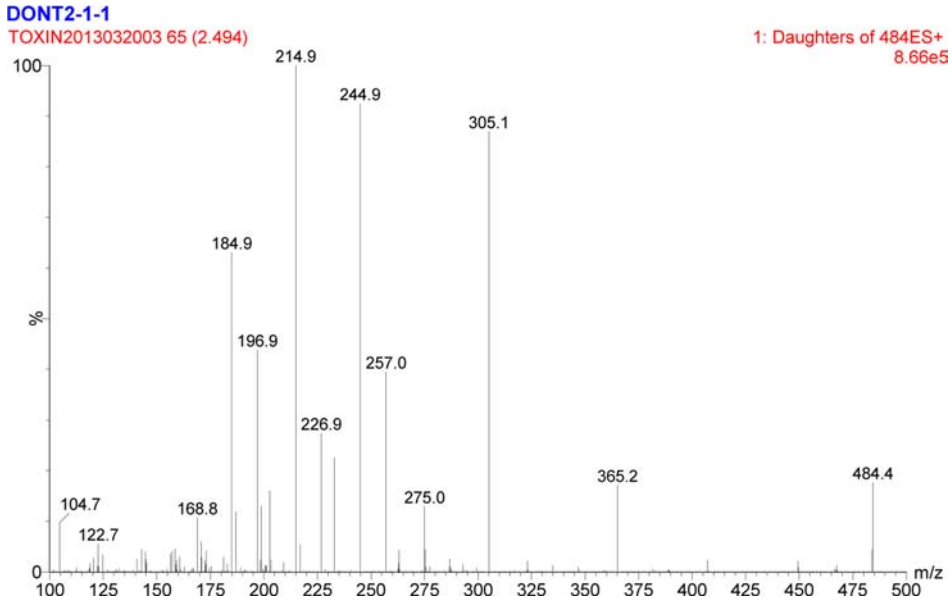

Figure 2. MS/MS spectrum of T-2 toxin $[M + NH_4]^+$.

hybrioma cells ($5-10 \times 10^6$ cell) were injected intraperitoneally into a mouse, and the anti-T-2 toxin mAb was prepared from the ascites fluid.

Principle and the Procedure of ELISA. The ELISA procedure for T-2 toxin determination was performed previously described.[31] 3-HS-T-2-OVA was performed as the coating antigen and the anti-T-2 toxin mAb working solution was prepared at a dilution of 1/6000 in PBS. Each well was individually analyzed, and the values were plotted to yield the calibration curve.

Calibration curves were prepared at 11 concentration levels with the initial concentration at 10 000 ng/mL. The following concentrations were one-third of the previous in turn. Each concentration was run in triplicate, and standard curves were fitted with a four-parameter logistic equation by using Origin version 7.0 (OriginLab, Northampton, MA, U.S.).

Sample Preparaton for ELISA Analysis. Two grams of rice samples were weighed into 50 mL polypropylene centrifuge tubes. After that, 20 mL of ethyl acetate was added for extraction. Then the mixture was vortexed for 3 min and centrifuged at 5000 rpm for 15 min at 4 °C. Ten milliliter aliquots of the supernatant of each sample were drawn to other centrifuge tubes and dried under a gentle stream of nitrogen at 60 °C. The residue was redissolved by 1 mL of 10% methanol and filtered through a 0.22 μm membrane. Fifty microliter aliquots of the supernatant of each sample were added to a 96-well plate for ELISA analysis.

Accuracy and Precision. Negative rice samples, which were previously confirmed by UPLC-MS/MS analyses, were spiked with T-2 toxin at concentrations 40, 200, and 1000 μg/kg. Analysis was performed according to the developed protocol with five replicates each (n = 5), and accuracy and precision were calculated on the basis of the standard curve.

UPLC-MS/MS Method. Results obtained from the developed ELISA protocol were verified and confirmed by an UPLC-MS/MS method. An Acquity BEH C18 column was applied in a Waters Acquity UPLC system for T-2 toxin separation, with the oven temperature maintained at 30 °C. A Micromass Quattro Premier XE triple quadrupole mass spectrometer detector was coupled to the UPLC system via an ESI interface. The analysis was performed in positive ionization mode. The optimized chromatographic conditions were as follows: Mobile phase, 0.005 mM ammonia−water/acetonitrile (40:60, v/v); isocratic elution with the flow rate, 0.3 mL/min; and injection volume, 10 μL.

For monitoring T-2 toxin, Multiple Reaction Monitoring mode was adopted. Quadrupoles 1 and 2 were set to transmit the precursor molecular ion ($[M + NH_4]^+$) of T-2 toxin (m/z 484) and the product ions, respectively. In this research, we choose m/z 484 as the precursor ion and m/z 214.9 and m/z 244.9 as the product ions (Figure 2).

RESULTS AND DISCUSSION

mAb Preparation and Characterization. In this research, the anti-T-2 toxin mAb produced in this research showed high titer with a low LOD value. In order to characterize the specificity of the mAb, another 9 mycotoxins (SI Figure S1) were determined by this developed ELISA protocol. The cross-reactivity (CR) values were calculated using the following equation.

$$\mathrm{CR}(\%) = \frac{\mathrm{IC50\ of\ T\text{-}2\ toxin}}{\mathrm{IC50\ of\ analogue}} \times 100\%$$

where IC_{50} is half maximal inhibitory concentration of a substance.

The selectivity of T-2 toxin and its analogues is shown in Table 1. It can be concluded that mAb shows a negligible CR value to most of the mycotoxins investigated in this research, including HT-2 toxin. The CR value and IC_{50} value of HT-2 toxin was 3.08% and 717 ng/mL, respectively. Considering the negligible CR value for other mycotoxins, this developed mAb could specially recognize T-2 toxin.

Table 1. IC50 and Cross-Reactivity (CR) Value of T-2 Toxin Analogues

no.	analogue	IC50 (ng/mL)	CR (%)
1	T-2	22.09	100
2	HT-2	717	3.08
3	T-2 triol	14 000	<0.1
4	T-2 tetraol	>100 000	<0.01
5	NEO	>100 000	<0.01
6	NIV	>100 000	<0.01
7	DON	>100 000	<0.01
8	DOM-1	>100 000	<0.01
9	3-AcDON	>100 000	<0.01
10	15-AcDON	>100 000	<0.01

dx.doi.org/10.1021/jf404818r | J. Agric. Food Chem. 2014, 62, 1492−1497

Sample Pretreatment. The extract efficiency from a complicated biological matrix depends on the structure of the target analyte. In the previous researches, acetonitrile/water (85:15, v/v) was the most common extraction solvent for T-2 toxin extraction.[24,35,36] Besides, dichloromethane, ethyl acetate, methanol, and PBS have been adopted as the extraction solvent.[37−40] On the basis of the previous research, ethyl acetate with high volatility and low toxicity was adopted as the extraction solvent in this research. On the basis of the previous report, ethyl acetate was adopted as the extraction solvent because of its high volatility and low toxicity. Then the supernatant was condensed in order to wipe off the organic solvent and get a lower LOD (limit of detection).

Sensitivity. To evaluate to sensitivity of the proposed ELISA protocol, IC_{50} and LOD (measured by IC_{10}) were obtained from the sigmoidal standard curve (Figure 3). LOD

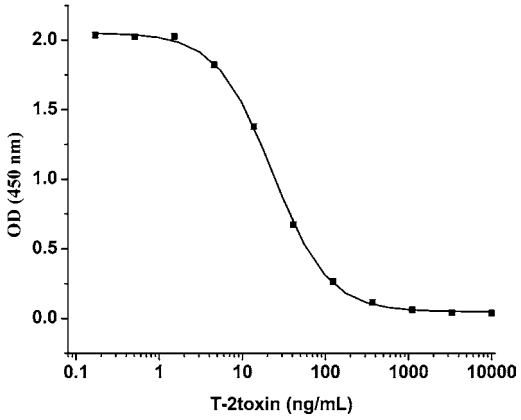

Figure 3. Standard curve of ELISA for T-2 toxin.

for T-2 toxin was 5.8 μg/kg, while IC50 was 23 μg/kg. Compared to the published colorimetric ELISA methods,[31] this research exhibited a higher sensitivity for T-2 toxin. Besides, published immunoassays for T-2 toxin mainly focused on the sum of T-2 toxin and HT-2 toxin. This is mainly due to the similar structure between T-2 toxin and HT-2 toxin, and the broad specificity mAb used in those methods could not distinguish one from another.[41−46] In this research, a high specific antibody was produced, which could recognize T-2 toxin specifically. The developed ELISA using this mAb could detect T-2 toxin in rice specifically, rather than the sum of T-2 toxin and HT-2 toxin.

Accuracy and Precision. Recoveries of T-2 toxin in fortified samples were calculated, and accuracy and precision were evaluated with five replicates each on three validation days. The fortified levels were 40, 200, and 1000 μg/kg. The mean recovery of T-2 toxin in spiked samples ranged from 72.0% to 108.5% for rice samples, and the intraday and interday variation were less than 16.8 and 13.7%, respectively (Table 2).

Table 2. Accuracy and Precision of T-2 Toxin in Rice with Five Replicates Each (n = 5) on Three Validation Days (n = 3)

matrix	analyte	spiked level (μg/kg)	recovery (%)	interday RSD (%)	intraday RSD (%)
rice	T-2 toxin	40	74.8−91.9	1.27−8.97	8.16
		200	77.9−108.5	3.15−16.8	13.7
		1000	72.0−100.7	1.73−10.8	12.4

Comparison of the ELISA and UPLC-MS/MS Analyses. Figure 4 demonstrates the correlation between the developed

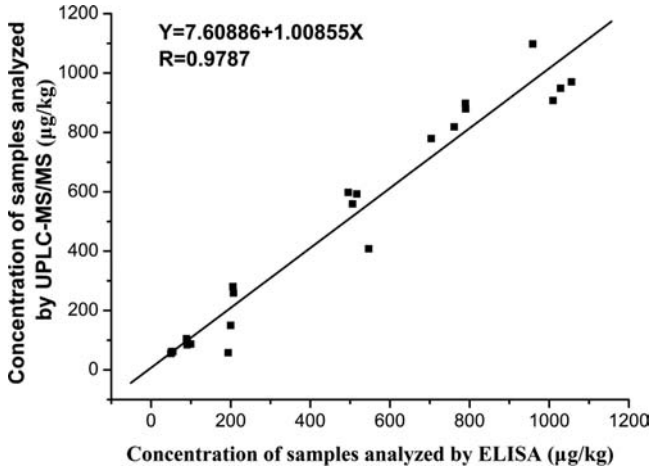

Figure 4. Correlation of T-2 toxin assay between the confirmatory UPLC-MS/MS and the ELISA method in rice samples obtained from T-2 toxin spiked at levels of 50, 100, 200, 500, 750, and 1000 μg/kg (n = 4).

ELISA protocol and the confirmatory UPLC-MS/MS method. Rice samples were prepared with T-2 toxin spiked levels of 50, 100, 200, 500, 750, and 1000 μg/kg with four replicates each concentration. The linear regression equation between the two methods was Y = 7.60886 + 1.00855X. The two methods exhibited significant correlation at the various fortified levels with the correlation at 0.9787.

Analysis of T-2 Toxin in Commercial Rice Samples. Commercial rice samples were purchased from local supermarkets in order to verify the applicability of this developed ELISA method. Samples were processed and analyzed according to the established ELISA protocol as well as the UPLC-MS/MS procedure. From all 20 commercial rice samples, 5 were detected with trace amount of T-2 toxin (Table 3). It is well-known that UPLC-MS/MS is a confirmatory method for quantification. The results in Table 3 showed a good correlation between this developed ELISA method and the UPLC-MS/MS method. It can be concluded that these specific ELISA methods could be applied for T-2 toxin detection in rice.

In conclusion, a specific anti-T-2 toxin mAb was produced and characterized in the present study. By the use of this mAb, an ELISA method was developed for the determination of T-2 toxin in rice. The results of the analysis were confirmed by UPLC-MS/MS, and significant correlation was obtained between the two methods. The proposed format offers the advantage of simplicity, rapidity, and cost-effectiveness. With respect to its overall sensitivity and specificity, the method is superior to most reported immunoassays for T-2 toxin in rice. What's more important is that this developed protocol could be specifically applied for T-2 toxin detection rather than the sum of T-2 toxin and HT-2 toxin. This newly developed procedure could be a suitable tool for specific, rapid, semiquantitative, and quantitative detection of T-2 toxin in rice, which will contribute to the control of contamination by this fungal toxin.

Table 3. Analysis of Commercial Rice Samples (n = 3)

sample code	ELISA (mean ± SD, μg/kg)	UPLC-MS/MS (mean ± SD, μg/kg)	sample code	ELISA (mean ± SD, μg/kg)	UPLC-MS/MS (mean ± SD, μg/kg)
01	ND	ND	11	ND	ND
02	11.2 ± 0.6	13.6 ± 1.9	12	9.6 ± 1.9	16.2 ± 1.7
03	ND	ND	13	ND	ND
04	ND	ND	14	35.2 ± 1.8	33.4 ± 3.1
05	15.8 ± 1.5	18.8 ± 1.6	15	ND	ND
06	ND	ND	16	ND	ND
07	ND	ND	17	28.1 ± 1.9	30.9 ± 2.6
08	ND	ND	18	ND	ND
09	ND	ND	19	ND	ND
10	ND	ND	20	ND	ND

■ ASSOCIATED CONTENT

Supporting Information

Table S1: Immune procedure for T-2 toxin. Figure S1: Chemical structures of T-2 toxin and its analogues. This material is available free of charge via the Internet at http://pubs.acs.org.

■ AUTHOR INFORMATION

Corresponding Authors

*Tel: +86-0535-6902638; e-mail: yizhanwangpai@163.com (Y.L.).

*Tel: +86 10 62733289; fax: +86 10 62731032; e-mail: suxia@cau.edu.cn (S.Z.).

Author Contributions

Y.L. and X.L. contributed equally to this work.

Notes

The authors declare no competing financial interest.

■ ACKNOWLEDGMENTS

This work was financially supported by National Basic Research Program of China (973 program; Grant No. 2009CB118801).

■ ABBREVIATIONS USED

15-AcDON, 15-Acetyl-deoxynivalenol; 3-AcDON, 3-Acetyl-deoxynivalenol; ATA, Alimentary Toxic Aleukia; BSA, Bovine Serum Albumin; CR, Cross-Reactivity; DON, Deoxynivalenol; ELISA, Enzyme-Linked Immunosorbent Assay; EU, European Union; FID, Flame Ionization Detector; FLD, Fluorescence Detector; FICA, Freund's incomplete adjuvant; FCA, Freund's complete adjuvant; GC, Gas chromatography; KBD, Kashin-Beck Disease; LC-MS/MS, Liquid chromatography-tandem mass spectrometry; mAb, Monoclonal antibody; NEO, Neosolaniol; NIV, Nivalenol; OVA, Ovalbumin; PBS, Phosphate buffer; UPLC-MS/MS, Ultrahigh performance liquid chromatography-tandem mass spectrometry

■ REFERENCES

(1) Li, Y.; Wang, Z.; Beier, R. C.; Shen, J.; De Smet, D.; De Saeger, S.; Zhang, S. T-2 Toxin, A Trichothecene Mycotoxin: Review of Toxicity, Metabolism, and Analytical Methods. *J. Agric. Food Chem.* **2011**, *59*, 3441−3453.

(2) Wu, Q.; Dohnal, V.; Huang, L.; Kuca, K.; Yuan, Z. Metabolic Pathways of Trichothecenes. *Drug Metab. Rev.* **2010**, *42*, 250−267.

(3) Foroud, N. A.; Eudes, F. Trichothecenes in Cereal Grains. *Int. J. Mol. Sci.* **2009**, *10*, 147−173.

(4) Mateo, J. J.; Mateo, R.; Jimenez, M. Accumulation of Type A Trichothecenes in Maize, Wheat and Rice by *Fusarium sporotrichioides* Isolates under Diverse Culture Conditions. *Int. J. Food Microbiol.* **2002**, *72*, 115−123.

(5) Schollenberger, M.; Muller, H. M.; Rufle, M.; Suchy, S.; Planck, S.; Drochner, W. Survey of Fusarium Toxins in Foodstuffs of Plant Origin Marketed in Germany. *Int. J. Food Microbiol.* **2005**, *97*, 317−326.

(6) Adejumo, T. O.; Hettwer, U.; Karlovsky, P. Occurrence of Fusarium species and Trichothecenes in Nigerian maize. *Int. J. Food Microbiol.* **2007**, *116*, 350−357.

(7) Milanez, T. V.; Valente-Soares, L. M.; Baptista, G. G. Occurrence of Trichothecene Mycotoxins in Brazilian Corn-Based Food Products. *Food Control* **2006**, *17*, 293−298.

(8) Reports on Tasks for Scientific Cooperation: Report of Experts Participation in Task 3.2.10. Part A: Trichothecenes. 2003, pp 20−22.

(9) Sudakin, D. L. Trichothecenes in the Environment: Relevance to Human Health. *Toxicol. Lett.* **2003**, *143*, 97−107.

(10) Islam, Z.; Nagase, M.; Ota, A.; Ueda, S.; Yoshizawa, T.; Sakato, N. Structure-Function Relationship of T-2 Toxin and Its Metabolites in Inducing Thymic Apoptosis in Vivo in Mice. *Biosci. Biotechnol. Biochem.* **1998**, *62*, 1492−1497.

(11) Fairhurst, S.; Marrs, T. C.; Parker, H. C.; Scawin, J. W.; Swanston, D. W. Acute Toxicity of T2 Toxin in Rats, Mice, Guinea Pigs, And Pigeons. *Toxicology* **1987**, *43*, 31−49.

(12) Glavits, R.; Vanyi, A.; Fekete, S.; Tamas, J. Acute Toxicological Experiment of T-2 Toxin in Rabbits. *Acta. Vet. Hung.* **1989**, *37*, 75−79.

(13) Velazco, V.; Faifer, G. C.; Godoy, H. M. Differential Effects of T-2 Toxin on Bone Marrow and Spleen Erythropoiesis in Mice. *Food Chem. Toxicol.* **1996**, *34*, 371−375.

(14) Shifrin, V. I.; Anderson, P. Trichothecene Mycotoxins Trigger a Ribotoxic Stress Response That Activates c-Jun N-Terminal Kinase and p38 Mitogen-Activated Protein Kinase and Induces Apoptosis. *J. Biol. Chem.* **1999**, *274*, 13985−13992.

(15) Doi, K.; Shinozuka, J.; Sehata, S. T-2 Toxin and Apoptosis. *J. Toxicol. Pathol.* **2006**, *19*, 15−27.

(16) Paterson, R. R.; Lima, N. Toxicology of Mycotoxins. In *Molecular, Clinical and Environmental Toxicology*; Springer: New York, 2010; pp 31−63.

(17) Sokolovic, M.; Garaj-Vrhovac, V.; Simpraga, B. T-2 Toxin: Incidence and Toxicity in Poultry. *Arh. Hig. Rada. Toksikol.* **2008**, *59*, 43−52.

(18) Shinozuka, J.; Suzuki, M.; Noguchi, N.; Sugimoto, T.; Uetsuka, K.; Nakayama, H.; Doi, K. T-2 Toxin-Induced Apoptosis in Hematopoietic Tissues of Mice. *Toxicol. Pathol.* **1998**, *26*, 674−681.

(19) Doi, K.; Ishigami, N.; Sehata, S. T-2 Toxin-Induced Toxicity in Pregnant Mice and Rats. *Int. J. Mol. Sci.* **2008**, *9*, 2146−2158.

(20) Dohnal, V.; Jezkova, A.; Jun, D.; Kuca, K. Metabolic Pathways of T-2 Toxin. *Curr. Drug Metab.* **2008**, *9*, 77−82.

(21) Trebstein, A.; Seefelder, W.; Lauber, U.; Humpf, H. U. Determination of T-2 and HT-2 Toxins in Cereals Including Oats after Immunoaffinity Cleanup by Liquid Chromatography and Fluorescence Detection. *J. Agric. Food Chem.* **2008**, *56*, 4968−4975.

(22) Visconti, A.; Lattanzio, V. M.; Pascale, M.; Haidukowski, M. Analysis of T-2 and HT-2 Toxins in Cereal Grains by Immunoaffinity

Clean-up and Liquid Chromatography with Fluorescence Detection. *J. Chromatogr. A* **2005**, *1075*, 151−158.
(23) Pascale, M.; Haidukowski, M.; Visconti, A. Determination of T-2 Toxin in Cereal Grains by Liquid Chromatography with Fluorescence Detection after Immunoaffinity Column Clean-up and Derivatization with 1-Anthroylnitrile. *J. Chromatogr. A* **2003**, *989*, 257−264.
(24) Klotzel, M.; Gutsche, B.; Lauber, U.; Humpf, H. U. Determination of 12 Type A and B Trichothecenes in Cereals by Liquid Chromatography-Electrospray Ionization Tandem Mass Spectrometry. *J. Agric. Food Chem.* **2005**, *53*, 8904−8910.
(25) Lattanzio, V. M.; Solfrizzo, M.; Visconti, A. Determination of Trichothecenes in Cereals and Cereal-Based Products by Liquid Chromatography-Tandem Mass Spectrometry. *Food Addit. Contam. Part A, Chem. Anal. Control Expo. Risk Assess.* **2008**, *25*, 320−330.
(26) Sagawa, N.; Takino, T.; Kurogochi, S. A Simple Method with Liquid Chromatography/Tandem Mass Spectrometry for the Determination of the Six Trichothecene Mycotoxins in Rice Medium. *Biosci. Biotech. Biochem.* **2006**, *70*, 230−236.
(27) European Community Commission. 2002/657/EC: Commission Decision of 12 August 2002, Regulation (EC) No. 3044/2002. Off. J. Eur. Communities 2002, L221, 8.
(28) Eke, Z.; Kende, A.; Torkos, K. Simultaneous Detection of A and B Trichothecenes by Gas Chromatography with Flame Ionization or Mass Selective Detection. *Microchem. J.* **2004**, *78*, 211−216.
(29) Turner, N. W.; Subrahmanyam, S.; Piletsky, S. A. Analytical Methods for Determination of Mycotoxins: A Review. *Anal. Chim. Acta* **2009**, *632*, 168−180.
(30) Schollenberger, M.; Muller, H. M.; Rufle, M.; Suchy, S.; Dejanovic, C.; Frauz, B.; Oechsner, H.; Drochner, W. Simultaneous Determination of a Spectrum of Trichothecene Toxins out of Residuals of Biogas Production. *J. Chromatogr. A* **2008**, *1193*, 92−96.
(31) Yoshizawa, T.; Kohno, H.; Ikeda, K.; Shinoda, T.; Yokohama, H.; Morita, K.; Kusada, O.; Kobayashi, Y. A Practical Method for Measuring Deoxynivalenol, Nivalenol, and T-2 + HT-2 Toxin in Foods by an Enzyme-Linked Immunosorbent Assay Using Monoclonal Antibodies. *Biosci. Biotechnol. Biochem.* **2004**, *68*, 2076−2085.
(32) Schwake-Anduschus, C.; Langenkamper, G.; Unbehend, G.; Dietrich, R.; Martlbauer, E.; Munzing, K. Occurrence of Fusarium T-2 and HT-2 Toxins in Oats from Cultivar Studies in Germany and Degradation of the Toxins during Grain Cleaning Treatment and Food Processing. *Food Addit. Contam. Part A, Chem. Anal. Control Expo. Risk Assess.* **2010**, *27*, 1253−1260.
(33) Fan, T. S.; Xu, Y. C.; Chu, F. S. Simultaneous Analysis of T-2 Toxin and HT-2 Toxin by an Indirect Enzyme-Linked Immunosorbent Assay. *J. Assoc. Off. Anal .Chem.* **1987**, *70*, 657−661.
(34) Nakazawa, M.; Mukumoto, M.; Miyatake, K. Production and Purification of Monoclonal Antibodies. In *Immunoelectron Microscopy*; Springer: New York, 2010; pp 75−91.
(35) Jestoi, M.; Ritieni, A.; Rizzo, A. Analysis of the Fusarium Mycotoxins Fusaproliferin and Trichothecenes in Grains Using Gas Chromatography-Mass Spectrometry. *J. Agric. Food Chem.* **2004**, *52*, 1464−1469.
(36) Haubl, G.; Berthiller, F.; Hametner, C.; Rechthaler, J.; Jaunecker, G.; Freudenschuss, M.; Krska, R.; Schuhmacher, R. Characterization of (^{13}C24) T-2 Toxin and Its Use As an Internal Standard for the Quantification of T-2 Toxin in Cereals with HPLC-MS/MS. *Anal. Bioanal. Chem.* **2007**, *389*, 931−940.
(37) Delmulle, B.; De Saeger, S.; Adams, A.; De Kimpe, N.; Van Peteghem, C. Development of a Liquid Chromatography/Tandem Mass Spectrometry Method for the Simultaneous Determination of 16 Mycotoxins on Cellulose Filters and in Fungal Cultures. *Rapid Commun. Mass Spectrom.* **2006**, *20*, 771−776.
(38) Lattanzio, V. M.; Solfrizzo, M.; Visconti, A. Enzymatic Hydrolysis of T-2 Toxin for the Quantitative Determination of Total T-2 and HT-2 Toxins in Cereals. *Anal. Bioanal. Chem.* **2009**, *395*, 1325−1334.
(39) Lippolis, V.; Pascale, M.; Maragos, C. M.; Visconti, A. Improvement of Detection Sensitivity of T-2 and HT-2 Toxins Using Different Fluorescent Labeling Reagents by High-Performance Liquid Chromatography. *Talanta* **2008**, *74*, 1476−1483.
(40) Dall'Asta, C.; Galaverna, G.; Biancardi, A.; Gasparini, M.; Sforza, S.; Dossena, A.; Marchelli, R. Simultaneous Liquid Chromatography-Fluorescence Analysis of Type a and Type B Trichothecenes As Fluorescent Derivatives via Reaction with Coumarin-3-carbonyl Chloride. *J. Chromatogr. A* **2004**, *1047*, 241−247.
(41) Goftman, V. V.; Beloglazova, N. V.; Njumbe Ediage, E.; De Saeger, S.; Dietrich, R.; Märtlbauer, E.; Goryacheva, I. Rapid Immunochemical Tests for Qualitative and Quantitative Determination of T-2 and HT-2 Toxins. *Anal. Methods* **2012**, *4*, 4244−4249.
(42) Meneely, J.; Ricci, F.; Vesco, S.; Abouzied, M.; Sulyok, M.; Krska, R.; Elliott, C. T. A Comparative Study of Qualitative Immunochemical Screening Assays for the Combined Measurement of T-2/HT-2 in Cereals and Cereal-Based Products. *World Mycotoxin J.* **2011**, *4*, 385−394.
(43) Lippolis, V.; Pascale, M.; Valenzano, S.; Pluchinotta, V.; Baumgartner, S. A Rapid Fluorescence Polarization Immunoassay for the Determination of T-2 and HT-2 Toxins in Wheat. *Anal. Bioanal. Chem.* **2011**, *401*, 2561−2571.
(44) Julie, P.; Ricci, M. R. Current Methods of Analysis for the Determination of Trichothecene Mycotoxins in Food. *Trends in Anal. Chem.* **2011**, *30*, 192−203.
(45) Wang, J.; Duan, S.; Zhang, Y.; Wang, S. Enzyme-Linked Immunosorbent Assay for the Etermination of T-2 Toxin in Cereals and Feedstuff. *Microchim. Acta* **2010**, *169*, 137−144.
(46) Julie, P.; Sulyok, M.; Baumgartner, S.; Krska, R.; Elliott, C. T. A Rapid Optical Immunoassay for the Screening of T-2 and HT-2 Toxin in Cereals and Maize-Based Baby Food. *Talanta* **2010**, *81*, 630−636.

were among the earliest to discuss EMA and allergen labeling concerns in 1989 and apply ELISA, SDS−PAGE, and fast protein liquid chromatography (LC) to detect soy proteins in bovine milk.[30,31] Detection limits ranged from 1 to 5%. Cattaneo et al. spiked cheese with soy protein, extracted samples with tetraborate-EDTA buffer, and performed analyses using gel-permeation chromatography, isoelectric focusing, and SDS−PAGE.[32] The respective limits of detection (LODs) were 0.6, 3, and 0.06% soy by weight. Lopez-Tapia et al. determined the LOD of soy and pea protein in milk powder to be 1% in an interlaboratory SDS−CE assay validation study.[10,33] The Lopez-Tapia study confirmed observations by Cattaneo et al. that tetraborate-EDTA buffer efficiently extracts soy proteins from milk proteins.[32,33] The outstanding selectivity of this buffer was also used to concentrate soy and pea proteins from milk for LC−MS/MS analysis in an experimental EMA model.[13,34] In an interlaboratory ELISA study, where tetraborate-EDTA extraction buffer was not used, soy, pea, and wheat proteins spiked in milk were detected at the 1% level.[11] The detection of plant proteins in milk products using HPLC−UV, NIR, SPR, perfusion chromatography, and flow cytometry have also been reported without using tetraborate-EDTA buffer.[5,9,12,35−38] These studies commonly accept 1% by weight as a nominal level above which EMA is practical. However, dilution of adulterated products during blending in complex distribution chains may require even more sensitive assays.

These methods may be useful for detecting specific foreign proteins or authenticating food samples, but none of them are especially well suited to performing low cost screening to detect the economically motivated adulteration of SMP with a variety of inexpensive plant proteins. Long electrophoretic or chromatographic separation times, the complicating effects of food processing and matrices on immunochemical assay and chemometric model performance, requirements for multiple different antibodies, and in some cases, expensive instrumentation contribute to this problem. However, the selectivity of tetraborate-EDTA buffer for extracting plant proteins from milk can be put to use in another way to address this problem. In this work, we demonstrate a rapid screening assay using tetraborate-EDTA buffer to prepare SMP for the turbidimetric detection of insoluble plant proteins. It is based on an intrinsic property of normal milk powder, namely, the absence of a visible precipitate upon extraction.

EXPERIMENTAL PROCEDURES

Materials. Reference samples were donated by the USP (Rockville, MD, USA), and their names are followed by USP-assigned identification codes: medium heat SMP (S085), soy protein isolate (A027), pea protein isolate (A011), rice protein isolate (A019), wheat protein isolate (A028), whey (A044), egg whites (A045), high molecular weight fish gelatin (A013), chitosan (A035), sorbitol (A122). Liquid and powdered soy milk products and powdered partially hydrolyzed (bovine whey) infant formula were purchased at a local market. Sequencing grade trypsin was purchased from Promega. Lo-bind microcentrifuge tubes (2 mL) were purchased from Eppendorf. "Fisherbrand" nonsterile, clear, flat-bottom polystyrene 96-well plates were used.

Methods. *Preparation of SMP Samples Containing Plant Proteins.* Plant protein isolate (PI) powders were individually dry blended with SMP to yield mixtures containing 0.03, 0.10, 0.30, 1.00 and 3.00% PI/SMP by weight. SMP and SMP/PI blends were brought up in buffer (30 mM sodium tetraborate/40 mM EDTA/pH 8.3) to 300 mg/mL. Individual PI solutions, without SMP, were prepared in buffer at 15 mg/mL.

Extraction and Turbidimetric Analysis in 96-Well Plates. Immediately after vortex mixing, SMP solution and PI/SMP suspensions in buffer (300 μL, 300 mg/mL) were loaded in 96-well plate column 1 wells, rows B−G, using a multichannel pipettor to deliver 90 mg of SMP test sample and progressively diluted 2-fold with buffer (150 μL) in columns 2−3, to respectively deliver 45 and 22.5 mg of each SMP test sample. Rows B through G were respectively loaded with test samples containing 0−3% PI/SMP. A schematic of the 96-well plate sample layout is provided as Supplemental Figure S1 in the Supporting Information. Wells in columns 4−6, 7−9, and 10−12 were similarly used to prepare replicates of samples prepared in columns 1−3 (rows B−G). Row A was used to prepare duplicate standard curves using only the plant PI without any SMP. Immediately after vortexing, PI solution (300 μL, 15 mg/mL) was deposited in wells A1 and A7. These test portions were progressively diluted 3-fold with buffer in columns A2−6 and A8−12. Buffer was added to produce a final volume of 300 μL in all wells. Solvent blank wells in row H were filled with 300 μL of buffer. Two 96-well plates were prepared for each type of PI/SMP mixture to provide 8 data points at each spike level and 4 data points at each PI (alone) concentration. Plates were centrifuged (Sorvall Evolution RC, Thermo Electron Corporation) at 1,500 rpm (466*g*) for 5 min at 20 °C in a swinging microplate carrier. Supernatants were removed taking care not to disturb sample pellets. Pellets were resuspended in fresh buffer (150 μL) by pipetting them up and down three times using aerosol barrier pipet tips. Samples were centrifuged again, and the supernatants were removed. This washing process was repeated three times. Pellets were finally resuspended in fresh buffer (150 μL), and the absorbance (360 ± 2 nm) was promptly measured, without shaking, for 1 s per well using a VERSAmax microplate reader (Molecular Devices, Sunnyvale, CA) at 20 °C.

Plant Protein Isolate Turbidimetric Standard Curves. Individual plant PI powders without SMP were suspended in buffer (5 mg/mL) and serially diluted 2-fold in 96-well plates so that 300 μL aliquots delivered 0−1.5 mg (dry powder weight). Four technical replicate wells were prepared at 12 concentrations. Test portions were not extracted before measuring the absorbance. Standard curves were prepared by linear regression of the baseline corrected absorbance data, limited to values approximately less than 1 OD unit. The LOD was estimated as three times the ratio of the standard error of the absorbance divided by the slope. The limit of quantitation (LOQ) was estimated as ten times this ratio. Standard curves were used to estimate the recovery of adulterants from samples extracted with tetraborate-EDTA buffer.

Fourier Transform Infrared Spectroscopy. Transmission Fourier transform infrared (FT-IR) measurements were carried out on an Agilent Technologies Inc. (Wilmington, DE; formerly Varian, Randolph, MA) FTS 7000e IR spectrometer operating with Resolution Pro 4.0 software. The optical bench included a Michelson interferometer with an air bearing moving mirror, a KBr substrate beam splitter, and a linearized mercury cadmium telluride liquid N_2 cooled detector. In the absence of a test sample, a 3 min data collection at 4 cm^{-1} resolution from 2200 to 2000 cm^{-1} yielded a peak-to-peak noise level <0.0005 OD. Test samples (~2 mg) were measured as KBr pellets. Test sample single-beam spectra were measured relative to an open beam (air). Spectra were collected from 4000 to 700 cm^{-1} at a resolution of 4 cm^{-1} and 32 scans were coadded and signal averaged.

SDS−PAGE. Pellets extracted from SMP containing 0 and 3% (w/w) protein isolate were suspended in Laemmli buffer containing 5 mM β-mercaptoethanol, heated (100 °C) in a steam bath (10 min), and cooled on ice. Precision Plus Protein Dual Xtra (Bio-Rad, Hercules, CA) protein ladder and samples were loaded onto a 4−20% SDS−PAGE gel (Bio-Rad, precast Criterion), and run in pH 8.3 Tris (89 mM)/Borate (89 mM)/EDTA (2 mM) buffer at 180 V for 60 min. Gels were stained with Gel Code Blue (Thermo Fisher Scientific). Gel images were acquired using a Syngene G:Box (Synoptic Group, Frederick, MD).

Reduction, Alkylation, and Digestion of Proteins. Solvent (200 μL: 94.9% water, 5% CH_3CN, 0.1% HCOOH) was added to single wells containing pellets from extracted SMP, plant protein isolate, or

plant protein adulterant in SMP from a 96-well plate loaded with 90 mg of test sample. Resuspended pellets were diluted with 50 mM ammonium bicarbonate containing 5 mM dithiothreitol (DTT) and heated (100 °C) in a steam bath for 10 min. After rapid cooling on ice, iodoacetamide (IAA) was added to a final concentration of 14 mM and samples were incubated in the dark for 30 min. DTT was added in 1.3-fold stoichiometric excess to IAA, and test portions were incubated in the dark for 15 min. Alkylated test samples were digested with trypsin at 37 °C overnight at a 1:50 (w/w) ratio. Digestions were acidified to a final 0.1% HCOOH by the addition of 10% HCOOH.

nLC–MS/MS Analysis. Digested samples (~125–200 ng) were analyzed using an LTQ-XL (Thermo Fisher Corp.) equipped with a CaptiveSpray (Bruker) electrospray source operated in the positive ionization mode. Collision-induced dissociation (CID) spectra were acquired in a data-dependent mode from the most abundant nine ions detected in survey scans. Chromatographic conditions: nano-Acquity LC system (Waters Corp., Milford, MA, USA), loop volume = 5 μL, C18 MAGIC column (0.1 × 50 mm, Bruker), flow rate = 1 μL/min, sample compartment temperature = 4 °C, column temperature 20 °C, run time = 60 min; mobile phases, A = 99.9% H_2O/0.1% HCOOH, B = 99.9% CH_3CN/0.1% HCOOH; gradient conditions started at 5% B and were held for 30 s, then linear gradient to 10% B at 1 min, then linear gradient to 60% B at 46 min, then linear gradient to 80% at 46 min and hold for 2 min, then linearly return to 5% B at 48 min and hold for 12 min.

Peptide Identification. LTQ-XL mass spectrometer .raw data files were converted to .mgf files using ProteoWizard's freely available software program MSConvert.[39] MASCOT search engine (2.3.02) was used to query .mgf files against the SwissProt database 20110214 (525,997 sequences, 185E6 residues) using the following parameters: mass values = monoisotopic; protein mass = unrestricted; enzyme = trypsin; max. missed cleavages = 2; variable modifications = oxidation (M), carbamidomethyl (C), Gln > pyro-Glu (N-terminal Q), Glu > pyro-Glu (N-terminal E); peptide charge = +2, +3; peptide and MS/MS tol. = ±0.8 Da; instrument type = ESI-trap. Individual proteins were inferred to be present if at least two different peptide sequences exceeding the critical peptide MASCOT score were detected.

RESULTS AND DISCUSSION

Soy, pea, rice, and wheat protein isolates extracted from SMP/PI suspensions in 96-well plates were turbidimetrically detected using a semitargeted technique for the rapid screening of milk powder for EMA with insoluble foreign proteins. Because previous reports described adulterant concentration as a percentage of the total sample weight, soy data are initially presented using this metric to facilitate comparison with published work.[5,13,33] Extracted sample absorbance in Figure 1 linearly increased with the addition of soy adulterant to SMP from ~0.1–1.0 OD units. Liquid and soy beverage powder added to SMP at 5% by weight yielded strong positive results with absorbance values ranging from 0.4 to 1.2 OD (data not shown). By contrast, negative control samples extracted from 5% sorbitol, chitosan, gelatin, whey, egg protein, and infant formula containing partially hydrolyzed whey in SMP were turbidimetrically and visually indistinguishable from the SMP blank. The observed lack of a pellet in these samples demonstrates that the extraction method is to some degree selective for plant proteins over other sources of added protein, polysaccharides, or monosaccharides potentially encountered in EMA schemes. Instead of longer visible wavelengths often used in turbidimetric assays, 360 nm was used because it was empirically found to yield the strongest signal.

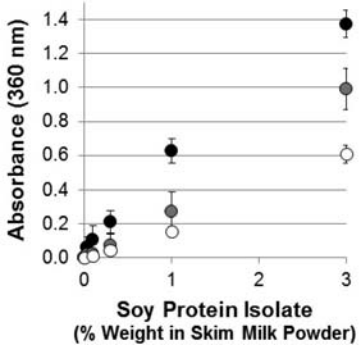

Figure 1. Turbidimetric detection of soy protein isolate extracted from skim milk powder in 96-well plates. Powder sample weight loaded: 22.5 mg (open circles), 45 mg (shaded circles), 90 mg (filled circles). Data points represent the mean (n = 8) ± one sample standard deviation.

It is more direct to specify the weight of spiked adulterant, instead of a weight percentage, because different SMP sample weights were used to explore the assay's dynamic range. The spiked adulterant weight and extracted sample absorbance data for soy in Figure 1 are replotted in Figure 2, along with pea, rice, and wheat protein isolate data. In Figure 2, absorbance begins to exhibit nonlinearity with increases in the theoretical amount of plant protein deposited above ~900 μg (assuming 100% extraction efficiency). This parallels the onset of nonlinearity in Figure 1 above 1% soy in 90 mg SMP samples.

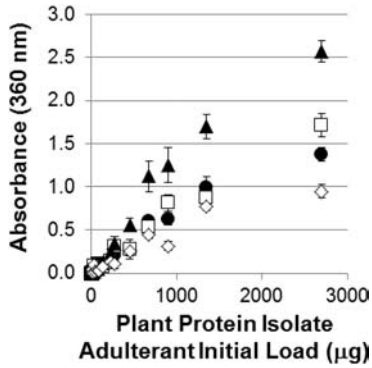

Figure 2. Turbidimetric detection of soy, pea, rice, and wheat protein isolates extracted from 22.5 to 90 mg of skim milk powder samples spiked with 0–3% plant protein isolate by weight. Data points represent the mean (n = 8) ± one sample standard deviation. Protein isolate symbol legend: rice (triangles), pea (squares), soy (closed circles), wheat (diamonds).

Extraction Efficiency. Plant protein extraction efficiency and gel formation can be affected by intra- and intermolecular protein interactions.[40–42] Changes in the resuspended particle size distribution could affect turbidimetric responses because light scattering is a function of particle size.[43] To survey for the influence of these effects and measure extraction efficiencies, absorbance differences between nonextracted and extracted plant adulterant standards alone (without SMP) and extracted adulterant-spiked SMP (Figure 2) were compared. Linear regression of adulterant weight versus absorbance data was performed from 0.1 to 1.0 OD. The extracted to nonextracted sample linear regression slope ratio was multiplied by 100 to calculate adulterant extraction efficiency in the presence and absence of SMP. Linear regression, LOD, LOQ, and extraction efficiency results are presented in Table 1. Recovery estimates were constrained to absorbance values nominally equal to the LOD (~200 μg of plant protein isolate). LODs were similar for

Table 1. Turbidimetric Assay Performance Metrics for Detection of Protein Isolates

protein isolate	slope (OD 360 nm/mg)	*Y*-intercept (OD)	R^2	LOD[a] (% wt)	LOD (μg)	LOQ (μg)	recovery (%) with SMP	recovery (%) without SMP
soy	0.7	0.0020	0.9829	0.2	190	575	50	65
rice	1.6	−0.0472	0.9728	0.1	115	350	100	96
wheat	0.6	0.0015	0.9296	0.2	191	580	25	47
pea	0.7	0.014	0.9525	0.2	204	618	90	46

[a]90 mg powder sample basis.

all isolates, ranging from 0.1 to 0.2% by weight (for 90 mg SMP load), and corresponded to 115−205 μg of spiked protein (independently of SMP load). This analytical sensitivity is comparable to or better than that offered by other reported ELISA, SDS−PAGE, and CE assays for detecting dairy product EMA with plant proteins and is achieved more rapidly using less equipment.[30−33,44] The extraction efficiencies of soy and rice proteins were not substantially affected by presence of SMP matrix in Table 1. However, wheat and pea protein extraction efficiencies were respectively decreased and increased by 50% in the presence of SMP. Soy extraction efficiency independence from SMP is consistent with HPLC−fluorescence data reported by Luykx, but, for unknown reasons, the dependency of pea extraction is not.[13] The 96-well plate assay format detected adulteration of 90 mg SMP samples spiked with ∼200 μg of plant protein isolate, a level (0.2% by weight) generally considered satisfactory for EMA detection. If adulterated samples are blended in complex supply chains, detection at even lower concentrations may be required.

A Larger Capacity Microcentrifuge Assay Format. Linear relationships between the protein spike concentration and absorbance in Figure 1 indicate that even lower amounts of adulterant, on a percentage of sample weight basis, could be detected by extracting larger amounts of sample. However, the maximum amount of SMP that could be precisely loaded in a single 96-well plate well was limited by three factors: solution viscosity, bubble formation, and well volume. The viscosity of nonspiked SMP solutions exceeding ∼600 mg/mL interfered with pipetting, and these samples formed bubbles. Aerosolization occurred when bubbles burst during pipetting of even lower concentration samples and gradually led to deposit accumulation inside the pipettor. The use of aerosol barrier pipet tips eliminated this problem. Because sensitivity is limited by the amount of SMP loaded in a well, a microcentrifuge tube assay format was briefly examined to increase the maximum sample load from 90 mg (300 μL of 300 mg of solids/mL) in the 96-plate format to 540 mg (1.8 mL × 300 mg of solids/mL). Photographs of pellets extracted using the 96-well plate and microcentrifuge tube assay formats are provided as Supplemental Figures S2 and S3 in the Supporting Information. Resuspended microcentrifuge pellet aliquots were transferred to 96-well plates to measure absorbance. The same linear dependence of absorbance on the amount of protein isolate spiked was observed in the microcentrifuge tube assay format without change in the SMP baseline signal. LODs in the microcentrifuge tube format ranged from 100 to 200 μg as was observed in the 96-well plate assay format in Figure 1. The microcentrifuge tube format is useful for detecting adulteration at low percent weight concentrations due to the more readily visible pellet obtained from larger samples. This enables spot tests to be performed if a microplate reader is not available. Although not explored here, larger samples could be used to achieve LODs at even lower % spike concentrations. Changes in extraction efficiency, baseline absorbance of SMP, and the optimal number of pellet washes need to be investigated to extend analyses to lower adulterant concentrations.

Effects Extraction Buffer Composition on Pellet Washing. The sequential extraction of storage proteins from plant sources by adjusting salt concentrations, pH, and organic solvent composition, known as Osborne fractionation, has been extensively studied, but mechanism(s) are not known through which EDTA-tetraborate buffer selectively precipitates plant proteins from dairy samples.[13,32,42] The formation of insoluble protein−boronate complexes via carbohydrate modified plant proteins and dissociation of casein micelles by EDTA may be involved.[45,46] On the basis of HPLC−fluorescence analysis of soy and pea protein isolate extracted from SMP, storage protein hydrophobicity may also be responsible.[13] Studies of protein extraction from soybean meal do not support isoelectric precipitation as being involved at pH 8.3.[47] To determine the optimal number of pellet washes and the effect of extraction buffer composition during assay development, SMP samples (n = 4) spiked with 0 and 2.5% soy protein isolate were extracted with water, EDTA (40 mM, pH 8.3), tetraborate (30 mM, pH 8.3), or EDTA (40 mM)/tetraborate (30 mM)/pH 8.3. The average resuspended pellet absorbance (n = 4) after each of five successive washes is presented in Supplemental Figure S4 in the Supporting Information. Water alone failed to yield differences between SMP and spiked sample absorbance after five washes. Tetraborate alone failed to yield significant ($p < 0.05$) differences between SMP and spiked test samples until the third wash. The absorbance of both samples continued to decrease in the fifth wash. EDTA alone and EDTA-tetraborate buffer were both very effective for extracting plant proteins and worked equally well. Large stable differences between SMP and spiked samples were apparent after the first wash. No changes occurred after the third wash, where absorbance of SMP-only samples decreased to 0.10 ± 0.00 OD (average ± SD). Three washes also produced optimal results in SMP samples spiked with pea protein isolate (data not shown). The insolubility of soy protein isolate at pH 8.3 in 30−40 mM salt solutions due to hydrophobicity, instead of boronate−plant protein complex insolubility, appears to more significantly contribute to the effectiveness of this extraction technique.[41] SMP solutions prepared in water exhibit a characteristic milky white appearance, but addition of EDTA under conditions of the assay produces transparent colorless solutions. Collapse of milk casein micelles due to EDTA chelation of Ca^{2+} minimizes light scattering, produces transparent SMP solutions, and enables the visual and turbidimetric detection of insoluble material that is otherwise obscured.[48] Detailed EDTA−SMP titration studies were not performed, but this process can be saturated by SMP to produce samples of varying turbidity in the absence of plant proteins, unless EDTA is maintained at some undetermined stoichiometric excess of Ca^{2+}. This is important if the amount of SMP loaded in the assay is increased.

Other Analytical Tools. To determine the composition of pellets detected in the turbidimetric assay and demonstrate a general work-flow for characterization of EMA with insoluble foreign proteins, additional SDS−PAGE, FT-IR, and LC−MS/MS analyses were performed. SDS−PAGE gel images of SMP and spiked (3% by weight) SMP test samples before and after extraction are presented in Figure 3. Nonextracted samples

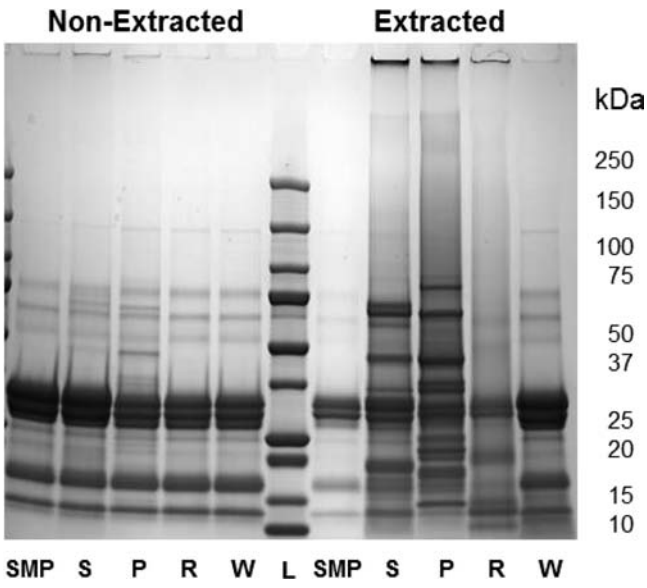

Figure 3. Reducing SDS−PAGE analysis of skim milk powder samples spiked with 3% plant protein isolate by weight before and after extraction with tetraborate-EDTA buffer. SMP = skim milk powder. Plant protein isolates: soy (S), pea (P), rice (R), wheat (W), molecular weight ladder (L).

(lanes 1−5) are dominated by intense bands (25−37 kDa) that correspond to milk proteins (α-S1, α-S2, and β-caseins) known to comprise ∼72% of normal milk protein. All nonextracted samples also exhibit bands (10−20 kDa) corresponding to β-lactoglobulin and α-lactalbumin that normally contribute a total of ∼15% to all milk protein. Nonextracted soy and pea spiked SMP samples (lanes 2 and 3) exhibit additional faint bands (50−75 kDa) that are also observed in extracted spiked samples (lanes 8 and 9) and the corresponding individual protein isolate standards analyzed without SMP (Supplemental Figure S5 in the Supporting Information). These bands are interpreted as being plant protein-specific proteins and are indicative of the protein isolate spike. This contrasts with nonextracted rice and wheat (lanes 4 and 5) where there are no clear differences from nonspiked SMP (lane 1). Comparison of nonextracted (lanes 1−5) and extracted (lanes 7−10) samples in Figure 3 shows that extraction produces distinct banding pattern changes and enables discrimination of spiked from nonspiked samples. The appearance of Figure 3 is consistent with previously reported SDS−PAGE data for soy and pea samples prepared using tetraborate-EDTA precipitation.[13]

Transmission FT-IR of Extracted SMP. Rapid screening of SMP using mid- and near-IR spectroscopy and chemometrics to detect EMA with low and high molecular weight compounds (e.g., melamine and soy protein isolate) is an active research area.[5,6] This is an appealing strategy because the NIR analysis of dry powder does not require samples to be dissolved or extracted. This lends itself to high sample throughput and automation. However, if seasonal or other manufacturing related factors (e.g., heat treatment, storage time) yield sufficiently large SMP matrix variability and compromise chemometric detection models, sample processing may be required to improve adulterant detection. Removal of milk components and concentration of plant proteins via tetraborate-EDTA extraction is expected to simplify IR spectra and facilitate the detection of insoluble foreign proteins but at the cost of lowering assay throughput. The FT-IR spectra of SMP, soy protein isolate, and extracted soy protein isolate are presented in Figure 4. Extracted protein isolate pellets exhibit

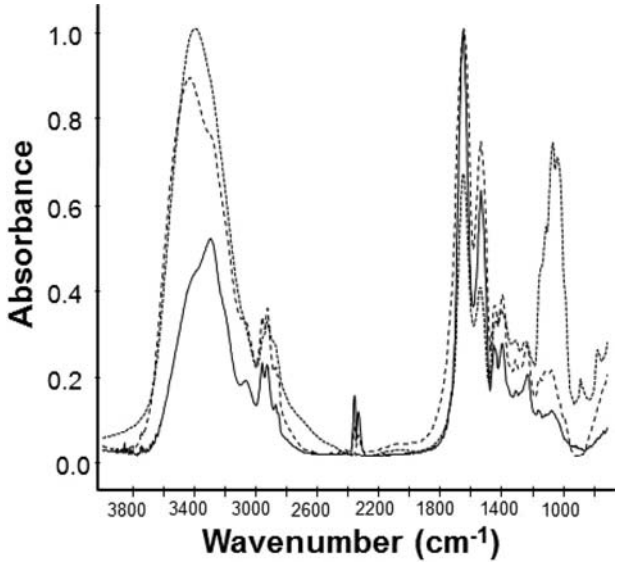

Figure 4. FT-IR KBr pellet transmission spectra of nonextracted skim milk powder and soy protein isolate reference samples, and a pellet extracted from skim milk powder spiked with soy protein isolate at 0.1% by weight. The atmospheric CO_2 stretching band (2360 cm^{-1}) appears as an artifact of the analyte to background single-beam normalization process. Nonextracted reference samples: skim milk powder (top dotted line), soy protein isolate (middle dashed line). Extracted pellet: skim milk powder spiked with soy protein isolate (bottom solid line).

strong amide I (1600−1700 cm^{-1}) and amide II (1500−1600 cm^{-1}) bands and the loss of the intense C−O stretching bands (1000−1200 cm^{-1}) that are uniquely characteristic of milk lactose and detected only in nonextracted SMP. The corresponding pea and rice data are provided as Supplemental Figures S6 and S7 in the Supporting Information. Subtle differences in protein bands between extracted soy, pea, and rice pellets were observed. These data principally indicate that extraction removes soluble lactose and milk proteins and yields pellets from spiked samples that exhibit IR spectra confirming the presence of insoluble proteins. The analysis of pellets using SDS−PAGE and LC−MS/MS, discussed below and in related work by Luykx et al., further indicates that these characteristic amide absorbance bands do not substantially arise from coprecipitated milk proteins.[13] The spectrum of nonextracted SMP in Figure 4 is similar to a published spectrum.[49]

LC−MS/MS Identification of Peptides and Detection of Proteins. To identify peptides and detect proteins in extracted pellets, trypsin digested samples were analyzed by nLC−MS/MS and protein database searching. Table 2 presents a list of proteins detected in the pellet obtained from SMP spiked with soy protein isolate. These soy storage proteins account for ∼70% of all seed protein.[27] Virtually identical lists

Table 2. Proteins Detected in Pellets Isolated from SMP Spiked with Soy Protein Isolate

Uniprot protein accession name	protein	MASCOT protein score	protein mass	protein sequence coverage (%)	no. of peptide sequences exceeding MASCOT identity score
GLYG2_SOYBN	glycinin G2	1112	54357	49.3	10
GLYG1_SOYBN	glycinin G1	973	55672	40.2	11
GLCA_SOYBN	β-conglycinin, α-chain	669	70250	40.8	9
GLYG4_SOYBN	glycinin G4	504	63548	29.7	7
GLCB_SOYBN	β-conglycinin, β-chain	463	50521	41.2	6
GLYG3_SOYBN	glycinin G3	454	54208	37	6
SBP_SOYBN	sucrose-binding protein	426	60485	31.5	7
GLYG5_SOYBN	glycinin G5	375	57921	21.5	5
LOX3_SOYBN	seed lipoxygenase-3	340	96698	16.9	4
GLCAP_SOYBN	β-conglycinin, α-chain	295	74280	20.2	4
LOX2_SOYBN	seed lipoxygenase-2	240	97085	11.4	5
ITRA_SOYBN	trypsin inhibitor A	198	23990	28.2	5
LOX1_SOYBN	seed lipoxygenase-1	159	94310	9.9	5
7SB1_SOYBN	basic 7S globulin	118	46363	15.7	2
2SS_SOYBN	2S albumin	95	18448	13.9	2

of soy proteins were previously reported in tetraborate-EDTA extracted pellets from different soy isolate samples, except that α-S1-casein and β-lactoglobulin were not detected in the present study.[13,34] This is presumably due to more extensive washing of the pellet in the 96-well plate assay format presented here. The corresponding protein detection data for pea and rice isolate-spiked SMP samples are presented in Supplemental Tables SI and SII in the Supporting Information. A corresponding abundance of pea and rice storage proteins were detected in these pellets, and the pea list matched those reported in earlier studies.[13,34] The detection of extracted soy, pea, and rice storage proteins amid little to no milk protein confirms the selectivity of tetraborate-EDTA buffer reported in this and previous studies. MASCOT search results for extracted soy, pea, and rice spiked SMP pellets are provided as Supplemental Data Files in the Supporting Information. Analysis of pellets from SMP spiked with wheat protein isolate failed to identify wheat peptides. The addition of glutamine and asparagine deamidation as variable modifications to protein database searches did not improve search results. Wheat storage proteins are generally less soluble in low salt aqueous conditions than soy, pea, and rice and contain many fewer trypsin cleavage sites. The use of more effective organic solvent (alcohol) and endoproteases (e.g., chymotrypsin) that yield a larger number of wheat peptide sequences for MS detection may be required to address this problem in future studies.

Turbidimetric detection of plant proteins extracted from SMP samples offers an inexpensive, fast, and simple procedure to detect a class of foreign proteins suspected of being used in EMA schemes. This is a semitargeted screening approach in that it is not plant-specific and relies on an intrinsic property of SMP, namely, the failure to form a precipitate under assay conditions. It does not require chemometric treatment of data, special equipment, or expertise. It exploits the use of EDTA to render adulterated opaque milk solutions transparent and the insolubility of plant protein isolates to rapidly produce samples for measurement by optical absorbance. The assay is scalable in that different amounts of SMP can be used to achieve different LODs on a percent weight basis. Other plant protein (e.g., zein, lupin, sorghum, millet) sources are expected to yield comparable turbidimetric results due to chemical similarities among storage proteins. Although SMP was studied, other imported high dairy protein concentration products such as milk protein concentrate, whey protein concentrate, and caseinates along with high value finished products such as quark, skyr, and greek yogurt are of special interest. Even without the use of a 96-well plate reader, the addition of as little as 0.1−0.2% by weight of plant protein isolate to SMP was visually detected. These features potentially make the assay useful for performing spot tests in resource poor environments. Very small, portable and inexpensive centrifuges that accommodate 2 mL sample tubes can be purchased for less than $300 (US). Hand-held spectrophotometers suitable for field deployment can be purchased for less than ~$2000 (US). Although data reported here were acquired in a laboratory, the simplicity of the assay should make it possible to obtain comparable results using these less expensive tools in field applications. Given the ubiquitous presence of smart phones, their adaptation to enable even lower cost absorbance measurements in the field is expected.[50] It has been pointed out that it is not possible to "test your way to absolute food safety."[3] However the selective application of this simple assay to the riskiest high protein dairy products may act as a deterrent and mitigate EMA risk imposed by insoluble and potentially allergenic proteins.

■ ASSOCIATED CONTENT

Supporting Information

The 96-well plate sample template, photographs of pellets extracted using the 96-well plate and microcentrifuge tube turbidimetric assay formats, a figure presenting the effect of extraction buffer composition and wash number on turbidimetric response, two tables listing peptides identified in pellets extracted from SMP spiked with pea and rice protein isolates, and MASCOT .dat files (converted to .csv format). This material is available free of charge via the Internet at http://pubs.acs.org.

AUTHOR INFORMATION

Corresponding Author

*Phone: (240) 402-2167. Fax: (301) 436-2624. E-mail: peter.scholl@fda.hhs.gov.

Notes

The authors declare no competing financial interest.

ACKNOWLEDGMENTS

The authors are grateful to Jeffery Moore at the USP for providing materials from the USP library of standards and helpful discussions. Further thanks are extended to Jonathan DeVries of the Medallion Laboratories at General Mills and John Sheehan of the US FDA for many helpful discussions.

ABBREVIATIONS USED

CE, capillary electrophoresis; CID, collision-induced dissociation; DTT, dithiothreitol; EDTA, ethylenediaminetetraacetic acid; ELISA, enzyme-linked immunosorbent assay; EMA, economically motivated adulteration; FALCPA, Food Allergen Labeling and Consumer Protection Act; FT-IR, Fourier transform infrared; IAA, iodoacetamide; LC, liquid chromatography; LOD, limit of detection; LOQ, limit of quantitation; NIR, near-infrared; NFDM, nonfat dry milk powder; PI, plant protein isolate; PPI, pea protein isolate; RPI, rice protein isolate; SDS−PAGE, sodium dodecyl sulfate−polyacrylamide gel electrophoresis; SMP, skim milk powder; SPI, soy protein isolate; SPR, surface plasmon resonance; USP, United States Pharmacopia; WPI, wheat protein isolate

REFERENCES

(1) Xin, H.; Stone, R. Tainted milk scandal. Chinese probe unmasks high-tech adulteration with melamine. *Science* **2008**, *322*, 1310−1311.

(2) Everstine, K.; Spink, J.; Kennedy, S. Economically Motivated Adulteration (EMA) of Food: Common Characteristics of EMA Incidents. *J. Food Protect.* **2013**, *76*, 723−735.

(3) Kennedy, S. Epidemiology. Why Can't We Test Our Way to Absolute Food Safety? *Science* **2008**, *322*, 1641−1643.

(4) Moore, J.; DeVries, J.; Lipp, M.; Griffiths, J.; Abernethy, D. Total Protein Methods and Their Potential Utility to Reduce the Risk of Food Protein Adulteration. *Compr. Rev. Food Sci. Food Saf.* **2010**, *9*, 330−357.

(5) Moore, J.; Ganguly, A.; Smeller, J.; Botros, L.; Mossoba, M.; Bergana, M. Standardisation of non-targeted screening tools to detect adulterations in skim milk powder using NIR spectroscopy and chemometrics. *NIR news* **2012**, *23*, 9−11.

(6) Botros, L. L.; Jablonski, J.; Chang, C.; Bergana, M. M.; Wehling, P.; Harnly, J. M.; Downey, G.; Harrington, P.; Potts, A. R.; Moore, J. C. Exploring authentic skim and nonfat dry milk powder variance for the development of nontargeted adulterant detection methods using near-infrared spectroscopy and chemometrics. *J. Agric. Food. Chem.* **2013**, *61*, 9810−9818.

(7) Ellis, D. I.; Brewster, V. L.; Dunn, W. B.; Allwood, J. W.; Golovanov, A. P.; Goodacre, R. Fingerprinting food: current technologies for the detection of food adulteration and contamination. *Chem. Soc. Rev.* **2012**, *41*, 5706−5727.

(8) Moore, J.; Spink, J.; Lipp, M. Development and Application of a Database of Food Ingredient Fraud and Economically Motivated Adulteration from 1980 to 2010. *J. Food Sci.* **2012**, *77*, R108−R116.

(9) Maraboli, A.; Cattaneo, T. M. P.; Giangiacomo, R. Detection of vegetable proteins from soy, pea and wheat isolates in milk powder by near infrared spectroscopy. *J. Near Infrared Spectrosc.* **2002**, *10*, 63−69.

(10) Manso, M. A.; Cattaneo, T. M.; Barzaghi, S.; Olieman, C.; Lopez-Fandino, R. Determination of vegetal proteins in milk powder by sodium dodecyl sulfate-capillary gel electrophoresis: Interlaboratory study. *J. AOAC Int.* **2002**, *85*, 1090−1095.

(11) Sanchez, L.; Perez, M. D.; Puyol, P.; Calvo, M.; Brett, G. Determination of vegetal proteins in milk powder by enzyme-linked immunosorbent assay: Interlaboratory study. *J. AOAC Int.* **2002**, *85*, 1390−1397.

(12) Haasnoot, W.; Marchesini, G. R.; Koopal, K. Spreeta-based biosensor immunoassays to detect fraudulent adulteration in milk and milk powder. *J. AOAC Int.* **2006**, *89*, 849−855.

(13) Luykx, D. M. A. M.; Cordewener, J. H. G.; Ferranti, P.; Frankhuizen, R.; Bremer, M. G. E. G.; Hooijerink, H.; America, A. H. P. Identification of plant proteins in adulterated skimmed milk powder by high-performance liquid chromatography-mass spectrometry. *J. Chromatogr., A* **2007**, *1164*, 189−197.

(14) Xu, Q.; Wei, H. P.; Du, S.; Li, H. B.; Ji, Z. P.; Hu, X. Y. Detection of Subnanomolar Melamine Based on Electrochemical Accumulation Coupled with Enzyme Colorimetric Assay. *J. Agric. Food Chem.* **2013**, *61*, 1810−1817.

(15) Gao, F.; Ye, Q. Q.; Cui, P.; Zhang, L. Efficient Fluorescence Energy Transfer System between CdTe-Doped Silica Nanoparticles and Gold Nanoparticles for Turn-On Fluorescence Detection of Melamine. *J. Agric. Food Chem.* **2012**, *60*, 4550−4558.

(16) Turnipseed, S.; Casey, C.; Nochetto, C.; Heller, D. N. Determination of melamine and cyanuric acid residues in infant formula using LC-MS/MS. *US FDA Laboratory Information Bulletin*; Laboratory Information Bulletin, LIB No. 4421; 2008; Vol. *24*.

(17) Abernethy, G.; Higgs, K. Rapid detection of economic adulterants in fresh milk by liquid chromatography−tandem mass spectrometry. *J. Chromatogr., A* **2013**, *1288*, 10−20.

(18) MacMahon, S.; Begley, T. H.; Diachenko, G. W.; Stromgren, S. A. A liquid chromatography-tandem mass spectrometry method for the detection of economically motivated adulteration in protein-containing foods. *J. Chromatogr., A* **2012**, *1220*, 101−107.

(19) ISOIDF, Technical specification 15495: Milk, milk products and infant formulae--Guidelines for the Quantitative determination of melamine and cyanuric acid by LC-MS/MS. In ISO: 2010.

(20) *Soybeans: Chemistry, Production, Processing, and Utilization*; AOCS Press: Urbana, IL, USA, 2008.

(21) Morr, C. V. Technical Problems and Opportunities in Using Vegetable Proteins in Dairy-Products. *J. Am. Oil Chem. Soc.* **1979**, *56*, 383−385.

(22) Kolar, C. W.; Cho, I. C.; Watrous, W. L. Vegetable Protein Application in Yogurt, Coffee Creamers and Whip Toppings. *J. Am. Oil Chem. Soc.* **1979**, *56*, 389−391.

(23) Sanchez-Monge, R.; Lopez-Torrejon, G.; Pascual, C. Y.; Varela, J.; Martin-Esteban, M.; Salcedo, G. Vicilin and convicilin are potential major allergens from pea. *Clin. Exp. Allergy* **2004**, *34*, 1747−1753.

(24) Satoh, R.; Nakamura, R.; Komatsu, A.; Oshima, M.; Teshima, R. Proteomic analysis of known and candidate rice allergens between non-transgenic and transgenic plants. *Regul. Toxicol. Pharmacol.* **2011**, *59*, 437−444.

(25) Goggin, D. E.; Mir, G.; Smith, W. B.; Stuckey, M.; Smith, P. M. Proteomic analysis of lupin seed proteins to identify conglutin β as an allergen, Lup an 1. *J. Agric. Food Chem.* **2008**, *56*, 6370−6377.

(26) Schoonderwoerd, M.; Misra, V. Detection and Quantitation of Pea and Soy-Derived Proteins in Calf Milk Replacers. *J. Dairy Sci.* **1989**, *72*, 157−161.

(27) Saz, J. M.; Marina, M. L. High performance liquid chromatography and capillary electrophoresis in the analysis of soybean proteins and peptides in foodstuffs. *J. Sep. Sci.* **2007**, *30*, 431−451.

(28) Reid, L. M.; O'Donnell, C. P.; Downey, G. Recent technological advances for the determination of food authenticity. *Trends Food Sci. Technol.* **2006**, *17*, 344−353.

(29) De la Fuente, M. A.; Juarez, M. Authenticity assessment of dairy products. *Crit. Rev. Food Sci. Nutr.* **2005**, *45*, 563−585.

(30) Hewedy, M. M.; Smith, C. J. Detection of soy milk in pasteurized bovine milk. *Food Hydrocolloids* **1989**, *3*, 399−405.

(31) Hewedy, M.; Smith, C. Modified immunoassay for the detection of soy milk in pasteurized skimmed bovine milk. *Food Hydrocolloids* **1990**, *3*, 485−490.

(32) Cattaneo, T. M. P.; Feroldi, A.; Toppino, P. M.; Olieman, C. Sample Preparation for Selective and Sensitive Detection of Soya Proteins in Dairy-Products with Chromatographic and Electrophoretic Techniques. *Neth. Milk Dairy J.* **1994**, *48*, 225−234.
(33) Lopez-Tapia, J.; Garcia-Risco, M. R.; Manso, M. A.; Lopez-Fandino, R. Detection of the presence of soya protein in milk powder by sodium dodecyl sulfate capillary electrophoresis. *J. Chromatogr., A* **1999**, *836*, 153−160.
(34) Cordewener, J. H. G.; Luykx, D. M. A. M.; Frankhuizen, R.; Bremer, M. G. E. G.; Hooijerink, H.; America, A. H. P. Untargeted LC-Q-TOF mass spectrometry method for the detection of adulterations in skimmed-milk powder. *J. Sep. Sci.* **2009**, *32*, 1216−1223.
(35) Krusa, M.; Torre, M.; Marina, M. L. A reversed-phase high-performance liquid chromatographic method for the determination of soya bean proteins in bovine milks. *Anal. Chem.* **2000**, *72*, 1814−1818.
(36) Haasnoot, W.; Olieman, K.; Cazemier, G.; Verheijen, R. Direct biosensor immunoassays for the detection of nonmilk proteins in milk powder. *J. Agric. Food Chem.* **2001**, *49*, 5201−5206.
(37) García, M.; Marina, D. M. Rapid detection of the addition of soybean proteins to cheese and other dairy products by reversed-phase perfusion chromatography. *Food Addit. Contam.* **2006**, *23*, 339−347.
(38) Haasnoot, W.; du Pre, J. G. Luminex-based triplex immunoassay for the simultaneous detection of soy, pea, and soluble wheat proteins in milk powder. *J. Agric. Food Chem.* **2007**, *55*, 3771−3777.
(39) Chambers, M. C.; Maclean, B.; Burke, R.; Amodei, D.; Ruderman, D. L.; Neumann, S.; Gatto, L.; Fischer, B.; Pratt, B.; Egertson, J.; Hoff, K.; Kessner, D.; Tasman, N.; Shulman, N.; Frewen, B.; Baker, T. A.; Brusniak, M. Y.; Paulse, C.; Creasy, D.; Flashner, L.; Kani, K.; Moulding, C.; Seymour, S. L.; Nuwaysir, L. M.; Lefebvre, B.; Kuhlmann, F.; Roark, J.; Rainer, P.; Detlev, S.; Hemenway, T.; Huhmer, A.; Langridge, J.; Connolly, B.; Chadick, T.; Holly, K.; Eckels, J.; Deutsch, E. W.; Moritz, R. L.; Katz, J. E.; Agus, D. B.; MacCoss, M.; Tabb, D. L.; Mallick, P. A cross-platform toolkit for mass spectrometry and proteomics. *Nat. Biotechnol.* **2012**, *30*, 918−920.
(40) Utsumi, S.; Kinsella, J. E. Structure-Function-Relationships in Food Proteins - Subunit Interactions in Heat-Induced Gelation of 7s, 11s, and Soy Isolate Proteins. *J. Agric. Food Chem.* **1985**, *33*, 297−303.
(41) Hayakawa, S.; Nakai, S. Relationships of Hydrophobicity and Net Charge to the Solubility of Milk and Soy Proteins. *J. Food Sci.* **1985**, *50*, 486−491.
(42) Mills, E. N. C.; Jenkins, J. A.; Bannon, G. A. Plant Seed Globulin Allergens. In *Plant Food Allergens*; Mills, E. N. C., Ed.; Blackwell Publishing: Bodmin, Cornwall, U.K., 2004; pp 141−157.
(43) Kolthoff, I. M.; Sandell, E. B. *Textbook of Quantitative Inorganic Analysis*; Macmillan Co.: New York, NY, USA, 1967.
(44) Sanchez, L.; Perez, M. D.; Puyol, P.; Calvo, M.; Brett, G. Determination of vegetal proteins in milk powder by enzyme-linked immunosorbent assay: interlaboratory study. *J. AOAC Int.* **2002**, *85*, 1390−1397.
(45) Sengupta, C.; Deluca, V.; Bailey, D. S.; Verma, D. P. S. Post-translational processing of 7S and 11S components of soybean storage proteins. *Plant Mol. Biol.* **1981**, *1*, 19−34.
(46) Vaia, B.; Smiddy, M. A.; Kelly, A. L.; Huppertz, T. Solvent-mediated disruption of bovine casein micelles at alkaline pH. *J. Agric. Food Chem.* **2006**, *54*, 8288−8293.
(47) Wolf, W. J. Soybean Proteins - Their Functional, Chemical, and Physical Properties. *J. Agric. Food Chem.* **1970**, *18*, 969−976.
(48) Griffin, M. C. A.; Lyster, R. L. J.; Price, J. C. The Disaggregation of Calcium-Depleted Casein Micelles. *Eur. J. Biochem.* **1988**, *174*, 339−343.
(49) Kher, A.; Udabage, P.; McKinnon, I.; McNaughton, D.; Augustin, M. A. FTIR investigation of spray-dried milk protein concentrate powders. *Vib. Spectrosc.* **2007**, *44*, 375−381.
(50) Choodum, A.; Kanatharana, P.; Wongniramaikul, W.; Daeid, N. N. Using the iPhone as a device for a rapid quantitative analysis of trinitrotoluene in soil. *Talanta* **2013**, *115*, 143−149.

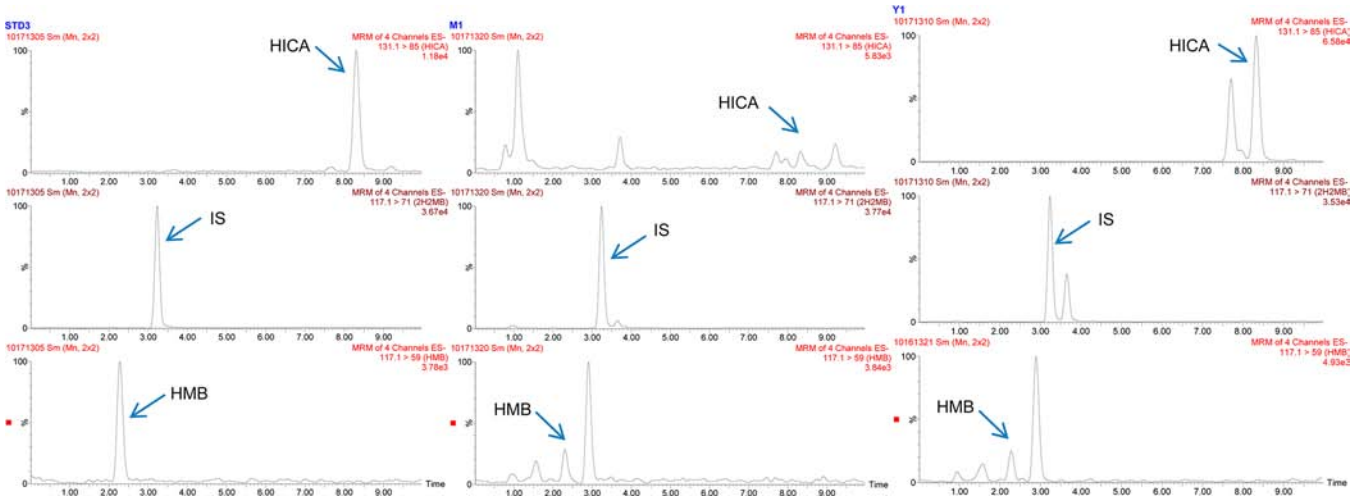

Figure 2. Multiple reaction monitoring (MRM) chromatograms of HMB, IS, and HICA in neat standard (left), whole milk (center), and yogurt (right).

Besides some early reports of qualitative identification of HICA in certain fermented foods (reviewed by Mero et al.[26]), analytical methods for HICA in various biological fluids, e.g., plasma and serum,[36−38] urine,[39,40] amniotic fluid,[41] and in cell culture[42] have been reported in the literature. These analyses were based on GC/MS after derivatization,[36−40] ammonia chemical ionization GC/MS without derivatization,[41] or preparative column chromatography with ultraviolet detection.[42] Some of these methods[36−38] have employed an in-house synthesized stable isotope labeled internal standard. Stable isotope labeled internal standards for HMB and HICA are not available commercially.

The presence of naturally occurring levels of HMB and HICA in milk and fermented dairy products has not been reported to date. Because milk and fermented dairy products are widely consumed, they are potentially suitable media for fortification with HMB and/or HICA in order to deliver the above-described physiological benefits.

This paper describes the development and comprehensive validation of a quantitative and confirmatory method based on liquid chromatography−mass spectrometry for both HMB and HICA in bovine whole milk and fermented dairy products such as yogurt. The method's applicability was demonstrated by analyzing a set of commercial bovine whole milk and yogurt samples for HMB and HICA.

MATERIALS AND METHODS

Safety. Solvents (methanol, acetonitrile) and acids (formic, hydrochloric) should be dispensed in a hood, and appropriate laboratory safety glasses, coat, and gloves should be worn.

Chemicals and Reagents. β-Hydroxy-β-methylbutyric acid (aka β-hydroxyisovaleric acid) (≥95%), α-hydroxyisocaproic acid (aka 2-hydroxyisocaproic acid) (99%), α-hydroxy-α-methylbutyric acid (aka 2-hydroxy-2-methylbutyric acid) (98%), and formic acid (≥96%) were purchased from Sigma-Aldrich Corp. (St. Louis, MO). The purity of β-hydroxy-β-methylbutyric acid was determined by the method of Baxter et al.[35] and was found to be 93.2%. Methanol (LC/MS grade) and hydrochloric acid (34−37% HCl) were purchased from Fisher Scientific (Fair Lawn, NJ). Acetonitrile (LC/MS grade) was from Honeywell Burdick & Jackson (Muskegon, MI).

Stock Solutions and Calibration Standards. Individual stock solutions of β-hydroxy-β-methylbutyric acid (HMB), α-hydroxyisocaproic acid (HICA), and α-hydroxy-α-methylbutyric acid (internal standard, IS) were prepared at concentrations of 2000, 400, and 400 mg/L, respectively, in 0.1 M HCl in 90/10 (v/v) water−acetonitrile. Stock solutions were prepared fresh every two weeks and were determined to be stable when stored at +5 °C during this time period. A mixed intermediate stock solution containing 1 mg/L of HMB and 0.25 mg/L of HICA was prepared in 0.1 M HCl in 90/10 (v/v) water−acetonitrile. A 4 mg/L intermediate stock solution of IS was also prepared in 0.1 M HCl in 90/10 (v/v) water−acetonitrile. Mixed calibration standards containing, respectively, 1, 2, 5, 10, 50, and 100 μg/L of HMB, 0.25, 0.5, 1.25, 2.5, 12.5, and 25 μg/L of HICA, and 10 μg/L each of IS were prepared in 0.1 M HCl in 90/10 (v/v) water−acetonitrile.

Samples. Bovine whole milk (3.3% fat) and plain, low-fat (1−2% fat) yogurt was purchased from supermarkets in the Columbus, OH, metropolitan area.

Sample Preparation. Yogurt was mixed well with a spatula prior to sampling. One-half milliliter (0.5 mL) of whole milk (undiluted) or yogurt (undiluted or 50-fold diluted with water) or water (for method blanks) was pipetted into a 2 mL Eppendorf centrifuge tube. Appropriate aliquots of spiking solution were added (for QC accuracy determination), followed by 25 μL of the 4 mg/L solution of internal standard. After brief vortexing, 1 mL of 0.15 M HCl in acetonitrile was added. The tube was capped, shaken for 30 s, and centrifuged at 3000 rpm for 5 min at ambient temperature. A 150 μL portion of the supernatant was transferred to a clean 2 mL Eppendorf centrifuge tube, followed by addition of 850 μL of 0.1 M HCl in water. The tube was vortexed briefly, and its content was filtered through a 0.2 μm pore size PTFE syringe filter into a 2 mL autosampler vial.

For confirmatory analysis on a hydrophilic interaction chromatography (HILIC) column, 900 μL of acetonitrile were added to a 2 mL Eppendorf centrifuge tube, followed by 100 μL of whole milk or 50-fold yogurt dilution. The tube was capped and shaken briefly, and its content was filtered through a 0.2 μm pore size PTFE syringe filter into a 2 mL autosampler vial.

Instrumentation. Analysis was performed on a Waters ACQUITY Ultra Performance LC coupled to a Xevo-TQS triple quadrupole mass spectrometer. Chromatographic separation was carried out on a Waters ACQUITY UPLC BEH C18 column (1.7 μm, 2.1 mm × 100 mm) maintained at 40 °C, according to the following gradient program: 0−2 min 90% A, switch to 85% A and maintain between 2−10 min, switch to 0% A and maintain between 10−12.5 min, and finally switch to 90% A and maintain between 12.5−16 min (A = 0.1% formic acid in water, B = 0.1% formic acid in methanol). Flow rate was 0.3 mL/min. Injection volume was 10 μL.

The mass spectrometer was operated in the negative electrospray (ESI−) mode with both quadrupoles tuned for unit resolution. Selected operating parameters were: capillary voltage 3.5 kV, desolvation temperature 350 °C, desolvation gas (N_2) 800 L/h,

dx.doi.org/10.1021/jf500026s | J. Agric. Food Chem. 2014, 62, 1506−1511

Table 1. Mean Accuracy and Precision (Within-Day, Between-Day, and Total) of Analysis of HMB and HICA in Whole Milk Across Three Validation Runs

					precision (%)		
analyte	QC level	conc (μg/L)	acceptance rate[a]	accuracy (%)	within-day	between-day	total
HMB	QC1	26[b]			13.9	12.8	18.9
	QC2	50	18/18	97	8.8	0.0	8.6
	QC3	200	18/18	107	6.4	1.4	6.6
	QC4	1500	18/18	105	3.7	4.7	6.0
HICA	QC1	5	18/18	100	5.5	3.6	6.5
	QC2	15	18/18	96	5.3	4.7	7.1
	QC3	50	18/18	111	4.0	4.8	6.2
	QC4	400	17/18	111	3.2	4.1	5.2

[a]Number of QCs which were between 80 and 120% of expected values. [b]Incurred concentration.

Table 2. Summary of Method Ruggedness Parameters Across Three Validation Runs

analyte	validation run no.	R^2	highest residual (%)	slope	RT[a] reproducibility RSD (%) (n = 24)	IS[b] peak area reproducibility RSD (%) (n = 24)
HMB	1	0.999	12.2	0.238	0.35	6.9
	2	0.999	12.9	0.240	0.27	3.2
	3	0.998	20.0	0.239	0.40	3.2
HICA	1	0.999	12.4	4.37	0.00	6.9
	2	0.998	9.7	4.41	0.05	3.2
	3	0.999	12.4	4.35	0.05	3.2

[a]Retention time. [b]Internal standard.

cone gas (N_2) 250 L/h, collision gas (Ar) (0.15 mL/min). One multiple reaction monitoring (MRM) transition was recorded for each compound as follows: HMB 117.1 > 59.0, IS 117.1 > 71.0, and HICA 131.1 > 85.0. Cone voltage and collision energy were 20 V and 10 eV, respectively, for all transitions. Dwell times were 0.2 s for HMB and IS and 0.4 s for HICA. The solvent flow was diverted to waste between 10 and 16 min of each run.

For confirmatory analysis, a Waters ACQUITY UPLC HILIC column (1.7 μm, 2.1 mm × 150 mm) was used. Mobile phase was 10 mM ammonium acetate in 85.5/14.5 acetonitrile–water (isocratic) at 0.3 mL/min and 40 °C. Mass spectrometer conditions were as described above (the flow diversion valve was not used).

RESULTS AND DISCUSSION

Method Development. Sample preparation consisted of a two-step dilute-and-shoot approach, i.e., protein precipitation with acetonitrile, followed by further dilution to achieve compatibility with the starting mobile phase composition. Hydrochloric acid was used in both steps at a concentration of 0.1 M in order to ensure complete dissociation of the calcium salt of HMB which could be potentially present, as described previously.[35] The injection solvent for both sample extracts and calibration standards was 0.1 M HCl in 90/10 (v/v) water–acetonitrile.

The internal standard α-hydroxy-α-methylbutyric acid was selected based on structural similarity with HMB and HICA. Whole milk and yogurt samples were first screened for the presence of a peak at the expected retention time of the internal standard. A small peak was indeed present; however, its intensity was <5% of the intensity of the internal standard peak at the concentration used (200 μg/L) and hence it did not adversely affect quantitation.

Chromatography was carried out on a sub-2 μ reverse phase column with a water–methanol (0.1% formic acid) mobile phase system. It was found that isocratic programming was necessary to resolve both HMB and HICA from closely eluting matrix peaks. HMB was eluted at ca. 2.3 min with 10% methanol in the mobile phase, at which point the percentage of methanol was increased to 15% to speed up elution of HICA at ca. 8.3 min. Finally, the column was flushed with 100% methanol and re-equilibrated to the starting conditions. The internal standard was eluted at ca. 3.2 min. A matrix peak was

Table 3. Results of Survey of Concentrations of HMB and HICA in Commercial Samples of Whole Milk

sample no.	HMB (μg/L)	HICA (μg/L)
1	26	<5
2	21	<5
3	<20	<5
4	28	<5
5	25	<5
6	22	<5
7	24	<5
8	<20	<5
9	25	<5
10	23	<5
11	22	<5
12	25	<5
13	22	<5
14	29	<5

Table 4. Results of Survey of Concentrations of HMB and HICA in Commercial Samples of Yogurt

sample no.	HMB (μg/L)	HICA (mg/L)
1	37	6.7
2	37	15.2
3	33	9.5
4	32	3.0

dx.doi.org/10.1021/jf500026s | J. Agric. Food Chem. 2014, 62, 1506–1511

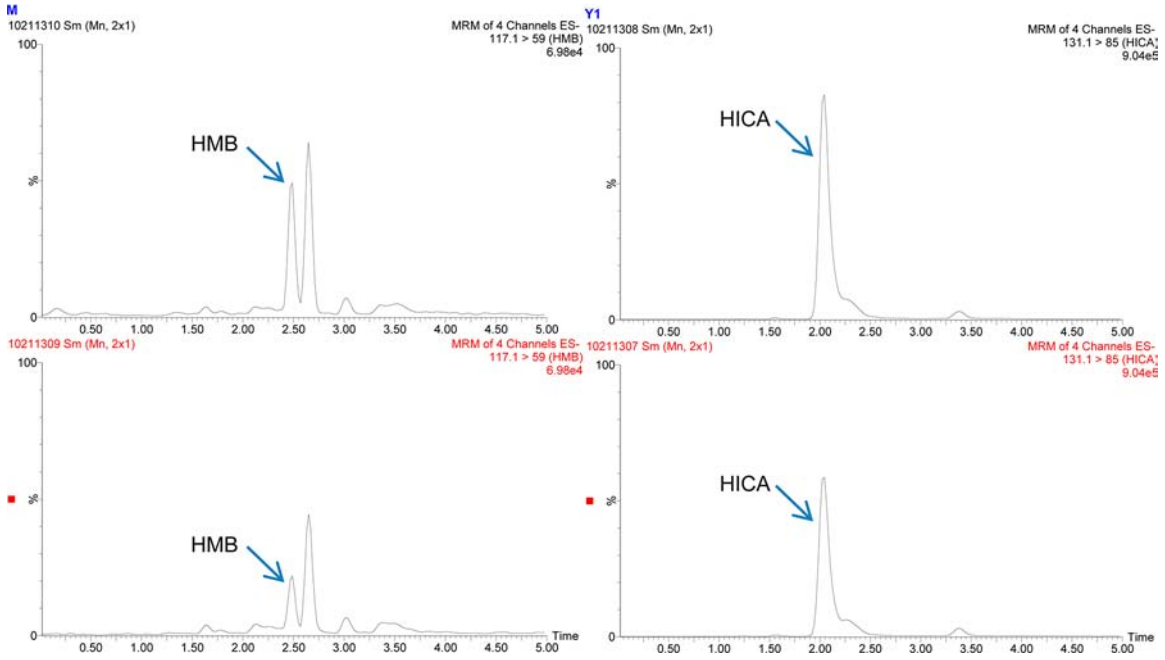

Figure 3. Confirmation of HMB in whole milk and HICA in yogurt (50-fold dilution) on a hydrophilic interaction (HILIC) column (bottom, sample extracts; top, sample extracts spiked with 20 μg/L HMB and 100 μg/L HICA, respectively).

present in the immediate vicinity of the internal standard peak in yogurt samples; however, the two peaks were fully resolved (Figure 2).

Both HMB and HICA are low molecular weight carboxylic acids (118 and 132 Da, respectively), which are amenable for detection in the negative electrospray ion mode. Because of limited fragmentation pathways associated with such low molecular weights, only one multiple reaction monitoring (MRM) transition could be monitored for each compound. Given the limited specificity of MRM transitions used and the expected presence of numerous amino acid metabolites with structures similar to HMB and HICA in milk, the presence of matrix peaks in the chromatograms is not surprising.

Method Validation. Three validation runs consisting of six replicates each at four QC spiking levels were conducted on three separate days. Calibration standards were analyzed at the beginning and at the end of each run. A linear regression model (1/x-weighted) was used for both HMB and HICA. Coefficients of determination (R^2) were ≥0.99. Residuals were ≤20% at the lowest calibration level and ≤15% at all other levels. Up to 25% of all calibration points could be rejected as needed while ensuring that at least one is maintained at each level.

A blank whole milk matrix in which both HMB and HICA were absent could not be found. Most samples of whole milk which were screened contained HMB at quantifiable levels. A small nonquantifiable peak at the retention time of HICA was also present (Figure 2).

The QC1 level for HMB was the incurred concentration (no spike) and for HICA the limit of quantitation (5 μg/L). The QC2, QC3, and QC4 spiking levels are listed in Table 1. All QC data points were within 80−120% of expected values (sum of incurred and spiked concentrations), with one single exception for HICA at the QC4 level. The latter data point was rejected. Mean accuracy, within-day precision, between-day precision, and total precision were calculated as described in ref 43 and are summarized in Table 1. Mean accuracy was 90−110% for HMB and 85−115% for HICA at all QC levels. Total precision for both HMB and HICA was <10% RSD at all QC levels with the exception of HMB at the QC1 level (<20% RSD). The consistent performance of the method over three validation runs established its ruggedness. Method ruggedness parameters are summarized in Table 2.

Limits of quantitation (LOQ) for HMB and HICA in whole milk were 20 and 5 μg/L, respectively. These concentrations corresponded to the lowest calibration levels used for each compound after accounting for the 20-fold dilution incurred during sample preparation.

Process stability was determined by reanalyzing an entire validation run after maintaining the samples on the autosampler tray for 48 h at ambient temperature. The run met accuracy and precision criteria outlined above.

Survey of HMB and HICA in Commercial Bovine Whole Milk and Yogurt. Fourteen samples of bovine whole milk and four samples of commercial plain yogurt were analyzed for their HMB and HICA content by the above-described validated method. Results of this survey (averages of duplicate analyses) are summarized in Tables 3 and 4.

All samples of whole milk contained a trace of HMB ranging from <LOQ (20 μg/L) to 29 μg/L. HICA was not present other than a small nonquantifiable peak and is being reported as <LOQ (5 μg/L) in all samples. A serendipitous finding was the progressive formation of HICA in certain samples of whole milk which were stored in the refrigerator (+5 °C) past their expiration dates. This is not entirely surprising because HICA has been reported previously in fermented foods (reviewed by Mero et al.[26]).

The above finding prompted further investigation of the potential presence of HICA in fermented dairy products such as yogurt. Samples of yogurt which were subjected to analysis contained significant concentrations of HICA between 3.0 and 15.2 mg/L. A 50-fold dilution of yogurt with water prior to analysis was necessary in order to bring concentrations of HICA within the method's quantitative range. Samples of

dx.doi.org/10.1021/jf500026s | J. Agric. Food Chem. 2014, 62, 1506−1511

yogurt were also analyzed for HMB (without dilution). Concentrations of HMB in yogurt were between 32 and 37 μg/L, slightly higher than in whole milk.

Confirmatory Analysis of HMB and HICA by Orthogonal Chromatography. Given that only one multiple reaction monitoring (MRM) transition was available for both HMB and HICA and the limited specificity of these transitions (as evidenced from the presence of matrix peaks in the chromatograms), further confirmation of the positive findings for HMB in whole milk and HICA in yogurt was undertaken. Hydrophilic interaction chromatography (HILIC) which is orthogonal to reversed phase chromatography was employed for this purpose. Both HMB in whole milk and HICA in yogurt have been confirmed by their respective retention times at 2.5 and 2.0 min, respectively (Figure 3). Because the internal standard α-hydroxy-α-methylbutyric acid did not show acceptable retention behavior on the HILIC column, and superior peak shape and retention were achieved for both HMB and HICA on the reversed phase column, the latter was retained for method validation and routine analysis.

In conclusion, a rugged, quantitative, and confirmatory method based on liquid chromatography−mass spectrometry was developed and comprehensively validated for the analysis of HMB and HICA in bovine whole milk and yogurt. The method was successfully applied to survey the concentrations of HMB and HICA in commercial samples of bovine whole milk and yogurt. To our knowledge, this is the first report in the scientific literature of naturally occurring (endogenous) concentrations of HMB in bovine whole milk and yogurt and of HICA in yogurt and also the first report of a quantitative and confirmatory analytical method for HICA in foods. On the basis of existing clinical studies and largely musculoskeletal outcome measures, the endogenous concentrations of HMB and HICA found by this study are insufficient by large margins to deliver any physiological benefits. Hence the opportunity arises for the fortification of milk, milk-based nutritional products, and fermented dairy products with HMB and/or HICA.

AUTHOR INFORMATION

Corresponding Author

*Phone: +1 614 6246309. Fax: +1 614 7276309. E-mail: stefan.ehling@abbott.com.

Author Contributions

†S.E. and T.M.R. contributed equally to this work.

Notes

The authors declare no competing financial interest.

ACKNOWLEDGMENTS

We thank Daniel Schmitz, Director of Analytical Research and Services, Abbott Nutrition, for his guidance and support, and Dr. Jeffrey Baxter, Dr. Sean Garvey, and Paul Johns for helpful discussions during the preparation of the manuscript.

ABBREVIATIONS USED

ESI, electrospray ionization; GC/MS, gas chromatography−mass spectrometry; HCl, hydrochloric acid; HICA, α-hydroxyisocaproic acid; HILIC, hydrophilic interaction chromatography; HMB, β-hydroxy-β-methylbutyric acid; IS, internal standard; LC/MS, liquid chromatography−mass spectrometry; LOQ, limit of quantitation; MRM, multiple reaction monitoring; PTFE, polytetrafluoroethylene; QC, quality control; RSD, relative standard deviation

REFERENCES

(1) Nissen, S.; Haymond, M. Effects of fasting on flux and interconversion of leucine and alpha-ketoisocaproate in vivo. *Am. J. Physiol.* **1981**, *241*, E72−E75.

(2) Liebich, H.; Forst, C. Hydroxycarboxylic and oxocarboxylic acids in urine: products from branched-chain amino acid degradation and from ketogenesis. *J. Chromatogr.* **1984**, *309*, 225−242.

(3) Wilkinson, D. J.; Hossain, T.; Hill, D. S.; Phillips, B. E.; Crossland, H.; Williams, J.; Loughna, P.; Churchward-Venne, T. A.; Breen, L.; Phillips, S. M.; Etheridge, T.; Rathmacher, J. A.; Smith, K.; Szewczyk, N. J.; Atherton, P. J. Effects of leucine and its metabolite β-hydroxy-β-methylbutyrate on human skeletal muscle protein metabolism. *J. Physiol.* **2013**, *591*, 2911−2923.

(4) Hao, Y.; Jackson, J. R.; Wang, Y.; Edens, N.; Pereira, S. L.; Alway, S. E. β-Hydroxy-β-methylbutyrate reduces myonuclear apoptosis during recovery from hind limb suspension-induced muscle fiber atrophy in aged rats. *Am. J. Physiol.: Regul. Integr. Comp. Physiol.* **2011**, *301*, R701−R715.

(5) Russell, S.; Tisdale, M. Mechanism of attenuation by β-hydroxy-β-methylbutyrate of muscle protein degradation induced by lipopolysaccharide. *Mol. Cell. Biochem.* **2009**, *330*, 171−179.

(6) Eley, H. L.; Russell, S. T.; Baxter, J. H.; Mukerji, P.; Tisdale, M. J. Signaling pathways initiated by β-hydroxy-β-methylbutyrate to attenuate the depression of protein synthesis in skeletal muscle in response to cachectic stimuli. *Am. J. Physiol.: Endocrinol. Metab.* **2007**, *293*, E923−E931.

(7) Pimentel, G.; Rosa, J.; Lira, F.; Zanchi, N.; Ropelle, E.; Oyama, L.; Oller do Nascimento, C.; de Mello, M.; Tufik, S.; Santos, R. beta-Hydroxy-beta-methylbutyrate (HMbeta) supplementation stimulates skeletal muscle hypertrophy in rats via the mTOR pathway. *Nutr. Metab.* **2011**, *8*, 11.

(8) Aversa, Z.; Bonetto, A.; Costelli, P.; Minero, V.; Penna, F.; Baccino, F.; Lucia, S.; Rossi, F.; Muscaritoli, M. beta-Hydroxy-beta-methylbutyrate (HMB) attenuates muscle and body weight loss in experimental cancer cachexia. *Int. J. Oncol.* **2011**, *38*, 713−720.

(9) Smith, H. J.; Mukerji, P.; Tisdale, M. J. Attenuation of Proteasome-Induced Proteolysis in Skeletal Muscle by β-Hydroxy-β-methylbutyrate in Cancer-Induced Muscle Loss. *Cancer Res.* **2005**, *65*, 277−283.

(10) Kovarik, M.; Muthny, T.; Sispera, L.; Holecek, M. Effects of β-hydroxy-β-methylbutyrate treatment in different types of skeletal muscle of intact and septic rats. *J. Physiol. Biochem.* **2010**, *66*, 311−319.

(11) Alway, S. E.; Pereira, S. L.; Edens, N. K.; Hao, Y.; Bennett, B. T. β-Hydroxy-β-methylbutyrate (HMB) enhances the proliferation of satellite cells in fast muscles of aged rats during recovery from disuse atrophy. *Exp. Gerontol.* **2013**, *48*, 973−984.

(12) Park, B.-S.; Henning, P. C.; Grant, S. C.; Lee, W. J.; Lee, S.-R.; Arjmandi, B. H.; Kim, J.-S. HMB attenuates muscle loss during sustained energy deficit induced by calorie restriction and endurance exercise. *Metabolism* **2013**, *62*, 1718−1729.

(13) Kreider, R.; Ferreira, M.; Wilson, M.; Almada, A. Effects of calcium beta-hydroxy-beta-methylbutyrate (HMB) supplementation during resistance-training on markers of catabolism, body composition and strength. *Int. J. Sports Med.* **1999**, *20*, 503−509.

(14) Nissen, S.; Sharp, R.; Ray, M.; Rathmacher, J. A.; Rice, D.; Fuller, J. C.; Connelly, A. S.; Abumrad, N. Effect of leucine metabolite β-hydroxy-β-methylbutyrate on muscle metabolism during resistance-exercise training. *J. Appl. Physiol.* **1996**, *81*, 2095−2104.

(15) Nissen, S.; Van Koevering, M.; Webb, D. Analysis of β-hydroxy-β-methyl butyrate in plasma by gas chromatography and mass spectrometry. *Anal. Biochem.* **1990**, *188*, 17−19.

(16) Townsend, J. R.; Fragala, M. S.; Jajtner, A. R.; Gonzalez, A. M.; Wells, A. J.; Mangine, G. T.; Robinson, E. H.; McCormack, W. P.; Beyer, K. S.; Pruna, G. J.; Boone, C. H.; Scanlon, T. M.; Bohner, J. D.; Stout, J. R.; Hoffman, J. R. β-Hydroxy-β-methylbutyrate (HMB)-free

acid attenuates circulating TNF-α and TNFR1 expression postresistance exercise. *J. Appl. Physiol.* **2013**, *115*, 1173−1182.
(17) Wilson, J. M.; Lowery, R. P.; Joy, J. M.; Walters, J. A.; Baier, S. M.; Fuller, J. C. J.; Stout, J. R.; Norton, L. E.; Sikorski, E. M.; Wilson, S. M. C.; Duncan, N. M.; Zanchi, N. E.; Rathmacher, J. β-Hydroxy-β-methylbutyrate free acid reduces markers of exercise-induced muscle damage and improves recovery in resistance-trained men. *Br. J. Nutr.* **2013**, *110*, 538−544.
(18) Portal, S.; Zadik, Z.; Rabinowitz, J.; Pilz-Burstein, R.; Adler-Portal, D.; Meckel, Y.; Cooper, D.; Eliakim, A.; Nemet, D. The effect of HMB supplementation on body composition, fitness, hormonal and inflammatory mediators in elite adolescent volleyball players: a prospective randomized, double-blind, placebo-controlled study. *Eur. J. Appl. Physiol.* **2011**, *111*, 2261−2269.
(19) Fuller, J. C.; Baier, S.; Flakoll, P.; Nissen, S. L.; Abumrad, N. N.; Rathmacher, J. A. Vitamin D Status Affects Strength Gains in Older Adults Supplemented With a Combination of β-Hydroxy-β-methylbutyrate, Arginine, and Lysine: A Cohort Study. *JPEN, J. Parenter. Enteral Nutr.* **2011**, *35*, 757−762.
(20) Flakoll, P.; Sharp, R.; Baier, S.; Levenhagen, D.; Carr, C.; Nissen, S. Effect of β-hydroxy-β-methylbutyrate, arginine, and lysine supplementation on strength, functionality, body composition, and protein metabolism in elderly women. *Nutrition* **2004**, *20*, 445−451.
(21) Vukovich, M. D.; Stubbs, N. B.; Bohlken, R. M. Body Composition in 70-Year-Old Adults Responds to Dietary β-Hydroxy-β-methylbutyrate Similarly to That of Young Adults. *J. Nutr.* **2001**, *131*, 2049−2052.
(22) Baier, S.; Johannsen, D.; Abumrad, N.; Rathmacher, J. A.; Nissen, S.; Flakoll, P. Year-long Changes in Protein Metabolism in Elderly Men and Women Supplemented With a Nutrition Cocktail of β-Hydroxy-β-methylbutyrate (HMB), L-Arginine, and L-Lysine. *JPEN, J. Parenter. Enteral Nutr.* **2009**, *33*, 71−82.
(23) Hsieh, L. C.; Chow, C. J.; Chang, W. C.; Liu, T. H.; Chang, C. K. Effect of beta-hydroxy-beta-methylbutyrate on protein metabolism in bed-ridden elderly receiving tube feeding. *Asia Pac. J. Clin. Nutr.* **2010**, *19*, 200−208.
(24) Stout, J. R.; Smith-Ryan, A. E.; Fukuda, D. H.; Kendall, K. L.; Moon, J. R.; Hoffman, J. R.; Wilson, J. M.; Oliver, J. S.; Mustad, V. A. Effect of calcium β-hydroxy-β-methylbutyrate (CaHMB) with and without resistance training in men and women 65+ yrs: a randomized, double-blind pilot trial. *Exp. Gerontol.* **2013**, *48*, 1303−1310.
(25) Deutz, N.; Pereira, S.; Hays, N.; Oliver, J.; Edens, N.; Evans, C.; Wolfe, R. Effect of β-hydroxy-β-methylbutyrate (HMB) on lean body mass during 10 days of bed rest in older adults. *Clin. Nutr.* **2013**, *32*, 704−712.
(26) Mero, A. A.; Ojala, T.; Hulmi, J. J.; Puurtinen, R.; Karila, T. A.; Seppala, T. Effects of alpha-hydroxy-isocaproic acid on body composition, DOMS and performance in athletes. *J. Int. Soc. Sports Nutr.* **2010**, *7*, 1.
(27) Lang, C. H.; Pruznak, A.; Navaratnarajah, M.; Rankine, K. A.; Deiter, G.; Magne, H.; Offord, E. A.; Breuille, D. Chronic alpha-hydroxyisocaproic acid treatment improves muscle recovery after immobilization-induced atrophy. *Am. J. Physiol.: Endocrinol. Metab.* **2013**, *305*, E416−E428.
(28) Zhang, Z.; Rathmacher, J.; Coates, C.; Nissen, S. Occurrence of b-hydroxy-b-methylbutyrate in foods and feeds. *FASEB J.* **1994**, *8*, A464 (Abstract 2685)..
(29) Smit, B. A.; Engels, W. J. M.; Wouters, J. T. M.; Smit, G. Diversity of L-leucine catabolism in various microorganisms involved in dairy fermentations, and identification of the rate-controlling step in the formation of the potent flavour component 3-methylbutanal. *Appl. Microbiol. Biotechnol.* **2004**, *64*, 396−402.
(30) Deshpande, P.; Jie, Z.; Subbarayan, R.; Mamidi, V. K.; Chunduri, R. H. B.; Das, T.; Shreeram, S. Development and validation of LC-MS/MS method for the estimation of β-hydroxy-β-methylbutyrate in rat plasma and its application to pharmacokinetic studies. *Biomed. Chromatogr.* **2013**, *27*, 142−147.
(31) Horvath, T.; Matthews, N.; Stratton, S.; Mock, D.; Boysen, G. Measurement of 3-hydroxyisovaleric acid in urine from marginally biotin-deficient humans by UPLC-MS/MS. *Anal. Bioanal. Chem.* **2011**, *401*, 2805−2810.
(32) Watanabe, T.; Oguchi, K.-I.; Ebara, S.; Fukui, T. Measurement of 3-Hydroxyisovaleric Acid in Urine of Biotin-Deficient Infants and Mice by HPLC. *J. Nutr.* **2005**, *135*, 615−618.
(33) Mock, D.; Jackson, H.; Lankford, G.; Mock, N.; Weintraub, S. Quantification of urinary 3-hydroxyisovaleric acid using deuterated 3-hydroxyisovaleric acid as internal standard. *Biomed. Environ. Mass Spectrom.* **1989**, *18*, 652−656.
(34) Jakobs, C.; Sweetman, L.; Nyhan, W.; Packman, S. Stable isotope dilution analysis of 3-hydroxyisovaleric acid in amniotic fluid: contribution to the prenatal diagnosis of inherited disorders of leucine catabolism. *J. Inherited Metab. Dis.* **1984**, *7*, 15−20.
(35) Baxter, J.; Phillips, R.; Dowlati, L.; Goehring, K.; Johns, P. Direct Determination of β-Hydroxy-β-methylbutyrate (HMB) in Liquid Nutritional Products. *Food Anal. Methods* **2011**, *4*, 341−346.
(36) Hoffer, L. J.; Taveroff, A.; Robitaille, L.; Mamer, O. A.; Reimer, M. L. alpha-Keto and alpha-hydroxy branched-chain acid interrelationships in normal humans. *J. Nutr.* **1993**, *123*, 1513−1521.
(37) Mamer, O. A.; Laschic, N. S.; Scriver, C. R. Stable isotope dilution assay for branched chain alpha-hydroxy-and alpha-ketoacids: serum concentrations for normal children. *Biomed. Environ. Mass Spectrom.* **1986**, *13*, 553−558.
(38) Mamer, O. A.; Montgomery, J. A. Determination of branched-chain 2-hydroxy and 2-keto acids by mass spectrometry. *Methods Enzymol.* **1988**, *166*, 27−38.
(39) Kuhara, T.; Shinka, T.; Inoue, Y.; Matsumoto, M.; Yoshino, M.; Sakaguchi, Y.; Matsumoto, I. Studies of urinary organic acid profiles of a patient with dihydrolipoyl dehydrogenase deficiency. *Clin. Chim. Acta* **1983**, *133*, 133−140.
(40) Spaapen, L. J.; Ketting, D.; Wadman, S. K.; Bruinvis, L.; Duran, M. Urinary D-4-hydroxyphenyllactate, D-phenyllactate and D-2-hydroxyisocaproate, abnormalities of bacterial origin. *J. Inherited Metab. Dis.* **1987**, *10*, 383−390.
(41) Jakobs, C.; Sweetman, L.; Nyhan, W. L. Hydroxy acid metabolites of branched-chain amino acids in amniotic fluid. *Clin. Chim. Acta* **1984**, *140*, 157−166.
(42) Yoshida, I.; Sweetman, L.; Nyhan, W. L. Metabolism of branched-chain amino acids in fibroblasts from patients with maple syrup urine disease and other abnormalities of branched-chain ketoacid dehydrogenase activity. *Pediatr. Res.* **1986**, *20*, 169−174.
(43) *Watson LIMS 7.3 User Manual r1*; Thermo Electron Corporation: Waltham, MA, 2006; p 365.

Spectral inspection indicates that there is a considerable number of interfering compounds that absorb in the UV−vis region. These compounds make it difficult to confirm the identical nature of the individual pigment peaks.

Anthocyanins are able to capture free radicals by donation of phenolic hydrogen atoms.[10,11] Acylation of the anthocyanin molecule improves their stability through intramolecular and/or intermolecular copigmentation and self-association reactions. Therefore, sources of acylated anthocyanins of the *S. scabrum* and *S. burbankii* berries may ensure the desirable stability for food applications. The anthocyanins with acylating substituents are more stable during processing and storage than the unacylated pigments.

The antioxidative activity of phenolic compounds, especially anthocyanin, was studied by different chemical methods. The Folin−Ciocalteu method, the oxygen radical absorbance capacity (ORAC) assay, and the Trolox equivalent antioxidant capacity (TEAC) assay are the most considered methods. Kilmartin et al.[13] developed an electrochemical method for the characterization of the antioxidant properties of wine and wine phenolics. Recently, Janeiro et al.[14] studied the redox behavior of anthocyanins by voltammetric techniques and found that all the phenolic hydroxyl groups can be oxidized electrochemically. Also differences in electroactive substituents on analogous structures can lead to characteristic differences in their voltammetric behavior.[15] Pereira at al.[16] studied the effects of substitution for the hydroxyl group at position C4′ in the B-ring of the flavylium cation, which indicated that the para-position of the ring B is important for the increase in the delocalization of π-electrons in the chromophore. Electrochemical studies reveal general trends in the electron-donating abilities of flavonoids. Cren-Olivé at al.[17] shown the importance the catechol group in the B-ring, which is more easily oxidizable than the resorcinol group in the A-ring. They indicated that the 4′-OH is the group that deprotonates preferentially in the flavylium cation of cyanidin and cyanidin-3-*O*-glucoside.[17]

The purpose of this research was to tentatively identify and quantify phenolic compounds, main flavonoids, phenolic acids, and anthocyanins for better characterization of *S. scabrum* and *S. burbankii* berries. Additionally, the study was aimed at monitoring the changes in the antioxidant activity by spectrometric methods (ABTS and FRAP assay) and an electrochemical technique, cyclic voltammetry. These rapid analytical techniques are very useful in determining the antioxidant activity, which is a consequence of the ability of an antioxidant to donate electrons around the potential of the anodic wave.

MATERIALS AND METHODS

Reagents and Standard. Acetonitrile and methanol for UPLC and LC/MS purity, formic acid, leucine enkephalin, 2,2-azinobis(3-ethylbenzothiazoline-6-sulfonic acid (ABTS), 6-hydroxy-2,5,7,8-tetramethylchroman-2-carboxylic acid (Trolox), 2,4,6-tri(2-pyridyl)-*s*-triazine (TPTZ), ammonium formate, and methanol were purchased from Sigma-Aldrich (Steinheim, Germany). Quercetin-3-*O*-glucoside and -3-*O*-rutinoside; peonidin, delphinidin and petunidin aglycon; *p*-coumaric acid; and sinapic acid were purchased from Extrasynthese (Lyon, France). Chlorogenic acid, neochlorogenic acid, and cryptochlorogenic acid were purchased from TRANS MIT GmbH (Giessen, Germany).

UPLC-grade water, prepared by using an HLP SMART 1000s system (Hydrolab, Gdańsk, Poland), was additionally filtered through a 0.22 μm membrane filter immediately before use.

Plant Material. *S. scabrum* and *S. burbankii* berries were collected in 2011 from the Garden of Medicinal Plants herbarium at the Medical University in Wroclaw, Poland, by cultivation in the University's experimental field. The fruits were harvest successively during 10 days and after harvest, the berries (100 g per day, finally 1 kg) were immediately frozen and stored at −20 °C until used for analysis.

Extraction Procedure. The extraction procedure of polyphenols was carried out as described previously by Oszmiański et al.[18] The frozen berries were quick thawed in a microwave oven and heated only to 20 °C and then directly crushed in a laboratory mill (IKA A11). This extraction procedure was applied because use of the microwave oven was previously found to be the best extraction method when berries were exposed for 1 min. Polyphenols were isolated from berries by maceration with water containing 200 mg/L SO_2 and subsequently extracted in a ultrasonic bath at 20 °C for 15 min. The ratio of this solvent to berries was 10:1 (v/v). The homogenized mixture was then centrifuged for 5 min (4000 rpm; MPW 360R; Warsaw, Poland), and the extraction was repeated twice. The experiment were performed in triplicate.

Four milliliters of the extract was passed through a C18 Sep-Pak cartridge (360 mg/0.7 mL; Waters) preconditioned with 5 mL of ethyl acetate, 5 mL of methanol, and 5 mL of 0.01 N HCl. The loaded cartridge was washed with 3 mL of 0.01% HCl and then the cartridge was dried with a flow of nitrogen gas for 3 min. Phenolic compounds other than anthocyanins were eluted with 20 mL of ethyl acetate. The solvent was removed using a rotary vacuum evaporator at 20 °C, and the phenolic residue was dissolved in 20% acetonitrile for UPLC-PDA−MS analysis. Anthocyanins adsorbed in the Sep-Pak C18 were eluted with methanol containing 0.5% HCOOH, and the anthocyanin fraction was analyzed by the UPLC-PDA−MS method.

Absorption Spectra of Berry Extracts. Berry extract was used for measurement of absorption spectra, which were recorded in the visible wavelength range from 450 to 600 nm. These spectra were measured using a PC 2401 UV−vis spectrophotometer (Shimadzu; Tokyo, Japan) in a 10-mm path length cell, with buffer solutions as a reference. Buffer solutions of two different pH values (pH 2.5 and 7.5) were prepared by mixing 50 mM ammonium formate with acetonitrile (50/50; v/v). pH was adjusted with ammonium hydroxide. All experiments were repeated in triplicate.

Identification of Polyphenols by the UPLC-PDA−Q/TOF-MS Method. Identification of polyphenol of *S. scabrum* and *S. burbankii* berry extracts was carried out using an ACQUITY ultra-performance LC system (UPLC) with binary solvent manager (Waters Corp.; Milford, MA) and a Micromass Q-Tof Micro mass spectrometer (Waters; Manchester, UK) equipped with an electrospray ionization (ESI) source operating in negative and positive mode. Separations of individual polyphenols were carried out using a UPLC BEH C18 column (1.7 μm, 2.1 × 100 mm, Waters Corp.; Milford, MA) at 30 °C. Samples (10 μL) were injected, and elution was completed in 15 min with a sequence of linear gradients and isocratic flow rates of 0.45 mL min^{-1}. The mobile phase was composed of solvent A (4.5% formic acid, v/v) and solvent B (100% acetonitrile). The program began with isocratic elution with 99% A (0−1 min), and then a linear gradient was used until 12 min, lowering A to 0%; from 12.5 to 13.5 min, the initial composition (99% A) was used and then held constant to re-equilibrate the column. Analysis was carried out using full scan, data-dependent MS scanning from m/z 100 to 1500. Leucine enkephalin was used as the internal reference compound during ESI-MS accurate mass experiments and was permanently introduced via the LockSpray channel using a Hamilton pump. The lock mass correction was ±1.000 for the mass window. All quadrupole time-of-flight mass spectrometry (Q/TOF-MS) chromatograms are displayed as base peak intensity (BPI) chromatograms and scaled to 12 400 counts per second (cps) (=100%). The effluent was led directly to an electrospray source with a source block temperature of 130 °C, desolvation temperature of 350 °C, capillary voltage of 2.5 kV, and cone voltage of 30 V. Nitrogen was used as desolvation gas at flow rate 300 L h^{-1}.

The characterization of the single components was carried out via the retention time and the accurate molecular masses. Each compound was optimized to its estimated molecular mass $[M - H]^-$ in the

Table 1. Qualitative and Quantitative (mg/100 g dm) Characterization of *S. scabrum* and *S. burbankii* Phenolic Compound Profiles with UPLC-PDA–MS/MS[a]

peak	compd	t_R (min)	λ_{max} (nm)	$[M + H]^+/[M - H]^-$ (m/z) and MS/MS fragments in ESI-MS-Q-TOF	*S. burbankii*	*S. scabrum*
1	3-caffeoylquinic acid	2.27	323	$[M - H]^-$ 353.0870 (100%) 191.0555 (100%)/173.0446 (43%)/135.0452 (62%)	0.83 ± 0.03	0.82 ± 0.04
2	delphinidin-3-*O*-rutinoside-5-*O*-glucoside	3.33	525	$[M + H]^+$ 773.2146 (100%) 611.1609 (26%)/465.1017 (21%)/303.0496 (100%)	0.24 ± 0.01	1.37 ± 0.08
3	5-caffeoylquinic acid	3.61	324	$[M - H]^-$ 707.1823 (100%) 353.0875 (88%)/191.0558 (100%)	47.64 ± 2.47	7.81 ± 1.50
4	4-caffeoylquinic acid	4.16	324	$[M - H]^-$ 353.0879 (100%) 191.0555 (84%)/173.0449 (100%)	0.29 ± 0.10	0.20 ± 0.04
5	petunidin-3-*O*-rutinoside-5-*O*-glucoside	4.43	529	$[M + H]^+$ 787.2300 (100%) 625.1765 (35%)/479.1188 (25%)/317.0671 (100%)	2.11 ± 0.26	7.80 ± 1.07
6	malonyl-caffeoylquinic acid	4.66	325	$[M - H]^-$ 439.0872 (100%) 353.0879 (20%)/233.0660 (100%)/191.0555 (32%)/173.0449 (20%)	15.95 ± 0.85	14.24 ± 1.51
7	malvidin-3-*O*-rutinoside-5-*O*-glucoside	5.53	526	$[M + H]^+$ 801.2440 (100%) 639.1934 (42%)/493.1325 (30%)/331.0814 (100%)	2.56 ± 0.41	nd[b]
8	malonyl-caffeoylquinic acid	5.76	325	$[M - H]^-$ 439.0872 (100%) 395.0979 (29%)/353.0879 (20%)/233.0665 (97%)/191.0555 (25%)/173.0453 (100%)	6.10 ± 1.20	5.67 ± 1.01
9	acetylo-*p*-coumaroylquinic acid	6.24	310	$[M - H]^-$ 379.1031 (100%) 319.0818 (31%)/163.0386 (245%)/145.0296 (46%)	0.44 ± 0.04	0.38 ± 0.05
10	quercetin-3-*O*-rutinoside	8.30	352	$[M - H]^-$ 609.1432 (100%) 301.0277 (86%)	4.96 ± 0.87	1.62 ± 0.11
11	delphinidin-3-*O*-*p*-coumaroyl-rutinoside-5-*O*-glucoside	8.37	528	$[M + H]^+$ 919.2509 (100%) 757.1982 (70%)/465.1034 (46%)/303.0496 (100%)	2.37 ± 0.12	0.24 ± 0.07
12	quercetin-3-*O*-glucoside	8.44	351	$[M - H]^-$ 463.0887 (100%) 301.0277 (100%)/173.0447 (30%)	1.69 ± 0.15	1.68 ± 0.13
13	delphinidin-3-*O*-feruoyl-rutinoside-5-*O*-glucoside	8.89	529	$[M + H]^+$ 949.2607 (100%) 787.2077 (85%)/465.1032 (55%)/303.0496 (100%)	7.71 ± 0.64	21.08 ± 0.68
14	sinapoyl malic acid	9.10	328	$[M - H]^-$ 339.0716 (100%) 223.0606 (100%)/149.0241 (57%)	0.98 ± 0.06	0.84 ± 0.07
15	petunidin-3-*O*-*p*-coumaroyl-hexoside-5-*O*-hexose	9.30	531	$[M + H]^+$ 933.2642 (100%) 771.2128 (99%)/479.1187 (59%)/317.0671 (100%)	63.26 ± 5.75	156.87 ± 3.87
16	petunidin-3-*O*-feruoyl-hexoside-5-*O*-hexose	9.82	532	$[M + H]^+$ 963.2780 (100%) 801.2242 (100%)/479.1100 (87%)/317.0671 (86%)	0.91 ± 0.17	13.67 ± 1.17
17	malvidin-3-*O*-*p*-coumaroyl-hexoside-5-*O*-hexose	10.28	532	$[M + H]^+$ 947.2829 (100%) 785.2296 (99)/493.1341 (55%)/331.0814 (100%)	2.66 ± 0.11	3.82 ± 0.66
18	malvidin-3-*O*-feruoyl-hexoside-5-*O*-hexose	10.75	532	$[M + H]^+$ 977.2892 (100%) 815.2397 (100%)/613.3407 (86%)/493.1344 (54%)/331.0814 (97%)	0.24 ± 0.04	1.37 ± 0.11
	total phenolics (mg/100 g)				160.95***	239.35***

[a]Results represent mean values of triplicated determinations ± standard deviation ($p < 0.001$). [b]nd: not detected.

dx.doi.org/10.1021/jf4045233 | J. Agric. Food Chem. 2014, 62, 1512−1519

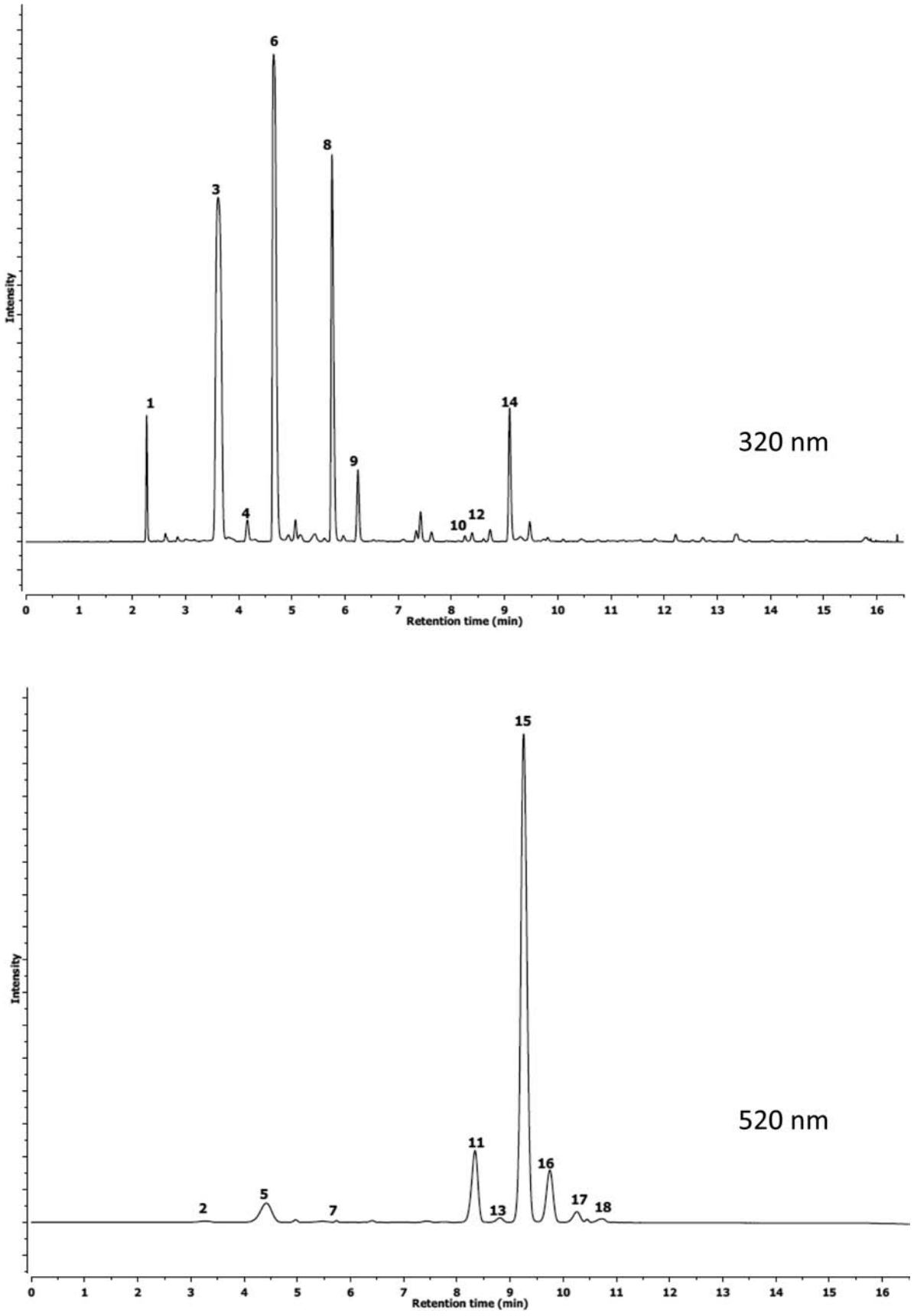

Figure 1. UPLC profile at 320 nm (phenolic acid and quercetin derivative) and 520 nm (anthocyanins) of *Solanum* berry extracts. For abbreviations of the peak labels, see Table 1

dx.doi.org/10.1021/jf4045233 | *J. Agric. Food Chem.* 2014, 62, 1512−1519

negative and positive mode before and after fragmentation. The data obtained from UPLC/MS were subsequently entered into the MassLynx 4.0 ChromaLynx Application Manager software. On the basis of these data, the software is able to scan different samples for the characterized substances.

The runs were monitored at the following wavelengths: hydroxycinnamates at 320 nm, flavonol glycosides at 360 nm, and anthocyanins at 520 nm. Photodiode detector (PDA) spectra were measured over the wavelength range 200−600 nm in steps of 2 nm. Retention times and spectra were compared with those of pure standards within 200−600 nm. Calibration curves were run for the external standards 3-, 4-, and 5-*O*-caffeoylquinic acids, *p*-coumaric acid, quercetin-3-*O*-rutinoside and -3-*O*-glucoside, peonidin-3-*O*-rutinoside, delphinidin-3-*O*-rutinoside, and petunidin-3-*O*-rutinoside at concentrations ranging from 0.05 to 5 mg/mL. Amounts of 3-, 4-, and 5-*O*-caffeoylquinic acids were calculated for the quantification of the neochlorogenic, cryptochlorogenic, and chlorogenic acids and their isomers. The concentrations of *p*-coumaric and sinapic acid containing compounds were calculated by using *p*-coumaric and sinapic acid, respectively. The concentrations of delphinidin-, petunidin-, and malvidin-containing compounds were calculated by using delphinidin, petunidin, and malvidin aglycons, respectively. Obtained results was express as milligrams per 100 g of dry matter (dm).

Analysis of Antioxidant Activity. The protocols for analysis were prepared as described previously by Wojdyło et al.[19] The $ABTS^{\bullet+}$ activity of the sample was used for measurement of antioxidant activity. The total antioxidant potential of the sample was determined using a ferric reducing ability of plasma (FRAP) assay. For all analyses, a standard curve was prepared using different concentrations of Trolox. All determinations were performed in triplicate using a Shimadzu UV-2401 PC spectrophotometer (Kyoto, Japan). The results were corrected for dilution and are expressed in millimole of Trolox per 100 g dm.

Cyclic Voltammograms. The mixture of 50 mM ammonium formate (pH 7.4) and acetonitrile (50/50, v/v) was prepared as the supporting electrolyte. All experiments were performed on a ROXY EC system (Antec; Zoeterwoude, The Netherlands). Electrochemical conversions were accomplished in an electrochemical thin-layer cell (ReactorCell, Antec). The reactor cell consisted of a three-electrode arrangement including a working electrode, an auxiliary electrode, and a reference electrode. Glassy carbon was used as working electrode material. The accessible area of the working electrode was 15.1 mm^2. The inlet block of the cell was employed as auxiliary electrode and the HyREF (Antec) electrode was used as reference electrode. The working electrode and the auxiliary electrode inlet block were separated by a 50-μm spacer, giving a cell volume of approximately 750 nL. Potentials (0−3000 mV) were applied using a purposive potentiostat (ROXY potentiostat, Antec). Shredded *S. scabrum* and *S. burbankii* berry extracts (~2.5 g) were mixed with 3 mL of ammonium formate and then centrifuged for 10 min at 15 000 rpm (20.878*g*; MPW-360R; Warsaw, Poland). Prior to each run, the surface of the glassy carbon electrode was freshly abraded with 12 μm flattening plate and rinsed with redistilled water and methanol. The scan was taken in the potential range between 0 and 3000 mV with a scan rate 50 mVs^{-1}. Samples were pumped through the cell at a flow rate of 5 μL/min by a syringe pump model 74900 (Cole Parmer; Vernon Hills, IL). Cyclic voltammograms were also recorded for 0.25 mM cyanidin, malvidin, and pelargonidin aglycon standards solutions.

RESULTS AND DISCUSSION

Characterization and Quantification of Phenolic Compounds. The data for retention times (t_R), wavelengths of maximum absorbance (λ_{max}), protonated/deprotonated molecules ($[M + H]^+/[M - H]^-$), diagnostic fragments, and identification for each peak of the phenolic compound detected in the *S. scabrum* and *S. burbankii* berry extracts are listed in Table 1. The compounds were characterized according to their retention time at 320 nm for phenolic acid derivatives, 360 nm for quercetin derivatives, and at 520 nm for anthocyanins and are shown in Figure 1, respectively.

Eighteen phenolic acid derivatives and flavonoids were detected in the *S. scabrum* and *S. burbankii* berry extracts. Among them, there were three nonacylated anthocyanin hexosides and six acylated anthocyanin hexosides.

Nine compounds other than antocyanin phenolic ones were tentatively identified in the *S. scabrum* and *S. burbankii* berry extracts for the first time. Among them, there were seven phenolic acid derivatives and two flavonol hexosides.

Chlorogenic acid (5-caffeoylquinic acid, compound **1**) and its isomers were found at different t_R, showing the deprotonated molecule $[M - H]^-$ (m/z 353) and the ion corresponding to the deprotonated quinic acid (m/z 191) in the full scan mode. Reference substances neochlorogenic acid (3-caffeoylquinic acid, compound **3**) and cryptochlorogenic (4-caffeoylquinic acid, compounds **4**) were confirmed by injection of standards and the subfractions in neutral loss of m/z 162, which also corresponds to the loss of a caffeic acid unit. Several isomers of chlorogenic acid have been found in other plant sources.[20,21]

Compounds **6** and **8** possessing two malonyl-caffeoylquinic acid derivatives were detected in full-scan experiments showing m/z 439, 191, and 173 at the t_R of 4.66 and 5.76 min in decreasing concentrations. The mass spectra of the peaks in full scan mode showed the typical fragmentation of the malonyl acid and quinic acid of chlorogenic acid derivatives at m/z 86 and 191, respectively.

Acetylo-*p*-coumaroylquinic acid (**9**) and sinapoyl-malic acid (**14**) were found in the analyzed berries as well. The compound **9** (t_R 6.24 min, λ_{max} 310 nm) produced the parent ion at m/z 163 and compound **14** (t_R 9.10 min, λ_{max} 328 nm) produced an ion at m/z 233, corresponding to *p*-coumaric acid and sinapic acid, respectively. The chemical nature of the nonphenolic acid side chains was established using high resolution in source fragmentation experiments in a negative ion mode showing fragment ions with the neutral losses of 60 amu (m/z 379 − 60 = 319) and 116 amu (m/z 339 − 116 = 223) for the acetyl and maloyl residues, respectively (Table 1).

Two glucosides of quercetin, namely, quercetin-3-*O*-rutinoside (**10**, rutin) and quercetin-3-*O*-glucoside (**12**, isoquercitrin), were identified. Quercetin-3-*O*-rutinoside was detected at the t_R of 8.30 min, whereas quercetin-3-*O*-glucoside was found at the t_R of 8.44 min, both of them exhibiting a mass spectrum in full-scan mode with m/z 609 and 463, respectively, and a precursor ion scan m/z 301 as quercetin aglycon. Comparison of the mass spectra and t_R with those of the respective standards confirmed the occurrence of these glycosylated flavonols in the *S. scabrum* and *S. burbankii* berry extracts. The fragmentation pathway of *O*-glycosylated flavonoids starts with the cleavage of the glycosydic bonds and elimination of the sugar moieties with charge retention on the aglycon. In compounds containing two or more sugars at the same aglycon carbon, ions arising from the cleavage of the glycosidic bonds between sugar units are weak. Compounds such as quercetin-3-*O*-glucosyl-rutinoside and quercetin-3-*O*-rutinoside were typical for the Solanaceae family and have been previously reported in potato.[22] Quercetin, a major representative of the flavonol subclass found at high concentrations in fruit and vegetables, has recently received considerable attention. This flavonoid displays the ability to prevent the oxidation of LDL by scavenging free radicals and chelating transition metal ions. As a result, quercetin may aid in the prevention of certain diseases, such as cancer, atherosclerosis, and chronic inflammation by

retarding oxidative degradation and inducing enzymes that detoxify carcinogens and also by blocking cancer formation by deactivating at least 30 types of potentially carcinogenic agents.[23,24]

The UPLC method was applied for short run times combined with a photodiode array detector (PDA), and a quadrupole/time-of-flight mass spectrometer (Q/TOF-MS) enables better characterization of individual compounds, especially with high molecular mass, i.e., acetylated anthocyanins. Three nonacylated anthocyanins were presented as delphinidin-*O*-3-rutinoside-*O*-5-glucoside (**2**; *m*/*z* 773, $[M + H]^+$), petunidin-3-*O*-rutinoside-5-*O*-glucoside (**5**; *m*/*z* 787, $[M + H]^+$), and malvidin-3-*O*-rutinoside-5-*O*-glucoside (**7**; *m*/*z* 801, $[M + H]^+$). Malvidin-3-*O*-rutinoside-5-*O*-glucoside was detected only in *S. burbankii* berry extract. The ESI mass spectrum of pigments showed fragment ions at $[M - 162 (glucose)]^+$ corresponding *m*/*z* 611, 625, and 639, respectively, and the next fragment ions at $[M - 146 (hexoside, probably rhamnoside)]^+$ *m*/*z* 465, 479, and 493, respectively. The last fragment ions at $[M - 162 (hexoside, probably glucoside)]^+$ *m*/*z* 303 (dephinidin), 317 (petunidin) and 331 (malvidin) were aglycons, as listed in Table 1. Seven other compounds **11** and **13**−**18** (t_R 8.37−10.78 min; molecular weights *m*/*z* 918−976 amu) were also clearly detected in *Solanum* berry extracts (Table 1). Acylated anthocyanin glycosides were easily identified on the basis of the increase in the mass of the parent ions and the wavelength maxima (330−336 nm) of their UV−vis spectra. Thus, peaks with the t_R at 8.37, 8.89, 9.30, 9.82, 10.28, and 10.75 min were identified as 3-*O*-*p*-coumaroyl-hexoside-5-*O*-hexoside (**11**) and 3-*O*-feruoyl-hexoside-5-*O*-hexoside (**13**) of delphinidin, 3-*O*-*p*-coumaroyl-hexoside-5-*O*-hexoside (**15**) and 3-*O*-feruoyl-hexoside-5-*O*-hexoside (**16**) of petunidin, and 3-*O*-*p*-coumaroyl-hexoside-5-*O*-hexoside (**17**) and 3-*O*-feruoyl-hexoside-5-*O*-hexoside (**18**) of malvidin, respectively. The ESI mass spectrum of the acylated pigment compound **11** showed a flavylium cation at *m*/*z* 919 $[M + H]^+$ together with a fragment ion at *m*/*z* 757 $[M - 162 (glucose)]^+$. On the basis of observations of two additional fragment ions at *m*/*z* 465 [M − 292 (the presence of hexoside, probably rhamnose, and *p*-coumaric acid)], and *m*/*z* 303 derived from successive losses of 162 amu, the presence of glucose moiety was confirmed, for structural elucidation. Similar fragmentation ions were observed for the remaining acetylated anthocyanins (Table 1). Although these compounds have already been presented in earlier works,[1,2] to enable their complete identification, their structures should be fully elucidated by means of NMR or by comparison with authentic compounds, if existing.

In addition, nonacylated anthocyanins were shown to be the most abundant compounds in wild species of berry and other fruits.[25,26] The presence of acylated anthocyanins is typical of grapes, blueberry, blackberry, and some vegetables, i.e., red cabbage, radish, and red-fleshed potato.[27]

Recent research has shown that anthocyanins with acylating substituents are more stable during processing and storage than other natural pigments.[6,9,27] Brouillard et al.[28] explain that the effect of the improved stabilization of the acylated anthocyanins has been attributed to the stacking of the acyl groups with the pyrylium ring of the flavylium cation, thereby reducing the susceptibility of a nucleophile attack of water and subsequent formation of intramolecular copigmentation of a pseudobase or a chalcone.

The concentrations of low molecular weight flavonols (quercetin) and hydroxycinnamic acid conjugates (caffeic, *p*-coumaric and sinapic acid) were higher in the *S. burbankii* berries (78.89 mg/100 g) than in the *S. scabrum* berries (33.13 mg/100 g) (Table 1). In both berries, 3-caffeoylquinic acid was dominant, and the concentration of 5-caffeoylquinic acid was higher than that of 4-caffeoylquinic acid. The content of acylated derivatives of anthocyanins showed the largest differences between the investigated berries. *S. scabrum* berries were much more richer sources of anthocyanins (206.22 mg/100 g) than *S. burbankii* berries (82.06 mg/100 g). Price et al.[2] found more anthocyanin compounds in *S. scabrum* berries (350 mg/100 g). The concentration of acylated antocyanins was higher than that of the nonacylated antocyanins in *Solanum* berries. Petunidin-3-*O*-*p*-coumaroyl-rutinoside-5-*O*-glucoside was the dominant acylated antocyanin in the investigated berries.

Figure 2 shows the spectral character of *S. scabrum* (A) and *S. burbankii* (B) berry extracts at pH 2.5 and 7.5, indicating that

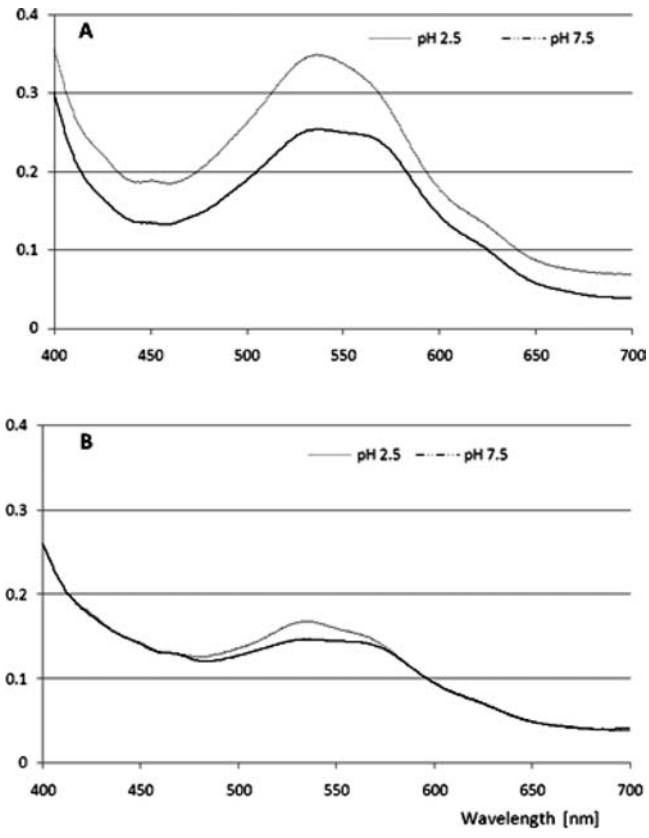

Figure 2. Spectral character of *S. scabrum* (A) and *S. burbankii* (B) berry extracts at pH 2.5 and 7.5.

these berries contain acylated anthocyanin. Changing the pH from 2.5 to 7.5 did not result in any significant reduction in absorbance at a wavelength of 530 nm, as is observed in the case of nonacylated anthocyanins. The variation of pH values influences anthocyanin properties, such as color, stability, spectral shape, and absorption peak.[29] In our research, it could be observed from Figure 2 that the anthocyanin extracts from *S. scabrum* (A) and *S. burbankii* (B) berries had the maximum absorption around 530 nm at pH 2.5 and 7.5. Anthocyanin solutions, at both pH values, exhibited bright red-violet color, and their absorbances at 530 nm varied slightly. Acylated

anthocyanins are also more resistant to color fading with increased pH than their unacylated analogs. Unacylated anthocyanins are only stable at pH values where the flavylium cation dominates. Cevallos-Casals et al.[6] showed that vegetables such as sweet potato and purple carrot, which contain acylated anthocyanins, were more resistant to the solution pH than red grape rich, which is in unacylated anthocyanins. Other researchers confirmed the unusual stability of acylated anthocyanins at pH >5.0.[7,8]

Antioxidant Activity and Cyclic Voltammetry of Solanum Berries. The antioxidant activity of *S. scabrum* (a) and *S. burbankii* (b) berries was tested by measuring their activity to scavenge radical (Table 2). The ABTS radical

Table 2. Antioxidant Activity (mmol Trolox/100 g dm) of *Solanum* Fruits

	S. scabrum	*S. burbankii*
ABTS	2.89 ± 0.37	2.07 ± 0.42
FRAP	1.65 ± 0.09	0.71 ± 0.06

Mean values with standard deviation of $n = 3$.

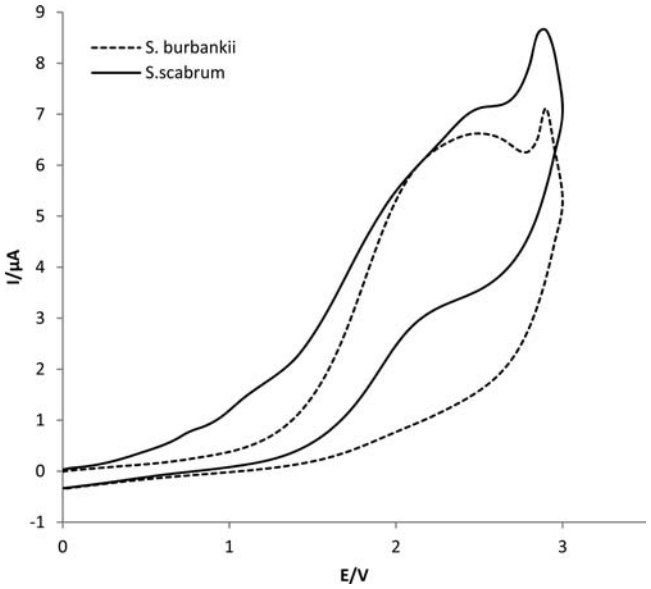

Figure 3. Cyclic voltammograms of *S. burbankii* and *S. scabrum*.

scavenging activity was higher in *S. scabrum* berry extract [2.89 mmol Trolox equiv (TE)/100 g dm] than in *S. burbankii* berry extract (2.07 mmol TE/100 g dm). After comparing the $ABTS^{\bullet+}$ activity of the *Solanum* berries with that of known food products we found that they exhibited a lower antioxidant activity than that of blueberries (4.59 mmol TE/100g dm), which constitute one of the richest reported sources of antioxidants.[30] But, still, *S. scabrum* berry extract had a higher antioxidant activity than *Rubus* species (0−2.53 mmol TE/100 g dm), which have been recommended as improving the nutritive value due to its high antioxidant activities.[31] In regard to the FRAP activity, *S. scabrum* had 1.65 mmol TE/100 g dm and *S. burbankii* had 0.71 mmol TE/100g dm, respectively. The differences in polyphenols between *Solanum* varieties could be preliminarily attributed to their different contents of antioxidant activity. *S. scabrum* berry extract contained much more phenolic compounds than *S. burbankii* berry extract.

The cyclic voltammetric technique (CV) was employed to study the electrochemical behavior of *S. scabrum* and *S. burbankii* berry polyphenol extracts, and results are presented in Figure 3. The major current peak appears at approximately 2.4 V for *S. scabrum* and at 2.1 V for *S. burbankii*. According to literature data, this peak may be attributed to powerful, low formal potential phenolics characterized by an *o*-hydroxyphenol or di- or trihydroxyphenol group. Petuninidin and delphinidin anthocyanin derivatives were the main compounds of *Solanum* berry, but higher contents of these compounds were determined in *S. scabrum*. These anthocyanins possess three and two catechol groups on the B-ring. Cevallos-Casals at al.[6] explained that oxidation of phenolic compounds involved the formation of a stable quinone, which can be reduced in the reverse scan, this process appearing as a cathodic peak of the current response. In the return scan, the electrochemical behavior of *S. burbankii* extract is irreversible. Yakovleva et al.[32] present the irreversible oxidation of some phenolic acids and flavones in plants. However Tamura et al.[12] found that anthocyanins acylated by *p*-coumaric acid are much better antioxidants than α-tocopherol or (+)-catechin. Besides the color and antioxidant activity, anthocyanins have free radical scavenging activity. The anthocyanin radical is more stable than other radicals generated in the human body; hence the duration of this radical is longer.[12]

In both cultivars, the major compound was found to be the anthocyanin petunidin-3-(*p*-coumaroyl-rutinoside)-5-glucoside. Eight additional anthocyanins in *S. burbankii* berries and 11 in *S. scabrum* berries were identified as petunidin, delphinidin, and malvidin with the same glycosidic substitution pattern as the major pigment and varying degrees of acylation with *p*-coumaric and ferulic acids. The presence of seven phenolic acid mainly caffeoylquinic derivatives and two quercetin derivatives was reported for the first time. *S. scabrum* extracts are richer in anthocyanins but have less phenolic acid than *S. burbankii*. This study demonstrated the usability of fast and effective electrochemical measurements and a spectrophotometric technique for determination of the phenolic content as well as antioxidant activity of *Solanum* berry extracts. *S. scabrum* exhibited the highest TEAC values according to both CV and ABTS and FRAP assay.

From the consumers' point of view, the analyzed fruits are good sources of bioactive compounds and colorants to be used in the food industry.

AUTHOR INFORMATION

Corresponding Author

*Tel./fax: +48 71 320 7706. E-mail: aneta.wojdylo@up.wroc.pl.

Notes

The authors declare no competing financial interest.

REFERENCES

(1) Francis, F. J.; Harborne, J. B. Anthocyanins of the garden huckleberry *Solanum guineense*. *J. Food Sci.* **1966**, *31*, 524−528.

(2) Price, C. L.; Wrolstad, R. E. Anthocyanin pigments of royal Okanogan huckleberry juice. *J. Food Sci.* **1995**, *60*, 369−374.

(3) Manoko, M. L. K.; Van den Berg, R. G.; Feron, R. M. C.; Van der Weerden, G. M.; Mariani, C. Genetic diversity of the African hexaploid species *Solanum scabrum* Mill. and *Solanum nigrum* L. (Solanaceae). *Genet. Resour. Crop Evol.* **2008**, *55* (3), 409−41.

(4) D'Arcy, W. G. The Solanaceae since 1976 with a review of its biogeography in Solanaceae III: Taxonomy chemistry and evolution (Hawkes, J. G., Lester, R. N., Nee, M., Estrada, N. R. , Eds.; Academic Press: London, 1991; pp 75−137.

(5) Rao, G. R. Role of fruit pigments in understanding the interrelationships and mechanism of evolution of higher chromosomal forms of the species of the *Solanum nigrum* L complex. *Acta Bot. Indica* **1978**, *6* (Suppl), 41−47.
(6) Cevallos-Casals, B. A.; Cisneros-Zevallos, L. Stability of anthocyanin-based aqueous extracts of Andean purple corn and red-fleshed sweet potato compared to synthetic and natural colorants. *Food Chem.* **2004**, *86*, 69−77.
(7) IdakaE. (Suntory Ltd.) Acylated anthocyanin and process for producing the same as well as pigment composition containing the same. Patent US 4999423 A, 1991.
(8) Delgado-Vargas, F.; Jimenez, A. R.; Paredes-Lopez, O. Natural pigments: Carotenoids, anthocyanins and betalains-characteristics, biosynthesis, processing and stability. *Crit. Rev. Food Sci. Nutr.* **2000**, *40* (3), 173−289.
(9) Fossen, T.; Ŕvstedal, D. O.; Slimestad, R.; Andersen, Ř. M. Anthocyanins from a Norwegian potato cultivar. *Food Chem.* **2003**, *81*, 433−437.
(10) Chen, Z. Y.; Chan, P. T.; Ho, K. Y.; Fung, K. P.; Wang, J. Antioxidant activity of natural flavonoids is governed by number and location of their aromatic hydroxyl groups. *Chem. Phys. Lipids* **1996**, *79* (2), 157−163.
(11) Rice-Evans, C. A.; Miller, N. J.; Paganga, G. Structure−antioxidant activity relationships of flavonoids and phenolic acids. *Free Radical Biol. Med.* **1996**, *20* (7), 933−956.
(12) Tamura, H.; Yamagami, A. Antioxidative activity of monoacylated anthocyanins isolated from Muscat Bailey grape. *J. Agric. Food Chem.* **1994**, *42*, 1612−1615.
(13) Kilmartin, P. A.; Hsu, C. F. A cyclic voltammetry method suitable for characterizing antioxidant properties of wine and wine phenolics. *J. Agric. Food Chem.* **2001**, *49*, 1957−1965.
(14) Janeiro, P.; Oliveira, B. A. M. Redox behaviour of anthocyanins present in *Vitis vinifera* L. *Electroanalysis* **2007**, *19*, 1779−1786.
(15) Mazza, G.; Brouillard, R. Recent developments in the stabilization of anthocyanins in food products. *Food Chem.* **1987**, *25*, 207−225.
(16) Pereira, G. K.; Donate, P. M.; Galembeck, S. E. Effects of substitution for hydroxyl in the B-ring of the flavylium cation. *J. Mol. Struct.* **1997**, *392*, 169−179.
(17) Cren-Olivé, C.; Hapiot, P.; Pinson, J.; Rolando, C. Free radical chemistry of flavan-3-ols: Determination of thermodynamic parameters and of kinetic reactivity from short (ns) to long (ms) time scale. *J. Am. Chem. Soc.* **2002**, *124*, 14027−14038.
(18) Oszmiański, J.; Lee, C. Y. Isolation and HPLC determination of phenolic compounds in red grapes. *Am. J. Enol. Vitic.* **1990**, *41*, 204−206.
(19) Wojdyło, A.; Oszmiański, J.; Laskowski, P. The polyphenolic compounds and antioxidant activity of new and old apple varieties. *J. Agric. Food Chem.* **2008**, *56*, 6520−6530.
(20) Narváez-Cuenca, C.-E.; Vincken, J.-P.; Gruppen, H. Identification and quantification of (dihydro) hydroxycinnamic acids and their conjugates in potato by UHPLC−DAD−ESI-MS^n. *Food Chem.* **2012**, *130*, 730−738.
(21) Schmidt, S.; Zietz, M.; Schreiner, M.; Rohn, S.; Kroh, L. W.; Krumbein, A. Identification of complex naturally occurring flavonoid glycosides in kale (*Brassica oleracea* var. sabellica) by high-performance liquid chromatography diode-array detection/electrospray ionization multi-stage mass spectrometry. *Rapid Commun. Mass Spectrom.* **2010**, *24*, 2009−2022.
(22) Shakya, R.; Navarre, D. A. Rapid screening of ascorbic acid glycoalkaloids and phenolics in potato using high-performance liquid chromatography. *J. Agric. Food Chem.* **2006**, *54*, 5253−5260.
(23) Ackland, M. L.; Van de Waarsenburg, S.; Jones, R. Synergistic antiproliferative action of the flavonols quercetin and kaempferol in cultured human cancer cell lines. *In Vivo* **2005**, *19*, 69−76.
(24) Fresco, P.; Borges, F.; Marques, M. P. M.; Diniz, C. The anticancer properties of dietary polyphenols and its relation with apoptosis. *Curr. Pharm. Des.* **2010**, *16*, 114−134.
(25) Liang, Z.; Yang, Y.; Cheng, L.; Zhong, G. Polyphenolic composition and content in the ripe berries of wild *Vitis* species. *Food Chem.* **2012**, *132*, 730−738.
(26) Wu, X.; Prior, R. L. Systematic identification and characterization of anthocyanins by HPLC−ESI-MS/MS in common foods in the United States: Fruits and berries. *J. Agric. Food Chem.* **2005**, *53*, 2589−2599.
(27) Giusti, M. M.; Rodriguez-Saona, L. E.; Griffin, D.; Wrolstad, R. E. Electrospray and tandem mass spectroscopy as tools for anthocyanin characterization. *J. Agric. Food Chem.* **1990**, *47*, 4657−4664.
(28) Brouillard, R.; Chassaing, S.; Fougerousse, A. Why are grape/fresh wine anthocyanins so simple and why is it that red wine color lasts so long? *Phytochemistry* **2003**, *64*, 1179−1186.
(29) Dao, L. T.; Takeoka, G. R.; Edwards, R. H.; Berrios, J.; De, J. Improved method for stabilization of anthocyanidins. *J. Agric. Food Chem.* **1996**, *46*, 3569−3654.
(30) Kaur, C. K.; Kapoor, H. C. Antioxidants in fruits and vegetables—The millennium's health. *Inter. J. Food Sci. Technol.* **2001**, *36*, 703−725.
(31) Deighton, N.; Brennan, R.; Finn, C.; Davies, H. V. Antioxidant properties of domesticated and wild *Rubus* species. *J. Agric. Food Chem.* **2000**, *80*, 1307−1313.
(32) Yakovleva, L. E.; Kurzeev, S. A.; Stepanova, E. V.; Fedorova, T. V.; Kuznetsov, B. A.; Koroleva, O. V. Characterization of plant phenolic compounds by cyclic voltammetry. *Applied Biochem. Microbiol* **2007**, *43*, 661−668.

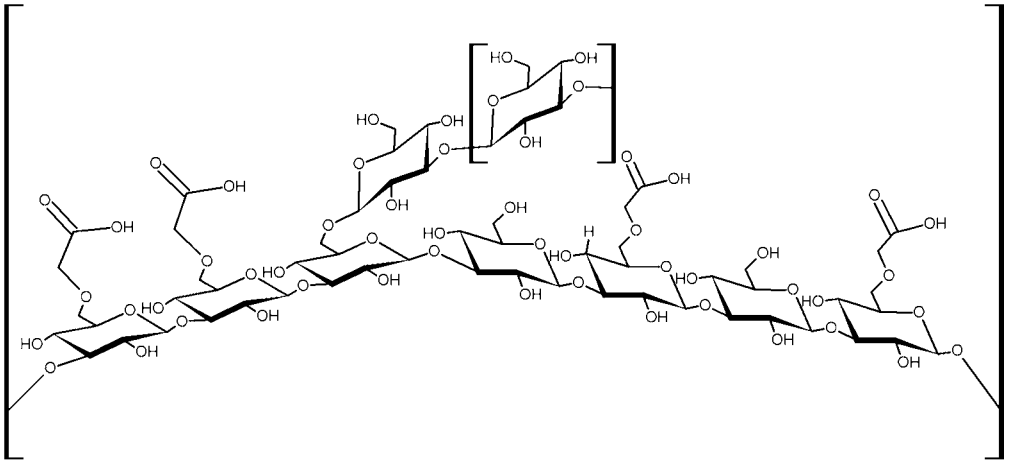

Figure 2. Carboxymethylated-(1,3/1,6)-β-D-Glucan chemical structure.

storage stability under wet and light stresses within 10 days. Furthermore, the authors demonstrated that no chemical modification occurs on resveratrol, which retains unaltered antioxidant and physicochemical properties following encapsulation in yeasts.

In this paper we aimed at studying a new association of resveratrol with a high molecular weight polysaccharide, the carboxymethylated (1,3/1,6)-β-D-glucan (CM-glucan), to be used in liquid formulations (Figure 2). β-Glucans are a class of natural polysaccharides that are endowed with well-known pharmacological activities and are increasingly utilized in pharmaceutical applications and in the food industry.[13] The term β-glucans indicates noncellulosic polymers of β-glucose, with glycosidic bonds in position $\beta(1\rightarrow3)$ and with a significant portion of $\beta(1\rightarrow6)$-bound glucose molecules. They are isolated from fungi, cereals, bacteria, or seaweeds.[14−16] The most important quality of β-glucans, and the reason so much attention has been devoted to these compounds, is that they are typical biological response modifiers with pronounced immunomodulating activity, which confer anticancer, antioxidant, antiviral, and wound-healing capacities to these molecules.[13,17] These biopolymers are also widely utilized in view of their structural and drug delivery properties for the nanoencapsulation of lipophilic pharmaceutical compounds and for poorly bioavailable drugs.[18,19]

However, despite their very interesting pharmaceutical and pharmacological profile, β-glucans have limited applications in liquid formulations due to their poor water solubility. Hence, for our aims we opted for the use of the carboxymethylated derivative of β-glucan, CM-glucan, showing a higher degree of solubility in water due to the presence of the easily ionizable carboxyl residues (Figure 2).[20] This chemical modification does not affect the pharmaceutical and pharmacological properties of the product, which still exerts outstanding anticancer and antioxidant properties.[21,22]

The purpose of the present investigation was to evaluate the effect of CM-glucan on the long-term stability and solubility of resveratrol in aqueous solutions. To this purpose, we have developed a liquid formulation in which resveratrol is complexed with CM-glucan and resuspended in a buffered saline solution. The stability and antioxidant activity of resveratrol were further confirmed with spectroscopic methods.

MATERIALS AND METHODS

Reagents. *trans*-Resveratrol was purchased from Shanghai Novanat Co., Ltd. (Shanghai, China) and CM-glucan from Nutraceutica s.r.l. (Bologna, Italy). 2,2-Diphenyl-1-picrylhydrazyl (DPPH) and benzalkonium chloride were purchased from Sigma-Aldrich (Milan, Italy). Gradient grade solvents used for chromatographic analyses were purchased from Carlo Erba Reagents (Milan, Italy). All other reagents were analytical grade products from Sigma-Aldrich.

Sample Preparation. Samples for the stability study were prepared by dissolving resveratrol at a final concentration of 0.05% in different aqueous solvents (0.9% NaCl or phosphate-buffered saline (PBS)) containing 0.1% CM-glucan. Sonication or extensive magnetic stirring was employed for evenly dispersing the preparations. The samples were prepared in triplicate and then split in two aliquots, one of which was maintained at 25 °C and the other at 40 °C for accelerated stability determinations. Samples were stored in the dark at over a relative humidity (RH) range of 40−45%. At different times, an aliquot of each sample was taken and analyzed for resveratrol content. In a similar manner, control solutions were prepared without CM-glucan to evaluate the stability of 0.05% resveratrol, which was brought in solution by using surfactant agents, such as 0.5% PEG and 0.1% Tween-20. Benzalkonium chloride (0.04%) was employed as a preserving agent to inhibit microbial growth during long-term storage in stability analyses both in samples and in controls. For specific purposes, such as for spectrofluorometric measurements, samples were centrifuged at 12000*g* for 10 min before analysis.

HPLC Determination and Quantification of Resveratrol. The HPLC consisted of a Waters apparatus equipped with a 600 pump and pump controller, a Waters autosampler model 717, a Symmetry C18 column (reversed phase, 3.9 × 150 mm, 5 μm particle size, with a 10 mm guard column of the same material matrix), and a UV−visible photodiode array detector model 2996. Solvent A was 10% acetic acid in water, and solvent B was acetonitrile. The elution was performed in isocratic conditions at a flow rate of 1 mL/min at 25 °C with 80% A and 20% B. Resveratrol had a retention time of ≃7.0 min, and its quantitation was performed by automatic peak area integration using dedicated software (*Millennium*,[32] Waters). Before the analysis, each sample was resuspended, diluted in mobile phase 1:10, and filtered onto 0.2 μm filters, and then 50 μL was injected onto the column.

Stock solutions of resveratrol were freshly prepared immediately before use in DMSO at a concentration of 20 mM. Working solutions were prepared by diluting stock resveratrol solutions to the desired concentration in appropriate solvents. Calibration curves in the range of 1−12 nmol were prepared by replicate autosampler injections of different volumes of a standard solution of 0.219 mM resveratrol. The curves (six data points, in duplicate) were linear with R^2 values of ≃1.00. Peak detection was carried out at 306 nm, and the purity of the peak was checked with the diode array detector to verify the characteristic absorption spectrum of the polyphenol. The limit of

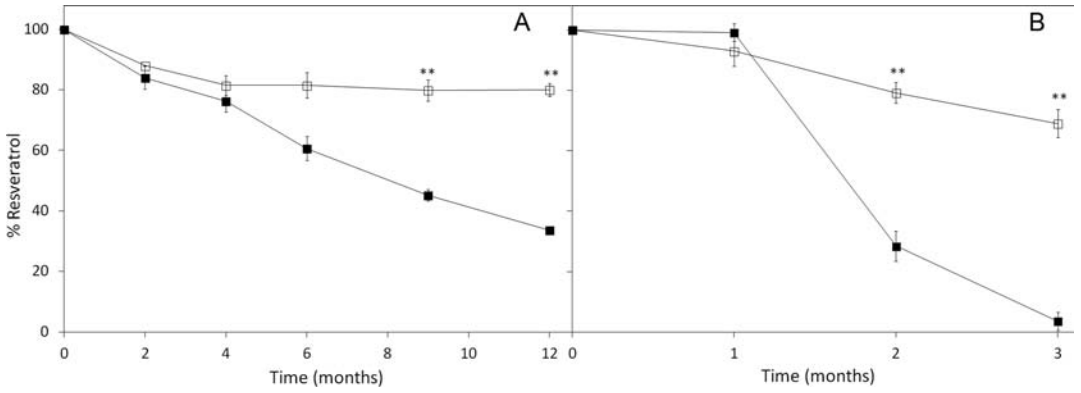

Figure 3. Stability analyses of the resveratrol/CM-glucan suspension. (A) Long-term stability at 25 °C: 0.05% resveratrol was resuspended in aqueous solutions in the presence (white squares) or in the absence (black squares) of 0.1% CM-glucan. Data points at 9 and 12 months are significantly different between resveratrol and resveratrol with CM-glucan (** = $p < 0.01$). (B) Accelerated stability at 40 °C: 0.05% resveratrol was resuspended in aqueous solutions in the presence (white squares) or in the absence (black squares) of 0.1% CM-glucan. Data points at 2 and 3 months are significantly different between resveratrol and resveratrol with CM-glucan (** = $p < 0.01$).

detection (4 pmol) was calculated as the analyte concentration giving a signal 3 times higher than the baseline value.

Fourier Transform Infrared Spectroscopy (FT-IR). FT-IR spectra were measured with a Nicolet Magna 760 (Thermo Scientific, Waltham, MA, USA) infrared spectrometer equipped with an ARK attenuated total reflectance device. The internal reflection element was ZnSe. Spectra were recorded at 4 cm^{-1} resolution with a DTGS detector. Samples were evaporated onto the ATR crystal by N_2 stream. The IR spectrum of the preserving agent utilized in the long-term measurements (i.e., benzalkonium chloride) was subtracted from spectrum of each sample analyzed.

Spectrofluorometric Analyses. Fluorescence emission spectra were recorded on a SPEX-Fluoromax spectrofluorometer (Horiba Scientific, Horiba Ltd., Kyoto, Japan) from 360 to 500 nm with excitation at 350 nm using a 0.1 cm path length quartz cuvette, under continuous stirring. The excitation and emission slits were both set to 5 nm, and scan speed was 120 nm/min.

Free Radical Scavenging Assay. Samples were tested for their free radical scavenging capacity by using the DPPH• test. DPPH•, a stable nitrogen-centered free radical, shows an absorption maximum at 517 nm, which decreases in the presence of H-donor molecules. Ten microliters of each sample was added to 1 mL of 30 μM DPPH• in ethanol, vortexed, and left for 15 min in the dark. Absorbance was measured at 517 nm on a Hitachi U-2000 spectrophotometer (Hitachi Ltd., Tokyo, Japan). The DPPH radical scavenging activity was estimated as described by Shi et al.[12]

Statistical Analyses. Experiments were repeated at least in triplicate, and all of the results are expressed as the mean value ± standard deviation (SD). Statistical comparison between groups was made using Student's t test. p values <0.05 were regarded as significant.

RESULTS

Long-Term and Accelerated Stability Analyses. To assess whether CM-glucan is able to stabilize resveratrol, we analyzed the shelf life of this compound in aqueous solutions in various storage conditions and at different times.

Data obtained from HPLC analyses of 0.05% resveratrol dissolved in PBS or in 0.9% NaCl solutions containing 0.1% CM-glucan show that the stability of this polyphenol is highly improved, with respect to the samples in which resveratrol is dispersed in saline solutions without CM-glucan. In the former case the loss of resveratrol is about 20% within 12 months; in the latter. this compound quickly undergoes oxidative and degradation processes with a loss of about 70% within 12 months (Figure 3A). Accelerated stability measurements at 40 °C confirm these data, indicating that in aqueous solutions without CM-glucan, resveratrol undergoes a rapid degradation and that this phenomenon is counteracted by CM-glucan (Figure 3B).

Further evidence of the stabilizing effect of CM-glucan on resveratrol is supported by the analysis of the absorbance spectra of the resveratrol peak (t_r = 7 min), as obtained by photodiode array detector. The results show that when resveratrol is in association with CM-glucan, it maintains its characteristic absorbance spectrum after 12 months at 25 °C, with a maximum at 306 nm and a shoulder around 320 nm, whereas preparations containing only resveratrol in aqueous solution show a peak at 270 nm and a shoulder at 305 nm, the absorbance of which is markedly lower than that of the unmodified compound (Figure 4).

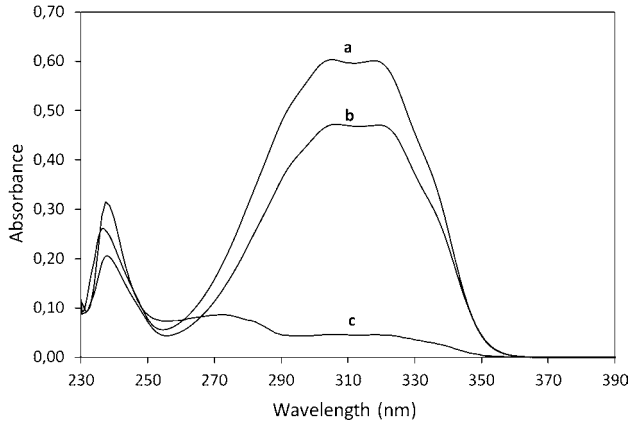

Figure 4. UV−visible spectra of the resveratrol peak (retention time = 7 min) isolated by HPLC from various samples: (a) freshly prepared 0.05% resveratrol in aqueous solution; (b) 0.05% resveratrol in 0.1% CM-glucan after 12 months at 25 °C; (c) 0.05% resveratrol in aqueous solutions after 12 months at 25 °C.

FT-IR. The spectra of resveratrol, CM-glucan, and their association were analyzed by FT-IR immediately after sample preparation and after 1 year of storage at room temperature to ascertain the concordances or the differences and to eventually verify the integrity or the degradation of resveratrol. As shown in Figure 5, the spectrum of isolated CM-Glucan (a) shows absorption bands at 1600, 1421, 1328, and 1047 cm^{-1} corresponding to the asymmetrical stretch of COOH, the

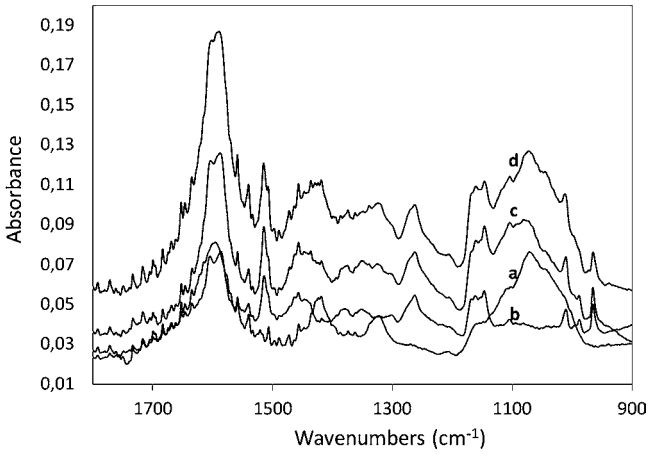

Figure 5. FT-IR spectra of resveratrol within the CM-glucan matrix. FT-IR-ATR spectra of 0.05% resveratrol embedded within 0.1% CM-glucan matrix are reported immediately after preparation (d) and after 12 months at 25 °C (c), in the region from 1800 to 900 cm^{-1}. Spectra of freshly prepared resveratrol (a) and CM-glucan (b) are also reported. All spectra were recorded at 25 °C, as thin layers over a ZnSe ATR reflection element.

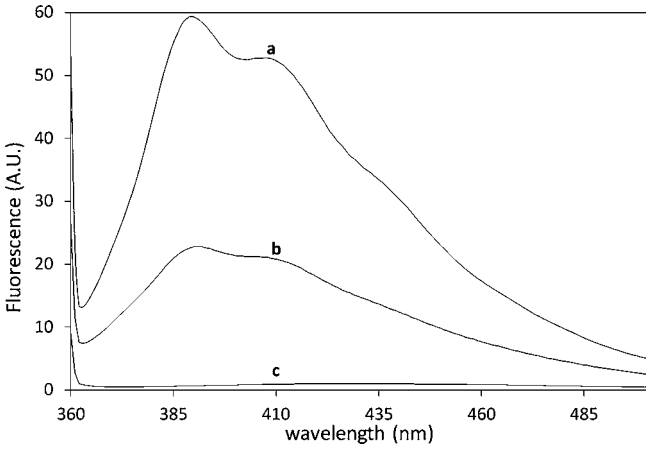

Figure 6. Fluorescence spectra of resveratrol or resveratrol/CM-glucan suspension. Resveratrol (0.05%) resuspended in aqueous solutions in the presence (b) or in the absence (a) of 0.1% CM-glucan was excited at 350 nm. Fluorescence spectra were recorded between 360 and 500 nm. CM-glucan in water (0.1%) (c) was used as a blank.

symmetrical stretch of COOH, and C−O and C−C stretches, respectively.[20] The resveratrol spectrum (b) shows a typical aromatic stretch at 1614 cm^{-1} that overlaps with asymmetrical COOH stretching of the CM-glucan. Resveratrol has also characteristic absorption bands at 1270 and 1150 cm^{-1} in the fingerprint region, corresponding to the in plane aromatic bending. Additional resveratrol bands occur at 1010, 988, and 966 cm^{-1}, corresponding to the three phenolic C−O stretches of the three hydroxyl groups on the aromatic rings. The same features observed in the isolated compounds are also present when resveratrol is complexed with CM-glucan. Interestingly, the spectrum of the mixture, recorded after 12 months at 25 °C (c), shows that there are no differences with respect to the spectrum of the freshly prepared solution (d).

Fluorescence Spectroscopy Analyses. To analyze whether resveratrol is able to interact with CM-glucan, we carried out spectrofluorometric analyses. When excited at 350 nm, resveratrol shows an emission spectrum with a maximum at 390 nm and a shoulder at 410 nm (Figure 6).[23] No significant spectral shift was noticed in the fluorescence spectrum of resveratrol after the addition of CM-glucan; however, a quenching effect was evident. The quenching effect on resveratrol by CM-glucan was calculated using the equation

$$Q\% = (1 - F/F_0) \times 100\%$$

where $Q\%$ represents the quenching fraction (%) and F_0 and F are the fluorescence intensities read at emission maximum of resveratrol (390 nm) in the absence or in the presence of CM-glucan, respectively. In our experimental conditions, CM-glucan is able to quench resveratrol intrinsic fluorescence by about 65−70%.

DPPH Radical Quenching by Resveratrol. DPPH• radical scavenging activity is widely used by many authors to measure the antioxidant activity of phenolic compounds.[24−26] This method was used to assess the radical scavenging activity of resveratrol solutions, either freshly prepared or aged in the presence or absence of CM-glucan.

The results of the radical scavenging capacity are expressed as percent of scavenging activity versus the intrinsic scavenging activity of the freshly prepared resveratrol samples (Figure 7). The higher the inhibition rate, the greater the hydrogen-donating ability and thus the higher the antioxidant activity. In our experimental conditions the association of resveratrol and CM-glucan has the same DPPH• scavenging activity with respect to freshly prepared resveratrol, and this activity is maintained after 12 months of storage at 25 °C, with only a partial loss of activity. On the contrary, aged resveratrol samples without CM-glucan or samples of CM-glucan have no significant antioxidant activity.

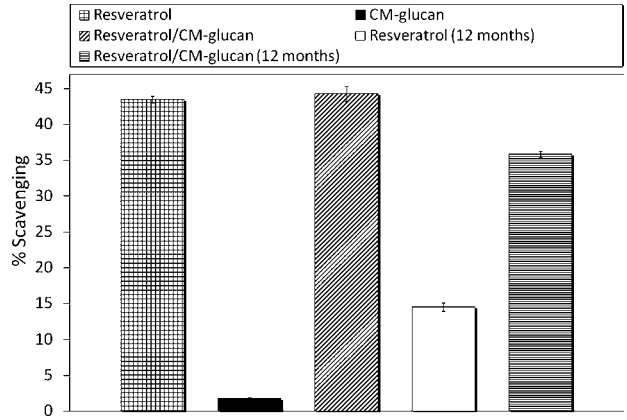

Figure 7. DPPH radical scavenging activity of resveratrol or resveratrol/CM-glucan suspension. DPPH scavenging activity was measured by determining the decrease in absorbance at 517 nm of a DPPH ethanolic solution taken as 100%.

DISCUSSION

Despite great interest in resveratrol and its multiple pharmacological properties, to date no pharmaceutical preparations are available on the market except for various food supplements or nutraceuticals. Resveratrol is unstable in aqueous solutions, and therefore the development of a liquid formulation useful for pharmacological applications is a significant challenge. The goal of our work was to develop a new liquid formulation by combining resveratrol with a

dx.doi.org/10.1021/jf404155e | J. Agric. Food Chem. 2014, 62, 1520−1525

polysaccharide able to stabilize this polyphenol over the long term.

One of the most interesting properties of CM-glucan is its structure-forming capacity, which, combined with its pharmacological activity, makes this compound ideal for the formulation of pharmaceutical preparations, which simultaneously take advantage of both properties. Gao and co-workers successfully encapsulated the anticancer drug Epirubicin in carboxymethyl Curdlan (a polysaccharide having a structure very similar to that of glucan) and demonstrated that compared with the free drug, Epirubicin-loaded Curdlan particles showed a higher anticancer activity.[27]

The evidence that glucan biopolymers may simultaneously act as a carrier of insoluble compounds and exert immunomodulatory and antioxidant activities prompted us to develop a new formulation in which resveratrol was combined with CM-glucan. This latter compound could act in synergistic action with resveratrol against a variety of pathogens (virus, bacteria) and could counteract its degradation in aqueous solutions. Recently, a combination of resveratrol and β-glucan has been described by Vetvika and co-workers in a number of publications in which the authors tested the synergistic effect of these two components in different model systems.[28−30] However, they did not aim at developing a new formulation or at assessing its shelf life.

Long-term stability studies, up to 12 months at 25 °C, demonstrated that the association with CM-glucan protected resveratrol from the fast degradation in aqueous medium. However, within the first 3 months the stability of resveratrol is only slightly affected by CM-glucan presence and is quite similar to the control sample, most probably because not all of the resveratrol molecules are bound to CM-glucan. The accelerated stability analyses at 40 °C further confirmed that the combination of resveratrol and CM-glucan shows a higher stability compared to resveratrol alone in solution.

In long-term stability analyses in the absence of CM-glucan, resveratrol shows a shift in its absorption spectrum, from 306 to 270 nm. This spectral feature can be correlated to the degradation or the oxidation of resveratrol[31] and cannot be attributed to the formation of *cis*-resveratrol, which has a λ_{max} of 284 nm and a retention time of 11.5 min in our experimental conditions.

HPLC analysis and the FT-IR spectra support the idea of a stable complex formation, as no modification of the UV−vis and IR spectra are observed during storage time. FT-IR, spectrophotometric, and stability data are in good agreement and overall clearly indicate that the CM-glucan matrix exerts a strong stabilizing effect on the polyphenolic molecule.

Furthermore, in our experiments, we observed that resveratrol stabilization by CM-glucan was independent of the method utilized for resuspension; that is, the mechanical dissolution by vortexing gave similar results compared to sonication or extensive magnetic stirring (data not shown). This indicates that the interaction between CM-glucan and resveratrol is of a chemical nature and independent of any physical or mechanical action that may favor the interaction of these two molecules.

The evaluation of the antioxidant potential of resveratrol by the DPPH assay further supports the HPLC and FT-IR data, as the CM-glucan completely prevents the loss of antioxidant activity of resveratrol due to prolonged storage of the preparations. In our experimental conditions the association of resveratrol and CM-glucan has the same $DPPH^{\bullet}$ scavenging activity with respect to resveratrol control samples, and this activity is maintained after 12 months of storage at 25 °C, even though there is a partial loss of activity, which exactly matches the 20% reduction in resveratrol amount observed by HPLC. On the contrary, CM-glucan alone or aged solutions of resveratrol have a low antioxidant activity in contrast to freshly prepared resveratrol samples.

As widely described in the literature, resveratrol is an extremely unstable molecule, easily undergoing oxidative and degradative processes when solubilized in water. The stabilization of the polyphenolic molecule by CM-glucan may be due to various factors. First, CM-glucan may exert a physical barrier by encapsulating resveratrol and protecting it from the environment, acting with a β-cyclodextrin-like mechanism.[6] This hypothesis is supported by spectrofluorometric measurements, in which we observed a quenching of resveratrol fluorescence without any significant modification of the emission spectrum or spectral shift. These data indicate that CM-glucan does not induce any obvious changes in resveratrol conformation, most likely due to a dynamic interaction. The decrease of fluorescence may indicate that the microenvironment of resveratrol molecules was altered due to the interaction with the biopolymer. These data suggest that the chemical environment created by CM-glucan can protect the polyphenol from degradation processes. It can be hypothesized that CM-glucan can establish a weak electrostatic interaction with resveratrol, contributing to the stabilization of the molecule by counteracting oxidative processes of hydroxyl groups and hampering the formation of quinonoid species. Indeed, another possible mechanism by which CM-glucan may exert a stabilizing effect on resveratrol may be due to its antioxidant activity, which can limit resveratrol autoxidation in solution, thereby hampering the formation of oxidation and degradation products of this compound. CM-glucan antioxidant activity was extensively studied by many authors, and this compound is largely utilized in many cosmetic preparations as it protects skin cells against ultraviolet A (UV-A) irradiation and promotes keratinocytes growth, thus enhancing the renewal rate of the stratum corneum.[21,32−34] In our experimental conditions CM-glucan shows a low antioxidant activity, most likely due to the low amount of sample used to highlight the differences in the scavenging activity of resveratrol among the various samples.

At present, a search of the clinicaltrials.gov database reveals that there are a total of 68 studies on resveratrol, of which 28 are ongoing trials. This is strong evidence of the great interest of the scientific community in this molecule; however, there is compelling evidence for the need of improved and more suitable formulations to get better clinical outcomes and reach clinical effectiveness. Our data provide evidence of the possibility to formulate resveratrol in liquid suspensions, overcoming its chemical instability and the consequent loss of biological activity and pharmacological efficacy.

AUTHOR INFORMATION

Corresponding Author

*(L.M.) Phone: +39 06 49910923. Fax: +39 06 4440062. E-mail: luciana.mosca@uniroma1.it.

Funding

This work was supported by NOOS srl.

Notes

The authors declare the following competing financial interest(s): A.F. and L.M. serve as consultants to NOOS srl.

ABBREVIATIONS USED

CM-glucan, carboxymethylated (1,3/1,6)-β-D-glucan; DPPH, 2,2-diphenyl-1-picrylhydrazyl; FT-IR, Fourier transformed infrared spectroscopy; HPLC, high-performance liquid chromatography; PBS, phosphate-buffered saline; PEG, polyethylene glycol; RH, relative humidity; t_r, retention time; UV-A, ultraviolet A light

REFERENCES

(1) Neves, A. R.; Lucio, M.; Lima, J. L. C.; Reis, S. Resveratrol in medicinal chemistry: a critical review of its pharmacokinetics, drug-delivery, and membrane interactions. *Curr. Med. Chem.* **2012**, *19*, 1663−1681.

(2) Baur, J. A.; Sinclair, D. A. Therapeutic potential of resveratrol: the in vivo evidence. *Nat. Rev. Drug Discov.* **2006**, *5*, 493−506.

(3) Amri, A.; Chaumeil, J. C.; Sfar, S.; Charrueau, C. Administration of resveratrol: what formulation solutions to bioavailability limitations? *J. Controlled Release* **2012**, *158*, 182−193.

(4) Francioso, A.; Mastromarino, P.; Masci, A.; d'Erme, M.; Mosca, L. Chemistry, stability and bioavailability of resveratrol. *Med. Chem.* **2014**, *10*, in press.

(5) Ansari, K. A.; Vavia, P. R.; Trotta, F.; Cavalli, R. Cyclodextrin-based nanosponges for delivery of resveratrol: in vitro characterisation, stability, cytotoxicity and permeation study. *AAPS PharmSciTech* **2011**, *12*, 279−286.

(6) Das, S.; Lin, H. S.; Ho, P. C.; Ng, K. Y. The impact of aqueous solubility and dose on the pharmacokinetic profiles of resveratrol. *Pharm. Res.* **2008**, *25*, 2593−2600.

(7) Das, S.; Ng, K. Y. Resveratrol-loaded calcium-pectinate beads: effects of formulation parameters on drug release and bead characteristics. *J. Pharm. Sci.* **2010**, *99*, 840−860.

(8) Das, S.; Ng, K. Y. Colon-specific delivery of resveratrol: optimization of multi-particulate calcium-pectinate carrier. *Int. J. Pharm.* **2010**, *385*, 20−28.

(9) Scognamiglio, I.; De Stefano, D.; Campani, V.; Mayol, L.; Carnuccio, R.; Fabbrocini, G.; Ayala, F.; La Rotonda, M. I.; De Rosa, G. Nanocarriers for topical administration of resveratrol: a comparative study. *Int. J. Pharm.* **2013**, *440*, 179−187.

(10) Wegiel, L. A.; Mauer, L. J.; Edgar, K. J.; Taylor, L. S. Crystallization of amorphous solid dispersions of resveratrol during preparation and storage-Impact of different polymers. *J. Pharm. Sci.* **2013**, *102*, 171−84.

(11) Silva, F.; Figueiras, A.; Gallardo, E.; Nerin, C.; Domingues, F. C. Strategies to improve the solubility and stability of stilbene antioxidants: a comparative study between cyclodextrins and bile acids. *Food Chem.* **2014**, *145*, 115−125.

(12) Shi, G. R.; Rao, L. Q.; Yu, H. Z.; Xiang, H.; Yang, H.; Ji, R. Stabilization and encapsulation of photosensitive resveratrol within yeast cell. *Int. J. Pharm.* **2008**, *349*, 83−93.

(13) Lehtovaara, B. C.; Gu, F. X. Pharmacological, structural, and drug delivery properties and applications of 1,3-β-glucans. *J. Agric. Food Chem.* **2011**, *59*, 6813−6828.

(14) Sutherland, I. W. Microbial polysaccharides from Gram-negative bacteria. *Int. Dairy J.* **2001**, *11*, 663−674.

(15) Wasser, S. P. Medicinal mushrooms as a source of antitumor and immunomodulating polysaccharides. *Appl. Microbiol. Biotechnol.* **2002**, *60*, 258−274.

(16) Wiater, A.; Paduch, R.; Pleszczynska, M.; Prochniak, K.; Choma, A.; Kandefer-Szerszen, M.; Szczodrak, J. α-(1→3)-D-Glucans from fruiting bodies of selected macromycetes fungi and the biological activity of their carboxymethylated products. *Biotechnol. Lett.* **2011**, *33*, 787−795.

(17) Magnani, M.; Castro-Gomez, R. H.; Aoki, M. N.; Gregorio, E. P.; Libos, F.; Morimoto, H. K.; Reiche, E. M. V.; Watanabe, M. A. E. Analysis of peripheral T cells and the CC chemokine receptor (CCR5) delta32 polymorphism in prostate cancer patients treated with carboxymethyl-glucan (CM-G). *Nat. Prod. Res.* **2012**, *26*, 945−951.

(18) Kanke, M.; Katayama, H.; Nakamura, M. Application of curdlan to controlled drug-delivery. 2. In-vitro and in-vivo drug-release studies of theophylline-containing Curdlan tablets. *Biol. Pharm. Bull.* **1995**, *18*, 1104−1108.

(19) Li, L.; Gao, F. P.; Tang, H. B.; Bai, Y. G.; Li, R. F.; Li, X. M.; Liu, L. R.; Wang, Y. S.; Zhang, Q. Q. Self-assembled nanoparticles of cholesterol-conjugated carboxymethyl Curdlan as a novel carrier of epirubicin. *Nanotechnology* **2010**, *21*, DOI: 10.1088/0957-4484/21/26/265601.

(20) Sandula, J.; Kogan, G.; Kacurakova, M.; Machova, E. Microbial (1→3)-β-D-glucans, their preparation, physico-chemical characterization and immunomodulatory activity. *Carbohydr. Polym.* **1999**, *38*, 247−253.

(21) Babincova, M.; Bacova, Z.; Machova, E.; Kogan, G. Antioxidant properties of carboxymethyl glucan: comparative analysis. *J. Med. Food* **2002**, *5*, 79−83.

(22) Wang, J.; Zhang, L.; Yu, Y.; Cheung, P. C. Enhancement of antitumor activities in sulfated and carboxymethylated polysaccharides of *Ganoderma lucidum*. *J. Agric. Food Chem.* **2009**, *57*, 10565−10572.

(23) Vitrac, X.; Monti, J. P.; Vercauteren, J.; Deffieux, G.; Merillon, J. M. Direct liquid chromatographic analysis of resveratrol derivatives and flavanonols in wines with absorbance and fluorescence detection. *Anal. Chim. Acta* **2002**, *458*, 103−110.

(24) Foti, M. C.; Daquino, C. Kinetic and thermodynamic parameters for the equilibrium reactions of phenols with the dpph(•) radical. *Chem. Commun.* **2006**, 3252−3254.

(25) Laghari, A. H.; Ali Memon, A.; Memon, S.; Nelofar, A.; Khan, K. M.; Yasmin, A. Determination of free phenolic acids and antioxidant capacity of methanolic extracts obtained from leaves and flowers of camel thorn (*Alhagi maurorum*). *Nat. Prod. Res.* **2012**, *26*, 173−176.

(26) Villano, D.; Fernandez-Pachon, M. S.; Moya, M. L.; Troncoso, A. M.; Garcia-Parrilla, M. C. Radical scavenging ability of polyphenolic compounds towards DPPH free radical. *Talanta* **2007**, *71*, 230−235.

(27) Gao, F. P.; Li, L.; Zhang, H. Z.; Yang, W. Z.; Chen, H. L.; Zhou, J.; Zhou, Z. M.; Wang, Y. S.; Cai, Y. Y.; Li, X. M.; Liu, L. R.; Zhang, Q. Q. Deoxycholic acid modified-carboxymethyl Curdlan conjugate as a novel carrier of epirubicin: In vitro and in vivo studies. *Int. J. Pharm.* **2010**, *392*, 254−260.

(28) Vetvicka, V.; Vetvickova, J. Glucan-resveratrol-vitamin C combination offers protection against toxic agents. *Toxins* **2012**, *4*, 1301−1308.

(29) Vetvicka, V.; Vetvickova, J. Combination of glucan, resveratrol and vitamin C demonstrates strong anti-tumor potential. *Anticancer Res.* **2012**, *32*, 81−87.

(30) Vetvicka, V.; Volny, T.; Saraswat-Ohri, S.; Vashishta, A.; Vancikova, Z.; Vetvickova, J. Glucan and resveratrol complex − possible synergistic effects on immune system. *Biomed. Pap. Med. Fac. Univ. Palacky, Olomouc* **2007**, *151*, 41−46.

(31) Bravo, M. N.; Feliciano, R.; Silva, S.; Coelho, A. V.; Boas, L. V.; Bronze, M. R. Analysis of *trans*-resveratrol: comparison of methods and contents in Muscatel fortified wines from Setubal region in Portugal. *J. Food Compos. Anal.* **2008**, *21*, 634−643.

(32) Shin, J. Y.; Lee, S.; Bae, I. Y.; Yoo, S. H.; Lee, H. G. Structural and biological study of carboxymethylated *Phellinus linteus* polysaccharides. *J. Agric. Food Chem.* **2007**, *55*, 3368−3372.

(33) Wang, Y. J.; Yu, Y. Z.; Mao, J. W. Carboxymethylated β-glucan derived from *Poria cocos* with biological activities. *J. Agric. Food Chem.* **2009**, *57*, 10913−10915.

(34) Zulli, F.; Suter, F.; Biltz, H.; Nissen, H. P. Improving skin function with CM-glucan, a biological response modifier from yeast. *Int. J. Cosmet. Sci.* **1998**, *20*, 79−86.

the TLRs, TLR2 is known to recognize several molecules from Gram-positive bacteria and mycobacteria, such as lipoteichoic acid, lipopeptides, and peptidoglycan,[11] whereas TLR4 is a transmembrane protein that plays an essential role in the recognition of LPS, which is the main component of the outer membrane of Gram-negative bacteria.[12] Both of these receptors have been demonstrated to play important roles in recognition of mushroom compounds that possess bioactive properties and active TLR-mediated signaling pathways that enhance the immune response.[13,14]

In the present study, a novel immune-activating protein, *T. fuciformis* immunomodulatory protein (TFP), which was isolated from the dried fruiting bodies of *T. fuciformis*, was demonstrated to induce macrophage activation. We demonstrated that TFP induces macrophage activation through NF-κB. Furthermore, our data revealed that TFP enhances proinflammatory gene expression and induces M1-type polarization of macrophages through a TLR4-dependent pathway.

MATERIALS AND METHODS

Mice. BALB/c and C57BL6 mice that were 8−10 weeks of age were purchased from the National Laboratory Animal Center, Taipei, Taiwan. TLR4-deficient mice ($TLR4^{-/-}$, strain C57BL/10ScN) were purchased from Jackson Laboratory (Bar Harbor, ME) and maintained in our animal facility under specific pathogen-free conditions. All mice were fed a standard mice diet (LabDiet, Richmond, IN). All experimental procedures were approved by the Institutional Animal Care and Use Committee of National Taiwan University (NTU-IACUC-95-139).

Cell Preparation. Peritoneal macrophages were obtained from BABL/c, C57BL/6J, and $TLR4^{-/-}$ mice 3 days after i.p. injection of 1.8 mL of sterile 3% thioglycollate (Sigma, St. Louis, MO). Macrophages were harvested by sacrificing mice and flushing ∼6 mL of cold phosphate-buffered saline (PBS) into the mouse peritoneal cavity twice. The fluid containing the macrophages was centrifuged and resuspended in Dulbecco's modified Eagle's medium (DMEM) (Hyclone, Logan, UT) with 10% (v/v) fetal bovine serum (FBS) (Life Technologies, Grand Island, NY). The cells were counted, plated in 24-well (2×10^6 cells/well) or 12-well (4×10^6 cells/well) flat-bottom culture plates (Costar, Cambridge, MA), and incubated for 2 h in a humidified atmosphere of 5% CO_2 at 37 °C. After the incubation, the supernatants were removed, and the cells were washed with warm PBS to remove nonadherent cells. The cells were further incubated in DMEM containing 10% FBS before and during all experiments.

Purification of TFP. One kilogram of weighed dried fruiting bodies of *T. fuciformis* that were obtained from a local market were soaked in water for 2 h for rehydration and then soaked in a 5% (v/v) acetic acid solution containing 50 mM 2-mercaptoethanol at 4 °C overnight. After soaking, the fruiting bodies were homogenized and centrifuged at 8500*g* for 50 min. The soluble proteins in the supernatant were precipitated by adding ammonium sulfate from 60% saturation and centrifuging at 8500*g* for 50 min to collect the precipitates. The precipitates were dialyzed in 20 mM Tris-HCl buffer (pH 8.2) for 96 h with at least eight changes of the dialysis buffer. The main active fractions in the dialysate, which was capable of increasing TNF-α production by RAW 264.7 macrophages, were fractionated and purified using a fast protein liquid chromatography (FPLC) system with a Resource-Q anion exchange column (GE Healthcare, Uppsala, Sweden) in 10 mM Tris-HCl buffer containing 0.5 M NaCl (pH 8.0). Each fraction was analyzed with denaturing sodium dodecyl sulfate polyacrylamide gel electrophoresis (SDS-PAGE), and the fraction containing a single 24 kDa protein was chosen for activity analysis. The 24 kDa protein that could induce RAW264.7 macrophages to produce TNF-α was our target protein, TFP. The fraction containing TFP was further dialyzed and concentrated optimally for the subsequent analysis and in vitro experiments.

Molecular Weight Determination and Amino Acid Sequencing. The purity and molecular weight of TFP were analyzed by SDS-PAGE using a Bio-Rad mini protein III gel apparatus (Bio-Rad Laboratories, Hercules, CA). The gels were stained with Coomassie brilliant blue R250 or periodic acid-Schiff reagent (Sigma). The molecular mass of the protein was compared with those of standard proteins in the range of 10−170 kDa (Fermentas Life Sciences, Glen Burnie, MD). The molecular weight of TFP was further estimated using an FPLC system with a Superdex gel filtration column (GE Healthcare), equilibrated, and eluted with 50 mM phosphate buffer (pH 7.0) containing 0.15 M NaCl. The column was calibrated using the same parameters with protein standards (Amersham Biosciences, Uppsala, Sweden) consisting of ovalbumin, carbonic anhydrase, trypsin inhibitor, and lysozyme (Supplemental Figure 1 in the Supporting Information). The TFP sample was separated by SDS-PAGE and electrotransferred onto a poly(vinylidene difluoride) (PVDF) Immobilon P membrane (Millipore, Billerica, MA) using a Trans-Blot cell system (Bio-Rad) with transfer buffer. The TFP protein band was cut out from the membrane, and its N-terminal peptide sequence was determined using automated Edman degradation and sequence analysis (Mission, Taipei, Taiwan).

Molecular Cloning of the Gene and cDNA Encoding TFP. The total RNA of *T. fuciformis* fruiting bodies was extracted using an RNeasy Plant Mini Kit (Qiagen, Germantown, MD) according to the manufacturer's protocol. First-strand cDNA was synthesized from total RNA by reverse-transcription polymerase chain reaction (RT-PCR) using a Thermoscript RT-PCR system (Invitrogen, Carlsbad, CA) with a 3′-SMART RACE cDNA Amplification Kit (Clontech, Mountain View, CA). The 3′-RACE TFP primer and the TFP-specific forward degenerate primer 3T36, which was designed on the basis of the partial N-terminal amino acid sequence with the lowest degeneracy of the genetic code, were paired for PCR amplification of the *tfp* gene. The resulting 600 bp PCR product (3T36-600) was ligated into the pGEM-T easy vector (Promega, Madison, WI), transformed into *Escherichia coli*, and sequenced. The 5′ end of TFP was obtained by using a 5′-SMART RACE cDNA Amplification Kit (Clontech). The 5′-RACE TFP primer was paired with the reverse primer Fru5T1, which is specific for the 3T36-600 fragment, for PCR amplification. A 400 bp PCR product (Fru5T1-400 fragment) was sequenced by the same method. The full-length sequence of TFP cDNA was obtained by alignment of the 3T36-600 and Fru5T1-400 fragments. After synthesis of cDNA from the total RNA of *T. fuciformis* fruiting bodies as the template, the sequence was confirmed via PCR amplification with gene-specific primer pairs that were designed on the basis of the full-length sequence of TFP.

Expression and Purification of Recombinant TFP. The cDNA synthesized from the total RNA of *T. fuciformis* fruiting bodies was used to amplify the TFP gene for expression. The primers used for PCR amplification of TFP were 5′-CCATGGTCGTCCAGAGGGATGACACA-3′ and 5′-CTCGAGATCAAACGCCTAGTCGAACTC-3′. After purification, the PCR products were digested with *Nco*I and *Xho*I (New England Biolabs, Beverly, MA). Double-digested PCR products were ligated into pET30a(+) vector and transformed into *E. coli* BL-21 competent cells (Bioman, Taipei, Taiwan) for protein expression. A single BL-21 colony containing the pET30-TFP vector was inoculated into LB/ampicillin medium overnight and then induced with 1 mM IPTG for 3 h at 37 °C. The cultures were centrifuged at 6500 rpm for 30 min and rinsed twice with PBS. After collection, the bacteria were sonicated for 30 min and then centrifuged at 6500 rpm for 30 min. The supernatants were collected for FPLC purification with a HiTrap chelating HP column (GE Healthcare). Before loading of the supernatants, the 1 mL Hitrap chelating column was prepared according to the manufacturer's instructions and equilibrated with binding buffer (0.02 M sodium phosphate, 0.5 M NaCl, 5 mM imidazole, pH 7.4) by washing with five column volumes. The column was loaded with supernatants containing His-tagged TFP protein and washed with five column volumes of binding buffer to remove nonbinding protein. His-tagged TFP protein was eluted with elution buffer (0.02 M sodium phosphate, 0.5 M NaCl, 0.5 M imidazole, pH 7.4) in the final fractions. The purities of the fractions containing His-tagged TFP protein were identified by SDS-PAGE and Western blotting analysis with monoclonal antibodies (mAbs) specific

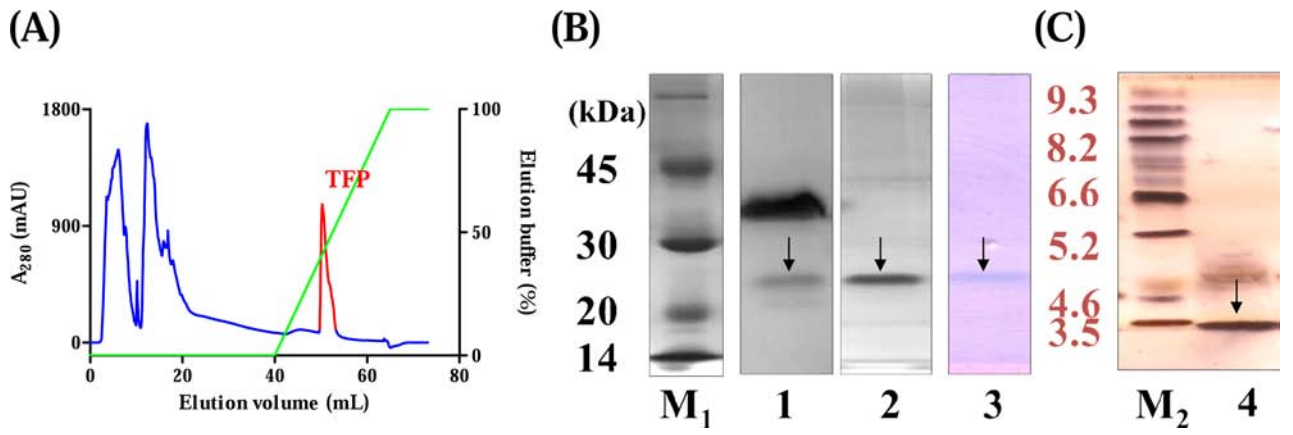

Figure 1. Chromatographic purification and electrophoretic analysis of native TFP. (A) The elution profile of the ammonium sulfate precipitates of a *T. fuciformis* dried fruiting body from FPLC using a Resource Q column displayed a single peak of TFP. (B) SDS-PAGE analysis of the crude protein from *T. fuciformis* (lane 1), purified TFP (lane 2), and purified TFP with periodic acid/Schiff's staining (lane 3) indicated that TFP had a mobility similar to that of a 24 kDa protein that did not contain carbohydrates. (C) Isoelectric focusing analysis (lane 4) indicated that the pI of TFP is 3.45.

for TFP and the His tag. The His tag was removed from the recombinant His-tagged TFP protein using EKMax enterokinase (Invitrogen) to yield recombinant TFP. All of the proteins were dialyzed with PBS and further concentrated optimally for the subsequent analysis.

Determination of Cytokine Production. The production of the cytokines TNF-α, IL-1β, IL-10, and IL-12p70 in cell-culture supernatants was determined by sandwich enzyme-linked immunosorbent assay (ELISA) using mouse TNF-α, IL-1β, and IL-10 ELISA kits (eBioscience, San Diego, CA) and a DuoSet mouse IL-12p70 ELISA Kit (R&D Systems, Minneapolis, MN) according to each manufacturer's protocols.

Quantitative Real-Time PCR. The cells were lysed using TRIzol reagent (Invitrogen), and the total RNA was extracted from the cell lysate according to the manufacturer's protocols. The quality and concentration of RNA were determined using a NanoDrop ND-1000 spectrophotometer (NanoDrop Technologies, Wilmington, DE). The total RNA was used as a template to synthesize the first-strand cDNA with a ThermoScript RT-PCR system (Invitrogen) for evaluation of the expression of genes implicated in TFP-induced activation in macrophages. The expression differences of individual genes were measured using real-time PCR. The primers were based on macrophage-specific cytokines, chemokines, and transcription factor sequences from NCBI and designed for SYBR green probes with Probe Design software (Roche, Mannheim, Germany) (Supplemental Table 1). Gene amplifications were normalized to the β-actin housekeeping gene. Real-time PCR was performed using a Bio-Rad MyiQ single-color detection system (Bio-Rad). The expression level of the individual target genes was quantified with the relative levels of the specific mRNA using cycling threshold (Ct) analysis. The relative expression value of significantly different expression in the gene should be higher than 4-fold relative to the 0 h control.

Electrophoretic Mobility Shift Assay. The DNA−protein interaction was determined using a LightShift Chemiluminescent EMSA kit (Pierce, Rockford, IL) according to the manufacturer's protocol. The nuclear protein extracts were prepared using NE-PER nuclear and cytoplasmic extraction reagents (Pierce) and incubated with biotinylated double-stranded NF-κB probes. The DNA−protein complexes were analyzed using a native 6% polyacrylamide gel and electrotransferred onto nylon membranes. When the transfer was completed, the biotinylated NF-κB−DNA complexes were detected using a chemiluminescent substrate kit (Pierce) with peroxidase-conjugated streptavidin.

Fluorescence-Activated Cell Sorting (FACS) Analysis. The expressions of surface CD80, CD86, and MHC-II on mouse peritoneal macrophages that were cultured with TFP for 24 h were detected using a FACScan flow cytometer (BD Biosciences, Franklin Lakes, NJ) with fluorescein isothiocyanate (FITC)-conjugated antibodies specific for mouse CD80, CD86, and MHC-II (eBioscience). The cells were harvested with PBS, centrifuged at 1500*g*, and resuspended with PBS containing 2% bovine serum albumin and 0.1% sodium azide (FACS buffer). Antibody was added to the cell suspensions, which were then incubated at 4 °C for 30 min. After the treatments, the cells were washed with FACS buffer to remove the unbound antibodies.

For phagocytosis experiments, the cells were incubated with TFP for 24 h, collected, centrifuged, and resuspended in FACS buffer. The phagocytosis ability of macrophages was analyzed using a Vybrant Phagocytosis Assay Kit (Molecular Probes) according to the manufacturer's protocol. After addition of the fluorescent *E. coli* BioParticles, cells (10^6 cells/mL) were incubated at 4 °C as a negative control and for 37 °C for 1 h. Antibody-stained or *E. coli*-treated cells were analyzed to determine the mean fluorescence intensity (MFI) and percentage of positive fluorescent cells using a FACScan flow cytometer with CellQuest software (BD Biosciences). The peak fluorescence intensities of the control and experiment groups were compared.

Statistical Analysis. All data are presented as means ± standard deviations of three independent experiments (n = 3) performed in triplicate. The statistical comparisons were executed by analysis of variance (ANOVA). When the P value was below 0.05 (i.e., $P < 0.05$), the differences were considered to be statistically significant.

RESULTS

Purification of TFP. To isolate the bioactive protein from *T. fuciformis*, the crude protein of the dry fruiting body that was obtained from homogenization and ammonium sulfate precipitation was subjected to FPLC using a Resource Q anion exchange column with a linear gradient of sodium chloride (0−0.5 M in 20 mM Tris-HCl buffer, pH 8.2). Measuring absorbance at 280 nm revealed a remarkable peak in the elution profile (Figure 1A). With this procedure, we were able to collect around 61 mg of this purified protein from 100 g of the dry fruiting bodies. The protein of this peak was then collected, and its activity was investigated by coculturing with RAW 264.7 macrophages. Significant TNF-α production was observed in the supernatant of RAW 264.7 cells that were cultured with the peak fraction (Supplemental Figure 2). This active fraction was analyzed with SDS-PAGE and displayed a single protein with an observed molecular mass of approximately 24 kDa (Figure 1B). This bioactive protein was designated TFP. The endotoxin level in the TFP sample which as determined with a ToxinSensor Chromogenic LAL Endotoxin Assay Kit was around 0.14 EU/μg (data not

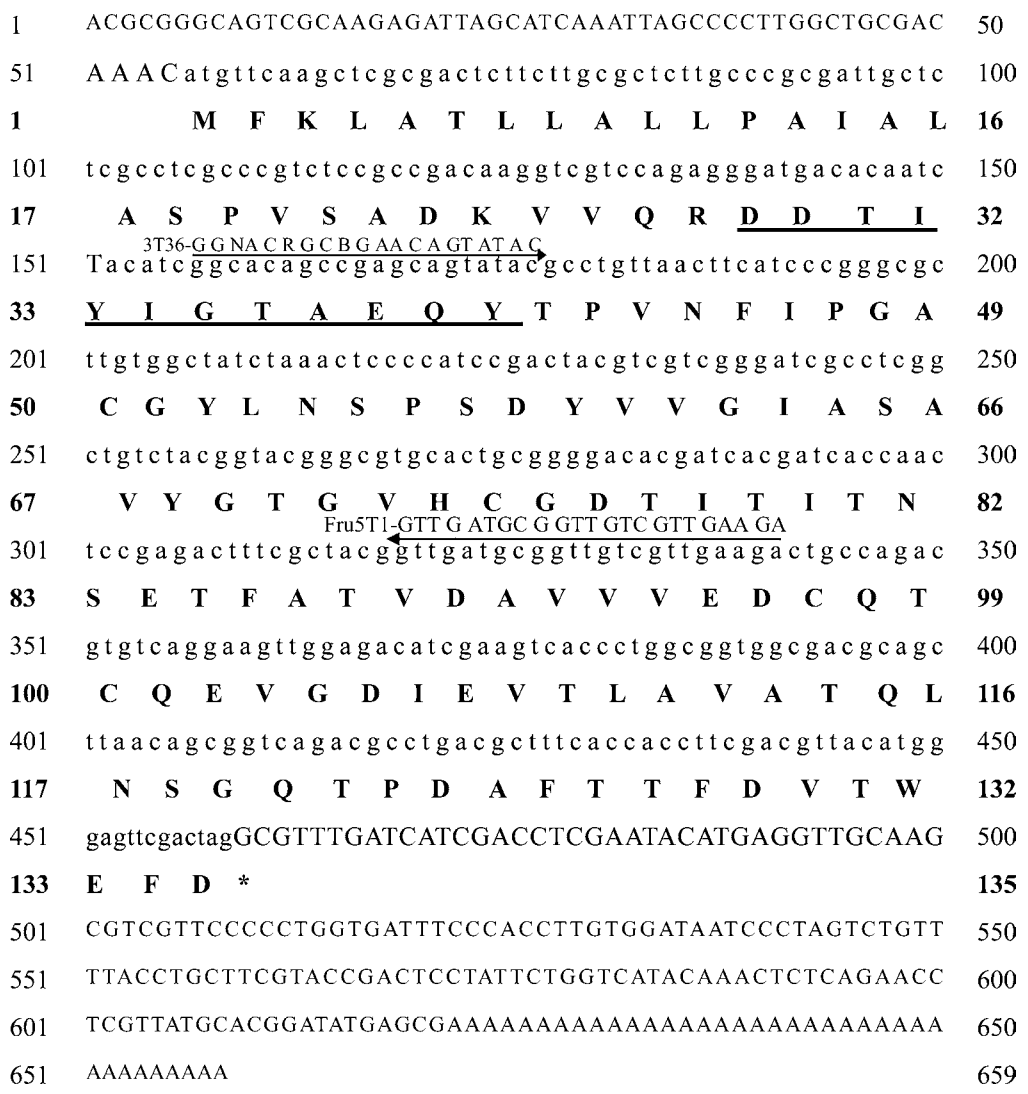

Figure 2. Nucleotide and translated amino acid sequence of TFP. The N-terminal amino acid sequence obtained by Edman degradation is underlined, and the signal peptide of TFP is shown in bold. The forward degenerate primer (3T36) based on the TFP N-terminal sequence (GTAEQY) and used in 3′-RACE PCR is indicated above the right-pointing arrow. The DNA sequence of the reverse degenerate primer (Fru5T1) used in 5′-RACE with the 3′-RACE product sequence (VDACCCED) is shown above the left-pointing arrow. The full-length sequence of TFP reported in this paper has been deposited in the GenBank database (accession number EF152774).

shown). To further analyze the biochemical characteristics of TFP, we used carbohydrate staining and isoelectric focusing electrophoresis to determine that TFP was not a glycoprotein (Figure 1B and Supplemental Figure 3) and that its pI value was 3.45 (Figure 1C), respectively.

Cloning of TFP. To clone the full-length cDNA sequence of TFP, we used N-terminal amino acid analysis and RACE by RT-PCR. First, the TFP after electrophoretic analysis with SDS-PAGE was immobilized onto a PVDF membrane and then subjected to N-terminal amino acid analysis. The sequence of the 15 N-terminal amino acid residues, DDTIYIGTAEQYTPV, was obtained from Edman degradation and analysis. This sequence exhibited low similarity to any known protein based on an NCBI database search with BLASTP. Next, we designed degenerate primers for RACE according to the TFP N-terminal amino acid sequence. The full-length DNA sequence was determined by a combination of RT-PCR and 3′/5′-RACE PCR with degenerate oligonucleotide primers. The 3′-RACE primer was designed by selecting the codon with the highest frequency based on the NCBI codon usage table of the *Tremella encephala* β-tubulin (tub2) gene. We obtained a 600 bp sequence of the 3′-RACE product (3T36-600), and its translated amino acid sequence was highly similar to the N-terminal sequence of TFP. On the basis of this 3′-RACE product, the primer Fru5T1 was then designed and used for the 5′-RACE PCR, which further generated a 400 bp fragment, Fru5T1-400, that encoded the same starting amino residues (DDTIYIGTAEQYTPV) as native TFP. By merging the two open reading frames of 3T36-600 and Fru5T1-400, we obtained the full-length sequence of TFP (GenBank accession number EF152774). A conceptual translation and analysis of the 336 bp open reading frames of the 408 bp TFP transcript suggested that this gene encodes a 112 aa protein with a predicted molecular mass of 11.34337 kDa (Figure 2).

Native TFP Exists as a Homodimer. According to the gene sequence of TFP, its predicted molecular mass (11 kDa) is approximately half of the mass of native TFP from the SDS-PAGE (24 kDa) (Figure 1B, lane 2). To clarify the conflict in the values of the molecular mass from the prediction and the SDS-PAGE observations, we determined the mobility of

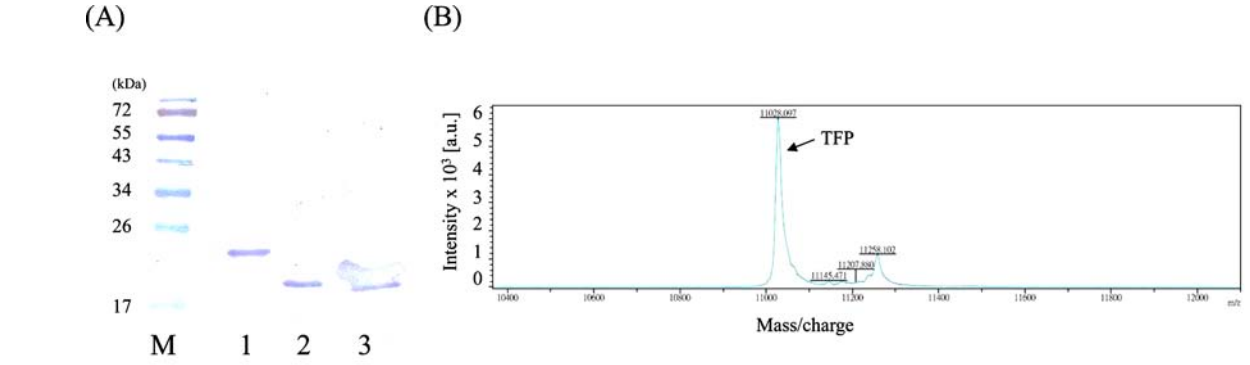

Figure 3. TFP is a homodimer protein. (A) Western blotting using an mAb against recombinant His-tagged TFP (lane 1), the enterokinase-digested product of His-tagged TFP (lane 2), and native TFP (lane 3). (B) The MALDI-TOF MS spectrum obtained from a purified TFP sample indicated a protein mass/charge ratio of between 10 400 and 12 000. The TFP peak is marked.

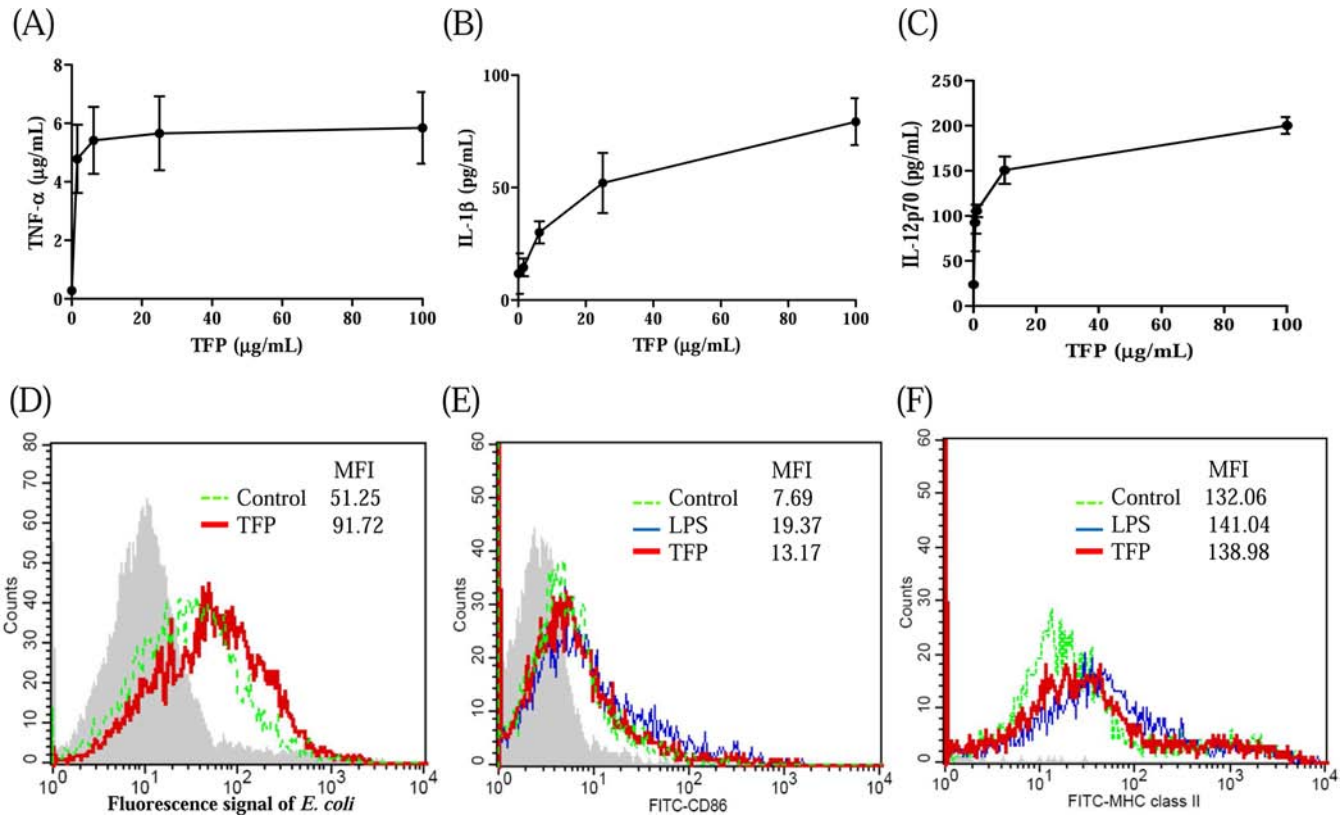

Figure 4. Effect of TFP on cytokine production and activation in mouse peritoneal macrophages. (A–C) Peritoneal macrophages freshly prepared from BALB/c mice were cultured in the presence of TFP at the indicated concentrations for 24 h. TFP induced (A) TNF-α, (B) IL-1β, and (C) IL-12p70 production. (D–F) Peritoneal macrophages stimulated with TFP (6 μg/mL) or LPS (1 μg/mL) for 24 h were analyzed, and the TFP-stimulated cells displayed enhanced (D) phagocytosis activity, (E) CD86 expression, (F) and MHC class II expression. The shaded areas indicate unstained controls, the green dotted lines indicate cells without stimulation, the thin blue solid lines indicate LPS-stimulated cells, and the thick red lines indicate TFP-stimulated cells.

recombinant TFP (rTFP) and its mass spectrum. To produce rTFP, the cDNA sequence encoding TFP from Asp[25] to the stop codon, containing 110 amino acids, was cloned into a pET-30a(+) vector and then transformed into the bacteria host *E. coli* BL21 with the constructed plasmid. Interestingly, transformant-expressed rTFP exhibited the mobility of a 24 kDa protein even though the inserted gene was predicted to translate an 11 kDa protein (Figure 3A), implying that TFP from the fruiting body of *T. fuciformis* could natively form a homodimer. Furthermore, to establish the molecular mass of TFP, the protein was analyzed with MALDI-TOF mass spectrometry. As shown in Figure 3B, TFP had a molecular mass of 11 033 Da, which is approximately the same as the predicted molecular mass from the TFP gene analysis. In addition, in the presence of a high percentage of β-mercaptoethanol, the mobility of TFP in SDS-PAGE still equaled that of a 24 kDa protein in the SDS-PAGE (Supplemental Figure 4). According to these results, we assume that the TFP dimer results not from disulfide bonds but rather from other protein interactions. Furthermore, we

dx.doi.org/10.1021/jf403835c | J. Agric. Food Chem. 2014, 62, 1526–1535

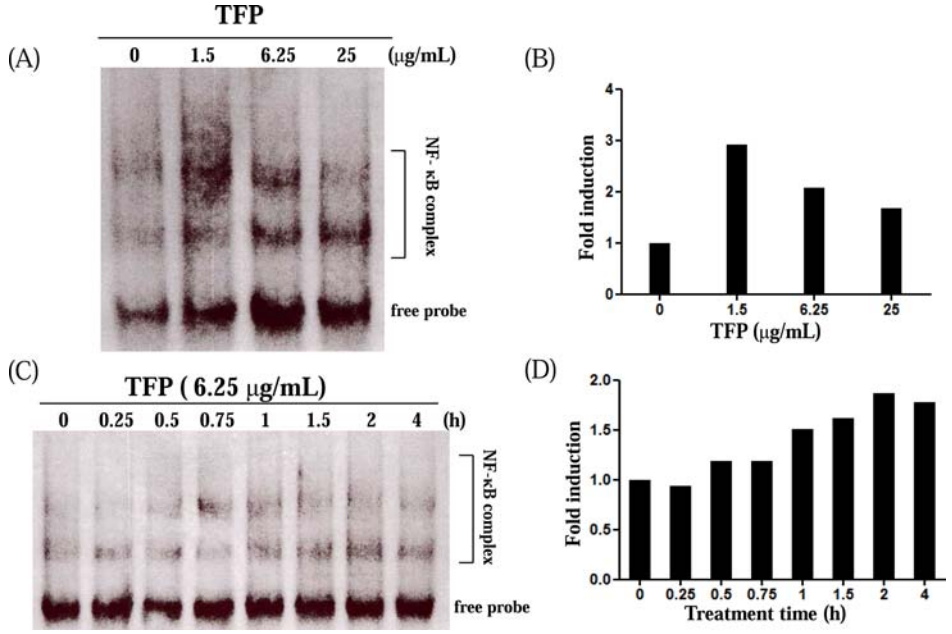

Figure 5. Effect of TFP on NF-κB activity in peritoneal macrophages. TFP-induced nuclear NF-κB DNA binding in mouse peritoneal macrophages occurred in a dose- and time-dependent manner. Nuclear NF-κB activity was determined by EMSA after the binding of nuclear extract to the labeled oligonucleotide corresponding to the NF-κB binding site. The biotin-labeled NF-κB DNA binding complex was visualized using chemiluminescence detection. (A) TFP-induced NF-κB DNA binding varied with the treatment concentration. The cells were cultured with the indicated concentration of TFP for 1.5 h, collected for nuclear protein extraction, and analyzed with EMSA. (B) The results of the densitometry analyses were compared with that for untreated cells (0 μg/mL TFP). (C) TFP initiated nuclear NF-κB DNA binding after 1 h of TFP treatment. The cells were treated by TFP (6.25 μg/mL) for the indicated times. (D) The results of the densitometry analyses were compared with that for the untreated time point (0 h).

used the COTH software,[15] a web service for protein complex structure prediction, to identify the complex structure of TFP from its primary amino acid sequence (Supplemental Figure 5). Taken together, these data suggest that the observed TFP is an 11 kDa protein and that it mostly forms natural homodimers.

TFP Activates the NF-κB Pathway in Mouse Peritoneal Macrophages. We then investigated the influence of TFP on cytokine production in mouse peritoneal macrophages to explore the activating capability of TFP in innate immune systemic cells. The peritoneal macrophages were cultured with medium that contained TFP at different concentrations ranging from 1.5 to 100 μg/mL. The supernatants were harvested to analyze the production of TNF-α, IL-1β, and IL-12p70. The macrophages cultured in the presence of TFP displayed dose-dependent upregulation of TNF-α, IL-1β, and IL-12p70 (Figure 4A−C). In addition, we investigated the effects of TFP on the phagocytic activity and activation marker expression in macrophages with flow cytometry. In the phagocytic activity assay, TFP significantly enhanced the phagocytosis of mouse peritoneal macrophages (Figure 4D). The MFI value of the TFP-induced cells (91.72; red thick line) was significantly higher ($P < 0.05$) than that of the control cells (51.25; green dotted line). Similarly, the cells cultured in the presence of TFP expressed more CD86 and MHC class II molecules than the control cells (Figure 4E,F). However, TFP treatment did not induce CD80 expression in the macrophages (Supplemental Figure 6). These results suggest that TFP can activate the phagocytic and antigen-presentation capabilities of mouse macrophage cells.

NF-κB, one of the most essential transcription factors in the generation of host defense and the innate immune system, has an important role in the induction of TNF-α and IL-12p40 gene expression in macrophages.[16] In the present study, we investigated whether TFP induces the activation of NF-κB, resulting in upregulation of the production of the previously described cytokines. As shown in Figure 5A,B, TFP directly induced an increase of NF-κB in the cell nucleus, and stimulation with different concentrations of TFP could enhance the NF-κB activation. In addition, the activation of NF-κB displayed a time-dependent pattern with the TFP treatment (Figure 5C,D). These results reveal that TFP can induce NF-κB activation and further modulate cellular immune responses.

TFP Induces M1-Type Polarization in Mouse Peritoneal Macrophages. Polarization is an important method of differentiation of function and phenotype in macrophages and has been broadly classified into types M1 and M2 on the basis of functional property differences.[17] Given the high levels of pro-inflammatory cytokine expression in TFP-induced mouse peritoneal macrophages, we examined some of the known markers of activated M1 macrophages.[18,19] We performed real-time PCR assays to determine the cytokine gene expression in macrophages that were treated with 6.25 μg/mL TFP for 8 h. As shown in Figure 6, TFP treatment increased the mRNA expression of TNF-α, IL-1β, IL-6, and IL-12p35, all of which are M1-type cytokines, but not IL-10, which is an M2-type cytokine. In addition, we observed that TFP-induced cells displayed enhanced mRNA expression of M1-type chemokines, including CCL3 and CXCL10 (Figure 7A,D). The CCL4 and CCL5 expression levels were unaffected (Figure 7B,C). However, the mRNA expression levels of CCL17 and CCL24, which are M2-type chemokines, were not changed during 8 h of 6.25 μg/mL TFP treatment (Figure 7E,F). These results indicate that TFP might upregulate the expression of M1-type cytokines and chemokine mRNA expression and therefore may induce M1 polarization of mouse macrophages.

dx.doi.org/10.1021/jf403835c | J. Agric. Food Chem. 2014, 62, 1526−1535

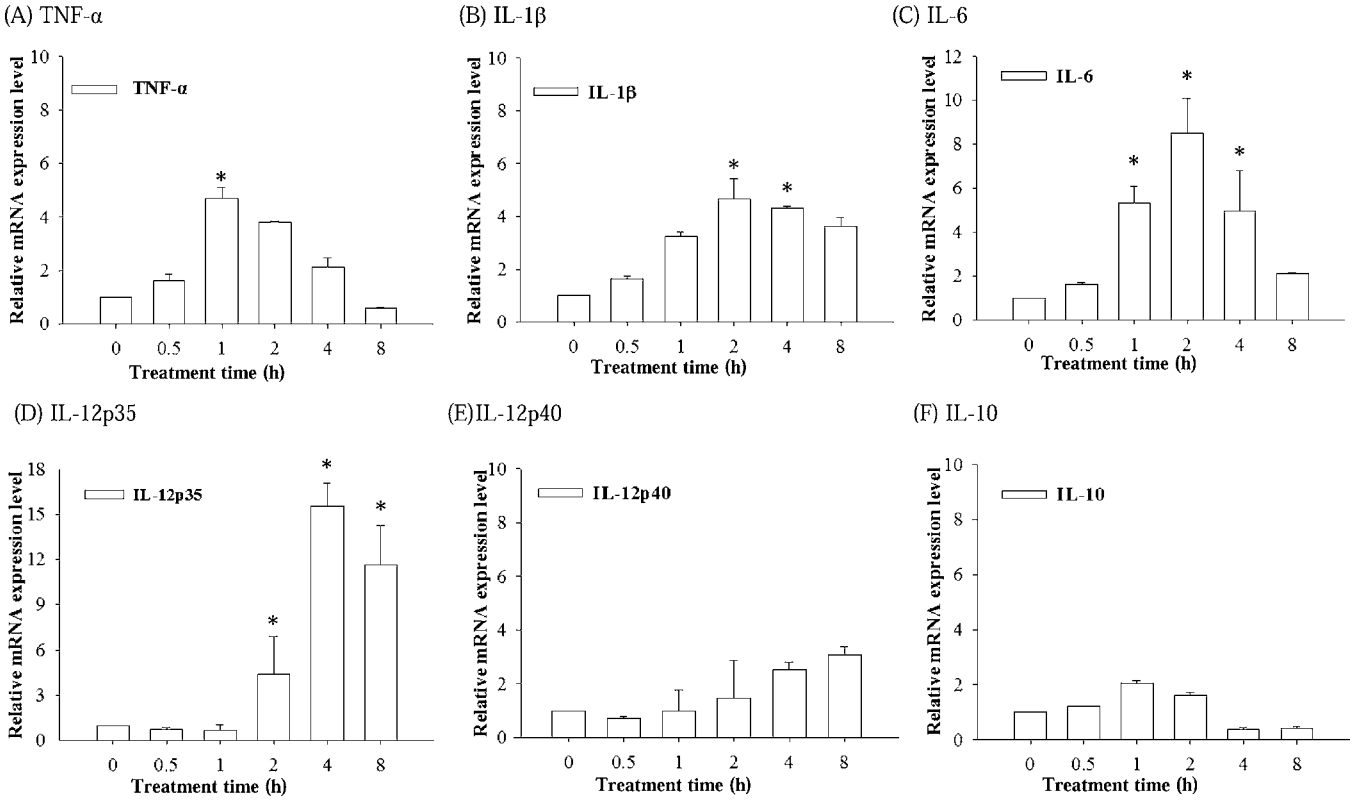

Figure 6. Effect of TFP on cytokine gene expression in peritoneal macrophages. A time course evaluation of cytokine mRNA expression in TFP-induced macrophages is shown. The cells were cultured in the presence of TFP (6.25 μg/mL) for the indicated times and collected for total RNA extraction. The expression of (A) TNF-α, (B) IL-1β, (C) IL-6, (D) IL-12p40, (E) IL-12p35, and (F) IL-10 mRNA was analyzed with quantitative real-time PCR. The mRNA expression level in each case was calculated on the basis of the Ct value and is shown as the ratio of the product to β-actin expression level. The relative mRNA expression of each time event is presented as the fold change relative to the 0 h time point. Asterisks indicate that the mRNA expression was 4-fold higher than that of the 0 h control.

TLR4 Is Associated with the Stimulation of TFP in Macrophages. The activation of TLR4 is believed to promote a Th1 response and induce the production of Th1-associated cytokines, specifically IL-12p70.[20] Therefore, we investigated whether TFP promotes activation through TLR4 in mouse peritoneal macrophages. Preliminary experiments were performed by using the anti-mouse TLR4 mAb to neutralize the TLR4-related activation in the cells. The TFP-induced TNF-α production was inhibited in the TLR4-neutralized cells (Figure 8A). To further confirm this result, we measured the TNF-α production in TFP-treated macrophages from TLR4-deficient mice (TLR4$^{-/-}$, C57BL/10ScN). As expected, the TNF-α secretion in wild-type (WT) macrophages was not observed in TLR4$^{-/-}$ cells (Figure 8B). On the basis of these results, we concluded that TLR4 is involved in TFP-mediated activation in mouse peritoneal macrophages.

DISCUSSION

In this work, we first identified that TFP, an immune-activating protein from *T. fuciformis*, is capable of enhancing Th1 cytokine secretion, phagocytic activity, co-stimulatory molecule expression, and M1 polarization of macrophages via the TLR4 signaling pathway. The cloned TFP cDNA sequence was dissimilar to those of other fungi or any other species (Supplemental Table 2). After biochemical and genetic analysis, we demonstrated that TFP consists of 112 amino acid residues (Figure 2) and lacks a glycosylation in *T. fuciformis* (Figure 1). In addition, TFP might lack a carbohydrate moiety linking the polypeptide through O- and N-glycosylation according to the predictions using NetNGlyc 1.0 and DictyOGlyc 1.1 software (Supplemental Figures 7 and 8).

Moreover, we found that TFP exists as a homodimeric molecule in the experiments. Dimerization of proteins could be related to many biological functions and could be a key process in the control a variety of cellular actions.[21] For the previously mentioned proteins, the formation of the homodimer through the N-terminal α-A-helix is necessary for recognition by their receptors on the cell surface and their immunomodulatory activities.[22−24] The method of Garnier[25] was used to predict the secondary structure of TFP, and the TFP was determined not to contain the N-terminal α-A-helix structure (Supplemental Figure 9), which differed from fungal immunomodulatory proteins (FIPs). Many proteins that have been purified from edible mushrooms have been classified as lectins and FIPs on the basis of their biochemical activities and conserved amino acid sequences.[23,24,26,27] Fip-*vvo* was classed as a lectin because of its hemagglutination and cell proliferation activity.[24] Lectins, known as carbohydrate-binding proteins, can agglutinate red blood cells and can recognize a wide variety of pathogens, and they consequently play an important role in innate immunity.[9,27] As shown in Supplemental Figure 10, the purified TFP (0.03125−1 mg/mL) lacked the ability to agglutinate mouse red blood cells. Moreover, the amino acid sequence of TFP exhibited low homology to any known FIP that has been classified as lectin (Supplemental Figure 11). Taken together,

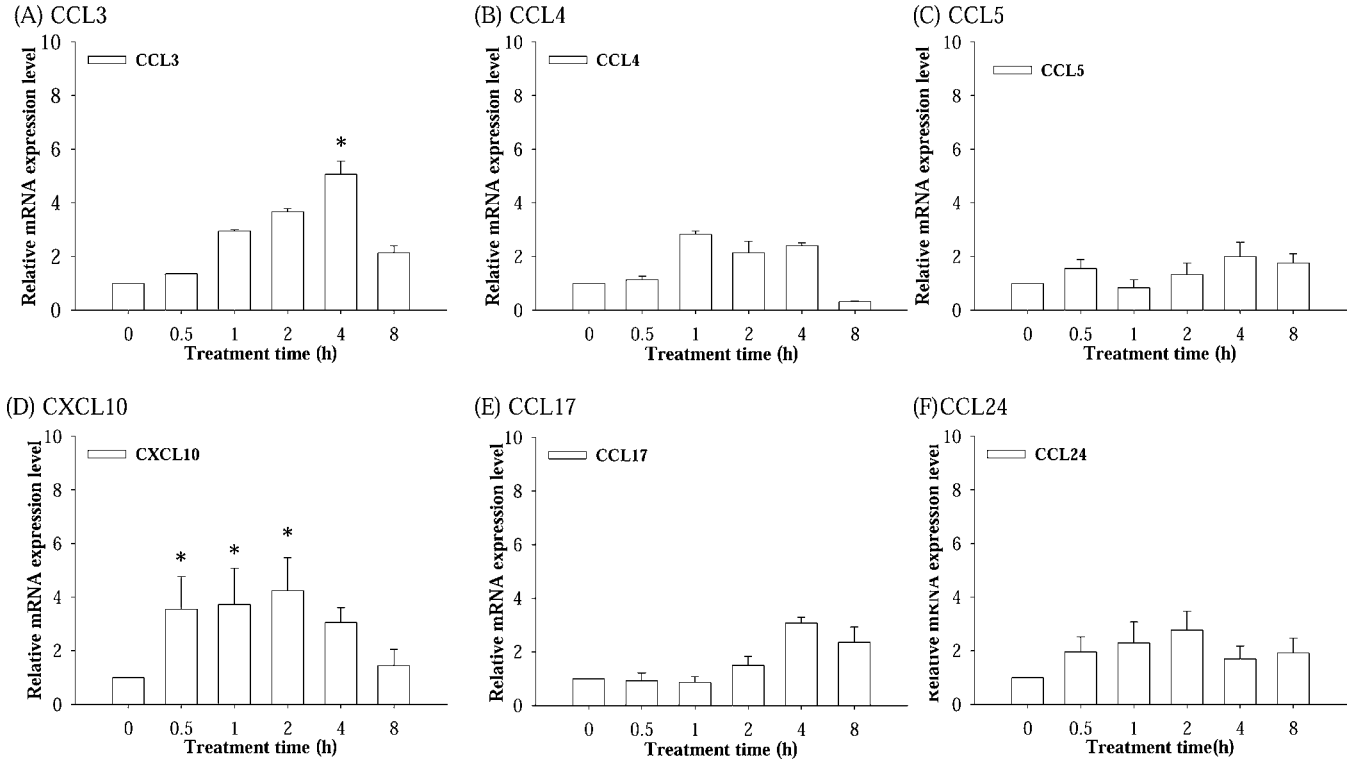

Figure 7. Time course evaluation of chemokine mRNA expression in TFP-induced macrophages. The cells were cultured in the presence of TFP (6.25 μg/mL) for the indicated times and collected for total RNA extraction. The expression of (A) CCL3, (B) CCL4, (C) CCL5, (D) CXCL10, (E) CCL17, and (F) CCL24 mRNA was analyzed with quantitative real-time PCR. The mRNA expression level in each case was calculated on the basis of the Ct value and is shown as the ratio of the product to the β-actin expression level. The relative mRNA expression of each time event is presented as the fold change relative to the 0 h time point. Asterisks indicate that the mRNA expression was 4-fold higher than that of the 0 h control.

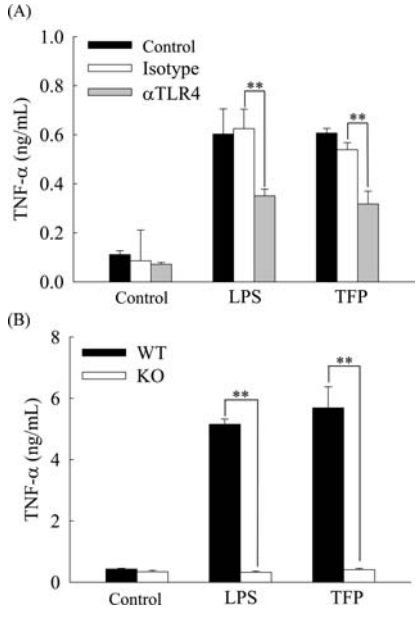

Figure 8. TFP-mediated activation of mouse peritoneal macrophages involves TLR4. (A) WT macrophages were pretreated with control (isotype) or anti-TLR4 mAb 30 min before incubation with 1 μg/mL ultrapurified LPS or 6.25 μg/mL TFP for 18 h. (B) TLR4$^{-/-}$ macrophages were incubated with 1 μg/mL ultrapurified LPS or 6.25 μg/mL TFP for 24 h. The supernatants were collected to determine the TNF-α production by macrophages using ELISA. **, $P < 0.01$ vs the isotype control.

these results show that TFP is different from those FIPs in regard to amino acid composition and biological activity.

As shown in Supplemental Table 2, the two known proteins identified in mushroom-forming fungi that are most similar to TFP, according to the NCBI nr database, are the noncatalytic module family EXPN protein (expressed by the wood-degrading fungus *Schizophyllum commune*)[28] and an expansin family protein (secreted by the ectomycorrhizal fungus *Laccaria bicolor*).[29] The noncatalytic module family EXPN proteins with high similarity (max identity >50%) from *S. commune* and *L. bicolor* are both classified as expansin superfamily proteins.[28,29] Expansins, the plant cell-wall-loosening proteins involved in plant cell growth processes, are not only found in plants but also secreted by mycorrhizal fungi, which develop symbiotic tissues in plant root tissues by using expansins to induce extension in the cell wall of roots.[30] As *T. fuciformis* is a wood-degrading fungus, the role of TFP may be associated with wood digestion and fungi development. As shown in Supplemental Figure 12, one of the TFP-similar proteins (max identity 37%) that is distinct from the expansins was found in *L. bicolor*, a riboflavin-aldehyde-forming enzyme that functions as an upregulator of the expanding sporophores.[31] It is possible that TFP plays an important role in the growth and development of *T. fuciformis*. Nevertheless, *T. fuciformis* genomics data remain sparse, and the physiological function of TFP in *T. fuciformis* remains unclear and requires further investigation.

TFP directly activates macrophages accompanying the enhanced macrophage immune functions in the innate immune responses as an immune modulator. It is well-known that

dx.doi.org/10.1021/jf403835c | J. Agric. Food Chem. 2014, 62, 1526−1535

macrophages rely on phagocytosis to eliminate exogenous pathogens and the production of cytokines to further improve the differentiation of T cells in adaptive immunity.[32−34] We demonstrated that TFP-activated macrophages display an increased phagocytosis ability and secrete a high level of TNF-α, IL-1β, and IL-12. TNF-α can promote the M1 polarization of macrophages, which leads to the tissue macrophages giving rise to classically activated macrophages. Subsequently, those macrophages produced more IL-12, which enhanced Th1 cell development.[32,33] Furthermore, we observed that TFP can induce the expression of M1 chemokines such as CCL3, CCL4, and CXCL10 but not M2 chemokines such as CCL17 and CCL24. These results suggest that TFP-mediated macrophage activation is associated with M1 polarization, which could further upregulate the Th1-response-integrated macrophages that are involved in type I inflammation, resulting in the killing of intracellular microorganisms and tumor resistance.[19] The TFP-activated macrophages exposed to TFP increased the expression of CD86, which is a well-known activation marker of macrophages and a considerable T cell co-stimulatory molecule involved in proliferation, cytokine production, and cytotoxic T lymphocyte generation during adaptive immune responses.[35] Therefore, we theorize that TFP might be a potent macrophage activator that drives the activation and M1 polarization of macrophages to promote innate immune responses.

TLRs are critical for the recognition of pathogen components and play important roles in eliciting innate immune responses, especially TLR4.[16,19] TLR4 has been reported to be capable of recognizing several pathogen molecules, including LPS from bacteria and mycobacteria, glycoinositolphospholipids from parasites, mannan from fungus, and structural proteins from viruses.[16] Using an anti-TLR4 mAb neutralization experiment and TLR4-deficient mice ($TLR4^{-/-}$), we demonstrated that TLR4 could be a major TFP-recognition receptor for macrophages and that blocking TLR4 causes macrophages to decrease TNF-α secretion. In addition, it is known that MyD88 and TIR-domain-containing adaptor protein (TIRAP) play necessary roles in the production of inflammatory cytokines such as TNF-α and IL-12p40 after the stimulation of TLR4.[10,36] Through the TLR4-mediated MyD88-dependent signaling pathway, recruited IRAK activates TRAF6 to trigger the activation of the IκB kinase (IKK) complex, leading to the translocation of NF-κB and expression of inflammatory cytokines.[10,36] We observed that TFP-mediated macrophage activation is related to the activation of NF-κB. This observation suggests that TFP regulates macrophage activation via the TLR4-NF-κB signaling pathway. Furthermore, NF-κB regulates the transcriptional program of inflammatory-response-related gene expression as the mediator of innate responses and promotes specific gene expression involving the recruitment and survival of leukocytes as an initiator of adaptive immune responses.[37,38] It was demonstrated previously that TFP induces the production of IL-12p70 and the expression of IL-12p35 and IL-12p40, which have been reported as bridges between the innate and adaptive immune responses.[37] It has also been reported that IL-12 has the ability to induce the production of IFN-γ, the differentiation of Th1 and NK cells, and the generation of cytotoxic T lymphocytes and LAK cells.[38] Taken together, these data suggest that TFP might utilize the TLR4-NF-κB signaling pathway to stimulate macrophages that have the potential to enhance the adaptive immune response.

In conclusion, TFP is a novel immune-activating protein and may be an important bioactive molecule from *T. fuciformis*. The current study is the first to provide evidence that TFP activates mouse macrophages (promoting M1-type polarization) via the TLR4-NF-κB pathway and might promote a further Th1 response. This research has revealed the potential for the use of TFP in the development of health foods and pharmaceutical products.

■ ASSOCIATED CONTENT

Supporting Information

Gel filtration chromatogram of TFP; effects of TFP on the production of TNF-α in RAW264.7 macrophages; PAS glycosylation analysis of TFP; effects of TFP on the expression of CD80 in mouse peritoneal macrophages; NetNGlyc 1.0 prediction results for TFP; DictyOGlyc 1.1 prediction results for TFP; GOR secondary structure prediction for TFP; hemagglutinating activity of TFP; SDS-PAGE of TFP with different percentages of β-mercaptoethanol in the sample dye; COTH prediction results for TFP; alignment of the amino acid sequences of LZ8, Fip-fve, Fip-vvo, and TFP; alignment of the amino acid sequences of extensin family protein (*L. bicolor* S238N-H82) and TFP; primers used in this study; and the 26 best results obtained in the NCBI Blast searches with the nr database. This material is available free of charge via the Internet at http://pubs.acs.org.

Accession Codes

The nucleotide sequence data reported for TFP from *Tremella fuciformis* have been submitted to the GenBank Nucleotide Sequence Database under accession number EF152774.

■ AUTHOR INFORMATION

Corresponding Author

*E-mail: fsheu@ntu.edu.tw. Tel.: 886-2-33664846. Fax: 886-2-23673103.

Funding

This work was supported by grants from the National Science Council (NSC), Taiwan (99-2628-B-002-003-MY3) to F.S.

Notes

The authors declare no competing financial interest.

■ ABBREVIATIONS USED

MHC, major histocompatibility complex; LPS, lipopolysaccharide; FPLC, fast protein liquid chromatography; RACE, rapid amplification of cDNA ends; RT-PCR, reverse-transcription polymerase chain reaction; TNF-α, tumor necrosis factor-α; IL, interleukin; EMSA, electrophoretic mobility shift assay; CXCL, chemokine (C-X-C motif) ligand; CCL, chemokine (C−C motif) ligand 1; Th1, T helper 1; TLR, Toll-like receptor.

■ REFERENCES

(1) Cheung, P. C. K. The Hypocholesterolemic Effect of Two Edible Mushrooms: *Auricularia auricula* (Tree-Ear) and *Tremella fuciformis* (White Jelly-Leaf) in Hypercholesterolemic Rats. *Nutr. Res. (N.Y.)* **1996**, *16*, 1721−1725.

(2) Cheng, H.-H.; Hou, W.-C.; Lu, M.-L. Interactions of Lipid Metabolism and Intestinal Physiology with *Tremella fuciformis* Berk Edible Mushroom in Rats Fed a High-Cholesterol Diet with or without Nebacitin. *J. Agric. Food Chem.* **2002**, *50*, 7438−7443.

(3) Kiho, T.; Tsujimura, Y.; Sakushima, M.; Usui, S.; Ukai, S. Polysaccharides in Fungi. XXXIII. Hypoglycemic Activity of an Acidic

Polysaccharide (AC) from *Tremella fuciformis*. *Yakugaku Zasshi* **1994**, *114*, 308−315.
(4) Ukai, S.; Hirose, K.; Kiho, T.; Hara, C.; Irikura, T. Antitumor Activity on Sarcoma 180 of the Polysaccharides from *Tremella fuciformis* Berk. *Chem. Pharm. Bull. (Tokyo)* **1972**, *20*, 2293−2294.
(5) Gao, Q.; Seljelid, R.; Chen, H.; Jiang, R. Characterisation of Acidic Heteroglycans from *Tremella fuciformis* Berk with Cytokine Stimulating Activity. *Carbohydr. Res.* **1996**, *288*, 135−142.
(6) Ma, L.; Lin, Z. B. [Effect of Tremella Polysaccharide on IL-2 Production by Mouse Splenocytes]. *Yao Xue Xue Bao* **1992**, *27*, 1−4.
(7) Guo, F. C.; Kwakkel, R. P.; Williams, B. A.; Parmentier, H. K.; Li, W. K.; Yang, Z. Q.; Verstegen, M. W. Effects of Mushroom and Herb Polysaccharides on Cellular and Humoral Immune Responses of *Eimeria tenella*-Infected Chickens. *Poult. Sci.* **2004**, *83*, 1124−1132.
(8) Sica, A.; Mantovani, A. Macrophage Plasticity and Polarization: In Vivo Veritas. *J. Clin. Invest.* **2012**, *122*, 787−795.
(9) Trinchieri, G.; Sher, A. Cooperation of Toll-like Receptor Signals in Innate Immune Defence. *Nat. Rev. Immunol.* **2007**, *7*, 179−190.
(10) Takeda, K.; Akira, S. Toll-like Receptors in Innate Immunity. *Int. Immunol.* **2005**, *17*, 1−14.
(11) Yoshimura, A.; Lien, E.; Ingalls, R. R.; Tuomanen, E.; Dziarski, R.; Golenbock, D. Cutting Edge: Recognition of Gram-Positive Bacterial Cell Wall Components by the Innate Immune System Occurs Via Toll-Like Receptor 2. *J. Immunol.* **1999**, *163*, 1−5.
(12) Fujihara, M.; Muroi, M.; Tanamoto, K.; Suzuki, T.; Azuma, H.; Ikeda, H. Molecular Mechanisms of Macrophage Activation and Deactivation by Lipopolysaccharide: Roles of the Receptor Complex. *Pharmacol. Ther.* **2003**, *100*, 171−194.
(13) Lee, J. Y.; Kim, J. Y.; Lee, Y. G.; Rhee, M. H.; Hong, E. K.; Cho, J. Y. Molecular Mechanism of Macrophage Activation by Exopolysaccharides from Liquid Culture of *Lentinus edodes*. *J. Microbiol. Biotechnol.* **2008**, *18*, 355−364.
(14) Chang, H.-H.; Yeh, C.-H.; Sheu, F. A Novel Immunomodulatory Protein from *Poria cocos* Induces Toll-like Receptor 4-Dependent Activation within Mouse Peritoneal Macrophages. *J. Agric. Food Chem.* **2009**, *57*, 6129−6139.
(15) Mukherjee, S.; Zhang, Y. Protein−Protein Complex Structure Predictions by Multimeric Threading and Template Recombination. *Structure* **2011**, *19*, 955−966.
(16) Kawai, T.; Akira, S. Toll-like Receptors and Their Crosstalk with Other Innate Receptors in Infection and Immunity. *Immunity* **2011**, *34*, 637−650.
(17) Benoit, M.; Desnues, B.; Mege, J.-L. Macrophage Polarization in Bacterial Infections. *J. Immunol.* **2008**, *181*, 3733−3739.
(18) Chan, G.; Bivins-Smith, E. R.; Smith, M. S.; Smith, P. M.; Yurochko, A. D. Transcriptome Analysis Reveals Human Cytomegalovirus Reprograms Monocyte Differentiation toward an M1 Macrophage. *J. Immunol.* **2008**, *181*, 698−711.
(19) Mantovani, A.; Sica, A.; Sozzani, S.; Allavena, P.; Vecchi, A.; Locati, M. The Chemokine System in Diverse Forms of Macrophage Activation and Polarization. *Trends Immunol.* **2004**, *25*, 677−686.
(20) Re, F.; Strominger, J. L. Toll-like Receptor 2 (TLR2) and TLR4 Differentially Activate Human Dendritic Cells. *J. Biol. Chem.* **2001**, *276*, 37692−37699.
(21) Jones, S.; Thornton, J. M. Protein−Protein Interactions: A Review of Protein Dimer Structures. *Prog. Biophys. Mol. Biol.* **1995**, *63*, 31−59.
(22) Ou, C.-C.; Hsiao, Y.-M.; Wang, W.-H.; Ko, J.-L.; Lin, M.-Y. Stability of Fungal Immunomodulatory Protein, FIP-Gts and FIP-Fve, in IFN-γ Production. *Food Agric. Immunol.* **2009**, *20*, 319.
(23) Lin, W.-H.; Hung, C.-H.; Hsu, C.-I.; Lin, J.-Y. Dimerization of the N-Terminal Amphipathic α-Helix Domain of the Fungal Immunomodulatory Protein from *Ganoderma tsugae* (Fip-gts) Defined by a Yeast Two-Hybrid System and Site-Directed Mutagenesis. *J. Biol. Chem.* **1997**, *272*, 20044−20048.
(24) Hsu, H. C.; Hsu, C. I.; Lin, R. H.; Kao, C. L.; Lin, J. Y. Fip-vvo, a New Fungal Immunomodulatory Protein Isolated from *Volvariella volvacea*. *Biochem. J.* **1997**, *323*, 557−565.
(25) Garnier, J.; Gibrat, J.-F.; Robson, B. GOR Method for Predicting Protein Secondary Structure from Amino Acid Sequence. *Methods Enzymol.* **1996**, *266*, 540−553.
(26) Ko, J.-L.; Hsu, C.-I.; Lin, R.-H.; Kao, C.-L.; Lin, J.-Y. A New Fungal Immunomodulatory Protein, FIP-fve, Isolated from the Edible Mushroom *Flammulina velutipes* and Its Complete Amino Acid Sequence. *Eur. J. Biochem.* **1995**, *228*, 244−249.
(27) Fujita, T.; Matsushita, M.; Endo, Y. The Lectin-Complement Pathway—Its Role in Innate Immunity and Evolution. *Immunol. Rev.* **2004**, *198*, 185−202.
(28) Ohm, R. A.; de Jong, J. F.; Lugones, L. G.; Aerts, A.; Kothe, E.; Stajich, J. E.; de Vries, R. P.; Record, E.; Levasseur, A.; Baker, S. E.; Bartholomew, K. A.; Coutinho, P. M.; Erdmann, S.; Fowler, T. J.; Gathman, A. C.; Lombard, V.; Henrissat, B.; Knabe, N.; Kues, U.; Lilly, W. W.; Lindquist, E.; Lucas, S.; Magnuson, J. K.; Piumi, F.; Raudaskoski, M.; Salamov, A.; Schmutz, J.; Schwarze, F. W. M. R.; vanKuyk, P. A.; Horton, J. S.; Grigoriev, I. V.; Wosten, H. A. B. Genome Sequence of the Model Mushroom *Schizophyllum commune*. *Nat. Biotechnol.* **2010**, *28*, 957−963.
(29) Martin, F.; Aerts, A.; Ahren, D.; Brun, A.; Danchin, E. G. J.; Duchaussoy, F.; Gibon, J.; Kohler, A.; Lindquist, E.; Pereda, V.; Salamov, A.; Shapiro, H. J.; Wuyts, J.; Blaudez, D.; Buee, M.; Brokstein, P.; Canback, B.; Cohen, D.; Courty, P. E.; Coutinho, P. M.; Delaruelle, C.; Detter, J. C.; Deveau, A.; DiFazio, S.; Duplessis, S.; Fraissinet-Tachet, L.; Lucic, E.; Frey-Klett, P.; Fourrey, C.; Feussner, I.; Gay, G.; Grimwood, J.; Hoegger, P. J.; Jain, P.; Kilaru, S.; Labbe, J.; Lin, Y. C.; Legue, V.; Le Tacon, F.; Marmeisse, R.; Melayah, D.; Montanini, B.; Muratet, M.; Nehls, U.; Niculita-Hirzel, H.; Oudot-Le Secq, M. P.; Peter, M.; Quesneville, H.; Rajashekar, B.; Reich, M.; Rouhier, N.; Schmutz, J.; Yin, T.; Chalot, M.; Henrissat, B.; Kues, U.; Lucas, S.; Van de Peer, Y.; Podila, G. K.; Polle, A.; Pukkila, P. J.; Richardson, P. M.; Rouze, P.; Sanders, I. R.; Stajich, J. E.; Tunlid, A.; Tuskan, G.; Grigoriev, I. V. The Genome of *Laccaria bicolor* Provides Insights into Mycorrhizal Symbiosis. *Nature* **2008**, *452*, 88−92.
(30) Sampedro, J.; Cosgrove, D. J. The Expansin Superfamily. *Genome Biol.* **2005**, *6*, No. 242.
(31) Sreenivasaprasad, S.; Eastwood, D. C.; Browning, N.; Lewis, S. M. J.; Burton, K. S. Differential Expression of a Putative Riboflavin-Aldehyde-Forming Enzyme (raf) Gene during Development and Post-Harvest Storage and in Different Tissue of the Sporophore in *Agaricus bisporus*. *Appl. Microbiol. Biotechnol.* **2006**, *70*, 470−476.
(32) Mosser, D. M.; Edwards, J. P. Exploring the Full Spectrum of Macrophage Activation. *Nat. Rev. Immunol.* **2008**, *8*, 958−969.
(33) Iwasaki, A.; Medzhitov, R. Regulation of Adaptive Immunity by the Innate Immune System. *Science* **2010**, *327*, 291−295.
(34) Plüddemann, A.; Mukhopadhyay, S.; Gordon, S. Innate Immunity to Intracellular Pathogens: Macrophage Receptors and Responses to Microbial Entry. *Immunol. Rev.* **2011**, *240*, 11−24.
(35) Lanier, L.; O'Fallon, S.; Somoza, C.; Phillips, J.; Linsley, P.; Okumura, K.; Ito, D.; Azuma, M. CD80 (B7) and CD86 (B70) Provide Similar Costimulatory Signals for T Cell Proliferation, Cytokine Production, and Generation of CTL. *J. Immunol.* **1995**, *154*, 97−105.
(36) Takeuchi, O.; Akira, S. MyD88 as a Bottle Neck in Toll/IL-1 Signaling. *Curr. Top. Microbiol. Immunol.* **2002**, *270*, 155−167.
(37) Dev, A.; Iyer, S.; Razani, B.; Cheng, G. NF-κB and Innate Immunity. *Curr. Top. Microbiol. Immunol.* **2011**, *349*, 115−143.
(38) Trinchieri, G. Interleukin-12 and the Regulation of Innate Resistance and Adaptive Immunity. *Nat. Rev. Immunol.* **2003**, *3*, 133−146.

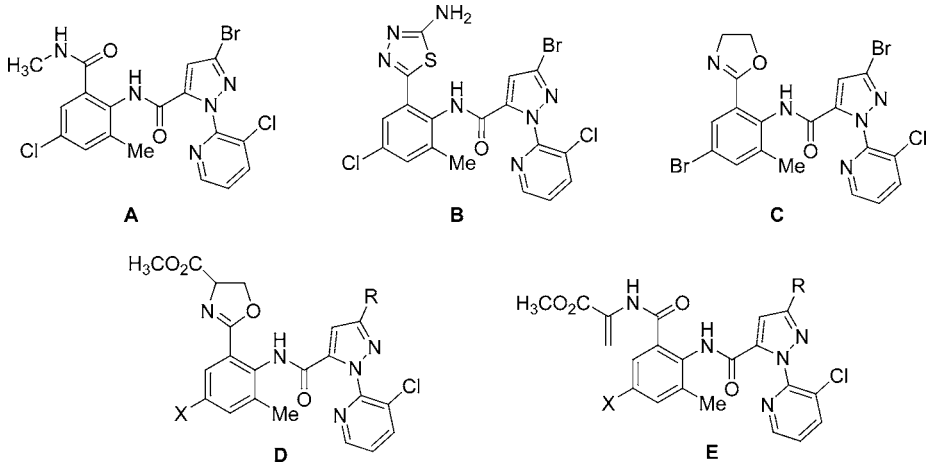

Figure 1. Chemical structures of compounds **A**–**E**.

Scheme 1[a]

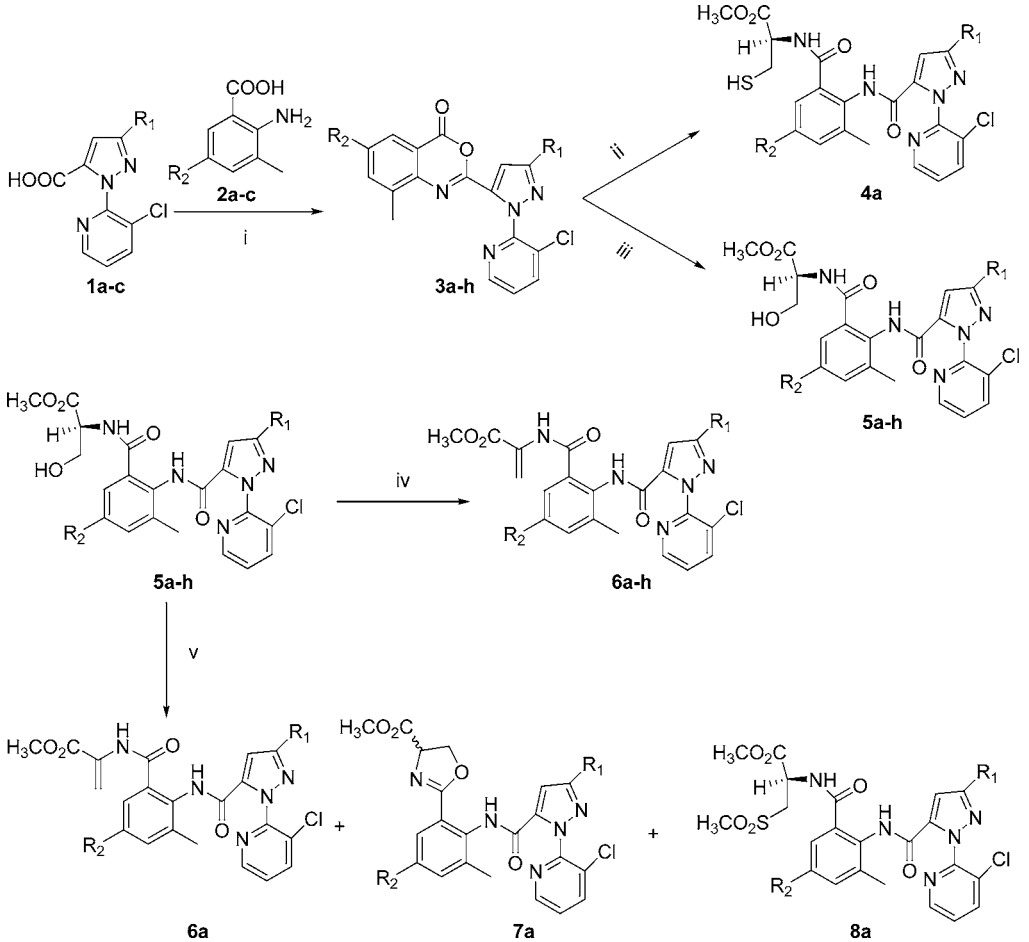

1a: R_1= Br;1b: R_1=CF_3; 2a: R_2=Cl; 2b: R_2=Br; 2c: R_2=CN; 3a: R_1=Br R_2=Cl; 3b: R_1=Br R_2=Br; 3c: R_1=Br R_2=CN; 3d: R_1=CF_3 R_2=Cl; 3e: R_1=CF_3 R_2=Br; 3f: R_1=CF_3 R_2=CN; 3g: R_1=OCH_2CF_3 R_2=Cl; 3h: R_1=OCH_2CF_3 R_2=Br; 4a: R_1=Br R_2=Cl; 5a: R_1=Br R_2=Cl;5b: R_1=Br R_2=Br; 5c: R_1=Br R_2=CN; 5d: R_1=CF_3 R_2=Cl; 5e: R_1=CF_3 R_2=Br; 5f: R_1=CF_3 R_2=CN; 5g: R_1=OCH_2CF_3 R_2=Cl; 5h: R_1=OCH_2CF_3 R_2=Br; 6a: R_1=Br R_2=Cl; 6b: R_1=Br R_2=Br; 6c: R_1=Br R_2=CN; 6d: R_1=CF_3 R_2=Cl; 6e: R_1=CF_3 R_2=Br; 6f: R_1=CF_3 R_2=CN; 6g: R_1=OCH_2CF_3 R_2=Cl; 6h: R_1=OCH_2CF_3 R_2=Br; 7a: R_1=Br R_2=Cl; 8a: R_1=Br R_2=Cl;

[a]Reagents and conditions: (i) CH_3CN, pyridine, CH_3SO_2Cl, room temperature; (ii) CH_3CN, L-cysteine methyl ester hydrochloride, Et_3N, room temperature, 10 min, then reflux; (iii) CH_3CN, L-serine methyl ester hydrochloride, Et_3N, room temperature, 10 min, then reflux; (iv) THF, $SOCl_2$, 0 °C; (v) CH_2Cl_2, CH_3SO_2Cl, Et_3N, 0 °C, then room temperature.

dx.doi.org/10.1021/jf500003d | J. Agric. Food Chem. 2014, 62, 1536–1542

Scheme 2. Proposed Formation of 6a, 7a, and 8a

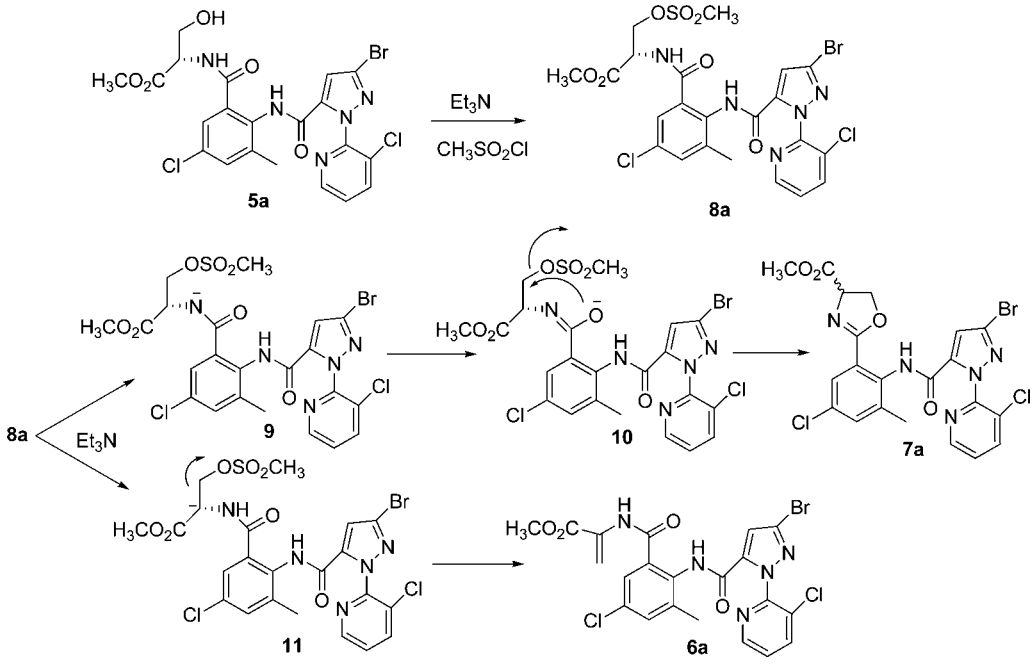

MATERIALS AND METHODS

Instruments. The measurement of melting points was conducted on a Yanaco MP-500 micromelting point apparatus without calibration. ^{1}H NMR spectra were recorded on a Bruker AC-400 instrument in $CDCl_3$ as solvent and Me_4Si as internal standard. Chemical shifts were reported as δ values in parts per million (ppm). Elemental analysis was performed on a Yanaco CHN Corder MF-3 automatic elemental analyzer. All chemical reagents and solvents were of analytical grade.

Compounds **1a−c** were synthesized according to the method reported by our previous work.[15−17] 2-Amino-5-substuituted-3-methylbenzoic acids (**2a−c**) were prepared by referring to the known procedure.[15,16] The intermediates **3a−h** were synthesized according to the literature.[18] The title compounds were prepared as shown in Scheme 1.

General Procedure for the Synthesis of Compounds 4 and 5.[19] L-Cysteine methyl ester hydrochloride (1.0 mmol) was added to 20 mL of acetonitrile under stirring, followed by the addition of triethylamine (1.2 mmol). After stirring for 0.5 h at room temperature, **3a** (1.0 mmol) was added and the resulting mixture was refluxed for a further 12 h (monitored by TLC). After completion of the reaction, the solvent was evaporated in vacuum and the residue was purified on silica gel, eluting with petroleum/ethyl acetate (v/v, 1:1), and **4a** was obtained.

Compounds **5a−f** were prepared following the same procedures described in the preparation of compound **4a** using L-serine methyl ester hydrochloride instead of L-cysteine methyl ester hydrochloride.

General Procedure for the Synthesis of Compounds 6−8.[20] To an ice-cold solution of **5** (1 mmol) in 20 mL of dichloromethane were added successively triethylamine (3 mmol) and methanesulfonyl chloride (1.5 mmol) with stirring. Then the reaction mixture was allowed to warm to room temperature and stirred until the reaction completed, monitored by TLC. After completion, the mixture was then washed with dilute hydrochloric acid solution and brine and dried with magnesium sulfate. The solvent was evaporated in a vacuum, the residue was purified on silica gel with petroleum/ethyl acetate (v/v, 4:1), and **6a**, **7a**, and **8a** were obtained.

Compound **5** (1 mmol) was dissolved in 20 mL of tetrahydrofuran and cooled in an ice bath. With constant agitation, thionyl chloride (2 mmol) was added dropwise, and the reaction mixture was stirred at 0 °C until the reaction completed, monitored by TLC. After the reaction, saturated sodium bicarbonate solution (30 mL) was then added to quench the excess amount of thionyl chloride. The resulting mixture was extracted with ethyl acetate (3 × 20 mL), and then the combined organic extracts were washed with brine and dried with magnesium sulfate. The solvent was evaporated in a vacuum, and the residue was purified on silica gel with petroleum/ethyl acetate (v/v, 4:1) to give **6a**.[21]

X-ray Diffraction. The crystal structure of compound **6g** was determined, and X-ray intensity data were recorded on a Bruker SMART 1000 CCD diffraction meter using graphite monochromated Mo Kα radiation (λ = 0.71073 Å). All calculations were refined anisotropically. All hydrogen atoms were located from a difference Fourier map and were placed at calculated positions and were included in the refinements in the riding mode with isotropic thermal parameters.

Biological Assay. Insecticidal activities against oriental armyworm (*Mythimna separata*) and diamondback moth (*Plutella xylostella*) were performed on test organisms reared in a greenhouse. The bioassay was replicated at 25 ± 1 °C according to statistical requirements. Assessments were made on a dead/alive basis, and mortality rates were corrected applying Abbott's formula.[22] Evaluation was based on a percentage scale of 0−100, where 0 equals no activity and 100 equals total kill. Error of the experiments was 5%. For comparative purposes, chlorantraniliprole was tested as control under the same conditions.

Larvicidal Activity against Oriental Armyworm (*M. separata*). The insecticidal activities of compounds **4a−8a** and chlorantraniliprole were evaluated using the reported procedure.[23] For the foliar armyworm tests, individual corn leaves were placed on moistened pieces of filter paper in Petri dishes. The leaves were then sprayed with the test solution and allowed to dry. The dishes were infested with 10 fourth-instar oriental armyworm larvae. Percentage mortalities were evaluated 2 days after treatment. Each treatment was performed three times.

Larvicidal Activity against Diamondback Moth (*P. xylostella*). The larvicidal activities of compounds **4a−8a** and chlorantraniliprole were tested by the leafdip method. First, a solution of each test sample in DMSO (AR, purchased from Alfa Aesar) at a concentration of 200 mg/L was prepared and then diluted to the required concentration with water (distilled). Leaf disks (6 cm × 2 cm) were cut from fresh cabbage leaves and then were sprayed with the test solution for 3 s and allowed to dry. The resulting leaf disks were placed individually into glass tubes. Each disk was infested with 30 second-

dx.doi.org/10.1021/jf500003d | J. Agric. Food Chem. 2014, 62, 1536−1542

instar diamondback moth larvae. Percentage mortalities were evaluated 2 days after treatment. Each treatment was performed in triplicate.

Calcium Imaging. Calibration of the fluorescence signal was obtained using the procedure of Iakahashi et al. with minor modifications.[24,25] The attached neurons were rinsed in standard physiological saline [(mM) 150 NaCl, 4 KCl, 2 $MgCl_2$, 2 $CaCl_2$, 10 HEPES, buffered to pH 7.0] and then incubated in the dark at 28 °C in standard external saline containing the dye Fluo-3 AM (Sigma, 10 μM). After dye loading, cells were again rinsed in physiological saline twice.

To block IP3Rs, cells were incubated with heparin for 10 min. Calcium ratio imaging studies were conducted using the imaging system coupled to an inverted fluorescence microscope with a Fluor 40× oil immersion objective (Olympus IX71). Cells excited at 488 and 530 nm under fluorescence emission were acquired by using a CCD (Image Pri-6.0).

Each experiment was replicated at least six times. The data were analyzed by using SPSS Inc., version 17.0, and Microcal Origin, version 8.0 (Origin Lab Corp., Northampton, MA, USA). Results were expressed as the mean ± SD (n = number of cells). Statistical significance was determined by Student's paired or unpaired t test. Fluorescence values were expressed as F/F_0, with F_0 being the resting (or baseline) fluorescence and F the change in fluorescence from baseline after drug application.[26]

RESULTS AND DISCUSSION

Chemistry. Compounds **5a**–**h** were prepared by treating compounds **3a**–**h** with L-serine methyl ester hydrochloride using triethylamine as alkali in acetonitrile, affording the desired product in good yields. Compound **4a** was prepared following the same procedures described in the preparation of compounds **5a**–**h** using L-cysteine methyl ester hydrochloride instead of L-serine methyl ester hydrochloride.

In the initial step,[20] we attempted to treat **5a** with methanesulfonyl chloride in the presence of triethylamine to prepare **7a**. Surprisingly, the elimination product **6a** was obtained as the main product, together with compounds **7a** and **8a** in low yields as shown in Scheme 1. On the basis of the literature previously reported, a mechanism that can possibly explain the formation of **6a**, **7a**, and **8a** was proposed and is illustrated in Scheme 2. In the presence of methanesulfonyl chloride in dichoromethane, compound **5a** first undergoes initial mesylation to give the intermediate **8a** and then generates nitrogen anion **9** and carbanion **11**. The nitrogen anion **9** subsequent isomerizes to **10**, which undergoes intramolecular nucleophilic attack to form the oxazoline ring closure compound **7a**, whereas compound **6a** is obtained by elimination of **11**.

Due to the low insecticidal activities of **7a**, the synthesis of this derivative was not further processed. Another alternative synthetic route was explored to prepare the target compound **6a**[21] by using thionyl chloride in tetrahydrofuran at 0 °C, which resulted in high yields and purity of **6a**.

Crystal Structure Analysis. Compound **6g** was recrystallized from a mixture of dichloromethane and petroleum ether (60–90 °C) to give colorless crystals (0.22 mm × 0.14 mm × 0.12 mm) suitable for X-ray single crystal diffraction as shown in Figure 2 with the following crystallographic parameters: a = 15.005(2) Å, b = 15.005(2) Å, c = 21.630 (4) Å, α = 90°, β = 90°, γ = 120°, V = 4217.8 (12) Å^3, Z = 6, D_c = 1.553 g cm^{-3}, μ = 0.486 mm^{-1}, $F(000)$ = 2004, R = 0.0498, T = 113 (2) K, wR = 0.0988, final R factor = 4.63%.

Structure–Activity Relationship (SAR). The larvicidal activity of compounds **4a**–**8a** against oriental armyworms is summarized in Table 1. The bioassay results indicated that

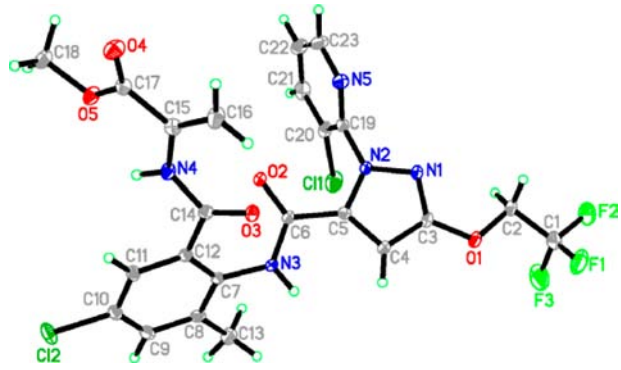

Figure 2. Crystal structure of compound **6g**.

some compounds have excellent larvicidal activities against oriental armyworm. Compounds **4a** and **5a**–**h** containing an amino acid methyl ester displayed moderate activities against oriental armyworm; the insecticidal activities were below 100% at 100 mg/L except for compound **4a**, which showed 60% at 50 mg/L. Compound **7a** containing oxazoline-4-carboxylate also showed low larvicidal activity against oriental armyworm; the mortality was only 60% at 200 mg/L. The larvicidal activity of mesylation product **8a** at a concentration of 10 mg L^{-1} was 50%, much higher than that of **5a**, indicating that the introduction of a mesyl in the hydroxyl group has a positive effect on larvicidal activities. The elimination products containing methyl acrylate substructure **6a**–**h** showed excellent insecticidal activities against oriental armyworm, especially compounds **6g** and **6h**, which showed 100% larvicidal activities at the concentration of 2.5 mg/L. Activities varied significantly depending upon the types of substituents on the 3-position of pyrazole. Compared with 3-Br and 3-CF_3 in pyrazole, compounds with 3-OCH_2CF_3 substituents showed higher insecticidal activities against oriental armyworm, which suggests that the introduction of the 2,2,2-trifluoroethoxy groups in the 3-position of pyrazole has a positive effect on the larvicidal activities. The substituents on the aromatic ring showed no significant effect on the activity.

The larvicidal activity of compounds **6a**–**h** against diamondback moth was evaluated as shown in Table 2. Most of them had excellent larvicidal activity against diamondback moth; all of the compounds showed 100% activity at 1 mg/L. Compounds with 3-Br substituents on the 3-position of pyrazole showed higher insecticidal activities against diamondback moth, which was different from the activities against oriental armyworm. For instance, the larvicidal activities of **6a**–**c** at 0.01 mg/L were 100, 57, and 43%, respectively, whereas **6d**–**h** had no more than 43% at the same dosage. In particular, compound **6a** had 100% mortality at the concentration of 0.005 mg/L, equal to that of chlorantraniliprole, but its LC_{50} was 0.0008 mg/mL, still higher than that of chlorantraniliprole (0.00009 mg/mL, Table 3).

Previously, the neurons of *S. exigua* were used for studying the mechanism of diamide insecticides, and we also found the increase of $[Ca^{2+}]_i$ was positive for the insecticidal activity against oriental armyworm. To determine whether compounds **6a**–**h** might be involved in calcium signaling transduction, we examined the effects of several novel compounds on the central neurons of *S. exigua* on the calcium homeostasis with calcium imaging technique after neuron loading with Fluo-3 AM. Figure 3 shows the change of $[Ca^{2+}]_i$ versus recording time when the neurons were treated with compounds **6a**, **6d**, **6g**, and **6h** in the

dx.doi.org/10.1021/jf500003d | J. Agric. Food Chem. 2014, 62, 1536–1542

Table 1. Insecticidal Activities of Compounds 4a, 5a–h, 6a–h, 7a, and 8a and Chlorantraniliprole against Oriental Armyworm

	larvicidal activity (%) at a concentration of						
compd	200 mg/L	100 mg/L	50 mg/L	10 mg/L	5 mg/L	2.5 mg/L	1 mg/L
4a	100	100	60				
5a	100	80					
5b	100	50					
5c	100	40					
5d	100	60					
5e	100	30					
5f	100	80					
5g	100	70					
5h	100	100	40				
6a	100	100	100	100	100	60	
6b	100	100	100	100	80		
6c	100	100	100	100	40		
6d	100	100	100	100	73.3		
6e	100	100	100	100	60		
6f	100	100	100	100	50		
6g	100	100	100	100	100	100	40
6h	100	100	100	100	100	100	40
7a	60						
8a	100	100	100	50			
chlorantraniliprole	100	100	100	100	100	100	100

Table 2. Insecticidal Activities of Compounds 6a–h and Chlorantraniliprole against Diamondback Moth

	larvicidal activity (%) at a concentration of						
compd	10 mg/L	1 mg/L	0.1 mg/L	0.01 mg/L	0.005 mg/L	0.001 mg/L	0.0005 mg/L
6a	100	100	100	100	100	57	29
6b	100	100	86	57			
6c	100	100	71	43			
6d	100	100	100	43			
6e	100	100	100	29			
6f	100	100	43	0			
6g	100	100	43	0			
6h	100	100	86	29			
chlorantraniliprole	100	100	100	100	100	90	80

Table 3. LC_{50} Values of Compound 6a and Chlorantraniliprole against Diamondback Moth

compd	$y = a + bx$	LC_{50} (mg/L)	R
6a	$y = 13.28 + 2.65x$	0.0008	0.99
chlorantraniliprole	$y = 9.66 + 1.07x$	0.00009	0.93

absence of extracellular calcium. Application of 1000 mg/L compound **6** and chlorantraniliprole to isolated *S. exigua* neurons caused an increase in the cytosolic calcium concentration. The peak of $[Ca^{2+}]_i$ was increased to 104.13 ± 2.88% (n = 9), 103.6 ± 3.10% (n = 16), 106.00 ± 2.17% (n = 12), 106.59 ± 2.41% (n = 15), and 115.42 ± 2.37% (n = 12) of the initial value after the neurons were treated with compounds **6a**, **6d**, **6g**, and **6h** for <10 s, respectively. Thus, calcium released from the calcium store elevated the cytosolic calcium levels. The calcium concentration in the neurons elevated by compounds **6a** and **6h** (Figure 4) is in a concentration-dependent manner, the same as previously reported for diamide insecticides by our research group.

When external Ca^{2+} was free, IP3 receptors were blocked by using heparin, and the increase of $[Ca^{2+}]_i$ was only attributed to the release by RyRs. Preincubated by heparin, the effect of compound **6h** on F/F_0 was reduced to 103.63 ± 2.04% (n =

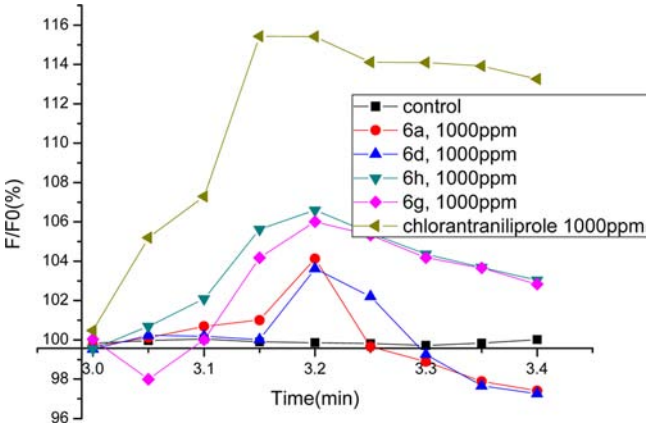

Figure 3. Effects of different concentrations of compounds **6a**, **6d**, **6g**, and **6h** on $[Ca^{2+}]_i$ in the central neurons of *S. exigua* when extracellular Ca^{2+} was absent (EGTA replaced Ca^{2+}). The central neurons of *S. exigua* third-instar larvae were dyed by loading with Fluo-3 AM.

13) (Figure 5). Inhibiting IP3Rs with heparin can activate the RyRs, meaning that using heparin can actually cause an increase in calcium. Figure 5 demonstrates compound **6h** could activate IP3Rs and RyRs, so it is elucidated that these compounds have

dx.doi.org/10.1021/jf500003d | J. Agric. Food Chem. 2014, 62, 1536–1542

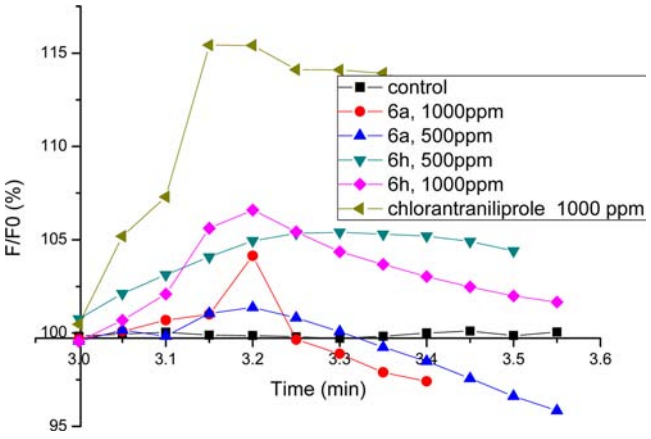

Figure 4. Effects of different concentrations of compounds **6a** and **6h** on $[Ca^{2+}]_i$ in the central neurons of *S. exigua* when extracellular Ca^{2+} was absent (EGTA replaced Ca^{2+}). The central neurons of *S. exigua* third-instar larvae were dyed by loading with Fluo-3 AM.

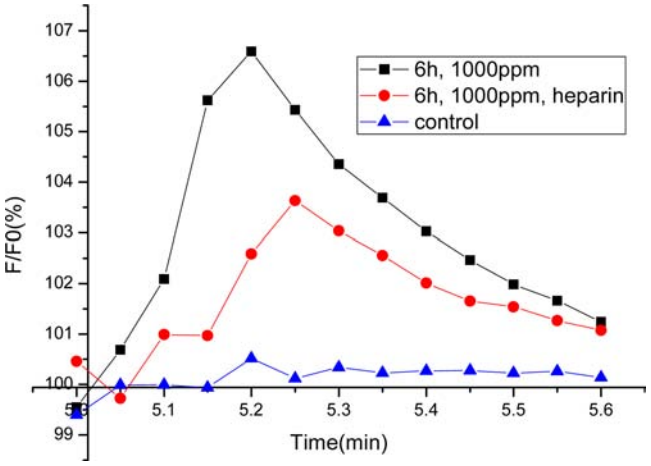

Figure 5. Effects of **6h** on $[Ca^{2+}]_i$ in the central neurons of *S. exigua* when the neurons were preincubated by heparin and thapsigargin. The central neurons of *S. exigua* third-instar larvae were dyed by loading with Fluo-3 AM.

a different mechanism from chlorantraniliprole, and we speculate that this difference affected the insecticidal activity.

In conclusion, a series of novel *N*-pyridylpyrazolecarboxamides containing an amino acid methyl ester and analogous substructures in the *ortho*-position were designed and synthesized. The bioassays showed that compounds **6** containing methyl acrylate substructure exhibited excellent insecticidal activities against oriental armyworm (*M. separata*) and diamondback moth (*P. xylostella*). Especially, compound **6a** showed 100% larvicidal activity against *P. xylostella* at the concentration of 0.005 mg/L, whereas the activities of compounds **6g** and **6h** against *M. separata* were 100% at 2.5 mg/L. More importantly, we concluded that the different mechanism of these novel compounds may decrease the insecticidal activity against Lepidoptera pests.

■ ASSOCIATED CONTENT

Supporting Information

^{1}H NMR, melting points, yields, and elemental analysis data for **4a**, **5a**−**h**, **6a**−**h**, **7**am and **8a**; ^{13}CNMR data for **6a**−**h**, **7**am and **8a**. This material is available free of charge via the Internet at http://pubs.acs.org.

■ AUTHOR INFORMATION

Corresponding Author

*(Z.-M.L.) E-mail: nkzml@vip.163.com.

Funding

This work has been supported by the National Basic Research Program of China (973 Project 2010CB126106), the National Natural Science Foundation of China (NNSFC 31370039), and the National Key Technologies Research and Development Program (2011BAE06B05).

Notes

The authors declare no competing financial interest.

■ REFERENCES

(1) DuPont Rynaxypyr_insect ontrol Technical Bulletin: http://www2.dupont.com/Production_Agriculture/en_US/assets/downloads/pdfs/Rynaxypyr_Tech_Bulletin.pdf.

(2) Lahm, G. P.; Cordova, D.; Barry, J. D. New and selective ryanodine receptor activators for insect control. *Bioorg. Med. Chem.* **2009**, *17*, 4127−4133.

(3) Finkelstein, B. L.; Lahm, G. P.; Mccann, S. F.; Song, Y.; Stevenson, T. M. Substituted anthranilamides for controlling invertebrate. WO Patent 200303016284 A1, 2003.

(4) Hughes K. A.; Lahm, G. P.; Selby, T. P.; Stevenson, T. M. Cyano anthranilamide insecticides. WO Patent 2004067528 A1, 2004.

(5) Hall, R. G.; Loiseleur, O.; Pabba, J.; Pal, S.; Jeanguenat, A.; Edmunds, A.; Stoller, A. Novel insecticieds. WO Patent 2009010260 A2, 2009.

(6) Li, B.; Xiang, D.; Chai, B. S.; Yuan, J.; Yang, H. B.; Zhang, H.; Wu, H. F.; Yu, H. B. Benzamide compounds and application thereof. WO Patent 2008134969 A1, 2008.

(7) Feng, Q.; Liu, Z. L.; Xiong, L. X.; Wang, M. Z.; Li, Y. Q.; Li, Z. M. Synthesis and insecticidal activities of novel anthranilicdiamides containing modified *N*-pyridylpyrazoles. *J. Agric. Food Chem.* **2010**, *58*, 12327−12336.

(8) Zhao, Y.; Li, Y. Q.; Xiong, L. X.; Wang, H. X.; Li, Z. M. Design, synthesis and biological activities of novel anthranilic diamide insecticide containing trifluoroethyl ether. *Chin. J. Chem.* **2012**, *30*, 1748−1758.

(9) Mao, M. Z.; Li, Y. X.; Liu, Q. X.; Zhou, Y. Y.; Zhang, X. L.; Xiong, L. X.; Li, Y. Q.; Li, Z. M. Synthesis and insecticidal evaluation of novel *N*-pyridylpyrazolecarboxamides containing cyano substituent in the *ortho*-position. *Bioorg. Med. Chem. Lett.* **2013**, *23*, 42−46.

(10) Wu, J.; Song, B. A.; Hu, D. Y.; Yue, M.; Yang, S. Design, synthesis and insecticidal activities of novel pyrazole amides containing hydrazone substructures. *Pest Manag Sci.* **2012**, *68*, 801−810.

(11) Clark, D. A.; Finkelstein, B. L.; Lahm, G. P.; Selby, T. P.; Stevenson, T. M. *Ortho*-heterocyclic substituted aryl amides for controlling invertebrate pests. WO Patent 2003016304 A1, 2003.

(12) Zhang, X. N.; Zhu, H. J.; Tan, H. J.; Li, Y. H.; Ni, J. P.; Shi, J. J.; Zeng, X.; Liu, L.; Zhang, Y. N.; Zhou, Y. L.; He, H. B.; Feng, H. M.; Wang, N. Preparation of heterocycles as insecticides. CN 101845043, 2010.

(13) Ni, J. P.; Zhang, Y. N.; Zhang, X. N.; Tan, H. J.; Zeng, X. Research on insecticidal activity of JS 9117 against five kinds of *Lepidoptera*. *Modern Agrochemicals* **2010**, *9*, 21−25 (in Chinese)..

(14) Kang, Z.; Lei, D. W.; Wang, J. F.; Peng, Y. W.; Cui, D. L.; Yang, H. B.; Sun, B. X.; Xu, J. D. Preparation of 4,5-dihydrooxazolylaniline derivatives as insecticides. CN 101863884 A1, 2010.

(15) Dong, W. L.; Xu, J. Y.; Xiong, L. X.; Liu, X. H.; Li, Z. M. Synthesis, structure and biological activities of some novel anthranilic acid esters containing *N*-pyridylpyrazole. *Chin. J. Chem.* **2009**, *27*, 579−586.

(16) Chai, B. S.; He, X. M.; Wang, J. F.; Li, Z. N; Liu, C. L. Synthesis of cyantraniliprole and its bioactivity. *Agrochemicals* **2010**, *49*, 167−169 (in Chinese)..

(17) Li, Z. M.; Wang, B. L.; Zhang, J. F.; Xu, J. Y.; Xiong, L. X.; Li, Y. Q. Zhao, Y.; Wang, G. (Pyrazolecarbonyl)thiourea derivatives as

agricultural insecticides and their preparation, agricultural compositions and use in the control of insects. WO Patent 2012163095 A1, 2012.
(18) Gnamm, C.; Jeanguenat, A.; Dutton, A. C.; Grimm, C.; Kloer, D. P.; Crossthwaite, A. J. Novel diamide insecticides: sulfoximines, sulfonimidamides and other new sulfonimidoyl derivatives. *Bioorg. Med. Chem. Lett.* **2012**, *22*, 3800−3806.
(19) Liu, C. L.; Chai, B. S.; Guan, A. Y.; Zhang, H.; Peng, Y. W.; Wang, J. F.; Li, H. C.; Li, Z. N. Anthranilamide compounds and the use thereof. WO Patent 2008134970 A1, 2008.
(20) White, D. E.; Stewart, I. C.; Seashore-Ludlow, B. A.; Grubbs, R. H.; Stoltz, B. M. A general enantioselective route to the chamigrene natural product family. *Tetrahedron* **2010**, *66*, 4668−4686.
(21) Dietz, F. R.; Gröger, H. Asymmetric synthesis of all stereoisomers of α-methylthreonine using an organocatalytic Steglich rearrangement reaction as a key step. *Synthesis* **2009**, *24*, 4208−4218.
(22) Abbott, W. S. A method of computing the effectiveness of an insecticide. *J. Econ. Entomol.* **1925**, *18*, 265−267.
(23) Chen, L.; Huang, Z. Q.; Wang, Q. M.; Shang, J.; Huang, R. Q.; Bi, F. C. Insecticidal benzoylphenylurea-S-carbamate: a new propesticide with two effects of both benzoylphenylureas and carbamates. *J. Agric. Food Chem.* **2007**, *55*, 2659−2663.
(24) Li, Y. X.; Mao, M. Z.; Li, Y. M.; Xiong, L. X.; Li, Z. M.; Xu, J. Y. Modulations of high-voltage activated Ca^{2+} channels in the central neurones of *Spodoptera exigua* by chlorantraniliprole. *Physiol. Entomol.* **2011**, *36*, 230−234.
(25) Takahashi, A.; Camacho, P.; Lechleiter, J. D.; Herman, B. Measurement of intracellular calcium. *Physiol. Rev.* **1999**, *79*, 1089−1125.
(26) Seo, M. D.; Velamakanni, S.; Ishiyama, N.; Stathopulos, P. B.; Rossi, A. M.; Khan, S. A.; Dale, P.; Li, C.; Ames, J. B.; Ikura, M.; Taylor, C. W. Structural and functional conservation of key domains in InsP3 and ryanodine receptors. *Nature* **2012**, *483*, 108−112.

Therefore, we studied, using an in vitro model simulating human gastrointestinal digestion, the bioaccessibility of phenolic compounds, vitamins, and total antioxidant capacity in durum wheat bran fractions rich in aleurone layer obtained by micronization. Moreover, the ultramicronization was applied to the fractions in order to investigate the effect of the particle size reduction as a possible way to further improve the bioaccessibility of these compounds.

MATERIALS AND METHODS

Chemicals. Ferulic acid, *p*-hydroxybenzoic acid, *p*-coumaric acid, caffeic acid, sinapic acid, nicotinic acid, thiamine, pepsin from porcine gastric mucosa, pancreatin from porcine pancreas (3xUSP), and taka diastase from *Aspergillus oryzae* were purchased from Sigma-Aldrich (Steinheim, Germany). Spectra/Por dialysis membrane tubes were from Spectrum Laboratories Inc. (Rancho Dominguez, CA, USA). All chemicals used in the study were of analytical grade. Ultrapure water from a Milli-Q system (Millipore, Bedford, MA, USA) was used throughout the experiments.

Wheat Bran Fractions. The durum wheat bran fractions were provided by Barilla G. e R. F.lli, Parma, Italy. Durum wheat (*Triticum turgidum* L. subsp. *durum*) grains underwent three subsequent steps of debranning (DECO 420R from TAE, Italy) in an industrial durum mill (capacity 13 ton/h, traditional milling by roller-millers, plansichters, and purifiers). The material produced from the third debranning step was processed through a micronization technique (Micronizer KMX-875, Separ Microsystem, Italy), followed by an air separation step (Air Separator SX-1.000, Separ Microsystem, Italy) to obtain two different bran fractions: the IN sample (the inner part of aleurone, Barilla Aleurone A) and the OUT sample (the outer part of aleurone, containing also a residue of tissue cells coming from the outer layer close to the aleurone, Barilla Aleurone B). The extraction yield of IN and OUT samples was 0.75% and 1.25% of wheat, respectively. The IN (particle sizes <100 μm) and OUT (particle sizes ranging 300−425 μm) fractions were subsequently ultramicronized by jet milling (Fluid Jet Mill Plant J-125, Tecnologia Meccanica Srl, Italy) to obtain the IN ultramicronized (IN-M) (particle sizes <20 μm) and the OUT ultramicronized (OUT-M) (particle sizes <100 μm) fractions, respectively.

Moreover, a standard wheat bran fraction (BRAN) (particle sizes 100−600 μm) was used as a control in this work. The BRAN was produced with a standard milling process (capacity 10 ton/h, traditional milling by roller-miller, plansichter, and purifiers).

Proximate Composition of Wheat Bran Fractions. All fractions were analyzed for starch (%, AOAC method 996.11), protein (% N × 5.70, AOAC method 992.23), lipid (%, AOAC method 922.06), fiber (%, AOAC method 985.29), and ash content (%, AOAC method 923.03).

For the analysis of minerals, samples were digested using a closed-vessel microwave digestion system (Milestone ETHOS PLUS with HPR-1000/10S high-pressure rotor). Raw and retained samples were weighted to proper Teflon digestion vessels. A mixture of concentrated nitric acid and hydrogen peroxide was carefully added, vessels were properly closed and introduced into the microwave oven. Vessels were thereafter cooled to room temperature and digested samples were diluted with deionized water for subsequent determination of minerals. An inductively coupled plasma atomic emission spectrometer (ULTIMA 2 ICP-AES HORIBA Jobin Yvon, France) with a radial configuration was used for Fe, Cu, Zn, and Mg determinations. Measurements were performed at the following emission lines (nm): Zn 213.856, Cu 324.754, Fe 259.940, Zn 213.856, and Mg 280.270.

In Vitro Digestion. All in vitro digestions were performed in triplicate for each wheat bran fraction, following the method described by Amrein et al.[8] with some modifications. Prior to digestion, the wheat fractions were mixed with water to obtain a mixture with ≈40% moisture, obtaining a homogeneous dough. The in vitro gastrointestinal model was set up as follows: 8 g of humidified samples was suspended in phosphate buffer (20 mmol L^{-1}) and incubated at 37 °C stepwise with human saliva for 2 min at pH 6.9, and porcine pepsin (2500 U) for 2 h at pH 2.0−2.5. Each sample was then transferred into 20-cm dialysis tubing strips (12 000 Da molecular weight cutoff) with 100 mg of pancreatin from porcine pancreas (3xUSP), sealed with plastic clamps, and incubated for 24 h at pH 6.9 into 1000-mL sealed containers containing 500 mL of phosphate buffer.

The dialyzed and retained solutions were collected after dialysis and the volumes were carefully measured. The dialyzed solution contained free low molecular weight compounds that are potentially absorbed during digestion, whereas the solution retained within the dialysis tube contained the portion of sample that is ideally not fully digested and absorbed in the upper gastrointestinal tract. The bioaccessibility of a specific compound was calculated considering the quantity of compound dialyzed with respect to the initial quantity in the sample before digestion (100%).

The analyses of total antioxidant capacity, phenolic acids, and vitamins were carried out in triplicate on the undigested, retained, and dialyzed solutions of all wheat bran fractions.

Extraction of Antioxidant Compounds and Phenolic Acids. For the preparation of soluble extracts, 50 mg of raw sample was extracted with 6 mL of water under agitation for 20 min at room temperature, followed by centrifugation at 9200*g* for 10 min, and the supernatant was collected. For the extraction of the bound phenolic compounds, the residue was further hydrolyzed with 1.5 mL of 2 mol L^{-1} sodium hydroxide at room temperature for 1 h. After alkaline hydrolysis, the pH of the mixture was adjusted to 3 by adding 1.35 mL of 3 mol L^{-1} citric acid. The bound phenolic samples were then extracted with 6 mL of ethyl acetate. The ethyl acetate extracts were evaporated to dryness under a stream of nitrogen at room temperature and the residue was dissolved in methanol. Retained samples were centrifuged at 9200*g* for 10 min, and the supernatant was collected and treated as soluble extract. The residue underwent the extraction of bound phenolic compounds as reported for raw samples. Dialyzed samples did not undergo extraction. Soluble and bound extracts and dialyzed samples were kept at −20 °C in the dark and filtered (0.45-μm nylon filters) prior to analysis.

Extraction of Vitamins. For the extraction of vitamins in undigested (i.e., raw samples) and retained fractions, about 1 g of undigested samples and 5−9.4 g of retained fractions (according to moisture of the sample) corresponding to 1 g of dried sample were extracted with 20 mL of water in the presence of 300 mg of taka diastase at pH 4.5 for 1 h at 37 °C, followed by centrifugation at 9200*g* for 10 min, and the supernatant was collected. The extraction was performed following the method described in a specific kit for vitamin analysis in cereal products (VitaFast Vitamin B3, VitaFast Vitamin B1, R-Biopharm, Italy).

Total Antioxidant Capacity (TAC). The total antioxidant capacity was measured by ferric reducing antioxidant power (FRAP) assay.[13]

LC-MS^n Analyses. Phenolic acids, thiamine and nicotinic acid in wheat bran fractions, dialyzed and retained solutions were analyzed using an Accela UHPLC 1250 equipped with linear ion-trap-mass spectrometer (LTQ XL, Thermo Fisher Scientific Inc., San Jose, CA, USA) fitted with a heated-electrospray ionization probe (H-ESI-II; Thermo Fisher Scientific Inc.). The separation was performed using a Hypersil Gold column (50 × 2.1 mm), 1.9 μm particle size (Thermo Fisher Scientific Inc.).

Phenolic Acids. The phenolic acids analysis was carried out in negative ionization mode, using the following conditions. The MS worked with a capillary temperature equal to 275 °C, while the source heather temperature was set to 45 °C. The sheath gas flow was 40 units, while auxiliary and sweep gases were set to 5 and 2 units, respectively. The source voltage was 4 kV. The capillary voltage and tube lens were −21.00 and −57.71 V, respectively. For separation of the analytes, phase A was aqueous formic acid (0.1% v/v) and phase B was methanol/water (98:2 v/v). The mobile phase, pumped at a flow rate of 0.3 mL/min, was kept for 10 min in linear gradient of 7% to 40% of B. Analyses were carried out using Selected Reaction Monitoring; *p*-hydroxybenzoic acid (m/z 137) was fragmented using a pure helium (99.999%) collision-induced dissociation (CID) of 36, generating a fragment ion with m/z 93; *p*-coumaric acid (m/z 163) was fragmented with CID 30, generating the corresponding fragment ion at m/z 119; caffeic acid (m/z 179)

yielded the corresponding fragment ion at m/z 135, using a CID of 29; ferulic acid (m/z 193) generated three daughter ions at m/z 134, 149, and 178, using a CID of 28; sinapic acid (m/z 223) generated three fragment ions at m/z 164, 179, and 208, with a CID of 25. The quantification of each phenolic acid was performed through a calibration curve with the respective commercial standard. The R^2 of the curves of standard compounds ranged from 0.992 to 0.998.

Thiamine and Nicotinic Acid. The analysis of thiamine and nicotinic acid was carried out in positive ionization mode, using the following conditions. The MS worked with capillary temperature equal to 275 °C, while the source heather temperature was set to 200 °C. The sheath gas flow was 40 units, while auxiliary gas was set to 5 units. The source voltage was 3.5 kV. The capillary voltage and tube lens were 24 and 85 V, respectively. For the separation of the analytes, phase A was aqueous formic acid (0.1% v/v) and phase B was acetonitrile in 0.1% formic acid (v/v). The mobile phase, pumped at a flow rate of 0.2 mL/min, was kept at 100% phase A up to 2 min, and then from 2 to 6 min linear gradient to 40% phase B. The analysis of nicotinic acid (m/z 124) was carried out using Selected Reaction Monitoring (SRM), with CID 55, generating the corresponding fragment ions at m/z 78, 80, 94, 96, 106. Thiamine (m/z 265) was analyzed by Consecutive Reaction Monitoring, with CID equal to 18, generating the corresponding fragment ion at m/z 122. This fragment was further fragmented with a CID of 42, generating fragment ions at m/z 81, 95, 105. The quantification of each vitamin was performed through a calibration curve with the respective commercial standards.

Statistical Analysis. All experiments were performed in triplicate. Means and standard deviations (SD) were calculated with SPSS Version 19.0 statistical software (SPSS Inc., Chicago, IL, USA). One-way analysis of variance followed by LSD posthoc test ($p < 0.05$) was used to identify differences among different fractions.

RESULTS

Proximate Composition and Analyses of Wheat Bran Fractions. *Macro- and Micronutrients.* The composition in macro- and micronutrients of the different wheat fractions is reported in Table 1. The OUT fraction was characterized by a higher fiber content, equal to 55%, with respect to 15 and 36% in the IN and BRAN samples, respectively. The IN fractions showed a higher content in starch, proteins, lipids, and ash. Regarding minerals, we limited the analysis to iron, copper, zinc, and magnesium because of their reported relevant concentration in wheat. The distribution among the fractions was similar for all the analyzed minerals, with slightly higher levels observed in the IN and IN-M fractions. Thiamine was higher in the IN and IN-M fractions, whereas the distribution of niacin was uniform.

Total Antioxidant Capacity. The TAC of the wheat bran fractions is reported in Figure 1. The OUT fractions showed the highest total antioxidant capacity values (11.69 and 11.04 mmol Fe^{2+}/100 g for OUT and OUT-M, respectively), followed by BRAN (8.73 mmol Fe^{2+}/100 g). The IN fractions showed the lowest TAC values (5.27 and 5.07 mmol Fe^{2+}/100 g in IN and IN-M, respectively). The ultramicronized and regular-sized samples showed comparable TAC values. The main TAC contributors to the OUT and OUT-M fractions TAC were bound compounds (88% and 84% of the global TAC, respectively), whereas the IN and IN-M fractions presented a high proportion of antioxidant capacity related to free compounds (≈ 50%).

Phenolic Acids. Figure 1 reports the phenolic acid profile of the wheat fractions. In each fraction, five phenolic acids were detected and quantified: ferulic, *p*-coumaric, sinapic, caffeic, and *p*-hydroxybenzoic acids. Ferulic acid was the main phenolic acid, with a concentration ranging between 50.2 and 210.4 mg/100 g, whereas *p*-coumaric, sinapic, caffeic and *p*-hydroxybenzoic acids were present in the different fractions in the range of 3.4−8.7,

Table 1. Macro- and Micronutrient Composition of Wheat Bran Fractions[a]

	starch	protein	lipid	fiber	ash	iron	copper	zinc	magnesium	thiamine	niacin
BRAN	24.42 ± 1.56	15.38 ± 0.48	6.00 ± 0.30	36.00 ± 0.23	3.40 ± 0.11	11.24 ± 0.10	2.37 ± 0.04	7.36 ± 0.04	391.66 ± 1.61	7.42 ± 1.63	19.53 ± 5.39
OUT	14.23 ± 0.30	12.64 ± 0.35	8.68 ± 0.20	55.57 ± 0.33	4.84 ± 0.10	11.51 ± 0.08	2.19 ± 0.01	8.51 ± 0.27	297.96 ± 5.61	6.79 ± 0.46	15.38 ± 4.76
OUT-M	12.63 ± 0.83	12.64 ± 0.35	8.68 ± 0.20	55.57 ± 0.33	4.84 ± 0.10	12.19 ± 0.25	2.22 ± 0.03	8.42 ± 0.56	295.63 ± 1.81	4.44 ± 0.98	14.15 ± 6.44
IN	40.28 ± 1.08	18.07 ± 0.47	11.04 ± 0.32	15.00 ± 1.00	6.90 ± 0.08	17.63 ± 0.20	2.80 ± 0.03	11.88 ± 0.41	602.78 ± 4.83	24.59 ± 1.08	21.86 ± 1.87
IN-M	34.52 ± 1.40	18.07 ± 0.47	11.04 ± 0.32	15.00 ± 1.00	6.90 ± 0.08	19.59 ± 0.17	3.00 ± 0.04	12.39 ± 0.54	676.24 ± 8.05	27.84 ± 4.34	17.08 ± 3.45

[a]Values are presented as means ± SD and are expressed on dry weight basis. Data of starch, protein, lipid, fiber, and ash are expressed as g/100 g, and those of minerals and vitamins are expressed as mg/100 g.

dx.doi.org/10.1021/jf404522a | J. Agric. Food Chem. 2014, 62, 1543−1549

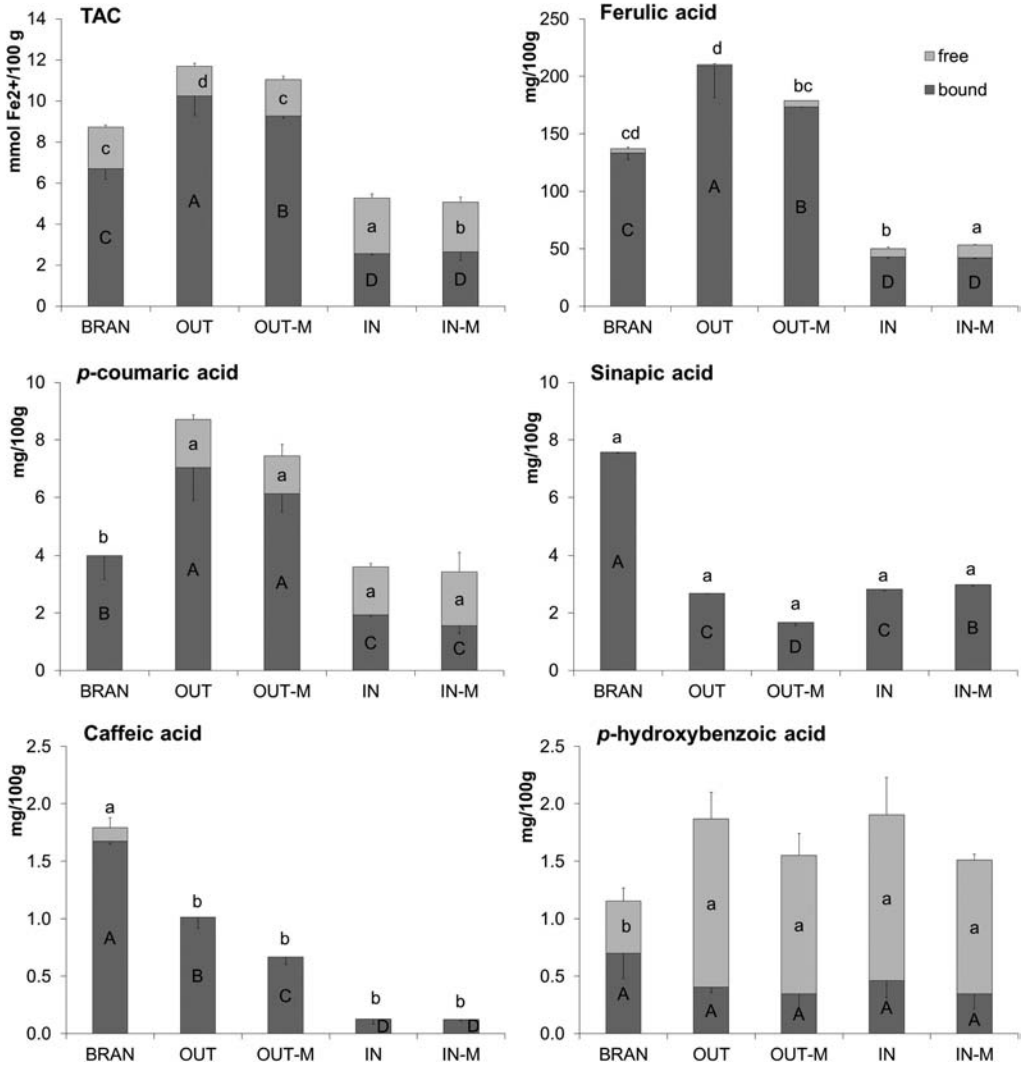

Figure 1. Total antioxidant capacity (mmol Fe^{2+}/100 g dry weight) and phenolic acids content (mg/100 g dry weight) of the wheat bran fractions. Different lowercase letters in the same panel correspond to significant ($p < 0.05$) differences in soluble portion among the fractions. Different capital letters in the same panel correspond to significant ($p < 0.05$) differences in bound portion among the fractions.

1.7−7.6, 0.1−1.8, and 1.2−1.9 mg/100 g dry weight, respectively. Ferulic, sinapic, and caffeic acids were present almost completely bound to the fiber fraction. Peculiarly, *p*-coumaric acid was present mainly in the bound form in BRAN, OUT, and OUT-M fractions, but its free form was close to the 50% in the IN and IN-M samples. Finally, *p*-hydroxybenzoic acid showed to be prevalently free in all samples.

Bioaccessibility of the Wheat Bran Fractions. *Total Antioxidant Capacity.* Figure 2 reports the percentage of absorbed TAC calculated as the amount of TAC found in the dialyzed solution divided by the initial TAC value of each wheat bran fractions. Antioxidant compounds contributing to the TAC were more bioaccessible in the IN and IN-M fractions, with bioaccessibility values of 60 and 65%, respectively, whereas the relative bioaccessibility in the other fractions was lower (≈ 20% in the OUT and OUT-M and 33% in BRAN), and not significantly different among these fractions. TAC values in retained and dialyzed samples are reported in Table 2. The retained samples of BRAN, OUT, and OUT-M, representing the non-bioaccessible components, showed a higher TAC level, mainly attributable to bound antioxidant compounds, than that of the dialyzed solutions. Conversely, the IN and IN-M fractions showed the lowest TAC in retained, unabsorbable portion, with a complementary high TAC of the dialyzed solution.

Phenolic Acids. The bioaccessibility of phenolic acids after digestion is reported in Figure 2. The percentage of absorbed compounds was different for the five phenolic acids and among fractions. Ferulic acid absorption did not show any significant difference among fractions, with values ranging from 32 to 51%. In addition, ferulic acid content in retained and dialyzed samples is presented in Table 2. Compared with the other fractions, IN and IN-M showed a lower content in dialyzed and retained ferulic acid, in accordance with their lower original content. Among the minor acids, *p*-hydroxybenzoic presented the highest percentage of absorption (84−99%), whereas for *p*-coumaric, sinapic, and caffeic acids the bioaccessibility was widely variable among the fractions.

Vitamins. Vitamin content in the retained fractions and bioaccessibility values are described in Table 3. Thiamine was extremely bioaccessible, with IN and IN-M fractions reaching the highest values (≈ 99%), followed by OUT-M, OUT, and BRAN. On the contrary, niacin was highly retained within the dialysis membrane, with slightly higher bioaccessibility values for the IN and IN-M fractions.

dx.doi.org/10.1021/jf404522a | *J. Agric. Food Chem.* 2014, 62, 1543−1549

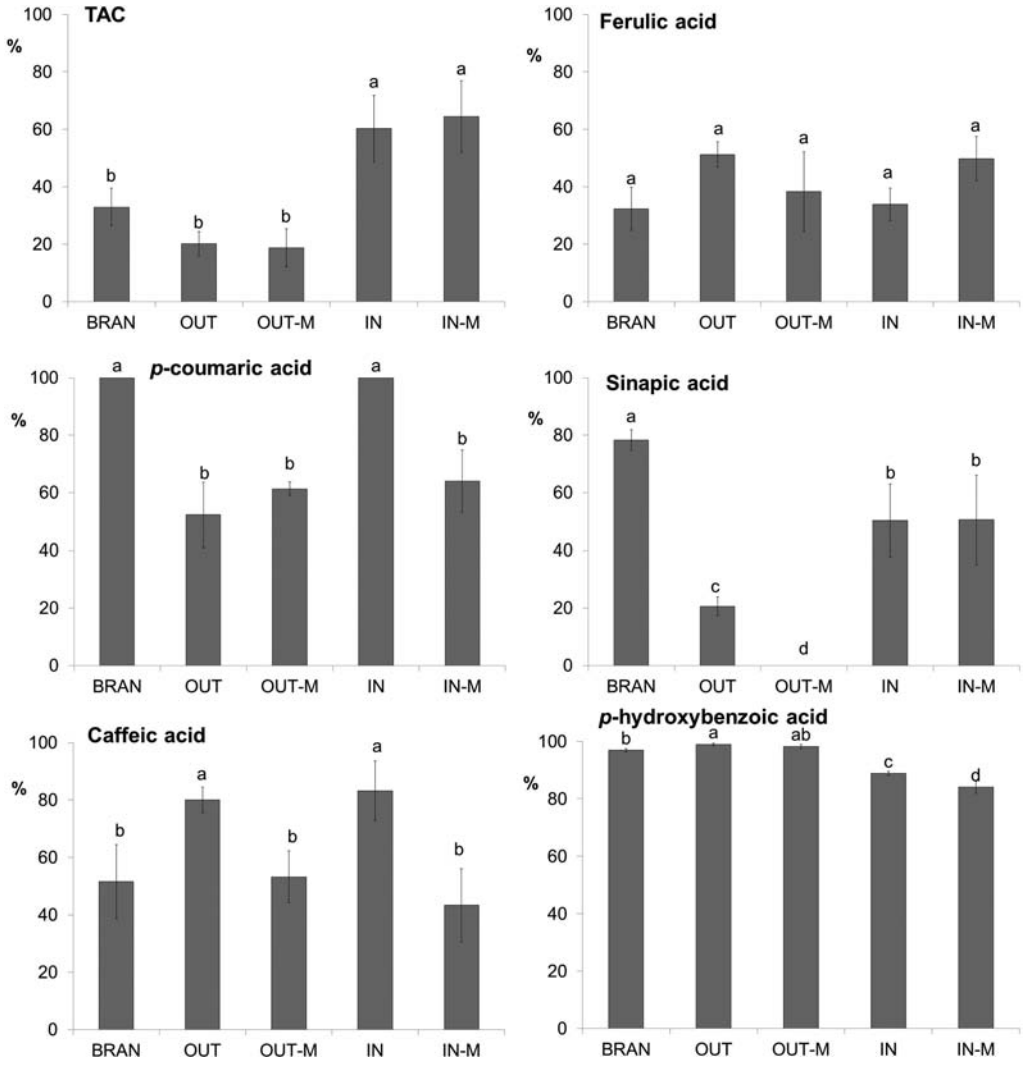

Figure 2. Bioaccessibility (%) of antioxidant compounds and phenolic acids of the wheat bran fractions. Different letters in the same panel correspond to significant ($p < 0.05$) differences among the fractions.

Table 2. TAC and Ferulic Acid Content in Retained and Dialyzed Samples after Digestion[a]

	TAC retained				ferulic retained			
	free	bound	total	TAC dialyzed	free	bound	total	ferulic dialyzed
BRAN	0.50 ± 0.03 b	5.96 ± 0.71 c	6.47 ± 0.74 c	2.88 ± 0.57 a	0.32 ± 0.04 c	92.43 ± 14.61 a	92.75 ± 14.58 a	44.38 ± 14.58 bc
OUT	0.37 ± 0.01 c	9.43 ± 0.55 a	9.86 ± 0.56 a	2.36 ± 0.49 a	0.45 ± 0.07 bc	102.03 ± 9.21 a	102.47 ± 9.13 a	107.89 ± 9.13 a
OUT-M	0.46 ± 0.02 b	7.96 ± 1.30 b	8.42 ± 1.32 b	2.07 ± 0.74 a	0.83 ± 0.26 b	109.30 ± 35.20 a	110.13 ± 24.71 a	68.59 ± 24.71 b
IN	0.67 ± 0.12 a	2.82 ± 0.29 d	3.49 ± 0.21 d	3.17 ± 0.61 a	0.49 ± 0.14 bc	32.68 ± 2.71 b	33.17 ± 2.81 b	17.01 ± 2.81 c
IN-M	0.67 ± 0.08 a	3.13 ± 0.14 d	3.80 ± 0.06 d	3.27 ± 0.89 a	1.36 ± 0.35 a	25.38 ± 4.15 b	26.74 ± 4.11 b	26.54 ± 4.11 c

[a]Values are presented as means ± SD. Data of TAC are expressed as mmol Fe^{2+}/100 g of undigested fraction on dry weight basis. Data of ferulic acid are expressed as mg/100 g of undigested fraction on dry weight basis. Different letters in column correspond to significantly ($p < 0.05$) different samples.

DISCUSSION

The present work aimed to study the nutritional characteristics of two innovative wheat aleurone fractions, in order to evaluate their potential use as functional ingredients in cereal-based foods. In particular, the bioaccessibility of vitamins, antioxidants, and phenolic compounds was evaluated in different wheat bran fractions by means of an in vitro digestive process, and in function of an ultramicronization treatment influencing their particle size. The aleurone fractions were obtained through an industrial process and do not correspond to a specific histological separation, making this work novel, and the results hardly comparable with those obtained with aleurone fractions obtained with different milling techniques analyzed in other studies.[14,15]

The compositional analysis of the investigated samples showed that the outer aleurone fraction is for a great extent fibrous, whereas the inner aleurone is mainly composed of intracellular material, containing more starch, proteins, and lipids. The higher mineral and vitamin content in the latter fraction might be explained by their compartmentalization within the cells.[7]

dx.doi.org/10.1021/jf404522a | J. Agric. Food Chem. 2014, 62, 1543−1549

Table 3. Thiamine and Niacin Content in Retained Samples and Bioaccessibility after Digestion[a]

	thiamine		niacin	
	content	bioaccessibility	content	bioaccessibility
BRAN	2.77 ± 0.95 a	62.64 ± 12.83 d	13.98 ± 2.41 a	28.41 ± 12.38 b
OUT	1.36 ± 0.37 b	79.95 ± 5.55 c	12.71 ± 0.35 a	17.34 ± 2.27 b
OUT-M	0.58 ± 0.19 bc	86.96 ± 4.33 bc	12.65 ± 1.84 a	10.61 ± 5.21 b
IN	0.33 ± 0.20 c	98.65 ± 0.84 ab	10.96 ± 0.82 a	49.84 ± 3.78 a
IN-M	0.16 ± 0.08 c	99.42 ± 0.29 a	7.53 ± 2.40 b	55.94 ± 14.05 a

[a]Values are presented as means ± SD and are expressed on dry weight basis. The content in retained is expressed as mg/100 g of undigested fraction on dry weight basis, the bioaccessibility is expressed as %. Different letters in column correspond to significantly ($p < 0.05$) different samples.

In accordance with the literature,[16,17] the most relevant contribution to the TAC was attributable to bound compounds, with the OUT fraction showing the highest bound and overall TAC, and the IN fraction showing the lowest, in good agreement with their content of fiber. This was expected, as fiber-bound phenolics represent the major TAC contributors in cereals.[14]

Ferulic acid was the predominant phenolic compound measured in the bran and aleurone fractions, as already reported.[10] This phenolic compound has been previously identified as the main contributor to aleurone TAC[14] and it constitutes a structural component of the cell wall. It is mostly esterified to arabinoxylans, as previously described by Beaugrand et al.,[18] who reported a strong correlation between arabinoxylans and ferulic acid content in wheat bran. In agreement with these observations, ferulic acid, together with *p*-coumaric acid, was present in a greater extent in the OUT fraction, which is richer in cell wall fiber. Conversely, *p*-hydroxybenzoic and sinapic acids contents were comparable in inner and outer aleurone layers, as they are mainly located in the aleurone intracellular compartment.[12]

The ultramicronized samples showed a TAC value comparable with their respective regular size fractions. Moreover, such process did not cause significant modifications to phenolic acid composition, with the only exception of a slight but significant increase in free ferulic acid. Conversely, previous works[19,20] observed that the ultrafine grinding increased the antioxidant capacity of wheat bran. These different results might be linked to the different analytical methods used for analyzing samples, as Zhou et al.[19] measured only free antioxidant compounds, whereas Rosa et al.[20] measured TAC with a direct method,[21] in which the reduction of particle size leads to a higher exposure of cell wall phenolic acids.

After the in vitro digestion, the inner aleurone layers showed the highest bioaccessibility and the highest in vitro absorbed TAC values. A higher antioxidant capacity of the bioaccessible aleurone fraction with respect to bran has been already reported by Mateo Anson et al.[15] Interestingly, in the present study, despite the inner aleurone fraction containing less antioxidant compounds, its TAC was released more efficiently during digestion, possibly because phenolics were present in large proportion in the free and more bioaccessible form. Actually, Adam et al.[22] observed that the rate of release of the esterified ferulic acid from a complex matrix within the digestive tract appears dependent on the nature of the fibers to which it is linked, with nonstarch polysaccharides in endosperm cell walls being more extensively broken down than their pericarp counterparts. Therefore, phenolic compounds bound to endosperm arabinoxylans might be more easily released with respect to phenolics linked to the pericarp or the outer aleurone layer.

In the present study, phenolic acids were differently released during digestion among the fractions. In particular, *p*-hydroxybenzoic acid presented the highest bioaccessibility in all the fractions, likely because of its predominant free form in the undigested fractions. The previous studies regarding the bioaccessibility of phenolic acids in cereals and cereal products have shown a very low bioavailability of ferulic acid from cereals in humans, with figures as low as 3%.[23] Mateo Anson et al.[24] reported that in a dynamic in vitro system the bioaccessibility of this compound from bran and aleurone was lower than 1%, assuming that the sole free fraction is a significant contributor. In the present study, the bioaccessibility of ferulic acid measured by an in vitro digestive model was observed to be higher, with all the free form absorbed, but also with a relevant percentage of the bound fraction able to become available for absorption after digestion. The micronization process could have partially improved the bioaccessibility of phenolic compounds.

The bioaccessibility of thiamine resulted high in all the fractions, as previously suggested by Roth-Maier and colleagues,[25] reporting a high prececal bioavailability of thiamine from wheat bran (92%) in pigs. Yu and Kies[26] observed that particle size is able to influence thiamine absorption. In the present study, the proportion of absorbed thiamine was BRAN < OUT < IN, with ultramicronized samples showing slightly higher values.

Niacin was less bioaccessible than thiamine, with values ranging between 10 and 55% in OUT-M and IN-M, respectively. In good agreement to this observation, in a study conducted on pigs treated with ileo-rectal anastomosis and fed wheat, the prececal digestibility of niacin was nearly 50−60%.[27] In aleurone, niacin forms inclusions with proteins, which can influence its bioaccessibility.

There is growing evidence indicating that the consumption of wholemeal cereals and wholemeal cereal-based products with respect to refined ones contributes to the prevention of chronic diseases. For this reason, the 2010 Dietary Guidelines for Americans recommended a consumption of at least 3 ounce-equivalents of wholemeal cereals per day.[28] In many western countries, the consumption of wholegrain products is estimated to be low, under the recommended intake; indeed, on average, Americans eat less than 1 ounce-equivalent per day of wholegrain products.[28] One barrier to a major consumption probably is the expected low sensory quality. The isolation and use of selected fractions in the formulation of new cereal based products could be a strategy for improving the offer of wholegrain products. In particular, aleurone fractions can be promising in replacing a part of the flour in the formulation of new products with wholegrain nutritional characteristics and that look and taste like a refined grain product. Moreover, the utilization of these fractions allows to valorize the milling byproducts, and to reduce wastes.

On the basis of the present results, wheat aleurone fractions analyzed in this study could represent a nutritionally relevant ingredient in the preparation of wheat-based products, bringing

together a high fiber content and an excellent bioaccessibility of vitamins and minor phytochemicals generally associated with nutritional benefits. Moreover, these nutritional characteristics are present in inner and outer aleurone layer fractions also without any further ultramicronization treatment, permitting obtaining nutritionally interesting ingredients without additional processing costs. In particular, IN fraction presented the most interesting characteristics among the analyzed fractions, suggesting that it can be used in the formulation of new wheat-based products. These promising results obtained with an in vitro model suggest proceeding with a human study to evaluate the bioaccessibility and bioavailability of aleurone-enriched foods.

AUTHOR INFORMATION

Corresponding Author

*E-mail: nicoletta.pellegrini@unipr.it. Telephone: +39 0521 903907. Mail: Department of Food Science, University of Parma, Parco Area delle Scienze 47/A, 43124 Parma, Italy.

Author Contributions

§Authors M.Z. and F.S. contributed equally.

Notes

The authors declare no competing financial interest.

ACKNOWLEDGMENTS

This work has been supported by Barilla G. and R. F.lli company.

ABBREVIATIONS USED

BRAN, wheat bran fraction; CID, collision induced dissociation; FRAP, ferric reducing antioxidant power; IN, inner part of aleurone; IN-M, IN micronized; OUT, the outer part of aleurone; OUT-M, OUT micronized; TAC, total antioxidant capacity

REFERENCES

(1) Ye, E. Q.; Chacko, S. A.; Chou, E. L.; Kugizaki, M.; Liu, S. Greater whole-grain intake is associated with lower risk of type 2 diabetes, cardiovascular disease, and weight gain. *J. Nutr.* **2012**, *142*, 1304−1313.

(2) de Munter, J. S. L.; Hu, F. B.; Speigelman, D.; Franz, M.; van Dam, R. M. Whole grain, bran, and germ intake and risk of type 2 diabetes; A prospective cohort study and systematic review. *PLoS Med.* **2007**, *4*, 1385−1395.

(3) Larsson, S. C.; Giovannucci, E.; Bergkvist, L.; Wolk, A. Whole grain consumption and risk of colorectal cancer: A population-based cohort of 60 000 women. *Br. J. Cancer* **2005**, *92*, 1803−1807.

(4) Chan, J. M.; Wang, F.; Holly, E. A. Whole grains and risk of pancreatic cancer in a large population-based case-control study in the San Francisco Bay Area, California. *Am. J. Epidemiol.* **2007**, *166*, 1174−1185.

(5) Okarter, N.; Liu, R. H. Health benefits of whole grain phytochemicals. *Crit. Rev. Food Sci. Nutr.* **2010**, *50*, 193−208.

(6) Fardet, A. New hypotheses for the health-protective mechanisms of whole-grain cereals: what is beyond fibre? *Nutr. Res. Rev.* **2010**, *23*, 65−134.

(7) Brouns, F.; Hemery, Y.; Price, R.; Mateo Anson, N. Wheat aleurone: Separation, composition, health aspects, and potential food use. *Crit. Rev. Food Sci. Nutr.* **2012**, *52*, 553−568.

(8) Amrein, T. M.; Gränicher, P.; Arrigoni, E.; Amadò, R. In vitro digestibility and colonic fermentability of aleurone isolated from wheat bran. *LWT−Food Sci. Technol.* **2003**, *36*, 451−460.

(9) Lillioja, S.; Neal, A. L.; Tapsell, L.; Jacobs, D. R., Jr. Whole grains, type 2 diabetes, coronary heart disease, and hypertension: Link to the aleurone preferred over indigestible fiber. *Biofactors* **2013**, *39*, 242−258.

(10) Li, L.; Shewry, P. R.; Ward, J. L. Phenolic acids in wheat varieties in the Healthgrain diversity screen. *J. Agric. Food Chem.* **2008**, *56*, 9732−9739.

(11) Vitaglione, P.; Napolitano, A.; Fogliano, V. Cereal dietary fibre: A natural functional ingredient to deliver phenolic compounds into the gut. *Trends Food Sci. Technol.* **2008**, *19*, 451−463.

(12) Hemery, Y. M.; Mateo Anson, N.; Havenaar, R.; Haenen, G. R. M. M.; Noort, M. W. J.; Rouau, X. Dry-fractionation of wheat bran increases the bioaccessibility of phenolic acids in breads made from processed bran fractions. *Food Res. Int.* **2010**, *43*, 1429−1438.

(13) Benzie, I. F. F.; Strain, J. J. Ferric reducing/antioxidant power assay: Direct measure of total antioxidant activity of biological fluids and modified version for simultaneous measurement of total antioxidant power and ascorbic acid concentration. *Methods Enzymol.* **1999**, *299*, 15−27.

(14) Mateo Anson, N.; van den Berg, R.; Havenaar, R.; Bast, A.; Haenen, G. R. M. M. Ferulic acid from aleurone determines the antioxidant potency of wheat grain (*Triticum aestivum* L.). *J. Agric. Food Chem.* **2008**, *56*, 5589−5594.

(15) Mateo Anson, N.; Havenaar, R.; Bast, A.; Haenen, G. R. M. M. Antioxidant and anti-inflammatory capacity of bioaccessible compounds from wheat fractions after gastrointestinal digestion. *J. Cereal Sci.* **2010**, *51*, 110−14.

(16) Adom, K. K.; Liu, R. H. Antioxidant activity of grains. *J. Agric. Food Chem.* **2002**, *50*, 6182−6187.

(17) Fardet, A.; Rock, E.; Rémésy, C. Is the *in vitro* antioxidant potential of whole grain cereals and cereals products well reflected *in vivo*? *J. Cereal Sci.* **2008**, *48*, 258−276.

(18) Beaugrand, J.; Crônier, D.; Debeire, P.; Chabbert, B. Arabinoxylans and hydroxycinnammate content of wheat bran in relation to endoxylanase susceptibility. *J. Cereal Sci.* **2004**, *40*, 223−230.

(19) Zhou, K.; Laux, J. J.; Yu, L. Comparison of Swiss red wheat grain and fractions for their antioxidant properties. *J. Agric. Food Chem.* **2004**, *52*, 1118−1123.

(20) Rosa, N. N.; Barron, C.; Gaiani, C.; Dufour, C.; Micard, V. Ultra-fine grinding increases the antioxidant capacity of wheat bran. *J. Cereal Sci.* **2013**, *57*, 84−90.

(21) Serpen, A.; Gökmen, V.; Pellegrini, N.; Fogliano, V. Direct measurement of the total antioxidant capacity of cereals products. *J. Cereal Sci.* **2008**, *48*, 816−820.

(22) Adam, A.; Crespy, V.; Levrat-Verny, M. A.; Leenhardt, F.; Leuillet, M.; Demigné, C.; Rémésy, C. The bioavailability of ferulic acid is governed primarily by the food matrix rather than its metabolism in intestine and liver in rats. *J. Nutr.* **2002**, *132*, 1962−1968.

(23) Kern, S. M.; Bennett, R. N.; Mellon, F. A.; Kroon, P. A.; Garcia-Conesa, M. T. Absorption of hydroxycinnamates in humans after high-bran cereal consumption. *J. Agric. Food Chem.* **2003**, *51*, 6050−6055.

(24) Mateo Anson, N.; van den Berg, R.; Havenaar, R.; Bast, A.; Haenen, G. R. M. M. Bioavailability of ferulic acid is determined by its bioaccessibility. *J. Cereal Sci.* **2009**, *49*, 296−300.

(25) Roth-Maier, D. A.; Wild, S. I.; Erhardt, W.; Henke, J.; Kirchgessner, M. Investigations on the intestinal availability of native thiamin in selcted foods and feedstuffs. *Eur. J. Nutr.* **1999**, *38*, 241−246.

(26) Yu, B. H.; Kies, C. Niacin, thiamine, and pantothenic-acid bioavailability to humans from maize bran as affected by milling and particle size. *Plant Foods Hum. Nutr.* **1993**, *43*, 87−95.

(27) Wauer, A.; Stangl, G. I.; Kirchgessner, M.; Erhardt, W.; Henke, J.; Henning, U.; Roth-Maier, D. A. A comparative evaluation of ileo-rectal anastomosis techniques for the measurement of apparent precaecal digestibilities of folate, niacin and pantothenic acid. *J. Anim. Physiol. Anim. Nutr.* **1999**, *82*, 80−87.

(28) U.S. Department of Agriculture and U.S. Department of Health and Human Services. *Dietary Guidelines for Americans, 2010*, 7th ed.; U.S. Government Printing Office: Washington, DC, December 2010.

pulverized using a mortar and pestle. The resulting powders were then stored at −80 °C for 5 months until use.

Extraction of Pistachio Bioactives. Free carotenoids, chlorophylls, and tocols in 0.1 g of pulverized whole pistachios, nutmeat, and skins (0.1 g) were extracted twice for 24 h at 4 °C with 5 mL of methanol, hexane, or acetone/methanol (75:25) with or without 0.5 g of Na_2CO_3. After centrifugation for 5 min at 3000 rpm (1200*g*), the supernatants were transferred and combined. Aliquots of the supernatants were dried under N_2 air and reconstituted for HPLC analyses. The solid residues yielded after the extractions of free lipophilic constituents were saponified with 5 mL of methanol containing 0.5 mol/L KOH for 15 min at 60 °C, 30 min at 60 °C, 45 min at 60 °C, 60 min at 60 °C, 60 min at 70 °C, 60 min at 80 °C, or 24 h at 4 °C. After the saponification, the released carotenoids, chlorophylls, and tocols were extracted twice for 24 h at 4 °C with three solutions separately to find the optimal extract solvent: (1) 2 mL of H_2O and 5 mL of hexane, (2) 7 mL of methyl *tert*-butyl ether (MTBE), and (3) 7 mL of diethyl ether. After centrifugation for 5 min at 3000 rpm (1200*g*), organic supernatants were transferred, combined, dried under N_2 air, and reconstituted for HPLC analyses. In order to simplify the extraction, the effect of combining the organic solvent supernatant of these two steps on the extraction efficiency of bioactives in pistachios was also investigated. The concentration of bioactives in extracts obtained using different extraction methods was calculated using standard curves constructed with authentic standards. Subsequently, the best extraction method was selected on the basis of the concentration of determined bioactives. All samples were analyzed in triplicate.

Phenolics, including phenolic acids and flavonoids (excluding anthocyanins), were determined according to the method of Bolling et al. with slight modifications.[12] Briefly, bioactives in 0.2 g of pulverized sample (whole pistachios, nutmeat, and skins) were extracted sequentially twice with 5 mL acidified methanol (50% methanol, 3.7% acetic acid) at 4 °C for ≥18 h. After centrifugation, the combined supernatant was aliquoted, dried under N_2 air, and reconstituted for HPLC analysis. The dry residue was incubated with 50% methanol containing 0.1 M HCl for 2 h at 90 °C to cleave conjugated glycosidic moieties of flavonoids,[13] followed by centrifugation, solvent removal, and reconstitution for HPLC analysis. All extractions were performed in triplicate.

The extraction of anthocyanins was performed according to the method of de Rosso and Mercadante with slight modifications.[14] Briefly, anthocyanins in 0.1 g of pulverized sample (whole pistachios, nutmeat, and skins) were extracted sequentially twice for 24 h at 4 °C with 5 mL of methanol containing 1% HCl. After centrifugation, the resulting supernatant was transferred, combined, dried under N_2 gas, and reconstituted for LC−MS/MS analysis. All the extractions were performed in triplicate.

Bioaccessibility of Pistachio Bioactives. The bioaccessibility of pistachio bioactives was assessed using the gastrointestinal mimic (GI) protocol of Chen and Blumberg.[15] Briefly, bioactives in 0.2 g of pulverized sample (whole pistachios, nutmeat, and skins) were mixed first with 18 mL of saline buffer and then acidified to pH 2 with HCl. After the addition of 500 μL pepsin solution, the resulting mixture was incubated at 37 °C for 1 h. At the end of the first gastric incubation, pH was titrated to pH 6.9 using $NaHCO_3$, followed by the addition of 2.5 mL of pancreatin-bile solution and incubation at 37 °C for 2 h. Subsequently, 500 μL of GI extract was mixed with 500 μL of 100% methanol. After centrifugation, 800 μL of supernatant was transferred, dried under N_2 gas, and reconstituted for HPLC analyses. All the extractions were performed in triplicate.

Quantification of Pistachio Bioactives. Lipophilic compounds were determined using a reversed-phase HPLC method according Cho et al. with slight modifications.[16] The HPLC system includes two Waters 515 pumps (Waters, Milford, MA), a Waters 717 plus autosampler, a Waters 2996 UV/visible detector, and a ProntoSIL 200-3-C30 column (3 μm, 4.6 mm × 150 mm, Leonberg, Germany). Lipophilic constituents in the extracts were separated with a gradient elution mode at a flow rate of 1 mL/min. The composition of mobile phases was 0.3 g of ammonium acetate dissolved in 830 mL of methanol, 150 mL of MTBE, and 20 mL of HPLC water for mobile phase A and 0.2 g of ammonium acetate in 80 mL of methanol, 900 mL of MTBE, and 20 mL of HPLC water for mobile phase B. The following gradient profile was used (percent mobile phase B): 0% (0−1 min), 0−30% (1−8 min), 30% (8−13 min), 30−55% (13−22 min), 55% (22−24 min), 55−95% (24−34 min), 95% (34−38 min), 95−0% (38−40 min), 0% (40−62 min). Tocols and lutein were monitored at 290 and 450 nm, respectively. Their concentration in the unknown samples was calculated on the basis of standard curves constructed with authentic standards. All samples were analyzed in triplicate.

The contents of phenolic acids and flavonoids were detected using an HPLC system equipped with an electrochemical detector (ECD) (ESA Inc., Chelmsford, MA) and an Agilent ZORBAX SB-C18 column (5 μm, 4.6 mm × 250 mm, Santa Clara, CA), according to the method of Chen et al.[17] Concentrations of phenolic acids and flavonoids in the unknown samples were calculated on the basis of the standard curves constructed with authentic standards. All samples were analyzed in triplicate.

Anthocyanins were quantified according to the LC−MS/MS method of Milbury et al. with slight modifications.[18] Briefly, anthocyanins in the extracts were eluted in a Phenomenex Synergy Max-RP C18 analytical column (4 μm, 250 × 4.6 mm, Torrance, CA) with 0.1% formic acid (mobile phase A) and 0.1% formic acid in acetonitrile (mobile phase B) at a flow rate of 0.3 mL/min in a gradient mode. The following gradient profile was used (percent mobile phase B): 5−10% (0−12 min), 10−15% (12−27 min), 15−100% (27−29 min), and 100−5% (29−40 min). Anthocyanins were monitored with an electrospray interface operated in the positive ion mode with their concentrations calculated on the basis of standard curves of authentic anthocyanin standards. The samples were determined in triplicate.

Statistical Analysis. The results are expressed as mean ± SD. One-way analysis of variance (ANOVA) was performed to evaluate differences between extraction methods, followed by the HSD Tukey's test. All statistical tests were performed using SPSS (v 16.0 program). $P < 0.05$ value was considered statistically significant.

RESULTS

Optimization of extraction method. *Solvent Selection for Free Lipophilic Bioactives.* Hexane, acetone/methanol, and methanol were employed to test extraction efficiency for dominant tocols, carotenoids, and chlorophylls (Figure 1). While methanol and hexane displayed comparable extraction efficiency for lutein, methanol was the most effective solvent for the extraction of free γ-tocopherol and chlorophylls, followed by acetone/methanol. Methanol extracted 114, 32, and 29% more γ-tocopherol, chlorophyll *a*, and chlorophyll *b* than acetone/methanol, respectively ($P < 0.05$)

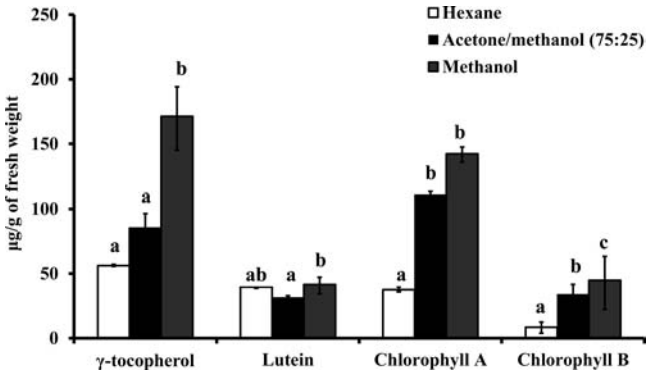

Figure 1. The effect of solvent on the extraction efficiency of lipophilic bioactives. Means bearing different letters within each nutrient differ ($n = 3$); $P < 0.05$, tested by one-way ANOVA, followed by the HSD Tukey's test.

dx.doi.org/10.1021/jf4046864 | J. Agric. Food Chem. 2014, 62, 1550−1556

Saponification and Extraction of Esterified Lipophilic Bioactives. Saponification was tested under seven conditions with different combinations of temperature (4, 60, 70, 80 °C) and duration (15, 30, 45, and 60 min and 24 h). As α-tocopherol and β-carotene exist mostly in an esterified form in pistachios (Supporting Information, Supplemental Table 1), we assessed the effect of saponification on their de-esterification (Figure 2). We found the optimal saponification condition was

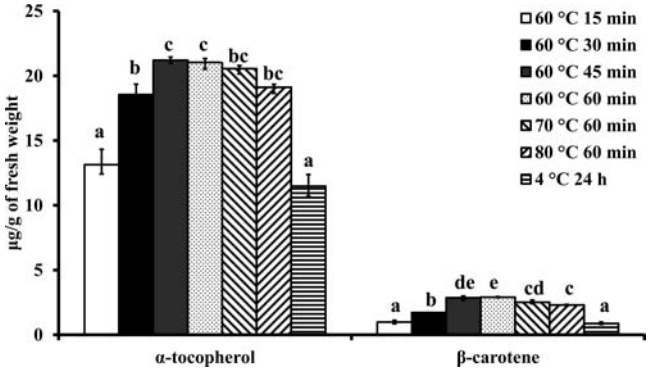

Figure 2. The effect of saponification conditions (temperature and duration) on the release of the esterified lipophilic bioactives. Means bearing different letters within each nutrient differ (n = 3); P < 0.05, tested by one-way ANOVA, followed by the HSD Tukey's test.

the incubation for 45−60 min at 60 °C (P < 0.05). Two conditions, 24 h at 4 °C and 15 min at 60 °C, were the least effective in de-estertifying α-tocopherol and β-carotene (P < 0.05). Saponification at 60 °C and 45 min was employed in the study.

Hexane, MTBE, and diethyl ether were selected to assess the efficiency for the extraction of de-esterified α-tocopherol and β-carotene (Figure 3). Both hexane and diethyl ether exhibited a

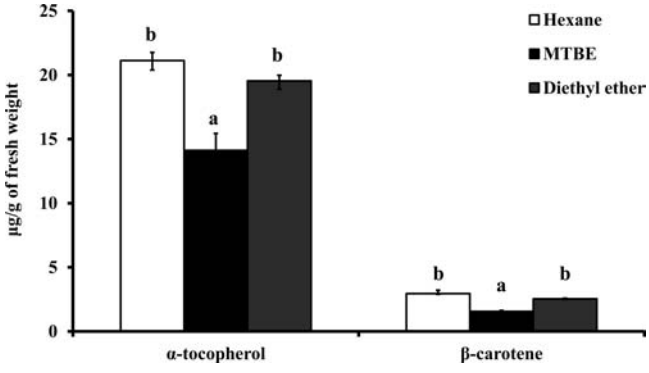

Figure 3. The effect of solvent on the extraction efficiency of esterified lipophilic bioactives. Means bearing different letter within each nutrient differ (n = 3); P < 0.05, tested by one-way ANOVA, followed by the HSD Tukey's test.

comparable efficiency and were ≥38.5 and 62.7% larger than MTBE, respectively (P < 0.05). As hexane extracted slightly more of these two compounds than diethyl ether, hexane was selected for the study.

Optimal Extraction Condition for Chlorophylls. Anhydrous Na_2CO_3 has been employed in the extraction of chlorophylls to prevent their conversion to pheophytins.[19] The addition of Na_2CO_3 to methanol decreased the amount of extractable chlorophylls as compared to methanol alone (Figure 4A,B)

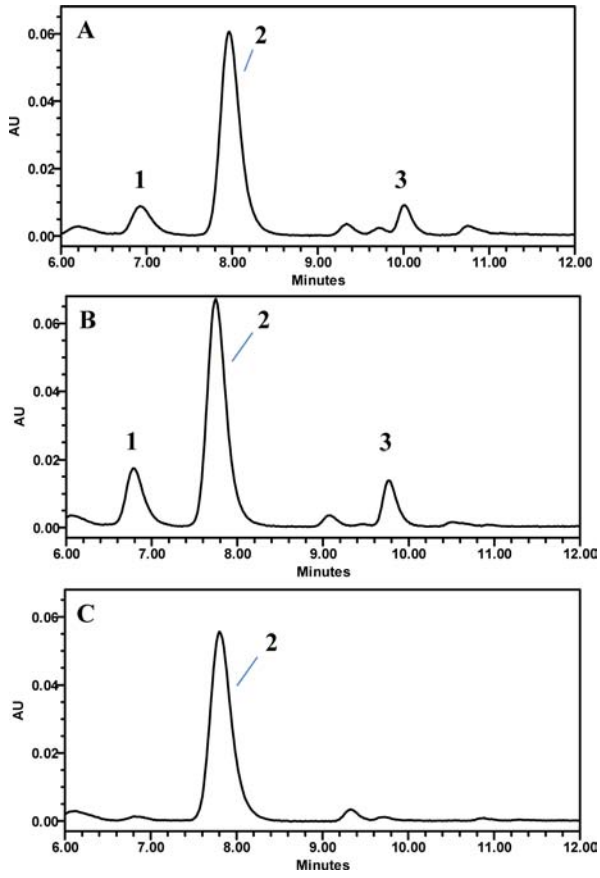

Figure 4. The effect of the alkaline condition as a result of the addition of Na_2CO_3 or KOH used in the saponification of recovery rate of chlorophyll a (peak 1), lutein (peak 2), and chlorophyll b (peak 3), as shown in the chromatographic 450 nm trace: (A) the addition of Na_2CO_3 to the extraction solvent, methanol; (B) methanol; and (C) the combination of methanol and saponification extracts.

with the area under the curve value of chlorophyll a and b being 42.6 and 36.0% smaller. Similarly, this method decreased the amount of extractable lutein by 15.3% (Figure 4C). Thus, the final extraction protocol for lipophilic nutrients in pistachios did not employ Na_2CO_3. The concentrations of the lipophilic bioactives in methanol and saponified extracts were quantified in two separated HPLC runs. The total content of each lipophilic compound in pistachios was obtained as the calculated sum of free and esterified forms.

Quantification of Lipophilic Compounds in Pistachios. A total of nine lipophilic compounds were quantified in pistachio skins, nutmeat, and whole pistachios (Table 1). Whole pistachios were comprised of 6% skin and 94% nutmeat by weight. The dominant carotenoid was lutein, chlorophyll was chlorophyll a, and tocol was γ-tocopherol. The content of the nine compounds in whole pistachios ranked as γ-tocopherol > chlorophyll a > chlorophyll b > lutein > α-tocopherol > γ-tocotrienol > β-carotene > zeaxanthin > α-carotene. The concentration of α-tocopherol and γ-tocotrienol were at least 81% lower than that of γ-tocopherol. While all nine compounds were detected in pistachio skins, their contribution to whole pistachios was minimal, ranging from 5.3% for α-carotene to 0.1% for chlorophyll A. The calculated sum of each lipophilic compound in the skin (6%) and the nutmeat (94%) was 21 ± 8% lower than the value obtained in whole pistachios, ranging from 4% (α-carotene) to 31% (chlorophyll a).

dx.doi.org/10.1021/jf4046864 | J. Agric. Food Chem. 2014, 62, 1550−1556

Table 1. Content (μg/g FW) of Carotenoids, Chlorophylls, and Tocopherols in Skins, Nutmeat, and Whole Nuts[a]

bioactives	skins	skins (GI)[b]	nutmeat	nutmeat (GI)	whole nuts	whole nuts (GI)
			Carotenoids			
α-carotene	0.26 ± 0.02 (5.3%)[d] a	ND[c]	0.29 ± 0.02 a	ND	0.30 ± 0.04 a	ND
β-carotene	1.24 ± 0.08 (3.3%) a	ND	2.34 ± 0.12 b	ND	2.94 ± 0.24 c	ND
lutein	4.17 ± 0.24 (0.8%) a	ND	35.43 ± 3.36 b	2.61 ± 0.11 a	42.35 ± 5.88 b	2.80 ± 0.11 a
zeaxanthin	0.76 ± 0.03 (5.5%) a	ND	0.98 ± 0.09 a	ND	1.66 ± 0.20 b	ND
			Chlorophylls			
chlorophyll *a*	4.59 ± 0.28 (0.1%) a	ND	104.28 ± 10.76 b	ND	142.24 ± 20.78 c	ND
chlorophyll *b*	2.26 ± 0.20 (0.4%) a	ND	34.78 ± 3.76 b	ND	44.74 ± 6.49 c	ND
			Tocols			
α-tocopherol	22.02 ± 2.28 (5%) a	ND	26.51 ± 0.87 b	ND	34.26 ± 2.02 c	ND
γ-tocopherol	42.14 ± 9.34 (1.6%) b	ND	165.72 ± 14.09 c	7.42 ± 0.52 a	182.20 ± 24.67 c	9.65 ± 0.48 ab
γ-tocotrienol	6.23 ± 0.22 (3%) a	ND	12.67 ± 1.19 b	ND	16.68 ± 2.50 c	ND

[a]Results are expressed as mean ± SD, $n = 3$. Means bearing different letters within a row differ; $P < 0.05$, tested by one-way ANOVA, followed by the HSD Tukey's test. [b]GI: gastrointestinal digestion mimic. [c]ND: not detected. [d]The percent contribution of the bioactives in the skins to those in whole nuts was calculated on the basis of the following equation: (amount of bioactives in skins × 0.06)/[(amount of bioactives in nutmeat × 0.94) + (the amount of bioactives in skins × 0.06)] × 100%.

Table 2. Content (μg/g FW) of Phenolics in Skins, Nutmeat, and Whole Nuts[a]

bioactives	skins	skins (GI)[b]	nutmeat	nutmeat (GI)	whole nuts	whole nuts (GI)
gallic acid	197.4 ± 14.1 (51.2%)[d] e	136.8 ± 7.2 e	11.9 ± 2.8 c	0.44 ± 0.04 a	36.5 ± 1.4 d	3.3 ± 0.1 b
protocatechuic acid	90.0 ± 7.4 (71.1%) f	46.7 ± 2.9 e	2.3 ± 0.1 b	0.92 ± 0.10 a	14.0 ± 0.5 d	4.8 ± 0.6 c
catechin	1774.2 ± 74.2 (84.0%) e	324.7 ± 43.7 d	21.5 ± 0.6 b	ND[c]	199.2 ± 22.2 c	4.7 ± 0.3 a
epicatechin	229.1 ± 15.5 (100%) d	57.1 ± 4.7 c	ND	ND	26.2 ± 2.6 b	1.1 ± 0.1 a
rutin	57.6 ± 3.4 (100%) b	15.3 ± 1.2 a	ND	ND	ND	ND
eriodictyol	59.2 ± 2.5 (100%) d	16.1 ± 0.6 b	ND	ND	26.3 ± 2.6 c	1.0 ± 0.0 a
total quercetin	144.4 ± 10.4 (41.4%) c	8.1 ± 0.8 a	13.0 ± 1.0 a	ND	43.5 ± 1.7 b	ND
quercetin (M)[e]	43.4 ± 0.9 b	–	ND	–	4.7 ± 0.0 a	–
quercetin (H)[f]	101.0 ± 9.8 c	–	13.0 ± 1.0 a	–	38.8 ± 1.7 b	–
total luteolin	52.8 ± 2.5 (2%) a	ND	204.9 ± 5.3 b	ND	217.9 ± 6.1 b	ND
luteolin (M)	37.3 ± 1.6 b	–	ND	–	5.8 ± 1.1 a	–
luteolin (H)	15.4 ± 3.3 a	–	204.9 ± 5.3 b	–	212.1 ± 5.8 b	–
total myricetin	68.2 ± 4.7 (3.0%) a	ND	140.6 ± 3.3 b	ND	135.2 ± 5.4 b	ND
myricetin (M)	ND	–	ND	–	–	–
myricetin (H)	68.2 ± 2.6 a	–	140.6 ± 3.3 b	–	135.2 ± 5.4 b	–
cyanidin-3-galactoside	876.5 ± 52.1 (100%) d	77.7 ± 5.7 c	ND	ND	38.3 ± 2.2 b	1.2 ± 0.1 a
cyanidin 3-glucoside	212.7 ± 17.7 (100%) d	23.8 ± 1.4 c	ND	ND	9.2 ± 1.5 b	0.5 ± 0.0 a

[a]Results are expressed as mean ± SD, $n = 3$. Means bearing different letters within a row differ; $P < 0.05$, tested by one-way ANOVA, followed by the HSD Tukey's test. [b]GI: gastrointestinal digestion mimic. [c]ND: not detected. [d]The percent contribution of the bioactives in the skin to those in whole nuts was calculated on the basis of the following equation: (amount of bioactives in skin × 0.06)/[(amount of bioactives in nutmeat × 0.94) + (the amount of bioactives in skin ×0.06)] × 100%. [e]M: Concentration obtained after acidified methanol extraction. [f]H: Concentration obtained after acid hydrolysis treatment.

We employed the in vitro GI mimic digestion mimic to estimate the bioaccessibility of the lipophilic nutrients. As the efficiency of the extraction appeared low for lipophilic compounds, these nutrients were not detected in the skin. Only lutein and γ-tocopherol were quantifiable in the GI mimic extract of nutmeat and whole pistachios. Their concentrations were 93 and 95% lower than those quantified after the extraction using the organic solvents described above.

Quantification of Phenolics in Pistachios. Eleven phenolic compounds were detected and quantified in pistachios (Table 2). All 11 compounds were detected in the skin, but only 6 were found in the nutmeat. The dominant phenolics in the skins with the concentration ≥100 μg/g FW were catechin, cyanidin-3-galactoside, epicatechin, cyanidin-3-glucoside, gallic acid, and quercetin, in descending order. The nutmeat was rich in luteolin and myricetin, with concentrations ≥140 μg/g. The percentage contribution of the phenolics in the skins to whole pistachios ranged from 2% for luteolin to 100% for epicatechin, rutin, eriodictyol, cyanidin-3-galactoside, and cyanidin-3-glucoside. The glycon form of quercetin, luteolin, and myricetin was quantified after the acidified hydrolysis. Myricetin was present exclusively as the glycone form in the skins and nutmeat. Quercetin and luteolin were found in the glycon form in the nutmeat and were present as the glycon and aglycon in the skins. The calculated sum of each nonanthocyanin compound in the skins (6%) and the nutmeat (94%) was 40 ± 24% lower than the value in whole pistachios, ranging from 1% (myricetin) to 86% (eriodictyol). The calculated sum of cyanidin-3-galactoside and cyanidin-3-glucoside was 37 and 39% larger than their value obtained in whole pistachios, respectively.

With the in vitro GI mimic digestion, only gallic and protocatechuic acids were detected, with their concentration ≤1 μg/g in the nutmeat. In the skins, except for luteolin and myricetin, the other nine compounds were all detected with their concentration being 30−94% lower than the corresponding value found in the acidified methanol extract. Only seven

dx.doi.org/10.1021/jf4046864 | J. Agric. Food Chem. 2014, 62, 1550−1556

compounds were detected in whole pistachios after the GI mimic extraction. Their total content were ≤10% that obtained from the acidified methanol extraction. Gallic and protocatechuic acids and catechin were the main compounds liberated from whole pistachios during the GI mimic digestion.

DISCUSSION

A variety of low-polarity solvents has been employed for extraction of carotenoids, chlorophylls, and tocols in pistachios. Mandalari et al., Bellomo and Fallico, and Ballistreri et al. used hexane for carotenoids and tocopherols.[9,19,20] Bellomo and Fallico employed acetone/methanol (75:25) for extraction of chlorophylls in pistachios, as compared to the study of Henriques et al. showing that methanol was the most suitable solvent for chlorophylls in marine microalga.[19,21] Contrary to Mandalari et al., Bellomo and Fallico, and Ballistreri et al.,[9,19,20] we found that methanol was superior to hexane and acetone/methanol (75:25) for the extraction of chlorophylls and nonesterified γ-tocopherol. While hexane and methanol displayed comparable extraction efficiency for lutein in our study, Craft and Soares indicated that lutein was the least soluble in hexane among all tested organic solvents.[22] As lutein is the dominant carotenoid in pistachios, we suggest that methanol is the most suitable solvent for extraction of nonesterified carotenoids and tocols and chlorophylls in pistachios.

Anhydrous Na_2CO_3 has been added to the extraction solvents with the intention of preventing the conversion of chlorophylls to pheophytins.[19] However, our results do not support the use of Na_2CO_3, in contrast to the reports from Bellomo et al. (for Italian pistachios) and Fuke et al. (for Kiwi fruit).[19,23] In addition to the reduction in the extracted chlorophyll contents, Na_2CO_3 resulted in a lower recovery rate of lutein. Thus, the use of Na_2CO_3 for the maximum extraction efficiency for chlorophylls may depend on climate, soil, or genetic conditions of the cultivars.

An adequate de-esterifying protocol is necessary to liberate esterified lipophilic bioactives to their free counterparts. On the basis of our results (data not shown), 62% of α-tocopherol in pistachios was present in the esterified form, as well as all α- and β-carotene. The effectiveness of saponification to de-esterify bioactives depends on incubation temperature and duration when the KOH concentration in methanol is fixed. There is a diversity of saponification conditions described in the literature, e.g., 30 min at 80 °C for 10 different nuts (including pistachios),[24] 10 min at 85 °C for soybeans,[25] and 5 min at 50 °C for sausages,[26] and 30 min at 70 °C for human serum and rat liver.[27] We found that saponification at 60 °C for 30 min appears optimal for tocols and carotenoids in pistachios, which is slightly different from the conditions employed by Kornsteiner et al. for their analysis of nuts.[24] Hexane, MTBE, and diethyl ether are usually employed as the extraction solvent of choice after the saponification.[24,28,29] However, we found that hexane is the most suitable one for tocols and carotenoids.

The phytochemical composition of pistachios has not been comprehensively examined for over 30 years,[30] even though such information is important to understanding the mechanisms of action by which pistachio consumption may reduce the risk of cardiovascular disease.[31] Consistent with the work of Tomaino et al.,[32] we found that most lipophilic compounds exist in the nutmeat, while most hydrophilic compounds are present in the skins. The dominant compounds characterized in our study include γ-tocopherol, chlorophylls *a* and *b*, lutein, cyanidin-3-galactoside, catechin, quercetin, luteolin, and myricetin, with their content being ≥38 μg/g FW. Interestingly, the calculated sum of each compound in the skins and nutmeat was generally lower than that quantified in whole pistachios. We speculate the difference was attributed to the reciprocal protection of antioxidants in pistachios against degradation during the extraction and the storage before analysis.

γ-Tocopherol is the dominant tocol in pistachios.[3,9,24] Consistent to the literature, we found γ-tocopherol is the main tocol in California pistachios, followed by α-tocopherol and γ-tocotrienol. Kornsteiner et al. reported that δ-tocopherol was detected at a concentration of 5 μg/g FW, while α-tocopherol was not detected.[24] However, Mandalari et al. found all three forms.[9] The α- and γ-tocopherol content of pistachios has been reported to range from 0 to 11 and 105 to 293 μg/g FW, respectively.[2,9,24] The content of γ-tocopherol [182.2 μg/g fresh weight (FW)] found in our study is within this range, while α-tocopherol (34.3 μg/g FW) is about 2-fold larger. The well-appreciated factors determining phytochemical contents, including cultivar, harvest season, cultivation practice, irrigation, growing region, soil, maturity level, and postharvest processing, may all contribute to the difference in the tocol contents of pistachios, as well as other phytochemicals.

Carotenoids are found in pistachios and other tree nuts with the exception of Brazil nuts and macadamias.[33] We found α- and β-carotene, lutein, and zeaxanthin mainly in the nutmeat of pistachios, as compared to lutein, violaxanthin, neoxanthin, luteoxanthin, and β-carotene reported by Giuffrida et al.[34] The other three studies of pistachios reported only the presence of lutein and/or β-carotene.[9,24,30] The reported content of β-carotene and lutein in pistachios ranges from 0 to 7 μg/g and 17 to 52 μg/g FW, respectively.[2,9,24,30,34] The content of β-carotene (2.94 μg/g) and lutein (42.35 μg/g) found in this study are within these ranges.

Chlorophylls are a conjugated tetrapyrrole ring that allows them to absorb light, thereby contributing to photosynthesis, color, and oxidative stability of plants.[34] Chlorophylls may also play a role in human health due to their antioxidant and antimutagenic activities.[35,36] Pistachios and pine nuts are the only two tree nuts containing chlorophylls.[33] Chlorophyll *a* and *b* in pistachios harvested in Italy, Turkey, Greece, and Iran ranged from 18.3 to 150.6 and 7.1 to 49.7 μg/g, respectively.[19,34] We found similar concentrations of chlorophyll in California pistachios. It is worth noting that Na_2CO_3 was employed in the extraction of chlorophylls in the studies by Bellomo and Fallico and Giuffrida et al.[19,34] Our results establish an adverse effect of Na_2CO_3 on chlorophylls during extraction. Further, methanol is proved a better extraction solvent than the hexane and acetone/methanol (75:25) solvents used in these two studies, respectively.[19,34] Thus, the chlorophyll contents reported in these studies might be underestimated.

Pistachios contain a variety of phenolic compounds, e.g., anthocyanins, flavonols, and isoflavones.[33] Consistent with a general understanding,[30] we found pistachio phenolics are mainly present in the skins, with cyanidin-3-galactoside, catechin, quercetin, luteolin, and myricetin being the main compounds. According to the USDA flavonoid database, pistachios contain 68.5 μg/g flavanols, 14.6 μg/g flavonols, and 60.6 μg/g anthocyanins. While the content of anthocyanins in pistachios found in this study are 22% lower than the USDA value, the contents of flavanols and flavonols are 1.3- and 16.6-fold larger. The main difference in flavonols is attributed to the

presence of myricetin. The wide variation is not unexpected, because phenolic contents in plant foods are subject to influence by growing location, season, cultivar, and food processing.[6,9,10,20,32]

In this study, we also tested in vitro bioaccessibility of pistachio bioactives in whole nuts using an upper GI mimic digestion protocol. It is worth noting that this protocol cannot fully reflect the mechanic and biochemical processes during human digestion. We observed that, as compared to the acidified methanol extraction, most phenolics found in pistachios were not readily accessible during the mimic digestion, with 5% phenolics being released, except protocatechuic and gallic acids. It is interesting to note that quercetin glycosides dominantly present in the skins were not released during the mimic digestion. As expected, fat-soluble nutrients in pistachios were not readily released to the aqueous GI mimic solvents, and only lutein and γ-tocopherol were found to be <7% in the GI mimic extract. Our data appear inconsistent with the Mandalari et al. study[9] in which gallic and procatechuic acids, luteolin, eriodyctiol, tocols, and lutein were >90% accessible during an in vitro digestion using a more sophisticated system. Kay et al. reported in a dose−response trial that consumption of diets containing 10% (32−63 g/d) or 20% (64−126 g/d) daily calories from California pistachios for 4 weeks increased circulating β-carotene, lutein, and γ-tocopherol in hypercholesterolemic adults, suggesting bioavailability of the lipophilic bioactives. Thus, more clinical studies are needed to validate the bioaccessibility and bioavailability of other pistachio bioactives.[37]

Lipophilic bioactives, including four carotenoids, two chlorophylls, and three tocols, in California pistachios were methodically characterized, as their quantification was performed after extraction protocols were optimized with solvents, saponification condition, and Na_2CO_3 addition. Further, 11 hydrophilic bioactives (2 phenolic acids, 9 flavonoids) were characterized. The most dominant bioactives were lutein, chlorophyll *a*, γ-tocopherol, catechins, luteolin, myricetin, and cyanidin-3-galactose in each nutrient category. γ-Tocotrienol, zeaxanthin, α-carotene, and myricetin were quantified in pistachios for the first time.

California pistachios are good source of antioxidants, e.g., tocols, carotenoids, and phenolics. Thus, pistachios incorporated into healthy diets shall help enhance health by prevention of cancers and cardiovascular diseases. Bioactive contents in pistachios and other nuts shall be systematically assessed so that health benefits of nut consumption can be fully appreciated.

■ ASSOCIATED CONTENT

Ⓢ Supporting Information

Supplemental Table 1, a list of the content of free and esterified lipophilic bioactives in whole pistachios. This material is available free of charge via the Internet at http://pubs.acs.org.

■ AUTHOR INFORMATION

Corresponding Author

*Tel: 617-556-3128. Fax: 617-556-3344. E-mail: Oliver.Chen@tufts.edu.

Author Contributions

Y.L. conducted the experiments, performed statistical analysis, and prepared the manuscript. J.B.B. contributed to data interpretation and manuscript preparation. C.-Y.O.C. contributed to study design, data interpretation, and manuscript preparation.

Funding

This work was supported by the American Pistachio Growers and the U.S. Department of Agriculture (USDA)/Agricultural Research Service (Cooperative Agreement No. 58-1950-0-014).

Notes

The contents of this publication do not necessarily reflect the views or policies of the USDA nor does mention of trade names, commercial products or organizations imply endorsement by the U.S. government.

The authors declare no competing financial interest.

■ ABBREVIATIONS USED

MTBE, methyl *tert*-butyl ether; BHT, butylated hydroxytoluene; HPLC, high-performance liquid chromatography; LC−MS/MS, liquid chromatography−mass spectrometry/mass spectrometry; ECD, gastrointestinal mimic; GI, electrochemical detector.

■ REFERENCES

(1) USDA/DHHS. Report of the dietary guidelines advisory committee on the dietary guidelines for Americans. (http://www.cnpp.usda.gov/DGAs2010-DGACReport.htm), June 15, 2010.

(2) Dreher, M. L. Pistachio nuts: Composition and potential health benefits. *Nutr. Rev.* **2012**, *70*, 234−240.

(3) Gentile, C.; Tesoriere, L.; Butera, D.; Fazzari, M.; Monastero, M.; Allegra, M.; Livrea, M. A. Antioxidant activity of Sicilian pistachio (*Pistacia vera* L. var. Bronte) nut extract and its bioactive components. *J. Agric. Food Chem.* **2007**, *55*, 643−648.

(4) Bisignano, C.; Filocamo, A.; Faulks, R. M.; Mandalari, G. In vitro antimicrobial activity of pistachio (*Pistacia vera* L.) polyphenols. *FEMS Microbiol. Lett.* **2013**, *341*, 62−67.

(5) Gentile, C.; Allegra, M.; Angileri, F.; Pintaudi, A. M.; Livrea, M. A.; Tesoriere, L. Polymeric proanthocyanidins from Sicilian pistachio (*Pistacia vera* L.) nut extract inhibit lipopolysaccharide-induced inflammatory response in RAW 264.7 cells. *Eur. J. Nutr.* **2012**, *51*, 353−363.

(6) Martorana, M.; Arcoraci, T.; Rizza, L.; Cristani, M.; Bonina, F. P.; Saija, A.; Trombetta, D.; Tomaino, A. In vitro antioxidant and in vivo photoprotective effect of pistachio (*Pistacia vera* L., variety Bronte) seed and skin extracts. *Fitoterapia* **2013**, *85*, 41−48.

(7) Rajaei, A.; Barzegar, M.; Mobarez, A. M.; Sahari, M. A.; Esfahani, Z. H. Antioxidant, anti-microbial and antimutagenicity activities of pistachio (*Pistachia vera*) green hull extract. *Food Chem. Toxicol.* **2010**, *48*, 107−112.

(8) Halvorsen, B. L.; Carlsen, M. H.; Phillips, K. M.; Bøhn, S. K.; Holte, K.; Jacobs, D. R.; Blomhoff, R. Content of redox-active compounds (i.e., antioxidants) in foods consumed in the United States. *Am. J. Clin. Nutr.* **2006**, *84*, 95−135.

(9) Mandalari, G.; Bisignano, C.; Filocamo, A.; Chessa, S.; Sarò, M.; Torre, G.; Faulks, R. M.; Dugo, P. Bioaccessibility of pistachio polyphenols, xanthophylls, and tocopherols during simulated human digestion. *Nutrition* **2013**, *29*, 338−344.

(10) Seeram, N. P.; Zhang, Y.; Henning, S. M.; Lee, R.; Niu, Y.; Lin, G.; Heber, D. Pistachio skin phenolics are destroyed by bleaching resulting in reduced antioxidative capacities. *J. Agric. Food Chem.* **2006**, *54*, 7036−7040.

(11) Wu, X.; Prior, R. L. Identification and characterization of anthocyanins by high-performance liquid chromatography−electrospray ionization-tandem mass spectrometry in common foods in the United States: Vegetables, nuts, and grains. *J. Agric. Food Chem.* **2005**, *53*, 3101−3113.

(12) Bolling, B. W.; Blumberg, J. B.; Chen, C. Y. The influence of roasting, pasteurisation, and storage on the polyphenol content and

antioxidant capacity of California almond skins. *Food Chem.* **2010**, *123*, 1040−1047.
(13) Dehkharghanian, M.; Adenier, H.; Vijayalakshmi, M. A. Study of flavonoids in aqueous spinach extract using positive electrospray ionisation tandem quadrupole mass spectrometry. *Food Chem.* **2010**, *121*, 863−870.
(14) de Rosso, V. V.; Mercadante, A. Z. Evaluation of colour and stability of anthocyanins from tropical fruits in an isotonic soft drink system. *Innovative Food Sci. Emerging Technol.* **2007**, *8*, 347−352.
(15) Chen, C. Y.; Blumberg, J. B. In vitro activity of almond skin polyphenols for scavenging free radicals and inducing quinone reductase. *J. Agric. Food Chem.* **2008**, *56*, 4427−4434.
(16) Cho, Y. S; Yeum, K. J; Chen, C. Y; Beretta, G.; Tang, G. W.; Krinsky, N. I., 2; Yoon, S.; Lee-Kim, Y. C.; Blumberg, J. B.; Russell, R. Phytonutrients affecting hydrophilic and lipophilic antioxidant activities in fruits, vegetables and legumes. *J. Sci. Food Agric.* **2007**, *87*, 1096−1107.
(17) Chen, C. Y.; Milbury, P. E.; Lapsley, K.; Blumberg, J. B. Flavonoids from almond skins are bioavailable and act synergistically with vitamins C and E to enhance hamster and human LDL resistance to oxidation. *J. Nutr.* **2005**, *135*, 1366−1373.
(18) Milbury, P. E.; Vita, J. A.; Blumberg, J .B. Anthocyanins are bioavailable in humans following an acute dose of cranberry juice. *J. Nutr.* **2010**, *140*, 1099−104.
(19) Bellomo, M. G.; Fallico, B. Anthocyanins, chlorophylls and xanthophylls in pistachio nuts (*Pistacia vera*) of different geographic origin. *J. Food Compos. Anal.* **2007**, *20*, 352−359.
(20) Ballistreri, G.; Arena, E.; Fallico, B. Influence of ripeness and drying process on the polyphenols and tocopherols of *Pistacia vera* L. *Molecules* **2009**, *14*, 4358−4369.
(21) Henriques, M.; Silva, A.; Rocha, J. Extraction and quantification of pigments from a marine microalga: A simple and reproducible method. In *Communicating Current Research and Educational Topics and Trends in Applied Microbiology*; Méndez-Vilas, A., Ed.; Formatex: Badajoz, Spain, 2007; vol. 2, pp 586−593.
(22) Craft, N. E.; Soares, J. H. Relative solubility, stability, and absorptivity of lutein and β-carotene in organic solvents. *J. Agric. Food Chem.* **1992**, *40*, 431−434.
(23) Fuke, Y.; Sasago, K.; Matsuoka, H. determination of chlorophylls in kiwi fruit and their changes during ripening. *J. Food Sci.* **1985**, *50*, 1220−1223.
(24) Kornsteiner, M.; Wagner, K. H.; Elmadfa, I. Tocopherols and total phenolics in 10 different nut types. *Food Chem.* **2006**, *98*, 381−387.
(25) Slavin, M.; Yu, L. A single extraction and HPLC procedure for simultaneous analysis of phytosterols, tocopherols and lutein in soybeans. *Food Chem.* **2012**, *135*, 2789−2795.
(26) Oliver, J.; Palou, A.; Pons, A. Semi-quantification of carotenoids by high-performance liquid chromatography: Saponification-induced losses in fatty foods. *J. Chromatogr. A* **1998**, *829*, 393−399.
(27) Hosotani, K.; Kitagawa, M. Improved simultaneous determination method of β-carotene and retinol with saponification in human serum and rat liver. *J. Chromatogr. B* **2003**, *791*, 305−313.
(28) Lee, H. S.; Castle, W. S.; Coates, G. A. High-performance liquid chromatography for the characterization of carotenoids in the new sweet orange (Earlygold) grown in Florida, USA. *J. Chromatogr. A* **2001**, *913*, 371−377.
(29) Pott, I.; Breithaupt, D. E.; Carle, R. Detection of unusual carotenoid esters in fresh mango (*Mangifera indica* L. cv. 'Kent'). *Phytochemistry* **2003**, *64*, 825−829.
(30) Saitta, M.; Giuffrida, D.; Bella, G. D.; La Torre, G. L.; Dugo, G. Compounds with antioxidant properties in pistachio (*Pistacia vera* L.) seeds. In *Nuts and Seeds in Health and Disease Prevention*; Preedy, V. R., Watson, R. R., Patel, V. B., Eds.; Academic Press: New York, 2011; pp 909−918.
(31) Gebauer, S. K.; West, S. G.; Kay, C. D.; Alaupovic, P.; Bagshaw, D.; Kris-Etherton, P. M. Effects of pistachios on cardiovascular disease risk factors and potential mechanisms of action: A dose−response study. *Am. J. Clin. Nutr.* **2008**, *88*, 651−659.
(32) Tomaino, A.; Martorana, M.; Arcoraci, T.; Monteleone, D.; Giovinazzo, C.; Saija, A. Antioxidant activity and phenolic profile of pistachio (*Pistacia vera* L., variety Bronte) seeds and skins. *Biochimie* **2010**, *92*, 1115−1122.
(33) Bolling, B. W.; McKay, D. L.; Blumberg, J. B. The phytochemical composition and antioxidant actions of tree nuts. *Asia Pac. J. Clin. Nutr.* **2010**, *19*, 117−123.
(34) Giuffrida, D.; Saitta, M.; La Torre, G. L.; Bombaci, L.; Dugo, G. Carotenoid, chlorophyll and chlorophyll-derived compounds in pistachio kernels (*Pistacia vera* L.) from Sicily. *Ital. J. Food Sci.* **2006**, *3*, 313−320.
(35) Fernandes, T. M.; Gomes, B. B.; Lanfer-Marquez, U. M. Apparent absorption of chlorophyll from spinach in an assay with dogs. *Innovative Food Sci. Emerging Technol.* **2007**, *8*, 426−432.
(36) Ferruzzi, M. G.; Böhm, V.; Courtney, P. D.; Schwartz, S. J. Antioxidant and antimutagenic activity of dietary chlorophyll derivatives determined by radical scavenging and bacterial reverse mutagenesis assays. *J. Food Sci.* **2002**, *67*, 2589−2595.
(37) Kay, C. D.; Gebauer, S. K.; West, S. G.; Kris-Etherton, P. M. Pistachios increase serum antioxidants and lower serum oxidized-LDL in hypercholesterolemic adults. *J. Nutr.* **2010**, *140*, 1093−1098.

oxygen species (ROS) production, and in modifying redox-sensitive molecular pathways.

MATERIALS AND METHODS

Chemicals. Tomatoes (*Solanum lycopersicum* L.) were obtained from a local market. Methanol (MeOH), methyl *tert*-butyl ether (MTBE), tetrahydrofuran (THF), and all others solvents used were of HPLC grade. A Millipore Milli-Q purification system (Millipore GmbH, Schwalbach, Germany) was used to obtain HPLC-grade water (18 MΩ). Carotenoids used were obtained from CaroteNature (Ostermundigen, Switzerland). Di(acetoxymethyl ester) analogue (C-2938) 6-carboxy-2′,7′-dichlorodihydrofluorescein diacetate (DCF) (Molecular Probes, Inc., Eugene, OR). Ethylene diamine tetraacetic acid (EDTA), DL-dithiothreitol (DTT), poly(deoxyinosinic-deoxycytidylic) acid (Poly(dI-dC)), and T4 polynucleotide kinase were obtained from Sigma-Aldrich at highest quality available (95−99%). Buffer salts and all other chemicals were of analytical grade. The concentrations of the carotenoid standard solutions were determined using standard spectrophotometric methods.[24]

Dry Tomato Peel (DTP) Preparation. Tomato peel was separated from the pulp using a tomato processing machine after cleaning with fresh water, then peel was freeze-dried in a Virtis lyophilizer (model FM12XL). DTP were grounded with a mill (particle size 0.025−0.05 mm) and stored in darkness at −30 °C until use.

Tomato Powder (TP) Preparation. Tomatoes were cleaned, ground, and centrifuged at 6000 *g* by 10 min at 5 °C. Supernatant was eliminated, and the pellet was dried in a Virtis lyophilizer (model FM12XL). The TP was ground with a mill (0.025−0.05 mm particle size) and stored in darkness at −30 °C until use.

E-Beam Treatment. Both tomato products were packed (1 g weigh) into laminated bags of low permeability (35 cm^3/24 h m^2 bar for oxygen, 150 cm^3/24 h m^2 bar for CO_2), vacuum-packaged, and transported in refrigeration to the irradiation plant (IONISOS Ibérica SA, Tarancón, Spain). This type of film is industrially used to manufacture vacuum packaged foods and guarantee the vacuum during storage of our samples. The treatment was performed with an electron accelerator which operated at 10 MeV. Doses of 4 kGy were applied which have been found to be effective to ensure spoilage and pathogen microbiota control.[22,23] Cellulose triacetate dosimeters were used to check the actual dose absorbed.[25] Experiments were made in triplicate and at a temperature of 15−18 °C. The temperature increased in the product less than 2 °C during E-beam treatment. DTP and TP were always protected from the light.

The samples were under refrigerated conditions (4 °C) during transport, and subsequently they were stored at −30 °C until analysis. Both irradiated and nonirradiated samples were analyzed as follows.

Analysis of Lycopene Composition and Quantification. Lycopene isomer composition as well as contents of lycopene were analyzed using a gradient C30-HPLC method using a Merck−Hitachi HPLC system (Darmstadt, Germany) and a Jetstream Plus column oven (JASCO, Groß-Umstadt, Germany).[25] For quantification of lycopene, a sample extract of 500 mg was diluted in 25 mL of methanol/methyl *tert*-butyl ether (MTBE) (20/80 v/v). *β*-apo-8-Carotenal was used as internal standard. A C_{30} column Trentec Stability 100 C30 PEEK (250 mm × 4.6 mm, 5 μm) (Trentec, Rutesheim, Germany), preceded by a C_{18} ProntoSil 120−5-C18 H (10 mm × 4.0 mm, 5 μm) column (Bischoff, Leonberg, Germany) was used. As mobile phase (1.0 mL/min), a gradient procedure consisting of MeOH (solvent A) and MTBE (solvent B) was used. Column temperature was 10 ± 1 °C and detection wavelength 470 nm. Lycopene contents were quantified using (*all-E*)-lycopene as external standard. For lycopene isomers, a different HPLC method was used: mobile phase (1.0 mL/min), MTBE/methanol/ethylacetate (50/45/5 v/v/v); column, polymeric C30 (250 mm × 4.6 mm, 5 μm) column (YMC Europe, Dinslaken, Germany); column temperature, 32 ± 1 °C; detection wavelength, 470 nm. Retention time of (*Z*)-isomer) in relation to that of (*all-E*)-lycopene was used to identify lycopene isomers. As only very low amounts of samples were available for HPLC of lycopene isomers, peak areas were used to calculate isomer ratios. Thus, exact contents of different lycopene isomers were not determined.

Cell Culture. RAT-1 fibroblasts have been used because they are a cellular line successfully used to study the antioxidant activity of lycopene.[26] The RAT-1 fibroblasts (American Type Culture Collection, Rockville, MD) were grown in Minimun Essential Medium Eagle (MEM) with streptomycin 100 μg/mL, penicillin 100 μg/mL, and supplemented with 10% fetal calf serum and 2 mM glutamine. Cells were maintained in log phase by seeding twice a week at density of 3×10^5 cells/mL at 3 °C under 5% CO_2 air atmosphere.

One milliliter of tetrahydrofuran (THF) was added to DTP and TP (0.5 g), and 2 μL of these solutions were added per 1 mL of MEM medium containing 10^6 cells for 24 h, and ROS production was measured after 30 and 60 min of incubation in the absence or in the presence of 100 μM H_2O_2. The solutions with THF were prepared immediately before each experiment in order to avoid lost of lycopene. After the addition of tomato extracts, the medium was not further replaced throughout the experiments. Control cultures received an equal amount of solvent (THF) but without tomato extracts. Experiments were routinely carried out on triplicate cultures. Intracellular radical species were detected by measuring the fluorescence intensity values due to oxidation of DCF (see below).

Measurement of ROS. Cells were harvested to evaluate the ROS production using the di(acetoxymethyl ester) analogue (C-2938) of 6-carboxy-2′,7′-dichlorodihydrofluorescein diacetate.[27] Before the addition of the fluorescent probes, 2×10^6 cells were washed to eliminate the amount of tomato products not cell-associated. Fluorescent units were measured in each well after 30 min incubation with DCF (10 μM) by use of a Cytofluor 2300/2350 fluorescence measurement system (Millipore Corp., Bedford, MA). Tomato products did not alter the basal fluorescence of DCF. Then cells were treated with 100 μM H_2O_2 for 30−60 min in order to amplify ROS production.

Western Blot Analysis of p38 and p-p38, ERK1/2, pERK1/2, JNK, p-JNK, Nox-4, and Cox-2 Expression. Cells (10×10^6) were harvested, lysed, and centrifuged. The supernatants were used for Western blot analysis.[28] The anti-p38 (clone C-20, catalogue no. SC-535), anti p-p38 (clone D-8, catalogue no. 7973), anti-ERK1/2 (clone K-23, catalogue no. SC-94), anti p-ERK1/2 (clone E-4, catalogue no. SC-7383), anti-JNK (clone C-17, catalogue no. SC-474), anti-p-JNK (clone G-7, catalogue no. SC-6254), anti-Nox-4 (clone N-15, catalogue no. sc-21860), and anti-Cox-2 (clone C-20, catalogue no. 1745) monoclonal antibodies, and the antihsp 70 (clone K-20, catalogue no. sc-1060) and the anti-hsp90*α* (clone C-20, catalogue no. sc-8262 goat) polyclonal antibodies were purchased from Santa Cruz Biotechnology (Santa Cruz, CA). The blots were washed and exposed to horseradish peroxidase-labeled secondary antibodies (Amersham Pharmacia Biotech, Arlington Heights, IL) for 45 min at room temperature. The immunocomplexes were visualized by the enhanced chemiluminescence detection system and quantified by densitometric scanning.

Electrophoretic Mobility Shift Assay. Frozen cell pellets were processed to obtain nuclear extracts. The pellet was treated as previously indicated by Joo et al.[29] Binding reactions containing 5 μg of nuclear extracts, 10 mM Tris-HCl (pH 7.6), 5% glycerol, 1 mM EDTA, 1 mM DTT, 50 mM NaCl, and 3 mg poly(dI-dC) were incubated for 30 min with 5000 cpm of α-^{32}P-end-labeled double-stranded oligonucleotide in a total volume of 20 μL. The probe was 5′-AGTTGAGGGGACTTTCCCAGGC3′. Labeling of the probe was obtained by incubating 5 pmol of oligonucleotide with 10 pmol [α-^{32}P] ATP and 3U T4 polynucleotide kinase for 30 min at 37 °C. The probe was then purified with MicroBIO-Spin P-30 columns. Complexes were separated on 60 g/L polyacrylamide gels with 45 mM Tris-borate, 1 mM EDTA, pH 8, buffer. After drying under vacuum, gels were exposed on phosphor screens which were then analyzed by phosphor/fluorescence imager STORM 840 (Molecular Dynamics, Sunnyvale, CA). The intensity of the revealed bands were directly quantified by Image QuaNT software (Molecular Dynamics, Sunnyvale, CA).

Table 1. Lycopene Isomers in Dry Tomato Peel (DTP) Tomato Powder (TP) Following Irradiation[a]

	ratios of (*all-E*)-lycopene to the different (*Z*) isomers			
	DTP	irradiated DTP	TP	irradiated TP
all-E/5*Z*	14.4 ± 0.5[a]	7.3 ± 0.4[b]	12.5 ± 0.8[c]	10.7 ± 0.5[d]
all-E/5*Z*,9*Z*	42.8 ± 1.2[a]	32.3 ± 1.3[b]	30.2 ± 0.7[c]	26.9 ± 1.4[d]
all-E/5*Z*,9′*Z*	728.0 ± 2.1[c]	317.0 ± 1.5[d]	1360.0 ± 1.6[a]	1051.0 ± 2.5[b]
all-E/9*Z*	57.8 ± 0.9[a]	33.4 ± 2.1[d]	61.4 ± 1.5[b]	56.0 ± 1.9[c]
all-E/13*Z*	4.6 ± 0.7[c]	3.0 ± 0.3[d]	10.6 ± 0.6[a]	8.8 ± 0.3[b]

[a]Values not sharing the same letter were significantly different ($P < 0.05$, Fisher's test).

Analysis of p65 Protein. Nuclear extracts, 25−30 μg of protein, were separated by sodium dodecyl sulfate polyacrylamide gel electrophoresis with 40−120 g/L Bis-Tris gels (NOVEX, San Diego, CA) and transferred to Immobilon-P membranes (Millipore Corp, Bedford, MA) with the use of a semidry system. Membranes were blocked overnight at 4 °C in 50 g/L dried milk in PBS, pH 7.4, plus 0.05% Tween 20. Blots were incubated with polyclonal primary antibodies to p65 (Santa Cruz, Biotechnology, CA, clone 49.Ser 311, catalogue no. SC-135769) in PBS plus 0.05% Tween 20 for 1−2 h at room temperature. The blots were visualized as described in Western blotting assay.

Statistical Analysis. Values were presented as means ± standard error of the mean (SEM). One-way ANOVA was used to determine differences between different treatments (control and irradiated and nonirradiated tomato samples) in ROS production (Figure 1), MAPK expression (Figure 3) in NF-κB activation (Figure 4), and Cox-2 and Nox-4 expression (Figure 5). A posthoc comparison of means was made, using Fisher's test, when significant values ($P < 0.05$) were found. Multifactorial two-way analysis of variance (ANOVA) was adopted to assess any differences among the treatments and the doses (Figure 2). A posthoc comparison of means was made, using the Tukey's Honestly Significant Differences test, when significant values ($P < 0.05$) were found. Differences were analyzed using Minitab Software (Minitab, Inc., State College, PA).

RESULTS AND DISCUSSION

Influence of irradiation on lycopene concentration was measured. The dry tomato peel showed almost double lycopene content (0.2 ± 0.02 mM) compared to tomato powder (0.1 ± 0.01 mM). Irradiation exposure consumed the carotenoid by almost 50% for both extracts (0.10 ± 0.01 and 0.06 ± 0.01 mM to DTP and TP, respectively). A decrease in lycopene content by E-beam irradiation has been reported in grapefruit;[30] these authors discussed evidence that lycopene levels decreased as the E-beam dose increased.

The HPLC analyses revealed a reduction of (*all-E*)-lycopene with increasing peaks of lycopene (*Z*)-isomers following irradiation (Table 1). This effect was significantly stronger in the DTP samples than in TP. Lycopene has 11 conjugated double bonds, and each of them could be either in an *E* or *Z* configuration. *all-E*-Lycopene is the predominant isomer in plants, representing about 80−97% of total lycopene in tomatoes and related products.[31] In the human body fluids and tissues such as plasma, breast milk, prostate, testis, and skin, 25−70% of lycopene is found in various *Z* forms.[32,33] Shi and Le Maguer[31] indicated that the biological potency of *Z*-lycopene isomers is different from that of the *all-E* form. In terms of bioefficacy, some *Z*-isomers had a stronger in vitro antioxidant activity than the *all-E* form.[34] These data may be particularly interesting in view of the high concentrations of *Z*-isomers in vivo.

The antioxidant activity of DTP and TP extracts, before and after irradiation, was analyzed in RAT-1 fibroblasts in the absence and in the presence of the well-known prooxidant agent H_2O_2. Antioxidant tomato efficiency was evaluated as inhibition of intracellular reactive oxygen species (ROS) production induced spontaneously or in the presence of the prooxidant (Figure 1). In the absence of the prooxidant, a very

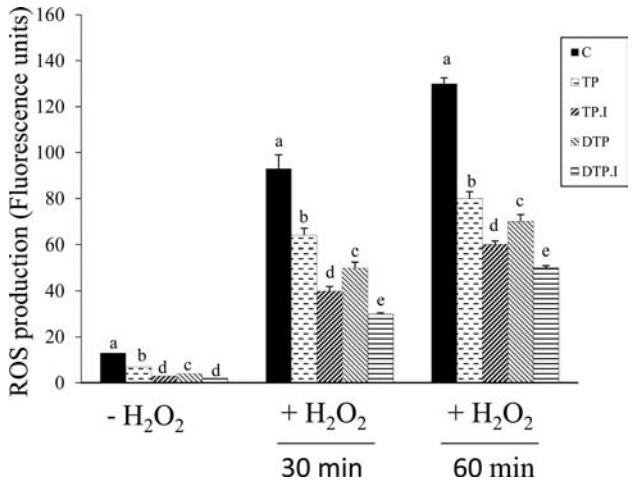

Figure 1. ROS production in RAT-1 fibroblasts incubated, without tomato products (C), tomato powder (TP), and dry tomato peel (DTP), pretreated (I) or untreated with E-beam, as indicated in Materials and Methods section. Spontaneous ($-H_2O_2$) and H_2O_2-induced ROS production in control cells and in treated cells, exposed, as indicated, to 100 μM H_2O_2 for 30−60 min. Values were the means ± SEM of three experiments. The treatment interaction was significant ($P < 0.05$). Values not sharing the same letter were significantly different ($P < 0.005$, Tukey's test).

small amount of ROS production was observed but it increased significantly in the presence of H_2O_2. Treatment of RAT-1 fibroblasts with the different tomato extracts caused a significant decrease in ROS production with respect to control cells (C), which was remarkably evidenced during the incubation with H_2O_2. A weak, but significant inhibition of ROS production in the absence of H_2O_2 was also observed following tomato extracts treatment. Such an effect was more remarkable for DTP than for TP extracts and more evident for irradiated samples than for unirradiated ones. Such effects were specific for both extracts because cells treated with H_2O_2 and THF alone as a vehicle did not differ in ROS expression from cells treated with H_2O_2 alone (data not shown).

The antioxidant effects of tomato extracts were clearly dose-dependent as can be observed by the progressive decrease of H_2O_2-induced ROS production after the addition of increasing concentrations of the different tomato extracts to RAT-1 fibroblasts (Figure 2).

The possible modulation of the MAPK cascade was analyzed in macrophages pretreated with the different tomato extracts to investigate intracellular redox signal transduction in RAT-1 cells

dx.doi.org/10.1021/jf4048012 | J. Agric. Food Chem. 2014, 62, 1557−1563

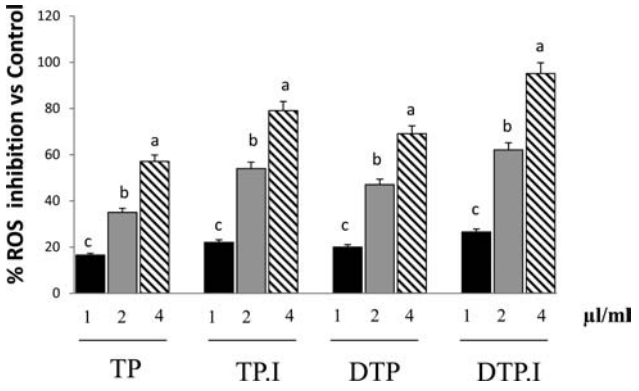

Figure 2. H_2O_2-induced ROS production in the presence of varying concentrations (1−4 μL/mL) of tomato powder (TP) and dry tomato peel (DTP) or without tomato products (C), pretreated (I) or untreated with E-beam, as indicated in Materials and Methods section. RAT-1 fibroblasts were exposed to 100 μM H_2O_2 for 60 min. Values were the means ± SEM of three experiments. The treatment/dose interaction was significant ($P < 0.05$). Values were the means ± SEM of three experiments. Values not sharing the same letter were significantly different ($P < 0.002$, Tukey's test).

(Figure 3). These kinases have been reported to be activated by various stress stimuli, including an overproduction of ROS, and they have been also implicated in the modulation of several intracellular redox functions. Remarkable levels of the phosphorylated forms of ERK1/2 (p-ERK1/2) (Figure 3A, B), JNK (p-JNK) (Figure 3C, D), and p-38 (p-p38) (Figure 3E, F) were observed in control cells after 3 h. Such levels were all decreased significantly by the addition of the different tomato extracts. Such inhibitions were more remarkable for DTP than for TP and more evident for irradiated samples than for unirradiated ones.

These data are not surprising in view of evidence showing that lycopene is a powerful in vitro antioxidant. Among naturally occurring carotenoids, lycopene has shown to possess ability in scavenging free radicals and in interacting with ROS, preventing ROS-induced cell damage.[35] Accordingly, several epidemiological studies have evaluated the role of lycopene and tomato products as potential in vivo antioxidants. Although the data are sometimes controversial, using tomatoes or tomato products, numerous studies have demonstrated decreased DNA damage,[36] decreased susceptibility to oxidative stress in lymphocytes,[37] and decreased LDL oxidation[5] or lipid peroxidation.[38] Moreover, tomato extracts acted in this study as a potent inhibitor of the phosphorylation of MAPKs, which are reported to be activated by ROS. These data are in agreement with previous observations showing that lycopene, alone or in combination with other natural products, modulate MAPK phosphorylation.[39] In particular, the carotenoid was reported to attenuate the phenotypic and functional maturation of murine bone marrow dendritic cells, especially in lipopolysaccharide (LPS)-induced DC maturation.[40] The carotenoid was also able to inhibit platelet derived growth factor (PDGF)-BB-induced signaling and migration in human fibroblasts by inhibiting the activation of extracellular signal-regulated kinase (ERK)1/2, p38, and jun N-terminal kinase (JNK).[41]

In view of recent studies suggesting that NF-κB plays an important role in regulating redox signaling, the involvement of this redox-sensitive transcription factor in THP-1 macrophages following the different tomato extracts was investigated (Figure 4A). In control cells, a net enhancement of nuclear trans-

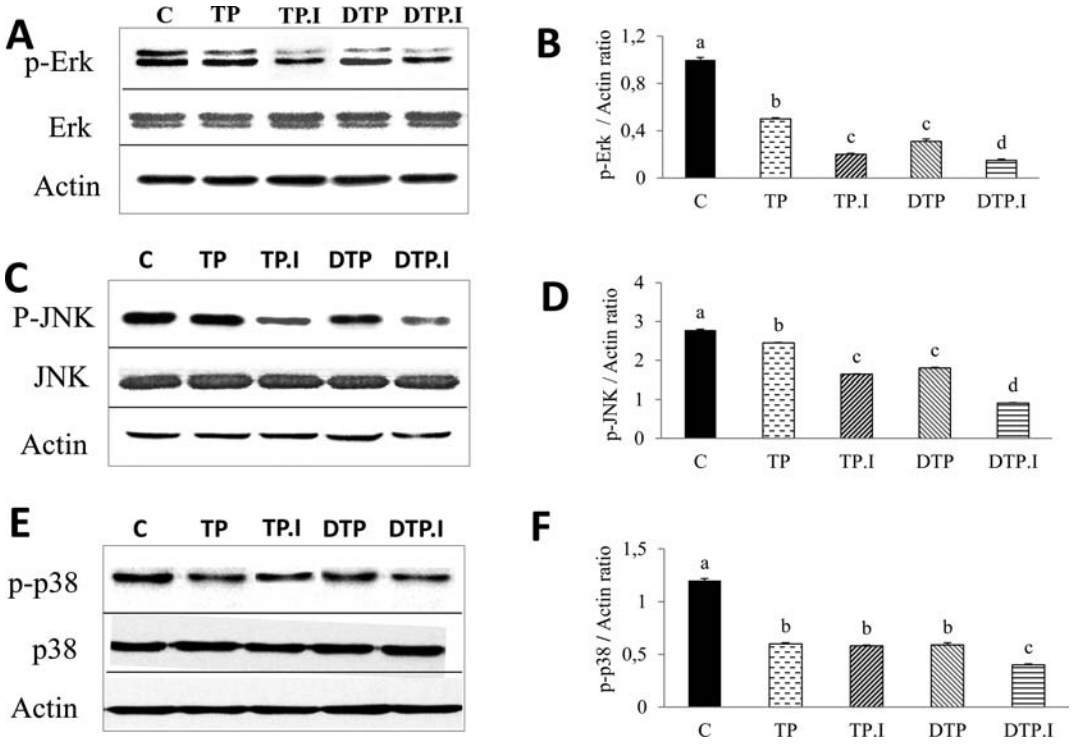

Figure 3. MAPK expression in RAT-1 fibroblasts pre-incubated with tomato powder (TP) and dry tomato peel (DTP) or without tomato products (C), pretreated (I) or untreated with E-beam, as indicated in Materials and Methods section. (A, C, E) Representative Western blotting analyses. (B, D, F) Densitometric analyses. Values were the means ± SEM of three experiments. Values not sharing the same letter were significantly different ($P < 0.05$, Fisher's test).

dx.doi.org/10.1021/jf4048012 | J. Agric. Food Chem. 2014, 62, 1557−1563

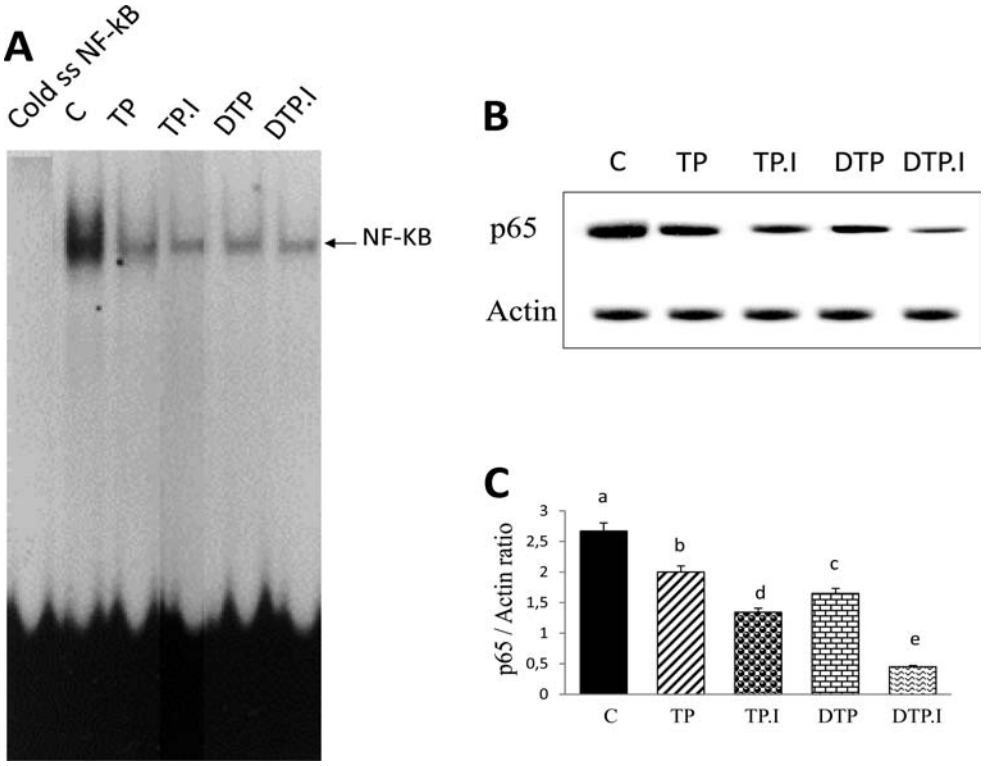

Figure 4. NF-κB activation in THP in RAT-1 fibroblasts pre-incubated with tomato powder (TP) and dry tomato peel (DTP) or without tomato products (C), pretreated (I) or untreated with E-beam, as indicated in Materials and Methods section. (A) DNA binding activities of NF-κB subunits complexes. After treatment, the binding activities of NF-κB subunits to DNA were determined using EMSA. The specifity was demonstrated by using excess unlabeled NF-κB oligonucleotides (= cold ssNF-κB), which competed away binding. (B) Representative Western blotting analyses of p65 subunits. (C) Densitometric analyses. Values were the means ± SEM of three experiments. Values not sharing the same letter were significantly different ($P < 0.05$, Fisher's test).

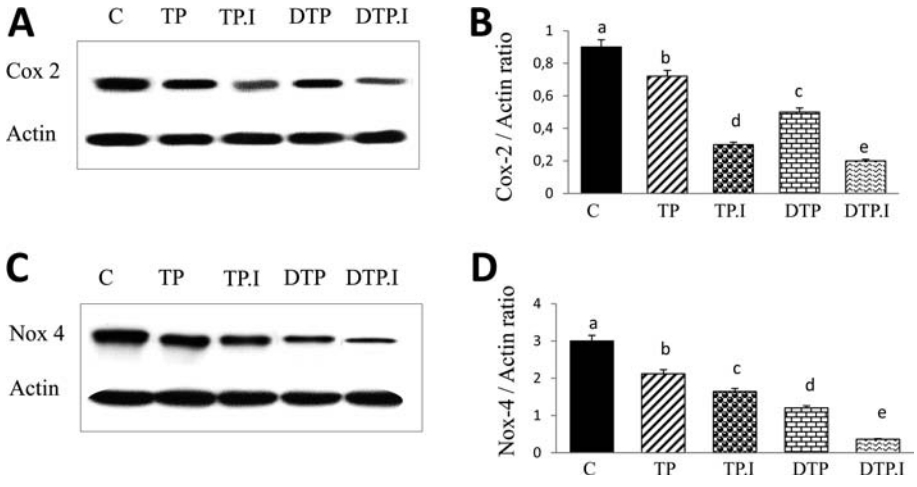

Figure 5. Cox-2 and Nox-4 expression in RAT-1 fibroblasts pre-incubated with tomato powder (TP) and dry tomato peel (DTP) or without tomato products (C), pretreated (I) or untreated with E-beam, as indicated in Materials and Methods section. (A, C) Representative Western blotting analyses and (B, D) densitometric analyses. Values were the means ± SEM of three experiments. Values not sharing the same letter were significantly different ($P < 0.05$, Fisher's test).

location was evident at 3 h treatment. However, the up-regulation of NF-κB nuclear binding was prevented by the addition of the different tomato extracts. In agreement with the previous results, the reductions were significantly higher for DTP extract than for TP extract and more evident for irradiated samples than for unirradiated ones. Similar results were found when nuclear extracts were prepared from fibroblasts treated with the different tomato extracts and nuclear translocation of the NF-κB p65 subunit was detected by Western blotting (Figure 4B, C). In control cells, a nuclear translocation of the NF-κB subunit p65 was evidenced within 3 h. Such an effect was inhibited by the addition of the different tomato extracts and, once again, the inhibition was significantly greater for DTP than for TP extract and also was significantly affected by irradiation.

dx.doi.org/10.1021/jf4048012 | J. Agric. Food Chem. 2014, 62, 1557−1563

In recent studies from our laboratory, lycopene suppressed both MAPK phosphorylation and NF-κB activation in oxysterol-stimulated macrophages as well as in prostatic cancer cells.[42] In addition, in this study, tomato extracts also inhibited H_2O_2-induced NF-κB activation, which has been reported to be the first eukaryotic transcription factor shown to respond directly to oxidative stress.[43] It has been found that lycopene inhibited the binding activity of NF-κB in human hepatoma cells[44] and in THP-1 cells exposed to cigarette smoke extract.[45] Such inhibition was mediated by the down-regulation of IκB phosphorylation, NF-κB expression, and NF-κB p65 subunit translocation from cytosol to nucleus.[46] Moreover, tomato lycopene extract prevented LPS-induced pro-inflammatory gene expression by blocking NF-κB signaling.[29]

Because it has been reported that cyclooxygenase-2 (Cox-2) and nicotinamide adenine dinucleotide phosphate oxidase (Nox) are proteins involved in oxidative stress, the expression of both of them in RAT-1 fibroblasts following the different tomato extracts was measured (Figure 5). The addition of all tomato extracts decreased significantly the expression of both Cox-2 and Nox-4 with respect to untreated control cells. The inhibition was significantly greater for DTP than for TP extract, and a significant influence of irradiation was observed showing irradiated samples a greater inhibition.

Tomato extracts inhibited the expression of proteins involved in stress signaling, such as Nox-4, one of the homologues of NADPH oxidase, and Cox-2. These results confirming those obtained in THP-1 cells[47] and in RAW 264.7 macrophages.[48]

The obtained results demonstrate that DTP had significantly ($p < 0.05$) higher concentration of total lycopene than TP. The higher lycopene content of DTP compared to the TP could probably explain its better antioxidant activity in our cell model. These results are not surprising because it has been reported that tomato peel can contain up to 5 times more lycopene than the whole tomato.[49]

Our study confirms the potency of tomato extracts containing lycopene in inhibiting oxidative stress in a cell model. In fact, all the extracts studied were able to counteract the effects of H_2O_2 on ROS formation and on redox-sensitive molecular targets involved in cell signaling, including MAPK and NF-κB, and on the expression of redox-sensitive proteins, including Nox-4 and Cox-2. All these events occurred in a range of carotenoid concentrations which can be reached in vivo after lycopene or tomato supplementation.[36]

The present study shows that E-beam treatment increased the antioxidant ability of both DTP and TP in inhibiting H_2O_2-induced oxidative stress. Concomitantly, it reduced the content of *all-E*-lycopene and increased the levels of *Z*-lycopene. The addition of the two irradiated tomato products (DTP or TP) could be suitable to manufacture meat functional products, improving their antioxidant capacity.

AUTHOR INFORMATION

Corresponding Author

*Phone: +34 915492300. Fax: +34 916644853. E-mail: mmcalvo@ictan.csic.es.

Funding

This research was funded by Project CONSOLIDER-Ingenio 2010 (ref. CSD2007-00016) and Group of Investigation BSCH-UCM no. 920276 (ref GR58/08).

Notes

The authors declare no competing financial interest.

ACKNOWLEDGMENTS

M.C. Gámez has been awarded a grant of personal mobility from the Spanish Ministerio de Educación y Ciencia.

REFERENCES

(1) Agarwal, S.; Rao, A. V. Tomato lycopene and its role in human health and chronic diseases. *Can. Med. Assoc. J.* **2000**, *163*, 739−744.

(2) Blum, A.; Monir, M.; Wirsansky, I.; Ben-Arzi, S. The beneficial effects of tomatoes. *Eur. J. Intern. Med.* **2005**, *16*, 402−404.

(3) Willcox, J. K.; Catignani, G. L.; Lazarus, S. Tomatoes and cardiovascular health. *Crit. Rev. Food Sci. Nutr.* **2003**, *43*, 1−18.

(4) Giovannucci, E. Tomatoes, tomato-based products, lycopene, and cancer: review of the epidemiologic literature. *J. Natl. Cancer Inst.* **1999**, *91*, 317−331.

(5) Agarwal, S.; Rao, A. V. Tomato lycopene and low density lipoprotein oxidation a human dietary intervention study. *Lipids* **1998**, *33*, 981−984.

(6) Ahuja, K. D. K.; Pittaway, J. K.; Ball, M. J. Effects of olive oil and tomato lycopene combination on serum lycopene, lipid profile, and lipid oxidation. *Nutrition* **2006**, *22*, 259−265.

(7) Sahin, N.; Akdemir, F.; Orhan, C.; Kucuk, O.; Hayirli, A.; Sahin, K. Lycopene-enriched quail egg as functional food for humans. *Food Res. Int.* **2008**, *41*, 295−300.

(8) Candogan, K. The effect of tomato paste on some quality characteristics of beef patties during refrigerated storage. *Eur. Food Res. Technol.* **2002**, *215*, 305−309.

(9) Deda, M. S.; Bloukas, J. G.; Fista, G. A. Effect of tomato paste and nitrite level on processing and quality characteristics of frankfurters. *Meat Sci.* **2007**, *76*, 501−508.

(10) Kim, S.; Sang-Keun, J.; Kumar, M. P. Quality of low-fat pork sausages with tomato powder as colour and functional additive during refrigerated storage. *J. Food Sci. Technol.* **2011**, *48*, 591−597.

(11) Yilmaz, I.; Simsek, O.; Isikli, M. Fatty acid composition and quality characteristics of low-fat cooked sausages made with beef and chicken meat, tomato juice and sunflower oil. *Meat Sci.* **2002**, *62*, 253−258.

(12) Calvo, M. M.; Rodríguez. M. J.; Santa-María. J. G.; Selgas, M. D.; García, M. L. Productos cárnicos y de la pesca enriquecidos en licopeno mediante la adición de piel de tomate. Patent P200701670, 2007.

(13) Calvo, M. M.; García, M. L.; Selgas, M. D. Dry fermented sausages enriched with lycopene from tomato peel. *Meat Sci.* **2008**, *80*, 167−172.

(14) García, M. L.; Calvo, M. M.; Selgas, M. D. Beef hamburgers enriched in lycopene using dry tomato peel as an ingredient. *Meat Sci.* **2009**, *83*, 45−49.

(15) *Facts about Food Irradiation*; ICGFI International Consultative Group on Food Irradiation: Geneva, 1999; https://apps.who.int/fsf/whopb3.htm#ICGFI.

(16) Cambero, M. I.; Cabeza, M. C.; Escudero, R.; Manzano, S.; Ordoñez, J. A. Sanitation of selected ready-to-eat intermediate-moisture foods of animal origin by E-beam irradiation. *Foodborne Pathog. Dis.* **2012**, *9*, 594−599.

(17) Hocaoglu, A.; Demirci, A. S.; Gumus, T.; Demirci, M. Effect of gamma irradiation on chemical, microbial quality and shelf life of shrimp. *Radiat. Phys. Chem.* **2012**, *81*, 1923−1929.

(18) Antonio, A. L.; Carocho, M.; Bento, A.; Quintana, B.; Botelho, M. L.; Ferreira, I. C. F. R. Effects of gamma radiation on the biological, physico-chemical, nutritional and antioxidant parameters of chestnuts—a review. *Food Chem. Toxicol.* **2012**, *50*, 3234−4242.

(19) Fernandes, A.; Antonio, A. L.; Oliveira, M. B. P. P.; Martins, A.; Ferreira, I. C. F. R. Effect of gamma and electron beam irradiation on the physico-chemical and nutritional properties of mushrooms: A review. *Food Chem.* **2012**, *135*, 641−650.

(20) Dempster, J. F. Radiation preservation of meat and meat products—a review. *Meat Sci.* **1985**, *12*, 61−89.

(21) Hoz, L.; Cambero, M. I.; Cabeza, M. C.; Herrero, A. M.; Ordoñez, J. A. Elimination of *Listeria monocytogenes* from vacuum-

packed dry-cured ham by E-beam radiation. *J. Food Protect.* **2008**, *71*, 2001−2006.
(22) Selgas, M. D.; García, M. L.; Calvo, M. M. Effect of irradiation and storage on the physico-chemical and sensory properties of hamburgers enriched with lycopene. *Int. J. Food Sci .Technol.* **2009**, *44*, 1983−1998.
(23) Gámez, M. C.; García, M. L.; Selgas, M. D.; Calvo, M. M. Irradiation of ready-to-eat sausages containing lycopene. *Ital. J. Food Sci.* **2011**, *23*, 260−269.
(24) Müller, L.; Goupy, P.; Fröhlich, K.; Dangles, O.; Caris-Veyrat, C.; Böhm, V. Comparative study on antioxidant activity of lycopene (*Z*)-isomers in different assays. *J. Agric. Food Chem.* **2011**, *59*, 4504−4511.
(25) *Standard Practice for Use of Cellulose Acetate Dosimetry Systems, E1650−97e1*; Standards on disc; ASTM American Society for Testing and Materials: West Conshohocken, PA, 2000; Vol. *12.02*.
(26) Lorenz, M.; Stangl, V.; Jacob, C.; Daemen, K.; Böhm, V.; Fröhlich, K.; Baumann, G.; Stangl, K.; Simone, R.; Palozza, P. Delivery of lycopene to physiologically relevant vascular cells. *J. Food Lipids* **2009**, *16*, 259−272.
(27) Palozza, P.; Piccioni, E.; Avanzi, L.; Vertuani, S.; Calviello, G.; Manfredini, S. Design, synthesis, and antioxidant activity of FeAOX-6, a novel agent deriving from a molecular combination of the chromanyl and polyisoprenyl moieties. *Free Radical Biol. Med.* **2002**, *33*, 1724−1735.
(28) Palozza, P.; Sheriff, A.; Serini, S.; Boninsegna, A.; Maggiano, N.; Ranelletti, F. O.; Calviello, G.; Cittadini, A. Lycopene induces apoptosis in immortalized fibroblast exposed to tobacco smoke condensate through arresting cell cycle and down regulating cyclin D1, pAKT and pBad. *Apoptosis* **2005**, *10*, 1445−1456.
(29) Joo, Y. E.; Karrasch, T.; Mühlbauer, M.; Allard, B.; Narula, A.; Herfarth, H. H.; Jobin, C. Tomato lycopene extract prevents lipopolysaccharide-induced NF-kappaB signaling but worsens dextran sulfate sodium-induced colitis in NF-kappaBEGFP mice. *PloS One* **2009**, *4*, 4562−4573.
(30) Girennavar, B.; Jayaprakasha, G. K.; Mclin, S. C.; Maxim, J.; Yoo, K. S.; Patil, B. S. Influence of electron-beam irradiation on bioactive compounds in grapefruits (*Citrus paradise* Macf.). *J. Agric. Food Chem.* **2008**, *56*, 10941−10946.
(31) Shi, J.; Le Maguer, M. Lycopene in tomatoes: chemical and physical properties affected by food processing. *Crit. Rev. Biotechnol.* **2000**, *20*, 293−334.
(32) Stahl, W.; Sies, H. Uptake of lycopene and its geometrical isomers is greater from heat-processed than from unprocessed tomato juice in humans. *J. Nutr.* **1992**, *122*, 2161−2166.
(33) Ferreira, A. L.; Yeum, K.-J.; Russell, R. M.; Krinsky, N. I.; Tang, G. W. Enzymatic and oxidative metabolites of lycopene. *J. Nutr. Biochem.* **2004**, *15*, 493−502.
(34) Böhm, V.; Puspitasari-Nienaber, N. L.; Ferruzzi, M. G.; Schwartz, S. J. Trolox equivalent antioxidant capacity of different geometrical isomers of α-carotene, β-carotene, lycopene, and zeaxanthin. *J. Agric. Food Chem.* **2002**, *50*, 221−226.
(35) Palozza, P.; Parrone, N.; Catalano, A.; Simone, R. Tomato lycopene and inflammatory cascade: basic interactions and clinical implications. *Curr. Med. Chem.* **2010a**, *17*, 2547−2563.
(36) Bowen, P.; Chen, L.; Stacewicz-Sapuntzakis, M.; Duncan, C.; Sharifi, R.; Ghosh, L.; Kim, H. S.; Christov-Tzelkov, K.; van Breemen, R. Tomato sauce supplementation and prostate cancer: lycopene accumulation and modulation of biomarkers of carcinogenesis. *Exp. Biol. Med* **2002**, *227*, 886−893.
(37) Riso, P.; Visioli, F.; Grande, S.; Guarnieri, S.; Gardana, C.; Simonetti, P.; Porrini, M. Effect of a tomato-based drink on markers of inflammation, immunomodulation, and oxidative stress. *J. Agric. Food Chem.* **2006**, *54*, 2563−2566.
(38) Bub, A.; Watzl, B.; Abrahamse, L.; Delincée, H.; Adam, S.; Wever, J.; Müller, H.; Rechkemmer, G. Moderate intervention with carotenoid-rich vegetable products reduces lipid peroxidation in men. *J. Nutr.* **2000**, *130*, 2200−2206.
(39) Sarkar, F. H.; Li, Y.; Wang, Z.; Kong, D. Cellular signaling perturbation by natural products. *Cell Signalling* **2009**, *21*, 1541−1547.
(40) Kim, G. Y.; Kim, J. H.; Ahn, S. C.; Lee, H. J.; Moom, D. O.; Lee, C. M.; Park, Y. M. Lycopene suppresses the lipopolysaccharide-induced phenotypic and functional maturation of murine dendritic cells through inhibition of mutagen-activated protein kinases and nuclear factor-kappa B. *Immunol.* **2004**, *113*, 203−211.
(41) Chan, C. M.; Fang, J. Y.; Lin, H. H.; Yang, C. Y.; Hung, C. Lycopene inhibits PDGF-BB-induced retinal pigment epithelial cell migration by suppression of PI3K Akt and MAPK pathways. *Biochem. Biophys. Res. Commun.* **2009**, *388*, 172−176.
(42) Palozza, P.; Simone, R.; Catalano, A.; Boninsegna, A.; Böhm, V.; Fröhlich, K.; Mele, M. C.; Monego, G.; Ranelletti, F. O. Lycopene prevents 7-ketocholesterol-induced oxidative stress, cell cycle arrest and apoptosis in human macrophages. *J. Nutr. Biochem.* **2010b**, *21*, 34−46.
(43) Schrek, R.; Bauerle, P. A. Reactive oxygen intermediates as apparently widely used messengers in the activation of NF-κB transcription factor and HIV-1. *Trends Cell Biol.* **1991**, *1*, 39−42.
(44) Huang, C. S.; Fan, Y. E.; Lin, C. Y.; Hu, M. L. Lycopene inhibits matrix metalloproteinase-9 expression and down-regulates the binding activity of nuclear factor-kappa B and stimulatory protein-1. *J. Nutr. Biochem.* **2007**, *18*, 449−456.
(45) Simone, R. E.; Russo, M.; Catalano, A.; Monego, G.; Froehlich, K.; Boehm, V.; Palozza, P. Lycopene inhibits NF-κB-mediated IL-8 expression and changes redox and PPARγ signaling in cigarette smoke-stimulated macrophages. *PloS One* **2011**, *6*, e19652.
(46) Hung, C. F.; Huang, T. F.; Chen, B. H.; Shieh, J. M.; Wu, P. H.; Wu, W. B. Lycopene inhibits TNF-alpha-induced endothelial ICAM-1 expression and monocyte-endothelial adhesion. *Eur. J. Pharmacol.* **2008**, *586*, 275−282.
(47) Palozza, P.; Simone, R.; Catalano, A.; Parrone, N.; Monego, G.; Ranelletti, F. O. Lycopene regulation of cholesterol synthesis and efflux in human macrophages. *J. Nutr. Biochem.* **2011**, *22*, 971−978.
(48) De Stefano, D.; Maiuri, M. C.; Simeon, V.; Grassia, G.; Soscia, A.; Cinelli, M. P.; Carnuccio, R. Lycopene, quercetin and tyrosol prevent macrophage activation induced by gliadin and IFN-γ. *Eur. J. Pharmacol.* **2007**, *566*, 192−199.
(49) Sharma, S. K.; Le Maguer, M. Lycopene in tomatoes and tomato pulp fractions. *Ital. J. Food Sci.* **1996**, *2*, 107−113.

Anchovy (*Engraulis japonicus*) is a schooling marine fish of the family *Engraulidae*. The estimated annual harvest of this fish in China is 700−800 t.[19]Anchovies are rich in proteins and oil, but because of their small bodies and rapid autolysis and spoilage soon after capture induced by endogenous protease, this species is underutilized.[20] Boiled-dried anchovies are a traditional Chinese seafood known as "haiyan". They are a potentially untapped source of bioactive peptides and value-added food production because of their high protein content and the digestive proteolytic enzymes that are distributed in the fish intestine. AMPs derived from boiled-dried anchovies might be natural and safe antimicrobial agents.

In this work, a new antibacterial peptide was rapidly purified from boiled-dried anchovies through immobilized bacterial membrane liposome chromatography (IBMLC) based on the peptide−membrane interaction. In addition, the attributes of the peptide including antimicrobial spectrum, hemolysis effect, and membrane permeability activity of the peptide were also studied.

MATERIALS AND METHODS

Materials. Boiled-dried anchovies (*Engraulis japonicus*) were purchased from a local aquatic wholesale market (Qingdao, China) and stored at −20 °C until use. Calcein, propidium iodide (PI), melittin (≥85%), acetonitrile (ACN), formic acid, and trifluoroacetic acid (TFA) for HPLC were purchased from Sigma (St. Louis, MO). Macroporous spherical silica (particle diameter 5 μm, pore diameter 120 Å) was supplied by Sepax Technologies (Suzhou, China). All other chemicals and reagents used were of analytical grade.

Bacterial Strains and Cultivation Conditions. *Escherichia coli* ATCC 25922, *Shigella dysenteriae* ATCC 51302, *Pseudomonas aeruginosa* ATCC 27853, *Salmonella typhimurium* ATCC 50013, *Staphylococcus aureus* ATCC 25923, *Bacillus subtilis* ATCC 9372, and *Streptococcus pneumoniae* ATCC 49619 were provided by Wuxi Center for Disease Prevention and Control (Wuxi, China). *E. coli* ATCC 25922 was cultured in Luria−Bertani (LB) agar at 37 °C unless otherwise specified. Other strains were cultured in nutrient agar at 37 °C. All tested strains were maintained at −80 °C in 20% (v/v) glycerol. Throughout the experiments, the strains were subcultured every 2 weeks on agar media to keep the microorganisms viable and kept at 4 °C. The cultures were propagated twice in liquid media overnight before use.

Peptide Extraction from Boiled-Dried Anchovies. Peptides were extracted from boiled-dried anchovies according to the method of Zhu et al. with some modifications.[21] Boiled-dried anchovies (20 g) were ground to uniformity with 100 mL of 0.01 M HCl and centrifuged at 10000*g* for 20 min at 4 °C. The supernatant was filtered by 0.45-μm membrane and then added to 3 volumes of ethanol to remove the protein fraction. The sample was kept for 20 min at 4 °C and then centrifuged at 10000*g* for 20 min at 4 °C. The supernatant was dialyzed against Milli-Q water using a 100-Da cutoff membrane (Spectrum, Spectra/Por cellulose acetate membrane, Los Angeles, CA), concentrated in a rotatory evaporator, and lyophilized.

Total Lipid Extraction of *E. coli* Membranes. Total lipid extraction of membranes of *E. coli* was conducted according to the method of Dennison et al. with some modifications.[22] *E. coli* ATCC 25922 was grown in LB broth at 37 °C to produce an inoculum population of about 10^9 colony-forming units per milliliter (CFU/mL). About 10 g of wet cells was harvested from 2.5 L of the medium by centrifugation (3000*g*, 5 min). The obtained cell pellets were then resuspended in 60 mL of Tris buffer (25 mM, pH 7.5), and then, 180 mL of a 1:2 (v/v) chloroform/methanol mixture was added to the cell suspension. The cell/solvent sample was then stirred for 90 min. After stirring, an additional 60 mL of chloroform and 60 mL of distilled water were added, and the whole mixture was vortexed for 20 min. The chloroform phase was separated, and then the solvent was removed in a rotary evaporator under a vacuum.

Preparation of Immobilized Bacterial Membrane Liposome Chromatography (IBMLC) Stationary Phase. Macroporous spherical silica was activated with 20% (v/v) hydrochloric acid for 6 h by reflux. It was then washed with deionized water to neutrality, dried at 120 °C, and kept dry until use. The lipid film was dissolved in chloroform/methanol (19:1, v/v). Activated silica (3.5 g) was added to the solution and shaken for 45 min at 4 °C. Then, the solvent was removed by rotary evaporation. The dried material was treated with nitrogen and kept under a vacuum overnight to remove the remaining solvent. The bacterial lipid film coated porous silica gel was swollen in Tris buffer (10 mM, pH 7.2) for 6 h to form liposome. The supernatant was removed by centrifugation (1000*g*, 5 min). To remove nonimmobilized bacterial lipid, the silica gel was washed with Tris buffer until no phosphorus was detected in the supernatant. Phosphorus was determined by Fiske and SubbaRow reagent according to the method of Bartlett.[23]

Calcein Fluorescence Release from IBMLC Stationary Phase. Ten milliliters of calcein (1 μg/mL) and 0.5 g of lyophilized IBMLC stationary phase were added to a centrifuge tube and incubated overnight at ambient temperature. Then, the supernatant was removed by centrifugation (10000*g*, 5 min), and the precipitate was repeatedly washed with Tris buffer with the same volume (10 mL). Each washing was followed by centrifugation at 10000*g* for 5 min. The supernatant after each centrifugation was collected and analyzed by a fluorescence spectrophotometer (F-7000 FL Spectrophotometer, Hitachi, Tokyo, Japan) at excitation and emission wavelengths of 490 and 515 nm, respectively. The stationary phase was washed until no fluorescence was detected. After that, 500 μL of methanol was injected into the centrifuge tube containing stationary phase. The procedures of washing with buffer and fluorescence determination were then repeated.

IBMLC of Anchovy Antimicrobial Peptide. The obtained IBMLC stationary phase was packed into a stainless steel column with dimensions of 250 mm × 4.6 mm i.d. using the slurry packing method. The column was equilibrated with phosphate-buffered saline (PBS; 10 mM, pH 7.2) containing 50 mM NaCl. Anchovy peptide sample (5 mg/mL, 60 μL) was run on the column at a flow rate of 0.5 mL/min. The eluate absorbance was monitored at 215 nm with a diode-array UV/vis detector (Agilent 1260 series, Agilent Technologies, Santa Clara, CA, USA). PBS (10 mM, pH 7.2) containing 50 mM NaCl was used as the mobile phase for an isocratic elution system with a fraction volume of 0.5 mL at 25 ± 2 °C. Thirty repeated injections were conducted to obtain sufficient quantities of the sample for analysis. The peaks were collected, lyophilized, and evaluated for their antibacterial activities against *E. coli* ATCC 25922 at identical concentrations. The peptide concentration was determined by monitoring its UV absorbance at 215 and 225 nm using the equation concentration (mg/mL) = $(A_{215} - A_{225}) \times 0.144$.[9,24] The same concentration of different fractions was obtained by dilution. The fraction with the highest activity was rechromatographed to RP-HPLC (Symmetry C18 column, 250 × 4.6 mm, 5 μm, Waters, Dublin, Ireland). The eluents were (A) 0.05% (v/v) trifluoroacetic acid (TFA) and (B) 100% acetonitrile. The elution program consisted of a gradient system (5−100% B in 40 min) at a flow rate of 0.5 mL/min at 30 ± 2 °C.

Analysis of Amino Acid Sequence of Anchovy Antimicrobial Peptide. The molecular mass and amino acid sequence of the purified peptide from IBMLC were analyzed by ultraperformance liquid chromatography tandem matrix-assisted laser desorption/ionization quadrupole time-of-flight mass spectrometry (UPLC MALDI Q-TOF MS) coupled with an electrospray ionization (ESI) source. UPLC was performed on an ACQUITY UPLCTM system (Waters, Milford, MA) using a reverse-phase column (BEH C18 2.1 × 150 mm, 1.7 μm, Waters, Milford, MA). The gradient elution was performed at a flow rate of 0.3 mL/min with eluent A as 100% ACN and eluent B as 0.1% formic acid. The flow gradient was as follows: 0−0.1 min, 100% B; 0.1−15 min, 100−60% B; 15−20 min, 60−0% B. The column temperature was maintained at 45 °C. Positive ion pattern (ESI+) was employed for ionization in TOF MS. In the experiments, the following parameters were used: capillary voltage, 3.5 kV; cone voltage, 40 V; source block temperature, 100 °C; desolvation temperature, 300 °C;

desolvation gas flow, 300 L/h; cone gas flow, 500 L/h; collision energy, 6 eV; detector voltage, 1700 V.

Peptide Synthesis. The analyzed peptide and nisin A were chemically synthesized on a model 432A peptide synthesizer (Applied Biosystems, Foster City, CA) using the standard 9-fluorenylmethyloxycarbonyl (FMOC) strategy. The purification of the crude peptides was conducted by RP-HPLC on a C18 column, and then the molecular mass and sequence of the purified peptide (>98% homogeneity) were confirmed by mass spectroscopy analysis.

Assay of Antimicrobial Activity. The antimicrobial activity during peptide purification was examined by liquid growth inhibition assay according to the method of Xiao and Zhang.[13] The antimicrobial activity was calculated using the equation antimicrobial activity (%) = $(A_0 - A)/A_0 \times 100$, where A and A_0 represent the absorbance of the sample and control, respectively. *E. coli* ATCC 25922 was used as the test organism throughout the peptide purification procedure.

Minimum inhibitory concentrations (MICs) were determined by microdilution assays. Briefly, microorganisms were collected during their midlogarithmic phase and resuspended in PBS (pH 7.2, 10 mM) to obtain a final microbial density of about 10^5 CFU/mL. Then, 100 μL of the cell suspension was placed in sterile flat-bottomed 96-well plates, after which 50 μL of peptides serially diluted 2-fold in the same buffer and 100 μL of media were added. The samples were then incubated at 37 °C for 18 h. MICs of the peptide against reference microorganisms were obtained by measuring the optical density at 600 nm (OD600) using a microplate reader (Multiskan MK3, Thermo Fisher Scientific, Waltham, MA). The lowest peptide concentration that completely inhibited the growth of bacteria was defined as the MIC. [25]

Assay of Hemolysis Activity. Hemolytic activity of the peptide was measured on C57BL/6 mouse red blood cells (MRBc).[26] Serial dilutions of the peptide were used to incubate with MRBc suspension for 30 min at 37 °C. Then the sample was centrifugated for 10 min at 400*g* to remove the cells. The absorbance of the supernatants was assessed at 595 nm. PBS (10 mM, pH 7.2) and 0.1% Triton X-100 were used as the negative and positive controls, respectively. The experiments were performed in triplicate.

Analysis of Nucleotide Leakage. The midlogarithmic *E. coli* ATCC 25922 cells grown in M9 minimal medium were adjusted to a final density of 10^7 CFU/mL with the same medium. Then the cells were incubated with the peptide at 2 × MIC for 0.5, 1.0, 2.0, 4.0, 6.0, 8.0, and 10.0 h. The cells incubated in M9 minimal medium without the peptide were used as the control. The cultures were centrifugated at 10000*g* for 1 min. Then the supernatant was filtered through a 0.22-μm membrane to remove the bacteria cells. The filtrate was diluted appropriately, and the OD value at 260 nm was recorded (UV-2800, Unico) at room temperature.[27] The experiments were performed in triplicate.

Scanning Electron Microscopy (SEM). The effect of the purified antimicrobial peptide on the morphology of *E. coli* ATCC 25922 cell was assessed by SEM (SU1510, Hitachi, Tokyo, Japan). The cells were prepared as follows: Midlogarithmic cells were obtained by centrifugation and then washed twice with PBS (10 mM, pH 7.2). The pellet was resuspended with PBS (10 mM, pH 7.2) and incubated with the active peptide (1 × MIC) at 37 °C for 30 min. Then the cells were washed twice with PBS (10 mM, pH 7.2), fixed with 2.5% glutaraldehyde for 4 h, and washed again with PBS. The fixed cells were dehydrated in ethanol gradients (30% × 10 min, 50% × 10 min, 70% × 10 min, 85% × 10 min, 90% × 10 min, and twice with 100% × 10 min, respectively). Dried cells were coated with gold and visualized by SEM. The control was performed in a similar manner except that the cells were incubated with PBS instead of the peptide.

Confocal Laser Scanning Microscopy (CLSM) Image Analysis. For the CLSM assay, *E. coli* ATCC 25922 cell suspensions were adjusted to (1−2) × 10^9 CFU/mL. The peptide-treated cells suspension (200 μL, 1 × MIC) was incubated with 50 μL of PI (final concentration of 50 μg/mL) for 30 min at 4 °C in darkness and then washed twice with 10 mM PBS (pH 7.2) and resuspended in the same buffer. Control cells were not treated with the peptide. Then 20 μL of the cell suspension was pipetted into glass bottom dishes. Images were captured on a LSM 710 confocal microscope (Carl Zeiss, Oberkochen, Germany) with ZEN 2011 software (Carl Zeiss, Oberkochen, Germany).

Statistical Analysis. The data were analyzed using SPSS 18.0 statistical software. The results are expressed as mean ± standard deviation (SD). The MALDI Q-TOF MS results were input into Mass Lynx4.1 software (Waters, Milford, MA) to obtain accurate molecular masses and amino acid sequences of the peptides. The matched peptides were verified manually. Peptide amino acid sequence homology search and analysis of biochemical properties were performed in the Antimicrobial Peptide Database (APD, http://aps.unmc.edu/AP/main.html) and NCBI database (http://www.ncbi.nlm.nih.gov/).

RESULTS AND DISCUSSION

Calcein Fluorescence Release. The content of phosphorus bound to the silica was determined to be 6.8 μM/g of silica. The bilayer structure of the liposome formed on the silica was further confirmed by calcein fluorescence leakage. Fluorescent calcein preferentially partitions into the hydrophobic environment. Therefore, the liposome with its characteristic bilayer structure can encapsulate calcein. However, when the liposome is disrupted by destructing reagent, calcein is released, and the fluorescent signal can be detected. The IBMLC stationary phase incubating with calcein was first washed repeatedly until no fluorescent signal was detected. However, the fluorescence intensity of the eluent substantially increased to 3514 fluorescence units after methanol was injected (Figure 1). This result

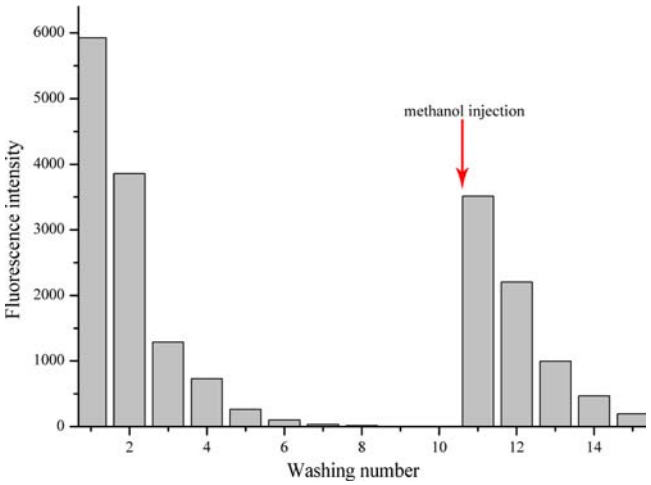

Figure 1. Fluorescence intensity change of the eluent of the calcein-entrapped IBMLC stationary phase induced by the injection of 500 μL of methanol. The fluorescent signal was monitored with excitation at 490 nm and emission at 515 nm.

indicates that the liposome with the lipid bilayer was formed on the silica. Yang et al. also confirmed the integrity of the bilayers of immobilized liposomes by determination of the release of liposome-entrapped calcein.[28]

Isolation of Antibacterial Peptide by IBMLC. Extracts of boiled-dried anchovies were fractionated (F1−6) by IBMLC, and the fractions were assayed for antimicrobial activity against *E. coli* at the same concentration (14.9 μg/mL). As shown in Figure 2, fractions eluting after 15 min exhibited antimicrobial activity, whereas those eluting before 15 min promoted the growth of the microorganism. The nitrogenous matter and phosphates in these fractions might provide further nutrients available for the growth. F6, which had the longest retention time, showed the highest antimicrobial activity among all of the fractions. A longer retention time suggests a greater interaction

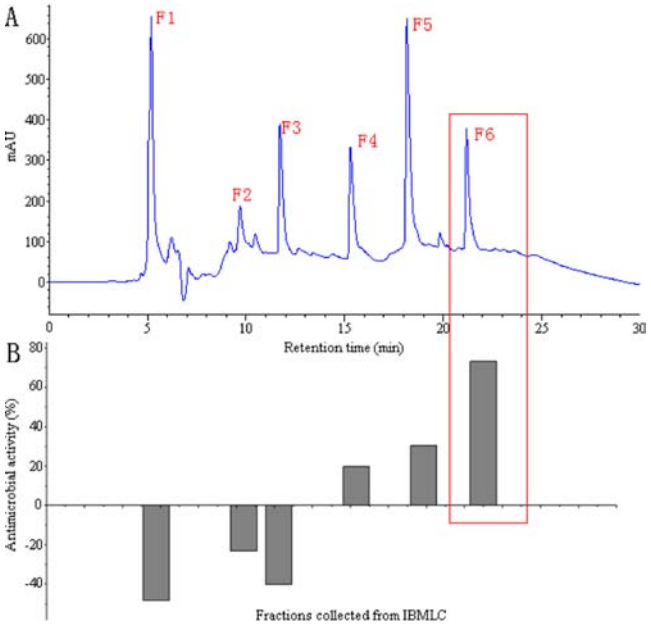

Figure 2. (A) Separation of antimicrobial peptide from boiled-dried anchovies by IBMLC. The column was equilibrated with PBS (10 mM, pH 7.2) containing 50 mM NaCl. Peptides were eluted with an isocratic elution at 25 ± 2 °C. The flow rate was 0.5 mL/min, the fraction volume was 0.5 mL, and the injection number was 60 μL. The peaks were combined and lyophilized. (B) Antimicrobial activities against *E. coli* of the fractions (14.9 μg/mL) obtained by IBMLC. The activity was evaluated according to a liquid growth inhibition assay.

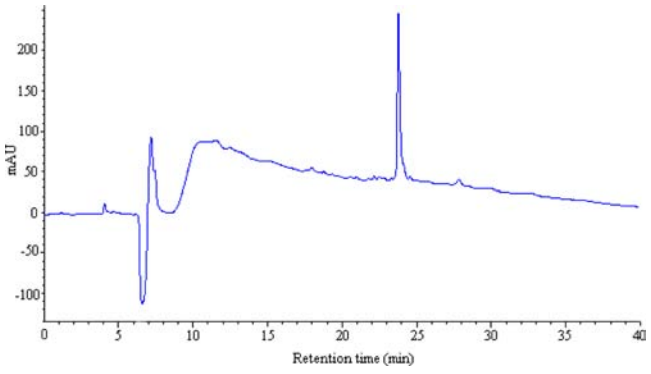

Figure 3. RP-HPLC of F6 from IBMLC. The sample was applied to an Agilent 1260 HPLC system (Symmetry C18 column, 250 × 4.6 mm, 5 μm, Waters, Dublin, Ireland). Elution was carried out using a gradient system [A, 0.05% (v/v) trifluoroacetic acid; B, 100% acetonitrile; 5−100% B in 40 min] at a flow rate of 0.5 mL/min at 30 ± 2 °C.

between the stationary phase and the solute.[29] This result indicates that the retention of a peptide in the IBMLC stationary phase might have a certain relationship with its activity because of the interaction with the bacterial membrane liposome, which is driven by electrostatics and hydrophobicity.[30] The reproducibility of the separation of the sample by IBMLC was also tested. The mean value and relative standard deviation (RSD) of the retention time of each peak were calculated. The RSD of the retention time of each peak was less than 1% (n = 6). F6 was pooled and further applied to RP-HPLC. A major single peak of absorbance at 215 nm was observed (Figure 3). As this method involved only one-step chromatography, it might be more time-saving and cost-effective than other AMP screening protocols that include multiple-step chromatography. The retention behavior of the AMP in the IBMLC reflects the interaction between the AMP and the bacterial cell membrane.

Identification of Antibacterial Peptides by MALDI Q-TOF MS. The fraction of F6 with the highest antimicrobial activity was collected and subjected to MALDI Q-TOF MS coupled with an ESI source to identify the molecular mass and amino acid sequence. m/z 974.12 was selected as the precursor ion for further analysis (Figure 4). The molecular mass of the peptide was 973.11 Da according to the analysis by Mass Lynx4.1, and the amino acid sequence was determined to be GLARCLAGTL (Gly-Leu-Ala-Arg-Cys-Leu-Ala-Gly-Thr-Leu) (Figure 5). The targeted antimicrobial peptide is a cationic decapeptide, with a total net charge of 1+ and a total hydrophobic ratio of 60%. The theoretical pI is 8.25. The prediction of Apep10 in APD showed that it might form α-helices and had at least five residues on the same hydrophobic surface. These features facilitate its affinity binding to the negatively charged bacterial cell membrane surface.[9] The results further support the previous conclusion that most antimicrobial peptides are hydrophobic and less than 10 kDa in molecular weight, with an overall net positive charge.[1] Searches in the APD and NCBI

Table 1. Minimal Inhibitory Concentrations (MICs) of Antimicrobial Peptide Apep10

species	Gram staining	MIC (μg/mL)
Escherichia coli ATCC 25922	−	8
Shigella dysenteriae ATCC 51302	−	16
Pseudomonas aeruginosa ATCC 27853	−	8
Salmonella typhimurium ATCC 50013	−	16
Staphylococcus aureus ATCC 25923	+	64
Bacillus subtilis ATCC 9372	+	8
Streptococcus pneumoniae ATCC 49619	+	16

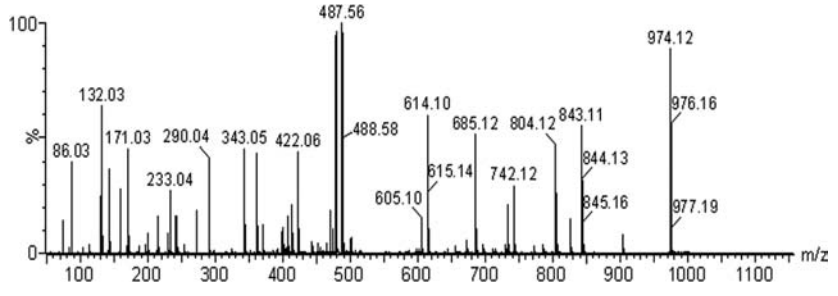

Figure 4. MALDI-TOF MS analysis of the pooled active peak fraction F6. Sample was ionized by positive-ion patter. Peaks marked with m/z values represent fragments of F6.

dx.doi.org/10.1021/jf4052286 | J. Agric. Food Chem. 2014, 62, 1564−1571

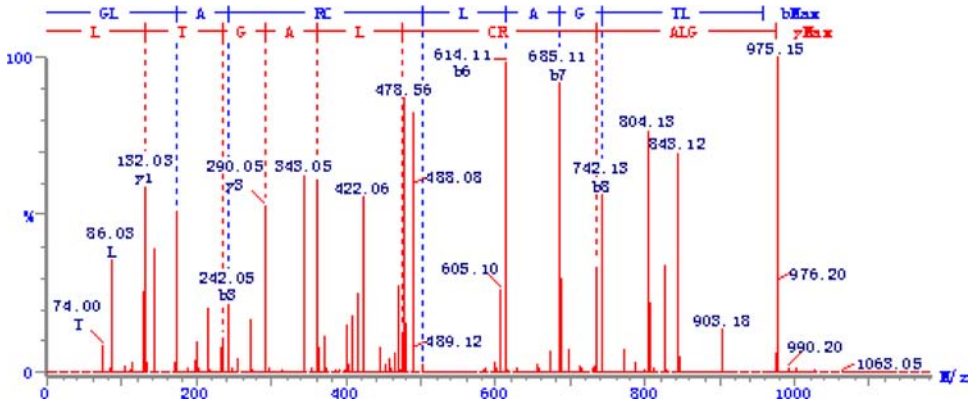

Figure 5. MS/MS spectrum of component at m/z 974.12. Peptide sequence was analyzed by Mass Lynx4.1 software.

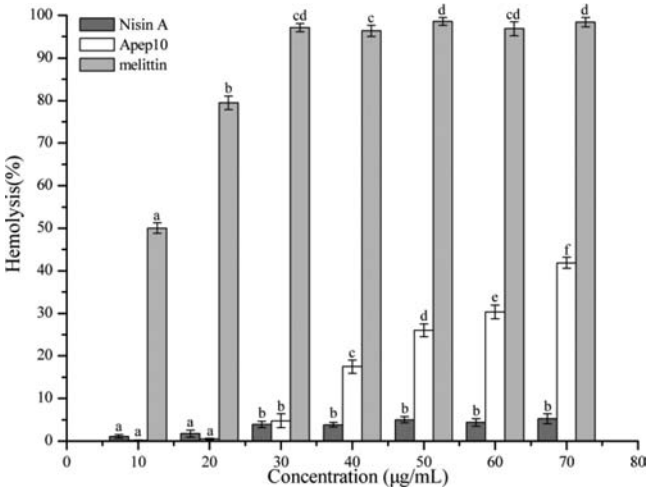

Figure 6. Hemolysis assay of Apep10, nisin, and melittin against C57BL/6 mouse erythrocytes at concentrations from 0 to 70 μg/mL. PBS (10 mM, pH 7.2) and 0.1% Triton X-100 were used as negative and positive controls, respectively. Values represent means ± SD (n = 3). Values in the column with different letters are significantly different (P < 0.05). The letter a denotes the lowest value.

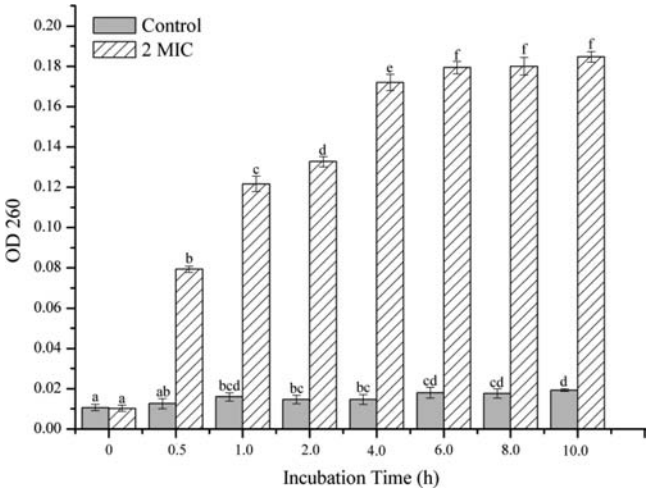

Figure 7. Total nucleotide leakage from *E. coli* cells treated with Apep10. Cells cultured in M9 minimal medium were used as the control. Values represent means ± SD (n = 3). Values in the column with different letters are significantly different (P < 0.05). The letter a denotes the lowest value.

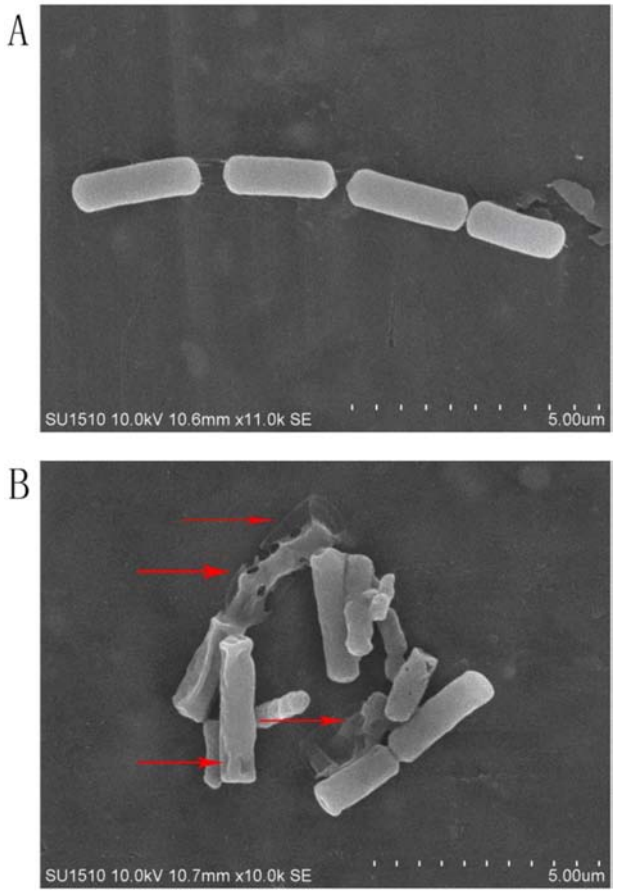

Figure 8. Morphology changes of *E. coli* cells treated by Apep10 and detected by SEM (10000×): (A) control cells incubated with PBS (10 mM, pH 7.2), (B) cells incubated with 1 × MIC Apep10 at 37 °C for 30 min. Holes, wrinkles, and ghostlike appearance indicated by arrows.

databases found no match, suggesting that it is a novel peptide, which we have named "Apep10".

Antimicrobial Activity. Apep10 extracted from boiled-dried anchovies was found to have antimicrobial activity against all of the tested bacteria, with MIC values ranging from 8 to 64 μg/mL (Table 1). The synthetic peptide was equally active against the tested strains. These bacteria are common pathogens or food-spoilage-related bacteria, suggesting a promising strategy to control some harmful strains by Apep10. The most susceptible bacteria were *E. coli*, *P. aeruginosa*, and *B. subtilis*, with a

dx.doi.org/10.1021/jf4052286 | J. Agric. Food Chem. 2014, 62, 1564−1571

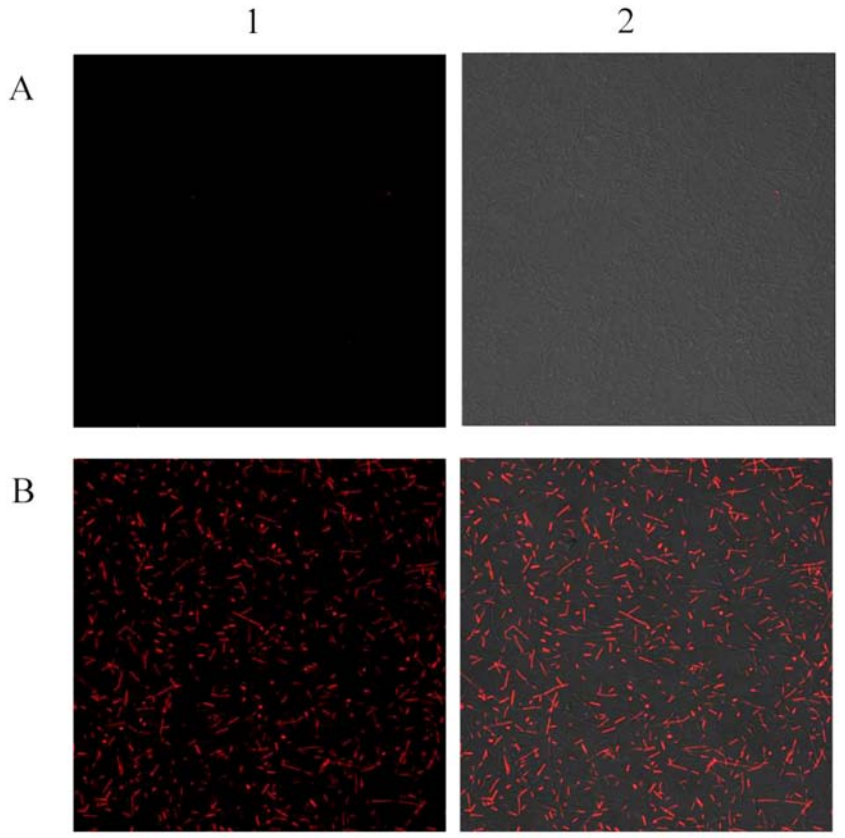

Figure 9. Confocal laser scanning microscopy images of Apep10-treated *E. coli*: (A) control *E. coli* cells, (B) *E. coli* cells treated with Apep10 (1 × MIC) for 60 min at 37 °C; (1) fluorescence images obtained by fluorescent field microscopy, (2) images obtained by fluorescent-field and bright-field micrososcopy.

MIC of 8 μg/mL. Although the liposome used to screen Apep10 was constructed from *E. coli*, Apep10 exhibited antibacterial activity against both Gram-negative (*E. coli*, *S. dysenteria*, *P. aeruginosa*, and *S. typhimurium*) and Gram-positive bacteria (*S. aureus*, *B. subtilis*, and *S. pneumoniae*). This might be because it could interact with the cell envelope of both Gram-negative and Gram-positive bacteria by electrostatic and hydrophobic interactions.[31] In addition to the negatively charged phospholipids, negatively charged teichoic acids (for Gram-positive bacteria) on the outer surface of the peptidoglycan and the negatively charged lipid A of lipopolysacharide (for Gram-negative bacteria) in the real bacteria might also contribute to the electrostatic interaction.[9] In addition, the peptide could interact with the bacterial membrane, with the hydrophobic face toward the lipid components and the polar residues binding to the phospholipid head. The differences in activity against the tested bacteria might be due to the diversity of lipids and other components among the microorganisms.

Hemolytic Activity. Typically, antibacterial peptides exhibiting no/low hemolytic activity can be considered for application in practice. The hemolytic activities of Apep10, nisin, and melittin against C57BL/6 mouse erythrocytes following 30 min of incubation were compared (Figure 6). Following a 30-min exposure to concentrations of 10 and 20 μg/mL, nisin A showed <2.0% hemolysis, and Apep10 exhibited <0.52% hemolysis, in contrast to the hemolysis of more than 50% for melittin at the same concentrations. When the concentrations were higher than 30 μg/mL, Apep10 induced a higher percentage of hemolysis than nisin A. For melittin, almost complete hemolysis was observed at concentrations higher than 30 μg/mL. It can be concluded that Apep 10 almost did not exert a cytotoxic effect against mouse erythrocytes below 20 μg/mL, a concentration higher than most MICs of the tested bacteria in Table 1 (except *S. aureus*). These results suggest that Apep10 might be a promising candidate for food preservative and antimicrobial drug.

Activity on Membrane Permeability. Membrane binding is thought to be the first step in the interaction between antimicrobial peptides and bacterial membranes.[32] Previous work has also indicated that membrane permeability is a key step in the antimicrobial mechanism of cationic peptides.[33,34] In this work, a membrane permeability assay was conducted to explore whether the permeabilization occurred when the peptide bound to the cell membrane. Nucleotides can release from the cells when the plasma membrane is permeable. As nucleotides have strong UV absorption at 260 nm, OD260 was used to determine the membrane permeability. As shown in Figure 7, the total nucleotide leakage content from *E. coli* cells induced by Apep10 was time-dependent. Compared with the control, a fast increase to 0.172 of OD260 in the first 4 h was observed. Slight change was observed afterward. However, the control showed very little increase in OD 260 in 10 h. The results indicate that Apep10 could cause membrane permeabilization and result in nucleotide leakage.

Typical SEM images of the effects of Apep10 on the morphology of *E. coli* are shown in Figure 8. The control *E. coli* cells (not incubated with Apep10) had a rodlike shape with a regular, intact, and smooth surface (Figure 8A). After treatment with Apep10, the *E. coli* cells exhibited significant abnormalities,

dx.doi.org/10.1021/jf4052286 | J. Agric. Food Chem. 2014, 62, 1564−1571

including noticeable holes or wrinkles on their surfaces, the collapse of the cell structure, and a ghostlike appearance in which the cells seemed transparent and looked empty (Figure 8B). These cell abnormalities suggest that the peptide might have caused pore formation and induced the release of cytoplasmic components. This result indicates that Apep10 can directly interact with the bacterial membrane and damage its integrity. This type of morphological effect on microorganisms has previously been shown for other antimicrobial peptides. Some researchers observed morphological changes such as a shrunken appearance on the surface of *Klebsiella pneumoniae* treated with cecropin B and its analogues.[35] Park et al. found that *Pseudomonas aeruginosa* treated with P5 and melittin showed cell surface disruption.[36] Tomasinsig et al. also observed that incubation with BMAP-28 caused extensive surface blebbing on *Prototheca wickerhamii* cells, with release of intracellular material.[37]

For more precise observation of the cytoplasmic-membrane-perturbing activity of Apep10, PI was used as a fluorescent probe in combination with CLSM. PI has been proposed in previous research as an appropriate probe in the assessment of membrane permeabilization, as it is supposed to penetrate cells and stain them only when the membrane is disrupted.[38,39] Indeed, when *E. coli* cells were incubated with the probe without pretreatment with Apep10, no appreciable fluorescent signal was observed, as visualized by comparing bright-field and fluorescence microscopy images (Figure 9A), suggesting that the intact membrane of the control *E. coli* prevented the uptake of PI. In contrast, the cells emitted a red fluorescence after exposure to 1 × MIC Apep10 as the result of PI uptake (Figure 9B), indicating that the peptide increased the permeability of the bacterial membrane. This finding was confirmed by SEM images (Figure 8). These results together demonstrate that Apep10 can interact with a bacterial membrane, which is the basis of IBMLC.

The present data demonstrate that immobilized bacterial membrane liposome chromatography can be employed to screen AMPs, which is much faster than conventional protocols using multiple-step chromatography. In addition, the activity on the bacterial membrane permeability of the peptide provides further insight into the interaction between AMPs and bacterial membranes.

AUTHOR INFORMATION

Corresponding Author

*Phone: +86-13921177990. Fax: +86-510-853-29099. E-mail: zhanghui@jiangnan.edu.cn.

Funding

This study was supported financially by the National Nature Science Foundation of China (NSFC, No. 31271934), the National High-tech Research and Development Program of China (863 Program, Nos. 2013AA102207 and 2013AA102203-07), and the Project of the Priority Academic Program Development of Jiangsu Higher Education Institutions (PAPD).

Notes

The authors declare no competing financial interest.

REFERENCES

(1) Reddy, K.; Yedery, R.; Aranha, C. Antimicrobial peptides: Premises and promises. *Int. J. Antimicrob. Agents* **2004**, *24*, 536−547.

(2) Parisien, A.; Allain, B.; Zhang, J.; Mandeville, R.; Lan, C. Novel alternatives to antibiotics: Bacteriophages, bacterial cell wall hydrolases, and antimicrobial peptides. *J. Appl. Microbiol.* **2008**, *104*, 1−13.

(3) Faccone, D.; Veliz, O.; Corso, A.; Noguera, M.; Martínez, M.; Payes, C.; Semorile, L.; Maffía, P. C. Antimicrobial activity of *de novo* designed cationic peptides against multi-resistant clinical isolates. *Eur. J. Med. Chem.* **2014**, *71*, 31−35.

(4) Zasloff, M. Antimicrobial peptides of multicellular organisms. *Nature* **2002**, *415*, 389−395.

(5) Brogden, K. A. Antimicrobial peptides: Pore formers or metabolic inhibitors in bacteria? *Nat. Rev. Microbiol.* **2005**, *3*, 238−250.

(6) Pellegrini, A. Antimicrobial peptides from food proteins. *Curr. Pharm. Des.* **2003**, *9*, 1225−1238.

(7) Pichu, S.; Ribeiro, J. M. C.; Mather, T. N. Purification and characterization of a novel salivary antimicrobial peptide from the tick, *Ixodes scapularis*. *Biochem. Biophys. Res. Commun.* **2009**, *390*, 511−515.

(8) Iijima, N.; Tanimoto, N.; Emoto, Y.; Morita, Y.; Uematsu, K.; Murakami, T.; Nakai, T. Purification and characterization of three isoforms of chrysophsin, a novel antimicrobial peptide in the gills of the red sea bream, *Chrysophrys major*. *Eur. J. Biochem.* **2003**, *270*, 675−686.

(9) Thammasirirak, S.; Pukcothanung, Y.; Preecharram, S.; Daduang, S.; Patramanon, R.; Fukamizo, T.; Araki, T. Antimicrobial peptides derived from goose egg white lysozyme. *Comp. Biochem. Physiol. C* **2010**, *151*, 84−91.

(10) Salampessy, J.; Phillips, M.; Seneweera, S.; Kailasapathy, K. Release of antimicrobial peptides through bromelain hydrolysis of leatherjacket (*Meuchenia sp.*) insoluble proteins. *Food Chem.* **2010**, *120*, 556−560.

(11) Chan, D. I.; Prenner, E. J.; Vogel, H. J. Tryptophan- and arginine-rich antimicrobial peptides: Structures and mechanisms of action. *Biochim. Biophys. Acta, Biomembr.* **2006**, *1758*, 1184−1202.

(12) Xiao, J.; Zhang, H.; Niu, L.; Wang, X. Efficient screening of a novel antimicrobial peptide from *Jatropha curcas* by cell membrane affinity chromatography. *J. Agric. Food Chem.* **2011**, *59*, 1145−1151.

(13) Xiao, J.; Zhang, H. An *Escherichia coli* cell membrane chromatography-offline LC-TOF-MS method for screening and identifying antimicrobial peptides from *Jatropha curcas* meal protein isolate hydrolysates. *J. Biomol. Screening* **2012**, *17*, 752−760.

(14) Kamimori, H.; Hall, K.; Craik, D. J.; Aguilar, M. I. Studies on the membrane interactions of the cyclotides kalata B1 and kalata B6 on model membrane systems by surface plasmon resonance. *Anal. Biochem.* **2005**, *337*, 149−153.

(15) Oren, Z.; Lerman, J. C.; Gudmundsson, G. H.; Agerberth, B.; Shai, Y. Structure and organization of the human antimicrobial peptide LL-37 in phospholipid membranes: Relevance to the molecular basis for its non-cell-selective activity. *Biochem. J.* **1999**, *341*, 501−513.

(16) Dathe, M.; Wieprecht, T. Structural features of helical antimicrobial peptides: Their potential to modulate activity on model membranes and biological cells. *Biochim. Biophys. Acta, Biomembr.* **1999**, *1462*, 71−87.

(17) Peetla, C.; Stine, A.; Labhasetwar, V. Biophysical interactions with model lipid membranes: Applications in drug discovery and drug delivery. *Mol. Pharmaceutics* **2009**, *6*, 1264−1276.

(18) Osterberg, T.; Svensson, M.; Lundahl, P. Chromatographic retention of drug molecules on immobilised liposomes prepared from egg phospholipids and from chemically pure phospholipids. *Eur. J. Pharm. Sci.* **2001**, *12*, 427−439.

(19) Wang, F.; Ning, Z.; Lan, D.; Liu, Y.; Yang, B.; Wang, Y. Biochemical properties of recombinant leucine aminopeptidase II from *Bacillus stearothermophilus* and potential applications in the hydrolysis of Chinese anchovy (*Engraulis japonicus*) proteins. *J. Agric. Food Chem.* **2012**, *60*, 165−172.

(20) Ahsan, M. N.; Watabe, S. Kinetic and structural properties of two isoforms of trypsin isolated from the viscera of Japanese anchovy, *Engraulis japonicus*. *J. Protein Chem.* **2001**, *20*, 49−58.

(21) Zhu, C.-Z.; Zhang, W.-G.; Zhou, G.-H.; Xu, X.-L.; Kang, Z.-L.; Yin, Y. Isolation and identification of antioxidant peptides from Jinhua ham. *J. Agric. Food Chem.* **2013**, *61*, 1265−1271.

(22) Dennison, S. R.; Howe, J.; Morton, L. H. G.; Brandenburg, K.; Harris, F.; Phoenix, D. A. Interactions of an anionic antimicrobial

peptide with *Staphylococcus aureus* membranes. *Biochem. Biophys. Res. Commun.* **2006**, *347*, 1006−1010.
(23) Bartlett, G. R. Phosphorus assay in column chromatography. *J. Biol. Chem.* **1959**, *234*, 466−468.
(24) Su, Y. Isolation and identification of pelteobagrin, a novel antimicrobial peptide from the skin mucus of yellow catfish (*Pelteobagrus fulvidraco*). *Comp. Biochem. Phys. B* **2011**, *158*, 149−154.
(25) Park, S.-C.; Kim, M.-H.; Hossain, M. A.; Shin, S. Y.; Kim, Y.; Stella, L.; Wade, J. D.; Park, Y.; Hahm, K.-S. Amphipathic α-helical peptide, HP (2−20), and its analogues derived from *Helicobacter pylori*: Pore formation mechanism in various lipid compositions. *Biochim. Biophys. Acta, Biomembr.* **2008**, *1778*, 229−241.
(26) Hou, F.; Li, J.; Pan, P.; Xu, J.; Liu, L.; Liu, W.; Song, B.; Li, N.; Wan, J.; Gao, H. Isolation and characterisation of a new antimicrobial peptide from the skin of *Xenopus laevis*. *Int. J. Antimicrob. Agents* **2011**, *38*, 510−515.
(27) Tang, Y.-L.; Shi, Y.-H.; Zhao, W.; Hao, G.; Le, G.-W. Discovery of a novel antimicrobial peptide using membrane binding-based approach. *Food Control* **2009**, *20*, 149−156.
(28) Yang, Q.; Liu, X.-Y.; Ajiki, S.-i.; Hara, M.; Lundahl, P.; Miyake, J. Avidin−biotin immobilization of unilamellar liposomes in gel beads for chromatographic analysis of drug−membrane partitioning. *J. Chromatogr. B* **1998**, *707*, 131−141.
(29) Österberg, T.; Svensson, M.; Lundahl, P. Chromatographic retention of drug molecules on immobilised liposomes prepared from egg phospholipids and from chemically pure phospholipids. *Eur. J. Pharm. Sci.* **2001**, *12*, 427−439.
(30) Seelig, J. Thermodynamics of lipid−peptide interactions. *Biochim. Biophys. Acta, Biomembr.* **2004**, *1666*, 40−50.
(31) Papo, N.; Shai, Y. Can we predict biological activity of antimicrobial peptides from their interactions with model phospholipid membranes? *Peptides* **2003**, *24*, 1693−1703.
(32) Anderson, R. C.; Hancock, R. E.; Yu, P.-L. Antimicrobial activity and bacterial-membrane interaction of ovine-derived cathelicidins. *Antimicrob. Agents Chemother.* **2004**, *48*, 673−676.
(33) Hawrani, A.; Howe, R. A.; Walsh, T. R.; Dempsey, C. E. Thermodynamics of RTA3 peptide binding to membranes and consequences for antimicrobial activity. *Biochim. Biophys. Acta, Biomembr.* **2010**, *1798*, 1254−1262.
(34) Epand, R. M.; Vogel, H. J. Diversity of antimicrobial peptides and their mechanisms of action. *Biochim. Biophys. Acta, Biomembr.* **1999**, *1462*, 11−28.
(35) Chan, S. C.; Yau, W. L.; Wang, W.; Smith, D. K.; Sheu, F. S.; Chen, H. M. Microscopic observations of the different morphological changes caused by anti-bacterial peptides on *Klebsiella pneumoniae* and HL-60 leukemia cells. *J. Pept. Sci.* **1998**, *4*, 413−425.
(36) Park, Y.; Lee, D. G.; Jang, S.-H.; Woo, E.-R.; Jeong, H. G.; Choi, C.-H.; Hahm, K.-S. A Leu−Lys-rich antimicrobial peptide: Activity and mechanism. *Biochim. Biophys. Acta, Proteins Proteomics* **2003**, *1645*, 172−182.
(37) Tomasinsig, L.; Skerlavaj, B.; Scarsini, M.; Guida, F.; Piccinini, R.; Tossi, A.; Zanetti, M. Comparative activity and mechanism of action of three types of bovine antimicrobial peptides against pathogenic *Prototheca spp*. *J. Pept. Sci.* **2012**, *18*, 105−113.
(38) Pagán, R.; Mackey, B. Relationship between membrane damage and cell death in pressure-treated *Escherichia coli* cells: Differences between exponential- and stationary-phase cells and variation among strains. *Appl. Environ. Microb.* **2000**, *66*, 2829−2834.
(39) Liao, H.; Zhang, F.; Liao, X.; Hu, X.; Chen, Y.; Deng, L. Analysis of *Escherichia coli* cell damage induced by HPCD using microscopies and fluorescent staining. *Int. J. Food Microbiol.* **2010**, *144*, 169−176.

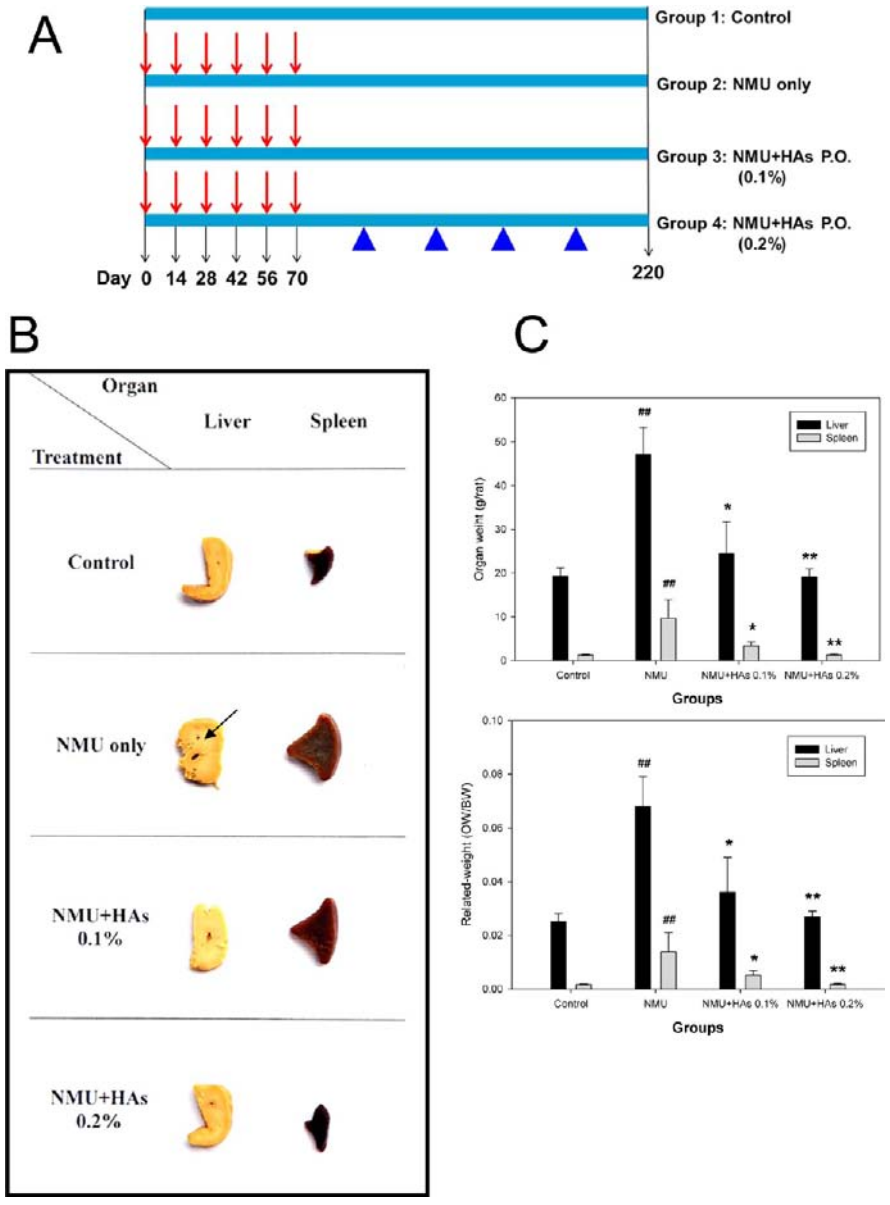

Figure 1. Effect of HAs on gross appearance and organ weight of NMU-treated rats. (A) Protocol of the animal model (experimental design). Rats were injected with NMU every 2 weeks for 6 times (arrow). The day of the first injection is designated day 0. HAs were given orally at day 0 every day until sacrifice. NMU at 35 mg/kg iv and animals after iv injection were monitored for blood data every 30−40 days from the caudal vein (triangle). The details were as described under Materials and Methods. (B) All of the animals were sacrificed, and the livers and spleens were immediately fixed in 6% formaldehyde for specimen preparation. The arrows indicate cancer cell invasion in liver tissue shown with a gray-white hyalinized look. (C) Data represented as net weight of organ (liver or spleen)/body weight (OW/BW). The indicated days are counted after iv NMU and recorded once about 30−40 days. These values were expressed as the mean ± SD, $n = 12$. (#) $p < 0.01$ and (##) $p < 0.001$, compared with control group. (∗) $p < 0.05$ and (∗∗) $p < 0.005$, compared with NMU-treated group.

acid (a phenolic acid extract from roselle) was reported to inhibit LDL oxidation induced by copper or a NO donor.[16] (ii) Antihyperlipidemia and antiatherosclerosis effects of roselle extract reduced foam cell formation, reduced smooth muscle cell migration, and lowered calcification in the blood vessels of treated rabbits.[17] HAs markedly inhibited oxidation of oxLDL by $CuSO_4$, perhaps by CD36 down-regulation in vitro.[18,19] (iii) Hepatoprotection effect of roselle extract was shown to exert the hypolipidemic effect via inhibiting lipogenesis and promoting hepatic lipid clearance.[20] (iv) Anticancer inhibitory effect of roselle extracts on carcinogenesis demonstrated that it possesses potential as a cancer chemopreventive agent against apoptosis evasion, insensitivity to antigrowth signals, tissue invasion, and metastasis.[21,22] (v) Antidiabetes effects roselle extracts are worthy of further investigation toward development as an adjunct therapy for diabetes or metabolic syndromes.[23,24] (vi) Other activities of *H. sabdariffa* polyphenols (HPE) give them potential as anti-inflammatory agents.[25] Recently, Pen et al. and Lee et al. illustrated the anti-insulin resistance properties of HPE and its effect on hypoglycemia, hypolipidemia, and antioxidation.[26,27] The demonstration of the beneficial effects of dietary polyphenols on health is becoming an important issue. Although most cellular studies have proven their biological effects at the in vitro level, the correlation between the in vivo observed effects and the presence of the responsible metabolites is still unclear. Therefore, the aim of this study

dx.doi.org/10.1021/jf405235j | J. Agric. Food Chem. 2014, 62, 1572−1580

was to characterize the antileukemia effect of the methanol extract of roselle, especially anthocyanins (HAs), using an animal model.

MATERIALS AND METHODS

Reagents. MPO (n1578), LSAB2 System-HRP, and the liquid DAB substrate chromogen system were purchased from Dako Corp. (Carpinteria, CA, USA). *N*-Methyl-*N*-nitrosourea (NMU) was purchased from Sigma (St. Louis, MO, USA). NMU was stored in a refrigerator at 4 °C. NMU solution (0.5 g/100 mL) was freshly prepared, dissolved immediately before use in physiologic saline. The PD-10 column was purchased from Amersham Biosciences (Uppsala, Sweden).

Preparation of HAs. The extraction of HAs was performed as previously described.[28] Briefly, 20 g of the dried flower *H. sabdariffa* L. with methanol (2 L) containing 1% HCl was kept for 1 day at 4 °C. The extract was filtered and concentrated; then, the precipitate was collected and stood on an Amberlife Diaion HP-20 resin column for 24 h. After that, distilled water (5 L) containing 0.1% HCl solution was used to clean, and the components of interest were eluted with methanol. The filtrate was collected and then lyophilized to obtain approximately 2 g of HAs and stored at −20 °C before use. A stock solution of HAs in ddH_2O at a concentration of 100 mg/mL was prepared and protected from light and stored at 4 °C.

Animal Treatment. The experimental design is presented in Figure 1A Male Sprague−Dawley rats (at 7 weeks old) were purchased from the National Laboratory Animal Breeding Research Center (Taipei, Taiwan) and acclimatized for 1 week. These animals were housed in an environmentally controlled animal room (at 25 °C with a 12 h light−dark cycle). Animal food (basal diet CE2) and water were provided ad libitum. The current study was approved by the Chung Shan Medical University Institutional Animal Care and Use Committee (IACUC, CSMU). Animals were randomly housed 3 per cage and divided into four experimental groups of 12 rats each. The first group served as control (untreated), and the second group received intravenous (iv) administration of NMU. Group 1: control, Sprague−Dawley rats fed the standard diet, without any treatment. Group 2: NMU only, iv injected with 35 mg/kg of NMU, fed the standard diet. Group 3: NMU+HAs oral administration (per os, po) (0.1%), fed 0.1 g/kg/day HAs in the standard diet and iv injected with 35 mg/kg NMU. Group 4: NMU+HAs po (0.2%), fed 0.2 g/kg/day HAs in the standard diet and iv injected with 35 mg/kg NMU. HAs extract been mixed with the feed, and the animals were dosed each day for 220 days. The dose of HAs was the amount of lyophilized powder per kilogram of body weight. A total of 12 rats (NMU group) were given a series of six iv injection of NMU, at 35 mg/kg of body weight, at biweekly intervals as described by Huggins et al.[29] with some modification. NMU was injected in a caudal vein; the day of the first injection was designated day 0, and HAs was administered orally to each assigned group at the same time. After carcinogen treatment, they were kept on basal diet and water ad libitum until sacrifice at 220 days of the experiment. The animals were individually observed daily for mortality and weekly for clinical signs throughout the study period. Body weights were measured weekly. Blood samples were collected in blood tubes every 30−40 days before sacrifice. The hepatic and splenic tissues were immediately fixed in 6% formaldehyde for specimen preparation and histochemical staining analysis.

Hematology and Blood Biochemistry. Blood was freshly obtained for hematological examination at intervals of 30−40 days after final NMU administration; 0.5−1.0 mL of blood was drawn on occasion without foaming or hemolysis. The lateral tail vein is usually used, and 0.1−2 mL of blood can be obtained per sample depending on the size of the rat. Whole blood samples were collected in tubes coated with an anticoagulant, 0.3 M EDTA-2K (ethylenediaminetetraacetic acid). Complete blood count (CBC) analysis included WBC (white blood cell) count, RBC (red blood cell) count, PLT (platelet) count, Hb (hemoglobin) concentration, and WBC differential count. Measurements were carried out by a fully automated hematology analyzer (model XE-2100, Sysmex). Blood smears were stained with Liu and Papanicolaou stain for cytological examination.

Biochemical Data Measurement. Analyses of all biochemical parameters in serum were examined with an autoanalyzer (Olympus AU2700, Olympus) using commercial reagent kits. The aspartate aminotransferase (AST/GOT), alanine aminotransferase (ALT/GPT), and uric acid were measured by enzymatic methods (AST, ALT, kinetic UV test; and UA, enzymatic color test).

Pathological Examination. Biopsies of liver and spleen were immediately obtained after the animals were sacrificed (day 220). A portion of them was fixed in 10% formalin solution, processed using routine histology procedures, embedded in paraffin, cut in 5 μm sections, and placed on a glass microscope slide for analysis. The samples were stained with hematoxylin and eosin (H&E) for morphological evaluation and then examined microscopically.

Immunohistochemistry. Immunohistochemical investigations were carried out on paraffin-embedded sections. Sections were dried in an oven at 50 °C overnight, deparaffinized in xylene, rehydrated in a graded alcohol series, immersed in citrate buffer (pH 6.0), and incubated in an autoclave for 25 min. Sections were then removed, allowed to cool at room temperature for 20 min, and rinsed with running water and distilled water for a total of 10 min. They were then blocked for the endogenous peroxidase measurement by incubating in a solution of 3% hydrogen peroxide (H_2O_2) for 10 min. Tissue sections were washed with PBS and then immunostained with primary antibodies for 30 min. The antigen−antibody complex was visualized by an avidin−biotin−peroxidase complex method followed by diaminobenzidine tetrahydrochloride (DAB) as a chromogen. After washing, sections were counterstained with Gill's hematoxylin, washed with tap water, mounted with Permount (Merck, Darmstadt, Germany), and examined by light microscopy. For confirmation that the immunocystochemical procedure was performing correctly, antibodies against MPO were tested.

Statistical Analysis. All data are presented as means ± SD. The statistically significant differences compared with the untreated control group or NMU group were calculated by Student's *t* test. Differences with probability value <0.05 were considered significant.

RESULTS

Anthocyanin Content in *H. sabdariffa* L. Extract. Our previous yield of HAs was approximately 2 g.[28] Spectrophotometer analysis of HAs showed that the purity of HAs was approximately 85−95%. According to calibration standards, the major components of HAs were delphinidin (3.7%) and cyanidin (0.9%) as analyzed by HPLC.[18] The phytochemical profile and HPLC analysis of the calyx extract of *H. sabdariffa* L. were previously performed by another research group.[30,31] The HPLC chromatogram shows the presence of several unidentified peaks.

Effect of HAs on Weights of Visceral Organs. Several papers have indicated that NMU can induce thymic lymphoma and myelogenous leukemia.[32,33] We first observed the gross evaluation of these four groups in Sprague−Dawley rats. Each group had 12 individuals. Normal spleens appeared dark brown in color, but the enlarged spleens with infiltrative tumors induced by NMU appeared paler. NMU-treated livers showed a gray-white hyalinized appearance with the presence of cancer cells. Invaded cells are indicated with arrows in Figure 1B. Gross visual examination of the livers and spleens from the NMU-exposed rats revealed that these organs were abnormally enlarged in appearance, whereas both organs appeared nearly normal upon administration of HAs (Figure 1B).

The effects of HAs on body weight and relative weights of liver and spleen of NMU-exposed rats were analyzed. The body weight gain of each rat was determined every day by comparing the current weight with the weight on day 0. The four groups of

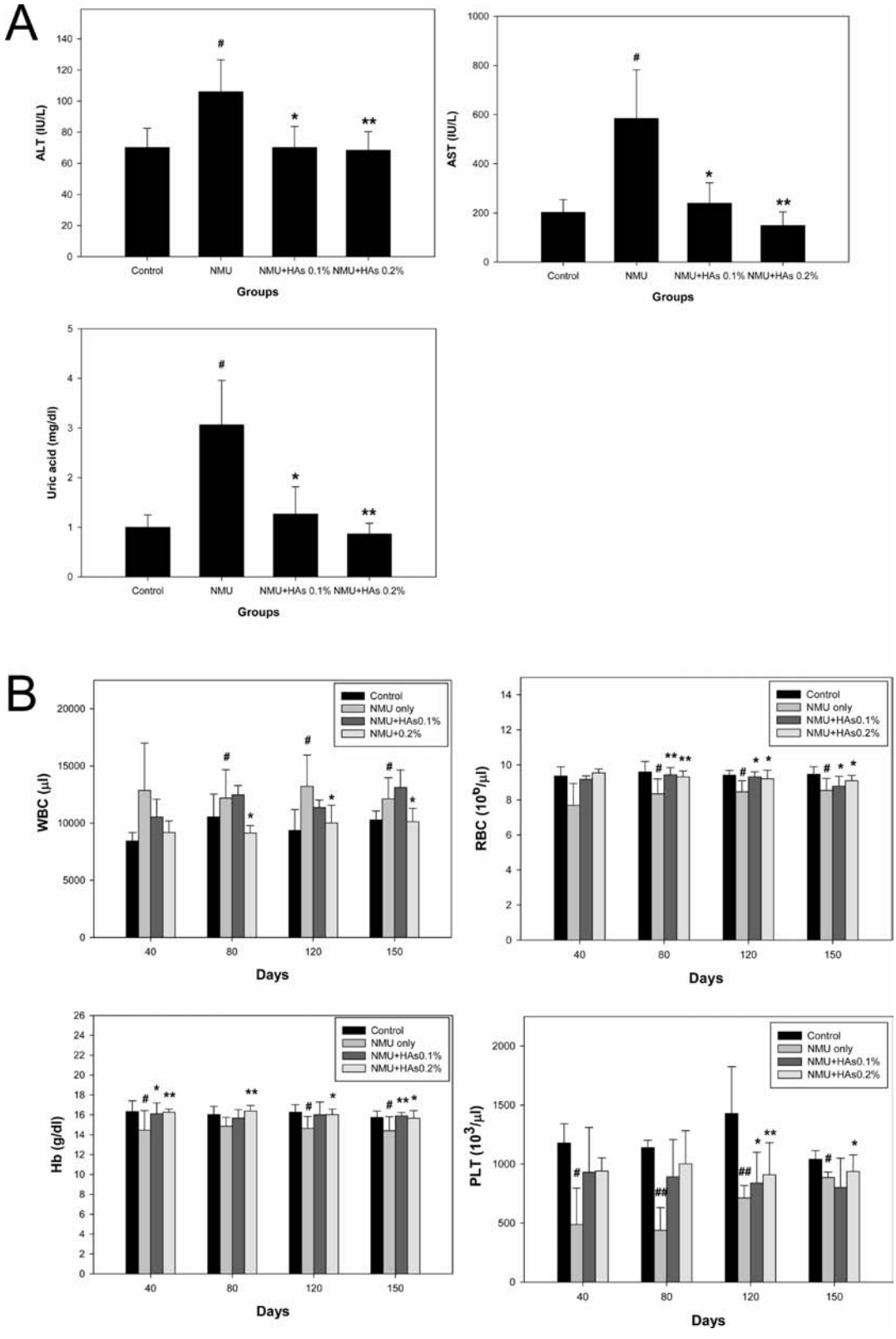

Figure 2. Effect of HAs on the serum biochemical analysis and complete blood count in Sprague−Dawley rats: (A) levels of alanine aminotransferase (ALT), aspartate aminotransferase (AST), and uric acid; (B) count of white blood cell (WBC), red blood cell (RBC), hemoglobin (Hb), and platelet (PLT). The indicated days are counted after iv NMU and recorded once about 30−40 days. Values are expressed as the mean ± SD, $n = 12$. (#) $p < 0.05$ and (##) $p < 0.005$, compared with control group. (∗) $p < 0.05$ and (∗∗) $p < 0.005$, compared with NMU-treated group.

rats had an average body weight gain during the whole experimental period. There was a remarkable increase (more than untreated group) in liver and spleen weight of NMU-induced leukemia rats. After oral treatment with HAs at two different doses (0.1 and 0.2%), the liver and spleen weights were significantly reduced dose dependently compared to the

dx.doi.org/10.1021/jf405235j | J. Agric. Food Chem. 2014, 62, 1572−1580

NMU group (Figure 1C). The mean liver and spleen weights in the 0.2% HAs groups were 19.11 ± 1.89 and 1.25 ± 0.27 g, respectively (*, $p < 0.05$; **, $p < 0.005$). Furthermore, the weights of liver and spleen, relative to body weight of rats after HAs administration, were also found to be significantly reduced, compared with rats in the NMU-treated group (Figure 1C). In the 0.2% HAs group, the mean values of relative liver and relative spleen weights were 0.027 ± 0.002 and 0.0017 ± 0.00040 g, respectively (*, $p < 0.05$; **, $p < 0.005$). Figure 1 illustrates that HAs treatment attenuated the elevated liver and spleen weight values in NMU-exposed rats.

Effect of HAs on Serum Biochemical Analyses. The effects of HAs on aspartate aminotransferase (AST), alanine aminotransferase (ALT), and uric acid level in the plasma of NMU-exposed rats are presented in Figure 2A. The hepatic function test was used to evaluate the liver for injury, infection, inflammation, or abdominal swelling. Increased permeability of the hepatocellular membrane caused by injury or disease results in a release of serum transaminase (ALT and AST). A high level of the soluble enzymes released into the bloodstream may be a sign of liver damage, cancer, or other diseases. Thus, the degree of liver cell damage can be estimated from the level of serum ALT and AST. Activities of ALT and AST enzymes were increased after NMU administration in rats as compared with the untreated control group (approximately 110 and 600 IU/L, respectively). Treatment with HAs (0.2%) resulted in significant inhibition of ALT (approximately 70 IU/L) and AST (approximately 180 IU/L), as compared with rats treated with NMU (Figure 2A). In addition, uric acid (UA) is the end product of purine nucleotide metabolism in humans. Determining the level of serum uric acid is useful in detecting hyperuricemia and in diagnosing leukemia,[34] gout, polycythemia, and renal dysfunction. Treatment of HAs at two tested concentrations caused significant decreases in the levels of uric acid compared to NMU treatment only (Figure 2A). HAs at 0.2% decreased from 3.07 ± 0.89 to 0.87 ± 0.22 mg/dL at the end of the study, which shows a decrease of 70%. These results confirmed that taking HAs can significantly diminish serum ALT and AST as well as uric acid level in rats exposed to NMU.

Effect of HAs on Complete Blood Count. Leukemia is a malignant disorder of the blood that is sometimes discovered during a routine blood test in an asymptomatic individual. More often, patients have constitutional complaints arising from leukocytosis (or neutropenia), anemia, or thrombocytopenia. The values of RBC and Hb decreased in the NMU-treated group, indicating a tendency to anemia; likewise, low platelet count of blood was considered as thrombocytopenia. WBC count was elevated significantly in the NMU-treated group, as compared with the control group, indicating the production of leukemia blasts induced by NMU in rats. On the other hand, the WBC count was decreased significantly after HAs (0.2%) treatment as compared with NMU ($10 \times 10^3/\mu L$ versus $13 \times 10^3/\mu L$) (Figure 2B). In contrast, other hematological data of HAs-treated rats were higher (mean of $9.6 \times 10^6/\mu L$ for RBC counts; $938 \times 10^3/\mu L$ for PLT counts; and 16.8 g/dL for Hb concentration at 0.2%) when compared to NMU-exposed rats ($7.5 \times 10^6/\mu L$, $613 \times 10^3/\mu L$, and 14.5 g/dL, respectively) (Figure 2B). In this study, we observed that the RBC, Hb, and PLT values were lower, whereas WBC values were higher in the HAs-treated group compared to the NMU-induced group (*, $p < 0.05$; **, $p < 0.005$). These data imply that HAs may improve anemia, leukocytosis, or thrombocytopenia. Hence, these results suggest that the administration of HAs decreased the NMU-induced increases in WBC counts.

Effect of HAs on Cytological Morphology Features. Figure 3 shows that Liu-stained smears in the NMU-induced group were cellular and revealed a markedly polymorphous mixture of small to large cells. A greater proportion of large, dark staining, blast-like promyelocytes and metamyelocytes, and dysplastic granulocytes were present in NMU-treated rats. The smaller cells were mature neutrophils. Most neutrophils were normal or occasionally dysplastic in the progression of the leukemia. The large cells were primitive and had abnormal nuclear maturation. The overall cytomorphological picture posed serious difficulties in differentiating this condition from those of the peripheral blood smear. In addition, the original staining procedure was developed by Papanicolaou to visualize

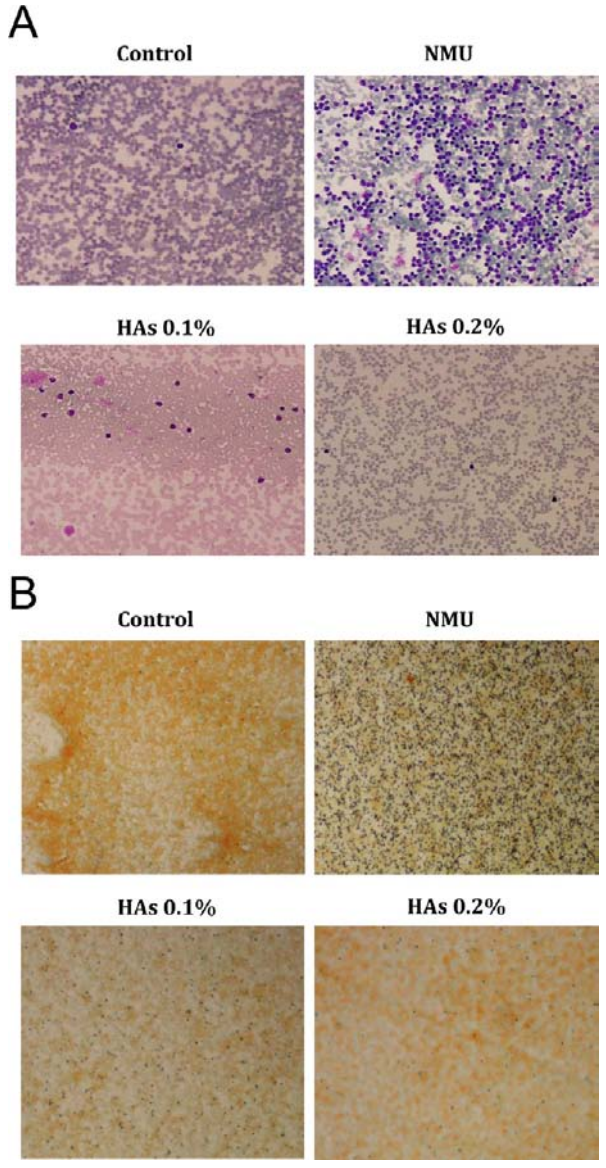

Figure 3. Hematology analysis for whole blood cells by Liu (A) and Papanicolaou (B) staining. After animals were treated with NMU alone (35 mg/kg) for 220 days or with HAs (0.1 and 0.2%) given orally for at least 150 days, animals were killed and blood was collected, which showed fewer malignant cells. All experiments were done in duplicate, and photographs were taken at 100× magnification.

dx.doi.org/10.1021/jf405235j | J. Agric. Food Chem. 2014, 62, 1572−1580

cancer cells, for example, cervical cancer. Papanicolaou's is the most important staining method in cytology because it enhances differentiation between malignant and nonmalignant cells and also allows critical examination of nuclei and cytoplasmic components. The Papanicolaou stain method revealed more atypical single cells in the NMU group than in the control group (Figure 3B). These atypical cells were round, dark blue in color, and approximately 2−3 times the size of lymphocytes. Abnormal leukemia cells equivalent to immature white blood cells were verified in smears from the NMU-induced group. Remarkably, the smears showed normal number and shape of blood cells in HAs administration (0.2% HAs group of Figure 3). These results show that HAs given orally to rats at a dose of 0.2% exhibited a potent antileukemia activity in all of the treated animals.

Effect of HAs on Histopathological Features. The effect of HAs on NMU-induced leukemia was evaluated. Liver and spleen samples of NMU-injected and HAs-fed rats were submitted for routine histological analysis to characterize their morphological aspects. Panels A and B of Figure 4 show the histological findings using H&E stain on the different organs. The spleen and liver were frequently enlarged in all cases (NMU group) and showed leukemic cell infiltration. Because the portal vein brought much more blood to the liver, cancer cells (arrows) infiltrated the portal area and sinusoids in the NMU-induced group (Figure 4A). In the spleen, the normal architecture of red and white pulp was destroyed in NMU-treated rats with a massive spread of undifferentiated cells (Figure 4B). The spleen showed marked red/white pulp diffusely infiltrated by leukemic cells induced by NMU. HAs effectively abrogated NMU-induced leukemic cell infiltration and subsequent tissue damage (0.2% HAs group of Figure 4A,B). Histopathological examination revealed 91.7% leukemia incidence by NMU. In the HAs groups (especially at the high dose of 0.2%), the incidence of leukemia was reduced by 33.3% (Table 1). Also, at the end of the experiment, the number of dead rats was 0 (0/12), 6 (6/12), 3 (3/12), and 1 (1/12) for control (rats with no manipulation), rats treated with NMU, and rats treated with HAs of 0.1 and 0.2%, respectively. It is clear that the mortality rate of rats that were given a high dosage of HAs was less than the mortality in the NMU group. In the 0.2% HAs-treated rats, four developed leukemia and one died. All control rats that were not given leukemia cells were still alive at the end of the study. HAs treatment reduced NMU-induced liver and spleen injury in a dose-dependent manner.

Effect of HAs on Immunohistochemical Analysis. The myeloperoxidase (MPO) stain distinguishes the immature cells in acute myeloblastic leukemia (cells stain positive) from those in acute lymphoblastic leukemia (cells stain negative).[35] In rat liver sections, immunohistochemical staining of MPO showed that there was a dark purple reaction product in NMU-exposed rats, indicating that this is a myeloid leukemia. Weak MPO expression was observed in control and HAs-treated groups (Figure 4C). These findings suggest that myeloperoxidase activity was increased in NMU-induced blast cells. Treatment with HAs may have had an anti-inflammatory effect consistent with no staining or weak staining.

DISCUSSION

Leukemia is cancer of the blood or bone marrow. It begins in the bone marrow and is characterized by an abnormal increase of immature white blood cells (called blasts). Cases of leukemia are classified into different types mainly on the basis of the kind

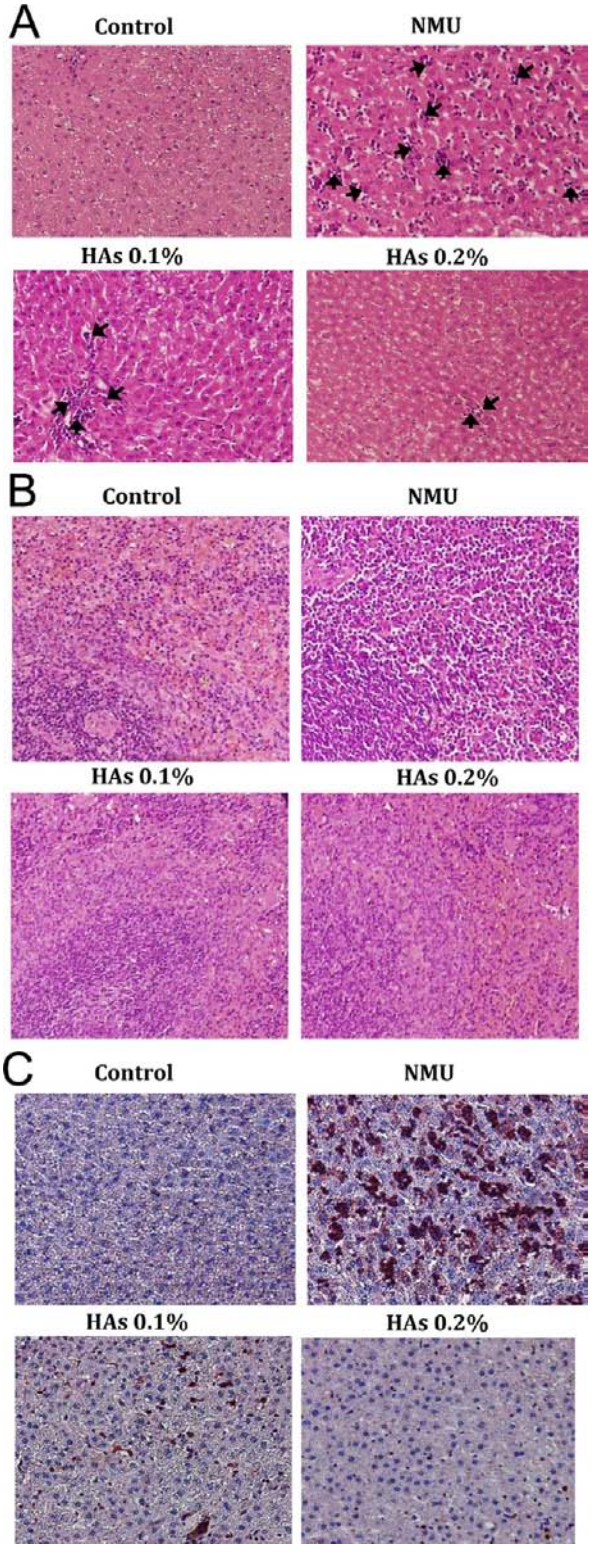

Figure 4. Histopathological examinations of organs in Sprague−Dawley rats. Paraffin-embedded sections of representative liver tissues (A) and spleen tissues (B) were stained by H&E staining. (C) The liver tissues were stained by MPO staining (immunohistochemical analysis). Animals were treated with NMU alone (35 mg/kg), which showed marked infiltrative cells in the NMU group. HAs (0.1 and 0.2%) were given orally for at least 150 days, which showed fewer infiltrative cells in the HAs-treated group. The arrows indicate malignant cells. All experiments were done in duplicate, and photographs were taken at 100× magnification.

Table 1. Inhibitory Effects of HAs on NMU-Induced Rats Tumorigenesis

treatment[a]	leukemia tumor incidence[b] (%)	ratio of death
control	0/12 (0%)	0/12 (0%)
NMU only	11/12 (91.7%)	6/12 (50%)
NMU + HAs 0.1%	7/12 (58.3%)	3/12 (25%)
NMU + HAs 0.2%	4/12 (33.3%)	1/12 (8.3%)

[a]First time iv NMU and treated various concentrations of HAs (0.1 and 0.2%) on the same day. [b]Tumor incidence is equal to the number of dead rats that had leukemia combined with the number of tumor rats.

of progression. Leukemia can be divided into four common types: chronic lymphocytic leukemia (CLL), chronic myeloid leukemia (CML), acute lymphocytic leukemia (ALL), and acute myeloid leukemia (AML). *N*-Methyl-*N*-nitrosourea (NMU), a DNA alkylating agent, acts as a potent carcinogen and mutagen to various tissues. O^6-Methylguanine adducts have been proposed to be the critical lesion in a variety of NMU-induced tumors. In particular, Huggins et al. found that NMU specifically elicited a high incidence of leukemia in Sprague–Dawley rats.[36] Therefore, NMU is a broad-spectrum carcinogen capable of inducing tumors in various target organs, including leukemia. According to a previous paper, blood samples were collected and used to evaluate cytological examination (through Liu and Papanicolaou stains) and morphological changes of rat livers and spleens by histological evaluation (through H&E staining) and to classify the leukemia of poorly differentiated blasts (through an immunohistochemical analysis).[37] The results showed that the NMU-induced group was positive for MPO, but negative for CD3, CD15, CD20, and CD34. NMU-induced leukemogenesis in a S-D rat suggests a more definite way to classify leukemia M3 (APL, acute promyelocytic leukemia). NMU characteristically induces an early and high incidence of leukemia and malignant lymphomas in young rats when provided at relatively high doses, resulting in a high mortality rate of the animals and limiting the conduct of long-term experimental studies.[38] In this study, we used the animal model of NMU-induced leukemia to detect the influence of HAs. Mortality rates varied from 50% in the NMU-only group to 8.3% with the HAs 0.2% group through the whole course (Table 1). NMU-related macroscopic observations included pale liver, heart, kidney, and bone marrow and enlargement of the spleen, thymus, and mandibular and mesenteric lymph nodes, which correlated with the diagnosis of lesions of the hematopoietic system.[39] Figure 1B shows that the livers and spleens from the NMU-exposed rats were abnormally enlarged, but with treatment of HAs both organs were significantly restored to nearly normal. Subsequently, we detected the count of ALT, AST, WBC, RBC, PLT, and Hb levels in the blood. These results display that HAs can significantly diminish elevated serum ALT and AST as well as complete blood count levels in rats exposed to NMU (Figure 2). Finally, we investigated the presence of leukemic cells in the peripheral smear using Liu and Papanicolaou stains; in addition, the severity of tissue injury resulting from leukemic cell infiltration was also assessed by histological detection (H&E and MPO assay). We found HAs can effectively abrogate NMU-induced leukemic cell infiltration and subsequent tissue damage (Figures 3 and 4). Thus, evaluation of the protective effect of anthocyanin extract of roselle on leukemia might shed light on drug discovery or alternative therapy.

Anthocyanins are a large group of polyphenols widely distributed in our diet. The intake of anthocyanins has been estimated at >180 mg/day in humans.[40] Anthocyanins have received considerable attention because of their wide range of potential health-promoting properties,[41] including cancer-prevention effects.[42] Indeed, intact anthocyanin forms (glycosides) have been detected in rat and human plasma as well as in urine after oral administration.[43] However, low bioavailability of anthocyanins, much less than 0.1% of intake, was suggested by the low concentration measured in plasma and urine after anthocyanin ingestion in some short-term studies.[44] Therefore, we wanted to ensure a sufficiently high intake and, thus, selected a daily dose of HAs of 100–200 mg/kg (approximately equal to 0.1–0.2%). On the other hand, our purpose was to assess the influence of HAs in rats fed an anthocyanin-rich diet for a relatively long period. This study was to evaluate the potential chemoinhibitory effects of HAs on leukemia. In this 220 day study we observed that dietary supplementation of 0.1 and 0.2% HAs decreased the WBC counts and uric acid levels by 30–70% in a dose-dependent manner. Our data demonstrate that an anthocyanin-rich diet (HAs) in fact is sufficient to enhance the antileukemia response, which is consistent with other studies. For instance, anthocyanin-rich berry extract significantly inhibits leukemia cell proliferation at 10–100 μg/mL, which corresponds to anthocyanin concentrations between 10^{-6} and 10^{-5} M.[45] There is some controversy about its bioavailabilty, but recent evidence indicates that despite low bioavailability, plasma concentrations of anthocyanins appear sufficient to induce changes in gene expression and signal transduction in vivo[46] in a manner suggesting a positive role in physiological functions and health outcomes. Several in vivo studies have provided evidence that plant foods have a notable impact on the absorption and metabolism of anthocyanins. In view of the above lower bioavailability of anthocyanins in patients, this was ascribed to the plasma or urinary recovery. For example, Harada et al. and Oki et al. found that 0.01–0.03% of purple sweet potato anthocyanins given by oral administration can be absorbed into plasma of both rat and human.[47,48] Ohnishi et al. pointed out that the recovery of administered cranberry juice anthocyanins in the urine of humans was estimated as 5%,[49] whereas other researchers recovered between 1.8 and 2% of strawberry anthocyanins.[50] Moreover, a previous study of 15 patients with coronary artery disease tested for total urinary recovery of administered cranberry juice anthocyanins. The recovery was in the range of 0.078–3.2% among the volunteers.[46] Although anthocyanin bioavailability appears low, it could have been underestimated, because the metabolites and breakdown products of anthocyanins have not yet been identified.[44] In addition, some research is needed to determine if anthocyanins alone or from their synergistic interactions with other phenolic compounds play a role in the inhibition of cancer. We believe such questions will be answered through continuing investigations in future decades.

The present results demonstrated that the HAs induced significant anticancer activity in a NMU-induced rat leukemia model. Although a cancer cell killing mechanism for HAs in human leukemia (HL-60) cells has been suggested,[9,28,51,52] clinical trials evaluating the use of roselle as a chemopreventive or therapeutic agent are lacking. Separation of the phenolic compounds of the roselle extract and in vivo experiments to determine whether HAs could be an effective anticancer agent for leukemia are important. Hence, this is the first report of the

antileukemic activity of HAs in vivo. Although further studies are needed to examine the mechanisms in detail, this study supports the contention that dietary intake of bioactive food compounds such as HAs may prevent cancer and reduce cancer risk.

AUTHOR INFORMATION

Corresponding Author

*(C.-J.W.) Mail: Institute of Biochemistry and Biotechnology, Chung Shan Medical University, No. 110, Sec. 1, Jianguo N. Road, South District, Taichung 402, Taiwan. Phone: +886 4 24730022, ext. 11670. Fax: +886 4 23248167. E-mail: wcj@csmu.edu.tw.

Author Contributions

‖Y.-C.C. and C.-J.W. contributed equally to the main findings of the manuscript.

Funding

This work was supported by grants from the National Science Council (NSC 98-2313-B-040-005-MY2) and Chung Shan Medical University, Antai Tian-Sheng Memorial Hospital (CSMU-TSMH-101-01), Taiwan.

Notes

The authors declare no competing financial interest.

ACKNOWLEDGMENTS

We thank all of our colleagues who participated in the present project.

ABBREVIATIONS USED

HAs, *Hibiscus* anthocyanin; NMU, *N*-nitrosomethylurea; AST, aspartate aminotransferase; ALT, alanine aminotransferase; H&E stain, hematoxylin and eosin stain; IHC stain, immunohistochemical stain; MPO stain, myeloperoxidase stain; CBC, complete blood count; WBC, white blood cell; RBC, red blood cell; PLT, platelet; Hb, hemoglobin; AST, aspartate aminotransferase; ALT, alanine aminotransferase; O^6-meG, O^6-methylguanine

REFERENCES

(1) Kufe, D. W.; Pollock, R. E.; Weichselbaum, R. R.; Bast, R. C.; Gansier, T. S.; Holland, J. F.; Frei, E. R. *Cancer Medicine*, 6th ed.; B. C. Decker: Hamilton, ON, Canada, 2003.

(2) Yang, H. L.; Chang, W. H.; Chia, Y. C.; Huang, C. J.; Lu, F. J.; Hsu, H. K.; Hseu, Y. C. *Toona sinensis* extracts induces apoptosis via reactive oxygen species in human premyelocytic leukemia cells. *Food Chem. Toxicol.* **2006**, *44*, 1978−1988.

(3) Chen, C.; Kong, A. N. Dietary cancer-chemopreventive compounds: from signaling and gene expression to pharmacological effects. *Trends Pharmacol. Sci.* **2005**, *26*, 318−326.

(4) Strohle, A.; Wolters, M.; Hahn, A. Folic acid and colorectal cancer prevention: molecular mechanisms and epidemiological evidence (review). *Int. J. Oncol.* **2005**, *26*, 1449−1464.

(5) Vasudeva, N.; Sharma, S. K. Post-coital antifertility activity of *Hibiscus rosa-sinensis* Linn. roots. *Evidence-Based Complement. Alternat. Med.* **2008**, *5*, 91−94.

(6) Chewonarin, T.; Kinouchi, T.; Kataoka, K.; Arimochi, H.; Kuwahara, T.; Vinitketkumnuen, U.; Ohnishi, Y. Effects of roselle (*Hibiscus sabdariffa* Linn.), a Thai medicinal plant, on the mutagenicity of various known mutagens in *Salmonella typhimurium* and on formation of aberrant crypt foci induced by the colon carcinogens azoxymethane and 2-amino-1-methyl-6-phenylimidazo[4,5-*b*]pyridine in F344 rats. *Food Chem. Toxicol.* **1999**, *37*, 591−601.

(7) Haji Faraji, M.; Haji Tarkhani, A. The effect of sour tea (*Hibiscus sabdariffa*) on essential hypertension. *J. Ethnopharmacol.* **1999**, *65*, 231−236.

(8) Jung, E.; Kim, Y.; Joo, N. Physicochemical properties and antimicrobial activity of roselle (*Hibiscus sabdariffa* L.). *J. Sci. Food Agric.* **2013**, DOI: 10.1002/jsfa.6256.

(9) Ali, B. H.; Al Wabel, N.; Blunden, G. Phytochemical, pharmacological and toxicological aspects of *Hibiscus sabdariffa* L.: a review. *Phytother. Res.* **2005**, *19*, 369−375.

(10) Olvera-Garcia, V.; Castano-Tostado, E.; Rezendiz-Lopez, R. I.; Reynoso-Camacho, R.; Gonzalez de Mejia, E.; Elizondo, G.; Loarca-Pina, G. *Hibiscus sabdariffa* L. extracts inhibit the mutagenicity in microsuspension assay and the proliferation of HeLa cells. *J. Food Sci.* **2008**, *73*, T75−81.

(11) Adigun, M. O.; Ogundipe, O. D.; Anetor, J. I.; Odetunde, A. O. Dose-dependent changes in some haematological parameters during short-term administration of *Hibiscus sabdariffa* calyx aqueous extract (Zobo) in Wistar albino rats. *Afr. J. Med. Med. Sci.* **2006**, *35*, 73−77.

(12) Wong, P. K.; Yusof, S.; Ghazali, H. M.; Che-Man, Y. B. Physicochemical characteristics of roselle (*Hibiscus sabdariffa* L.). *Nutr. Food Sci.* **2002**, *32*, 68−73.

(13) Wahabi, H. A.; Alansary, L. A.; Al-Sabban, A. H.; Glasziuo, P. The effectiveness of *Hibiscus sabdariffa* in the treatment of hypertension: a systematic review. *Phytomedicine* **2010**, *17*, 83−86.

(14) Ajiboye, T. O.; Salawu, N. A.; Yakubu, M. T.; Oladiji, A. T.; Akanji, M. A.; Okogun, J. I. Antioxidant and drug detoxification potentials of *Hibiscus sabdariffa* anthocyanin extract. *Drug Chem. Toxicol.* **2011**, *34*, 109−115.

(15) Hirunpanich, V.; Utaipat, A.; Morales, N. P.; Bunyapraphatsara, N.; Sato, H.; Herunsale, A.; Suthisisang, C. Hypocholesterolemic and antioxidant effects of aqueous extracts from the dried calyx of *Hibiscus sabdariffa* L. in hypercholesterolemic rats. *J. Ethnopharmacol.* **2006**, *103*, 252−260.

(16) Lee, M. J.; Chou, F. P.; Tseng, T. H.; Hsieh, M. H.; Lin, M. C.; Wang, C. J. Hibiscus protocatechuic acid or esculetin can inhibit oxidative LDL induced by either copper ion or nitric oxide donor. *J. Agric. Food Chem.* **2002**, *50*, 2130−2136.

(17) Chen, C. C.; Hsu, J. D.; Wang, S. F.; Chiang, H. C.; Yang, M. Y.; Kao, E. S.; Ho, Y. C.; Wang, C. J. *Hibiscus sabdariffa* extract inhibits the development of atherosclerosis in cholesterol-fed rabbits. *J. Agric. Food Chem.* **2003**, *51*, 5472−5477.

(18) Chang, Y. C.; Huang, K. X.; Huang, A. C.; Ho, Y. C.; Wang, C. J. Hibiscus anthocyanins-rich extract inhibited LDL oxidation and oxLDL-mediated macrophages apoptosis. *Food Chem. Toxicol.* **2006**, *44*, 1015−1023.

(19) Kao, E. S.; Tseng, T. H.; Lee, H. J.; Chan, K. C.; Wang, C. J. Anthocyanin extracted from hibiscus attenuate oxidized LDL-mediated foam cell formation involving regulation of CD36 gene. *Chem. Biol. Interact.* **2009**, *179*, 212−218.

(20) Yang, M. Y.; Peng, C. H.; Chan, K. C.; Yang, Y. S.; Huang, C. N.; Wang, C. J. The hypolipidemic effect of *Hibiscus sabdariffa* polyphenols via inhibiting lipogenesis and promoting hepatic lipid clearance. *J. Agric. Food Chem.* **2010**, *58*, 850−859.

(21) Lin, H. H.; Chen, J. H.; Kuo, W. H.; Wang, C. J. Chemopreventive properties of *Hibiscus sabdariffa* L. on human gastric carcinoma cells through apoptosis induction and JNK/p38 MAPK signaling activation. *Chem.−Biol. Interact.* **2007**, *165*, 59−75.

(22) Lin, H. H.; Chen, J. H.; Chou, F. P.; Wang, C. J. Protocatechuic acid inhibits cancer cell metastasis involving the down-regulation of Ras/Akt/NF-kappaB pathway and MMP-2 production by targeting RhoB activation. *Br. J. Pharmacol.* **2011**, *162*, 237−254.

(23) Wang, S. C.; Lee, S. F.; Wang, C. J.; Lee, C. H.; Lee, W. C.; Lee, H. J. Aqueous extract from *Hibiscus sabdariffa* Linnaeus ameliorate diabetic nephropathy via regulating oxidative status and Akt/Bad/14-3-3gamma in an experimental animal model. *Evidence-Based Complement. Alternat. Med.* **2011**, *2011*, 938126.

(24) Huang, C. N.; Chan, K. C.; Lin, W. T.; Su, S. L.; Wang, C. J.; Peng, C. H. *Hibiscus sabdariffa* inhibits vascular smooth muscle cell proliferation and migration induced by high glucose − a mechanism

involves connective tissue growth factor signals. *J. Agric. Food Chem.* **2009**, *57*, 3073−3079.
(25) Kao, E. S.; Hsu, J. D.; Wang, C. J.; Yang, S. H.; Cheng, S. Y.; Lee, H. J. Polyphenols extracted from *Hibiscus sabdariffa* L. inhibited lipopolysaccharide-induced inflammation by improving antioxidative conditions and regulating cyclooxygenase-2 expression. *Biosci., Biotechnol., Biochem.* **2009**, *73*, 385−390.
(26) Lee, C. H.; Kuo, C. Y.; Wang, C. J.; Wang, C. P.; Lee, Y. R.; Hung, C. N.; Lee, H. J. A polyphenol extract of *Hibiscus sabdariffa* L. ameliorates acetaminophen-induced hepatic steatosis by attenuating the mitochondrial dysfunction in vivo and in vitro. *Biosci., Biotechnol., Biochem.* **2012**, *76*, 646−651.
(27) Peng, C. H.; Chyau, C. C.; Chan, K. C.; Chan, T. H.; Wang, C. J.; Huang, C. N. Hibiscus sabdariffa polyphenolic extract inhibits hyperglycemia, hyperlipidemia, and glycation-oxidative stress while improving insulin resistance. *J. Agric. Food Chem.* **2011**, *59*, 9901−9909.
(28) Chang, Y. C.; Huang, H. P.; Hsu, J. D.; Yang, S. F.; Wang, C. J. Hibiscus anthocyanins rich extract-induced apoptotic cell death in human promyelocytic leukemia cells. *Toxicol. Appl. Pharmacol.* **2005**, *205*, 201−212.
(29) Huggins, C. B.; Grand, L.; Ueda, N. Specific induction of erythroleukemia and myelogenous leukemia in Sprague-Dawley rats. *Proc. Natl. Acad. Sci. U.S.A.* **1982**, *79*, 5411−5414.
(30) Beltran-Debon, R.; Alonso-Villaverde, C.; Aragones, G.; Rodriguez-Medina, I.; Rull, A.; Micol, V.; Segura-Carretero, A.; Fernandez-Gutierrez, A.; Camps, J.; Joven, J. The aqueous extract of *Hibiscus sabdariffa* calices modulates the production of monocyte chemoattractant protein-1 in humans. *Phytomedicine* **2010**, *17*, 186−191.
(31) Rodriguez-Medina, I. C.; Beltran-Debon, R.; Molina, V. M.; Alonso-Villaverde, C.; Joven, J.; Menendez, J. A.; Segura-Carretero, A.; Fernandez-Gutierrez, A. Direct characterization of aqueous extract of *Hibiscus sabdariffa* using HPLC with diode array detection coupled to ESI and ion trap MS. *J. Sep. Sci.* **2009**, *32*, 3441−3448.
(32) Drescher, B.; Ehm, I.; Fey, F. Characterization of an RNA-directed DNA polymerase from mouse spleen infected with leukaemia virus activated during *N*-methyl-*N*-nitroso urea-induced leukaemogenesis. *Acta Virol.* **1982**, *26*, 41−49.
(33) Seidel, H. J.; Kreja, L. Leukemia induction by methylnitrosourea (MNU) in selected mouse strains. Effects of MNU on hemopoietic stem cells, the immune system and natural killer cells. *J. Cancer Res. Clin. Oncol.* **1984**, *108*, 214−220.
(34) Hafiz, M. G.; Islam, A. Extensive skeletal lesions in childhood acute lymphoblastic leukemia. *Mymensingh Med. J.* **2009**, *18*, 88−94.
(35) Chuang, S. S.; Li, C. Y. Useful panel of antibodies for the classification of acute leukemia by immunohistochemical methods in bone marrow trephine biopsy specimens. *Am. J. Clin. Pathol.* **1997**, *107*, 410−418.
(36) Huggins, C. B.; Ueda, N. Regression of myelocytic leukemia in rats after hypophysectomy. *Proc. Natl. Acad. Sci. U.S.A.* **1984**, *81*, 598−601.
(37) Chang, Y. C.; Hsu, J. D.; Lin, W. L.; Lee, Y. J.; Wang, C. J. High incidence of acute promyelocytic leukemia specifically induced by *N*-nitroso-*N*-methylurea (NMU) in Sprague-Dawley rats. *Arch. Toxicol.* **2012**, *86*, 315−327.
(38) Mizoguchi, M.; Naito, H.; Kurata, Y.; Shibata, M. A.; Tsuda, H.; Wild, C. P.; Montesano, R.; Fukushima, S. Influence of aging on multi-organ carcinogenesis in rats induced by *N*-methyl-*N*-nitrosourea. *Jpn. J. Cancer Res.* **1993**, *84*, 139−146.
(39) Hoivik, D. J.; Allen, J. S.; Wall, H. G.; Nold, J. B.; Miller, R. T.; Santostefano, M. J. Studies evaluating the utility of *N*-methyl-*N*-nitrosourea as a positive control in carcinogenicity studies in the p53± mouse. *Int. J. Toxicol.* **2005**, *24*, 349−356.
(40) Hertog, M. G.; Hollman, P. C.; Katan, M. B.; Kromhout, D. Intake of potentially anticarcinogenic flavonoids and their determinants in adults in The Netherlands. *Nutr. Cancer* **1993**, *20*, 21−29.
(41) Prior, R. L.; Wu, X. Anthocyanins: structural characteristics that result in unique metabolic patterns and biological activities. *Free Radical Res.* **2006**, *40*, 1014−1028.
(42) Malik, M.; Zhao, C.; Schoene, N.; Guisti, M. M.; Moyer, M. P.; Magnuson, B. A. Anthocyanin-rich extract from *Aronia meloncarpa* E induces a cell cycle block in colon cancer but not normal colonic cells. *Nutr. Cancer* **2003**, *46*, 186−196.
(43) McGhie, T. K.; Walton, M. C. The bioavailability and absorption of anthocyanins: towards a better understanding. *Mol. Nutr. Food Res.* **2007**, *51*, 702−713.
(44) Manach, C.; Williamson, G.; Morand, C.; Scalbert, A.; Remesy, C. Bioavailability and bioefficacy of polyphenols in humans. I. Review of 97 bioavailability studies. *Am. J. Clin. Nutr.* **2005**, *81*, 230S−242S.
(45) Kochling, J.; Schmidt, M.; Rott, Y.; Sagner, M.; Ungefroren, H.; Wittig, B.; Henze, G. Can anthocyanins improve maintenance therapy of Ph(+) acute lymphoblastic leukaemia? *Eur. J. Haematol.* **2013**, *90*, 291−300.
(46) Milbury, P. E.; Vita, J. A.; Blumberg, J. B. Anthocyanins are bioavailable in humans following an acute dose of cranberry juice. *J. Nutr.* **2010**, *140*, 1099−1104.
(47) Oki, T.; Suda, I.; Terahara, N.; Sato, M.; Hatakeyama, M. Determination of acylated anthocyanin in human urine after ingesting a purple-fleshed sweet potato beverage with various contents of anthocyanin by LC-ESI-MS/MS. *Biosci., Biotechnol., Biochem.* **2006**, *70*, 2540−2543.
(48) Harada, K.; Kano, M.; Takayanagi, T.; Yamakawa, O.; Ishikawa, F. Absorption of acylated anthocyanins in rats and humans after ingesting an extract of *Ipomoea batatas* purple sweet potato tuber. *Biosci., Biotechnol., Biochem.* **2004**, *68*, 1500−1507.
(49) Ohnishi, R.; Ito, H.; Kasajima, N.; Kaneda, M.; Kariyama, R.; Kumon, H.; Hatano, T.; Yoshida, T. Urinary excretion of anthocyanins in humans after cranberry juice ingestion. *Biosci., Biotechnol., Biochem.* **2006**, *70*, 1681−1687.
(50) Carkeet, C.; Clevidence, B. A.; Novotny, J. A. Anthocyanin excretion by humans increases linearly with increasing strawberry dose. *J. Nutr.* **2008**, *138*, 897−902.
(51) Tseng, T. H.; Kao, T. W.; Chu, C. Y.; Chou, F. P.; Lin, W. L.; Wang, C. J. Induction of apoptosis by hibiscus protocatechuic acid in human leukemia cells via reduction of retinoblastoma (RB) phosphorylation and Bcl-2 expression. *Biochem. Pharmacol.* **2000**, *60*, 307−315.
(52) Hou, D. X.; Tong, X.; Terahara, N.; Luo, D.; Fujii, M. Delphinidin 3-sambubioside, a hibiscus anthocyanin, induces apoptosis in human leukemia cells through reactive oxygen species-mediated mitochondrial pathway. *Arch. Biochem. Biophys.* **2005**, *440*, 101−109.

two diverse pathways. The extrinsic pathway is initiated by the interaction of the ligands with their death receptors, which lead to activate caspase-8 and -3. The intrinsic pathway for programmed cell death requires the destabilization of the mitochondrial membrane and release of related apoptotic proteins like cytochrome *c*. Cytosolic cytochrome *c* together with Apaf-1 activates caspase-9, and the latter then activates caspase-3, resulting in apoptosis.[19] This process is controlled by the Bcl-2 family of proteins, which regulate the permeability of mitochondrial membrane. [20] According to previous studies, the effects of natural polysaccharide on apoptosis are likely to be through the intrinsic pathway. Currently, the importance of the mitochondrial pathway in cancer is being investigated.

To further identify the bioactivity and molecular mechanism of PSG-1, we analyzed the abilities of PSG-1 to inhibit tumor growth in CT26-bearing mice and activate immune responses. In addition, the molecular mechanism of PSG-1 inhibited tumor growth was elucidated. We found that PSG-1 could induce the apoptosis of CT26 colon carcinoma cells through an intrinsic apoptotic pathway and enhance the host antitumor immune response. These findings suggest the possibility of PSG-1 to be a promising drug candidate or functional food, and supply a theoretical basis for further exploring.

MATERALS AND METHODS

Materials. *G. atrum* was cultivated and gathered in Ganzhou, Jiangxi Province, China. The species identification was carried out by Prof. Zhihong Fu, from Jiangxi University of Chinese Medicine. PSG-1 was purified according to a previously published protocol.[13] 3-(4,5-Dimethylthiazol-2-yl)-2,5-diphenyltetrazolium bromide (MTT) and 5-fluorouracil (5-Fu) were products of Sigma-Aldrich (St. Louis, MO, USA). Annexin V-FITC/PI assay kit was purchased from KeyGEN Biotech (Nanjing, China). Caspase-3 and -9 activity assay kits, Rhodamine 123 (Rh123), and reactive oxygen species assay kits were products of Beyotime Biotech (Jiangsu, China). The antibodies against Bcl-2, Bax, and cytochrome *c* were from Cell Signaling Technology (Danvers, MA). Anti-voltage-dependent anion channel (VDAC) 1 and anti-α-tubulin antibodies were purchased from Abcam (Cambridge, MA). Cytokine (TNF-α, IL-2, and IFN-γ) ELISA kits were from R & D Systems (Minneapolis, MN, USA).

Cells and Animals. CT26.WT mouse colon cell line was provided by Type Culture Collection of Chinese Academy of Sciences, Shanghai, China. The cells were cultured in RPMI-1640, 10% fetal bovine serum (FBS), and 1% P/S (100 units/mL penicillin and 100 units/mL streptomycin) under 37 °C, 5% CO_2 humidified conditions. BALB/c mice (male, 18−22 g) aged 6−8 weeks (SPF Certificate; No. SCXK (jing) 2009−0004, Beijing, China), were provided by Beijing HFK Biotechnology Company (Beijing, China). The animals were kept according to the Guide for the Care and Use of Laboratory Animals (NRC 2011), and all experimental protocols were in accordance with Nanchang University Medical College Animal Care Review Committee guidelines.

Cell Proliferation Assay. CT26 cells (2×10^4 cells/well) were plated into culture plates (Costar, Corning, NY) and incubated for 48 h in the absence or presence of different concentrations (0−320 μg/mL) of PSG-1. Then 20 μL MTT (5 mg/mL) solutions were added to each well. After incubation for 4 h, the optical density was measured at 570 nm in each well by using a microplate reader (Thermo, Shanghai, China) following removal of the medium and dissolution of the formazan crystals in the DMSO. Triplicate experiments were performed in a parallel manner for each concentration.

In Vivo Antitumor Activity. Mouse model of CT26 was established by inoculating 0.2 mL 5×10^6 cells/mL into the right hind groin of each mouse. After 24 h, the mice were divided into five groups (eight mice in each group) at random. The three groups of PSG-1-treated mice received different dosages (50, 100, and 200 mg/kg body weight), respectively. The positive control group was treated with 5-Fu (20 mg/kg), and the model control group was administered 0.9% saline solution. PSG-1 or saline solution was administered by using intragastric perfusion, and 5-Fu was administered by intraperitoneal injection once daily. On the 15th day, the mice were weighed and sacrificed by cervical dislocation. The spleen, tumor, and thymus were immediately excised and weighed. Thymus and spleen indexes were calculated as the weight of thymus and spleen relative to body weight. The inhibition rate was expressed as follows:

$$\text{tumor inhibitory rate}\ (\%) = (W_{\text{control}} - W_{\text{treated}})/W_{\text{control}} \times 100\%$$

W_{treated} and W_{control} were the average tumor weight of the treated and control mice, respectively.

The blood samples of mice in each group were centrifuged at 3,500 rpm for 10 min, and the serum was collected to detect the levels of TNF-α, IFN-γ, and IL-2 using commercial ELISA kits (R & D, Minneapolis, MN, USA). The absorbance was measured in an automatic ELISA plate reader (Thermo, Shanghai, China) at 450 nm.

Analysis of Apoptotic Cells. Flow cytometry can be used to quantitatively measure the apoptotic rate. The tumor tissue was isolated from CT26-bearing mice and chopped into small pieces with sterile scissors. Single cell suspension was prepared with a sterile filter screen. The suspension was washed twice and adjusted to the concentration of 1×10^6 cells/mL with cold PBS. Then the Annexin V-FITC and propidium iodide (PI) were added and incubated for 10−15 min away from light. Ten thousand events were collected for each sample. Stained cells were analyzed by flow cytometry (FACSCalibur, Becton Dickinson, Franklin Lakes, NJ, USA) in the FL1-H and FL2-H channels.

Determination of Mitochondrial Transmembrane Potential ($\Delta\Psi_m$). $\Delta\Psi_m$ was assessed by Rhodamine 123 (Rh123) probe (Beyotime Biotech, Jiangsu, China). Cells were collected and adjusted to a density of 0.5×10^6 cells/mL with RPMI 1640 medium and then incubated with 2 μM Rh123 at 37 °C for 20 min. The relative fluorescence intensities were measured by flow cytometry (FACSCalibur, Becton Dickinson) assay with the excitation and emission wavelengths of 488 and 530 nm, respectively.

Western Blot Analysis. The fresh tumor tissues were collected from tumor-bearing mice and fractionated into mitochondrial and cytoplasmic compartments with a Mitochondrial/Cytosol Fractionation Kit (Biovision, Mountain View, CA). Equal protein concentrations of lysate (containing 50 μg of proteins) were separated by SDS−PAGE in 12% gels, and then the proteins were electrotransferred to 0.22 μm nitrocellulose membranes. Membranes were preincubated with TBS buffer containing 5% BSA and 0.05% Tween 20 (TBST) for 2 h at room temperature and then incubated with anti-p53, anti-cytochrome *c*, anti-Bcl-2, or anti-Bax antibody (Cell Signaling Technology, Beverly, MA, USA) overnight at 4 °C. Immunoreactive bands were then incubated with peroxidase-conjugated secondary antibodies (ZSGB-Bio, Beijing, China) and detected by an enhanced chemiluninescence detection kit (ECL, Beyotime Biotech). β-Actin, α-tubulin, and VDAC1 were used as loading controls.

Assay for Caspase Activity. The activities of caspase-3 and -9 in cells were detected using caspase activity assay kits (Beyotime Biotech, Jiangsu, China) according to the manufacturer's protocols. The equal amounts of cells (1×10^5 cells/mL) from each sample were preincubated with cell lysis buffer for 10 min on ice and centrifuged for 8 min in a microcentrifuge at 10000*g*. The supernatant (100 μg of protein) was incubated with each caspase substrate (LEHD-AFC for caspase-9 and DEVD-AFC for caspase-3) at 37 °C for 1.5 h. Formation of ρ-nitroanilide was measured by ELISA Microplate Reader (Thermo, Shanghai, China) at 405 nm.

Intracellular Reactive Oxygen Species (ROS) Analysis. The intracellular levels of reactive oxygen species were monitored using the fluorescent probe DCFH-DA. 1×10^6 CT26 cells were isolated from tumor tissue, seeded in a 6-well plate, and then directly treated with 10 μM DCFH-DA dissolved in RPMI 1640 (1 mL) without FBS at 37 °C for 20 min. After the cells were washed with medium, the fluorescence intensity was measured with excitation wavelength at 488 nm and emission wavelength at 525 nm.

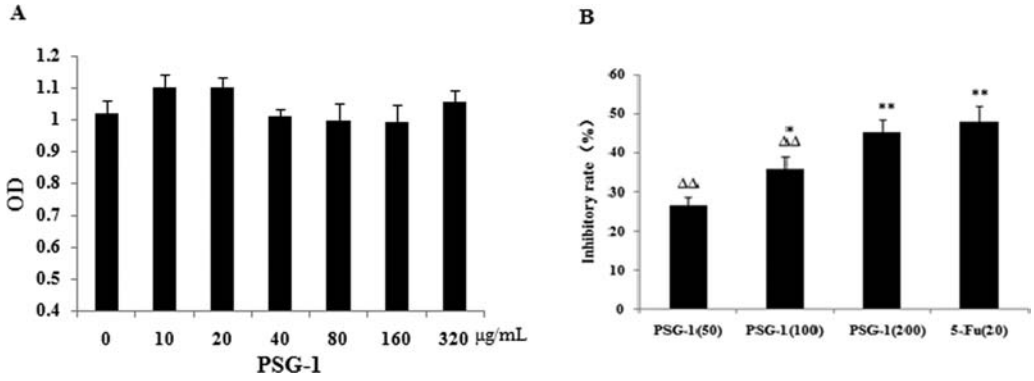

Figure 1. Antitumor effects of PSG-1 in vitro and in vivo. (A) Growth inhibitory effect of PSG-1 on CT26 cells. The effects of PSG-1 on the growth of CT26 cells were determined by the MTT method. The data presented are averages derived from at least triplicate experiments. (B) The tumor growth inhibitory rates of 5-Fu (20 mg/kg) and PSG-1 (50, 100, and 200 mg/kg) treated groups. Each data point is the average from 8 mice ($n = 8$). $^{*}P < 0.05$ and $^{**}P < 0.01$ vs control group; $\Delta\Delta$ $P < 0.01$ vs 5-Fu group.

Splenocyte Proliferation. Splenocytes were collected from tissue by homogenizing spleens; and then separated mononuclear cells were suspended in RPMI 1640 medium. The splenocytes were set up into the 96-well microplates at a density of 5×10^5 cells/well in RPMI 1640 medium, and then Con A (final concentration, 5 μg/mL) or LPS (final concentration, 10 μg/mL) was added to the wells. Plates were kept for 48 h at 37 °C with 5% CO_2. Cell proliferation was measured by MTT assay. The absorbance of each well was measured with an automatic microplate reader (Thermo, Shanghai, China) at 570 nm wavelength filter.

Statistical Analysis. All results were analyzed by one-way ANOVA using SPSS to determine the significance of differences between treatment groups and presented as the mean ± SEM. P values more than 0.05 were considered to be statistically insignificant.

Table 1. Effects of PSG-1 on Thymus Index and Spleen Index in CT26-Bearing Mice[a]

group	concn (mg/kg)	thymus index (mg/g)	spleen index (mg/g)
CT26 control		$1.341 \pm 0.263^{\Delta\Delta}$	$7.362 \pm 1.523^{\Delta\Delta}$
5-Fu	20	$0.421 \pm 0.114^{**}$	$3.982 \pm 1.375^{**}$
PSG-1	50	$1.610 \pm 0.325^{*\Delta\Delta}$	$8.397 \pm 1.564^{**\Delta\Delta}$
	100	$1.892 \pm 0.341^{**\Delta\Delta}$	$9.884 \pm 2.061^{**\Delta\Delta}$
	200	$2.746 \pm 0.385^{**\Delta\Delta}$	$10.253 \pm 3.226^{**\Delta\Delta}$

[a]Data are expressed as mean ± SEM of eight mice. $^{*}P < 0.05$, $^{**}P < 0.01$ vs CT26 control group. $^{\Delta}P < 0.05$, $^{\Delta\Delta}P < 0.01$ vs 5-Fu group.

RESULTS

Effect of PSG-1 on the Proliferation of CT26 Cells in Vitro. To investigate the effects of PSG-1 on the proliferation of CT26 cells, the cells were cultivated with different concentrations of PSG-1. MTT assays showed that PSG-1 exhibited no growth inhibitory activity on CT26 cells at concentrations of 20−320 μg/mL (Figure 1A).

PSG-1 Inhibited the Growth of Transplantable Tumors. After the 14 day treatment, PSG-1 (50, 100, and 200 mg/kg) and 5-Fu (20 mg/kg) had significant inhibitory effects on the growth of inoculated CT26 in mice. Figure 1B shows the inhibition ratio of tumor growth for different treatments in tumor-bearing mice. The data suggested that PSG-1 could inhibit the tumor growth in vivo.

Effect of PSG-1 Treatment on Thymus and Spleen Indexes. As shown in Table 1, after the treatment of PSG-1, the thymus and spleen indexes were significantly raised in CT26-bearing mice compared with the control group.

PSG-1 Promoted Apoptosis of CT26 Cells in Vivo. To investigate whether the inhibition of tumor growth may be caused by induced apoptosis in vivo, CT26 cells were prepared and then analyzed using Annexin V-FITC/PI double-straining. The results showed that the number of both necrotic cells and apoptotic cells was dramatically increased in the tumor administered with PSG-1 compared with control group (Figure 2). After treatment with PSG-1 for 2 weeks, the early and median apoptotic cells (lower right section of the fluorocytogram) were upregulated from 1.48% to 3.16%, 3.92%, and 5.01%, respectively. The late and apoptotic and necrotic cells (upper right section of the fluorocytogram) were also improved markedly (from 1.2% to 2.97%, 5.25%, and 8.51%). These data confirmed that PSG-1 induced the apoptosis of tumor cells of CT26-bearing mice.

Effect of PSG-1 on the Mitochondrial Transmembrane Potential ($\Delta\Psi_m$) in the Tumor of CT26-Bearing Mice. The disruption of mitochondrial integrity is an initial and irreversible event that occurs following induction of apoptosis through the mitochondrial pathway. To assess whether PSG-1 affects the function of mitochondria, the mitochondrial transmembrane potential were investigated by using the mitochondria probe, Rhodamine 123. With the increase of PGS-1 concentration, a remarkable attenuation of $\Delta\Psi_m$ was observed (Figure 3A,B). PSG-1 administration led to the $\Delta\Psi_m$ collapse.

PSG-1 Increased Release of Cytochrome *c* and Apoptosis-Associated Protein Expression in the Tumor of CT26-Bearing Mice. A critical step in the intrinsic apoptotic pathway is the liberation of mitochondrial intermembrane proteins into the cytosol, most notably cytochrome *c*, which plays a pivotal role in the activation of the caspase cascade.[21] Western-blotting results revealed that the level of cytosolic cytochrome *c* protein was unregulated dose-dependently (Figure 4B). In contrast, PSG-1 caused a slight decrease in protein level of cytochrome *c* in the mitochondrial fraction in 100 and 200 mg/kg body weight treated mice. These results indicated that PSG-1 led to the release of cytochrome *c* from the mitochondria to the cytosol.

The p53 is a potent tumor suppressor, which plays an important role in apoptosis signaling. A great many stress signals converge on p53, which responds to them by triggering cell cycle arrest and/or cell death by apoptosis.[22] The p53 directly binds to and inhibits antiapoptotic protein Bcl-2, and

dx.doi.org/10.1021/jf4053012 | J. Agric. Food Chem. 2014, 62, 1581−1589

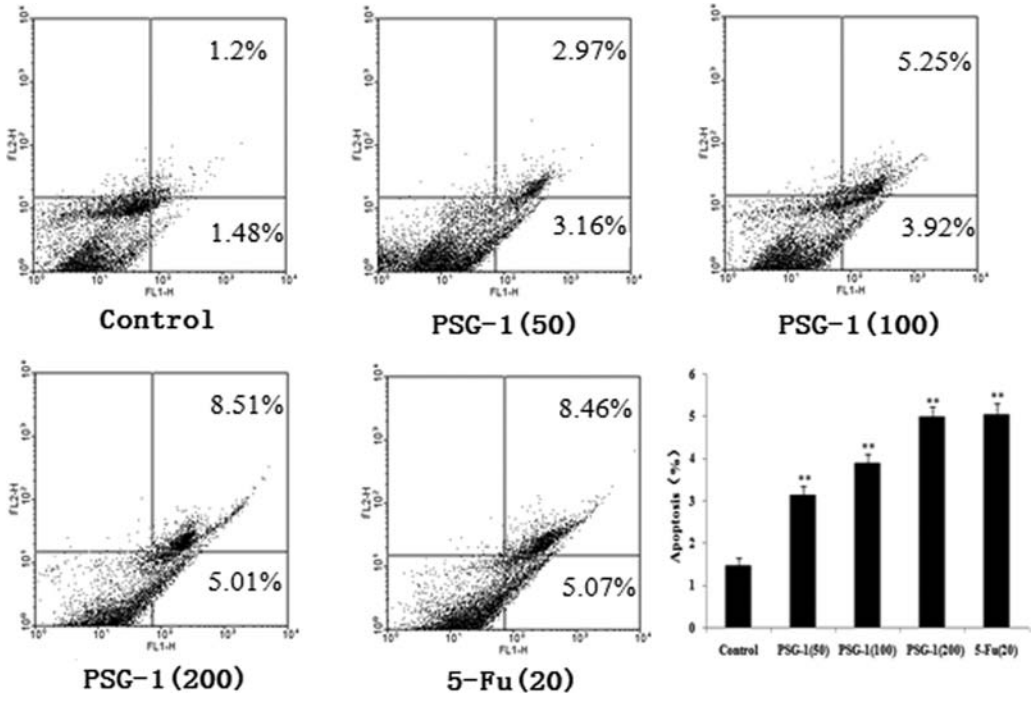

Figure 2. PSG-1 induced apoptosis in CT26 cells from CT26-bearing mice. CT26 tumor cells stained with AnnexinV-FITC and PI labeling and analyzed by flow cytometry.

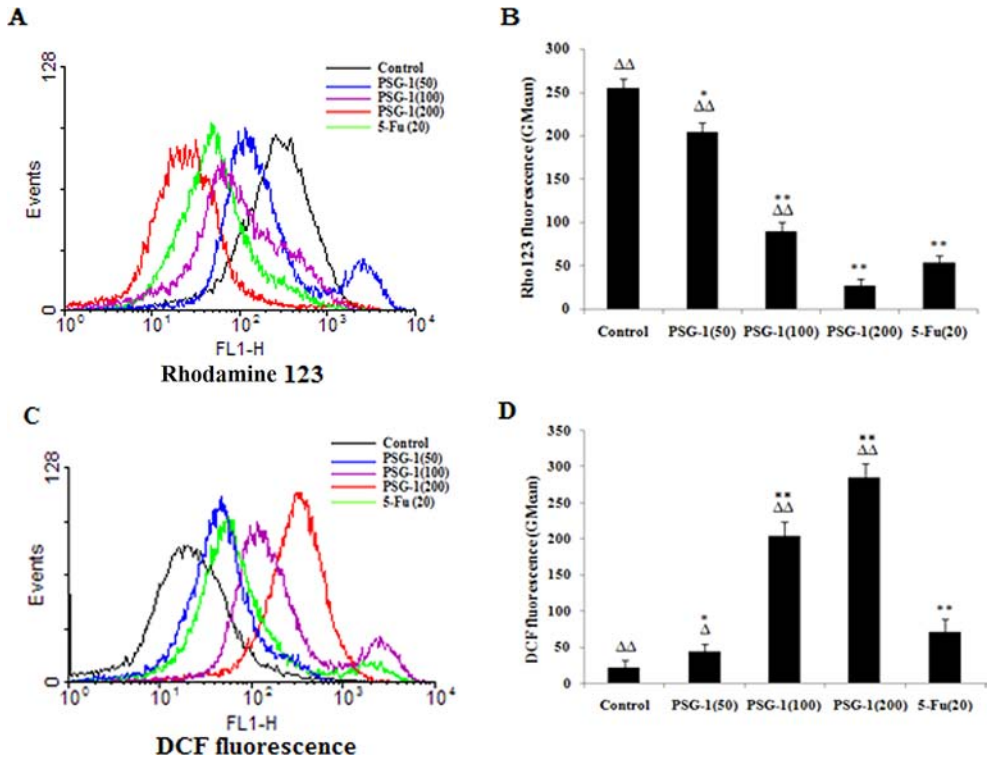

Figure 3. Effects of PSG-1 on the loss of $\Delta\Psi_m$ and generation of ROS. (A) The loss of $\Delta\Psi_m$ was evaluated by Rh123 staining. (B) Column chart of cell fluorescence for Rh123. (C) Intracellular ROS levels were measured by flow cytometry using an oxidation-sensitive fluorescent probe, DCFH-DA, which is oxidized to DCF in the presence of ROS. (D) Column chart of cell fluorescence for DCF. Values are mean ± SEM of eight mice. *P < 0.05 and **P < 0.01 vs control group; Δ P < 0.05 and ΔΔ P < 0.01 vs 5-Fu group.

also can trigger oligomerization of proapoptotic protein Bax, which are necessary for the disruption of mitochondria and release of cytochrome *c* from mitochondria into cytosol, stirring up the activation of the mitochondria-dependent apoptotic signaling pathway.[23] The Bcl-2 family members are important regulators of the mitochondrial apoptotic pathway. In order to clarify the mechanism of PSG-1-induced apoptosis, this study examined the expression of p53, Bax, and Bcl-2 proteins. Western blotting testing revealed that protein levels of both Bax and p53 increased dramatically in the 100 and 200 mg/kg PSG-

dx.doi.org/10.1021/jf4053012 | J. Agric. Food Chem. 2014, 62, 1581−1589

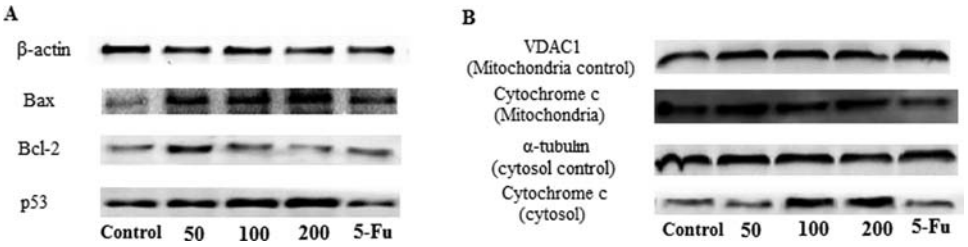

Figure 4. Western blot analysis of cytochrome *c* release and the expression of Bcl-2 family in tumor. (A) Total protein extracts were prepared and then analyzed by Western blotting with antibodies to p53, Bax, Bcl-2, and *β*-actin. (B) The cytosolic and mitochondrial proteins were analyzed by Western blotting with anti-cytochrome *c*, anti-VDAC1, and anti-*α*-tubulin antibodies. Western blots were representative of three independent experiments.

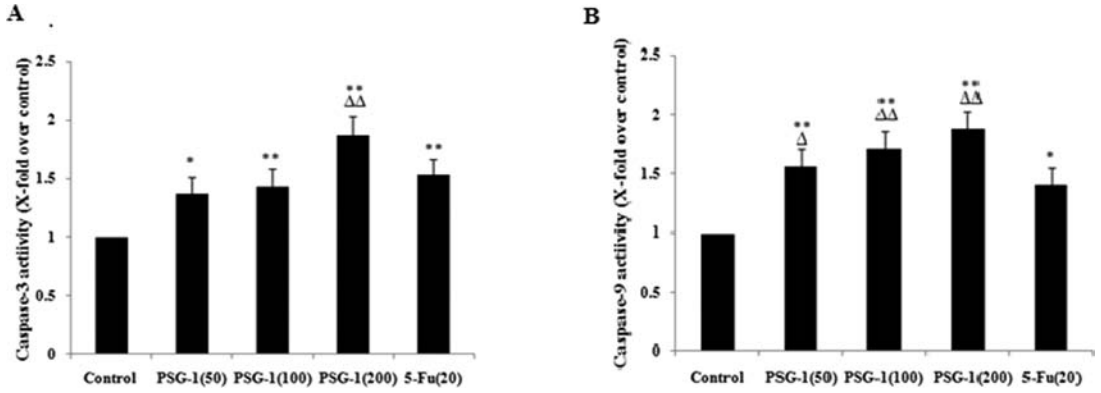

Figure 5. Effects of PSG-1 on the activation of caspase in the tumor of CT26-bearing mice. Quantitative analysis of caspase-3 and -9 activities in the tumor cells of CT26-bearing mice. Values are mean ± SEM of eight mice. $^{*}P < 0.05$, $^{**}P < 0.01$ vs control group; $^{\Delta}P < 0.05$ and $^{\Delta\Delta}P < 0.01$ vs 5-Fu group.

1-treated tumor-bearing groups, compared with control group, whereas the protein expression level of Bcl-2 was decreased in a dose-dependent manner (Figure 4A).

Effect of PSG-1 on Caspase Activity in the Tumor of CT26-Bearing Mice. Caspases are at the core of apoptotic machinery and play essential roles in the execution of apoptosis. According to the results of apoptosis assay, we hypothesized that PSG-1 might promote the activation of the caspase-dependent cell apoptosis pathway. We therefore set out to analyze the ability of PSG-1 to modulate caspase-3 and caspase-9 activities. Both caspase-3 and caspase-9 activities were elevated by treatment of PSG-1 in the CT26-bearing mice (Figure 5A,B). Taken together, all these lines of evidence suggested that PSG-1 could activate caspase-3 and caspase-9, and induce caspase-dependent apoptosis in the tumor of CT26-bearing mice.

Effect of PSG-1 on ROS Production in the Tumor of CT26-Bearing Mice. ROS generation are closely related to mitochondrial depolarization and apoptosis induction.[24] The level of ROS was detected to test whether oxidative stress went into effect in PSG-1-induced apoptosis in the tumor of CT26-bearing mice. As shown in Figure 3C,D, PSG-1 led to a remarkable increase in intracellular ROS level compared with control group. Therefore, the elevation of ROS production may be a major cause of PSG-1-induced apoptosis.

Effect of PSG-1 on Lymphocyte Proliferation and Cytokine Production in Serum of CT26-Bearing Mice. A wide variety of polysaccharides hold up antitumor activities and are side-effect-free in vivo. Most studies proved that fungus polysaccharides could exert the antitumor function through stimulating the immune response of the host organism. Furthermore, many mushroom polysaccharides were regarded as biological response modifiers. In this study, the normal murine lymphocyte proliferation rate induced by Con A or LPS was investigated. As shown in Table 2, there was a marked increase in the Con A- or LPS-induced proliferation of splenic cells in PSG-1 treated groups. As shown in Figure 6, TNF-*α*, IL-2, and IFN-*γ* concentrations in serum of 5-Fu treated CT26-bearing mice were lower than in control group. In contrast, administration of PSG-1 significantly increased TNF-*α*, IL-2, and IFN-*γ* levels in serum of tumor-bearing mice.

Table 2. Effects of PSG-1 on Immunomodulatory Activity in CT26-Bearing Mice[a]

group	concn (mg/kg)	A_{570} (OD) Con A	A_{570} (OD) LPS
CT26 control		$0.735 \pm 0.034^{\Delta}$	$0.699 \pm 0.023^{\Delta}$
5-Fu	20	$0.537 \pm 0.020^{*}$	$0.602 \pm 0.031^{*}$
PSG-1	50	$0.671 \pm 0.038^{*\Delta}$	$0.746 \pm 0.040^{*\Delta\Delta}$
	100	$0.809 \pm 0.033^{**\Delta\Delta}$	$0.832 \pm 0.037^{**\Delta\Delta}$
	200	$0.946 \pm 0.035^{**\Delta\Delta}$	$0.889 \pm 0.042^{**\Delta\Delta}$

[a]Data are expressed as mean ± SEM of eight mice. $^{*}P < 0.05$, $^{**}P < 0.01$ vs CT26 control group.$^{\Delta}P < 0.05$, $^{\Delta\Delta}P < 0.01$ vs 5-Fu group.

DISCUSSION

Bioactive polysaccharides have been found in a large number of natural resources, including plants, fungi, and bacteria, and have attracted more and more attention in the biochemistry and medical areas. Among them, the antitumor activity of polysaccharides from medical fungi were most attractive owing to their low cytotoxicity to normal cells and no obvious

dx.doi.org/10.1021/jf4053012 | J. Agric. Food Chem. 2014, 62, 1581−1589

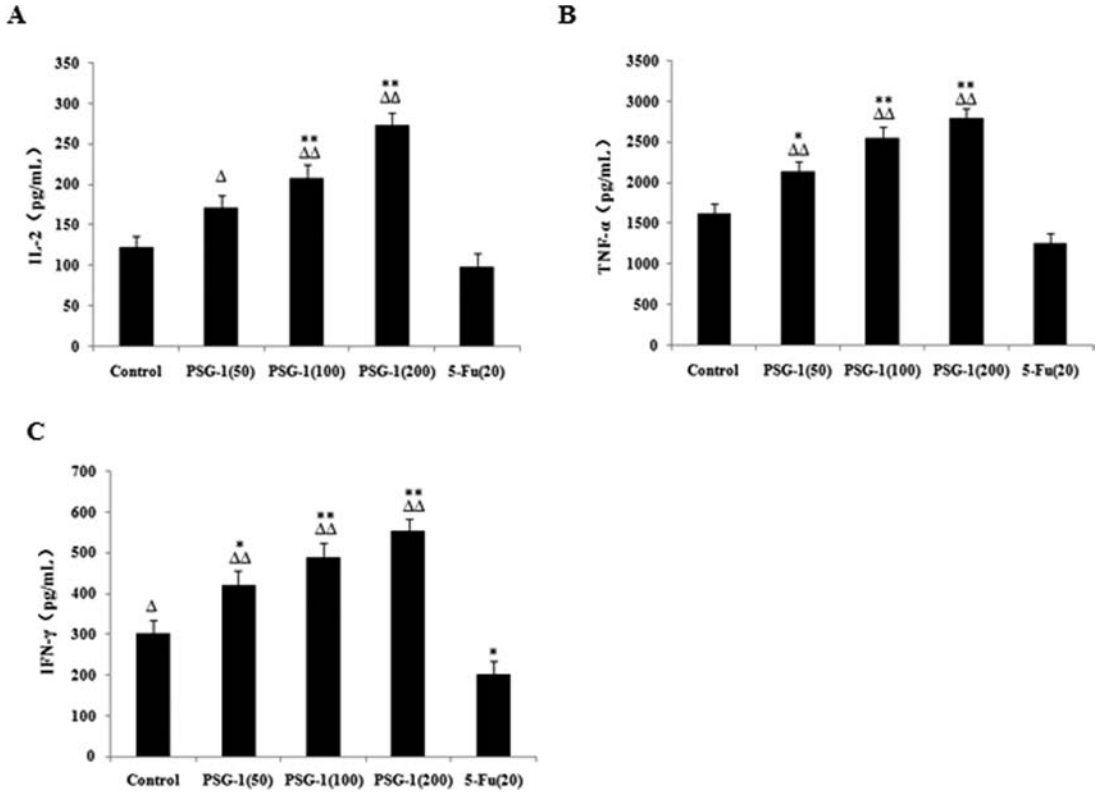

Figure 6. Effects of PSG-1 on levels of TNF-α, IL-2, and IFN-γ in serum of CT26-bearing mice: (A) IL-2, (B) TNF-α, and (C) IFN-γ. Concentrations of TNF-α, IL-2, and IFN-γ were determined by ELISA. Values are expressed as means ± SEM of eight mice for each group. *P < 0.05 and **P < 0.01 vs control group; Δ P < 0.05 and ΔΔ P < 0.01 vs 5-Fu group.

side effects in patients.[25] Lentinan from *Lentinus edodes* and PS-K/PS-P from *Coriolus versicolor* and *G. lucidum* polysaccharide are the most efficient and powerful fungal polysaccharides that have been extensively employed in antitumor action.[26] Recently, many kinds of polysaccharides displaying cyctoxic activity on tumor cells have been revealed, and some of these bioactive polysaccharides were possessed of potent apoptosis-inducing activities.

PSG-1 is a novel fungal polysaccharide purified from *G. atrum* and possesses excellent inhibitory activities against the proliferation of many kinds of tumor cells in vivo. Our previous studies have demonstrated that PSG-1 could inhibit S180 tumor growth, and improve immune system function through the TLR4 mediated-NF-κB and MAPKs signaling pathway.[27] Moreover, oral administration of PSG-1 could significantly prevent and inhibit CT26 solid tumor formation in BALB/c mice via TLR4-dependent signaling pathway.[15] In this study, we further assessed the apoptosis-inducing effect of PSG-1 on CT26 cells, and investigated the mechanism of tumor growth inhibition by PSG-1.

Apoptosis is always considered as the main pathway by which cytotoxic drugs induce tumor cell death and also a critical process that makes a contribution to both drug sensitivity and resistance in tumor cells.[28] Defective apoptosis would promote carcinogenesis and tumor progression as many antitumor therapies work by inducing apoptosis in tumor cells. In the present study, the results showed that PSG-1 induced CT26 cells apoptosis in vivo. We further explored the possible mechanism of apoptosis induced by PSG-1. The apoptotic process is often considered to be mediated by two separate mechanisms, mitochondrial and nonmitochondrial pathways. Mitochondrial outer membrane permeabilization is a decisive event in apoptosis which is mediated by Bcl-2 family proteins.[19,29] At present, existing data demonstrate that elimination of potentially malignant cells often relays on mitochondria apoptotic pathway.[30] Moreover, our previous study also found that the mitochondrial apoptotic pathway was closely related to the antitumor effect of (−)-epigallocatechin-3-gallate (EGCG) on human hepatoma cells.[31] Thus, we detected several apoptosis associated parameters of mitochondrial apoptotic pathway in our research.

$\Delta\Psi_m$, the loss of mitochondrial membrane potential, is one of the crucial parameters of mitochondrial dysfunction and could lead to an irreversible event during the process of cell apoptosis.[32] The disruption of $\Delta\Psi_m$ could result in the release of some apoptogenic proteins, activating the cascade of events that lead to the activation of caspases in the mitochondrial dependent apoptotic pathway.[33] In the present study, a very significant depletion of $\Delta\Psi_m$ was revealed by flow cytometry in PSG-1 treated groups. As could be judged from the loss of $\Delta\Psi_m$, PSG-1 is most likely to elicit marked changes in these mitochondrial functions.

The disruption of $\Delta\Psi_m$ in mitochondria could cause not only an uncoupling of the respiratory chain but also the efflux of some proteins as well as small molecules (e.g., cytochrome *c* and calcium). When cytochrome *c* is released into the cytosol, cytochrome *c* would bind to Apaf-1 to produce apoptosome accelerating the activation of caspase-9 and then caspase-3 for caspase-dependent apoptosis.[34] The dissipation of $\Delta\Psi_m$ prompted us to investigate the effect of PSG-1 on the release of cytochrome *c*. In the present study, we revealed that PSG-1 was able to induced the release of cytochrome *c*. Caspases are a

ubiquitous family of cysteine proteases that modulate the apoptotic response. Particularly, the activation of caspase-3 is one of the most common involvements in the apoptosis of various cell types.[35] Caspase-3, which might be activated by caspase-9, typically functions in the downstream of other caspases and directly activates enzymes that are responsible for DNA fragmentation in the mitochondrial apoptosis pathway. Lots of microtubule inhibitors such as vincristine, paclitaxel, colchicines, and vinblastine induce growth arrest, subsequent inactivation of Bcl-2, and finally apoptotic cell death through the caspase-9-dependent pathway.[36] Our current results were consistent with previous studies that the activities of caspase-9 and caspase-3 were markedly elevated in the PSG-1 treated group. These results suggested that PSG-1 exhibited the antitumor effect via induction of apoptosis mediated by mitochondrial pathways.

In cancer cells, ROS have been broadly reported to play a crucial part in apoptosis induction in both pathological and physiological processes. It has been detected as an early signal that initiates and mediates cellular apoptosis.[37] Interestingly enough, mitochondria are both the major source of and target of ROS. It could lead to the breakdown of membrane phospholipids, inactivation of enzymes, and destruction of mitochondrial function, which contribute to the intermembrane proteins, such as cytochrome *c*, to be released out of the mitochondria and eventually initiate caspase-3 activation. Recent evidence suggested that another cause of PSG-1-induced apoptosis may be ROS overproduction. The production of ROS in CT26 cells from CT26-bearing mice was determined by the oxidation-sensitive fluorescence dye, DCFH-DA. The data showed that PSG-1 elevated the level of ROS generation, suggesting that ROS production is relevant to PSG-1-induced mitochondria-mediated apoptosis.

The mitochondria-mediated apoptotic pathway was under the control of multiple layers of regulation, one of the most important players being members of Bcl-2 family.[38] Two most important members of Bcl-2 family, the antiapoptotic protein Bcl-2 and the proapoptotic protein Bax, are key regulators of this progress. The main function of them is to control mithochondrial permeability. Bax can promote cell death. Conversely, Bcl-2 proteins cause resistance to chemotherapeutic agents and radiation therapy, while reducing Bcl-2 expression could promote apoptotic responses to antitumor agents.[39] Triterpene extract was found to be able to modulate the expression of Bcl-2 and Bax in many types of tumor cell lines.[40] In addition, tumor suppressor p53 has been identified as an effector of apoptosis signals. Reactivating p53 provides a general strategy in conquering cancer specifically.[41] It is a regulator of cell cycle arrest progression and the mediator of apoptosis in various cases. To further analyze the possible mechanism underlying the PSG-1-induced apoptosis, we assessed the expression of these proteins. The results revealed that Bcl-2 expression was downregulated while Bax and p53 expression levels were strikingly increased, suggesting that upregulation of p53 and Bcl-2 family proteins might be another important mechanism contributing to mitochondrial pathway of apoptosis induced by PSG-1.

Taken together, our results suggest that PSG-1 may induce tumor apoptosis through mitochondrial death pathways. Downregulation of the death antagonist Bcl-2 and upregulation of p53 and the death agonist Bax, which lead to the collapse of $\Delta\Psi_m$, may promote the mitochondria-related cytochrome *c* release and lead to the activation of caspase-9, followed by caspase-3, thus paving the way for PSG-1-induced apoptosis.

To the best of our knowledge, PSG-1 is also a good immune-regulated agent. It could increase macrophage phagocytosis and the levels of cytokines and nitride oxide and elicit its antitumor effect by improving immune system functions through TLR4 mediated-NF-κB and MAPK signaling pathway. The inhibition rate of PSG-1 on S180-bearing mice is about 46.52%.[27] In the present research, PSG-1 showed a better antitumor effect on the CT26-bearing mice, reaching up to 47.83%. We supposed that PSG-1 not only induced the tumor apoptosis through mitochondrial pathway but also stimulated the host immune system. To support this hypothesis, we evaluated the immunomodulatory activity of PSG-1 on CT26-bearing mice. Many effects of polysaccharides are related to the potentiation of precursor T cells after recognition of malignant cells.[42] The occurrence, development, and prognosis of tumor has a close relationship to the immune condition of the cancer patients. So we further investigated the effect of PSG-1 on immune function in CT26-bearing mice. PSG-1 was found to cause an increase in the thymus and spleen indexes dramatically. Protective immunity against tumor can be separated into two branches: cellular and humoral immunity. Immune responses play a key role in eliminating the locally growing and circulating tumor cells and, hence, lead to the suppression of growth and metastasis of tumors. In this research, cell-mediated immune defense was likely to be mediated specifically by T- and B-cells. The results of the present study suggested that PSG-1 significantly enhanced spleen lymphocyte proliferation.

In addition to the action on immune cells, another crucial function of polysaccharides is the augmentation of the cytokine level. Cytokines play a vital role in mediating the host defense, and regulate communication between antigen-presenting cells (APCs), lymphocytes, and other host effector cells during the immune response. The data of the present study clearly indicated that PSG-1 was a potent inducer of the cytokines, TNF-α, IL-2, and IFN-γ. It might also explain the enhancement of cytotoxicity of splenocytes by PSG-1 administration. Therefore, it is suggested that PSG-1 might elicit its antitumor effect by promoting immunity and killer activities.

In conclusion, PSG-1 has been shown to exhibit prominent antitumor activity in vivo, at least in part by inducing apoptosis through the mitochondrial pathway and enhancement of host immune system function. To the best of our knowledge, our results have provided new evidence to support clinical trials of PSG-1 in cancer patients in the future. PSG-1 could be a safe and effective antitumor bioactive agent or food material.

AUTHOR INFORMATION

Corresponding Author

*Tel and fax: +86-791-88304452. E-mail: spnie@ncu.edu.cn.

Funding

This study was supported by Key Program of National Natural Science Foundation of China (No. 31130041), and National Natural Science Foundation of China (31071532), National Key Technology R & D Program of China (2012BAD33B06), the Program for New Century Excellent Talents in University (NCET-12-0749) and Research Project of State Key Laboratory of Food Science and Technology (SKLF-ZZA-201301, SKLF-TS-201107).

Notes

The authors declare no competing financial interest.

ABBREVIATIONS USED

BSA, bovine serum albumin; 5-Fu, 5-fluorouracil; $\Delta\Psi_m$, mitochondrial transmembrane potential; ρNA, ρ-nitroanilide; PBS, phosphate-buffered saline; PI, propidium iodide; PSG-1, *Ganoderma atrum* polysaccharide; Rh123, Rhodamine 123; ROS, reactive oxygen species; TBS, Tris-buffered saline; VDAC, voltage-dependent anion channel

REFERENCES

(1) Boyle, P.; Levin, B. *World Cancer Report*; World Health Organization Press: 2008.

(2) Rein, D. T.; Kurbacher, C. M. The role of chemotherapy in invasive cancer of the cervix uteri: current standards and future prospects. *Anti-Cancer Drugs* **2001**, *12*, 787−795.

(3) Kim, J.; Park, E. J. Cytotoxic anticancer candidates from natural resources. *Curr. Med. Chem.: Anti-Cancer Agents* **2002**, *2*, 485−537.

(4) Chihara, G.; Maeda, Y.; Hamuro, J.; Sasaki, T.; Fukuoka, F. Inhibition of mouse sarcoma 180 by polysaccharides from Lentinus edodes (Berk.) sing. *Nature* **1969**, *222*, 687−688.

(5) Kobayashi, H.; Yoshida, R.; Kanada, Y.; Fukuda, Y.; Yagyu, T.; Inagaki, K.; Kondo, T.; Kurita, N.; Suzuki, M.; Kanayama, N.; Terao, T. Suppressing effects of daily oral supplementation of beta-glucan extracted from Agaricus blazei Murill on spontaneous and peritoneal disseminated metastasis in mouse model. *J. Cancer Res. Clin. Oncol.* **2005**, *131*, 527−538.

(6) Nakazato, H.; Koike, A.; Saji, S.; Ogawa, N.; Sakamoto, J. Efficacy of immunochemotherapy as adjuvant treatment after curative resection of gastric cancer. Study Group of Immunochemotherapy with PSK for Gastric Cancer. *Lancet* **1994**, *343*, 1122−1126.

(7) Shin, J. Y; Song, J. Y.; Yun, Y. S.; Yang, H. O.; Rhee, D. K.; Pyo, S. Immunostimu-lating effects of acidic polysaccharides extract of Panax ginseng on macrophage function. *Immunopharmacol. Immunotoxicol.* **2002**, *24*, 469−482.

(8) Sliva, D. Cellular and physiological effects of Ganoderma lucidum (Reishi). *Mini-Rev. Med. Chem.* **2004**, *4*, 873−879.

(9) Eo, S. K.; Kim, Y. S.; Lee, C. K.; Han, S. S. Antiherpetic activities of various protein bound polysaccharides isolated from Ganoderma lucidum. *J. Ethnopharmacol.* **1999**, *68*, 175−181.

(10) Gao, Y. H.; Zhou, S. F.; Wen, J. B.; Huang, M.; Xu, A. L. Mechanism of the antiulcerogenic effect of Ganoderma lucidum polysaccharides on indomethacin-induced lesions in the rat. *Life Sci.* **2002**, *72*, 731−45.

(11) Xu, Z. T.; Chen, X. P.; Zhong, Z. F.; Chen, L. D.; Wang, Y. T. Ganoderma lucidum polysaccharides: Immunomodulation and potential anti-tumor activities. *Am. J. Chin. Med.* **2011**, *39*, 15−27.

(12) Gao, Y.; Chan, E.; Tang, W.; Xu, A.; Yang, H.; Huang, M.; Lan, J.; Li, X.; Duan, W.; Xu, C.; Zhou, S. Antitumor activity and underlying mechanisms of ganopoly, the refined polysaccharides extracted from Ganoderma lucidum in mice. *Immunol. Invest.* **2005**, *34*, 171−198.

(13) Chen, Y.; Xie, M. Y.; Wang, Y. X.; Nie, S. P.; Li, C. Analysis of the monosaccharide composition of purified polysaccharides in Ganoderma atrum by capillary gas chromatography. *Phytochem. Anal.* **2009**, *20*, 503−510.

(14) Zhang, H.; Li, W. J.; Nie, S. P.; Chen, Y.; Wang, Y. X.; Xie, M. Y. Structural characterisation of a novel bioactive polysaccharide from *Ganoderma atrum*. *Carbohydr. Polym.* **2012**, *88*, 1047−1054.

(15) Zhang, S. S.; Nie, S. P.; Huang, D. F.; Li, W. J.; Xie, M. Y. Immunomodulatory effect of Ganoderma atrum polysaccharide on CT26 tumor bearing mice. *Food Chem.* **2013**, *136*, 3−4.

(16) Li, W. J.; Nie, S. P.; Chen, Y.; Wang, Y. X.; Li, C.; Xie, M. Y. Enhancement of cyclophosphamide-induced antitumor effect by a novel polysaccharide from Ganoderma atrum in sarcoma 180-bearing mice. *J. Agric. Food Chem.* **2011**, *59*, 3707−3716.

(17) Takano, Y.; Okudaira, M.; Harmon, B. V. Apoptosis induced by microtubule disrupting drugs in cultured human lymphoma cells. Inhibitory effects of phorbol ester and zinc sulphate. *Pathol. Res. Pract.* **1993**, *189*, 197−203.

(18) Khan, N.; Adhami, V. M.; Mukhtar, H. Apoptosis by dietary agents for prevention and treatment of cancer. *Biochem. Pharmacol.* **2008**, *76*, 1333−1339.

(19) Cui, Z.; Piao, J.; Rehman, M. U.; Ogawa, R.; Li, P.; Zhao, Q. L.; Kondo, T.; Inadera, H. Molecular mechanisms of hyperthermia-induced apoptosis enhanced by withaferin A. *Eur. J. Pharmacol.* **2014**, *723*, 99−107.

(20) Green, D. R.; Kroemer, G. The pathophysiology of mitochondrial cell death. *Science* **2004**, *305*, 626−629.

(21) Green, D. R.; Reed, J. C. Mitochondria and apoptosis. *Science* **1998**, *281*, 1309−1312.

(22) Vogelstein, B.; Lane, D.; Levine, A. J. Surfing the p53 network. *Nature* **2000**, *408*, 307−310.

(23) Choi, H. S.; Cho, M. C.; Lee, H. G.; Yoon, D. Y. Indole-3-carbinol induces apoptosis through p53 and activation of caspase-8 pathway in lung cancer A549 cells. *Food Chem. Toxicol.* **2010**, *48*, 883−890.

(24) Simon, H. U.; Haj-Yehia, A.; Levi-Schaffer, F. Role of reactive oxygen species (ROS) in apoptosis induction. *Apoptosis* **2000**, *5*, 415−418.

(25) Furusawa, E.; Chou, S. C.; Furusawa, S.; Hirazami, A.; Dang, Y. Anti-tumor activity of Ganoderma lucidum, an edible mushroom, on intraperitoneally implanted Lewis lung carcinoma in synergenic mice. *Phytother. Res.* **1992**, *6*, 300−304.

(26) Wang, S. Y.; Hsu, M. L.; Hsu, H. C.; Tzeng, C. H.; Lee, S. S.; Shiao, M. S.; Ho, C. K. The anti-tumor effect of Ganoderma lucidum is mediated by cytokines released from activated macrophages and T lymphocytes. *Int. J. Cancer* **1997**, *70*, 699−705.

(27) Zhang, S. S.; Nie, S. P.; Huang, D. F.; Huang, J. Q.; Wang, Y. X.; Xie, M. Y. Polysaccharide from Ganoderma atrum evokes antitumor activity via Toll-like receptor 4-mediated NF-κB and mitogen-activated protein kinase signaling pathways. *J. Agric. Food Chem.* **2013**, *61*, 3676−3682.

(28) Modark, D. E.; Gold, D. V.; Goldenberg, D. M. Sphingolipid targets in cancer therapy. *Mol. Cancer. Ther.* **2006**, *5*, 200−208.

(29) Pinton, P.; Giorgi, C.; Pandolfi, P. P. The role of PML in the control of apoptotic cell fate: a new key player at ER−mitochondria sites. *Cell Death Differ.* **2011**, *18*, 1450−1456.

(30) Ghosh, J. C.; Dohi, T.; Raskett, C. M.; Kowalik, T. F.; Altieri, D. C. Activated checkpoint kinase 2 provides a survival signal for tumor cells. *Cancer Res.* **2006**, *66*, 11576−11579.

(31) Li, W. J.; Nie, S. P.; Qu, Q.; Xie, M. Y. (-)-Epigallocatechin-3-gallate induces apoptosis of human hepatoma cells by mitochondrial pathways related to reactive oxygen species. *J. Agric. Food Chem.* **2009**, *57*, 6685−6691.

(32) Zhou, Q.; Li, Y.; Jin, J.; Lang, L. W.; Zhu, Z. X.; Fang, W. S.; Chen, X. G. Lx2−32c, a novel taxane derivative, exerts anti-resistance activity by initiating intrinsic apoptosis pathway in vitro and inhibits the growth of resistant tumor in vivo. *Biol. Pharm. Bull.* **2012**, *35*, 2170−2179.

(33) Nakazato, T.; Ito, K.; Ikeda, Y.; Kizaki, M. Green tea component, catechin, induces apoptosis of human malignant B cells via production of reactive oxygen species. *Clin. Cancer Res.* **2005**, *11*, 6040−6049.

(34) Kim, R. Recent advances in understanding the cell death pathways activated by anticancer therapy. *Cancer* **2005**, *103*, 1551−1560.

(35) Mancini, M.; Nicholson, D. W.; Roy, S.; Thornberry, N. A.; Peterson, E. P.; Casciola-Rosen, L. A.; Rosen, A. The caspase-3 precursor has a cytosolic and mitochondrial distribution: implications for apoptotic signaling. *J. Cell Biol.* **1998**, *140*, 1485−1495.

(36) Wang, L. G.; Liu, X. M.; Kreis, W.; Budman, D. R. The effect of antimicrotubule agents on signal transduction pathways of apoptosis: a review. *Cancer Chemother. Pharmacol.* **1999**, *44*, 355−361.

(37) Cort, A.; Timur, M.; Dursun, E.; Kucuksayan, E.; Aslan, M.; Ozben, T. Effects of N-acetylcystein on bleomycin-induced apoptosis in malignant testicular germ cell tumors. *J. Physiol. Biochem.* **2012**, *68*, 555−562.

(38) Gogvadze, V.; Orrenius, S.; Zhivotovsky, B. Multiple pathways of cytochrome c release from mitochondria in apoptosis. *Biochim. Biophys. Acta* **2006**, *1757*, 639−647.
(39) Portt, L.; Norman, G.; Clapp, C.; Greenwood, M.; Greenwood, M. T. Anti-apoptosis and cell survival: a review. *Biochim. Biophys. Acta* **2011**, *1813*, 238−259.
(40) Choudhuri, T.; Pal, S.; Agwarwal, M. L.; Das, T.; Sa, G. Curcumin induces apoptosis in human breast cancer cells through p53-dependent Bax induction. *FEBS Lett.* **2002**, *512*, 334−340.
(41) Chen, F.; Wang, W.; El-Deiry, W. S. Current strategies to target p53 in cancer. *Biochem. Pharmacol.* **2010**, *80*, 724−730.
(42) Borchers, A. T.; Stern, J. S.; Hackman, R. M.; Keen, C. L.; Gershwin, M. E. Mushrooms, tumors, and immunity. *Proc. Soc. Exp. Biol. Med.* **1999**, *221*, 281−293.

MATERIALS AND METHODS

Ethical Approval. The animal protocol followed in this study was reviewed and approved by the Bioethical Committee of our University, and guidelines for the use and care of laboratory animals of the University were followed.

Animals and Experimental Design. Virgin female Wistar rats (Charles River Laboratories Spain, SA, Barcelona, Spain), housed at 22 °C with a period of light/dark of 12 h each (lights on from 08:00 to 20:00) and with free access to food and water, were mated with male rats. The day of conception (day 0 of pregnancy) was determined by examination of vaginal smears for the presence of sperm, and then female rats were single caged. Pregnant rats were supplemented with 30% of the normal caloric intake of a group of dams fed ad libitum in the form of different fat sources (refined olive oil, margarine, or butter) during late pregnancy and lactation (from day 14 of pregnancy to day 21 of lactation), as previously described.[19] The fatty acid profile of the different fat sources has been previously described[20] and is shown in Table 1. Supplementation of the different fat sources was carried out by gavage once a day. As described,[19] no differences were observed in the total amount of kilocalories ingested by dams during the supplementation period among fat-supplemented groups. Thus, different outcomes observed in the offspring may be attributed to the different fat sources of maternal supplementation and not to the intake of different amount of calories. The offspring of these animals are referred to as olive oil, margarine, and butter groups, respectively. The offspring of dams fed ad libitum (control group) were also followed. At day 1 after delivery, excess pups in each litter were removed to keep 10 pups per dam.

Table 1. Fatty Acid Composition of Fat Sources Used in the Experimental Design[19,a]

fatty acid	olive oil	margarine	butter
C10:0	nd	nd	2.06
C12:0	nd	4.56	6.44
C14:0	0.63	1.54	15.7
C16:0	12.7	13.9	36.9
C18:0	0.91	1.28	10.7
C20:0	nd	nd	0.77
C23:0	nd	nd	0.86
SFAs	**14.3**	**21.2**	**73.5**
C16:1n7	1.05	nd	1.53
C18:1n7	1.87	1.04	0.42
C18:1n9c	70.6	20.9	16.5
C24:1	nd	1.72	0.61
MUFAs	**74.0**	**23.8**	**19.8**
C18:2n6	7.70	41.9	1.17
C18:3n6	nd	nd	0.64
C18:3n3	1.02	5.52	0.75
CLA 9,11	nd	nd	0.79
C20:3n6	nd	nd	0.12
C22:5n3	nd	1.48	0.52
PUFAs	**8.72**	**49.0**	**3.99**
n-6	**7.70**	**42.0**	**1.93**
n-3	**1.02**	**7.01**	**1.27**

[a]Data are the means of three different measurements expressed as a percentage of total fat. SFAs = saturated fatty acids, MUFAs = monounsaturated fatty acids, PUFAs = polyunsaturated fatty acids, and nd = nondetectable levels. The bold numbers indicate the total of each category of fatty acid in each fat source.

At weaning animals were fed a standard diet until the age of 4 months; then they were divided into two groups: one group continued under a normal-fat (NF) diet (standard diet containing 3.2 kcal/g, with 8% calories from fat), and the other group was exposed to a high-fat (HF) diet (containing 4.7 kcal/g, with 45% calories from fat, Research Diets, Inc., New Brunswick, NJ). The HF diet contained 5.5% calories from soybean oil and 39.5% from lard. Body mass and food intake were followed until the age of 6 months. At this age, the body fat content (by EchoMRI-700, Echo Medical Systems, LLC, Houston, TX) was recorded and blood samples were collected (in heparinized containers) from the saphenous vein, under fasting—animals deprived of food for 12 h. All groups include at least seven animals (n = 7−12).

At the age of 6 months, the animals were killed by decapitation under fed conditions, during the first 2 h of the beginning of the light cycle. The liver and various WAT depots—gonadal, retroperitoneal, mesenteric, and inguinal—were rapidly removed. All samples were weighed, immediately frozen in liquid nitrogen, and stored at −70 °C. The retroperitoneal was the depot selected as representative of the WAT to perform mRNA expression. Blood was also collected and centrifuged at 1000g for 10 min to collect the plasma, which was stored at −20 °C until analysis.

Quantification of Insulin and Glucose Concentration and Calculation of the Homeostatic Model Assessment for Insulin Resistance. The blood glucose concentration was measured with an Accu-Chek glucometer (Roche Diagnostics, Barcelona, Spain). The plasma insulin concentration was measured using a rat insulin enzyme-linked immunosorbent assay (ELISA) kit (Mercodia AB, Uppsala, Sweden) following standard procedures.

The homeostatic model assessment for insulin resistance (HOMA-IR) was used to assess insulin resistance. It was calculated from the fasting insulin and glucose concentrations using the formula of Matthews et al.:[21] HOMA-IR = [fasting glucose concentration (mmol/L) × fasting insulin concentration (mU/L)]/22.5.

Quantification of Plasma Levels of Triglycerides, Nonesterified (or Free) Fatty Acids, and β-Hydroxybutyrate and Hepatic Lipid Content. Commercial enzymatic colorimetric kits were used for the determination of plasma triglyceride (Sigma, Madrid, Spain), nonesterified (or free) fatty acids (NEFAs) (Wako Chemicals GmbH, Neuss, Germany), and 3-hydroxybutyrate (BEN S.r.l.-Biochemical enterprise) levels. Total lipids were extracted from about 600 mg of hepatic tissue and quantified by the method of Folch et al.[22]

Histological Studies. A histological study was performed on the liver. A piece of fresh dissected liver (n = 6) was fixed by immersion in 4% paraformaldehyde in 0.1 M phosphate buffer (pH 7.4) overnight at 4 °C. The samples were then washed in phosphate buffer and dehydrated in a graded series of ethanol, cleared in xylene, and embedded in paraffin blocks. Sections of the tissues 5 μm thick were stained with hematoxylin and eosin. Liver sections were classified into four grades depending on fat accumulation following the Burnt et al. classification.[23] Grade 0 was assigned when no fat accumulation was found in the liver, grade 1 when fat vacuoles were seen in less than 33% of hepatocytes, grade 2 when 33−66% of hepatocytes were affected by fat vacuoles, and grade 3 when fat vacuoles were found in more than 66% of hepatocytes. Liver images from light microscopy were digitalized and analyzed using Axio Vision software (Carl Zeiss Imaging Solutions).

RNA Extraction. Total RNA was extracted from the liver and retroperitoneal WAT by an E.Z.N.A. RNA purification system (Omega Biotek, Inc., Norcross, GA) according to the manufacturer's instructions. Isolated RNA was quantified using the NanoDrop ND-1000 spectrophotometer (NadroDrop Technologies Wilmington, DE) and its integrity confirmed using agarose gel electrophoresis.

RT-qPCR Analysis. Real-time polymerase chain reaction was used to measure mRNA expression levels of selected genes in the liver and retroperitoneal WAT in the offspring of the different groups of animals at the age of 6 months: specifically, CD36, sterol regulatory element binding protein 1c (SREBP1c), fatty acid synthase (FAS), stearoyl coenzyme A desaturase 1 (SCD1), peroxisome proliferator activated receptor α (PPARα), fibroblast growth factor 21 (FGF21), liver carnitine palmitoyltransferase 1a (CPT1L), pyruvate dehydrogenase kinase 4 (PDK4), glucokinase (GK), pyruvate kinase 4 (PK), insulin

Table 2. Body Mass, Fat Content, and Mass of Different WAT Depots and Liver of 6 Month Old Male Offspring of Dams Supplemented with 30% of the Normal Caloric Intake with Different Fat Sources (Olive Oil, Margarine, or Butter) during Late Pregnancy and Lactation[a]

		Control	Olive oil	Margarine	Butter	ANOVA
Body weight (g)	NF	450 ± 12	442 ± 10	439 ± 9	462 ± 14	D
	HF	485 ± 19	491 ± 16 *	462 ± 13	486 ± 13	
Body fat content (%)	NF	15.8 ± 1.3	17.0 ± 0.8	17.1 ± 1.6	17.6 ± 1.5	D
	HF	22.9 ± 1.7 *	23.0 ± 1.2 (ab) *	21.1 ± 1.6 (b)	25.9 ± 1.0 (a) *	
Adiposity index (%)	NF	6.07 ± 0.40	7.02 ± 0.36	6.79 ± 0.64	7.11 ± 0.67	D
	HF	9.96 ± 0.81 *	9.85 ± 0.60 *	9.40 ± 0.59 *	10.8 ± 0.41 *	
Inguinal WAT(g)	NF	6.44 ± 0.3	8.49 ± 0.49 ↑	8.09 ± 0.63↑	9.22 ± 1.07↑	D
	HF	12.7 ± 1.4 *	12.6 ± 0.89 (ab)*	9.75 ± 0.81 (a)	13.5 ± 1.2 (b)*	T
Mesenteric WAT(g)	NF	4.24 ± 0.60	4.78 ± 0.42	4.12 ± 0.36	4.92 ± 0.68	D
	HF	6.73 ± 0.71 *	6.86 ± 0.69*	5.70 ± 0.41*	7.42 ± 0.54*	
Retroperitoneal WAT(g)	NF	7.93 ± 0.67	9.15 ± 0.79	8.97 ± 1.05	8.99 ± 1.19	D
	HF	14.8 ± 1.7 *	14.7 ± 1.1 *	13.7 ± 1.2*	15.9 ± 1.2*	
Epididymal WAT(g)	NF	9.32 ± 0.93	9.50 ± 0.60	9.23 ± 0.93	10.7 ± 1.2	D
	HF	15.7 ± 2.1 *	15.6 ± 1.7*	13.8 ± 0.9*	17.2 ± 1.3*	
Liver (g)	NF	14.1 ± 0.8	14.1 ± 0.4	13.9 ± 0.5	14.9 ± 0.7	
	HF	13.8 ± 0.7	14.7 ± 0.9	13.3 ± 0.3	14.2 ± 0.6	

[a]Animals were fed a standard NF diet until the age of 4 months and then an NF or HF diet until the age of 6 months. The double vertical line indicates that the ANOVA analysis was assessed without the control group. Data are means ± SEM (n = 7−12). Statistics: D, effect of diet (NF or HF); T, effect of maternal supplementation ($p < 0.05$, two-way ANOVA). a ≠ b, LSD post hoc analysis. Key: *, different from their respective NF-diet-fed group ($p < 0.05$, Student's t test); ↑, different versus the control ($p < 0.05$, Student's t test).

receptor (INSR), and insulin receptor substrate 1 (IRS1) in the liver and lipoprotein lipase (LPL), CD36, muscle CPT1, adipose triglyceride lipase (ATGL), glucose transporter 4 (GLUT4), hexokinase II (HK), PPARγ2, SREBP1c, FAS, acetyl coenzyme A carboxylase (ACC), glycerol-3-phosphate acyltransferase (GPAT), and InsR in WAT. 18S (in liver) and β-actin (in WAT) were used as reference genes.

A 0.25 μg of total RNA (in a final volume of 5 μL) was denatured at 65 °C for 10 min and then reverse transcribed to cDNA using MuLV reverse transcriptase (Applied Biosystems, Madrid, Spain) at 20 °C for 15 min and 42 °C for 30 min with a final step of 5 min at 95 °C in an Applied Biosystems 2720 thermal cycler (Madrid, Spain). Each polymerase chain reaction (PCR) was performed from diluted (1/20) cDNA template, forward and reverse primers (1 μM each), and Power SYBER Green PCR Master Mix (Applied Biosystems, Foster City, CA). Primers, obtained from Sigma (Madrid, Spain), for the different genes are described in ref 24. Real-time PCR was performed using the Applied Biosystems StepOnePlus real-time PCR system with the following profile: 10 min at 95 °C, followed by a total of 40 two-temperature cycles (15 s at 95 °C and 1 min at 60 °C). To verify the purity of the products, a melting curve was produced after each run according to the manufacturer's instructions. The threshold cycle (Ct) was calculated by the instrument's software (StepOne Software v2.0), and the relative expression of each mRNA was calculated as previously described.[25]

Western Blot Analysis of ATGL in Retroperitoneal WAT. The amount of ATGL in retroperitoneal WAT was determined by Western blot. This protein was chosen because it is considered to be the main triacylglycerol lipase in adipose tissue and catalyzes the first step of lipid hydrolysis.[26] Briefly, tissue was homogenized at 4 °C in 1:5 (w/v) in RIPA buffer containing Halt protease and phosphatase inhibitor cocktail (Thermo Fisher, Rockford, IL). Western blot was performed in a 4−15% Criterion TGX precast gel (BioRad, Madrid, Spain), transferred to a nitrocellulose membrane. ATGL antibody was obtained from Cayman Chemical (Ann Arbor, MI). Membranes were also incubated with anti-β-actin antibody (Cell Signaling, Inc., Hercules, CA) to ensure the equal loading. Specific infrared (IR)-dyed secondary anti-IgG antibodies (LI-COR Biosciences, Lincoln, NE) were used. For IR detection, membranes were scanned in an Odyssey imager (LI-COR); the bands were quantified using the software Odyssey v3.0 (LI-COR).

Statistical Analysis. All data are expressed as the mean ± SEM (n = 7−12). Multiple comparisons were assessed by repeated measures ANOVA and two-way ANOVA to determine the effects of different factors (maternal fatty acid source supplementation and type of diet). Differences between groups were assessed by one-way ANOVA followed by least significant difference (LSD) post hoc comparison to assess statistical differences between the groups. Single comparisons were assessed by Student's t test or pair t test analysis. Principal component analysis (PCA) was performed to assess relationships between the adiposity of the animals, the lipid content in the liver, and the expression levels of the genes measured in the liver and WAT (a total of 27 variables). Two PCA models were constructed, one for all samples receiving the NF diet and another for all those receiving the HF diet. The score plot of PC1 versus PC2 was used to examine the potential contribution of these components to discriminate the four groups of animals (control, olive oil, margarine, and butter). The analyses were performed with SPSS for Windows (SPSS, Chicago, IL). The threshold of significance was defined at $p < 0.05$.

RESULTS

Body Mass, Body Fat, and Hepatic Lipid Content. As previously described for the same cohort of animals,[19] no significant differences were found regarding the body mass of

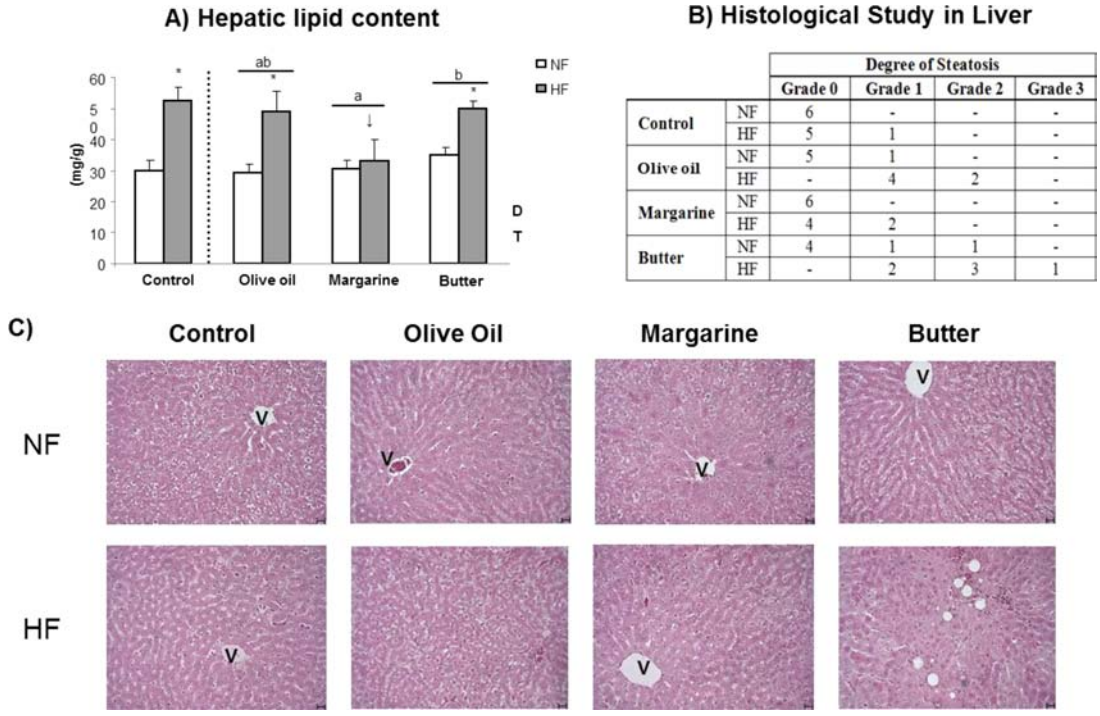

Figure 1. (A) Hepatic lipid content, (B) numerical grading of NASH in liver biopsies, and (C) representative hematoxylin and eosin staining of histological liver samples from 6 month old male offspring of dams supplemented with 30% of the normal caloric intake with different fat sources (olive oil, margarine, or butter) during late pregnancy and lactation. Animals were fed a standard NF diet until the age of 4 months and then an NF or HF diet until the age of 6 months. Scale bar = 20 μm. V = terminal hepatic venule. The dotted line indicates that the ANOVA analysis was assessed without the control group. Data are the mean ± SEM (n = 7−12). Statistics: D, effect of diet (NF or HF); T, effect of maternal supplementation ($p < 0.05$, two-way ANOVA). a ≠ b, LSD post hoc analysis. Key: *, different from their respective NF-diet-fed group ($p < 0.05$, Student's t test); ↓, different versus the control ($p < 0.05$, Student's t test).

Table 3. Circulating Glucose, Insulin, Nonesterified Fatty Acid (NEFA), Triglyceride, and β-Hydroxybutyrate Levels and HOMA-IR in Male Offspring of Dams Supplemented with 30% of the Normal Caloric Intake with Different Fat Sources (Olive Oil, Margarine, or Butter) during Late Pregnancy and Lactation, at 6 months of Age under ad Libitum Feeding Conditions, and after 12 h of Fasting[a]

	Control		Olive oil		Margarine		Butter	
	NF	HF	NF	HF	NF	HF	NF	HF
Glucose (mg/dL)								
Ad libitum	123 ± 9	142 ± 6	137 ± 6	130 ± 4	126 ± 7	136 ± 7	122 ± 6	141 ± 6 *
12-h Fasting	82 ± 5 #	83 ± 7 #	75 ± 5 #	77 ± 3 #	81 ± 5 #	79 ± 3 #	80 ± 3 #	78 ± 2 #
Insulin (ug/L)								
Ad libitum	4.24 ± 1.04	5.37 ± 0.75	7.69 ± 0.72	5.98 ± 0.83	5.99 ± 1.24	5.91 ± 1.03	6.43 ± 0.75	5.62 ± 0.78
12-h Fasting	0.87 ± 0.10 #	1.75 ± 0.49 #	1.00 ± 0.27 #	1.35 ± 0.31 #	1.84 ± 0.58 #	1.80 ± 0.60 #	1.45 ± 0.44 #	1.02 ± 0.30 #
HOMA-IR								
12-h Fasting	4.30 ± 0.61	8.50 ± 2.39	4.25 ± 1.07	6.03 ± 1.35	8.99 ± 2.86	9.06 ± 3.56	6.98 ± 2.17	4.61 ± 1.31
NEFAs (mMol/L)								
Ad libitum	0.72 ± 0.10	1.20 ± 0.12 *	0.69 ± 0.06	1.29 ± 0.08 *	0.78 ± 0.22	1.53 ± 0.17 *	0.65 ± 0.04	1.19 ± 0.19 *
12-h Fasting	1.63 ± 0.12 #	1.30 ± 0.14	1.61 ± 0.08 #	1.24 ± 0.16	1.37 ± 0.27	0.81 ± 0.06 # ↓	1.35 ± 0.09 #	1.10 ± 0.08 *
Triglycerides (mg/mL)								
Ad libitum	2.21 ± 0.11	3.07 ± 0.25 *	2.29 ± 0.11	3.00 ± 0.13 *	2.47 ± 0.28	2.94 ± 0.26	2.31 ± 0.13	3.51 ± 0.44 *
12-h Fasting	1.88 ± 0.18 #	1.74 ± 0.07 #	2.23 ± 0.13 (a)	2.09 ± 0.14 # (x)	1.79 ± 0.07 # (b)	1.61 ± 0.12 # (y)	2.20 ± 0.12 (a)	1.97 ± 0.09 # (x)
β-hydroxybutyrate (mg/dL)								
Ad libitum	1.52 ±0.32	2.88 ± 0.58	1.40 ± 0.20 (a)	2.45 ± 0.46 *	2.97 ± 0.17 (b) ↑	3.45 ± 0.37	2.45 ± 0.33 (b)	3.34 ± 0.17 *
12-h Fasting	2.11 ± 0.58	4.75 ± 0.45 *	3.81 ± 0.82	5.19 ± 0.78 #	5.06 ± 0.55 # ↑	5.84 ± 0.58 #	3.24 ± 0.75	4.43 ± 0.51

[a]Animals were fed a standard NF diet until the age of 4 months and then an NF or HF diet until the age of 6 months. The double vertical line indicates the ANOVA analysis was assessed without the control group. Data are means ± SEM (n = 7−12). Statistics: within normal-fat conditions, a ≠ b, LSD post hoc analysis; within high-fat conditions, y ≠ x, LSD post hoc analysis. Key: #, different from their respective ad-libitum-fed group ($p <$ 0.05. paired t test); *, different from their respective NF-diet-fed group ($p < 0.05$. Student's t test); ↑/↓, different versus the control ($p < 0.05$, Student's t test).

dx.doi.org/10.1021/jf405161e | J. Agric. Food Chem. 2014, 62, 1590−1601

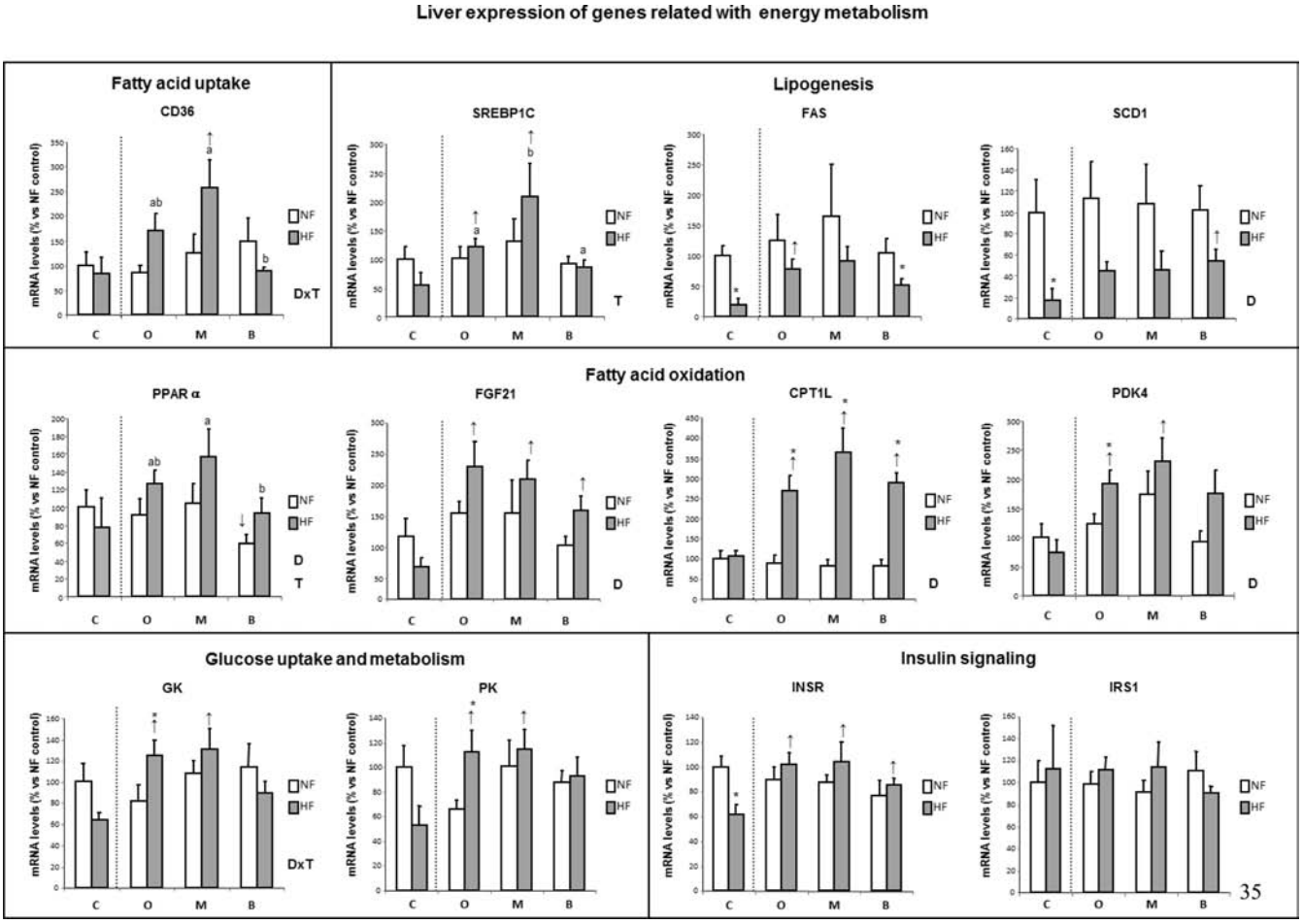

Figure 2. Expression of genes related to energy metabolism (FA uptake and oxidation, lipogenesis, glucose uptake and metabolism, and insulin signaling) in liver of 6 month old male offspring of dams supplemented with 30% of the normal caloric intake with different fat sources (olive oil, margarine, or butter) during late pregnancy and lactation. C = control, O = olive oil, M = margarine, and B = butter. Animals were fed a standard NF diet until the age of 4 months and then an NF or HF diet until the age of 6 months. The dotted line indicates that the ANOVA analysis was assessed without the control group. Data are means ± SEM (n = 7−12). Genes determined were CD36, sterol regulatory element binding protein 1c (SREBP1c), fatty acid synthase (FAS), stearoyl coenzyme A desaturase 1 (SCD1), peroxisome proliferator activated receptor α (PPARα), fibroblast growth factor 21 (FGF21), liver carnitine palmitoyltransferase 1a (CPT1L), pyruvate dehydrogenase kinase 4 (PDK4), glucokinase (GK), pyruvate kinase 4 (PK), insulin receptor (INSR), and insulin receptor substrate 1 (IRS1). Statistics: D, effect of diet (NF or HF); T, effect of maternal supplementation; D×T, interaction between diet and maternal supplementation ($p < 0.05$, two-way ANOVA). a ≠ b, LSD post hoc analysis. Key: *, different from their respective NF-diet-fed group ($p < 0.05$, Student's t test); ↑, different versus the control ($p < 0.05$, Student's t test).

the different groups of animals at the age of 6 months, depending on maternal fat supplementation, under either an NF or an HF diet (Table 2). As expected, the body mass of animals under an HF diet was higher than that of animals under an NF diet ($p < 0.05$, two-way ANOVA), the difference being higher and significant by Student's t test in the olive oil group. Animals exposed to an HF diet presented higher body fat content, higher adiposity index (calculated as the percentage of the sum of the four fat depots measured—inguinal, mesenteric, retroperitoneal, and epididymal—divided by the mass of the animal), and greater mass of the individual fat depots ($p < 0.05$, two-way ANOVA). Nevertheless, the body fat content and mass of the inguinal WAT in the margarine group under an HF diet were not different compared to their NF-diet-fed counterparts (by Student's t test), and the values were significantly lower than those of the butter group. The offspring of all fat-supplemented groups displayed greater mass of the inguinal WAT under NF diet conditions compared to the control group ($p < 0.05$, Student's t test), but no differences were found under the HF diet. No differences between groups were found in liver mass, under either the NF or HF diet.

Figure 1A shows the hepatic lipid content in the different groups of animals. Animals exposed to the HF diet presented higher hepatic lipid content compared to animals maintained under the NF diet ($p < 0.05$, Student's t test), with the exception of animals in the margarine group. Notably, within animals exposed to the HF diet, animals in the margarine group presented lower hepatic lipid content compared to the controls ($p < 0.05$, Student's t test). Moreover, the margarine groups (NF and HF analyzed together) showed lower hepatic lipid content compared to the butter groups ($p < 0.05$, LSD post hoc).

Histological analysis of the liver (Figure 1B,C) revealed evidence of NAFLD in animals exposed to the HF diet, especially in the olive oil and butter groups. The control and margarine groups showed a lower incidence of steatosis. In addition, although the control and margarine groups did not show evidence of hepatic steatosis under NF diet conditions,

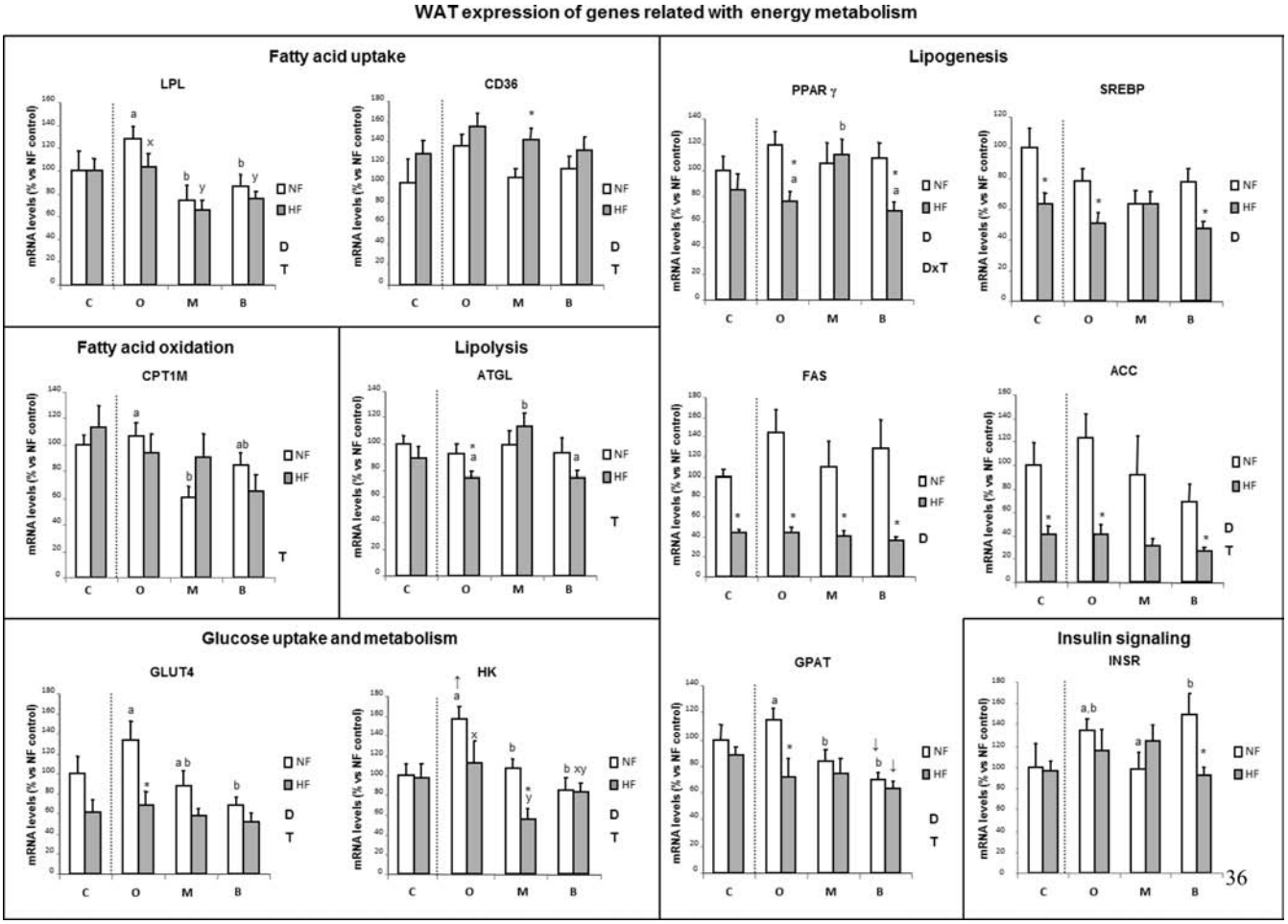

Figure 3. Expression of genes related to energy metabolism (FA uptake and oxidation, lipolysis, glucose uptake and metabolism, lipogenesis, and insulin signaling) in the retroperitoneal white adipose tissue (rpWAT) of 6 month old male offspring of dams supplemented with 30% of the normal caloric intake with different fat sources (olive oil, margarine, or butter) during late pregnancy and lactation. C = control, O = olive oil, M = margarine, and B = butter. Animals were fed a standard NF diet until the age of 4 months and then an NF or HF diet until the age of 6 months. The dotted line indicates that the ANOVA analysis was assessed without the control group. Data are means ± SEM (n = 7−12). Genes determined were lipoprotein lipase (LPL), CD36, muscle carnitine palmitoyltransferase 1a (CPT1m), adipose triglyceride lipase (ATGL), glucose transporter 4 (GLUT4), hexoquinase II (HK), peroxisome proliferator activated receptor γ 2 (PPARγ2), sterol regulatory element binding protein 1c (SREBP1c), fatty acid synthase (FAS), acetyl coenzyme A carboxylase (ACC), glycerol-3-phosphate acyltransferase (GPAT), and insulin receptor (INSR). Statistics: D, effect of diet (NF or HF); T, effect of maternal supplementation; D×T, interaction between diet and maternal supplementation (p < 0.05, two-way ANOVA). a ≠ b, x ≠ y, LSD post hoc analysis. Key: *, different from their respective NF-diet-fed group (p < 0.05, Student's t test); ↑/↓, different versus control (p < 0.05, Student's t test).

some evidence of steatosis was already seen at this age in the olive oil group and particularly in the butter group.

Glucose, Insulin, NEFA, TG, and β-Hydroxybutyrate Circulating Levels. Table 3 shows circulating parameters in the different groups of animals fed an NF or HF diet and under ad libitum and 12 h fasting conditions. As expected, the glucose and insulin levels decreased with fasting in all groups (p < 0.05, repeated measures analysis and pair t test). No differences were observed in the glucose and insulin levels as an effect of maternal fat supplementation, under either the NF or HF diet. Notably, animals in the butter group exposed to an HF diet presented higher glucose levels under ad libitum feeding conditions compared to their NF-diet-fed counterparts (p < 0.05, Student's t test). No significant differences were found in HOMA-IR.

Regarding circulating NEFA, no significant differences were found under ad libitum feeding conditions between the different groups of animals. In all of them, circulating levels were higher under the HF diet conditions compared to those under the NF diet conditions (p < 0.05, Student's t test). In addition, in animals exposed to the NF diet, an increase in NEFA levels was observed as an effect of fasting (p < 0.05, pair t test), except in the margarine group, where differences did not reach statistical significance; however, under the HF diet, NEFA levels remained unchanged with fasting, with the exception of the animals in the margarine group, which showed lower levels under fasting conditions compared to the feeding state (p < 0.05, pair t test).

Concerning TGs, all groups showed increased triglyceridemia under the HF diet compared to the NF diet (p < 0.05, Student's t test), with the exception of the margarine group, where differences did not reach statistical significance. Fasting produced a decrease in TG levels in the margarine group, similar to the controls, under both NF and HF diet conditions (p < 0.05, pair t test); however, this decrease was not observed in the olive oil and butter groups fed the NF diet. Animals in

dx.doi.org/10.1021/jf405161e | J. Agric. Food Chem. 2014, 62, 1590−1601

the margarine group, under either the NF or HF diet, displayed lower fasting TG levels compared to the olive oil and butter groups ($p < 0.05$, one-way ANOVA).

Regarding ketone bodies, NF-diet-fed animals in the margarine and butter groups showed higher β-hydroxybutyrate (BHB) levels than the olive oil group (one-way ANOVA), under ad-libitum-fed conditions; the margarine group also presented higher levels than the controls, under both fed and fasting conditions ($p < 0.05$, Student's t test). Under fed conditions, the HF-diet-fed olive oil and butter groups showed increased BHB levels compared to their NF-diet-fed counterparts ($p < 0.05$, Student's t test). Fasting produced a significant increase in BHB levels in HF-diet-fed animals in the olive oil group and in the margarine group, under both NF and HF diet conditions ($p < 0.05$, pair t test), but no changes were found in the other groups.

Expression of Genes Related to Energy Metabolism in the Liver. Results showing the expression of selected genes involved in nutrient handling and metabolism in the liver are summarized in Figure 2. HF diet feeding differently affected CD36 expression levels in the distinct fat-supplemented groups (interactive effect between diet and maternal treatment, $p < 0.05$, two-way ANOVA). Whereas levels tended to increase in the olive oil and margarine groups as an effect of the HF diet (with levels in the latter being higher compared to those of the control and butter groups), they tended to decrease in the butter group. Concerning lipogenesis-related genes, HF-diet-fed animals in the margarine group showed higher mRNA levels of SREBP1c than the olive oil and butter groups, and both the olive oil and margarine groups also showed higher levels than the controls. FAS and SCD1 mRNA expression levels were decreased in control animals under HF diet conditions, but only SCD1 showed a significant decrease in the fat-supplemented groups, and the decrease was not as marked as in the control group. Compared to the controls, HF-diet-fed animals in the olive oil group and in the butter group showed higher mRNA levels of FAS and SCD1, respectively.

The expression levels of genes related to fatty acid oxidation (PPARα, FGF21, CPT1L, and PDK4) increased in the fat-supplemented groups as an effect of the HF diet but not in the control animals ($p < 0.05$, two-way ANOVA). Therefore, under the HF diet, all fat-supplemented groups revealed a greater expression of FGF21, CPT1L, and PDK4 compared to the controls (with the exception of the butter group for the latter gene). The increase in gene expression as an effect of HF diet feeding was particularly remarkable for CPT1L, and especially in the margarine group, which showed a 2.45-fold increase. Under the HF diet, animals in the margarine group also showed higher mRNA levels of PPARα compared to the butter group ($p < 0.05$, one-way ANOVA). Under the NF diet, animals in the butter group displayed lower expression levels of PPARα compared to the controls ($p = 0.06$, Student's t test).

GK and PK mRNA expression levels followed a similar pattern in the different groups of animals. Compared to the controls, the HF-diet-fed olive oil and margarine groups presented higher GK and PK mRNA levels ($p < 0.05$, Student's t test). These animals, together with the HF-diet-fed animals of the butter group, also showed higher INSR mRNA levels than the controls ($p < 0.05$, Student's t test). No significant changes were found concerning IRS1 between the different groups of animals

Expression of Genes Related to Energy Metabolism in WAT. The retroperitoneal fat pad was chosen as representative of WAT because it is a major internal fat pad present in rats and is involved in the development of insulin resistance and type 2 diabetes.[27] Results showing the expression of selected genes involved in nutrient handling and metabolism in this fat depot are summarized in Figure 3.

Animals in the olive oil group showed higher LPL mRNA levels compared to the other fat-supplemented groups, under both NF and HF diets ($p < 0.05$, one-way ANOVA). Concerning CD36, their mRNA levels were higher in the fat-supplemented groups under the HF diet compared to their NF diet counterparts ($p < 0.05$; two-way ANOVA), with higher significant differences by Student's t test in the margarine group. Concerning lipolysis and fatty acid oxidation genes, under HF diet conditions, animals in the margarine group showed higher ATGL mRNA expression levels than the olive oil and butter groups, whereas, under the NF diet, they presented lower CPT1M mRNA levels compared to animals in the olive oil group ($p < 0.05$, one-way ANOVA). Regarding ATGL, differences similar to those of the mRNA levels were also found in their protein levels, although in this case differences did not reach statistical significance (Figure 4).

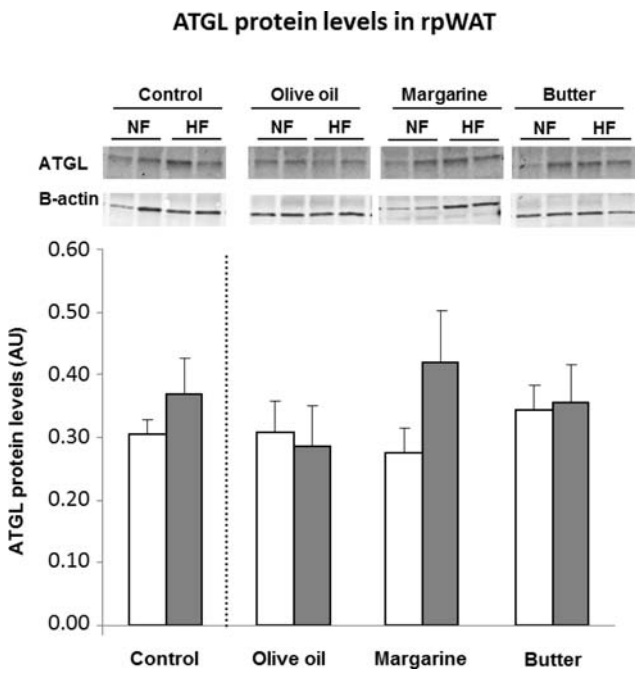

Figure 4. ATGL protein levels (measured by Western blotting) in retroperitoneal white adipose tissue (rpWAT) of 6 month old male offspring of dams supplemented with 30% of the normal caloric intake with different fat sources (olive oil, margarine, or butter) during late pregnancy and lactation. Animals were fed a standard NF diet until the age of 4 months and then an NF or HF diet until the age of 6 months. The dotted line indicates that the ANOVA analysis was assessed without the control group. Representative results are shown in the top panels. In the bottom panels, results represent the mean ± SEM (n = 7−12) expressed in arbitrary units (AU).

Animals of the fat-supplemented groups showed lower GLUT4 and HK mRNA levels under the HF diet compared to their NF-diet-fed counterparts ($p < 0.05$, two-way ANOVA), with a higher significant difference by Student's t test in the olive oil group (for both genes) and in the margarine group (for the latter gene). No significant changes were found in the control group as an effect of HF diet feeding, although a

A) Principal Component Analysis

	Normal Fat		High Fat	
	PC1	PC2	PC1	PC2
Adiposity index	0.172	-0.141	-0.042	-0.532*
Hepatic lipid content	-0.048	-0.023	-0.328	-0.631*
Gene expression in rpWAT:				
PPARγ	0.334	-0.237	0.167	0.857*
FAS	0.305	-0.084	0.276	0.148
ACC	0.164	0.448	-0.336	0.131
ATGL	-0.179	0.024	-0.048	0.898*
CD36	-0.226	0.745*	-0.106	0.332
GLUT4	0.161	0.399	0.125	0.351
CPT1M	-0.118	-0.126	-0.044	0.177
HK	-0.238	0.001	0.047	-0.112
LPL	-0.093	0.734*	-0.096	-0.054
SREBP	0.206	-0.411	-0.081	0.613*
GPAT	0.321	-0.017	-0.099	0.428
INSR	-0.107	-0.127	0.211	0.730*
FGF21	0.419	-0.090	-0.014	-0.105
Gene expression in Liver:				
CPT1L	0.542	0.714*	0.627*	0.290
PPARα	0.441	0.635*	0.406	0.251
SREBP1c	0.801*	-0.028	0.513	0.414
FAS	0.767*	0.206	0.795*	0.250
CD36	0.514	-0.048	0.245	0.174
SCD	0.788*	0.259	0.715*	-0.128
PDK4	0.269	0.653*	0.626*	0.257
FGF21	0.010	0.809*	0.765*	0.137
GK	0.551	-0.053	0.697*	0.144
PK	0.895*	0.099	0.685*	-0.192
INSR	0.430	0.627*	0.366	-0.031
IRS1	0.494	0.540	0.013	-0.246
Portion of variance (%)	25	18	27	20
Cumulative variance (%)	25	43	27	47

B) The score plot of PC1 versus PC2

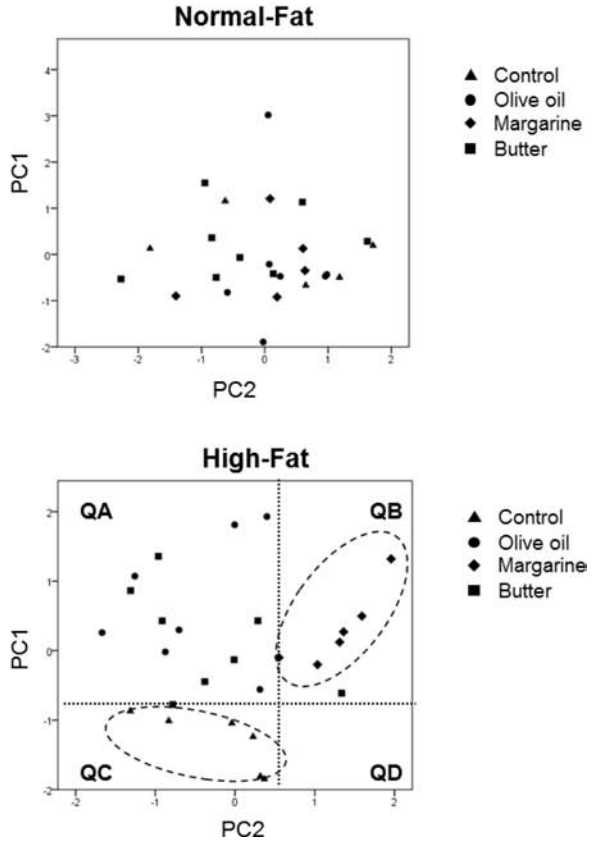

Figure 5. (A) Principal component loadings for the first two principal components (PCs). Data were spread by diet to assess possible relationships between gene expression in the tissues studied (liver and rpWAT) and the adiposity index and the hepatic lipid content under both dietary conditions (NF and HF diets). The most significant loadings are indicated with an asterisk. (B) Score plot representation.

tendency to lower levels was found concerning GLUT4. Notably, animals in the olive oil group displayed the highest mRNA levels of these genes under NF diet conditions, and these levels were significantly higher compared to those of the butter group (for GLUT4) and those of both the margarine and butter groups (for HK).

Under an HF diet, animals of the fat-supplemented groups showed lower mRNA expression levels of the adipogenic factor SREBP1c and of genes related to the synthesis of fatty acids (ACC1 and FAS) and TG (GPAT) with respect to those found under an NF diet ($p < 0.05$, two-way ANOVA), with some differences between groups. Specifically, HF-diet-fed animals in the margarine group did not show significant differences (by Student's t test) compared to their NF-diet-fed counterparts concerning SREBP1c, ACC, and GPAT mRNA levels, as also occurred for the latter in the animals in the butter group. A pattern similar to that of the SREBP1c gene was found for the other adipogenic factor, PPARγ. HF-diet-fed animals in the olive oil and butter groups showed lower mRNA levels compared to their NF-diet-fed counterparts ($p < 0.05$, Student's t test), while no changes were found in the margarine group as an effect of the HF diet. Control animals also showed a significant decrease in the expression levels of SREBP1c, ACC, and FAS under the HF diet, but no changes were observed concerning PPARγ and GPAT ($p < 0.05$, Student's t test), compared to their NF-diet-fed counterparts. Animals in the olive oil group fed an NF diet showed higher mRNA levels of GPAT with respect to animals in the margarine and butter groups ($p < 0.05$, one-way ANOVA).

Concerning the insulin receptor, animals in the butter group presented higher mRNA levels than animals in the margarine group under the NF diet ($p < 0.05$, one-way ANOVA), but their expression levels were decreased when these animals were fed the HF diet ($p < 0.05$, Student's t test). No significant changes were found in the other groups of animals as an effect of HF diet feeding.

Principal Component Analyses. The results of principal component analysis (PCA) of 27 variables are shown in Figure 5A. The data were spread by diet to assess possible relationships between gene expression in the studied tissues (liver and WAT) and the adiposity index and the hepatic lipid content under both dietary conditions (NF and HF diets). The first and second components were responsible for over 40% of the total variance in both conditions (43% in samples under the NF diet and 47% in those under the HF diet). Under NF diet conditions, PC1 was mainly characterized by liver transcripts related to glycolysis and lipogenesis, such as PK (0.895), SREBP1c (0.801), SCD1 (0.788), and FAS (0.767). Under the HF diet, the same transcripts mentioned above were important in the PC1, but other liver transcripts related to fat oxidation such as FGF21 (0.765), CPT1L (0.627), and PDK4 (0.626) were also of great importance. Concerning PC2, under the NF diet, the variables with higher loadings were liver transcripts related to fat oxidation [FGF21 (0.809), CPT1L (0.714), PDK4 (0.653), PPARα (0.635)] and insulin signaling [INSR

(0.627)] and WAT transcripts related to fat uptake [CD36 (0.745) and LPL (0.734)]. Under the HF diet, PC2 was mainly characterized by hepatic lipid content (−0.631), adiposity index (−0.532), and WAT transcripts, such as ATGL (0.898), PPARγ (0.857), INSR (0.730), and SREBP (0.613).

The score plots of PC1 versus PC2 of all the samples in both dietary conditions are shown in Figure 5B. As can be seen, no discriminant model was found for animals of the different groups under an NF diet. In contrast, under an HF diet, control animals were separated from the animals of the fat-supplemented groups and were located in quadrant C, with the lowest scores for PC1. Animals in the margarine group were located in quadrant B, completely separate from the control animals. The olive oil and butter groups were mainly located in quadrant A, and no discrimination between these two groups was achieved.

DISCUSSION

Maternal intake of excess fat during pregnancy and lactation in rodents has been reported to be associated with negative outcomes on metabolic health in offspring, increasing the susceptibility to develop obesity and other related metabolic diseases.[8] Studies performed in this respect are generally based on saturated fat sources. However, we previously described that maternal supplementation with excess fat during late pregnancy and lactation may have different outcomes in offspring depending on the source of fat. In particular, margarine, compared to other fats such as olive oil and butter, was shown to program the offspring for increased leptin sensitivity and a lower preference for fat food in adulthood.[19] Here, by using the same cohort of animals, we also aimed to assess whether maternal lipid oversupply (with margarine, olive oil, or butter) during late pregnancy and lactation may also differently affect the metabolic health of offspring and hence the risk of obesity-related metabolic diseases, particularly the development of hepatic steatosis.

We show here that although maternal supplementation with the different fat sources did not result in significant differences regarding body mass in the adult offspring, margarine supplementation conferred partial protection against the increase in body fat content, particularly subcutaneous fat, observed in the other groups when exposed to an HF diet. This protection was not seen under NF diet conditions, where the three fat-supplemented groups showed higher subcutaneous fat content than the control group. Concerning hepatic lipid content, HF-diet-fed animals from the different groups showed increased lipid accumulation compared to their NF-diet-fed counterparts with the exception of animals in the margarine group, which seemed to present a certain protection against lipid accumulation in the liver. Histological analyses of liver samples essentially confirmed the results obtained from lipid quantification, but showed little incidence of hepatic steatosis signs in HF-diet-fed control animals, which was similar to that of animals in the margarine group under the HF diet. On the other hand, although animals in the olive oil and butter groups under the HF diet presented hepatic lipid levels similar to those of the control animals, histological analysis unveiled that these animals presented a more advanced form of the disease, particularly the animals in the butter group. Indeed, even under an NF diet, some animals in the olive oil group and more acutely in the butter group presented histological signs of NAFLD, suggesting that maternal olive oil and particularly butter oversupply during critical periods of development may affect offspring susceptibility to develop this disease, with different degrees of severity depending on the type of diet they are exposed to in adulthood.

HF diet conditions in adulthood have been previously described to lead to increased hepatic content of lipids.[28] However, perinatal conditions have also been proved to be determinant. In fact, Bruce et al. showed that HF diet exposure during both development and postweaning periods was worse than HF diet exposure in the postweaning period alone,[16] and a maternal HF diet led to the development of NAFLD later in life, even if a control diet was given in the postweaning period.[16,17] Thus, maternal HF diet during early periods of development may increase susceptibility to hepatic steatosis and inflammation in adult offspring, which may result in a more severe form when animals are also exposed to adult nutritional insults.[16] Interestingly, we show here that this effect depends not only on the ingestion of fat per se but also on the maternal source of fat during the early stage of life.

To ascertain which metabolic pathway could be responsible for the observed effects of maternal supplementation with different fat sources, we analyzed the expression levels of selected genes involved in energy metabolism in liver and WAT of adult animals, under both NF and HF diet conditions. The results revealed that differences between the groups were made particularly evident when animals were exposed to HF diet conditions in adulthood. Under an HF diet, we observed increased hepatic expression levels of β-oxidation-related genes, such as PPARα, FGF21, CPT1L, and PDK4, in the offspring of all fat-supplemented groups, and the increase for most of them was more marked in the margarine group. HF-diet-fed animals in the margarine group also presented higher expression levels of CD36 compared to animals in the butter group and the controls, which suggests increased hepatic uptake of fatty acids. An increase in the fatty acid influx to the liver has been related to the development of hepatic steatosis;[28] however, this does not appear to be the case in these conditions, suggesting that fatty acids taken up by the liver may be efficiently oxidized, in accordance with the increased levels in ketone bodies found in the margarine group compared to the other groups, particularly animals in the olive oil and control groups. This assumed increase in the uptake and oxidation of fatty acids by the liver in animals in the margarine group could be a mechanism to avoid increased circulating levels of NEFA, which has been related to insulin resistance progression.[29] In fact, animals in the margarine group seemed to be protected against the increased triglyceridemia observed in the other groups under an HF diet and showed lower circulating levels of NEFA than the other groups under these conditions. This could be indicative of lower WAT lipolytic capacity, but contrasts with the presence in this tissue of higher mRNA levels (and to some extent also of the protein) of the key rate-limiting enzyme for lipolysis, ATGL, compared to those of the other fat-supplemented groups. Therefore, it is plausible that although WAT in these animals appears to have a greater capacity to release NEFA under fasting conditions, other tissues, as seen for the liver, could be more efficient in removing them from circulation. All in all, these results suggest that animals in the margarine group are programmed to be more efficient in the processing and handling of lipids under HF diet conditions, in relation to a better lipid clearance from circulation, and hence are protected against the ectopic accumulation of fat in tissues other than adipose tissue.

According to previous results,[28,30] exposure of control animals to HF diet conditions brings about a decrease in the expression of lipogenic genes (FAS and SCD1) in the liver; however, this decrease was diminished in the offspring of all fat-supplemented groups. This lower downregulation could be related to the increased mRNA levels of INSR, suggesting higher insulin signaling, and to higher mRNA levels of the transcription factor SREBP1c, also occurring in these animals with the exception of those in the butter group. SREBP1c mediates the effects of insulin on the expression of different lipogenic genes, such as GK, ACC, FAS, ELOVL6, SCD1, and GPAT.[18] In fact, HF-diet-fed animals in the olive oil and margarine groups showed increased expression levels of hepatic GK and PK compared to the controls. This may suggest a higher rate of fatty acid synthesis from glucose. Hence, lower downregulation of de novo lipogenesis under HF diet conditions may lead to higher hepatic accumulation of TG, as found in animals in the olive oil and butter groups. Animals in the margarine group, despite having increased lipogenesis capacity compared to the controls, appear to be more efficient in burning this excess fat supply and would better respond against hepatic steatosis under an HF diet. Therefore, increased β-oxidation capacity in spite of the higher capacity of de novo fatty acid synthesis appears to be responsible for the protection against hepatic steatosis in animals in the margarine group under HF diet conditions. This response seems to be different from that occurring in control animals under these obesogenic conditions, because they did not show increased lipogenic capacity in the liver, but in turn fatty acid oxidation capacity was not activated.

Differences in the expression of lipogenic genes, depending on maternal fat supplementation, were also observed in WAT. PPARγ is a master transcriptional regulator of adipogenesis. Animals in the margarine group did not show the down-regulation in the expression levels of PPARγ and SREBP occurring in the other groups of animals under HF diet conditions. This indicate that these animals may have a greater lipogenesis capacity in the WAT than the other fat-supplemented groups, but this could be counterbalanced with the increased ATGL mRNA expression levels in WAT of these animals compared to the other fat-supplemented groups under HF diet conditions.

Hepatic steatosis has been associated with insulin resistance, and several rodent models have shown that a decrease in the hepatic TG pool correlates with improved insulin sensitivity.[31,32] Here we did not find clear evidence of insulin resistance (in terms of serum parameters and HOMA-IR) in any group of animals, not even in those presenting signs of hepatic steatosis. Nevertheless, it should be mentioned that animals in the butter group fed an HF diet presented decreased expression levels of INSR in WAT compared to their NF-diet-fed counterparts, suggesting that these animals, which also presented the more advanced form of NAFLD, may be more prone to developing insulin resistance. Conversely, animals in the olive oil group, particularly under NF diet conditions, appear to be more efficient in the glucose clearance from circulation, since they showed the highest mRNA levels of GLUT4 and HK in WAT. This might indicate that animals in the olive oil group are metabolically better programmed for a correct glucose metabolism when under an NF diet. However, with the challenge of an HF diet, these animals do not seem to be that metabolically flexible and hence displayed a higher increase in body fat content than animals in the margarine group and presented signs of liver steatosis. The predictive adaptative response hypothesis proposes that the degree of mismatch between the pre- and postnatal environments is an important determinant of subsequent diseases.[8] Notably, we previously described that the intake of excess olive oil by dams during late pregnancy and lactation was associated with decreased adipogenesis and increased thermogenic capacity in weaned animals, affecting body mass gain and body fat during the suckling period.[20] According to the mentioned hypothesis, later effects of this type of fat during the perinatal period appear to be dependent on postweaning diet and conditions.

To figure out what changes in gene expression patterns (in the liver and WAT) were more related with two parameters related to metabolic health, such as adiposity and hepatic lipid content, a PCA was performed. This analysis showed that, under an HF diet, adiposity and lipid content in the liver were highly associated (in a negative way) with transcript levels in WAT related to lipolysis (ATGL) and to insulin sensitivity and adipogenesis (INSR, PPARγ, and SERBP). Thus, it can be interpreted that increased expression levels of these genes under an HF diet may be relevant to avoid excessive adiposity and TG accumulation in tissues other than WAT, particularly the liver. Interestingly, these variables were characteristic of principal component 2, and the margarine group was the one with the highest values of this component. In addition, PCA also showed the significance of the liver transcripts related to energy uptake and adipogenesis (GH, PK, and FAS) and also to fat oxidation (CPT1L, PDK4, and FGF21), all these transcripts with high scores in PC1 (in both dietary conditions). Curiously, control animals under an HF diet presented low values of this component compared to all the other groups. Therefore, although the distribution of animals under the NF diet was disperse, among HF-diet-fed animals, the control and the margarine groups were clearly distinguished between each other and from the olive oil and butter groups.

The specific factors underlying the effects of maternal supplementation with different fat sources are not known. Differences described in milk fatty acid composition depending on the type of maternal fat during lactation [20] could influence the different outcomes. In addition, the putative involvement of the leptin protein in the beneficial effects of margarine oversupply compared to other fat sources may be considered, taking into account that margarine-supplemented dams (in the same cohort of dams) were described to present higher milk leptin concentration compared to olive oil dams at day 12 of lactation.[19] Leptin is present in maternal milk,[33] and its intake during the suckling period has been described to exert protecting effects against the development of later obesity and related metabolic pathologies, such as hepatic steatosis, under obesogenic conditions.[25,34] It could be speculated that the greater supply of milk-borne leptin to animals in the margarine group could account for some of the beneficial effects found in this group of animals compared to the other fat-supplemented groups. However, further studies need to be done to confirm the involvement of milk-borne leptin and to ascertain whether other factors may be involved.

In conclusion, maternal HF diet feeding during pregnancy and lactation affects offspring susceptibility to metabolic diseases, but the consequences depend not only on the intake of fat per se but also on the type of fat supplied. That is, maternal supplementation with excess fat from margarine during late gestation and lactation, in comparison with other types of fat, appears to program the offspring for healthier lipid

partitioning and handling and in turn prevents, to some extent, hepatic steatosis under obesogenic conditions. This effect seems to be associated with an activation of the metabolic pathways related to adipogenesis and lipolysis in WAT, as well as with increased fatty acid oxidation in the liver. Conversely, butter oversupply during this critical period of development may promote hepatic steatosis in the offspring, even when animals are fed a balanced diet after weaning.

AUTHOR INFORMATION

Corresponding Author

*Phone: +34 971173170. Fax: +34 971173426. E-mail: andreu.palou@uib.es.

Author Contributions

†M.L. and J.S. contributed equally to this work.

Funding

This work was supported by the Spanish Government (Grants AGL2009-11277 and AGL2012-33692), the European Union (BIOCLAIMS, Grant FP7-244995), and the Instituto de Salud Carlos III, Centro de Investigación Biomédica en Red Fisiopatología de la Obesidad y Nutrición, CIBERobn. Our Laboratory is a member of the European Research Network of Excellence NuGO (The European Nutrigenomics Organization; EU Contract FP6-506360).

Notes

The authors declare no competing financial interest.

ACKNOWLEDGMENTS

We thank E. Ceresi for his work in the liver histological analysis.

ABBREVIATIONS USED

ACC, actetyl coenzyme A carboxylase; ATGL, adipose triglyceride lipase; BHB, β-hydroxybutyrate; CPT1, carnitine palmitoyltransferase; FAS, fatty acid synthase; FGF21, fibroblast growth factor 21; GPAT, glycerol-3-phosphate acyltransferase; GK, glucokinase; GLUT4, glucose transporter 4; HK, hexokinase II; HF, high fat; INSR, insulin receptor; IRS1, insulin receptor substrate 1; LPL, lipoprotein lipase; NAFLD, nonalcoholic fatty liver disease; NASH, nonalcoholic steatohepatitis; NEFA, nonesterified (or free) fatty acid; NF, normal fat; PPAR, peroxisome proliferator activated receptor; PCA, principal component analysis; PDK4, pyruvate dehydrogenase kinase 4; PK, pyruvate kinase 4; SCD1, stearoyl coenzyme A desaturase 1; SREBP1c, sterol regulatory element binding protein 1c; TG, triglyceride; WAT, white adipose tissue

REFERENCES

(1) Barker, D. J.; Eriksson, J. G.; Forsen, T.; Osmond, C. Fetal origins of adult disease: strength of effects and biological basis. *Int. J. Epidemiol.* **2002**, *31*, 1235−9.

(2) Ravelli, G. P.; Stein, Z. A.; Susser, M. W. Obesity in young men after famine exposure in utero and early infancy. *N. Engl. J. Med.* **1976**, *295*, 349−53.

(3) Garcia, A. P.; Palou, M.; Priego, T.; Sanchez, J.; Palou, A.; Pico, C. Moderate caloric restriction during gestation results in lower arcuate nucleus NPY- and αMSH-neurons and impairs hypothalamic response to fed/fasting conditions in weaned rats. *Diabetes, Obes. Metab.* **2010**, *12*, 403−13.

(4) Garcia, A. P.; Palou, M.; Sanchez, J.; Priego, T.; Palou, A.; Pico, C. Moderate caloric restriction during gestation in rats alters adipose tissue sympathetic innervation and later adiposity in offspring. *PLoS One* **2011**, *6*, e17313.

(5) Palou, M.; Priego, T.; Sanchez, J.; Palou, A.; Pico, C. Sexual dimorphism in the lasting effects of moderate caloric restriction during gestation on energy homeostasis in rats is related with fetal programming of insulin and leptin resistance. *Nutr. Metab.* **2010**, *7*, 69.

(6) Pico, C.; Palou, M.; Priego, T.; Sanchez, J.; Palou, A. Metabolic programming of obesity by energy restriction during the perinatal period: different outcomes depending on gender and period, type and severity of restriction. *Front. Physiol.* **2012**, *3*, 436.

(7) Bayol, S. A.; Simbi, B. H.; Stickland, N. C. A maternal cafeteria diet during gestation and lactation promotes adiposity and impairs skeletal muscle development and metabolism in rat offspring at weaning. *J. Physiol.* **2005**, *567*, 951−61.

(8) Armitage, J. A.; Taylor, P. D.; Poston, L. Experimental models of developmental programming: consequences of exposure to an energy rich diet during development. *J. Physiol.* **2005**, *565*, 3−8.

(9) Bayol, S. A.; Simbi, B. H.; Fowkes, R. C.; Stickland, N. C. A maternal "junk food" diet in pregnancy and lactation promotes nonalcoholic fatty liver disease in rat offspring. *Endocrinology* **2010**, *151*, 1451−61.

(10) Guo, F.; Jen, K. L. High-fat feeding during pregnancy and lactation affects offspring metabolism in rats. *Physiol. Behav.* **1995**, *57*, 681−6.

(11) Buckley, A. J.; Keseru, B.; Briody, J.; Thompson, M.; Ozanne, S. E.; Thompson, C. H. Altered body composition and metabolism in the male offspring of high fat-fed rats. *Metabolism* **2005**, *54*, 500−7.

(12) Taylor, P. D.; McConnell, J.; Khan, I. Y.; Holemans, K.; Lawrence, K. M.; Asare-Anane, H.; Persaud, S. J.; Jones, P. M.; Petrie, L.; Hanson, M. A.; Poston, L. Impaired glucose homeostasis and mitochondrial abnormalities in offspring of rats fed a fat-rich diet in pregnancy. *Am. J. Physiol. Regul. Integr. Comp. Physiol.* **2005**, *288*, R134−9.

(13) Karnik, H. B.; Sonawane, B. R.; Adkins, J. S.; Mohla, S. High dietary fat feeding during perinatal development of rats alters hepatic drug metabolism of progeny. *Dev. Pharmacol. Ther.* **1989**, *14*, 135−40.

(14) Khan, I. Y.; Taylor, P. D.; Dekou, V.; Seed, P. T.; Lakasing, L.; Graham, D.; Dominiczak, A. F.; Hanson, M. A.; Poston, L. Gender-linked hypertension in offspring of lard-fed pregnant rats. *Hypertension* **2003**, *41*, 168−75.

(15) Langley-Evans, S. C. Intrauterine programming of hypertension in the rat: nutrient interactions. *Comp. Biochem. Physiol., A: Physiol.* **1996**, *114*, 327−33.

(16) Bruce, K. D.; Cagampang, F. R.; Argenton, M.; Zhang, J.; Ethirajan, P. L.; Burdge, G. C.; Bateman, A. C.; Clough, G. F.; Poston, L.; Hanson, M. A.; McConnell, J. M.; Byrne, C. D. Maternal high-fat feeding primes steatohepatitis in adult mice offspring, involving mitochondrial dysfunction and altered lipogenesis gene expression. *Hepatology* **2009**, *50*, 1796−808.

(17) Gregorio, B. M.; Souza-Mello, V.; Carvalho, J. J.; Mandarim-de-Lacerda, C. A.; Aguila, M. B. Maternal high-fat intake predisposes nonalcoholic fatty liver disease in C57BL/6 offspring. *Am. J. Obstet. Gynecol.* **2010**, *203*, 495 e1−8.

(18) Postic, C.; Girard, J. Contribution of de novo fatty acid synthesis to hepatic steatosis and insulin resistance: lessons from genetically engineered mice. *J. Clin. Invest.* **2008**, *118*, 829−38.

(19) Sanchez, J.; Priego, T.; Garcia, A. P.; Llopis, M.; Palou, M.; Pico, C.; Palou, A. Maternal supplementation with an excess of different fat sources during pregnancy and lactation differentially affects feeding behavior in offspring: putative role of the leptin system. *Mol. Nutr. Food Res.* **2012**, *56*, 1715−28.

(20) Priego, T.; Sanchez, J.; Garcia, A. P.; Palou, A.; Pico, C. Maternal dietary fat affects milk Fatty Acid profile and impacts on weight gain and thermogenic capacity of suckling rats. *Lipids* **2013**, *48*, 481−95.

(21) Matthews, D. R.; Hosker, J. P.; Rudenski, A. S.; Naylor, B. A.; Treacher, D. F.; Turner, R. C. Homeostasis model assessment: insulin resistance and beta-cell function from fasting plasma glucose and insulin concentrations in man. *Diabetologia* **1985**, *28*, 412−9.

(22) Folch, J.; Lees, M.; Sloane Stanley, G. H. A simple method for the isolation and purification of total lipides from animal tissues. *J. Biol. Chem.* **1957**, *226*, 497−509.
(23) Brunt, E. M.; Janney, C. G.; Di Bisceglie, A. M.; Neuschwander-Tetri, B. A.; Bacon, B. R. Nonalcoholic steatohepatitis: a proposal for grading and staging the histological lesions. *Am. J. Gastroenterol.* **1999**, *94*, 2467−74.
(24) Palou, M.; Sanchez, J.; Rodriguez, A. M.; Priego, T.; Pico, C.; Palou, A. Induction of NPY/AgRP orexigenic peptide expression in rat hypothalamus is an early event in fasting: relationship with circulating leptin, insulin and glucose. *Cell. Physiol. Biochem.* **2009**, *23*, 115−24.
(25) Pico, C.; Oliver, P.; Sanchez, J.; Miralles, O.; Caimari, A.; Priego, T.; Palou, A. The intake of physiological doses of leptin during lactation in rats prevents obesity in later life. *Int. J. Obes.* **2007**, *31*, 1199−209.
(26) Zimmermann, R.; Strauss, J. G.; Haemmerle, G.; Schoiswohl, G.; Birner-Gruenberger, R.; Riederer, M.; Lass, A.; Neuberger, G.; Eisenhaber, F.; Hermetter, A.; Zechner, R. Fat mobilization in adipose tissue is promoted by adipose triglyceride lipase. *Science* **2004**, *306*, 1383−6.
(27) Gabriely, I.; Ma, X. H.; Yang, X. M.; Atzmon, G.; Rajala, M. W.; Berg, A. H.; Scherer, P.; Rossetti, L.; Barzilai, N. Removal of visceral fat prevents insulin resistance and glucose intolerance of aging: an adipokine-mediated process? *Diabetes* **2002**, *51*, 2951−8.
(28) Priego, T.; Sanchez, J.; Pico, C.; Palou, A. Sex-differential expression of metabolism-related genes in response to a high-fat diet. *Obesity* **2008**, *16*, 819−26.
(29) Despres, J. P.; Lemieux, I. Abdominal obesity and metabolic syndrome. *Nature* **2006**, *444*, 881−7.
(30) Sanchez, J.; Palou, A.; Pico, C. Response to carbohydrate and fat refeeding in the expression of genes involved in nutrient partitioning and metabolism: striking effects on fibroblast growth factor-21 induction. *Endocrinology* **2009**, *150*, 5341−50.
(31) Dentin, R.; Benhamed, F.; Hainault, I.; Fauveau, V.; Foufelle, F.; Dyck, J. R.; Girard, J.; Postic, C. Liver-specific inhibition of ChREBP improves hepatic steatosis and insulin resistance in ob/ob mice. *Diabetes* **2006**, *55*, 2159−70.
(32) Savage, D. B.; Choi, C. S.; Samuel, V. T.; Liu, Z. X.; Zhang, D.; Wang, A.; Zhang, X. M.; Cline, G. W.; Yu, X. X.; Geisler, J. G.; Bhanot, S.; Monia, B. P.; Shulman, G. I. Reversal of diet-induced hepatic steatosis and hepatic insulin resistance by antisense oligonucleotide inhibitors of acetyl-CoA carboxylases 1 and 2. *J. Clin. Invest.* **2006**, *116*, 817−24.
(33) Casabiell, X.; Pineiro, V.; Tome, M.; Peino, R.; Dieguez, C.; Casanueva, F. Presence of leptin in colostrum and/or breast milk from lactating mothers: a potential role in the regulation of neonatal food intake. *J. Clin. Endocrinol. Metab.* **1997**, *82*, 4270−3.
(34) Priego, T.; Sanchez, J.; Palou, A.; Pico, C. Leptin intake during the suckling period improves the metabolic response of adipose tissue to a high-fat diet. *Int. J. Obes.* **2010**, *34*, 809−19.

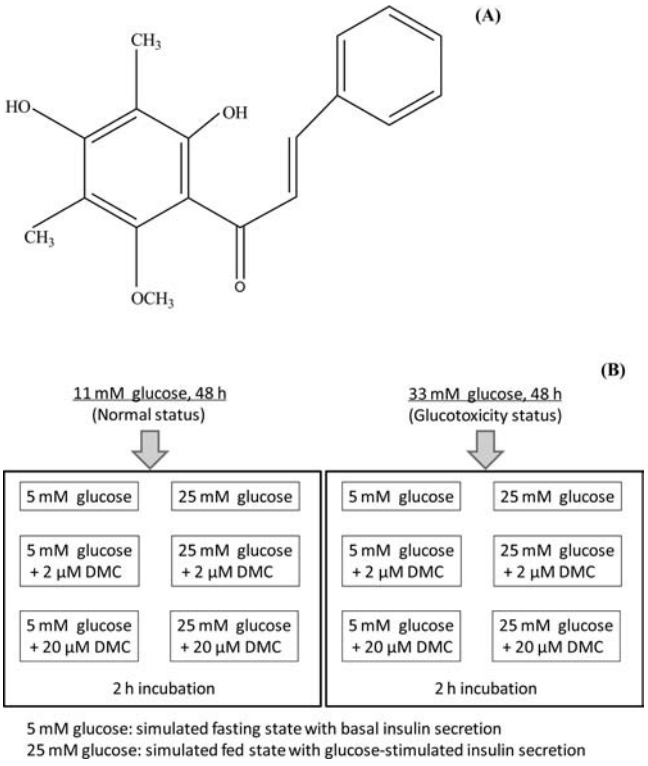

Figure 1. (A) Chemical structure of DMC. (B) Experiment design of insulin stimulation assay.

Although the hypoglycemic effects of *Cleistocalyx operculatus* flower bud aqueous extracts and DMC have been demonstrated in in vitro and animal models in the literature, and the mechanism of insulin enhancement has been illustrated in H_2O_2-damaged pancreatic cells, the effects and underlying mechanism of DMC against more physiologically relevant glucotoxicity conditions remains unclear. In this study, the effects of DMC on glucotoxicity induced insulin secretion impairment of RIN-5F cells and its corresponding mechanism were investigated.

MATERIALS AND METHODS

Reagents. DMC was isolated from the dried flower buds of *Cleistocalyx operculatus* as previous described.[16] Cell counting kit 8 (CCK-8) was purchased from Dojindo Molecular Technologies, Inc. (Tabaru, Japan), and dimethyl sulfoxide (DMSO) from Merck (Gibbstown, NJ, USA). All the primers were synthesized by Life Technologies (Carlsbad, CA, USA). Cell culture reagents were acquired from Life Technologies as well. All other chemicals were analytical reagent grade acquired from Sigma Aldrich (St. Louis, MO, USA).

Cell Culture. RIN-5F cells derived from rat pancreatic β-cells were purchased from American Type Culture Collection (ATCC, Manassas, VA). RIN-5F cells were maintained in RPMI-1640 containing 11 mM glucose, supplemented with 10% fetal bovine serum (FBS), and 1% penicillin/streptomycin under a condition of saturated humidity atmosphere containing 5% CO_2 at 37 °C. The medium was renewed every 3 days.

Measurements of Insulin Secretion and Cell Viability. RIN-5F cells (from 8 to 13 passages) were seeded in 24-well plates at a density of 2×10^5 cells/well. After 2 days, the cells were preincubated in RPMI-1640 medium at either a maintenance glucose condition (11 mM) or a high glucose condition (33 mM) for 48 h, and then the cells were used for insulin stimulation experiment. In detail, RIN-5F cells were washed twice with Krebs−Ringer bicarbonate buffer (KRB buffer, pH 7.4) containing 25 mM HEPES, 115 mM NaCl, 24 mM $NaHCO_3$, 5 mM KCl, 2.5 mM $CaCl_2$, and 1 mM $MgCl_2$ supplemented with 0.1% bovine serum albumin (BSA). Subsequently, the medium was replaced by 0.5 mL of KRB containing 5 mM glucose (simulated fasting state with basal insulin secretion) or 25 mM glucose (simulated fed state with glucose-stimulated insulin secretion) with or without DMC (2 μM and 20 μM), and the cells were incubated for 2 h at 37 °C as indicated respectively (Figure 1B). The supernatant was collected for measurement of secreted insulin using a high range rat insulin ELISA kit (Mercodia Inc., Uppsala, Sweden), and the attached cells were used for viability test by CCK-8 according to the manufacturer's instructions.

RNA Isolation and Quantitative RT-PCR. Total RNA from each well was extracted from RIN-5F cells using the RNeasy mini kit (Qiagen NV, Venlo, The Netherlands), and complementary DNAs (cDNAs) were synthesized using PrimeScript first strand DNA synthesis kit (TaKaRa Biotech, Japan) according to the manufacturer's instructions. Quantitative reverse transcription PCR (qRT-PCR) was done using SYBR Premix ExTaq kit (Takara Biotech, Dalian, China) and the ABI Prism 7500 sequence detection system (Applied Biosystems, Foster City, CA, USA) to determine the gene expression level. Each PCR was performed in a 20 μL solution containing 0.8 μL (10 μM) of each pair of forward and reverse primers, 10 μL of Premix Ex Taq DNA polymerase, 0.4 μL of ROX reference dye, 6 μL of dH_2O, and 2 μL of reverse transcription reaction products. The qRT-PCR primers used in the experiment are shown in Table 1. All experiments were done in triplicate. Relative expression was determined by the $2^{-\Delta Ct}$ method using GAPDH as the internal control, and fold change was calculated in comparison with the corresponding control group.

Determination of PDX-1 Protein Expression by Western Blotting. Pancreatic duodenum homeobox-1 (PDX-1) protein expression in RIN-5F cells was examined using Western blotting. Cells were seeded in 12-well plates at a density of 4×10^5 cells/well. Following the treatment with 11 and 33 mM glucose, with or without DMC (at 2 μM and 20 μM) for 48 h, cells were washed with ice-cold PBS before lysis in 200 μL of CelLytic-M cell lysis reagents (Sigma Aldrich). Then, samples were centrifuged at 14000 *g* for 15 min at 4

Table 1. Primer Sequences of the Selected Genes Involved in Key Pathways of Insulin Secretion in Rat Pancreatic β-Cells RIN-5F

		primer	
gene	full name	forward	reverse
GAPDH	glyceraldehyde-3-phosphate dehydrogenase	GGCAAGTTCAATGGCACAGT	TGGTGAAGACGCCAGTAGACTC
PRE-INS	preinsulin	TCTTCTACACACCCATGTCCC	GGTGCAGCACTGATCCAC
GLP-1R	glucagon-like peptide-1 receptor	GGGTCTCTGGCTACATAAGGACAAC	AAGGATGGCTGAAGCGATGAC
GLUT2	glucose transporter type 2	TTAGCAACTGGGTCTGCAAT	GGTGTAGTCCTACACTCATG
PDX-1	pancreatic duodenum homeobox-1	AAACGCCACACACCAAGGAGAA	AGACCTGGCGGTTCACATG
GCK	glucokinase	GCTTTTGAGACCCGTTTCGT	CGCACAATGTCGCAGTCG
iNOS	inducible nitric oxide synthase	CACCTTGGAGTTCACCCAGT	ACCACTCGTACTTGGGATGC
MCP-1	monocyte chemoattractant protein-1	GCAATCAATGCCCCAGTCA	GCCTCTGCACTGAGATCTTCCT

°C, the supernatant was collected, and the total protein was determined using a BCA assay (Pierce, Rockford, IL, USA). For Western blotting, equal amounts of total cellular protein (8 μg) were resolved by SDS−PAGE and transferred onto polyvinylidene difluoride (PVDF) membranes (Bio-Rad, Hercules, CA, USA) with a Bio-Rad Transblot apparatus, and probed with a primary antibody against PDX-1 overnight at 4 °C, followed by incubation with a horseradish peroxidase (HRP)-conjugated secondary antibody (all antibodies were from Cell Signaling Technologies, Beverly, MA, USA) for 1 h. The immune complexes of bound antibody were visualized with an enhanced chemiluminescence (ECL) system according to the manufacturer's instructions (GE Healthcare, Piscataway, NJ, USA). Equal loading was confirmed by analysis of the internal control of GAPDH, and bands were quantified using densitometry by the Image J Software (NIH, Bethesda, MD, USA).

Measurement of NO Release by Griess Assay. The quantity of NO produced during the experiment was estimated spectrophotometrically as formed nitrite (NO_2^-). After the 48 h treatment with 11 and 33 mM glucose, with or without DMC (at 2 μM and 20 μM), culture medium was collected for NO measurement. In brief, 50 μL of the culture medium and 50 μL of the sulfanilamide solution reagent (1% sulfanilamide in 5% phosphoric acid) were sequentially added to a 96-well microplate (Corning, Corning, NY, USA) in triplicate. After 10 min of incubation at room temperature, 50 μL of the NED solution (0.1% *N*-1-naphthylethylenediamine dihydrochloride in water) was added to all wells for another 10 min of incubation. Then, the optical density (OD) of the reaction mixture was determined by a Safire 2 microplate reader (Tecan, Mannedorf, Switzerland) at 540 nm. The nitrite content was calculated based on a standard curve constructed with sodium nitrite (Promega, Madison, WI, USA).

Statistics. Results were expressed as mean ± SEM. The data were analyzed by one-way analysis of variance (ANOVA) followed by Tukey's or Dunnett's post hoc comparisons to determine the significant differences between groups. Differences with $P < 0.05$ were considered statistically significant.

RESULTS

Glucose-Stimulated Insulin Secretion and Cell Viability of RIN-5F Cells. RIN-5F cells were exposed to 33 mM glucose for a sustained period of 48 h to induce impaired glucose-stimulated insulin secretion (GSIS). As shown in Figure 2A, high glucose-exposed RIN-5F cells had a blunted insulin secretory response when glucose was raised from 5 to 25 mM, with a 1.2-fold increase of insulin secretion compared with a 1.6-fold increase in normal control RIN-5F cells maintained in 11 mM glucose. Culturing RIN-5F cells at high glucose concentration of 33 mM decreased insulin content (3.05 vs 7.57 ng/mL insulin for RIN-5F cells cultured at 33 and 11 mM glucose, respectively; $P < 0.05$) when stimulated with 25 mM glucose. And, DMC improved the impaired insulin secretion (33 mM glucose for 48 h) with glucose stimulation (25 mM glucose for 2 h) in a concentration-dependent manner ($P < 0.05$ vs control group); it increased insulin secretion by 1.94 and 4.38 ng/mL (63 and 143%, respectively) at the concentration of 2 and 20 μM, respectively. However, DMC did not show significant insulin secretion enhancing effect at basal insulin secretion condition under 5 mM glucose. Under the condition of normal status of 11 mM glucose, the addition of DMC did not increase insulin secretion without glucose stimulation. When responding to an acute stimulation of 25 mM glucose, the insulin secretion rose from 7.57 to 9.30 and 9.94 ng/mL with the treatment of 2 and 20 μM DMC, respectively ($P < 0.05$). Thus, DMC maintained the GSIS potential of RIN-5F cells chronically exposed to high glucose levels.

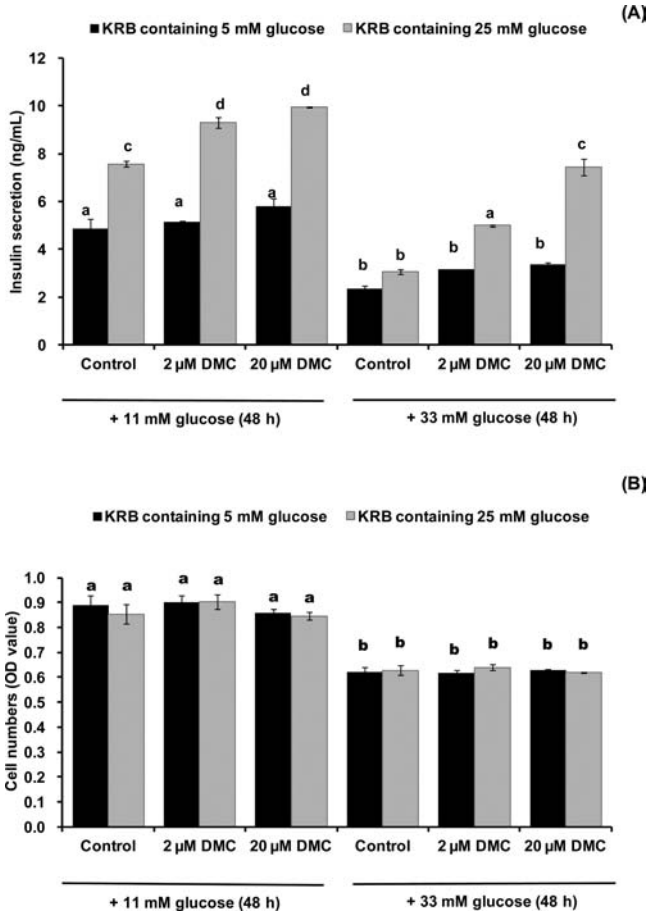

Figure 2. The effect of DMC on basal (5 mM glucose) and glucose-stimulated (25 mM glucose) (A) insulin secretion and (B) cell viability under maintenance glucose (11 mM) and glucotoxicity (33 mM) status. Values are presented as mean ± SEM ($n = 6$), duplicate by means of three independent experiments. The data values were analyzed by one-way ANOVA followed by Tukey's post hoc multiple comparison tests, and significant differences between groups are indicated by the lack of common letter annotations of a, b, c, d at $P < 0.05$.

To test the effects of high glucose and various concentrations of DMC on the viability of RIN-5F cells, CCK-8 assay was performed after the glucose stimulated insulin secretion assay. The results showed that the viability of RIN-5F cells treated with 33 mM glucose was reduced by 28% when compared with that of the control group with 11 mM glucose (Figure 2B). DMC, applied at different concentrations, did not affect the viability of RIN-5F cells compared with the corresponding controls (Figure 2B).

DMC Regulated β-Cell Function via GLP-1R, PDX-1, PRE-INS, GLUT2, and GCK at Gene Expression Level. In order to determine which step, from glucose sensing to insulin exocytosis, is impaired in glucotoxicity status in RIN-5F cells and the effect of DMC on glucotoxicity, we compared the gene expression levels of a series of regulators of insulin secretion process in pancreatic β-cells. The mRNA levels of glucagon-like peptide-1 receptor (GLP-1R), insulin transcription factor PDX-1, preinsulin (PRE-INS), glucose transport 2 (GLUT2), and glucokinase (GCK) were determined by qPCR. As shown in Figure 3, semiquantitative RT-PCR analysis showed that 33 mM glucose significantly downregulated the transcription levels of the tested genes compared with the normal glucose level of

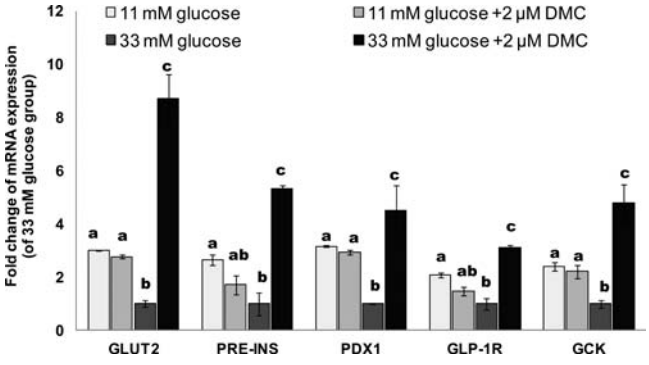

Figure 3. Relative mRNA expression of GLUT2, PRE-INS, PDX-1, GLP-1R, and GCK at glucose dose of 11 and 33 mM with or without the treatment of 2 μM DMC, fold change compared with 33 mM glucose control group. Values are shown as mean ± SEM (n = 3), triplicate by means of three independent experiments. The data values were analyzed by one-way ANOVA followed by Tukey's post hoc multiple comparison tests, and significant differences between groups are indicated by different letters of a, b, c at $P < 0.05$.

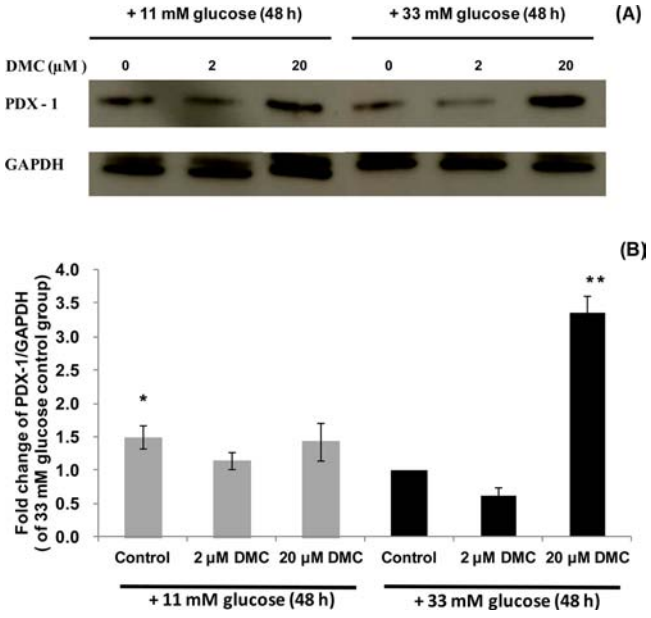

Figure 4. Effect of DMC on the glucose induced PDX-1 expression in RIN-5F cells. (A) A representative image of protein expression of GAPDH and PDX-1 measured by Western blot. (B) Quantification of PDX-1 protein expression. The level of PDX-1 expression was normalized against GAPDH, and the results were expressed as relative fold change compare to 33 mM glucose control. Values are shown as mean ± SEM (n = 3) by means of three independent experiments. The data values were analyzed by one-way ANOVA followed by Dunnett's post hoc: compare all columns vs 33 mM glucose control column tests, and significant differences between groups are indicated by * at $P < 0.05$ and ** at $P < 0.01$.

11 mM ($P < 0.05$). Under the treatment of 11 mM glucose, none of the tested target gene expression was statistically altered by 2 μM DMC. Under the condition of 33 mM glucose, 2 μM DMC significantly increased the expression levels of GLP-1R, PDX-1, PRE-INS, GLUT2, and GCK ($P < 0.05$) to a level beyond those at 11 mM glucose status (Figure 3).

PDX-1 Was Involved in Insulin Release at Protein Level. PDX-1 is involved in β-cell differentiation and functional maintenance and regulates the transcription of insulin and other insulin secretion related genes.[49] To confirm whether DMC stimulates the expression of PDX-1 at the protein level based on the results of mRNA investigation, Western blotting analysis was employed upon RIN-5F cells cultured at 11 and 33 mM glucose for 48 h. The high glucose control (33 mM) reduced the protein expression of PDX-1 compared with the maintenance glucose (11 mM) condition ($P < 0.05$). Application of 20 μM DMC effectively reversed the suppression of PDX-1 after prolonged high glucose incubation (Figure 4A,B) ($P < 0.01$), and resulted in ~3.3-fold enhancement in PDX-1 expression which was even stronger than that under maintenance glucose condition, whereas, 2 μM of DMC was not effective in regulating PDX-1 expression at the protein level, but it significantly increased its gene expression level; the possible reason was that 2 μM DMC induced PDX-1 mRNA changes were not strong enough to alter its protein expression level or needed more time to see the alteration.

DMC Inhibited NO Release under Glucotoxicity Condition. Since the half-life of NO is very short, the concentration of nitrite was measured using Griess reagents. As shown in Figure 5A, 33 mM glucose treatment significantly enhanced nitrite content compared with the treatment of maintenance glucose concentration of 11 mM ($P < 0.05$). Under the condition of glucotoxicity (33 mM glucose), DMC remarkably suppressed the increase of nitrite content dose-dependently ($P < 0.05$). Meanwhile, there was no significant difference among control and DMC treatment groups under the 11 mM glucose maintenance level. The results indicated that DMC could protect β-cells from damage caused by overproduction of NO.

DMC Suppressed the Expression of iNOS and MCP-1 at mRNA Level. As shown in Figure 5B, under conditions of glucotoxicity (33 mM glucose), the mRNA levels of iNOS and MCP-1 reached 2- and 2.8-fold of the maintenance level. At the glucotoxicity state, treatment with DMC at 2 and 20 μM decreased the mRNA level of iNOS by 86 and 88%, respectively ($P < 0.05$ vs control group), but did not show significant difference between these two concentrations ($P > 0.05$). With the concentration of 2 and 20 μM DMC, the mRNA levels of MCP-1 were decreased by 77 and 96%, respectively ($P < 0.05$ vs control group). While at the maintenance condition of 11 mM glucose, treatment with DMC at 2 and 20 μM did not cause a significant reduction of the mRNA level of iNOS and MCP-1.

■ DISCUSSION

Pancreatic islet cells are more susceptible to oxidative stress than cells in other tissue as they produce less antioxidant enzymes.[5] Damage of pancreatic islets leads to decreased insulin secretion, resulting in hyperglycemic condition and continuous generation of additional oxidative stress, forming a vicious cycle. Pretreatment of aqueous extract of *Cleistocalyx operculatus* flower buds has been demonstrated to restore the pancreatic islets insulin secretion injury of streptozotocin-induced diabetic rats.[14] Also, pretreatment of DMC was shown to protect the damage of H_2O_2-induced glucose responded insulin secretion of MIN6 cells[47] by conferring antioxidant and antiapoptotic effects through improved mitochondrial function in our previous work.[48] In the present study, we investigated the effect of DMC on RIN-5F cells under glucotoxicity condition and its underlying mechanism. Induction of glucotoxicity was achieved by incubating cells with 33 mM glucose for a duration of time, as previously reported.[50] Our

dx.doi.org/10.1021/jf405365d | J. Agric. Food Chem. 2014, 62, 1602−1608

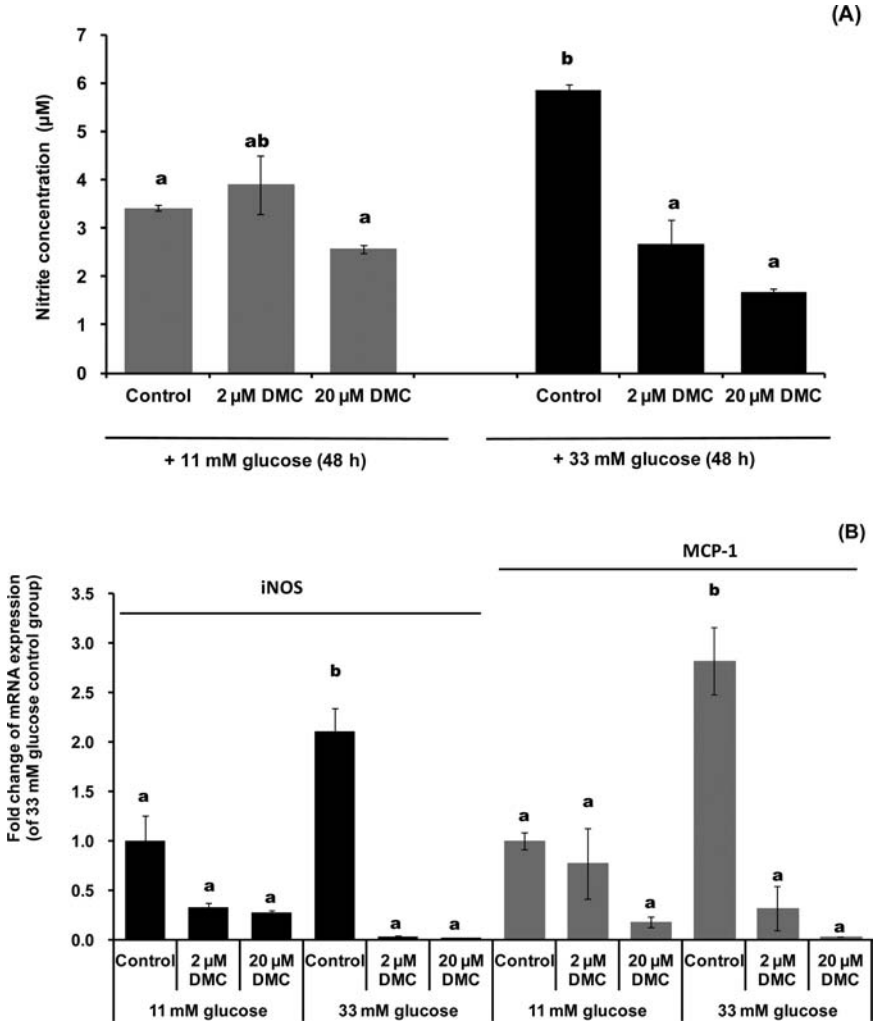

Figure 5. Effect of various concentrations of DMC on (A) NO release and (B) relative mRNA expression of iNOS and MCP-1 in RIN-5F cells under the maintenance and glucotoxicity conditions. Values are expressed as mean ± SEM (n = 3), triplicate by means of three independent experiments. The data values were analyzed by one-way ANOVA followed by Tukey's post hoc multiple comparison tests, and significant differences between groups are indicated by different letters of a, b at $P < 0.05$.

current study showed that incubation with 33 mM glucose for 48 h significantly impaired the basal and glucose-induced insulin secretion in RIN-5F cells. Treatment with DMC (2 and 20 μM) caused a significant increase of glucose-induced insulin secretion in a dose-dependent manner compared with control under conditions of glucotoxicity. As no impact on cell viability was observed, such effect could, at least in part, be attributed to the enhanced insulin secretion capacity.

There are two main signaling pathways impacting insulin secretion. In the first pathway glucose is transported into pancreatic β-cells by GLUT2, and then metabolized by GCK to glucose-6-phosphate, resulting in ATP production, which in turn induces Ca^{2+} influx, followed by the release of insulin (Figure 6).[51] Under simulated chronic glucotoxicity, the expression of GLUT2 and GCK in RIN-5F cells was decreased in the present study, accompanied with a reduction of insulin secretion, an observation which was in line with the existing literature.[52] In the present study, DMC was observed to reverse the decrease in glucose-stimulated insulin secretion by RIN-5F cells under glucotoxic conditions and to boost glucose-stimulated insulin secretion under normal conditions. At the same time, the mRNA levels of GLUT2 and GCK were

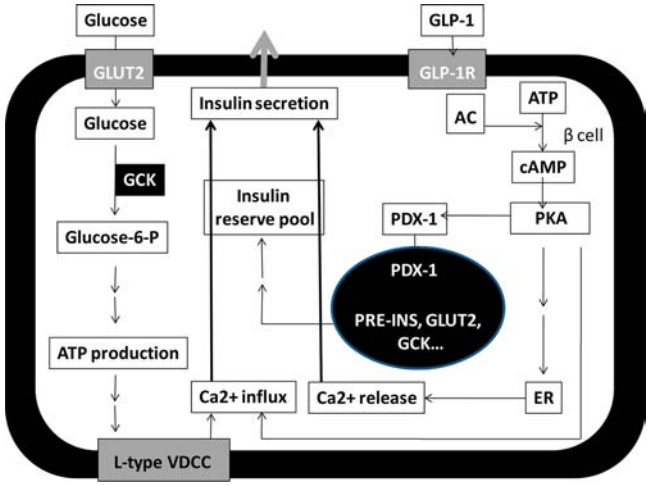

Figure 6. Schematic representation of the major intracellular steps that lead to insulin secretion. The signal pathways include glucose-induced and GLP-1-induced insulin secretion. The targets written in white color were tested in the present study.

dx.doi.org/10.1021/jf405365d | J. Agric. Food Chem. 2014, 62, 1602−1608

elevated by DMC, suggesting that the entire glucose-stimulated insulin release pathway was affected.

The second recognized signaling route affecting insulin secretion is mediated by GLP-1. GLP-1 is produced in the intestine and binds to a specific receptor (GLP-1R) located on the membrane of pancreatic β-cells. The interaction between GLP-1 and GLP-1R leads to activation of adenylate cyclase (AC) and production of cAMP as a secondary messenger. Followed by protein kinase A (PKA) activation and PDX-1 translocation to the nucleus, PRE-INS expression is induced (Figure 6).[51] In our study, DMC enhanced the gene expression of GLP-1R compared with control in the glucotoxicity assay. Thus, we concluded that DMC might mimic the effect of GLP-1, enhance the expression of GLP-1R, and promote insulin secretion. As GLP-1 stimulates the expression of GLUT2 and GCK to help to confer glucose sensitivity to β-cells,[53] DMC may mimic GLP-1 and stimulate GLP-1R to increase the expression of GLUT2 and GCK.

The gene expression levels of GLP-1R, PDX-1, PRE-INS, GLUT2, and GCK were only significantly elevated by DMC under glucotoxic conditions in the study, but not at normal conditions, suggesting that pancreatic cells might only be susceptible to DMC under the condition of elevated glucose (33 mM in this study). The upregulation of multiple genes by DMC may indicate potentiated glucose stimulation of multiple elements of the insulin secretion pathway. PDX-1 is recognized as a key regulation factor in the cascade regulating insulin secretion[49] (Figure 6); therefore, we quantified the impact of DMC on increasing the protein expression via Western blotting analysis, with results showing increased PDX-1 level as well. Since PDX-1 is a transcription factor that acts by translocation into the nucleus, we hypothesized that increased amount of PDX-1 would also enable stronger downstream gene expression activation.

We addressed the potential protective effect of DMC against oxidative and inflammatory damage induced by glucotoxicity. The incubation of RIN-5F cells with 33 mM glucose led to elevated levels of NO production and MCP-1 expression, contributing to oxidative stress and inflammatory damage. DMC treatment dramatically alleviated such impact, which could partially explain the restored insulin secretion ability observed in RIN-5F cells.

In conclusion, the present study provided evidence that DMC could ameliorate glucotoxicity-induced impairment of insulin secretion by RIN-5F cells. The mechanism was likely to involve potentiating GLP-1R mediated PDX-1 translocation, the elevated expression of GLUT2 and GCK, and protection against detrimental oxidative and inflammatory damage by DMC.

AUTHOR INFORMATION

Corresponding Author

*Tel: + 86-21-64251185. Fax: + 86-21-64251185. E-mail: luyanhua@ecust.edu.cn.

Funding

This work was supported by "the Fundamental Research Funds for the Central Universities", and partially supported by Shanghai Leading Academic Discipline Project (B505), the National Special Fund for State Key Laboratory of Bioreactor Engineering (2060204).

Notes

The authors declare no competing financial interest.

ABBREVIATIONS USED

DMC, 2′,4′-dihydroxy-6′-methoxy-3′,5′-dimethylchalcone; PKA, protein kinase A; GAPDH, glyceraldehyde-3-phosphate dehydrogenase; GLP-1R, glucagon-like peptide-1 receptor; PDX-1, pancreatic duodenum homeobox-1; GLUT2, glucose transporter 2; PPAR-γ, peroxisome proliferator-activated receptor-γ; GCK, glucokinase; GSIS, glucose-stimulated insulin secretion; iNOS, inducible nitric oxide synthase; PRE-INS, preinsulin; MCP-1, monocyte chemoattractant protein-1; CCK-8, cell counting kit-8

REFERENCES

(1) Kaiser, N.; Leibowitz, G.; Nesher, R. Glucotoxicity and beta-cell failure in type 2 diabetes mellitus. *J. Pediatr. Endocrinol. Metab.* **2003**, *16*, 5−22.

(2) Solomon, T. P. J.; Knudsen, S. H.; Karstoft, K.; Winding, K.; Holst, J. J.; Pedersen, B. K. Examining the effects of hyperglycemia on pancreatic endocrine function in humans: evidence for in vivo glucotoxicity. *J. Clin. Endocrinol. Metab.* **2012**, *97*, 4682−4691.

(3) Brownlee, M. A radical explanation for glucose-induced beta cell dysfunction. *J. Clin. Invest.* **2003**, *112*, 1788−1790.

(4) Marchetti, P.; Del Prato, S.; Lupi, R.; Del Guerra, S. The pancreatic beta-cell in human Type 2 diabetes. *Nutr. Metab. Cardiovasc. Dis.* **2006**, *16* (Suppl. 1), S3−6.

(5) Robertson, R.; Zhou, H.; Zhang, T.; Harmon, J. S. Chronic oxidative stress as a mechanism for glucose toxicity of the beta cell in type 2 diabetes. *Cell Biochem. Biophys.* **2007**, *48*, 139−146.

(6) Bonora, E. Protection of pancreatic beta-cells: is it feasible? *Nutr. Metab. Cardiovasc. Dis.* **2008**, *18*, 74−83.

(7) Chang-Chen, K. J.; Mullur, R.; Bernal-Mizrachi, E. Beta-cell failure as a complication of diabetes. *Rev. Endocr. Metab. Disord.* **2008**, *9*, 329−343.

(8) Lee, S. H.; Park, M. H.; Park, S. J.; Kim, J.; Kim, Y. T.; Oh, M. C.; Jeong, Y.; Kim, M.; Han, J. S.; Jeon, Y. J. Bioactive compounds extracted from Ecklonia cava by using enzymatic hydrolysis protects high glucose-induced damage in INS-1 pancreatic β-cells. *Appl. Biochem. Biotechnol.* **2012**, *167*, 1973−1985.

(9) Chakraborty, D.; Samadder, A.; Dutta, S.; Khuda-Bukhsh, A. R. Antihyperglycemic potentials of a threatened plant, Helonias dioica: antioxidative stress responses and the signaling cascade. *Exp. Biol. Med. (Maywood)* **2012**, *237*, 64−76.

(10) Palsamy, P.; Subramanian, S. Ameliorative potential of resveratrol on proinflammatory cytokines, hyperglycemia mediated oxidative stress, and pancreatic beta-cell dysfunction in streptozotocin-nicotinamide-induced diabetic rats. *J. Cell. Physiol.* **2010**, *224*, 423−432.

(11) Ekelund, M.; Qader, S. S.; Jimenez-Feltstrom, J.; Salehi, A. Selective induction of inducible nitric oxide synthase in pancreatic islet of rat after an intravenous glucose or intralipid challenge. *Nutrition* **2006**, *22*, 652−660.

(12) Yuan, H. D.; Chung, S. H. Fermented ginseng protects streptozotocin-induced damage in rat pancreas by inhibiting nuclear factor-kappaB. *Phytother. Res.* **2010**, *24* (Suppl. 2), S190−195.

(13) Dung, N. T.; Kim, J. M.; Kang, S. C. Chemical composition, antimicrobial and antioxidant activities of the essential oil and the ethanol extract of *Cleistocalyx operculatus* (Roxb.) Merr and Perry buds. *Food Chem. Toxicol.* **2008**, *46*, 3632−3639.

(14) Mai, T. T.; Yamaguchi, K.; Yamanaka, M.; Lam, N. T.; Otsuka, Y.; Chuyen, N. V. Protective and anticataract effects of the aqueous extract of *Cleistocalyx operculatus* flower buds on beta-cells of streptozotocin-diabetic rats. *J. Agric. Food Chem.* **2010**, *58*, 4162−4168.

(15) Ye, C. L.; Lu, Y. H.; Wei, D. Z. Flavonoids from *Cleistocalyx operculatus*. *Phytochemistry* **2004**, *65*, 445−447.

(16) Min, B. S.; Thu, C. V.; Dat, N. T.; Dang, N. H.; Jang, H. S.; Hung, T. M. Antioxidative flavonoids from *Cleistocalyx operculatus* buds. *Chem. Pharm. Bull.* **2008**, *56*, 1725−1728.

(17) Min, B. S.; Cuong, T. D.; Lee, J. S.; Shin, B. S.; Woo, M. H.; Hung, T. M. Cholinesterase inhibitors from *Cleistocalyx operculatus* buds. *Arch. Pharm. Res.* **2010**, *33*, 1665−1670.
(18) Woo, A. Y. H.; Waye, M. M. Y.; Kwan, H. S.; Chan, M. C. Y.; Chau, C. F.; Cheng, C. H. K. Inhibition of ATPases by *Cleistocalyx operculatus*. A possible mechanism for the cardiotonic actions of the herb. *Vasc. Pharmacol.* **2002**, *38*, 163−168.
(19) Mai, T. T.; Thu, N. N.; Tien, P. G.; Van Chuyen, N. Alpha-glucosidase inhibitory and antioxidant activities of Vietnamese edible plants and their relationships with polyphenol contents. *J. Nutr. Sci.Vitaminol.* **2007**, *53*, 267−276.
(20) Mai, T. T.; Chuyen, N. Van Anti-Hyperglycemic Activity of an Aqueous Extract from Flower Buds of *Cleistocalyx operculatus* (Roxb.) Merr and Perry. *Biosci., Biotechnol., Biochem.* **2007**, *71*, 69−76.
(21) Ko, H.; Kim, Y. J.; Amor, E. C.; Lee, J. W.; Kim, H. C.; Kim, H. J.; Yang, H. O. Induction of autophagy by dimethyl cardamonin is associated with proliferative arrest in human colorectal carcinoma HCT116 and LOVO cells. *J. Cell Biochem.* **2011**, *112*, 2471−2479.
(22) Li, D. D.; Wu, X. Q.; Tang, J.; Wei, X. Y.; Zhu, X. F. ON-III inhibits erbB-2 tyrosine kinase receptor signal pathway and triggers apoptosis through induction of Bim in breast cancer cells. *Cancer Biol. Ther.* **2009**, *8*, 739−743.
(23) Ye, C. L.; Liu, Y.; Wei, D. Z. Antioxidant and anticancer activity of 3′-formyl-4′, 6′-dihydroxy-2′-methoxy-5′-methylchalcone and (2S)-8-formyl-5-hydroxy-7-methoxy-6-methylflavanone. *J. Pharm. Pharmacol.* **2007**, *59*, 553−559.
(24) Ye, C. L.; Qian, F.; Wei, D. Z.; Lu, Y. H.; Liu, J. W. Induction of apoptosis in K562 human leukemia cells by 2′,4′-dihydroxy-6′-methoxy-3′,5′-dimethylchalcone. *Leuk. Res.* **2005**, *29*, 887−892.
(25) Zhu, X.; Xie, B.; Zhou, J.; Feng, G.; Liu, Z.; Wei, X.; Zhang, F.; Liu, M.; Zeng, Y. Blockade of vascular endothelial growth factor receptor signal pathway and antitumor activity of ON-III (2′,4′-dihydroxy-6′-methoxy-3′,5′-dimethylchalcone), a Component from Chinese herbal medicine. *Mol. Pharmacol.* **2005**, *67*, 1444−1450.
(26) Ye, C. L.; Liu, J. W.; Wei, D. Z.; Lu, Y. H.; Qian, F. In vivo antitumor activity by 2′,4′-dihydroxy-6′-methoxy-3′,5′-dimethylchalcone in a solid human carcinoma xenograft model. *Cancer Chemother. Pharmacol.* **2005**, *55*, 447−452.
(27) Ye, C. L.; Liu, J. W.; Wei, D. Z.; Lu, Y. H.; Qian, F. In vitro anti-tumor activity of 2′,4′-dihydroxy-6′-methoxy-3′,5′-dimethylchalcone against six established human cancer cell lines. *Pharmacol. Res.* **2004**, *50*, 505−510.
(28) Huang, H.; Niu, J.; Lu, Y. Multidrug resistance reversal effect of DMC derived from buds of *Cleistocalyx operculatus* in human hepatocellular tumor xenograft model. *J. Sci. Food Agric.* **2012**, *92*, 135−140.
(29) Huang, H.; Niu, J.; Zhao, L.; Lu, Y. Reversal effect of 2′,4′-dihydroxy-6′-methoxy-3′,5′-dimethylchalcone on multi-drug resistance in resistant human hepatocellular carcinoma cell line BEL-7402/5-FU. *Phytomedicine* **2011**, *18*, 1086−1092.
(30) Qian, F.; Ye, C. L.; Wei, D. Z.; Lu, Y. H.; Yang, S. L. In vitro and in vivo reversal of cancer cell multidrug resistance by 2′,4′-dihydroxy-6′-methoxy-3′,5′-dimethylchalcone. *J. Chemother.* **2005**, *17*, 309−314.
(31) Kim, Y. J.; Ko, H.; Park, J. S.; Han, I. H.; Amor, E. C.; Lee, J. W.; Yang, H. O. Dimethyl cardamonin inhibits lipopolysaccharide-induced inflammatory factors through blocking NF-kappaB p65 activation. *Int. Immunopharmacol.* **2010**, *10*, 1127−1134.
(32) Dung, N. T.; Bajpai, V. K.; Yoon, J. I.; Kang, S. C. Anti-inflammatory effects of essential oil isolated from the buds of *Cleistocalyx operculatus* (Roxb.) Merr and Perry. *Food Chem. Toxicol.* **2009**, *47*, 449−453.
(33) Martínez, A.; Conde, E.; Moure, A. Natural Product Research: Formerly Natural Product Letters Protective effect against oxygen reactive species and skin fibroblast stimulation of Couroupita guianensis leaf extracts. *Nat. Prod. Res.* **2012**, 37−41.
(34) Su, M. Y.; Huang, H. Y.; Li, L.; Lu, Y. H. Protective effects of 2′,4′-dihydroxy-6′-methoxy-3′,5′-dimethylchalcone to PC12 cells against cytotoxicity induced by hydrogen peroxide. *J. Agric. Food Chem.* **2011**, *59*, 521−527.
(35) Maisuthisakul, P.; Suttajit, M.; Pongsawatmanit, R. Assessment of phenolic content and free radical-scavenging capacity of some Thai indigenous plants. *Food Chem.* **2007**, *100*, 1409−1418.
(36) Yu, W. G.; Qian, J.; Lu, Y. H. Hepatoprotective effects of 2′,4′-dihydroxy-6′-methoxy-3′,5′-dimethylchalcone on CCl_4-induced acute liver injury in mice. *J. Agric. Food Chem.* **2011**, *59*, 12821−12829.
(37) Amor, E. C.; Villaseñor, I. M.; Ghayur, M. N.; Gilani, A. H.; Choudhary, M. I. Spasmolytic flavonoids from Syzygium samarangense (Blume) Merr. & L.M. Perry. *Z. Naturforsch., C* **2005**, *60*, 67−71.
(38) Ghayur, M. N.; Gilani, A. H.; Khan, A; Amor, E. C.; Villaseñor, I. M.; Choudhary, M. I. Presence of calcium antagonist activity explains the use of Syzygium samarangense in diarrhoea. *Phytother. Res.* **2006**, *20*, 49−52.
(39) Salem, M. M.; Werbovetz, K. A. Antiprotozoal compounds from Psorothamnus polydenius. *J. Nat. Prod.* **2005**, *68*, 108−111.
(40) Gafner, S.; Wolfender, J. L.; Mavi, S.; Hostettmann, K. Antifungal and antibacterial chalcones from Myrica serrata. *Planta Med.* **1996**, *62*, 67−69.
(41) Dao, T. T.; Tung, B. T.; Nguyen, P. H.; Thuong, P. T.; Yoo, S. S.; Kim, E. H.; Kim, S. K.; Oh, W. K. C-Methylated Flavonoids from *Cleistocalyx operculatus* and Their Inhibitory Effects on Novel Influenza A (H1N1) Neuraminidase. *J. Nat. Prod.* **2010**, *3423*, 1636−1642.
(42) Amor, E. C.; Villaseñor, I. M.; Yasin, A.; Choudhary, M. I. Prolyl endopeptidase inhibitors from Syzygium samarangense (Blume) Merr. & L. M. Perry. *Z. Naturforsch., C* **2004**, *59*, 86−92.
(43) Resurreccion-Magno, M. H.; Villaseñor, I. M.; Harada, N.; Monde, K. Antihyperglycaemic flavonoids from Syzygium samarangense (Blume) Merr. and Perry. *Phytother. Res.* **2005**, *19*, 246−251.
(44) Jin, X. H.; Wei, X. Y.; Huang, Z. W.; Wu, D. H. Identify and Characterize the PPAR-γ Ligand-binding Activity of Extracts of *Cleistocalyx operculatus*. *J. Anhui Agric. Sci.* **2008**, *36*, 9106−9109.
(45) Lu, Y.; Du, C.; Wu, Z.; Ye, C.; Liu, J.; Wei, D. Protective effects of *Cleistocalyx operculatus* on lipid peroxidation and trauma of neuronal cells. *Zhongguo Zhongyao Zazhi* **2003**, *28*, 964−966.
(46) Su, M. Y.; Huang, H. Y.; Li, L.; Lu, Y. H. Protective effects of 2′,4′-dihydroxy-6′-methoxy-3′,5′-dimethylchalcone to PC12 cells against cytotoxicity induced by hydrogen peroxide. *J. Agric. Food Chem.* **2011**, *59*, 521−527.
(47) Hu, Y. C.; Luo, Y. D.; Li, L.; Joshi, M. K.; Lu, Y. H. In vitro investigation of 2′,4′-dihydroxy-6′-methoxy-3′,5′-dimethylchalcone for glycemic control. *J. Agric. Food Chem.* **2012**, *60*, 10683−10688.
(48) Luo, Y. D.; Lu, Y. H. 2′,4′-Dihydroxy-6′-methoxy-3′,5′-dimethylchalcone inhibits apoptosis of MIN6 cells via improving mitochondrial function. *Pharmazie* **2012**, *67*, 798−803.
(49) Kaneto, H.; Miyatsuka, T.; Kawamori, D.; Matsuoka, T. A. Pleiotropic Roles of PDX-1 in the Pancreas. *Rev. Diabetic Stud.* **2007**, *4*, 209−225.
(50) Cai, E. P.; Lin, J. K. Epigallocatechin gallate (EGCG) and rutin suppress the glucotoxicity through activating IRS2 and AMPK signaling in rat pancreatic beta cells. *J. Agric. Food Chem.* **2009**, *57*, 9817−9827.
(51) Dalle, S.; Burcelin, R.; Gourdy, P. Specific actions of GLP-1 receptor agonists and DPP4 inhibitors for the treatment of pancreatic β-cell impairments in type 2 diabetes. *Cell. Signalling* **2013**, *25*, 570−579.
(52) Jonas, J. C.; Bensellam, M.; Duprez, J.; Elouil, H.; Guiot, Y.; Pascal, S. M. A. Glucose regulation of islet stress responses and beta-cell failure in type 2 diabetes. *Diabetes, Obes. Metab.* **2009**, *11* (Suppl. 4), 65−81.
(53) Ding, S. Y.; Nkobena, A.; Kraft, C. A.; Markwardt, M. L.; Rizzo, M. A. Glucagon-like peptide 1 stimulates post-translational activation of glucokinase in pancreatic beta cells. *J. Biol. Chem.* **2011**, *286*, 16768−16774.

some other antihypertensive peptides are expected to be identified and isolated still from LF hydrolyzates.[12]

In a previous work, proteolytic yeast strains of *Debaryomyces hansenii*, *Kluyveromyces lactis* and *K. marxianus* isolated from cheeses[13] were screened for their ability to grow in media with LF as the sole nitrogen source and to produce LF hydrolyzates containing ACE-inhibitory peptides. *K. marxianus* Km2 strain grown on LF produced the most potent hydrolyzate which, when orally administered to SHRs, exerted antihypertensive effect.[14]

The objective of the present study was to identify the LF-derived peptides produced by *K. marxianus* Km2 and characterize their antihypertensive effects. For this purpose, a *K. marxianus* LF permeate enriched in peptides of molecular weight lower than 3 kDa (pLFH) was fractionated and the main peptides present in the ACE-inhibitory fractions were identified by using an ion trap mass spectrometer. Selected peptides were evaluated for their inhibitory effects on ACE activity, their antihypertensive effects in SHRs and their stability against simulated gastrointestinal digestion. Finally the *in vivo* effect of peptides on SHRs blood ACE activity as well as angiotensin II and aldosterone levels are discussed.

MATERIALS AND METHODS

Materials. Bovine LF was provided by FrieslandCampina Domo (Zwolle, The Netherlands). ACE from porcine kidney, captopril, and bicinchoninic acid protein assay kit were purchased from Sigma (St. Louis, MO). Glucose was obtained from Panreac (Barcelona, Spain), bacteriological peptone was purchased from Cultimed (Barcelona, Spain) and yeast extract and agar were acquired from Pronadisa (Madrid, Spain). ACE substrate *o*-aminobenzoylglycyl-*p*-nitrophenylalanylproline was provided by Bachem Feinchemikalien (Bubendorf, Switzerland). Corolase PP (porcine pancreatic extract) was from AB enzymes (Darmstadt, Germany). Diazepam and ketamine were purchased from Roche Farma (Madrid, Spain) and Parke-Davis (Alcobendas, Madrid, Spain), respectively. An ACE colorimetric kit was acquired from Bühlmann Laboratories (Schönenbuch, Switzerland). An AssayMax Angiotensin II ELISA kit was from AssayPro (Saint Charles, MI) and a Coat-A-Count Aldosterone ^{125}I RIA kit was provided by Siemens Medical Solutions Diagnostics (Los Angeles, CA).

Preparation of *K. marxianus* Lactoferrin Permeate (pLFH) and Fractionation by Reversed-Phase High-Performance Liquid Chromatography (RP-HPLC). *K. marxianus* LF hydrolyzate was prepared as previously described, and it was subjected to ultrafiltration through a VivaFlow 50 3 kDa cutoff polyethersulfone membrane (Vivascience, Sartorius Stedim Biotech, Aubagne, France). Resulting permeate (pLFH), enriched in peptides of molecular weight lower than 3 kDa, showed an IC_{50} value of 50.2 ± 2.7 μg/mL. [14]

Fractionation of pLFH was carried out by RP-HPLC using a Waters system (Waters Corporation, Milford, MA) equipped with a 1525 Binary HPLC pump, a 2996 Photodiode Array Detector and a 717 plus Autosampler in combination with a Fraction Collector III. For this purpose, pLFH was applied to a Prep Nova-Pak HR C18, 60 Å, 6 μm, 7.8 × 300 mm column (Waters). The column was developed at a flow rate of 4 mL/min. Elution was performed with a linear gradient of solvent B (acetonitrile with 0.05% TFA) in solvent A (water with 0.05% TFA) from 0 to 20% B in 70 min. Samples of the whole permeate and the fractions (20 mL) were freeze-dried and kept at −20 °C until reconstitution with distilled water for determination of the protein content and *in vitro* ACE-inhibitory effect, as explained below.

Peptide Sequencing by Reversed-Phase High-Performance Liquid Chromatography Tandem Mass Spectrometry (RP-HPLC-MS/MS). RP-HPLC-MS/MS analysis of pLFH fractions was performed as described by Sánchez-Rivera et al.[15] with minor changes. The flow rate was 0.2 mL/min and the injection volume 50 μL. Peptides were eluted using a linear gradient from 0 to 45% of solvent B (acetonitrile:formic acid; 1000:0.1, v/v) and 55% of solvent A (water:formic acid; 1000:0.1% v/v) in 120 min. Data Analysis (version 4.0; Bruker Daltoniks) was used to process and transform spectra to representing mass values. BioTools (version 3.2; Bruker Daltoniks) was used to process the MSn spectra, to perform peptide sequencing and to calculate theoretical masses.

Main peptides identified in the pLFH were ordered at >90% purity from GenScript Corporation (Piscataway, NJ) wherein they were synthesized by solid phase methods using *N*-(9-fluorenyl) methoxycarbonyl (Fmoc) chemistry.

***In vitro* Assay of ACE-Inhibitory Activity.** *In vitro* ACE-inhibitory activity of pLFH fractions and synthetic peptides was measured using the fluorescent method described by Sentandreu and Toldrá[16] based on the hydrolysis of the internally quenched fluorescent substrate *o*-aminobenzoylglycyl-*p*-nitrophenylalanylproline by the action of ACE. Protein content of peptide fractions was estimated by the bicinchoninic acid method (BCA) using bovine serum albumin as standard.[7] Synthetic peptide concentration was based on the dry weight of the peptides.

The IC_{50} value was defined as the protein/peptide concentration required to inhibit 50% of the ACE activity, and the value for each experiment was estimated by nonlinear regression of the experimental data to a four-parameter logistic curve using the software package SigmaPlot v 10.0 (SPSS Inc., Chicago, IL).

***In vivo* Assay of Antihypertensive Effect in SHRs.** Experimental procedures were conducted in accordance with the Spanish legislation on 'Protection of Animals used for Experimental and other Scientific Purposes' and to the Directives of the European Community on this subject. The study was approved by the 'Ethics Committee for Animal Welfare' of 'La Fe' Hospital to be carried out in its accredited animal research facility.

Male SHRs weighing 230−330 g (Charles River Laboratories, Barcelona, Spain) were housed in temperature-controlled rooms (23 °C) with 12 h light/dark cycles and consumed tap water and standard diets *ad libitum*. To minimize the impact of light cycle and feeding on circadian rhythms of blood pressure,[17] the experiments always started at the same time in the morning (9:00 a.m.) in fasted rats. Indirect measurement of systolic blood pressure (SBP) was carried out in 18 awake restrained rats by the noninvasive tail-cuff method using computer-assisted Non-Invasive Blood Pressure equipment (LE5001 unit with LE5160R cuff and transducer, Panlab Harvard Apparatus, Cornellá, Barcelona, Spain). Peptides (up to 10 mg/kg) were orally administered by gastric intubation in 650 μL of physiological saline. Before the measurements, rats were kept at 37 °C during 15 min to make the pulsations of the tail artery detectable. The SBP was measured before peptide intake (zero time) and 1, 2, 3, 4, and 24 h after intake. Physiological saline (650 μL) and captopril (50 mg/kg) served as negative and positive controls, respectively. Each value of SBP was obtained by averaging at least three consecutive and successful measurements without disturbance of the signal. Changes in SBP were calculated as the absolute difference (in mm Hg) with respect to the basal values of measurements obtained just before peptide administration.

***In vitro* Simulated Gastrointestinal Digestion and Analysis of Digests by RP-HPLC.** Peptides were subjected to a two-stage simulated gastrointestinal digestion process as previously described.[10] Briefly, pepsin (0.2 mg) was added to aqueous solutions of peptides (10 mL; 1 mM) adjusted at pH 2.0 using 1 N HCl and incubated at 37 °C. After 90 min, the pH was adjusted to 7.5 adding 10 mL of 0.4 M sodium phosphate buffer at pH 7.5. Corolase PP, a proteolytic enzyme preparation that contains trypsin, chymotrypsin, and amino and carboxypeptidase activities, was added (0.2 mg), and the sample was further incubated at 37 °C for 150 min. The reaction was stopped by heating at 80 °C for 10 min in a water bath, followed by cooling at room temperature. Each sample was stored at −20 °C until further analysis by RP-HPLC.

Analysis of gastrointestinal digests was performed in the same RP-HPLC system specified above using a Symmetry C18 column (4.6 × 150 mm, 5 μm, Waters) kept at 40 °C. The column was developed at a flow rate of 1 mL/min. Peptides were eluted with a linear gradient of

Table 1. Identification of Peptides Contained in the F6, F7 and F11 RP-HPLC Fractions of the *K. marxianus* Lactoferrin Permeate (pLFH)

fraction[a]	ion for MS/MS (m/z)[b]	observed mass[c]	theoretical mass	protein fragment	identified sequence
F6	755.397	754.390	754.372	f(601−607)	SDRAAHV
	779.362	778.354	778.361	f(652−658)	GGRPTYE
	646.390	645.382	645.333	f(335−340)	AEEVKA
	676.329	675.322	675.308	f(261−266)	**DGKEDL**[d]
	624.367	623.360	623.303	f(283−287)	SRSFQ
	638.438	637.431	637.355	f(611−615)	LLHQQ
	668.412	667.405	667.340	f(602−607)	DRAAHV
	607.349	606.341	606.276	f(68−72)	GRDPY
	439.113	438.105	438.211	f(319−322)	YLGS
	722.407	721.400	721.376	f(276−281)	EKFGKN
F7	908.426	907.419	907.404	f(652−659)	GGRPTYEE
	575.214	574.206	574.260	f(536−541)	DVGDVA
	714.516	713.509	713.480	f(435−441)	AVAVVKK
	775.417	774.409	774.376	f(260−266)	VDGKEDL
	504.075	503.068	503.223	f(536−540)	DVGDV
	851.407	850.400	850.382	f(653−659)	GRPTYEE
	548.256	547.249	548.226	f(503−508)	ALCAGD
	636.454	635.447	635.375	f(338−342)	VKARY
	582.226	581.219	581.270	f(660−664)	YLGTE
	572.331	571.324	571.333	f(28−33)	KLGAPS
	496.155	495.148	495.244	f(283−286)	SRSF
	779.466	778.459	778.434	f(98−104)	VKKGSNF
	861.351	860.344	860.366	f(86−92)	**ESPQTHY**[d]
F11	848.427	847.420	847.455	f(68−74)	GRDPYKL
	823.472	822.465	822.387	f(224−229)	RDQYEL
	693.239	692.232	692.281	f(189−194)	YFGYSG
	743.382	742.375	742.386	f(141−147)	SLEPLQG
	773.499	772.492	772.460	f(71−76)	**PYKLRP**[d]
	907.415	906.408	906.420	f(563−569)	NLNREDF
	780.312	779.305	779.345	f(101−107)	GSNFQLD
	677.293	676.286	676.318	f(445−450)	GLTWNS
	676.510	675.503	675.407	f(72−76)	**YKLRP**[d]
	555.428	554.421	554.354	f(130−134)	**GILRP**[d]
	888.482	887.475	887.487	f(70−76)	**DPYKLRP**[d]
	414.156	413.149	413.227	f(144−147)	PLQG

[a]Fractions are termed as in Figure 1. [b]Charge of precursor ion: 1. [c]Calculated monoisotopic mass. [d]Chemically synthesized peptides are labeled in bold.

solvent B (acetonitrile with 0.1% TFA) in solvent A (water with 0.1% TFA) from 0 to 40% in 20 min and detected at 214 nm. Peptides LRP and KLRP were quantified in gastrointestinal digests of DPYKLRP, PYKLRP and YKLRP in accordance to standard curves in water.

Determination of Blood Components of the Renin-Angiotensin System. Twenty-two rats were anaesthetized by intraperitoneal injection of 5 mg/kg diazepam and 100 mg/kg ketamine. Blood samples were collected to obtain both serum and plasma which were kept frozen at −80 °C until the determination of ACE activity, angiotensin II and aldosterone levels.

Direct quantitative *in vitro* determination of ACE activity was carried out by using the Bühlmann ACE colorimetric kit according to the manufacturer's instructions. Briefly, it is a kinetic enzymatic assay in which ACE catalyzes the cleavage of the synthetic substrate (FAPGG) into an amino acid derivative and a dipeptide. The kinetic of this cleavage reaction is measured by recording the decrease in absorbance at 340 nm.

Quantitative *in vitro* measurement of angiotensin II was carried out by using the AssayMax Angiotensin II ELISA kit according to the manufacturer's instructions. Briefly, this assay employs a quantitative sandwich enzyme immunoassay technique in which a polyclonal antibody specific for angiotensin II is precoated onto a microplate. The angiotensin II in standards and samples is sandwiched by the immobilized antibody and biotinylated polyclonal antibody specific for angiotensin II, which is recognized by a streptavidin-peroxidase conjugate. A peroxidase enzyme substrate is added and intensity of developed color is measured.

Quantitative *in vitro* measurement of aldosterone was carried out by using the Coat-A-Count Aldosterone ^{125}I RIA kit according to the manufacturer's instructions. Briefly, it is a solid-phase radioimmunoassay, based on aldosterone-specific antibody immobilized to the wall of the assay tube. ^{125}I-labeled aldosterone competes for a fixed time with aldosterone in the sample for antibody sites.

RESULTS

Fractionation of *K. marxianus* pLFH: ACE-Inhibitory Activity of Resulting Fractions and Identification of Major Peptides. *K. marxianus* pLFH was subjected to semipreparative RP-HPLC and the total chromatogram was divided into 11 fractions which showed IC_{50} values ranging from 49 to 288 μg/mL. The three most active fractions (F6, F7 and F11) with IC_{50} values of 68, 74, and 49 μg/mL, respectively, were analyzed by HPLC-MS/MS, and the major peptide components were sequenced (35 peptides on total, Table 1).

dx.doi.org/10.1021/jf4053868 | J. Agric. Food Chem. 2014, 62, 1609−1616

Table 2. Inhibitory Potency of Selected LF-Derived Peptides on ACE Activity

peptide	IC_{50} (μM)[a]
DPYKLRP	30.5 ± 1.4 (c)
PYKLRP	10.2 ± 1.2 (b)
YKLRP	16.5 ± 0.7 (b)
KLRP	91.6 ± 4.0 (d)
LRP	0.35 ± 0.03 (a)
GILRP	90.7 ± 5.0 (d)

[a]Inhibitory potency is expressed as IC_{50} and data are mean ± SEM of at least 3 independent experiments. Data with the same letter are not significantly different, $P > 0.05$ (one way ANOVA followed by Student−Newman−Keuls test).

ACE-Inhibitory Activity of LF-Derived Peptides. A total of 6 peptides (labeled in Table 1) from those identified in fractions F6, F7 and F11 were chemically synthesized. These included four sequences (DGKEDL, ESPQTHY, YKLRP and DPYKLRP) that, being among the most abundant in each fraction, also fulfilled the common structural features described for many ACE-inhibitory peptides derived from food proteins.[18] Since the role of specifically C-terminal P residue in enhancing inhibition has been highlighted in most effective antihypertensive sequences derived from milk proteins,[1] the peptides PYKLRP and GILRP identified in the most active fraction (F11) were also included in the study despite not being abundant. Interestingly, the yeast proteolytic system produced the set of sequences DPYKLRP, PYKLRP and YKLRP differing in the amino acidic residue at the N-terminal end. With the aim of establishing sequence-inhibitory potency relationships, the peptides KLRP and LRP were also synthesized.

Only the six peptides having a P residue at the C-terminal end showed detectable inhibitory activity at 20 μM under our *in vitro* assay conditions. Further concentration response curves allowed the determination of IC_{50} values (Table 2) which varied over a 200-fold range. The higher potency as indicated by lower IC_{50} value corresponded to the tripeptide LRP.

Antihypertensive Effect of LF-Derived Peptides. The antihypertensive effect of the six ACE-inhibitory peptide sequences was characterized in SHRs. Average SBP, measured by the tail-cuff method in awake SHRs, was 200 ± 1 mmHg (n = 58). Oral administration of the six LF-derived peptides at 10 mg/kg induced significant reductions in SBP as shown in Figure 1, together with the lack of effect of oral saline and the antihypertensive effect of captopril (50 mg/kg). Similar to the effect caused by captopril, the antihypertensive effect of sequences DPYKLRP, GILRP and LRP remained significant up to 24 h post administration. Antihypertensive effects ranged from −26.8 mmHg for both DPYKLRP and LRP until −13.2 mmHg for KLRP. Reductions in SBP caused by DPYKLRP (−26.8 ± 2.4 mmHg; 1 h post administration) and LRP (−26.8 ± 1.3 mmHg; 2 h) were comparable to that of the captopril control (−27.9 ± 2.1 mmHg; 1 h) (one-way ANOVA; $P > 0.05$).

The heptapeptide DPYKLRP and the tripeptide LRP were further studied for dose-dependent antihypertensive effects. Both peptides induced significant dose-dependent (3, 7, and 10 mg/kg) reductions in SBP at each time point from 1 to 24 h after oral administration (Figure 2).

Resistance of LF-Derived Peptides to Gastrointestinal Enzymes. The six antihypertensive peptides were subjected to a hydrolysis process which simulates gastrointestinal digestion due to the action of gastric and pancreatic enzymes. The

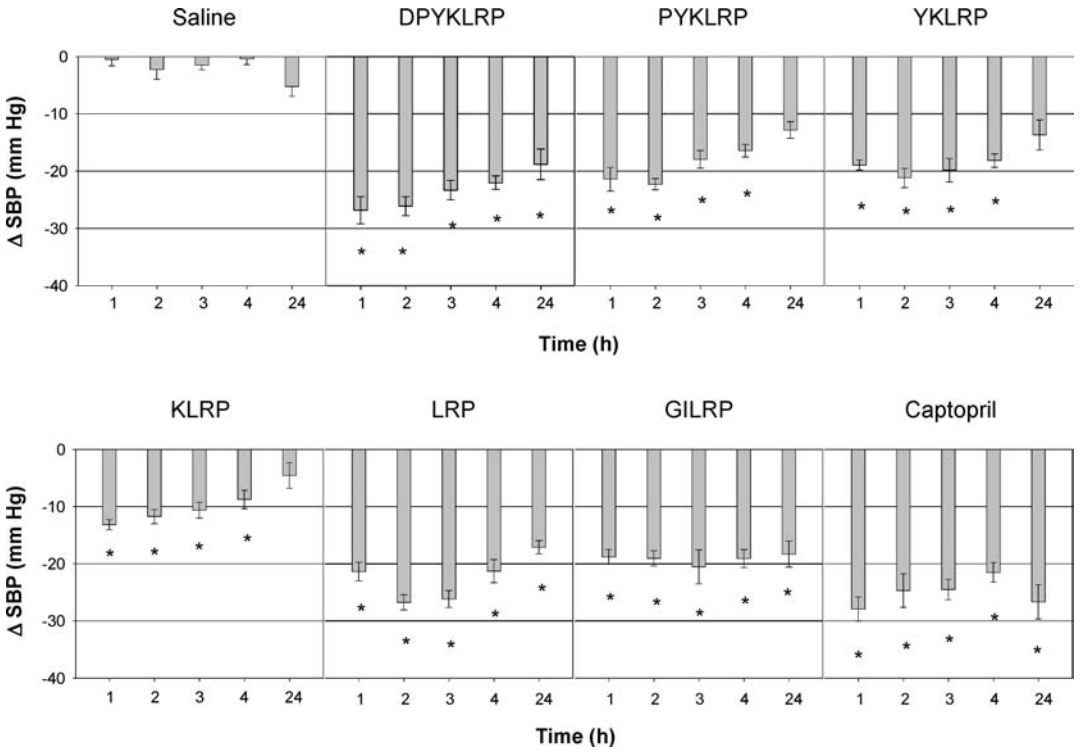

Figure 1. Time course of systolic blood pressure (SBP) changes after oral administration of physiological saline, captopril (50 mg/kg) and LF-derived peptides (10 mg/kg) to SHRs. Pressure changes (ΔSBP) are expressed in absolute values (mm Hg) and data are expressed as mean ± SEM from 6 to 7 determinations. *$P < 0.01$ versus control saline group (one-way ANOVA followed by Dunnett multiple comparison tests).

dx.doi.org/10.1021/jf4053868 | J. Agric. Food Chem. 2014, 62, 1609−1616

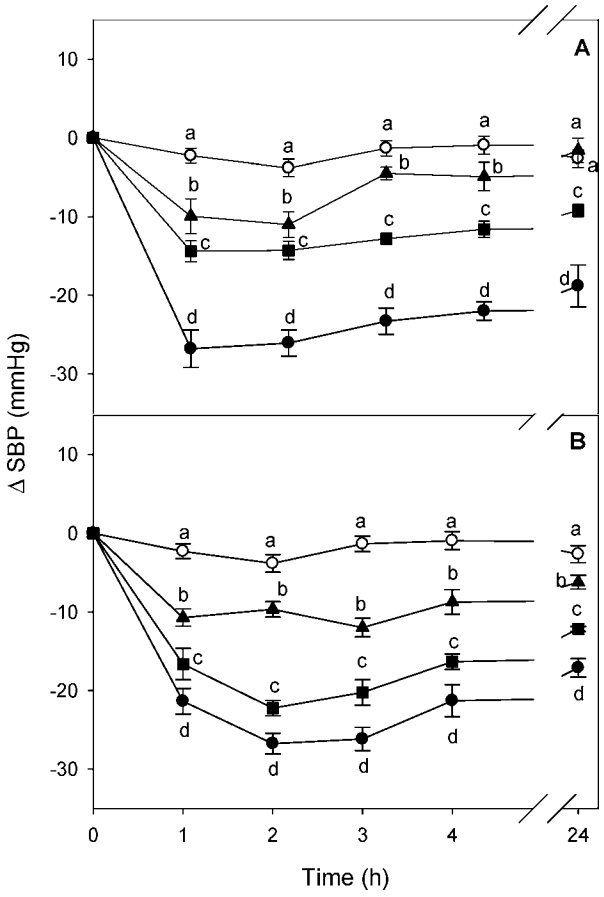

Figure 2. Time course of systolic blood pressure (SBP) changes after oral administration of increasing doses of (A) DPYKLRP and (B) LRP to SHRs. Physiological saline (○), 3 mg/kg (▲), 7 mg/kg (■), 10 mg/kg (●). Pressure changes are expressed in absolute values (mm Hg) and data are expressed as mean ± SEM from 5 to 8 determinations. Different letters indicate significant differences among doses at each time point (one-way ANOVA followed by Student−Newman−Keuls multiple comparison tests, $P < 0.05$).

analysis of digests by RP-HPLC (Figure 3) showed that the longer sequences, DPYKLRP and PYKLRP, were completely hydrolyzed releasing several fragments. A partial hydrolysis was observed for the pentapeptide YKLRP (approximately 60% of the initial concentration of the input peptide). In the conditions tested, sequences KLRP and GILRP were slightly hydrolyzed (approximately 6 and 12% decrease from the initial concentrations) whereas LRP was resistant to gastrointestinal enzymes. Noteworthy, in the gastrointestinal digests of the hydrolyzed peptides, the sequences LRP and KLRP were detected among others. LRP at concentrations of 525, 600 and 465 μM were detected in the digests of DPYKLRP, PYKLRP and YKLRP, respectively. Also, a minor quantity of LRP (3 μM) was detected in the KLRP digest. In the conditions tested, the sequence LRP was not detected in the GILRP digest. With respect to KLRP, concentrations of 550 and 140 μM were detected in the digests of DPYKLRP and PYKLRP. Also the sequence KLRP was detected at a concentration of 17 μM in the YKLRP digest.

Effects of LF-Derived Peptides on Blood Components of the Renin-Angiotensin System. The effects of DPYKLRP and LRP (10 mg/kg) on serum ACE activity and angiotensin II levels, and on plasma aldosterone levels were studied in SHRs. Captopril (50 mg/kg) was also included as a positive control.

The average serum ACE activity for all measurements carried out in the three experimental groups before treatment intake was 111.4 ± 1.8 U/L (n = 22). As shown in Figure 4A, ACE activity was significantly reduced in SHRs treated with DPYKLRP, LRP and captopril at 1 and 4 h post administration, and reverted to initial values after 24 h. At 1 h postadministration, when maximum effects were observed, the reduction in ACE activity induced by DPYKLRP (48.1 ± 2.5%) was similar to that caused by captopril (43.4 ± 3.1%) and significantly higher than the reduction induced by LRP (19.1 ± 2.7%) in SHRs (one way ANOVA followed by Student−Newman−Keuls test).

SHRs showed an average serum angiotensin II level of 71.2 ± 1.3 pg/mL (n = 22) before treatment intake. Angiotensin II levels in SHRs were significantly reduced by the three treatments at 1 h post administration (Figure 4B). The effect of LRP reverted at 4 h post administration whereas the reductions caused by the heptapeptide and captopril reverted at 24 h. When maximum effects were observed (1 h), the effects caused by DPYKLRP (27.1 ± 0.6% reduction in angiotensin II levels) and captopril (33.2 ± 1.3%) were similar and higher than that provoked by LRP treatment to SHRs (14.8 ± 1.9%; one way ANOVA followed by Student−Newman−Keuls test).

By contrast to that observed in serum ACE activity and angiotensin II levels, plasma aldosterone level of SHRs (244.7 ± 1.9 pg/mL; n = 22) was not significantly affected by any of the treatments (data not shown).

DISCUSSION

Yeast products have been used for many years as ingredients and additives in food processing, although their potential bioactivity has been less investigated.[19] *K. marxianus*, considered a GRAS (Generally Recognized As Safe) microorganism, has been isolated from a great variety of habitats, which results in a high metabolic diversity. Therefore, different biotechnological applications of this yeast including production of enzymes, of single cell-protein, and of aroma compounds as well as production of bioingredients from cheese-whey have been described.[20] Moreover, the beneficial properties of *K. marxianus* as a human probiotic have been recently assessed.[21]

In this study, we have identified four novel LF-derived peptides which are reported as ACE-inhibitory and antihypertensive sequences for the first time. To the best of our knowledge, DPYKLRP, PYKLRP, YKLRP and GILRP produced by the proteolytic system of *K. marxianus* Km2 strain when grown in LF as sole nitrogen source, are the first peptides with antihypertensive effects after oral administration to SHRs produced by a food-isolated yeast strain. Novel sequences identified here could at least in part contribute to the ACE inhibiting and antihypertensive effects of *K. marxianus* pLFH.[14]

The four *K. marxianus* ACE-inhibitory peptides have a C-terminal P residue. It has been described that the rigid structure of this amino acid may lock the carboxyl group into a conformation favorable for interaction with the positively charged residue at the active site of the enzyme.[22] Also the four sequences share the C-terminal tripeptide LRP. Interestingly LRP, which can be found in three different regions of LF sequence, was pointed out as the sequence responsible of the *in silico* high ACE-inhibitory activity of different peptide sequences in LF, and in accordance with our results, an IC_{50}

dx.doi.org/10.1021/jf4053868 | J. Agric. Food Chem. 2014, 62, 1609−1616

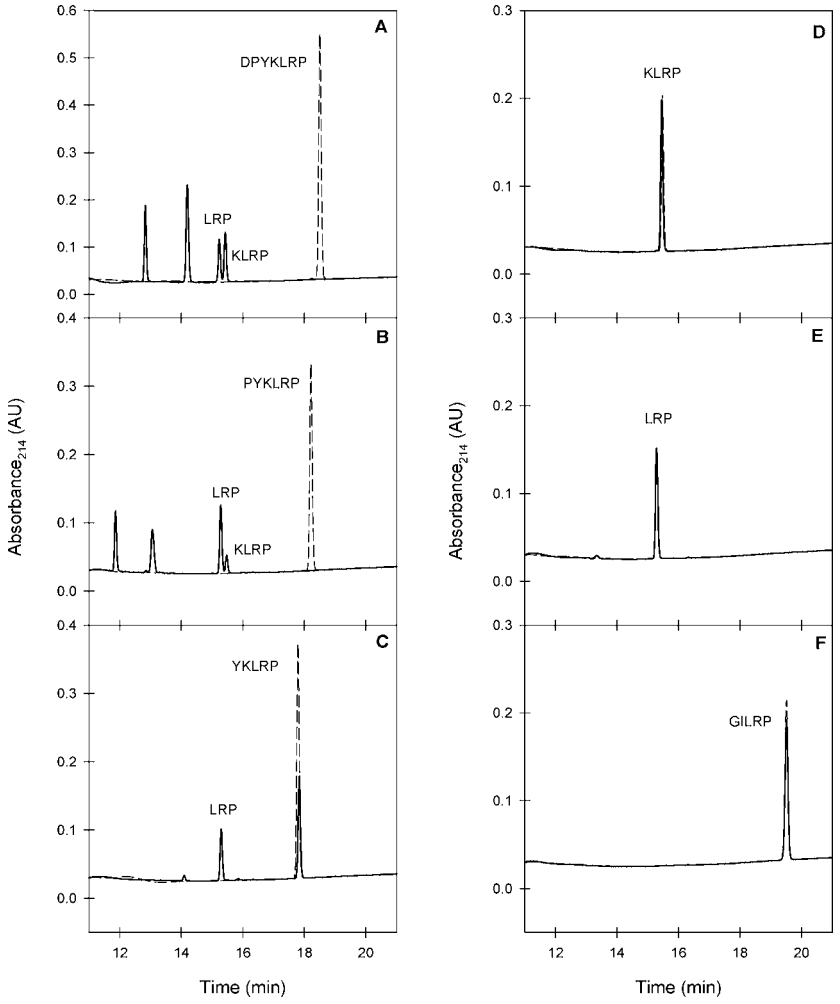

Figure 3. RP-HPLC chromatograms of peptides before (dashed line) and after (solid line) being submitted to a simulated gastrointestinal digestion. (A) DPYKLRP, (B) PYKLRP, (C) YKLRP, (D) KLRP, (E) LRP, (F) GILRP.

value of 0.27 μM was described for the tripeptide.[12] The sequence LIWKL was the most potent LF-derived peptide described so far (IC_{50} = 0.47 ± 0.01 μM).[8] Here, LRP was the most potent sequence with an IC_{50} value (IC_{50} = 0.35 ± 0.03 μM) slightly lower than that of LIWKL. Our results suggest that N-terminal elongations decrease *in vitro* inhibitory potency, although it might not result in lower antihypertensive effects (see below). Moreover, elongations at the C-terminal end of the tripeptide also provoked a decrease of inhibitory potency since an IC_{50} value of 4.14 μM was described for the sequence LRPVAA.[23]

Our results in SHRs show a complex relationship between the *in vitro* ACE-inhibitory potency and the *in vivo* antihypertensive effects after oral administration suggesting a role for gastrointestinal digestion in the formation and degradation of antihypertensive peptides. When subjected to hydrolysis with gastrointestinal enzymes all of the peptides tested in this study were hydrolyzed to different degrees with the exception of LRP. Remarkably this sequence was found in most of the digests suggesting that the tripeptide might contribute to the *in vivo* effects of parental peptides. Further work will be needed to clarify the physiological relevance of LRP as well as of the other digestion fragments that could also contribute to the blood pressure-lowering effects of parental peptides.

Although the IC_{50} values of LF-derived peptides were by far higher than that of ACE-inhibitory drug captopril (0.022 μM),[24] in the conditions tested, oral administration of DPYKLRP and LRP resulted in a significant decrease in SBP (13.4% reduction from baseline) similar to that of captopril (14% reduction). These results are also in agreement with the previously reported antihypertensive effect of the LF-derived peptide LIWKL (12.1% reduction).[8] It has been reported that food-derived ACE-inhibitory peptides might possess higher *in vivo* effects than expected from *in vitro* inhibitory potencies due to their higher affinity to target tissues and their slower elimination.[25]

It has been also postulated that other mechanisms of action apart from ACE inhibition might underlie *in vivo* antihypertensive effect of ACE-inhibitory peptides, including short-term vasoactive mechanisms as well as long-term-antioxidant and anti-inflammatory mechanisms.[26] In this context the sequence GILRP isolated here is part of the sequences GILRPY and GILRPYL identified in a proteinase K LF hydrolyzate which exerted *in vivo* antihypertensive effect. Both the hydrolyzate and GILRPY showed significant endothelin converting enzyme (ECE)-inhibitory effects.[9] ECE is a key peptidase in the endothelin system that cleaves precursor inactive big endothelin-1 to produce active endothelin-1 which has powerful vasoconstrictor and pressor properties.[27] The

dx.doi.org/10.1021/jf4053868 | J. Agric. Food Chem. 2014, 62, 1609−1616

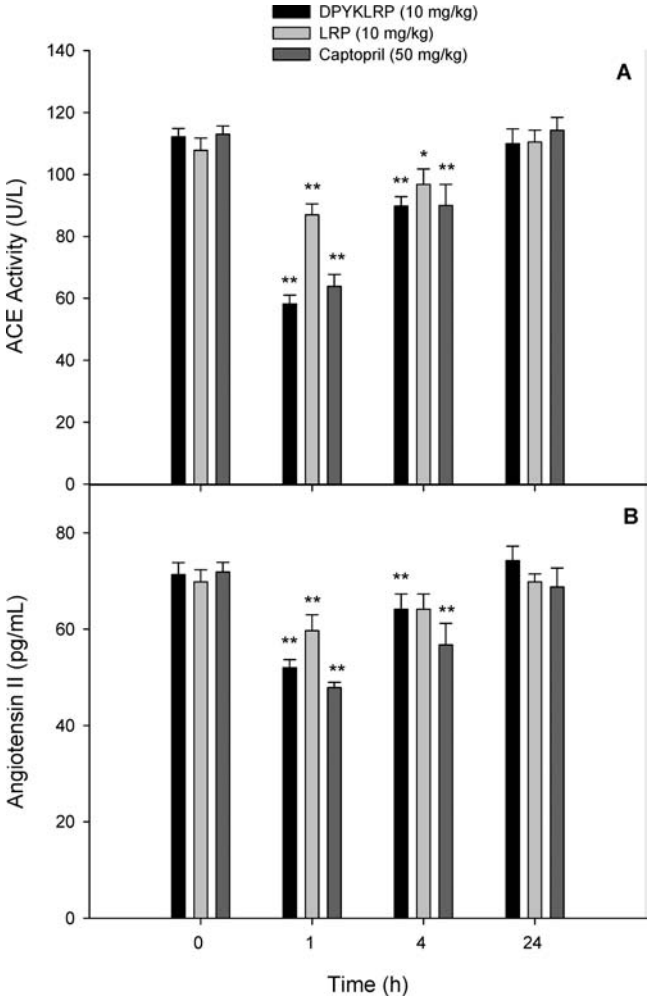

Figure 4. Time course of changes produced in the levels of blood components of the renin-angiotensin system after oral administration of DPYKLRP (10 mg/kg), LRP (10 mg/kg) and captopril (50 mg/kg) to SHRs. (A) Serum angiotensin I-converting enzyme (ACE) activity. (B) Serum angiotensin II levels. Data are mean ± SEM from 4 to 10 determinations. *P < 0.05 versus baseline values at time 0 h, **P < 0.01 versus baseline values at time 0 h (one-way ANOVA followed by Dunnett multiple comparison tests).

endothelin system has an increasingly recognized role in blood pressure regulation and has also been targeted for hypertension drug treatment. Moreover, we described a set of peptides derived from LF which showed inhibitory effects on ACE and ECE activities.[28] Also the ACE-inhibitory peptide lactokinin can modulate endothelin-1 release by endothelial cells.[29] Whether the antihypertensive effect showed by GILRP in this study might be also due to ECE inhibition deserves further studies.

Dose-dependent antihypertensive effects of DPYKLRP and LRP prompted us to look for a mechanism of action responsible for the graded *in vivo* responses of the LF-derived peptides. Determinations of blood RAS components support ACE inhibition as an *in vivo* antihypertensive mechanism in SHRs. *In vivo* ACE-inhibitory effect can be assessed by measuring tissue membrane-anchored or soluble, circulating ACE activities, and confirmed by measuring circulating levels of angiotensin II.[30] Our results show that serum ACE activity is reduced in SHRs after oral administration of both peptides. Moreover, inhibition of ACE was confirmed in peptide treated SHRs by the reduction in angiotensin II level. We have previously reported that long-term administration to SHRs of an antihypertensive bovine LF pepsin hydrolyzate enriched in low molecular weight peptides reduced circulating ACE activity, angiotensin II and aldosterone levels.[10] By contrast, in the present study, the level of serum aldosterone, the adrenal endocrine component downstream angiotensin II in the renin-angiotensin axis,[2] was not affected by single-dose treatments with DPYKLRP and LRP. *In vivo* ACE inhibition has been also pointed out as the mechanism underlying the blood pressure reduction of the tripeptide IQP derived from the blue algae *Spirulina platensis* since serum ACE and angiotensin II levels were significantly reduced in SHRs after one-week treatment.[31] Nonetheless, the identification of other *in vivo* mechanisms beyond ACE inhibition underlying antihypertensive effects of the LF-derived peptides identified in this study should be further investigated.

Our results point out *K. marxianus* as a feasible GRAS microorganism for the production of novel LF-derived peptides with ACE-inhibitory and antihypertensive effects. The LF-derived peptides produced by *K. marxianus*, DPYKLRP, PYKLRP, YKLRP and GILRP, effectively decreased arterial blood pressure in SHRs and could, at least in part, be responsible for the antihypertensive properties previously described for *K. marxianus* LF hydrolyzate. Also, data reported here suggest ACE inhibition as an *in vivo* mechanism for the antihypertensive effects of the sequences DPYKLRP and LRP in particular, although other mechanisms cannot be discarded.

AUTHOR INFORMATION

Corresponding Author

*Tel.: 34-96-3900022. Fax: 34-96-3636301. E-mail: pmanz@iata.csic.es.

Funding

This work was supported by grant AGL2010−21009 from 'Ministerio de Educación y Ciencia - FEDER', Consolider Ingenio 2010, Fun-C-Food, CSD2007−00063 and RETICS INVICTUS RD12/0014/0004 from 'Instituto de Salud Carlos III'. A.G.-T. is the recipient of a predoctoral fellowship from 'Ministerio de Educación y Ciencia' (BES-2011−044424).

Notes

The authors declare no competing financial interest.

ACKNOWLEDGMENTS

We thank José Javier López-Díez and Sonia Ruiz-Piquer for technical assistance.

ABBREVIATIONS USED

ACE, angiotensin I-converting enzyme; BCA, bicinchoninic acid method; ECE, endothelin converting enzyme; LF, bovine lactoferrin; GRAS, generally recognized as safe; LAB, lactic acid bacteria; pLFH, lactoferrin permeate enriched in peptides of molecular weight lower than 3 kDa; RAS, renin-angiotensin system; RP-HPLC, reversed-phase high-performance liquid chromatography; RP-HPLC-MS/MS, reversed-phase high-performance liquid chromatography tandem mass spectrometry; SBP, systolic blood pressure; SHRs, spontaneously hypertensive rats; TFA, trifluoroacetic acid

REFERENCES

(1) Martínez-Maqueda, D.; Miralles, B.; Recio, I.; Hernández-Ledesma, B. Antihypertensive peptides from food proteins: a review. *Food Function* **2012**, *3*, 350−361.

(2) Carey, R. M.; Siragy, H. M. Newly recognized components of the renin-angiotensin system: potential roles in cardiovascular and renal regulation. *Endocrine Rev.* **2003**, *24*, 261−271.

(3) Vermeirssen, V.; van Camp, J.; Verstraete, W. Bioavailability of angiotensin I converting enzyme inhibitory peptides. *Br. J. Nutr.* **2004**, *92*, 357−366.

(4) Turpeinen, A. M.; Järvenpää, S.; Kautiainen, H.; Korpela, R.; Vapaatalo, H. Antihypertensive effects of bioactive tripeptides-random effects meta-analysis. *Ann. Med.* **2013**, *45*, 51−56.

(5) Hernández-Ledesma, B.; Contreras, M. M.; Recio, I. Antihypertensive peptides: production, bioavailability and incorporation into foods. *Adv. Colloid Interface Sci.* **2011**, *165*, 23−35.

(6) Hamme, V.; Sannier, F.; Piot, J.-M.; Didelot, S.; Bordenave-Juchereau, S. Crude goat whey fermentation by *Kluyveromyces marxianus* and *Lactobacillus rhamnosus*: contribution to proteolysis and ACE inhibitory activity. *J. Dairy Res.* **2009**, *76*, 152−157.

(7) Chaves-López, C.; Tofalo, R.; Serio, A.; Paparella, A.; Sacchetti, G.; Suzzi, G. Yeasts from colombian Kumis as a source of peptides with angiotensin-I converting enzyme (ACE) inhibitory activity in milk. *Int. J. Food Microbiol.* **2012**, *159*, 39−46.

(8) Ruiz-Giménez, P.; Salom, J. B.; Marcos, J. F.; Vallés, S.; Martínez-Maqueda, D.; Recio, I.; Torregrosa, G.; Alborch, E.; Manzanares, P. Antihypertensive effect of a bovine lactoferrin pepsin hydrolysate: identification of novel active peptides. *Food Chem.* **2012**, *131*, 266−273.

(9) Fernández-Musoles, R.; Salom, J. B.; Martínez-Maqueda, D.; López-Díez, J. J.; Recio, I.; Manzanares, P. Antihypertensive effects of lactoferrin hydrolysates: inhibition of angiotensin- and endothelin-converting enzymes. *Food Chem.* **2013**, *139*, 994−1000.

(10) Fernández-Musoles, R.; Manzanares, P.; Burguete, M. C.; Alborch, E.; Salom, J. B. *In vivo* angiotensin I-converting enzyme inhibition by long-term intake of antihypertensive lactoferrin hydrolysate in spontaneously hypertensive rats. *Food Res. Int.* **2013**, *54*, 627−632.

(11) Ruiz-Giménez, P.; Ibáñez, A.; Salom, J. B.; Marcos, J. F.; López-Díez, J. J.; Vallés, S.; Torregrosa, G.; Alborch, E.; Manzanares, P. Antihypertensive properties of lactoferricin B-derived peptides. *J. Agric. Food Chem.* **2010**, *58*, 6721−6727.

(12) Vermeirssen, V.; van der Bent, A.; van Camp, J.; van Amerongen, A.; Verstraete, W. A quantitative *in silico* analysis calculates the angiotensin I converting enzyme (ACE) inhibitory activity in pea and whey protein digests. *Biochimie* **2004**, *86*, 231−239.

(13) Padilla, B.; Manzanares, P.; Belloch, C. Yeast species and genetic heterogeneity within *Debaryomyces hansenii* along the ripening process of traditional ewes' and goats' cheeses. *Food Microbiol.* **2014**, *38*, 160−166.

(14) García-Tejedor, A.; Padilla, B.; Salom, J. B.; Belloch, C.; Manzanares, P. Dairy yeasts produce milk protein-derived antihypertensive hydrolysates. *Food Res. Int.* **2013**, *53*, 203−208.

(15) Sánchez-Rivera, L.; Recio, I.; Ramos, M.; Gómez-Ruiz, J. A. Peptide profiling in cheeses packed using different technologies. *J. Dairy Sci.* **2013**, *96*, 3551−3557.

(16) Sentandreu, M. A.; Toldrá, F. A rapid, simple and sensitive fluorescence method for the assay of angiotensin-I converting enzyme. *Food Chem.* **2006**, *97*, 546−554.

(17) van den Buuse, M. Circadian rhythms of blood pressure and heart rate in conscious rats: effects of light cycle shift and timed feeding. *Physiol. Behav.* **1999**, *68*, 9−15.

(18) Murray, B. A.; FitzGerald, R. J. Angiotensin converting enzyme inhibitory peptides derived from food proteins: biochemistry, bioactivity and production. *Curr. Pharm. Des.* **2007**, *13*, 773−791.

(19) Abbas, C. A. Production of antioxidants, aromas, colours, flavours and vitamins by yeasts. In *Yeasts in food and beverages*; Querol, A., Fleet, G. H., Eds.; Springer: New York, 2006; pp 285−334.

(20) Fonseca, G. G.; Heinzle, E.; Wittmann, C.; Gombert, A. K. The yeast *Kluyveromyces marxianus* and its biotechnological potential. *Appl. Microbiol. Biotechnol.* **2008**, *79*, 339−354.

(21) Maccaferri, S.; Klinder, A.; Brigidi, P.; Cavina, P.; Costabile, A. Potential probiotic *Kluyveromyces marxianus* B0399 modulates the immune response in Caco-2 cells and peripheral blood mononuclear cells and impacts the human gut microbiota in an *in vitro* colonic model system. *App. Environ. Microbiol.* **2012**, *78*, 956−964.

(22) Cushman, D. W.; Cheung, H. S.; Sabo, E. F.; Ondetti, M. A. Design of potent competitive inhibitors of angiotensin-converting enzyme. Carboxyalkanoyl and mercaptoalkanoyl amino acids. *Biochem.* **1977**, *16*, 5484−5491.

(23) Lee, N.-Y.; Cheng, J.-T.; Enomoto, T.; Nakamura, I. The antihypertensive activity of angiotensin-converting enzyme inhibitory peptide containing in bovine lactoferrin. *Chin. J. Physiol.* **2006**, *49*, 67−73.

(24) Ondetti, M. A.; Rubin, B.; Cushman, D. W. Design of specific inhibitors of angiotensin-converting enzyme: new class of orally active antihypertensive agents. *Science* **1977**, *196*, 441−444.

(25) Fujita, H.; Yoshikawa, M. LKPNM: a pro-drug type ACE-inhibitory peptide derived from fish protein. *Immunopharmacology* **1999**, *44*, 123−127.

(26) Marques, C.; Amorim, M. M.; Pereira, J. O.; Pintado, M. E.; Moura, D.; Calhau, C.; Pinheiro, H. Bioactive peptides: are there more antihypertensive mechanisms beyond ACE inhibition? *Curr. Pharm. Des.* **2012**, *18*, 4706−4713.

(27) Schiffrin, E. L. Vascular endothelin in hypertension. *Vasc. Pharmacol.* **2005**, *43*, 19−29.

(28) Fernández-Musoles, R.; López-Díez, J. J.; Torregrosa, G.; Vallés, S.; Alborch, E.; Manzanares, P.; Salom, J. B. Lactoferricin B-derived peptides with inhibitory effects on ECE-dependent vasoconstriction. *Peptides* **2010**, *31*, 1926−1933.

(29) Maes, W.; van Camp, J.; Vermeirssen, V.; Hemeryck, M.; Ketelslegers, J. M.; Schrezenmeir, J.; van Oostveldt, P.; Huyghebaert, A. Influence of the lactokinin Ala-Leu-Pro-Met-His-Ile-Arg (ALPM-HIR) on the release of endothelin-1 by endothelial cells. *Reg. Peptides* **2004**, *118*, 105−109.

(30) Coates, D. The angiotensin converting enzyme (ACE). *Int. J. Biochem. Cell Biol.* **2003**, *35*, 769−773.

(31) Lu, J.; Sawano, Y.; Miyakawa, T.; Xue, Y.-L.; Cai, M.-Y.; Egashira, Y.; Ren, D.-F.; Tanokura, M. One-week antihypertensive effect of Ile-Gln-Pro in spontaneously hypertensive rats. *J. Agric. Food Chem.* **2011**, *59*, 559−563.

promising host for heterologous gene expression, was already successfully used for the production of β-galactosidase from *Lactobacillus delbrueckii*[21] and chitinase from *Bacillus licheniformis*.[22] Available inducible expression systems[23] are based on quorum-sensing mechanisms involved in the production of sakacins A and P.[24−26] More recently, the erythromycin antibiotic resistance gene (*erm*) was replaced by the homologous alanine racemase gene (*alr*), and an alanine racemase-deficient host strain was constructed that obviates the undesirable fermentation in the presence of antibiotics and is suitable for applications in the food industry.[19]

In this study we present the heterologous expression of the L-AI and D-XI-encoding genes from the food grade microorganism *L. reuteri* in *E. coli*, the most commonly used organism for heterologous protein production, and the characterization of these novel enzymes.[27] *L. reuteri*, a heterofermentative and symbiotic species, is well adapted to colonize human and animal gastrointestinal tracts. Among probiotic microorganisms *L. reuteri* is unique due to its ability to produce and secrete the antimicrobial substance reuterin.[28] Furthermore, we coexpressed the genes in the food grade host *L. plantarum* using two different expression systems and performed comprehensive studies on the conversion of D-glucose and D-galactose, respectively.

MATERIALS AND METHODS

Chemicals and Enzymes. All chemicals were of the highest purity available and purchased from Sigma-Aldrich (St. Louis, MO, USA), unless otherwise stated. Restriction endonucleases, T4 DNA ligase, and Phusion High-Fidelity DNA polymerase were obtained from Thermo Fisher Scientific Biosciences (St. Leon-Rot, Germany), whereas GoTaq DNA polymerase was from Promega (Madison, WI, USA). Phenylmethanesulfonyl fluoride (PMSF) was obtained from Fluka (Buchs, Switzerland), and chromatographic materials were obtained from GE Healthcare (Chalfont St. Giles, UK).

Bacterial Strains and Culture Conditions. The bacterial strains and plasmids used in this study are listed in Table 1. *Lactobacillus reuteri* DSMZ 17509 (strain designation 100-23) was obtained from the German Collection of Microorganisms and Cell Cultures (DSMZ, Braunschweig, Germany). *Lactobacillus* strains were cultivated in deMan−Rogosa−Sharpe (MRS) medium at 30 °C without agitation. *E. coli* strain NEB5α (New England Biolabs, Ipswich, MA, USA), MB2159 (D-alanine auxotrophe), and BL21 Star (DE3) (Invitrogen, Carlsbad, CA, USA) were grown in Luria−Bertani (LB) medium at 37 °C with shaking at 125 rpm. When needed, media were supplemented with ampicillin at a concentration of 100 μg/mL and erythromycin at concentrations of 5 and 200 μg/mL for *L. plantarum* and *E. coli*, respectively. *E. coli* MB2159 and *L. plantarum* strain TLG02 were cultivated by adding 200 μg/mL D-alanine to the respective media. Solid media were prepared by adding 1.5% agar to the respective media.

DNA Amplification and Subcloning. DNA amplification was performed with Phusion High-Fidelity DNA Polymerase according to the manufacturer's instructions. The oligonucleotide primers were obtained from VBC Biotech (Vienna, Austria) and are listed in Table 2. PCR products and restriction enzyme digested DNA were purified with GFX PCR DNA and a Gel Band Purification Kit (GE Healthcare) as recommended by the supplier. When needed, the PCR fragments were subcloned into the pJET1.2 vector (CloneJET PCR cloning kit, Thermo Fisher Scientific Biosciences), and *E. coli* was used as host for plasmid propagation before transformation into *Lactobacillus*. The amplified sequences were verified by a commercial sequencing service (LGC Genomics, Berlin, Germany).

The *araA* gene (NCBI reference sequence for the genome: NZ_AAPZ02000002.1) was amplified by colony-PCR using the primers araA_LbReu_fwd1 and araA_LbReu_rev1. The *xylA* gene was amplified with the primer pair xylA_LbReu_fwd1 and xylA_LbReu_rev1. Each PCR product was ligated into the pJET1.2 vector as recommended by the supplier, resulting in plasmids pPW116 and pPW114, respectively. Each plasmid was transformed into chemically competent *E. coli* NEB5α cells according to the manufacturer's instructions.

Table 1. Strains and Plasmids Used in This Work[a]

strain or plasmid	relevant characteristics	ref
strains		
L. reuteri		
DSMZ 17509	source for L-AI and D-XI encoding genes	DSMZ
L. plantarum		
WCFS1	wild type	49
TLG02	Δalr, D-alanine auxotroph	19
E. coli		
MB2159	D-alanine auxotroph, cloning host	50
NEB5α	cloning host	New England Biolabs
BL21 Star (DE3)	expression host	Invitrogen
plasmids		
pET-21a(+)	Amp^r, T7 promoter, C-terminal His-Tag	Novagen
pSIP409	Erm^r, pSIP401 derivative, P_{sppQ}	25
pSIP609	pSIP409 derivative, *alr* replaced with *erm*	19
pPW002	L-AI from *L. reuteri* in pET-21a(+)	this work
pPW004	D-XI from *L. reuteri* in pET-21a(+)	this work
pPS1	pSIP609 derivative, *Nco*I replaced with *Nhe*I	this work
pPW-015	pSIP409 derivative, *Nco*I replaced with *Nhe*I	this work
pPS2	L-AI and D-XI from *L. reuteri* in pPS1	this work
pPS3	L-AI and D-XI from *L. reuteri* in pPW-015	this work
pPW116	L-AI from *L. reuteri* in pJET1.2	this work
pPW114	D-XI from *L. reuteri* in pJET1.2	this work

[a]Amp^r, ampicillin resistance; Erm^r, erythromycin resistance; *alr*, alanine racemase encoding gene; *erm*, erythromycin resistance gene.

Plasmid Construction and Expression in *E. coli*. The *araA* and *xylA* genes were amplified using the primer pairs AraReu*Nhe*I_fwd1/AraReu*Eco*RI_His6 and XylReuNheI_fwd1/XylReu*Eco*RI_His6 as well as pPW116 and pPW114 as templates, respectively. The resulting PCR fragments were cut with the restriction enzymes *Nhe*I and *Eco*RI and ligated into the equally treated expression vector pET21-a(+) (Novagen, Darmstadt, Germany) in frame with the C-terminal His_6-tag encoded by the vector. The resulting plasmids pPW002 and pPW004 were transformed into electrocompetent *E. coli* BL21 Star (DE3) according to the method of Inoue et al.[29]

Plasmid Construction and Expression in *L. plantarum*. The *Nco*I restriction site on the pSIP609 and pSIP409 vector, respectively, was replaced by a *Nhe*I restriction site by site-directed mutagenesis.[30] A PCR was peformed using the primer pair pSIP_SD_NheI_fwd1 and pSIP409_SD_NheI_rev1. Subsequent digestion with *Dpn*I and transformation into *E. coli* resulted in the plasmids pPS1 (pSIP609 derivative) and pPW015 (pSIP409 derivative), respectively.[30] The fusion of the *araA* and the *xylA* genes was performed according to the overlap extension method.[31] PCR reactions were done with the primer pairs XylReu_OE_fwd1/XylReu_OE_rev1 (pPW114 as template) and AraReuNheI_fwd1/AraReu_OE_rev1 (pPW116 as template). The resulting PCR products were purified and used as templates for a third reaction with the primers AraReu*Nhe*I_fwd1 and XylReu_OE_rev1. The resulting amplicon was digested with *Nhe*I and *Eco*RI and

Table 2. Primers Used in This Study[a]

primer	sequence (5′−3′)
araA_LbReu_fwd1	ATGGATATTAAGAATTACGAATTTTGGTTT
araA_LbReu_rev1	CTATTCAATAAAATCAACTTTAACA
xylA_LbReu_fwd1	TCATCATGATAAGGATAAAGTTTTGG
xylA_LbReu_rev1	ATTGCAATCGTTGTTCCATAAAGCCAATC
pSIP_SD_*Nhe*I_fwd1	TACGTCCTGTAGAAACCCCAAC
pSIP409_SD_*Nhe*I_rev1	CTACAGGACGTAGCTAGCCTAAAATCTCCTTGT
AraReu*Nhe*I_fwd1	TTTTCGCTAGCATGGATATTAAGAATTACG
AraReu*Eco*RI_His6	AACGCGAATTCGTTTCAATAAAATCAACTT
XylReu*Nhe*I_fwd1	ATTTTGCTAGCATGGCTGATTTATGGA
XylReu*Eco*RI_His6	CCGTGGAATTCGTCTTAGCAAGCGTTTC
AraReu_OE_rev1	TAAAACTCCTGAACTAGTGGTGGTGGTGGTGGTGTTCAATAAAATCAAC
XylReu_OE_fwd1	TTCAGGAGATTTTAATGGCTGATTTATGGAATAA
XylReu_OE_rev1	CGAATGAATTCTTAGTGGTGGTGGTGGTGCTTAGCAAGCGTTTC

[a]The restriction sites are underlined.

ligated into the equally treated vectors pPS1 and pPW-015, resulting in plasmids pPS2 and pPS3, respectively. These plasmids were transformed into *E. coli* MB2159 and NEB5α, respectively, for plasmid propagation. Competent cells of *E. coli* MB2159 were prepared and transformed according to the method of Inoue et al.[29] The isolated plasmids were transformed into electrocompetent *L. plantarum* TLG02 and WCFS1 cells, respectively, according to the method of Josson et al.[32]

Sequence Analysis. The translated amino acid sequences were analyzed using the programs Translate and Compute pI/MW at http://www.expasy.org/.[33]

Expression in *E. coli*. *E. coli* BL21 Star (DE3) carrying the plasmids pPW002 and pPW004, respectively, was grown overnight at 37 °C and 125 rpm in 3 mL of LB medium containing 100 μg/mL ampicillin. Two hundred milliliters of Terrific-Broth (TB) medium supplemented with 100 μg/mL in 1 L baffled shaking flasks were inoculated with 1 mL of the starter culture. The cells were incubated at 37 °C until an optical density at 600 nm (OD_{600}) between 0.4 and 0.6 was reached. Lactose in a final concentration of 5 g/L was added to the culture for induction of the heterologous expression, and the cultures were incubated further at 25 °C for 20 h. Cells were then harvested by centrifugation (4000*g*, 20 min, 4 °C), resuspended in buffer A (50 mM sodium phosphate buffer, 500 mM NaCl, 5 mM imidazole, pH 6.0) supplemented with 5.7 mM PMSF, and disrupted by using a French press (Aminco, Silver Spring, MD, USA). Cell debris was removed by centrifugation (30000*g*, 30 min, 4 °C), and the supernatant was recovered as crude extract.

Expression in *L. plantarum*. *L. plantarum* carrying the plasmids pPS2 and pPS3, respectively, was grown overnight at 37 °C in 10 mL of MRS medium containing 5 μg/mL erythromycin in the case of the latter. These starter cultures were used to inoculate 1 L of the same media. The cultures were incubated at 30 °C until an OD_{600} between 0.3 and 0.4 was reached. Heterologous expression was induced by adding 25 ng/mL of the peptide pheromone IP-673 (supplied by the Molecular Biology Unit, University of Newcastle-upon-Tyne, UK). The cultures were incubated further at 30 °C for 20 h. Cells were washed twice by buffer A, and the cell pellet was resuspended in the same buffer containing 5.7 mM PMSF. The cells were homogenized by using a French press, and the cell debris was removed by centrifugation to obtain the crude extract.

Protein Purification. The crude extract was purified by one-step immobilized metal affinity chromatography (IMAC) on a prepacked 20 mL HisPrep FF 16/10 column (GE Healthcare). The column was pre-equilibrated with buffer A (see above), and the crude extract was applied at a rate of 2.5 mL/min. After an additional washing step (3 column volumes), the enzyme was eluted at the same rate by using a linear gradient of 5 mM−1 M imidazole in 10 column volumes. Active fractions were pooled, desalted, and concentrated in 50 mM sodium phosphate buffer (pH 6.0) using Amicon Ultra-15 centrifugal filter units (30 kDa cutoff; Millipore, Billerica, MA, USA) and stored at 4 °C. D-XI containing fractions were concentrated in 50 mM sodium acetate buffer (pH 5.0).

Protein Quantification, Electrophoresis, and Molecular Mass Determination. Protein concentration was determined according to the method of Bradford[34] using a BSA standard curve and a prefabricated assay solution (Bio-Rad). SDS-PAGE was carried out using Mini-PROTEAN TGX precast gradient gels (4−15%) and Precision Plus Protein Unstained Standard. Bio-Safe Coomassie was used for visualization of the protein bands (Bio-Rad). The theoretical mass was derived from the ExPASy ProtParam tool (http://web.expasy.org/protparam/) and confirmed by size exclusion chromatography (SEC) using a 190 mL Sephacryl S300 column (GE Healthcare) equilibrated with 50 mM potassium phosphate buffer (pH 7.0) containing 150 mM NaCl and the molecular weight marker kit for gel filtration (Sigma-Aldrich).

Enzyme Assays and HPLC Analysis. L-AI activity was measured by determing the amount of formed L-ribulose or D-tagatose. The reaction mixture contained 50 mM L-arabinose or D-galactose, 1 mM $CoCl_2$, 0.5 mM $MnCl_2$, 50 μL of 0.5−1.0 mg/mL enzyme preparation, and 50 mM sodium phosphate buffer (pH 6.0) to bring the final volume to 0.5 mL. The reaction mixture was incubated at 65 °C for 10 min followed by heating the mixture to 95 °C for 5 min to stop the reaction. The amount of L-ribulose or D-tagatose was determined either by HPLC analysis or colorimetrically using the cysteine−carbazole−sulfuric-acid method[35] with slight modifications. Fifty microliters of freshly prepared 1.5% (w/v) L-cysteine−HCl was added to 250 μL of reaction mixture (in a suitable dilution), 1.5 mL of ≈70% sulfuric acid and 50 μL of 0.12% (w/v) carbazole in ethanol were added, and the absorbance at 560 nm was measured after 1 h of incubation at room temperature. HPLC analysis was performed on a Dionex Summit HPLC system (Thermo Fisher Scientific) fitted with a Shodex RI-101 refractive index detector (Shoko Scientific, Yokohama, Japan) using an Aminex HPX 87-K column (Bio-Rad) with a guard column. Samples and standards were eluted at 80 °C with 1 g/L boric acid (pH 8.5, 0.5 mL/min). For calculation of the reaction product(s) L-arabinose, D-galactose, L-ribulose, and D-tagatose standards were included in the run. One unit of L-arabinose isomerase activity is defined as the amount of enzyme needed to produce 1 μmol of L-ribulose or D-tagatose per minute under the assay conditions.

D-XI activity was measured by the determination of the amount of formed D-xylulose (or D-fructose). The reaction mixture contained 50 mM D-xylose, 0.5 mM $CoCl_2$, 0.5 mM $MnCl_2$, 50 μL of 1 mg/mL enzyme preparation, and 50 mM sodium acetate buffer (pH 5.0) to bring the final volume to 0.5 mL. The reaction mixture was incubated at 65 °C for 10 min, and the reaction was stopped by heating the mixture at 95 °C for 5 min. For assaying the glucose isomerase activity, the reaction mixture contained 400 mM D-glucose, 5 mM $CoCl_2$, 5 mM $MnCl_2$, 5 mM $MgSO_4$, 50 μL of 5 mg/mL enzyme preparation, and 50 mM sodium acetate buffer (pH 5.0) to bring the final volume to 0.5 mL. The reaction mixture was incubated at 60 °C for 10 min.

The amount of D-xylulose or D-fructose was determined either by HPLC analysis or using the cysteine−carbazole−sulfuric-acid method[35] with slight modifications (see above). For HPLC analysis and calculation of the reaction products D-xylose, D-glucose, D-xylulose, and D-fructose standards were included in the run. One unit of D-xylose isomerase activity is defined as the amount of enzyme needed to produce 1 μmol of D-xylulose or D-fructose per minute under the assay conditions.

Effect of Temperature, pH, and Divalent Metal Ions on Enzyme Activity. The temperature optimum was measured by assaying the enzyme samples over the range of 30−90 °C, at pH 5 (D-XI) and pH 6 (L-AI). Three buffer systems (sodium acetate/sodium phosphate/Tris-HCl) were used for measuring the pH optimum of enzyme activity at 65 °C with D-xylose (D-XI) and L-arabinose (L-AI) as substrate. The effects of various metal ions were determined by the addition of 1 mM $MgSO_4$, $CoCl_2$, or $MnCl_2$ (or more than one in various concentrations) and assaying D-XI and L-AI activity, respectively, under standard conditions without 0.5 mM $MnCl_2$ and 0.5 mM $CoCl_2$ (D-XI) and without 0.5 mM $MnCl_2$ and 1 mM $CoCl_2$ (L-AI).

Determination of Kinetic Parameters. The kinetic paramters of L-AI were determined in 50 mM sodium phosphate buffer (pH 6.0) containing 0.5 mM $MnCl_2$ and 1 mM $CoCl_2$ and 5−800 mM L-arabinose (10−800 mM D-galactose). The reaction mixtures were incubated for 10 min at 65 °C. The kinetic parameters of D-XI were determined in 50 mM sodium acetate buffer (pH 5.0) containing 0.5 mM $MnCl_2$, 0.5 mM $CoCl_2$ (5 mM $CoCl_2$, 5 mM $MnCl_2$, 5 mM $MgSO_4$), and 1−500 mM D-xylose (25−1500 mM D-glucose). The reaction mixtures were incubated for 10 min at 65 °C (60 °C). The observed data were fitted to the Michaelis−Menten equation, and kinetic constants were calculated by nonlinear least-squares regression. Using the molecular mass, turnover numbers (k_{cat}) and catalytic efficiencies (k_{cat}/K_m) were calculated.

Enzymatic Conversion of D-Galactose to D-Tagatose. The conversion was carried out at 60 °C with 0.8 and 1.4 U of purified enzyme (i.e., 1.0 mg of L-AI produced in *E. coli* and 0.9 mg of L-AI expressed in *L. plantarum*), respectively, in a total volume of 1 mL. The conversion medium contained 500 mM D-galactose, 1 mM $CoCl_2$, and 0.5 mM $MnCl_2$ in 50 mM sodium phosphate buffer (pH 6.0). Samples were taken regularly for the analysis of D-galactose and D-tagatose by HPLC. The conversion rate represents the ratio between the formed D-tagatose and the initial D-galactose.

Enzymatic Conversion of D-Glucose to D-Fructose. The conversion was carried out at 60 °C with 2.1 and 1.1 U of purified enzyme (i.e., 1.9 mg of D-XI produced in *E. coli* and 0.9 mg of D-XI expressed in *L. plantarum*), respectively, in a total volume of 1 mL. The conversion media contained 500 mM D-glucose, 5 mM $CoCl_2$, 5 mM $MnCl_2$, and 5 mM $MgSO_4$ in 50 mM sodium acetate buffer (pH 5.0). Samples were taken regularly for the analysis of D-glucose and D-fructose by HPLC. The conversion rate represents the ratio between the formed D-fructose and the initial D-glucose.

RESULTS AND DISCUSSION

Heterologous Expression of the L-AI and D-XI Encoding Gene in *E. coli*. The L-AI encoding gene from *L. reuteri* DSMZ 17509 was successfully expressed in *E. coli* BL21(DE3). The nucleotide sequence contains an open reading frame of 1422 bp encoding a polypeptide of 473 amino acids. On the basis of the DNA sequence, two modified oligonucleotide primers containing restriction sites for in-frame ligation into the pET21-a(+) were designed and used to reamplify the *araA* sequence and to construct the expression vector pPW002. The L-AI encoding sequence was fused in frame with the C-terminal His_6-tag encoded by the vector, and the construct was expressed under the control of the lactose- or IPTG-inducible T7 promoter. Approximately 137.9 U of L-AI activity/L fermentation medium was produced under the described conditions with a volumetric activity of 1.6 U/mL and a specific activity of 0.18 U/mg using D-galactose as substrate. The D-XI encoding gene from *L. reuteri* DSM 17509 contains an open reading frame of 1350 bp encoding a polypeptide of 449 amino acids. The *xylA* sequence was fused in frame with the C-terminal His_6-tag encoded by the vector, and the heterologous expression resulted in approximately 780.5 U of D-XI activity/L fermentation medium with a volumetric activity of 8.9 U/mL and a specific activity of 0.57 U/mg using D-glucose as substrate.

Due to the use of an ampicillin resistance marker, the potential of the pET21-a(+) expression system is limited to food applications. Furthermore, the use of *E. coli* strains is not permitted in the food industry in most countries,[36] due to possible endotoxin production.[37]

Coexpression of L-AI and D-XI Encoding Gene(s) in *L. plantarum*. The resulting expression vector contains the *araA* gene fused with a C-terminal His_6-tag (CAC_6) and a stop-codon (TAG). The following ribosomal binding site (RBS)[38] was flanked downstream (5′) with TTC (three nucleotides downstream from the RBS) and upstream with the nucleotides ATTTTA (six nucleotides upstream of the RBS).[26,39] The *xylA* gene was also fused with a His_6-tag followed by the stop-codon (TAA). Approximately 28.6 U (18.3 U) of L-AI activity/L fermentation medium with a volumetric activity of 0.8 U/mL (0.5 U/mL) and a specific activity of 0.15 U/mg (0.08 U/mg) with D-galactose as substrate was produced in *L. plantarum* using the pSIP609 (pSIP409) vector. The coexpression of the *xylA* gene allowed production of approximately 32.3 U (55.9 U) of GI activity/L fermentation medium with a volumetric activity of 0.9 U/mL (1.6 U/mL) and a specific activity of 0.17 U/mg (0.23 U/mg) using the pSIP609 (pSIP409) expression system.

A food grade LAB strain was chosen as expression host as demonstrated by Rhimi et al.[40] and Salonen et al.[3] Although expression yields in *E. coli* are much higher, the combination of the (homologous) alanine racemase gene (*alr*) as selection marker and the safe cell factory *L. plantarum* has considerable potential for the production of ingredients and additives for the food industry.[19] Compared to the erythromycin-dependent expression system pSIP409, the expression yield of the (first) *araA* gene was higher; in the case of the (second) *xylA* gene, the induction/expression worked less efficiently. However, the antibiotic-independent expression system pSIP609 allowed the successful coexpression of the genes *araA* and *xylA* from *L. reuteri* DSMZ 17509. The slightly higher yields with the pSIP609 system (alanine racemase as selection marker in combination with a suitable deficient host strain) are in agreement with previous data and can be explained by the avoidance of antibiotic detoxification and subsequently reduced plasmid loss.[19]

Purification of Recombinant L-AI and D-XI. The recombinant enzymes were purified to apparent homogeneity from cell extracts by a single-step purification protocol using immobilized metal affinity chromatography (Figure 1).

The specific activities of the purified enzymes were 0.9 U/mg for L-AI and 1.1 U/mg for D-XI with *E. coli* as expression host and D-galactose and D-glucose, respectively, as substrate. The use of *L. plantarum* as expression host resulted in 1.6 U/mg (in the case of pSIP609 and 409) for L-AI and 1.2 U/mg (pSIP609) and 1.8 (pSIP409) for D-XI after purification. Although the coexpressed genes contained the same affinity tag, the resulting proteins are separated successfully and elute in different fractions.

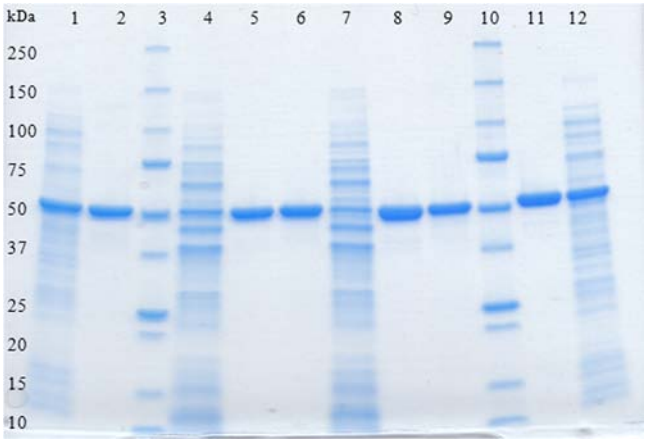

Figure 1. SDS-PAGE analysis of recombinant L-AI and D-XI from *L. reuteri*. Lanes: 1, L-AI-containing crude extract from *E. coli*; 2, purified L-AI (*E. coli*); 3, Precision Protein standard (Bio-Rad); 4, L-AI-containing crude extract from *L. plantarum* (pSIP609); 5, purified L-AI (pSIP609); 6, purified D-XI (pSIP609); 7, D-XI-containing crude extract from *L. plantarum* (pSIP409); 8, purified L-AI (pSIP409); 9, purified D-XI (pSIP409); 10, Precision Protein standard (Bio-Rad); 11, purified D-XI (*E. coli*); 12, D-XI-containing crude extract from *E. coli*.

Molecular masses of approximately 300 kDa (L-AI) and 190 kDa (D-XI) were determined using size exclusion chromatography. Considering the calculated molecular masses of 53.6 kDa (L-AI) and 51.04 kDa (D-XI), these data suggest that L-AI is naturally active as a homohexamer and D-XI is a tetramer. The hexameric quaternary structure of the L-AI from *L. reuteri* is also observed in the enzymes from *E. coli*[41] and *L. plantarum* NC8,[42] whereas many other L-AIs exhibit tetrameric structures.[9,42] The tetrameric quaternary structure of the D-XI from *L. reuteri* is the most common form of D-XIs,[43] but dimeric and trimeric forms are also described.[11]

Effect of Temperature, pH, and Divalent Metal Ions on Enzyme Activity. The temperature profile of purified L-AI and D-XI (expressed in *E. coli*), respectively, was determined from 30 to 90 °C using the standard assay according to Dische and Borenfreund.[35] L-AI exhibited maximum activity at 65 °C, with 90 and 97% activity at 60 and 70 °C, respectively (Figure 2). The enzyme D-XI exhibited the same temperature optimum (65 °C) and retained 85% of its maximum activity at 60 and 70 °C, respectively (Figure 2). For industrial production of D-tagatose and D-fructose, respectively, an isomerization at elevated temperature of 60−65 °C resulted in higher conversion yields, better sugar solubility, and lower risk of microbial contamination. Higher temperatures above 70 °C resulted in the formation of undesired byproducts and browning effects.[1,44]

The standard assay was performed using different buffers with pH ranging from 4 to 10. The pH optimum of L-AI and D-XI was found in the slightly acidic pH range (6.0 and 5.0, respectively) (Figure 3). Acidic conditions avoid the formation of undesired byproducts, a great advantage for industrial purposes.[3,44]

The L-AI enzyme activity was assayed at 65 °C and pH 6.0 in the presence of various cations and D-galactose as substrate (Table 3). The activity was increased by the addition of 1 mM Co^{2+} (3.7-fold) and 1 mM Mn^{2+} (1.4-fold). A mixture of 1 mM Co^{2+} and 0.5 mM Mn^{2+} increased the enzyme activity 3.9-fold. The D-XI enzyme activity was assayed at 65 °C and pH 5.0 in the presence of various cations and D-xylose as substrate (Table 3). The activity was increased by the addition of 1 mM Co^{2+} (1.9-fold) and 1 mM Mn^{2+} (2.9-fold). A mixture of 0.5 mM Co^{2+} and 0.5 mM Mn^{2+} increased the enzyme activity 3.2-fold. Glucose isomerase activity was assayed at 60 °C and pH 5.0 and was maximally enhanced by the addition of 5 mM Co^{2+}, 5 mM Mn^{2+}, and 5 mM Mg^{2+} (data not shown).

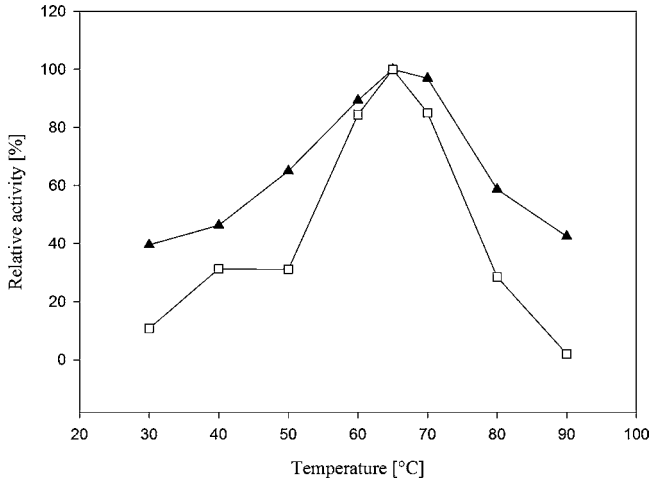

Figure 2. Effect of temperature on L-AI (solid triangles) and D-XI (open squares) activity. Relative activities are presented as functions of temperature with L-arabinose and D-xylose, respectively, as substrate. The reaction mixtures were incubated for 10 min.

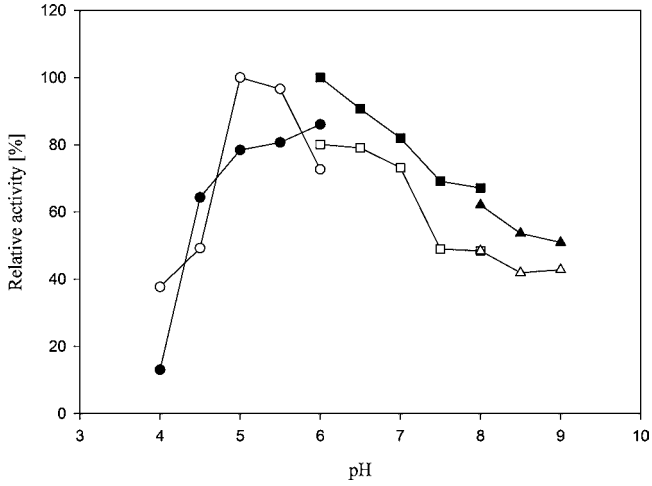

Figure 3. Effect of pH on L-AI (solid symbols) and D-XI (open symbols) activity. Relative activities are presented as functions of pH with L-arabinose and D-xylose, respectively, as substrate. The reaction mixtures were incubated for 10 min. The buffers used were acetate (circles), phosphate (squares), and tris (triangles).

Table 3. Effect of Metal Ions on L-AI and D-XI Activity[a]

metal ion	L-AI relative activity (%)	D-XI relative activity (%)
none	26	32
Co^{2+}	94	62
Mg^{2+}	25	36
Mn^{2+}	41	93
Co^{2+} + Mn^{2+}	100	100

[a] $CoCl_2$, $MgSO_4$, and $MnCl_2$ were added to the enzyme reaction mixture at a final concentration of 1 mM. The mixture of $CoCl_2$ and $MnCl_2$ was added at a final concentration of 1 or 0.5 mM (in the case of L-AI) and 0.5 or 0.5 mM (in the case of D-XI), respectively.

dx.doi.org/10.1021/jf404785m | J. Agric. Food Chem. 2014, 62, 1617−1624

A number of L-arabinose and D-xylose isomerases require metal ions for (maximal) activity (and stability).[4,11] The use of metal cofactors, especially Co^{2+}, increases downstream processing costs as they have to be removed from the final product.[9] For industrial purposes, independence from or a very low requirement for metal ions is advantageous.[3]

Kinetic Parameters/Properties. The apparent K_m, V_{max}, k_{cat}, and catalytic efficiency (k_{cat}/K_m) of L-AI using D-galactose as substrate were 647 ± 109 mM, 11 ± 1 U/mg, 59 ± 5 s^{-1}, and 0.09 mM^{-1} s^{-1}, respectively. For L-arabinose the apparent K_m, V_{max}, k_{cat}, and catalytic efficiency (k_{cat}/K_m) were estimated to be 633 ± 69 mM, 179 ± 10 U/mg, 959 ± 55 s^{-1}, and 1.5 mM^{-1} s^{-1}, respectively.

The high K_m value for D-galactose is comparable with that of the enzyme from *Bifidobacterium longum*[3] and *L. pentosus*,[7,45] whereas enzymes from other *Lactobacillus* strains exhibit up to 10 times lower K_m values.[1,9,42] The low affinity for L-arabinose is comparable with the enzyme from *Pediococcus pentosaceus* PC-5, which shows no activity for this substrate.[10]

The apparent K_m, V_{max}, k_{cat}, and catalytic efficiency (k_{cat}/K_m) of D-XI using D-glucose as substrate were 1099 ± 98 mM, 4.6 ± 0.2 U/mg, 15.5 ± 0.8 s^{-1}, and 0.014 mM^{-1} s^{-1}, respectively. For D-xylose the apparent K_m, V_{max}, k_{cat}, and catalytic efficiency (k_{cat}/K_m) were estimated to be 177.4 ± 5.6 mM, 43.1 ± 0.6 U/mg, 146.6 ± 1.9 s^{-1}, and 0.83 mM^{-1} s^{-1}, respectively.

The lower K_m value for D-xylose than for D-glucose is in agreement with the natural function of the D-XI to produce xylulose for the pentose phosphate or phosphoketolase pathway.[46] The high K_m value for D-glucose is compareable to that from *L. brevis*.[47]

Conversion Experiments. L-AI converted D-galactose to D-tagatose at a conversion ratio of approximately 35% after 25 h of incubation at 60 °C (Figure 4). The use of L-AI (120 U) from the related organism *L. plantarum* SK-2 resulted in a conversion rate of 39% after 96 h at 35 °C,[45] whereas the enzyme from strain NC8 showed a yield of 30% after 6 h at 60 °C. A similar equilibrium was observed by using D-AI from *L. sakei* as biocatalyst (36% after 7 h at 40 °C),[9] whereas a higher conversion yield (55% after 96 h at 65 °C) can be obtained by using the enzyme (9.98 U) from *L. fermentum* CGMCC2921 and 50 mM substrate.[1]

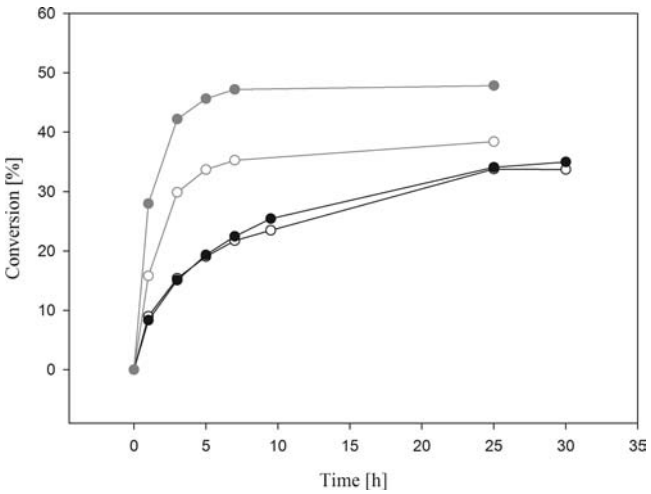

Figure 4. Time course of D-tagatose (black symbols) and D-fructose (gray symbols) production during L-AI- and D-XI-catalyzed isomerization of D-galactose and D-glucose, respectively: black, open circle) conversion curve at 60 °C performed with 0.9 mg of L-AI (expressed in pSIP609 *L. plantarum*); (black, solid circle) conversion curve at 60 °C performed with 1.0 mg of L-AI (expressed in pET21-a(+) *E. coli*); (gray, open circle) conversion curve at 60 °C performed with 0.9 mg of D-XI (expressed in pSIP609 *L. plantarum*); (gray, solid circle) conversion curve at 60 °C performed with 1.9 mg of D-XI (expressed in pET21-a(+) *E. coli*).

The conversion of D-glucose resulted in approximately 48% D-fructose after 25 h of incubation and the use of D-XI produced in the expression host *E. coli* (Figure 4). Using D-XI produced in *L. plantarum* resulted in approximately 38% D-fructose after 25 h of incubation (Figure 4) when approximately 1 unit (approximately 1 mg) of purified protein was used for the conversion experiment. After an incubation of 3 h, conversion rates of approximately 42% (*E. coli*) and 30% (*L. plantarum*) were obtained; thus, the reaction reached its equilibrium after 3 h. A reaction temperature at 40 °C for 3 h resulted in conversion rates of approximately 30 and 9% (data not shown). For industrial purposes an operating temperature of 60 °C is favorable due to the reasons mentioned above (i.e., limited color formation and byproduct formation). HPLC analysis revealed that no byproducts were formed, either in the conversion of D-galactose or in the case of D-glucose (data not shown).

In summary, this study demonstrates the successful expression of the L-arabinose isomerase and D-xylose isomerase encoding genes from *L. reuteri* in *E. coli* as well as the coexpression of both genes in the food grade microorganism *L. plantarum*. Small-scale conversion experiments demonstrate the principal suitability of both enzymes for isomerization of D-galactose and D-glucose, the hydrolysis products of lactose, under preferred industrial conditions (acidic pH and 60 °C). Neither enzyme is ideally suited for the envisaged application due to their rather unfavorable K_m values as well as their dependence on divalent metal cations. However, enzymes with more favorable properties can be screened from a large number of organisms that are considered safe, or an improvement of these properties by enzyme engineering methods[48] may be an alternative. The expression system based on the pSIP vector series is suitable for other lactic acid bacteria as well, and construction of alanine racemase-deficient strains containing no foreign DNA has been shown to be straightforward for organisms that are amenable to transformation.[19] Higher yields can be achieved by expression in *E. coli* and presumably also by expression of the single genes; however, the presented coexpression of two enzymes in a food grade host−vector system offers the possibility of cost-efficient production of enzyme preparations for the conversion of mixed substrates.

■ ASSOCIATED CONTENT

Supporting Information

Additional figures. This material is available free of charge via the Internet at http://pubs.acs.org.

■ AUTHOR INFORMATION

Corresponding Author

*(C.K.P.) Phone: +43 1 47654 6144. Fax: +43 1 47654 6199. E-mail: clemens.peterbauer@boku.ac.at.

Funding

This work was supported by the Austrian Science Fund FWF (Grant P22094 to C.K.P.).

Notes

The authors declare no competing financial interest.

■ ACKNOWLEDGMENTS

We thank Dr. Martin Tangney for kindly supplying *E. coli* MB2159 and Cindy Lorenz for technical assistance and performing the HPLC analysis.

■ ABBREVIATIONS USED

L-AI, L-arabinose isomerase; D-XI, D-xylose isomerase; GI, glucose isomerase; *L.*, *Lactobacillus*; HCFS, high-fructose corn syrup

■ REFERENCES

(1) Xu, Z.; Qing, Y.; Li, S.; Feng, X.; Xu, H.; Ouyang, P. A novel L-arabinose isomerase from *Lactobacillus fermentum* CGMCC2921 for D-tagatose production: gene cloning, purification and characterization. *J. Mol. Catal. B: Enzymatic* **2011**, *70* (1−2), 1−7.

(2) Rhimi, M.; Messaoud, E. B.; Borgi, M. A.; Khadra, K. B.; Bejar, S. Co-expression of L-arabinose isomerase and D-glucose isomerase in *E. coli* and development of an efficient process producing simultaneously D-tagatose and D-fructose. *Enzyme Microb. Technol.* **2007**, *40* (6), 1531−1537.

(3) Salonen, N.; Nyyssölä, A.; Salonen, K.; Turunen, O. *Bifidobacterium longum* L-arabinose isomerase overexpression in *Lactococcus lactis*, purification, and characterization. *Appl. Biochem. Biotechnol.* **2012**, *168* (2), 392−405.

(4) Oh, D. K. Tagatose: properties, applications, and biotechnological processes. *Appl. Microbiol. Biotechnol.* **2007**, *76* (1), 1−8.

(5) Roh, H. J.; Yoon, S. H.; Kim, P. Preparation of L-arabinose isomerase originated from *Escherichia coli* as a biocatalyst for D-tagatose production. *Biotechnol. Lett.* **2000**, *22* (3), 197−199.

(6) Kim, P.; Yoon, S. H.; Seo, M. J.; Oh, D. K.; Choi, J. H. Improvement of tagatose conversion rate by genetic evolution of thermostable galactose isomerase. *Biotechnol. Appl. Biochem.* **2001**, *34* (2), 99−102.

(7) Ibrahim, O. O.; Spradlin, J. E. Process for manufacturing D-tagatose USA. U.S. Patent 6,057,135, 2000.

(8) Kim, P. Current studies on biological tagatose production using L-arabinose isomerase: a review and future perspective. *Appl. Microbiol. Biotechnol.* **2004**, *65* (3), 243−249.

(9) Rhimi, M.; Ilhammami, R.; Bajic, G.; Boudebbouze, S.; Maguin, E.; Haser, R.; Aghajari, N. The acid tolerant L-arabinose isomerase from the food grade *Lactobacillus sakei* 23K is an attractive D-tagatose producer. *Bioresour. Technol.* **2010**, *101* (23), 9171−9177.

(10) Men, Y.; Zhu, Y.; Zhang, L.; Kang, Z.; Izumori, K.; Sun, Y.; Ma, Y. Enzymatic conversion of D-galactose to D-tagatose: cloning, overexpression and characterization of L-arabinose isomerase from *Pediococcus pentosaceus* PC-5. *Microbiol. Res.* **2014**, *169*, 171−178.

(11) Bhosale, S. H.; Rao, M. B.; Deshpande, V. V. Molecular and industrial aspects of glucose isomerase. *Microbiol. Rev.* **1996**, *60* (2), 280−300.

(12) Mrabet, N. T.; Van Den Brande, I.; Van Den Broeck, A. One-step purification of *Actinoplanes missouriensis* D-sylose isomerase by high-performance immobilized copper-affinity chromatography: functional analysis of surface histidine residues by site-directed mutagenesis. *Biochemistry* **1992**, *31* (10), 2690−2702.

(13) Boguslawski, G.; Rynski, M. J. Novel strain of *Bacillus licheniformis* useful in production of glucose isomerase and method of screening *Bacillus* mutants for the ability to produce glucose isomerase in the absence of xylose. U.S. Patent 4,355,103, 1982.

(14) Vuolanto, A.; Uotila, S.; Leisola, M.; Visuri, K. Solubility and crystallization of xylose isomerase from *Streptomyces rubiginosus*. *J. Cryst. Growth* **2003**, *257* (3−4), 403−411.

(15) Jørgensen, F.; Hansen, O. C.; Stougaard, P. Enzymatic conversion of D-galactose to D-tagatose: heterologous expression and characterisation of a thermostable L-arabinose isomerase from *Thermoanaerobacter mathranii*. *Appl. Microbiol. Biotechnol.* **2004**, *64* (6), 816−822.

(16) Peterbauer, C.; Maischberger, T.; Haltrich, D. Food-grade gene expression in lactic acid bacteria. *Biotechnol. J.* **2011**, *6* (9), 1147−1161.

(17) Spath, K.; Heinl, S.; Egger, E.; Grabherr, R. *Lactobacillus plantarum* and *Lactobacillus buchneri* as expression systems: evaluation of different origins of replication for the design of suitable shuttle vectors. *Mol. Biotechnol.* **2012**, *52* (1), 40−48.

(18) Giraffa, G.; Chanishvili, N.; Widyastuti, Y. Importance of lactobacilli in food and feed biotechnology. *Res. Microbiol.* **2010**, *161* (6), 480−487.

(19) Nguyen, T. T.; Mathiesen, G.; Fredriksen, L.; Kittl, R.; Nguyen, T. H.; Eijsink, V. G. H.; Haltrich, D.; Peterbauer, C. K. A food-grade system for inducible gene expression in *Lactobacillus plantarum* using an alanine racemase-encoding selection marker. *J. Agric. Food Chem.* **2011**, *59* (10), 5617−5624.

(20) Spath, K.; Heinl, S.; Grabherr, R. Direct cloning in *Lactobacillus plantarum*: electroporation with non-methylated plasmid DNA enhances transformation efficiency and makes shuttle vectors obsolete. *Microb. Cell Factories* **2012**, *11*, 141.

(21) Nguyen, T. T.; Nguyen, H. A.; Arreola, S. L.; Mlynek, G.; Djinović-Carugo, K.; Mathiesen, G.; Nguyen, T. H.; Haltrich, D. Homodimeric β-galactosidase from *Lactobacillus delbrueckii* subsp. *bulgaricus* DSM 20081: expression in *Lactobacillus plantarum* and biochemical characterization. *J. Agric. Food Chem.* **2012**, *60* (7), 1713−1721.

(22) Nguyen, H. A.; Nguyen, T. H.; Nguyen, T. T.; Peterbauer, C. K.; Mathiesen, G.; Haltrich, D. Chitinase from *Bacillus licheniformis* DSM13: expression in *Lactobacillus plantarum* WCFS1 and biochemical characterisation. *Protein Express. Purif.* **2012**, *81* (2), 166−174.

(23) Mathiesen, G.; Sørvig, E.; Blatny, J.; Naterstad, K.; Axelsson, L.; Eijsink, V. G. H. High-level gene expression in *Lactobacillus plantarum* using a pheromone-regulated bacteriocin promoter. *Lett. Appl. Microbiol.* **2004**, *39* (2), 137−143.

(24) Sørvig, E.; Grönqvist, S.; Naterstad, K.; Mathiesen, G.; Eijsink, V. G. H.; Axelsson, L. Construction of vectors for inducible gene expression in *Lactobacillus sakei* and *L. plantarum*. *FEMS Microbiol. Lett.* **2003**, *229* (1), 119−126.

(25) Sørvig, E.; Mathiesen, G.; Naterstad, K.; Eijsink, V. G. H.; Axelsson, L. High-level, inducible gene expression in *Lactobacillus sakei* and *Lactobacillus plantarum* using versatile expression vectors. *Microbiology* **2005**, *151* (7), 2439−2449.

(26) Mathiesen, G.; Huehne, K.; Kroeckel, L.; Axelsson, L.; Eijsink, V. G. H. Characterization of a new bacteriocin operon in sakacin P-producing *Lactobacillus sakei*, showing strong translational coupling between the bacteriocin and immunity genes. *Appl. Environ. Microbiol.* **2005**, *71* (7), 3565−3574.

(27) Terpe, K. Overview of bacterial expression systems for heterologous protein production: from molecular and biochemical fundamentals to commercial systems. *Appl. Microbiol. Biotechnol.* **2006**, *72* (2), 211−222.

(28) Casas, I. A.; Dobrogosz, W. J. Validation of the probiotic concept: *Lactobacillus reuteri* confers broad-spectrum protection against disease in humans and animals. *Microb. Ecol. Health Dis.* **2000**, *12* (4), 247−285.

(29) Inoue, H.; Nojima, H.; Okayama, H. High efficiency transformation of *Escherichia coli* with plasmids. *Gene* **1990**, *96* (1), 23−28.

(30) Li, S.; Wilkinson, M. F. Site-directed mutagenesis: a two-step method using PCR and DpnI. *BioTechniques* **1997**, *23* (4), 588−590.

(31) Ho, S. N.; Hunt, H. D.; Horton, R. M.; Pullen, J. K.; Pease, L. R. Site-directed mutagenesis by overlap extension using the polymerase chain reaction. *Gene* **1989**, *77* (1), 51−59.

(32) Josson, K.; Scheirlinck, T.; Michiels, F.; Platteeuw, C.; Stanssens, P.; Joos, H.; Dhaese, P.; Zabeau, M.; Mahillon, J. Characterization of a Gram-positive broad-host-range plasmid isolated from *Lactobacillus hilgardii*. *Plasmid* **1989**, *21* (1), 9−20.

(33) Artimo, P.; Jonnalagedda, M.; Arnold, K.; Baratin, D.; Csardi, G.; De Castro, E.; Duvaud, S.; Flegel, V.; Fortier, A.; Gasteiger, E.; Grosdidier, A.; Hernandez, C.; Ioannidis, V.; Kuznetsov, D.; Liechti,

R.; Moretti, S.; Mostaguir, K.; Redaschi, N.; Rossier, G.; Xenarios, I.; Stockinger, H. ExPASy: SIB bioinformatics resource portal. *Nucleic Acids Res.* **2012**, *40* (W1), W597−W603.
(34) Bradford, M. M. A rapid and sensitive method for the quantitation of microgram quantities of protein utilizing the principle of protein dye binding. *Anal. Biochem.* **1976**, *72* (1−2), 248−254.
(35) Dische, Z.; Borenfreund, E. A new spectrophotometric method for the detection and determination of keto sugars and trioses. *J. Biol. Chem.* **1951**, *192* (2), 583−587.
(36) Fox, P. F.; McSweeney, P. L. H. *Advanced Dairy Chemistry: Vol. 3: Lactose, Water, Salts and Minor Constituents*, 3rd ed.; Springer: New York, 2009.
(37) Kaswurm, V.; Nguyen, T. T.; Maischberger, T.; Kulbe, K. D.; Michlmayr, H. Evaluation of the food grade expression systems NICE and pSIP for the production of 2,5-diketo-D-gluconic acid reductase from *Corynebacterium glutamicum*. *AMB Express* **2013**, *3* (1), 1−11.
(38) Elagöz, A.; Abdi, A.; Hubert, J. C.; Kammerer, B. Structure and organisation of the pyrimidine biosynthesis pathway genes in *Lactobacillus plantarum*: a PCR strategy for sequencing without cloning. *Gene* **1996**, *182* (1−2), 37−43.
(39) Pouwels, P. H.; Leer, R. J. Genetics of lactobacilli: plasmids and gene expression. *Antonie van Leeuwenhoek, Int. J. Gen. Mol. Microbiol.* **1993**, *64* (2), 85−107.
(40) Rhimi, M.; Chouayekh, H.; Gouillouard, I.; Maguin, E.; Bejar, S. Production of D-tagatose, a low caloric sweetener during milk fermentation using L-arabinose isomerase. *Bioresour. Technol.* **2011**, *102* (3), 3309−3315.
(41) Manjasetty, B. A.; Chance, M. R. Crystal structure of *Escherichia coli* L-arabinose isomerase (ECAI), the putative target of biological tagatose production. *J. Mol. Biol.* **2006**, *360* (2), 297−309.
(42) Chouayekh, H.; Bejar, W.; Rhimi, M.; Jelleli, K.; Mseddi, M.; Bejar, S. Characterization of an L-arabinose isomerase from the *Lactobacillus plantarum* NC8 strain showing pronounced stability at acidic pH. *FEMS Microbiol. Lett.* **2007**, *277* (2), 260−267.
(43) Umemoto, Y.; Shibata, T.; Araki, T. D-Xylose isomerase from a marine bacterium, *Vibrio* sp. strain XY-214, and D-xylulose production from *β*-1,3-xylan. *Mari. Biotechnol.* **2012**, *14* (1), 10−20.
(44) Liu, S. Y.; Wiegel, J.; Gherardini, F. C. Purification and cloning of a thermostable xylose (glucose) isomerase with an acidic pH optimum from *Thermoanaerobacterium* strain JW/SL-YS 489. *J. Bacteriol.* **1996**, *178* (20), 5938−5945.
(45) Zhang, H.; Jiang, B.; Pan, B. Purification and characterization of L-arabinose isomerase from *Lactobacillus plantarum* producing D-tagatose. *World J. Microbiol. Biotechnol.* **2007**, *23* (5), 641−646.
(46) Ravikumar, S.; Vikramathithan, J.; Srikumar, K. Purification and characterization of a novel thermostable xylose isomerase from *Opuntia vulgaris* Mill. *Appl. Biochem. Biotechnol.* **2011**, *164* (5), 593−603.
(47) Yamanaka, K. Purification, crystallization and properties of the D-xylose isomerase from *Lactobacillus brevis*. *Biochim. Biophys. Acta−Enzymol.* **1968**, *151* (3), 670−680.
(48) Hong, Y. H.; Lee, D. W.; Pyun, Y. R.; Lee, S. H. Creation of metal-independent hyperthermophilic L-arabinose isomerase by homologous recombination. *J. Agric. Food Chem.* **2011**, *59* (24), 12939−12947.
(49) Kleerebezem, M.; Boekhorst, J.; Van Kranenburg, R.; Molenaar, D.; Kuipers, O. P.; Leer, R.; Tarchini, R.; Peters, S. A.; Sandbrink, H. M.; Fiers, M. W. E. J.; Stiekema, W.; Klein Lankhorst, R. M.; Bron, P. A.; Hoffer, S. M.; Nierop Groot, M. N.; Kerkhoven, R.; De Vries, M.; Ursing, B.; De Vos, W. M.; Siezen, R. J. Complete genome sequence of *Lactobacillus plantarum* WCFS1. *Proc. Natl. Acad. Sci. U.S.A.* **2003**, *100* (4), 1990−1995.
(50) Strych, U.; Penland, R. L.; Jimenez, M.; Krause, K. L.; Benedik, M. J. Characterization of the alanine racemases from two *Mycobacteria*. *FEMS Microbiol. Lett.* **2001**, *196* (2), 93−98.

surfactants are relatively stable to droplet growth when the storage temperature is 25−70 °C below the PIT. On the other hand, O/W emulsions stored close to the PIT are highly prone to coalescence, which has been attributed to the ultralow interfacial tension.[16] It is therefore postulated that the storage stability of emulsions that are susceptible to coalescence can be improved by increasing the cloud point or PIT. Studies have shown that the cloud point of nonionic surfactant solutions increases with addition of ionic surfactants[17−20] which was attributed to the generation of electrostatic repulsion between the mixed micelles formed.[20] Addition of ionic surfactants to emulsions stabilized by nonionic surfactants has also been reported to increase their stability to droplet growth.[15,21−23] The purpose of this study was therefore to examine the influence of cosurfactant addition (nonionic, anionic, or cationic) on the thermal and storage stability of nanoemulsions formed in the presence of cosurfactants, and to determine the dominant instability mechanisms.

Previous studies, suggest that there are two main instability mechanisms contributing to the breakdown of vitamin E acetate nanoemulsions (VE-nanoemulsions) containing nonionic surfactants and cosolvents: Ostwald ripening and coalescence.[8,9] We therefore investigated the influence of posthomogenization cosurfactant addition on the stability on VE-nanoemulsions. Recently, it has been shown that this approach can improve the stability of oil-in-water nanoemulsions formed by the PIT method to droplet growth.[15] Cosurfactants may improve nanoemulsion stability by altering the spontaneous curvature of the surfactant monolayer and/or by generating repulsive interactions between droplets (Figure 1). The results of this study should be useful for designing vitamin-enriched delivery systems for utilization in foods, beverages, or pharmaceuticals.

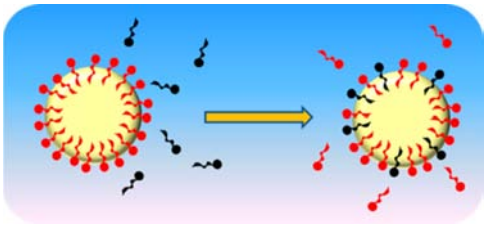

Figure 1. Schematic representation of the surfactant displacement approach: A nanoemulsion is created with one kind of surfactant, and then this is partially displaced by mixing it with another surfactant.

MATERIALS AND METHODS

Materials. Vitamin E acetate (VE, >96% purity) was kindly donated by BASF (Ludwigshafen, Germany). Nonionic surfactants (Tween 80 and 20) and sodium dodecyl sulfate (SDS, 99% purity) were purchased from Sigma-Aldrich Co. (St. Louis, MO). Lauric arginate (LAE) was obtained from Vedeqsa (Vedeqsa Inc., New York, NY). Citric acid and sodium benzoate were provided by PepsiCo (Valhalla, NY). Ethanol (99%) was purchased from Fisher Scientific Co. (Springfield, NJ). Double distilled water was used in the preparation of all solutions and nanoemulsions. All concentrations are expressed as a mass percentage (w/w %) of whole emulsion.

Nanoemulsion Preparation. Nanoemulsion formation was carried out using a method based on a spontaneous emulsification procedure described in the previous study.[9] In brief, spontaneous emulsification was performed by addition of an organic phase to an aqueous phase while magnetically stirring (600 rpm) the system at 25 °C. The organic phase consisted of different amounts of VE and surfactant, while the aqueous phase was a buffer solution (pH 3.0, 0.8% citric acid, 0.08% sodium benzoate) that contained ethanol. The initial nanoemulsions were prepared with the following composition: 10% vitamin E acetate, 10% Tween 80, 20% ethanol, and 60% buffer solution (pH 3). In these samples, the oil (10 g) and surfactant (10 g) were first mixed together and then the mixture was slowly poured into 80 g of aqueous phase over a 15-min period with continuous stirring.

Surfactant Displacement. Surfactant displacement was carried out using a method described previously[15] with a slight modification. Vitamin E nanoemulsions were prepared using the spontaneous emulsification method as described above and then diluted 2-fold using solutions of either nonionic (Tween 20) or ionic (SDS and/or lauric arginate) cosurfactants containing different cosurfactant concentrations.

Particle Size and Charge Measurements. Particle size distributions were measured using a dynamic light scattering instrument (Zetasizer Nano ZS, Malvern Instruments, Malvern, UK). This instrument determines the particle size from intensity−time fluctuations of a laser beam (633 nm) scattered from a sample at an angle of 173°. Each individual measurement was an average of 13 runs. To avoid multiple scattering effects, samples were diluted (× 500) before the particle size measurements using buffer solution (pH 3.0). The mean droplet radius (Z-average) was calculated from the particle size distribution. All measurements were conducted at ambient temperature.

The ζ-potential of the droplets in the emulsions was measured using a particle electrophoresis instrument (NanoZS, Malvern Instruments, Malvern, UK). This instrument calculates the ζ-potential of the particles from measurements of the direction and velocity that the droplets moved in the applied electric field. Conversion of electrophoretic mobility measurements into ζ-potential values was conducted by the software using the Smoluchowsky model. To avoid the multiple scattering, nanoemulsion was diluted before the particle charge measurement using buffer solution (pH 3.0, 0.8% citric acid, 0.08% sodium benzoate).

Turbidity Measurements and Cloud Point Calculation. The influence of temperature on nanoemulsion turbidity was determined using a UV−visible spectrophotometer with temperature scanning capabilities (Evolution Array, Thermo Scientific). The absorbance (A) at 600 nm was measured as the temperature was increased from 20 to 90 °C at 1 °C per minute. The *turbidity increase* was calculated as $A(T) - A(T_0)$, where $A(T)$ is the turbidity at temperature T and $A(T_0)$ is the turbidity at the starting temperature, T_0 (20 °C). The cloud point was determined by fitting the turbidity increase versus temperature data using graphical software (SigmaPlot, Systat Software Inc.). The cloud point was defined as the temperature at which the turbidity increase first reached 1 cm^{-1}.

Statistical Analysis. All experiments were carried out two or three times using two freshly prepared samples, and the results are reported as the calculated mean and standard deviation of these measurements. Statistical analysis was performed through subjection of data to analysis of variance (ANOVA) using statistics software (version 12.0; SPSS, Inc., Chicago, IL). Means were subjected to Duncan's test and a P-value of <0.05 was considered statistically significant.

RESULTS AND DISCUSSION

Effect of Cosurfactants on Thermal Stability. Knowledge of the thermal stability of a nanoemulsion-based delivery system is of particular importance as they are often exposed to elevated temperatures during their manufacture, storage, and utilization. Thermal stability measurements may also be useful as an accelerated test for predicting the stability of nanoemulsions during long-term storage.[9] Therefore, oil-in-water nanoemulsions containing 10% vitamin E acetate (VE), 10% Tween 80, 20% ethanol, and 60% aqueous phase were prepared using the spontaneous emulsification method, and then diluted 2-fold using buffer solutions containing different concentrations of cationic (lauric arginate), ionic (SDS), or nonionic (Tween

20) cosurfactants. This led to nanoemulsions with a final composition of 5% VE, 5% Tween 80, 10% ethanol, and 0−1% cosurfactant.

The dependence of the turbidity on temperature for buffer solution containing 5% (w/w) Tween 80 and 10% (w/w) ethanol and nanoemulsions containing a similar amount of Tween 80 and ethanol and different types and amounts of cosurfactants were determined during heating from 20 to 90 °C. The results for the buffer solution containing Tween 80 and ethanol and nanoemulsions containing different levels of lauric arginate are shown in Figure 2a and b, respectively. Similar

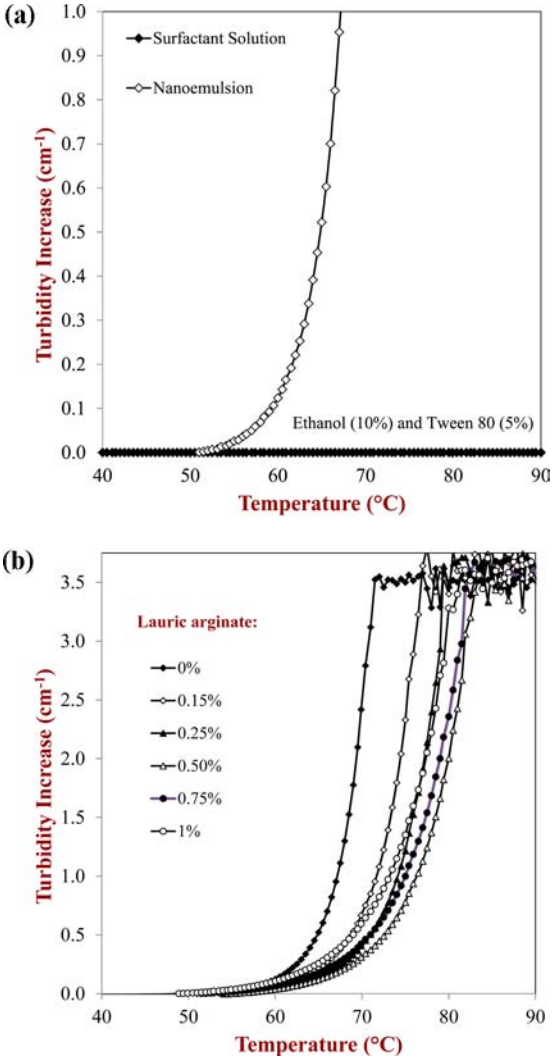

Figure 2. (a) Effect of temperature on the turbidity of surfactant solution containing 5% surfactant, 10% ethanol (pH 3.0) and nanoemulsion containing 5% vitamin E acetate, 5% surfactant, 10% ethanol, and 80% buffer solution (pH 3.0). (b) Effect of lauric arginate on the temperature dependence of the turbidity of nanoemulsions containing 5% oil phase (vitamin E acetate), 5% surfactant (Tween 80), 10% cosolvent (ethanol), and 80% buffer solution (pH 3).

results were also obtained for the nanoemulsions containing SDS or Tween 20 (data not shown). In general, the turbidity of the VE-nanoemulsions was relatively small at low temperatures, increased steeply above a particular temperature (the "cloud point"), and then remained high upon further heating (Figure 2b). Initially, we compared the cloud points of the nanoemulsion and the buffer solution both containing 5% Tween 80 and 10% ethanol (Figure 2a). The turbidity of the buffer solution containing Tween 80 and ethanol did not change over the temperature range of 20−90 °C, suggesting that the cloud point was higher than the range of temperatures studied. However, a steep increase in turbidity was observed at 65 °C for the nanoemulsion (containing no cosurfactant). This result suggests that the presence of the oil phase appreciably decreased the cloud point, presumably by altering the optimum curvature of the system. The presence of the cosurfactants in the nanoemulsions also altered their cloud points, with steep increases in turbidity occurring at 66−74, 71−83, and 75−89 °C for Tween 20, lauric arginate, and SDS, respectively. The observed increase in *turbidity* upon heating can be related to the progressive dehydration of the polar head groups of the nonionic surfactant molecules with increasing temperature.[24,25] The dehydration of the polar head groups of the nonionic surfactants alters their packing parameter ($p = A_T/A_H$), and thereby changes the optimum curvature of the surfactant monolayer. Here, A_T and A_H are the effective cross-sectional areas of the surfactant tail group and headgroup, respectively. At low temperatures, the packing parameter favors the formation of stable oil-in-water nanoemulsions ($A_H > A_T$). As the temperature increases, the headgroup becomes dehydrated (lower A_H) and so the packing parameter moves toward unity, which leads to an ultralow interfacial tension and accelerated droplet coalescence.[26] In addition, surfactant dehydration decreases the steric repulsion between the oil droplets thereby allowing the droplets to come closer together and coalesce. The turbidity increase versus temperature profiles were used to determine the *cloud points* of the nanoemulsions so that we could establish the influence of cosurfactant type and concentration on their thermal behavior.

We defined the cloud point practically as the temperature at which the *turbidity increase* during heating first exceeded 1 cm^{-1}. In general, the cloud point initially increased with increasing cosurfactant concentration, but then it decreased once a particular cosurfactant concentration was exceeded (Figure 3). The highest cloud points obtained for the three cosurfactants were ∼81, 76, and 69 °C at 0.5% SDS, 0.5% lauric arginate, and 0.25% Tween 20, respectively, which compared to a value of ∼67 °C measured in the absence of cosurfactant.

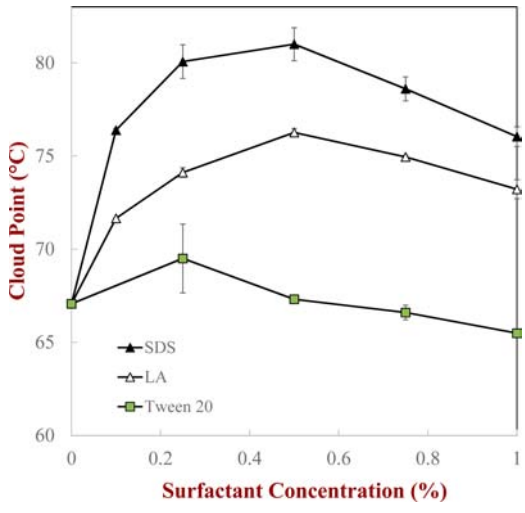

Figure 3. Effect of cosurfactants on the cloud point of nanoemulsions containing 5% oil phase (vitamin E acetate), 5% surfactant (Tween 80), 10% cosolvent (ethanol), and 80% buffer solution (pH 3).

dx.doi.org/10.1021/jf404182b | J. Agric. Food Chem. 2014, 62, 1625−1633

Significantly ($p < 0.05$) higher cloud points were observed in the presence of ionic cosurfactants than in the presence of the nonionic one.

The addition of 0.25% Tween 20 to the VE-nanoemulsions slightly increased the cloud point, but the addition of higher amounts of this cosurfactant caused a slight decrease (Figure 3). Previous studies have reported that Tween 20 has a lower cloud point (~ 79 °C) than Tween 80 (~ 95 °C),[27] which would account for the observed reduction in cloud point at higher Tween 20 levels. Tween 80 and Tween 20 both have similar polar head groups, but the nonpolar tail-groups are different. Tween 20 has a 12-carbon fully saturated hydrocarbon chain ($C_{12:0}$) that would be expected to be linear, whereas Tween 80 has an 18-carbon unsaturated hydrocarbon chain ($C_{18:1}$) that would be expected to be kinked. Consequently, adsorption of Tween 20 to the surfaces of oil droplets initially stabilized by Tween 80 may have changed the optimum curvature of the surfactant monolayer, and thereby altered the PIT and cloud point of the nanoemulsions.

The addition of ionic surfactants (SDS or lauric arginate) to the VE-nanoemulsions also caused an appreciable increase in the cloud point at relatively low levels (0–0.5%), but then caused an appreciable decrease at higher levels (Figure 3). This effect can be attributed to the ability of the ionic surfactants to adsorb to the droplet surfaces and alter the optimum curvature of the surfactant monolayer, as well as increasing the electrostatic repulsion between the oil droplets.

Effect of Cosurfactants on Droplet Charge. Information about the ability of the cosurfactants to adsorb to oil droplet surfaces can be established using droplet charge measurements. In addition, droplet charge plays a key role in determining the stability of nanoemulsions to aggregation: if the droplet charge is sufficiently high, the droplets are prevented from aggregation due to electrostatic repulsion.[28] We therefore measured the droplet charge of VE-nanoemulsions containing different concentrations of ionic and nonionic cosurfactants (Figure 4). The initial nanoemulsions stabilized by Tween 80 had a ζ-potential that was slightly negative (~ −0.8 mV). As expected, addition of different concentrations of nonionic cosurfactant (Tween 20) caused little change in droplet charge (~ −0.8 to −1.1 mV). The small negative charge on the droplet surfaces stabilized by the nonionic surfactants can be attributed to the presence of impurities such as free fatty acids in the surfactant or oil, or preferential adsorption of anions (such as hydroxyl ions) from the water.[29] Addition of increasing amounts of cationic surfactant (lauric arginate) to the VE-nanoemulsions increased the positive charge on the droplets until the ζ-potential reached a relatively constant value (~ +9 mV). Conversely, adding increasing amounts of an anionic surfactant (SDS) to the VE-nanoemulsions increased the negative charge on the droplets until the ζ-potential reached a relatively constant value (~ −11 mV). These results suggested that the ionic surfactants adsorbed to the surfaces of the droplets in the VE-nanoemulsions and altered their electrical characteristics, which would help account for the observed influence of ionic cosurfactants on the thermal stability of the nanoemulsions (Figure 3).

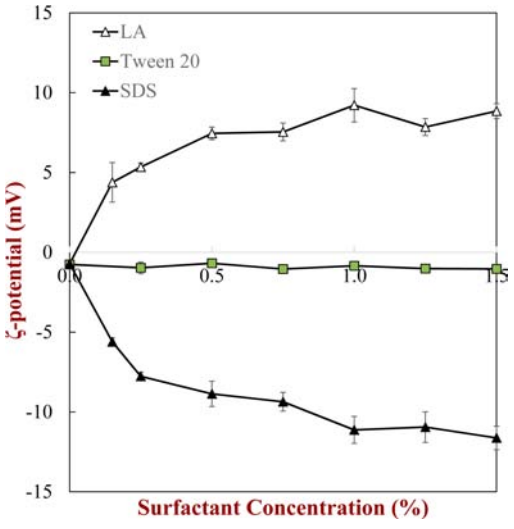

Figure 4. Effect of cosurfactant on the zeta potential of oil droplets in nanoemulsion containing 5% oil phase (vitamin E acetate), 5% surfactant (Tween 80), 10% cosolvent (ethanol), and 80% buffer solution (pH 3).

Effect of Cosurfactants on Storage Stability. Commercial food and beverage products containing emulsion-based delivery systems are required to have good long-term stability during storage, transport, and utilization. Nanoemulsions are thermodynamically unstable systems that may undergo a variety of breakdown processes, including flocculation, coalescence, Ostwald ripening, and gravitational separation.[1,10,28] As mentioned earlier, the two main instability mechanisms in VE-nanoemulsions containing cosolvents are droplet coalescence and Ostwald ripening.[8,9] We therefore examined the possibility of using a surfactant displacement approach for increasing the storage stability of VE-nanoemulsions (containing 20% cosolvent) against droplet growth through these mechanisms. In this approach, VE-nanoemulsions were formed using 10% Tween 80 and 20% ethanol and then diluted (1:1) with aqueous solutions containing different cosurfactants. Three different VE-nanoemulsions were prepared with final concentrations of 5% VE, 5% Tween 80, 10% ethanol, 0.5% cosurfactant, and 79.5% buffer solution. This cosurfactant concentration was selected because it was close to the level where the highest cloud points were observed in the thermal stability studies for the two ionic surfactants (Figure 3). The influence of storage time and holding temperature on their mean droplet sizes was then measured (Figure 5).

In the absence of cosurfactants (control), there was only a slight increase in the mean droplet radius over time for VE-nanoemulsions stored at 5 °C for 1 month, but there was an appreciable increase for those stored at 20 and 37 °C (Figure 5): r increasing from ~22 nm initially to ~25 nm at 5 °C (about 9% increase), ~30 nm at 20 °C (about 30% increase), and ~48 nm at 37 °C (about 112% increase). The droplet size distribution of the VE-nanoemulsions containing no cosurfactant remained monomodal at all storage temperatures, but the peak maximum occurred at larger droplets sizes with increasing storage temperature (Figure 6a). These results indicate that the droplet growth rate increased with increasing holding temperature. Droplet growth may have occurred due to droplet coalescence (merging together of two or more droplets) or Ostwald ripening (diffusion of oil molecules between droplets), which is discussed in Potential Physicochemical Mechanisms.

We found that the addition of the cosurfactants to the VE-nanoemulsions did not improve their isothermal storage stability (Figure 5), even those that appreciably increased the cloud points (Figure 3). Indeed, some of the cosurfactants actually decreased the isothermal stability of the nanoemulsions

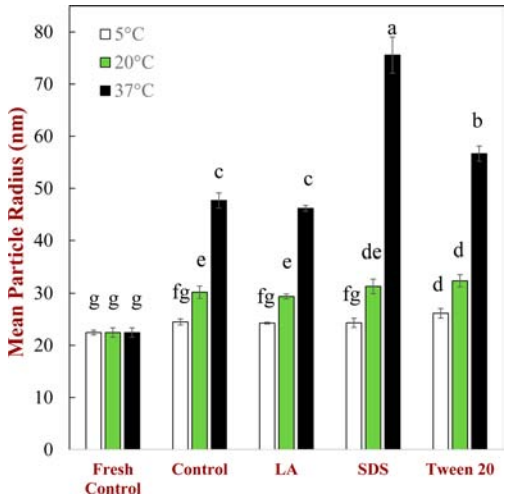

Figure 5. Effect of cosurfactant on mean particle diameter of nanoemulsions (5% vitamin E acetate), 5% surfactant (Tween 80), 10% cosolvent (ethanol), 0.5% cosurfactant, and 79.5% buffer solution) after storage at different holding temperatures for one month. Results are compared with controls (containing no cosurfactant) after 0 days ("fresh") and one month storage. Means with different superscripts are significantly ($P < 0.05$) different.

at elevated holding temperatures, e.g., droplet growth was faster in the nanoemulsions containing SDS than in the control at 37 °C. Like the controls, the particle size distributions of the VE-nanoemulsions in the presence of all three cosurfactants were monomodal at all storage temperatures and times, but with an increase in the location of the maximum at higher storage temperatures (e.g., see Figure 6b for nanoemulsions containing SDS).

Potential Physicochemical Mechanisms. There are a number of possible mechanisms that might be responsible for the observed increase in mean particle size in the nanoemulsions during storage, including flocculation, coalescence, and Ostwald ripening.[2,6,30] We do not believe that flocculation was important in the nanoemulsions used in this study since flocculated droplets were not observed in the systems using an optical microscope. In general, the growth of the individual droplets within a nanoemulsion may occur through either coalescence and/or Ostwald ripening mechanisms.[31] In practice, it is often difficult to distinguish between these two mechanisms, and to precisely establish the relative importance of each mechanism in particular systems. In this section, we present a brief overview of the mechanisms underlying Ostwald ripening and coalescence, and discuss how they may be influenced by cosurfactant addition.

Ostwald Ripening. Ostwald ripening (OR) is the process whereby larger droplets grow at the expense of smaller droplets due to diffusion of disperse phase molecules through the intervening continuous phase.[32] The driving force for this mechanism is the higher chemical potential of the disperse phase within the smaller droplets due to their higher curvature.[33] OR can be divided into two regimes that can be distinguished by the nature of the evolution of the particle size distribution (PSD) during storage: *transient* and *steady state* regimes.[33] Initially, the shape of the PSD depends on the method used to prepare the nanoemulsion. In the transient regime, the shape of the PSD changes over time due to diffusion of oil molecules from the small to the large droplets. Eventually, the PSD attains a characteristic shape (determined

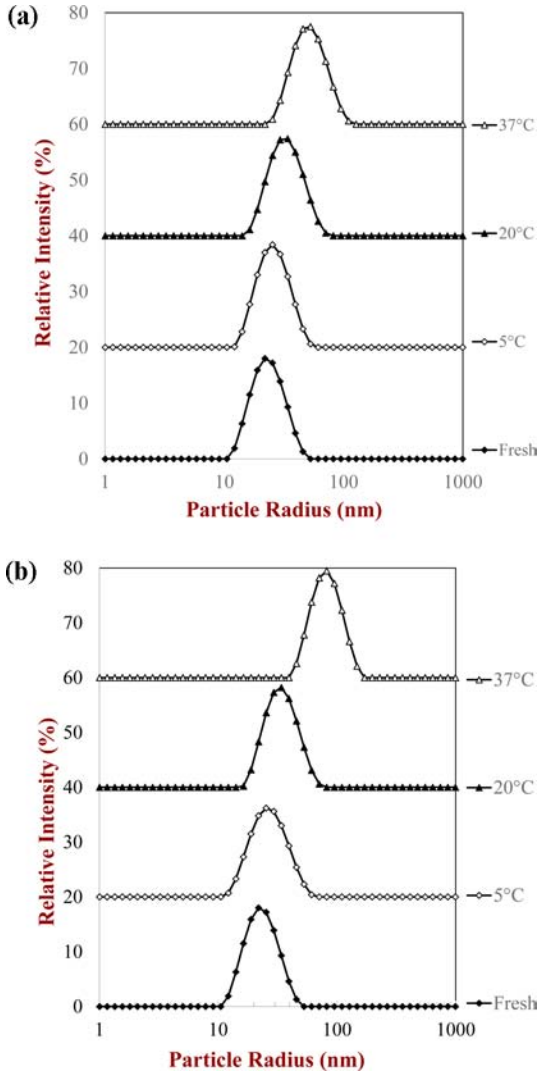

Figure 6. (a) Influence of storage temperature on particle size distribution of nanoemulsions produced using 5% oil phase (vitamin E), 5% surfactant phase (Tween 80), 10% ethanol, and 80% buffer solution immediately after formation ("Fresh") and after storage at different temperatures for one month. (b) Influence of storage temperature on particle size distribution of nanoemulsions produced using 5% oil phase (vitamin E), 5% surfactant phase (Tween 80), 10% ethanol, 0.5% cosurfactant (SDS) and 79.5% buffer solution immediately after formation ("Fresh") and after storage at different temperatures for one month.

by the size-dependence of droplet dissolution and growth processes), which signifies the beginning of the steady-state regime.[33] The PSD then retains this characteristic shape over time, but it moves up the particle size axis as the average size of the droplets continues to increase. In the steady-state regime, the mean droplet radius (r) should vary with time (t) according to the following expression:[33]

$$r^3 - r_0^3 = \omega_{OR} t = \frac{8\gamma V_m^2 c_\infty D}{9RT} t \quad (1)$$

Here, r_0 is the initial droplet radius, ω_{OR} is the Ostwald ripening rate, γ is the oil–water interfacial tension, V_m is the molar volume of the oil, c_∞ is the solubility of the oil in the aqueous phase, D is the diffusion coefficient of the oil molecules through the aqueous phase, R is the gas constant, and T is the

dx.doi.org/10.1021/jf404182b | J. Agric. Food Chem. 2014, 62, 1625–1633

absolute temperature. This theory suggests that the OR rate should increase as the water-solubility of the oil increases, the interfacial tension increases, or the diffusion coefficient increases. Equation 1 indicates that the cube of the mean droplet radius (r^3) should increase linearly with time for nanoemulsions undergoing Ostwald ripening. We therefore calculated r^3 versus time profiles for nanoemulsions at different storage temperatures, e.g., the data at 20 and 37 °C are shown in Figure 7. At 5 °C, we saw little change in the particle size with time, and therefore this data is not shown. The droplet growth rate (ω) for each of the nanoemulsions was calculated from the slope of r^3 versus time by linear regression analysis (Table 1).

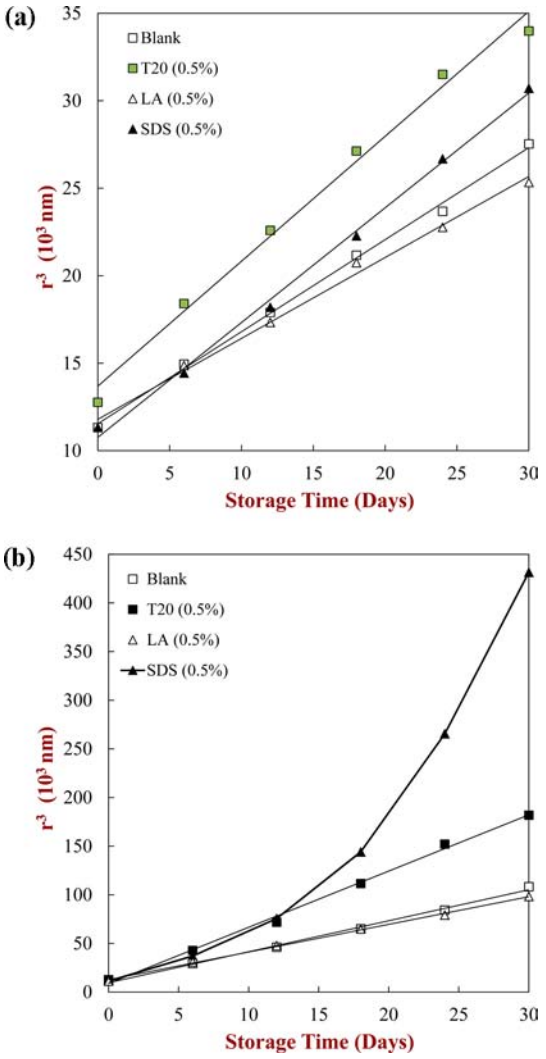

Figure 7. Effect of cosurfactant and storage time on droplet radius cubed of nanoemulsion containing 5% oil phase (vitamin E), 5% surfactant phase (Tween 80), 10% cosolvent (ethanol), 0.5% cosurfactant, and 79.5% buffer solution at storage temperatures of 20 °C (a) and 37 °C (b).

There were linear relationships between r^3 and time for VE-nanoemulsions that contained no cosurfactant, lauric arginate, and Tween 20 at all storage temperatures, and for the VE-nanoemulsions containing SDS at 5 and 20 °C. However, the relationship was not linear for the VE-nanoemulsions containing SDS at 37 °C (Figure 7). It is often assumed that a linear relationship between r^3 and time and a time-invariant particle size distribution is indicative of OR, but this is not generally the case.[31] Theoretical studies have shown that for certain types of coalescence mechanisms the PSD may also reach a constant shape at longer times, and that the cube of the droplet radius may also increase linearly with time, such as Brownian-motion induced coalescence, e.g., see Coalescence section below.[34] At relatively high surfactant concentration (10% Tween 80) in the VE-nanoemulsions studied there may have been appreciable amounts of free surfactant micelles present that could transfer oil molecules between droplets through an Ostwald ripening mechanism[35]or promote droplet aggregation through a depletion mechanism.[36] Further, we experimentally observed that the droplet growth rate increased with increasing temperature, and depended somewhat on cosurfactant addition (Table 1).

A number of physical properties of the system may influence the OR rate as the temperature increases. First, the aqueous phase viscosity decreases with increasing temperature (and therefore D increases), which would increase the OR rate. However, this effect would be expected to be fairly small since the shear viscosity of water only changes from about 1.5 to 0.69 mPa s when the temperature is increased from 5 to 37 °C (CRC Handbook of Chemistry and Physics). Second, the interfacial tension of nonionic surfactant monolayers decreases with increasing temperature due to progressive dehydration of the surfactant head groups,[37] which should decrease the OR rate. The change in interfacial tension with temperature may be appreciable, particularly near the phase inversion temperature (PIT) where the interfacial tension becomes ultralow, and therefore one would expect this effect to play an important role. Third, the solubility of the vitamin E acetate in the aqueous phase is likely to change with temperature. To our knowledge there are no published data on the solubility of vitamin E acetate in aqueous 20% ethanol solutions at different temperatures. We tried to measure this parameter by mixing excess vitamin E acetate with aqueous 20% ethanol solutions and storing the resulting systems at 5, 20, and 37 °C for 72 h. We then used UV−visible spectrophotometry to try to measure the concentration of vitamin E acetate present in the resulting solutions at saturation, using the published wavelength maximum (λ = 292 nm) and extinction coefficient (ε = 3260 M^{-1} cm^{-1}) of this compound.[38] However, the levels of vitamin

Table 1. Calculated Growth Rates of Nanoemulsions Containing Different Cosurfactants (0.5%) at Various Storage Temperatures (Correlation Coefficients Are Shown in Brackets)

	growth rates (nm^3 per day)			
storage temperature	control	+ LA	+ SDS	+ Tween 20
5 °C	106 (0.974)	91 (0.964)	104 (0.994)	154 (0.953)
20 °C	526 (0.999)	463 (0.997)	656 (0.999)	714 (0.995)
37 °C	3190 (0.998)	2840 (0.999)	13600 (0.948)	5780 (0.999)

dx.doi.org/10.1021/jf404182b | J. Agric. Food Chem. 2014, 62, 1625−1633

E acetate present were so small that we could not measure them, i.e., no maximum was observed at the expected wavelength and the UV-signal was close to the baseline.

The solubility of vitamin E acetate in pure water reported in a chemical database (www.scifinder.com) was therefore used to provide a rough prediction of the expected rate of Ostwald ripening in the system: $c_\infty = 2 \times 10^{-6}$ kg m^{-3} or 4.64×10^{-6} mol m^{-3} at 25 °C. The other parameters needed to calculate the OR rate using eq 1 were also taken from this database or measured in our laboratory: $V_m = 0.431$ kg mol^{-1}, $D = 3.9 \times 10^{-10}$ m^2 s^{-1}, $\gamma = 30$ mJ m^{-2}, $R = 8.31$ J K^{-1} mol^{-1}, and $T = 298.1$ K. The droplet growth rate was estimated to be around 4.2×10^5 nm^3/day, which is appreciably higher than the measured droplet growth rates particularly at the higher storage temperatures (Table 1). In addition, the above calculations have ignored the influence of ethanol on the predicted growth rate, and studies have shown that the solubility of vitamin E (α-tocopherol) increases over 5-fold when the ethanol concentration is increased from 0 to 20% in aqueous ethanol solutions.[39] There therefore seems to be a contradiction between the experimental measurements and the theoretical predictions made using the OR theory. There are a number of possible reasons for this discrepancy. First, some of the physicochemical parameters used in the calculations may have been incorrect. In particular, the solubility of the vitamin E acetate in the aqueous phase was predicted using a mathematical model from a chemical database, which may have been incorrect. Second, the influence of surfactant molecules adsorbed to the oil−water interface on the OR rate was ignored. Surfactants are known to decrease the interfacial tension (particularly near the PIT), which would reduce the OR rate considerably.[40] Third, there may have been some highly hydrophobic impurities within the vitamin E acetate preparation used in this study that acted as ripening inhibitors.[32,40]

Coalescence. Coalescence is the process whereby two or more droplets come into close contact and then merge together.[16,26] The rate at which this process occurs depends on the frequency and duration of encounters between droplets, as well as the colloidal and hydrodynamic interactions between them. The following expression has been derived to describe the increase in mean droplet radius with time due to Brownian-motion induced coalescence:[34]

$$r^3 - r_0^3 = \omega_C t = \frac{4.258 r_0^3 N_0 kT(\hat{\mu} + 1)E}{\mu(3\hat{\mu} + 2)} t \approx \frac{\varphi kT(\hat{\mu} + 1)E}{\mu(3\hat{\mu} + 2)} t \quad (2)$$

Here, ω_C is the coalescence droplet growth rate, N_0 is the total number density of droplets in the initial system, ϕ is the disperse phase volume fraction, μ is the viscosity of the continuous phase, $\hat{\mu}$ is the dispersed-to-continuous phase viscosity ratio (μ'/μ), k is Boltzmann's constant, and E is the collision efficiency. The collision efficiency depends on the nature of the colloidal and hydrodynamic interactions between the droplets and typically has a value <1.0. This theory suggests that the coalescence rate (ω_C) should increase as the droplet concentration and collision efficiency increases. Like the OR theory, it predicts that the droplet growth rate should increase linearly with the cube of the droplet radius. For certain initial particle size distributions, this theory also predicts that the PSD should maintain a constant shape at longer storage times, and should just move up the particle size axis with time.[34] The fact that changes in the mean particle size and PSD with time may be similar for OR and coalescence means that it is often difficult to distinguish between these two different growth mechanisms. To estimate the potential contribution of coalescence in the nanoemulsions we calculated the droplet growth rate using eq 2 and the physicochemical properties of the system ($\phi = 0.05$: $\eta = 0.001$ Pa s; $\eta' = 2.95$ Pa s) and assumed that every collision led to coalescence ($E = 1$). We estimated a droplet growth rate of 2400 nm^3/day using eq 2, which is fairly close to the values measured at the higher temperatures. The relatively low growth rates measured at lower temperatures may have been because the collision efficiency was much less than unity, due to the presence of repulsion colloidal interactions operating between the droplets in the nanoemulsions (such as steric or electrostatic repulsion).[24] These calculations suggest that coalescence may play an important role in determining the overall rate of droplet growth in the nanoemulsions during storage, particularly at elevated temperatures near the cloud point.

Experimentally, we observed that the rate of droplet growth increased appreciably with temperature and depended somewhat on cosurfactant addition (Figure 7, Table 1). Previous studies have shown that the rate of droplet coalescence increases as the temperature moves toward the PIT of the system due to changes in the optimum curvature of the surfactant monolayer at the droplet surfaces.[16] When the optimum curvature is close to unity the interfacial tension is very low, which leads to rapid droplet coalescence.[26] For example, Shinoda and Saito[14] showed that O/W emulsions stabilized by nonionic surfactants were relatively stable to droplet growth at storage temperatures well below the PIT, but were highly prone to coalescence at temperatures near the PIT. One might therefore expect that cosurfactants that increase the PIT would improve the coalescence stability of nanoemulsions at elevated temperatures. In addition, one would expect that cosurfactants that increased the repulsive interactions between droplets (decreased the collision efficiency) would reduce the coalescence rate.[34] Nevertheless, we did not find any correlation between increasing effects of cosurfactant on the cloud point (and thereby PIT) and the corresponding storage stability. The origin of this phenomenon is currently unknown, and it would be useful in future studies to identify its molecular basis. In particular, it would be useful to establish the physicochemical origin of the differences in the impact of the different surfactants on the droplet growth rates.

In this study, we investigated the effect of cosurfactants on the thermal and isothermal stability of VE-nanoemulsions (containing ethanol as cosolvent). These systems were highly unstable to droplet growth, which was attributed to droplet coalescence and/or Ostwald ripening. Addition of a nonionic cosurfactant (0.5% Tween 20) has little influence on the cloud point of VE-nanoemulsions, however addition of ionic surfactants (0.5% lauric alginate or SDS) caused an appreciable increase in the cloud point. On the other hand, addition of cosurfactants did not increase the long-term stability of VE-nanoemulsions under isothermal conditions, particularly at elevated temperatures. Theoretical calculations suggested that both coalescence and Ostwald ripening may be important, with coalescence being particularly important at high storage

temperatures. Overall, this study indicated that addition of nonionic or ionic surfactants did not have a major impact on the isothermal storage stability of nanoemulsions, but did alter their phase inversion temperatures.

AUTHOR INFORMATION

Corresponding Author

*Tel: 413-545-1019. Fax: 413-545-1262. E-mail: mcclements@foodsci.umass.edu.

Notes

Disclaimer. The opinions expressed in this manuscript are those of the authors and do not represent statements of position, intention or strategy of PepsiCo Inc.

The authors declare no competing financial interest.

ACKNOWLEDGMENTS

This material is based upon work supported by the Cooperative State Research, Extension, Education Service, United State Department of Agriculture, Massachusetts Agricultural Experiment Station and United States Department of Agriculture, CREES, NRI, and AFRI Grants. We also thank William Mutilangi of PepsiCo for useful advice and discussions on this research.

REFERENCES

(1) McClements, D. J.; Rao, J. Food-grade nanoemulsions: Formulation, fabrication, properties, performance, biological fate, and potential toxicity. *Crit. Rev. Food Sci. Nutr.* **2011**, *51*, 285−330.

(2) Tadros, T.; Izquierdo, P.; Esquena, J.; Solans, C. Formation and stability of nano-emulsions. *Adv. Colloid Interface Sci.* **2004**, *108*−*109*, 303−318.

(3) Anton, N.; Benoit, J. P.; Saulnier, P. Design and production of nanoparticles formulated from nano-emulsion templates - A review. *J. Controlled Release* **2008**, *128*, 185−199.

(4) Solans, C.; Solé, I. Nano-emulsions: Formation by low-energy methods. *Curr. Opin. Colloid Interface Sci.* **2012**, *17*, 246−254.

(5) Ostertag, F.; Weiss, J.; McClements, D. J. Low-energy formation of edible nanoemulsions: Factors influencing droplet size produced by emulsion phase inversion. *J. Colloid Interface Sci.* **2012**, *388*, 95−102.

(6) McClements, D. J. Edible nanoemulsions: Fabrication, properties, and functional performance. *Soft Matter* **2011**, *7*, 2297−2316.

(7) Saberi, A. H.; Fang, Y.; McClements, D. J. Fabrication of vitamin E-enriched nanoemulsions: Factors affecting particle size using spontaneous emulsification. *J. Colloid Interface Sci.* **2013**, *391*, 95−102.

(8) Saberi, A. H.; Fang, Y.; McClements, D. J. Effect of glycerol on formation, stability, and properties of vitamin-E enriched nanoemulsions produced using spontaneous emulsification. *J. Colloid Interface Sci.* **2013**, *411*, 105−113.

(9) Saberi, A. H.; Fang, Y.; McClements, D. J. Fabrication of vitamin E-enriched nanoemulsions by spontaneous emulsification: Effect of propylene glycol and ethanol on formation, stability, and properties. *Food Res. Int.* **2013**, *54*, 812−820.

(10) McClements, D. J. Critical review of techniques and methodologies for characterization of emulsion stability. *Crit. Rev. Food Sci. Nutr.* **2007**, *47*, 611−649.

(11) Friberg, S.; Larsson, K.; Sjoblom, J. *Food Emulsions*; Marcel Dekker: New York, 2004.

(12) Shinoda, K.; Arai, H. Correlation between phase inversion temperature in emulsion + cloud point in solution of nonionic emulsifier. *J. Phys. Chem.* **1964**, *68*, 3485−3490.

(13) Sunderland, V. B.; Enever, R. P. The influence of formulation variables on phase inversion temperatures of emulsions as determined by a programmed viscometric technique. *J. Pharm. Pharmacol.* **1972**, *24*, 804−814.

(14) Shinoda, K.; Saito, H. Stability of O/W type emulsions as functions of temperature and HLB of emulsifiers - emulsification by PIT-method. *J. Colloid Interface Sci.* **1969**, *30*, 258−263.

(15) Rao, J.; McClements, D. J. Stabilization of phase inversion temperature nanoemulsions by surfactant displacement. *J. Agric. Food Chem.* **2010**, *58*, 7059−7066.

(16) Leal-Calderon, F.; Schmitt, V.; Bibette, J. *Emulsion Science: Basic Principles*; Springer Verlag: Duesseldorf, 2007.

(17) Marszall, L. Cloud point of mixed ionic-nonionic surfactant solutions in the presence of electrolytes. *Langmuir* **1988**, *4*, 90−93.

(18) Schott, H.; Royce, A. E. Effect of inorganic additives on solutions of nonionic surfactants VI: Further cloud point relations. *J. Pharm. Sci.* **1984**, *73*, 793−799.

(19) Gu, T.; Qin, S.; Ma, C. The effect of electrolytes on the cloud point of mixed solutions of ionic and nonionic surfactants. *J. Colloid Interface Sci.* **1989**, *127*, 586−588.

(20) Valaulikar, B. S.; Manohar, C. The mechanism of clouding in triton X-100: The effect of additives. *J. Colloid Interface Sci.* **1985**, *108*, 403−406.

(21) Avranas, A.; Stalidis, G. Interfacial properties and stability of oil-in-water emulsions stabilized with binary mixtures of surfactants: II. Effect of a cationic surfactant on a nonionic surfactant stabilized emulsion. *J. Colloid Interface Sci.* **1991**, *143*, 180−187.

(22) Stalidis, G.; Avranas, A.; Jannakoudakis, D. Interfacial properties and stability of oil-in-water emulsions stabilized with binary mixtures of surfactants. *J. Colloid Interface Sci.* **1990**, *135*, 313−324.

(23) Wang, L.; Tabor, R.; Eastoe, J.; Li, X.; Heenan, R. K.; Dong, J. Formation and stability of nanoemulsions with mixed ionic-nonionic surfactants. *Phys. Chem. Chem. Phys.* **2009**, *11*, 9772−8.

(24) Israelachvili, J. *Intermolecular and Surface Forces*, 3rd ed.; Academic Press: London, UK, 2011.

(25) Shinoda, K.; Friberg, S. *Emulsions and Solubilization*; Wiley Interscience: New York, 1986.

(26) Kabalnov, A.; Wennerstrom, H. Macroemulsion stability: The oriented wedge theory revisited. *Langmuir* **1996**, *12*, 276−292.

(27) Chawla, J.; Mahajan, R. K. Cloud point studies of Tween and glycol in the presence of salts. *J. Dispersion Sci. Technol.* **2011**, *32*, 822−827.

(28) McClements, D. J. *Food Emulsions: Principles, Practice, and Techniques*, 2nd ed.; CRC Press: Boca Raton, FL, 2005.

(29) Ziani, K.; Barish, J. A.; McClements, D. J.; Goddard, J. M. Manipulating interactions between functional colloidal particles and polyethylene surfaces using interfacial engineering. *J. Colloid Interface Sci.* **2011**, *360*, 31−38.

(30) Mason, T. G.; Wilking, J. N.; Meleson, K.; Chang, C. B.; Graves, S. M. Nanoemulsions: Formation, structure, and physical properties. *J. Phys.: Condens. Matter* **2006**, *18*, R635−R666.

(31) Nazarzadeh, E.; Anthonypillai, T.; Sajjadi, S. On the growth mechanisms of nanoemulsions. *J. Colloid Interface Sci.* **2013**, *397*, 154−162.

(32) Taylor, P. Ostwald ripening in emulsions. *Adv. Colloid Interface Sci.* **1998**, *75*, 107−163.

(33) Kabalnov, A. S.; Shchukin, E. D. Ostwald Ripening Theory - Applications to Fluorocarbon Emulsion Stability. *Adv. Colloid Interface* **1992**, *38*, 69−97.

(34) Wang, H.; Davis, R. H. Droplet growth due to Brownian, gravitational, or thermocapillary motion and coalescence in dilute dispersions. *J. Colloid Interface Sci.* **1993**, *159*, 108−118.

(35) McClements, D. J.; Dungan, S. R. Factors that affect the rate of oil exchange between oil-in-water emulsion droplets stabilized by a nonionic surfactant: Droplet size, surfactant concentration, and ionic strength. *J. Phys. Chem.* **1993**, *97*, 7304−7308.

(36) McClements, D. J. Ultrasonic determination of depletion flocculation in oil-in-water emulsions containing a non-ionic surfactant. *Colloids Surf., A* **1994**, *90*, 25−35.

(37) Fujiu, K. B.; Kobayashi, I.; Neves, M. A.; Uemura, K.; Nakajima, M. Effect of temperature on production of soybean oil-in-water emulsions by microchannel emulsification using different emulsifiers. *Food Sci. Technol. Res.* **2011**, *17*, 77−86.

(38) Dahot, M. U.; Memon, M. A.; Memon, M. A. UV-spectrophotometric determination of α-tocopherol acetate in pharmaceutical preparations. *Pak. J. Pharm. Sci.* **1990**, *3*, 53−59.
(39) Dubbs, M. D.; Gupta, R. B. Solubility of vitamin E (alpha-tocopherol) and vitamin K-3 (menadione) in ethanol-water mixture. *J. Chem. Eng. Data* **1998**, *43*, 590−591.
(40) Kabalnov, A. S.; Pertzov, A. V.; Shchukin, E. D. Ostwald ripening in 2-component disperse phase systems - Application to emulsion stability. *Colloids Surf.* **1987**, *24*, 19−32.

tension. After adjustment to the same protein concentration, the heated SPI was used to prepare emulsions using a high-shear homogenizer. We examined the effects of homogenizer rotating speed and ionic strength on soy protein aggregates' adsorption. Results of the study could provide more information as to the effects of heating conditions on the emulsifying properties of soy proteins.

MATERIALS AND METHODS

Materials. Low-denatured, defatted soy flakes were kindly provided by Shandong Gushen Industrial & Commercial Co., Ltd. (Dongying, Shandong, China). For the preparation of the emulsions, soybean oil was obtained from a local supermarket and purified with Florisil (60−100 mesh, Sigma-Aldrich) to remove surface-active impurities. All other reagents and chemicals were of analytical grade.

Preparation of Soy Proteins. The defatted soy flakes were dispersed in 15-fold distilled water and adjusted to pH 7.0 with 2 M NaOH. After stirring for 1 h, the suspension was centrifuged at 15500*g* for 30 min at 4 °C, and then the supernatant was subjected to isoelectric precipitation by adjusting the pH to 4.5 with 2 M HCl and centrifuged at 4 °C for 1 h. The protein precipitate was washed twice with distilled water and then adjusted to pH 7.0 by 2 M NaOH. This protein suspension was centrifuged at 15500*g* for 30 min at 4 °C (CR-21G, Hitachi, Japan), and the supernatant was then freeze-dried and ground to yield soy proteins. Protein content of the prepared soy protein was 90.6% (w/w) as determined by using the micro-Kjeldahl method with a nitrogen conversion factor of 6.25.

Native soy protein (NSP) solution with concentrations of 1, 3, and 5% (w/v) were prepared by dissolving soy proteins prepared as above in 10 mM sodium phosphate buffer and stored at 4 °C overnight. The final pH was adjusted to 7.0 by adding 1 M NaOH or 1 M HCl. The protein dispersions were filtered to remove the insoluble particles through 0.45 μm filters (Φ50 mm × 0.45 μm, low protein binding, Sinopharm Chemical Reagent Co., Ltd.), using a sand core filter device by vacuum extraction filtering method. The filtrates were heated in a 95 °C water bath for 30 min and cooled to room temperature in an ice bath to obtain H1, H3, and H5, which was heated at protein concentrations 1, 3, and 5%, respectively. The protein concentration of the final solutions was checked by using the Lowry method.[14] In our experiment, high-purity native soy protein was used as a protein standard. The high-purity native soy protein was prepared in this laboratory and has a protein content of 99.0% as determined by the micro-Kjeldahl method.

High-Performance Size Exclusion Chromatography (HPSEC). The molecular weight distribution was determined according to the method of Wu et al.[15] Native and heated soy protein solutions were filtered through a cellulose acetate membrane with a pore size of 0.45 μm (Sartorius Co., Ltd., Gottingen, Germany). A Waters 2690 liquid chromatograph system (Waters Chromatography Division, Milford, MA, USA) equipped with a Shodex protein KW-804 column (Shodex Separation and HPLC Group, Tokyo, Japan) was used. The elution was performed with 50 mM phosphate buffer (pH 7.0, including 0.3 M NaCl) at a flow rate of 1.0 mL/min. About 20 μL of protein solutions was injected into the column, and the fluent was monitored at 280 nm. The relative amount of the aggregates was expressed as the percentage of its peak areas (PA) as related to the total area (TA) (eq 1). The content of non-aggregated fraction was calculated by taking the difference in relative protein content reading in the whole solution and the aggregates (eq 2).

$$C_{\text{aggregates}} = \frac{\text{PA}_{\text{aggregates}}}{\text{TA}} \times C_{\text{solution}} \quad (1)$$

$$C_{\text{non-aggregates}} = C_{\text{solution}} - C_{\text{aggregates}} \quad (2)$$

Dynamic Light Scattering. Apparent hydrodynamic radius (Rh) was determined according to method of Wang et al.[6] To avoid multiple particle effects, protein samples were diluted to 1.0 mg/mL with 10 mM phosphate buffer (pH 7.0), and the native proteins were filtered through a 0.45 μm filter. The appropriate viscosity and refractive index parameters for each solution were set. DLS analysis was carried out at a fixed angle of 173° using a Zetasizer Nano-ZS instrument (Malvern Instruments, British) at 25 °C. All measurements were performed in at least duplicate at room temperature, and the results reported are averaged over three readings.

Surface Hydrophobicity. Surface hydrophobicity of protein samples was determined according to the method of Wang et al.[6] The aliquots (1.0 mL) of protein solutions (0.2 mg/mL) were placed in the cell of an F7000 fluorescence spectrophotometer (Hitachi Co., Japan), and aliquots (10 μL) of 1-anilino-8-naphthalenesulfonate (ANS; 5 mM in 10 mM phosphate buffer, pH 7.0) were titrated to reach a final concentration of 50 μM. The molar coefficient (5000 M^{-1} cm^{-1} at 350 nm) was used to calculate ANS concentration. The relative fluorescence intensity (F) was measured at 390 nm (excitation; slit width, 5 nm) and 470 nm (emission; slit width, 5 nm). Data were elaborated using the Lineweaver−Burk equation (eq 3)

$$1/F = 1/F_{\max} + (K_d/L_0)(1/F_{\max}) \quad (3)$$

where L_0 is the fluorescent probe concentration (μM), $F_{\max}$ is the maximum fluorescence intensity of the ANS probe (at saturating probe concentration), and K_d is the apparent dissociation constant of a supposedly monomolecular protein/ANS complex. $F_{\max}$ can be calculated by standard linear regression fitting procedures.

Interfacial Tension. The interfacial tensions between soybean oil and 10 mM phosphate buffer or the protein solutions were measured according to the Wilhelmy plate method,[16] using a dynamic contact angle meter and tensiometer (DCAT21, Dataphysics, Germany), at 25 °C. The aqueous phase was water or SPI solution (0.3%, w/v) in water, pH adjusted to 7.0.

Emulsion Preparation. Two different series of emulsions were prepared. In the first series, the pH (7.0) and the salt addition level (0 M) were kept constant, whereas the homogenizer rotating speed was varied between 10000 and 22000 rpm. In the second series, the homogenizer rotating speed (16000 rpm) and the pH (7.0) were kept constant, whereas the salt addition level was adjusted to 0, 0.1, 0.2, 0.3, and 0.4 M, respectively. All protein samples were diluted to 0.3% (w/v) using 10 mM sodium phosphate buffer, pH 7.0, containing 0.02% sodium azide as an antimicrobial agent. Emulsions were prepared by mixing 10% soybean oil with 90% SPI solution and emulsified using a high-shear homogenizer (FA25 model, Fluko Equipment Co., Ltd., Shanghai, China) for 2 min at room temperature. Each emulsion was prepared at least three times to check for processing repeatability and stored at 4 °C for further analysis (within 2 h).

Mean Particle Size of Emulsion. The particle size distribution of the emulsion was determined using a Mastersizer 2000 laser particle-size analyzer (Malvern Instruments, Malvern, U.K.). The refractive indices of soybean oil and phosphate buffer were taken as 1.472 and 1.330, respectively; absorption index, 0.001; obscuration value, 15%. Half a milliliter of fresh emulsion was taken and diluted in 10 mL of 1% SDS solution (1% SDS in 10 mM phosphate buffer). The particle sizes measured are reported as the area-weighted mean diameter, d_{32}.

Determination of Protein Concentration at the O/W Interface. The concentration of protein adsorbed at the O/W interface was determined according to the method described by Keerati-u-rai et al.[1] with some modifications. Emulsions were centrifuged twice at 15500*g* at 4 °C for 45 min. The serum phase (unadsorbed protein) was withdrawn carefully using a syringe, and the protein concentration was determined according to the method of Lowry et al.[14]

The aggregates (A) or non-aggregates (NA) remaining in serum phase were determined using high-performance size exclusion chromatography (HPSEC).[15] The serum phase was concentrated by ultrafiltration tubes to about 3 mg/mL before the HPSEC experiment.

The surface load (Γ) was obtained by relating the adsorbed amount to the specific surface area of the emulsion.[13,17] Equation 4 was used to calculate the surface load (Γ) in this study:[13]

$$\Gamma\ (\text{mg/m}^2) = \frac{d_{32}(C_{\text{INI}} - C_{\text{SER}})(1 - \Phi)}{6\Phi} \quad (4)$$

dx.doi.org/10.1021/jf404464z | J. Agric. Food Chem. 2014, 62, 1634−1642

C_{INI} and C_{SER} are the protein concentration in the initial solution (prior to emulsification) and the concentration in the aqueous phase after the centrifugation procedure, respectively. Φ is the volume fraction of oil phase.

Statistical Analysis. Experiment data were analyzed by analysis of variance (ANOVA) using the SAS 9.1 package (SAS 2005). A least significant difference (LSD) test with a confidence interval of 95% was used to compare the means. All treatments were run in triplicate. Data were expressed as the mean ± SD (n = 3).

RESULTS AND DISCUSSION

Characterization of Soy Proteins. Heat treatment above the denaturation temperature caused protein unfolding and subsequent protein aggregation. As shown in Figure 1, native soy proteins (NSP) resulted in two peaks at 9−10 and 11−12 min, corresponding to molecular weights of 150 kDa (20−630 kDa) and 14.1 kDa (2−20 kDa). Elution profiles for heated soy proteins revealed that protein aggregates' peak emerged at about 6 min, and heating at higher protein concentration resulted in more aggregates. Protein aggregates' content increased from 0 to 1.92 mg/mL for H5, whereas the non-aggregated protein decreased from 2.78 to 0.857 mg/mL. Ratios of non-aggregated proteins to protein aggregates were approximately 1:2, 1:1, and 2:1 for H1, H3, and H5, respectively. At the same time, R_h values also increased with the heating concentration of proteins (Table1). These findings are well in agreement with previous studies.[8,18,19]

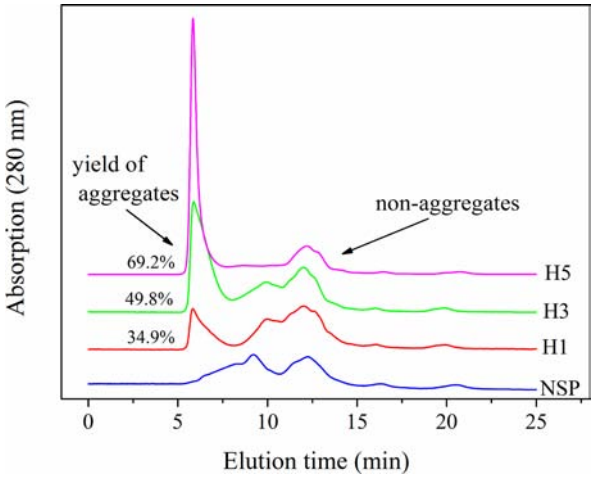

Figure 1. HPSEC profiles of native and heat-denatured soy proteins.

Surface hydrophobicity of protein has long been used to characterize the structural changes and recognized as a related factor controlling surface activity of protein. Table 1 summarizes the surface hydrophobicity data of native and heated soy proteins. The surface hydrophobicity of all heated proteins was significantly (p < 0.05) higher than that of NSP. Several previous studies had also reported that heat-treated soy protein possessed higher surface hydrophobicity than the native protein.[20,21] These changes might be induced by a modification of the native structure of soy proteins during heat treatment: more hydrophobic group clusters in the interior of molecule transferred to protein's surface as a consequence of heat-induced protein unfolding.[22] Furthermore, the heated proteins that were heated at higher concentration possessed more surface hydrophobicity. This may seem surprising because aggregation of heat-denatured proteins was thought to take place through hydrophobic interactions between nonpolar groups; thus, more aggregates mean fewer exposed hydrophobic groups. Semisotnov et al.[23] pointed out that protein−ANS binding was not only affected by accessibility of hydrophobic area but also influenced by the protein structure. Most probably, soy proteins heated at higher concentrations were more "molten globule" like and had higher β-structure, both of which displayed a higher affinity to ANS. The interfacial tension of the soybean oil−phosphate buffer (10 mM) was 18.1 mN/m. When soy protein (0.3%) was added to the aqueous phase, the interfacial tension of the O/W interface substantially decreased. However, heat treatment induced only a slight decrease in interfacial tension of soy proteins (Table 1). Possibly in addition to hydrophobicity, the interfacial tension is also related to properties such as molecular size and flexibility.[24,25]

Table 1. Surface Hydrophobicity (F_{max}), Interfacial Tension (σ), and Hydrodynamic Radius (R_h) of NSP or Heat-Denatured Soy Proteins[a]

sample	F_{max}	σ (mN m^{-1})	R_h (nm)
NSP	299.2c	12.1a	7.45d
H1	680.1b	11.1b	14.0c
H3	714.3b	10.9b	18.1b
H5	759.2a	11.7a	23.0a

[a]Letters (a−d) following each value indicate significant differences at the 0.05 level (n = 3).

Adsorption of Soy Protein at the O/W Interface As Affected by Homogenizer Rotating Speed. *Droplet Size Distribution of the Emulsions.* As shown in Figure 2, homogenizer rotating speed was a major factor determining the droplet size of emulsions. According to Walstra,[26] the size of an emulsion's drops depended mainly on the average power density in the emulsification chamber. This could explain why droplet sizes of emulsions stabilized by different proteins decreased in almost the same pattern. Heat treatment of soy proteins also affected droplet size of emulsions. For every rotating speed, NSP-stabilized emulsions possessed larger droplet sizes than emulsions stabilized by heated proteins. Li et al.[5] reported that heated soy proteins yielded smaller droplet

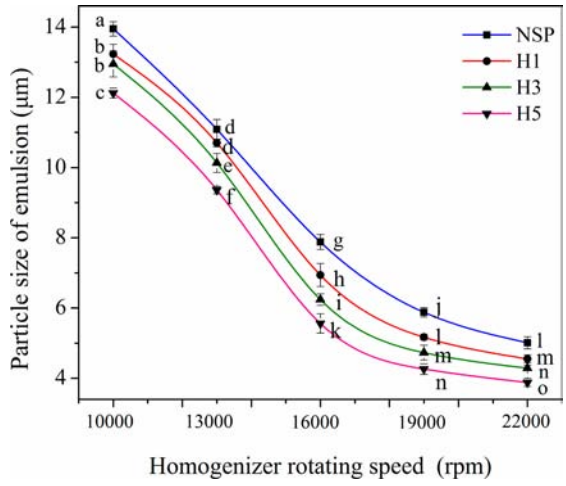

Figure 2. Mean particle size of emulsion (μm) at various homogenizer rotating speeds and zero salt addition. Letters (a−o) following each point indicate significant differences at the 0.05 level (n = 3).

sizes, whereas Keerati-u-rai et al.[1] found that heated soy proteins resulted in larger sized droplets. Li-Chan et al.[27] considered that emulsifying and fat-binding properties of heated proteins were improved under the conditions favoring combinations of high solubility and hydrophobicity. Because surface hydrophobicity of heated soy proteins increased substantially and protein solubility remained unchanged in this experiment, it was found that heated proteins displayed better emulsifying property than NSP. This was in agreement with previous studies, which have reported that increasing the heat-induced aggregate concentration resulted in the formation of emulsions with smaller droplet size.[3] The marked difference in emulsifying behavior among H1, H3, and H5 could not be solely explained by the surface hydrophobicity. Instead, a difference in the content of protein aggregates was found to parallel the changes in droplet size of emulsions (Figure 2). Different adsorption behaviors for aggregates and non-aggregates are considered in the following parts.

Adsorption of Total Proteins at the O/W Interface. Protein surface loads obtained in this study (Figure 3) were much

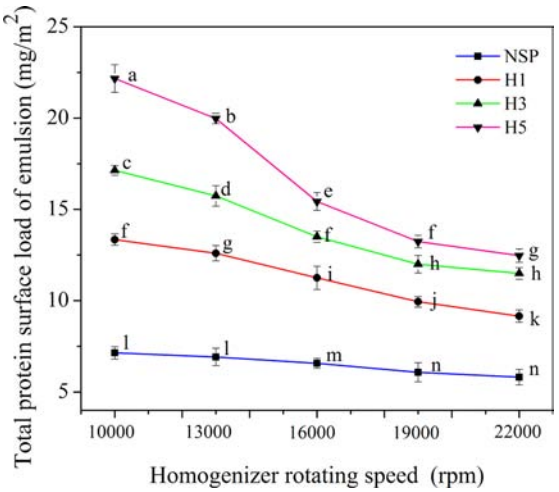

Figure 3. Total protein surface load (mg/m^2) of emulsion at various homogenizer rotating speeds and zero salt addition. Letters (a–n) following each point indicate significant differences at the 0.05 level (n = 3).

higher than the typical globular protein monolayer (about 1–3 mg/m^2).[16] The values of all heated samples were >9.16 mg/m^2. High protein surface load values were also reported by Puppo et al.[28] (>9.0 mg/m^2) and Waninge et al.[29] (4–5 mg/m^2) on emulsifying properties of soy protein and milk protein, respectively. As shown in Figure 3, heat treatment enhanced the surface load of soy protein; the protein surface load of H5 (22.2 mg/m^2) was almost doubled compared to that of H1 (13.3 mg/m^2) at the homogenizer rotating speed of 10000 rpm. Nilsson and Bergenståhl[30] considered that diffusional transport of polymers to the interface became less important; instead, convective transport would dominate during homogenization conditions. In the homogenization shear field, transportation to the O/W interface of large molecules was favored over small ones, leading to higher surface loads by causing jamming at the interface. Tcholakova et al.[13] attributed the much higher protein surface load at the O/W interface to the presence of aggregates in their study. From Figure 3, it could also be noted that the increasing rotating speed decreased the surface protein loads of all emulsions to various degrees. The protein adsorption at the O/W interface would be expected to increase at higher homogenizer rotating speed if there were enough proteins in the system. In the present systems, however, increase of rotating speed resulted in emulsions with small droplet size (larger interface area), at the expense of surface protein load.

Good linear relationships were found when protein surface loads (Γ) were plotted against concentrations of unadsorbed proteins in the aqueous phase (C_{SER}) under the respective homogenizer rotating speed (Figure 4). Thus, adsorption of soy

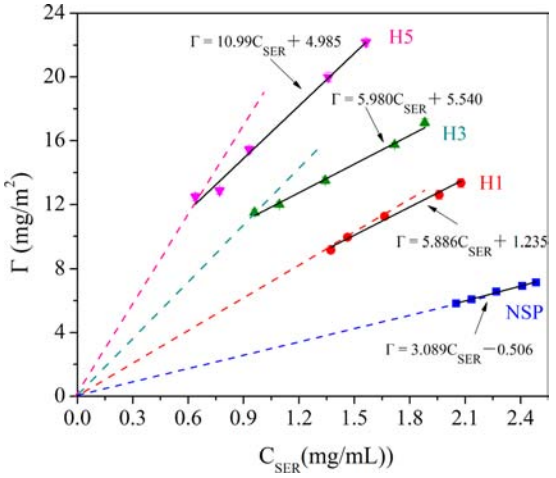

Figure 4. Linear relationships of protein surface loads (Γ) and unadsorbed proteins in the aqueous phase (C_{SER}) at various homogenizer rotating speeds.

proteins at the O/W interface could be described by a simple linear equation. Tcholakova et al.[13] also used an empirical equation to describe protein adsorption behavior at the O/W interface after an unsuccessful attempt of fitting data with those well-known adsorption isotherms. Unfortunately, there were no data describing adsorption behavior when the protein concentration approached 0. To simplify discussion, a linear adsorption isotherm was also assumed in this range (as represented by dashed lines in Figure 4).

In the linear Henry isotherm equation (eq 5)

$$\Gamma = kc \tag{5}$$

The amount of surface adsorbate was proportional to the unadsorbed protein concentrations in the aqueous phase. Therefore, a two-stage Henry isotherm was proposed to describe the adsorption of soy proteins at the O/W interface. The first stage, starting from the origin and ending at the point obtained at a homogenizer rotating speed of 22000 rpm, was assumed to be the adsorption of insufficient proteins relative to large interface area. The second stage, represented by the original fitted line, was the adsorption of excess proteins relative to small interface area. The Henry isotherm constant (k) was the adsorbed protein quantity corresponding to unit concentration of unadsorbed proteins and revealed the affinity of the adsorbate to the adsorbent. For both adsorption stages, k values changed according to the order H5 > H3 > H1 > NSP, again suggesting that proteins heated at higher concentration were prone to be adsorbed at the O/W interface. If k values of different adsorption stages were compared, we could find that for heated proteins, k values of the first stage were higher than those of the second stage. For NSP, however, k values for the

dx.doi.org/10.1021/jf404464z | J. Agric. Food Chem. 2014, 62, 1634–1642

Table 2. Adsorption Percentages of Aggregates (A) or Non-aggregates (NA) at the O/W Interface at Different Homogenizer Rotating Speeds[a]

	NSP	H1		H3		H5	
homogenizer rotating speed (rpm)	NA (%)	NA (%)	A (%)	NA (%)	A (%)	NA (%)	A (%)
10000	12.1u	27.0n	17.4r	23.7o	35.5k	10.7v	58.5g
13000	14.7s	29.5m	28.1m	28.0n	45.8h	13.2t	67.1e
16000	19.7q	34.4k	48.3h	32.4l	68.8e	19.70	84.2c
19000	24.4o	38.02j	62.9f	37.3j	85.3b	22.9p	96.4a
22000	27.4n	40.6i	72.5d	40.8i	90.4b	24.4o	99.8a

[a]Letters (a−u) following each value indicate significant differences at the 0.05 level (n = 3).

two stages were not remarkably different. Due to the much higher surface protein load than the monolayer adsorption, multilayer adsorption was expected for all emulsions. The different k values between stages 1 and 2 suggested that the adsorption behavior of NSP toward the oil surface was not substantially different from that toward the adsorbed protein layer. On the contrary, heated soy proteins, especially those heated at higher concentrations, showed much stronger affinity toward the oil surface than that toward the adsorbed protein layer.

Adsorption of Aggregates and Non-aggregates at the O/W Interface. The adsorption behavior of aggregated and non-aggregated proteins in heated soy proteins was studied. It was found that protein aggregates had higher adsorption percentages than non-aggregated proteins (Table 2). Furthermore, aggregates formed at higher concentrations had higher possibility to be adsorbed at the O/W interface (H5 > H3 > H1). However, non-aggregates formed by heating in lower concentrations were more extensively adsorbed by the O/W interface (H1 > H3 > H5).

Higher adsorption percentage for aggregates than for non-aggregates could be related to their difference in structure. As revealed in previous studies, heat-induced aggregation of soy proteins was a consequence of several steps, including dissociation, unfolding, reassociation, and aggregation.[10] Unfolding of heat-dissociated polypeptides from glycinin and conglycinin resulted in the loss of α-helical structure, whereas much of the β-sheet structure remained. Because the transition of structure and the exposure extent of hydrophobic sites for the protein molecules were closely related, the surface hydrophobicity increased.[10] Specific associations between basic polypeptides or between basic polypeptides and β-subunits through disulfide bonds or noncovalent bonds have been reported.[9] When soy proteins were heated at gradually increased concentrations, aggregation of unfolded polypeptides and reassociated oligomers would have more chances to occur and, as a result, those proteins with more hydrophilic nature would be left as non-aggregates. In addition to hydrophobicity, electric charge frequency and molecular flexibility[31] were important for protein function at an interface.

With the increase of homogenizer rotating speed, adsorption percentages for both aggregated and non-aggregated proteins rose. For aggregated proteins of H5, adsorption percentage increased from 58.5% at 10000 rpm to nearly 100% at 22000 rpm. However, under no circumstance did adsorption percentages of non-aggregated proteins exceed 40.8%. The low adsorption percentages suggested the low affinity of non-aggregated proteins toward the oil phase. On the other hand, the adsorption of larger sized protein aggregates was limited by the diffusion rate at low rotating speed, but effectively enhanced at higher speed. Nilsson et al.[32] reported that the high molar mass components in the polymer were selectively adsorbed in dynamic homogenization condition, which favored transport to the interface of the high molar mass polymers in the sample.

Next, surface protein loads for aggregated and non-aggregated soy proteins were studied (Figure 5) as a function of concentration of the corresponding unadsorbed protein species in the aqueous phases (Figure 6). Intriguingly, the behavior for aggregates in both H3 and H5 resulted in downward convex curves, whereas that for non-aggregates in both H1 and H3 showed upward concave curves. The adsorption energy of the convex type adsorption isotherm decreases as surface load increases, whereas that of concave type increases as surface load increases. Thus, the adsorbed aggregates expelled the adsorbing aggregates, possibly due to the steric effects, whereas the adsorbed non-aggregates attracted the adsorbing non-aggregates, probably because of the hydrophobic interactions between unfolded polypeptides. The adsorption behavior of H1 aggregates and H5 non-aggregates was abnormal because the Γ_A for H1 in the high C_{SER} region decreased, whereas Γ_N for H5 was exceptionally low. This phenomenon could be a demonstration of the interaction between two protein fractions: for H1, the adsorption of aggregates was suppressed by non-aggregates, but for H5 the reverse may be the case.

Adsorption of Soy Proteins at the O/W Interface As Affected by Ionic Strength. *Particle Size and Total Protein Surface Load of the Emulsions.* Soy protein stabilized emulsions were prepared with different levels of NaCl addition. Variation in oil droplet sizes and protein surface loads for heated and unheated soy protein stabilized emulsions followed the same pattern with the increase of NaCl concentration, although the effects differed quantitatively. At low salt concentration (<0.1 M), the addition of salt reduced droplet sizes. A gradual increase in droplet sizes was noted between NaCl concentrations of 0.1 and 0.3 M and then leveled off (Figure 7A). Some studies reported different ranges of emulsion droplet size as a function of salt concentrations. Dickinson[33] and Onsaard[34] found that the initial average droplet sizes and creaming behavior for emulsions stabilized by milk protein remained relatively stable at NaCl concentrations ≤0.1 M. Tcholakova et al.[35] observed that mean drop sizes remained almost constant (about 40 μm) in the electrolyte concentration range of 5−1000 mM (pH 6.2.). However, other studies[36−38] reported that droplet sizes of dairy protein stabilized emulsions increased at a much lower ionic concentration. In addition, emulsifying activities of some vegetable protein stabilized emulsions were reported to increase in the ionic strength range of 0−0.2 M,[39] some even in 0−0.4 M,[39,40] but reduced afterward with further increase in NaCl concentration. The lower sizes of emulsions at 0.1 M NaCl in this study might be partially because low ionic strength

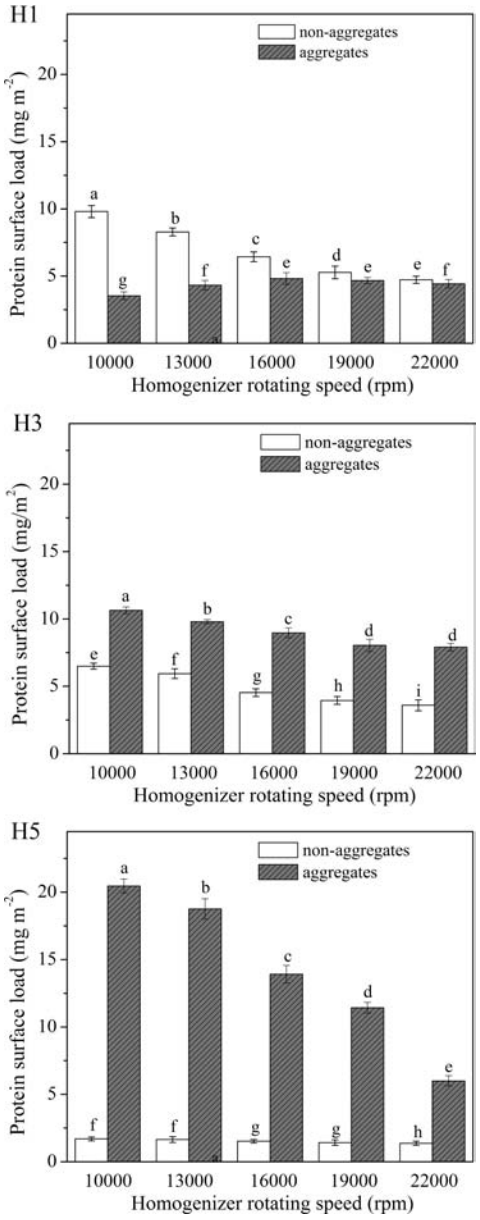

Figure 5. Protein surface load of aggregates and non-aggregates in emulsions at various homogenizer rotating speeds. Letters (a–i) above each column indicate significant differences at the 0.05 level (n = 3).

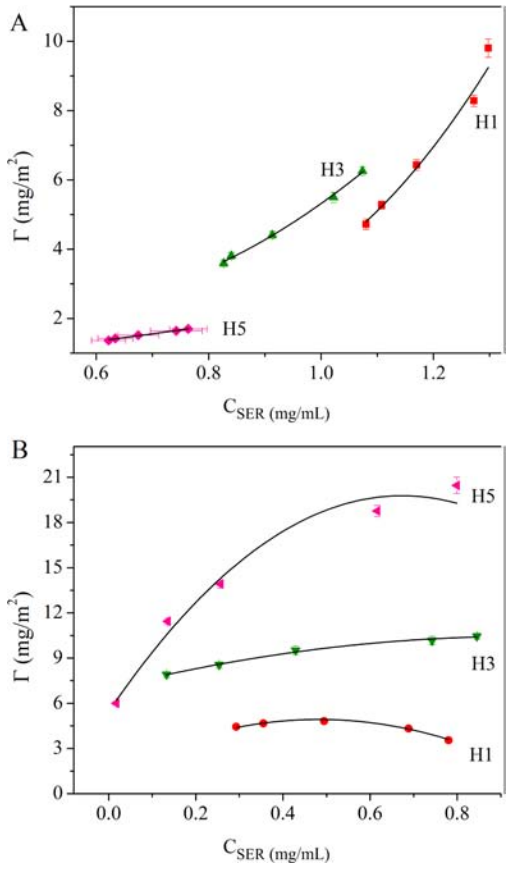

Figure 6. Relationships of surface load for non-aggregates (Γ_N) or aggregates (Γ_A) of heated proteins and the respective unadsorbed protein concentrations in aqueous phases (C_{SER}): (A) non-aggregates; (B) aggregates.

encouraged unfolding of protein molecules and subsequent increase in protein solubility. Lawal et al.[39] considered that such an increase in protein solubility enhanced a rapid migration to the O/W interface and improved the emulsifying activity of the protein. With further increase in ionic strength (>0.1 M), screening of the surface charges increased and this encouraged protein–protein interaction but reduced protein–oil interaction.

Protein surface loads were also influenced markedly by increasing ionic strength (Figure 7B). More proteins, whether heated or unheated, were found to be adsorbed at the O/W interface with increasing of NaCl concentration. Tcholakova et al.[35] also found that the protein surface loads of emulsions stabilized by β-lactoglobulin (0.02 or 0.1%, w/v) increased with increasing NaCl concentration (5–1000 mM, pH 6.2.) In this study, the enhanced Γ was probably due to the electrostatic screening, which reduced electrostatic repulsion with increasing concentration of NaCl and facilitated the adsorption of soy proteins at the interface.

Adsorption of Aggregated and Non-aggregated Proteins at the O/W Interface at Different Ionic Strengths. Addition of salt was very effective in enhancing the adsorption of aggregated proteins. In fact, >95% of aggregated proteins were found to transfer to the O/W interface at a salt concentration of ≥0.2 M. Adsorptions of non-aggregated proteins as well as the unheated soy proteins displayed similar increasing trends, but the maximum adsorption percentage was much lower than that of aggregates. In contrast to the effect of homogenizer rotating speed, salt enhanced adsorption percentages of non-aggregates of H5 more effectively than other proteins (Table 3). It seems that adsorption of non-aggregates of H5 was more severely hindered by electrical repulsion, and the screening of electric charges on proteins resulted in a more remarkable increase in adsorption percentage. It was clear that aggregate/non-aggregate profiles on the O/W interfaces did not change substantially as a result of increasing salt concentration (Figure 8). With the elevation of salt concentration, aggregates in H5 remained as predominantly adsorbed components but both protein fractions contributed to the adsorbed layer for H1- and H3-stabilized emulsions. On the other hand, increase in NaCl concentration effected a marked decrease of Γ_A/Γ_N for H5 emulsions, from 8.21 to 3.66, whereas Γ_A/Γ_N was observed to increase from 0.76 to 1.17 for H1-stabilized emulsion.

dx.doi.org/10.1021/jf404464z | J. Agric. Food Chem. 2014, 62, 1634–1642

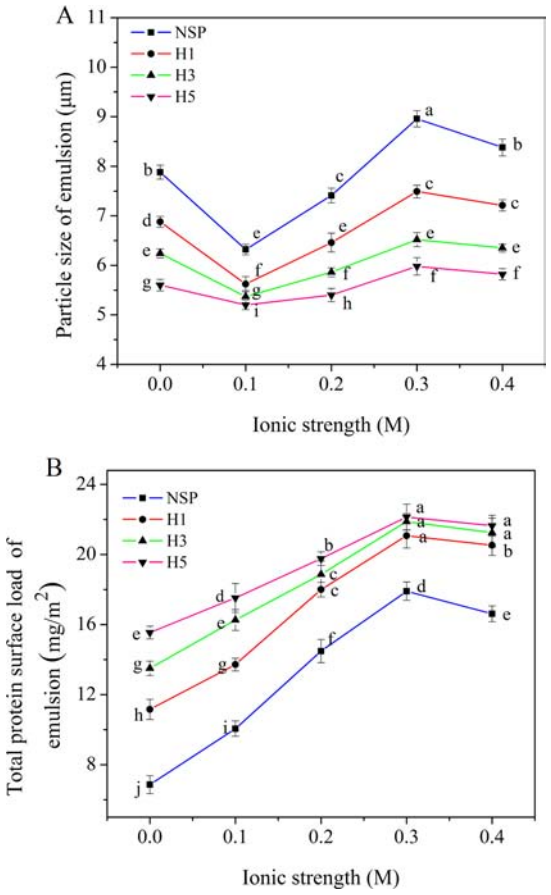

Figure 7. Mean particle size of emulsion (μm) at various ionic strengths and constant homogenizer rotating speed of 16000 rpm (A); total protein surface load (mg/m^2) of emulsion at various ionic strengths and constant homogenizer rotating speed of 16000 rpm (B). Letters (a–j) following each point indicate significant differences at the 0.05 level (n = 3).

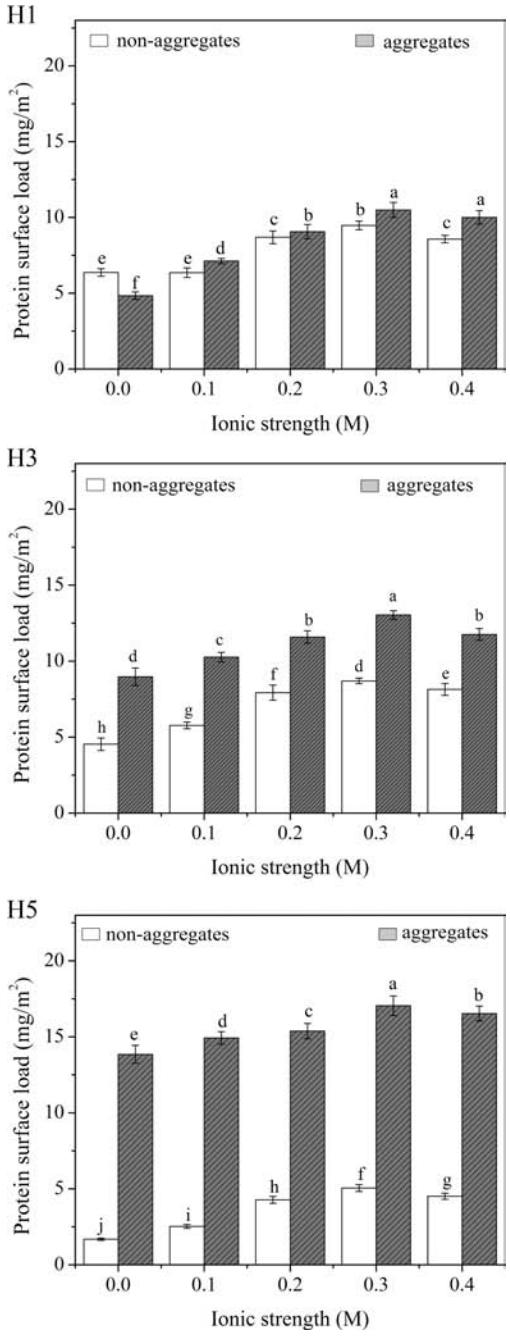

Figure 8. Protein surface load of aggregates and non-aggregates in emulsions at various ionic strengths and constant homogenizer rotating speed of 16000 rpm. Letters (a–j) above each column indicate significant differences at the 0.05 level (n = 3).

In summary, the present study showed that not only the heat treatment but also the heating concentration affected the emulsifying properties of soy proteins. Better emulsifying properties, as judged from droplet size, adsorption percentage, and surface load, could be obtained by heating soy proteins at higher concentrations. Levels of protein aggregates in heated samples were more important than other variables in affecting adsorption properties of proteins at the O/W interface. Adsorption properties of total proteins at the O/W interface as a function of homogenizer rotating speed or salt concentration seem to follow a similar trend, regardless of the use or not of heating and the heating concentrations. However, if aggregated and non-aggregated proteins were

Table 3. Adsorption Percentages of Aggregates (A) or Non-aggregates (NA) at the O/W Interface at Different Ionic Strengths[a]

	NSP	H1		H3		H5	
ionic strength (M)	NA (%)	NA (%)	A (%)	NA (%)	A (%)	NA (%)	A (%)
0	19.7l	33.7j	48.3g	34.7j	69.1d	23.9k	86.7c
0.1	37.5i	43.2h	87.0c	53.3f	91.8b	39.0i	99.6a
0.2	46.1g	50.9f	96.3a	66.6d	95.0a	61.1e	99.8a
0.3	47.2g	51.9f	96.2a	66.6d	96.1a	63.6e	99.9a
0.4	47.4 g	52.5f	96.8a	65.9d	96.8a	64.0e	99.9a

[a]Letters (a–l) following each value indicate significant differences at the 0.05 level (n = 3).

dx.doi.org/10.1021/jf404464z | J. Agric. Food Chem. 2014, 62, 1634–1642

considered separately, different adsorption behaviors that depended on heating concentrations could be observed. Thus, the adsorption of soy proteins at the O/W interface could not be considered as the sum of the independent adsorption of aggregates and non-aggregates.

AUTHOR INFORMATION

Corresponding Author

*Postal address: State Key Laboratory of Food Science and Technology, Jiangnan University, 1800 Lihu Avenue, Wuxi 214122, Jiangsu Province, PR China. Phone/fax: 0510-85329091. E-mail: yfhua@jiangnan.edu.cn.

Funding

We gratefully acknowledge financial support received from the National High Technology Research and Development Program of China (2013AA102204-3) and the Key Project in the National Science and Technology Pillar Program during the Eleventh Five-year Plan Period (2012BAD34B04-1).

Notes

The authors declare no competing financial interest.

REFERENCES

(1) Keerati-u-rai, M.; Corredig, M. Heat-induced changes in oil-in-water emulsions stabilized with soy protein isolate. *Food Hydrocolloids* **2009**, *23*, 2141−2148.

(2) Palazolo, G. G.; Mitidieri, F. E.; Wagner, J. R. Relationship between interfacial behaviour of native and denatured soybean isolates and microstructure and coalescence of oil in water emulsions − effect of salt and protein concentration. *Food Sci. Technol. Int.* **2003**, *9*, 409−419.

(3) Liu, F.; Tang, C. H. Soy protein nanoparticle aggregates as Pickering stabilizers for oil-in-water emulsions. *J. Agric. Food Chem.* **2013**, *61*, 8888−8898.

(4) Palazolo, G. G.; Sobral, P. A.; Wagner, J. R. Freeze-thaw stability of oil-in-water emulsions prepared with native and thermally-denatured soybean isolates. *Food Hydrocolloids* **2011**, *25*, 398−409.

(5) Li, F.; Kong, X.; Zhang, C.; Hua, Y. Effect of heat treatment on the properties of soy protein-stabilised emulsions. *Int. J. Food Sci. Technol.* **2011**, *46*, 1554−1560.

(6) Wang, J.; Xia, N.; Yang, X.; Yin, S.; Qi, J.; He, X.; Yuan, D.; Wang, L. Adsorption and dilatational rheology of heat-treated soy protein at the oil-water interface: relationship to structural properties. *J. Agric. Food Chem.* **2012**, *60*, 3302−3310.

(7) Keerati-u-rai, M.; Corredig, M. Heat-induced changes occurring in oil/water emulsions stabilized by soy glycinin and β-conglycinin. *J. Agric. Food Chem.* **2010**, *58*, 9171−9180.

(8) Keerati-u-rai, M.; Miriani, M.; Iametti, S.; Bonomi, F.; Corredig, M. Structural changes of soy proteins at the oil-water interface studied by fluorescence spectroscopy. *Colloids Surf. B−Biointerfaces* **2012**, *93*, 41−48.

(9) Wagner, J. R.; Gueguen, J. Surface functional properties of native, acid-treated, and reduced soy glycinin. 2. Emulsifying properties. *J. Agric. Food Chem.* **1999**, *47*, 2181−2187.

(10) Utsumi, S.; Matsumura, Y.; Mori, T. Structure-function relations of soy proteins. In *Food Proteins and Their Application*; Damodaran, S., Paraf, A., Eds.; Dekker: New York, 1997; pp 268−276.

(11) Kinsella, J. E.; Mulvihill, D. M. Gelation characteristics of whey proteins and β-lactoglobulin. *Food Technol.* **1987**, *41*, 102−111.

(12) Damodaran, S.; Razumovsky, L. Role of surface area-to-volume ratio in protein adsorption at the air-water interface. *Surf. Sci.* **2008**, *602*, 307−315.

(13) Tcholakova, S.; Denkov, N. D.; Sidzhakova, D.; Ivanov, I. B.; Campbell, B. Interrelation between drop size and protein adsorption at various emulsification conditions. *Langmuir* **2003**, *19*, 5640−5649.

(14) Lowry, O. H.; Rosebrough, N. J.; Farr, A. L.; Randall, R. J. Protein measurement with the Folin phenol reagent. *J. Biol. Chem.* **1951**, *193*, 265−275.

(15) Wu, W.; Wu, X.; Hu, Y. Structural modification of soy protein by the lipid peroxidation product acrolein. *LWT−Food Sci. Technol.* **2010**, *43*, 133−140.

(16) Sakuno, M. M.; Matsumoto, S.; Kawai, S.; Taihei, K.; Matsumura, Y. Adsorption and structural change of β-lactoglobulin at the diacylglycerol-water interface. *Langmuir* **2008**, *24*, 11483−11488.

(17) Nilsson, L.; Osmark, P.; Fernandez, C.; Andersson, M.; Bergenstahl, B. Competitive adsorption of water soluble plasma proteins from egg yolk at the oil/water interface. *J. Agric. Food Chem.* **2006**, *54*, 6881−6887.

(18) Mills, E. N. C.; Huang, L.; Noel, T. R.; Gunning, A. P.; Morris, V. J. Formation of thermally induced aggregates of the soya globulin β-conglycinin. *Biochim. Biophys. Acta−Protein Struct. Mol. Enzymol.* **2001**, *1547*, 339−350.

(19) Li, X.; Li, Y.; Hua, Y.; Qiu, A.; Yang, C.; Cui, S. Effect of concentration, ionic strength and freeze-drying on the heat-induced aggregation of soy proteins. *Food Chem.* **2007**, *104*, 1410−1417.

(20) Sorgentini, D.; Wagner, J.; Anon, M. Effects of thermal treatment of soy protein isolate on the characteristics and structure-function relationship of soluble and insoluble fractions. *J. Agric. Food Chem.* **1995**, *43*, 2471−2479.

(21) Wang, Y.; Sun, X. S.; Wang, D. Effects of preheating treatment on thermal property and adhesion performance of soy protein isolates. *J. Adhes. Sci. Technol.* **2007**, *21*, 1469−1481.

(22) Mahmoudi, N.; Axelos, M. A. V.; Riaublanc, A. Interfacial properties of fractal and spherical whey protein aggregates. *Soft Matter* **2011**, *7*, 7643−7654.

(23) Semisotnov, G. V.; Rodionova, N. A.; Razgulyaev, O. I.; Uversky, V. N.; Gripas, A. F.; Gilmanshin, R. I. Study of the "molten globule" intermediate state in protein folding by a hydrophobic fluorescent probe. *Biopolymers* **1991**, *31*, 119−128.

(24) Rao, C.; Damodaran, S. Is interfacial activation of lipases in lipid monolayers related to thermodynamic activity of interfacial water? *Langmuir* **2002**, *18*, 6294−6306.

(25) Dickinson, E.; Radford, S.; Golding, M. Stability and rheology of emulsions containing sodium caseinate: combined effects of ionic calcium and non-ionic surfactant. *Food Hydrocolloids* **2003**, *17*, 211−220.

(26) Walstra, P. Principles of emulsion formation. *Chem. Eng. Sci.* **1993**, *48*, 333−349.

(27) Li-Chan, E.; Nakai, S.; Wood, D. F. Relationship between functional (fat binding, emulsifying) and physicochemical properties of muscle proteins. Effects of heating, freezing, pH and species. *J. Food Sci.* **1985**, *50*, 1034−1040.

(28) Puppo, M. C.; Beaumal, V.; Chapleau, N.; Speroni, F.; Lamballerie, M.; Añóna, M. C.; Anton, M. Physicochemical and rheological properties of soybean protein emulsions processed with a combined temperature/high-pressure treatment. *Food Hydrocolloids* **2008**, *22*, 1079−1089.

(29) Waninge, R.; Walstra, P.; Bastiaans, J.; Nieuwenhuijse, H.; Nylander, T.; Paulsson, M.; Bergenståhl, B. Competitive adsorption between β-casein or β-lactoglobulin and model milk membrane lipids at oil−water interfaces. *J. Agric. Food Chem.* **2005**, *53*, 716−724.

(30) Nilsson, L.; Bergenståhl, B. Adsorption of hydrophobically modified starch at oil/water interfaces during emulsification. *Langmuir* **2006**, *22*, 8770−8776.

(31) Akio, K.; Noriko, T.; Naotoshi, M.; Kunihiko, K.; Shuryo, N. Effects of partial denaturation on surface properties of ovalbumin and lysozyme. *Biol. Chem.* **1981**, *45*, 2755−2760.

(32) Nilsson, L.; Leeman, M.; Wahlund, K.; Bergenståhl, B. Competitive adsorption of a polydisperse polymer during emulsification: experiments and modeling. *Langmuir* **2007**, *23*, 2346−2351.

(33) Dickinson, E.; Semenova, M.; Antipova, A. S. Salt stability of casein emulsions. *Food Hydrocolloids* **1998**, *12*, 227−225.

(34) Onsaard, E.; Vittayanont, M.; Srigam, S.; McClements, D. J. Properties and stability of oil-in-water emulsions stabilized by coconut skim milk proteins. *J. Agric. Food Chem.* **2005**, *53*, 5747−5753.
(35) Tcholakova, S.; Denkov, N. D.; Sidzhakova, D.; Ivanov, I. B.; Campbell, B. Effects of electrolyte concentration and pH on the coalescence stability of *β*-lactoglobulin emulsions: experiment and interpretation. *Langmuir* **2005**, *21*, 4842−4855.
(36) Demetriades, K.; Coupland, J. N.; McClements, D. J. Physical properties of whey protein stabilized emulsions as related to pH and NaCl. *J. Food Sci.* **1997**, *62*, 342−347.
(37) Ye, A.; Singh, H. Interfacial composition and stability of sodium caseinate emulsions as induenced by calcium ions. *Food Hydrocolloids* **2001**, *15*, 195−207.
(38) Kulmyrzaev, A. A.; Schubert, H. Influence of KCl on the physicochemical properties of whey protein stabilized emulsions. *Food Hydrocolloids* **2004**, *18*, 13−19.
(39) Lawal, O. S. Functionality of African locust bean (*Parkia biglobossa*) protein isolate: effects of pH, ionic strength and various protein concentrations. *Food Chem.* **2004**, *86*, 345−355.
(40) Adebowale, K. O.; Lawal, O. S. Comparative study of the functional properties of bambarra groundnut (*Voandzeia subterranean*), jack bean (*Canavalia ensiformis*) and mucuna bean (*Mucuna pruriens*) flours. *Food Res. Int.* **2004**, *37*, 355−365.

to 300 °C, and baking time varied between 5 and 30 min.[8−15] Under these baking kinetics, a variety of complex physical and chemical phenomena would happen, including the important nonenzymatic browning reaction resulting in brown color and bakery flavor development. During cookie baking, α-dicarbonyls may be produced via caramelization, Maillard reaction, and lipid peroxidation. Their high reactivity with protein poses health risks associated with pathological events and carcinogenicity.[10] Cookies are also rich sources of dietary AGEs, which can be produced with α-dicarbonyls as precursors and are implicated in the development of oxidative stress and inflammation-associated diseases. On the basis of the above discussions, cookies would be suitable food models to examine the antioxidant and antiglycation activities of dietary polyphenols under thermal processing.

The current study prepared cookies fortified with five representative dietary polyphenols (naringenin, quercetin, epicatechin, chlorogenic acid, and rosmarinic acid), respectively. Examination of the antioxidant capacity of fortified cookies would allow characterization of how thermal treatment affected phenolics' antioxidant activity in the cookie system. The antiglycation potential of polyphenols in cookie was also assessed with reference to the formation of both total fluorescent AGEs and their important precursors, the reactive carbonyl intermediates. Finally, the practicality of polyphenol fortification was evaluated on the basis of the influence of phenolic addition on the color and other quality attributes of cookies.

MATERIALS AND METHODS

Reagents and Chemicals. Epicatechin was purchased from Biopurify Phytochemicals Ltd. (Chengdu, China). Naringenin, quercetin, chlorogenic acid, rosmarinic acid, sodium chloride, sodium carbonate, sodium bicarbonate, trolox, ABTS [2,2′-azinobis(3-ethylbenzothiazoline-6-sulfonic acid)], potassium peroxosulfate, OPD (*o*-phenylenediamine), quinoxaline, 2-methylquinoxaline, Tween-20, SDS (sodium dodecyl sulfate), Tris, and β-mercaptoethanol were all purchased from Sigma-Aldrich (St. Louis, MO, USA). The ingredients for cookie preparation including salt, sugar, baking powder, canola oil, and white flour were purchased at a local supermarket. All solvents and acids used were of analytical or HPLC grade and obtained from BDH Laboratory Supplies (Poole, UK).

Cookie Model. The cookie recipe consisted of double-deionized water (1.5 mL), salt (0.1 g), baking powder (0.12 g), sugar (3.5 g), canola oil (1.5 mL), and white flour (7.5 g). The ingredients were thoroughly mixed with 0.25% (w/w) of individual phenolic compound (naringenin, quercetin, epicatechin, chlorogenic acid, and rosmarinic acid). Dough was rolled and baked in an electronic baking oven (Kenwood, China) at 200 °C for 10 min. After baking, the cookie samples were cooled to room temperature and kept at −20 °C until further analysis.

Measurement of Color, Texture, Moisture, and pH of Cookie Samples. The three chromatic coordinates L^*, a^*, and b^* of ground cookie were measured by a colorimeter (CR-400, Konica Minolta, Japan). The coordinate L^* indicates the lightness of color ($L^* = 0$ yields black and $L^* = 100$ means diffuse white); a^* characterizes the position between red and green (negative values indicate green, and positive values indicate red); b^* suggests the position between yellow and blue (negative values indicate blue, and positive values indicate yellow). Chroma value was calculated as $(a^{*2} + b^{*2})^{1/2}$; E index was calculated as $(L^{*2} + a^{*2} + b^{*2})^{1/2}$.

The textural analysis was conducted by a texture analyzer (TA-XT2, stable micro system, Surrey, UK) equipped with a cylindrical probe of 20 mm in diameter. The mode was set as "measure force in compression", and the compression distance was 1 mm. Hardness of the cookies was estimated by the maximum force (g). The moisture content of cookie was measured by a moisture analyzer (HB43-S, Mettler Toledo, USA). Around 3 g of ground cookie was heated at 120 °C until stable weight, and the moisture content was calculated according to the weight loss. For measurement of pH, 0.4 g of ground cookie was vortexed in 20 mL of water for 3 min and then held for 1 h at room temperature. The pH of the supernatant layer was taken by a pH meter (pHI510, Beckman Coulter, USA).

Measurement of Antioxidant Capacity. The antioxidant capacity was quantified by Trolox equivalent antioxidant capacity (TEAC) assay.[16] The stock radical solution was prepared by reacting 7 mM ABTS solution with 2.45 mM potassium peroxosulfate in the dark for 16 h at room temperature. Working radical solution was freshly prepared by diluting stock radical solution with Milli-Q water to have an absorbance of 0.7 ± 0.05 at 734 nm. Ground cookie was dispersed in water and 30, 50, and 70% ethanol with a final concentration of 100 mg/mL. The samples were extracted by sonication for 30 min and then centrifuged at 5100*g* for 20 min. Fifty microliters of supernatant or Trolox standard was mixed with 1.9 mL of working radical solution, and absorbance at 734 nm was read by a spectrophotometer (UV-1206, Shimadzu, Japan) after 6 min of incubation. The results were expressed as nanomoles of Trolox per milligram of cookie.

Investigation of Thermal Products of Quercetin after Cookie Baking Process. Ten grams of ground cookie was weighed in a 100 mL volumetric flask, and extraction was conducted by 70% methanol under sonication for 1 h. The extract was filtered, and the filtrate was analyzed by HPLC-DAD and LC-MS/MS. The Shimadzu HPLC system is composed of a separation module (LC-20AT), an autosampler (SIL-20A), a degasser (DGU-20A3), and a photodiode array detector (SPD-M20A). The separation of reaction products was achieved on a YMC-pack Pro column (5 μm, i.d. 2.1 × 150 mm). The mobile phases were water with 0.1% formic acid (A) and acetonitrile (B), and gradient flow was as follows: 0 min, 3% B; 5 min, 3% B; 45 min, 50% B; 55 min, 80% B; 60 min, 90% B; back to 3% B in 1 min and held for 14 min. The total run time was 75 min, and flow rate was 0.2 mL/min. The injection volume was 10 μL. UV detection wavelength for quercetin was 366 nm.

The LC-MS/MS instrument was equipped with an electrospray ionization (ESI) source interfaced to a 3200 Qtrap mass spectrometer (AB Sciex, Canada). Liquid chromatography was performed on an Agilent 1290 UHPLC system with a binary pump (G4420A) and a thermostated autosampler (G4226A). The separation of the reaction products was performed in the same conditions as described above. The MS parameters were as follows: negative ion mode; spray voltage, −4300 V; scan range, 100−1000 Da; temperature, 450 °C; declustering potential (DP), −65 V; collision energy (CE), −30 eV.

Determination of Glyoxal (GO) and Methylglyoxal (MGO). The two typical representatives of reactive carbonyls, GO and MGO, were quantified by a derivatization HPLC-DAD method.[10] Two grams of ground cookie was extracted by 20 mL of 50% methanol under sonication for 1 h. After centrifugation, the supernatant was filtered, and 15 mL of filtrate was concentrated by rotary evaporation. The extract was redissolved in 2 mL of 50% methanol. Derivatization was conducted by mixing 600 μL of cookie extract with 200 μL of OPD (10 mM) and afterward incubating the solutions for 3 h at 70 °C in an oven. After cooling, 200 μL of acetic acid was added to the derivatized mixture. The samples were then filtered by a 0.45 μm membrane before HPLC-DAD analysis.

After derivatization with OPD, GO and MGO could be measured as quinoxaline (Q) and 2-methylquinoxaline (2-MQ) correspondingly detectable by UV absorbance at 315 nm. The same Shimadzu HPLC system is used as described above. Separation was conducted on an ACE C18 column (5 μm, 250 × 4.6 mm, Advanced Chromatography Technologies, Aberdeen, UK). Elution was performed with a mixture of (A) 0.5% (v/v) acetic acid in water and (B) methanol, and gradient flow was as follows: 0 min, 16% B; 2 min, 16% B; 22 min, 32% B; 37 min, 80% B; 42 min, 80% B; 43 min, 16% B; 53 min, 16% B. Flow rate was 0.8 mL/min, and injection volume equaled 10 μL. Quantitative interpolation was facilitated by calibration curves constructed by Q and 2-MQ standard.

Table 1. Impacts of Dietary Polyphenols on the Color of Cookies[a]

	L^*	a^*	b^*	chroma value	E index
control	41.75 ± 1.91	3.55 ± 0.10	12.28 ± 0.44	12.78 ± 0.39	43.66 ± 1.94
naringenin	41.51 ± 0.34	3.87 ± 0.23	13.67 ± 0.36a	14.21 ± 0.41a	43.88 ± 0.23
quercetin	38.67 ± 1.69	2.03 ± 0.19b	16.70 ± 1.13a	16.82 ± 1.10a	42.17 ± 1.98
epicatechin	40.22 ± 1.65	4.09 ± 0.11a	11.78 ± 0.50	12.47 ± 0.49	42.11 ± 1.72
chlorogenic acid	42.46 ± 0.42	2.78 ± 0.03b	14.25 ± 0.08a	14.52 ± 0.08a	44.88 ± 0.43
rosmarinic acid	43.35 ± 0.88	2.75 ± 0.08b	13.64 ± 0.43a	13.92 ± 0.43a	45.53 ± 0.97

[a]"a" marks values significantly higher than control value, whereas "b" marks values significantly lower than control value ($P < 0.05$).

Measurement of Fluorescent AGEs. To extract the protein from cookie samples, 250 mg of ground cookie was extracted by 4.75 mL of extraction buffer (0.05% Tween-20, 1% SDS, 5% β-mercaptoethanol, 50 mM Tris-HCl at pH 7.4).[14] Extraction was performed overnight at room temperature under gentle agitation. The supernatant containing extracted protein was collected after centrifugation. One hundred microliters of extracted protein solution from cookies was pippeted to each well of a 96-well plate, and fluorescent AGEs were indicated by fluorescence with excitation wavelength of 355/40 nm and emission wavelength of 405/10 nm (Victor X4 Multilabel Plate Reader, PerkinElmer, USA).

Statistical Analysis. Statistical analyses were carried out by Graphpad Prism 5 software package (GraphPad Software, Inc., La Jolla, CA, USA). Data are expressed as the mean ± standard error of triplicate determinations, and differences with $P < 0.05$ were considered to be statistically significant.

RESULTS AND DISCUSSION

Polyphenol Addition Alters Selected Quality Attributes. One key consideration in the utilization of dietary polyphenols as functional food ingredients is whether the polyphenols will adversely influence the appearance, flavor, taste, and other sensory or quality attributes of fortified foods. Green tea and grape seed extract fortification have been illustrated to alter the color of baked bread on the basis of instrumental analysis.[4,17] In this study, the potential of polyphenol addition to cause colorimetric changes of cookie was examined. As shown in Table 1, cookies prepared with 0.25% (w/w) quercetin, chlorogenic acid, and rosmarinic acid showed decreased redness and increased yellowness; epicatechin or naringenin could induce a positive shift in the redness or yellowness of cookies, respectively. For a comprehensive analysis combining lightness, redness, and yellowness values, the chroma value of cookies fortified with naringenin, quercetin, chlorogenic acid, and rosmarinic acid was significantly higher than control, whereas no obvious effects were observed on the E index. The above observed colorimetric changes might be attributed to colorants originated from thermal transformation of polyphenols or newly formed unknown colorants from reactions between polyphenol and the nutritional components in cookies.

Table 2 summarizes the influence of dietary polyphenol addition on three commonly used quality descriptive indices. In textural analysis, phenolics were found to cause no significant change in cookie hardness at the specific addition level used in the study. A 0.1−0.7 decrease in pH value, however, was recorded as a result of polyphenol addition, which is probably a result of acidic compound formation. Tested polyphenols resulted in 0.1−0.4% fluctuation in cookies' moisture content, and the decrease in the moisture content induced by epicatechin or rosmarinic acid fortification might favor the shelf life of cookies.[18]

Table 2. Impacts of Dietary Polyphenols on the Selected Quality Attributes of Cookies[a]

	hardness (g)	pH	moisture (%)
control	11613 ± 3448.6	9.62 ± 0.038	2.20 ± 0.065
naringenin	8270 ± 1407.3	9.49 ± 0.015b	2.25 ± 0.072
quercetin	6273 ± 1257.8	9.02 ± 0.017b	2.64 ± 0.061a
epicatechin	8745 ± 421	9.11 ± 0.017b	1.85 ± 0.023b
chlorogenic acid	9653 ± 792.3	8.88 ± 0.092b	2.10 ± 0.031
rosmarinic acid	8596 ± 1763.6	9.27 ± 0.031b	2.07 ± 0.006b

[a]"a" marks values significantly higher than control value, whereas "b" marks values significantly lower than control value ($P < 0.05$).

Polyphenol Fortification Enhances Antioxidant Capacity, but Primary Compounds Are Thermally Converted to Other Products. As shown in Figure 1, the antioxidant capacity of cookie extract, which was prepared by extraction with solvents of different polarity, was significantly elevated with phenolics fortification. The increase in the antioxidant capacity, however, was much lower than that carried by the quantity of polyphenol originally added to the cookie recipe (denoted polyphenol equivalent in Figure 1), especially in the cases of quercetin and epicatechin fortification. This observation was consistent with early findings that quercetin and epicatechin were relatively sensitive to thermal processing and suffered from obvious thermal loss of their antioxidant activity.[2] Naringenin and quercetin were selected for further quantitative analysis (70% methanol extraction followed by HPLC/DAD quantification) of remaining primary polyphenol compound after baking process. Surprisingly, results showed that even after a 10 min short baking time, a >30% decrease in naringenin amount was found, and in quercetin's case, there was around an 88% loss of detectable UV absorption signal of

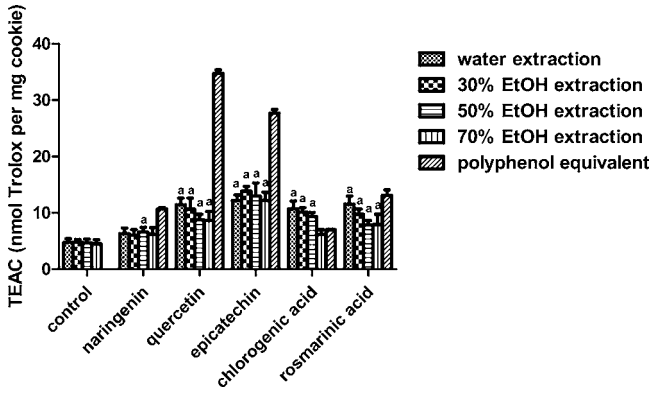

Figure 1. Antioxidant capacity of cookie extracts with or without addition of polyphenols and polyphenol equivalents. Extract with antioxidant capacity significantly higher than control is marked with "a" ($P < 0.05$).

dx.doi.org/10.1021/jf4045827 | J. Agric. Food Chem. 2014, 62, 1643−1648

primary compound. Quercetin has been previously reported to be thermally unstable after long heating: heating quercetin at 100 °C in aqueous solution caused a 25% decrease after 300 min at pH 5, whereas an alkalinic pH of 8 resulted in much more severe thermal loss that left no quercetin after 240 min of heating.[19] Our results indicate that in a low-moisture environment with heating temperature elevated to 200 °C, it took a very short time for quercetin to transform to other compounds.

Further investigation was made into the thermal transformation of quercetin. On the basis of the total ion chromatogram comparison of cookie extract without or with quercetin, three major additional peaks were identified in quercetin-fortified cookie extract, the information of which is summarized in Table 3. Remaining primary quercetin (m/z 301) was eluted at 28.7 min. Compound **I** (retention time = 20.2 min) showed UV λ_{max} at 290 nm and two main ions at m/z 349 and 331 during enhanced mass spectrometry (EMS) analysis, indicating easy loss of one molecule of water. Enhanced product ion (EPI) analysis of the ion at m/z 331 further elucidated a product ion at m/z 299, which may be the $[M - H]^-$ ion of oxidized quercetin, and the neutral loss was likely a molecule of methanol (32 Da).[20] Neutral loss of 28 Da from the ion at m/z 299, probably corresponding to a CO, gave rise to a product ion at m/z 271, whereas the same loss of CO from quercetin produced an ion at m/z 273. The product ion spectrum of both quercetin and its deprotonated ion at m/z 299 showed two ions at m/z 179 and 151. On the basis of the agreements on the UV absorption and LC-MS/MS data, compound **I** is likely to be 2-(3,4-dihydroxyphenyl)-3,3,5,7-tetrahydroxy-2-methoxy-2,3-dihydrochromen-4-one, which was identified by LC-MS/MS and NMR as the reaction product of quercetin and 2,2-diphenyl-1-picrylhydrazyl (DPPH) in methanol.[20] The compound has also been reported by Buchner et al.[19] to be present in the methanol solution of thermally processed quercetin at 100 °C.

Table 3. LC-MS/MS Data of Three Major Additional Compounds in Quercetin-Fortified Cookie Extract

peak	retention time (min)	m/z $[M - H]^-$	MS/MS	suggested structure
1	20.2	349, 331	299, 271, 179, 151	2-(3,4-dihydroxyphenyl)-3,3,5,7-tetrahydroxy-2-methoxy-2,3-dihydrochromen-4-one
2	24.4	363, 331	299, 271, 179, 151	2-(3,4-dihydroxyphenyl)-3,5,7-trihydroxy-2,3-dimethoxy-2,3-dihydrochromen-4-one
3	28.7	301	273, 179, 151, 107	quercetin

The maximum UV absorption wavelength of compound **II** (retention time = 24.4 min) is 293 nm, and the main ions found from the mass spectrum were at m/z 363, 331, and 299. The base ion at m/z 363 was of low abundance and may be unstable to readily lose a molecule of methanol (32 Da) to m/z 331. The neutral loss from m/z 331 to 299 could represent a second molecule of methanol. The following fragmentation pattern was analogous to that of compound **I**, giving rise to product ions at m/z 271, 179, and 151. Therefore, compound **II** might be the reaction product of oxidized quercetin incorporating two molecules of methanol, namely, 2-(3,4-dihydroxyphenyl)-3,5,7-trihydroxy-2,3-dimethoxy-2,3-dihydrochromen-4-one as previously identified by Hvattum et al.[20] In all, during the high-temperature baking process, quercetin was possibly degraded to very small molecules beyond detection of current LC/MS-MS methodology or transformed to unstable oxidized compounds, which readily react with methanol during extraction, forming compounds **I** and **II**.

In addition to degradation or oxidation loss of primary polyphenol structure carrying antioxidant activity, thermal processing likely favors reaction of phenolics with other nutritional components in cookie recipes, such as sugar fragments originated from caramelization and Maillard reaction, and thereafter affects the antioxidants' content.[2,21] Therefore, it seems to be necessary to consider the phenolics' thermal stability and reactivity in the food matrix when the food product is fortified with phenolics for the purpose of increasing the level of health-beneficial antioxidants.

Polyphenols Inhibit the Formation of Glycation Intermediates and Endproducts. The α-dicarbonyl compounds are important intermediate products originated from either sugar/lipid oxidation or thermal degradation of Schiff base or Amadori rearrangement products. GO and MGO are two major α-dicarbonyls that can react with amino groups on the protein backbone and contribute to the formation of AGEs.[10,22] The GO and MGO levels in model cookie control were 12.6 and 16.9 mg/kg, respectively, which are comparable to the values reported for commercial cookies.[10] Selected polyphenols, including tea catechins and theaflavins, chalcones represented by phloretin and phloridzin, stilbenes, and genistein, have been reported to trap these two reactive carbonyls in physiological conditions.[23] Our results suggested that under baking conditions, all five tested polyphenols were effective in reducing the amount of GO but not MGO in cookies (Figure 2). Furthermore, the inhibitory activity against glyoxal formation was positively correlated with polyphenols' antioxidant activity (R^2 = 0.975). This phenomenon led to a hypothesis that the inhibitory activity of tested phenolics against glyoxal formation during cookie baking might be attributable to the phenolics' free radical scavenging capability. Quercetin was most effective against fluorescent AGEs formation (>80% inhibition), followed by naringenin, rosmarinic acid, and epicatechin (Figure 2). Chlorogenic acid showed no significant inhibition.

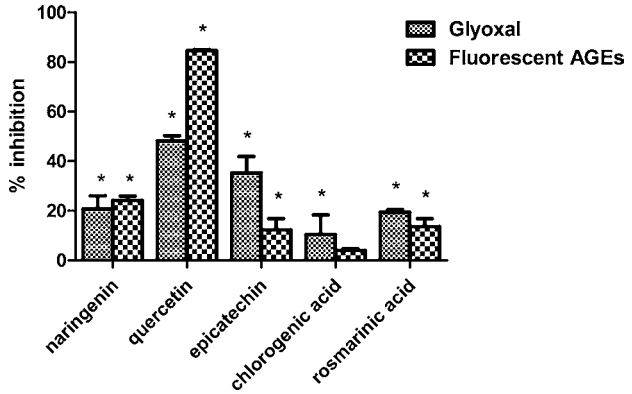

Figure 2. Inhibitory activity of polyphenols on the formation of glyoxal and fluorescent AGEs in a cookie model. Bars with an asterisk indicate significant difference from control ($P < 0.05$).

It has been suggested that the food ingredient profile has substantial effects on AGE formation and, compared with

sucrose, the lipid composition might play a more important role in AGE production in sponge cake.[7] The model cookie was rich in canola oil, which is a kind of edible oil containing a high proportion of unsaturated fatty acids including oleic acid, linoleic acid, and α-linolenic acid. Glyoxal is a prominent product of lipid peroxidation, and phenolics are able to inhibit lipid peroxidation via free radical scavenging capability. Therefore, it is likely that the tested dietary polyphenols reduced glyoxal generation by inhibiting lipid peroxidation. In agreement with earlier studies' viewpoints, the antiglycation effect of dietary polyphenols possibly relied on their free radical scavenging activity in the oxidative stage of glycation, when reactive carbonyl species are produced from sugar/lipid/Amadori product oxidation.[4,7]

In this paper, the antioxidant and antiglycation activities of five selected dietary polyphenols in a cookie model were discussed. Further to their potential to induce changes in cookies' color, pH, and moisture content, polyphenols were capable of increasing the health-beneficial antioxidants content in fortified cookies. The antiglycation activity of dietary polyphenols during cookie baking was indicated by lower levels of glyoxal and total fluorescent AGEs, which might be attributed to phenolics' free radical scavenging capacity. Compared with other tested polyphenols at the same mass-based fortification level, quercetin is suggested to be the most promising functional cookie additive given its significant promotion of antioxidant capacity together with strong inhibition against glycation toxicants formation.

The fate of dietary polyphenols during thermal food processing is of high research significance because the thermal conversion of chemical structure, which is associated with destruction of some primary compounds and introduction of many new compounds, would lead to alterations in foods' organoleptic properties and, more importantly, biological activities. The suggested reaction products of oxidized quercetin, for example, might be potential antioxidative and chemopreventive agents or in contrast be harmful to human health, which need further investigations. The current work suggests that during future functional food development by means of dietary polyphenol fortification before food processing, cautious measures are required to efficiently retain the primary chemical structure and the structure-associated health-beneficial bioactivities of polyphenols during thermal treatment; on the other hand, research efforts are expected elucidating the complex array of chemical conversions taking place during heating and characterizing the structure and bioactivity of reaction products formed.

■ ASSOCIATED CONTENT

Supporting Information

LC-MS total ion chromatograms of control cookie extract and quercetin-fortified cookie extract (showing the first 30 min only). This material is available free of charge via the Internet at http://pubs.acs.org.

■ AUTHOR INFORMATION

Corresponding Author

*(M.W.) Phone: +852-22990338. Fax: +852-22990348. E-mail: mfwang@hku.hk.

Notes

The authors declare no competing financial interest.

■ ABBREVIATIONS USED

ABTS, 2,2′-azinobis(3-ethylbenzothiazoline-6-sulfonic acid); AGEs, advanced glycation endproducts; CE, collision energy; CEL, carboxyethyllysine; CML, carboxymethyllysine; DP, declustering potential; DPPH, 2,2-diphenyl-1-picrylhydrazyl; EMS, enhanced mass spectrometry; EPI, enhanced product ion; ESI, electrospray ionization; GO, glyoxal; GSE, grape seed extract; MGO, methylglyoxal; 2-MQ, 2-methylquinoxaline; OPD, *o*-phenylenediamine; Q, quinoxaline; SDS, sodium dodecyl sulfate; TEAC, Trolox equivalent antioxidant capacity

■ REFERENCES

(1) Han, X.; Shen, T.; Lou, H. Dietary polyphenols and their biological significance. *Int. J. Mol. Sci.* **2007**, *8*, 950−988.

(2) Zhang, X.; Chen, F.; Wang, M. Impacts of selected dietary polyphenols on caramelization in model systems. *Food Chem.* **2013**, *141*, 3451−3458.

(3) Xu, B.; Chang, S. K. C. Total phenolics, phenolic acids, isoflavones, and anthocyanins and antioxidant properties of yellow and black soybeans as affected by thermal processing. *J. Agric. Food Chem.* **2008**, *56*, 7165−7175.

(4) Peng, X.; Ma, J.; Cheng, K.; Jiang, Y.; Chen, F.; Wang, M. The effects of grape seed extract fortification on the antioxidant activity and quality attributes of bread. *Food Chem.* **2010**, *119*, 49−53.

(5) Dewanto, V.; Wu, X.; Adom, K. K.; Liu, R. H. Thermal processing enhances the nutritional value of tomatoes by increasing total antioxidant activity. *J. Agric. Food Chem.* **2002**, *50*, 3010−3014.

(6) Patras, A.; Brunton, N.; Da Pieve, S.; Butler, F.; Downey, G. Effect of thermal and high pressure processing on antioxidant activity and instrumental colour of tomato and carrot purees. *Innovative Food Sci. Emerging Technol.* **2009**, *10*, 16−22.

(7) Srey, C.; Hull, G. L. J.; Connolly, L.; Elliott, C. T.; Castillo, M. D. D.; Ames, J. M. Effect of inhibitor compounds on N^{ϵ}-(carboxymethyl)-lysine (CML) and N^{ϵ}-(carboxyethyl)lysine (CEL) formation in model foods. *J. Agric. Food Chem.* **2010**, *58*, 12036−12041.

(8) Ameur, L. A.; Mathieu, O.; Lalanne, V.; Trystram, G.; Birlouez-Aragon, I. Comparison of the effects of sucrose and hexose on furfural formation and browning in cookies baked at different temperatures. *Food Chem.* **2007**, *101*, 1407−1416.

(9) Arribas-Lorenzo, G.; Fogliano, V.; Morales, F. J. Acrylamide formation in a cookie system as influenced by the oil phenol profile and degree of oxidation. *Eur. Food Res. Technol.* **2009**, *229*, 63−72.

(10) Arribas-Lorenzo, G.; Morales, F. J. Analysis, distribution, and dietary exposure of glyoxal and methylglyoxal in cookies and their relationship with other heat-induced contaminants. *J. Agric. Food Chem.* **2010**, *58*, 2966−2972.

(11) Charissou, A.; Ait-Ameur, L.; Birlouez-Aragon, I. Kinetics of formation of three indicators of the Maillard reaction in model cookies: influence of baking temperature and type of sugar. *J. Agric. Food Chem.* **2007**, *55*, 4532−4539.

(12) Gokmen, V.; Acar, O. C.; Koksel, H.; Acar, J. Effects of dough formula and baking conditions on acrylamide and hydroxymethylfurfural formation in cookies. *Food Chem.* **2007**, *104*, 1136−1142.

(13) Palermo, M.; Fiore, A.; Fogliano, V. Okara promoted acrylamide and carboxymethyl-lysine formation in bakery products. *J. Agric. Food Chem.* **2012**, *60*, 10141−10146.

(14) Tregoat, V.; Brohee, M.; Cordeiro, F.; Hengel, A. J. v. Immunofluorescence detection of advanced glycation end products (AGEs) in cookies and its correlation with acrylamide content and antioxidant activity. *Food Agric. Immunol.* **2009**, *20* (3), 253−268.

(15) Zhu, F.; Cai, Y.; Ke, J.; Corke, H. Dietary plant materials reduce acrylamide formation in cookie and starch-based model systems. *J. Sci. Food Agric.* **2011**, *91*, 2477−2483.

(16) Cheng, K.; Chen, F.; Wang, M. Inhibitory activities of dietary phenolic compounds on heterocyclic amine formation in both chemical model system and beef patties. *Mol. Nutr. Food Res.* **2007**, *51*, 969−976.

(17) Wang, R.; Zhou, W.; Isabelle, M. Comparison study of the effect of green tea extract (GTE) on the quality of bread by instrumental analysis and sensory evaluation. *Food Res. Int.* **2007**, *40*, 470−479.
(18) Zoulias, E.; Oreopoulou, V.; Kounalaki, E. Effect of fat and sugar replacement on cookie properties. *J. Sci. Food Agric.* **2002**, *82*, 1637−1644.
(19) Buchner, N.; Krumbein, A.; Rohn, S.; Kroh, L. W. Effect of thermal processing on the flavonols rutin and quercetin. *Rapid Commun. Mass Spectrom.* **2006**, *20*, 3229−3235.
(20) Hvattum, E.; Stenstrom, Y.; Ekeberg, D. Study of the reaction products of flavonols with 2,2-diphenyl-1-picrylhydrazyl using liquid chromatography coupled with negative electrospray ionization tandem mass spectrometry. *J. Mass Spectrom.* **2004**, *39*, 1570−1581.
(21) Ma, J.; Peng, X.; Ng, K.; Che, C.; Wang, M. Impact of phloretin and phloridzin on the formation of Maillard reaction products in aqueous models composed of glucose and L-lysine or its derivatives. *Food Funct.* **2012**, *3*, 178−186.
(22) Silvan, J. M.; Assar, S. H.; Srey, C.; Castillo, M. D. d.; Ames, J. M. Control of the Maillard reaction by ferulic acid. *Food Chem.* **2011**, *128*, 208−213.
(23) Wang, Y.; Ho, C. Flavour chemistry of methylglyoxal and glyoxal. *Chem. Soc. Rev.* **2012**, *41*, 4140−4149.

Table 1. Composition of Mixtures Prepared from Milk and 10 mg/mL NaCas−Thymol Dispersions Used in Anti-Listerial Experiments

	volume of constituents (mL)			fat content of mixture (%)	overall thymol concentration (mg/mL)
	milk volume and type	thymol dispersion	sterile water		
A	9, skim	1		<0.05	1
B	5.5, 2% reduced-fat	4.5		~1.14	4.5
C	4, full fat	4.5	1.5	~1.33	4.5
D	4.5, full fat	4.5	1	~1.49	4.5
E	5.5, full fat	4.5		~1.83	4.5
control	same volume and type of milk as in A−E		10 minus milk volume		

and milk. Milk with different fat contents was studied as model food systems to investigate the impacts of binding with proteins and lipids on antilisterial properties of thymol. To further understand the binding between thymol and milk components, the second objective was to characterize thymol content in the milk serum to correlate antimicrobial properties observed in growth media and milk.

MATERIALS AND METHODS

Chemicals. NaCas was purchased from Sigma-Aldrich Corp. (St Louis, MO). The product had a purity of over 90% w/w according to the vendor. Thymol (>99% purity), pyrene, and sodium azide were purchased from Sigma-Aldrich Corp. SSPS was a commercial product from Fuji Oil Corp. (Osaka, Japan). Ultrahigh temperature-processed skim milk, 2% reduced-fat milk, and full (3.3%) fat milk were products of Simple Truth Organic (San Diego, CA).

Encapsulation. NaCas was hydrated at 5% w/w in deionized water overnight at room temperature (21 °C). The pH of the solution was 6.8. Thymol was mixed in the NaCas solution at 0, 5, 10, 15, and 20 mg/mL. The mixture was homogenized at 15000 rpm for 2 min using a Cyclone I.Q. microprocessor homogenizer (VirTis Co., Gardiner, NY).

Determination of Encapsulation Efficiency in Transparent Dispersions. The concentration of thymol encapsulated by NaCas was determined by UV−vis. spectroscopy. The dispersions as prepared above were centrifuged at 6000*g* for 10 min (Minispin plus, Eppendorff, Hamburg, Germany). The upper transparent supernatant was transferred and diluted 100 (for dispersions prepared with 5 and 10 mg/mL thymol) or 200 (for dispersions prepared with 15 and 20 mg/mL thymol) times in volume using hexane. After vortexing for 5 min, the mixture was allowed to stand until two separate transparent phases formed. The upper organic phase was taken to measure the absorbance at 275 nm to determine thymol concentration based on a calibration curve established previously using standard solutions with 0.01−0.1 mg/mL thymol dissolved in hexane. Three independent emulsion replicates were measured. The encapsulation efficiency was calculated based on the total thymol (g) used in encapsulation, the mass in the transparent dispersion, and the amount truly dissolved (eq 1). To quantify the amount of thymol truly dissolved in water (not encapsulated in casein nanoparticles), the dispersion prepared with 10 mg/mL thymol was acidified to pH 4.6 using 6 M HCl to precipitate casein nanoparticles (with encapsulated thymol) and was centrifuged at 10000*g* for 5 min. The supernatant was filtered through a 0.22 μm polyvinyl difluoride filter (Fisher Scientific, Co., Pittsburgh, PA), then 300 μL of the permeate was mixed with 1.5 mL of hexane and the thymol concentration determined as above.

$$\text{encapsulation efficiency \%} = \frac{\text{dispersed thymol} - \text{dissolved thymol}}{\text{total thymol} - \text{dissolved thymol}} \times 100\% \quad (1)$$

Particle Size and ζ Potential. The hydrodynamic diameter (D_h) was measured using a Delsa Nano analyzer (Beckman Coulter, Atlanta, GA). Samples were diluted 30 times with 10 mM phosphate buffer at pH 7.0. The scattering angle was fixed at 165°. The ζ potential of thymol dispersion, SSPS, and their mixture at pH 3.0−7.0 was also measured using the Delsa Nano analyzer. The dispersion, prepared with 10 mg/mL thymol, was diluted 100 times to a casein concentration of 0.05% using deionized water and adjusted to pH 3.0−7.0 using 1 and 0.25 M HCl. Solutions with 0.05% w/v SSPS and the mixture of the thymol dispersion and SSPS with same biopolymer concentrations at pH 3.0−7.0 were prepared similarly for ζ potential measurements.

Atomic Force Microscopy (AFM). The topography of NaCas nanoparticles before and after encapsulation of thymol was characterized using AFM. A 5% w/w NaCas dispersion and the dispersion prepared with 10 mg/mL thymol were diluted to a NaCas concentration of 10 mg/L using deionized water. Then 10 μL of each diluted sample was spread evenly onto a freshly cleaved mica sheet mounted on a sample disk (Bruker Corp., Santa Barbara, CA). A rectangular cantilever having an aluminum reflective coating on the backside and a quoted force constant of 2.80 N/m (FESPA, Bruker Corp.) were used on a Multimode VIII microscope (Bruker AXS, Billerica, MA). The tapping mode was used to scan the sample, and topography images were generated with a preset scan area of 2.0 μm × 2.0 μm at a scanning speed of 1 Hz.

Storage Stability. The storage stability of dispersions prepared with 0, 5, and 10 mg/mL thymol was determined by measuring the D_h during storage at room temperature (21 °C) for 30 d. The dispersion without thymol was added with 0.02% w/w sodium azide to prevent microbial spoilage.

Stabilization of Dispersions at pH 4.6 Using SSPS. The dispersion prepared with 5% NaCas and 10 mg/mL thymol was diluted to a NaCas concentration of 0.25% and mixed with 0−0.5% SSPS. The pH was adjusted to 4.6 with 0.25 M HCl. Samples were heated at 88 °C for 2 min, and the absorbance was measured at 400 nm as an indicator of turbidity before and after heating, with deionized water as the blank.

Fluorescence Spectroscopy. The interactions between thymol and NaCas were studied by fluorescence spectroscopy using a spectrofluorometer (model RF-1501, Shimadzu Corp., Kyoto, Japan). Briefly, thymol stock solution was prepared at 1.0% w/v in 95% aqueous ethanol and was diluted to 0−7.5 mg/L (10−50 μM) in 0.01 mg/mL aqueous NaCas (pH 7.0) and incubated at room temperature (21 °C) for at least 2 h before measurement. Fluorescent spectroscopy was carried out with excitation wavelength of 280 or 295 nm and emission spectra were recorded from 290 to 550 nm. The slit width for excitation and emission was set at 10 nm. The fluorescence intensity of thymol dissolved in 10% aqueous ethanol was used as background fluorescence for calibrating the spectra. Three replicates were performed at each condition.

Minimum Inhibitory Concentration (MIC) and Minimum Bactericidal Concentration (MBC) of Encapsulated Thymol. An antimicrobial microbroth dilution assay in 96-well microtiter plates was used to determine the MIC and MBC of encapsulated and free thymol against *L. monocytogenes* Scott A.[15,16] *L. monocytogenes* strain was from the culture collection of the Department of Food Science and Technology at the University of Tennessee. The stock *L. monocytogenes* culture, stored in glycerol at −20 °C, was transferred in tryptic soy broth (TSB) at 32 °C for two consecutive days to activate bacteria. *L. monocytogenes* was grown for 18 h in TSB at the

dx.doi.org/10.1021/jf4055402 | J. Agric. Food Chem. 2014, 62, 1649−1657

same temperature before use and diluted in TSB to ca. 7 log CFU/mL as a working culture. Free thymol stock solution was prepared in 95% ethanol at a concentration of 100 mg/mL, which was then diluted to 4 mg/mL with TSB as the working solution. The 4 mg/mL working solution was further diluted in TSB to 0.1−2 mg/mL thymol with 0.1 mg/mL increments. Thymol (10 mg/mL) encapsulated in NaCas was prepared and diluted to the same range as free thymol. The diluted thymol or thymol−NaCas samples (120 μL) were mixed with 120 μL of the working culture in the 300 μL wells of the microtiter plate, resulting in overall thymol concentrations of 0.05−1 mg/mL. Microtiter plates were then incubated at 32 or 21 °C for 24 h. The MIC was determined as the lowest thymol concentration that produced no visible growth.[15,16] To determine the MBC, 20 μL of the culture broth from each well showing no visible growth was transferred onto tryptic soy agar plates and incubated for another 48 h at 32 or 21 °C. The lowest concentration of thymol corresponding to the complete absence of *L. monocytogenes* growth on the agar surface was defined as the MBC. Experiments were performed in triplicate using three independent fresh working cultures.

Antilisterial Activity of Thymol in Milk with Different Fat Levels. Fat content is a dominant parameter impacting the effectiveness of lipophilic antimicrobials in milk.[17] Skim, 2% reduced fat, or whole milk were mixed with different volumes of the 10 mg/mL aqueous NaCas−thymol dispersion and sterile water to a total volume of 10 mL to obtain different fat levels (Table 1) so that the findings can be applied not only in fluid milk but also other dairy and relevant products with varying fat contents. Because liquid thymol dispersion was used to mix milk, it was not possible to simulate full fat (3.3%) milk. The overall concentration of thymol was 1 mg/mL in skim milk and 4.5 mg/mL in other milk treatments. These two concentrations were chosen because preliminary experiments showed complete inhibition of *L. monocytogenes* in skim milk within 4 h by 4.5 mg/mL of both free and encapsulated thymol, with no recovery in 7 days, while 1 mg/mL thymol in milk with 1% or higher fat corresponded to no inhibition of *L. monocytogenes*. For free thymol, thymol crystals were weighed and added directly into the milk at the same concentrations as the encapsulated thymol (Table 1). Sterile water was used to make up the total volume of 10 mL, followed by mixing using an end-to-end shaker for 30 min at room temperature. The 100 μL working culture with ca. 8 log CFU/mL *L. monocytogenes* was inoculated in the final milk mixture to an overall population of ca. 6 log CFU/mL using the method described previously.[18] After incubation at room temperature (~21 °C) for up to 7 d, *L. monocytogenes* was enumerated using the tryptic soy agar pour plating method with a detection limit of 1 log CFU/mL. Experiments were performed in triplicate using three independent fresh working cultures.

Quantification of Thymol Dissolved in the Aqueous Phase of Milk. The amount of thymol dissolved in the aqueous phase of milk was quantified as follows. Free thymol and encapsulated thymol samples were prepared in milk as described above except that the 0.1 mL of bacterial culture was replaced with 0.1 mL of deionized water. After incubation at room temperature (21 °C) for 0 and 48 h, samples were adjusted to pH 4.6 using 6 M HCl to precipitate caseins, followed by centrifugation at 10,000*g* for 5 min and filtration of the supernatant through a 0.22 μm polyvinyl difluoride membrane filter. The 300 μL of permeate was mixed with 1.5 mL of hexane to determine thymol concentration using the procedures described previously. Duplicate samples were measured.

Solubility of Thymol in Water at Room Temperature. The solubility of thymol in water was measured by adding an excess amount of thymol crystals to deionized water (2 mg/mL). After stirring overnight at room temperature (21 °C), the aqueous phase with dissolved thymol was mixed with hexane to determine thymol concentration, as described above. Two independent sample replicates were tested.

Statistical Analysis. Statistical analyses were performed using the JMP program (JMP Statistical Software, SAS Institute, Cary, NC). One-way analysis of variance was carried out. Differences between means were determined using a Fisher's least significant difference test. The significance level was set at 0.05.

RESULTS AND DISCUSSION

Encapsulation Efficiency. Transparent samples were observed after homogenizing thymol at overall concentrations of 5 and 10 mg/mL, which was well above its water solubility at 21 °C (0.75 mg/mL). Conversely, thymol crystals were visible after homogenization at overall thymol concentrations of 15 and 20 mg/mL (not shown), which indicated that 5% w/v NaCas reached its encapsulation capacity under the conditions studied. The dissolved thymol concentration determined in the transparent dispersion with 10 mg/mL thymol was 0.74 mg/mL, similar to the water solubility of thymol crystals. The efficiency of encapsulating thymol in transparent dispersions was determined according to eq 1 and listed in Table 2. There was no significant difference between samples with 5 and 10 mg/mL thymol, with encapsulation efficiency of 89% and 92.3%. The encapsulation efficiency as determined decreased to around 72% when thymol was emulsified at overall concentrations of 15 and 20 mg/mL.

Table 2. Encapsulation Efficiency of Dispersions Prepared with 5% w/v NaCas and Different Thymol Concentrations

overall thymol concentration (mg/mL)	encapsulation efficiency (%)[a]
5	89.0 ± 3.1[a]
10	92.3 ± 2.2[a]
15	72.1 ± 1.4[b]
20	72.4 ± 1.3[b]

[a]Numbers are mean ± standard deviation from triplicate samples. Different superscripts indicate differences in the means ($P < 0.05$).

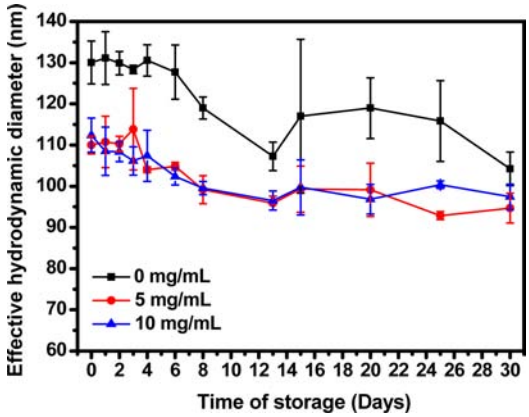

Figure 1. Effective hydrodynamic diameter of 5% w/v sodium caseinate dispersions homogenized with 0, 5, and 10 mg/mL thymol during storage at room temperature (21 °C).

Physical Properties of Transparent Dispersions. Because thymol was not completely encapsulated at an overall concentration of 15 and 20 mg/mL, only samples with 5 and 10 mg/mL thymol were characterized for storage stability. The D_h of transparent dispersions prepared with 5 and 10 mg/mL thymol during storage at room temperature for 30 days is shown in Figure 1. There was no significant increase of D_h during storage. The D_h of NaCas, also sheared at homogenization conditions, was around 130 nm, and the dispersion after encapsulating 5 or 10 mg/mL thymol had a D_h of about 110 nm. The smaller dimension of casein particles after encapsulation was also observed in AFM (Figure 2). The smaller dimension of particles measured in AFM than D_h may be the result of drying of particles during sample preparation

dx.doi.org/10.1021/jf4055402 | J. Agric. Food Chem. 2014, 62, 1649−1657

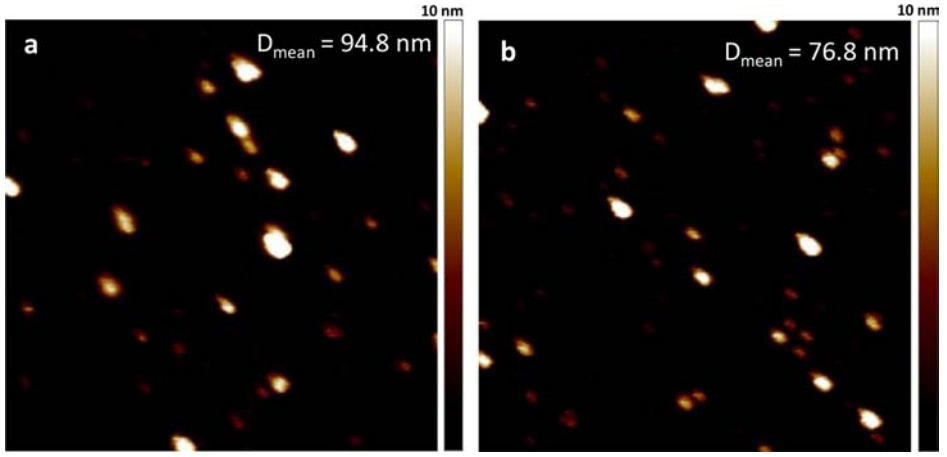

Figure 2. AFM topography images of NaCas (a) without or (b) with thymol. The dispersion was prepared with 10 mg/mL thymol and 5% NaCas before dilution for AFM. The NaCas only dispersion was also homogenized before dilution for AFM. Mean diameter of the particles was measured using the instrument software. Image dimension is 2 μm × 2 μm. The scale on the right is for particle height.

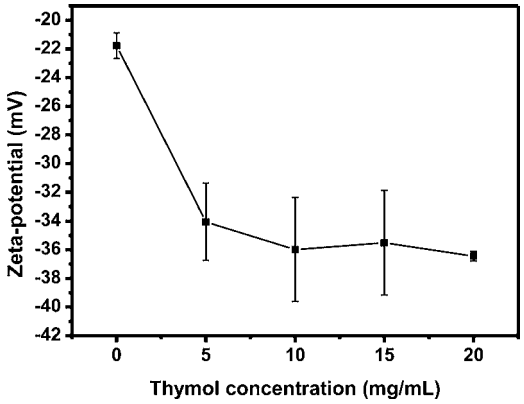

Figure 3. ζ potential of the dispersions prepared with 5% NaCas and different concentrations of thymol at pH 7.0. The dispersions were centrifuged, and the supernatant was collected and diluted before measurement.

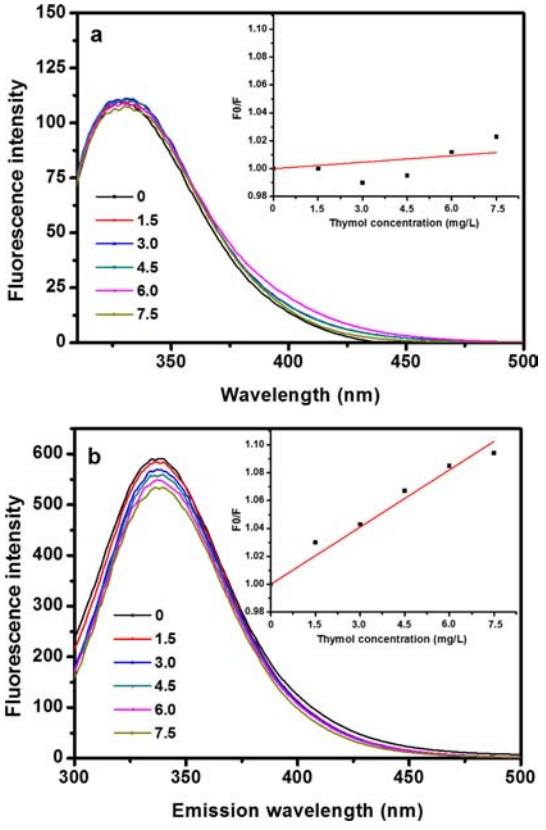

Figure 4. Fluorescence emission spectra of NaCas at excitation wavelength of (a) 295 nm and (b) 280 nm in 10 mM phosphate buffer at pH 7.0, after interacting with 0−7.5 mg/L (0−50 μM) thymol. The plot of F_0/F versus thymol concentration is shown in the inset, with the lines showing the linear fit of data with an intercept of 1.

for AFM. The reduction of casein nanoparticle dimension after encapsulation with thymol may be the result of enhanced packing of casein molecules due to hydrophobic attraction by thymol. Furthermore, the stable D_h during storage indicates the insignificance of Ostwald ripening as has been observed by others for dispersions prepared with small-molecule surfactants like Tween 80.[19]

NaCas dispersions with thymol had a much higher magnitude of ζ potential when compared with NaCas alone, and the thymol concentration did not affect the ζ potential significantly (Figure 3). The p*I*s of α_{s1}-, α_{s2}-, β-, and κ-casein are 4.94, 5.23, 5.14, and 5.90, respectively, with respective net charges of −21.9, −17.1, −13.3, and −2.0 at pH 6.6. [20] Theoretically, a more negative ζ potential is expected for smaller casein particles because of a smaller quantity of κ-casein per particle. The ζ potential results in Figure 3 therefore agree with this expectation based on particle dimension (Figures 1 and 2). The high magnitude of ζ potential can prevent particle aggregation during storage (Figure 1).

Interactions between Thymol and NaCas. Binding between proteins and small molecules in aqueous solutions can be conveniently studied using intrinsic fluorescence properties of proteins.[13] Figure 4 shows the emission spectra of NaCas with different concentrations of thymol. Figure 4a shows little change of the fluorescence intensity of NaCas after interacting with various amounts of thymol at the excitation wavelength of 295 nm, which reflects the binding near tryptophan (Trp) residues.[21] Conversely, the fluorescence intensity of NaCas excited at 280 nm, due to both Trp and tyrosine (Tyr) residues,[21] decreased with an increase in thymol concentration (Figure 4b). Therefore, thymol binds with caseins at Tyr or other residues away from Trp of caseins, effectively quenching the fluorescence excited at 280 nm.

dx.doi.org/10.1021/jf4055402 | J. Agric. Food Chem. 2014, 62, 1649−1657

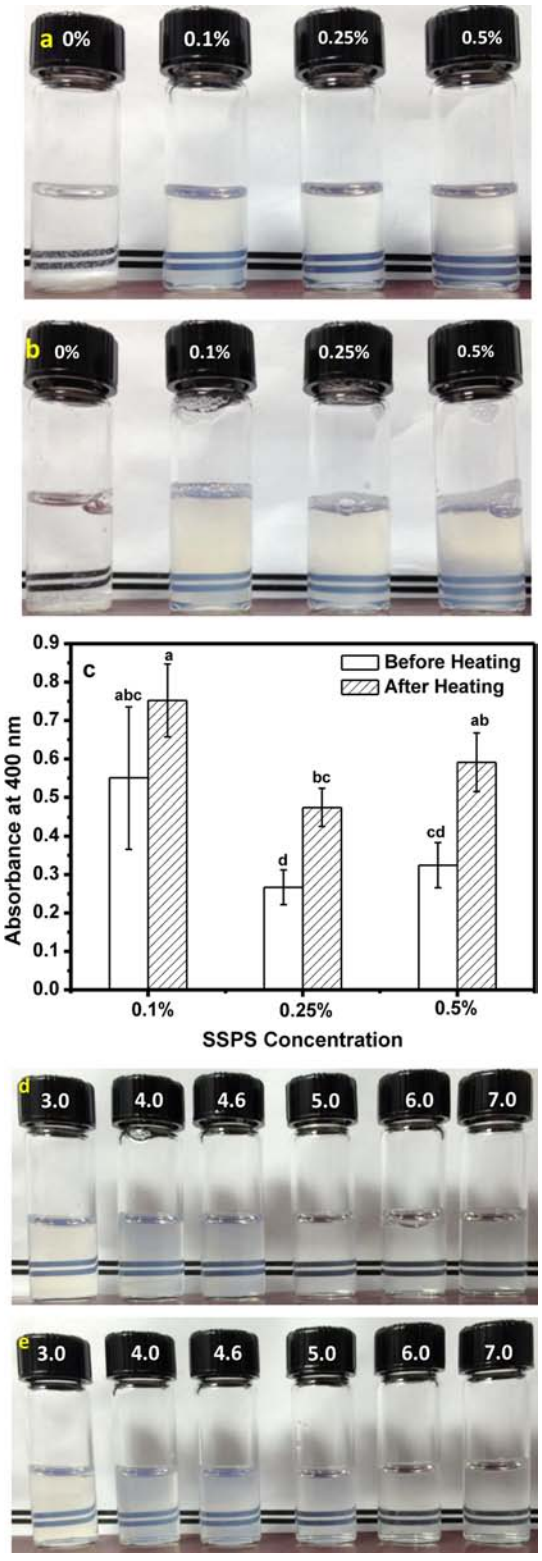

Figure 5. Appearance of thymol-containing dispersions containing 0.25% NaCas, diluted from the dispersion prepared with 5% NaCas and 10 mg/mL thymol, with 0%, 0.1%, 0.25%, and 0.5% SSPS (as labeled on vial caps) at pH 4.6, (a) before and (b) after being heated at 88 °C for 2 min. The absorbance at 400 nm is shown in panel (c), where different letters above bars indicate significant difference ($P < 0.05$) in the mean. Photos (d) and (e) show the respective samples, with 0.25% NaCas and 0.25% SSPS adjusted to pH 3.0–7.0 before and after heating at 88 °C for 2 min.

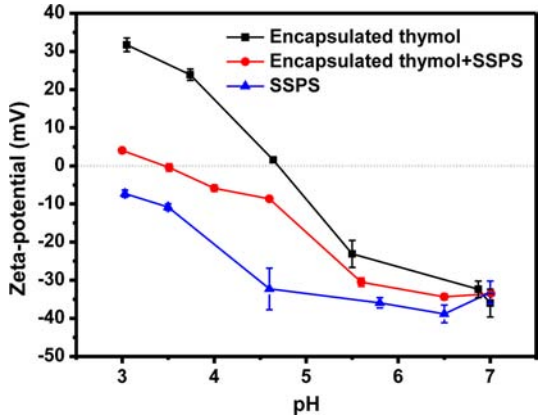

Figure 6. ζ potential of thymol dispersion, SSPS, and their mixture (with equal mass of NaCas and SSPS) at pH 3.0–7.0.

The intrinsic fluorescence was further analyzed using the Stern–Volmer equation[22]

$$F_0/F = 1 + k_q \times \tau_0 \times [Q] = 1 + K_{sv} \times [\text{thymol}] \quad (2)$$

where F_0 and F are fluorescence intensities in the absence and presence of a quencher, [Thymol] is the concentration of thymol (M), k_q is the fluorescence quenching rate constant, τ_0 is the lifetime of fluorophore fluorescence in absence of quenchers and equals 10^{-8} s, and K_{sv} is the Stern–Volmer quenching constant which can be determined by linear fit of F_0/F plot against [Thymol].[23] The linear plots of F_0/F as a function of [Thymol] excited at 295 and 280 nm are given in the inset of parts a and b of Figure 4, respectively. The good linear fit of data to eq 2 ($R^2 > 0.99$) showed the applicability of the Stern–Volmer model, and the obtained K_{sv} values were 100 ± 212 M^{-1} and 1900 ± 141 M^{-1} at the excitation wavelength of 295 and 280 nm, respectively. The K_{sv} at excitation wavelength of 295 nm is not statistically different from 0 ($P > 0.05$), which indicates no interactions between thymol and Trp. Fluorescence quenching can result from collision (dynamic quenching) or complex formation (static quenching) between biopolymers and quenchers.[22] The k_q at excitation wavelength of 280 nm is 1.9×10^{11} M^{-1} s^{-1}, which is about 10-fold higher than the maximum dynamic quenching constant (2×10^{10} M^{-1} s^{-1}) for quenchers interacting with biopolymers.[24] The results suggest the fluorescence quenching is static, and therefore complexes are formed when thymol binds with caseins at low NaCas concentrations.

Stabilization of Thymol Dispersions at pH 4.6 Using SSPS. The dispersion prepared with 10 mg/mL thymol was diluted to an overall NaCas concentration of 0.25% w/v and mixed with 0–0.5%w/v SSPS. After adjusting to pH 4.6, samples were heated at 88 °C for 2 min, equivalent thermal processing conditions for acidic beverages (pH < 4.6),[25] and the absorbance at 400 nm before and after heating was measured to indicate turbidity (presented in Figure 5). Without SSPS, the dispersion showed precipitation both before and after heating. With 0.1–0.5% SSPS, dispersions were stable before and after heating. The dispersion with 0.1% SSPS had higher absorbance than the other two SSPS treatments (Figure 5c), possibly because of insufficient SSPS to prevent particle aggregation. There is no significant difference ($P > 0.05$) between the dispersions with 0.25% and 0.5% SSPS, which indicates SSPS is able to stabilize equal mass of NaCas at pH 4.6.

dx.doi.org/10.1021/jf4055402 | J. Agric. Food Chem. 2014, 62, 1649–1657

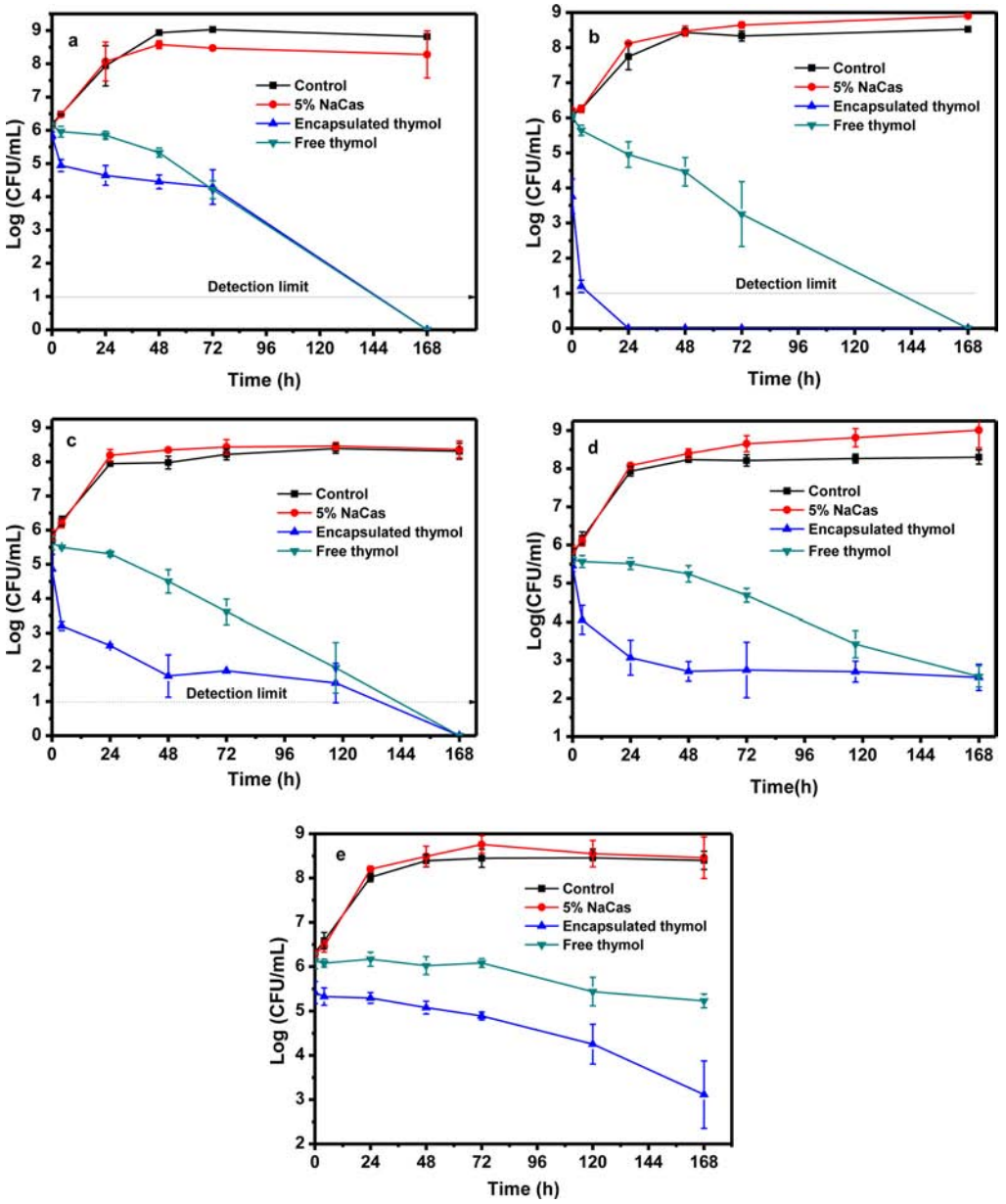

Figure 7. Growth of *Listeria monocytogenes* Scott A in milk prepared to different fat levels at room temperature (~21 °C) treated by different concentrations of free or capsulated thymol: (a) 1 mg/mL thymol in skim milk; 4.5 mg/mL thymol in milk with (b) 1.14%, (c) 1.33%, (d) 1.49%, and (e) 1.83% fat. Milk compositions are listed in Table 1. The control was the treatment with milk added with sterile water and culture only. The 5% NaCas treatment was conducted by adding 5% NaCas solution at the same volume as encapsulated thymol into milk. Error bars are standard deviations (n = 3).

The forces stabilizing colloidal particles from aggregation include electrostatic and steric repulsions.[12,26] At neutral pH, caseins are highly negatively charged and electrostatic repulsion itself is strong enough to prevent particle aggregation, as indicated in Figure 1 for stable D_h during storage. To understand the stabilization of dispersions by SSPS at pH 4.6, the ζ potential of SSPS, the thymol dispersion, and their mixture at pH 3.0−7.0 was measured and is presented in Figure 6. The lowest ζ potential magnitude of thymol dispersion was observed at around pH 4.6, the pI of caseins and the weakened electrostatic repulsion caused the aggregation and precipitation of casein capsules, as discussed above. The ζ potential of SSPS alone was negative at pH 3.0−7.0, with a smaller magnitude at a lower pH. After mixing thymol dispersion with SSPS, the ζ potentials were in between the individual components, with the magnitude being close to zero at pH 3.5, suggesting complex formation between SSPS and casein particles.[14] Because dispersions were stable at pH 3.0−7.0, even after heating at 88 °C for 2 min (Figures 5d and 5e), both electrostatic and steric interactions contributed to the stability of mixture system, with steric interactions being dominant at acidity near the pI of caseins. Therefore, SSPS stabilized thymol dispersions similarly to acidified milk by providing steric repulsion after adsorbing on free casein or casein-coated thymol particles,[14] as discussed previously. This enables the application of casein-based encapsulation systems in various acidic conditions.

Antilisterial Properties and Correlation to Solubility. The MICs and MBCs of free and encapsulated thymol against *L. monocytogenes* were 0.2 and 0.3 mg/L, respectively, at both 21 and 32 °C. These concentrations are below the water

dx.doi.org/10.1021/jf4055402 | J. Agric. Food Chem. 2014, 62, 1649−1657

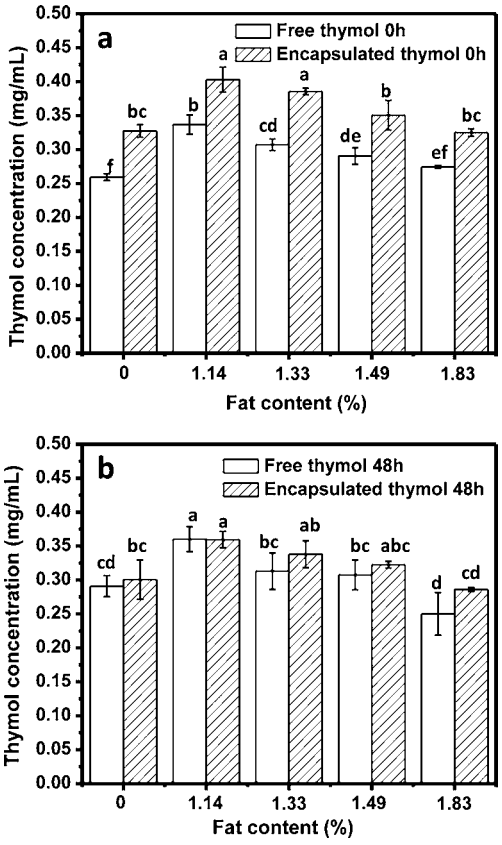

Figure 8. Concentration of thymol in the continuous phase of model milk systems with different fat contents after (a) 0 h and (b) 48 h at room temperature (21 °C). Different letters above bars indicate significant difference ($P < 0.05$) in the mean.

solubility limit of 0.75 mg/mL, and the similar MIC and MBC of encapsulated and free thymol suggest that the binding between thymol and caseins does not affect the activity of thymol interacting with bacteria. Similar results were previously reported for thymol against *Staphylococcus aureus* ATCC 25923 and *Escherichia coli* ATCC 25922 after encapsulation in methylcellulose/ethylcellulose.[27]

Figure 7 presents the growth activity of *L. monocytogenes* in milk with different fat levels in the presence of free and encapsulated thymol. The *L. monocytogenes* growth curves were similar for the control (no treatment) and NaCas control, indicating that NaCas alone has no antimicrobial activity. In skim milk (Figure 7a), encapsulated thymol has slightly better antilisterial activity (ca. 1 log CFU/ml) than free thymol in the first 48 h, while no difference was observed at 72 or 168 h. The concentration of thymol in the aqueous phase of milk at 0 h was significantly higher for encapsulated thymol than for free thymol (Figure 8a). The delay in antilisterial activity of free thymol may be due to the slow dissolution process of thymol from crystals compared to the encapsulated form that enabled faster distribution into the milk matrix.[28] The concentration of thymol (1 mg/mL) required to inhibit *L. monocytogenes* in skim milk is higher than the MIC and MBC of free and encapsulated thymol in TSB. Furthermore, the respective thymol concentration in the aqueous phase of skim milk at 0 h was 0.26 to 0.33 mg/mL for free and encapsulated thymol, which was much lower than the water solubility of 0.75 mg/mL, and reduced after 48 h (Figure 8a). This suggests that the reduced thymol activity in skim milk is due to binding by proteins and fat globules (<0.5% in skim milk).

To study effects of fat content on antilisterial properties, 4.5 mg/mL thymol was added to milk adjusted to 1.1−1.8% fat (Table 1). As shown in Figure 7b−e, the inactivation of *L. monocytogenes* was slower at a higher fat level and the encapsulated thymol consistently reduced the *L. monocytogenes* population to a lower level in a shorter time than free thymol. With 1.14% (Figure 7b) and 1.33% (Figure 7c) fat, both free and encapsulated thymol reduced *L. monocytogenes* to below the detection limit of 1 log CFU/mL in 168 h. With 1.49% fat (Figure 7d), *L. monocytogenes* was reduced to about 2.5 log CFU/mL in 168 h by free and encapsulated thymol. The greater than 3 log reduction after 48 h in milk with 1.14−1.49% fat is in agreement with thymol concentrations in the milk serum higher than the MBC (0.3 mg/mL) at both 0 and 48 h (Figure 8). At 1.83% fat (Figure 7e), the encapsulated and free thymol used at an overall concentration of 4.5 mg/mL was detected at 0.28 and 0.25 mg/mL in the aqueous phase of milk (Figure 8b), respectively, at 48 h. Because these concentrations were above the MIC (0.2 mg/mL) but below the MBC (0.3 mg/mL), inactivation of *L. monocytogenes* to a lesser extent was observed than in milk with lower fat levels, with the encapsulated thymol being more effective (Figure 7e).

Figures 7 and 8 indicate the significant effects of fat on the activity of hydrophobic antimicrobials like thymol. The antimicrobial activity of hydrophobic essential oil components is enabled after dissolution in phospholipids of the bacterial cell membrane to a sufficient quantity to result in substantial changes in membrane structures and cell metabolism.[29] The cell membrane of bacteria is covered by structures including peptidoglycan that can prevent the direct access of caseins and thymol enclosed in nanocapsules. Therefore, only the truly dissolved thymol may be able to diffuse into the cell membrane. For thymol binding with/encapsulated in caseins, the partitioning to the continuous water phase is expected, which is expected to further partition with bacterial cells. Because bacterial cells have phospholipids that are more hydrophobic than water-soluble caseins, the partitioning of lipophilic thymol to bacteria may be more favorable than binding with caseins and may become irreversible because of the much higher polarity of the continuous water phase. This may have resulted in the same MIC (0.2 mg/mL) and MBC (0.3 mg/mL) of free and encapsulated thymol, both of which are well below the water solubility of thymol (0.75 mg/mL). For the dispersion with 10 mg/mL thymol, the amount of truly dissolved thymol (after precipitation of casein capsules at pH 4.6, eq 1) is 0.74 mg/mL, which is close to the water solubility, while the rest is being dissolved/dispersed in casein nanocapsules. When the thymol dispersion is mixed with milk, the truly dissolved thymol is expected to decrease and the encapsulated thymol is again expected to be partitioning with the continuous water phase. The dissolved thymol also can diffuse into porous casein micelles[30] and bind with fat globules in milk. Analogous to bacterial cells, fat globules in milk are covered by membranes composed of phospholipids and proteins,[31] may be more favorable than caseins and water phase, and therefore reduce the amount of thymol that can potentially be dissolved in the continuous water phase and subsequently the bacterial membrane. For skim milk (with <0.5% fat), the impacts of binding by fat globules are not as significant, as 1 mg/mL thymol, ∼3 times higher than the MBC (0.3 mg/mL), is sufficient to inhibit *L. monocytogenes* (Figure 7a). As fat

concentration increases in milk, the binding by fat globules becomes more and more significant, reducing the amount of truly dissolved thymol (Figure 8) and therefore antilisterial activity (Figure 7) despite the higher overall thymol usage level (4.5 mg/mL). Findings from the present study agree with the speculations based on physics and mass transport.[28,32]

In conclusion, 5%w/v NaCas enabled the encapsulation of 1% w/v thymol as transparent dispersions that were stable at neutral pH during 30-day storage at room temperature. The encapsulation reduced the dimension of NaCas and increased the ζ potential. Thymol selectively binds with Tyr and possibly other amino acids not close to Trp of NaCas based on fluorescence spectroscopy. Under acidic conditions, the adsorption of SSPS on thymol-loaded casein particles provided steric repulsion and effectively prevented the aggregation and precipitation of casein capsules, even at pH 4.6. Lastly, encapsulation of thymol in casein nanocapsules enabled the fast and even distribution and increased the solubility and antilisterial activity of lipophilic antimicrobials in milk with different fat levels. Findings from the present study indicate the potential of the studied antimicrobial delivery system to improve the microbiological safety of complex food matrices such as Spanish cheeses.

AUTHOR INFORMATION

Corresponding Author

*Phone: (865) 974-6196. Fax: (865) 974-7332. E-mail: qzhong@utk.edu.

Funding

The present study was supported by the University of Tennessee, the U.S. Department of Agriculture, and Dairy Research Institute (Rosemont, IL).

Notes

The authors declare no competing financial interest.

REFERENCES

(1) Datta, A. R., *Listeria monocytogenes*. In *International Handbook of Foodborne Pathogens*, 1st ed.; Miliotis, M. D., Bier, J. W., Eds.; Marcel Dekker: New York, 2003; Vol. *125*, pp 105−121.

(2) Garcia, M. T.; Canamero, M. M.; Lucas, R.; Ben Omar, N.; Pulido, R. P.; Galvez, A. Inhibition of *Listeria monocytogenes* by enterocin EJ97 produced by *Enterococcus faecalis* EJ97. *Int. J. Food Microbiol.* **2004**, *90*, 161−170.

(3) Tippayatum, P.; Chonhenchob, V. Antibacterial activities of thymol, eugenol and nisin against some food spoilage bacteria. *Kasetsart J.: Nat. Sci.* **2007**, *41*, 319−323.

(4) Johny, A. K.; Darre, M. J.; Donoghue, A. M.; Donoghue, D. J.; Venkitanarayanan, K. Antibacterial effect of *trans*-cinnamaldehyde, eugenol, carvacrol, and thymol on Salmonella enteritidis and *Campylobacter jejuni* in chicken cecal contents in vitro. *J. Appl. Poult. Res.* **2010**, *19*, 237−244.

(5) Myers, H. B.; Thienes, C. H. The fungicidal activity of certain volatile oils and stearoptens—their comparative toxicity on a pathogenic yeastlike organism: report of clinical utilization in related infections. *JAMA, J. Am. Med. Assoc.* **1925**, *84*, 1985−1986.

(6) Griffin, S. G.; Wyllie, S. G.; Markham, J. L.; Leach, D. N. The role of structure and molecular properties of terpenoids in determining their antimicrobial activity. *Flavour Fragrance J.* **1999**, *14*, 322−332.

(7) Xu, J.; Zhou, F.; Ji, B. P.; Pei, R. S.; Xu, N. The antibacterial mechanism of carvacrol and thymol against *Escherichia coli*. *Lett. Appl. Microbiol.* **2008**, *47*, 174−179.

(8) Bhavini, S.; Davidson, P. M.; Qixin, Z. Nanocapsular dispersion of thymol for enhanced dispersibility and increased antimicrobial effectiveness against *Escherichia coli* O157:H7 and *Listeria monocytogenes* in model food systems. *Appl. Environ. Microbiol.* **2012**, *78*, 8448−8453.

(9) Brugman, S.; Klatter, F.; Visser, J.; Bos, N.; Elias, D.; Rozing, J. Neonatal oral administration of DiaPep277, combined with hydrolysed casein diet, protects against type 1 diabetes in BB-DP rats. An experimental study. *Diabetologia* **2004**, *47*, 1331−1333.

(10) Pan, K.; Zhong, Q. Improving clarity and stability of skim milk powder dispersions by dissociation of casein micelles at pH 11.0 and acidification with citric acid. *J. Agric. Food. Chem.* **2013**, *61*, 9260−9268.

(11) Udabage, P.; McKinnon, I. R.; Augustin, M. A. The use of sedimentation field flow fractionation and photon correlation spectroscopy in the characterization of casein micelles. *J. Dairy Res.* **2003**, *70*, 453−459.

(12) Walstra, P.; Jenness, R., Casein micelles. In *Dairy Chemistry and Physics*, 1st ed.; Walstra, P., Jenness, R., Eds.; John Wiley & Sons: Hoboken, NJ, 1984; Vol. *1*, pp 229−253.

(13) Pan, K.; Zhong, Q.; Baek, S. J. Enhanced dispersibility and bioactivity of curcumin by encapsulation in casein nanocapsules. *J. Agric. Food. Chem.* **2013**, *61*, 6036−6043.

(14) Nakamura, A.; Furuta, H.; Kato, M.; Maeda, H.; Nagamatsu, Y. Effect of soybean soluble polysaccharides on the stability of milk protein under acidic conditions. *Food Hydrocolloids* **2003**, *17*, 333−343.

(15) Basile, A.; Senatore, F.; Gargano, R.; Sorbo, S.; Del Pezzo, M.; Lavitola, A.; Ritieni, A.; Bruno, M.; Spatuzzi, D.; Rigano, D.; Vuotto, M. L. Antibacterial and antioxidant activities in *Sideritis italica* (Miller) Greuter et Burdet essential oils. *J. Ethnopharmacol.* **2006**, *107*, 240−248.

(16) Dung, N. T.; Kim, J. M.; Kang, S. C. Chemical composition, antimicrobial and antioxidant activities of the essential oil and the ethanol extract of *Cleistocalyx operculatus* (Roxb.) Merr and Perry buds. *Food Chem. Toxicol.* **2008**, *46*, 3632−3639.

(17) Shah, B.; Davidson, P. M.; Zhong, Q. X. Nanodispersed eugenol has improved antimicrobial activity against *Escherichia coli* O157:H7 and *Listeria monocytogenes* in bovine milk. *Int. J. Food Microbiol.* **2013**, *161*, 53−59.

(18) Xiao, D.; Davidson, P. M.; Zhong, Q. X. Spray-dried zein capsules with coencapsulated nisin and thymol as antimicrobial delivery system for enhanced antilisterial properties. *J. Agric. Food Chem.* **2011**, *59*, 7393−7404.

(19) Chang, Y. H.; McLandsborough, L.; McClements, D. J. Physical properties and antimicrobial efficacy of thyme oil nanoemulsions: influence of ripening inhibitors. *J. Agric. Food Chem.* **2012**, *60*, 12056−12063.

(20) O'Connell, J. E.; Flynn, C., The manufacture and applications of casein-derived ingredients. In *Handbook of Food Products Manufacturing*, 1st ed.; Hui, Y. H., Ed.; John Wiley & Sons: Hoboken, NJ, 2007; Vol. *1*, pp 557−591.

(21) Liang, L.; Tajmir-Riahi, H. A.; Subirade, M. Interaction of beta-lactoglobulin with resveratrol and its biological implications. *Biomacromolecules* **2008**, *9*, 50−56.

(22) Zhang, Y.; Li, J.-H.; Ge, Y.-S.; Liu, X.-R.; Jiang, F.-L.; Liu, Y. Biophysical studies on the interactions of a classic mitochondrial uncoupler with bovine serum albumin by spectroscopic, isothermal titration calorimetric and molecular modeling methods. *J. Fluoresc.* **2011**, *21*, 475−485.

(23) Lakowicz, J. R., *Principles of Fluorescence Spectroscopy*, 3rd ed.; Springer: New York, 2009.

(24) Lange, D. C.; Kothari, R.; Patel, R. C.; Patel, S. C. Retinol and retinoic acid bind to a surface cleft in bovine beta-lactoglobulin: a method of binding site determination using fluorescence resonance energy transfer. *Biophys. Chem.* **1998**, *74*, 45−51.

(25) Pontius, A. J.; Rushing, J. E.; Foegeding, P. M. Heat resistance of *Alicyclobacillus acidoterrestris* spores as affected by various pH values and organic acids. *J. Food Prot.* **1998**, *61*, 41−46.

(26) Walstra, P., Colloidal interactions. In *Physical Chemistry of Foods*, 1st ed.; Walstra, P., Ed.; Marcel Decker: New York, 2002; Vol. *121*, pp 484−486.

(27) Wattanasatcha, A.; Rengpipat, S.; Wanichwecharungruang, S. Thymol nanospheres as an effective anti-bacterial agent. *Int. J. Pharm.* **2012**, *434*, 360−365.
(28) Gaysinsky, S.; Taylor, T. M.; Davidson, P. M.; Bruce, B. D.; Weiss, J. Antimicrobial efficacy of eugenol microemulsions in milk against *Listeria monocytogenes* and *Escherichia coli* O157:H7. *J. Food Prot.* **2007**, *70*, 2631−2637.
(29) Burt, S. Essential oils: their antibacterial properties and potential applications in foods—a review. *Int. J. Food Microbiol.* **2004**, *94*, 223−253.
(30) Slattery, C. W.; Evard, R. A model for the formation and structure of casein micelles from subunits of variable composition. *Biochim. Biophys. Acta* **1973**, *317*, 529−538.
(31) Salton, M. Studies of the bacterial cell wall: IV. The composition of the cell walls of some Gram-positive and Gram-negative bacteria. *Biochim. Biophys. Acta* **1953**, *10*, 512−523.
(32) Terjung, N.; Loffler, M.; Gibis, M.; Hinrichs, J.; Weiss, J. Influence of droplet size on the efficacy of oil-in-water emulsions loaded with phenolic antimicrobials. *Food Funct.* **2012**, *3*, 290−301.

Bacterial Cultures and Materials. *S. thermophilus* NBRC 13957 (National Institute of Technology and Evaluation Biological Resource Center, Chiba, Japan) and the commercially available lactic acid bacteria starter culture, YO-MIX505, from Danisco USA Inc. (Wilmington, DE, USA) were used in this study. The starter culture, which consisted of *S. thermophilus* and *L. delbrueckii* subsp. *bulgaricus*, was freeze-dried and stored at −20 °C and was used according to the manufacturer's description. *S. thermophilus* NBRC 13957 was stored at −80 °C in an MRS broth with 30% (v/v) sterile glycerol and was cultured in an MRS broth for 16−24 h at 37 °C. The bacterial cells of *S. thermophilus* NBRC 13957 were washed twice with saline and were used for subsequent experiments. Commercially available pasteurized milk (Meiji Holdings Co., Ltd., Tokyo, Japan) and commercially available sterilized unprepared soymilk (Kikkoman Corporation, Tokyo, Japan) were used to produce fermented milk and soymilk, respectively. Soymilk whey solution was obtained from sterilized soymilk using a microfiltration module with a pore size of 1.0 μm (Asahi Kasei Chemicals Corp., Tokyo, Japan).

Fermentation Conditions. The commercially available starter culture, YO-MIX505, and *S. thermophilus* NBRC 13957 were cultured at 37 °C for 16 h in all the samples that were used in this study. A total of 128 mg of powdered YO-MIX505 starter was suspended in 5 mL of sterile water, and the 0.05% (v/v) of the starter solution was then inoculated into each sample. Casamino acids were sterilized as a 10% solution and then aseptically added to soymilk whey (final concentrations of 0.05%, 0.1%, and 0.5% (v/v)) before fermentation. Each amino acid solution (100 mM) was sterilized with filtration using 0.2 μm pore size membrane filter unit (Toyo Roshi Kaisha, Ltd., Tokyo, Japan) and then added to the soymilk whey to create a final concentration of 1.0 mM before fermentation.

Gas Chromatography and Mass Spectrometry Analysis. Ten grams of fermented soymilk whey samples were weighed into headspace vials, and 5.0 g of fermented soymilk was diluted with 5.0 g of sterile water and added to the headspace vials. Volatiles of each of the fermented products were equilibrated in the vials by heating for 20 min at 60 °C under strong agitation, and they were then injected onto a gas chromatography (GC) column with G1888 Network headspace sampler (Agilent Technologies, Inc., Santa Clara, CA, USA). The concentrations of diacetyl, acetoin, and acetoaldehyde in the fermented samples were quantified with the standard addition method with a HP 5973 mass spectrometry (MS) detector (Hewlett-Packard Company, Palo Alto, CA, USA). Briefly, four samples were prepared in the vials separately; next, each authentic preparation was added to each sample to result in the concentrations of 0, 1, 5, 10, and 20 ppm (v/v). The standard curve was prepared within the relative peak area against the concentration.

Isolation and Purification of Bacterial RNA. One milliliter of cultured soymilk whey with *S. thermophilus* NBRC 13957 was obtained in the middle of the logarithmic growth phase, and 2.0 mL of RNAprotect bacteria reagent (QIAGEN KK, Tokyo, Japan) was added. The cell pellets from the mixture of the cultured soymilk whey and the RNAprotect bacteria reagent were obtained by centrifugation at 8000*g* and 4 °C for 10 min, and the cell pellets were stored at −20 °C until RNA isolation. The cell pellets were lysed with lysozyme and proteinase K using an RNeasy Kit (QIAGEN KK) as per the manufacturer's instructions. Subsequently, RNA was isolated by phenol-chloroform extraction using TRIzol reagent (Life Technologies Corporation, Grand Island, NY, USA) in accordance with the manufacturer's instructions. The quantity and quality of isolated RNA were checked using a ND-1000 photospectrometer (Nanodrop Products, Wilmington, DE, USA), and RNA samples with an A260/A280 ratio over 1.8 and a clear two-peak (16S and 23S rRNA) pattern were included in the real-time quantitative polymerase chain reaction (RT-qPCR) analysis.

cDNA Synthesis and Real-Time Quantitative PCR. A total of 0.5 μg of total RNA was reverse transcribed into cDNA using a PrimeScript RT Reagent Kit (Takara Bio Inc., Shiga, Japan). Briefly, reverse transcription was performed in the Mastercycler gradient (Eppendorf AG, Hamburg, Germany) as follows: 37 °C for 15 min and 85 °C for 5 s in one cycle. The primers for the RT-qPCR were designed using the Primer 3 software (http://primer3plus.com) and are listed in Table 1. RT-qPCR was performed as per the following program: initial denaturation at 95 °C for 10 s, which was followed by 40 cycles of amplification at 95 °C for 5 s and at 60 °C for 20 s. The reaction mixture contained 2 μL of the reverse transcription product, 12.5 μL of SYBR *Premix Ex Taq* II (2×), 0.5 μL of ROX Reference Dye II (Takara Bio Inc.), 0.4 μL of forward primer (10 μM), 0.4 μL of reverse primer (10 μM), and 9.2 μL of RNase-free water. The reverse transcription product was replaced with RNase-free water for negative controls. Individual RT-qPCR was performed in triplicate for each gene.

Table 1. Oligonucleotide Sequences Used for PCR

gene	primer	sequences (5′-3′)	product size
als			144
	forward	AAGCACGTAACTGGAATGCTGA	
	reverse	GAATAGCGGGCAAAAGCAAG	
aldB			145
	forward	CGGTGTGAGTGTTGCTGGTT	
	reverse	GTCTTGAACTGGGAAGCGTTG	
ilvC			147
	forward	GGCAGTCAAACCACCACAAA	
	reverse	GCCACAGGTAACGCTAAAGACA	

Sensory Evaluation of Fermented Soymilk with Lactic Acid Bacteria. The sensory properties of fermented soymilk were evaluated with a method described previously.[14] Briefly, for the triangle difference test, a series of three samples were presented to nine untrained panelists. One sample was fermented soymilk alone; the other two samples were fermented soymilk with 1.0 mM L-valine. For the preference test, two samples with and without 1.0 mM of L-valine were prepared, and 30 untrained assessors selected the preferred sample. In each test, the panelists selected a sample based on sniffing alone. All samples were fermented with *S. thermophilus* NBRC 13957 at 37 °C for 16 h and were kept at approximately 10 °C. Each fermented soymilk sample was coded with three random digit numbers.

Statistical Analysis. The statistical significance of the differences between the experimental groups was determined with a two-tailed Student's *t*-test for unpaired data, with *P* values less than 0.05 considered significant.

RESULTS AND DISCUSSION

Comparison of the Flavor Components in Fermented Milk and Fermented Soymilk with Commercially Available Starter Culture. *S. thermophilus* and *L. delbrueckii* subsp. *bulgaricus* are defined as yogurt starter strains by Codex Alimentarius. In milk, *S. thermophilus* grows and produces formic acid, folic acid, and carbon dioxide. *L. delbrueckii* subsp. *bulgaricus*, which has high proteolytic activity, grows simultaneously by consuming these organic acids and digests casein to produce peptides and amino acids, which are advantageous for the further growth of *S. thermophilus*.[15,16] These species establish a symbiotic relationship in milk and usually produce flavorful yogurt. However, in soymilk, only *S. thermophilus* can grow because *L. delbrueckii* subsp. *bulgaricus* cannot utilize sucrose, the main carbon source in soymilk. In other words, the mutual stimulation between these species does not occur during fermentation in soymilk.

To analyze the flavor difference between fermented milk and fermented soymilk, a commercially available starter culture, which contained only *S. thermophilus* and *L. delbrueckii* subsp. *bulgaricus*, was inoculated in crude unprepared ultrahigh

temperature treated milk and sterilized unprepared soymilk with the same fermentation conditions (37 °C, 16 h). The total ion chromatograms of fermented milk and fermented soymilk were obtained with the headspace sampler and GC-MS, as described in the Materials and Methods (Figure 1). Most of the

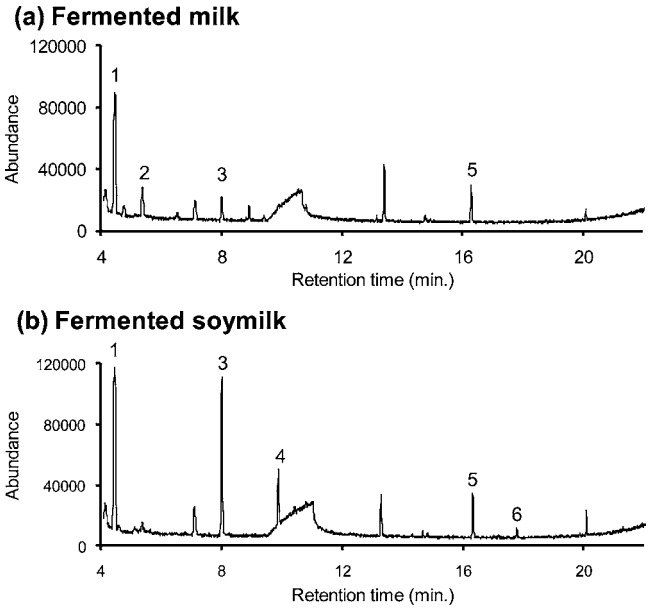

Figure 1. Total ion chromatograms of (a) fermented milk and (b) fermented soymilk with commercially available starter culture (*S. thermophilus* and *L. delbrueckii* subsp. *bulgaricus*) obtained from headspace gas chromatography−mass spectrometry. The fermentation conditions were the same (37 °C, 16 h). Each number in TIC indicates the following: (1) acetaldehyde, (2) acetone, (3) diacetyl, (4) 2,3-pentanedione, (5) acetoin, and (6) 1-hexanol.

flavors extracted, such as acetaldehyde, diacetyl, and acetoin, were qualitatively similar between fermented milk and fermented soymilk. However, the concentration of diacetyl was higher in fermented soymilk than in fermented milk, and 2,3-pentanedione was detected only in fermented soymilk. These compounds are vicinal diketones, and it is known that diacetyl has a much lower odor threshold than 2,3-pentanedione. Although these compounds are responsible for key aromas of dairy products,[17,18] the sensory test of this study suggested that the addition of a standard preparation of diacetyl, and not that of 2,3-pentanedione, contributed an unpleasant odor to fermented soymilk. In addition, it was suggested that the balance of the flavor compounds collapsed due to excess diacetyl production in fermented soymilk. In alcoholic beverages such as wine, beer, and Japanese sake, vicinal diketones, particularly diacetyl, contribute to off-flavors above a certain concentration.[19−22] We demonstrated that excess diacetyl could be one of the major off-flavors generated with *S. thermophilus* in fermented soymilk.

Influence of the Different Carbon Sources and Nitrogen Sources on Diacetyl Levels after Fermentation by *S. thermophilus* NBRC 13957 in Milk and Soymilk. To produce flavorful fermented soymilk, we first attempted to determine how diacetyl was excessively produced by *S. thermophilus* in soymilk. The main carbon sources of milk and soymilk are lactose and sucrose, respectively. Excess diacetyl was not detected in fermented milk. Thus, sucrose may have induced the generation of diacetyl by *S. thermophilus*. We measured the concentration of diacetyl was produced in a chemically defined medium whose carbon source was sucrose or lactose. The approximate amount of diacetyl generated was detected in both media (data not shown). Therefore, it was suggested that the diacetyl levels generated by *S. thermophilus* did not depend on the carbon source. Next, we focused on the differences in the nitrogen source between soymilk and milk. Previous reports have shown that *S. thermophilus* grows in milk by utilizing the peptides and amino acids derived from the proteolysis of casein by *L. delbrueckii* subsp. *bulgaricus*. However, the proteolytic activity of *L. delbrueckii* subsp. *bulgaricus* would be restricted in soymilk because it has no capability of growing in soymilk due to the carbon source. Therefore, it was hypothesized that free amino acids formed in the hydrolysis of casein are important for regulating the generation of diacetyl by *S. thermophilus*. On the basis of this hypothesis, we investigated the effects of casamino acid supplementation on the generation of diacetyl. In this experiment, we used soymilk whey instead of soymilk itself because we found that *S. thermophilus* could grow in soymilk whey and that it generated approximately the same amount of diacetyl compared to that in soymilk itself (data not shown). Therefore, it was suggested that insoluble soy proteins, such as 7S globulin and 11S globulin, were not implicated in the production of diacetyl by *S. thermophilus*. Ten percent of casamino acid solution was supplemented in the soymilk whey to produce a final concentration of 0.05%, 0.1%, and 0.5%, and diacetyl levels were then investigated in the cultured soymilk whey with *S. thermophilus*. As a result, the concentration of diacetyl in fermented soymilk whey with 0.05% casamino acids added was significantly decreased compared with that in fermented soymilk alone. In addition, fermented soymilk whey with 0.5% casamino acids had significantly lower diacetyl levels than the others (Figure 2). These results indicated that casamino acids had an effect on diacetyl production during fermentation by *S. thermophilus* although they were not sources of carbon.

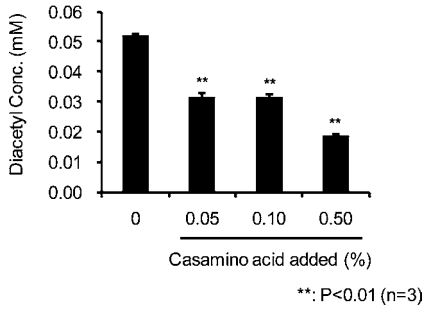

Figure 2. Evaluation of the diacetyl concentrations in fermented soymilk whey with each concentration of casamino acid added. The error bars indicate the standard deviations (SD) of the triplicate samples of the experiments. The statistical significance comparing the results from each concentration of casamino acid added to no casamino acid added is indicated (**$P < 0.01$). The error bars indicate the SD of the triplicate samples of experiments.

Influence of the 20 Essential Amino Acids on Diacetyl Levels after Lactic Acid Fermentation by *S. thermophilus*. The addition of casamino acids in soymilk whey had some impact on decreasing the diacetyl levels during fermentation. Therefore, to understand which amino acid mainly regulated diacetyl levels, each of the 20 essential amino acids was

separately added to soymilk whey to produce a concentration of 1.0 mM. Of the 20 amino acids added, L-valine had a strong effect on decreasing the diacetyl levels in fermented soymilk whey (Figure 3). L-Cysteine, L-threonine, L-tryptophan, L-

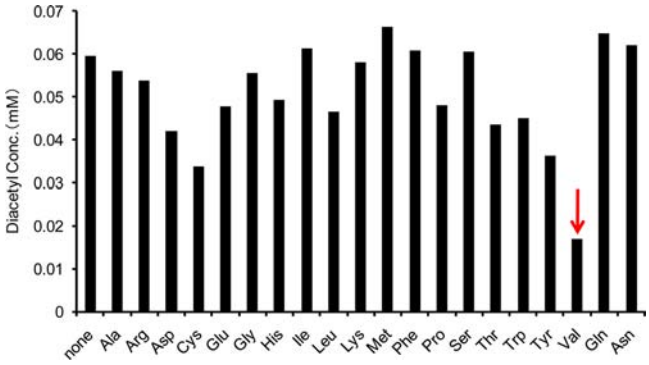

Figure 3. Concentration of diacetyl (mM) in soymilk whey fermented with *S. thermophilus* in the presence of 1.0 mM of each amino acid.

leucine, and L-tyrosine also had small effects on reducing diacetyl. The other amino acids did not any influence diacetyl levels. In previous studies, it has been reported that the supplementation of L-valine regulates the production of diacetyl due to the inhibition of 2-acetolactate synthase and the activation of acetolactate decarboxylase in *Escherichia coli*.[23,24] In addition, Ott et al. suggested an interconnection between the metabolism of L-valine and diacetyl in lactic acid bacteria.[25] The results of this study supported the findings of these reports.

Gene Expression Analysis of Metabolic Enzymes Related to the L-Valine Metabolic Pathway. Next, to investigate the effects of L-valine on the decline of diacetyl levels in fermented soymilk whey, the levels of expression of the *als*, *aldB*, and *ilvC* genes of *S. thermophilus* NBRC 13957 were examined with and without L-valine added in the middle of the exponential growth phase. The proposed schematic of the metabolic pathways involved in the biosynthesis of L-valine and diacetyl is shown in Figure 4. First, pyruvate is converted to α-acetolactate, which is an unstable compound. Then α-acetolactate is decarboxylated to diacetyl in the presence of oxygen without any enzymatic activity. With the addition of 1.0 mM of L-valine, the levels of expression of the *als* and *aldB* genes were significantly increased (Figure 5A,B), whereas the levels of expression of the *ilvC* gene were significantly repressed

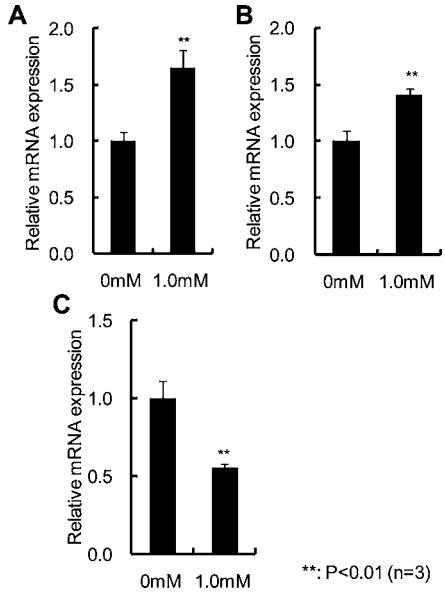

Figure 5. Comparison of the levels of expression of the *als* (A), *aldB* (B), and *ilvC* (C) genes that are involved in the biosynthesis of L-valine, diacetyl, and acetoin in the presence of 1.0 mM of L-valine. The error bars indicate the SD of triplicate samples of the experiments. The statistical significance of the comparisons of the results for each concentration of L-valine added compared with no L-valine added is indicated (**$P < 0.01$). The error bars indicate the SD of the triplicate samples of the experiments.

(Figure 5C). Acetolactate decarboxylase (*aldB*) catalyzes the conversion of α-acetolactate to acetoin, and acetohydroxy acid isomeroreductase (*ilvC*) catalyzes the conversion of α-acetolactate to the precursor of valine, 2,3-dihydroxy isovalerate.[25] Goupil et al. have shown that diacetyl is accumulated in fermented milk by a *Lactococcus lactis aldB* mutant, whose acetolactate decarboxylase activity was suppressed, more than that in the wild type.[26] On the basis of these results, it was suggested that supplementing L-valine into soymilk whey shifted the metabolic flux to produce more acetoin from α-acetolactate rather than the nonenzymatic oxidation from α-acetolactate to diacetyl in *S. thermophilus*.

Quantification of the Flavor Compounds of Acetaldehyde, Diacetyl, and Acetoin Produced by *S. thermophilus* with the Supplementation of L-Valine into Soymilk. The expression analysis of this study suggested that the

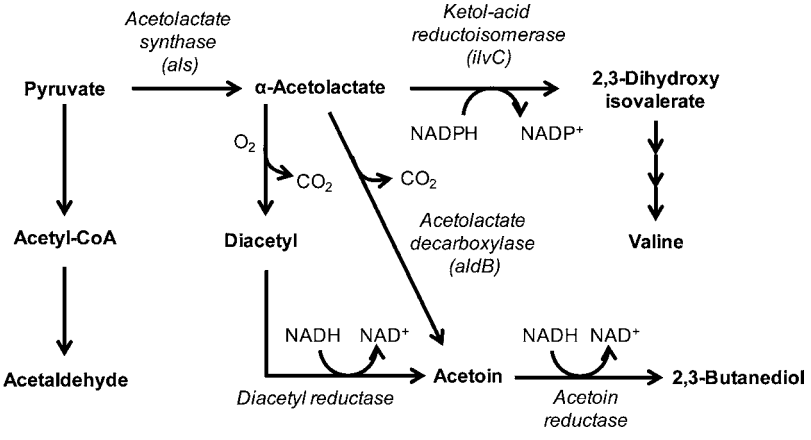

Figure 4. Proposed schematic of the metabolic pathways involved in the biosynthesis of L-valine and diacetyl from pyruvate.

dx.doi.org/10.1021/jf404567e | J. Agric. Food Chem. 2014, 62, 1658−1663

metabolic flux might shift from the biosynthesis of L-valine to acetoin by the addition of L-valine. In addition, according to the database of the complete genome sequence, *S. thermophilus* lacks metabolic enzymes of both diacetyl reductase and acetoin reductase, which catalyze the conversion of diacetyl to acetoin and acetoin to 2,3-butanediol, respectively. Therefore, it was hypothesized that acetoin would accumulate in fermented soymilk in response to the addition of L-valine instead of the decline of diacetyl concentration. In addition to acetoin and diacetyl, the concentration of acetaldehyde, which is one of the important flavor compounds in yogurt, was determined in fermented soymilk in response to the addition of L-valine because acetaldehyde is also produced from pyruvate by acetyl-coA. Figure 6 shows the concentration of acetaldehyde, diacetyl, and acetoin in fermented soymilk with *S. thermophilus* in the presence of increasing amounts of L-valine (0.0, 0.5, 1.0, and 5.0 mM). In the presence of L-valine, the concentration of diacetyl was decreased, whereas acetoin accumulated in fermented soymilk. The concentration of acetaldehyde stayed constant with the addition of L-valine. Chaves et al. have previously shown that the supplementation of the growth medium with L-threonine led to an increase in acetaldehyde production and that the differences in acetaldehyde formation were correlated with the differences in threonine aldolase activity.[27] Acetaldehyde is also generated by *S. thermophilus* through other metabolic pathways from citrate, which is already contained in soymilk itself. These findings suggested that the addition of L-valine had no effect on acetaldehyde production in soymilk. Like diacetyl, acetoin is characterized as having a butter-like aroma and it is important for the flavor of cheese. However, the odor threshold of acetoin is much higher than that of diacetyl. Therefore, fermented soymilk with L-valine added was expected to have fewer off-flavors than the one without L-valine supplementation.

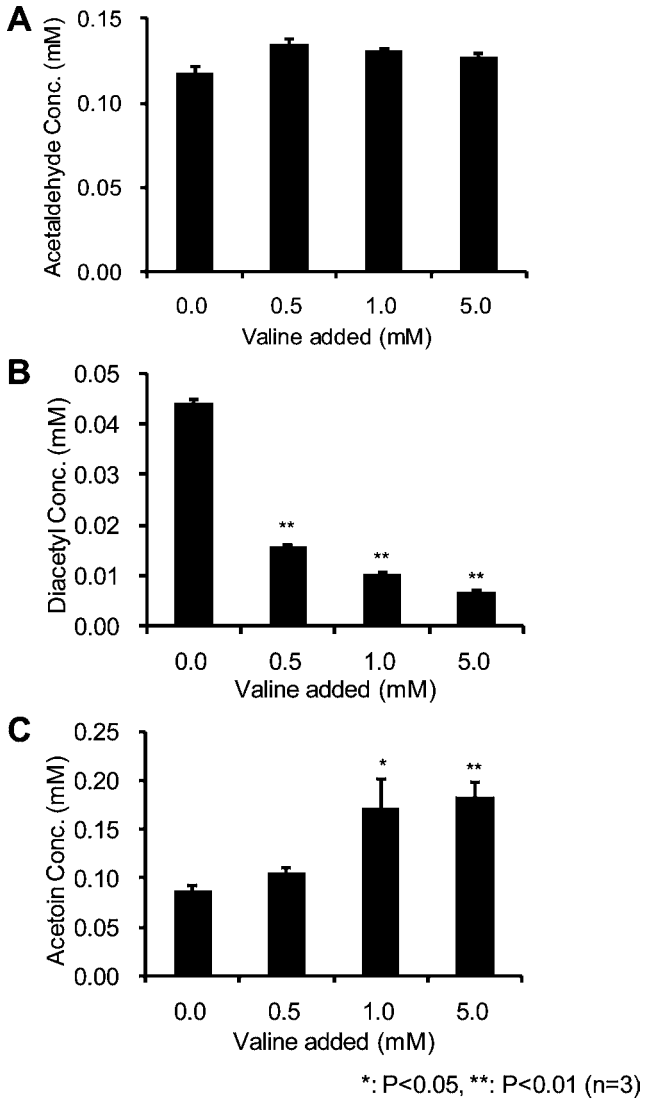

Figure 6. The concentrations of acetaldehyde (A), diacetyl (B), and acetoin (C) in fermented soymilk with *S. thermophilus* in the presence of increasing amounts of L-valine (0.0, 0.5, 1.0, and 5.0 mM). The statistical significance of the comparisons of the results for each concentration of L-valine added compared with no L-valine added is indicated (*$P < 0.05$, **$P < 0.01$). The error bars indicate the SD of the triplicate samples of the experiments.

Sensory Evaluation. The sensory properties of fermented soymilk were evaluated by an untrained panel of nine assessors with a triangle difference test and 30 assessors with a preference test. The experimental design was outlined in the Materials and Methods. As a result, six of the nine assessors could identify the flavor difference between fermented soymilk with and without L-valine supplementation. This result suggested that these two samples were significantly different. In the preference test, 27 of 30 assessors preferred fermented soymilk with L-valine added for its decreased off-flavor compared to the one without L-valine added.

On the basis of the results that were obtained in this study, we suggest that some natural ingredients consisting of highly concentrated branched-chain amino acids, such as powdered sugar beets, could be used for the enrichment of L-valine in soymilk instead of directly adding L-valine. In addition, the supplementation of a little protease (or peptidase)-treated soymilk could have enough L-valine to regulate diacetyl generation by *S. thermophilus*. Although it is well-known that a small amount of diacetyl is necessary for flavorful dairy yogurt, this study is the first to indicate that diacetyl could contribute an off-flavor in the case of fermented soymilk. Moreover, the present study showed that some metabolisms of lactic acid bacteria were controllable by modifying the amino acid compositions without the use of genetically modified lactic acid bacteria strains.

AUTHOR INFORMATION

Corresponding Author

*E-mail: dkaneko@mail.kikkoman.co.jp.

Notes

The authors declare no competing financial interest.

ACKNOWLEDGMENTS

We gratefully acknowledge Dr. A. Matsuyama and Dr. N. Kajiyama for their helpful advice and discussions, Y. Shimaoka for the helpful technical assistance, and all the colleagues who participated in the sensory panels.

REFERENCES

(1) Golbitz, P. Traditional soyfoods: processing and products. *J. Nutr.* **1995**, *125*, 570S−572S.

(2) Messina, M. J.; Persky, V.; Setchell, K. D.; Barnes, S. Soy intake and cancer risk: a review of the in vitro and in vivo data. *Nutr. Cancer* **1994**, *21*, 113−131.

(3) Lopez-Lazaro, M.; Akiyama, M. Flavonoids as anticancer agents: structure−activity relationship study. *Curr. Med. Chem. Anti- Cancer Agents* **2002**, *2*, 691−714.
(4) Kitawaki, R.; Nishimura, Y.; Takagi, N.; Iwasaki, M.; Tsuzuki, K.; Fukuda, M. Effects of *Lactobacillus* fermented soymilk and soy yogurt on hepatic lipid accumulation in rats fed a cholesterol-free diet. *Biosci., Biotchnol., Biochem.* **2009**, *73* (7), 1484−1488.
(5) Kobayashi, M.; Hirahata, R.; Egusa, S.; Fukuda, M. Hypocholesterolemic effects of lactic acid-fermented soymilk on rats fed a high cholesterol diet. *Nutrients* **2012**, *4* (9), 1304−16.
(6) Lai, L. R.; Hsieh, S. C.; Huang, H. Y.; Chou, C. C. Effect of lactic fermentation on the total phenolic, saponin and phytic acid contents as well as anti-colon cancer cell proliferation activity of soymilk. *J. Biosci. Bioeng.* **2013**, *115* (5), 552−556.
(7) Kano, M.; Takayanagi, T.; Harada, K.; Sawada, S.; Ishikawa, F. Bioavailability of isoflavones after ingestion of soy beverages in healthy adults. *J. Nutr.* **2006**, *136*, 2291−2296.
(8) Izumi, T.; Piskula, M. K.; Osawa, S.; Obata, A.; Tobe, K.; Saito, M.; Kataoka, S.; Kubota, Y.; Kikuchi, M. Soy Isoflavone Aglycones Are Absorbed Faster and in Higher Amounts than Their Glucosides in Humans. *J. Nutr.* **2000**, *Feb*, 1695−1699.
(9) Mellor, N.; Bligh, F.; Chandler, I.; Hodgman, C. Reduction of Off-Flavor Generation in Soybean Homogenates: A Mathematical Model. *J. Food Sci.* **2010**, *75* (7), R131−138.
(10) Feussner, I.; Wasternack, C. The lipoxygenase pathway. *Annu. Rev. Plant Biol.* **2002**, *53*, 275−297.
(11) Zhang, Y.; Guo, S.; Liu, Z.; Chang, S. K. C. Off-Flavor Related Volatiles in Soymilk As Affected by Soybean Variety, Grinding, and Heat-Processing Methods. *J. Agric. Food Chem.* **2012**, *60*, 7457−7462.
(12) Lv, Y. C.; Song, H. L.; Li, X.; Wu, L.; Guo, S. T. Influence of blanching and grinding process with hot water on beany and non-beany flavor in soymilk. *J. Food Sci.* **2011**, *Jan-Feb;76* (1), S20−825.
(13) Yuan, S. H.; Chang, S. K. Selected odor compounds in cooked soymilk as affected by soybean materials and direct steam injection. *J. Food Sci.* **2007**, *Sep;72* (7), S481−S486.
(14) Donkor, O. N.; Henriksson, A.; Vasiljevic, T.; Shah, N. P. Rheological Properties and Sensory Characteristics of Set-Type Soy Yogurt. *J. Agric. Food Chem.* **2007**, *55*, 9868−9876.
(15) Sieuwerts, S.; Molenaar, D.; van Hijum, S. A.; Beerthuyzen, M.; Stevens, M. J. A.; Janssen, P. W. M.; Ingham, C. J.; de Bok, F. A. M.; de Vos, W. M.; van Hylckama; Vlieg, J. E. T. Mixed-culture transcriptome analysis reveals the molecular basis of mixed-culture growth in *Streptococcus thermophilus* and *Lactobacillus bulgaricus*. *Appl. Environ. Microbiol.* **2010**, *76* (23), 7775−7784.
(16) O'Leary, V. S.; Woychik, J. H. Utilization of lactose, glucose, and galactose by a mixed culture of *Strepotoccocus thermophilus* and *Lactobacillus bulgaricus* in milk treated with lactase enzyme. *Appl. Environ. Microbiol.* **1976**, *32* (1), 89−94.
(17) Imhof, R.; Glattli, H.; Bosset, J. O. Volatile organic compounds produced by thermophilic and mesophilic single strain dairy starter cultures. *Lebensm.-Wiss.-Technol.* **1995**, *28*, 78−86.
(18) Ott, A.; Fay, L. B.; Chaintreau, A. Determination and origin of the aroma impact compounds of yogurt flavor. *J. Agric. Food Chem.* **1997**, *45*, 850−858.
(19) Horie, K.; Oba, T.; Motomura, S.; Isogai, A.; Yoshimura, T.; Tsuge, K.; Koganemaru, K.; Kobayashi, G.; Kitagaki, H. Breeding of a low pyruvate-producing sake yeast by isolation of a mutant resistant to ethyl α-transcyanocinnamate, an inhibitor of mitochondrial pyruvate transport. *Biosci., Biotechnol., Biochem.* **2010**, *74* (4), 843−847.
(20) Hugenholtz, J. Citrate metabolism in lactic acid bacteria. *FEMS Microbiol. Rev.* **1993**, *12*, 165−178.
(21) Blomqvist, K.; Suihko, M. L.; Knowles, J. K. C.; Penttila, M. E. Chromosomal integration and expression of two bacterial α-acetolactate decarboxylase genes in brewer's yeast. *Appl. Environ. Microbiol.* **1991**, *57*, 2796−2803.
(22) Dasari, S.; Kölling, R. Cytosolic Localization of Acetohydroxyacid Synthase Ilv2 and Its Impact on Diacetyl Formation during Beer Fermentation. *Appl. Environ. Microbiol.* **2011**, *77* (3), 727−731.
(23) Vyazmensky, M.; Sella, C.; Barak, Z.; Chipman, D. M. Isolation and characterization of subunits of acetohydroxy acid synthase isozyme III and reconstitution of the holoenzyme. *Biochemistry* **1996**, *35*, 10339−10346.
(24) Phalip, V.; Monnet, C.; Schmitt, P.; Renault, P.; Godon, J. J.; Diviès, C. Purification and properties of the α-acetolactate decarboxylase from *Lactococcus lactis* subsp. *lactis* NCDO 2118. *FEBS Lett.* **1994**, *351*, 95−99.
(25) Ott, A.; Germond, J. E.; Chaintreau, A. Vicinal diketone formation in yogurt: ^{13}C precursors and effect of branched-chain amino acids. *J. Agric. Food Chem.* **2000**, *48* (3), 724−731.
(26) Goupil, N.; Corthier, G.; Ehrlich, S. D.; Renault, P. Imbalance of leucine flux in *Lactococcus lactis* and its use for the isolation of diacetyl-overproducing strains. *Appl. Environ. Microbiol.* **1996**, *62* (7), 2636−2640.
(27) Chaves, A.; Fernandez, M.; Lerayer, A.; Mierau, I.; Kleerebezem, M.; Hugenholtz, J. Metabolic Engineering of Acetaldehyde Production by *Streptococcus thermophilus*. *Appl. Environ. Microbiol.* **2002**, *68* (11), 5656−5662.

chloroform for chromatographic analysis of the lipid fraction. The acetone-extracted sample was then extracted with hot water (100 mL, 3 h at 100 °C) to determine the water-soluble material. Klason lignin content was estimated as the residue after sulphuric acid hydrolysis of the pre-extracted material, corrected for ash and protein content, according to the TAPPI method T222 om-88.[16] The acid-soluble lignin was determined, after the insoluble lignin was filtered off (Duran filter crucible 4; nominal pore size max. 10−16 μm), by UV-spectroscopic determination at 205 nm wavelength using 110 L cm^{-1} g^{-1} as the extinction coefficient. Holocellulose was isolated from the pre-extracted fibers by delignification for 4 h using the acid chlorite method.[17] The α-cellulose content was determined by removing the hemicelluloses from the holocellulose by alkali extraction.[17] Ash content was estimated as the residue after 6 h of heating at 575 °C according to the TAPPI method T211 om-02.[16] Three replicates were used for each sample.

Table 1. Abundance of the Main Constituents (% Dry-Weight) of Wheat Bran

constituent	content[a]
water-soluble extractives	2.4 ± 0.1
lipids	2.0 ± 0.1
Klason lignin[b]	12.1 ± 0.8
acid-soluble lignin	8.5 ± 1.0
carbohydrates	64.0 ± 1.0
(α-cellulose)	(30 ± 1.0)
proteins[c]	9.9 ± 1.0
ash	1.1 ± 0.1

[a]Average of three replicates. [b]Corrected for proteins and ash. [c]Determined indirectly by subtracting the other components to 100%.

GC and GC-MS Analyses. The lipophilic extractives (0.8 mg) were silylated with 0.250 mL bis(trimethylsilyl)trifluoroacetamide (BSTFA, from Supelco) in the presence of 0.050 mL pyridine at 70 °C for 2 h before GC and GC-MS analyses. An HP 5890 gas chromatograph (Hewlett-Packard, Hoofddorp, Netherlands) equipped with a split−splitless injector and a flame ionization detector (FID) was used for GC analyses. The injector and the detector temperatures were set at 300 and 350 °C, respectively. Samples were injected in the splitless mode at a concentration of 7.5 mg/mL. Helium was used as the carrier gas. The capillary column used was a high temperature, polyimide coated fused silica tubing DB5-HT (5 m x 0.25 mm I.D., 0.1 μm film thickness; J&W Scientific). The oven was temperature-programmed from 100 °C (1 min) to 350 °C (3 min) at 15 °C min^{-1}. Peaks were quantified by area, and a mixture of different standards, such as octadecane (Sigma-Aldrich, 99%), palmitic acid (Sigma-Aldrich, 99%), sitosterol (Calbiochem, 98%), cholesteryl stearate (Sigma-Aldrich, 99%), sitosteryl 3β-D-glucopyranoside (Matreya LLC, a mixture of three steryl glucosides of 98% purity, of which 56% correspond to sitosteryl glucoside) and triheptadecanoin (Sigma-Aldrich, 99%), with a concentration range between 0.1 and 1 mg/mL, was used to elaborate calibration curves. The correlation coefficient was higher than 0.99 in all cases. Quantification was obtained using response factors of the same or similar compounds (in the case of alkylresorcinols, they were quantified against sitosterol). The data from the three replicates were averaged. In all cases, the standard deviations from replicates were below 10% of the mean values. The total amounts of the different lipid families were determined by adding up the amounts of their constituent compounds.

The GC-MS analyses were performed on a Varian Star 3400 gas chromatograph (Varian, Walnut Creek, CA) coupled with an ion-trap detector (Varian Saturn 400) equipped with a high-temperature capillary column (DB-5HT, 15 m × 0.25 mm i.d., 0.1 μm film

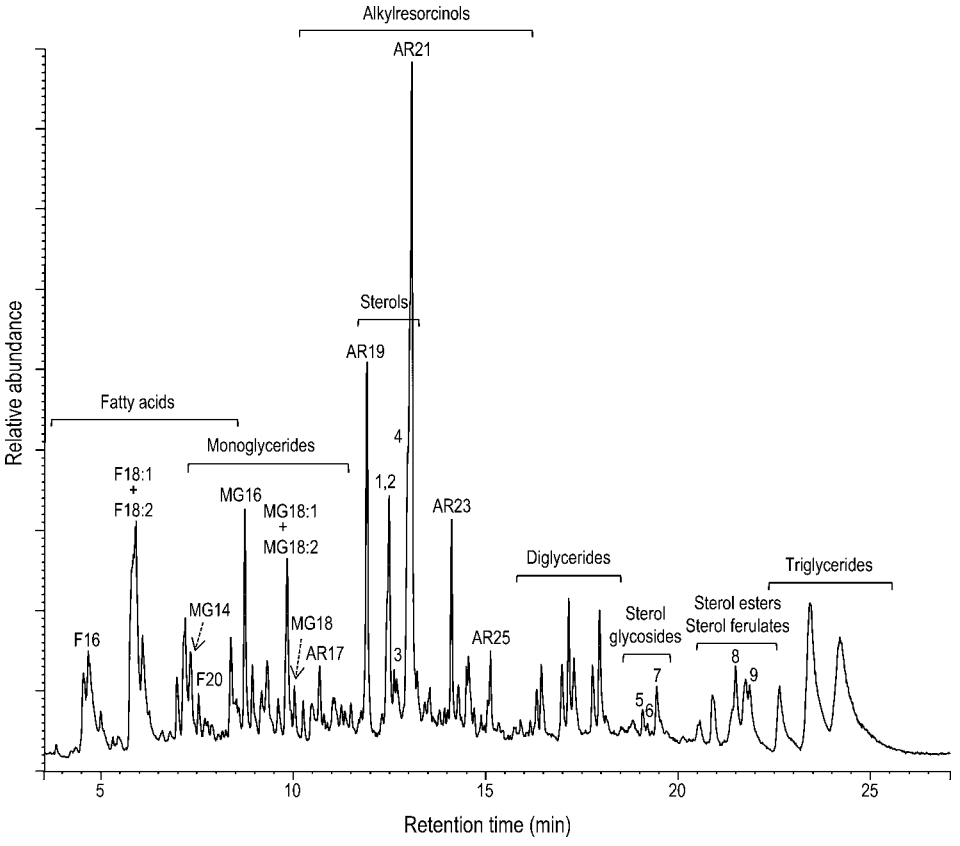

Figure 1. GC-MS chromatogram of the lipid extracts from wheat bran (as TMS-ether derivatives). F(n): n-fatty acid series; MG(n): monoglycerides; AR(n): n-alkylresorcinols; n denotes the total carbon atom number. Other compounds reflected are as follows: 1: campesterol; 2: campestanol; 3: stigmasterol; 4: sitosterol; 5: campesteryl 3β-D-glucopyranoside; 6: stigmasteryl 3β-D-glucopyranoside; 7: sitosteryl 3β-D-glucopyranoside; 8: campestanyl ferulate; and 9: stigmastanyl ferulate.

Table 2. Composition and Abundance (mg/kg Fiber, d.a.f.) of Main Lipids Identified in the Extracts of Wheat Bran

compound	abundance
n-fatty acids	6620
n-tetradecanoic acid	40
n-pentadecanoic acid	32
n-hexadecanoic acid	1595
n-heptadecanoic acid	42
cis,*cis*-octadeca-9,12-dienoic acid	1500
cis-octadec-9-enoic acid	1590
n-octadecanoic acid	720
n-nonadecanoic acid	33
n-eicosanoic acid	190
n-heneicosanoic acid	23
n-docosanoic acid	285
n-tricosanoic acid	66
n-tetracosanoic acid	180
n-pentacosanoic acid	35
n-hexacosanoic acid	130
n-heptacosanoic acid	8
n-octacosanoic acid	98
n-nonacosanoic acid	3
n-triacontanoic acid	23
n-hentriacontanoic acid	2
n-docotriacontanoic acid	20
n-tritriacontanoic acid	2
n-tetratriacontanoic acid	3
monoglycerides	2580
2,3-dihydroxypropyl tetradecanoate	20
2,3-dihydroxypropyl pentadecanoate	6
2,3-dihydroxypropyl hexadecanoate	930
2,3-dihydroxypropyl heptadecanoate	7
2,3-dihydroxypropyl octadec-9,12-dienoate	500
2,3-dihydroxypropyl octadec-9-enoate	785
2,3-dihydroxypropyl octadecanoate	200
2,3-dihydroxypropyl nonadecanoate	3
2,3-dihydroxypropyl eicosanoate	14
2,3-dihydroxypropyl heneicosanoate	2
2,3-dihydroxypropyl docosanoate	20
2,3-dihydroxypropyl tricosanoate	6
2,3-dihydroxypropyl tetracosanoate	25
2,3-dihydroxypropyl pentacosanoate	8
2,3-dihydroxypropyl hexacosanoate	32
2,3-dihydroxypropyl heptacosanoate	3
2,3-dihydroxypropyl octacosanoate	15
2,3-dihydroxypropyl nonacosanoate	1
2,3-dihydroxypropyl triacontanoate	3
diglycerides	2150
1,2-dipalmitin	50
1,3-dipalmitin	172
1,2-palmitoyl linolein	140
1,2-palmitoyl olein	210
1,2-palmitoyl stearin	50
1,3-palmitoyl linolein	154
1,3-palmitoyl olein	280
1,3-palmitoyl stearin	90
1,2-dilinolein	70
1,2-linoleoyl olein	95
1,2-linoleoyl stearin + 1,2-diolein	120
1,2-oleoylstearin	50
1,2-distearin	50
1,3-dilinolein	95
1,3-linoleoyl olein	120
1,3-linoleoyl stearin + 1,3-diolein	250
1,3-oleoyl stearin	64
1,3-distearin	90
triglycerides	1960
tripalmitin	10
dipalmitoyl linolein	150
dipalmitoyl olein	110
dilinoleoyl palmitin	480
linoleoyloleoyl palmitin	300
dioleoyl palmitin	20
trilinolein	250
dilinoleoyl olein	400
dilinoleoyl stearin	200
tristearin	40
n-alkanes	40
n-tricosane	2
n-pentacosane	5
n-hexacosane	1
n-heptacosane	10
n-octacosane	1
n-nonacosane	14
n-triacontane	1
n-hentriacontane	5
n-tritriacontane	1
sterols	510
campesterol	120
campestanol	45
stigmasterol	35
sitosterol	290
stigmastanol	20
sterol glycosides	135
campesteryl-β-D-glucopyranoside	42
stigmasteryl-β-D-glucopyranoside	8
sitosteryl-β-D-glucopyranoside	85
sterol esters	240
campesteryl hexadecanoate	20
campestanyl hexadecanoate	13
stigmasteryl hexadecanoate	3
sitosteryl hexadecanoate	60
stigmastanyl hexadecanoate	20
campesteryl octadec-9,12-dienoate	33
campestanyl octadec-9,12-dienoate	7
stigmasteryl octadec-9,12-dienoate	3
sitosteryl octadec-9,12-dienoate	70
stigmastanyl octadec-9,12-dienoate	11
sterol ferulates	105
campestanyl ferulate	67
stigmastanyl ferulate	38
steroid hydrocarbons	60
ergostatriene	5
ergostadiene	10
stigmasta-4,22-diene	5
stigmasta-3,5,22-triene	20
stigmasta-3,5-diene	20
steroid ketones	80
stigmasta-4,22-dien-3-one	15
stigmasta-3,5-dien-7-one	45
stigmast-4-en-3-one	20
n-alkylresorcinols	2250
5-*n*-pentadecylresorcinol	5
5-*n*-heptadecylresorcinol	80
5-*n*-nonadecylresorcinol	660
5-*n*-heneicosylresorcinol	1140
5-*n*-tricosylresorcinol	270
5-*n*-pentacosylresorcinol	90
5-*n*-heptacosylresorcinol	5

dx.doi.org/10.1021/jf404772b | J. Agric. Food Chem. 2014, 62, 1664−1673

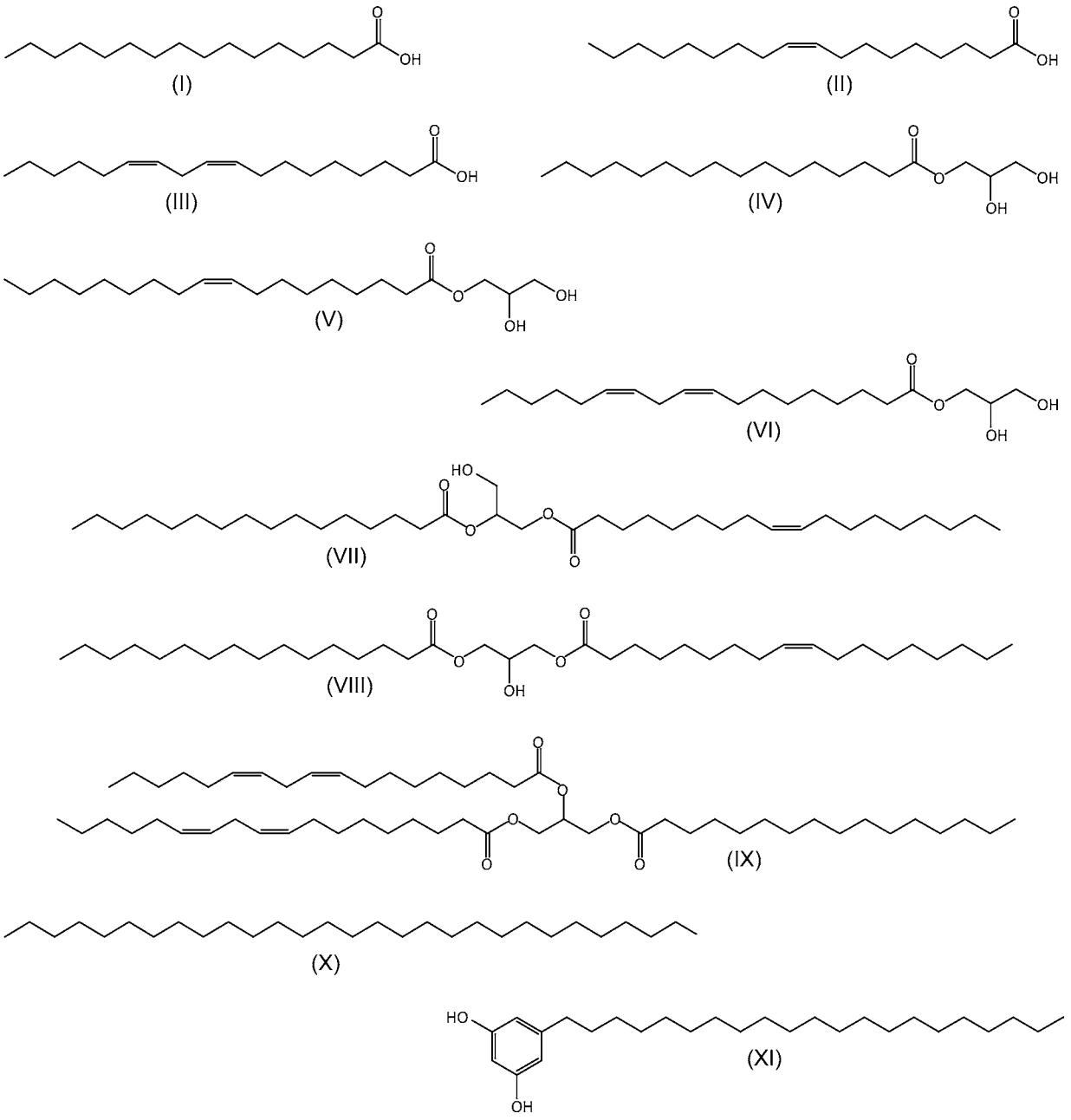

Figure 2. Structures representative of the main aliphatic lipophilic compounds identified in the extracts of wheat bran and referred in the text. (**I**) hexadecanoic (palmitic) acid; (**II**) 9-octadecenoic (oleic) acid; (**III**) 9,12-octadecadienoic (linoleic) acid; (**IV**) 2,3-dihydroxypropyl hexadecanoate (1-monopalmitin); (**V**) 2,3-dihydroxypropyl octadecenoate (1-monoolein); (**VI**) 2,3-dihydroxypropyl octadecadienoate (1-monolinolein); (**VII**) 1,2-palmitoyl olein; (**VIII**) 1,3-palmitoyl olein; (**IX**) dilineoylpalmitin; (**X**) *n*-nonacosane; and (**XI**) 5-*n*-heneicosylresorcinol.

thickness; J&W Scientific). Helium was used as carrier gas at a rate of 2 mL/min. The samples, at concentrations of 2.5 mg/mL, were injected with an autoinjector (Varian 8200) directly onto the column using a SPI (septum-equipped programmable injector) system. The temperature of the injector during the injection was 60 °C, and 0.1 min after injection was programmed to 380 °C at a rate of 200 °C min^{-1} and held for 10 min. The oven was heated from 120 °C (1 min) to 380 °C (5 min) at 10 °C min^{-1}. The temperature of the transfer line was set at 300 °C. Compounds were identified by comparing their retention times and mass spectra with authentic standards, except for alkylresorcinols and sterol ferulates, which were tentatively identified by comparing their mass spectra with those reported in the literature. Single ion chromatographic profiles were used to estimate compound abundances when two peaks partially overlapped.

RESULTS AND DISCUSSION

Lipid Composition of Wheat Bran. The destarched wheat bran sample selected for this study is mostly composed of carbohydrates (64.0% of the whole material, among which 30% corresponds to α-cellulose), lignin (20.6%), and proteins (9.9%), as seen in Table 1. Minor amounts of water-soluble extractives (2.4%), lipids (2.0%), and ash (1.1%) were also present in this sample. The detailed analysis of the chemical composition of the lipids was accomplished by GC and GC-MS (after preparation of the trimethylsilyl (TMS)-ether derivatives) according to the method previously described.[15] The chromatographic conditions used for the analyses, by using short- and medium-length high-temperature capillary columns with thin

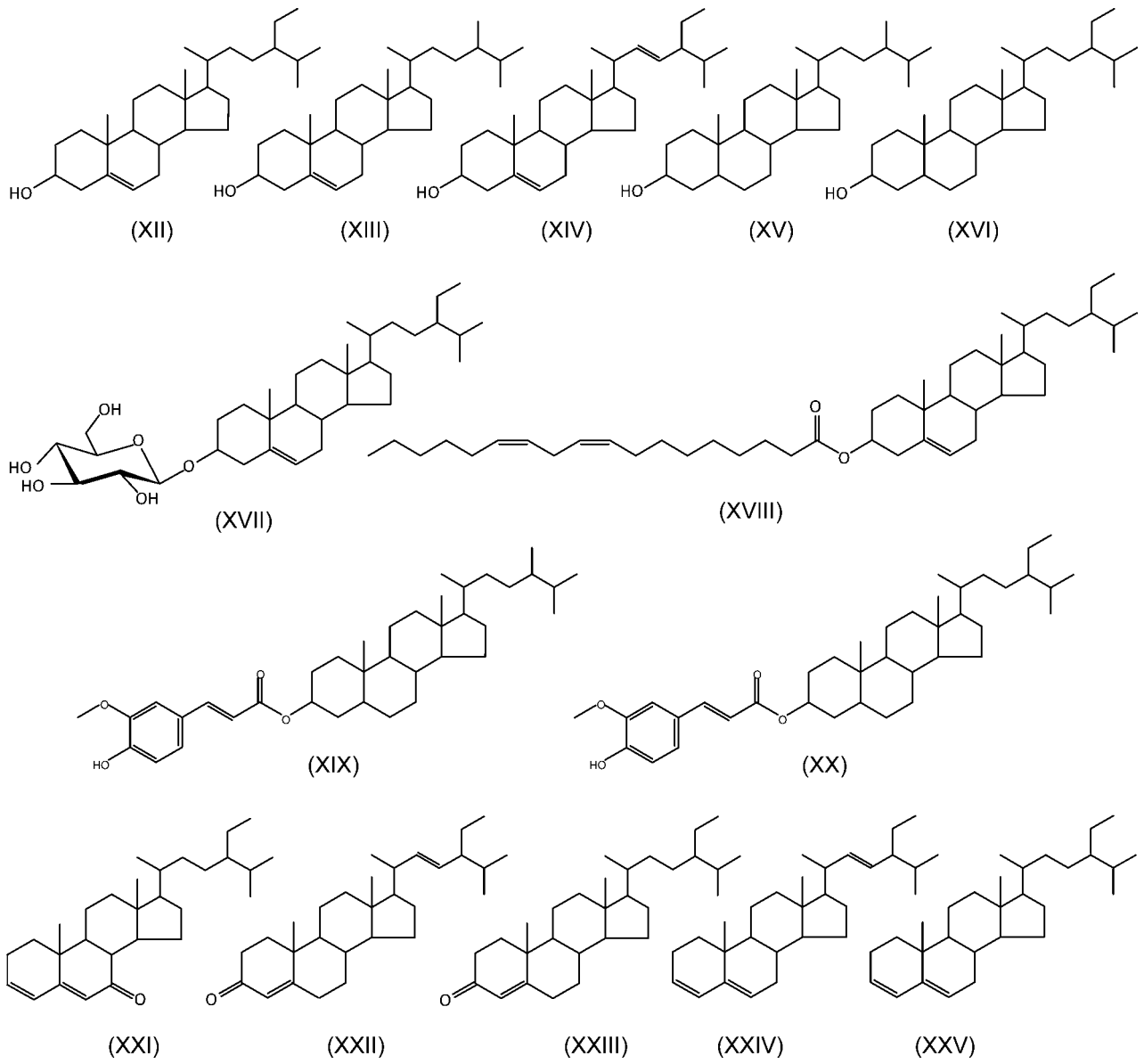

Figure 3. Structures of the main steroid compounds identified in wheat bran and referred in the text. (**XII**) sitosterol; (**XIII**) campesterol; (**XIV**) stigmasterol; (**XV**) campestanol; (**XVI**) stigmastanol; (**XVII**) sitosteryl 3β-D-glucopyranoside; (**XVIII**) sitosteryl linoleate; (**XIX**) campestanyl ferulate; (**XX**) stigmastanyl ferulate; (**XXI**) stigmasta-3,5-dien-7-one; (**XXII**) stigmasta-4,22-dien-3-one; (**XXIII**) stigmasta-4-en-3-one; (**XXIV**) stigmasta-3,5,22-triene; and (**XXV**) stigmasta-3,5-diene.

films, allow for the elution of a wide range of compounds, from low molecular weight free fatty acids and sterols to intact high molecular weight lipids such as sterol esters, sterol glycosides, or triglycerides, that are usually biased in more standard GC conditions.

Figure 1 shows the GC-MS chromatogram of the lipids (as their TMS-ether derivatives) extracted from wheat bran. A large number of compounds were identified and quantified. The identities and abundances (mg/kg fiber, dry, ash-free basis) of the main lipid compounds identified in the extracts of wheat bran are listed in Table 2. Structures representative of the main lipid families identified in wheat bran, including aliphatic and steroid compounds, are shown in Figure 2 and Figure 3. The results demonstrated that the predominant lipids identified among the extracts of this wheat bran sample were series of free fatty acids, accounting for around 40% of all identified compounds, followed by series of acylglycerols (40% in total), that included mono-, di- and triglycerides. Important amounts of alkylresorcinols (13% of all identified compounds) were also found among the lipids of wheat bran. Alkylresorcinols have been the most widely reported lipids in wheat bran.[9,11−13] Steroid compounds (including hydrocarbons, ketones, free sterols, sterol glycosides, sterol esters, and sterol ferulates) were also present among the lipids of wheat bran in important amounts (7% of all identified lipids). Only free sterols and sterol ferulates were previously reported among the lipids of wheat bran.[9,12,18] Lower amounts of other aliphatic series such as *n*-alkanes, were also observed. The distributions of the main aliphatic series (fatty acids, *n*-alkanes, monoglycerides, and *n*-alkylresorcinols) are represented in the histograms of Figure 4.

Aliphatic Series. Free fatty acids (6620 mg/kg) were the most abundant family of identified lipids. The series of free fatty acids was found in the range from tetradecanoic acid (C_{14}) to tetratriacontanoic acid (C_{34}), with a predominance of the even

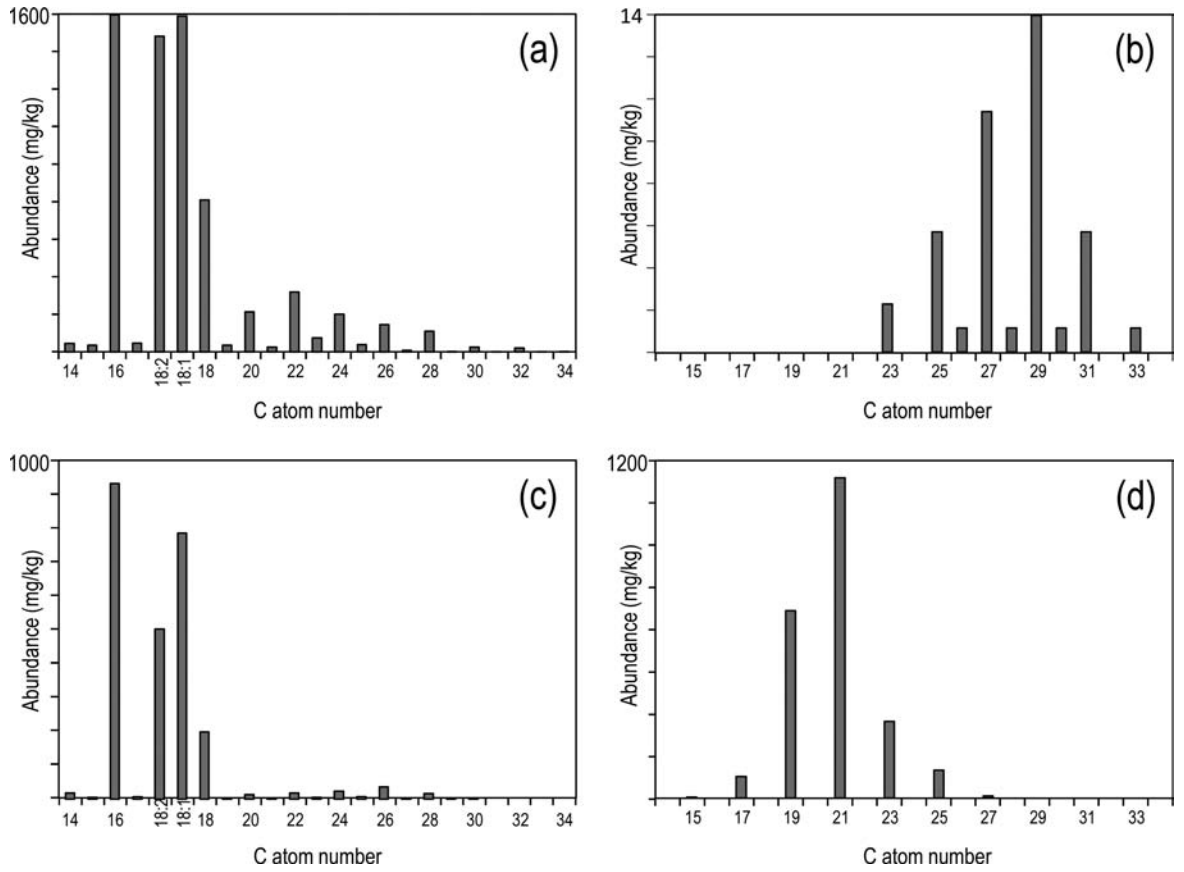

Figure 4. Distribution of the main aliphatic series identified in the extracts of wheat bran. (a) *n*-Fatty acids; (b) *n*-alkanes; (c) monoglycerides; and (d) *n*-alkylresorcinols. The histograms are scaled up to the abundance of the major compound in the series.

carbon atom number homologues. Hexadecanoic acid (palmitic acid, **I**) was the most abundant free fatty acid (1595 mg/kg), together with the unsaturated *cis*-9-octadecenoic acid (oleic acid, **II**) (1590 mg/kg) and *cis*,*cis*-9,12-octadecadienoic acid (linoleic acid, **III**) (1500 mg/kg). High amounts of the saturated octadecanoic acid (stearic acid) (720 mg/kg) were also found, while the rest of fatty acids were present in minor amounts. Despite the high abundance of fatty acids identified in wheat bran, a detailed analysis of their occurrence has not been performed so far, and there is a substantial gap in the information reported in the literature. The major free fatty acids previously reported in wheat bran were linolenic ($C_{18:3}$) and linoleic ($C_{18:2}$) acids,[9] which substantially differ from our results.

Acylglycerols (including mono-, di-, and triglycerides) were also found among the lipids of wheat bran in important amounts, accounting for a total of 6490 mg/kg, with monoglycerides being the predominant ones. However, and despite this abundance, the detailed analyses of their components have not been performed so far, and only the occurrence of the diglyceride dilinoleoylglycerol was previously reported.[9] Monoglycerides in wheat bran accounted for 2580 mg/kg, and were identified in the range from 2,3-dihydroxypropyl tetradecanoate (C_{14}) to 2,3-dihydroxypropyl triacontanoate (C_{30}), with a strong predominance of the even carbon atom number homologues. 1-Monopalmitin (**IV**) was the most abundant monoglyceride (930 mg/kg), followed by the unsaturated 1-monoolein (**V**, 785 mg/kg) and 1-monolinolein (**VI**, 500 mg/kg), and the saturated 1-monostearin (200 mg/kg). To our knowledge, this is the first time that the series of monoglycerides has been reported in wheat bran. The distribution of esterified fatty acids occurring as monoglycerides roughly matches that of the free fatty acids, as seen in the histograms of Figure 4. Diglycerides were also found in important amounts (2150 mg/kg) among the lipids in wheat bran. The most abundant diglycerides identified were 1,2-palmitoyl olein (**VII**) (210 mg/kg) and 1,3-palmitoyl olein (**VIII**) (280 mg/kg), with a predominance of the 1,3-isomers, as also occurs in other grasses.[19,20] Palmitic and linoleic acids were the most important esterified fatty acids occurring as diglycerides, as also occurred in the case of monoglycerides. A previous work only identified dilineoylglycerol (although it did not report the substitution pattern), but these compounds are minor components in our study. Triglycerides were also identified in high amounts among the lipids of wheat bran, accounting for 1960 mg/kg, (Table 2) and, although their occurrence was previously reported,[9] this is the first time that the identification of individual triglycerides was achieved by GC-MS. Dilinoleoyl palmitin (**IX**) was the most abundant triglyceride in the wheat bran sample (480 mg/kg) followed by dilinoleoyl olein (400 mg/kg), linoleyloleyl palmitin (300 mg/kg), and trilinolein (250 mg/kg). Palmitic and linoleic acids were the most abundant esterified fatty acids present as triglycerides, as also occurred in the case of mono- and diglycerides.

A series of *n*-alkanes could also be identified among the lipids of wheat bran, although in lower amounts (40 mg/kg). The series of *n*-alkanes was found in the range from *n*-tricosane (C_{23}) to *n*-tritriacontane (C_{31}), with a strong odd-over-even atom carbon number predominance. Nonacosane (**X**) was the main compound of this series, accounting for 14 mg/kg, followed by

dx.doi.org/10.1021/jf404772b | J. Agric. Food Chem. 2014, 62, 1664−1673

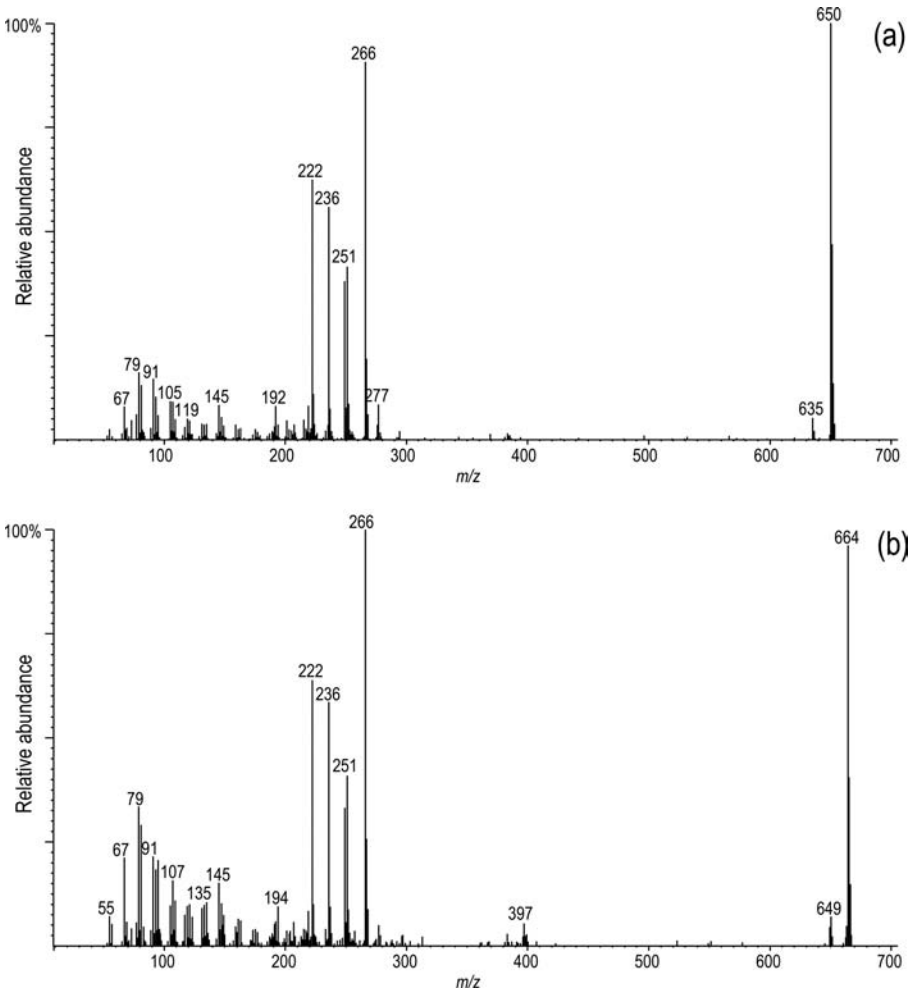

Figure 5. Mass spectra of (a) campestanyl ferulate, and (b) stigmastanyl ferulate, (as TMS ethers).

heptacosane (10 mg/kg). The rest of the alkanes were identified in very minor amounts.

Steroid Compounds. Different families of steroid compounds were identified among the lipids in wheat bran, including steroid hydrocarbons, steroid ketones, free sterols, sterol glycosides, sterol esters, and sterol ferulates. Free sterols, accounting for 510 mg/kg, were the major family of steroid compounds present in wheat bran, with sitosterol (**XII**) occurring at the highest level (290 mg/kg), followed by campesterol (**XIII**) (120 mg/kg). In addition, lower amounts of stigmasterol (**XIV**) and the saturated campestanol (**XV**) and stigmastanol (**XVI**) were also identified. Sterols conjugated with carbohydrates forming sterol glycosides or with long chain fatty acids or ferulic acid forming sterol esters were also identified. Important amounts of sterol glycosides (135 mg/kg) were identified among the lipids of wheat bran by comparison with the mass spectra and relative retention times of authentic standards.[21] As far as we know, this is the first time that sterol glycosides are reported as constituents of wheat bran lipids. Sitosteryl 3β-D-glucopyranoside (**XVII**) was the most predominant sterol glycoside in wheat bran (85 mg/kg) with lower amounts of campesteryl and stigmasteryl 3β-D-glucopyranosides, as usually observed in other grasses.[19,20] Sterol esters of long chain fatty acids corresponding to campesterol, campestanol, stigmasterol, sitosterol, and stigmastanol esterified with different fatty acids were also found (240 mg/kg). Each sterol ester series identified showed two major peaks due to the esterification with the C_{16} (palmitic acid) and with the unsaturated linoleic acid.

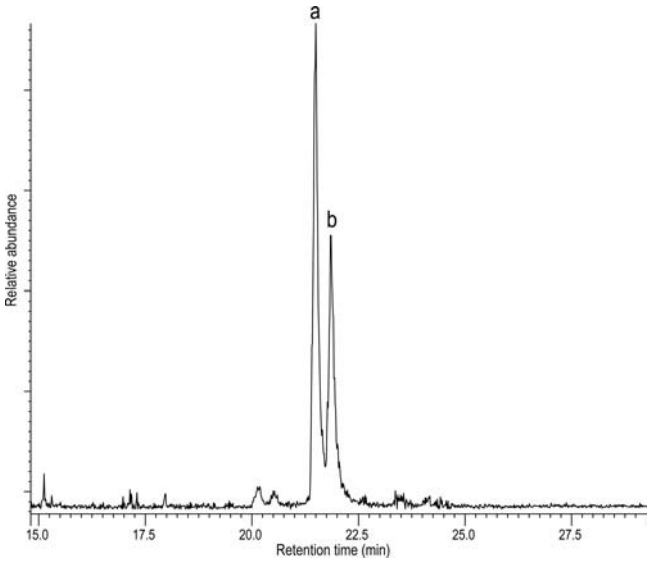

Figure 6. Single ion chromatogram (m/z 266) showing the distribution of sterol ferulates (as TMS ethers) identified in the extracts of wheat bran. (a) Campestenyl ferulate; and (b) stigmastanyl ferulate.

Sitosteryl linoleate (**XVIII**) was the most predominant (70 mg/kg) sterol ester in wheat bran, followed by sitosteryl hexadecanoate (60 mg/kg), as also occurs in other cereals.[22]

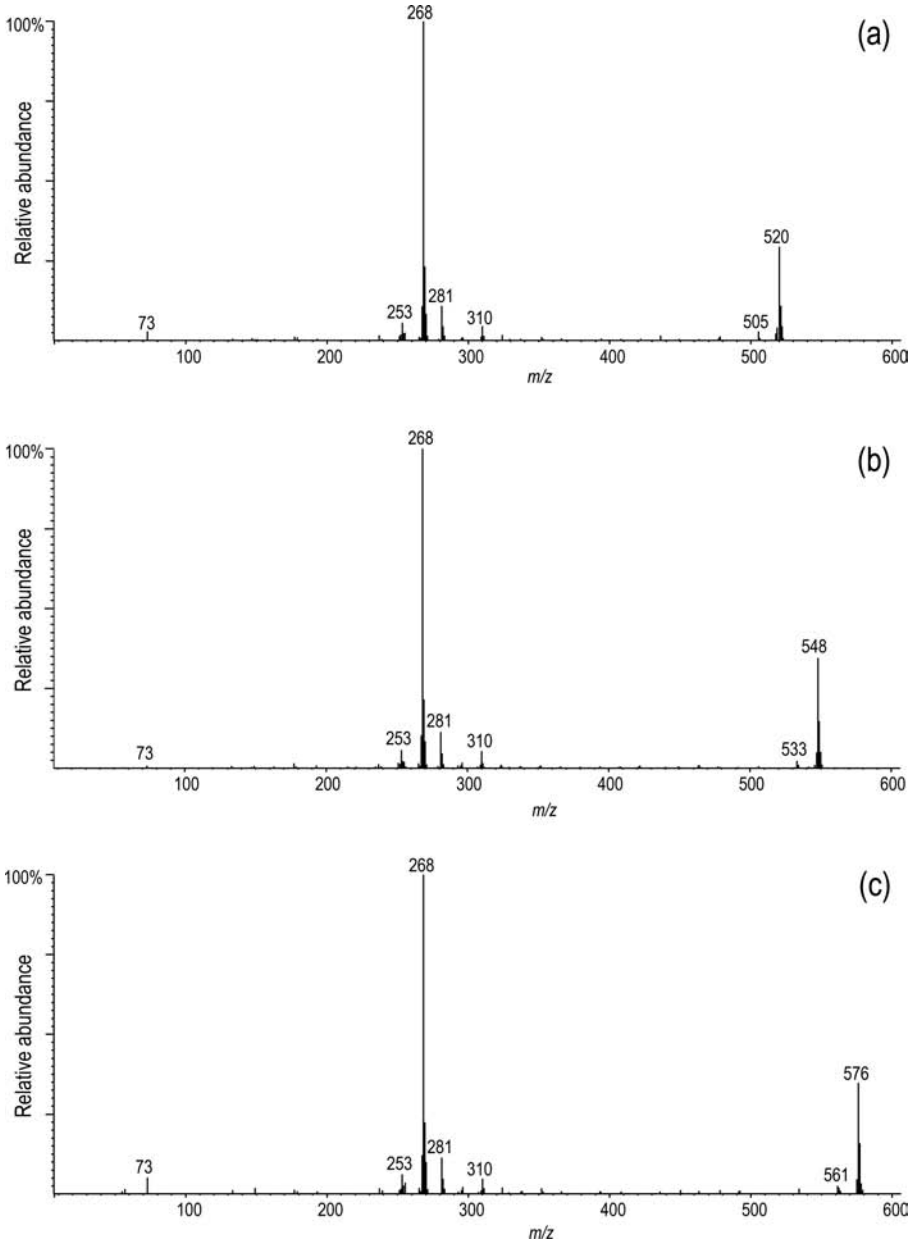

Figure 7. Mass spectra of selected alkylresorcinols (as TMS ethers): (a) 5-*n*-nonadecylresorcinol, (b) 5-*n*-heneicosylresorcinol, and (c) 5-*n*-tricosylresorcinol.

Sterol ferulates were also identified among the lipids of wheat bran (105 mg/kg), and consisted exclusively of the saturated campestanyl ferulate (**XIX**) and sitostanyl ferulate (**XX**). The identification of sterol ferulates was obtained from the mass spectra of their TMS ethers that show a characteristic base peak ion at *m*/*z* 266, typical of these molecules, together with the molecular ions at *m*/*z* 650 and *m*/*z* 664 for campestanyl and stigmastanyl ferulates, respectively.[23] The mass spectra of these sterol ferulates are shown in Figure 5, whereas Figure 6 displays the single ion chromatogram (*m*/*z* 266) showing the distribution of the series of sterol ferulates present among the lipids of wheat bran. The identification of these compounds is consistent with previous observations in several cereal bran oils.[12] Different steroid ketones, namely stigmast-3,5-dien-7-one (**XXI**), stigmasta-4,22-dien-3-one (**XXII**) and stigmast-4-en-3-one (**XXIII**), were also identified in lower amounts (80 mg/kg) among the lipids of wheat bran. Steroid hydrocarbons were also found, albeit in low amounts (60 mg/kg), and included stigmasta-3,5,22-triene (**XXIV**) and stigmasta-3,5-diene (**XXV**). The important amounts of steroid compounds present in wheat bran, and particularly the high content of free and conjugated sterols, makes wheat bran a good source of valuable phytosterols.

Alkylresorcinols. A series of 5-*n*-alkylresorcinos was identified among the lipids of wheat bran in important amounts (2250 mg/kg). The identification of 5-*n*-alkylresorcinols was achieved from their mass spectra that show a base peak due to the McLafferty rearrangement at *m*/*z* 268, characteristic of these molecules.[14,24] The mass spectra of three representative 5-*n*-alkylresorcinols are shown in Figure 7, with the characteristic base peak at *m*/*z* 268 and the molecular ions at *m*/*z* 520, *m*/*z* 548, and *m*/*z* 576 for the TMS ether derivatives of 5-*n*-nonadecyl-, 5-*n*-heneicosyl-, and 5-*n*-tricosylresorcinols, respectively. Figure 8 displays the single ion chromatogram (*m*/*z* 268) showing the distribution of the series of

dx.doi.org/10.1021/jf404772b | J. Agric. Food Chem. 2014, 62, 1664−1673

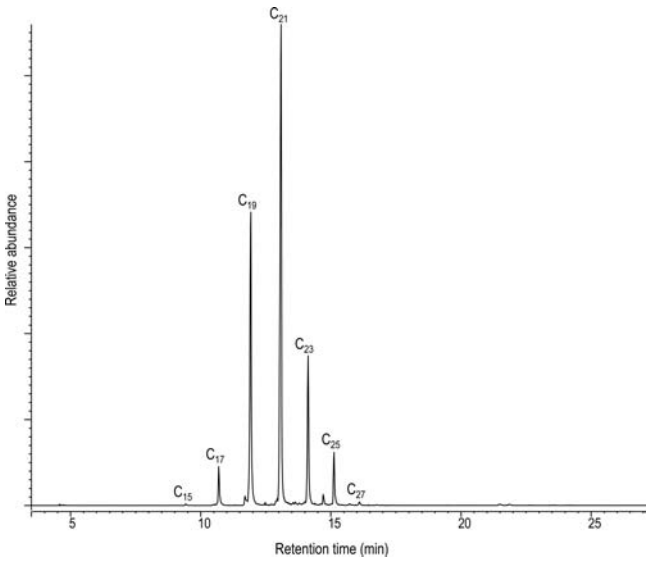

Figure 8. Single ion chromatogram (m/z 268) showing the distribution of the series of *n*-alkylresorcinols (as TMS ethers) identified in the extracts of wheat bran. C_n indicates the carbon length of the alkyl chain.

5-*n*-alkylresorcinols present among the lipids of wheat bran. The 5-*n*-alkylresorcinols ranged from 5-*n*-pentadecyl (C_{15}) to 5-*n*-heptacosylresorcinol (C_{27}), with the sole occurrence of the odd carbon atom-numbered homologues, and with 5-*n*-heneicosylresorcinol (C_{21}, **XI**) being the most abundant one (1140 mg/kg), followed by 5-*n*-nonadecylresorcinol (660 mg/kg). Alkylresorcinols are known to occur in cereal grains and their occurrence in wheat bran has been widely reported.[9,11−14,25] The distribution of alkylresorcinols identified is similar to that found in previous works,[9,11−14,25] although in the present work we have extended the series of identified alkylresorcinols up to C_{27}.

Possible Uses and Benefits of Wheat Bran Lipids. The study shown here indicates that wheat bran is a promising source of phytochemicals, such as fatty acids, triglycerides, phytosterols, and alkylresorcinols. These compounds have a wide range of nutraceutical, pharmaceutical, and cosmetic properties and are also of interest for other industrial sectors. The particularly high content of free fatty acids (40%) and acylglycerols (40%) in wheat bran extracts makes this material an interesting feedstock for biodiesel production, which is nowadays essentially produced from oil seed crops.[26] The potential use of cereal brans, such as rice bran, as useful feedstocks for biodiesel production, has recently being reported,[27] although there could be some considerations if the material used in animal diets are diverted to fuel production. Among the fatty acids, wheat bran also contains important amounts of linoleic acid, an essential unsaturated omega-6 fatty acid that must be consumed for proper health and is of interest for the food industry. Moreover, linoleic acid is also used in pharmaceutical and cosmetic products and is considered to influence the metabolic processes in the skin and to promote the activity of vitamins A and E and recovery barrier properties of stratum corneum.[28] On the other hand, phytosterols, which are also present in important amounts in wheat bran, when used as functional ingredients in foods, reduce blood cholesterol levels by interfering with intestinal cholesterol absorption.[29,30] The efficacy of phytosterols as cholesterol-lowering agents have been shown when incorporated into fat spreads as well as other food matrices. In addition, phytosterols have been combined with other beneficial dietary components to enhance their effect on risk factors of cardiovascular disease. Phytosterols appear not only to play an important role in the regulation of cardiovascular disease, but also to exhibit anticancer properties.[30] Hence, phytosterols, especially sitosterol, are suggested to have a protective effect against the most common cancers in the developed countries including colon, prostate, and breast.[12] In addition, sterol ferulates present anti-inflammatory effects and are also effective antitumor-promoters.[31] Finally, the important amounts of alkylresorcinols present in wheat bran are of special value since they are involved in multiple biological activities, including antimicrobial,[32] antiparasitic,[33,34] antioxidant,[13,14,35] and antimutagenic activities.[9,11,12,36]

In conclusion, we report a comprehensive description of the chemical composition of lipids in wheat bran that opens up new possibilities for a more complete industrial utilization of this side-stream in the context of a wheat bran biorefinery. Due to the large amounts produced annually worldwide, wheat bran can be viewed as an unexploited and promising source of highly valuable phytochemicals with potential health benefits and biological activities. Variations in the chemical composition of the lipids, however, can be expected to occur among different wheat bran samples from differences in wheat cultivars and milling procedures; the screening and analysis of additional wheat bran samples are therefore needed in order to evaluate the divergences in the composition and content of lipids among samples from different sources.

AUTHOR INFORMATION

Corresponding Author

*Tel: +34-95-4624711; Fax: +34-95-4624002; E-mail: delrio@irnase.csic.es.

Funding

This study has been funded by the Spanish project AGL2011−25379 and the EU-project LIGNODECO (KBBE-244362). Pepijn Prinsen thanks the Spanish Ministry of Science and Innovation for a FPI fellowship.

Notes

The authors declare no competing financial interest.

ACKNOWLEDGMENTS

We thank Jorge Rencoret for technical assistance in the GC-MS analyses.

REFERENCES

(1) Shewry, P. R.; Piironen, V.; Lampi, A.; Edelmann, M.; Kariluoto, S.; Nurmi, T.; Fernandez-Orozco, R.; Ravel, C.; Charmet, G.; Andersson, A. A. M.; Aman, P.; Boros, D.; Gebruers, K.; Dornez, E.; Courtin, C. M.; Delcour, J. A.; Rakszegi, M.; Bedo, Z.; Ward, J. L. The HEALTHGRAIN Wheat Diversity Screen: Effects of Genotype and Environment on Phytochemicals and Dietary Fiber Components. *J. Agric. Food Chem.* **2010**, *58*, 9291−9298.

(2) Fardet, A. New Hypotheses for the Health-Protective Mechanisms of Whole-Grain Cereals: What Is beyond Fibre? *Nutr. Res. Rev.* **2010**, *23*, 65−134.

(3) Reisinger, M.; Tirpanalan, Ö.; Prückler, M.; Huber, F.; Kneifel, W.; Novalin, S. Wheat Bran Biorefinery—A Detailed Investigation on Hydrothermal and Enzymatic Treatment. *Bioresour. Technol.* **2013**, *144*, 179−185.

(4) Swennen, K.; Courtin, C. M.; Lindemans, G. C. J. E.; Delcour, J. A. Large-Scale Production and Characterisation of Wheat Bran Arabinoxylooligosaccharides. *J. Sci. Food Agric.* **2006**, *86*, 1722−1731.

(5) Mandalari, G.; Faulds, C. G.; Sancho, A. I.; Saija, A.; Bisignano, G.; LoCurto, R.; Waldron, K. W. Fractionation and Characterisation of

Arabinoxylans from Brewers' Spent Grain and Wheat Bran. *J. Cereal Sci.* **2005**, *42*, 205−212.
(6) Anderson, J. W. Whole Grains and Coronary Heart Disease: The Whole Kernel of Truth. *Am. J. Clin. Nutr.* **2004**, *80*, 1459−1460.
(7) Montonen, J.; Knekt, P.; Jarvinen, R.; Aromaa, A.; Reunanen, A. Whole-Grain and Fiber Intake and the Incidence of Type 2 Diabetes. *Am. J. Clin. Nutr.* **2003**, *77*, 622−629.
(8) Landberg, R.; Kamal-Eldin, A.; Andersson, S.; Johansson, J.; Zhang, J.; Hallmans, G.; Aaman, P. Reproducibility of Plasma Alkylresorcinols during a 6-Week Rye Intervention Study in Men with Prostate Cancer. *J. Nutr.* **2009**, *139*, 975−980.
(9) Liu, L.; Winter, K. M.; Stevenson, L.; Morris, C.; Leach, D. N. Wheat Bran Lipophilic Compounds with in Vitro Anticancer Effects. *Food Chem.* **2012**, *130*, 156−164.
(10) Sang, S.; Ju, J.; Lambert, J. D.; Lin, Y.; Hong, J.; Bose, M.; Wang, S.; Bai, N.; He, K.; Reddy, B. S.; Ho, C. T.; Li, F.; Yang, C. S. Wheat Bran Oil and Its Fractions Inhibit Human Colon Cancer Cell Growth and Intestinal Tumorigenesis in Apc(min/+) Mice. *J. Agric. Food Chem.* **2006**, *54*, 9792−9797.
(11) Zhu, Y.; Conklin, D. R.; Chen, H.; Wang, L.; Sang, S. 5-Alk(en)ylresorcinols as the Major Active Components in Wheat Bran Inhibit Human Colon Cancer Cell Growth. *Bioorg. Med. Chem.* **2011**, *19*, 3973−3982.
(12) Iwatsuki, K.; Akihisa, T.; Tokuda, H.; Ukiya, M.; Higashihara, H.; Mukainaka, T.; Iizuka, M.; Hayashi, Y.; Kimura, Y.; Nishino, H. Sterol Ferulates, Sterols, And 5-Alk(en)ylresorcinols from Wheat, Rye, And Corn Bran Oils and Their Inhibitory Effects on Epstein-Barr Virus Activation. *J. Agric. Food Chem.* **2003**, *51*, 6683−6688.
(13) Gunenc, A.; HadiNezhad, M.; Tamburic-Ilincic, L.; Mayer, P. M.; Hosseinian, F. Effects of Region and Cultivar on Alkylresorcinols Content and Composition in Wheat Bran and Their Antioxidant Activity. *J. Cereal Sci.* **2013**, *57*, 405−410.
(14) Gunenc, A.; Tavakoli, H.; Setharaman, K.; Mayer, P. M.; Fairbanks, D.; Hosseinian, F. Stability and Antioxidant Activity of Alkylresorcinols in Breads Enriched with Hard and Soft Wheat Brans. *Food Res. Int.* **2013**, *51*, 571−578.
(15) Gutiérrez, A.; del Río, J. C.; González-Vila, F. J.; Martín, F. Analysis of Lipophilic Extractives from Wood and Pitch Deposits by Solid-Phase Extraction and Gas Chromatography. *J. Chromatogr. A* **1998**, *823*, 449−455.
(16) *Tappi Test Methods 2004−2005*; Tappi Press: Norcoss, GA, 2004.
(17) Browning, B. L. *Methods of Wood Chemistry, Vol. II*; Wiley-Interscience Publishers: New York, 1967.
(18) Dutta, P.; Appelqvist, L. -Å. Saturated Sterols (Stanols) In Unhydrogenated and Hydrogenated Edible Vegetable Oils and in Cereal Lipids. *J. Sci. Food Agric.* **1996**, *71*, 383−391.
(19) del Río, J. C.; Prinsen, P.; Gutiérrez, A. Chemical Composition of Lipids in Brewerś Spent Grain: A Promising Source of Valuable Phytochemicals. *J. Cereal Sci.* **2013**, *58*, 248−254.
(20) del Río, J. C.; Prinsen, P.; Gutiérrez, A. A Comprehensive Characterization of Lipids in Wheat Straw. *J. Agric. Food Chem.* **2013**, *61*, 1904−1913.
(21) Gutiérrez, A.; del Río, J. C. Gas Chromatography/Mass Spectrometry Demonstration of Steryl Glycosides in Eucalypt Wood, Kraft Pulp and Process Liquids. *Rapid Commun. Mass Spectrom.* **2001**, *15*, 2515−2520.
(22) Esche, R.; Scholz, B.; Engel, K. -H. Online LC-GC Analysis of Free Sterols/Stanols and Intact Steryl/Stanyl Esters in Cereals. *J. Agric. Food Chem.* **2013**, *61*, 10932−10939.
(23) Evershed, R. P.; Spooner, N.; Prescott, M. C.; Goad, L. J. Isolation and Characterisation of Intact Steryl Ferulates from Seeds. *J. Chromatogr. A* **1988**, *440*, 23−35.
(24) Zarnowski, R.; Suzuki, Y.; Yamaguchi, I. Alkylresorcinols in Barley (*Hordeum vulgare* L. distichon) Grains. *Z. Naturforsch.* **2002**, *57c*, 57−62.
(25) Athukorala, Y.; Hosseinian, F. S.; Mazza, G. Extraction and Fractionation of Alkylresorcinols from Triticale Bran by Two-Step Supercritical Carbon Dioxide. *LWT—Food Sci. Technol.* **2010**, *43*, 660−665.
(26) Singh Nigam, P.; Singh, A. Production of Liquid Biofuels from Renewable Resources. *Prog. Energ. Combust. Sci.* **2011**, *37*, 52−68.
(27) Zhang, Y.; Wong, W. -T.; Yung, K. -F. One-Step Production of Biodiesel from Rice Bran Oil Catalyzed by Chlorosulfonic Acid Modified Zirconia via Simultaneous Esterification and Transesterification. . *Bioresour. Technol.* **2013**, *147*, 59−64.
(28) Huang, F. C.; Ju, Y. H.; Chiang, J. C. Gamma-Linolenic Acid-Rich Triacylglycerols Derived from Borage Oil via Lipase-Catalyzed Reactions. *J. Am. Oil Chem. Soc.* **1999**, *76*, 833−837.
(29) Quílez, J.; García-Lorda, P.; Salas-Salvadó, J. Potential Uses and Benefits of Phytosterols in Diet: Present Situation and Future Directions. *Clin. Nutr.* **2003**, *22*, 343−351.
(30) Jones, P. J.; AbuMweis, S. S. Phytosterols as Functional Food Ingredients: Linkages to Cardiovascular Disease and Cancer. *Curr. Opin. Clin. Nutr. Metab. Care* **2009**, *12*, 147−51.
(31) Akihisa, T.; Yasukawa, K.; Yamaura, M.; Ukiya, M.; Kimura, Y.; Shimizu, N.; Arai, K. Triterpene Alcohol and Sterol Ferulates from Rice Bran and Their Anti-Inflammatory Effects. *J. Agric. Food Chem.* **2000**, *48*, 2313−2319.
(32) Reiss, J. Influence of Alkylresorcinols from Rye and Related Compounds on the Growth of Food-Borne Moulds. *Cereal Chem.* **1989**, *66*, 491−493.
(33) Kozubek, A.; Tyman, J. H. P. Resorcinol Lipids, The Natural Non-Isoprenoid Phenolic Amphiphiles and Their Biological Activity. *Chem. Rev.* **1999**, *99*, 1−25.
(34) Suresh, M.; Raj, R. K. Cardol: Antifilarial Principle from *Anacardium occidentale*. *Curr. Sci.* **1990**, *59*, 477−479.
(35) Hładyszowski, J.; Zubik, L.; Kozubek, A. Quantum Mechanical and Experimental Oxidation Studies of Pentadecylresorcinol, Olivetol, Orcinol and Resorcinol. *Free Radical Res.* **1998**, *28*, 359−368.
(36) Gasiorowski, K.; Brokos, B.; Kulma, A.; Ogorzałek, A.; Skórkowska, K. Impact of Four Antimutagens on Apoptosis in Genotoxically Damaged Lymphocytes in Vitro. *Cell. Mol. Biol. Lett.* **2001**, *6*, 649−675.

and pears were found to contain twice the amount of total phenolics as found in the peeled fruits.[5,23]

Major advances have been achieved in recent years in understanding the absorption and metabolism of most other classes of phenolic compounds. These studies have focused on anthocyanins, flavanones, catechins, proanthocyanidins, and the hydroxybenzoic and hydroxycinnamic acids.[24]

Some additives that can preserve the natural properties of foods are simple sugars. A number of mechanisms have been suggested for the explanation of sugar's effectiveness on preservation. These include sugar's ability to form glass, to lock in compounds, to mimic the hydrogen-bonding character of water, to increase the surface tension of the bulk solvent, to prevent thermotropic phase separations in lipid bilayers, and to prevent the fusion of membranes.[25,26]

The objective of this study was to investigate the influence of several simple sugar additions at levels of 1 and 5% on the polyphenol content and antioxidative activity of apple purée processed by freezing and freeze-drying and stored for 6 months.

MATERIALS AND METHODS

Chemicals. Folin−Ciocalteu reagent was purchased from Kemika (Zagreb, Croatia); 2,6-dichlorophenol indophenols, phloretin, catechin, epicatechin, rutin, quercetin, chlorogenic acid, caffeic acid were obtained from Sigma Chemical Co. (St. Louis, MO, USA); 2,2′-azinobis(3-ethylbenzothiazoline-6-sulfonate), 2,2-diphenyl-1-picrylhydrazyl, and procyanidin B2 were from Fluka (St. Louis, MO, USA); phlorizin was from Aldrich (St. Louis, MO, USA); and methanol (HPLC grade) and orthophosphoric acid (85%) were obatined from Panareac (Barcelona, Spain).

Apple Cultivars Used for Experiment. Actual apple cultivars 'Idared' and 'Fuji' were purchased from the Agricultural Institute (Osijek, Croatia). Both apple varieties were stored under regular atmosphere (RA) at 2−6 °C before they were purchased for study. During apple purée preparation the core area was removed and two opposite cuts of each fruit were pureed and mixed with simple sugars (S, sucrose; G, glucose; F, fructose; and T, trehalose). Sixteen variants of mixed purees were prepared: 1 and 5% of each sugar were mixed with both apple cultivars. Prepared samples were used for processing, freezing, and freeze-drying.

Physical and Chemical Analysis. Apples were held at room temperatures for ca. 1 h before preparation for analysis. Before the apple fruits were disintegrated using a Braun Multiquick Professional 600 W Turbo for the analysis, the core was removed. The content of soluble solids of apples was measured with a tabletop Abbe refractometer and given in Brix (°Brix). Acids were measured by titration with 0.1 M NaOH and phenolphthalein as an indicator and given as grams per 100 g of malic acid. Reducing and total sugars were determined by Luff Schoorl's method,[27] and vitamin C (L-ascorbic acid) was determined by a volumetric method: titration using dichlorophenol indophenol (DCPIP).[28]

Freezing and Freeze-Drying. Apple purée samples used for freezing were placed in plastic bags and frozen in a laboratory freezer. Samples were maintained at −18 °C. Apple purée samples used for freeze-drying were placed into plastic bags and frozen at −18 °C for 12 h before freeze-drying in a laboratory freeze-dryer (Christ Freeze-Dryer, Gamma 2-20, Germany). Drying conditions were as follows: freezing temperature, −55 °C; temperature of sublimation, −35 to 0 °C; vacuum level, 0.220 mbar. The temperature of isothermal desorption varied from 0 to 22 °C under the vacuum of 0.060 mbar. Freeze-drying lasted until the total solids content was 94−98%, which was about 48 h.

Extraction of Phenolics. The extraction of polyphenols for the determination of TPC and AOA was performed as follows: disintegrated apple parts (peel, peel + flesh, flesh), freeze-dried, and frozen apple purée were homogenized with methanol containing hydrochloric acid (1% v/v) (1 g of sample in 10 mL of 1% HCl methanol). The samples were held at ambient temperature for 1 h. After 1 h, the mixture was filtered through pleated Whatman no. 2 filter paper (Whatman International Limited, Kent, UK), and permeates were used for analysis. Before the identification of polyphenols, fresh and frozen samples were freeze-dried as described earlier. Phenolics were extracted from freeze-dried samples using 80% aqueous methanol. The mixture was sonicated for 15 min and centrifuged at room temperature for 15 min. Extracted samples were filtered through a 0.45 Rm poly(tetrafluoroethylene) syringe-tip filter (Chromafil Xtra, Macherey-Nagel GmbH & Co. KG), and extracts were used for HPLC analysis. The amount of phenolics was expressed as milligrams per 100 g of fresh weight (FW).

Table 1. Physicochemical Parameters of 'Idared' and 'Fuji' Apple Varieties, n^a = 20

parameter	'Idared'	'Fuji'
av fruit wt (g)	209.24 ± 24.760	193.25 ± 29.310
hardness (kg/cm^2)	8.60 ± 0.423	9.96 ± 0.185
moisture (%)	83.76 ± 0.133	84.46 ± 0.550
soluble solids (°Brix)	13.27 ± 0.152	13.10 ± 0.173
L-ascorbic acid (mg/100 g)	5.58 ± 0.230	6.16 ± 0.230
acids (g/100 g of malic acid)	0.25 ± 0.020	0.15 ± 0.001
pH	3.43 ± 0.006	3.76 ± 0.017
sugars		
reducing	8.40 ± 0.091	9.10 ± 0.144
total	11.64 ± 0.057	12.35 ± 0.075
color parameters		
L^*	39.65 ± 0.990	42.96 ± 0.134
a^*	3.4 ± 0.053	−2.74 ± 0.020
b^*	15.48 ± 0.100	15.77 ± 0.210
total polyphenols content (g GAE/kg)		
peel	5.72 ± 0.182	3.28 ± 0.082
peel + flesh	1.16 ± 0.009	0.85 ± 0.022
flesh	1.06 ± 0.027	0.62 ± 0.002
antioxidant activity		
ABTS assay (mmol trolox/100 mL)		
peel	15.75 ± 0.338	34.86 ± 0.270
peel + flesh	12.72 ± 0.558	10.36 ± 0.258
flesh	3.22 ± 0.250	6.77 ± 0.480
DPPH assay (mmol trolox/100 mL)		
peel	6.02 ± 0.104	5.13 ± 0.231
peel + flesh	2.46 ± 0.060	2.69 ± 0.080
flesh	1.67 ± 0.044	2.09 ± 0.042

[a] n, number of fruits under study.

Determination of Total Polyphenol Content. The total phenols content was determined according to the modified colorimetric Folin−Ciocalteu method.[29] A 0.2 mL of apple extract and 1.8 mL of deionizer water were added to a 23 mL test tube. Ten milliliters of Folin−Ciocalteu reagent (1:10) was added to the solution, and finally 8 mL of 7.5% sodium carbonate (Na_2CO_3) solution was transferred into the test tubes. The color was developed in 120 min, and the absorbance was read at 765 nm by a spectrophotometer (Jenway 6300, Bibby Scientific, UK). The measurements were performed in triplicates for each sample, and the average value was interpolated on a gallic acid calibration curve and expressed as grams of gallic acid per kilogram of sample equivalents (g GAE/kg).

Antioxidant Activity Determination. The ABTS assay followed the method of Arnao et al. with some modifications.[30] The results were expressed as millimoles of trolox equivalents (TE) per 100 mL of sample. Additional dilution was needed if the measured ABTS value was over the linear range of the standard curve. For the DPPH assay 0.2 mL of the apple extract was diluted with methanol (2 mL), and 1 mL of DPPH solution (0.5 mM) was added. After 15 min, the absorbance was measured at 517 nm.[31] The results were expressed as

Table 2. Polyphenol Compounds in 'Idared' and 'Fuji' Apple Varieties (Milligrams per 100 g FW)[a]

part of fruit		polyphenol	'Idared'	'Fuji'
flesh		procyanidin B2	3.13 ± 0.027a	nd[b]
		phloridzin	0.72 ± 0.021a	0.57 ± 0.012b
		(−)-epicatchin	0.45 ± 0.012a	1.16 ± 0.078b
		phloretin xyloglucoside	nd	nd
		chlorogenic acid	8.05 ± 0.083a	3.82 ± 0.024b
peel + flesh		procyanidin B2	12.41 ± 0.433a	9.48 ± 0.348b
		phloridzin	1.54 ± 0.093a	0.87 ± 0.026b
		(−)-epicatchin	1.12 ± 0.021b	1.70 ± 0.049a
		phloretin xyloglucoside	nd	nd
		chlorogenic acid	9.16 ± 0.133a	4.69 ± 0.029b
	quercetin glycoside[c]	24.416	0.30 ± 0.016a	0.13 ± 0.005b
		24.997	nd	0.17 ± 0.005a
		25.243	0.68 ± 0.025a[a]	0.09 ± 0.005b
		rutin	2.93 ± 0.050a	0.95 ± 0.020b
peel		procyanidin B2	23.47 ± 0.013b	31.41 ± 0.131a
		phloridzin	4.32 ± 0.127a	nd
		(−)-epicatchin	3.33 ± 0.036b	6.39 ± 0.094a
		phloretin xyloglucoside	nd	nd
		chlorogenic acid	2.54 ± 0.064a	nd
		caffeic acid	nd	nd
	quercetin glycoside[c]	24.181	0.56 ± 0.048b	3.88 ± 0.004a
		24.440	0.11 ± 0.001b	0.95 ± 0.002a
		24.997	1.16 ± 0.078b	5.53 ± 0.012a
		25.213	0.51 ± 0.007b	2.66 ± 0.009a
		rutin	3.26 ± 0.058b	8.33 ± 0.136a
		quercetin	0.08 ± 0.001a	nd

[a]Each value is expressed as the mean ± standard deviation (n = 3). Within the same row, means followed by different letters are significantly different at $p \leq 0.05$ (ANOVA, Fisher's LSD). [b]nd, not detectable. [c]Quercetin glycosides retention times (min): peaks of quercetin-3-glucoside, galactoside, arabinoside, xyloside, and rhamnoside.

millimoles of trolox equivalents (TE) per 100 mL of sample. Additional dilution was needed if the measured DPPH value was over the linear range of the standard curve.

Identification of Phenolics. The analytical HPLC system employed consisted of a Varian LC system (Agilent, Avondale, PA, USA) equipped with a ProStar 230 solvent delivery module and a ProStar 330 PDA detector. Phenolic compound separation was done with an OmniSpher C18 column (250 × 4.6 mm inner diameter, 5 μm, Agilent, USA) protected with a guard column (ChromSep 1 cm × 3 mm, Varian, USA). The data were collected and analyzed on an IBM computing system equipped with Star Chromatography Workstation software (version 5.52). The same solvents and gradient elution program were used in the determination of phenolic acids and flavonols. Solvent A was 0.1% phosphoric acid, and solvent B was 100% HPLC grade methanol. The elution conditions were as follows: 0−30 min from 5 to 80% B; 30−33 min, 80% B; 33−35 min, from 80 to 5% B; with a flow rate = 0.8 mL/min.[32] Phenolic standards were used to generate characteristic UV−vis spectra and calibration curves. Individual phenolics in the sample were tentatively identified by comparison of their UV−vis spectra and retention times with spiked input of polyphenolic standard. Three replicated HPLC analyses were performed for each sample.

Color Measurement. The color of the apple purée was determined by using a colorimeter (Minolta CR-300) prior to the chemical analysis. Color values, for each fruit, were calculated using the averaging mode with five replications. The color measurements were made using the $L^*a^*b^*$ system. L^* measures lightness and varies from 100 for perfect white to zero for black, approximately as the eye would evaluate it. The a^* parameter measures redness when positive and greenness when negative, and b^* measures yellowness when positive and blueness when negative.

Statistical Analysis. All measurements were done in triplicate, and data were expressed as the mean ± standard deviation. The experimental data were subjected to a one-way analysis of variance (ANOVA), and Fisher's LSD values were calculated to detect significant differences ($p \leq 0.05$) between mean values. Statistical analyses were performed with the statistical program MS Excel (Microsoft Office 2007 Professional).

RESULTS AND DISCUSSION

The physicochemical parameters of both apple varieties are shown in Table 1. The water content of the total fresh weight of both apple varieties was ca. 84%, and the content of soluble solids ca. 13 °Brix. pH value differed from 3.4 ± 0.006 ('Idared') to 3.8 ± 0.017 ('Fuji'). 'Idared' apples had a higher acidity (0.3 ± 0.020 g 100 g^{-1} of malic acid) than 'Fuji' apples (0.2 ± 0.001 g 100 g^{-1} of malic acid), whereas the amount of ascorbic acid was higher in 'Fuji' apples (8.4 mg 100 g^{-1}). Mean values of ascorbic acid and soluble solids content were at a range of those reported for other commercial apple cultivars.[33] The total sugar content ranged from 11.6 mg ('Idared') to 12.4 mg ('Fuji') (Table 1). The total sugar contents were slightly lower than those obtained in studies on apple cultivars grown in, for example, Slovenia and Brazil.[34,35] Color parameters of 'Fuji' apples indicated that the flesh was lighter green (a^* parameter was negative) and the coordinate b^* indicates a slight yellow color, whereas 'Idared' apples had a light red flesh (a^* parameter was positive).

In both apple varieties, TPC was highest in the peel, followed by the flesh + peel and the flesh, which is in accordance with the results of other researchers.[36,37] However, 'Idared' apple peel had a higher TPC than 'Fuji' (5.7 ± 0.182 and 3.3 ± 0.082 g GAE/kg of peel, respectively).

Table 3. Total Polyphenol Content and Antioxidant Activity in Processed Apple Purée during Storage[a]

	frozen			freeze-dried		
	0 days	30 days	180 days	0 days	30 days	180 days
			'Idared'			
TPC (g GAE/L)	0.27 ± 0.005b	0.30 ± 0.012a	0.27 ± 0.004b	0.30 ± 0.009c	0.34 ± 0.008a	0.32 ± 0.011b
DPPH (mmol trolox/100 mL)	0.81 ± 0.003a	0.70 ± 0.021b	0.57 ± 0.019c	1.67 ± 0.007a	0.70 ± 0.047b	0.65 ± 0.010b
ABTS (mmol trolox/100 mL)	3.42 ± 0.349a	3.48 ± 0.073a	3.78 ± 0.134a	1.99 ± 0.385c	3.29 ± 0.031b	3.73 ± 0.233a
			'Fuji'			
TPC (g GAE/L)	0.25 ± 0.005c	0.37 ± 0.005a	0.33 ± 0.009b	0.32 ± 0.010a	0.32 ± 0.004a	0.34 ± 0.022a
DPPH (mmol trolox/100 mL)	0.92 ± 0.001a	0.68 ± 0.081b	0.24 ± 0.039c	0.69 ± 0.005a	0.71 ± 0.014a	0.52 ± 0.062b
ABTS (mmol trolox/100 mL)	0.77 ± 0.031c	2.34 ± 0.081b	2.85 ± 0.131a	2.45 ± 0.406b	3.24 ± 0.146a	3.65 ± 0.042a

[a]Each value is expressed as the mean ± standard deviation (n = 3). Within the same row, means followed by different letters are significantly different at $p \leq 0.05$ (ANOVA, Fisher's LSD).

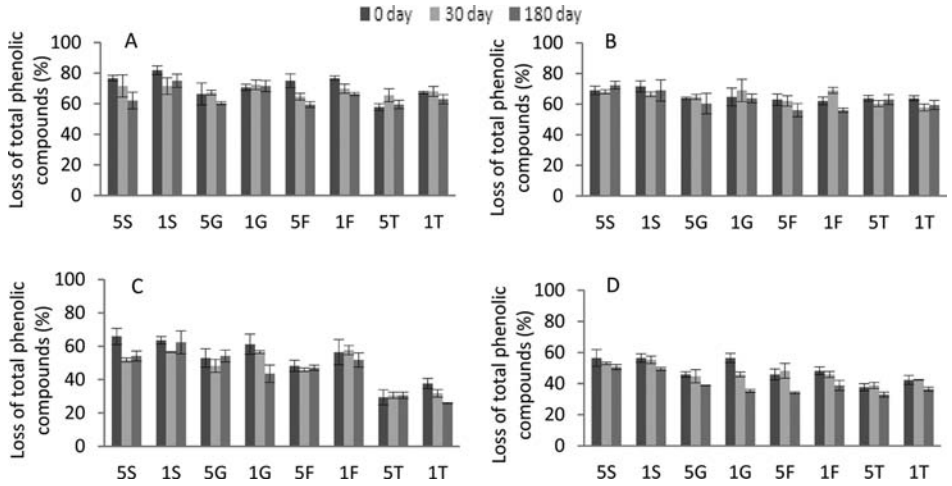

Figure 1. Loss of total polyphenols (%) in frozen (A, 'Idared'; C, 'Fuji') and freeze-dried (B, 'Idared'; D, 'Fuji') apple purée, prepared with an addition of sugars (S, sucrose; G, glucose; F, fructose; T, trehalose; 5, 5%; 1, 1%): black bars, immediately after preparation; light gray bars, after 3 months of storage; dark gray bars, after 6 months of storage. Error bars represent standard deviations of each data (n = 3).

Antioxidant activity in both ABTS and DPPH assays was positively correlated with TPC in the peel, flesh + peel, and flesh. Ki Won et al. found that quercetin, epicatechin, and procyanidin B2 significantly contribute to the total antioxidant activity of apples.[37] As shown in Table 2 the phenolics in apple flesh consisted of four main compounds, procyanidin B2, phloridzin, (−)-epicatchin, and chlorogenic acid. The apple peels contained additional quercetin glycoside such as glucoside, galactoside, xyloside, arabinoside, rhamnoside, and rutinoside. The main quercetin glycoside in the peel of both apple varieties was quercetin rutinoside (rutin). Mean values of phenolic compounds presented in Table 2 were at the range of those reported by Carbone et al. and Ceymann et al. for other commercial apple cultivars.[38,39] Differences in extraction procedures or quantification methods could explain the different results for the same cultivar as could be influenced by pre- and postharvest factors.[40] A difference in the levels of TPC between fresh and processed apple purées was detected, as shown in Table 3. The content of TPC in unprocessed apple fruit ranged from 0.9 g GAE/kg ('Fuji' apples) to 1.2 g GAE/kg ('Idared' apples). The highest retention of TPC in processed frozen samples was observed in (unprocessed 100% TPC) 'Fuji' apple purée: 29.4, 43.5, and 38.3% on days 0, 30, and 180 respectively. Retention of TPC in (unprocessed 100% TPC) 'Idared' apples purée was slightly lower at 23.3, 25.9, and 23.9% on days 0, 30, and 180, respectively. In freeze-dried samples, retention of TPC was 37.7, 37.7, and 40.0% for 'Fuji' apple purée and 25.9, 29.3, and 27.6 for 'Idared' apple purée on days 0, 30, and 180, respectively. In general, the highest levels of polyphenols were lost in the apple flesh (without peel) followed by flesh + peel, and peel (data not shown).

Significant losses during processing can be explained by the oxidation of phenolic compounds during the slow freezing process achieved in a laboratory freezer (−18 °C). These losses were detected also in freeze-dried samples. In some samples an increase of polyphenols during storage occurred. The higher amount of polyphenols during storage in frozen apple purée (peel + flesh) may be attributed to better extraction efficiency of polyphenols from frozen apple purée than from fresh apple fruit (purée) because of cellular disruption during freezing and thawing.[41]

It is known that AOA is influenced not only by the content of the polyphenols but also by phenolic compositions. The results of antioxidant activity (Table 3) obtained with the use of the $ABTS^{\cdot+}$ radical were higher compared to the results of assays performed using the DPPH radical (Table 3), which is in accordance with ref 1. The results obtained by the DPPH method (Table 3) indicate a decrease of AOA during storage of the samples of both apple varieties. This was not the case with AOA measured with the ABTS method. The AOA determined with the ABTS method increased during storage. This can be explained by the nature of the two radicals applied. Like $ABTS^{\bullet+}$, DPPH reacts with both electron and hydrogen donors, although more slowly, and as result of that, the DPPH radical can

Table 4. Polyphenolic Profile of Freeze-Dried Apple Purée with Addition of Sugars after 6 Months of Storage (Milligrrams per 100 g FW)[a]

		control	5S	1S	5G	1G	5F	1F	5T	1T
					'Idared'					
(+)-catechin		2.84 ± 0.018bc	4.63 ± 0.038a	3.85 ± 0.021a	3.19 ± 0.017ab	2.67 ± 0.014bc	2.56 ± 0.018c	2.58 ± 0.024c	3.11 ± 0.018bc	3.27 ± 0.026bc
(−)-epicatchin		0.91 ± 0.026b	0.58 ± 0.003h	0.81 ± 0.001d	0.69 ± 0.006f	0.75 ± 0.007e	0.64 ± 0.002g	0.86 ± 0.007c	0.55 ± 0.005i	1.06 ± 0.018a
chlorogenic acid		0.54 ± 0.005h	0.67 ± 0.010g	1.28 ± 0.014b	1.03 ± 0.009e	1.18 ± 0.012c	1.09 ± 0.002d	1.03 ± 0.015e	0.91 ± 0.001f	1.64 ± 0.014a
caffeic acid		0.09 ± 0.001bc	0.03 ± 0.022e	0.10 ± 0.001ab	0.08 ± 0.011c	0.06 ± 0.003d	0.08 ± 0.001c	0.08 ± 0.016c	0.02 ± 0.001e	0.11 ± 0.001a
rutin		4.59 ± 0.004i	6.66 ± 0.013f	7.18 ± 0.012c	6.44 ± 0.031g	7.02 ± 0.021d	6.82 ± 0.004e	7.90 ± 0.019b	5.17 ± 0.024h	8.02 ± 0.016a
quercetin glycosides[b]	23.867	0.41 ± 0.007c	0.41 ± 0.002c	0.54 ± 0.003b	0.30 ± 0.001e	0.40 ± 0.001d	0.25 ± 0.001f	0.54 ± 0.006b	0.22 ± 0.007g	1.01 ± 0.011a
	24.664	0.50 ± 0.049c	0.48 ± 0.006c	0.67 ± 0.004b	0.40 ± 0.004d	0.49 ± 0.004c	0.36 ± 0.001e	0.65 ± 0.001b	0.31 ± 0.002f	0.73 ± 0.002a
	24.912	0.33 ± 0.009bc	0.29 ± 0.020d	0.34 ± 0.001b	0.23 ± 0.001e	0.23 ± 0.001e	0.21 ± 0.001f	0.32 ± 0.001c	0.24 ± 0.002e	0.41 ± 0.004a
quercetin		0.14 ± 0.001a	nd[c]	nd	nd	nd	nd	nd	nd	nd
					'Fuji'					
(+)-catechin		nd	1.90 ± 0.027c	nd	2.72 ± 0.016a	nd	2.58 ± 0.017b	nd	nd	nd
(−)-epicatchin		0.44 ± 0.004h	0.47 ± 0.011g	0.38 ± 0.006i	1.33 ± 0.014a	0.56 ± 0.001d	0.70 ± 0.006c	0.50 ± 0.004f	1.09 ± 0.016b	0.53 ± 0.002e
chlorogenic acid		0.60 ± 0.001g	0.63 ± 0.012f	0.55 ± 0.007i	0.89 ± 0.007b	0.68 ± 0.004e	0.73 ± 0.004d	0.79 ± 0.001c	0.97 ± 0.001a	0.58 ± 0.006h
caffeic acid		nd	nd	nd	nd	nd	nd	0.08 ± 0.001b	0.10 ± 0.001a	0.05 ± 0.001c
rutin		3.90 ± 0.016i	6.87 ± 0.021d	5.63 ± 0.022h	6.82 ± 0.019e	6.16 ± 0.016g	6.73 ± 0.027f	7.03 ± 0.024c	7.44 ± 0.026b	11.10 ± 0.024a
quercetin glycosides[b]	23.867	0.26 ± 0.004g	0.35 ± 0.004e	0.33 ± 0.002f	0.52 ± 0.005a	0.42 ± 0.001b	0.35 ± 0.001e	0.38 ± 0.006c	0.36 ± 0.011d	0.52 ± 0.008a
	24.664	0.35 ± 0.003h	0.08 ± 0.001i	0.44 ± 0.003g	0.73 ± 0.007a	0.51 ± 0.006d	0.48 ± 0.001f	0.54 ± 0.009c	0.50 ± 0.010e	0.62 ± 0.004b
	24.912	0.19 ± 0.001i	0.47 ± 0.001a	0.21 ± 0.001h	0.34 ± 0.001b	0.22 ± 0.004g	0.24 ± 0.004f	0.26 ± 0.004e	0.27 ± 0.007d	0.35 ± 0.004c
quercetin		nd	nd	nd	nd	nd	nd	nd	nd	nd

[a]Each value is expressed as mean ± standard deviation (n = 3). Within the same row, means followed by different letters are significantly different at $p \leq 0.05$ (ANOVA, Fisher's LSD). [b]Quercetin glycoside retention times peaks of quercetin-3-glucoside, galactoside, arabinoside, xyloside, and rhamnoside. [c]nd, not detectable.

dx.doi.org/10.1021/jf405003u | J. Agric. Food Chem. 2014, 62, 1674−1682

underestimate fast reactors. DPPH is also more selective than $ABTS^{\bullet+}$ in the reaction with H-donors. For instance, the inhibition coefficient *f* for a series of tea catechins was found to be almost equal to the number of active OH-groups inherent in catechol and pyrogallol fragments.[42] In contrast to $ABTS^{\bullet+}$, DPPH does not react with flavonoids, which contain no OH-groups in the B-ring as well as with aromatic acids containing only one OH-group.[43,44] With regard to $ABTS^{\bullet+}$, nonspecific side reactions are common and could cause an overestimation of antioxidant activity. $ABTS^{\bullet+}$ reacts with any hydroxylated aromatics independently of their real antioxidative potential.[44] Some examples may verify this statement. The AOA of resorcinol determined with microsomal model was found to be less than that of catechol and *p*-hydroquinone by 150- and 10-fold, respectively. At the same time, AOA measured with the ABTS method for resorcinol (2.49) was significantly superior to those for catechol (1.43) and *p*-hydroquinone (1.33).[45]

In more recent years research on the influence of sugars upon polyphenols has focused on anthocyanins and color stability of fruit and vegetable products. Numerous studies have been performed to elucidate such effects, however, revealing contradictory results. Increased loss of anthocyanin color or uninfluenced anthocyanin color in the presence of saccharides was reported by Malien-Aubert et al., Dyrby et al., and Hubbermann et al.[46−48] In contrast, improved pigment stability upon sugar addition was reported by Kopjar et al., Ścibisz and Mitek, and Kopjar et al.[26,49,50]

In our research, the loss of TPC in all apple samples, determined immediately after sugar addition and after processing, was smaller compared to the findings in the samples without sugar addition (Figure 1).

The apple polyphenol profile was mostly preserved in the freeze-dried samples with sugar addition during 6 months of storage (Table 4). In the 'Idared' apple samples we observed a reduction of quercetin aglycon and an increase of quercetin glycosides, which is observed in all 'Idared' samples with added sugars.

In the freeze-dried apple samples the highest impact on (+)-catechin preservation had S 5% ('Idared') and G 5% ('Fuji') 4.6 and 2.7 mg/100 g FW, respectively. The highest impact on (−)-epicatechin preservation had T 1% ('Idared') and G 5% ('Fuji') 1.1 and 1.3 mg/100 g FW, respectively, whereas that on the phenolic acids (chlorogenic acid and caffeic acid) had T 1% ('Idared') and T 5% ('Fuji'). Addition of T 1% had the highest impact on flavonol preservation in both apple cultivars. Flavonols were present in the ranges from 6.0 to 10.2 mg/100 g FW and from 1.2 to 12.5 mg/100 g FW in 'Idared' and 'Fuji' apple samples, respectively. Rutin accounted for most of the flavonols, 4.6−8.0 and 0.4−11.0 mg/100 g FW in 'Idared' and 'Fuji' apple samples, respectively. Results obtained by an HPLC method showed that the samples in which T 1% was added had the highest levels of polyphenols in both apple cultivars 'Idared' and 'Fuji' (16.3 and 13.7 mg/100 g FW, respectively).

In the frozen samples after 6 months of storage, a different polyphenolic profile was identified (Table 5). It consists only of quercetin glycosides, of which rutin had the largest share. It can be seen that samples of both apple varieties, 'Idared' and 'Fuji', had the highest proportion of quercetin glycosides with addition of T 5% (12.2 and 16.7 mg/100 g FW, respectively) detected by HPLC.

As in the case of apple samples without sugars, there was an increase of AOA measured with the ABTS method during storage in all 'Idared' apple samples, whereas in 'Fuji' apple samples the increase of AOA during storage was noted in

Table 5. Polyphenolic Profile of Frozen Apple Purée with Addition of Sugars after 6 Months of Storage (Milligrams per 100 g FW)[a]

		control	5S	1S	5G	1G	5F	1F	5T	1T
					'Idared'					
quercetin glycosides[b]	rutin	7.28 ± 0.008e	9.23 ± 0.021a	5.33 ± 0.011g	8.17 ± 0.021c	4.07 ± 0.014h	7.68 ± 0.016d	5.85 ± 0.011f	9.21 ± 0.021a	8.44 ± 0.017b
	23.867	0.53 ± 0.001e	0.74 ± 0.005c	0.31 ± 0.004i	0.38 ± 0.006h	0.43 ± 0.004g	0.71 ± 0.004d	0.46 ± 0.004f	1.06 ± 0.009a	0.81 ± 0.003b
	24.664	nd[c]	0.67 ± 0.010b	nd	nd	nd	nd	nd	nd	1.40 ± 0.010a
	24.912	0.96 ± 0.009b	nd	0.81 ± 0.003e	0.73 ± 0.001g	0.90 ± 0.009d	1.24 ± 0.001a	0.74 ± 0.006f	0.92 ± 0.001c	0.73 ± 0.004g
	25.213	nd	0.58 ± 0.009bc	nd	nd	0.41 ± 0.001c	0.76 ± 0.005ab	0.75 ± 0.008ab	0.99 ± 0.001a	nd
					'Fuji'					
quercetin glycosides[b]	rutin	5.01 ± 0.021h	10.10 ± 0.027b	7.25 ± 0.015f	8.23 ± 0.012d	7.98 ± 0.018e	5.46 ± 0.015g	8.25 ± 0.018d	15.36 ± 0.021a	9.10 ± 0.025c
	23.867	0.48 ± 0.005de	0.55 ± 0.009c	0.33 ± 0.005g	0.49 ± 0.004d	0.47 ± 0.005e	0.33 ± 0.014g	0.60 ± 0.011b	0.42 ± 0.017f	0.79 ± 0.003a
	24.664	nd	nd	nd	nd	0.18 ± 0.001b	nd	nd	nd	0.20 ± 0.004a
	24.912	0.46 ± 0.002h	0.70 ± 0.001d	0.43 ± 0.006i	0.60 ± 0.004e	0.81 ± 0.003c	0.52 ± 0.001g	0.87 ± 0.007b	0.57 ± 0.001f	1.36 ± 0.016a
	25.213	0.35 ± 0.001d	0.45 ± 0.001c	0.20 ± 0.004e	0.36 ± 0.003d	0.35 ± 0.003d	0.44 ± 0.009c	0.51 ± 0.005b	0.36 ± 0.001d	0.61 ± 0.008a

[a]Each value is expressed as the mean ± standard deviation ($n = 3$). Within the same row, means followed by different letters are significantly different at $p \leq 0.05$ (ANOVA, Fisher's LSD). [b]Quercetin glycoside retention time peaks of quercetin-3-glucoside, galactoside, arabinoside, xyloside, and rhamnoside. [c]nd, not detectable.

dx.doi.org/10.1021/jf405003u | J. Agric. Food Chem. 2014, 62, 1674−1682

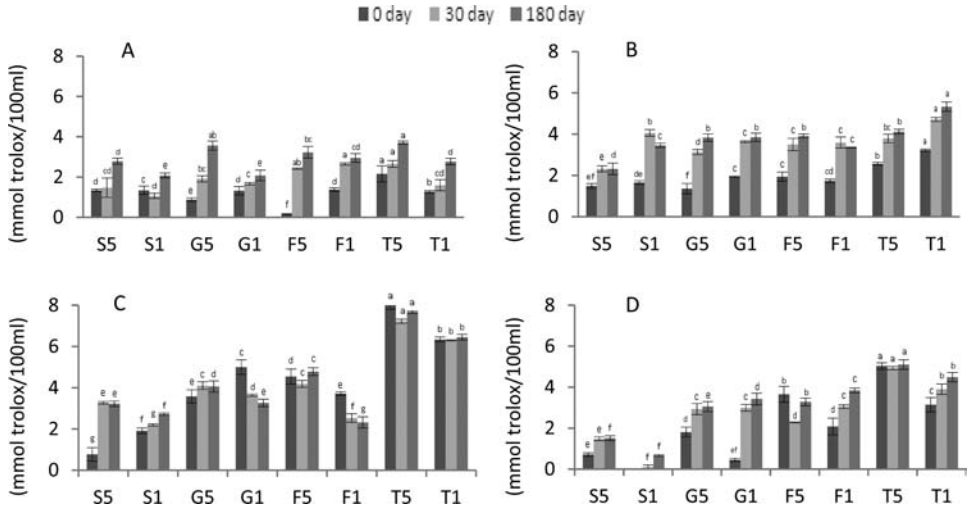

Figure 2. Antioxidative activity measured with ABTS method (mmol trolox/100 mL) for 'Idared' frozen (A) and freeze-dried (B) and 'Fuji' frozen (C) and freeze-dried (D) (S, sucrose; G, glucose; F, fructose; T, trehalose; 5, 5%; 1, 1%): black bars, immediately after preparation; light gray bars, after 3 months of storage; dark gray bars, after 6 months of storage. Each value is expressed as the mean ± standard deviation (n = 3). Among the different sugars within the same period of storage, different letters are significantly different at $p \leq 0.05$ (ANOVA, Fisher's LSD).

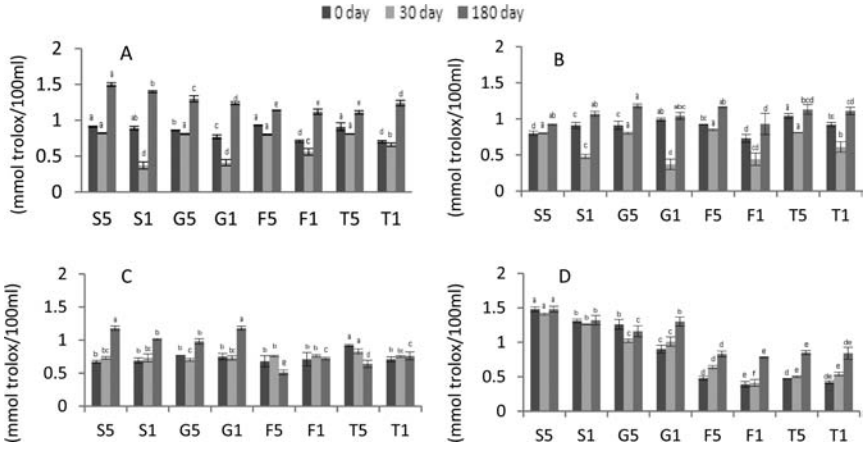

Figure 3. Antioxidative activity measured with DPPH method (mmol trolox/100 mL) for 'Idared' frozen (A) and freeze-dried (B) and 'Fuji' frozen (C) and freeze-dried (D) (S, sucrose; G, glucose; F, fructose; T, trehalose; 5, 5%; 1, 1%): black bars, immediately after preparation; light gray bars, after 3 months of storage; dark gray bars, after 6 months of storage. Each value is expressed as the mean ± standard deviation (n = 3). Among the different sugars within the same period of storage, different letters are significantly different at $p \leq 0.05$ (ANOVA, Fisher's LSD).

samples with addition of S 5%, S 1%, and G 5%. In frozen 'Idared' apple purée, antioxidative activity was the highest in the samples with an addition of T 5% and in freeze-dried samples with an addition of T 1% (3.71 and 5.33 mmol trolox/100 mL, respectively). Those results are equivalent to polyphenol content measured by HPLC.[51] The highest antioxidative activities measured in 'Fuji' apple purée with the addition of T 5%, in both frozen and freeze-dried samples, were 6.7 and 5.1 mmol trolox/100 mL, respectively. With addition of sucrose the AOA in freeze-dried 'Fuji' apple samples decreased (Figure 2).

During the first 30 days of frozen and freeze-dried 'Idared' apple purée storage, high AOA preservation after addition of S 5%, G 5%, F 5%, and T 5% was noted. In frozen 'Fuji' apple purée during the first 30 days of storage the highest preservation of AOA was noted in samples with added T 5%. However, in freeze-dried 'Fuji' apple purée during the first 30 days of storage the highest preservation ability of AOA was noted in samples with added S 5%. After the storage, the highest AOA in both frozen and freeze-dried 'Fuji' and 'Idared' apple purées was with addition of S 5% and G 5%, respectively (Figure 3).

In this study, the highest effect on polyphenol retention in freeze-dried apple purées was observed in the samples with addition of T 1%, whereas in frozen samples higher preservation of polyphenols was in samples with addition of T 5%.

The difference in the extent of the effect of sugars on TPC and AOA preservation in the particular apple variety could also depend on the complex apple matrix. In such complex natural systems, in which the presence of other compounds can lead to numerous reactions, the stability of the system will be limited by the extent to which physicochemical reactions can occur. Because the degradation mechanisms of polyphenols in the presence of sugars are still unknown, further investigations on processing (in this case freezing and freeze-drying) that induce degradation of polyphenols and the effect of different sugars on its preservation are needed.

AUTHOR INFORMATION

Corresponding Author

*(A.L.) Phone: (385) 91 576 6066. Fax: (385) 31 207 115. E-mail: ante.loncaric@ptfos.hr.

Funding
This research was supported by the Croatian Ministry of Science, Education and Sport.

Notes
The authors declare no competing financial interest.

■ ACKNOWLEDGMENTS

We thank the Agricultural Institute (Osijek, Croatia) for providing the raw materials required for experiments. We also thank Hayashibara Co. for providing a trehalose.

■ ABBREVIATION USED

TPC, total polyphenol content; AOA, antioxidant activity; ABTS, 2,2′-azinobis(3-ethylbenzothiazoline-6-sulfonate); DPPH, 2,2-diphenyl-1-picrylhydrazyl; DCPIP, 2,6-dichlorophenol indophenols

■ REFERENCES

(1) Chodak, A. D.; Tarko, T.; Satora, P.; Sroka, P.; Yński, T. T. The profile of polyphenols and antioxidant properties of selected apple cultivars grown in Poland. *J. Fruit Ornamental Plant Res.* **2010**, *18*, 39−50.

(2) Henríquez, C.; Speisky, H.; Chiffelle, I.; Valenzuela, T.; Araya, M.; Simpson, R.; Almonacid, S. Development of an ingredient containing apple peel, as a source of polyphenols and dietary fiber. *J. Food Sci.* **2010**, *75*, H172−H181.

(3) Valdenegro, M.; Henríquez, C.; Lutz, M.; Almonacid, S.; Simpson, R. Apple peels, a promising value-added food ingredient. *Food Innovation* **2010**, 1−3.

(4) Zhang, G.; Ji, B.; Chen, G. Antioxidant activities and phenolic composition of apple peel, core and flesh extracts on selected apple cultivars. *Adv. Mater. Res.* **2012**, *554- 556*, 1103−1109.

(5) Wolfe, K.; Wu, X.; Liu, R. H. Antioxidant activity of apple peels. *J. Agric. Food Chem.* **2003**, *51*, 609−614.

(6) Boyer, J.; Liu, R. H. Apple phytochemicals and their health benefits. *J. Nutr.* **2004**, *3* (5), 1−15.

(7) Qing, L. W.; Khanizadeh, S.; Clément, V. Preharvest ways of enhancing the phytochemical content of fruits and vegetables. *Stewart Postharvest Rev.* **2007**, *3*, 1−8.

(8) Khanizadeh, S.; Ding, L.; Tsao, R.; Rekika, D.; Yang, R.; Charles, M.-T.; Vigneault, C.; Vasantha Rupasinghe, H. P. Phytochemical distribution among selected advanced apple genotypes developed for fresh market and processing. *J. Agric. Food Environ. Sci.* **2007**, *1*.

(9) Van Sluis, A. A.; Dekker, M.; Skrede, G.; Jongen, W. M. F. Activity and concentration of polyphenolic antioxidants in apple juice. 1. Effect of existing production methods. *J. Agric. Food Chem.* **2002**, *50*, 7211−7219.

(10) Mahdavi, R.; Nikniaz, Z.; Rafraf, M.; Jouyban, A. Determination and comparison of total polyphenol and vitamin C contents of natural fresh and commercial fruit juices. *Pakistan J. Nutr.* **2010**, *9*, 968−972.

(11) Häkkinen, S. H.; Kärenlampi, S. O.; Mykkänen, H. M.; Törrönen, A. R. Influence of domestic processing and storage on flavonol contents in berries. *J. Agric. Food Chem.* **2000**, *48*, 2960−2965.

(12) Markowski, J.; Płocharski, W. Determination of phenolic compounds in apples and processed apple products. *J. Fruit Ornam. Plant Res.* **2006**, *14*, 133−142.

(13) Burda, S.; Oleszek, W.; Lee, C. Y. Phenolic compounds and their changes in apples during maturation and cold storage. *J. Agric. Food Chem.* **1990**, *38*, 945−948.

(14) Van Sluis, A. A.; Dekker, M.; De Jager, A.; Jongen, W. M. F. Activity and concentration of polyphenolic antioxidants in apple, effect of cultivar, harvest year, and storage conditions. *J. Agric. Food Chem.* **2001**, *49*, 3606−3613.

(15) Napolitano, A.; Cascone, A.; Graziani, G.; Ferracane, R.; Scalfi, L.; Di Vaio, C.; Ritieni, A.; Fogliano, V. Influence of variety and storage on the polyphenol composition of apple flesh. *J. Agric. Food Chem.* **2004**, *52*, 6526−6531.

(16) Golding, J. B.; Mcglasson, W. B.; Wyllie, S. G.; Leach, D. N. Fate of apple peel phenolics during cool storage. *J. Agric. Food Chem.* **2001**, *49*, 2283−2289.

(17) Mareczek, A.; Leja, M.; Ben, J. Total phenolics, anthocyanins and antioxidant activity in the peel of the stored apples. *J. Fruit Ornamental Plant Res.* **2000**, *8*, 59−64.

(18) Awad, M. A.; De Jager, A. Flavonoid and chlorogenic acid concentrations in skin of 'Jonagold' and 'Elstar' apples during and after regular and ultra low oxygen storage. *Postharvest Biol. Technol.* **2000**, *20*, 15−24.

(19) Lattanzio, V.; Di Venere, D.; Linsalata, V.; Bertolini, P.; Ippolito, A.; Salerno, M. Low temperature metabolism of apple phenolics and quiescence of *Phlyctaena vagabunda*. *J. Agric. Food Chem.* **2001**, *49*, 5817−5821.

(20) Kozłowicz, K.; Kluza, F. Experimental characteristics of freezing of apple-pear purée with sweetening substances addition. *Acta Agrophys.* **2006**, *7*, 105−112.

(21) Genin, N.; René, F. Analyse du rôle de la transition vitreuse dans les procédés de conservation agroalimentaires. *J. Food Eng* **1995**, *26*, 391−408.

(22) Desai, K. G. H.; Park, H. J. Recent developments in microencapsulation of food ingredients. *Dry Technol.* **2005**, *23*, 1361−1394.

(23) Denis, M. C.; Furtos, A.; Dudonne, S.; Montoudis, A.; Garofalo, C.; Desjardins, Y.; Delvin, E.; Levy, E. Apple peel polyphenols and their beneficial actions on oxidative stress and inflammation. *PLoS One* **2013**, *8*, e53725.

(24) Balasundram, N.; Sundram, K.; Samman, S. Phenolic compounds in plants and agri-industrial by-products, antioxidant activity, occurrence, and potential uses. *Food Chem.* **2006**, *99*, 191−203.

(25) Komes, D.; Lovric, T.; Kovacevic Ganic, K. Aroma of dehydrated pear products. *LWT−Food Sci. Technol.* **2007**, *40*, 1578−1586.

(26) Kopjar, M.; Pilizota, V.; Hribar, J.; Simcic, M.; Zlatic, E.; Nedic Tiban, N. Influence of trehalose addition and storage conditions on the quality of strawberry cream filling. *J. Food Eng.* **2008**, *87*, 341−350.

(27) Egan, H.; Kirk, R.; Sawyer, R. The Luff Schoorl method. Sugars and preserves. In *Pearson's Chemical Analysis of Foods*, 8th ed.; Longman Scientific and Technical: Harlow, UK, 1981; pp 152−153.

(28) Tee, E. S.; Siti Mizura, S.; Kuladevan, R.; Young, S. I.; Khor, S. C.; Chin, S. K. *Laboratory Procedures in Nutrient Analysis of Foods*; Tee, E. S., Siti Mizura, S., Kuladevan, R., Young, S. I., Khor, S. C., Chin, S. K., Eds.; Division of Human Nutrition, Institute for Medical Research: Kuala Lumpur, Malaysia, 1987; pp 47−54.

(29) Ough, C. S.; Amerine, M. A. Phenolic compounds. In *Methods for Analysis of Musts and Wines*; Ough, C. S., Amarine, M. A., Eds.; Wiley: New York, 1998; pp 196−221.

(30) Arnao, M. B.; Cano, A.; Acosta, M. The hydrophilic and lipophilic contribution to total antioxidant activity. *Food Chem.* **2001**, *73*, 239−244.

(31) Brand-Williams, W.; Cuvelier, M. E.; Berset, C. Use of a free radical method to evaluate antioxidant activity. *Lebensm. Wiss. Technol.* **1995**, *28*, 25−30.

(32) Jakobek, L.; Šeruga, M.; Novak, L.; Medvidović-Kosanović, M. Flavonols, phenolic acids and antioxidant activity of some red fruit. *Dtsch. Lebensm.-Rundsch.* **2007**, *103*, 369−378.

(33) Planchon, V.; Lateur, M.; Dupont, P.; Lognay, G. Ascorbic acid level of Belgian apple genetic resources. *Sci. Hortic.* **2004**, *100*, 51−61.

(34) Mikulic, P. M.; Stampar, F.; Veberic, R. Parameters of inner quality of the apple scab resistant and susceptible apple cultivars *Malus domestica* Borkh. *Sci. Hortic.* **2007**, *114*, 37−44.

(35) Vieira, F. G. K.; Borges, G. D. S. C.; Copetti, C.; Amboni, R. D. D. M. C.; Denardi, F.; Fett, R. Physico-chemical and antioxidant properties of six apple cultivars *Malus domestica* Borkh, grown in southern Brazil. *Sci. Hortic.* **2009**, *122*, 421−425.

(36) Ayala-Zavala, J. F.; Rosas-Dominguez, C.; Vega-Vega, V.; Gonzalez-Aguilar, G. A. Antioxidant enrichment and antimicrobial

protection of fresh-cut fruits using their own byproducts, looking for integral exploitation. *J. Food Sci.* **2010**, *75*, R175−R181.
(37) Ki Won, L.; Young, J. K.; Dae-Ok, K.; Hyong, J. L.; Chang, Y. L. Major phenolics in apple and their contribution to the total antioxidant capacity. *J. Agric. Food Chem.* **2003**, *51*, 6516−6520.
(38) Carbone, K.; Giannini, B.; Picchi, V.; Lo Scalzo, R.; Cecchini, F. Phenolic composition and free radical scavenging activity of different apple varieties in relation to the cultivar, tissue type and storage. *Food Chem.* **2011**, *127*, 493−500.
(39) Ceymann, M.; Arrigoni, E.; Scharer, H.; Bozzinising, A.; Hurrell, R. F. Identification of apples rich in health-promoting flavan-3-ols and phenolic acids by measuring the polyphenol profile. *J. Food Compos. Anal.* **2012**, *26*, 128−135.
(40) Lamperi, L.; Chiuminatto, U.; Cincinelli, A.; Galvan, P.; Giordani, E.; Lepri, L.; Del Bubba, M. Polyphenol levels and free radical scavenging activities of four apple cultivars from integrated and organic farming in different Italian areas. *J. Agric. Food Chem.* **2008**, *56*, 6536−6546.
(41) De Ancos, B.; Gonzlez, E. M.; Pilar Cano, M. Ellagic acid, vitamin C, and total phenolic contents and radical scavenging capacity affected by freezing and frozen storage in raspberry fruit. *J. Agric. Food Chem.* **2000**, *48*, 4565−4570.
(42) Nanjo, F.; Mori, M.; Goto, K.; Hara, Y. Radical scavenging activity of tea catechines and their related compounds. *Biosci., Biotechnol., Biochem.* **1999**, *63*, 1621−1623.
(43) Yokozawa, T.; Chen, C. P.; Dong, E.; Tanaka, T.; Nonaka, G.-I.; Nishioka, I. Study on the inhibitory effect of tannins and flavonoids against 1,1-diphenyl-2-picrylhydrazyl radical. *Biochem. Pharmacol.* **1998**, *56*, 213−222.
(44) Roginsky, V.; Lissi, E. A. Review of methods to determine chain-breaking antioxidant activity in food. *Food Chem.* **2005**, *92*, 235−254.
(45) Arts, M. J. T. J.; Dallinga, J. S.; Voss, H. O.; Haenen, G. R. M. M.; Bast, A. Critical appraisals of the use of antioxidant capacity (TEAC) assay in defining optimal antioxidant structures. *Food Chem.* **2003**, *80*, 409−414.
(46) Malien-Aubert, C.; Dangles, O.; Amiot, M. J. Color stability of commercial anthocyanin-based extracts in relation to the phenolic composition. Protective effects by intra- and intermolecular copigmentation. *J. Agric. Food Chem.* **2001**, *49*, 170−176.
(47) Dyrby, M.; Westergaard, N.; Stapelfeldt, H. Light and heat sensitivity of red cabbage extract in soft drink model systems. *Food Chem.* **2001**, *72*, 431−437.
(48) Hubbermann, E. M.; Heins, A.; Stockmann, H.; Schwarz, K. Influence of acids, salt, sugars and hydrocolloids on the colour stability of anthocyanin rich black currant and elderberry concentrates. *Eur. Food Res. Technol.* **2006**, *223*, 83−90.
(49) Ścibisz, I.; Mitek, M. Effect of processing and storage conditions on phenolic compounds and antioxidant capacity of highbush blueberry jams. *Pol. J. Food Nutr. Sci.* **2009**, *59*, 45−52.
(50) Kopjar, M.; Nedic Tiban, N.; Pilizota, V.; Babic, J. Stability of anthocyanins, phenols and free radical scavenging activity through sugar addition during frozen storage of blackberries. *J. Food Process. Preserv.* **2009**, *33*, 1−11.
(51) Escarpa, A.; González, M. C. Approach to the content of total extractable phenolic compounds from different food samples by comparison of chromatographic and spectrophotometric methods. *Anal. Chim. Acta* **2001**, *427*, 119−127.

oil−water interface plays an important role in the stability of the resultant emulsion.[18] The pH-shifting process, namely, subjecting the protein solution to an extreme acidic or alkaline pH condition and then to a neutral pH environment, allows the protein to undergo partial unfolding and then refolding to assume a molten globule conformation that has unique surface properties.[19] In our previous investigation, we applied the pH-shifting process to modify the structure of soy globulins for improved functionality. We showed that glycinin and β-conglycinin globulins subjected to such treatments lose much of their tertiary structure but retain considerable amounts of α-helical structure, embodying a molten globule state.[18,20] Typically, flexible polymers often assume "train", "loop", and "tail" configurations at the oil−water interface.[21] The tails and loops have the propensity to protrude into the aqueous phase, and the segments in the train configuration anchor into the lipid phase.[22] Both β-conglycinin (7S) and glycinin (11S) after the pH-shifting treatment appear to resume such an interfacial configuration.[23] The shear force during emulsion preparation is another important factor affecting protein load to the oil−water interface.[24] By varying the operating pressure and the geometry of the pressure cell, a certain shear force is generated to produce emulsion droplets with different sizes, thereby allowing the investigation of interfacial distribution of proteins and their possible role as antioxidants.

Pea protein, an emerging agricultural product, has great potential as a functional ingredient in the food industry.[25] Pea protein is relatively low in sulfur-containing amino acids but otherwise has an amino acid profile similar to that of other commonly consumed legumes.[26,27] According to Aluko et al.,[28] pea protein is a better emulsifier and foaming agent than soy protein at neutral pH. Proteins forming the interfacial membrane may act as a physical barrier that separates lipid molecules from pro-oxidants in the aqueous phase. Hence, the structure of adsorbed proteins and the droplet size influence the rate of lipid oxidation. On the other hand, the chemical nature of the antioxidant mechanism, including neutralization of radicals and chelation of metal ions by reactive amino acid residue side-chain groups, would further complement the physical effect and enhance the overall antioxidant activity of proteins.

The purpose of the present study was to test the hypothesis that structural modification aimed at improving protein interfacial adsorption and biophysical behavior can give rise to an O/W emulsion that is less prone to oxidation. Because pea protein having a molten globule structure induced by pH-shifting treatment is able to adsorb efficiently at the oil−water interface, it was used as the model protein surfactant. Here, we describe the evidence that physical barriers formed around oil droplets contribute to the overall oxidative stability of O/W emulsions.

MATERIALS AND METHODS

Materials. Pea protein isolate (PPI) was prepared from yellow field pea seeds (*Pisum sativum*) purchased from a local supermarket. Peas were milled and protein was extracted from the milled flour in 10 volumes (v/w) of a pH 8.0 solution and then precipitated by adjusting the pH to 4.5 as described previously.[23] The isoelectrically precipitated protein was redissolved by bringing the solution pH to 7.0 and lyophilized. All chemicals used were reagent or higher grade purchased from Sigma Chemicals (St. Louis, MO) or Fisher Scientific (Pittsburgh, PA).

pH-Shifting Treatment. Structurally modified protein was prepared by alkaline pH treatment as described previously.[23] Briefly, PPI (20 mg/mL, pH 7.0) solution was titrated to pH 12 with 2 M NaOH at 20 °C, held at this pH for 1 h to induce partial unfolding, and then titrated back to 7.0 with 2 N HCl to allow refolding. The residual salt was negligible (<0.03 in ionic strength) and therefore was not removed before lyophilization. This alkaline pH-treated sample was referred to as "APP", and the untreated (native) protein was defined as "NPP".

Evaluation of Antioxidant Activity. The prepared APP and NPP as comparison were subjected to the ABTS [2,2′-azinobis(3-ethylbenzothiazoline-6-sulfonic acid)] assay[29] to establish radical-quenching capability and the TBARS (thiobarbituric acid-reactive substances) analysis to validate the efficacy in a liposome system. The liposome was prepared from 0.2 mg/mL soybean phosphatidylcholine by sonication.[30] Prepared liposome was mixed with 3 mg/mL APP and NPP, stored in the dark at 37 °C, and analyzed for TBARS production during storage using the colorimetric thiobarbituric acid−malonaldehyde adduct assay.[31]

In addition, transmission electron microscopy (TEM) was applied to delineate the structural feature of liposome that might indicate the physical protective action of proteins under oxidative stress. Accordingly, one drop of liposome solution and one drop of staining solution (2% phosphotungstic acid) were applied onto a copper grid with 200 mesh and allowed to stabilize for 10 min. Images were captured using an ES500W Erlangshen charge-coupled device (CCD) camera (Gatan, Inc., Pleasanton, CA) mounted to a JEM-2100 electron microscope (JEOL, Tokyo, Japan).

Emulsion Preparation. Oil-in-water (O/W) emulsions were prepared from the mixture of 25% (v/v) sunflower oil and 75% (v/v) 10 mg/mL PPI (pH adjusted to 7.0 by titration) by initial dispersion with an Ultra-Turrax blender (Ika T18 Basic, Staufen, Germany) at 13 500 rpm for three bursts of 40 s each and then by homogenization twice with a high-pressure homogenizer at three pressure levels (30, 70, and 120 MPa) (AH2010, ATS Engineering, Inc., Shanghai, China). To prevent microbial growth, sodium azide (3 mM) was added to all samples.

Microstructure of Emulsion Droplets. Confocal laser scanning microscopy (CLSM) was applied to visualize the microstructure of emulsions and evidence the formation of protein coating around lipid droplets.[32] The oil phase in the emulsions was stained with Nile Red dye (0.1%), and the protein was stained with fluorescein isothiocyanate dye (0.1%). The dye-treated samples were placed in small cylindrical containers (10 μL) and kept in the dark for 20 min. Fluorescence was produced by excitation with a blue light (488 nm) and emission in the green region (514 nm) using a model LSM 710 CLSM machine (Carl Zeiss AG, Dresden, Germany).

Distribution and Characteristics of Interfacial Proteins. Emulsions were centrifuged at 15 000*g* for 30 min. After the removal of the cream phase (upper), the subnatant (serum) was collected and filtered through 0.22 μm pores (Stericup-GV, Minipore) to analyze the unadsorbed protein. The amount of protein present in the original cream phase and that in the serum were measured using Lowry's method. The distribution coefficient was calculated from the equation $[1 - (W_a/W_t)] \times 100\%$, where W_a is the protein (mg) in the aqueous phase and W_t is the total amount of protein (mg) in the emulsion. The cream phase was suspended in deionized water (equivalent in volume to the original serum phase) by gently stirring and then centrifuged under the same condition as described previously to recover the interfacial proteins.

The washed cream was then spread onto a Whatman No. 50 filter to dewater. The dehydrated cream containing membrane (adsorbed) proteins, as well as the serum proteins collected, were submitted to sodium dodecyl sulfate−polyacrylamide gel electrophoresis (SDS−PAGE) to identify the composition of adsorbed proteins in the emulsions according to Laemmli using a 3% acrylamide stacking gel and 10% acrylamide separation gel.[33] Both the serum and cream samples were dissolved in an equal volume of SDS−PAGE sample buffer; the protein concentration was not standardized so that the relative distribution of polypeptides between the samples can be compared.

Emulsion Droplet Stability. Because the O/W emulsions made with APP and NPP under different pressure conditions would have different particle sizes, they might vary in flocculation behavior during storage and affect the oxidative stability. To test the tendency to flocculate, emulsion samples were placed in test tubes (22 mm diameter × 43 mm height) sealed with Teflon-coated caps and kept in the dark in a 37 °C incubator to track the formation of the cream layer during storage up to 14 days. The droplet size (d_{32}) of the emulsion samples taken at different times, after 10-fold dilution with deionized water, was measured using a Mastersizer Nano-ZS instrument (Malvern Instruments, Worcestershire, U.K.).

Whipped Cream Characterization. Whipped creams are products commonly prepared from tempered O/W emulsions. To investigate the influence of the type of protein surfactants (APP versus NPP) on the physical characteristics of such products, cream-type emulsions were prepared from the mixture of 18% hydrogenated palm oil, 16% corn syrup, 1% sodium caseinate, 0.2% xanthan, 0.1% guar gums, and 2% pea protein. The mixture was homogenized at 30 MPa as previously described, and the resultant emulsions were quickly frozen (−18 °C), thawed at 4 °C, and then blended with a KitchenAid to produce whipped creams.

For microstructural evaluation, the procedure described by Chang and Hartel was followed.[34] Briefly, samples of whipped creams placed in specimen capsules were quickly frozen by immersion in liquid nitrogen (−198 °C) and then fractured with a knife. Sublimation of ice crystals occurred under high vacuum at −115 °C. The cryo-etched samples were sputter-coated with gold and then observed in a model S-4800 Hitachi cryo-scanning electron microscope (SEM) (Tokyo, Japan).

Emulsion Oxidative Stability. We have previously shown that alkaline pH-treated soy protein, which has a markedly increased surface hydrophobicity, adsorbs more efficiently than native soy protein to the oil−water interface.[18] The peptide segments showing strong hydrophobicity have a propensity to stabilize radicals.[35] Therefore, we surmised that APP would contribute to the oxidative stability of emulsions and tested the hypothesis on stored emulsion samples. Freshly prepared emulsions were placed in Teflon-capped test tubes and incubated in the dark at 37 °C for different time periods up to 14 days. The primary and secondary products of lipid oxidation were measured as peroxides (POV) and TBARS using the procedures of AOCS[36] and Mei et al.,[31] respectively.

Statistical Analysis. The experiment was replicated 3 times (n = 3) as independent trials each with triplicate sample analyses. Data were subjected to analysis of variance using the linear model procedure of the Statistix software 9.0 (Analytical Software, Tallahassee, FL). Significant differences (P < 0.05) between means were identified by Tukey HSD all-pairwise multiple comparisons.

RESULTS AND DISCUSSION

Evidence of Antioxidative Activity of APP. When exposed to varying pH conditions, proteins undergo conformational and spectroscopic changes, a process referred to as the Tanford transition.[37] For example, shifting the pH by as little as 2 units can alter ligand-binding (and -releasing) efficiency of β-lactoglobulin due to protein structural change.[38] Upon the extreme alkaline pH (12) process, the surface hydrophobicity of resulting pea protein (APP) increased by 62% (result not shown), indicating the exposure of nonpolar amino acid residue side-chains and the attainment of a molten globule state.[18] According to Pownall et al.,[35] hydrophobic amino acids account for 40.6% of total pea protein content, and the peptide segments rich in hydrophobic and aromatic amino acids (i.e., Pro, Val, Leu, Ile, and Phe) have particularly strong radical-scavenging and metal-chelating activities. For intact proteins, His, Arg, Lys, Pro, Met, and Cys are the most common targets of oxidants due to their easy accessibility.[39] Yet, once unfolded, newly exposed hydrophobic amino acids could readily react with radicals, and, by virtue of stabilizing radicals, they accomplish the role as sacrificing antioxidants. Indeed, based on the ABTS$^{\bullet+}$ scavenging assay, antiradical activity of APP is 60% greater than that of NPP (Figure 1, lower panel). In

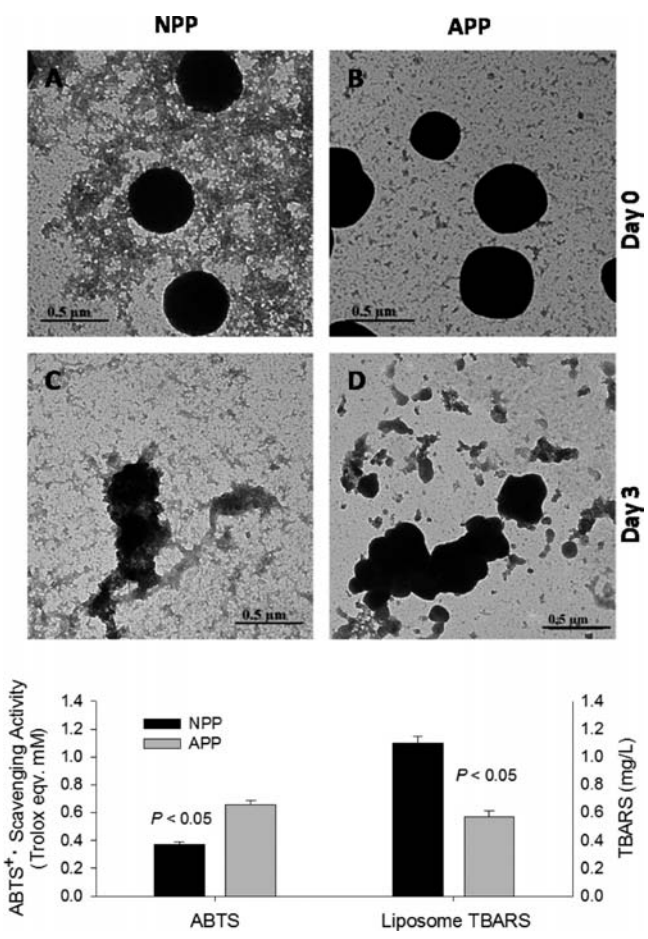

Figure 1. Transmission electron microscopic images of liposomes with native (NPP) and alkali-treated (APP) pea protein at different storage times (upper panel). Evidence of radical-scavenging activity (ABTS$^{+\bullet}$) and inhibition TBARS formation in liposome solution is shown in the lower panel.

agreement, in the oxidizing liposome model system, APP is nearly twice as effective as NPP in inhibiting the TBARS formation. Therefore, the results confirm APP as a more favorable chemical antioxidant than NPP. The stronger efficacy when compared with NPP is attributed to the protein conformational changes that expose proton/electron donors of specific hydrophobic groups.

Electron microscopy of liposome solution suggests possible physical effects of pea protein as well. Pea protein is a large globular polypeptide composed of multiple subunits.[18,35] Variations in protein−protein interaction and the effect on liposomal membrane under oxidative stress can be viewed (Figure 1, upper panel). In the process of pH-shifting, legume protein subunits are dissociated[40] and well-dispersed in aqueous solutions.[23] Therefore, proteins are largely invisible in the liposome system with APP (Figure 1B). In contrast, with their relatively intact quaternary and tertiary structures, NPP molecules in the continuous phase appear to form an interactive network surrounding liposomes (Figure 1A). The main driving force involved in the interaction between globally

dx.doi.org/10.1021/jf405190h | J. Agric. Food Chem. 2014, 62, 1683−1691

anionic liposomes and protein is believed to be electrostatic compensation, but hydrophobic contribution is also present.[41,42] In the liposome, the phosphatidylcholine head group contains a positively charged choline moiety and a negatively charged phosphate group. At pH 7.0, pea protein carries a net negative charge, and the dominant anionic groups can form charge pairing with the choline group so as to enable protein adsorption on liposomes via ionic forces. Moreover, due to the alkali-induced exposure of more nonpolar residues, hydrophobic interactions between nonpolar segments of pea polypeptides and liposome could be improved, leading to an enhanced physical protection of liposome particles against oxidation.

Because of the discrepant protein−phospholipid interaction, there are significant morphological differences between liposome particles with the presence of APP and those with NPP as well as their susceptibility to oxidation. The surface of fresh liposome particles in the NPP solution appears to be slightly rough when compared with that of liposomes dispersed in the APP solution. Liposome particles with NPP are very sensitive to oxidation, and the spherical structure is totally destroyed, forming clusters and fusion in an elongated manner, reminiscent of fibrillar aggregates (Figure 1C). While oxidized liposomes in the presence of APP also form aggregates with shrunk vesicles, some of the original structure, i.e., globes, appears to be partially preserved (Figure 1D).

Emulsion Oxidative Stability. The efficacy of APP to protect emulsions from autoxidative processes through serving as an oil droplet coating was assessed by monitoring the formation of primary (peroxides) and secondary (TBARS) products from oxidized lipids during storage. The relationship between POV (y) and storage time (x) is successfully fitted to the power-law model, $y = a(1 + x)^b$ (Figure 2, upper panel). While the a value is fairly constant, the power-law index, b, is significantly larger for emulsions prepared with NPP when compared with APP emulsions, indicating not only a greater rate but also a higher extent of autoxidation. The production of TBARS over time follows a sigmoidal curve pattern, and the most rapid accumulation of TBARS appears to occur between day 4 and day 10. Similar to the POV evolution, APP provides a stronger protection of the O/W emulsions than NPP. However, for emulsions prepared with NPP, the results are best fitted to a sigmoidal−logistic model, differing from the emulsions with APP that is perfectly fitted in a sigmoidal−Chapman equation. The subtle difference in curve fitting indicates that the mode of stabilization against oxidation has shifted and is dependent upon the protein surfactants used.

The influence of homogenization pressure on the emulsion oxidative stability cannot be ignored. In general, the most extensive autoxidation is induced at 120 MPa, whereas the difference between 30 and 70 MPa is variable and small (Figure 2). Because under the same pressure the NPP emulsion is always more susceptible to oxidation than the APP emulsion, the structure of parent proteins (i.e., before high-pressure homogenization) is an important controlling factor.[10] Aside from the elicited radical-scavenging power (Figure 1), physical shielding through increased adsorption and interfacial distribution (results described later) of the alkali-treated protein appears to impart a steric mechanism to the protection of the emulsion during storage.

As reported by Desrumaux and Marcand,[24] from 60 to 100 MPa, the viscosity and the amount of adsorbed protein in an O/W emulsion increases as the average droplet size decreases.

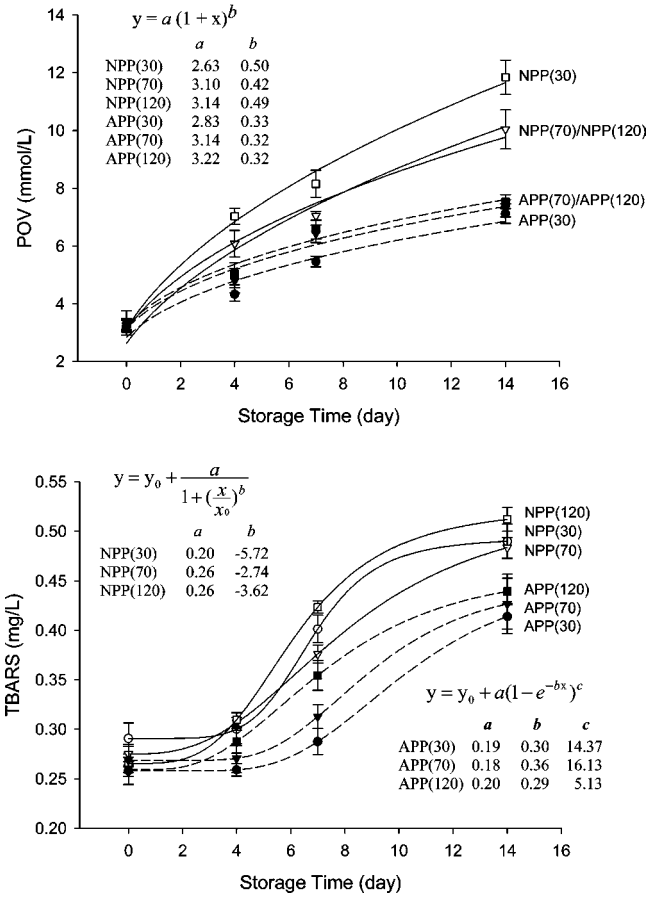

Figure 2. Oxidative stability (POV, TBARS) of O/W emulsions prepared under different pressures (values in parentheses, MPa) with native (NPP) and alkali-treated (APP) pea protein during storage (37 °C). The curves were fitted to the power-law model for POV (upper panel) and the sigmoidal−logistic/Chapman model for TBARS (lower panel).

At above 100 and up to about 210 MPa, d_{32} increases and then reaches a plateau, manifestating an "overprocessing" phenomenon. The total surface area increase due to particle size reductions leads to a rapid increase of the fraction of adsorbed proteins, i.e., a higher protein-to-lipid ratio. This also explains why the oxidative stability is improved in the presence of APP. Nakaya et al.[43] studied the oxidation of O/W emulsions with TAG and sucrose lauryl ester as the emulsifier, noting that fine-particle emulsions were more resistant to oxidation than large-particle emulsions.

CLSM. To elucidate the structural role of APP in the oxidative stability of emulsions, a series of morphological and physical analyses were performed. The CLSM image of pea protein-stabilized emulsions illuminated with two different fluorescent dyes demonstrates the coverage of oil droplets by proteins (dyed red). The microstructure of the emulsion containing NPP (Figure 3A) is very inhomogeneous. This emulsion has a broad droplet size distribution with a larger mean droplet diameter up to ~4 μm (data not shown). After 3 days of storage, many droplets form clusters with small droplets being attached to the surface of the larger ones, and some clusters appear to loosely connect with each other (Figure 3C). However, there is no apparent fusion or coalescence of the emulsion particles. In comparison, a different morphological image is observed for emulsions stabilized with APP where not

dx.doi.org/10.1021/jf405190h | J. Agric. Food Chem. 2014, 62, 1683−1691

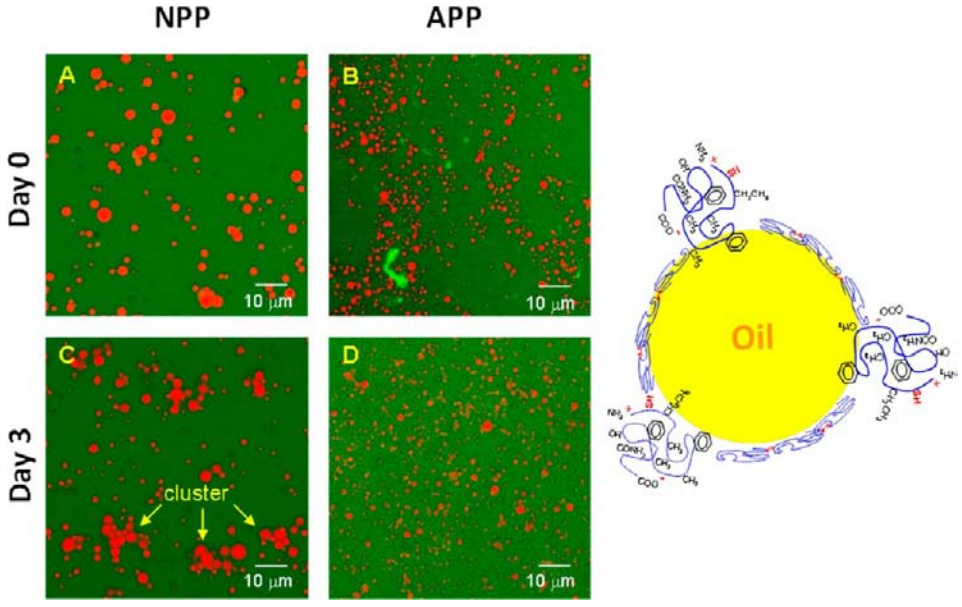

Figure 3. Representative confocal image of O/W emulsions prepared under 30 MPa with native (NPP) and alkali-treated (APP) pea protein at different storage times. The drawing on the right depicts hypothetical oil droplets with a protein membrane.

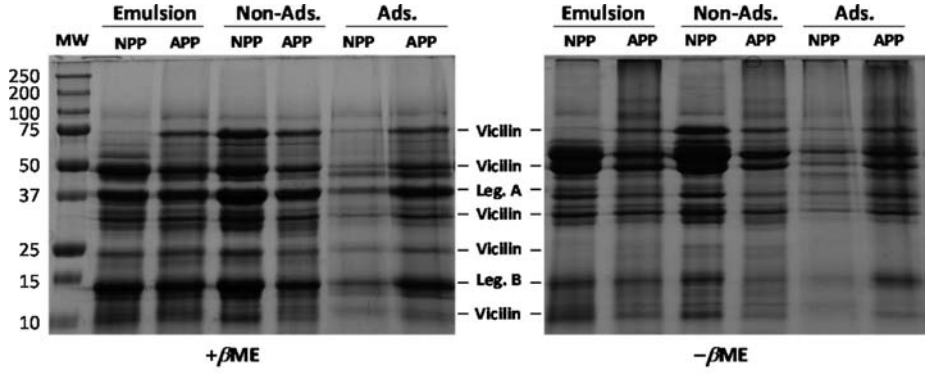

Emulsifier	Total protein (mg/mL)	Aqueous phase (%)	Cream phase (%)	Distribution coefficient
NPP	7.5	56.1	43.9	0.44
APP	7.5	33.3	66.7	0.67

Figure 4. Protein distribution in the aqueous and cream phases (lower panel) and the compositional profiles of nonadsorbed (Non-Ads.) and adsorbed (Ads.) proteins (upper panel) for O/W emulsions prepared under 30 MPa with native (NPP) and alkali-treated (APP) pea protein. MW, molecular weight (kDa); βME, β-mercaptoethanol. In each lane 30 μL of sample was loaded.

only are the oil droplets much smaller but also they are more homogeneous and uniform (Figure 3B). The result indicates a greater coating efficiency of alkali-treated (pH-shifting) protein on the oil droplets due to higher emulsifying activity, which would contribute to the oxidative stability of the O/W emulsion systems.

Furthermore, the emulsion with APP appears to be very stable, and the spherical droplets remain well-separated, showing no apparent flocculation after 3 days (Figure 3D). On the basis of our preliminary study on soy globulins, pH-shifting treatment induces a molten globular structure that has an improved surface activity and thus more efficient loading at the oil−water interface.[18] In the present case, partially unfolded pea polypeptides are more easily adsorbed to the surfaces of oil droplets through hydrophobic interactions, forming a multilayered thicker protein membrane capable of withstanding emulsion droplet coalescence when compared with the emulsion created with NPP. This would explain the improved oxidative stability of APP emulsions. Although in the present study the thickness of adsorbed protein layers is not known, Delahaije et al.,[44] using a β-lactoglobulin film model, have estimated that a film with an equilibrium thickness of ∼40 nm can form at the interface in the absence of salt. At the emulsion pH (7.0), pea legumin and vicilin carry net negative charges[45] and, therefore, will repel each other, counteracting the van der Waals attraction between membrane nonpolar groups. The greater thickness of the charged protein layer surrounding oil droplets would also compensate for the interparticle hydrophobic attraction, thereby contributing to the emulsion stability based on the DLVO theory.[46] As illustrated in the drawn diagram in Figure 3, for emulsion droplets coated with APP, the larger hydrodynamic volume of membrane molten globular

dx.doi.org/10.1021/jf405190h | J. Agric. Food Chem. 2014, 62, 1683−1691

protein molecules would impart steric hindrances to prevent particle aggregation.

Identification of Interfacial Proteins. In the process of homogenizing fat in an aqueous solution in the presence of amphiphilic molecules like proteins, a membrane quickly forms around the fat globule. This membrane acts to lower the interfacial tension (surface free energy) between oil and water and, depending on the amount of surfactant adsorbed, can increase the density of the fat globule.[10] In the emulsion prepared with NPP, 44% of the protein is distributed in the cream phase, compared to 67% for the emulsion prepared with APP (Figure 4, lower panel). The greater interfacial distribution for APP is attributed to the increased amphiphilicity of pea polypeptides as well as increased structural flexibility as a result of pH-induced structural change, similar to that observed on soy protein.[18] It must be noted, however, that the larger total surface area due to smaller droplet size for the APP emulsion should account for the greater interfacial distribution of protein.

To determine the specific polypeptides adsorbed on the fat globules, the cream phase was washed to remove unbound proteins, and the bound proteins were then desorbed and subjected to SDS−PAGE. In comparison with NPP-stabilized emulsions, significantly higher amounts (band intensity) of proteins are recovered from the membrane of APP-stabilized emulsions (Figure 4, upper panel), in agreement with the above distribution data. The more effective coverage of the fat globule by APP results in, reciprocally, lesser amounts of polypeptides in the nonadsorbed protein fraction. Because of the reduction of particle size as shown in Figure 3B, the interfacial area in APP-stabilized emulsions is larger; therefore, the protein load at the interface is higher.

An advantage of SDS−PAGE analysis is that it is possible to monitor the preferential adsorption of native and pH-treated proteins. Indeed, a detailed comparison of the electrophoretic patterns indicates discrepant protein subunit adsorptions of NPP and APP. Legumin, a hexameric protein, consists of acidic (Leg. A, 38−40 kDa) and basic (Leg. B, 19−22 kDa) peptides linked by S−S bonds.[47] Because disulfide bonds are mostly cleaved during alkaline pH treatments,[20] the dissociated legumin subunits with increased structural mobility are able to diffuse and subsequently adsorb more efficiently to the fat globule surface. A number of studies have shown that free cysteine groups participate in intra- and interdroplet sulfhydryl−disulfide interchanges during emulsification.[48,22] Comparison of the lanes of adsorbed APP (pH 12) samples shows a significant recovery of the legumin basic subunit (Leg. B) after the sample is treated with βME, suggesting that newly formed legumin polymers in APP contribute to the emulsion formation and its stability. This phenomeon is largely absent in NPP emulsions. Furthermore, the protein samples recovered from washed fat globules noticeably contain higher amounts of legumin (A and B) when compared with nonadsorbed protein, which is comprised of abundant vicilin subunits (Figure 4, $-\beta$ME). The differential adsorption is obviously promoted by pH-induced structural changes in legumin, which is a more efficient surfactant having a superior emulsifying activity over vicilin.[49]

Particle Size and Stability. The pressure applied to prepare O/W emulsions was varied to produce emulsions with different droplet sizes to enable the investigation of the influence of the protein-to-fat ratio in a given oil droplet on emulsion properties. As shown in Figure 5, while the average particle size (Sauter d_{32}) of freshly prepared emulsions is

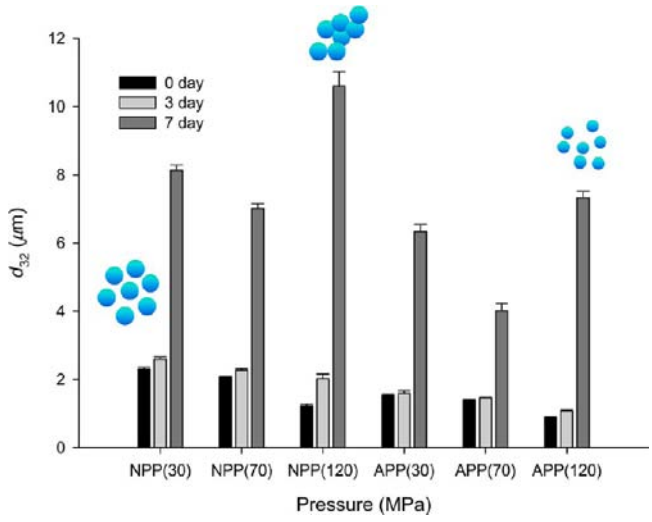

Figure 5. Average particle size (d_{32}) and storage-induced changes of O/W emulsions prepared with native (NPP) and alkali-treated (APP) pea protein under different pressures (30, 70, and 120 MPa).

reduced with increasing homogenization pressure (30 → 70 → 120 MPa), the pH treatment allows the pea protein to perform more effectively to disrupt oil into smaller droplets when compared with native protein. A smaller droplet size is obtained with a more efficient protein adsorption at the interface, and the result confirms the particle size variation observed under CLSM (Figure 3). By considering the protein distribution in the cream phase (Figure 4) and the average emulsion droplet size (Figure 5), it can be calculated that there are at least three times as many droplets (1.34×10^{10} vs 3.92×10^{9}) per mL in fresh APP emulsions (d_{32} = 1.53 μm) as in NPP emulsions (d_{32} = 2.30 μm) prepared at 30 MPa. Although the derived interfacial protein coverage based on the calculation is essentially identical (51.0 mg/m^2 for APP compared to 50.1 mg/m^2 for NPP), the substantially larger protein load per volume of an oil droplet for APP emulsions (1.99×10^{8} mg/m^3) compared to that for NPP emulsions (1.32×10^{8} mg/m^3) due to the particle size disparity would clearly favor the APP emulsion stability.

Although the mean particle size difference between freshly prepared APP and NPP emulsions is well within 1 μm, the NPP emulsion particles becomes noticeably larger during storage and the size increases 4−9-fold after 7 days, depending on the homogenization pressure. In comparison, the accretion of the APP emulsion particles is slower and the final size (by day 7) grows much less. Hydrophobic agglomeration of protein-coated oil droplets rather than fusion is responsible for the droplet size increases during storage (Figure 3). As reported by Floury et al.,[50] from 20 to 100 MPa, the diameter of whey protein-stabilized emulsion particles decreased, and, when the pressure exceeded 100 MPa, the viscosity of adsorbed protein rose significantly. The average particle sizes of the emulsions prepared with native and pH-treated pea protein at 120 MPa both increase remarkably after 7 days, ostensibly resulting from the association of the oil droplets through viscous membrane proteins.

Consequent to particle aggregation, O/W emulsions during storage are gradually separated into two phases: the cream phase (supernatant) and the serum phase (subnatant) (Figure 6). The emulsion with NPP begins showing signs of phase boundary after 1 day storage. Over the observation period, the

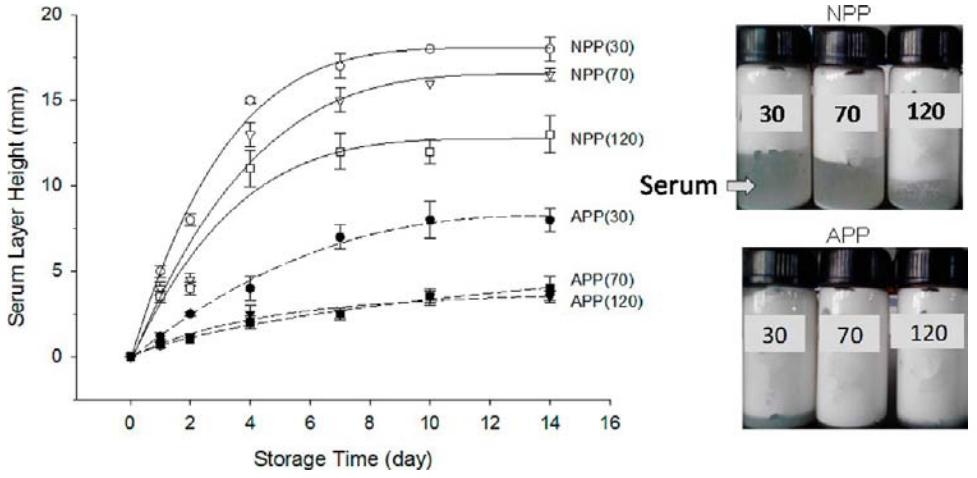

Figure 6. Storage-induced phase separation (right picture, 14 days) and resulting serum layer height (left plots) of O/W emulsions prepared with native (NPP) and alkali-treated (APP) pea protein under different pressures (30, 70, and 120 MPa).

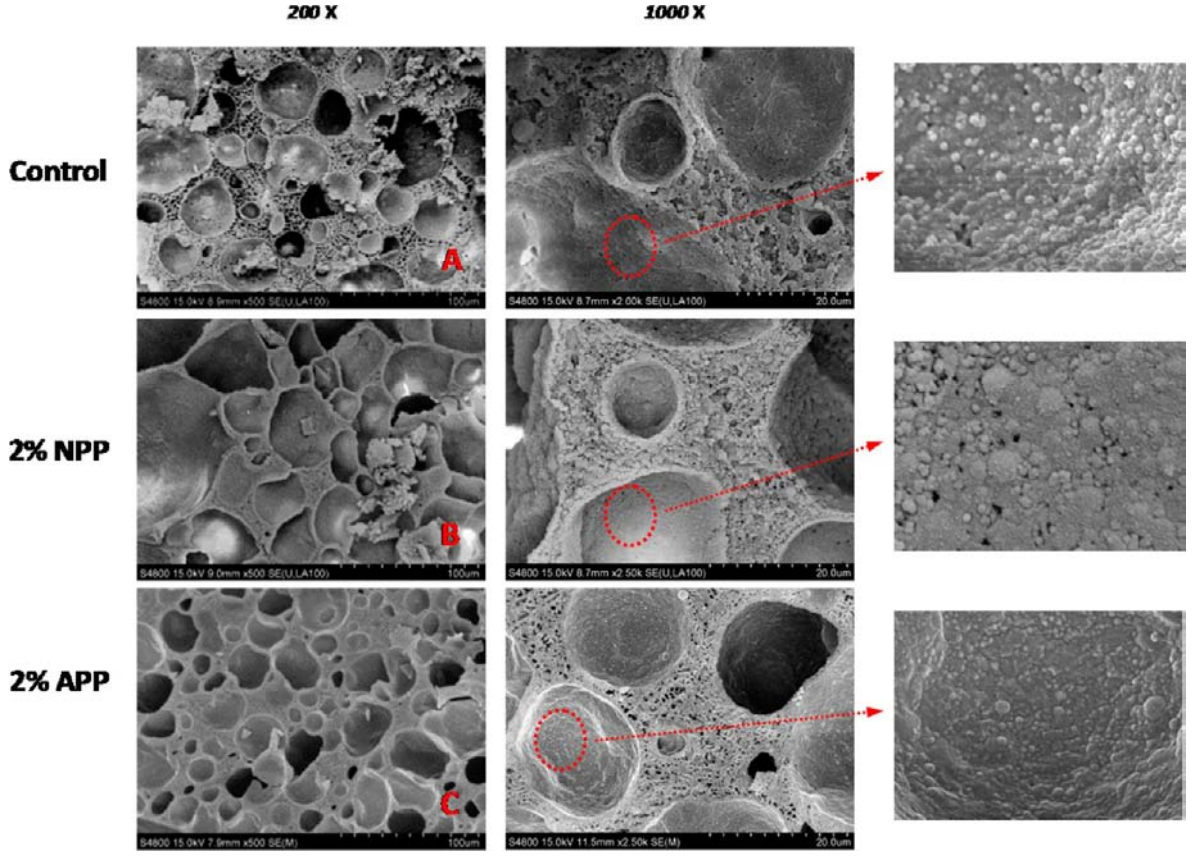

Figure 7. Cryo-scanning electron micrograph of the structure of whipped creams prepared with 18% fat without pea protein (Control); 18% fat with 2% native pea protein (NPP); and 18% fat with 2% alkali-treated pea protein (APP).

boundary line gradually becomes clearer and the height of the serum phase grows substantially within 7 days, while there is no appreciable further change between 7 and 14 days. In contrast, the emulsion with APP shows a remarkable storage stability, and the serum layer maintains a relatively low level except for samples prepared at 30 MPa, where it grows significantly taller ($P < 0.05$) after 14 days. The physical stability of a protein-based emulsion is largely attributed to the properties of the protein membrane. The fact that with APP there is a more efficient interfacial protein coverage than with NPP (Figure 4), allowing the formation of finer (Figure 5), less creaming-prone (Figure 6) and less oxidizable (Figure 2) emulsion particles, underscores the steric role of pea protein in the emulsion oxidative stability.

As also illustrated in Figure 6, the emulsion stability increases with the homogenization pressure, corresponding to the particle size reduction (Figure 5). This occurs in spite of the more rapid particle size growth in emulsions prepared at 120 MPa than in those prepared at other pressures after 7 days (Figure 5). It seems that, during storage, charge and steric repulsions are maintained between emulsion aggregates and clusters to prevent coalescence. For APP-stabilized emulsions,

dx.doi.org/10.1021/jf405190h | J. Agric. Food Chem. 2014, 62, 1683−1691

the stability is independent of the homogenization pressure at 70 and 120 MPa, suggesting that the increased particle size at 120 MPa after 7 days (Figure 5) is due to emulsion droplet flocculation. As a result of flocculation, there is an increased opportunity for the oil droplets (which ascend to the surface of the container) to be in contact with molecular oxygen. This would explain why, in the emulsion formed with NPP at 120 MPa, which consists of large particles or aggregates, there are more abundant peroxides and secondary aldehydes being produced during storage than in other emulsions (Figure 2).

Microstructure of Whipped Creams. The steric effect of pea protein at the interface was also tested in a whipped cream model system where two types of interfaces, i.e., oil−water and air−water, coexist and can influence each other. The fat content of a typical commercial whipped cream is ∼25−40% to necessitate the foam stability.[51] Foaming properties could be compromised if the fat content is reduced. In our study, we prepared whipped creams with 18% oil (which are more foamy than with a higher amount of fat) to investigate the structural role of pH-treated pea protein. Prepared emulsions after the aging, freezing, hardening, and thawing processes were blended to build a complex foam texture.

The matrix structures of three types of whipped creams (containing no added pea protein or containing 2% NPP or 2% APP) are presented in Figure 7. Each microstructure displays vivid air cells immobilized within a network consisting of protein and tiny fat globules. The control cream with 18% fat still maintains some degree of structure, but the foam stability is poor. The incorporation of NPP slightly improves the appearance of the whipped cream, but it still exhibits broad and flat large surface areas instead of regular-shaped air pockets, which are basically fracture planes along the largest dimension of the air cell. In contrast, with the presence of APP, the cream displays a uniform texture filled with air cells that are small and regular in shape. Moreover, the intricate underside of the "dome" of the air cells (pointed to by an arrow) in the APP-stabilized cream exhibits a somewhat fused layer of fat droplets immobilized with a continuous protein coating. The formation of such fat globule clusters and agglomerates in whipped creams has been described as "partial coalescence", which is responsible for surrounding and stabilizing air cells and creating a semicontinuous network or matrix of fat throughout the product.[52] Although weakening of the fat globule membrane through tempering and whipping is a necessary process for the creation of an agglomerated structure, partially coalesced fat globules with APP still maintain a superior aggregated network throughout the volume. Consequently, the air cells within the APP-fortified whipped cream are uniformly distributed and effectively entrapped. In comparison, the relatively weak adsorption of NPP at the oil−water interface seems to render the emulsion vulnerable to extensive coalescence during whipping, which is evidenced by the presence of large and discrete fat globules, resulting in a less stable cream product with numerous pinholes.

In conclusion, the properties of O/W emulsions formulated with sunflower oil and pea protein are significantly affected by the protein surfactant and the homogenization procedure that employs different pressures. The emulsions prepared with structurally modified pea protein by the alkaline pH-shifting process (APP) are distinctly more stable against coalescence and resistant to oxidation than emulsions formed with native pea protein (NPP). Evidence from confocal microscopy and electrophoresis suggests that increased adsorptions of APP molecules, particularly legumin, onto the fat globules and their accumulation at the oil−water interface are the primary mechanism for the physicochemical stability of the emulsions. High-pressure homogenization up to 70 MPa disrupts oil into fine droplets that are then stabilized by an interfacial protein coating capable of minimizing the interfacial tension and free energy. Attributed to steric repulsions, fine and small emulsion droplets with a viscoelastic membrane made up of structurally flexible APP are more resistant to lipid oxidation than large emulsion droplets formed with NPP. However, the lack of reliable correlations between particle size and oxidation rates suggests that the nature and properties of the interfacial protein rather than the particle size are a more important determinant of the oxidative stability of oil emulsions. Hence, it is entirely possible, through modifying the conformation of a protein surfactant (e.g., pH-shifting for pea protein as in the present case), to produce an O/W emulsion with desirable surface properties and oxidative stability thereby allowing the emulsion droplets to function as carriers for nutrients, bioactive compounds, and other food or pharmaceutical additives.

AUTHOR INFORMATION

Corresponding Authors

*E-mail: yunfa.liu@gmail.com. Tel.: +86-13861768813. Fax: +(86)-138-6176-8813.

*E-mail: ylxiong@uky.edu. Tel.: +001-859-257-3822. Fax: +001-859-257-5318.

Notes

The authors declare no competing financial interest.

ACKNOWLEDGMENTS

The study was supported by the Ministry of Science and Technology, China (Grant Nos. 2012BAD28B04 and 2013AA102103), the National Natural Science Foundation, China (Grant No. 30471225), and the USDA Agriculture and Food Research Initiative, USA (Grant No. 2008-35503-18790).

REFERENCES

(1) Rao, J.; McClements, D. J. Food-grade microemulsions and nanoemulsions: Role of oil phase composition on formation and stability. *Food Hydrocolloids* **2012**, *29*, 326−334.

(2) Yang, Y.; Marshall-Breton, C.; Leser, M. E.; Sher, A. A.; McClements, D. J. Fabrication of ultrafine edible emulsions: Comparison of high-energy and low-energy homogenization methods. *Food Hydrocolloids* **2012**, *29*, 398−406.

(3) McClements, D. J. Edible nanoemulsions: Fabrication, properties, and functional performance. *Soft Matter* **2011**, *7*, 2297−2316.

(4) Dickinson, E. Flocculation of protein-stabilized oil-in-water emulsions. *Colloids Surf., B* **2010**, *81*, 130−140.

(5) Dalgleish, D. G. Food emulsions—Their structures and structure-forming properties. *Food Hydrocolloids* **2006**, *20*, 415−422.

(6) Zhai, J.; Hoffmann, S. V.; Day, L.; Lee, T. H.; Augustin, M. A.; Aguilar, M. I.; Wooster, T. J. Conformational changes of α-lactalbumin adsorbed at oil−water interfaces: Interplay between protein structure and emulsion stability. *Langmuir* **2012**, *28*, 2357−2367.

(7) Miriani, M.; Keerati-u-rai, M.; Corredig, M.; Iametti, S.; Bonomi, F. Denaturation of soy proteins in solution and at the oil−water interface: A fluorescence study. *Food Hydrocolloids* **2011**, *25*, 620−626.

(8) Wong, B. T.; Zhai, J.; Hoffmann, S. V.; Aguilar, M. I.; Augustin, M.; Wooster, T. J.; Day, L. Conformational changes to deamidated wheat gliadins and β-casein upon adsorption to oil−water emulsion interfaces. *Food Hydrocolloids* **2012**, *27*, 91−101.

(9) Poon, S.; Clarke, A. E.; Schultz, C. J. Effect of denaturants on the emulsifying activity of proteins. *J. Agric. Food Chem.* **2001**, *49*, 281−286.

(10) Damodaran, S. Protein stabilization of emulsions and foams. *J. Food Sci.* **2005**, *70*, R54−66.
(11) Zhai, J. L.; Day, L.; Aguilar, M. I.; Wooster, T. J. Protein folding at emulsion oil/water interfaces. *Curr. Opin. Colloid Interface Sci.* **2013**, *5*, 257−271.
(12) Hu, M.; McClements, D. J.; Decker, E. A. Lipid oxidation in corn oil-in-water emulsions stabilized by casein, whey protein isolate, and soy protein isolate. *J. Agric. Food Chem.* **2003**, *51*, 1696−1700.
(13) Ma, Y.; Xiong, Y. L.; Zhai, J.; Zhu, H.; Dziubla, T. Fractionation and evaluation of radical scavenging peptides from *in vitro* digests of buckwheat protein. *Food Chem.* **2010**, *118*, 582−588.
(14) Elias, R. J.; Kellerby, S. S.; Decker, E. A. Antioxidant activity of proteins and peptides. *Crit. Rev. Food Sci. Nutr.* **2008**, *48*, 430−441.
(15) Xiong, Y. L. Antioxidant peptides. In *Bioactive Proteins and Peptides as Functional Foods and Nutraceuticals*; Mine, Y., Jiang, B., Li-Chan, E., Eds.; Wiley-Blackwell: Hoboken, NJ, 2010; pp 29−42.
(16) Korhonen, H.; Pihlanto, A. Food-derived bioactive peptides—Opportunities for designing future foods. *Curr. Pharm. Des.* **2003**, *9*, 1297−1308.
(17) Kikugawa, K.; Kato, T.; Hayasaka, A. Formation of dityrosine and other fluorescent amino acids by reaction of amino acids with lipid hydroperoxides. *Lipids* **1991**, *26*, 922−929.
(18) Jiang, J.; Chen, J.; Xiong, Y. L. Structural and emulsifying properties of soy protein isolate subjected to acid and alkaline pH-shifting processes. *J. Agric. Food Chem.* **2009**, *57*, 7576−7583.
(19) Goto, Y.; Calciano, L. J.; Fink, A. L. Acid-induced folding of proteins. *Proc. Natl. Acad. Sci. U.S.A.* **1990**, *87*, 573−577.
(20) Jiang, J.; Xiong, Y. L.; Chen, J. Role of β-conglycinin and glycinin subunits in the pH-shifting-induced structural and physicochemical changes of soy protein isolate. *J. Food Sci.* **2011**, *76*, C293−C302.
(21) Israelachvili, J. N. *Intermolecular and Surface Forces*; Academic Press: New York, 1992; pp 176−178.
(22) Damodaran, S.; Anand, K. Sulfhydryl-disulfide interchange-induced interparticle protein polymerization in whey protein-stabilized emulsions and its relation to emulsion stability. *J. Agric. Food Chem.* **1997**, *45*, 3813−3820.
(23) Jiang, J.; Xiong, Y. L.; Chen, J. pH shifting alters solubility characteristics and thermal stability of soy protein isolate and its globulin fractions in different pH, salt concentration, and temperature conditions. *J. Agric. Food Chem.* **2010**, *58*, 8035−8042.
(24) Desrumaux, A.; Marcand, J. Formation of sunflower oil emulsions stabilized by whey proteins with high-pressure homogenization (up to 350 MPa): Effect of pressure on emulsion characteristics. *Intl. J. Food Sci. Technol.* **2002**, *37*, 263−269.
(25) Aluko, R. Bioactive peptides. In *Functional Foods and Nutraceuticals*; Springer: New York, 2012; pp 37−61.
(26) Wang, T. L.; Domoney, C.; Hedley, C. L.; Casey, R.; Grusak, M. A. Can we improve the nutritional quality of legume seeds? *Plant Physiol.* **2003**, *131*, 886−891.
(27) Iqbal, A.; Khalil, I. A.; Ateeq, N.; Sayyar Khan, M. Nutritional quality of important food legumes. *Food Chem.* **2006**, *97*, 331−335.
(28) Aluko, R. E.; Mofolasayo, O. A.; Watts, B. M. Emulsifying and foaming properties of commercial yellow pea (*Pisum sativum* L.) seed flours. *J. Agric. Food Chem.* **2009**, *57*, 9793−9800.
(29) Pellegrini, N.; Re, R.; Yang, M.; Rice-Evans, C. Screening of dietary carotenoids and carotenoids-rich fruit extracts for antioxidant activities applying 2,2′-azinobis(3-ethylenebenzothiazoline-6-sulfonic acid) radical cation decolorization assay. *Methods Enzymol.* **1999**, *299*, 379−389.
(30) Decker, E. A.; Hultin, H. O. Factors influencing catalysis of lipid oxidation by the soluble fraction of mackerel muscle. *J. Food Sci.* **1990**, *55*, 947−950.
(31) Mei, L.; Decker, E. A.; McClements, D. J. Evidence of iron association with emulsion droplets and its impact on lipid oxidation. *J. Agric. Food Chem.* **1998**, *46*, 5072−5077.
(32) Kerstens, S.; Murray, B. S.; Dickinson, E. Microstructure of β-lactoglobulin-stabilized emulsions containing non-ionic surfactant and excess free protein: Influence of heating. *J. Colloid Interface Sci.* **2006**, *296*, 332−334.
(33) Laemmli, U. K. Cleavage of structural proteins during the assembly of the head of bacteriophage T4. *Nature* **1970**, *277*, 680−685.
(34) Chang, Y.; Hartel, R. W. Development of air cells in a batch ice cream freezer. *J. Food Eng.* **2002**, *55*, 71−78.
(35) Pownall, T. L.; Udenigwe, C. C.; Aluko, R. E. Amino acid composition and antioxidant properties of pea seed (*Pisum sativum* L.) enzymatic protein hydrolysate fractions. *J. Agric. Food Chem.* **2010**, *58*, 4712−4718.
(36) AOCS. Official method Cd 8−53. Peroxide value acetic acid−chloroform method. In *Official Methods and Recommended Practices of AOCS*, 5th ed.; American Oil Chemists' Society: Champaign, IL, 1999.
(37) Tanford, C.; Bunville, L. G.; Nozaki, Y. The reversible transformation of β-lactoglobulin at pH 7.5. *J. Am. Chem. Soc.* **1959**, *81*, 4032−4036.
(38) Qin, B. Y.; Bewley, M. C.; Creamer, L. K.; Baker, H. M.; Baker, E. N.; Jameson, G. B. Structural basis of the Tanford transition of bovine β-lactoglobulin. *Biochemistry* **1998**, *37*, 14014−14023.
(39) Stadtman, E. R. Oxidation of free amino acids and amino acid residues in proteins by radiolysis and by metal-catalyzed reactions. *Annu. Rev. Biochem.* **1993**, *62*, 797−821.
(40) Wagner, J. R.; Gueguen, J. Surface functional properties of native, acid-treated, and reduced soy glycinin. 2. Emulsifying properties. *J. Agric. Food Chem.* **1999**, *47*, 2181−2187.
(41) Sabín, J.; Prieto, G.; Ruso, J. M.; Messina, P. V.; Salgado, F. J.; Nogueira, M.; Costas, M.; Sarmiento, F. Interactions between DMPC liposomes and the serum blood proteins HSA and IgG. *J. Phys. Chem. B.* **2009**, *113*, 1655−1661.
(42) Di Foggia, M.; Bonora, S.; Tugnoli, V. DSC and Raman study on the effect of lysozyme and bovine serum albumin on phospholipids liposomes. *J. Therm Anal. Calorim.* **2013**, *111*, 1871−1880.
(43) Nakaya, K.; Ushio, H.; Matsukawa, S.; Shimizu, M.; Ohshima, T. Effects of droplet size on the oxidative stability of oil-in-water emulsions. *Lipids* **2005**, *40*, 501−507.
(44) Delahaije, R. J.; Wierenga, P. A.; van Nieuwenhuijzen, N. H.; Guiseppin, M. L.; Gruppen, H. Protein concentration and protein exposed hydrophobicity as dominant parameters determining flocculation of protein stabilized oil-in-water emulsions. *Langmuir* **2013**, DOI: 10.1021/la401314a.
(45) Popello, I. A.; Suchkov, V. V.; Grinberg, V. Y.; Tolstoguzov, V. B. Effects of pH upon the liquid−liquid phase equilibria in solutions of legumins and vicilins from broad beans and peas. *Food Hydrocolloids* **1992**, *6*, 147−152.
(46) Dickinson, E. Flocculation of protein-stabilized oil-in-water emulsions. *Colloids Surf., B* **2010**, *81*, 130−140.
(47) Shand, P. J.; Ya, H.; Pietrasik, Z.; Wanasundara, P. K. J. P. D. Physicochemical and textural properties of heat-induced pea protein isolate gels. *Food Chem.* **2007**, *102*, 1119−1130.
(48) Monahan, F. J.; McClements, D. J.; Kinsella, J. E. Polymerization of whey proteins in whey protein-stabilized emulsions. *J. Agric. Food Chem.* **1993**, *41*, 1826−1829.
(49) Koyoro, H.; Powers, J. R. Functional properties of pea globulin fractions. *Cereal Chem.* **1987**, *64*, 97.
(50) Floury, J.; Desrumaux, A.; Lardieres, J. Effect of high-pressure homogenization on droplet size distributions and rheological properties of model oil-in-water emulsions. *Innov. Food Sci. Emerg.* **2000**, *1*, 127−134.
(51) Cash, M. J.; Erazo-Majewicz, P.; Politis, J. K. Cream compositions and food foams made therefrom; Pub. No.: US 2007/0071874 A1.
(52) Goff, H. D. Instability and partial coalescence in whippable dairy emulsions. *J. Dairy Sci.* **1997**, *80*, 2620−2630.

the membrane disturbance assumed to explain the proven activity of lysozyme against some Gram-negative strains.[15−17]

Molecules that provoke bacterial membrane disruption are mostly positively charged, amphipathic, and hydrophobic.[4] Lysozyme possesses these physicochemical criteria at physiological pH. However, lysozyme activity against Gram-negative bacteria remains limited, but when lysozyme is modified by fusion with a chemical moiety,[18−23] heat denaturation,[24−26] or enzymatic hydrolysis,[27,28] its antimicrobial activity is enhanced. One relevant question is then to investigate the antibacterial activity against Gram-negative bacteria of lysozyme modified to increase its positive charge and/or amphipathicity and/or hydrophobicity. Dry-heating of lysozyme has been described as an easy process resulting in different lysozyme isoforms, some of them being especially more positive and more hydrophobic than native hen egg white lysozyme.[29] This modified lysozyme could then be an opportunity to create a new efficient antimicrobial, simply using a safe physical treatment.

MATERIALS AND METHODS

Materials. Native lysozyme powder (pH 3.2) was obtained from Liot (Annezin, 62-France); it was heated for 7 days at 80 °C in hermetically closed glass tubes to obtain dry-heated lysozyme. *Micrococcus lysodeikticus*, ATCC no. 4698, Trisma base, potassium phosphate monobasic, potassium phosphate dibasic, potassium chloride, ampicillin, chloramphenicol, (*o*-nitrophenyl)galactoside (ONPG), 3,3′-dipropylthiadicarbocyanine iodide ($DiSC_3$), 4-(2-hydroxyethyl)-1-piperazineethanesulfonic acid, 4-(2-hydroxyethyl)-1-piperazineethanesulfonic acid (HEPES), and glucose were obtained from Sigma-Aldrich (Saint-Quentin, France).

Nitrocefin, a standard solution of potassium (1000 mg/L), casein peptone, and yeast extract were obtained from Merck Chemicals (Darmstadt, Germany). Tryptic soy broth (TSB) was from AES (Bruz, France).

Bacterial Strains. Three different *E. coli* strains have been used (Table 1). *E. coli* K12 was obtained from the Institut Pasteur (Paris, France). *E. coli* MG1655 *ivy*::*Cm* was kindly provided by C. Michiels (Centre of Food and Microbial Technology, KU Leuven, Belgium); this bacterial strain no longer expresses the lysozyme inhibitor Ivy. The bacterial strain *E. coli* ML-35p (*LacI*$^-$ *LacY*$^-$ *LacZ*$^+$, plasmid pBR322) was kindly provided by R. Lehrer (Department of Medicine, University of California, Los Angeles) and transmitted to our laboratory by D. Destoumieux-Garzon (UMR 5119, Ecologie des systèmes marins côtiers, University of Montpellier, France). *E. coli* ML-35p lacks lactose permease and expresses *β*-lactamase and *β*-galactosidase in the periplasm and cytoplasm, respectively.

Table 1. Presence (+) or Absence (−) of Ivy, *β*-Lactamase, *β*-Galactosidase, and Lactose Permease in the Different Bacterial Strains Used for the Present Study

	Ivy	*β*-lactamase	*β*-galactosidase	Lactose permease
E. coli K12	+	−	+	+
E. coli ML-35p	+	+	+	−
E. coli MG1655 *ivy*::*Cm*	−	−	+	+

Growth Assays with *E. coli* K12 and *E. coli* MG1655 *ivy*::*Cm*. The bacterial culture *E. coli* K12 or *E. coli* MG1655 *ivy*::*Cm* was grown overnight (18 h) at 37 °C under stirring (130 rpm) in TSB containing 50 *μ*g/mL ampicillin or 30 *μ*g/mL chloramphenicol, respectively. After the incubation period, the cultures contained about 10^9 CFU/mL *E. coli*, from which 10^5 CFU/mL bacterial suspensions were prepared by performing four 10-fold serial dilutions in LB05 (Luria broth containing 10 g/L peptone of casein, 5 g/L yeast extract, and 0.5 g/L NaCl). After solubilization in demineralized water, lysozyme (native or dry-heated) was added at 0.25 or 3.7 g/L to the bacterial suspension, before incubation at 37 °C under stirring (130 rpm) for 24 h; 3.7 g/L is the natural concentration of lysozyme in hen egg white. Cell enumeration was performed by colony count after 2, 4, 6, and 24 h as previously described by Baron et al.[30] The results for cell counts are based on nine replicates (three biological replicates, each with three technical replicates).

Outer and Inner Membrane Permeability Measurements. Outer and inner membrane permeability was measured using the Lehrer method,[31] modified as described by Derde et al.[32] The *E. coli* ML-35p culture was grown overnight (18 h) in TSB containing 50 *μ*g/mL ampicillin at 37 °C under stirring (130 rpm). The bacterial culture was washed twice in 50 mM Tris−HCl buffer, pH 7.0 (5000*g*, 10 min), and diluted to obtain about 10^7 CFU/mL in solutions containing 0.25 or 3.7 g/L native or dry-heated lysozyme.

To test outer membrane permeability, 0.015 mg/mL nitrocefin (substrate of *β*-lactamase) was added to the sample solutions. When the outer membrane was permeabilized, the periplasmic *β*-lactamase hydrolyzed nitrocefin into the hydrolysis product of nitrocefin (HP-nitrocefin). HP-nitrocefin absorbance was measured at 486 nm (Spectramax M2, Molecular Devices, United Kingdom), at 37 °C under stirring.

To test inner membrane permeability, 0.7 mg/mL ONPG (substrate of *β*-galactosidase) was added to the sample solutions. When the inner membrane was permeabilized, the cytoplasmic *β*-galactosidase hydrolyzed ONPG into *o*-nitrophenol (ONP). ONP absorbance was measured at 420 nm (Spectramax M2, Molecular Devices, United Kingdom), at 37 °C under stirring.

Two parameters could then be determined: maximal slope and lag time. The maximal slope determined the maximal velocity of the enzymatic reaction of either *β*-lactamase or *β*-galactosidase. The maximal velocity is directly related to the concentration of accessible enzyme and thus to the permeability of the outer or inner membrane, respectively. The lag time was the time between outer and inner membrane permeabilization, estimated by the delay between both enzymatic reactions.

The results of lysozyme activity on membrane permeability are based on three replicates. The results were corrected for reference absorbance, i.e., the absorbance of the microplate and of the buffer solution.

Detection of *β*-Lactamase and *β*-Galactosidase Leakage out of Bacterial Cells. After overnight growth (18 h) in TSB containing 50 *μ*g/mL ampicillin at 37 °C under stirring (130 rpm), the *E. coli* ML-35p culture was washed twice with 50 mM Tris−HCl buffer, pH 7.0 (5000*g*, 10 min), and diluted to obtain 10^7 CFU/mL bacterial suspensions. These suspensions were added with lysozyme (0.25 or 3.7 g/L, native or dry-heated lysozyme) and incubated for 5 h at 37 °C under stirring, before centrifugation at 5000*g* for 10 min. *β*-Lactamase and *β*-galactosidase activities were then tested in the supernatants by adding 0.05 g/L nitrocefin and 1 g/L ONPG, respectively. The initial reaction rates of both enzymatic reactions (v_0 = ΔAU/min) were determined at 25 °C from absorbance curves (Multiskan Go, Thermo Fisher Scientific, Illkirch, France) at 486 and 420 nm, respectively.

Measurement of the Bacterial Membrane Potential Disruption. The disruption of the bacterial membrane potential was measured according to the method proposed by Wu et al.[33] The *E. coli* K12 culture was grown for 3.5 h in TSB at 37 °C under stirring (130 rpm) to reach a midlog phase. The culture was washed twice with 5 mM HEPES buffer at pH 7.2 containing 5 mM glucose (5000*g*, 10 min) and diluted to obtain an absorbance of around 0.06 at 620 nm. A 1 *μ*M concentration of $DiSC_3$ and 100 mM KCl were added to the diluted bacterial suspension, before incubation for 1 h at 30 °C in the dark. Then lysozyme (0.25 or 3.7 g/L, native or dry-heated) was added to the bacterial cells, and the samples were incubated for 30 min at 30 °C in the dark. Fluorescence was then measured at 670 nm with a fluorimeter, Perkin-Elmer LS55 (Perkin-Elmer, Courtaboeuf, France), after excitation at 622 nm; the slit width was 2.5 nm/2.5 nm, and the integration time was 6.2 s. The results are based on nine replicates (three biological replicates, each with three technical replicates).

Potassium Leakage Measurement. The measurement of potassium leakage was performed according to the method described by Orlov et al.[34] After overnight growth (18 h) in TSB at 37 °C under stirring (130 rpm), the *E. coli* K12 culture was washed twice with 10 mM Tris−acetate buffer, pH 7.0, containing 100 mM NaCl (5000*g*, 10 min), and diluted to obtain 10^8 CFU/mL bacterial suspensions. Lysozyme (0.25 or 3.7 g/L, native or dry-heated) was added to the bacterial solutions, and then the samples were incubated for 3 h at 37 °C under stirring, centrifugated (5000*g* for 10 min), and filtered with 0.22 μm filters. The K^+ concentration was measured in the filtrates using a potassium-selective electrode (DX239-K) coupled to an S50 SevenMulti meter (Mettler Toledo, Viroflay, France) and recorded with an ISE meter previously calibrated with six standard solutions containing 5.15, 10.3, 77.6, 103, 1330, and 11700 μM potassium, respectively. Calibration and measurements were performed at 25 °C.

Optical Microscopy and Atomic Force Microscopy (AFM). The *E. coli* K12 culture was grown overnight (18 h) in TSB at 37 °C under stirring (130 rpm). After the incubation period, the culture contained about 10^9 CFU/mL *E. coli*, from which 10^5 CFU/mL bacterial suspensions were prepared by performing four 10-fold serial dilutions in LB05. Then lysozyme (0.25 or 3.7 g/L, native or dry-heated) was added to the bacterial suspension before incubation at 37 °C under stirring (130 rpm) for 24 h. Samples were washed in a 0.85% NaCl solution (3000*g*, 10 min) before optical microscopy and AFM were performed.

Optical microscopy observations were performed with an Olympus BX51 (enlargement 100×). Images were taken with a digital camera, Olympus Camedia C-5050.

Samples were deposited on freshly cleaved mica. To avoid accumulation of bacteria, a dipper (Nima Technology, Cambridge, U.K.) was used to gently remove the mica from the sample solution at 2 mm/min while the solution was being stirred. The mica plate was then dried at room temperature, and shortly after that, AFM imaging was performed. Images were recorded with a Pico-plus atomic force microscope (Molecular Imaging, Phoenix, AZ) operating in tapping mode. A scanner of 100 μm was used for the measurements. Topographic and phase images, illustrating cell topography and cell heterogeneity,[35] were acquired simultaneously using silicon nitride tips (AppNano, Silicon Valley, CA) with a resonance frequency of 145−230 kHz and a nominal spring constant of 20−95 mN/m. Transversal cross sections of the bacteria were performed to illustrate height and surface roughness. The images presented in the present study are representative of several samples.

Statistical Analysis. All experiments were performed at least in triplicate. Statistical analysis was performed with R 2.15.2. Significance levels were at least 95%. Data from the normal distribution and with equal variances were treated with parametric tests. In this case, for the comparison of means the Student *t* test was used. Data from other distributions or with unequal variances were treated with non-parametric tests. In this case, for the comparison of means the Wilcoxon rank sum test was used.

RESULTS

Growth of *E. coli* in the Presence of Lysozyme. The growth of *E. coli* K12 is disturbed in the presence of both native (N-L) and dry-heated (DH-L) lysozyme during the first hours of growth (Figure 1A), but after 24 h of incubation at 37 °C, no significant difference is observed between the samples with or without lysozyme. The growth of *E. coli* K12 shows the same pattern when N-L is added, whatever the concentration (0.25 or 3.7 g/L), and when DH-L is added at low concentration (0.25 g/L): the bacterial growth is inhibited for 2 h, before it recovers, and cell counts similar to those in the control sample (without lysozyme) are finally reached. On the contrary, the addition of 3.7 g/L DH-L induces a different pattern of the *E. coli* K12 growth: 1 log reduction of the bacterial cells is observed after 2 h of incubation, after which the growth rate recovers; with up to 6 h of incubation, the *E. coli* K12 population remains lower than in the other samples (control sample and samples with N-L or low-concentration DH-L).

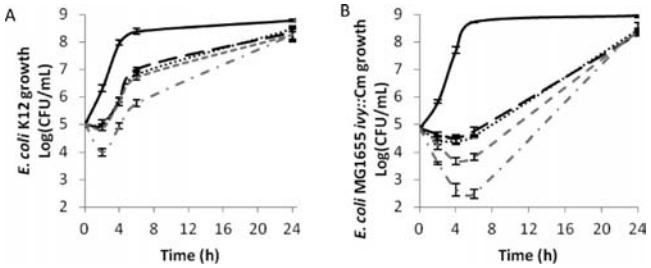

Figure 1. Growth curves of *E. coli* K12 (A) and of *E. coli* MG1655 *ivy*::*Cm* (B) in LB05 medium in the absence of lysozyme (—) or in the presence of 0.25 g/L N-L (− − −), 0.25 g/L DH-L (···), 3.7 g/L N-L (---,) or 3.7 g/L DH-L (-·-). The results are based on nine replicates.

When the same tests are performed on the *E. coli* MG1655 *Ivy*::*Cm* strain, which lacks the periplasmic lysozyme inhibitor Ivy, the impact of lysozyme on the bacterial growth pattern is stronger as compared to that for *E. coli* K12, for both N-L and DH-L and both concentrations (0.25 and 3.7 g/L) (Figure 1B). The modification of the growth pattern is dose-dependent: the higher the N-L or DH-L concentration, the higher the population decrease observed in the first hours of incubation. At high concentration (3.7 g/L), DH-L causes a population decrease which is 1.3 log higher than that of N-L, whereas no difference is observed between both types of lysozyme at low concentrations (0.25 g/L). However, the number of bacterial cells suitable for growth is the same after 24 h of incubation with N-L and DH-L.

Membrane State of *E. coli* in the Presence of Lysozyme. N-L and DH-L induce similar overall permeabilization of the outer membrane whatever the concentration, as measured by the total β-lactamase activity (Figure 2A), but externalized β-lactamase activity, i.e., activity in the supernatant resulting from centrifugation of the bacterial culture incubated with lysozyme, is higher with DH-L than with N-L at both lysozyme concentrations (Figure 2B). Moreover, it is noticeable

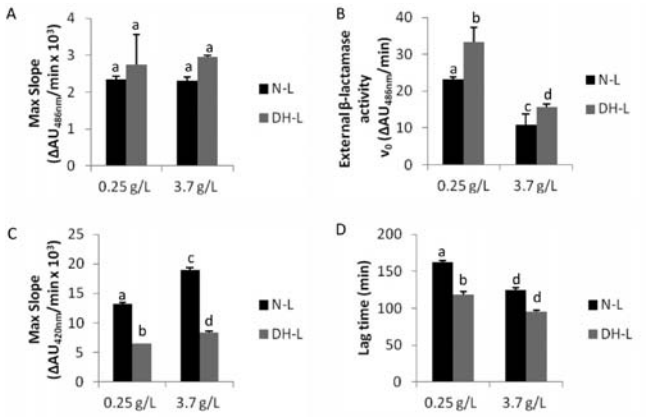

Figure 2. Comparison of the permeabilization of *E. coli* ML-35p outer (A, B) and inner (C, D) membranes by native (N-L) or dry-heated (DH-L) lysozyme as evidenced by β-lactamase and β-galactosidase activity, respectively. Different letters (a, b, c, d) indicate significant difference obtained from the Student *t* test (A, C, D) ($p < 0.01$) or Wilcoxon rank sum test (B) ($p < 0.01$).

that a high concentration (3.7 g/L) of N-L and DH-L causes lower externalized β-lactamase activity than a low concentration (0.25 g/L) (Figure 2B).

Figure 2C shows that permeabilization of the inner membrane is stronger with N-L than with DH-L at either 0.25 or 3.7 g/L. On the other hand, the lag time before detection of the inner membrane permeabilization is shorter with DH-L than with N-L at both concentrations (Figure 2D). The intensity of inner membrane permeabilization and lag time are lysozyme concentration-dependent for both N-L and DH-L.

Disturbance of the inner membrane has also been investigated by measurement of changes of the membrane potential. N-L and DH-L similarly disturb the membrane potential of *E. coli* when added at 0.25 g/L in the bacterial culture. On the contrary, at higher concentration (3.7 g/L lysozyme), DH-L causes a stronger disruption of the membrane potential than N-L, as indicated by the 2-fold higher relative fluorescence of $DiSC_3$ (Figure 3A). For both N-L and DH-L, a dose−response effect is observed.

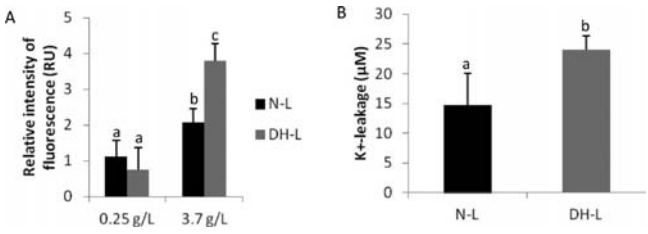

Figure 3. (A) Disruption of the membrane potential of *E. coli* K12 caused by native (N-L) or dry-heated (DH-L) lysozyme at 0.25 and 3.7 g/L. Different letters (a, b, c) indicate significant difference obtained from the Student *t* test ($p < 0.01$). Results are based on nine replicates. (B) K^+ leakage of *E. coli* K12 in the presence of 3.7 g/L N-L or DH-L after 3 h of incubation. Different letters (a, b) indicate significant difference obtained from the Student *t* test ($p < 0.01$). Results are based on six replicates.

Finally, the measurement of intracellular K^+ leakage has been used as an indicator of inner membrane disruption. K^+ leakage is not detectable in *E. coli* cultures containing 0.25 g/L N-L or DH-L (data not shown), but significant K^+ leakage is measured in the presence of 3.7 g/L lysozyme. The extent of the K^+ leakage is 75% higher with DH-L than with N-L (Figure 3B).

Morphology of *E. coli* K12 in the Presence of Lysozyme. *E. coli* K12 incubated for 24 h in the presence of 0.25 g/L lysozyme exhibits differences in cell morphology in comparison to the control sample, as shown by optical microscopy images (Figure 4). Abnormally elongated bacterial cells are observed after treatment with lysozyme; such modified bacteria are present in a larger number when DH-L is added as compared to N-L (Figure 4B,C). These elongated cells could not be observed at high concentration (3.7 g/L) of N-L and DH-L (data not shown).

Topographic AFM enables determination of the size and characterization of the shape and the surface topology of bacteria. Nontreated bacteria are about 2 μm long, with a diameter of 500 nm; the surface is smooth and regular, and flagella are observed (Figure 5A). When bacteria are treated with N-L, the size is not modified (Figure 5B,D), whereas abnormally elongated cells without a visible septum are observed when the bacteria are treated with 0.25 g/L DH-L (Figure 5C). With high-concentration N-L treatment (Figure 5D), depressions can be observed on the bacterial cells, but the bacterial morphology is more strongly disturbed when the bacteria are treated with DH-L (Figure 5C,E), with an especially irregular cell surface and depressions; the depth and the diameter of these depressions increase when the DH-L concentration increases: around 15 nm depth at 0.25 g/L DH-L versus around 26 nm at 3.7 g/L and around 128 nm diameter versus 160 nm. When the bacteria are treated with either 3.7 g/L N-L or both concentrations of DH-L, cell debris is also observed (data not shown).

Phase AFM enables visualization of homogeneity or heterogeneity of the cell surface composition.[35] Thus, the nontreated bacteria appear homogeneous (Figure 6A), whereas heterogeneity can be observed with all the treated samples, with either N-L or DH-L, and at both concentrations (Figure 6B−E). However, higher heterogeneity is observed when the bacteria are treated with DH-L as compared to N-L.

DISCUSSION

The capability of native hen egg white lysozyme to permeabilize the outer and inner membranes of *E. coli* has been previously established by Derde et al.[32] Moreover, some structural modifications of lysozyme proved to be efficient to enhance the antibacterial activity of this protein.[8] Modifying lysozyme to design a novel antimicrobial with enhanced membrane activity and thus improved antibacterial activity against *E. coli* then seems relevant. Because membrane activity of antimicrobial proteins or peptides is highly dependent on the physicochemical properties of the molecules, dry-heating could be an interesting process for lysozyme design. Indeed, dry-heated lysozyme is more hydrophobic and more surface-active, and it contains isoforms that are more positively charged than native lysozyme.[29] To test the hypothesis that dry-heated lysozyme is more active than native lysozyme against *E. coli*, because of an increased membrane activity, a comparative study is proposed.

Native Lysozyme Causes *E. coli* K12 Growth Latency. In the presence of low and high concentrations of N-L, the inhibition of *E. coli* K12 growth is observed for 2 h (Figure 1A). Lysozyme is undoubtedly the cause of this phenomenon, regarding the fact that the control sample (without lysozyme) does not induce any lag time before bacterial growth starts (Figure 1A). However, the N-L effect is rather short, and bacterial growth resumes. A bacterial concentration similar to that in the control sample is reached after 24 h of incubation (Figure 1A). This could be explained by several hypotheses: damage repair by the bacteria, activation of adaptation and defense mechanisms, and/or depletion of lysozyme in the growth medium by irreversible interaction with the bacteria.

The first possibility is that N-L causes minor damage to the bacterial cells. This damage does not lead to cell death, but the bacterial cell needs to repair the obtained cell structures. For these repair mechanisms, energy is needed and cell growth is thus retarded.

E. coli also have several defense mechanisms. The first defense mechanism of Gram-negative bacteria is the outer membrane. However, lysozyme has been shown to cross this hurdle.[32] Another present defense mechanism in *E. coli* is the lysozyme inhibitor Ivy, which neutralizes N-L in the periplasm.[36] When N-L reaches the periplasm of *E. coli*, Ivy binds to N-L. This makes N-L harmless for the *E. coli* cells (Figure 1). Enterobacteriaceae are also known for the presence of proteases on their outer membrane. *E. coli* K12 carries a protease, OmpT, which combines characteristics of serine and aspartate proteases. The OmpT of *E. coli* K12 has been

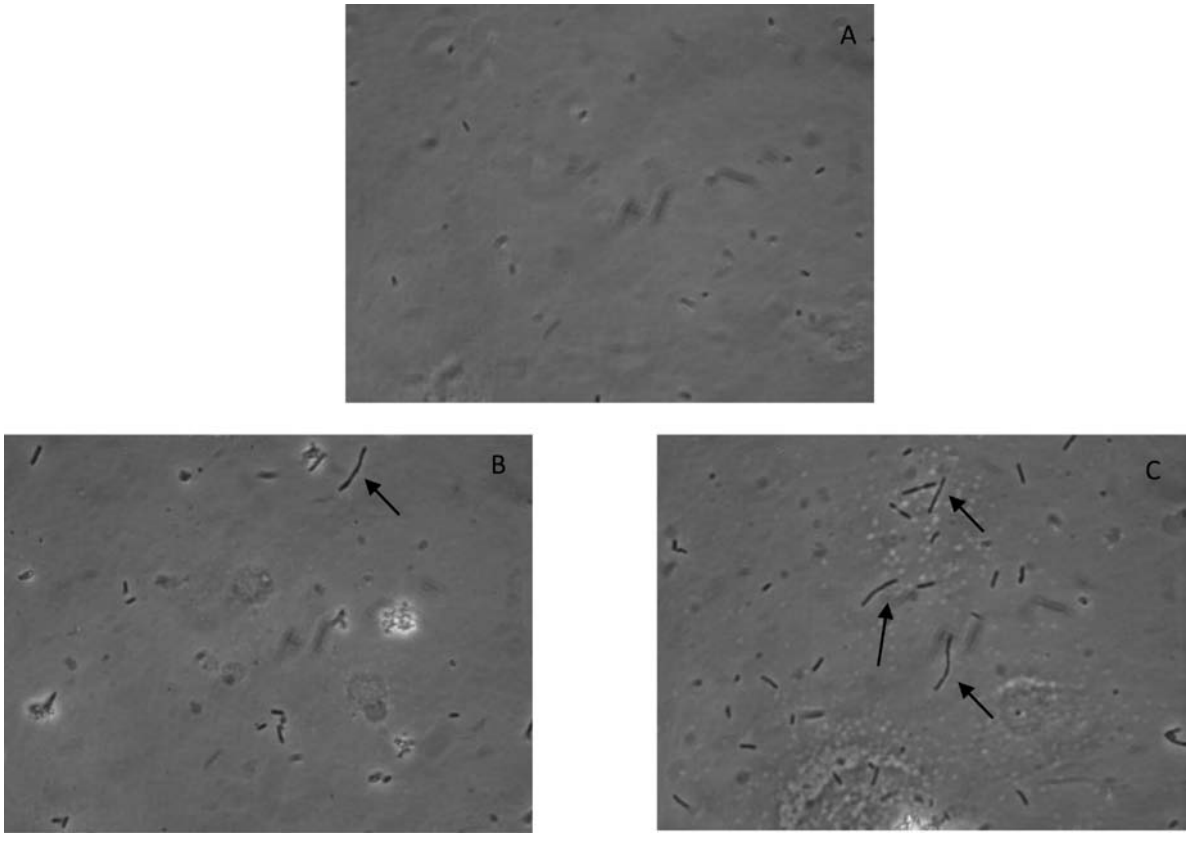

Figure 4. Observations of *E. coli* K12 with optical microscopy after 24 h of incubation in the absence of lysozyme (A) and in the presence of 0.25 g/L native lysozyme (N-L) (B) and dry-heated lysozyme (DH-L) (C).

reported to degrade the antimicrobial peptide protamine.[37] It is thus possible that OmpT also hydrolyzes lysozyme molecules. Besides the above-mentioned defense mechanisms, *E. coli* is also able to modify the lipopolysaccharides of the outer membrane, protecting the outer membrane from permeabilization and neutralizing negative charges of the lipid A moiety.[37] Finally, all these defense mechanisms could protect *E. coli* from N-L and would delay the bacterial growth in the first moments after N-L addition.

Another assumption is that lysozyme concentration in the culture medium progressively decreases until it drops below a critical concentration, because of irreversible interaction between the protein and the bacterial cell membranes.[32] Because of its amphiphilic nature, and its surface-active properties, N-L could insert itself into the outer bacterial membrane, in which it could be irreversebly entrapped, causing depletion of N-L in the medium. Moreover, regarding the N-L molecules that could pass the outer membrane, binding to the peptidoglycan and/or to the inner membrane could decrease the lysozyme concentration in the culture medium. When this decrease results in a lysozyme concentration lower than the lowest active concentration, bacterial growth will resume.

Dry-Heated Lysozyme at High Concentration (3.7 g/L) Causes an Early-Stage Population Decrease. At low concentration (0.25 g/L), DH-L acts similarly to N-L at low and high concentrations: *E. coli* growth is inhibited whether Ivy is present or not (Figure 1), but bacterial growth resumes afterward, and the same bacterial levels as in the control sample are attained after 24 h. As suggested above, three assumptions can be proposed: damage repair by the bacteria, activation of defense and adaptation mechanisms, and/or depletion of lysozyme in the growth medium by irreversible interaction with bacteria.

On the contrary, high-concentration DH-L (3.7 g/L) causes a population decrease (~1 log) in the early stages of growth. Thus, it is noticeable that whereas the presence of the Ivy inhibitor completely removes the population decrease observed when *E. coli* is treated with 3.7 g/L N-L, a slight decrease is still observed in the presence of the Ivy inhibitor when *E. coli* is treated with 3.7 g/L DH-L, even when the muramidase activity of DH-L is 22% lower than that of N-L (data not shown). This indicates that the Ivy inhibitor is not enough to defend *E. coli* cells against the effect of DH-L and that DH-L undoubtedly acts in different way compared to N-L. The physicochemical differences between both lysozymes could be responsible for such different activities. Especially, DH-L has been described more surface-active, more positively charged, and more hydrophobic than N-L.[29] This indicates that DH-L is more membrane active than N-L. To confirm this hypothesis, the *E. coli* membrane state has been tested in the presence of either DH-L or N-L.

Membrane Disruption Differs between Native and Dry-Heated Lysozyme. Both N-L and DH-L pass the outer bacterial membrane and reach the periplasm, consistently with the increased lysozyme effect in the absence of the lysozyme inhibitor Ivy (Figure 1B). Actually, the passage of N-L through the outer bacterial membrane has already been described.[32] In the present study, it is demonstrated that N-L and DH-L permeabilize the outer membrane (Figure 2A), but when *E. coli* is treated with DH-L, more β-lactamase is released from the bacterial cell than when it is treated with N-L (Figure 2B),

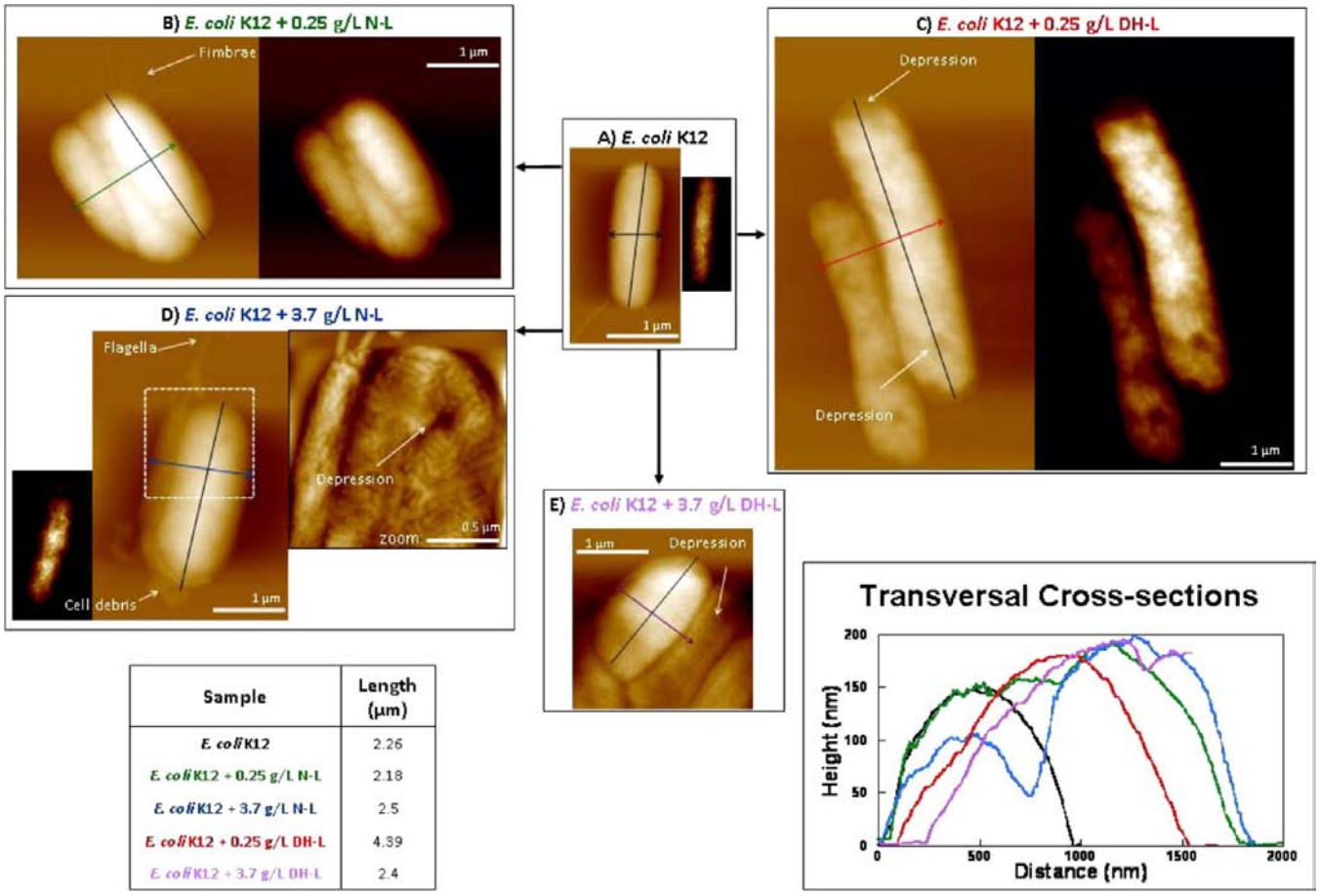

Sample	Length (µm)
E. coli K12	2.26
E. coli K12 + 0.25 g/L N-L	2.18
E. coli K12 + 3.7 g/L N-L	2.5
E. coli K12 + 0.25 g/L DH-L	4.39
E. coli K12 + 3.7 g/L DH-L	2.4

Figure 5. Topographical AFM observations: nontreated *E. coli* K12 cells (A); cells treated with native lysozyme at 0.25 g/L (B) or 3.7 g/L (D); cells treated with dry-heated lysozyme at 0.25 g/L (C) or 3.7 g/L (E). Topographical AFM images have a *z*-range from 0 to 400 nm for full-scale images and from 0 to 15 nm for the 3.7 g/L N-L zoom. Bacterial lengths and cross sections are measured as indicated by full lines on the AFM images. AFM images shown here are representative of the whole sample.

meaning that DH-L causes either larger pores or more pores in the outer membrane as compared to N-L.

Outer membrane permeabilization intensity is independent of the concentration of N-L or DH-L administered to the bacteria (Figure 2A), but higher concentrations of N-L or DH-L (3.7 g/L) cause less β-lactamase leakage in the medium (Figure 2B). This could result from a large insertion of lysozyme molecules into the outer membrane and/or surrounding of the bacteria in high-concentration conditions, causing more difficult diffusion of β-lactamase.

The permeabilization of the inner membrane by DH-L is less intense as compared to that by N-L when measured by the maximal rate of β-galactosidase activity (Figure 2C), but permeabilization occurs faster with DH-L than with N-L (Figure 2D). In both cases, β-galactosidase activity could not be observed in the medium (data not shown), meaning that neither N-L nor DH-L causes pores large enough in the inner membrane to release this cytoplasmic enzyme. High-concentration DH-L also causes higher membrane potential disturbance and K^+ leakage than N-L (Figure 3). Inner membrane disruption is also dose-dependent: the higher the lysozyme concentration, the more severe (Figures 2C and 3) and the faster (Figure 2D) the inner membrane disruption.

It thus seems that, at high concentration, the DH-L activity on *E. coli* could be related to its enhanced activity on the outer and inner membranes. DH-L forms large and/or a lot of pores in the outer membrane; afterward it penetrates into the periplasm where it could either hydrolyze the peptidoglycan layer or diffuse through this layer to finally reach the inner membrane. Once it has arrived at the inner membrane, DH-L causes severe membrane potential disturbance and cytosol leakage (K^+ leakage). These latter phenomena suggest ion channel formation, which has already been reported for native lysozyme and lysozyme-derived peptides by Kimelberg and Papahadjopoulos[38] and Ibrahim et al., respectively.[28] The presented study thus suggests that DH-L forms more ion channels in the cytoplasm membrane than N-L. Moreover, membrane potential disturbance is known to cause cellular division disturbance.[39] In combination with the pore formation, this could explain the morphological modifications observed here.

The Impact of DH-L on the Membrane Integrity of *E. coli* Is Confirmed by Severe Morphological Modifications Observed in Vivo. Not only can the effect of lysozyme, and especially of DH-L, on the membrane integrity of *E. coli* be shown in vitro as described above, it can also be highlighted in vivo. DH-L causes severe disruptions of cellular division observed by optical and atomic force microscopy: elongated cells of about 4.5 μm long could be observed without any sign of septum formation (Figures 4 and 5), as well as depressions which could be pores in the outer membrane and lateral depression which can be related to the activity of an

dx.doi.org/10.1021/jf405155p | J. Agric. Food Chem. 2014, 62, 1692−1700

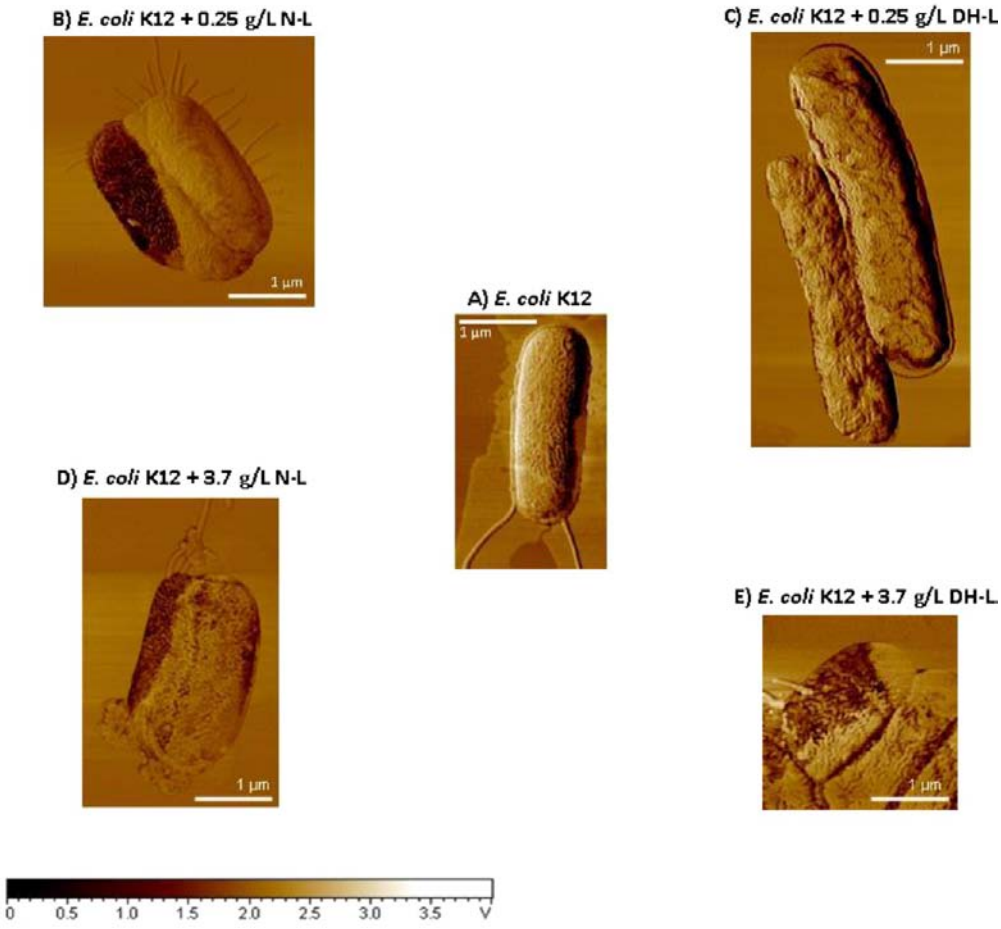

Figure 6. AFM phase imaging: nontreated *E. coli* K12 cells (A); cells treated with native lysozyme at 0.25 g/L (B) or 3.7 g/L (D); cells treated with dry-heated lysozyme at 0.25 g/L (C) or 3.7 g/L (E). The *z*-range is from 0 to 4 V. AFM images shown here are representative of the whole sample.

antimicrobial as reported by Meincken et al.[40] and Li et al.[41] (Figure 5). DH-L also homogenizes the ribs present on the bacterial cell surface at high concentrations (3.7 g/L), which could be the result of protein insertion into the bacterial cell wall as seen for *E. coli* cells treated with PGLa.[40] Then cell division and cell morphology are known to depend on the proton motive force, which itself depends on the bacterial membrane integrity.[39] In Figure 6, it is also noticeable that N-L or DH-L (0.25 and 3.7 g/L) alters the bacterial surface heterogeneity, resulting in the appearance of more rigid zones.[35,40]

These morphological modifications are consistent with the membrane integrity disturbances. Thus, the depressions formed in the presence of DH-L (Figure 5) are consistent with the higher leakage of β-lactamase, as compared to that in bacterial cells treated with N-L (Figure 2B). Perturbated cell division (Figures 4 and 5) is consistent with membrane potential disruption (Figure 3A), as recently reported by Strahl et al.[39]

To explain the differences observed between N-L and DH-L against *E. coli* membrane integrity, some assumptions can be proposed. Especially, the physicochemical modifications induced by dry-heating, and previously described by Desfougères et al.,[29] could be responsible for higher affinity of DH-L with outer and inner membranes and/or for more severe membrane disruptions. Because DH-L is more positively charged than N-L, interactions with LPS could be increased. Moreover, the higher hydrophobicity of DH-L could make it easier to interact with the lipid parts of bacterial membranes, and its higher flexibility could improve lysozyme insertion into the membranes. At last, the higher positive charge of DH-L could modify the membrane potential to a larger extent than N-L, when adsorbed on the inner membrane. However, more research has to be performed to identify the prevalent parameters responsible for the improved antibacterial activity of DH-L as compared to N-L. This is in progress by studying the behavior of DH-L at 2D model interfaces mimicking bacterial membranes.

AUTHOR INFORMATION

Corresponding Author

*E-mail: melanie.derde@agrocampus-ouest.fr.

Funding

This research was funded by Conseil Régional de Bretagne.

Notes

The authors declare no competing financial interest.

ACKNOWLEDGMENTS

We thank Delphine Destoumieux-Garzon and Chris Michiels for kindly providing the *E. coli* ML-35p strain and *E. coli* MG1655 *ivy*::Cm, respectively.

ABBREVIATIONS USED

ONPG, (*o*-nitrophenyl)galactoside; ONP, *o*-nitrophenol; DiSC3, 3,3′-dipropylthiadicarbocyanine; HEPES, 4-(2-hydrox-

yethyl)-1-piperazineethanesulfonic acid; TSB, tryptic soy broth; LB, Luria broth; HP-nitrocefin, hydrolysis product of nitrocefin; AFM, atomic force microscopy; N-L, native lysozyme; DH-L, dry-heated lysozyme

REFERENCES

(1) World Health Organization (WHO). *Overcoming Antimicrobial Resistance*; WHO: Geneva, Switserland, 2000.

(2) Bruhn, C. M. Consumer attitudes toward food additives. In *Food Additives*, 2nd ed.; Branen, A. L., Davidson, P. M., Salminen, S., Thorngate, J. H., Eds.; Marcel Dekker Inc.: New York, 2002; pp 111−119.

(3) *Special Eurobarometer 354: Food-Related Risks*; conducted by TNS Opinion & Social at the request of the European Food Safety Authority (EFSA): Parma, Italy, 2010.

(4) Nguyen, L. T.; Haney, E. F.; Vogel, H. J. The expanding scope of antimicrobial peptide structures and their modes of action. *Trends Biotechnol.* **2011**, *29* (9), 464−472.

(5) Peschel, A.; Sahl, H. G. The co-evolution of host cationic antimicrobial peptides and microbial resistance. *Nat. Rev. Microbiol.* **2006**, *4* (7), 529−536.

(6) Jolles, P.; Jolles, J. Whats new in lysozyme research—always a model system, today as yesterday. *Mol. Cell. Biochem.* **1984**, *63* (2), 165−189.

(7) *European Parliament and Council Directive No 95/2/EC of 20 February 1995 on Food Additives Other Than Coulors and Sweeteners*; European Union: Brussels, Belgium, 1995.

(8) Masschalck, B.; Michiels, C. W. Antimicrobial properties of lysozyme in relation to foodborne vegetative bacteria. *Crit. Rev. Microbiol.* **2003**, *29* (3), 191−214.

(9) Bera, A.; Herbert, S.; Jakob, A.; Vollmer, W.; Götz, F. Why are pathogenic staphylococci so lysozyme resistant? The peptidoglycan O-acetyltransferase OatA is the major determinant for lysozyme resistance of *Staphylococcus aureus*. *Mol. Microbiol.* **2005**, *55* (3), 778−787.

(10) Zipperle, G. F., Jr.; Ezzell, J. W., Jr.; Doyle, R. J. Glucosamine substitution and muramidase susceptibility in *Bacillus anthracis*. *Can. J. Microbiol.* **1984**, *30* (5), 553−559.

(11) Nikaido, H. Molecular basis of bacterial outer membrane permeability revisited. *Microbiol. Mol. Biol. Rev.* **2003**, *67* (4), 593−656.

(12) Callewaert, L.; Masschalck, B.; Deckers, D.; Nakimbugwe, D.; Atanassova, M.; Aertsen, A.; Michiels, C. W. Purification of Ivy, a lysozyme inhibitor from *Escherichia coli*, and characterisation of its specificity for various lysozymes. *Enzyme Microb. Technol.* **2005**, *37* (2), 205−211.

(13) Callewaert, L.; Aertsen, A.; Deckers, D.; Vanoirbeek, K. G.; Vanderkelen, L.; Van Herreweghe, J. M.; Masschalck, B.; Nakimbugwe, D.; Robben, J.; Michiels, C. W. A new family of lysozyme inhibitors contributing to lysozyme tolerance in Gram-negative bacteria. *PloS Pathog.* **2008**, *4* (3), e000019.

(14) Deckers, D.; Masschalck, B.; Aertsen, A.; Callewaert, L.; Van Tiggelen, C. G. M.; Atanassova, M.; Michiels, C. W. Periplasmic lysozyme inhibitor contributes to lysozyme resistance in *Escherichia coli*. *Cell. Mol. Life Sci.* **2004**, *61* (10), 1229−1237.

(15) Pellegrini, A.; Thomas, U.; Vonfellenberg, R.; Wild, P. Bactericidal activities of lysozyme and aprotinin against Gram-negative and Gram-positive bacteria related to their basic character. *J. Appl. Bacteriol.* **1992**, *72* (3), 180−187.

(16) Pellegrini, A.; Thomas, U.; Wild, P.; Schraner, E.; von Fellenberg, R. Effect of lysozyme or modified lysozyme fragments on DNA and RNA synthesis and membrane permeability of *Escherichia coli*. *Microbiol. Res.* **2000**, *155* (2), 69−77.

(17) Wild, P.; Gabrieli, A.; Schraner, E. M.; Pellegrini, A.; Thomas, U.; Frederik, P. M.; Stuart, M. C. A.; Vonfellenberg, R. Reevaluation of the effect of lysoyzme on *Escherichia coli* employing ultrarapid freezing followed by cryoelectronmicroscopy or freeze substitution. *Microsc. Res. Tech.* **1997**, *39* (3), 297−304.

(18) Ibrahim, H. R.; Kato, A.; Kobayashi, K. Antimicrobial effects of lysozyme against Gram-negative bacteria due to covalent binding of palmitic acid. *J. Agric. Food Chem.* **1991**, *39* (11), 2077−2082.

(19) Ibrahim, H. R.; Yamada, M.; Kobayashi, K.; Kato, A. Bactericidal action of lysozyme against Gram-negative bacteria due to insertion of a hydrophobic pentapeptide into its C-terminus. *Biosci., Biotechnol., Biochem.* **1992**, *56* (8), 1361−1363.

(20) Ibrahim, H. R.; Kobayashi, K.; Kato, A. Length of hydrocarbon chain and antimicrobial action to Gram-negative bacteria of fatty acylated lysozyme. *J. Agric. Food Chem.* **1993**, *41* (7), 1164−1168.

(21) Li, C. P.; Ibrahim, H. R.; Sugimoto, Y.; Hatta, H.; Aoki, T. Improvement of functional properties of egg white protein through phosphorylation by dry-heating in the presence of pyrophosphate. *J. Agric. Food Chem.* **2004**, *52* (18), 5752−5758.

(22) Amiri, S.; Ramezani, R.; Aminlari, M. Antibacterial activity of dextran-conjugated lysozyme against *Escherichia coli* and *Staphylococcus aureus* in cheese curd. *J. Food Prot.* **2008**, *71* (2), 411−415.

(23) Ibrahim, H. R.; Hatta, H.; Fujiki, M.; Kim, M.; Yamamoto, T. Enhanced antimicrobial action of lysozyme against Gram-negative and Gram-positive bacteria due to modification with perillaldehyde. *J. Agric. Food Chem.* **1994**, *42* (8), 1813−1817.

(24) Ibrahim, H. R.; Higashiguchi, S.; Juneja, L. R.; Kim, M.; Yamamoto, T. A structural phase of heat-denatured lysozyme with novel antimicrobial action. *J. Agric. Food Chem.* **1996**, *44* (6), 1416−1423.

(25) Ibrahim, H. R.; Higashiguchi, S.; Sugimoto, Y.; Aoki, T. Role of divalent cations in the novel bactericidal activity of the partially unfolded lysozyme. *J. Agric. Food Chem.* **1997**, *45* (1), 89−94.

(26) Ibrahim, H. R.; Higashiguchi, S.; Koketsu, M.; Juneja, L. R.; Kim, M.; Yamamoto, T.; Sugimoto, Y.; Aoki, T. Partially unfolded lysozyme at neutral pH agglutinates and kills Gram-negative and Gram-positive bacteria through membrane damage mechanism. *J. Agric. Food Chem.* **1996**, *44* (12), 3799−3806.

(27) Mine, Y.; Ma, F. P.; Lauriau, S. Antimicrobial peptides released by enzymatic hydrolysis of hen egg white lysozyme. *J. Agric. Food Chem.* **2004**, *52* (5), 1088−1094.

(28) Ibrahim, H. R.; Thomas, U.; Pellegrini, A. A helix-loop-helix peptide at the upper lip of the active site cleft of lysozyme confers potent antimicrobial activity with membrane permeabilization action. *J. Biol. Chem.* **2001**, *276* (47), 43767−43774.

(29) Desfougeres, Y.; Jardin, J.; Lechevalier, V.; Pezennec, S.; Nau, F. Succinimidyl residue formation in hen egg-white lysozyme favors the formation of intermolecular covalent bonds without affecting its tertiary structure. *Biomacromolecules* **2011**, *12* (1), 156−166.

(30) Baron, F.; Cochet, M. F.; Wilfried, A.; Noël, G.; Madec, M. N.; Gonnet, F.; Jan, S.; Gautier, M. Rapid and cost-effective method for micro-organism enumeration based on miniaturization of the conventional plate-counting technique. *Lait* **2006**, *86* (3), 251−257.

(31) Lehrer, R. I.; Barton, A.; Ganz, T. Concurrent assessment of inner and outer-membrane permeabilization and bacteriolysis in *Escherichia coli* by multiple-wavelength spectrophotometry. *J. Immunol. Methods* **1988**, *108* (1−2), 153−158.

(32) Derde, M.; Lechevalier, V.; Guerin-Dubiard, C.; Cochet, M. F.; Jan, S.; Baron, F.; Gautier, M.; Vié, V.; Nau, F. Hen egg white lysozyme permeabilizes the *Escherichia coli* outer and inner membranes. *J. Agric. Food Chem.* **2013**, *61* (41), 9922−9929.

(33) Wu, M.; Maier, E.; Benz, R.; Hancock, R. E. Mechanism of interaction of different classes of cationic antimicrobial peptides with planar bilayers and with the cytoplasmic membrane of *Escherichia coli*. *Biochemistry* **1999**, *38* (22), 7235−7242.

(34) Orlov, D. S.; Nguyen, T.; Lehrer, R. I. Potassium release, a useful tool for studying antimicrobial peptides. *J. Microbiol. Methods* **2002**, *49* (3), 325−328.

(35) Camesano, T.; Natan, M.; Logan, B. Observation of changes in bacterial cell morphology using tapping mode atomic force microscopy. *Langmuir* **2000**, *16* (10), 4563−4572.

(36) Abergel, C.; Monchois, V.; Byrne, D.; Chenivesse, S.; Lembo, F.; Lazzaroni, J. C.; Claverie, J. M. Structure and evolution of the Ivy

protein family, unexpected lysozyme inhibitors in Gram-negative bacteria. *Proc. Natl. Acad. Sci. U.S.A.* **2007**, *104* (15), 6394−6399.
(37) Gruenheid, S.; Le Moual, H. Resistance to antimicrobial peptides in Gram-negative bacteria. *FEMS Microbiol. Lett.* **2012**, *330* (2), 81−89.
(38) Kimelberg, H. K.; Papahadjopoulos, D. Interactions of basic proteins with phospholipid membranes: binding and changes in the sodium permeability of phosphatidylserine vesicles. *J. Biol. Chem.* **1971**, *246* (4), 1142−1148.
(39) Strahl, H.; Hamoen, L. W. Membrane potential is important for bacterial cell division. *Proc. Natl. Acad. Sci. U.S.A.* **2010**, *107* (27), 12281−12286.
(40) Meincken, M.; Holroyd, D. L.; Rautenbach, M. Atomic force microscopy study of the effect of antimicrobial peptides on the cell envelope of *Escherichia coli*. *Antimicrob. Agents Chemother.* **2005**, *49* (10), 4085−4092.
(41) Li, A.; Lee, P.; Ho, B.; Ding, J.; Lim, C. Atomic force microscopy study of the antimicrobial action of Sushi peptides on Gram-negative bacteria. *Biochim. Biophys. Acta, Biomembr.* **2007**, *1768* (3), 411−418.

in aged red wine as a result of ethanol oxidation. In summary, from a mechanistic point of view, the two key parameters leading to the formation of pyranoanthocyanins in red wine are the acidity, which controls the addition of ethanal on flavanols or procyanidins, as well as the cycloaddition of a vinyl group on the anthocyanin skeleton, and the oxygen level for the oxidative aromatization of pyranic ring D.

Pyranoanthocyanins linked directly to flavanol monomers and dimers have been detected and identified in different aged Port wine (i.e., from 2 to 6 year-old). In those wines pyranoanthocyanin−procyanidin dimers appear to be more abundant and more stable than pyranoanthocyanin−flavanol monomers.[22]

Thus the aim of this work was to estimate the impact of acidity and oxygen level in dry red wine on the formation of pyranomalvidin-3-*O*-glucoside-procyanidin dimers. For this purpose, the pH of a dry red wine has been adjusted at 3, 3.5, and 4, and each pH has been submitted to four different levels of oxygen (i.e., 0, 2, 8, and 20 mg/L). The occurrence in dry red wine of these two pyranomalvidin−procyanidin dimers, as well as their kinetics of formation, has been followed by HPLC-UV-MS.

MATERIALS AND METHODS

General. Distilled water was obtained from an ELGA system, and Milli-Q (Millipore) water used for HPLC-UV-MS separation and analysis was prepared using a Sartorius-arium 611 system. Acetonitrile (HPLC grade quality, > 99.8%) was purchased from VWR (Strasbourg, France).

Wine Sample. The wine used was a Merlot vintage 2011 from the "Entre deux mers" region of Bordeaux. The chemical characteristics of the red wine were as follows: a total polyphenolic index (TPI) of 61, a pH of 3.78, a total condensed tannins (i.e., estimated by Ribereau-Gayon and Stonestreet procedure) of 3.22 ± 0.25 g/L, total anthocyanins (i.e., determined using the SO_2 bleaching method) of 603 ± 1.2 mg/L, molecular anthocyanins content (i.e., anthocyanins quantified by HPLC-UV at 520 nm) of 347 ± 11.9 mg/L, and a condensed tannins mean degree of polymerization (mDP; i.e., determined by phloroglucinolysis method) of 4.38 ± 0.04. All of these parameters were determined using similar procedure as described in Chira et al.[23]

Experimental Conditions. The wine was placed in 5 L glass containers, which were closed as tightly as possible, using proper stoppers (i.e., silicone stopper with small septum in order to collect the sample and add oxygen without opening the containers), with addition of vacuum grease around the caps. Each 5 L glass container was flushed with N_2 prior to red wine filling in order to exclude incorporation of oxygen during filling. The wine was split in three pH groups: pH 3, pH 3.5, and pH 4. The pH was adjusted with NaOH (5 M) and/or sulphuric acid (99%). For each pH group, four quantities of oxygen were added: 0, 2, 8, and 20 mg/L. The oxygen was added into the bottles with a syringe filled with pure oxygen. As red wine consumes oxygen quite fast, oxygen was readjusted to 0, 2, 8, and 20 mg/L each week in order to keep constant levels during the four months. Each modality was performed in triplicate.

After four months, 1 mL of each separate sample was filtrated on a 0.45 μm membrane and then injected in the HPLC-UV-MS for identification and quantification. For the quantitative analyses, 900 μL of sample was mixed with 100 μL of chlorogenic acid (500 mg/L) used as internal standard.

Identification of the Pyranoanthocyanin−Procyanidin Dimers by HPLC-UV-MS/MS. These analyses were performed on two different systems. The first one was a Thermo-Finnigan Surveyor HPLC-UV system composed of a UV−vis detector (Surveyor PDA Plus), an autosampler (Surveyor autosampler Plus), and a quaternary pump system (Surveyor LC pump Plus) and controlled by a Xcalibur data treatment system. These analyses were carried out on a 250 × 4.6 mm, 5 μm Lichrospher 100 RP 18 column. The solvents used for the gradient were as follows: solvent A, water with 0.5% of formic acid, and solvent B, acetonitrile with 0.5% formic acid. The gradient used was as follows: from 100 to 85% of A in 5 min, from 85 to 70% of A in 30 min, from 70 to 0% of A in 1 min, then 0% of A during 4 min. The flow rate was set at 1 mL/min, and the tray temperature was fixed at 12 °C. The wavelengths used were 280 and 520 nm. This HPLC-UV system was also coupled to a Thermo-Finnigan LCQ Advantage spectrometer equipped with an electrospray ionization source and an ion trap mass analyzer. The electrospray ionization mass spectrometry detection was performed in positive mode with the following optimized parameters: capillary temperature 300 °C, capillary voltage 5 V, nebulizer gas flow 1.75 L/min, desolvation gas flow 1 L/min, and spray voltage 5 kV. The collision energy was set at 30% for the MS^2 analyses on the ion [M] = 1093 and MS^3 on the ion [M] = 931. The pyranoanthocyanin-procyanidin dimers were identified according to their mass spectra and fragmentation.

The molecular formula of the molecular ion [M] = 1093 as well as the fragment detected during MS/MS analyses with the ion trap were confirmed by injection on a high resolution Q-TOF mass spectrometer. The UHPLC system used was an Agilent 1290 Infinity Series which consisted of a quaternary pump, a solvent degasser, an autosampler, and a diode-array detector. These analyses were carried out on 2.1 × 100 mm, 1.8 μm Eclipse Plus C18. The solvents used for the gradient were: solvent A, water with 0.1% formic acid, and solvent B methanol with 0.1% formic acid at a flow rate of 400 μL/min. The gradient was as follows: 94% of A during 30 s; 94 to 5% of A during 13.5 min; 5% of A during 3 min. This UHPLC system was coupled to an ESI-Q-TOF-MS Agilent 6530 Series Accurate with an electrospray ion source with Agilent Jet Stream Technology. The mass spectrometer was operated in extended dynamic range of 2 GHz with the mass range up to 1700 Th, with a drying gas flow and temperature respectively set at 9 L/min and 300 °C. The nebulizer pressure was set at 25 psi, and the sheath gas flow and temperature were respectively set at 11 L/min and 350 °C. The capillary voltage was of 4 kV. The collision energy was set at 5, 15, and 30% for MS^2 analysis. The fragmentation voltage was set at 150 V. The reference masses used were $[M+H]^+$ = 121.050873, 322.048121, and 1221.990637. The software used for the determination of the exact molecular formula of the pyranoanthocyanin-procyanidin dimers molecular ions, as well as their fragments was MassHunter Qualitative Analysis.

Quantification of the Pyranoanthocyanin−Procyanidin Dimers by HPLC-UV-MS. The quantification of the pyranoanthocyanin−procyanidin dimers was performed by HPLC-UV-MS using the same HPLC Thermo Finnigan Surveyor system coupled to the ion-trap mass apparatus as described above. The pigment has been quantified using pure malvidin-3-*O*-glucoside as standard and chlorogenic acid as internal standard. The calibration curve was accomplished by injecting solutions with increasing concentrations of malvidin-3-*O*-glucoside ranging from 1 to 256 mg/L and containing 50 mg/L of chlorogenic acid. The response factor was established by plotting the concentrations ratios versus the peak-area ratios of malvidin-3-*O*-glucoside ion (i.e., m/z 493) to the internal standard ion (i.e., m/z 355). The R^2 obtained was 0.9998. The quantification of the pyranoanthocyanin-procyanidin dimers was realized using their molecular ion $[M]^+$ = 1093.

RESULTS AND DISCUSSION

The first part of our study was to identify pyranoanthocyanin−procyanidin dimers in Merlot red wine since these pigments have only been detected in aged Port red wine which is a sweet red wine.[22] This identification has been realized by HPLC-UV-MS using both low and high resolution HPLC-MS analysis. During the investigation on Merlot red wine, two peaks with a molecular ion of $[M]^+$ = 1093 have been detected which could be the two pyranomalvidin-3-*O*-glucoside-procyanidin dimers as previously described in aged Port wine.[11,22,24,25] MS^n analysis

with an ion trap mass spectrometer has been conducted to confirm this assignation. Fragmentation pattern in MS^2 of the molecular ion m/z 1093 leads to the formation of a single ion at m/z 931 which can result of the loss of a glucose moiety (i.e., loss of 162 amu). Then, a MS^3 analysis performed on the m/z 931 ion led to the formation of three main fragments at m/z 779, 641, and 623 (Figure 1). The fragment at m/z 641

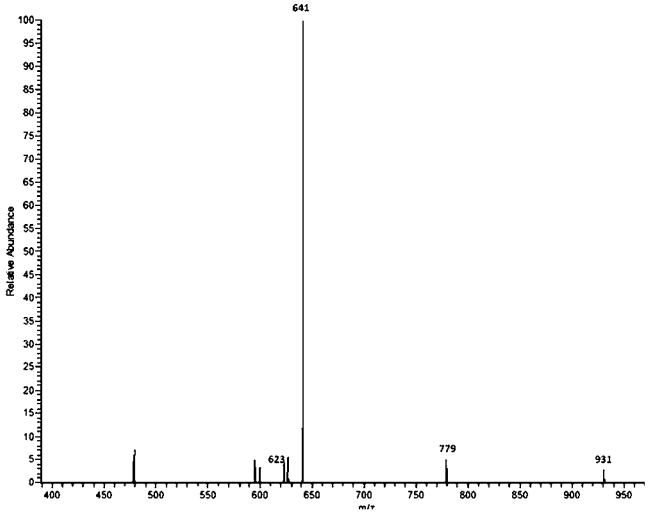

Figure 1. MS^3 fragmentation of the $[M]^+$ = 1093 compound.

resulted from the direct cleavage of the interflavanoid linkage from the pyranomalvidin-procyanidin-dimer aglycone (i.e., m/z 931). This fragment m/z 641 can then undergo a water elimination to form a new fragment at m/z 623. Another important fragmentation pattern of the ion at m/z 931 was attributable to the RDA (Retro-Diels–Alder) ring fission of the C-ring of the upper flavanol unit leading to an ion at m/z 779. This RDA ring fission was a key fragmentation for the structure elucidation, proving the presence of the procyanidin moieties in the molecule. Such fragmentation patterns (Figure 2) are in accordance with the fragmentation pattern of the pyranomalvidin–procyanidin dimer detected in Port wine.[22]

To confirm this assignation of both the molecular ion as well as the observed fragments, HPLC-UV-MS analysis using a high resolution Q-TOF mass spectrometer has been performed (Figure 3). This analysis clearly showed that the molecular ion of both peaks had a chemical formula of $C_{55}H_{49}O_{24}$ with a very high identity score and an extremely low difference (i.e., 0.34 ppm) between the measured mass and the calculated one (Table 1). Similarly, the identification and chemical formulas of the fragments have also been confirmed by high resolution mass analysis since the mass differences between the measured and the calculated masses were around 5 ppm. These investigations in HPLC-UV-MS confirmed the identification in dry red wine of two pyranomalvidin–3-*O*-glucoside-procyanidin dimers.

Following this first identification in dry red wine, a quantification method by HPLC-UV-MS using chlorogenic acid as internal standard has been developed and used to estimate the impact of acidity and oxygen levels in wine on the formation of these two pyranomalvidin–3-*O*-glucoside-procyanidin dimers. As shown in Figure 4, the quantification of both pyranomalvidin–procyanidin dimers showed similar trends among the different studied modalities (i.e., three pH 3, 3.5, and 4 as well as four different level oxygen 0, 2, 8, and 20 mg/L). Among the same pH, it clearly appeared that the amounts of the quantified compounds constantly increased from 0 to 20 mg/L of oxygen. In the modality without oxygen at pH 3, these compounds were present at the lowest concentration (i.e., around 2 mg/L), while in the modalities with 2, 8, and 20 mg/L of oxygen, the concentrations were respectively of 5.5, 14.5, and 19.7 mg/L. Following a similar trend, for a same quantity of oxygen, the amounts of the pyranomalvidin–procyanidin dimers increased along with the acidity of the red wine. Indeed, for the modality with the highest oxygen concentration, the amounts were 19.7, 12.5, and 4.6 mg/L from pH 3 to pH 4. However, for all studied pH, the lowest level was observed for the modality without oxygen, with concentrations of 2.0, 1.7, and 1.9 mg/L for the pH 3, 3.5, and 4, respectively. A similar trend has been previously observed from pyranomanthocyanins deriving from a vinyl cycloaddition mechanism in red wine with a single oxygen level and with three different pH.[26]

The observed formation trends according to pH and oxygen levels were of interest and confirmed these key parameters in the mechanism leading to the formation of pyranomalvidin–procyanidin dimers in red wine. Indeed, without oxygen the lowest level of pyranomalvidin–procyanidin dimers were similar for each pH which confirmed that oxygen is absolutely needed for the oxidative aromatization of the newly formed pyranic ring D of the pyranoanthocyanins. Similarly, the acidity of the red wine also appeared to be an important feature since the highest concentrations of pyranomalvidin–procyanidin dimers were observed for the lowest pH in the presence of oxygen.

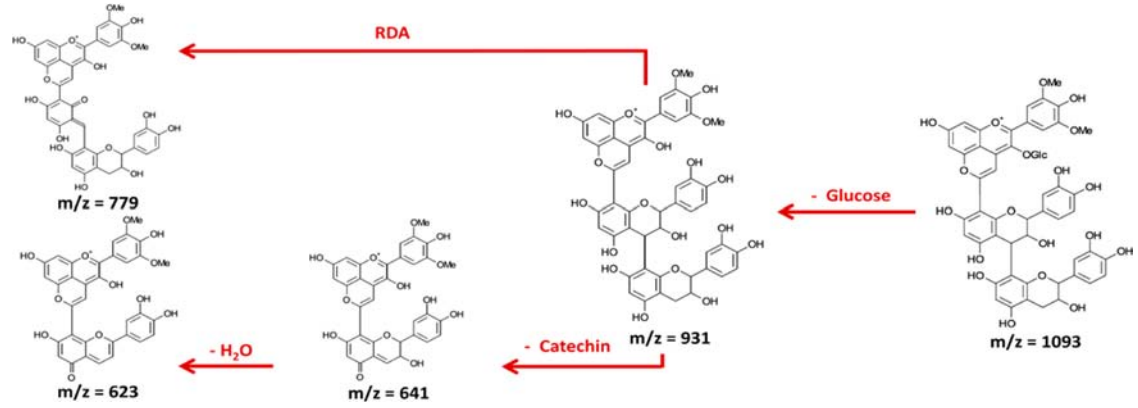

Figure 2. Fragmentation pattern of the pyranomalvidin–3-*O*-glucoside-procyanidin dimer.

dx.doi.org/10.1021/jf4052754 | *J. Agric. Food Chem.* 2014, 62, 1701–1705

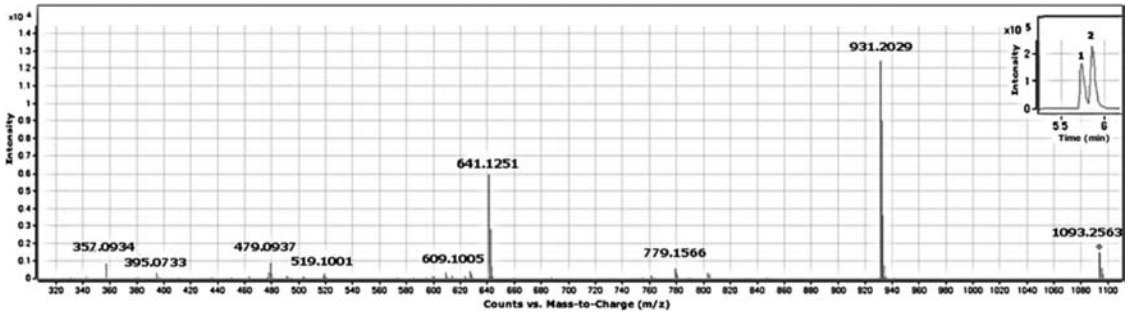

Figure 3. Extract ion chromatogram (EIC) of $[M]^+$ = 1093 compound (right corner) and ion spectrum after MS/MS fragmentation with Q-TOF.

Table 1. Accurate Mass Analyses of the Fragments

fragment $[M]^+$	chemical formula	mass difference (ppm)	score[b]	corresponding fragment
1093.2607	$C_{55}H_{49}O_{24}$	0.34	99.11	pyranomalvidin−procyanidin dimer
931.2026	$C_{49}H_{39}O_{19}$	5.82	X	glucose
779.1569	$C_{41}H_{31}O_{16}$	4.88	X	RDA ring fission[a]
641.1256	$C_{34}H_{25}O_{13}$	5.28	X	glucose, catechin

[a]RDA: (Retro-Diels−Alder) ring fission of the C-ring of the upper flavanol. [b]Score represent a percentage of identity between the calculate molecular formula and the analyzed mass taking in too account the obtained mass as well as the isotopic abondances.

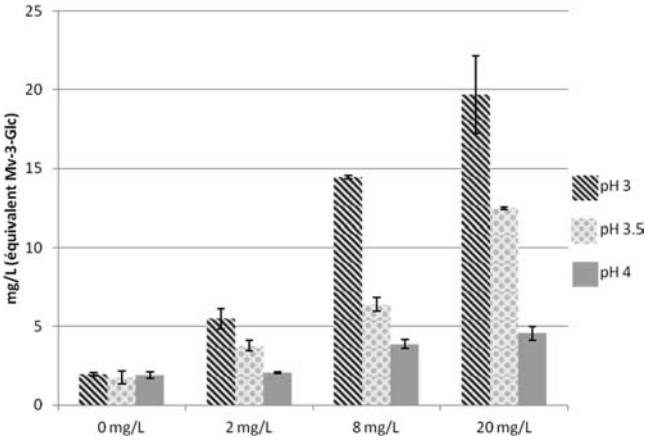

Figure 4. Evolution of the pyranomalvidin−-3-*O*-glucoside-procyanidin dimer content in red wine according to pH and oxygen level.

From an oenological point of view, the key involvement of red wine acidity in the formation of pyranoanthocyanins is an important parameter for red wine color stabilization since over the last two decades, red wine acidity tends to decrease due to the global warming. Such decrease in wine acidity might result in a diminution of pyranoanthocyanins contents, which are an important contributor to red wine color stability. Further studies on the impact of pH and oxygen levels on the formation of the other pyranoanthocyanins are actually under investigation.

AUTHOR INFORMATION

Corresponding Author

*Tel: (+33)557575850. Fax: (+33)557575813. E-mail: p.teissedre@u-bordeaux2.fr.

Funding

L.P. is supported by two French financial grants of Agricultural french Ministry FAM (France Agrimer) Nos. 2011-1162 and 2012-1025 and by a French financial grant of CIVB (Conseil Interprofessionnel des Vins de Bordeaux) No. 30566 (2011-2014). The authors gratefully thank CIVB (Conseil Interprofessionnel des Vins de Bordeaux) and the Region Aquitaine for providing funds for the acquisition of the HPLC-MS(n)-UV/Fluo material.

Notes

The authors declare no competing financial interest.

ACKNOWLEDGMENTS

The authors gratefully thank Christian POUPOT for his help with the wine oxygen delivery experiments.

REFERENCES

(1) Glories, Y.; Maujean, A.; Dubourdieu, D.; Ribéreau-Gayon, P. *Traité d'oenologie: Tome 2, Chimie du vin, stabilisation et traitement*; 5th ed.; Dunod, 2004.

(2) Arnold, R. A.; Noble, A. C.; Singleton, V. L. Bitterness and astringency of phenolic fractions in wine. *J. Agric. Food Chem.* **1980**, *28*, 675−678.

(3) Bakker, J.; Timberlake, C. F. The distribution of anthocyanins in grape skin extracts of port wine cultivars as determined by High Performance Liquid Chromatography. *J. Sci. Food Agric.* **1985**, *36*, 1315−1324.

(4) Bakker, J.; Timberlake, C. F. The distribution and content of anthocyanins in young port wines as determined by High Performance Liquid Chromatography. *J. Sci. Food Agric.* **1985**, *36*, 1325−1333.

(5) Brouillard, R.; Dubois, J.-E. Mechanism of the structural transformations of anthocyanins in acidic media. *J. Am. Chem. Soc.* **1977**, *99*, 1359−1364.

(6) Remy, S.; Fulcrand, H.; Labarbe, B.; Cheynier, V.; Moutounet, M. First confirmation in red wine of products resulting from direct anthocyanin−tannin reactions. *J. Sci. Food Agric.* **2000**, *80*, 745−751.

(7) Salas, E.; Atanasova, V.; Poncet-Legrand, C.; Meudec, E.; Mazauric, J. .; Cheynier, V. Demonstration of the occurrence of flavanol−anthocyanin adducts in wine and in model solutions. *Anal. Chim. Acta* **2004**, *513*, 325−332.

(8) Timberlake, C. F.; Bridle, P. Interactions between anthocyanins, phenolic compounds, and acetaldehyde and their significance in red wines. *Am. J. Enol. Vitic.* **1976**, *27*, 97−105.

(9) Rivas-Gonzalo, J. C.; Bravo-Haro, S.; Santos-Buelga, C. Detection of compounds formed through the reaction of malvidin 3-monoglucoside and catechin in the presence of acetaldehyde. *J. Agric. Food Chem.* **1995**, *43*, 1444−1449.

(10) Fulcrand, H.; Santos, P.-J. C.; dos Sarni-Manchado, P.; Cheynier, V.; Favre-Bonvin, J. Structure of new anthocyanin-derived wine pigments. *J. Chem. Soc. Perkin Trans. 1* **1996**, 735−739.

(11) Mateus, N.; Silva, A. M. S.; Santos-Buelga, C.; Rivas-Gonzalo, J. C.; de Freitas, V. Identification of anthocyanin-flavanol pigments in

red wines by NMR and Mass Spectrometry. *J. Agric. Food Chem.* **2002**, *50*, 2110−2116.
(12) Mateus, N.; Silva, A. M. S.; Rivas-Gonzalo, J. C.; Santos-Buelga, C.; de Freitas, V. A new class of blue anthocyanin-derived pigments isolated from red wines. *J. Agric. Food Chem.* **2003**, *51*, 1919−1923.
(13) Cameira-dos-Santos, P.-J.; Brillouet, J.-M.; Cheynier, V.; Moutounet, M. Detection and partial characterisation of new anthocyanin-derived pigments in wine. *J. Sci. Food Agric.* **1996**, *70*, 204−208.
(14) Atanasova, V.; Fulcrand, H.; Le Guernevé, C.; Cheynier, V.; Moutounet, M. Structure of a new dimeric acetaldehyde malvidin 3-glucoside condensation product. *Tetrahedron Lett.* **2002**, *43*, 6151−6153.
(15) Es-Safi, N.-E.; Le Guernevé, C.; Fulcrand, H.; Cheynier, V.; Moutounet, M. New Polyphenolic compounds with xanthylium skeletons formed through reaction between (+)-catechin and glyoxylic acid. *J. Agric. Food Chem.* **1999**, *47*, 5211−5217.
(16) Francia-Aricha, E. M.; Rivas-Gonzalo, J. C.; Santos-Buelga, C. Effect of malvidin-3-monoglucoside on the browning of monomeric and dimeric flavanols. *Z. Für Leb. Forsch. A* **1998**, *207*, 223−228.
(17) Chassaing, S.; Lefeuvre, D.; Jacquet, R.; Jourdes, M.; Ducasse, L.; Galland, S.; Grelard, A.; Saucier, C.; Teissedre, P.-L.; Dangles, O.; Quideau, S. Physicochemical studies of new anthocyano-ellagitannin hybrid pigments: About the origin of the influence of oak *C*-glycosidic ellagitannins on wine color. *Eur. J. Org. Chem.* **2010**, *2010*, 55−63.
(18) Oliveira, J.; Azevedo, J.; Silva, A. M. S.; Teixeira, N.; Cruz, L.; Mateus, N.; de Freitas, V. Pyranoanthocyanin dimers: A new family of turquoise blue anthocyanin-derived pigments found in port wine. *J. Agric. Food Chem.* **2010**, *58*, 5154−5159.
(19) Bakker, J.; Timberlake, C. F. Isolation, identification, and characterization of new color-stable anthocyanins occurring in some red wines. *J. Agric. Food Chem.* **1997**, *45*, 35−43.
(20) Freitas, V.; Mateus, N. Formation of pyranoanthocyanins in red wines: A new and diverse class of anthocyanin derivatives. *Anal. Bioanal. Chem.* **2011**, *401*, 1463−1473.
(21) Es-Safi, N.-E.; Fulcrand, H.; Cheynier, V.; Moutounet, M. Studies on the acetaldehyde-induced condensation of (−)-epicatechin and malvidin 3-*O*-glucoside in a model solution system. *J. Agric. Food Chem.* **1999**, *47*, 2096−2102.
(22) He, J.; Santos-Buelga, C.; Mateus, N.; de Freitas, V. Isolation and quantification of oligomeric pyranoanthocyanin-flavanol pigments from red wines by combination of column chromatographic techniques. *J. Chromatogr. A* **2006**, *1134*, 215−225.
(23) Chira, K.; Jourdes, M.; Teissedre, P.-L. Cabernet sauvignon red wine astringency quality control by tannin characterization and polymerization during storage. *Eur. Food Res. Technol.* **2012**, *234*, 253−261.
(24) Asenstorfer, R. E.; Hayasaka, Y.; Jones, G. P. Isolation and structures of oligomeric wine pigments by bisulfite-mediated ion-exchange chromatography. *J. Agric. Food Chem.* **2001**, *49*, 5957−5963.
(25) Vivar-Quintana, A. M.; Santos-Buelga, C.; Francia-Aricha, E.; Rivas-Gonzalo, J. C. Formation of anthocyanin-derived pigments in experimental red wines. *Food Sci. Technol. Int.* **1999**, *5*, 347−352.
(26) Kountoudakis, N.; Gonzalez, E.; Gil, M.; Esteruelas, M.; Fort, F.; Canals, J. M.; Zamora, F. Influence of wine pH on changes in color and polyphenol composition induced by micro-oxygenation. *J. Agric. Food Chem.* **2011**, *59*, 1974−1984.

The leaf EOs of the cinnamaldehyde-type *C.o.* have been proved to have excellent bioactivities, such as antifungal,[16] antibacterial,[17] antipathogenic,[18] anti-inflammatory,[19] antihyperuricemia,[20] antidyslipidemic,[21] and mosquito larvicidal activities.[22] Although there are so many bioactivities in the cinnamaldehyde-type *C.o.*, the information related to the coumarin contents of this species is very limited. To seek an alternative source for safe cinnamons without harvesting trees, the leaves of the cinnamaldehyde-type *C.o.* might have a great potential for this purpose. The objective of this study was to identify the coumarin level of this indigenous cinnamon. Samples from different geographical regions in Taiwan were collected, and the major constituents of essential oils from these samples were compared. Cassia cinnamon samples from local markets were also included in the comparison.

MATERIALS AND METHODS

Plant Materials. Leaves of *Cinnamomum osmophloeum* ct. cinnamaldehyde (*C.o.*) from sixteen individual clones were collected from six different geographic sites in Taiwan in 2006 and 2010, and the trees were about 20 years old when harvested. All samples were identified by Sheng-Yu Lu and Yen-Ray Hsui, Taiwan Forestry Research Institute. Voucher specimens were deposited with the Laboratory of Wood Chemistry (School of Forestry and Resource Conservation, National Taiwan University). Table 1 lists the detailed information of the *C.o.* leaf samples. The sites where these *C.o.* leaves harvested are also indicated in Figure 1. To compare the differences of flavoring constituents between Cassia cinnamon and *C.o.*, three additional bark samples of *Cinnamomum cassia* (*C.c.*), commonly sold in the local markets, were used for comparison. Two *C.c.* leaf samples were also collected for comparison (Table 1). All samples were air-dried at ambient temperature (23 °C) and stored at 4 °C for further experiments.

Table 1. Detailed Information of *Cinnamomum osmophloeum* ct. cinnamaldehyde (*C.o.*) and *Cinnamomum cassia* (*C.c.*) Collected

species	geographic site[a] or source	sample type	no. of samples	sample ID	time collected[b] or purchased
C.o.	A	leaf	5	CoL1−5	2010
	B	leaf	5	CoL6−10	2006
	C	leaf	2	CoL11−12	2010
	D	leaf	1	CoL13	2010
	E	leaf	1	CoL14	2010
	F	leaf	2	CoL15−16	2010
C.c.	G	leaf	2	CcL1−2	2010
	commercial source	bark (powder)	1	CcBP	2011
	commercial source	bark (twig)	1	CcTB	2011
	commercial source	bark (stem)	1	CcSB	2011

[a]Please refer to Figure 1 for the geographic sites. [b]Samples were collected between October and November.

Chemicals. The authentic compounds used to verify the flavoring constituents in current study, including *trans*-cinnamaldehyde, *trans*-cinnamyl acetate, *trans*-cinnamic acid, coumarin, and eugenol, are from TCI (Japan), Acros (Belgium), or Sigma-Aldrich (USA). The purities of these compounds are more than 95%.

Distillation of Essential Oils. About 200 g of air-dried samples with 1000 mL of water were hydrodistilled for 6 h in a Clevenger-type apparatus. The essential oils were stored in airtight brown bottles at 4 °C before further GC or GC−MS analyses.

Figure 1. Geographic sites of *Cinnamomum osmophloeum* ct. cinnamaldehyde (*C.o.*) and *Cinnamomum cassia* (*C.c.*) samplings. A: Fushan. B: Lileng. C: Hualian. D: Changhua. E: Lugu. F: Puli. G: Sinsian.

Instrumentation. A Thermo Trace GC Ultra system (Thermo Scientific, Waltham, MA, USA) was used to quantify the major flavoring constituents of different samples. GC was performed on a 30 m DB-5 ms column (J&W Scientific, Folsom, CA, USA) with 0.25 μm film thickness and 0.25 mm inner diameter. The injection port was set to 250 °C, and the flame ionization detector (FID) was set to 300 °C. The helium flow was 1 mL/min, and the splitting ratio was 10:1. After a 1 min isothermal heating at 60 °C, the oven temperature was programmed at 4 °C/min to 220 °C, held for 2 min, increased at 20 °C/min to 250 °C, and held isocratic for 2 min. The peak areas of the target compounds were used to quantify the absolute contents (mg/kg of EO) compared to that of calibration samples with known concentrations.

The same Thermo Trace GC Ultra system with a PolarisQ MSD mass spectrometer (Thermo Scientific, Waltham, MA, USA) was used for the compound authentication. The column and method used for GC−MS analysis were the same as those in the GC analysis, except the ion source was adjusted to 230 °C. Mass spectra were recorded from m/z 50 to 400 with an electron ionization of 70 eV. The compound authentication was achieved by the search results from NIST Mass Spectral Search Program V. 2.0 (National Institute of Standards and Technology, USA) and Wiley 7.0 mass database. Coinjection of the authentic compounds and calculation of the Kovats indices (KI)[23] were also used for the compound authentication.

Statistics. Different groups were compared all together by multiple means comparisons (Tukey HSD test, $\alpha = 0.05$) to test for significant differences among groups (SAS 9.3, SAS Institute Inc., USA). All data are expressed as mean ± SE ($n = 3$).

RESULTS AND DISCUSSION

Comparison of Main Compounds from the Essential Oils of *C.o.* Leaves and *C.c.* Samples. To know whether the

dx.doi.org/10.1021/jf405312q | J. Agric. Food Chem. 2014, 62, 1706−1712

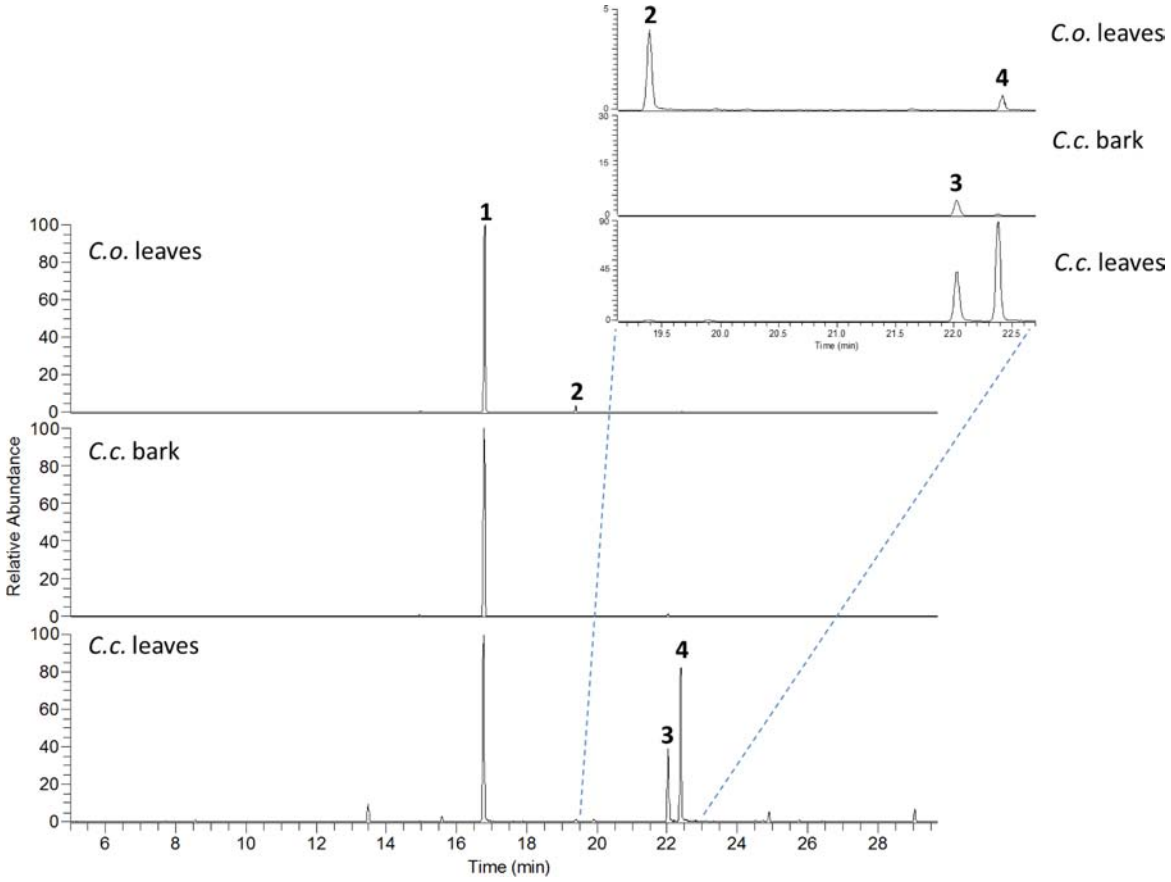

Figure 2. GC−MS chromatograms of essential oils from *C.o.* leaves, *C.c.* bark, and *C.c.* leaves. **1**: Cinnamaldehyde. **2**: Eugenol. **3**: Coumarin. **4**: Cinnamyl acetate.

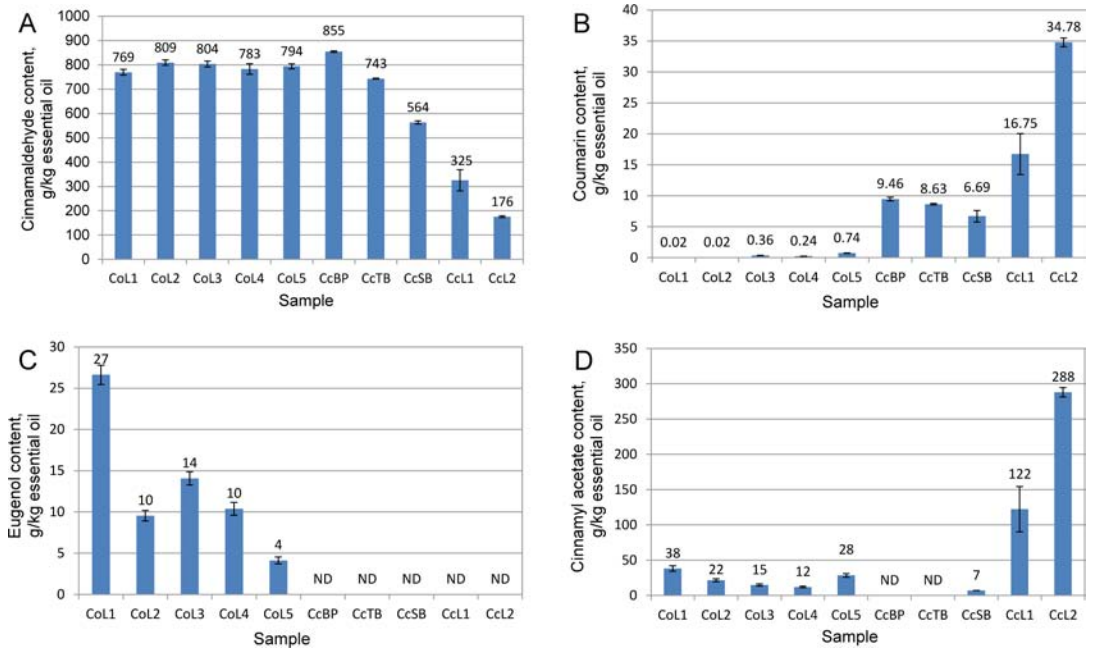

Figure 3. Variations of the main compounds from the essential oils of *C.o.* leaves (CoL) and *C.c.* samples (CcBP, bark powder; CcTB, twig bark; CcSB, stem bark; CcL, leaves). (A) Cinnamaldehyde. (B) Coumarin. (C) Eugenol. (D) Cinnamyl acetate. ND: not detected. All data are mean ± SE (n = 3). Please refer to Table 1 for the sample ID.

essential oils of *C.o.* leaves contain high levels of coumarin, *C.o.* leaves from five individual trees in one location (site A, Figure 1) were collected and the major compounds of their essential oils were compared with that of the essential oils from *C.c.* samples. The typical chromatograms of the essential oils from *C.o.* leaves, *C.c.* bark, and *C.c.* leaves are shown in Figure 2. The

dx.doi.org/10.1021/jf405312q | J. Agric. Food Chem. 2014, 62, 1706−1712

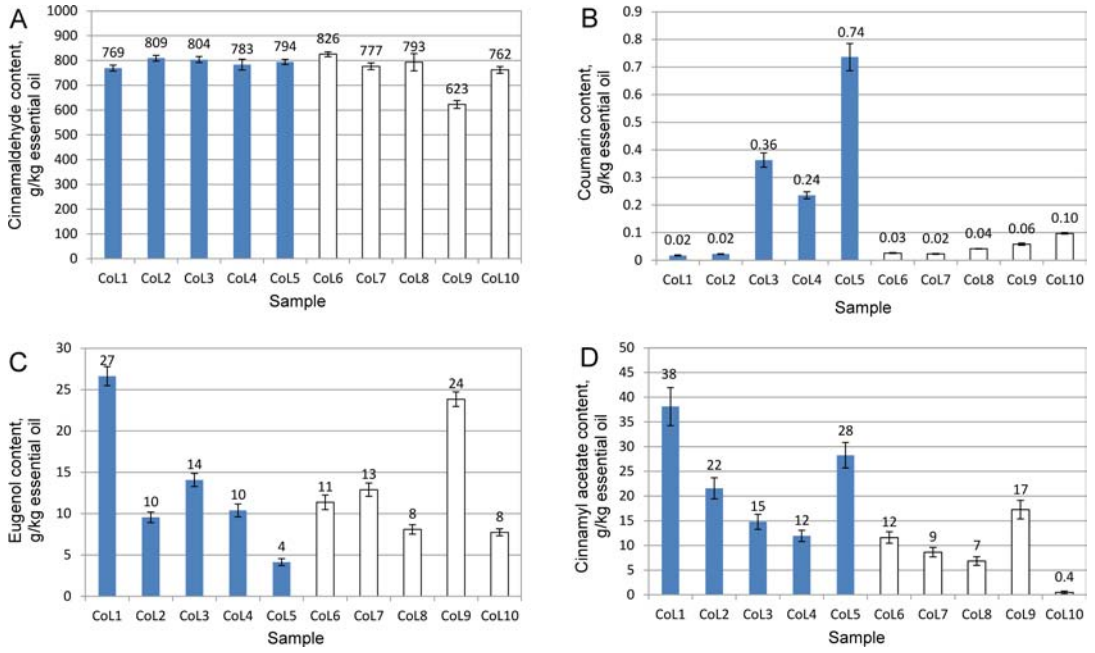

Figure 4. Variations of the main compounds from the essential oils of *C.o.* leaves in the same site. Solid bar: site A. Open bar: site B. (A) Cinnamaldehyde. (B) Coumarin. (C) Eugenol. (D) Cinnamyl acetate. All data are mean ± SE (n = 3). Please refer to Table 1 for the sample ID and site.

major compounds of essential oils from *C.o.* leaves (CoL1−CoL5 in Figure 3) detected by GC−MS are cinnamaldehyde, coumarin, eugenol, and cinnamyl acetate. About 80% (w/w) of the *C.o.* leaf EOs are composed of cinnamaldehyde (Figure 3A), and these values ranged from 769 to 809 g/kg of EOs, which correspond to about 8.9−26.1 g/kg of sample. The cinnamaldehyde contents from *C.o.* leaf EOs are rather comparable to that from *C.c.* bark EOs, ranging from 564 g/kg of EO for the *C.c.* stem bark (CcSB in Figure 3A) to 855 g/kg of EO for the *C.c.* bark powder (CcBP in Figure 3A). These values would be 23.6−33.8 g/kg based on sample weights. Woehrlin et al. reported that the cinnamaldehyde contents of *C.c.* powders were 12.0−42.6 g/kg of sample and that those of *C.c.* sticks were 8.93−54.3 g/kg of sample.[6] Similar cinnamaldehyde contents (15.4−22.3 g/kg) were also reported by Wang et al. when they analyzed *C.c.* bark samples.[4] Both results are consistent with our measurements. The cinnamaldehyde contents of the *C.c.* leaf EOs (CcL1 and CcL2 in Figure 3A) are 325 g/kg of EO and 176 g/kg of EO, respectively. Both are much lower than the cinnamaldehyde contents of the *C.o.* leaf EOs and the *C.c.* bark EOs, indicating that *C.c.* leaves are not a good source for cinnamaldehyde flavoring materials. Researchers have pointed out that a good quality cinnamon would contain 60−90% of cinnamaldehyde as the major constituent in its volatile oil.[3] *C.o.* leaf EOs contain about 80% of cinnamaldehyde as the major constituent, and hence *C.o.* leaves can be considered a good quality and also a great potential cinnamon substitute source to replace commercial bark cinnamons.

The coumarin contents of the *C.o.* leaf EOs are about 0.02−0.74 g/kg of EOs (Figure 3B), which correspond to 0.29−13.99 mg/kg leaf samples. The coumarin contents of the *C.c.* bark EOs are 6.69−9.46 g/kg of EOs (Figure 3B) and correspond to 94.1−374.6 mg/kg bark samples. The coumarin contents of the *C.c.* leaf EOs are 16.75−34.78 g/kg of EOs, however these values correspond to 26.8−97.4 mg/kg leaf samples due to very low EO yields of the *C.c.* leaf samples. Cassia cinnamon bark is known to contain a certain amount of coumarin,[4−7,24] and the amounts vary by research ranging from 40 to 12180 mg/kg of sample. These amounts of coumarin far exceed 2 mg/kg of sample, the maximum limits of coumarin for food in general set by the Council of European Communities in 1988.[11] Our results also confirmed that the *C.c.* bark samples contain high level of coumarin, whereas the *C.o.* leaf samples contain rather low levels of coumarin. Furthermore, the coumarin contents of the two *C.o.* leaf samples, CoL1 and CoL2, are remarkably lower than 2 mg/kg of sample, and they are 0.29 and 0.72 mg/kg of sample, respectively. Identifying *C.o.* clones with low-coumarin and high-cinnamaldehyde contents in their leaves as a potential source for bark cinnamon substitution would be very beneficial for reducing the coumarin-induced hepatotoxicity to certain groups of the populations.

Eugenol (Figure 3C) constitutes about 4−27 g per kg of the *C.o.* leaf EOs (i.e., 118−455 mg/kg leaf sample), but was not detected for all *C.c.* samples tested. Cassia cinnamon was often reported to be without eugenol.[4,6] Eugenol, the principal ingredient of cloves and their products, is widely used in agricultural industries as a food additive to protect foods from microbes during storage, and it is also routinely used in dental clinics as an antiseptic and analgesic.[25] Although eugenol appears to induce cytotoxicity at levels far greater than those occurring in foods,[26] when it is used as a food additive, it is listed as "generally recognized as safe (GRAS)" by the US Food and Drug Administration.[27] Yeh et al. reported that *C.o.* leaf EOs containing eugenol have a longer shelf life and thermostability compared to those without eugenol.[28] Bevilacqua et al. also pointed out that the combination of eugenol and cinnamaldehyde has excellent antimicrobial activity and is good for food product preservation.[29] This indicates that the shelf life of *C.o.* leaf samples could be longer than that of *C.c.* bark samples due to the existence of both eugenol and cinnamaldehyde within *C.o.* leaf EOs.

dx.doi.org/10.1021/jf405312q | J. Agric. Food Chem. 2014, 62, 1706−1712

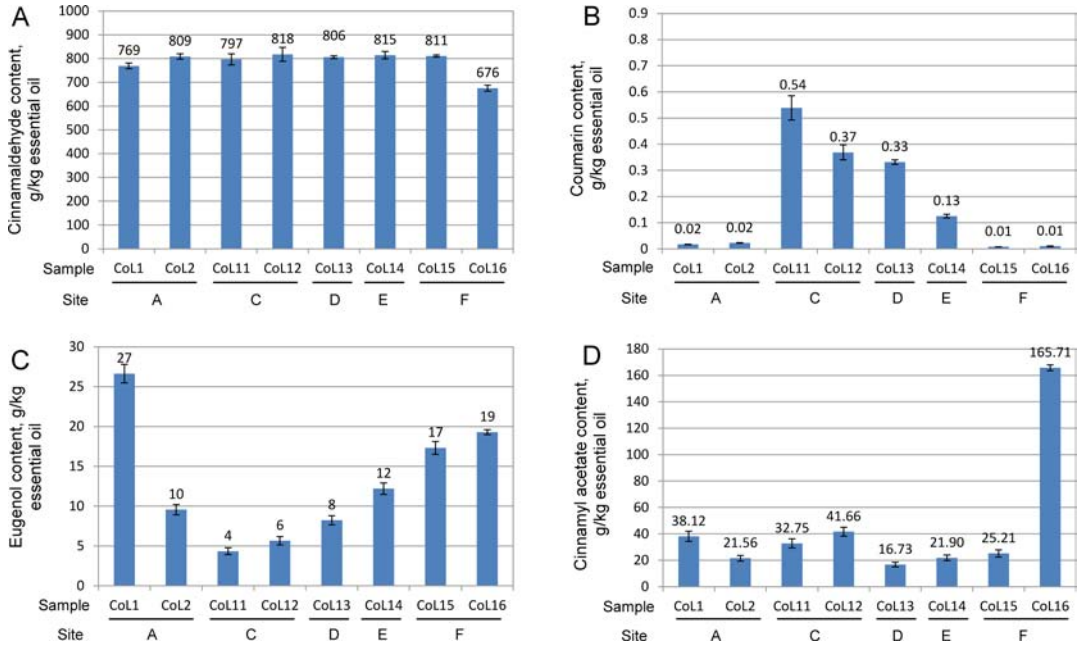

Figure 5. Variations of the main compounds from the essential oils of *C.o.* leaves from different geographic sites. (A) Cinnamaldehyde. (B) Coumarin. (C) Eugenol. (D) Cinnamyl acetate. All data are mean ± SE (n = 3). Please refer to Table 1 for the sample ID and site.

Cinnamyl acetate (Figure 3D) constitutes about 12−38 g/kg of EOs of the *C.o.* leaves (i.e., 136−694 mg/kg of *C.o.* leaf samples). The *C.c.* stem bark sample contains cinnamyl acetate in the level of about 7 g/kg of bark EO (i.e., 290 mg/kg of *C.c.* stem bark sample), and this level is higher in the *C.c.* leaf samples, about 122−288 g/kg of leaf EOs (i.e., 195−807 mg/kg of *C.c.* leaf samples). We did not detect any cinnamic acid (data not show) in the *C.o.* leaves' EOs, however, we did detect cinnamic acid of 88 and 132 g/kg of EOs (i.e., 960 and 5506 mg/kg of sample) from the *C.c.* twig bark and stem bark samples.

Clonal Variations of Essential Oils in *C.o.* Leaves from the Same Site. To know the clonal variations of the essential oils in *C.o.* leaves from the same geographic region, 5 additional *C.o.* clone samples from the second site (site B) were compared and the compositions of their leaf EOs were analyzed (Figure 4). The results showed that the cinnamaldehyde contents of the *C.o.* leaves within the same site, either site A or site B, are quite similar (Tukey HSD test, α = 0.05). They are all about 80% (w/w) of EOs in Figure 4A, except for that of CoL9 sample in site B. Although the cinnamaldehyde content of CoL9 sample is in the margin of 62.3% EO, it is still more than 60% of EO, which can also be considered as a good quality cinnamon source.

The clonal variations of the coumarin contents in *C.o.* leaves showed significant difference within site A (Tukey HSD test, α = 0.05), except for CoL1 and CoL2 samples (Figure 4B), whereas this big variation was less significant between different samples from site B (0.03−0.10 g/kg of EOs), indicating that the coumarin contents of the *C.o.* clones in site B are generally low-coumarin clones compared to that from site A. If *C.o.* clones from site A will be selected for future massive propagation for commercial purposes, a further coumarin screening for individual clones will be needed to ensure low-coumarin *C.o.* clones are selected for propagation to reduce the potential risk of coumarin-induced toxicity.

The clonal variations of eugenol and cinnamyl acetate contents from either site A or site B show differences within the same site (Tukey HSD test, α = 0.05). The eugenol content variations of the *C.o.* clones in site A range between 4 and 27 g/kg of EOs, and those of clones in site B range between 8 and 24 g/kg of EOs (Figure 4C). The *C.o.* leaves from site A contain 12−38 g of cinnamyl acetate per kg of EOs, however, those from site B contain 0.4−17 g of cinnamyl acetate per kg of EOs (Figure 4C). Franz pointed out that composition variation within a species seems to be the principle in essential oil crops,[30] and hence the variation seen within site A or site B is likely under the individual genetic variability of the *C.o.* plant itself.

Variations of Main Compounds from the EOs of *C.o.* Leaves from Different Geographic Sites. Additional samples from 4 different geographic sites were collected and compared with the low-coumarin clones (CoL1 and CoL2) from site A. The results showed that the cinnamaldehyde contents in the *C.o.* leaves from different sites were no different under Tukey HSD test at α = 0.05 level (Figure 5A), indicating that cinnamaldehyde contents of the *C.o.* leaves were quite consistent and stable between different geographic sites. The cinnamaldehyde contents of the *C.o.* leaves from different sites were all above 60% EO, which meets the criterion as a good quality cinnamon source indicated by Poole and Poole.[3]

The *C.o.* leaves from sites C, D, and E show relatively higher level of coumarin contents compared to those from sites A (CoL1 and CoL2) and F (CoL15 and CoL16) (Figure 5B). The coumarin contents of the *C.o.* leaves do vary by different geographic sites (Tukey HSD test, α = 0.05). The coumarin contents of the *C.o.* leaves from sites A (CoL1 and CoL2) and F (CoL15 and CoL16) were all around 0.01−0.02 g/kg of EOs. If we calculate them on the basis of leaf sample weight, they are all significantly lower than 2 mg/kg of sample, and are 0.29, 0.72, 0.13, and 0.15 mg/kg of leaf samples, respectively. The coumarin contents of many cinnamon species including *C. cassia*, *C. verum*, *C. burmannii*, *C. loureiroi*, *Cinnamomum*

dx.doi.org/10.1021/jf405312q | J. Agric. Food Chem. 2014, 62, 1706−1712

wilsonii, and *Cinnamomum japonicum* have been reported by many researchers,[3,4,6,7] and only *C. verum* samples (Ceylon cinnamon) might contain coumarin lower than 2 mg/kg of sample. All other samples were reported to exceed the 2 mg of coumarin per kg of sample regulation.[3,4,6,7] Our samples show that specific *C.o.* clones from some areas did show very low coumarin contents (lower than 2 mg/kg of sample).

The eugenol contents of the *C.o.* leaves from different geographic regions were from 4 to 27 g/kg of EOs (Figure 5C), and showed no significant difference between different sites except that from site C (Tukey HSD test, $\alpha = 0.05$). However the eugenol contents from all *C.o.* leaf samples were higher than those from the *C.c.* samples (Figure 3C), indicating that the shelf life of the *C.o.* leaf samples could be longer compared to that of the *C.c.* samples. The cinnamyl acetate contents of the *C.o.* leaves from different geographic sites showed no significant difference between different sites (Tukey HSD test, $\alpha = 0.05$) (Figure 5D).

Our results clearly suggested that leaves of *Cinnamomum osmophloeum* ct. cinnamaldehyde could be a potential renewable source for a better cinnamon substitute due to its low coumarin content. It will be worth selecting the high-cinnamaldehyde, low-coumarin, and eugenol-containing clones from the specific sites, and conducting further field tests using clonal propagations in different sites to test if these high-cinnamaldehyde, low-coumarin, and eugenol-containing clones are stable over different geographic regions and seasons. This will promote these special clones for further commercial purposes.

AUTHOR INFORMATION

Corresponding Author

*Phone: +886-2-33664626. Fax: +886-2-23654520. E-mail: peter@ntu.edu.tw.

Funding

This study was sponsored part by a grant (101AS-13.2.2-FB-e1) from the Forestry Bureau, Council of Agriculture, Taiwan.

Notes

The authors declare no competing financial interest.

ACKNOWLEDGMENTS

The authors gratefully acknowledge Sheng-Yu Lu and Yen-Ray Hsui of Taiwan Forestry Research Institute for their supports in sample identification and Li-Yuan Liu of National Taiwan University for her technical assistance.

REFERENCES

(1) Liu, Y. C.; Lu, F. Y.; Ou, C. H. *Trees of Taiwan*; College of Agriculture, National Chung-Hshing University: Taichung, Taiwan, 1994.

(2) Hu, T. W.; Lin, Y. T.; Ho, C. K. Natural variation of chemical components of the leaf oil of *Cinnamomum osmophloeum* Kaneh. In *Proceedings of the Annual Meeting of Agricultural Associations of the Republic of China*, December, 1985; Taichung, Taiwan; pp 45–62.

(3) Poole, S. K.; Poole, C. F. Thin-layer chromatographic method for the determination of the prinicpal polar aromatic flavour compounds of the cinnamons of commerce. *Analyst* **1994**, *119*, 113–120.

(4) Wang, Y. H.; Avula, B.; Nanayakkara, N. P. D.; Zhao, J. P.; Khan, I. A. Cassia cinnamon as a source of coumarin in cinnamon-flavored food and food supplements in the United States. *J. Agric. Food Chem.* **2013**, *61*, 4470–4476.

(5) Sproll, C.; Ruge, W.; Andlauer, C.; Godelmann, R.; Lachenmeier, D. W. HPLC analysis and safety assessment of coumarin in foods. *Food Chem.* **2008**, *109*, 462–469.

(6) Woehrlin, F.; Fry, H.; Abraham, K.; Preiss-Weigert, A. Quantification of flavoring constituents in cinnamon: high variation of coumarin in cassia bark from the German retail market and in authentic samples from Indonesia. *J. Agric. Food Chem.* **2010**, *58*, 10568–10575.

(7) He, Z. D.; Qiao, C. F.; Han, Q. B.; Cheng, C. L.; Xu, H. X.; Jiang, R. W.; But, P. P. H.; Shaw, P. C. Authentication and quantitative analysis on the chemical profile of cassia bark (*Cortex cinnamomi*) by high-pressure liquid chromatography. *J. Agric. Food Chem.* **2005**, *53*, 2424–2428.

(8) Clark, G. S. Coumarin, an aroma chemical profile. *Perfum. Flavor.* **1995**, *20*, 23–34.

(9) Lake, B. G. Coumarin metabolism, toxicity and carcinogenicity: Relevance for human risk assessment. *Food Chem. Toxicol.* **1999**, *37*, 423–453.

(10) Hazleton, L. W.; Tusing, T. W.; Zeitlin, B. R.; Thiessen, R.; Murer, H. K. Toxicity of coumarin. *J. Pharmacol. Exp. Ther.* **1956**, *118*, 348–358.

(11) Council of the European Communities. On the approximation of the laws of the Member States relating to flavourings for use in foodstuffs and to source materials for their production. *Council Directive 88/388/EEC* 1988, *L184*, 61–66.

(12) European Food Safety Authority. Opinion of the scientific panel on food additives, flavourings, processing aids and materials in contacts with food (AFC) on a request from the commission related to coumarin. *EFSA J.* **2004**, *104*, 1–36.

(13) European Food Safety Authority. Coumarin in flavourings and other food ingredients with flavouring properties. *EFSA J.* **2008**, *793*, 1–15.

(14) Fotland, T. O.; Paulsen, J. E.; Sanner, T.; Alexander, J.; Husoy, T. Risk assessment of coumarin using the bench mark dose (BMD) approach: Children in Norway which regularly eat oatmeal porridge with cinnamon may exceed the TDI for coumarin with several folds. *Food Chem. Toxicol.* **2012**, *50*, 903–912.

(15) Abraham, K.; Wohrlin, F.; Lindtner, O.; Heinemeyer, G.; Lampen, A. Toxicology and risk assessment of coumarin: Focus on human data. *Mol. Nutr. Food Res.* **2010**, *54*, 228–239.

(16) Lee, H. C.; Cheng, S. S.; Chang, S. T. Antifungal property of the essential oils and their constituents from *Cinnamomum osmophloeum* leaf against tree pathogenic fungi. *J. Sci. Food Agric.* **2005**, *85*, 2047–2053.

(17) Chang, S. T.; Chen, P. F.; Chang, S. C. Antibacterial activity of leaf essential oils and their constituents from *Cinnamomum osmophloeum*. *J. Ethnopharmacol.* **2001**, *77*, 123–127.

(18) Cheng, S. S.; Chung, M. J.; Chen, Y. J.; Chang, S. T. Antipathogenic activities and chemical composition of *Cinnamomum osmophloeum* and *Cinnamomum zeylanicum* leaf essential oils. *J. Wood Chem. Technol.* **2011**, *31*, 73–87.

(19) Chao, L. K.; Hua, K. F.; Hsu, H. Y.; Cheng, S. S.; Lin, I. F.; Chen, C. J.; Chen, S. T.; Chang, S. T. Cinnamaldehyde inhibits pro-inflammatory cytokines secretion from monocytes/macrophages through suppression of intracellular signaling. *Food Chem. Toxicol.* **2008**, *46*, 220–231.

(20) Wang, S. Y.; Yang, C. W.; Liao, J. W.; Zhen, W. W.; Chu, F. H.; Chang, S. T. Essential oil from leaves of *Cinnamomum osmophloeum* acts as a xanthine oxidase inhibitor and reduces the serum uric acid levels in oxonate-induced mice. *Phytomedicine* **2008**, *15*, 940–945.

(21) Lin, T. Y.; Liao, J. W.; Chang, S. T.; Wang, S. Y. Antidyslipidemic activity of hot-water extracts from leaves of *Cinnamomum osmophloeum* Kaneh. *Phytother. Res.* **2011**, *25*, 1317–1322.

(22) Cheng, S. S.; Liu, J. Y.; Tsai, K. H.; Chen, W. J.; Chang, S. T. Chemical composition and mosquito larvicidal activity of essential oils from leaves of different *Cinnamomum osmophloeum* provenances. *J. Agric. Food Chem.* **2004**, *52*, 4395–4400.

(23) Adams, R. P. *Identification of Essential Oil Components by Gas Chromatography/Mass Spectrometry*; Allured Pub Corp: Carol Stream, IL, 2007.

(24) Lv, G. P.; Huang, W. H.; Yang, F. Q.; Li, J.; Li, S. P. Pressurized liquid extraction and GC-MS analysis for simultaneous determination of seven components in *Cinnamomum cassia* and the effect of sample preparation. *J. Sep. Sci.* **2010**, *33*, 2341−2348.
(25) Kamatou, G. P.; Vermaak, I.; Viljoen, A. M. Eugenol-from the remote Maluku Islands to the international market place: A review of a remarkable and versatile molecule. *Molecules* **2012**, *17*, 6953−6981.
(26) Maralhas, A.; Monteiro, A.; Martins, C.; Kranendonk, M.; Laires, A.; Rueff, J.; Rodrigues, A. S. Genotoxicity and endoreduplication inducing activity of the food flavouring eugenol. *Mutagenesis* **2006**, *21*, 199−204.
(27) Code for Federal Regulations. Part 182 substances generally recognized as safe. In *Title 21 Food and Drugs*; U.S. Government Printing Office: Washington, DC, 2013; Vol. 3.
(28) Yeh, H. F.; Luo, C. Y.; Lin, C. Y.; Cheng, S. S.; Hsu, Y. R.; Chang, S. T. Methods for thermal stability enhancement of leaf essential oils and their main consituents from indigenous cinnamon (*Cinnamomum osmophloeum*). *J. Agric. Food Chem.* **2013**, *61*, 6293−6298.
(29) Bevilacqua, A.; Corbo, M. R.; Sinigaglia, M. Combining eugenol and cinnamaldehyde to control the growth of *Alicyclobacillus acidoterrestris*. *Food Control* **2010**, *21*, 172−177.
(30) Franz, C. Genetics. In *Volatile Oil Crops: Their Biology, Biochemistry and Production*; Hay, R. K. M., Waterman, P. G., Eds.; Longman: Harlow, U.K., 1993; pp 63−96.

MS). Also, the modification effects of the enzyme on the wheat proteins were investigated in the current work.

MATERIALS AND METHODS

Materials. Three wheat varieties (Annong0950, Yang13, and Yang15) bred in China were used in this study. These cultivars were milled into flour using a Brabender experimental mill (Brabender, Duisburg, Germany) according to AACC approved method 26-21A. The flours were stored at 4 °C until further use.

High-purity α-[4-pyridyl 1-oxide]-*N*-*tert*-butyl nitrone (POBN) and high-quality linoleic acid (LA), linolenic acid (ALA), arachidonic acid (AA), eicosapentaenoic acid (EPA), and docosahexaenoic acid (DHA) were purchased from Sigma Chemical Co. Ethanol, acetonitrile (ACN), and tetrahydrofuran (THF) were of HPLC grade. Purified ana-rLOX (activity = 30000 IU/mg) was prepared in our laboratory.

Measurement of Radical Formation with ESR. Enzyme reactions were performed in 1 mL of 50 mM Tris-HCl buffer (pH 8). The reaction mixture containing 1 mM linoleic acid (linolenic acid, arachidonic acid, eicosapentaenoic acid, and docosahexaenoic acid), 20 mM POBN, and 8×10^3 IU/mL ana-rLOX was incubated at 16 °C without light. After 30 min, the reaction product was injected for ESR to detect the peroxidation radical.

ESR spectra were obtained with a Bruker ElexSys E500 spectrometer equipped with a super high Q cavity operating at 9.78 GHz and room temperature. The ESR spectrometer settings were as follow: modulation frequency, 100 kHz; modulation amplitude, 1.0 G; microwave power, 20 mW; receiver gain, 10^6; time constant, 0.6 s; and magnetic field scan, 70 G.

Determination of Radical Species from ana-rLOX with MS. The above mixture of enzyme reaction was terminated by ACN after 30 min, and the reaction products were separated with a centrifuge (Thermo, USA) at 10^4 rpm. The supernatant was kept and concentrated by evaporation. Finally, the concentrated sample was filtered by using a 0.45 μL membrane filter and injected for MS analysis.

MS detection of lipid peroxidation radicals was carried out with a Finnigan LCQ ion trap mass spectrometer (Thermo, USA) using an electrospray ionization (ESI) and Finnigan X calibur software (version 1.2). ESI in positive ion mode was employed. The conditions were as follows: sheath gas flow, 35 arbitrary units; capillary temperature, 80 °C; capillary voltage, 17 V; and spray voltage, 4.5 kV. Samples were infused into the mass spectrometer at 5 μL/min.

Separation of Wheat Proteins and Their Modification with ana-rLOX/LA. Wheat protein (albumin, globulin, and gluten) was extracted from wheat flour using a classical Osborne procedure based on protein solubility with modification.[22] The protein extracts were further purified through dialysis and lyophilization and stored at 4 °C for further use. Protein content was assayed according to the colorimetric Bradford method using BSA as a standard.[23]

Wheat proteins modified with ana-rLOX were dissolved in 1% protein solution (w/v) containing 0.05% LA in 200 mL at 16 °C, with thermostatic shaking at 180 rpm for 2 h. The wheat proteins after enzyme reaction were extracted with acetone, and the extracts were dried through vacuum evaporation.

Determination of Functional Properties, Particle Size Distribution, and Morphological Observation of Wheat Proteins Modified with ana-rLOX/LA. Functional properties such as the foam capacity (FC) and foam stability (FS) of wheat proteins prepared were determined according to the following Makri method.[24] FC was measured in terms of volume increase on whipping expressed as percentage of original volume of the liquid. FS was expressed as percentage of foam volume remaining in relation to initial foam volume at room temperature after 0, 5, 10, 20, and 30 min. The emulsifying activity index (EAI), and emulsifying stability index (ESI) were tested according to Dipak's method.[25] The mixture of 140 mL modified protein and 60 mL oil was homogenized at 10000 rpm for 1 min, room temperature A sample of 0.02 mL of the emulsion was respectively taken out from the bottom of the vessel at 0 and 20 min, then diluted with 1 mL of 0.1% SDS solution. The light absorption of the emulsions at 500 nm was measured in a spectrophotometer with blank of 0.1% SDS solution.

Average particle size and specific surface area of proteins (albumin-, globulin-, gluten-soluble proteins) before and after ana-rLOX/LA enzymatic reaction, were measured by an integrated-laser light scattering instrument (Mastersizer 2000, Malvern Instruments Co. Ltd., Worcestershire, UK). Relative refractive index and absorption were set at 1.414 and 0.001, respectively. The particle size and specific surface area of proteins were analyzed using Malvern Mastersizer software (version 5.12c, Malvern Instruments Co. Ltd.).

The protein was frozen and lyophilized according to the same method as previously described. Protein texture was observed by using a scanning electron microscope (SEM). The images were taken by using the SEM with a 6 kV acceleration voltage. The micrographs were taken using the same magnification.

Effect of ana-rLOX on Texture of Wheat Flours. The ana-rLOX was added into 300 g of three kinds of wheat flours (Annong0950, Yang13, and Yang15), reaching final enzyme activities of 10, 20, 30, and 40 IU/g flour, respectively. Then, they were mixed in a Brabender Farinograph (mixer bowl 300 g, Brabender OHG, Duisburg, Germany) at 63 rpm and 30 °C for 10 min. Texture parameters including springiness (SP), gumminess (GU), cohesiveness (CO), and resilience (RE) of dough were evaluated using a textural analyzer (TA-XT plus, Stable Micro System Ltd., UK) equipped with a cylindrical probe of P20 (20 mm in diameter). The tested parameters for the instrument were set as follows: pretest speed, 2.0 mm/s; crosshead speed, 1 mm/s; post-test speed, 10.0 mm/s; rupture test distance, 1%; distance, 50%; and time, 5.00 s. The loaves were cut into slices of 15 mm, and the ends were discarded. All tests were conducted in triplicate

Statistical Analysis. Data were reported as means ± standard deviations (SD) for triplicate treatments. One-way analysis of variance (ANOVA) and orthogonal design were performed using SPSS (SPSS for Windows, version 10.0.5, SPSS Inc., Chicago, IL, USA). Statistical significance was declared at $P < 0.05$.

RESULTS AND DISCUSSION

Radical Formation of PUFA Peroxidation by ana-rLOX. LOX-catalyzed PUFA peroxidation is a complex biochemical event that generate a series of free radicals.[6,7] However, there is limited direct evidence about the reactive and short-lived PUFA-derived free radicals due to the lack of an appropriate methodology. An ESR spectroscopy approach, with spin trapping, was taken here to investigate the dynamic behavior of fatty acids catalyzed by ana-rLOX with POBN. To

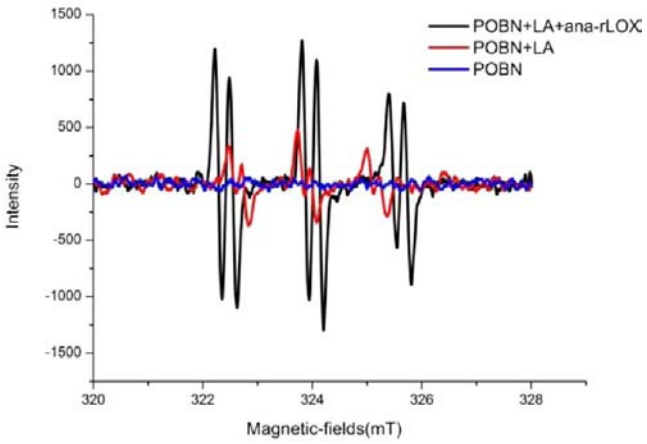

Figure 1. ESR spectra of POBN radical adducts from ana-rLOX/LA oxidation. The reaction mixture contained 20 mM POBN, 0.1 M LA, and 8×10^3 IU/mL ana-rLOX.

Table 1. Identification of POBN Adducts and Oxygenated Positions in ana-rLOX/PUFA Reaction

PUFA				
linoleic acid	α-linolenic acid	arachidonic acid	eicosapentaenoic acid	docosahexaenoic acid
MS Identification (m/z)				
474.7 POBN-LA	473.3 POBN-LOA	499.3 POBN-AA	496.6 POBN-EPA	522.7 POBN-DHA
508.8 POBN-LA$(OH)_2$	489.3 POBN-LOAO	515.1 POBN-AAO	512.8 POBN-EPAO	538.9 POBN-DHAO
490.1 POBN-LAO	502.7 POBN-LOAO_2	531.2 POBN-AAO_2	528.9 POBN-EPAO_2	557.0 POBN-DHA$(OH)_2$
266.0 POBN-C_5H_{11}	506.9 POBN-LOA$(OH)_2$	532.9 POBN-AA$(OH)_2$	531.3 POBN-EPA$(OH)_2$	555.0 POBN-DHAO_2
418.0 POBN-$C_{13}H_{19}O_3$	443.5 POBN-$C_{16}H_{25}O_2$	265.8 POBN-C_5H_{11}	224.2 POBN-C_2H_5	303.6 POBN-C_8H_{13}
	459.9 POBN-$C_{16}H_{25}O_2$-O	427.6 POBN-$C_{15}H_{21}O_2$	467.7 POBN-$C_{18}H_{25}O_2$	413.8 POBN-$C_{14}H_{19}O_2$
	475.8 POBN-$C_{16}H_{25}O_2$-O_2	443.8 POBN-$C_{15}H_{21}O_2$-O	484.3 POBN-$C_{18}H_{25}O_2O$	446.1 POBN-$C_{14}H_{19}O_2$-O_2
	477.6 POBN-$C_{16}H_{25}O_2(OH)_2$	459.8 POBN-$C_{15}H_{21}O_2$-O_2	502.1 POBN-$C_{18}H_{25}O_2(OH)_2$	449.4 POBN-$C_{14}H_{19}O_2(OH)_2$
	420.0 POBN-$C_{13}H_{21}O_2$-O	461.9 POBN-$C_{15}H_{21}O_2(OH)_2$	263.7 POBN-C_5H_9	383.6 POBN-$C_{14}H_{21}$
	436.0 POBN-$C_{13}H_{21}O_2$-O_2	306.2 POBN-C_8H_{15}	427.6 POBN-$C_{15}H_{21}O_2$	333.9 POBN-$C_8H_{11}O_2$
	437.6 POBN-$C_{13}H_{21}O_2(OH)_2$	404.0 POBN-$C_{12}H_{17}O_2$-O	444.3 POBN-$C_{15}H_{21}O_2$-O	268.1 POBN-$C_3H_5O_2$
	378.5 POBN-$C_{11}H_{19}O_2$	420.2 POBN-$C_{12}H_{17}O_2$-O_2	460.1 POBN-$C_{15}H_{21}O_2$-O_2	466.0 POBN-$C_{19}H_{23}$-O
	289.9 POBN-C_7H_{11}	346.2 POBN-$C_{11}H_{19}$	461.9 POBN-$C_{15}H_{21}O_2(OH)_2$	481.5 POBN-$C_{19}H_{23}$-O_2
	322.0 POBN-C_7H_{11}-O_2	348.1 POBN-$C_9H_{13}O_2$	304.5 POBN-C_8H_{13}	308.1 POBN-$C_6H_9O_2$
		364.3 POBN-$C_9H_{13}O_2$-O	403.7 POBN-$C_{12}H_{17}O_2$-O	426.9 POBN-$C_{16}H_{23}O$
		379.7 POBN-$C_9H_{13}O_2$-O_2	420.0 POBN-$C_{12}H_{17}O_2$-O_2	444.0 POBN-$C_{16}H_{23}(OH)_2$
		380.5 POBN-$C_9H_{13}O_2(OH)_2$	321.9 POBN-$C_7H_{11}O_2$	389.9 POBN-$C_{12}H_{19}O_2$
		269.4 POBN-$C_3H_6O_2$	401.9 POBN-$C_{13}H_{19}$-O_2	362.1 POBN-$C_{10}H_{13}(OH)_2$
		415.0 POBN-$C_{17}H_{16}$	403.7 POBN-$C_{13}H_{19}(OH)_2$	
		431.0 POBN-$C_{17}H_{16}$-O	361.7 POBN-$C_{10}H_{15}O_2$	
		446.8 POBN-$C_{17}H_{16}$-O_2	330.0 POBN-$C_{10}H_{15}$	
		449.1 POBN-$C_{17}H_{16}(OH)_2$	364.3 POBN-$C_{10}H_{15}$-O_2	
		309.1 POBN-$C_6H_{10}O_2$	361.7 POBN-$C_{10}H_{15}(OH)_2$	
		400.9 POBN-$C_{14}H_{22}$-O	401.9 POBN-$C_{13}H_{19}O_2$	
		417.0 POBN-$C_{14}H_{22}$-O_2	289.8 POBN-C_7H_{11}	
		419.4 POBN-$C_{14}H_{22}(OH)_2$	306.4 POBN-$C_7H_{11}O$	
		345.0 POBN-$C_{11}H_{18}$	321.9 POBN-$C_7H_{11}O_2$	
		349.1 POBN-$C_9H_{14}O_2$	324.2 POBN-$C_7H_{11}(OH)_2$	
		360.7 POBN-$C_{11}H_{18}$-O		
		377.0 POBN-$C_{11}H_{18}O_2$		
		379.0 POBN-$C_{11}H_{18}(OH)_2$		
Regiospecific				
C-13	C-13, C-16	C-9, C-12, C-15	C-12, C-15, C-18	C-14, C-16

Table 2. Effect of ana-rLox on Physical Properties of Wheat Proteins[a]

protein	FC (V_0)	FS (V_{30})	EAI (m^2g^{-1})	ESI (min)
albumin	320 ± 4a	149 ± 3a	4948 ± 16a	22 ± 1a
albumin (R)	360 ± 5b	181 ± 6b	5826 ± 23b	26 ± 1b
globulin	292 ± 5a	171 ± 4a	5838 ± 10a	26 ± 0a
globulin (R)	310 ± 2b	188 ± 6b	6019 ± 5b	30 ± 1b
gluten	362 ± 3a	125 ± 5a	3336 ± 12a	25 ± 0a
gluten (R)	385 ± 4b	190 ± 7b	3299 ± 19a	34 ± 1b

[a]FC, foaming capacity; FS, foam stability; EAI, emulsifying activity index; ESI, emulsifying stability index; V_0, enzymatic reaction at 0 min; V_{30}, enzymatic reaction for 30 min; (R), adding ana-rLOX/LA.

facilitate comparison, all samples were tested at the same condition (a^N = 15.7G and a^H = 2.8G). In Figure 1, six peaks of the radical species in the ESR spectrum are displayed in the reaction system by adding ana-rLOX with LA and POBN or LA with POBN, indicating that the free radical of lipid oxidation and POBN adducts existed. The POBN was used to trap free radicals during the reaction. It could be assumed that the oxidation of the LA fatty acid promoted the formation of transient unpaired-spin-density species, after reacting with POBN, generating the stable radicals displayed in the ESR spectrum.[26] A similar six peaks were found in soybean LOX.[27]

In addition, it was found that the spectrum of adding ana-rLOX was significantly different from that of nonenzyme, and the intensity of the peak with ana-rLOX was markedly increased. In comparison, the intensity of the peak without ana-rLOX was much lower, which indicated that ana-rLOX promoted the formation of LA peroxidation free radicals (Figure 1). Lipid peroxyl radicals resulted from the peroxidation of polyunsaturated fatty acids by soybean lipoxygenase.[28] The increase of the intensity of the peak with ana-rLOX might be because ana-rLOX promoted more free radicals during the lipid peroxidation.

Identification of the Oxygenated Position and Peroxidation Species Catalyzed by ana-rLOX. ESR alone cannot provide molecular structures and identities from hyperfine coupling constants, particularly those from spin adducts. Here, the combination with spin trapping and mass spectrometry (MS) was utilized to characterize PUFA-derived peroxidation radicals generated by ana-rLOX and to provide direct proof of the formation of PUFA peroxidation.

The position oxygenated and the radical species formed on five PUFA (LA, ALA, AA, EPA, and DHA) are shown in Table 1. By the ESI/MS analysis of oxidation ion fragments, the

dx.doi.org/10.1021/jf405425c | J. Agric. Food Chem. 2014, 62, 1713−1719

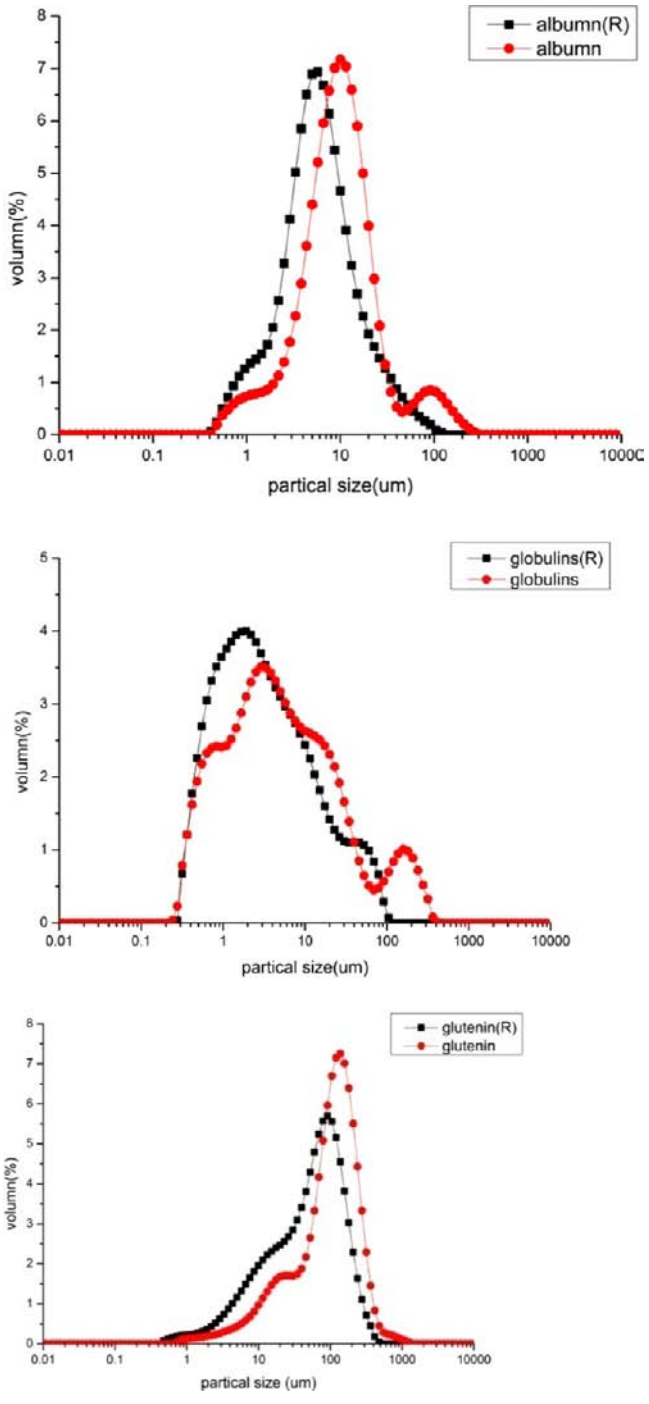

Figure 2. Effect of ana-rLOX on particle size distribution of wheat protein. (R), with ana-rLOX/LA.

oxygenation position on LA was C-13; C-13 and C-16 on ALA; C-9, C-13 and C-15 on AA; C-12, C-15 and C-18 on EPA; C-14 and C-16 on DHA, respectively. These results indicated that the positions oxygenated by ana-rLOX could vary with different PUFA. LA, as a substrate molecular oxygen, can be introduced either at carbon 9 (9-LOX) or at carbon 13 (13-LOX) of the hydrocarbon backbone, which led to the formation of 9-hydroperoxy and 13-hydroperoxy derivatives of LA (9- and 13-HPODE), respectively.[29]

In mammals, LOXs are similarly classified according to their positional specificity of arachidonic acid oxygenation, which can take place either at position C-5, C-8, C-9, C-11, C-12, or C-15.[30] The ana-rLOX did not oxygenate on the sites C-5, C-8, and C-11, but did on sites C-14, C-16, and C-18, which were not reported in latest published papers, neither from animals nor from plants or bacteria. We should note that the different positions LOXs acted on would create different novel compounds; this result may have a special application in the food and clinical fields.

Table 3. Effect of ana-rLOX/LA on the Particle Size of Wheat Protein[a]

protein	$D[4,3]$ (μm)	$D[3,2]$ (μm)	SSA (m^2/mg)
albumin	18.20	5.79	1.04
albumin (R)	9.91	3.92	1.53
globulin	23.16	2.10	2.86
globulin (R)	9.14	1.75	3.43
gluten	136.34	31.74	0.19
gluten (R)	79.12	15.62	0.38

[a]Volume mean diameter ($D[4,3]$); surface area mean diameter ($D[3,2]$); specific surface area (SSA) of protein. (R), adding ana-rLOX/LA.

In the radical adducts and their m/z of PUFA with ana-rLOX, totals of 7, 14, 30, 28, and 18 radical adducts for LA, ALA, AA, EPA, and DHA were respectively identified by ESI/MS. LOX-catalyzed PUFA peroxidation is a well-known free radical chain reaction. Peroxyl radical is generated from the reaction of oxygen and can also be converted into other types of free radicals through H abstraction; Fe^{2+} converted into Fe^{3+} through electron transfer.[31] As the result of chain reaction with peroxyl radical, many secondary radicals were produced and further induced more reactions. These new radicals can be metabolized to form new leukotrienes, lipoxins, jasmonic acids, green leaf volatiles, and lactones.[32]

Effect of ana-rLOX/LA on Funtional Properties of Wheat Protein. The use of soybean flour for commercial production of white bread has been well documented, and its main uses include bleaching flour, improving dough rheology, and increasing loaf volume. However, the effect of ana-rLOX/LA on wheat protein has not been well reported. Table 2 presents FC and FS of wheat proteins as albumin, globulin, and gluten with or without ana-rLOX/LA.

By adding ana-rLOX/LA in wheat proteins, FC and FS were significantly increased. The FC of albumin, globulin, and gluten solution respectively increased from 320, 292, and 360 mL before the enzymatic reaction to 360, 310, and 385 mL, and the FS of albumin, globulin, and gluten solution respectively increased from 149, 170, and 120 mL before the enzymatic reaction to 189, 188, and 190 mL, which suggested that the structural modification of wheat proteins had occurred and the physical properties had been changed during ana-rLOX enzymatic reaction. The proteins might generate two disulfide bonds through thiol oxidation with radicals initialized from ana-rLOX/LA, from which protein aggregation was produced, and finally the FC and FS increased.

As shown in Table 2, the EAI and ESI of wheat proteins were significantly enhanced with the ana-rLOX/LA reaction system. The EAI of albumin and globulin solution respectively increased from 4948 and 5838 to 5838 and 6019 m^2 g^{-1}, but there was no significant change in the EAI for gluten. The ESI of albumin, globulin, and gluten solution increased from 22, 26, and 25 to 26, 30, and 34 min, respectively. The increase of EAI and ESI may result in the change of hydrophilic groups and hydrophobic groups related to emulsibility of protein. In the

dx.doi.org/10.1021/jf405425c | J. Agric. Food Chem. 2014, 62, 1713−1719

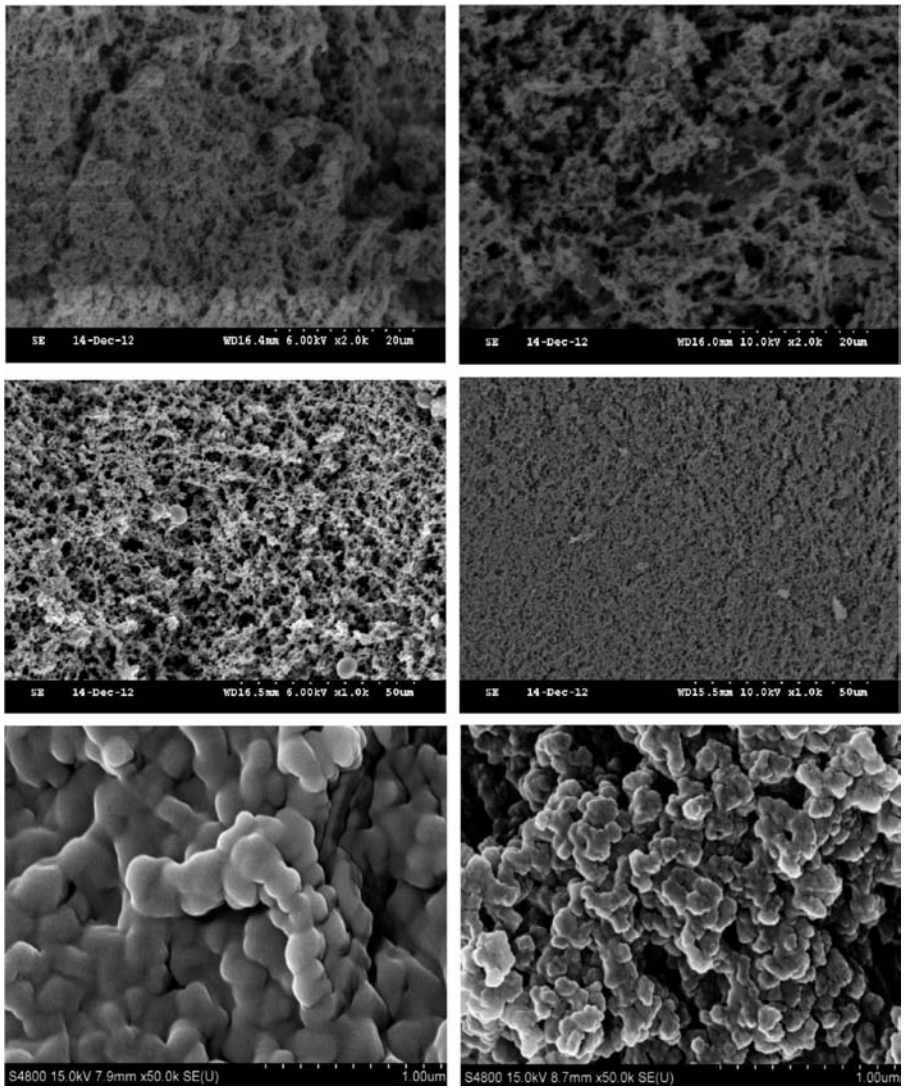

Figure 3. Effect of ana-rLOX on micrographic structure of wheat flour by scanning electron micrograph: (left) no ana-rLOX/LA; (right) adding ana-rLOX/LA.

Table 4. Modification Effects of ana-rLOX on Different Wheat Flours

variety	ana-rLOX (U/g)	springiness	cohesiveness	gumminess	resilience
Annong0950	0	0.32 ± 0.01a	0.27 ± 0.01c	23.90 ± 1.32a	0.073 ± 0.011a
	10	0.34 ± 0.01b	0.30 ± 0.01b	22.72 ± 1.45a	0.068 ± 0.015b
	20	0.34 ± 0.01b	0.30 ± 0.01b	25.06 ± 1.63b	0.065 ± 0.012b
	30	0.35 ± 0.02b	0.31 ± 0.01b	38.98 ± 2.25c	0.066 ± 0.017b
	40	0.34 ± 0.01 b	0.28 ± 0.01a	29.27 ± 1.97b	0.063 ± 0.012c
Yang13	0	0.35 ± 0.01a	0.30 ± 0.01a	29.17 ± 1.92a	0.061 ± 0.016a
	10	0.36 ± 0.01a	0.30 ± 0.01a	30.10 ± 1.18a	0.072 ± 0.014b
	20	0.39 ± 0.01b	0.38 ± 0.02c	58.65 ± 2.73d	0.079 ± 0.016c
	30	0.39 ± 0.02b	0.31 ± 0.01a	31.54 ± 1.85a	0.061 ± 0.011a
	40	0.37 ± 0.01b	0.33 ± 0.01b	32.41 ± 1.76b	0.076 ± 0.018b
Yang15	0	0.40 ± 0.01a	0.30 ± 0.01a	31.74 ± 1.50a	0.061 ± 0.012a
	10	0.41 ± 0.01a	0.33 ± 0.01d	49.70 ± 3.05c	0.071 ± 0.014b
	20	0.43 ± 0.02b	0.32 ± 0.01b	27.67 ± 1.92a	0.075 ± 0.016b
	30	0.45 ± 0.02b	0.40 ± 0.01c	38.14 ± 2.86b	0.095 ± 0.015d
	40	0.43 ± 0.01b	0.41 ± 0.01c	63.59 ± 4.65d	0.078 ± 0.015c

dx.doi.org/10.1021/jf405425c | J. Agric. Food Chem. 2014, 62, 1713−1719

work, the conformation of wheat protein was changed in the oxidation process, caused by enzymatic reaction, and hydrophobic groups were exposed, which improved the lipophilicity of protein. Therefore, the emulsifying properties of proteins were improved. Through increasing EAI and ESI of wheat protein, the original dough of incompatibility of dispersed phase system becomes more homogeneous, and all kinds of materials in the dough were mixed evenly. Therefore, the quality of products is even and stable.[33]

Effect of ana-rLOX/LA on Particle Size and Surface Structure of Wheat Proteins. The particle size of wheat proteins in solution ranged broadly from 1 to 1000 μm (Figure 2). It was found that there were significant differences in the volume mean diameter ($D[4,3]$), the surface area mean diameter ($D[3,2]$), and the specific surface area (SSA) by addition of ana-rLOX/LA in protein solutions. The average particle size $D[3,2]$ of albumin, globulin, and gluten solution decreased from 5.79, 2.10, and 31.74 to 3.92, 1.75, and 15.62 μm after the enzymatic reaction, respectively (Table 3). These results might be attributed to the modified reaction that was caused by ana-rLOX/LA, which made the protein structure more compact and led to the decrease of average particle size of wheat proteins. In addition, lipid peroxidation radicals could also induce S−S bond formation. The results indicated that all kinds of wheat protein were cross-linked by lipid peroxidation radicals.

To confirm the above explanation, wheat proteins with or without ana-rLOX/LA were observed by scanning electron microscopy (SEM). The outer topography and inner structure of protein modified with or without ana-rLOX/LA are presented in Figure 3. Proteins modified by enzymatic reaction were in regular shape with a denser and tighter surface in comparison with nonenzymatic reaction. The wheat albumin, globulin, and gluten appeared to be tighter network structures, and wheat albumin presented the membrane-like structure by cross-linking of the radicals reaction after the addition of ana-rLOX/LA. The results indicated that the structure of wheat proteins became tighter and more compact due to the oxidation of proteins after the addition of ana-rLOX/LA. Therefore, the particle size of wheat proteins became smaller. All of the above changes of wheat proteins showed that the free radical yielded from the lipid oxidation affect the formation of the network of wheat protein. These results suggested that ana-rLOX might be useful in food industries to improve textural and leavening characteristics of bread, cakes, or toppings and confectionery products in which foaming properties are important, similar to that reported by Mirsaeedghazi.[34]

Modification Effect of ana-rLOX on Different Wheat Flours. It has been reported that LOX increases mixing tolerance and generally enhances dough rheological properties,[35] suggesting that LOX could be utilized as a natural food improver. In this study, three wheat flours, Annong0950, Yang13, and Yang15, which are weak-, medium-, and strong-gluten wheat flours, were used to determine whether ana-rLOX could effectively improve dough quality.

Table 4 shows that the dough processing characteristics of the three wheat flours, such as springiness (SP), cohesiveness (CO), gumminess (GU), and resilience (RE), were improved after the addition of ana-rLOX in flours.

The ana-rLOX had a positive impact on SP for three doughs. SP of three doughs with 30 IU/g ana-rLOX increased significantly by 8.4, 9.9, and 13.1%, respectively. A similar trend was shown in weak-, medium-, and strong-gluten flours (Table 4).

The ana-rLOX positively affected CO in three doughs, too (Table 4). For weak-gluten flour, the dough's CO increased by 13.3% at 30 IU/g of ana-rLOX and then decreased after the addition of more ana-rLOX. The same trend was also shown in medium-gluten flour with a maximum of 26.7% increase at 20 IU/g ana-rLOX. However, the dough's CO of strong-gluten flour increased with more addition of ana-rLOX, and the maximum value of 37.7% was observed at 40 U/g ana-rLOX.

ana-rLOX enhanced the dough's GU in three flours. For weak-gluten flour, the dough's GU increased by 63.1% at 30 IU/g of ana-LOX, followed by a decrease after additional ana-LOX. The same trend was also shown in medium-gluten flour with a maximum of 101% increase at 20 IU/g ana-LOX. For strong-gluten flour, dough GU increased with more addition of ana-LOX, and the maximum of 100% increase was observed at 40 IU/g ana-rLOX (Table 4).

Table 4 also shows different effects of ana-LOX on the dough's RE among three flours. The dough's RE of weak-gluten flour significantly decreased by 13.7% at 40 IU/g ana-rLOX as ana-rLOX increased. For medium-gluten flour, RE increased by 29.5% at 20 IU/g, but decreased thereafter. For strong-gluten flour, the maximum of the dough's RE is 55.7% increase at 30 IU/g ana-rLOX. The results supported that ana-LOX-treated bread volume improved by 16.8%, the loaf height increased by 10.3%, and the specific volume increased by 18.2%.

When LOX was added into dough, the increased number of formed disulfide bonds enhanced the ability of dough to retain gas.[36] In American baking practices, the main purpose for adding enzyme-active soy flour into wheat flour is to improve dough properties.[37] Overall, the additional ana-rLOX in the flours was able to improve wheat dough's processing characteristics including SP, CO, GU, and RE to different degrees except RE for low-gluten flour. Although the activity of adding ana-rLOX for reaching the best effect of improving dough quality was different, these results provided clear evidence that ana-rLOX from *Anabaena* sp. PCC7120 could effectively improve the quality of wheat flour and explained why the enzyme increased loaf height, bread volume, and specific volume,[22] suggesting that it could be not only applied to baking practices but also used as a natural flour improver for wheat-based food.

AUTHOR INFORMATION

Corresponding Author

*(Z. Lu) Phone/fax: +86-25-84396583. E-mail: fmb@njau.edu.cn.

Funding

This work was funded by the National Natural Science Foundation of China (31071605; 31201423), Chinese "863 High-Tech" Program (2012AA022207), Science and Technology Support Program of Jiangsu Province (BE2011390), and a project funded by the Priority Academic Program Development of Jiangsu Higher Education Institutions (PAPD).

Notes

The authors declare no competing financial interest.

REFERENCES

(1) Ahmad, M. K.; Naqshbandi, A.; Fareed, M.; Mahmood, R. Oral administration of a nephrotoxic dose of potassium bromate, a food additive, alters renal redox and metabolic status and inhibits brush border membrane enzymes in rats. *Food Chem.* **2012**, *134*, 980−985.

(2) Dunnewind, B.; van Vliet, T.; Orsel, R. Effect of oxidative enzymes on bulk rheological properties of wheat flour doughs. *J. Cereal Sci.* **2002**, *36*, 357−366.
(3) Vemulapalli, V.; Miller, K. A.; Hoseney, R .C. Glucose oxidase in breadmaking systems. *Cereal Chem.* **1998**, *75*, 439−442.
(4) Bonet, A.; Rosell, C. M.; Caballero, P. A. Glucose oxidase effect on dough rheology and bread quality: a study from macroscopic to molecular level. *Food Chem.* **2006**, *99*, 408−415.
(5) Rakotozafy, L.; Mackova, B.; Delcros, J. Effect of adding exogenous oxidative enzymes on the activity of three endogenous oxidoreductases during mixing of wheat flour dough. *Cereal Chem.* **1999**, *76*, 213−218.
(6) Liavonchanka, A.; Feussner, I. Lipoxygenases: occurrence, functions and catalysis. *Plant Physiol.* **2006**, *163*, 348−357.
(7) Porta, H.; Rocha-Sosa, M. Plant lipoxygenases. Physiological and molecular features. *Plant Physiol.* **2002**, *130*, 15−21.
(8) Xu, Y.; Gu, Y.; Qian, S. Y. An advanced electron spin resonance (ESR) spin-trapping and LC/(ESR)/MS technique for the study of lipid peroxidation. *Int. J. Mol. Sci.* **2012**, *13*, 14648−14666.
(9) Alexandra, A.; Ivo, F. Lipoxygenases − structure and reaction mechanism. *Phytochemistry* **2009**, *70*, 13−14.
(10) Brash, A. R. Lipoxygenases: occurrence, functions, catalysis, and acquisition of substrate. *J. Biol. Chem.* **1999**, *274*, 23679−23682.
(11) Hamberg, M.; Su, C.; Oliw, E. Manganese lipoxygenase − discovery of a bisallylic hydroperoxide as product and intermediate in a lipoxygenase reaction. *J. Biol. Chem.* **1998**, *273*, 13080−13088.
(12) Prigge, S. T.; Boyington, J. C.; Faig, M.; Doctor, K. S.; Gaffney, B. J.; Amzel, L. M. Structure and mechanism of lipoxygenases. *Biochemie* **1997**, *79*, 629−636.
(13) Su, C.; Oliw, E. H. Manganese lipoxygenase − purification and characterization. *J. Biol. Chem.* **1998**, *273*, 13072−13079.
(14) Taner, B.; Aslihan, D. Lipoxygenase in fruits and vegetables: a review. *Enzyme Microb. Technol.* **2007**, *40*, 491−496.
(15) Whitehead, T. P.; Robinson, D.; Allaway, S.; Syms, J.; Hale, A. Effect of red wine ingestion on the antioxidant capacity of serum. *Clin. Chem.* **1995**, *41*, 32−35.
(16) Hughes, R. K.; Wu, Z. C.; Robinson, D. S.; Hardy, D.; West, S. I.; Fairhurst, S. A.; Casey, R. Characterization of authentic recombinant peaseed lipoxygenases with distinct properties and reaction mechanisms. *Biochem. J.* **1998**, *333*, 33−43.
(17) Casey, R.; West, S. I.; Hardy, D.; Robinson, D. S.; Wu, Z. C.; Hughes, R. K. New frontiers in food enzymology: recombinant lipoxygenases. *Trends Food Sci. Technol.* **1999**, *10*, 297−302.
(18) Lindsay, M. P.; Skerritt, J. H. The glutenin macropolymer of wheat flour doughs: structure-function perspectives. *Trends Food Sci. Technol.* **1999**, *10*, 247−253.
(19) Shewry, P. R.; Popineau, Y.; Lafiandra, D.; Belton, P. Wheat glutenin subunits and dough elasticity: findings of the Eurowheat Project. *Trends Food Sci. Technol.* **2001**, *11*, 433−441.
(20) Junqueira, R. M.; Cocato, M. L.; Colli, C.; Castro, I. A. Synergism between lipoxygenase-active soybean flour and ascorbic acid on rheological and sensory properties of wheat bread. *J. Sci. Food Agric.* **2008**, *88*, 194−198.
(21) Zhang, C.; Tao, T. T.; Ying, Q.; Zhang, D. L.; Lu, F. X.; Bie, X. M.; Lu, Z. X. Extracellular production of lipoxygenase from *Anabaena* sp. PCC 7120 in *Bacillus subtilis* and its effect on wheat protein. *Appl. Microbiol. Biotechnol.* **2012**, *94*, 949−958.
(22) Zhang, C.; Zhang, S.; Lu, Z. X.; Bie, X. M.; Zhao, H. Z.; Wang, X. M.; Lu, F. X. Effects of recombinant lipoxygenase on wheat flour, dough and bread properties. *Food Res. Int.* **2013**, *54*, 26−32.
(23) Sun, X. D.; Arntfield, S. D. Gelation properties of salt-extracted pea protein isolate induced by heat treatment: effect of heating and cooling rate. *Food Chem.* **2011**, *124*, 1011−1016.
(24) Markri, E.; Papalamprou, E.; Doxastakis, G. Study of functional properties of seed storage proteins from indigenous European legume crops (lupin, pea, broad bean) in admixture with polysaccharides. *Food Hydrocolloids* **2005**, *19*, 583−594.
(25) Dipak, K. D.; Kumar, D. M. Functional properties of rapeseed protein products with varying phytic acid contents. *J. Agric. Food Chem.* **1986**, *34*, 775−780.
(26) Qian, S. Y.; Yue, G. H.; Kenneth, B. T.; Mason, R. P. Identification of all classes of spin-trapped carbon-centered radicals in soybean lipoxygenase-dependent lipid peroxidations of ω-6 polyunsaturated fatty acids via LC/ESR, LC/MS, and tandem MS. *Free Radical Biol. Med.* **2003**, *34*, 1017−1028.
(27) Anna, R.; Serafina, C.; Manuela, P.; Enzo, P.; Giovanni, S.; Luigi, S. Amino acids as modulators of lipoxygenase oxidation mechanism. The identification and structural characterization of spin adducts intermediates by electron spin resonance and tandem mass spectrometry. *Food Chem.* **2010**, *119*, 533−538.
(28) Walee, C. S.; Ronald, P. M. Lipid peroxyl radical intermediates in the peroxidation of polyunsaturated fatty acids by lipoxygenase. *J. Biol. Chem.* **1989**, *264* (35), 20968−20973.
(29) Liavonchanka, A.; Feussner, I. Lipoxygenases: occurrence, functions and catalysis. *J. Plant Physiol.* **2006**, *163*, 348−357.
(30) Schneider, C.; Pratt, D. A.; Porter, N. A.; Brash, A. R. Control of oxygenation in lipoxygenase and cyclooxygenase catalysis. *J. Chem. Biol.* **2007**, *14*, 473−488.
(31) Sharon, H. S. Hydrogen tunneling and protein motion in enzyme reactions. *Acc. Chem. Res.* **2006**, *39*, 93−100.
(32) Joo, Y. C.; Oh, D. K. Lipoxygenases: potential starting biocatalysts for the synthesis of signaling compounds. *Biotechnol. Adv.* **2012**, *30* (6), 1524−1532.
(33) Dickinson, E. Properties of emulsions stabilized with milk proteins: overview of some recent developments. *Dairy Sci.* **1997**, *80*, 2607−2619.
(34) Mirsaeedghazi, H.; Zahra, E. D.; Mousavi, S. M. A. Rheometric measurement of dough rheological characteristics and factors affecting it. *Int. J. Agric. Biol.* **2008**, *10*, 112−119.
(35) Larisa, C. *The Effect of Selected Enzymes on the Quality and Structural Attributes of White Salted and Yellow Alkaline Asian Noodles*. B.Sc. Food Sci. (hons), Victoria University, 2005.
(36) Larisa, C.; Andrew, L. H.; Darryl, M. S. Measurement of lipoxygenase in Australian white wheat flour: the effect of lipoxygenase on the quality properties of white salted noodles. *J. Sci. Food Agric.* **2006**, *86*, 1670−1678.
(37) Pablo, D. R.; Salvador, F. A.; Martin, H. M.; Gabriela, T. P.; Dante, M. B.; Alberto, E. L. Production of gluten-free bread using soybean flour. *J. Sci. Food Agric.* **2004**, *84*, 1969−1974.

One of the main advantages of nanoemulsions over microemulsions is that they require considerably less surfactant to form them. Food-grade nanoemulsions can be formed by high-energy methods (such as high-pressure homogenization or sonication) or low-energy methods (such as phase inversion temperature, spontaneous emulsification, or emulsion phase inversion).[23,26] In this study, we examined the utilization of spontaneous emulsification for forming food-grade ω-3 fatty acid delivery systems suitable for utilization in transparent foods and beverages. This method involves simply injecting an oily phase (typically consisting of a hydrophilic surfactant, a carrier oil, and a lipophilic bioactive) into an aqueous phase (typically consisting of water and cosolvent) with continuous stirring.[27] We have recently shown that this method can be used to successfully encapsulate vitamin E in nanoemulsion-based delivery systems.[27−30] An advantage of using low-energy methods to form nanoemulsions is that no expensive processing equipment (such as a high-pressure homogenizer or sonicator) is required.

MATERIALS AND METHODS

Materials. Fish oil (Denomega 100) was kindly donated by Denofa (Brighton, CO, USA). Lemon oil (SC 020207, lot 2894308) was kindly donated by International Flavors and Fragrances (Union Beach, NJ, USA). The supplier reported that this oil contained ≈60% limonene, <18% citral + citral acetate, and <15% γ-terpinene. Medium-chain triglyceride (MCT) oil (*MIGLYOL* 812) was purchased from Warner Graham Co. (Sasol Germany GmbH). Nonionic surfactant (Tween 80), citric acid, sodium benzoate, and propylene glycol were purchased from Sigma-Aldrich Co. (St. Louis, MO, USA). Glycerol was purchased from Fisher Scientific (Pittsburgh, PA, USA). Ethanol was purchased from Pharmco−Aaper (Brookfield, CT, USA). Double-distilled water was used in the preparation of all solutions and emulsions.

Sample Preparation. Nanoemulsions were prepared by spontaneous emulsification using the method described previously.[27] In brief, an organic phase was added by a micropipet in an aqueous phase with continuous stirring of the system at 25 °C and 500 rpm using a magnetic stirrer (PC-410 D, Corning Instruments, Corning, NY, USA). The organic phase consisted of a mixture of different amounts of fish oil (0−10 wt %), MCT or lemon oil (0−10 wt %), and nonionic surfactant (2.5−10 wt %), whereas the aqueous phase was a buffer solution (pH 3.0, 0.8% citric acid, 0.08% sodium benzoate) mixed with different amounts of propylene glycol, glycerol, or ethanol (0−50 wt %). The low pH of the buffer was designed to imitate the aqueous phase of commercial beverage products. An organic phase was prepared by mixing oils and surfactant together for 30 min (750 rpm), and then 20 g of this organic phase was slowly injected into 80 g of aqueous phase over a 15 min period using a micropipet with continuous stirring (500 rpm).

Particle Size Measurements. The particle size distributions of nanoemulsions and emulsions produced by spontaneous emulsification were measured using either a dynamic light-scattering instrument (Zetasizer Nano ZS, Malvern Instruments, Malvern, UK) or a static light-scattering instrument (Mastersizer 2000, Malvern Instruments). Dynamic light scattering was used for samples with relatively small particle diameters (d < 3000 nm), whereas static light sattering was used for samples with larger droplets.

Dynamic Light Scattering. The particle size distribution was determined by measuring the frequency shift of a laser beam (633 nm) scattered from a sample at an angle of 173°.[27] To avoid multiple scattering effects, all of the samples were diluted before the measurements (×500) with citric buffer. The mean particle diameter (Z-average) and polydispersity index (PDI) were calculated from the particle size distribution. The PDI provides a measure of the narrowness of the particle size distribution, with values ≤0.1 indicating a very narrow distribution.

Static Light Scattering. The particle size distribution was determined by measuring the angular dependence of the intensity of light scattered from the emulsions. Mean particle diameters (d_{32}) were calculated from the particle size distribution. All samples were diluted with citric buffer prior to making the measurements to avoid multiple scattering effects. This was achieved by adding a few drops of nanoemulsions into approximately 125 mL of citric buffer in the sample chamber of the instrument until an obscuration of 11−15% was obtained.

Turbidity Measurements. The influence of temperature on the turbidity of the nanoemulsions was determined using a UV−visible spectrophotometer with temperature-scanning capabilities (Evolution Array, Thermo Scientific, Madison, WI, USA). The turbidity was measured at 600 nm as the temperature was increased form 20 to 90 °C at 1 °C/min and then decreased back to 20 °C.

Statistical Analysis. All experiments were carried out twice with two samples being analyzed for each trial. The results are reported as the calculated mean and standard deviation of these measurements.

RESULTS AND DISCUSSION

The overall aim of this study was to identify optimum conditions to prepare stable ω-3-enriched nanoemulsions that were optically transparent. We therefore systematically examined the influence of a number of factors on the formation and stability of the nanoemulsions.

Influence of Carrier Oil. Preliminary experiments indicated that nanoemulsions with small droplets could not be formed using fish oil alone as the oil phase. We therefore examined the influence of mixing fish oil with a carrier oil (either MCT or lemon oil). Previous studies with vitamin E have shown that this approach can be used to produce nanoemulsions containing small droplets.[27] In this series of experiments, the composition of the oil phase was varied, whereas the total oil (10%), surfactant (10%), and buffer (80%) contents were kept constant.

Static light scattering (SLS) was used for these experiments because many of the samples formed after spontaneous emulsification had relatively large particle sizes (d > 1000 nm). The influence of carrier oil type and oil phase composition on the particle size of the systems formed by spontaneous emulsification is shown in Figures 1 and 2. The mean particle diameter was relatively small (d < 200 nm) for both carrier oils when the fish oil concentration in the oil phase remained relatively low (≤40% for MCT and ≤50% for lemon oil). On the other hand, there was a steep increase in the mean particle diameter when the fish oil concentration was higher than these values (Figure 1). At low fish oil concentrations, the nanoemulsions had relatively narrow monomodal particle size distributions for both lemon oil and MCT.

Ideally, one would like to have small droplet sizes but also a high loading capacity, that is, a relatively high concentration of fish oil within the oil phase. The nanoemulsions prepared using the lemon oil were more suitable for this purpose, because they still had relatively small droplet diameters at relatively high fish oil contents. For example, when the oil phase contained 50% lemon oil and 50% fish oil, the mean droplet diameter was 112 ± 3 nm when measured by static light scattering. This value was close to the mean droplet diameter of 106.0 ± 0.5 nm determined by dynamic light scattering on the sample. We therefore decided to utilize lemon oil as the carrier oil in the remainder of the study. Another advantage of using lemon oil is that it can mask any off-flavors associated with fish oil.

Influence of Surfactant Concentration. Previous studies have shown that the size of the droplets produced by low-

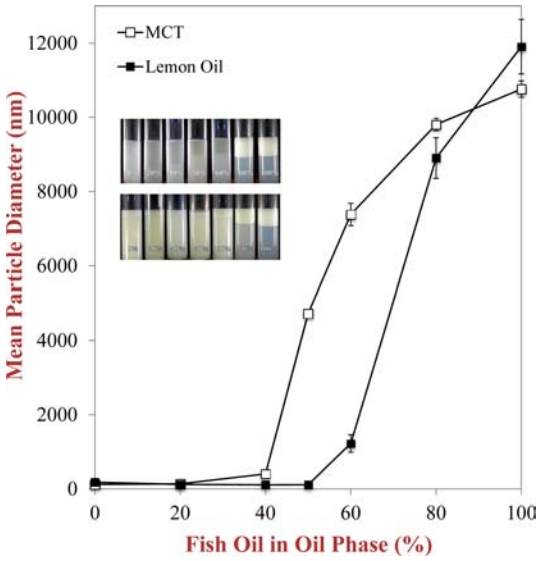

Figure 1. Influence of oil phase composition on the mean particle diameter. The oil phase contained different amounts of fish oil and carrier oil (MCT or lemon oil). (Inset) Photographs of the emulsions. Measurements were made after 24 h of storage at ambient temperature.

energy methods, such as the spontaneous emulsification and emulsion phase inversion methods, depends on the surfactant-to-oil ratio (SOR).[27,28,31,32] We therefore examined the influence of SOR on the size of the droplets produced in this study. The total oil content was maintained constant (10%) while the ratio of surfactant to buffer solution was varied. Polyoxyethylene-20-sorbitan-monooleate (Tween 80) was used as a food-grade hydrophilic nonionic surfactant (hydrophile–lipophile balance = 15). A 50% fish oil and 50% lemon oil mixture was used as the oil phase because this value gave small droplets with a high ω-3 acid content (see previous section).

As shown in Figure 3, the mean particle diameter was large (d > 1000 nm) at relatively low surfactant levels (SOR < 0.75), but small (<200 nm) at higher surfactant levels (SOR ≥ 0.75). Dynamic light scattering (DLS) measurements could not be carried out on emulsions at low SOR because they were out of the range of the instrument. However, there was excellent agreement between the mean particle diameters measured by DLS and SLS at higher SOR values (Figure 3). For example, at a SOR of 1 the mean droplet diameter was ≈108 ± 8 nm for DLS and ≈114 ± 2 nm for SLS. The particle size distrutions were monomodal at this SOR value (data not shown), with a narrow polydispersity index (PDI ≈ 0.18).

The physicochemical origin of the dependence of particle size on SOR may be related to the amount of surfactant required to cover the droplet surfaces formed. The minimum concentration of surfactant (C) required to cover all of the droplet surfaces in an emulsion is given by the relationship[33]

$$C = \frac{6\varphi\Gamma_S}{d_{32}} \quad (1)$$

where ϕ is the disperse phase volume fraction, d_{32} is the surface-weighted mean droplet diameter, and Γ_S is the surface load.[34] The surface load of Tween 80 has previously been reported to be about 3.1 mg m^{-2}.[35] Assuming ϕ = 0.1, d_{32} = 100 nm, and Γ_S = 3.1 mg m^{-2}, a surfactant concentration of around 1.9 wt % was calculated to be required to cover all of

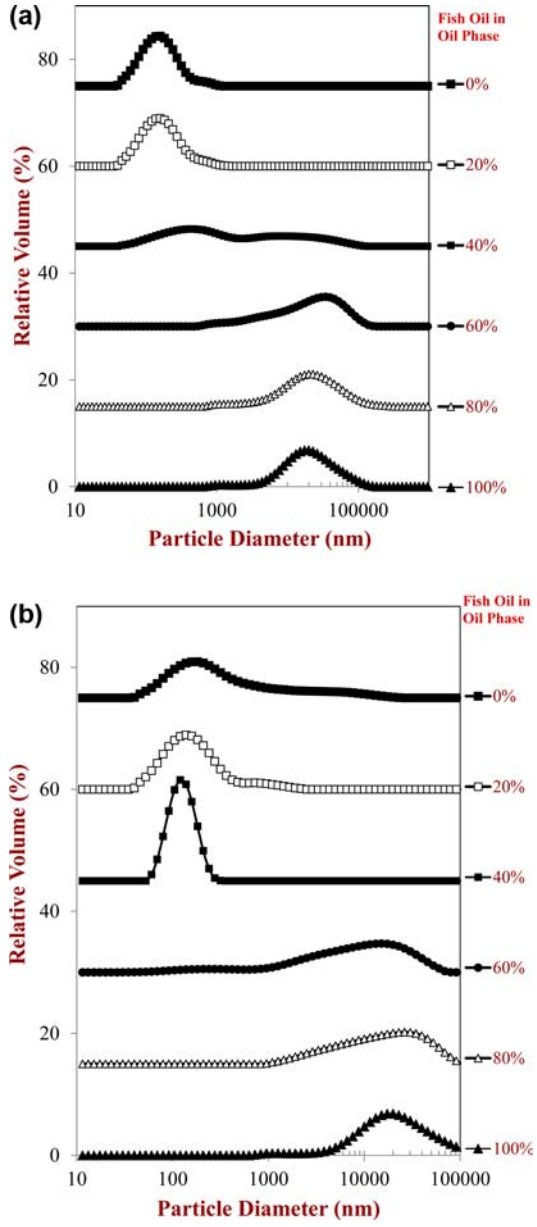

Figure 2. Particle size distributions of nanoemulsions and emulsions formed by spontaneous emulsification using oil phases with different compositions (a, MCT and fish oil; b, lemon oil and fish oil).

the droplets formed, which corresponds to an SOR of about 0.2. The experimental measurements show that a much higher SOR is required to form nanoemulsions with this droplet diameter (Figure 3), which suggests that the particle size is not limited by the amount of surfactant present. Instead, it must be related to the physicochemical events that occur at the boundary between the oil/surfactant and aqueous phases when they are brought into contact.

Influence of Cosolvent Type and Concentration. To produce optically transparent nanoemulsions, it is improtant that the droplet diameter is as small as possible. We therefore examined the influence of cosolvent type and concentration on the particle size of the droplets produced by spontaneous emulsification. Three short-chain alcohols (ethanol, propylene glycol, and glycerol) were used as water-soluble cosolvents in this study. The total oil content (10%) and surfactant content (10%) were kept constant in this study, with 50% fish oil/50%

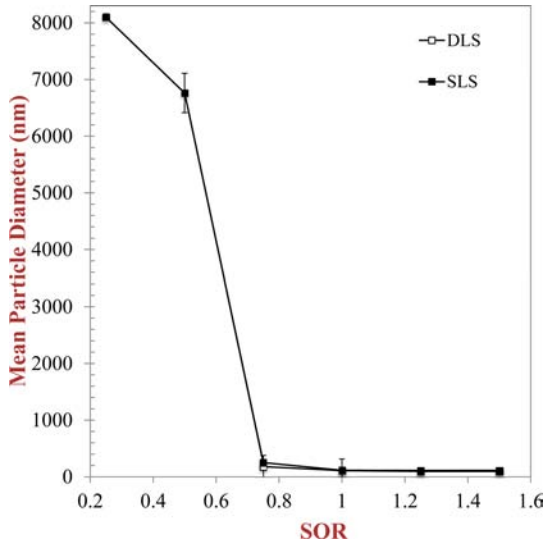

Figure 3. Influence of surfactant-to-oil ratio (SOR) on the mean particle diameter produced by spontaneous emulsification. All systems had the same total oil phase content (10%), which consisted of 50% fish oil and 50% lemon oil. Particle sizes were measured after 24 h of storage at ambient temperature.

lemon oil being used as the oil phase and Tween 80 being used as the surfactant. The amount of the different cosolvents in the aqueous buffer solution was systematically varied.

Incorporation of ethanol (10−50%) into the aqueous phase led to an increase in mean particle size and the formation of emulsions that were highly unstable to phase separation, and so this cosolvent was not studied further. Incorporation of propylene glycol (PG) into the aqueous phase led to a complex dependence of the particle size on cosolvent concentration. There was an increase in mean particle diameter with increasing PG concentration from 0 to 35%, but then a decrease from 35 to 40%, and then a steep increase from 35 to 45% (Figure 4a). The smallest droplets were formed in the systems containing 40% PG: $d \approx 99 \pm 2$ nm; PDI $\approx 0.22 \pm 0.01$. The physicochemical origin of this effect is currently unknown, but is presumably due to the nature of the structures formed at the boundary between the surfactant/oil and aqueous phases at particular cosolvent concentrations. Incorporation of glycerol into the aqueous phase could be used to cause an appreciable decrease in the mean droplet size of the nanoemulsions produced by spontaneous emulsification. The droplet size remained relatively constant from 0 to 20% glycerol, but decreased appreciably from 20 to 40% glycerol (Figure 4b). The smallest droplets were formed in the systems containing 40% glycerol: $d \approx 51 \pm 4$ nm; PDI $\approx 0.15 \pm 0.03$. In addition, these nanoemulsions appeared optically transparent in their nondiluted form (Figure 4b, inset). Optical transparency may have been due to the fact that glycerol addition reduced the refractive index contrast between the oil droplets and the surrounding aqueous phase or because it reduced the droplet size.[18] The DLS measurements were made after the nanoemulsions had been highly diluted with an aqueous solution containing no glycerol, and so the optical clarity of these systems can be at least partly attributed to their reduced light-scattering efficiency of the smaller droplets.

Presumably, the presence of the glycerol molecules in the aqueous phase altered the nature of the colloidal structures formed at the oil/surfactant and aqueous phase boundary when

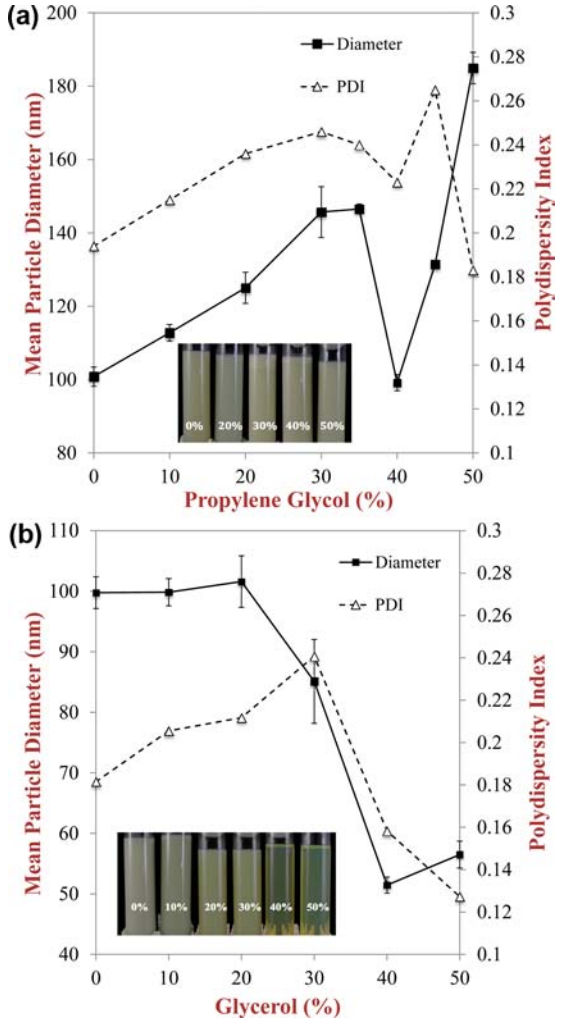

Figure 4. Influence of (a) propylene glycol content and (b) glycerol content in the aqueous phase on the mean particle diameter produced by spontaneous emulsification. All systems contained 10% oil phase (50% fish oil/50% lemon oil) and 10% surfactant (Tween 80). Particle sizes were measured after 24 h of storage at ambient temperature.

the two phases were brought into contact. For example, they may have been able to penetrate into the surfactant monolayer and alter its optimum curvature and flexibility.[36] As a result, the spontaneous formation of ultrafine droplets at the boundary may have been facilitated.

Thermal Stability. Nanoemulsions stabilized by nonionic surfactants are often unstable to coalescence when they are heated close to their phase inversion temperatures, and so we examined the influence of heating on nanoemulsion stability. A nanoemulsion was initially prepared by spontaneous emulsification that contained 10% oil phase (50% fish oil/50% lemon oil), 10% surfactant (Tween 80), and 80% aqueous phase (40% glycerol in citrate buffer). The turbidity of this nanoemulsion was then measured as the sample was heated from 20 to 90 °C (Figure 5).

The turbidity of the nanoemulsions remained relatively small from around 20 to 50 °C, indicating that they were relatively stable to droplet growth in this temperature range. However, there was a steep increase in turbidity from around 50 to 68 °C, which can be attributed to droplet growth due to coalescence. The turbidity of the samples then decreased steeply from 68 to 70 °C and remained relatively low until around 74 °C. Visual

dx.doi.org/10.1021/jf4054808 | J. Agric. Food Chem. 2014, 62, 1720−1725

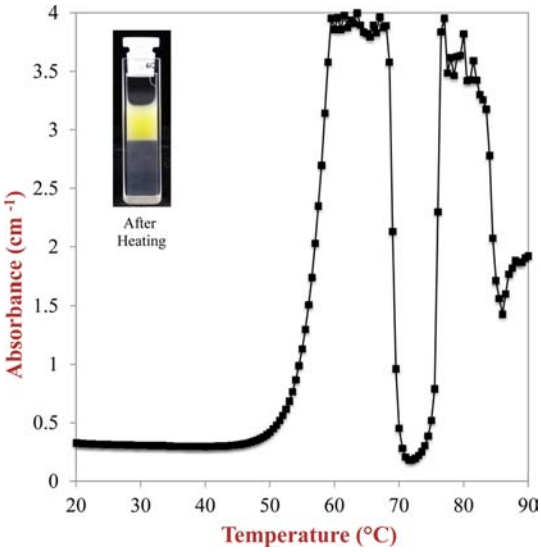

Figure 5. Influence of heating on the turbidity of nanoemulsions produced by spontaneous emulsification. All systems contained 10% oil (50% fish oil/50% lemon oil), 10% surfactant (Tween 80), and 80% aqueous phase (40% glycerol in citrate buffer solution). (Inset) Photograph of the sample after heating.

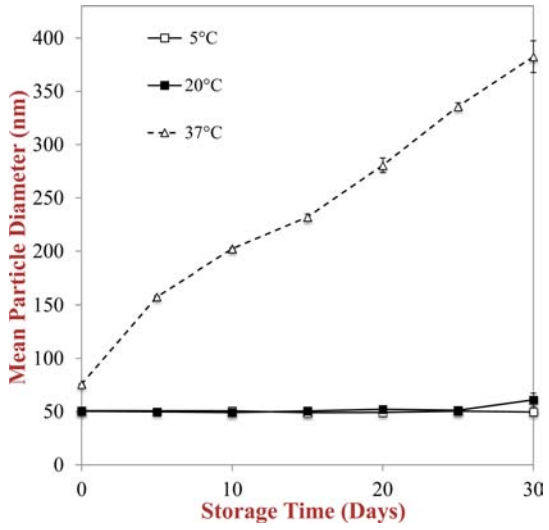

Figure 6. Influence of storage temperature on the mean particle diameter of nanoemulsions. All systems contained 10% oil (50% fish oil/50% lemon oil), 10% surfactant (Tween 80), and 80% aqueous phase (40% glycerol in citrate buffer solution).

observation of these samples showed that they were homogeneous and optically transparent. We propose that a single isotropic microemulsion phase was formed in this narrow temperature range, corresponding to the phase inversion temperature. When the samples were further heated, there was a steep increase in turbidity, which can be attributed to the formation of a water-in-oil emulsion and the corresponding increase in particle size. The reason that the emulsions go from an oil-in-water system at low temperatures to a microemulsion at intermediate temperatures to a water-in-oil system at high temperatures can be attributed to surfactant dehydration.[37,38] When the samples were cooled to ambient temperature inside the instrument (which occurred relatively slowly), they underwent phase separation (Figure 5, inset).

Isothermal Stability. For commercial applications, it is important that nanoemulsion-based delivery systems remain physically stable during storage. Nanoemulsions become physically unstable through numerous physicochemical processes, including flocculation, coalescence, Ostwald ripening, and gravitational separation.[23] We therefore examined the influence of isothermal storage on the stabilty of the nanoemulsions to droplet growth and phase separation. As before, nanoemulsions were prepared using the spontaneous emulsification method that contained 10% oil phase (50% fish oil/50% lemon oil), 10% surfactant (Tween 80), and 80% aqueous phase (40% glycerol in citrate buffer). These samples were then diluted in buffer solution, and their mean particle diameter and appearance were measured after they were stored at three storage temperatures for different times (Figure 6).

The nanoemulsions stored at 5 and 20 °C appeared to be stable to droplet growth with no change in mean particle diameter or appearance during 30 days of storage. On the other hand, the nanoemulsions stored at 37 °C showed an appreciable increase in mean particle diameter during storage and became cloudy in appearance. Indeed, after 30 days, they phase separated into a white cream layer on top of a clear serum layer. Presumably, droplet growth occurred due to enhanced coalescence when the nanoemulsions were held at temperatures close to their phase inversion temperature. Around these temperatures, there is a decrease in interfacial tension, which makes the surfactant monolayers more flexible and more prone to coalescence.[23]

This study has shown that stable transparent nanoemulsions containing relatively high levels of fish oil can be formed using a low-energy method (spontaneous emulsification). The size of the droplets in these nanoemulsions can be controlled by manipulating the surfactant-to-oil ratio, oil composition, and aqueous phase composition. A major advantage of the spontaneous emulsification method is that no sophisticated or expensive equipment is required to form the nanoemulsions. On the other hand, a major disadvantage of the method is that a relatively high surfactant concentration is required to form them. For example, about 250 mg of surfactant would be required to incorporate around 250 mg of fish oil into a commercial product. This level of surfactant may cause problems due to economic, flavor, or regulatory considerations. For example, the U.S. Food and Drug Administration puts legal limits on the use of Tween 80 in various food applications, for example, < 475 mg/day in fat-soluble vitamin preparations (www.fda.gov).

AUTHOR INFORMATION

Corresponding Author

*(D.J.M.) Phone: (413) 545-1019. Fax: (413) 545-1262. E-mail: mcclements@foodsci.umass.edu.

Funding

This material is based upon work supported by the U.S. Department of Agriculture competitive grants program (NRI-AFRI).

Notes

The authors declare no competing financial interest.

REFERENCES

(1) Ruxton, C. H. S.; Reed, S. C.; Simpson, M. J. A.; Millington, K. J. The health benefits of omega-3 polyunsaturated fatty acids: a review of the evidence. *J. Hum. Nutr. Diet.* **2004**, *17* (5), 449–459.

(2) Ruxton, C. H. S.; Reed, S. C.; Simpson, M. J. A.; Millington, K. J. The health benefits of omega-3 polyunsaturated fatty acids: a review of the evidence. *J. Hum. Nutr. Diet.* **2007**, *20* (3), 275−285.
(3) Siddiqui, R. A.; Shaikh, Sr.; Sech, L. A.; Yount, H. R.; Stillwell, W.; Zaloga, G. P. Omega 3-fatty acids: health benefits and cellular mechanisms of action. *Mini-Rev. Med. Chem.* **2004**, *4* (8), 859−871.
(4) Jacobsen, C. Omega-3s in food emulsions: overview and case studies. *Agro Food Ind. Hi-Tech* **2008**, *19* (5), 9−12.
(5) Orchard, T. S.; Pan, X. L.; Cheek, F.; Ing, S. W.; Jackson, R. D. A systematic review of omega-3 fatty acids and osteoporosis. *Br. J. Nutr.* **2012**, *107*, S253−S260.
(6) Tur, J. A.; Bibiloni, M. M.; Sureda, A.; Pons, A. Dietary sources of omega 3 fatty acids: public health risks and benefits. *Br. J. Nutr.* **2012**, *107*, S23−S52.
(7) Waraho, T.; McClements, D. J.; Decker, E. A. Mechanisms of lipid oxidation in food dispersions. *Trends Food Sci. Technol.* **2011**, *22* (1), 3−13.
(8) McClements, D. J.; Decker, E. A. Lipid oxidation in oil-in-water emulsions: impact of molecular environment on chemical reactions in heterogeneous food systems. *J. Food Sci.* **2000**, *65* (8), 1270−1282.
(9) Arab-Tehrany, E.; Jacquot, M.; Gaiani, C.; Imran, M.; Desobry, S.; Linder, M. Beneficial effects and oxidative stability of omega-3 long-chain polyunsaturated fatty acids. *Trends Food Sci. Technol.* **2012**, *25* (1), 24−33.
(10) Berton-Carabin, C.; Genot, C.; Gaillard, C.; Guibert, D.; Ropers, M. H. Design of interfacial films to control lipid oxidation in oil-in-water emulsions. *Food Hydrocolloids* **2013**, *33* (1), 99−105.
(11) Poyato, C.; Navarro-Blasco, I.; Calvo, M. I.; Cavero, R. Y.; Astiasaran, I.; Ansorena, D. Oxidative stability of O/W and W/O/W emulsions: effect of lipid composition and antioxidant polarity. *Food Res. Int.* **2013**, *51* (1), 132−140.
(12) Salminen, H.; Herrmann, K.; Weiss, J. Oil-in-water emulsions as a delivery system for n-3 fatty acids in meat products. *Meat Sci.* **2013**, *93* (3), 659−667.
(13) Matalanis, A.; Decker, E. A.; McClements, D. J. Inhibition of lipid oxidation by encapsulation of emulsion droplets within hydrogel microspheres. *Food Chem.* **2012**, *132* (2), 766−772.
(14) Djordjevic, D.; Cercaci, L.; Alamed, J.; McClements, D. J.; Decker, E. A. Chemical and physical stability of citral and limonene in sodium dodecyl sulfate-chitosan and gum arabic-stabilized oil-in-water emulsions. *J. Agric. Food Chem.* **2007**, *55* (9), 3585−3591.
(15) Augustin, M. A.; Sanguansri, L. Polyunsaturated fatty acids: delivery, innovation and incorporation into foods. *Food Aust.* **2003**, *55* (7), 294−296.
(16) McClements, D. J. Theoretical prediction of emulsion color. *Adv. Colloid Interface Sci.* **2002**, *97* (1−3), 63−89.
(17) McClements, D. J. Colloidal basis of emulsion color. *Curr. Opin. Colloid Interface Sci.* **2002**, *7* (5−6), 451−455.
(18) Chantrapornchai, W.; Clydesdale, F. M.; McClements, D. J. Influence of relative refractive index on optical properties of emulsions. *Food Res. Int.* **2001**, *34* (9), 827−835.
(19) Mozaffarian, D.; Wu, J. H. Y. Omega-3 fatty acids and cardiovascular disease effects on risk factors, molecular pathways, and clinical events. *J. Am. Coll. Cardiol.* **2011**, *58* (20), 2047−2067.
(20) Velikov, K. P.; Pelan, E. Colloidal delivery systems for micronutrients and nutraceuticals. *Soft Matter* **2008**, *4* (10), 1964−1980.
(21) Wooster, T. J.; Golding, M.; Sanguansri, P. Impact of oil type on nanoemulsion formation and Ostwald ripening stability. *Langmuir* **2008**, *24* (22), 12758−12765.
(22) Acosta, E. Bioavailability of nanoparticles in nutrient and nutraceutical delivery. *Curr. Opin. Colloid Interface Sci.* **2009**, *14* (1), 3−15.
(23) McClements, D. J. Edible nanoemulsions: fabrication, properties, and functional performance. *Soft Matter* **2011**, *7* (6), 2297−2316.
(24) McClements, D. J. Emulsion design to improve the delivery of functional lipophilic components. *Annu. Rev. Food Sci. Technol.* **2010**, *1* (1), 241−269.
(25) McClements, D. J. Nanoemulsions versus microemulsions: terminology, differences, and similarities. *Soft Matter* **2012**, *8* (6), 1719−1729.
(26) Solans, C.; Sole, I. Nano-emulsions: formation by low-energy methods. *Curr. Opin. Colloid Interface Sci.* **2012**, *17* (5), 246−254.
(27) Saberi, A. H.; Fang, Y.; McClements, D. J. Fabrication of vitamin E-enriched nanoemulsions: factors affecting particle size using spontaneous emulsification. *J. Colloid Interface Sci.* **2013**, *391*, 95−102.
(28) Yang, Y.; Marshall-Breton, C.; Leser, M. E.; Sher, A. A.; McClements, D. J. Fabrication of ultrafine edible emulsions: comparison of high-energy and low-energy homogenization methods. *Food Hydrocolloids* **2012**, *29* (2), 398−406.
(29) Saberi, A. H.; Fang, Y.; McClements, D. J. Effect of glycerol on formation, stability, and properties of vitamin-E enriched nanoemulsions produced using spontaneous emulsification. *J. Colloid Interface Sci.* **2013**, *411*, 105−113.
(30) Saberi, A. H.; Fang, Y.; McClements, D. J. Fabrication of vitamin E-enriched nanoemulsions by spontaneous emulsification: effect of propylene glycol and ethanol on formation, stability, and properties. *Food Res. Int.* **2013**, *54*, 812−820.
(31) Mayer, S.; Weiss, J.; McClements, D. J. Vitamin E-enriched nanoemulsions formed by emulsion phase inversion: factors influencing droplet size and stability. *J. Colloid Interface Sci.* **2013**, *402*, 122−130.
(32) Ostertag, F.; Weiss, J.; McClements, D. J. Low-energy formation of edible nanoemulsions: factors influencing droplet size produced by emulsion phase inversion. *J. Colloid Interface Sci.* **2012**, *388*, 95−102.
(33) McClements, D. J. Critical review of techniques and methodologies for characterization of emulsion stability. *Crit. Rev. Food Sci. Nutr.* **2007**, *47* (7), 611−649.
(34) Dickinson, E. *An Introduction to Food Colloids*; Oxford Science Publishers: Oxford, UK, 1992.
(35) Yang, Y.; Leser, M. E.; Sher, A. A.; McClements, D. J. Formation and stability of emulsions using a natural small molecule surfactant: quillaja saponin (Q-Naturale (R). *Food Hydrocolloids* **2013**, *30* (2), 589−596.
(36) Yaghmur, A.; Aserin, A.; Garti, N. Phase behavior of microemulsions based on food-grade nonionic surfactants: effect of polyols and short-chain alcohols* 1. *Colloids Surf., A* **2002**, *209* (1), 71−81.
(37) Israelachvili, J. *Intermolecular and Surface Forces*, 3rd ed.; Academic Press: London, UK, 2011.
(38) Wennerstrom, H.; Olsson, U. Microemulsions as model systems. *C. R. Chim.* **2009**, *12* (1−2), 4−17.

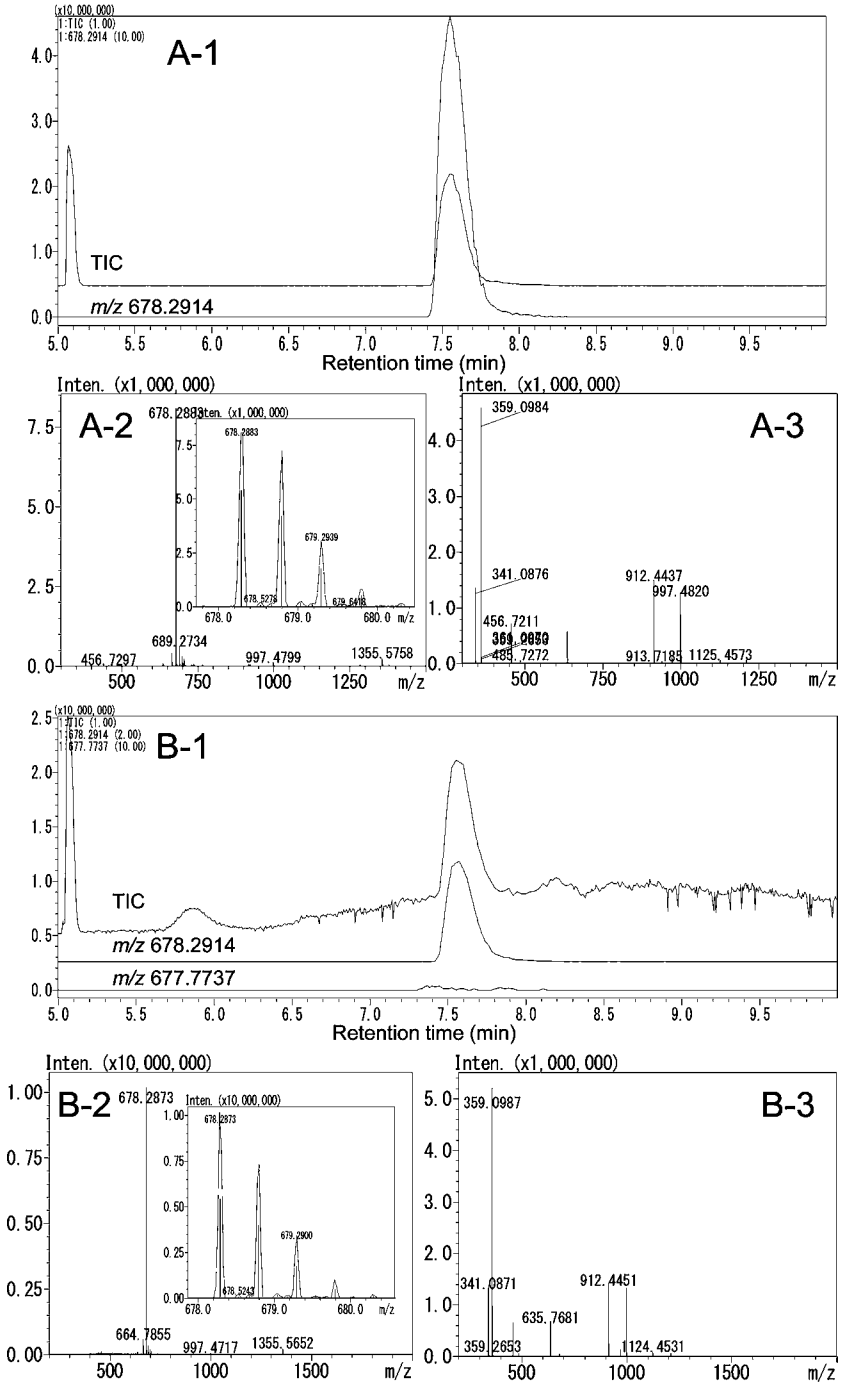

Figure 1. LC/ESI–MS/MS chromatograms of authentic B_{12} and the B_{12} compounds purified from the lion's mane mushroom sample G. B_{12} was analyzed using an LCMS-IT-TOF system (Shimadzu), as described in the text. Panels A-1 and B-1 show the total ion chromatograms (TICs) and the chromatograms (*m/z* 678.2914) of authentic B_{12} and the purified B_{12} compounds from lion's mane mushroom sample G, respectively. The mass spectra of authentic B_{12} and the B_{12} compounds purified from mushroom sample G at 7.55 min are shown in panels A-2 and B-2, respectively (the magnified spectrum range from *m/z* 678 to *m/z* 680 is shown as an insert in each panel). The MS/MS spectra for *m/z* 678.2883 peak of authentic B_{12} and the B_{12} compounds purified from the mushroom sample G are shown in panels A-3 and B-3, respectively.

known as alkali-resistant factors. Because *L. delbrueckii* ATCC 7830 can utilize both deoxyribosides and deoxyribonucleotides (alkali-resistant factors) as well as B_{12}, the amount of B_{12} was calculated by subtracting the values of the alkali-resistant factor from the values of total B_{12}. The B_{12} assay was performed in triplicate.

In the case of B_{12} assay using vitamin B_{12}-dependent *Escherichia coli* 215, each B_{12} compound was spotted onto a filter paper (circle, 6 mm), which was placed on 1.5% (w/v) agar containing a basal medium of *E. coli* 215 and incubated at 30 °C for approximately 20 h.[9] The gel plate was sprayed with a methanol solution containing 2,3,5-triphenyltetrazolium salt to enable visualization of the B_{12} compounds, indicating *E. coli* growth.

Identification of Mushroom B_{12} Compounds by LC/ESI–MS/MS. *H. erinaceus* fruiting body samples (each 50 g dry weight) were homogenized in a mixer (TML160; Tokyo, Japan). Each homogenate was added to 500 mL of distilled water, 50 mL of 0.57 mol/L acetic buffer, pH 4.5, with 0.77 mmol KCN, and boiled for 30 min to extract B_{12} compounds. The extraction procedures were performed in a draft chamber (Dalton Co., Tokyo, Japan). The boiled suspension was filtered with a cotton cloth, and the filtrate was centrifuged at 10 000*g*

dx.doi.org/10.1021/jf404463v | J. Agric. Food Chem. 2014, 62, 1726–1732

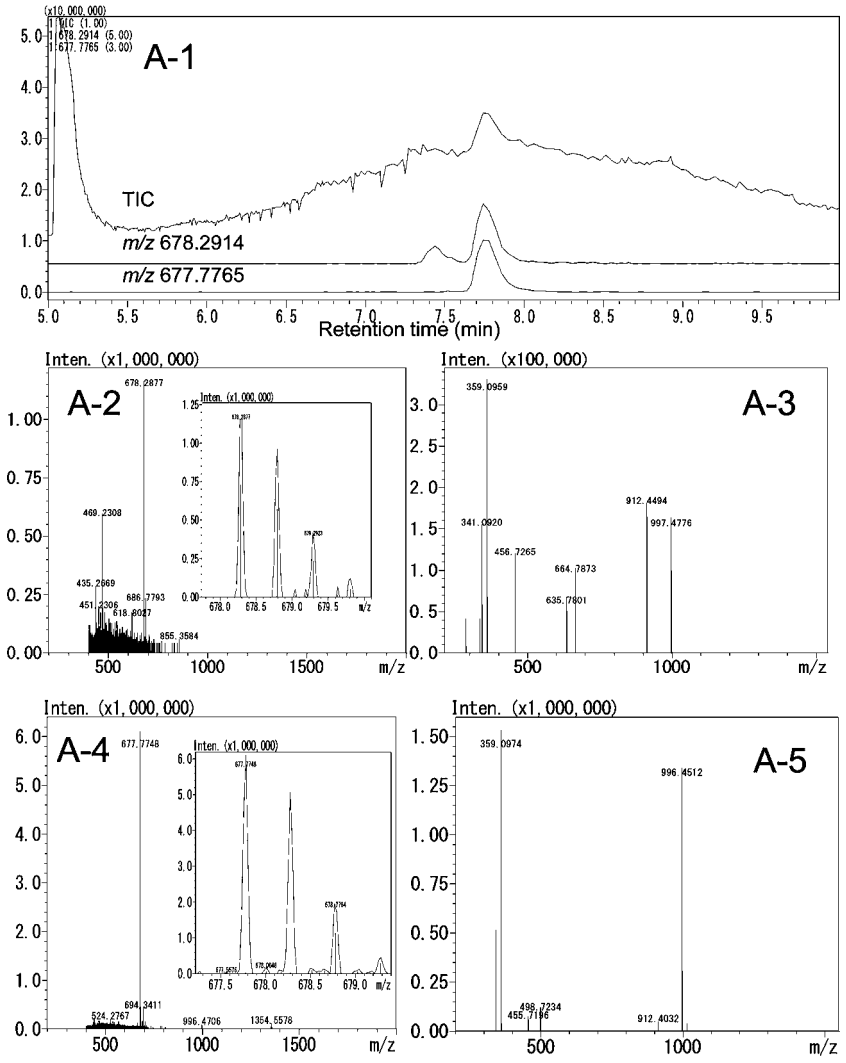

Figure 2. LC/ESI−MS/MS chromatograms of the B_{12} compounds purified from the lion's mane mushroom sample C. Panel A-1 shows the total ion chromatograms (TICs) and the chromatograms of *m/z* 678.2914 and *m/z* 677.7765 in the purified B_{12} compounds from mushroom sample C. The mass spectra of the *m/z* 678.2914 (at 7.45 min) and *m/z* 677.7765 (at 7.7 min) peaks of the B_{12} compounds purified from mushroom sample C are shown in panels A-2 and A-4 (the magnified spectrum range from *m/z* 678 to *m/z* 680 is shown as an insert in each panel), respectively. The MS/MS spectra for the *m/z* 678.2877 and *m/z* 677.7748 peaks of the B_{12} compounds purified from the mushroom sample C are shown in panels A-3 and A-5, respectively.

Table 1. Vitamin B_{12} Contents of Various Types of Dried Lion's Mane Mushroom (*Hericium erinaceus*)

sample	vitamin B_{12} content (μg/100 g dry weight)
A	0.04
B	0.36
C	0.56
D	0.10
E	0.27
F	0.20
G	1.04
mean ± SD	0.37 ± 0.34

for 10 min. Aliquots (approximately 200 mL) of the supernatant were placed in Sep-Pak Vac 20-cc (5-g) C18 cartridges (Waters Corp.), which had been washed with 75% (v/v) ethanol and equilibrated with distilled water. The C18 cartridges were washed with 30 mL of distilled water, and B_{12} compounds were eluted using 30 mL of 75% (v/v) ethanol. The remaining supernatant was treated in a similar manner. The combined eluates were evaporated to dryness under reduced pressure and the residual fraction was dissolved in 5 mL of distilled water and centrifuged at 10 000*g* for 10 min to remove any insoluble material. The supernatant fraction was loaded onto an immunoaffinity column (EASI-EXTRACT B_{12} Immunoaffinity Column (P80) R-Biopharm AG, Darmstadt, Germany), and B_{12} compounds were purified according to the manufacturer's protocol. The purified mushroom B_{12} compounds and authentic B_{12} were dissolved in 0.1% (v/v) acetic acid and filtered using a Nanosep MF centrifuge device (0.4 μm; Pall Corp., Tokyo, Japan) to remove small particles. We analyzed an aliquot (2 μL) of the filtrate using an LCMS-IT-TOF system coupled to an Ultra-Fast LC system (Shimadzu, Kyoto, Japan). Each purified sample was injected into an InertSustain column (3 μm, 2.0 × 100 mm; GL Science, Tokyo, Japan) and equilibrated with 85% solvent A (0.1% (v/v) acetic acid) and 15% solvent B (100% methanol) at 40 °C. B_{12} compounds were eluted using a linear gradient of methanol (15% solvent B for 0−5 min, 15−90% solvent B for 5−11 min, and 90−15% solvent B for 11−15 min). The flow rate was 0.2 mL/min. The electrospray ion (ESI) conditions were determined by injecting authentic B_{12} into the MS detector to identify the optimum parameters for detecting the parent and daughter ions of the B_{12} compound. ESI−MS was operated in the positive ion mode using argon as the collision gas. The identification of B_{12} (*m/z*

dx.doi.org/10.1021/jf404463v | J. Agric. Food Chem. 2014, 62, 1726−1732

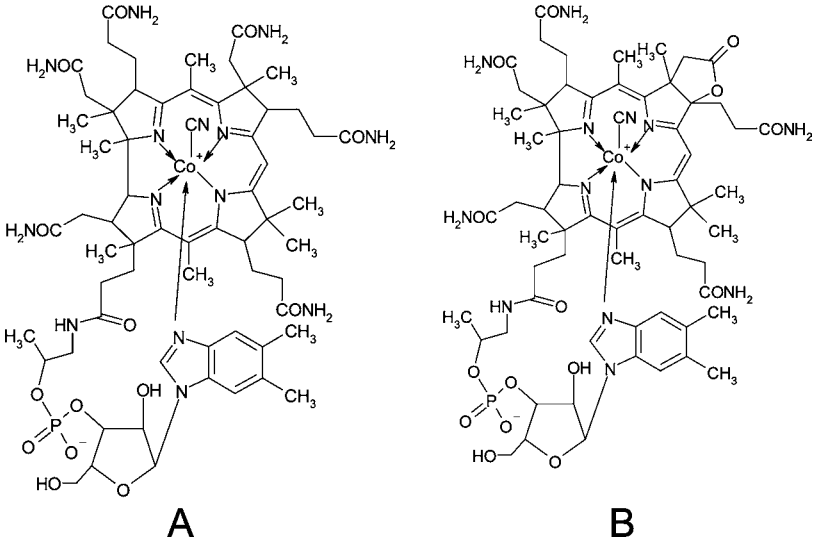

Figure 3. Structures of B_{12} and B_{12}[*c*-lactone]: (A) B_{12} and (B) B_{12}[*c*-lactone].

Table 2. R_f Values and Retention Times of Authentic B_{12} and Prepared B_{12}[*c*-lactone] during TLC and HPLC

	silica gel 60 TLC (R_f)		reversed-phase HPLC
compound	solvent I	solvent II	(min)
authentic B_{12}	0.57	0.21	8.4
B_{12}[*c*-lactone]	0.58	0.29	12.2

678.2914) representing $[M + 2H]^{2+}$was confirmed by comparing the observed molecular ions and their retention times.

Preparation of B_{12}[c-lactone]. B_{12}[*c*-lactone] was synthesized according to the method of Pathare et al.[10] In brief, B_{12}(cyanocobalamin, 0.5 g), was dissolved in 150 mL of distilled water, and 7.5 mL of acetic acid was added. Sodium iodide (50 mg) and *N*-chlorosuccinimide (90 mg) were then added, and the reaction mixture was stirred at 25 °C for 16 h in the dark. After the reaction mixture was desalted using Sep-Pak Vac 20-cc (5-g) C18 cartridges, the desalted solution was evaporated to dryness under reduced pressure and then dissolved in a small amount of distilled water. The solution was further purified using a reversed-phase HPLC column (Wakosil-II 5C18RS, 4.6 × 150 mm; 5-μm particle size; Wako Pure Chemical Industries, Osaka, Japan). B_{12}[*c*-lactone] was isocratically eluted with 20% (v/v) methanol solution containing 1% (v/v) acetic acid at 40 °C and monitored by measuring the absorbance at 280 nm. The flow rate was 1 mL/min. A main peak with a retention time of 12.2 min was recovered and treated as B_{12}[*c*-lactone] in the experiments. B_{12}[*c*-lactone] concentration was determined using the molar extinction coefficient ($\varepsilon = 2.63 \times 10^4$) at an absorbance of 359 nm as described previously.[10]

Analytical TLC and HPLC. Concentrated solutions of prepared B_{12}[*c*-lactone] and authentic B_{12} were spotted onto the silica gel 60 TLC sheet and developed at 25 °C in the dark using 2-propanol/NH_4OH (28%)/water (7:1:2 v/v) and 1-butanol/2-propanol/water (10:7:10 v/v) as solvents I and II, respectively. After drying the TLC sheet, the R_f values of the red spots were measured. In HPLC analysis, prepared B_{12}[*c*-lactone], authentic B_{12}, or a reaction mixture was analyzed using a reversed-phase HPLC column (Wakosil-II 5C18RS, 4.6 × 150 mm; 5-μm particle size; Wako Pure Chemical Industries, Osaka, Japan). Corrinoids were isocratically eluted with 20% (v/v) methanol solution containing 1% (v/v) acetic acid at 40 °C and monitored by measuring the absorbance at 361 nm. The flow rate was 1 mL/min. The retention times of authentic B_{12} and prepared B_{12}[*c*-lactone] were 8.4 and 12.2 min, respectively.

Conversion of B_{12} to B_{12}[c-lactone] by Chloramine-T. The reaction mixture contained 10 μmol/L B_{12} (cyanocobalamin), 10 μmol/L chloramine-T, and 100 mmol/L citrate buffer (pH range 3.0−6.0), 2-(*N*-morpholino)ethane sulfonic acid buffer (pH range 5.0−8.0), 4-(2-hydroxyethyl)-1-piperazine ethane sulfonic acid buffer (pH range 7.0−9.0), or borate buffer (pH range 8.0−10.0). After leaving the reaction mixture for 24 h at 25 °C in the dark, each mixture was immediately analyzed using the reversed-phase HPLC system, as described above. The relative concentrations of B_{12} and B_{12}[*c*-lactone] were calculated based on the peak areas with the identical retention times of B_{12} and B_{12}[*c*-lactone], respectively. B_{12}[*c*-lactone] formation was represented as the percentage of B_{12}[*c*-lactone] versus the sum of B_{12} and B_{12}[*c*-lactone].

RESULTS AND DISCUSSION

The B_{12} contents were determined in seven samples of dried lion's mane mushroom (*H. erinaceus*) fruiting body using a microbiological assay method based on *L. delbrueckii* ATCC 7830 (Table 1). Trace levels (0.04−0.36 μg/100 g dry weight) of B_{12} were found in most samples (A, B, D, E, and F), and samples C and G contained 0.56 and 1.04 μg/100 g dry weight of B_{12}, respectively. As these cultured and dried lion's mane mushroom fruiting body samples were obtained from different manufacturers as food items, precise strains of the tested lion's mane mushrooms, culture conditions, and postharvest processing methods (probably heat-drying and then storage at an ambient temperature) of their fruiting bodies are not available. Thus, we have little information on why such differences in B_{12} contents occurred among these dried fruiting bodies.

L. delbrueckii ATCC 7830 can utilize deoxyribosides and deoxyribonucleotides (known as alkali-resistant factors) as well as B_{12}. High levels (0.51−4.03 μg as B_{12} equivalent/100 g dry weight) of the alkali-resistant factor were found in all mushroom fruiting body samples.

Corrinoids were purified from the extracts of dried lion's mane mushroom fruiting bodies using an immunoaffinity column and identified by LC/ESI−MS/MS (Figure 1). Authentic B_{12} was eluted as a peak with a retention time of 7.55 min (Figure 1A-1). The mass spectrum of authentic B_{12} mainly contained a doubly charged ion with an m/z of 678.2883 $[M + 2H]^{2+}$ (Figure 1A-1 and A-2). Its exact mass was calculated from its formula ($C_{63}H_{88}CoN_{14}O_{14}P$), i.e. 1354.5674, and the isotope distribution data showed that B_{12} mainly existed as a doubly charged ion under LC/ESI−MS conditions. The MS/MS spectrum of B_{12} indicated that a monovalent ion with an m/z of 359.0984 predominated, which was mainly attributable to the nucleotide moiety of B_{12} (Figure 1A-3). The compounds purified from dried lion's mane

dx.doi.org/10.1021/jf404463v | J. Agric. Food Chem. 2014, 62, 1726−1732

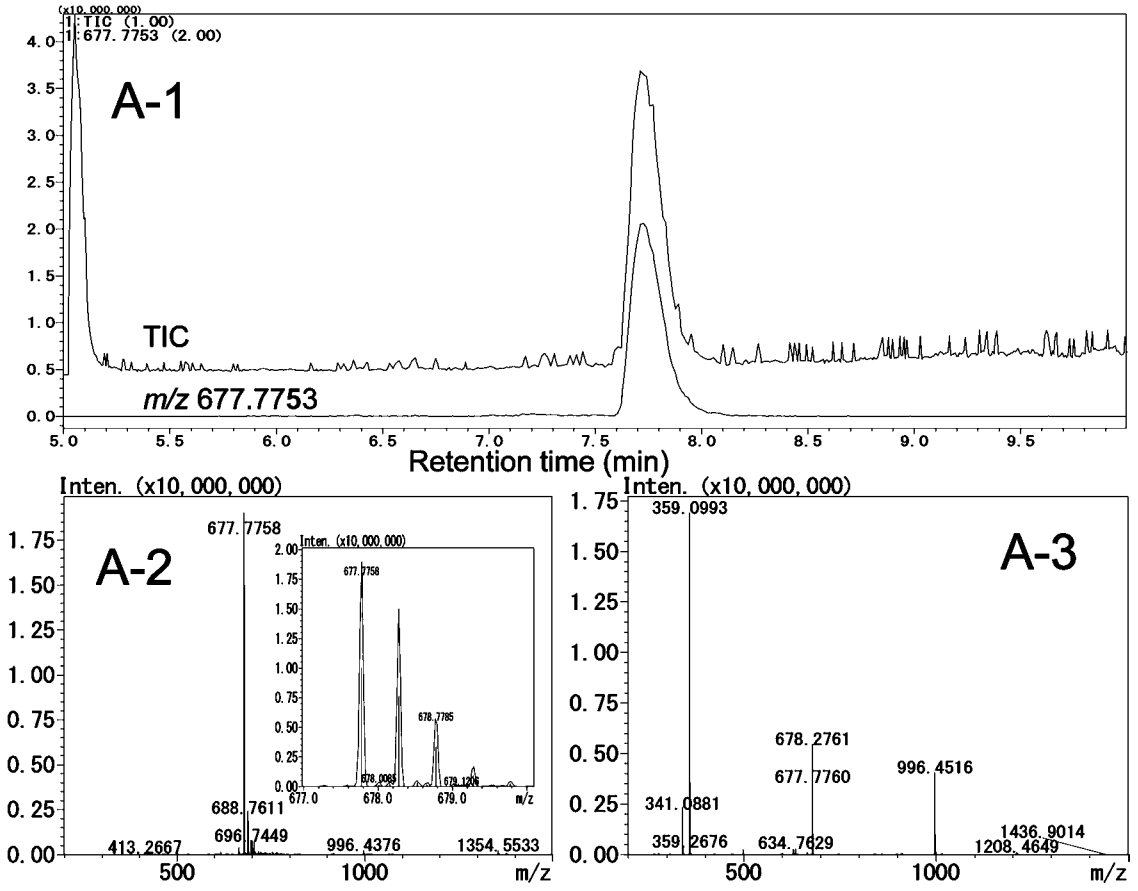

Figure 4. LC/ESI–MS/MS chromatograms of prepared B_{12}[*c*-lactone]. Panel A-1 shows the total ion chromatograms (TICs) and the chromatogram (*m*/*z* 677.7753) of prepared B_{12}[*c*-lactone]. The mass spectrum of prepared B_{12}[*c*-lactone] at 7.7 min is shown in panel A-2 (the magnified spectrum range from *m*/*z* 678 to *m*/*z* 680 is shown as an insert in each panel). The MS/MS spectra for the *m*/*z* 677.7758 peak of prepared B_{12}[*c*-lactone] is shown in panel A-3.

mushroom sample G were eluted as several ion peaks, which indicated that impurities were still present. The mass spectrum of the main peak had a retention time of 7.55 min in the purified sample (Figure 1B-1), where the B_{12} doubly charged ions had an *m*/*z* value of 678.2873 (Figure 1B-2). The MS/MS spectrum of the compound was identical to that of B_{12} (Figure 1B-3). These results indicated that dried lion's mane mushroom sample G contained B_{12} but not inactive corrinoid compounds. Similar LC/ESI–MS/MS chromatograms were obtained for the samples B, D, and F. No spectrum was obtained for mushroom sample A because it only had a trace level of B_{12}.

However, the compounds purified from mushroom sample C were eluted as two ion peaks in the chromatogram of *m*/*z* values of 678.2914 (Figure 2A-1). The mass spectrum of the minor ion peak had a retention time of 7.45 min in the purified compounds, where the B_{12} doubly charged ions had *m*/*z* values of 678.2877 (Figure 2A-2). The MS/MS spectrum of the compound was identical to that of B_{12} (Figure 2A-3). The mass spectrum of the major ion peak had a retention time of 7.7 min in the purified compounds (Figure 2A-1). The mass spectrum of the major peak had a doubly charged ion with an *m*/*z* of 677.7748 $[M + 2H]^{2+}$ (Figure 2A-4). The MS/MS spectrum of the major peak indicated that a monovalent ion with an *m*/*z* of 359.0974 (the nucleotide moiety of B_{12}) predominated (Figure 2A-5). The identical spectra were also obtained with sample E. These results indicated that dried lion's mane mushroom samples C and E contained another B_{12} compound as well as B_{12}.

Chloramine-T, an antimicrobial agent, has widespread uses in medical, dental, veterinary, food processing, and agricultural fields because of its low cytotoxicity.[11] Bonnett et al.[12] reported that chloramine-T is a source of electrophilic chlorine and it reacts with B_{12} to form B_{12}[*c*-lactone], which contains no halogen, at pH 4.0 (Figure 3). Thus, B_{12}[*c*-lactone] was synthesized according to the method of Pathare et al.[10] and then analyzed using the silica gel 60TLC and reversed-phase HPLC (Table 2). Although B_{12} and B_{12}[*c*-lactone] showed similar R_f values on TLC, B_{12}[*c*-lactone] was eluted as a single peak with different retention time of B_{12} during HPLC.

To identify the mushroom B_{12} compound with a doubly charged ion with an *m*/*z* of 677.7748 $[M + 2H]^{2+}$, B_{12}[*c*-lactone] was prepared and analyzed by LC/ESI–MS/MS (Figure 4). The prepared B_{12}[*c*-lactone] was eluted as a peak with a retention time of 7.7 min (Figure 4A-1). The mass spectrum of B_{12}[*c*-lactone] mainly had a doubly charged ion with an *m*/*z* of 677.7758 $[M + 2H]^{2+}$ (Figure 4A-1 and A-2). Its exact mass was calculated from its formula ($C_{63}H_{87}CoN_{14}O_{14}P$), i.e. 1353.5674. The MS/MS spectra of B_{12}[*c*-lactone] indicated that a monovalent ion with an *m*/*z* of 359.0993 predominated (the nucleotide moiety of B_{12}) (Figure 4A-3). These data were identical to those of the unidentified B_{12} compound found in mushroom C, which indicated that mushroom samples C and E contained an unnatural B_{12} compound, B_{12}[*c*-lactone]. To the best of our knowledge, this is the first report on the occurrence of B_{12}[*c*-lactone] in food.

We have no information on precise strains of the tested lion's mane mushrooms and their culture conditions and postharvest

dx.doi.org/10.1021/jf404463v | J. Agric. Food Chem. 2014, 62, 1726–1732

processes because the tested fruiting body samples were obtained as food items. Therefore, the reasons for such differences in B_{12} contents and occurrence of B_{12}[*c*-lactone] among the individual dried fruiting bodies is unclear. Previously, we demonstrated that the dried fruiting bodies of wild mushrooms (black trumpet and golden chanterelle) contained higher amounts (1.09−2.65 μg/100 g dry weight) of B_{12} than those of the cultured lion's mane mushrooms,[7] but B_{12}[*c*-lactone] was not detected in these dried wild mushroom fruiting bodies.

It is known that mushrooms neither have the ability to synthesize B_{12} *de novo* nor contain any B_{12}-dependent enzymes. Thus, mushroom B_{12} was probably derived from B_{12} sources outside the mushrooms, probably sawdust substrate (but no evidence of any B_{12}-containing substrates), or it was derived from B_{12} synthesized by bacteria living on the surfaces of the mushroom fruiting body. It is unclear at the present time whether such B_{12}-synthesizing bacteria can grow symbiotically with the mushroom during growth of its fruiting body or they are contaminated during preparation and storage of the dried mushroom fruiting body. However, occurrence of B_{12}[*c*-lactone] suggests that the antimicrobial agent chloramine-T was used during postharvest processing of the mushroom fruiting body.

Figure 5 shows the effects of varying pH on the conversion of B_{12} to B_{12}[*c*-lactone]. The formation of B_{12}[*c*-lactone] was

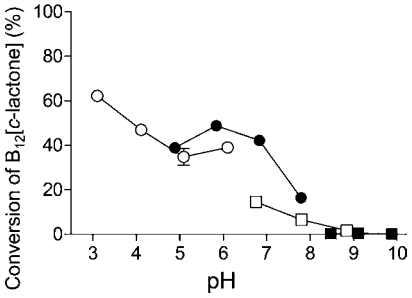

Figure 5. Effects of varying pH on the conversion of B_{12} to B_{12}[*c*-lactone]. B_{12}[*c*-lactone] formation is represented as the percentage of B_{12}[*c*-lactone] versus the sum of B_{12} and B_{12}[*c*-lactone]. Citrate buffer (○), 2-(*N*-morpholino)ethane sulfonic acid buffer (●), 4-(2-hydroxyethyl)-1-piperazine ethane sulfonic acid buffer (□), or borate buffer (■). The values represent the mean ± SD from three independent experiments.

highest at pH 3.0 in the experimental conditions, but considerable (approximately 40−50%) B_{12}[*c*-lactone] was also produced at neutral pH values (pH 6.0−7.0). These results indicate that B_{12}[*c*-lactone] is simple to be produced by incubating B_{12} with chloramine-T at a varying pH values (3.0−7.0).

We investigated whether B_{12}[*c*-lactone] exhibited any B_{12} activity in two B_{12}-dependent bacteria, which are used in microbiological B_{12} assays. B_{12}[*c*-lactone] was completely inactive in *E. coli* 215 (Figure 6A) and *L. delbrueckii* ATCC 7830 (Figure 6B). These results suggest that the lower B_{12} contents of mushroom samples C and E (Table 1) were due to the presence of B_{12}[*c*-lactone]. Stabler et al.[13] demonstrated that hydroxo (OH)-B_{12}[*c*-lactone] binds very weakly to the most specific B_{12}-binding protein, intrinsic factor. When OH-B_{12}[*c*-lactone] was injected into a rat blood vessel using an osmotic pomp, the indices of B_{12} deficiency (the serum methylmalonic acid and homocysteine levels) significantly increased because methylmalonyl-CoA mutase and methionine synthase were strongly inhibited by the addition of OH-B_{12}[*c*-lactone].

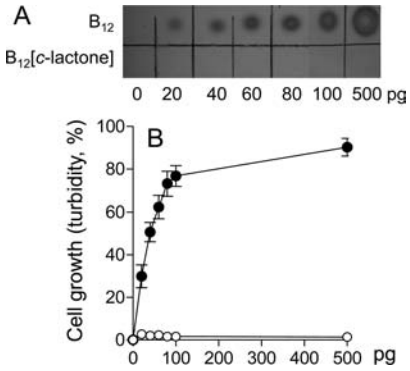

Figure 6. Effects of B_{12}[*c*-lactone] on two B_{12}-dependent bacteria used in microbiological B_{12} assay methods. (A) *E. coli* 215 and (B) *L. delbrueckii* ATCC 7830: Authentic B_{12} (○) and prepared B_{12}[*c*-lactone] (●). The values represent the mean ± SD from three independent experiments.

This study indicates that the use of the antimicrobial agent chloramine-T in food processing and agricultural fields readily promotes the formation of B_{12}[*c*-lactone] in food materials. Because nutritional values of foods treated with chloramine-T are reduced significantly, it would be necessary to make a detailed survey on the occurrence of B_{12}[*c*-lactone] in various foods.

The consumption of approximately 240 g of dried mushroom (even dried lion's mane mushroom sample G; 1.04 μg/100g dry weight) could provide the recommended dietary allowance for adults (2.4 μg/day),[14] although they would not be able to ingest such large amounts of this dried mushroom daily. Thus, dried lion's mane mushroom is not suitable for use as a B_{12} source by vegetarians because of its low B_{12} contents and the occasional presence of B_{12}[*c*-lactone] which is inactive in humans.

AUTHOR INFORMATION

Corresponding Author

*Tel/Fax: +81-857-31-5412. E-mail: watanabe@muses.tottori-u.ac.jp.

Notes

The authors declare no competing financial interest.

REFERENCES

(1) Shang, X.; Tan, Q.; Liu, R.; Yu, K.; Li, P.; Zhao, G. P. In vitro anti-*Helicobacter pylori* effects of medicinal mushroom extracts, with special emphasis on the lion's mane mushroom, *Hericium erinaceus* (higher Basidiomycetes). *Int. J. Med. Mushrooms* **2013**, *15*, 165−174.

(2) Wong, K. H.; Naidu, M.; David, R. P.; Bakar, R.; Sabaratnam, V. Neuroregenerative potential of lion's mane mushroom, *Hericium erinaceus* (Bull.:Fr.) Per. (higher Basidiomycetes), in the treatment of peripheral nerve injury (review). *Int. J. Med. Mushrooms* **2012**, *14*, 427−446.

(3) Scheider, Z.; Stroiński, A. Biosynthesis of vitamin B_{12}. In *Comprehensive B_{12}*; Schneider, Z, Stroiński, A., Eds.; Walter de Gruyter: Berlin, 1987: pp 93−110.

(4) Watanabe, F. Vitamin B_{12} sources and bioavailability. *Exp. Biol. Med.* **2007**, *232*, 1266−1274.

(5) Millet, P.; Guilland, J. C.; Fuchs, F.; Klepping, J. Nutrient intake and vitamin status of healthy French vegetarians and nonvegetarians. *Am. J. Clin. Nutr.* **1989**, *50*, 718−727.

(6) Scalabrino, G. The multi-faced basis of vitamin B_{12} (cobalamin) neurotrophism in adult central nervous system: Lessons learned from its deficiency. *Prog. Neurobiol.* **2009**, *88*, 203−220.

(7) Watanabe, F.; Schwarz, J.; Takenaka, S.; Miyamoto, E.; Ohnishi, N.; Nelle, E.; Hochstrasser, R.; Yabuta, Y. Characterization of vitamin B_{12} compounds in the wild edible mushrooms black trumpet

(*Craterellus cornucopioides*) and golden chanterelle (*Cantharellus cibarius*). *J. Nutr. Sci. Vitaminol.* **2012**, *58*, 438−441.
(8) Resources Council, Science and Technology Agency. *Standard Tables of Food Composition in Japan−Vitamin K, B6, and B12*; Resource Council, Science and Technology Agency: Tokyo, 1995; pp 16−56.
(9) Tanioka, Y.; Yabuta, Y.; Miyamoto, E.; Inui, H.; Watanabe, F. Analysis of vitamin B_{12} in food by silica gel 60 TLC and bioautography with vitamin B_{12}-dependent *Escherichia coli* 215. *J. Liq. Chromatogr. Relat. Technol.* **2008**, *31*, 1977−1985.
(10) Pathare, P. M.; Wilbur, D. S.; Heusser, S.; Quadros, E. V.; McLoughlin, P.; Morgan, A. C. Synthesis of cobalamin-biotin conjugates that vary in the position of cobalamin coupling. Evaluation of cobalamin derivative binding to transcobalamin II. *Bioconjugate Chem.* **1996**, *7*, 217−232.
(11) Steverink, A. T. G.; Steunenberg, H. Determination of chromamine-T in foodstuffs. *J. Agric. Food Chem.* **1979**, *27*, 932−934.
(12) Bonnett, R. The chemistry of the vitamin B_{12} group. *Chem. Rev.* **1963**, *63*, 573−605.
(13) Stabler, S. P.; Brass, E. P.; Marcell, P. D.; Allen, R. H. Inhibition of cobalamin-dependent enzymes by cobalamin analogues in rats. *J. Clin. Invest.* **1991**, *87*, 1422−1430.
(14) Institute of Medicine. *Dietary Reference Intakes for Thiamin, Riboflavin, Niacin, Vitamin B6, Folate, Vitamin B12, Pantothenic Acid, Biotin, and Choline*; Institute of Medicine, National Academy Press: Washington, DC, 1998; pp 306−356.

methods for TCC residue detection and screening in routine assays is still a research demand.

Immunochemical assays could be an alternative to meet all those requirements, as detection of low concentrations of TCC residues in many samples in a short time and in some cases avoiding long and tedious sample pretreatment steps may be possible. In fact, several approaches of competitive ELISA format assays have been already developed for the analysis of TCCs, being applied in most of the cases to milk samples.[1,15−17] Assuming that a majority of samples analyzed may not be contaminated by any of the TCCs, sample screening methods providing a reliable "yes/no" binary response related to a preset concentration threshold are of increasing interest in food control. Screening systems give mainly qualitative or semiquantitative information as they are focused on identifying and selecting a group of samples that contain one or more analytes above a preset concentration or threshold level.[18,19] In this context, the high selectivity and sensitivity typically provided by immunological methods are particularly suitable for the development of such screening strategies.

The use of quantum dots (QDs) as fluorescent labels in bioassays has been increasing due to their advantageous features, including excellent photostability and chemical stability, long fluorescence lifetimes, intense and narrow emission spectra, and size- and composition-tunable properties.[20] Furthermore, the possibility of attaching QDs to biomolecules keeping their functionality has allowed development of different formats of immunoassays such as microarrays[21] or Western blotting[22] as well as luminescent sensors for the analysis of health-risk environmental pollutants (e.g., based on molecular imprinted polymers[23]). However, the development of fluorescent immunoassay can report an additional benefit over the ELISA immunoassays, that is, saving time and costs in avoiding the final step of enzymatic reaction.

In this context, a QD-based immunoassay for direct screening of four TCCs in bovine muscle tissue is here described. The fluorescent probe consists of QDs bioconjugated to oxytetracycline−BSA conjugate (Oxy−BSA−QD), prepared following the carbodiimide chemistry. Due to the small size of the TCCs (haptens with only one site for binding to the antibody), the immunoassay design is restricted to a competitive format. So, competition for antibody binding sites between free antigen of the sample (unlabeled TCC) and the bioconjugates (Oxy−BSA−QD) is established.

MATERIALS AND METHODS

Reagents, materials, and instrumentation used through the work are available in the Supporting Information.

Characterization of Oxy−BSA conjugates. The synthesis and purification of Oxy−BSA conjugates are based on a commercial kit, and a detailed description about the procedure is collected in the Supporting Information. Once Oxy−BSA conjugates are obtained, an exhaustive characterization step is mandatory. A Bradford test[24] was used to determine the BSA concentration in the Oxy−BSA conjugate. The test correlates the ratio between absorbance of the samples measured at 465 and 595 nm (595/465) with the BSA (protein) concentration. According to a linear regression, BSA concentration in the conjugate was then calculated.

Molecular weight and stoichiometry of the conjugate were evaluated by MALDI-MS. A solution of 5 mg/mL of sinapinic acid in 30% of acetonitrile, containing 0.1% of trifluoroacetic acid, was prepared. An amount of 1−10 pmol of protein in the sample was needed, being 2.42 pmol in this case. As the sample has to be ideally clean of salts and the Oxy−BSA conjugate was stored in a 28 mM Na_3PO_4, 300 mM NaCl, and 33 mM sorbitol buffer (PBS), a previous cleanup step was carried out (sample desalting by Zip Tips). A solution of 1 mg/mL of BSA standard in water was used as reference. The MALDI plate was loaded with standards, matrix, and/or samples, and when the spots had been dried (at least after 30 min), the MALDI-MS analysis was performed.

Finally, following a strategy previously developed in our lab[25] based on the combination of the information provided by the Bradford test and the MALDI analysis, the final concentration of Oxy in the conjugate can be calculated. Such information is necessary to further optimize the bioconjugation of Oxy−BSA to QDs.

Synthesis and Characterization of the Immunoprobe: Oxy−BSA−QD Bioconjugate. The fluorescent labels used for labeling the Oxy−BSA conjugate giving rise to the tracer of the immunoassay are the CdSe/ZnS QDs. A brief description about their synthesis and solubilization are presented in the Supporting Information. The bioconjugation strategy used to synthesize the fluorescent tracer was based on a coupling procedure between −COOH groups from outer polymeric layers of QDs and $-NH_2$ groups from the BSA of the Oxy−BSA conjugate owing to the catalytic activity of EDC.[26] After stirring of the mixture of reagents during 2 h at room temperature, a purification step is needed to separate the bioconjugate from the rest of undesirable products (e.g., excess of reagents). The purification step is based on differences in molecular weights between the Oxy−BSA conjugate (71.2 kDa) and the Oxy−BSA−QD bioconjugate (>150 kDa). So, it can be carried out by ultrafiltration (UHF) using a 100 kDa membrane filter. Experimental conditions used for UHF were 3000 g, 5 min, making 3 washes with 100 mM PBS buffer at pH 7.4 at 4 °C.

The characterization of this bioconjugate consists on the evaluation of the fluorescent properties of QDs after the reaction and the stability in time of the tracer. These studies were carried out using fluorescent measurements.

Competitive Immunoassay Protocol. In a conventional immunoassay analysis the following experimental procedure was performed. First, the microtiter plate is coated with 100 μL/well of a 1 μg/mL antibody solution and is incubated at 37 °C for 2 h. In this step the antibody is immobilized on the microtiter plate wells by absorption over the surface of the support of polystyrene. Antibody solution is then removed and a blocking step is performed by adding 200 μL/well of 3% casein solution in water, in order to minimize further unspecific bindings. The microtiter plate is then incubated overnight at 4 °C. In a further step, the microtiter plate is washed three times using a washing solution (200 μL/well of 10 mM PBS pH 7.4 + 0.05% Tween20) to remove the excess of reagents. Then, the competition is established by the addition of a mixture of the standard (or the sample) and a known amount of the tracer (Oxy−BSA−QD) in a total volume of 150 μL/well. The reaction is incubated at 37 °C for 2 h. After the corresponding washing step, the fluorescence emission of the QDs from the Oxy−BSA−QD recognized by the antibody is measured.

Cross Reactivity Calculation. Cross reactivity (CR) is generally defined as the necessary amount of mass or concentration of interference able to produce an equal signal as when the analyte is assayed to provoke a signal inhibition of 50%.[27] Therefore, in this work CR rates, in terms of percentage (%), were calculated according to the expression (eq 1)

$$CR = [(IC_{50}(\text{analyte})/IC_{50}(\text{interference}))] \times 100 \quad (1)$$

where IC_{50} is the necessary concentration of species (analyte or interference) to induce a signal inhibition of 50%.

Screening Theory and Determination of the Unreliability Region. A screening system provides mainly qualitative or semiquantitative information. In this type of analysis it is not possible to express uncertainty in the same way as in quantitative analysis. For that reason it is necessary to define new concepts that characterize screening methods. Thus, "reliability" of a screening test is defined as the "proportion of correct yes/no responses from a large number of tests carried out on 'n' aliquots of the same sample". On the other hand, the term "uncertainty" should be replaced by "unreliability", that is the concentration range of the analyte around the limit where false

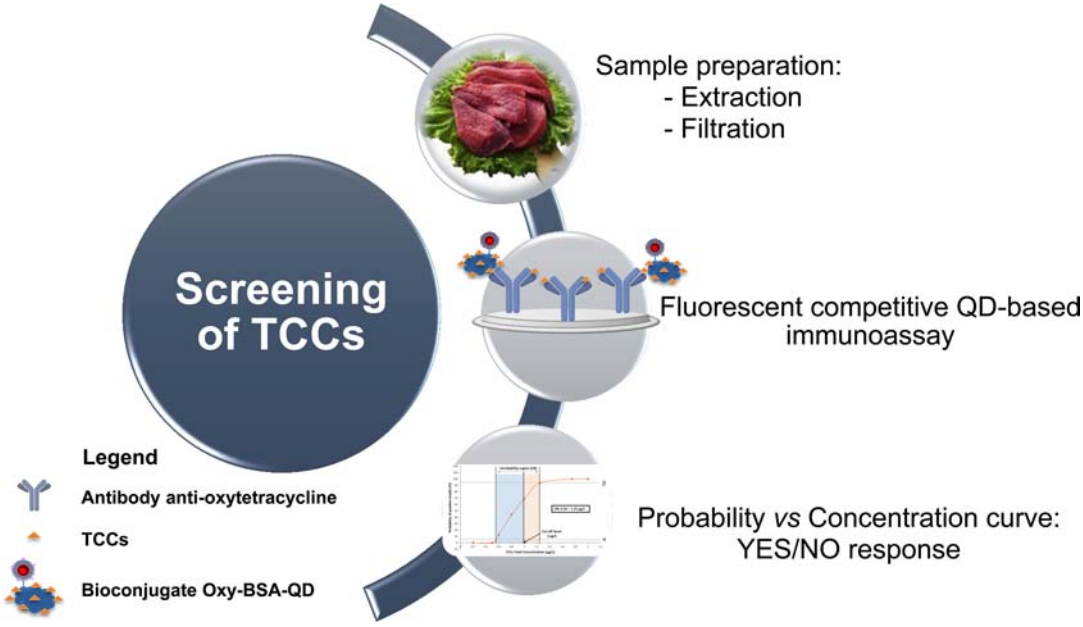

Figure 2. Work-flow diagram of the TCC screening in bovine muscle samples by fluorescent competitive QD-based immunoassay.

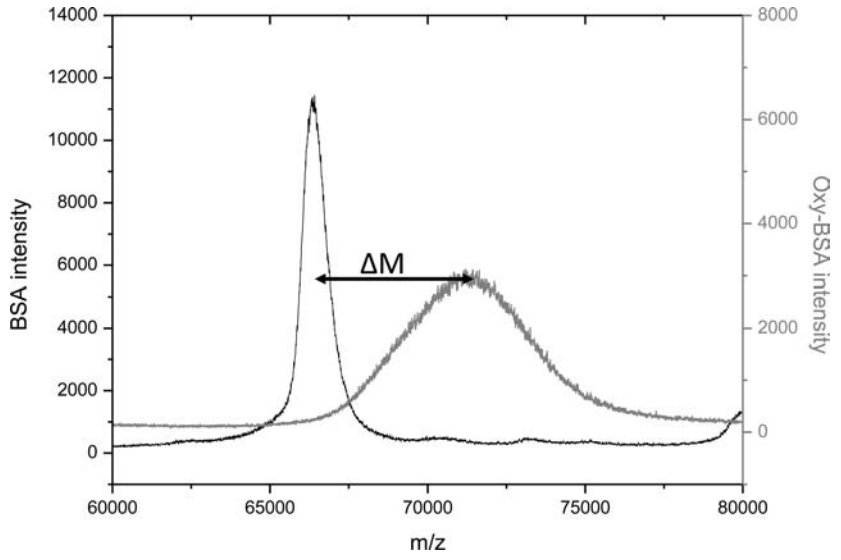

Figure 3. MALDI-MS characterization of the synthesized Oxy−BSA conjugate. The mass spectra were obtained using sinapic acid as matrix. BSA standard (black line) and Oxy−BSA conjugate (gray line) mass spectra are represented, showing clearly the mass shift between both (ΔM).

positives, false negatives, and dubious results are obtained.[18,28] In order to determine the unreliability region (UR) in the screening procedures, the cutoff level must be defined. The UR is finally calculated from the probability−concentration curve established for the screening test. In this work the limits defining the UR were determined as the levels of false positives (probability that a negative sample is classified as positive, also called α error) and false negatives (probability that a positive sample is classified as negative, also called β error).[29]

In this work, to obtain the probability vs concentration graph, 20 assays (random samples containing variable concentrations of the individual TCC but ensuring the same total antibiotic concentration) were carried out for each point of the curve, and the relative proportion (in terms of percentage) of "yes/no" answers was determined. In all cases, the binary "yes/no" response was obtained from the analytical signal (fluorescent intensity measured at the final step of the immunoassay) and was classified as "negative" or "positive" after its comparison with the fluorescence intensity signal registered for the corresponding cutoff concentration (I_0).

Analysis of Bovine Muscle Samples. Bovine muscle samples from noncontaminated cows were extracted following the Oka et al. procedure,[30] blending successively the meat samples (5 g) with three successive portions of 20, 20, and 10 mL of 0.1 M Na_2EDTA-McIlvaine buffer pH 4.0, centrifuging the mixture (at 850*g* for 5 min), and collecting and combining the supernatants by decanting. As no detectable levels of TCC residues were found in the meat samples, 5 g of chopped meat was spiked with the appropriate amount of TCC mixtures (see Table S1 in the Supporting Information for details of the concentrations of each TCC) and carefully stirred manually during 5 min. The samples were kept at 4 °C for 1 h. Afterward, the McIlvaine buffer was added and the Oka et al. procedure[30] was then followed. However, additional ultrafiltration steps were needed to remove the color that remains in the extract, which can interfere in the fluorescence measurements. For that reason, ultrafiltration with Amicon membrane filter of 10 kDa followed by ultrafiltration with Amicon membrane filter of 3 kDa (centrifuged at 12000*g* for 15 min in both cases) was performed, collecting the filtered solution. Two-hundred microliter aliquots of such solution were then used in the

immunoassays. A work-flow diagram of the complete process for the analysis of TCCs in bovine muscle samples is shown in Figure 2.

RESULTS AND DISCUSSION

Characterization of the Oxy−BSA Conjugate. As it is not possible to purchase commercial Oxy−BSA conjugate, it is necessary to synthesize it as described in Materials and Methods. A complete characterization of synthesized Oxy−BSA conjugate was performed following the strategy developed by Trapiella-Alfonso et al.[25] The molecular weight of the conjugate, the stoichiometry, and the concentration of Oxy and BSA in the conjugate are obtained.

Based on results obtained from a Bradford assay, BSA concentration was calculated to 335 ± 9 μg/mL. Molecular weight and stoichiometry were investigated by MALDI-MS. Results from MALDI experiments were used to calculate the molecular weight of the conjugate, being 71223 ± 99 Da (n = 15). Comparing the mass spectrum of BSA standard with the Oxy−BSA spectrum (see Figure 3), a mass shift (ΔM) is noticed, and this can only be attributed to the incorporation of the Oxy in the BSA structure.

If Oxy molecular weight is considered as 460.434 Da, dividing the ΔM observed by the Oxy molecular weight, the number of Oxy per BSA can be estimated. For this case, the found value was close to 10, leading to a ratio of Oxy:BSA of 10:1. Finally, applying eq 2 the final concentration of Oxy in the conjugate can be estimated.[25]

$$C_{Oxy} = 10C_{BSA}(MW_{Oxy}/MW_{BSA}) \quad (2)$$

where C_{Oxy} is the concentration of oxytetracycline in the conjugate, 10 is the Oxy:BSA ratio, C_{BSA} is the concentration of BSA in the conjugate obtained by the Bradford test, and MW_{Oxy} and MW_{BSA} are the molecular weights of oxytetracycline and BSA respectively.

Synthesis and Characterization of Oxy−BSA−QD Bioconjugate. The molar ratios used to carry out the bioconjugation reaction were optimized by varying the ratios QDs:Oxy−BSA from 1:1 to 3:1 (always with an excess of EDC in a ratio of 1500 mol per mol of biomolecule to ensure that bioconjugation is completed). Optimum molar ratio values were observed for 2:1:1500 (QDs:Oxy−BSA:EDC) attending to the highest fluorescence intensity signals measured, indicating a high efficiency on the labeling of the Oxy−BSA conjugate with the nanoparticles. According to Trapiella-Alfonso et al.[31] the concentration of Oxy and BSA in the tracer and the bioconjugation yield can be calculated.

In order to characterize the purified bioconjugate, fluorescence measurements were performed to check that QD emission is not interfered with the bioconjugation reaction. As can be seen in Figure 4, the Oxy−BSA−QD bioconjugate does not modify significantly QD emission wavelength or fluorescence intensity; therefore, it is possible to develop a fluorescent immunoassay with this tracer.

Finally, the stability of the immunoprobe (utility valid period of the tracer for immunoassays) was evaluated attending to the stability of the fluorescence emission and the ability of the antibody to recognize the tracer. It was observed that 10 days was established as the maximum period where the Oxy−BSA−QD is stable and suitable for immunosensing, being stored at 4 °C. In the Supporting Information, Figure S1 shows data from a stability study. It is observed that the fluorescence emission of the immunoprobe is reduced more than 50% after 10 days, limiting its utility in the immunoassay.

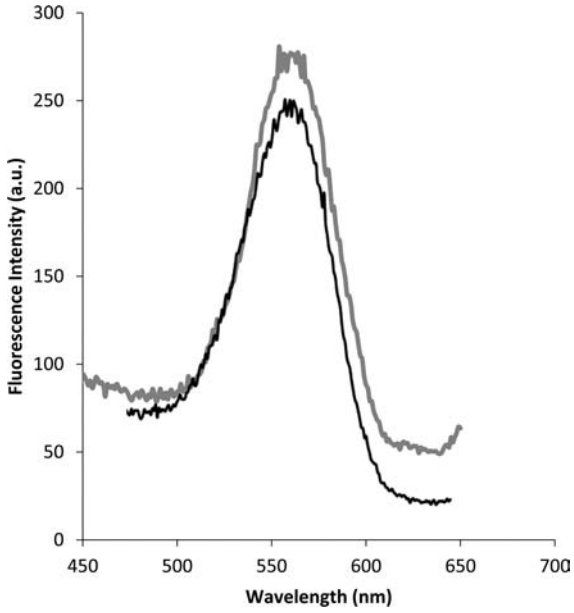

Figure 4. QDs (gray line) and Oxy−BSA−QD bioconjugate (black line) fluorescence emission spectra in buffer 10 mM PBS (pH = 7.4).

Development of the Competitive Fluorescent Immunoassay and Analytical Performance Characteristics. The immunoassay format consists of a competitive fluorescent immunoassay where nanoparticles are used as antigen labels. In this format, sample antigen and tracer (Oxy−BSA−QD) compete for the limited binding sites of the immobilized antibody.

First, the concentration of anti-Oxy antibody used for coating the well-plate and immunoprobe concentration added in the competition step were optimized for the development of the immunoassay. Optimum conditions (referring to the highest fluorescence intensity, the lowest signal deviation, and the best inhibition curve) were achieved with 1 μg/mL of the antibody solution and 10 μg/mL of the tracer (Oxy−BSA−QD) solution, ensuring a 1:1 volume ratio between the sample and the immunoprobe involved in the competition (see Table 1).

Table 1. Optimized Experimental Conditions of the Immunoassay Based on QDs

step/condition	optimized value
coating	100 μL/well Ab_{oxy} (1 μg/mL)
blocking	200 μL/well 3% casein
[Oxy] in the bioconjugate	10 μg/mL
sample:bioconjugate ratio	1:1

The analytical performance characteristics are assessed by the analysis of a series of Oxy standard solutions at different concentration levels, using the optimized QD-based immunoassay. The corresponding inhibition curve was fitted using a four-parameter equation with SOFTmax Pro software (see Figure 5). The principal parameters (see Table 2) are defined by different inhibitory concentration (IC) values calculated from the inhibition curve. Thus, a linear relationship was achieved ranging from 0.26 to 3.53 μg/L (IC_{20}−IC_{80}) enabling Oxy trace determination in bovine muscle. The detection limit (IC_{10}) was 0.12 μg/L of Oxy and the sensitivity of the assay (IC_{50}) was 0.96 μg/L of Oxy in aqueous media.

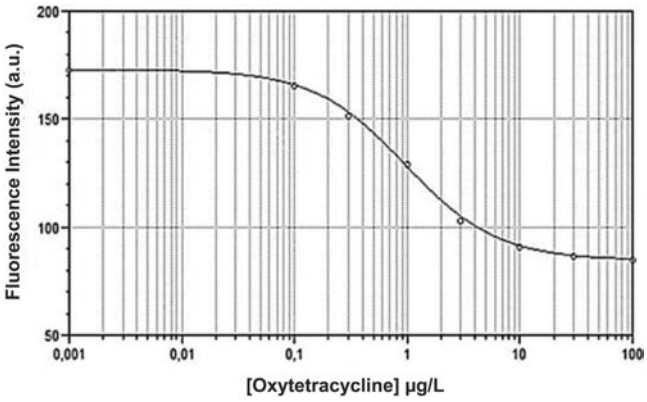

Figure 5. Fluorescent inhibition curve obtained for the analysis of TCCs in bovine muscle samples using oxytetracycline labeled with QDs as tracer in the competitive immunoassay. All the points that plot the curve exhibit a RSD < 5%.

Table 2. Analytical Characteristics of the Inhibition Curve for the Analysis of TCCs in Bovine Muscle

analytical parameter	obtained value
limit of detection (IC_{10})	0.12 μg/L
limit of quantification (IC_{20})	0.26 μg/L
linear range (IC_{20}–IC_{80})	0.26–3.53 μg/L
sensitivity (IC_{50})	0.96 μg/L
R^2	0.999

The here developed competitive QD-based fluoroimmunoassay shows some attractive features that make it advantageous over the established conventional immunoassays for the analysis of TCCs in bovine meat (in general competitive ELISA formats). Such advantages include a lower detection limit (<1.5 μg/kg), less time consumption (avoiding some steps required in the enzyme-linked immunosorbent assay), and low-cost assays (due to the smaller number of reagents used).[1,15,17,32] In addition, comparing with other analysis techniques, such as chromatographic methods, immunochemical techniques have the advantage that up to 96 samples can be analyzed within 2 h (in the best of the cases up to 24 samples can be analyzed by LC–MS[33]).

Cross Reactivity Test. A study of the cross reactivity was evaluated in order to test the performance of the antibody anti-Oxy rabbit IgG reaction with the other selected members of the TCC family under scrutiny (TC, Chlor, and Doxy). The selection of these TCCs was based on EU Commission Regulation[7] on pharmacologically active substances and their classification regarding maximum residue limits in foodstuffs of animal origin.

Different inhibition curves (corresponding to the different selected TCCs) were registered, employing the same optimized conditions as those used in the case of the Oxy determinations, and deviations from the standard curve were investigated. IC_{50} values for each analyte were determined and the cross reactivity rates were calculated applying the eq 1 given in Materials and Methods. Results obtained are collected in Table 3. Considering the high values observed for the four analytes, it is confirmed that anti-Oxy could be an appropriate antibody for the design of a screening test able to detect the presence of any of the four selected TCCs.

Additivity Studies. The immunoassay based screening system under development aims at recognizing the presence of total TCCs in the samples over a preset concentration level (e.g., the maximum residue level authorized for such family of antibiotics). Therefore, fluorescence signals from the different TCCs that could be present in the sample should be expected as additive.

Table 3. Cross Reactivity Test Using as Antibody Rabbit Anti-Oxytetracycline IgG

antigens assayed (TCC family)	CR (%)
tetracycline	89
chlortetracycline	90
doxytetracycline	82

To evaluate whether the analytical signals from the TCCs are additive, sets of aqueous samples containing only a single type of tetracyclines, as well as binary, ternary, and quaternary mixtures of the TCCs under study, were prepared and analyzed by the QD-based immunoassay. In all cases solutions contained 2 μg/L of TCC total concentration. The samples were analyzed according to the general procedure described above, and results are shown in Figure 6. A good agreement between experimental concentrations extracted from immunoassay fluorescence measurements and expected concentrations were observed. This is a proof of the analytical potential of the immunochemical method proposed for the development of the intended screening system of TCCs.

Characterization of the Screening System for TCC Detection. In order to characterize the here-developed screening test, and thus obtain the UR region, a screening curve for TCC detection was designed and characterized in aqueous media. For this purpose, a probability versus concentration graph was elaborated selecting a cutoff level of 1 μg/L total concentration of TCCs, according to the maximum sensitivity reached by the immunoassay methodology (IC_{50} factor extracted from the inhibition curve was 0.96 μg/L). The limits defining the UR of our method were determined by calculating the concentrations of TCCs that produce a probability of 5% to obtain a false positive and a probability of having a 95% of positive response (α, β errors) as it is explained in Materials and Methods. According to these patterns, the experimental unreliability region obtained was in the range between 0.56 and 1.25 μg/L total TCC concentration (see Figure 7).

This means that the presence of TCCs in aqueous media can be confirmed reliably by the proposed screening system for concentrations higher than 1.25 μg/L and, on the other hand, samples giving total concentration of TCCs below 0.56 μg/L can be reliably considered as noncontaminated.

Application to Bovine Muscle Samples. The applicability of this QD-based immunochemical method for the screening of TCC residues in contaminated bovine meat samples was finally evaluated. As no TCCs were detected by immunoassay in the scrutinized samples, they were spiked with known amounts of TCCs and then screened following the general procedure above-described.

In order to get a validation of the used methodology for the extraction of analytes from bovine muscle, a high-performance liquid chromatography (HPLC) with spectrophotometric detection for the determination of TCCs in bovine tissues was carried out. Bovine meat samples were extracted and then analyzed following the Cinquina et al. procedure.[34] The analyses were performed using a mobile phase of 0.01 M oxalic acid:acetonitrile:methanol (60:25:15 in volume) on a

dx.doi.org/10.1021/jf500118x | J. Agric. Food Chem. 2014, 62, 1733–1740

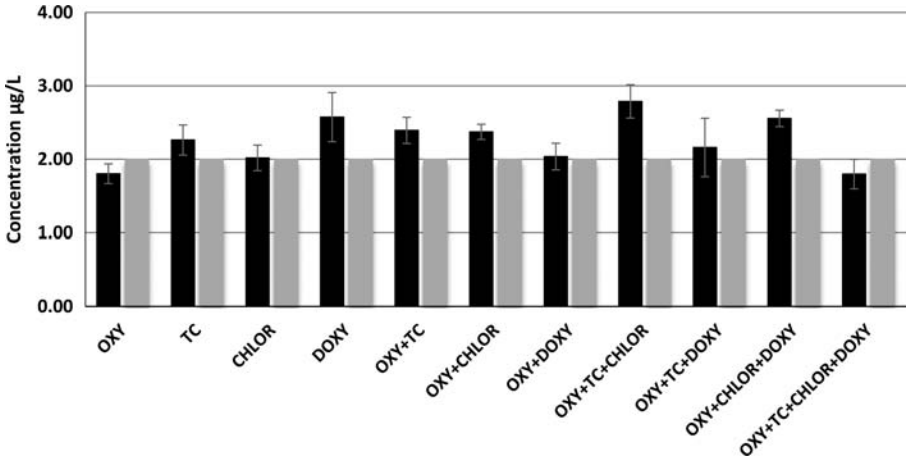

Figure 6. Additive study. In the graphic are represented the fluorescent signal intensities from different TCC mixtures (bars in black) compared with the expected signal for the concentration assayed (2 μg/L; bars in gray). As can be seen the results are in agreement.

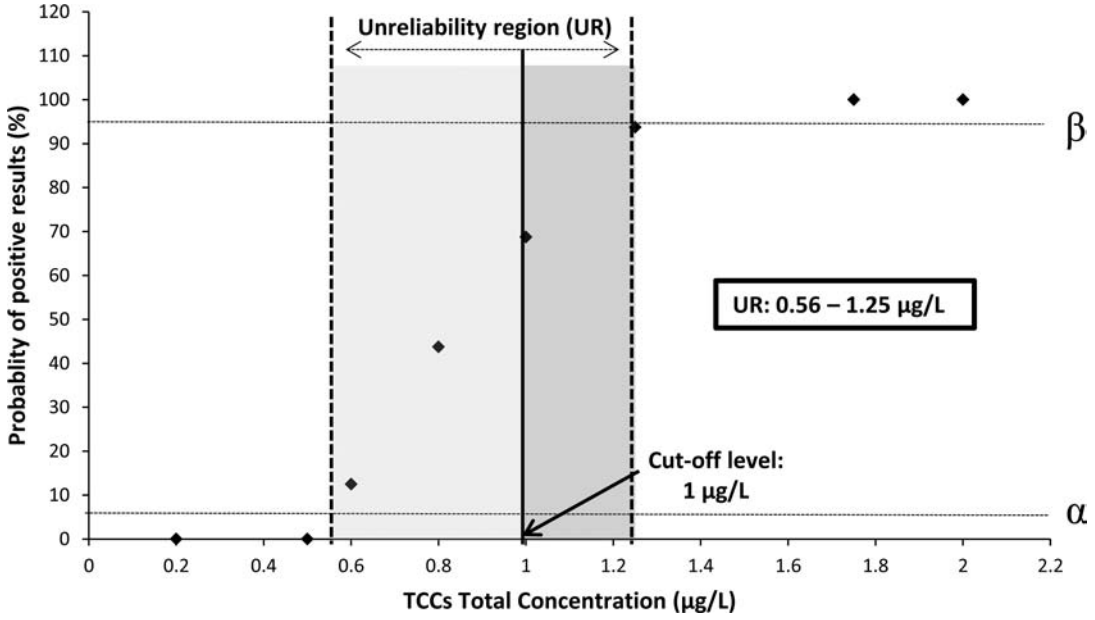

Figure 7. Experimental probability–concentration graph for the screening of TCCs in aqueous solution for a cutoff concentration value of 1 μg/L.

reversed-phase C_8 column. The recoveries were obtained by spiking bovine muscle samples at three different concentrations (50, 100, and 150 μg/kg) of the TCC quaternary mixture and then by analyzing the samples with reference to the blank. Good recoveries (average recoveries were higher than 95%) were observed in all cases, validating the selected sample pretreatment strategy here used.

A 1 μg/L total concentration of TCCs was set out as cutoff level considering the analyzed bovine muscle sample amount taken and the dilution carried out eventually before analysis, corresponding to 10 μg/kg in the bovine muscle. Results obtained for the screening in the bovine muscle samples using the proposed QD-based immunoassay are collected in Table 4. Results were classified as positive or negative, depending on their values in comparison to the cutoff one. Good agreement between expected and experimental results was obtained. This confirms that the immunoassay developed is suitable for TCC screening of bovine meat samples. Moreover, the here-developed screening methodology may provide rigorous and reliable analytical results in the case that legislation on these contaminants turns stricter in the future due to the lowest detection limit (10-fold lower than the current MRL given by European Legislation) and the selectivity achieved by this method for the TCC family compared to those developed up to now for similar purposes.[18,33] In addition, compared with other TCC screening luminescent approaches recently proposed[18]

Table 4. Screening of Bovine Muscle Samples Spiked with TCCs

[TCCs] μg/kg	screening result	expected screening result
0[a]	negative	negative
3	negative	negative
4	negative	negative
9	uncertain	negative
10	cutoff	cutoff
11	uncertain	positive
18	positive	positive
19	positive	positive

[a]Blank.

and HPLC methodologies,[14] the QD-based immunoassay presents some benefits including the possibility of analyzing a high number of samples simultaneously in a short time (up to 96 samples/plate in 2 h), as well as the nonexistence of some problems related to phosphorescent labels (e.g., deoxygenation). The drawback of the proposed methodology is the need to carry out a sample preparation step in order to extract the analyte from the bovine muscle and make the sample colorless (filtration step) because the coloration can interfere in the final fluorescence emission of QDs. Nevertheless, the designed procedure is simple and up 10 samples can be prepared in 30 min.

■ ASSOCIATED CONTENT

Ⓢ Supporting Information

Additional details of materials and methods including reagents and materials; instrumentation; synthesis and solubilization of CdSe/ZnS quantum dots; and preparation of Oxy−BSA conjugates. This material is available free of charge via the Internet at http://pubs.acs.org.

■ AUTHOR INFORMATION

Corresponding Author

*E-mail: asm@uniovi.es. Tel: +34 985 103474.

Funding

The authors are grateful for financial support from the Spanish Ministry of Education and Science (CTQ2010-16636 and MAT2010-20921-C02-01) and the European FEDER program. Finally, L.T.-A. acknowledges the FPU program (ref: AP2008-01504) from the Spanish Education Ministry for the predoctoral fellowship.

Notes

The authors declare no competing financial interest.

■ REFERENCES

(1) Pastor-Navarro, N.; Maquieira, A.; Puchades, R. Review on immunoanalytical determination of tetracycline and sulfonamide residues in edible products. *Anal. Bioanal. Chem.* **2009**, *395*, 907−920.

(2) Griffin, M. O.; Fricovsky, E.; Ceballos, G.; Villarreal, F. Tetracyclines: a pleitropic family of compounds with promising therapeutic properties. Review of the literature. *Am. J. Physiol.* **2010**, *299*, C539−C548.

(3) Jeon, M.; Kim, J.; Paeng, K.-J.; Park, S.-W.; Paeng, I. Biotin−avidin mediated competitive enzyme-linked immunosorbent assay to detect residues of tetracyclines in milk. *Microchem. J.* **2008**, *88*, 26−31.

(4) FAO/WHO Food Standards Codex Alimentarius (2007). Veterinary drug residues in food. Maximum residue limits. URL (http://www.codexalimentarius.net/mrls/vetdrugs/jsp/vetd_q-e.jsp) (accessed 25 September 2013).

(5) US Food and Drug Administration (1975). Titled 21 − Food and drugs. Chapter I −Food and Drugs Administration Department of Health and Human Services, Subchapter E − Animal drugs, feed and related products. Part 556. Tolerances for residues of new animal drugs in food. URL (http://www.accessdata.fda.gov/scripts/cdrh/cfdocs/cfcfr/cfrsearch.cfm?fr=556.500) (accessed 25 September 2013).

(6) Japanese Ministry of Health Welfare and Labor (2008). *Food safety information*. URL (http://www.mhlw.go.jp/english/topics/foodsafety/index.html) (accessed 25 September 2013).

(7) Commission Regulation (EU) No 37/2010 of 22 December 2009.

(8) Kurittu, J.; Lönnberg, S.; Virta, M.; Karp, M. A Group-Specific Microbiological Test for the Detection of Tetracycline Residues in Raw Milk. *J. Agric. Food Chem.* **2000**, *48*, 3372−3377.

(9) Virolainen, N. E.; Pikkemaat, M. G.; Alexander Elferink, J. W.; Karp, M. T. Rapid Detection of Tetracyclines and Their 4-Epimer Derivatives from Poultry Meat with Bioluminescent Biosensor Bacteria. *J. Agric. Food Chem.* **2008**, *56*, 11065−11070.

(10) Kanda, M.; Kusano, T.; Osonai, T.; Ushiyama, K.; Takeba, K.; Sakamoto, M.; Hayashi, H.; Igusa, K.; Ibe, A.; Nagayama, T. Rapid determination of residues of 4 tetracyclines in meat by microbiological screening, HPLC and LC/MS/MS. *J. Food Hyg. Soc. Jpn.* **2008**, *49*, 37−44.

(11) Goudin, V.; Hedou, C.; Rault, A.; Verdon, E. Validation of a five plate test, the STAR protocol, for the screening of antibiotic residues in muscle from different animal species according to European Decision 2002/657/EC. *Food Addit. Contam., Part A* **2010**, *27*, 935−952.

(12) Miranda, J. M.; Rodríguez, J. A.; Galán-Vidal, C. A. Simultaneous determination of tetracyclines in poultry muscle by capillary zone electrophoresis. *J. Chromatogr., A* **2009**, *1216*, 3366−3371.

(13) Önal, A. Overview on liquid chromatographic analysis of tetracycline residues in food matrices. *Food Chem.* **2011**, *127*, 197−203.

(14) Rodríguez, C.; Granados, F.; Sánchez, J.; García, F. A novel Green chemistry method for non-aqueous extraction and HPLC detection of first-, second-, and third-generation tetracyclines, 4-epitetracycline, and tylosin in aninal feeds. *J. Agric. Food Chem.* **2012**, *60*, 7121−7128.

(15) Pastor-Navarro, N.; Morais, S.; Maquieira, A.; Puchades, R. Synthesis of haptens and development of a sensitive immunoassay for tetracycline residues: Application to honey samples. *Anal. Chim. Acta* **2007**, *594*, 211−218.

(16) Adrian, J.; Fernandez, F.; Sanchez-Baeza, F.; Marco, M. P. Preparation of antibodies and development of an enzyme-linked immunosorbent assay (ELISA) for the determination of doxycycline antibiotic in milk samples. *J. Agric. Food Chem.* **2012**, *60*, 3837−3846.

(17) Zhang, Y. L.; Lu, S. X.; Liu, W.; Zhao, C. B.; Xi, R. M. Preparation of anti-tetracycline antibodies and development of an indirect heterologous competitive enzyme-linked immunosorbent assay to detect residues of tetracycline in milk. *J. Agric. Food Chem.* **2007**, *55*, 211−218.

(18) Traviesa-Alvarez, J. M.; Costa-Fernández, J. M.; Pereiro, R.; Sanz-Medel, A. Direct screening of tetracyclines in water and bovine milk using room temperature phosphorescence detection. *Anal. Chim. Acta* **2007**, *589*, 51−58.

(19) Valcárcel, M.; Cárdenas, S. Current and future screening systems. *Anal. Bioanal. Chem.* **2005**, *381*, 81−83.

(20) Chan, W. C. W.; Maxwell, D. J.; Gao, X.; Bailey, R. E.; Han, M.; Nie, S. Luminescent quantum dots for multiplexed biological detection and imaging. *Curr. Opin. Biotechnol.* **2002**, *13*, 40−46.

(21) Nichkova, M.; Dosev, D.; Davies, A. E.; Gee, S. J.; Kennedy, I. M.; Hammock, B. D. Quantum Dots as Reporters in Multiplexed Immunoassays for Biomarkers of Exposure to Agrochemicals. *Anal. Lett.* **2007**, *40*, 1423−1433.

(22) Xu, H.; Xu, J.; Wang, X.; Wu, D.; Chen, Z.; Georgia, W.; Andrew, Y. Quantum dot-based, quantitative, and multiplexed assay for tissue staining. *ACS Appl. Mater. Interfaces* **2013**, *5*, 2901−2907.

(23) Xie, M-X; Chen, Y.; Wang, D.; Yin, Y.; Wang, L.; Wang, X. Quantum dots capped with dummy molecularly imprinted film as luminescent sensor for determination of tetrabromobisphenol A in water and soils. *J. Agric. Food Chem.* **2012**, *60*, 10472−10479.

(24) Bradford, M. A rapid and sensitive method for the quantitation of microgram quantities of protein utilizing the principle of protein-dye binding. *Anal. Biochem.* **1976**, *72*, 248−254.

(25) Trapiella-Alfonso, L.; Costa-Fernández, J. M.; Pereiro, R.; Sanz-Medel, A. Synthesis and characterization of hapten-quantum dots bioconjugates: application to development of a melamine fluorescent immunoassay. *Talanta* **2013**, *106*, 243−248.

(26) Sun, B.; Xie, W.; Yi, G.; Chen, D.; Zhou, Y.; Cheng, J. Microminiaturized immunoassays using quantum dots as fluorescent

label by laser confocal scanning fluorescence detection. *J. Immunol. Methods* **2001**, *249*, 85−89.
(27) Mikkelsen, S. R.; Cortón, E. Chapter 6: Quantitative immunoassays with labels. *Bioanalytical Chemistry*; John Wiley & Sons, Inc.: Hoboken, NJ, 2004.
(28) Simonet, B. M.; Ríos, A.; Valcárcel, M. Unreliability of screening methods. *Anal. Chim. Acta* **2004**, *516*, 67−74.
(29) Trullols, E.; Ruisánchez, I.; Rius, F. X. Validation of qualitative analytical methods. *TrAC, Trends Anal. Chem.* **2004**, *23*, 137−145.
(30) Oka, H.; Ikai, Y.; Ito, Y.; Hayakawa, J.; Harada, K.; Suzuki, M.; Odani, H.; Maeda, K. Improvement of chemical analysis of antibiotics: XXIII. Identification of residual tetracyclines in bovine tissues by electrospray high-performance liquid chromatography−tandem mass spectrometry. *J. Chromatogr., B* **1997**, *693*, 337−344.
(31) Trapiella-Alfonso, L.; Costa-Fernández, J. M.; Pereiro, R.; Sanz-Medel, A. Development of a quantum dot-based fluorescent immunoassay for progesterone determination in bovine milk. *Biosens. Bioelectron.* **2011**, *26*, 4753−4759.
(32) Gao, F.; Zhao, G. X.; Zhang, H. C.; Wang, P.; Wang, J. P. Production of monoclonal antibody against doxycycline for immunoassay of seven tetracyclines in bovine muscle and milk. *J. Environ. Sci. Health, Part B* **2013**, *48*, 92−100.
(33) Granelli, K.; Elgerud, C.; Lundström, A.; Ohlsson, A.; Sjöberg, P. Rapid multi-residue analysis of antibiotics in muscle by liquid chromatography−tandem mass spectrometry. *Anal. Chim. Acta* **2009**, *637*, 87−91.
(34) Cinquina, A. L.; Longo, F.; Anastasi, G.; Giannetti, L.; Cozzani, R. Validation of a high-performance liquid chromatography method for the determination of oxytetracycline, tetracycline, chlortetracycline and doxycycline in bovine milk and muscle. *J. Chromatogr., A* **2003**, *987*, 227−233.

Table 1. Abbreviation, Source, and Mass Spectral Tag[a]

volatile compound	abbreviation	mass spectral tag (retention index, target ion)	standard source
1-butanol	1-butanol	661.1, 56	Sigma-Aldrich
1-hexanol	1-hexanol	877.3, 56	Sigma-Aldrich
1-pentanol	1-pentanol	760.5, 55	Sigma-Aldrich
1-propanol	1-propanol	559.6, 31	J.T. Baker
2-ethyl-1-hexanol	2-eth 1-hex	1027.2, 57	Sigma-Aldrich
2-methyl-1-butanol	2-meth 1-but	743.2, 57	Sigma-Aldrich
2-methyl-1-propanol	2-meth 1-pro	622.9, 43	Sigma-Aldrich
2-methylbutyl acetate	2-MB ace	881.8, 43	Sigma-Aldrich
2-methylbutyl butanoate	2-MB but	1056.5, 71	synthesized
2-methylbutyl propanoate	2-MB Prop	971.1, 57	synthesized
2-methylpropyl acetate	2-MP ace	775.1, 56	Sigma-Aldrich
4-allylanisole	estragole	1198.8, 148	Sigma-Aldrich
6-methyl-5-hepten-2-ol	6M5H2Ol	992, 95	Sigma-Aldrich
6-methyl-5-hepten-2-one	6M5H2One	983.6, 108	Sigma-Aldrich
acetaldehyde	acet	462.4, 29	Sigma-Aldrich
acetone	acetone	508.8, 43	Sigma-Aldrich
benzaldehyde	benz	963.1, 106	Sigma-Aldrich
butyl 2-methylbutyrate	but 2-MB	1039.8, 103	Sigma-Aldrich
butyl acetate	but ace	818.2, 43	Sigma-Aldrich
butyl butyrate	but but	993.8, 71	Sigma-Aldrich
butyl hexanoate	but hex	1186.1, 117	Sigma-Aldrich
butyl propanoate	but pro	908, 57	Sigma-Aldrich
butyric acid	butyric	837.9, 60	Sigma-Aldrich
decanal	decanal	1203.2, 57	Sigma-Aldrich
ethanol	ethanol	516.7, 31	Decon
ethyl 2-methylbutyrate	eth 2-MB	852.8, 102	Sigma-Aldrich
ethyl acetate	eth ace	613.9, 43	Fischer
ethyl butyrate	eth but	805.2, 71	Sigma-Aldrich
ethyl hexanoate	eth hex	996, 88	Sigma-Aldrich
ethyl octanoate	eth oct	1190.8, 88	Sigma-Aldrich
ethyl pentanoate	eth pen	900.4, 101	synthesized
ethyl propionate	eth pro	711.9, 57	Sigma-Aldrich
heptanal	heptanal	899.6, 70	Sigma-Aldrich
hexanal	hexanal	799.6, 56	Sigma-Aldrich
hexyl 2-methylbutyrate	hex 2-MB	1231.6, 103	Sigma-Aldrich
hexyl acetate	hex ace	1011, 56	Sigma-Aldrich
hexyl butyrate	hex but	1187.9, 89	Sigma-Aldrich
hexyl propanoate	hex pro	1100.6, 57	Sigma-Aldrich
methyl 2-methylbutyrate	meth 2-MB	777.2, 88	Sigma-Aldrich
methyl acetate	meth ace	531.6, 74	Sigma-Aldrich
methyl butyrate	meth but	721.8, 74	Sigma-Aldrich
methyl hexanoate	meth hex	924, 74	Sigma-Aldrich
nonanal	nonanal	1102.3, 57	Sigma-Aldrich
octanal	octanal	1000, 84	Sigma-Aldrich
pentanal	pentanal	701.1, 44	Sigma-Aldrich
pentyl acetate	pen ace	913.8, 43	Sigma-Aldrich
propyl 2-methylbutanoate	prop 2-MB	945.8, 103	synthesized
propyl acetate	pro ace	714, 61	Sigma-Aldrich
propyl butyrate	pro but	898.1, 71	Sigma-Aldrich
propyl hexanoate	pro hex	1091.1, 99	Sigma-Aldrich
propyl propanoate	pro pro	811.9, 57	Sigma-Aldrich

[a]Synthesized volatiles produced using modification of methods in Fischer et al., 1895.[31]

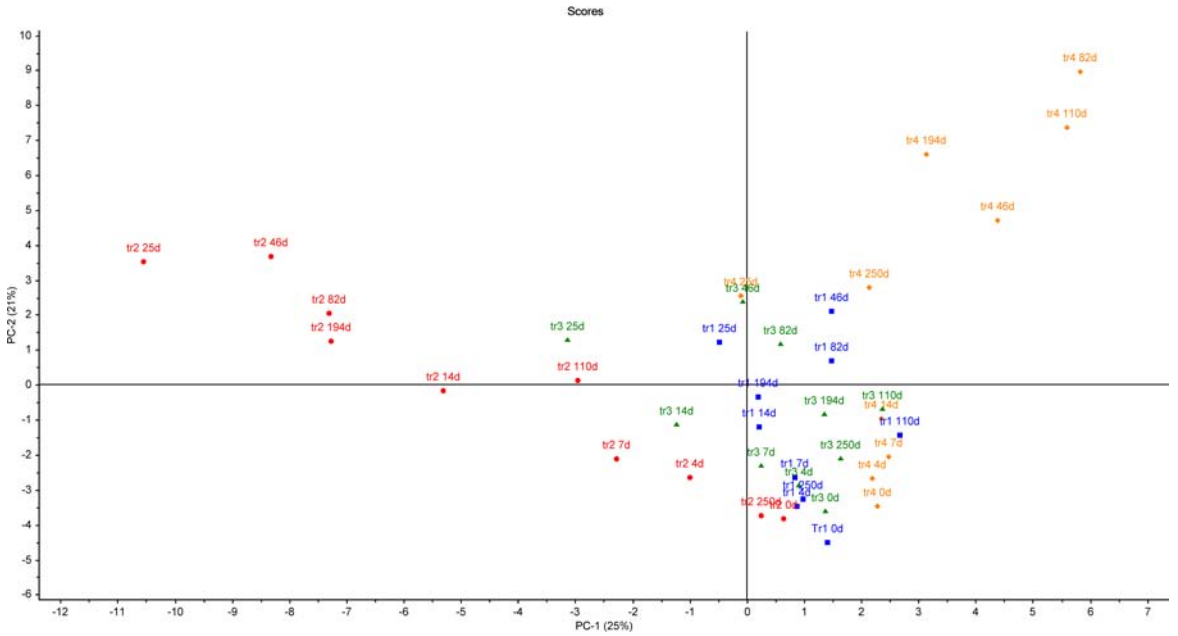

Figure 1. Principal Components Analysis plot of headspace volatile compounds collected during storage of 'Scarlett Spur Red Delicious' apple fruit. Gas samples collected from 3 replicate storage chambers for each atmosphere were analyzed by GC-MS. Red: 0.3 kPa O_2. Green: 0.8 kPa O_2. Blue: 1.6 kPa O_2. Orange: air. CO_2 in all low O_2 atmospheres was 1 kPa. All fruit stored at 0.5 °C.

(Hewlett-Packard, Avondale, PA) equipped with a 50 cm long × 0.32 cm internal diameter glass column packed with 80−100 mesh Porapak Q (Supelco, Bellafonte, PA). The injector, oven, and detector temperatures were 100 °C, 130 °C, and 200 °C, respectively. Gas flows for air, N_2 carrier, and H_2 were 5.0, 0.5, and 0.5 mL s^{-1}, respectively. Firmness was analyzed with a Mohr Digitest 1.25 penetrometer (Mohr and Associates, Richland, WA) equipped with an 11 mm tip. Starch hydrolysis was visually assessed on a full width tissue slice cut from the fruit equator using a 1−6 scale (1 = no hydrolysis, all tissue black, 6 = hydrolysis complete, tissue unstained) after staining with a 0.024 M I−KI solution.[28] Fresh juice prepared using a Champion juicer (Plastaket Mfg., Lodi, CA) was used to measure SSC with a

dx.doi.org/10.1021/jf405267b | J. Agric. Food Chem. 2014, 62, 1741−1754

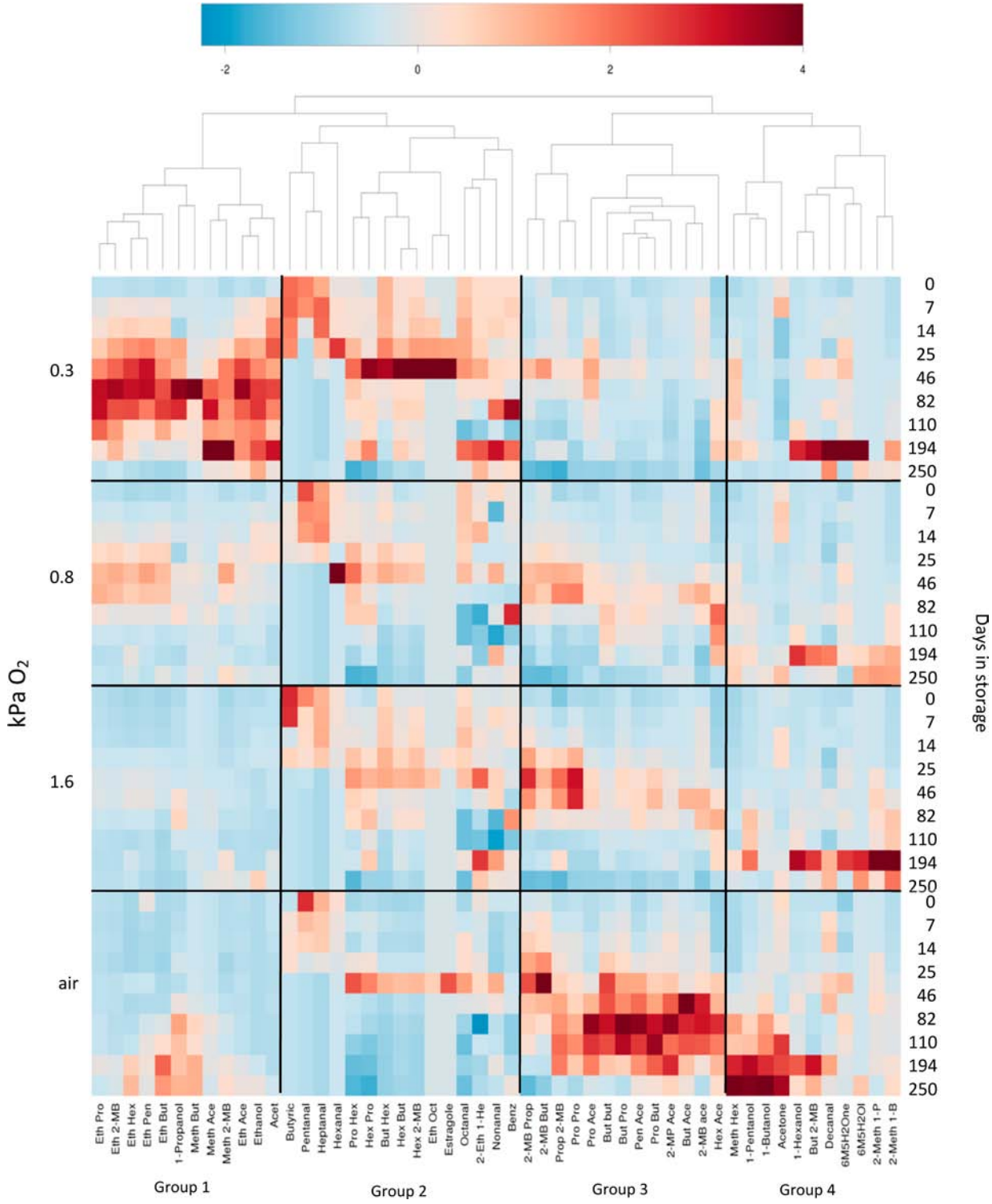

Figure 2. Heatmap of 'Scarlett Spur Red Delicious' volatile accumulation during cold storage. Gas samples collected from three replicate storage chambers for each atmosphere were analyzed by GC-MS. Storage temperature was 0.5 °C and storage chamber atmospheres were air or 0.3, 0.8, or 1.6 kPa O_2 with 1 kPa CO_2. Volatile compounds were hierarchically clustered using Pearson's correlation and Ward's linkage algorithm. Atmosphere treatment indicated on the left *y*-axis by colored bars, storage duration (days) indicated on the right *y*-axis. Compound concentration increases with blue to red color change. Compound abbreviations presented in Table 1.

hand-held refractometer (ATAGO, Tokyo), and TA by titrating 10 mL juice with 0.1 M KOH to pH 8.2 using an autotitrator (TIM850, Radiometer Analytical, Copenhagen, Denmark).

Fruit (18 fruit/pressed paper tray) were stored in air for 3 days at 0.5 °C before being weighed and placed into 0.145 m^3 stainless steel CA chambers with Plexiglas doors, four trays per chamber. CA chamber atmospheres were established over two days using compressed air and CO_2 plus N_2 from a membrane generator (Permea, St. Louis, MO). Chamber gas composition was analyzed every 90 min and automatically corrected as necessary (Techni-Systems, Chelan, WA); therefore, chamber atmospheres were static except when adjustments were conducted.[29] Fruit chlorophyll fluorescence measured with the

dx.doi.org/10.1021/jf405267b | J. Agric. Food Chem. 2014, 62, 1741−1754

Table 2. Group 1 'Scarlett Spur Red Delicious' Volatile Accumulation (ηmol L^{-1}) During Controlled Atmosphere or Air Storage[a]

		days in storage									
group 1 compd.	atm	0	4	7	14	25	46	82	110	194	250
ethyl propanoate	0.3	0.082D	0.512aD	0.774aD	1.28aCD	2.21aC	3.67aA	3.65aA	2.64aAB	0.811aD	0.048D
	0.8	0.060D	0.270abCD	0.530aCD	1.03aB	1.54aA	1.68bA	0.760bBC	0.263bCD	0.034bD	0.137D
	1.6	0.015	0.054b	0.095b	0.268b	0.402b	0.429bc	0.211b	0.054b	0.013b	0.049
	air	0.050B	0.029bB	0.040bB	0.015bB	0.090bB	0.096cB	0.159bB	0.160bB	0.574aA	0.199B
ethyl 2-methylbutyrate	0.3	0.127D	0.496aCD	0.703aCD	1.11aBC	1.57aAB	2.28aA	1.70aAB	1.21aBC	0.972aBC	0.195D
	0.8	0.093C	0.244bC	0.385bBC	0.729bAB	1.06aA	0.944bA	0.374bBC	0.204bC	0.105cC	0.125C
	1.6	0.031	0.064b	0.087c	0.189c	0.270b	0.282bc	0.172b	0.078b	0.078c	0.107
	air	0.090ABC	0.063bBC	0.074cBC	0.032cC	0.110bABC	0.101cABC	0.093bABC	0.108bABC	0.325bA	0.294AB
ethyl hexanoate	0.3	0.008aD	0.028aCD	0.041aBCD	0.066aABCD	0.094aAB	0.106aA	0.088aABC	0.037aBCD	0.029CD	0.007bD
	0.8	0.004abC	0.011bC	0.017bBC	0.030bABC	0.048abA	0.042abAB	0.024bABC	0.011bC	0.023ABC	0.018bBC
	1.6	0.002b	0.005b	0.006b	0.013b	0.020b	0.023b	0.014b	0.006b	0.016	0.012b
	air	0.003abB	0.002bB	0.002bB	0.002bB	0.012bB	0.005bB	0.008bB	0.011bB	0.041A	0.050aA
ethyl pentanoate	0.3	0.000C	0.001aBC	0.002aBC	0.004aAB	0.006aA	0.006aA	0.004aAB	0.002aBC	0.001BC	0.000aC
	0.8	0.000D	0.001bD	0.001bCD	0.002abBC	0.003abA	0.002bAB	0.001bCD	0.001bcD	0.000D	0.000abD
	1.6	0.000	0.000b	0.000bc	0.001bc	0.001b	0.001b	0.001b	0.000c	0.000	0.000b
	air	0.001	0.000b	0.000c	0.000c	0.001b	0.000b	0.001b	0.001ab	0.001	0.001a
ethyl butyrate	0.3	0.122E	0.517aCDE	0.726aBCD	1.03aBC	1.23aAB	1.63aA	1.71aA	1.06aBC	0.460bDE	0.052E
	0.8	0.099C	0.280abABC	0.471aABC	0.743aAB	0.922aA	0.855bA	0.425bABC	0.200cBC	0.170bcBC	0.419ABC
	1.6	0.041	0.088b	0.124b	0.259b	0.336b	0.321bc	0.169b	0.059c	0.072c	0.053
	air	0.103C	0.074bC	0.083bC	0.039bC	0.111bC	0.142cC	0.375bC	0.626bBC	1.49aA	1.18AB
1-propanol	0.3	0.021	0.058	0.000c	0.261	0.232	0.559	0.449	0.136	0.078	0.000
	0.8	0.017	0.034	0.062a	0.000	0.106	0.095	0.133	0.037	0.008	0.039
	1.6	0.008C	0.026BC	0.025bcC	0.038BC	0.049BC	0.124AB	0.162A	0.056BC	0.021C	0.000C
	air	0.010	0.022	0.031b	0.059	0.022	0.104	0.262	0.210	0.202	0.238
methyl butyrate	0.3	0.003	0.008	0.012	0.021a	0.026	0.397	0.053ab	0.039a	0.039b	0.005
	0.8	0.004B	0.008AB	0.015AB	0.019aAB	0.035A	0.025AB	0.016bcAB	0.008bAB	0.009bAB	0.025AB
	1.6	0.001	0.003	0.004	0.005ab	0.008	0.011	0.009c	0.003b	0.011b	0.005
	air	0.004B	0.002B	0.003B	0.001bB	0.006B	0.016AB	0.064aAB	0.047aAB	0.104aA	0.102A
methyl acetate	0.3	0.001C	0.006C	0.012C	0.038C	0.073aBC	0.195aABC	0.266aAB	0.144aABC	0.340aA	0.041C
	0.8	0.001B	0.008AB	0.011AB	0.008AB	0.023bAB	0.014bAB	0.043bA	0.015bAB	0.017bAB	0.012AB
	1.6	0.000	0.000	0.000	0.001	0.004b	0.021b	0.021b	0.007b	0.007b	0.028
	air	0.000B	0.000B	0.000B	0.001B	0.003bAB	0.010bAB	0.039bA	0.028bAB	0.029bAB	0.016AB
methyl 2-methylbutyrate	0.3	0.003B	0.010B	0.014B	0.026aB	0.055aAB	0.054aAB	0.048aAB	0.044aAB	0.103aA	0.019B
	0.8	0.004B	0.009B	0.013B	0.023aAB	0.044aA	0.023bAB	0.010bB	0.006bB	0.010bB	0.026AB
	1.6	0.001	0.003	0.004	0.006b	0.009b	0.009b	0.006b	0.003b	0.021b	0.017
	air	0.004BC	0.004BC	0.005BC	0.000bC	0.003bBC	0.006bABC	0.012bABC	0.009bABC	0.019bAB	0.024A
ethyl acetate	0.3	0.276E	2.23aE	3.04aDE	6.00aCD	9.81aAB	13.1aA	8.83aBC	6.87aBC	6.86aBC	2.98DE
	0.8	0.346	0.867b	0.963b	2.08b	2.47b	2.03b	1.67b	0.906b	0.360b	1.70
	1.6	0.051	0.202bc	0.265bc	0.515c	0.445b	0.557b	0.378b	0.121b	0.045b	1.45
	air	0.191AB	0.099cB	0.183cAB	0.086cB	0.359bAB	0.232bAB	0.327bAB	0.331bAB	1.54bAB	2.16A
ethanol	0.3	0.671C	9.64aBC	9.23aBC	17.2aABC	22.9aAB	31.5aA	32.1aA	23.8aAB	29.1aA	18.3ABC
	0.8	0.945B	5.04bAB	8.93aA	9.17bA	6.19bAB	5.70bAB	3.73bAB	3.65bAB	2.41bB	4.07AB

dx.doi.org/10.1021/jf405267b | J. Agric. Food Chem. 2014, 62, 1741−1754

Table 2. continued

group 1 compd.	atm	days in storage										
		0	4	7	14	25	46	82	110	194	250	
acetaldehyde	1.6	0.550	1.60c	2.76b	3.46c	0.976b	1.03b	1.13b	0.678b	0.768b	12.6	
	air	0.284B	0.220cB	0.358cB	0.205 dB	0.261bB	0.282bB	0.267bB	0.281bB	3.13bAB	7.31A	
	0.3	0.227C	1.02aBC	1.58aABC	1.96aAB	1.28aABC	2.10aAB	1.61aABC	0.965aBC	2.52aA	0.503C	
	0.8	0.199BC	0.247bBC	0.545bAB	0.695bA	0.263bBC	0.313bBC	0.156bC	0.000bC	0.000bC	0.288BC	
	1.6	0.081	0.094b	0.159bc	0.185c	0.155b	0.123b	0.000b	0.000b	0.338b	0.281	
	air	0.156AB	0.148bABC	0.096cBCD	0.034cCD	0.023bD	0.076bBCD	0.000bD	0.000bD	0.000bD	0.238A	

[a]Headspace gas samples collected from 3 replicate storage chambers for each atmosphere were analyzed by GC-MS. Chambers were maintained at 0.3, 0.8, or 1.6 kPa CO_2 with 1 kPa O_2 or air. All fruit was stored at 0.5 °C. Storage duration and atmosphere differences are denoted by upper and lowercase letters, respectively, and values with the same letter are not significantly different ($P \leq 0.05$, Tukey's HSD).

HarvestWatch system (Satlantic Inc., Halifax, NS) was used to determine the lowest pO_2 set-point based on changes in fruit chlorophyll fluorescence as pO_2 decreased.[30] Fruit were stored at 0.5 °C in air or CA (0.3, 0.8, or 1.6 kPa O_2, 1 kPa CO_2) with four chambers for each atmosphere: three for sampling volatile compounds (volatile chambers) and one from which fruit were periodically removed and assessed for quality (quality chambers).

After 1, 2, 4, and 8 months in storage, one tray was removed from each quality chamber. Fruit were examined for external disorders and then held at 20 °C in air for 7 days. On day 7, the rate of ethylene evolution was determined. Evolved ethylene was analyzed in gas samples collected from 4 replicates, 4 fruit each, from each storage atmosphere placed into 3.79 L glass jars with Teflon lids (Berghof/America, Coral Springs, FL) fitted with Tygon and Teflon tubing. Compressed air was passed through Purafil (Purafil Inc., Atlanta), calcium hydroxide, a carbon filter (Agilent Technologies, Santa Clara, CA), and Tenax TA (80−100 mesh, Alltech Associates, Deerfield, IL) before flowing through the jars. The purified air was passed through the jars for 60 min, then a 1 mL gas sample was collected at the outlet from each jar and 0.5 mL injected into the 5880A GC-FID (Hewlett-Packard, Avondale, PA) described previously. The incidence of internal and external disorders (superficial scald, decay, internal browning) was also recorded. Chamber ethylene concentration was determined by collecting a gas sample from each storage chamber into a 1 L Tedlar bag (SKC Inc., Eighty Four, PA). Ethylene in a 0.5 mL sample from each bag was analyzed using the 5880A GC-FID previously described. After 9 months storage plus 7 days at 20 °C, apples from the volatile chambers were assessed for internal and external disorders.

Volatile compounds were collected directly from each storage chamber 0, 4, 7, 14, 25, 46, 82, 110, 194, and 250 d after chambers were sealed. Tygon tubing was attached to an outlet gas port on the side of each chamber and gas samples (0.25−1 L) were drawn through a 17.8 cm Tenax TA Glass TD Tube (Supelco, Bellefonte, PA) containing 60 mm/180 mg Tenax using a pump and volume was measured using a digital flow meter. Traps were thermally desorbed (TDS3 and TDSA2, Gerstel, Linthicum, MD) using a temperature program of 20 °C for 30 s, increased at 1 °C s^{-1} to 250 °C and held for 360 s. Desorbed compounds were cryogenically trapped at −130 °C (CIS-3, Gerstel) using the Gerstel Maestro Global Analytical System. Following the transfer of desorbed compounds from the TDS, the cryotrap temperature was increased 10 °C s^{-1} to 250 °C and held for 120 s as compounds were transferred to a Hewlett-Packard 5890A-5971A GC-MSD system (Hewlett-Packard, Palo Alto, CA) equipped with a DB-5MS column (Agilent Technologies, Santa Clara, CA) 30 m long × 0.25 mm internal diameter with 0.25 μm film thickness. The oven initial temperature (35 °C) was held 600 s, increased at 0.17 °C s^{-1} to 250 °C, then held 180 s. Linear gas velocity of the He carrier gas was 33.9 cm s^{-1}. Mass spectra were recorded with a Hewlett-Packard Enhanced Chemstation (G1701BA Version B.01.00; Agilent Technologies, Santa Clara, CA). Using MSD Chemstation Data Analysis (Agilent Technologies, Santa Clara, CA), AMDIS GC/MS Analysis, and NIST MS Search 2.0 (NIST, Gaithersburg, MD), compounds were identified by comparing sample retention times and spectra with those of standards (Table 1). Sample compounds were quantified by comparing base peak abundances of selected ions with those for standards of known concentration. Standards were obtained from Sigma-Aldrich (Milwaukee, WI) except 1-propanol (J.T. Baker, Center Valley, PA), ethyl acetate (Fischer Scientific, Pittsburgh, PA), and ethanol (Decon Laboratories, King of Prussia, PA). Esters synthesized[31] included 2-methylbutyl butyrate, 2-methylbutyl propanoate, ethyl pentanoate, and propyl 2-methylbutryate. For each compound, synthesis was performed using 5 g of the organic acid and excess alcohol (at least two times the molar equivalent of the organic acid) refluxed for 1 h with 3 mL of concentrated sulfuric acid at the boiling point of the alcohol. The resulting mixture was partitioned against 50 mL water three times; then, the nonaqueous phase was purified by distillation. Purity was assessed using the GC-MS method previously described.

Chromatographic data was mean centered and scaled according to the standard deviation. MetaboAnalyst[32] was used to generate

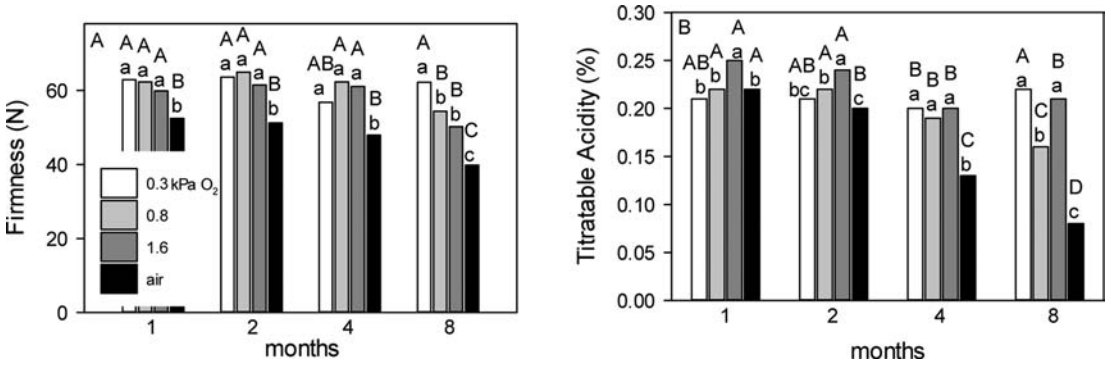

Figure 3. 'Scarlett Spur Red Delicious' apple firmness (A), and titratable acidity (B) of fruit previously stored in a controlled atmosphere (CA) or air at 0.5 °C. CA kPa O_2 concentrations were 0.3, 0.8, or 1.6, all with 1 kPa CO_2. Apples were removed from storage and analyzed after 7 days at 20 °C. Values are means of 18 individual fruit. Storage duration and atmosphere differences are denoted by upper and lowercase letters, respectively, and values with the same letter are not significantly different ($P \leq 0.05$, Tukey's HSD).

heatmaps from the normalized data analyzed by hierarchical clustering analysis using Pearson's correlation and Ward's linkage algorithm. Principal Components Analyses were performed using UnscramblerX 10.1 (CAMO Software, Woodbridge, NJ). The predictive models were created using cross-validation and outliers were removed. Statistical analyses were conducted using SAS 9.3 (SAS Institute, Cary, NC). Fruit quality data was analyzed by ANOVA, and means were separated using Tukey's HSD ($P < 0.05$). Non-normalized volatile compound data was analyzed using a GLM with storage duration as a repeated measure, and means were separated using Tukey's HSD ($P < 0.05$).

RESULTS AND DISCUSSION

Values for fruit maturity and quality at harvest were weight 223 ± 7 g, firmness 70.3 ± 0.9 N, internal ethylene 0.91 ± 0.33 μL L^{-1}, starch index 2.2 ± 0.2, SSC 11.9 ± 0.2%, and TA 0.278 ± 0.007%.

Principal Components Analysis (PCA) generated a model with principal components accounting for 25, 21, 17, and 10% (total: 72%) of the variance (Figure 1). The model identified storage duration and storage atmosphere effects on sample variation, with atmospheres diverging during the first 2 weeks storage. Volatile compound accumulation among storage atmospheres was the most similar during the first two and final 20 weeks storage. Atmosphere treatment differences were greatest on days 25, 46, and 82. The lack of significant atmosphere treatment effects at the end of storage suggests fruit volatile production was similar metabolically, possibly due to decreased metabolic rates and/or a lack of substrate for volatile production.[11,33] At 250 days, chamber volatile content was lower compared to previous dates for all atmospheres (Figure 2) indicating analysis of volatile accumulation in storage after 6 months may not be useful for monitoring anaerobic oxygen conditions imposed early in storage.

The hierarchical clustering procedure identified four main groups of volatile compounds. Volatiles in group 1, including many that are products of fermentation, were significantly highest from day 4 through day 194 in chambers where O_2 was 0.3 kPa (Table 2). The PCA loading plot (not shown) also associated fermentative volatiles with the 0.3 kPa O_2 atmosphere. The increase in fermentative compounds indicates the 0.3 kPa O_2 atmosphere induced oxygen stress and anaerobic metabolism.[7] Ethanol was the most abundant compound accumulating at 0.3 kPa O_2 followed by ethyl acetate. Ethanol accumulation was higher in 0.3 and 0.8 kPa O_2 chambers compared with 1.6 kPa O_2 and air chambers. The increase in ethanol likely provided substrate for ethyl ester production[34] and was accompanied by decreased butyl and hexyl ester content, consistent with previous reports.[10,13] Day 14 ethanol concentrations were significantly different among atmospheres, and ethanol increased with decreased pO_2. Ethyl esters also accumulated in chambers held at 0.8 kPa O_2, but concentrations in these chambers were significantly lower (ethyl propanoate, days 46–194; ethyl acetate, days 4–194; ethyl 2-methylbutyrate, days 4–14 and 46–194; ethyl hexanoate, days 4–14, 82 and 110; ethyl pentanoate, days 4,7, and 46–110; ethyl butyrate, days 46–110) compared with chambers held at 0.3 kPa O_2. Several volatiles began accumulating in significantly higher concentrations in the air chambers during the latter storage period (days 84–250) including ethyl hexanoate, ethyl pentanoate, ethyl butyrate, and methyl butyrate. The air stored fruit was riper compared with CA fruit during this period and had begun to senesce based on firmness, titratable acidity, and internal breakdown incidence in air stored fruit (Figures 3, 4) resulting in the production of volatiles typical of overripe fruit.[35,36]

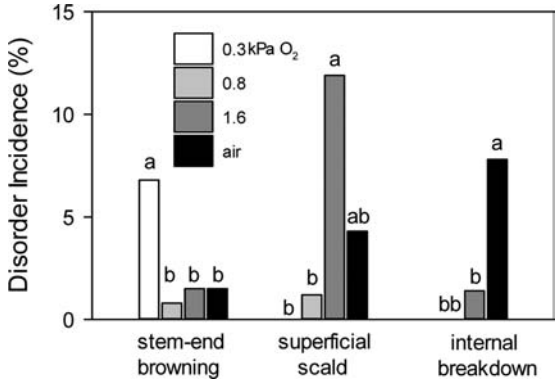

Figure 4. 'Scarlett Spur Red Delicious' apple physiological disorders after 9 months storage in a controlled atmosphere (CA) or air at 0.5 °C. CA kPa O_2 concentrations were 0.3, 0.8, or 1.6, all with 1 kPa CO_2. Fruit were evaluated after removal from cold storage plus 7 days at 20 °C. Values are means of 216 fruit for each storage treatment. Within each disorder, columns with the same letters are not significantly different ($P \leq 0.05$, Tukey's HSD).

Comparing days within storage atmospheres, most volatiles in group 1 were significantly highest during days 25–110. Ethanol concentration, however, did not significantly decrease in chambers held at 0.3 kPa O_2. This lack of change may indicate that the rates of fruit ethanol production and its metabolism to

Table 3. Group 2 'Scarlett Spur Red Delicious' Volatile Accumulation (ηmol L^{-1}) During Controlled Atmosphere or Air Storage[a]

		days in storage									
group 2 compd.	atm	0	4	7	14	25	46	82	110	194	250
butyric acid	0.3	0.010abA	0.011abA	0.009aA	0.009A	0.000B	0.000B	0.000B	0.000B	0.000B	0.000B
	0.8	0.000b	0.003b	0.003b	0.002	0.000	0.000	0.000	0.000	0.000	0.000
	1.6	0.013aA	0.013aA	0.001bB	0.004AB	0.000B	0.000B	0.000B	0.000B	0.000B	0.000B
	air	0.000b	0.003b	0.003ab	0.003	0.000	0.000	0.000	0.000	0.000	0.000
pentanal	0.3	0.006A	0.006A	0.001B	0.000B	0.000B	0.000B	0.000B	0.000B	0.000B	0.000B
	0.8	0.008A	0.006A	0.005AB	0.002BC	0.000C	0.000C	0.000C	0.000C	0.000C	0.000C
	1.6	0.006A	0.003AB	0.002B	0.002B	0.000B	0.000B	0.000B	0.000B	0.000B	0.000B
	air	0.008A	0.004B	0.003B	0.001B	0.000B	0.000B	0.000B	0.000B	0.000B	0.000B
heptanal	0.3	0.003AB	0.004aA	0.004A	0.002aBC	0.001CD	0.000D	0.000D	0.000D	0.000D	0.000D
	0.8	0.003A	0.003abA	0.003A	0.002abB	0.000C	0.000C	0.000C	0.000C	0.000C	0.000C
	1.6	0.003A	0.003abA	0.003A	0.002abB	0.000C	0.000C	0.000C	0.000C	0.000C	0.000C
	air	0.003A	0.002bAB	0.002AB	0.001bBC	0.000C	0.000C	0.000C	0.000C	0.000C	0.000C
hexanal	0.3	0.030B	0.051AB	0.048AB	0.234A	0.000bB	0.000B	0.000B	0.000B	0.000B	0.004B
	0.8	0.052B	0.046B	0.045B	0.000B	0.431aA	0.000B	0.000B	0.000B	0.000B	0.003B
	1.6	0.045A	0.041AB	0.035B	0.024C	0.008bD	0.000D	0.000D	0.000D	0.002D	0.003D
	air	0.052A	0.034AB	0.030AB	0.013BC	0.006bC	0.000C	0.000C	0.000C	0.000C	0.000C
propyl hexanoate	0.3	0.003B	0.004B	0.004B	0.005AB	0.007A	0.005AB	0.004B	0.003B	0.004aB	0.000C
	0.8	0.003D	0.003CD	0.004CD	0.005B	0.007A	0.005B	0.004BC	0.003DE	0.002bE	0.001F
	1.6	0.003BC	0.003BC	0.003AB	0.005AB	0.006A	0.004AB	0.004AB	0.002BC	0.003abBC	0.001C
	air	0.002B	0.003AB	0.002B	0.003AB	0.007A	0.003AB	0.002B	0.002B	0.001bB	0.001B
hexyl propanoate	0.3	0.003AB	0.003AB	0.003AB	0.003AB	0.009A	0.003AB	0.004abAB	0.004aAB	0.006aAB	0.001B
	0.8	0.003C	0.003BC	0.003ABC	0.003ABC	0.004A	0.003ABC	0.004aAB	0.003abC	0.002abC	0.001D
	1.6	0.002BC	0.003ABC	0.003ABC	0.004ABC	0.005A	0.003ABC	0.004aA	0.003abABC	0.004bcAB	0.002C
	air	0.002AB	0.003AB	0.002AB	0.003AB	0.006A	0.002AB	0.002bAB	0.001bB	0.001cB	0.000B
butyl hexanoate	0.3	0.007aAB	0.008aAB	0.007aAB	0.010aAB	0.015A	0.004aB	0.003aB	0.002aB	0.002aB	0.000B
	0.8	0.004bBCD	0.005bBC	0.004bCD	0.006bAB	0.008A	0.002bCDE	0.002bDE	0.000bE	0.000bE	0.000E
	1.6	0.005abB	0.006abB	0.006aB	0.007abA	0.008A	0.003abC	0.003aC	0.001bD	0.001bD	0.000D
	air	0.001cB	0.002cAB	0.001bB	0.002cAB	0.007A	0.001cB	0.000cB	0.000bB	0.000bB	0.000B
hexyl butyrate	0.3	0.001aAB	0.001aAB	0.001aAB	0.002aAB	0.005A	0.001aAB	0.001aAB	0.001aAB	0.001aAB	0.000B
	0.8	0.000bcCD	0.001bBC	0.000bCD	0.001bB	0.002A	0.001bBC	0.001bBC	0.000bCD	0.000bCD	0.000D
	1.6	0.001abDE	0.001abCDE	0.001aCD	0.001abB	0.002A	0.001aCDE	0.001aBC	0.000bEF	0.001bDE	0.000F
	air	0.000cB	0.000cB	0.000bB	0.000cAB	0.002cA	0.000cB	0.000cB	0.000bB	0.000bB	0.000B
hexyl 2-methylbutyrate	0.3	0.008aAB	0.010aAB	0.012aAB	0.016aAB	0.037A	0.008aAB	0.010aAB	0.006aAB	0.007aAB	0.001B
	0.8	0.004bCD	0.006bBC	0.005bBCD	0.008bAB	0.011A	0.004bBCD	0.004bBCD	0.001bD	0.001bD	0.000D
	1.6	0.005bEF	0.008abCD	0.009aBC	0.012abAB	0.014A	0.006abDE	0.008aCD	0.003bFG	0.003bG	0.001G
	air	0.001cB	0.002cAB	0.001bB	0.003cAB	0.013A	0.002cAB	0.001cB	0.000bB	0.000bB	0.000B
ethyl octanoate	0.3	0.000	0.000	0.000	0.000	0.000	0.000	0.000	0.000	0.000	0.000
	0.8	0.000	0.000	0.000	0.000	0.000	0.000	0.000	0.000	0.000	0.000
	1.6	0.000B	0.000B	0.000B	0.000B	0.000A	0.000B	0.000B	0.000B	0.000B	0.000B
	air	0.000	0.000	0.000	0.000	0.000	0.000	0.000	0.000	0.000	0.000
estragole	0.3	0.000	0.000	0.000	0.000	0.000	0.000	0.000	0.000	0.000	0.000
	0.8	0.000	0.000	0.000	0.000	0.000	0.000	0.000	0.000	0.000	0.000

dx.doi.org/10.1021/jf405267b | J. Agric. Food Chem. 2014, 62, 1741−1754

Table 3. continued

		days in storage									
group 2 compd.	atm	0	4	7	14	25	46	82	110	194	250
	1.6	0.000	0.000	0.000	0.000	0.000	0.000	0.000	0.000	0.000	0.000
	air	0.000	0.000	0.000	0.000	0.000	0.000	0.000	0.000	0.000	0.000
octanal	0.3	0.001aAB	0.001AB	0.001aAB	0.001aAB	0.001A	0.001AB	0.001AB	0.000B	0.001A	0.001AB
	0.8	0.001aA	0.001A	0.001abA	0.001abA	0.001A	0.000AB	0.000B	0.000B	0.001AB	0.000B
	1.6	0.001abA	0.001A	0.001abA	0.001abA	0.001A	0.000AB	0.000B	0.000B	0.001AB	0.000B
	air	0.000bAB	0.000AB	0.001bAB	0.001bAB	0.001A	0.001AB	0.000B	0.000B	0.000B	0.000B
2-ethyl 1-hexanol	0.3	0.002BC	0.002BC	0.002BC	0.002aABC	0.002AB	0.002BC	0.001BC	0.001C	0.003A	0.002aAB
	0.8	0.002	0.002	0.002	0.001b	0.002	0.001	0.001	0.001	0.001	0.002ab
	1.6	0.002	0.002	0.002	0.002ab	0.003	0.002	0.001	0.001	0.003	0.002ab
	air	0.002A	0.002A	0.001A	0.002abA	0.002A	0.002A	0.000B	0.001A	0.001AB	0.001bA
nonanal	0.3	0.001	0.001	0.001	0.001	0.001	0.001	0.002	0.001	0.002	0.001
	0.8	0.001AB	0.000AB	0.001AB	0.001AB	0.001A	0.001AB	0.001AB	0.000B	0.001A	0.001AB
	1.6	0.001AB	0.001AB	0.001AB	0.001AB	0.001AB	0.001AB	0.000B	0.000B	0.001A	0.001AB
	air	0.001	0.001	0.001	0.001	0.001	0.001	0.001	0.001	0.001	0.001
benzaldehyde	0.3	0.001	0.001a	0.001a	0.001a	0.001a	0.001	0.003	0.000	0.002a	0.001
	0.8	0.001	0.001ab	0.001ab	0.001ab	0.001b	0.001	0.003	0.000	0.001b	0.001
	1.6	0.001	0.001ab	0.001a	0.001ab	0.001b	0.001	0.002	0.000	0.001ab	0.001
	air	0.001AB	0.001bAB	0.001bAB	0.001bAB	0.001bAB	0.001AB	0.000B	0.000B	0.001bAB	0.001A

[a]Headspace gas samples collected from 3 replicate storage chambers for each atmosphere were analyzed by GC-MS. Chambers were maintained at 0.3, 0.8, or 1.6 kPa O_2 with 1 kPa CO_2 or air. All fruit was stored at 0.5 °C. Storage duration and atmosphere differences are denoted by upper and lowercase letters, respectively, and values with the same letter are not significantly different ($P \leq 0.05$, Tukey's HSD).

dx.doi.org/10.1021/jf405267b | J. Agric. Food Chem. 2014, 62, 1741−1754

Table 4. Group 3 'Scarlett Spur Red Delicious' Volatile Accumulation (ηmol L^{-1}) during Controlled Atmosphere or Air Storage[a]

		days in storage									
group 3 compd.	atm	0	4	7	14	25	46	82	110	194	250
2-methylbutyl propanoate	0.3	0.002AB	0.002AB	0.002AB	0.002AB	0.004A	0.003AB	0.003AB	0.002AB	0.002AB	0.000B
	0.8	0.002BCD	0.002BC	0.003BC	0.003B	0.004A	0.005A	0.003B	0.002CD	0.001DE	0.000E
	1.6	0.002BC	0.003BC	0.003ABC	0.005AB	0.007A	0.005AB	0.004ABC	0.002BC	0.002BC	0.000C
	air	0.002	0.003	0.004	0.005	0.007	0.004	0.004	0.003	0.002	0.000
2-methylbutyl butyrate	0.3	0.002AB	0.002AB	0.002AB	0.002AB	0.004A	0.002AB	0.001AB	0.001B	0.002AB	0.000B
	0.8	0.002BC	0.002BC	0.002BC	0.003ABC	0.003A	0.003AB	0.002BC	0.002C	0.001CD	0.000D
	1.6	0.001BC	0.002BC	0.002ABC	0.003AB	0.003A	0.003AB	0.002ABC	0.001BC	0.002BC	0.001C
	air	0.002AB	0.002AB	0.003AB	0.004AB	0.007A	0.003AB	0.002AB	0.002AB	0.001B	0.001B
propyl 2-methylbutyrate	0.3	0.032AB	0.047A	0.045A	0.044A	0.052A	0.044A	0.031bAB	0.025bAB	0.044abA	0.007AB
	0.8	0.027CD	0.038CD	0.045C	0.050BC	0.074AB	0.086A	0.042abC	0.027bCD	0.025bCD	0.015D
	1.6	0.019C	0.031BC	0.037ABC	0.061ABC	0.094A	0.082AB	0.051abABC	0.031bBC	0.055abABC	0.011C
	air	0.032	0.036	0.046	0.050	0.061	0.076	0.084a	0.094a	0.090a	0.036
propyl propanoate	0.3	0.012CD	0.013CD	0.012CD	0.015C	0.032A	0.027AB	0.017bBC	0.015bC	0.004bDE	0.000E
	0.8	0.010DE	0.016CDE	0.021CD	0.026C	0.053B	0.072A	0.022abCD	0.012bCDE	0.005bE	0.003E
	1.6	0.008C	0.018BC	0.026ABC	0.055ABC	0.106A	0.100AB	0.028abABC	0.011bC	0.006bC	0.000C
	air	0.012B	0.016B	0.024AB	0.024AB	0.035AB	0.041AB	0.055aAB	0.068aA	0.046aAB	0.007B
propyl acetate	0.3	0.054DE	0.116CD	0.137CD	0.244aAB	0.325A	0.285A	0.152bBC	0.139bCD	0.093bCDE	0.010E
	0.8	0.046C	0.081BC	0.101ABC	0.135abABC	0.196AB	0.202A	0.124bABC	0.056bC	0.026cC	0.065C
	1.6	0.039AB	0.065AB	0.076AB	0.122abAB	0.217A	0.229A	0.157bAB	0.072bAB	0.036bcAB	0.009B
	air	0.056B	0.056B	0.083B	0.074bB	0.144B	0.304AB	0.664aA	0.527aA	0.403aAB	0.116B
butyl butyrate	0.3	0.015AB	0.014AB	0.014AB	0.015bAB	0.034bA	0.020bAB	0.022bAB	0.022bAB	0.027AB	0.003bB
	0.8	0.018AB	0.017AB	0.019AB	0.024abAB	0.035bAB	0.046abAB	0.056abA	0.051abA	0.036AB	0.007bB
	1.6	0.014CD	0.015BCD	0.016BCD	0.021abABC	0.030bAB	0.033abA	0.031bA	0.024bABC	0.023ABC	0.005bD
	air	0.017B	0.025AB	0.031AB	0.055aAB	0.110aAB	0.104aAB	0.129aA	0.108aAB	0.058AB	0.023aB
butyl propanoate	0.3	0.012AB	0.011AB	0.009AB	0.008AB	0.022A	0.011AB	0.011bAB	0.009bAB	0.006bAB	0.000bB
	0.8	0.012AB	0.013AB	0.014AB	0.014AB	0.020AB	0.025A	0.029bA	0.025bAB	0.010bAB	0.002abB
	1.6	0.010BCD	0.015ABCD	0.017ABCD	0.024ABC	0.037A	0.032AB	0.022bABCD	0.012bBCD	0.006bCD	0.001bD
	air	0.014C	0.020C	0.027BC	0.036BC	0.061ABC	0.072ABC	0.135aA	0.119aAB	0.042aBC	0.006aC
pentyl acetate	0.3	0.009DE	0.016BCD	0.019BCD	0.023AB	0.030A	0.020BC	0.017bBCD	0.012bCD	0.011bCDE	0.002bE
	0.8	0.009C	0.014BC	0.018ABC	0.022ABC	0.028ABC	0.032AB	0.037bA	0.026abABC	0.020bABC	0.008abC
	1.6	0.007C	0.012C	0.014BC	0.021ABC	0.032AB	0.038A	0.038bA	0.020bABC	0.013bBC	0.003bC
	air	0.008B	0.011B	0.015B	0.025B	0.057AB	0.076AB	0.118aA	0.092aAB	0.065aAB	0.029aAB
propyl butyrate	0.3	0.024A	0.025A	0.023AB	0.025A	0.041A	0.040A	0.036bA	0.029bA	0.035bA	0.004bB
	0.8	0.020B	0.027B	0.033AB	0.035AB	0.054AB	0.095A	0.076bAB	0.070bAB	0.056bAB	0.024abB
	1.6	0.015B	0.028B	0.037B	0.068AB	0.122A	0.147A	0.070bAB	0.038bB	0.034bB	0.007bB
	air	0.027C	0.040C	0.058C	0.079BC	0.123ABC	0.179ABC	0.328aAB	0.360aA	0.249aABC	0.084aBC
2-methylpropyl acetate	0.3	0.017	0.023	0.021	0.018	0.023	0.012	0.010b	0.007b	0.012b	0.006
	0.8	0.020	0.024	0.025	0.020	0.022	0.028	0.028b	0.016b	0.011b	0.023
	1.6	0.014	0.019	0.019	0.023	0.032	0.031	0.032b	0.017b	0.024b	0.007
	air	0.025B	0.027B	0.035B	0.030B	0.049AB	0.088AB	0.126aA	0.082aAB	0.104aAB	0.044AB
butyl acetate	0.3	0.091ABC	0.116A	0.112A	0.098bAB	0.118bA	0.060CD	0.064bBCD	0.044bDE	0.033bDE	0.009E
	0.8	0.091	0.111	0.117	0.100b	0.129b	0.627	0.197b	0.128b	0.072b	0.150

dx.doi.org/10.1021/jf405267b | J. Agric. Food Chem. 2014, 62, 1741−1754

Table 4. continued

group 3 compd.	atm	days in storage									
		0	4	7	14	25	46	82	110	194	250
2-methylbutyl acetate	1.6	0.075	0.097	0.095	0.110b	0.181b	0.747	0.168b	0.080b	0.038b	0.014
	air	0.092B	0.121B	0.170B	0.193aB	0.279aAB	2.05A	1.50aAB	1.27aAB	0.632aAB	0.300AB
	0.3	0.188A	0.250A	0.231A	0.223A	0.246A	0.186A	0.115bB	0.076bB	0.065bB	0.047B
	0.8	0.226ABCD	0.213ABCD	0.232ABCD	0.159BCD	0.253ABC	0.384A	0.278bAB	0.149bBCD	0.076bD	0.101CD
	1.6	0.160BC	0.223ABC	0.225ABC	0.229ABC	0.228ABC	0.379A	0.349abAB	0.204bABC	0.137abC	0.070C
	air	0.157	0.203	0.231	0.235	0.281	0.626	0.641a	0.537a	0.244a	0.141
hexyl acetate	0.3	0.028D	0.050aCD	0.059CD	0.081CD	0.137abBC	0.134BC	0.218AB	0.210AB	0.256A	0.043bCD
	0.8	0.024D	0.036abD	0.045D	0.068D	0.124bCD	0.221BCD	0.438A	0.366AB	0.292ABC	0.082bD
	1.6	0.021E	0.032abDE	0.039DE	0.046DE	0.119bCD	0.196BC	0.316A	0.221AB	0.219B	0.075bDE
	air	0.017B	0.025bB	0.031B	0.076AB	0.253aAB	0.309AB	0.532A	0.408AB	0.295AB	0.206aAB

[a]Headspace gas samples collected from 3 replicate storage chambers for each atmosphere were analyzed by GC-MS. Chambers were maintained at 0.3, 0.8, or 1.6 kPa O_2 with 1 kPa CO_2 or air. All fruit was stored at 0.5 °C. Storage duration and atmosphere differences are denoted by upper and lowercase letters, respectively, and values with the same letter are not significantly different ($P \leq 0.05$, Tukey's HSD).

esters and other compounds was similar during this period in storage. Acetaldehyde, also a product of fermentative metabolism, is metabolized first to ethanol and then to ethyl esters.[10,37] Low oxygen CA storage reduces fruit metabolic rate including activity of the terminal enzyme in ester synthesis alcohol acyltransferase[8] such that ester production decreases as storage duration increases.[5,11,12,25,26,28,29,37] Methyl acetate, methyl 2-methylbutyrate, and acetaldehyde were all significantly highest at day 194. Although methanol was not detected, the presence of methyl esters indicates methanol was likely present as a substrate for ester synthesis.[34]

The group 1 volatiles associated with fermentative metabolism in 'Delicious' may be useful indicators for monitoring the occurrence of anaerobic conditions during CA storage. An ideal indicator would have a marked concentration change soon after low oxygen conditions occur, and many of the group 1 volatiles are significantly highest in the 0.3 kPa O_2 chambers by day 4. The increase in ethanol concentration during the days after 0.3 kPa O_2 was established may indicate its utility as an early indicator of low O_2 stress due to the higher rate of increase between ultralow oxygen and more typical (1.6 kPa) O_2 CA conditions. The increase in ethanol at 0.8 kPa O_2 for which low oxygen injury development was similar to that occurring in fruit stored at 1.6 kPa O_2 or in air indicates a threshold concentration associated with injury risk may need to be identified to enable ethanol monitoring in storage room headspace as an indicator of low O_2 injury risk.

Amounts of the group 2 compounds butyl hexanoate, hexyl butyrate, and hexyl 2-methylbutyrate were significantly highest in 0.3 and 1.6 kPa O_2 through day 82 and at 0.3 kPa O_2 on days 110 and 194 (Table 3). On the same dates, the concentrations of these compounds were lowest in air chambers. Hexyl propanoate (days 82−194), benzaldehyde (days 4−25, 194), and heptanal (days 4, 14) were highest in 0.3 kPa O_2 and lowest in air. Amounts of butyric acid, pentanal, hexanal, ethyl octanoate, estragole, octanal, 2-ethyl-1-hexanol, nonanal, and propyl hexanoate were unaffected by storage conditions. Within atmospheres, butyric acid, pentanal, heptanal, and hexanal accumulated during the first 7 days of storage then significantly decreased during days 14−25. Aldehydes present in preclimacteric fruit are responsible for the 'green/unripe' aroma and, as ripening occurs, the volatile profile shifts to esters and a 'fruity' aroma.[34,38] Many group 2 volatiles were significantly highest on day 25 and significantly decreased by day 82 including propyl hexanoate, hexyl propanoate, butyl hexanoate, hexyl butyrate, hexyl 2-methylbutyrate, and octanal. This pattern indicates high production of these compounds occurred relatively early in the ripening process. Amounts of ethyl octanoate, estragole, 2-ethyl 1-hexanol, nonanal, and benzaldehyde did not change with storage duration. Lack of atmosphere treatment differences for these compounds indicates production was unaffected by storage atmospheres and ripening metabolism, while volatiles unaffected by storage duration were unrelated to the progression of ripening.

Group 3 volatiles accumulated in significantly higher concentrations in air chambers, while fruit stored in 0.3 kPa O_2 produced the lowest amounts of these compounds (Table 4). These volatiles, including propyl acetate, butyl butyrate, butyl propanoate, pentyl acetate, propyl butyrate, 2-methylpropyl acetate, butyl acetate, and 2-methylbutyl acetate, are compounds produced during typical climacteric ripening of 'Delicious' apples.[10] Due to fermentative metabolism in the 0.3 and 0.8 kPa O_2 stored fruit, ethanol accumulation provided substrate to favor

Table 5. Group 4 'Scarlett Spur Red Delicious' Volatile Accumulation (ηmol L^{-1}) During Controlled Atmosphere or Air Storage[a]

		days in storage									
group 4 compd.	atm	0	4	7	14	25	46	82	110	194	250
methyl hexanoate	0.3	0.000B	0.000AB	0.001aAB	0.001aAB	0.002aA	0.002A	0.002abA	0.001bAB	0.002bA	0.001bAB
	0.8	0.000D	0.000CD	0.000abCD	0.001abBCD	0.001abABC	0.001ABCD	0.001abABC	0.001bcABCD	0.001bAB	0.002abA
	1.6	0.000B	0.000B	0.000bB	0.000bB	0.000bB	0.000B	0.001bB	0.000cB	0.001bA	0.001bAB
	air	0.000C	0.000C	0.000bC	0.000bC	0.000abC	0.001C	0.002aABC	0.002aBC	0.004aAB	0.005aA
1-pentanol	0.3	0.007abB	0.008B	0.009B	0.007B	0.008B	0.009B	0.021AB	0.018AB	0.033A	0.007B
	0.8	0.008a	0.008	0.009	0.008	0.007	0.014	0.024	0.022	0.031	0.019
	1.6	0.006bC	0.007C	0.008C	0.008C	0.010C	0.018C	0.046B	0.043B	0.078A	0.012C
	air	0.008aBC	0.007BC	0.009BC	0.011BC	0.018C	0.020BC	0.039AB	0.048ABC	0.115A	0.130ABC
1-butanol	0.3	0.190ABC	0.232AB	0.233AB	0.254A	0.190abABC	0.124BC	0.150bABC	0.122bBC	0.224bAB	0.104C
	0.8	0.195	0.207	0.222	0.199	0.135b	0.162	0.213b	0.174ab	0.234b	0.442
	1.6	0.160BC	0.171BC	0.175BC	0.183BC	0.125bC	0.195BC	0.368bA	0.285abAB	0.278bAB	0.083C
	air	0.236	0.207	0.246	0.355	0.370a	0.719	1.26a	1.39a	2.08a	3.21
acetone	0.3	0.088AB	0.165A	0.000bC	0.000bC	0.041BC	0.007C	0.000bC	0.012bBC	0.048bBC	0.044BC
	0.8	0.098AB	0.142AB	0.133aAB	0.041abB	0.046B	0.051B	0.038abB	0.050bB	0.080bAB	0.156A
	1.6	0.067	0.051	0.112ab	0.112a	0.062	0.051	0.044ab	0.062b	0.074b	0.103
	air	0.120AB	0.095B	0.091abB	0.085abB	0.051B	0.047B	0.115aAB	0.292aAB	0.278aAB	0.353A
1-hexanol	0.3	0.013B	0.019B	0.022B	0.041B	0.084B	0.065B	0.075B	0.330aB	1.07A	0.030bB
	0.8	0.012B	0.017B	0.023B	0.036B	0.077B	0.093B	0.103B	0.312aB	1.02A	0.067bB
	1.6	0.013B	0.013B	0.014B	0.026B	0.046B	0.105B	0.157B	0.227abB	1.22A	0.063bB
	air	0.014B	0.019B	0.016B	0.032B	0.129B	0.228B	0.104B	0.130bB	0.876A	0.302aB
butyl 2-methylbutyrate	0.3	0.002B	0.002B	0.002B	0.002B	0.006B	0.002B	0.003abB	0.003aB	0.020A	0.002bB
	0.8	0.002B	0.002B	0.002B	0.002B	0.003B	0.002B	0.003aB	0.002abB	0.014A	0.004abB
	1.6	0.002D	0.002CD	0.002CD	0.003BCD	0.003BC	0.003BCD	0.003aBCD	0.002abCD	0.017A	0.004abB
	air	0.001B	0.002B	0.002B	0.002B	0.004B	0.002B	0.001bB	0.001bB	0.020A	0.010aAB
decanal	0.3	0.000B	0.000B	0.001B	0.000B	0.001B	0.001B	0.001B	0.000B	0.002aA	0.001AB
	0.8	0.000B	0.000B	0.000B	0.000B	0.000B	0.000B	0.001B	0.000B	0.001abA	0.001B
	1.6	0.000	0.000	0.000	0.000	0.000	0.001	0.001	0.000	0.001b	0.001
	air	0.000	0.001	0.001	0.001	0.001	0.001	0.000	0.001	0.001b	0.001
6-methyl-5-hepten-2-one	0.3	0.002abB	0.003B	0.003B	0.005aB	0.005B	0.004B	0.003B	0.004B	0.013aA	0.002B
	0.8	0.002ab	0.003	0.003	0.003ab	0.004	0.003	0.004	0.004	0.004b	0.002
	1.6	0.002aB	0.003B	0.003B	0.003abB	0.004B	0.003B	0.004B	0.003B	0.009abA	0.003B
	air	0.002b	0.002	0.002	0.003b	0.005	0.003	0.005	0.004	0.003b	0.003
6-methyl-5-hepten-2-ol	0.3	0.000B	0.000B	0.000B	0.000B	0.000B	0.000B	0.000B	0.000B	0.004aA	0.001B
	0.8	0.000B	0.000AB	0.000AB	0.000AB	0.000A	0.000AB	0.000A	0.000AB	0.001bA	0.001B
	1.6	0.000C	0.000C	0.000C	0.000C	0.000C	0.000C	0.000C	0.000C	0.003abA	0.002B
	air	0.000	0.000	0.000	0.000	0.000	0.000	0.000	0.000	0.000b	0.001
2-methyl 1-propanol	0.3	0.000	0.000	0.000	0.000	0.000	0.000	0.000	0.000	0.000	0.013
	0.8	0.000	0.000	0.000	0.000	0.000	0.000	0.000	0.000	0.039	0.054
	1.6	0.000	0.000	0.000	0.000	0.017	0.028	0.020	0.015	0.176	0.019
	air	0.000	0.000	0.000	0.015	0.015	0.023	0.009	0.010	0.012	0.000
2-methyl 1-butanol	0.3	0.005abD	0.008D	0.012D	0.020D	0.047CD	0.060CD	0.087bBC	0.090BC	0.338bA	0.133B
	0.8	0.005ab	0.007	0.010	0.016	0.038	0.070	0.160ab	0.155	0.302bc	0.327

dx.doi.org/10.1021/jf405267b | J. Agric. Food Chem. 2014, 62, 1741−1754

Table 5. continued

group 4 compd.	atm	days in storage										
		0	4	7	14	25	46	82	110	194	250	
	1.6	0.004bC	0.007C	0.009C	0.017C	0.043C	0.106C	0.241aBC	0.228BC	0.830aA	0.423B	
	air	0.007a	0.010	0.015	0.028	0.061	0.104	0.092b	0.084	0.139c	0.173	

[a]Headspace gas samples collected from 3 replicate storage chambers for each atmosphere were analyzed by GC-MS. Chambers were maintained at 0.3, 0.8, or 1.6 kPa O_2 with 1 kPa CO_2 or air. All fruit was stored at 0.5 °C. Storage duration and atmosphere differences are denoted by upper and lowercase letters, respectively, and values with the same letter are not significantly different ($P \leq 0.05$, Tukey's HSD).

ethyl-ester synthesis and decreased butyl and hexyl ester production, consistent with previous reports.[10,13] Amounts of these compounds increased regardless of storage atmosphere from 25 to 82 days, however, these compounds continued to accumulate in air chambers until 194 days storage and had significantly higher levels compared with the CA chambers from 82 days until the end of storage. Amounts of propyl 2-methylbutyrate and propyl propanoate were significantly higher in air chambers compared with some or all CA treatments from 82 to 194 days storage. Within atmospheres, all group 3 volatiles were significantly higher on day 25 and/or day 46 compared to other sampling dates. High amounts of group 3 compounds in the air chambers and relatively lower levels in CA chambers indicates reduced ester production occurs during as well as following CA storage compared to fruit stored in air.[39,11,4]

Group 4 compounds methyl hexanoate, 1-butanol, and acetone were significantly higher in air compared to CA chambers (Table 5), and amounts increased for the entire storage duration. 2-Methyl-1-butanol concentration was significantly higher in chambers held at 1.6 kPa O_2 on days 82 and 194 compared with amounts in air or 0.3 kPa O_2 chambers. Accumulation of 2-methyl-1-butanol may have been lower in air storage due to its metabolism to 2-methylbutyl acetate.[40] No consistent atmosphere treatment effects were observed for 1-pentanol, 1-hexanol, butyl 2-methylbutyrate, 2-methyl-1-propanol, decanal, 6-methyl-5-hepten-2-one, and 6-methyl-5-hepten-2-ol. Amounts of all group 4 compounds except 1-butanol were higher on day 250 and/or day 194 compared with most/all other days for most atmospheres. As stated previously, alcohols are substrates for ester production and are actively converted to esters. However, by the end of storage, ester production decreases as ripening progresses and alcohols that could serve as substrates for ester synthesis (1-propanol, 1-butanol, 2-methyl-1-butanol, and 1-pentanol) accumulate.

Atmosphere−day interactions were significant for 31 of 51 volatiles detected. 1-Propanol, methyl butyrate, pentanal, propyl hexanoate, hexyl propanoate, butyl hexanoate, hexyl butanoate, hexyl 2-methylbutyrate, estragole, octanal, 2-ethyl-1-hexanol, nonanal, benzaldehyde, 2-methylbutyl propanoate, 2-methylbutyl butyrate, propyl 2-methylbutyrate, hexyl acetate, 1-hexanol, butyl 2-methylbutyrate, and decanal did not have a significant atmosphere−day interaction. Several of these volatiles (estragole, octanal, 2-ethyl-1-hexanol, nonanal, benzaldehyde, 1-hexanol, butyl 2-methylbutyrate, and decanal) were not affected by storage conditions, implying that their production is also unrelated to the progression of fruit ripening.

Dynamics of apple fruit volatile production following storage have been characterized[25,26] but information regarding production dynamics during storage is lacking. Argenta et al. (2004)[7] reported 'Fuji' apple volatile production 24 h after removal from 8 months in 0.5 kPa O_2 storage was less than that of fruit previously stored in air. Production of 1-butanol, 1-pentanol, and 1-hexanol and the corresponding esters for each alcohol was reduced following low oxygen storage, while amounts of ethanol, ethyl acetate, and ethyl esters increased. Higher oxygen CA storage also results in reduced poststorage alcohol, hexyl- and butyl ester emission with increased ethanol, ethyl acetate and acetaldehyde compared with fruit stored in air.[11,41] Diminution of post-storage volatile emission also increases with increasing storage duration and decreased CA oxygen content.[11] Imposition of anaerobic storage conditions following 4−5 months CA storage also results in enhanced

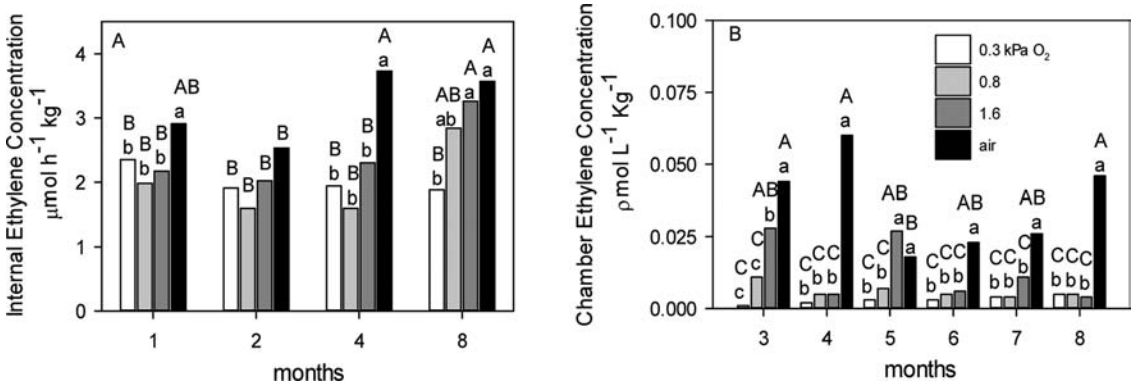

Figure 5. 'Scarlett Spur Red Delicious' fruit internal ethylene (A) and storage chamber ethylene concentration (B). All fruit stored at 0.5 °C. Controlled atmosphere kPa O_2 concentrations were 0.3, 0.8, or 1.6, all with 1 kPa CO_2. Internal ethylene values are means (n = 4) of apples (~ 1 kg) for each storage atmosphere, measured after removal from cold storage plus 7 days at 20 °C. Storage chamber ethylene was measured in gas samples removed from storage chambers (n = 3 per atmosphere) containing 72 fruit each. Time and treatment differences are denoted by upper or lowercase letters, respectively. Within each month or treatment, columns with the same letter are not significantly different (P < 0.05, Tukey's HSD).

acetaldehyde, ethanol, and ethyl ester production with reduced hexyl and butyl ester production.[10]

The current results indicate accumulation of many alcohols and esters is also reduced during low oxygen CA storage compared to fruit stored in air. Hexyl ester accumulation, however, was not affected by low O_2 storage conditions in this study. Fermentative volatile accumulation during storage was similar to that reported for fruit held in air after removal from CA.

Fruit ethylene production after storage increased relative to values at harvest regardless of storage atmosphere (Figure 5), and fruit stored in air consistently had the highest ethylene production. Ethylene production by fruit previously stored in 0.3 kPa O_2 did not change with storage duration but fruit stored in air, 0.8 kPa O_2, or 1.6 kPa O_2 significantly increased by months 4 and/or 8 compared to month 2. Ethylene content was significantly higher in storage chambers maintained with air compared to chambers with 0.3 or 0.8 kPa O_2 at 6, 7, and 8 months and 1.6 kPa O_2 chambers at 6 and 8 months. However, within atmospheres, storage duration did not significantly impact ethylene content with only 1.6 kPa O_2 having significant differences in ethylene content between 5 and 8 months.

The increase in ethylene production from harvest to month 1 indicates climacteric ripening was ongoing. Apple volatile production during storage increased in the first 3 months, also consistent with apple ripening. CA gas composition appeared to have no effect on the timing of ripening but did impact the amounts of ethylene and volatile production. Volatile accumulation among atmospheres was the most different during 1−3 months storage, confirming that gas composition had a large effect on the metabolic rates of ripening processes that impact volatile production. In addition, anaerobic conditions caused further changes in volatile production during the first 3 months in storage as indicated by the increased distance between the 0.3 kPa O_2 and the 0.8 and 1.6 kPa O_2 results in Figure 1. As expected, the rise in ethylene and volatile production was also accompanied by a gradual decrease in firmness and titratable acidity[42] (Figure 3). The lower ethylene levels in all CA treatments accompanying decreased losses in firmness and titratable acidity reflects the requirement for ethylene to promote ripening during cold storage.

At 9 months, internal breakdown incidence was significantly higher in air than in all CA treatments (Figure 4). The higher cortex browning and internal breakdown in air stored apples indicates that those fruit had become senescent. Consistent with previous studies, superficial scald levels were significantly higher in 1.6 kPa O_2 than in 0.3 or 0.8 kPa O_2 stored fruit. This indicates ultralow O_2 storage was able to reduce scald incidence.[15−17] However, 0.3 kPa O_2 stored fruit was negatively affected by the anaerobic conditions, resulting in significantly higher levels of stem browning and fermentative volatiles.

In summary, storage duration and O_2 concentration quantitatively impacted volatile production during long-term storage. Differences due to storage atmosphere were greatest during the first 6 months, and volatile production measured during CA storage was similar to measuring production after storage. Butyl and propyl ester production was inhibited by CA storage conditions and anaerobic oxygen storage promoted fermentative volatile production. CA storage prolonged storage life by reducing ethylene production, disorder incidence, and losses in firmness, and titratable acidity.

The rate of ethanol production increased with decreasing kPa O_2 and could be useful in monitoring for low O_2 stress during storage. Monitoring production of other fermentative volatiles such as acetaldehyde and ethyl acetate could also have potential as stress indicators. Fermentative volatile production was significantly different among atmospheres as early as day 4, so monitoring can begin early in storage.

AUTHOR INFORMATION

Corresponding Author

*Tel.: 509-664-2280. E-mail: James.Mattheis@ars.usda.gov.

Present Address

§(C.L.) Western Colorado Research Center, Colorado State University, Grand Junction, CO 81503-9621, United States

Funding

Supplemental funding for this research was received from the Washington Tree Fruit Research Commission. Mention of trade names or commercial products is solely for the purpose of providing specific information and does not imply recommendation or endorsement by the U.S. Department of Agriculture.

Notes

The authors declare no competing financial interest.

■ ACKNOWLEDGMENTS

We thank David Buchanan, Janie Countryman, and Rachel Leisso for excellent technical assistance.

■ REFERENCES

(1) Watkins, C. B.; Kupferman, E.; Rosenberger, D. A. Apple. In *The Commercial Storage of Fruits, Vegetables, and Florist and Nursery Stocks*, Agricultural Handbook 66; Gross, K. C., Wang, C. Y., Saltviet, M., Eds.; USDA: Washington DC, 2004. http://www.ba.ars.usda.gov/hb66/contents.html.

(2) Burg, S. P.; Burg, E. A. Molecular requirements for the biological activity of ethylene. *Plant Physiol.* **1967**, *42*, 144−152.

(3) Hertog, M.L.A.T.M.; Nicholson, S. E.; Banks, N. H. The effect of modified atmospheres on the rate of firmness change in 'Braeburn' apples. *Postharvest Biol. Technol.* **2001**, *23*, 175−184.

(4) Rudell, D. R.; Mattinson, D. S.; Mattheis, J. P.; Wyllie, S. G.; Fellman, J. K. Investigations of aroma volatile biosynthesis under anoxic conditions and in different tissues of "Redchief Delicious" apple fruit (*Malus domestica Borkh*). *J. Agric. Food Chem.* **2002**, *50*, 2627−2632.

(5) Echeverría, G.; Fuentes, M. T.; Graell, J.; López, M. L. Relationships between volatile production, fruit quality and sensory evaluation of Fuji apples stored in different atmospheres by means of multivariate analysis. *J. Sci. Food Agric.* **2003**, *84*, 5−20.

(6) Gran, C. D.; Beaudry, R. M. Determination of the low oxygen limit for several commercial apple cultivars by respiratory quotient breakpoint. *Postharvest Biol. Technol.* **1993**, *3*, 259−267.

(7) Argenta, L. C.; Mattheis, J. P.; Fan, X.; Finger, F. L. Production of volatile compounds by Fuji apples following exposure to high CO_2 or low O_2. *J. Agric. Food Chem.* **2004**, *52*, 5957−5963.

(8) Ke, D.; Zhou, L.; Kader, A. A. Mode of oxygen and carbon dioxide action on strawberry ester biosynthesis. *J. Amer. Soc. Hort. Sci.* **1994**, *119*, 971−975.

(9) Gorny, J. R.; Kader, A. A. Regulation of ethylene biosynthesis in climacteric apple fruit by elevated CO_2 and reduced O_2 atmospheres. *Postharvest Biol. Technol.* **1996**, *9*, 311−323.

(10) Mattheis, J. P.; Buchanan, D. A.; Fellman, J. K. Change in apple fruit volatiles after storage in atmospheres inducing anaerobic metabolism. *J. Agric. Food Chem.* **1991**, *39*, 1602−1605.

(11) Brackmann, A.; Streif, J.; Bangerth, F. Relationship between a reduced aroma production and lipid metabolism of apples after long-term controlled-atmosphere storage. *J. Amer. Soc. Hort. Sci.* **1993**, *118*, 243−247.

(12) Fellman, J. K.; Mattinson, D. S.; Bostick, B. C.; Mattheis, J. P.; Patterson, M. E. Ester biosynthesis in "Rome" apples subjected to low-oxygen atmospheres. *Postharvest Biol. Technol.* **1993**, *3*, 201−214.

(13) Yahia, E. M. Apple flavor. *Hortic. Rev.* **1994**, *16*, 197−234.

(14) Ingle, M.; D'Souza, M. C. Physiology and control of superficial scald of apples: A review. *HortScience* **1989**, *24*, 28−31.

(15) Lau, O. L. Efficacy of diphenylamine, ultra-low oxygen, and ethylene scrubbing on scald control in 'Delicious' apples. *J. Amer. Soc. Hort. Sci.* **1990**, *115*, 959−961.

(16) Fan, X.; Mattheis, J. P. Development of apple superficial scald, soft scald, core flush, and greasiness is reduced by MCP. *J. Agric. Food Chem.* **1999**, *47*, 3063−3068.

(17) Ghahramani, F.; Scott, K. J.; Holmes, R. Effects of alcohol vapors and oxygen stress on superficial scald and red color of stored 'Delicious' apples. *HortScience* **2000**, *35*, 1292−1293.

(18) Wang, Z.; Dilley, D. R. Initial low oxygen stress controls superficial scald of apples. *Postharvest Biol. Technol.* **2000**, *18*, 201−213.

(19) Zanella, A. Control of apple superficial scald and ripening—A comparison between 1-methylcyclopropene and diphenylamine postharvest treatments, initial low oxygen stress and ultra low oxygen storage. *Postharvest Biol. Technol.* **2003**, *27*, 69−78.

(20) Thomas, M. The production of ethyl alcohol and acetaldehyde by apples in relation to the injuries occurring in storage. Part 1: Injuries to apples occurring in the absence of oxygen and in certain mixtures of carbon dioxide and oxygen. *Ann. Appl. Biol.* **1928**, *16*, 444−457.

(21) Kupferman, E. Controlled atmosphere storage of apples and pears. *Acta Hort.* **2003**, *600*, 729−735.

(22) Ferguson, I.; Volz, R.; Woolf, A. Preharvest factors affecting physiological disorders of fruit. *Postharvest Biol. Technol.* **1999**, *15*, 255−262.

(23) Streif, J.; Saquet, A. A.; Xuan, H. CA-related disorders of apples and pears. *Acta Hort.* **2003**, *600*, 223−230.

(24) Rudell, D. R.; Mattheis, J. P.; Hertog, M.L.A.T.M. Metabolic change precedes apple superficial scald symptoms. *J. Agric. Food Chem.* **2009**, *57*, 8459−8466.

(25) Streif, J.; Bangerth, F. Production of volatile aroma substances by 'Golden Delicious' apple fruits after storage for various times in different CO_2 and O_2 concentrations. *J. Hort. Sci.* **1988**, *63*, 193−199.

(26) Mattheis, J. P.; Buchanan, D. A.; Fellman, J. K. Volatile compound production by Bisbee Delicious apples after sequential atmosphere storage. *J. Agric. Food Chem.* **1995**, *43*, 194−199.

(27) Zerbini, P. E.; Grassi, M.; Rizzolo, A. Influence of water scrubbing on the production of volatile compounds and on sensory characteristics of 'Golden Delicious' apples stored in controlled atmosphere. *Postharvest Biol. Technol.* **1996**, *9*, 7−17.

(28) Brookfield, P.; Murphy, P.; Harker, R.; MacRae, E. Starch degradation and starch pattern indices: Interpretation and relationship to maturity. *Postharvest Biol. Technol.* **1997**, *11*, 23−30.

(29) Mattheis, J. P.; Buchanan, D. A.; Fellman, J. K. Volatile compounds emitted by 'Gala' apples following dynamic atmosphere storage. *J. Amer. Soc. Hort. Sci.* **1998**, *123*, 426−432.

(30) Prange, R. K.; DeLong, J. M.; Leyte, J. C.; Harrison, P. A. Oxygen concentration affects chlorophyll fluorescence in chlorophyll-containing fruit. *Postharvest Biol. Tech.* **2002**, *24*, 201−205.

(31) Fischer, E.; Speier, A. Representation of the esters. *Chemistry* **1895**, *28*, 3252−3258.

(32) Xia, J.; Mandal, R.; Sinelnikov, I. V.; Broadhurst, D.; Wishart, D. S. MetaboAnalyst 2.0—A comprehensive server for metabolomics data analysis. *Nucleic Acids Res.* **2012**, DOI: 10.1093/nar/gks374.

(33) Patterson, B. D.; Hatfield, D. G. S.; Knee, M. Residual effects of controlled atmosphere storage on the production of volatile compounds by two varieties of apples. *J. Sci. Food Agric.* **1974**, *25*, 843−849.

(34) Berger, R. G.; Drawert, F. Changes in the composition of volatiles by post-harvest application of alcohols to Red Delicious apples. *J. Sci. Food Agric.* **1984**, *35*, 1318−1325.

(35) Panasiuk, O.; Talley, F. B.; Sapers, G. M. Correlation between aroma and volatile composition of McIntosh apples. *J. Food Sci.* **1980**, *45*, 989−991.

(36) Vanoli, M.; Visai, C.; Rizzolo, A. The influence of harvest date on the volatile composition of 'Starkspur Golden' apples. *Postharvest Biol. Technol.* **1995**, *6*, 225−234.

(37) Dixon, J.; Hewett, E. W. Factors affecting apple aroma/flavor volatile concentration: A review. *N.Z. J. Crop Hort. Sci.* **2000**, *28*, 155−173.

(38) Fellman, J. K.; Miller, T. W.; Mattinson, D. S. Factors that influence biosynthesis of volatile flavor compounds in apple fruits. *HortScience* **2000**, *35*, 1026−1033.

(39) Willaert, G. A.; Dirinck, P. J.; De Pooter, H. L.; Schamp, N. N. Objective measurement of aroma quality of Golden Delicious apples as a function of controlled-atmosphere storage time. *J. Agric. Food Chem.* **1983**, *31*, 809−813.

(40) Knee, M.; Hatfield, S. G. S. The metabolism of alcohols by apple fruit tissue. *J Sci. Food Agric.* **1981**, *32*, 593−600.

(41) Lara, I.; Graell, J.; López, M. L.; Echeverría, G. Multivariate analysis of modifications in biosynthesis of volatile compounds after CA storage of 'Fuji' apples. *Postharvest Biol. Technol.* **2006**, *39*, 19−28.

(42) Bouzayen, M.; Latché, A.; Nath, P.; Pech, J. C. Mechanism of fruit ripening. In *Plant Developmental Biology −Biotechnological Perspectives*; Pua, E. C.; ,Davey, M. R., Eds.; Springer: New York, 2010; Vol. *1*, pp 319−339.

The object of this work was to prepare biodegradable films using potato starch, PVA, and AsA as a plasticizer and a casting method. We also evaluated the effect of AsA content and heat curing time and temperature on the optical and physical properties of the prepared films such as tensile strength, elongation at break, water resistance, and water vapor absorption, thermal properties, and biodegradability in soil.

EXPERIMENTAL SECTION

Materials. Potato starch (PS) was purchased from Samyang Genex Co. Polyvinyl alcohol (PVA), ascorbic acid (AsA), glycerol (GL), and xylitol (XL) were purchased from Aldrich Chemical Co., Inc. (Milwaukee, WI). PVA was 99% hydrolyzed with an average molecular weight of 89000−98000. Distilled water (DW) was used in all experiments.

Preparation of Cross-Linked PS/PVA Blend Films. Cross-linked PS/PVA blend films were obtained by the casting method. At first, a PVA solution was prepared by dissolving PVA in hot water (90 °C). PS and plasticizers (GL, XL, and AsA) were mixed together with water using a KitchenAid mixer (Anymix, Hyun-woo Star, Seoul, Korea) for 15 min. Formulations contained 10, 20, 30, 40, and 50 wt % GL, XL, and AsA. The PVA solution and PS/plasticizer mix were kept at 95 °C for 10 min. Then, the mixture was blended to form a homogeneously gel-like solution with a mechanical stirrer (600 rpm) at room temperature for 60 min. Bubbles, the byproduct of preparation, were removed by using an aspirator. The mixing composition is shown in Table 1. The gel-like solution thus prepared

Table 1. Compositions of Gel-like Solutions Used To Prepare PS/PVA Blend Films

sample	PS (g)	PVA (g)	glycerol (wt %)	xylitol (wt %)	ascorbic acid (wt %)	DW (g)
PSP	5	5	–	–	–	100
PSPG1	5	5	10	–	–	100
PSPG2	5	5	20	–	–	100
PSPG3	5	5	30	–	–	100
PSPG4	5	5	40	–	–	100
PSPG5	5	5	50	–	–	100
PSPX1	5	5	–	10	–	100
PSPX2	5	5	–	20	–	100
PSPX3	5	5	–	30	–	100
PSPX4	5	5	–	40	–	100
PSPX5	5	5	–	50	–	100
PSPA1	5	5	–	–	10	100
PSPA2	5	5	–	–	20	100
PSPA3	5	5	–	–	30	100
PSPA4	5	5	–	–	40	100
PSPA5	5	5	–	–	50	100

was poured onto a prewarmed (60 °C) Teflon mold (200 mm × 200 mm × 1 mm). Water was evaporated from the molds in a ventilated oven at 50 °C for 24 h. Dried films were put in open polyethylene bags and stored at 25 °C and 53% relative humidity (RH) for 1 week. The prepared films were then cured in a vacuum oven at 95 ± 2, 120 ± 2, 140 ± 2, or 160 ± 2 °C for 30, 60, 90, 120, 180, 240, and 300 min at atmospheric pressure. After being heat cured, films were conditioned again at 53% RH and 25 °C for 1 week before the measurements were taken. The surfaces of the prepared films with and without heat curing were investigated via scanning electron microscopy (SEM) (S-4700, Hitachi, Tokyo, Japan), at an acceleration voltage of 5 kV.

Mechanical Properties of Biodegradable Films. Tensile strength (TS) and elongation at break (%E) were evaluated for each film using an Instron 6012 testing machine. Five dumbbell-shaped specimens with a width of 15 mm (ASTM D-421) were cut from each film. Each piece was measured for thickness in three places along the test length using a mechanical scanner (digital thickness gauge "Mitutoyo") at 15 random positions around the film. The specimen's average thickness was ~0.12 ± 0.003 mm. The gauge length and grip distance were both 50.0 mm. The crosshead speed was 20 mm/min, and the load cell was 250 kg_f. The tests were conducted at constant values of 25 °C and 53% RH.

Fourier Transform Infrared (FT-IR). The FT-IR spectra of the noncured films and cured films with and without AsA were recorded on an FT-IR spectrometer (JASCO FT/IR-430). The samples were thoroughly dried in a vacuum oven at 50 °C, and 16 scans were taken for each sample.

Dynamic Thermogravimetric Measurements. Thermogravimetric measurements were taken on a Mettler-Toledo (Zurich, Switzerland) TGA/SDTA 851e thermal system from 25 to 600 °C in a N_2 environment (flow rate, 20 mL/min) at a heating rate of 10 °C/min. The sample size was between 10 and 12 mg.

Optical Properties. Each film specimen was cut into a rectangle piece and placed directly into a UV−visible spectrophotometer (Optizen 2120UV, Mecasys Co., Ltd.) test cell. All measurements were performed using air as the reference. A spectrum of each film was obtained at wavelengths between 200 and 800 nm. The transparency at 600 nm (T_{600}) was calculated with eq 1:[26]

$$T_{600} = -\log T_{600}/x \text{ or } A_{600}/x \quad (1)$$

where %T is percentage transmittance and x is the film thickness (millimeters).

The opacity of the films was obtained using eq 2 according to the method of Gontard and Guilbert.[27]

$$\text{opacity} = \text{absorbance at 500 nm} \times \text{film thickness (mm)} \quad (2)$$

Degree of Swelling and Solubility of Films. The degree of swelling (DS) and solubility (S) of the films were measured by applying the following method. The dried films were immersed in distilled water at room temperature (25 °C). After equilibrium had been reached (24 h), moisture on the surface of the film was removed, and the weight of the films was measured. DS in films was calculated as

$$\text{DS} = \frac{W_e - W_0}{W_0} \quad (3)$$

where W_e is the weight of the film at the adsorbing equilibrium and W_0 is the first dry weight of the film.

The swollen films were dried again for 24 h at 60 °C, and their solubility (S) was calculated with eq 4:

$$S = \frac{W_0 - W_d}{W_d} \quad (4)$$

where W_0 is the first dry weight of the film and W_d is the dry weight of the swelled film.

Water Vapor Absorption. The pieces of prepared films were cut into small pieces (5 cm × 5 cm), and the weights of pieces were measured immediately. They were then dried in an oven at 60 °C overnight and weighed. The water content (k) of starch/PVA composite films was calculated with eq 5

$$k = \frac{W_f - W_0}{W_0} \quad (5)$$

where W_0 is the mass of the dried sample and W_f is the mass of the sample before it had been dried. Water vapor adsorption of the films were evaluated after being stored in desiccator chambers over the salt solution of $MgCl_2$ (54% RH) and $Mg(NO_3)_2$[28] for 10 days at 25 °C.

The nitrogen adsorption and desorption isotherms at 77 K were measured in the relative pressure range of 10^{-5} to 0.99, using the volumetric adsorption analyzer (Micromeritics, ASAP 2020) to characterize the geometrical structures of the films with and without heat curing. Prior to the measurement, ~0.2 g of the sample was outgassed at 373 K under vacuum for 24 h to remove the moisture content as well as the impurities. The textural properties such as the specific surface area [Brunauer−Emmett−Teller (BET)] and pore volume [total pore volume at P/P_0 = 0.99 and Barrett−Joyner−

dx.doi.org/10.1021/jf4024855 | J. Agric. Food Chem. 2014, 62, 1755−1764

Halenda (BJH) for the mesopore size distribution] were calculated from the nitrogen adsorption isotherm data. AFM was also employed to assess the topography and roughness value of the surface of the films. AFM imaging was performed with a Multimode IV instrument (Veeco), and the images were scanned in tapping mode (noncontact mode) using silicon cantilevers. All measurements were taken under atmospheric conditions and at room temperature.

Soil Burial Degradation Test. Soil burial degradation was conducted as described by Devi et al.[29] and in our previous work[30] with a slight modification. Garden pots with an approximate volume of 10 L were filled with soil taken from a culture field in Gangjin Gun, Korea. The samples were cut into 3 cm × 3 cm pieces and buried in the soil at a depth of 10 cm. The pots were placed in an uncovered gazebo. The soil was kept moist by being sprinkled with water at a regular time interval to maintain 30−50% humidity. The excess water drained through the hole at the bottom of the pot. The degradation of the specimen was determined at a regular time interval (15 days) by taking the specimen carefully from the soil and washing it gently with distilled water to remove the soil. The specimen was dried in an oven until a constant weight was obtained. The loss of weight of the specimen with time was used to indicate the degradation rate in the soil burial test.

RESULTS AND DISCUSSION

Mechanical Properties of Films. The measurement of mechanical properties such as tensile strength (TS) and elongation at break (%*E*) of biodegradable films plays an important role in various fields for application and modification. In addition, curing has a significant effect on mechanical properties. The methods of curing are gamma and electron beam irradiation,[31,32] UV irradiation,[33−35] and heat curing.[36,37] The mechanical properties and water resistance for the films are improved by the use of these methods.

Figure 1a shows the FT-IR spectra obtained for noncured films and cured films with and without AsA at different curing times. The strong peaks observed at 990−998, 1015−1020, and 1080 cm^{-1} are characteristic of the anhydroglucose ring like that found in starch. The broad band at 3265−3280 cm^{-1} was due to hydrogen-bonded hydroxyl groups (O−H). This band is of great importance because it indicates the presence of hydrogen bonding in the polymer. Higher-frequency shifts were observed when the heat curing time increased (~3280 cm^{-1}). This result is closely related to an increase in the level of hydrogen bonding among PS, PVA, and AsA hydroxyl groups, provoking an improvement in the mechanical properties and a decrease in the water solubility of the blended films.[38] AsA is easily hydrolyzed by heat or light. To verify hydrolysis of AsA, the AsA was boiled in the DW at 90 °C, which was the same preparation condition used for the films. Figure 1b clearly shows the results of the FT-IR spectra before and after the AsA treatment. The results indicate that the hydrolysis of AsA did not occur under the synthesis conditions of the films. As shown in Figure 2b for the typical FT-IR spectrum of AsA, the spectra of C═O, C−O−C, and O−H groups appeared at 1757, 1678, and 2920−3525 cm^{-1}, respectively.

Figure 2 shows the effect of heat curing time and temperature on the TS and %*E* of a nonplasticizer film and an AsA-added film. As shown in Figure 2a, TS slightly increased with increasing heat curing time whereas %*E* decreased until 120 min. However, when the curing time exceeded 150 min, TS increased and %*E* decreased rapidly because the films were discolored and oxidized. TS and %*E* of films with heat curing temperature are shown in Figure 2b. With an increasing curing temperature, TS slightly increased and %*E* drastically decreased. When heat curing was conducted at 120 °C, discoloration of

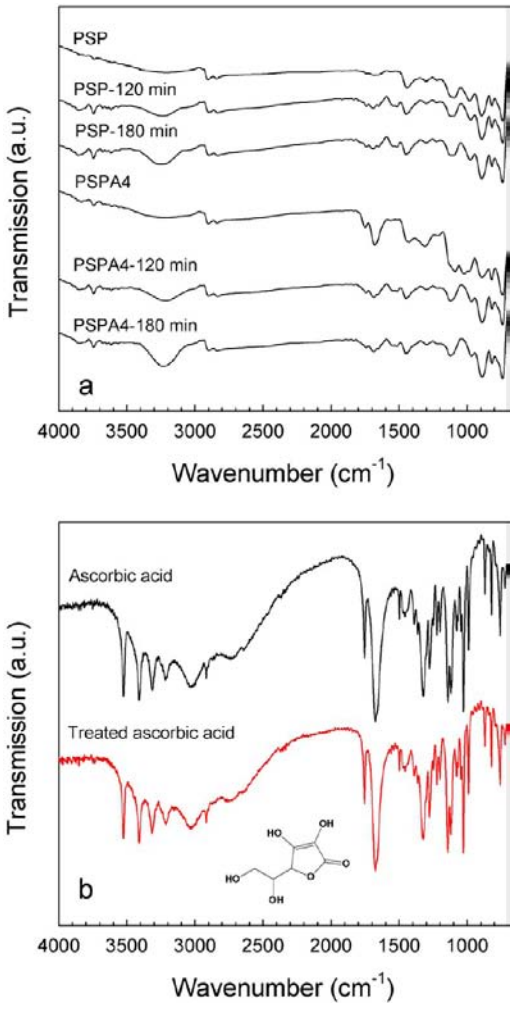

Figure 1. (a) FT-IR spectra of noncured and cured films with and without ascorbic acid (AsA). (b) FT-IR spectra of AsA and AsA treated with heat curing.

films occurred when heat curing lasted more than 150 min. When heat curing was performed for 120 min, discoloration of the film occurred after the temperature had reached ≥140 °C. Taking these results into consideration, we prepared the cross-linked PS/PVA blend films by heat curing at 120 °C for 120 min using glycerol (GL), xylitol (XL), and AsA as plasticizers. In addition, the results of the effects on heat curing revealed that TS of cured films was improved ~1.5 times compared with that of films without heat curing.

Panels a and b of Figure 3 show TS and %*E* for cured films with plasticizers (GL, XL, and AsA). Each plasticizer is added from 0 to 50 wt % on a mass percent ratio to total CS and PVA weight basis. As the content of GL, XL, and AsA increased, TS decreased and %*E* increased. A comparison of functional groups of plasticizers indicated that TS of a film with added XL with five hydroxyl groups was higher than that of a film with added GL with three hydroxyl groups. However, TS of a film with added AsA with four hydroxyl groups was highest of all the films because AsA has not only four hydroxyl groups but also one ether and one ketone. In other words, TS of an AsA-added film was improved because of the existence of the functional groups, i.e., hydroxyl, ether, and ketone groups, which can combine with starch and PVA molecules. In addition, the %*E* values indicated that GL-added films have higher values than

dx.doi.org/10.1021/jf4024855 | J. Agric. Food Chem. 2014, 62, 1755−1764

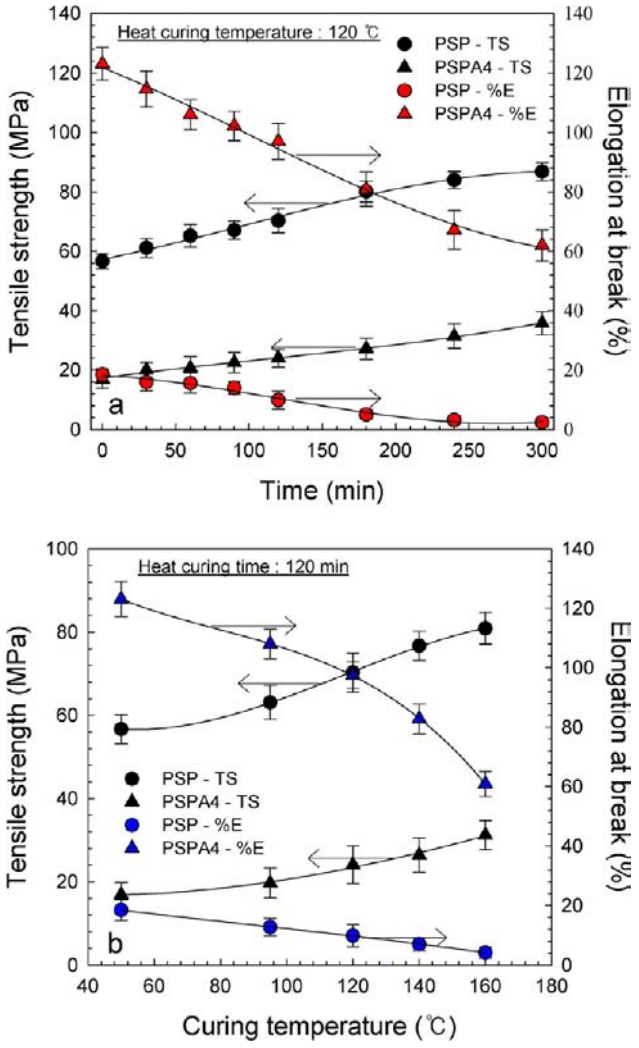

Figure 2. Tensile strength (TS) and elongation at break (%*E*) for a nonplasticizer film and an AsA-added film vs heat curing time (a) and temperature (b).

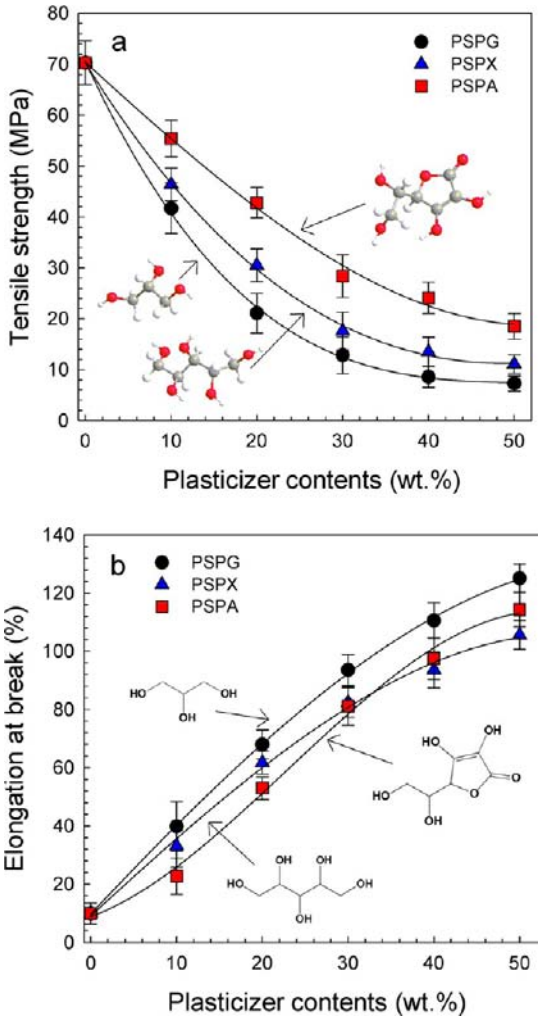

Figure 3. (a) Tensile strength (TS) and (b) elongation at break (%*E*) vs cured film glycerol (GL), xylitol (XL), and ascorbic acid (AsA) content.

XL-added films or AsA-added films. The %*E* values of XL-added films were higher than those of AsA-added films when <30 wt % plasticizers were added. However, when >30 wt % plasticizers were added, the %*E* values of AsA-added films were higher than those of XL-added films. A possible explanation of this phenomenon is that when >30 wt % AsA was added, the effect of inter-intramolecular reaction of one ether and one ketone as functional groups of AsA takes place between the components of PS, PVA, and plasticizer films.

Figure 4 presents the effect of heat curing on the SEM images of the surface of films to which 40 wt % plasticizers had been added. The surface of the noncured film without plasticizers appeared to be quite homogeneous and smooth (Figure 4a). However, as shown in panels c, e, and g of Figure 4, the noncured films to which 40 wt % plasticizers (GL, XL, and AsA) had been added appeared to be somewhat rough and agglomerated because of the combination of PS, PVA, and plasticizers for the formation of blended films. SEM images of the surface of the cured films with and without added plasticizers showed no agglomeration, cracks, or pores (Figure 4b,d,f,h).

Thermal Analysis of Films. Figure 5 shows the results of thermogravimetric analysis (TGA) of noncured and cured films with and without plasticizers. The effects of heat curing on the film without a plasticizer and the AsA-added film are shown in Figure 5a. Physical properties such as tensile properties, water resistance, and thermal stability are generally improved via the use of heat curing.[32] As shown in Figure 5a, the TGA curve of the cured films with and without AsA shifted toward the high-temperature region. It means that the thermal properties of cured films are improved by heat curing, which improved the mutual reaction of inter-intramolecular combinations. In other words, heat curing treatment of the film slightly decreased the degree of thermal decomposition. This may be due to the cross-linking of the films, which increases the resistance to thermal decomposition. The thermal properties are closely related to mechanical properties. Comparison of the noncured films and cured films showed that the TS value of the film without a plasticizer increased from 55.6 to 69.2 MPa, and at the same time, the thermal stability was also improved. The TS value of the noncured AsA-added film increased from 15.6 to 20.1 MPa when the film was treated with heat curing. The degree of thermal decomposition of the cured film without AsA was higher than that of the cured AsA-added films because the strong interaction between PS and PVA was weakened by addition of AsA as the plasticizer. Because PS and plasticizers (GL, XL, and AsA) are especially sensitive to thermal

dx.doi.org/10.1021/jf4024855 | J. Agric. Food Chem. 2014, 62, 1755−1764

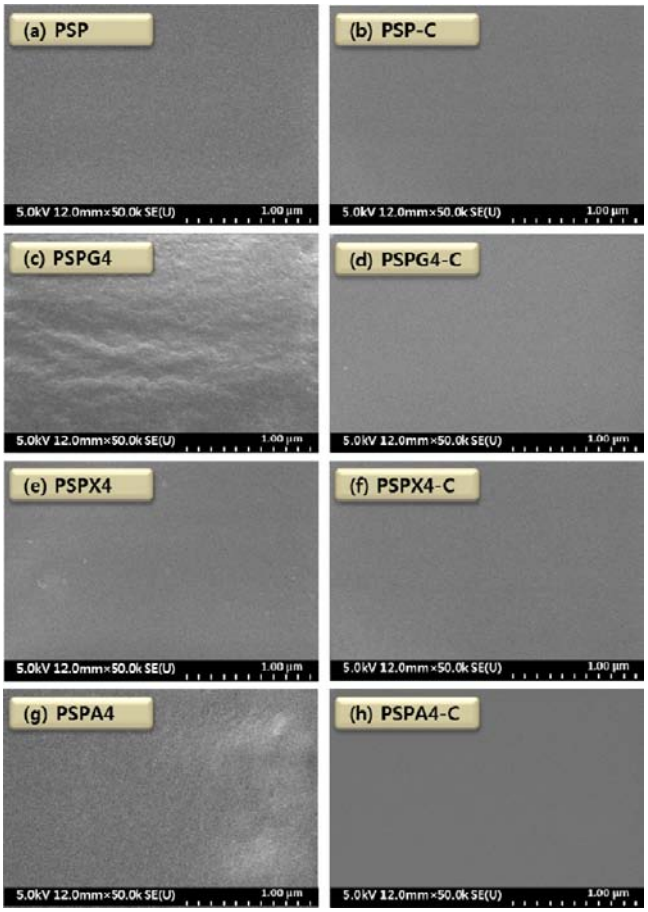

Figure 4. Scanning electron microscope image of the surface of PS/PVA blend films with added 40 wt % GL, XL, and AsA with and without heat curing. (a) Noncured film without added plasticizer. (b) Cured film without added plasticizer. (c) Noncured film with added 40 wt % GL. (d) Cured film with added 40 wt % GL. (e) Noncured film with added 40 wt % XL. (f) Cured film with added 40 wt % XL. (g) Noncured film with added 40 wt % AsA. (h) Noncured film with added 40 wt % AsA. Noncured films are denoted PSP, PSPG4, PSPX4, and PSPA4, and cured films are denoted PSP-C, PSPG4-C, PSPX4-C, and PSPA4-C.

decomposition, the incorporation of plasticizers into a PS/PVA blend film intensifies its thermal decomposition. Panels b and c of Figure 5 show the TGA curves for the cured films with added 20, 40, and 50 wt % AsA and the cured films with added 40 wt % GL, XL, and AsA. As shown in Figure 5b, the degree of thermal decomposition increased but TS decreased (see Figure 3a) because the mobility between the components of the films is increased by the addition of AsA as the plasticizer. Furthermore, the flexibility of AsA-added films also increased. Figure 5c shows the TGA curves of the cured films with the same ratio of GL, XL, and AsA added (40 wt %). The changes in the rate of thermal decomposition in the cured films indicate that the thermal stability of the AsA-added film is superior to those of other GL- or XL-added films. In addition, the reversed phenomenon is observed above 350 °C because strong interactions among PS, PVA, and plasticizer are formed by the heat curing process and the addition of plasticizers.

Degree of Swelling and Solubility of Films. The evaluation of the degree of swelling (DS) and solubility (*S*) of the prepared films plays an important role in the characterization of the degree of incorporation and cross-

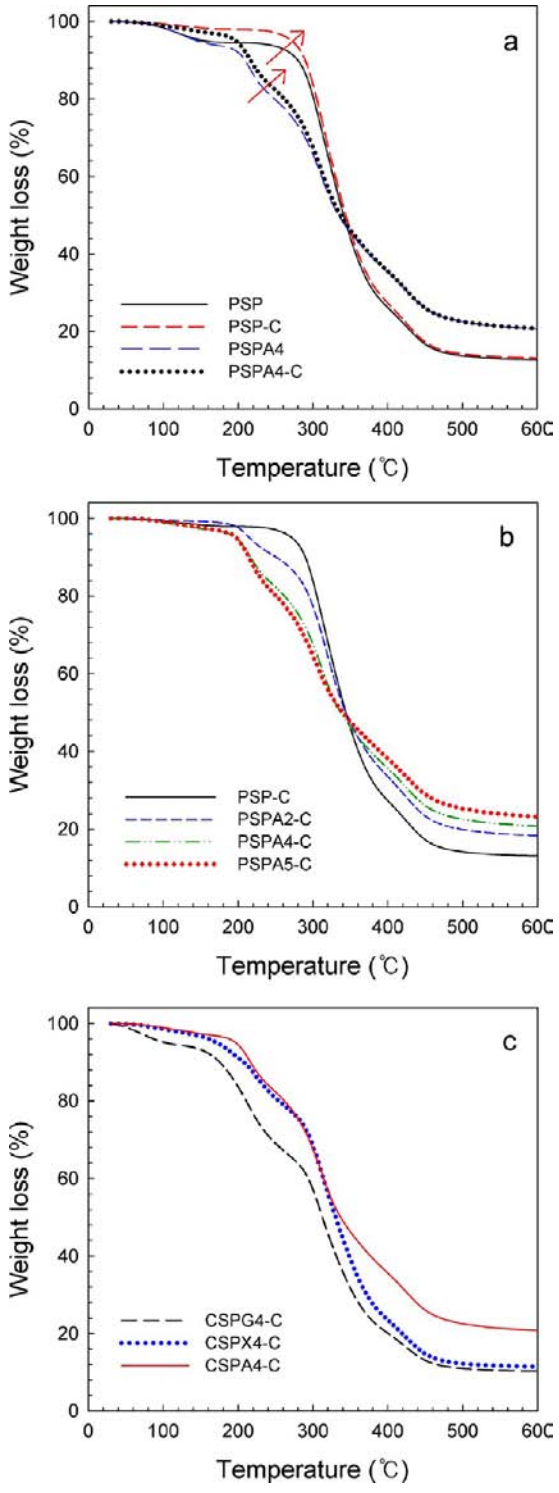

Figure 5. Thermogravimetric analysis (TGA) of noncured and cured films with and without plasticizers. (a) TGA curves of noncured and cured films with and without added AsA. (b) TGA curves of cured films with 20, 40, and 50 wt % AsA. (c) TGA curves of cured films with added 40 wt % GL, XL, and AsA.

linking between the constituents of films as well as water resistance.[39] Figure 6 shows the effect of heat curing time and temperature on the DS and *S* of the film without a plasticizer and those of the AsA-added film. As shown in Figure 6a, with an increasing heat curing time, DS values of the film without a plasticizer gradually decreased for 300 min until the end of

dx.doi.org/10.1021/jf4024855 | J. Agric. Food Chem. 2014, 62, 1755−1764

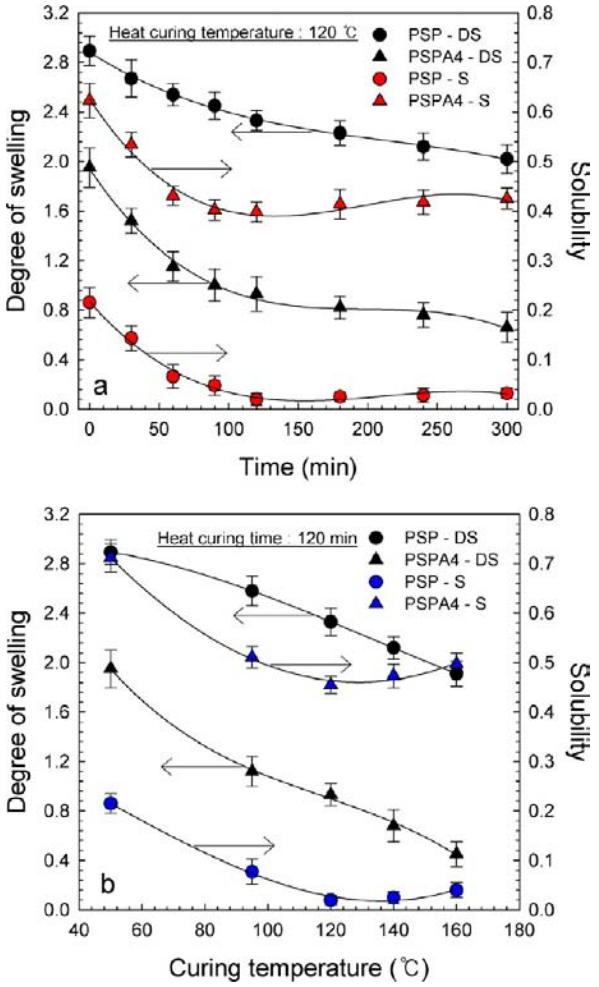

Figure 6. Degree of swelling (DS) and solubility (*S*) for a film without a plasticizer and an AsA-added film vs (a) heat curing time and (b) temperature.

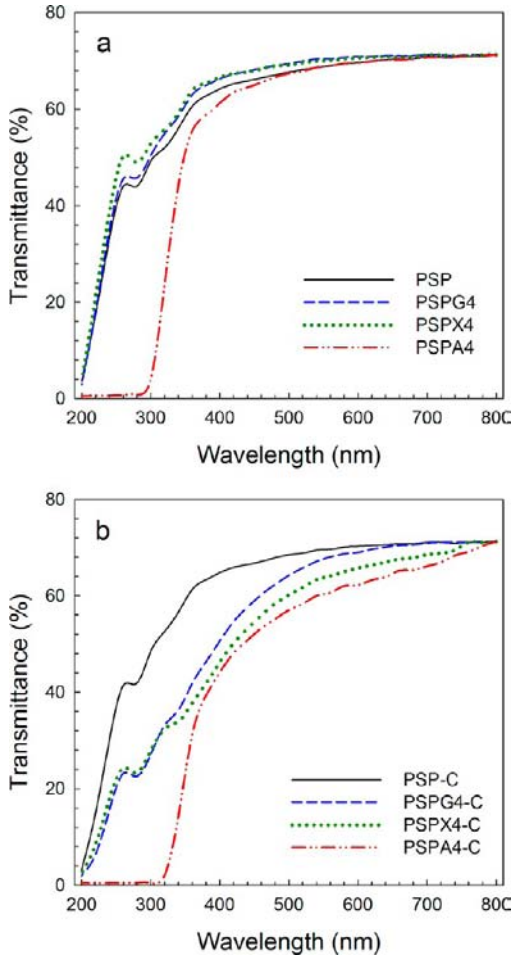

Figure 7. Transmittance (%) of non-cured and cured films added various plasticizers. (a) Transmittance (%) of non-cured films with/without added 40 wt.% plasticizers. (b) Transmittance (%) of cured films with/without added 40 wt.% plasticizers.

Table 2. Degree of Swelling and Solubility of Cured PS/PVA Blend Films in Terms of Plasticizer (GL, XL, and AsA) Content

sample	degree of swelling (g/g)	solubility (g/g)
PSP	2.330 ± 0.061	0.020 ± 0.021
PSPG1	1.642 ± 0.069	0.212 ± 0.019
PSPG2	1.183 ± 0.072	0.325 ± 0.024
PSPG3	0.725 ± 0.053	0.388 ± 0.019
PSPG4	0.575 ± 0.089	0.436 ± 0.018
PSPG5	0.473 ± 0.070	0.460 ± 0.030
PSPX1	1.783 ± 0.075	0.182 ± 0.026
PSPX2	1.280 ± 0.051	0.311 ± 0.022
PSPX3	0.962 ± 0.063	0.370 ± 0.020
PSPX4	0.752 ± 0.066	0.425 ± 0.018
PSPX5	0.607 ± 0.072	0.451 ± 0.021
PSPA1	1.931 ± 0.058	0.169 ± 0.019
PSPA2	1.516 ± 0.081	0.302 ± 0.015
PSPA3	1.154 ± 0.072	0.352 ± 0.017
PSPA4	0.930 ± 0.066	0.398 ± 0.017
PSPA5	0.814 ± 0.087	0.430 ± 0.025

Table 3. Opacity and Transparency of Noncured and Cured PS/PVA Blend Films with Various Plasticizers

sample	opacity	transparency
PSP	0.0185 ± 0.0055	1.4289 ± 0.26
PSP-C	0.0180 ± 0.0049	1.3839 ± 0.30
PSPG4	0.0169 ± 0.0059	1.3478 ± 0.26
PSPG4-C	0.0213 ± 0.0039	1.4681 ± 0.31
PSPX4	0.0180 ± 0.0051	1.3755 ± 0.27
PSPX4-C	0.0241 ± 0.0035	1.6667 ± 0.29
PSPA4	0.0198 ± 0.0040	1.4301 ± 0.25
PSPA4-C	0.0277 ± 0.0055	1.8456 ± 0.24

experiment but the *S* values drastically decreased until 120 min and increased again when the film was cured for >150 min. In the AsA-added film, DS and *S* values decreased rapidly until the sample had been cured for 120 min, but after curing had been conducted for ≥150 min, DS values slowly decreased and *S* values increased. These results indicate that the inter-intra-molecular interaction among PS, PVA, and plasticizer is improved until the sample is cured for 120 min, but when the sample had been heat cured for >150 min, the properties of the film markedly deteriorated, with discoloration and oxidation of the film. As for the effects of heat curing temperature, DS values gradually decreased until the final heat curing stage of 160 °C, but *S* values decreased rapidly up to 120 °C and then increased up to 160 °C (Figure 6b). These results suggest that these combinations between the constituents of films were

dx.doi.org/10.1021/jf4024855 | J. Agric. Food Chem. 2014, 62, 1755−1764

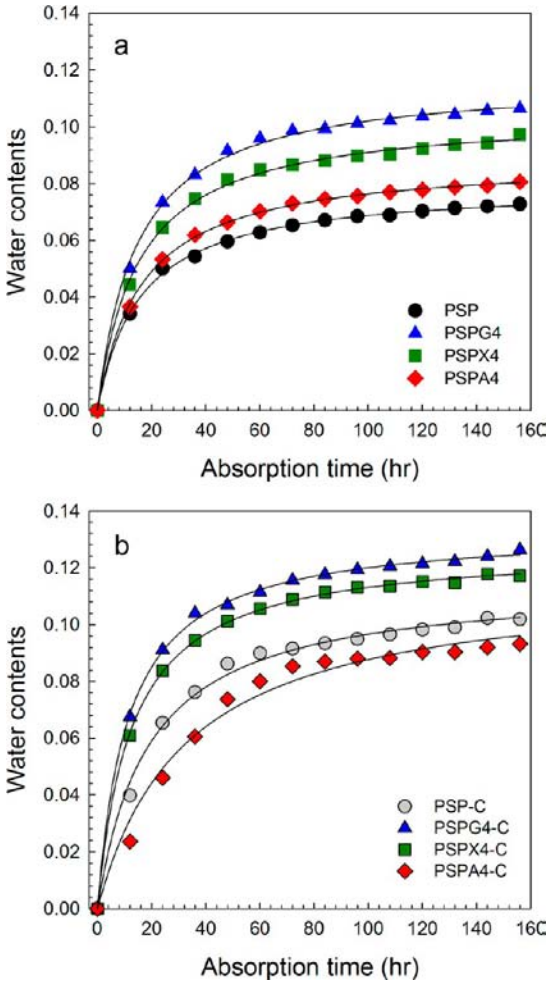

Figure 8. Water contents of non-cured and cured PS/PVA blend films with/without added 40 wt.% GL, XL, and AsA. (a) Water contents of non-cured films with/without added 40 wt.% GL, XL, and AsA in terms of adsorption time (hr). (b) Water contents of cured films with/without added 40 wt.% GL, XL, and AsA in terms of adsorption time (hr).

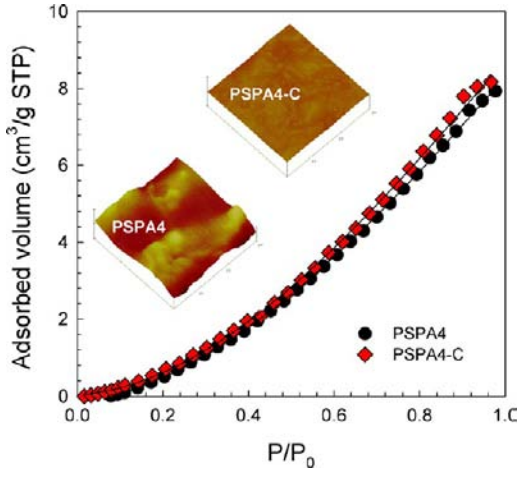

Figure 9. Nitrogen adsorption and desorption isotherms and atomic force microscopy (AFM) images of noncured and cured films with added 40 wt % AsA.

Table 4. Comparison of Specific Surface Areas, Pore Volumes, and Pore Diameters with and without Heat Curing

	specific surface area (m^2/g)	pore volume (cm^3/g)	average pore diameter (nm)
PSPA4	9.01	0.0139	5.39
PSPA4-C	9.89	0.0163	4.99

destroyed by high temperatures. From the results, the changes in DS and *S* indicate that the water resistance was improved by heat curing.

Table 2 lists DS and *S* values of cured films to which various plasticizers (GL, XL, and AsA) had been added. As the plasticizer content increased, DS values decreased but *S* values increased. DS values increased in the following order: GL-added film < XL-added film < AsA-added film. *S* values increased in the following order: AsA-added film < XL-added film < GL-added film. The GL-added films had the lowest DS value and the highest *S* value. This means that the GL-added film has a relatively weak bond strength. In contrast, the AsA-added films showed the highest DS value and the lowest *S* value, which indicates that the degree of combination among PS, PVA, and AsA is stronger than in the films with added GL or XL.

Optical Properties. One of the demands of biodegradable polymers such as edible and packing materials is that they should protect materials from the effects of light, i.e., ultraviolet radiation. Figure 7 shows the light transmission characterization of noncured and cured films with various added plasticizers. Cured films had lower transmittance (percent) than noncured films, suggesting that cured films had improved light barrier properties as a result of heat curing. In addition, films with added AsA had the lowest transmittance (percent) compared with those of the films with added GL, XL, and AsA. It means that AsA-added films have a good barrier to ultraviolet light. The opacity and transparency of noncured and cured films with GL, XL, and AsA are listed in Table 3. The results indicate that the opacity and transparency values had a tendency to increase because of the improvement of the inter-intramolecular adhesion among PS, PVA, and plasticizers by heat curing. It could confirm that the opacity and transparency values of prepared films in this study are lower compared with the reported values of synthetic films. The results obtained seem to indicate that the AsA-added films are clear enough to be used as packaging or coating materials when their values are compared with values reported by Shiku et al.[40]

Water Vapor Absorption. The water absorption property of starch-based polymers is one of their notable defects. Enhancement of water resistance is also an important issue. Therefore, we investigated the water contents of the noncured films and cured films to which GL, XL, and AsA had been added as a plasticizer. The influence of humidity on the prepared films was also evaluated because PS/PVA blend films are highly sensitive to humidity. Figure 8 shows the effect of water content on noncured films and cured films to which 40 wt % plasticizers had been added. The measurements of water content for the noncured films and the cured films with and without various plasticizers were taken at the same 55% RH. The water contents are highly dependent on the plasticizers regardless of their treatment conditions. The equilibrium water contents of noncured films were in the following order: GL-added film (0.1044) > XL-added film (0.0937) > AsA-added film (0.0788) > the film without a plasticizer (0.0714) (Figure

dx.doi.org/10.1021/jf4024855 | J. Agric. Food Chem. 2014, 62, 1755−1764

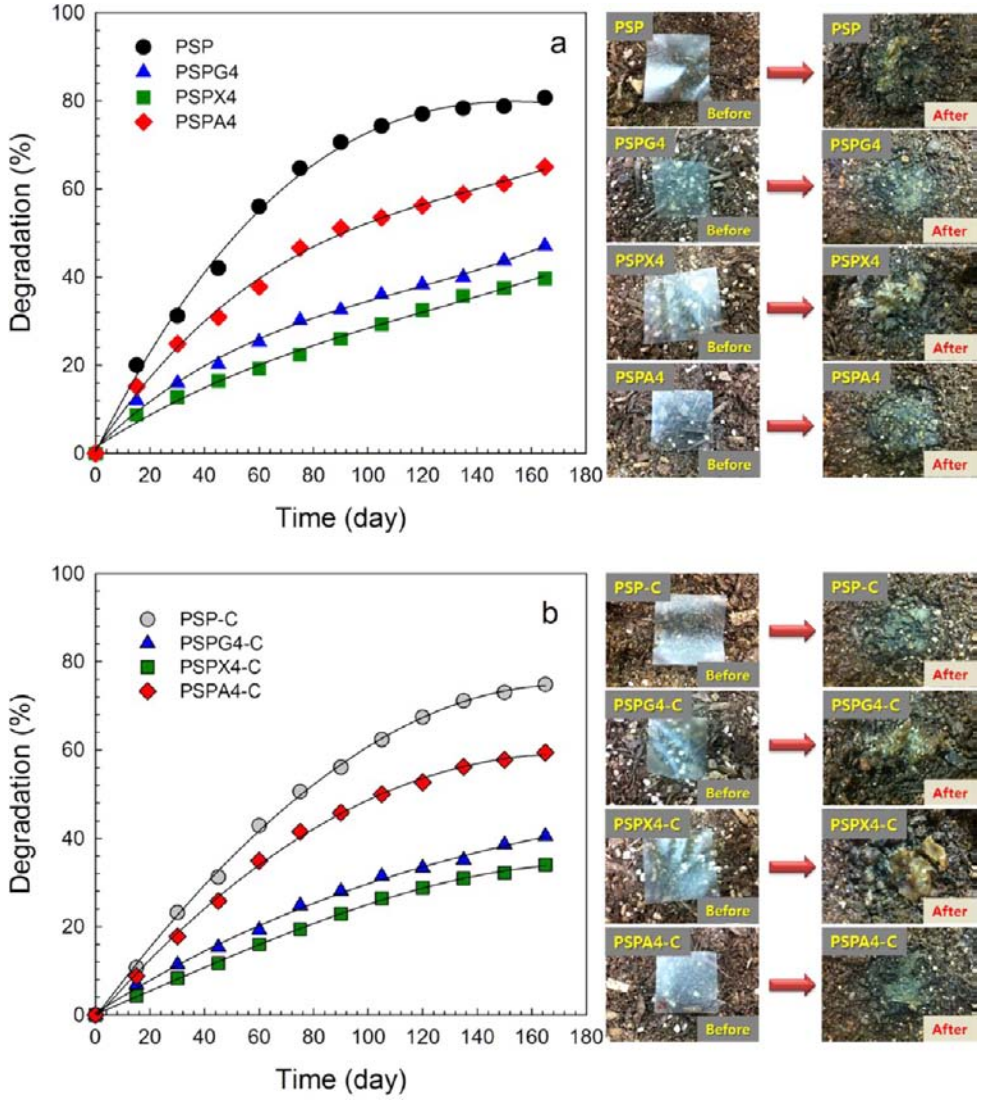

Figure 10. Biodegradation of non-cured and cured films with/without added 40 wt.% GL, XL, and AsA. (a) Biodegradation of non-cured films with/without added 40 wt.% GL, XL, and AsA. (b) Biodegradation of cured films with/without added 40 wt.% GL, XL, and AsA.

8a). However, as shown in Figure 8b, the water contents of the cured films, which were greater than those of the noncured films, were 0.1222 (GL-added film), 0.1147 (XL-added film), 0.0903 (AsA-added film), and 0.0990 (none plasticizer). The water content of the cured films was higher than that of noncured films. The hydrophilic properties of plasticizers are closely connected to the water resistance of starch-based blend films.[20] From these results, the water content of the GL-added film and the XL-added film was higher than that of the AsA-added film, which shows that GL and XL are more hydrophilic than AsA. The results of water vapor absorption in the prepared films indicated that the water resistance of the AsA-added film was better than that of the GL-added film and XL-added film.

It is important to note that the water content of the cured films is higher than that of noncured films. To confirm this phenomenon, we conducted a BET experiment and AFM analysis on the specific surface area, pore volume, and topography of both the noncured film and the cured films to which 40 wt % AsA had been added. Figure 9 shows the nitrogen adsorption and desorption isotherms and AFM images of the films. The nitrogen adsorption and desorption isotherms of the prepared films seemed to belong to type V according to the IUPAC classification. The adsorption behaviors of the prepared films were similar to each other. However, the adsorbed amount of the cured film was larger than that of the noncured film. The detailed properties of the films such as the surface area, pore volume, and average pore size are listed in Table 4. The results of AFM analysis also confirmed that the surface roughness of the cured film is decreased by heat curing, and pores that can absorb H_2O molecules are formed.

Soil Burial Degradation. The biodegradability of the noncured films and the cured films to which 40 wt % GL, XL, and AsA had been added as plasticizers was estimated by using a soil burial method. As shown in panels a and b of Figure 10, the degree of biodegradation of the films was investigated by the loss of weight of the films with time. In all the films, a rapid degradation occurred in the initial 60 days, followed by a slow degradation until the end of the experiment (165 days). The degree of biodegradation of the cured films was slightly lower than that of the noncured films because of the influence of cross-linking by the treatment of heat curing. In addition, different plasticizers showed different degrees of biodegradability. The degree of biodegradation of the AsA-added films was higher than that of the GL-added films and XL-added films.

dx.doi.org/10.1021/jf4024855 | J. Agric. Food Chem. 2014, 62, 1755−1764

The biodegradability of the GL-added films and XL-added films is low because GL and XL as plasticizers play a role as antibacterial agents.

Conclusions. Biodegradable films were successfully prepared by using potato starch, PVA, and ascorbic acid (AsA) as plasticizers and by heat curing treatment. The tensile strength (TS), elongation at break (%*E*), degree of swelling (DS), solubility (*S*), optical properties, water vapor absorption, thermal characteristics, and biodegradability of the prepared films were investigated. The results of the evaluation of the physical properties of noncured films and cured films indicated that the TS, %*E*, thermal properties, and water resistance of cured films were improved up to 65−295% by the use of heat curing. In addition, the optical properties of cured films were lower than those of noncared films. In particular, the optical properties of AsA-added films were superior to those of the other films. The water vapor absorption of cured films was slightly higher than that of noncured films. To verify this phenomenon, we investigated the specific surface area, pore volume, and topography of films with and without heat curing by using the BET experiment and AFM analysis. The results indicated that the nitrogen adsorption−desorption behavior of the prepared films was similar. However, the adsorbed amount of the cured film was larger than that of the noncured film. The results of AFM analysis verified that the surface roughness of the cured film was decreased by the heat curing process and that pores that can absorb H_2O molecules are formed. Compared to the properties of the films with various plasticizers (GL, XL, and AsA), the mechanical, thermal, and water barrier properties of a film with added AsA with four hydroxyl groups, one ether, and ketone groups were superior to those of the other films with added GL and XL with only hydroxyl groups.

The soil burial biodegradation test showed that the prepared films were degraded by ∼35−80% after 165 days. The degree of biodegradation of cured films, however, was lower than that of noncured films. In addition, the biodegradability was different with different plasticizers. The degree of biodegradation of AsA-added films was higher than that of GL-added films and XL-added films. Using the results of this study, we found that AsA could be used as an alternative plasticizer of biodegradable polymers.

AUTHOR INFORMATION

Corresponding Author

*Telephone: +82-61-659-7297. Fax: +82-61-653-3659. E-mail: yunsd03@chonnam.ac.kr.

Funding

This study was financially supported by Chonnam National University.

Notes

The authors declare no competing financial interest.

REFERENCES

(1) Kołodziejska, I.; Piotrowska, B. The water vapour permeability, mechanical properties and solubility of fish gelatin−chitosan films modified with transglutaminase or 1-ethyl-3-(3-dimethylaminopropyl) carbodiimide (EDC) and plasticized with glycerol. *Food Chem.* **2007**, *103*, 295−300.

(2) Chaudhary, A. L.; Miler, M.; Torley, P. J.; Sopade, P. A.; Halley, P. J. Amylose content and chemical modification effects on the extrusion of thermoplastic starch from maize. *Carbohydr. Polym.* **2008**, *74*, 907−913.

(3) Zhang, J. F.; Sun, X. Mechanical properties of poly(lactic acid)/starch composites compatibilized by maleic anhydride. *Biomacromolecules* **2004**, *5*, 1446−1451.

(4) Funke, U.; Bergthaller, W.; Lindhauer, M. G. Processing and characterization of biodegradable products based on starch. *Polym. Degrad. Stab.* **1998**, *59*, 293−296.

(5) Angellier, H.; Molina-Boisseau, S.; Dole, P.; Dufresne, A. Thermoplastic starch-waxy maize starch nanocrystals nanocomposites. *Biomacromolecules* **2006**, *7*, 531−539.

(6) Lourdin, D.; Valle, G. D.; Colonna, P. Influence of amylose content on starch films and foams. *Carbohydr. Polym.* **1995**, *27*, 261−270.

(7) van Soest, J. J. G.; Benes, K.; De Wit, D. The influence of starch molecular mass on the properties of extruded thermoplastic starch. *Polymer* **1996**, *37*, 3543−3552.

(8) Ma, X.; Jian, R.; Chang, P. R.; Yu, J. Fabrication and characterization of citric acid-modified starch nanoparticles/plasticized-starch composites. *Biomacromolecules* **2008**, *9*, 3314−3320.

(9) Liao, H. T.; Wu, C. S. Preparation and characterization of ternary blends composed of polylactide, poly(e-caprolactone) and starch. *Mater. Sci. Eng., A* **2009**, *515*, 207−214.

(10) Guana, J.; Eskridgeb, K. M.; Hannaa, M. A. Acetylated starch-polylactic acid loose-fill packaging materials. *Ind. Crops Prod.* **2005**, *22*, 109−123.

(11) Huneault, M. A.; Li, H. Morphology and properties of compatibilized polylactide/thermoplastic starch blends. *Polymer* **2007**, *48*, 270−280.

(12) Ren, J.; Fu, H.; Ren, T.; Yuan, W. Preparation, characterization and properties of binary and ternary blends with thermoplastic starch, poly(lactic acid) and poly(butylene adipate-co-terephthalate). *Carbohydr. Polym.* **2009**, *77*, 576−582.

(13) Lawton, J. W.; Fanta, G. F. Glycerol-plasticized films prepared from poly(vinyl alcohol) mixtures: Effect of poly (ethylene-co-acrylic acid). *Carbohydr. Polym.* **1994**, *23*, 275−280.

(14) Liu, Z. Q.; Feng, Y.; Yi, X. S. Thermoplastic starch/PVAI compounds: Preparation, processing and properties. *J. Appl. Polym. Sci.* **1999**, *74*, 2667−2673.

(15) Lourdin, D.; Coignard, L.; Bizot, H.; Colonna, P. Influence of equilibrium relative humidity and plasticizer concentration on the water content and glass transition of starch materials. *Polymer* **1997**, *38*, 5401−5406.

(16) Park, H. R.; Chough, S. H.; Yun, Y. H.; Yoon, S. D. Properties of starch/PVA blend films containing citric acid as additive. *J. Polym. Environ.* **2005**, *13*, 375−382.

(17) Westhoff, R. P.; Kwolek, W. F.; Otey, F. H. Starch-polyvinyl alcohol films effect of various plasticizers. *Starch* **1979**, *31*, 163−165.

(18) Tudorachi, N.; Cascaval, C. N.; Rusu, M.; Pruteanu, M. Testing of polyvinyl alcohol and starch mixtures as biodegradable polymeric materials. *Polym. Test.* **2000**, *19*, 785−799.

(19) Yoon, S. D.; Chough, S. H.; Park, H. R. Effects of additives with different functional groups on the physical properties of starch/PVA blend film. *J. Appl. Polym. Sci.* **2006**, *100*, 3733−3740.

(20) Zou, G. X.; Jin, P. Q.; Xin, L. Z. Extruded starch/PVA composites: Water resistance, thermal properties, and morphology. *J. Elastomers Plast.* **2008**, *40*, 303−316.

(21) Zhou, X. Y.; Cu, Y. F.; Jia, D. M.; Xie, D. Effect of a complex plasticizer on the structure and properties of the thermoplastic PVA/starch blends. *Polym.-Plast. Technol. Eng.* **2009**, *48*, 489−495.

(22) Dai, H.; Chang, P. R.; Geng, F.; Yu, J.; Ma, X. Preparation and properties of starch-based film using N,N-bis(2-hydroxyethyl)-formamide as a new plasticizer. *Carbohydr. Polym.* **2010**, *79*, 306−311.

(23) Dai, H.; Chang, P. R.; Yu, J.; Ma, X. N,N-Bis(2-hydroxyethyl)-formamide as a new plasticizer for thermoplastic starch. *Starch* **2008**, *60*, 676−684.

(24) Thiagarajan, S.; Chen, S. M. Preparation and characterization of PtAu hybrid film modified electrodes and their use in simultaneous determination of dopamine, ascorbic acid and uric acid. *Talanta* **2007**, *74*, 212−222.

(25) Arrigoni, O.; De Tullio, M. C. Ascorbic acid: Much more than just an antioxidant. *Biochim. Biophys. Acta* **2002**, *1569*, 1−9.
(26) Han, J. H.; Floros, J. D. Casting antimicrobial packaging films and measuring their physical properties and antimicrobial activity. *J. Plast. Film Sheeting* **1997**, *13*, 287−298.
(27) Gontard, N.; Guilbert, S. Biopackaging: Technology and properties of edible and/or biodegradable material of agricultural origin. In *Food Packaging and Preservation*; Mathlouthi, M., Ed.; Blackie Academic & Professional: New York, 1994; pp 159−181.
(28) Labuza, T. P.; Kaanane, A.; Chen, J. Y. Effect of temperature on the moisture sorption isotherms and water activity shift of two dehydrated foods. *J. Food Sci.* **1985**, *50*, 385−391.
(29) Thakore, I. M.; Desai, S.; Sarawade, B. D.; Devi, S. Studies on biodegradability, morphology and thermomechanical properties of LDPE/modified starch blends. *Eur. Polym. J.* **2001**, *37*, 151−60.
(30) Yun, Y. H.; Wee, Y. J.; Byun, H. S.; Yoon, S. D. Biodegradability of Chemically Modified Starch (RS4)/PVA Blend Films: Part 2. *J. Polym. Environ.* **2008**, *16*, 12−18.
(31) Zhai, M. L.; Yoshii, F.; Kume, T.; Hashim, K. Syntheses of PVA/starch grafted hydrogels by irradiation. *Carbohydr. Polym.* **2002**, *50*, 295−303.
(32) Zhai, M. L.; Yoshii, F.; Kume, T. Radiation modification of starch-based plastic sheets. *Carbohydr. Polym.* **2003**, *52*, 311−317.
(33) Rhim, J. W.; Gennadios, A.; Handa, A.; Weller, C. L.; Hanna, M. A. Solubility, tensile, and color properties of modified soy protein isolate films. *J. Agric. Food Chem.* **2000**, *48*, 4937−4941.
(34) Kaczmarek, H.; Podgorski, A. The effect of UV-irradiation on poly(vinyl alcohol) composites with montmorillonite. *J. Photochem. Photobiol., A* **2007**, *191*, 209−215.
(35) Dintcheva, N. T.; La Mantia, F. P. Durability of a starch-based biodegradable polymer. *Polym. Degrad. Stab.* **2007**, *92*, 630−634.
(36) Miller, K. S.; Chiang, M. T.; Krochta, J. M. Heat curing of whey protein films. *J. Food Sci.* **1997**, *62*, 1189−1193.
(37) Kim, K. M.; Weller, C. L.; Hanna, M. A.; Gennadios, A. Heat curing of soy protein films at selected temperatures and pressures. *LWT—Food Sci. Technol.* **2002**, *35*, 140−145.
(38) Elizondo, N. J.; Sobral, P. J. A.; Menegalli, F. C. Development of films based on blends of *Amaranthus cruentus* flour and poly(vinyl alcohol). *Carbohydr. Polym.* **2009**, *75*, 592−598.
(39) Chen, L.; Remondetto, G.; Rouabhia, M.; Subirade, M. Kinetics of the breakdown of cross-linked soy protein films for drug delivery. *Biomaterials* **2008**, *29*, 3750−3756.
(40) Shiku, Y.; Hamaguchi, P. Y.; Benjakul, S.; Visessanguan, W.; Munehiko, T. Effect of surimi quality on properties of edible films based on Alaska pollack. *Food Chem.* **2004**, *86*, 493−499.

■ NOTE ADDED AFTER ASAP PUBLICATION

The authorship has been changed in the version of this paper published on August 20, 2013. The corrected version published August 28, 2013.

EXPERIMENTAL SECTION

Materials. SPSR and AN were acquired from Henan Shizhong Shuye Ltd. (Henan, China) and Tianjin Fu Chen Chemical Reagents (Tianjin, China), respectively. Methanol, hydroxylamine hydrochloride, VC, and DMF were obtained from Tianjin Chemical Reagents (Tianjin, China). HMTA, bromoacetyl bromide, dimethylacetamide (DMAc), pyridine, LiCl, and La(0) powder were purchased from Aladdin Chemistry.

Methods. Infrared spectra (IR) were collected on a Perkin-Elmer Spectrum 2000 FTIR. The surface morphologies were studied using a scanning electron microscope, JSF5600LV, JEOL, Japan.

Preparation of AO BSPS-*g*-PAN. SPSR was bromoactylated using the method described in the literature[33] to prepare the bromoactylated sweet potato starch (BSPS). SI-SET-LRP of AN on the modified BSPS surface was achieved in DMF in the presence of VC with La(0) powder as catalyst and HMTA as ligand. The graft polymer BSPS-*g*-PAN was obtained. The modified resin (AO BSPS-*g*-PAN) was prepared by the reaction of BSPS-*g*-PAN with hydroxylamine hydrochloride ($NH_2OH{\cdot}HCl$).

Adsorption Characteristics of AO BSPS-*g*-PAN for Hg(II). The concentration of Hg(II) was determined by atomic adsorption spectroscopy. AO BSPS-*g*-PAN adsorbent was added to a buffered Hg(II) solution of certain pH to discuss adsorption behavior. Adsorption efficiency under situations mimicking real conditions was studied with the initial concentration of Hg(II) at 1.7×10^{-5} mol·L^{-1}, which was close to the levels found in industrial wastewater samples.[34]

RESULTS AND DISCUSSION

Surface-Initiated SET-LRP on the Bromoactylated Sweet Potato Starch Surface. Polymerization of AN via SI-SET-LRP initiated by BSPS was carried out in DMF with La(0) powder as the catalyst in the presence of VC at 65 °C (Scheme 1). The novel catalyst system based on La(0)/HMTA

Scheme 1. Modification of BSPS Macroinitiator and Polymerization of AN on BSPS Surface by SI-SET-LRP

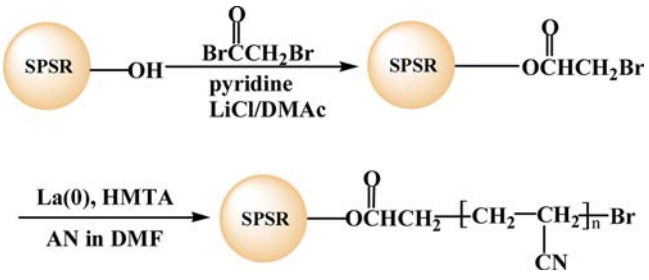

had been developed by our laboratory, and proven to be superior to the traditional catalyst system.[35] In addition, we had also reported that the addition of a small amount of VC to the reaction mixture significantly increased the reaction rate and the controllability of the polymer.[36] The monomer conversion (C%) increased reaching about 23% within 24 h. Figure 1 shows kinetic plots of $\ln([M]_0/[M])$ versus reaction time. The apparent rate constant for SET-LRP of AN was calculated to be 2.9×10^{-6} s^{-1}. The linearity of the plot indicated that the polymerization was approximately first-order with respect to the monomer concentration.

Characterization. Figure 2 shows the infrared spectra of the (a) SPSR, (b) macroinitiator, (c) BSPS-*g*-PAN, and (d) AO BSPS-*g*-PAN. As shown in Figure 2c, the spectrum of the modified resins exhibits two absorption peaks at 1636 and 920 cm^{-1}, corresponding to the stretching vibrations of C−N and N−O bonds of AO groups, respectively. In Figure 2d, the band at 2244 cm^{-1} related to the CN group is absent. Compared

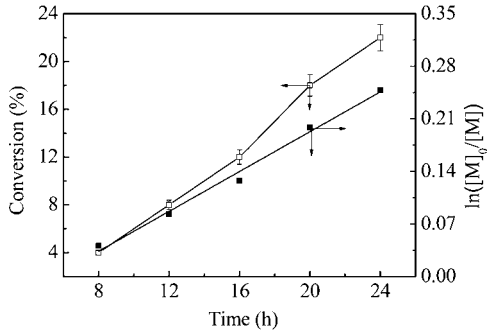

Figure 1. First-order kinetic plots for the SI-SET-LRP of AN.

with SPSR (Figure 2a), the FT-IR spectrum of BSPS (Figure 2b) shows a very sharp absorption band at 1749 cm^{-1} attributable to the carbonyl groups after esterification. A sharp peak at 2244 cm^{-1}, corresponding to the stretching of the CN bond, is present in Figure 2c but absent in Figure 2b. This indicates that PAN has been grafted onto BSPS using SET-LRP.

The SEM images of (a) SPS, (b) macroinitiator, (c) BSPS-*g*-PAN, and (d) AO BSPS-*g*-PAN are shown in Figure 3. Significant changes in morphology can be seen from PAN-*g*-BSPS (Figure 3c) to AO BSPS-*g*-PAN (Figure 3d), indicating successful modification. Moreover, the surface of BSPS changed significantly after the esterification reaction, which demonstrated the success of the grafting reaction. Compared with the macroinitiator, the surface of BSPS-*g*-PAN is rougher, confirming that organic moieties were anchored successfully on the surface. All these results indicated that PAN adsorbent was successfully prepared.

Adsorption Properties. *Effect of pH on Adsorption.* Figure 4 shows the effect of pH on the adsorption of Hg(II) by AO BSPS-*g*-PAN. With increasing pH of the adsorption medium, the uptake value increased and then decreased. When the pH was at 4.0, the uptake value reached a maximum of 4.03 mmol·g^{-1}. This maximum Hg(II) adsorption capacity value is higher than that for sulfur-containing Hg(II)-imprinted thiol-functionalized mesoporous sorbent (0.39 mmol·g^{-1})[37] and that for silica gel supported amidoxime adsorbents (1.28 mmol·g^{-1}).[38] The decrease of the uptake in the acidic media may be attributed to the protonation of nitrogen, hindering the complex formation. When the pH reached about 5 or higher, this condition is often not optimal. It was doubtful to attribute this decrease to the formation of metal hydroxide species.[39]

Adsorption Kinetics. As shown in Figure 5, the kinetic curves at four different temperatures follow an ascending trend with time, especially at the beginning. Then the increase becomes gentle and finally reaches equilibrium at around 4 h. In the temperature range from 15 to 45 °C, higher temperature corresponds to higher adsorption. This suggests that the adsorption was an endothermic process.

Adsorption Efficiency under Situations Mimicking Real Conditions. As shown in Figure 6, the adsorption of Hg(II) per unit weight of adsorbent decreases with increasing adsorbent load. When the amount of adsorbent reached 0.10 g, the percent adsorption maximized at approximately 100%.

The pseudo-first- and -second-order models were used to describe the adsorption process of Hg(II) on AO BSPS-*g*-PAN, as expressed in eq 1 and eq 2.

dx.doi.org/10.1021/jf4048397 | J. Agric. Food Chem. 2014, 62, 1765−1770

Figure 2. FTIR spectra of (a) SPS, (b) BSPS, (c) BSPS-*g*-PAN, and (d) AO BSPS-*g*-PAN.

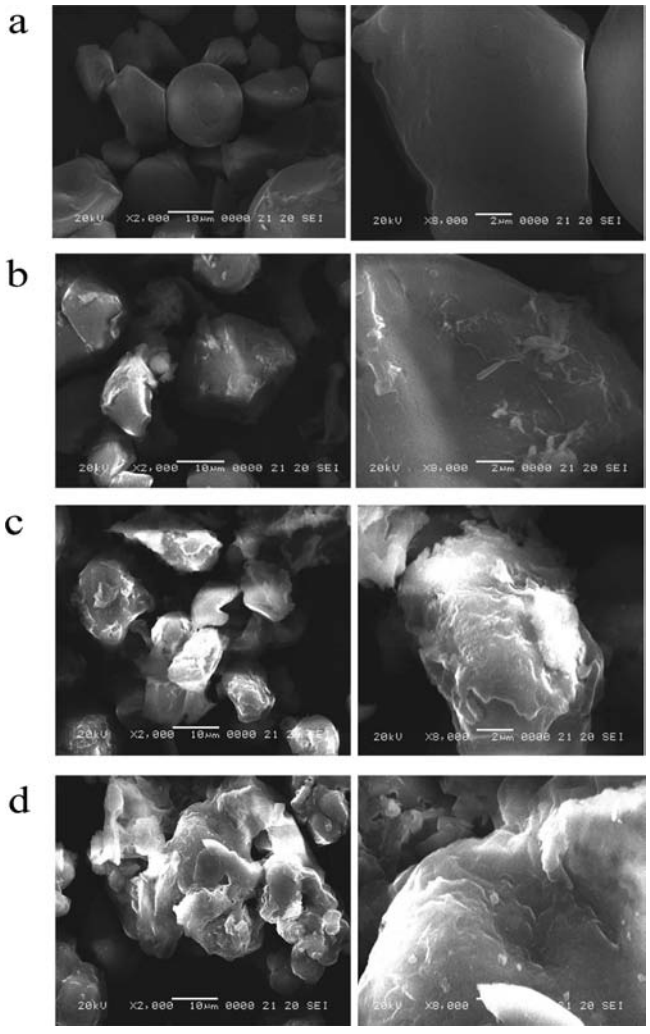

Figure 3. SEM photographs of (a) SPS, (b) BSPS, (C) BSPS-*g*-PAN, and (d) AO BSPS-*g*-PAN.

$$\ln \frac{(q_e - q_t)}{q_e} = - k_1 t \quad (1)$$

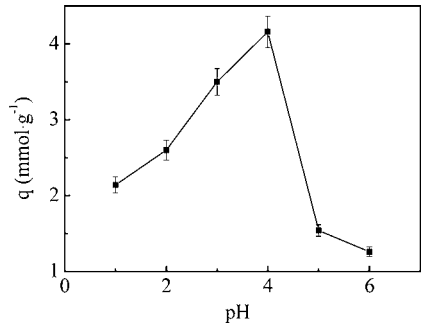

Figure 4. Effect of pH on the adsorption of AO BSPS-*g*-PAN for Hg(II).

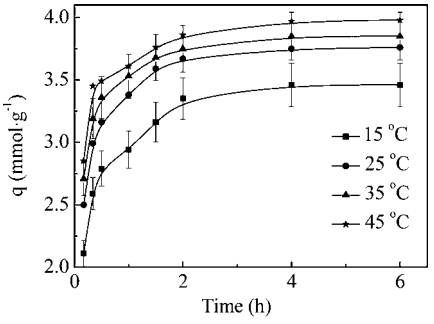

Figure 5. Adsorption kinetics of Hg(II) on AO BSPS-*g*-PAN.

$$\frac{t}{q_t} = \frac{1}{k_2 q_e^{\,2}} + \frac{t}{q_e} \quad (2)$$

where k_1 and k_2 are the pseudo-first-order and the pseudo-second-order rate constants (min^{-1}), respectively; q_e and q_t ($mmol \cdot g^{-1}$) are the amounts of Hg(II) adsorbed at equilibrium and time t (min), respectively. The value of $\ln(q_e - q_t)$ was calculated from the experimental results and plotted against t (min). The slope and intercept of the linear plot t/q_t versus t yielded the values of q_e and k_2.

The pseudo-first-order kinetic plots and pseudo-second-order kinetic plots for the adsorption of Hg(II) onto AO PAN-*g*-BSPS are shown in Figures 7 and 8, respectively, and the fitting results are summarized in Table 1. Results suggest that

dx.doi.org/10.1021/jf4048397 | J. Agric. Food Chem. 2014, 62, 1765−1770

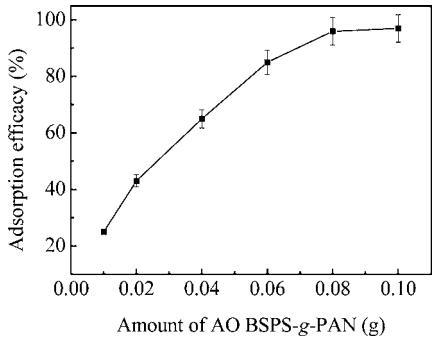

Figure 6. Effect of the amount of adsorbent on percent adsorption of Hg(II) ions.

the pseudo-second-order model was more suitable to describe the adsorption process.

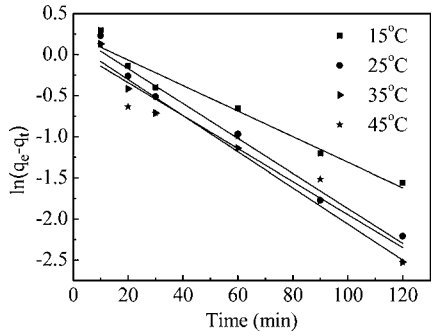

Figure 7. Pseudo-first-order kinetic plots for the adsorption of Hg(II) onto AO BSPS-*g*-PAN.

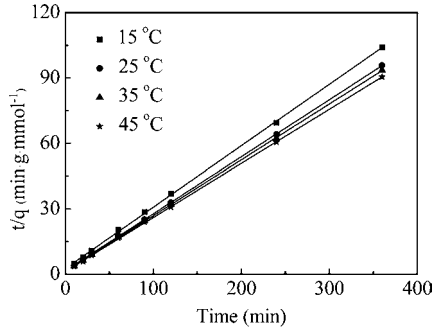

Figure 8. Pseudo-second-order kinetic plots for the adsorption of Hg(II) onto AO BSPS-*g*-PAN.

Adsorption isotherms. The adsorption experimental data were analyzed by Langmuir model (eq 3) and Freundlich model (eq 4), respectively.

$$\frac{Ce}{q_e} = \frac{Ce}{q_0} + \frac{1}{q_0 K_L} \quad (3)$$

$$\ln q_e = \ln K_F + \frac{1}{n} \ln Ce \quad (4)$$

where q_e is the adsorption capacity, mmol·g^{-1}; Ce is the equilibrium concentration of Hg(II), mol·cm^{-3}; q_0 is the adsorption capacity, mmol·g^{-1}; K_L is an empirical parameter; K_F is the binding energy constant reflecting the affinity of the adsorbents to Hg(II); and n is the Freundlich exponent related to adsorption intensity.

The adsorption isotherms of AO BSPS-*g*-PAN for Hg(II) in the temperature range from 15 to 45 °C are presented in Figure 9. The figures and parameters of the Langmuir and Freundlich

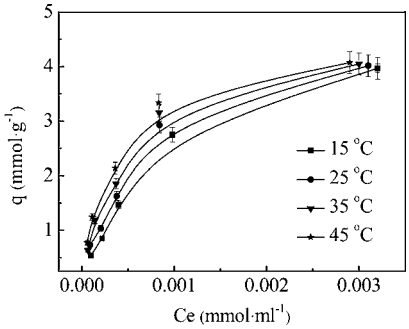

Figure 9. Adsorption isotherms of AO BSPS-*g*-PAN beads for Hg(II).

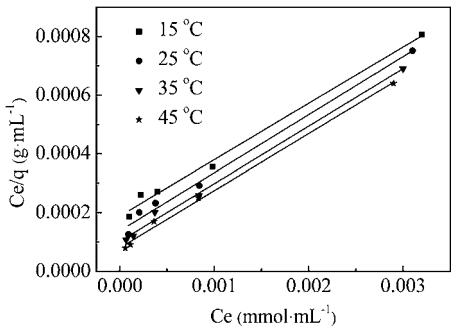

Figure 10. Langmuir isotherms of Hg(II) adsorbed on AO BSPS-*g*-PAN at different temperatures.

models are shown in Figure 10, Figure 11, and Table 2. The Langmuir model fits the experimental results better than Freundlich model as the values of R_L^2 are higher than those of R_F^2. The uptake of metal ions is applicable to homogeneous adsorption, where each molecule of adsorbate on the surface has equal adsorption activation energy. Thus, the adsorptions of

Table 1. Kinetic Parameters for Hg(II) Adsorption onto AO BSPS-*g*-PAN at Different Temperatures

		pseudo-first-order kinetics			pseudo-second-order kinetics		
T (°C)	q_e(exp) (mmol·g^{-1})	k_1 (min^{-1})	q_e(cal) (mmol·g^{-1})	R_1^2	k_2 (g·mmol^{-1}·min^{-1})	q_e(cal) (mmol·g^{-1})	R_2^2
15	3.46	0.0156	1.27	0.9527	0.031	3.55	0.9996
25	3.76	0.0213	1.28	0.9757	0.043	3.83	0.9999
35	3.85	0.0220	1.15	0.9723	0.052	3.91	0.9999
45	3.98	0.0201	1.06	0.9099	0.051	4.04	0.9999

dx.doi.org/10.1021/jf4048397 | J. Agric. Food Chem. 2014, 62, 1765−1770

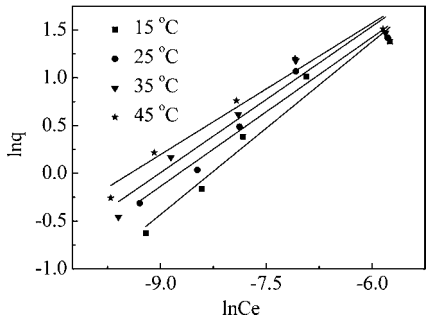

Figure 11. Freundlich isotherms of Hg(II) adsorbed on AO BSPS-*g*-PAN at different temperatures.

Table 2. Langmuir and Freundlich Constants for Hg(II) Adsorption on AO BSPS-*g*-PAN at Different Temperatures

	Langmuir params			Freundlich params		
T (°C)	q_0(mmol·g^{-1})	K_L	R_L^2	K_F	$1/n$	R_F^2
15	5.21	1019	0.9902	147	0.6028	0.9582
25	4.87	1526	0.9897	88	0.5128	0.9484
35	4.68	2218	0.9952	85	0.4929	0.9254
45	4.53	3077	0.9979	61	0.4348	0.9346

Hg(II) on AO BSPS-*g*-PAN follow the mechanism of monolayer adsorption.

Adsorption Selectivity. A series of representative binary metal ions of Hg(II)−Ag(I), Hg(II)−Pb(II), and Hg(II)−Ni(II) systems were chosen to investigate the adsorption selectivity of AO PAN-*g*-BSPS for Hg(II), and the results are shown in Table 3. As shown in Table 3, Hg(II) can be readily

Table 3. The Adsorption Selectivity of AO BSPS-*g*-PAN for Hg(II) in Binary Ions Systems at 25 °C

system	metal ion	adsorption capacity (mmol·g^{-1})
Hg(II)−Ag(I)	Hg(II)	4.02
	Ag(I)	0.41
Hg(II)−Pb(II)	Hg(II)	4.07
	Pb(II)	0.45
Hg(II)−Ni(II)	Hg(II)	3.99
	Ni(II)	0.36

adsorbed by AO BSPS-*g*-PAN in the binary systems of Hg(II)−Ag(I), Hg(II)−Pb(II), and Hg(II)−Ni(II). The percent adsorptions for Hg(II) are more than 98%, indicating that AO BSPS-*g*-PAN exhibited good selectivity for Hg(II).

AUTHOR INFORMATION

Corresponding Author

*Tel: +86 535 6697933. Fax: +86 535 6696162. E-mail: lduchenhou@hotmail.com.

Funding

The authors are grateful for the financial support by the National Natural Scientific Foundation of China (No. 20904018), the Program for New Century Excellent Talents in University (No. NCET-11-1028), the Natural Science Foundation for Distinguished Young Scholars of Shandong province (No. JQ201203), the Shandong Provincial Natural Science Foundation of China (No. ZR2010BQ007), and the Program for Scientific Research Innovation Team in Colleges and universities of Shandong Province.

Notes

The authors declare no competing financial interest.

REFERENCES

(1) Abegunde, O. K.; Mu, T. H.; Chen, J. W.; Deng, F. M. Physicochemical characterization of sweet potato starches popularly used in Chinese starch industry. *Food Hydrocolloids* **2013**, *33*, 169−177.

(2) Sun, M. J.; Mu, T. H.; Zhang, M.; Arogundade, L. A. Nutritional assessment and effects of heat processing on digestibility of Chinese sweet potato protein. *J. Food Compos. Anal.* **2012**, *26*, 104−110.

(3) Zhang, Y. Y.; Mu, T. H.; Zhang, M. Optimisation of acid extraction of pectin from sweet potato residues by response surface methodology and its antiproliferation effect on cancer cells. *Int. J. Food Sci. Technol.* **2013**, *48*, 778−785.

(4) Meng, T.; Gao, X.; Zhang, J.; Yuan, J. Y.; Zhang, Z. J.; He, S. Graft copolymers prepared by atom transfer radical polymerization (ATRP) from cellulose. *Polymer* **2009**, *50*, 447−454.

(5) Bruzzano, S.; Sieverling, N.; Wieland, C.; Jaeger, W. Cationic polymer grafted starch from nonsymmetrically substituted macro-initiators. *Macromolecules* **2005**, *38*, 7251−7261.

(6) Bruyn, H. D.; Sprong, E.; Gaborieau, M.; David, G.; Roper, J. A.; Gilbert, R. G. Starch-graft- copolymer latexes initiated and stabilized by ozonolyzed amylopectin. *J. Polym. Sci., Polym. Chem.* **2006**, *44*, 5832−5845.

(7) Aziz, N. H; Mohsen, G. I. Bioconversion of acid- and gamma-ray-treated sweet potato residue to microbial protein by mixed cultures. *J. Microbiol. Biotechnol.* **2002**, *29*, 264−267.

(8) Wani, D. A.; Sogi, D. S.; Gill, B. S. Physicochemical properties of acetylated starches from some Indian kidney bean (Phaseolus vulgaris L.) cultivars. *Int. J. Food Sci. Technol.* **2012**, *47*, 1993−1999.

(9) Kim, Y. N.; Min Park, K.; Jun Choi, S. Optimizing conditions for TEMPO/NaOCl-mediated chemoselective oxidation of primary alcohols in sweet potato residue Pahn-Shick chang. *Food Bioprocess Technol.* **2013**, *6*, 690−698.

(10) Suwanmala, P.; Hemvichian, K.; Hoshina, H.; Srinuttrakul, W.; Seko, N. Preparation of metal adsorbent from poly(methyl acrylate)-grafted-cassava starch via gamma irradiation. *Radiat. Phys. Chem.* **2012**, *81*, 982−985.

(11) Guo, L.; Li, G. Y.; Liu, J. S.; Meng, Y. F.; Tang, Y. F. Adsorptive decolorization of methylene blue by crosslinked porous starch. *Carbohydr. Polym.* **2013**, *93*, 374−379.

(12) Qin, H.; Zhou, S.; Zhang, Y. Z. Characterization and expression analysis of starch branching enzymes in sweet potato. *J. Integr. Agric.* **2013**, *12*, 1530−1539.

(13) Zhang, P.; Chen, C. F.; Shen, Y. H.; Ding, T. L.; Ma, D. F.; Hua, Z. C.; Sun, D. X. Starch saccharification and fermentation of uncooked sweet potato roots for fuel ethanol production. *Bioresour. Technol.* **2013**, *128*, 835−838.

(14) Lian, X. J.; Li, L.; Zhang, K. S.; Xu, Y.; Lu, J. X. A new proposed sweet potato starch granule structure-pomegranate concept. *Int. J. Biol. Macromol.* **2012**, *50*, 471−475.

(15) Deligöz, H.; Erdem, E. Comparative studies on the solvent extraction of transition metal cations by calixarene, phenol and ester derivatives. *J. Hazard. Mater.* **2008**, *154*, 29−32.

(16) Ruparelia, J. P.; Duttagupta, S. P.; Chatterjee, A. K.; Mukherji, S. Potential of carbon nanomaterials for removal ofheavymetals from-water. *Desalination* **2008**, *232*, 145−156.

(17) Sonmez, H. B.; Senkala, B. F.; Sherringtonb, D. C.; Bicaka, N. Atom transfer radical graft polymerization of acrylamide from N-chlorosulfonamidated polystyrene resin, and use of the resin in selective mercury removal. *React. Funct. Polym.* **2003**, *55*, 1−8.

(18) Kawai, T.; Saito, K.; Sugita, K. Comparison of amidoxime adsorbents prepared by cografting methacrylic acid and 2-hydroxyethyl methacrylate with acrylonitrile onto polyethylene. *Ind. Eng. Chem. Res.* **2000**, *39*, 2910−2915.

(19) Peng, F. M. *Encyclopedia of polymer science and engineering*; Wiley: New York, 1985; p 426.

(20) Percec, V.; Guliashvili, T. J.; Ladislaw, S.; Wistrand, A.; Stjerndahl, A.; Sienkowska, M. J.; Monteiro, M. J.; Sahoo, S. Ultrafast synthesis of ultrahigh molar mass polymers by metal-catalyzed living radical polymerization of acrylates, methacrylates, and vinyl chloride mediated by set at 25°C. *J. Am. Chem. Soc.* **2006**, *128*, 14156−14165.
(21) Percec, V.; Aopov, A. V.; Ramirez-Castillo, E.; Monteiro, M.; Weichold, O.; Mitchell, C. M. Aqueous room temperature metal-catalyzed living radical polymerization of vinyl chloride. *J. Am. Chem. Soc.* **2002**, *124*, 4940−4941.
(22) Nguyen, N. H.; Sun, H. J.; Levere, M. E.; Fleischmann, S.; Percec, V. Where is Cu(0) generated by disproportionation during SET-LRP? *Polym. Chem.* **2013**, *4*, 1328−1332.
(23) Nguyen, N. H.; Percec, V. SET-LRP of methyl acrylate catalyzed with activated Cu(0) wire in methanol in the presence of air. *J. Polym. Sci., Polym. Chem.* **2011**, *49*, 4756−4765.
(24) Rosen, B. M.; Jiang, X.; Wilson, C. J.; Nguyen, N.; Monteiro, M. J.; Percec, V. The disproportionation of Cu(I)/X mediated by ligand and solvent into Cu(0) and Cu(II)/X_2 and its implications for SET-LRP. *J. Polym. Sci., Polym. Chem.* **2009**, *47*, 5606−5628.
(25) Isse, A. A.; Gennaro, A.; Hodgson, J. L.; Coote, M. L.; Guliashvili, T. Mechanism of carbon-halogen bond reductive cleavage in activated alkyl halide initiators relevant to living radical polymerization: theoretical and experimental study. *J. Am. Chem. Soc.* **2011**, *133*, 6254−6264.
(26) Lligadas, G.; Rosen, B. M.; Monteiro, M. J.; Percec, V. Solvent choice differentiates SET-LRP and Cu-mediated radical polymerization with non-first-order kinetics. *Macromolecules* **2008**, *41*, 8360−8364.
(27) Levere, M. E.; Nguyen, N. H.; Percec, V. No reduction of $CuBr_2$ during Cu (0)-catalyzed living radical polymerization of methyl acrylate in DMSO at 25 °C. *Macromolecules* **2012**, *45*, 8267−8274.
(28) Fleischmann, S.; Rosen, B. M.; Percec, V. SET-LRP of acrylates in air. *J. Polym. Sci., Polym. Chem.* **2010**, *48*, 1190−1196.
(29) Nguyen, N. H.; Levere, M. E. R.; Kulis, J.; Monteiro, M. J.; Percec, V. Where is Cu(0) generated by disproportionation during SET-LRP. *Macromolecules* **2012**, *45*, 4606−4622.
(30) Nguyen, N. H.; Rosen, B. M.; Jiang, X.; Fleischmann, S.; Percec, V. New efficient reaction media for SET-LRP produced from binary mixtures of organic solvents and H_2O. *J. Polym. Sci., Polym. Chem.* **2009**, *47*, 5577−5590.
(31) Nguyen, N. H.; Levere, M. E.; Percec, V. SET-LRP of methyl acrylate to complete conversion with zero termination. *J. Polym. Sci., Polym. Chem.* **2012**, *50*, 860−873.
(32) Levere, M. E.; Nguyen, N. H.; Leng, X. F.; Percec, V. Visualization of the crucial step in SET-LRP. *Polym. Chem.* **2013**, *4*, 1635−1647.
(33) Moghaddam, P. N.; Fareghi, A. R.; Entezami, A. A.; Mehr, M. A. G. Synthesis of biodegradable thermoplastic copolymers based on starch by atom transfer radical polymerization (ATRP): Monolayer chain growth on starch. *Starch* **2013**, *65*, 210−218.
(34) Sreedhar, M. K.; Anirudhan, T. S. Preparation of an adsorbent by graft polymerization of acrylamide onto coconut husk for mercury(II) removal from aqueous solution and chloralkali industry wastewater. *J. Appl. Polym. Sci.* **2000**, *75*, 1261−1269.
(35) Zhang, J.; Hao, Z. H.; Chen, H. Single electron transfer-living radical polymerization of acrylonitrile catalyzed by lanthanum powder. *J. Polym. Sci., Polym. Chem.* **2013**, *51*, 3323−3327.
(36) Hao, Z. H.; Zhang, J.; Chen, H.; Liu, D. L.; Wang, D. J.; Qu, H. Y.; Lang, J. M. Preparation of polyacrylonitrile via SET-LRP catalyzed by lanthanum powder in the presence of VC. *J. Polym. Sci., Polym. Chem.* **2013**, *51*, 4088−4094.
(37) Fan, Z. F. Hg(II)-imprinted thiol-functionalized mesoporous sorbent micro-column preconcentration of trace mercury and determination by inductively coupled plasma optical emission spectrometry. *Talanta* **2006**, *70*, 1164−1169.
(38) Chen, J.; Qu, R. J.; Zhang, Y.; Sun, C. M.; Wang, C. H.; Ji, C. N.; Yin, P.; Chen, H.; Niu, Y. Z. Preparation of silica gel supported amidoxime adsorbents for selective adsorption of Hg(II) from aqueous solution. *Chem. Eng. J.* **2012**, *209*, 235−244.
(39) Zhang, Y.; Qu, R. J.; Sun, C. M.; Wang, C. H.; Ji, C. N.; Chen, H.; Yin, P. Chemical modification of silica-gel with diethylenetriamine via an end-group protection approach for adsorption to Hg(II). *Appl. Surf. Sci.* **2009**, *255*, 5818−5826.

Table 1. Sampling Sites and Characterization of the Soils Studied

soil site[a]	particle size			pH[b]	C_{org} (%)	CEC[c] (%)	TN[d](g/kg)	TP[e](g/kg)
	sand (%)	silt (%)	clay (%)					
Guizhou Guiyang	21.0	62.0	17.0	4.8	1.797	18.6	1.4	0.4
Guangxi Nanning	8.5	38.8	52.7	5.2	2.192	11.4	1.6	0.5
Anhui Hefei	6.8	37.9	55.3	7.8	3.809	18.2	2.1	0.6
Heilongjian Harbin	3.7	31.6	64.7	8.5	4.348	24.3	3.9	0.8

[a]Sites in China. [b]Suspension of soil in water, 1:2.5 (w/w). [c]Cation exchange capacity. [d]Total nitrogen. [e]Total phosphorus.

to be different depending on the plant species. *rac*-Glufosinate and L-glufosinate were metabolized in nontransgenic and transgenic plant cell cultures, whereas D-glufosinate was not metabolized. Furthermore, the absorption rate of D-glufosinate was substantially lower than that of *rac*- or L-glufosinate in sugar beet.[24,25] Thus, considering the effect of chiral pesticides on the environment, enantioselectivity is an important factor that should not be ignored.[26,27]

Some methods for the achiral analysis and residue determination of dufulin in various matrices have been reported. However, information related to the degradation of dufulin enantiomers is limited. To evaluate the enantioselective degradation of dufulin enantiomers in the environment, it is necessary to understand dufulin enantiomer degradation in different soils under agricultural cultivation. Therefore, we investigated the enantioselective degradation of *rac*-dufulin and its two enantiomers in four types of soil.

MATERIALS AND METHODS

Chemicals and Reagents. *rac*-Dufulin (purity > 99%) was synthesized in pure form. The products were unequivocally characterized by nuclear magnetic resonance spectral and elemental analyses. Enantiopure enantiomers of dufulin were prepared on an Agilent HPLC system with a semipreparative chiral column. The purity of both enantiomers was >99%. Water was purified using a Milli-Q system. All other chemicals and solvents were analytical reagents or of HPLC grade and were obtained from common commercial sources. The chiral analytical column amylose tris(3,5-dimethylphenylcarbamate) (Chiralpak IA, 4.6 mm × 250 mm i.d., 5 μm) was purchased from Daicel (Tokyo, Japan).

Electronic Circular Dichroism (ECD) Spectroscopy. ECD spectroscopy was carried out using a Jasco-J810 spectropolarimeter at room temperature. The spectra were obtained from 200 to 330 nm at a scan speed of 50 nm/min.

ECD Calculations. The optimized geometry of the two dufulin enantiomers was obtained by Gaussian 09 with density functional theory (DFT) at the B3LYP/6-31G* level. ECD calculations of the two enantiomers of dufulin were obtained by Gaussian 09 with time-dependent density functional theory (TDDFT) methods at the B3LYP/6-311++G (2d, 2p) level following reported protocols.[28,29]

Soil Samples. Four types of soil were collected using a 0−20 cm plow layer from geographically distinct agricultural regions of China. The level of dufulin in these soil samples was lower than the limit of detection (LOD). All samples were air-dried at room temperature, homogenized, passed through a 2 mm sieve, and stored in the dark for several days until use. More details on soil sites and specific physicochemical characteristics are presented in Table 1.

Incubation of Dufulin in Soils under Nonsterile Conditions. Separate incubation experiments with pure (better biological activity)[30] *S*-(+)-dufulin and *R*-(−)-dufulin and with racemic compounds in soils were conducted in 50 mL polypropylene centrifuge tubes covered with aluminum foil. Approximately 5.0 g of soil (dry weight equivalent) was fortified with 30 μg (50 μL of 600 μg/mL stock solution in acetone) of *S*-(+)- or *R*-(−)-dufulin or 60 μg of *rac*-dufulin (*S*:*R* = 1:1), and they were set to air-dry for 5 min before thorough homogenization. The soil samples were then rehydrated by adding 1.2 mL of purified water (about 60% of the field holding capacity (w/w)) and incubated at 25 °C in the dark. To compensate for water loss throughout the experiments, the samples were weighed regularly and purified water was added. Triplicate samples were removed from each treatment at different time intervals (0, 1, 3, 5, 7, 10, 14, 21, 28, 49, 63, and 91 days) and immediately transferred to a freezer (−40 °C).

Incubation of Dufulin in Soils under Sterile Conditions. To determine if enantioselective degradation was a result of microbe-mediated transformations, portions of 5.0 g of soil set in 50 mL polypropylene centrifuge tubes were subjected to sterilization treatment, which was achieved by autoclaving the samples twice at 121 °C for 40 min 24 h apart. On a clean bench, the sterilized samples were treated with 30 μg of *S*-(+)- or *R*-(−)-dufulin or 60 μg of *rac*-dufulin (*S*:*R* = 1:1), and sterile water was added. The samples were then covered with glass paper to maintain sterile conditions.

Extraction of Soil Samples. Samples were thawed at room temperature, and 10 mL of water was added to each polypropylene centrifuge tube containing 5.0 g of soil. To extract the dufulin residues, 25 mL of acetonitrile, 1.5 g of NaCl, and 6 g of anhydrous $MgSO_4$ were added to the samples. Then the tube was stirred on a vortex shaker for 3 min, ultrasonically extracted for 10 min, and centrifuged at 6000 rpm for 5 min. A portion of 20 mL of supernatant was transferred and concentrated using a rotary evaporator and a nitrogen blow-dry instrument. The residue was dissolved in 1.0 mL of methanol for analysis.

Chromatographic Measurements. Analytical HPLC was performed using an Agilent 1200 series apparatus consisting of a quaternary pump, an autosampler, a diode array detector, a vacuum degasser, a column oven, and Agilent Chemstation software. After filtration, 5 μL of the sample was injected into a Daicel Chiralpak IA column. The temperature of the column was adjusted to 25 °C. The flow rate of the mobile phase, *n*-hexane/ethanol (90:10 by volume), was 1 mL/min.

Method Validation. For this study, a series of dufulin standard working solutions (12−1200 μg/mL) were prepared for determining the linearity of the two enantiomers by HPLC analysis. Calibration curves were generated by plotting the peak area versus concentration for each enantiomer. Linear regression analysis was performed using Microsoft Excel 2010. The LODs and the limits of quantitation (LOQs) were defined as signal-to-noise (S/N) ratios of 3:1 and 10:1, respectively.

Precision and accuracy of the methods were evaluated by recovery studies using spiked samples at three concentration levels (0.6, 1.2, and 6.0 μg/g for each dufulin enantiomer based on five replicates). For method recovery studies, samples without residue (5.0 g) were spiked prior to extraction by the addition of appropriate volumes of the pesticide standard solution in acetone. The treated samples were analyzed following the described procedure, and the recoveries were calculated. The method precision was assessed by determining repeatability and reproducibility, and both were expressed as relative standard deviation (RSD). Repeatability (RSD_r) was measured by comparing the SD of the recovery percentage of spiked samples run on the same day. Reproducibility (RSD_R) was determined by analyzing spiked samples from three different days.

Kinetic Analysis and Calculation. For all treatment conditions, data were assumed to follow the first-order kinetics model. The corresponding rate constant *k* for (+)-enantiomer and (−)-enantiomer was calculated on the basis of eq 1 by regression analysis. The starting

point was the maximum value of the concentration, which declined in subsequent days. The half-life ($t_{1/2}$, days) was determined on the basis of eq 2:

$$C_t = C_0 \times e^{-kt} \quad (1)$$

$$t_{1/2} = \ln 2/k \quad (2)$$

C_t and C_0 refer to the concentration of the *S*-(+)- or *R*-(−)-enantiomer at time t and time 0, respectively.

The enantiomer fraction (EF) was used to express enantioselectivity as defined by the equation EF = peak area of the (+)-enantiomer/[(+)-enantiomer + (−)-enantiomer]. EF values ranged from 0 to 1, with an EF value of 0.5 indicating racemic mixture.[31,32]

RESULTS AND DISCUSSION

Optical Isomerism Characteristics of Dufulin. The individual enantiomers of dufulin were stereochemically analyzed by ECD spectroscopy, and almost mirror-image ECD curves were obtained. The overall curves of ECD obtained by TDDFT calculations (Figure 2a) and experimental

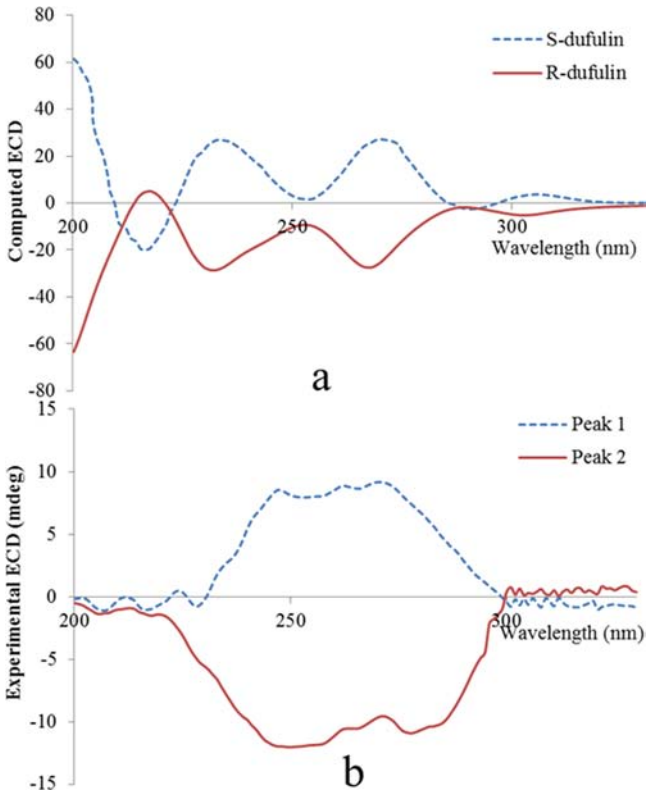

Figure 2. Calculation (a) and experimental measurement (b) of the ECD spectra of dufulin enantiomers in methanol (12 μg/mL).

ECD (Figure 2b) are similar. By comparison of the absolute configurations from computed ECD, the configurations of dufulin enantiomers eluted from the columns could be correctly assigned. As shown in Figure 2a, enantiomers with peaks 1 and 2 in Figure 2b are assigned to *S*-(+)-dufulin and *R*-(−)-dufulin, respectively.

Method Validation. Calibration curves were obtained over a concentration range of 12−1200 μg/mL (n = 7) for the *S*-(+)-enantiomer (y = 12.1432x + 12.8549, R^2 = 1.0000) and *R*-(−)-enantiomer (y = 12.0948x + 16.1483, R^2 = 0.9999) of *rac*-dufulin. The chromatogram of *rac*-dufulin in the standard solution is shown in Figure 3a. The precision data for *S*-(+)-

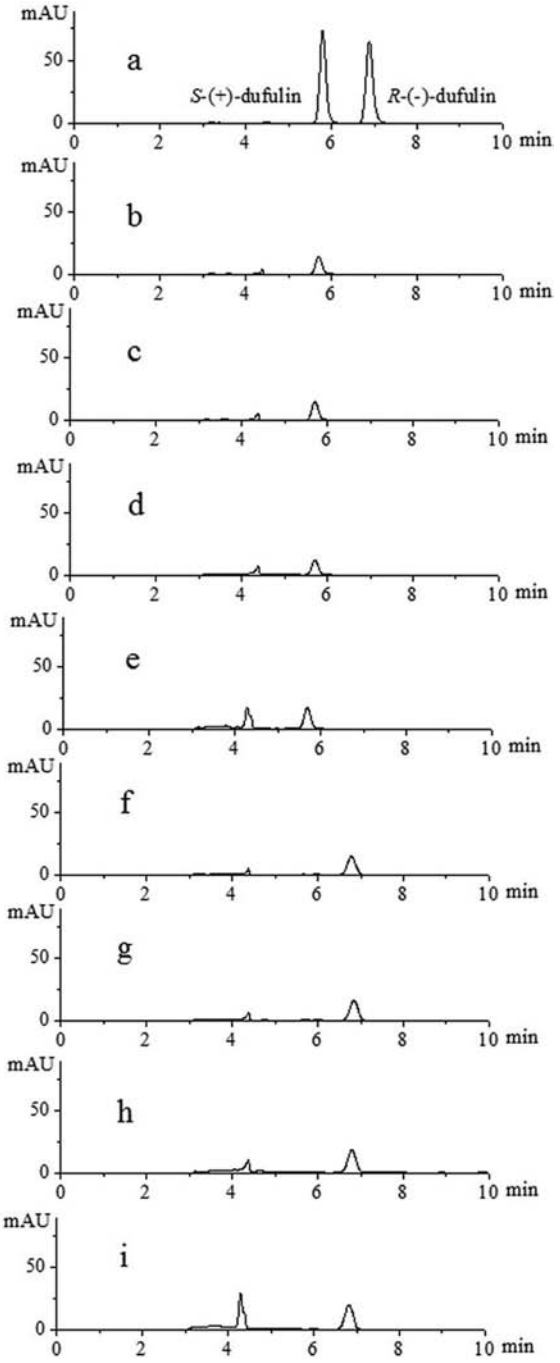

Figure 3. Chromatograms of the *S*-(+)- and *R*-(−)-dufulin enantiomers in the standard solution (a) and degradation experiments with the *S*-(+)-isomer for (b) Guiyang, (c) Nanning, (d) Hefei, and (e) Harbin soils and with *R*-(−)-isomer for (f) Guiyang, (g) Nanning, (h) Hefei, and (i) Harbin soils after 21 days of incubation under nonsterile condition.

and *R*-(−)-enantiomers of *rac*-dufulin are summarized in Table S1 in the Supporting Information. For both enantiomers, the recoveries obtained were in the acceptable range of 77.21−109.95%, whereas repeatability (RSD_r) ranged from 2.13 to 13.09% and reproducibility (RSD_R) ranged from 2.19 to 10.57% (Supporting Information Table S2). The LODs were 0.004 μg/g and the LOQs were 0.013 μg/g for both dufulin enantiomers.

dx.doi.org/10.1021/jf404130d | J. Agric. Food Chem. 2014, 62, 1771−1776

Degradation of Racemic Dufulin, Enantiopure *S*-(+)-Dufulin, and *R*-(−)-Dufulin in Four Soil Types under Sterile Conditions. No significant difference in enantioselectivity was found for *rac*-dufulin degradation in four soils under sterile conditions. The concentrations of the two enantiomers of dufulin in sterile soils were determined. The EF values of dufulin in four sterile soils were approximately 0.5 after treatment (Supporting Information Figure S2f). Degradation of each enantiomer in the four soil types generally fit a first-order kinetics decay model (Table 2). Data from experiments involving sterilized soils are plotted in Figure S2c,d in the Supporting Information. Half-life ($t_{1/2}$) values of dufulin in the four sterile soils (Guiyang, Nanning, Hefei, and Harbin) were about 77.9, 64.2, 63.3, and 56.2 days, respectively.

Table 2. Degradation Rate Constant (k), Half-Life ($t_{1/2}$), and Correlation Coefficient (R^2) Values for the Degradation of *rac*-Dufulin in Four Types of Soil

condition	incubated compound	dufulin enantiomer	k (day^{-1})	$t_{1/2}$ (days)	R^2
Guizhou Guiyang Soil					
nonsterile	*rac*-dufulin	*S*	0.0181	38.30	0.9987
		R	0.0182	38.09	0.9982
sterile	*rac*-dufulin	*S*	0.0087	79.67	0.9858
		R	0.0091	76.17	0.9892
Guangxi Nanning Soil					
nonsterile	*rac*-dufulin	*S*	0.0201	34.48	0.9965
		R	0.0204	33.98	0.9961
sterile	*rac*-dufulin	*S*	0.0108	64.18	0.9930
		R	0.0108	64.18	0.9933
Anhui Hefei Soil					
nonsterile	*rac*-dufulin	*S*	0.0213	32.54	0.9910
		R	0.0200	34.66	0.9884
sterile	*rac*-dufulin	*S*	0.0107	64.78	0.9920
		R	0.0112	61.89	0.9955
Heilongjiang Harbin Soil					
nonsterile	*rac*-dufulin	*S*	0.0259	26.76	0.9746
		R	0.0268	25.86	0.9724
sterile	*rac*-dufulin	*S*	0.0127	54.58	0.9950
		R	0.0120	57.76	0.9965

The degradation rates of enantiopure *S*-(+)-dufulin and *R*-(−)-dufulin were also similar (Supporting Information Figure S3c,d). No interversion between the two enantiomers was observed. Rate constants (k), half-lives ($t_{1/2}$), and correlation coefficients (R^2) were calculated (Table 3). Half-life ($t_{1/2}$) values in the four sterile soils (Guiyang, Nanning, Hefei, and Harbin) were about 82.52, 78.68, 60.27, and 50.97 days for *S*-(+)-dufulin and 83.51, 79.67, 59.24, and 51.73 days for *R*-(−)-dufulin, respectively.

Soil pH may play an important role in the degradation of various compounds in sterile soils.[33] Higher overall microbial activity in the soil with a high pH, high organic matter (OM), and high cation exchange capacity (CEC) was also the main reason for the fast degradation. Consistent with this theory we found that degradation $t_{1/2}$ of *rac*-dufulin in Harbin soil with the highest pH (8.5), OM (4.348%), and CEC (24.3%) was 56.2 days, which was shorter compared to those in Hefei, Nanning, and Guiyang soils (Table 2). Therefore, dufulin possibly degrades more efficiently in an alkaline soil with high CEC and high OM.

Table 3. Degradation Rate Constant (k), Half-Life ($t_{1/2}$), and Correlation Coefficient (R^2) Values for the Degradation of *S*-(+)- and *R*-(−)-Dufulin in Four Types of Soil

condition	incubated compound	k (day^{-1})	$t_{1/2}$ (days)	R^2
Guizhou Guiyang Soil				
nonsterile	*S*-(+)-dufulin	0.0245	28.29	0.9966
	R-(−)-dufulin	0.0120	57.76	0.9841
sterile	*S*-(+)-dufulin	0.0088	82.52	0.9974
	R-(−)-dufulin	0.0083	83.51	0.9976
Guangxi Nanning Soil				
nonsterile	*S*-(+)-dufulin	0.0263	26.36	0.9901
	R-(−)-dufulin	0.0136	50.97	0.9718
sterile	*S*-(+)-dufulin	0.0091	78.68	0.9972
	R-(−)-dufulin	0.0087	79.67	0.9967
Anhui Hefei Soil				
nonsterile	*S*-(+)-dufulin	0.0289	23.98	0.9987
	R-(−)-dufulin	0.0172	40.30	0.9938
sterile	*S*-(+)-dufulin	0.0115	60.27	0.9969
	R-(−)-dufulin	0.0117	59.24	0.9964
Heilongjiang Harbin Soil				
nonsterile	*S*-(+)-dufulin	0.0339	20.45	0.9935
	R-(−)-dufulin	0.0201	34.48	0.9954
sterile	*S*-(+)-dufulin	0.0164	50.97	0.9994
	R-(−)-dufulin	0.0134	51.73	0.9987

Degradation of Racemic Dufulin, Enantiopure *S*-(+)-Dufulin, and *R*-(−)-Dufulin in Four Soil Types under Nonsterile Conditions. The plots of concentration of *rac*-dufulin from nonsterile experiments versus incubation time (t) are shown in Figure S2a,b in the Supporting Information. The half-life ($t_{1/2}$) values of *S*-(+)-enantiomer were 38.30, 34.48, 32.54, and 26.76 days in Guiyang, Nanning, Hefei, and Harbin soils, respectively. The half-life ($t_{1/2}$) values of *R*-(−)-enantiomer were 38.09, 33.98, 34.66, and 25.86 days in Guiyang, Nanning, Hefei, and Harbin soils, respectively. Thus, degradation of dufulin was faster in Harbin soil, which had the highest organic carbon content and alkalinity, compared to the other three soils.

Our results revealed that degradation of dufulin under sterile conditions is much slower than under nonsterile conditions. In addition, besides abiotic degradation, dufulin degradation can also be attributed to microbial community activity in agricultural soils. Microorganisms in the soil may play important roles in the enantioselective metabolism of many chiral compounds. The enantioselective degradation behavior could be conducted by comparing the half-life ($t_{1/2}$) of each enantiomer. However, the half-life ($t_{1/2}$) of each enantiomer of dufulin was found to be approximately the same in the four soils from nonsterile conditions in our study. Moreover, EF values for *rac*-dufulin degradation in the four soils from nonsterile conditions were calculated to be approximately 0.5 after treatment (Supporting Information Figure S2e). This indicated that there was no significant enantioselectivity during degradation, which was the same as the degradation of *rac*-malathion in Nanchang soil,[20] but differed from other chiral pesticides.[21,32] Some studies suggested that soil properties such as texture, pH, and OM content could have major impacts on the activity of the soil microbial community and then could influence chiral signatures in soils.[12,20,21,34] Therefore, the activity of the microbial community might be distinguished in the four tested soils which had differing textures, pH values, and OM contents (Table 1). The degradation of *rac*-dufulin should

dx.doi.org/10.1021/jf404130d | J. Agric. Food Chem. 2014, 62, 1771−1776

be enantioselective in one or more soils, but the actual degradations of *rac*-dufulin in all tested soils were non-enantioselective. This result assumed that the microorganisms could not conduct the enantioselective degradation of *rac*-dufulin in soil. This phenomenon is possibly due to some interactions between the two enantiomers in *rac*-dufulin such as the mutual promotion effects, which led to the similar degradation rates of two dufulin enantiomers in soils.

During the degradation of enantiopure *S*-(+)- or *R*-(−)-enantiomer in nonsterile soils, no interconversion of *S*-(+)- to *R*-(−)-enantiomer or vice versa was detected. This indicated that the enantiomer was configurationally stable in these four soil types. The chromatograms of *S*-(+)-dufulin and *R*-(−)-dufulin after 21 days of incubation in the four soil types we tested are shown in Figure 3. We plotted data from the degradation of enantiopure *S*-(+)-dufulin and *R*-(−)-dufulin in four nonsterile soils (Supporting Information Figure S3a,b). Unlike the degradation study in sterile soils, the difference in degradation rate between enantiopure *S*-(+)-dufulin and *R*-(−)-dufulin was obvious. The half-life ($t_{1/2}$) values of *S*-(+)-dufulin and *R*-(−)-dufulin were 28.29 and 57.76 days, 26.36 and 50.97 days, 23.98 and 40.30 days, and 20.45 and 34.48 days in Guiyang, Nanning, Hefei, and Harbin soils, respectively (Table 3). Degradation rates for the enantiomers in the incubation with the single pure enantiomers were higher than in the incubations with the raceme; this phenomenon was consistent with the results reported by Zipper.[35] The degradation rate of *S*-(+)-dufulin incubations with single pure enantiomers was approximately 1.68−2.04 times higher than that of its antipode in the four types of soils tested. This result was also consistent with the results reported by Sun that enantiopure *R*-malathion degraded more rapidly than enantiopure *S*-malathion in Nanchang soil.[20] However, no enantiomerization was observed. These results differed from the degradation study of enantiopure malathion that converted between *R*-(+)-malathion and *S*-(−)-malathion in different soils.[20] No interaction between enantiomers existed during the degradation process of enantiopure dufulin in soil. This suggests that the microbial community in agricultural soils may decompose enantiopure *S*-(+)-dufulin more efficiently than *R*-(−)-dufulin, but not lead to the enantiomerization of the two dufulin enantiomers.

In conclusion, we investigated the enantioselective degradation of *rac*-dufulin and its two enantiopure enantiomers in four types of soil. We initially determined the absolute configuration of dufulin enantiomers on the basis of a combination of calculated and experimental ECD spectra. We found no significant enantioselectivity in the degradation of *rac*-dufulin in the four soil types tested under sterile and nonsterile conditions. However, enantiopure *S*-(+)-dufulin degraded much more quickly than its antipode *R*-(−)-dufulin in all nonsterile soils, which suggests that microorganisms degrade enantiopure *S*-(+)-dufulin more efficiently than they do *R*-(−)-dufulin.

Future studies should aim to identify the primary metabolites and metabolic processes of dufulin in soil and water to adequately assess the environmental risk associated with dufulin use.

■ ASSOCIATED CONTENT

Supporting Information

Figures of calibration curves of two enantiomers of *rac*-dufulin (Figure S1), figures of concentration−time curves *rac*-dufulin, *S*-(+)-dufulin and *R*-(−)-dufulin in nonsterile soils and sterile soils (Figures S2 and S3), tables of precision, accuracy, and recovery data for the determination of dufulin on three different days (Tables S1 and S2). This material is available free of charge via the Internet at http://pubs.acs.org.

■ AUTHOR INFORMATION

Corresponding Author

*(B.-A.S.) Phone: +86(851)362-0521. Fax: +86(851)362-2211. E-mail: songbaoan22@yahoo.com.

Funding

We gratefully acknowledge financial support from the National Key Program for Basic Research (no. 2010CB126105), the Key Technologies R&D Program (no. 2011BAE06B05-6), and the National Natural Science Foundation of China (no. 21132003).

Notes

The authors declare no competing financial interest.

■ REFERENCES

(1) Lintunen, T.; Yli-Kauhaluoma, J. T. Synthesis of aminophosphonate haptens for an aminoacylation reaction between methyl glucoside and a β-alanyl ester. *Bioorg. Med. Chem. Lett.* **2000**, *10*, 1749−1750.

(2) Boukallaba, K.; Elachqar, A.; El Hallaoui, A.; Alami, A.; Elhajji, S.; Labriti, B.; Martinez, J.; Rolland, V. Synthesis of new α-heterocyclic-α-aminophosphonates. *Phosphorus Sulfur* **2006**, *181*, 819−823.

(3) Shi, D. Q.; Chen, R. Y. Synthesis and biological activities of abscisic amide derivatives containing α-aminophosphonate. *Chin. J. Appl. Chem.* **2002**, *19*, 780−782.

(4) Jin, L. H.; Song, B. A.; Zhang, G. P.; Xu, R. Q.; Zhang, S. M.; Gao, X. W.; Hu, D. Y.; Yang, S. Synthesis, X-ray crystallographic analysis, and antitumor activity of *N*-(benzothiazole-2-yl)-1-(fluorophenyl)-*O*,*O*-dialkyl-α-aminophosphonates. *Bioorg. Med. Chem. Lett.* **2006**, *16*, 1537−1543.

(5) Zhang, G. P.; Song, B. A.; Xue, W.; Jin, L. H.; Hu, D. Y.; Wan, Q. Q.; Lu, P.; Yang, S.; Li, Q. Z.; Liu, G. Synthesis and biological activities of novel dialkyl 1-(4-trifluoro methylphenylamino)-1-(4-trifluoromethyl or 3-fluorophenyl)methylphosphonate. *J. Fluorine Chem.* **2006**, *127*, 48−53.

(6) Hu, D. Y.; Wan, Q. Q.; Yang, S.; Song, B. A.; Bhadury, P. S.; Jin, L. H.; Yan, K.; Liu, F.; Chen, Z.; Xue, W. Synthesis and antiviral activities of amide detivatives containing the α-aminophosphonates moiety. *J. Agric. Food Chem.* **2008**, *56*, 998−1001.

(7) Song, B. A.; Zhang, G. P.; Yang, S.; Hu, D. Y.; Jin, L. H. Synthesis of *N*-(4-bromo-2-trifluoromethylphenyl)-1-(2-fluorophenyl)-*O*,*O*-dialkyl-α-aminophosphonates under ultrasonic irradiation. *Ultrason. Sonochem.* **2006**, *2*, 139−142.

(8) Song, B. A.; Wu, Y. L.; Huang, R. M. Synthesis of plant virucidal fluorine contain α-aminophosphonates. CN 1432573, 2003, Patent approval certificate ZL02113252.6; *Chem Abstr.* **2005**, *142*, 482148.

(9) Song, B. A.; Zhang, G. P.; Hu, D. Y.; Pang, L.; Yang, S.; Liu, G.; Wang, H. N-substituted benzothiazolyl-1-substitutedphenyl-O, O-dialkyl-alpha- aminophosphonate ester derivatives preparation and application. CN 1687088, 2005, Patent approval certificate ZL0200510003041.7; *Chem Abstr.* **2006**, *145*, 145879.

(10) Hu, D. Y.; Wan, Q. Q.; Yang, S.; Song, B. A.; Bhadury, P. S.; Jin, L. H.; Yan, K.; Liu, F.; Chen, Z.; Xue, W. Synthesis and antiviral activity of amide derivatives containing the α-aminophosponate moiety. *J. Agric. Food Chem.* **2008**, *56*, 998−1001.

(11) Garrison, A. W. Probing the enantioselectivity of chiral pesticides. *Environ. Sci. Technol.* **2006**, *40*, 16−23.

(12) Jarman, J. L.; Jones, W. J.; Howell, L. A.; Garrison, A. W. Application of capillary electrophoresis to study the enantioselective transformation of five chiral pesticides in aerobic soil slurries. *J. Agric. Food Chem.* **2005**, *53*, 6175−6182.

(13) Li, Z. Y.; Zhang, Z. C.; Zhou, Q. L.; Wang, Q. M.; Gao, R. Y.; Wang, Q. S. Stereo- and enantioselective determination of pesticides in

soil by using achiral and chiral liquid chromatography in combination with matrix solid-phase dispersion. *J. AOAC Int.* **2003**, *86*, 521−528.
(14) Pantelelis, I.; Karpouzas, D. G.; Menkissoglu-Spiroudi, U.; Tsiropoulos, N. Influence of soil physicochemical and biological properties on the degradation and adsorption of the nematicide fosthiazate. *J. Agric. Food. Chem.* **2006**, *54*, 6783−6789.
(15) Kurihara, N.; Miyamoto, J.; Paulson, G. D.; Zeeh, B.; Skidmore, M. W.; Hollingworth, R. M.; Kuiper, H. A. Chirality in synthetic agrochemicals: bioactivity and safety consideration. *Pure Appl. Chem.* **1997**, *69*, 1335−1348.
(16) Lewis, D. L.; Garrison, A. W.; Wimmack, K. E.; Whittemore, A.; Sreudler, P.; Melillo, J. Influence of environmental changes on degradation of chiral pollutants in soils. *Nature* **1999**, *401*, 898−901.
(17) Liu, W. P.; Gan, J. Y.; Schlenk, D.; Jury, W. A. Enantioselectivity in environmental safety of current chiral insecticides. *Proc. Natl. Acad. Sci. U.S.A.* **2005**, *102*, 701−706.
(18) Williams, A. Opportunities for chiral agrochemicals. *Pestic. Sci.* **1996**, *46*, 3−9.
(19) Li, Z.; Zhang, Y.; Luo, X.; Guo, J.; Wang, W. Enantioselective degradation characteristics of chiral organophosphorus insecticides in soil. *Ecol. Environ. Sci.* **2009**, *18*, 1247−1250.
(20) Sun, M. J.; Liu, D. H.; Zhou, G. X.; Li, J. D.; Qiu, X. X.; Zhou, Z. Q.; Wang, P. Enantioselective degradation and chiral stability of malathion in environmental samples. *J. Agric. Food Chem.* **2012**, *60*, 372−379.
(21) Xu, Y. X.; Zhang, H.; Zhuang, S. L.; Yu, M.; Xiao, H.; Qian, M. R. Different enantioselective degradation of pyraclofos in soils. *J. Agric. Food Chem.* **2012**, *60*, 4173−4178.
(22) Sekhon, B. S. Chiral pesticides. *J. Pestic. Sci.* **2009**, *34*, 1−12.
(23) Liu, W. P.; Ye, J.; Jin, M. Q. Enantioselective phytoeffects of chiral pesticides. *J. Agric. Food Chem.* **2009**, *57*, 2087−2095.
(24) Müller, B. P.; Zumdick, A.; Schuphan, I.; Schmidt, B. Metabolism of the herbicide glusinateammonium in plant cell cultures of transgenic (rhizomania-resistant) and non-transgenic sugarbeet (*Beta vulgaris*), carrot (*Daucus carota*), purple foxglove (*Digitalis purpurea*) and thorn apple (*Datura stramonium*). *Pest Manag. Sci.* **2001**, *57*, 46−56.
(25) Ruhland, M.; Engelhardt, G.; Pawlizki, K. A comparative investigation of the metabolism of the herbicide glufosinate in cell cultures of transgenic glufosinate-resistant and non-transgenic oilseed rape (*Brassica napus*) and corn (*Zea mays*). *Environ. Biosaf. Res.* **2002**, *1*, 29−37.
(26) Nollos, M. G.; Gana, J.; Schlenk, D. J. Chirality of organophosphorus pesticides: analysis and toxicity. *J. Chromatogr., B* **2010**, *878*, 1277−1284.
(27) Walker, A.; Hollis, J. M. Prediction of pesticide mobility in soils and their potential to contaminate surface and groundwater. In *Comparing Glasshouse and Field Pesticide Performance*; BCPC Monograph 59; BCPC: Surrey, UK, 1994; pp 211−224.
(28) Ding, S.; Jia, L.; Durandin, A.; Crean, C.; Kolbanovskiy, A.; Shafirovich, V.; Broyde, S.; Geacintov, N. E. Absolute configurations of spiroiminodihydantoin and allantoin stereoisomers: comparison of computed and measured electronic circular dichroism spectra. *Chem. Res. Toxicol.* **2009**, *22*, 1189−1193.
(29) Stephens, P. J.; McCann, D. M.; Devlin, F. J.; Cheeseman, J. R.; Frisch, M. J. Determination of the absolute configuration of $[3_2](1,4)$barrelenophanedicarbonitrile using concerted time-dependent density functional theory calculations of optical rotation and electronic circular dichroism. *J. Am. Chem. Soc.* **2004**, *126*, 7514−7521.
(30) Zhang, Y. P.; Song, B. A.; Bhadury, P. S.; Hu, D. Y.; Yang, S.; Shi, X.; Liu, D. M.; Jin, L. H. Analytical and semi-preparative enantioseparation of organic phosphonates on a new immobilized amylose based chiral stationary phase. *J. Sep. Sci.* **2008**, *31*, 2946−2952.
(31) Shen, Z. G.; Zhu, W. T.; Liu, D. H.; Xu, X. Y.; Zhang, P.; Zhou, Z. Q. Stereoselective degradation of tebuconazole in rat liver microsomes. *Chirality* **2012**, *24*, 67−71.
(32) Buerge, I. J.; Poiger, T.; Muller, M. D.; Buser, H. R. Enantioselective degradation of metalaxyl in soils: chiral preference changes with soil pH. *Environ. Sci. Technol.* **2003**, *37*, 2668−2674.
(33) Yang, H. Y.; Xue, B.; Li, L.; Zhou, S. S.; Tu, Y. J.; Lin, C. M. Hydrolysis and soil sorption of insecticide pyraclofos. *J. Environ. Sci. Health B* **2008**, *43*, 219−223.
(34) Li, Z. Y.; Zhang, Z. C.; Zhang, L.; Leng, L. Enantiosellective degradation and chiral stability of phenthoate in soil. *Bull. Environ. Contam. Toxicol.* **2007**, *79*, 153−157.
(35) Zipper, C.; Bolliger, C.; Fleischmann, T.; Suter, M. J. F.; Angst, W.; Müller, M. D.; Kohler, H. P. E. Fate of the herbicides mecoprop, dichlorprop, and 2,4-D in aerobic and anaerobic sewage sludge as determined by laboratory batch studies and enantiomer-specific analysis. *Biodegradation* **1999**, *10*, 271−278.

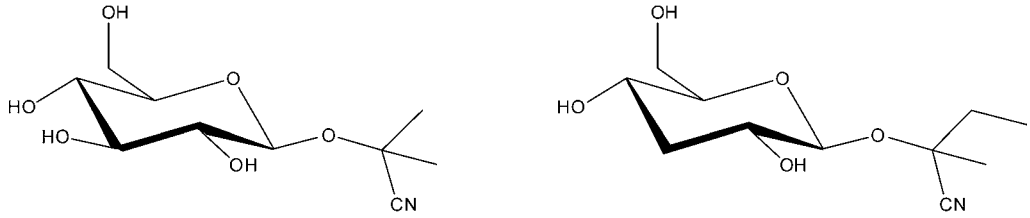

Figure 1. Structures of standards, linamarin (**1**) and lotaustralin (**2**), isolated from *Trifolium repens* aerial parts.

and they were harvested on July 8 (23 species), 18 (25 species), and 29 (14 species) and August 18th (26 species). A list of examined *Trifolium* species, their origins, and voucher specimens is reported in Table 1.

Extraction and Purification. Powdered aerial parts of *Trifolium* species were defatted with chloroform in Soxhlet apparatus. After removal of chlorophyll the samples (100 mg each) were extracted in an automated accelerated solvent extractor ASE 200 (Dionex, Sunnyvale, CA) using 80% aqueous MeOH (23 mL) at 40 °C and 1500 psi working pressure. Extracts were evaporated to dryness (at 40 °C). Residues were dissolved in Milli-Q water and purified by solid-phase extraction (SPE) using water preconditioned 1 mL, 360 mg C18 Sep-Pak cartridges (Waters Corp., Milford, MA). After loading the samples, cartridges were washed with water (1 mL) to remove carbohydrates; cyanogenic glycosides were eluted with 20% (v/v) MeOH (6 mL). Fractions were concentrated under reduced pressure and dissolved in 1 mL of 20% (v/v) MeOH for analyses. Three independent extraction and purification procedures were performed for each species, and data were presented as mean values with standard deviations (Table 2).

Isolation of Standards. Linamarin, **1**, and lotaustralin, **2** (Figure 1), used as standards for analysis, were isolated from *T. repens* L. cultivar 'Haifa'. The specimen (Voucher number 7/2010) has been deposited at the Department of Biochemistry and Crop Quality, Institute of Soil Science and Plant Cultivation, State Research Institute, Pulawy, Poland.

Plant material was defatted with chloroform and extracted three times with 75% (v/v) MeOH at room temperature for 24 h using an ultrasonic bath. Extracts were concentrated under reduced pressure and lyophilized. Then they were dissolved in water and loaded onto a 100 × 60 mm LiChroprep RP-18, 40−63 μm vacuum liquid chromatography column (Merck, Darmstadt, Germany). The column was washed with water, and cyanogenic glycosides were eluted with 20% (v/v) MeOH. Cyanogenic glycosides fraction was chromatographed with a semipreparative high-performance chromatograph Gilson HPLC equipped with a PrepELS II evaporative light-scattering detector and RP-18 column (10 × 250 mm; 5 μm; Kromasil C18, Eka Chemicals AB, Sweeden) at a flow rate of 5.0 mL/min using a 0.5% (v/v) HOAc−MeCN gradient as the mobile phase. Fractions containing pure compounds were precipitated in ethyl acetate. Single compounds were identified by NMR analysis, which was consistent with reported data. Purity of the standards linamarin, **1**, and lotaustralin, **2**, was 99.0 and 99.8%, respectively.

UPLC-MS/MS Analysis. A Waters ACQUITY UPLC system equipped with a binary solvent manager and coupled to a Waters ACQUITY TQD (tandem quadruple mass detector) with an electrospray ionization (ESI) source was used for quantitation. All data were acquired and processed using Waters MassLynx 4.1 and QuanLynx software. A Waters BEH C18 column (1 × 100 mm, 1.7 μm particles) was used to separate analytes. The elution program used for chromatographic separation consisted of solvents A (Milli-Q water containing 0.1% (v/v) HCOOH) and B (MeCN containing 0.1% (v/v) HCOOH) delivered as follows: 0.0−0.5 min (7% B), 8.0 min (25% B), 11.5 min (60% B), 12.0 min (80% B), 13.0 min (80% B), 13.1 min (7% B), and finished at 15.0 min. The flow rate was 0.15 mL/min, and the column temperature was 50 °C. The injection wash solvents were MeCN/H_2O (5:95, v/v) and MeOH/H_2O (5:95, v/v) for weak (900 μL) and strong wash (300 μL), respectively. A 1 μL sample was injected for analysis. For MS detection, negative ESI was used as the ionization mode. Nitrogen was used as the desolvation and cone gas with a flow rate of 800 and 80 L/h, respectively. Argon was used as the collision gas at a flow rate of 0.2 mL/min. The optimal MS parameters were as follows: capillary, 3.0 kV; extractor and radiofrequency voltage were fixed to 3.0 and 0.1 V, respectively; source temperature, 140 °C; desolvation temperature, 350 °C; cone voltage varied from 19 to 23 V; collision energies varied from 13 to 15 eV. Quantitation was performed using the selected reaction monitoring (SRM) mode; parent > daughter transitions were m/z 292 > 161 and m/z 306 > 161 for linamarin and lotaustralin, respectively.

Statistical Analysis. Statistical and cluster analyses (K-means clustering) were performed using the XLSTAT 2012 program.

RESULTS AND DISCUSSION

Analysis of cyanogenic glucosides in plant material creates some analytical problems. Older methods of analysis were based on sodium picrate or Feigl-Anger reagent.[16] Both tests depended on the release of HCN by enzymatic or nonenzymatic hydrolysis of cyanogenic glucosides. They were very sensitive but not always proper due to the fact that some other plant components (glucosinolates) could produce misleading information. Improvement in cyanogenic glucosides analysis was the application of high-performance liquid chromatography with refractive index detection.[15] The method provided more objective data, but its sensitivity was low, and some plants with trace amounts of compounds could be classified as non-cyanogenic. In the present research HPLC combined with the mass detector was applied in selected reaction monitoring (SRM) mode. This gave high sensitivity and precision of analysis, and both compounds could be detected even at very low concentration in plants (Figure 2).

Analysis of 88 species, originating from different parts of the globe but grown at the same site, provided interesting results. All analyzed species with respect to the content of cyanogenic glycosides could be grouped in five clusters (Table 2). As a criteria for clustering the presence of linamarin and lotaustralin and the linamarin/lotaustralin ratio were considered. The majority of 37 species belonged to cluster C1, which was characterized by the absence of cyanogenic glucosides. The second cluster C2 of 22 species grouped those, which contained only lotaustralin as a sole cyanogenic glucoside ranging from trace amounts of 0.85 (*T. alexandrinum*) to 121.47 μg/g (*T. incarnatum*) of dry weight. The third cluster C3 of 14 species was characterized by the presence of both linamarin and lotaustralin, but the linamarin occurred at a very low level; the linamarin/lotaustralin ratio ranged from 0.01 to 0.08, and the total concentration ranged from 13.26 (*T. ochroleucon* Huds.) to 424.77 μg/g (*T. resupinatum* L. var. *majus* Boiss.).

Similarly, the fourth cluster C4 of 13 species also contained both linamarin and lotaustralin, but the ratio of linamarin/lotaustralin ranged from 0.11 to 0.61, and the total

Table 1. List of Examined *Trifolium* Species

no.	species (subspecies, variety)	origin	herbarium voucher
1	*T. alexandrinum* L.	unknown	TRIF 10
2	*T. alexandrinum* L.	India	TRIF 30
3	*T. alexandrinum* L.	unknown	TRIF 45
4	*T. alexandrinum* L.	unknown	TRIF 47
5	*T. alexandrinum* L.	Albania	TRIF 269
6	*T. alexandrinum* L.	Italy	TRIF 312
7	*T. alexandrinum* L.	Greece	TRIF 1237
8	*T. alpestre* L.	unknown	TRIF 201
9	*T. ambiguum* M. Bieb.	unknown	TRIF 178
10	*T. angustifolium* L.	France	TRIF 139
11	*T. apertum* Bobrov.	unknown	TRIF 44
12	*T. argutum* Sol.	unknown	TRIF 80
13	*T. arvense* L.	unknown	TRIF 40
14	*T. bocconei* Savi	Portugal	TRIF 81
15	*T. campestre* Schreb.	Sweden	TRIF 99
16	*T. cernuum* Brot.	Portugal	TRIF 52
17	*T. cherleri* Jusl.	unknown	TRIF 74
18	*T. clussii* Godr. & Green. var. *clussii*	unknown	TRIF 57
19	*T. clypeatum* L.	Israel	TRIF 129
20	*T. dubium* Sibth.	Germany	TRIF 103
21	*T. echinatum* M.Bieb. var. *carmeli* (Boiss.) Gibelli & Belli	Israel	TRIF 100
22	*T. echinatum* M.Bieb. var. *echinatum*	Romania	TRIF 104
23	*T. fragiferum* L.	Bulgaria	TRIF 1151
24	*T. fragiferum* L. ssp. *bonanni* (Presl) Sojak	Ukraine	TRIF 197
25	*T. fragiferum* L. ssp. *Fragiferum*	United States	TRIF 1241
26	*T. fragiferum* L. ssp. *bonanni* (Presl) Sojak	Hungary	TRIF 208
27	*T. fragiferum* L. ssp. *Fragiferum*	unknown	TRIF 37
28	*T. glomeratum* L.	Morocco	TRIF 107
29	*T. heldreichianum* Hausskn.	unknown	TRIF 149
30	*T. hirtum* All.	unknown	TRIF 213
31	*T. hybridum* L.	unknown	TRIF 6
32	*T. hybridum* L.	United States	TRIF 155
33	*T. hybridum* L.	Finland	TRIF 194
34	*T. hybridum* L.	Denmark	TRIF 1177
35	*T. hybridum* L. var. *hybridum*	Norway	TRIF 1242
36	*T. hybridum* L. var. *hybridum*	Canada	TRIF 1243
37	*T. incarnatum* L.	Czechoslovakia	TRIF 82
38	*T. incarnatum* L.	Poland	TRIF 86
39	*T. incarnatum* L.	United States	TRIF 247
40	*T. incarnatum* L.	Italy	TRIF 1141
41	*T. incarnatum* L.	United States	TRIF 1189
42	*T. incarnatum* L. var. Molinerii (Balb. ex Hornem.) Ser.	France	TRIF 280
43	*T. isthmocarpum* Brot.	Portugal	TRIF 77
44	*T. lappaceum* L.	unknown	TRIF 55
45	*T. leucanthum* M. Bieb.	Israel	TRIF 131
46	*T. ligusticum* Balb.	Portugal	TRIF 113
47	*T. medium* L.	unknown	TRIF 281
48	*T. medium* L. var. *medium*	unknown	TRIF 32
49	*T. medium* L. var. *medium*	unknown	TRIF 35
50	*T. medium* L. var. *sarosiense* (Hazsl.) Savul. & Rayss	unknown	TRIF 179
51	T. *michelianum* Savi	unknown	TRIF 79
52	*T. michelianum* Savi var. *balansae* (Boiss.) Azn.	Bulgaria	TRIF 145
53	*T. miegeanum* Maire	Portugal	TRIF 116
54	*T. montanum* L.	unknown	TRIF 147
55	*T. nigrescens* Viv. ssp. *Nigrescens*	Portugal	TRIF 117
56	*T. obscurum* Savi	Denmark	TRIF 133
57	*T. ochroleucon* Huds.	Slovakia	TRIF 173
58	*T. palidum* Waldst. et Kit.	Italy	TRIF 253
59	*T. pannonicum* Jacq.	unknown	TRIF 8
60	*T. pannonicum* Jacq.	unknown	TRIF 9
61	*T. phleoides* Pourr. ex. Willd.	unknown	TRIF 132
62	*T. pratense* L.	Poland	TRIF 1482
63	*T. pratense* L.	United States	TRIF 1491
64	*T. pratense* L.	Sweden	TRIF 1745
65	*T. pratense* L.	Austria	TRIF 2016
66	*T. pratense* L.	Belgium	TRIF 2536
67	*T. pratense* L.	Netherlands	TRIF 2561
68	*T. purpureum* Lois. var. *desvauxii* (Boiss. & Blanche) Post	United States	TRIF 143
69	*T. repens* L.	unknown	TRIF 15
70	*T. repens* L.	Poland	TRIF 1156
71	*T. repens* L.	United States	TRIF 1157
72	*T. repens* L. var. *biasoletti* (Stend. & Hochst.) Asch. & Graebn.	France	TRIF 254
73	*T. repens* L. *gigantem* Lagr.-Foss.	Hungary	TRIF 229
74	*T. repens* L. var. *biasoletti* (Steud. & Hochst.) Asch. & Graebn.	France	TRIF 255
75	*T. resupinatum* L. var. *majus* Boiss.	United States	TRIF 224
76	T. *resupinatum* L. var. *majus* Boiss.	Germany	TRIF 1135
77	*T. resupinatum* L. var. *resupinatum*	United States	TRIF 59
78	*T. resupinatum* L. var. *resupinatum*	Turkey	TRIF 1134
79	*T. resupinatum* L. var. *majus* Boiss.	Iran	TRIF 61
80	*T. resupinatum* L. var. *resupinatum*	unknown	TRIF 43
81	*T. scabrum* L.	Portugal	TRIF 120
82	*T. spumosum* L.	unknown	TRIF 67
83	*T. squarrosum* L.	unknown	TRIF 122
84	*T. stellatum* L.	Croatia	TRIF 215
85	*T. striatum* L.	France	TRIF 70
86	*T. subterraneum* L. ssp. *Subterraneum*	United States	TRIF 259
87	*T. tomentosum* L. var. *tomentosum*	Portugal	TRIF 218
88	*T. tomentosum* L. var. *curvisepalum* (Täckh.) Thiebaut	unknown	TRIF 53

concentration varied from 4.97 (*T. repens* L.) to 1877.33 μg/g (*T. montanum* L.). Finally, the fifth cluster C5 contained only two species: *T. repens* L. and *T. repens* L. *giganteum* Lagr.-Foss with a relatively low total concentration of both cyanogenic glucosides (27.73 and 68.27 μg/g, respectively), but in these plants linamarin was the dominating compound and the linamarin/lotaustralin ratio was 3.25 and 3.75, respectively.

Considering the total concentration of cyanogenic glucosides it should be noticed that all samples were collected at the beginning of flowering, the period when most of the secondary metabolites are most intensively biosynthesized.[17] On the other hand, plants were harvested during the summer period (July–August) when, as shown with white clover varieties, cyanogenic glucoside content was the lowest,[13] which corresponded with the general view that cyanogen concentration increases at low temperatures.[18] For white clover in Europe the Swiss cultivar 'Milkanova' was accepted as a reference variety as regards the cyanogen content to be safe for grazing animals. This cultivar in Swiss conditions synthesizes about 370 mg of HCN/kg of dry matter. In these circumstances the concentration of cyanogens

dx.doi.org/10.1021/jf4056659 | J. Agric. Food Chem. 2014, 62, 1777–1782

Table 2. Concentrations (μg/g dm ± SD) of Cyanogenic Glucosides in 88 *Trifolium* Species

species	linamarin	lotaustralin	total	Lin/Lot ratio
cluster C1[a]				
cluster C2				
2	ND[b]	0.85 ± 0.05	0.85	
23	ND	0.93 ± 0.21	0.93	
4	ND	1.33 ± 0.31	1.31	
20	ND	1.57 ± 0.48	1.57	
48	ND	2.47 ± 0.31	2.47	
58	ND	3.60 ± 0.29	3.60	
51	ND	5.63 ± 0.29	5.63	
6	ND	7.50 ± 0.16	7.50	
61	ND	8.53 ± 0.69	8.53	
15	ND	11.10 ± 0.22	11.10	
16	ND	14.03 ± 0.37	14.03	
45	ND	16.50 ± 0.50	16.50	
9	ND	17.60 ± 0.56	17.60	
10	ND	18.17 ± 0.34	18.17	
5	ND	28.17 ± 0.90	28.17	
63	ND	28.23 ± 0.12	28.23	
46	ND	33.93 ± 0.79	33.93	
14	ND	42.17 ± 0.57	42.17	
47	ND	71.60 ± 1.15	71.60	
56	ND	78.67 ± 1.73	78.67	
12	ND	99.57 ± 0.37	99.57	
38	ND	121.47 ± 0.68	121.47	
cluster C3				
57	1.03 ± 0.34	12.23 ± 0.12	13.26	0.08
39	0.20 ± 0.00	24.30 ± 0.24	24.50	0.01
25	1.23 ± 0.05	25.97 ± 0.37	27.20	0.05
52	0.40 ± 0.10	40.97 ± 0.23	41.37	0.01
67	2.53 ± 0.24	49.50 ± 0.65	52.03	0.05
49	0.87 ± 0.17	53.60 ± 0.73	54.47	0.02
cluster C3				
26	1.13 ± 0.42	108.47 ± 1.74	109.60	0.01
87	6.43 ± 0.21	113.37 ± 0.88	119.80	0.06
13	10.33 ± 0.21	139.30 ± 0.65	149.63	0.07
83	1.17 ± 0.12	152.20 ± 0.29	153.37	0.01
18	12.07 ± 0.72	204.73 ± 1.84	216.80	0.06
22	7.47 ± 0.30	212.17 ± 0.47	219.64	0.04
43	21.17 ± 1.60	338.47 ± 13.65	359.64	0.06
75	22.00 ± 0.64	402.77 ± 1.09	424.77	0.05
cluster C4				
71	1.40 ± 0.08	4.97 ± 0.09	6.37	0.28
53	6.37 ± 0.25	21.63 ± 0.26	28.00	0.29
29	2.87 ± 0.29	25.70 ± 0.08	28.57	0.11
44	9.20 ± 0.08	23.87 ± 0.84	33.07	0.38
30	4.73 ± 0.53	30.60 ± 0.64	35.33	0.15
35	13.77 ± 0.25	24.93 ± 0.54	38.70	0.55
11	22.87 ± 0.33	106.47 ± 0.99	129.34	0.21
60	36.33 ± 0.45	255.50 ± 2.24	291.83	0.14
40	35.63 ± 1.54	195.53 ± 1.31	340.76	0.18
74	90.00 ± 0.79	252.83 ± 1.93	342.83	0.36
55	59.07 ± 3.27	443.27 ± 10.17	502.34	0.13
72	571.00 ± 2.48	932.30 ± 3.48	1503.30	0.61
54	593.00 ± 0.71	1284.33 ± 8.81	1877.30	0.46
cluster C5				
69	21.20 ± 0.43	6.53 ± 0.12	27.73	3.25
73	53.90 ± 0.57	14.37 ± 1.51	68.27	3.75

[a]In cluster C1 (species 3, 7, 8, 17, 19, 21, 24, 27, 28, 31, 32, 33, 34, 36, 37, 41, 42, 50, 59, 62, 64, 65, 66, 68, 70, 76, 77, 78, 79, 80, 81, 82, 84, 85, 86, 88), no linamarin, **1**, or lotaustralin, **2**, was detected. [b]ND – not detected.

in plants of clusters C2, C3, and C5 should be considered as rather low. Cluster C4 contained species with concentrations comparable to cited 'Milkanova' cultivar. Only two species, *T. repens* var. *biasoletti* (Stend & Hochst.) Asch. & Graebn. and *T. montanum* showed extremely high cyanogen concentration (1505.30 and 1877.30 μg/g of dry matter, respectively). This has a concentration comparable to the content of linamarin and lotaustralin in cassava tubers where they accumulate up to 1.5 g/kg dry weight.[19,20] However, in cassava tubers the linamarin/lotaustralin ratio was approximately 97:3, whereas in most of the *Trifolium* species lotaustralin has been the dominant glucoside.

There was no regularity observed regarding the genus-dependent occurrence of cyanogenic glucosides. For these genera, which were represented by several species or subspecies of different origin, their distribution between different clusters was observed. Out of the six samples of widely cultivated red clover (*T. pratense*), four were free of cyanogenic glucosides, one had only lotaustralin, and one possessed both linamarin and lotaustralin. It is interesting to notice that *T. pretense* originating from Belgium (66) was free of cyanogens, while the same species originating from Netherlands (67) contained both linamarin and lotaustralin. White clover (*T. repens*) was also represented by six samples of different origin, and five of them contained both linamarin and lotaustralin. The total cyanogen concentration in these samples ranged between 6.37 and 1503.30 μg/g. The highest concentration was observed for samples originating from France: 342.83 (74) and 1503.30 μg/g (72). This finding correlates with previous reports, showing that in the Mediterranean region the frequency of cyanogenesis in white clover populations was 100%, while in other European regions it was decreasing when moving to the northeast, and in Central Russia the populations were noncyanogenic.[21] This was correlated with the mean temperature of January and preferential grazing of noncyanogenic plantlets by snails. Only the sample originating from Poland (70) was free of cyanogens. This finding confirmed previous data showing that old Polish cultivar 'Podkowa' bred from local population was non-cyanogenic.[14]

Similar trends were observed in the case of *T. incarnatum*. Three of the five samples were free of cyanogens, one (38) contained only lotaustralin, and one (39) contained both linamarin and lotaustralin. In contrast, white clover *T. incarnatum* originating from France was free of cyanogens, while the sample originating from Poland had the highest content of these glycosides.

In the case of *T. hybridum*, out of six samples five did not contain cyanogens and only the sample originating from Norway (35) possessed linamarin and lotaustralin at a relatively low level of 38.70 μg/g of dry matter.

The species *T. resupinatum* were differentiated in cyanogen content as well. Out of six tested samples five were noncyanogenic and one originating from the United States contained both linamarin and lotaustralin at a relatively high level of 424.77 μg/g.

dx.doi.org/10.1021/jf4056659 | J. Agric. Food Chem. 2014, 62, 1777−1782

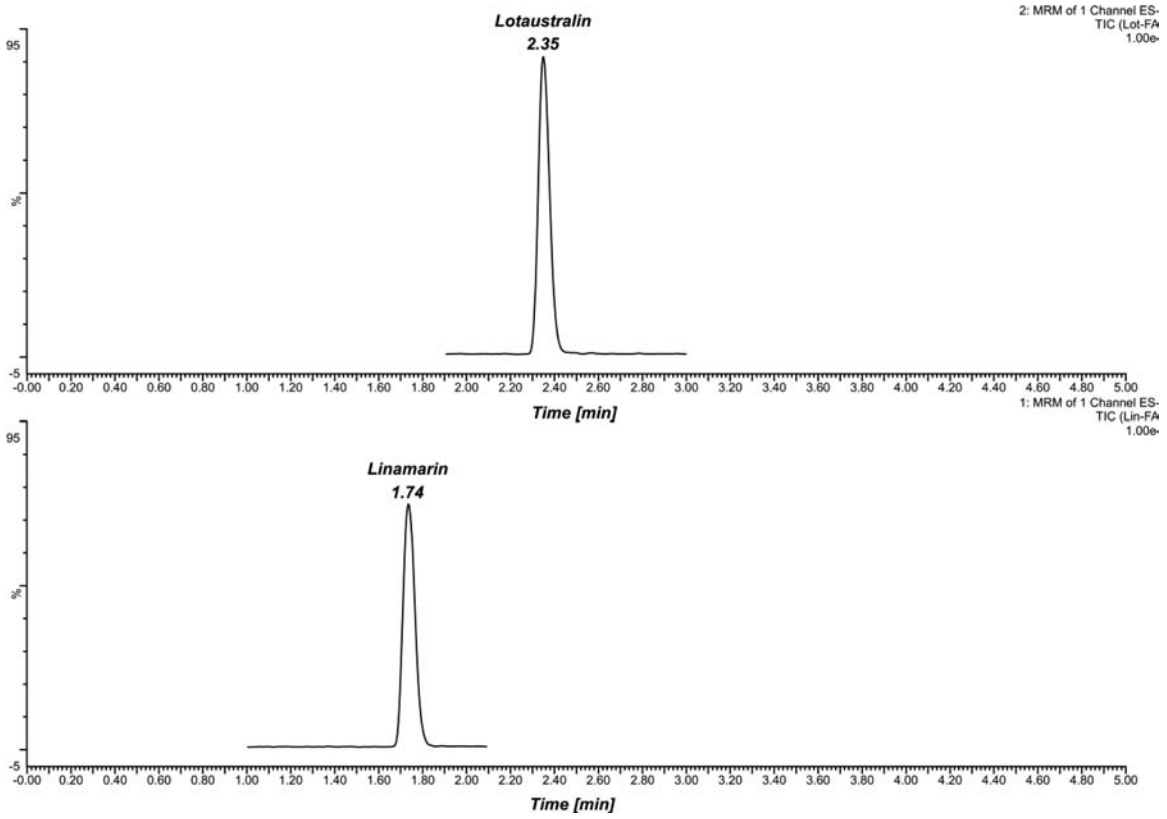

Figure 2. UPLC ESI-MS/MS ion chromatograms of linamarin (**1**) and lotaustralin (**2**) quantified in *T. repens* var. *biasoletti* (Steud. & Hochst.) Asch. & Graebn. were obtained with selected reaction monitoring (SRM).

The presence or absence of both glycosides is regulated by alleles of a single gene, designated Ac, whereas the presence or absence of the enzyme *linamarase* is governed by alleles or another, independently inherited gene (Li). Only plants possessing dominant functional alleles of both genes liberate HCN when damaged.[13,22] Biosynthesis of linamarin, **1**, and lotaustralin, **2**, the valine and isoleucine-derived cyanogenic glucosides has been recently extensively studied. The biosynthetic pathway that includes enzymes and corresponding genes has been fully identified in *Sorghum bicolor*, synthesizing aromatic cyanogenic glucoside dhurrin.[23] The CYP79 enzymes converting amino acids into oximes have been known in several plant species. For some species (great millet and cassava) the enzymes converting oximes to cyanohydrins have also been identified.[24−26] In particular, identification of *CYP71E1* and *CYP71E7* in cassava synthetizing aliphatic cyanogenic glucoside may aid as a probe for isolation of their paralogs in *Trifolium* species. Our present findings may help in selection of species/subspecies for these studies. The full recognition of the enzymes involved in biosynthesis, transport, and degradation of these compounds has been of crucial value for breeding purposes.

It is experimentally demonstrated that the acyanogenic plants have a competitive advantage over the cyanogenic ones (the relative fitness, i.e., biomass production and the number of flowers per plant are higher).[13] Screening, which was carried out, revealed the cyanogenic and acyanogenic species. Obtained data can be used for their future safe nutritive use or clover-breeding programs, and they can have a chemotaxonomic significance.

■ ASSOCIATED CONTENT

Supporting Information

NMR data and structures of standards (linamarin and lotaustralin) used for analysis; ESI-MS/MS spectra of linamarin and lotaustralin obtained with selected reaction monitoring (SRM). This material is available free of charge via the Internet at http://pubs.acs.org.

■ AUTHOR INFORMATION

Corresponding Author

*Phone: +48 8188 63421, ext 205. Fax: +48 8188 63421, ext 295. E-mail: asf@iung.pulawy.pl.

Funding

This work was supported by the European Community seventh Framework Program project PROFICIENCY (Contract No. 245751) and OSCAR (Contract No. 289277).

Notes

The authors declare no competing financial interest.

■ REFERENCES

(1) Bisby, F. A.; Buckingham, J.; Harborne, J. B. In *Phytochemical Dictionary of Leguminosae*; Chapman and Hall: London, 1994.

(2) Smetham, M. A review of subterranean clover (*Trifolium subterraneum* L.) its ecology, and use in Australasia. *Adv. Agron.* **2003**, *79*, 303−350.

(3) Drenin, A. A.; Botirov, E.Kh.; Petrulyak, E. V. Two new isoflavonoid monogalactosides from *Trifolium pratense* roots. *Chem. Nat. Compd.* **2008**, *44*, 24−27.

(4) Foo, L. Y.; Lu, Y.; Molan, A. L.; Woodfield, D. R.; McNabb, W. C. The phenols and prodelphinidins of white clover flowers. *Phytochemistry* **2000**, *54*, 539−548.

(5) Oleszek, W.; Stochmal, A.; Janda, B. Concentration of isoflavones and other phenolics in the aerial parts of *Trifolium* species. *J. Agric. Food Chem.* **2007**, *55*, 8095−8100.
(6) Oleszek, W.; Stochmal, A. Triterpene saponins and flavonoids in the seeds of *Trifolium* species. *Phytochemistry* **2002**, *61*, 165−170.
(7) Simonet, A. M.; Stochmal, A.; Oleszek, W.; Macias, F. A. Saponins and polar compounds from *Trifolium resupinatum*. *Phytochemistry* **1999**, *51*, 1065−1067.
(8) Godevac, D.; Zdunic, G.; Savikin, K.; Vajs, V.; Menkovic, N. Antioxidant activity of nine Fabaceae species growing in Serbia and Montenegro. *Fitoterapia* **2008**, *79*, 185−187.
(9) Parvu, E. *Trifolium pratense* for breast disease: a case series. *Homeopathy* **2004**, *93*, 45−50.
(10) De Nicola, G. R.; Leoni, O.; Malaguti, L.; Bernardi, R.; Lazzeri, L. A simple analytical method for dhurrin content evaluation in cyanogenic plants for their utilization in fodder and biofumigation. *J. Agric. Food Chem.* **2011**, *59*, 8065−8069.
(11) Zagrobelny, M.; Bak, S.; Myller, B. L. Cyanogenesis in plants and arthropods. *Phytochemistry* **2008**, *69*, 1457−1468.
(12) Ly, J. Use of Cassava roots for pigs: Antinutritional factors. *Rev. Comput. Prod. Porcina* **1998**, *5*, 1−28.
(13) Vetter, J. Plant cyanogenic glycosides. *Toxicon* **2000**, *38*, 11−36.
(14) Stochmal, A.; Oleszek, W. Changes of cyanogenic glucosides in white clover (*Trifolium repens* L.) during the growing season. *J. Agric. Food Chem.* **1997**, *45*, 4333−4336.
(15) Stochmal, A.; Oleszek, W. Determination of cyanogenic glucosides in white clover (*Trifolium repens* L.) by high-performance liquid chromatography. *Phytochem. Anal.* **1994**, *5*, 271−271.
(16) Nahrestedt, A., Erb, N., Zinsmeister, H. D. Methods of liberating and estimating hydrocyanic acid from cyanogens plant material. *Cyanide in biology*; Academic Press: London, 1981.
(17) Harborne, J. B. *Introduction to Ecological Biochemistry*; Academic Press: London, 1992.
(18) Baker, M. J., Williams, M. W. *White clover*; AAB International: Aberystwyth, 1987.
(19) Bokanga, M. Processing of cassava leaves for human consumption. *Acta Hortic.* **1994**, *375*, 203−207.
(20) Jorgensen, K.; Bak, S.; Busk, P. K.; Sorensen, C.; Olsen, C.; Puonti-Kaerlas, J.; Moller, B. L. Cassava plants with a depleted cyanogenic glucoside content in leaves and tubers. Distribution of cyanogenic glucosides, their site of synthesis and transport, and blockage of the biosynthesis by RNA interference technology. *Plant Physiol.* **2005**, *139*, 363−374.
(21) Jones, D. A. Cyanogenic glycosides and their function. *Phytochemical ecology*; Academic Press, London, 1972.
(22) Noitsakis, B.; Jaquard, P. Competition between cyanogenic and acyanogenic morphs of *Trifolium repens*. *Theor. Appl. Genet.* **1992**, *83*, 443−450.
(23) Jones, D. A. Why are so many food plants cyanogenic? *Phytochemistry* **1998**, *47*, 155−162.
(24) Halkier, B. A.; Nielsen, H. L.; Koch, B.; Moller, B. L. Purification and characterization of recombinant cytochrome P450TYR expressed at high levels in *Escherichia coli*. *Arch. Biochem. Biophys.* **1995**, *322*, 369−377.
(25) Bak, S.; Kahn, R. A.; Nielsen, H. L.; Moller, B. L.; Halkier, B. A. Cloning of three A-type cytochromes P450, CYP71E1, CYP98 and CYP99 from *Sorghum bicolor* (L.) Moench by PCR approach and identification by expression in *Escherichia coli* of CYP71E1 as multifunctional cytochrome P450 in the biosynthesis of the cyanogenic glucoside dhurrin. *Plant Mol. Biol.* **1998**, *36*, 393−405.
(26) Jorgensen, K.; Morant, A. V.; Morant, M.; Jensen, N. B.; Olsen, C. E.; Kannangara, R.; Motawia, M. S.; Moller, B. L.; Bak, S. Biosynthesis of the cyanogenic glucosides linamarin and lotaustralin in cassava: Isolation, biochemical characterization, and expression pattern of CYP71E7, the oxime-metabolizing cytochrome P450 enzyme. *Plant Physiol.* **2011**, *155*, 282−292.

strategies reducing malnutrition in developing countries.[16] It has been reported that inoculation of bacteria (*Providencia sp.* PW5) resulted in a significant increase of Fe, Mn, and Cu in wheat grain.[16]

Recently, endophytic bacteria colonizing the internal tissues of metal hyperaccumulator or accumulator plants have been gaining increasing attention.[17] Endophytic bacteria promoted plant growth, increased heavy metal accumulation, and available heavy metal in the rhizosphere soil. Inoculation of plants with endophytes, which were isolated from metal-resistant or hyperaccumator plant species, is extensively used for phytoremediation of metalliferous soils.[18−20] However, there are few reports on whether the bacteria isolated from hyperaccumulator could survive in a crop system and their potential use in biofortification of micronutrients in crop plants. In the present study, five endophytic strains, *Burkholderia sp.* SaZR4, *Burkholderia sp.* SaMR10, *Sphingomonas sp.* SaMR12, *Variovorax sp.* SaNR1, and *Enterobacter sp.* SaCS20, were isolated from *Sedum alfredii* Hance, a Zn hyperaccumulator native to China.[21,22] Our previous studies showed that inoculation of the isolated endophytic bacterial strains back to sterilized plants of the hyperaccumulator *S. alfredii* resulted in elevated biomass and Zn concentrations in both shoots and roots.[23] The endophytic microbia were also harmless to crops according to pathogenic detection of tobacco leaf.[23] The objective of the study is to investigate the possibility of Zn biofortification in rice grains by inoculation with the endophytic strains isolated from *S. alfredii*.

MATERIALS AND METHODS

Bacteria, Plasmids, and Plants. Five single bacterial strains (SaZR4, SaMR10, SaNR1, SaMR12, and SaCS20) used in this study were isolated from *S. alfredii* as described by Zhang et al.[24] The bacterial strains were identified as *Burkholderia sp.* SaZR4, *Burkholderia sp.* SaMR10, *Sphingomonas sp.* SaMR12, *Variovorax sp.* SaNR1, and *Enterobacter sp.* SaCS20 based on their 16S rRNA gene sequences and carbon source utilization profiles determined using Biolog GN2 microplates (Biolog Inc., Hayward, CA, USA). SaZR4, SaMR12, SaNR1, and SaCS20 transconjugants constitutively expressing green fluorescent protein (GFP) were obtained by triparental mating with the vector plasmid pHC60 and helper phage pRK2013.[23] Bacterial physiology including indole-3-acetic acid (IAA) and siderophore production and phosphate solubilization (except SaNR1) was determined according to Lin et al.[25]

Japonica rice (*Oryza sativa* L.) variety Nipponbare obtained from Zhejiang Academy of Agricultural Sciences was used for this study. Surface-sterilized rice seeds were germinated at 30 °C in the dark. After germination, plantlets were sown in a sterile pot that was filled with sterilized quartz sand in a growth chamber. Uniform seedlings at three-leaf stage were transplanted to a 2.5 L black plastic pot with nutrient solution containing (in mM) NH_4NO_3, 1.43; $CaCl_2{\cdot}2H_2O$, 1.00; $MgSO_4{\cdot}7H_2O$, 1.64; $NaH_2PO_4{\cdot}2H_2O$, 0.32; and K_2SO_4, 1.32; and (in μM) $MnCl_2{\cdot}4H_2O$, 5.0; $CuSO_4{\cdot}5H_2O$, 0.2; $(NH4)_6Mo_7O_{24}{\cdot}4H_2O$, 0.075; H_3BO_3, 1.90; Fe-EDTA, 20.0; and $ZnSO_4{\cdot}7H_2O$, 2.0.[26] The nutrient solutions were replaced every 3 days and adjusted to pH 5.5 ± 0.1 every day. Plants were grown in a growth chamber under a photo flux density of 400 μmol m^{-2} s^{-1}, a light/dark period of 16/8 h, day/night temperatures of 30/25 °C, and day/night relative humidities of 75%/85%.

Inoculation with Endophytic Microbia under Hydroponic Conditions. The five isolated endophytic strains were used in the hydroponic experiment. A single bacterial strain was grown in liquid Luria broth (LB) medium for 48 h at 30 °C on a rotating shaker. Cells were harvested by centrifugation, washed twice with phosphate buffered saline (PBS), and suspended in biological saline (0.85% NaCl), then the inoculum density was adjusted to 10^8 colony-forming units mL^{-1}, and the resulting suspensions were used for inoculation.

Roots of rice seedling at five-leaf stage were surface sterilized with 3% chloride for 2 min and four washes with sterile water. A total of 5 mL of bacterial inocula were carefully introduced into 2.5 L of nutrient solution using a pipet avoiding contamination of the above-ground rice tissues. Plants were grown in a growth chamber, and treatments were arranged randomly with four replications. Rice plants were harvested at 30 d after inoculation (DAI).

Inoculation with Endophytic Microbia under Soil Conditions. In a separate experiment, the effects of the endophytic strains on rice growth and grain Zn accumulation were further investigated under soil conditions in a greenhouse. Two strains (SaMR12 and SaCS20) selected from the hydroponic experiment were used in the pot experiment. The silty loam soil used in this experiment was collected from the experimental field of Zhejiang University, Zhejiang Province, China. The physical−chemical properties of the experimental soil were pH 6.5, available N, P, and K of 67.7, 37.6, and 62.5 mg kg^{-1}, respectively, DTPA-extractable Zn 4.33 mg kg^{-1}. Soil was air-dried, sieved to 5 mm, and homogenized before filling the pot, each of which contained 8.0 kg of dry soil. Recommended levels of NPK fertilizers were supplied (in mg per kg of dry soil) to each pot at a rate of 160 mg of N (70% as basal and 30% at panicle initiation), 50 mg of P_2O_5, and 90 mg of K_2O before transplanting.

Roots of rice seedlings at five-leaf stage were sterilized as described above, and every six seedlings were inoculated by soaking the roots in 500 mL of single bacterial suspension (10^8 colony-forming units mL^{-1}) for 2 h and then transplanted to each pot. Rice was additionally treated with 20 mL of the bacterial cell suspensions (10^8 colony-forming units mL^{-1}) by spraying on the plant rhizosphere soil at tillering stage and flowering stage, respectively. The same volume of sterilized deionized water was used as control. Treatments were arranged randomly with four replications. Water content of each pot was maintained at 75% (w/w) with deionized water daily. Plants were grown in greenhouse with day/night temperatures of 30 ± 2 °C/23 ± 2 °C under natural light conditions from June to Oct., 2012, at Zhejiang Province, China.

Laser Scanning Confocal Microscopy (LSCM). For hydroponic experiments, rice roots for LSCM were excised from plants at 2, 4, and 6 DAI, and a random sample of root system was assessed for microbial colonization. For pot experiments, rice roots and root with less rhizosphere soil were excised at 3 and 7 DAI for LSCM. LSCM was performed according to Lin et al.[25]

Root Morphology and Root System Formation. Roots of harvest plants were analyzed with a root automatism scan apparatus (MIN MAC STDI600+, Tokyo, Japan) equipped with the WinRHIZO software (Regent instruments Inc., Quebec, Canada).[20] Root system formation of the rice was observed by using a stereomicroscope (Leica MZ9.5) with a DCF300 camera. Individual root was sampled randomly and cut into 10 mm fragments from root tips. Images were captured with a Leica application suite (LAS) software (Leica, Bannockburn, IL).

Elemental Determination. At 30 DAI under hydroponic conditions, roots of rice cultured hydroponically were submerged into a 1.0 L bath containing 1.0 mM $LaCl_3$ and 0.05 mM $CaCl_2$ for 10 min to remove apoplastic Zn.[27] Plants were separated into roots, stems, and leaves and cleaned with ultrapure water (resistivity ≥ 18.2 MΩ cm^{-2}). Rice plants cultured under soil conditions were harvested at maturity and separated into grains, flag leaves, leaves, and stems. All plant samples were rinsed thoroughly with ultrapure water, oven-dried at 65 °C for 72 h, weighed, and ground with an MM301 (Retsch, Germany) with agate ball and internal wall. Samples were digested in a diacid mixture of HNO_3−$HClO_4$ (v/v, 4:1), and the digest was transferred to a 50 mL volumetric flask, made up to volume, and filtered. Samples were digested in triplicate, and Zn concentration was determined using an inductively coupled-plasma mass spectrometer (ICP-MS, Agilent 7500a, CA, USA). DTPA-extractable Zn in the rhizosphere soil was analyzed by ICP-MS (Agilent 7500a, CA), and soil pH was measured in a soil slurry (soil/water ratio = 1:2.5).[28]

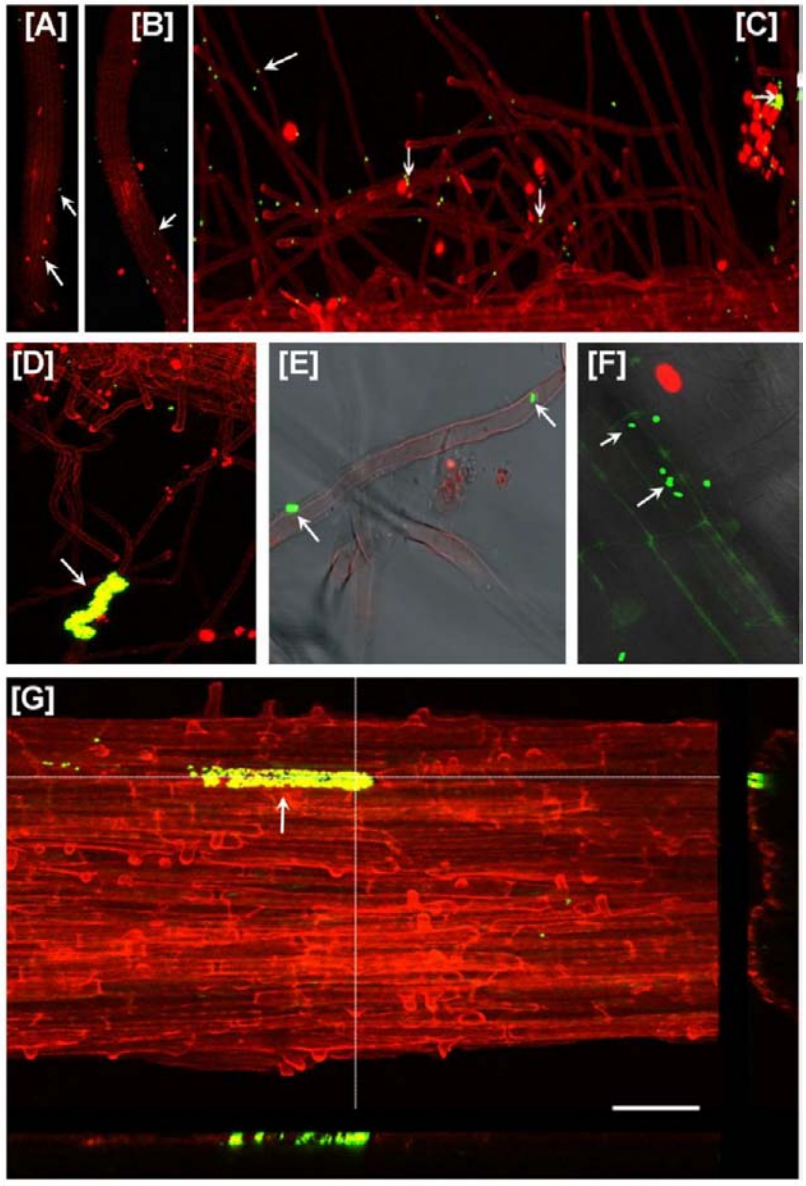

Figure 1. GFP-tagged *Burkholderia sp*. SaMR12 strain colonized on and in the roots of rice. LSCM images present bacterial GFP fluorescence in green and root autofluorescence in red. SaMR12 cells colonized on root cap (A), lateral root (B), and root hairs (C) at 2 DAI. SaMR12 cells colonized at root hairs (D), entered root hair cells (E) and cortical intercellular spaces (F) at 4 DAI. SaMR12 invaded vascular tissues of the primary root (G) at 7 DAI, and arrowhead points to bacterial aggregates. The *xy* crosshairs present the positions for orthogonal sectioning through the *z*-strack. The top right orthogonal view presents the *yz* section of the *z*-stack; the bottom orthogonal view presents the *xz* section of the *z*-strack. Bars: 50 μm in panels A–D and G and 5 μm in panels E and F. DAI, days after inoculation.

SRXRF Analysis. Micro-X-ray fluorescence imaging of Zn in rice root and rhizosphere soil was carried out on beamline BL15U at the Shanghai Synchrotron Radiation Facility (SSRF), Shanghai, China. At 30 DAI, root together with its adjacent rhizosphere soil (0.20 cm) was carefully cut with a razor blade. *In situ* micro-XRF mapping of Zn was analyzed according to Lu et al.[29] The electron energy in the storage ring was 3.5 GeV with a current range from 200 to 300(5) mA. The brilliance of the beam in BL15U was 0.5×10^{12} photons s^{-1} mm^{-2} $mrad^{-2}$ $(0.1\%\ BW)^{-1}$. The microfocused beam of 3.5 μm was provided by a Kirkpatrick–Baez mirror pair (Xradia Inc.) with the sample at 45° to the incident X-ray beam. The fluorescence yield was detected using a seven-element Si (Li) solid state detector, positioned at 90° to the beamline. Dwell time per point was 0.5 s. The step size was set to 10 μm. Scanning areas of the samples were selected and observed using a microscope. BL15U saves full XRF spectrum data at each pixel. Elemental distributions are achieved by windowing on the elements of interest in the XRF spectra. The windows can be applied during data collection or during data analysis since the full XRF spectrum is saved for each pixel. The beam energy was set to 13 keV during mapping. The fluorescence energy windows for this investigation were Zn, Fe, K, Ca, and Mn. The fluorescence data are presented as color maps, and pixel brightness is displayed in RGB, with the brightest spots corresponding to the highest element fluorescence.

Statistical Analysis. All data were statistically analyzed using the SPSS package (version 11.0). Analysis of variance (ANOVA) was performed on the data sets, and the mean and SE of each treatment as well as LSD ($P < 0.05$ and $P < 0.01$) for each set of corresponding data were calculated. The figures were made using the software Origin 8.0.

RESULTS

Root Colonization Patterns of GFP-Tagged Endophytic Bacteria. The GFP-tagged endophytic bacteria were inoculated as the treatment of endophytic inoculation for

dx.doi.org/10.1021/jf404152u | J. Agric. Food Chem. 2014, 62, 1783–1791

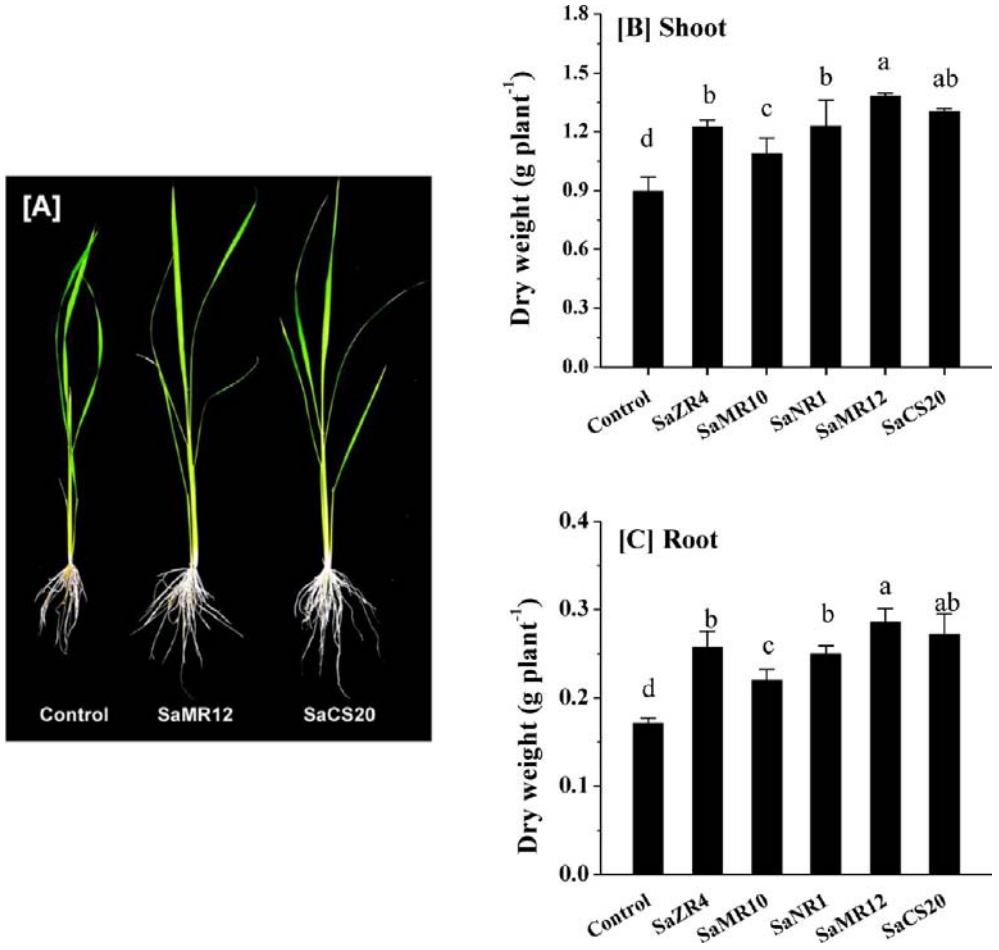

Figure 2. Plant growth (A) and biomass (B, shoot; C, root) of rice after 30 days inoculation with different endophytic bacteria isolated from *S. alfredii*. Different letters indicate statistically significant difference ($P < 0.05$) among treatments. Error bars indicate standard deviations of three replicate determinations.

Table 1. Root Morphology of Rice after 30 Days Hydroponic Inoculation of the Endophytes[a]

treatments	tips	forks	length (cm)	diameter (mm)	surface area (cm^2)	volume (cm^3)
control	7051 ± 468d	13284 ± 601a	1659 ± 136b	0.34 ± 0.04b	253 ± 34b	2.4 ± 0.3b
SaZR4	7480 ± 473cd	12956 ± 591a	1893 ± 167a	0.43 ± 0.02a	280 ± 43ab	3.1 ± 1.1a
SaMR10	8457 ± 451a	12400 ± 463a	1877 ± 189a	0.46 ± 0.02a	269 ± 34b	3.0 ± 0.4a
SaNR1	7359 ± 253d	13085 ± 449a	1933 ± 158a	0.48 ± 0.04a	267 ± 29b	3.3 ± 0.3a
SaMR12	7845 ± 465b	13336 ± 355a	1976 ± 195a	0.46 ± 0.04a	272 ± 38b	3.3 ± 0.6a
SaCS20	8084 ± 231a	12905 ± 399a	1920 ± 382a	0.45 ± 0.03a	310 ± 67a	3.4 ± 0.6a

[a]Values are presented as mean value ± standard deviation of four replicates. Means followed by different letters in the same column indicate significant difference between the treatments at $P < 0.05$.

determination of bacterial populations at different days after inoculation (DAI) under hydroponic conditions. Root colonization patterns of other GFP-tagged endophytic bacteria were quite similar to that of SaMR12, which is shown in Figure 1. At 2 DAI, GFP-tagged SaMR12 had successfully colonized the surface of lateral roots (Figure 1A) and primary roots from root caps (Figure 1B) to root hairs (Figure 1C). From 2 to 4 DAI, SaMR12 cells formed biofilm-like structures on the root surface (Figure 1D) and entered into root hair cells and cortical intercellular spaces (Figure 1E,F). By 7 DAI, SaMR12 had invaded vascular tissues of the primary root (Figure 1G). The GFP-tagged SaMR12 heavily colonized the roots of rice after 2 weeks of inoculation (data not shown). There was no fluorescent bacteria observed on or in the uninoculated roots of rice.

Plant Growth, Root Morphology, and Zn Uptake of Rice Modulated by Endophytic Bacteria. Modulation of plant growth, root morphology, and Zn uptake of rice plants by endophytic bacteria were investigated hydroponically. Five endophytic strains (SaZR4, SaMR10, SaMR12, SaNR1, and SaCS20) isolated from *S. alfredii* were inoculated in the rice roots of Nipponbare under hydroponic condition for 30 d. As shown in Figure 2, inoculation with endophytic bacteria, especially SaMR12 and SaCS20, significantly improved the rice growth. Both root and shoot biomass increased markedly with inoculation with each individual endophytic strain, by 29.4−70.6% in root and 21.1−53.3% in shoot. Among the five

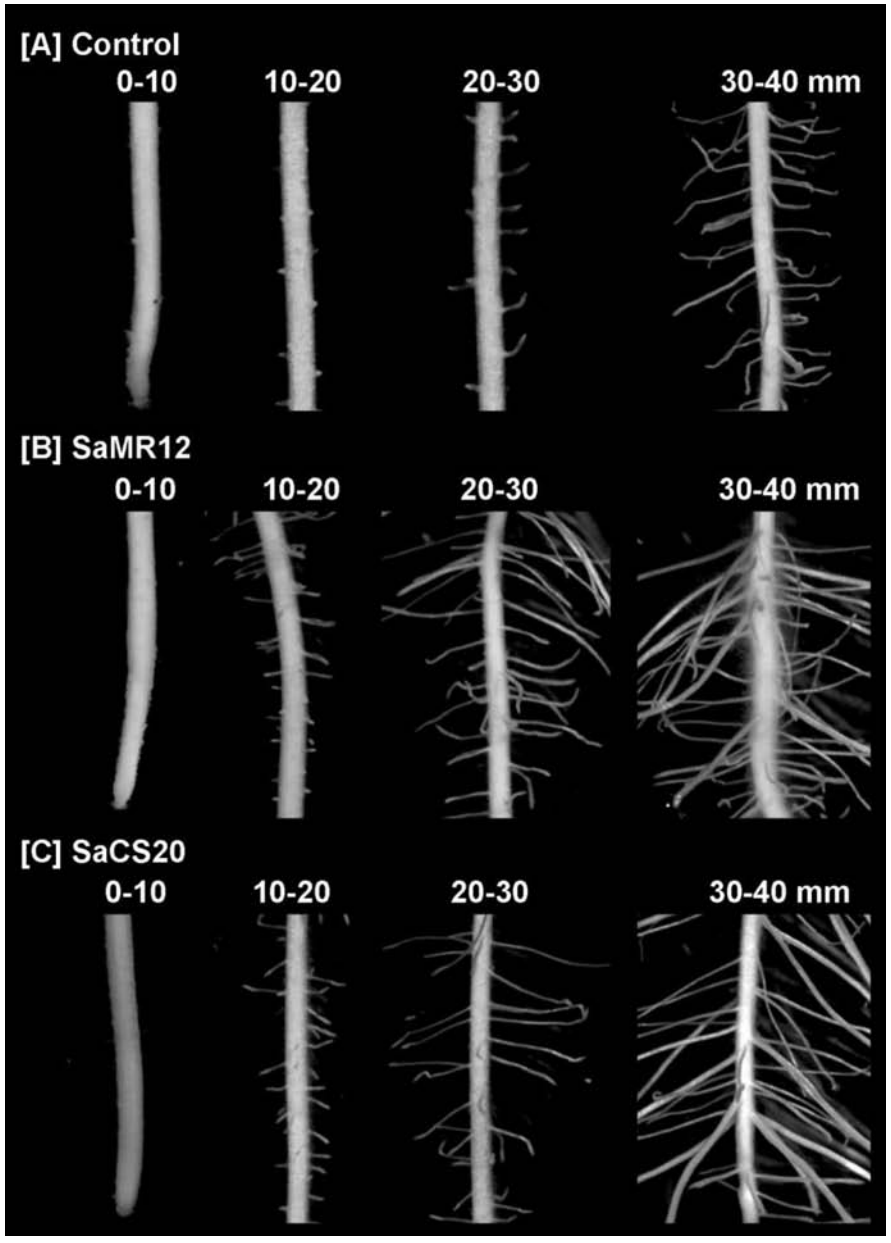

Figure 3. Root tips of rice after 30 days inoculation without (A) or with different endophytic bacteria, SaMR12 (B) and SaCS20 (C), isolated from *S. alfredii*.

endophytic strains, the most pronounced effect of inoculation on growth promotion was observed with SaMR12, followed by SaCS20.

Significant variation of root morphology was observed for rice plants with endophytic inoculation, especially by SaMR12 and SaCS20 (Table 1). Root length and diameter of inoculated seedlings significantly increased by 11.5−16.4% and 23.9−35.2%, respectively, compared with the controls, although no differences were recorded among the five strains. After inoculation with individual bacterial strain, root tips significantly increased by 11.3% and 14.7% at the presence of SaMR12 and SaCS20, although no significant difference of root forks was noted. Significantly increased (22.5%) root surface area was also observed with SaCS20 inoculation. Stereomicroscope imaging of single roots showed that endophytic inoculation of SaMR12 and SaCS20 significantly stimulated root hair production, especially at the 30−40 mm fragment, compared with the controls (Figure 3).

Elevated Zn uptake by rice was observed after inoculation with the five individual endophytic strains, among which the effects of SaMR12 and SaCS20 were mostly pronounced (Figure 4). Inoculation with SaMR12 and SaCS20 raised shoot Zn concentration of rice by 44.4% and 51.1%, respectively, compared with the controls (Figure 4A), and also increased Zn concentration in roots by 73.6% and 83.4%, respectively (Figure 4B). Root Zn concentration increased up to 48.1 and 50.8 $\mu g\ g^{-1}$, respectively, after SaMR12 and SaCS20 inoculation. Calculated from the biomass and Zn concentration, Zn accumulation in shoots and roots of rice increased by approximately 100% and 200%, respectively, in the presence of either SaMR12 or SaCS20.

Improved Grain Yield and Zn Accumulation by SaMR12/SaCS20 Inoculation. Since SaMR12 and SaCS20

dx.doi.org/10.1021/jf404152u | J. Agric. Food Chem. 2014, 62, 1783−1791

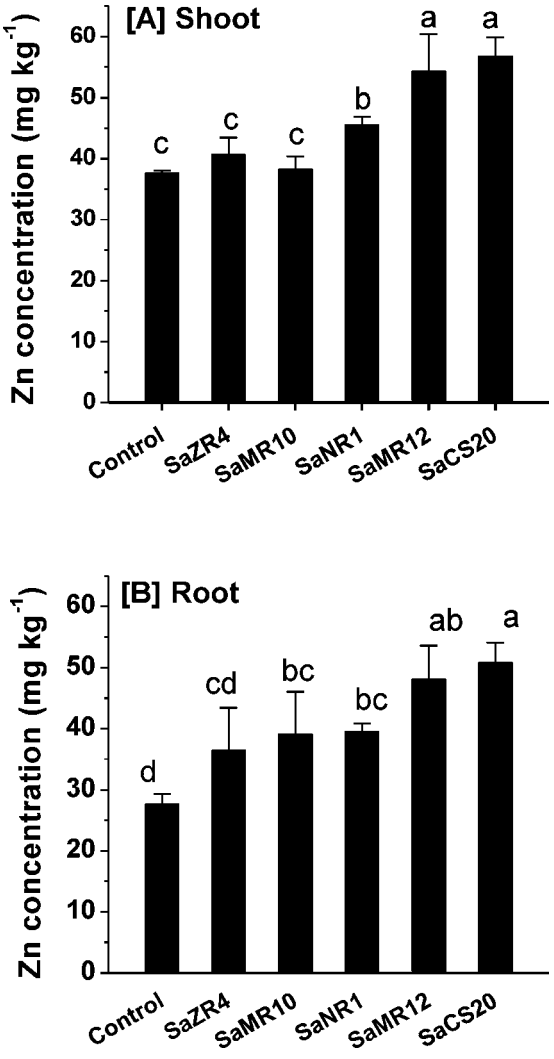

Figure 4. Zn concentrations in shoots (A) and roots (B) of rice after 30 days inoculation with different endophytic bacteria isolated from *S. alfredii*. Different letters indicate statistically significant difference ($P < 0.05$) among treatments. Error bars indicate standard deviations of three replicate determinations.

were of most effective for promotion of plant growth, root morphology, and Zn uptake of rice in solution, their impacts on grain yield and Zn accumulation in rice were further investigated under soil conditions. As shown in Figure 5, SaMR12 began to colonize root rhizosphere soil and root surface at 3 DAI and entered into root cortical intercellular spaces at 7 DAI. SaCS20 showed a similar colonization pattern to that of SaMR12 (data not shown).

Endophytic inoculation with SaMR12 and SaCS20 significantly affected the values of yield components and improved grain yields (Table 2). Although no variation of thousand-grain weight (TGW) and grain setting rate was observed, among all the treatments, significant elevation of panicles and grain per spike was noted by inoculation with the endophytes. When compared with the controls, grain yields increased by 25.5% and 26.9%, respectively, after endophytic inoculation with SaMR12 and SaCS20.

Inoculation with either SaMR12 or SaCS20 also resulted in significant increase of Zn densities in both brown rice and polished rice (Table 3). For instance, Zn concentrations in brown rice reached up to 30 mg kg^{-1} with SaMR12 and

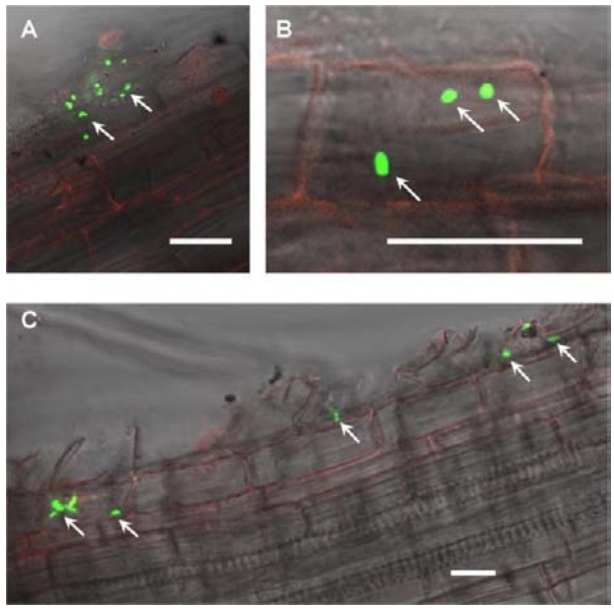

Figure 5. GFP-tagged *Burkholderia sp*. SaMR12 strain colonized in the roots of rice in soil. LSCM images present bacterial GFP fluorescence in green and root autofluorescence in red. SaMR12 cells colonized on root surface (A) and root cells (B, C) at 3 DAI. Bars: 10 μm.

SaCS20 inoculation. Accordingly, the total Zn accumulation in both brown rice and polished rice increased by 50.9−54.4% and 39.4−41.8%, as the result of endophytic inoculation of SaMR12 and SaCS20, respectively. Due to the elevated biomass, Zn accumulation in plant tissues (stems, leaves, flag leaf) was also significantly improved by inoculation with the two endophytic strains, although no variation of Zn concentrations was observed for leaves and stems (Table 3).

Alteration of Rhizosphere Zn by SaMR12/SaCS20 Inoculation. The impacts of SaMR12 and SaCS20 on soil pH and rhizosphere Zn were analyzed for rice cultured in pot experiments. Bacterial inoculation did not change soil pH in the rhizosphere zone cultured with rice plants (Figure 6A). However, in the presence of SaMR12 or SaCS20, rhizosphere soils contained a higher concentration of DTPA-Zn by 10.4−20.6% compared with the controls (Figure 6B).

To further investigate the impacts of endophytic bacterial inoculation on rhizosphere Zn of rice, microscanning XRF mapping of elemental distributions was performed on rice roots and rhizosphere soil nearby with or without SaMR12 inoculation. The integrated intensity for Zn was calculated from the spectrum and normalized by the intensity of the Compton scattering peak. Elemental mapping for the measurement area was obtained from the normalized intensity for the element. The elemental distribution maps of Zn in the scanned area of rhizosphere zone are presented in Figure 7, together with photographs taken using an optical microscope. The XRF maps indicate the relative distribution of Zn, and the normalized X-ray fluorescence intensities are scaled from red (maximum, 1000 counts s^{-1}) to purple (minimum, 0 counts s^{-1}). The XRF image of the controls (Figure 7A) revealed that Zn intensities were very low in the rhizosphere zone nearby the rice roots, while higher intensities of Zn were observed in both roots of rice and their adjacent rhizosphere zone with inoculation with SaMR12 at 30 DAI (Figure 7B). On the basis of the intensity of Zn signal (Figure 7B), the concentration of Zn in the rhizosphere zone in presence of

Table 2. Plant Growth and Yield Parameters of Rice Cultivar at Harvest with Two Different Endophytic Inoculation Treatments[a]

treatments	panicles per pot	grain per spike (grain per^{-1})	grain setting (%)	TGW (g)	shoot biomass (g pot^{-1})	grain yield (g pot^{-1})
control	18 ± 3b	57.3 ± 4.1b	0.79 ± 0.03a	25.9 ± 0.7a	32.6 ± 5.6b	21.6 ± 2.9b
SaMR12	22 ± 2a	63.4 ± 3.5a	0.75 ± 0.02a	26.2 ± 0.9a	45.12 ± 6.9a	27.1 ± 3.0a
SaCS20	20 ± 3ab	66.9 ± 5.8a	0.79 ± 0.04a	25.8 ± 0.8a	46.6 ± 5.7a	27.4 ± 6.2a

[a]Values are presented as mean value ± standard deviation of four replicates. TGW, thousand-grain weight. Means followed by different letters in the same column indicate significant difference between the treatments at $P < 0.05$.

Table 3. Zn Concentration (μg g^{-1}) and Zn Accumulation (μg pot^{-1}) of Different Parts of Rice Cultivar at Harvest with Two Different Endophytic Inoculation Treatments[a]

treatments	stem	leaf	flag leaf	brown rice	polished rice
			Zn Concentration (μg g^{-1})		
control	40.3 ± 3.8ab	47.6 ± 3.2a	37.6 ± 4.0a	25.1 ± 2.9b	20.5 ± 0.4b
SaMR12	49.3 ± 6.0a	48.4 ± 2.8a	40.3 ± 3.6a	30.2 ± 2.4a	23.3 ± 0.5a
SaCS20	37.6 ± 4.2b	44.6 ± 2.6a	38.2 ± 2.0a	30.6 ± 2.9a	22.8 ± 0.4a
			Zn Accumulation (μg pot^{-1})		
control	983.2 ± 24.6c	568.2 ± 26.1b	45.8 ± 2.3b	433.3 ± 24.3b	311.8 ± 19.5b
SaMR12	1481.3 ± 35.3a	715.0 ± 32.7a	60.5 ± 3.0a	653.9 ± 39.0a	442.2 ± 30.4a
SaCS20	1166.8 ± 32.4b	681.2 ± 31.1a	59.2 ± 4.3a	668.8 ± 40.5a	434.5 ± 25.9a

[a]Values are presented as mean value ± standard deviation of four replicates. Means followed by different letters in the same column indicate significant difference between the treatments at $P < 0.05$.

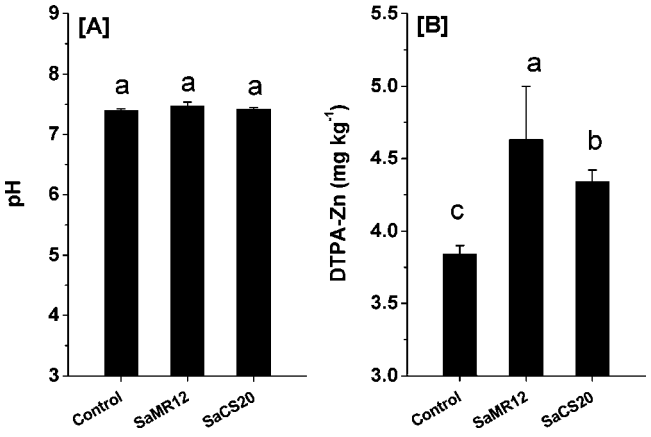

Figure 6. Variations of soil pH and DTPA-Zn (mg kg^{-1}) in rice rhizosphere soil with inoculation of SaMR12 and SaCS20. Different letters indicate statistically significant difference ($P < 0.05$) among treatments. Error bars indicate standard deviations of four replicate determinations.

SaMR12 was likely to be many times higher than that of the controls.

DISCUSSION

Plant growth-promoting rhizobacteria (PGPR) are beneficial bacteria that colonize the rhizosphere and contribute to enhanced plant growth and yield of crop plants.[30] The most important characteristic of PGPR is the ability to colonize the roots of host plants.[31] Different plant hosts have different ability for the stains to be colonized.[32] The present study clearly showed successful colonization of endophytic microbial isolates from the Zn hyperaccumulator *S. alfredii*,[23] resulting in significantly plant growth promotion of rice plants (Figures 1 and 2). It has been reported that the survival of PGPR in soil was greatly influenced by external parameters including water content, pH, soil type, composition of root exudates, and other microorganisms;[33] their survival and colonization in soils are still doubtful even if the microbe could colonize the host plants in hydroponic conditions. Here we also clarified by pot experiments that the isolated endophytic strains from *S. alfredii* could succeed in surviving in paddy soils and colonize rice root cortical intercellular spaces (Figure 5). These results suggested that these endophytic microbial strains isolated from *S. alfredii* had a significant effect on plant growth promotion either under hydroponic or soil conditions.

Recent investigation on PGPR suggests its promotion of growth by a wide variety of mechanisms, including phytohormone production, rhizosphere engineering, phosphate solubilization, etc.[13,16] The main characteristic of PGPR is to promote the growth of plant roots, and this is confirmed by the bacteria-improved root morphology and enhanced root hair production in this study (Figure 2; Table 1). Most commonly, endophytic bacteria synthesize IAA to promote root growth and root length.[34] Zhang et al.[23] suggested that bacterial IAA production was likely involved in the plant-promoting effects on *S. alfredii* in hydroponic culture. IAA production of the endophytic microbes ranged from 0.51 to 82.99 μg mL^{-1},[24] with higher IAA production observed for SaMR12 and SaCS20. Although not determined in this study, it is possible that IAA production may be responsible for the enhanced plant growth of rice induced by SaMR12 and SaCS20 inoculation.

Distiguished from normal PGPR, endophytic microbial strains applied in this study were isolated from a Zn hyperaccumualtor *S. alfredii*, which has an extraordinary ability to take up Zn from soils and accumulate large amounts of Zn in its aerial parts.[21,22] The endophytic microbial strains were able to increase Zn accumulation in plants of their original host *S. alfredii*.[23] It is therefore not surprising that inoculation of the endophytic microbial strains (SaMR12 and SaCS20) to rice plants not only resulted in promotion of plant growth and grain yields (Table 2) but also elevated Zn densities in rice grains (Table 3). Reduced yield and low harvest index resulting from increased mineral concentrations in the edible parts is a general problem for micronutrient biofortification of crops.[35] The positive responses of both rice grains yields and Zn densities

dx.doi.org/10.1021/jf404152u | J. Agric. Food Chem. 2014, 62, 1783−1791

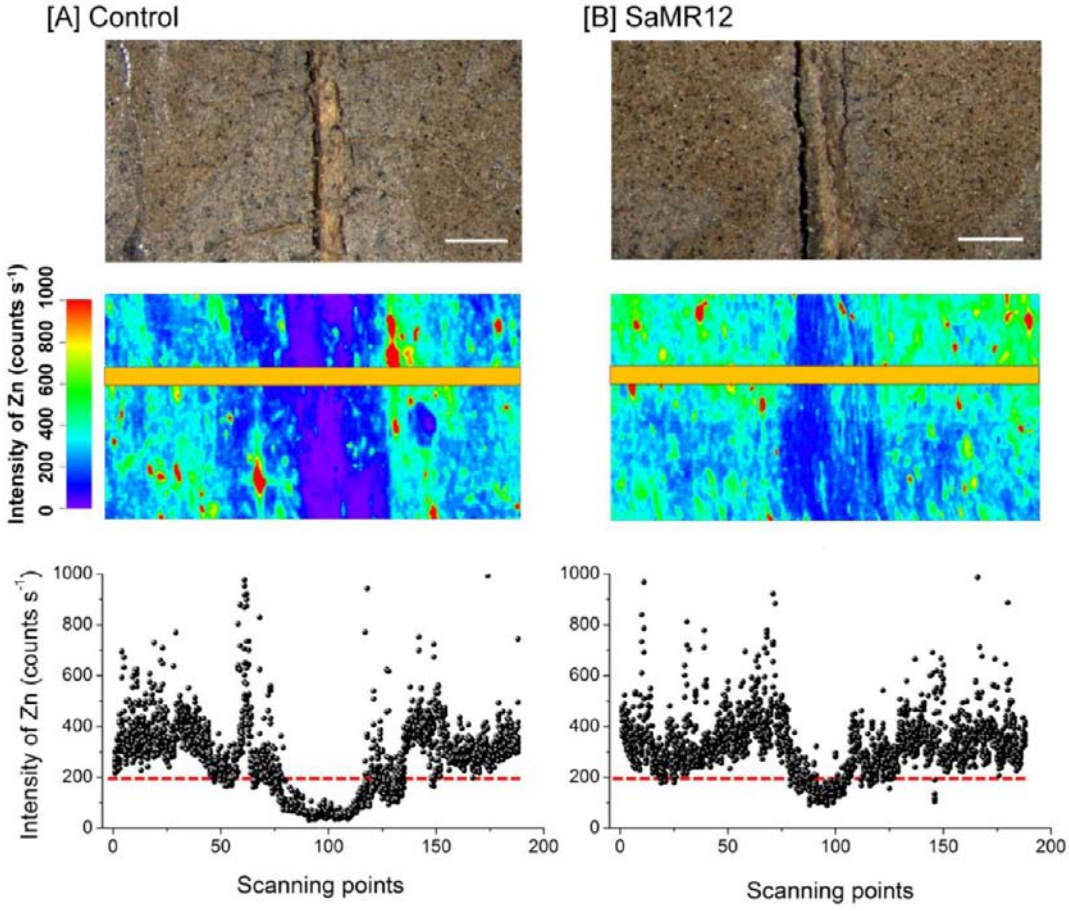

Figure 7. μ-XRF elemental maps for Zn of rice root and rhizosphere soil treated with control (A) and SaMR12 strain inoculation (B) for 30 DAI.

with SaMR12 and SaCS20 inoculation suggested that application of the endophytes could be an efficient strategy for Zn biofortification in rice grains. Millions of hectares of cropland are affected by Zn deficiency, and approximately one-third of the human population suffers from an inadequate intake of Zn.[36] To the best of our knowledge, the present study for the first time reported the potential use of endophytes isolated from hyperaccumulators on Zn biofortification of rice plants.

The possible mechanisms involved in the enhanced Zn accumulation in rice by endophytic inoculation, however, are not well-known. The results in the present study suggested modulation of root morphology might be one of the strategies involved in endophyte-enhanced metal uptake and accumulation in rice plants. In nutrient efficiency conditions, roots play the most important role in nutrient acquisition;[37] root morphology (length, surface, volume, and diameter) are of key importance for acquisition of nutrients. In hydroponic experiments, in the presence of endophytic bacteria, root length, surface, volume, and diameter of rice roots were significantly increased (Table 1; Figure 3). The enhancement of root morphology with endophytic inoculation might result in higher Zn uptake by rice plants. Another possible mechanism for enhanced Zn accumulation in rice plants is the alteration of rhizosphere Zn under soil conditions. Biofortification of Zn for food crops is largely dependent on the size of plant-available Zn pools in soil.[7] DTPA-Zn is regarded as a mixture of both mobile and potentially mobilizable species and represented the pool of bioavailable Zn in soils. The inoculation of endophytic bacteria increased the root surface area (Table 1) and DTPA-Zn content in the rhizosphere soil (Figure 6), the same as reported by Orhan et al.,[38] further facilitating Zn acquisition by the plants (Table 3). The XRF images (Figure7) further confirmed higher intensities of Zn observed in both roots of rice and their adjacent rhizosphere zone after inoculation of SaMR12 for 30 DAI, compared with the controls. The alteration of rhizosphere Zn was not due to the soil acidification since soil pH did not changed with inoculation of the endophytes.

In conclusion, the present study suggest that colonization with the endophytic microbial isolates from hyperaccumulators to rice plants could result in improved root morphology and plant growth, increased Zn bioavailability in rhizosphere soils, and elevated grain yields and Zn densities in both brown rice and polished rice, thus providing a potential strategy for Zn biofortification of rice grains.

AUTHOR INFORMATION

Corresponding Author

*Dr. Lingli Lu. Mailing address: Department of Plant Nutrition, College of Environmental & Resources Science, Nongshenghuan Building B-517 Zhejiang University, Zijingang Campus, Hangzhou, 310058, P.R. China. Tel: +86-13588356620. Fax: +86-0571-88982907. E-mail: lulingli@zju.edu.cn, linglilulu@gmail.com.

Funding

This research work was financially supported by the HarvestPlus-China Program (Grant 8271), the National Natural

Science Foundation of China (Grant 31300040), and the Department of Science & Technology of Zhejiang Province (Grant 2011C22077).

Notes

The authors declare no competing financial interest.

■ ACKNOWLEDGMENTS

Liao Haibing is gratefully acknowledged for ICP-MS analysis.

■ REFERENCES

(1) Ishimaru, Y.; Bashir, K.; Nishizawa, N. K. Zn uptake and translocation in rice plants. *Rice* **2011**, *4*, 21−27.
(2) Gibson, R. Zinc: The missing link in combating micronutrient malnutrition in developing countries. *Proc. Nutr. Soc.* **2006**, *65*, 51−60.
(3) Chasapis, C. T.; Loutsidou, A. C.; Spiliopoulou, C. A.; Stefanidou, M. E. Zinc and human health: An update. *Arc. Toxicol.* **2012**, *86*, 521−534.
(4) Maret, W.; Sandstead, H. H. Zinc requirements and the risks and benefits of zinc supplementation. *J. Trace Elem. Med. Biol.* **2006**, *20*, 3−18.
(5) Fitzgerald, M. A.; McCouch, S. R.; Hall, R. D. Not just a grain of rice: The quest for quality. *Cell* **2009**, *14*, 133−139.
(6) Palmgren, M. G.; Clemens, S.; Williams, L. E.; U, K.; Borg, S.; Schjørring, J. K.; Sanders, D. Zinc biofortification of cereals: Problems and solutions. *Trends Plant Sci.* **2008**, *13*, 464−473.
(7) Cakmak, I. Enrichment of cereal grains with zinc: Agronomic or genetic biofortification? *Plant Soil* **2008**, *302*, 1−17.
(8) Hussain, S.; Maqsood, M. A.; Rengel, Z.; Aziz, T. Biofortification and estimated human bioavailability of zinc in wheat grains as influenced by methods of zinc application. *Plant Soil* **2012**, *361*, 279−290.
(9) Gao, X.; Hoffland, E.; Stomph, T.; Grant, C.; Zou, C.; Zhang, F. Improving zinc bioavailability in transition from flooded to aerobic rice. A review. *Agron. Sustainable Dev.* **2012**, *32*, 465−478.
(10) Impa, S. M.; Johnson-Beebout, S. Mitigating zinc deficiency and achieving high grain Zn in rice through integration of soil chemistry and plant physiology research. *Plant Soil* **2012**, *361*, 3−41.
(11) Rehman, H.-u.; Aziz, T.; Farooq, M.; Wakeel, A.; Rengel, Z. Zinc nutrition in rice production systems: A review. *Plant Soil* **2012**, *361*, 203−226.
(12) Miransari, M. Soil microbes and plant fertilization. *Appl. Microbiol. Biotechnol.* **2011**, *92*, 875−885.
(13) Bhattacharyya, P. N.; Jha, D. K. Plant growth-promoting rhizobacteria (PGPR): Emergence in agriculture. *World J. Microbiol. Biotechnol.* **2012**, *28*, 1327−50.
(14) Sturz, A. V.; Christie, B. R.; Nowak, J. Bacterial endophytes: Potential role in developing sustainable systems of crop production. *Crit. Rev. Plant Sci.* **2000**, *19*, 1−30.
(15) Peng, S. B.; Biswas, J. C.; Ladha, J. K.; Gyaneshwar, P.; Chen, Y. Z. Influence of rhizobial inoculation on photosynthesis and grain yield of rice. *Agron. J.* **2002**, *94*, 925−929.
(16) Rana, A.; Joshi, M.; Prasanna, R.; Shivay, Y. S.; Nain, L. Biofortification of wheat through inoculation of plant growth promoting rhizobacteria and cyanobacteria. *Eur. J. Soil Biol.* **2012**, *50*, 118−126.
(17) Weyens, N.; van der Lelie, D.; Taghavi, S.; Vangronsveld, J. Phytoremediation: Plant-endophyte partnerships take the challenge. *Curr. Opin. Biotechnol.* **2009**, *20*, 248−254.
(18) Luo, S.; Xu, T.; Chen, L.; Chen, J.; Rao, C.; Xiao, X.; Wan, Y.; Zeng, G.; Long, F.; Liu, C.; Liu, Y. Endophyte-assisted promotion of biomass production and metal-uptake of energy crop sweet sorghum by plant-growth-promoting endophyte *Bacillus sp*. SLS18. *Appl. Microbiol. Biotechnol.* **2011**, *93*, 1745−1753.
(19) Sheng, X.; Sun, L.; Huang, Z.; He, L.; Zhang, W.; Chen, Z. Promotion of growth and Cu accumulation of bio-energy crop (*Zea mays*) by bacteria: Implications for energy plant biomass production and phytoremediation. *J. Environ. Manage.* **2012**, *103*, 58−64.
(20) Zhang, X.; Lin, L.; Chen, M.; Zhu, Z.; Yang, W.; Chen, B.; Yang, X.; An, Q. A nonpathogenic *Fusarium oxysporum* strain enhances phytoextraction of heavy metals by the hyperaccumulator *Sedum alfredii* Hance. *J. Hazard. Mater.* **2012**, *229*−*230*, 361−370.
(21) Tian, S. K.; Lu, L. L.; Yang, X. E.; Labavitch, J. M.; Huang, Y. Y.; Brown, P. Stem and leaf sequestration of zinc at the cellular level in the hyperaccumulator *Sedum alfredii*. *New Phytol.* **2009**, *182*, 116−126.
(22) Yang, X. E.; Long, X. X.; Ni, W. Z.; Fu, C. X. *Sedum alfredii* H: A new Zn hyperaccumulating plant first found in China. *Chin. Sci. Bull.* **2002**, *47*, 1634−1637.
(23) Zhang, X.; Lin, L.; Zhu, Z.; Yang, X. E.; Wang, Y.; An, Q. Colonization and modulation of host growth and metal uptake by endophytic bacteria of *Sedum alfredii*. *Int. J. Phytorem.* **2012**, *15*, 51−64.
(24) Zhang, X. Isolation and identification of endophytes from *Sedum alfredii* and the mechanisms of their enhancement on heavy metal hyperaccumulation. Ph.D. Thesis, Zhejiang University, 2012.
(25) Lin, L.; Guo, W.; Xing, Y.; Zhang, X.; Li, Z.; Hu, C.; Li, S.; Li, Y.; An, Q. The actinobacterium *Microbacterium sp.* 16SH accepts pBBR1-based pPROBE vectors, forms biofilms, invades roots, and fixes N_2 associated with micropropagated sugarcane plants. *Appl. Microbiol. Biotechnol.* **2011**, *93*, 1185−1195.
(26) Yang, X.; Romheld, V.; Marschner, H.; Chaney, R. L. Application of chelator-buffered nutrient solution technique in studies on zinc nutrition in rice plant (*Oryza-sativa* L). *Plant Soil* **1994**, *163*, 85−94.
(27) Wu, C. Y.; Lu, L. L.; Yang, X. E.; Feng, Y.; Wei, Y. Y.; Hao, H. L.; Stoffella, P. J.; He, Z. L. Uptake, translocation, and remobilization of zinc absorbed at different growth stages by rice genotypes of different Zn densities. *J. Agric. Food Chem.* **2010**, *58*, 6767−6773.
(28) Lu, R. K. *Analysis Method of Soil Agricultural Chemistry*; Chinese Agricultural Science & Technology Press: Beijing, 2000.
(29) Lu, L. L.; Tian, S. K.; Liao, H. B.; Zhang, J.; Yang, X. E.; Labavitch, J. M.; Chen, W. R. Analysis of metal element distributions in rice (*Oryza sativa* L.) seeds and relocation during germination based on X-Ray fluorescence imaging of Zn, Fe, K, Ca, and Mn. *PLoS One* **2013**, *8*, No. e57360.
(30) Dutta, S.; Podile, A. R. Plant growth promoting rhizobacteria (PGPR): The bugs to debug the root zone. *Critl. Rev. Microbiol.* **2010**, *36*, 232−244.
(31) Rajkumar, M.; Sandhya, S.; Prasad, M. N.; Freitas, H. Perspectives of plant-associated microbes in heavy metal phytoremediation. *Biotechnol. Adv.* **2012**, *30*, 1562−1574.
(32) Rosenblueth, M.; Martinez-Romero, E. Bacterial endophytes and their interactions with hosts. *Mol. Plant−Microbe Interact.* **2006**, *19*, 827−837.
(33) Ahmad, F.; Husain, F. M.; Ahmad, I. Rhizosphere and root colonization by bacterial inoculants and their monitoring methods: A critical area in PGPR research. In *Microbes and Microbial Technology: Agricultural and Environmental Applications*; Ahmad, I., Ahmad, F., Pichtel, J., Eds.; Springer: New York: 2011; pp 363−391.
(34) Vessey, J. K. Plant growth promoting rhizobacteria as biofertilizers. *Plant Soil* **2003**, *255*, 571−586.
(35) White, P. J.; Broadley, M. R. Biofortifying crops with essential mineral elements. *Trends Plant Sci.* **2005**, *10*, 586−593.
(36) Alloway, B. J. Soil factors associated with zinc deficiency in crops and humans. *Environ. Geochem. Health* **2009**, *31*, 537−548.
(37) Marschener, H. Role of root growth, arbuscular mycorrhiza, and root exudates for the efficiency in nutrient acquisition. *Field Crop. Res.* **1998**, *56*, 203−207.
(38) Orhan, E.; Esitken, A.; Ercisli, S.; Turan, M.; Sahin, F. Effects of plant growth promoting rhizobacteria (PGPR) on yield, growth and nutrient contents in organically growing raspberry. *Sci. Hortic. (Amsterdam, Neth.)* **2006**, *111*, 38−43.

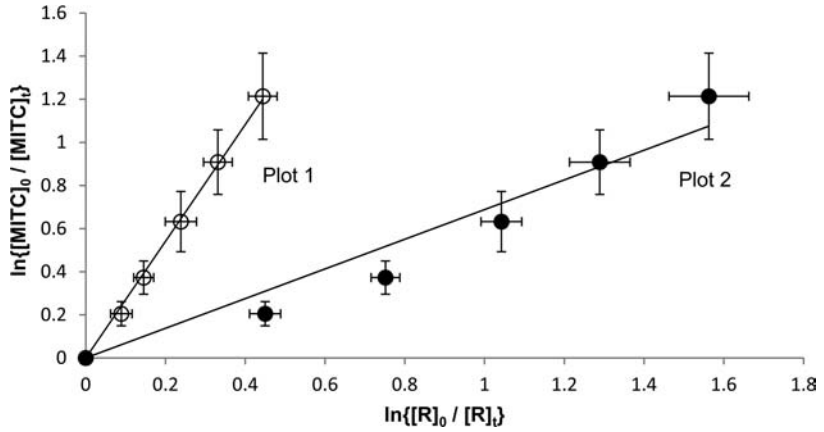

Figure 1. Plots of eq 5 for MITC using toluene (plot 1) and *m*-xylene (plot 2) as reference chemicals.

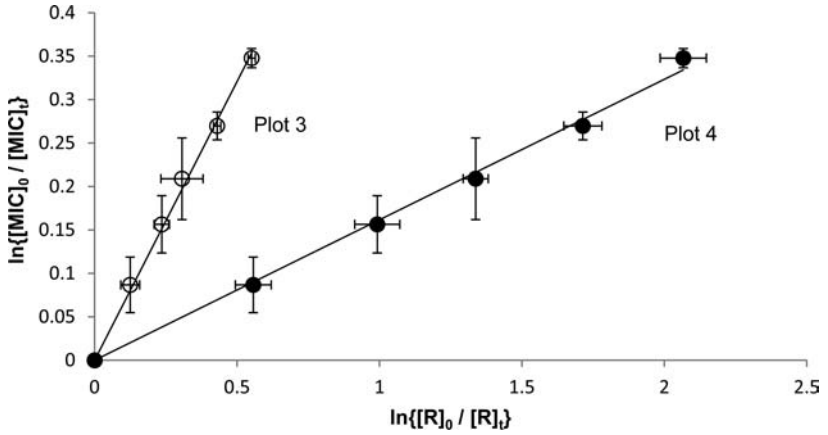

Figure 2. Plots of eq 5 for MIC using toluene (plot 3) and *m*-xylene (plot 4) as reference chemicals.

$$-\frac{d[T]}{dt} = k_1[OH][T] \quad (1)$$

$$-\frac{d[R]}{dt} = k_2[OH][R] \quad (2)$$

where k_1 and k_2 refer to the OH radical rate constants of the test compound and the reference chemical, respectively. Integrations can be made to both sides of eqs 1 and 2:

$$\int_0^c \left\{\frac{d[T]}{[T]}\right\} = -k_1[OH]\int_0^t dt \quad (3)$$

$$\int_0^c \left\{\frac{d[R]}{[R]}\right\} = -k_2[OH]\int_0^t dt \quad (4)$$

Finally, eq 5 is derived from the combination of eqs 3 and 4:

$$\ln\left\{\frac{[T]_0}{[T]_t}\right\} = \frac{k_1}{k_2}\ln\left\{\frac{[R]_0}{[R]_t}\right\} \quad (5)$$

where $[T]_0$ and $[R]_0$ refer to the concentrations of the test compound and the reference chemical at the beginning time of the experiment, t = 0, respectively; $[T]_t$ and $[R]_t$ are their concentrations measured at each time point as the experiment proceeds. A plot of $\ln\{[T]_0/[T]_t\}$ versus $\ln\{[R]_0/[R]_t\}$ will yield a straight line with a slope of k_1/k_2, assuming that there are no other reactions occurring.

Rate Constant Determination. The test procedures were performed in a 100 L Tedlar bag (SKC, Inc., Eighty Four, PA) with the irradiation of 9 Q-PANEL UVA-351 lamps (Q-LAB, Co., Westlake, OH). A fan was used to provide a stream of air to eliminate heating caused by the irradiation, and a temperature of 293 ± 2 K was measured around the bag. Carbon tetrachloride (CCl_4) was added as a stable tracer to demonstrate that the OH radical reaction is the predominant reaction causing the loss of the reactants in the bag. Certain amounts of CH_3ONO, CCl_4, MITC or MIC, toluene, and *m*-xylene were first injected into a glass gas sampling tube using a gastight syringe. The contents of the gas sampling tube were then passed into the Tedlar bag using a constant stream of air, which carried the volatile compounds into the bag until 90 L of air was added. The initial concentrations of each component in the bag were as follows: CH_3ONO, ∼400 ppm; MITC or MIC, ∼20 ppm; CCl_4, ∼20 ppm, toluene and *m*-xylene, ∼20 ppm.

The bag was first placed in the dark irradiation chamber for 1 h, which allowed each volatile compound to mix thoroughly. The loss of each substance in the irradiated bag was determined by sampling the bag every 10 min using a Supelco solid-phase microextraction (SPME) fiber (75 μm CAR/PDMS, Sigma−Aldrich Co. LLC.). The SPME sampling was performed for 30 s followed by 10 s desorption onto the inlet of a Hewlett−Packard 6890-5972 gas chromatography−mass spectrometry (GC-MS) system (Agilent Technologies, Inc., Santa Clara, CA) equipped with a 30 m × 0.25 mm DB-624 capillary column (Agilent Technologies). The oven temperature of the gas chromatograph was first held at 70 °C for 0.5 min; then, the temperature ramped from 70 to 150 °C at a rate of 15 °C/min. The mass spectrometer was operated in the selected ion monitoring (SIM) mode to screen mass-to-charge ratios (m/z) of 72 for MITC, 57 for MIC, 91 for toluene, 106 for *m*-xylene, and 117 for CCl_4. The MITC−OH and MIC−OH reaction experiments were replicated three times, respectively.

Conversion of MITC to MIC. A solution was prepared by dissolving the same mass of MITC and MIC in *o*-xylene. The solution was then analyzed by GC-MS to yield the peak area ratio of MITC to MIC.

dx.doi.org/10.1021/jf404526t | J. Agric. Food Chem. 2014, 62, 1792−1795

RESULTS AND DISCUSSION

OH Radical Reaction Rate Constants of MITC and MIC. Samples taken and analyzed using GC-MS every 15 min for 1 h in the dark indicated that there was no significant loss of either the test compound or the reference chemicals in the Tedlar bag during this period.

When the lamps were turned on, about 50% of the initial concentration of *m*-xylene was observed to be lost within 10 min, consistent with an observation of Biermann and co-workers.[11] As discussed in this previous study, a series of complex photoreactions induced by a small amount of impurity in CH_3ONO added could be one possible reason accounting for this phenomenon.[11] Thus, for these experiments, the samples taken at 10 min after turning on the lamps were used as the time 0 samples, since samples taken earlier showed a high level of inconsistency.

Concentrations of the test compound and the reference chemicals obtained from each sampling time point during the 1 h irradiation period were plotted based on eq 5 with standard deviations from three replications (Figures 1 and 2). Relevant index of the plots is shown in Table 1.

Table 1. Index of MITC and MIC OH Radical Reaction Data Plots

plots of eq 5	reference chemical	equation	R^2
plot 1	toluene	$y = 2.71x$	0.998
plot 2	*m*-xylene	$y = 0.688x$	0.943
plot 3	toluene	$y = 0.641x$	0.996
plot 4	*m*-xylene	$y = 0.162x$	0.996

A consistent, but small curvilinear response was observed for MITC, but not for MIC, when *m*-xylene was used as the reference chemical (see Figure 1), suggesting that some additional mechanism for loss of MITC exists, in addition to reaction with OH radicals. Previous research has indicated that MITC does undergo direct photolysis, although the photochemical reaction is slower than the OH radical reaction.[12] The reason for the observed lack of linearity may be due to a small contribution from direct photolysis, since while the lamps have a maximum emission at 351 nm, this is a broad band emission and emits light of shorter wavelengths. The relatively greater loss of MITC in those plots is consistent with this suggestion.

OH radical rate constants of 5.48×10^{-12} cm^3 molecule^{-1} s^{-1} for toluene and 23.0×10^{-12} cm^3 molecule^{-1} s^{-1} for *m*-xylene reported by Atkinson were used in this study.[13] Thus, according to eq 5, multiplying the slope of a linear plot by the rate constant of its corresponding reference chemical gives the OH radical rate constant of MITC and/or MIC (Table 2).

For determining the rate of loss of chemicals in the atmosphere from OH radical reactions, the concentration of OH radicals is required. Since the OH radical concentration varies at different times in a day, an average concentration of 8.0×10^5 molecules cm^{-3} is commonly utilized for estimating the rate of OH radical reactions.[5] The calculated half-lives of MITC and MIC using this average concentration are shown in Table 3.

Photolysis is also observed when MITC is exposed to midsummer sunlight, with a half-life on the order of 30 h of continuous exposure (including nighttime).[12] While direct comparisons using these results are only approximate, the results of the previous study on photolysis of MITC and the present study indicate that OH radical reactions are about twice as important as direct photolysis for transformation of MITC. MIC was also observed during the photolysis reactions, although it presumably went through a photochemically produced intermediate, methyl isocyanide, which was then oxidized to MIC.[14] The possibility that the OH radical was created during the direct photolysis studies also cannot be excluded.

Table 2. OH Radical Reaction Rate Constants of MITC and MIC

test compd	reference chemical	k_1/k_2[a]	k_1 ($\times 10^{-12}$ cm^3 molecule^{-1} s^{-1})	k_1 ($\times 10^{-12}$ cm^3 molecule^{-1} s^{-1})[b]
MITC	toluene	2.71	14.9 ± 2.66	15.4
	m-xylene	0.688	15.8 ± 2.98	
MIC	toluene	0.641	3.52 ± 0.152	3.62
	m-xylene	0.162	3.73 ± 0.0823	

[a]OH radical rate constant ratio, mean value from three replications using each reference chemical. [b]Average OH radical rate constants, mean value from three replications and for each of the two reference chemicals.

Table 3. Estimated Half-lives of MITC and MIC

test compd	half-life (h)[a]
MITC	15.6
MIC	66.5

[a]Half-lives calculated by using the average OH radical rate constants in Table 2 and an average OH radical concentration of 8.0×10^5 molecules cm^{-3}.

Molar Conversion Ratio of MITC to MIC. At the same weight per volume concentration, the GC peak area ratio of MITC to MIC was determined to be 1.98 to 1. The calculated disappearance rate of MIC in the first 30 min of the irradiation of the MIC−OH reaction was approximately 14%. Since the MIC formed in the MITC−OH reaction also reacts with OH radicals to degrade at the same time, a correction of 14% should be made to the increased peak area of MIC measured during the first 30 min irradiation period of MITC−OH reaction. Thus, molar conversion ratio of MITC to MIC can be calculated by combining their peak area ratio, molecular weights (M_r) and the changed peak area (ΔA_{peak}) of MITC and MIC obtained in the first 30 min of the irradiation, respectively:

$$\text{Molar conversion ratio} = \frac{\Delta A_{peak(MIC)} \times (1 + 14\%) \times 1.98}{\Delta A_{peak(MITC)}} \cdot \frac{M_{r(MITC)}}{M_{r(MIC)}} \quad (6)$$

Finally, a molar conversion ratio of MITC to MIC during the first 30 min irradiation period of the MITC−OH reaction is estimated to be 67% ± 8% based on eq 6, indicating that MIC is a primary product of MITC in the OH radical reaction.

OH radical reaction rate constants measured in this work are 15.36×10^{-12} cm^3 molecule^{-1} s^{-1} for MITC and 3.62×10^{-12} cm^3 molecule^{-1} s^{-1} for MIC. The result of MITC is comparable to that of the former work done by Sommerlade, employing a smog chamber−mass spectrometer system.[5] Results obtained in this work demonstrate that MIC is a primary transformation product of MITC and it disappears approximately 4 times slower than MITC in the presence of OH radicals. Due to the large consumption of metam sodium in U.S. agriculture[1] and the important health concern of MIC,[9] this study will provide useful information for the exposure assessments for use of the

dx.doi.org/10.1021/jf404526t | J. Agric. Food Chem. 2014, 62, 1792−1795

fumigant metam sodium and other pesticides in which MITC serves as the active fumigant.

AUTHOR INFORMATION

Corresponding Author

*Phone: (775) 784-4108; fax: (775) 784-1142; e-mail: gcmiller@unr.edu.

Notes

The authors declare no competing financial interest.

ACKNOWLEDGMENTS

We thank Dr. Jeff Angermann for providing the liquid nitrogen container. We also appreciate the helpful advice given by Dr. Roger Atkinson.

ABBREVIATIONS USED

MITC, methyl isothiocyanate; MIC, methyl isocyanate; OH radical, hydroxyl radical; SPME, solid-phase microextraction; GC-MS, gas chromatography−mass spectrometry; T, test compound; R, reference chemical; $[T]_0$, concentration of test compound at the beginning time of the experiment; $[R]_0$, concentration of reference chemical at the beginning time of the experiment; $[T]_t$, concentration of test compound measured at each time point as the experiment proceeds; $[R]_t$, concentration of reference chemical measured at each time point as the experiment proceeds; k_1, hydroxyl radical reaction rate constant of test compound; k_2, hydroxyl radical reaction rate constant of reference chemical; R^2, coefficient of determination; ΔA_{peak}, changed peak area; M_r, molecular weight

REFERENCES

(1) Cox, C. Metam sodium. *J. Pestic. Reform* **2006**, *26*, 12−16.

(2) California Environmental Protection Agency. *Risk Characterization Document Methyl Isothiocyanate (MITC) Following the Agricultural Use of Metam Sodium*; Medical Toxicology Branch, Department of Pesticide Regulation: Sacramento, CA, 2003.

(3) Leistra, M.; Crum, S. J. H. Emission of methyl isothiocyanate to the air after application of metham-sodium to greenhouse soil. *Water, Air, Soil Pollut.* **1990**, *50*, 109−121.

(4) Atkinson, R.; Aschmann, S. M.; Winer, A. M.; Pitts, J. N., Jr. Rate constants for the reaction of OH radicals with a series of alkanes and alkenes at 299 ± 2 K. *Int. J. Chem. Kinet.* **1982**, *14*, 507−516.

(5) Sommerlade, R.; Ekici, P.; Parlar, H. Gas phase reaction of selected isothiocyanates with OH radicals using a smog chamber-mass analyzer system. *Atmos. Environ.* **2006**, *40*, 3306−3315.

(6) Dash, M. R.; Rajakumar, B. Experimental and theoretical rate coefficients for the gas phase reaction of β-pinene with OH radical. *Atmos. Environ.* **2013**, *79*, 161−171.

(7) Atkinson, R. Kinetics and mechanisms of gas-phase reactions of the hydroxyl radical with organic compounds. *J. Phys. Chem. Ref. Data, Monogr.* **1989**, *1*, 1−246.

(8) Aschmann, S. M.; Arey, J.; Atkinson, R. Reaction of OH radicals with 5-hydroxy-2-pentanone: Formation yield of 4-oxopentanal and its OH radical reaction rate constant. *Environ. Chem.* **2013**, *10*, 145−150.

(9) U.S. Environmental Protection Agency. *Health and Environmental Effects Profile for Methyl Isocyanate*; Environmental Criteria and Assessment Office, Office of Health and Environmental Assessment, Office of Research and Development: Washington, DC, 1986.

(10) Taylor, W. D.; Allston, T. D.; Moscato, M. J.; Fazekas, G. B.; Kozlowski, R.; Takacs, G. A. Atmospheric photodissociation lifetimes for nitromethane, methyl nitrite, and methyl nitrate. *Int. J. Chem. Kinet.* **1980**, *7*, 231−240.

(11) Biermann, H. W.; Mac Leod, H.; Atkinson, R.; Winer, A. M.; Pitts, J. N., Jr. Kinetics of the gas-phase reactions of the hydroxyl radical with naphthalene, phenanthrene, and anthracene. *Environ. Sci. Technol.* **1985**, *19*, 244−248.

(12) Geddes, J. D.; Miller, G. C.; Taylor, G. E., Jr. Gas phase photolysis of methyl isothiocyanate. *Environ. Sci. Technol.* **1995**, *29*, 2590−2594.

(13) Atkinson, R.; Aschmann, S. M. Rate constants for the gas-phase reactions of the OH radical with a series of aromatic hydrocarbons at 296 ± 2 K. *Int. J. Chem. Kinet.* **1989**, *21*, 355−365.

(14) Alvarez, R. A.; Moore, C. B. Quantum yield for production of CH_3NC in the photolysis of CH_3NCS. *Science* **1994**, *263*, 205−207.

deaminates cytosine in single-stranded DNA are known to restrict HIV infection through deamination induced mutational inactivation.[16] A similar enzyme APOBEC3C (A3C) is known to restrict herpes viruses in mammalian cells.[17] APOBEC1 is known to initiate diversity in gene expression by deaminating dC to dU on single-stranded DNA and RNA.[18]

There are very limited reports on DCDs of terrestrial plants available so far and therefore in order to find out the prospective of their application, it is important to characterize the biochemical and functional properties of plant DCDs as studied in their mammalian counterpart. In this study, recombinant BoDCD was cloned and expressed in an *Escherichia coli* host system and the ability of the recombinant BoDCD to confer host resistance against cytarabine, a dC analog, was determined. The enzyme was further purified to homogeneity and characterized for their kinetic and physiological properties. Characteristics of BoDCD gives a novel insight on the functions of plant DCDs as it is the only resistance related DCD in plants reported and characterized so far.

MATERIALS AND METHODS

All the chemicals were purchased from Sigma-Aldrich (St. Louis, MO) unless stated otherwise.

Bacterial Strain and Growth Media. The *E. coli* Rosetta DE3 (provided by Dr. Ruey-Yi Chang, National Dong Hwa University, Taiwan) cells with recombinant and nonrecombinant PCR 2.1 plasmid were cultured in Luria−Bertani media containing 50 mg mL^{-1} kanamycin sulfate.

Cloning of BoDCD mRNA. The BoDCD was induced in *B. oleracea* plants and the BoDCD cDNA was amplified as described previously.[10] The primers used were 5′-GAATTCATGGAAGAA-GCTAAAGTGGAAGCA-3′ (sense) and 5′-CTCGAGGTATAA-ACGGAACTTCTCCTTGGT-3′ (antisense). The primers were designed from the nucleotide sequence of BoDCD (GenBank accession no. AEX58668). The sense primer contained the recognition sequences for *Eco*RI restriction endonuclease and N-terminal region of the BoDCD, and the antisense primer contained the recognition sequences for *Xho*I restriction endonuclease and the coding sequences of the C-terminal region of BoDCD. The amplified cDNAs were ligated into a PCR 2.1 vector by using the TOPO TA cloning kit (Invitrogen, Carlsbad, CA, USA) and transferred into $CaCl_2$-mediated competent *E. coli* TOP10 cells according to the manufacturer's instructions. The positive BoDCD transformants were screened by PCR, and the PCR 2.1-BoDCD plasmids from them were isolated and sequenced by using the commercial sequencing service from Protech Technology Enterprise Co., Ltd., Taipei, Taiwan (Republic of China).

Construction of Recombinant Expression Vector pET28a-BoDCD. The BoDCD insert from the PCR 2.1-BoDCD vector was collected by double digestion with *Eco*RI and *Xho*I restriction enzymes. The BoDCD fragments obtained (558 + 11 bp) were analyzed with 1.5% agarose gel electrophoresis and recovered with the Qiaquick gel extraction kit (Qiagen, Valencia, CA, USA). Similarly, the expression vector pET28a (+) (5369 bp) was also digested with *Eco*RI and *Xho*I (Promega, Madison, WI, USA), and the linear plasmid was recovered and purified after separating by electrophoresis in a 1% agarose gel. The digested pET28a vector and the BoDCD insert were constructed as a pET28a-BoDCD expression vector by ligating them with T4 DNA ligase (Promega, Annandale, NSW, Australia). The recombinant expression vector construct was transformed into *E. coli* DH5α host, and the positive recombinant clones were further detected by PCR and verified by DNA sequencing.

Induction and Expression of the Recombinant BoDCD. The recombinant BoDCD was overexpressed in *E. coli* Rosetta cells that provide suitable eukaryotic codons to facilitate universal translation. Specifically, screened single colonies of pET28a-BoDCD transformant *E. coli* cells were used for overexpression, and the transformant cells with pET28a plasmid without BoDCD insert were used as a control.

One milliliter of cultured cell suspension was inoculated into a culture flask with 100 mL of LB−kanamycin medium and incubated at 37 °C at 200 rpm until the OD_{600} reached 0.6−0.8. The cells were induced by adding100 μL of 1 M isopropyl-β-D-thiogalactopyranoside (IPTG) and incubated at 28 °C and 150 rpm for 7 h. The cell suspension was then centrifuged at 12000*g* for 10 min to pellet the cells, and the pellet was washed twice with pH 7.4 phosphate-buffered saline (PBS) buffer. The cells were then suspended in 100 μL of protein extraction buffer [50 mM Tris-HCl (pH 7.4), 0.1% (v/v) Tween 20, 1 mM phenylmethanesulfonyl fluoride (PMSF), and 10% glycerol (v/v)] and sonicated on ice using the Microson XL2000 sonicator (Misonix, Farmingdale, NY, USA) at 5 W for 5 min with an intermittent 30 s interval every 30 s. The lysate was then centrifuged for 10 min at 12000*g*, and the soluble and insoluble proteins were respectively isolated from the supernatant and the pellet. The supernatant was loaded to a HisTrap HP 1 mL column (GE Healthcare, Little Chalfont, UK) and purified using an ATKA prime plus FPLC system (GE Healthcare) by eluting with an imidazole linear gradient of 20−500 mM. The eluted protein was desalted by a HiTrap desalting column (GE Healthcare). Purified BoDCD was visualized by Coomassie-stained 12% SDS-PAGE analysis and protein concentration determined using a Bradford Protein Assay Kit (Bio-Rad).

Antibacterial Activity. The agar disk diffusion method was performed to determine the resistance exerted by the BoDCD transformants to cytarabine.[19] One milliliter of culture with 1×10^7 colony-forming units (CFUs) of *E. coli* was plated on the Luria−Bertani agar on which filter papers of 8 mm diameter, blotted with various concentrations of 50 μL of cytarabine, were placed on the middle of the cultured plates. Kanamycin sulfate (50 μg mL^{-1}) disks served as a positive control. After incubation at 30 °C for 24 h, the zone of inhibition around each disk was measured. Experiment was done with triplicates.

DCD Assays. Enzymatic activity was determined spectrophotometrically at 27 °C by following the decrease in absorption at 282 nm.[20] The reaction was performed in 300 μL of 50 mM Tris-HCl, pH 7.5, 50 mM NaCl, 0.2 mM substrate, and the BoDCD enzyme. One enzyme unit is defined as the amount of enzyme that catalyzes the deamination of 1 μM of dC per minute at 27 °C.

Enzyme Characterization. The protein concentration was determined according to the bicinchoninic acid (BCA) method using bovine serum albumin (BSA) as the standard.[21] Optimal temperature (T_{opt}) of the purified BoDCD (1 U) was determined by measuring the activity at different temperatures (from 15 to 45 °C). To determine the optimal pH (pH_{opt}) for the enzyme activity, the activity was measured in 0.5 M phosphate buffer, pH 5−9. K_m and V_{max} values of BoDCD for different substrates (dC, cytidine, and cytarbine) were determined from the initial velocities and substrate concentration. To evaluate the effects of different metal ions, the DCD activity of the purified enzyme was determined in the presence of 1 mM concentrations of different metal ions ($CaCl_2$, $MnCl_2$, $MgCl_2$, $HgCl_2$, $CoCl_2$, $CuCl_2$, $FeCl_3$, KCl, Na-EDTA) in 0.5 M phosphate buffer (pH 7.5).

RESULTS AND DISCUSSION

Enhancement of Resistance to Cytarabine in Transformant *E. coli* Cells. Like the mammalian DCDs, BoDCD also can potentially convert toxic dC analogues into relatively less toxic uridine derivatives and therefore provide resistance to infection-related hypersensitivity in plants.[10,22] To investigate this functional property, BoDCD was characterized for its ability to detoxify cytarabine, a cytosine base with an arabinose sugar, which is known to interfere with DNA synthesis.[23,24] Cytarabine is rapidly converted to cytarabine triphosphate, which damages DNA by incorporating into the DNA during the S phase. Cytarabine also inhibits both polymerase enzymes

and nucleotide reductase enzymes that are essential for DNA synthesis.[24,25]

The ability of an *E. coli* BoDCD transformant to resist cytarabine toxicity was comparatively assessed to find the potential of the recombinant BoDCD to neutralize cytidine analogues (Figure 1). Cytarabine inhibited the growth of

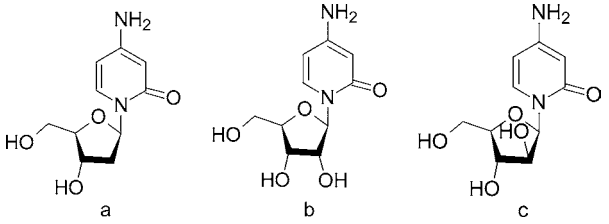

Figure 1. Structures of three substrates of BoDCD: 2′-deoxycytidine (a); cytidine (b); cytarabine (c).

control *E. coli* cells at all tested concentrations. The inhibition was found to increase with increasing concentration, but the transformed colonies were found to be resistant and were protected from the cytarabine toxicity. However, at a higher concentration of 2 μM cytarabine, the BoDCD transformants showed a slight inhibition (Figure 2).

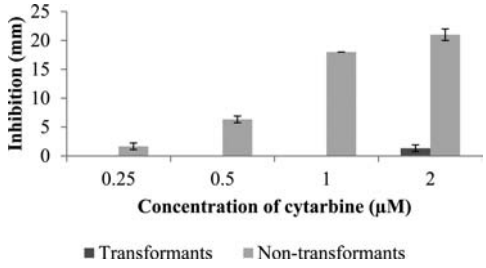

Figure 2. BoDCD mediated resistance to cytarabine toxicity and bacteriostatic effect of cytarabine on the BoDCD transformant and the control *E. coli*. Error bars indicate standard error of the mean (n = 3).

Catalytic Activity of the Recombinant BoDCD. To find the substrate specificity of BoDCD, the enzyme was overexpressed and purified as a C-terminal His-tagged soluble fusion protein, and its catalytic properties were determined. The size of the fusion protein (191 amino acid length) was determined as 20.8 kDa on the basis of 10% SDS-PAGE analysis (Figure 3). The theoretical mass of the native BoDCD without the His-tag was calculated as 20.01 kDa. The specific activity of BoDCD in the soluble portion of the total extract for its natural substrate dC was 54.6 U mg^{-1}, and that of the purified enzyme (96.6% yield) was 61 U mg^{-1} (Table 1).

Kinetic Parameters and Catalytic Properties of BoDCD. Although there are only a few reports on the characterization of plant DCDs so far, reports on plant cytidine deaminase (EC 3.5.4.5, CDA), an enzyme with a similar biochemical function, are available. The kinetic parameters of plant CDAs have been determined and reported previously. K_m and V_{max} of a previously known *Arabidopsis thaliana* CDA for dC have been reported as 49.3 and 24.4 μM, respectively.[26] CDA also deaminates known cytidine analogues such as cytarabine, 5-azacytidine, and 5-methylcytidine that are formed as a product of lipoxidation and targets nucleosides and dsDNA, causing severe damage to the DNA.[20] The substrate specificity and the kinetic properties show that BoDCD is

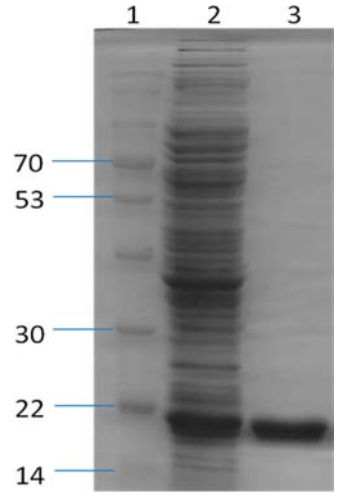

Figure 3. SDS-PAGE analysis of the overexpressed and purified recombinant BoDCD. An aliquot of sample containing 20 μg of protein was loaded for separation. Lanes: 1, molecular weight markers; 2, total soluble proteins from bacterial lysate after overexpression; 3, purified recombinant BoDCD.

Table 1. Purification of Recombinant *B. oleracea* Deoxycytidine Deaminase

purification step	total protein (mg)	total activity (U)[a]	specific activity (U mg^{-1})[a]	yield (%)
soluble lysate	30	1639	54.6	100
affinity column	26	1583.5	61	96.6%

[a]One enzyme unit (U) is defined as the amount of enzyme that catalyzes the deamination of 1 μM 2′-deoxycytidine (dC) min^{-1} at 27 °C.

functionally more active in metabolizing dC adducts such as cytarabine and comparatively less effective in deaminating dC to dU in nuclei acids and metabolizing cytidine to uridine for the pyrimidine pool. The conserved functional DCD domain (AA 27−AA 105) of BoDCD is a zinc binding region, which plays a central role in the proposed catalytic mechanism by activating a water molecule to form a hydroxide ion that performs a nucleophilic attack on the substrate. As three-dimensional structures of similar DCDs have not been determined so far, the specific characteristics of the catalytic domain that are responsible for the difference in substrate specificity were not established. However, upon analysis of the structures of all three substrates used, the difference in the functional group at the 2′ carbon and their spatial configurations appear to determine the enzyme−substrate binding and activity.

The K_m and the V_{max} of BoDCD for the substrate dC were detrermined as 91.3 μM and 1.475 mM, respectively; for cytidine the values were 368 μM and 0.599 mM, and for cytarabine the values were 63 μM and 2.072 mM (Table 2). The K_m of cytidine was >3-fold higher and the V_{max} was almost 1.5-fold lower than those of dC, whereas the K_m of cytarabine was almost 0.45 times lower and the V_{max} was 0.4-fold higher than those of dC (Table 2). On the basis of their respective k_{cat}/K_m values, the BoDCD was relatively more active when cytarabine was used as a substrate and was less active with cytidine as the substrate (Table 2). The higher BoDCD activity to cytarabine and dC can be attributed to the close structural

Table 2. Kinetic Parameters and Substrate Specificity of the Recombinant *B. oleracea* Deoxycytidine Deaminase

substrate	K_m (μM)	V_{max} (mM min^{-1})	k_{cat}/K_m (μM S^{-1})
2′-deoxycytidine	91.3 ± 5.6	1.475 ± 0.3	0.342
cytidine	368 ± 18.2	0.599	0.034
cytarabin	63 ± 12.2	2.072 ± 0.2	0.697

similarity of these two substrates. The k_{cat}/K_m values of BoDCD were 0.342, 0.034, and 0.697 μM S^{-1} for dC, cytidine, and cytarabine, respectively. The higher affinity and higher reaction rate of BoDCD to cytarabine, according to the kinetic parameters, suggest that the enzyme binds and metabolizes cytarabine comparatively more swiftly than it binds and metabolizes cytosine. This can be also theoretically interpreted that BoDCD potentially neutralizes cytarabine in less concentration during the early stages of cytarabine accumulation but maintains a higher threshold level before dC and cytidine metabolism. Therefore, BoDCD is more sensitive and active in the detoxification mechanism than dC and cytidine metabolism. Furthermore, although BoDCD can metabolize dC and cytidine, a function contributing to DNA synthesis and expression, the fact that they are known to be induced only during three-way interaction shows that they contribute more during cytotoxic challenges and potentially provide protection by neutralizing dC analogues to protect macromolecules from adducts.[10]

Optimal Conditions for BoDCD Activity. Optimal conditions for the activity of plant CDAs have been determined previously, and their T_{opt} and pH_{opt} ranges were found to vary greatly. At-cda1, a CDA from *A. thaliana*, is found to be active between pH 3.0 and 10.5, beyond which the enzyme was inactive irreversibly.[20] A CDA from *A. thaliana* was found to be active between pH 6 and 11 with a slight maximum at pH 7.5−8. The enzyme was inactive at pH 4.[27] The optimal temperature of the BoDCD was determined as 27 °C. The enzyme activity was found to be inhibited below 25 °C and above 30 °C (Figure 4). BoDCD was highly active at pH 7.5, and the activity

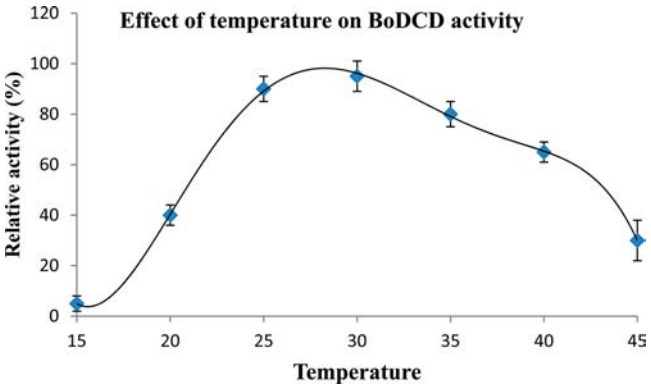

Figure 4. Influence of temperature on the activity of the recombinant BoDCD.

dropped significantly beyond this range (Figure 5). As the normal pH in the cytoplasm of most higher plants is slightly alkaline (7.4−7.5), the pH_{opt} of BoDCD suggests that they are potentially active during normal cytoplasm conditions without proton fluxes.[28] The ability of dC deamination by BoDCD was strongly inhibited in the presence of 1 mM Hg^{2+} and substantially inhibited in the presence of Cu^{2+} and Fe^{3+} ions.

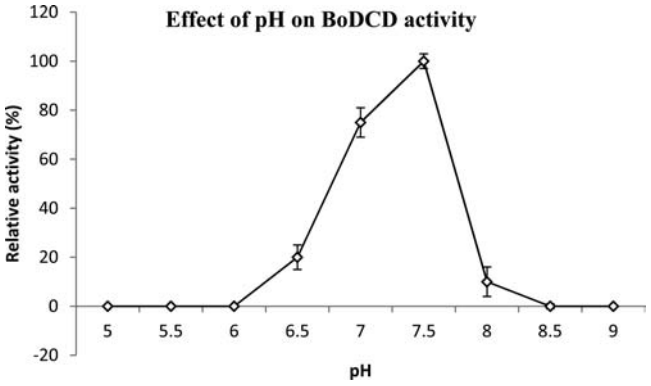

Figure 5. Influence of pH on the activity of the recombinant BoDCD.

This may be due to the presence of thiol groups in amino acids C90, C101, C107, C110, M112, and C113 located in the catalytic motif. All other metal ions relatively inhibited BoDCD activity by 5−30% (Table 3).

Table 3. Effect of Metal Ions on the *B. oleracea* Deoxycytidine Deaminase Activity

metal ion[a]	relative activity (%)	metal ion[a]	relative activity (%)
none	100	EDTA	80
$MnCl_2$	70	KCl	98
$CoCl_2$	85	$MgCl_2$	95
$CuCl_2$	15	$HgCl_2$	0
$CaCl_2$	88	$FeCl_3$	15

[a]Final concentration of the various agents was 1 mM.

The biochemical and physiological functions of plant DCDs were so far not characterized and were considered as the enzymes for pyrimidine metabolism and gene expression diversity. The deduced biochemical property of BoDCD justifies previous evidence on the role of DCD in plant resistance.[10] Enhancement of systemic resistance in plants to pathogens occurs due to two different mechanisms. The systemic acquired resistance (SAR) is mediated by a salicylic acid-dependent pathway and involves the role of pathogenesis-related proteins. SAR develops either locally or systemically according to the pathogen challenged, as a result of a successful infection or a hypersensitive response. The induced systemic resistance (ISR) is a response to colonization of plant roots by certain rhizosphere microorganisms. They are mediated by jasmonic acid/ethylene pathways. The biocontrol agent, *Trichoderma*, is commonly known as an inducer of ISR by root colonization.[29] As BoDCD is an enzyme induced during three-way interaction between *B. oleracea*, *T. harzianum* ETS 323, and *R. solani* that also involves hypersensitivity, the possibility of BoDCD being a cross talk between SAR and ISR is evident.

The functional properties of BoDCD, apart from revealing the antimicrobial potential of BoDCD, show that BoDCD can be used in other possible applications such as in ameliorating the adverse effect of dC analogues during chemotherapy. Normal intestinal florae help to maintain intestinal structure, function, and defense. Cytotoxic chemotherapeutic drugs such as cytarabine are detrimental to such protective florae. When the ecological balance of the intestine is damaged, a lot of bacteria and endotoxin enter into the circulation by the portal system and cause intestinal endotoxemia; under certain

dx.doi.org/10.1021/jf4048513 | J. Agric. Food Chem. 2014, 62, 1796−1801

conditions it can also stimulate a chain reaction of the cytokines and other inflammatory mediators and cause systemic organ damage.[30−34] The DCD enzymes can be effectively used to neutralize the side effects of cytotoxic cytidine adducts that are employed as drugs. As the affinity of BoDCD to cytarabine is greater than to its natural substrate DCD, the enzyme can be potentially considered for providing resistance to intestinal florae against cytidine analogues. Engineered microbes with BoDCD expression can be used as probiotics to counter the effects of cytarabine.[35] Further exploration on BoDCD will reveal interesting insights and applications.

AUTHOR INFORMATION

Corresponding Author

*(K.-C.P.) Phone: +886 3 863 3635. Fax: +886 3 863 3630. E-mail: kcpeng@mail.ndhu.edu.tw. (S.-Y.L.) Phone: 886 4 8511 888 ext. 4256. Fax: 886 4 8511 326. E-mail: syliu@mail.dyu.edu.tw.

Funding

This work was partly supported by grants from the National Science Council, Taiwan (NSC 99-2313-B-212-001-MY3 and NSC 102-2313-B-259 -003). This work is part of the Ph.D. thesis of M. A. Shibu, who was financially supported by the Taiwan scholarship awarded by the Ministry of Foreign Affairs of the Republic of China and from the Department of Life Science, National Dong Hwa University.

Notes

The authors declare no competing financial interest.

ACKNOWLEDGMENTS

We thank B. Y. Huang, H. N. Shih, and F. J. Tsai from K.-C. Peng's laboratory for all their help that facilitated this work.

REFERENCES

(1) Benitez, T.; Rincon, A. M.; Limon, M. C.; Codon, A. C. Biocontrol mechanisms of *Trichoderma* strains. *Int. Microbiol.* **2004**, *7*, 249−260.

(2) Liu, S. Y.; Lo, C. T.; Chen, C.; Liu, M. Y.; Chen, J. H.; Peng, K. C. Efficient isolation of anthraquinone-derivatives from *Trichoderma harzianum* ETS 323. *J. Biochem. Biophys. Methods* **2007**, *70*, 391−395.

(3) Yang, C. A.; Cheng, C. H.; Lee, J. W.; Lo, C. T.; Liu, S. Y.; Peng, K. C. Monomeric L-amino acid oxidase-induced mitochondrial dysfunction in *Rhizoctonia solani* reveals a novel antagonistic mechanism of *Trichoderma harzianum* ETS 323. *J. Agric. Food Chem.* **2012**, *60*, 2464−2471.

(4) Liu, S. Y.; Shibu, M. A.; Jhan, H. J.; Lo, C. T.; Peng, K. C. Purification and characterization of novel glucanases from *Trichoderma harzianum* ETS 323. *J. Agric. Food Chem.* **2010**, *58*, 10309−10314.

(5) Cheng, C. H.; Yang, C. A.; Peng, K. C. Antagonism of *Trichoderma harzianum* ETS 323 on *Botrytis cinerea* mycelium in culture conditions. *Phytopathology* **2012**, *102*, 1054−1063.

(6) Tseng, S. C.; Liu, S. Y.; Yang, H. H.; Lo, C. T.; Peng, K. C. Proteomic study of biocontrol mechanisms of *Trichoderma harzianum* ETS 323 in response to *Rhizoctonia solani*. *J. Agric. Food Chem.* **2008**, *56*, 6914−6922.

(7) Yang, H. H.; Yang, S. L.; Peng, K. C.; Lo, C. T.; Liu, S. Y. Induced proteome of *Trichoderma harzianum* by *Botrytis cinerea*. *Mycol. Res.* **2009**, *113*, 924−932.

(8) Yang, C. A.; Cheng, C. H.; Lo, C. T.; Liu, S. Y.; Lee, J. W.; Peng, K. C. A novel L-amino acid oxidase from *Trichoderma harzianum* ETS 323 associated with antagonism of *Rhizoctonia solani*. *J. Agric. Food Chem.* **2011**, *59*, 4519−4526.

(9) Yang, C. A.; Cheng, C. H.; Liu, S. Y.; Lo, C. T.; Lee, J. W.; Peng, K. C. Identification of antibacterial mechanism of L-amino acid oxidase derived from *Trichoderma harzianum* ETS 323. *FEBS J.* **2011**, *278*, 3381−3394.

(10) Shibu, M. A.; Lin, H. S.; Yang, H. H.; Peng, K. C. *Trichoderma harzianum* ETS 323-mediated resistance in *Brassica oleracea* var. *capitata* to *Rhizoctonia solani* involves the novel expression of a glutathione S-transferase and a deoxycytidine deaminase. *J. Agric. Food Chem.* **2012**, *60*, 10723−10732.

(11) Lam, E.; Kato, N.; Lawton, M. Programmed cell death, mitochondria and the plant hypersensitive response. *Nature* **2001**, *411*, 848−853.

(12) Heath, M. C. Hypersensitive response-related death. *Plant Mol. Biol.* **2000**, *44*, 321−334.

(13) Govrin, E. M.; Levine, A. The hypersensitive response facilitates plant infection by the necrotrophic pathogen *Botrytis cinerea*. *Curr. Biol.: CB* **2000**, *10*, 751−757.

(14) Mancini, W. R. The role of deoxycytidine-metabolizing enzymes in the cytotoxicity induced by 3′-amino-2′,3′-dideoxycytidine and cytosine arabinoside. *Cancer Chemother. Pharmacol.* **1992**, *30*, 139−144.

(15) Sigmond, J.; Honeywell, R. J.; Postma, T. J.; Dirven, C. M. F.; de Lange, S. M.; van der Born, K.; Laan, A. C.; Baayen, J. C. A.; Van Groeningen, C. J.; Bergman, A. M.; Giaccone, G.; Peters, G. J. Gemcitabine uptake in glioblastoma multiforme: potential as a radiosensitizer. *Ann. Oncol.* **2009**, *20*, 182−187.

(16) Love, R. P.; Xu, H.; Chelico, L. Biochemical analysis of hypermutation by the deoxycytidine deaminase APOBEC3A. *J. Biol. Chem.* **2012**, *287*, 30812−30822.

(17) Suspene, R.; Aynaud, M. M.; Koch, S.; Pasdeloup, D.; Labetoulle, M.; Gaertner, B.; Vartanian, J. P.; Meyerhans, A.; Wain-Hobson, S. Genetic editing of herpes simplex virus 1 and Epstein-Barr herpesvirus genomes by human APOBEC3 cytidine deaminases in culture and in vivo. *J. Virol.* **2011**, *85*, 7594−7602.

(18) Conticello, S. G. The AID/APOBEC family of nucleic acid mutators. *Genome Biol.* **2008**, *9*, 229.

(19) Almeida, A. A.; Farah, A.; Silva, D. A.; Nunan, E. A.; Gloria, M. B. Antibacterial activity of coffee extracts and selected coffee chemical compounds against enterobacteria. *J. Agric. Food Chem.* **2006**, *54*, 8738−8743.

(20) Vincenzetti, S.; Cambi, A.; Neuhard, J.; Schnorr, K.; Grelloni, M.; Vita, A. Cloning, expression, and purification of cytidine deaminase from *Arabidopsis thaliana*. *Protein Express. Purif.* **1999**, *15*, 8−15.

(21) Smith, P. K.; Krohn, R. I.; Hermanson, G. T.; Mallia, A. K.; Gartner, F. H.; Provenzano, M. D.; Fujimoto, E. K.; Goeke, N. M.; Olson, B. J.; Klenk, D. C. Measurement of protein using bicinchoninic acid. *Anal. Biochem.* **1985**, *150*, 76−85.

(22) Letourneau, S.; Palerme, J. S.; Delisle, J. S.; Beausejour, C. M.; Momparler, R. L.; Cournoyer, D. Coexpression of rat glutathione S-transferase A3 and human cytidine deaminase by a bicistronic retroviral vector confers in vitro resistance to nitrogen mustards and cytosine arabinoside in murine fibroblasts. *Cancer Gene Ther.* **2000**, *7*, 757−765.

(23) Kufe, D. W.; Major, P. P. Studies on the mechanism of action of cytosine arabinoside. *Med. Pediatr. Oncol.* **1982**, *10* (Suppl. 1), 49−67.

(24) Carbone, G. M.; Catapano, C. V.; Fernandes, D. J. Imbalanced DNA synthesis induced by cytosine arabinoside and fludarabine in human leukemia cells. *Biochem. Pharmacol.* **2001**, *62*, 101−110.

(25) Perry, M. C. *The Chemotherapy Source Book*, 4th ed.; Wolters Kluwer Health/Lippincott Williams & Wilkins: Philadelphia, PA, USA, 2008; p xvi, 779 pp.

(26) Kafer, C.; Thornburg, R. *Arabidopsis thaliana* cytidine deaminase 1 shows more similarity to prokaryotic enzymes than to eukaryotic enzymes. *J. Plant Biol.* **2000**, *43*, 162−170.

(27) Faivre-Nitschke, S. E.; Grienenberger, J. M.; Gualberto, J. M. A prokaryotic-type cytidine deaminase from *Arabidopsis thaliana* gene expression and functional characterization. *Eur. J. Biochem./FEBS* **1999**, *263*, 896−903.

(28) Gout, E.; Bligny, R.; Douce, R. Regulation of intracellular pH values in higher plant cells. Carbon-13 and phosphorus-31 nuclear magnetic resonance studies. *J. Biol. Chem.* **1992**, *267*, 13903−13909.
(29) Harman, G. E.; Howell, C. R.; Viterbo, A.; Chet, I.; Lorito, M. *Trichoderma* species − opportunistic, avirulent plant symbionts. *Nat. Rev. Microbiol.* **2004**, *2*, 43−56.
(30) Camera, A.; Andretta, C.; Villa, M. R.; Volpicelli, M.; Picardi, M.; Rossi, M.; Rinaldi, C. R.; Della Cioppa, P.; Ciancia, R.; Selleri, C.; Rotoli, B. Intestinal toxicity during induction chemotherapy with cytarabine-based regimens in adult acute myeloid leukemia. *Hematol. J.* **2003**, *4*, 346−350.
(31) van Vliet, M. J.; Tissing, W. J.; Dun, C. A.; Meessen, N. E.; Kamps, W. A.; de Bont, E. S.; Harmsen, H. J. Chemotherapy treatment in pediatric patients with acute myeloid leukemia receiving antimicrobial prophylaxis leads to a relative increase of colonization with potentially pathogenic bacteria in the gut. *Clin. Infect. Dis.* **2009**, *49*, 262−270.
(32) Rudnick, S. A.; Cadman, E. C.; Capizzi, R. L.; Skeel, R. T.; Bertino, J. R.; McIntosh, S. High dose cytosine arabinoside (HDARAC) in refractory acute leukemia. *Cancer* **1979**, *44*, 1189−1193.
(33) Wang, W. S.; Tzeng, C. H.; Chiou, T. J.; Liu, J. H.; Hsieh, R. K.; Yen, C. C.; Chen, P. M. High-dose cytarabine and mitoxantrone as salvage therapy for refractory non-Hodgkin's lymphoma. *Jpn. J. Clin. Oncol.* **1997**, *27*, 154−157.
(34) Muller, A.; Florek, M. 5-Azacytidine/azacitidine. *Recent Results Cancer Res.* **2010**, *184*, 159−170.
(35) Paton, A. W.; Morona, R.; Paton, J. C. Bioengineered microbes in disease therapy. *Trends Mol. Med.* **2012**, *18*, 417−425.

chemical reagents were obtained from Sigma-Aldrich (Milwaukee, WI, USA) with the highest purity available.

Biochar Production. Feedstock property and pyrolysis conditions were described in detail previously.[13,17] Briefly, cottonseed hull (CH25) was used as received from Planters Cotton Oil Mill (Pine Bluff, AK, USA).[13] Broiler litter (BL25) was obtained from a USDA-ARS facility (Starkville, MS, USA) and was milled and pelletized.[17] Feedstock was pyrolyzed at 350, 500, 650, and 800 °C under 1600 mL min^{-1} N_2 flow rate for 1 h (for BL25) or 4 h (for CH25) using a laboratory-scale box furnace (22 L void volume) with a retort (Lindberg, type 51662-HR, Watertown, WI, USA). Biochar products were allowed to cool to room temperature overnight under N_2 atmosphere. Biochars are hereby denoted by the feedstock abbreviation and pyrolysis temperature, for example, cottonseed hull feedstock (CH25) and biochars produced at 350 (CH350) and 500 °C (CH500).

Extraction Procedures. To understand the solubility of different phosphorus species, each biochar sample was exposed to increasingly more rigorous extraction procedures (abbreviations in parentheses will be used throughout the text): DDW (water), Mehlich 3 (M3), basic EDTA (NaOH−EDTA), acidic ammonium oxalate (oxalate), and microwave digestion (total). Each extraction was performed independently, rather than sequentially. At the end of each extraction procedure, filtrate was acidified to 4 vol % nitric acid (trace metal grade, Sigma-Aldrich) for the determination of soluble P, K, Ca, Mg, Al, Fe, and Na concentrations using inductively coupled plasma atomic emission spectrometer (ICP-AES; Profile Plus, Teledyne/Leeman Laboratories, Hudson, NH, USA). Blanks, blank spikes, and matrix spikes were included for the quality assurance and control for the ICP-AES analysis.[18]

Except for sizing, all biochars were extracted without modifications. For M3, oxalate, and water extractions, biochars were ground and sieved to <2 mm. Total and NaOH−EDTA extractions employed 44 μm (325 mesh) sized biochars corresponding to the silt fraction (0.002−0.05 mm) having higher surface area and reactivity than the larger fractions.[2]

Water extracts were obtained by shaking 0.5 g of biochar in 30 mL of DDW end-over-end for 16 h at room temperature. The suspension was then centrifuged at 10000*g* for 15 min and vacuum filtered (0.45 μm Millipore filter paper; Millipore, Billerica, MA, USA). Mehlich 3 extraction followed the literature protocol.[19] Briefly, 2.5 mL of 2 mm sieved sample was extracted in 25 mL of 1 mM EDTA extraction fluid at pH 2.5 (0.2 M acetic acid + 0.25 M ammonium nitrate + 0.015 M ammonium fluoride + 0.13 M nitric acid + 0.001 M EDTA) for 5 min and then filtered through Whatman no. 2 filter paper. The Mehlich 3 method[19] determines extractable P on the sample volume, rather than the weight basis. To convert P concentration to units of milligrams per gram biochar, the density of biochar was determined by weighing dry biochar sample packed in a 2.5 mL volumetric flask. Acid ammonium oxalate extraction followed the literature procedure.[20] Briefly, 0.5 g of sample was shaken in 25 mL of 0.2 M ammonium oxalate at pH 3.5 for 4 h in the dark and then centrifuged and 0.45 μm filtered. Total P contents of cottonseed hull feedstock and biochars were determined by microwave-assisted (Ethos EZ microwave digester, Milestone, Inc., Shelton, CT, USA) digestion (concentrated HNO_3/HCl + 30% H_2O_2) following U.S. EPA method 3052;[21] values for broiler litter samples were obtained from the literature.[14] Electric conductivity (EC), pH, and total organic carbon (TOC) of 16 h hot (80 °C) water extracts[12] and proximate analysis[13,14] results were obtained from the literature.

^{31}P NMR Analysis. For each feedstock and biochar, 5 g of sample was shaken in 250 mM NaOH + 5 mM EDTA for 16 h and then centrifuged at 900*g* for 30 min and filtered through Whatman no. 42 filter paper.[22] An aliquot was kept for P concentration measurement by ICP-AES. To concentrate samples for the ^{31}P NMR analysis,[22] remaining filtrate was freeze-dried. The NMR sample was obtained by dissolving 100 mg of freeze-dried sample in 0.6 mL of 1 M NaOH in 10% D_2O. As described in detail previously,[7] ^{31}P NMR spectra were obtained using an Alpha 600 FT NMR spectrometer (JEOL, Tokyo, Japan) with a 5 mm probe. Spectra were recorded at 242.85 MHz using a pulse width of 10.00 μs (90°), an acquisition time of 0.4522 s, and broadband proton decoupling at 30 °C. The pulse delay time of 2 s was employed.[23] Each spectrum was scanned 30000 times, and a broadening factor of 5.00 Hz was used in the Fourier transform procedure. Chemical shifts (ppm) were determined with respect to 85% H_3PO_4 solution (0 ppm). The total signal intensity and the fraction contributed by each P compound were calculated by integration of the spectral signals using Alice 2 for Windows version 5.1.1 (JEOL).

RESULTS AND DISCUSSION

Soluble Phosphorus Content of Plant and Manure Biochars. To highlight the contrasting properties of plant (cottonseed hull; CH) and manure (broiler litter; BL) biochars employed in this study, Table 1 presents the pH, electric conductivity (EC), and total organic carbon (TOC) of 16 h hot (80 °C) water extracts at biochar/DDW (w/w) = 1:10;[12] ash, fixed carbon, volatile matter (VM), and moisture contents;[13,14] and density of feedstocks (CH25 and BL25) and biochars pyrolyzed at 350, 500, 650, and 800 °C. Manure biochars contained higher water-soluble inorganic salts (EC) as well as organic carbon (TOC) than plant biochars. Table 1 also presents total (microwave digestion in concentrated HNO_3/HCl + 30% H_2O_2), NaOH−EDTA (250 mM NaOH + 5 mM EDTA for 16 h), oxalate (200 mM oxalate at pH 3.5 for 4 h), M3 (1 mM EDTA at pH 2.5 for 5 min), and water-extractable (16 h at room temperature) P concentrations in milligrams per kilogram biochar on a dry weight basis. Values in parentheses provide percent extractable P (relative to total by microwave digestion) in NaOH−EDTA, oxalate, M3, and water extracts. Phosphorus-containing compounds vaporize near 760 °C.[24] Progressive increase in total P content of BL and CH biochars (Table 1) indicates that temperature-induced condensation of P on the solid biochar product outweighed the volatilization loss at pyrolysis temperatures as high as 800 °C. The "ash" component of biochar is a complex mixture of amorphous, semicrystalline, and crystalline inorganic phases as well as organic (char) components.[25] These ash components may be originally present in the manure feedstock or thermochemically produced. Common phosphorus minerals in biomass are calicum, iron, potassium, and magnesium phosphates.[26] Thermal treatment of biomass produces silicates, carbonates, halides, phosphates, sulfates, oxides, and hydroxides.[27] The organic carbon fraction of biochar likely stabilizes these inorganic phases by various organomineral interactions, for example, by serving as a template for the formation of nanocrystals during pyrolysis.[28] Limited solubility of P and Ca in 500 °C manure and food waste biochars was attributed to whitlockite ($(Ca,Mg)_3(PO_4)_2$).[29] More soluble struvite ($MgNH_4PO_4{\cdot}6H_2O$) was observed by XRD analysis of biochars produced from a mixture of cattle manure and wood chips.[30]

In Table 1, compared to the total (microwave digestible) P, percent extractable P of plant (CH) biochars increased in the following order (except for disproportionately high oxalate-extractable P of CH25): M3 < oxalate ≈ water < NaOH−EDTA. The following order was observed for manure (BL) biochars: water < M3 < NaOH−EDTA < oxalate. Of five extraction methods, total, oxalate, and M3 employed strongly acidic conditions (pH ≤3.5), whereas NaOH−EDTA solution was strongly basic. The pH of water extracts depended on the pH of biochar (Table 1). Especially for BL biochars, negligible P in water extract at ≥650 °C likely resulted from high pH in the absence of chelating agents. For the M3 extracts, low P concentrations likely resulted from the short (5 min) extraction

dx.doi.org/10.1021/jf4053385 | J. Agric. Food Chem. 2014, 62, 1802−1809

Table 1. Bulk Parameters for Cottonseed Hull (CH) and Broiler Litter (BL) Feedstock and Biochars Pyrolyzed at 350, 500, 650, and 800 °C: pH, Electric Conductivity (EC), and Total Organic Carbon (TOC) of Hot Water Extracts (80 °C for 16 h); Density; Ash, Fixed Carbon, Volatile Matter (VM), and Moisture[a]

					proximate analysis (wt $\%_{dry}$)[b]				extractable P in mg kg^{-1}_{dry} (% extracted)				
biochar	pH[c]	EC[c] (mS cm^{-1})	TOC[c] (ppm C)	density[d] (g L^{-1})	ash	fixed C	VM	moisture	total[c,f]	NaOH−EDTA	oxalate[f]	M3[f]	water
cottonseed hull													
CH25	7.4	0.0	6766	104	3	23	75	12	3180	802 (25%)	2003 (63%)	201 (6.3%)	424 (13%)
CH350	8.2	2.6	521	306	6	56	37	7	3405	2383 (70%)	554 (16%)	27 (0.8%)	908 (27%)
CH500	9.6	2.5	72	423	8	72	20	7	5124	2024 (40%)	931 (18%)	36 (0.7%)	1139 (22%)
CH650	9.6	5.1	52	293	9	77	14	8	16816	2717 (16%)	1735 (10%)	119 (0.7%)	1173 (7%)
CH800	9.6	5.8	0	540	10	77	13	10	37560	2829 (8%)	2119 (6%)	80 (0.2%)	577 (2%)
broiler litter													
BL25	5.0	0.3	9310	509	29	12	58	20	22022	16566 (75%)	19261 (87%)	800 (3.6%)	2053 (9%)
BL350	7.6	9.9	1724	614	35	28	37	3	31319	15187 (48%)	27309 (87%)	770 (2.5%)	0
BL500	9.3	9.4	126	623	50	31	19	3	39240	18859 (48%)	34810 (89%)	343 (0.9%)	325 (1%)
BL650	9.7	10.0	32	655	54	34	12	5	40879	16910 (41%)	37537 (92%)	554 (1.4%)	0
BL800	10.0	9.1	5	694	58	32	10	7	41371	13832 (33%)	39273 (95%)	400 (1.0%)	0

[a]Soluble phosphorus concentrations determined by different extraction procedures: total (by microwave digestion), NaOH-EDTA, oxalate, Mehlich 3 (M3), and water; values in parentheses are % extractable P (relative to total by microwave digestion) in NaOH-EDTA, oxalate, M3, and water extracts. [b]References 13 and 14. [c]Refereence 12. [d]Mean for triplicate (SD < 0.09 g L^{-1}). [e]Reference 14 for BL samples. [f]Mean for duplicate.

period, as observed previously.[31] For different extraction procedures, a greater degree of carbonization often leads to lower concentrations of labile P species. For example, Mehlich I (50 mM HCl + 12.5 mM H_2SO_4 for 5 min) P values were similar for 400 and 500 °C poultry litter biochars and decreased after steam activation of these biochars.[32] Pyrolysis at 450 °C decreased the water-soluble P fraction of sewage sludge from >60 to <20%.[8] Calcium-bound P phases (HCl-extractable) increased to >30% in the char fraction, whereas Fe/Al-bound fractions (NaOH extractable) did not change significantly.[8] In a separate study, nearly an order of magnitude greater Colwell (8.5 sodium bicarbonate) P content was observed in 450 °C poultry litter biochar than in the steam-activated 550 °C biochar.[33]

Distinctive feedstock and temperature dependence was observable for oxalate and NaOH−EDTA extractions in Table 1. Especially at ≥650 °C, oxalate was nearly as effective as microwave digestion for extracting P from manure biochars, but not from plant biochars. On the other hand, NaOH−EDTA was particularly effective for dissolving P in 350−500 °C plant biochars (Table 1). Table S1 of the Supporting Information provides stability constants for the 1:1 complex of oxalate, EDTA, and phosphate with Ca^{2+}, Fe^{3+}, and other selected cations.[34] EDTA has far greater stability constants for Ca^{2+}, Fe^{3+}, and other phosphate-binding metals than oxalate (Table S1). Greater P solubility of 350−500 °C plant biochars in NaOH−EDTA indicates the dominance of P species that are strongly interacting with the organic C fraction of biochar and/or associated with iron/aluminum hydroxides and other mineral surfaces and are resistant to acid dissolution. For manure biochars, greater P dissolution in acidic media containing weaker ligand (oxalate) suggests the acid dissolution of calcium phosphate phases. Oxalate is able to release P from calcium phosphate phases by forming insoluble calcium oxalate[35] having the solubility product constant (K_{SO}) of $10^{-8.75}$.[34] For both manure and plant biochars, Ca concentration in NaOH−EDTA was consistently higher than in oxalate extracts (Table S2, Supporting Information). Lower Ca concentration in the oxalate extract was set by the K_{SO} of calcium oxalate.

^{31}P NMR Analysis of Plant and Manure Biochar Extracts. To understand the individual P species contributing to extractable P concentrations in Table 1, NaOH−EDTA extracts were analyzed using solution-phase ^{31}P NMR. This extraction fluid (0.25 M NaOH + 0.05 M Na_2EDTA) is widely utilized to enhance P extraction from soil while minimizing the hydrolysis of organic P to inorganic P.[1] EDTA is used to release P from paramagnetic ions (see stability constant for Fe in Table S1), thereby decreasing line broadening.[2] To our knowledge, no prior liquid-phase ^{31}P NMR study systematically investigated the feedstock and pyrolysis temperature dependence. Figure 1 presents ^{31}P NMR spectra for manure (left) and plant (right) feedstocks and biochars pyrolyzed at 350, 500, 650, and 800 °C. Spectra for manure biochars (left) indicate the dominance of inorganic orthophosphate (PO_4^{3-} at 6.2 ppm) especially at higher temperatures. In contrast, pyrophosphate ($P_2O_7^{4-}$ at −4.1 ppm) persisted in plant biochars (Figure 1, right). Pyrophosphate is produced by heating orthophosphate above 300 °C.[36]

Figure 2 presents Figure 1 with an expanded *x*-axis to visualize the monoester region (3−7 ppm). Both cottonseed hull and broiler litter feedstocks showed four peaks corresponding to phytate: 5.9 ppm (attributable to the P_2

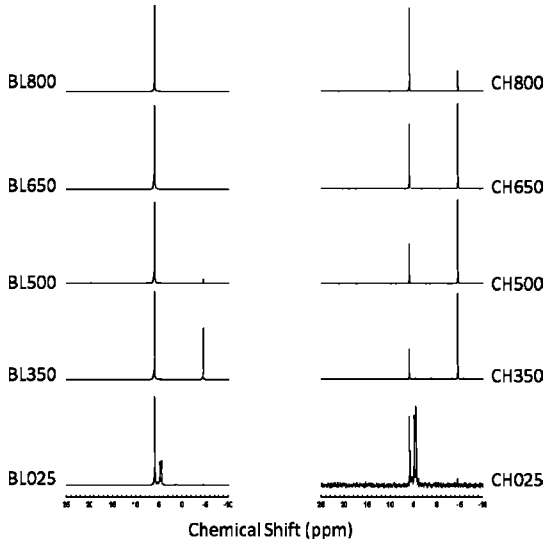

Figure 1. ^{31}P NMR spectra of broiler litter (BL25, left) and cottonseed hull (CH25, right) feedstock and biochar (pyrolyzed at 350, 500, 650, and 800 °C) extracts. Extraction method: 5 g of sample was shaken in 250 mM NaOH + 5 mM EDTA for 16 h. Chemical shifts (ppm) were determined with respect to 85% H_3PO_4 solution (0 ppm).

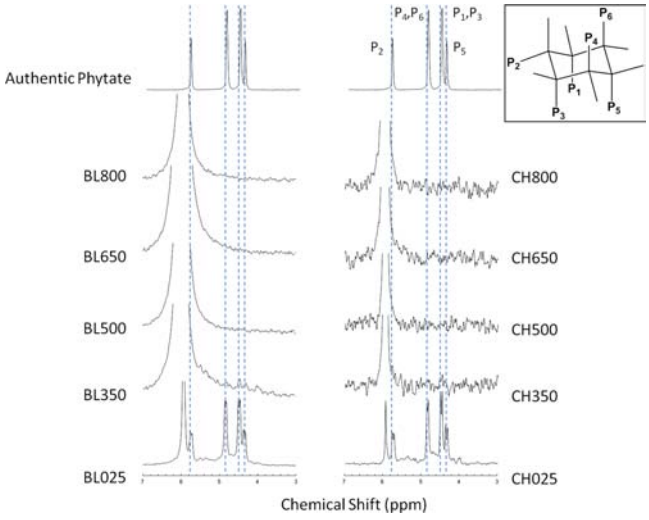

Figure 2. Figure 1 with expanded *x*-axis to visualize the monoester region (3−7 ppm). Top spectra show authentic phytate having 5.9 ppm (attributable to the P_2 position of phytate structure shown), 4.9 ppm (P_4 and P_6), 4.6 ppm (P_1 and P_3), and 4.4 ppm (P_5) peaks.

position of phytate structure in Figure 2), 4.9 ppm (P_4 and P_6), 4.6 ppm (P_1 and P_3), and 4.4 ppm (P_5).[2] An authentic spectrum of phytate is shown in Figure 2 (top) for comparison. Above pH 9.5, phytate exists in a sterically hindered form having one equatorial (P_2 in Figure 2) and five axial positions[37] as shown in Figure 2. The majority of the phytate peaks disappeared upon pyrolysis at ≥350 °C (Figure 2). Additional minor peaks in manure feedstock (BL25) are attributable to diesters: alkali-stable phospholipids and teichoic acid at 0.3−2.1 ppm and DNA at −1.5 to −0.13 ppm in Figure 1.[22,38] Polyphosphate (−20 ppm)[2] was not observable in the spectra showing the entire −30 to 30 ppm region (Figure S1, Supporting Information).

Table 2 presents ^{31}P NMR peak integration results for inorganic (orthophosphate, pyrophosphate, and total inorganic P) and organic P species (phytate, lipids, DNA, and total organic P), based on Figures 1, 2, and S1. The monoester region was integrated as a whole because of well-documented signal overlap at 3−7 ppm.[39] Absolute values in Table 2 are given in milligrams per kilogram biochar on a dry weight basis. These values were calculated by multiplying the fraction of integrated area (with respect to the total area) by total NaOH−EDTA extractable P in Table 1. Values in parentheses represent percent contribution of each P species to the total P extracted by NaOH−EDTA (Table 1). Broiler litter feedstock was dominated by phytate (58%) followed by inorganic orthophosphate (39%). Pyrolysis of broiler litter at 350 °C decreased phytate to 1%, and inorganic orthophosphate (63%) and pyrophosphate (36%) became dominant. Orthophosphate was the only species observable in 500, 650, and 800 °C broiler litter biochars (except for 3% pyrophosphate in BL500). In summary, pyrolysis of broiler litter transformed organic P dominance to inorganic P, and orthophosphate was the sole species at ≥500 °C. Cottonseed hull biochars showed a distinctively different temperature trend from the broiler litter biochars. Cottonseed hull feedstock was primarily (87%) phytate with lower orthophosphate fraction (12%) than BL25. At 350 °C, phytate decreased to zero, and pyrophosphate became the dominant species (71%); orthophosphate (27%) was much lower than BL350. The dominance of pyrophosphate continued until 650 °C: 68% pyrophosphate and 32% orthophosphate at 500 °C; 54% pyrophosphate and 46% orthophosphate at 650 °C (Table 2). Orthophosphate became the dominant species only at the highest temperature (800 °C): 81% orthophosphate and 19% pyrophosphate. In conclusion, EDTA was required to sufficiently dissolve P of plant biochar (Table 1) that was predominantly pyrophosphate (Table 2). The results suggest that pyrophosphate was stabilized by forming complexes with ash components (see stability constants in Table S1) or by interacting with organic C by electrostatic and hydrogen bonding interactions[40] and other organomineral interactions.[28] In contrast, orthophosphate was the dominant soluble P species of manure biochars (Table 2) and almost completely dissolved in acidic ammonium oxalate (Table 1). This observation suggests that soluble P of manure biochar consists of amorphous calcium phosphate, rather than the stable minerals such as apatite.

Literature reviews on the XRD analyses of manure, biochar, and ash indicated the presence of apatite in ashed[41] and gasified[42] manures, but not in the slow-pyrolysis manure biochars[29,30] containing as much as >40% C on a dry weight basis. Removal of organic matter by combustion is likely necessary to thermally form crystalline hydroxyapatite ($Ca_{10}(PO_4)_6(OH)_2$; OH may be replaced by F or Cl) and other stable calcium phosphate minerals. Calcination (heating in air) and other high-temperature processing are commonly employed to produce crystalline apatite, especially for the synthesis of biomaterials.[43] Thermal stability of apatite is controlled by the Ca/P ratio, degree of substitution by carbonate and other ions, and heating atmosphere.[43] In addition, pyrolysis produces reactive nanometer-sized precipitates on the biochar surface.[42,44] These nanosized crystals can contain P and other nutrient elements that may be released into the aqueous phase in a more controlled fashion.[45,46] Such nanomaterials are reactive sorbents for inorganic (e.g., heavy metals) and organic (e.g., agrochemicals) solutes[44] and will add further complexity to the chemical interactions within rhizospheres that will ultimately influence crop growth.

dx.doi.org/10.1021/jf4053385 | J. Agric. Food Chem. 2014, 62, 1802−1809

Table 2. Phosphorus Speciation of NaOH−EDTA (250 mM NaOH + 5 mM EDTA for 16 h) Extracts Determined by ^{31}P NMR[a]

	inorganic P in mg kg$^{-1}_{dry}$ (% total)			organic P in mg kg$^{-1}_{dry}$ (% total)			
biochar	orthophosphate	pyrophosphate	total	phytate	lipids	DNA	total
cottonseed hull							
CH25	93 (12%)	9 (1%)	101 (13%)	701 (87%)	0	0	701 (87%)
CH350	654 (27%)	1692 (71%)	2346 (98%)	0	37 (2%)	0	37 (2%)
CH500	646 (32%)	1379 (68%)	2024 (100%)	0	0	0	0
CH650	1251 (46%)	1466 (54%)	2717 (100%)	0	0	0	0
CH800	2286 (81%)	542 (19%)	2828 (100%)	0	0	0	0
broiler litter							
BL25	6445 (39%)	66 (0.4%)	6511 (39%)	9573 (58%)	346 (2%)	136 (1%)	10055 (61%)
BL350	9551 (63%)	5410 (36%)	14961 (99%)	226 (1%)	0	0	226 (1%)
BL500	18241 (97%)	618 (3%)	18859 (100%)	0	0	0	0
BL650	100%	0	16910 (100%)	0	0	0	0
BL800	100%	0	13832 (100%)	0	0	0	0

[a]Values in parentheses represent percent contribution of each P species to the total P in NaOH−EDTA extracts (Table 1 provides absolute values in mg kg$^{-1}_{dry}$.)

Table 3. Pearson's Correlation ($r > 0.878$ for $N = 5$, $p = 0.05$) between Phosphorus Species in NaOH−EDTA Extracts (Table 2) and Bulk Property of Cottonseed Hull and Broiler Litter Biochars (Table 1)[a]

		[P] by ^{31}P NMR (mg kg$^{-1}_{dry}$)				
		orthophosphate	pyrophosphate	total inorganic	phytate	total organic
		Cottonseed Hull Biochars				
	EC (mS cm^{-1})	X		X		
proximate analysis	ash			X		
(wt %$_{dry}$)	TOC					X
	VM					X
	moisture					
extracted [P]	total	X				
(mg kg$^{-1}_{dry}$)	NaOH−EDTA			X		
	water		X			
		Broiler Litter Biochars				
	EC (mS cm^{-1})			X		
proximate analysis	ash					
(wt %$_{dry}$)	TOC				X	X
	VM					
	moisture				X	X
extracted [P]	total	X				
(mg kg$^{-1}_{dry}$)	NaOH−EDTA					
	water				X	X

[a]Separate correlation was observed between the phosphorus species and total, NaOH−EDTA, and water-extractable P concentrations.

Observed predominance of phytate in both plant and manure feedstocks and decomposition at ≥350 °C (Table 2) are in agreement with the reported properties of phytate. Phytic acid forms during ripening of seeds and cereal grains and composes 60−80% of total P in cereals, oilseeds, and legumes.[47] Poorly digestible phytate composes >60% P in swine and poultry (nonruminant) feed.[47] Phytate can hydrolyze in water[1] but is stabilized by forming complexes with metal cations.[48] Compared to phosphate monoesters, diesters are more mobile because of lower charge.[1] Mononucleotides and other monophosphate esters degrade within hours of release, whereas inositol phosphate is stabilized by interacting with iron/aluminum oxides and becomes the major organic P in soil.[49] However, phytate nonenzymatically decomposes at ≥150 °C within an hour.[50] Phytic acid visually darkened at 150 °C and lost C and H at 380 °C.[50]

Orthophosphate can be formed by hydrolysis and thermal degradation of phytate.[24,51] In general, more condensed P in a polyphosphate mixture reacts with water to form less condensed P, for example, from pyrophosphate to orthophosphate.[52] Thermal treatment of orthophosphate in turn forms less soluble polyphosphate species;[51] pyrophosphate is an intermediate species in this process. The 350−650 °C plant biochars were primarily composed of pyrophosphate (Table 2), and polyphosphate was not observed (Figure S1). Subsequent discussions aim to elucidate the mechanisms favoring the formation of pyrophosphate from phytate or orthophosphate during pyrolysis of cottonseed hulls (Table 2).

Polyphosphate is a food additive for meat and dairy products, partly to sequester Ca.[53] When triphosphate-treated cheese spread was cooked, the product became enriched with pyrophosphate.[54] In addition, pyrophosphate was more resistant to hydrolysis than triphosphate.[53] The authors hypothesized that after heat-induced hydrolysis of triphosphate, pyrophosphate product became stabilized by forming complexes with Ca as well as protein in cheese.[54] Similar enrichment of pyrophosphate product was observed when commercial polyphosphate was hydrolyzed by heating without

dx.doi.org/10.1021/jf4053385 | J. Agric. Food Chem. 2014, 62, 1802−1809

Table 4. Pearson's Correlation ($r > 0.878$ for $N = 5$, $p = 0.05$) between P and Fe, Ca, Mg, Al, K, or Na in Total, NaOH−EDTA, Oxalate, and Water Extracts[a]

		total						NaOH−EDTA	oxalate				
		Fe	Ca	Mg	Al	K	Na	Al	Ca	Mg	Al	K	Na
Cottonseed Hull Biochars													
mg kg^{-1}_{dry} extracted [P]	total P												
	NaOH−EDTA P							X					
	oxalate P										X		
[P] by ^{31}P NMR	orthophosphate								X			X	X
	total inorganic							X					
Broiler Litter Biochars													
mg kg^{-1}_{dry} extracted [P]	total P	X	X	X	X	X	X						
	NaOH−EDTA P												
	oxalate P									X	X	X	X
[P] by ^{31}P NMR	orthophosphate	X								X		X	X
	total inorganic			X									X

[a]Separate correlation was observed between (i) orthophosphate or total inorganic P in NaOH−EDTA extracts by ^{31}P NMR and (ii) Fe, Ca, Mg, Al, K, or Na in different extracts.

a food product.[53] In addition to pyrophosphate, the formation of trimetaphosphate ring product was catalyzed by Ca^{2+} when commercial polyphosphate was heated at >120 °C.[53]

Pyrophosphate (P_2) can form nonenzymatically at neutral and alkaline pH and room temperature via coupled exergonic hydrolysis of polyphosphate (P_3) and endergonic condensation of orthophosphate (P): $P_3 + P = 2P_2$;[55] this reaction can be catalyzed by Ca^{2+} and other cations. Surface catalysis lowers the temperature at which high-energy phosphoanyhydride bonds can form nonenzymatically between orthophosphate to produce pyrophosphate.[56] Orthophosphate was converted to pyrophosphate on dry SiO_2 and $CaPO_4$ surfaces at 70 °C.[56] Similarly, the surface of cottonseed hull biochars may catalyze the formation of pyrophosphate from orthophosphate (Table 2).

Because water is the product of condensation reaction to form the phosphoric anhydride (P−O−P) bond,[57] drying alone can alter the P speciation.[38,56] Air-drying decreased water-extractable (labile) P in feed by 13−61%, primarily by decreasing orthophosphate.[38] In contrast, drying increased NaOH−EDTA extractable P by as much as 48%[38] In summary, thermal degradation of phytate produces orthophosphate, which thermally converts to pyrophosphate. Pyrophosphate was likely stabilized by forming complexes on the biochar surface and did not convert to polyphosphate. It must be noted that pyrophosphate has an order of magnitude higher water solubility (0.5 M) than phytate (0.07 M; both Na salts) (SciFinder Scholar).

Pearson's Correlation between P Species and Bulk Properties of Biochar. To understand the feedstock- and temperature-dependent origins of different P species, Pearson's correlation was conducted between P species (Table 2) and bulk parameters of biochar samples (Table 1). Table 3 presents parameters that showed positive correlation ($r > 0.878$ for $N = 5$, $p = 0.05$) with orthophosphate, pyrophosphate, total inorganic P, phytate, or total organic P determined by the ^{31}P NMR method: EC, ash, TOC, VM, and moisture. For the plant biochars, (i) orthophosphate correlated with EC; (ii) total inorganic P correlated with EC and ash; and (iii) total organic P correlated with TOC and VM. For the manure biochars, (i) total inorganic P correlated with EC, similarly to the plant biochars; and (ii) both phytate and total organic P correlated with TOC as well as the moisture content. In summary, bulk property for the inorganic component (EC and ash) correlated with inorganic P species. Bulk property for organic carbon (TOC and VM) correlated with organic P species. Hydrophilicity (moisture content) of manure biochars may contribute to the release of organic P species in NaOH−EDTA.

Table 3 shows a separate correlation between (i) the same series of P species in NaOH−EDTA extracts and (ii) total, NaOH−EDTA, and water-extractable P concentrations of plant and manure biochars. Interestingly, most labile (water-extractable) P fraction correlated with the signature P species in each feedstock category: pyrophosphate for plant biochars; phytate and total organic P for manure biochars (Table 3; note that water-extractable P was zero for BL350, 650, and 800 in Table 1). Total P (determined by the most rigorous microwave digestion method) correlated with orthophosphate for both plant and manure biochars. Plant biochars also showed a correlation between the total inorganic P and NaOH−EDTA extractable P (Table 3).

Pearson's Correlation between P and Other Extractable Elements. Phosphorus species are stabilized in aqueous systems by binding Al, Ca, Mg, Fe, and K (Table S1); these elements often dissolve together during extraction procedures.[7] For example, Mg^{2+} may dissolve together with orthophosphate from struvite ($MgNH_4PO_4{\cdot}6H_2O$) in poultry litter.[3] Alum (aluminum sulfate), lime, and iron sulfate are often intentionally added to poultry litter to decrease P runoff.[4] The Ca stability constant for a 1:1 complex increases from 2.66 for orthophosphate, to 8.1 for triphosphate, to approximately 22 for phytate (25 °C and zero ionic strength).[34] In contrast, the stability constant for Ca is similar for different phosphorus species containing one phosphate group: orthophosphate (2.66), $CH_3-O-PO_3^{2-}$ (1.47), and phenyl−O−PO_3^{2-} (1.45) (Table S1).

Table 4 presents observed correlation ($r > 0.878$ for $N = 5$, $p = 0.05$) between P and Fe, Ca, Mg, Al, K, or Na in total, NaOH−EDTA, and oxalate extracts. Overall, total P of broiler litter biochars correlated with total Fe, Ca, Mg, Al, K, and Na. Similarly, oxalate-extractable P correlated with oxalate-extractable Mg, Al, K, and Na of broiler litter biochars. In contrast, no

dx.doi.org/10.1021/jf4053385 | J. Agric. Food Chem. 2014, 62, 1802−1809

correlation was observed between EDTA-extractable P and these elements. Table 4 also shows observed correlations between (i) Fe, Ca, Mg, Al, K, and Na in different extracts and (ii) orthophosphate or total inorganic P in NaOH−EDTA extracts determined by ^{31}P NMR. Orthophosphate correlated with oxalate-extractable Mg, K, and Na for broiler litter biochars and Ca, K and Na for cottonseed hull biochars. Of different elements composing biochar ash, alkali metals (Na, K) dissolve in water most readily.[10] Alkaline earth metals (Ca, Mg) exist as sulfate, phosphate, and carbonate phases and dissolved in acidic oxalate solution (Table 4). At respective pyrolysis temperature, manure biochar contained >2-fold greater total Ca (by microwave digestion) than the plant biochar (Table S2). The persistence of pyrophosphate in cottonseed hull (but not broiler litter, Table 2) biochar having lower Ca (compared to manure biochars, Table S2) suggests the interaction of pyrophosphate with the organic C fraction of plant biochars. Strong chelating agent EDTA at elevated pH (Table 2) was necessary to compete with this interaction to release pyrophosphate from the biochar surface.

■ ASSOCIATED CONTENT

Ⓢ Supporting Information

Stability constants for phosphate, carboxylate, and amino-carboxylate ligands, entire ^{31}P NMR spectra for plant and manure biochars, and total, NaOH−EDTA, and oxalate-extractable elements for Table 4. This material is available free of charge via the Internet at http://pubs.acs.org.

■ AUTHOR INFORMATION

Corresponding Author

*(M.U.) Fax: (504) 286-4367. Phone: (504) 286-4356. E-mail: sophie.uchimiya@ars.usda.gov.

Notes

The authors declare no competing financial interest.

■ ACKNOWLEDGMENTS

We thank Dr. Isabel Lima for providing the broiler litter biochar samples and Lynda Wartelle for laboratory assistance. Mention of trade names or commercial products in this publication is solely for the purpose of providing specific information and does not imply recommendation or endorsement by the U.S. Department of Agriculture.

■ REFERENCES

(1) Koopmans, G. F.; Chardon, W. J.; McDowell, R. W. Phosphorus movement and speciation in a sandy soil profile after long-term animal manure applications. *J. Environ. Qual.* **2007**, *36*, 305−315.

(2) Cade-Menun, B. J. Characterizing phosphorus in environmental and agricultural samples by ^{31}P nuclear magnetic resonance spectroscopy. *Talanta* **2005**, *66*, 359−371.

(3) Hunger, S.; Sims, J. T.; Sparks, D. L. Evidence for struvite in poultry litter: effect of storage and drying. *J. Environ. Qual.* **2008**, *37*, 1617−1625.

(4) Seiter, J. M.; Staats-Borda, K. E.; Ginder-Vogel, M.; Sparks, D. L. XANES spectroscopic analysis of phosphorus speciation in alum-amended poultry litter. *J. Environ. Qual.* **2008**, *37*, 477−485.

(5) Novotny, E. H.; Auccaise, R.; Velloso, M. H. R.; Corrêa, J. C.; Higarashi, M. M.; Abreu, V. M. N.; Rocha, J. D.; Kwapinski, W. Characterization of phosphate structures in biochar from swine bones. *Pesqui. Agropecu. Bras.* **2012**, *47*, 672−676.

(6) Streube, J. D.; Collins, H. P.; Tarara, J. M.; Cochran, R. L. Biochar produced from anaerobically digested fiber reduces phosphorus in dairy lagoons. *J. Environ. Qual.* **2012**, *41*, 1166−1174.

(7) Ohno, T.; Hiradate, S.; He, Z. Phosphorus solubility of agricultural soils: a surface charge and phosphorus-31 NMR speciation study. *Soil Sci. Soc. Am. J.* **2011**, *75*, 1704−1711.

(8) Bridle, T. R.; Pritchard, D. Energy and nutrient recovery from sewage sludge via pyrolysis. *Water Sci. Technol.* **2004**, *50*, 169−175.

(9) Cantrell, K. B.; Hunt, P. G.; Uchimiya, M.; Novak, J. M.; Ro, K. S. Impact of pyrolysis temperature and manure source on physicochemical characteristics of biochar. *Bioresour. Technol.* **2012**, *107*, 419−428.

(10) Wu, H.; Yip, K.; Kong, Z.; Li, C. Z.; Liu, D.; Yu, Y.; Gao, X. Removal and recycling of inherent inorganic nutrient species in mallee biomass and derived biochars by water leaching. *Ind. Eng. Chem. Res.* **2011**, *50*, 12143−12151.

(11) Silber, A.; Levkovitch, I.; Graber, E. R. pH-dependent mineral release and surface properties of cornstraw biochar: agronomic implications. *Environ. Sci. Technol.* **2010**, *44*, 9318−9323.

(12) Uchimiya, M.; Ohno, T.; He, Z. Pyrolysis temperature-dependent release of dissolved organic carbon from plant, manure, and biorefinery wastes. *J. Anal. Appl. Pyrol.* **2013**, *104*, 84−94.

(13) Uchimiya, M.; Wartelle, L. H.; Klasson, K. T.; Fortier, C. A.; Lima, I. M. Influence of pyrolysis temperature on biochar property and function as a heavy metal sorbent in soil. *J. Agric. Food Chem.* **2011**, *59*, 2501−2510.

(14) Uchimiya, M.; Bannon, D. I.; Wartelle, L. H.; Lima, I. M.; Klasson, K. T. Lead retention by broiler litter biochars in small arms range soil: impact of pyrolysis temperature. *J. Agric. Food Chem.* **2012**, *60*, 5035−5044.

(15) Uchimiya, M.; Wartelle, L. H.; Boddu, V. M. Sorption of triazine and organophosphorus pesticides on soil and biochar. *J. Agric. Food Chem.* **2012**, *60*, 2989−2997.

(16) Uchimiya, M.; Wartelle, L. H.; Lima, I. M.; Klasson, K. T. Sorption of deisopropylatrazine on broiler litter biochars. *J. Agric. Food Chem.* **2010**, *58*, 12350−12356.

(17) Lima, I. M.; Boateng, A. A.; Klasson, K. T. Pyrolysis of broiler manure: char and product gas characterization. *Ind. Eng. Chem. Res.* **2009**, *48*, 1292−1297.

(18) U.S. EPA Method 200.7. *Trace Elements in Water, Solids, and Biosolids by Inductively Coupled Plasma-Mass Spectrometry*, revision 5.0; EPA-821-R-01-010; U.S. Environmental Protection Agency, Office of Research and Development: Cincinnati, OH, USA, 2001.

(19) Mehlich, A. Mehlich 3 soil test extractant: a modification of Mehlich 2 extractant. *Commun. Soil Sci. Plan.* **1984**, *15*, 1409−1416.

(20) Iyengar, S. S.; Zelazny, L. W.; Martens, D. C. Effect of photolytic oxalate treatment on soil hydroxy-interlayered vermiculites. *Clays Clay Miner.* **1981**, *29*, 429−434.

(21) U.S. EPA Method 3052. *Microwave Assisted Acid Digestion of Siliceous and Organically Based Matrice*; U.S. Environmental Protection Agency: Washington, DC, USA, 1996.

(22) Turner, B. L.; Mahieu, N.; Condron, L. M. Phosphorus-31 nuclear magnetic resonance spectral assignments of phosphorus compounds in soil NaOH-EDTA extracts. *Soil Sci. Soc. Am. J.* **2003**, *67*, 497−510.

(23) Turner, B. L.; Condron, L. M.; Richardson, S. J.; Peltzer, D. A.; Allison, V. J. Soil organic phosphorus transformations during pedogenesis. *Ecosystems* **2007**, *10*, 1166−1181.

(24) Knicker, H. How does fire affect the nature and stability of soil organic nitrogen and carbon? A review. *Biogeochemistry* **2007**, *85*, 91−118.

(25) Vassilev, S. V.; Baxter, D.; Andersen, L. K.; Vassileva, C. G. An overview of the composition and application of biomass ash. Part 1. Phase-mineral and chemical composition and classification. *Fuel* **2013**, *105*, 40−76.

(26) Vassilev, S. V.; Baxter, D.; Andersen, L. K.; Vassileva, C. G.; Morgan, T. J. An overview of the organic and inorganic phase composition of biomass. *Fuel* **2012**, *94*, 1−33.

(27) Thy, P.; Yu, C.; Jenkins, B. M.; Lesher, C. E. Inorganic composition and environmental impact of biomass feedstock. *Energy Fuels* **2013**, *27*, 3969−3987.

(28) Uchimiya, M. Changes in nutrient content and availability during the slow pyrolysis of animal wastes. In *Applied Manure and*

Nutrient Chemistry for Sustainable Agriculture and Environment; He, Z., Zhang, H., Eds.; Springer: New York, in press.
(29) Zhao, L.; Cao, X.; Wang, Q.; Yang, F.; Xu, S. Mineral constituents profile of biochar derived from diversified waste biomasses: Implications for agricultural applications. *J. Environ. Qual.* **2013**, *42*, 545−552.
(30) Wang, T.; Camps-Arbestain, M.; Hedley, M.; Bishop, P. Predicting phosphorus bioavailability from high-ash biochars. *Plant Soil* **2012**, *357*, 173−187.
(31) Warnock, D. D.; Mummey, D. L.; McBride, B.; Major, J.; Lehmann, J.; Rillig, M. C. Influences of non-herbaceous biochar on arbuscular mycorrhizal fungal abundances in roots and soils: results from growth-chamber and field experiments. *Appl. Soil Ecol.* **2010**, *46*, 450−456.
(32) Gaskin, J. W.; Steiner, C.; Harris, K.; Das, K. C.; Bibens, B. Effect of low-temperature pyrolysis conditions on biochar for agricultural use. *Trans. ASABE* **2008**, *51*, 2061−2069.
(33) Chan, K. Y.; Van Zwieten, L.; Meszaros, I.; Downie, A.; Joseph, S. Using poultry litter biochars as soil amendments. *Aust. J. Soil Res.* **2008**, *46*, 437−444.
(34) Martell, A. E.; Smith, R. M.; Motekaitis, R. J. *Critically Selected Stability Constants of Metal Complexes Database*, version 8.0; U.S. Department of Commerce, National Institute of Standards and Technology: Gaithersburg, MD, USA, 2004.
(35) Horner, H. T.; Cervantes-Martinez, T.; Healy, R.; Reddy, M. B.; Deardorff, B. L.; Bailey, T. B.; Al-Wahsh, I.; Massey, L. K.; Palmer, R. G. Oxalate and phytate concentrations in seeds of soybean cultivars [*Glycine max* (L.) Merr.]. *J. Agric. Food Chem.* **2005**, *53*, 7870−7877.
(36) Miller, S. L.; Parris, M. Synthesis of pyrophosphate under primitive earth conditions. *Nature* **1964**, *204*, 1248−1250.
(37) Bauman, A. T.; Chateauneuf, G. M.; Boyd, B. R.; Brown, R. E.; Murthy, P. P. N. Conformational inversion processes in phytic acid: NMR spectroscopic and molecular modeling studies. *Tetrahedron Lett.* **1999**, *40*, 4489−4492.
(38) McDowell, R. W.; Dou, Z.; Toth, J. D.; Cade-Menun, B. J.; Kleinman, P. J. A.; Soder, K.; Saporito, L. A comparison of phosphorus speciation and potential bioavailability in feed and feces of different dairy herds using ^{31}P nuclear magnetic resonance spectroscopy. *J. Environ. Qual.* **2008**, *37*, 741−752.
(39) Vestergren, J.; Vincent, A. G.; Jansson, M.; Persson, P.; Ilstedt, U.; Gröbner, G.; Giesler, R.; Schleucher, J. High-resolution characterization of organic phosphorus in soil extracts using 2D 1H-^{31}P NMR correlation spectroscopy. *Environ. Sci. Technol.* **2012**, *46*, 3950−3956.
(40) Fang, Q.; Chen, B.; Lin, Y.; Guan, Y. Aromatic and hydrophobic surfaces of wood-derived biochar enhance perchlorate adsorption via hydrogen bonding to oxygen-containing organic groups. *Environ. Sci. Technol.* **2014**, *48*, 279−288.
(41) Herrera, D.; Harris, W. G.; Nair, V. D.; Josan, M.; Staples, C. R. Effect of dietary modifications of calcium and magnesium on reducing solubility of phosphorus in feces from lactating dairy cows. *J. Dairy Sci.* **2010**, *93*, 2598−2611.
(42) Ksawery, K.; John, G. R.; Gorm, P. T.; Baiq Emielda, Y. The composition and dissolution in citric extractants of ash from the thermal gasification of pig manure. *Chem. Eng. J.* **2010**, *163*, 1−9.
(43) Tõnsuaadu, K.; Gross, K. A.; Pluduma, L.; Veiderma, M. A review on the thermal stability of calcium apatites. *J. Therm. Anal. Calorim.* **2012**, *110*, 647−659.
(44) Zhang, M.; Gao, B.; Yao, Y.; Xue, Y.; Inyang, M. Synthesis of porous MgO-biochar nanocomposites for removal of phosphate and nitrate from aqueous solutions. *Chem. Eng. J.* **2012**, *210*, 26−32.
(45) Yao, Y.; Gao, B.; Chen, J.; Yang, L. Engineered biochar reclaiming phosphate from aqueous solutions: mechanisms and potential application as a slow-release fertilizer. *Environ. Sci. Technol.* **2013**, *47*, 8700−8708.
(46) Qian, T.; Zhang, X.; Hu, J.; Jiang, H. Effects of environmental conditions on the release of phosphorus from biochar. *Chemosphere* **2013**, *93*, 2069−2075.
(47) Maguire, R. O.; Sims, J. T.; Saylor, W. W.; Turner, B. L.; Angel, R.; Applegate, T. J. Influence of phytase addition to poultry diets on phosphorus forms and solubility in litters and amended soils. *J. Environ. Qual.* **2004**, *33*, 2306−2316.
(48) Crea, F.; De Stefano, C.; Milea, D.; Sammartano, S. Formation and stability of phytate complexes in solution. *Coordin. Chem. Rev.* **2008**, *252*, 1108−1120.
(49) Turner, B. L.; Mahieu, N.; Condron, L. M. The phosphorus composition of temperate pasture soils determined by NaOH-EDTA extraction and solution ^{31}P NMR spectroscopy. *Org. Geochem.* **2003**, *34*, 1199−1210.
(50) Daneluti, A. L. M.; Matos, J. R. Study of thermal behavior of phytic acid. *Braz. J. Pharm. Sci.* **2013**, *49*, 275−283.
(51) Cade-Menun, B. J.; Berch, S. M.; Preston, C. M.; Lavkulich, L. M. Phosphorus forms and related soil chemistry of Podzolic soils on northern Vancouver Island. II. The effects of clear-cutting and burning. *Can. J. Forest Res.* **2000**, *30*, 1726−1741.
(52) McBeath, T. M.; Lombi, E.; McLaughlin, M. J.; Bünemann, E. K. Isotopic exchangeability, hydrolysis and mobilization reactions of pyrophosphate in soil. *Soil Sci. Soc. Am. J.* **2008**, *72*, 1337−1343.
(53) Rulliere, C.; Perenes, L.; Senocq, D.; Dodi, A.; Marchesseau, S. Heat treatment effect on polyphosphate chain length in aqueous and calcium solutions. *Food Chem.* **2012**, *134*, 712−716.
(54) Rulliere, C.; Rondeau-Mouro, C.; Raouche, S.; Dufrechou, M.; Marchesseau, S. Studies of polyphosphate composition and their interaction with dairy matrices by ion chromatography and ^{31}P NMR spectroscopy. *Int. Dairy J.* **2013**, *28*, 102−108.
(55) Etaix, E.; Buvet, R. Conditions of occurrence for primeval processes of transphosphorylations. *Origins Life* **1975**, *6*, 175−183.
(56) Georgelin, T.; Jaber, M.; Onfroy, T.; Hargrove, A. A.; Costa-Torro, F.; Lambert, J. F. Inorganic phosphate and nucleotides on silica surface: condensation, dismutation, and phosphorylation. *J. Phys. Chem. C* **2013**, *117*, 12579−12590.
(57) Hong, J.; Yoshida, N.; Chong, S. H.; Lee, C.; Ham, S.; Hirata, F. Elucidating the molecular origin of hydrolysis energy of pyrophosphate in water. *J. Chem. Theory Comput.* **2012**, *8*, 2239−2246.

elucidation of the geographic origin of volatile compounds should lead to a better understanding of factors causing aroma differences between teas. To effectively organize and explain the results from the volatile component, some chemometric tools [such as cluster analysis (CA) and principal component analysis (PCA)] provide more objective interpretations. CA and PCA can be used to explain similarities and differences in data and discover natural groupings of samples.[13] Recently, on the basis of CA and PCA, many food products have been successfully discriminated according to variety and geographical origin.[14,15] For tea, quality control data obtained by the volatile component have been used to discriminate the different types,[16,17] different fermentation degrees,[18] and different grades of tea[19,20] by using CA and PCA. However, no studies have been reported for the determination of the aroma characteristics and discrimination model between Pu-erh and Fuzhuan teas based on their volatile components through using CA and PCA.

Previously developed methods for extracting the volatile compounds of tea mainly used simultaneous distillation extraction (SDE).[21−24] However, this approach is a lengthy process (e.g., 3−5 h) and consumes large amounts of both samples (e.g., 50−200 g) and organic solvents. Because headspace−solid phase microextraction (HS-SPME) is a simple, fast, and solvent-free analytical technology, it can help consumers to understand the authentic aroma components of tea.[12] Many studies have proved that HS-SPME has many enormous advantages compared with SDE;[25] HS-SPME coupled with GC-MS also has been successfully used to analyze volatile compounds of different tea samples.[18,26,27]

In our previous studies, fully automatic HS-SPME was investigated for the determination of aroma components from Pu-erh ripe tea and black tea, showing good repeatability, sensitivity, and selectivity.[28,29] However, these studies compared the aroma components of only a limited number of tea samples and did not use multivariate statistical methods, so the obtained results were not representative and persuasive. In this work, we report for the first time the discrimination or classification of Pu-erh and Fuzhuan teas, through their comprehensive volatile compound profiling by fully automatic HS-SPME combined with GC-MS analysis; multivariate statistical analysis such as PCA and CA was employed. To our knowledge, this is the first attempt of classification and differentiation of CDTs in accordance with production area through CA and PCA.

MATERIALS AND METHODS

Tea Samples. Thirteen Pu-erh tea samples, numbered from YP1 to YP13, were collected from five representative Pu-erh tea geographical protection areas (Puer, Xishuangbanna, Lincang, Dali, and Baoshan) in Yunnan province, and 13 Fuzhuan tea samples, numbered from HF1 to HF13, were collected from a local market in Anhua country of Hunan province and produced by Yiqingyuan Tea Ltd., Inc. All 26 dark teas were processed in 2012 and stored in a dry place.

HS-SPME Analysis. A 100 μm polydimethylsiloxane (PDMS) fiber, a 65 μm polydimethylsiloxane/divinylbenzene (PDMS/DVB) fiber, and a 75 μm carboxen/polydimethylsiloxane (CAR/PDMS) fiber were used in this work (Supelco, Bellefonte, PA, USA). The fiber used for analysis was previously kept in the GC-MS injection port for 30 min at 250 °C and used immediately to prevent subsequent contamination.

The 26 dark tea samples were ground into fine powder and passed through a 30−60 mesh. The ground tea sample (2.0 g) was introduced into a 20 mL sealed headspace bottle and infused with 5 mL of boiling water; the temperature of the headspace bottle was kept at 80 °C with a hot plate. A 65 μm PDMS/DVB fiber was then exposed to the sample headspace while the tea powder was continuously stirred (250 rpm) for 60 min. All of the volatile components absorbed on the SPME fiber were desorbed at the GC-MS injection port (250 °C for 3.5 min) and subsequently analyzed by GC-MS, separately.

GC-MS Analysis. An Agilent 7890A GC system, coupled with an Agilent 5975C MSD mass spectrometer (Agilent, Santa Clara, CA, USA), was used to identify volatile compounds of all tea samples. An Agilent HP-5MS capillary column (30 m × 0.25 mm i.d. × 0.25 μm film thickness) was employed, helium (purity > 99.999%) was used as the carrier gas, and the flow rate was 1 mL/min. The injector temperature was 250 °C, and injection mode was performed in splitless. The GC oven temperature was held at 50 °C for 5 min, then increased to 210 °C at a rate of 3 °C/min, maintained at 210 °C for 3 min, and finally increased to 230 °C at a rate of 15 °C/min. The mass spectrometer conditions were as follows: ionization energy, 70 eV; ion source temperature, 230 °C; quadrupole temperature, 150 °C; quadrupole mass spectrometer scan range, 30−500 atomic mass units (amu); solvent delay time, 2.8 min.

Data Analysis. Identifications of the peaks were made by searching the National Institute of Standards and Technology (NIST) 08.L GC-MS database, and the retention indices (RI) were compared with the published data.[30−33] The relative contents of the aroma compounds were calculated by peak area normalization. The GC Kovats RI for each compound was determined by using 1 μL of *n*-alkanes (C8−C40; Sigma-Aldrich, St. Louis, MO, USA) under the identical GC-MS experimental conditions. Significant differences between Pu-erh and Fuzhuan teas for each of the volatile compounds were determined by independent samples *t*-test analysis using the SPSS statistical package (version 17.0 for Windows, SPSS, Inc., Chicago, IL, USA). CA and PCA were performed using SIMCA-P12 software (Umetrics, Umea, Sweden).

RESULTS AND DISCUSSION

Optimization of HS-SPME Parameters. In this work, three key experimental parameters (type of fiber, extraction temperature, and extraction time) for fully automatic HS-SPME were examined. Pu-erh tea sample YP-1 was used as optimized sample under different conditions. In general, the effective SPME fibers included three polymeric materials: a liquid PDMS for the less polar components and two solid DVB and CAR for the more polar components. First, three types of fiber (100 μm PDMS, 65 μm PDMS/DVB, and 75 μm CAR/PDMS) were studied for the extraction of volatile compounds from the YP-1 sample. Each fiber can absorb volatile components under the same temperature and time. The SPME fiber adsorption yield was evaluated in terms of total amount of volatile components from the YP-1 sample. Results showed the 65 μm PDMS/DVB fiber can absorb 71 volatile components and obtain maximum peak area, whereas the 100 μm PDMS and 75 μm CAR/PDMS fibers can absorb only 49 and 60 volatile components, respectively. Therefore, the 65 μm PDMS/DVB fiber was used as the most optimal fiber for the HS-SPME method. Second, the extraction temperature and extraction time of SPME were investigated by varying the extraction temperature (50, 60, 70, 80, 90, and 100 °C) and time (30, 40, 50, 60, 70, and 80 min) when the SPME fiber was set as 65 μm PDMS/DVB. Figure 1 shows the sum of total peak area in the extraction temperature and time studied. As shown in Figure 1A, the total peak area of the YP-1 sample was gradually increased from 50 to 80 °C but slightly decreased above 80 °C. For extraction time, the total peak area of the YP-1 sample was gradually increased from 30 to 60 min. However, as the extraction time was extended, the total peak area of the YP-1 sample showed little change (Figure 1B). Because the extraction time was 60 min, the adsorption of aroma components by SPME fiber reached a dynamic equilibrium.

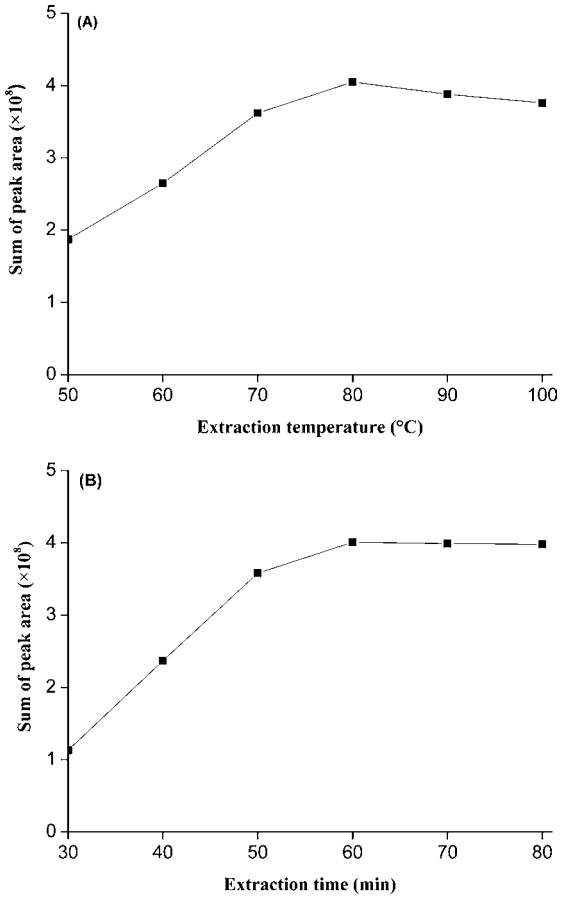

Figure 1. Effect of extraction temperature (A) and time (B) on extraction of volatile compounds from the YP-1 sample according to the sum of the total peak area.

Therefore, in this work, extraction temperature and extraction time were selected at 80 °C and 60 min, respectively.

Analysis of Volatile Compounds. Twenty-six samples of Pu-erh and Fuzhuan teas were analyzed by the fully automatic headspace GC-MS method. TICs are presented in Figure 2. The identified components and their relative percentage contents (%) are summarized in Table 1. The relative percentage contents of these identified aroma components were presented as "% average (range)". A total of 93 aroma components, including 23 hydrocarbons, 21 alcohols, 14 ketones, 11 methoxyphenolic compounds, 7 esters, 7 aldehydes, 4 furans, 2 nitrogen compounds, 2 lactones, 1 acid, and 1 phenol compound, were identified in 26 dark tea samples. Among these identified volatiles, methoxyphenolic compounds (31.77%), alcohols (15.50%), and hydrocarbons (14.63%) were the major volatile components in 13 Pu-erh teas, whereas ketones (25.42%), alcohols (19.14%), and hydrocarbons (15.58%) were the major volatile components in 13 Fuzhuan teas. The most abundant compounds in Pu-erh teas were 1,2,3-trimethoxybenzene, hexadecanoic acid, 1,2,4-trimethoxybenzene, and dihydroactinidiolide, whereas the most abundant compounds in Fuzhuan teas were caffeine, β-ionone, geranyl acetone, and dihydroactinidiolide.

A total of 23 hydrocarbon compounds were identified in 26 dark teas. There were no significant differences ($P > 0.05$) in the content of hydrocarbon compounds in these two kinds of dark tea samples. However, these identified volatile components were mostly saturated hydrocarbons, such as hexadecane,

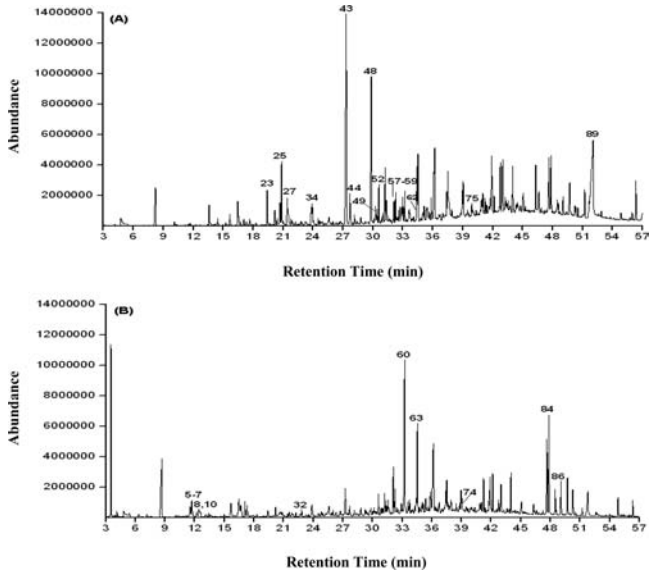

Figure 2. TIC of Pu-erh tea (A, sample YP-1) and Fuzhuan tea (B, sample HF-1). Twenty-six volatile compounds with significant differences ($P < 0.01$) in Pu-erh and Fuzhuan teas are denoted by the numbers shown in Table 1.

heptadecane, 2,6,10,14-tetramethylpentadecane, and 2,6,10,14-tetramethyhexadecane. Only five kinds of unsaturated hydrocarbons were identified, and the average contents of these compounds in Pu-erh and Fuzhuan teas were only 1.77 and 3.16%, respectively. Saturated hydrocarbons generally have no effect on flavor, whereas unsaturated hydrocarbons play an important role in giving the tea flavor.[34,35] In our results, limonene was present at a relatively high level in Fuzhuan teas, whereas β-guaiene was present at a relatively high level in Pu-erh teas. Qiao et al.[31] found limonene at the greatest concentrations (90.85%) in fruit juice but it did not exhibit the strongest aroma activity, although it had an orange odor in gas chromatography−olafactometry (GC-O). β-Guaiene was considered to be an important feature of aroma compounds and endowed with a unique woody scent for Pu-erh tea.[33] In short, the unsaturated hydrocarbons generally having a woody and fruit fragrance in Fuzhuan teas were in higher proportion than in Pu-erh teas, which may have special contribution to the flavor of Fuzhuan teas.

A total of 21 alcohol compounds were identified in 26 dark tea samples. Among them, 10 alcohols were common to all of the tea samples. Linalool oxides were the most abundant alcohols in Pu-erh teas (5.39%) and Fuzhuan teas (3.77%), followed by phytol and isophytol. As shown in Table 1, linalool, reported as an abundant volatile constituent in various green teas,[32] oolong teas,[23] and black teas,[36] was present at a relatively low level in Pu-erh teas (0.72%) and Fuzhuan teas (1.85%), but the content of linalool oxides increased sharply. This indicated that linalool underwent a significant oxygenation effect during the postfermentation process with microbial activity. The level of α-terpineol in Pu-erh teas (1.60%) had a significant difference ($P < 0.001$) compared to Fuzhuan teas (0.32%). Similar to our results, many studies have shown linalool oxides and α-terpineol, which have a unique floral and sweet odor, were the most abundant alcohol constituents in Pu-erh tea, and their formation may be mostly related to the postfermentation process with the microbial activity.[37] Phytol and isophytol, with a camphoraceous odor, were present at a relatively high content

Table 1. Volatile Compounds and Their Relative Contents in Pu-erh and Fuzhuan Teas[a]

no.	RI[b]	compound[c]	ID[d]	relative percentage content [% (range)] YP(n = 13)	HF(n = 13)	P value[e]
1	803	2,3-butanediol	MS	0a[f]	0.05 (0−0.28)a	0.097
2	861	hexyl alcohol	MS, RI	0a	0.08 (0−0.49)a	0.085
3	884	2-heptanone	MS, RI	0a	0.14 (0−0.45)b	0.011
4	957	benzaldehyde	MS, RI	0.16 (0−0.36)a	0.30 (0−0.52)b	0.012
5	**979**	**1-octen-3-ol**	**MS, RI**	**0.02 (0−0.14)a**	**0.10 (0−0.20)b**	**0.003**
6	**985**	**6-methyl-5-hepten-2-one**	**MS, RI**	**0.04 (0−0.16)a**	**0.62 (0.16−1.19)b**	**0.000**
7	**989**	**2-pentylfuran**	**MS, RI**	**0.16 (0−0.36)a**	**0.83 (0.40−1.63)b**	**0.000**
8	**998**	***cis*-2-(2-pentenyl)furan**	**MS, RI**	**0a**	**0.22 (0−0.54)b**	**0.001**
9	1018	1,2,3-trimethylbenzene	MS, RI	0a	0.02 (0−0.15)a	0.166
10	**1026**	**limonene**	**MS, RI**	**0.03 (0−0.12)a**	**0.24 (0.13−0.38)b**	**0.000**
11	1030	2-ethylhexanol	MS, RI	0.10 (0−0.89)a	0a	0.202
12	1034	benzyl alcohol	MS, RI	0.02 (0−0.14)a	0.10 (0−0.59)a	0.085
13	1042	phenyl acetaldehyde	MS, RI	0.03 (0−0.21)a	0.04 (0−0.20)a	0.720
14	1048	1-ethyl-1*H*-pyrrole-2-carbaldehyde	MS, RI	0.16 (0−0.54)a	0.11 (0−0.84)a	0.469
15	1064	acetophenone	MS, RI	0.05 (0−0.25)a	0.13 (0−0.35)a	0.062
16	1072	linalool oxide I	MS, RI	1.01 (0.51−2.27)a	0.95 (0.28−2.14)a	0.783
17	1087	linalool oxide II	MS, RI	2.13 (1.26−3.37)a	1.99 (0.78−3.51)a	0.620
18	1092	(*E*,*E*)-3,5-octadien-2-one	MS	0.06 (0−0.16)a	0.17 (0−0.73)a	0.164
19	1098	linalool	MS, RI	0.72 (0.30−2.43)a	1.85 (0.87−3.18)b	0.011
20	1104	nonanal	MS, RI	0.15 (0−0.76)a	0a	0.061
21	1110	phenylethyl alcohol	MS, RI	0.33 (0−0.99)a	0.72 (0−2.25)a	0.092
22	1137	2,5-pyrrolidinedione, 1-ethyl-	MS, RI	0.04 (0−0.19)a	0.10 (0−0.28)a	0.061
23	**1149**	**1,2-dimethoxybenzene**	**MS, RI**	**1.40 (0.90−2.01)a**	**0.61 (0.17−2.21)b**	**0.000**
24	1169	linalool oxide III	MS, RI	0.51 (0.22−1.00)a	0.38 (0−1.28)a	0.294
25	**1175**	**linalool oxide IV**	**MS, RI**	**1.65 (0.63−3.73)a**	**0.45 (0.26−1.20)b**	**0.000**
26	1178	naphthalene	MS, RI	0.44 (0−3.05)a	0.29 (0.14−0.37)a	0.496
27	**1188**	**α-terpineol**	**MS, RI**	**1.60 (0.84−3.17)a**	**0.32 (0.17−0.59)b**	**0.000**
28	1190	methyl salicylate	MS, RI	0.44 (0−0.98)a	1.41 (0.27−5.67)b	0.034
29	1196	safranal	MS, RI	0.13 (0−0.34)a	0.28 (0.16−0.53)b	0.012
30	1200	dodecane	MS, RI	0.04 (0−0.21)a	0.14 (0−0.48)a	0.069
31	1205	decanal	MS, RI	0.25 (0−0.68)a	0.34 (0−0.63)a	0.212
32	**1218**	**β-cyclocitral**	**MS, RI**	**0.12 (0−0.30)a**	**0.60 (0.28−0.78)b**	**0.000**
33	1228	nerol	MS, RI	0.05 (0−0.27)a	0.03 (0−0.22)a	0.633
34	**1241**	**3,4-dimethoxytoluene**	**MS, RI**	**0.83 (0−1.79)a**	**0b**	**0.001**
35	1256	geraniol	MS, RI	0.43 (0.13−0.98)a	0.83 (0.21−2.40)a	0.061
36	1260	2-methoxybenzylalcohol	MS, RI	0.05 (0−0.20)a	0b	0.045
37	1265	3,5-dimethoxytoluene	MS, RI	0.08 (0−0.24)a	0b	0.019
38	1287	2-methylnaphthalene	MS, RI	0.19 (0−0.37)a	0.30 (0−0.51)b	0.045
39	1294	2-undecanone	MS	0.09 (0−0.31)a	0.10 (0−0.44)a	0.806
40	1300	tridecane	MS, RI	0a	0.07 (0−0.46)a	0.116
41	1302	1-methylnaphthalene	MS, RI	0.17 (0−0.36)a	0.29 (0−0.47)a	0.064
42	1304	isopropyl salicylate	MS, RI	0a	0.18 (0−2.39)a	0.337
43	**1316**	**1,2,3-trimethoxybenzene**	**MS, RI**	**14.75 (7.25−27.43)a**	**1.71 (0.53−2.82)b**	**0.000**
44	**1325**	**4-ethyl-1,2-dimethoxybenzene**	**MS, RI**	**2.22 (0.31−4.93)a**	**0.32 (0−0.72)b**	**0.000**
45	1334	2,6,6-trimethyl-1-cyclohexene-1-ethanol	MS	0.05 (0−0.42)a	0.03 (0−0.38)a	0.619
46	1351	2,6-dimethoxyphenol	MS, RI	0.30 (0−0.67)a	0.66 (0.21−2.78)a	0.071
47	1362	γ-nonanolactone	MS	0a	0.19 (0−0.65)b	0.016
48	**1375**	**1,2,4-trimethoxybenzene**	**MS, RI**	**6.53 (2.14−11.79)a**	**0b**	**0.000**
49	**1387**	**β-guaiene**	**MS, RI**	**0.49 (0−0.91)a**	**0.09 (0−0.58)b**	**0.001**
50	1397	*cis*-jasmone	MS, RI	0.32 (0−0.64)a	0.67 (0.27−2.78)a	0.076
51	1400	tetradecane	MS, RI	0.42 (0.21−0.56)a	0.71 (0.34−1.42)b	0.011
52	**1406**	**1,2,3-trimethoxy-5-methylbenzene**	**MS, RI**	**3.15 (0.27−8.00)a**	**0.67 (0−1.33)b**	**0.004**
53	1409	α-cedrene	MS, RI	0.81 (0−1.44)a	1.52 (0.35−3.40)b	0.022
54	1417	β-caryophyllene	MS	0.04 (0−0.49)a	0.96 (0−2.96)b	0.012
55	1428	α-ionone	MS, RI	0.77 (0.38−1.45)a	2.00 (0.19−3.69)b	0.014
56	1438	dihydro-β-ionone	MS, RI	0.13 (0−0.36)a	0.22 (0−0.62)a	0.230
57	**1442**	**1-methoxynaphthalene**	**MS**	**0.60 (0.26−1.04)a**	**0b**	**0.000**
58	**1447**	**2-methoxynaphthalene**	**MS**	**0.74 (0.46−1.23)a**	**0b**	**0.000**
59	**1449**	**1,2,3,4-tetramethoxybenzene**	**MS, RI**	**1.02 (0.32−1.59)a**	**0.18 (0−0.96)b**	**0.000**

dx.doi.org/10.1021/jf405237u | J. Agric. Food Chem. 2014, 62, 1810−1818

Table 1. continued

no.	RI[b]	compound[c]	ID[d]	relative percentage content [% (range)] YP(n = 13)	HF(n = 13)	P value[e]
60	**1455**	**geranyl acetone**	**MS, RI**	**1.41 (0.54−2.45)a**	**6.45 (3.03−13.55)b**	**0.000**
61	1468	5-methoxy-6,7-dimethylbenzofuran	MS	0a	0.44 (0−1.64)b	0.019
62	**1483**	**4-(2,6,6-trimethylcyclohexa-1,3-dienyl)-but-3-en-2-one**	**MS**	**2.69 (0−6.52)a**	**0.86 (0.32−1.68)b**	**0.008**
63	**1487**	***β*-ionone**	**MS, RI**	**2.65 (1.47−4.33)a**	**7.18 (4.62−9.88)b**	**0.000**
64	1492	2-tridecanone	MS	0.32 (0−1.70)a	0a	0.089
65	1497	methyl isoeugenol	MS, RI	0.45 (0−0.96)a	0.22 (0−0.92)a	0.231
66	1500	pentadecane	MS, RI	0.60 (0.35−0.98)a	0.72 (0.47−1.29)a	0.121
67	1506	dibenzofuran	MS, RI	0.52 (0−1.09)a	0.69 (0.38−1.04)a	0.151
68	1508	*α*-farnesene	MS, RI	0.40 (0−1.14)a	0.35 (0−2.94)a	0.824
69	1528	dihydroactinidiolide	MS, RI	4.38 (2.27−6.51)a	5.45 (2.85−9.41)a	0.086
70	1554	nerolidol	MS, RI	1.18 (0−2.86)a	2.93 (0.70−18.94)a	0.252
71	1572	fluorene	MS, RI	0.69 (0−1.10)a	0.90 (0−1.85)a	0.278
72	1598	cedrol	MS, RI	0.95 (0−3.38)a	2.78 (0.67−7.43)b	0.014
73	1600	hexadecane	MS, RI	1.65 (0.86−2.57)a	1.33 (0.50−2.95)a	0.282
74	**1649**	**methyl jasmonate**	**MS, RI**	**0a**	**0.99 (0.60−2.05)b**	**0.000**
75	**1653**	***α*-cadinol**	**MS, RI**	**1.04 (0.65−1.29)a**	**0.74 (0.48−1.14)b**	**0.000**
76	1659	2,2′,5,5′-tetramethyl-1,1′-biphenyl	MS	0.54 (0−1.23)a	1.09 (0−3.68)a	0.085
77	1664	2-methylhexadecane	MS, RI	0.40 (0.19−0.79)a	0.38 (0.22−0.61)a	0.709
78	1700	heptadecane	MS, RI	1.46 (0.40−3.29)a	1.23 (0.49−2.78)a	0.435
79	1706	2,6,10,14-tetramethylpentadecane	MS, RI	2.34 (0.87−4.49)a	2.35 (1.09−3.24)a	0.971
80	1765	anthracene	MS, RI	1.25 (0.71−2.24)a	0.79 (0.30−1.84)b	0.018
81	1800	octadecane	MS, RI	1.20(0.35−3.60)a	0.80(0.31−1.39)a	0.175
82	1809	2,6,10,14-tetramethylhexadecane	MS, RI	1.43 (0.43−3.32)a	0.93 (0.33−1.91)a	0.093
83	1828	isopropyl myristate	MS, RI	0a	0.53 (0−4.96)a	0.177
84	**1840**	**caffeine**	**MS**	**3.86 (0.83−8.07)a**	**10.91 (5.16−16.03)b**	**0.000**
85	1846	6,10,14-trimethyl-2-pentadecanone	MS, RI	3.54 (2.15−8.25)a	5.34 (0.94−7.85)b	0.022
86	**1918**	**farnesyl acetone**	**MS, RI**	**0.50 (0−1.35)a**	**1.54 (0.51−2.45)b**	**0.000**
87	1927	hexadecanoic acid methyl ester	MS, RI	0.54 (0.19−0.72)a	0.93 (0.28−2.30)b	0.027
88	1949	isophytol	MS, RI	1.27 (0.38−2.16)a	1.09 (0.38−5.35)a	0.651
89	**1975**	**hexadecanoic acid**	**MS, RI**	**9.29 (3.91−16.92)a**	**4.47 (2.12−8.12)b**	**0.001**
90	2000	eicosane	MS, RI	0.24 (0−0.68)a	0.08 (0−0.50)b	0.039
91	2093	methyl linoleate	MS, RI	0.07 (0−0.32)a	0.15 (0−0.78)a	0.286
92	2099	methyl linolenate	MS, RI	0.40 (0−1.15)a	0.49 (0−1.49)a	0.464
93	2122	phytol	MS, RI	2.39 (0.82−6.99)a	3.72 (0.97−10.34)a	0.138

[a]Twenty-six volatile compounds with significant differences ($P < 0.01$) in Pu-erh and Fuzhuan teas are indicated in bold type. [b]RI, retention indices as determined on HP-5MS column using the homologous series of *n*-alkanes (C_8−C_{40}). [c]Compounds are listed in order of retention time. [d]Method of identification: MS, identified by comparison with mass spectra; RI, identified by retention indices. [e]Two-sample *t*-test significant values at a level of 0.05. [f]The same letter in the same row indicates no significant difference ($P < 0.05$).

in both Pu-erh and Fuzhuan teas and are considered common among plant volatiles, because they are hydrolysis products of the alcohol moiety of chlorophyll;[38] their aroma activity and contribution to tea flavor needed to be further elucidated. These results indicated that these alcohol compounds contributed unique flavor for each kind of dark tea with different concentrations, and the concentration differences of these compounds were often determined by different production processes.

A total of 11 methoxyphenolic compounds were identified in 26 dark tea samples. Among them, 3,4-dimethoxytoluene, 3,5-dimethoxytoluene, 4-ethyl-1,2-dimethoxybenzene, 1,2,4-trimethoxybenzene, 1-methoxynaphthalene, and 2-methoxynaphthalene were detected only in Pu-erh teas, and 1-methoxynaphthalene and 2-methoxynaphthalene were reported here for the first time as volatiles of Pu-erh tea. It was worth noting that the level of methoxyphenolic compounds was significantly higher ($P < 0.001$) among Pu-erh teas (31.77%) than among Fuzhuan teas (3.53%). These methoxyphenolic compounds with a higher level appear to be the unique characteristic volatile compounds in Pu-erh teas. Our results are consistent with those of other studies for the high level of methoxyphenolic compounds coexisting in Pu-erh teas, mainly including 1,2,3-trimethoxybenzene and 1,2,4-trimethoxybenzene, and these methoxyphenolic compounds had an important effect in the unique "stale" flavor of Pu-erh tea.[27,33] Meanwhile, some studies have reported that *Aspergillus niger* was the major microorganism responsible for the formation of Pu-erh special flavor through the methylation effect of phenolic hydroxyl compounds.[39] Therefore, we conclude that the formation of these methoxyphenolic compounds may have great relation to *A. niger* activity in the postfermentation process. The degradation and hydrolysis of tannins and (−)-epigallocatechin gallate (EGCG) by microbial enzymes were considered to be related to these results.[40]

A total of 14 ketone compounds were identified in 26 dark tea samples. There were significant differences ($P < 0.001$) in the content of ketones between Pu-erh teas (12.57%) and Fuzhuan teas (25.42%). Among these ketones, *β*-ionone, geranyl acetone, farnesyl acetone, and 6-methyl-5-hepten-2-

one were the most abundant compounds in the Fuzhuan teas and had very significant differences compared with Pu-erh teas ($P < 0.001$). It is well-known that these ketone compounds are very important volatile compounds in various teas, providing a special floral and woody odor, and appear to be the unique volatile compounds in Fuzhuan teas. In particular, β-ionone, with low human odor perception thresholds, significantly contributes to the flavor of tea.[11] These ketone compounds were probably derived from the oxidation and condensation of carotenoids (phytoene or phytofluene) and oxidative breakdown products of β-carotene,[41] which may greatly dependent on *Eurotium* spp. activity in the postfermentation process of Fuzhuan tea.[42] The carotenoid degradation pathway also was considered to be a key route for the formation of aroma compounds in many plants and plant products.[43] A possible formation mechanism of these volatile components is shown in Figure 3. In short, the contents of these carotenoid degradation products in Fuzhuan teas were relatively higher than in Pu-erh teas.

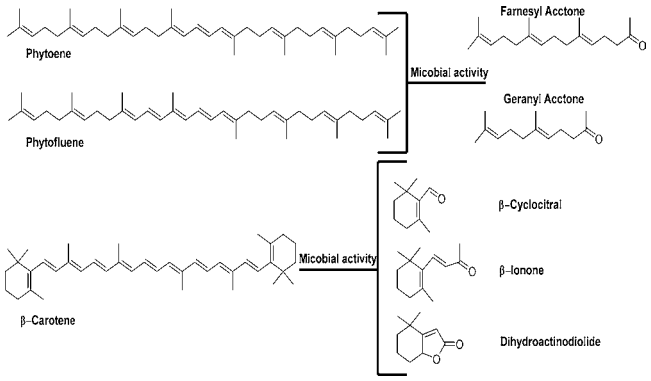

Figure 3. Carotenoids (left) are possibly degraded into some volatile compounds (right) in dark tea.

A total of 7 aldehydes and 7 esters were identified in 26 dark tea samples. The contents of aldehyde compounds were relatively low in Fuzhuan teas (1.00%) and Pu-erh teas (1.67%), mainly including β-cyclocitral, safranal, and benzaldehyde. Among them, β-cyclocitral had a very significant difference in these two kinds of dark teas ($P < 0.001$). Our results have some differences with the previous investigations; that is, Lv et al.[33] found 3,4,5-trimethoxybenzaldehyde was the dominant compound in Pu-erh teas, and Xu et al.[44] found aldehyde compounds were dominant and represented 51% of the identified volatile components in postfermented Fuzhuan dark tea. These differences could be accounted for by the difference of tea samples and extraction methods used in the analysis. The contents of ester compounds in Fuzhuan teas (4.68%) were relatively higher than in Pu-erh teas (1.45%). Among them, methyl jasmonate was detected only in Fuzhuan teas (0.99%), providing a special sweet floral, tenacious jasmine-like odor for black tea.[45] Methyl salicylate and isopropyl salicylate, which had a holly oil herbal fragrance, also were detected with a relatively high level in Fuzhuan teas compared Pu-erh teas. These compounds may give a unique contribution to the flavor of the Fuzhuan tea. In addition, hexadecanoic acid methyl ester, methyl linoleate, and methyl linolenate were formed from higher fatty acid and lower alcohol, in which these ester components had poor volatility, and thus, had no effect on the flavor of the tea.[46]

As for the rest of the identified compounds, hexadecanoic acid and caffeine were found at high levels in both Pu-erh and Fuzhuan teas. These compounds also were previously reported in other teas, but their aroma activities and contribution to tea flavor were not described.[47−49] In addition, dihydroactinidiolide existed at a high level in both Pu-erh and Fuzhuan teas in the present study and was found to be an important aroma compound, likely having a special contribution to the woody flavor of tea.[33] 2-Pentylfuran and *cis*-2-(2-pentenyl)furan with a burnt and sweet odor were found at a high level in Fuzhuan teas compared to Pu-erh teas ($P < 0.001$), and their formation may related to amino acids and sugars through Maillard and Strecker degradation reactions,[34] which is probably responsible for a special contribution to the flavor of Fuzhuan tea.

Although the microbial fermentation leads to a significant change of volatile flavor components in dark tea, very little is known about the microorganism group involved in the pile fermentation process and its effects on the chemical and biological transformation of the tea leaf ingredients. For this reason, the formation mechanism of volatile aroma components during the postfermentation process is urgently needed to be studied for explaining the dynamic process by microbial enzymes in subsequent studies. In addition, the distinct aroma of dark tea is a reflection of hundreds of chemicals, rather than a single flavor-active compound; thus, the odor threshold of identified compounds was not considered in this study. In future studies, novel analytical investigations will focus on determining the interactions between tea volatile matrices and flavor-active compounds and the human influence on odorant perception.

Cluster Analysis. In the present study, all percentage quantitative data of 93 volatile compounds were used for CA model. Objects will be gathered in terms of their nearness or

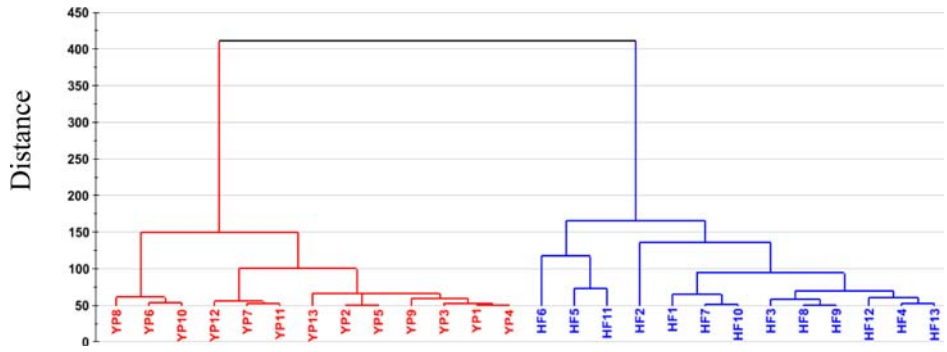

Figure 4. CA dendrogram of 26 dark tea samples.

dx.doi.org/10.1021/jf405237u | J. Agric. Food Chem. 2014, 62, 1810−1818

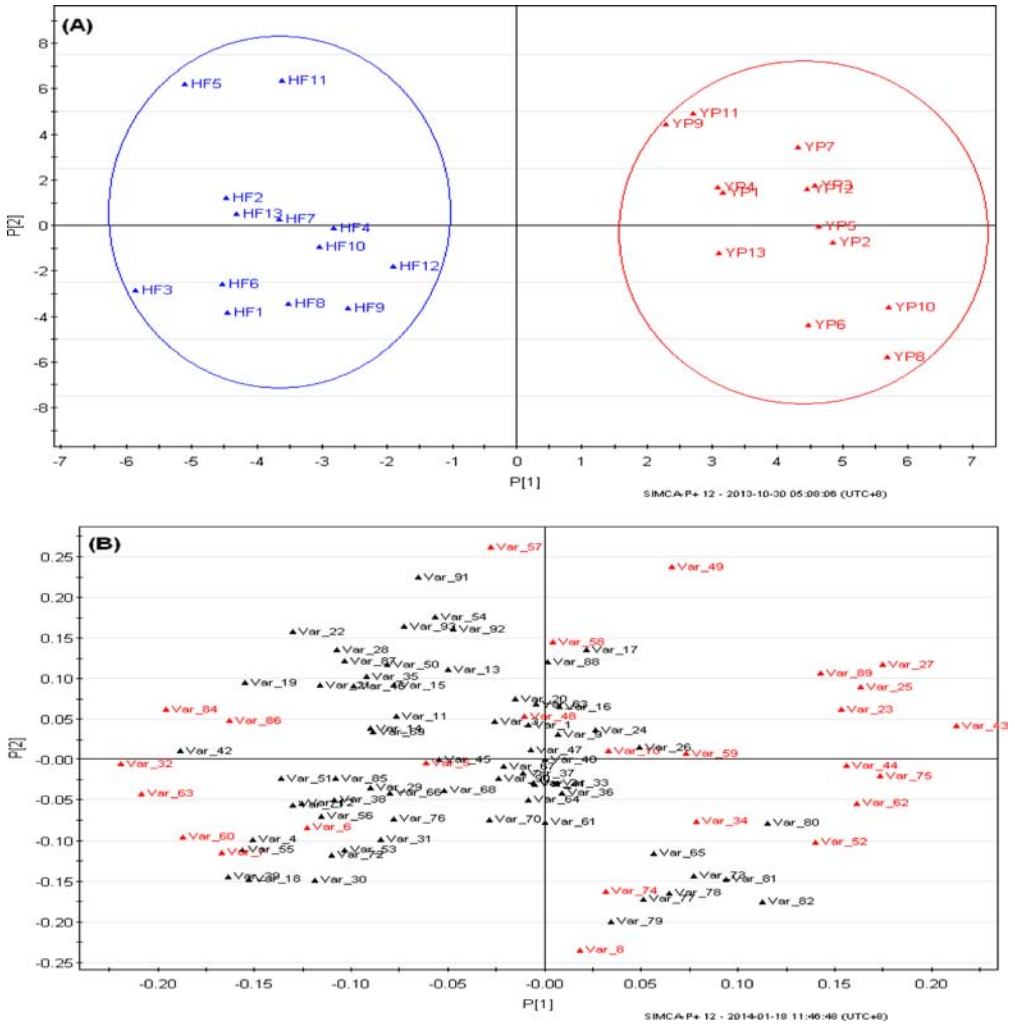

Figure 5. PCA score (A) and loading (B) plots derived from 93 volatile compounds of 26 dark tea samples: (A) YP indicated by red color represents Pu-erh tea from Yunnan province and HF indicated by blue color indicates Fuzhuan tea from Hunan province; (B) red color represents 26 volatile compounds with significant differences ($P < 0.01$) in Pu-erh and Fuzhuan teas based on the results given in Table 1.

similarity, and the objects with minimum variance were clustered preferentially. In this work, sample similarities were calculated on the basis of the Euclidean distance and Ward's method was used as an amalgamation rule.[50] As shown in Figure 4, there was a clear division between dark tea samples according to their respective production areas, and two clusters were observed: the first one was composed of 13 Yunnan Pu-erh teas, and the second main cluster was constituted by 13 Hunan Fuzhuan teas.

Principal Component Analysis. PCA is an unsupervised statistical method used to investigate the differences between sample groups by reduction of the dimension of principal components and has become a hot research field in recent years.[14,51,52] The score plot shows the differences/similarities between various tea samples, which is based on comprehensive volatile compounds. The loading scatter plot shows which volatile compounds contribute to the differences/similarities. PCA (Figure 5) was determined using the same data as used in the CA model. Figure 5A shows the score plot on the two first principal components (PC1 and PC2), representing 73.62% of the total variability. Figure 5B shows the loading scatter plot that established the relative importance of each variable, and it was useful for the study of relationships between variables and tea samples. As shown in Figure 5A, 13 Pu-erh teas were clearly distinguished from 13 Fuzhuan teas in the PCA model. As can be seen from Figure 5B, some variables that explained maximum variance in the data were given higher loading values and were considered as important for discrimination samples (corresponding with score plot and not close to the origin). These variables including 1,2-dimethoxybenzene (V23), linalool oxide IV (V25), α-terpineol (V27), 1,2,3-trimethoxybenzene (V43), 4-ethyl-1,2-dimethoxybenzene (V44), 1,2,3-trimethoxy-5-methylbenzene (V52), 4-(2,6,6-trimethylcyclohexa-1,3-dienyl)-but-3-en-2-one (V62), α-cadinol (V75), and hexadecanoic acid (V89) had high positive values on PC1 and mainly affected the discrimination of Pu-erh tea samples from dark tea samples. Other variables including β-cyclocitral (V32), isopropyl salicylate (V42), geranyl acetone (V60), β-ionone (V63), caffeine (V64), and farnesyl acetone (V86) had high negative values on PC1 and mainly were considered as important compounds for the discrimination of Fuzhuan teas from Pu-erh teas. In addition, *cis*-2-(2-pentenyl) furan (V8, having high negative values on PC2) was detected only in Fuzhuan teas, and β-guaiene (V49) and 1-methoxynaphthalene (V57), having high positive values on PC2, were present at higher contents in Pu-erh teas. These results in PCA were almost consistent with the significant result given in Table 1. PCA provided similar classification of Pu-erh and Fuzhuan

teas, showing that the volatile chemical compounds of teas analyzed by fully automatic HS-SPME can be used for quality evaluation based on chemometric and statistical methods using CA or PCA models.

In addition, we found that PCA results also showed some differences among the same types of tea samples. Because tea aroma is a complex colligation character, this may relate to the raw material selection, cultivation measures, and environment factors of tea. However, this result is a feasibility study because the number of dark tea samples is relatively small for classification. To improve the reliability of the clustering model, the increased variables by collecting various analytical data and extended number by adding dark tea samples are recommended.

In conclusion, this study reported for the first time an attempt to compare and differentiate dark tea samples from different production areas. The result obtained from the HS-SPME/GC-MS combined with CA and PCA has shown that this method can be useful to discriminate dark samples from Yunnan and Hunan. The HS-SPME coupled with GC-MS method showed obvious differences between Pu-erh tea and Fuzhuan tea with regard to volatile constituents. The abundant methoxyphenolic compounds existing in Pu-erh teas and the abundant ketone compounds existing in Fuzhuan teas represent their special characteristic aroma components. Combined with chemometric analysis, this HS-SPME/GC-MS technology can successfully differentiate different production areas of dark teas by their volatile compounds.

AUTHOR INFORMATION

Corresponding Author

*(Q.M.) Phone: +86-871-65920541. Fax: +86-871-65920570. E-mail: qxmeng@scbg.ac.cn.

Funding

This work was supported by the National Natural Science Foundation of China (no. 3100960) and the Natural Science Foundation of Yunnan Province (no. 2010ZC054).

Notes

The authors declare no competing financial interest.

REFERENCES

(1) Aditi, J.; Chanchal, M.; Shrey, K.; Darshika, N.; Vibha, R. Tea and human health: the dark shadows. *Toxicol. Lett.* **2013**, *220*, 82−87.

(2) Xie, G.; Ye, M.; Wang, Y.; Ni, Y.; Su, M.; Huang, H.; Qiu, M.; Zhao, A.; Zheng, X.; Chen, T.; Jia, W. Characterization of Pu-erh tea using chemical and metabolic profiling approaches. *J. Agric. Food Chem.* **2009**, *57*, 3046−3054.

(3) Xu, A.; Wang, Y.; Wen, J.; Liu, P.; Liu, Z.; Li, Z. Fungal community associated with fermentation and storage of Fuzhuan brick-tea. *Int. J. Food Microbiol.* **2011**, *146*, 14−22.

(4) Lv, H. P.; Zhang, Y. J.; Lin, Z.; Liang, Y. R. Processing and chemical constituents of Pu-erh tea: a review. *Food Res. Int.* **2013**, *53*, 608−618.

(5) Mo, H.; Zhu, Y.; Chen, Z. Microbial fermented tea − a potential source of natural food preservatives. *Trends Food Sci. Technol.* **2008**, *19*, 124−130.

(6) Zhang, L.; Zhang, Z. Z.; Zhou, Y. B.; Ling, T. J.; Wan, X. C. Chinese dark teas: postfermentation, chemistry and biological activities. *Food Res. Int.* **2013**, *53*, 600−607.

(7) Ling, T. J.; Wan, X. C.; Ling, W. W.; Zhang, Z. Z.; Xia, T.; Li, D. X.; Hou, R. Y. New triterpenoids and other constituents from a special microbial-fermented tea − Fuzhuan brick tea. *J. Agric. Food Chem.* **2010**, *58*, 4945−4950.

(8) Zhang, H.; Wang, C.; Shen, S.; Wang, G.; Liu, P.; Liu, Z.; Wang, Y.; Du, S.; Liu, Z.; Deng, Z. Antioxidant phenolic compounds from Pu-erh tea. *Molecules* **2012**, *17*, 14037−14045.

(9) Ghasemi-Varnamkhasti, M.; Mohtasebi, S. S.; Siadat, M. Biomimetic-based odor and taste sensing systems to food quality and safety characterization: an overview on basic principles and recent achievements. *J. Food Eng.* **2010**, *100*, 377−387.

(10) Bhattacharyya, R.; Tudu, B.; Das, S. C.; Bhattacharyya, N.; Bandyopadhyay, R.; Pramanik, P. Classification of black tea liquor using cyclic voltammetry. *J. Food Eng.* **2012**, *109*, 120−126.

(11) Yang, Z.; Baldermann, S.; Watanabe, N. Recent studies of the volatile compounds in tea. *Food Res. Int.* **2013**, *53*, 585−599.

(12) Lee, J.; Chambers, D.; Chambers, E.; Adhikari, K.; Yoon, Y. Volatile aroma compounds in various brewed green teas. *Molecules* **2013**, *18*, 10024−10041.

(13) Cheng, H.; Qin, Z. H.; Guo, X. F.; Hu, X. S.; Wu, J. H. Geographical origin identification of propolis using GC−MS and electronic nose combined with principal component analysis. *Food Res. Int.* **2013**, *51*, 813−822.

(14) Wu, S. B.; Meyer, R. S.; Whitaker, B. D.; Litt, A.; Kennelly, E. J. A new liquid chromatography−mass spectrometry-based strategy to integrate chemistry, morphology, and evolution of eggplant (*Solanum*) species. *J. Chromatogr., A* **2013**, *1314*, 154−172.

(15) Kim, N. S.; Lee, J. H.; Han, K. M.; Kim, J. W.; Cho, S.; Kim, J. Discrimination of commercial cheeses from fatty acid profiles and phytosterol contents obtained by GC and PCA. *Food Chem.* **2014**, *143*, 405−407.

(16) Togari, N.; Kobayashi, A.; Aishima, T. Pattern recognition applied to gas chromatographic profiles of volatile components in three tea categories. *Food Res. Int* **1995**, *28*, 495−502.

(17) Ye, N.; Zhang, L.; Gu, X. Discrimination of green teas from different geographical origins by using HS-SPME/GC−MS and pattern recognition methods. *Food Anal. Methods* **2012**, *5*, 856−860.

(18) Wang, L. F.; Lee, J. Y.; Chung, J. O.; Baik, J. H.; So, S.; Park, S. K. Discrimination of teas with different degrees of fermentation by SPME−GC analysis of the characteristic volatile flavour compounds. *Food Chem.* **2008**, *109*, 196−206.

(19) Pongsuwan, W.; Fukusaki, E.; Bamba, T.; Yonetani, T.; Yamahara, T.; Kobayashi, A. Prediction of Japanese green tea ranking by gas chromatography/mass spectrometry-based hydrophilic metabolite fingerprinting. *J. Agric. Food Chem.* **2007**, *55*, 231−236.

(20) Jumtee, K.; Komura, H.; Bamba, T.; Fukusaki, E. Predication of Japanese green tea (Sen-cha) ranking by volatile profiling using gas chromatography mass spectrometry and multivariate analysis. *J. Biosci. Bioeng.* **2011**, *112*, 252−255.

(21) Shimoda, M.; Shigematsu, H.; Shiratsuchi, H.; Osajima, Y. Comparison of the odor concentrates by SDE and adsorptive column method from green tea infusion. *J. Agric. Food Chem.* **1995**, *43*, 1616−1620.

(22) Rawat, R.; Gulati, A.; Kiran Babu, G. D.; Acharya, R.; Kaul, V. K.; Singh, B. Characterization of volatile components of Kangra orthodox black tea by gas chromatography-mass spectrometry. *Food Chem.* **2007**, *105*, 229−235.

(23) Pripdeevech, P.; Machan, T. Fingerprint of volatile flavour constituents and antioxidant activities of teas from Thailand. *Food Chem.* **2011**, *125*, 797−802.

(24) Hu, C. D.; Liang, Y. Z.; Guo, F. Q.; Li, X. R.; Wang, W. P. Determination of essential oil composition from osmanthus fragrans tea by GC-MS combined with a chemometric resolution method. *Molecules* **2010**, *15*, 3683−3693.

(25) Su, X. G.; Jiang, Y. M.; Wang, X. H.; Duan, J.; Mi, S. Q.; Wang, N. S. Application of solid phase microextraction on the oolong tea (*Camellia sinensis* cv. Fenghuangdancong) aroma analysis. *Food Sci.* **2005**, *26*, 213−216 (in Chinese).

(26) Schuh, C.; Schieberle, P. Characterization of the key aroma compounds in the beverage prepared from Darjeeling black tea: quantitative differences between tea leaves and infusion. *J. Agric. Food Chem.* **2006**, *54*, 916−924.

(27) Du, L.; Wang, C.; Li, J.; Xiao, D.; Li, C.; Xu, Y. Optimization of headspace solid-phase microextraction coupled with gas chromatography−mass spectrometry for detecting methoxyphenolic compounds in Pu-erh tea. *J. Agric. Food Chem.* **2012**, *61*, 561−568.
(28) Lv, S.; Jiang, D.; Yang, F.; Zhou, J.; Lian, M.; Meng, Q. Analysis of aroma components between Pu-erh ripe tea and Anhua dark tea by headspace solid-phase microectraction and GC-MS. *J. Trop. Crop* **2013**, *34*, 1583−1591 (in Chinese).
(29) Lv, S.; Jiang, D.; Liu, C.; Huang, W.; Meng, Q. Comparison of aroma components between special Zijuan black tea and Dianhong tea. *J. Food Sci. Biotechnol.* **2013**, *32*, 734−742 (in Chinese).
(30) Msaada, K.; Hosni, K.; Taarit, M. B.; Chahed, T.; Kchouk, M. E.; Marzouk, B. Changes on essential oil composition of coriander (*Coriandrum sativum* L.) fruits during three stages of maturity. *Food Chem.* **2007**, *102*, 1131−1134.
(31) Qiao, Y.; Xie, B.; Zhang, Y.; Zhang, Y.; Fan, G.; Yao, X.; Pan, S. Characterization of aroma active compounds in fruit juice and peel oil of Jinchen sweet orange fruit (*Citrus sinensis* (L.) Osbeck) by GC-MS and GC-O. *Molecules* **2008**, *13*, 1333−1344.
(32) Lin, J.; Dai, Y.; Guo, Y. N.; Xu, H. R.; Wang, X. C. Volatile profile analysis and quality prediction of Longjing tea (*Camellia sinensis*) by HS-SPME/GC-MS. *J. Zhejiang Univ. Sci. B* **2012**, *13*, 972−980.
(33) Lv, H. P.; Zhong, Q. S.; Lin, Z.; Wang, L.; Tan, J. F.; Guo, L. Aroma characterisation of Pu-erh tea using headspace-solid phase microextraction combined with GC/MS and GC−olfactometry. *Food Chem.* **2012**, *130*, 1074−1081.
(34) Alasalvar, C.; Topal, B.; Serpen, A.; Bahar, B.; Pelvan, E.; Gökmen, V. Flavor characteristics of seven grades of black tea produced in Turkey. *J. Agric. Food Chem.* **2012**, *60*, 6323−6332.
(35) Toldrá, F.; Flores, M.; Sanz, Y. Dry-cured ham flavour: enzymatic generation and process influence. *Food Chem.* **1997**, *59*, 523−530.
(36) Qin, Z.; Pang, X.; Chen, D.; Cheng, H.; Hu, X.; Wu, J. Evaluation of Chinese tea by the electronic nose and gas chromatography−mass spectrometry: correlation with sensory properties and classification according to grade level. *Food Res. Int.* **2013**, *53*, 864−874.
(37) Xu, X.; Yan, M.; Zhu, Y. Influence of fungal fermentation on the development of volatile compounds in the Puer tea manufacturing process. *Eng. Life Sci.* **2005**, *5*, 382−386.
(38) Byju, K.; Anuradha, V.; Rosmine, E.; Kumar, N. C.; Nair, S. M. Chemical characterization of the lipophilic extract of *Hydrilla verticillata*: a widely spread aquatic weed. *J. Plant Biochem. Biotechnol.* **2013**, *22*, 304−311.
(39) Abe, M.; Takaoka, N.; Idemoto, Y.; Takagi, C.; Imai, T.; Nakasaki, K. Characteristic fungi observed in the fermentation process for Puer tea. *Int. J. Food Microbiol.* **2008**, *124*, 199−203.
(40) Lu, H.; Lin, Z.; Gu, J.; Guo, L.; Tan, J. Study on the gallic acid in Pu-erh tea. *Tea Sci.* **2007**, *27*, 104−110 (in Chinese).
(41) Waché, Y.; Bosser-DeRatuld, A.; Lhuguenot, J. C.; Belin, J. M. Effect of cis/trans isomerism of β-carotene on the ratios of volatile compounds produced during oxidative degradation. *J. Agric. Food Chem.* **2003**, *51*, 1984−1987.
(42) Mapari, S. A.; Nielsen, K. F.; Larsen, T. O.; Frisvad, J. C.; Meyer, A. S.; Thrane, U. Exploring fungal biodiversity for the production of water-soluble pigments as potential natural food colorants. *Curr. Opin. Biotechnol.* **2005**, *16*, 231−238.
(43) Lewinsohn, E.; Sitrit, Y.; Bar, E.; Azulay, Y.; Meir, A.; Zamir, D.; Tadmor, Y. Carotenoid pigmentation affects the volatile composition of tomato and watermelon fruits, as revealed by comparative genetic analyses. *J. Agric. Food Chem.* **2005**, *53*, 3142−3148.
(44) Xu, X.; Mo, H.; Yan, M.; Zhu, Y. Analysis of characteristic aroma of fungal fermented Fuzhuan brick-tea by gas chromatography/mass spectrophotometry. *J. Sci. Food Agric.* **2007**, *87*, 1502−1504.
(45) Shimoda, M.; Shigematsu, H.; Shiratsuchi, H.; Osajima, Y. Comparison of volatile compounds among different grades of green tea and their relations to odor attributes. *J. Agric. Food Chem.* **1995**, *43*, 1621−1625.
(46) Chen, C. S.; Zhang, Y. G.; Zhong, Q. S.; Chen, R. B. Analysis of aroma compounds on four Taiwang oolong tea using simultaneous distillation extraction. *Food Ferment. Ind.* **2011**, *37*, 165−171 (in Chinese).
(47) Pongsuwan, W.; Bamba, T.; Yonetani, T.; Kobayashi, A.; Fukusaki, E. Quality prediction of Japanese green tea using pyrolyzer coupled GC/MS based metabolic fingerprinting. *J. Agric. Food Chem.* **2008**, *56*, 744−750.
(48) Sereshti, H.; Samadi, S.; Jalali-Heravi, M. Determination of volatile components of green, black, oolong and white tea by optimized ultrasound-assisted extraction-dispersive liquid−liquid microextraction coupled with gas chromatography. *J. Chromatogr., A* **2013**, *1280*, 1−8.
(49) Jacques, R. A.; Santos, J. G.; Dariva, C.; Oliveira, J. V.; Caramão, E. B. GC/MS characterization of mate tea leaves extracts obtained from high-pressure CO_2 extraction. *J. Supercrit. Fluids* **2007**, *40*, 354−359.
(50) Moreda-Piñeiro, A.; Fisher, A.; Hill, S. J. The classification of tea according to region of origin using pattern recognition techniques and trace metal data. *J. Food Compos. Anal.* **2003**, *16*, 195−211.
(51) Wu, S. B.; Dastmalchi, K.; Long, C.; Kennelly, E. J. Metabolite profiling of jaboticaba (*Myrciaria cauliflora*) and other dark-colored fruit juices. *J. Agric. Food Chem.* **2012**, *60*, 7513−7525.
(52) Ma, C.; Dastmalchi, K.; Flores, G.; Wu, S. B.; Pedraza-Peñalosa, P.; Long, C.; Kennelly, E. J. Antioxidant and metabolite profiling of North American and neotropical blueberries using LC-TOF-MS and multivariate analyses. *J. Agric. Food Chem.* **2013**, *61*, 3548−3559.

that are concentrated just before the detector using an external electromagnet device. The introduction into the flow system of the surfactant Triton X-100, together with ALP, gives rise to the lysis of the liposomes, the "in-situ" development of the enzymatic reaction, and the fluorometric detection of the substrate product.

The new method for ALP determination has been applied to the analysis of raw and commercial milk samples. The results have been compared with those obtained using a method based on the same enzymatic reaction, but involving the retention of the reaction product on a resin placed in the cell flow.[23] Although several methods have been described for the determination of ALP activity in milk samples,[24−26] the above-mentioned method was chosen because it also involves the use of MUP and a flow system, which enables an effective assessment of the MLs on the system. The usefulness of the method has been also checked by its application to study the milk pasteurization process by monitoring the degradation of ALP.

MATERIALS AND METHODS

Apparatus and Instruments. A Cary Eclipse Varian spectrofluorometer (Walnut Creek, CA, USA; http://www.varianinc.com) was used. A desktop laboratory MPW-350R centrifuge (MPW Med. Instrument, Warsaw, Poland) with a cooled rotating chamber and equipped with an angle rotor HSL-11199 (45°, 12 × 12 × 1.5 mL, maximum speed = 18000 rpm, 24088 RCF, and $r_{min/max}$ = 3.5/6.25) was used. A VorTemp 56 LA-S2056 shaking incubator (Labnet International, Woodbrige, NJ, USA) and an ultrasound bath were used. A Büchi rotavapor R-205 (Flawil, Switzerland) was used to evaporate the organic solvent and form the liposomes.

The characterization of the synthesized nanomaterials was performed by conventional and both transmission (TEM) and scanning (SEM) electron microscopy. Images were acquired in the first case using a bright-field UIS2 optical system microscope (Olympus, Hamburg, Germany; http://www.olympus.de/microscopy/, BX51, model U MDOB3) equipped with a DP20 digital camera, which provided high-precision images of 2 megapixels in UXGA (1600 × 1200), operating at 15 frames per second. TEM images were obtained using a CM-10 Philips microscope (Philips Research, Eindhoven, The Netherlands; http://www.research.philips.com) with 0.5 × 0.34 nm resolution and equipped with a digital megaview III camera. Copper grids (200C-FC) coated with a Formvar carbon film 200 mesh supplied by Aname (Madrid, Spain; http://www.aname.es) were used as support in TEM experiments. The XPS measurements of Fe_3O_4@AuNPs-DT were carried out using a Specs Phoibos 150 MCD instrument equipped with a monochromatized AlK (12 kV). The morphology and elemental composition of these NPs were studied by SEM, using a microscope (JEOL JSM 6300) operating at 20 kV, which was also equipped with an energy dispersive detector (EDX).

Reagents. All chemicals used were of analytical grade. 1,2-Diacyl-*sn*-glycerol-3-phosphatidylcholine (DSPC), 3-*sn*-phosphatidylethanolamine (DOPE) (type II-S from sheep brain), cholesterol (CH), tetrachloroauric acid ($HAuCl_4$) trihydrate, 1-dodecanethiol (DT), Triton X-100, 4-methylumbelliferyl-phosphate disodium salt (MUP), alkaline phosphatase (ALP), and sodium hydroxide were purchased from Sigma-Aldrich (Steinheim, Germany). Trisodium citrate dihydrate, iron(II) chloride, and other common reagents were also purchased from Merck, and iron(III) chloride was from Panreac. A buffer solution containing 50 mM tris(hydroxymethyl)aminomethane hydrochloride (Tris) (Merck) and adjusted to a pH of 9.8 was used. Methanol and chloroform were used for preparing the liposomes. Aqueous solutions were prepared using deionized water purified with a Milli-Q system (Millipore, Bedford, MA, USA).

Synthesis and Characterization of the Nanomaterial. Hydrophobic NPs (Fe_3O_4@AuNPs-DT) were prepared using a procedure previously reported,[27] which was modified to introduce the DT. Briefly, 25 mL of an aqueous solution containing 0.8 M iron(III) chloride, 0.4 M iron(II) chloride, and 40 mM hydrochloric acid was dropwise added into 250 mL of 1.5 M sodium hydroxide solution under vigorous stirring using a nonmagnetic stirrer. Black-brown Fe_3O_4NPs were immediately formed, which were separated using a commercial neodymium magnet (NdFeB) and washed three times with deionized water. The Fe_3O_4 NPs were collected by centrifugation at 5352.80*g* for 15 min and dispersed again in 100 mL of deionized water. The NPs concentration of this solution was about 100 mM,[18] which was stored refrigerated at 4 °C for further use.

The preparation of Fe_3O_4@AuNPs-DT was carried out by adding 2.2 mL of $HAuCl_4 \cdot 3\ H_2O$ (2.0 mg mL^{-1}) to 22.5 mL of deionized water and heated to boiling for 5 min. Then, 2 mL of the above prepared Fe_3O_4 NPs solution was added to the reaction mixture followed by the addition of 0.5 mL of sodium citrate (80 mM) and 5 mL of DT, and the mixture was vigorously mixed under stirring. The color of the solution gradually changed from brown to burgundy. The reaction mixture was boiled under stirring for 40 min.

TEM images were obtained by dropping the resulting Fe_3O_4@AuNPs-DT on a carbon-coated copper grid and setting a completely dried drop by the oven. XPS spectra were also obtained to identify the presence of a particular element and distinguish the different forms in the NPs. Also, SEM-EDX measurements were made to determine the elemental composition of the NPs.

Preparation, Separation, and Characterization of Magneto-liposomes. Liposomes containing MNPs and the enzyme substrate MUP were prepared using the rapid solvent evaporation (RSE) method.[28] Briefly, 100 μL of a lipid mixture containing DSPC, DOPE, and CH (75:12.5:12.5) was diluted to 1.0 mL with a chloroform/methanol (880:120) mixture and was put into a 50 mL round-bottom flask. Then, a mixture containing 3 mL of an about 7 mM Fe_3O_4@AuNPs-DT suspension, 2.5 mL of 40 mM MUP solution, and 3.5 mL of deionized water was carefully added along the flask wall. The organic solvent was removed in the rotary evaporator at 40 °C and 300 rpm under vacuum pressure. After 20 min, a pale brown opalescent fluid was obtained, which contained a wide variety of liposomes. The liposome population was homogenized by using two physical treatments, mechanical shaking and sonication. A volume (10 mL) of the liposome suspension was shaken in a shaking incubator at 40 °C, which is close to the transition temperature, and at 250 rpm for 30 min, stopping each 10 min for 2 min. After this treatment, the liposomes were resized by sonication. This liposome suspension was partially submerged in a bath sonicator and treated for a period of 10 min, stopping each 2 min for 10 s. The suspension changed in its appearance from milky to a clear suspension.

The separation of filled liposomes from empty liposomes, phospholipid residues, and untrapped magnetic NPs was carried out using conventional centrifugation at 20073*g* for 30 min. Filled liposomes, which showed a brown appearance, were located in the intermediate zone, whereas empty liposomes and untrapped NPs appeared in the top and bottom zones, respectively. After separation, filled liposomes were washed four times with deionized water. These liposomes were stable for at least 30 days.

Procedure for the Determination of ALP Activity. Figure 1 depicts the hydrodynamic arrangement used for the determination of ALP activity (A) and the process time schedule (B). A suspension of MLs containing MUP, prepared in Tris buffer solution (50 mM, pH 9.8), was injected through the injection valve IV_1 at a flow rate of 0.4 mL min^{-1}. The liposomes were retained before the detector, using an electromagnet device, for a time (retention time, Δt_1) of 200 s. A solution containing Triton X-100 and ALP standard or diluted milk sample solution, with an ALP activity in the range of the calibration graph, was then injected using the injection valve IV_2. The surfactant provided the liposome lyse and the release of the enzyme substrate, which was hydrolyzed by ALP, obtaining a transitory fluorescence signal that was monitored at λ_{ex} 365 nm and λ_{em} 449 nm, using a 10/5 slit ratio and a detector gain of 600 V. As Figure 1B shows, the system takes about 120 s (release time, Δt_2) to achieve the baseline. Each standard or sample solution was assayed in triplicate.

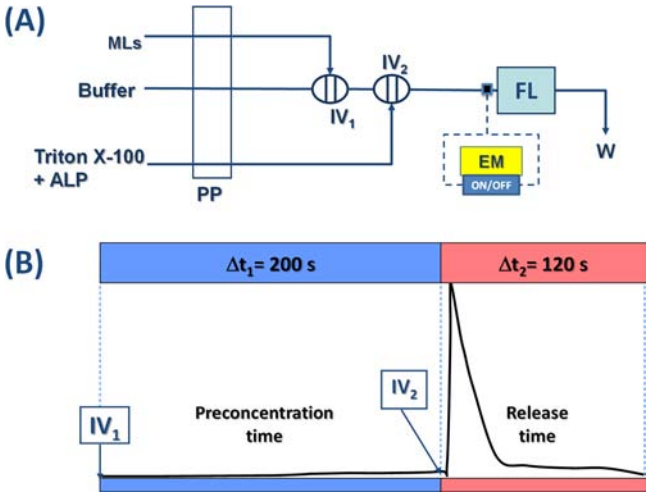

Figure 1. (A) Scheme of the flow injection system used for the determination of ALP activity. (B) Time schedule of the process. PP, peristaltic pump; IV_1 and IV_2, sample and reagent injection valves, respectively; EM, electromagnet device; FL, fluorescence detector; W, waste.

The same enzymatic reaction was assayed using a flow injection system in the absence of liposomes, with the aim of comparing the features of both methods. For this purpose, a solution containing 10 mM MUP prepared in Tris buffer solution (50 mM, pH 9.8) was pumped at a flow rate of 0.4 mL min^{-1} and mixed with the same buffer solution in which the ALP solution was injected. A transitory fluorescence signal (λ_{ex} 365 nm, λ_{em} 449 nm, 10/5 slit ratio, detector gain of 600 V) was obtained when the mixed reaction plug passed through the detector. The area of the peak was used as the analytical parameter.

Analysis of Food Samples. Several raw and commercial milk samples were processed to determine ALP activity. The raw samples were treated with bronopol as preservative and stored at −15 °C until use. The samples were adequately diluted using 50 mM Tris buffer solution (pH 9.8) and analyzed as described above.

Comparison Method. The results obtained by applying the new method to the analysis of milk samples were compared with those obtained using a flow-through method previously described.[23] This method involves the hydrolysis of MUP (0.4 mM) in the presence of ALP, the transient immobilization of the reaction product on a resin (Dowex-1 strongly basic anion exchange resin) packed in the flow cell, and the use of the fluorescence intensity as the analytical parameter. A solution containing EDTA (100 mM) and sodium chloride (150 mM) is used to remove the product of the reaction from the support. This method reaches a detection limit of 0.05 U L^{-1} ALP.

Statistical Analysis. All experiments were replicated three times. Statistical analyses were performed with Statgraphics Plus 5.1 software (Statistical Graphics Corp.). The paired *t* test was used to compare the results obtained for the analysis of milk samples using both the new method and the previously reported method.[23]

RESULTS AND DISCUSSION

Study of the Features of Hydrophobic Magnetic Nanoparticles. As indicated above, several methods have been described to protect the surface of Fe_3O_4 NPs against oxidation and corrosion and to improve their reactivity. The use of gold to coat magnetic NPs is frequently chosen because these core/shell NPs show adequate magnetic properties and chemical stability, and their surface can be easily modified using the well-developed Au−S chemistry.[15,16] After the synthesis of Fe_3O_4@-AuNPs, their surface was covered with DT to obtain hydrophobic MNPs and facilitate their entrapment into the internal medium of the liposomes. These Fe_3O_4@AuNPs-DT, characterized by TEM (Figure 2A), exhibited spherical structures with an average diameter of 30 ± 10 nm. Also, it was checked that they can be easily separated from the solution when an external magnetic field is applied.

The chemical composition of the hydrophobic magnetic NPs was studied using XPS and SEM-EDX. The XPS spectrum (Figure 2B) indicates the presence of Fe, Au, C, S, and O in the NPs. As can be seen in this figure, Fe(2p) electrons show binding energy (BE) at 725 and 712 eV, respectively, whereas the Au(4f) electrons BE correspond to 84 and 89 eV, respectively, which also indicate the presence of iron and gold in the Fe_3O_4@AuNPs-DT nanocomposites. In addition, the small peaks at 162 and 164 eV correspond to the S(2p3/2) and S(2p1/2) electrons, whereas the strongest peak obtained at 532 eV corresponds to the O(1s) electron.

Figure 2C depicts the image acquired using SEM-EDX, the results of which indicate the presence of Fe, Au, and S in the

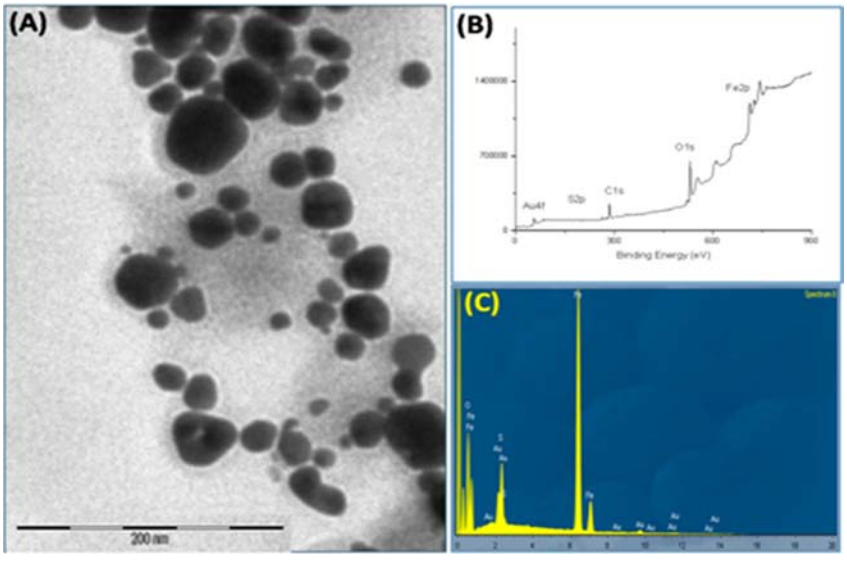

Figure 2. (A) TEM image, (B) XPS and (C) SEM-EDX measurements obtained for Fe_3O_4@AuNPs-DT nanocomposites.

dx.doi.org/10.1021/jf5004804 | J. Agric. Food Chem. 2014, 62, 1819−1825

Fe_3O_4@AuNPs-DT nanocomposites. The EDX diagram also provides a semiquantitative chemical composition of 64:8:6 from the Fe/Au/S distribution that confirms the composition of the hydrophobic MNPs. The absorption spectrum obtained for these NPs showed the typical band at 530−550 nm corresponding to the surface plasmon resonance of AuNPs.

Optimization of Variables. The variables affecting the synthesis of MLs containing MUP and those involved in the development of the method for ALP determination were studied using the univariate method. Tables 1 and 2 summarize the variables studied, the ranges assayed, and the values chosen.

Table 1. Optimization of Variables Affecting the Magnetoliposomes Synthesis

type of variable	variable	range studied	optimal value
hydrophobic MNP formation	$HAuCl_4$, mM	0.23−2.27	1.13
	Fe_3O_4−NPs, mM	5−25	15
	sodium citrate, mM	1.5−6.2	3.1
	dodecanethiol, mL	1−10	5
liposome formation	phosphatidylcholine (DSPC), mM	0.45−0.72	0.68
	phosphatidylethanolamine (DOPE), mM	0.045−0.135	0.11
	cholesterol (CH), M	0.045−0.135	0.11
	deionized water, mL		3.5
	chloroform, μL	600−900	880
	methanol, μL	100−200	120
	MUP, mM	0.2−20	10
	hydrophobic MNPs, mM	0.1−7	2.1
	temperature, °C	30−60	40
	evaporation time, min	5−30	20
	rotatory speed, rpm	5−500	300
shaking treatment	temperature, °C	20−100	40
	time, min	5−40	30

Table 2. Optimization of Variables Affecting the Enzymatic Reaction

type of variable	variable	range studied	optimal value
hydrodynamic	flow rate, mL min^{-1}	0.2−0.8	0.4
	sample injection, μL	50−200	150
	reagent injection, mL	0.3−2.0	1.3
	retention time, s	5−300	200
	release time, s	5−300	120
instrumental	λ_{ex}, nm	200−800	360
	λ_{em}, nm	200−800	449
	excitation slit, nm	2.5−10	5
	emission slit, nm	2.5−10	10
	PMT gain, V	450−800	600
chemical	pH	8−12	9.8
	Tris buffer, mM	20−200	50
	Triton X-100, mM	5−150	10

Variables Affecting the Synthesis of Magnetoliposomes Containing the Enzymatic Substrate. The optimization study was carried out to obtain adequate structural features (size, shape, and magnetic efficiency) of the hydrophobic MNPs[27] and maximum encapsulation efficiency for the synthesis of the liposomes.[28]

The synthesis of Fe_3O_4@AuNPs was carried out using $HAuCl_4$ and sodium citrate,[16] and the surface of these NPs was modified with DT to improve their hydrophobicity and the efficiency of their encapsulation into liposomes. The experimental conditions used to obtain these NPs are summarized in Table 1.

Liposomes containing hydrophobic MNPs and MUP were prepared using the RSE method and homogenized by shake/ultrasound treatments. A method previously described,[11] which was modified with respect to the type of phospholipids and the internalized material, was used to obtain these liposomes. The composition of the phospholipid mixture and the chloroform and methanol volume ratio are critical variables in the synthesis process. As Table 1 shows, the best results were obtained using a phospholipid mixture (100 μL) composed by DSPC, DOPE, and CH (75:12.5:12.5), which was diluted to 1 mL with a chloroform/methanol (880:120) mixture. This solution was mixed with a solution containing 3 mL of about 7 mM hydrophobic MNPs, 2.5 mL of 40 mM MUP, and 3.5 mL of deionized water.

The influence of the temperature in the RSE method was studied in the range of 30−60 °C, which covered the transition temperature of the phospholipids used. The percentage of liposomes increased up to a temperature of 40 °C, remaining constant at higher temperature values. The study of the stability of the liposome suspension showed that it increased when the suspension was refrigerated at 4 °C.

The purification of the liposome suspension, to separate filled liposomes from empty liposomes, phospholipid residues, and untrapped MNPs, was carried out using conventional centrifugation, in which the suspension (10 mL) was treated at different centrifugation speeds, between 2007.3*g* and 20073*g* at 4 °C, assaying also variable centrifugation times, between 15 and 30 min. A centrifugation of 20073*g* for 30 min provided the best results. Filled liposomes, which showed a brown appearance, were located in the intermediate zone, whereas empty liposomes and untrapped NPs appeared in the top and bottom zones, respectively. The liposomes were washed by 100 mL of deionized water four times.

Variables Affecting the Enzymatic Reaction. The method was developed by using a flow injection system in which a Tris buffer solution was used as the carrier to transport, first, the MLs containing the enzymatic substrate and, second, the ALP and Triton X-100 mixture. Hydrodynamic, instrumental, and chemical variables were optimized, as shown in Table 2, which includes the ranges assayed and the values chosen for each variable. All of the assays were carried out at 25 °C to avoid degradation of the liposomes.

The injection volumes chosen to introduce MLs (IV_1) and ALP (IV_2) solutions into the system were 1.3 mL and 150 μL, respectively, using a flow rate of 0.4 mL min^{-1}. The influence of the MLs retention and release times on the system is shown in Figure 3A, selecting 200 and 120 s, respectively, as the optimal values. A pH of 9.8 was chosen, which was adjusted using 50 mM Tris buffer solution. Figure 3B shows the influence of Triton X-100 concentration on the analytical signal, in which it can be seen that a 10 mM concentration is suitable to obtain the maximum peak area value. The influence of the enzymatic substrate on the system was studied by assaying different MLs synthesized in the presence of solutions containing different MUP concentrations. As Figure 3C shows, a maximum signal

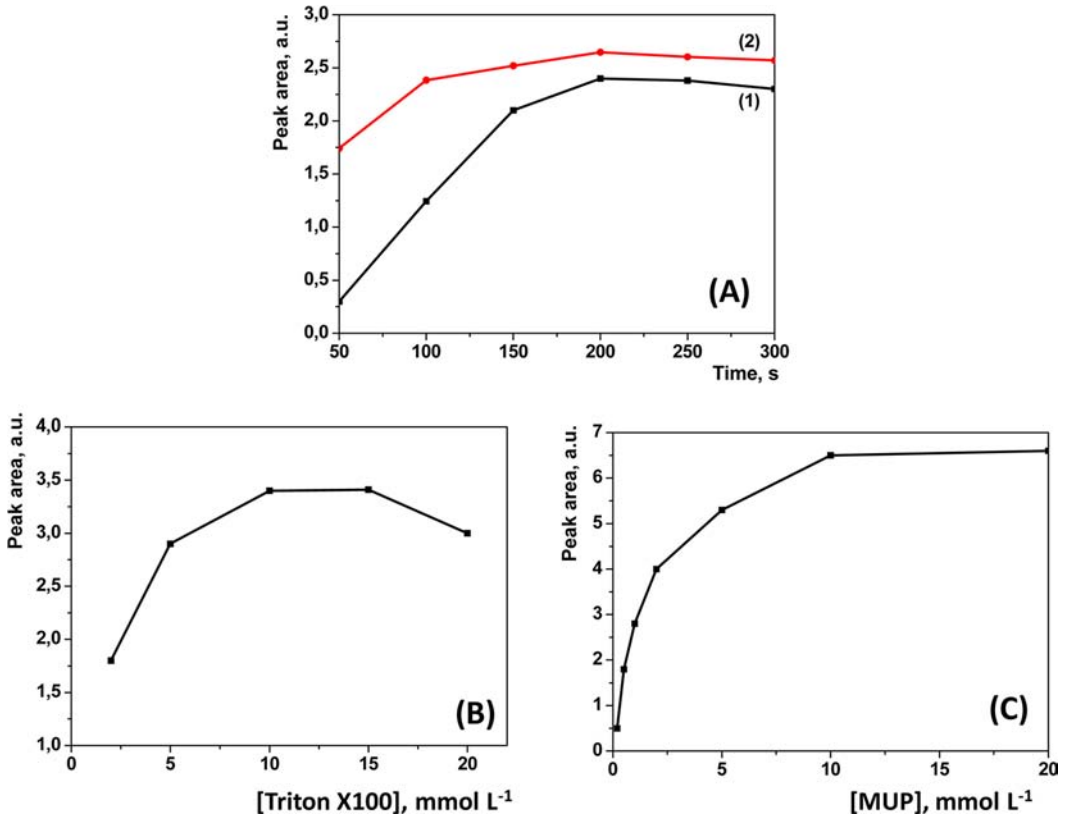

Figure 3. Influence of experimental variables on the flow system: (A) retention time of the MLs by the magnet (1) integration time of the analytical signal (2); (B) Triton X-100 and (C) MUP concentrations. pH 9.8; [ALP] = 50 mU L^{-1}; [MUP] = 2 mM in (A) and (B); [Triton X-100] = 3 mM in (A) and 10 mM in (C).

was obtained when the MUP concentration was 10 mM MUP, remaining constant for higher substrate concentrations.

Features of the Method. The area of the peak obtained in the flow injection scheme depicted in Figure 1A was used as the analytical parameter to obtain the figures of merit of the method. The same system was studied in the absence of MLs with the aim of checking the positive effect of the use of MLs on the ALP determination. Table 3 summarizes the features of both approaches. As can be seen, the dynamic range of the calibration graph in the presence of MLs is 6.4×10^{-3}–0.250 U L^{-1} ALP, and the limit of detection (LOD)[29] is 1.9×10^{-3} U L^{-1}, which is 58 times lower than that obtained in the absence of MLs (0.11 U L^{-1}). Also, the LOD is 26 times lower that that reached by retaining the product of the enzymatic reaction in a resin placed in the flow cell (0.05 U L^{-1}).[23] Table 3 also shows the repeatability ($n = 7$, $r = 3$) and reproducibility ($n = 5$, $r = 3$) data, expressed as RSD%, obtained in the presence and absence of liposomes. As can be seen, the precision values are better in the first case.

Application of the Method. The ALP activity in milk samples from farms and commercial local markets was determined using the new method, and the results were evaluated by comparison with the flow method involving the retention of the enzymatic reaction product above-described.[23] The standard addition method was used to carry out the analysis. Table 4 lists the content found in the samples using both methods. The paired t test was applied to the results at a 5% significance level. It was found that there were not significant differences in the results provided by both methods, which confirms the practical utility of the new method to the analysis of these samples. A recovery study was carried out by adding two different amounts of ALP to each sample and subtracting the results obtained from similarly treated unspiked samples. Table 4 shows the recovery percentages, which ranged from 87.5 to 104.6%. This internal validation also confirms the usefulness of the developed MLs method for the analysis of real samples.

The utility of the new method was also checked for milk pasteurization verification, in which ALP is used as a thermal

Table 3. Features of the Method

	FI method	
calibration graph	with liposomes	without liposomes
equation parameters		
a	2.9 (±0.7)	0.64 (±0.03)
b	1.10 (±0.01)	0.805 (±0.004)
r^2	0.9930	0.9990
LOD, U L^{-1}	1.9×10^{-3}	0.11
linear range, U L^{-1}	6.4×10^{-3}–0.25	0.35–10
repeatability[a] ($n = 7$, $r = 3$)		
low level	2.4	8.7
high level	0.7	0.9
reproducibility[a] ($n = 5$, $r = 3$)		
low level	2.8	8.8
high level	1.2	3.6

[a]RSD% values at 6.4×10^{-3} and 0.023 U L^{-1} ALP activity for low and high concentration levels, respectively, in the presence of liposomes, and at 0.35 and 4.8 U L^{-1} ALP activity for low and high concentration levels, respectively, in the absence of liposomes.

dx.doi.org/10.1021/jf5004804 | J. Agric. Food Chem. 2014, 62, 1819–1825

Table 4. Application of the Method

				comparison method[23]	MLs method		
						recovery %[a]	
sample	type of milk		dilution factor	[ALP], mU L^{-1}	[ALP], mU L^{-1}	first add	second add
1	raw	goat	1000	3995 ± 42	3800 ± 3	88.2	100.4
2	raw	goat	1000	4487 ± 10	4400 ± 8	89.2	90.8
3	raw	goat	1000	3934 ± 25	3818 ± 6	100.1	89.7
4	raw	goat	1000	2730 ± 49	2284 ± 1	94.0	104.1
5	raw	cow	1000	6211 ± 41	6818 ± 4	90.9	104.1
6	raw	cow	1000	5491 ± 20	5291 ± 17	94.0	90.9
7	raw	cow	1000	6058 ± 9	6001 ± 24	95.8	90.9
8	raw	cow	1000	5709 ± 3	6110 ± 20	96.1	87.5
9	pasteurized	whole	100		18.2 ± 0.5	100.0	104.6
10	pasteurized	skimmed	100		11.6 ± 0.5	88.7	99.6

[a]First add, 10 mU L^{-1}; second add, 50 mU L^{-1}.

marker.[22] U.S. and EU regulations specify that pasteurized dairy products may contain <350 mU L^{-1} ALP.[30,31] The thermal degradation of the ALP activity in goat's and cow's milk samples after heating at 59 °C for different times was studied. Figure 4 shows the evolution of the degradation process studied

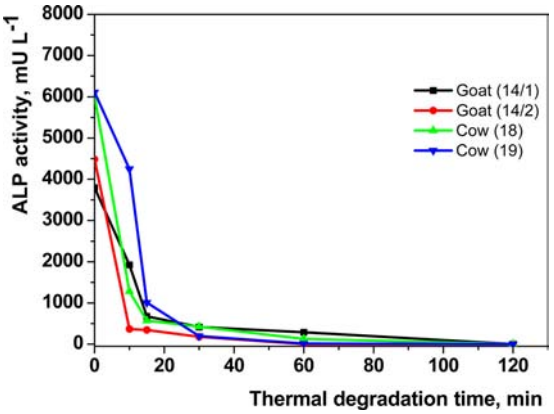

Figure 4. Study of the thermal degradation of milk samples.

using two samples of each milk type. As can be seen, the degradation process is slightly lower for cow's milk samples, which agrees with the results previously described using a similar thermal treatment.[32]

The results obtained show the practical usefulness of MLs containing the enzymatic substrate MUP as enhancement reagents for the determination of ALP activity in milk samples. The positive effect of the retention of the MLs before the detection system, using an external magnet, is mainly shown by the improvement of the LOD and the precision. Also, the flow system allows the automation of the method, obtaining analytical results in only a few minutes.

AUTHOR INFORMATION

Corresponding Author

*(A.G.-H.) Phone: +34 957 218645. Fax: +34 957 218644. E-mail: qa1gohea@uco.es.

Funding

We gratefully acknowledge financial support from the Spanish MICINN (Ministerio de Ciencia e Innovación) (Grant CTQ2012-32941/BQU), the Junta de Andalucía (Grant PO9-FQM-4933), and the FEDER-FSE program.

Notes

The authors declare no competing financial interest.

ACKNOWLEDGMENTS

We gratefully acknowledge Central Laboratories Service (University of Córdoba) for providing electronic microscopy (TEM and SEM-EDX) and additional spectroscopic (XPS) techniques.

ABBREVIATIONS USED

AuNPs, gold nanoparticles; ALP, alkaline phophatase; DT, 1-dodecanethiol; PET, positron emission tomography; MNPs, magnetic nanoparticles; MLs, magnetoliposomes; MUP, 4-methylumbelliferyl-phosphate disodium salt; TEM, transmission electron microscopy; SEM-EDX, scanning electron microscopy − energy dispersive detector; $HAuCl_4$, tetrachloroauric acid; Tris, tris(hydroxymethyl)aminomethane hydrochloride; RSE, rapid solvent evaporation

REFERENCES

(1) Taylor, T. M.; Davidson, P. M.; Bruce, B. D.; Weiss, J. Liposomal nanocapsules in food science and agriculture. *J. Crit. Rev. Food Sci. Nutr.* **2005**, *45*, 587−605.

(2) Peng, H.; Li, W.; Ning, F.; Yao, L.; Luo, M.; Zhu, X.; Zhao, Q.; Xiong, H. Amphiphilic chitosan derivatives-based liposomes: synthesis, development and properties as a carrier for sustained release of salidroside. *J. Agric. Food Chem.* **2014**, *62*, 626−633.

(3) Shin, G. H.; Chung, S. K.; Kim, J. T.; Joung, H. J.; Park, H. J. Preparation of chitosan-coated nanoliposomes for improving mucoadhesive property of curcumin using the ethanol injection method. *J. Agric. Food Chem.* **2013**, *61*, 11119−11126.

(4) Gulseren, I.; Corredig, M. Storage stability and physical characteristics of tea polyphenol bearing nanoliposomes prepared with milk fat globule membrane phospholipids. *J. Agric. Food Chem.* **2013**, *61*, 3242−3251.

(5) Tan, C.; Xia, S.; Xue, J.; Xie, J.; Feng, B.; Zhang, X. Liposomes as vehicles for lutein: preparation, stability, liposomal membrane dynamics and structure. *J. Agric. Food Chem.* **2013**, *61*, 8175−8184.

(6) Were, L. M.; Bruce, B. D.; Davidson, P. M.; Weiss, J. Size, stability, and entrapment efficiency of phospholipid nanocapsules containing polypeptide antimicrobials. *J. Agric. Food Chem.* **2003**, *51*, 8073−8079.

(7) Smith, A. M.; Jaime-Fonseca, M. R.; Grover, L. M.; Bakalis, S. Alginate-loaded liposomes can protect encapsulated alkaline phosphatase functionality when exposed to gastric pH. *J. Agric. Food Chem.* **2010**, *58*, 4719−4724.

(8) Liu, W.; Liu, J.; Liu, W.; Li, T.; Liu, C.. Improved physical and in vitro digestion stability of a polyelectrolyte delivery system based on

layer-by-layer self-assembly alginate-chitosan coated nanoliposomes. *J. Agric. Food Chem.* **2013**, *61*, 4133−4144.
(9) Gómez-Hens, A.; Fernández-Romero, J. M. The role of liposomes in analytical processes. *Trends Anal. Chem.* **2005**, *24*, 1−19.
(10) Edwards, K. A.; Bolduc, O. R.; Baeumner, A. J. Miniaturized bioanalytical systems: enhanced performance through liposomes. *Curr. Opin. Chem. Biol.* **2012**, *16*, 1−9.
(11) Román-Pizarro, V.; Fernández-Romero, J. M.; Gómez-Hens, A. Gold nanoparticle-biotinylated liposome hybrids as analytical reagents for biotin determination using a competitive assay and resonance light scattering detection. *Talanta* **2012**, *99*, 538−543.
(12) Beveridge, J. S.; Stephens, J. R.; Williams, M. E. The use of magnetic nanoparticles in analytical chemistry. *Annu. Rev. Anal. Chem.* **2011**, *4*, 251−273.
(13) Wang, G.; Su, X. The synthesis and bio-applications of magnetic and fluorescent bifunctional composite nanoparticles. *Analyst* **2011**, *136*, 1783−1798.
(14) Rios, A.; Zougagh, M.; Bouri, M. Magnetic (nano)materials as an useful tool for sample preparation in analytical methods. A review. *Anal. Methods* **2013**, *5*, 4558−4573.
(15) Qiu, J. D.; Xiong, M.; Liang, R. P.; Peng, H. P.; Liu, F. Synthesis and characterization of ferrocene modified Fe_3O_4@Au magnetic nanoparticles and its application. *Biosens. Bioelectron.* **2009**, *24*, 2649−2653.
(16) Cui, Y. R.; Hong, C.; Zhou, Y. L.; Li, Y.; Gao, X. M.; Zhang, X. X. Synthesis of orientedly bioconjugated core/shell Fe_3O_4@Au magnetic nanoparticles for cell separation. *Talanta* **2011**, *85*, 1246−1252.
(17) Bakandritsos, A.; Fatourou, A. G.; Fatouros, D. G. Magneto-liposomes and their potential in the intelligent drug-delivery field. *Ther. Deliv.* **2012**, *3*, 1469−1482.
(18) Faria, M. R.; Cruz, M. M.; Gonçalves, M. C.; Carvalho, A.; Feio, G.; Martins, M. B. F. Synthesis and characterization of magneto-liposomes for MRI contrast enhancement. *Int. J. Pharm.* **2013**, *446*, 183−190.
(19) Fattahi, H.; Laurent, S.; Liu, F.; Arsalani, N.; Elst, L. V.; Muller, R. N. Magnetoliposomes as multimodal contrast agents for molecular imaging and cancer nanotheragnostics. *Nanomedicine (London)* **2011**, *6*, 529−544.
(20) Soenen, S. J. H.; Hodenius, M.; De Cuyper, M. Magneto-liposomes: versatile innovative nanocolloids for use in biothechnology and biomedicine. *Nanomedicine (London)* **2009**, *4*, 177−191.
(21) Veiseh, O.; Gunn, J.; Zhang, M. Design and fabrication of magnetic nanoparticles for targeted drug delivery and imaging. *Adv. Drug Delivery Rev.* **2010**, *62*, 284−304.
(22) Rankin, S. A.; Christiansen, A.; Lee, W.; Banavara, D. S.; Lopez-Hernandez, A. The application of alkaline phosphatase assays for the validation of milk product pasteurization. *J. Dairy Sci.* **2010**, *93*, 5538−5551.
(23) Sánchez-Cabezudo, M.; Fernández-Romero, J. M.; Luque de Castro, M. D. Fluorimetric determination of alkaline phosphatase activity in human serum by use of a flow-through biosensor. *J. Biotechnol.* **1994**, *37*, 143−149.
(24) Vega-Warner, A. V.; Gandhi, H.; Smith, D. S.; Ustunol, Z. Polyclonal-antibody-based ELISA to detect milk alkaline phosphatase. *J. Agric. Food Chem.* **2000**, *48*, 2087−2091.
(25) Fenoll, J.; Jourquin, G.; Kauffmann, J. M. Fluorimetric determination of alkaline phosphatase in solid and fluid dairy products. *Talanta* **2002**, *56*, 1021−1026.
(26) Park, L.; Bae, H.; Kim, Y. T.; Lee, J. H. Rapid monitoring of alkaline phosphatase in raw milk using 1,1′-oxalyldiimidazole chemiluminescence detection. *Anal. Methods* **2011**, *3*, 156−160.
(27) Rudakovskaya, P.; Beloglazkina, E.; Majouga, A.; Zyk, N. V. Synthesis and characterization of terpyridine-type ligand-protected gold-coated Fe_3O_4 nanoparticles. *Mendeleev Commun.* **2010**, *20*, 158−160.
(28) Sánchez-López, V.; Fernández-Romero, J. M.; Gómez-Hens, A. Evaluation of liposome populations using a sucrose density gradient centrifugation approach coupled to a continuous flow system. *Anal. Chim. Acta* **2009**, *645*, 79−85.
(29) Long, G. L.; Winefordner, J. D. Limit of detection: a closer look at the IUPAC definition. *Anal. Chem.* **1983**, *55*, 712A−724A.
(30) U.S. Department of Health and Human Services. Publication 229, Pasteurized Milk Ordinance, 2005.
(31) Commission Regulation (EC) No. 1664/2006. *Off. J. Eur. Union* **2006**, *320*, 13.
(32) Vamvakaki, A. N.; Zoidou, E. G.; Moatsou, G.; Bokari, M.; Anifantakis, E. Residual alkaline phosphatase activity after heat treatment of ovine and caprine milk. *Small Ruminant Res.* **2006**, *65*, 237−241.

Apparatus. Cell culture plates and 96-well polystyrene microtiter plates were purchased from Costar (Corning, NY, USA). A direct heat CO_2 incubator, an automated plate washer (Wellwash 4 MK2), and a microplate reader were purchased from Thermo (Franklin, MA, USA). An electric heating constant-temperature incubator was purchased from Tianjin Zhonghuan Experiment Electric Stove Co. Ltd. An ultrasonic cleaner (KH-500E, Jiangsu, China) was purchased from Kunshan Hechuang Ultrasonic Apparatus Co. Ltd. Syringe filters (25 mm, 0.2 μm, and 0.45 μm pore size, Acrodisc) and filter unit (Acrocap) were purchased from Pall (Ann Arbor, MI, USA).

Medium. DMEM containing 10−20% (v/v) FBS was supplemented with 0.2 M glutamine, 50000 units/L penicillin, and 50 mg/L streptomycin. The standard medium was used for growing of myeloma and hybridoma cells.

Buffers and Solutions. Buffers and solutions included the following: (1) coating buffer (0.05 M carbonate buffer, pH 9.6); (2) phosphate-buffered saline (PBS) (0.1 M phosphate buffer containing 0.9% NaCl, pH 7.5); (3) PBS with 0.1% (v/v) Tween-20 (PBST); (4) PBST containing 0.5% (w/v) gelatin (PBSTG); (5) PBSTG containing 10% (w/v) methanol; (6) citrate−phosphate buffer (0.01 M citric acid and 0.03 M Na_2HPO_4, pH 5.5); (7) substrate solution (4 μL of 30% H_2O_2 added to 10 mL of citrate−phosphate buffer containing 2 mg/mL OPD); (8) stop solution (2 M H_2SO_4).

Myeloma Cell Line. The HAT-sensitive BALB/c mouse myeloma cell line SP2/0-Ag14 obtained from the Chinese Institute of Veterinary Drug Control (Beijing, China) was used in fusion experiments.

Synthesis of Hapten−Protein Conjugate. The synthetic route of the immunogen and coating antigen is presented in Figure 1. The

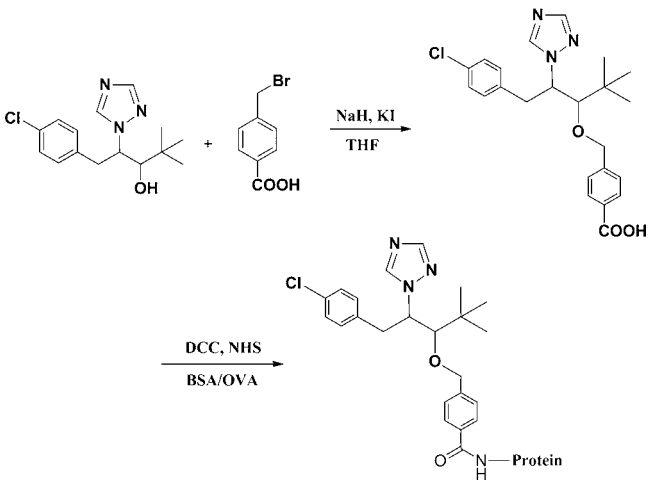

Figure 1. A general synthesis schematic and chemical structure of immunogen and coating antigen.

hapten, 4-(((1-(4-chlorophenyl)-4,4-dimethyl-2-(1*H*-1,2,4-triazol-1-yl)pentan-3-yl)oxy)methyl)benzoic acid, was synthesized through substitution reaction at the hydrogen group of PBZ. Briefly, 1.0 g (3.4 mmol) of PBZ and 0.73 g (3.4 mmol) of 4-(bromomethyl)-benzoic acid were dissolved in 20 mL of distilled tetrahydrofuran (THF) at 0 °C. The solution was stirred on an ice bath for 30 min after 0.3 g of NaH was added. After stirring at room temperature for an additional 30 min, 0.056 g of KI (0.34 mmol) was added. The solution was then heated to reflux overnight. The reaction solution was cooled to room temperature and quenched slowly by addition of 10 mL of distilled water. The mixture was acidified to pH 5 with 2 M HCl; and most THF was removed by rotary evaporation, followed by extraction of the organic layer three times with 20 mL of ethyl acetate. After the ethyl acetate extract had been dried over anhydrous Na_2SO_4, the solvent was evaporated. The residual product was eluted with a mixture of petroleum ether (boiling range: 60−90 °C)/ethyl acetate (4:1 v/v) from a silica gel column (30 g, 25 cm). The eluent was concentrated to give 0.70 g of hapten, in 48% yield. HRMS (ESI) calculated for $C_{23}H_{27}ClN_3O_3$: 428.17355, found m/z 428.17338 [M^+ + H] by Bruker Apex IV FTMS. ^{1}H NMR (300 MHz, $CDCl_3$): δ 0.89 (s, 9, *tert*-butyl), 3.16−3.34 (m, 2, Ar-CH_2CH), 3.44 (d, 1, J = 2.7 Hz, CHC*H*C(CH_3)), 4.69 (s, 2, OCH_2-Ar), 4.84−4.91(m, 1, CH_2C*H*CH), 6.97 (d, 2, J = 8.3 Hz Ar-H_a), 7.19 (d, 2, J = 8.3 Hz Ar-H_b), 7.43 (d, 2, J = 8.2 Hz Ar-H_c), 7.86 (s, 1, Ar-H_e), 8.12 (d, 2, J = 8.2 Hz Ar-H_d), 8.53 (s, 1, Ar-H_f), 10.54 (s, 1, COOH). ^{14}C NMR ($CDCl_3$, 75 MHz): δ 26.5, 36.5, 40.4, 63.7, 76.3, 87.3, 126.8, 128.9, 129.9, 130.0, 130.4, 133.0, 135.0, 142.8, 144.2, 149.2, 169.4.

The hapten (54.5 mg), NHS (10.3 mg), and DCC (14.8 mg) were dissolved in 1 mL of dimethylformamide. The activation reaction was carried out for 1 h at ambient temperature and then 18 h at 4 °C. After centrifugation, the supernatant was divided into two equal aliquots and added dropwise to protein solution (130.0 mg of BSA or 88.0 mg of OVA in 10.0 mL of carbonate buffer, 50 mM, pH 9.6). The reaction mixtures were stirred overnight at 4 °C followed by dialysis against PBS with five changes in 3 days. The dialyzed conjugate solutions were lyophilized, and then the powders were stored at −20 °C. The conjugates of hapten−OVA and hapten−BSA were used as a coating and immunogen antigen, respectively. The molar ratios of hapten-to-BSA and hapten-to-OVA were 10:1 and 9:1, respectively, which were determined through the UV−vis method.[15]

Immunization Protocol, Monoclonal Antibody Production, Purification, and Characterization. Six female BALB/c mice, 8 weeks old, were immunized with the immunogen (hapten−BSA) .The protocols of immunization, fusion, antibody production, and purification were the same as described previously.[16] All the experiments were approved by Beijing Experimental Animal Management Office and performed in compliance with the regulation of Animals Welfare Act of the U.S. Department of Agriculture.

icELISAs. The procedure of icELISA was applied in the screening of the best-performance sera, positive clones, and assay condition. First, a microplate was coated with the coating antigen (100 μL per well in coating buffer), at 37 °C for 3 h. After four washes with PBS, each well was blocked with 200 μL of 3% nonfat dry milk in PBS for 30 min at 37 °C. After the plate was washed with PBST, to each well was pipetted 50 μL of analytes which were diluted in PBSTG containing 10% (w/v) methanol and 50 μL of antisera, supernatant, or mAbs, which were diluted in PBSTG; this was followed by incubation for 30 min at 37 °C. The plate was washed with PBST four times. An aliquot of 100 μL per well of goat anti-mouse IgG−HRP conjugate diluted in PBSTG was added. Likewise, after being incubated at 37 °C for 30 min, the plate was washed four times. To each well was added 100 μL of substrate solution for color development. Finally, the reaction was terminated with 50 μL of 2 M H_2SO_4. The absorbance was read at 492 nm on the microplate reader. The calibration curve data were imported into OriginPro 8.5 (OriginLab) and fit to a sigmoidal logistical equation.

Preparation and Extraction of Samples. PBZ (300.0 mg/L, a recommended use concentration of the commercial product) aqueous solution was sprayed on wheat seedlings which were cultivated in an outdoor experimental field of China Agricultural University. On the harvest day, sixty days after PBZ spraying, eight kernel samples were randomly collected at multiple sites in the experimental field and PBZ-free wheat kernels for recovery study were collected from the unsprayed control field. All kernel samples were stored under an ambient dry condition prior to test.

PBZ was fortified at varying concentrations in PBZ-free kernel samples (10.0 g) for recovery studies. The fortified samples (10.0 g) in triplicate were finely powdered in liquid nitrogen. After crushing, to 10.0 g of finely powered kernel was added 0, 0.4, 1, 2, 5, 10, 20, and 50 μL of 50.0 μg/mL PBZ standard solution in HPLC grade methanol to obtain fortification levels of 0, 2.0, 5.0, 10.0, 25.0, 50.0, 100.0, and 250.0 ng/g, respectively. The spiked samples were allowed to stand at room temperature overnight prior to extraction. The samples were then extracted with 20 mL of methanol under sonication (5 min, room temperature, ultrasonic frequency 40 Hz, ultrasonic power 500 W) followed by centrifugation at 10000g for 5 min. The extraction and centrifugation were repeated three more times. Solids were removed by filtration through filter paper. All supernatants were combined in a 100 mL triangular flask. Five grams of anhydrous Na_2SO_4 was added

to remove H_2O in the supernatants. After filtration through a filter paper the solution was evaporated to near dryness in a 40 °C water bath. The rest of the supernatants were then diluted in 4 mL of HPLC grade methanol and transferred to a 10 mL volume centrifuge tube. After storage at −40 °C for 30 min the supernatants were centrifuged at 10000*g* for 1 min at 4 °C to separate out most of the lipids. The supernatants were transferred to a 5 mL volume centrifuge tube and further dried under a gentle nitrogen stream. The residues reconstituted in 1 mL of PBSTG containing 10% methanol through vigorous vortexing for 2 min. The solution was further diluted 10-fold in PBSTG containing 10% methanol and then was analyzed with the icELISA.

The extraction procedure of kernel samples from PBZ-sprayed seedlings was the same as the recovery study. The residue dried under nitrogen was dissolved in 4 mL of HPLC grade methanol. The solution was divided into two equal aliquots. One aliquot was passed through a 0.22 μm Xiboshi cellulose filter (Envta, Beijing, China) prior to direct injection into the LC−electrospray ionization (ESI)-MS system. The other aliquot was dried with a gentle nitrogen stream and reconstituted in 1 mL of PBSTG containing 10% methanol for icELISA anlaysis.

LC−ESI-MS. PBZ in extracts was also analyzed on a Waters Acquity UPLC H-class bio system (Waters, MA, USA) interfaced to a Thermo Scientific Q-Exactive hybrid quadrupole-Orbitrap mass spectrometer (Thermo Fisher, Franklin, MA, USA) at the State Key Laboratory of Plant Physiology and Biochemistry of China Agricultural University. PBZ in extracts was separated on an Inspire C18 column (100 mm × 2.1 mm i.d., 3 μm) (Dikma, Beijing, China) by gradient elution. The mobile phase was started with 40% acetonitrile in distilled water containing 0.1% formic acid and gradually increased to 95% acetonitrile in 4 min. After 4 min at 95% acetonitrile, acetonitrile percentage was decreased to 40% in 6 s and remained at 40% acetonitrile for 4 min prior to the next sample injection. The flow rate was 300 μL/min. The sample injection volume was 5 μL. The retention time of PBZ was at 3.8 min.

RESULTS AND DISCUSSION

Characteristics of Monoclonal Antibody. Six monoclonal hybridomas which were positive to PBZ were obtained, and mAb6H73C9 was the best in sensitivity and selectivity (data not shown). The titer (the maximum serum dilution that gave an absorbance of 1.0 at the noncompetitive assay conditions) of the ascites was $2-4 \times 10^4$. The dissociation constant (K_d) of the mAb was determined with the method of Zhang et al.[15] The K_d value was 2.8×10^{-10} M. The mAb is IgG1 isotype that has κ light chains.

Optimization of icELISA. Organic solvents, ionic strengths, and pH values are the most frequently studied factors that affect the ELISA performance.[17−19] High concentrations of organic solvent were often used to assist the hydrophobic analytes to dissolve in ELISA sample buffer,[19] while 20% methanol in sample buffer, for example, can cause a decrease in sensitivity due to the nonspecific binding and higher background.[20] We assessed effects of methanol, acetone, and DMSO as described previously.[17] The result demonstrated that over 20% acetone caused measurement errors and severe sensitivity decrease and 10% DMSO led to serious antibody deactivation. Sensitivity was notably decreased as concentrations of methanol in PBSTG increased from 5%, 10%, to 20%, which IC_{50} values increased around 2-fold (data not shown). Similar tests were carried out to examine effects of ionic strengths (0.1−0.4 M Na^+), pH (4.5−9.5), and assay buffer concentrations (0.01−0.4 M PBSTG contain 0.14 M Na^+), respectively, and no significant effects were observed. Consequently, the optimal assay solution used in the study was 0.01 M PBSTG buffer containing 0.14 M sodium chloride (pH 7.4) and 10% methanol. MAb6H73C9 was characterized by icELISA using a two-dimensional checkerboard method. The optimum working dilutions for the coating antigen (1.0 mg/mL), purified mAb (1.0 mg/mL), and IgG−HRP conjugate (1.0 mg/mL) were at a ratio of 1:16,000, 1:32,000, and 1:1,000, respectively. Figure 2 shows the standard sigmoidal inhibition curve of PBZ using the optimum reagent dilutions. The calibration curve showed good linearity with a correlation coefficient ≥0.999. The IC_{50} value and quantification detection range (between 80% and 20% B/B_0) were 8.7 ng/mL and 2.0−50.4 ng/mL, respectively. The IC_{50} value was lower than the reported LOD of GC−MS (10 ng/mL).[21]

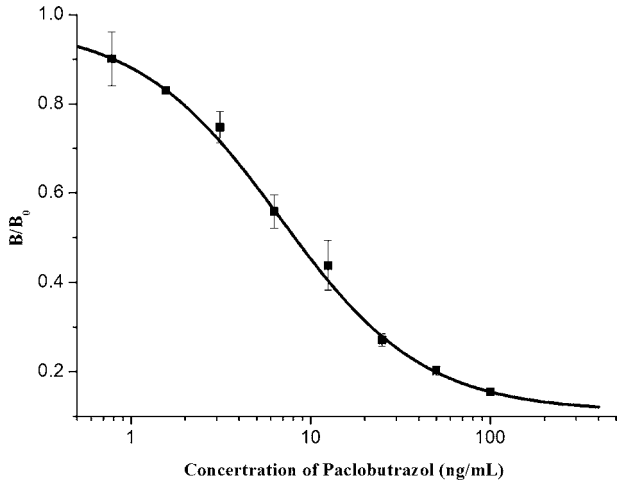

Figure 2. Standard inhibition curve of paclobutrazol by icELISA, obtained under optimized conditions. B_0 and B were absorbance in the absence and presence of competitors, respectively. Concentrations causing 20% and 50% inhibition by paclobutrazol were 2.0 and 8.7 ng/mL, respectively. Each value represents the mean of three replicates.

Cross-Reactivity Studies. The choice and design of the hapten are critical for the production of highly selective antibodies. The strategy to link PBZ with a carrier protein through the hydroxyl group by O-alkylation or O-succinylation as described previously[22] failed, probably due to steric hindrance of the hydroxyl group. Table 1 shows the IC_{50} values and cross-reactivity of 12 triazole compounds. Although most triazoles share the same moieties: a 1,2,4-triazolyl group, a mono- or dichlorinated phenyl group, the cross reactivity of mAb6H73C9 with uniconazole and triadimefon was approximately 0.7% or less. No inhibition was observed up to 4,000 ng/mL of the other 9 analytes. The cross-reactivity result suggested good specificity of mAb6H73C9 to PBZ.

Analyses of Paclobutrazol in Spiked Kernel Samples. Table 2 shows the average recoveries of PBZ fortified in PBZ-free wheat kernels. The matrix interference was almost inevitable for ELISA analysis.[23] The quantitation of hydrophobic compounds such as triazoles requires minimizing matrix interference, which is often a bottleneck in foodstuff analysis by ELISA.[19,22,24] A common method to minimize matrix interference was dilution or appropriate sample pretreatment. In the present study, most lipids were separated out in a small volume of methanol at low temperature, and the −40 °C treatment of concentrated extract solution and centrifugation have most effectively decreased the matrix interference in the optimized icELISA. It is noteworthy that Szekacs et al.[25] studied further cleanup to minimize the interference effects, but

Table 1. Cross-Reactivity of Paclobutrazol and Other Triazole Compounds

Analyte	Structure	IC_{50} (ng/mL)	Cross-reactivity[a] (%)
Paclobutrazol	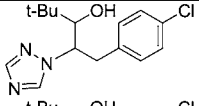	8.7 ± 0.6[b]	100 ± 6.9
Uniconazole	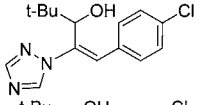	1,252 ± 14	0.7 ± 0.005
Triadimenol	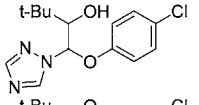	> 4,000	< 0.2
Triadimefon	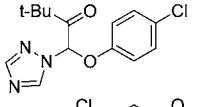	NI[c]	0
Difenoconazole	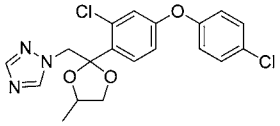	NI	0
Flutriafol	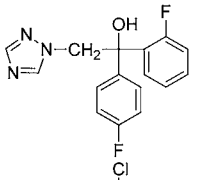	NI	0
Hexaconazole	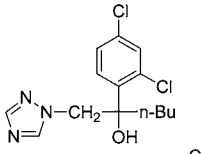	NI	0
Tebuconazole	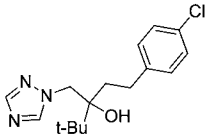	NI	0
Cyproconazole	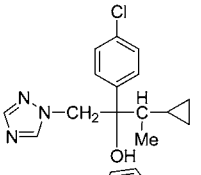	NI	0
Epoxiconazole	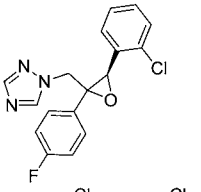	NI	0
Propiconazole	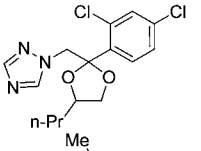	NI	0
Tricyclazole	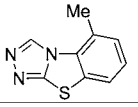	NI	0

[a]Cross-reactivity (%) = (IC_{50} of paclotrabuzol/IC_{50} of other compound) × 100. [b]Values were mean of triplicate determinations ± SD (standard deviation). [c]No inhibition was observed up to 4,000 ng/mL of the analytes.

the average recoveries of the target analytes were not significantly improved. Therefore, the sample extracts were not further cleaned up in the present study. The average recoveries were between 84.3% and 118.9% and the standard deviations were between 3.9 and 14.2% for the seven concentrations. Based on the quantification detection range of icELISA and the recovery study, the LOD of the assay was 2.0 ng/g, which was below the MRLs set by China (500 ng/g) and EU (20 ng/g).

dx.doi.org/10.1021/jf404905w | J. Agric. Food Chem. 2014, 62, 1826−1831

Table 2. Average Recoveries of Paclobutrazol from Wheat Kernels

spiked concns (ng/g)	mean recoveries (%, n = 3)[a]
0	0 ± 0[b]
2.0	118.9 ± 6.3
5.0	114.3 ± 6.3
10.0	101.3 ± 10.5
25.0	118.2 ± 6.2
50.0	99.2 ± 14.2
100.0	89.2 ± 3.9
250.0	84.3 ± 9.2

[a]Data were the means of triplicate samples. Each extract was diluted 10-fold in PBSTG containing 10% methanol before detection. [b]Not detected.

Analyses of Paclobutrazol Residues in Wheat Kernel Samples. The icELISA was applied to monitor PBZ residues in wheat kernels (Table 3). PBZ residues were detectable in all eight kernel samples of which the seedlings were sprayed with PBZ, indicating that PBZ could be transferred from vegetable organs to kernels. The results by icELISA agreed well with those by LC−ESI-MS. The PBZ concentration in the kernel samples varied from 1.5 to 7.3 ng/g, which may be due to uneven sprays of PBZ solution, different efficiencies of absorption and transportation, and metabolic rate in PBZ treated wheat seedlings.

Table 3. Comparison between icELISA and LC−MS Analyses for Paclobutrazol Residues in Wheat Kernels

	concns of PBZ residues (ng/g)	
samples	icELISA	LC−MS
1	7.4 ± 1.1[a]	7.3 ± 0.7
2	5.7 ± 0.8	5.6 ± 0.4
3	3.2 ± 0.7	3.4 ± 0.5
4	2.8 ± 0.4	3.1 ± 0.3
5	2.6 ± 0.7	2.7 ± 0.6
6	2.4 ± 0.8	2.3 ± 0.3
7	<2.0[b]	1.6 ± 0.1
8	<2.0	1.5 ± 0.2

[a]Data were means of triplicate samples. [b]Data were below the LOD of 2.0 ng/g.

We also analyzed PBZ residues with the developed icELISA in commercially available wheat flour samples purchased from different provinces of China including Beijing, Shandong, Shanxi, Anhui, Hebei, and Inner Mongolia. All residues were below the icELISA LOD level or not detected in these 20 samples (Figure 3). ELISA methods have advantages of high throughput and low costs, making it possible to analyze a large number of samples, and the assay we developed can be applied in routine analysis for screening of residue levels in large numbers of wheat flour samples. Samples that appear to exceed the MRL would then be subjected to a confirmatory analysis by HPLC−MS/MS methods.

According to the US Environmental Protection Agency (EPA) memorandum of Paclobutrazol Human Health Risk Assessment, PBZ is allowed for uses on nonfood crops and fruits, while in China, PBZ is widely used on crops or fruits such as wheat, rice, rape, soybean, peanut, orange, longan, litchi, and mango due to its obvious advantages on seedling height decrease while yield increases. Therefore, there is an urgent need to screen PBZ residues in agricultural produce. Our study proved that the developed icELISA could satisfactorily measure PBZ residues in wheat kernels and the LOD was 10-fold below the EU MRL.

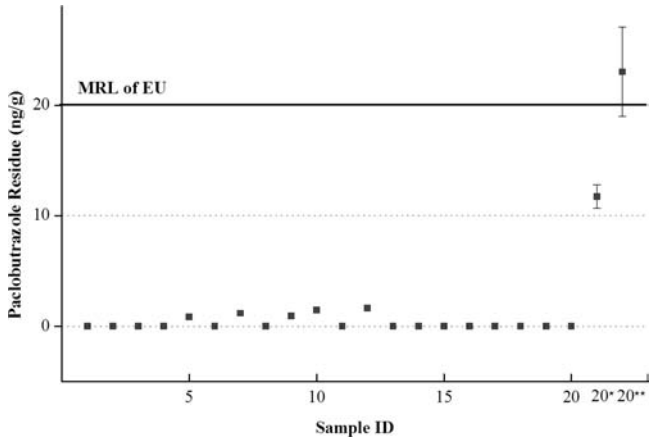

Figure 3. Result of paclobutrazol detection in twenty commercial wheat flour samples by icELISA. Samples 5, 7, 10, 12, and 19 contained paclobutrazol less than 2 ng/g. Residues were not detected in the other samples. Samples 20* and 20** represents sample 20 spiked with 10 ng/g and 20 ng/g paclobutrazol, respectively. Each value represents the mean of three replicates.

AUTHOR INFORMATION

Corresponding Author

*B.W.: tel, +86 10 6273 1305; fax, +86 10 6273 2567; e-mail, wbaomin@263.net. G.T.: tel, +86-10-62731070; e-mail: guiyu-0401@163.com.

Funding

The project was supported in part by the US National Institute of Occupational Safety and Health Grant 2U54OH007550.

Notes

The authors declare no competing financial interest.

ACKNOWLEDGMENTS

We would like to thank Prof. Huizhu Yuan of Institute of Plant Protection, Chinese Academy of Agricultural Sciences, for kindly providing triazole compounds.

ABBREVIATIONS USED

PBZ, paclobutrazol; ELISA, enzyme-linked immunosorbent assay; icELISA, indirect competitive ELISA; mAb, monoclonal antibody; IC_{50}, half-maximum inhibition concentration; LC−ESI-MS, liquid chromatography combined with electrospray ionization quadrupole Orbitrap mass spectrometry; MRL, maximum residue limit; EU, European Union; GC, gas chromatography; LC, liquid chromatography; HPLC, high performance liquid chromatography; MS, mass spectrometry; LOD, limit of detection; BSA, bovine serum albumin; OVA, ovalbumin; OPD, *o*-phenylenediamine; NHS, *N*-hydroxysuccinimide; DMSO, dimethyl sulfoxide; DCC, dicyclohexylcarbodiimide; IgG−HRP, IgG−horseradish peroxidase; DMEM, Dulbecco's modified Eagle's medium; FBS, fetal bovine serum; PBS, phosphate-buffered saline; PBST, PBS with 0.1% (v/v) Tween-20; PBSTG, PBST containing 0.5% (w/v) gelatin; THF, tetrahydrofuran

REFERENCES

(1) Keever, G. J.; Cox, D. A. Growth inhibition in marigold following drench and foliar-applied paclobutrazol. *HortScience* **1989**, *24*, 390.

(2) El-Khoreiby, A. M.; Unrath, C. R.; Lehman, L. J. Paclobutrazol spray timing influences apple tree growth. *HortScience* **1990**, *25*, 310−312.

(3) Berova, M.; Zlatev, Z.; Stoeva, N. Effect of paclobutrazol on wheat seedlings under low temperature stress. *Bulg. J. Plant Physiol.* **2002**, *28*, 75−84.

(4) Espindula, M. C.; Rocha, V. S.; Grossi, J.; Souza, M. A.; Souza, L. T.; Favarato, L. F. Use of growth retardants in wheat. *Planta Daninha* **2009**, *27*, 379−387.

(5) Yeshitela, T.; Robbertse, P. J.; Stassen, P. Paclobutrazol suppressed vegetative growth and improved yield as well as fruit quality of 'Tommy Atkins' mango (Mangifera indica) in Ethiopia. *N. Z. J. Crop Hort. Sci.* **2004**, *32*, 281−293.

(6) Witchard, M. A simplified technique for detection of paclobutrazol in plant sap extracts, using HPLC. *J. Plant Growth Regul.* **1997**, *16*, 213−214.

(7) Bicchi, C.; Cordero, C.; Rubiolo, P.; Occelli, A. Simultaneous determination of six triazolic pesticide residues in apple and pear pulps by liquid chromatography with ultraviolet diode array detection. *J. AOAC Int.* **2001**, *84*, 1543−1550.

(8) LeDoux, M. Analytical methods applied to the determination of pesticide residues in foods of animal origin. A review of the past two decades. *J. Chromatogr., A* **2011**, *1218*, 1021−1036.

(9) Hedden, P.; Graebe, J. E. Inhibition of gibberellin biosynthesis by paclobutrazol in cell-free homogenates ofCucurbita maxima endosperm andMalus pumila embryos. *J. Plant Growth Regul.* **1985**, *4*, 111−122.

(10) Mol, H. G. J.; van Dam, R. C. J.; Vreeken, R. J.; Steijger, O. M. Determination of daminozide in apples and apple leaves by liquid chromatography-mass spectrometry. *J. Chromatogr., A* **1999**, *833*, 53−60.

(11) Sancho, J. V.; Pozo, Ó. J.; Zamora, T.; Grimalt, S.; Hernández, F. Direct determination of paclobutrazol residues in pear samples by liquid chromatography-electrospray tandem mass spectrometry. *J. Agric. Food Chem.* **2003**, *51*, 4202−4206.

(12) Xu, Z. L.; Xie, G. M.; Li, Y. X.; Wang, B. F.; Beier, R. C.; Lei, H. T.; Wang, H.; Shen, Y. D.; Sun, Y. M. Production and characterization of a broad-specificity polyclonal antibody for O,O-diethyl organophosphorus pesticides and a quantitative structure-activity relationship study of antibody recognition. *Anal. Chim. Acta* **2009**, *647*, 90−96.

(13) Aston, L. S.; Seiber, J. N. Methods for the comparative analysis of organophosphate residues in four compartments of needles of Pinus ponderosa. *J. Agric. Food Chem.* **1996**, *44*, 2728−2735.

(14) Hu, Y.; Shen, G.; Zhu, H.; Jiang, G. A class-specific enzyme-linked immunosorbent assay based on magnetic particles for multiresidue organophosphorus pesticides. *J. Agric. Food Chem.* **2010**, *58*, 2801−2806.

(15) Zhang, Q.; Wang, L.; Ahn, K. C.; Sun, Q.; Hu, B.; Wang, J.; Liu, F. Hapten heterology for a specific and sensitive indirect enzyme-linked immunosorbent assay for organophosphorus insecticide fenthion. *Anal. Chim. Acta* **2007**, *596*, 303−311.

(16) Zhao, J.; Li, G.; Yi, G. X.; Wang, B. M.; Deng, A. X.; Nan, T. G.; Li, Z. H.; Li, Q. X. Comparison between conventional indirect competitive enzyme-linked immunosorbent assay (icELISA) and simplified icELISA for small molecules. *Anal. Chim. Acta* **2006**, *571*, 79−85.

(17) Cui, Y.; Liu, K.; Xu, C.; Liu, F.; Li, Q. X.; Liu, S.; Wang, B. Development of a sensitive monoclonal antibody-based indirect competitive enzyme-linked immunosorbent assay for analysing chlorantraniliprole residues. *Food Chem.* **2014**, *143*, 293−299.

(18) Marco, M. P.; Gee, S. J.; Cheng, H. M.; Liang, Z. Y.; Hammock, B. D. Development of an enzyme-linked immunosorbent assay for carbaryl. *J. Agric. Food Chem.* **1993**, *41*, 423−430.

(19) Jiang, X.; Shi, H.; Wu, N.; Wang, M. Development of an enzyme-linked immunosorbent assay for diniconazole in agricultural samples. *Food Chem.* **2011**, *125*, 1385−1389.

(20) Li, B.; Shi, H.; Wang, M. An enzyme-linked immunosorbent assay for the detection of bifenthrin. *Fenxi Huaxue* **2008**, *36*, 34−38.

(21) Sharma, D.; Awasthi, M. D. Uptake of soil applied paclobutrazol in mango (Mangifera indica L.) and its persistence in fruit and soil. *Chemosphere* **2005**, *60*, 164−169.

(22) Manclus, J. J.; Moreno, M. J.; Plana, E.; Montoya, A. Development of monoclonal immunoassays for the determination of triazole fungicides in fruit juices. *J. Agric. Food Chem.* **2008**, *56*, 8793−8800.

(23) Cairoli, S.; Arnoldi, A.; Pagani, S. Enzyme-Linked Immunosorbent Assay for the Quantitation of the Fungicide Tetraconazole in Fruits and Fruit Juices. *J. Agric. Food Chem.* **1996**, *44*, 3849−3854.

(24) Szekacs, A.; Hammock, B. D. ELISA for the detection of the triazole fungicide myclobutanil. *J. Agric. Food Chem.* **1995**, *43*, 2083−2091.

(25) Szekacs, A.; Cairoli, S.; Le, H. M.; Pagani, S. Comparative studies on enzyme-immunoassays for triazole fungicides tetraconazole and myclobutanil. *Acta Phytopathol. Entomol. Hung.* **1996**, *31*, 293−301.

Early quantitation of water using gas chromatography consisted of methods using packed molecular sieve columns, and these methods used direct detection with thermal conductivity detectors (TCD)[33−35,37,39] and indirect detection methods (acetylene produced from water reacting with calcium carbide) with a flame ionization detector.[31] These methods yielded poor peak symmetry, poor sensitivity, and poor efficiency due to the strong adsorption of water to the stationary phase. To improve peak symmetry, capillary GC columns were used;[36] however, virtually all GC stationary phases are degraded by water, although bonded and cross-linked varieties are somewhat more stable.[50]

The aim of this work is to develop a method for the simultaneous quantitation of ethanol and water that is simple, accurate, precise, rapid, and cost-effective. This is done by using the response of water or ethanol to normalize reproducibility from injection to injection instead of using an internal standard. The use of water in the gas chromatographic quantitation of commercial products that contain both water and ethanol has been ignored mainly due to the high concentrations of water present in most samples. The concentration of water can exceed the linearity of the detectors, and it can be observed by only a few detectors.[51]

Gas chromatography detectors suitable for water detection are thermal conductivity detectors and ionization detectors that can produce energies higher than 12.6 eV (the ionization energy of water). Helium ionization detectors[52] and barrier discharge ionization detectors (BID)[53] are examples of GC ionization detectors. The detectors used in this study were the thermal conductivity detector and a new barrier discharged ionization detector. The TCD is widely used and available. The BID is chosen because of its high sensitivity to water and because it is optimally designed to reduce baseline fluctuation.[53] It was reported that the BID is 100 times more sensitive to water than the TCD.[54] It is known that TCDs are nonlinear at high concentrations of water and ethanol.[51] The degree of linearity of the BID response to water and ethanol has not been reported.

Column considerations for water analysis consist of column stability, peak efficiency and symmetry, and selectivity between water and ethanol. Armstrong et al. showed that new ionic liquid (IL) based GC capillary columns have far superior selectivity and stability toward water in all solvents tested as compared to traditional commercial columns.[55−62] In addition, the IL column containing bis(3-hydroxyalkylimidazolium)-polyethylene glycol triflate (SLB-IL107) is shown to have good peak shape and symmetry for water.[55]

Herein we outline an effective and accurate method for the quantitation of both ethanol and water at any/all levels in commercial products. Typical run times are just over 3 min. This paper examines the determination of ethanol and water in commercial products using their individual responses rather than an internal standard to improve method precision. Examination of the responses of water and ethanol over a broad range of concentrations with the TCD and BID GC detectors is performed. To our knowledge this is the first study that uses (a) the responses of both water and ethanol to maintain method precision, (b) a nonlinear-based calibration, (c) IL-based GC capillary columns, and (d) a BID in the simultaneous determination of ethanol and water in a variety of commercial products.

MATERIALS AND METHODS

Materials. *Chemicals.* Anhydrous 200 proof ethanol was purchased from Sigma-Aldrich (Milwaukee, WI, USA). Deionized water was produced by a Milli-Q system (Billerica, MA, USA).

Standards. Standard reference materials were purchased from the National Institute of Standards and Technology (NIST, Gaithersburg, MD, USA): 1847, ethanol−water solution set. The *NIST2* sample contained 1.55 ± 0.02 mass % ethanol, *NIST6* contained 6.04 ± 0.04 mass % ethanol, and *NIST25* contained 25.2 ± 0.2 mass % ethanol. Ethanol reference standards also were purchased from Sigma-Aldrich: E2385, ethanol standards 10% (v/v); this sample was identified in this work as *Sigma10*. Sigma-Aldrich reported *Sigma10* to contain 7.7 mass % ethanol.

Samples. The commercial products used, such as beer, wine, liquor, mouthwash, and flavor extracts, were Bud Light (Anheuser-Busch Inc., St. Louis, MO, USA), chardonnay (Gallo Family Vineyards, Modesto, CA, USA), Crown Royal (The Crown Royal Co., Norwalk, CT, USA), Scope Mint (Procter & Gamble Co., Cincinnati, OH, USA), and pure almond extract (Penzeys Spices, Arlington, TX, USA).

Gas Chromatography-TCD. Gas chromatography was performed with an Agilent 6890N gas chromatograph equipped with a thermal conductivity detector and a 7683B series autosampler (Agilent Technologies, Inc., Santa Clara, CA, USA).

Gas Chromatography-BID. Gas chromatography was performed using a Shimadzu Tracera GC system consisting of a Shimadzu barrier discharge ionization detector coupled with a Shimadzu GC-2010 Plus capillary gas chromatograph and a Shimadzu AOC-5000 liquid GC injection system (Shimadzu Scientific Instruments, Inc., Columbia, MD).

Gas Chromatography Column. The column selected for all analyses was bis(3-hydroxyalkylimidazolium)-polyethylene glycol triflate: SLB-IL107, 30 m × 0.25 mm i.d. × 0.20 μm (Supelco, Bellefonte, PA, USA).

Software. The chromatographic software analysis was performed on an Agilent ChemStation rev. B.01.03 (Agilent Technologies, Inc.) and Shimadzu GCsolution version 2.41 (Shimadzu Corp.). The nonlinear regression was completed using Microsoft Excel 2013 (Microsoft Corp., Redmond, WA, USA). The calculations for solving the polynomials was performed using Wolfram Mathematica 9 (Wolfram Research, Champaign, IL, USA).

Methods. *Gas Chromatography-TCD.* Instrumental conditions were isothermal at 110 °C, constant flow at 1 mL/min, 0.1 μL injection, split 100:1 or 200:1, and TCD and inlet at 250 °C.

Gas Chromatography-BID. Instrumental conditions were isothermal at 110 °C, flow at 1 mL/min, 0.1 μL injection, split 100:1 or 200:1, and BID and inlet at 250 °C.

Standards. Ethanol and water standards for calibration were made gravimetrically using anhydrous ethanol and water with the concentration in mass percent (m/m). Conversion of concentration to volume percent (v/v) was performed by density values at measured temperatures.

Samples. All commercial samples and standards were injected neat.

Calculations. The retention factor (k) was calculated using $k = (t_r - t_o)/t_r$, where t_r is the retention time and t_o is the dead time, which is determined by the air peak in TCD and BID. Selectivity (α) was calculated by $\alpha = k_2/k_1$, where k_1 and k_2 are the retention factors of the first and second species, respectively. The resolution (R_s) was determined using $R_s = 2(t_{r2} - t_{r1})/(w_1 + w_2)$, where w_1 and w_2 are the base peak width of the first and second species, respectively. Efficiency or plate count, N, was determined by $N = 16\,(t_r/w_b)^2$ where w_b is the width at the base of the peak and t_r is the retention time of the analyte. Peak symmetry factor, A_s, was determined by $A_s = b/a$, where b is the distance from the point at peak midpoint to the trailing edge of the peak measured at 10% of peak height and a is the distance from the leading edge of the peak to the midpoint of the peak measured at 10% of peak height.

dx.doi.org/10.1021/jf4050167 | J. Agric. Food Chem. 2014, 62, 1832−1838

RESULTS AND DISCUSSION

The separation of ethanol and water standards was obtained in under 3.5 min (Figure 1) using a capillary ionic liquid column

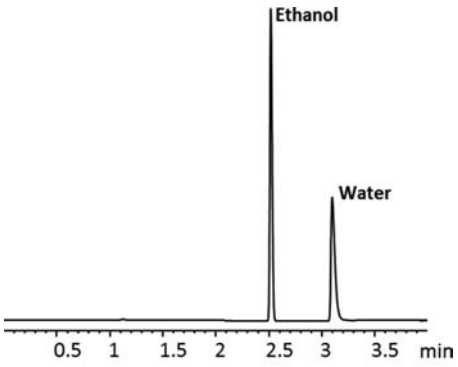

Parameter	Ethanol	Water
Retention Factor (*k*)	0.7	1.1
Plate Count (*N*)	64000	33000
Peak Symmetry Factor (A_s)	0.95	1.30
*Selectivity (α)	1.6	
*Resolution (R_s)	6.4	

Figure 1. Chromatographic separation and data of ethanol and water using a thermal conductivity detector. Standard sample analyzed is 60% ethanol and 40% water (m/m). See Materials and Methods for method details and equations of retention factor (k), plate count (N), peak asymmetry factor (A_s), selectivity (α), and resolution (R_s). *Selectivity and resolution are calculated using the ethanol and the water peak.

at isothermal conditions of 110 °C. Chromatographic data are shown in Figure 1. Peak symmetry factors (A_s) for ethanol and water were 0.95 and 1.3, respectively. Selectivity (α) between ethanol and water is 1.6, and resolution (R_s) between ethanol and water is 6.4. The chromatographic data show excellent selectivity between ethanol and water and excellent method resolution. Injector considerations are important when water is a large component of the injected sample. Water can cause inlet backflash given its large expansion volume.[50] The direct injection of water requires small injection volumes and appropriate inlet liner selection. The inlet liner used is a cup style liner with glass wool that allows turbulent flow for adequate sample vaporization and mixing. Injection volume was chosen to be 0.1 μL to avoid backflash and error in quantitation. The split ratio was adjusted between 100:1 and 200:1. The calibration and quantitation used a split ratio of 200:1. To investigate column stability a standard consisting of 10% by mass ethanol and 90% by mass water was injected 800 times on the SLB-IL107 ionic liquid capillary column. The chromatogram at injection 1 is overlaid with the chromatogram at injection 800 (Figure 2). No changes in column performance can be seen.

Method Range. The method range can be seen in Figure 3. The concentrations of water and ethanol are usually high in commercial products such as beer, wine, liquor, mouthwash, and flavor extracts. Consequently, an examination of the method response to water and ethanol over a broad range of concentrations was performed.

Analysis using TCD, shown in Figure 3A, produced a nonlinear plot of the peak area of water versus concentration of water (m/m) at a split ratio of 200:1, whereas ethanol shows

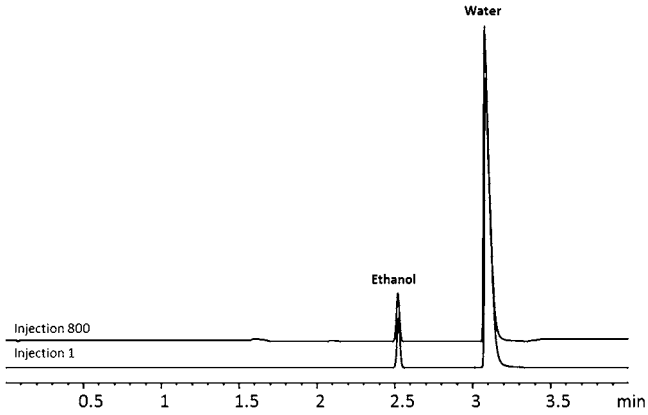

Figure 2. Column stability after 800 injections of a sample containing 10% by mass ethanol and 90% by mass water. Chromatographic separation was performed using a thermal conductivity detector. See Materials and Methods for method details.

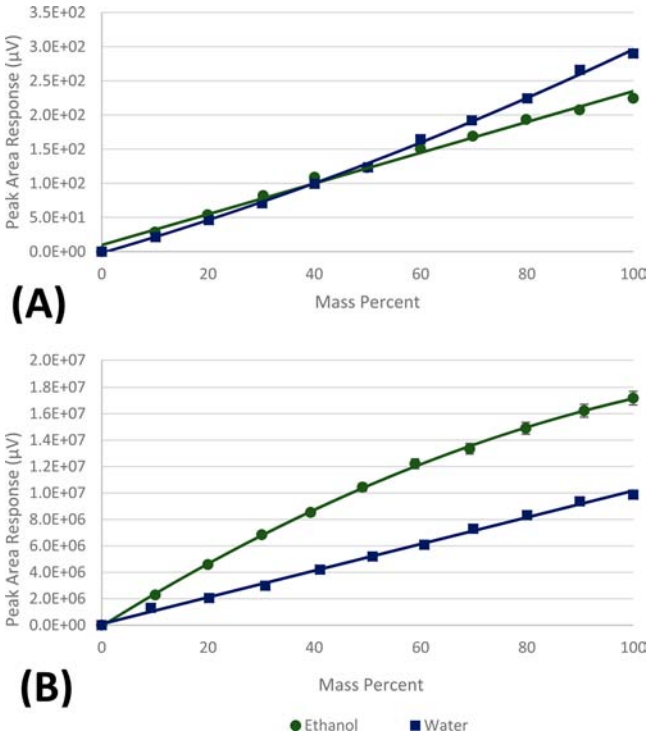

Figure 3. (A) Thermal conductivity detector (TCD) experimental linear range of peak area response versus mass percent of ethanol and water. TCD was set at 250 °C. Water showed a nonlinear response that yielded a polynomial best fit equation $y = 0.0072x^2 + 2.2633x - 2.0212$ with a square correlation coefficient of 0.9984. Ethanol showed a linear response that yielded a best fit equation $y = 2.2523x + 9.4708$ with a square correlation coefficient of 0.993. (B) Barrier discharge ionization detector (BID) experimental linear range of peak area response versus mass percent of ethanol and water. BID was set at 250 °C. Water showed a linear response that yielded a best fit equation $y = 100786x + 88459$ with a square correlation coefficient of 0.997. Ethanol showed a nonlinear response that yielded a polynomial best fit equation $y = -797.35x^2 + 251945x - 76451459$ with a square correlation coefficient of 0.9996. For both panels A and B, the standards consisted of a binary solution of water and ethanol that ranged in concentration from 0 to 100 mass %. See Materials and Methods for method details.

dx.doi.org/10.1021/jf4050167 | J. Agric. Food Chem. 2014, 62, 1832−1838

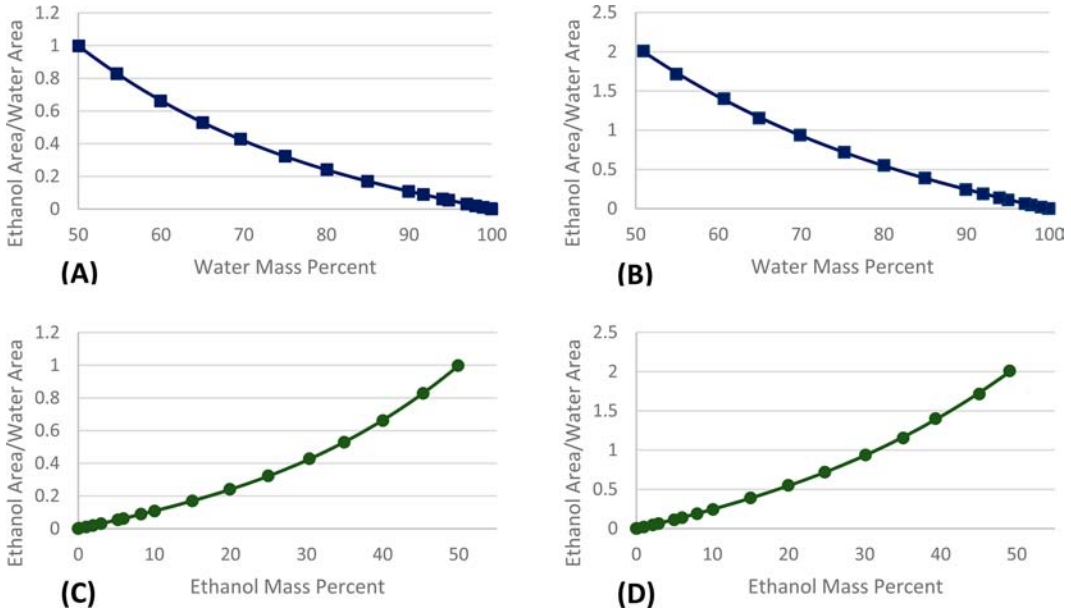

Figure 4. (A) Thermal conductivity detector (TCD) calibration plot of ethanol peak area divided by water peak area versus mass percent of water. The standards consisted of a binary solution of water and ethanol that ranged in concentration from 50 to 100 mass % water. (B) Barrier discharge ionization detector (BID) calibration plot of ethanol peak area divided by water peak area versus mass percent of water. The standards consisted of a binary solution of water and ethanol that ranged in concentration from 50 to 100 mass % water. (C) TCD calibration plot of ethanol peak area divided by water peak area versus mass percent of ethanol. The standards consisted of a binary solution of water and ethanol that ranged in concentration from 0 to 50 mass % ethanol. (D) BID calibration plot of ethanol peak area divided by water peak area versus mass percent of ethanol. BID was set at 250 °C. The standards consisted of a binary solution of water and ethanol that ranged in concentration from 0 to 50 mass % ethanol. See Materials and Methods for method details.

linearity through all concentrations. The TCD nonlinear response of water is due to the high concentration of water saturating the TCD flow cell, and this causes a positive deviation from linearity. In addition, the response of water is linear at concentrations lower than approximately 50% by mass.

Performing the same analysis using a BID (see Materials and Methods and Figure 3B) shows a nonlinear plot for the peak area of ethanol versus concentration at a split ratio of 200:1, whereas water shows a linear range through all concentrations. The BID nonlinear response of ethanol is due to the ionizability of water as compared to ethanol. The ionization energies of water and ethanol are 12.6 and 10.6 eV, respectively. The ionization energy of water is higher compared to that of ethanol, and thus the BID is more sensitive to ethanol than to water. The nonlinear response of ethanol using the BID is due to the saturation of the detector causing a negative deviation from linearity due to the ease of ionizability of ethanol. The linearity in the BID detectors also is dependent on the gas phase concentration of ethanol or water in the detector cell. In addition, the BID response to ethanol is linear at concentrations lower than approximately 30% by mass.

A study was performed to observe changes in the linear range in the TCD and BID by adjusting the split ratio from 200:1 to 100:1 (see Figures S1 and S2 in the Supporting Information and Figure 3). The decrease in the split ratio to 100:1 reduced the linear range of both the TCD response to water and the BID response to ethanol by almost 10 mass %.

Calibration and Quantitation. Calibration can be accomplished by the response of ethanol divided by the response of water (or vice versa) plotted against the concentration range of a series of ethanol and water standards, and no internal standard is needed. This is possible by taking advantage of two things. One is the volatile components of beer, wine, liquor, mouthwash, and flavor extracts of commercial products consisting mainly of a binary solvent mixture of a total concentration greater than approximately 99.5% (m/m) (determined gas chromatographically by total trace volatile component presence)[63] and eliminates the need for an internal standard. The other is that the use of nonlinear calibration corrects for the nonlinear response of the detectors.

All calibrations are shown in Figure 4. The calibration process can be described via an approach that is analogous to external calibration with the addition of the response of water and ethanol normalizing injection reproducibility. This shortens the analysis time. In addition, this process shows a nonlinear plot. This is due to detector response of ethanol and water at high concentrations as previously described. Nonlinear calibration is possible as long as the reproducibility of the calibration is assured.[64,65] Quantitation is simplified by solving a polynomial equation of a nonlinear calibration curve using mathematical software.

The standards for calibration consisted of binary solutions of water and ethanol that ranged in concentration from 0 to 50 mass % ethanol and from 50 to 100 mass % water. All of the calibration curves (Figure 4) could be described with third-order polynomials created in Microsoft Excel using the response data to obtain the best fit model. The GC split ratio of 200:1 was chosen for the calibration and quantitation. Figure 4A shows the TCD calibration plot of water (ethanol peak area divided by water peak area vs mass percent of water), and the calibration plot (Figure 4A) yielded a polynomial best fit equation $y = -4 \times 10^{-6}x^3 + 0.0011x^2 - 0.1234x + 4.821$ with a square correlation coefficient of 0.9999. Figure 4B shows the BID calibration plot of water (ethanol peak area divided by water peak area vs mass percent of water), and the calibration plot (Figure 4B) yielded a polynomial best fit equation $y = -5$

Table 1. Reported and Calculated Values of Ethanol and Water Concentration by Mass Percent[a]

	reported value[b]		TCD		BID	
sample	ethanol, mass %	water, mass %	ethanol, mass %	water, mass %	ethanol, mass %	water, mass %
NIST2	1.55 ± 0.02	98.4	1.5 ± 0.1	99 ± 2	1.5 ± 0.1	98 ± 4
NIST6	6.04 ± 0.04	94.0	5.8 ± 0.2	94 ± 2	6.0 ± 0.3	94 ± 6
NIST25	25.2 ± 0.2	74.8	24.7 ± 0.3	75 ± 1	25.0 ± 0.2	75 ± 1
Sigma 10	7.7	92.3	7.6 ± 0.1	92 ± 1	7.7 ± 0.3	92 ± 3
almond extract	25.3	74.7	24.4 ± 0.4	76 ± 1	24.9 ± 0.8	75 ± 3
Bud Light	3.3	96.7	3.2 ± 0.2	97 ± 7	3.3 ± 0.1	97 ± 2
Scope Mint	15.0	85.0	15.5 ± 0.2	84 ± 1	15.5 ± 0.1	85 ± 1
chardonnay	10.6	87.1[c]	11.0 ± 0.3[c]	88 ± 3[c]	11.1 ± 0.2[c]	88 ± 2[c]
Crown Royal	34.5	65.5	32.8 ± 0.5	67 ± 2	33.4 ± 0.6	67 ± 2

[a]Calculated values were extrapolated from the calibration curves. Chromatographic conditions were isothermal at 110 °C, flow = 1 mL/min, 0.1 μL injection, split 200:1, thermal conductivity detector (TCD), barrier discharge ionization detector (BID), and inlet at 250 °C, column SLB-IL107 (30 m × 0.25 mm i.d. × 0.20 μm). See Materials and Methods for descriptions of samples. [b]Deviation of the reported values is listed only for NIST samples. Other manufacturers did not provide a deviation for the values shown. The reported value for water was determined from the difference of the concentration of ethanol from 100%. [c]Adjusted for nonvolatile component. Nonvolatile component mass percent is determined by weight of residue after drying from an initial weight of consumer product.

$\times 10^{-6}x^3 + 0.0016x^2 - 0.1977x + 8.496$ with a square correlation coefficient of 0.9999. Figure 4C shows the TCD calibration plot of ethanol (ethanol peak area divided by water peak area vs mass percent of ethanol), and the calibration plot (Figure 4C) yielded a polynomial best fit equation $y = 4 \times 10^{-6}x^3 + 2 \times 10^{-6}x^2 + 0.0105x - 0.0006$ with a square correlation coefficient of 0.9999. Figure 4D shows the BID calibration plot of ethanol (ethanol peak area divided by water peak area vs mass percent of ethanol), and the calibration plot (Figure 4D) yielded a polynomial best fit equation $y = 5 \times 10^{-6}x^3 + 0.0001x^2 + 0.0233x - 0.0041$ with a square correlation coefficient of 0.9999. For a faster calibration, a two to three point linear calibration within a short concentration range of the consumer product being analyzed can be performed. The BID and TCD showed good intraday reproducibility of the method. The BID showed good interday reproducibility. However, interday reproducibility is limited for the TCD due to the dependence to the response of the TCD to humidity.

Standard reference materials were purchased for validation of method accuracy (see Materials and Methods; Table 1). The samples chosen for quantitation of water and ethanol commercial products consisted of beer, wine, liquor, mouthwash, and flavor extract. These samples are used to illustrate the range of applicability of this method to different commercial products. Table 1 lists the reported values from the manufacturer and the calculated concentrations with GC-TCD and GC-BID analysis of ethanol and water. The value of water in the reported values column in Table 1 was calculated by the difference of the concentration of ethanol reported from the manufacture from 100. The calculated values were determined by solving for x with the calibration polynomial in Wolfram Mathematica 9 by the input of the response of ethanol divided by the response of water as the variable, y (see Materials and Methods). Both TCD and the BID yielded results in agreement with the standard reference materials (Table 1).

Figure 5 shows a chromatogram of the commercial almond extract sample analyzed using the BID. This chromatogram shows the method's effectiveness in the analysis of the commercial products with ample efficiency and selectivity for water and ethanol and no trace components observed. The overall water and ethanol content determined for the commercial products was similar to the values stated by the

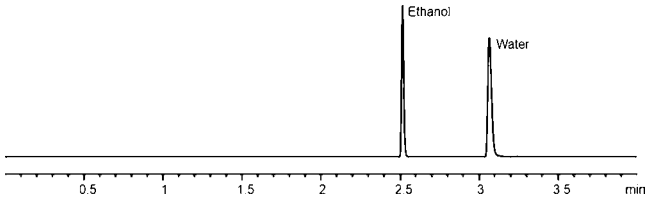

Figure 5. Chromatogram of commercial almond extract sample analyzed with barrier discharge ionization detection. The method for the analysis can be seen under Materials and Methods.

manufacturers. However, initial analysis of the wine sample, chardonnay, resulted in a low value for ethanol (8.3% mass) compared to the manufacturer's reported value (10.6% mass). It was found that this deviation was due to the presence of nonvolatiles, such as sugar, in the wine sample. Adjustment for nonvolatile components can be made by weight analysis of the residue by drying. The nonvolatile component mass percent was determined by the measurement of the weight of residue after drying from an initial weight of the wine product. The wine was found to consist of 2.3% mass of nonvolatiles. The final value of the ethanol and water mass percent was adjusted using the residue value, and the adjusted results agreed with the manufacturer's reported values. The uncertainties in the measurements of the water analysis compared to ethanol analysis were slightly larger. This was due to the high concentration of water in the samples and the dependency on humidity. To reduce the error, all samples and standards were parafilm sealed and stored at 4 °C. In addition, all samples and standards were minimally exposed to the atmosphere when opened.

A method for the quantitation of both ethanol and water that is simple, rapid, cost-effective, precise, and accurate has been developed. Simplicity, reduction of cost, and decreased analysis time have been accomplished by the removal of the internal standard method. This was accomplished by using the response of ethanol divided by the response of water (or vice versa) plotted against the concentration range of a series of ethanol and water standards. Using capillary ionic liquid gas chromatography, a fast analysis with high selectivity and resolution of the water and ethanol was obtained. This method shows both ethanol and water can be determined at all concentrations in commercial products. This method is

transferable to other binary solvent systems other than ethanol and water. The BID is linear at all concentrations of water with the described method. This makes it advantageous for development of external calibration methods for water analysis that cannot be performed with a TCD.

■ ASSOCIATED CONTENT

Supporting Information

Figures S1 and S2. This material is available free of charge via the Internet at http://pubs.acs.org.

■ AUTHOR INFORMATION

Corresponding Author

*(D.W.A.) E-mail: sec4dwa@uta.edu.

Notes

The authors declare no competing financial interest.

■ ACKNOWLEDGMENTS

We thank the Welch Foundation (Y-0026) for supporting this work, Shimadzu Scientific Instruments, Inc., and Dr. Zhuangzhi Wang, senior product specialist (GC/GCMS), of Shimadzu Scientific Instruments, Inc.

■ ABBREVIATIONS USED

GC, gas chromatography; TCD, thermal conductivity detector; BID, barrier ionization detector; IL, ionic liquid; SLB, Supelco Low Bleed; NIST, National Institute of Standards and Technology

■ REFERENCES

(1) *Offical Methods of Analysis of the AOAC*, 13th ed.; Horwitz, W., Ed.; Association of Offical Analytical Chemists: Washington, DC, USA, 1980.

(2) Brereton, P.; Hasnip, S.; Bertrand, A.; Wittkowski, R.; Guillou, C. Analytical methods for the determination of spirit drinks. *Trends Anal. Chem.* **2003**, *22*, 19−25.

(3) Castritius, S.; Kron, A.; Schafer, T.; Radle, M.; Harms, D. Determination of alcohol and extract concentration in beer samples using a combined method of near-infrared (NIR) spectroscopy and refractometry. *J. Agric. Food Chem.* **2010**, *58*, 12634−12641.

(4) Gerogiannaki-Christopoulou, M.; Kyriakidis, N. V.; Athanasopoulos, P. E. New refractive index method for measurement of alcoholic strength of small volume samples. *J. AOAC Int.* **2003**, *86*, 1232−1235.

(5) Bouthilet, R. J.; Caputi, A.; Ueda, M. Analysis of ethanol in wine by gas-liquid partition chromatography. *J. Assoc. Off. Agric. Chem.* **1961**, *44*, 410−414.

(6) Caputi, A.; Wright, D. Alcoholic beverages. Collaborative study of the determination of ethanol in wine by chemical oxidation. *J.−Assoc. Off. Anal. Chem.* **1969**, *52*, 85−88.

(7) Fernandes, E. N.; Reis, B. F. Automatic flow procedure for the determination of ethanol in wine exploiting multicommutation and enzymatic reaction with detection by chemiluminescence. *J. AOAC Int.* **2004**, *87*, 920−926.

(8) Mason, M. Ethanol determination in wine with an immobilized enzyme electrode. *Am. J. Enol. Vitic.* **1983**, *34*, 173−175.

(9) Ethanol determination via immobilized enzyme. *J. Am. Soc. Brew. Chem.* **1983**, *41*, 89−90.

(10) McCloskey, L. P.; Replogle, L. L. Evaluation of an enzymic method for estimating ethanol in wines using an enzyme kit. *Am. J. Enol. Vitic.* **1974**, *25*, 194−197.

(11) Sanford, C. L.; Mantooth, B. A.; Jones, B. T. Determination of ethanol in alcohol samples using a modular Raman spectrometer. *J. Chem. Educ.* **2001**, *78*, 1221−1225.

(12) Baumgarten, G. F. The determination of alcohol in wines by means of near infrared technology. *S. Afr. J. Enol. Vitic.* **1987**, *8*, 75−77.

(13) Gallignani, M.; Garrigues, S.; de la Guardia, M. Direct determination of ethanol in all types of alcoholic beverages by near-infrared derivative spectrometry. *Analyst* **1993**, *118*, 1167−1172.

(14) Van, D. B.; Van, O.; Smilde, A. K. Process analytical chemistry in the distillation industry using near-infrared spectroscopy. *Process Control Qual.* **1997**, *9*, 51−57.

(15) Collins, T. S.; Miller, C. A.; Altria, K. D.; Waterhouse, A. L. Development of a rapid method for the analysis of ethanol in wines using capillary electrophoresis. *Am. J. Enol. Vitic.* **1997**, *48*, 280−284.

(16) Martin, E.; Iadaresta, V.; Giacometti, J. C.; Vogel, J. Determination of ethanol by high-performance liquid chromatography (HPLC). *Mitt. Geb. Lebensmittelunters. Hyg.* **1986**, *77*, 528−534.

(17) Yarita, T.; Nakajima, R.; Otsuka, S.; Ihara, T.; Takatsu, A.; Shibukawa, M. Determination of ethanol in alcoholic beverages by high-performance liquid chromatography-flame ionization detection using pure water as mobile phase. *J. Chromatogr., A* **2002**, *976*, 387−391.

(18) Wang, M.-L.; Choong, Y.-M.; Su, N.-W.; Lee, M.-H. A rapid method for determination of ethanol in alcoholic beverages using capillary gas chromatography. *Yaowu Shipin Fenxi* **2003**, *11*, 133−140.

(19) Antonelli, A. Ethanol determination by packed GLC: a quick method with small sample amount and high sensitivity. *Wein−Wiss.* **1994**, *49*, 165−167.

(20) Caputi, A.; Mooney, D. P. Gas chromatographic determination of ethanol in wine: collaborative study. *J.−Assoc. Off. Anal. Chem.* **1983**, *66*, 1152−1157.

(21) Cutaia, A. J. Malt beverages and brewing materials: gas chromatographic determination of ethanol in beer. *J.−Assoc. Off. Anal. Chem.* **1984**, *67*, 192−193.

(22) Stackler, B.; Christensen, E. N. Quantitative determination of ethanol in wine by gas chromatography. *Am. J. Enol. Vitic.* **1974**, *25*, 202−207.

(23) Naviglio, D.; Ramano, R.; Attanasio, G. Rapid determination of ethanol content in spirits and in beer by high resolution gas chromatography. *Ind. Bevande* **2001**, *30*, 113−115.

(24) Wang, M.-L.; Wang, J.-T.; Choong, Y.-M. Simultaneous quantification of methanol and ethanol in alcoholic beverage using a rapid gas chromatographic method coupling with dual internal standards. *Food Chem.* **2004**, *86*, 609−615.

(25) Mattos, I. L.; Sartini, R. P.; Zagatto, E. A. G.; Reis, B. F.; Gine, M. F. Spectrophotometric flow injection determination of ethanol in distilled spirits and wines involving permeation through a silicon tubular membrane. *Anal. Sci.* **1998**, *14*, 1005−1008.

(26) Taniai, T.; Sukuragawa, A.; Okutani, T. Fluorometric determination of ethanol in liquor samples by flow-injection analysis using an immobilized enzyme-reactor column with packing prepared by coupling alcohol oxidase and peroxidase onto chitosan beads. *J. AOAC Int.* **2001**, *84*, 1475−1483.

(27) Wagner, K.; Bilitewski, U.; Schmid, R. D. Flow injection analysis of wine − accomplishments and needs. *Microchem. J.* **1992**, *45*, 114−120.

(28) Trachman, H. Determination of ethanol in beer by gas chromatography. *Wallerstein Lab. Commun.* **1969**, *32*, 111−114.

(29) Sun, H.; Wang, B.; DiMagno, S. G. A method for detecting water in organic solvents. *Org. Lett.* **2008**, *10*, 4413−4416.

(30) Streim, H. G.; Boyce, E. A.; Smith, J. R. Determination of water in 1,1-dimethylhydrazine, diethylenetriamine, and mixtures. *Anal. Chem.* **1961**, *33*, 85−89.

(31) Knight, H. S.; Weiss, F. T. Determination of traces of water in hydrocarbons. A calcium carbide gas-liquid chromatography method. *Anal. Chem.* **1962**, *34*, 749−751.

(32) Quiram, E. R. Wide-diameter open tubular columns in gas chromatography. *Anal. Chem.* **1963**, *35*, 593−595.

(33) Hogan, J. M.; Engel, R. A.; Stevenson, H. F. Versatile internal standard technique for the gas chromatographic determination of water in liquids. *Anal. Chem.* **1970**, *42*, 249−252.

(34) MacDonald, J. C.; Brady, C. A. Substitute method for the Karl Fischer titration. Gas chromatographic determination of water in ketonic solvents by use of the method of standard addition. *Anal. Chem.* **1975**, *47*, 947−948.
(35) Houston, T. E. Methods for the determination of water in coatings. *Met. Finish.* **1997**, *95*, 36−38.
(36) Jalbert, J.; Gilbert, R.; Tetreault, P. Determination of the analytical performance of a headspace capillary gas chromatographic technique and Karl Fischer coulometric titration by system calibration by using oil samples containing known amounts of moisture. *Anal. Chem.* **1999**, *71*, 3283−3291.
(37) Nussbaum, R.; Lischke, D.; Paxmann, H.; Wolf, B. Quantitative GC determination of water in small samples. *Chromatographia* **2000**, *51*, 119−121.
(38) Lee, C.-T.; Chang, S.-Y. A GC-TCD method for measuring the liquid water mass of collected aerosols. *Atmos. Environ.* **2002**, *36*, 1883−1894.
(39) O'Keefe, W. K.; Ng, F. T. T.; Rempel, G. L. Validation of a gas chromatography/thermal conductivity detection method for the determination of the water content of oxygenated solvents. *J. Chromatogr., A* **2008**, *1182*, 113−118.
(40) De, J.; Huizenga, J. R.; Wolthers, B. G.; Jansen, H. G.; Uges, D. R. A.; Hindriks, F. R.; Gips, C. H. Comparison of the precision of seven analytical methods for the water concentration in human serum and urine. *Clin. Chim. Acta* **1987**, *166*, 187−194.
(41) Jamin, E.; Guerin, R.; Retif, M.; Lees, M.; Martin, G. J. Improved detection of added water in orange juice by simultaneous determination of the oxygen-18/oxygen-16 isotope ratios of water and ethanol derived from sugars. *J. Agric. Food Chem.* **2003**, *51*, 5202−5206.
(42) Fischer, K. A new method for the analytical determination of the water content of liquids and solids. *Angew. Chem.* **1935**, *48*, 394−396.
(43) Scholz, E. Karl Fischer titrations of aldehydes and ketones. *Anal. Chem.* **1985**, *57*, 2965−2971.
(44) Vornheder, P. F.; Brabbs, W. J. Moisture determination by near-infrared spectrometry. *Anal. Chem.* **1970**, *42*, 1454−1456.
(45) Li, M.; Pacey, G. E. Spectrophotometric determination of trace water in organic solvents with a near infrared absorbing dye. *Talanta* **1997**, *44*, 1949−1958.
(46) Zhou, X.; Hines, P. A.; White, K. C.; Borer, M. W. Gas chromatography as a reference method for moisture determination by near-infrared spectroscopy. *Anal. Chem.* **1998**, *70*, 390−394.
(47) Pinheiro, C.; Lima, J. C.; Parola, A. J. Using hydrogen bonding-specific interactions to detect water in aprotic solvents at concentrations below 50 ppm. *Sensors Actuators B: Chem.* **2006**, *114*, 978−983.
(48) Isengard, H. D.; Striffler, U. Karl Fischer titration in boiling methanol. *Fresenius' J. Anal. Chem.* **1992**, *342*, 287−291.
(49) Scholz, E. *Karl Fischer Titration: Determination of Water*; Springer: Berlin, Germany, 1984.
(50) Kuhn, E. R. Water injections in GC − how wet can you get? *LCGC North Am.* **2002**, *20*, 474−475, 478.
(51) Patterson, P. L.; Gatten, R. A.; Kolar, J.; Ontiveros, C. Improved linear response of the thermal conductivity detector. *J. Chromatogr. Sci.* **1982**, *20*, 27−32.
(52) Andrawes, F.; Greenhouse, S. Applications of the helium ionization detector in trace analysis. *J. Chromatogr. Sci.* **1988**, *26*, 153−159.
(53) Shinada, K.; Horiike, S.; Uchiyama, S.; Takechi, R.; Nishimoto, T. Development of new ionization detector for gas chromatography by applying dielectric barrier discharge. *Shimadzu Hyoron* **2012**, *69*, 255−263.
(54) Frink, L. A.; Weatherly, C. A.; Armstrong, D. W. Water determination in active pharmaceutical ingredients using ionic liquid headspace gas chromatography and two different detection protocols. *J. Pharm. Biomed. Anal.* **2014**, in press.
(55) Jayawardhana, D. A.; Woods, R. M.; Zhang, Y.; Wang, C.; Armstrong, D. W. Rapid, efficient quantification of water in solvents and solvents in water using an ionic liquid-based GC column. *LCGC North Am.* **2012**, *30*, 142,144, 146, 148, 150, 152, 154, 157−158.
(56) Armstrong, D. W.; He, L.; Liu, Y.-S. Examination of ionic liquids and their interaction with molecules, when used as stationary phases in gas chromatography. *Anal. Chem.* **1999**, *71*, 3873−3876.
(57) Anderson, J. L.; Ding, J.; Welton, T.; Armstrong, D. W. Characterizing ionic liquids on the basis of multiple solvation interactions. *J. Am. Chem. Soc.* **2002**, *124*, 14247−14254.
(58) Anderson, J. L.; Armstrong, D. W. High-stability ionic liquids. A new class of stationary phases for gas chromatography. *Anal. Chem.* **2003**, *75*, 4851−4858.
(59) Anderson, J. L.; Armstrong, D. W. Immobilized ionic liquids as high-selectivity/high-temperature/high-stability gas chromatography stationary phases. *Anal. Chem.* **2005**, *77*, 6453−6462.
(60) Anderson, J. L.; Ding, R.; Ellern, A.; Armstrong, D. W. Structure and properties of high stability geminal dicationic ionic liquids. *J. Am. Chem. Soc.* **2005**, *127*, 593−604.
(61) Huang, K.; Han, X.; Zhang, X.; Armstrong, D. W. PEG-linked geminal dicationic ionic liquids as selective, high-stability gas chromatographic stationary phases. *Anal. Bioanal. Chem.* **2007**, *389*, 2265−2275.
(62) Armstrong, D. W.; Payagala, T.; Sidisky, L. M. The advent and potential impact of ionic liquid stationary phases in GC and GCxGC. *LCGC North Am.* **2009**, *27*, 596, 598, 600−602, 604−605.
(63) Restek. Analyzing alcoholic beverages by gas chromatography, http://www.restek.com/pdfs/59462.pdf (accessed Nov 7, 2013).
(64) Hinshaw, J. V. Non-linear calibration. *LC-GC Eur.* **2002**, *15*, 722−724, 726−727.
(65) Hinshaw, J. V. Non-linearity in a chromatographic system. *LC-GC Eur.* **2002**, *15*, 406, 408−409.

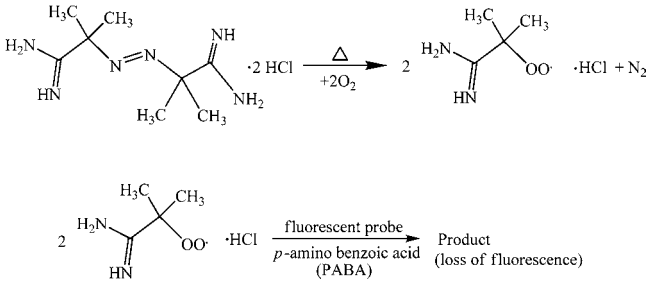

Figure 1. Scheme of competitive reactions showing the decomposition of AAPH, generation of peroxyl radicals, and conversion of the PABA probe to non-fluorescent products.

would be observed. As the reaction proceeds, the antioxidants are consumed by the constant flux of ROO• and the oxidation of the probe would progress at a slower rate when compared to the control (i.e., absence of antioxidant compounds). When the antioxidants are depleted, the rate of oxidation of the probe is similar to that of the control.[2]

The oxygen radical absorbance capacity (ORAC) assay is one of the most common methods for assessing ROO• scavenging activity based on the fluorescence intensity decrease of the ORAC probe with time under a reproducible and constant flux of ROO•, generated from the thermal decomposition of AAPH in aqueous buffer. The area under the fluorescence decay curve (AUC) is the parameter used to analyze the results in conventional ORAC tests. In the presence of chain-breaking antioxidants, the decay of fluorescence is inhibited.[11] The protein isolated from *Porphyridium cruentum*, β-PE, was initially used as the fluorescent probe, which reacts with ROO• to form a non-fluorescent product.[12] However, some shortcomings were observed with this probe, such as large lot-to-lot variability of production, photobleaching of β-PE after exposure to excitation light, and interaction with polyphenols by non-specific protein binding.[13] To overcome these limitations, the synthetic non-protein fluorescent probe, FL, has replaced the original β-PE,[14] but FL has also been criticized to undergo fluorescence quenching, side reactions, and undesired interactions.[15] The conventional ORAC method is limited to the measurement of hydrophilic chain-breaking antioxidants but ignores lipophilic ones. The application to both lipophilic and hydrophilic chain-breaking antioxidants was carried out using a mixture of acetone/water containing 7% randomly methylated β-cyclodextrin (M-β-CD) oligosaccharide as a water solubility enhancer,[16] but such high concentrations of oligosaccharides may not release the tested antioxidants to undergo oxidation because of the formation of relatively stable inclusion complexes.

The total radical-trapping antioxidant parameter (TRAP) assay was based on the measurement of the time period in which oxygen uptake was inhibited by plasma during a controlled ROO• peroxidation reaction.[17] TRAP measures oxygen consumption during controlled lipid oxidation induced by thermal decomposition of AAPH as the radical generator and R-phycoerythrin (PE) as the fluorescent probe and reports results in micromoles of peroxyl radical deactivated per liter of solution.[17] In the crocin bleaching assay, which has found limited applications in food and biochemistry, the ability of antioxidant compounds to protect the carotenoid derivative crocin from oxidation by ROO• is measured.[18]

The selectivity of a probe for ROO• detection mainly depends upon its standard redox potential. Although ROO• has a wide range of reduction potentials ($E°$) ranging between 0.77 and 1.44 V, the $E°$ of alkyl peroxyl radicals derived from polyunsatured fatty acids (PUFA) is 1.00 V at pH 7.0.[19] On the other hand, in strongly to weakly acidic solutions, the oxidation peak potentials of the *p*-aminobenzoic acid (PABA) probe (on a carbon paste electrode) vary in the range of 0.84−0.98 V.[20] With other modified electrodes (e.g., with crown ethers), the PABA oxidation potential may rise up to 1.055 V. Thus, it may be envisaged that ROO• can oxidize PABA, whereas $O_2^{\bullet -}$ ($E°$ = 0.940 V), $^1O_2$ ($E°$ = 0.650 V), PUFA alkyl radicals ($E°$ = 0.600 V), and H_2O_2 ($E°$ = 0.320 V)[21] may not easily do so. The oxidation potential of the ORAC probe, FL, was reported as 0.78 and 1.21 V versus saturated calomel electrode (SCE) in protonated and deprotonated forms, respectively, corresponding to 1.024 and 1.45 V calculated potentials versus standard hydrogen electrode (SHE),[22] and consequently, FL was characterized as "prone to be oxidized by several reactive species into a non-fluorescent product".[23] Thus, the PABA probe is expected to be a right choice for ROO• detection.

We report herein the development of a novel fluorescence probe for ROO•, PABA, which can specifically detect ROO• and measure its scavenging activity in terms of an increase of fluorescence in the presence of a scavenger compound. ROO• scavenging activity of several pure compounds (thiol-type antioxidants, glutathione (GSH), cysteine, *N*-acetyl-cysteine (NAC), homocysteine, 1,4-dithioerythritol (DTE), and cysteamine; amino acids, methionine, serine, and proline; plasma antioxidants, albumin, bilirubin, uric acid, and ascorbic acid) and tissue homogenates (kidney, liver, and heart) was determined by the proposed method in comparison to the classical ORAC method.

MATERIALS AND METHODS

Reagents and Apparatus. Bilirubin, serine, cysteamine, homocysteine, uric acid, GSH, AAPH, N-acetyl-L-cysteine, and dithioerythritol were purchased from Sigma-Aldrich (St. Louis, MO). Ascorbic acid, albumin from bovine serum, and proline were donated from Merck (Darmstadt, Germany), and PABA, cysteine, methionine, and FL were obtained from Fluka (Buchs, Switzerland). All other reagents used were of analytical grade.

The fluorescence spectra were measured in quartz cuvettes using a Varian Cary Eclipse model spectrofluorometer (Mulgrave, Victoria, Australia). A Waters Breeze 2 model high-performance liquid chromatography (HPLC) system (Milford, MA) equipped with a 2998 photodiode array detector (Chelmsford, MA) was used for chromatographic measurements.

Preparation of Solutions. For the PABA method, the following solutions were prepared: PABA solution (20 μM) and AAPH (20 mM) were prepared in pure distilled water (Millipore Simpak 1 Synergy 185, Billerica, MA). For the classical ORAC method, FL (78 nM) and AAPH (221 mM) were prepared in phosphate buffer (pH 7.4). This buffer (7.5×10^{-2} M NaH_2PO_4−Na_2HPO_4 equimolar mixture) was prepared in distilled water. All scavengers were freshly prepared in distilled water from 1.0×10^{-5} to 5.0×10^{-5} M concentrations, except uric acid and bilirubin, which were initially prepared in 0.5 M NaOH solution and then diluted with distilled water for the PABA method. The original uric acid and bilirubin solutions in 0.5 M aqueous NaOH were diluted with phosphate buffer (pH 7.4) for the classical ORAC assay.

Preparation of Tissue Homogenates. Male, 8−10-week-old, Wistar rats (weight range of 290−310 g) were supplied by the animal facility from the Faculty of Veterinary Medicine of Istanbul University. The rats were housed in polycarbonate cages (450 cm^2 area per animal), acclimatized for 2 weeks under laboratory conditions (21 ± 2 °C, humidity of 60 ± 5%, and 12 h light/dark cycle), and fed with water and standard rat chow *ad libitum*. Liver, heart, and kidney tissues

were isolated after sacrifice by decapitation of the rat. The tissue samples were washed with 0.9% (w/v) NaCl solution, weighed (10%, w/v), and homogenized by adding cold 1.15% (w/v) KCl solution in a glass homogenizer. Homogenates were immediately frozen in liquid nitrogen and kept at −80 °C until analysis.[24] Homogenates were centrifugated at 12 000 rpm for 15 min at 4 °C and filtered through a 0.45 μm membrane filter before analysis.

PABA Assay (Proposed Method). To a test tube were added 0.5 mL of 20 μM PABA (probe), 0.5 mL of scavenger solution (at different concentrations), 2.0 mL of distilled water, and 2.0 mL of 2.0×10^{-2} M AAPH in this order. The reaction started by adding AAPH solution. The mixture in a total volume of 5.0 mL was incubated for 30 min in a water bath kept at 37 °C. At the end of this period, the fluorescence intensity (λ_{ex} = 267 nm, and λ_{em} = 334 nm) of the reaction mixture was recorded. The half-maximal inhibitory concentration (IC_{50}) values of the scavengers (i.e., defined as the concentration of the scavenger antioxidant that results in 50% inhibition of the fluorescence-decay reaction caused by peroxyl radicals) were determined with the use of PABA by means of a linear plot of inhibition percentage as a function of $C_{scavenger}$, where I_0 is the initial fluorescence intensity of the original PABA solution and I_1 and I_2 are the fluorescence intensities of PABA subjected to peroxyl radical action in the absence and presence of a scavenger compound (having a molar concentration, C), respectively. The IC_{50} values were then compared to those found with the classical ORAC method. The fluorescence intensity of PABA was higher in the presence of ROO• scavengers; therefore, a higher intensity of the reaction mixture was an indication of enhanced ROO• scavenging activity.

ROO• scavenging activity was calculated using the following equation:

$$\text{inhibition ratio } (\%) = 100[(I_2 - I_1)/(I_0 - I_1)] \quad (1)$$

The inhibition percentage (y) can be linearly correlated to the concentration of the scavenger antioxidant (x)

$$y \approx mx + n \quad (2)$$

where m and n are the slope and intercept of this line, respectively.

IC_{50} can then be calculated for 50% inhibition by substituting an ordinate (y) value of 50.

$$y = 50 = m(IC_{50}) + n \quad \text{or} \quad IC_{50} = (50 - n)/m \quad (3)$$

Classical ORAC Assay. The ORAC method, using FL as the fluorescent probe, was carried out as described by Ou et al.[14] Briefly, to a test tube were added 2.0 mL of 78 nM FL, 2.0 mL of scavenger solution (at different concentrations), and 1.0 mL of 221 μM AAPH rapidly in this order. The reaction was started by adding AAPH solution. The reaction was performed at 37 °C through the thermal decomposition of AAPH because of the sensitivity of FL to pH.[13] The mixture in a total volume of 5.0 mL was incubated for 10 min in a water bath kept at 37 °C. At the end of this period, the fluorescence intensity (λ_{ex} = 493 nm, and λ_{em} = 515 nm) of the reaction mixture was recorded. ROO• scavenging activity was calculated using eqs 1−3.

HPLC Assay. The chromatographic analysis was carried out on a Waters Breeze 2 model HPLC system (Milford, MA), equipped with a 2998 model photodiode array detector (Chelmsford, MA). A total of 20 μL of incubation solution was injected into a reverse-phase ACE C18 column (4.6 × 250 mm, 5 μm particle size) (Milford, MA), and the separation was performed by gradient elution. The mobile phase consisting of a mixture of (A) 5% methanol/94% water (v/v) and 1% acetic acid and (B) 55% methanol, 44% water, and 1% acetic acid was delivered to the column at a flow rate of 1.0 mL min^{-1}. The gradient elution program for the analysis of the incubation mixture was 0−3 min, mobile phase A (slope 1.0); 3−8 min, gradient to 100% mobile phase B (slope 1.0); 8−23 min, mobile phase B (slope 1.0); 23−23 min, and linear gradient to 100% mobile phase A (slope 1.0).[25] The detection wavelength was set at 286 nm with a total run time of 23 min. Data acquisition and handling were performed by Empower PRO (Waters Associates, Milford, MA).

ROO• scavenging activity was calculated using a modified version of eq 1

$$\text{inhibition ratio } (\%) = 100[(A_2 - A_1)/(A_0 - A_1)] \quad (4)$$

where A_1 and A_2 are the peak areas of the PABA probe in the absence and presence of the ROO• scavenger, respectively, and A_0 is the peak area of the PABA probe at the initial concentration in the reaction mixture.

Statistical Analysis. The two-way analysis of variance (ANOVA) was used for data evaluation, and the significance of the difference between means was determined (p = 0.05) using SPSS software for Windows (version 13).[26] Results were reported as the mean ± standard deviation (SD) by carrying out measurements for at least three replicates of each scavenger compound or biological sample.

RESULTS AND DISCUSSION

Optimization of the PABA Assay Parameters. In this study, we developed a rapid and sensitive ROO• scavenging activity assay for pure antioxidant compounds (i.e., amino acids, thiol-type antioxidants, and plasma antioxidants) and biological fluids. PABA has first been used as a specific probe for the determination of ROO• scavenging activity. The PABA assay measures ROO• scavenging potential based on the ability of a compound to protect the oxidative probe PABA from oxidation by ROO•. In the competitive reaction, ROO• generated by thermal dissociation of AAPH attacks both the PABA probe and scavengers to form non-fluorescent products. The attenuation in the fluorescence intensity loss of the PABA probe is dependent upon the ROO• scavenging activity of the tested compound or sample. With the aid of PABA fluorescence values recorded in the presence and absence of scavengers, the ROO• scavenging activity of scavenger compounds can be calculated.

Although the non-fluorescent oxidation products were not identified under the same conditions of this assay, photochemical oxidation products were detected by Shaw et al., which may give some idea about the nature of such products.[27] Rapid discoloration of the photolyzed sample was observed when PABA was irradiated in aerated solution. Although a number of products were detected under these conditions, the three most abundant stable compounds have been isolated and identified [by nuclear magnetic resonance (NMR) spectroscopy] as 4-amino-3-hydroxybenzoic acid, 4-aminophenol, and 4-(4′-hydroxyphenyl)aminobenzoic acid. Likewise, a rapid reaction of singlet oxygen with PABA was reported by Allen et al.,[28] but oxidation products were not identified.

Under the optimized conditions, the molar fluorescence coefficient for PABA in the proposed method was $\varepsilon = 1.0 \times 10^8$ M^{-1} cm^{-1} and the linear range of relative fluorescence intensity versus the concentration of PABA was in the interval of 0.5−5.0 μM, with a correlation coefficient (r) of 0.992 (N = 3), within which the relative standard deviation (RSD) was 3.1%. The limit of detection (LOD) and limit of quantification (LOQ) of the proposed method were calculated using the equations: $LOD = 3s_{bl}/m$ and $LOQ = 10s_{bl}/m$, respectively, where s_{bl} is the standard deviation of a blank and m is the slope of the calibration line. LOD and LOQ were found to be 0.09 and 0.30 μM, respectively. Assay precision and accuracy were assessed by analyzing two spiked homogenates (i.e., liver and kidney) at clinical relevant concentrations of 1, 2, and 5 μM analyzed (Table 1). The precision data of the proposed assay (expressed as the percent RSD values) was approximately 4.14%. Recovery values from 97.5 to 105.0% were obtained. Reproducibility studies were carried out in five replicates for PABA at 2.0 μM.

Table 1. Precision and Recovery of the Proposed Method

PABA additions to tissue homogenates	added concentration (μM)	mean (μM)	SD[a]	RSD (%)[b]	REC (%)[c]
liver	1.0	1.02	0.04	4.14	101.5
	2.0	2.08	0.05	2.16	104.3
	5.0	5.01	0.03	0.52	100.2
kidney	1.0	1.05	0.03	3.05	105.0
	2.0	1.95	0.03	1.32	97.5
	5.0	4.98	0.07	1.36	99.5

[a]SD = standard deviation. [b]RSD = relative standard deviation. [c]REC = recovery (N = 3).

The intraday and interday precisions of the developed method, expressed as the RSD for the analyte, were 0.98 and 2.27% (N = 5), respectively.

For comparison, time-dependent fluorescence intensity changes were recorded using final mixture solutions (PABA, PABA + AAPH, and PABA + AAPH + cysteine) incubated under identical conditions (Figure 2). There was no noteworthy change in intensity of the PABA standard solution within the 0−35 min time interval (Figure 2). It was observed that the fluorescence intensity response in the presence of cysteine decreased with the increase in incubation time from 0 to 30 min and reached a plateau after 30 min. Therefore, 30 min was chosen as the optimal measurement time. Thus, because of the high conversion yield of PABA, IC_{50} values of the studied scavengers could be relatively rapidly and precisely determined by recording the relative intensities within 30 min. On the other hand, for a typical human serum sample using the ORAC assay system originally used by Cao et al.,[12] oxidation of β-PE was reported to reach completion within about 90 min.

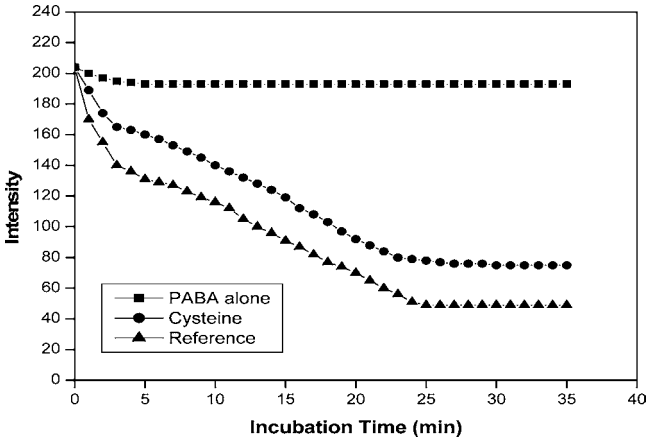

Figure 2. Fluorescence intensity versus incubation time curves of PABA alone and PABA subjected to peroxyl radical in the absence (reference) and presence (5.0×10^{-5} M cysteine) of a scavenger.

The fluorescence spectra of PABA, recorded in aqueous solutions at pH 7.0 with varying cysteine concentrations, are shown in Figure 3, where the maximal decrease in fluorescence intensity of PABA was due to ROO• oxidation of the probe without competition and its relative increase from the baseline level was proportional to the scavenging ability of the competitive scavenger. Upon mixing PABA (2.0 μM) with ROO• in the presence of cysteine at various concentrations (1.0−5.0 μM), the fluorescence intensities of PABA (remaining intact after ROO• attack) at 334 nm were greater than that of the reference (containing no cysteine) because of the competitive scavenging effect of cysteine. The results indicate that PABA is converted into non-fluorescent products with ROO• and also there is a proportional increase of 334 nm peak heights (Figure 3) with an increasing concentration of scavenger (cysteine). With the aid of PABA fluorescence intensity values recorded in the presence and absence of scavengers at varying concentrations, the IC_{50} values of scavengers and tissue homogenates can be calculated.

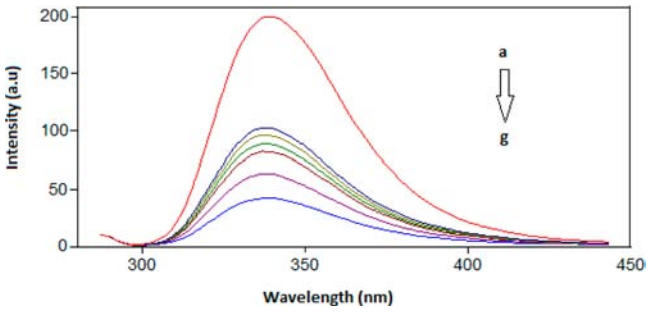

Figure 3. Fluorescence spectra of the remaining PABA in the absence and presence of cysteine: (a) 2 μM PABA, (b) 5 μM cysteine, (c) 4 μM cysteine, (d) 3 μM cysteine, (e) 2 μM cysteine, (f) 1 μM cysteine, and (g) 0 μM cysteine (reference).

HPLC Results of the Tested Scavengers. The developed method for measurement of ROO• scavenging activity was validated by quantifying the probe (PABA) and its oxidation product(s) by the HPLC method, followed by statistically comparing the results. Conversion of the PABA probe to products and inhibition of this reaction with a scavenger (i.e., NAC) were followed by the proposed and HPLC methods. As shown in Figure 4, the peak area of the PABA probe (retention time of PABA of 8.8 min) was higher in the presence of a ROO• scavenger, such as NAC, compared to its absence under identical conditions of radical attack (AAPH). The concentrations of PABA (in μg mL^{-1}) remaining after ROO• attack to PABA in the presence of NAC (3.0×10^{-4} M) measured by the proposed method and HPLC method were 6.76 ± 0.03 (N = 3) and 6.62 ± 0.07 (N = 3), respectively, where the initial concentration of PABA was 13.71 ± 0.09 (N = 3). The results obtained using these two methods were quite close, and the proposed method was verified (Figure 4b). As a result of the incubation reaction, the conversion ratio of the original probe to products in the absence of scavenger (reference) were found to be 78.9 and 81.1% with respect to the HPLC and proposed methods, respectively.

Evaluation of Results for Synthetic Scavengers. The PABA assay results for ROO• activity measurement were compared to those of the ORAC assay. Albumin had the lowest IC_{50} value among the studied antioxidants [i.e., highest peroxyl radical scavenging (PRS) activity] with respect to both the developed fluorometric (PABA) and ORAC methods. IC_{50} values of albumin were found to be 0.6 and 2.8 μM, respectively (Table 2). Zulueta et al. reported that,[29] in terms of PRS activity, albumin, a very powerful chain-breaking and transition-metal-binding extracellular antioxidant,[30] was the most effective antioxidant among plasma antioxidants, in accordance with the findings of the proposed method. Inspection of IC_{50} values of amino acids reveals that the highest scavenging activity was found for methionine (i.e., an amino acid not containing a free thiol group) and the lowest scavenging activity was found for serine with respect to classical ORAC and PABA methods

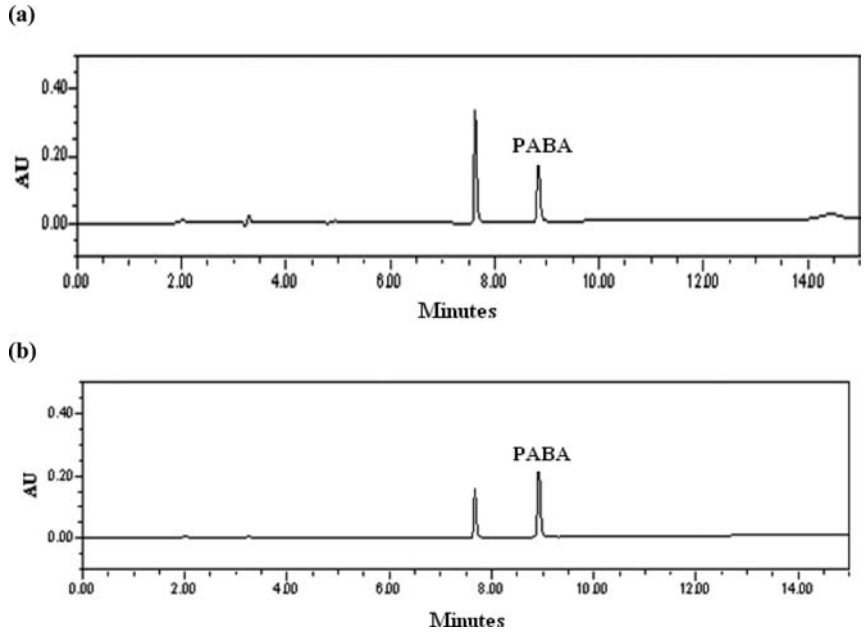

Figure 4. HPLC chromatograms for remaining PABA after AAPH reaction in the absence (reference) and presence of NAC (λ = 280 nm): (a) reference (0.5 mL of 1.0 × 10^{-3} M PABA + 2.5 mL of water + 2.0 mL of 0.4 M AAPH) and (b) 0.5 mL of 1.0 × 10^{-3} M PABA + 0.5 mL of 3.0 × 10^{-4} M NAC + 2.0 mL of water + 2.0 mL of 0.4 M AAPH.

Table 2. ROO• Scavenging Activity of Various Scavengers Measured by the PABA Method in Comparison to the ORAC Method (IC_{50} Values Were Calculated with Respect to Equations 1 and 4; N = 4 or 5 Data Points)[a]

peroxyl scavengers	IC_{50} value with respect to the PABA method (μM)	IC_{50} value with respect to the ORAC method (μM)
	Thiol-Type Antioxidants	
GSH	6.5 ± 0.3	16.2 ± 1.0
NAC	8.7 ± 0.4	9.3 ± 0.4
cysteine	6.7 ± 0.3	24.9 ± 1.1
homocysteine	5.7 ± 0.2	14.2 ± 0.4
DTE	12.1 ± 1.4	13.0 ± 1.2
cysteamine	121 ± 12	197 ± 19
	Amino Acids	
methionine	97.9 ± 8.2	21.9 ± 2.5
serine[b]	136 ± 15	338 ± 39
proline[b]	129 ± 9	326 ± 30
	Plasma Antioxidants	
albumin	0.6 ± 0.1	2.8 ± 0.1
uric acid	11.6 ± 1.1	9.6 ± 0.3
ascorbic acid	5.6 ± 0.4	10.7 ± 1.3
bilirubin	6.2 ± 0.3	10.8 ± 1.1

[a]Data presented as the mean ± SD (N = 3). All tested samples: $1.98IC_{50(PABA)} - 6.91 = IC_{50(ORAC)}$ (r = 0.882). Excluding amino acids: $1.61IC_{50(PABA)} + 1.09 = IC_{50(ORAC)}$ (r = 0.993). [b]IC_{50} values were calculated in millimolar.

(Table 2). The IC_{50} values for NAC (8.7 ± 0.4) and DTE (12.1 ± 1.4) obtained by the proposed method were similar to those of the classical ORAC assay (9.3 ± 0.4 and 13.0 ± 1.2, respectively). It is also noteworthy from Table 2 that cysteamine exhibited a much greater IC_{50} value (therefore lower peroxyl scavenging activity) than cysteine, having a similar structure. Cysteamine has less electron donation ability through the −SH group than cysteine because the electronegative N atom of the amine group in cysteamine counterbalances the effect of thiol. Although cysteine and cysteamine have quite close rate constants for radical disulfide anion formation in pulse radiolysis[31] and exhibited very close trolox equivalent antioxidant capacities (TEAC) in the ABTS/persulfate assay,[32] these two thiol compounds may behave differently against lipid peroxidation. Aruoma et al. have shown that, although cysteamine is an excellent scavenger of hydroxyl radicals and hypochlorous acid, it reacts slowly with hydrogen peroxide and does not react at an appreciable rate with superoxide anion radicals.[33] As a general drawback for the measurement thiols, the original ORAC method suffers a limitation from protein −SH, because the antioxidant action of plasma proteins was included in the total radical-trapping antioxidant parameter (TRAP) calculation independent of their thiol groups[34] and the ORAC values found for GSH with the two probes (β-PE and FL) of the assay greatly differ by a ratio of 1:2.[14] Some researchers even found zero ORAC value for cysteine in water or acetone−water solvents using the classical ORAC assay with the FL probe.[35]

Lussignoli et al. reported that both ascorbic and uric acids exhibited high PRS activities,[5] again compatible with the results of the PABA method, because the IC_{50} values obtained by the developed method for ascorbic acid and uric acid were 5.6 and 11.6 μM, respectively (in a microplate-based crocin bleaching assay of ROO• scavenging, the IC_{50} values of ascorbic and uric acids were reported as 3.97 and 8.15 μM, respectively).[5] Using the classical ORAC method, the IC_{50} values for ascorbic and uric acids were found to be 10.7 and 9.6 μM, respectively (Table 2). The differences between the types of assays and their conditions (pH, temperature, etc.) may compensate for the different activities reported. Both thiol-type antioxidants and plasma antioxidants with lower IC_{50} values had higher ROO• scavenging activity than non-thiol amino acids with respect to the PABA method, and this finding is in accordance with the results of other antioxidant activity assays, regardless of the mode of action, i.e., HAT- or electron transfer (ET)-based reactions.[33,36,37]

dx.doi.org/10.1021/jf405464v | J. Agric. Food Chem. 2014, 62, 1839−1845

The findings for the 13 ROO• scavengers (IC_{50} values) were statistically compared to those of classical ORAC using the two-way ANOVA test. It is concluded that there was no significant difference between the precisions of these two methods at the 95% confidence level ($p = 0.05$; $F_{exp} = 2.416$; $F_{crit} = 4.747$; and $F_{exp} < F_{crit}$). For IC_{50} values of all of the tested samples, PABA correlated linearly with ORAC ($r = 0.882$); by exclusion of the values for amino acids, this correlation was higher ($r = 0.993$). Thus, the proposed methodology was validated against the classical ORAC method of wide use.

Application of the Proposed Method to Some Tissue Homogenates. The PRS activity of heart homogenate as inhibition percentage versus dilution ratio is shown in Figure 5, where the inhibition percentage was curvilinearly correlated to the homogenate dilution ratio within the interval of 1:50–1:600 dilution.

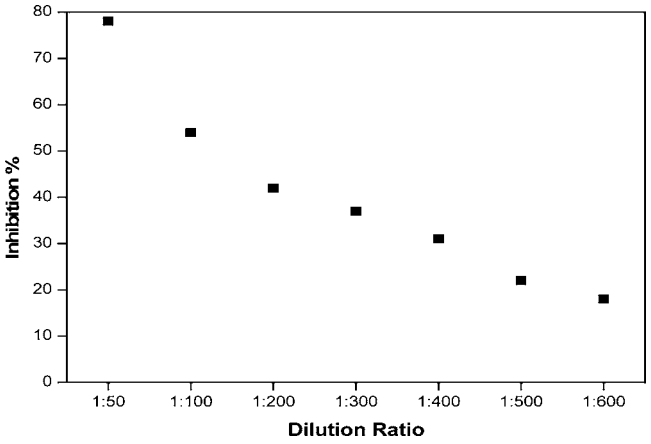

Figure 5. Inhibition percentage of tissue homogenates (heart) as a function of the homogenate dilution ratio using the PABA method.

The proposed method was successfully applied to tissue homogenate samples. The ROO• scavenging activity values measured with the proposed PABA and classical ORAC methods are comparatively depicted in a bar diagram (Figure 6), and the percentage inhibitions of identical tissue homogenates found with PABA were very close in relative intensity to those measured with the reference method. The ROO• scavenging activity of liver tissue homogenate was found to be higher than that of kidney and heart homogenate with respect to both methods. Since the liver was described as the most important organ involved in the regulation of the redox metabolism because of the synthesis of key enzymes responsible for ROS clearance and the production of GSH,[38] this result is acceptible. Linear regression analysis of PRS activity data presented in Figure 6 found with the PABA assay showed that this assay correlated well with the classical ORAC assay. The correlation equation between PABA and classical ORAC methods was calculated ($y = 0.940x + 12.98$; $r = 0.991$; and $N = 3$), with the closeness of the slope to unity showing one-to-one correspondence between results. Thus, the proposed methodology was validated for real samples.

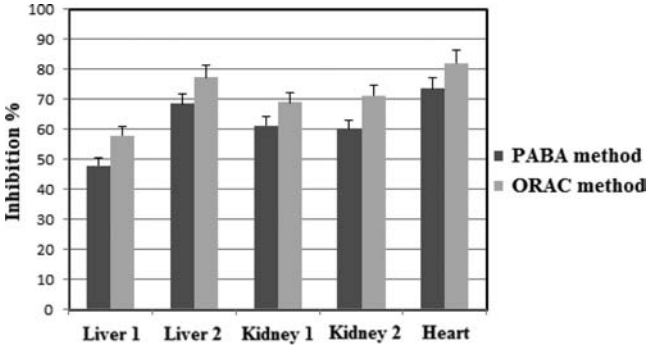

Figure 6. Inhibition percentage of some tissue homogenates calculated with the PABA method in comparison to the classical ORAC method (1:50 diluted homogenate). Data are presented as the mean ± SD (error bars) ($N = 3$) ($p = 0.05$; $F_{exp} = 0.584$; $F_{crit(table)} = 7.709$; and $F_{exp} < F_{crit(table)}$).

Because the existing ROO• scavenging assays require much labor and strictly optimized conditions, new assay development using the PABA probe may be useful for more comparable applications in food and biochemical research. ORAC as the most widely used PRS measurement assay has used two probes since it was first launched. The initial probe, β-PE, showed variable performance from one production cycle to another, undesired photobleaching, and non-specific protein binding to polyphenols. Thus, it was replaced with FL, but this latter probe showed rather high ORAC values, some photobleaching and undesired side reactions, and inconsistent findings with thiols. As alternative peroxyl scavenging measurement methods, TRAP uses a lag phase detection of antioxidants, but not all antioxidants possess a lag phase, giving rise to difficulties in comparison of end-point detection. The less frequently used crocin bleaching assay suffers from the initial color of crocin in the presence of other carotenoids and colored compounds, and there are no standard formats for expressing results.[39] In regard to redox potential data, the new PABA probe is expected to be more specific for ROO•, because the R-PE and β-PE protein probes of TRAP and ORAC assays, respectively, have been claimed to respond to more than one ROS. Moreover, PABA responds relatively quickly (i.e., within 30 min) to ROO• scavengers, such as cysteine, in reaching a plateau of fluorescence intensity, whereas the classical ORAC assay generally requires longer times for completion of the oxidation reaction for most antioxidants. It is envisaged that future research in HAT-based antioxidant assays (preferentially showing comparable results to those of one or more ET-based assays) should be directed to the design of "turn-on" fluorescence/absorbance probes for selectively detecting a given reactive species [ROS/reactive nitrogen species (RNS)] at a time. It is also preferable to develop probes not affected from side reactions with compounds not having genuine antioxidant status.

AUTHOR INFORMATION

Corresponding Author

*Telephone: +90-212-473-7070/17627. Fax: +90-212-473-7180. E-mail: mozyurek@istanbul.edu.tr.

Funding

Gülşah Kıbrıslıoğlu thanks the Istanbul University Research Fund, Bilimsel Arastirma Projeleri (BAP) Yurutucu Sekreterligi, for the support given to her M.Sc. Thesis Project 29739 and Istanbul University, Institute of Pure and Applied Sciences (I.U. Fen Bilimleri Enstitüsü), for the support given to her M.Sc. thesis work with the title: "Development of Spectrofluorometric Methods for Measurement of Peroxyl Radical Scavenging Activity in Biological Samples". The authors express their

gratitude to T. R. Ministry of Development for the Advanced Research Project of Istanbul University (2011K120320).

Notes

The authors declare no competing financial interest.

REFERENCES

(1) MacDonald-Wicks, L. K.; Wood, L. G.; Garg, M. L. Methodology for the determination of biological antioxidant capacity *in vitro*: A review. *J. Sci. Food Agric.* **2006**, *86*, 2046−2056.
(2) Halliwell, B.; Murcia, M. A.; Chirico, S.; Aruoma, O. I. Free radicals and antioxidants in food and *in vivo*: What they do and how they work. *Crit. Rev. Food Sci. Nutr.* **1995**, *35*, 7−20.
(3) Laguerre, M.; Lecomte, J.; Villeneuve, P. Evaluation of the ability of antioxidants to counteract lipid oxidation: Existing methods, new trends and challenges. *Prog. Lipid Res.* **2007**, *46*, 244−282.
(4) Roginsky, V.; Lissi, E. A. Review of methods to determine chain-breaking antioxidant activity in food. *Food Chem.* **2005**, *92*, 235−254.
(5) Lussignoli, S.; Fraccaroli, M.; Andrioli, G.; Brocco, G.; Bellavite, P. A microplate-based colorimetric assay of the total peroxyl radical trapping capability of human plasma. *Anal. Biochem.* **1999**, *269*, 38−44.
(6) Valkonen, M.; Kuusi, T. Spectrophotometric assay for total radical-trapping antioxidant potential in human serum. *J. Lipid Res.* **1997**, *38*, 823−833.
(7) Cabrini, L.; Barzanti, B.; Cipollone, M.; Fiorentini, D.; Grossi, G.; Tolomelli, B.; Zambonin, L.; Landi, L. Antioxidants and total peroxyl radical-trapping ability of olive and seed oils. *J. Agric. Food Chem.* **2001**, *49*, 6026−6032.
(8) Handelman, G. J.; Cao, G.; Walter, M. F.; Nightingale, Z. D.; Paul, G. L.; Prior, R. L.; Blumberg, J. B. Antioxidant capacity of oat (*Avena sativa* L.) extracts. 1. Inhibition of low-density lipoprotein oxidation and oxygen radical absorbance capacity. *J. Agric. Food Chem.* **1999**, *47*, 4888−4893.
(9) Niki, E. Free radical initiators as source of water- or lipid-soluble peroxyl radicals. *Methods Enzymol.* **1990**, *186*, 100−108.
(10) Yeum, K.-J.; Russell, R. M.; Krinsky, N. I.; Aldini, G. Biomarkers of antioxidant capacity in the hydrophilic and lipophilic compartments of human plasma. *Arch. Biochem. Biophys.* **2004**, *430*, 97−103.
(11) Glazer, A. N. Phycoerythrin fluorescence-based assay for reactive oxygen species. *Methods Enzymol.* **1990**, *186*, 161−168.
(12) Cao, G.; Alessio, H. M.; Cutler, R. G. Oxygen-radical absorbance capacity assay for antioxidants. *Free Radical Biol. Med.* **1993**, *14*, 303−311.
(13) Huang, D.; Ou, B.; Prior, R. L. The chemistry behind antioxidant capacity assays. *J. Agric. Food Chem.* **2005**, *53*, 1841−1856.
(14) Ou, B.; Hampsch-Woodill, M.; Prior, R. L. Development and validation of an improved oxygen radical absorbance capacity assay using fluorescein as the fluorescent probe. *J. Agric. Food Chem.* **2001**, *49*, 4619−4626.
(15) Apak, R.; Gorinstein, S.; Böhm, V.; Schaich, K. M.; Özyürek, M.; Güçlü, K. Methods of measurement and evaluation of natural antioxidant capacity/activity. *Pure Appl. Chem.* **2013**, *85*, 957−998.
(16) Huang, D.; Ou, B.; Hampsch-Woodill, M.; Flanagan, J. A.; Deemer, E. K. Development and validation of oxygen radical absorbance capacity assay for lipophilic antioxidants using randomly methylated cyclodextrin as the solubility enhancer. *J. Agric. Food Chem.* **2002**, *50*, 1815−1821.
(17) Wayner, D. D. M.; Burton, G. W.; Ingold, K. U.; Locke, S. Quantitative measurement of the total peroxyl radical-trapping antioxidant capability of human blood plasma by controlled peroxidation: The important contribution made by plasma proteins. *FEBS Lett.* **1985**, *187*, 33−37.
(18) Bors, W.; Michel, C.; Saran, M. Inhibition of bleaching of the carotenoid crotin, a rapid test for quantifying antioxidant activity. *Biochim. Biophys. Acta* **1984**, *796*, 312−319.
(19) Koppenol, W. H. Oxyradical reactions: From bond-dissociation energies to reduction potentials. *FEBS Lett.* **1990**, *264*, 165−167.
(20) Kotkar, R. M.; Srivastava, A. K. Voltammetric determination of *para*-aminobenzoic acid using carbon paste electrode modified with macrocyclic compounds. *Sens. Actuators, B* **2006**, *119*, 524−530.
(21) Buettner, G. R. The pecking order of free radicals and antioxidants: lipid peroxidation, α-tocopherol, and ascorbate. *Arch. Biochem. Biophsy.* **1993**, *300*, 535−543.
(22) Urano, Y.; Kamiya, M.; Kanda, K.; Ueno, T.; Hirose, K.; Nagano, T. Evolution of fluorescein as a platform for finely tunable fluorescence probes. *J. Am. Chem. Soc.* **2005**, *127*, 4888−4894.
(23) Gomes, A.; Fernandes, E.; Lima, J. L. F. C. Fluorescence probes used for detection of reactive oxygen species. *J. Biochem. Biophys. Methods* **2005**, *65*, 45−80.
(24) Alía, M.; Horcajo, C.; Bravo, L.; Goya, L. Effect of grape antioxidant dietary fiber on the total antioxidant capacity and the activity of liver antioxidant enzymes in rats. *Nutr. Res. (N. Y., NY, U. S.)* **2003**, *23*, 1251−1267.
(25) Szoke, A.; Hayton, W. L.; Schultz, I. R. Quantification of benzocaine and its metabolites in channel catfish tissues and fluids by HPLC. *J. Pharm. Biomed. Anal.* **1997**, *16*, 69−75.
(26) Miller, J. C.; Miller, J. N. *Statistics for Analytical Chemists*, 3rd ed.; Ellis Horwood and Prentice Hall: New York, 1993.
(27) Shaw, A. A.; Wainschel, L. A.; Shetlar, M. D. The photochemistry of *p*-aminobenzoic acid. *Photochem. Photobiol.* **1992**, *55*, 647−656.
(28) Allen, J. M.; Engenolf, S.; Allen, S. K. Rapid reaction of singlet molecular oxygen ($^1O_2$) with *p*-aminobenzoic acid (PABA) in aqueous solution. *Biochem. Biophys. Res. Commun.* **1995**, *212*, 1145−1151.
(29) Zulueta, A.; Esteve, M. J.; Frigola, A. ORAC and TEAC assays comparison to measure the antioxidant capacity of food products. *Food Chem.* **2009**, *114*, 310−316.
(30) Halliwell, B. Albumin—An important extracellular antioxidant? *Biochem. Pharmacol.* **1988**, *37*, 569−571.
(31) Mezyk, S. P. Direct rate constant measurement of radical disulphide anion formation for cysteine and cysteamine in aqueous solution. *Chem. Phys. Lett.* **1995**, *235*, 89−93.
(32) Walker, R. B.; Everette, J. D. Comparative reaction rates of various antioxidants with ABTS radical cation. *J. Agric. Food Chem.* **2009**, *57*, 1156−1161.
(33) Aruoma, O. I.; Halliwell, B.; Hoey, B. M.; Butler, J. The antioxidant action of taurine, hypotaurine and their metabolic precursors. *Biochem. J.* **1988**, *256*, 251−255.
(34) Ghiselli, A.; Serafini, M.; Maiani, G.; Azzini, E.; Ferro-Luzzi, A. A fluorescence-based method for measuring total plasma antioxidant capability. *Free Radical Biol. Med.* **1995**, *18*, 29−36.
(35) Pérez-Jiménez, J.; Saura-Calixto, F. Effect of solvent and certain food constituents on different antioxidant capacity assays. *Food Res. Int.* **2006**, *39*, 791−800.
(36) Suzuki, N.; Kochi, M.; Wada, N.; Mashiko, S.; Nomoto, T.; Yoda, B. Antioxidative activity of amino acids and sulfur-containing compounds to superoxide: measurement by quenching the chem-iluminescence of a cypridina luciferin analogue. *Biosci., Biotechnol., Biochem.* **1992**, *56*, 409−411.
(37) Güngör, N.; Özyürek, M.; Güçlü, K.; Demirci Cekic, S.; Apak, R. Comparative evaluation of antioxidant capacities of thiol-based antioxidants measured by different *in vitro* methods. *Talanta* **2011**, *83*, 1650−1658.
(38) Moreno, I.; Pichardo, S.; Jos, A.; Gomez-Amores, L.; Mate, A.; Vazquez, C. M.; Camean, A. M. Antioxidant enzyme activity and lipid peroxidation in liver and kidney of rats exposed to microcystin-LR administered intraperitoneally. *Toxicon* **2005**, *45*, 395−402.
(39) Prior, R. L.; Wu, X.; Schaich, K. Standardized methods for the determination of antioxidant capacity and phenolics in foods and dietary supplements. *J. Agric. Food Chem.* **2005**, *53*, 4290−4302.

substrate, also considering the clinical and experimental data reported above.

MATERIALS AND METHODS

Chemicals. The commercial sources of proteases were as follows: pepsin (from porcine gastric mucosa; EC 3.4.23.1; commercial code P6887), trypsin (from bovine pancreas; EC 3.4.21.4; commercial code T1426), chymotrypsin (from bovine pancreas; EC 3.4.21.1; commercial code C4129), and flavourzyme (from *Aspergillus oryzae*; EC 232.752.2; commercial code P6110) from Sigma-Aldrich (St. Louis, MO, USA), corolase PP (from porcine pancreas; EC 3.4.21.4; commercial code 89082) from AB Enzymes (Darmstadt, Germany), and umamizyme (from *Aspergillus oryzae*; EC not specified; declared activity of 74.3 U/g) from Amano Enzyme Inc. (Nagoya, Japan). Amicon Ultra-0.5 filters (centrifuge tubes) were bought from Millipore (Billerica, MA, USA). HPLC-grade water was prepared with a Milli-Q purification system (Millipore). Bio-Safe Coomassie and Precision Plus Protein Standards Dual Color marker for SDS-PAGE were from Biorad (Biorad Laboratories Inc., Hercules, CA). All other chemicals (reagents and solvents) were from Sigma-Aldrich.

Sampling. Lupin seeds of the species *L. albus* (cultivar Ares) were provided by Terrena (Matrignè-Ferchaud, France), *L. angustifolius* (cultivar Boregine) by Fraunhofer institute IVV (Freising, Germany), and *L. luteus* (cultivar Mister) by Prof. Biagina Chiofalo (University of Messina, Messina, Italy).

TPE Preparation. The total protein extracts (TPEs) of the lupin seeds were obtained as previously reported[17] and stored at −20 °C. Briefly, proteins were extracted from defatted flour with 100 mM Tris-HCl/0.5 M NaCl buffer, pH 8.2, for 2 h at 4 °C. The solid residue was eliminated by centrifugation at 6500*g* for 20 min at 4 °C, and the supernatant was dialyzed against 100 mM Tris-HCl buffer, pH 8.2, for 24 h at 4 °C. The protein content was assessed according to Bradford, using bovine serum albumin (BSA) as standard.[18]

Enzymatic Hydrolysis. TPEs were dissolved in Tris-HCl buffer 100 mM, pH 8. The pH value were adjusted to the optimal hydrolysis conditions for each enzyme with the addition of 1 M NaOH or 1 M HCl, if necessary. The enzymes were dissolved in appropriate solutions: 30 mM NaCl for pepsin, and 1 mM HCl for trypsin, chymotrypsin, and corolase PP. Umamizyme was added as a powder to the TPEs, whereas flavourzyme was a ready-to-use solution.

Both enzyme solutions and the umamizyme powder were directly added to the TPE solutions. Reaction mixtures were incubated at a fixed temperature for different reaction times. For the two-stage digestion with pepsin + trypsin, TPEs were initially incubated with pepsin at pH 2 for 4 h, the pH was adjusted to 8 with 1 M NaOH, and trypsin was added to the reaction mixture.

Finally, pepsin was inactivated by adjusting the pH to 7 with 1 M NaOH, whereas all other enzymes were inactivated by heating the solutions at 100 °C for 10 min. Then the solutions were cooled and stored at −20 °C.

SDS-PAGE. Drawings were taken at various intervals and analyzed by SDS-PAGE. They were separated on 15% SDS-polyacrylamide gel using Mini Protean 3 Cell (Biorad Laboratories Inc., Hercules, CA). Electrophoresis was performed at a constant voltage of 80 V for stacking and 120 V for separation. Gels were stained with Bio-Safe Coomassie (Biorad), scanned with Versa Doc 3000 (Biorad), and analyzed with Quantity One 4.6.8 Software (Biorad).

Ultrafiltration. After the hydrolysis, all low-molecular-weight peptides were separated from intact enzymes, proteins, and high-molecular-weight polypeptides by ultrafiltration through 3000 Da cutoff centrifuge filters (Amicon Ultra-0.5, Millipore, Billerica, MA, USA) at 12000*g* for 30 min at 4 °C. The permeates were then stored at −20 °C.

Determination of Peptide Concentration. The peptide concentration in the hydrolyzed samples was measured according to literature methods[19,20] based on chelating the peptide bonds by Cu(II) in alkaline media and monitoring the change of absorbance at 330 nm. In brief, a solution of X μL peptide mixture, (500 − X) μL of water, 500 μL of 6% (w/w) NaOH in water, and 50 μL of active reagent (containing 0.6 M sodium citrate, 0.9 M sodium carbonate, and 0.07 M copper sulfate, 2.4 M NaOH, pH 10.6) was prepared. The reaction mixture was carefully mixed, incubated for 15 min at 20 °C, and then the absorbance was measured at 330 nm. A sterile solution of peptone from casein at 10 mg/mL in water was used as standard for the calibration curve; the assay is linear in the range 100−1000 μg of peptides in cuvette.

ACE-Inhibitory Activity Assay. After hydrolysis and filtration, all samples were tested for determining their ACE-inhibitory activity, as recently reported.[16] Briefly, 100 μL of 2.5 mM hippuryl-histidyl-leucine (HHL) in buffer 1 (100 mM Tris-HCOOH, 300 mM NaCl pH 8.3) was mixed with 30 μL of sample in buffer 1 at different concentrations. Usually, six concentrations were used for each sample, and each solution was tested twice. Samples were preincubated at 37 °C for 15 min, then 15 μL of ACE solution, corresponding to 3 mU of enzyme in buffer 2 (100 mM Tris-HCOOH, 300 nM NaCl, 10 μM $ZnCl_2$, pH 8.3), were added; samples were incubated for 60 min at 37 °C. The reaction was stopped with 125 μL of 0.1 M HCl. The aqueous solution was extracted twice with 600 μL of ethyl acetate; the solvent was evaporated at 95 °C and the residue was dissolved in 500 μL of buffer 1 and then analyzed by HPLC.

HPLC analyses were performed with a HPLC 1200 series equipped with an autosampler (Agilent Technologies, Santa Clara, US) with a Lichrospher 100, C18 column (4.6 mm × 250 mm, 5 μm; Grace, Italy) using water and acetonitrile as solvent and following the gradient: 0 min 5% acetonitrile, 10 min 60% acetonitrile, 12 min 60% acetonitrile, 15 min 5% acetonitrile. Injection volume was 10 μL, wavelength 228 nm, flow 0.5 mL/min. The evaluation of ACE inhibition was based on the comparison between the concentrations of HA (hippuric acid) in the presence or absence of an estimated inhibitor. The phenomenon of autolysis of HHL to give HA was evaluated by a reaction blank, i.e., a sample with the higher evaluated inhibitor concentration and without the enzyme. The percentage of ACE inhibition was computed considering the area of HA peak with the following formula:

$$\%\ \text{ACE inhibition} = \left[\frac{(A_{IB} - A_N)}{(A_{IB} - A_{RB})}\right] \times 100$$

where A_{IB} is the area of HA in inhibitor blank (IB) sample (i.e., sample with enzyme but without any estimated inhibitor), A_N is the area of HA in the *n* samples containing different amounts of the estimated inhibitor (in our case the hydrolyzate), and A_{RB} is the area of HA in the reaction blank (RB) sample (i.e., sample without enzyme and with the estimated inhibitor at the highest concentration).

The percentages of ACE inhibition were plotted vs the peptide concentrations. When the maximum ACE-inhibition concentration was over 50%, the percentages of ACE-inhibition were plotted vs the $\log_{10}$ peptide concentrations obtaining a sigmoid curve. This curve permitted to calculate the inhibitory concentration 50% (IC_{50}), i.e., the concentration needed to observe a 50% inhibition of ACE activity. The IC_{50} values were obtained testing independently each sample three times and are expressed as mean value ± standard deviation. The most active peptides have the lowest IC_{50} values.

Statistical Analysis. Statistical analyses were performed with Statgraphics Plus (version 2.1 for Windows). The data were evaluated using one-way analysis of variance followed by Fisher's least significant difference (LSD) procedure; values with different letters are significantly different for $p < 0.05$.

RESULTS AND DISCUSSION

In a preliminary part of the present investigation, we tested the total protein extract from the seeds of *L. albus* before hydrolysis. As expected, it resulted to be inactive as ACE-inhibitor, according to literature.[13,21] In fact, owing to the dimension of the active site of the enzyme, the interaction may take place only when bioactive peptides are released from the parent protein by enzymatic or hydrolytic reactions, such as digestion, or industrial processing, such as fermentation.

Preparation of Enzymatic Hydrolyzates. The first part of the experimental work was devoted to establish the best reaction conditions for each proteolytic enzyme. Drawings were taken at various intervals and analyzed by SDS-PAGE in order to evaluate the hydrolysis efficiency, changing the following parameters: enzyme/substrate (E/S) ratio, pH, temperature, and reaction time. In the case of pepsin, the best pH was 2, the temperature 37 °C, the E/S ratio 1/100, and 18 hours were necessary to complete the reaction. Figure 1a shows the SDS-PAGEs of the drawings of the hydrolysis of *L. albus* (A) and *L. luteus* (L) proteins collected immediately after the enzyme addition (A_0 and L_0), after 1 h (A_{1h} and L_{1h}), and after 18 h (A_{18h} and L_{18h}).

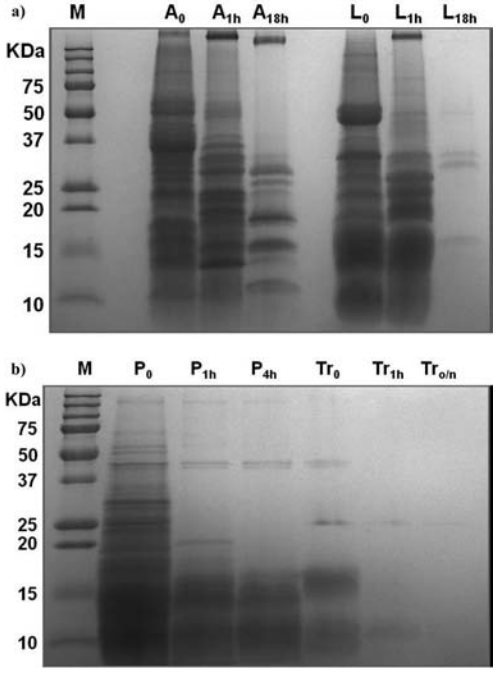

Figure 1. SDS-PAGE obtained after digestion of: a) *Lupinus albus* (A) and *Lupinus luteus* (L) proteins with pepsin, at 37 °C with enzyme/substrate (E/S) ratio 1/100; drawings collected immediately after enzyme addition (A_0 and L_0), after 1 h (A_{1h} and L_{1h}), and after 18 h (A_{18h} and L_{18h}). b) *Lupinus angustifolius* proteins digested with pepsin + trypsin drawings collected immediately after pepsin addition (P_0), after 1 h (P_{1h}), after 4 h (P_{4h}), immediately after trypsin addition (Tr_o), after 1 h (Tr_{1h}), after 24 h (overnight, $Tr_{o/n}$). M is the marker.

In general, the optimal conditions for using trypsin are 37 °C and pH 7−8; in our experience, the best pH value for hydrolyzing lupin proteins is 8. With an E/S ratio of 1/100, the digestion was complete after 18 h. The same conditions were used also for chymotrypsin. The double digestion with the sequence pepsin + trypsin was performed treating with pepsin at pH 2 for 4 h and then, after changing the pH value to 8, adding trypsin and incubating for 24 h. Figure 2b shows the SDS-PAGE of the two-step digestion.

For corolase PP digestion, better results were obtained by changing the E/S ratio to 1/50. For flavourzyme and umamizyme, several changes were performed; the reaction time was extended to 24 h and the E/S ratio was changed to 1/20 because both 1/50 and 1/100 ratios were ineffective. In addition, the incubation temperatures were increased to 45 and 60 °C, respectively. Table 1 reports the final conditions used for producing the samples used in the following experimentations.

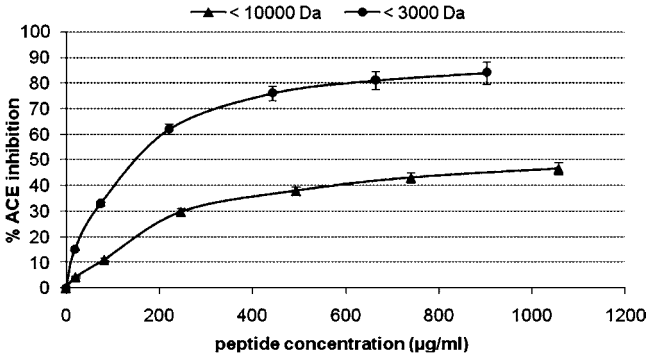

Figure 2. Total protein extract of *Lupinus albus* seed digested with pepsin: comparison between the ACE inhibition curves obtained filtering with 10000 and 3000 Da cutoff membranes.

Table 1. Optimized Parameters for the Hydrolysis of the Lupin Total Protein Extract: Enzyme, pH, Temperature (°C), Enzyme/Substrate Ratio (E/S ratio), and Time (h)

enzyme	pH	temperature (°C)	E/S ratio (w/w)	time (h)
pepsin	2	37	1/100	18
trypsin	8	37	1/100	18
chymotrypsin	8	37	1/100	18
corolase PP	8	37	1/50	18
umamizyme	7	45	1/20	24
flavourzyme	7	60	1/20	24

After the digestion, the samples were ultrafiltered in order to separate low-molecular-weight peptides from high-molecular ones and intact enzymes.

To select the best filtration conditions for maximizing the ACE-inhibitory activity, the digested mixture obtained by hydrolyzing *L. albus* protein with pepsin was ultrafiltered either with 10000 or 3000 Da cutoff membranes. Figure 2 shows two ACE inhibition curves obtained by plotting the peptide concentration vs the percentage ACE-inhibition for the samples with molecular weight (MW) lower than 3000 or 10000 Da, respectively. Whereas the latter sample did not reach the 50% ACE-inhibition even at the highest tested concentration (1110 μg/mL), the former, having molecular weight less than 3000 Da, was much more active, showing a 87% ACE-inhibition at the concentration of 893 μg/mL. A possible explanation is that the sample having MW lower than 10000 Da contains numerous inactive peptides (with MW in the range 3000 and 10000 Da), which decrease the concentration of the active peptides. Low MW peptides, usually under 3000 Da, are known as ACE-inhibitors in vivo because they can be absorbed at gut level.[21] After these results, all subsequent experimentation was performed on hydrolyzed mixtures filtered through a 3000 Da cutoff membrane.

Evaluation of ACE-Inhibitory Activity. The ACE-inhibitory activity assays were performed after having equalized the peptide concentrations of all samples. The peptide concentration was determined by using a literature colorimetric assay optimized for peptides.[19,20] In our opinion, the evaluation of the peptide concentrations and their equalization before performing the ACE-inhibitory test are of outmost importance in order to get a reliable comparison of their activities.

The results of the ACE inhibition assays (maximum percentage of ACE inhibition and IC_{50} value) of the peptide mixtures from *L. albus*, *L. angustifolius*, and *L. luteus* are reported in Tables 2, 3, and 4, respectively.

dx.doi.org/10.1021/jf4039056 | J. Agric. Food Chem. 2014, 62, 1846−1851

Table 2. Results of ACE Inhibition Assay for *Lupinus albus* Proteins: Digestion Enzyme, Highest Inhibitor Concentration (μg/mL), Maximum ACE Inhibition (%), and IC_{50} Value (μg/mL)[a]

enzyme	highest inhibitor concentration (μg/mL)	max ACE inhibition (%)	IC_{50} (μg/mL)
pepsin	856	76 ± 6.3	197 ± 1.6a
trypsin	939	67 ± 4.3	427 ± 16.8c
pepsin + trypsin	908	84 ± 2.5	205 ± 4.5a
chymotrypsin	989	73 ± 3.0	301 ± 4.8b
corolase PP	1039	60 ± 4.7	488 ± 42.8c
umamizyme	1066	58 ± 2.6	1053 ± 77.8e
flavourzyme	1037	51 ± 0.6	930 ± 3.71d

[a]IC_{50} values are reported as mean value ± standard deviation of three independent experiments; values with different letters are significantly different ($p < 0.05$).

Table 3. Results of ACE Inhibition Assay for *Lupinus angustifolius* Proteins: Digestion Enzyme, Highest Inhibitor Concentration (μg/mL), Maximum ACE Inhibition (%), and IC_{50} Value (μg/mL)[a]

enzyme	highest inhibitor concentration (μg/mL)	max ACE inhibition (%)	IC_{50} (μg/mL)
pepsin	723	80 ± 3.9	185 ± 13.3a
trypsin	614	58 ± 3.2	446 ± 17.5b
pepsin + trypsin	1047	82 ± 3.2	210 ± 1.9a
chymotrypsin	894	79 ± 4.6	203 ± 5.9a
corolase PP	953	67 ± 2.3	470 ± 27.5b
umamizyme	990	53 ± 1.5	933 ± 0.7d
flavourzyme	1151	55 ± 2.8	827 ± 41.9c

[a]IC_{50} values are reported as mean value ± standard deviation of three independent experiments; values with different letters are significantly different ($p < 0.05$).

Table 4. Results of ACE Inhibition Assay for *Lupinus luteus* Proteins: Digestion Enzyme, Highest Inhibitor Concentration (μg/mL), Maximum ACE Inhibition (%), and IC_{50} Value (μg/mL)[a]

enzyme	highest inhibitor concentration (μg/mL)	max ACE inhibition (%)	IC_{50} (μg/mL)
pepsin	1014	84 ± 3.7	176 ± 2.3a
trypsin	999	72 ± 3.5	343 ± 28.1b
pepsin + trypsin	999	83 ± 4.0	181 ± 2.4a
chymotrypsin	1014	87 ± 4.3	136 ± 4.5a
corolase PP	896	66 ± 2.6	533 ± 5.7c
umamizyme	1232	67 ± 3.9	608 ± 64.1d
flavourzyme	1081	54 ± 3.8	1009 ± 33.0e

[a]IC_{50} values are reported as mean value ± standard deviation of three independent experiments; values with different letters are significantly different ($p < 0.05$).

IC_{50} values range from 136 μg/mL in the case of the *L. luteus* sample treated with chymotrypsin to 1053 μg/mL in the case of the *L. albus* sample treated with umamizyme.

Comparing the three species, generally, the effects of the enzymes on the three lupin species are comparable: pepsin, followed by pepsin + trypsin, and chymotrypsin samples give the lowest IC_{50} values, i.e., the highest ACE-inhibitory activities, whereas corolase PP gives intermediate IC_{50} values and umamizyme and flavourzyme give the least active samples (Tables 2, 3, 4).

Pepsin gives always peptide mixtures with the highest ACE-inhibitory activity, with a mean IC50 value among the three species of 186 ± 10 μg/mL. When a trypsin treatment follows the pepsin one, for mimicking the physiological digestion, the ACE inhibition does not improve, but instead slightly decreases (mean value 198 ±16 μg/mL), even if no significant differences are revealed towards pepsin digestion (same letter in the statistical analysis for each species in Tables 2, 3, 4). Also chymotrypsin gives samples with good ACE-inhibitory activities with a mean value of 213 ± 83 μg/mL. Lower activities were observed treating the proteins with trypsin and corolase PP, with mean IC50 values of 405 ± 54 μg/mL and 497 ± 32 μg/mL, respectively. The other two enzymes gave even less satisfactory results: umamizyme gave a mean IC50 value of 865 ± 230 μg/mL and flavourzyme of 922 ± 91 μg/mL.

Figure 3 enables a direct comparison of the three species. The statistical analysis indicates that the treatment of the proteins of the three lupin species with pepsin and corolase PP produces peptide mixtures whose activities do not depend on the species, whereas by treating with trypsin, pepsin + trypsin as well as with chymotrypsin, significant differences are observed, the peptides from *L. luteus* being the most active. Also with umamyzime, the peptides from *L. luteus* were significantly the most active, whereas the peptides from *L. angustifolius* were the best after proteolysis with flavourzyme.

The comparison of data from different papers is a complex task because the differences in the ACE-inhibitory activity may be related to several different causes such as the protein extraction procedure, the enzyme selected for the proteolysis, the parameters of the digestion process (substrate/enzyme ratio, pH, time, temperature), or the different analytical method used for the determination of the ACE-inhibitory activity.[22]

As already indicated in the introduction, very few data are available on ACE-inhibitory activity of lupin proteins. In a previous paper by our group, *L. albus* and *L. angustifolius* proteins were digested with pepsin showing an ACE-inhibitory activity similar to soybean and higher than other legumes (pea, common bean, lentils, chickpea).[16]

Bioactive peptides are usually formed by sequences of 3−20 amino acids encrypted within the primary sequence of proteins. During food processing, fermentation, and/or gastrointestinal digestion, they are released through proteolysis of the parent protein. Although the complexity of the tested hydrolyzates impairs their direct comparison, it is clear that the observed activities reflect the different specificities of the tested enzymes. Pepsin and chymotrypsin are specific endopeptidases, which mainly break the peptidic bonds involving hydrophobic and aromatic amino acids; for this reason they produce peptides having a hydrophobic and/or aromatic amino acid as terminal group, preferably, proline, tryptophan, phenylalanine, or tyrosine. These features are particularly suitable for interacting with the ACE catalytic site, thus permitting the inhibition.[21] Trypsin, instead, is a specific endopeptidase that cleaves mainly peptidic bonds involving basic amino acids.[23] Combining pepsin + trypsin in a two-stage process resulted in a small overall reduction of ACE-inhibitory activity. Possibly, the active peptides formed during the pepsin digestion are in part degraded by trypsin. The same explanation was proposed for other sequential enzymatic treatments impairing the ACE-inhibitory activity: in particular, the two-step digestion with

dx.doi.org/10.1021/jf4039056 | J. Agric. Food Chem. 2014, 62, 1846−1851

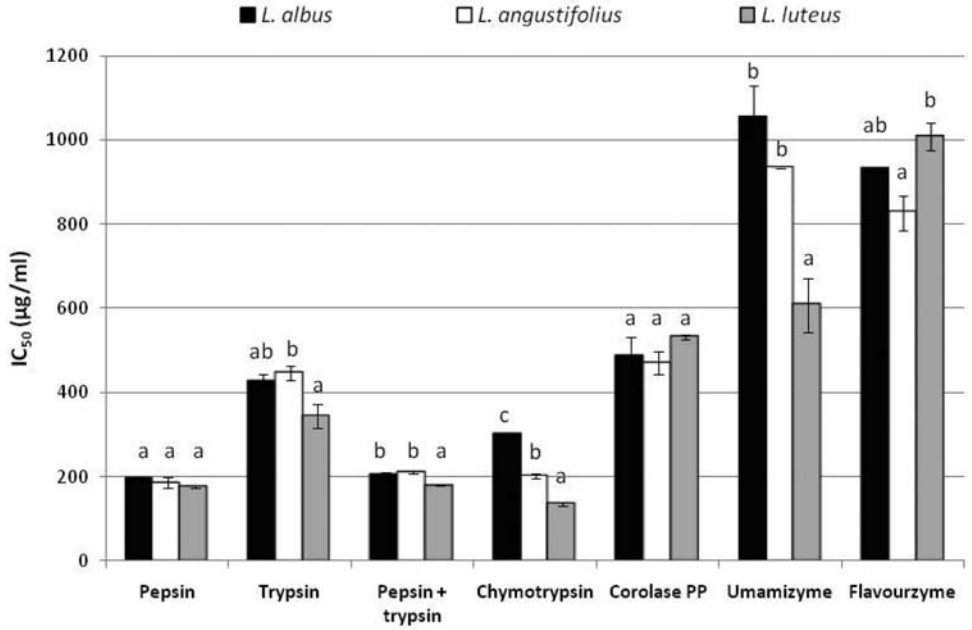

Figure 3. Comparison of mean values of ACE-inhibition IC_{50} values (expressed in μg/mL) of peptides mixtures obtained from *Lupinus albus*, *Lupinus angustifolius*, and *Lupinus luteus* proteins digested with pepsin, trypsin, pepsin + trypsin, chymotrypsin, corolase PP, umamizyme, and flavourzyme. Values with different letters are significantly different ($p < 0.05$).

alcalase and flavourzyme performed on common bean protein and chicken protein isolates.[24,25]

Corolase PP, a patented enzymatic complex used to simulate the in vitro protein digestion in the intestinal tract, consists of a mixture of proteolytic enzymes from pig pancreas, containing trypsin and chymotrypsin, together with other aminopeptidases and carboxypeptidases. Its moderate ACE-inhibitory activity may be related to the absence of pepsin that seems to be the best enzyme to produce lupin peptides with good ACE-inhibitory activity. Obviously, this enzyme may give good results with other proteins; for example, satisfactory results were obtained on sea cucumber proteins digested with pepsin and subsequently with corolase PP.[26]

Flavourzyme and umamizyme are "generally recognized as safe" (GRAS) enzymes used in the food industry. They are food-grade fungal protease/peptidase complexes produced by submerged fermentation of a strain of *Aspergillus oryzae*, exhibiting both endoprotease and exopeptidase activities. They were tested with the final aim of a large-scale production of hydrolyzates to be used as food supplements production but did not provided useful results. In the literature, flavourzyme digestion was applied to cowpea proteins, giving peptides with IC_{50} values in the large range 0.04−170.6 μg/mL and to rapeseed protein producing peptides with an ACE-inhibitory activity of about 50%.[27,28] Moreover a double digestion with alcalase/flavourzyme on two different chickpea varieties gave peptide mixtures with IC_{50} values of 316 and 228 μg/mL, while on yellow pea proteins gave an IC_{50} value of 412 μg/mL.[22] Umamizyme was used to digest canola meal proteins, giving peptide mixtures with low ACE-inhibitory activity.[29] Unfortunately, with lupin proteins, they give lower ACE-inhibitory activity than the other tested enzymes.

In conclusion, this investigation confirms that lupin seed may be a valuable source of ACE-inhibitory peptides, possibly explaining the activity observed in experimental and clinical studies.[5−8] This may foresee their future applications into either functional foods or dietary supplements.

Of course, this is only a first step in the study of ACE-inhibitory activity of lupin peptides because other studies are necessary to determine their stability and bioavailability. In fact, an open question is their capability to survive to the gastrointestinal digestion and to be absorbed in order to reach the bloodstream in their active form. Indeed, the literature shows that peptides from other food sources (for example milk) are systemically distributed.[21,30] The problem could be overcome also by using new emerging technologies, such as micro- or nanoencapsulation, that may offer feasible solutions for improving the stability of peptides in various food products and during digestion.[21,30] The bioavailability of ACE-inhibitory peptides may also be increased by cross-linking the target peptide to protein transduction domains or by means of specific peptide carriers able to deliver biologically active peptides into cells. Moreover, peptide permeation may be achieved by chemical enhancers and surfactant-like agents.[31] Finally, further studies are needed to determine the composition of active peptide mixtures, to isolate the peptide(s) responsibles for ACE-inhibitory activity, and to confirm their activity through in vitro and in vivo studies.

AUTHOR INFORMATION

Corresponding Author

*Phone: +39-02-50318210. Fax: +39-02-50318202. E-mail: giovanna.boschin@unimi.it.

Notes

The authors declare no competing financial interest.

ACKNOWLEDGMENTS

We are grateful to Mariantonietta Loredana Mesce for her precious help in experimental work, Biagina Chiofalo for *L. luteus* seeds, the Fraunhofer Institute IVV for *L. angustifolius* seeds, Terrena for *L. albus* seeds, AB enzymes for the gift of corolase PP, Giovanna Speranza for the gift of umamizyme and

flavourzyme, and Andrea Meregaglia for enzymatic digestions advices.

■ ABBREVIATIONS USED

ACE, angiotensin-converting enzyme; BSA, bovine serum albumin; E/S, enzyme/substrate ratio; HA, hippuric Acid; HHL, hippuryl-histidyl-leucine; HL, histidyl-leucine; IC_{50}, inhibitory concentration 50%; MW, molecular weight; PP, from porcine pancreas; SDS-PAGE, sodium dodecyl sulfate−polyacrylamide gel electrophoresis; TPE, total protein extract

■ REFERENCES

(1) Sujak, A.; Kotlarz, A.; Strobel, W. Compositional and nutritional evaluation of several lupin seeds. *Food Chem.* **2006**, *98*, 711−719.
(2) Boschin, G.; Arnoldi, A. Legumes are valuable sources of tocopherols. *Food Chem.* **2011**, *127*, 1199−1203.
(3) Boschin, G.; D'Agostina, A.; Annicchiarico, P.; Arnoldi, A. Effect of genotype and environment on fatty acid composition of *Lupinus albus* L. seed. *Food Chem.* **2008**, *108*, 600−606.
(4) Boschin, G.; Annicchiarico, P.; Resta, D.; D'Agostina, A.; Arnoldi, A. Quinolizidine alkaloids in seeds of lupin genotypes of different origins. *J. Agric. Food Chem.* **2008**, *56*, 3657−3663.
(5) Pilvi, T. K.; Jauhiainen, T.; Cheng, Z. J.; Mervaala, E. M.; Vapaatalo, H.; Korpela, R. Lupin protein attenuates the development of hypertension and normalises the vascular function of NaCl-loaded Goto−Kakizaki rats. *J. Physiol. Pharmacol.* **2006**, *57*, 167−176.
(6) Novicka, G.; Klosiewicz-Latoszek, L.; Sirtori, C. R.; Arnoldi, A.; Naruszewicz, M. Lupin proteins in the treatment of hypercholesterolemia. *Atheroscler. Suppl.* **2006**, *7*, 477.
(7) Belski, R.; Mori, T. A.; Puddey, I. B.; Sipsas, S.; Woodman, R. J.; Ackland, T. R.; Beilin, L. J.; Dove, E. R.; Carlyon, N. B.; Jayaseena, V.; Hodgson, J. M. Effects of lupin-enriched foods on body composition and cardiovascular disease risk factors: a 12-month randomized controlled weight loss trial. *Int. J. Obes.* **2011**, *35*, 810−819.
(8) Lee, Y. P.; Mori, T. A.; Puddey, I. B.; Sipsas, S.; Ackland, T. R.; Beilin, L. J.; Hodgson, J. M. Effects of lupin kernel flour-enriched bread on blood pressure: a controlled intervention study. *Am. J. Clin. Nutr.* **2009**, *89*, 766−772.
(9) Aronow, W. S. Treatment of systemic hypertension. *Am. J. Cardiovasc. Dis.* **2012**, *2*, 160−170.
(10) Yang, H.-Y. T.; Erdos, E. G.; Levin, Y. Dipeptidyl carboxypeptidase that converts angiotensin I and inactivates bradykinin. *Biochim. Biophys. Acta, Protein Struct.* **1970**, *214*, 374−376.
(11) Nakamura, Y.; Yamamoto, N.; Sakai, K.; Takano, T. Antihypertensive effect of sour milk and peptides isolated from it that are inhibitors to angiotensin I-converting enzyme. *J. Dairy Sci.* **1995**, *78*, 1253−1257.
(12) Wu, J.; Ding, X. Characterization of inhibition and stability of soy-protein-derived angiotensin I-converting enzyme inhibitory peptides. *Food Res. Int.* **2002**, *35*, 367−375.
(13) Aluko, R. E. Determination of nutritional and bioactive properties of peptides in enzymatic pea, chickpea, and mung bean protein hydrolysates. *J. AOAC Int.* **2008**, *91*, 947−956.
(14) Guang, C.; Phillips, R. D. Plant food-derived angiotensin I converting enzyme inhibitory peptides. *J. Agric. Food Chem.* **2009**, *57*, 5113−5120.
(15) Roy, F.; Boye, J. I.; Simpson, B. K. Bioactive proteins and peptides in pulse crops: pea, chickpea and lentil. *Food Res. Int.* **2010**, *43*, 432−442.
(16) Boschin, G.; Scigliuolo, G. M.; Resta, D.; Arnoldi, A. ACE-inhibitory activity of enzymatic protein hydrolysates from lupin and other legumes. *Food Chem.* **2014**, *145*, 34−40.
(17) Brambilla, F.; Resta, D.; Isak, I.; Zanotti, M.; Arnoldi, A. A label-free internal standard method for the differential analysis of bioactive lupin proteins using nano HPLC-chip coupled with ion trap mass spectrometry. *Proteomics* **2009**, *9*, 272−286.
(18) Bradford, M. M. A rapid and sensitive method for the quantitation of microgram quantities of protein utilizing the principle of protein−dye binding. *Anal. Biochem.* **1976**, *72*, 248−254.
(19) Levashov, P. A.; Sutherland, D. S.; Besenbacher, F.; Shipovskov, S. A robust method of determination of high concentrations of peptides and proteins. *Anal. Biochem.* **2009**, *395*, 111−112.
(20) Goa, J. A micro biuret method for protein determination. Determination of total protein in cerebrospinal fluid. *Scand. J. Clin. Lab. Invest.* **1953**, *5*, 218−222.
(21) Vermeirssen, V.; van Camp, J.; Verstraete, W. Bioavailability of angiotensin I converting enzyme inhibitory peptides. *Br. J. Nutr.* **2004**, *92*, 357−366.
(22) Roberts, P. R.; Burney, J. D.; Black, K. W.; Zaloga, G. P. Effect of chain length on absorption of biologically active peptides from the gastrointestinal tract. *Digestion* **1999**, *60*, 332−337.
(23) Rui, X.; Boye, J. I.; Simpson, B. K.; Prasher, S. O. Angiotensin I-converting enzyme inhibitory properties of *Phaseolus vulgaris* bean hydrolysates: effects of different thermal and enzymatic digestion treatments. *Food Res. Int.* **2012**, *49*, 739−746.
(24) Pedroche, J.; Yust, M. M.; Giron-Calle, J.; Alaiz, M.; Millan, F.; Vioque, J. Utilisation of chickpea protein isolates for production of peptides with angiotensin I-converting enzyme (ACE)-inhibitory activity. *J. Sci. Food Agric.* **2002**, *82*, 960−965.
(25) Barbana, C.; Boye, J. I. Angiotensin I-converting enzyme inhibitory activity of chickpea and pea protein hydrolysates. *Food Res. Int.* **2010**, *43*, 1642−1649.
(26) Pérez-Vega, J. A.; Olivera-Castillo, L.; Gómez-Ruiz, J. Á.; Hernández-Ledesma, B. Release of multifunctional peptides by gastrointestinal digestion of sea cucumber (*Isostichopus badionotus*). *J. Funct. Foods* **2013**, *5*, 869−877.
(27) Segura Campos, M. R.; Chel Guerrero, L. A.; Betancur Ancona, D. A. Angiotensin-I converting enzyme inhibitory and antioxidant activities of peptide fractions extracted by ultrafiltration of cowpea *Vigna unguiculata* hydrolysates. *J. Sci. Food Agric.* **2010**, *90*, 2512−2518.
(28) He, R.; Alashi, A.; Malomo, S. A.; Girgih, A. T.; Chao, D.; Ju, X.; Aluko, R. E. Antihypertensive and free radical scavenging properties of enzymatic rapeseed protein hydrolysates. *Food Chem.* **2013**, *141*, 153−159.
(29) Wu, J.; Aluko, R. E.; Muir, A. D. Production of angiotensin I-converting enzyme inhibitory peptides from defatted canola meal. *Biores. Technol.* **2009**, *100*, 5283−5287.
(30) Korhonen, H. Milk-derived bioactive peptides: from science to applications. *J. Funct. Foods* **2009**, *1*, 177−187.
(31) Hong, F.; Ming, L.; Yi, S.; Zhanxia, L.; Yongquan, W.; Chi, L. The antihypertensive effect of peptides: a novel alternative to drugs? *Peptides* **2008**, *29*, 1062−1071.

MATERIALS AND METHODS

Materials. Quercetin dihydrate (90%) was purchased from VWR Scientific (Seattle, WA, USA). Polyoxyethylene (20) sorbitan monooleate (Tween 80), ethanol, ferric chloride ($FeCl_3 \cdot 6H_2O$), hydrochloric acid, AAPH (2,2′-azobis(2-amidinopropane) dihydrochloride), Trolox (6-hydroxy-2,5,7,8-tetramethylchroman-2-carboxylic acid), and methanol were purchased from Sigma-Aldrich Co. (St. Louis, MO, USA). Maltodextrin (MaltrinM100) was provided from Grain Processing Corp. (Muscatine, IA, USA). DPPH (1,1-diphenyl-2-picrylhydrazyl), TPTZ (2,4,6-tripyridyl-s-triazine), and sodium fluorescein were purchased from Fluka (Buchs, Switzerland). Milli-Q water (18.3 MΩ) was used in all experiments.

High-Pressure Homogenization Processing. Quercetin (0.5%, w/w) was dispersed in either water or water−Tween 80 mixtures and held on an oil bath for 20 min at 70 °C. The suspensions were subjected to premilling treatments to reduce quercetin particle sizes to the micrometer range by high-speed homogenization (HSH) (high-speed homogenizer, Ultra-Turrax T-25 basic, IKA Works Inc., Wilmington, NC, USA) at 24000 rpm for 5 min. After filtration (cellulose filters, 6 μm mesh, grade 3, Whatman), the mixture was kept on a magnetic stirrer overnight at room temperature. The next day, the water that was either evaporated or lost during filtration was reconstituted, and the samples were homogenized at 24000 rpm for an additional 5 min (the samples referred to as cycle 0). The quercetin suspensions were further homogenized by high-pressure homogenizer (HPH) (EmulsiFlex-C3, 90 Avestin Inc., Ottowa, Canada) at pressure levels ranging from 50 to 200 MPa and for up to 40 HPH cycles. The process temperature of HPH was kept constant at 25 °C.

Lyophilization. The quercetin nanosuspension was frozen at −20 °C overnight and lyophilized using a Freezone 4.5 freeze-dry system (Labconco, Kansas City, MO, USA).

Spray-Drying. Maltodextrin with a final concentration of 30% (w/w) was utilized as the carrier for quercetin, and powder was retrieved by a spray-drying technique applied with Yamato Pulvis Mini-Spray GA32 (Yamato Scientific Co., Ltd., Tokyo, Japan). Quercetin suspensions were passed at a spray rate of 4 mL/min, with inlet temperature and outlet temperature fixed at 200 and 120 °C, respectively. Dry air flow was set at 800 L/h, and the atomization pressure was set at 1.5 bar.

CHARACTERIZATION

Particle Size Measurements. Particle sizes of quercetin dispersions were measured by photon correlation spectroscopy (PCS) based BIC 90 plus particle size analyzer equipped with a Brookhaven BI-9000AT digital correlator (Brookhaven Instrument Corp., New York, NY, USA). The light source of the particle size analyzer is a solid state laser operating at 658 nm with 30 mW power, and the signals were detected by a high-sensitivity avalanche photodiode detector. All measurements were made at a fixed scattering angle of 90° and temperature of 25.0 ± 0.1 °C. The mean diameter, or z-diameter, was determined by cumulant analysis of the intensity−intensity autocorrelation function, $G(q,t)$.[19−23]

Solubility Test. Saturation solubility was measured through ultraviolet−visible (UV−vis) absorbance determination at 373 nm using a Cary Eclipse UV−vis spectrophotometer with a 1 cm optical path length. The suspensions prepared in water and Tween 80 solutions as described above were subjected to HPH process, and the samples were collected at predetermined pressures and cycles. Afterward, they were centrifuged for 10 min at 10000 rpm prior to analysis, and the upper phase was extracted with ethanol. All measurements were completed on the same day for each cycle at predetermined pressure. Quercetin concentration was determined by the calibration curve ($R^2 = 0.999$; $y = 0.069x - 0.041$) which was linear within the range of 2−15 ppm. It should be mentioned that the presence of residual fine solid particles, if not sedimented by the centrifugation method applied, may affect the UV−vis measurement. Nevertheless, particle size measurements after centrifugation showed that the mean sizes of residual solid particles dispersed in the liquid were always <300 nm for all tested samples.

Dissolution Rate Measurements. Dissolution rate shows how fast dried particles redisperse into submicrometer suspensions upon rehydration. Dried powder of maltodextrin-entrapped quercetin was prepared for dissolution experiments with a typical formulation of 0.5 g of powder in 5 mL of distilled water. The samples held in independent flasks were agitated at 140 rpm on an ital shaker for different time periods. At definite times, a flask was collected from the shaker, the content was filtered through Whatman no. 4 and centrifuged at 10000 rpm for 10 min, and supernatant was assayed through UV−vis absorbance determination at 373 nm.

Atomic Force Microscopy (AFM). The image of quercetin nanoparticles was collected by using a commercial Nanoscope IIIa Multi-Mode AFM (Veeco Instruments, Camaillo, CA, USA) equipped with a J scanner, which was operated in tapping mode using a silicon cantilever. The quercetin nanosuspension sample for AFM imaging was prepared by treating the mixture of 0.5% (w/w) quercetin in water with 20 cycles of high pressure homogenization at 150 MPa. A drop of quercetin submicrometer suspension was deposited on a precleaned silicon wafer surface and evaporated naturally.

Differential Scanning Calorimetry (DSC) Measurements. The thermal properties of HPH-treated quercetin powder were investigated in comparison to the thermal properties of pure quercetin, with DSC (model Q10, TA Instruments, New Castle, DE, USA). Powder samples were placed in aluminum sealed pans at an amount of 5−10 mg. The thermal analyses were performed, with a temperature scanning range from 25 to 400 °C and a heating rate of 10 °C/min. Nitrogen was used as blanket gas.

Antioxidant Activity Assays. All samples (0.5 g of HPH-treated and nontreated spray-dried powders) were dissolved in water (5 mL) and then centrifuged at 10000 rpm for 10 min, and supernatant was used for further antioxidant assays. Maltodextrin was used as blank.

2,2-Diphenyl-1-picrylhydrazyl Hydrate Free Radical Scavenging Activity Assay. The DPPH assay was done according to the method of Brand-Williams et al.,[24] with little modifications. DPPH solution (6×10^{-5} M) was prepared in methanol; 2.9 mL of DPPH solution was mixed with 100 μL of sample, and the reaction mixture was incubated in the dark at room temperature for 30 min. Absorbance was taken at 517 nm against blank solution. The radical scavenging activity was calculated using the following equation:

$$\text{scavenging activity (\%)} = \left(\frac{A_{\text{blank at 517 nm}} - A_{\text{sample at 517 nm}}}{A_{\text{blank at 517 nm}}} \right) \times 100 \quad (1)$$

Ferric Reducing/Antioxidant Power (FRAP) Assay. The FRAP assay was done according to the method of Benzie et al.,[25] with little modifications. The working solution was prepared by mixing 25 mL of acetate buffer (pH 3.6), 2.5 mL of 10 mM TPTZ solution in 40 mM HCl, and 2.5 mL of 20 mM ferric chloride solution. Three milliliters of working solution was mixed with 40 μL of sample. The increase in absorbance at

593 nm was measured after 4 min, and higher absorbance values indicate higher reduction ability of samples.

Oxygen Radical Antioxidant Capacity (ORAC) Assay. The ORAC procedure used an automated plate reader (Synergy HT Multi-Mode Microplate Reader; BioTek Instruments, Inc., Winooski, VT, USA) with 96-well plates.[26] Analyses were conducted in 75 mM phosphate buffer (pH 7.4) at 37 °C. Peroxyl radical was generated using AAPH, which was prepared fresh for each run. Fluorescein was used as the substrate. Fluorescence conditions were as follows: excitation was performed at 485 nm with a 20 nm bandpass, and emission was measured at 520 nm with a 25 nm bandpass. The plate reader was controlled by Gen5 Data Analysis software (BioTek Instruments, Inc.). The standard curve was linear between 0 and 100 mM Trolox. Results are expressed as micromoles of Trolox equivalents (TE) per gram of powder (μmol TE/g).

Briefly, AAPH (0.2069 g) was dissolved in 5 mL of 75 mM phosphate buffer (pH 7.4), and a fluorescein stock solution (4 μM) was made in 75 mM phosphate buffer (pH 7.4) and stored in foil at 4 °C. Immediately prior to use, the stock solution was diluted 1:50 with phosphate buffer. In all experimental wells, 150 μL of sodium fluorescein working solution was added. In addition, blank wells received 25 μL of 75 mM phosphate buffer (pH 7.4), whereas standards received 25 μL of Trolox dilution and samples received 25 μL of sample. The plate was then allowed to equilibrate by incubation for a minimum of 30 min at 37 °C. Reactions were initiated after pipetting each well with 25 μL of AAPH solution for a final reaction volume of 200 μL. The fluorescence was then monitored kinetically with data taken every minute for a duration of 120 min.[26]

Scanning Electron Microscopy (SEM). The morphology of pure nontreated quercetin crystals and lyophilized HPH-treated quercetin was observed using a scanning electron microscope (JSM-5410- SEM, Jeol Co., Japan). Prior to analysis, the samples were diluted with water to obtain a suitable concentration. Then, the samples were mounted onto separate, adhesive-coated aluminum pin stubs, dried naturally, and sputtered with gold. The SEM was operated at high vacuum with an accelerating voltage of 10 kV. Images were taken at 3500 magnification.

Statistical Analysis. All measurements were repeated at least three times using duplicate samples. Means and standard deviations were calculated from these measurements using Excel (Microsoft, Redmond, WA, USA).

RESULTS AND DISCUSSION

Effect of High-Pressure Conditions on Particle Size. The suspension of quercetin, surfactant, and water is forced through a valve having a narrow orifice under pressure. According to Bernoulli's equation, the flow volume of liquid in a closed system per cross section is constant. That means that when the liquid is in the homogenizer gap, the reduction in the diameter leads to a tremendous increase in the dynamic pressure and simultaneous decrease in static pressure to maintain constant energy. A liquid boils when its vapor pressure is equal to the air/static pressure of the environment. In the gap, the static pressure falls below the vapor pressure of water, causing the boiling of water at room temperature. This is followed by the formation of gas bubbles, which implode vigorously, and the cleavage along the drug crystal is caused by cavitation, fluid shear, and particle collision against each other. As the suspension leaves the gap, the pressure suddenly rises to normal air pressure again.[11,13,20,27]

Altough the implosion forces in this instantaneous progress are sufficiently high to break down the drug microparticles into nanoparticles, the energy generated in such a short time (generally within miliseconds) is not sufficient to break down all particles into uniform nanocrystals even at the higher applied pressures. The increased homogenization cycles provided more energy to break down the crystalline structure. Therefore, homogenization often is performed in 5, 10, or more cycles that depend on the hardness of the drug and the desired particle size.[11,18]

Figure 1 shows the effect of the number of cycles on the mean particle sizes and polydispersity of quercetin suspensions

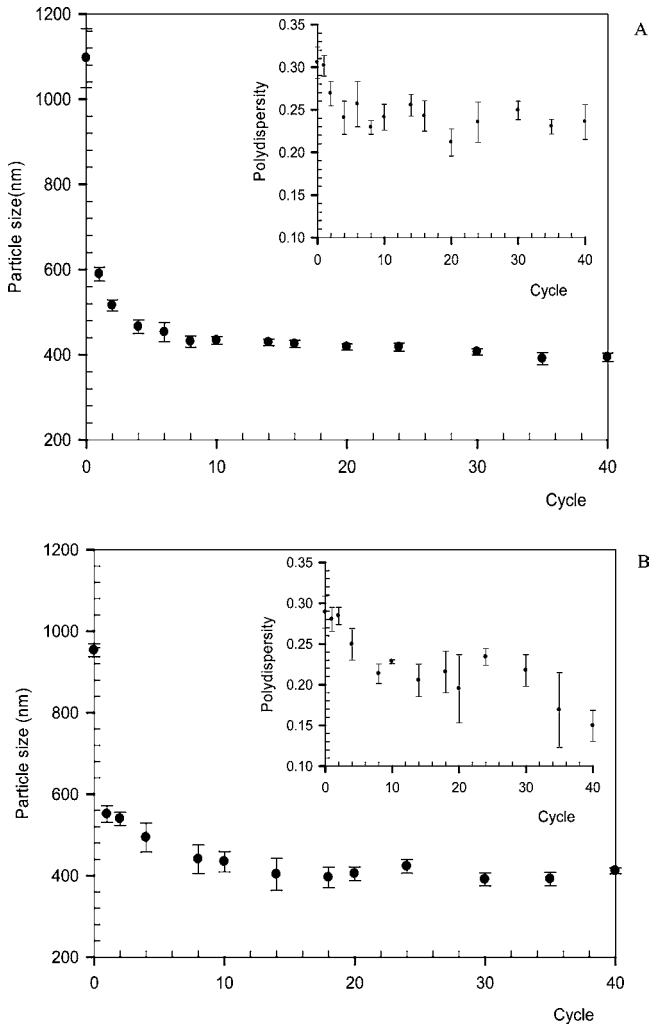

Figure 1. Change in particle size and polydispersity of quercetin in water (A) and in 1% Tween 80 (w/w) solution (B) as a function of HPH cycle. HPH pressure and processing temperature were fixed at 150 MPa and 25 °C, respectively. Duplicate samples were prepared, and the results are reported as the mean and standard deviation of three measurements made per sample.

at a fixed operating pressure of 150 MPa and 25 °C inlet temperature. The mean particle sizes of quercetin crystals in water and 1% Tween 80 (T80) solution (w/w) exhibited around 50% reduction after only two cycles. Reduction rate decreased with the following cycles and got a steady value (~430 nm) after 10 cycles. After that point, increasing the

dx.doi.org/10.1021/jf404065p | J. Agric. Food Chem. 2014, 62, 1852−1859

number of cycles did not change the particle size, which was in agreement with previous studies.[19,20] The polydispersity of samples reached a value of 0.2 for samples after around 10 cycles, but between cycles it showed fluctations, which could indicate a slightly reversible formation of aggregates that were disaggregated in the subsequent cycles (Figure 1).

Generally, the energy delivered into the system is proportional to the homogenization pressure, because higher pressure causes higher velocity of the fluid in the gap; as a result, static pressure will drop to a larger extent, leading to generation of more bubbles eventually to comminute the particles. Thus, it is anticipated that the higher the homogenization pressure, the smaller the particle size obtained as is observed in Figure 2.

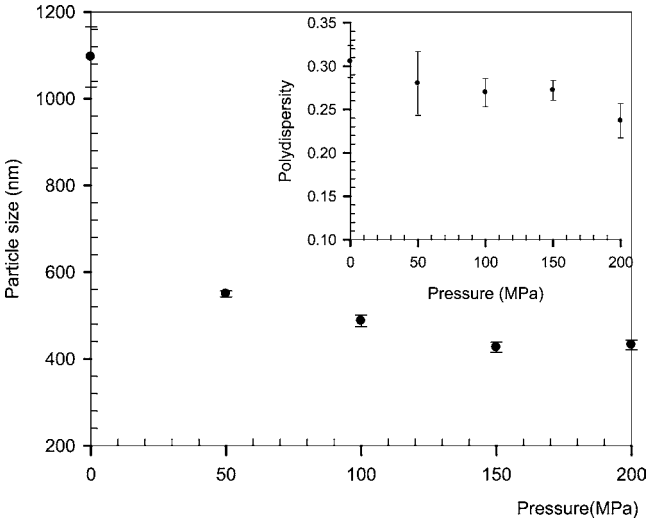

Figure 2. Change in particle size and polydispersity of quercetin in water as a function of homogenization pressure. HPH cycle and processing temperatures were fixed at 20 and 25 °C, respectively. Duplicate samples were prepared, and the results are reported as the mean and standard deviation of three measurements made per sample.

However, it should be noted that there is no linear relationship between increase in pressure and decrease in size. Because the HPH process breaks the particles/crystals preferentially at weaker points, that is, imperfections, and by decreasing the size, the number of imperfections becomes less and the remaining crystals become more perfect. If the force in the homogenizer is equal to the interaction forces in the crystal, the particles will not diminish further, even if additional cycles are applied. The force required to break down the crystals seems to increase rather exponentially with decreasing particle size.[27]

The smallest particle size achieved at the end of 30 cycles does not depend on the concentration of stabilizer (Table 1), but the polydispersity index of the system using Tween 80 has lower values, which indicates that having surfactant in the system provides fineness of particle (Figure 1). The role of surfactant in emulsion and suspension systems is theorotically different. In the case of emulsions, the stabilizer/surfactant reduces the interfacial tension between the oil and the water phase. Consequently, the required energy to produce nanoemulsion decreases because the energy is equal to surface area × interfacial tension. On the other hand, in a suspension, the main energy is utilized to break the crystal itself, which means overcoming the binding forces in the crystal lattice.

The presence of nanosized quercetin particles was confirmed by an AFM height image suggesting that most particles were

Table 1. Water Dispersity of HPH-Treated Quercetin Nanosuspensions in Different T80 Concentrations for Cycles 0 and 30 at 25 °C and 150 MPa Pressure

Tween 80 concn % (w/w)	quercetin dispersitiy in water (mg/L)	particle size (nm)	polydispersity
	Cycle 0		
0	2.4 ± 0.1	751.1 ± 28.3	0.31 ± 0.02
0.5	65.3 ± 0.5	657.1 ± 30.1	0.28 ± 0.02
1	135.5 ± 6.8	662.6 ± 27.2	0.24 ± 0.01
1.5	209.8 ± 1.8	651.6 ± 19.2	0.23 ± 0.01
2	270.5 ± 13.2	664.7 ± 18.1	0.27 ± 0.04
	Cycle 30		
0	7.3 ± 0.03	426.6 ± 11.8	0.27 ± 0.01
0.5	147.4 ± 6.2	424.3 ± 9.2	0.21 ± 0.02
1	204.8 ± 7.01	427.8 ± 18.1	0.23 ± 0.02
1.5	304.3 ± 3.8	430.6 ± 4.5	0.23 ± 0.02
2	302.1 ± 3.9	421.2 ± 11.2	0.22 ± 0.05

mainly irregularly shaped (Figure 3A). Panels B and C of Figure 3 show the SEM images of pure nontreated quercetin and lyophilized HPH-treated quercetin nanosuspension, respectively. Pure quercetin showed lack of particle size uniformity and relatively larger size. On the other hand, HPH-treated particles exhibited particle size uniformity and lack of larger needle-type crystalline structures.

Effect of High-Pressure Conditions on Water Dispersity. In general, the water solubility of a particle increases with a decrease of particle size because it causes a linear increase of the specific surface area, which is in an inverse relationship with the particle diameter. The relationship between particle size and water dispersity can be axplained by Ostwald−Freundlich theory[11,13]

$$\log \frac{C_s}{C_\infty} = \frac{2\sigma V}{2.303RT\rho r} \quad (2)$$

where C_s is the solubility, C_∞ is the solubility of the solid consisting of large particles, σ is the interfacial tension substance, V is the molar volume of the particle material, R is the gas constant, T is the absolute temperature, ρ is the density of the solid, and r is the radius. It is obvious that the solubility (C_s) of the drug increases with a decrease of particle size (r). However, this effect is pronounced for materials that have mean particle size of <1 μm.[11]

Another possible explanation for the enhancement in the solubility is the creation of high-energy surfaces when the drug microcrystals are disrupted to nanoparticles. Hence, by raising the interfacial area through particle size reduction, the transition among different polymorphic forms occurs.[19] The increase in water solubility of quercetin by increase in number of cycles and the level of pressure (Figures 4 and 5) can be explained by the application of higher energy during HPH processing to the quercetin system causing more transitions from crystal to amorphous phase; however, the DSC thermogram in Figure 6 shows the preservation of a part of crystal structure of original quercetin.

To further visualize the improved solubility of quercetin nanosuspension after HPH, photographs of quercetin suspensions prepared in water and in 1% Tween 80 (w/w) solution treated by 40 cycles of HPH at 150 MPa as well as nontreated quercetin (undissolved parts were removed by filtration) were taken and are presented in Figure 4. The nontreated quercetin suspension in water was nearly colorless; however, HPH

dx.doi.org/10.1021/jf404065p | J. Agric. Food Chem. 2014, 62, 1852−1859

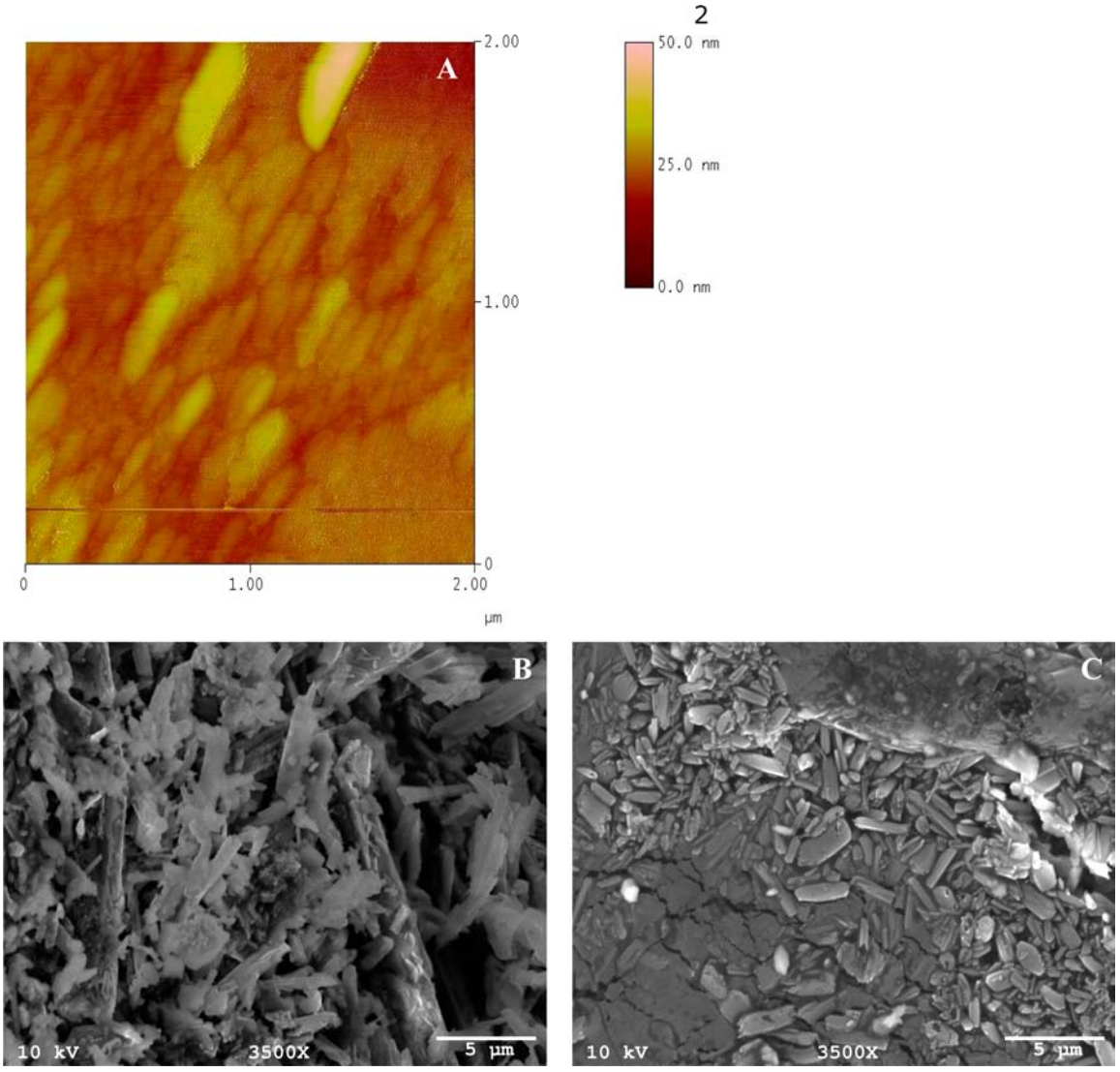

Figure 3. AFM height image (A) of HPH-treated quercetin nanosuspension deposited on a precleaned silicon surface; SEM images of pure quercetin (B) and lyophilized HPH-treated quercetin (C) nanosuspension. HPH was carried at 150 MPa for 20 cycles at 25 °C. Pictures were taken at ×3500 magnification.

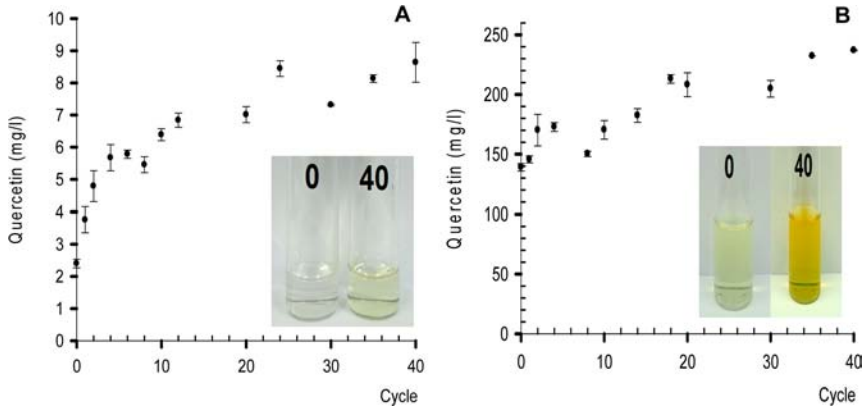

Figure 4. Water solubility of quercetin nanosuspensions in water (A) and in 1% T80 (w/w) solution (B) as a function of cycle at 150 MPa and 25 °C. Photographs show the quercetin nanosuspensions in water (left) and in 1% T80 (w/w) solution (right) for cycles 0 and 40 at 150 MPa and 25 °C; the insoluble part of quercetin was removed by ultracentrifugation.

treatment provided a yellowish color. When Tween 80 was added to the system, the color difference became more pronounced. The presence of Tween 80 in the solution increased the quercetin solubility in both HPH-processed and

dx.doi.org/10.1021/jf404065p | J. Agric. Food Chem. 2014, 62, 1852−1859

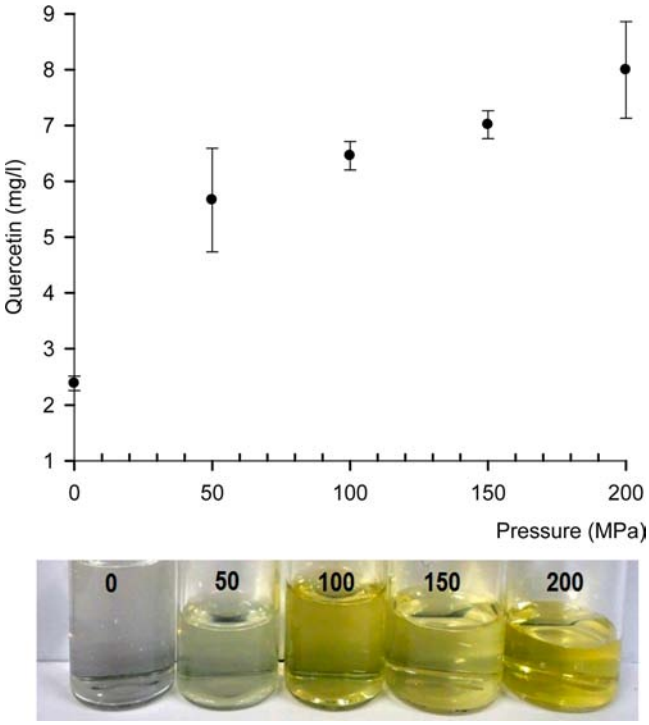

Figure 5. Water solubility of HPH-treated quercetin nanosuspensions in water at different pressures for cycle 20 at 25 °C. The insoluble part of quercetin was removed by ultracentrifugation.

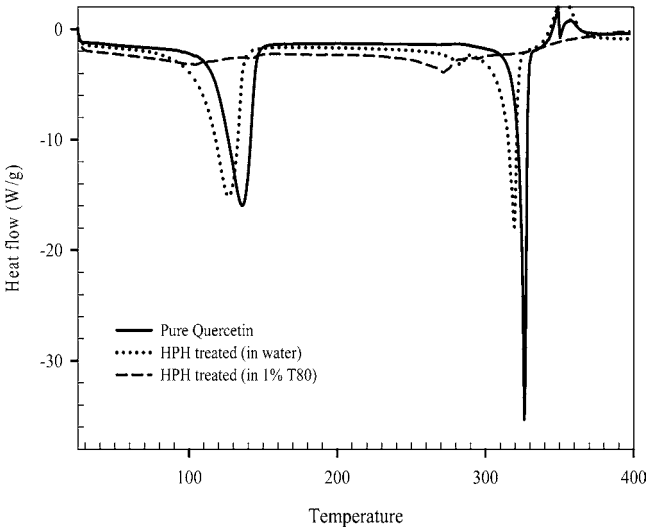

Figure 6. DSC thermograms of pure quercetin crystals and lyophilized HPH-treated quercetin nanosuspensions prepared in water and in 1% T80(w/w) solution. HPH was carried at 150 MPa for 20 cycles at 25 °C.

nonprocessed suspensions depending on its concentration (Table 1). The utility of the surfactant systems in solubilization is well-known. Due to its amphilphilic nature, the presence of Tween 80 improved quercetin solubility by forming micelles and providing regions for hydrophobic interactions in solution.[28] As a surfactant, Tween 80 provides particle wetting and it would adsorb onto the surface and decrease the interfacial tension between water and quercetin particles, and thus water can penetrate into the pores of quercetin particles, which would facilitate the dispersion of particles.

Although according to Ostwald ripening theory, increased solubility of dispersed solid particles would facilitate particle size growth during storage, in our study an increase in the amount of the micellar solubilized drug did not have a significant effect on the particle size on the day of preparation. A similar result was also pointed out in another study in which the role of stabilizers on Ostwald ripening in nanosuspensions was investigated and no effect of the amount of solubilized drug on Ostwald ripening was observed.[15]

Thermal Properties of Quercetin before and after HPH Treatment. Thermograms of pure nontreated quercetin and lyophilized HPH-treated quercetin samples with scanning temperatures ranging from 25 to 400 °C are presented in Figure 6. The curve of quercetin showed two endothermic peaks: a broad endotherm peak centered at around 120 °C corresponds to the loss of bound water; the other was a sharp endothermic peak at 325 °C indicating the melting point of quercetin. This result was consistent with other reports.[20,21] The melting peak of HPH-treated quercetin suspensions shifted to lower temperature values, which was the indication of reduced particle size and having surfactant in the system. Enthalpies of fusion, proportional to the amount of crystallinity, of pure quercetin and HPH-treated samples were different. They might be considered as the loss of crystalline structure; however, the appearance of recrystallization peaks indicates the maintenance of the initial crystalline state. It was also reported that HPH application had slightly reduced the crystallinity of querctin nanocrystals,[20] and when the HPH method was compared with the evaporative precipitation into aqueous solution method, the crystalline structure of quercetin had been partly retained through HPH cycles.[21]

Dissolution Rate. HPH-treated (at 150 MPa for 20 cycles at 25 °C) quercetin suspensions in the presence of carrier matrix of maltodextrin (30%, w/w) were obtained by the spray-drying technique. The obtained powder is convenient for handling and storage and is ready for redispersion in water. Figure 7 shows the plot of the water solubility of HPH-treated quercetin powders as a function of agitation time. The dissolution times (time to reach the concentration plateau) for spray-dried samples were nearly the same within a 10 min period. The effect of spray-drying on water solubility can be evaluated by comparing the final values of water solubility after complete powder dissolution to the solubility of the original quercetin suspension. For the HPH-treated sample prepared in water, spray-drying caused a certain increase of water solubility, from 9 to ~15 mg/L. The effect of spray-drying on the increasing water solubility of quercetin can be attributed to the reduced crystallinity of the quercetin powder through the incorporation of maltodextrins.[29,30]

Antioxidant Assays. The 2,2-diphenyl-1-picrylhydrazyl hydrate (DPPH) radical scavenging assay is routinely practiced for the assessment of the antioxidant activity of single compounds and their mixtures. The DPPH radical is stable at room temperature and produces a deep purple solution in organic solvents. The method is based on the discoloration due to the reaction that occurs between radical and antioxidant, which can be determined spectrophotometrically.[31]

The FRAP assay is based on the ability of phenolics to reduce yellow ferric tripyridyltriazine complex (Fe(III)−TPTZ) to blue ferrous complex (Fe(II)−TPTZ) by the action of electron-donating antioxidants. The resulting blue color measured spectrophotometrically at 593 nm is taken as linearly

dx.doi.org/10.1021/jf404065p | J. Agric. Food Chem. 2014, 62, 1852−1859

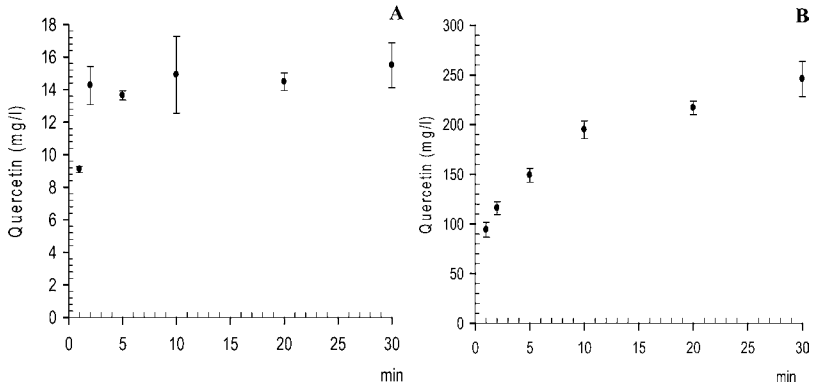

Figure 7. Dissolution of HPH-treated quercetin powder spray-dried with MD in water as a function of the agitation time: predried suspension prepared in water (A) and in 1% T80 (w/w) solution (B). HPH was carried at 150 MPa for 20 cycles at 25 °C.

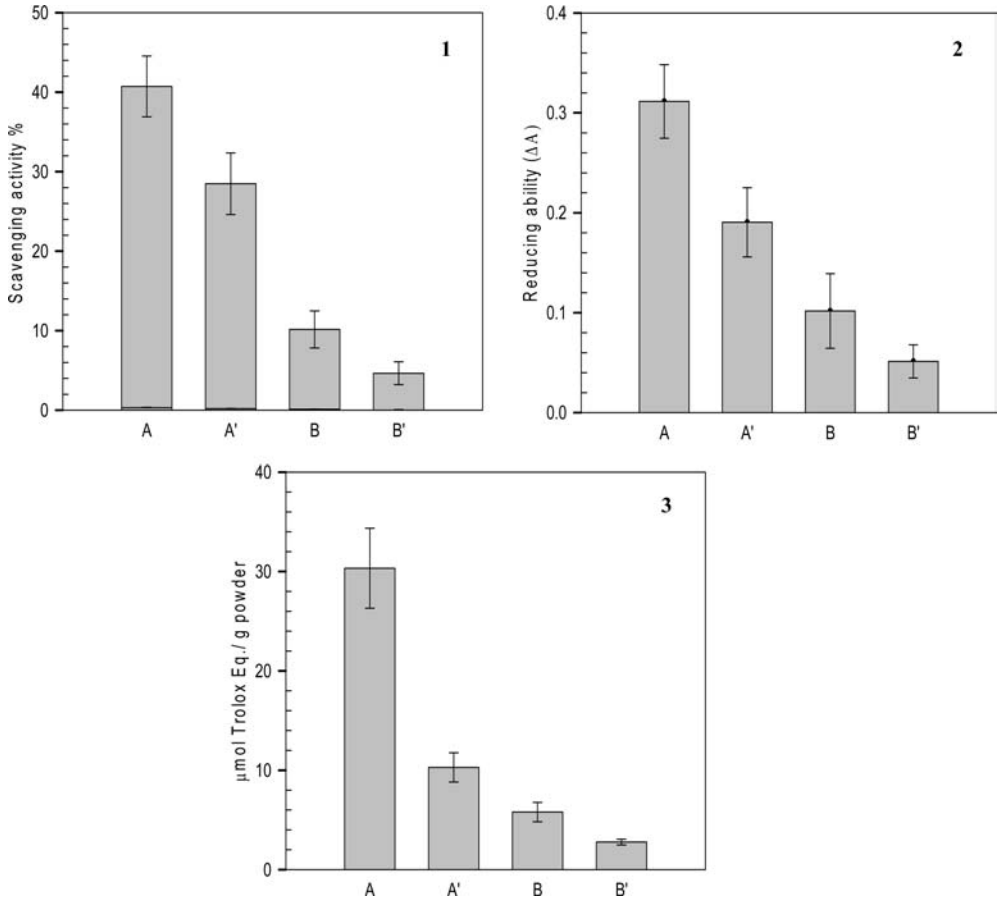

Figure 8. Scavenging activities (1), reducing abilities (2), and oxygen radical absorbing capacities (3) of spray-dried quercetin suspension powders prepared in 1% T80 (w/w) solution [(A) HPH treated and (A′) nontreated] and prepared in water [(B) HPH treated and (B′) nontreated samples].

related to the total reducing capacity of electron-donating antioxidants.[31]

In our study, spray-dried samples were first dissolved in water followed by the removal of undissolved portion by ultracentrifugation; after that, the supernatant was extracted with methanol. The radical scavenging activities and reducing abilities of spray-dried HPH-treated and nontreated quercetin powders are exhibited in Figure 8. Consistent with increased water solubility of quercetin by the application of high pressure, the HPH-treated powders scavenged more DPPH radical in the reaction medium and showed higher reducing power.

The ORAC assay as originally designed is limited to measurement of hydrophilic chain-breaking antioxidant capacity. To solve this disadvantage, the method is modified by using a solubility enhancer, that is, methylated β-cyclodextrin.[31] In our study, the ORAC assay was done as originally designed, although quercetin is a hydropohobic antioxidant and has very poor water solubility. Because one of the goals in our study was the enhancement of the water solubility of quercetin, we expected an increase in ORAC values depending on HPH treatment, which is also presented in Figure 8.

In summary, high-pressure homogenization was used to increase the water solubility of quercetin crystals, and very fine suspensions in the nanometric range were produced. The effects of the pressure, number of cycles, and concentration of stabilizer (Tween 80) on particle size, water solubility, and structure were examined. Particle size reduction rate was decreased by increasing the number of cycles and reached a steady value (~430 nm) after 10 cycles. The force required to break down the crystals seemed to increase rather exponentially with decreasing particle size. The smallest particle size achieved did not depend on the concentration of stabilizer, but the polydispersity index of the systems using Tween 80 had lower values, which indicated that having surfactant in the system provides fineness of particle by preventing agglomeration during HPH cycles. Furthermore, the formation of nanosized particles was confirmed by AFM and SEM images showing uniformity in size and lack of large needle-type crsytals. DSC thermograms also showed the loss of crystallinity through shifting to lower melting temperature and enthalpy of fusion values of HPH-treated samples. Easily water redispersible powders were fabricated by using a spray-drying process when maltodextrin was used as a carrier agent. HPH-treated spray-dried powders showed higher antioxidant activity than nontreated powders through increased water solubility in terms of radical scavenging activity, reducing ability, and oxygen radical absorbance capacity determinations. HPH has been proven to be an appropriate method to produce readily dispersible quercetin powders with high water dispersity, which is of vital importance for enhancement of the oral bioavailability.

AUTHOR INFORMATION

Corresponding Author

*(Q.H.) Phone: (848) 932-5514. Fax: (732) 932-6776. E-mail: qhuang@aesop.rutgers.edu.

Notes

The authors declare no competing financial interest.

REFERENCES

(1) Hollman, P. C. H.; van Trijp, J. M. P.; Mengelers, M. J. B.; de Vries, J. H. M.; Katan, M. B. Bioavailability of the dietary antioxidant flavonol quercetin in man. *Cancer Lett.* **1997**, *114*, 139−140.

(2) Wach, A.; Pyrzynska, K.; Biesaga, M. Quercetin content in some food and herbal samples. *Food Chem.* **2007**, *100*, 699−704.

(3) Formica, J. V.; Regelson, W. Review of the biology of quercetin and related bioflavonoids. *Food Chem. Toxicol.* **1995**, *33*, 1061−1080.

(4) Erlund, I. Review of the flavonoids quercetin, hesperetin, and naringenin. Dietary sources, bioactivities, bioavailability, and epidemiology. *Nutr. Res. (N.Y.)* **2004**, *24*, 851−874.

(5) Casagrande, R.; Georgetti, S.; Verri, W.; Jabor, J.; Santos, A.; Fonseca, M. Evaluation of functional stability of quercetin as a raw material and in different topical formulations by its antilipoperoxidative activity. *AAPS PharmSciTech* **2006**, *7*, E64−E71.

(6) Boots, A. W.; Haenen, G. R. M. M.; Bast, A. Health effects of quercetin: from antioxidant to nutraceutical. *Eur. J. Pharmacol.* **2008**, *585*, 325−337.

(7) Li, H.; Zhao, X.; Ma, Y.; Zhai, G.; Li, L.; Lou, H. Enhancement of gastrointestinal absorption of quercetin by solid lipid nanoparticles. *J. Controlled Release* **2009**, *133*, 238−244.

(8) Gao, Y.; Wang, Y.; Ma, Y.; Yu, A.; Cai, F.; Shao, W.; Zhai, G. Formulation optimization and in situ absorption in rat intestinal tract of quercetin-loaded microemulsion. *Colloid Surf. B: Biointerfaces* **2009**, *71*, 306−314.

(9) Zheng, Y.; Haworth, I. S.; Zuo, Z.; Chow, M. S. S.; Chow, A. H. L. Physicochemical and structural characterization of quercetin-β-cyclodextrin complexes. *J. Pharm. Sci.* **2005**, *94*, 1079−1089.

(10) Huang, Q.; Yu, H.; Ru, Q. Bioavailability and delivery of nutraceuticals using nanotechnology. *J. Food Sci.* **2010**, *75*, R50−R57.

(11) Müller, R. H.; Peters, K. Nanosuspensions for the formulation of poorly soluble drugs: I. Preparation by a size-reduction technique. *Int. J. Pharm.* **1998**, *160*, 229−237.

(12) Liu, P.; Rong, X.; Laru, J.; van Veen, B.; Kiesvaara, J.; Hirvonen, J.; Laaksonen, T.; Peltonen, L. Nanosuspensions of poorly soluble drugs: preparation and development by wet milling. *Int. J. Pharm.* **2011**, *411*, 215−222.

(13) Gao, L.; Zhang, D.; Chen, M. Drug nanocrystals for the formulation of poorly soluble drugs and its application as a potential drug delivery system. *J. Nanopart. Res.* **2008**, *10*, 845−862.

(14) Rabinow, B. E. Nanosuspensions in drug delivery. *Nat. Rev. Drug Discov.* **2004**, *3*, 785−796.

(15) Verma, S.; Kumar, S.; Gokhale, R.; Burgess, D. J. Physical stability of nanosuspensions: investigation of the role of stabilizers on Ostwald ripening. *Int. J. Pharm.* **2011**, *406*, 145−152.

(16) Tan, C. P.; Nakajima, M. β-Carotene nanodispersions: preparation, characterization and stability evaluation. *Food Chem.* **2005**, *92*, 661−671.

(17) Krause, K. P.; Müller, R. H. Production and characterisation of highly concentrated nanosuspensions by high pressure homogenisation. *Int. J. Pharm.* **2001**, *214*, 21−24.

(18) Jacobs, C.; Kayser, O.; Müller, R. H. Nanosuspensions as a new approach for the formulation for the poorly soluble drug tarazepide. *Int. J. Pharm.* **2000**, *196*, 161−164.

(19) Donsì, F.; Wang, Y.; Li, J.; Huang, Q. Preparation of curcumin sub-micrometer dispersions by high-pressure homogenization. *J. Agric. Food Chem.* **2010**, *58*, 2848−2853.

(20) Sahoo, N. G.; Kakran, M.; Shaal, L. A.; Li, L.; Müller, R. H.; Pal, M.; Tan, L. P. Preparation and characterization of quercetin nanocrystals. *J. Pharm. Sci.* **2011**, *100*, 2379−2390.

(21) Gao, L.; Liu, G.; Wang, X.; Liu, F.; Xu, Y.; Ma, J. Preparation of a chemically stable quercetin formulation using nanosuspension technology. *Int. J. Pharm.* **2011**, *404*, 231−237.

(22) Anarjan, N.; Mirhosseini, H.; Baharin, B. S.; Tan, C. P. Effect of processing conditions on physicochemical properties of astaxanthin nanodispersions. *Food Chem.* **2010**, *123*, 477−483.

(23) Stepanek, P. *Data Analysis in Dynamic Light Scattering*; Oxford University Press: Oxford, UK, 1993; pp 177−241.

(24) Brand-Williams, W.; Cuvelier, M. E.; Berset, C. Use of a free radical method to evaluate antioxidant activity. *LWT−Food Sci.Technol.* **1995**, *28*, 25−30.

(25) Benzie, I. F. F.; Strain, J. J. The ferric reducing ability of plasma (FRAP) as a measure of "antioxidant power": the FRAP assay. *Anal. Biochem.* **1996**, *239*, 70−76.

(26) Huang, D.; Ou, B.; Hampsch-Woodill, M.; Flanagan, J. A.; Prior, R. L. High-throughput assay of oxygen radical absorbance capacity (ORAC) using a multichannel liquid handling system coupled with a microplate fluorescence reader in 96-well format. *J. Agric. Food Chem.* **2002**, *50*, 4437−4444.

(27) Keck, C. M.; Müller, R. H. Drug nanocrystals of poorly soluble drugs produced by high pressure homogenisation. *Eur. J. Pharm. Biopharm.* **2006**, *62*, 3−16.

(28) Narang, A. S.; Delmarre, D.; Gao, D. Stable drug encapsulation in micelles and microemulsions. *Int. J. Pharm.* **2007**, *345*, 9−25.

(29) Vogt, M.; Kunath, K.; Dressman, J. B. Dissolution enhancement of fenofibrate by micronization, cogrinding and spray-drying: comparison with commercial preparations. *Eur. J. Pharm. Biopharm.* **2008**, *68*, 283−288.

(30) Chaubal, M.; Popescu, C. Conversion of nanosuspensions into dry powders by spray drying: a case study. *Pharm. Res.* **2008**, *25*, 2302−2308.

(31) Karadag, A.; Ozcelik, B.; Saner, S. Review of methods to determine antioxidant capacities. *Food Anal. Methods* **2009**, *2*, 41−60.

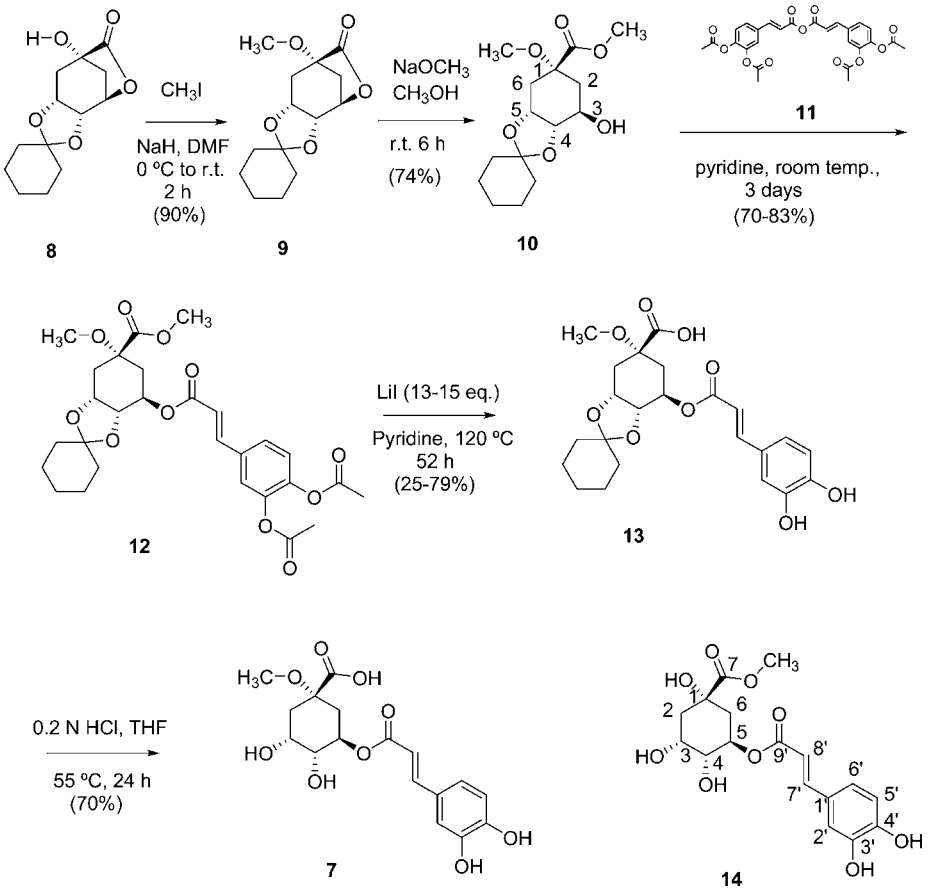

Figure 2. Synthesis of 1-*O*-methylchlorogenic acid, **7**.

and C-4 hydroxyl groups of chlorogenic acid, **7** and **6**, respectively. Evaluation of these compounds revealed strong antioxidant properties in standard tests with compound **7** showing activity superior to that of chlorogenic acid and compound **6** in both the DPPH scavenging assay and the iron-induced rat microsomal lipid peroxidation system.[32] Compound **7** was reported to possess unique antioxidant properties, including induction of heme oxygenase-1 mRNA and protein and providing protection of bovine aortic pulmonary endothelial cells against ROS-mediated necrosis when challenged with the oxidant *tert*-butyl hydroperoxide.[33] Further studies have shown that this compound also induces additional selected phase II genes including ferretin, γ-glutamylcysteine lygase, glutathione reductase, and glutathione transferase at the micromolar level.[34] Lastly, the compound assigned structure **7** was shown to enhance ultraviolet A-mediated apoptosis via activation of p21 in HaCaT keratinocytes, potentially leading to prevention of sunlight-induced photocarcinogenesis.[35]

Our interest in this class of compounds is coupled to recent reports showing that the presence of compounds containing the *o*-diphenol functionality during ensilage of dairy cow forages, containing either naturally occurring or plants transfected with polyphenoloxidase (PPO),[36] results in enhanced protein preservation of the stored forage. Thus, our interest lies in securing sufficient quantities of naturally occurring *o*-diphenols to evaluate them as PPO substrates and allow investigation of the mechanism by which these compounds alter forage protein composition toward rumen digestion. We have initiated a program to produce naturally occurring caffeoyl-containing *o*-diphenols[37] and examine their ability to serve as substrates for PPO and protein preservations.[38] The extraordinary activities reported for **7**, abbreviated as MCGA3 in reports of subsequent studies, prompted us to develop a laboratory synthesis of this compound.

MATERIALS AND METHODS

General Experimental. ^{1}H and ^{13}C NMR spectra were obtained on a Bruker Avance 360 instrument operating at 360 MHz (^{1}H) and 90 MHz (^{13}C), respectively. Spectra (presented in Supporting Information) obtained were referenced to the residual signals: for acetone-d_6 at 2.04 and 29.8 ppm; for methanol-d_4 at 3.30 and 49.0 ppm; for ^{1}H and ^{13}C, respectively. Mass spectra were obtained on a Waters LCT instrument. Melting points were obtained on a Fisher-Johns melting point apparatus and are uncorrected. IR spectra were obtained on a Shimadzu IRPrestige-21 spectrometer operating in the ATR mode. Elemental analyses were performed by Midwest Microlabs, LLC, Indianapolis, IN. Optical rotations were determined on a Rudolph Research (Flanders, NJ) Autopol III Automatic Polarimeter. Thin-layer chromatography was performed on precoated DC-Fertigplatten SIL G-25 UV254 plates (Alltech, Deerfield, IL). Flash chromatography was conducted on silica gel, Merck, grade 9385, 230−400 mesh, 60 Å. Pyridine was dried over activated 4 Å sieves. For clarity in interpretation of NMR assignments, all assignments are made according to numbered structure **14** in Figure 2. Mention of trade names or commercial products in this article is solely for the purpose of providing specific information and does not imply recommendation or endorsement by the U.S. Department of Agriculture.

Synthesis of 1-*O*-Methyl-3,4-cyclohexylidenequinic Acid Lactone, 9. To a 50 mL, two-necked, round-bottomed flask equipped with a magnetic stir bar, an equalizing addition funnel, and a septum were added sodium hydride (193 mg, 8.02 mmol, 60% in mineral oil) and anhydrous DMF (10 mL), and the flask was placed under an argon atmosphere using a gas inlet adapter. The stirring suspension

dx.doi.org/10.1021/jf4042112 | J. Agric. Food Chem. 2014, 62, 1860−1865

was cooled in an ice bath, and a mixture of (−)-4,5-cyclohexylidenequinic acid lactone, **8** (1.36 g, 5.35 mmol), and iodomethane (1.14 g, 8.02 mmol) in anhydrous DMF (15 mL) was added dropwise via the addition funnel over a 30 min period. The mixture was allowed to slowly warm to room temperature over 2 h. The mixture was cautiously quenched by adding it to a stirred solution of half-saturated aqueous ammonium chloride and ethyl acetate (50 mL each). The layers were separated, the aqueous layer was extracted with ethyl acetate (2 × 50 mL), and the combined organic extracts were washed with water (3 × 50 mL) and brine (20 mL), dried (Na_2SO_4), filtered, and concentrated to give an off-white solid. This material was recrystallized from hexanes (10 mL/g of residue) to give 1.30 g (90%) of an off-white solid. R_f = 0.45 (7:3 hexanes/EtOAc), $[\alpha]_D^{25}$ = +1.4 (*c* = 1.02, $CHCl_3$), mp 95.5−97 °C (hexanes), ^{1}H NMR (360 MHz, acetone-d_6) δ 4.68 (dd, 1, *J* = 6.3, 2.5 Hz, H5), 4.56 (m, 1, H3), 4.30 (ddd, 1, *J* = 6.4, 2.4, 1.2 Hz, H4), 3.30 (s, 3, OCH_3), 2.57 (dddd, 1, *J* = 11.7, 6.2, 2.3, 1.3 Hz, H6a), 2.33 (d, 1, *J* = 11.7, H6b), 2.30 (ddd, 1, *J* = 14.6, 7.7, 2.4 Hz, H2a), 2.04 (dd, 1, *J* = 14.6, 3.0 Hz, H2b), 1.66−1.72 (m, 2), 1.56−1.66 (m, 4), 1.48−1.56 (m, 2), 1.35−1.42 (m, 2). ^{13}C NMR (90 MHz, acetone-d_6) δ 175.8 (C═O), 110.6 (acetal C), 77.6 (C1), 75.6 (C5), 72.9 (C4), 71.8 (C3), 52.0 (OCH_3), 37.6, 36.8 (C2), 34.3, 29.9 (C6), 25.7, 24.7, 24.2 ppm. IR (ATR) ν_{max} 2926, 2842, 1777, 1653, 1452, 1163, 1085, 983, 913 cm^{-1}. Anal. Calcd for $C_{14}H_{20}O_5$: C: 62.67; H: 7.51. Found: C; 62.99, H; 7.58.

Synthesis of Methyl 1-*O*-Methyl-3,4-cyclohexylidenequinate, 10. To a 100 mL, pear-shaped, one-necked flask equipped with a magnetic stir bar and a ground glass stopper were added compound **9** (1.26 g, 4.69 mmol) and anhydrous methanol (28 mL). To this stirring solution was added freshly prepared 1.0 M sodium methoxide in methanol (14.0 mL, 14.0 mmol, 2.98 equiv) dropwise over ∼2 min at room temperature. After 21 h of being stirred at room temperature, the reaction was quenched through the addition of glacial acetic acid (1.70 mL, 29.6 mmol), diluted with EtOAc (150 mL), and washed with water (50 mL). The layers were separated, the aqueous layer extracted with EtOAc (50 mL), and the combined EtOAc extracts were washed with water (50 mL), saturated $NaHCO_3$ (50 mL), and brine (25 mL) and dried (Na_2SO_4). The mixture was filtered, concentrated, and dried to give a white solid residue. The residue was purified via flash chromatography on silica gel (80 g) using 9:1 $CHCl_3$/ acetone as eluent to give 1.08 g (76%) of a white solid. R_f = 0.23 (9:1 $CHCl_3$/acetone); $[\alpha]_D^{25}$ = −16.7 (*c* = 0.86, $CHCl_3$), ^{1}H NMR (360 MHz, acetone-d_6) δ 4.37 (dd, 1, *J* = 10.6, 5.2 Hz, H3), 4.08 (d, 1, *J* = 4.5 Hz, C3-O*H*), 3.99 (m, 1, H5), 3.88 (t, 1, *J* = 6.2 Hz, H4), 3.69 (s, 3, CO_2CH_3), 3.19 (s, 3, OCH_3), 2.22 (dd, 1, *J* = 15.1, 5.2 Hz, H6a), 2.14 (ddd, 1, *J* = 15.1, 4.7, 1.6 Hz, H6b), 1.99 (ddd, 1, *J* = 13.5, 4.0, 1.6 Hz, H2a), 1.70 (dd, 1, *J* = 13.5, 10.5 Hz, H2b), 1.53−1.66 (m, 4), 1.49−1.53 (m, 4), 1.30−1.40 (m, 2H). ^{13}C NMR (90 MHz, acetone-d_6) δ 174.1 (C7, C═O), 109.5 (acetal C), 80.8 (C4), 79.9 (C1), 73.5 (C5), 68.4 (C3), 52.3 (OCH_3), 52.2 (CO_2CH_3), 39.1 (C2), 39.0, 35.9, 31.2 (C6), 25.8, 24.8, 24.5. IR (ATR) ν_{max} 3203, 2938, 2851, 1721, 1450, 1436, 1160, 1078, 1066 cm^{-1}. Anal. Calcd for $C_{15}H_{24}O_6$: C: 59.98; H: 8.05. Found: C; 60.04, H; 7.97.

Synthesis of Methyl 1-*O*-Methyl-3,4-cyclohexylidene-5-*O*-bis(3′,4′-*O*-acetylcaffeoyl)quinate, 12. To a pear-shaped, one-necked flask equipped with a magnetic stir bar and a septum were added ester alcohol **10** (855 mg, 2.85 mmol) and pyridine (12 mL). To this stirred solution was added caffeic acid anhydride tetraacetate (**11**, 2.17 g, 4.27 mmol, 1.5 equiv) in one portion, and the resulting mixture was capped with a septum and stirred at room temperature for 72 h. The mixture was diluted with EtOAc (350 mL) and transferred to a 500 mL separatory funnel. The mixture was washed with 2 N aqueous HCl (2 × 75 mL, second washing acidic w/litmus), saturated aqueous $NaHCO_3$ (4 × 60 mL), brine (50 mL) and dried ($MgSO_4$). The solution was filtered, concentrated, and dried to give an off-white foam (2.0 g). The residue was purified via chromatography on flash silica gel (200 g) using 96:4 $CHCl_3$/acetone (1.5 L) followed by 9:1 $CHCl_3$/acetone (500 mL) as eluent to afford 1.10 g (71%) of an off-white foam. $[\alpha]_D^{25}$ = −28.3 (*c* = 1.05, $CHCl_3$), ^{1}H NMR (360 MHz, acetone-d_6) δ 7.67 (d, 1, *J* = 16.0 Hz, H7′), 7.64−7.60 (m, 2, H2′, H6′), 7.31 (d, 1, *J* = 7.9 Hz, H5′), 6.54 (d, 1, *J* = 16.0 Hz, H8′), 5.34 (ddd, 1, *J* = 11.5, 7.5, 4.2 Hz, H5), 4.48 (ddd, 1, *J* = 5.3, 5.3, 2.9 Hz, H3), 4.17 (dd, 1, *J* = 7.3, 5.8 Hz, H4), 3.70 (s, 3, CO_2CH_3), 3.27 (s, 3, OCH_3), 2.43 (br d, 1, *J* = 15.8 Hz, H2a), 2.27−2.17 (m, 8, H2b, H6a, O_2CCH_3, O_2CCH_3), 1.82 (dd, 1, *J* = 13.2, 11.3 Hz, H6b), 1.71−1.65 (m, 2), 1.60−1.50 (m, 6), 1.40−1.25 (m, 2) ppm. ^{13}C NMR (90 MHz, acetone-d_6) δ 173.6 (COOH), 168.6 (O_2CCH_3), 168.5 (O_2CCH_3), 166.2 (C9′), 145.0 (C3′ or C4′), 143.9 (C3′ or C4′), 134.0 (C1′), 127.3 (C6′), 125.0 (C5′), 123.9 (C2′), 120.0 (C8′), 110.1 (acetal C), 80.0 (C1), 77.2 (C4), 73.7 (C3), 72.2 (C5), 52.6 (OCH_3), 52.5 (CO_2CH_3), 38.8, 36.0, 35.4 (C2), 31.1 (C6), 25.7, 24.7, 24.5, 20.5 (O_2CCH_3), 20.4 (O_2CCH_3) ppm. IR (ATR) ν_{max} 2930, 2853, 1770, 1710, 1635, 1505, 1368, 1199, 1166, 1111, 1070, 1008, 903 cm^{-1}. HRMS: Calcd for $C_{28}H_{34}O_{11}$ $[M + NH_4]^+$: 564.2440 *m*/*z*. Found: 564.2445 *m*/*z*.

Synthesis of 1-*O*-Methyl-3,4-cyclohexylidene-5-*O*-caffeoylquinic Acid, 13. To an 8 mL vial equipped with a magnetic stir bar and a screw cap were added compound **12** (200 mg, 0.366 mmol) and anhydrous pyridine (5.0 mL). To this solution was added LiI (740 mg 5.53 mmol) in one portion, and the mixture was degassed by bubbling Ar gas through the solution for 2 min by which time the LiI had completely dissolved. The vial was sealed and heated in an oil bath at 120 °C for 52 h. The cooled reaction mixture was diluted with EtOAc (70 mL) and washed with 1 N aqueous HCl (30 mL). The aqueous layer was extracted with EtOAc (30 mL), and the combined EtOAc extracts were washed with 0.5 M aqueous sodium thiosulfate (2 × 30 mL), water (30 mL), brine (30 mL) and dried ($MgSO_4$). The solution was filtered, concentrated, and dried to give a light tan foam. This residue was purified via column chromatography on flash silica gel (30 g) using 92:8:1 CH_2Cl_2/CH_3OH/AcOH as eluent to give 131 mg (79%) of an off-white foam. R_f = 0.25 (92:8:1 CH_2Cl_2/CH_3OH/AcOH); $[\alpha]_D^{25}$ = −37.2 (*c* = 1.04, MeOH), mp 118−120 °C. ^{1}H NMR (360 MHz, acetone-d_6) δ 7.55 (d, 1, *J* = 15.9 Hz, H7′), 7.16 (d, 1, *J* = 2.0 Hz, H2′), 7.04 (dd, 1, *J* = 8.2, 2.0 Hz, H6′), 6.86 (d, 1, *J* = 8.2 Hz, H5′), 6.27 (d, 1, *J* = 15.9 Hz, H8′), 5.34 (ddd, 1, *J* = 11.5, 7.5, 4.2 Hz, H5), 4.49 (m, 1, H3), 4.17 (dd, 1, *J* = 7.4, 5.7 Hz, H4), 3.32 (s, 3, OCH_3), 2.41 (m, 1, H2a), 2.29−2.22 (m, 2, H2b, H6a), 1.83 (dd, 1, *J* = 13.2, 11.3 Hz, H6b), 1.70−1.60 (m, 2), 1.60−1.50 (m, 6), 1.45−1.30 (m, 2). ^{13}C NMR (90 MHz, acetone-d_6) δ 174.2 (CO_2H), 166.8 (C9′), 148.7 (C4′), 146.3 (C3′), 145.9 (C7′), 127.6 (C1′), 122.6 (C6′), 116.3 (C5′), 115.7 (C8′), 115.2 (C2′), 110.0 (acetal C), 79.9 (C1), 77.3 (C4), 73.8 (C3), 71.7 (C5), 52.6 (OCH_3), 38.8, 36.0, 35.5 (C6), 31.2 (C2), 25.7, 24.7, 24.5. IR (ATR) ν_{max} 3255, 2878, 1770, 1684, 1596, 1514, 1269, 1154, 810 cm^{-1}. HRMS: Calcd for $C_{23}H_{28}O_9$ $[M + H]^+$: 449.1807 *m*/*z*. Found: 449.1799 *m*/*z*.

Synthesis of 1-*O*-Methyl-5-*O*-caffeoylquinic Acid (1-*O*-Methylchlorogenic Acid), 7. To an 8 mL vial containing acetal **13** (20.8 mg, 0.0463 mmol) was added tetrahydrofuran (5 mL) followed by 0.2 M aqueous HCl (600 μL). The resulting solution was degassed by bubbling Ar gas through the solution for 1 min, and the vial was sealed with a screw cap and placed in a 55 °C oil bath for 24 h. The resulting mixture was cooled to room temperature, diluted with ethyl acetate (40 mL), washed with water (5 mL) and 80% brine (2 × 5 mL), and dried ($MgSO_4$). The solution was filtered and concentrated to give a light brown residue. The residue was diluted with water (1 mL) to provide a suspension which was frozen in liquid nitrogen and freeze-dried on a vacuum line to give 12.0 mg (70%) of a fluffy white solid. Attempted melting point determination of this hygroscopic material resulted in formation of a glass below 140 °C. $[\alpha]_D^{25}$ = −16.1 (*c* = 0.55, MeOH), ^{1}H NMR (360 MHz, CD_3OD) δ 7.52 (d, 1, *J* = 15.9 Hz, H7′), 7.04 (d, 1, *J* = 1.9 Hz, H2′), 6.94 (dd, 1, *J* = 8.2, 1.9 Hz, H6′), 6.76 (d, 1, *J* = 8.0 Hz, H5′), 6.21 (d, 1, *J* = 15.9 Hz, H8′), 5.13, (m, 1, H5), 4.11 (m, 1, H3), 3.75 (m, 1, H4), 3.31 (s, 3, OCH_3), 2.32−2.24 (m, 2, H2a, H6a), 2.11 (m, 1, H6b), 2.01 (m, H2b) ppm. ^{13}C NMR (90 MHz, CD_3OD) δ 175.0 (COOH), 168.4 (C9′), 149.6 (C4′), 147.2 (C7′), 146.8 (C3′), 127.8 (C1′), 123.0 (C6′), 116.4 (C5′), 115.2 (C2′), 115.1 (C8′), 81.2 (C1), 72.2 (C4), 72.0 (C5), 69.7 (C3), 52.2 (OCH_3), 35.9 (C2), 34.2 (C6) ppm. IR (ATR) ν_{max} 2951, 2906 1700, 1595, 1516, 1436, 1254, 1151, 1111, 976, 808 cm^{-1}. HRMS: Calcd for $C_{17}H_{20}O_{\backslash 9}$ + Na $[M + Na]^+$: 391.1000 *m*/*z*. Found: 391.1013 *m*/*z*.

dx.doi.org/10.1021/jf4042112 | J. Agric. Food Chem. 2014, 62, 1860−1865

Table 1. Comparison of ^{1}H NMR Data for MCGA3,[32] for Methyl Chlorogenate from the Current Study and from Kancheva et al.,[43] and for Compound 7

MCGA3 (Kweon et al.)[32]	methyl chlorogenate (current study, **14**)	methyl chlorogenate (Kancheva et al)[43]	compound **7**
7.51 (d, 1, J = 15.9 Hz, H7′)	7.52 (d, 1, J = 15.9 Hz, H7′)	7.52 (d, 1, J = 15.9 Hz)	7.52 (d, 1, J = 15.9 Hz, H7′)
7.04(d, 1, J = 2.0 Hz, H2′)	7.04 (d, 1, J = 1.9 Hz, H2′)	7.04 (d, 1, J = 2.0 Hz)	7.04 (d, 1, J = 1.9 Hz, H2′)
6.94 (dd, 1, J = 8.2, 2.0 Hz, H6′)	6.94 (dd, 1, J = 8.2, 1.9 Hz, H6′)	6.95 (dd, 1, J = 8.2, 2.0 Hz)	6.94 (dd, 1, J = 8.0, 1.2 Hz, H6′)
6.77 (d, 1, J = 8.4 Hz, H5′)	6.78 (d, 1, J = 8.2 Hz, H5′)	6.78 (d, 1, J = 8.2 Hz)	6.76 (d, 1, J = 8.0 Hz, H5′)
6.20 (d, 1, J = 15.9 Hz, H8′)	6.21 (d, 1, J = 15.9 Hz, H8′)	6.21 (d, 1, J = 15.9 Hz)	6.21 (d, 1, J = 15.9 Hz, H8′)
5.26−5.30 (m, 1, H5)	5.27 (m, 1, H5)	5.27 (m, 1)	5.13 (m, 1, H5)
4.12−4.15 (m, 1, H3)	4.13, (dt, 1, J = 6.6, 3.3 Hz, H3)	4.13 (m, 1)	4.11 (m, 1, H3)
3.71 (dd, 1, J = 7.5, 3.1 Hz, H4)	3.73 (dd, 1, J = 7.5, 3.1 Hz, H4)	3.73 (m, 1)	3.75 (m, 1, H4)
3.70 (s, 3, OCH_3)	3.69 (s, 3, OCH_3)	3.69 (s, 3, OCH_3)	3.31 (s, 3, OCH_3)
1.93−2.23 (m, 4, H2, H6)	2.23−2.19 (m, 3)	2.23−2.11 (m, 3)	2.32−2.24 (m, 2, H2a, H6a)
	2.00 (dd, 1, J = 13.4, 6.8 Hz, H2a)	2.03−1.99 (m, 1)	2.11 (m, 1, H6b)
			2.01 (m, 1, H2b)

RESULTS AND DISCUSSION

The approach taken for the production of MCGA3 was similar in design to a previous report outlining a synthesis of a closely related derivative.[39] However, detailed synthetic procedures were not presented in this communication. Previous reports have indicated that alkylation of the C-1 hydroxyl of the 4,5-ketal-protected quinic acid lactone can be accomplished with iodomethane.[39] Reaction of lactone **8** with methyl iodide and sodium hydride in DMF afforded methyl ether **9** in 90% yield after recrystallization from hexanes (Figure 2). Hydroxide opening of lactone **9** afforded the corresponding hydroxyl carboxylate. In our hands, acylation of this carboxylate with acetate-protected caffeoyl chloride and imidazole derivatives[39] resulted in poor isolated yields from complex mixtures. We opted to examine the feasibility of unmasking the lactone functionality to the hydroxyl methyl ester **10**. Reaction of lactone **9** with freshly prepared sodium methoxide (Na, CH_3OH)[40] afforded hydroxy ester **10** in 74% yield after chromatographic purification. The caffeoyl moiety was introduced through acylation of the secondary alcohol using caffeic acid anhydride tetraacetate, **11**,[37] a reagent developed specifically for construction of caffeoyl-containing compounds, and afforded the fully protected target compound **12**. The methyl ester functionality was cleaved with lithium iodide in pyridine (120 °C, 52 h)[41] which also resulted in concomitant loss of the caffeoyl acetate protecting groups to give the intermediate acetal **13** in 79% yield after chromatographic purification. Completion of the first synthesis of 1-*O*-methyl chlorogenic acid, **7**, was accomplished after treatment of acetal **13** with aqueous HCl in THF (70%).

Extensive NMR examination of **7** (^{1}H, ^{13}C, HSQC, and HMBC) confirmed the structure as assigned. Conclusive evidence for the assigned structure comes from diagnostic absorption in the HMBC spectrum of compound **7** where, as predicted, the methyl ether protons show only a single cross-peak interaction with the assigned C-1 carbon atom. The C-5 hydrogen atom shows three-bond correlations with C-1, C-3, and the carbonyl carbon of the caffeoyl group, as the expected arrangement for the C-5 attachment of the caffeoyl group to the quinic acid unit.

However, these spectroscopic absorptions differ significantly from those reported for MCGA3.[32] Unfortunately, an authentic sample or spectroscopic data of MCGA3 is not available for comparison purposes. No response was received through attempted contact (e-mail) with the corresponding author of the original isolation/activity paper.[32] The corresponding author of another laboratory which utilized MCGA3 in additional studies[34,35] indicated that they are not in possession of any authentic sample of the isolated MCGA3 and have no spectroscopic data for the compound. After closer examination of the reported spectroscopic data, we surmised that the CH_3 signal at 3.7 ppm in the reported ^{1}H NMR data for MCGA3 was most likely arising from a methyl ester and not an aliphatic methyl ether (typically absorbing at 3.2−3.3 ppm) and that the ^{1}H NMR data as a whole was strikingly similar to that reported for methyl chlorogenate. Literature NMR spectroscopic data appearing both before[42] and after[43] the initial structure assignment disclosure[32] supports these observations. To verify this conjecture, we converted commercially available chlorogenic acid to methyl chlorogenate, **14**, in methanolic HCl[11] at room temperature. Comparison of reported ^{1}H and ^{13}C NMR absorption data for MCGA3 with the data obtained for **14** and **7** in CD_3OD are given in Tables 1 and 2. Both the ^{1}H and ^{13}C NMR data of methyl chlorogenate from the published literature

Table 2. Comparison of ^{13}C NMR Data for MCGA3,[32] for Methyl Chlorogenate from the Current Study and from Deyama et al.,[42] and for Compound 7

MCGA3, Kweon et al.[32] (assignment)	methyl chlorogenate, **14**, current study (assignment)	methyl chlorogenate, Deyama et al.[42] (assignment)	compound **7**, current study (assignment)
175.4 (COOR)	175.6 (COOR)	175.3 (COOR)	175.0 (COOR)
168.3 (C-9′)	168.5 (C-9′)	168.3 (C-9′)	168.4 (C-9′)
149.7 (C-3′)	149.8 (C-4′)	149.4 (C-4′)	149.6 (C-4′)
147.2 (C-4′)	147.4 (C-7′)	147.0 (C-3′ or C-7′)	147.2 (C-7′)
146.8 (C-7′)	147.0 (C-3′)	146.6 (C-3′ or C7′)	146.8 (C-3′)
127.7 (C-6′)	127.8 (C-1′)	127.7 (C-1′)	127.8 (C-1′)
123.0 (C-1′)	123.2 (C-6′)	122.9 (C-6′)	123.0 (C6′)
116.5 (C-5′)	116.7 (C-5′)	116.5 (C-5′)	116.4 (C-5′)
115.1 (C-2′)	115.3 (C-2′)	115.2 (C2′ or C8′)	115.2 (C-2′)
115.1 (C-8′)	115.1(C-8′)	115.2 (C2′ or C8′)	115.1 (C-8′)
75.8 (C-4)	75.8 (C-1)	76.0 (C-1)	81.2 (C-1)
72.6 (C-1)	72.6 (C-4)	73.0 (C-5 or C-4)	72.2 (C-4)
72.1 (C-5)	72.1 (C-5)	72.0 (C-5 or C-4)	72.0 (C-5)
70.3 (C-3)	70.3 (C-3)	70.7 (C-3)	69.7 (C-3)
53.0 (OCH_3)	53.0 (OCH_3)	53.0 (OCH_3)	52.2 (OCH_3)
38.1 (C-2)	38.1 (C-2)	38.2 (C-2 or C-6)	35.9 (C-2)
37.8 (C-6)	37.8 (C-6)	38.2 (C-2 or C-6)	34.2 (C-6)

dx.doi.org/10.1021/jf4042112 | J. Agric. Food Chem. 2014, 62, 1860−1865

values and the authentic sample correlate well with the data reported from the isolation paper[32] for MCGA3, leading to the conclusion that the compound isolated from bamboo (*Phyllostachys edulis*) leaves is instead methyl chlorogenate, **14**. In addition, subsequent reports[33−35] detailing the biological activities of MCGA3 need to be amended to indicate the correct structural formula.

■ ASSOCIATED CONTENT

Supporting Information

^{1}H and ^{13}C NMR spectra for compounds **9**, **10**, **12**, and **13**, along with ^{1}H, ^{13}C, $^{1}H-^{13}C$ HSQC, and $^{1}H-^{13}C$ HMBC NMR spectra for compounds **7** and **14**. This material is available free of charge via the Internet at http://pubs.acs.org.

■ AUTHOR INFORMATION

Corresponding Author

*Phone: 608-890-0071. Fax: 608-890-0076. E-mail: Wayne.Zeller@ars.usda.gov.

Funding

Purchase of the Waters LCT instrument in 2000 was partially funded by NSF award no. CHE9974839 to the Department of Chemistry, University of Wisconsin—Madison.

Notes

The authors declare no competing financial interest.

■ ACKNOWLEDGMENTS

The author thanks Dr. Paul Schatz for helpful discussions, for preparation of the Supporting Information, and for the preparation of lactone **8**. The author also thanks Professor Steve Burke and Alex Clemens of the Department of Chemistry at the University of Wisconsin—Madison for assistance in obtaining optical rotations, and Professor Mukhtar of the Department of Dermatology at the University of Wisconsin—Madison for his assistance in our attempt to locate an authentic sample and spectroscopic data for MCGA3.

■ REFERENCES

(1) Weng, C.-J.; Yen, G.-C. Chemopreventive effects of dietary phytochemicals against cancer invasion and metastasis: Phenolic acids, monophenol, polyphenol, and their derivatives. *Cancer Treat. Rev.* **2012**, *38*, 76−87.

(2) Evans, D. A.; Hirsch, J. B.; Dushenkov, S. Phenolics, inflammation and nutrigenomics. *J. Sci. Food Agric.* **2006**, *86*, 2503−2509.

(3) Vita, J. A. Polyphenols and cardiovascular disease: effects on endothelial and platelet function. *Am. J. Clin. Nutr.* **2005**, *81*, 292S−297S.

(4) Clifford, M. N. Chlorogenic acids and other cinnamates-nature, occurrence and dietary burden. *J. Sci. Food Agric.* **1999**, *79*, 362−372.

(5) Shahidi, F.; Chandrasekara, A. Hydroxycinnamates and their in vitro and in vivo antioxidant activities. *Phytochem. Rev.* **2010**, *9*, 147−170.

(6) Petersen, M.; Simmonds, M. S. J. Molecules of interest: Rosmarinic acid. *Phytochemistry* **2003**, *62*, 121−125.

(7) Zeng, H.-W.; Locatelli, M.; Bardelli, C.; Amoruso, A.; Coisson, J. D.; Travaglia, F.; Arlorio, M.; Brunelleschi, S. Anti-inflammatory properties of clovamide and *Theobroma cacao* phenolic extracts in human monocytes: Evaluation of respiratory burst, cytokine release, NF-κB activation, and PPARγ modulation. *J. Agric. Food Chem.* **2011**, *59*, 5342−5350.

(8) Zhang, X.; Ishida, R.; Yuhara, Y.; Kamiya, T.; Hatano, T.; Okamoto, G.; Arimoto-Kobayashi, S. Anti-genotoxic activity of *Vitis coignetiae* Pulliat towards heterocyclic amines and isolation and identification of caftaric acid as an antimutagenic component from the juice. *Mut. Res.* **2011**, *723*, 182−189.

(9) Robinson, W. E., Jr.; Reinecke, M. G.; Abdel-Malek, S.; Jia, Q.; Chow, S. A. Inhibitors of HIV-1 replication that inhibit HIV integrase. *Proc. Natl. Acad. Sci. U.S.A.* **1996**, *93*, 6326−6331.

(10) McDougall, B.; King, P. J.; Wu, B. W.; Hostomsky, Z.; Reinecke, M. G.; Robinson, W. E., Jr. Dicaffeoylquinic and dicaffeoyltartaric acids are selective inhibitors of human immunodeficiency virus type 1 integrase. *Antimicrob. Agents Chemother.* **1998**, *42*, 140−146.

(11) Reinke, R. A.; King, P. J.; Victoria, J. G.; McDougall, B. R.; Ma, G.; Mao, Y.; Reinecke, M. G.; Robinson, W. E., Jr. Dicaffeoyltartaric acid analogues inhibit human immunodeficiency virus type 1 (HIV-1) integrase and HIV-1 replication at nontoxic concentrations. *J. Med. Chem.* **2002**, *45*, 3669−3683.

(12) Lin, Z.; Neamati, N.; Zhoa, H.; Kiryu, Y.; Turpin, J. A.; Aberham, C.; Strebel, K.; Kohn, K.; Witvrouw, M.; Pannecouque, C.; Debyser, Z.; De Clercq, E.; Rice, W. G.; Pommier, Y.; Burke, T. R., Jr. Chicoric acid analogues as HIV-1 integrase inhibitors. *J. Med. Chem.* **1999**, *42*, 1401−1414.

(13) Tazaki, H.; Ito, M.; Miyoshi, M.; Kawabata, J.; Fukushi, E.; Fujita, T.; Motouri, M.; Furuki, T.; Nabeta, K. Subulatin, an antioxidic caffeic acid derivative isolated from the *in vitro* cultured liverworts *Jungermannia subulata*, *Lophocolea heterophylla*, and *Scapania parvitexta*. *Biosci. Biotechnol. Biochem.* **2002**, *66*, 255−261.

(14) Maruta, Y.; Kawabata, J.; Niki, R. Antioxidative caffeoylquinic acid derivatives in the roots of burdock (*Arctium lappa* L.). *J. Agric. Food Chem.* **1995**, *43*, 2592−2595.

(15) Sato, Y.; Itagaki, S.; Kurokawa, T.; Ogura, J.; Kobayashi, M.; Hirano, T.; Sugawara, M.; Iseki, K. *In vitro* and *in vivo* antioxidant properties of chlorogenic acid and caffeic acid. *Int. J. Pharm.* **2011**, *403*, 136−138.

(16) Wang, M.; Simon, J. E.; Aviles, I. F.; He, K.; Zheng, Q.-Y.; Tadmor, Y. Analysis of antioxidative phenolic compounds in artichoke (*Cynara scolymus* L.). *J. Agric. Food Chem.* **2003**, *51*, 601−608.

(17) Chen, J. H.; Ho, C.-T. Antioxidant activities of caffeic acid and its related hydroxycinnamic acid compounds. *J. Agric. Food Chem.* **1997**, *45*, 2374−2378.

(18) Ohnishi, M.; Morishita, H.; Iwahashi, H.; Toda, S.; Shirataki, Y.; Kimura, M.; Kido, R. Inhibitory effects of chlorogenic acids on linoleic acid peroxidation and haemolysis. *Phytochemistry* **1994**, *36*, 579−583.

(19) Mubarak, A.; Bondonno, C. P.; Liu, A. H.; Considine, M. J.; Rich, L.; Mas, E.; Croft, K. D.; Hodgson, J. M. Acute effects of chlorogenic acid on nitric oxide status, endothelial function, and blood pressure in healthy volunteers: A randomized trial. *J. Agric. Food Chem.* **2012**, *60*, 9130−9136.

(20) Belkaid, A.; Currie, J.-C.; Desgagnés, J.; Annabi, B. The chemopreventive properties of chlorogenic acid reveal a potential new role for the microsomal glucose-6-phosphate translocase in brain tumor progression. *Cancer Cell Int.* **2006**, *6*, 7.

(21) Kang, N. J.; Lee, K. W.; Kim, B. H.; Bode, A. M.; Lee, H.-J.; Heo, Y.-S.; Boardman, L.; Limburg, P.; Lee, H. J.; Dong, Z. Coffee phenolic phytochemicals suppress colon cancer metastasis by targeting MEK and TOPK. *Carcinogenesis* **2011**, *32*, 921−928.

(22) Kasai, H.; Fukada, S.; Yamaizumi, Z.; Sugie, S.; Mori, H. Action of chlorogenic acid in vegetables and fruits as an inhibitor of 8-hydroxydeoxyguanosine formation *in vitro* and in a rat carcinogenesis model. *Food Chem. Toxicol.* **2000**, *38*, 467−471.

(23) Lou, Z.; Wang, H.; Zhu, S.; Ma, C.; Wang, Z. Antibacterial activity and mechanism of action of chlorogenic acid. *J. Food Sci* **2011**, *76*, M398−M403.

(24) Niggeweg, R.; Michael, A. J.; Martin, C. Engineering plants with increased levels of the antioxidant chlorogenic acid. *Nat. Biotechnol.* **2004**, *22*, 746−754.

(25) Nakatani, N.; Kayano, S.; Kikuzaki, H.; Sumino, K.; Katagiri, K.; Mitani, T. Identification, quantitative determination, and antioxidative activities of chlorogenic acid isomers in prune (*Prunus domestica* L.). *J. Agric. Food Chem.* **2000**, *48*, 5512−5516.

(26) Iwai, K.; Kishimoto, N.; Kakino, Y.; Mochida, K.; Fujita, T. In vitro antioxidative effects and tyrosinase inhibitory activities of seven

hydroxycinnamoyl derivatives in green coffee beans. *J. Agric. Food Chem.* **2004**, *52*, 4893−4898.
(27) Takeoka, G. R.; Dao, L. T. Antioxidant constituents of almond [*Prunus dulcis* (Mill.) D.A. Webb] hulls. *J. Agric. Food Chem.* **2003**, *51*, 496−501.
(28) Xia, D.; Shi, J.; Gong, J.; Wu, X.; Yang, Q.; Zhang, Y. Anitoxidant activity of Chinese mei (*Prunus mume*) and its active phytochemicals. *J. Med. Plants Res.* **2010**, *4*, 1156−1160.
(29) Lee, S. G.; Lee, H.; Nam, T. G.; Eom, S. H.; Heo, H. J.; Lee, C. Y.; Kim, D.-O. Neuroprotective effects of caffeoylquinic acids from *Artemisia princeps* Pampanini against oxidative stress-induced toxicity in PC-12 cells. *J. Food Sci.* **2011**, *76*, C250−C256.
(30) Nishizawa, M.; Izuhara, R.; Kaneko, K.; Koshihara, Y.; Fujimoto, Y. 5-Lipoxygenase inhibitors from Gardeniae fructus. *Chem. Pharm. Bull.* **1988**, *36*, 87−95.
(31) Matsuse, I. T.; Nakabayashi, T.; Lim, Y. A.; Hussein, G M. E.; Miyashiro, H.; Kakiuchi, N.; Hattori, M.; Stardjo, S.; Shimotohno, K. A human immunodeficiency virus protease inhibitory substance from *Swietenia mahagoni*. *Phytother. Res.* **1997**, *11*, 433−436.
(32) Kweon, M.-H.; Hwang, H.-J.; Sung, H.-C Identification and antioxidant activity of novel chlorogenic acid derivatives from bamboo (*Phyllostachys edulis*). *J. Agric. Food Chem.* **2001**, *49*, 4646−4655.
(33) Kweon, M.-H.; Jung, M.-J.; Sung, H.-C. Cytoprotective effects of heme oxygenase-1 induction by 3-O-caffeoyl-1-methylquinic acid. *Free Radicals Biol. Med.* **2004**, *36*, 40−52.
(34) Kweon, M.-H.; Park, Y. I.; Sung, H.-C.; Mukhtar, H. The novel antioxidant 3-O-caffeoyl-1-methylquinic acid induces Nrf2-dependent phase II detoxifying genes and alters intracellular glutathione redox. *Free Radicals Biol. Med.* **2006**, *40*, 1349−1361.
(35) Kweon, M.-H.; Afaq, F.; Bhat, K. M. R.; Setaluri, V.; Mukhtar, H. A novel antioxidant 3-O-caffeoyl-1-methylquinic acid enhances ultraviolet A-mediated apoptosis in immortalized HaCaT keratinocytes via Sp1-dependent transcriptional activation of $p21^{WAF1/Cip1}$. *Oncogene* **2007**, *26*, 3559−3571.
(36) Sullivan, M. L.; Hatfield, R. D. Polyphenol oxidase and *o*-diphenols inhibit postharvest proteolysis in red clover and alfalfa. *Crop Sci.* **2006**, *46*, 662−670.
(37) Zeller, W. E. Synthesis of (+)- and (−)-phaselic acid. *Synth. Commun.* **2013**, *43*, 1345−1350.
(38) Sullivan, M. L.; Zeller, W. E. Efficacy of various naturally occurring caffeic acid derivatives in preventing post-harvest protein losses in forages. *J. Sci. Food Agric.* **2013**, *93*, 219−226.
(39) Hemmerle, H.; Burger, H.-J.; Below, P.; Schubert, G.; Rippel, R.; Schindler, P. W.; Paulus, E.; Herling, A. W. Chlorogenic acid and synthetic chlorogenic acid derivatives: Novel inhibitors of hepatic glucose-6-phosphate translocase. *J. Med. Chem.* **1997**, *40*, 137−145.
(40) Lange, G. L.; Humber, C. C.; Manthorpe, J. M. [2 + 2] Photoadditions with chiral 2,5-cyclohexadienone synthons. *Tetrahedron: Asymmetry* **2002**, *13*, 1355−1362.
(41) Brummond, K. M.; DeForrest, J. E. Synthesis of the naturally occurring (−)-1,3,5-tri-*O*-caffeoylquinic acid. *Synlett* **2009**, *9*, 1517−1519.
(42) Deyama, T.; Ikawa, T.; Kitagawa, S.; Nishibe, S. The constituents of *Eucommia ulmoides* Oliv. V. Isolation of dihydroxydehydroconiferyl alcohol isomers and phenolic compounds. *Chem. Pharm. Bull.* **1987**, *35*, 1785−1789.
(43) Kancheva, V. D.; Saso, L.; Angelova, S. E.; Foti, M. C.; Slavova-Kasakova, A.; Daquino, C.; Enchev, V.; Firuzi, O.; Nechev, J. Antiradical and antioxidant activities of new bio-antioxidants. *Biochimie* **2012**, *94*, 403−415.

Table 1. The Primer Sequences

serial no.	name	sequences	length (bp)
NM_001047088.1	GPR120	forward: ACTTCCCTTTCTTCTCGGATGT	97
		reverse: AGCAGTGAGACCACAAAGATGA	
NM_001039713.1	FTO	forward: TAAGAGCAGAGCAGCCTACAAC	137
		reverse: TGTCCACCAAGTTCTCGTCAT	
NM_013196.1	PPARα	forward: CAGAGGTCCGATTCTTCCACT	150
		reverse: AGTAGGCTTCATACACACCGTA	
NM_013124.3	PPARγ	forward: CCTCCCTGATGAATAAAGATGG	125
		reverse: CACAGCAAACTCAAACTTAGGC	
NM_019354.2	UCP2	forward: AGATGTGGTAAAGGTCCGCTTC	90
		reverse: GCAATGGTCTTGTAGGCTTCG	
NM_013076.3	Leptin	forward: GGCTTTGGTCCTATCTGTCCTA	123
		reverse: ATACCGACTGCGTGTGTGAAAT	
NM_144744.3	Adiponectin	forward: TCACCTACGACCAGTATCAGGA	122
		reverse: GAGTCCATTGTTGTCCCCTTC	
NM_031144	β-actin	forward: CCCATCTATGAGGGTTACGC	150
		reverse: TTTAATGTCACGCACGATTTC	

Shanghai, China. We prepared the CTMSs used in this work in our laboratory via a previously reported procedure.[8,15] The microparticles were approximately 600−1000 nm in size. All other reagents and solvents were of analytical grade.

CCMS Preparation. CCMSs were prepared as follows. Briefly, CAP was dissolved in distilled water containing Tween-80, and CTS was dissolved in 1% ethylic acid solution. The CAP and CTS solutions were mixed using a magnetic stirrer, and the desired microspheres were spontaneously obtained upon addition of an aqueous basic solution of sodium tripolyphosphate (TPP) to the CAP-CTS solution. After 30 min, a CCMS suspension was obtained. Factors affecting drug entrapment efficiency, including CTS concentration, TPP concentration, CAP concentration, pH, and CTS/TPP composition ratio were investigated. The suspension was dried by spray drying to yield CCMSs as a powder. The effects of input temperature, flow rate, and hot air flow rate on particle size and microsphere yield were investigated.

CAP Determination in CCMS. The CAP in the CCMS was extracted by methanol from the CCMS powder and determined by HPLC. A Diamonsil C_{18} (250 mm × 4.6 mm, 5 μm) column was used for this procedure. The mobile phase was 32% H_2O in methanol (V/V), and the detection wavelength was 281 nm.

CCMS Characterization. The particle size and ζ potential of the CCMSs were determined with a laser diffraction size analyzer. The surface morphology of the CCMSs was investigated by SEM (S3700N). HPLC was used to analyze the drug entrapment efficiency and drug loading capacity of the microspheres. The CCMSs were mixed with 25 mL of methanol for ultrasound extraction. CAP in the supernatant was analyzed by HPLC after high-speed centrifugation, and the results obtained were used to calculate the drug entrapment efficiency and drug loading capacity of the products.

Antiobesity Activity of CCMS in Male SD Rats. The SD obese rat model was used in animal studies. A total of 90 male SD rats aged 4 weeks were purchased from Guangdong Medical Laboratory Animal Center (Guangzhou, China). All of the animal protocols were approved by the Institutional Animal Care and Use Committee of the Guangdong Pharmaceutical University (Guangzhou, China) (Protocol no. SPF2013100). All of the rats were housed under standard conditions at 23 ± 2 °C, a 12 h light and dark cycle, and relative humidity of 55%. Food and water were provided ad libitum throughout the experiment.

Experimental Design. Ten rats were randomly separated as (1) the normal diet (standard rodent chow) group (NF); this group was fed with a standard diet. The remaining 80 rats were fed with a high-fat diet to obtain the obesity model. This high-fat diet comprised 60% basic feed, 10% lard, 10% egg yolk powder, 2.5% cholesterol, 0.5% bile salts, 5% sucrose, 5% peanut, 5% milk powder, and 2% salt. After a 4 week high-fat diet, the obesity model was considered complete when the average weight of the rats fed a high-fat diet was greater than 20% that of the rats fed a normal diet. The 80 rats were then randomly divided into eight groups by weight: (2) high-fat feeding group (FF), (3) CTS group (CTS), (4) Orlistat group (Orlistat), (5) CTMS group (CTMS), (6) CAP group (CAP), (7) CCMS high-dose group (H-CCMS), (8) CCMS middle-dose group (M-CCMS), and (9) CCMS low-dose group (L-CCMS). The corresponding "drugs" were administered orally by gavage at a dose of 1 mL/100 g per day at the same time for 5 weeks. The "drugs" were suspended in water. The doses of "drugs" for each group were as follows: CTS, 440 mg/kg/d; CTMS, 440 mg/kg/d; Orlistat, 75 mg/kg/d; CAP, 30 mg/kg/d; H-CCMS, 3382 mg/kg/d (containing 30 mg CAP); M-CCMS, 1128 mg/kg/d (10 mg CAP); L-CCMS, 367 mg/kg/d (3 mg CAP). All rats were weighed every week, and food intake levels for each group were recorded every day. During the experimental period, no rat died and no untoward effects were observed. At the end of the experiment, the rats were fasted overnight, and blood samples were withdrawn from the orbital vein using a capillary after ether anesthesia. The rats were then subjected to ether anesthesia, sacrificed, and necropsied. The liver, heart, white subcutaneous adipose tissues, and mesenteric adipose tissues were quickly removed and weighed on ice. Tissues were stored at −80 °C until biopsy.

Serum Lipid Determination. The serum was prepared, and lipid levels in the blood samples were detected. The levels of TC, TG, HDL-C, and LDL-C were measured with commercial assay kits using an automated biochemistry analyzer BC200 instrument (Beijing Precil Instrument Co. Ltd., Beijing, China).

Quantitative RT-PCR. Total RNA was extracted from the rat livers using TRIzol reagent (Invitrogen). First-strand cDNA was generated using a commercial Bestbio RT kit (Bestbio, Shanghai, China). The cDNA product was amplified by real-time RT-PCR using a Takara SYBR Premix EX Taq kit (TaKaRa, Otsu, Shiga, Japan) and Bio-Rad IQ5 real-time PCR instrument and analysis software (Applied Biosystems, Foster City, CA). The primer sequences (Table 1) used in the PCR were designed by Sangon Biotech (Shanghai) Co., Ltd.

The relative quantification of gene expression was analyzed by the $2^{-\Delta\Delta Ct}$ method. If the average gene expression of the experimental groups was considered lower than that of the FF group. If $2^{-\Delta\Delta Ct} > 1$, the average gene expression of the experimental groups was considered higher than that of the FF group. PCR was performed as follows: 94 °C for 30 s, 61 °C for 30 s, and 72 °C for 15 s after a 5 min warm-up. The system was then cooled to 72 °C for 5 min and finally heated from 65 to 95 °C (1 °C/s and 36 cycles).

ELISA. The concentrations of obesity factors in the serum were measured using an ELISA kit (R&D Systems China Co. Ltd., Shanghai, China), and the ELISAs were read with a multifunctional microplate reader (Berthold Mithras LB 940; Berthold Technologies GmbH & Co. KG, Germany).

Statistical Analysis. All of the data are expressed as means ± SE. Differences between groups were determined by one-way ANOVA using SPSS for Windows, version 16.0 (SPSS Inc., Chicago, IL, USA). Student−Newman−Keuls Multiple-Range Test comparisons at $P < 0.05$ were carried out to determine significant differences among means.

RESULTS

CCMS Preparation. On the basis of the results of single-factor experiments (the effects of the concentration of CTS, sodium TPP, and CAP, the pH of the reaction system, and the mass ratio of CTS/TPP are not presented here), we selected the factors that had the greatest influence on the encapsulation efficiency for orthogonal experiments (Table 2A). The key factors were encapsulation efficiency and drug loading. Parts B and C of Table 2 clearly indicate that the order of influence is pH > concentration of CTS > ratio of CTS/TPP. The optimum conditions for preparation are as follows: CTS concentration, 1 mg/mL; pH 4.5; CTS/TPP ratio, 4:1.

CCMS Optimization. Spray drying is a key technique in preparing samples for the present study. Parts D−F of Table 2 show the effects of inlet temperature, flow rate, and hot air flow on the particle size and microsphere yield. On the basis of the results, we selected 160 °C as the inlet temperature, 600 mL/h as the flow rate, and 32 m^3/h as the hot air flow rate for CCMS preparation.

Characterization. Parts A and B of Figure 1 show the particle distribution and ζ distribution of the resultant products, respectively; the mean particle size and ζ potential of the CCMSs were 4.5 μm and +3.48 mV, respectively. SEM images of the CCMSs (Figure 1C) showed a spherical morphology with uniform diameters. The mean entrapment efficiency of the CCMSs was 85.17%, and the mean drug loading was 8.87% [entrapment efficiency = (total amount of CAP − free amount of CAP)/total amount of CAP, drug loading = (total amount of CAP − free amount of CAP)/microsphere weight].

Pharmacodynamics Study. *Body Weight, Lee's Index, Food Intake, Organ Index, and Proportion of Body Fat.* Body weight was recorded each week. Figure 2 shows the changes in body weight, food intake, Lee's index (body $mass^{1/3}$ × 1000/body length), liver index (liver mass × 100/body mass), and proportion of body fat.

Among the treatments studied, high doses of CCMSs best controlled weight gain (Figure 2B), ΔLee's index (Figure 2C), liver index (Figure 2D), and proportion of body fat (Figure 2F) without affecting food intake (Figure 2A). The ability of the CCMSs to control body weight and ΔLee's index was better than that of Orlistat. While high doses of CCMSs controlled obesity indices favorably, no differences were observed in terms of ΔLee's index, organ index, and proportion of body fat between the H-CCMS and M-CCMS groups. Therefore, 3382 mg/kg/d is an efficient CCMS dosage for controlling obesity in rats. The CCMSs exhibited better obesity control than either the CTMSs or CAP alone; this finding indicates that cooperation may occur between the CTMS and the CAP.

Serum Lipid Determination. Lipid levels in serum were detected using an automatic biochemical analyzer, and the results are shown in Figure 3. TC, TG, and LDL levels in the CCMS group were similar to those in the normal group, but HDL levels were higher in the former than in the latter. Orlistat, CTS, CTMS, CAP, and CCMS showed good control of TC levels. TG levels were lower and HDL levels were higher in the FF group than in any of the other groups. Compared with the TG and HDL levels of the normal group, the Orlistat, CTS, CTMS, and CCMS groups shows varying degrees of reduction in TG levels and increases in HDL levels. The CCMS groups showed higher HDL levels than the CTMS or CAP groups. These results indicate that CCMSs exhibit potential as an antihyperlipidemic for decreasing TC.

Table 2. Result of Preparation of CCMS: Orthogonal Experiments Factors and Levels (A), Arrangement and Results of Orthogonal Experiments (B), Analysis of Variance (C), and the Effect of the Inlet Temperature (D), Flow Rate (E), and Hot Air Flow (F) on the Particle Size and Microsphere Yield

(A)

	factors		
levers	A CTS concentration (mg/mL)	B pH	C CTS/TPP
1	1.0	4.0	3
2	1.5	4.5	4
3	2.0	5.0	5

(B)

	factors						
no.	A	B	C	D	DEE (%)	EPR (%)	score
1	1	1	1	1	53.29	5.96	59.88
2	1	2	2	2	55.67	6.50	62.17
3	1	3	3	3	51.19	6.39	57.58
4	2	1	2	3	55.07	4.56	59.63
5	2	2	3	1	54.28	4.32	58.60
6	2	3	1	2	49.42	3.75	53.17
7	3	1	3	2	55.10	3.40	58.50
8	3	2	1	3	55.01	2.95	57.96
9	3	3	2	1	50.19	2.98	53.17
K_1	59.88	59.34	57.00	57.22			
K_2	57.13	59.58	58.32	57.95			
K_3	56.54	54.64	58.23	58.39			
R	3.33	4.94	1.32	1.17			

(C)

factors	SS	f	F	F*	significance
A	18.99	2	9.02	9.00	$P < 0.1$
B	46.49	2	22.07	9.00	$P < 0.1$
C	3.25	2	1.54	9.00	
error	2.11	2			

D

inlet temperature (°C)	particle size (μm)	yield (%)
140	4.4 ± 0.2	56.7 ± 1.4
160	4.6 ± 0.4	59.6 ± 1.9
180	4.5 ± 0.1	59.8 ± 1.2

(E)

flow rate (mL/h)	particles size (μm)	yield (%)
400	4.2 ± 0.3	60.1 ± 1.8
600	4.8 ± 0.5	59.8 ± 1.3
800	7.2 ± 0.2	44.5 ± 1.7

(F)

hot air flow (m^3/h)	particle size (μm)	yield (%)
28	4.2 ± 0.2	41.3 ± 1.1
32	4.1 ± 0.2	58.9 ± 1.6
36	4.6 ± 0.3	59.2 ± 1.4

Antiobesity Mechanism Study. *Quantitative RT-PCR.* To identify the mechanism by which CCMSs exert their antiobesity effects, adiponectin, leptin, PPARα, PPARγ, FTO,

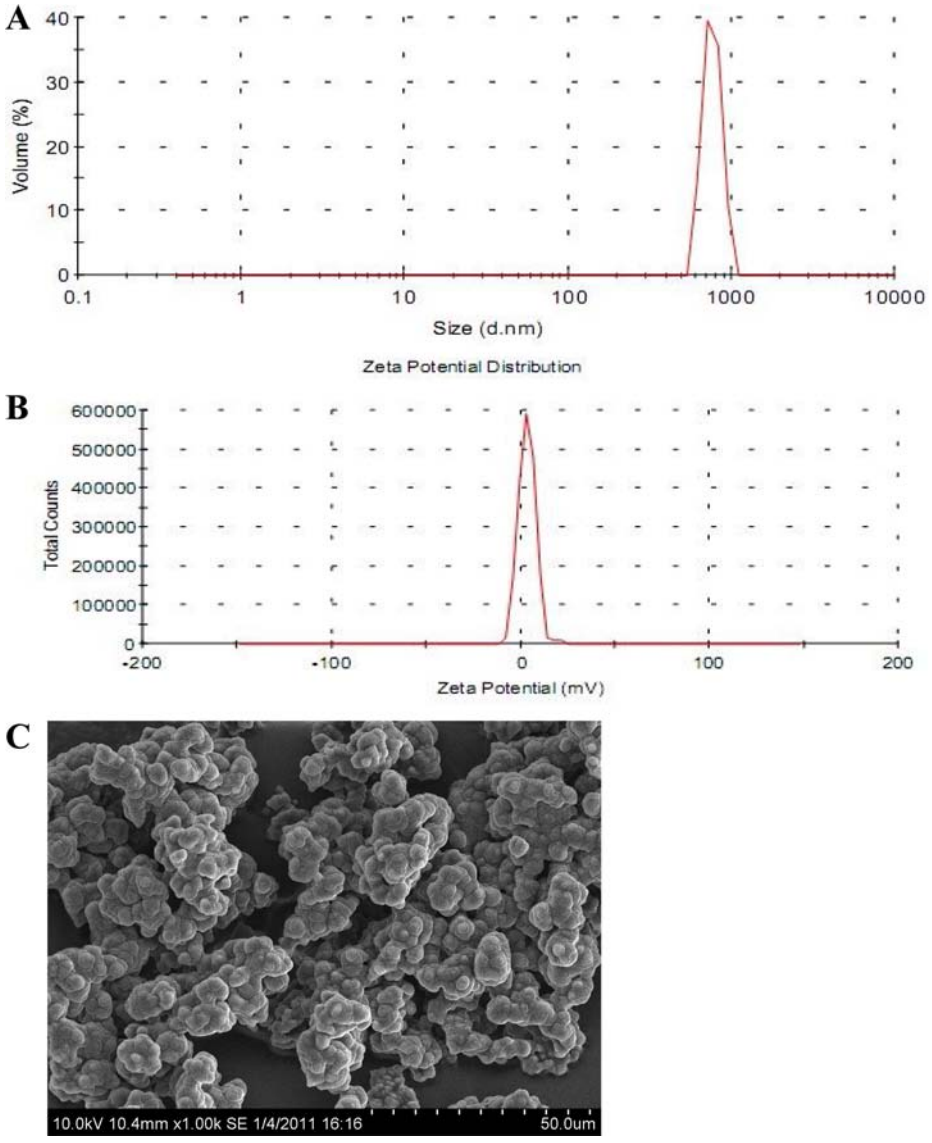

Figure 1. Characterization of CCMS. Particle distribution (A), ζ potential (B), and SEM (C) of CCMS. The particle distribution and ζ potential of the CCMS were determined with a laser diffraction size analyzer, and the surface morphology of the CCMS was studied by SEM (S3700N).

GPR120, and UCP2 were selected for RT-PCR detection (Figure 4A). The mRNA expression of adiponectin, PPARα, PPARγ, FTO, GPR120, and UCP2 increased among the groups to varying degrees, and the mRNA expression of LE decreased. The CCMS and CTMS groups showed significantly increased expression of AD, PPARα, and UCP2 and decreased expression of LE. In the CAP group, the expression of AD, PPARα, and UCP2 was upregulated while the expression of LE was slightly downregulated. The H-CCMS and M-CCMS groups showed better regulation of AD, PPARα, leptin, and UCP2 mRNA expression than the CTMS, CAP, and Orlistat groups. This finding may be attributed to the improved obesity control afforded by CCMSs in rats.

ELISA. RT-PCR analysis results indicated that the key obesity factors are AD, LE, PPARα, and UCP2 mRNA. Therefore, we detected the protein expression of these obesity factors in the serum by ELISA; the results are shown in Figure 4B−F. The AD, UCP2, and HL contents in serum from CCMS groups were much higher than those in the HF group. No significant difference in the expression of PPARα was found between the CCMS and HF groups. HL results showed that the HL may possibly be one of the reasons of CCMS for controlling obesity. RT-PCR and ELISA study results indicate that CTMSs and CCMSs affect the protein expression of AD, UCP2, and LE by exerting effects on obesity-associated genes.

Slices of Different Tissues. Tissue sections were stained with hematoxylin and eosin (H&E), and H&E images of different tissues are shown in Figure 5. The heart slices (Figure 5A) showed no myocardial hypertrophy in the NF, M-CCMS, and L-CCMS groups. The myofibers were in order, the stripes and muscle space were clear, and the nucleus was not enlarged. Figure 5B clearly shows that the liver cells of the fat group underwent vacuolation. The cells contained a pale, watery cytoplasm. Several differently shaped lipids and a large number of both small and large cytoplasmic lipid droplets were present. Large fat droplets were fairly noticeable. Spotty and focal necrosis occurred in the liver cells of the fat group, and an inflammatory cell infiltrate was observed in the normal group. Compared with the CTS, CAP, CTMS, and CCMS groups, the fatty liver-like Fat group was much better than the Fat group. In Figure 5C, the adipocytes of the Fat group were larger than those of other groups, except for the M-CCMS and L-CCMS

dx.doi.org/10.1021/jf4040628 | J. Agric. Food Chem. 2014, 62, 1866−1874

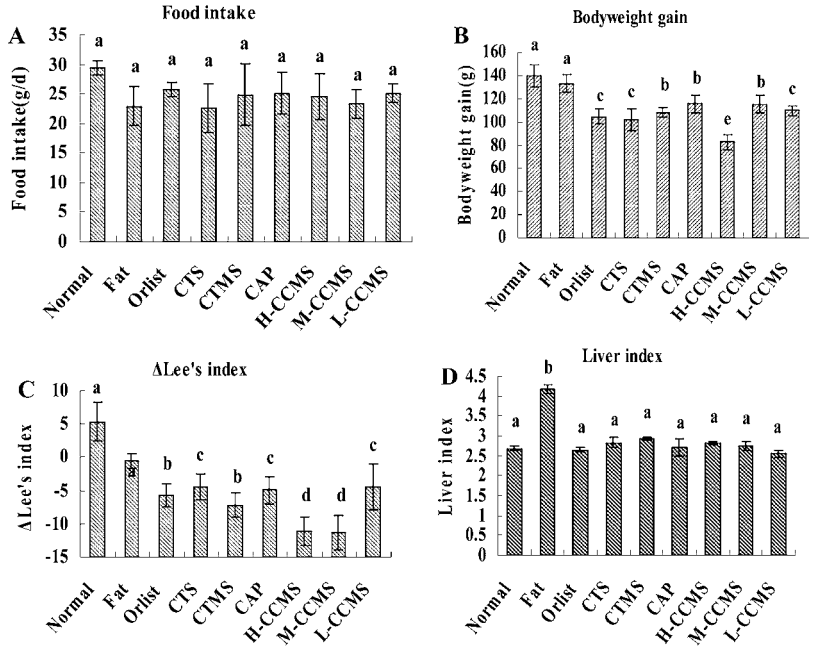

Figure 2. The main antiobese index of CCMS ($P < 0.05$). Changes in the body weight (A), food intake (B), Lee's index (C), liver index (D), body fat (E), and ratio of the body fat and weight (F) after 5 weeks treatment. Lee's index (body mass$^{1/3}$ × 1000/body length), Liver index (liver mass × 100/body mass), a low value of Lee's index, or liver index means that it is better at controlling obesity. The data are the means ± SE ($n = 10$). $P < 0.05$.

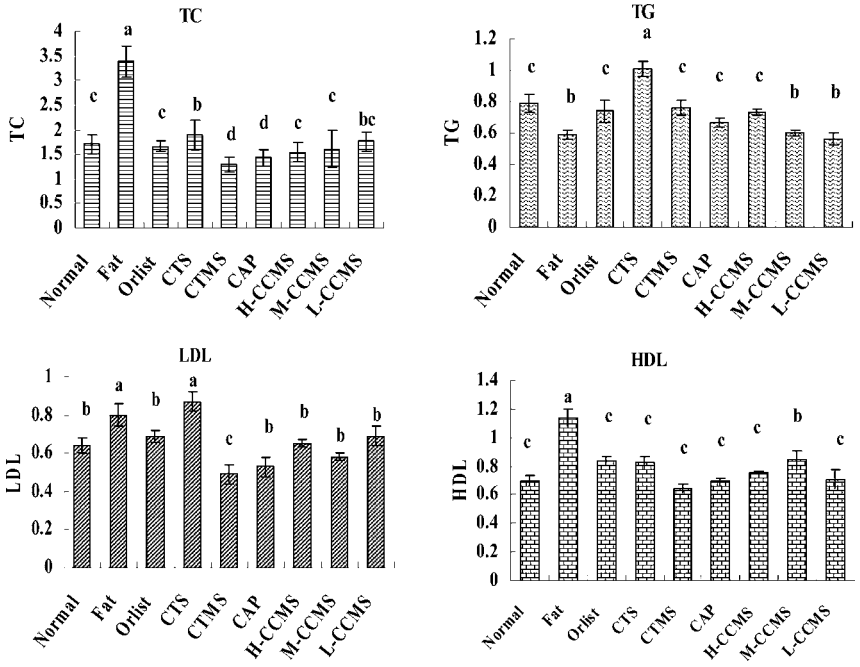

Figure 3. The serum lipid levels in rats ($P < 0.05$). The levels of TC, TG, LDL, and HDL in each group after 5 weeks treatment. The data are the means ± SE ($n = 10$). $P < 0.05$.

groups. Treatment with Orlistat, CTS, and high doses of CCMS clearly inhibited the proliferation of adipocytes. The same phenomena were observed in the mesentery fatty tissue slices (Figure 5D). In summary, the CCMSs are beneficial to the fatty liver and cardiac hypertrophy, which are caused by obesity.

DISCUSSION

Obesity is associated with a number of diseases and metabolic disturbances, including type 2 diabetes, hypertension, dyslipidemia, gallbladder disease, and some cancers.[17−19] Developing new types of antiobesity drugs is thus rapidly becoming an urgent necessity. Natural products, such as *Cassia* mimosoides, CTS, and CAP, and some types of food show promising antiobesity activities.[20−22]

dx.doi.org/10.1021/jf4040628 | J. Agric. Food Chem. 2014, 62, 1866−1874

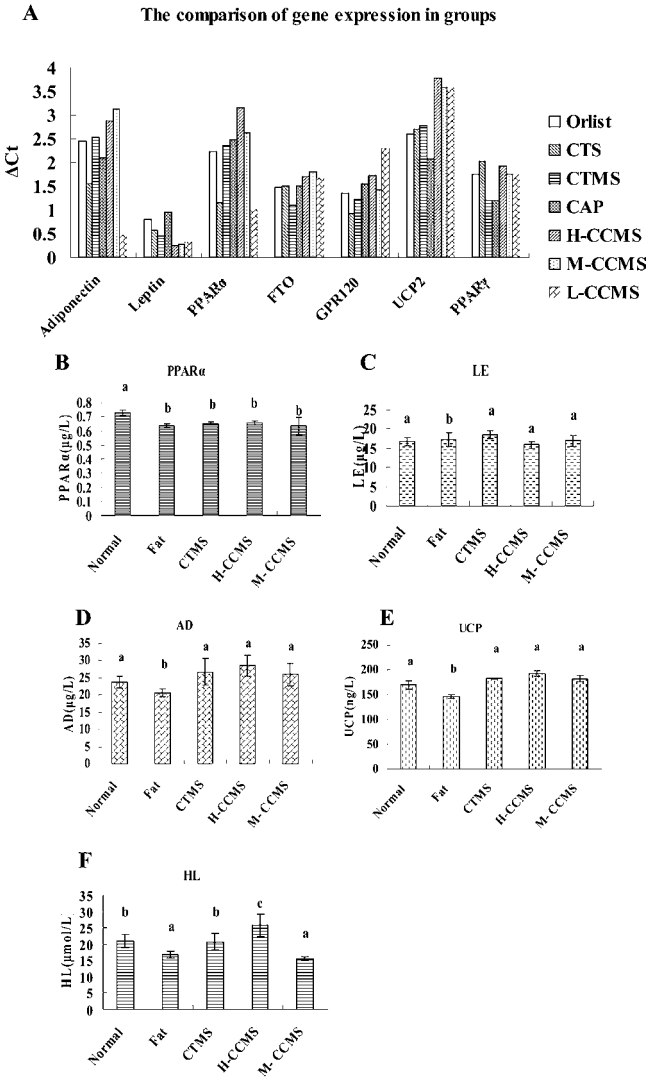

Figure 4. Gene expression and protein expression comparisons in the different treatment groups. The expression of adiponectin, leptin, PPARα, FTO, GPR120, UCP2, and PPARγ mRNA (A) in different treatment groups after 5 weeks of treatment. The level of mRNA was detected by Q-PCR. The changes of protein expression of adiponectin (B), leptin (C), PPARα (D), UCP2 (E), and hepatic lipase (F) in different treatment groups were detected by ELISA. Δ^{Ct} is the average value of 10 samples in the formulation (average gene expression of experiment groups/average gene expression of FF groups) = $2^{-\Delta\Delta Ct} = 2^{(-\Delta Ct_{control} - \Delta Ct_{FF})}$. If $2^{-\Delta\Delta Ct} < 1$, the average gene expression of the experiment groups is lower than that in the FF group. If this value is higher than 1, the average gene expression of the experiment groups is higher than that in the FF group.

CAP is a natural active substance extracted from red pepper.[23] The substance has been shown to be effective for weight loss and exhibited antihyperlipidemic activity in both animal and human studies.[15,24−27] However, CAP has limited use because of its pungency. This current study provides a solution that may partially eliminate this problem. During CCMS administration, the rats showed better tolerance toward the CCMSs than toward CAP (the compliance of the CCMS groups was better than that of the CAP group). The antiobesity activity of the CCMSs was also better than that of the CAP and CTMS groups, which may be attributed to the fact that CAP absorption is promoted by the CTMSs and additive effects exist between CAP and the CTMSs.

CTS is a polysaccharide material extracted from shell; it is generally considered a good excipient because of its biocompatibility.[28−30] CTS-based nanoparticles have been widely studied as drug carrier systems for many years,[31−33] and relevant studies show that these nanoparticles could improve the intestinal absorption of a drug in vivo.[34−36] Our research showed that CTMSs were significantly lowered blood lipid levels.[12] Combining microspheres with CAP may thus present a good solution to compensate for limitations associated with CAP use.

In this study, we prepared CCMSs by cross-linking and spray drying. CTS and TPP were combined by chemical bonding, and CAP was encapsulated inside the sphere. Many experiments have demonstrated that CTS has active functions in weight control and may be used as an antiobesity agent.[6,37,38] Therefore, CCMSs may be more functionally active than either CTS or CAP alone. The CCMSs may be applied as a future drug for weight loss.

The oral LD_{50} values of CAP were 118.84 and 97.40 mg/kg for male and female rats, respectively.[39] Prior to this research, we carried out a brief experiment to determine the highest dosage. No deaths occurred with 10-fold dosage of CCMS (CAP) in mice, which indicates that CCMSs may reduce CAP toxicity.

Compared with the CTMS, CAP, and Orlistat groups, the CCMSs grouped showed better inhibition of increases in rat body weight, body mass index, organ index, body fat, and proportion of fat to body weight (Figure 2). CCMSs maintained these parameters at normal or lower levels in rats and exhibited no effect on the appetite of rats. Rats treated with CCMSs showed more controlled body weight gains than rats treated with CAP or CTMS. Additive effects were also observed. Treatment with CCMSs significantly reduced the TC, TG, and LDL of rats to normal levels, and these decreases were lower than those shown by either CTMSs or CAP alone (Figure 3). The CCMSs could potentially lower blood lipids, but they are not as effective as the CTMSs, CTS, or CAP. While many studies have shown that CTS or chitin has potential use as an antiobesity agent and lowering lipid levels, concerns regarding CTS/chitin use remain. Low-molecular-weight CTS is easily absorbed,[40] and its small size exhibits great effects on body weight.[9] CCMSs, which are composed of small particles, may be easily absorbed and exhibit good antiobesity activity.

The mechanism of obesity is complex, and various genes have different effects on obesity.[41] In this study, we selected seven significant genes associated with obesity or hyperlipidemia for analysis. In the study of the antiobesity mechanism of CCMS, the expression of PPARα, PPARγ, leptin, adiponectin, UCP2, GPR120, and FTO genes was assayed by real-time RT-PCR at the mRNA level (Figure 4A). Genome-wide association studies have shown a strong correlation between a single nucleotide polymorphism in the first intron of the FTO gene with increased body mass index and obesity risk.[42] Adiponectin is an adipokine that antagonizes excess lipid storage in the liver and protects against inflammation and fibrosis.[43] GPR120 dysfunction has been demonstrated to cause obesity in mice and humans.[44] UCP2 is a key regulator of energy balance and mediates proton leaks across the inner membrane via the uncoupling of substrate oxidation from ATP synthesis.[45] Obese individuals have high circulating levels of leptin, which is a hormone secreted by adipose tissue and is involved in energy homeostasis.[46] PPARs

dx.doi.org/10.1021/jf4040628 | J. Agric. Food Chem. 2014, 62, 1866−1874

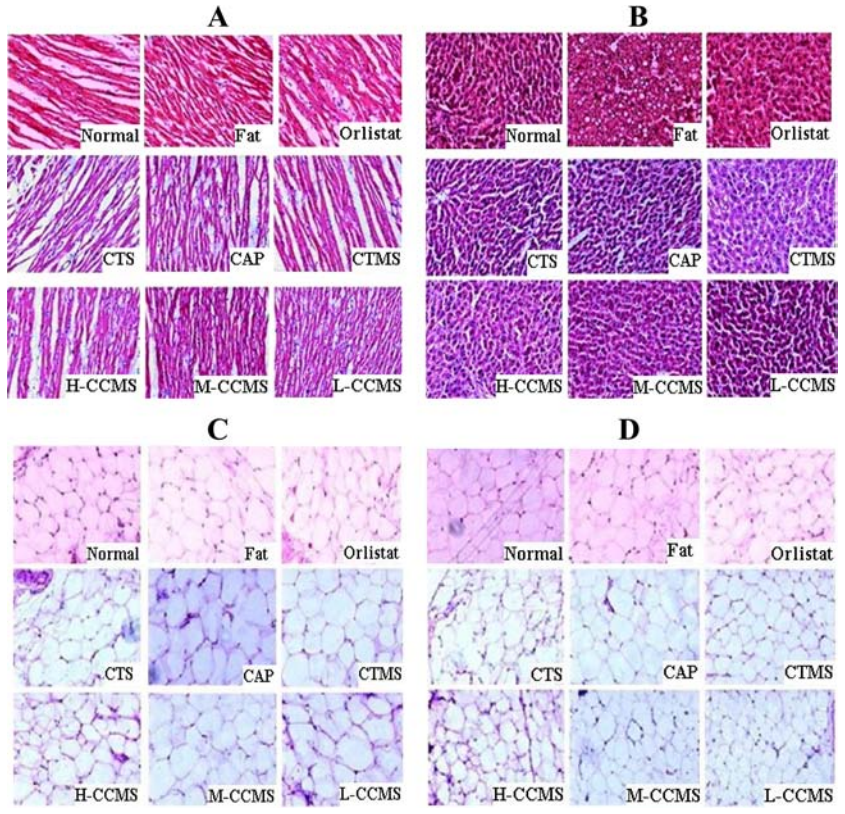

Figure 5. The tissue slices from different organs (200×). Heart slices (A), liver slices (B), subcutaneous fatty tissue slices (C), and mesentery fatty tissue slices (D). Tissue sections were stained with hematoxylin and eosin (H&E).

are important in the control of lipid metabolism.[47] The CCMSs were found to upregulate the expression of PPARα, UCP2, and adiponectin genes and downregulate the expression of the leptin gene. These results were confirmed by the serum protein contents determined using ELISA. The results of genes and protein (Figure 4 B−F) showed that PPARα, UCP2, leptin, and HL and were the key reasons of CCMS for controlling obesity.

Tissue slices showed that the rats fed with CCMSs had thinner myocardial and liver cells than the model group (Figure 5). Moreover, fewer inflammatory cell infiltrates and fatty degeneration of hepatocytes were observed in the heart and liver cells, respectively, of the CCMS-treated rats. The CCMS-treated groups also showed smaller subcutaneous and mesentery fat cells. Hsu demonstrated that CAP efficiently induces apoptosis and inhibits adipogenesis in 3T3-L1 preadipocytes and adipocytes.[48] Overall, the CCMSs possessed good efficacy in reducing weight and have potential therapeutic effects on fatty liver and myocardial hypertrophy caused by obesity. The CCMSs also inhibited the growth of fat cells to a certain extent.

On the basis of the results of the present study, CCMSs could be used as "natural products" with good ability to control obesity and hyperlipidemia. CCMSs may achieve weight loss effects by increasing the mRNA and protein expression of PPARα, UCP2, and adiponectin genes and downregulating the expression of leptin. The antiobesity activity of CCMSs was better than those of either CTMS or CAP. This result indicates that an additive effect exists between CTMSs and CAP.

AUTHOR INFORMATION

Corresponding Authors

*For J.G.: E-mail, wshxalb@163.com.

*For Z.S.: phone/fax, +86 20 39352067; E-mail, suzhq@scnu.edu.cn.

Author Contributions

‡S.T. and B.G. equally contributed to this work.

Funding

This project was financially supported by The National Natural Science Foundation of China (no. 81173107), the Science and Technology Planning Project of Guangzhou, China (no. 2011J4300064), and the Science and Technology Planning Project of Zhongshan, China (no. 2009H017).

Notes

The authors declare no competing financial interest.

ACKNOWLEDGMENTS

We are grateful to all our colleagues at the Guangdong TCM Key Laboratory for Metabolic Diseases. Acknowledgements are also made to Prof. Jiao Guo for providing the platform for this research.

ABBREVIATIONS USED

CTS, chitosan; CAP, capsaicin; CTMS, chitosan microsphere; CCMS, capsaicin−chitosan microspheres; ELISA, enzyme linked immunosorbent assay; PPAR, peroxisome proliferator-activated receptor; UCP, uncoupling protein; TC, total cholesterol; TG, triacylglyceride; LDL-C, low-density lipoprotein; HDL-C, high-density lipoprotein; TPP, sodium tripolyphosphate; HPLC, high performance liquid chromatography; SEM, scanning electron microscope; NF, normal diet group; FF, high-fat feeding group; AD, adiponectin; LE, leptin; HL, hepaticlipase; FTO, fat mass and obesity associated gene;

GPR120, G-protein-coupled receptor 120; LD_{50}, median lethal dose

REFERENCES

(1) *The World Health Report 1997—Conquering Suffering, Enriching Humanity*; World Health Organization: Geneva, 1998.

(2) Hill, J. O.; Peters, J. C. Environment contributions to the obesity epidemic. *Science* **1998**, *280*, 1371−1374.

(3) *Obesity: Preventing and Managing the Global Epidemic*; World Health Organization: Geneva, 2000.

(4) Hsu, Y. W.; Chu, D. C.; Ku, P. W.; Liou, T. H.; Chou, P. Pharmacotherapy for obesity: past, present and future. *J. Exp. Clin. Med.* **2010**, *2*, 118−123.

(5) Zhang, J.; Liu, J.; Li, L.; Xia, W. Dietary chitosan improves hypercholesterolemia in rats fed high-fat diets. *Nutr. Res. (N. Y.)* **2008**, *6*, 383−390.

(6) Jull, A. B.; Ni Mhurchu, C.; Bennett, D. A.; Dunshea-Mooij, C. A.; Rodgers, A. Chitosan for overweight or obesity. *Cochrane Database Syst. Rev.* **2008**, *3*, CD003892.

(7) Ni Mhurchu, C.; Poppitt, S. D.; McGill, A. T.; Leahy, F. E.; Benett, D. A.; Lin, R. B.; Ormrod, D.; Ward, L.; Strik, C.; Rodgers, A. The effect of the dietary supplement, chitosan, on body weight: a randomized controlled trial in 250 overweight and obese adults. *Int. J. Obes.* **2004**, *28*, 1149−1156.

(8) Zhang, H. L.; Tao, Y.; Guo, J.; Hu, Y. M.; Su, Z. Q. Hypolipidemic effects of chitosan nanoparticles in hyperlipidemia rats induced by high fat diet. *Int. Immunopharmacol.* **2011**, *11*, 457−461.

(9) Tao, Y.; Zhang, H. L.; Gao, B.; Guo, J.; Hu, Y. M.; Su, Z. Q. Water-Soluble Chitosan Nanoparticles Inhibit Hypercholesterolemia Induced by Feeding a High-Fat Diet in Male Sprague−Dawley Rats. *J. Nanomater.* **2011**, *2011*, 6.

(10) Zhang, H. L.; Wu, S. H.; Tao, Y.; Zang, L. Q.; Su, Z. Q. Preparation and Characterization of Water-Soluble Chitosan Nanoparticles as Protein Delivery System. *J. Nanomater.* **2010**, *2010*, 1.

(11) Gao, B.; Wu, S. H.; Zhang, H. L.; Tao, Y.; Su, Z. Q. Study on the lipid-lowering effect of water-soluble chitosan nanoparticles and microspheres in vitro. *Adv. Mater. Res.* **2011**, *217*, 306−310.

(12) Tan, S. R.; Wu, S. H.; Gao, B.; Xiao, J. R.; Guo, Z. Y.; Long, S. Y.; Bai, Y.; Su, Z. Q. Experimental investigation on the lipid-lowering activity of three novel antilipidemic materials in vitro. *Adv. Mater. Res.* **2012**, *399*, 1568−1572.

(13) Tao, Y.; Wu, S. H.; Zhang, H. L.; Zhang, W. Y.; Chen, H. C.; Su, Z. Q. Study on the effects of chitosan nanoparticles and microspheres on binding capacities of lipids and bile salts in vitro. *Food Sci. Technol.* **2010**, *35*, 271−274,279.

(14) Zhang, H. L.; Zhong, X. B.; Tao, Y.; Wu, S. H.; Su, Z. Q. Effect of chitosan and water-soluble chitosan micro- and nanoparticles in obese rats fed a high-fat diet. *Int. J. Nanomedicine* **2012**, *7*, 4069−4076.

(15) Diepvens, K.; Westerterp, K. R.; Westerterp-Plantenga, M. S. Obesity and thermogenesis related to the consumption of caffeine, ephedrine, capsaicin, and green tea. *Am. J. Physiol.: Regul. Integr. Comp. Physiol.* **2007**, *9*, 77−85.

(16) Smeets, A. J.; Westerterp-Plantenga, M. S. The acute effects of a lunch containing capsaicin on energy and substrate utilization, hormones, and satiety. *Eur. J. Nutr.* **2009**, *48*, 229−234.

(17) Snitker, S.; Fujishima, Y.; Shen, H.; Ott, S.; Pi-Sunyer, X.; Furuhata, Y.; Sato, H.; Takahashi, M. Effects of novel capsinoid treatment on fatness and energy metabolism in humans: possible pharmacogenetic implications. *Am. J. Clin. Nutr.* **2009**, *89*, 45−50.

(18) Hsu, Y. W.; Chu, D. C.; Ku, P. W.; Liou, T. H.; Chou, P. Pharmacotherapy for obesity: past, present and future. *J. Exp. Clin. Med.* **2010**, *2*, 118−123.

(19) Khandekar, M. J.; Cohen, P.; Spiegelman, B. M. Molecular mechanisms of cancer development in obesity. *Nature Rev. Cancer* **2011**, *11*, 886−895.

(20) Mcbride, D. New research provides insight into the link between obesity and cancer. *ONS Connect.* **2012**, *27*, 21.

(21) Vermaak, I.; Viljoen, A. M.; Hamman, J. H. Natural products in anti-obesity therapy. *Nat. Prod. Rep.* **2011**, *28*, 1493−1533.

(22) Yun, J. W. Possible anti-obesity therapeutics from nature. *Phytochemistry* **2010**, *71*, 1625−1645.

(23) Heber, D. Herbal preparations for obesity: are they useful? *Primary Care* **1999**, *30*, 441−463.

(24) Wachtel, R. E. Capsaicin. *Reg. Anesth. Pain Med.* **1999**, *24*, 361−363.

(25) Kobayashi, A.; Osaka, T.; Namba, Y.; Inoue, S.; Lee, T. H.; Kimura, S. Capsaicin activates heat loss and heat production simultaneously and independently in rats. *Am. J. Physiol.: Regul. Integr. Comp. Physiol.* **1998**, *275*, 92−98.

(26) Shin, K. O.; Moritani, T. Alterations of autonomic nervous activity and energy metabolism by capsaicin ingestion during aerobic exercise in healthy men. *J. Nutr. Sci. Vitaminol.* **2007**, *53*, 124−132.

(27) Watanabe, T.; Kawada, T.; Yamamoto, M.; Iwai, K. Capsaicin, a pungent principle of hot red pepper, evokes catecholamine secretion from the adrenal medulla of anesthetized rats. *Biochem. Biophys. Res. Commun.* **1987**, *142*, 259−264.

(28) Mahmmoud, Y. A. Capsaicin stimulates uncoupled ATP hydrolysis by the sarcoplasmic reticulum calcium pump. *J. Biol. Chem.* **2008**, *283*, 21418−21426.

(29) Kean, T.; Thanou, M. Biodegradation, biodistribution and toxicity of chitosan. *Adv. Drug. Delivery Rev.* **2010**, *62*, 3−11.

(30) De Souza, R.; Zahedi, P.; Allen, C. J. Biocompatibility of injectable chitosan−phospholipid implant systems. *Biomaterials* **2009**, *30*, 3818−3824.

(31) Wang, X. H.; Yu, X.; Yan, Y. N.; Zhang, R. J. Liver tissue responses to gelatin and gelatin chitosan gels. *J. Biomed. Mater. Res. A.* **2008**, *87*, 62−68.

(32) Hejazi, R.; Amiji, M. Chitosan-based gastrointestinal delivery systems. *J. Controlled Release* **2003**, *89*, 151−165.

(33) Hsu, S. H.; Chang, Y. B.; Tsai, C. L.; Fu, K. Y.; Wang, S. H.; Tseng, H. J. Characterization and biocompatibility of chitosan nanocomposites. *Colloids Surf., B: Biointerfaces* **2011**, *85*, 198−206.

(34) Lee, D.; Mohapatra, S. S. Chitosan nanoparticle-mediated gene transfer. *Methods Mol. Biol.* **2008**, *433*, 127−140.

(35) Pan, Y.; Li, Y. J.; Zhao, H. Y.; Zheng, J. M.; Xu, H.; Wei, G.; Hao, J. S.; Cui, F. D. Bioadhesive polysaccharide in protein delivery system: chitosan nanoparticles improve the intestinal absorption of insulin in vivo. *Int. J. Pharm.* **2002**, *249*, 139−147.

(36) Lin, Y. H.; Mi, F. L.; Chen, C. T. Preparation and characterization of nanoparticles shelled with chitosan for oral insulin delivery. *Biomacromolecules* **2007**, *8*, 146−152.

(37) Wu, S. H.; Tao, Y.; Zhang, H. L.; Su, Z. Q. Preparation and characterization of water-soluble chitosan microparticles loaded with insulin using the polyelectrolyte complexation method. *J. Nanomater.* **2011**, *2011*, ArticleID 404523 DOI: 10.1155/2011/404523.

(38) Jull, A. B.; Ni Mhurchu, C.; Bennett, D. A. Chitosan for overweight or obesity. *Cochrane Database Syst. Rev.* **2008**, *3*, CD003892.

(39) Wydro, P.; Krajewska, B.; Hac-Wydro, K. Chitosan as a lipid binder: a Langmuir monolayer study of chitosan−lipid interactions. *Biomacromolecules* **2007**, *8*, 2611−2617.

(40) Chae, S. Y.; Jang, M. K.; Nah, J. W. Influence of molecular weight on oral absorption of water soluble chitosan. *J. Controlled Release* **2005**, *102*, 383−394.

(41) Saito, A.; Yamanoto, M. Acute oral toxicity of capsaicin in mice and rats. *J. Toxicol. Sci.* **1996**, *21*, 195−200.

(42) Dina, C.; Meyre, D.; Gallina, S.; Durand, E.; Korner, A.; Jacobson, P.; Carlsson, L.; Kiess, W.; Vatin, V.; Lecoeur, C.; Delplanque, J.; Vaillant, E.; Pattou, F.; Ruiz, J.; Weill, J.; Levy-Marchal, C.; Horber, F.; Potoczna, N.; Hercberg, S.; Stunff, C. L.; Bougneres, P.; Kovacs, P.; Marre, M.; Balkau, B.; Cauchi, S.; Chevre, J.; Froguel, P. Variation in FTO contributes to childhood obesity and severe adult obesity. *Nature Genet.* **2007**, *39*, 724−726.

(43) Buechler, C.; Wanninger, J.; Neumeier, M. Adiponectin, a key adipokine in obesity related liver diseases. *World J. Gastroenterol.* **2011**, *23*, 2801−2811.

(44) McLarnon, A. Obesity: GPR120 dysfunction can cause obesity in mice and humans. *Nature Rev. Gastroenterol. Hepatol.* **2012**, *4*, 187.
(45) Zhang, C. Y.; Baffy, G.; Perret, P.; Krauss, S.; Peroni, O.; Grujic, D.; Hagen, T.; Vidal-Puig, A.; Boss, O.; Kim, Y.; Zheng, X. X.; Wheeler, M.; Shulman, G.; Chan, C.; Lowell, B. Uncoupling protein-2 negatively regulates insulin secretion and is a major link between obesity, beta cell dysfunction, and type 2 diabetes. *Cell.* **2011**, *105*, 745−755.
(46) Leshan, R. L.; Greenwald-Yarnell, M.; Patterson, C. M.; Gonzalez, I. E.; Myers, M. G. Leptin action throuph hypothalamic nitric oxide synthase-1-expressing neurons controls energy balance. *Nature Med.* **2012**, *18*, 2.
(47) Djouadi, F.; Brandt, J. M.; Weinheimer, C. J. The role of the peroxisome proliferators-activated receptor alpha(PPAR alpha) in the control of cardiac lipid metabolism. *Prostaqlandins, Leukotrienes Essent. Fatty Acids* **1999**, *5*, 339−343.
(48) Hsu, C. L.; Yen, G. C. Effects of capsaicin on induction of apotosis and inhibition of adipogenesis in 3T3-L1 cells. *J. Agric. Food Chem.* **2007**, *55*, 1730−1736.

Garlic and sprouted garlic were minced, ground, and extracted with 10 volumes of 100% ethanol as a solvent. The extract was prepared by removing the solvent with rotary evaporation. The sample solution was prepared by redissolving the extract in ethanol at 40 mg/mL and diluting, if necessary, before use. The garlic extract was further fractionated with *n*-hexane, ethyl acetate, butanol, and water consecutively for use in the 2,2-diphenyl-1-picrylhydrazyl (DPPH) radical scavenging assay.

Determination of the Total Phenolic Content. The total phenolic content was measured using the Folin−Ciocalteu reagent.[23] Briefly, 100 μL of extract was mixed with 50 μL of sodium bicarbonate (10%, w/v) solution; 15 μL of the Folin−Ciocalteu reagent, which was diluted by 5-fold with distilled water, was then added. After 5 min at room temperature, the sample mixture was transferred to a 96-well microplate, followed by measuring the absorbance at 593 nm using a microplate reader (Sunrise, Tecan Retisoft, Inc., Mississauga, Ontario, Canada). The total phenolics were expressed as gallic acid equivalents (GAE).

DPPH Radical Scavenging Activity Assay. The DPPH radical scavenging activity assay was performed following a published method, with some modifications.[24] Briefly, 50 μL of each sample was mixed with 200 μL of 200 μM DPPH methanolic solution in a 96-well plate, followed by gentle shaking. After incubation at 37 °C for 30 min, the absorbance was measured at 515 nm. The sample-dissolving solvent and Trolox were used as negative and positive controls, respectively.

Oxygen Radical Absorbance Capacity (ORAC) Assay. The peroxyl radical scavenging capacity of the sample extracts was evaluated by an ORAC assay system.[25] All data were expressed as micromoles of Trolox equivalents (TE), and 1 ORAC unit was equivalent to the net protection by 1 μM Trolox.

Neuroprotective Effect of SGE. HT22 mouse hippocampal neuronal cells were routinely maintained in Dulbecco's modified Eagle's medium (DMEM) with 10% FBS and 100 units/mL penicillin and streptomycin in a humidified CO_2 incubator (MCO-19-AIC, Sanyo, Osaka, Japan) at 37 °C and 5/95% CO_2/air.

The cells were seeded in a 96-well culture dish in DMEM supplemented with 10% FBS at a density of 2×10^3 cells per well. The next day, various doses of SGE and 5 mM glutamate were added to the cells.[26] After cells were cultured for 20 h, the cell survival rate was determined using the 3-(4,5-dimethylthiazol-2-yl)-2,5-diphenyltetrazolium bromide (MTT) cell proliferation assay. The cell viability was presented as the percentage of the untreated control.

Assessment of Intracellular Reactive Oxygen Species (ROS). The intracellular ROS level was determined by a previously reported method.[27] HT22 cells (2×10^3 cells/well) were seeded in a 96-well black culture plate and cultured for 24 h. After cells were attached on the culture plate, the cells were incubated in the presence of 5 mM glutamate and garlic samples for 6 h. The cells were then washed with phosphate-buffered saline (PBS), incubated for 30 min with DCFDA dissolved in DMEM (final concentration of 30 μM), and then washed with PBS. The fluorescence generated by the interaction of the ROS with dichlorofluorescein (DCF) was observed and photographed under a fluorescence microscope (Eclipse 80i, Nikon, Tokyo, Japan).

Ultraperformance Liquid Chromatography Quadruple Time-of-Flight Mass Spectrometry (UPLC-Q-TOF-MS) Analysis of SGEs. To analyze the metabolites of garlic and sprouted garlic, ethanolic extracts from garlic and sprouted garlic were redissolved in ethanol. The metabolites were analyzed using an Acquity UPLC system (Waters, Milford, MA) equipped with a Waters Micromass Q-TOF Premier mass spectrometer and an Acquity UPLC BEH C18 column (100 × 2.1 mm, 1.7 μm, Waters, Milford, MA). Two solvents, 0.1% formic acid (v/v) and acetonitrile containing 0.1% (v/v) formic acid, were used as the mobile phase. The elution was initiated with the mobile phase containing 5% acetonitrile that was maintained for 1 min, gradually increased to 100% acetonitrile over 10 min, remained at 100% acetonitrile for 1 min, and decreased to 5% acetonitrile for 1 min. The sample (5 μL) was injected, while the flow rate was maintained at 0.3 mL/min. Electron spray ionization was conducted in the negative and positive modes within a m/z range of 100−1000. The ion source and desolvation temperatures were 200 and 250 °C, respectively. The capillary and cone voltages were 3.0 kV and 30 V, respectively. The cone gas flow was 50 L/h. Leucine enkephalin was used as the lock mass (m/z 554.2615) at a concentration of 0.5 ng/μL and a flow rate of 3.0 μL/min.

Data Processing, Multivariate Analysis, and Tentative Identification of Discriminative Variables. The DataBridge program in the MassLynx software package (version 4.1, Waters) was used to export raw data sets to the net CDF file format, in which the net CDF files were automatically aligned using the XCMS package in R 3.0.1 (www.bioconductor.org). The result .txt file, which included the sample name, peak area, and retention time as a variable, was processed using SIMCA-P software 12.0 (Umetrics, Umea, Sweden) for multivariate statistical analysis. The data sets were autoscaled (unit variance scaling) and log-transformed before principal component analysis (PCA) modeling. To identify the different metabolites, we used partial least-squares discriminant analysis (PLS-DA, data not shown) models and created box-and-whisker plots with the mean data using STATISTICA (version 7.0, StatSoft, Inc., Tulsa, OK). We selected metabolites based on the variable important to projection (VIP) values (VIP > 1.0) and p values ($p < 0.05$) and tentatively identified them by comparing their molecular weights to those in the 2008 *Dictionary of Natural Products* (CRC Press, Taylor and Francis Group, Boca Raton, FL) and related references. In addition, the accurate mass from TOF-MS was matched with the elemental composition and the theoretical isotope distribution (i-FIT).

Statistical Analysis. Data were assessed by analysis of variance, followed by Duncan's multiple range test, using SPSS software (SPSS, Inc., Chicago, IL). The significance level was set at $p < 0.05$.

RESULTS

Total Phenolic Contents. Plant polyphenols are multifunctional; they can act as reducing agents, hydrogen-donating antioxidants, and singlet oxygen quenchers. As shown in Figure 1, the total phenolic content in garlic increased slightly during sprouting but there was no significant difference when garlic was sprouted for different periods.

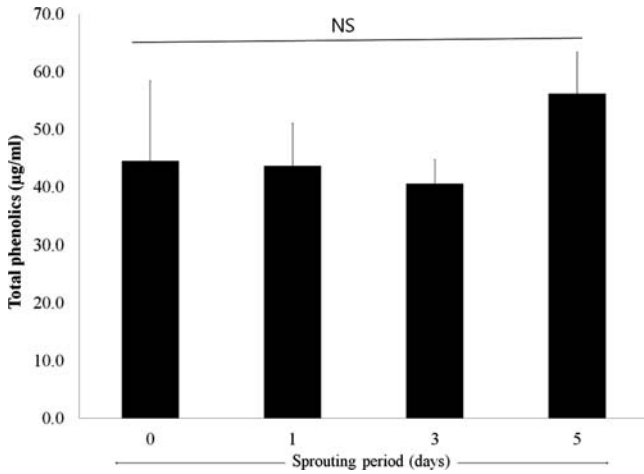

Figure 1. Total phenolic content of SGE. Data are expressed as the mean ± standard deviation (SD) of four independent experiments. NS = no significant difference between the groups.

DPPH Radical Scavenging Activity of Sprouted Garlic. The antioxidant activities of garlic and sprouted garlic are shown in Figure 2 as the percentage of DPPH radical scavenging activity in the control. The DPPH radical scavenging activity of sprouted garlic was higher than that of unsprouted garlic. Of the extracts from samples sprouted 0, 1, 3, or 5 days, the ethanol extract from garlic sprouted for 5 days showed the highest DPPH radical scavenging activity; the

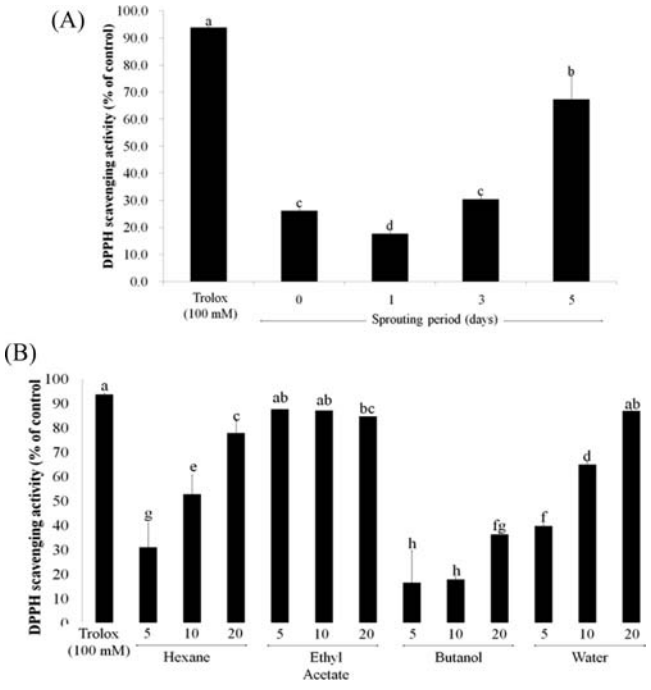

Figure 2. DPPH radical scavenging activity of (A) SGE and (B) solvent fractions. Data are expressed as the mean ± SD of four independent experiments. Values not sharing a common letter differ significantly from each other ($p < 0.05$).

scavenging activity of the 10 mg/mL extract was 80−100% of the control (Figure 2).

ORAC of Sprouted Garlic. The ORAC assay measures the loss of fluorescence caused by the oxidative degradation of fluorescein, a fluorescent molecule, when mixed with 2,2′-azobis(2-amidinopropane) dihydrochloride (AAPH) (final concentration of 11.4 mM), a peroxyl radical generator (Figure 3). The presence of an antioxidant suppresses or slows the loss of fluorescence, resulting in a high ORAC value. Extracts from garlic sprouted for 5 days suppressed the generation of the peroxy radical more than extracts from raw garlic and garlic sprouted for shorter times, consistent with the results of the other antioxidant assays.

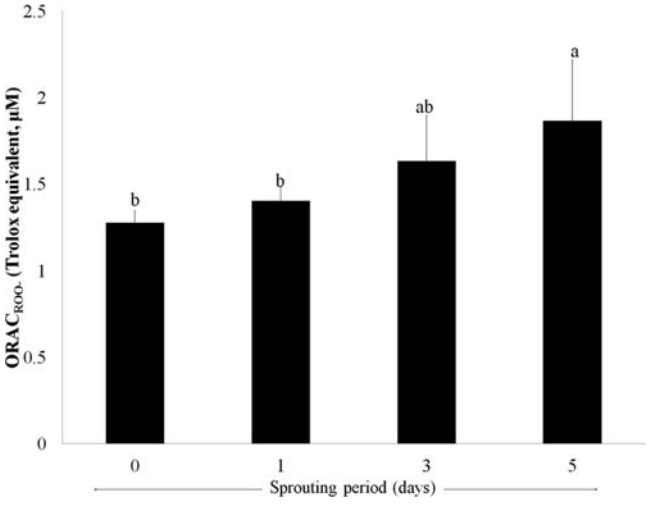

Figure 3. Oxygen radical absorbance activity of SGE. All data are expressed as micromoles of TE. One ORAC unit is equivalent to the net protection area provided by 1 μM Trolox. Values not sharing a common letter differ significantly from each other ($p < 0.05$).

Suppression of Intracellular ROS Generation by SGE in Mouse Hippocampus Cells. We investigated the inhibitory effect of SGE on ROS generation using the oxidant-reactive fluorescent dye DCFDA. SGE prevented glutamate-induced cytotoxicity in the HT22 mouse hippocampal neuronal cell line (Figure 4), whereas raw garlic extract had a limited protective effect. Furthermore, ROS generation mediated by glutamate treatment in HT22 cells was significantly suppressed by the ethanolic extract from garlic sprouted for 4−5 days. These results confirm that sprouted garlic has higher antioxidant potential than non-sprouted garlic (Figure 5).

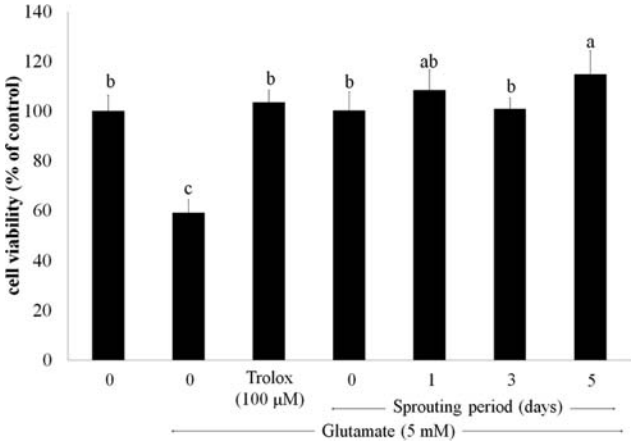

Figure 4. Inhibition of glutamate-induced cell death by SGE in HT22 cells. Cells were treated with 5 mM glutamate in the absence and presence of sprouted garlic samples for 24 h. Cell viability was measured with the MTT assay. The cell survival rate is presented as the percentage of the untreated control. Values not sharing a common letter differ significantly from each other ($p < 0.05$).

Multivariate Analysis of Raw and Sprouted Garlic Metabolites. After aligning the UPLC-Q-TOF-MS spectral data, we obtained 1098 and 1904 variables with the negative and positive detection modes, respectively. The aligned data were presented as two-dimensional PCA (Figure 6) score plots: vector t[1] explained 37.99 and 40.62% of the variation, and vector t[2] explained 16.55 and 22.77% of the variation in the positive and negative modes, respectively. The PCA score plots demonstrated that the metabolite profiles of garlic differed depending upon the sprouting period. In particular, in PC1 of the positive and negative analyses, the metabolite profile of garlic that sprouted for 5 and 6 days (group 1) differed from the metabolite profile of garlic that sprouted for <5 days (group 2). The metabolites that discriminated between the two groups were identified on the basis of the criteria of $p < 0.05$ and VIP > 1.0 (Table 1). Among these metabolites, we identified isoguanosine (or 1-aminoinosine) (**2**), γ-glutamyl-*S*-*trans*-1-propenyl cysteine, glucoside (**3**), 8,11,12-trihydroxy-9-octadecenoic acid (**5**), and spirostane-3,6-diol, 6-*O*-D-glucopyranoside (**7**). These metabolites increased during the sprouting period (Figure 7).

DISCUSSION

Garlic (*Allium sativum*) has long been used for medicinal purposes, owing to its immune-enhancing functions and

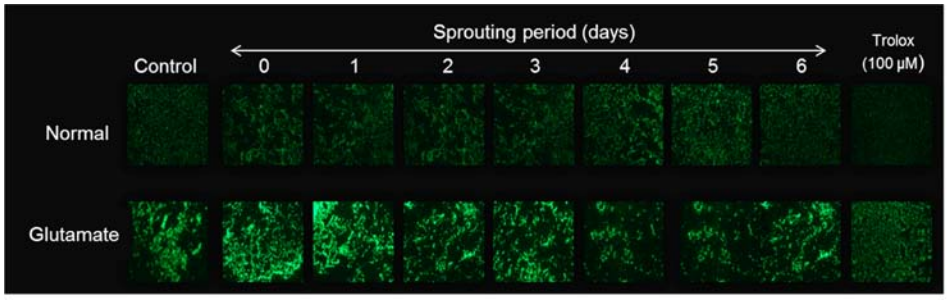

Figure 5. Inhibition of glutamate-induced ROS production by SGE in HT22 cells. The cells (2×10^3 cells/well) were seeded in a 96-well black-bottom plate and cultured for 24 h. After cell attachment, the cells were incubated in the presence of 5 mM glutamate and garlic samples for 6 h. The treated cells were washed with PBS, incubated for 30 min with DCFDA dissolved in DMEM (final concentration of 30 μM), and then washed with PBS. The fluorescence generated by the interaction of ROS with DCF was visualized under a fluorescence microscope.

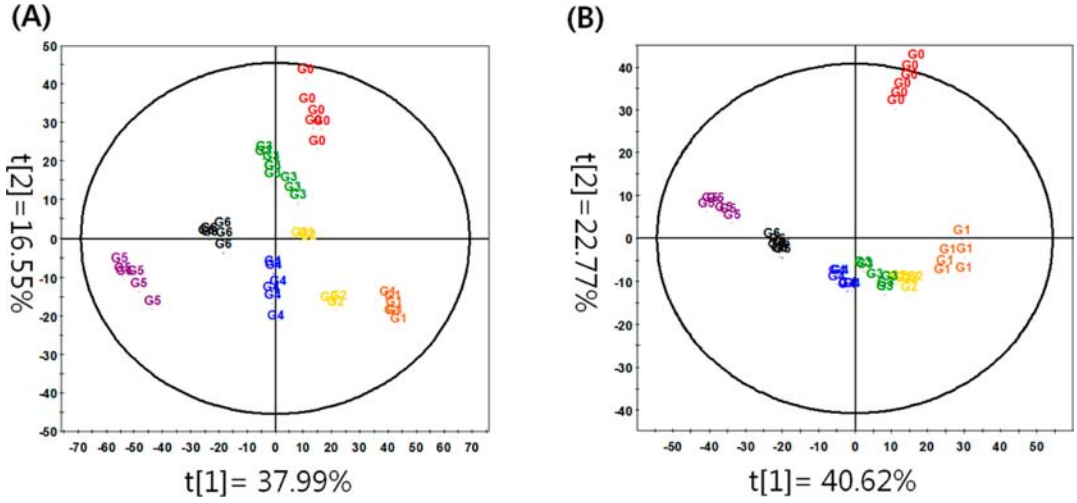

Figure 6. PCA score scatter plots of the first two components for UPLC-Q-TOF-MS analysis in (A) positive and (B) negative modes. Sprouting time: red, 0 days; orange, 1 day; yellow, 2 days; green, 3 days; blue, 4 days; purple, 5 days; and black, 6 days.

Table 1. Tentative Identification of Significant Variables Distinguished by Groups 1 and 2 in UPLC-Q-TOF-MS

		UPLC-Q-TOF-MS							
number	t_R[a] (min)	negative	error (ppm)	positive	error (ppm)	MW	tentative compound	p value[b]	reference
1	0.79	131.0827					NI[c]	1.03×10^{-7}	
2	1.31	282.0851	4.6	284.1007	4.2	283	isoguanosine or 1-aminoinosine	2.92×10^{-12}	
3	3.05	451.1385	−0.2	453.1532	1.1	452	γ-glutamyl-*S*-*trans*-1-propenylcysteine, glucoside	5.84×10^{-5}	29
4	5.59			325.2287			NI	2.51×10^{-7}	
5	5.90	329.2328	0.0	353.2299	−8.2	330	8,11,12-trihydroxy-9-octadecenoic acid	4.11×10^{-12}	31
6	6.19			257.0114			NI	1.23×10^{-8}	
7	6.84	593.3707	2.9	595.3843	−0.5	594	spirostane-3,6-diol, 6-*O*-D-glucopyranoside	7.15×10^{-10}	30
8	8.47	614.3359		616.3417		615	NI	1.55×10^{-12}	
9	8.51	311.1681					NI	3.41×10^{-5}	
10	8.78			496.3370			NI	5.01×10^{-13}	

[a] t_R = retention time. [b] Significance was determined by the t test. Components with a p value of ≤0.05 indicate moderate evidence of a statistically significant effect. [c] NI = not identified.

antibacterial, antifungal, antiviral, and anticancer activities. Garlic prevents platelet aggregation, and it has hypotensive and cholesterol- and triglyceride-lowering effects.[28]

We found that sprouting enhanced the DPPH radical scavenging activity and ORAC of garlic. Sprouting also increased the capacity of garlic to suppress intracellular ROS induced by hydrogen peroxide in HT22 cells. The HT22 mouse hippocampal cell line, a subclone of the original HT4 clone, is sensitive to amyloid-β (Aβ) and particularly vulnerable to glutamate; thus, HT22 cells provide a good model system with which to study neuronal cell degeneration and screen for potential agents, such as antioxidants, that prevent Aβ- or glutamate-induced cell death.[19,26,29,30] Glutamate reduced the viability of HT22 cells, but viability was restored by treatment with an extract from garlic sprouted for 5 days. Furthermore, the same effect was observed with extracts prepared from garlic at an early stage of sprouting, suggesting that certain

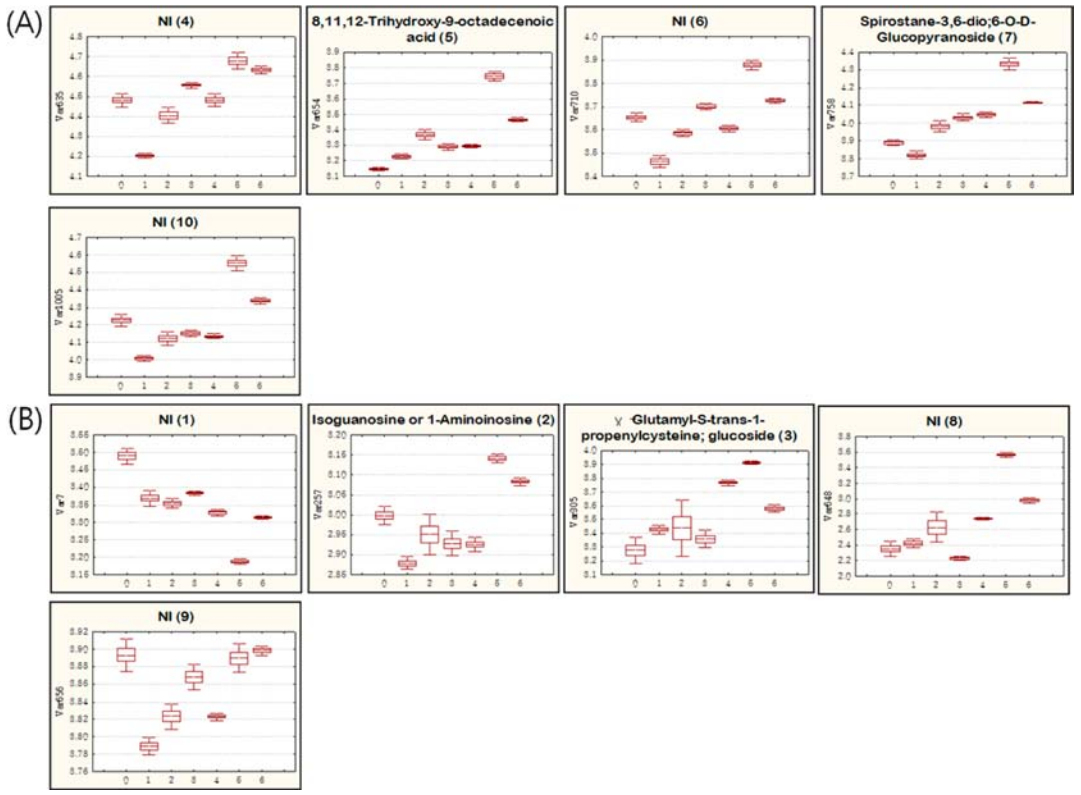

Figure 7. Box-and-whisker plots of changes in metabolite levels with sprouting time when mass spectrometry was run in (A) positive and (B) negative modes.

antioxidants or neuroprotective compounds like flavonoids are produced during the early stage of sprouting.

Although the increased neuroprotective effect could be ascribed to the enhanced antioxidant capacity of sprouted garlic, it is not clear which components in sprouted garlic are primarily responsible for the increased antioxidant capacity. Furthermore, sprouting did not increase the total phenolic content of garlic, suggesting that phenolics are not associated with the increased antioxidant activity and neuroprotective effect of SGE.

The health benefits of garlic are attributed to organosulfur compounds that mainly derive from alliin. Alliin is quickly converted into allicin through extremely reactive intermediates, sulfenic acids (R-SOH), by the enzyme alliinase (alliin lyase EC.4.4.1.4) when garlic is physically damaged. Alliin, allyl disulfide, and allyl cysteine scavenge hydroxyl radicals, whereas allicin does not.[18] In our multivariate analysis, the metabolite patterns differed depending upon the sprouting period and correlated closely with the antioxidant activities. Moreover, the PCA score plots were different before and after 4 sprouting days. Among the 10 metabolites that influenced the multivariate analysis, γ-glutamyl-*S*-*trans*-1-propenyl cysteine; glucoside (**3**) and spirostane-3,6-diol, 6-*O*-D-glucopyranoside (**7**) were previously detected in their derivative forms, γ-glutamyl-*S*-*trans*-1-propenyl cysteine (GSPC)[31] and steroidal oligoglycoside,[32] respectively, in *Allium* species. GSPC is a major metabolite[33] in garlic and a precursor of isoalliin, which has antioxidant activity. Spirostane-3,6-diol, 6-*O*-D-glucopyranoside is a steroidal oligoglycoside and an antineoplastic agent. Although there is no information on the antioxidant activities of these two compounds in their glycosidic forms, the glucosidic forms of flavonoids have a similar level of antioxidant activity as the aglycone forms.[34] Furthermore, it has been reported that certain glycosidic forms could be hydrolyzed into aglycones by intracellular glucosidases in neuronal tissues.[35] However, further studies are required to define the antioxidative potential of the compounds that increased in sprouted garlic and to characterize the components responsible for the antioxidative and neuroprotective activities.

In conclusion, sprouting could be a useful way to increase the antioxidative potential of garlic and thereby expand its use.

AUTHOR INFORMATION

Corresponding Author

*Telephone: 82-53-950-5752. Fax: 82-53-950-6750. E-mail: vision@knu.ac.kr.

Author Contributions

†Alexandra Zakarova and Ji Yeon Seo contributed equally to this work.

Funding

This work was supported by a grant from Korea Institute of Planning and Evaluation for Technology in Food, Agriculture, Forestry and Fisheries (IPET) (High Value-Added Food Technology Development Program, 2012, 112066-3), Ministry for Food, Agriculture, Forestry and Fisheries, Republic of Korea.

Notes

The authors declare no competing financial interest.

REFERENCES

(1) Tattelman, E. Health effects of garlic. *Am. Fam. Physician* **2005**, *72*, 103−106.

(2) Weik, R.; Francky, A.; Striedner, G.; Raspor, P.; Bayer, K.; Mattanovich, D. Recombinant expression of alliin lyase from garlic

(*Allium sativum*) in bacteria and yeasts. *Planta Med.* **1998**, *64*, 387−388.
(3) Borek, C. Antioxidant health effects of aged garlic extract. *J. Nutr.* **2001**, *131*, 1010S−1015S.
(4) Reeve, V. E.; Bosnic, M.; Rozinova, E.; Boehm-Wilcox, C. A garlic extract protects from ultraviolet B (280−320 nm) radiation-induced suppression of contact hypersensitivity. *Photochem. Photobiol.* **1993**, *58*, 813−817.
(5) Chang, H. S.; Yamato, O.; Yamasaki, M.; Maede, Y. Modulatory influence of sodium 2-propenyl thiosulfate from garlic on cyclo-oxygenase activity in canine platelets: Possible mechanism for the anti-aggregatory effect. *Prostaglandins, Leukotrienes Essent. Fatty Acids* **2005**, *72*, 351−355.
(6) Ali, M. Mechanism by which garlic (*Allium sativum*) inhibits cyclooxygenase activity. Effect of raw versus boiled garlic extract on the synthesis of prostanoids. *Prostaglandins, Leukotrienes Essent. Fatty Acids* **1995**, *53*, 397−400.
(7) Block, E. The chemistry of garlic and onions. *Sci. Am.* **1985**, *252*, 114−119.
(8) Sangeetha, T.; Quine, S. D. Protective effect of S-allyl cysteine sulphoxide (alliin) on glycoproteins and hematology in isoproterenol induced myocardial infarction in male Wistar rats. *J. Appl. Toxicol.* **2008**, *28*, 710−716.
(9) Ortuno Sahagun, D.; Marquez-Aguirre, A. L.; Quintero-Fabian, S.; Lopez-Roa, R. I.; Rojas-Mayorquin, A. E. Modulation of PPAR-γ by nutraceutics as complementary treatment for obesity-related disorders and inflammatory diseases. *PPAR Res.* **2012**, *2012*, 318613.
(10) Moriguchi, T.; Matsuura, H.; Itakura, Y.; Katsuki, H.; Saito, H.; Nishiyama, N. Allixin, a phytoalexin produced by garlic, and its analogues as novel exogenous substances with neurotrophic activity. *Life Sci.* **1997**, *61*, 1413−1420.
(11) Kim, H. J.; Suh, H. J.; Lee, C. H.; Kim, J. H.; Kang, S. C.; Park, S.; Kim, J. S. Antifungal activity of glyceollins isolated from soybean elicited with *Aspergillus sojae*. *J. Agric. Food Chem.* **2010**, *58*, 9483−9487.
(12) Takahashi, M.; Shibamoto, T. Chemical compositions and antioxidant/anti-inflammatory activities of steam distillate from freeze-dried onion (*Allium cepa* L.) sprout. *J. Agric. Food Chem.* **2008**, *56*, 10462−10467.
(13) Alvarez-Jubete, L.; Wijngaard, H.; Arendt, E. K.; Gallagher, E. Polyphenol composition and in vitro antioxidant activity of amaranth, quinoa buckwheat and wheat as affected by sprouting and baking. *Food Chem.* **2010**, *119*, 770−778.
(14) Randhir, R.; Lin, Y. T.; Shetty, K. Stimulation of phenolics, antioxidant and antimicrobial activities in dark germinated mung bean sprouts in response to peptide and phytochemical elicitors. *Process Biochem.* **2004**, *39*, 637−646.
(15) Kim, H. J.; Suh, H. J.; Kim, J. H.; Park, S.; Joo, Y. C.; Kim, J. S. Antioxidant activity of glyceollins derived from soybean elicited with *Aspergillus sojae*. *J. Agric. Food Chem.* **2012**, *58*, 11633−11638.
(16) Bozin, B.; Mimica-Dukic, N.; Samojlik, I.; Goran, A.; Igic, R. Phenolics as antioxidants in garlic (*Allium sativum* L., Alliaceae). *Food Chem.* **2008**, *111*, 925−929.
(17) Ichikawa, M.; Ide, N.; Ono, K. Changes in organosulfur compounds in garlic cloves during storage. *J. Agric. Food Chem.* **2006**, *54*, 4849−4854.
(18) Chung, L. Y. The antioxidant properties of garlic compounds: allyl cysteine, alliin, allicin, and allyl disulfide. *J. Med. Food* **2006**, *9*, 205−213.
(19) Behl, C.; Skutella, T.; Lezoualc'h, F.; Post, A.; Widmann, M.; Newton, C. J.; Holsboer, F. Neuroprotection against oxidative stress by estrogens: Structure−activity relationship. *Mol. Pharmacol.* **1997**, *51*, 535−541.
(20) Herrera, F.; Martin, V.; Garcia-Santos, G.; Rodriguez-Blanco, J.; Antolin, I.; Rodriguez, C. Melatonin prevents glutamate-induced oxytosis in the HT22 mouse hippocampal cell line through an antioxidant effect specifically targeting mitochondria. *J. Neurochem.* **2007**, *100*, 736−746.
(21) Sucontphunt, A.; De-Eknamkul, W.; Nimmannit, U.; Dan Dimitrijevich, S.; Gracy, R. W. Protection of HT22 neuronal cells against glutamate toxicity mediated by the antioxidant activity of *Pueraria candollei* var. *mirifica* extracts. *J. Nat. Med.* **2011**, *65*, 1−8.
(22) Huang, W. Y.; Chao, X. J.; Ouyang, Y.; Liu, A. M.; He, X. X.; Chen, M. H.; Wang, L. H.; Liu, J.; Yu, S. W.; Rapposelli, S.; Pi, R. B. Tacrine-6-ferulic acid, a novel multifunctional dimer against Alzheimer's disease, prevents oxidative stress-induced neuronal death through activating Nrf2/ARE/HO-1 pathway in HT22 cells. *CNS Neurosci. Ther.* **2012**, *18*, 950−951.
(23) Singleton, V. L.; Rossi, J. A. Colorimetry of total phenolics with phosphomolybdic−phosphotungstic acid reagents. *Am. J. Enol. Vitic.* **1965**, *16*, 15.
(24) Hatano, T.; Kagawa, H.; Yasuhara, T.; Okuda, T. Two new flavonoids and other constituents in licorice root: Their relative astringency and radical scavenging effects. *Chem. Pharm. Bull.* **1988**, *36*, 2090−2097.
(25) Kurihara, H.; Fukami, H.; Asami, S.; Toyoda, Y.; Nakai, M.; Shibata, H.; Yao, X. S. Effects of oolong tea on plasma antioxidative capacity in mice loaded with restraint stress assessed using the oxygen radical absorbance capacity (ORAC) assay. *Biol. Pharm. Bull.* **2004**, *27*, 1093−1098.
(26) Behl, C.; Widmann, M.; Trapp, T.; Holsboer, F. 17-β estradiol protects neurons from oxidative stress-induced cell death in vitro. *Biochem. Biophys. Res. Commun.* **1995**, *216*, 473−482.
(27) Wang, H.; Joseph, J. A. Quantifying cellular oxidative stress by dichlorofluorescein assay using microplate reader. *Free Radical Biol. Med.* **1999**, *27*, 612−616.
(28) Iciek, M.; Kwiecien, I.; Wlodek, L. Biological properties of garlic and garlic-derived organosulfur compounds. *Environ. Mol. Mutagen.* **2009**, *50*, 247−265.
(29) Li, B.; Jeong, G. S.; Kang, D. G.; Lee, H. S.; Kim, Y. C. Cytoprotective effects of lindenenyl acetate isolated from *Lindera strychnifolia* on mouse hippocampal HT22 cells. *Eur. J. Pharmacol.* **2009**, *614*, 58−65.
(30) Howes, M. J.; Perry, E. The role of phytochemicals in the treatment and prevention of dementia. *Drugs Aging* **2011**, *28*, 439−468.
(31) Kamel, A.; Saleh, M. Recent studies on the chemistry and biological activities of the organosulfur compounds of garlic (*Allium sativum*). *Stud. Nat. Prod. Chem.* **2000**, *23*, 455−486.
(32) Ikeda, T.; Tsumagari, H.; Nohara, T. Steroidal oligoglycosides from the seeds of *Allium tuberosum*. *Chem. Pharm. Bull.* **2000**, *48*, 362−365.
(33) Xu, Q. M.; Liu, Y. L.; Li, X. R.; Li, X.; Yang, S. L. Three new fatty acids from the roots of *Boehmeria nivea* (L.) Gaudich and their antifungal activities. *Nat. Prod. Res.* **2011**, *25*, 640−647.
(34) Lee, C. H.; Yang, L.; Xu, J. Z.; Yeung, S. Y. V.; Huang, Y.; Chen, Z. Y. Relative antioxidant activity of soybean isoflavones and their glycosides. *Food Chem.* **2005**, *90*, 735−741.
(35) Lee, P.; Lee, J.; Choi, S. Y.; Lee, S. E.; Lee, S.; Son, D. Geniposide from *Gardenia jasminoides* attenuates neuronal cell death in oxygen and glucose deprivation-exposed rat hippocampal slice culture. *Biol. Pharm. Bull.* **2006**, *29*, 174−176.

scavenging functions, germination, development, photosynthesis, carbon and nitrogen metabolism, flowering, stress responses, and senescence.[13] Finally, previous experiments demonstrated that also application of the amino acid methionine, as a biosynthetic precursor, led to enhanced GLSs contents in radish as well as in broccoli heads.[14,15]

The aim of this study was to investigate the effect of the most active elicitors found in the literature, the JA,[16] methyl jasmonate,[17,18] salicylic acid,[18] glucose,[19] sucrose,[20,21] and DL-methionine,[18] using 5 days of treatment from 3- to 8-day of sprouting under controlled growth conditions of *B. oleraceae* (broccoli), *B. napus* (rutabaga), *B. rapa* (turnip), and *R. sativus* (China rose and red radishes), rich in aliphatic and indolic GLSs because their young physiological state, in order to provide fresh, safe, and ready-to-eat sprouts, maximizing their health-promoting compounds.

MATERIAL AND METHODS

Chemicals. Jasmonic acid, sucrose, and glucose were obtained from Sigma-Aldrich Co. (St. Louis, MO, USA); methyl jasmonate was purchased from SAFC (St. Louis, MO, USA); salycilic acid and ethanol absolute were obtained from Panreac S.A. (Barcelona, Spain). DL-Methionine was from Alfa Aesar GmbH & Co. (Karlsruhe, Germany). Formic acid (98−100%) for analysis was obtained from EMSURE, ACS, Reag. Ph Eur, Merck, KGaA (Darmstadt, Germany). Trifluoroacetic acid for optima LC/MS was purchased from Fisher Scientific Co. (New Jersey, USA). Methanol and acetonitrile were LC-MS grade from HiPerSolv Chromanorm, BDH Prolabo (Leuven, Belgium). Sinigrin monohydrate was obtained from Phytoplan (Germany).

Plant Material and Germination Conditions. Seeds provided by Intersemillas S.A. (Valencia, Spain) were of commercial quality for ready-for-sprouting lines. Five varieties from the *Brassicaceae* family were used: broccoli (*B. oleracea* L. var. *italica*), rutabaga (*B. napus* L. var. *napobrassica*), turnip (*B. rapa* L. subsp. *rapa*), China rose radish (*R. sativus* L. cv. China rose), and red radish (*R. sativus* L. cv. Rambo). Seeds were rinsed in distilled water and immersed in 5 $g{\cdot}L^{-1}$ sodium hypochlorite under aeration for 24 h. After pouring off the soaking water, the seeds were weighed (day 0) and spread evenly on trays (5 g per tray) lined with cellulose growth pad (CN Seeds, U.K.) and irrigated everyday with Milli-Q water with 5 $g{\cdot}L^{-1}$ sodium hypochlorite. Aliquots of 5 g of seeds were frozen in liquid nitrogen and stored at −80 °C pending phytochemical analysis.

The three replicates (trays) per sample were germinated for 2 days in a controlled dark chamber at 28 °C, for increasing the stem elongation of sprouts. Then, trays were transferred to a controlled environment chamber with a 16 h light/8 h dark cycle and air temperatures of 25 and 20 °C, respectively. The relative humidity (RH) was 60% (day) and 80% (night). Photosynthetically active radiation (PAR) of 400 $\mu mol\ m^{-2}\ s^{-1}$ was provided by a combination of fluorescent tubes (Philips TLD 36 W/83, Hamburg, Germany; Sylvania F36W/GRO, Danvers, MA, USA) and metal halide lamps (Osram HQI.T 400 W, Munich, Germany). Three replicates per treatment of *Brassicaceae* sprouts samples were rapidly and gently collected at day 8 after germination, in the middle of the light period, for analysis. All samples were weighed (fresh mass), collected separately, flash frozen in liquid nitrogen, and stored at −80 °C prior to analyses.

Treatments with Elicitors. The phytohormones jasmonic acid (JA) (150 μM), methyl jasmonate (MeJA) (25 μM), and salicylic acid (SA) (100 μM), the oligosaccharides glucose (277 mM) and sucrose (146 mM), and the amino acid DL-methionine (5 mM) were selected as elicitors according to a literature review. JA, MeJA, and SA were dissolved in 0.2% ethanol in Milli-Q water. Sucrose and glucose were also dissolved in Milli-Q water. DL-Methionine was dissolved in 0.04% ethanol in Milli-Q water. Elicitors were applied as exogenous spraying on the cotyledons (not as soaking or irrigation solution) with 30 mL of test solution per sample (10 mL per tray) from day 3 to day 7 of sprouting (5 days of treatment) using Milli-Q water as control.

Extraction and Determination of Glucosinolates. *Sample Extraction.* Freeze-dried samples (100 mg) were extracted with 1.5 mL of methanol 70% V/V in a US bath for 10 min, then heated at 70 °C for 30 min in a heating bath, with shaking every 5 min using a vortex stirrer, and centrifuged (17 500 × *g*, 15 min, 4 °C). Supernatants were collected, and methanol was completely removed using a rotary evaporator. The dry material obtained was redissolved in 1 mL of ultrapure water and filtered through a 0.45 μm Millex-HV13 filter (Millipore, Billerica, MA, USA).

HPLC-DAD-ESI-MS^n Qualitative and Quantitative Analysis of Glucosinolates. First, the separate intact GLSs were identified from the extracted samples following their MS^2 $[M-H]^-$ fragmentations in HPLC-DAD-ESI-MS^n, carried out on a Luna C18 100A column (150 × 1.0 mm, 3 μm particle size; Phenomenex, Macclesfield, U.K.). Water:formic acid (99:1, v/v) and acetonitrile were used as mobile phases A and B, respectively, with a flow rate of 20 μL/min. The linear gradient started with 1% of solvent B, reaching 17% solvent B at 15 min up to 17 min, 25% at 22 min, 35% at 30 min, 50% at 35 min, which was maintained up to 45 min. The injection volume was 3 μL. Chromatograms were recorded at 227 nm. HPLC-DAD-ESI/MS^n analyses were carried out in an Agilent HPLC 1200 (Agilent Technologies, Waldbronn, Germany) and coupled to a mass detector in series. The HPLC system consisted of a binary capillary pump (model G1376A), an autosampler (model G1377A), a degasser (model G1379B), a sample cooler (model G1330B), and a photodiode array detector (model G1315D) and controlled by ChemStation software (v.B.0103-SR2). The mass detector was a Bruker, model UltraHCT (Bremen, Germany), ion trap spectrometer equipped with an electrospray ionization interface (ESI) and controlled by Bruker Daltonic Esquire software (v.6.1). Ionization conditions were adjusted at 350 °C and 4 kV for capillary temperature and voltage, respectively. The nebulizer pressure and flow rate of nitrogen were 65.0 psi and 11 L/min, respectively. The full-scan mass covered the range from m/z 50 to 600. Collision-induced fragmentation experiments were performed in the ion trap using helium as the collision gas with voltage ramping cycles from 0.3 up to 2 V. Mass spectrometry data were acquired in the negative ionization mode for glucosinolates. MS^n was carried out in the automatic mode on the more abundant fragment ion in MS$^{(n-1)}$. Then, the extracted samples (20 μL) were analyzed and quantified in a Water HPLC-DAD system (Waters Cromatografia S.A., Barcelona, Spain) as previously described by Pérez-Balibrea et al.[22] Intact GLSs were identified following their UV spectra and the order of elution previously described for the acquisition conditions. Glucosinolates were quantified using sinigrin as external standard, because of the similar structure to the glucosinolates in the sample.[22,23]

Statistical Methods. All assays were conducted by triplicate. Data were processed using the SPSS 15.0 software package (LEAD Technologies, Inc., Chicago, IL, USA). We carried out a multifactorial analysis of variance (ANOVA) and the Ducan's Multiple Range Test to determine significant differences at P values < 0.05.

RESULTS AND DISCUSSION

Biomass. The weight of seeds and sprouts was collected on day 0 (embebed seeds) and day 8. The ratio of fresh weight between sprouts and seeds as an indication of biomass production (Table 1) showed the expected increase in weight over sprouting and served as a quality index to select species with higher biomass production. Growing plants are exposed to a range of genetic, environmental, biotic, and abiotic factors which affect their growth and yield.[24] The biomass of the *Brassicaceae* sprouts treated with sucrose increased significantly over other treatments, ranging from about 15% in turnip and China rose radish to 80% in Red radish (Table 1), in agreement with results of Guo et al.[25] using a 146 mM sucrose treatment. Stewart et al.[26] explained that sucrose (88 mM) alters the growth rate and causes a dramatic increase in hypocotyl length.

Table 1. Biomass of Sprouts:Seeds Ratio in Cruciferous Edible Sprouts on a Fresh Weight Basis

species	broccoli	rutabaga	turnip	china rose radish	red radish
control	2.62[a]c	4.34b	2.69c	3.29b	1.45b
methyl jasmonate	2.24 cd	5.59a	2.71 cd	3.78b	1.61b
jasmonic acid	1.33e	3.15c	1.37e	2.14c	2.28a
salicylic acid	1.50de	4.24b	1.54de	2.50c	1.59b
glucose	0.95e	3.94bc	1.03e	2.38c	1.92a
sucrose	4.21a	6.43a	3.17a	3.70b	2.65a
DL-methionine	3.47b	4.18b	2.81b	5.15a	2.54a
$LSD_{0.05}$ [B](ANOVA $P < 0.001$)	0.22[b]***	0.27**	0.47*	0.15***	0.21***

[a]Mean values ($n = 3$) comparing species for each elicitor treatment, followed by different lowercase letters are significantly different at $P < 0.05$. a–h, Different lowercase letters mean statistically significant differences among elicitor treatments ($p < 0.05$). [b]Least significant difference (LSD) for separating means in the respective column. The LSD was computed only after analysis of variance indicating a significant ($p < 0.05$) entry effect. Levels of significance for each sampling day between species. Nonsignificant at $P > 0.05$ (n.s.); significant at $P < 0.05$ (*); significant at $P < 0.01$ (**); significant at $p < 0.001$ (***).

Sucrose could supply a balanced carbon source for cell growth by hydrolysis of invertase and sucrose synthase, with the resulting hexose directly participating in the glycolytic and pentose phosphate pathway (required for cells to synthesize nucleic acids and quickly replicate).[27] Stressful conditions such as starvation or hypoxia result in low energy status in the cell; Smeekens et al.[28] showed that sugars repressed the bZIP growth regulatory system activity in a concentration-dependent manner; therefore, our employed dose (5g/100 mL) was appropriate for biomass increase in sucrose treatment sprouts but not in the case of glucose, also in accord with Mirnezhad.[29]

DL-Methionine also showed a positive effect, increasing the fresh weight of sprouts in almost all varieties, 30% in broccoli, 4% in turnip, 57% in China rose radish, and 75% in red radish, except for rutabaga, agreeing with previous reports.[30,31] Gigolashvili et al.[32] reported a relationship between the overexpression of the HAG1/MYB28 gene, specific for methionine-derived GLSs (aliphatics), and strongest growth phenotype in *Arabidopsis thaliana*. On the other hand, glucose and the phytohormones (JA, MeJA, and SA) did not increase the fresh weight of sprouts and even reduced the size as for the control, as happened in broccoli, turnip, and China rose radish, founding a decrease around 60% in JA- and SA-treated sprouts, as also found by Kastell et al.[33] MeJA and SA regulate the overexpression of the OBP2 transcription factor involved in GLS biosynthesis, which altered the phenotype of *A. thaliana*, with smaller leaves,[34] supporting our result. In red radish sprouts, nonsignificant differences were found between the glucose- and phytohormones-treated sprouts and the controls. Higher values of biomass ratio not only means better growth (data not shown) but also higher fresh weight, making the sprouts more palatable. Concentration of elicitor and interval between treatment and harvest induce different responses characteristic of plant species, making it necessary to find the required effective dose and time empirically.[35]

Glucosinolate Profiles of *Brassicaceae* Sprouts. Identification and quantification of individual GLSs in seeds and 8-day-old sprouts of the five *Brassicaceae* cultivars are presented in Tables 2–5. The molecular ion $[M - H]^-$ (m/z) of GLSs, their fragment ion pattern, and retention times allowed identification of 16 different compounds.[3] The MS^2 fragmentation of aglycone side chain produces the most consistent ion at m/z 259, and the MS^3 fragmentation of this ion gives rise to fragments at m/z 97 (corresponding to the sulfate group) by disassociation of GLSs in the ion trap mass spectrometer, constituting a very useful preliminary screening method for determining the presence of GLSs in sprouts.[36] Sixteen GLSs, belonging to the aliphatic, indolic, and aromatic classes based on their different side chain structure, were detected. Results showed significant differences of the characteristic GLSs profile among cruciferous seeds and sprouts (Tables 2–5). The aliphatic GLSs were the major group in *B. oleraceae*, *B. napus*, and *R. sativus* sprouts, corresponding to 60% in *Brassica* and 90% in *Raphanus* varieties. In contrast, *B. rapa* sprouts showed higher amount of indolic GLSs, corresponding to 65% of the total (Table 4). Seeds exhibited the largest amount of GLSs being the nutrient reservoir organ, containing ranging concentrations from 563.79 to 1731.32 mg·100 g^{-1} F.W. in turnip and broccoli, respectively (Table 2), of interest for the composition of the sprouts during germination. According to Pérez-Balibrea et al.,[18,22] the major source of glucoraphanin are broccoli seeds and sprouts (987.02 and 182.46 mg·100 g^{-1} F.W., respectively) (Tables 2 and 3), which has been intensively studied because of its derived product sulforaphane, a potential chemopreventive beneficial compound against cancer, cardiovascular, and neurological diseases.[4] Turnip and rutabaga seeds and sprouts showed the antinutrient progoitrin as the major GLS, and glucoraphanin and gluconasturtiin were absent in the sprouts, probably degraded or diluted during germination.[22] In radish cultivars, specific GLSs in seeds were found as well (traces of the aromatic glucoberteroin). The major characteristic GLS in this species is glucoraphenin, containing 1051.88 and 32.78 mg·100 g^{-1} F.W. in China rose radish and 887.20 and 166.93 mg·100 g^{-1} F.W. in red radish in seeds and sprouts, respectively (Table 5). The bioactive sulforaphene, like sulphoraphane, is a potential anticancer agent.[8] In *Brassica* species, in addition to the parent indole GLS glucobrassicin, 4-hydroxyglucobrassicin, 4-methoxyglucobrassicin, and neoglucobrassicin were also detected in the samples (Tables 2–5). Only the indole 4-hydroxiglucobrassicin GLS was present in all species, being also one of the major compounds in seeds (from 152.49 to 358.34 mg·100 g^{-1} F.W. in China rose radish and broccoli, respectively). On the contrary, in *Raphanus* sprouts only 4-hydroxiglucobrassicin and 4-methoxyglucobrassicin were detected.[6]

Phytohormones as Elicitors. The jasmonates are signal compounds in the elicitation process leading to de novo transcription, translation, and, ultimately, biosynthesis of secondary metabolites in plant cell cultures. Methyl jasmonate (MeJA) is believed to be, at least, partially hydrolyzed by endogenous esterases to free jasmonic acid (JA) within the plant tissue.[12] MeJA elicitor (25 μM) was found highly effective for almost all the 8-day-old *Brassicaceae* sprouts, increasing by 84%, 50%, 123%, 25%, and 23% the total GLSs amount in broccoli, turnip, rutabaga, China rose radish, and red radish, respectively, increasing the indoles more than the aliphatic GLSs (Tables 3–5). After MeJA treatments, the broccoli sprouts showed significantly much more glucoraphanin, glucobrassicin, 4-methoxyglucobrassicin, and neoglucobrassicin by 60%, 241%, 48%, and 247%, respectively, associated with

dx.doi.org/10.1021/jf404876z | J. Agric. Food Chem. 2014, 62, 1881–1889

Table 2. List of Individual Glucosinolates (mg 100 g^{-1} F.W.) Detected in the Seeds of *Brassicaceae* Varieties

				seeds					
peak	compound	GLS semisystematic name	class	broccoli	rutabaga	turnip	china rose radish	red radish	
1	glucoiberin	3-methylsulfinylpropyl-gls	aliphatic	26.0 ± 3.43[a]	n.d.	n.d.	n.d.	n.d.	
2	progoitrin	(*R*)-2-hydroxy-3-butenyl-gls	aliphatic	n.d.	1278 ± 65.5	177 ± 0.36	n.d.	n.d.	
3	glucoraphenin	4-methylsulfinyl-3-butenyl-gls	aliphatic	n.d.	n.d.	n.d.	1052 ± 16.8	887 ± 49.6	
4	glucoraphanin	4-methylsulfinylbutyl-gls	aliphatic	987 ± 51.4	40.6 ± 2.66	28.7 ± 1.42	n.d.	n.d.	
5	glucoalyssin	5-methylsulfinylpentyl-gls	aliphatic	10.1 ± 12.1	n.d.	2.30 ± 1.02	n.d.	n.d.	
6	gluconapoleiferin	(*R*)-2-hydroxy-4-pentenyl-gls	aliphatic	n.d.	11.9 ± 2.32	Tr	n.d.	n.d.	
7	gluconapin	3-butenyl-gls	aliphatic	n.d.	95.8 ± 4.62	44.9 ± 10.9	n.d.	n.d.	
8	4-hydroxiglucobrassicin	4-hydroxy-3-indolylmethyl-gls	indolic	358 ± 48.2	239 ± 23.5	290 ± 24.3	152.5 ± 19.4	223 ± 8.60	
9	glucobrassicanapin	4-pentenyl-gls	aliphatic	n.d.	Tr	Tr	n.d.	n.d.	
10	glucoerucin	4-methylthiobutyl-gls	aliphatic	324 ± 43.7	n.d.	n.d.	3.56 ± 0.36	n.d.	
11	dehydroerucin	4-methylthio-3-butenyl-gls	aliphatic	n.d.	n.d.	n.d.	85.1 ± 5.18	31.3 ± 2.23	
12	glucobrassicin	3-indolylmethyl-gls	aliphatic	14.9 ± 4.61	1.79 ± 0.05	14.3 ± 7.57	n.d.	n.d.	
13	gluconasturtin	2-phenylethyl-gls	aromatic	Tr	Tr	Tr	n.d.	n.d.	
14	4-methoxyglucobrassicin	4-methoxy-3-indolylmethyl-gls	indolic	6.23 ± 4.16	Tr	Tr	n.d.	n.d.	
15	*n*-hexyl	*n*-hexyl-gls	aliphatic	Tr	n.d.	n.d.	n.d.	n.d.	
16	neoglucobrassicin	*N*-methoxy-3-indolylmethyl-gls	indolic	7.36 ± 1.47	Tr	7.14 ± 3.56	n.d.	n.d.	
			total	1731a	1666a	564d	1293b	1142c	46.1^{be} ($LSD_{0.05}$)

[a]Mean values ($n = 3 \pm SD$). Tr, traces, not quantified. n.d., not detected. a–d, Different lowercase letters mean statistically significant differences in the total glucosinolates content between species. [b]Least significant difference (LSD) for separating means in the respective row. The LSD was computed only after analysis of variance indicated a significant ($p < 0.05$) entry effect. ANOVA p value. [c](*) $p < 0.05$. [d](**) $p < 0.01$. [e](***)$p < 0.001$; n.s. $p > 0.05$.

dx.doi.org/10.1021/jf404876z | J. Agric. Food Chem. 2014, 62, 1881−1889

Table 3. List of Individual and Total Glucosinolates (mg 100 g^{-1} F.W.) in Broccoli (*B. oleraceae*) Sprouts under Elicitor Treatments

		broccoli							
peak	compound	control	MeJA	JA	SA	glucose	sucrose	DL-methionine	$LSD_{0.05}$ [b]
1	glucoiberin	10.8[a]a	7.68ab	9.33a	3.41b	6.35ab	11.9a	11.5a	1.86[c]
2	progoitrin	Tr	Tr	Tr	Tr	Tr	Tr	Tr	
3	glucoraphenin	n.d.	n.d.	n.d.	n.d.	n.d.	n.d.	n.d.	
4	glucoraphanin	183c	294a	265ab	288ab	297a	253b	200c	13.2[e]
5	glucoalyssin	0.46b	Tr	0.70a	Tr	Tr	Tr	Tr	0.16[c]
6	gluconapoleiferin	n.d.	n.d.	n.d.	n.d.	n.d.	n.d.	n.d.	
7	gluconapin	Tr	Tr	Tr	Tr	Tr	Tr .	Tr	
8	4-hydroxiglucobrassicin	39.9bc	40.1bc	32.4c	42.4b	54.7a	44.7b	55.6a	3.09[e]
9	glucobrassicanapin	n.d.	n.d.	n.d.	n.d.	n.d.	n.d.	n.d.	
10	glucoerucin	39.1	31.7	36.5	39.1	36.8	41.0	37.8	4.35nd
11	dehydroerucin	n.d.	n.d.	n.d.	n.d.	n.d.	n.d.	n.d.	
12	glucobrassicin	55.2 cd	188.5a	86.4b	43.0d	53.8 cd	92.3b	74.2bc	8.66[e]
13	gluconasturtin	Tr	Tr	Tr	Tr	Tr	Tr	Tr	
14	4-methoxyglucobrassicin	28.7c	42.7ab	49.2a	39.8b	43.4ab	45.4ab	40.2b	2.47[e]
15	*n*-hexyl	Tr	Tr	Tr	Tr	Tr	Tr	Tr	
16	neoglucobrassicin	30.9c	107.0a	95.6a	25.5c	43.1bc	61.2b	43.1bc	6.69[e]
	total	388e	712a	575b	481 cd	536bc	549b	463d	21.1[e]

[a]Mean values (n = 3). Tr, traces, not quantified. n.d., not detected. a–d, Different lowercase letters mean statistically significant differences between treatments (for each variety). [b]Least significant difference (LSD) for separating means in the respective row. The LSD was computed only after analysis of variance indicated a significant ($p < 0.05$) entry effect. ANOVA p value. [c](*) $p < 0.05$. [d](**) $p < 0.01$. [e](***) $p < 0.001$; n.s. $p > 0.05$.

potential health benefits due to the biological activity of their products.[4] The enhancement of the aliphatic GLS glucoraphenin in China rose and red radish sprouts after MeJA treatment was 278% and 35%, respectively. Indole GLSs in turnip, rutabaga, red radish, and China rose radish sprouts were also higher than the controls and increased by 109%, 223%, 54%, and 200%, respectively. The JA (150 μM) also produced an increase of total GLSs, especially in broccoli (by 50%), rutabaga (by 95%), and turnip (by 24%), having a higher effect on the indoles than on the aliphatic GLSs (Tables 3 and 4). In contrast, scarce differences were found in total GLSs in the treated radish sprouts compared to control samples (Table 5). Salicylic acid (SA) caused an increase of 20% in total GLSs in broccoli and radish sprouts, with aliphatic GLSs being the most affected (Tables 3 and 5), and no effects were found in turnip or rutabaga sprouts (Table 4). This phytohormone produced an increase in glucoraphanin in broccoli (by 58%) as well as in glucoraphenin (by 50% and 14%) and dehydroerucin (by 18% and 29%) in China rose and red radish sprouts, respectively (Tables 3 and 5).

Biosynthesis of glucosinolates can be drastically induced by wounding, hormone application, and pathogen or herbivore attack. Berger[34] demonstrated the induction of several pathway genes after phytohormones spraying application in *A. thaliana*, where IQD1 protein, OBP2 transcription factor, and ATR1/MYB34 and HIG1/MYB51 genes were overexpressed and regarded as a regulator with respect to increased concentrations of major indole GLSs. Nevertheless, the genes respond differently to biotic stress conditions in time and the site of metabolites accumulation in the plant.[34] These treatments increased the concentration of individual health-promoting glucosinolates (such as glucoraphanin, glucoraphenin, dehydroerucin, and indole GLSs) and also of great interest had not effect or even decreased the concentrations of the antinutrient progoitrin by JA and MeJA, present in rutabaga and turnip sprouts (Tables 3–5). Similar induction of GLSs by exogenous application of phytohormones as elicitors has been previously found by different authors, particularly, increased indole-GLSs.[16−18,33,34] Consistent with Brader et al.,[37] MeJA is able to trigger accumulation of the indole GLSs by inducting the tryptophan biosynthesis as demonstrated in *A. thaliana*, in contrast to SA, which seems to play a minor role in this response. The above-mentioned treatments, particularly, JA and its ester MeJA, were highly effective elicitors in *Brassica* sprouts. On the other hand, SA was more effective in radish sprouts than JA, with the MeJA solution being an interesting common elicitor to enrich in GLSs all species studied.

Sugars as Elicitors. Nonstructural carbohydrates, both sucrose and glucose, used as elicitors, enhanced the total GLSs amount in all sprouts under study, in accordance with some studies on broccoli, cabbage, and radish sprouts.[19,20] Sucrose (146 mM) showed higher effects in *Brassica* species, increasing by 42%, 31%, and 159% the total GLSs in broccoli, turnip, and rutabaga, respectively (Tables 3 and 4). By contrast, total GLSs in radish sprouts were increased higher after glucose treatment (277 mM) by 22% and 26% in China rose and red radish, respectively (Table 5). It must be emphasized the elicitation effect observed in broccoli sprouts, where glucoraphanin was increased by 40% and 60% under sucrose and glucose treatments, respectively (Table 3). Glucoraphanin was enhanced as well, by 50% and 30%, under both sucrose and glucose spray in China rose and red radish, respectively (Table 5). The other major aliphatic GLS from radish, dehydroerucin, was increased by the glucose treatment by 22% and 33% in China rose and red radish, respectively. In contrast to what was found by Wei et al.,[19] who showed a decrease in this compound. These results were consistent with those previously reported by Guo et al.,[25] indicating that the *Bo-Elong* gene involved in the aliphatic GLSs pathway was up-regulated by sucrose. Gigolashvili et al.[32] described glucose as an important signaling molecule that may induce transcriptional regulatory mechanisms, integrating carbohydrate availability and hormone action, regulating this class of GLSs by the HAG1/MYB28 gene, in response to carbohydrate availability, in *A. thaliana*.

Table 4. List of Individual and Total Glucosinolates (mg 100 g^{-1} F.W.) in Turnip (*B. rapa*) and Rutabaga (*B. napus*) Sprouts under Elicitor Treatments

		turnip								rutabaga							
peak	compound	control	MeJA	JA	SA	glucose	sucrose	DL-metionine	$LSD_{0.05}$ [b]	control	MeJA	JA	SA	glucose	sucrose	DL-metionine	$LSD_{0.05}$ [b]
1	glucoiberin	n.d.	n.d.	n.d.	n.d.	n.d.	n.d.	n.d.		n.d.	n.d.	n.d.	n.d.	n.d.	n.d.	n.d.	
2	progoitrin	41.9[a]bc	27.5c	5.69d	40.7bc	50.5ab	63.8a	43.5b	4.92[e]	185e	292c	240d	198e	253d	444a	343b	8.64[e]
3	glucoraphenin	n.d.	n.d.	n.d.	n.d.	n.d.	n.d.	n.d.		n.d.	n.d.	n.d.	n.d.	n.d.	n.d.	n.d.	
4	glucoraphanin	n.d.	n.d.	n.d.	n.d.	n.d.	n.d.	n.d.		n.d.	n.d.	n.d.	n.d.	n.d.	n.d.	n.d.	
5	glucoalyssin	1.09	0.96	Tr	Tr	Tr	0.99	1.27	0.23nd	n.d.	n.d.	n.d.	n.d.	n.d.	n.d.	n.d.	
6	gluconapoleiferin	Tr	Tr	Tr	Tr	Tr	Tr	Tr		Tr	Tr	Tr	Tr	Tr	Tr	Tr	
7	gluconapin	7.81	0.38	1.50	5.19	1.06	0.92	1.41	2.34 [nd]	15.8b	17.8ab	5.36 cd	1.22d	Tr	11.8bc	24.0a	2.51[e]
8	4-hydroxiglucobrassicin	23.6bc	25.5ab	31.9a	17.6c	32.0a	30.5ab	23.8bc	2.28[d]	17.1c	21.5b	22.7b	17.0c	23.8b	28.7a	14.8c	1.24[e]
9	glucobrassicanapin	Tr	Tr	Tr	Tr	Tr	Tr	Tr		Tr	Tr	Tr	Tr	Tr	Tr	Tr	
10	glucoerucin	n.d.	n.d.	n.d.	n.d.	n.d.	n.d.	n.d.		n.d.	n.d.	n.d.	n.d.	n.d.	n.d.	n.d.	
11	dehydroerucin	n.d.	n.d.	n.d.	n.d.	n.d.	n.d.	n.d.		n.d.	n.d.	n.d.	n.d.	n.d.	n.d.	n.d.	
12	glucobrassicin	23.4c	91.0a	41.1b	18.6c	26.1c	37.7b	25.0c	3.26[e]	29.6e	186a	158b	24.2e	46.4e	132c	94.6d	8.22[e]
13	gluconasturtin	n.d.	n.d.	n.d.	n.d.	n.d.	n.d.	n.d.		n.d.	n.d.	n.d.	n.d.	n.d.	n.d.	n.d.	
14	4-methoxyglucobrassicin	22.4b	22.3b	42.8a	23.0b	25.0b	23.9b	18.5b	2.08[e]	37.8de	61.9bc	33.6de	25.2e	48.3 cd	93.6a	73.5b	5.03[e]
15	*n*-hexyl	n.d.	n.d.	n.d.	n.d.	n.d.	n.d.	n.d.		n.d.	n.d.	n.d.	n.d.	n.d.	n.d.	n.d.	
16	neoglucobrassicin	24.2 cd	48.8a	56.7a	28.0bcd	41.4ab	31.4bc	12.7d	5.22[e]	33.9d	131b	162a	47.9d	73.8c	116b	38.4d	5.53[e]
	total	150 cd	216a	180b	133d	176bc	189b	126d	9.13[e]	319e	710b	621c	314e	445d	826a	588c	12.3[e]

[a]Mean values (n = 3). Tr, traces, not quantified. n.d., not detected. a–d, Different lowercase letters mean statistically significant differences between treatments (for each variety). [b]Least significant difference (LSD) for separating means in the respective row. The LSD was computed only after analysis of variance indicated a significant ($p < 0.05$) entry effect. ANOVA p value. [c](*) $p < 0.05$. [d](**) $p < 0.01$. [e](***) $p < 0.001$; n.s. $p > 0.05$.

dx.doi.org/10.1021/jf404876z | J. Agric. Food Chem. 2014, 62, 1881−1889

Table 5. List of Individual and Total Glucosinolates (mg 100 g^{-1} F.W.) in China Rose Radish and Red Radish (*R. sativus*) Sprouts under Elicitor Treatments

		China rose radish								red radish							
peak	compound	control	MeJA	JA	SA	glucose	sucrose	DL-methionine	$LSD_{0.05}$ [b]	control	MeJA	JA	SA	glucose	sucrose	DL-methionine	$LSD_{0.05}$ [b]
1	glucoiberin	n.d.	n.d.	n.d.	n.d.	n.d.	n.d.	n.d.		n.d.	n.d.	n.d.	n.d.	n.d.	n.d.	n.d.	
2	progoitrin	n.d.	n.d.	n.d.	n.d.	n.d.	n.d.	n.d.		n.d.	n.d.	n.d.	n.d.	n.d.	n.d.	n.d.	
3	glucoraphenin	32.8[A]d	124a	88.7b	50.5c	51.4c	50.6c	31.6d	3.18[e]	167 cd	227a	185bc	191ab	210ab	226a	146d	12.8[d]
4	glucoraphanin	n.d.	n.d.	n.d.	n.d.	n.d.	n.d.	n.d.		n.d.	n.d.	n.d.	n.d.	n.d.	n.d.	n.d.	
5	glucoalyssin	n.d.	n.d.	n.d.	n.d.	n.d.	n.d.	n.d.		n.d.	n.d.	n.d.	n.d.	n.d.	n.d.	n.d.	
6	gluconapoleiferin	n.d.	n.d.	n.d.	n.d.	n.d.	n.d.	n.d.		n.d.	n.d.	n.d.	n.d.	n.d.	n.d.	n.d.	
7	gluconapin	n.d.	n.d.	n.d.	n.d.	n.d.	n.d.	n.d.		n.d.	n.d.	n.d.	n.d.	n.d.	n.d.	n.d.	
8	4-hydroxiglucobrassicin	15.2b	22.6a	22.5a	16.1b	16.1b	12.7b	12.8b	1.31[e]	27.3b	44.2a	31.2b	21.1c	22.2c	41.7a	27.0b	1.42[e]
9	glucobrassicanapin	n.d.	n.d.	n.d.	n.d.	n.d.	n.d.	n.d.		n.d.	n.d.	n.d.	n.d.	n.d.	n.d.	n.d.	
10	glucoerucin	1.95b	10.9a	0.59b	1.61b	0.98b	1.73b	1.95b	0.67[e]	Tr	Tr	Tr	Tr	Tr	Tr	Tr	
11	dehydroerucin	411bc	434b	370c	489b	502a	439b	403c	9.33[e]	172c	182bc	180bc	222ab	229a	183bc	150c	14.4[c]
12	glucobrassicin	n.d.	n.d.	n.d.	n.d.	n.d.	n.d.	n.d.		n.d.	n.d.	n.d.	n.d.	n.d.	n.d.	n.d.	
13	gluconasturtin	n.d.	n.d.	n.d.	n.d.	n.d.	n.d.	n.d.		n.d.	n.d.	n.d.	n.d.	n.d.	n.d.	n.d.	
14	4-methoxyglucobrassicin	27.2ab	19.8c	15.5d	30.8a	25.9b	17.8 cd	29.0ab	1.31[e]	Tr	Tr	Tr	Tr	Tr	Tr	Tr	
15	*n*-hexyl	n.d.	n.d.	n.d.	n.d.	n.d.	n.d.	n.d.		n.d.	n.d.	n.d.	n.d.	n.d.	n.d.	n.d.	
16	neoglucobrassicin	n.d.	n.d.	n.d.	n.d.	n.d.	n.d.	n.d.		n.d.	n.d.	n.d.	n.d.	n.d.	n.d.	n.d.	
	total	488bc	611a	498bc	588a	596a	520b	478.c	12.1[e]	366d	452ab	396c	431b	461a	451ab	323e	8.04[e]

[a]Mean values (n = 3). Tr, traces, not quantified. n.d., not detected. a–d, Different lowercase letters mean statistically significant differences between treatments (for each variety). [b]Least significant difference (LSD) for separating means in the respective row. The LSD was computed only after analysis of variance indicated a significant ($p < 0.05$) entry effect. ANOVA p value. [c](*) $p < 0.05$. [d](**) $p < 0.01$. [e](***) $p < 0.001$; n.s. $p > 0.05$.

dx.doi.org/10.1021/jf404876z | J. Agric. Food Chem. 2014, 62, 1881−1889

As for the indole-GLSs, no effects were found on radish sprouts, while both sucrose and glucose highly and significantly enhanced 4-hydroxiglucobrassicin, 4-methoxyglucobrassicin, and neoglucobrassicin in *Brassica* species, with the glucobrassicin being mainly increased by sucrose (Tables 3 and 4). Sivanandhan et al.[38] showed that the type and concentration of carbon source induces profound effects on growth and quality of the metabolites produced. Sugars serve as the carbon and energy source and also affect the osmotic pressure of the medium, which stimulates mitochondrial activity and, hence, energy production for metabolites synthesis.[39] The secondary product formation after sugar application could be attributed to a certain level of osmotic stress, which initiated the signal perception through a receptor in the cell membrane to activate the signal transduction network. This activates the transcription factors, which regulates gene expression involved in biosynthesis of the target metabolites.[38,40]

DL-Methionine as Elicitor. Aliphatic GLSs, such as glucoraphanin and glucoiberin, are secondary metabolites derived from amino acids, mainly methionine.[31] The effect of the exogenous spray application of this amino acid (5 mM) has been studied in order to increase the amount of GLSs in sprouts, mainly aliphatic ones.[17,18] In the biosynthesis of glucosinolates, first, methionine is transaminated to the corresponding α-keto-acids, and subsequently, the side-chain elongation of the amino acid is produced, followed by formation of the GLS core structure mediated by cytochrome P450 mono-oxygenase.[32] Only in broccoli and rutabaga sprouts a significant effect after application of this amino acid was found, where the total GLSs were increased by 19% and 85%, respectively (Tables 3 and 4). China rose radish sprouts remained without changes in GLSs contents, while turnip and red radish sprouts showed a small decrease in total GLSs after the DL-methionine applications (Tables 4 and 5). Opposite to our first hypothesis, aliphatic GLSs were not affected to a higher degree than indole GLSs upon DL-methionine treatment, probably resulting from expression of HAG1/MYB28 in young sprouts, reported by Gigolashvili et al.[32] Broccoli-treated sprouts showed a weak increase of 7% and 28% in aliphatic (glucoiberin and glucoraphanin) and indole GLSs (4-hydroxiglucobrassicin, glucobrassicin, 4-methoxyglucobrassicin), respectively. Rutabaga sprouts registered a significant increase (by 85%) in both aliphatic (progoitrin and gluconapin) and indole GLSs (glucobrassicin and 4-methoxyglucobrassicin). Some authors reported that application of methionine to growing broccoli plants increased not only their aliphatic GLSs content but also the indolic GLSs.[41] Few reports on the effect of methionine elicitor have been found, and based on our results we may conclude that low concentrations of methionine, such as 5 and 10 mM applied by Pérez-Balibrea et al.,[18] allowed a certain increase of total GLSs (23% and 21% respectively) than higher concentrations, such as 200 mM applied by Scheuner et al.,[41] where a similar increase by 28% was found in broccoli at the time of head formation, while no significant impact on total GLSs was found in broccoli heads or radish hypocotyls.

All elicitors promoted the accumulation of GLSs in *Brassicaceae* sprouts. Detected differences in the quantified total and individual GLSs between controls and treated sprouts were not only due to cultivar differences but also due to the specific elicitor nature used. Indole GLSs in all species were found to either increase or remain stable after elicitor treatments. The total GLSs performed in similar way. Major desirable aliphatic GLSs, such as glucoraphanin, glucoraphenin, and dehydroerucin, were increased by elicitors, except with DL-methionine. Only undesirable aliphatic progoitrin and the glucoiberin decreased after the treatments, and minor GLSs, such as glucoerucin or gluconapin, were not affected. Elicitation practices, particularly using MeJA, could be established as an effective treatment to enrich in health-promoting GLSs cruciferous sprouts, for natural functional foods, a source of bioactive ingredients. The increase in the production of desirable healthy GLSs (glucoraphanin, glucoraphenin, dehydroerucin, and indole-GLSs) is important in order to enhance the intake of beneficial phytochemicals on a daily basis. Understanding the changes in the metabolism of sprouts is crucial to design strategies that would enhance the biosynthesis of secondary metabolites as novel cost-effective tools for nutrition and health applications that guarantee further research.

■ ASSOCIATED CONTENT

Supporting Information

Intact glucosinolates identified by HPLC-DAD-ESI-MSn in the Brassicaceae sprouts under study. This material is available free of charge via the Internet at http://pubs.acs.org.

■ AUTHOR INFORMATION

Corresponding Author

*Phone: +34 968 396369. Fax: +34 968 396213. E-mail: dmoreno@cebas.csic.es.

Funding

This work was supported by the Spanish Ministerio de Ciencia e Innovación CICYT (AGL2012-40175-C02-01) and by the Seneca Foundation-Regional Agency for Science and Technology of the Autonomous Community of the Murcia Region (CARM; Project ref. 08753/PI/08, Excellence in research 04486/GERM/06). N. Baenas was funded by a FPU (Formación Profesorado Universitario) grant of the Fellowship Programme from the Spanish Ministry of Education.

Notes

The authors declare no competing financial interest.

■ REFERENCES

(1) Pérez-Balibrea, S.; Moreno, D. A.; García-Viguera, C. Influence of light on health-promoting phytochemicals of broccoli sprouts. *J. Sci. Food Agric.* **2008**, *88*, 904−910.

(2) Zieliński, H.; Frias, J.; Piskuła, M.; Kozłowska, H.; Vidal-Valverde, C. Vitamin B1 and B2, dietary fiber and minerals content of Cruciferae sprouts. *Eur. Food Res. Technol.* **2005**, *221*, 78−83.

(3) Baenas, N.; Moreno, D. A.; García-Viguera, C. Selecting sprouts of *Brassicaceae* for optimum phytochemical composition. *J. Agric. Food Chem.* **2012**, *60*, 11409−11420.

(4) Dinkova-Kostova, A. T.; Kostov, R. V. Glucosinolates and isothiocyanates in health and disease. *Trends Mol. Med* **2012**, *18*, 337−347.

(5) Valgimigli, L.; Iori, R. Antioxidant and pro-oxidant capacities of ITCs. *Environ. Mol. Mutagen.* **2009**, *50*, 222−237.

(6) De Nicola, G. R.; Bagatta, M.; Pagnotta, E.; Angelino, D.; Gennari, L.; Ninfali, P.; Rollin, P.; Iori, R. Comparison of bioactive phytochemical content and release of isothiocyanates in selected *brassica* sprouts. *Food Chem.* **2013**, *141*, 297−303.

(7) Cartea, M.; Velasco, P. Glucosinolates in *Brassica* foods: bioavailability in food and significance for human health. *Phytochem. Rev.* **2008**, *7*, 213−229.

(8) Papi, A.; Orlandi, M.; Bartolini, G.; Barillari, J.; Iori, R.; Paolini, M.; Ferroni, F.; Grazia Fumo, M.; Pedulli, G. F.; Valgimigli, L.

Cytotoxic and antioxidant activity of 4-methylthio-3-butenyl isothiocyanate from Raphanus sativus L. (Kaiware Daikon) sprouts. *J. Agric. Food Chem.* **2008**, *56*, 875−883.
(9) Choi, H. S.; Cho, M. C.; Lee, H. G.; Yoon, D. Y. Indole-3-carbinol induces apoptosis through p53 and activation of caspase-8 pathway in lung cancer A549 cells. *Food Chem. Toxicol.* **2010**, *48*, 883−890.
(10) Angelova, Z.; Georgiev, S.; Roos, W. Elicitation of plants. *Biotechnol. Biotechnol. Equip.* **2006**, *20*.
(11) Poulev, A.; O'Neal, J. M.; Logendra, S.; Pouleva, R. B.; Timeva, V.; Garvey, A. S.; Gleba, D.; Jenkins, I. S.; Halpern, B. T.; Kneer, R.; Cragg, G. M.; Raskin, I. Elicitation, a new window into plant chemodiversity and phytochemical drug discovery. *J. Med. Chem.* **2003**, *6*, 2542−2547.
(12) Gundlach, H.; Müller, M. J.; Kutchan, T. M.; Zenk, M. H. Jasmonic acid is a signal transducer in elicitor-induced plant cell cultures. *Proc. Natl. Acad. Sci. U.S.A.* **1992**, *89*, 2389−2393.
(13) Bolouri-Moghaddam, M. R.; Le Roy, K.; Xiang, L.; Rolland, F.; Van Den Ende, W. Sugar signalling and antioxidant network connections in plant cells. *FEBS J.* **2010**, *277*, 2022−2037.
(14) Moreno, D. A.; López-Berenguer, C.; Martínez-Ballesta, M. C.; Carvajal, M.; García-Viguera, C. Basis for the new challenges of growing broccoli for health in hydroponics. *J. Sci. Food Agric.* **2008**, *88*, 1472−1481.
(15) Schreiner, M. Vegetable crop management strategies to increase the quantity of phytochemicals. *Eur. J. Nutr.* **2005**, *44*, 85−94.
(16) Bodnaryk, R. P. Potent effect of jasmonates on indole glucosinolates in oilseed rape and mustard. *Phytochemistry* **1994**, *35*, 301−305.
(17) Schreiner, M.; Krumbein, A.; Knorr, D.; Smetanska, I. Enhanced glucosinolates in root exudates of *Brassica rapa* ssp. rapa mediated by salicylic acid and methyl jasmonate. *J. Agric. Food Chem.* **2011**, *59*, 1400−1405.
(18) Pérez-Balibrea, S.; Moreno, D. A.; García-Viguera, C. Improving the phytochemical composition of broccoli sprouts by elicitation. *Food Chem.* **2011b**, *129*, 35−44.
(19) Wei, J.; Miao, H.; Wang, Q. Effect of glucose on glucosinolates, antioxidants and metabolic enzymes in *Brassica* sprouts. *Sci. Hortic.* **2011**, *129*, 535−540.
(20) Guo, R.; Yuan, G.; Wang, Q. Effect of sucrose and mannitol on the accumulation of health-promoting compounds and the activity of metabolic enzymes in broccoli sprouts. *Sci. Hortic.* **2011a**, *128*, 159−165.
(21) Tretter, D.; Galensa, R.; Feucht, W.; Schmid, P. P. S. Flavanone glucosides in callus and phloem of Prunus avium: Identification and stimulation of their synthesis. *Physiol. Plantarum.* **1985**, *65*, 95−101.
(22) Pérez-Balibrea, S.; Moreno, D. A.; García-Viguera, C. Genotypic effects on the phytochemical quality of seeds and sprouts from commercial broccoli cultivars. *Food Chem.* **2011a**, *125*, 348−354.
(23) Hernández-Hierro, J. M.; Valverde, J.; Villacreces, S.; Reilly, K.; Gaffney, M.; González-Miret, M. L.; Heredia, F. J.; Downey, G. Feasibility Study on the Use of Visible−Near-Infrared Spectroscopy for the Screening of Individual and Total Glucosinolate Contents in Broccoli. *J. Agric. Food Chem.* **2012**, *60*, 7352−7358.
(24) Jahangir, M.; Abdel-Farid, I. B.; Kim, H. K.; Choi, Y. H.; Verpoorte, R. Healthy and unhealthy plants: The effect of stress on the metabolism of *Brassicaceae*. *Environ. Exp. Bot.* **2009**, *67*, 23−33.
(25) Guo, R.; Yuan, G.; Wang, Q. Sucrose enhances the accumulation of anthocyanins and glucosinolates in broccoli sprouts. *Food Chem.* **2011b**, *129*, 1080−1087.
(26) Stewart, J. L.; Maloof, J. N.; Nemhauser, J. L. PIF genes mediate the effect of sucrose on seedling growth dynamics. *PLoS ONE* **2011**, *6*.
(27) Stepan-Sarkissian, G.; Fowler, M. W. The metabolism and utilization of carbohydrates by suspension cultures of plant cells. In *Carbohydrate metabolism in cultured cells*; Morgan, M. J., Ed.; Plenum: New York, 1986; pp 151−182.
(28) Smeekens, S.; Ma, J.; Hanson, J.; Rolland, F. Sugar signals and molecular networks controlling plant growth. *Curr. Opin. Plant Biol.* **2010**, *13*, 274−279.
(29) Mirnezhad, M. Effect of sugar spraying on host plant resistance to western flower thrips in tomato. Doctoral thesis, Leiden University, 2011; Chapter 6.
(30) Chen, M.; Cheng, B.; Zhang, Q.; Ding, Y.; Yang, Z.; Liu, P. Effects of applying L-methionine, L-phenylalanine and L-tryptophan on Zea mays growth and its nutrient uptake. *Ying Yong Sheng Tai Xue Bao* **2005**, *16*, 1033−1037.
(31) Thompson, J. F.; Madison, J. T.; Waterman, M. A.; Muenster, A. M. E. Effect of methionine on growth and protein composition of cultured soybean cotyledons. *Phytochemistry* **1981**, *20*, 941−945.
(32) Gigolashvili, T.; Yatusevich, R.; Berger, B.; Muller, C.; Flugge, U. I. The R2R3-MYB transcription factor HAG1/MYB28 is a regulator of methionine-derived glucosinolate biosynthesis in *Arabidopsis thaliana*. *Plant J.* **2007**, *51*, 247−261.
(33) Kastell, A.; Smetanska, I.; Ulrichs, C.; Cai, Z.; Mewis, I. Effects of phytohormones and jasmonic acid on glucosinolate content in hairy root cultures of Sinapis alba and *Brassica rapa*. *Appl. Biochem. Biotechnol.* **2013**, *169*, 624−635.
(34) Berger, B. The role of HIG1/MYB51 in the regulation of indolic glucosinolates biosynthesis. Inaugural Dissertation. University of Köln, Germany, 2007.
(35) Vasconsuelo, A.; Boland, R. Molecular aspects of the early stages of elicitation of secondary metabolites in plants. *Plant Sci.* **2007**, *172* (5), 861−875.
(36) Velasco, P.; Francisco, M.; Moreno, D. A.; Ferreres, F.; Garcia-Viguera, C.; Cartea, M. E. Phytochemical fingerprinting of vegetable *Brassica oleracea* and *Brassica napus* by simultaneous identification of glucosinolates and phenolics. *Phytochem. Anal.* **2011**, *22*, 144−152.
(37) Brader, G.; Tas, E.; Palva, E. T. Jasmonate-dependent induction of indole glucosinolates in *Arabidopsis* by culture filtrates of the nonspecific pathogen *Erwinia carotovora*. *Plant Physiol.* **2001**, *126*, 849−860.
(38) Sivanandhan, G.; Kapil Dev, G.; Jeyaraj, M.; Rajesh, M.; Muthuselvam, M.; Selvaraj, N.; Manickavasagam, M.; Ganapathi, A. A promising approach on biomass accumulation and withanolides production in cell suspension culture of *Withania somnifera* (L.) Dunal. *Protoplasma* **2013**, *250*, 885−898.
(39) Su, W. W. Bioprocessing technology for plant cell suspension cultures. *Appl. Biochem. Biotechnol.* **1995**, *50*, 189−230.
(40) Zhao, J.; Davis, L. C.; Verpoorte, R. Elicitor signal transduction leading to production of plant secondary metabolites. *Biotechnol. Adv.* **2005**, *23*, 283−333.
(41) Scheuner, E. T.; Krumbein, A.; Schonhof, I.; Schreiner, M. Increasing the alkyl glucosinolate level in Broccoli by leafstalk infusion of methionine. *J. Appl. Bot. Food Qual.* **2005**, *79*, 175−178.

Cell Culture. Pheochromocytoma PC12 cells, a cell line derived from rat adrenal medulla, were obtained from American Type Culture Collection (ATCC, Manassas, VA, USA). The cells were maintained in Dulbecco's modified Eagles medium (DMEM) supplemented with 6% fetal bovine serum (FBS), 6% horse serum (HS), 100 U/mL penicillin, and 100 μg/mL streptomycin at 37 °C in a water-saturated 7.5% CO_2 incubator. Fresh medium was supplied every other day. Reagents for cell cultures were purchased from Invitrogen Technologies (Carlsbad, CA, USA).

Neurite Outgrowth Assay. The determination of neurite outgrowth in cell cultures was performed according to a previous paper.[17] Briefly, PC12 cells (5×10^4 cells/well) were seeded into a 6-well plate. After 24 h, the cells were changed with DMEM containing 1% FBS, 1% HS, 100 U/mL penicillin, and 100 μg/mL streptomycin for 3 h. Cultured PC12 cells were treated with the jujube extract (2.0 mg/mL) in the absence or presence of H89 for 72 h and changed with medium containing jujube extract every 24 h. NGF (Alomone Laboratories, Jerusalem, Israel) at a concentration of 50 ng/mL was used as positive control routinely. After treatment, cells were fixed with ice-cold 4% paraformaldehyde. A light microscope (Diagnostic Instruments, Sterling Heights, MI, USA) equipped with a phase-contrast condenser, 10× objective lens, digital camera, and SPOT imaging software was used to capture and analyze the neurite presence and neurite length, and approximately 100 cells were counted from at least 10 randomly chosen visual fields for each culture. The cells were scored as differentiated if one or more neurites were longer than the diameter of the cell body and also classified according to their neurite length in <15, 15−30, and >30 μm.

Sodium Dodecyl Sulfate−Polyacrylamide Gel Electrophrosesis (SDS-PAGE). For the study on the expression of neurofilament, PC12 cells (8×10^4 cells/mL) were seeded into 12-well plates in normal serum medium for 24 h and then transferred to low serum (1% FBS, 1% HS, 100 U/mL penicillin, and 100 μg/mL streptomycin) as indicated for 3 h prior to exposure of the jujube extract in the absence or presence of H89. After 72 h of treatment, the cultures were collected in high salt lysis buffer (1 M NaCl, 10 mM HEPES, pH 7.5, 1 mM EDTA, 1 mM EGTA, 0.5% Triton X-100), followed by centrifugation at 16100 *g* for 10 min at 4 °C. Total protein content was measured by using Bradford's method with a kit from Bio-Rad Laboratories (Hercules, CA, USA). Samples of equal amounts of total protein were treated with 2× direct lysis buffer (0.125 M HCl, pH 6.8, 4% SDS, 20% glycerol, 2% 2-mercaptoethanol, and 0.02% bromophenol blue) and boiled for 10 min before an 8% gel electrophrosesis was performed.

Protein Phosphorylation on PC12 Cells. PC12 cells were seeded onto a 12-well plate. After the degree of confluence reached to >90%, the culture medium was changed to DMEM without serum over 5 h. The cells were treated with jujube extract or forskolin at different time points in the absence or presence of H89 (0, 5, 10, and 20 min). Then, the cells were harvested, digested with 200 μL of 2× direct lysis buffer, and boiled for 10 min before an 8% gel electrophrosesis was performed.

Western Blot Analysis. Following the electrophoresis, proteins that were separated on an 8% SDS-PAGE were transferred to the nitrocellulose membrane, using a Mini Trans-Blot cell at 40 V and 0.1 A for 16 h in 1× transfer buffer containing 24 mM Tris, 192 mM glycine, 15% ethanol, and 0.1% SDS. Transfer and equal loading of the samples were confirmed by staining with Ponceau-S. The nitrocellulose was blocked with 5% fat-free milk in Tris-buffer saline/0.1% Tween 20 (TBS-T) and then incubated in the primary antibody diluted in 2.5% fat-free milk in TBS-T overnight in a cold room (4 °C). The primary antibodies used were antineurofilament 200 (NF200; Sigma, St. Louis, MO, USA), anti-NF160 (Sigma), anti-NF68 (Sigma), antiphospho-CREB (Cell Signaling Technology, Beverly, MA, USA), antitotal CREB (Cell Signaling Technology), and antiglyceraldehyde 3-phosphate dehydrogenase (GAPDH; Abcam Ltd., Cambridge, UK). Following that, the nitrocellulose was rinsed with TBS-T and incubated for 2 h at room temperature in horseradish peroxidase (HRP)-conjugated anti-mouse secondary antibody (Invitrogen) diluted in the 2.5% fat-free milk in TBS-T. After intensive washing with TBS-T, the immune complexes were visualized using the enhanced chemiluminescence (ECL) method (GE Healthcare, Piscateway, NJ, USA). The intensities of the bands in the control and different samples running on the same gel and under strictly standardized ECL conditions were compared on an image analyzer, using a calibration plot constructed from a parallel gel with serial dilutions of one of the samples.

Statistical Analysis. Individual data were expressed as the mean ± standard error of the mean (SEM). Statistical tests were performed with *t* test (version 13.0, SPSS, IBM Corp., Armonk, NY, USA). Statistically significant changes were classified as significant (∗) when $p < 0.05$, more significant (∗∗) when $p < 0.01$, and highly significant (∗∗∗) when $p < 0.001$.

RESULTS

Jujube Induces the Neurite Outgrowth of PC12 Cells. Before the application of jujube extract onto cell cultures, the water extract was chemically standardized.[15] The amounts of nucleobases, including uracil, xanthine, hypoxanthine, guanine, and/or adenine in water extract, should be no less than 80 μg/g of dried extract. The amounts of nucleosides, including cytidine, uridine, and/or guanosine in jujube extract should be no less than 150 μg/g. The amounts of cyclic nucleotides, including cGMP and cAMP, in the extract should be no less than 100 μg/g. The amounts of flavonoids, including quercetin 3-*O*-rutinoside, quercetin 3-*O*-galactoside, quercetin 3-*O*-β-D-glucoside, and kaempferol 3-*O*-rutinoside, in jujube extract should be no less than 35 μg/g. In addition, the extraction efficiency of the extract was 77.3 ± 0.1% (w/w, mean ± SEM, $n = 4$).

PC12 cells are a widely employed model for the study of neuronal differentiation.[18] To investigate the efficacies of jujube on PC12 differentiation, water extract of jujube was applied onto cultured PC12 cells for 72 h before examination under microscope. As shown in Figure 1A, the water extract of jujube induced neurite outgrowth of PC12 cells. To quantify the change of morphology, 10 areas in the cultures were randomly selected, and then the number of differentiated cells and neurite length were calculated. The results indicated that after the treatment with water extract on PC12 cells for 3 days, the differentiated cells were counted to about 25% of the total cells in cultures (Figure 1B, upper panel). The length of neurite was also measured. The number of cells possessing neurite length at 15−30 μm was more significantly increased in water extract-treated cells (Figure 1B, lower panel).

In addition to the morphological exploration, the differentiation could also be evaluated by a biochemical analysis in determining the expression of neurofilament that is the neuronal cell-specific cytoskeleton proteins, including NF68 (at ∼68 kDa), NF160 (at ∼160 kDa), and NF200 (at ∼200 kDa). NGF served as positive control, which could induce the expression of neurofilament in a dose-dependent manner (Supporting Information Figure S1). As for jujube water extract, the treatment of 72 h at various concentrations (0.75, 1.5, and 3.0 mg/mL) induced the expressions of NF68, NF160, and NF200, with the highest induction by ∼150, 150, and 100%, respectively (Figure 2).

PKA Signaling Mediates Jujube-Induced Neuronal Differentiation on PC12 Cells. An activation of the cAMP pathway is essential for neuronal differentiation on PC12 cells.[19] Thus, the potency of jujube extract in stimulating neurite outgrowth and neurofilament expression via the cAMP pathway was investigated. Forskolin, a CREB phosphorylation inducer, was reported to induce neurite outgrowth and protein

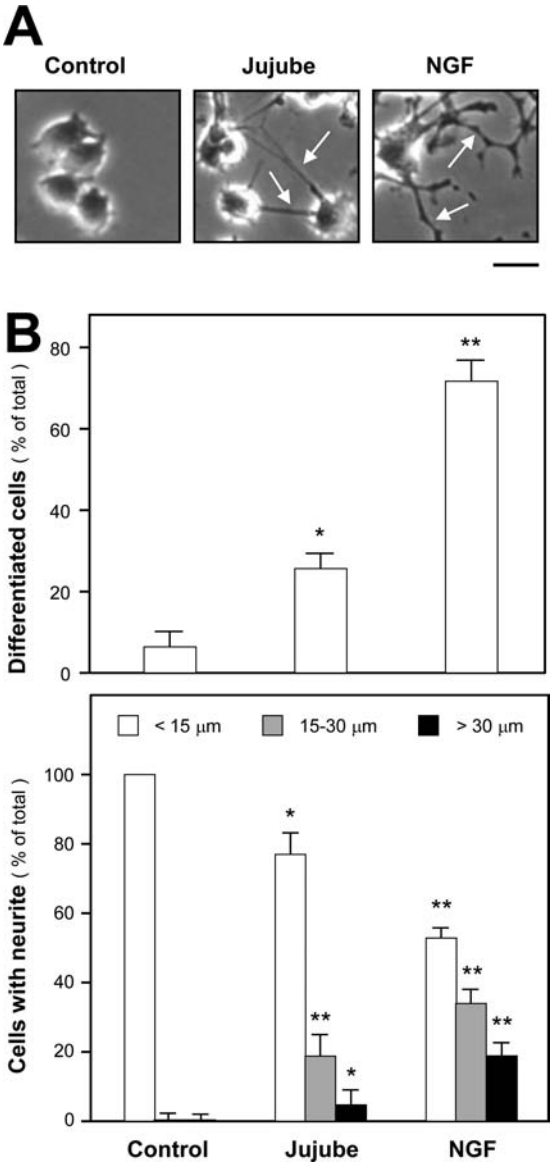

Figure 1. Jujube induces neurite outgrowth in cultured PC12 cells. (A) Jujube water extract (2.0 mg/mL) was applied into cultured PC12 cells for 72 h, with fresh medium or jujube extract every 24 h. NGF (50 ng/mL) served as the positive control. Cells were fixed with ice-cold 4% paraformaldehyde, and then the neurite outgrowth was examined under microscope. Representative images are shown, $n = 5$. Bar = 20 μm. Arrowheads indicate cell neurite. (B) To quantify the differentiation effect, the percentage of differentiated cell numbers (upper panel) and length of neurite (lower panel) were counted as described under Materials and Methods. Data are expressed as the percentage of cells in 100 counted cells, mean ± SEM, $n = 5$. Statistical comparison was made with the control; (∗) $p < 0.05$; (∗∗) $p < 0.01$.

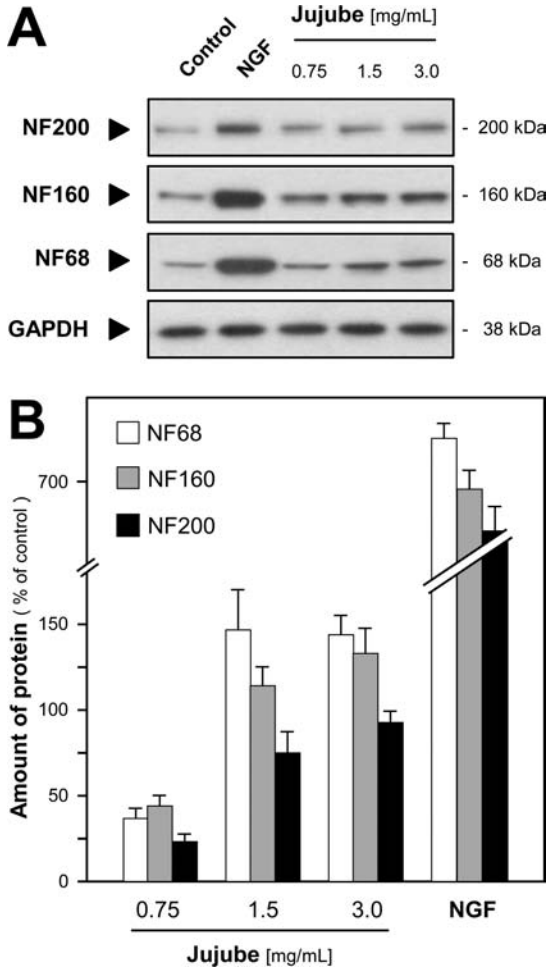

Figure 2. Jujube induces the expression of neurofilament on cultured PC12 cells. (A) Cultured PC12 cells were treated with jujube water extracts (0.75−3.0 mg/mL) for 72 h. The cell lysates were collected to determine the expressions of NF68, NF160, and NF200. NGF (50 ng/mL) served as the positive control. GAPDH served as loading control. (B) Quantification plot is shown in histograms. Values are expressed as the percentage of increase to basal reading (untreated culture), mean ± SEM, $n = 5$.

phosphorylation on PC12 cells. The effect of forskolin could be inhibited by H89, a cyclic AMP-dependent[20] and a marketed selective PKA inhibitor. To explore the possible mechanism of jujube-induced neuronal differentiation, PC12 cells were pretreated with H89 for 3 h. Then, the culture was treated with jujube extract for 72 h. Their effects on neurite outgrowth and neurofilament expression were evaluated. The forskolin-induced neurite outgrowth and neurofilament expression were inhibited by H89 (Figures 3 and 4). Similarly, the jujube-induced neurite outgrowth could be blocked by H89 (Figure 3). In addition, neurofilament expressions, induced by jujube, were also attenuated by H89 (Figure 4). The blockage did not apply to the induction by NGF. Besides, the application of H89 did not fully abolish the jujube effect in both cases of neurite outgrowth and neurofilament expression.

The nuclear transcription factor CREB has been well-documented to play a crucial role in neuronal differentiation on PC12 cells.[21] The phosphorylated CREB recruiting the coactivator CREB-binding protein allows its binding at the promoter and further stimulates target gene transcription that leads to neuronal differentiation. Therefore, the role of jujube in inducing the phosphorylation of CREB was investigated. As indicated in Figure 5A, the jujube extract could induce the phosphorylation of CREB at ∼43 kDa, and its inductive role could be fully abolished by H89 (Figure 5B).

On the basis of the aforementioned studies, the jujube extract has been demonstrated to induce neuronal differentiation in terms of neurite outgrowth and neurofilament expression. Still it is less known which active component accounts for the neuronal differentiation. On the one hand, cAMP was found in jujube.[22] Interestingly, its content was determined to be much higher in comparison with all other horticultural fruits, that is,

dx.doi.org/10.1021/jf405093f | J. Agric. Food Chem. 2014, 62, 1890−1897

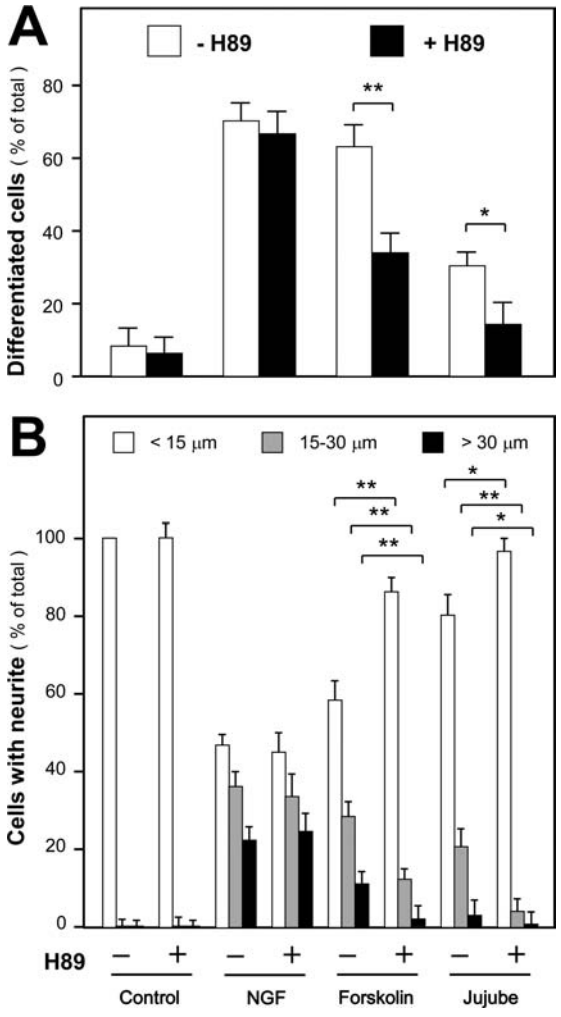

Figure 3. Inhibition of PKA signaling attenuates jujube-induced neurite outgrowth on cultured PC12 cells. Cultured PC12 cells were pretreated with or without H89 (5 μM; a PKA inhibitor) for 3 h and then treated with forskolin (10 μM), NGF (50 ng/mL), and jujube extract (2.0 mg/mL) for 72 h, with fresh medium or extract every 24 h. Cells were fixed with ice-cold 4% paraformaldehyde, and then the neurite outgrowth was examined under a microscope. To quantify the differentiation effect, the percentage of differentiated cell numbers (A) and length of neurite (B) were counted as described in Figure 1. Data are expressed as the percentage of cells in 100 counted cells, mean ± SEM, n = 5. Statistical comparison was made with the H89-treated group; (∗) $p < 0.05$; (∗∗) $p < 0.01$.

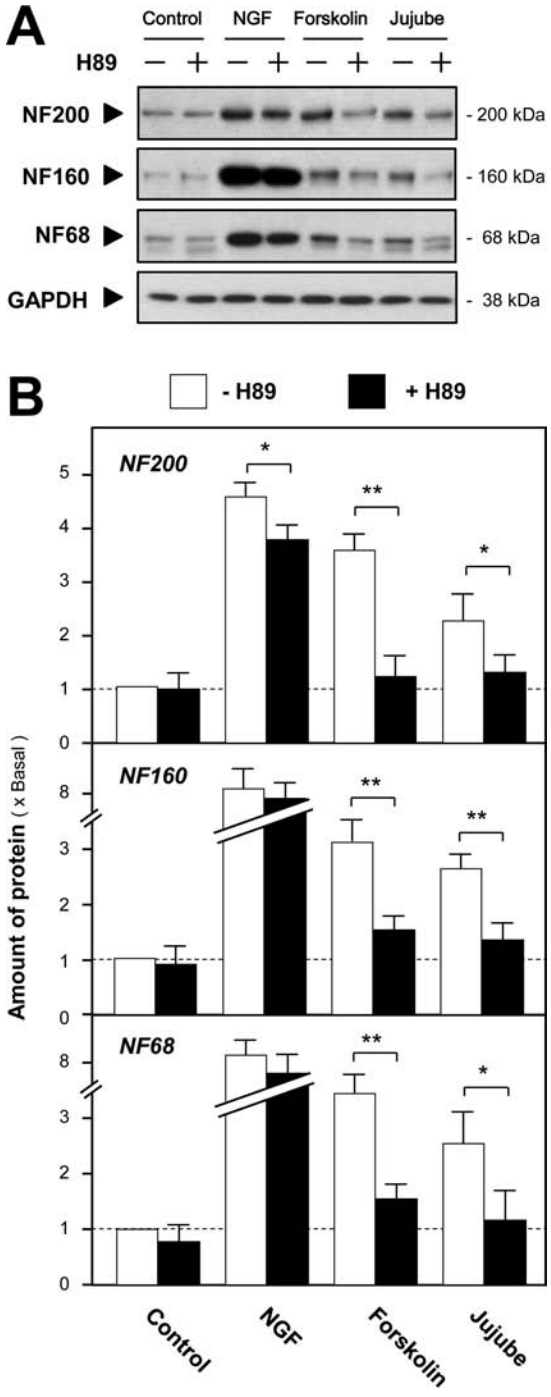

Figure 4. Inhibition of PKA signaling suppresses jujube-induced neurofilament expression on cultured PC12 cells. (A) Cultured PC12 cells were pretreated with or without H89 (5 μM; a PKA inhibitor) for 3 h and then treated with forskolin (10 μM), NGF (50 ng/mL), and jujube extract (2.0 mg/mL) for 72 h. The cell lysates were collected to determine the expressions of NF68, NF160, and NF200. GAPDH served as loading control. (B) Quantification plot (NF68, NF160, and NF200) is shown in histograms. Data are expressed as the fold of change (× Basal) against the control (no treatment; set as 1), mean ± SEM, n = 5. Statistical comparison was made with the H89-treated group; (∗) $p < 0.05$; (∗∗) $p < 0.01$.

apple and pear.[15,23,24] On the other hand, it is well-known that the increase in cAMP level could activate PKA and subsequently phosphorylate CREB. Thus, we speculated that the cAMP in the jujube extract might contribute to its effect on neuronal differentiation. Here, cAMP at 2 μM (approximately the amount in 2 mg/mL extract) was applied to PC12 cells. As shown in Figures 6 and 7, it could also induce both neurite outgrowth and neurofilament expression on cultured PC12 cells. In comparison with cAMP, the effect of jujube extract was better than that of cAMP in inducing neurite outgrowth, especially in neurite length between 15 and 30 μm (Figure 6). In addition, other possible ingredients including cGMP and a flavonoid mixture containing (−)-catechin, procyanidin B2, (−)-epicatechin, quercetin 3-*O*-galactoside, quercetin 3-*O*-rutinoside, quercetin 3-*O*-β-D-glucoside, and kaempferol 3-*O*-rutinoside (approximately the amount in 2 mg/mL extract) were also investigated, yet no significant effect was observed (Figure 6). The jujube extract performed better effect on the expression of NF200 than that of cAMP, whereas cAMP possessed better activity in the expression of NF160 than jujube

dx.doi.org/10.1021/jf405093f | J. Agric. Food Chem. 2014, 62, 1890−1897

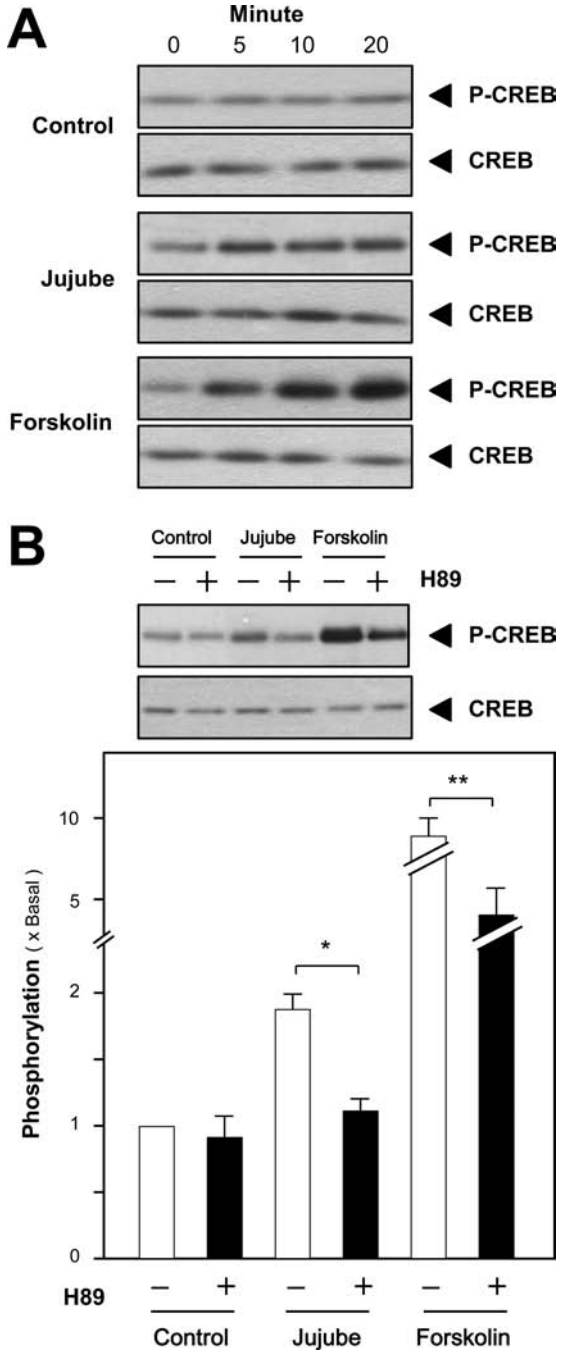

Figure 5. Jujube extract promotes CREB phosphorylation on PC12 cells. (A) Cultured PC12 cells were serum starved over 5 h before treatment with jujube (2 mg/mL) or forskolin (10 μM) for different times. Total CREB and phosphorylated CREB (both at ~43 kDa) were revealed by using specific antibodies. (B) Cultured PC12 cells, serum starved for over 5 h, were pretreated with or without H89 (5 μM; a PKA inhibitor) for 3 h prior to treatment with forskolin (10 μM) and jujube (2.0 mg/mL) for 10 min. Total CREB and phosphorylated CREB were revealed by using specific antibodies (upper panel). Quantification plot is shown in histograms (lower panel). Data are expressed as the fold of change (× Basal) against the control (no treatment; set as 1), mean ± SEM, n = 5. Statistical comparison was made with the H89-treated group; (∗) $p < 0.05$; (∗∗) $p < 0.01$.

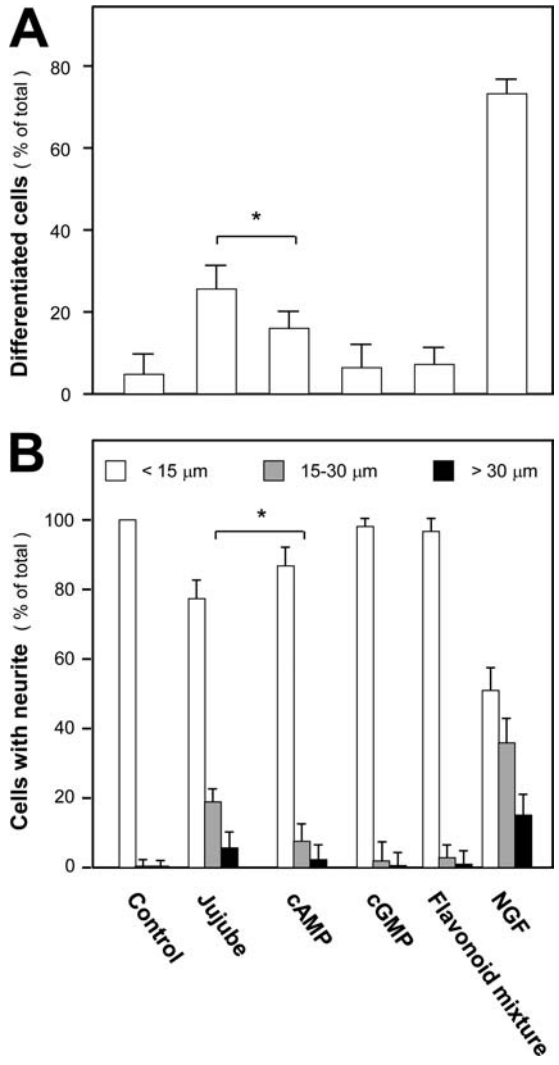

Figure 6. cAMP found in jujube induces neurite outgrowth in cultured PC12 cells. Jujube extract (2 mg/mL), cAMP at 2 μM, cGMP at 1.2 μM, or flavonoid mixture including (−)-catechin (52 nM), procyanidin B2 (49 nM), (−)-epicatechin (40 nM), quercetin 3-*O*-galactoside (2 nM), quercetin 3-*O*-rutinoside (157 nM), quercetin 3-*O*-β-D-glucoside (6 nM) and kaempferol 3-*O*-rutinoside (4 nM) was applied into cultured PC12 cells for 72 h, with fresh medium or drugs every 24 h. The concentrations of cAMP, cGMP, and flavonoids were the same as in 2 mg/mL of jujube extract. NGF (50 ng/mL) served as the positive control. Cells were fixed with ice-cold 4% paraformaldehyde, and then the neurite outgrowth was examined under a microscope. To quantify the differentiation effect, the percentage of differentiated cell numbers (A) and length of neurite (B) were counted as described under Materials and Methods. Data are expressed as the percentage of cells in 100 counted cells, mean ± SEM, n = 5. Statistical comparison was made between extract and cAMP; (∗) $p < 0.05$.

extract. No significant difference was found on NF68 between the extract and cAMP (Figure 7).

■ DISCUSSION

In the developing neuron, neuronal differentiation is a vital and first stage of development, in which the axon and neurite are promoted to prepare for synapse formation. Recently, morphological observation and biochemical detection were considered as the main approaches to evaluate neuronal differentiation. Here, we found that treatment with jujube extract in cultured PC12 cells could robustly stimulate the expression levels of NF68 and NF160. Both NF68 and NF160 are protein markers for the early stage of the differentiation. In

dx.doi.org/10.1021/jf405093f | J. Agric. Food Chem. 2014, 62, 1890−1897

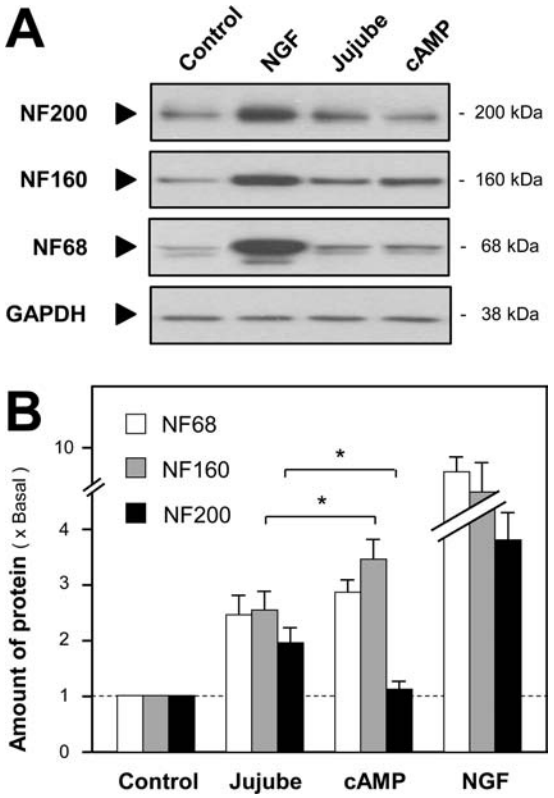

Figure 7. cAMP found in jujube induces the expression of neurofilament on cultured PC12 cells. (A) Cultured PC12 cells were treated with jujube extract (2 mg/mL) and cAMP (2 μM) for 72 h. The cell lysates were collected to determine the expressions of NF68, NF160, and NF200. NGF (50 ng/mL) served as the positive control. GAPDH served as loading control. (B) Quantification plot is shown in histograms. Data are expressed as the fold of change (× Basal) against the control (no treatment; set as 1), mean ± SEM, $n = 5$. Statistical comparison was made between extract and cAMP; (*) $p < 0.05$.

contrast, the expression of NF200, a marker for the late stage of neuron differentiation,[24] was also altered but to a lesser extent. Thus, the involvement of jujube in neuronal differentiation could be mainly at the early stage, but might not fully support the entire differentiation process at late stage.[17] In addition to neurofilament expression, the jujube-induced neurite outgrowth on PC12 cells was also observed morphologically, which was in line with the role of neurofilaments being the structural components of differentiated neurons.[25] In the cases of other neurite-inducing agents, however, the robust inductive effect on neurofilament expression was not consistent with neurite outgrowth, suggesting that the neurofilament expression and the neurite outgrowth could be two independent events.[17]

An increase of cAMP level activates PKA, followed by subsequent CREB phosphorylation, and the transcription factor binding on the promoter finally triggers target gene expression and leads to neurite outgrowth.[26] Here, we found that the inhibition of PKA signaling by H89 suppressed the jujube-induced neuronal differentiation, but not that of NGF-treated cultures. Our study was in good agreement with a previous report that NGF-induced neurite outgrowth could not be blocked by H89.[20] This implied that the differentiation mechanisms could be different between the inductions triggered by jujube and NGF.[27] Further study also revealed that jujube could also promote the phosphorylation of CREB. The aforementioned studies therefore elucidated the involvement of PKA−CREB signaling in jujube-induced neuronal differentiation on PC12 cells.

As reported previously, the water extract contained a higher amount of cyclic nucleotides, as well as their derivatives,[15] which could be one of the crucial ingredients in contributing to the jujube-induced beneficial effect. In addition, cyclic nucleotides and their derivatives also have been reported to participate in the regulation and modulation of numerous physiological processes in the human body.[28−32] In parallel, 20 of these chemicals have been identified from jujube.[33] Among many of these chemicals, cAMP showed a relatively high amount in jujube, and interestingly its content was much higher than in other horticultural fruits, that is, apple and pear.[15,22−24] In line with this notion, the amount of cAMP at approximately the amount contained in 2 mg/mL of jujube extract possessed neuronal differentiation, that is, neurite outgrowth and neurofilament expression. This strongly suggested that jujube cAMP played a role in neuronal differentiation, at least in cultured PC12 cells. In support of this hypothesis, a study revealed that the jujube extract could increase the level of cAMP in the plasma and hippocampus of jujube-treated animals.[34] However, the amount of cAMP within jujube did not fully account for its functions, as the jujube extract showed better neuronal differentiation function when compared to the same amount of cAMP. Thus, other active ingredients of jujube should not be eliminated.

Flavonoids have been reported to possess biological activities in promoting neuronal differentiation.[17] The flavonoids within jujube, including (−)-catechin, (−)-epicatechin, kaempferol 3-*O*-rutinoside, and quercetin 3-*O*-rutinoside, were also included in this screening study, yet no effect was found among them, which suggested that flavonoids were not the active ingredients for jujube-induced neuronal differentiation. Furthermore, the water extract of jujube was found to contain a higher amount of cGMP; however, it did not induce differentiation. Thus, the effect of other possible ingredients in jujube should not be eliminated. We speculated that other chemicals such as saponins might also contribute to the effect of jujube, which will be investigated in the future.

■ ASSOCIATED CONTENT

Supporting Information

Dose-dependent effect of NGF in neuronal differentiation on cultured PC12 cells. (A) Cultured PC12 cells were treated with NGF (0.5−50 ng/mL) for 72 h. The cell lysates were collected to determine the expressions of NF68, NF160, and NF200. GAPDH served as loading control. (B) Quantification plot (NF68, NF160 and NF200) is shown in histograms. Data are expressed as the fold of change (× Basal) against the control (no treatment; set as 1), mean ± SEM, $n = 4$ (Figure S1). This material is available free of charge via the Internet at http://pubs.acs.org.

■ AUTHOR INFORMATION

Corresponding Author

*(K.W.K.T.) Mail: Division of Life Science and Center for Chinese Medicine, The Hong Kong University of Science and Technology, Clear Water Bay Road, Hong Kong, China. Phone: +852-2358 7332. Fax: +852-2358 1559. E-mail: botsim@ust.hk.

Funding

This research was supported by the Hong Kong Research Grants Council Theme-based Research Scheme (T13-607/12R), GRF (661110, 662911, 663012, 662713), and the Foundation of the Awareness of Nature (TAON12SC01) to K.W.K.T. J.C. received a scholarship from the Hong Kong Chiu Chow Chamber of Commerce.

Notes

The authors declare no competing financial interest.

■ ABBREVIATIONS USED

PKA, protein kinase A; H89, *N*-[2-(*p*-bromocinnamylaminl)-ethyl]-5-isoquinolinesulfonamide; cAMP, adenosine 3′,5′-cyclic monophosphate; cGMP, guanosine 3′,5′-cyclic monophosphate; CREB, cAMP responsive element binding protein; SDS-PAGE, sodium dodecyl sulfate−polyacrylamide gel electrophrosesis; NFs, neurofilaments; NGF, nerve growth factor; GAPDH, glyceraldehyde 3-phosphate dehydrogenase

■ REFERENCES

(1) Lin, C. W.; Wu, M. J.; Liu, I. Y. C.; Su, J. D.; Yen, J. H. Neurotrophic and cytoprotective action of luteolin in PC12 cells through ERK-dependent induction of Nrf2-driven HO-1 expression. *J. Agric. Food Chem.* **2010**, *58*, 4477−4486.

(2) Dorrell, M. I.; Aguilar, E.; Jacobson, R.; Yanes, O.; Gariano, R.; Heckenlively, J.; Banin, E.; Ramirez, G. A.; Gasmi, M.; Bird, A.; Siuzdak, G.; Friedlander, M. Antioxidant or neurotrophic factor treatment preserves function in a mouse model of neovascularization-associated oxidative stress. *J. Clin. Invest.* **2009**, *119*, 611−623.

(3) Weissmiller, A. M.; Wu, C. Current advances in using neurotrophic factors to treat neurodegenerative disorders. *Transl. Neurodegener.* **2012**, *1*, 14.

(4) Li, J. W.; Fan, L. P.; Ding, S. D.; Ding, X. L. Nutritional composition of five cultivars of Chinese jujube. *Food Chem.* **2007**, *103*, 454−460.

(5) U.S. Department of Agriculture, ARS. USDA National Nutrient Database for Standard Reference, release 25, 2012.

(6) Chang, S. C.; Hsu, B. Y.; Chen, B. H. Structural characterization of polysaccharides from *Zizyphus jujuba* and evaluation of antioxidant activity. *Int. J. Biol. Macromol.* **2010**, *47*, 445−453.

(7) Choi, S. H.; Ahn, J. B.; Kozukue, N.; Levin, C. E.; Friedman, M. Distribution of free amino acids, flavonoids, total phenolics, and antioxidative activities of jujube (*Ziziphus jujuba*) fruits and seeds harvested from plants grown in Korea. *J. Agric. Food Chem.* **2011**, *59*, 6594−6604.

(8) Zhao, Z. H.; Li, J.; Wu, X. M.; Dai, H.; Gao, X. M.; Liu, M. J.; Tu, P. F. Structures and immunological activities of two pectic polysaccharides from the fruits of *Ziziphus jujuba* Mill. cv. *jinsixiaozao* Hort. *Food Res. Int.* **2006**, *39*, 917−923.

(9) Zhao, Z. H.; Dai, H.; Wu, X. M.; Chang, H. T.; Gao, X. M.; Liu, M. J.; Tu, P. F. Characterization of a pectic polysaccharide from the fruit of *Ziziphus jujuba*. *Chem. Nat. Compd.* **2007**, *43*, 374−376.

(10) Zhao, Z. H.; Liu, M. J.; Tu, P. F. Characterization of water soluble polysaccharides from organs of Chinese jujube (*Ziziphus jujuba* Mill. cv. *dongzao*). *Eur. Food Res. Technol.* **2008**, *226*, 985−989.

(11) Xue, Z. P.; Feng, W. H.; Cao, J. K.; Cao, D. D.; Jiang, W. B. Antioxidant activity and total phenolic contents in peel and pulp of Chinese jujube (*Ziziphus jujuba* Mill.) fruits. *J. Food Biochem.* **2009**, *33*, 613−629.

(12) Li, J. W.; Shan, L.; Liu, Y. F.; Fan, L. P.; Ai, L. Z. Screening of a functional polysaccharide from *Zizyphus jujuba* cv. *jinsixiaozao* and its property. *Int. J. Biol. Macromol.* **2011**, *49*, 255−259.

(13) Jiang, J. G.; Huang, X. J.; Chen, J.; Lin, Q. S. Comparison of the sedative and hypnotic effects of flavonoids, saponins, and polysaccharides extracted from Semen Ziziphus Jujube. *Nat. Prod. Res.* **2007**, *21*, 310−320.

(14) Cao, J. X.; Zhang, Q. Y.; Cui, S. Y.; Cui, X. Y.; Zhang, J. A.; Zhang, Y. H.; Bai, Y. J.; Zhao, Y. Y. Hypnotic effect of jujubosides from Semen Ziziphi Spinosae. *J. Ethnopharmacol.* **2010**, *130*, 163−166.

(15) Chen, J. P.; Li, Z. G.; Maiwulanjiang, M.; Zhang, W. L.; Zhan, J. Y. X.; Lam, C. T. W.; Zhu, K. Y.; Yao, P.; Choi, R. C. Y.; Lau, D. T. W.; Dong, T. X. X.; Tsim, K. W. K. Chemical and biological assessment of *Ziziphus jujuba* fruits from China: different geographical sources and developmental stages. *J. Agric. Food Chem.* **2013**, *61*, 7315−7324.

(16) Guo, S.; Duan, J. A.; Tang, Y. P.; Zhu, Z. H.; Qian, Y. F.; Yang, N. Y.; Shang, E. X.; Qian, D. W. Characterization of nucleosides and nucleobases in fruits of *Ziziphus jujuba* by UPLC-DAD-MS. *J. Agric. Food Chem.* **2010**, *58*, 10774−10780.

(17) Xu, S. L.; Choi, R. C. Y.; Zhu, K. Y.; Leung, K. W.; Guo, A. J. Y.; Bi, D.; Xu, H.; Lau, D. T. W.; Dong, T. T. X.; Tsim, K. W. K. Isorhamnetin, a flavonol aglycone from *Ginkgo biloba* L., induces neuronal differentiation of cultured PC12 cells: potentiating the effect of nerve growth factor. *Evidence-Based Complement. Altern. Med.* **2012**, 278273, DOI: 10.1155/2012/278273.

(18) Greene, L. A.; Aletta, J. M.; Rukenstein, A.; Green, S. H. PC12 pheochromocytoma cells: culture, nerve growth growth factor treatment, and experimental exploitation. *Methods Enzymol.* **1987**, *147*, 207−216.

(19) Ravni, A.; Vaudry, D.; Gerdin, M. J.; Eiden, M. V.; Falluel-Morel, A.; Gonzalez, B. J.; Vaudry, H.; Eiden, L. E. A cAMP-dependent, protein kinase A-independent signaling pathway mediating neuritogenesis through Egr1 in PC12 cells. *Mol. Pharmacol.* **2008**, *73*, 1688−1708.

(20) Chijiwa, T.; Mishima, A.; Hagiwara, M.; Sano, M.; Hayashi, K.; Inoue, T.; Naito, K.; Toshioka, T.; Hidaka, H. Inhibition of forskolin-induced neurite outgrowth and protein-phosphorylation by a newly synthesized selective inhibitor of cyclic AMP-dependent protein kinase, *N*-[2-(*p*-bromocinnamylaminl)ethyl]-5-isoquinolinesulfonamide (H-89), of PC12D pheochromocytoma cells. *J. Biol. Chem.* **1990**, *265*, 5267−5272.

(21) Ginty, D. D.; Bonni, A.; Greenberg, M. E. Nerve growth factor activates a Ras-dependent protein kinase that stimulates c-fos transcription phosphorylation of CREB. *Cell* **1994**, *77*, 713−725.

(22) Cyong, J. C.; Hanabusa, K. Cyclic adenosine monophosphate in fruits of *Zizyphus jujuba*. *Phytochemistry* **1980**, *19*, 2747−2748.

(23) Hanabusa, K.; Cyong, J.; Takahashi, M. High level of cyclic AMP in the jujube plum. *Planta Med.* **1981**, *42*, 380−384.

(24) Liu, M.; Wang, Y. cAMP contents of *Zizyphus jujuba* Mill., *Zizyphus spinosus* Hu. and other twelve horticultural plants. *J. Agric. Univ. Hebei* **1991**, *14*, 20−23.

(25) Schimmelpfeng, J.; Weibezahn, K. F.; Dertinger, H. Quantification of NGF-dependent neuronal differentiation of PC-12 cells by means of neurofilament-L mRNA expression and neuronal outgrowth. *J. Neurosci. Methods* **2004**, *139*, 299−306.

(26) Richter-Landsberg, C.; Jastorff, B. The role of cAMP in nerve growth factor-promoted neurite outgrowth in PC12 cells. *J. Cell Biol.* **1986**, *102*, 821−829.

(27) Vaudry, D.; Stork, P. J. S.; Lazarovici, P.; Eiden, L. E. Signaling pathways for PC12 cell differentiation: making the right connections. *Science* **2002**, *296*, 1648−1649.

(28) Conti, J. B.; Belardinelli, L.; Utterback, D. B.; Curtis, A. B. Endogenous adenosine is an antiarrhyhmic agent. *Circulation* **1995**, *91*, 1761−1767.

(29) Schmidt, A. P.; Lara, D. R.; Maraschin, J. D.; Perla, A. D.; Souza, D. O. Guanosine and GMP prevent seizures induced by quinolinic acid in mice. *Brain Res.* **2000**, *864*, 40−43.

(30) Urushitani, M.; Inoue, R.; Nakamizo, T.; Sawada, H.; Shibasaki, H.; Shimohama, S. Neuroprotective effect of cyclic GMP against radical-induced toxicity in cultured spinal motor neurons. *J. Neurosci. Res.* **2000**, *61*, 443−448.

(31) Anfossi, G.; Russo, I.; Massucco, P.; Mattiello, L.; Cavalot, F.; Balbo, A.; Trovati, M. Adenosine increases human platelet levels of cGMP through nitric oxide − possible role in its antiaggregating effect. *Thromb. Res.* **2002**, *105*, 71−78.

(32) Shah, D. I.; Singh, M. Possible role of exogenous cAMP to improve vascular endothelial dysfunction in hypertensive rats. *Fundam. Clin. Pharmacol.* **2006**, *20*, 595−604.
(33) Guo, S.; Duan, J. A.; Qian, D. W.; Wang, H. Q.; Tang, Y. P.; Qian, Y. F.; Wu, D. W.; Su, S. L.; Shang, E. X. Hydrophilic interaction ultra-high performance liquid chromatography coupled with triple quadrupole mass spectrometry for determination of nucleotides, nucleosides and nucleobases in *Ziziphus* plants. *J. Chromatogr., A* **2013**, *1301*, 147−155.
(34) Tian, J. S.; Gao, S.; Cui, Y. L.; Wang, Q. S.; Liu, L. P.; Zhang, Z. G. The cyclic AMP content with time variation after oral administration of the extract of Fructus Jujubae in mice. *Chinese J. Exp. Tradit. Med. Formulae* **2010**, *16*, 102−104.

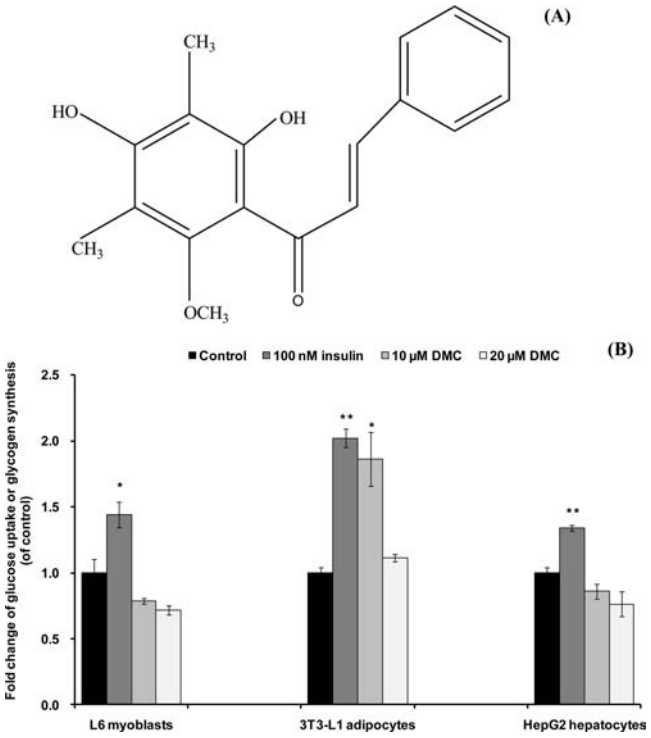

Figure 1. (A) Chemical structure of DMC. (B) Effect of DMC on glucose uptake in L6 myoblasts and 3T3-L1 adipocytes and on glycogen synthesis in HepG2 hepatocytes. Values are presented as the mean ± SEM (n = 3). Significant differences between groups and the control are indicated by ∗ for $P < 0.05$, and by ∗∗ for $P < 0.01$.

The hypoglycemic effects of *C. operculatus* flower bud aqueous extract and DMC have been demonstrated by several studies. However, the focuses were more on pancreatic islets, and studies of DMC in insulin-sensitive organs are rare. In the present study, the effects of DMC on glucose uptake in insulin-sensitive 3T3-L1 adipocytes and L6 skeleton muscle cells, as well as glycogen synthesis in HepG2 hepatocytes, were investigated, with its effects and mechanism on lipid accumulation in 3T3-L1 adipocytes unveiled.

MATERIALS AND METHODS

Reagents. DMC (purity is 98%) was isolated from the dried flower buds of *C. operculatus* as previously described.[16] Bicinchoninic acid (BCA) Protein Assay Kit was purchased from Pierce (Rockford, IL, USA), and dimethyl sulfoxide (DMSO) was purchased from Merck (Gibbstown, NJ, USA). All of the primers used in this study were synthesized by Life Technologies (Carlsbad, CA, USA). Cell culture reagents were acquired from Life Technologies as well. All other chemicals were of analytical reagent grade and acquired from Sigma-Aldrich (St. Louis, MO, USA).

Cell Culture and Differentiation for Glucose Uptake Assessments. L6 myoblasts were derived from rat skeletal muscle. L6 myoblast cell line was obtained from the Cell Bank of Type Culture Collection of the Chinese Academy of Sciences (Shanghai, China) and maintained in DMEM, supplemented with 10% fetal bovine serum (FBS) and 1% penicillin/streptomycin under a condition of saturated humidity atmosphere containing 5% CO_2 at 37 °C. When the cells reached 90% confluence, the medium was switched to DMEM containing 2% FBS and 1% penicillin/streptomycin. Cells were allowed to differentiate into myotubes for 7 days with medium changed every other day. 3T3-L1 preadipocytes were purchased from American Type Culture Collection (ATCC, Manassas, VA, USA) and were grown to confluence in DMEM containing 25 mM glucose, 10% FBS, and 1% penicillin/streptomycin at 5% CO_2 at 37 °C. Two days after confluence, cells were placed in DMEM containing 25 mM glucose, 0.5 mM isobutylmethylxanthine (IBMX), 1 μM dexamethasone, 10 μg/mL insulin, 10% FBS, and 1% penicillin/streptomycin (day 0) for 2 days of induction and then in DMEM that contained 25 mM glucose, 10 μg/mL insulin, 10% FBS, and 1% penicillin/streptomycin for 2 days for continuous differentiation. Thereafter, cells were maintained and refed every 2 days with DMEM containing 25 mM glucose, 10% FBS, and 1% penicillin/streptomycin until subjected to glucose uptake experiments (7 days from induction). The HepG2 cell line (ATCC) derived from human hepatocellular carcinoma was maintained in DMEM supplemented with 10% FBS and 1% penicillin/streptomycin under a condition of saturated humidity atmosphere containing 5% CO_2 at 37 °C.

Glucose Uptake Assays. Glucose uptake assay was performed on fully differentiated L6 myoblasts or 3T3-L1 adipocytes in 96-well plates. In detail, after differentiation, cells were serum-starved in DMEM with 0.2% bovine serum albumin (BSA; Sigma-Aldrich) overnight and treated with or without DMC (10 and 20 μM) in the same medium for 24 h. After that, 100 μL of Krebs−Ringer phosphate (KRP)/HEPES buffer (pH 7.4) containing 128 mM NaCl, 4.7 mM KCl, 1.65 mM $CaCl_2$, 2.5 mM $MgSO_4$, and 5 mM Na_2HPO_4, with or without 100 nM insulin, was placed in each well after three washings with KRP/HEPES and incubated for 30 min at 37 °C. Subsequently, 50 μL of KRP/HEPES containing 2 μCi/mL 2-deoxy-D-[^{3}H] glucose (China Isotope Co., Beijing, China) was added to the wells, and the plate was incubated for 20 min at 37 °C. Then, cells were solubilized in lysis buffer (0.5 M NaOH and 0.1% SDS) after three washings with ice-cold PBS. After 100 μL of optiphase supermix (PerkinElmer Life and Analytical Sciences, Boston, MA, USA) was added and thoroughly mixed, the relative radioactivity in the cells was measured in a Microbeta liquid scintillation counter (PerkinElmer).

Glycogen Synthesis Assay. HepG2 cells were seeded in 24-well plates at a density of 4×10^5 cells/well in DMEM supplemented with 10% FBS. After 24 h, the cells were serum-starved for 24 h. Then, insulin (100 nM) or DMC (10 and 20 μM) together with 0.5 μCi/mL of D-[^{3}H] glucose (China Isotope Co.) was added directly, and the incubation was continued for 2 h. After that, cell medium was replaced with 200 μL of 0.2 N KOH containing 1 mg of glycogen (5 mg/mL final concentration), and cells were incubated for 40 min at 60 °C. Then, cells were solubilized in lysis buffer, and the cell lysates were transferred to tubes, followed by 1 h of incubation at 60 °C. Subsequently, the tubes were placed on ice, and 1 mL of cold ethanol was added. Glycogen was separated by centrifugation at 5000 g for 5 min, and the pellets were washed twice with cold ethanol containing 0.1% LiBr and 0.2 N KOH. The final precipitable radioactivity was counted with MicroBeta.

Lipid Accumulation in 3T3-L1 Adipocytes. 3T3-L1 preadipocytes were seeded in a 24-well plate at a density of 5×10^4 cells/well. 3T3-L1 cells were differentiated as described above, with or without the addition of various concentrations of DMC or pioglitazone (1 μM) in the culture medium during the differentiation process for 7 days. After differentiation, the supernatant was collected for measurement of secreted adiponectin by a quantitative adiponectin mouse ELISA kit (Abcam, Cambridge, UK) according to the manufacturer's instructions. The cells were stained with Oil Red O for neutral lipid (mainly triglycerides and cholesteryl oleate) using a method adopted from the literature and modified.[41] In detail, cells were washed once by PBS and fixed by 10% formalin (3.7% formaldehyde) for 10 min. After removal of the fixation liquid and a washing with 60% isopropyl alcohol, 200 μL of Oil Red O solution (0.05% in 70% ethanol) was added to each well for 30 min of incubation. Then, cells were washed with dH_2O four times and extracted by 100% isopropyl alcohol. The extraction was transferred to a 96-well plate, and optical density (OD) was determined by a Safire 2 microplate reader (Tecan, Mannedorf, Switzerland) at a wavelength of 500 nm.

RNA Isolation and Quantitative RT-PCR. 3T3-L1 preadipocytes were seeded in 12-well plates at a density of 1×10^5 cells/well and differentiated as well as treated as above. Total RNA from each well was extracted and purified using the RNeasy mini kit (Qiagen NV, Venlo, The Netherlands). Complementary DNAs (cDNAs) were

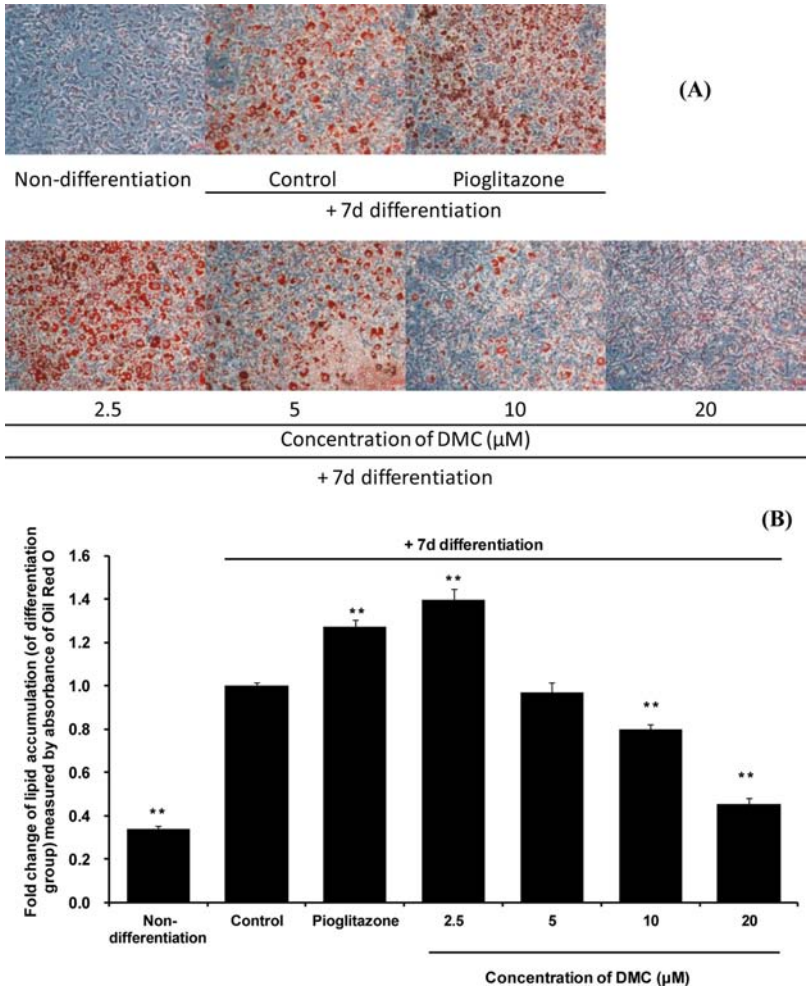

Figure 2. Paradoxical effect of DMC on 3T3-L1 adipocyte differentiation: (A) photographed representative lipid droplet stained with Oil Red O; (B) corresponding absorbance values of Oil Red O staining. Values are shown as the mean ± SEM (n = 3). The data values in (B) are compared versus 7 day differentiation control, with significant differences indicated by ∗ for $P < 0.05$ and by ∗∗ for $P < 0.01$.

synthesized using a primescript first-strand DNA synthesis kit (Takara Biotech, Shiga, Japan) according to the manufacturer's instruction. Quantitative reverse transcription PCR (qRT-PCR) was carried out using the kit of SYBR Premix ExTaq (Takara) and an ABI Prism 7500 sequence detection system (Applied Biosystems, Foster City, CA, USA) to determine the gene expression level. Each PCR was performed in a total of 20 μL of solution containing 0.8 μL (10 μM) of each pair of forward and reverse primers, 10 μL of Premix Ex Taq DNA polymerase, 0.4 μL of ROX reference dye, 6 μL of dH_2O, and 2 μL of reverse transcription reaction products. The primer sequences used in the experiment were as follows: PPAR-γ (forward) 5′-GGCCGAGAAGGAGAAGCTGTTG-3′ and (reverse) 5′-TGGCCACCTCTTTGCTCTGCTC-3′; C/EBP-α (forward) 5′-CCGGGAGAACTCTAACTC-3′ and (reverse) 5′-GATGTAGGCGCTGATGT-3′. All experiments were done in triplicate. Relative expression was determined by the $2^{(-\Delta ct)}$ method using GAPDH as the internal control, and fold change was calculated in comparison to the control group.

Determination of PPAR-γ Protein Expression by Western Blotting. PPAR-γ protein expression level in 3T3-L1 adipocytes was examined using Western blotting. Following the same culture, differentiation, and treatment regimen as described above, cells were washed twice with ice-cold PBS before lysis in 200 μL of CelLytic-M cell lysis reagents (Sigma-Aldrich). The lysate was centrifuged at 14000 g for 15 min at 4 °C, with supernatant collected and total protein determined using a BCA assay. For Western blotting, equal amounts of total cellular protein (10 μg) were resolved by SDS-PAGE and transferred onto polyvinylidene difluoride (PVDF) membranes (Bio-Rad, Hercules, CA, USA) with a Bio-Rad Transblot apparatus and probed with primary antibodies against PPAR-γ and GAPDH overnight at 4 °C, followed by 1 h of incubation with a horseradish peroxidase (HRP)-conjugated secondary antibody (all antibodies were from Cell Signaling Technologies, Beverly, MA, USA). The immune complexes of bound antibody were visualized with an enhanced chemiluminescence (ECL) system according to the manufacturer's instructions (GE Healthcare, Piscataway, NJ, USA). Equal loading was confirmed by analysis of the internal control of GAPDH, and bands were quantified using densitometry by Image J software (NIH, Bethesda, MD, USA).

Statistics. Results were expressed as the mean ± SEM. The data were analyzed by one-way analysis of variance (ANOVA) followed by Dunnett's post hoc comparisons to determine the significant differences between treatment groups and the control group. Differences with $P < 0.05$ were considered statistically significant.

RESULTS

DMC-Promoted Glucose Uptake in 3T3-L1 Adipocytes. To determine the effect of DMC on glucose uptake in skeletal muscle and fat, ^{3}H-labeled 2-deoxyglucose was measured in a differentiated L6 rat skeleton muscle cell and 3T3-L1 mouse adipocytes, respectively. As shown in Figure 1B, 100 nM insulin significantly increased glucose uptake in L6 and 3T3-L1 cells by 44 and 102%, respectively ($P < 0.05$ vs control group), as expected. Interestingly, 10 μM DMC treatment also

remarkably promoted glucose uptake in 3T3-L1 adipocytes by 78% ($P < 0.05$ vs control group), but 20 μM DMC did not show statistical significance. DMC (10 and 20 μM) was not effective for glucose uptake in L6 myoblasts. Glycogen synthesis by detecting ^{3}H-labeled D-glucose was measured in HepG2 hepatocytes. Insulin (100 nM) significantly increased glycogen synthesis by 34% ($P < 0.05$ vs control group), but DMC (10 and 20 μM) did not show significant difference compared to control group.

Paradoxical Effect of DMC on Lipid Accumulation in 3T3-L1 Adipocytes. First, we examined the effects of DMC on the differentiation of 3T3-L1 adipocytes through the microscopic examination of Oil Red O-stained lipid droplets (Figure 2A), and the results were further verified by the spectrophotometric quantification of the Oil Red O extracted from the cells (Figure 2B). Differentiation was initiated in induction medium and continued in differentiation medium by treating the cells with or without pioglitazone (1 μM) or in the presence of various doses of DMC (0, 2.5, 5, 10, or 20 μM). On day 8, it was found that 3T3-L1 cells were significantly differentiated compared to the nondifferentiation group with a 3-fold increase ($P < 0.01$) in Oil Red O staining for intracellular neutral lipids (Figure 2B). Pioglitazone was used as positive control, and 3T3-L1 cells markedly promoted lipid production by 27% ($P < 0.01$ vs differentiation control group). DMC promoted lipid accumulation of 3T3-L1 cells in a dose-dependent manner, and its effect was paradoxical compared with control. A low concentration DMC (2.5 μM) enhanced lipid content in 3T3-L1 cells by 39% ($P < 0.01$ vs differentiation control group), whereas 5 μM DMC did not lead to a significant difference (Figure 2B). However, high concentrations DMC (10 and 20 μM) markedly diminished lipid accumulation by 55 and 20%, respectively ($P < 0.01$ vs differentiation control group). On the other hand, DMC had no effect on cell proliferation or viability, and DMC alone did not affect lipid accumulation in nondifferentiation 3T3-L1 cells (data not shown).

Paradoxical Effect of DMC on Adiponectin Production in 3T3-L1 Adipocytes. As shown in Figure 3, the adiponectin level in 3T3-L1 cells treated with a well-established standard adipocyte differentiation protocol was increased about 50-fold compared with the nondifferentiation group. Pioglitazone (1 μM), as a positive control, enhanced the adiponectin level by 59% ($P < 0.01$ vs differentiation control group). DMC (2.5−20 μM) increased adiponectin production during cell differentiation dose-dependently, but their effects were paradoxical compared with the differentiation control group. DMC, at dosages of 2.5 and 5 μM, enhanced the production of adiponectin in 3T3-L1 cells by 56 and 30%, respectively ($P < 0.01$ vs differentiation control group); at concentrations of 10 and 20 μM, DMC markedly suppressed adiponectin level by 53 and 85%, respectively ($P < 0.01$ vs differentiation control group), whereas under nondifferentiated conditions, DMC did not show a significant effect compared with control (data not shown).

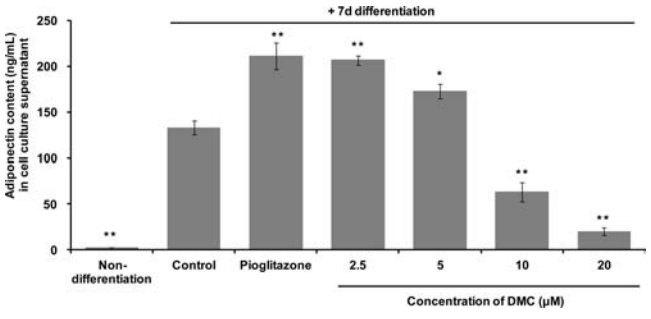

Figure 3. Paradoxical effect of DMC on adiponectin production in 3T3-L1 adipocytes. Values are shown as the mean ± SEM ($n = 3$). All values were compared versus 7 day differentiation control, and significant differences are indicated by * for $P < 0.05$ and by ** for $P < 0.01$.

Quantification of C/EBP-α and PPAR-γ at Gene Expression Level. To study the effect and the corresponding mechanism of DMC in 3T3-L1 adipocyte differentiation, the gene expression levels of C/EBP-α and PPAR-γ were determined as adipocyte differentiation markers. Semiquantitative RT-PCR analysis data showed that differentiated 3T3-L1 expressed C/EBP-α and PPAR-γ, whereas neither was detectable in the nondifferentiation group (Figure 4A). Pioglitazone (1 μM) significantly increased the mRNA expression of C/EBP-α and PPAR-γ by 1.8- and 1.5-fold compared with the differentiation control group ($P < 0.05$). DMC at a concentration of 2.5 μM markedly enhanced both gene expressions compared with the differentiation control (4.4-fold for C/EBP-α; 3.9-fold for PPAR-γ, $P < 0.01$), which was even higher than pioglitazone. On the contrary, treatments with high concentrations of DMC (20 and 10 μM) down-regulated these two gene expressions compared with differentiation control group (0.3/0.5-fold for C/EBP-α; 0.2/0.3-fold for PPAR-γ, $P < 0.05$), and 5 μM DMC treatment did not show significant effects in the gene expressions (Figure 4A).

Determination of PPAR-γ at Protein Level. PPAR-γ is involved in adipocyte differentiation by stimulating adipogenesis and glucose metabolism. To investigate the effect of DMC on the expression of PPAR-γ, Western blot analysis was employed in 3T3-L1 adipocytes. The protein expression of PPAR-γ in the differentiation group was significantly enhanced compared with the nondifferentiation condition ($P < 0.01$). DMC (2.5−20 μM) treatment decreased the protein expression level of PPAR-γ in a dose-dependent fashion, and its effect was paradoxical compared with the differentiation control group. DMC at a dosage of 2.5 μM significantly enhanced the protein expression of PPAR-γ by 40%, which was comparable to pioglitazone by 30% ($P < 0.01$ vs differentiation control group). However, 5 μM DMC treatment did not show a significant effect compared with the differentiation control group. Surprisingly, application of 20 and 10 μM DMC effectively decreased 3T3-L1 adipocyte differentiation by suppression of PPAR-γ after an extensive period of treatment, accompanied with around 8- and 3-fold decreases in PPAR-γ protein expression, respectively ($P < 0.01$ vs differentiation control group) (Figure 4B,C).

DISCUSSION

For diabetes, two major mechanisms contribute to hyperglycemia. One is a shortage of insulin release in the pancreas; the other is insulin resistance in key glucose-metabolizing organs such as the liver, fat, and cardiac and skeletal muscles. The effects of an aqueous extract of *C. operculatus* flower buds[2] and DMC[32,33] on the protection of pancreatic islets and MIN6 cells and insulin release have been demonstrated, but the effects on insulin target tissues are rare. Physiologically, insulin secreted from the pancreas reduces glucose output from the liver and enhances glucose uptake by skeletal muscle and fat

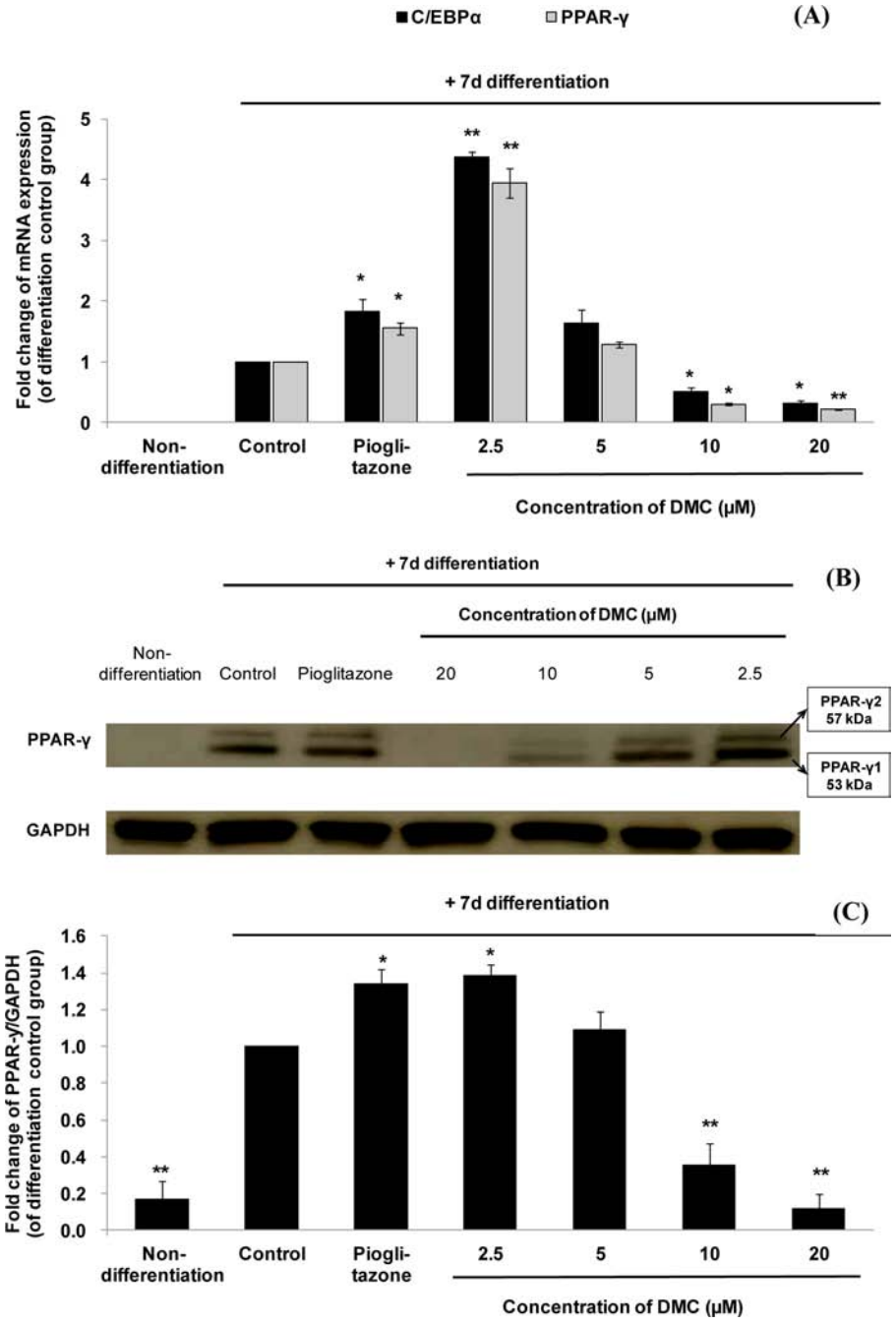

Figure 4. (A) Relative mRNA expression of C/EBP-α and PPAR-γ under different treatments in 3T3-L1 adipocytes. (B) Effect of DMC on PPAR-γ protein expression in 3T3-L1 adipocytes: representative image of protein expression of PPAR-γ and GAPDH measured by Western blot. (C) Quantification of PPAR-γ protein expression. The level of PPAR-γ expression was normalized against GAPDH, and the results were expressed as relative fold change compared to 7 day differentiation control. Values in (A) and (C) are shown as the mean ± SEM (n = 3). Significant differences between treatment groups and the differentiation control are indicated by ∗ for $P < 0.05$ and by ∗∗ for $P < 0.01$.

tissue.[42] In diabetes, insulin-sensitive tissues are functionally impaired, as manifested by a reduction in glucose uptake, lipid accumulation, and glycogen synthesis.[42] In the present study, we evaluated the effect of DMC on glucose uptake in differentiated L6 skeleton muscle cells and 3T3-L1 adipocytes, as well as glycogen synthesis in HepG2 hepatocytes. Our studies showed that DMC, at a dose of 10 μM, but not 20 μM, had the effect in 3T3-L1 adipocytes of remarkably enhanced glucose uptake, and it was aligned with the report that DMC improved glucose uptake in adipocytes.[34] At the same time, DMC showed no direct insulin mimicking effect on glucose uptake in L6 skeleton muscle cells or on glycogen synthesis in HepG2 hepatocytes.

3T3-L1 is a well-studied cell line that could provide an in vitro model for adipogenic differentiation from preadipose to adipose.[43] In this study, DMC was demonstrated to have paradoxical effects on cell differentiation and lipid accumulation in this cell line. High concentrations of DMC (10 and 20 μM) markedly diminished lipid accumulation, whereas a low dose (2.5 μM) enhanced lipid content in 3T3-L1 cells ($P < 0.05$ vs differentiation control group). To further understand the mechanism, we explored relevant terminal differentiation

dx.doi.org/10.1021/jf405368q | J. Agric. Food Chem. 2014, 62, 1898−1904

markers PPAR-γ and C/EBP-α.[44] PPAR-γ is the core of the adipogenesis and forms a feedback loop with C/EBP-α.[35] Similar paradoxical effects of DMC were observed in adipocyte differentiation by examining the gene expressions of PPAR-γ and C/EBP-α. Also, the protein level of PPAR-γ by Western blotting was consistent with our previous findings of lipid accumulation in differentiation 3T3-L1 cells. Therefore, we postulated that DMC may play a role as a key modulator affecting 3T3-L1 adipocyte differentiation (lipid accumulation) via regulating PPAR-γ. It was reported that DMC was a ligand of PPAR-γ,[34] yet it cannot explain why high concentrations of DMC decreased the expression of PPAR-γ. We hypothesize that high doses of DMC stimulated and low doses suppressed the expression of PPAR-γ, leading to a paradoxical effect on cell differentiation and fat accumulation in 3T3-L1 adipocytes. DMC was capable of inhibiting adipocyte differentiation and diminishing lipid accumulation with concomitant down-regulation of PPAR-γ at high dose.

Adiponectin, also known as the adipocyte complement-related protein, is mainly expressed in adipose tissue. DMC showed similar paradoxical effects on the production of adiponectin as on lipid accumulation and PPAR-γ expression in 3T3-L1 adipocytes. Because PPAR-γ activation leads to increased adiponectin gene expression and protein production and PPAR-γ and adiponectin have overlapping effects on downstream metabolic pathways,[45] we postulated that the adiponectin increasing and decreasing effect of different doses of DMC resulted from parallel regulation on PPAR-γ.

In conclusion, the present study provided evidence that DMC improved glucose uptake in differentiated 3T3-L1 adipocytes at 10 μM, but not at 20 μM, and that it had paradoxical effects on lipid accumulation during the process of adipocyte differentiation by controlling the expression of PPAR-γ. At a low dose, DMC promoted lipid production, whereas it suppressed the differentiation from preadipocytes to adipocytes at high concentrations. The study suggested the potential application of certain levels of DMC in the management of hyperglycemia. At the same time, the molecular mechanisms underlying the apparently paradoxical dose–response remain to be unveiled.

AUTHOR INFORMATION

Corresponding Author

*(Y.-H.L.) Phone: + 86-21-64251185. Fax: + 86-21-64251185. E-mail: luyanhua@ecust.edu.cn.

Funding

This work was supported by The Fundamental Research Funds for the Central Universities and partially supported by Shanghai Leading Academic Discipline Project (B505) and the National Special Fund for State Key Laboratory of Bioreactor Engineering (2060204).

Notes

The authors declare no competing financial interest.

ABBREVIATIONS USED

DMC, 2′,4′-dihydroxy-6′-methoxy-3′,5′-dimethylchalcone; C/EBP, CCAAT/enhancer binding protein; GAPDH, glyceraldehyde-3-phosphate dehydrogenase; aP2, adipocyte lipid-binding protein; CD36, cluster of differentiation 36; LPL, lipoprotein lipase; PPAR-γ, peroxisome proliferator-activated receptor-γ; PEPCK, phosphoenolpyruvate carboxykinase

REFERENCES

(1) Dung, N. T.; Kim, J. M.; Kang, S. C. Chemical composition, antimicrobial and antioxidant activities of the essential oil and the ethanol extract of *Cleistocalyx operculatus* (Roxb.) Merr and Perry buds. *Food Chem. Toxicol.* **2008**, *46*, 3632–3639.

(2) Mai, T. T.; Yamaguchi, K.; Yamanaka, M.; Lam, N. T.; Otsuka, Y.; Chuyen, N. V. Protective and anticataract effects of the aqueous extract of *Cleistocalyx operculatus* flower buds on β-cells of streptozotocin-diabetic rats. *J. Agric. Food Chem.* **2010**, *58*, 4162–4168.

(3) Ye, C. L.; Lu, Y. H.; Wei, D. Z. Flavonoids from *Cleistocalyx operculatus*. *Phytochemistry* **2004**, *65*, 445–447.

(4) Min, B. S.; Thu, C.; Van Dat, N. T.; Dang, N. H.; Jang, H. S.; Hung, T. M. Antioxidative flavonoids from *Cleistocalyx operculatus* buds. *Chem. Pharm. Bull.* **2008**, *56*, 1725–1728.

(5) Min, B. S.; Cuong, T. D.; Lee, J. S.; Shin, B.-S.; Woo, M. H.; Hung, T. M. Cholinesterase inhibitors from *Cleistocalyx operculatus* buds. *Arch. Pharm. Res.* **2010**, *33*, 1665–1670.

(6) Woo, A. Y. H.; Waye, M. M. Y.; Kwan, H. S.; Chan, M. C. Y.; Chau, C. F.; Cheng, C. H. K. Inhibition of ATPases by *Cleistocalyx operculatus*. A possible mechanism for the cardiotonic actions of the herb. *Vasc. Pharmacol.* **2002**, *38*, 163–168.

(7) Mai, T. T.; Thu, N. N.; Tien, P. G.; Van Chuyen, N. α-Glucosidase inhibitory and antioxidant activities of Vietnamese edible plants and their relationships with polyphenol contents. *J. Nutr. Sci. Vitaminol.* **2007**, *53*, 267–276.

(8) Mai, T. T.; Chuyen, N. V. Anti-hyperglycemic activity of an aqueous extract from flower buds of *Cleistocalyx operculatus* (Roxb.) Merr and Perry. *Biosci., Biotechnol., Biochem.* **2007**, *71*, 69–76.

(9) Ko, H.; Kim, Y. J.; Amor, E. C.; Lee, J. W.; Kim, H. C.; Kim, H. J.; Yang, H. O. Induction of autophagy by dimethyl cardamonin is associated with proliferative arrest in human colorectal carcinoma HCT116 and LOVO cells. *J. Cell Biochem.* **2011**, *112*, 2471–2479.

(10) Li, D.; Wu, X.; Tang, J.; Wei, X.; Zhu, X. F. ON-III inhibits erbB-2 tyrosine kinase receptor signal pathway and triggers apoptosis through induction of Bim in breast cancer cells. *Cancer Biol. Ther.* **2009**, 739–743.

(11) Ye, C. L.; Liu, Y.; Wei, D. Z. Antioxidant and anticancer activity of 3′-formyl-4′,6′-dihydroxy-2′-methoxy-5′-methylchalcone and (2*S*)-8-formyl-5-hydroxy-7-methoxy-6-methylflavanone. *J. Pharm. Pharmacol.* **2007**, *59*, 553–559.

(12) Ye, C.; Qian, F.; Wei, D.; Lu, Y.; Liu, J. Induction of apoptosis in K562 human leukemia cells by 2′,4′-dihydroxy-6′-methoxy-3′,5′-dimethylchalcone. *Leuk. Res.* **2005**, *29*, 887–892.

(13) Zhu, X.; Xie, B.; Zhou, J.; Feng, G.; Liu, Z.; Wei, X.; Zhang, F.; Liu, M.; Zeng, Y. Blockade of vascular endothelial growth factor receptor signal pathway and antitumor activity of ON-III (2′,4′-dihydroxy-6′-methoxy-3′,5′-dimethylchalcone), a component from Chinese herbal medicine. *Mol. Pharmacol.* **2005**, *67*, 1444–1450.

(14) Ye, C. L.; Liu, J. W.; Wei, D. Z.; Lu, Y. H.; Qian, F. In vivo antitumor activity by 2′,4′-dihydroxy-6′-methoxy-3′,5′-dimethylchalcone in a solid human carcinoma xenograft model. *Cancer Chemother. Pharmacol.* **2005**, *55*, 447–452.

(15) Ye, C. L.; Liu, J. W.; Wei, D. Z.; Lu, Y. H.; Qian, F. In vitro anti-tumor activity of 2′,4′-dihydroxy-6′-methoxy-3′,5′-dimethylchalcone against six established human cancer cell lines. *Pharmacol. Res.* **2004**, *50*, 505–510.

(16) Huang, H.; Niu, J.; Lu, Y. Multidrug resistance reversal effect of DMC derived from buds of *Cleistocalyx operculatus* in human hepatocellular tumor xenograft model. *J. Sci. Food Agric.* **2012**, *92*, 135–140.

(17) Huang, H.; Niu, J.; Zhao, L.; Lu, Y. Reversal effect of 2′,4′-dihydroxy-6′-methoxy-3′,5′-dimethylchalcone on multi-drug resistance in resistant human hepatocellular carcinoma cell line BEL-7402/5-FU. *Phytomedicine* **2011**, *18*, 1086–1092.

(18) Qian, F.; Ye, C. L.; Wei, D. Z.; Lu, Y. H.; Yang, S. L. In vitro and in vivo reversal of cancer cell multidrug resistance by 2′,4′-dihydroxy-6′-methoxy-3′,5′-dimethylchalcone. *J. Chemother.* **2005**, *17*, 309–314.

(19) Kim, Y. J.; Ko, H.; Park, J. S.; Han, I. H.; Amor, E. C.; Lee, J. W.; Yang, H. O. Dimethyl cardamonin inhibits lipopolysaccharide-induced

inflammatory factors through blocking NF-κB p65 activation. *Int. Immunopharmacol.* **2010**, *10*, 1127−1134.
(20) Dung, N. T.; Bajpai, V. K.; Yoon, J. I.; Kang, S. C. Anti-inflammatory effects of essential oil isolated from the buds of *Cleistocalyx operculatus* (Roxb.) Merr and Perry. *Food Chem. Toxicol.* **2009**, *47*, 449−453.
(21) Martínez, A.; Conde, E.; Moure, A. Protective effect against oxygen reactive species and skin fibroblast stimulation of *Couroupita guianensis* leaf extracts. *Nat. Prod. Res.* **2012**, 37−41.
(22) Su, M. Y.; Huang, H. Y.; Li, L.; L., Y. Protective effects of 2′,4′-dihydroxy-6′-methoxy-3′,5′-dimethylchalcone to PC12 cells against cytotoxicity induced by hydrogen peroxide. *J. Agric. Food Chem.* **2011**, *59*, 521−527.
(23) Maisuthisakul, P.; Suttajit, M.; Pongsawatmanit, R. Assessment of phenolic content and free radical-scavenging capacity of some Thai indigenous plants. *Food Chem.* **2007**, *100*, 1409−1418.
(24) Yu, W. G.; Qian, J.; Lu, Y. H. Hepatoprotective effects of 2′,4′-dihydroxy-6′-methoxy-3′,5′-dimethylchalcone on CCl_4-induced acute liver injury in mice. *J. Agric. Food Chem.* **2011**, *59*, 12821−12829.
(25) Amor, E. C.; Villaseñor, I. M.; Ghayur, M. N.; Gilani, A. H.; Choudhary, M. I. Spasmolytic flavonoids from *Syzygium samarangense* (Blume) Merr. & L.M. Perry. *Z. Naturforsch., C* **2005**, *60*, 67−71.
(26) Ghayur, M. N.; Gilani, A. H.; Khan, A.; Amor, E. C.; Villaseñor, I. M.; Choudhary, M. I. Presence of calcium antagonist activity explains the use of *Syzygium samarangense* in diarrhoea. *Phytother. Res.* **2006**, *20*, 49−52.
(27) Salem, M. M.; Werbovetz, K. Antiprotozoal compounds from *Psorothamnus polydenius*. *J. Nat. Prod.* **2005**, *68*, 108−111.
(28) Gafner, S.; Wolfender, J. L.; Mavi, S.; Hostettmann, K. Antifungal and antibacterial chalcones from *Myrica serrata*. *Planta Med.* **1996**, *62*, 67−69.
(29) Dao, T. T.; Tung, B. T.; Nguyen, P. H.; Thuong, P. T.; Yoo, S. S.; Kim, E. H.; Kim, S. K.; Oh, W. K. C-Methylated flavonoids from *Cleistocalyx operculatus* and their inhibitory effects on novel influenza A (H1N1) neuraminidase. *J. Nat. Prod.* **2010**, *3423*, 1636−1642.
(30) Amor, E. C.; Villaseñor, I. M.; Yasin, A.; Choudhary, M. I. Prolyl endopeptidase inhibitors from *Syzygium samarangense* (Blume) Merr. & L. M. Perry. *Z. Naturforsch., C* **2004**, *59*, 86−92.
(31) Resurreccion-Magno, M. H. C.; Villaseñor, I. M.; Harada, N.; Monde, K. Antihyperglycaemic flavonoids from *Syzygium samarangense* (Blume) Merr. and Perry. *Phytother. Res.* **2005**, *19*, 246−251.
(32) Hu, Y. C.; Luo, Y. D.; Li, L.; Joshi, M. K.; Lu, Y. H. In vitro investigation of 2′,4′-dihydroxy-6′-methoxy-3′,5′-dimethylchalcone for glycemic control. *J. Agric. Food Chem.* **2012**, *60*, 10683−10688.
(33) Luo, Y.; Lu, Y. H. 2′,4′-Dihydroxy-6′-methoxy-3′,5′-dimethylchalcone inhibits apoptosis of MIN6 cells via improving mitochondrial function. *Pharmazie* **2012**, *67*, 798−803.
(34) Jin, X. H.; Wei, X. Y.; Huang, Z. W.; Wu, D. H. Identify and characterize the PPAR-γ ligand-binding activity of extracts of *Cleistocalyx operculatus*. *J. Anhui Agric. Sci.* **2008**, *36*, 9106−9109.
(35) Tontonoz, P.; Spiegelman, B. M. Fat and beyond: the diverse biology of PPARγ. *Annu. Rev. Biochem.* **2008**, *77*, 289−312.
(36) Yang, M. H.; Avula, B.; Smillie, T.; Khan, I. A.; Khan, S. I. Screening of medicinal plants for PPARα and PPARγ activation and evaluation of their effects on glucose uptake and 3T3-L1 adipogenesis. *Planta Med.* **2013**, *79*, 1084−1095.
(37) Goto, T.; Kim, Y. I.; Takahashi, N.; Kawada, T. Natural compounds regulate energy metabolism by the modulating the activity of lipid-sensing nuclear receptors. *Mol. Nutr. Food Res.* **2013**, *57*, 20−33.
(38) Kuroda, M.; Mimaki, Y.; Sashida, Y.; Mae, T.; Kishida, H.; Nishiyama, T.; Tsukagawa, M.; Konishi, E.; Takahashi, K.; Kawada, T.; Nakagawa, K.; Kitahara, M. Phenolics with PPAR-γ ligand-binding activity obtained from licorice (*Glycyrrhiza uralensis* roots) and ameliorative effects of glycyrin on genetically diabetic KK-A(y) mice. *Bioorg. Med. Chem. Lett.* **2003**, *13*, 4267−4272.
(39) Salam, N. K.; Huang, T. H.-W.; Kota, B. P.; Kim, M. S.; Li, Y.; Hibbs, D. E. Novel PPAR-γ agonists identified from a natural product library: a virtual screening, induced-fit docking and biological assay study. *Chem. Biol. Drug Des.* **2008**, *71*, 57−70.
(40) Katsukawa, M.; Nakata, R.; Takizawa, Y.; Hori, K.; Takahashi, S.; Inoue, H. Citral, a component of lemongrass oil, activates PPARα and γ and suppresses COX-2 expression. *Biochim. Biophys. Acta* **2010**, *1801*, 1214−1220.
(41) Ramírez-Zacarías, J. L.; Castro-Muñozledo, F.; Kuri-Harcuch, W. Quantitation of adipose conversion and triglycerides by staining intracytoplasmic lipids with Oil red O. *Histochemistry* **1992**, *97*, 493−497.
(42) Stumvoll, M.; Goldstein, B. J.; van Haeften, T. W. Type 2 diabetes: principles of pathogenesis and therapy. *Lancet* **2005**, *365*, 1333−1346.
(43) Zebisch, K.; Voigt, V.; Wabitsch, M.; Brandsch, M. Protocol for effective differentiation of 3T3-L1 cells to adipocytes. *Anal. Biochem.* **2012**, *425*, 88−90.
(44) Fajas, L.; Fruchart, J. C.; Auwerx, J. Transcriptional control of adipogenesis. *Curr. Opin. Cell. Biol.* **1998**, *10*, 165−173.
(45) Astapova, O.; Leff, T. Adiponectin and PPARγ: cooperative and interdependent actions of two key regulators of metabolism. *Vitam. Horm.* **2012**, *90*, 143−162.

(C_4mim·Cl) was an efficient system for hydrolyzing lignocellulosic biomass. These authors attributed the excellent behavior of the system to the dispersion of most of the cellulose and hemicellulose molecules within the ionic liquid. Amarasekara et al.[18] successfully immobilized the sulfonic acid functionalized ionic liquid, C_4mim·Cl, on a silica surface to synthesize a silica-supported acid catalyst, showing that an effective heterogeneous acid catalyst can be produced by tethering an imidazolium moiety functionalized by attachment of a sulfonic acid group to a solid support. To better understand the mechanism of cellulose solvation by the above-mentioned ionic liquid, Remsing et al.[19] conducted a study and found that there was a 1:1 stoichiometry for the hydrogen-bonded interaction between the hydroxyl protons of carbohydrate and the chloride ions of ionic liquid. The chloride concentration in this system was as high as 20%. To expand on this bifunctional strategy, we have produced a unique artificial catalyst that mimics the structure of not only the catalytic active sites found in homogeneous acid catalysis but also the active sites of enzymes in the biocatalytic transformation of lignocellulose. In this present study, sucralose was chosen as a satisfactory carbonaceous material for the introduction of chlorine groups in carbon-based solid acid catalysts that can be prepared expediently by carbonization and sulfonation of various sugar in a manner that gives a relatively stable solid acid catalyst for hydrolyzing cellulose to glucose (**2**).[14] The incorporation ability of hydrophilic molecules will make it more easy for a cellulose chain in solution to be in contact with the $-SO_3H$ groups in the carbon material, thus giving rise to higher catalytic performance.[20] We propose that this study will enable the future rational design of new catalytic strategies by bonding chloride as a functional group to promote binding of cellulose to catalysts to overcome the intrinsic bottleneck of biomass hydrolysis, the severe mass-transfer limitation hampering progress, and thus enable the development of methods for processing widely available water-insoluble polymeric biomass under heterogeneous conditions.

EXPERIMENTAL SECTION

Materials. Sucralose (**4**) (biological reagent grade) was purchased from Shiyuanye Co., Ltd. (Shanghai, China). Sucrose was purchased from Jinhuada Chemical Reagent Co., Ltd. (Guangzhou, China). Microcrystalline cellulose (Avicel PH101) was obtained from FMC (Philadelphia, PA), and its degree of polymerization (DP) was 220. Starch (29.0% amylose content), was supplied by Huanglong Food Industry Co., Ltd. (Jilin, China). Rice straw and hardwood obtained locally was mechanically powdered to a particle size of 50−400 μm. C_4mim·OAc was from Lanzhou Institute of Chemical Physics (Lanzhou, China). Cellulase from *Trichoderma reesei* (6 U/mg) was bought from Sigma (St. Louis, MO, USA). All other chemicals were obtained from commercial sources and were of the highest grade available.

Catalyst Preparation and Characterization. The SUCRA-SO_3H catalyst and SUCRO-SO_3H catalysts were prepared from sucralose (**4**) and sucrose (**5**), respectively, according to a method similar to that reported previously by Hara et al.[14] Characterization of the carbon-based solid acid catalysts was carried out by a combination of Fourier transform infrared spectroscopy (FT-IR), X-ray photoelectron spectroscopy (XPS), Branauer−Emmett−Teller analysis (BET), scanning electron microscopy (SEM), temperature-programmed desorption of ammonia anaysis (NH_3-TPD), and acid−base titration.

Hydrolysis of Cellobiose and Cellulose. The standard reaction conditions for the hydrolysis reactions were as follows: cellobiose (**1**) (0.1 g) or cellulose (0.05 g), catalyst (0.1 g) or 1 mL of 4% dilute sulfuric acid and water (4 mL) were loaded into a 10 mL flask with a suitable rubber plug sealed with an aluminum cap to prevent loss of water by evaporation. After stirring (500 rpm) for 1 min the mixture was heated for 0−48 h to the temperature specified for each reaction. The flask was then placed into a mixture of ice and water for 10 min to stop reaction, and the mixtures (1−1.5 mL) were transferred into a 2 mL microcentrifuge tube and separated by centrifugation (1150*g*, 10 min) . Aliquots (100 μL) were withdrawn from the supernatant prior to HPLC analysis. The residual solids in the pipet, microcentrifuge tube, and flask were all collected together by filtration. Reasonable leaching water volume was heated to 80 °C to elute the remaining sugars adsorbed on the surface of the catalyst. The resultant liquor volume was concentrated down to 2 mL for subsequent HPLC analysis. In the reactions containing sulfuric acid, the solution was neutralized with $CaCO_3$ powder after the reaction, the $CaSO_4$ precipitate was removed by centrifugation, and the supernatant solution was analyzed. All reactions were performed in duplicate, and yields of glucose (**2**) had margins of error of up to ±3.4%.

Saccharide Adsorption Capacity of the Prepared Catalysts. Glucose (**2**) (600 mg) or cellobiose (**1**) (600 mg) was added into 12 mL of water and vortexed. The mixture was divided into 12 equal portions in microtubes. Then 100 mg of the catalyst was loaded into each microtube, and the contents were mixed well. All microtubes were kept at room temperature and vortexed for 2 min every 5 min. One microtube was taken and centrifuged at each of the following reaction times: 10, 20, 30, 60, 90, and 120 min. **2** and **1** in the supernatant were determined via high performance ion chromatograph to calculate the adsorption capacity of the catalyst. Other catalysts were treated in the same manner with a reaction time of for 2 h to investigate their adsorptive properties. Error bars represent standard deviations from three experiments.

Hydrolysate Analysis. Glucose (**2**) and cellobiose (**1**) were determined using an HPLC system consisting of a Waters 515 HPLC pump, a Bio-Rad organic acid column, and a Waters 2410 refractive index detector. The column used was a 300 mm × 7.8 mm i.d., Aminex HPX-87H (BIO-RAD Laboratories, Hercules, CA, USA). The mobile phase consisted of 5 mmol/L sulfuric acid aqueous solution with a flow rate of 0.5 mL/min. The column temperature was 65 °C. The cellulose and xylan contents were calculated from glucose (**2**) and xylose (**3**) contents multiplied by conversion factors of 0 0.90 and 0.88, respectively. The concentration of each compound in the liquid phase was determined using calibration curves obtained by analyzing standard solutions with known concentrations. TOC (total organic carbon), which is mostly composed of water-soluble polysaccharide and products from the dehydration of saccharides, was analyzed using a model 5000A TOC Analyzer (Shimadu, Tokyo, Japan). Y_{WSOC}, which represents the yield of total amount of water-soluble organic compounds in the reaction liquid, was calculated based on the data from TOC analysis. Concentration curves ranging from 1 to 150 ppm were prepared from a TOC standard solution (100 ppm) purchased from Sigma with a resulting R^2 value of 0.998.

Glucose yields were calculated as follows:

$$\text{glucose yield (\%)} = \{[\text{mol of glucose (produced)}] / (\text{theoretical yield of glucose in mol})\} \times 100$$

Glucose selectivity was calculated on the basis of TOC results as follows:

$$\text{glucose selectivity (\%)} = (\text{mol of carbon present in the form of glucose}) / (\text{mol of total water} - \text{soluble organic carbon})$$

Estimation of the Activation Energy of Glycosidic Bond Cleavage. The activation energy of cellobiose (**1**) hydrolysis using the sucralose- and sucrose-derived carbon-based solid acid catalysts was studied by comparing the reaction rate at four temperatures (373 K, 383 K, 393 K, and 403 K). Results were plotted as Arrhenius plots in the form of rate constants at each temperature, and activation

energies were calculated by multiplying the slope by the gas constant *R*.

Reuse Experiment. The catalyst reuse experiments were performed at 393 K. Reaction conditions were as follows: 0.1 g of cellobiose, 0.1 g of catalyst, 4 mL of deionized water, and reaction time 3 h, reaction temperature 393 K. The solid catalysts were washed by filtration with distilled water until sulfate ions could no longer be detected in the washings, after which the catalyst was reused in the next cycle of the reaction.

RESULTS AND DISCUSSION

Fourier transform infrared (FT-IR) spectra of the catalysts displayed peaks at approximately 1180 cm^{-1} and 1030 cm^{-1}, which are typically attributable to the stretching modes of SO_3H groups. X-ray photoelectron spectroscopy (XPS) revealed only one peak at 168 eV, assigned to the SO_3H groups, implying that all sulfur in the carbon catalyst is contained in the SO_3H groups. The elemental compositions of the catalysts were measured using the XPS data in order to determine the content of sulfonic acid group. The amount of sulfur per gram of catalyst was 0.28 mmol for the sucralose-derived catalyst (SUCRA-SO_3H), 0.47 mmol for the sucrose-derived catalyst (SUCRO-SO_3H), and 0.67 mmol for the sulfonated sucralose. As expected, the carbonized sucralose contained no detectable sulfur. The specific surface area of SUCRA-SO_3H catalyst was 0.317 m^2/g, which was similar to the 0.282 m^2/g measured for the SUCRO-SO_3H catalyst. Sulfonated sucralose showed a clear advantage in the amount of sulfonyl group attachment compared to other catalysts, indicating that both the carbonization and sulfonation processes cause a decrease in chloride group content, negatively affecting adsorption ability and reaction results. Here, we evaluated the best catalyst among different materials that were capable of hydrolyzing polysaccharide. Both SUCRO-SO_3H and SUCRA-SO_3H catalysts are composed of irregular shaped amorphous carbon particles with layer structures, and the size of catalyst particles was between 0.4 and 1.0 mm. However, there were no obvious mesoporous or microporous particles observed in the SEM micrographs. The acidic properties of SUCRO-SO_3H, SUCRA-SO_3H, and carbonated sucralose were investigated by temperature-programmed desorption of ammonia analysis. Both samples of SUCRO-SO_3H and SUCRA-SO_3H show a distinct broad peak at around 473 K due to the presence of abundant hydroxyl groups. The curve of incompletely carbonated sucralose shows a little higher intensity and desorption in the temperature range of 723–923 K than the other two samples, due to the more severe decomposition of the solid sample. Both SUCRO-SO_3H and SUCRA-SO_3H catalysts showed the presence of medium acid sites, as their respective desorption temperatures are around 623 K, which corresponded to the carboxyl groups.

Initially, we tested the capacity of the catalysts to hydrolyze β-1,4-glycosidic bonds by using cellobiose (**1**) as the substrate, which is commonly used as model compound for cellulose. Figure 1 shows time courses for D-glucose (**2**) formation from cellobiose (**1**) by the SUCRA-SO_3H catalyst. As a comparison, the results for the SUCRO-SO_3H catalyst are also included. Conversion of cellobiose (**2**) reached 100% after 3 h with both catalysts. Taking the sulfur content of the catalysts into account, which based on the XPS results equates to the content of sulfonic acid groups in the catalysts, the SUCRA-SO_3H catalyst (containing 0.28 mmol/g of sulfur) performs much better than the higher sulfur content SUCRO-SO_3H catalyst (containing 0.47 mmol/g of sulfur).

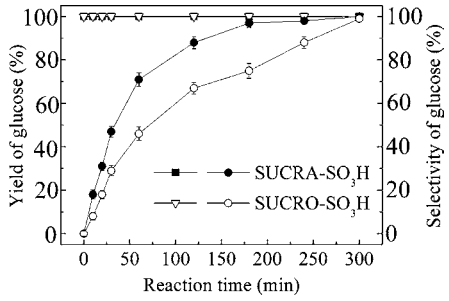

Figure 1. Time courses for D-glucose formation from cellobiose.Yield of glucose (**2**) (circular symbols) and selectivity of glucose (**2**) (square symbols and triangles) during hydrolysis of cellobiose (**1**) over SUCRA-SO_3H (closed symbols) and SUCRO-SO_3H (open symbols).

To investigate the performance of the new catalysts in comparison to other catalytic systems, their performance was compared with that of sulfonated sucralose, sulfonated sucrose, Amberlyst-15, and niobic acid (Figure 2). Only trace amounts

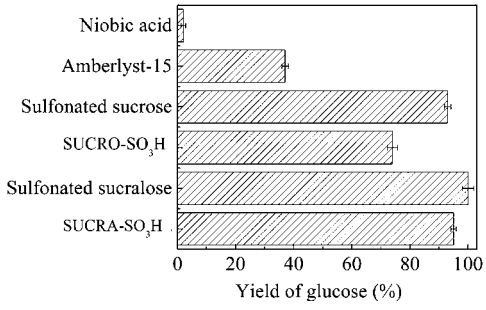

Figure 2. Hydrolysis of cellobiose (**1**) catalyzed by various catalysts.

of cellobiose (**1**) were converted over niobic acid, presumably due to the lack of efficient acid catalytic sites,[21] while the catalysts bearing Brønsted acid sites (Amberlyst-15 and the sulfonated carbon materials) generally exhibited good catalytic performance. Furthermore, the addition of halogen as cellulose binding sites in SUCRA-SO_3H significantly enhanced the reaction activity compared to the SUCRO-SO_3H catalyst, which does not contain halogen.

This encouraging progress could be attributed to increases in adsorption capacity. Catalysts with cellulose binding sites are thought to be superior at adsorbing cellobiose (**1**) (the shortest β-1,4-linked polysaccharide, which is often used to model the cellulose hydrolysis reaction) and **2** (the expected product), since the chloride group is a strong hydrogen bond acceptor that may enter into hydrogen bonding with the hydroxyl groups on cellulose, cellobiose (**1**), and glucose (**2**). To confirm this conjecture, 0.1 g portions of the solid catalyst were added to separate 2 mL aliquots of aqueous cellobiose (**1**) and glucose (**2**) solutions (50 g/L), and the mixture was oscillated at room temperature (298 K). As shown in Figure 3, 21.5% of the added cellobiose (**1**) was absorbed by the SUCRA-SO_3H catalyst within 2 h, which was higher than the value of 18% absorbed by the SUCRO-SO_3H catalyst, and the Cl-bearing catalyst SUCRA-SO_3H required a shorter time before adsorption equilibrium was reached compared to the Cl-free SUCRO-SO_3H catalyst. Similarly, the SUCRA-SO_3H catalyst absorbed 8.5% of the added glucose (**2**), which was more than the 5% absorbed by the SUCRO-SO_3H catalyst and agrees with the

dx.doi.org/10.1021/jf405712b | J. Agric. Food Chem. 2014, 62, 1905–1911

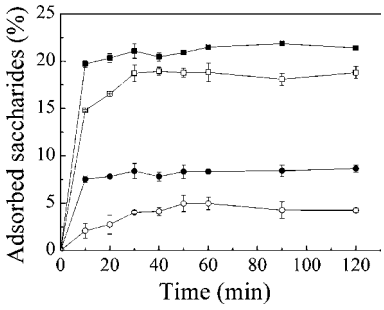

Figure 3. Adsorption curve of glucose (**2**) (circular symbols) and cellobiose (**1**) (square symbols) onto SUCRA-SO_3H catalyst (closed symbols) and SUCRO-SO_3H catalyst (open symbols) in aqueous solution. 100% adsorption would correspond to binding of 50 mg of carbohydrate to 100 mg of catalyst in a volume of 1 mL.

results of Suganuma et al.[21] and Shuai et al.[16] The ability of the catalysts to take up large amounts of saccharides is likely caused by the simultaneous incorporation of water and adsorption of saccharides. It is possible that the formation of hydrogen bonds occurs between the hydroxyl groups of cellulose and not only the chloride groups but also the hydroxyl groups on catalyst as minor electronegative groups. Furthermore, the stronger electrophilicity of surface chloride groups than hydroxyl groups on the carbon affords better adsorption capacity.

Further, the adsorption capacity of the SUCRA-SO_3H catalyst was compared with those achieved with other heterogeneous catalysts (Figure 4). Among the range of

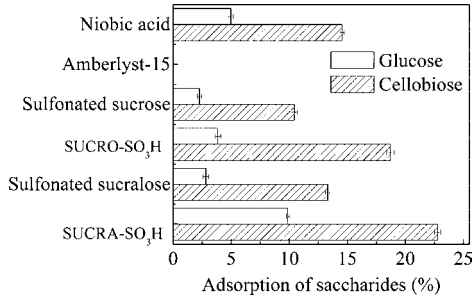

Figure 4. The adsorption capacity of the tested catalysts. 100% adsorption would correspond to binding of 50 mg of carbohydrate to 100 mg of catalyst in a volume of 1 mL.

catalysts tested, the sulfonated sucralose shows the best adsorption ability, which correlates with its highest chloride group loading. Although niobic acid showed the third greatest saccharide-binding capacity, possibly caused by swelling of the solid acid catalyst, it exhibited poor catalysis presumably owing to its low acidity (70% that of sulfuric acid). However, Amberlyst-15, with its strong acid groups, performed conversely, indicating that only when a certain amount of acid groups and requisite electron pair acceptor are present on the catalyst will a highly effective catalyst result.[22]

Catalytic activity was further investigated by examining the effectiveness of the catalysts for cellulose and starch hydrolysis. Compared to starches, cellulose is more difficult to hydrolyze due to its crystalline form and the abundant hydrogen bonding present in the cellulose molecule, and the β-glycosidic linkage of cellobiose (**1**) among the various types of simple disaccharides is one of the most recalcitrant bonds to acid hydrolysis compared to maltose, sucrose, lactose, and xylobiose.[23] As shown in Table 1, in the case of starch, the carbon-based catalyst SUCRA-SO_3H showed a glucose (**2**) yield of approximately 90%, with an equivalent amount of fructose observed after a 6 h reaction. For hydrolysis of unpretreated cellulose, however, only 4% glucose (**2**) yield was achieved after 24 h of reaction. Nonetheless, the glucose (**2**) yield from this reaction could be increased to 53% by converting the water-soluble polysaccharide in the resulting reaction liquid through a 48 h enzyme hydrolysis, and 48% saccharide was detected in the final product according to the TOC result based on mass.

To improve the accessibility of the catalytic sites of the catalyst to the β-1,4-glycosidic bond in cellulose, we pretreated cellulose with the ionic liquid C_4mim·OAc and then regenerated it with water. It is generally accepted that the primary mechanism for dissolution of cellulose by ionic liquids proceeds through disruption of the interstrand hydrogen-bonding network between adjacent polymer chains, and C_4mim·OAc has been found to be an efficient ionic liquid for reducing the crystallinity of cellulose.[24] XRD analysis indicated that the amorphous region increased greatly in the regenerated cellulose, and thereby it is possible that the glycosidic bonds in the substrates become more exposed to the catalysts. Three diffraction peaks, at around 2θ of 16°, 22°, and 34°, respectively, for untreated microcrystalline cellulose, but only one weak peak remained at around 22° after treatment with C_4mim·OAc. The most important result of pretreatment is that it enables maximum sugar yield and minimizes the loss of sugars and the subsequent formation of inhibitory products. The yield of glucose (**2**) increased up to 55% with a 98%

Table 1. Hydrolytic Degradation of Polysaccharides to Glucose Using Various Catalysts

entry	catalyst	substrate	time[a] (h)	temp (K)	Y_{Glu}[b] (%)	Y_{WSOC}[c] (%)	S_{Glu}[d] (%)
1	SUCRA-SO_3H	cellulose (Avicel PH101)	24	393	4	48	8
2	SUCRA-SO_3H	IL-pretreated cellulose	24	393	55	56	98
3	SUCRA-SO_3H	IL-pretreated cellulose	24	413	46	63	73
4	SUCRA-SO_3H	IL-pretreated cellulose	24	423	41	67	61
5	SUCRA-SO_3H	starch	6	383	92	96	47
6	SUCRO-SO_3H	cellulose (Avicel PH101)	24	393	3	26	11
7	SUCRO-SO_3H	IL-pretreated cellulose	24	393	49	49	97
8	Amberlyst-15	IL-pretreated cellulose	24	393	–	3	–
9	niobic acid	IL-pretreated cellulose	24	393	–	–	–
10	dilute sulfuric acid	IL-pretreated cellulose	30	393	25	34	75

[a]The optimum reaction time for the hydrolysis. [b]Y_{Glu} was the yield of glucose. [c]Y_{WSOC} was the yield of water-soluble organic compounds determined via a TOC analyzer. [d]S_{Glu} was the selectivity of glucose on tested catalysts. – represents "not detected".

dx.doi.org/10.1021/jf405712b | J. Agric. Food Chem. 2014, 62, 1905−1911

selectivity for regenerated cellulose using SUCRA-SO_3H catalyst at an optimum reaction time of 24 h and 393 K, which was superior to that with SUCRO-SO_3H catalyst (49%) at an optimum reaction time of 24 h and 393 K and that with dilute sulfuric acid (25%) at an optimum reaction time of 30 h and 393 K (Table 1). Additionally, in comparison with other liquid acid catalysts reported previously such as maleic acid[25] and phosphoric acid,[26] our prepared SUCRA-SO_3H catalyst gave a higher yield of glucose (**2**) in hydrolysis of cellulose. Figure 5A–C illustrates the effects of reaction time on

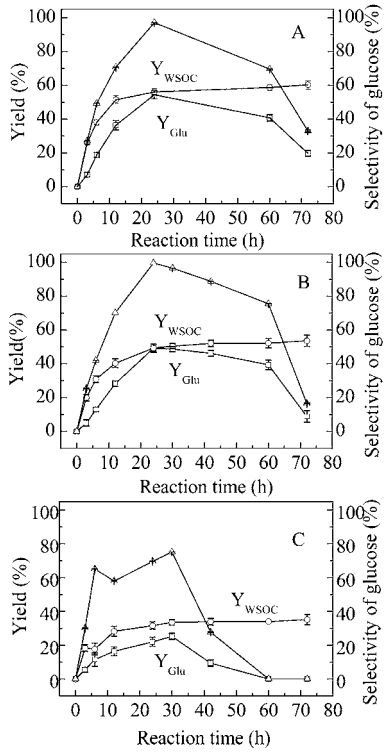

Figure 5. Hydrolysis of cellulose pretreated with C_4mim·OAc over various catalysts: (A) SUCRA-SO_3H, (B) SUCRO-SO_3H, and (C) dilute sulfuric acid.

hydrolysis of cellulose pretreated by ionic liquid with SUCRA-SO_3H, SUCRO-SO_3H, and dilute sulfuric acid as the catalyst, respectively. It was found that the reaction time had significant influence on yield of glucose (**2**), selectivity of glucose (**2**), and yield of water-soluble organic compounds (Y_{WSOC}) in hydrolysis of cellulose using various catalysts. The yield and selectivity of glucose (**2**) and the Y_{WSOC} with SUCRA-SO_3H increased clearly with increasing reaction time up to 24 h, but a further increase in reaction time resulted in a significant drop in the yield and selectivity of glucose (**2**) (Figure 5A). The Y_{WSOC} with SUCRA-SO_3H showed only slight increase when reaction time was more than 24 h, suggesting that there is a recalcitrant portion of insoluble cellulose present in the cellulose that is not accessible to hydrolysis. This similar trend was seen with increasing reaction time in hydrolysis of cellulose catalyzed by SUCRO-SO_3H (Figure 5B). Obviously, the optimum reaction time for hydrolysis of cellulose using SUCRA-SO_3H or SUCRO-SO_3H was 24 h. In the case of dilute sulfuric acid, the yield and selectivity of glucose (**2**) reached maximum values at reaction time of 30 h, being the optimum reaction time for the reaction. Similarly, no significant variation in the Y_{WSOC} was observed when reaction time was further prolonged. Although both carbon-based catalysts and dilute acid suffered from an undesirable side reaction, namely, the conversion of glucose (**2**) into hydroxymethyl furfural (HMF), the yield of glucose (**2**) showed a sharper decline with prolonged reaction time in the case of the dilute acid catalyst, in comparison with SUCRA-SO_3H and SUCRO-SO_3H. The result suggests that the formed glucose (**2**) from cellulosic biomass may be less converted into byproducts by the carbon-based catalysts. When reaction temperature was elevated, the formed glucose (**2**) was further converted into HMF with high concentrations, thus lowering the selectivity of glucose (**2**) (Table 1). We also performed the reaction using rice straw and hardwood (Table 2) as commercially significant lignocellulosic substrate to check the practicability of tested catalysts. When rice straw pretreated with C_4mim·OAc was hydrolyzed by the SUCRA-SO_3H catalyst, the obtained yield of glucose (**2**) was much less than that of hydrolysis of pure cellulose similarly pretreated under the same conditions. As evident from the data summarized in Table 2, rice straw was more easily degraded by the SUCRA-SO_3H and SUCRO-SO_3H catalysts than hardwood. SUCRA-SO_3H slightly surpassed SUCRO-SO_3H for hydrolysis of both rice straw and hardwood. Hemicellulose as an important component of ligincellulose can be hydrolyzed by our prepared solid acid catalysts as well as by liquid acid catalysts.[27] Interestingly, both the cabon-based catalysts preferentially hydrolyzed hemicellulose.

It has been reported that cellulose hydrolysis can be modeled based on a pseudo-first-order reaction followed by degradation of the generated glucose (**2**).[28] The reaction rate constant obeys modified Arrhenius equations, including effects of temperature and acid concentration. The advantage of adsorbing the substrate onto the catalyst surface is that it will increase the opportunity for the substrate to come into contact with the local acid moieties dispersed on the surface of the amorphous carbon sheet, thereby increasing the rate of the reaction associated by reducing activation energy (Figure 6). Kinetic studies showed that the apparent activation of cellobiose (**1**) hydrolysis was 94 kJ/mol at 373–403 K for

Table 2. Hydrolytic Degradation of Lignocellulose to Glucose Using SUCRA-SO_3H

	composition of regenerated lignincellulose (%)				yield (%)					
					SUCRA-SO_3H			SUCRO-SO_3H		
raw material	cellulose	hemic-ellulose	lignin	ash	Y_{Glu} [a]	Y_{Xyl} [b]	Y_{WSOC} [c]	Y_{Glu} [a]	Y_{Xyl} [b]	Y_{WSOC} [c]
rice straw	47.7	15.6	14.5	16.4	19.5	57.3	36.0	16.5	56.0	34.5
hardwood	54.3	16.5	14.4	1.3	12.7	44.4	32.0	11.2	39.8	29.8

[a] Y_{Glu} was the maximum yield of glucose based on the weight of cellulose in regenerated lignincellulose. [b] Y_{Xyl} was the maximum yield of xylose (**3**) based on the weight of hemicellulose in regenerated lignincellulose. [c] Y_{WSOC} was the yield of water-soluble organic compounds determined via a TOC analyzer.

dx.doi.org/10.1021/jf405712b | J. Agric. Food Chem. 2014, 62, 1905–1911

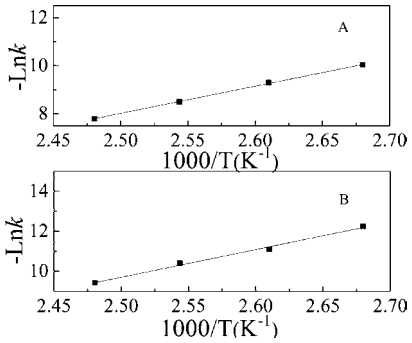

Figure 6. Arrhenius plot of cellobiose (**1**) hydrolysis over (A) SUCRA-SO_3H and (B) SUCRO-SO_3H. Rate constant k was calculated on the basis of the average rate during the initial reaction period (<50% conversion).

SUCRA-SO_3H catalyst (Figure 6A), which is significantly lower than values for microcrystalline cellulose-derived carbon catalyst (110 kJ/mol),[21] SUCRO-SO_3H catalyst (114 kJ/mol) (Figure 6B), and sulfuric acid (133 kJ/mol).[16]

Figure 7 shows the operational stability of the resulting solid catalysts by conducting sequential hydrolytic reactions with the same sample of catalyst using cellobiose (**1**) as substrate at 393 K for 3 h reaction time per cycle. The SUCRA-SO_3H catalyst showed no significant loss in activity after successive reuse of six batches, but an obvious loss in activity was observed after seven batches, and the SUCRA-SO_3H catalyst remained around 56% of the original activity after being repeatedly used for 10 batches, which was attributable to the partial leach of SO_3H groups from the catalyst with the increase of reuse batch. We subsequently detected the pH of the reaction system after the removal of the SUCRA-SO_3H catalyst by filtration during the course of each run, including those at the beginning and the end. The pH of the reaction system showed only a slight fall after successive reuse of six batches, but manifested a relatively obvious decrease after seven batches, particular at the end of the tenth batch, implying the partial leach of SO_3H groups into the reaction system to form free acids through possible self-hydrolysis of the sulfonated catalysts, which was also confirmed by analyzing the S content of the catalyst (data not shown). This could well explain the observation that the SUCRA-SO_3H catalyst indicated relative instability after seven batches of reuse. Moreover, as can be seen in Figure 7, the stability of the SUCRA-SO_3H catalyst prepared by carbonization and sulfonation was clearly superior to that of the sulfonated sucralose, possibly due to the increase of the COOH groups and the rigidity of the carbon skeleton structure in SUCRA-SO_3H by carbonization, which was similar to the observation reported by Siril et al.[29] In fact, it is known that aromatic carbon−SO_3H bonds in sulfoaromatic compounds bearing electron-withdrawing functional groups such as halogens, COOH, and phenol OH are more stable against loss of the sulfonyl group as a result of the increased electron density between the carbon and sulfur atoms. Moreover, the prepared SUCRA-SO_3H catalyst was incubated for 24 h at a relatively higher temperature of 413 K to evaluate its thermal stability, and still maintained more than 80% of its initial activity, showing good stability which was comparable to that of the catalyst Amberlyst 35.[23] A possible mechanism for the hydrolysis process over the solid acid catalysts prepared is that the stronger affinity for β-1,4-glucan of the novel carbon-based catalyst than the traditional solid acid catalysts may provide better access by reactants to the −SO_3H groups in the carbon material to cleave the β-1,4-glucosidic bonds. Catalysis over the tentative carbon catalyst with −SO_3H, −COOH, −Cl, and phenolic −OH groups thus resulted in high catalyst activity.

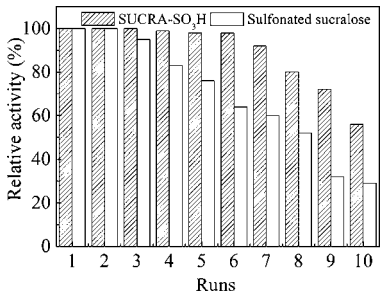

Figure 7. Reusability of SUCRA-SO_3H and sulfonated sucralose in hydrolysis of cellobiose. The relative activity for both catalysts tested prior to use is defined as 100%, and activity is shown after each cycle.

■ ASSOCIATED CONTENT

Ⓢ Supporting Information

Chlorine and sulfur content of the four catalysts (SUCRO-SO_3H, SUCRA-SO_3H, carbonized sucralose, and sulfonated sucralose) (Table S1). BET parameters of SUCRO-SO_3H and SUCRA-SO_3H (Table S2). Detail equation parameters of lnk-1/T curve (Table S3). The pH of the reaction system after removal of the catalyst for each run (Table S4). FT-IR spectra and S2p curves from XPS analysis of SUCRO-SO_3H catalyst and SUCRA-SO_3H catalyst (Figures S1 and S2). XRD analysis of cellulose substrate before and after pretreatment using ionic liquid (Figure S3). Nitrogen adsorption/desorption isotherms and scanning electron microscopy images of SUCRO-SO_3H and SUCRA-SO_3H (Figures S4 and S5). The NH_3-TPD profiles of SUCRO-SO_3H catalyst, SUCRA-SO_3H catalyst, and carbonized sucralose (Figure S6). Glucose (**2**) and xylose (**3**) yields of hydrolysis of IL-pretreated straw catalyzed by SUCRA-SO_3H and SUCRO-SO_3H with time (Figure S7). This material is available free of charge via the Internet at http://pubs.acs.org.

■ AUTHOR INFORMATION

Corresponding Author

*Tel: +86-20-22236669. Fax: +86-20-22236669. E-mail: wylou@scut.edu.cn.

Notes

The authors declare no competing financial interest.

■ ACKNOWLEDGMENTS

We wish to thank the National Science Found for Excellent Young Scholars (21222606), the State Key Program of National Natural Science Foundation of China (21336002), the National Key Basic Research Program of China (2013CB733500), and the Fundamental Research Funds for SCUT (2013ZG0003) for partially funding this work.

■ REFERENCES

(1) Chu, S.; Majumdar, A. Opportunities and challenges for a sustainable energy future. *Nature* **2012**, *488*, 294−303.

(2) Dhepe, P. L.; Fukuoka, A. Cellulose conversion under heterogeneous catalysis. *ChemSusChem* **2008**, *1*, 969−975.

(3) Geboers, J. A.; Vyver, S.; Van de; Ooms, R.; Beeck, B. Op de; Jacobs, P. A.; Sels, B. F. Chemocatalytic conversion of cellulose:

opportunities, advances and pitfalls. *Catal. Sci. Technol.* **2011**, *1*, 714−726.
(4) Mosier, N.; Sarikaya, S. A.; Ladisch, C. M.; Ladisch, M. R. Characterization of dicarboxylic acids for cellulose hydrolysis. *Biotechnol. Prog.* **2001**, *17* (3), 474−480.
(5) Berlin, A.; Maximenko, V.; Gilkes, N.; Saddler, J. Optimization of enzyme complexes for lignocellulose hydrolysis. *Biotechnol. Bioeng.* **2007**, *97*, 287−296.
(6) Zhang, Z.; Donaldson, A. A.; Ma, X. Advancements and future directions in enzyme technology for biomass conversion. *Biotechnol. Adv.* **2012**, *30*, 913−919.
(7) Shimizu, K.; Satsuma, A. Toward a rational control of solid acid catalysis for green synthesis and biomass conversion. *Energy Environ. Sci.* **2011**, *4*, 3140−3153.
(8) Kobayashi, H.; Ohta, H.; Fukuoka, A. Conversion of lignocellulose into renewable chemicals by heterogeneous catalysis. *Catal. Sci. Technol.* **2012**, *2*, 869−883.
(9) Takagaki, A.; Tagusagawa, C.; Domen, K. Glucose production from saccharides using layered transition metal oxide and exfoliated nanosheets as a water-tolerant solid acid catalyst. *Chem. Commun.* **2008**, *42*, 5363−5365.
(10) Onda, A.; Ochi, T.; Yanagisawa, K. Hydrolysis of cellulose selectively into glucose over sulfonated activated-carbon catalyst under hydrothermal conditions. *Top. Catal.* **2009**, *52*, 801−807.
(11) Muhammad, N.; Man, Z.; Khalil, M. A. B. Ionic liquid-a future solvent for the enhanced uses of wood biomass. *Eur. J. Wood Prod.* **2011**, *70*, 125−133.
(12) Ignatyev, I. A.; Van Doorslaer, C.; Mertens, P. G. N.; Binnemans, K.; De Vos, D. E. Reductive splitting of cellulose in the ionic liquid 1-butyl-3-methylimidazolium chloride. *ChemSusChem* **2010**, *3*, 91−96.
(13) Bansal, P.; Vowell, B. J.; Hall, M.; Realff, M. J.; Lee, J. H.; Bommarius, A. S. Elucidation of cellulose accessibility, hydrolysability and reactivity as the major limitations in the enzymatic hydrolysis of cellulose. *Bioresour. Technol.* **2012**, *107*, 243−250.
(14) Suganuma, S.; Nakajima, K.; Kitano, M.; Yamaguchi, D.; Kato, H.; Hayashi, S.; Hara, M. Synthesis and acid catalysis of cellulose-derived carbon-based solid acid. *Solid State Sci.* **2010**, *12*, 1029−1034.
(15) Van de Vyver, S.; Peng, L.; Geboers, J.; Schepers, H.; de Clippel, F.; Gommes, C. J.; Goderis, B.; Jacobs, P. A.; Sels, B. F. Sulfonated silica/carbon nanocomposites as novel catalysts for hydrolysis of cellulose to glucose. *Green Chem.* **2010**, *12*, 1560−1563.
(16) Shuai, L.; Pan, X. J. Hydrolysis of cellulose by cellulase-mimetic solid catalyst. *Energy Environ. Sci.* **2012**, *5*, 6889.
(17) Li, C. Z.; Wang, Q.; Zhao, Z. B. Acid in ionic liquid: An efficient system for hydrolysis of lignocellulose. *Green Chem.* **2008**, *10*, 177−182.
(18) Amarasekara, A. S.; Owereh, O. S. Synthesis of a sulfonic acid functionalized acidic ionic liquid modified silica catalyst and applications in the hydrolysis of cellulose. *Catal. Commun.* **2010**, *11* (13), 1072−1075.
(19) Remsing, R. C.; Swatloski, R. P.; Rogers, R. D.; Moyna, G. Mechanism of cellulose dissolution in the ionic liquid 1-*n*-butyl-3-methylimidazolium chloride: a 13C and 35/37Cl NMR relaxation study on model systems. *Chem. Commun.* **2006**, 1271−1273.
(20) Huang, Y. B.; Fu, Y. Hydrolysis of cellulose to glucose by solid acid catalysts. *Green Chem.* **2013**, *15*, 1095−1101.
(21) Suganuma, S.; Nakajima, K.; Kitano, M.; Yamaguchi, D.; Kato, H.; Hayashi, S.; Hara, M. Hydrolysis of cellulose by amorphous carbon bearing SO_3H, COOH, and OH groups. *J. Am. Chem. Soc.* **2008**, *130*, 12787−12793.
(22) Kitano, M.; Yamaguchi, D.; Suganuma, S.; Nakajima, K.; Kato, H.; Hayashi, S.; Hara, M. Adsorption-enhanced hydrolysis of β-1,4-glucan on graphene-based. *Langmuir* **2009**, *25* (9), 5068−5075.
(23) Kim, Y. R.; Hendrickson, N. M.; Ladisch, M. R. Plug-flow reactor for continuous hydrolysis of glucans and xylans from pretreated corn fiber. *Energy Fuels* **2005**, *19* (5), 2189−2200.
(24) Cheng, G.; Varanasi, P.; Arora, R.; Stavila, V.; Simmons, B. A.; Kent, M. S.; Singh, S. Impact of ionic liquid pretreatment conditions on cellulose crystalline structure using 1-ethyl-3-methylimidazolium acetate. *J. Phys. Chem. B* **2012**, *116* (33), 10049−10054.
(25) Mosier, N. S.; Ladisch, C. M.; Ladisch, M. R. Characterization of acid catalytic domains for cellulose hydrolysis and glucose degradation. *Biotechnol. Bioeng.* **2002**, *79*, 610−618.
(26) Palkovits, R.; Tajvidi, K.; Procelewska, J.; Rinaldi, R.; Ruppert, A. Hydrogenolysis of cellulose combining mineral acids and hydrogenation catalysts. *Green Chem.* **2010**, *12*, 972−978.
(27) Kim, Y.; Hendrickson, R.; Mosier, N.; Ladisch, M. R. Reaction mechanisms and kinetics of xylo-oligosaccharide hydrolysis by dicarboxylic acids. *AIChE J.* **2012**, *59* (1), 188−199.
(28) Vyver, S.; Van de; Geboers, J.; Jacobs, P. A.; Sels, B. F. Recent advances in the catalytic conversion of cellulose. *ChemCatChem* **2011**, *3*, 82−94.
(29) Siril, P. F.; Cross, H. E.; Brown, D. R. New polystyrene sulfonic acid resin catalysts with enhanced acidic and catalytic properties. *J. Mol. Catal. A: Chem.* **2008**, *279*, 63−68.

Table 1. Elemental Content of Poultry Manure (PM) and PM Chars Obtained at 350, 450, and 600 °C for Heating Times of 30, 60, 90, and 120 min[a]

sample	heating time (min)	C (%)	H (%)	N (%)	C/H
poultry manure (PM)		30 ± 2	4 ± 1	2.6 ± 0.3	7 ± 2
PM char at 350 °C	30	32 ± 2	2.6 ± 0.3	2.1 ± 0.1	12 ± 2
	60	34 ± 1	2.63 ± 0.03	2.4 ± 0.3	13.0 ± 0.3
	90	30 ± 2	2.4 ± 0.2	2.1 ± 0.2	12 ± 2
	120	31 ± 2	1.9 ± 0.2	2.3 ± 0.3	16 ± 3
PM char at 450 °C	30	27 ± 2	1.3 ± 0.2	1.62 ± 0.08	21 ± 4
	60	30 ± 1	1.4 ± 0.1	1.75 ± 0.06	21 ± 2
	90	29 ± 1	1.5 ± 0.1	1.88 ± 0.02	19 ± 2
	120	24 ± 1	0.9 ± 0.2	1.5 ± 0.2	27 ± 7
PM char at 600 °C	30	26 ± 7	0.6 ± 0.2	1.2 ± 0.4	42 ± 25
	60	24 ± 2	0.50 ± 0.01	1.08 ± 0.04	48 ± 5
	90	24 ± 1	0.64 ± 0.09	1.23 ± 0.02	37 ± 7
	120	25 ± 3	0.62 ± 0.06	1.24 ± 0.09	40 ± 8

[a]All values are uncorrected for ash and moisture contents.

and microbial recalcitrance, which is also the cause of their long mean residence time in soils.[33]

The physical characteristics of the charred materials also depend on the nature of the biomasses subjected to the thermal stress.[34,35] Indeed, plant species with many large-diameter cells in the stem tissues can lead to biochars containing larger amounts of macropores.[31] Macropores in biochar applied to soils may enhance soil-draining properties and the capacity to retain larger molecules such as phenolic compounds.[36]

On this basis, we can infer that understanding the char chemical and physical properties is crucial to address its agronomical and environmental uses and allow meaningful preapplication quality assessments.

The aim of the present paper is to report on the changes occurring in the structure of poultry manure biochar when it is obtained at different temperatures and heating times. For this reason we applied cross-polarization magic angle spinning (CPMAS) ^{13}C NMR spectroscopy and thermogravimetric analysis (TGA). Results will show that production temperature is more important than heating time in the chemical−physical characteristics of PM biochar. Our findings appear to confirm recent data obtained on other different animal and vegetal biomasses.[35,37]

MATERIALS AND METHODS

Sample Preparation. Poultry manure (PM) was collected from a Sicilian chicken farm, Conca d'Uovo, Misilmeri, Palermo, Italy (38°3′4″ N, 13°25′32″ E). After sampling, the material was air-dried to a maximum moisture content of 20%. The manure was then charred in 300 mL Pyrex flasks at atmospheric pressure by applying three temperatures: 350, 450, and 600 °C. At the beginning, residual air was still present in the system. Once the reaction started, oxygen was consumed and pyrolysis proceeded under anoxic conditions. The effectiveness of the pyrolysis was confirmed by the NMR analyses described below. For each temperature, heating times of 30, 60, 90, and 120 min were employed. PM chars were allowed to cool to room temperature after pyrolysis. They were then finely ground in a ceramic mortar and dried again at 105 °C overnight. The dried materials were stored in a desiccator until analyses.

Chemical Analyses of PM Chars. Elemental contents (C, H, N) for all samples were achieved by using a Vario MicroCUBE Elemental Analyzer (Elementar, Hanau, Germany). All of the results are reported in Table 1. C, H, and N values were not corrected for the ash and moisture contents.

CPMAS ^{13}C NMR Spectroscopy. A 7.05 T Varian UNITY INOVA (Varian Inc., Palo Alto, CA, USA), equipped with an Apex HX wide-bore probe operating at a ^{13}C frequency of 75.4 MHz, was used to acquire the ^{13}C NMR spectra. The samples were packed in 6 mm zirconium rotors with Teflon bottom and top spacers and Vespel drive tips. The temperature was kept constant at 25.0 ± 0.1 °C. Magic angle spinning was carried out at 8000 ± 1 Hz. A ^{1}H RF field strength of 50.3 kHZ and a ramp of 16 kHz to account for inhomogeneity of the Hartmann−Hahn condition were applied.[38] VNMRJ software (version 1.1 revision D, Varian Inc.) was used to acquire all of the free induction decays (FID). Spectra were processed by Mestre-C software (version 4.9.9.9, Mestrelab Research, Santiago de Compostela, Spain). All of the FIDs were transformed by applying first a 2K zero filling and then an exponential filter function with a line broadening (LB) of 50 Hz. Fully automatic baseline correction using a Bernstein algorithm was applied for baseline corrections.

Thermogravimetric Analyses. TGA was carried out using a Netzsch Simultaneous Thermal Analyzer STA 449 F3 Jupiter (Netzsch-Gerätebau GmbH, Selb, Germany). Alumina crucibles were used as sample holder. Prior to analyses, ground PM chars were equilibrated in a chamber with controlled humidity (relative humidity of 40%). For the thermoanalytical experiments, the following conditions were applied: heating rate of 10 °C min^{-1} from 30 to 1000 °C, under dynamic air atmosphere, flow rate of 50 mL min^{-1}, and sample mass about 10 mg (weighted with an accuracy of ±0.001 mg). The measurements were repeated three times for each sample. Data were analyzed using the Netzsch Star software (NETZSCH Proteus software). The TG curves were derivated (DTG) to improve their resolution with respect to the number of degradation steps and their onsets. The first derivative of the TG trace represents the mass loss rate (expressed as % min^{-1}) as a function of temperature. DTG curves are represented as a series of peaks, instead of an "integrate" stepwise curve (TG), in which the areas under the peaks are proportional to the total mass change of the sample.[39] In this way, even subtle mass changes, not evident in the TG curves, can be highlighted by a DTG peak.[39]

RESULTS AND DISCUSSION

CPMAS ^{13}C NMR Investigations. Figure 1 shows the CPMAS ^{13}C NMR spectra of the PM and Figure 2 its char derivatives produced at 350, 450, and 600 °C for charring times of 30, 60, 90, and 120 min.

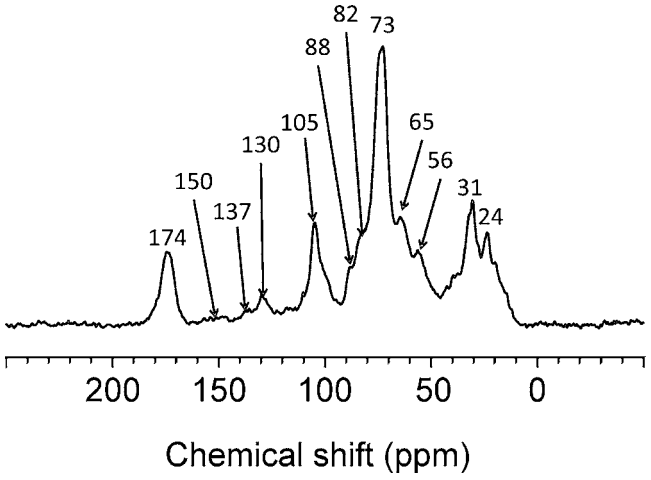

Figure 1. CPMAS ^{13}C NMR spectrum of the poultry manure.

The PM spectrum (Figure 1) reveals a signal pattern that is due to the typical plant material provided to chickens as food. In fact, signals in the region 0−50 ppm are traditionally attributed to alkyl systems. Here, a predominance of methylene ($-CH_2-$) chains (peaks at 24 and 31 ppm) due to lipids, cutin-like structures, and other aliphatic biomolecules can be observed.[40,41]

The region in the interval of 50−60 ppm is assigned to both nitrogenated and oxygenated alkyl systems. However, only a signal at 56 ppm is visible. The latter is usually attributed to methoxyl groups in lignin-like structures.[40,41]

The NMR signal pattern between 60 and 110 ppm is assigned to carbohydrates. Here, cellulose carbons resonate at 65 ppm (C-6), 73 ppm (C-2, C-3, C-5), 82 ppm (C-4 in amorphous cellulose, hemicellulose, and cellulose oligomers), and 88 ppm (C-4 of cellulose on fibril surfaces).[41] Finally, the anomeric carbon in cellulose appears at 105 ppm.[40,41]

The aromatic carbon spectral region is represented by the interval 110−160 ppm. The PM spectrum in Figure 1 reveals aromatic signals at 130, 137, and 150 ppm. Due to the aforementioned signal at 56 ppm, aromatic signals are most likely assigned to lignin-like systems.[41,42] In particular, the signal at 130 ppm is generated by *p*-hydroxyphenol derivatives, whereas those at 137 and 150 are by syringyl-like systems.[41]

The last signal at 174 ppm is assigned to carboxyl groups.

After pyrolysis at 350 °C, the chemical composition of PM drastically changed (Figure 2A). In fact, regardless of the muffle residence time, only two sets of broad bands are observed in the alkyl (0−45 ppm) and aromatic (110−160 ppm) regions. In particular, three main signals can be recognized in the alkyl interval of the spectra, whereas the aromatic carbons produce only one broad signal centered at 130 ppm (Figure 2A). The three main alkyl signals are placed at 14, 24, and 31 ppm. Whereas the latter two can be attributed to methylene chains as reported above, the former signal (14 ppm) is generated by methyl groups terminating alkyl chains. The presence of large amounts of alkyl carbons in the 350 °C charred PM (Figure 2A) shows that the temperature of 350 °C is not sufficient to completely pyrolyze the poultry manure. In particular, aliphatic chains and carbohydrates are converted partly to polycyclic aromatic systems and partly to shorter alkyl moieties. These can either be immobilized to bridge aromatic moieties or be methyl-containing linear substituents on aromatic rings.[17,31] At the longest residence time of 120 min, the signal at 31 ppm, which stems from $-CH_2-$ groups inside aliphatic chains, is noticeably reduced compared to the signals at 24 and 14 ppm. This indicates not only that the aliphatic content decreases with longer residence times but also that the chain length is reduced.

As reported in the literature,[31] the amount of alkyl carbons decreases while that of the aromatic moieties increases, as

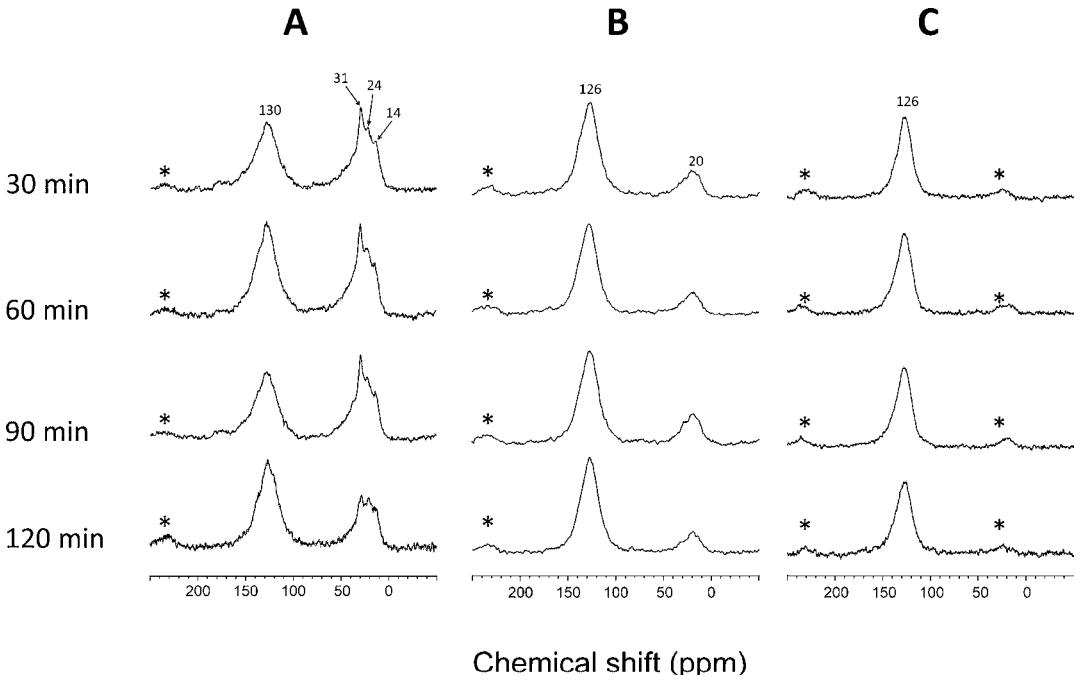

Figure 2. CPMAS ^{13}C NMR spectra of the poultry manure chars produced at 350 °C (A), 450 °C (B), and 600 °C (C) for heating times of 30, 60, 90, and 120 min. The positions of spinning side bands (SSBs) are marked with asterisks (*). Note that the high-field SSB is overlapped by the alkyl resonances in the chemical shift interval 0−50 ppm.

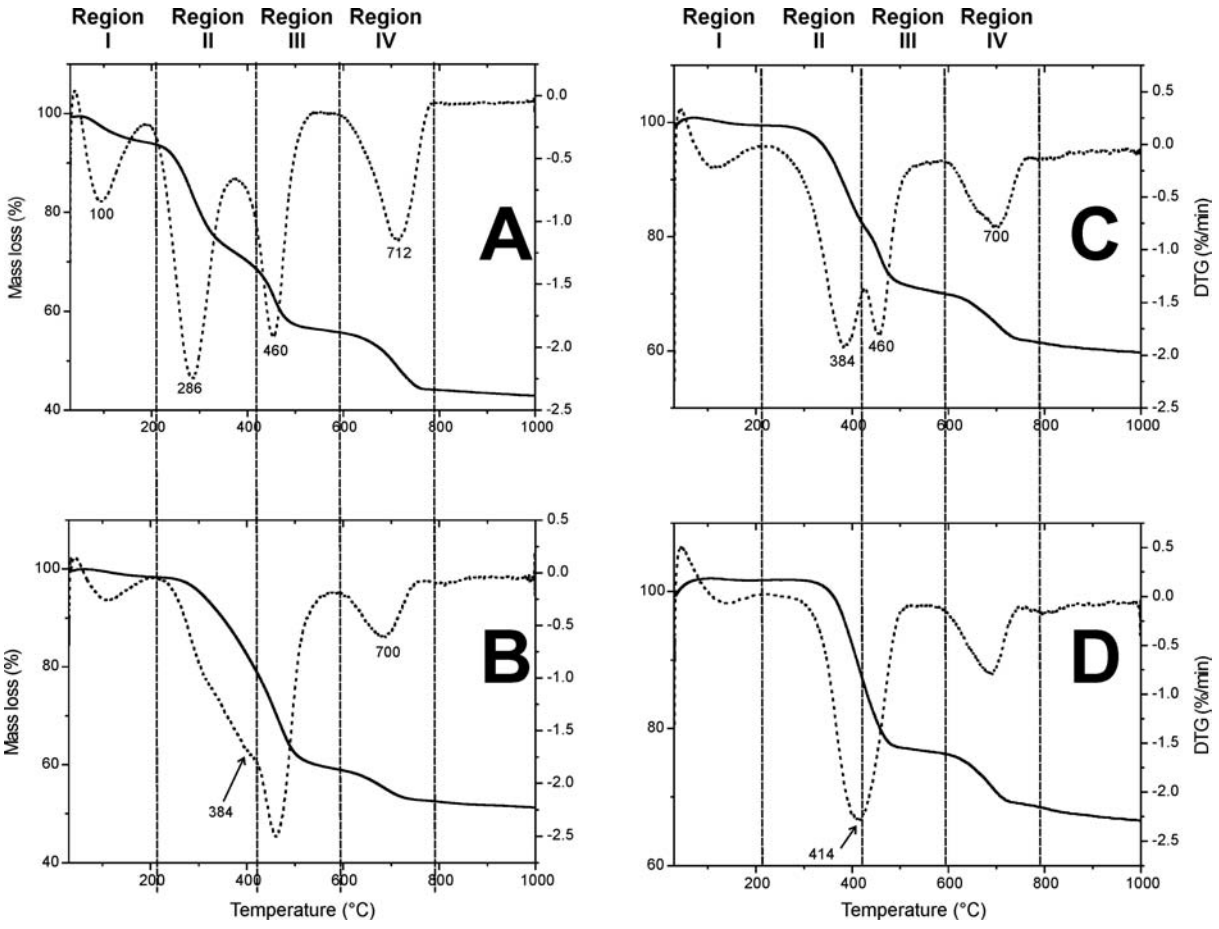

Figure 3. Thermograms (TG, solid lines) and first derivatives of the thermograms (DTG, dotted curves) for the poultry manure (A) and the chars obtained at 350 °C (B), 450 °C (C), and 600 °C (D) and heating time of 120 min. Four different regions can be identified. Region I refers to water removal, region II describes the mass loss due to thermal transformation of carbohydrates and alkyl labile systems, region III is associated with the thermal transformation of aromatic moieties; and region IV is due to transformation of the inorganic components of poultry manure chars.

charring temperature is raised. This is confirmed by the spectra of the poultry manure charred at 450 and 600 °C (Figure 2, panels B and C, respectively). The pyrolysis at 450 °C at all muffle residence times produces charred materials containing mainly aromatic carbons (broad band at 126 ppm in the spectra of Figure 2B). A strong reduction of the alkyl signal intensity is observed as compared to the spectra in Figure 2A. The comparison between the spectra in panels A and B of Figure 2 shows also a loss of resolution of the alkyl band in the spectrum of the biochar retrieved at 450 °C. This finding can be explained by the reduction of the number of methyl-rich linear substituents and the formation of methyl-free alkyl bridges between aromatic rings.

The alkyl signal completely disappears after pyrolysis at 600 °C (Figure 2C), thereby supporting previous results showing that aromatic carbons are the main components in char systems when they are produced with temperatures above 500 °C.[17,35]

It is worth noting that the NMR spectra of the chars obtained at each temperature were similar to each other regardless of the applied charring time (i.e., comparison of the spectra in Figure 2 from top to bottom along columns A, B, and C). However, a shift of 4 ppm of the aromatic carbon chemical shift value can be observed when the spectra in Figure 2 are compared at the same charring time for the different temperatures. In fact, the aromatic carbons resonate at 130 ppm in the spectrum of the PM charred at 350 °C, whereas they appear at 126 ppm in the spectra of the PM chars obtained at 450 and 600 °C. According to McBeath and Smernik,[43] the higher the heating temperature applied for PM charring, the lower is the chemical shift value for the resonance of the aromatic carbons. This is due to the enhancement of the aromatic polycondensation degree as the charring temperature is raised. The elemental content reported in Table 1 further confirms the results from CPMAS ^{13}C NMR experiments. In fact, on the one hand, no changes are observed in the elemental compositions of the chars retrieved at the different heating times when pyrolysis is done at the three temperatures of 350, 450, and 600 °C. This indicates that heating temperature is more important than heating time in affecting the chemical nature of PM chars, thereby confirming recent results by Wolf et al.[37] and Zhao et al.[35] on different char materials. On the other hand, the C/H ratio increases with increasing charring temperature (Table 1). The larger the C/H ratio, the higher the polycondensation degree of organic systems. This supports the conclusion that higher charring temperatures favor formation of polycondensed aromatic rings.[43]

TGA. Figure 3 reports the thermogravimetic (TG) records (solid lines) of the poultry manure and its char products together with the first-derivative curve (DTG, dotted lines). The latter curve reflects the rate of the thermo-oxidative degradation.[44] The chemical similarity among chars as evidenced by CPMAS ^{13}C NMR spectroscopy (see above) is

dx.doi.org/10.1021/jf405549z | J. Agric. Food Chem. 2014, 62, 1912−1918

also reflected in the TG/DTG curves reported in Figure 3. For this reason, only the TG/DTG profiles of the chars obtained at the heating time of 120 min are reported in Figure 3.

TG investigations revealed that mass loss (ML) was in the order $ML_{600\ °C} < ML_{450\ °C} < ML_{350\ °C} \approx ML_{PM}$ (Figure 3). This is expected because charring processes progressively reduce sample carbon, hydrogen, and nitrogen contents as heating temperature is increased.[45,46] Table 1 supports the latter findings. In fact, the carbon amount varied from a mean value of ≈30% in the PM and PM chars obtained at 350 °C to an average of ≈28% in the 450 °C PM chars and to an average of ≈25% in the chars retrieved at 600 °C. Reduction of H and N contents followed the same trend. In fact, they were in the orders $H_{PM} \approx H_{(PM\ chars\ at\ 350)} > H_{(PM\ chars\ at\ 450)} > H_{(PM\ chars\ at\ 600)}$ and $N_{PM} \approx N_{(PM\ chars\ at\ 350)} > N_{(PM\ chars\ at\ 450)} > N_{(PM\ chars\ at\ 600)}$, respectively.

Each TG/DTG curve has been operationally subdivided into four different mass loss steps at four specific temperature intervals (Figure 3).[44,47] The first interval, in the temperature range 40−210 °C (region I in Figure 3) with a progressive mass loss with the maximum rate around 100 °C, is common for all samples. It refers to the loss of moisture adsorbed on PM and chars during the equilibration stage (RH 40%) prior to analysis[44] (see Materials and Methods).

Region II spans a temperature interval from 210 to 420 °C, whereas region III includes the interval 420−570 °C (Figure 3). Poultry manure evidenced the maximum rate of the progressive mass loss at around 286 °C in region II. Conversely, the chars retrieved at 350 and 450 °C showed a maximum mass loss rate at around 384 °C in the same region. Moreover, both PM and PM chars produced at 350 and 450 °C revealed a maximum ML rate at around 460 °C in region III. Finally, the char sample retrieved at 600 °C showed only one DTG peak at around 414 °C placed between regions II and III (Figure 3). The last thermal region, IV, between 600 and 800 °C (Figure 3), with a DTG peak at around 700 °C in all of the samples, is attributed to the degradation of mineral and biogenic salts such as calcium and potassium carbonates usually present in poultry manure.[47,48]

Poultry manure has already been described as a complex mixture of alkyl moieties, sugars, aromatic systems, and acidic functions (see discussion above on CPMAS ^{13}C NMR spectroscopy). The TG/DTG curves reported in Figure 3A confirm those findings. In fact, region II in biomass thermograms is usually due to the thermo-oxidative degradation of labile alkyl systems, carbohydrates, and fatty acids.[47,49] Conversely, region III is mainly assigned to mass loss of more recalcitrant aromatic moieties.[47,49] The latter come from original structures and, partially, from structures that developed in previous stages during the degradation and recombination of aliphatic molecules.[50] In particular, the highly oxygenated degree of the organic PM systems favors mass loss at the temperature of 286 °C in region II (Figure 3A). Conversely, the larger chemical stability of aromatic systems is responsible for the thermal degradation at the temperature of 460 °C as evidenced in region III (Figure 3A).

Following pyrolysis at 350 and 450 °C, PM transforms into a char mainly made by alkyl and aromatic domains. All of the oxygenated functions are lost (see the CPMAS ^{13}C NMR spectroscopy discussion above). Alkyl systems are thermally more stable than the oxygen-rich moieties. For this reason, region II in Figure 3B,C reveals a mass loss at a temperature of 384 °C, which is around 100 °C higher than that observed in Figure 3A.

According to literature data,[44,49,51] linkages of recalcitrant aromatic moieties disrupt between 430 and 600 °C. This arises in region III at 460 °C in poultry manure (Figure 3A), and the chars retrieved at 350 °C (Figure 3B) and 450 °C (Figure 3C). Conversely, the aromatic systems of the chars obtained at 600 °C degraded at 414 °C (Figure 3D), which is a temperature 46 °C lower than that observed in Figure 3A−C and placed on the border of regions II and III.

To explain the thermo-oxidative instability of the aromatic domains of the 600 °C PM chars as compared to the thermo-oxidative stability of the same domains in PM and PM chars at 350 and 450 °C, differences in the conformational arrangements of the different molecular domains have been considered.[52] In fact, it is conceivable that the nonaromatic domains in poultry manure and its 350 and 450 °C chars are mainly displaced on the surface of highly condensed or strongly associated polyaromatic systems.[52] Due to this, the surficial nonaromatic components are degraded first during the TG investigation. The stable products obtained by this first degradation step[50,53] protect the inner aromatic constituents toward the thermo-oxidative degradation, thereby decelerating the effective heat flow and preventing the char particles from penetration of reactive atmosphere.[54] Conversely, the polyaromatic domain in the 600 °C PM chars is degraded at a lower temperature (≈400 °C in Figure 3C) than the other chars due to the absence of the protective effect of the nonaromatic components.

In conclusion, spectroscopic and thermal characterization of poultry manure and its char derivatives obtained at different temperatures and charring times revealed that char chemical nature is affected more by the former than by the latter. Although such a conclusion confirms findings from other authors,[35] our study showed in addition an unexpected stability of the aromatic systems in the low-temperature-retrieved materials than in those obtained at the highest temperature. This result was explained by hypothesizing that the alkyl domains in chars produced at 350 and 450 °C were mainly displaced on the surface of a rigid aromatic core. For this reason, the thermal destruction of the original aromatic core was retrieved only after the complete degradation of the products developed from the original alkyl systems.

Alkyl removal by charring poultry manure at 600 °C left the aromatic domain unprotected, thereby allowing thermal degradation of the aromatic systems at a temperature lower than that measured for the PM chars produced at the two lowest temperatures (350 and 450 °C).

Due to the knowledge that conformation has on the sorption properties of chars (e.g., kinetics and thermodynamics of char sorption or residence time of adsorbed species), the understanding of the role of alkyl and aromatic domains in these interactions is of great importance.

AUTHOR INFORMATION

Corresponding Author

*(P.C.) E-mail: pellegrino.conte@unipa.it. Phone: 0039 091 238 64673. Fax: 0039 091 484035.

Funding

This study was partially funded by Ateneo Italo-Tedesco/Deutsch-Italienisches Hochschulzentrum through Vigoni project 2010.

Notes

The authors declare no competing financial interest.

■ ABBREVIATIONS USED

PM, poultry manure; CPMAS, cross-polarization magic angle spinning; NMR, nuclear magnetic resonance; TGA, thermogravimetric analyses; DTG, derivative thermogravimetry; ML, mass loss

■ REFERENCES

(1) Roach, S.; Isenhart, L.; McKenna, L.; Cunningham, M. *Filthy Feed − The Risky and Unregulated Practice of Feeding Poultry Litter to Cattle*; FACT, Food Animal Concerns Trust: Chicago, IL, USA, 2009.

(2) Huang, G.; Wang, X.; Han, L. Rapid estimation of nutrients in chicken manure during plant-field composting using physicochemical properties. *Bioresour. Technol.* **2011**, *102*, 1455−1461.

(3) Chan, K. Y.; Van Zwieten, L.; Meszaros, I.; Downie, A.; Joseph, S. Using poultry litter biochars as soil amendments. *Aust. J. Soil Res.* **2008**, *46*, 437−444.

(4) Khaleel, R.; Reddy, K. P.; Overcash, M. R. Changes in soil physical properties due to waste applications: a review. *J. Environ. Qual.* **1981**, *10*, 133−141.

(5) Lal, R.; Kang, B. T. Management of organic matter in soils of the tropics and subtropics. *XII Congress International Society Soil Science*, New Delhi, India; CIRAD: Paris, France, 1982; pp 152−178.

(6) Metzger, L.; Yaron, B. Influence of sludge organic matter on soil physical properties. *Adv. Soil Sci.* **1987**, *7*, 141−163.

(7) Davies, D. B.; Payne, D. Management of soil physical properties. In *Russell's Soil Conditions and Plant Growth*, 11th ed.; Wild, A., Ed.; Longman: Harlow, Essex, UK, 1988.

(8) Sanchez, P. A.; Palm, C. A.; Szott, L. T.; Cuevas, E.; Lal, R. Organic input management in tropical agroecosystems. In *Dynamics of Soil Organic Matter in Tropical Ecosystems*; Coleman, D. C., Oades, J. M., Uehara, G., Eds.; University of Hawaii Press: Honolulu, HI, USA, 1989.

(9) Haynes, R. J.; Naidu, R. Influence of lime, fertilizer and manure applications on soil organic matter content and soil physical conditions: a review. *Nutr. Cycl. Agroecosyst.* **1998**, *51* (2), 123−137.

(10) Perkins, H. F.; Parker, M. B.; Walker, M. L. *Chicken Manure − Its Production, Composition, and Use as a Fertilizer*; Georgia Agricultural Experiment Stations Bulletin 123; 1964.

(11) Wilkinson, K. G.; Harapas, D.; Tee, E.; Tomkins, R. B.; Premier, R. *Strategies for the Safe Use of Poultry Litter in Food Crop Production.* Horticulture Australia Ltd.: Sidney, Australia, 2003.

(12) Chan, K. Y.; Van Zwieten, L.; Meszaros, I.; Downie, A.; Joseph, S. Assessing the agronomic values of contrasting char materials on Australian hardsetting soil. In *Proceedings of the Conference of the International Agrichar Initiative*, April 30−May 2, 2007, Terrigal, NSW, Australia; 2007.

(13) Gay, S. W.; Schmidt, D. R.; Clanton, C. J.; Janni, K. A.; Jacobson, L. D.; Weisberg, S. Odor, total reduced sulfur and ammonia emissions from animal housing facilities and manure storage units in Minnesota. *Appl. Eng. Agric.* **2003**, *19* (3), 347−360.

(14) Fan, Z. J.; Ai, Y. W.; Li, J. M.; Li, G. W. Discussion of controlling N loss from volatilization in animal manure. *J. Sichuan Normal Univ.* **2000**, *23* (5), 548−550.

(15) Shinogi, Y.; Kanri, Y. Pyrolysis of plant, animal and human waste: physical and chemical characterization of the pyrolytic products. *Bioresour. Technol.* **2003**, *90* (3), 241−247.

(16) Popov, V.; Itoh, H.; Brebbia, C. A.; Kungoles, A. *Waste Management and the Environment II*; WIT Press: Boston, MA, USA, 2004.

(17) De Pasquale, C.; Marsala, V.; Berns, A. E.; Valagussa, M.; Pozzi, A.; Alonzo, G.; Conte, P. Fast field cycling NMR relaxometry characterization of biochars obtained from an industrial thermochemical process. *J. Soil Sediment* **2012**, *2*, 1211−1221.

(18) Schmidt, M. W. I; Noack, A. G. Black carbon in soils and sediments: analysis, distribution, implications, and current challenges. *Global Biogeochem. Cy.* **2000**, *14* (3), 777−793.

(19) Gaunt, J. L.; Lehmann, J. Energy balance and emissions associated with biochar sequestration and pyrolysis bioenergy production. *Environ. Sci. Technol.* **2008**, *42*, 4152−4158.

(20) Matthews, J. A. Carbon negative biofuels. *Energy Policy* **2008**, *36*, 940−945.

(21) Lehmann, J.; Czimczik, C.; Laird, D.; Sohi, S. Stability of biochar in the soil. In *Biochar for Environmental Management: Science and Technology*; Lehmann, J., Joseph, S., Eds.; Earthscan: London, UK, 2009.

(22) Sohi, S. P.; Krull, E.; Lopez-Capel, E.; Bol, R. A review of biochar and its use and function in soil. *Adv. Agron.* **2010**, *105*, 47−82.

(23) Uchimiya, M.; Lima, I. M.; Klasson, K. T.; Chang, S.; Wartelle, L. H.; Rodgers, J. E. Immobilization of heavy metal ions (Cu^{II}, Cd^{II}, Ni^{II}, and Pb^{II}) by broiler litter-derived biochars in water and soil. *J. Agric. Food Chem.* **2010**, *58*, 5538−5544.

(24) Yuan, J. H.; Xu, R. K.; Wang, N.; Li, J. Y. Amendment of acid soils with crop residues and biochars. *Pedosphere* **2011**, *21* (3), 302−308.

(25) Kishimoto, S.; Sugiura, G. Charcoal as a soil conditioner. *Int. Achieve Future* **1985**, *5*, 12−23.

(26) Mikan, C. J.; Abrams, M. D. Altered forest composition and soil properties of historic charcoal hearths in southeastern Pennsylvania. *Can. J. For. Res.* **1995**, *25*, 687−696.

(27) Rondon, M. A.; Lehmann, J.; Ramirez, J.; Hurtado, M. Biological nitrogen fixation by common beans (*Phaseolus vulgaris* L.) increases with bio-char additions. *Biol. Fert. Soils* **2007**, *43*, 699−708.

(28) Rillig, M. C.; Wagner, M.; Salem, M.; Antunes, P. M.; George, C.; Ramke, H. G.; Titirici, M.-M.; Antonietti, M. Material derived from hydrothermal carbonization: effects on plant growth and arbuscular mycorrhiza. *Appl. Soil Ecol.* **2010**, *45* (3), 238−242.

(29) Conte, P.; Marsala, V.; De Pasquale, C.; Bubici, S.; Valagussa, M.; Pozzi, A.; Alonzo, G. Nature of water-biochar interface interactions. *GCB Bioenergy* **2013**, *5*, 116−121.

(30) Krull, E. S.; Baldock, J. A.; Skjemstad, J. O.; Smernik, R. J. Characteristics of biochar: organo-chemical properties. In *Biochar for Environmental Management: Science and Technology*; Lehmann, J., Joseph, S., Eds.; Earthscan: London, UK, 2009.

(31) Lehmann, J.; Joseph, S. Biochar for environmental management: an introduction. In *Biochar for Environmental Management: Science and Technology*; Lehmann, J., Joseph, S., Eds.; Earthscan: London, UK, 2009.

(32) Gundale, M. J.; De Luca, T. H. Temperature and source material influence ecological attributes of ponderosa pine and Douglas-fir charcoal. *For. Ecol. Manag.* **2006**, *231*, 86−93.

(33) Knicker, H. Pyrogenic organic matter in soil: its origin and occurrence, its chemistry and survival in soil environments. *Quat. Int.* **2011**, *243* (2), 251−263.

(34) Wiedner, K.; Rumpel, C.; Steiner, C.; Pozzi, A.; Maas, R.; Glaser, B. Chemical evaluation of chars produced by thermochemical conversion (gasification, pyrolysis and hydrothermal carbonization) of agro-industrial biomass on a commercial scale. *Biomass Bioenergy* **2013**, DOI: 10.1016/j.biombioe.2013.08.026 (article in press).

(35) Zhao, L.; Cao, X.; Mašek, O.; Zimmerman, A. Heterogeneity of biochar properties as a function of feedstock sources and production temperatures. *J. Hazard Mater.* **2013**, *256−257*, 1−9.

(36) Warnock, D. D.; Lehmann, J.; Kuyper, T. W.; Rilling, M. C. Mycorrhizal responses to biochar in soil − concepts and mechanisms. *Plant Soil* **2007**, *300*, 9−20.

(37) Wolf, M.; Lehndorff, E.; Wiesemberg, G. L. B.; Stockhausen, M.; Schwark, L.; Amelung, W. Towards reconstruction of past fire regimes from geochemical analysis of charcoal. *Org. Geochem.* **2013**, *55*, 11−21.

(38) Berns, A. E.; Conte, P. Effect of ramp size and sample spinning speed on CPMAS C-13 NMR spectra of soil organic matter. *Org. Geochem.* **2011**, *42*, 926−935.

(39) Wendlandt, W. W. M. *Thermal Analysis*; Wiley: New York, 1986.

(40) Gómez, X.; Diaz, M. C.; Cooper, M.; Blanco, D.; Morán, A.; Snape, C. E. Study of biological stabilization processes of cattle and poultry manure by thermogravimetric analysis and ^{13}C NMR. *Chemosphere* **2007**, *68*, 1889−1897.
(41) Conte, P.; De Pasquale, C.; Novotny, E. H.; Caponetto, G.; Laudicina, V. A.; Ciofalo, M.; Panno, M.; Palazzolo, E.; Badalucco, L.; Alonzo, G. CPMAS ^{13}C NMR characterization of leaves and litters from the reafforestated area of Mustigarufi in Sicily (Italy). *Open Magn. Reson. J.* **2010**, *3*, 89−95.
(42) Wilson, M. A. *N.M.R. Techniques and Applications in Geochemistry and Soil Chemistry*, 1st ed.; Pergamon Press: London, UK, 1987.
(43) McBeath, A. V.; Smernik, R. J. Variation in the degree of aromatic condensation of chars. *Org. Geochem.* **2009**, *40*, 1161−1168.
(44) Kucerik, J.; Kovar, J.; Pekar, M. Thermoanalytical investigations of lignite humic acid fractions. *J. Therm. Anal. Calorim.* **2004**, *76*, 55−65.
(45) Alèn, R.; Kuoppala, E.; Oesch, P. Formation of the main degradation compound groups from wood and its components during pyrolysis. *J. Anal. Appl. Pyrolysis* **1996**, *36*, 137−148.
(46) Gaskin, J. W.; Steiner, C.; Harris, K.; Das, K. C.; Bibens, B. Effect of low-temperature pyrolysis conditions on biochar for agricultural use. *Trans. ASAE* **2008**, *51*, 2061−2069.
(47) Dell'Abate, M. T.; Benedetti, A.; Sequi, P. Thermal methods of organic matter maturation monitoring during a composting process. *J. Therm. Anal. Calorim.* **2000**, *61* (2), 389−396.
(48) Liodakis, S.; Katsigiannis, G.; Kakali, G. Ash properties of some dominant Greek forest species. *Thermochim. Acta* **2005**, *437*, 158−167.
(49) Lopez-Capel, E.; Sohi, S. P.; Gaunt, J. L.; Manning, D. A. C. Use of thermogravimetry−differential scanning calorimetry to characterize modelable soil organic matter fractions. *Soil Sci. Soc. Am. J.* **2005**, *69*, 136−140.
(50) Kucerik, J.; Kamenarova, D.; Valkova, D.; Pekar, M.; Kislinger, J. The role of various compounds in humic acids stability studied by TG and DTA. *J. Therm. Anal. Calorim.* **2006**, *84* (3), 715−720.
(51) Melligan, F.; Dussan, K.; Auccaise, R.; Novotny, E. H.; Leahy, J. J.; Hayes, M. H. B.; Kwapinski, W. Characterization of the products from pyrolysis of residues after acid hydrolysis of *Miscanthus*. *Bioresour. Technol.* **2012**, *108*, 258−263.
(52) Conte, P.; Berns, A. E. Dynamics of cross polarization in solid state nuclear magnetic resonance experiments of amorphous and heterogeneous natural organic substances. *Anal. Sci.* **2008**, *24* (9), 1183−1188.
(53) Valkova, D.; Kislinger, J.; Pekar, M.; Kucerik, J. The kinetics of thermo-oxidative humic acids degradation studied by isoconversional methods. *J. Therm. Anal. Calorim.* **2007**, *89* (3), 957−964.
(54) Šesták, J. *Heat, Thermal Analysis and Society*; Nucleus HK Press: Hradec Kralove, Czech Republic, 2004.

environmentally controlled room (20−22 °C, 60% relative humidity, 12 h alternating light/dark cycle). Hamsters were acclimatized and given water and a rodent diet (LabDiet 5001, PMI International, Redwood, CA, USA; protein, 239 g/kg; fat, 50 g/kg; non-nitrogenous substances, 487 g/kg; crude fiber, 51 g/kg; ash, 70 g/kg; energy, 17 MJ/kg; and sufficient amounts of minerals and vitamins for healthy maintenance) ad libitum for 1 week prior to the initiation of the experimental diets. Hamsters were weighed and randomized into four groups of 10 hamsters each and fed HF diets ad libitum containing 10% (w/w) grape seed flours (Chardonnay (ChrSd), Cabernet Sauvignon (CabSd), Syrah (SyrSd) from Sonomaceuticals, LLC/WholeVine products, Santa Rosa, CA, USA) and a control diet containing 5% microcrystalline cellulose (MCC; Dyets Inc., Bethlehem, PA, USA) for 3 weeks (Table 1). MCC is an insoluble fiber that has little effect on sterol metabolism.[12] Grape pomace was sourced from coastal vineyards in Sonoma County, California. Seeds from the 2010 vintage were separated from skins and stems by screening and dried using hot air (55−70 °C). Oil was pressed from the seed, and the residual press cake was subsequently milled to pass through an 85 mesh sieve. Body weights were recorded weekly, and food intake was monitored twice per week. The study was approved by the Animal Care and Use Committee, Western Regional Research Center, USDA, Albany, CA, USA.

Table 1. Diet Composition (Grams)

ingredient	control	ChrSd	CabSd	SyrSd
butter	80.0	80.0	80.0	80.0
corn oil−vitamin E	100.0	67.3	70.5	71.3
fish-oil	20.0	20.0	20.0	20.0
cholesterol	1.0	1.0	1.0	1.0
grape seed flour	0.0	100.0	100.0	100.0
cellulose (0.95 solids)	52.5	52.5	52.5	52.5
casein	200.0	182.5	182.0	182.7
corn starch	495.5	445.6	443.0	441.5
DL-methionine	3.0	3.0	3.0	3.0
choline bitartrate	3.0	3.0	3.0	3.0
mineral mix	35.0	35.0	35.0	35.0
vitamin mix−vitamin E	10.0	10.0	10.0	10.0
total weight	1000.0	1000.0	1000.0	1000.0
calories/kg	4582.0	4461.4	4464.8	4463.3

Plasma and Tissue Collection. Hamsters were feed-deprived for 12 h and anesthetized with isoflurane (Phoenix Pharmaceutical, St. Joseph, MO, USA). Blood was collected by cardiac puncture with syringes previously rinsed with potassium EDTA solution (15 wt %/v). The plasma was separated after centrifugation at 2000*g* for 30 min at 4 °C. Livers, intestines, and adipose tissues (epididymal and perirenal adipose tissues) were collected, weighed, and immediately frozen in liquid nitrogen for analysis.

Extractable Flavonoid Content. A 0.2 g sample was extracted with 20 mL of MeOH for 30 min with shaking, followed by 10 min of sonication and then centrifuging. Supernatant was taken for HPLC and total phenolic analysis. Total phenols and flavonoid compounds were analyzed using the Folin−Ciocalteu and standard HPLC methods, respectively, as previously described.[13,14]

Plasma Lipids, Hepatic Lipids, and Glucose Analysis. Cholesterol in plasma lipoproteins was determined by size exclusion chromatography as previously described.[15] Briefly, an Agilent 1100 HPLC chromatograph with a Superose 6HR HPLC column (Pharmacia LKB Biotechnology, Piscataway, NJ, USA), a postcolumn derivatization reactor, consisting of a mixing coil (1615-50 Bodman, Aston, PA, USA) in a temperature-controlled water jacket (Aura Industrials, Staten, NY, USA), was employed. A Hewlett-Packard (Agilent, Palo Alto, CA, USA) HPLC pump 79851-A was used to deliver cholesterol reagent (Roche Diagnostics, Indianapolis, IN, USA) at a flow rate of 0.2 mL/min. Bovine cholesterol lipoprotein standards (Sigma-Aldrich, St. Louis, MO, USA) were used to calibrate the signal on the basis of peak areas. Lipoproteins were separated by injecting 15 μL of plasma onto the Superose column. The lipoproteins were eluted with a solution containing 0.15 M NaCl and 0.02% sodium azide at a flow rate of 0.5 mL/min. Liver lipids were prepared by grinding freeze-dried livers into a powder, weighing out about 0.2 g, and mixing with 2 mL of $CHCl_3$/MeOH (2:1), sonicated for 5 min, and then extracted overnight. The samples were centrifuged for 10 min × 1000 rpm, and the supernatant was removed with a glass pipet. Another 2 mL of $CHCl_3$/MeOH was added, sonicated, and allowed to stand overnight to extract. The solvent of the combined extracts was removed under nitrogen. After solvent extraction, hepatic total lipid contents were determined gravimetrically. Blood glucose concentration in feed-deprived hamsters was measured in tail vein samples using a OneTouch Ultrameter (LifeScan Inc., Milpitas, CA, USA).

Real-Time RT-PCR. Total RNA from livers, intestines, and adipose tissues was extracted using a TRIzol plus RNA purification kit (Invitrogen, Life Technologies, Carlsbad, CA, USA), and cDNA was synthesized using a GeneAmpRNA PCR kit (Applied Biosystems, Foster City, CA, USA) per the manufacturer's protocol. One microliter of diluted cDNA (1:10) was used in each real-time RT-PCR using SYBR Green Supermix (Bio-Rad, Hercules, CA, USA) with an Mx3000P instrument (Stratagene, Cedar Creek, TX, USA). The cycle conditions were as follows: 5 min at 95 °C followed by 40 cycles of incubation at 94 °C for 15 s, then 58−60 °C for 1 min, and 72 °C for 30 s. The sequences of the primers used for this study are shown in Table 2 and previous studies.[16−18] The primers were validated by size and sequencing of PCR products. No accumulation of nonspecific products and primer dimers was observed in a gel electrophoresis test of the PCR products. The results were analyzed using the software provided with the Stratagene Mx3000P QPCR system. Differences in mRNA expression for liver, intestines, and adipose tissue were calculated after normalization to β-actin or 36B4 mRNA expression.

Fecal Total Lipid Analysis. Feces were collected during the last 3 consecutive days of the feeding period and were lyophilized, milled, and stored at −20 °C. Fecal total lipid contents were determined gravimetrically after solvent extraction.

Statistical Analysis. All data are expressed as means ± SE. One-way analysis of variance (ANOVA) was performed to examine the effect of treatment on plasma biomarkers, lipid levels, and body and tissue weights using the JMP7 statistical program (SAS Institute, Cary, NC, USA). Tukey−Kramer HSD (honestly significant difference) tests were used to determine the significant differences in group means. Pearson correlation coefficients were calculated for investigating relationships between expression of hepatic gene and plasma cholesterol concentrations. Significance was defined at $P < 0.05$.

RESULTS

Procyanidin Content in Grape Seed Flour. The total methanol-extractable flavonoid content of the Chardonnay grape seed (ChrSd) flour was 1.4- and 1.9-fold greater, respectively, than those in Cabernet Sauvignon (CabSd) and Syrah (SyrSd). The total methanol-extractable catechin content of the ChrSd flour was also greater by 6.4- and 8.4-fold, respectively, compared to CabSd and SyrSd. Total catechins made up 13, 3, and 3% of the total flavan-3-ol content of ChrSd, CabSd, and SyrSd flours, respectively. Catechin content of the ChrSd flour was 5- and 8.7-fold greater, and the epicatechin content was 7.2- and 7.6-fold greater, respectively, than that of CabSd and SyrSd (Table 3). With the exception of ChrSd epigallocatechin, the content of the epicatechin gallate contents was <10 mg/100 g.

Metabolic Effects of Grape Seed Flour Supplementation. ChrSd supplementation into HF diet for 3 weeks lowered plasma very low density lipoprotein (VLDL)-, low-density lipoprotein (LDL)-, and total-cholesterol concentrations by 73, 56, and 38%, respectively, compared with the control diet ($P <$

Table 2. Sequences of PCR Primers

gene	product size (bp)	primer pair	5′−3′ primer sequence
ASBT	239	forward	TTGGAATCATGCCTCTCAC
		reverse	TGAGTCAACCCACATCTTG
ADPN	216	forward	GGAGATGCAGGTCTTCTTGGTC
		reverse	CTGTTGGTTGTAGAAGATCTTAGTAAAG
β-ACTIN	214	forward	CAGCCTTCCTTCCTGGGTATGG
		reverse	CAGGAGGAGCAATGATCTTGAT
DGAT2	145	forward	ACTGAGGTGCTGGAGGTGAA
		reverse	CTTTTAAATAACCCACAGACA
HMG-CoAR	132	forward	CAAGTGGTCCCACGAATGAAGAC
		reverse	ACGCTCCTTGAACACCTAGCATC
LBP	233	forward	ATGCTGCATCCAGAGAAGGCACA
		reverse	TACTGGACATTGGCACCC
LEPTIN	163	forward	TCCATCTGCTGGCCTTCTCC
		reverse	TCCAACTGTTGAAGAATGTCCTG
MCP-1	148	forward	TGGCCCAGCCAGACGCTGTTA
		reverse	TTGAGCTTGGTGATGAAAATCACAG
PPARγ2	158	forward	ACTGCCTATGAGCACTTCACAAG
		reverse	TGCTGGAGAAATCAACTGTGGTA
RAPTOR	150	forward	GGGCCACATCGTGAGTGTG
		reverse	TTCATGGAGCCACAGGCGAT
TNF-α	161	forward	GCCGCATTGCTGTGTCCTACG
		reverse	GGCACTGAGTCGGTCACCTTTCT

Table 3. Contents[a] of Flavonoids and Nutritional Composition in Grape Seed Flours[b]

	ChrSd	CabSd	SyrSd
polyphenol, mg/100 g			
total flavonoids	12000	8560	6280
total catechins	1610	252	191
catechin	701	135	80.4
epicatechin	732	102	96.4
epigallocatechin	145	<10.0	<10.0
nutritional composition, g/100 g			
protein	16.1	16.9	16.6
fat	11.66	8.88	8.41
carbohydrates	59.66	63.89	66.73
ash	4.74	4.01	4.49
moisture	7.84	6.32	3.77
total dietary fiber	31.3	46.9	50.5
total sugars	8.6	2.9	3.2

[a]The contents of epigallocatechin gallate, gallocatechin gallate, catechin gallate, and gallocatechin were all <10 mg/100 g. [b]ChrSd, Chardonnay seed; CabSd, Cabernet Sauvignon seed; SyrSd, Syrah seed.

0.05) (Figure 1). However, plasma lipoprotein cholesterol concentrations of the hamsters fed the CabSd and SyrSd diets were not different from the control diet (Figure 1) with the exception of lower HDL cholesterol by the CabSd diet. Although HDL was lowered by CabSd and tended to be lower by ChrSd and SyrSd, the LDL/HDL ratio was significantly improved only with the ChrSd diet (0.5) compared to 0.8 for the control diet and 1.2 and 1.0 for the CabSd and SyrSd diets, respectively. Hepatic total lipid concentration of the hamsters on the ChrSd diet was 24% lower than the control diet ($P < 0.05$) (Figure 1B). Fecal total lipid percent was not changed by the ChrSd diet (Figure 1C).

Hamsters on the HF diets supplemented with ChrSd gained 31% less weight than those on the HF control diet, although total energy intake was not significantly different (Table 4). Total energy intake by hamsters on the SyrSd diet was 12% greater than those on the control diet ($P < 0.05$) (Table 4). The liver weight of hamsters on the ChrSd diet was 38% lower compared to the control diet ($P < 0.05$) (Table 4). The ChrSd diet also significantly lowered the sum of the epididymal and perirenal adipose tissue weights by 23% when compared with control diet by *t* test (Table 4). Blood glucose concentration of the grape seed diets did not significantly differ from the control diet (Table 4).

Expression of Hepatic Genes Related to Cholesterol, Bile Acid, and Fatty Acid Metabolism. Hepatic expression of genes regulating the biosynthesis of cholesterol and bile acids was determined to understand the molecular basis for the observed cholesterol lowering by ChrSd supplementation. The mRNA levels of hepatic genes involved in cholesterol synthesis, SREBP-2 (sterol response element binding protein-2), HMG-CoAR (3-hydroxy-3-methylglutaryl CoA reductase), and

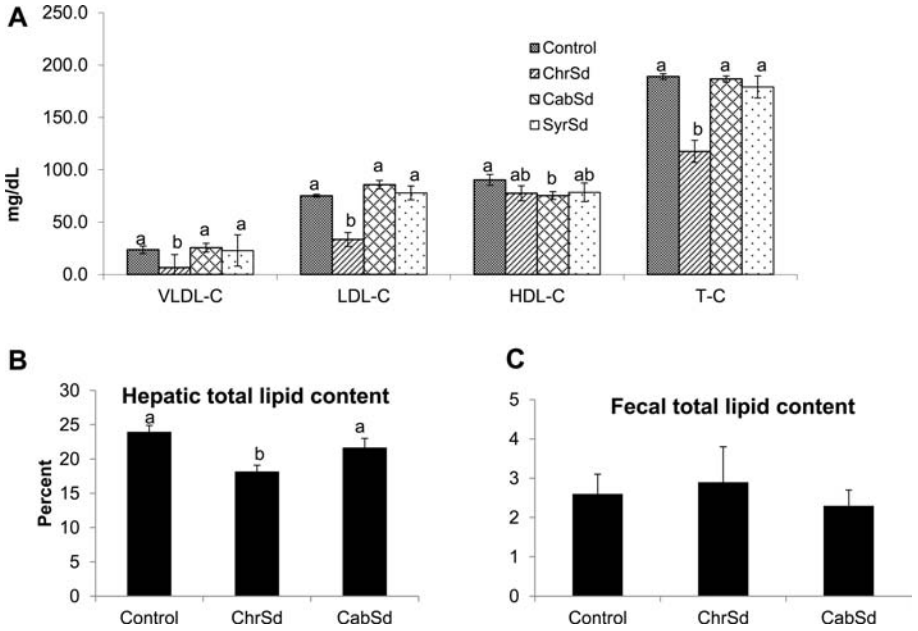

Figure 1. Effect of grape seed flour diets on concentration of plasma lipids (A), hepatic lipids (B), and fecal lipid contents (C). Male Golden Syrian hamsters were fed high-fat diets containing 10% (w/w) Chardonnay (ChrSd), Cabernet Sauvignon (CabSd), and Syrah (SyrSd) grape seed flours and 5% microcrystalline cellulose (MCC, control) for 3 weeks, and blood was collected in a food-deprived state. Data are expressed as means ± SE; n = 8−10/group. Different letters indicate significant difference at $P < 0.05$.

Table 4. Anthropometrics in Hamsters Fed MCC, ChrSd, CabSd, and SyrSd Diets for 3 Weeks[a]

	control	ChrSd	CabSd	SyrSd
body weight gain (g)	34.7 ± 1.9a	23.9 ± 1.9b	38.8 ± 1.9a	40.5 ± 2.2a
total energy intake (kcal)	750 ± 14.6a	809 ± 40.7ab	824 ± 16.6ab	849 ± 24.0b
feed efficiency ratio (g gain/g feed)	0.21 ± 0.01a	0.13 ± 0.01b	0.21 ± 0.01a	0.21 ± 0.01a
liver weight (g)	5.0 ± 0.2a	3.1 ± 0.1b	4.4 ± 0.2a	4.7 ± 0.1a
adipose tissue weight[b] (g)	3.0 ± 0.1ab	2.3 ± 0.1b	3.7 ± 0.2a	3.6 ± 0.3a
blood glucose (mg/dL)	96.0 ± 7.5a	87.0 ± 6.1a	92.7 ± 4.9a	111.8 ± 11.2a

[a]Values are means ± SE, n = 10. Different letters indicate significant difference at $P < 0.05$. [b]Sum of epididymal and perirenal adipose tissue weight.

CYP51 (lanosterol 14α-demethylase), were 1.6-, 1.6-, and 5.6-fold greater, respectively in the hamsters on the ChrSd diet than on the control diet (Figure 2). The mRNA level of ABCG5 (ATP binding cassette subfamily G member 5) was 4-fold lower in ChrSd diet than in the control diet (Figure 2). The mRNA levels of RAPTOR (regulatory associated protein of MTOR) and LDLR (LDL receptor) were greater by 1.4- and 1.5-fold, respectively, compared with the control diet (Figure 2).

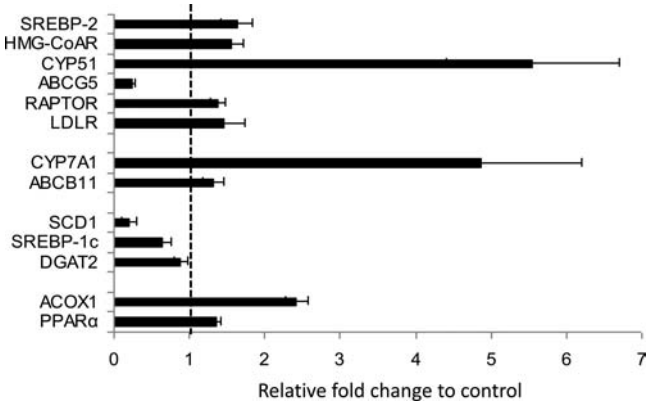

Figure 2. Relative hepatic expression of SREBP-2, HMG-CoAR, CYP51, ABCG5, RAPTOR, LDLR, CYP7A1, ABCB11, SCD-1, SREBP-1c, DGAT2, ACOX1, and PPARα genes. Male Golden Syrian hamsters were fed high-fat diets containing 10% (w/w) Chardonnay (ChrSd) and 5% microcrystalline cellulose (MCC, control) for 3 weeks. Data are expressed as means ± SE n = 6/group.

The expression of the gene controlling the rate-limiting step of bile acid synthesis from cholesterol, CYP7A1 (cytochrome P450 7A1), was 4.9-fold greater relative to the expression in livers of hamsters fed control diet (Figure 2). In addition, the mRNA level of ABCB11 (ATP-binding cassette, subfamily B member 11) was 1.3-fold greater in the ChrSd diet compared with the control diet (Figure 2).

Expression levels of SREBP-1c, a transcription factor for fatty acid synthesis and its target gene, SCD-1 (stearoyl-CoA desaturase-1), were 1.6- and 2-fold lower, respectively in the ChrSd diet compared with the control diet (Figure 2). In contrast, expression levels of PPARα, a transcription factor regulating fatty acid β-oxidation and its target gene, ACOX (acyl-CoA oxidase) 1, were 1.4- and 2.4-fold greater, respectively, in the ChrSd diet than in the control group. The expression of DGAT2 (diacylglycerol O-acyltransferase 2), the gene coding for the enzyme to catalyze the final step of triglyceride synthesis by forming an ester bond between a long-chain fatty acid and diacylglycerol, was not different from control. Expression of a gene regulating bile acid absorption in

the intestine, ileal apical sodium bile acid transporter (ASBT), was not affected by ChrSd diet (data not shown).

Expression of Adipose Tissue Genes Related to Lipid Metabolism and Inflammation. The relative expression of peroxisome proliferator-activated receptor (PPARγ2), a transcription factor for adipocyte differentiation, was lower by 1.8-fold in epididymal adipose tissue of hamsters fed the ChrSd diet compared with the control diet (Figure 3). The mRNA level of adipose ADPN (adiponectin) from ChrSd fed hamsters was not significantly different from in the control diet, but the expression level of leptin was 1.6-fold lower in the ChrSd diet (Figure 3). The expression levels of the inflammatory marker genes TNF-α and MCP-1 were 1.3- and 1.1-fold lower in the ChrSd diet than in the control diet (Figure 3). The expression level of LBP (lipopolysaccharide binding protein), a gene related to innate immune and inflammatory response, was lower by 1.3-fold in the ChrSd diet compared with the control diet (Figure 3).

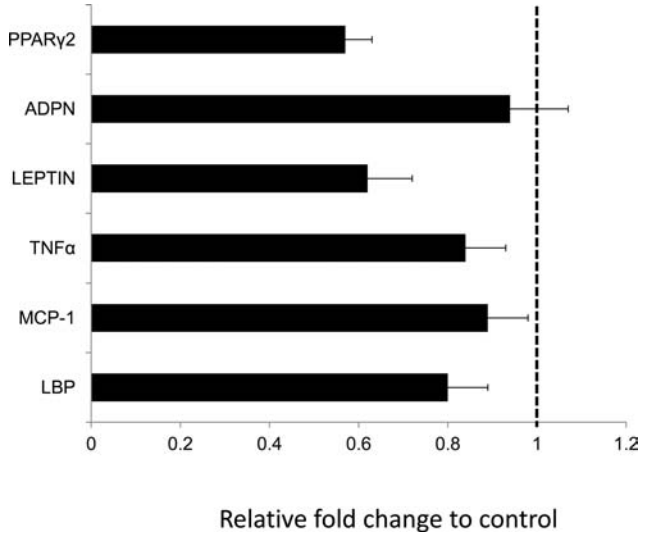

Figure 3. Relative expression of PPARγ2, adiponectin (ADPN), leptin, TNFα, MCP-1, and LBP genes in epididymal adipose tissue of hamsters fed HF diet supplemented with 10% (w/w) Chardonnay (ChrSd) and 5% microcrystalline cellulose (MCC, control) for 3 weeks. Data are expressed as means ± SE n = 5/group.

Correlation between Plasma Lipid and Hepatic Gene Expression. There were significant negative correlations between plasma concentrations of total-, VLDL-, LDL-, and HDL-cholesterol and hepatic expression of CYP51, CYP7A1, ABCB11, and LDLR genes (Table 5). There was a significant positive correlation between plasma VLDL-cholesterol concentration and mRNA levels of the cholesterol transporter ABCG5 (Table 5).

Table 5. Correlations between Plasma Cholesterol Concentrations and Expression of Hepatic Genes[a]

gene	total-C	VLDL-C	LDL-C	HDL-C
CYP51	−0.76***	−0.74***	−0.69**	−0.61*
CYP7A1	−0.44	−0.58*	−0.41	−0.12
ABCG5	0.48	0.52*	0.40	0.42
ABCB11	−0.26	−0.30	−0.24	−0.13
LDLR	−0.52*	−0.39	−0.50*	−0.41

[a]Values are Pearson correlation, n = 12. *, $P < 0.05$; **, $P < 0.01$; ***, $P < 0.005$.

DISCUSSION

Studies of cholesterol-lowering effects by grape seed flavonoids have been typically conducted with aqueous and/or alcoholic extracts. In a meta-analysis of nine human studies on the relationship between grape seed extract, blood pressure, and lipid concentration, it was concluded that the daily intake of 0.15−2.0 g flavonoids/day reduced systolic pressure but did not influence plasma cholesterol concentration.[19] The intake of a red grape pomace byproduct called GADF (grape antioxidant dietary fiber) lowered total plasma cholesterol but not LDL-cholesterol in hypercholesterolemic subjects.[20]

The present study showed for the first time, to our knowledge, that hamsters fed a HF and hypercholesterolemic diet supplemented with Chardonnay grape seed flour (ChrSd diet) significantly lowered plasma LDL-, VLDL-, and total-cholesterol concentrations, abdominal adipose tissue weight, and body weight gain in comparison to control diet. Although red wine is associated with lower plasma cholesterol in Mediterranean countries, cholesterol-lowering and antiobesity properties were not observed in CabSd and SyrSd diets containing red wine grape seed flours, possibly due to low content of flavonoids from the winemaking process. Lower plasma cholesterol levels were associated with higher total content of catechins in the grape seed diets, supporting the role of flavonoids as the bioactive component behind cholesterol-lowering and antiobesity effects of Chardonnay grape seed flour. The flavonoid contents of white and red wine grape seeds vary considerably due to varietal differences, viticultural regions, viticultural practices, and processing methods. In the production of red wines, the whole fruit, including the seed, is fermented; in typical white wine production, only the juice is fermented. The higher levels of flavonoids in red wines and lower levels in seeds are partly due to the ethanol extraction of flavonoids during fermentation.

Cholesterol-lowering and antiobesity effects of Chardonnay wine grape seed flours could be ascribed to the content of monomers, oligomers, and polymers. Chardonnay grape seed extract containing mainly monomers and oligomers induced cholesterol-lowering effects without changes in body weight. This effect was mediated via increased hepatic expression of CYP7A1 and enhanced fecal bile acid excretion in hamsters.[21] Chardonnay grape seed extract containing mostly polymeric flavonoids did display antiobesity effects in hamsters.[9] Grape seed polymeric tannins induced greater cholesterol-lowering properties and fecal bile acid excretion than those in grape seed monomeric tannins in rats.[22] Grape seed extract high in oligomers and polymers showed greater lipase inhibitor activity as well as increased fecal lipid excretion.[6,23] In contrast, monomeric catechin-rich grape seed extract supplementation did not change fecal lipid content compared with high-fat diet controls in C57BL/6J mice despite the presence of antiobesity effects.[24] In the present study, ChrSd diet did not affect fecal lipid content but did induce cholesterol-lowering and antiobesity effects, suggesting that ChrSd diet's beneficial effects possibly represent the effects of multiple constituents in Chardonnay grape seed flour. Calculated intakes of flavonoids from ChrSd, CabSd, and SyrSd diets are, respectively, about 1000, 700, and 600 mg/kg body wt/day and total epicatechin intakes of about 138, 21, and 18 mg/kg body wt/day.

The ChrSd diet may increase hepatic cholesterol and bile acid synthesis as well as hepatic LDL-cholesterol uptake by up-regulating expression of hepatic CYP7A1, CYP51, and LDLR genes. A result similar to ours was reported for catechins from green tea up-regulating CYP7A1 expression in HepG2 hepatocytes.[25] Epigallocatechin gallate (EGCG) was reported to up-regulate LDLR expression in HepG2 hepatocytes via enhanced LDLR mRNA stability.[26,27] These findings suggest that catechins in the ChrSd diet play a direct role in the regulation of hepatic genes (CYP7A1 and LDLR) by accelerating hepatic cholesterol uptake from the circulation and directing the use of hepatic cholesterol to synthesize bile acids. Additionally, the down-regulation of hepatic ABCG5 was observed, which retains hepatic cholesterol by limiting cholesterol efflux to the bile duct to compensate bile acid synthesis demand for cholesterol. Moreover, expression of ileal ASBT was not changed by ChrSd diet, indicating intestinal bile acid absorption was not affected. The ChrSd diet significantly down-regulated expression of ileal SRB1 and ABCG5, suggesting that reduced cholesterol reabsorption by the intestine plays a role in the overall cholesterol-lowering effect of ChrSd diet.

Catechin-rich grape seed extract supplementation up-regulated expression of genes related to fatty acid oxidation including ACOX1 and CPT-1 in livers of mice.[24,28] In accordance with this previous study, we also show that the catechin-rich ChrSd diet down-regulated genes related to fatty acid synthesis (SCD-1 and SREBP-1) while it up-regulated genes related to fatty acid β-oxidation (ACOX1 and PPARα) compared to control diet. As a result, ChrSd diet lowered hepatic lipid content, thus contributing to the potential beneficial effect on hepatic steatosis. We should note that this study did not determine enzymatic activities of fatty acid oxidation and synthesis. Changes in mRNA expression levels are not always a measure of pathway flux; however, previous studies have shown a linear relationship between fatty acid oxidation/synthesis activity and gene expression related to these fatty acid metabolic pathways. For example, dietary supplementation with tea catechins up-regulates both ACOX1 mRNA and fatty acid activity in the liver.[29]

Consumption of the ChrSd diet lowered the sum of epididymal and perirenal adipose tissue weights compared to the HF control diet. Relative expression of PPARγ2 and leptin was down-regulated by ChrSd diet, indicating inhibition of adipogenesis and HF-induced leptin resistance. In 3T3-L1 cell culture, catechin and epicatechin suppressed expression of PPARγ2, adipogenesis, and lipid accumulation.[30,31] These results indicate that monomeric catechins in Chardonnay grape seed flour are likely involved in its antiobesity effect. The low bioactivity of grape seed flavonoids in targeted tissues may be due to their poor bioavailability. However, a recent study has shown that by using ^{14}C-labeling, grape polyphenols or their metabolites were detected in the brain, suggesting possible biological activity in the brain.[32] Further studies are required to determine distribution of flavonoids in target tissues after consumption of grape seed flour.

In summary, flavonoid-rich Chardonnay grape seed flour (a potential byproduct of winemaking) attenuates HF-induced body weight gain, abdominal fat content, hepatic steatosis, hepatic cholesterol, and lipid metabolism. We have demonstrated that the improvements in plasma lipid profiles with the Chardonnay grape seed flours are linked to the regulation of bile acid, cholesterol, and fatty acid metabolism in the liver, which appears to be mediated through regulation of hepatic genes. Expression of genes associated with cholesterol and bile acid transport in and out of hepatocytes was also modified. An antiobesity effect appears to be associated with expression of genes related to adipogenesis and inflammatory markers of adipose tissue. This study supports the potential dietary use of Chardonnay grape seed flour as a flavonoid-rich whole food ingredient for the prevention or management of obesity-related metabolic diseases such as cardiovascular disease and fatty liver in populations consuming a Western diet.

AUTHOR INFORMATION

Corresponding Authors

*(H.K.) Mail: Department of Physiology, College of Veterinary Medicine, Konkuk University, Hwayang-dong, Gwangjin-gu, Seoul 143-701, South Korea. E-mail: hyunsk13@konkuk.ac.kr. Phone: +82 2 450 4154. Fax: +82 2 450 3037.

*(W.Y.) Mail: USDA, ARS, PWA, WRRC-PFR, 800 Buchannan St., Albany, CA 94710, USA. E-mail: Wally.Yokoyama@ars.usda.edu. Phone: (510) 559-5695. Fax: (510) 559-5777.

Funding

H.K. was supported by the KU Research Professor Program of Konkuk University.

Notes

The authors declare no competing financial interest.

ACKNOWLEDGMENTS

Many thanks to Sonomaceuticals, LLC/WholeVine Products and their sister company for contribution of pomace, grape seed flours, and compositional analysis.

REFERENCES

(1) Yang, J.; Xiao, Y. Y. Grape phytochemicals and associated health benefits. *Crit. Rev. Food Sci. Nutr.* **2013**, *53*, 1202−1225.

(2) Hsu, C. L.; Yen, G. C. Effect of gallic acid on high fat diet-induced dyslipidaemia, hepatosteatosis and oxidative stress in rats. *Br. J. Nutr.* **2007**, *98*, 727−735.

(3) Simonetti, P.; Ciappellano, S.; Gardana, C.; Bramati, L.; Pietta, P. Procyanidins from *Vitis vinifera* seeds: in vivo effects on oxidative stress. *J. Agric. Food Chem.* **2002**, *50*, 6217−6221.

(4) Shi, J.; Yu, J.; Pohorly, J. E.; Kakuda, Y. Polyphenolics in grape seeds − biochemistry and functionality. *J. Med. Food* **2003**, *6*, 291−299.

(5) Steffen, Y.; Schewe, T.; Sies, H. Epicatechin protects endothelial cells against oxidized LDL and maintains NO synthase. *Biochem. Biophys. Res. Commun.* **2005**, *331*, 1277−1283.

(6) Moreno, D. A.; Ilic, N.; Poulev, A.; Brasaemle, D. L.; Fried, S. K.; Raskin, I. Inhibitory effects of grape seed extract on lipases. *Nutrition* **2003**, *19*, 876−879.

(7) Ngamukote, S.; Makynen, K.; Thilawech, T.; Adisakwattana, S. Cholesterol-lowering activity of the major polyphenols in grape seed. *Molecules* **2011**, *16*, 5054−5061.

(8) Pinent, M.; Blade, M. C.; Salvado, M. J.; Arola, L.; Hackl, H.; Quackenbush, J.; Trajanoski, Z.; Ardevol, A. Grape-seed derived procyanidins interfere with adipogenesis of 3T3-L1 cells at the onset of differentiation. *Int. J. Obes. (London)* **2005**, *29*, 934−941.

(9) Decorde, K.; Teissedre, P. L.; Sutra, T.; Ventura, E.; Cristol, J. P.; Rouanet, J. M. Chardonnay grape seed procyanidin extract supplementation prevents high-fat diet-induced obesity in hamsters by improving adipokine imbalance and oxidative stress markers. *Mol. Nutr. Food Res.* **2009**, *53*, 659−666.

(10) Zhang, Z.; Wang, H.; Jiao, R.; Peng, C.; Wong, Y. M.; Yeung, V. S.; Huang, Y.; Chen, Z. Y. Choosing hamsters but not rats as a model

for studying plasma cholesterol-lowering activity of functional foods. *Mol. Nutr. Food Res.* **2009**, *53*, 921−930.
(11) Turley, S. D.; Spady, D. K.; Dietschy, J. M. Role of liver in the synthesis of cholesterol and the clearance of low density lipoproteins in the cynomolgus monkey. *J. Lipid Res.* **1995**, *36*, 67−79.
(12) Horton, J. D.; Cuthbert, J. A.; Spady, D. K. Regulation of hepatic 7α-hydroxylase expression by dietary psyllium in the hamster. *J. Clin. Invest.* **1994**, *93*, 2084−2092.
(13) Singleton, V. L.; Orthofer, R.; Lamuela-Raventós, R. M. Analysis of total phenols and other oxidation substrates and antioxidants by means of folin-ciocalteu reagent. *Methods Enzymol.* **1999**, *299*, 152−178.
(14) Lamuela-Raventós, R. M.; Waterhouse, A. L. A direct HPLC separation of wine phenolics. *Am. J. Enol. Vitic.* **1994**, *45*, 1−5.
(15) German, J. B.; Walzem, X. R.; Kinsella, R.; Knuckles, J. E.; Nakamura, B.; Yokoyama, W. H. Effect of dietary fats and barley fiber on total cholesterol and lipoprotein cholesterol distribution in plasma of hamsters. *Nutr. Res. (N.Y.)* **1996**, *16*, 1239−1249.
(16) Bartley, G. E.; Yokoyama, W.; Young, S. A.; Anderson, W. H.; Hung, S. C.; Albers, D. R.; Langhorst, M. L.; Kim, H. Hypocholesterolemic effects of hydroxypropyl methylcellulose are mediated by altered gene expression in hepatic bile and cholesterol pathways of male hamsters. *J. Nutr.* **2010**, *140*, 1255−1260.
(17) Field, F. J.; Born, E.; Mathur, S. N. Fatty acid flux suppresses fatty acid synthesis in hamster intestine independently of SREBP-1 expression. *J. Lipid Res.* **2003**, *44*, 1199−1208.
(18) Kim, H.; Bartley, G. E.; Young, S. A.; Seo, K. H.; Yokoyama, W. Altered hepatic gene expression profiles associated with improved fatty liver, insulin resistance, and intestinal permeability after hydroxypropyl methylcellulose (HPMC) supplementation in diet-induced obese mice. *J. Agric. Food Chem.* **2013**, *61*, 6404−6411.
(19) Feringa, H. H.; Laskey, D. A.; Dickson, J. E.; Coleman, C. I. The effect of grape seed extract on cardiovascular risk markers: a meta-analysis of randomized controlled trials. *J. Am. Diet. Assoc.* **2011**, *111*, 1173−1181.
(20) Jiménez, J. P.; Serrano, J.; Tabernero, M.; Arranz, S.; Díaz-Rubio, M. E.; García-Diz, L.; Goñi, I.; Saura-Calixto, F. Effects of grape antioxidant dietary fiber in cardiovascular disease risk factors. *Nutrition* **2008**, *24*, 646−653.
(21) Jiao, R.; Zhang, Z.; Yu, H.; Huang, Y.; Chen, Z. Y. Hypocholesterolemic activity of grape seed proanthocyanidin is mediated by enhancement of bile acid excretion and up-regulation of CYP7A1. *J. Nutr. Biochem.* **2010**, *21*, 1134−1139.
(22) Tebib, K.; Besancon, P.; Rouanet, J. M. Dietary grape seed tannins affect lipoproteins, lipoprotein lipases and tissue lipids in rats fed hypercholesterolemic diets. *J. Nutr.* **1994**, *124*, 2451−2457.
(23) Goncalves, R.; Mateus, N.; de Freitas, V. Study of the interaction of pancreatic lipase with procyanidins by optical and enzymatic methods. *J. Agric. Food Chem.* **2010**, *58*, 11901−11906.
(24) Ohyama, K.; Furuta, C.; Nogusa, Y.; Nomura, K.; Miwa, T.; Suzuki, K. Catechin-rich grape seed extract supplementation attenuates diet-induced obesity in C57BL/6J mice. *Ann. Nutr. Metab.* **2011**, *58*, 250−258.
(25) Lee, M. S.; Park, J. Y.; Freake, H.; Kwun, I. S.; Kim, Y. Green tea catechin enhances cholesterol 7α-hydroxylase gene expression in HepG2 cells. *Br. J. Nutr.* **2008**, *99*, 1182−1185.
(26) Goto, T.; Saito, Y.; Morikawa, K.; Kanamaru, Y.; Nagaoka, S. Epigallocatechin gallate changes mRNA expression level of genes involved in cholesterol metabolism in hepatocytes. *Br. J. Nutr.* **2013**, *107*, 769−773.
(27) Bursill, C. A.; Roach, P. D. Modulation of cholesterol metabolism by the green tea polyphenol (−)-epigallocatechin gallate in cultured human liver (HepG2) cells. *J. Agric. Food Chem.* **2006**, *54*, 1621−1626.
(28) Park, S. H.; Park, T. S.; Cha, Y. S. Grape seed extract (*Vitis vinifera*) partially reverses high fat diet-induced obesity in C57BL/6J mice. *Nutr. Res. Pract.* **2008**, *2*, 227−233.
(29) Murase, T.; Nagasawa, A.; Suzuki, J.; Hase, T.; Tokimitsu, I. Beneficial effects of tea catechins on diet-induced obesity: stimulation of lipid catabolism in the liver. *Int. J. Obes. Relat. Metab. Disord.* **2002**, *26*, 1459−1464.
(30) Furuyashiki, T.; Nagayasu, H.; Aoki, Y.; Bessho, H.; Hashimoto, T.; Kanazawa, K.; Ashida, H. Tea catechin suppresses adipocyte differentiation accompanied by down-regulation of PPARγ2 and C/EBPα in 3T3-L1 cells. *Biosci., Biotechnol., Biochem.* **2004**, *68*, 2353−2359.
(31) Hung, P. F.; Wu, B. T.; Chen, H. C.; Chen, Y. H.; Chen, C. L.; Wu, M. H.; Liu, H. C.; Lee, M. J.; Kao, Y. H. Antimitogenic effect of green tea (−)-epigallocatechin gallate on 3T3-L1 preadipocytes depends on the ERK and Cdk2 pathways. *Am. J. Physiol. Cell. Physiol.* **2005**, *288*, C1094−C1108.
(32) Janle, E. M.; Lila, M. A.; Grannan, M.; Wood, L.; Higgins, A.; Yousef, G. G.; Rogers, R. B.; Kim, H.; Jackson, G. S.; Ho, L.; Weaver, C. M. Pharmacokinetics and tissue distribution of ^{14}C-labeled grape polyphenols in the periphery and the central nervous system following oral administration. *J. Med. Food* **2010**, *13*, 926−933.

group is a long nonpolar alkyl group, and all the derivatives that lose it form a polar, colored chlorophyll derivative family and a suffix (-ide) is added to their names. Some processes call for a high-temperature blanching pretreatment (dipped in boiling water for a few seconds), which deactivates the chlorophyllase enzyme;[10] thus, chlorophyllides can no longer be formed from chlorophylls. The loss of the carboxymethoxy group at $C13^2$ is due to a decarboxymethylation reaction that happens during severe heat treatment such as canning.[11] This reaction eliminates the asymmetry at $C13^2$, and thus, no a′ and b′ derivative epimers can be formed. All the derivatives losing their carboxymethoxy group get a prefix (pyro-) added to their names. Another color-related transformation is the removal of chelated magnesium from the center of the porphyrin ring leading to derivatives with an olive-brown pigmentation. When plants are harvested leaf cell membranes break allowing sap acidic compounds to interact with chlorophylls. Acid conditions promote the loss of Mg^{2+} from the porphyrin ring, converting chlorophylls into olive-brown pheophytins. This conversion is the most frequent chlorophyll degradation, giving the product a brownish-greying surface color. Pheophytins can be formed through both dry-heating and moist-heating processes.[7] All the derivatives losing their chelating Mg^{2+} get a prefix (pheo-) added to their names. Finally, the formation of hydroxylchlorophylls and hydroxypheophytins caused by oxidation at $C13^2$ has been described in analytical studies on traditional Chinese herbs as well as other colored chlorophylls allomers like lactone derivatives.[12−14]

Chlorophylls and their derivatives have been extensively studied for both their implication in the color preservation in plants and for their reported biological activities.[15] Surface color is an important quality attribute of herbal products; that is why numerous studies have been conducted to investigate color changes or chlorophyll degradation during various processes such as blanching, drying, or heat-treatment. The bright green color of chlorophylls is more pleasing to the consumer than the olive-brown color brought on by certain derivatives. Browning and greying of culinary herbs during drying processes is the most obvious visible symptom. A challenge to culinary herb processors is to preserve the natural color associated with quality attributes in a particular herb.

Many publications in food process engineering and related fields deal with processes such as blanching, heat-treatment, or cooking that keep the plant wet at the end. However, culinary aromatic herbs such as oregano, basil, or dill are generally sold in a dried form to inhibit the growth of microorganism at ambient temperature. Freeze-drying, oven-drying, and sun-drying are the processes commonly used in the aromatic herb industry, but they must be used carefully so as to preserve as much of both the aroma and the color of the (fresh) raw material as possible. International standards for the quality specifications, including moisture content, of most culinary aromatic herbs are available, but none mention color specifications. Therefore, the drying treatment step is crucial to preserve the color quality of culinary herbs.

In this Article we focused our attention on chlorophylls and their colored derivatives (both polar and nonpolar) present in dried culinary herbs. The first objectives were to detect and quantitate the largest range of chlorophyll colored derivatives possible. From this work we developed a knowledge and understanding of the various degradation pathways responsible for color changes in the dried herbs. With these findings our next goal was to find a novel way of determining the global level of dried culinary herb quality in terms of color. We thus designed an interesting color degradation ladder enabling us to classify drying processes according to their impact on culinary herb surface color.

MATERIALS AND METHODS

Materials. Fresh spinach was obtained from a local store in Avignon. No commercial frozen spinach was used, because it is generally subjected to a blanching step leading to important epimerization of chlorophylls.[7] Culinary aromatic herbs were cultivated and dried in Turkey and Egypt. Fresh culinary herbs were obtained from fields in east-southern France and kept between 2 and 8 °C prior to analysis.

Chemicals. Analytical grade (acetone) and HPLC grade solvents (methanol, acetone, water) as well as all analytical grade chemicals (ammonium acetate, sodium citrate, hydrochloric acid, sodium hydroxide) were obtained from Sigma-Aldrich (St. Louis, MO). Nylon filters were obtained from Macherey-Nagel (Hoerdt, France).

Instrumentation. The HPLC system consisted of an Alltech Elite degassing system (Nicholasville, KY), a Thermo SpectraSystem P1000 pump (San Jose, CA), a Thermo Spectra Series AS100 autosampler equipped with a 20-μL loop, and a Kinetex stainless-steel column (100 × 4.6 mm i.d.) packed with XB-C18 (2.6-μm) from Phenomenex (Torrance, CA). A Thermo SpectraSystem UV6000LP diode array detector (DAD) was used to both monitor the separation and determine the absorption spectra of chlorophylls and their derivatives. Spectral data from the DAD system were recorded between 350 and 700 nm. For mass spectra, the HPLC described above was equipped with an AB-Sciex 4000 Q-trap mass spectrometer (MS) (Foster City, CA) with an electrospray ionization source.

A UV-1800 spectrophotometer from Shimadzu (Kyoto, Japan) was used.

An IKA T25 Ultra-Turrax homogenizer (Staufen, Germany) equipped with a stainless steel disperser (18 mm in diameter) and a Waring Lab blender (Winsted, CT) equipped with 1-L stainless-steel container were used to grind plant samples in solvents. A Retsch MM400 benchtop mixer mill (Haan, Germany) was used to grind dry plants.

A Minolta CR310 colorimeter (Osaka, Japan) was used to measure in the LCh° colorimetric space. Data reported are the average of 3 determinations.

Xlstat version 2012.4.03 from Addinsoft (Paris, France) was used for processing principal components analyses (PCA) and principal component regression (PCR).

Dehydration Processes. Several dehydration processes were used: sun-drying as the commonly used approach, freeze-drying as the reference in term of preserving green color, and last oven-drying. The latter two methods were used as control treatments. Two other proprietary types of dehydration processes were used and were named DP1 and DP2. DP1 is an innovation brought to the traditional sun-drying process. DP2 is a recently developed process designed to preserve the green appearance of aromatic herbs.

Preparation of Standard Solutions. Chlorophyll a and b standard solutions were extracted and prepared from fresh spinach leaves. The chlorophyll derivatives comprising the pheophorbides and pyropheophorbides, although available commercially,[16] were synthesized as deemed necessary.

Approximately 54 g of fresh spinach leaves were weighed into a 1-L container to which 200 mL of acetone was added. The mixture was homogenized for 1 min. Part of the extract was passed through a 0.45-μm nylon filter. The ratio of 54 g of spinach−200 mL acetone was prepared to obtain a final chlorophyll solution composed of 80:20 acetone−water. This solution was subjected to a 10-fold dilution with acetone−water 80:20 and used as the standard chlorophyll solution for realizing regression curves for external calibration. A pheophytin standard solution was prepared by acidification of the chlorophyll standard solution according to Schwartz et al.[17] Hydrochloric acid (1 N) was added dropwise to 100 mL of the chlorophyll standard solution, and the solution was shaken after each addition. The complete conversion was reached once the color of the solution turned

from green to olive brown. The absence of remaining chlorophylls could be confirmed by HPLC.

Chlorophyllides were prepared in situ by the action of chlorophyllase enzyme on chlorophylls as substrate.[10] Fresh spinach leaves were gently dehydrated for 48 h in an oven at 40 °C and finely ground with a mixer mill. This resulting powder contained both enzyme and substrate (the substrate was the chlorophyll already present in the spinach leaves). A 500 mg portion of the dried spinach leaf powder and 10 mL of a 50:50 acetone−aqueous citrate solution (0.04 M) were added. The mixture stood for 2 h at ambient temperature and was then passed through a 0.45-μm nylon filter.

Pheophorbides were obtained by using a chlorophyllase enzyme solution described below on the pheophytins substrate. Around 5 g of dry spinach leaf powder, dried according to the procedure above for chlorophyllides, was weighed on a glass Buchner filtration system with a round paper filter. All the glassware as well as the sample and 500 mL of acetone were kept in a freezer at −20 °C. Immediately after taking all the materials out of the freezer, the cold acetone was passed through the spinach leaf powder in the cold Büchner filtration system in order to remove the chlorophylls. Once the acetonic eluent became transparent, the sample was put in an oven at 37 °C for solvent evaporation. To 500 mg of the resulting powder was added 5 mL of neutralized standard pheophytin solution along with 5 mL of deionized water previously equilibrated to pH 8 with aqueous sodium hydroxide solution (0.1 N).

Pyrochlorophylls were obtained from the chlorophyll standard solution. Briefly, 10 mL of the chlorophyll standard solution was extracted with diethyl ether and the ether extract evaporated to dryness. The residue was dissolved in 20 mL of pyridine and heated under reflux in an oil bath at 100 °C for 2 h.[18] Pyridine was removed in a rotary evaporator, and 10 mL of an acetone−water 80:20 mixture was added. Pyropheophytins were prepared from the standard pheophytin solution using the same procedure with additional steps consisting of neutralization of the pheophytin solution with 0.1 M NaOH solution prior to evaporation. Pyropheophorbides were prepared from the pheophorbide solution using the protocol described above and time allotted to turn the chlorophylls into pyrochlorophylls. Finally, pyrochlorphillides were prepared from the chlorophillide solution using the same procedure described, but in this chemical preparation, no heat was necessary for the reaction to occur.

To summarize, a solution with chlorophylls and all the synthesized derivatives was prepared. The more acidic solutions (i.e., pheophytins and pheophorbides) were neutralized by a 0.1 N NaOH solution so that the chlorophylls and other derivatives with chelated magnesium remained stable. All solutions prepared were kept at −20 °C.

Extraction of Chlorophylls and Their Derivatives from Culinary Herb Samples. Approximately 1 g of fresh or dry herb was weighed into a 150 mL beaker to which 100 mL of an 80:20 acetone−sodium citrate solution (0.1M) was added. The mixture was homogenized for 8 min at medium speed. The homogenate was filtered on a nylon filter prior to chromatographic analysis. The mixture volume lost upon extraction was accurately measured for adjustment in the final calculations. A 10-fold dilution can be necessary for samples of fresh herbs or herbs subjected to efficient color-protective dehydration processes.

Preparation of the Stock and Working Solutions for External Calibration. Chlorophyll and pheophytin concentrations in the stock solutions were determined according to Vernon.[19] The pheophytin stock solution was neutralized with 0.1 M NaOH. Five working solutions containing chlorophylls and pheophytins (between 1 and 20 mg/L for chlorophyll a and pheophytin a) were prepared by mixing the stock solutions and dilution with acetone−water (80:20). The calibration curves were generated by plotting the five concentrations of each compound against peak area measured at 654 nm. A working solution was injected every five sample injections to check for drift effect on the calibration. Final results of pigment levels in herbs were expressed in mol/g on dry wt basis; therefore, the moisture content was measured for every sample.

Analysis of Chlorophylls and Their Derivatives by HPLC-DAD-MS. A solvent system of acetone−methanol−0.5 M NH_4OAc was used to separate chlorophylls and their breakdown compounds (see Table 1). The injection volume was 20 μL.

Table 1. Solvent Composition Evolution of the Elution Phase During the HPLC-DAD Analysis

time	MeOH	ammonium acetate 0.5 M	acetone	flow (mL/min)
0	80	20	0	0.5
2	80	20	0	0.5
15	65	5	30	1
18	65	5	30	1.2
24	30	5	65	1.2
26	30	5	65	1.2
28	0	0	100	1.2
30	0	0	100	1.2

Chlorophylls and their various derivatives were identified by retention time and by comparison of the absorption spectra between 350 and 700 nm of unknown peak with those in the literature, as well as with reference standards obtained by synthesis.

In addition, the pigments were confirmed for their molecular weight ($[M + H]^+$) by a quadrupole MS in positive mode with a 500−1000 Da scanning range. The source temperature was at 500 °C, ion spray voltage at 5500 V, curtain gas at 30 psi, declustering potential at 125 V, and the entrance potential at 10 V.

Moisture Content Determination. For culinary aromatic herbs the recommended method to measure the moisture content is by distillation with toluene according to ISO 939:1980.

Chlorophylls and Derivatives Breakdown: PCA and PCR Analyses. Using the experimental protocol described in this paper, chlorophylls and their derivatives were detected and quantified in 50 samples of diverse culinary herbs prepared fresh and after five different drying treatments described below. Herb samples included tarragon, coriander, parsley, dill, chive, oregano, mint, basil, and marjoram. All the samples were independent of each other. Drying treatments were the following: no process (fresh), sun-drying, freeze-drying, oven-drying, DP1 and DP2. The data (average of duplicate analyses) was evaluated using principal component analysis (PCA) and principal component regression (PCR) techniques.

RESULTS AND DISCUSSION

Extraction of Chlorophylls and Their Derivatives from Culinary Aromatic Herb Samples. An experimental design was carried out to optimize the parameters ruling the pigment extraction yields from fresh and dried herbs by means of an Ultra-Turrax homogenizer. The extraction mixture contained a 0.1 M sodium citrate solution to maintain a neutral pH while protecting the pigments against oxidation. The extraction time and the homogenizer rate of revolution were two key parameters. Other important factors were the extraction solution temperature and total molar contents of chlorophylls and their derivatives. The experimental design showed a strong interaction between the key parameters. For example, regardless the type of culinary herb or whether it was fresh or dry, the final optimized parameters were found to be an extraction time of 8 min at medium rotation speed.

Preparation of the Stock and Working Solutions for External Calibration. Internal standards like Fast green FCF or zinc-phtalocyanine were used in some publications with varying levels of success.[12,20] Chlorophyll and derivate quantitation was also realized using external calibration.[7]

The UV−vis absorption properties of chlorophylls and their derivatives can be attributed to three parameters: the primary porphyrin ring structure, the presence of chelated magnesium at its center, and the type of functional group or constituent at C7. With that in mind we could approximate to first order that both epimerization and decarboxymethylation at C13[2], and also

phytol loss at C17, do not affect the global UV−vis spectra of chlorophyll derivatives because $C13^2$ and C17 are not part of the porphyrin ring. Consequently, there are 4 types of UV−vis spectra: two groups for the green pigments (chlorophyll, chlorophyllide, pyrochlorophyllide, and pyrochlorophyll) according to the substituent at C7 (a or b) and likewise two groups for the olive-brown pigments (pheophytin, pheophorbide, pyropheophytin, and pyropheophorbide, a or b). This first approximation also takes into consideration the slight effect on the absorption spectra of the elution phase composition change throughout the chromatographic analysis. This effect is very low for the visible part of the spectrum, that is, why 654 nm was chosen as the quantitation wavelength for all green and olive-brown pigments. Furthermore, at this wavelength the carotenoid interferences are also eliminated. An external calibration method was used to quantitate each pigment. The two groups of green pigments were quantified using the calibration curve of chlorophyll a and b. Likewise, the 2 groups of olive-brown pigments were quantified using the calibration curves of pheophytin a and b.

With working solutions containing known concentrations of chlorophylls a and b and pheophytins a and b, 5 injections were sufficient to cover the quantitation of all 24 chlorophylls and derivatives. The calibration curves showed a high linearity, with a correlation coefficient ≥0.9993, as long as the concentration was below 25 mg/L (see Table 2).

Table 2. Analytical Parameters of Calibration Regression Curves

	chlorophyll a	chlorophyll b	pheophytin a	pheophytin b
conc range (mg/L)	1−19	05−10	1−22	0.5−13
slope ± SD (n = 6) (1×10^3 AU)[a]	315 ± 10	139 ± 6	140 ± 7	69 ± 4
r^2 (av, n = 6)	0.9993	0.9995	0.9997	0.9998

[a]AU = area units.

The final results of pigment contents in fresh or dried culinary herbs were expressed in mol/g on dry weight basis. In order to assess the global level of green pigment breakdown and to further estimate the visual color appearance of the herb product, the molar percentage of the green pigments was calculated (see equation below), with the remainder of the components representing the percentage of the olive-brown pigments.

$$\%\text{green pigments} = 100 \times \frac{\sum_{i=a,a'}^{b,b'} (\text{chlorophyll}_i + \text{pyrochlorophyll}_i + \text{chlorophyllide}_i + \text{pyrochlorophillide}_i)}{\sum_{i=a,a'}^{b,b'} (\text{chlorophyll}_i \text{ and derivates}_i)}$$

Analysis of Chlorophylls and Their Derivatives by HPLC-DAD-MS. In order to separate chlorophylls and their polar and nonpolar colored derivatives, a combination of two gradient mobile phases reported in previous studies was utilized.[9,12] Polar derivatives were separated using a solvent system of methanol/aqueous ammonium acetate (0.5 M).[9] These polar pigments are acidic pigments with pK_a ranging from 2 to 4.[21] Ammonium acetate was used in HPLC analysis because it provides excellent results in the separation of highly polar acidic chlorophyll derivatives. In addition, it buffers the elution phase at a pH around 7 and thus reduces the likelihood of porphyrin rings losing their chelating magnesium during analysis. Nonpolar derivatives were separated using a solvent system of methanol/acetone.[12]

Figure 2 shows the HPLC chromatogram of chlorophylls and their derivatives from a standard solution by employing a ternary solvent system of acetone/methanol/ammonium acetate (0.5 M). Following the described gradient program, good resolution of the chlorophyll derivative peaks was achieved.

All the peaks showing chlorophyll-like or pheophytin-like spectra were checked for their molecular weight by LC-MS. With a single injection and a 28 min run, a total of 24 pigments could be detected. The retention time increased in the order presented in Figure 2 in agreement with results reported previously for chlorophillide/pheophorbide/chlorophyll/pheophytin.[22] We noticed different clusters of peaks on the pigment chromatogram. Each cluster contains the peak of the main pigment (chlorophyll or chlorophillide or pheophytin or pheophorbide, either a or b), the peak of its epimer form, and the peak of the -pyro form. The -pyro form elutes last in each cluster likely due to the elimination of the carbomethoxy group. This slightly reduces the polarity of the pigments resulting in greater interactions with the C18 stationary phase, as well as a lower solubility in the eluent.[23] Therefore, the entire chromatogram in Figure 2 shows eight clusters of 3 peaks that make the final identification easier.

Chlorophylls and Derivatives Breakdown: PCA Analyses. In our study we decided to quantitate chlorophylls and their colored derivatives in fresh and dried culinary aromatic herbs subjected to different dehydration processes. There were 50 different herb samples. Of the 24 chlorophylls and their derivatives detected and identified by our method, only 14 of them were found in the different herb samples, namely the following: chlorophyll a and a′, chlorophyll b and b′, chlorophyllide a, pheophytin a and a′, pheophytin b and b′, pheophorbide a, pyrochlorophyll a and b, pyropheophytine a and b. No compounds were identified by MS as hydroxychlorophyll or hydroxypheophytin with a hydroxyl group at $C13^2$.

The raw data are presented in Table 3, and they were used to build Table 4. Chlorophyllide a and pheophorbide a were rarely found in the 50 samples (only in samples 3 and 1, respectively). Chlorophillide a appeared after a low-temperature blanching step on fresh herbs prior to dehydration which allowed the chlorophyllase to be activated. Chlorophyll epimers were present in highest concentrations in the samples with oven- and sun-drying processes. Table 4 shows that chlorophyll a′/chlorophyll a ratio is generally lower than chlorophyll b′/chlorophyll b ratio. Similar results were reported previously in cooked wet spinach.[20] In our study, these epimer ratios varied noticeably according to the type of treatment. Surprisingly, the pheophytin a′/pheophytin a ratio values were less dependent on the type of process used for drying the herbs. Pheophytin b′/pheophytin b ratio values (when detected) were high, showing that pheophytin b is subjected to a strong epimerization in every type of process.

In the plants with less degraded chlorophylls (freeze-drying, DP1, and DP2 treatments), chlorophyll a was in higher amounts than chlorophyll b, which was also mentioned elsewhere.[13]

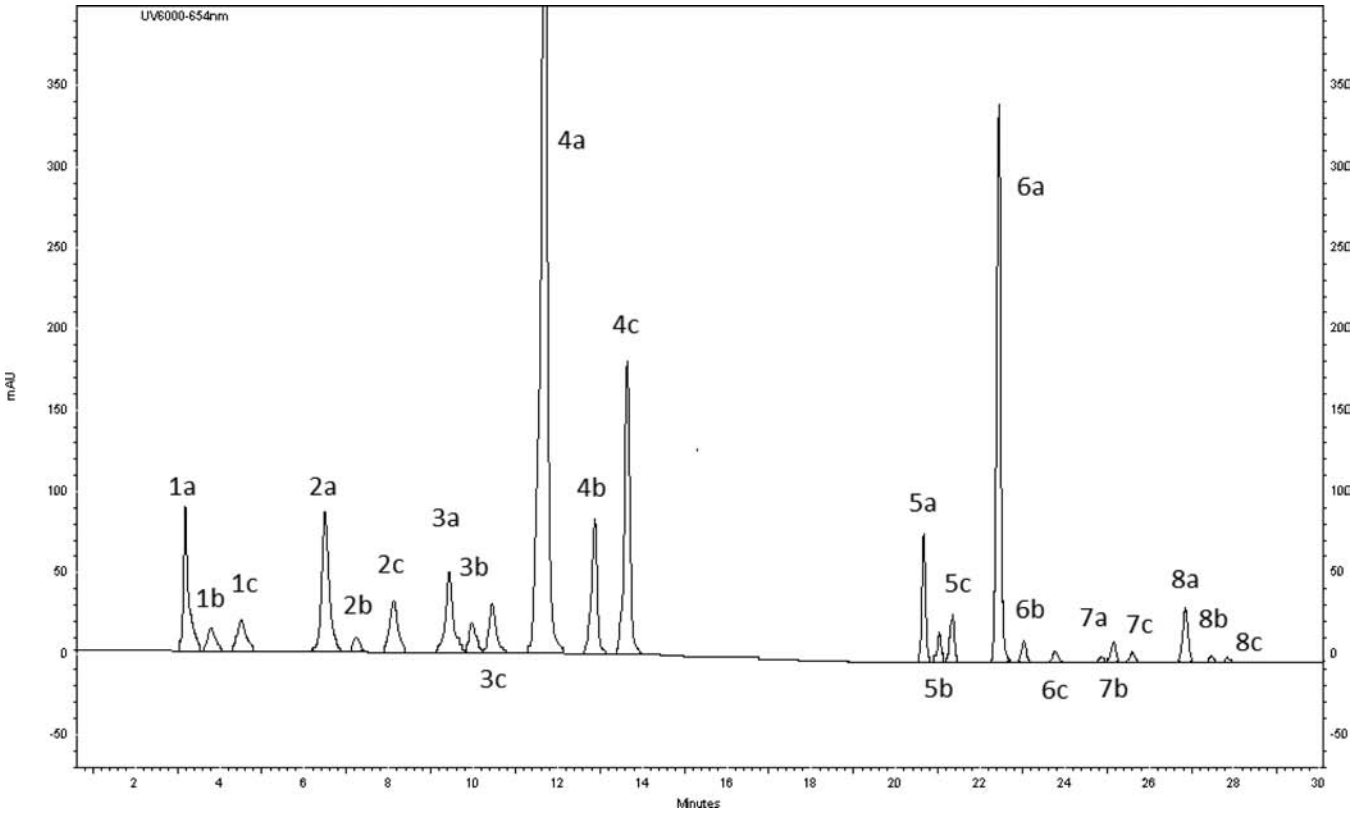

Figure 2. HPLC chromatogram of a mixture of chlorophylls and their colored derivatives. Chromatographic conditions described in the text. Peaks: 1a,b = chlorophyllide b,b′; 1c = pyrochlorophyllide b; 2a,b = chlorophyllide a,a′; 2c = pyrochlorophyllide a; 3a,b = pheophorbide b,b′; 3c = pyropheophorbide b; 4a,b = pheophorbide a,a′; 4c = pyropheophorbide a; 5a,b = chlorophyll b,b′; 5c = pyrochlorophyll b; 6a,b = chlorophyll a,a′; 6c = pyrochlorophyll a; 7a,b = pheophytin b,b′; 7c = pyropheophytin b; 8a,b = pheophytin a,a′; 8c = pyropheophytin a.

Pyrochlorophyll b was found in most of the samples, even in fresh herb samples, and the only degradation pathway available is from chlorophyll b. Fresh plants were kept several days in a refrigerator prior to analysis, and the degradation process may have already started, which could explain the presence of pyrochlorophyll b. This phenomenon has not been described elsewhere. As for pyrochlorophyll a, it has not been detected in fresh herb samples, nor after the DP2 process, the quickest process.

The presence of pheophytin b was not observed in fresh herbs or in DP2 processed samples. In the other processes, this pigment was not present all the time, except for samples subjected to sun-drying. Unlike pheophytin b, pheophytin a was detected in all 50 samples. It is well-known from numerous reports[11] that chlorophyll a is more susceptible to forming pheophytin than chlorophyll b. This slower conversion of chlorophyll b to pheophytin presents two aspects: on one hand, after the long sun-drying process that produces the highest level of chlorophyll breakdown, the concentration of chlorophyll a became lower than that of chlorophyll b. On the other hand, it allows an easier conversion of chlorophyll b into pyrochlorophyll b through decarboxymethylation, which is thus the dominant breakdown reaction for chlorophyll b. This degradation pathway is confirmed by looking at the pyrochlorophyll b/chlorophyll b + b′ ratio (Table 4) which is much higher than the pyrochlorophyll a/chlorophyll a + a′ ratio, except in the sun-drying process. Pyrochlorophyll b content was generally found to be higher than that of pyrochlorophyll a, except in the sun-dried herb samples. This unique sun-drying exception can be explained: it is a long process leading to further pigment degradation toward the appearance of pyropheophytins, with pyrochlorophylls and pheophytins as potential precursors. In that case, pyrochlorophyll b turns into pyropheophytin b more rapidly whereas pyrochlorophyll a tends to accumulate. This means that pheophytin b tends to accumulate as well, allowing an important conversion into pheophytin b′ that is well-observed for herbs subjected to sun-drying processes (Table 3). However, the presence of pyropheophytin a in measurable amounts, especially in sun-dried herb samples, suggests that it might have been formed from pheophytin a. These findings demonstrate that pyropheophytins cannot only be formed under relative severe heat treatment as previously described,[11] but also during long mild drying processes such as sun-drying. In conclusion, the total of pyroderivatives in the b series (pyrochlorophyll b + pyropheophytin b) is always higher than the total of pyroderivatives in the a series and contrary to what happens to chlorophylls a and b. This kinetic tendency in the pyroderivative formation has not been described elsewhere to date. Figure 3 attempts to describe the degradation pathways and the novel kinetic qualitative tendencies described above. Normally, the loss of Mg^{2+} ion is supposed to be the primary and direct way of chlorophyll breakdown, but in the case of dried aromatic herbs both Mg^{2+} removal and decarboxymethylation can be dominant reactions, depending on whether one considers the a or b chlorophyll form. The primary focus of literature references on chlorophyll degradation pathways includes wet plants (leaf senescence, cooking processes, fruit ripening) or vegetable oils.[2−11,16,17,19,20] For dried culinary herbs, the dehydration process is done rapidly after harvesting, and thus,

dx.doi.org/10.1021/jf4054947 | J. Agric. Food Chem. 2014, 62, 1926−1935

Table 3. Pigment Contents in the Culinary Aromatic Herb Samples

		green pigments (1×10^{-9} mol/g dry weight)[a]							olive-brown pigments (1×10^{-9} mol/g dry weight)[a]								
type of herb and sample number	no. on PCA	chlorophyll a	chlorophyll a′	chlorophyll b	chlorophyll b′	chlorophyllide a	pyrochlorophyll a	pyrochlorophyll b	pheophytin a	pheophytin a′	pheophytin b	pheophytin b′	pyropheophytin a	pyropheophytin b	pheophorbide a	chloro a/b[b]	% green[c]
								Oven-Drying									
parsley 1	1.1	470.3	88.4	165.2	44.7	ND	4.0	4.2	46.1	11.0	ND	ND	ND	ND	ND	2.85	93.2
tarragon 1	1.2	32.1	9.1	15.1	18.7	ND	1.0	13.8	6.6	1.3	ND	3.9	ND	3.2	ND	2.12	85.7
chive 1	1.3	140.6	33.0	108.2	31.8	ND	1.5	9.6	232.6	44.5	17.8	18.4	7.5	21.7	ND	1.30	48.7
dill 1	1.4	203.9	52.1	124.7	39.3	ND	ND	21.6	187.8	32.8	6.8	21.6	5.8	17.7	ND	1.63	61.8
tarragon 2	1.5	46.6	12.3	26.9	9.7	ND	1.4	20.8	11.0	2.4	6.3	5.7	4.6	ND	ND	1.74	79.7
coriander leaves 1	1.6	279.9	68.2	148.0	47.8	ND	2.3	18.0	162.8	35.7	10.8	25.5	14.5	17.7	ND	1.89	67.9
parsley 2	1.7	347.3	90.9	179.0	54.6	ND	2.8	18.2	203.5	41.5	ND	ND	19.3	ND	ND	1.94	72.4
coriander leaves 2	1.8	335.8	66.3	145.8	39.0	ND	1.0	7.3	90.3	19.3	ND	ND	ND	ND	ND	2.30	84.4
parsley 3	1.9	206.4	51.7	85.6	31.6	ND	2.7	23.2	61.7	11.5	ND	ND	3.0	ND	ND	2.41	84.0
parsley 4	1.10	269.1	64.7	108.4	38.7	ND	2.4	31.7	97.8	22.9	6.1	14.1	9.6	13.3	ND	2.48	75.9
coriander leaves 3	1.11	253.2	66.2	96.2	28.8	ND	4.9	19.7	71.4	14.8	ND	ND	8.0	ND	ND	2.63	83.3
								Freeze-Drying									
dill 2	2.1	927.4	86.7	374.9	67.8	ND	ND	35.0	46.4	7.6	8.5	7.8	ND	ND	ND	2.47	95.5
tarragon 3	2.2	245.2	15.6	101.4	18.8	ND	ND	13.9	6.7	1.2	ND	ND	ND	ND	ND	2.42	98.0
mint 1	2.3	566.3	33.8	243.6	25.7	ND	1.2	24.2	50.0	10.3	ND	ND	ND	ND	ND	2.32	93.7
basil 1	2.4	423.4	19.9	204.8	23.8	ND	1.3	27.0	49.0	8.2	20.1	17.1	ND	ND	ND	2.07	88.1
parsley 5	2.5	603.5	27.6	265.2	42.1	ND	ND	25.9	109.8	19.4	19.2	17.6	3.4	ND	ND	2.28	85.1
chive 2	2.6	504.6	16.8	242.3	16.0	9.8	ND	8.8	119.4	21.5	10.5	11.0	2.0	ND	27.7	2.08	80.6
								DP1									
oregano 1	3.1	77.4	ND	47.1	2.0	ND	1.4	2.1	34.6	6.5	2.2	9.7	0.4	8.1	ND	1.64	67.9
oregano 2	3.2	11.3	0.3	10.3	0.4	ND	ND	0.4	7.6	1.6	2.6	2.2	ND	ND	ND	1.10	61.8
marjoram 1	3.3	124.5	1.9	67.7	2.2	ND	ND	3.8	5.5	0.7	ND	4.0	ND	3.3	ND	1.84	93.6
basil 2	3.4	433.2	8.6	219.0	10.7	ND	ND	11.9	42.1	6.8	1.9	6.5	0.8	5.8	ND	1.98	91.4
marjoram 2	3.5	24.1	7.2	32.4	10.3	ND	0.1	2.1	65.6	13.0	8.7	6.9	2.0	3.6	ND	0.74	43.3
								DP2									
dill 3	4.1	772.7	81.3	263.3	47.0	ND	ND	9.7	37.5	10.4	ND	ND	13.3	ND	ND	2.94	95.0
oregano 3	4.2	204.0	21.9	103.6	17.5	ND	ND	ND	65.1	12.6	ND	ND	ND	ND	ND	1.97	81.7
parsley 6	4.3	808.0	19.1	334.4	19.9	ND	ND	7.5	18.2	3.8	ND	ND	ND	ND	ND	2.42	98.2
parsley 7	4.4	826.9	19.8	362.7	19.4	ND	ND	11.6	16.0	ND	ND	ND	ND	ND	ND	2.28	98.7
parsley 8	4.5	761.3	27.6	329.3	22.6	ND	ND	7.6	24.3	4.3	ND	ND	ND	ND	ND	2.31	97.6
parsley 9	4.6	813.6	31.3	355.4	23.1	ND	ND	7.7	36.1	5.3	ND	ND	1.6	ND	ND	2.29	96.6
coriander leaves 4	4.7	516.0	8.7	272.0	1.7	0.4	0.6	6.2	18.6	2.7	ND	ND	ND	ND	ND	1.90	97.4
								Sun-Drying									
mint 2	5.1	3.0	0.0	52.1	14.1	ND	0.7	1.4	199.6	36.1	32.9	20.1	12.3	4.8	ND	0.06	18.9
mint 3	5.2	0.6	0.6	19.1	5.1	ND	6.6	1.9	88.5	14.9	70.1	59.2	16.0	9.8	ND	0.03	11.6

dx.doi.org/10.1021/jf4054947 | J. Agric. Food Chem. 2014, 62, 1926−1935

Table 3. continued

type of herb and sample number	no. on PCA	green pigments (1×10^{-9} mol/g dry weight)[a]							olive-brown pigments (1×10^{-9} mol/g dry weight)[a]								
		chlorophyll a	chlorophyll a′	chlorophyll b	chlorophyll b′	chlorophyllide a	pyrochlorophyll a	pyrochlorophyll b	pheophytin a	pheophytin a′	pheophytin b	pheophytin b′	pyropheophytin a	pyropheophytin b	pheophorbide a	chloro a/b[b]	% green[c]
Sun-Drying																	
marjoram 3	5.3	1.2	0.3	22.5	6.5	ND	3.5	0.8	108.9	18.3	49.6	35.1	10.6	5.2	ND	0.05	13.2
basil 3	5.4	2.6	0.6	25.4	6.5	ND	8.6	4.0	190.2	27.5	84.3	70.0	10.9	3.1	ND	0.10	11.0
marjoram 4	5.5	2.8	0.6	24.5	7.3	ND	0.3	1.0	103.7	16.7	43.3	31.0	5.7	2.0	ND	0.11	15.3
oregano 4	5.6	1.3	0.5	10.0	3.1	ND	0.2	0.7	70.8	13.4	33.7	13.3	42.1	2.8	ND	0.13	8.2
oregano 5	5.7	2.6	4.1	30.7	8.8	ND	1.5	1.4	196.9	37.4	94.9	67.8	7.0	42.6	ND	0.09	9.9
oregano 6	5.8	3.0	1.0	15.7	4.8	ND	0.3	1.0	132.0	24.2	75.6	28.6	128.0	9.5	ND	0.19	6.1
basil 4	5.9	7.5	1.6	21.0	5.5	ND	0.4	1.6	155.3	22.5	83.1	62.6	13.3	6.0	ND	0.36	9.9
oregano 7	5.10	154.3	1.9	128.3	5.8	ND	1.1	5.9	94.9	18.0	5.7	20.2	0.9	17.4	ND	1.20	65.4
coriander leaves 5	5.11	63.6	9.9	32.1	6.2	ND	0.4	1.9	23.5	4.9	6.3	3.1	1.7	2.4	ND	1.98	73.1
marjoram 5	5.15	5.1	0.5	50.1	14.6	ND	3.4	2.7	199.4	36.2	32.2	34.1	6.8	23.7	ND	0.10	18.7
basil 5	5.16	4.7	0.5	48.1	13.8	ND	5.6	2.8	220.4	37.0	52.1	58.5	17.4	38.7	ND	0.10	15.1
chive 3	5.17	136.2	5.4	108.8	12.2	ND	1.2	4.7	164.5	27.1	10.2	32.7	5.8	27.2	ND	1.25	50.1
Fresh Herb																	
oregano 8	6.1	441.2	2.6	175.0	3.1	ND	ND	3.6	7.3	ND	ND	ND	ND	ND	ND	2.52	98.8
parsley 10	6.2	714.8	3.8	322.5	3.1	ND	ND	2.8	13.5	ND	ND	ND	ND	ND	ND	2.22	98.7
parsley 11	6.3	609.1	3.7	266.2	3.8	ND	ND	10.0	11.8	ND	ND	ND	ND	ND	ND	2.29	98.7
parsley 12	6.4	557.9	3.7	252.6	1.6	ND	ND	11.6	9.7	2.0	ND	ND	ND	ND	ND	2.21	98.6
parsley 13	6.5	643.9	3.9	272.6	3.1	ND	ND	3.8	10.3	0.6	ND	ND	ND	ND	ND	2.36	98.8
parsley 14	6.6	720.7	4.2	326.4	2.9	ND	ND	18.4	14.7	1.7	ND	ND	ND	ND	ND	2.21	98.5
coriander leaves 6	6.7	428.0	ND	181.0	ND	94.1	2.8	1.8	7.0	0.7	ND	ND	ND	ND	ND	2.36	98.9

[a]Mean of duplicate analyses. [b]Chloro a/b = chlorphyll a/chlorophyll b. [c]% green, percentage of total green pigments.

dx.doi.org/10.1021/jf4054947 | J. Agric. Food Chem. 2014, 62, 1926−1935

Table 4. Pigment Ratio Results (Means and Standard Deviations)

process	*n*	% green pigments[a]	chlorophyll a′/ chlorophyll a	chlorophyll b′/ chlorophyll b	pheophytin a′/ pheophytin a	pheophytin b′/ pheophytin b	pyrochlorophyll a/ chlorophyll (a + a′)	pyrochlorophyll b/ chlorophyll (b + b′)
oven-drying	11	75.6 ± 12.6	0.24 ± 0.03	0.40 ± 0.28	0.21 ± 0.02	1.96 ± 1.0	0,01 ± 0.008	0.18 ± 0.17
freeze-drying	6	90.7 ± 7.1	0.06 ± 0.02	0.14 ± 0.05	0.18 ± 0.01	0.93 ± 0.08	0.0008 ± 0.001	0.09 ± 0.03
DP1	5	71.9 ± 21.1	0.07 ± 0.13	0.10 ± 0.12	0.18 ± 0.03	2.37 ± 1.8	0.004 ± 0.008	0.05 ± 0.007
DP2	7	95.3 ± 5.5	0.05 ± 0.04	0.09 ± 0.06	0.16 ± 0.08		0.0002 ± 0.0004	0.02 ± 0.01
sun-drying	14	22.7 ± 22.4	0.32 ± 0.43	0.25 ± 0.08	0.17 ± 0.02	1.10 ± 1.0	0.95 ± 1,6	0.05 ± 0.03
fresh herb	7	98.7 ± 0.1	0.01 ± 0.002	0.01 ± 0.01	0.07 ± 0.08		0.0009 ± 0.003	0.03 ± 0.02

[a]% green pigments = percentage of total green pigments.

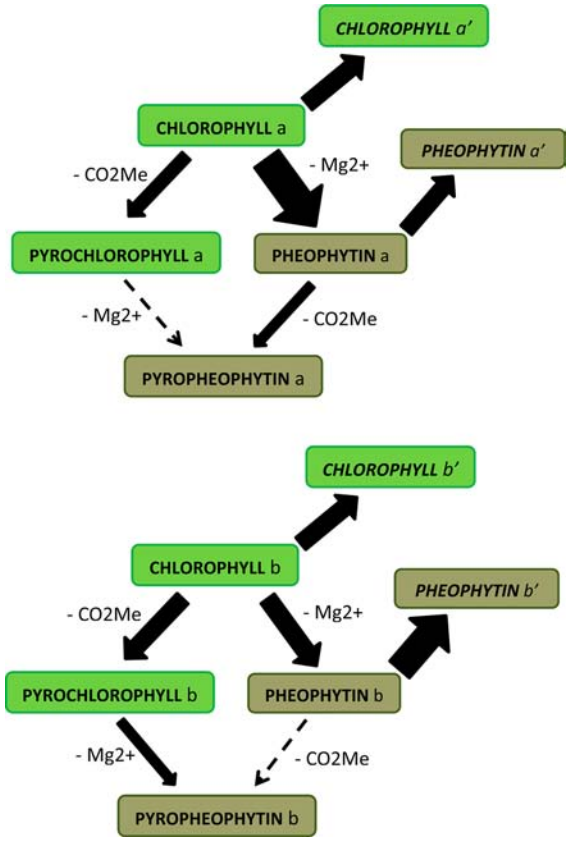

Figure 3. Chlorophyll a and b degradation pathways in culinary aromatic herbs during drying processes. Arrow width is proportional to the qualitative importance of the degradation pathway kinetic.

the final water activity ranges from 0.3 to 0.55. This low range significantly reduces the effect of enzymatic reactions involved in Mg-dechelatase, chlorophyllase, or enzymatic reduction of chlorophyll b.[24] Consequently, no chlorophyllide was detected in this study except in one product subjected to a blanching step prior to dehydration. Moreover, neither pyrochlorophyllides nor pyropheophorbides were detected, because both need the chlorophyllase action to occur somewhere in the chlorophyll degradation process. The chlorophyll catabolic pathway is stopped;[24] a simpler chemical degradation occurs instead. The raw data in Tables 3 and 4 and illustrated pathways in Figure 3 show how different dry culinary herb species chosen independently of each other can show similar behavior with respect to noncatabolic chlorophyll degradation. In those conditions, the type of process became an important factor for differentiation.

The raw data were evaluated by PCA, which is mainly a statistical treatment of the data. The objective was to present a maximum of information by converting a set of observations (herb samples) of possibly correlated variables (pigments) into a set of values of orthogonal variables called principal components. As explained above, the use of these variables did not aim to differentiate the types of dried herbs, but rather the types of processes they were subjected to. The first two components represent the plane of best fit through the data. As PCA is sensitive to the relative scaling of the original variables, observation values expressed in mol/g on dry wt basis were reduced and centered prior to calculations. In our case, there were 14 variables composed of the 14 detected chlorophylls and derivatives leading to a 14D space composed of the final orthogonal principal components. The 2D (F1, F2) principal plane with the orthogonal projections of the 14 initial variables as well as the scatterplot diagram with scores of the observations are displayed in Figure 4 showing an interesting cumulative variability: F1 and F2 axes account for 57% of the total variability, and the following principal components show Eigenvalues below 1.15.

On principal plane with the variable projections (Figure 4A), most of the variables are away from the plane center meaning that they were not that distorted by the projection. Chlorophyllide a and pheophorbide a have a low contribution to F1 and F2, but they were rarely found in the 50 samples. Apart from pyrochlorophyll a, all the relevant variable projections related to green pigments are on the left half of the plane. All the relevant variable projections related to olive-brown pigments are on the right half. This suggests that globally green and olive-brown pigments are negatively correlated along the F1 axis. In practical terms, it reflects the fact that a drop in the green pigment concentrations leads to an increase of the brown-olive ones. As pyrochlorophyll a tends to accumulate, its behavior is like that of the olive-brown pigments. That is why its projection is atypically in the right half of the (F1, F2) plane. Chlorophyll epimer variables (a′ and b′) point upward on the principal plane suggesting that samples subjected to mild processes will be placed rather at the top of this plane.

On the scatterplot (Figure 4B), observations coming from the same drying treatments were plotted so that they form clusters. As mentioned for the variable projection directions, fresh and freeze-dried plants, as well as the group of plants subjected to treatment DP2 (which is supposed to protect the green color effectively), are in the left half of the (F1, F2) plane considered as the region where green pigments are well-preserved. Treatment DP1 and oven-drying are more central, and sun-drying on the right part is driven by the olive-brown pigment variables. The freeze-drying cluster extends toward the upper-left portion of the (F1, F2) plane in the direction of the pyrochlorophyll b projection. Consequently, this process produces the highest levels of pyrochlorophyll b.

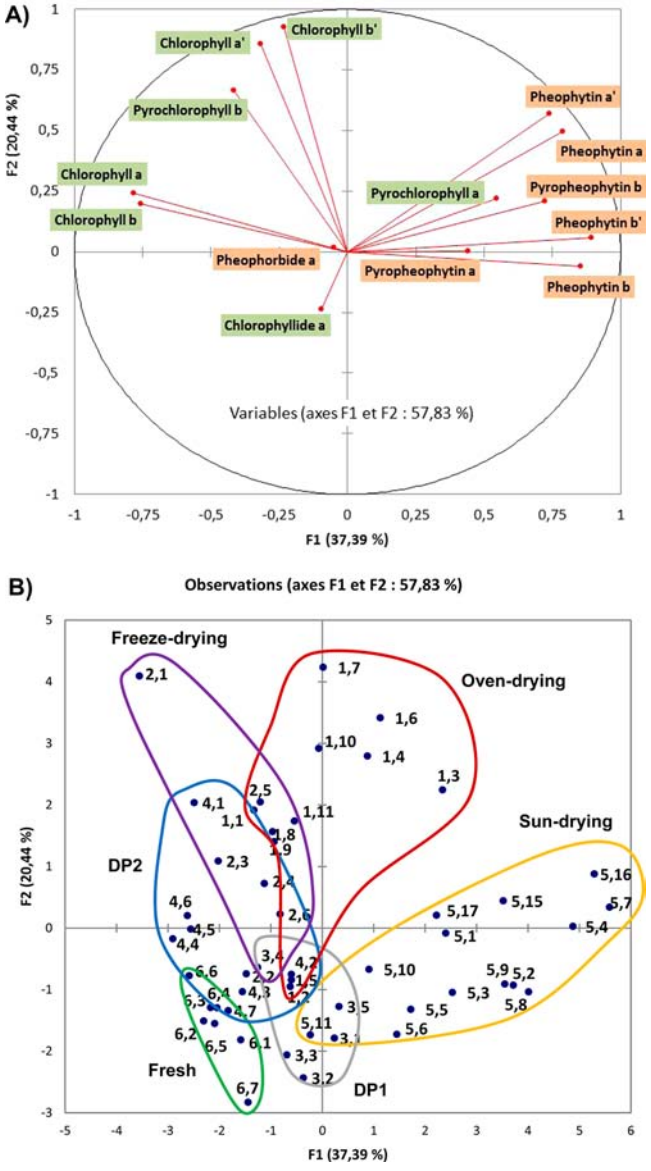

Figure 4. Projection of the pigment variables on (A) the principal (F1, F2) plane, and (B) scatterplot of the culinary herb samples on the first 2 principal component plane.

Oven-drying and sun-drying clusters are the most scattered groups of observations but elongate in different directions. For oven drying, higher energy is brought to the product in a medium period of time. High energy and medium time preserve relatively well the green color; that is why the cluster of oven-drying observations tends to extend toward the upper part of the (F1, F2) plane, the direction between the chlorophyll epimer and pheophytin projections. Thus, herbs subjected to this process showed that chlorophylls had been partly turned to both other green pigments and olive-brown pigments. The oven-drying cluster is scattered, presumably due to the impact of the oven temperature parameter on the color result.

As for sun-drying, a process with low energy and long delay time impacting chlorophyll breakdown, samples are situated on the right part of the plane. That is the consequence of a massive chlorophyll conversion into olive-brown derivatives such as pheophytin a, pheophytin b and b′ and moderately pheophytin a′, pyropheophytin a and pyrochlorophylls. The efficiency of this process on color preservation depends on numerous factors: cloudy or sunny conditions during drying, windy or calm, exposure to the sun light for long or short periods of time, high, low or moderate temperature fluctuations and, finally, whether or not a a pretedding step is included. The variability of these parameters can vary greatly and make the sun-drying cluster large.

On the F1 axis representing the greenness scale, the DP2 process (high energy, short time) cluster is the closest to the fresh herb cluster and elongates toward the pyrochlorophyll b and chlorophyll epimer in direction. Very few olive-brown pigments are thus produced.

Chlorophylls and Derivatives Breakdown: PCR Analyses. After the PCA treatment of the data we chose to extract quantitative information from the results. It was interesting to test if quantitative information could be forecasted for unknowns from the available measures. In that case, PCR (principal component regression) can help, since it calculates a single principal component regression model using the given number of principal components to predict unknown quantitative information (response) from available measurements (observations). The calculated orthogonal principal components from the PCA data were used to run the PCR model. Herb surface color was chosen as an interesting response for variables and especially the LCh° colorometric space according to three axes: lightness (L), chroma or saturation (C), and hue ($h°$). This colorometric space describes how well the human eye can perceive the different colors.

Unfortunately, no significant correlation was found between the variables and the 3 colorimetric responses. A slight linearity was observed for the hue $h°$ response. Additionally, the relationship between hue and the total green pigment content (on dry wt basis, mol/g) was plotted. Hue values ranged from 85° to 128°, which correspond to the yellow-green part of colorimetric space. The curve $h°$ as a function of total green pigment content reached rapidly an asymptote at $h° = 128°$ for contents above 4×10^{-7} mol/g. This interesting result shows that no surface color improvement can be realized by having greater concentrations of green pigments. It also tells us that below 4×10^{-7} mol/g the surface green color rapidly worsens.

Color Degradation Ladder. In order to understand the tendency for chlorophyll to degrade toward olive-brown derivatives, a degradation ladder was designed. The idea was to find a sole and easy-to-use indicator using the complex set of chlorophyll and derivative results in order to assess the plant material color after processing. This ladder was thus based on the percentage of total green pigments present (presented earlier in this paper), while understanding that green chlorophyll derivatives do not bring about any change in color insofar as the light absorption properties remain globally the same. This ladder was divided into four categories. Category limits were fixed according to the visual color estimation of each sample. Figure 5 shows the ladder visually and allows one to check whether the processing and treatment of a herb has an impact on the visual quality of the final product when dried. The various herb process treatments from Table 4 were evaluated with the ladder definitions. Fresh herbs, freeze-dried herbs, and DP2 treatment (high energy short time) of herbs belong to the category "no significant impact" with percentage of total green pigments above 90% on average with a well-preserved green appearance of the dried herb samples. Oven-drying (high energy medium time) and DP1 treatment (low energy long time) belong to the "low impact" category, with a percentage ranging from 65% to 90%. Sun-drying (low energy long time) falls into the fourth

dx.doi.org/10.1021/jf4054947 | J. Agric. Food Chem. 2014, 62, 1926−1935

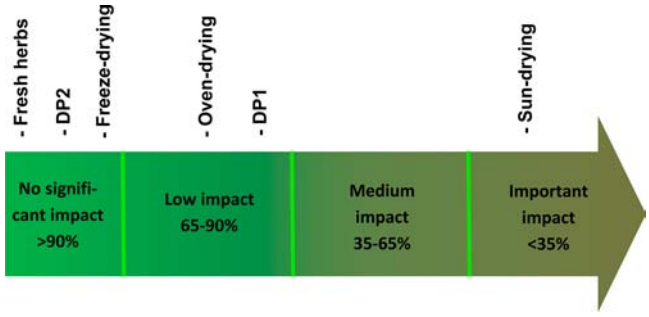

Figure 5. Color degradation ladder of culinary aromatic herbs. The percentages are the level of total green pigments (figure colors are arbitrary).

category, named "important impact", and characterized by an average percentage below 35%. Sun-drying is a commonly used process to dry herbs; however, the technique greatly impacts the global herb color.

AUTHOR INFORMATION

Corresponding Author

*Phone: +33 4 90 63 89 22. Fax: +33 4 90 63 89 82. E-mail: jlafeuille@fr.mccormick.com.

Notes

The authors declare no competing financial interest.

REFERENCES

(1) Matile, P.; Schellenberg, M.; Vicentini, F. Localization of chlorophyllase in the chloroplast envelope. *Planta* **1997**, *201*, 96−99.
(2) Schwartz, S. J.; Lorenzo, T. V. Chlorophylls in foods. *Food Sci. Nutr.* **1990**, *29* (1), 1−17.
(3) Matile, P.; Hörtensteiner, S. Chlorophyll degradation. *Annu. Rev. Plant Physiol. Plant Mol. Biol.* **1999**, *50*, 67−95.
(4) Ginsburg, S.; Matile, P. Identification of catabolites of chlorophyll-porphyrin in senescent rape cotyledons. *Plant Physiol.* **1993**, *102*, 521−527.
(5) Marangoni, A. G. Kinetic model for chlorophyll degradation in green tissue. 2. Pheophorbide degradation to colorless compounds. *J. Agric. Food Chem.* **1996**, *44*, 3735−3740.
(6) Yamauchi, Y.; Watada, A. E. Effectiveness of various phenolic compounds in degradation of chlorophyll by in vitro peroxydase-hydrogen peroxide system. *J. Jpn. Soc. Hortic. Sci.* **1994**, *63* (2), 439−444.
(7) Teng, S. S.; Chen, B. H. Formation of pyrochlorophylls and their derivatives in spinach leaves during heating. *Food Chem.* **1999**, *65*, 367−373.
(8) Yamauchi, N.; Watada, A. E. Pigment changes in parsley leaves during storage in controlled or ethylene containing atmosphere. *J. Food Sci.* **1993**, *58*, 616−618.
(9) Almela, L.; Fernandez-Lopez, J. A.; Roca, M. J. High-performance liquid chromatographic screening of chlorophyll derivatives produced during fruit storage. *J. Chromatogr. A* **2000**, *870*, 483−489.
(10) Holden, M. The breakdown of chlorophyll by chlorophyllase. *Biochem. J.* **1961**, *78*, 359−364.
(11) Schwartz, S. J.; Lorenzo, T. V. Chlorophyll stability during continuous aseptic processing and storage. *J. Food Sci.* **1991**, *56* (4), 1059−1062.
(12) Shioi, Y.; Tomita, N.; Tsuchiya, T.; Takamiya, K. Conversion of chlorophyllide to pheophorbide by Mg-dechelating substance in extracts of Chenopodium album. *Plant Physiol. Biochem.* **1996**, *34*, 41−47.
(13) Huang, S. C.; Hung, C. F.; Wu, B. H.; Chen, B. H. Determination of chlorophylls and their derivatives in *Gynostemma pentaphyllum* Makino by liquid chromatography−mass spectrometry. *J. Pharm. Biomed. Anal.* **2008**, *48* (1), 105−112.
(14) Kao, T. H.; Chen, C. J.; Chen, B. H. An improved high performance liquid chromatography-photodiode array detection-atmospheric pressure chemical ionization-mass spectrometer method for determination of chlorophylls and their derivates in freeze-dried and hot-air-dried *Rhinacanthus nasutus*. *Talanta* **2011**, *86*, 349−355.
(15) Lanfer-Marquez, U. M.; Barros, R. M. C.; Sinnecker, P. Antioxidant activity of chlorophylls and their derivatives. *Food Res. Int.* **2005**, *38*, 885−891.
(16) Yamauchi, N.; Harada, K.; Watada, A. E. In vitro chlorophyll degradation in stored broccoli (*Brassica oleracea* L. *var. italica* Plen.) florets. *Postharvest Biol. Technol.* **1997**, *12*, 239−245.
(17) Schwartz, S. J.; Woo, S. L.; von Elbe, J. H. High-performance liquid chromatography of chlorophylls and their derivatives in fresh and processed spinach. *J. Agric. Food Chem.* **1981**, *29*, 533−535.
(18) Pennington, F. C.; Strain, H. H.; Svec, W. A.; Katz, J. J. Preparation and properties of pyrochlorophyll *a*, methyl pyrochlorophyllide *a*, pyropheophytin *a*, and methyl pyropheophorbide *a* derived from chlorophyll by decarbomethoxylation. *J. Am. Chem. Soc.* **1964**, *86* (7), 1418−1426.
(19) Vernon, L. P. Spectrophotometric determination of chlorophylls and pheophytins in plants extracts. *Anal. Chem.* **1960**, *32* (9), 1144−1150.
(20) Bohn, T.; Walczyk, T. Determination of chlorophyll in plant samples by liquid chromatography using zinc−phthalocyanine as an internal standard. *J. Chromatogr. A.* **2004**, *1024*, 123−128.
(21) Mantoura, R. F. C.; Llewellyn, C. A. The rapid determination of algal chlorophyll and carotenoid pigments and their breakdown products in natural waters by reverse-phase high-performance liquid chromatography. *Anal. Chim. Acta* **1983**, *151*, 297−314.
(22) Canjura, F. L.; Schwartz, S. J. Separation of chlorophyll compounds and their polar derivatives by high-performance liquid chromatography. *J. Agric. Food Chem.* **1991**, *39*, 1102−1105.
(23) Suzuki, N.; Saitoh, K.; Adachi, K. Reversed-phase high-performance thin-layer chromatography and column liquid chromatography of chlorophylls and their derivatives. *J. Chromatogr. A.* **1987**, *408*, 181−190.
(24) Hörtensteiner, S.; Kräutler, B. Chlorophyll breakdown in higher plants. *Biochim. Biophys. Acta* **2011**, *1807*, 977−988.

promising method for natural compounds extraction, there are still some limitations (security, appropriate reactors, and craft determination, et al.) for its industrial applications. Therefore, further fundamental study on natural compounds extraction by MAE method is needed for large scale production.

In the present work, water-soluble pigments were quickly obtained from *C. mollissima* shells by water/ethanol (1:1, v/v) with microwave-assisted extraction, and purified by a two-step precipitation for the first time. The chemical composition and physical properties of the new pigments were subsequently determined by a combination method of spectroscopic techniques (UV, FT-IR, ^{13}C NMR), elemental analysis, and chromatographic techniques (HPAEC, GPC). Furthermore, the physical properties, DPPH radical scavenging capacity, antimicrobial activity, and the acute oral toxicity test were also investigated. The comprehensive and systematic knowledge of the new pigments from *C. mollissima* shells will help to maximize the exploitation of these agricultural residues for possible use in food additives production.

MATERIALS AND METHODS

Materials. Ten kg of *C. mollissima* fruit was collected from Qianxi, Hebei province, China. After peeling, about 1.47 kg of *C. mollissima* shells was obtained. The shells were washed extensively with distilled water. After drying at 55 °C for 16 h in an oven, the shells were smashed in an FZ120 plant shredder (Truelab, Shanghai, China), then sieved to 20−40 mesh. The resulting powder was stored in sealed bags (under N_2 atmosphere) at room temperature. All chemicals used were of analytical grade and purchased from Sigma Chemical Co. (Beijing, China).

Extraction and Purification of Pigments. The extraction and purification procedures of pigments are shown in Figure 1. MAE experiments were performed on an Ethos T microwave extractor (Milestone, Sorisole, Italy) with a maximum delivered power of 600 W at 70 °C for 30 min. Briefly, *C. mollissima* shell powder was submitted to aqueous ethanol/water (1:1, v/v) in a 2-L round-bottom flask with a solid to liquid ratio of 1:20 (g/mL) under magnetic stirring at 50% of nominal power. After centrifugation, 1500 mL of crude pigments supernatant was obtained and evaporated at 60 °C under reduced pressure (−0.09 MPa) until the final volume was 50 mL. The concentrated solution was then purified by a two-step precipitation method. First, the concentrated solution was poured into 3 volumes of 95% ethanol to remove hemicelluloses by precipitation. Second, the above solution was concentrated again and then the solubilized lignin could be removed by precipitating the solution into 10 volumes of deionized water.[15,16] After the two-step precipitation, the pigments were redissolved in the solution of ethanol/water (1:1, v/v), and successively extracted by 3 volumes of organic solvents (ethyl acetates, petroleum ether) for three times to remove lipids.[17] Finally, the water layer was freeze-dried overnight.

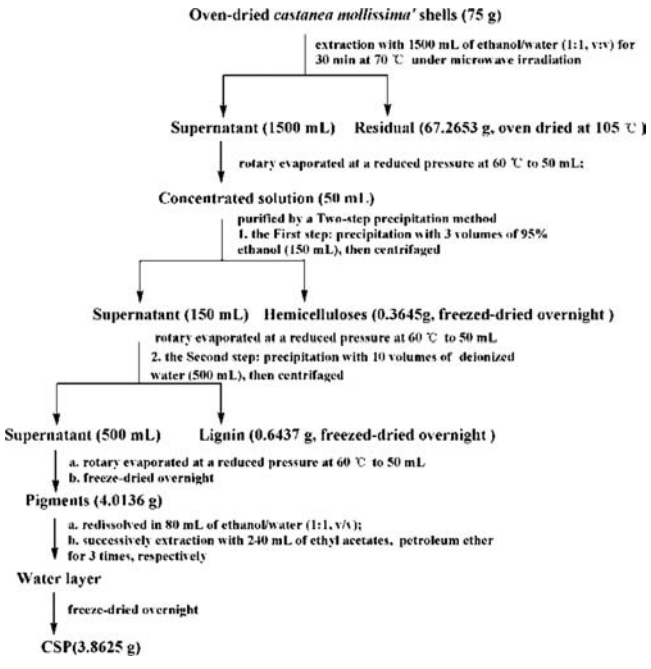

Figure 1. Extraction and purification procedures of CSP.

Chemical Composition and Structural Analysis. To analyze the associated sugars in pigments, sugar analyses were conducted by acid hydrolysis according to the procedures described in a previous paper.[18] Then the hydrolysate analyses were performed on a high-performance anion chromatography system (ICS3000, Dionex, Sunnyvale, CA) with pulsed amperometric detector and an ion exchange Carbopac PA-1 column (40 × 250 mm). The neutral sugars were separated in 18 mM NaOH (carbonate free and purged with nitrogen) with post column addition of 0.3 M NaOH at a rate of 0.5 mL/min. Run time was 45 min, followed by a 10-min elution with 0.2 M NaOH to wash the column and then a 15-min elution with 18 mM NaOH to reequilibrate the column. Calibration was performed with a standard solution of L-rhamnose, L-arabinose, L-glucose, L-galactose, D-mannose, and D-xylose. Measurements were conducted with two parallels, and reproducibility of the values was found within the range of 5%. The elemental composition of the pigments before and after acid hydrolysis was recorded on a Vario EL analyzer (Elementar Analysensysteme GmbH, Hanau, Germany). Infrared spectra of pigments were collected on a Thermo Scientific Nicolet iN 10 FT-IR Microscopy instrument (Thermo Nicolet Corp., Madison, WI) equipped with a liquid nitrogen-cooled MCT detector. The weight-average (M_w) and number-average (M_n) molecular weights of the pigments were determined by Agilent1200 gel permeation chromatography (Agilent, Santa Clara, CSA) on a 300 mm × 7.7 mm i.d., 10 μm, PL aquagel−OH column of the same material (Agilent, England), calibrated with PL pullulan polysaccharide standards (peak average molecular weights of 783, 12 200, 100 000, 1 600 000 g/mol, Polymer Laboratories Ltd.). ^{13}C NMR spectra of the pigments were recorded on a Bruker AVIII 400 MHz spectrometer (Germany) instrument at 25 °C and chemical shifts were referenced to solvent signal. The preparation of 100 mg of CSP was carried out using 0.5 mL of DMSO-d_6 (δ_C 39.5). ^{13}C NMR spectra were obtained in the pulse FT mode (100.6 MHz). A 30° pulse angle, a 9.2-μs pulse width, 1.89-s delay time, and 1.36-s acquired time between scans were used. All chemical shifts were expressed in ppm (δ_C) from TMS.

Physical Properties Determination. The solubility and stability studies of the pigments were based on the previous literature with minor alterations.[19] The solubility in water and other common solvents (benzene, chloroform, diethyl ether, acetone, ethyl acetate, petroleum ether, hexane, methanol, ethanol, acetic acid, DMSO, and alkaline solutions) was investigated by adding 0.05 g of the pigments in 5 mL of solvents with stirring at 25 °C for 1 h, and standing for 1 h. As for the stability, 0.005 g/100 mL water/ethanol (1:1, v/v) solution was used for studying the pigment stability of temperature (25, 50, 75, and 100 °C), light (natural light, ultraviolet light, and dark), and different kinds of metal ions (Ca^{2+}, Cu^{2+}, Na^{+}, Zn^{2+}, Al^{3+}, Mg^{2+}, Fe^{3+}, and K^{+}). All absorption coefficients of samples were determined at λ_{max} by a UV 2300 spectrophotometer (Techcomp, Shanghai, China). All the determinations were carried out in triplicate. The results are expressed as mean values and standard deviation (SD). Analysis of variance (ANOVA) was performed by using the data analysis tools in Microsoft Excel 2007, and a least significant difference (LSD) test was used to determine the differences of means. P values less than 0.05 were considered to be statistically significant.

Antioxidant Activity of the Pigments. The pigments were reacted with a stable free radical, 2,2′-diphenyl-1-picrylhydrazyl radical (DPPH), to evaluate antioxidant activity.[20] The DPPH radical scavenging capacity was estimated using the reported method.[21] The antioxidant activity was expressed as a percentage of reduction of the

DPPH radical: radical scavenging rate (SC%) = [1 − (absorbance of sample)/(absorbance of control)] × 100%. For comparison, the DPPH radical scavenging capacity of synthetic antioxidant butylated hydroxytoluene (BHT, 0.5 mg/mL) and butylated hydroxyanisole (BHA, 0.5 mg/mL) was also tested. The DPPH solution with no CSP added was used as control. The EC_{50} value (mg extract/mL), an effective concentration at which 50% radical was scavenging, was also calculated. All tests were performed in triplicate.

Antimicrobial Activity of the Pigments. To evaluate the antimicrobial activity of CSP, disc-diffusion assay was carried out using 6-mm filter disc.[22] Gram-negative bacteria strain *Escherichia coli* (CMCC (B) 44103) and gram-positive bacteria strains *Streptomyces somaliensis* (NBRC 12916 (T)), *Staphylococcus aureus* (ATCC 25923), *Bacillus subtilis* (CGMCC 3376), and fungus *Penicillium oxalicum* (CGMCC 13428), and *Aspergillus japonicus* (ATCC 204480) used were kindly given by the Institute of Microbiology, Beijing Forestry University, Beijing, China. After culturing, the microorganisms were adjusted with sterile saline to a concentration of 1.0×10^7 to 10^9 cfu/mL. The suspension was added to the top of the agar plates and dissolved in Petri dishes (20 μL/agar plate) with solid agar. The filter paper discs with pigment solution (concentrations of 0.05, 0.10, and 0.15 g/mL, 20 μL/disc) were placed on agar plates. After 24 h of incubation for bacteria and 3−4 days of incubation for fungus at 28 °C, the diameters of the growth inhibition zones were measured. Additionally, the 5% aqueous phenol as a positive control and 50% aqueous ethanol and water as negative controls were used. All tests were done in triplicate.

Acute Oral Toxicity Test of the Pigments. The acute toxicity of the pigments was determined according to the U.S. Food and Drug Administration (FDA) guidelines for toxicity tests IV C 2.[23] Briefly, the animals were divided into four groups (two groups of male and two groups of female), and same-sex animals were housed together in groups of three at room temperature (20 ± 2 °C), 30−60% relative humidity, and 12 h light−dark cycle. Prior to testing, the animals were starved for 4 h. After fasting, 200 mg/mL of pigments suspension (single dose of 5 g/kg body weight) was administered orally to the experimental groups, while the vehicle control groups were given distilled water (10 mL/kg). Food and water were provided 2 h later. Symptoms of toxicity and mortality were observed for 14 days after the administration. On day 14, all mice were sacrificed and subjected to necropsies. Kunming mice (17.5−20.0 g) used in the tests were purchased from the Laboratory Animal Center of the Academy of Military Medical Sciences (Beijing, China) and allowed to acclimate for 1 week prior to beginning experiment. All procedures used in this experiment were compliant with the local ethics committee.

RESULTS AND DISCUSSION

Yield and Sugar Analysis. Conventionally, pigments can be obtained by extracting for several hours or overnight using hot water, bases, acids, or some organic solvents. Compared with traditional extractive methods, MAE has been considered as an efficient and rapid process to extract pigments or antioxidants from plants with higher yield.[24] In this study, the polar ethanol/water (1:1, v/v) and the temperature of 70 °C accelerated the mass transfer of water-soluble pigments from chestnut shells. A two-step (by 95% ethanol, and water subsequently) precipitation method was first applied to remove hemicelluloses (0.3645 g/75 g dry weight) and lignin (0.6437 g/75 g) from the pigments. After purification, the total yield of pigments was 3.8625 g/75 g, which was a little higher than traditional extraction for 36 h by aqueous alkaline (Fr. 3, a yield of 2.7 g/100 g from chestnut shells), but much lower than that from tea leaves under the same condition (about 29%).[5,25] This phenomenon might be the result of severe purification and the high level of lignification of chestnut shells.

Table 1. Average Neutral Sugar Contents (%) (± 3%)[a] of CSP

	CSP-1 (%)	CSP-2 (%)	average (%)
ara	4.35	4.23	4.29
gal	1.69	1.75	1.72
glu	16.23	15.58	15.9
xyl	0.99	0.38	0.68
total	23.26	21.94	22.6

[a]Pooled standard error.

The sugar analysis of CSP was applied to estimate the associated neutral sugars. It is well-known that pigments are readily bound to proteins, polysaccharides, and lipids. To figure out the associated polysaccharides, CSP was hydrolyzed by acid and analyzed through HPAEC. The results of sugar analysis are listed in Table 1. Results showed that the total amount of the neutral sugars in CSP was 22.6%. The sugars in the isolated pigments demonstrated a predominance of glucose (70.35%), followed by arabinose, galactose, and xylose. This suggested that the main associated monosaccharide in CSP was glucose and it might attach to pigments to some extent.

Table 2. Elemental Composition and Molar Ratio of CSP

	elemental composition (wt%)				molar ratio		
	C	H	O	N	N/C	H/C	O/C
P1[a]	46.00	5.43	47.62	0.95	0.018	1.42	0.78
P2[b]	56.15	4.17	39.68	0	0	0.89	0.53

[a]The original CSP. [b]CSP after acid hydrolysis.

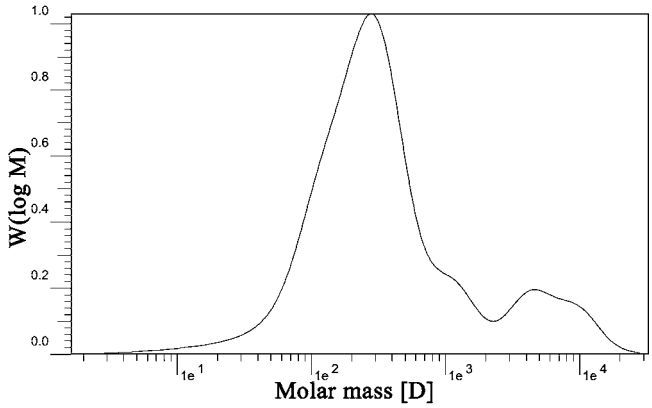

Figure 2. Actual gel permeation chromatograms of CSP.

Elemental Composition. The average elemental compositions for the pigments before (P1) and after (P2) acid hydrolysis are presented in Table 2. As noted, the original elemental composition of P1 was C = 46.00%, N = 0.95%, H = 5.43%, O = 47.62%, and the C element content increased while N element was in too trace a concentration to be detected after acid hydrolysis (P2). The H/C ratio (1.42) in P1 was high, which reflected a relatively high content of aliphatic chains. The low content of N element and N/C ratio in P1 suggested that the content of bounding protein was low and was comparable with the deproteinated samples extracted by alkaline.[5] In addition, a high ratio of O/C showed a high degree of oxygen substitution in the pigments, especially the bounding glycosides. This was in line with the sugar analysis aforementioned. After acid hydrolysis, both H/C and O/C ratios were decreased, suggesting that the linked sugars were almost removed during the hydrolysis. As the ether bonds in

Figure 3. FT-IR spectrum of CSP.

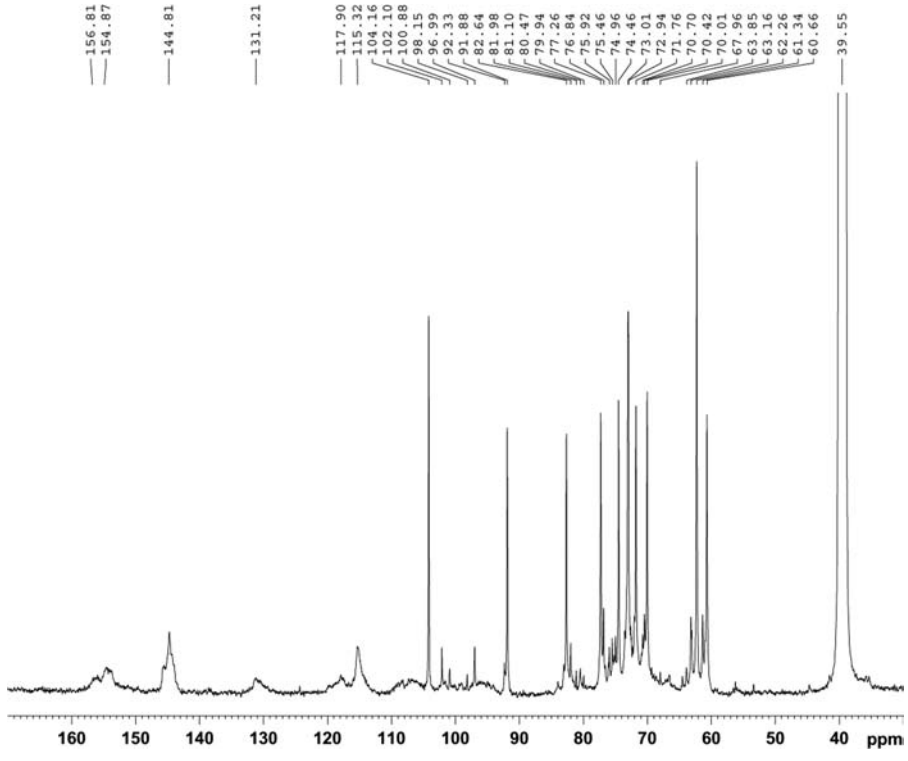

Figure 4. ^{13}C NMR spectrum (in DMSO-d_6) of CSP.

compounds are apt to cleave by acid, this probably inferred that the associated carbohydrates were attached to pigments via ether bonds. Furthermore, the disappearance of N element in P2 suggested the extracted pigment was lacking chlorophyll *a*, betacyanin, phycocyanobilin, or rubropunctamine, which are relatively rich in N element.[12]

Molecular Weight Distributions. The values of the weight-average (M_w) and number-average (M_n) molecular weights, estimated from GPC curves, and polydispersity indexes (M_w/M_n, PI) of the pigments extracted from chestnut's shells are shown in Figure 2. The M_w of pigments from chestnut shells was 1240 g/mol with a PI of 8.25, indicating an inhomogeneous molecular weight distribution of CSP.

FT-IR Analysis. FT-IR spectroscopy provides information on the main functional groups in the pigment structure. The FT-IR spectrum of the pigments is illustrated in Figure 3. As shown, a broad band at 3450 cm^{-1}, which is attributed to stretching vibrations of phenolic OH group, was evidently distinguished. The peak at 1442 cm^{-1} was indicative of a strong aliphatic character.[26] The 1607 cm^{-1} band was assigned to aromatic C═C stretching. The 1047 cm^{-1} band attributing to C−O stretching of polysaccharides suggested a certain amount of glycosidic bonds in the pigments. Moreover, the absorption peak at 1280 cm^{-1} represents bending vibration of hydroxyl.[27] The results of FT-IR spectrum demonstrated a certain amount of aliphatic chains in the pigments structure, accompanying OH

dx.doi.org/10.1021/jf4045414 | J. Agric. Food Chem. 2014, 62, 1936−1944

Table 3. Main Assignments[a] of CSP in the ^{13}C NMR Spectra Shown in Figure 4

chemical shift (ppm)	assignment
156.8	C-5 in procyanidin B3; C-2 in querctin-3-*O*-glycoside
154.9	C-7 in procyanidin B3
144.8	C-3′ in procyanidin B3; C-3′ in querctin-3-*O*-glycoside
131.2	C-1′ in procyanidin B3
117.9	C-8 in flavanol
115.3	C-2′ of the H ring of flavanol moiety in flavylium; C-2′ in querctin-3-*O*-glycoside
104.2	gl-1 in luteolin-5-*O*-glycoside and querctin-3-*O*-glycoside
102.1	C-4a in procyanidin B3
98.1	C-8 in luteolin-5-*O*-glycoside; C-6 in kaempferol and quercetin
97	C-6 in procyanidin B3
91.9	flavonoid glycoside
82.6/82.0	C-2 in procyanidin B3
81.1	C-17 in 5β-steroidal sapogenins
79.9	C-2′ in phenolic glycoside
77.3	gl-5 in querctin-3-*O*-glycoside
76.8	gl-3 in querctin-3-*O*-glycoside
75.9	C-4 in arabinoxylans
75.5	C-2 in β-glucose
74.5	gl-2 in querctin-3-*O*-glycoside
73/72.9	C-3 in procyanidin B3
71.8	flavonoid glycoside
70.7	C-4 in β-glucose
70.4	C-3,4 in α-galactose
70	C-4 in α,β-xylose
63.8	C-5 in the arabinoxylans
63.2	C-17 in 5β-steroidal sapogenins
62.3	C-5 in xylose
61.3	C-6 in β-glucose
60.7	flavonoid glycoside

[a]Signals were assigned by comparison with the literature.[20,23,36−40]

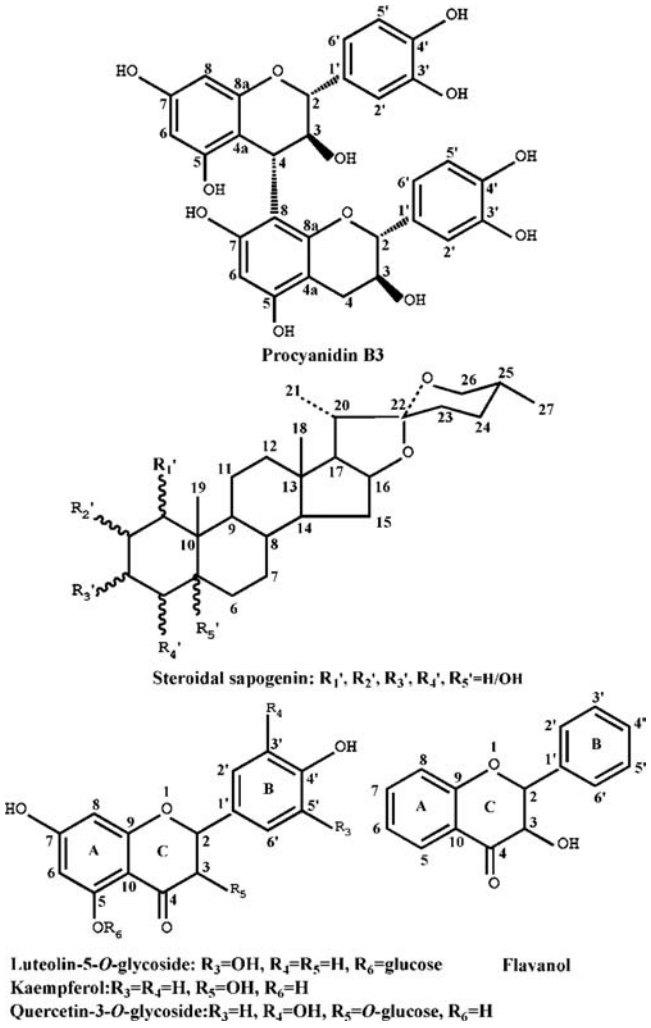

Figure 5. Main components of CSP, involving procyanidin B3, flavanol, kaempferol, quercetin, luteolin, and steroidal sapogenins identified by ^{13}C NMR.

and C−O groups. This was supported by the data of the elemental analysis.

^{13}C NMR Analysis. Application of ^{13}C NMR technique allows quick qualitative determination of different components in pigments. To further investigate the structural features and the main components in pigments, the pigments were analyzed by solution-state ^{13}C NMR. The ^{13}C NMR spectrum of the pigments is shown in Figure 4. The spectrum can be divided into aliphatic (δ_C 20−90) and aromatic (δ_C 90−160) regions.[28] The main signals in the ^{13}C NMR spectrum were assigned by comparison with the published literatures, and are listed in Table 3; the main components are depicted in Figure 5.[28−35]

The upfield signals ranging from δ_C 20 to 90 were due to the aliphatic carbons in pigments, which mainly resulted from the associated sugars and some micromolecule substances. As can be seen, Figure 4 apparently showed the spectral characteristic of sugars in this region. Based on the previous publications, the signals at δ_C 75.5, 76.8, 70.7, 77.3, 61.3 were assigned to carbon atoms 2, 3, 4, 5, and 6 in β-glucose, respectively.[30] The signals for atoms 5 and atoms 4 of xylose were discovered at δ_C 62.3 and 70.0. Signals resulted from α-galactose could be detected at δ_C 70.4.[31] Among these, signals from the β-glucose could be seen at higher contour levels, which indicates a higher amount of β-glucose in CSP. Weak signals at 102.1, 74.5, 75.9, and 63.8 ppm, which are assigned respectively to C-1, C-3, C-4, and C-5 positions of the arabinoxylan, suggested that the associated arabinose in CSP appeared in the form of arabinoxylan. Above all, β-glucose was the most predominant in CSP, followed by similar amounts of arabinose, xylose, and galactose, which was in agreement with the results obtained by sugar analysis. In addition, some interglycosidic linkages such as phenolic glycosides were also recognized in the sugar region of the spectrum. It has been reported that two signals at δ_C 79.9 and 74.5 are assigned to phenolic glycosides.[32] The most important glycosides found in the CSP might be flavonoids-*O*-glycosides, such as quercetin-3-*O*-glycoside, which had strong signals at δ_C 77.3, 76.8, 74.5, 70.7, 70.4, 68, and 61.3 in the sugar region.[33] Furthermore, some micromolecule substances were also distinguished. Interestingly, flavanoid procyanidin B3 (condensed tannin) was also revealed by the signals at 82.6, 82.0, 73.0, 72.9, and 68.0 ppm in this region.[28] It could be concluded that the condensed tannins in *C. mollissima* shells could be extracted by aqueous ethanol. Except for the flavonoids, signals at 81.1 and 63.2 ppm could be probably assigned to 5β-steroidal sapogenin.[29]

The aromatic region of the spectrum gave more useful information about different groups of flavonoids and some micromolecular substances present in the pigments. Most of the downfield signals at δ_C 156.8, 154.9, 144.8, 131.2, and 102.1, are caused by C-5, C-7, C-3′, C-1′, and C-4a positions of

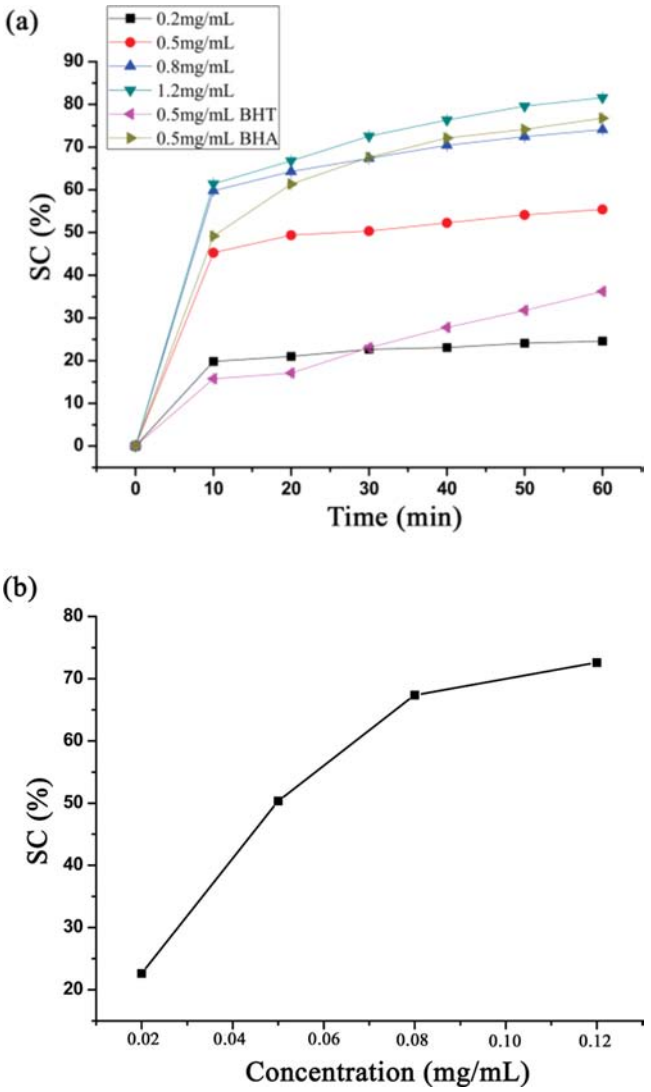

Figure 6. (a) Scavenging abilities of different concentrations of CSP, BHT (0.5 mg/mL), and BHA (0.5 mg/mL) on DPPH radical with increasing time. (b) DPPH radical scavenging rate of CSP with increasing concentration when the mixture was treated for 30 min. Error bars represent standard deviation of the means (n = 3); $P \leq 0.05$.

the procyanidin B3, respectively.[28] As for quercetin-3-*O*-glycoside, signals in this region were detected at δ_C 156.8, 144.8, 115.3, 104.2, 100.8, and 98.1. In addition, the luteolin-5-*O*-glycoside showed a prominent signal for glucose carbon atom 1 at δ_C 104.2. A weak signal at 98.1 ppm may originate from C-8 of luteolin-5-*O*-glycoside, C-6 of kaempfero,l and quercetin. Moreover, the signal at δ_C 117.9 was attributed to C-8 of flavonol.[34] In short, the ^{13}C NMR spectrum indicated that the main components in CSP were flavonoids, steroidal sapogenins, and the ether linked sugars which may be flavonoid glycosides, such as quercetin-3-*O*-glycoside and luteolin-5-*O*-glycoside. Flavanol and procyanidin were observed as the major flavonoids in CSP, whereas signals of kaempferol, free quercetin, and luteolin appeared in a trace amount.

Physical Properties Analysis. As the UV spectrum indicated, the absorption spectrum of the pigments exhibited strong optical absorbance in a spectral range from 270 to 290 nm, and relatively weak absorbance range from 290 to 650 nm. The wavelength of maximum absorption was 278.5 nm, which is a typical peak of flavonoids. Therefore, as the main components in pigments, the absorbance of flavonoids at 278.5 nm was selected as reference in the following experiments.

Solubility of CSP. The solubility results indicated that the pigments were scarcely soluble in benzene, chloroform, diethyl ether, acetone, ethyl acetate, petroleum ether, and hexane. However, the pigments could be dissolved in methanol, ethanol, and acetic acid. Furthermore, they displayed a good solubility in water, DMSO, and alkaline solutions (such as Na_2CO_3, NaOH, and NH_4OH). The solubility in water and DMSO may be due to the flavonids and water-soluble glycosides in CSP.

Stability of CSP. The effect of temperature on the CSP stability was evaluated to investigate the potential use as an antioxidant. The absorbance of the pigment solution at λ_{max} changed slightly from 25 to 50 °C after incubating in a thermostatically controlled bath for 3 h. On the contrary, the absorbance of CSP solution at 75 °C increased during the early incubation period, and decreased gradually to meet the initial value. This phenomenon was probably related to the thermal auto-oxidation and degradation of the flavonoids in CSP.[36,37] Unfortunately, the CSP was extremely unstable at the temperature of 100 °C, which might be correlated with the polarity of the CSP.[37] These results suggested that the pigments were stable when the temperature was below 75 °C.

To study the effect of light on CSP, the pigment solutions were performed under ultraviolet light, indoor natural light, and stored in a dark place for 1−10 d. Only 0.03 and 0.01 of absorbance were increased under natural light and dark after 10 days' treatment, respectively. However, the absorbance increased first and then decreased with the increasing irradiation time when the solution was irradiated under ultraviolet-light. After being treated for 3 days, about 0.07 of the absorbance was increased. These results indicated that the pigments were stable to the indoor natural light and under dark condition, while the ultraviolet light had a relatively strong effect on the light stability. This phenomenon might be explained by the degree of glucosylation in CSP, which has an important contribution to pigment stability for light.[7]

Table 4. Antibacterial Activity of CSP by Diameter of Inhibition Zones (mm)

	CSP			phenol	50% aqueous ethanol	sterile water
bacteria	1 mg/disc	2 mg/disc	3 mg/disc	1 mg/disc	20 μL/disc	20 μL/disc
E. coli	6.12 ± 0.03	7.21 ± 0.08	7.20 ± 0.05	7.50 ± 0.22	6.60 ± 0.04	n.a.[a]
S. somaliensis	10.60 ± 0.10	12.82 ± 0.27	13.68 ± 0.24	7.15 ± 0.06	n.a.	n.a.
S. aureus	6.57 ± 0.18	6.94 ± 0.02	7.02 ± 0.06	7.59 ± 0.09	8.68 ± 0.11	n.a.
B. subtilis	9.96 ± 0.15	11.62 ± 0.05	13.46 ± 0.22	9.63 ± 0.19	7.78 ± 0.14	n.a.

[a]n.a. The pigment was not active at the tested concentration.

dx.doi.org/10.1021/jf4045414 | J. Agric. Food Chem. 2014, 62, 1936−1944

Figure 7. Results of antibacterial activity against Gram-positive bacteria strain *Streptomyces somaliensis* and *Bacillus subtilis* of CSP in disc-diffusion method. (1) a: 1 mg/disc CSP; b: 1 mg/disc phenol; c: 50% aqueous ethanol; d: sterile water. (2) a: 2 mg/disc CSP; b: 1 mg/disc phenol; c: 50% aqueous ethanol; d: sterile water. (3) a: 3 mg/disc CSP; b: 1 mg/disc phenol; c: 50% aqueous ethanol; d: sterile water.

With regard to metal ions stability, it was apparent that the absorbance of the pigment solution diminished sharply when mixed with Zn^{2+} solution for 48 h, whereas the pigment solutions mixed with the other metal ions (Ca^{2+}, Cu^{2+}, Na^{+}, Zn^{2+}, Al^{3+}, Mg^{2+}, Fe^{3+}, and K^{+}) had no obvious change. Therefore, most of the metal ions aforementioned affected the pigments slightly.

DPPH Radical Scavenging Capacity of CSP. DPPH is a stable free radical, gives rise to the deep violet solution in ethanol, and has a strong absorption at 515 nm. When the solution is added with an antioxidant, the free radical of DPPH can be paired and reduce the amount of the free radical, resulting in a decrease in the absorbance of DPPH at 515 nm.[38] The scavenging ability of CSP, BHT, and BHA on DPPH radical is shown in Figure 6. As illustrated, the scavenging capacity of the pigments was increased with the increasing reaction time (Figure 6a) and concentration (Figure 6b). Compared with the synthetic antioxidant BHT, the CSP had a strong DPPH radical scavenging capacity, and was closed to BHA. At 0.2−1.2 mg/mL, CSP showed scavenging abilities of 22.6−72.6% on DPPH radicals in 60 min (Figure 6a), which was better than that of pigments from the seeds of *Osmanthus fragrant*.[21] Moreover, the EC_{50} value was 0.057 mg/mL (Figure 6b), which was significantly lower than that of polysaccharides isolated from *Ganoderma tsugae* and comparable to that of the flavonoid glycosides from *Daphniphyllum calycinum*, indicating a higher antioxidant activity of CSP.[39,40] The significant DPPH radical scavenging capacity of CSP may reflect a certain amount of substances with an available OH group,[41] such as tannins and procyanidin, which was verified by FT-IR and ^{13}C NMR spectra. These results implied that the 50% ethanol extracted and a two-step precipitation purified pigments from *C. mollissima* shells processed excellent DPPH scavenge capacity.

Antimicrobial Activity of CSP. With respect to the antimicrobial activity of CSP, the disc-diffusion method was used to test the diameter of inhibition zones effect on bacteria and fungus and the results are listed in Table 4. As shown, the pigments (1, 2, and 3 mg/disc) indicated an increased antibacterial activity with the increasing pigments content per disc. However, the pigments were not sensitive to the fungus (*P. oxalicum* and *A. japonicus*), which exhibited considerable antibacterial activity, especially the Gram-positive bacteria. This was in agreement with the antimicrobial activities of extracts from some other plants.[22] The highest inhibition zones could be obtained for *S. somaliensis*, which may refer to pathogens,[42] ranging from 10.60 to 13.68 mm. The pigment solution was active against *B. subtilis* as well, with inhibition zones of 9.96−13.46 mm (Figure 7). Moreover, the lowest inhibition zones (6.12−7.50 mm) were recorded for *E. coli*, while *S. aureus* possessed almost the same activity, with inhibition zones 6.57−7.59 mm.

The antimicrobial potential of pigments tested in the disc-diffusion method can be presented as *S. somaliensis* > *B. subtilis* > *S. aureus* > *E. coli* > fungus. Compared with the commercial antibiotic phenol, it was remarkable that the pigments showed stronger antibacterial potential toward *S. somaliensis*, while almost the same with regard to *B. subtilis*. The excellent antibacterial activity of CSP might be a good proof of the presence of the natural antioxidants procyanidin and quercetin-3-*O*-glycoside. The interesting results display the eminent antibacterial activity of CSP, which will broaden the potential applications of CSP as food additives.

Acute Toxicity Effect of CSP. Acute toxicity of CSP was assessed at a maximum dose of 5.0 g/kg of body weight. No treatment-related mortality, body weights, or clinical signs of toxicity including hair loss, scabbing, soft or mucoid feces,

decreased defecation or feces smaller than normal, wet yellow material in urogenital area, or vocalization upon handling, were observed for 14 days following the oral administration of CSP. All animals gained weight and appeared active and normal. After sacrifice on the 14th day, macroscopic and gross pathology observations conducted at the necropsy examination revealed no visible lesions in any animals. Relative weight of organs in mice of control and experimental groups did not show significant difference. These phenomena indicated that the mice could tolerate maximum dose at 5.0 g/kg of body weight of CSP, and the LD_{50} should be greater than 5.0 g/kg in both male and female mice according to the guidance for the safety assessment of botanicals and botanical preparations for use in food and food supplements.[43] Based on the toxicity classification proposed by Loomis and Hayes, substances with LD_{50} between 5000 and 15 000 mg/kg body weight are regarded as being practically nontoxic.[44] The present results suggested that CSP could be regarded as being practically nontoxic, which might be related to the quercetin-3-*O*-glycoside in CSP.[45]

In summary, the water-soluble pigments from *C. mollissima* shells extracted by 50% ethanol with microwave assisted were purified by a two-step precipitation method for the first time. The comprehensive and systematic evaluation of the pigments provided valuable results in relation to the chemical composition and characteristics of these natural pigments. It demonstrated a predominance of flavonoids (procyanidin B3) and ether-linked sugars (quercetin-3-*O*-glycoside), followed by a small amount of steroidal sapogenins. As a consequence, CSP was water-soluble, practically nontoxic, and exhibited wonderful DPPH radical scavenging ability and antibacterial activity. With respect to physical properties, CSP revealed good stability with temperature, natural light, and metal ions. However, CSP was not resistant to UV light. The detailed study of pigments from *C. mollissima* shells will shed light on the utilization of these agricultural residues.

AUTHOR INFORMATION

Corresponding Author

*Tel: +86-10-62336387. Fax: +86-10-62336903. E-mail: xfx315@bjfu.edu.cn.

Notes

The authors declare no competing financial interest.

ACKNOWLEDGMENTS

We gratefully acknowledge the financial support from National Science Foundation for Distinguished Young Scholars of China (31225005), National Science and Technology Program of the Twelfth Five-Year Plan Period (2012BAD32B06), and Chinese Ministry of Education (113014A).

REFERENCES

(1) Goodell, E. *Castanea mollissima*: A Chinese chestnut for the northeast. http://missourinutgrowers.org/pdf/Castanea%20Mollissima.pdf; 2013.9.28.

(2) Youngs, R. L. A right smart little jolt: Loss of the chestnut and a way of life. *J. For.* **2000**, *98*, 17−21.

(3) FAOSTAT. Country rank in the world, by commodity: China. http://faostat.fao.org/site/339/default.aspx; 2013.10.3)

(4) McCarthy, M. A.; Meredith, F. I. Nutrient data on chestnuts consumed in the United States. *Econ. Bot.* **1988**, *42*, 29−36.

(5) Yao, Z.; Qi, J.; Wang, L. Isolation, fractionation and characterization of melanin-like pigments from chestnut (*Castanea mollissima*) shells. *J. Food Sci.* **2012**, *77*, C671−C676.

(6) Qi, J. H.; Shi, Y.; Feng, T.; Wang, F.; Pang, M. X.; Xu, Y.; Yi, X. X. Characteristic of the pigments in *Castanea mollissina* shell. *Adv. Mater. Res.* **2013**, *602*, 874−878.

(7) Delgado-Vargas, F.; Jiménez, A. R.; Paredes-López, O. Natural pigments: Carotenoids, anthocyanins, and betalains-characteristics, biosynthesis, processing, and stability. *Crit. Rev. Food Sci.* **2000**, *40*, 173−289.

(8) Kim, D. H.; Kim, J. H.; Bae, S. E.; Seo, J. H.; Oh, T. K.; Lee, C. H. Enhancement of natural pigment extraction using *Bacillus* species xylanase. *J. Agric. Food Chem.* **2005**, *53*, 2541−2545.

(9) Cai, Z.; Wu, J.; Chen, L.; Guo, W.; Li, J.; Wang, J.; Zhang, Q. Purification and characterisation of aquamarine blue pigment from the shells of abalone (*Haliotis discus hannai Ino*). *Food Chem.* **2011**, *128*, 129−133.

(10) Mapari, S. A.; Nielsen, K. F.; Larsen, T. O.; Frisvad, J. C.; Meyer, A. S.; Thrane, U. Exploring fungal biodiversity for the production of water-soluble pigments as potential natural food colorants. *Curr. Opin. Biotech.* **2005**, *16*, 231−238.

(11) Vázquez, G.; Fernández-Agulló, A.; Gómez-Castro, C.; Freire, M. S.; Antorrena, G.; González-Álvarez, J. Response surface optimization of antioxidants extraction from chestnut (*Castanea sativa*) bur. *Ind. Crop Prod.* **2012**, *35*, 126−134.

(12) Mortensen, A. Carotenoids and other pigments as natural colorants. *Pure Appl. Chem.* **2006**, *78*, 1477−1491.

(13) Cai, Y. Z.; Sun, M.; Wu, H. X.; Huang, R. H.; Corke, H. Characterization and quantification of betacyanin pigments from diverse *Amaranthus* species. *J. Agric. Food Chem.* **1998**, *46*, 2063−2070.

(14) Rostagno, M. A.; Palma, M.; Barroso, C. G. Microwave assisted extraction of soy isoflavones. *Anal. Chim. Acta* **2007**, *588*, 274−282.

(15) Sun, R. C.; Tomkinson, J.; Ma, P. L.; Liang, S. F. Comparative study of hemicelluloses from rice straw by alkali and hydrogen peroxide treatments. *Carbohydr. Polym.* **2000**, *42*, 111−122.

(16) Björkman, A. Isolation of lignin from finely divided wood with neutral solvents. *Nature* **1954**, *174*, 1057−1058.

(17) Hung, Y. C.; Sava, V. M.; Makan, S. Y.; Chen, T. H. J.; Hong, M. Y.; Huang, G. S. Antioxidant activity of melanins derived from tea: Comparison between different oxidative states. *Food Chem.* **2002**, *78*, 233−240.

(18) You, T. T.; Mao, J. Z.; Yuan, T. Q.; Wen, J. L.; Xu, F. Structural elucidation of the lignins from stems and foliage of *Arundo donax* Linn. *J. Agric. Food Chem.* **2013**, *61*, 5361−5370.

(19) Tan, M. X.; Gan, D. H.; Wei, L. X.; Pan, Y. M.; Tang, S. Q.; Wang, H. S. Isolation and characterization of pigment from *Cinnamomum burmannii* peel. *Food Res. Int.* **2011**, *44*, 2289−2294.

(20) Blois, M. S. Antioxidant determinations by the use of a stable free radical. *Nature* **1958**, *181*, 1199−1200.

(21) Pan, Y.; Zhu, Z.; Huang, Z.; Wang, H.; Liang, Y.; Wang, K.; Lei, Q.; Liang, M. Characterisation and free radical scavenging activities of novel red pigment from *Osmanthus fragrans* seeds. *Food Chem.* **2009**, *112*, 909−913.

(22) Verpoorte, R.; Van Beek, T. A.; Thomassen, P. H. A. M.; Aandewiel, J.; Svendsen, A. B. Screening of antimicrobial activity of some plants belonging to the *Apocynaceae* and *Loganiaceae*. *J. Ethnopharmacol.* **1983**, *8*, 287−302.

(23) Food and Drug Administration (FDA). 1993 Draft Redbook II Toxicological principles for the safety assessment of direct food additives and color additives used in food: Chapter IV. Guidelines for Toxicity Tests. http://www.fda.gov/downloads/Food/GuidanceRegulation/GuidanceDocumentsRegulatoryInformation/IngredientsAdditivesGRASPackaging/UCM078734.pdf.

(24) Pasquet, V.; Chérouvrier, J. R.; Farhat, F.; Thiéry, V.; Piot, J. M.; Bérard, J. B.; Kaas, R.; Serive, B.; Patrice, T.; Cadoret, J. B.; Picot, L. Study on the microalgal pigments extraction process: Performance of microwave assisted extraction. *Process Biochem.* **2011**, *46*, 59−67.

(25) Pan, X. J.; Niu, G.; Liu, H. Microwave-assisted extraction of tea polyphenols and tea caffeine from green tea leaves. *Chem. Eng. Process.* **2003**, *42*, 129−133.
(26) Senesi, N.; Miano, T. M.; Martin, J. P. Elemental functional infrared and free radical characterization of humic acid-type fungal polymers (melanins). *Biol. Fert. Soils* **1987**, *5*, 120−125.
(27) Wang, X.; Li, Y.; Wei, J.; de Groot, K. Development of biomimetic nano-hydroxyapatite/poly (hexamethylene adipamide) composites. *Biomaterials* **2002**, *23*, 4787−4791.
(28) de Bruyne, T.; Pieters, L. A.; Dommisse, R. A.; Kolodziej, H.; Wray, V.; Domke, T.; Vlietinck, A. J. Unambiguous assignments for free dimeric proanthocyanidin phenols from 2D NMR. *Phytochemistry* **1996**, *43*, 265−272.
(29) Agrawal, P. K.; Jain, D. C.; Gupta, R. K.; Thakur, R. S. Carbon-13 NMR spectroscopy of steroidal sapogenins and steroidal saponins. *Phytochemistry* **1985**, *24*, 2479−2496.
(30) Zhou, Y.; Xie, Y. M.; Gan, D. N.; Yang, Z. Y.; Yang, H. T. Synthesis of condensed lignin model compound and formation mechanism of LCC during kraft cooking. *T. China Pulp Pap.* **2006**, 5−9.
(31) Mateus, N.; Silva, A. M.; Santos-Buelga, C.; Rivas-Gonzalo, J. C.; de Freitas, V. Identification of anthocyanin-flavanol pigments in red wines by NMR and mass spectrometry. *J. Agric. Food Chem.* **2002**, *50*, 2110−2116.
(32) Lu, Y.; Yeap Foo, L. Flavonoid and phenolic glycosides from *Salvia officinalis*. *Phytochemistry* **2000**, *55*, 263−267.
(33) Markham, K. R.; Ternai, B.; Stanley, R.; Geiger, H.; Mabry, T. J.. Carbon-13 NMR studies of flavonoids-III: Naturally occurring flavonoid glycosides and their acylated derivatives. *Tetrahedron* **1978**, *34*, 1389−1397.
(34) Ternai, B.; Markham, K. R. Carbon-13 NMR studies of flavonoids-I: Flavones and flavonols. *Tetrahedron* **1976**, *32*, 565−569.
(35) Van Loo, P.; De Bruyn, A.; Buděšínský, M. Reinvestigation of the structural assignment of signals in the ^{1}H and ^{13}C NMR spectra of the flavone apigenin. *Magn. Reson. Chem.* **1986**, *24*, 879−882.
(36) Das, N. P.; Pereira, T. A. Effects of flavonoids on thermal autoxidation of palm oil: Structure-activity relationships. *J. Am. Oil Chem. Soc.* **1990**, *67*, 255−258.
(37) Xiao, W.; Han, L.; Shi, B. Microwave-assisted extraction of flavonoids from *Radix Astragali*. *Sep. Purif. Technol.* **2008**, *62*, 614−618.
(38) Kim, D. O.; Lee, K. W.; Lee, H. J.; Lee, C. Y. Vitamin C equivalent antioxidant capacity (VCEAC) of phenolic phytochemicals. *J. Agric. Food Chem.* **2002**, *50*, 3713−3717.
(39) Tseng, Y. H.; Yang, J. H.; Mau, J. L. Antioxidant properties of polysaccharides from *Ganoderma tsugae*. *Food Chem.* **2008**, *107*, 732−738.
(40) Gamez, E. J. C.; Luyengi, L.; Lee, S. K.; Zhu, L. F.; Zhou, B. N.; Fong, H. H. S.; Pezzuto, J. M.; Kinghorn, A. D. Antioxidant flavonoid glycosides from *Daphniphyllum calycinum*. *J. Nat. Prod.* **1998**, *61*, 706−708.
(41) Mensor, L. L.; Menezes, F. S.; Leitão, G. G.; Reis, A. S.; Santos, T. C. D.; Coube, C. S.; Leitão, S. G. Screening of Brazilian plant extracts for antioxidant activity by the use of DPPH free radical method. *Phytotherapy Res.* **2001**, *15*, 127−130.
(42) Gooptu, S.; Ali, I.; Singh, G.; Mishra, R. N. Mycetoma foot. *J. Fam. Commun. Med.* **2013**, *20*, 136−138.
(43) Schilter, B.; Andersson, C.; Anton, R.; Constable, A.; Kleiner, J.; O'Brien, J.; Renwick, A. G.; Korver, O.; Smitand, F.; Walker, R. Guidance for the safety assessment of botanicals and botanical preparations for use in food and food supplements. *Food Chem. Toxicol.* **2003**, *41*, 1625−1649.
(44) Loomis, T. A.; Hayes, A. W. Toxicology testing methods. In *Loomis's Essentials of Toxicology*; Loomis, T. A., Hayes, A. W., Eds.; Academic Press: New York, 1996; pp 208−245.
(45) Akroum, S.; Bendjeddou, D.; Satta, D.; Lalaoui, K. Antibacterial activity and acute toxicity effect of flavonoids extracted from *Mentha longifolia*. *Am.-Eurasian J. Sci. Res.* **2009**, *4*, 93−96.

for 15 min using an ultrasonic bath (Tru-Sweep 275D, Crest Ultrasonic, Malaysia). The solution was delivered from an amber glass bottle, which was connected via a helium gas balloon to prevent oxygen contamination, through a tubular reactor comprising stainless steel tubing (0.75 mm i.d., 1.58 mm o.d.) immersed in a temperature-controlled silicone fluid bath using a high-performance liquid chromatography (HPLC) pump (LC-20AD, Shimadzu, Kyoto, Japan). The length of the reactor coil and the flow rate were adjusted to obtain the desired treatment times (40−1080, 20−340, 20−240, 10−80, and 5−30 s for 160, 180, 200, 220, and 240 °C, respectively). A thermocouple (type K) was connected via a tee connector near the initial part of the reactor (~10 cm under the fluid surface) to monitor the temperature of the solution inside the tube. After treatment, the solution flowed through a cooling coil immersed in an ice−water bath to rapidly stop the reaction. A miniature back-pressure regulator (P-880, Upchurch Scientific, WA, USA) was connected to the end of the tube to maintain a constant pressure of 5 MPa. This pressure was high enough to ensure that the solution remained in the liquid state throughout the temperature range.

HPLC-DAD Analysis of Caffeic Acid and Its Degradation Products. Caffeic acid and its degradation products in the treated solution were quantitatively analyzed using an HPLC system (Shimadzu, Kyoto, Japan) comprised of a solvent delivery unit (LC-20AD), a diode array detector (DAD; SPD-M20A), and a system controller (CBM-20A). The sample was chromatographically separated using an Inertsil ODS-3 column (4.6 mm × 150 mm, GL Sciences, Tokyo, Japan). The mobile phase consisted of 0.5% v/v aqueous acetic acid (A) and methanol (B), and the following gradient was used at a flow rate of 1.5 mL/min: 0−5 min, 5% B; 5−9 min, linear increase to 50% B; and 9−12 min, 50% B. The treated sample was filtered through a 0.45 μm nylon syringe filter, and 20 μL of sample was injected into the HPLC instrument. Caffeic acid and its degradation products were monitored at 280 nm with authentic caffeic acid as a calibration standard. However, since one of the major degradation products (4-vinylcatechol) is not commercially available, the concentrations of degradation products were estimated, after identification by liquid chromatography-diode array detection/mass spectrometry (LC-DAD/MS), using a calibration curve of caffeic acid corrected by the ratio of the molar absorptivities of caffeic acid (ε = 18 200 M^{-1} cm^{-1}) and the products, that is, 2951 M^{-1} cm^{-1} for hydroxytyrosol,[9] 10 233 M^{-1} cm^{-1} for protocatechuic aldehyde,[10] and 2692 M^{-1} cm^{-1} for 4-vinylcatechol.[11]

Identification of Degradation Products Using LC-DAD/MS. Agilent 1100 LC/MSD Trap SL (Agilent Technologies, CA, USA) equipped with a solvent delivery unit (G113A), a diode array detector (G1315D), and an ion-trap mass spectrometer (G2445D) with an electrospray ionization ion source was used to identify the degradation products. Chromatographic separation was accomplished using the same column described above. The mobile phase consisted of 0.5% v/v aqueous acetic acid and methanol (85:15 v/v) and flowed at a rate of 0.4 mL/min. The treated sample was filtered through a 0.45 μm nylon syringe filter, and 30 μL of sample was injected. Both positive and negative modes were performed over the m/z range 50−400.

Online HPLC-DPPH Assay. Evaluation of the DPPH radical scavenging activity of caffeic acid and each degradation product in the treated samples was conducted using an online HPLC-DPPH assay.[12] This method is based on the chromatographic separation of components in the sample and a postcolumn reaction with DPPH solution. In this study, only one DAD detector was used to monitor caffeic acid, the degradation products at 280 nm, and the negative peaks due to DPPH bleaching at 517 nm. A first pump was used to deliver the mobile phase that consisted of 0.5% v/v aqueous acetic acid and methanol (85:15 v/v) at a flow rate of 1 mL/min for separating the compound on the column described above, while another pump delivered 6 × 10^{-5} M DPPH in methanol or pure methanol at a flow rate of 0.8 mL/min through tubing that was connected via a tee connector to the column outlet. A reaction coil made with PEEK tubing (28.8 m) was connected to enable the compounds eluted from the column to react with DPPH for 47 s. Ascorbic acid (AA) was used for calibration of the DPPH radical scavenging assay via the negative peak area.

RESULTS AND DISCUSSION

Degradation Products of Caffeic Acid in Subcritical Water. A typical HPLC chromatogram of the solution treated under subcritical water conditions is shown in Figure S1 (Supporting Information). There were many compounds in the treated solution, but only the following three main compounds, which could be accurately identified by the LC-DAD/MS, are proposed to be degradation products of caffeic acid: hydroxytyrosol (3,4-dihydroxyphenylethanol), protocatechuic aldehyde (3,4-dihydroxybenzaldehyde), and 4-vinylcatechol (2-hydroxy-4-vinylphenol) (Figure 2). The mass/charge ratio (m/z) and maximum absorbance (λ_{max}) values were used to identify these compounds, as shown in Table 1. Only the standard

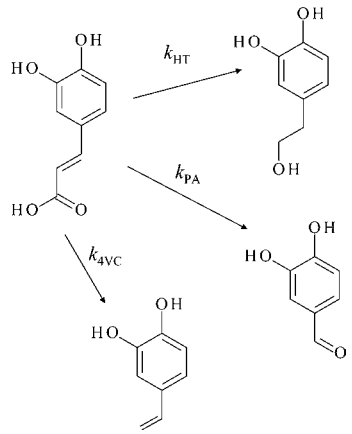

Figure 2. Proposed pathway of caffeic acid degradation in subcritical water.

Table 1. Characteristics of Caffeic Acid and Its Degradation Products Obtained by LC-DAD/MS

peak no.	compd	λ_{max} (nm)	$[M - H]^-$ m/z	negative ions m/z
1	hydroxytyrosol	220, 279	153	153 $[M - H]^-$
2	protocatechuic aldehyde	228, 278, 311	137	137 $[M - H]^-$; 108 $[M - CHO]^-$
3	caffeic acid	324	179	179 $[M - H]^-$; 135 $[M - COOH]^-$
4	4-vinylcatechol	259	135	135 $[M - H]^-$

caffeic acid was injected to confirm the accuracy of the mass spectrometer. Decarboxylated products are the main products of the degradation of phenolic acids under subcritical water conditions. For example, degradation of vanillic acid gave 2-methoxy-phenol,[5] whereas degradation of syringic acid gave syringol (1,3-dimethoxy-2-hydroxybenzene).[6] In this study, 4-vinylcatechol was detected as a decarboxylated product and was a main product in the treated solution (~38−57 mol %). It is known that 4-vinylcatechol can be formed through thermal degradation[13] and photodegradation[14] and can also be prepared by heating caffeic acid at 110 °C using a sodium acetate catalyst.[15] However, 4-ethylcatechol, which was also formed during pyrolysis, was not detected in this study. Hydroxytyrosol was found at moderate amounts in the treated solution (~14−43 mol %); this compound is an effective antioxidant that is naturally found in olive oil.[16] However, the pathway for the

dx.doi.org/10.1021/jf404850a | J. Agric. Food Chem. 2014, 62, 1945−1949

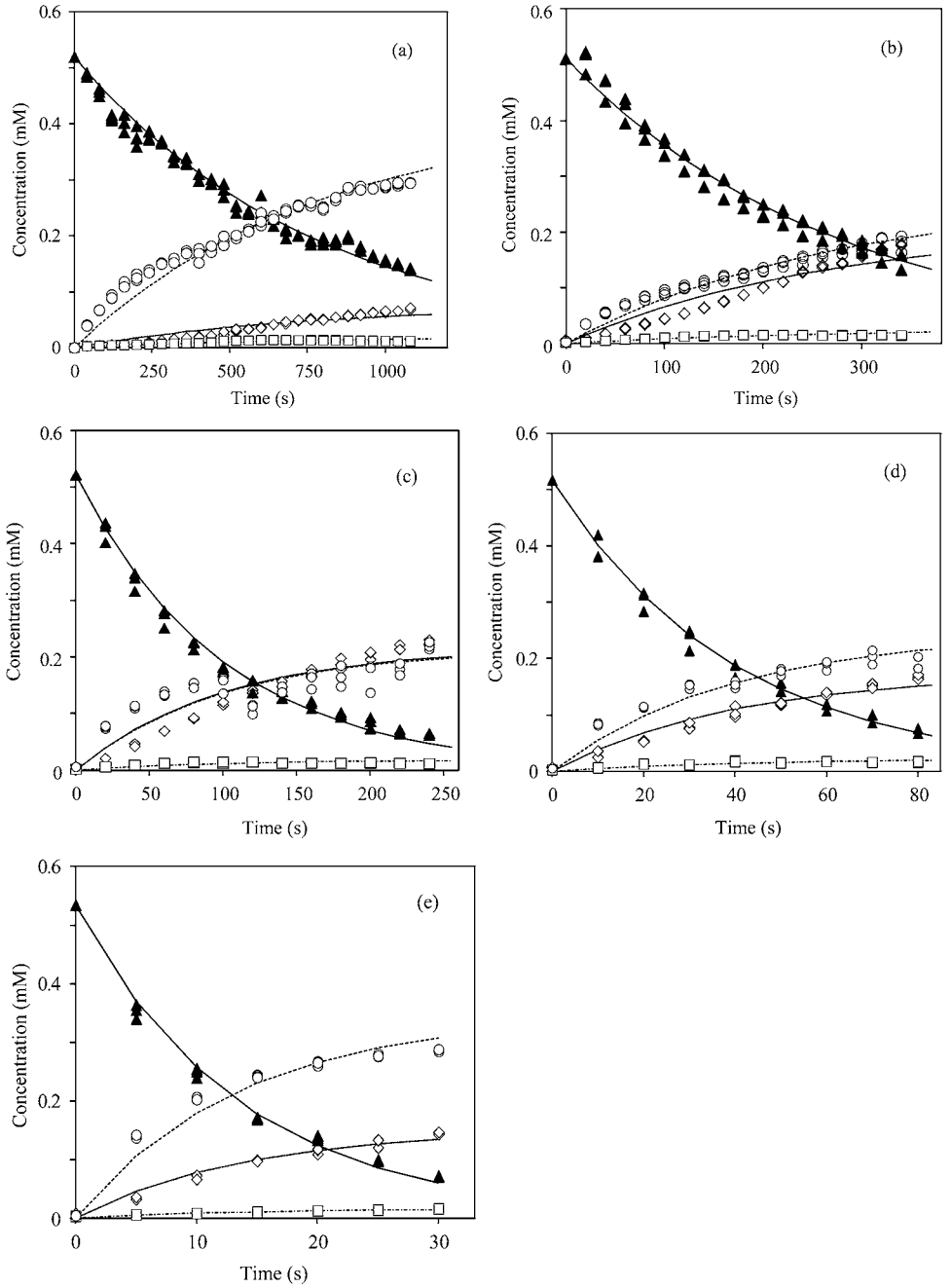

Figure 3. Caffeic acid degradation products at (a) 160, (b) 180, (c) 200, (d) 220, and (e) 240 °C. Caffeic acid (▲), hydroxytyrosol (◇), protocatechuic aldehyde (□), and 4-vinylcatechol (○).

formation of hydroxytyrosol from caffeic acid remains unclear. A small amount of protocatechuic aldehyde was also found in the treated solution. It has been reported that thermal degradation of chlorogenic acid, which is an ester of caffeic acid and quinic acid, can form a small amount of protocatechuic aldehyde.[17] In addition, protocatechuic aldehyde has been reported to be a main oxidation product of caffeic acid in the Fenton oxidation system.[18]

Kinetics analysis was performed along the pathways shown in Figure 2. The reactions can be described using the following first-order rate equations:

$$\frac{dC_{CA}}{dt} = -k_{HT}C_{CA} - k_{PA}C_{CA} - k_{4VC}C_{CA} \quad (1)$$

$$\frac{dC_{HT}}{dt} = k_{HT}C_{CA} \quad (2)$$

$$\frac{dC_{PA}}{dt} = k_{PA}C_{CA} \quad (3)$$

$$\frac{dC_{4VC}}{dt} = k_{4VC}C_{CA} \quad (4)$$

where C_{CA}, C_{HT}, C_{PA}, and C_{4VC} are the concentrations of caffeic acid, hydroxytyrosol, protocatechuic aldehyde, and 4-vinylcatechol, respectively, and the k terms are the rate constants for each reaction step. Equations 1−4 were solved by integration and substitution to generate the following equations:

dx.doi.org/10.1021/jf404850a | J. Agric. Food Chem. 2014, 62, 1945−1949

$$C_{CA} = C_{CA0}e^{-k_{total}t} \quad (5)$$

$$C_{HT} = \frac{k_{HT}}{k_{total}}C_{CA0}(1 - e^{-k_{total}t}) \quad (6)$$

$$C_{PA} = \frac{k_{PA}}{k_{total}}C_{CA0}(1 - e^{-k_{total}t}) \quad (7)$$

$$C_{4VC} = \frac{k_{4VC}}{k_{total}}C_{CA0}(1 - e^{-k_{total}t}) \quad (8)$$

where k_{total} is the overall degradation rate constant of caffeic acid and therefore equal to $k_{HT} + k_{PA} + k_{4VC}$, and C_{CA0} is the initial concentration of caffeic acid.

First, the overall degradation rate constant (k_{total}) was determined by nonlinear regression fitting of eq 5 to the changes in the caffeic acid concentration with time; then, eqs 6−8 were fitted to obtain the rate constants. All the reaction rate constants and their standard errors were estimated using the *nls* function in R statistical language;[19] the results are shown in Figure 3. The standard errors of the estimated rate constants were less than 5% in all cases. It is evident that the experimental results were in good agreement with the proposed reaction pathway. The overall degradation rate constants (k_{total}) increased with temperature and followed the Arrhenius relationship (Figure S2 in the Supporting Information) with an activation energy (E_a) of 93 kJ/mol and a pre-exponential factor (A) of 1.78×10^8 s^{-1}. This value is significantly higher than that for vanillic acid degradation (57 kJ/mol) in the temperature range 280−375 °C.[5] The formation rate constant for each product also obeyed the Arrhenius equation with E_a values of 103, 85, and 87 kJ/mol and A values of 8.24×10^8, 1.06×10^6, and 2.46×10^7 s^{-1} for hydroxytyrosol, protocatechuic aldehyde, and 4-vinylcatechol, respectively.

Online HPLC-DPPH Assay. The antioxidant activity of caffeic acid and its degradation products during subcritical water treatment at 240 °C were estimated using an online HPLC-DPPH assay. A typical chromatogram is shown in Figure 4. The seven peaks that were detected at 280 nm appeared as negative peaks at 517 nm, which indicates their ability to quench the DPPH radicals. Changes in the DPPH radical scavenging activity of each identified product are shown in Figure 5. The total radical scavenging activity of the treated solution, which was calculated from the areas of all seven negative peaks, was not affected by the treatment time (t test, $p \geq 0.05$) even though the caffeic acid content gradually decreased. We found that the radical scavenging activity changed linearly with the concentration of each compound; from these relationships, the DPPH radical scavenging activity of each compound was estimated to be ~88, 212, 230, and 292 g AA/mol for hydroxytyrosol, protocatechuic aldehyde, caffeic acid, and 4-vinylcatechol, respectively. However, because the concentrations of the degradation products were estimated, we can only conclude that protocatechuic aldehyde, caffeic acid, and 4-vinylcatechol showed higher DPPH radical scavenging activities than hydroxytyrosol. Obied et al. reported that caffeic acid was more active for DPPH radical scavenging than hydroxytyrosol.[20] It should be noted that the DPPH radical scavenging activities of these four compounds accounted for more than 90% of the overall activity.

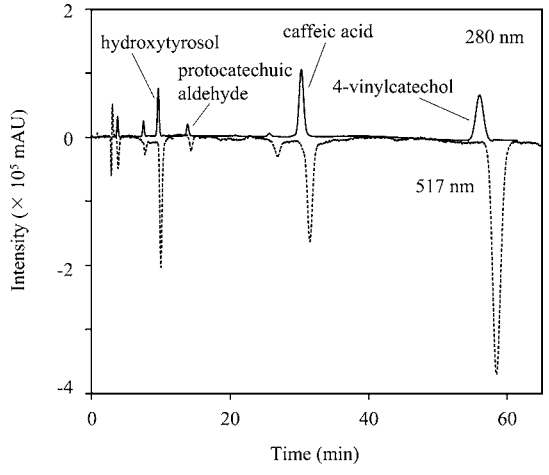

Figure 4. HPLC chromatogram of caffeic acid after subcritical water treatment detected at 280 and 517 nm. The negative peaks indicate DPPH radical scavenging activity.

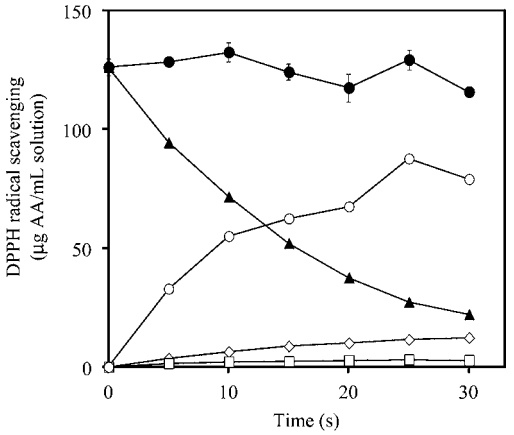

Figure 5. DPPH radical scavenging activity of caffeic acid (▲), hydroxytyrosol (◇), protocatechuic aldehyde (□), and 4-vinylcatechol (○) in the solution treated by subcritical water at 240 °C. The overall activity (●) was calculated from the summation of the areas of the negative peaks in Figure 5.

From these results, it can be expected that, during an extraction of plant materials containing phenolic compounds using the subcritical water technique, which is usually performed in a batch type extractor for longer periods, similar circumstances might occur for caffeic acid and other compounds as well. More complex reactions might also be possible because there are several compounds existing in sample matrices. This can be an advantage if degradation products possess some required bioactive activities or a disadvantage if undesirable or even toxic products are formed.

■ ASSOCIATED CONTENT

Supporting Information

HPLC chromatogram of caffeic acid after subcritical water treatment and Arrhenius plot of the reaction rates. This material is available free of charge via the Internet at http://pubs.acs.org.

■ AUTHOR INFORMATION

Corresponding Author

*Phone: +66-034-219361; fax: +66-034-272194; e-mail: kpramote@su.ac.th.

Funding

This work was supported by a cofunded project between the Thailand Research Fund, the Office of the Higher Education Commission, and the Faculty of Engineering and Industrial Technology, Silpakorn University (MRG5380123).

Notes

The authors declare no competing financial interest.

■ ACKNOWLEDGMENTS

PK thanks Associate Professor Dr. Rungnaphar Pongsawatmanit, Kasetsart University for her valuable discussion from the beginning of the project.

■ REFERENCES

(1) Herrero, M.; Cifuentes, A.; Ibañez, E. Sub- and supercritical fluid extraction of functional ingredients from different natural sources: Plants, food-by-products, algae and microalgae: A review. *Food Chem.* **2006**, *98*, 136−148.

(2) Wiboonsirikul, J.; Adachi, S. Extraction of functional substances from agricultural products or by-products by subcritical water treatment. *Food Sci. Technol. Res.* **2008**, *14*, 319.

(3) Singh, P. P.; Saldaña, M. D. A. Subcritical water extraction of phenolic compounds from potato peel. *Food Res. Int.* **2011**, *44*, 2452−2458.

(4) Vergara-Salinas, J. R.; Bulnes, P.; Zúñiga, M. C.; Pérez-Jiménez, J.; Torres, J. L.; Mateos-Martín, M. L.; Agosin, E.; Pérez-Correa, J. R. Effect of pressurized hot water extraction on antioxidants from grape pomace before and after enological fermentation. *J. Agric. Food Chem.* **2013**, *61*, 6929−6936.

(5) González, G.; Salvadó, J.; Montané, D. Reactions of vanillic acid in sub- and supercritical water. *J. Supercrit. Fluids* **2004**, *31*, 57−66.

(6) Lindquist, E.; Yang, Y. Degradation of benzoic acid and its derivatives in subcritical water. *J. Chromatogr. A* **2011**, *1218*, 2146−2152.

(7) Khuwijitjaru, P.; Plernjit, J.; Suaylam, B.; Samuhaseneetoo, S.; Pongsawatmanit, R.; Adachi, S. Degradation kinetics of some phenolic compounds in subcritical water and radical scavenging activity of their degradation products. *Can. J. Chem. Eng.* doi:10.1002/cjce.21898.

(8) Brand-Williams, W.; Cuvelier, M. E.; Berset, C. Use of a free radical method to evaluate antioxidant activity. *Lebensm.−Wiss. Technol. (1968−2004)* **1995**, *28*, 25−30.

(9) Owen, R. W.; Haubner, R.; Mier, W.; Giacosa, A.; Hull, W. E.; Spiegelhalder, B.; Bartsch, H. Isolation, structure elucidation and antioxidant potential of the major phenolic and flavonoid compounds in brined olive drupes. *Food Chem. Toxicol.* **2003**, *41*, 703−717.

(10) Achenbach, H.; Benirschke, G. Joannesialactone and other compounds from *Joannesia princeps*. *Phytochemistry* **1997**, *45*, 149−157.

(11) Albert, S.; Horbach, R.; Deising, H. B.; Siewert, B.; Csuk, R. Synthesis and antimicrobial activity of (E) stilbene derivatives. *Bioorg. Med. Chem.* **2011**, *19*, 5155−5166.

(12) Niederländer, H. A. G.; van Beek, T. A.; Bartasiute, A.; Koleva, I. I. Antioxidant activity assays on-line with liquid chromatography. *J. Chromatogr. A* **2008**, *1210*, 121−134.

(13) Stadler, R. H.; Welti, D. H.; Stämpfli, A. A.; Fay, L. B. Thermal decomposition of caffeic acid in model systems: Identification of novel tetraoxygenated phenylindan isomers and their stability in aqueous solution. *J. Agric. Food Chem.* **1996**, *44*, 898−905.

(14) Le Person, A.; Lacoste, A.-S.; Cornard, J.-P. Photo-degradation of trans-caffeic acid in aqueous solution and influence of complexation by metal ions. *J. Photochem. Photobiol., A* **2013**, *265*, 10−19.

(15) Terpinc, P.; Polak, T.; Šegatin, N.; Hanzlowsky, A.; Ulrih, N. P.; Abramovič, H. Antioxidant properties of 4-vinyl derivatives of hydroxycinnamic acids. *Food Chem.* **2011**, *128*, 62−69.

(16) Cornwell, D. G.; Ma, J. Nutritional benefit of olive oil: The biological effects of hydroxytyrosol and its arylating quinone adducts. *J. Agric. Food Chem.* **2008**, *56*, 8774−8786.

(17) Moon, J.-K.; Shibamoto, T. Formation of volatile chemicals from thermal degradation of less volatile coffee components: Quinic acid, caffeic acid, and chlorogenic acid. *J. Agric. Food Chem.* **2010**, *58*, 5465−5470.

(18) Antolovich, M.; Bedgood, D. R.; Bishop, A. G.; Jardine, D.; Prenzler, P. D.; Robards, K. LC-MS investigation of oxidation products of phenolic antioxidants. *J. Agric. Food Chem.* **2004**, *52*, 962−971.

(19) R Core Team. *R: A Language and Environment for Statistical Computing*; R Foundation for Statistical Computing: Vienna, Austria, 2013.

(20) Obied, H. K.; Prenzler, P. D.; Robards, K. Potent antioxidant biophenols from olive mill waste. *Food Chem.* **2008**, *111*, 171−178.

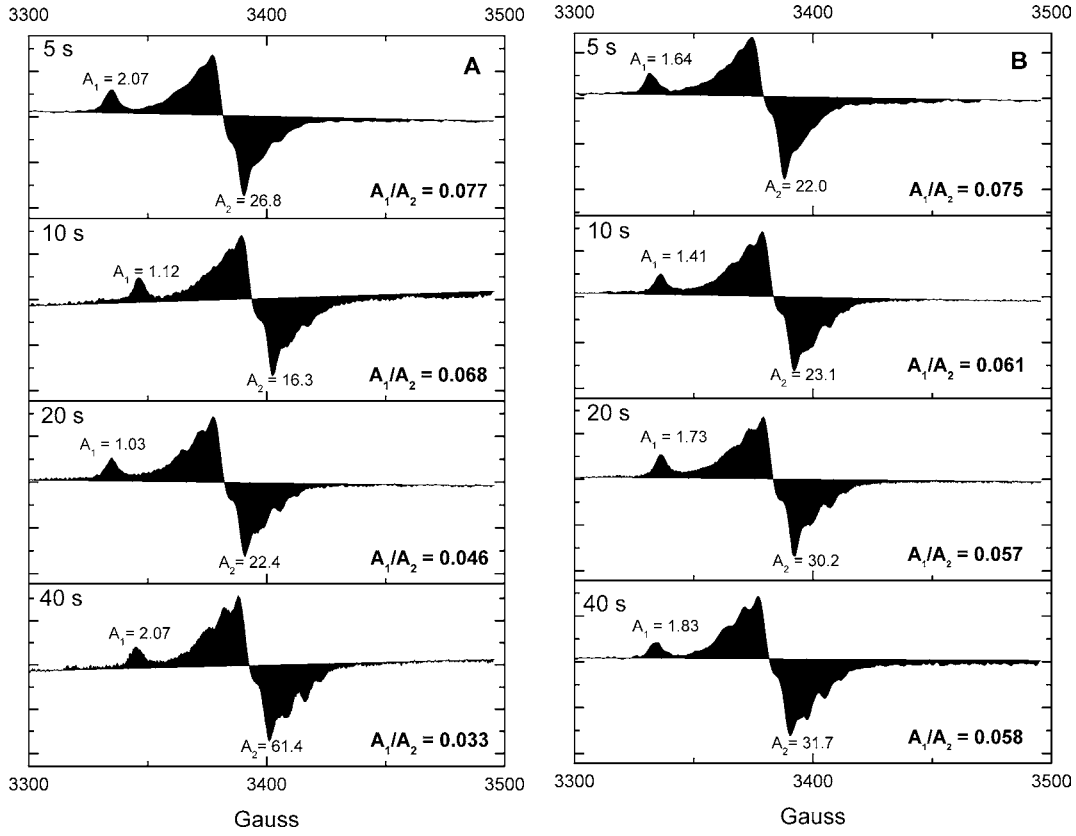

Figure 1. EPR spectra at 77 K of perferrylmyoglobin ($^{\bullet}$MbFe(IV)=O) during reduction to ferrylmyoglobin (MbFe(IV)=O) in aqueous solution of pH 7.4 at 25 °C saturated with CO (A) or in the absence of CO (B) at different aging times, as indicated using a stopped-flow freeze-quench technique. Each spectrum is from an independent experiment, and the decay of the tryptophan peroxyl radical (g_x = 2.036) is normalized relative to the tyrosine carbon-centered radical (g = 2.005). The ratio of the integrated signals A_1/A_2 is probing the tryptophan peroxyl radical decay.

After irradiation, the Rose Bengal was removed by filtering the solution through a Teflon membrane filter of 0.2 μM (Chromafil, Macharey-Nagel GmbH & Co., Dueren, Germany). The TrpOOH, tryptophan hydroperoxide derivatives, were further isolated from the reaction mixture by semipreparative liquid chromatography (HPLC20A Prominence system equipped with a DAD detector SPDM20A, Shimadzu Co., Kyoto, Japan) employing a Luna C18 reverse-phase column (250 mm × 7 mm × 10 μm; Phenomenex Inc., North Hill, CA, USA) with aqueous formic acid 0.05% containing 4% acetonitrile as isocratic mobile phase at a flow rate of 1 mL/min. The product peaks were collected in an ice bath protected from light and immediately lyophilized using a ModulyoD freeze-dryer (Thermo Electron Corp., São Paulo, Brazil). The hydroperoxide concentration was evaluated by the ferric-xylenol orange method (FOX) using H_2O_2 as a standard.[21] Typically, a yield of 10% for the high-purity TrpOOH derivative was obtained after the purification step.

NMR Spectroscopy. NMR analyses (^{1}H, COSY, and HSQC) were recorded at 25.0 °C on a Bruker AVANCE III, 14.1 T instrument (600 MHz for hydrogen frequency) equipped with an automatic sample changer, a cryo-probe TCI (^{1}H/^{13}C/^{15}N) of 5 mm with ATMA (automatic tuning matching) and z-field gradient (Bruker BioSpin, Rheinstetten, Germany). Aliquots of each isolated product were dissolved in D_2O containing 0.050% w/w TMSP-d_4 for NMR analysis. The ^{1}H NMR experiment was based on the 1D version of the NOESY sequence, using water suppression during the relaxation delay (2.40 s). The spectrum was acquired using 64K data points in a 12019.23 Hz spectral width, giving an acquisition time of 2.73 s. Processing was performed using exponential multiplication, applying a line broadening factor of 0.3 Hz. ^{1}H−^{1}H COSY experiments were performed using a spectral width of 12019.23 Hz, an acquisition time of 0.17 s, a relaxation delay of 1 s, and 16 scans for each increment (256 increments). The ^{1}H−^{13}C HSQC experiment employed spectral widths of 12019.23 Hz for the F2 (^{1}H) dimension and 36057.69 Hz for the F1 (^{13}C) dimension. The acquisition time was 0.17 s, the relaxation delay was 1 s, and 64 scans were performed for each increment (256 increments). TopSpin 3.0 software (Bruker BioSpin) was used for data acquisition and processing.

FT-IR Spectroscopy. Experiment type A: 2 mL of a solution of 2 × 10^{-4} mol L^{-1} of MbFe(III), or lactoperoxidase, or Fe(III)TPPS in aqueous phosphate buffer, pH 7.4 (0.16 M), was saturated with CO for 20 min in a half-filled cylindrical quartz cuvette (5 cm optical path), and the reaction was initiated by the addition of an equimolar quantity of H_2O_2. A blank solution without heme iron or iron compound was also investigated. The equilibrated gas-phase spectra were recorded after 1 h using a FT-IR IRAffinity-1 instrument (Shimadzu Co., Kyoto, Japan). Experiment type B: 2 mL of a solution of 2 × 10^{-4} mol L^{-1} of Fe(III)TPPS or Fe(II) or Fe(III) ions in aqueous formate buffer, pH 4.7 (0.16 M), was saturated with CO for 20 min in the half-filled cylindrical quartz cuvette (5 cm optical path), and the reaction was initiated by the addition of an equimolar quantity of TrpOOH. A blank solution without Fe(III)TPPS or iron salt was also investigated. The equilibrated gas-phase spectra were recorded after 1 h using a FT-IR IRAffinity-1 instrument. Experiment type C: 2 mL of a solution of 2 × 10^{-4} mol L^{-1} of preformed MbFe(IV)=O (H_2O_2 plus MbFe(III) after 10 min of reaction) in aqueous phosphate buffer pH 7.4 (0.16 M) was saturated with CO for 20 min in the half-filled cylindrical quartz cuvette (5 cm optical path), and the reaction was initiated by the addition of an equimolar quantity of TrpOOH. A blank solution without TrpOOH was also investigated. The equilibrated gas-phase spectra were recorded after 1 h using a FT-IR IRAffinity-1 instrument.

Freeze-Quench EPR Spectroscopy. An SFM-20 freeze-quench apparatus (Biologic Scientific Instruments, Claix, France) with a minimal aging time of 9 ms and an EMXplus X-band EPR instrument (Bruker Biospin GmbH, Karlsruhe, Germany) using a TM101 cylindrical cavity were used for freeze-quench kinetics. For this experiment, a solution containing 1.7 × 10^{-4} mol L^{-1} MbFe(III)

dx.doi.org/10.1021/jf4053176 | J. Agric. Food Chem. 2014, 62, 1950−1955

saturated or not with CO was loaded in syringe A and a solution of 7.7 × 10^{-4} mol L^{-1} of H_2O_2 was loaded in the opposite syringe B. The solutions of syringes A and B were mechanically pushed to the reaction chamber at a ratio of 1:1 at 25 °C and aged inside the calibrated aging loop for different reaction times from 5 to 40 s before being sprayed by the ejection nozzle into a cryogenic bath at 77 K. EPR spectrometer parameters: center field, 3395.58 G; sweep width, 200 G; MW power, 2.00 mW; MW frequency, ~9.52 GHz; modulation frequency, 100.00 kHz; modulation amplitude, 3.00 G; time constant, 81.92 ms; conversion time, 81.92 ms; temperature, 77 K. Each spectrum is an average of eight scans.

RESULTS AND DISCUSSION

Purified metmyoglobin (MbFe(III)) when reacting with hydrogen peroxide (H_2O_2), in neutral aqueous solution, forms perferrylmyoglobin (dot-MbFe(IV)═O), a protein radical of the iron(IV) heme pigment.[22] Perferrylmyoglobin decays to ferrylmyoglobin (MbFe(IV)═O), the iron(IV) pigment for ambient conditions with a half-life of 30 s at 25 °C and neutral pH.[23] The EPR spectrum of perferrylmyoglobin shows under aerobic conditions two features (see Figure 1), one assigned to a tryptophan peroxyl radical (g_x = 2.036, g_y = 2.008, g_z = 2.0028) and another septet EPR signal with g = 2.005 assigned to a carbon-centered tyrosyl radical.[23,24]

The tryptophan peroxyl radical of perferrylmyoglobin decays by reaction with external reductants or by slower intramolecular electron transfer.[15,16,21] The ratio between the two integrated signals, as shown in Figure 1, was used to follow the decay of the tryptophan peroxyl radical in aqueous solution at 25 °C in the absence of CO (Figure 1B) or for aqueous solution saturated with CO (Figure 1A), using a freeze-quench stopped-flow technique. The decay of the tryptophan peroxyl radical was found both in the absence and in the presence of CO to follow first-order kinetics (see Figure 2), but clearly the presence of CO accelerated the decay, as is seen for the values of the rate constant in the absence of CO, k = (5.3 ± 0.1) × 10^{-2} s^{-1}, and for water saturated with CO, k = (2.8 ± 0.1) × 10^{-1} s^{-1}. Formation of CO_2 was detected by FT-IR spectroscopy of the gas phase in equilibrium with aqueous solution (see Figure 3). The absorption maximum for CO_2 at 2335 and 2361 cm^{-1} increased for the reaction mixture as the one illustrated in Figure 3, for which the FT-IR spectrum is presented for a reaction time of 60 min.[25,26]

Tryptophan hydroperoxide, as a mixture of *cis* and *trans* isomers, was synthesized photochemically using Rose Bengal as a sensitizer for singlet-excited oxygen generation and isolated by HPLC employing a semipreparative C18 reverse-phase column (see Figure 4) and included as reactant with CO for comparison with activated myoglobin. The photolysis of an oxygen-saturated solution of 30 mM tryptophan in D_2O containing 8 μM Rose Bengal using 532 nm light from a green LED diode (5 mW) for 2 h at 0 °C resulted in the formation of mainly the tryptophan-derived hydroperoxides as *cis* and *trans* isomers, as may be seen in Figure 4. The identity of the compounds seen as peaks P_1 and P_2 was confirmed by 1D and 2D NMR analysis (^{1}H/COSY/HSQC) after isolation as the HSQC spectrum collected for peak P_2, the *cis*-TrpOOH isomer (Figure S1 in the Supporting Information). The *cis*- and *trans*-TrpOOH, after the purification step, were quantified using the ferric-xylenol orange method (FOX) and fully characterized by ^{1}H, COSY, and HSQC NMR experiments (Table 1); the obtained data were consistent with literature values for the proposed structures.[20,21] The most remarkable difference in the ^{1}H NMR spectrum for the *cis*- and *trans*-TrpOOH derivatives is

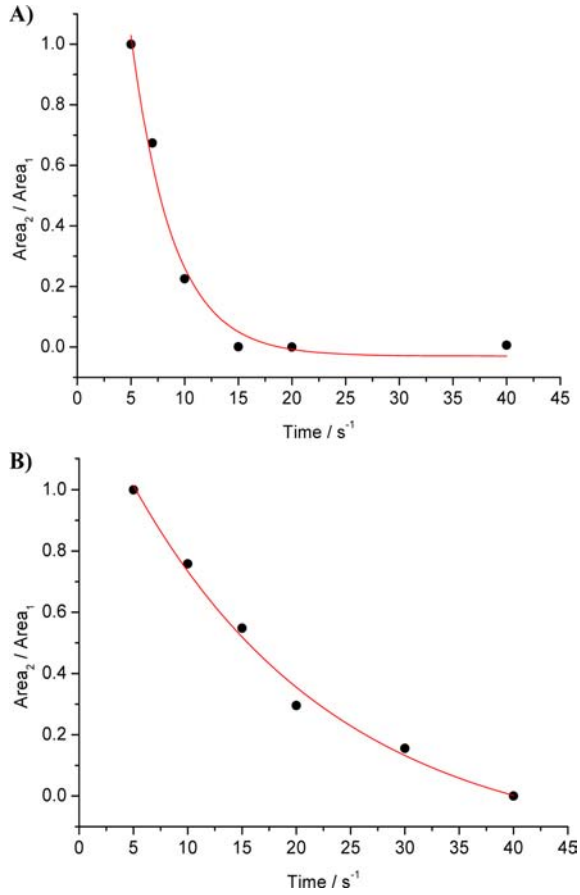

Figure 2. Decay of tryptophan peroxyl radical of perferrylmyoglobin (•MbFe(IV)═O) in aqueous solution of pH 7.4 at 25 °C saturated with CO (A) or in the absence of CO (B) as probed by the A_1/A_2 ratio from EPR spectra obtained by a stopped-flow freeze-quench technique (see Figure 1). Curves are exponential fits corresponding to first-order decay kinetics with observed rate constants of k_1 = 0.28 ± 0.04 s^{-1} (A) and k_1 = 0.05 ± 0.01 s^{-1} (B) to yield k_1 = 0.23 ± 0.04 s^{-1} for CO reduction of •MbFe(IV)═O.

associated with the C_3 methylene hydrogens. As may be seen from Table 1, for the *cis*-TrpOOH derivative, the C_3 methylene hydrogens are magnetically equivalent and appear as one doublet at 2.66 ppm. On the other hand, the C_3 methylene hydrogens for the *trans*-TrpOOH derivative show a double−doublet coupling pattern for nonequivalent hydrogens in an ABX system, the nonequivalent hydrogens being the AB part and the H_2 hydrogen the X part.

Tryptophan hydroperoxide did not react with CO to form CO_2 unless catalyzed by tetra(4-sulfonatophenyl)-porphyrinate iron(III) (Fe(III)TPPS) or by $FeSO_4$ or $FeCl_3$ as simple iron salts. The efficiency by which these and other reactant mixtures were oxidizing CO to CO_2 for comparable reaction conditions and reaction time is depicted in Figure 5 as the integrated FT-IR signal to provide a relative concentration of CO_2.

From the results presented in Figure 5, it is evident that H_2O_2 and CO do not produce CO_2 in buffered aqueous solution of pH 7.4 at 25 °C in the absence of iron salts or in the presence of Fe(III)TPPS. Solutions of tryptophan incubated with CO in the presence of hydrogen peroxide and in the absence of heme iron or iron salts do not produce CO_2. Tryptophan hydroperoxide plus CO likewise does not produce CO_2 in the absence of iron salts, but CO_2 is clearly produced when iron(II) or iron(III) is present and especially when

dx.doi.org/10.1021/jf4053176 | J. Agric. Food Chem. 2014, 62, 1950−1955

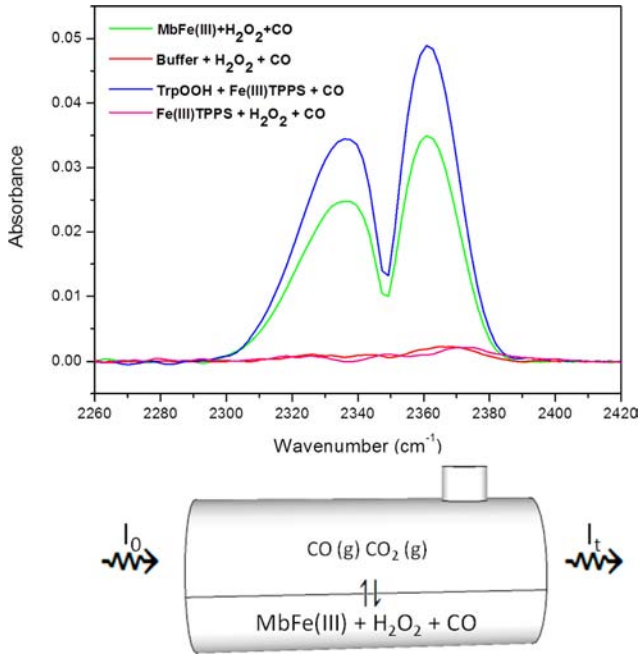

Figure 3. FT-IR spectra of equilibrated gas phase of aqueous solution of pH 7.4 with reactants shown in sketch of quartz cylindrical cuvette at 25 °C for metmyoglobin following 60 min of reaction and equilibration. [MbFe(III)] = 1×10^{-4} mol L^{-1}; [H_2O_2] = 1×10^{-4} mol L^{-1}; [CO] = 7×10^{-4} mol L^{-1}; [TrpOOH] = 1×10^{-4} mol L^{-1}; [Fe(III)TPPS] = 1×10^{-4} mol L^{-1}.

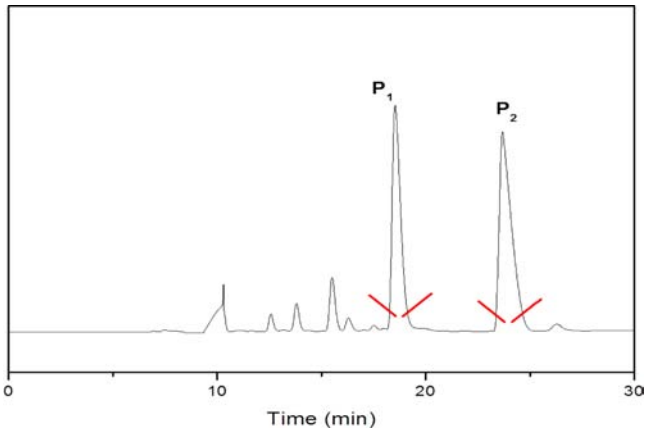

Figure 4. Separation and characterization of tryptophan hydroperoxide *trans*/*cis* isomers as formed by singlet oxygen addition to tryptophan in oxygen-saturated D_2O with Rose Bengal added as photosensitizer and exposed to green light (see Materials and Methods). HPLC separation of *trans* isomer (P_1) and *cis* isomer (P_2) is marked to indicate collection range.

Fe(III)TPPS is present. This identifies a tryptophan radical rather than tryptophan peroxide as the reactant for oxidation of CO to CO_2, as iron(III) and iron(II) may cleave hydroperoxides by oxidation or by reduction, respectively:

$$TrpOOH + Fe^{3+} \rightarrow TrpOO^{\bullet} + H^{+} + Fe^{2+} \quad (1)$$

$$TrpOOH + Fe^{2+} \rightarrow TrpO^{\bullet} + OH^{-} + Fe^{3+} \quad (2)$$

The tryptophan radicals will react with CO by oxygen atom transfer[27] according to

$$TrpOO^{\bullet} + CO \rightarrow TrpO^{\bullet} + CO_2 \quad (3)$$

$$TrpO^{\bullet} + CO \rightarrow Trp^{\bullet} + CO_2 \quad (4)$$

of which the reaction of $ROO^{\bullet}$ with CO has been reported to be faster than the reaction of $TrpO^{\bullet}$ with CO by a factor of 10^2.[27]

For perferrylmyoglobin, a similar reactivity is recognized, as activation of MbFe(III) by hydrogen peroxide prior to addition of CO yields no reaction compared to activation of MbFe(III) by hydrogen peroxide in the presence of CO, indicating that when $^{\bullet}$MbFe(IV)=O has decayed to MbFe(IV)=O, the reactivity toward CO will disappear. The presence of tryptophan hydroperoxide in experiments with preformed ferrylmyoglobin enhances the reaction moderately, showing that the heme iron may cleave the peroxide oxidatively corresponding to the reaction of eq 1 to yield reactive peroxyl radicals or that the tryptophan hydroperoxide may have reactivated ferrylmyoglobin to perferrylmyoglobin. Lactoperoxidase, as heme enzyme also with solvent-exposed tryptophan, included for comparison in the resting iron(III) form, showed less activity than MbFe(III) when both heme compounds were activated by H_2O_2 in the presence of CO.[28]

The reactivity of the two tryptophan radicals, $TrpOO^{\bullet}$ and $TrpO^{\bullet}$, in oxygen transfer reaction to CO finds a parallel in the activated MbFe(III). The solvent-exposed tryptophan of MbFe(III) becomes oxidized to $TrpOO^{\bullet}$ during the oxidation of MbFe(III) by H_2O_2 in aerated aqueous solution:

$$\begin{aligned} &MbFe(III) + H_2O_2 \\ &\quad \rightarrow {}^{\bullet+}MbFe(IV)=O + H_2O \\ &\quad \rightarrow {}^{\bullet}MbFe(IV)=O + H^{+} + H_2O \end{aligned} \quad (5)$$

$^{\bullet}$MbFe(IV)=O is a tryptophan peroxyl radical, as shown in eq 5 and will react with CO in a reaction similar to the reaction of eq 3 to yield CO_2, and the tryptophan alkoxyl radical still capable of transferring an oxygen atom to CO will react as in the reaction of eq 4. The carbon-centered tryptophan radical thus formed will decay by intramolecular reaction to form a carbon-centered tyrosine radical of higher stability, which may undergo an intermolecular reaction to form heme dimers. This reaction sequence as depicted in eq 5 accounts for the experimental observations related to CO_2 formation from the different reaction mixtures described in Figure 5 and also the EPR spectra of Figure 1. Notably, only $^{\bullet}$MbFe(IV)=O and not MbFe(IV)=O is capable of oxidizing CO to CO_2.

From the observed rate of disappearance of $^{\bullet}$MbFe(IV)=O in the presence of CO (saturated water corresponding to 0.7 mM CO in the reaction chamber), it becomes possible to estimate the rate constant for the bimolecular reaction between $^{\bullet}$MbFe(IV)=O and CO to have the value of 330 ± 60 L mol^{-1} s^{-1}. This seems to be the first value available for the rate constant for deactivation of perferrylmyoglobin by an external reductant. For the reaction of perferrylmyoglobin with the water-soluble carotenoid crocin, a lower limit for the rate constant was estimated to be 4×10^5 L mol^{-1} s^{-1},[17] and for the reaction with 2,2′-azinobis(3-ethylbenzthiazoline-6-sulfonic acid (ABTS) to form the $ABTS^{\bullet+}$ radical the lower limit was 6×10^5 L mol^{-1} s^{-1}.[18] The reaction with crocin is an electron-transfer reaction

$$\begin{aligned} {}^{\bullet}MbFe(IV) &= O + crocin \\ &\rightarrow {}^{-}MbFe(IV) \\ &= O + crocin^{\bullet+} \end{aligned} \quad (6)$$

dx.doi.org/10.1021/jf4053176 | J. Agric. Food Chem. 2014, 62, 1950−1955

Table 1. ^{1}H and ^{13}C NMR Chemical Shifts of the *cis*- and *trans*-Tryptophan Hydroperoxides in D_2O

	trans-TrpOOH				*cis*-TrpOOH			
	1H			13C	1H			13C
position	δ (ppm)	multiplicity	J_{xy} (Hz)	δ (ppm)	δ (ppm)	multiplicity	J_{xy} (Hz)	δ (ppm)
2	4.19	t	J_{23}=7.8	59.7	3.83	t	J_{23}=8.6	59.8
3	2.91	dd	J_{33}=14.3	35.8				
			J_{32}=7.8					
	2.52	dd	J_{33}=14.3		2.66	d	J_{32}=8.6	39.0
			J_{32}=7.8					
4	7.46	d	J_{45}=7.9	125	7.44	d	J_{45}=7.4	124
5	7.03	t	$J_{54,56}$=7.5	121	7.00	t	$J_{54,56}$=7.4	121
6	7.38	t	$J_{65,67}$=7.7	131	7.35	t	$J_{65,67}$=7.7	131
7	6.80	d	J_{76}=8.1	111	6.86	d	J_{76}=8.0	111
8a	5.72	s		79.5	5.54	s		79.2

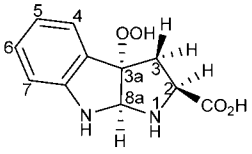

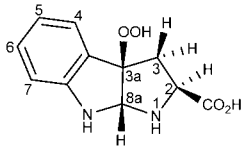

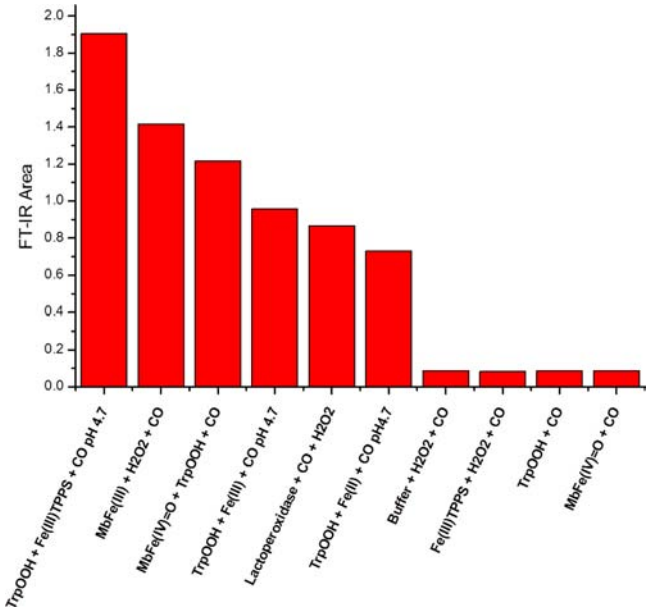

Figure 5. CO_2 production from reaction mixtures as indicated for experiments shown in Figure 3 using integrated absorption from 2280 to 2400 cm^{-1} as a relative measure of CO_2 concentration.

as in the reduction with ABTS, explaining the higher rate compared to the oxygen atom transfer for the reaction of eqs 3 and 4.

Activated myoglobin, which will be formed during digestion of red meat through reaction of MbFe(III) with peroxides, has been shown to be deactivated by reaction with CO. The reaction of CO involves oxygen atom transfer to form CO_2 in principle in two-reaction steps, eventually forming a heme dimer through a dityrosine linkage. The scavenging of activated myoglobin by CO may protect sensitive structures against oxidative damage involving proteins and unsaturated lipids. CO may in this respect function as an inherent antioxidant. Future experiments are required to investigate whether CO may act synergistically with dietary antioxidants such as polyphenols and carotenoids through binding to ferrous myoglobin or through a subsequent reduction of MbFe(IV)=O following the initial reduction of perferrylmyoglobin by CO.

■ ASSOCIATED CONTENT

Supporting Information

$^{1}H-^{13}C$ HSQC spectrum for the isolated *cis*-TrpOOH derivative. This material is available free of charge via the Internet at http://pubs.acs.org.

■ AUTHOR INFORMATION

Corresponding Authors

*(L.H.S.) E-mail: ls@food.ku.dk. Phone: + 45 35 33 32 21.
*(D.R.C.) E-mail: drcardoso@iqsc.usp.br. Phone: +55 16 33 73 99 76.

Funding

This research is part of the bilateral Brazilian/Danish Food Science Research Program "BEAM − Bread and Meat for the Future" supported by FAPESP (Grant 2011/51555-7) to D.R.C. and by the Danish Research Council for Strategic

Research (Grant 11-116064) to L.H.S. D.R.C. thanks CNPq for the research fellowship.

Notes

The authors declare no competing financial interest.

REFERENCES

(1) Maines, M. D. The heme oxygenase system: a regulator of second messenger gases. *Annu. Rev. Pharmacol. Toxicol.* **1997**, *37*, 517−554.

(2) Gibbons, S. J.; Farrugia, G. The role of carbon monoxide in the gastrointestinal tract. *J. Physiol.* **2004**, *556*, 325−336.

(3) Gibbons, S. J.; Verhulst, P. J.; Bharucha, A.; Farrugia, G. Review article: carbon monoxide in gastrointestinal physiology and its potential in therapeutics. *Aliment. Pharmacol. Ther.* **2013**, *38*, 689−702.

(4) Young, L. J.; Caughey, W. S. Autoreduction phenomena of bovine heart cytochrome-*c*-oxidase and other metalloproteins. *J. Biol. Chem.* **1987**, *262*, 15019−15025.

(5) Piantadosi, C. A. Biological chemistry of carbon monoxide. *Antioxid. Redox Signal.* **2002**, *4*, 259−270.

(6) Berne, J.-P.; Lauzier, B.; Rochette, L.; Vergely, C. Carbon monoxide protects against ischemia-reperfusion injury in vitro via antioxidant properties. *Cell. Physiol. Biochem.* **2012**, *29*, 475−484.

(7) Mikkelsen, A.; Skibsted, L. H. Acid-catalyzed reduction of ferrylmyoglobin − product distribution and kinetics of autoreduction and reduction by NADH. *Z. Lebensm. Unters. Forsch.* **1995**, *200*, 171−177.

(8) Pierre, F.; Tache, S.; Petit, C. R.; Van der Meer, R.; Corpet, D. E. Meat and cancer: haemoglobin and haemin in a low-calcium diet promote colorectal carcinogenesis at the aberrant crypt stage in rats. *Carcinogenesis* **2003**, *24*, 1683−1690.

(9) Ishikawa, S.-i.; Tamaki, S.; Ohata, M.; Arihara, K.; Itoh, M. Heme induces DNA damage and hyperproliferation of colonic epithelial cells via hydrogen peroxide produced by heme oxygenase: a possible mechanism of heme-induced colon cancer. *Mol. Nutr. Food Res.* **2010**, *54*, 1182−1191.

(10) Bax, M.-L.; Aubry, L.; Ferreira, C.; Daudin, J.-D.; Gatellier, P.; Remond, D.; Sante-Lhoutellier, V. Cooking temperature is a key determinant of in vitro meat protein digestion rate: investigation of underlying mechanisms. *J. Agric. Food Chem.* **2012**, *60*, 2569−2576.

(11) Yin, S.; Faustman, C.; Tatiyaborworntham, N.; Ramanathan, R.; Maheswarappa, N. B.; Mancini, R. A.; Joseph, P.; Suman, S. P.; Sun, Q. Species-specific myoglobin oxidation. *J. Agric. Food Chem.* **2011**, *59*, 12198−12203.

(12) Carlsen, C. U.; Moller, J. K. S.; Skibsted, L. H. Heme-iron in lipid oxidation. *Coord. Chem. Rev.* **2005**, *249*, 485−498.

(13) Lorrain, B.; Dangles, O.; Genot, C.; Dufour, C. Chemical modeling of heme-induced lipid oxidation in gastric conditions and inhibition by dietary polyphenols. *J. Agric. Food Chem.* **2010**, *58*, 676−683.

(14) Lorrain, B.; Dufour, C.; Dangles, O. Influence of serum albumin and the flavonol quercetin on the peroxidase activity of metmyoglobin. *Free Radical Biol. Med.* **2010**, *48*, 1162−1172.

(15) Sy, C.; Caris-Veyrat, C.; Dufour, C.; Boutaleb, M.; Borel, P.; Dangles, O. Inhibition of iron-induced lipid peroxidation by newly identified bacterial carotenoids in model gastric conditions: comparison with common carotenoids. *Food Funct.* **2013**, *4*, 698−712.

(16) Halliwell, B.; Zhao, K. C.; Whiteman, M. The gastrointestinal tract: a major site of antioxidant action? *Free Radical Res.* **2000**, *33*, 819−830.

(17) Jorgensen, L. V.; Andersen, H. J.; Skibsted, L. H. Kinetics of reduction of hypervalent iron in myoglobin by crocin in aqueous solution. *Free Radical Res.* **1997**, *27*, 73−87.

(18) Carlsen, C. U.; Skovgaard, I. M.; Skibsted, L. H. Pseudoperoxidase activity of myoglobin: kinetics and mechanism of the peroxidase cycle of myoglobin with H_2O_2 and 2,2-azino-bis(3-ethylbenzthiazoline-6-sulfonate) as substrates. *J. Agric. Food Chem.* **2003**, *51*, 5815−5823.

(19) Barley, M. H.; Takeuchi, K. J.; Meyer, T. J. Electrocatalytic reduction of nitrite to ammonia based on a water-soluble iron porphyrin. *J. Am. Chem. Soc.* **1986**, *108*, 5876−5885.

(20) Ronsein, G. E.; Oliveira, M. C. B.; Miyamoto, S.; Medeiros, M. H. G.; Di Mascio, P. Tryptophan oxidation by singlet molecular oxygen O-2 ($^1\Delta_g$): mechanistic studies using O-18-labeled hydroperoxides, mass spectrometry, and light emission measurements. *Chem. Res. Toxicol.* **2008**, *21*, 1271−1283.

(21) Gay, C.; Collins, J.; Gebicki, J. M. Hydroperoxide assay with the ferric-xylenol orange complex. *Anal. Biochem.* **1999**, *273*, 149−155.

(22) King, N. K.; Winfield, M. E. Mechanism of metmyoglobin oxidation. *J. Biol. Chem.* **1963**, *238*, 1520−1528.

(23) Svistunenko, D. A. Reaction of haem containing proteins and enzymes with hydroperoxides: the radical view. *Biochim. Biophys. Acta: Bioenerg.* **2005**, *1707*, 127−155.

(24) Irwin, J. A.; Ostdal, H.; Davies, M. J. Myoglobin-induced oxidative damage: evidence for radical transfer from oxidized myoglobin to other proteins and antioxidants. *Arch. Biochem. Biophys.* **1999**, *362*, 94−104.

(25) Seichter, F.; Wilk, A.; Woerle, K.; Kim, S.-S.; Vogt, J. A.; Wachter, U.; Radermacher, P.; Mizaikoff, B. Multivariate determination of (CO_2)-C-13/(CO_2)-C-12 ratios in exhaled mouse breath with mid-infrared hollow waveguide gas sensors. *Anal. Bioanal. Chem.* **2013**, *405*, 4945−4951.

(26) Young, L. J.; Caughey, W. S. Mitochondrial oxygenation of carbon-monoxide. *Biochem. J.* **1986**, *239*, 225−227.

(27) Denisov, E. T.; Shestakov, A. F. Reactions of alkoxy and peroxy radicals with carbon monoxide. *Kinet. Catal.* **2008**, *49*, 1−10.

(28) Fielding, A. J.; Singh, R.; Boscolo, B.; Loewen, P. C.; Ghibaudi, E. M.; Ivancich, A. Intramolecular electron transfer versus substrate oxidation in lactoperoxidase: investigation of radical intermediates by stopped-flow absorption spectrophotometry and (9−285 GHz) electron paramagnetic resonance spectroscopy. *Biochemistry* **2008**, *47*, 9781−9792.

Table 1. Content of Phenolic Compounds in the Rapeseed and Oil from Untreated Rapeseed by Cold Press as Mean with SD (n = 3)[a]

	content of phenolic compounds in rapeseed and oil samples [mg/100g]							
	sinapine	sinapic acid	caffeic acid	ferulic acid	cinnamic acid	canolol	TPCC [mg/100 g]	TPC [mg SA/100 g]
rapeseed	459.22 ± 13.27	76.80 ± 4.39	10.26 ± 0.59	2.17 ± 0.09	ND	14.07 ± 0.82	562.52 ± 13.27	1017.12 ± 46.22
oil	ND	2.73 ± 0.13	ND	0.05 ± 0.00	0.10 ± 0.00	17.06 ± 2.16	19.94 ± 2.16	28.53 ± 0.65

[a]Values are means ± standard deviation, n = 3. ND = not detected. TPCC = total phenolic compounds content as estimated by UPLC. TPC = total phenolic content as estimated by Folin-Ciocalteu method. SA = sinapic acid.

have provided free sinapic acid by hydrolysis during roasting.[22−24]

Microwave pretreatment of seeds is a simple and desirable method for production of high-quality vegetable oils. Using microwave radiation, a higher oil extraction yield by press can be obtained due to rupturing of the cell membrane and generation of permanent pores. In addition, microwave pretreatment of oilseeds can increase phytosterols, tocopherols, and phenolic compounds in the oil extracted by press and improve the oxidative stability of oil.[25−30] However, there is a lack of information in the literature on the effect of pretreatment with microwaves on phenolic compounds (sinapic, caffeic, ferulic, cinnamic acid, and canolol) and esterified sinapic acid derivatives (sinapine) content in rapeseed. Moreover, transfer of the phenolic to oil has not been determined when pressing the oil from rapeseed treated with microwave. It is not known whether there is similar transfer ratio for difference phenolic compounds. Thus, the objectives of this research were (1) to evaluate the effect of microwave treatment on phenolic compounds, including sinapine, sinapic, caffeic, ferulic, cinnamic acid, and canolol content in the rapeseed and (2) to investigate the differences in transfer of the difference phenolic compounds to the oil extracted from microwave-treated rapeseed by press.

MATERIALS AND METHODS

Materials. Double low rapeseed containing no erucic acid and low amounts of glucosinolates (11.67 μmol/g) was collected from the local market in China. All reagents were of analytical or HPLC grade. 4-Acetoxy-3,5-dimethoxystyrene (purity ≥ 99.0%) was purchased from Apin Chemicals Limited (Abingdon, Oxon, U.K.). Sinapic acid (purity ≥ 99.0%), sinapine (purity ≥ 98.0%), ferulic acid (purity ≥ 98.0%), cinnamic acid (purity ≥ 98.0%), and caffeic acid (purity ≥ 99.0%) were purchased from Sigma-Aldrich Co. (St. Louis, MO, USA). Chromatographic-grade methanol and acetic acid were purchased from Merck (Darmstadt, Germany). Other chemicals and reagents were purchased from Sinopharm Chemical Reagent Co., Ltd. (Shang-hai, China).

Methods. *Microwave Pretreatment of Rapeseed and Oil Extraction.* For each sample, 400 g of whole rapeseed were placed in eight Pyrex Petri dishes (9 cm diameter) inside a microwave (Model Mars, 800 W, CEM, USA). Samples were microwave treated at a frequency of 2450 MHz for a roasting period between 1 and 8 min (interval 1 min). Each microwave treatment was done with three replicates, and samples were collected and allowed to cool to ambient temperature prior to oil extraction by pressing. A rapeseed sample without microwave radiation (0 min radiation time) was used as a control sample.

Rapeseed was pressed at room temperature with a cold-pressing machine (CA59G, German Monforts Group, Moenchengladbach, North Rhine-Westphalia, Germany), and the oil was centrifuged at 8983 × g for 15 min. The oil was separated and stored in stoppered glass containers.

Synthesis of 2, 6-Dimethoxy-4-vinylphenol (Canolol). Canolol was synthesized according to the method described by Harbaum-Piayda et al.[31] Potassium hydroxide (250 mg) was dissolved in 1.25 mL of methanol and added to a solution of 250 mg of 4-acetoxy-3,5-dimethoxystyrene in 1.5 mL of methanol. The suspension was stored at ambient temperature overnight (15 h). Afterward, the suspension was acidified by acetic acid (250 μL) and extracted three times with ethylacetate (3 × 5 mL). The organic phase was washed with water (2.5 mL) and 5% sodium hydrogen carbonate solution (2.5 mL).

Identification of Canolol. Identification of canolol was carried out on the basis of nuclear magnetic resonance (NMR) and mass spectrometry (MS).

NMR Spectroscopy. The organic solvent of synthetic product was removed under vacuum, and the fraction was dissolved in deuterated chloroform. Proton (^{1}H) and carbon (^{13}C) NMR spectra were taken using an Oxford NMR (600 MHz) spectrophotometer (USA).

Liquid Chromatography-Mass Spectrometry (LC-MS) Spectroscopy. The MS used for analysis was a hybrid, triple-quadrupole/linear ion trap mass spectrometer, API 4000 Q-Trap, with an APCI interface (AB SCIEX, Foster City, CA, USA).

ESIMS/MS analysis was performed in the positive ionization mode. DP, CE, and CXP were optimized for production of precursor-to-production transitions. Other instrument parameters were also optimized for generating the highest signal intensities. The nebulizer gas pressure, drying gas pressure, curtain gas pressure, source voltage, and source temperature were set at 60 psi, 50 psi, 30 psi, 5.5 kV, and 500 °C, respectively.

UPLC-Diode Array Detector (DAD) Analysis for Quantification of Phenolic Compounds. Extraction Procedure. (1) For rapeseed sample: 0.1 g (accuracy 0.001 g) of grounded rapeseed sample and 4 mL of methanol−water (1:1 v/v) were transferred into a 10 mL centrifuge tube and shaken at room temperature for 20 min. Each sample was extracted in triplicate, and the residual rapeseed flour was separated by centrifugation (1383 × g, 10 min). Extracts were filtered through a 0.22 μm nylon filter and analyzed directly by UPLC. (2) For oil sample: 1.25 g (accuracy 0.001g) of oil sample was dissolved in 1.5 mL of hexane; the polar compounds were extracted into aqueous 80% methanol (3 × 1.5 mL) and centrifuged (2823 × g, 10 min). Pooled extracts were through a 0.22 μm nylon filter and analyzed directly by UPLC.

UPLC Analysis. Analysis was carried out using Acquity UPLC (Waters, Milford, USA), equipped with a degasser, two solvent delivery modules, an autosampler, a column oven, and a DAD. Separation was carried out using a 2.1 × 100 mm, 1.7 μm, Waters Acquity BEH RP18 column (Waters, Milford, USA) maintained at 30 °C. The injection volume was 3 μL, and compounds were eluted with 2% acetic acid in water (v/v) (mobile phase A) and 100% methanol (mobile phase B) at a flow rate of 0.21 mL/min. The gradient program was as follows: 0−25% B (7.40 min), 25−29% B (2.67 min), 29−36% B (6.66 min), 36−45% B (6.67 min), 45−5% B (2 min), 5% B−100% A (2 min), and 100% A (2.67 min).

Eluates were detected at 325 (sinapine, sinapic, caffeic, and ferulic acid), 295 (cinnamic acid), and 280 nm (canolol). Peak identities were confirmed from retention data and by spiking of extracts with six standards. Calibration curves: y = 16 700x −1460, y = 28 400x − 9140, y = 28 200x − 2370, y = 34 000x + 942, y = 29 100x − 829, and y = 19 030x − 25 134 with determination coefficients of R^2 = 0.9994, 0.9998, 0.9995, 0.9998, 0.9999, and 0.9999 in the concentration range 0.5−20.0 mg/L of standard solutions of sinapine and cinnamic acid, 0.5−100.0 mg/L of standard solutions of sinapic acid, 0.25−10.0 mg/L of standard solutions of caffeic acid, 0.5−20.0 mg/L of standard solutions of ferulic acid, and 5−500.0 mg/L of standard solutions of canolol

were obtained for quantification of individual phenolic compounds. Calculated values of the slope relative standard deviations (RSD = 0.4−2.9%, n = 5) and the average recovery rate (100.6−106.7%) indicate reasonable repeatability and accuracy of the UPLC method. Moreover, limits of detection and quantification ranged as follows: 0.065−0.114 and 0.224−0.381 mg/L, respectively, for UPLC analysis of all studied phenolic compounds.

Statistical Analysis. Analysis was performed in triplicate. Results were expressed as means with standard deviation (SD). An ANOVA test (using SPSS 18 statistical software; SPSS Inc., Chicago, IL) was used to compare the mean values of each treatment. Mean differences were considered significant at the $P < 0.05$ level. The Pearson correlation test was used to determine the correlations.

RESULTS AND DISCUSSION

Individual Phenolic Compounds in Seed and Cold-Pressed Oil from Rapeseed. Results of phenolic compounds in untreated rapeseeds and cold-pressed oils from them analyzed by the UPLC-DAD method are listed in Table 1. Five phenolic compounds (sinapine, sinapic acid, caffeic acid, ferulic acid, and canolol) were identified comparing the UV spectral data and retention time of standard. The main phenolic compound in rapeseed was sinapine (459.22 mg/100 g), while the content of ferulic acid was the lowest (2.17 mg/100 g). On the basis of various reports, the major phenolics in rapeseed are sinapine, sinapic acid, and sinapoylglucose.[4,11] Among them, sinapine is the most abundant species accounting for about 1−2% (w/w) in rapeseed.[32] A higher content of sinapine was found in the defatted rapeseed and canola cotyledons, on average, accounting for 2.67% and 2.85%, respectively.[33] Liu et al. found that sinapine contents ranged from 93 to 176 mg/100 g and from 1565 to 2188 mg/100 g in defatted rapeseed hulls and dehulled flours from 10 rapeseed varieties (*Brassica napus*) in China, respectively.[34] The differences in sinapine levels might arise from factors such as the cultivars, climate, growth conditions, degree of maturity, and method of analysis.

The main free phenolic acid found in rapeseed was sinapic acid, with its content being 76.80 mg/100 g (Table 1). This result was in agreement with the results obtained by Krygier et al. (73.2−80.1 mg/100 g),[7] whereas it is higher than the results obtained by Kozlowska et al. (41.3−51.6 mg/100 g),[8] Cai and Arntfield (34.0−49.0 mg/100 g),[11] Siger et al. (19.8−67.3 mg/100 g),[16] and Szydłowska-Czerniak et al. (17.4−36.4 mg/100 g).[35] Moreover, 10.26 mg/100 g of caffeic acid, 2.17 mg/100 g of ferulic acid, and 14.07 mg/100 g of canolol in our rapeseed sample were detected (Table 1). Our results were higher than those of Szydłowska-Czerniak et al.[35] Szydłowska-Czerniak et al. reported the six individual phenolic acid in seven rapeseed varieties: sinapic acid was the dominant phenolic acid, with concentrations from 17.4 to 36.4 mg/100 g, followed by gallic acid (0.97−1.97 mg/100 g), ferulic acid (0.10−1.96 mg/100 g), *p*-coumaric acid (0.57−0.92 mg/100 g), and caffeic acid (0.01−0.07 mg/100 g). Gallic acid and *p*-coumaric acid were not detected in our rapeseed sample. The high variability in the amounts of the individual phenolic compounds in rapeseed varieties has been widely reported and depends on several factors, such as genetic, agronomic, environmental, and extraction procedures.[6,11,13,16,35] The canolol content in our rapeseed sample was higher than those reported by Shrestha et al. (2.47 mg canolol/100 g)[23] and Spielmeyer et al. (0.58 mg canolol/100 g).[24] The total phenolic content determined by the Folin-Ciocalteu method was 1017.12 mg SA/100 g of rapeseed (Table 1). The obtained results of total phenolic content are similar to those reported by other authors.[11,13,35]

When pressing the oil from rapeseed, most of the phenolic compounds remain in the cold-pressed rapeseed cake, and only a small proportion is transferred to the crude oil (Table 1). However, approximately 56% of the canolol is transferred to the crude oil. There were differences in the phenolic compounds and contents between the rapeseeds and the cold-pressed oil from them. Only four phenolic compounds (sinapic acid, ferulic acid, cinnamic acid, and canolol) were detected, and canolol was the main phenolic compound in the oil from untreated rapeseed by press. The canolol content was 17.06 mg canolol/100 g of rapeseed oil. This result was higher than those reported by Spielmeyer et al.,[24] whereas it was lower than those of Koski et al.[5] Spielmeyer et al. reported that the canolol content ranged from 0.67 to 8.14 mg canolol per 100 g in 4 rapeseed kernel oils and 5 cold-pressed oils, and canolol was not detectable in 2 refined rapeseed oils. Koski et al. detected higher amounts of canolol: 62.9 and 29.7 mg caffeic acid/100 g in post-expelled crude turnip rapeseed and post-expelled crude oil, respectively, but only 4.8 mg of caffeic acid/100 g of canolol was detected in superdegummed oil.[5]

In rapeseed, phenolic acids consist mostly of sinapic acid;[4,6,11,14] therefore, sinapic acid is also the main phenolic acid in rapeseed oil. UPLC analyses revealed the presence of sinapic acid (2.73 mg/100 g), cinnamic acid (0.10 mg/100 g), and ferulic acid (0.05 mg/100 g) in the oil from untreated rapeseed by press (Table 1). In the rapeseed oil, sinapic acid accounts for about 95% of free phenolic acids, but that only accounts for about 9% of four phenolic compounds (three phenolic acids and canolol); thus, canolol is the main phenolic in the cold-pressed oil. The level of sinapic acid in our sample was higher when compared to the results obtained by Siger et al.[16] (0.24 mg/100 g for cold-pressed rapeseed oil), Vuorela et al.[36] (0−2.8 mg/100 g for commercial rapeseed oil, post-expelled crude rapeseed oil, pre-expelled crude rapeseed oil, and superdegummed rapeseed oil), and Harbaum-Piayda et al.[31] (0.09−1.94 mg/100 g for cold-pressed rapeseed oil). Moreover, the concentration of ferulic acid (0.0056 mg/100 g) reported by another author was also lower than that of our cold-pressed oil from rapeseed.[36] In minor amounts, sinapine (0.4−1.9 mg/100 g), *p*-hydroxybenzoic (0.0016 mg/100 g), syringic acid (0.68 mg/100g), *o*-coumaric, and *p*-coumaric acids (0.013 mg/100g) were identified in the cold-pressed rapeseed oil as well.[16−18,33]

The total phenolic compounds content calculated from UPLC data was 19.94 mg/100 g, whereas total phenolic content determined by the Folin-Ciocalteu method was 28.53 mg SA/100 g in cold-pressed rapeseed oil (Table 1). Our obtained result of total phenolic content was higher than that reported by Zacchi et al.,[37] Siger et al.,[16] and Koski et al.[17] Zacchi et al. found that the mixed oil (the pressed oil and the solvent-extracted oil coming from the same batch of seeds) contained 17.8 mg of sinapic acid/100 g of polyphenol compounds. Siger et al. determined the content of total phenolic compounds at a level of 1.31 mg/100 g caffeic acid equivalents in cold-pressed rapeseed oil.[16] Koski et al. reported that cold-pressed rapeseed oil contained only minor amounts (0.3−0.4 mg caffeic acid/100 g) of polar phenolics.[17] However, Koski et al. detected higher total amounts of phenolic compounds: 106.6, 73.0, 19.3, 4.4, and 1.6 mg caffeic acid/100 g in post-expelled crude turnip rapeseed, post-expelled crude oil, superdegummed oil, oil refined, bleached, and deodorized under modified, milder conditions, and refined, bleached, and deodorized oil, respectively.[5] The phenolic acid

content in rapeseed oil is the result of complex interactions among several factors, including the method of analysis, processing technology, rapeseed cultivar and ripening degree, and climate.

Influence of Microwave on Phenolic Compounds in Rapeseed. Tocopherols, photosterols, and phenolic compounds are minor components of rapeseed oils. Our previously published results revealed that total tocopherols content in the oil extracted by press first increased and then decreased depending on the period of microwave radiation, whereas phytosterols and total phenolics contents increased with increasing microwave time.[30] It has been reported that microwave pretreatment of rapeseed could increase the canolol content, and higher temperatures (>160 °C) can cause a reduction in the canolol content.[24] Canolol can be formed by thermal decarboxylation of the sinapic acid during the roasting process. Previous studies have indicated that the loss of free sinapic acid was far below the amount of sinapic acid converted into canolol, and esterified sinapic acid derivatives must have provided free sinapic acid by hydrolysis during roasting.[22−24] Thus, study on the changes of sinapine (the main esterified sinapic acid derivatives) in rapeseed during the microwave roasting process is necessary.

The amount of sinapine in the rapeseed sample first increased and then decreased ($p < 0.01$) depending on the microwave pretreatment time (Table 2). A 3 min microwave exposure period could increase the sinapine content of the rapeseed to the maximum (502.81 mg/100 g), and it was 43.59 mg/100 g higher than that of the untreated rapeseed. When the microwave time increased to 8 min, the sinapine content was the minimum; it was 409.20 mg/100 g, and 50.02 mg/100 g lower than the initial content. The decrease in sinapine content after roasting by microwave could be observed in Figure 1. Our results suggest that the microwave pretreatment may result in the reduced sinapine content with increased microwave time. This result must be due to a partial hydrolysis of sinapine by the elevated temperature from the relatively long period of microwave exposure.

Sinapic acid is the main phenolic acid in rapeseed. The unroasted samples possessed 76.80 mg per 100 g of rapeseed. As shown in Table 2, the trend seen was clear: similarly to sinapine, the content of sinapic acid first increased and then decreased depending on the period of microwave radiation ($p < 0.05$) too. When the rapeseed was treated for 2 min with microwaves, the sinapic acid content was the maximum (86.14 mg/100 g); it was 9.34 mg/100 g higher than that of the untreated sample. Microwave treatment of rapeseed sample for a period of 8 min could make the sinapic acid content decreased to the minimum (31.20 mg/100g) that it was 45.60 mg/100 g lower than that of the untreated sample, representing about 40% of its initial value (Figure 1). This fact can be explained by the fact that damage to the rapeseed cell membrane by microwave radiation favors the increase of extraction efficiency of sinapic acid in an earlier stage of the pretreatment. However, along with the extension of microwave treatment time, the temperature of the sample increased, the thermal decarboxylation of the sinapic acid naturally occurred, and canolol was formed in rapeseed.

The unroasted sample possessed 14.07 mg of canolol per 100 g of rapeseed (Table 2). The roasting treatment by microwave significantly increased the amount of canolol in rapeseed ($p < 0.001$). After exposure to a microwave treatment of 7 min duration, the canolol content increased from 14.07 mg/100 g to

Table 2. Phenolic Compounds Distribution and Content in Rapeseed and Oil Extracted from Rapeseed by Press as Mean with SD ($n = 3$)[a]

	microwave time							
sample	T_0 (0 min)	T_1 (1 min)	T_2 (2 min)	T_3 (3 min)	T_4 (4 min)	T_5 (5 min)	T_6 (6 min)	T_7 (7 min)	T_8 (8 min)
rapeseed									
sinapine	459.22 ± 13.27 b	457.76 ± 8.07 b, c	500.73 ± 14.78 c	502.81 ± 10.84 c	498.24 ± 15.37 c	498.43 ± 18.58 c	473.15 ± 34.09 b	463.41 ± 6.05 a	409.20 ± 26.37 a
sinapic acid	76.80 ± 4.39 e	76.10 ± 3.89 e	86.14 ± 3.06 f	83.11 ± 0.64 f	74.06 ± 1.62 e	65.14 ± 4.84 d	52.17 ± 3.54 c	38.09 ± 0.70 b	31.20 ± 1.24 a
caffeic acid	10.26 ± 0.58 d, f	10.87 ± 0.40 f	12.64 ± 0.55 g	12.61 ± 0.60 g	9.63 ± 0.28 c, d	8.92 ± 0.20 b, c	8.70 ± 0.39 a, b	8.90 ± 0.31 b, c	8.12 ± 0.09 a
ferulic acid	2.17 ± 0.09 d	2.14 ± 0.12 d	2.44 ± 0.18 e	2.60 ± 0.08 e	2.48 ± 0.09 e	2.21 ± 0.09 d	1.66 ± 0.12 c	1.11 ± 0.05 b	0.74 ± 0.05 a
cinnamic acid	ND	ND	ND	ND	ND	ND	ND	ND	ND
canolol	14.07 ± 0.82 a	14.78 ± 0.97 a	16.16 ± 0.40 a, b	19.65 ± 0.36 b	30.54 ± 1.58 c	49.21 ± 3.53 d	71.79 ± 2.44 e	89.89 ± 3.70 f	83.48 ± 1.87 g
oil									
sinapine	ND	ND	ND	ND	0.05 ± 0.00 a	0.10 ± 0.00 b	0.21 ± 0.00 c	0.65 ± 0.01 d	0.66 ± 0.05 d
sinapic acid	2.73 ± 0.08 b, c	2.59 ± 0.07 b	2.61 ± 0.03 b	2.62 ± 0.20 b	2.65 ± 0.08 b	2.90 ± 0.08 c	2.58 ± 0.17 b	1.95 ± 0.16 a	1.80 ± 0.12 a
caffeic acid	ND	ND	ND	ND	ND	ND	ND	ND	ND
ferulic acid	0.05 ± 0.00	0.05 ± 0.00	0.05 ± 0.00	0.05 ± 0.00	0.05 ± 0.00	0.05 ± 0.00	0.05 ± 0.00	0.04 ± 0.00	0.04 ± 0.00
cinnamic acid	0.10 ± 0.01 a	0.12 ± 0.00 a, b	0.16 ± 0.00 b, c	0.20 ± 0.01 c, d	0.22 ± 0.02 d	0.32 ± 0.02 e	0.46 ± 0.04 f	0.59 ± 0.05 g	0.59 ± 0.02 g
canolol	17.06 ± 2.16 a	19.75 ± 1.25 a	23.07 ± 1.12 a, b	30.88 ± 0.76 b	47.40 ± 1.62 c	79.79 ± 5.96 d	116.86 ± 3.74 e	162.71 ± 6.43 f	151.42 ± 11.19 g

[a]Values are means ± standard deviation, $n = 3$. Different letters within the same column indicate significant differences (one-way ANOVA and Duncan test, $p < 0.05$). ND = not detected.

dx.doi.org/10.1021/jf4054287 | J. Agric. Food Chem. 2014, 62, 1956−1963

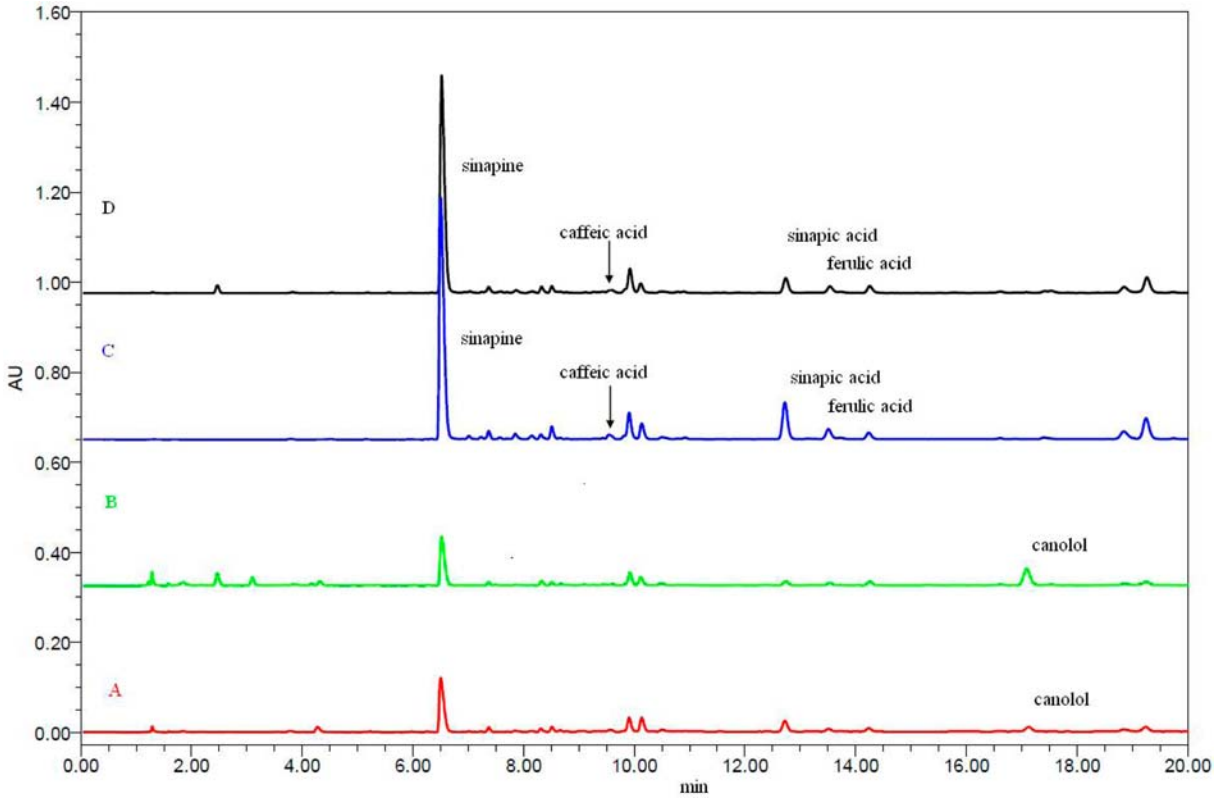

Figure 1. Reverse-phase UPLC chromatogram of the phenolic compounds: (A) unroasted seed measured at 280 nm, (B) 8 min roasted seed measured at 280 nm, (C) unroasted seed measured at 325 nm, and (D) 8 min roasted seed measured at 325 nm. Time axis is in minutes.

89.89 mg/100 g. The canolol content of 7 min microwave pretreatment rapeseed was approximately six times greater than that of the unroasted rapeseed. Spielmeyer et al. reported that the optimal roasting conditions (exposure to a microwave roasting of 7.5 min duration with a temperature of 160 °C) produced increased canolol content 120 times that found in the unroasted sample.[24] The increase in the amount of canolol content in our sample was lower than that reported by Spielmeyer et al., but the canolol content in 7 min microwave rapeseed was in accordance with the result presented by Spielmeyer et al.[24] Canolol was shown to be thermally unstable, and fast degradation during longer roasting was previously reported.[24] In our study, when the microwave time was extended to 8 min, the rapeseed sample possessed 83.48 mg of canolol per 100 g of rapeseed. This result concurs with previously published results.[24]

As shown in Table 2, when the microwave treatment time was 7 min, the decrease in sinapic acid content was 48.05 mg/100 g, compared with the content in 2 min microwave rapeseed, and the increase in canolol content was 67.77 mg/100 g in rapeseed. Thus, it was very clear: loss of sinapic acid was far below the amount of sinapic acid converted into canolol. This fact can be explained by the decrease in sinapine content: when the rapeseed was exposed to microwave radiation for 7 min, the sinapine content decreased from the maximum 502.81 mg/100 g to 463.21 mg/100 g and there was a 39.40 mg/100 g of decrease in sinapine content. Thus, hydrolysis of sinapine favors canolol formation during roasting. The amount of canolol formed was highly correlated with the content of sinapic acid and sinapine and also the loss of sinapic acid and sinapine during rapeseed roasting. The coefficients of correlation were −0.950 between the content of canolol and sinapic acid in the rapeseed treated by microwave for 0−8 min and 0.997 between the increase of canolol and loss of sinapic acid in the rapeseed treated by microwave for 2−8 min ($p < 0.001$). The coefficients of correlation were −0.828 between the content of canolol and sinapine in the rapeseed treated by microwave for 0−8 min and 0.952 between the increase of canolol and loss of sinapine in the rapeseed treated by microwave for 3−8 min ($p < 0.05$). The content of sinapic acid and sinapine in rapeseed was the maximum when microwave time was 2 and 3 min, respectively, as shown in Table 2. Previous studies have shown that the decrease in free sinapic acid (FSA) content and total sinapic acid content after basic hydrolysis (TSAH) content in rapeseed was 17.04 mg/100 g and 287 mg/100 g after roasting for 10 min at 160 °C, respectively. Furthermore, canolol formation was highly correlated with the initial FSA content, the residual FSA content after roasting, and also the loss of TSAH during seed roasting.[23]

Similarly to sinapine and sinapic acid, the content of caffeic and ferulic acid in the sample first increased and then decreased with increasing microwave time ($p < 0.01$) (Table 2). Caffeic, ferulic, and sinapic acids belong to hydroxycinnamic acids and have a similar molecular structure. It has been reported that 4-vinylguaiacol and 4-vinylphenol are formed from ferulic and *p*-coumaric acid during thermal treatment and by enzyme activity.[38,39] Moreover, the decarboxylation products of *p*-coumaric, caffeic, ferulic, and sinapic acids have been obtained by decarboxylation of 4-hydroxycinnamic acids.[40,41]Therefore, the decrease of caffeic and ferulic acid content can be explained by the thermal decarboxylation of them during rapeseed roasting by microwave.

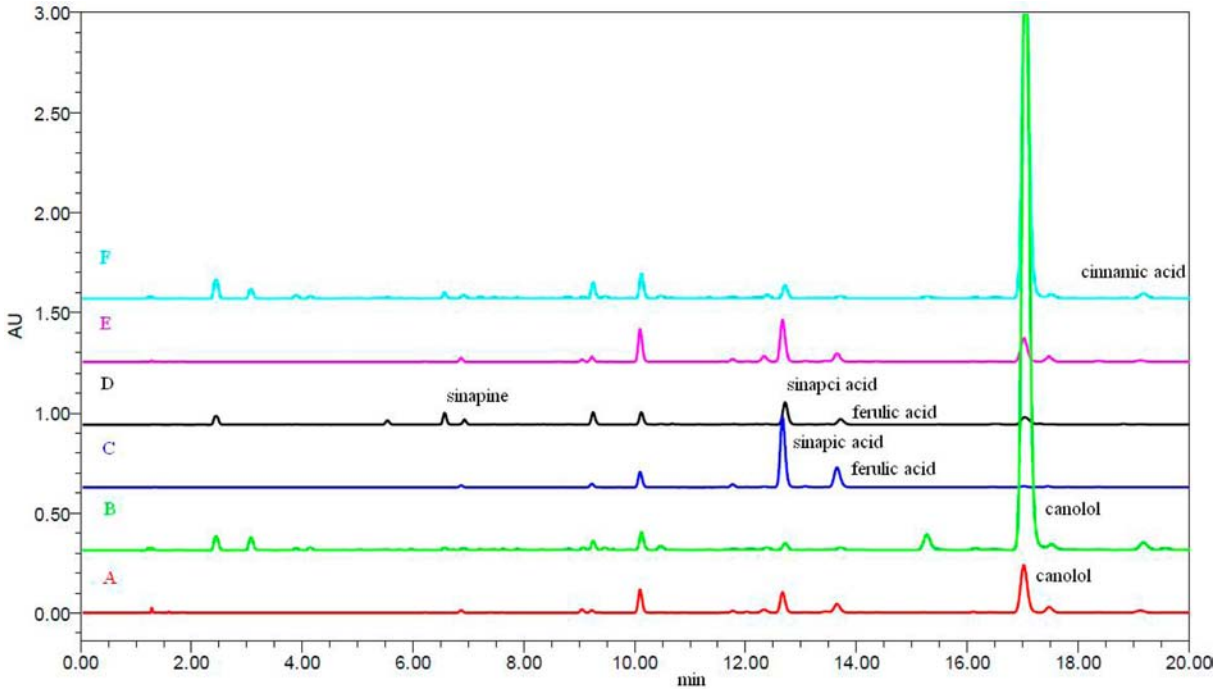

Figure 2. Reverse-phase UPLC chromatogram of the phenolic compounds: (A) oil from unroasted seed measured at 280 nm, (B) oil from 8 min roasted seed measured at 280 nm, (C) oil from unroasted seed measured at 325 nm, (D) oil from 8 min roasted seed measured at 325 nm, (E) oil from unroasted seed measured at 295 nm, (F) oil from 8 min roasted seed measured at 295 nm. Time axis is in minutes.

Transfer of Phenolic Compounds from Rapeseed to Oil by Press. Rapeseeds are much richer in phenolic compounds (Table 2). Most of these phenolics remain in the meal after pressing, and only a small proportion are transferred to the crude oil. However, owing to the difference in molecular structure, polarity, and fat solubility, there were differences in the quantities and transfer ratios of these phenolic compounds transferred to the crude oil.

The phenolic compounds of the studied rapeseeds and oil extracted from them by press by UPLC-DAD are presented in Table 2. Formation of canolol after roasting by microwave could be observed in Figure 2. As shown in Table 2, although the sinapine content in rapeseed up to about 500 mg/100 g it was not detected in the pressed oils from rapeseed by microwave pretreatment for 1−3 min, and sinapine content in the oils from rapeseed by microwave pretreatment for 4−8 min ranged from 0.05 mg/100 g to 0.66 mg/100 g and did not exceed 1 mg/100g. This result can be explained by the fact that sinapine is present in rapeseed in thiocyanate forms and is a water-soluble substance. Moreover, we observed that the content of sinapine in the oil sample increased with microwave time after roasting for 3 min ($p < 0.05$). This fact can be explained by the fact that the oil extraction yield by pressing increased with increasing microwave pretreatment time of rapeseed.[27−30]

We can see from Table 2 that the quantities of sinapic acid transferred to the pressed crude oil were few, and the transfer ratios increased with microwave pretreatment time: they were1.6%, 1.6%, 1.4%, 1.5%, 1.6%, 2.0%, 2.3%, 2.4%, and 2.7% when rapeseed was exposed for 0, 1, 2, 3, 4, 5, 6, 7, and 8 min, respectively. Table 2 shows that the content of sinapic acid in the oil first increased and then decreased depending on the period of microwave radiation ($p < 0.001$), similarly to the change of sinapic acid in the rapeseed. Small amounts of caffeic and ferulic acid were detected in the rapeseed samples (Table 2). Caffeic acid in the oil was not detected, and all of the caffeic acid remained in the meal after pressing, whereas a small amount of ferulic and cinnamic acid were detected in all oil samples. It was noteworthy that cinnamic acid was not detected in the rapeseed sample. The cinnamic acid content in the oil significantly increased with microwave time ($p < 0.001$), and the ferulic acid content in oil was not significantly different ($p > 0.05$). This result may be explained by the fact that there was a difference in the polarity of caffeic, ferulic, and cinnamic acids in the following order caffeic acid > ferulic acid > cinnamic acid.

However, the phenomenon of transferring in canolol was completely different from sinapic, caffeic, ferulic, and cinnamic acids: most of the canolol was transferred to the crude oil when pressing the oil from rapeseed, and the content and transfer ratio of canolol significantly increased depending on the period of microwave radiation ($p < 0.001$). This result may be due to the strong fat solubility of canolol. As shown in Table 2, the canolol content of oil pressed from 4 min microwave pretreatment rapeseed increased from 17.06 mg/100g to 47.40 mg/100g and was approximately three times greater than that of the oil pressed from untreated rapeseed. When the microwave time of rapeseed reached 7 min, the canolol content in the oil increased to 162.71 mg/100g and was approximately nine times greater than that of the oil from unroasted rapeseed. The transfer ratio of canolol transferred to the crude oil was 56%, 60%, 64%, 68%, 71%, 73%, 74%, 79%, and 83% when rapeseed was exposed for 0, 1, 2, 3, 4, 5, 6, 7, and 8 min, respectively. Shrestha et al. found that 49−56% of the canolol formed during seed roasting was transferred to the oil.[23] The transfer rates of canolol in our study were higher than the results obtained by Shrestha et al. The difference in transfer rate levels might arise from factors, such as the oil sample preparation and oil content of seed.

We observed that there was an inflection point of rapid increase in the canolol content of oil from rapeseed by roasting

dx.doi.org/10.1021/jf4054287 | J. Agric. Food Chem. 2014, 62, 1956−1963

for 5 min: the canolol content increased to 79.79 mg/100 g. Moreover, there was faster growth in the canolol content in the oil from rapeseed by roasting for 5−8 min than that for 1−4 min (Table 2). This result might arise from the following factor: the temperature of rapeseed increased with microwave pretreatment time and lead to an increase in the amount of sinapic acid and esterified sinapic acid derivatives, such as sinapine, converted into canolol. Moreover, more canolol transferred to the pressed crude oil as a result of an increase in the oil extraction yield with increasing microwave pretreatment time.

The induction period (IP, 110 °C) was 9.59, 9.72, 9.52, 10.00, 11.77, 14.27, 16.99, 28.77, and 30.15 h of the oil from rapeseed treated with microwaves for 0, 1, 2, 3, 4, 5, 6, 7, and 8 min, respectively. Thus, microwave pretreatment of rapeseed is a beneficial step for improving the oxidative stability of oil. Canolol has very good antioxidative activity. The IP was positively correlated with the canolol content in oil, and the correlation coefficient was 0.895, p = 0.001. The significant correlations between the amount of canolol formation and the loss of sinapic acid and sinapine during roasting were found. Engels et al. identified eight kinds of sinapic acid derivatives from mustard seed meal using UHPLC-DAD-ESI-MS^n.[42] The roles of these sinapic acid derivatives in canolol formation need further study.

AUTHOR INFORMATION

Corresponding Author

*Phone: +86 27 86827874. Fax: +86 27 86815916. E-mail: oiljgzx@gmail.com.

Notes

The authors declare no competing financial interest.

ACKNOWLEDGMENTS

We are grateful to the Special Fund for Agro-scientific Research in the Public Interest (201303072) and the Industry Technology System of Rapeseed in China for financial support.

REFERENCES

(1) Han-zhong, W. Review and future development of rapeseed industry in China [J]. *Chin. J. Oil Crop Sci.* **2010**, *2* (30), 300−302.

(2) Erkkilä, A.; de Mello, V. D.; Risérus, U.; Laaksonen, D. E. Dietary fatty acids and cardiovascular disease: an epidemiological approach. *Prog. Lipid Res.* **2008**, *47*, 172−187.

(3) Tarascou, I.; Souquet, J.; Mazauric, J.; Carrillo, S.; Coq, S.; Canon, F.; Fulcrand, H.; Cheynier, V. The hidden face of food phenolic composition. *Arch. Biochem. Biophys.* **2010**, *501*, 16−22.

(4) Naczk, M.; Amarowicz, R.; Sullivan, A.; Shahidi, F. Current research developments on polyphenolics of rapeseed/canola: a review. *Food Chem.* **1998**, *62*, 489−502.

(5) Koski, A.; Pekkarinen, S.; Hopia, A.; Wähälä, K.; Heinonen, M. Processing of rapeseed oil: effects on sinapic acid derivative content and oxidative stability. *Eur. Food Res. Technol.* **2003**, *217* (2), 110−114.

(6) Shahidi, F.; Naczk, M. An overview of the phenolics of canola and rapeseed: chemical, sensory and nutritional significance. *J. Am. Oil Chem. Soc.* **1992**, *69*, 917−924.

(7) Krygier, K.; Sosulski, F.; Hogge, L. Free, esterified, and insoluble-bound phenolic acids. 2. Composition of phenolic acids in rapeseed flour and hulls. *J. Agric. Food Chem.* **1982**, *30*, 334−336.

(8) Kozlowska, H.; Naczk, M.; Shahidi, F.; Zadernowski, R., Phenolic acids and tannins in rapeseed and canola. In *Canola and rapeseed; production, chemistry, nutrition andprocessing technology*; Shahidi, F., Ed.; Van Nostrand Reinhold: New York, 1990; pp 193−210.

(9) Amarowicz, R.; Naczk, M.; Shahidi, F. Antioxidant activity of crude tannins of canola and rapeseed hulls. *J. Am. Oil Chem. Soc.* **2000**, *77*, 957−961.

(10) Amarowicz, R.; Kolodziejczyk, P.; Pegg, R. Chromatographic Separation of Phenolic Compounds from Rapeseed by a Sephadex LH-20 Column with Ethanol as the Mobile Phase. *J. Liquid Chromatogr. Relat. Technol.* **2003**, *26*, 2157−2165.

(11) Cai, R.; Arntfield, S. A rapid high-performance liquid chromatographic method for the determination of sinapine and sinapic acid in canola seed and meal. *J. Am. Oil Chem. Soc.* **2001**, *78*, 903−910.

(12) Matthäus, B. Isolation, fractionation and HPLC analysis of neutral phenolic compounds in rapeseeds. *Food/Nahrung.* **1998**, *42*, 75−80.

(13) Matthäus, B. Antioxidant activity of extracts obtained from residues of different oilseeds. *J. Agric. Food Chem.* **2002**, *50*, 3444−3452.

(14) Siger, A.; Nogala-Kałucka, M.; Lampart-Szczapa, E.; Hoffmann, A. Phenolic compound contents in new rape varieties. *Oilseeds Plant.* **2004**, *25*, 263−274.

(15) Dabrowski, K. J.; Sosulski, F. W. Quantitation of free and hydrolyzable phenolic acids in seeds by capillary gas-liquid chromatography. *J. Agric. Food Chem.* **1984**, *32*, 123−127.

(16) Siger, A.; Nogala-Kalucka, M.; Lampart-Szczapa, E. The content and antioxidant activity of phenolic compunds in cold-pressed plant oils. *J. Food Lipids* **2008**, *15*, 137−149.

(17) Koski, A.; Psomiadou, E.; Tsimidou, M.; Hopia, A.; Kefalas, P.; Wähälä, K.; Heinonen, M. Oxidative stability and minor constituents of virgin olive oil and cold-pressed rapeseed oil. *Eur. Food Res. Technol.* **2002**, *214*, 294−298.

(18) Tuberoso, C. I.; Kowalczyk, A.; Sarritzu, E.; Cabras, P. Determination of antioxidant compounds and antioxidant activity in commercial oilseeds for food use. *Food Chem.* **2007**, *103*, 1494−1501.

(19) Wakamatsu, D.; Morimura, S.; Sawa, T.; Kida, K.; Nakai, C.; Maeda, H. Isolation, identification, and structure of a potent alkyl-peroxyl radical scavenger in crude canola oil, canolol. *Biosci., Biotechnol., Biochem.* **2005**, *69*, 1568−1574.

(20) Kuwahara, H.; Kanazawa, A.; Wakamatu, D.; Morimura, S.; Kida, K.; Akaike, T.; Maeda, H. Antioxidative and antimutagenic activities of 4-vinyl-2, 6-dimethoxyphenol (canolol) isolated from canola oil. *J. Agric. Food Chem.* **2004**, *52*, 4380−4387.

(21) Vuorela, S.; Kreander, K.; Karonen, M.; Nieminen, R.; Hämäläinen, M.; Galkin, A.; Laitinen, L.; Salminen, J.-P.; Moilanen, E.; Pihlaja, K. Preclinical evaluation of rapeseed, raspberry, and pine bark phenolics for health related effects. *J. Agric. Food Chem.* **2005**, *53*, 5922−5931.

(22) Wijesundera, C.; Ceccato, C.; Fagan, P.; Shen, Z. Seed roasting improves the oxidative stability of canola (B. napus) and mustard (B. juncea) seed oils. *Eur. J. Lipid Sci. Technol.* **2008**, *110*, 360−367.

(23) Shrestha, K.; Stevens, C. V.; De Meulenaer, B. Isolation and Identification of a Potent Radical Scavenger (Canolol) from Roasted High Erucic Mustard Seed Oil from Nepal and Its Formation during Roasting. *J. Agric. Food Chem.* **2012**, *60*, 7506−7512.

(24) Spielmeyer, A.; Wagner, A.; Jahreis, G. Influence of thermal treatment of rapeseed on the canolol content. *Food Chem.* **2009**, *112*, 944−948.

(25) Maheshwari, P.; Stanley, D.; Van De Voort, F.; Gray, J. Effect of microwave treatment on the microstructure of dehulled rapeseed. *Cereal Chem.* **1981**, *58* (5), 381−384.

(26) Anjum, F.; Anwar, F.; Jamil, A.; Iqbal, M. Microwave roasting effects on the physico-chemical composition and oxidative stability of sunflower seed oil. *J. Am. Oil Chem. Soc.* **2006**, *83*, 777−784.

(27) Azadmard-Damirchi, S.; Alirezalu, K.; Achachlouei, B. F. Microwave Pretreatment of Seeds to extract high quality vegetable oil. *World Acad. Sci., Eng. Technol.* **2011**, *81*, 513−516.

(28) Azadmard-Damirchi, S.; Habibi-Nodeh, F.; Hesari, J.; Nemati, M.; Achachlouei, B. F. Effect of pretreatment with microwaves on oxidative stability and nutraceuticals content of oil from rapeseed. *Food Chem.* **2010**, *121*, 1211−1215.

(29) Uquiche, E.; Jeréz, M.; Ortíz, J. Effect of pretreatment with microwaves on mechanical extraction yield and quality of vegetable oil from Chilean hazelnuts (*Gevuina avellana* Mol). *Innovative Food Sci. Emerging Technol.* **2008**, *9*, 495−500.
(30) Yang, M.; Huang, F.; Liu, C.; Zheng, C.; Zhou, Q.; Wang, H. Influence of microwave treatment of rapeseed on minor components content and oxidative stability of oil. *Food Bioprocess Technol.* **2013**, *6*, 3206−3216.
(31) Harbaum-Piayda, B.; Oehlke, K.; Sönnichsen, F. D.; Zacchi, P.; Eggers, R.; Schwarz, K. New polyphenolic compounds in commercial deodistillate and rapeseed oils. *Food Chem.* **2010**, *123*, 607−615.
(32) Khattab, R.; Eskin, M.; Aliani, M.; Thiyam, U. Determination of sinapic acid derivatives in canola extracts using high-performance liquid chromatography. *J. Am. Oil Chem. Soc.* **2010**, *87*, 147−155.
(33) Blair, R.; Reichert, R. D. Carbohydrate and phenolic constituents in a comprehensive range of rapeseed and canola fractions: nutritional significance for animals. *J. Sci. Food Agric.* **1984**, *35*, 29−35.
(34) Liu, Q.; Wu, L.; Pu, H.; Li, C.; Hu, Q. Profile and distribution of soluble and insoluble phenolics in Chinese rapeseed (*Brassica napus*). *Food Chem.* **2012**, *135*, 616−622.
(35) Szydłowska-Czerniak, A.; Trokowski, K.; Karlovits, G. r.; Szłyk, E. Determination of antioxidant capacity, phenolic acids, and fatty acid composition of rapeseed varieties. *J. Agric. Food Chem.* **2010**, *58*, 7502−7509.
(36) Vuorela, S.; Meyer, A. S.; Heinonen, M. Quantitative analysis of the main phenolics in rapeseed meal and oils processed differently using enzymatic hydrolysis and HPLC. *Eur. Food Res. Technol.* **2003**, *217*, 517−523.
(37) Zacchi, P.; Eggers, R. High-temperature pre-conditioning of rapeseed: A polyphenol-enriched oil and the effect of refining. *Eur. J. Lipid Sci. Technol.* **2008**, *110*, 111−119.
(38) Adler-Nissen, J.; Olsen, H. S. The influence of peptide chain length on taste and functional properties of enzymatically modified soy protein. *ACS Symposium Series 92*; ACS Publications: Washington, DC, 1979; pp 125−146.
(39) Rein, M. J.; Ollilainen, V.; Vahermo, M.; Yli-Kauhaluoma, J.; Heinonen, M. Identification of novel pyranoanthocyanins in berry juices. *Eur. Food Res. Technol.* **2005**, *220*, 239−244.
(40) Bernini, R.; Mincione, E.; Barontini, M.; Provenzano, G.; Setti, L. Obtaining 4-vinylphenols by decarboxylation of natural 4-hydroxycinnamic acids under microwave irradiation. *Tetrahedron* **2007**, *63*, 9663−9667.
(41) Terpinc, P.; Polak, T.; Šegatin, N.; Hanzlowsky, A.; Ulrih, N. P.; Abramovič, H. Antioxidant properties of 4-vinyl derivatives of hydroxycinnamic acids. *Food Chem.* **2011**, *128*, 62−69.
(42) Engels, C.; Schieber, A.; Gänzle, M. G. Sinapic acid derivatives in defatted Oriental mustard (*Brassica juncea L.*) seed meal extracts using UHPLC-DAD-ESI-MS n and identification of compounds with antibacterial activity. *Eur. Food Res. Technol.* **2012**, *234*, 535−542.

produces the CP4 EPSPS protein,[4] which allows for full vegetative and reproductive tissue glyphosate tolerance in the hybrid seed.

The research reported here compares the composition of grain and forage from MON 87427 and MON 87427 × MON 89034 × NK603 to the composition of near-isogenic conventional hybrid comparators. Compositional analysis is a key component of the comparative assessment process of new crops containing traits derived from modern agricultural biotechnology. It involves comparisons of levels of key nutrients, antinutrients, and secondary metabolites in the new biotech or genetically modified (GM) crop to levels in a near-isogenic conventional counterpart. Assessments of differences between the two comparators typically use statistical significance testing. Harrigan et al.[5] recently reviewed the results of GM crop composition studies conducted over multiple geographies and growing seasons and concluded that significant differences ($\alpha = 0.05$) in mean values between a GM crop and its near-isogenic comparator were typically of very small magnitudes and that these differences were considerably less than the differences resulting from germplasm and environmental factors. This has led to increased emphasis that statistical significance does not necessarily imply biological relevance[6] and that the well-documented sources of compositional variability and its influence on overall crop composition must be considered in comparative assessments. In this investigation, we highlight types of further evaluations to consider in the assessment of compositional outcomes in the context of natural variability.

MATERIALS AND METHODS

Maize Samples for Compositional Analyses. The control for MON 87427 was EXP262, a conventional maize hybrid, with a genetic background similar to that of MON 87427. The control for MON 87427 × MON 89034 × NK603 was MPA636B, a conventional maize hybrid, with a genetic background similar to that of MON 87427 × MON 89034 × NK603. Commercially available conventional reference hybrids were planted concurrently with the experimental (MON 87427 or MON 87427 × MON 89034 × NK603) and control hybrids to provide in-study data on the variability of each compositional component assessed.

Materials for composition analyses were generated in 2010 at eight locations within the primary maize-growing regions. For the MON 87427 study, hybrids were grown in Jackson county, Arkansas; Greene and Jefferson counties, Iowa; Clinton and Stark counties, Illinois; Boone county, Indiana; Pawnee county, Kansas; and York county, Nebraska. For the MON 87427 × MON 89034 × NK603 study, hybrids were grown in Jackson county, Arkansas; Clinton and Stark counties, Illinois; Jefferson county, Iowa; Pawnee county, Kansas; Shelby county, Missouri; York county, Nebraska; and Miami county, Ohio.

At each location, hybrids were planted in a randomized complete block design with four blocks. Within each block, plots (six rows × 6.1 m) were assigned randomly to experimental hybrid (MON 87427 or MON 87427 × MON 89034 × NK603), control (EXP262 or MPA636B), or one of the four of the conventional reference hybrids. For the MON 87427 study, a total of 24 unique reference hybrids were planted across the eight-site multilocation study. For the MON 87427 × MON 89034 × NK603 study, a total of 22 unique reference hybrids were planted across the eight-site multilocation study. These conventional reference hybrids were representative of maize hybrids typically grown at each specific location.

Standard agronomic practices for each region were followed. A single application of Roundup WeatherMAX (Roundup and Roundup WeatherMAX are registered trademarks of Monsanto Technology LLC) was applied, according to the label, at a rate of 1.0 lb ae/acre to the MON 87427 × MON 89034 × NK603 plots at approximately the V2−V4 growth stages for weed control. The genetic purity of MON 87427, MON 87427 × MON 89034 × NK603, control, and commercial reference maize was maintained by bagging the tassels and ear shoots at anthesis and hand-pollinating each plant.

Forage and grain harvest, sampling, shipping, storage and sample preparation protocols for compositional analysis were followed as previously described.[7] Event-specific polymerase chain reaction analysis[8] was conducted to confirm the genetic identity of the harvested grain. From the MON 87427 field production, one experimental sample from one location and a total of 11 samples of nine reference substances from six locations were excluded from compositional analyses due to the adventitious presence of unintended traits. From the MON 87427 × MON 89034 × NK603 field production, 15 samples of nine reference substances from seven locations were also excluded from analysis due to the adventitious presence of unintended traits.

Compositional Analysis Methods. Forage samples were analyzed for proximates (ash, fat, moisture, and protein), acid detergent fiber (ADF), neutral detergent fiber (NDF), and minerals (calcium and phosphorus).[9] Grain samples were analyzed for proximates, ADF, NDF, total dietary fiber (TDF), amino acids, fatty acids (FA), minerals (calcium, copper, iron, magnesium, manganese, phosphorus, potassium, sodium, and zinc), secondary metabolites [ferulic acid, 2-furaldehyde (furfural), and *p*-coumaric acid], antinutrients (phytic acid and raffinose), and vitamins [folic acid, vitamin A (β-carotene), niacin, vitamin B_1, vitamin B_2, vitamin B_6, and vitamin E]. Carbohydrate levels in forage and grain were determined by calculation, and moisture levels were measured for the re-expression of fresh weight values on a dry weight basis. The compositional analyses were conducted using industry standard analytical methods (AOAC, AOCS, or other published methods) that are used in routine compositional characterization of foods and feeds[3,10] at Covance Laboratories Inc. (Madison, WI, USA) and EPL Bio-Analytical Services (Niantic, IL, USA). Samples from each study were analyzed in a randomized order to reduce assay bias.

Statistical Analysis of Compositional Data. Statistical analysis of the data involved a comparison of MON 87427 to EXP262 and MON 87427 × MON 89034 × NK603 to MPA636B for every analyte across all sites to determine significant differences ($\alpha = 0.05$) using analysis of variance (ANOVA). To complete a statistical analysis for a component in each separate study, at least 50% of the values for an analyte had to be greater than the assay limit of quantitation (LOQ).[11] The following 13 analytes, which had >50% of observations less than the LOQs, were excluded from statistical analysis from both MON 87427 and MON 87427 × MON 89034 × NK603: capric acid, caprylic acid, lauric acid, myristic acid, myristoleic acid, pentadecanoic acid, pentadecenoic acid, heptadecenoic acid, γ-linolenic acid, eicosadienoic acid, eicosatrienoic acid, arachidonic acid, erucic, and furfural. In addition, heptadecanoic acid and sodium in MON 87427 were below the assay LOQ. The fatty acids reported above are present in only low amounts in maize grain, if present at all.[5] This investigation confirmed that this observation extended to MON 87427 and MON 87427 × MON 89034 × NK603.

For analytes with individual measurements less than the LOQ and with >50% of all of the values greater than the LOQ, a value equal to half of the LOQ was assigned prior to statistical analyses.[3] Assigned values for grain in the MON 87427 study included 127 values of palmitoleic acid, four values of behenic acid, and one value of calcium. For the MON 87427 × MON 89034 × NK603 study, assigned grain values included five values of palmitoleic acid, 102 values of heptadecanoic acid, two values of ecosenoic acid, 85 values of behenic acid, three values of copper, 95 values of sodium, 14 values of vitamin A, and 33 values of vitamin B_1.

A studentized PRESS residual test was applied to the adjusted data set to identify outliers. Data points that were outside the ±6 studentized PRESS residual range were considered for exclusion, as outliers, from the final statistical analysis on the basis of a biological assessment of the data point. For the MON 87427 study, one ash value was identified as an outlier and was removed from the statistical

Table 1. Summary of Maize Grain Fat and Fatty Acids (FA) for MON 87427, MON 87427 × MON 89034 × NK603 and the Respective Conventional Controls

	MON 87427	control EXP62	MON 87427 × MON 89034 × NK603	control MPA636B
	mean (SE)[c]	mean (SE)	mean (SE)	mean (SE)
component	range	range	range	range
total fat (% dwt)[a]	3.37 (0.089)	3.33 (0.089)	2.99 (0.14)	2.92 (0.14)
	2.69−3.82	2.74−3.78	1.96−3.98	1.59−3.75
palmitic[b]	11.34 (0.11)[d]	11.67 (0.11)	13.06 (0.39)	12.48 (0.39)
	10.84−12.14	10.87−13.26	11.22−22.74	10.76−18.48
palmitoleic[b]	0.12 (0.0084)	0.10 (0.0083)	0.16 (0.0065)	0.15 (0.0065)
	0.069−0.16	0.067−0.16	0.077−0.26	0.10−0.22
heptadecanoic[b]	<LOQ	<LOQ	0.083 (0.0057)	0.081 (0.0057)
			0.035−0.13	0.034−0.15
stearic[b]	2.01 (0.050)	2.00 (0.049)	2.47 (0.088)	2.29 (0.088)
	1.79−2.29	1.76−2.40	2.00−3.96	1.80−3.27
oleic[b]	22.86 (0.32)[d]	22.50 (0.32)	25.32 (0.44)	24.74 (0.44)
	21.39−25.96	20.22−24.01	22.19−32.00	21.66−29.31
linoleic[b]	61.66 (0.26)	61.69 (0.26)	56.76 (0.88)	58.14 (0.88)
	58.25−63.02	60.58−63.59	38.66−62.42	46.46−63.42
linolenic[b]	1.22 (0.024)	1.25 (0.024)	1.15 (0.043)	1.17 (0.043)
	1.08−1.45	1.15−1.53	0.47−1.46	0.77−1.65
arachidic[b]	0.41 (0.014)	0.41 (0.014)	0.55 (0.021)	0.51 (0.021)
	0.37−0.49	0.36−0.53	0.43−0.89	0.40−0.75
eicosenoic[b]	0.21 (0.0029)	0.21 (0.0029)	0.25 (0.011)	0.26 (0.011)
	0.19−0.23	0.18−0.24	0.037−0.61	0.20−0.34
behenic[b]	0.17 (0.0092)	0.17 (0.0091)	0.19 (0.017)	0.17 (0.017)
	0.14−0.23	0.069−0.25	0.067−0.52	0.069−0.30

[a]dwt = dry weight. [b]Percent total FA. [c]Mean (SE) = least-squares mean (standard error). [d]Statistically significant at 5% level ($\alpha = 0.05$).

analysis. Statistical analysis of the data from samples collected from each separate study was conducted at Certus International, Inc. (Chesterfield, MO, USA). Statistical analyses were conducted on forage and grain using a mixed model analysis of variance from the combination of all sites using the following model:

$$Y_{ijk} = U + T_i + L_j + B(L)_{jk} + LT_{ij} + e_{ijk}$$

Y_{ijk} is the unique individual observation, U is the overall mean, T_i is the substance effect, L_j is the random location effect, $B(L)_{jk}$ is the random block within location effect, LT_{ij} is the random location by substance interaction effect, and e_{ijk} is the residual error. Within grain and forage, data for each compositional component from the experimental hybrids (MON 87427 or MON 87427 × MON 89034 × NK603) were compared to data from their respective control (EXP262 or MPA636B). Statistically significant differences between the experimental hybrid values and the control values were declared at $\alpha = 0.05$. For both studies, the field designs included other experimental hybrids not related to this study but included in the overall ANOVA. The conventional reference hybrids were used to estimate natural compositional variation that can generally be attributed to differences in the germplasm and environment.

Variance components analysis (VCA) was also conducted for both studies (MON 87427 and MON 87427 × MON 89034 × NK603) separately to estimate the proportion of random effects contributing to the total variance. In this application, the effects of substance, location, location × substance interaction, and replication (block) in the ANOVA model were set as random effects. The SAS procedure PROC MIXED was employed to run the analysis. The output table of covariance parameter estimates from SAS PROC MIXED procedure gives estimates of the variance component parameters for each of model components.[12] The variance component parameters of each model component were divided by the total variance to get the variance proportions for each of the components (see Suppl. Tables 3 and 4 in the Supporting Information). For both studies, the field designs included other experimental substances not related to this work but included in the overall ANOVA and VCA.

RESULTS AND DISCUSSION

Comparisons of MON 87427 and MON 87427 × MON 89034 × NK603 to their respective near-isogenic conventional control were on data combined across all field sites from each separate study (Tables 1−5; Suppl. Table 1 in the Supporting Information) using ANOVA. The analysis from both studies showed few statistically significant differences ($\alpha = 0.05$). For MON 87427, differences were observed for histidine, methionine, proline, palmitic acid, oleic acid, and vitamin B_6 in grain (Tables 1, 2, and 5). No differences were observed for forage (Suppl. Table 1). For MON 87427 × MON 89034 × NK603 differences were observed for calcium, manganese, phosphorus, zinc, niacin, and *p*-coumaric acid in grain (Tables 2−4). No differences were observed for forage (Suppl. Table 1).

These results are consistent with numerous prior studies that have illustrated the lack of impact of transgenesis on composition and highlighted that compositional variability is dominated by germplasm and environmental factors. The purpose of the following section is (i) to further describe the compositional equivalence of the MON 87427 products to their near-isogenic comparators, (ii) to illustrate how well-documented influential sources of compositional variability can be considered in comparative assessments,[5] and (iii) to further explain how statistical significance does not imply biological relevance from a composition or food/feed perspective.[5,6] Evaluation of the differences observed in the combined-site analysis therefore focused on the following logic:

(1) Consideration of the magnitude of the mean difference between experimental hybrid (MON 87427 or MON 87427 × MON 89034 × NK603) and the respective control in the context of the variation observed

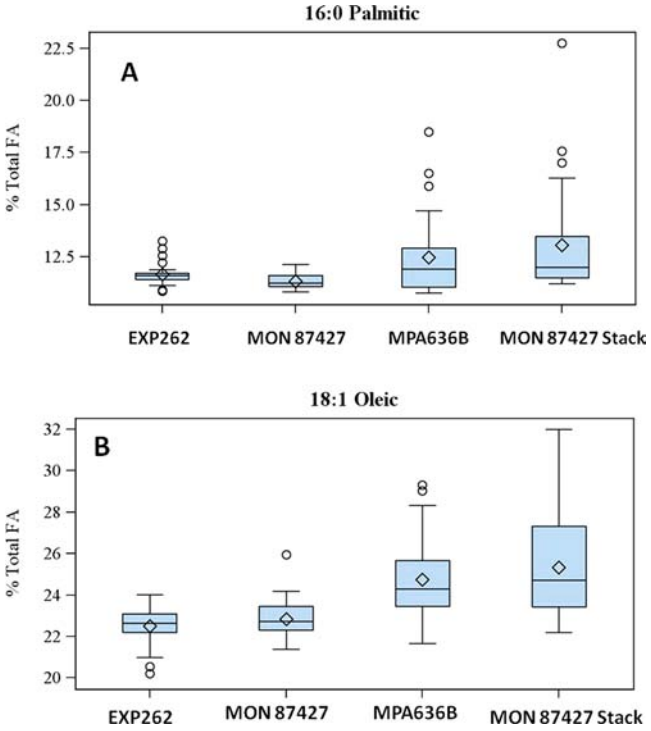

Figure 1. Box plot representing observed variability for palmitic acid and oleic acid values in MON 87427 and MON 87427 × MON 89034 × NK603 (MON 87427 Stack) and their respective conventional control. Each box extends from the lower (25th) to the upper (75th) quartile, and the line in each box represents the median. The whiskers extend to minimum and maximum data points. See Table 1 for details.

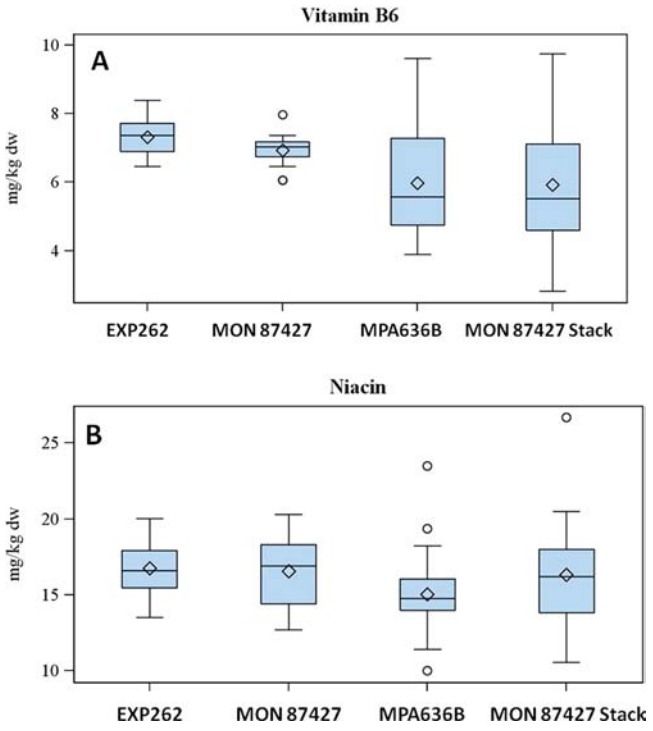

Figure 2. Box plot representing observed variability for niacin and vitamin B_6 values in MON 87427 and MON 87427 × MON 89034 × NK603 (MON 87427 Stack) and their respective conventional control. Legends are the same as described in Figure 1. See Table 2 for details.

(maximum value minus the minimum value) for the control. This allows a meaningful evaluation of the impact of transgene insertion relative to the environmental variability observed in a single genotype (with and without transgene). The individual replicate values of the experimental hybrid and control were also compared to each other to further demonstrate similarity. A significant difference in mean values between an experimental hybrid and the respective control values does not imply a meaningful difference from a compositional perspective, especially if the difference is much less than variation attributable to other sources (e.g., environmental influences).

(2) Comparison of the magnitude of the mean difference between the experimental hybrid (MON 87427 or MON 87427 × MON 89034 × NK603) and the respective control to variation in conventional maize as estimated

Table 2. Summary of Maize Grain Vitamins for MON 87427, MON 87427 × MON 89034 × NK603 and the Respective Conventional Controls

component (mg/kg dwt)[a]	MON 87427 mean (SE)[b] range	control EXP62 mean (SE) range	MON 87427 × MON 89034 × NK603 mean (SE) range	control MPA636B mean (SE) range
folic acid	0.32 (0.020)	0.32 (0.020)	0.99 (0.058)	0.91 (0.058)
	0.25−0.50	0.25−0.47	0.53−2.01	0.43−1.96
niacin	16.61 (0.56)	16.75 (0.56)	16.33 (0.60)[c]	15.06 (0.60)
	12.73−20.29	13.53−20.05	10.56−26.70	10.03−23.52
vitamin A	0.91 (0.036)	0.93 (0.036)	6.54 (0.49)	6.23 (0.49)
	0.66−1.17	0.77−1.12	3.40−9.11	3.03−9.38
vitamin B_1	2.58 (0.099)	2.53 (0.098)	2.48 (0.21)	2.57 (0.21)
	2.01−3.18	1.98−3.22	1.00−3.68	1.00−4.42
vitamin B_2	1.42 (0.043)	1.41 (0.043)	3.38 (0.19)	3.44 (0.19)
	1.05−1.81	1.04−1.83	1.92−5.46	1.72−5.96
vitamin B_6	6.92 (0.11)[c]	7.31 (0.11)	5.92 (0.30)	5.98 (0.30)
	6.05−7.97	6.45−8.39	2.81−9.75	3.90−9.61
vitamin E	18.34 (0.91)	18.62 (0.91)	16.41 (1.08)	15.60 (1.08)
	12.81−27.53	12.82−26.25	11.47−22.96	4.77−21.40

[a]dwt = dry weight. [b]Mean (SE) = least-squares mean (standard error). [c]Statistically significant at 5% level (α = 0.05).

dx.doi.org/10.1021/jf4041589 | J. Agric. Food Chem. 2014, 62, 1964−1973

Table 3. Summary of Maize Grain Carbohydrates by Calculation, Fibers, and Minerals for MON 87427, MON 87427 × MON 89034 × NK603 and the Respective Conventional Controls

component [a] (% dwt)	MON 87427 mean (SE)[b] range	control EXP62 mean (SE) range	MON 87427 × MON 89034 × NK603 mean (SE) range	control MPA636B mean (SE) range
carbohydrates by calculation	85.95 (0.23)	86.13 (0.23)	86.16 (0.36)	86.10 (0.36)
	84.75−87.61	84.93−88.12	84.54−88.41	84.36−88.66
acid detergent fiber	3.07 (0.095)	3.25 (0.094)	4.27 (0.073)	4.44 (0.073)
	2.27−4.10	2.18−4.36	3.60−4.79	3.80−4.87
neutral detergent fiber	10.54 (0.38)	10.74 (0.38)	11.51 (0.27)	11.52 (0.27)
	8.79−13.63	8.88−15.11	9.76−14.56	10.46−12.99
total dietary fiber	13.97 (0.45)	14.68 (0.45)	16.27 (0.45)	16.48 (0.45)
	10.39−16.57	11.64−17.68	12.36−19.35	13.70−18.67
ash	1.26 (0.040)	1.33 (0.040)	1.36 (0.025)	1.39 (0.025)
	0.98−1.59	0.96−1.86	1.11−1.50	1.15−1.51
calcium	0.0041 (0.00022)	0.0040 (0.00022)	0.0053 (0.00036)[c]	0.0048 (0.00036)
	0.0032−0.0054	0.0032−0.0053	0.0035−0.0077	0.0036−0.0066
copper (mg/kg dwt)	2.22 (0.059)	2.33 (0.059)	1.46 (0.071)	1.57 (0.071)
	1.79−2.73	1.78−3.34	1.04−2.24	0.98−2.42
iron (mg/kg dwt)	19.92 (0.55)	19.72 (0.55)	22.32 (0.62)	22.31 (0.62)
	16.97−23.51	16.97−24.07	18.60−26.99	17.11−29.39
magnesium	0.11 (0.0024)	0.11 (0.0024)	0.12 (0.0032)	0.12 (0.0032)
	0.099−0.13	0.096−0.13	0.088−0.14	0.098−0.15
manganese (mg/kg dwt)	6.70 (0.28)	6.63 (0.28)	7.53 (0.41)[c]	8.00 (0.41)
	5.01−8.25	5.10−8.45	4.05−9.15	4.61−11.46
phosphorus	0.31 (0.0056)	0.31 (0.0055)	0.31 (0.0069)[c]	0.33 (0.0069)
	0.27−0.33	0.25−0.35	0.24−0.40	0.27−0.39
potassium	0.32 (0.0093)	0.33 (0.0093)	0.36 (0.0079)	0.36 (0.0079)
	0.28−0.37	0.27−0.41	0.30−0.42	0.30−0.45
sodium (mg/kg dwt)	<LOQ	<LOQ	1.46 (0.21)	1.42 (0.21)
			0.35−6.25	0.34−8.60
zinc (mg/kg dwt)	24.91 (0.64)	24.92 (0.63)	25.14 (0.77)[c]	27.67 (0.77)
	20.43−29.36	20.14−29.94	18.67−30.37	20.87−36.63

[a]dwt = dry weight. [b]Mean (SE) = least-squares mean (standard error). [c]Statistically significant at 5% level (α = 0.05).

by in-study reference hybrid values, the scientific literature, and the ILSI Crop Composition Database (ILSI-CCDB). This provides further information that a difference in mean values between the experimental hybrids and respective controls does not imply a meaningful difference from a food and feed safety perspective, especially if the difference is much less than natural variation due to other sources (i.e., environmental and varietal influences).

(3) Evaluations of graphical representations of the compositional data. Proponents of graphical approaches consider that the "location, range, and distribution of numerical values[6a] within a data set should be understood" to provide context to results from significance testing. Box plots (Figures 1−4) are presented to compare the variation observed in the selected experimental hybrid and control components. Results from VCA are also presented to understand and convey sources of variation in the data (Figure 5; Suppl. Tables 3 and 4).

Total Fat and Fatty Acids. No significant differences (α = 0.05) between total fat mean values were observed between the MON 87427 products and their respective near-isogenic controls (Table 1) using ANOVA. Differences were observed for only two of 10 fatty acids assessed (palmitic and oleic acids, Table 1) in MON 87427, and no differences in fatty acids were observed for MON 87427 × MON 89034 × NK603. By evaluating the observed differences for palmitic and oleic acid in MON 87427 using the logic described above, these differences are shown to be irrelevant from a compositional and food/feed perspective. The mean palmitic acid value was 11.34% total FA for MON 87427 and 11.67% total FA for the control, a difference of −0.32% total FA. This difference was less than the range of the control values, 2.39% total FA (Table 1; Figure 1A) calculated from the minimum (10.87% total FA) and maximum (13.26% total FA) palmitic acid values. The mean oleic acid values were 22.86% total FA for MON 87427 and 22.50% total FA for the control, a difference of 0.36% total FA. This was less than the range of the control values, 3.79% total FA (Table 2; Figure 1B), calculated similarly to above from minimum and maximum oleic acid values. The mean differences in palmitic and oleic acid values between MON 87427 and the control were less than the ranges of the control values, indicating that MON 87427 does not affect levels more than natural variation within the control grown at multiple locations. The mean differences in palmitic acid and oleic acid were also less than the variation seen in the reference values (palmitic acid range = 9.27−14.17% total FA and oleic acid range = 21.23−34.93% total FA; Suppl. Table 2), and the MON 87427 mean values were within values observed in the literature and the ILSI-CCDB values[13] (Suppl. Table 5). Maize is known to exhibit extensive variability in total fat and fatty acid levels,[14] and these results are consistent with the literature. Figure 1 illustrates how the concepts of variability discussed

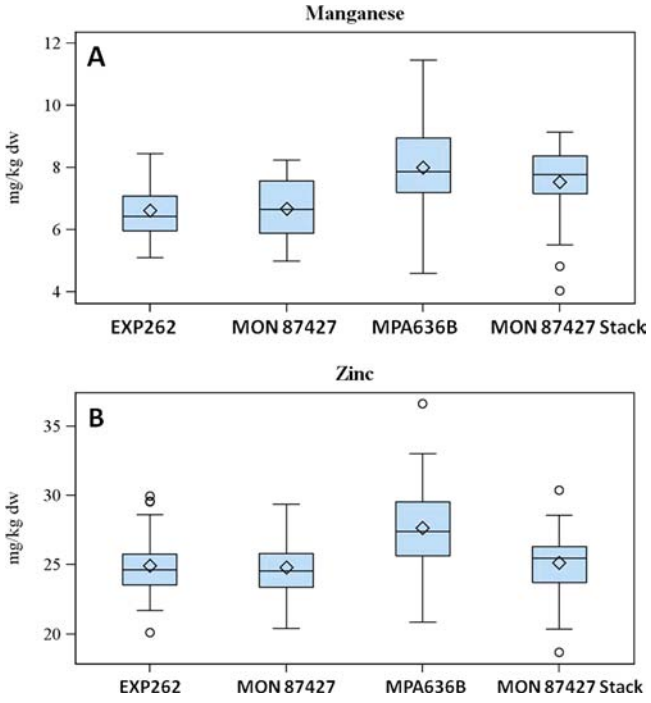

Figure 3. Box plot representing observed variability for manganese and zinc values in MON 87427 and MON 87427 × MON 89034 × NK603 (MON 87427 Stack) and their respective conventional control. Legends are the same as described in Figure 1. See Table 3 for details.

above can be presented graphically by comparing the observed variability in the experimental and control substances for palmitic and oleic acid. Figure 1 also demonstrates the similarities observed in values between the experimental and control hybrids. VCA results for all fatty acids are shown in the Supporting Information (Suppl. Tables 3 and 4). Overall, the greatest contributors to variation in both studies were location and residual error. Block and location × substance contributed least to variation in fat and fatty acid levels.

Vitamins. Significant differences (α = 0.05) between vitamin mean values were observed only for vitamin B_6 in MON 87427 compared to the near-isogenic control and for niacin in MON 87427 × MON 89034 × NK603 compared to the near-isogenic control (Table 2).

For vitamin B_6, the mean values were 6.92 mg/kg dwt for MON 87427 and 7.31 mg/kg dwt for the control, a difference of −0.39 mg/kg dwt. This difference was less than the range of the control values, 1.93 mg/kg dwt, indicating that MON 87427 does not affect levels of vitamin B_6 more than natural variation within the control grown at multiple locations. The corresponding range of values for MON 87427 was 1.92 mg/kg dwt (Table 2; Figure 2A).

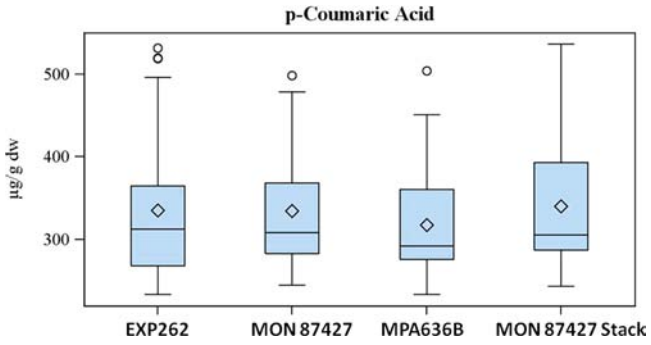

Figure 4. Box plot representing observed variability for *p*-coumaric acid values in MON 87427 and MON 87427 × MON 89034 × NK603 (MON 87427 Stack) and respective conventional control. Legends are the same as described in Figure 1. See Table 4 for details.

For niacin, the mean values were 16.33 mg/kg dwt for MON 87427 × MON 89034 × NK603 and 15.06 mg/kg dwt for the control, a difference of 1.27 mg/kg dwt. This difference was less than the range of the control values, 13.48 mg/kg dwt, indicating that MON 87427 × MON 89034 × NK603 does not affect levels of niacin more than natural variation within the control grown at multiple locations. The corresponding range of values for MON 87427 × MON 89034 × NK603 was 16.14 mg/kg dwt (Table 2; Figure 2B). The mean difference in vitamin B_6 and niacin was also less than the variation seen in the respective reference values (vitamin B_6 range in MON 87427 = 5.51−8.22 mg/kg dwt, niacin range in MON 87427 × MON 89034 × NK603 = 9.53−25.00 mg/kg dwt, respectively, Suppl. Table 2) and values observed in the literature and the ILSI-CCDB (Suppl. Table 5). Figure 2 compares the variation observed in experimental and control hybrids in individual values across sites for vitamin B_6 and niacin and emphasizes the observed similarities in values between experimental and control hybrids. VCA results for all vitamins are shown in Suppl. Tables 3 and 4 in the Supporting Information. Overall, the greatest contributions to variation in both studies were location and residual error. Block and location × substance overall contributed least to variation in vitamin levels.

Table 4. Summary of Maize Grain Antinutrients and Secondary Metabolites for MON 87427, MON 87427 × MON 89034 × NK603 and the Respective Conventional Controls

component (% dwt)[a]	MON 87427 (treated) mean (SE)[b] range	control EXP62 mean (SE) range	MON 87427 × MON 89034 × NK603 mean (SE) range	control MPA636B mean (SE) range
phytic acid	0.87 (0.020)	0.90 (0.020)	0.90 (0.021)	0.92 (0.021)
	0.73−0.97	0.66−1.01	0.71−1.10	0.70−1.10
raffinose	0.23 (0.0097)	0.24 (0.0096)	0.26 (0.011)	0.26 (0.011)
	0.18−0.28	0.19−0.28	0.20−0.34	0.22−0.32
ferulic acid (µg/g dwt)	2610.27 (102.62)	2574.27 (102.51)	3166.36 (105.26)	3093.29 (105.26)
	2120.18−3179.78	1943.50−3636.36	2709.97−3710.76	2560.99−3492.06
p-coumaric acid (µg/g dwt)	331.99 (28.49)	335.25 (28.48)	340.37 (27.71)[c]	317.80 (27.71)
	244.09−498.88	232.77−532.51	242.97−537.25	232.58−504.50

[a]dwt = dry weight. [b]Mean (SE) = least-squares mean (standard error). [c]Statistically significant at 5% level (α = 0.05).

dx.doi.org/10.1021/jf4041589 | J. Agric. Food Chem. 2014, 62, 1964−1973

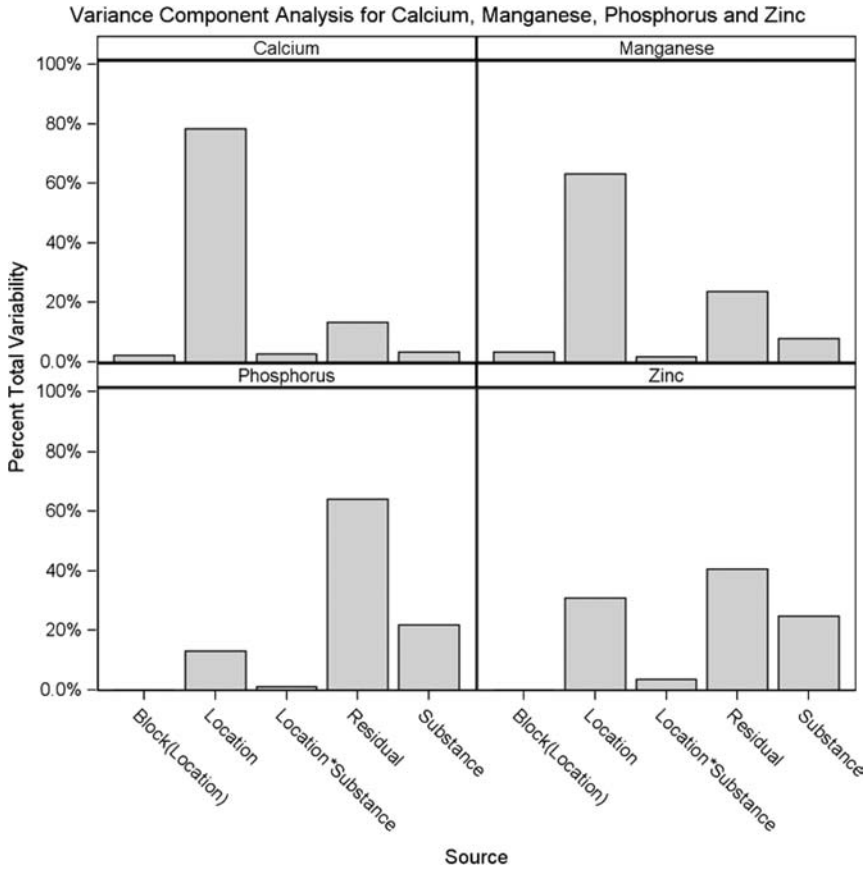

Figure 5. Sources of variation estimates from variance component analysis for calcium, manganese, phosphorus, and zinc values in MON 87427 × MON 89034 × NK603 (MON 87427 Stack).

Ash and Minerals. For MON 87427, no significant difference (α = 0.05) was observed for ash (Table 3) or minerals. For MON 87427 × MON 89034 × NK603, differences were observed for calcium, manganese, phosphorus, and zinc. Similar to the results observed for the fatty acids and vitamins discussed above, the logic applied above illustrated that observed significant mean differences (α = 0.05) for calcium, manganese, phosphorus, and zinc for MON 87427 × MON 89034 × NK603 were small relative to ranges of values observed for the control and reference hybrids as well as in the scientific literature. In other words, these data confirm that MON 87427 by itself or as part of a combined-stack product does not affect levels of minerals more than natural variation within the control grown at multiple locations. Mineral content in maize is known to vary by environment and germplasm.[15] Figure 3 compares the variation observed in experimental and control hybrids for manganese and zinc and highlights observed compositional similarity. VCA results for all minerals are shown in Suppl. Tables 3 and 4. Even though there were clear differences in the contribution of "location", "residual", and "substance" effects for different minerals, the greatest contributor to variation in both studies for most minerals was location. "Block" and "location × substance" overall contributed least to variation in mineral levels. Figure 5 shows results for calcium, manganese, phosphorus, and zinc from the MON 87427 × MON 89034 × NK603 study.

Antinutrient and Secondary Metabolites. Significant differences (α = 0.05) between antinutrient and secondary metabolite mean values were observed only for *p*-coumaric acid between MON 87427 × MON 89034 × NK603 and the near-isogenic control (Table 5). The mean *p*-coumaric acid values for MON 87427 × MON 89034 × NK603 were 340.37 and 317.80 μg/g dwt for the control, a difference of 22.57 μg/g dwt. This difference was much less than the range of the control values, 271.92 μg/g dwt, indicating that MON 87427 × MON 89034 × NK603 does not affect levels of *p*-coumaric acid more than natural variation observed within the control grown at multiple locations. The corresponding range of values from MON 87427 × MON 89034 × NK603 was 294.28 (Table 4; Figure 4). The mean difference was also less than the variation seen in the reference hybrid values (range = 104.18−608.45 μg/g dwt, Table 4) as well as the values observed in the literature and the ILSI-CCDB (Suppl. Table 5). Figure 4 shows the extensive variation associated with *p*-coumaric acid, and this variation can be attributed to location. The estimates of source of variation from variance component analysis are provided in Suppl. Tables 3 and 4 in the Supporting Information and highlight a major contribution (>75%) in both studies due to location.

Protein and Amino Acids. No significant differences (α = 0.05) in protein mean values were observed between the MON 87427 products and their respective near-isogenic controls (Table 5). The actual observed differences were small relative to the control; 2.33% for MON 87427 and −1.01% for MON 87427 × MON 89034 × NK603. To allow an assessment of the difference in amino acids in relation to a difference in protein, relative magnitudes of difference were expressed as a percent of control. Consistent with the changes observed with the protein values, the magnitudes of differences for amino acids were also small with statistical significance observed only for histidine,

Table 5. Summary of Maize Grain Protein and Amino Acids for MON 87427, MON 87427 × MON 89034 × NK603, and the Respective Conventional Controls

component (% dwt)[a]	MON 87427 mean (SE)[b] range	control EXP62 mean (SE) range	MON 87427 × MON 89034 × NK603 mean (SE)[b] range	control MPA636B mean (SE) range
protein	9.43 (0.20)	9.21 (0.20)	9.49 (0.38)	9.58 (0.38)
	8.25−10.74	7.44−10.51	7.47−11.14	6.79−11.90
alanine	0.70 (0.020)	0.68 (0.020)	0.73 (0.034)	0.73 (0.034)
	0.57−0.80	0.54−0.82	0.53−0.93	0.47−0.95
arginine	0.47 (0.0062)	0.47 (0.0062)	0.43 (0.012)	0.44 (0.012)
	0.43−0.53	0.42−0.53	0.35−0.49	0.34−0.52
aspartic acid	0.60 (0.011)	0.59 (0.011)	0.63 (0.025)	0.64 (0.025)
	0.52−0.66	0.52−0.65	0.48−0.79	0.43−0.79
cystine	0.20 (0.0040)	0.20 (0.0040)	0.21 (0.0061)	0.22 (0.0061)
	0.17−0.23	0.16−0.23	0.13−0.27	0.17−0.26
glutamic acid	1.71 (0.049)	1.65 (0.049)	1.88 (0.092)	1.89 (0.092)
	1.36−2.02	1.26−1.95	1.34−2.41	1.17−2.46
glycine	0.37 (0.0052)	0.36 (0.0052)	0.39 (0.0097)	0.40 (0.0097)
	0.34−0.40	0.31−0.41	0.32−0.44	0.32−0.45
histidine	0.27 (0.0048)[c]	0.26 (0.0048)	0.30 (0.0087)	0.31 (0.0087)
	0.23−0.29	0.19−0.30	0.24−0.35	0.23−0.37
isoleucine	0.33 (0.0090)	0.32 (0.0090)	0.35 (0.014)	0.35 (0.014)
	0.25−0.39	0.26−0.37	0.26−0.43	0.24−0.44
leucine	1.11 (0.040)	1.06 (0.040)	1.19 (0.064)	1.20 (0.064)
	0.83−1.31	0.76−1.31	0.83−1.53	0.73−1.60
lysine	0.26 (0.0043)	0.26 (0.0043)	0.31 (0.0079)	0.32 (0.0079)
	0.22−0.30	0.22−0.32	0.25−0.37	0.24−0.37
methionine	0.20 (0.0070)[c]	0.19 (0.0070)	0.23 (0.0086)	0.22 (0.0086)
	0.15−0.25	0.15−0.23	0.14−0.32	0.16−0.30
phenylalanine	0.47 (0.014)	0.45 (0.014)	0.51 (0.025)	0.52 (0.025)
	0.36−0.55	0.35−0.55	0.36−0.63	0.32−0.68
proline	0.82 (0.024)[c]	0.79 (0.024)	0.89 (0.035)	0.89 (0.035)
	0.62−0.95	0.57−0.95	0.67−1.08	0.60−1.11
serine	0.44 (0.0095)	0.43 (0.0094)	0.49 (0.020)	0.50 (0.020)
	0.38−0.53	0.34−0.51	0.37−0.60	0.35−0.63
threonine	0.34 (0.0053)	0.33 (0.0053)	0.37 (0.011)	0.38 (0.011)
	0.31−0.38	0.29−0.37	0.30−0.43	0.28−0.46
tryptophan	0.079 (0.0015)	0.079 (0.0015)	0.065 (0.0018)	0.067 (0.0018)
	0.072−0.087	0.068−0.097	0.057−0.072	0.053−0.077
tyrosine	0.36 (0.0092)	0.34 (0.0091)	0.26 (0.011)	0.27 (0.011)
	0.28−0.43	0.23−0.40	0.19−0.33	0.18−0.36
valine	0.44 (0.0080)	0.43 (0.0079)	0.46 (0.015)	0.47 (0.015)
	0.36−0.50	0.38−0.49	0.36−0.55	0.34−0.57

[a]dwt = dry weight. [b]Mean (SE) = least-squares mean (standard error). [c]Statistically significant at 5% level (α = 0.05).

methionine, and proline in the assessment of MON 87427 and no difference for MON 87427 × MON 89034 × NK603 (Table 5). The rationale applied above for other components reinforced how small these differences were by highlighting that MON 87427 did not affect levels of any amino acids acid more than natural variation within the control grown at multiple locations (Table 5). The mean histidine value was 0.27% dwt for MON 87427 and 0.26% dwt for the control, a difference of 0.0091% dwt. This difference was much less than range of the control values, 0.112% dwt (Table 1). Mean differences in methionine (0.011% dwt) and proline (0.032%) were also much less than the respective control ranges (0.081 and 0.383% dwt, respectively). The mean differences in histidine, methionine, and proline values were also less than the variation seen in the reference values (histidine range = 0.22−0.34% dwt, methionine range = 0.13−0.30% dwt, and proline range = 0.65−1.17% dwt; Suppl. Table 2), and the MON 87427 mean values were within values observed in the literature and the ILSI-CCDB (Suppl. Table 3). Together, these data confirm that the differences in mean values observed for the amino acids histidine, methionine, and proline in MON 87427 were not meaningful from a food/feed safety perspective. It is known that the levels of protein and amino acids in maize can vary widely depending on environmental conditions and agronomic practices.[4,16] The estimates of the source of variation for protein and amino acids from the VCA are provided in Suppl. Tables 3 and 4. The greatest sources of variation were "location" and "residual error".

Fibers and Carbohydrates by Calculation. No significant differences (α = 0.05) between carbohydrates and fiber mean values were observed between the MON 87427 and MON 87427 × MON 89034 × NK603 and their respective near-isogenic controls, respectively (Table 3).

Concluding Remarks. In summary, comprehensive compositional analysis shows that levels of key nutrients, antinutrients, and secondary metabolites in forage and grain of MON 87427, an inducible male sterile and tissue selective glyphosate-tolerant maize product, are comparable to the near-isogenic conventional control. Multiple sources (germplasm and location) of variation in the study were accounted for to aid in the interpretation of compositional outcomes. This methodology highlighted that differences between MON 87427 and the control were of small magnitude and inconsequential from a food/feed safety perspective. This study also highlights the fact that transgene insertion was a much smaller source of variation in the composition when compared to environmental effects. Results from analysis of MON 87427 × MON 89034 × NK603 confirm that this observation extends to the combined-trait product. With increasing global demand for food production, developments of new strategies for seed production are important to sustainable agriculture. MON 87427 offers a novel biotechnology-derived trait to produce hybrid seeds with decreased costs and labor while maintaining seed purity. The investigation reported here demonstrated that biotechnological approaches can be applied in enhancing hybrid maize seed production without affecting compositional quality.

■ ASSOCIATED CONTENT

Ⓢ Supporting Information

Summary of forage components, analyte ranges, VCA proportions, and literature and ILSI-CCDB ranges. This material is available free of charge via the Internet at http://pubs.acs.org.

■ AUTHOR INFORMATION

Corresponding Author

*(T.V.V.) E-mail t.v.venkatesh@monsanto.com.

Notes

The authors declare no competing financial interest.

■ ACKNOWLEDGMENTS

We thank the Monsanto Field Agronomy and Sample Management teams for production and preparation of the samples used in this study, the Monsanto Product Characterization group for the molecular analysis of the grain, EPL Bio-Analytical Services and Covance Laboratories Inc. for compositional analysis of the forage and grain samples, and Susan Riordan, Statistical Technology Centre and Certus International, Inc., for statistical analysis of the composition data. We also thank our colleagues Mark Groth, Regulatory Affairs Manager, LeAnna Stork, Lead, Statistics Technology Center, John Vicini, Lead, Scientific Affairs, and Cherian George, Composition Biology Center, for their critical review and feedback in improving the manuscript.

■ REFERENCES

(1) Bennetzen, J. L. H.; Hake, S. C. *Handbook of Maize, Genetics and Genomics*; Springer: New York, 2009.

(2) Feng, P. C. C.; Qi, Y.; Chiu, T.; Stoecker, M. A.; Schuster, C. L.; Johnson, S. C.; Fonseca, A. E.; Huang, J. Improving hybrid seed production in corn with glyphosate-mediated male sterility. *Pest Manage. Sci.* **2013**, n/a–n/a.

(3) Drury, S. M.; Reynolds, T. L.; Ridley, W. P.; Bogdanova, N.; Riordan, S.; Nemeth, M. A.; Sorbet, R.; Trujillo, W. A.; Breeze, M. L. Composition of forage and grain from second-generation insect-protected corn MON 89034 is equivalent to that of conventional corn (*Zea mays* L.). *J. Agric. Food Chem.* **2008**, *56* (12), 4623–4630.

(4) Ridley, W. P.; Harrigan, G. G.; Breeze, M. L.; Nemeth, M. A.; Sidhu, R. S.; Glenn, K. C. Evaluation of compositional equivalence for multitrait biotechnology crops. *J. Agric. Food Chem.* **2011**, *59* (11), 5865–5876.

(5) Harrigan, G. G.; Lundry, D.; Drury, S.; Berman, K.; Riordan, S. G.; Nemeth, M. A.; Ridley, W. P.; Glenn, K. C. Natural variation in crop composition and the impact of transgenesis. *Nat. Biotechnol.* **2010**, *28*, 402–404.

(6) (a) Harrigan, G. G.; Harrison, J. M. Assessing compositional variability through graphical analysis and Bayesian statistical approaches: case studies on transgenic crops. *Biotechnol. Genet. Eng. Rev.* **2012**, *28*, 15–32. (b) Herman, R. A.; Chassy, B. M.; Parrott, W. Compositional assessment of transgenic crops: an idea whose time has passed. *Trends Biotechnol.* **2009**, *27* (10), 555–557. (c) Mudge, J. F. Explicit consideration of critical effect sizes and costs of errors can improve decision-making in plant science. *New Phytol.* **2013**, *199* (4), 876–878. (d) Lovell, D. P. Biological importance and statistical significance. *J. Agric. Food Chem.* **2013**, *61* (35), 8340–8348. (e) EFSA. EFSA Scientific Committee. Statistical significance and biological relevance. *EFSA J.* **2011**, *9* (9), 17.

(7) Lundry, D. R.; Burns, J. A.; Nemeth, M. A.; Riordan, S. G. Composition of grain and forage from insect-protected and herbicide-tolerant corn, MON 89034 × TC1507 × MON 88017 × DAS-59122-7 (SmartStax), is equivalent to that of conventional corn (*Zea mays* L.). *J. Agric. Food Chem.* **2013**, *61* (8), 1991–1998.

(8) Saiki, R. K.; Innis, M. A.; Gelfand, D.; Sninsky, J. J.; White, T. J. In *PCR Protocols: A Guide to Methods and Applications*; Academic Press: New York, 1990; p 13.

(9) Drury, S. M.; Reynolds, T. L.; Ridley, W. P.; Bogdanova, N.; Riordan, S.; Nemeth, M. A.; Sorbet, R.; Trujillo, W. A.; Breeze, M. L. Composition of forage and grain from second-generation insect-protected corn MON 89034 is equivalent to that of conventional corn (*Zea mays* L.). *J. Agric. Food Chem.* **2008**, *56*, 4623–4630.

(10) (a) AOAC. AOAC International Method 923.03. In *Official Methods of Analysis of the AOAC International*, 18th ed.; Association of Official Analytical Chemists International: Gaithersburg, MD, USA, 2011. (b) ANKOM Technology. *ANKOM Technology Method 2*; Ankom Technology: Macedon, NY, USA, 2009. (c) Foss-Tecator. *Foss-Tecator Kjeltec 2400 Site Preparation, Installation, and Operating Guide*; Foss Tecator AB: Höganäs, Sweden, 1999. (d) AOAC. AOAC International Method 985.29. In *Official Methods of Analysis of the AOAC International*, 18th ed.; Association of Official Analytical Chemists International: Gaithersburg, MD, USA, 2011. (e) AOAC. AOAC International Method 923.03. In *Official Methods of Analysis of the AOAC International*, 18th ed.; Association of Official Analytical Chemists International: Gaithersburg, MD, USA, 2011. (f) Hong, J. L. Determination of amino acids by precolumn derivatization 6-aminoquinolyl-*N*-hydroxysuccinimidyl carbamate and ultra-performance liquid chromatography with ultraviolet detection. *J. Chromatogr., A* **1994**, *670* (1–2), 59–66. (g) AOAC. AOAC International Method 994.12. In *Official Methods of Analysis of the AOAC International*, 18th ed.; Association of Official Analytical Chemists International: Gaithersburg, MD, USA, 2011. (h) AOAC. AOAC International Method 939.05. In *Official Methods of Analysis of the AOAC International*, 18th ed.; Association of Official Analytical Chemists International: Gaithersburg, MD, USA, 2011. (i) AOCS. AOCS Method Ce 2-66. In *Official Methods and Recommended Practices of the AOCS*, 5th ed.; American Oil Chemists' Society: Champaign, IL, USA, 1997. (j) AOCS. AOCS Method Ce 2-66. In *Official Methods and Recommended Practices of the AOCS*, 5th ed.; American Oil Chemists' Society: Champaign, IL, USA, 1997. (k) AOCS. AOCS Method Ce 1e-91. In *Official Methods and Recommended Practices of the AOCS*, 5th ed.; American Oil Chemists' Society: Champaign, IL, USA, 2000. (l) AACC. AACC Method 86-80. In *Approved Methods of the American Association of Cereal Chemists*, 10th ed.; American Association of Cereal Chemists: St. Paul, MN, USA, 1999. (m) Weber, E. J. High performance liquid chromatography of the tocols in corn grain. *J.*

Am. Oil Chem. Soc. **1984**, *61.7*, 1231−1234. (n) Amaral, J. S. Simultaneous determination of tocopherols and tocotrienols in hazelnuts by a normal phase liquid chromatographic method. *Anal. Sci.* **2005**, *21*, 1545−1548. (o) AACC. AACC Method 86-47. In *Approved Methods of the American Association of Cereal Chemists*, 10th ed.; American Association of Cereal Chemists: St. Paul, MN, USA, 2000. (p) AOAC. AOAC International Method 986.11. In *Official Methods of Analysis of the AOAC International*, 18th ed.; AOAC International: Gaithersburg, MD, USA, 2011. (q) AACC. AACC Method 80-04. In *Approved Methods of the American Association of Cereal Chemists*, 10th ed.; American Association of Cereal Chemists: St. Paul, MN, USA, 2000. (r) Knapp, D. R. *Handbook of Analytical Derivatization Reactions*; Wiley: Somerset, NJ, USA, 1979. (s) Johansen, H. N.; Glisto, V.; Knudsen, K. E. B. Influence of extraction solvent and temperature on the quantitative determination of oligosaccharides from plant materials by high-performance liquid chromatography. *J. Agric. Food Chem.* **1996**, *44*, 1470−1474. (t) AOAC. AOAC International Method 999.11. In *Official Methods of Analysis of the AOAC International*, 18th ed.; Association of Official Analytical Chemists International: Gaithersburg, MD, USA, 2011. (u) AOAC. AOAC International Method 941.15. In *Official Methods of Analysis of the AOAC International*, 18th ed.; Association of Official Analytical Chemists International: Gaithersburg, MD, USA, 2011. (v) AACC. AACC Method 86-72. In *Approved Methods of the American Association of Cereal Chemists*, 10th ed.; American Association of Cereal Chemists: St. Paul, MN, USA, 1999. (w) AACC. AACC Method 86-51. In *Approved Methods of the American Association of Cereal Chemists*, 10th ed.; American Association of Cereal Chemists: St. Paul, MN, USA, 1999. (x) AACC. AACC Method 86-31. In *Approved Methods of the American Association of Cereal Chemists*, 10th ed.; American Association of Cereal Chemists: St. Paul, MN, USA, 1999. (y) Figueroa-Espinoza, M.-C.; Morel, M.-H.; Rouau, X. Effect of lysine, tyrosine, cysteine, and glutathione on the oxidative cross-linking of feruloylated arabinoxylans by a fungal laccase. *J. Agric. Food Chem.* **1998**, *46*, 2583−2589. (z) Krygier, K.; Sosulski, F.; Hogge, L. Free, esterified, and insoluble-bound phenolic acids. 1. Extraction and purification procedure. *J. Agric. Food Chem.* **1982**, *30*, 330−334. (aa) Classen, D.; Amason, J. T.; Serratos, J. A.; Lambert, J. D. H.; Nozzolillo, C.; Philogene, B. J. R. Correlation of phenolic acid content of maize to resistance to *Sitophilus zeamais*, the maize weevil, in CIMMYT'S collections. *J. Chem. Ecol.* **1990**, *16.2*, 301−315. (ab) Sosulski, F.; Krygier, K.; Hogge, L. Free, esterified, and insoluble-bound phenolic acids. 3. Composition of phenolic acids in cereals and potato flours. *J. Agric. Food Chem.* **1982**, *30*, 337−340. (ac) Bredie, W. L. P.; Mottram, D. S.; Guy, R. C. E. Aroma volatiles generated during extrusion cooking of maize flour. *J. Agric. Food Chem.* **1998**, *46*, 1479−1487. (ad) Buttery, R. G.; Stem, D. J.; Ling, L. C. Studies on flavor volatiles of some sweet corn products. *J. Agric. Food Chem.* **1994**, *42*, 791−795. (ae) Rogers, S. R.; Pesti, G. M. Determination of tryptophan from feedstuffs using reverse phase high-performance liquid chromatography. *J. Micronutr. Anal.* **1990**, *7.1*, 27−35.

(11) U.S. EPA. *Assigning Values to Non-Detected/Non-Quantified Pesticide Residues in Human Health Food Exposure Assessments*; U.S. Environmental Protection Agency, Office of Pesticide Programs: Washington, DC, 2000.

(12) Littell, R. C.; Milliken, G. A.; Stroup, W. W.; Wolfinger, R. D.; Schabenberger, O. *SAS for Mixed Models*; SAS Institute: Cary, NC, USA, 2006.

(13) ILSI. *Crop Composition Database*, version 4.1. International Life Sciences Institute: Washington, DC, 2010.

(14) (a) Miao, Y.; Mulla, D. J.; Robert, P. C.; Hernandez, J. A. Within-field variation in corn yield and grain quality responses to nitrogen fertilization and hybrid selection. *Agron. J.* **2006**, *98* (1), 129−140. (b) Thompson, D. L.; Jellum, M. D.; Young, C. T. Effect of controlled temperature environments on oil content and on fatty acid composition of corn oil. *J. Am. Oil Chem. Soc.* **1973**, *50* (12), 540−542.

(15) (a) Menkir, A. Genetic variation for grain mineral content in tropical-adapted maize inbred lines. *Food Chem.* **2008**, *110* (2), 454−464. (b) Singh, V.; Moreau, R. A.; Haken, A. E.; Eckhoff, S. R.; Hicks, K. B. Hybrid variability and effect of growth location on corn fiber yields and corn fiber oil composition. *Cereal Chem.* **2000**, *77* (5), 692−695. (c) Uribelarrea, M.; Below, F. E.; Moose, S. P. Grain composition and productivity of maize hybrids derived from the Illinois protein strains in response to variable nitrogen supply. *Crop Sci.* **2004**, *44* (5), 1593−1600. (d) Widdicombe, W. D.; Thelen, K. D. Row width and plant density effect on corn forage hybrids. *Agron. J.* **2002**, *94* (2), 326−330.

(16) (a) Harrigan, G. G.; Ridley, W. P.; Miller, K. D.; Sorbet, R.; Riordan, S. G.; Nemeth, M. A.; Reeves, W.; Pester, T. A. The forage and grain of MON 87460, a drought-tolerant corn hybrid, are compositionally equivalent to that of conventional corn. *J. Agric. Food Chem.* **2009**, *57* (20), 9754−9763. (b) Zhou, J.; Harrigan, G. G.; Berman, K. H.; Webb, E. G.; Klusmeyer, T. H.; Nemeth, M. A. Stability in the composition equivalence of grain from insect-protected maize and seed from glyphosate-tolerant soybean to conventional counterparts over multiple seasons, locations, and breeding germplasms. *J. Agric. Food Chem.* **2011**, *59* (16), 8822−8828.

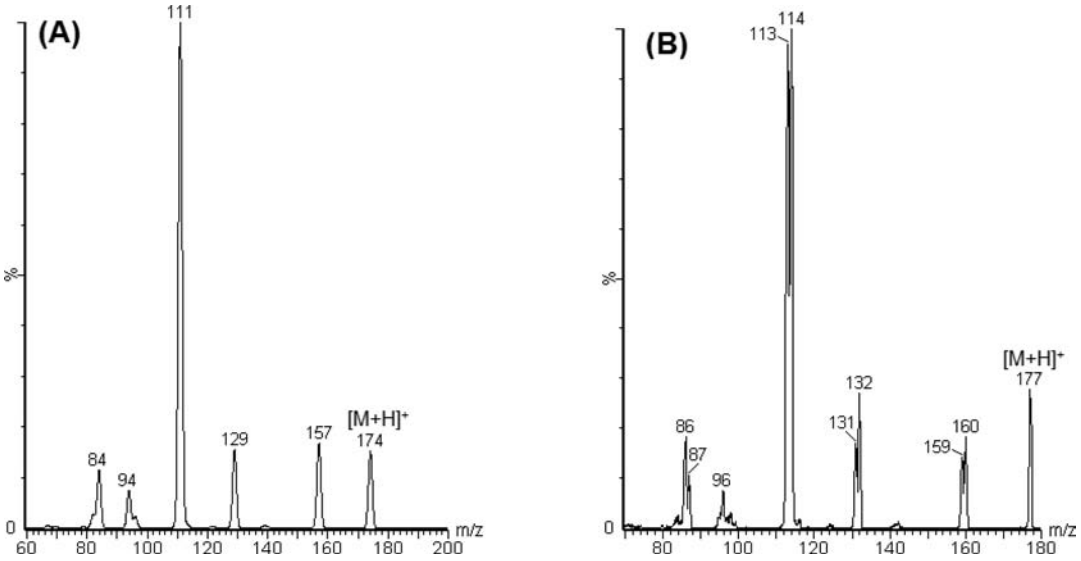

Figure 2. Tandem mass spectrometry fragmentation spectra of (A) indospicine and (B) D_3-L-indospicine.

times", and *I. linnaei* and *I. basedowii*, which are"preferred food plants".[18] Short-lived mass developments of forbs were reported to be seasonally utilized by camels, including *Indigofera* species in summer. Despite the reported dog poisoning incident,[16] the extent of indospicine (**2**) contamination of camel meat in Australia remains largely unknown. Consequently, this study was undertaken to develop and validate a high-throughput ultra-performance liquid chromatography–tandem mass spectrometry (UPLC–MS/MS) method to quantitate indospicine (**2**) in camel meat tissue. The validated method was then used to determine the concentrations of indospicine (**2**) in a number of collected camel meat samples obtained from a high camel density area of Australia, the Simpson Desert in the Northern Territory of Australia.

Indospicine (**2**) has previously been measured in plant material by amino acid analysis,[1,19,20] HPLC,[4,9] and, more recently, LC–MS/MS with phenylisothiocyanate derivitization.[21] Analysis of indospicine (**2**) in meat is more challenging due to the lower levels of toxin and the complex matrix. Indospicine (**2**) in animal tissues have previously been analyzed by lengthy (nearly 2 h) amino acid analysis[1,22] and by phenylisothiocyanate derivatization and UV detection, with resolution from other amino acids being problematic.[9] The incorporation of D_3-L-indospicine (**3**) (Figure 1) in this present study overcomes matrix effects noted in our previous LC–MS/MS analysis of camel tissues.[16]

MATERIALS AND METHODS

Indospicine Standards. Synthesized indospicine (**2**) and D_3-L-indospicine (**3**) were provided by Dr. James De Voss and Dr. Robert Lang, The University of Queensland.

Meat Materials. A total of 99 camels were sampled as part of a cull exercise under the Australian Feral Camel Management Project[23] in the Simpson Desert in central Australia. Rump muscle samples were excised from culled camels, placed in specimen containers, frozen, and transported to Health and Food Science Precinct, Brisbane, Australia. All of the samples were stored frozen (−30 °C) prior to extraction and analysis. Camel muscle samples free from indospicine (**2**) contamination (used for negative control and spike samples) were obtained from a pet food supplier, and these samples had been sourced from 200 km northwest of Rawlinna in Nullabor Plain, West Australia (an area relatively free from *Indigofera* species),[24] and stored frozen.

Indospicine Extraction. Prior to analysis, Amicon Ultra 0.5 mL, 3K centrifugal filter units (Merck Millipore, Kilsyth, Australia) were prerinsed and centrifuged (10 000 rpm, 20 min) with reverse osmosis water (2 × 300 μL) to remove glycerine and then inverted and spun for 1 min at 1000 rpm. Camel muscle samples were thawed, finely chopped, weighed (0.5 g), and mixed with 0.1% heptafluorobutyric acid (HFBA, 25 mL), follow by homogenization with a Polytron T25 Basic homogenizer (Labtek, Brendale, Australia) for 15 s. The homogenized samples were chilled (4 °C) for 20 min and then centrifuged at 4500 rpm for 20 min at 18 °C. Aliquots of supernatants (1.0 mL) spiked with the internal standard D_3-L-indospicine (**3**) (1 mg/L in 0.1% HFBA, 100 μL) were vortexed for 10 s. A portion (450 μL) was transferred into prerinsed Amicon Ultra 0.5 mL, 3K centrifugal filters, which were centrifuged (10 000 rpm, 20 min), with the filtrates transferred to a limited volume insert for UPLC–MS/MS analysis.

UPLC–MS/MS Equipment and Conditions. Sample data were collected by MassLynx 4.1 and processed by TargetLynx application managers. Separation of indospicine was done by a Waters ACQUITY UPLC system liquid chromatography (Waters, Rydalmere, Australia). LC separations were performed using a 100 mm × 2.1 mm i.d., 1.7 μm, BEH C18 column (Waters, Rydalmere, Australia) at 30 °C with flow rate of 0.2 mL/min. The mobile phase was a mixture of (A) H_2O with 0.1% HFBA (v/v) (pH 2.15) and (B) acetonitrile with 0.1% HFBA, which were prepared freshly for each analysis. The following gradient was used: 0 min, 99% A; 4 min, 70% A; 7 min, 70% A; 8 min, 99% A; 10 min, 99% A.

MS/MS detection was made using a Waters Micromass Quattro Premier triple quadrupole mass spectrometer with an electrospray ionization (ESI) source (Waters, Rydalmere, Australia), operated in the positive mode. Eluted indospicine (**2**) was quantitated by utilizing selected reaction monitoring (SRM) transitions of m/z 174.2 → 111.0 (verified by transition of m/z 174.2 → 157.1) for indospicine (**2**) and m/z 177.1 → 114.0 (verified by transition of m/z 177.1 → 113.0) for D_3-L-indospicine (**3**) as internal standard. The capillary voltage was 2.79 kV, cone gas flow was 50 L/h, and desolvation gas flow was 600 L/h. The source and desolvation temperatures were set at 150 and 350 °C, respectively. The argon gas collision energies for indospicine (**2**) (15 and 12 eV) and D_3-L-indospicine (**3**) (15 and 15 eV) were set with cone voltage at 25 V.

Synthesized indospicine (**2**) (external standard) and D_3-L-indospicine (**3**) (deuterium-labeled internal standard, >99% pure) were used in UPLC–MS/MS analysis. Internal (1 mg/L) and external standard (0.002–2 mg/L) solutions for indospicine (**2**) were prepared in H_2O with 0.1% HFBA. Solutions were frozen for no longer than 1 month.

Accurate Mass Analysis. Accurate mass analysis of both parent and daughter ions was performed on an AB SCIEX TripleTOF 5600+ system (AB SCIEX, Mt. Waverley, Australia) via direct injection and fragmentation of standard solutions of both indospicine and D_3-L-indospicine.

RESULTS AND DISCUSSION

UPLC−MS/MS Fragmentation of Indospicine and D_3-L-indospicine. Fragmentation of the protonated molecular ion of indospicine (**2**) ($[M + H]^+$ m/z 174) in positive-ion ESI mode produces a number of daughter ions, notably m/z 157 (loss of NH_3), m/z 129 (loss of NH_3 and CO), m/z 111 (loss of NH_3 and HCO_2H), and m/z 84 (loss of NH_3, CO_2H, and HCN), as seen in Figure 2. Accurate mass MS and MS/MS data confirmed the composition of each of the daughter ions, particularly the perhaps unexpected composition of m/z 129 as $C_6H_{13}N_2O$ (observed 129.1029, calculated 129.1028). We postulate then that the required loss of NH_3 and CO occurs via loss of NH_3 from the amidine group followed by formation of a cyclic lactone intermediate, from which it is possible to lose CO while retaining the second oxygen atom.

In the labeled standard D_3-L-indospicine (**3**), deuterium atoms are incorporated at C-5 (two deuterium) and C-6 (one deuterium), and this is evident in the fragmentation of the protonated molecular ion $[M + H]^+$ m/z 177, which produces corresponding daughter ions of m/z 160/159 (loss of NH_3/NH_2D), m/z 132/131 (loss of NH_3/NH_2D and CO), m/z 114/113 (loss of NH_3/NH_2D and H_2CO_2H), and m/z 86/87 (loss of NH_3/NH_2D, H_2CO_2H, and HCN), as seen in Figure 2. The fragmentation to almost equal proportion of each of these ion pairs is consistent with the proposed initial loss of NH_2 from the terminal amidine group with concomitant loss of either H or D from the monodeuterated C-6 position. Accurate mass MS and MS/MS data again confirmed that the composition of each of the daughter ions is consistent with the listed mass losses.

The most dominant daughter ion observed at m/z 111 was chosen as the transition (m/z 174 → 111) for quantitation of indospicine (**2**) using the selected reaction monitoring (SRM) program on the UPLC−MS/MS, with the m/z 157 daughter ion selected as the transition (m/z 174 → 157) for verification. The efficiency of the ionization and the detection of the precursor and fragments ions were optimized by adjusting collision energy (15 and 12 eV) and cone voltage (25 V). Similarly, the transition m/z 177 → 114 was selected for SRM quantitation of D_3-L-indospicine (**3**), with the transition m/z 177 → 113 for verification with optimized collision energy and cone voltage (15 eV and 25 V, respectively).

Development and Validation of a UPLC−MS/MS Method for Indospicine in Camel Meat Samples. The UPLC−MS/MS method reported here is a high-throughput yet sensitive analysis method for indospicine (**2**) in camel meat tissue, and this is the first reported indospicine analysis in unprocessed camel meat tissue based on the developed and validated UPLC−MS/MS method. The method involves a simple tissue extraction into aqueous solution followed by physical deproteinisation using centrifugal ultrafiltration before UPLC−MS/MS detection. The described UPLC separation on BEH C18 column eluting with water and acetonitrile (0.1% HFBA) gradients provides good peak shape and column retention. Heptafluorobutyric acid (HFBA) is an effective ion-pairing agent that is widely used in reverse-phase peptide/amino acid separations.[25] Concentrations of indospicine (**2**) in camel meat extracts (spiked samples and Simpson Desert samples) were determined by interpolating the relative intensity with a calibration curve. Calibration curves were constructed for each batch and involved plotting the ratio of the intensity of the positive-ion ESI SRM transition m/z 174 → 111 relative to the internal standard (D_3-L-indospicine, **3**) SRM transition m/z 177 → 114, versus the indospicine (**2**) concentrations for standard solutions of 0.002−2.00 mg/L. Seven-point calibration curves with the overlaid chromatograms of internal and external standards are shown in Figure 3.

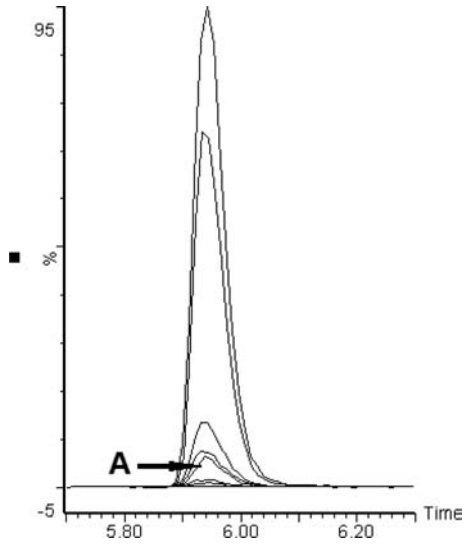

Figure 3. Overlaid SRM chromatograms of indospicine standards (0.002−2.00 mg/L) and internal standard (A) monitored by UPLC−MS/MS with ESI.

The limit of quantitation (LOQ) determined for this work was at least 9:1 for the peak-to-peak signal-to noise ratio for the quantitation transition (m/z 174 → 111). Both quantitation and qualification ions were monitored for each analysis. The average ratio of the quantitation peak to that of the qualification peak for spiked samples (n = 21) was 4.49. Confirmation of indospicine (**2**) was also carried out by examining the quantitation/qualification ion ratio, with the requirement that the ratio be within ±20%. Hence, only samples that have the ratio of 3.59 to 5.39 are considered to contain actual indospicine (**2**).

The calibration curves (n = 8) demonstrated good linearity with R^2 values of 0.9960 ± 0.004 throughout the analysis. Recovery efficiency and reproducibility of this analytical method were demonstrated by replicate analyses (n = 7) of the matrix spiked at three concentration levels: 2.5, 5.0, and 50.0 mg/kg indospicine-free camel meat. The spiked matrices were then extracted by the method described in indospicine (**2**) extraction. These spiking studies had recoveries of 106, 109, and 102%, respectively. The mean concentrations (standard deviation (SD), relative standard deviation (RSD)) of seven analyses for each spiked sample were 2.65 mg/kg (SD 0.24, RSD 9.06%), 5.43 mg/kg (SD 0.42, RSD 7.82%), and 51.01 mg/kg (SD 5.02, RSD 9.85%), respectively. The relative standard deviation was in all cases below 10% for three spiked samples, and this indicated that the method is reproducible with good precision. A significant clinical challenge with UPLC−MS/MS is the potential for matrix effects that cause interferences or impact ionization efficiency. The matrices of

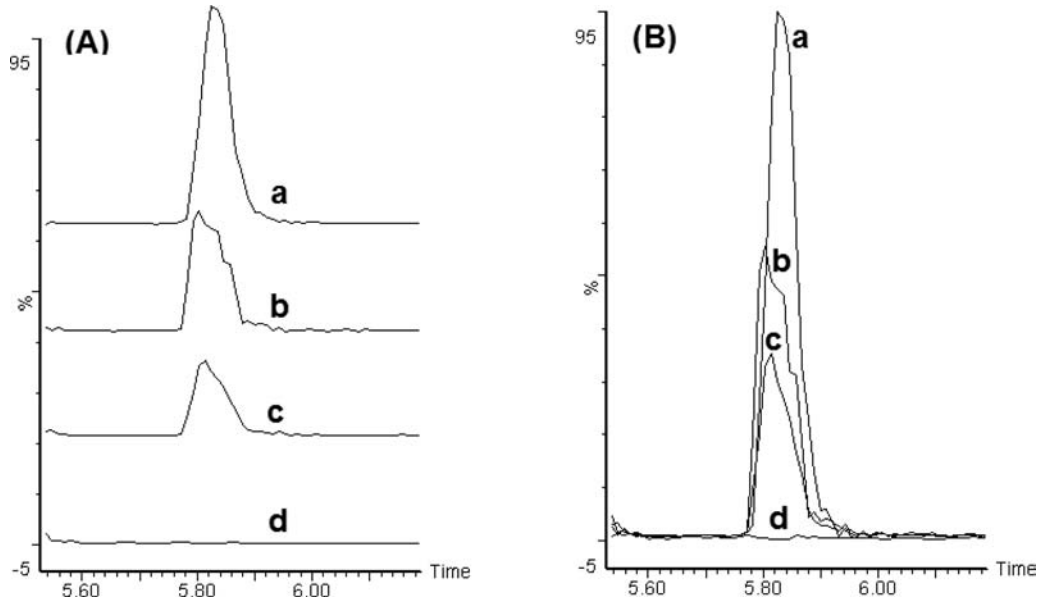

Figure 4. UPLC−MS/MS analysis of (A) individual and (B) overlaid SRM chromatograms for indospicine: (a) 0.05 mg/L standard, (b) 2.5 mg/L spiked sample, (c) Simpson Desert camel meat sample (SD_79) (1.41 mg/L), and (d) blank sample.

the extract can significantly ($p \leq 0.05$) suppress the indospicine and isotope-labeled internal standard responses. However, the use of stable isotope-labeled internal standards in this study to compensate for matrix effects and to increase accuracy resulted in the quantitation of matrix and matrix-free extracts having no substantial differences. Reagent spike recovery efficiency was not done due to this internal standard compensation principle. A blank matrix sample, spiked matrix samples, and spiked check samples were analyzed for each batch of analyses as part of the quality control for the validity of the analyses. The validity of indospicine (**2**) present in camel meat samples was ensured by spiked check samples being reported within 70% ≤ spike ≤130%. The study showed that the developed and validated method is reproducible with good recovery. Figure 4 shows UPLC−MS/MS analysis of individual and overlaid SRM chromatograms corresponding to indospicine (**2**), standard, spiked, real, and blank samples.

Trace amounts of glycerine present on the Amicon Ultra 0.5 mL, 3K centrifugal filter unit used in the extraction could interfere with the analysis by enhancing UPLC−MS/MS indospicine (**2**) responses. Hence, Amicon Ultra 0.5 mL, 3K centrifugal filter units are prerinsed twice to remove the interference. The response of indospicine (**2**) was then not significantly affected by the ultrafiltration step. To further minimize the effect of the Amicon Ultra 0.5 mL, 3K centrifugal filter, the internal standard was added prior to filtration in the sample preparation steps. While the use of an internal standard can correct for the effects of matrix on measured signals, as discussed earlier, an internal standard can also compensate for centrifugal filtration effects that occur when it cofilters with indospicine. In the method development process, recovery efficiency referrals to centrifugal filtered and noncentrifugal filtered external standards were carried out, and there was no significant difference between them. Therefore, the preparation of external standards for each batch of quantitation did not involve the ultrafiltration step. The indospicine (**2**) concentrations of the matrix spike samples were analyzed after 2 months of frozen storage and were still within standard deviation ranges. Thus, indospicine (**2**) is stable under cold storage conditions with low storage losses. This is in line with an indospicine stability study reported by Simpson and Hegarty.[22]

The current developed method is less time-consuming than the amino acid analyzer method,[2,19,20] more accurate and specific than the HPLC method,[9] and less tedious through the absence of derivatization in the sample preparation.[21] The indospicine (**2**) method reported here and the method developed by Gardner and Riet-Correa[21] are generally alike in their ease at achieving indospicine resolution from other components.

Indospicine in Camel Meat. To demonstrate the applicability of the developed and validated method, an analysis of a large number of meat samples from feral camel sampled as part of a cull exercise in the Simpson Desert was carried out. UPLC−MS/MS analysis of the feral camel meat samples revealed the presence of indospicine (**2**) at concentrations of 0−3.73 mg/kg. Figure 5 shows the number of contaminated camel meat samples by range of indospicine (**2**) concentrations.

The indospicine (**2**) concentrations have a skewed distribution toward a zero value. These results show that indospicine (**2**) does contaminate camel meat in central Australia and are consistent with the previous detection of indospicine (**2**) in minced camel meat.[16] However, more than 50% of the samples analyzed in this study have concentrations that are below the LOQ (0.1 mg/kg), while less than 5% of the samples have concentrations ≥1 mg/kg. Even so, several samples contained concentrations as high as 3.73 mg/kg. These results suggest caution, since a clinical investigation found that dietary exposure to an indospicine-contaminated pet food diet, of sweet potato/camel meat (2:1) containing indospicine at 2.1 mg/kg, could cause severe hepatic disease in dogs when consumed over extended time periods.[16] The camel meat used to make this diet would have contained 3 times this level (or 6.3 mg/kg), almost twice the maximal levels seen in the present study. The low prevalence of indospicine (**2**) residues in camels in this study may, however, have been affected by the below average and very much below average rainfall in central Australia for the past 12 months (April 2012−May 2013)[26]

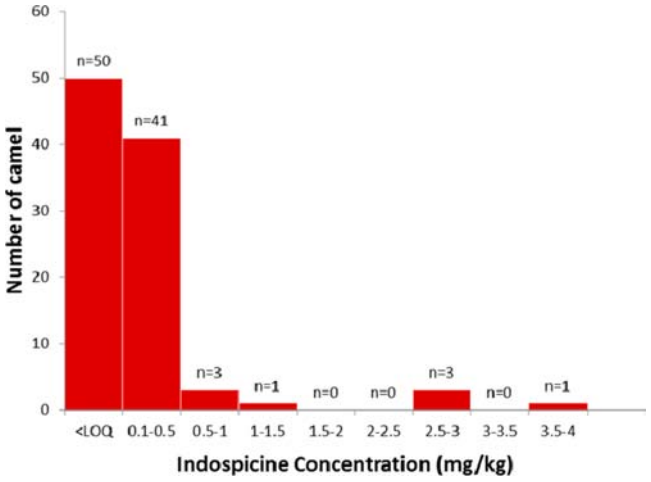

Figure 5. Number of camel meat samples contaminated by a range of indospicine concentrations (mg/kg).

before camel meat samples were being collected from Simpson Desert. *Indigofera* plants are known to be seasonally abundant, with the greatest density occurring after rain, which may lead to sporadic instances of higher *Indigofera* consumption by camels and potentially much higher indospicine (**2**) residues than found in the present study.

In conclusion, this is the first nonderivatized UPLC−MS/MS method developed and validated for the quantitation of indospicine (**2**) in camel meat samples, with a limit of detection down to 0.1 mg/kg. It was used for the definitive identification of indospicine (**2**) in feral camel meat samples collected from central Australia and has confirmed the presence of indospicine in them, but at levels far lower than has been previously associated with canine fatalities.[1,16]

AUTHOR INFORMATION

Corresponding Author

*Tel: +61 7 32766089. Fax: +61 7 326 6565. E-mail: mary.fletcher@uq.edu.au.

Funding

This study was partly funded by the Academic Training Scheme for Institutions of Higher Education (SLAI) Scholarship sponsored by the Malaysian Government.

Notes

The authors declare no competing financial interest.

ACKNOWLEDGMENTS

We are grateful for the support of the Australian Feral Camel Management Project, administered by NintiOne, and Jordan Hampton and Corissa Miller (Ecotone Wildlife Veterinary Services), who collected camel tissue samples. Dr. Maria Jose Gomez Ramos (The University of Queensland) performed accurate MS and MS/MS analysis, and UPLC−MS/MS technical advice was provided by Cindy Giles, Dennis Webber, and Warwick Turner (Department of Agriculture, Fisheries and Forestry, Queensland, Australia).

REFERENCES

(1) Hegarty, M. P.; Kelly, W. R.; McEwan, D.; Williams, O. J.; Cameron, R. Hepatotoxicity to dogs of horse meat contaminated with indospicine. *Aust. Vet. J.* **1988**, *65*, 337−40.

(2) Hegarty, M. P.; Pound, A. W. Indospicine, a hepatotoxic amino acid from *Indigofera spicata*: Isolation, structure, and biological studies. *Aust. J. Biol. Sci.* **1970**, *23*, 831−42.

(3) Charlwood, B. V.; Morris, G. S.; Grenham, M. J., A chemical database for the Leguminosae. In *Database in Systematics*, Alkin, R., Bisby, F. A., Eds.; Academic Press: London, 1984; pp 201−208.

(4) Ossedryver, S. M.; Baldwin, G. I.; Stone, B. M.; McKenzie, R. A.; van Eps, A. W.; Murray, S.; Fletcher, M. T. *Indigofera spicata* (creeping indigo) poisoning of three ponies. *Aust. Vet. J.* **2013**, *91*, 143−149.

(5) Morton, J. F. Creeping indigo (*Indigofera spicata* Forsk.) (Fabaceae): A hazard to herbivores in Florida. *Econ. Bot.* **1989**, *43*, 314−327.

(6) Wilson, P. G.; Rowe, R. A revision of the *Indigofereae* (Fabaceae) in Australia. 1. Indigastrum and the simple or unifoliolate species of *Indigofera*. *Telopea* **2004**, *10*, 651−682.

(7) Wilson, P. G.; Rowe, R. Three new species of *Indigofera* (Fabaceae: Faboideae) from Cape York Peninsula. *Telopea* **2008**, *12*, 285−292.

(8) Wilson, P. G.; Rowe, R. A revision of the *Indigofereae* (Fabaceae) in Australia. 2. *Indigofera* species with trifoliolate and alternately pinnate leaves. *Telopea* **2008**, *12*, 293−307.

(9) Pollitt, S.; Hegarty, M. P.; Pass, M. A. Analysis of the amino acid indospicine in biological samples by high performance liquid chromatography. *Nat. Toxins* **1999**, *7*, 233−240.

(10) Hegarty, M. P., Non-metallic chemical residues in toxic plants with potential importance to animal and human health. In *Vet Update '92*; Osborne, H. G., Ed.; University of Queensland. Continuing Professional Education: Brisbane, 1992; pp 323−332.

(11) Young, M. P. Investigation of the toxicity of horsemeat due to contamination by indospicine. Ph.D. Thesis, University of Queensland, Brisbane, Australia, 1992.

(12) AZRI, Arid Zone Research Institute. Indospicine in beef. In *Northern Territory Department of Primary Industries and Fisheries Technical Annual Report 1987−1988*; NTDPIF: Alice Springs, Australia, 1989; p 39.

(13) Pollitt, S. Residue implications of indospicine, a toxic, non-protein amino acid. Ph.D. Thesis, University of Queensland, Brisbane, Australia, 2001.

(14) Christie, G. S.; Wilson, M.; Hegarty, M. P. Effects on the liver in the rat of ingestion of *Indigofera spicata*, a legume containing an inhibitor of arginine metabolism. *J. Pathol.* **1975**, *117*, 195−205.

(15) Kelly, W. R.; Young, M. P.; Hegarty, M. P.; Simpson, G. D. The hepatotoxicity of indospicine in dogs. In *Poisonous Plants*; James, L. F., Keeler, R. F., Bailey, E. M., Cheeke, P. R., Hegarty, M. P., Eds.; Iowa State University Press: Ames, IA, 1992; pp 126−130.

(16) FitzGerald, L. M.; Fletcher, M. T.; Paul, A. E. H.; Mansfield, C. S.; O'Hara, A. J. Hepatotoxicosis in dogs consuming a diet of camel meat contaminated with indospicine. *Aust. Vet. J.* **2011**, *89*, 95−100.

(17) Edwards, G.; Zeng, B.; Saalfeld, W.; Vaarzon-Morel, P.; McGregor, M. *Managing the Impacts of Feral Camels in Australia: A New Way of Doing Business. DKCRC Report 47*; Desert Knowledge Cooperative Research Centre: Alice Springs, Australia, 2008.

(18) Dörges, B.; Heucke, J.; Dance, R. *The palatability of Central Australian plant species to camels. Technote No. 116*; Department of Primary Industry, Fisheries and Resources: Northern Territory Government, Alice Springs, Australia (www.nt.gov.au/d/Content/File/p/Technote/TN116.pdf), July 11, 2013.

(19) Aylward, J. H.; Court, R. D.; Haydock, K. P.; Strickland, R. W.; Hegarty, M. P. *Indigofera* species with agronomic potential in the tropics. Rat toxicity studies. *Aust. J. Agric. Res.* **1987**, *38*, 177−86.

(20) Miller, R. W.; Smith, C. R., Jr. Seeds of *Indigofera* species. Their content of amino acids that may be deleterious. *J. Agric. Food Chem.* **1973**, *21*, 909−12.

(21) Gardner, D. R.; Riet-Correa, F. Analysis of the toxic amino acid indospicine by liquid chromatography−tandem mass spectrometry. *IJPPR* **2011**, *1*, 20−27.

(22) Simpson, G. D.; Hegarty, M. P. Determination of indospicine in biological material. *Tropical Agronomy Technical Memorandum 57*;

CSIRO Australia, Division Tropical Crops and Pastures: Brisbane, Australia, 1987.
(23) Australia Feral Camel Management Project. http://www.feralcamels.com.au/ (Accessed October 14, 2013).
(24) The Council of Heads of Australasian Herbaria Australia's Virtual Herbarium. http://avh.chah.org.au (Accessed September 3, 2013).
(25) Guo, D.; Mant, C. T.; Hodges, R. S. Effects of ion-pairing reagents on the prediction of peptide retention in reversed-phase high-resolution liquid chromatography. *J. Chromatogr.* **1987**, *386*, 205−222.
(26) The Bureau of Meteorology Australia. http://www.bom.gov.au/ (Accessed October 11, 2013)

Table 1. Composition of Digestive Juices (1 L) Used for in Vitro Incubation of Meat Samples

digestion[a]													fermentation					
mouth			stomach			duodenum							colon					
saliva (pH 6.8)			gastric juice (pH 1.3)			duodenal juice (pH 8.1)			bile (pH 8.2)				SHIME medium[b] (pH 7.0)			cultured bacterial inoculum[c]		
Inorganic Solution																		
0.90	g	KCl	2.75	g	NaCl	7.01	g	NaCl	5.26	g	NaCl		6.8	g	KH_2PO_4	0.51	g	NaCl
0.2	g	KSCN	0.27	g	NaH_2PO_4	3.39	g	$NaHCO_3$	5.79	g	$NaHCO_3$		8.8	g	K_2HPO_4	0.01	g	KCl
0.9	g	NaH_2PO_4	0.82	g	KCl	0.08	g	KH_2PO_4	0.38	g	KCl					0.23	g	$Na_2HPO_4{\cdot}12H_2O$
0.57g	g	$NaSO_4$	0.40	g	$CaCl_2{\cdot}2H_2O$	0.56	g	KCl	0.15	mL	HCl 37%					0.02	g	KH_2PO_4
0.3	g	NaCl	0.31	g	NH_4Cl	0.05	g	$MgCl_2$										
1.6	g	$NaHCO_3$	6.50	mL	HCl 37%	0.18	mL	HCl 37%										
Organic Solution																		
0.20	g	urea	0.09	g	urea	0.10	g	urea	0.25	g	urea		1.0	g	arabinogalactan	0.06	g	$C_2H_3NaO_2S$
11.5	mg	uric acid	0.02	g	glucuronic acid	1.00	g	BSA					3.0	g	yeast extract	33.3	g	brain heart infusion
25.0	mg	mucin	0.65	g	glucose	9.00	g	pancreatin	1.80	g	BSA		0.4	g	glucose	0.45	g	L-cystein-HCl
2.50	IU	peroxidase[d]	0.33	g	glucosamine-HCl	1.50	g	lipase	30.0	g	bile		0.5	g	L-cystein-HCl	16.0	mL	fecal matter
			17.6	mg	ascorbic acid[f]								4.0	g	mucin	20.0	mL	glycerol
			1.00	g	BSA								2.0	g	pectin			
			2.50	g	pepsin								1.0	g	pepton			
			3.00	g	mucin								1.0	g	xylan			
													4.0	g	potato starch			
Add																		
6.90	mg	$NaNO_2$[e]	10.0	μL	H_2O_2 (30%)[g]	0.200	g	$CaCl_2{\cdot}2H_2O$	0.222	g	$CaCl_2{\cdot}2H_2O$							
			11.2	mg	$FeSO_4{\cdot}7H_2O$[h]													

[a]Digestion: based on Versantfoort et al.[20] unless otherwise indicated [b]SHIME medium: Molley et al.[26] [c]Bacterial inoculum was cultured under anaerobic conditions for 24 h at 37 °C and used immediately in the fermentation procedure. [d]Peroxidase: Güven et al.[21] [e]$NaNO_2$: Takahama et al.[22] [f]Ascorbic acid: Dabrowska-Ufniarz et al.[23] [g]H_2O_2: Nalini et al.[24] [h]$FeSO_4$: Nalini et al.[24]

dx.doi.org/10.1021/jf4057583 | J. Agric. Food Chem. 2014, 62, 1980−1988

nitrosative stress during digestion of meat. For this purpose, uncured and nitrite-cured cooked chicken, pork, and beef as low, medium, and high sources of heme-Fe, respectively, were subjected to a multicompartment in vitro digestion model. In the digests, the major toxic lipid oxidation products MDA and 4-HNE and the less toxic simple aldehydes pentanal, hexanal, heptanal, and nonanal were determined. During the oxidation of proteins, carbonylation is one of the most prominent protein modifications[19] and, hence, measurement of protein carbonyl compounds (PCC) was used to estimate protein oxidation during digestion. The NOC-specific DNA adduct O^6-carboxymethyl-guanine (O^6-C-MeG) was determined in digesta to estimate DNA damage induced by nitrosative stress. O^6-C-MeG is a far more specific end point than the commonly used "apparent total nitroso-compounds" (ATNC) because (i) it demonstrates DNA damage caused by alkylating NOCs and (ii) ATNC also include noncarcinogenic nitrosyl-Fe and nitrosothiols along with the carcinogenic NOCs.

MATERIALS AND METHODS

Experimental Setup. Uncured and nitrite-cured cooked chicken, pork, and beef were compared before and after mimicked duodenal and colonic digestion. Each incubation run included all treatments in quadruplicate, from which two duplicates underwent digestion until the duodenum and two until the colon step. Each incubation run was performed three times with fecal inoculum originating from three different human volunteers.

Manufacturing of Meat Samples. Lean meat samples from the *m. Pectoralis profundus* (chicken), *m. Longissimus dorsi* (pork), and *m. Biceps femoris* (beef) were purchased in a local supermarket. The meat was manually chopped into cubes of approximately 1−2 cm^3. To exclude a possible confounding effect of differences in fatty acid composition, 4% subcutaneous pork fat was added to the different lean meat sources. Meat samples with added fat were first minced in a grinder (Omega T-12) equipped with a 10 mm plate, followed by grinding through a 3.5 mm plate. Thereafter, nitrite curing was applied by adding 20 g of 0.6% nitrite salt/kg meat, corresponding to an added concentration of 120 mg nitrite/kg meat. All meat samples were heated in a warm water bath for 15 min after the core temperature had reached 65 °C. After manufacturing, all meat samples were homogenized in three 5 s bursts using a food processor (Moulinex DP700), vacuum packed, and stored at −20 °C until the start of the incubation.

Incubations. The in vitro digestions consisted of an enzymatic digestion simulating the mouth, stomach, and duodenum gastrointestinal tract compartments, followed by a simulation of colonic fermentation. For the enzymatic digestion, the protocol described by Versantfoort et al.[18] was adapted by adding oxidants and antioxidants that are normally present in digestive juices (Table 1). Hence, peroxidase[21] and $NaNO_2$[22] were added to the saliva juice, and ascorbic acid,[23] H_2O_2,[24] and ferrous iron[24] were added to the gastric juice. Meat samples (4.5 g) were sequentially incubated for 5 min with 6 mL of saliva, for 2 h with 12 mL of gastric juice, and for 2 h with 2 mL of bicarbonate buffer (1 M, pH 8.0), 12 mL of duodenal juice, and 6 mL of bile juice. These enzymatic incubations were performed in quadruplicate. After completion, two replicates were diluted with 44 mL of H_2O to obtain the same solid/liquid ratio as in the colonic digestion (see below) and homogenized with an Ultraturrax (9500 rpm). While stirring on a magnetic field in the dark, samples were subdivided in 1.3 mL aliquots and stored at −20 and −80 °C pending analysis. The two remaining replicates underwent the additional colonic fermentation stage according to the method of Van de Wiele et al.[25] Simulation of the human intestinal microbial ecosystem (SHIME) medium (22 mL)[26] and a human fecal inoculum (22 mL) (for preparation, see Preparation of Human Fecal Inoculum) were added to the digesta. The vessels were flushed with N_2 for 30 min to obtain an anaerobic environment. Anaerobic conditions in flasks with digesta in the colon phase were confirmed, using resazurin-saturated test strips. Subsequently, the vessels were incubated for 72 h with stirring at 37 °C. To evaluate the rate of bacterial fermentation, total anaerobic bacteria were counted after 72 h of fermentation. One milliliter of digesta was serially diluted (10-fold) using a sterile peptone solution (1 g/L peptone, 0.4 g/L agar, 8.5 g/L NaCl, and 0.5 g/L cystein), after which 0.1 mL was added on an reinforced clostridial medium (RCM) plate. After 48 h of incubation at 37 °C, colony-forming units (CFU) were counted and expressed as $\log_{10}$ CFU/mL digesta. As for the duodenal samples, colonic digestion samples were homogenized by Ultraturrax at 9500 rpm. While stirring on a magnetic field in the dark, samples were subdivided in 1.3 mL aliquots and stored at −20 and −80 °C until analyses. Undigested control samples were obtained in duplicate by homogenizing 4.5 g of meat in 82 mL of H_2O, mimicking the liquid/solid ratio in the digested samples.

Preparation of Human Fecal Inoculum. Fresh fecal material was collected from three volunteers without known gastrointestinal diseases and without intake of antibiotics for at least 6 months. All volunteers were male, nonvegetarians on a Western diet, and aged 49, 26, and 38 years, respectively. Fresh fecal material was diluted in preheated PBS solution (1:4; w/v), to which sodium thioglycolate (1 g/L) was added as a reducing agent. The fecal slurry was filtered by a 1 mm metal sieve to remove particulate matter. Afterward, the inocula were stored at −80 °C on a glycerol stock (20%) in different aliquots. Before use in the colonic fermentation phase, the bacterial inoculum was cultured during 24 h at 37 °C to obtain the necessary microbiotic culture. For this purpose, fecal inoculum was diluted with brain heart infusion (BHI) broth (37 g/L BHI and 0.5 g/L cysteine) at a 1:9 ratio. Subsequently, anaerobic conditions in the flask were reached by flushing the headspace with N_2 during 1 h.

Chemical Composition of the Meat Samples. Meat samples were analyzed for dry matter, crude protein, and crude fat content according to ISO 1442-1973, ISO 937-1978, and ISO 1444-1973 methods, respectively. Lipids were extracted using chloroform/methanol (2:1; v/v)[27] and subsequently, fatty acids (FA) were analyzed as described by Raes et al.[28] Briefly, FA were methylated and analyzed by gas chromatography (HP6890, Brussels, Belgium) using a CP-Sil88 column for fatty acid methyl esters (FAME; 100 m × 0.25 mm × 0.25 μm; Chrompack, Middelburg, The Netherlands). Peaks were identified, on the basis of their retention times corresponding with standards (NuChek Prep. Inc., Sigma, Bornem, Belgium). Nonadecanoic acid (C19:0) was used as an internal standard to quantify the individual and total FA. The fatty acid profiles were expressed in grams per 100 g of FAME. Residual nitrite concentrations were measured colorimetrically at 538 nm after diazotization with sulfanilamide and *N*-(1-naphthyl)ethylenediamine dihydrochloride (ISO 2918-1975). Nitrite concentrations were calculated on the basis of a standard curve obtained with sodium nitrite and expressed as milligrams of nitrite per kilogram of meat. Hematin was determined colorimetrically according to the method of Hornsey et al.[29] and converted to heme-Fe using the formula heme-Fe = hematin × atomic weight Fe/molecular weight hematin. Total Fe was determined by ICP-AES (Iris Intrepid II XSP, Thermo Electron Corp.) following destruction by Bunsen burner and dry incineration at 550 °C for 4 h, followed by dissolving in 3 mL of concentrated HNO_3, diluting to 10 mL of HNO_3, and filtration. Total Fe was calculated on the basis of a standard curve and expressed as milligrams per 100 g of meat.

Oxidation Products. MDA concentrations in digesta (−20 °C) were measured according to a modified method in accordance with Grotto et al.[30] TBARS were formed from the reaction of MDA with 2-thiobarbituric acid in an acid environment. After extraction in 1-butanol, the absorbance of the colored complex was measured colorimetrically at 532 nm. A standard curve with 1,1,3,3-tetramethoxypropane was used, and the concentration was expressed as nanomoles of MDA per milliliter of solution.

Levels of 4-HNE, pentanal, hexanal, heptanal, octanal, and nonanal were analyzed in digesta (−80 °C) through HPLC (Agilent 1200 series, provided with a degasser, autosampler, quaternary pump, column oven, fluorescence detector) using an adapted method of Holley et al.[31] All solutions were purified with activated carbon and

Table 2. Composition of the Meat Model Products Used in the in Vitro Digestion Experiment[a]

		uncured			nitrite-cured				*P* values		
	unit	chicken	pork	beef	chicken	pork	beef	RMSE	H	NC	H × NC
dry matter	%	30.1	31.9	30.6	31.3	31.9	30.0	0.45	**0.027**	**0.727**	0.040
protein	%	23.8	21.5	21.4	22.9	22.2	21.3	0.95	0.055	0.829	0.526
fat	%	4.7b	5.6a	5.3ab	4.1b	5.4a	4.6b	0.22	**<0.001**	**0.008**	0.414
SFA	g/100 g FAME	37.8	38.0	36.6	37.1	38.3	37.5	1.21	0.466	0.804	0.686
MUFA	g/100 g FAME	41.3ab	42.2a	39.6b	40.3ab	42.4a	38.2c	0.85	**0.004**	0.178	0.474
PUFA	g/100 g FAME	17.7a	16.0c	16.9b	17.5a	15.9b	16.3b*	0.20	**<0.001**	**0.021**	0.301
ALA	g/100 g FAME	0.80b	0.69c	0.90a	0.79b	0.65c	0.89a	0.015	**<0.001**	0.140	0.504
LC n-3 PUFA	g/100 g FAME	0.50b	0.29c	0.90a	0.53b	0.27c	0.91a	0.037	**<0.001**	0.919	0.568
LA	g/100 g FAME	14.1a	12.9b	12.7b	13.8a	12.8b	12.1c*	0.210	**<0.001**	**0.023**	0.252
LC n-6 PUFA	g/100 g FAME	1.43b	1.36b	1.75a	1.47b	1.38b	1.76a	0.055	**<0.001**	0.491	0.917
residual nitrite	mg/100 g				60.0a	36.4b	18.5c	0.58	**<0.001**		
total Fe	mg/100 g	0.43b	0.55b	1.38a	0.41b	0.49b	1.44a	0.079	**<0.001**	0.894	0.549
heme-Fe	mg/100 g	0.14b	0.25b	1.33a	0.15b	0.31b	1.34a	0.044	**<0.001**	0.433	0.844

[a]SFA, saturated fatty acids; MUFA, monounsaturated fatty acids; PUFA, polyunsaturated fatty acids; ALA, α-linolenic acid (C18:3, n-3); LC n-3 PUFA, long-chain omega-3 polyunsaturated fatty acids (C20:5, n-3; C22:5, n-3; C22:6, n-3); LA, linoleic acid (C18:2, n-6); LC n-6 PUFA, long chain omega-6 polyunsaturated fatty acids (C20:4, n-6; C22:4, n-6; C22:5, n-6); FAME, fatty acid methyl esters; RMSE, root-mean-square error; H, heme-Fe content; NC, nitrite-curing. Means for different heme-Fe content (within curing treatment) with different letters (a–c) are significantly different ($P < 0.05$); * , significantly different from uncured equivalent ($P < 0.05$).

filtered. For preparation of the cyclohexanedione (CHD) reagent, 10 g of ammonium sulfate and 0.29 mL of acetic acid were dissolved in 100 mL, adjusted to pH 5, and purified with activated carbon. After filtration, 0.25 g of CHD, dissolved in 2 mL of activated carbon purified MeOH, was added to the mixture. All glassware was cleaned with ethanol and H_2O and dried in a 100 °C oven to remove contaminating aldehydes. One milliliter of digest was mixed with 4 mL of $CHCl_3$/MeOH (2:1, v/v) and 0.4 mL of NaCl (9%). After a 30 s vortex, the mixture was centrifuged (5 min, 1100*g*) and the $CHCl_3$ phase was collected. The remaining aqueous solution was mixed again with 2 mL of $CHCl_3$/MeOH, and the $CHCl_3$ phase was collected as described before. The combined $CHCl_3$ phases were dried under a gentle N_2 stream. The dried residue was resolved in 0.1 mL of MeOH, 0.4 mL of H_2O, and 1 mL of CHD reagent. After 1 h of heating at 60 °C in a warm water bath, samples were filter sterilized (0.2 μm cellulose membrane filter) in dark HPLC vials. The injection volume was 80 μL and the flow rate, 1 mL/min. Separation was done on a Supelcosil LC-18 column (25 cm × 4.6 mm, 5 μm, catalog no. 58295, Supelco), using stepwise elution (50% tetrahydrofuran from 0 to 40 min). The derivatized aldehydes were detected by a fluorescence detector at an excitation wavelength of 380 nm and an emission wavelength of 446 nm. Aldehydes were quantified using a standard curve and expressed as picomoles of aldehyde per milliliter of solution.

The measurement of PCC following their covalent reaction with 2,4-dinitrophenylhydrazine (DNPH) was done according to the method of Ganhão et al.[32] This reaction leads to the formation of a stable 2,4-dinitrophenyl hydrazone product. Total carbonyl content was quantified colorimetrically at 370 nm, using a molar absorption coefficient of 21.0/(mM·cm) and expressed as nanomoles of DNPH per milligram of protein. Protein concentrations were measured at 280 nm after reaction with 2 M HCl instead of DNPH, quantified using a standard curve with BSA, and expressed as milligrams per milliliter of solution. Both PCC and protein concentrations were reported separately.

O^6-Carboxy-methylguanine (O^6-C-MeG). The internal standard O^6-methyl-d_3-guanine (O^6-d3-MeG) was obtained from Toronto Research Chemicals Inc. (Toronto, Canada). O^6-Carboxymethyl-deoxyguanosine (O^6-C-MedG) was a gift from S.A. Moore (Liverpool John Moores University, UK). The NOC-specific DNA adduct O^6-C-MeG was quantified using U-HPLC-MS/MS.[33] In brief, 182 μL of filter-sterilized sample was incubated for 18 h at 37 °C with 100 μg of calf thymus (CT)-DNA. After addition of the internal standard (50 μL, 20 ng/mL O^6-d3-MeG), the mixture was dissolved in 2 mL of 0.1 M formic acid and hydrolyzed by heating (80 °C for 30 min). The hydrolysate was cooled on ice and then applied to an Oasis HLB cartridge (SPE) (30 mg, 1 mL), which was conditioned with 2 mL of 100% MeOH and equilibrated with 2 mL of deionized water. After loading the hydrolysate, a vacuum suction was applied on the SPE cartridge, followed by the elution step with 2 mL of 100% MeOH. The collected fraction was evaporated to dryness (90 min, 20 °C) using a SpeedVac Plus (Savant, Holbrook, NY, USA). Finally, the dried residue was dissolved in a total volume of 100 μL of mobile phase consisting of 95:5 0.05% aqueous acetic acid/H_2O. Chromatographic separation of the DNA adducts was achieved by reversed phase chromatography and gradient elution. Separation of the DNA adducts was carried out on a Nucleodur C18 ISIS column (5 μm, 250 × 4 mm, Machery Nagel, Düren, Germany), kept at 30 °C. Analysis was performed on a triple-quadrupole mass analyzer (TSQ Vantage, Thermo Electron, San Jose, CA, USA), fitted with a heated electrospray ionization (HESI-II) source operating in the positive ion mode. A standard curve of O^6-C-MeG was made by derivatization of O^6-C-MedG with 0.1 M formic acid at 70 °C for 1 h.[34] O^6-C-MeG was quantified using the standard curve and the area ratio of internal standard O^6-D3-MeG and expressed as nanograms of O^6-C-MeG per milliliter of digesta.

Statistical Analysis. For the meat characteristics, a linear model ANOVA procedure (SAS enterprise guide 5) was used with the fixed effects of heme-Fe, nitrite, and heme-Fe × nitrite. Data on MDA, 4-HNE, simple aldehydes, PCC, and protein content were analyzed for the undigested meat, duodenum step, and colon step, separately. For the undigested meat, the same linear model as for the meat characteristics was used, whereas for the duodenum and colon phases a mixed model ANOVA procedure was used with the fixed effects heme-Fe, nitrite, and heme-Fe × nitrite and the random effect incubation run. Data on O^6-C-MeG were analyzed for each run (fecal inoculum) separately due to very high variation between the different applied inocula, using a linear model with the fixed effects heme-Fe, nitrite, and heme-Fe × nitrite. Tukey-adjusted post hoc tests were performed for all pairwise comparisons. $P < 0.05$ was considered significant.

RESULTS

Meat Characteristics. Characteristics of the used meats are shown in Table 2. Pork contained a marginally higher fat content compared to the other meats. The fatty acid profile showed no significant differences in SFA between the different meats, whereas minor differences were observed for total MUFA and PUFA. The beef sample contained significantly

Table 3. Lipid Oxidation in Uncured and Nitrite-Cured Chicken, Pork, and Beef before and after in Vitro Digestion[a]

		uncured			nitrite-cured				*P* values		
	step	chicken	pork	beef	chicken	pork	beef	RMSE	H	NC	H × NC
MDA	BD	5.7b	5.4b	15.1a	2.8b*	2.0b*	7.4a*	0.41	**<0.001**	**<0.001**	**<0.001**
(nmol/mL)	D	9.8c	14.8b	28.1a	8.7b	9.2b*	11.0a*	0.96	**<0.001**	**<0.001**	**<0.001**
	C	13.9c	17.7b	26.3a	12.8b	13.0b*	15.3a*	1.21	**<0.001**	**<0.001**	**<0.001**
4-HNE	BD	48.5c	221.2b	428.6a	8.8	nd	nd	48.08	**0.004**		
(pmol/mL)	D	20.4c	211.6b	521.2a	12.2	19.4*	19.8*	69.57	**<0.001**	**<0.001**	**<0.001**
	C	16.4b	20.2ab	23.6a	15.8	17.1	13.3*	2.90	**0.088**	**<0.001**	**<0.001**
pentanal	BD	65c	172b	331a	84a	32b*	37b*	10.8	**<0.001**	**<0.001**	**<0.001**
(pmol/mL)	D	130c	314b	697a	103	124*	107*	66.2	**<0.001**	**<0.001**	**<0.001**
	C	108	126	125	101	106	87*	14.03	**0.098**	**<0.001**	**<0.037**
hexanal	BD	287c	1162b	1391a	107*	77*	77*	32.4	**<0.001**	**<0.001**	**<0.001**
(pmol/mL)	D	299c	1017b	2652a	214	212*	232*	178.5	**< 0.001**	**< 0.001**	**< 0.001**
	C	178b	209ab	241a	176ab	211a	138b*	25.0	**0.011**	**<0.001**	**<0.001**
heptanal	BD	3.0c	18.4b	56.0a	1.9	nd	nd	2.24	**<0.001**		
(pmol/mL)	D	23.2bc	65.0b	147.8a	20.8	16.1	23.9*	34.22	**<0.001**	**<0.001**	**<0.001**
	C	84.2a	67.5a*	38.9b	99.1a	132.0a	69.5b	25.35	**<0.001**	**<0.001**	0.065
nonanal	BD	10.1	14.9	16.9	12.7	10.3	6.8	3.03	0.866	0.060	0.067
(pmol/mL)	D	21.6c	28.9b	52.2a	16.0b	16.9b*	24.3a*	3.12	**<0.001**	**<0.001**	**<0.001**
	C	8.5	7.8	14.1	10.0	8.8	13.3	3.75	**0.005**	0.682	0.754

[a]MDA, malondialdehyde; 4-HNE, 4-hydroxy-2-nonenal; BD, before digestion; D, duodenal stage; C, colonic stage; RMSE, root-mean-square error; H, heme-Fe content; NC, nitrite-curing. Means for different heme-Fe contents (within curing treatment) with different letters (a−c) are significantly different ($P < 0.05$); *, significantly different from uncured equivalent ($P < 0.05$); nd, not detected.

Table 4. Protein Oxidation in Uncured and Nitrite-Cured Chicken, Pork, and Beef before and after in Vitro Digestion[a]

		uncured			nitrite-cured				*P* values		
	step	chicken	pork	beef	chicken	pork	beef	RMSE	H	NC	H × NC
PCC	BD	1.57	1.85	2.17	0.65*	0.76*	0.88*	0.279	0.082	**<0.001**	0.562
(nmol DNPH/mg	D	2.47b	2.81b	4.87a	1.78	1.79*	1.97*	0.445	**<0.001**	**<0.001**	**<0.001**
protein)	C	3.11b	3.54ab	4.19a	2.93	3.10	3.71	0.517	**<0.001**	**0.043**	0.742
protein	BD	6.44	6.44	6.05	6.40	6.09	6.20	0.580	0.851	0.865	0.875
(mg/mL)	D	2.22	2.28	2.41	2.24	1.98	2.05	0.207	0.497	**0.017**	0.174
	C	1.54	1.36	1.38	1.32*	1.26	1.25	0.109	**0.020**	**<0.001**	0.332

[a]PCC, protein carbonyl compounds; BD, before digestion; D, duodenal stage; C, colonic stage; RMSE, root-mean-square error; H, heme-Fe content; NC, nitrite-curing. Means for different heme-Fe contents (within curing treatment) with different letters (a−c) are significantly different ($P < 0.05$); *, significantly different from uncured equivalent ($P < 0.05$).

more ALA, LC n-3 PUFA, and LC n-6 PUFA and less LA compared to the other meats, whereas the chicken sample contained significantly more ALA and LC n-3 PUFA compared to pork. A clearly lower amount of residual nitrite in cured meat samples was found, compared to the added amount (120 mg/kg meat). The lowest amount of residual nitrite was found in beef, followed by pork and chicken. Beef had significantly higher heme-Fe and total Fe compared to chicken and pork.

Lipid Oxidation. Table 3 shows the concentrations of lipid aldehydes before the digestion and after duodenal and colonic digestion of the meats. Uncured beef showed significantly higher amounts of all lipid oxidation products before digestion, except for nonanal, compared to pork, followed by chicken. Concentrations of lipid oxidation products were significantly lower when meats were nitrite-cured to even undetected for 4-HNE and heptanal. Compared to uncured chicken, nitrite-cured chicken had significantly lower MDA and hexanal concentrations, whereas 4-HNE and heptanal concentrations were hardly detectable. An increase in all oxidation products was observed in the duodenum step; however, this was less distinctive for 4-HNE. Also, after duodenal digestion, uncured beef resulted in significantly higher concentrations of lipid aldehydes compared to pork, followed by chicken. Hexanal concentrations in duodenal digested uncured beef increased 2-fold during digestion while the hexanal concentrations in the uncured chicken and pork remained similar. Nonanal increased 3-fold during digestion of uncured beef, but only 2-fold in uncured chicken and pork. After duodenal digestion of nitrite-cured meats, 4-HNE and heptanal were detected, but in accordance with the other lipid oxidation products in much lower concentrations compared to their uncured equivalents. Except for MDA, the concentration of lipid oxidation products was clearly lower after 72 h of colonic digestion compared to the duodenum step or before digestion. Similar significant

Table 5. NOC-Induced DNA Damage by Uncured and Nitrite-Cured Chicken, Pork, and Beef before and after in Vitro Digestion[a]

		uncured			nitrite-cured				*P* values		
	step	chicken	pork	beef	chicken	pork	beef	RMSE	H	NC	H × NC
O^6-C-MeG	BD	nd	nd	nd	nd	nd	nd				
(ng/mL)	D	nd	nd	nd	nd	nd	nd				
	C1	nd	nd	nd	nd	nd	nd				
	C2	10.8b	13.3ab	14.4a	11.9	11.9	11.9	0.89	0.071	0.121	0.066
	C3	539b	504b	762a	558b	620b	760a	45.4	**0.001**	0.143	0.225

[a] O^6-C-MeG, O^6-carboxy-methylguanine; BD, before digestion; D, duodenal stage; C1, C2, C3, colonic stage incubated with microbiota 1, 2, and 3; RMSE, root-mean-square error; H, heme-Fe content; NC, nitrite curing. Means for different heme-Fe contents (within curing treatment) with different letters (a–c) are significantly different ($P < 0.05$); nd, not detected.

effects of nitrite curing and heme-Fe content on most aldehyde concentrations were observed in the colon digestive samples. In contrast to other aldehydes in the colonic digestive fluids, heptanal was significantly lower in beef compared to chicken and pork and significantly higher in nitrite-cured meats compared to the uncured equivalents. Nitrite curing had no significant effect on nonanal in the colonic digestion samples. Octanal was not detected or close to no detection and hence was not included in the statistical analysis.

Protein Oxidation. Undigested nitrite-cured meats had significantly lower PCC concentrations than their uncured equivalents (Table 4). Higher PCC concentrations were observed after duodenal and colonic digestion with significantly higher PCC levels in uncured beef digests compared to chicken and pork after duodenum digestion and compared to chicken after colon digestion. Nitrite curing of the meat also resulted in lower protein oxidation in simulated duodenum and in marginally lower values in the colonic step.

A clear decrease in protein levels was observed starting from the nondigested meat to the duodenal and colonic digestive fluids (Table 4). No significant differences were observed between different meat samples before digestion. Cured meats had significantly lower protein levels in duodenum and colon compared to uncured equivalents. A marginal effect of heme-Fe was also observed in the colonic phase.

***O^6*-Carboxy-methylguanine.** No O^6-C-MeG was detected in meats before digestion or at the end of the duodenal phase (Table 5). In contrast to the other parameters, detection of O^6-C-MeG after 72 h of colonic digestion was highly dependent on the individual bacterial inoculum. Inoculum originating from the first test subject did not allow detection of O^6-C-MeG in any sample. When fermented using inoculum originating from the second and third test persons, O^6-C-MeG levels were low or very high, respectively. After 72 h of fermentation, a significant effect of heme-Fe concentration was observed. When fermented by inoculum 2, uncured beef had significantly more O^6-C-MeG than chicken, whereas no difference was seen in nitrite-cured meats. Fermentation by the third inoculum resulted in higher O^6-C-MeG formation in both uncured and nitrite-cured beef compared to chicken and pork. No significant effect of nitrite curing was found.

DISCUSSION

The objective of the present study was to test the involvement of heme-Fe and nitrite curing on the formation of toxic compounds during the digestion of meat. In uncured meats, the promoting effects of heme-Fe on oxidation and NOC-induced DNA damage during digestion were distinct. Our data confirm the importance of heme-Fe as catalyst of endogenous oxidation and nitrosation reactions, and hence it is likely to be involved in the association between red meat consumption and CRC. Curing with nitrite drastically inhibited the formation of the major toxic oxidation products MDA, 4-HNE, the minor toxic simple aldehydes, and PCC with no stimulating effect on the formation of NOC-specific DNA adducts. Consequently, nitrite curing of meat was not perceived as a risk factor in the presented study.

In accordance with our results, Hur et al.[11] already demonstrated a rise in TBARS during in vitro digestion of beef patties until duodenal digestion. Increased oxidation during digestion of meat under simulated duodenal conditions was confirmed in our study using more specific markers. Changes in 4-HNE concentrations before and after duodenal digestion were less distinct compared to other lipid oxidation products. However, measurable levels of 4-HNE were noted in nitrite-cured meat samples under simulated duodenal and colonic conditions, whereas it was not detected before digestion, indicating the formation of 4-HNE during digestion. Gorelik et al.[35] demonstrated absorption and accumulation of MDA in human plasma and urine after consumption of turkey cutlets. Increased plasma 4-hydroxy-2-hexenal (4-HHE) in mice after consumption of oxidized n-3 fatty acids was associated with oxidative stress and inflammation in the upper intestine.[36] Through systemic circulation, lipid oxidation products can reach sensitive tissues where MDA and 4-HNE can form adducts with DNA, increasing cancer risk.[37] In this way, higher plasma and tissue MDA in rats fed beef compared to chicken were associated with higher colonic DNA strand breaks.[38] In our experiment, the clearly lower concentrations of lipid oxidation products after colonic digestion, with an exception for MDA, could be attributed to degradation into volatile compounds and adduct formation with proteins or bacterial DNA. Oxidation of aldehydes by previously demonstrated aldehyde dehydrogenase activity of colonic bacteria[39] could also explain the observed decrease throughout colonic digestion. It should be noted that the fecal inocula likely also contained aldehydes. The net disappearance of the aldehydes during colonic digestion was thus probably underestimated.

The antioxidative effect of nitrite was clearly demonstrated in meats before and after digestion. Whereas high concentrations of the major cytotoxic 4-HNE were found in uncured beef, undetected to very low traces were observed for nitrite-cured beef. Nitrite curing of meat samples was performed by mixing with 0.6% nitrite salt. In contrast, adding salt without nitrite to meat increased TBARS and peroxides in meat.[40] Adding nitrite (1 g/L) in drinking water significantly reduced lipid oxidation in the colon of rats on a heme diet.[41] These results should be

interpreted with care because a dual role of •NO on oxidative stress has been described. Because a 1:1 ratio of •NO to ROS enhances lipid peroxidation whereas an excess of •NO inhibits oxidation,[17] consumption of oxidized nitrite-cured meat could result in a reversed effect. In contrast to other aldehydes in the colonic digests, heptanal was surprisingly lower in beef compared to chicken and pork and higher in nitrite-cured meats compared to their uncured equivalents. This unexpected result should be clarified in future experiments.

Because lipid oxidation products arise from PUFA, we aimed to exclude a possible confounding effect of different fatty acid profiles by adding 4% subcutaneous pork fat to the lean chicken, pork, and beef meats (approximately 1% intramuscular fat) of the present study. Despite this, there were some minor differences in the PUFA subgroups. Total PUFA was very similar across the different samples. 4-HNE and hexanal arise specifically from n-6 PUFA.[42] The small differences in n-6 PUFA content among the different meat samples in the present study are not expected to explain the large differences in 4-HNE and hexanal formation. LA, which belongs to the n-6 PUFA subgroup, was even higher in the chicken meat, but was associated with the lowest 4-HNE and hexanal formation.

Measurement of PCC as a marker for protein oxidation compared well with our observations on lipid oxidation. Higher heme-Fe concentrations in meats induced more protein oxidation, whereas nitrite curing prevented oxidation before and during in vitro digestion. It was previously demonstrated that CRC patients had higher plasma PCC levels than healthy controls.[43] The formation of PCC affects the nature and function of the protein, but the importance of dietary PCC to human health is still not completely clear. As protein oxidation is believed to be a free radical chain reaction,[44] it could be hypothesized that oxidized dietary proteins catalyze the oxidation of cellular proteins and hence induce cell damage.

The significantly lower PCC and protein levels in nitrite-cured meats compared to uncured meats during simulation of duodenum and colon digestion agree with Santé-Lhoutellier et al.,[45] who found a highly significant negative correlation between PCC concentrations and proteolytic susceptibility to pepsin. MDA and 4-HNE can also react with proteins, leading to the formation of Schiff bases, which are known to play a role in protein aggregation. Previously, it was shown that a higher amount of protein reaching the colon fermentation resulted in a higher formation of potentially toxic protein fermentation products such as ammonia, phenol, *p*-cresol, and indole. However, higher formation of these products was not associated with enhanced colon cancer promotion in rats.[46]

The increased O^6-C-MeG concentrations in colon samples when meats contained higher heme-Fe contents were in accordance with Bingham et al.,[8] who showed a dose-responsive increase in ATNC with consumption of red meat, whereas consumption of large amounts of white meat did not influence fecal ATNC. Cross et al.[9] showed that heme-Fe was responsible for endogenous intestinal N-nitrosation arising from red meat. Elevated O^6-C-MeG was also observed in colonic exfoliated cells of humans on a high red meat diet.[10] These observations are in agreement with extensive epidemiologic studies that showed a moderate but significantly increased CRC risk with high red meat consumption.[2,3] IJssennagger et al.[47] provided evidence for selective susceptibility of Gram-positive bacteria to heme cytotoxic fecal water, which was not observed for Gram-negative bacteria. Furthermore, heme-Fe increased colonic *Enterobacteria* and *Bacteroidetes* spp. and decreased *Lactobacilli* and *Firmicutes* spp.[47,48] Possibly, a bacterial shift induced by heme-Fe toxicity or heme-induced oxidative stress could alter the bacterial metabolic capacity and contribute to higher O^6-C-MeG formation in beef digesta. The pronounced differences in the detection of the NOC-specific DNA adduct O^6-C-MeG among the individual fecal inocula are most likely the result of variation in the gut bacterial composition of the fecal donor or varying concentrations of compounds in the fecal inoculum that are involved in formation of the DNA adduct O^6-C-MeG. More research is needed to clarify how and which bacterial species or compounds are responsible for the formation of O^6-C-MeG.

A higher formation of O^6-C-MeG when meats were nitrite-cured was not observed and, hence, our results do not support an earlier suggestion about the importance of nitrite curing on NOC formation.[5] Rats on a high heme-Fe diet displayed 3-fold higher fecal ATNC when drinking water contained sodium nitrate and nitrite (0.17 g/L $NaNO_2$ and 0.23 g/L $NaNO_3$).[41] However, because the increase in ATNC was mainly attributed to an increase of the nongenotoxic iron-nitrosyl, the authors concluded this was probably not associated with an increased colon cancer risk. Nitrite-cured meats also contain far less residual nitrite than many vegetables, which are not associated with increased risk in epidemiologic studies. Furthermore, nitrite is formed endogenously and recycled with the saliva. Santarelli et al.[49] showed clearly higher fecal ATNC in 1,2-dimethylhydrazin injected rats on a diet of dark, nitrite-cured, cooked, and oxidized meat. In contrast, no increase was observed in rats on a diet of dark, nitrite-cured, cooked, and anaerobically stored meat. Meats used in our experiment were stored anaerobically at −20 °C to prevent oxidation during storage. Our results did not show an increased O^6-C-MeG formation when nitrite-cured meats were stored properly.

In conclusion, our study presents a valuable in vitro tool to study oxidation and nitrosation processes during digestion of meat. Our results confirm an earlier-described catalyzing effect of heme-Fe in meat on oxidative stress and demonstrate NOC-induced DNA damage during digestion. Nitrite curing of meat resulted in a lower formation of toxic oxidation products, whereas no effect was observed on the formation of the NOC-specific DNA adduct O^6-C-MeG.

AUTHOR INFORMATION

Corresponding Author

*(S.D.S.) E-mail: stefaan.desmet@ugent.be. Phone: +329 264 90 03. Fax: +329 264 90 99.

Funding

This study was financed by the Federal Public Service Health, Food Chain Safety and Environment (Grant RF-11/625 MEATNOX). L.V. is supported by a postdoctoral fellowship from the Research Foundation − Flanders (FWO).

Notes

The authors declare no competing financial interest.

ACKNOWLEDGMENTS

We thank S. Lescouhier, D. Baeyens, and E. Claeys for the preparation and characterization of meat samples. We also thank C. Boterdaele for assistance during the incubations and L. Hemeryck for assistance in the analysis of the NOC-specific DNA adducts.

ABBREVATIONS USED

ALA, α-linolenic acid; ATNC, apparent total nitroso-compounds; CRC, colorectal cancer; FA, fatty acids; 4-HNE, 4-hydroxy-2-nonenal; LA, linoleic acid; MDA, malondialdehyde; MUFA, monounsaturated fatty acids; LC n-3 PUFA, long-chain n-3 polyunsaturated fatty acids; LC n-6 PUFA, long-chain n-6 polyunsaturated fatty acids; ·NO, nitric oxide; NOCs, *N*-nitroso-compounds; O^6-C-MeG, O^6-carboxy-methylguanine; O^6-MeG, O^6-methylguanine; PCC, protein carbonyl compounds; ROS, reactive oxygen species; SFA, saturated fatty acids; TBARS, thiobarbituric acid reactive substances

REFERENCES

(1) World Cancer Research Fund/American Institute for Cancer Research. *Food, Nutrition, Physical Activity, and the Prevention of Cancer: A Global Perspective*; American Institute for Cancer Research: Washington, DC, USA, 2007; 517 pp, www.dietandcancerreport.org/?p=ER (accessed Dec 24, 2013).

(2) Larsson, S. C.; Wolk, A. Meat consumption and risk of colorectal cancer: a meta-analysis of prospective studies. *Int. J. Cancer* **2006**, *119*, 2657−2664.

(3) Chan, D. S.; Lau, R.; Aune, D.; Vieira, R.; Greenwood, D. C.; Kampman, E.; Norat, T. Red and processed meat and colorectal cancer incidence: meta-analysis of prospective studies. *PLoS One* **2011**, *6*, e20456.

(4) Santarelli, R. L.; Pierre, F.; Corpet, D. E. Processed meat and colorectal cancer: a review of epidemiologic and experimental evidence. *Nutr. Cancer* **2008**, *60*, 131−144.

(5) Corpet, D. E. Red meat and colon cancer: should we become vegetarians, or can we make meat safer? *Meat Sci.* **2011**, *89*, 310−316.

(6) Pierre, F.; Freeman, A.; Taché, S.; Van der Meer, R.; Corpet, D. E. Beef meat and blood sausage promote the formation of azoxymethane-induced mucin-depleted foci and aberrant crypt foci in rat colons. *J. Nutr.* **2004**, *134*, 2711−2716.

(7) Pierre, F.; Peiro, G.; Taché, S.; Cross, A. J.; Bingham, S. A.; Gasc, N.; Gottardi, G.; Corpet, D. E.; Guéraud, F. New marker of colon cancer risk associated with heme intake: 1,4-dihydroxynonane mercapturic acid. *Cancer Epidemiol. Biomarkers Prev.* **2006**, *15*, 2274−2279.

(8) Bingham, S. A.; Hughes, R.; Cross, A. J. Effect of white versus red meat on endogenous N-nitrosation in the human colon and further evidence of a dose response. *J. Nutr.* **2002**, *132*, 3522S−3525S.

(9) Cross, A. J.; Pollock, J. R.; Bingham, S. A. Haem, not protein or inorganic iron, is responsible for endogenous intestinal N-nitrosation arising from red meat. *Cancer Res.* **2003**, *63*, 2358−2360.

(10) Lewin, M. H.; Bailey, N.; Bandaletova, T.; Bowman, R.; Cross, A. J.; Pollock, J.; Shuker, D. E. G.; Bingham, S. A. Red meat enhances the colonic formation of the DNA adduct O^6-carboxymethyl guanine: implications for colorectal cancer risk. *Cancer Res.* **2006**, *66*, 1859−1865.

(11) Hur, S. J.; Lim, B. O.; Park, G. B.; Joo, S. T. Effects of various fiber additions on lipid digestion during in vitro digestion of beef patties. *J. Food Sci.* **2009**, *74*, C653−C657.

(12) Kanner, J.; Lapidot, T. The stomach as a bioreactor: dietary lipid peroxidation in the gastric fluid and the effects of plant-derived antioxidants. *Free Radical Biol. Med.* **2001**, *31*, 1388−1395.

(13) Gorelik, S.; Ligumsky, M.; Kohen, R.; Kanner, J. The stomach as a "bioreactor": when red meat meets red wine. *J. Agric. Food Chem.* **2008**, *56*, 5002−5007.

(14) Nair, U.; Bartsch, H.; Nair, J. Lipid peroxidation-induced DNA damage in cancer-prone inflammatory diseases: a review of published adduct types and levels in humans. *Free Radical Biol. Med.* **2007**, *43*, 1109−1120.

(15) Kanner, J. Oxidative processes in meat and meat products: quality implications. *Meat Sci.* **1994**, *36*, 169−189.

(16) Honikel, K. O. The use and control of nitrate and nitrite for the processing of meat products. *Meat Sci.* **2008**, *78*, 68−76.

(17) Darley-Usmar, V.; Wiseman, H.; Halliwell, B. Nitric oxide and oxygen radicals: a question of balance. *FEBS Lett.* **1995**, *369*, 131−135.

(18) Espey, M. G.; Miranda, K. M.; Thomas, D. D.; Xavier, S.; Citrin, D.; Vitek, M. P.; Wink, D. A. A chemical perspective on the interplay between NO, reactive oxygen species, and reactive nitrogen oxide species. *Ann. N.Y. Acad. Sci.* **2002**, *962*, 195−206.

(19) Estévez, M. Protein carbonyls in meat systems: a review. *Meat Sci.* **2011**, *89*, 259−279.

(20) Versantfoort, C. H. M.; Oomen, A. G.; Van de Kamp, E.; Rompelberg, C. J. M.; Sips, A. J. A. M. Applicability of an in vitro digestion model in assessing the bioaccessibility of mycotoxins from food. *Food Chem. Toxicol.* **2005**, *43*, 31−40.

(21) Güven, Y.; Satman, I.; Dinççag, N.; Alptekin, S. Salivary peroxidase activity in whole saliva of patients with insulin-dependent (type-1) diabetes mellitus. *J. Clin. Periodontol.* **1996**, *23*, 879−88.

(22) Takahama, U.; Yamamoto, A.; Hirota, S.; Oniki, T. Quercetin-dependent reduction of salivary nitrite to nitric oxide under acidic conditions and interaction between quercetin and ascorbic acid during the reduction. *J. Agric. Food Chem.* **2003**, *51*, 6014−6020.

(23) Dabrowska-Ufniarz, E.; Dzieniszewski, J.; Jarosz, M.; Wartanowicz, M. Vitamin C concentration in gastric juice in patients with precancerous lesions of the stomach and gastric cancer. *Med Sci. Monit.* **2002**, *8*, CR96−CR103.

(24) Nalini, S.; Ramakrishna, B. S.; Mohanty, A.; Balasubramanian, K. A. Hydroxyl radical formation in human gastric juice. *J. Gastroenterol. Hepatol.* **1992**, *7*, 497−501.

(25) Van de Wiele, T.; Vanhaecke, L.; Boeckaert, C.; Peru, K.; Headley, J.; Verstraete, W.; Siciliano, S. Human colon microbiota transform polycyclic aromatic hydrocarbons to estrogenic metabolites. *Environ. Health Perspect.* **2005**, *113*, 6−10.

(26) Molly, K.; Woestyne, M. V.; Smet, I. D.; Verstraete, W. Validation of the simulator of the human intestinal microbial ecosystem (SHIME) reactor using microorganism-associated activities. *Microb. Ecol. Health D* **1994**, *7*, 191−200.

(27) Folch, J.; Lees, M.; Sloane-Stanley, G. H. A simple method for the isolation and purification of total lipids from animal tissues. *J. Biol. Chem.* **1957**, *226*, 497−509.

(28) Raes, K.; De Smet, S.; Demeyer, D. Effect of double-muscling in Belgian Blue young bulls on the intramuscular fatty acid composition with emphasis on conjugated linoleic acid and polyunsaturated fatty acids. *Anim. Sci.* **2001**, *73*, 253−260.

(29) Hornsey, H. The colour of cooked cured pork − estimation of the nitric oxide-haem pigments. *J. Sci. Food Agric.* **1956**, *7*, 534−547.

(30) Grotto, D.; Santa Maria, L. D.; Boeira, S.; Valentini, J.; Charão, M. F.; Moro, A. M.; Nascimento, P. C.; Pomblum, V. J.; Garcia, S. C. Rapid quantification of malondialdehyde in plasma by high performance liquid chromatography−visible detection. *J. Pharm. Biomed. Anal.* **2007**, *43*, 619−624.

(31) Holley, A. E.; Walker, M. K.; Cheeseman, K. H.; Slater, T. F. Measurement of *n*-alkanals and hydroxyalkenals in biological samples. *Free Radical Biol. Med.* **1993**, *15*, 281−289.

(32) Ganhão, R.; Morcuende, D.; Estévez, M. Protein oxidation in emulsified cooked burger patties with added fruit extracts: influence on colour and texture deterioration during chill storage. *Meat Sci.* **2010**, *85*, 402−409.

(33) Vanden Bussche, J.; Moore, S. A.; Pasmans, F.; Kuhnle, G. G. C.; Vanhaecke, L. An approach based on ultrahigh pressure liquid chromatography-tandem mass spectrometry to quantify O^6-methyl and O^6-carboxymethylguanine DNA adducts in intestinal cell lines. *J. Chromatogr., A* **2012**, *1257*, 25−33.

(34) Moore, S. A.; Xeniou, O.; Zeng, Z. T.; Humphreys, E.; Burr, S.; Gottschalg, E.; Bingham, S. A.; Shuker, D. E. Optimizing immunoslot blot assays and application to low DNA adduct levels using an amplification approach. *Anal. Biochem.* **2010**, *403*, 67−73.

(35) Gorelik, S.; Ligumsky, M.; Kohen, R.; Kanner, J. A novel function of red wine polyphenols in humans: prevention of absorption of cytotoxic lipid peroxidation products. *FASEB J.* **2008**, *22*, 41−46.

(36) Awada, M.; Soulage, C. O.; Meynier, A.; Debard, C.; Plaisancié, P.; Benoit, B.; Picard, G.; Loizon, E.; Chauvin, M.-A.; Estienne, M.;

Peretti, N.; Guichardant, M.; Lagarde, M.; Genot, C.; Michalski, M. C. Dietary oxidized n-3 PUFA induce oxidative stress and inflammation: role of intestinal absorption of 4-HHE and reactivity in intestinal cells. *J. Lipid Res.* **2012**, *53*, 2069−2080.

(37) Nair, U.; Bartsch, H.; Nair, J. Lipid peroxidation-induced DNA damage in cancer-prone inflammatory diseases: a review of published adduct types and levels in humans. *Free Radical Biol. Med.* **2007**, *43*, 1109−1120.

(38) Toden, S.; Belobrajdic, D. P.; Bird, A. R.; Topping, D. L.; Conlon, M. A. Effects of dietary beef and chicken with and without high amylose maize starch on blood malondialdehyde, interleukins, IGF-I, insulin, leptin, MMP-2, and TIMP-2 concentrations in rats. *Nutr. Cancer* **2010**, *62*, 454−465.

(39) Nosova, T.; Jokelainen, K.; Kaihovaara, P.; Jousimies-Somer, H.; Siitonen, A.; Heine, R.; Salaspuro, M. Aldehyde dehydrogenase activity and acetate production by aerobic bacteria representing the normal flora of human large intestine. *Alcohol Alcohol.* **1996**, *31*, 555−564.

(40) Gheisari, H. R.; Motamedi, H. Chloride salt type/ionic strength and refrigeration effects on antioxidant enzymes and lipid oxidation in cattle, camel and chicken meat. *Meat Sci.* **2010**, *86*, 377−383.

(41) Chenni, F. Z.; Taché, S.; Naud, N.; Guéraud, F.; Hobbs, D. A.; Kunhle, G. G.; Pierre, F. H.; Corpet, D. E. Heme-induced biomarkers associated with red meat promotion of colon cancer are not modulated by the intake of nitrite. *Nutr. Cancer* **2013**, *65*, 227−233.

(42) Esterbauer, H.; Schaur, R. J.; Zollner, H. Chemistry and biochemistry of 4-hydroxynonenal, malondialdehyde and related aldehydes. *Free Radical Biol. Med.* **1991**, *11*, 81−128.

(43) Yeh, C. C.; Lai, C. Y.; Hsieh, L. L.; Tang, R.; Wu, F. Y.; Sung, F. C. Protein carbonyl levels, glutathione S-transferase polymorphisms and risk of colorectal cancer. *Carcinogenesis* **2010**, *31*, 228−233.

(44) Lund, M. N.; Heinonen, M.; Baron, C. P.; Estevez, M. Protein oxidation in muscle foods: a review. *Mol. Nutr. Food Res.* **2011**, *55*, 83−95.

(45) Santé-Lhoutellier, V.; Astruc, T.; Marinova, P.; Greve, E.; Gatellier, P. Effect of meat cooking on physicochemical state and in vitro digestibility of myofibrillar proteins. *J. Agric. Food Chem.* **2008**, *56*, 1488−1494.

(46) Corpet, D. E.; Yin, Y.; Zhang, X. M.; Remesy, C.; Stamp, D.; Medline, A.; Thompson, L.; Bruce, W. R.; Archer, M. C. Colonic protein fermentation and promotion of colon carcinogenesis by thermolyzed casein. *Nutr. Cancer* **1995**, *23*, 271−276.

(47) IJssennagger, N.; Derrien, M.; van Doorn, G. M.; Rijnierse, A.; van den Bogert, B.; Müller, M.; Dekker, M.; Kleerebezem, M.; van der Meer, R. Dietary heme alters microbiota and mucosa of mouse colon without functional changes in host-microbe cross-talk. *PLoS One* **2012**, *7*, e49868.

(48) Schepens, M. A.; Vink, C.; Schonewille, A. J.; Dijkstra, G.; van der Meer, R.; Bovee-Oudenhoven, I. M. Dietary heme adversely affects experimental colitis in rats, despite heat-shock protein induction. *Nutrition* **2011**, *27*, 590−597.

(49) Santarelli, R. L.; Vendeuvre, J. L.; Naud, N.; Taché, S.; Guéraud, F.; Viau, M.; Genot, C.; Corpet, D. E.; Pierre, F. H. Meat processing and colon carcinogenesis: cooked, nitrite-treated, and oxidized high-heme cured meat promotes mucin-depleted foci in rats. *Cancer Prev. Res.* **2010**, *3*, 852−864.

develop analytical model systems that delineate plant constituent−therapeutic response relationships.

To meet this challenge, we developed a model system that compares the ^{1}H NMR spectra of relatively crude BR extracts with the cellular proliferation of HT-29 human colon cancer cells.

Our approach to modeling linked variable bioassay results to variation in plant sample extract secondary metabolite complements and employed multivariate statistical analyses to identify specific regions of the extract NMR spectra that were associated with the array of biological responses. Once spectral regions responsible for these relationships were identified by the model, compound structures were verified using 2D NMR methods, such as heteronuclear single-quantum coherence (HSQC)[16] and heteronuclear multiple-bond correlation (HMBC)[17] experiments.

To validate this approach, we first ensured that BR extract profile variability could be achieved by capitalizing upon the genetic and environmental influences on fruit composition.[18,19] In addition, we verified that specific signals within complex NMR profiles responsible for known chemical relationships could be identified through multivariate statistical analyses. Specifically, we regressed BR extract NMR profiles against standard biochemical analyses [total monomeric anthocyanin content (TMA) and antioxidant capacity assays, ferric-reducing antioxidant power (FRAP) and 2,2-diphenyl-1-picrylhydrazl (DPPH)].[20] This verification model successfully recognized the specific protons within the NMR spectra associated with anthocyanins that played significant roles in the activity of extracts in these assays. Furthermore, the model found structure−activity relationships to be statistically identifiable.

Here we have applied our system to model the biological relationship between bioactive compound variability among 73 BR extracts and their ability to inhibit HT-29 colon cancer cell proliferation. We previously reported the effects of these extracts on cancer cell cultures in this study.[21] The variable BR juice extracts inhibited HT-29 colon cancer cell growth broadly from 33 to 118% when included in the culture media at low and high doses of 0.6 or 1.2 mg extract/mL, respectively (Table S1 in the Supporting Information). Cell responses were dose-dependent, and the response arrays between doses were highly correlated. Although anthocyanins are known to contribute substantially to BR's chemoprotective properties,[2,5−8] extract anthocyanin concentrations as measured by TMA were not correlated to levels of growth inhibition, suggesting that nonanthocyanin components also contribute to BR extract bioactivity in the HT-29 colon cancer cell assay. Recently, we identified a cadre of nonanthocyanins present in our extracts, some of which had yet to be reported as BR constituents.[22]

In this paper, we present the description of anthocyanin as well as nonanthocyanin compounds identified by our modeling system that are responsible for the antiproliferative properties of BR extracts within the HT-29 colon cancer cell bioassay. Our model also indicates that compounds of various classes present in extracts over a broad concentration range may act together to affect cancer cell growth.

MATERIALS AND METHODS

Sample Acquisition and Extract Preparation. Marketable BR fruit samples of three cultivars ('Bristol', 'Jewel', or 'MacBlack') varying in ripeness (slightly under-ripe, ripe, or slightly over-ripe)[21] from seven Ohio commercial farms were obtained for this study. Fruit were hand-harvested in fiber-board containers and transported on ice to the Ohio Agricultural Research and Development Center. Sample extracts from 75 samples for both NMR and cell assay procedures were prepared as described by Johnson and coauthors.[21] This process included the following steps: sample handling, over-ripening fruit, sample storage, preparation of BR juices, isolation of secondary product constituent-rich methanolic extracts via solid phase extraction (SPE), evaporation of solvents under an N_2 stream, and freeze-drying of solvent-free SPE column eluates.

NMR Data Collection. All NMR studies of BR extract samples were performed with a Varian INOVA 750 MHz NMR spectrometer (Varian Inc., Palo Alto, CA, USA) using a Varian triple-resonance ^{1}H{^{13}C/^{15}N} pulsed field gradient cryoprobe. Solid materials derived from the column eluate were diluted with appropriate amounts of methanol-d_4/trifluoroacetic acid-d (95:5 v/v) and 5 mM 2,2-dimethyl-2-silapentane-5-sulfonate sodium salt (DSS) in methanol-d_4 to give 800 μL aliquots that contained 20 mg of dried berry extract and 0.5 mM DSS. The samples were filtered through glass wool and placed in 5 mm NMR tubes. All samples were stored at 4 °C prior to analysis. Two of the 75 samples were prepared incorrectly for NMR analysis and were excluded from further examination.

The spectra were collected at 25 °C over a spectral width of 9023 Hz using a 6.2 μs (90°) pulse. The acquisition time was 2.7 s, and 128 transients were accumulated with presaturation of the HDO resonance in the 4.91−5.07 ppm region. Data were processed with 0.5 Hz exponential line broadening and zero filled to 131,072 points before Fourier transformation.

NMR Data Binning. ^{1}H NMR free induction decays (FIDs) were processed as a batch, using KnowItAll Metabolomics software 8.1 (Bio-Rad Laboratories, Informatics Division, Philadelphia, PA, USA) with a Lorentzian apodization of 0.3 Hz, baseline correction with automatic base point detection, and spline fitting. The DSS reference peak was manually set to 0 ppm for each spectrum. After the region containing solvent (CD_3OD) resonances (3.257 −3.373 ppm) had been flat-lined, each spectrum was normalized against the DSS peak. Alignment macros were applied as a batch process to numerous specific locations along the spectrum to compensate for peak shifting due to variation in pH and in the constituent concentrations among samples. Prior to statistical analysis, binning/bucketing was conducted from 0.550 to 9.200 ppm using the Bio-Rad IntelliBucket method, where the bin width was automatically adjusted on the basis of the overlap density heatmap (ODH) consensus spectrum and a bin width setting of 0.004 ± 0.002 ppm. Regions that were excluded from binning were as follows: (1) 4.910−5.070 ppm (presaturation region for HDO); (2) 3.257−3.373 ppm (flat-lined for solvent); (3) highly overlapping peaks (3.220−4.000 ppm) of the saccharide region; and (4) regions throughout the spectrum of low signal/noise. However, all regions containing resonances for anomeric protons were included in the binning process. This resulted in a data set of 1003 bins from each of 73 BR extract samples that was further reduced to 464 bins by selecting bins with intensities above the analytically justified limit of quantitation[23] (LOQ, i.e., ≥10 times the standard deviation of intensity of bins from data representative of spectral noise).

PLS Modeling. The PLS regression-based predictive model building using Pirouette 4.0 (Infometrix, Bothell, WA, USA) started with the 464 bin data sets. Peak intensities of bins for each of the 73 BR samples were regressed against the bioassay responses[21] as shown in Table S1 in the Supporting Information. A maximum number of 15 factors and a probability threshold of 0.95 were set. Two-component orthogonal signal correction[24] (OSC) was used to remove components in our large X block that were orthogonal to the Y block, thus segregating the portion of the X block that was correlated. To aid the interpretation of chemical information from the regression models, one subset of relevant variables (NMR bins) was selected from the entire block of X-variables. The criteria for variable selection were software-dependent measures of fit [prediction residual error sum of squares (PRESS) and r]. The regression vector values from this subset of bins were then ranked from highest to lowest for the low- and high-dose bioassays, respectively.

RESULTS AND DISCUSSION

Classical biochemical studies of chemoprevention and cancer cell antiproliferation, in response to berry fruits and BR in particular, are challenging because several berry fractions and many specific secondary products have been shown to have some effect on the cancer cell performance, but no single fraction or compound can account for the efficacy of whole fruit or crude fruit extracts.[2,7] Our approach uses "omics" and bioinformatic procedures to identify active components by NMR spectroscopy and to link them to their impact on cell proliferation in HT-29 colon cancer cells in a manner similar to that described by Leiss et al.[25] and Gavaghan et al.[26] to determine important effectors of host-plant resistance and maize salt stress, respectively. Because many BR secondary compounds have been shown to have roles in BR regulation of cancer cell development, there exists a large body of data for the potential verification of the compounds identified by the model.

Modeling of secondary product chemistry, in conjunction with medical efficacy, provides an opportunity to examine complex mixtures of secondary products that are present in plant materials and determine how they affect cell health, chemoprevention, and/or cancer cell proliferation. NMR is a powerful method used to elucidate chemical structures of molecules; here we have used it to identify components of complex mixtures of small molecule metabolites simultaneously, at a high resolution. Moreover, samples were readily prepared in a reproducible manner without the need for additional separation techniques. Processing the data with KnowItAll statistical software permitted the BR components that play significant roles in the control of HT-29 cell proliferation to be identified.

Our model generated large blocks of data concerning the chemical nature of the extracts, which were evaluated against a complex series of chemical reactions that we monitored as cell proliferation. The impact of these secondary compounds on cell proliferation represents the sum of all of the reactions controlling cell growth, metabolism, and apoptosis that have been demonstrated by a host of research.[2,5,7,8,15]

^{1}H 1D-NMR Analyses. Model development was initiated by obtaining the ^{1}H NMR spectra of the 73 BR extracts. The spectra of three representative BR extract samples are shown in Figure 1 [a, slightly under-ripe sample (BR-2); b, ripe sample (BR-47); and c, slightly over-ripe sample (BR-28)]. In all ^{1}H spectra of BR extract samples, the HDO resonance from water that had been observed in the 4.91−5.07 ppm region was suppressed using a presaturation pulse sequence. The singlet peak at 0.0 ppm is from DSS, which was added as an internal standard for chemical shift measurement as well as a calibration standard for quantitation. The strong peaks centered at 3.31 ppm (quintet), 3.35 ppm (singlet), and 3.97 ppm (singlet) are attributed to the resonances of residual $C\underline{H}D_2OD$ from methanol-d_4, a solvent-like impurity, and an artifact compound, respectively. The resonances in the complex region, 4.00−3.22 ppm, are attributed to nonanomeric resonances from the saccharides that are attached to the phenolic structures. The suppression of these signals and the regions of low signal-to-noise ratios (see Materials and Methods) in the initial data sets were made to ensure a robust analysis.

The spectra of BR extract samples are dominated by the resonances from cyanidin 3-glycosides (**1**, Figure 2) as well as defining peaks for cyanidin 3-rutinoside (Cy 3-rut, **2**), cyanidin 3-xylosylrutinoside (Cy 3-xylrut, **3**), cyanidin 3-glucoside

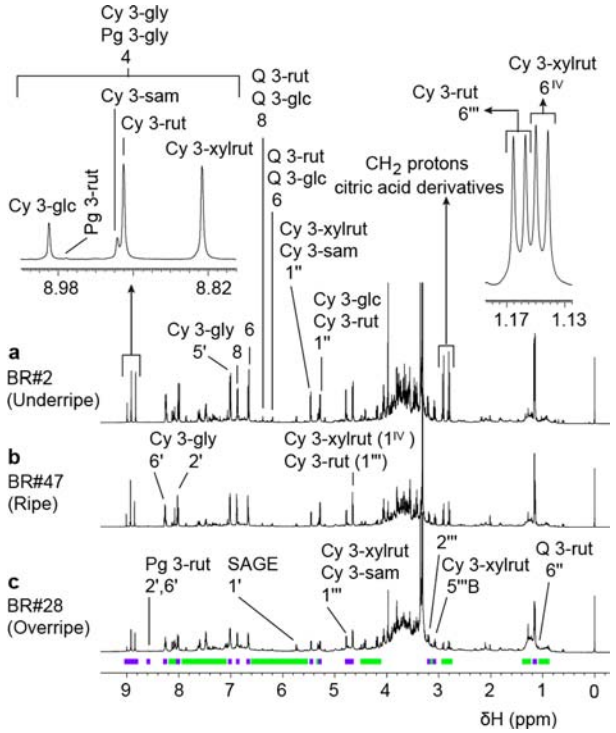

Figure 1. 750 MHz ^{1}H NMR spectra of three representative methanolic BR juice extract samples: (a) sample BR-2 from slightly under-ripe berries; (b) sample BR-47 from ripe berries; (c) sample BR-28 from slightly over-ripe berries. Resonances from anthocyanins are indicated in purple and those from nonanthocyanins are indicated in green bars above the chemical shift scale.

(Cy 3-glc, **4**), and cyanidin 3-sambubioside (Cy 3-sam, **5**), the major phenolic antioxidants of BR fruits.[19] The unique resonances from the minor anthocyanin, pelargonidin 3-rutinoside, are also detected. In Figure 1, the resonances from these anthocyanin phenolics are indicated in purple bars above the chemical shift scale.

Several resonances from nonanthocyanin metabolites and the aliphatic moieties associated with citric acid derivatives (**6**) were also observed (Figure 1, indicated in green bars above the chemical shift scale). The structures of nonanthocyanin phenolics, which were readily detected in the ^{1}H NMR spectra of BR extracts, are shown in Figure 3. Compounds based on the quercetin moiety (**7**, Q, where R_n = H) included quercetin 3-glucoside (Q 3-glc, **8**) and quercetin 3-rutinoside (Q 3-rut, **9**). Compound **11**, salicylic acid glucosyl ester (SAGE), where the glucose moiety is attached to a salicylic acid (SA, **10**), was also evident. Additional nonanthocyanin compounds that have been detected in the ^{1}H NMR spectra of BR extract samples are epicatechin (**12**), benzoic acid β-D-glucopyranosyl ester (BAGE, **13**), a salicylic acid derivative (SAD, **14**), *p*-coumaric acid (**15**), and methyl ellagic acid acetylpentose (MEAAP, **16**).

Although these minor metabolites are present at concentrations approximately 10^{-2}−10^{-3} times the concentrations of the cyanidin 3-glycosides,[5] some of their proton resonances are clearly visible in the ^{1}H NMR spectra of the BR extracts (Figure 1). For example, the H-8 and H-6 resonances from the quercetin glycosides, namely, Q 3-rut and Q 3-glc, are seen at 6.39 and 6.20 ppm, respectively. Likewise, for SAGE, one of the readily detected resonances is H-1′ (5.73 ppm), the anomeric proton resonance from the glucose attached to the phenolic structure via an ester linkage.

dx.doi.org/10.1021/jf404998k | J. Agric. Food Chem. 2014, 62, 1989−1998

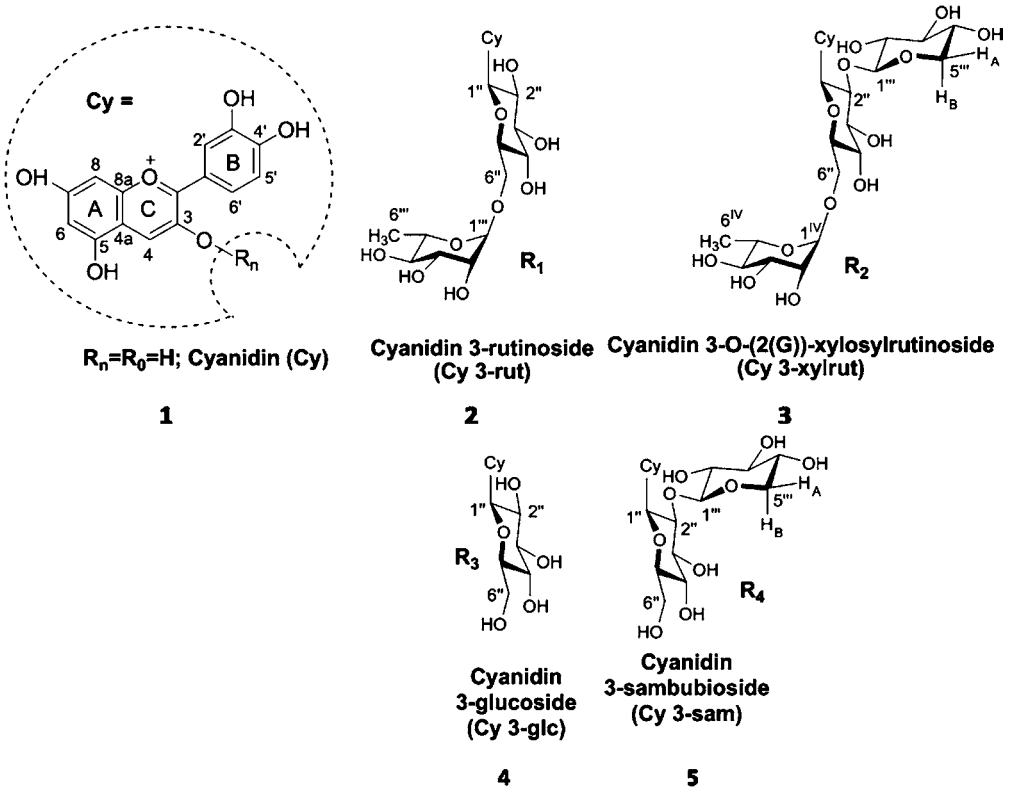

Figure 2. Structures of the cyanidin aglycone and four major anthocyanin phenolic compounds of black raspberry. **1**, cyanidin aglycone (Cy); **2**, cyanidin 3-rutinoside (Cy 3-rut); **3**, cyanidin 3-xylosylrutinoside (Cy 3-xylrut); **4**, cyanidin 3-glucoside (Cy 3-glc); and **5**, cyanidin 3-sambubioside (Cy 3-sam).

Our model simultaneously analyzed a number of regions of the 1D ^{1}H NMR spectra to ensure that participating components of the BR could be identified. This approach was demanding, because several proton resonances can be associated with one compound and intensities may differ depending on the number of protons in the compound structural unit. In addition, similarities in structures (e.g., phenolics) can result in overlapping peaks yielding complex spectral patterns. To verify structures, especially for compounds present at low concentrations, additional NMR experiments such as 1D selective total correlation spectroscopy, TOCSY, and 2D-NMR (gDQCOSY, gHSQCAD, and gHMBC) were conducted (Figures S1−S11 in the Supporting Information). Furthermore, during the statistical analysis, the NMR data were subjected to Pareto scaling,[27] where the square root of the standard deviation was used as a scaling factor. This minimized the effect of larger intensities in the presence of much smaller intensities.

To make regression modeling possible, we needed large amounts of variation in the extracts with a corresponding amount of variability in the cancer cell responses. This methodology differs from traditional medicinal chemistry approaches in which consistency in treatments is essential to understanding experimental outcomes. To verify the variability among our samples, the concentrations (μM) of cyanidin structures were obtained for all 73 spectra on the basis of the manual integration of the H-4 resonances using Bio-Rad's ProcessIt NMR application. Normalized peak areas were obtained relative to the integration of the CH_3 peak of DSS calibration standard at 0.0 ppm set to 100. These data revealed that the concentrations of the anthocyanin components in the 73 BR extract samples exhibited the desired high level of variability needed for our modeling efforts (Table S2 in the Supporting Information). In this study, Cy 3-xylrut was the most abundant phenolic component of the berry extracts (mean = 58 μM; CV = 34%), and the second most abundant component was Cy 3-rut (mean = 51 μM; CV = 31%). In general, the amounts of Cy 3-xylrut and Cy 3-rut were higher in ripe samples than in the under-ripe samples, whereas the amounts of Cy 3-glc and Cy 3-sam (mean = 24 μM, CV = 52%; and mean = 13 μM, CV = 40%, respectively) both decrease with increasing ripeness.

Bioactivity Model Development. Initially, a model of the low-dose assay was generated with a data set of 464 bins determined using Pareto scaling and leave-one-out cross-validation. NMR bins were ranked according to their regression vector values. Subsets of the highest ranked bins were then created and modeled against the low-dose bioassay to determine the best fit of the NMR spectra to the extract impact on cell proliferation. Figure 4a shows a plot of PRESS as well as r values against model sets with various numbers of X-variables. Figure 4b shows the corresponding line plot between model factors and number of bins. The arrows A_4 and A_5 represent the regions of minimum PRESS and maximum r, respectively. Because the maximum number of bins does not exceed 2 times the number of samples, the minimum value of PRESS, maximum value of r, and minimum number of model factors are the quality indices of a good model. A compromise among these quality indices indicated that the optimum number of bins for the low-dose bioassay was 125 (Figure 4, indicated by arrow A_5). The indicators of the fit for this five-factor model are shown in Table 1. This model has r and slope values approaching 1 and values of the standard error of cross-validation (SECV) and PRESS that approached their minima.

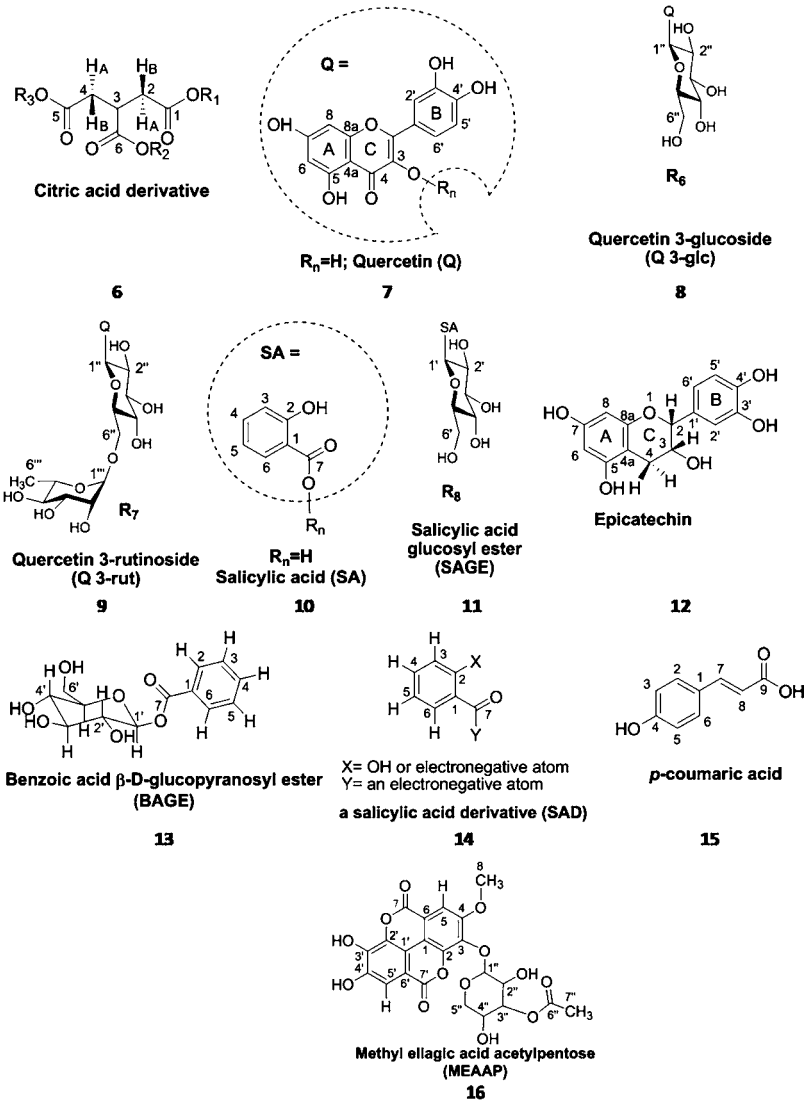

Figure 3. Structures of a citric acid derivative and nonanthocyanin phenolics detected in BR juice extract samples and their aglycones. **6**, citric acid derivatives; **7**, quercetin aglycone (Q); **8**, quercetin 3-glucoside (Q 3-glc); **9**, quercetin 3-rutinoside (Q 3-rut); **10**, salicylic acid aglycone; **11**, glucose ester of salicylic acid (SAGE); **12**, epicatechin; **13**, glucose ester of benzoic acid (BAGE); **14**, salicylic acid derivative (SAD); **15**, *p*-coumaric acid; and **16**, methyl ellagic acid acetylpentose (MEAAP).

In addition, Figure 5a shows the goodness of the *Y*-fit between predicted and measured values. The random distribution of the residuals (Figure 5b) also indicates that the assumption of linearity between the *X*- and *Y*-variables is warranted.

When the top 125 bins of this model were ranked according to their regression vector values, the contribution of specific compounds became evident. Because regression vectors are the weighted sum of loadings included in the model, they reveal the importance of each independent variable. These predictor variables are the basis for interpreting the effect of NMR bins (our independent variables), which carry the information about the chemical components, on the dependent variable, percent inhibition of cell proliferation. For the low-dose bioassay, Table 2 shows some of these compounds by their defining atom assignments and their rank/bin number, with corresponding atomic assignments being illustrated in Figures 2 and 3. The complete table of all 125 bin assignments can be found in Table S3 in the Supporting Information. In Table 2, specific bins corresponding to each of the four major anthocyanins in BR are shown to be important with Cy 3-xylrut and Cy 3-rut as the top-ranked. Cy 3-sam and Cy 3-glc also have an impact on bioassay results. A large number of bins were attributed to resonances of these cyanidin glycosides.

Bins corresponding to nonanthocyanin compounds were also shown to augment inhibition of cell proliferation in the HT29 low-dose bioassay (Table 2). BR anthocyanins and nonanthocyanin phenolic compounds share some similarities in structure (Figures 2 and 3); therefore, their ^{1}H NMR spectra (Figure 1) would be expected to contain some overlapping resonances. Although this overlap confounded compound identification, defining bins were found to be important for MEAAP, epicatechin, Q 3-rut, Q 3-glc, *p*-coumaric acid, SAGE, a salicylic acid derivative (SAD), BAGE, and citric acid derivatives.

When a model was calculated for the high-dose bioassay, similar but not identical results were obtained. This model was optimized at 100 bins (Figure S12 in the Supporting Information), and indicators of fit are shown in Table 1 and Figure 5c,d. When the 100 bins were ranked according to their regression vector values, a trend similar to the low-dose results was evident (Table 3 and Table S4 in the Supporting Information). The highest ranked

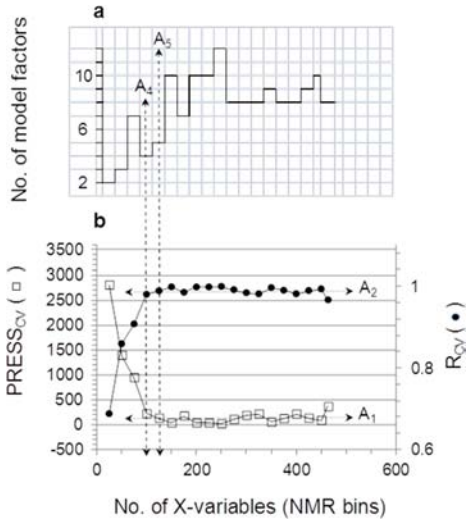

Figure 4. Partial least-squares (PLS) plots for the selection of *X*-variables (NMR bins): (a) number of factors; (b) indicators of fit. Arrow A_1 represents the regions of minimum prediction residual error sum of squares (PRESS) values, and arrow A_2 represents the regions of maximum *r* values. The vertical arrow indicated by A_5 represents the subset of optimum of *X*-variables and its PLS-derived low-dose model factors.

Table 1. Pirouette PLS-Derived Summary of Fit Measurements for the Low- and High-Dose Bioassay Activity of BRs

statistical parameter	low-dose bioassay[a]	high-dose bioassay[b]
no. of BR samples	73	73
no. of independent variables (NMR bins)	125	100
SECV[c]	1.3353	0.9338
PRESS[d]	130.1561	63.6579
r[e]	0.9878	0.9953
factors	5	5
slope	0.9897	0.9949
intercept	0.6496	0.4723

[a]Data are taken from the best PLS model with 125 highest ranked *X*-variables (NMR bins) from the first test model. [b]Data are taken from the best PLS model with 100 highest ranked *X*-variables (NMR bins) from the first test model. [c]SECV, standard error of cross-validation. [d]PRESS, prediction residual error sums of squares. [e]*r*, correlation coefficient.

bin corresponded to Cy 3-xylrut and a defining bin for Cy 3-rut was ranked 11th. Bins consistent with Cy 3-sam and Cy 3-glc were also evident as well as a large number of bins that corresponded to resonances of cyanidin glycosides. The same nonanthocyanin compounds that affected the low-dose model were also evident. However, the rankings of these compounds, especially a citric acid derivative, differed from those in the low-dose model (Table 3). In general, many of the nonanthocyanin constituents appeared to gain in predictive value in the high-dose model.

Overall, the importance of the nonanthocyanins was evident. As shown in Tables 2 and 3, of our original 1003 bins for each of 73 samples, the rankings of the NMR bins based on their regression vector values ranged from 30 to 121 for the low-dose bioassay and from 6 to 81 for the high-dose bioassay. Furthermore, error analyses of PLS models that were calculated using only anthocyanin-related bins proved to be less than optimal when compared to our PLS models containing both anthocyanin- and nonanthocyanin-related bins.

Model-Identified Cell Antiproliferative Compounds. As with other "omics" approaches, the cell assay (our *Y*-variable), provided a simple phenotypic-like response to the treatments, here, control of the HT-29 colon cancer cell proliferation. However, just as a simple phenotypic response is controlled by changes in many overlapping and/or independent biochemical pathways, cell proliferation reflects the combined impacts of the extract components on the stimulation of apoptosis, regulation of cell cycle gene expression, and the impact of BR extract components on overlapping and independent biochemical pathways. Therefore, the model must integrate all of these interactions to determine the impact of the extracts on cancer cell growth. This integration then provides data to identify compounds that affect any of a myriad of chemical reactions.

Cy 3-xylrut and Cy 3-rut were identified by the model as the most important contributors to the inhibition of proliferation of HT-29 colon cancer cells. Anthocyanins constitute a major group of phenolic antioxidants produced in most small fruits.[28] According to Stoner,[5] anthocyanins are present in BR at concentrations that exceed those of ellagic acid by approximately 15-fold and of all other phenolic materials by factors of 10^2 or 10^3. BR anthocyanins are known to effectively intercede against various forms of aerodigestive cancers[2,5−8] at several stages by initiating and maintaining the enzymatic defenses against oxidative stress, reducing inflammation, and inhibiting mutagenesis, as well as decreasing cell proliferation and stimulating apoptosis.[8] BR anthocyanins or anthocyanin-rich fractions affect these chemopreventive processes at cellular and subcellular levels by direct interaction or interaction with controlling elements of kinase-based signaling cascades that influence gene expression, mRNA translation, or enzymatic activity of key cancer-related factors.[2,4−8]

However, the model data also support our previous conclusion that the antiproliferative effectiveness of these BR extracts is not directly correlated with their TMA contents.[21] When we compared the NMR-determined concentrations of individual anthocyanins herein with the low- and high-dose bioassay data using a simple Pearson correlation analysis, only the Cy 3-rut correlation values ($r = -0.32$ and $r = -0.31$, respectively) were significant ($p < 0.01$). However, this relationship was weak, suggesting that the effects of BR extracts on HT-29 colon cancer cell proliferation arise from the activity of multiple compounds in concert. Moreover, bins associated with protons of nonanthocyanin constituents appeared to gain in importance in the anthocyanin-rich extract/high-dose assay PLS model over their position in the model constructed with low-dose assay data developed with extracts containing lower levels of anthocyanins. Together, these findings suggest that anthocyanins may reach a maximum effect on cells and that further increases in their total content or alterations in anthocyanin profiles may not increase the activity of the specific extract.

Supporting this contention, Seguin and co-workers[29] recently reported four temperate berries (BR, blueberry, red raspberry, strawberry) and a cyanidin-containing tropical fruit acai (*Euterpe oleraceae*), presumably with differing anthocyanin profiles, to be similar in their antiproliferative activities. In a study by Wang and co-workers,[7] dietary treatments with freeze-dried BR powder, an aqueous ethanol extract, and an anthocyanin-enriched subfraction of the extract were found to affect rat esophageal papilloma formation and mass, proteins associated with proliferation, and markers of apoptosis similarly.

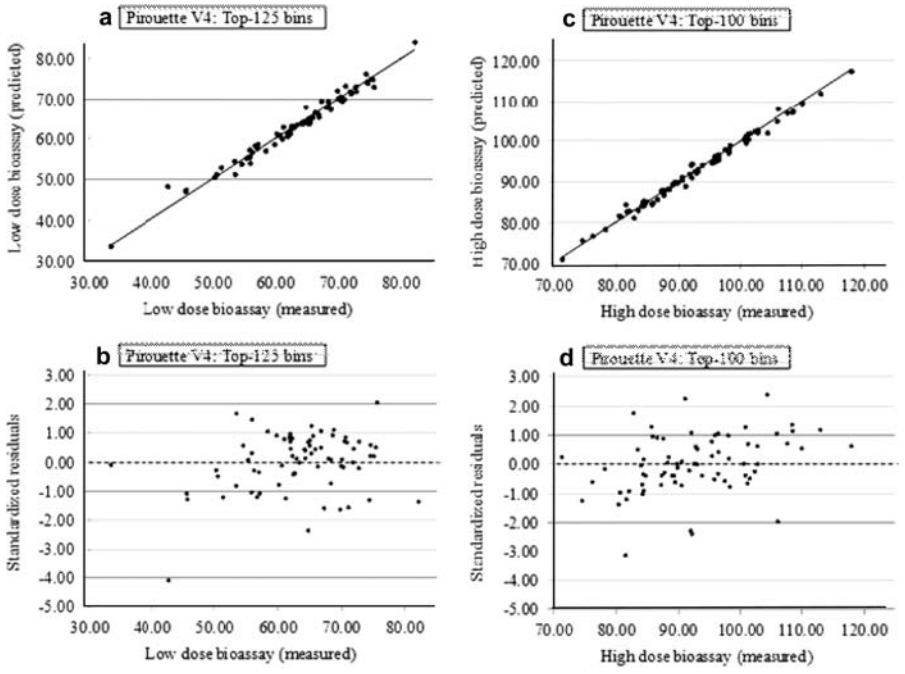

Figure 5. *Y*-fits and residual plots for the models produced with low-dose (a, b) and high-dose (c, d) bioassays.

Table 2. Pirouette PLS Model Developed with the Top 125 Bins Showing Bin Assignments, Chemical Shifts, and Rankings Based on Regression Vector Values for the Assessment of Low-Dose Bioassay Activity of Black Raspberry Extracts

species	group (atom no.)	δ^1H range (ppm)	rank/bin no.
Cy 3-xylrut (cyanidin 3-xylosylrutinoside)	CH_3 (6^{IV})	(1.147−1.142) (1.139−1.134)	1/425, 2/427
		(1.134−1.128) (1.142−1.139)	18/428, 36/426
	CH (4)	(8.848−8.842)	10/9
Cy 3-rut (cyanidin 3-rutinoside)	CH_3 (6‴)	(1.155−1.149) (1.163−1.158)	4/423, 9/421
		(1.158−1.155)	41/422
	CH (4)	(8.923−8.918)	19/5
Cy 3-sam (cyanidin 3-sambubioside)	CH (2‴)	(3.154−3.148)	99/313
Cy 3-glc (cyanidin 3-glucoside)	CH(1″)	(5.302−5.296)	103/196
SAGE (glucose ester of salicylic acid)	CH (3, 5)	(7.070−7.064) (7.099−7.097)	30/132, 79/130
		(7.061−7.059)	112/134
	CH (1′)	(5.739−5.733)	71/174
	CH (6)	(8.065−8.059) (8.069−8.065)	106/40, 119/39
		(8.055−8.049)	120/43
BAGE (glucose ester of benzoic acid)	CH (2,6)	(8.083−8.078) (8.089−8.083)	33/36, 59/35
	CH (4)	(7.626−7.622)(7.622−7.616)	53/70, 73/71
citric acid derivatives	CH_2 (2B,4B)	(2.806−2.800) (2.785−2.779)	42/350, 57/356
	CH_2 (2A, 4A)	(2.899−2.893) (2.920−2.915)	43/341, 62/335
methyl ellagic acid derivative	OCH_3	(4.055−4.050)	48/292
SAD (salicylic acid derivative)	CH (6)	(8.099−8.093) (8.128−8.125)	67/32, 109/25
epicatechin	CH (3 equiv)	(4.172−4.166) (4.189−4.183)	66/271, 85/265
p-coumaric acid	CH (8, olefinic)	(7.608−7.602)	94/75
Q 3-rut (quercetin 3-rutinoside)	CH (1‴)	(4.526−4.521)	50/238
	CH_3 (6‴)	(1.110−1.104) (1.104−1.098)	64/432, 80/433
		(1.118−1.112) (1.122−1.118)	91/430,121/429
	CH (6′)	(7.630−7.626)	63/69
Q-3-glc (quercetin 3-glucoside)	CH (6′)	(7.598−7.592)	100/78

dx.doi.org/10.1021/jf404998k | *J. Agric. Food Chem.* 2014, 62, 1989−1998

Table 3. Pirouette PLS Model Developed with Top 100 Bins Showing Bin Assignments, Chemical Shifts, and Rankings Based on Regression Vector Values for the Assessment of High-Dose Bioassay Activity of Black Raspberry Extracts

species	group (atom no.)	δ^1H range (ppm)	rank/bin no.
Cy 3-xylrut (cyanidin 3-xylosylrutinoside)	CH_3 (6^{IV})	(1.147−1.142) (1.139−1.134)	1/425, 3/427
		(1.134−1.128) (1.142−1.139)	30/428, 41/426
	CH (4)	(8.848−8.842)	10/9
Cy 3-rut (cyanidin 3-rutinoside)	CH_3 ($6'''$)	(1.155−1.149) (1.163−1.158)	11/423, 19/421
		(1.158−1.155)	90/422
	CH (4)	(8.923−8.918)	22/5
Cy 3-sam (cyanidin 3-sambubioside)	CH ($2'''$)	(3.154−3.148)	88/313
Cy 3-glc (cyanidin 3-glucoside)	CH ($1''$)	(5.302−5.296)	98/196
SAGE (glucose ester of salicylic acid)	CH (3, 5)	(7.070−7.064)	33/132
	CH (6)	(8.065−8.059)	77/40
BAGE (glucose ester of benzoic acid)	CH (2, 6)	(8.083−8.078) (8.089−8.083)	81/36, 57/35
citric acid derivatives	CH_2 (2B, 4B)	(2.806−2.800) (2.785−2.779)	6/350 12/356
	CH_2 (2A, 4A)	(2.899−2.893)	9/341
methyl ellagic acid derivative	OCH_3	(4.055−4.050)	60/292
SAD (salicylic acid derivative)	CH (6)	(8.099−8.093) (8.128−8.125)	51/32, 72/25
epicatechin	CH (3 equiv)	(4.172−4.166) (4.189−4.183)	56/271, 52/265
p-coumaric acid	CH (8, olefinic)	(7.608−7.602)	50/75
Q 3-rut (quercetin 3-rutinoside)	CH ($6'$)	(7.630−7.626)	68/69
Q-3-glc (quercetin 3-glucoside)	CH ($6'$)	(7.598−7.592)	45/78

Wang and co-workers[7] also noted similar antiproliferative properties associated with a diet formulated with the insoluble residue of the extraction with anthocyanin concentrations reduced by approximately 200-fold. These authors noted that among the potential nonanthocyanin constituents of the extract insoluble residue, ellagitannins (polymers of ellagic acid) were likely responsible for the chemoprotective effects of the residue diet. Due to their low solubility in methanol, ellagitannins were likely to be present at minimal concentrations in our extracts. However, our model clearly identified MEAAP as one of the important antiproliferative components of BR extracts. The metabolism and chemoprotective properties of ellagic acid and its polymers, derivatives, and colonic microflora-generated metabolites (urolithins, a series of bioactive dibenzopyran-6-one biomarkers of ellagic acid consumption) were recently reviewed by Landete.[30] Similar to other polyphenols, these compounds act chemoprotectively by reducing the activity of signaling cascades, limiting inflammatory responses, controlling cell cycling and proliferation, reducing angiogenesis, and stimulating apoptosis.[8,30]

Our model also identified epicatechin, Q 3-glc, Q 3-rut, SAGE, SAD, BAGE, and *p*-coumaric acids as important BR extract components in the control of HT-29 cell proliferation. Flavan-3-ols (e.g., epicatechin), flavonol glycosides (e.g., Q 3-glc, Q 3-rut), and salicylates (e.g., SAGE, SAD) are powerful phenolic antioxidants that have been shown to have chemopreventive properties against colon cancer[31−34] and other types of cancers.[3,6,31,32,34,35] In vitro cell assays and animal studies have shown these compounds inhibit proliferation or tumor growth by controlling cell cycle genes and enzymes and by promoting genes and enzymes associated with apoptosis. In a study of bioactive constituents isolated from freeze-dried strawberry, Zhang and co-workers[34] demonstrated that a *p*-coumaric acid glucose ester strongly inhibited proliferation in two colon cancer cell line assays. There is also evidence that hydroxycinnamic acids may play an active role in cancer cell regulation when acylated to anthocyanins.[36] The chemopreventive activity of hydroxybenzoic acids and their derivatives (e.g., protocatechuic acid) has also been extensively studied.[37] However, to our knowledge, this is the first report of a benzoic acid glucose ester (BAGE) showing antiproliferative potential against cancer cells.

Altered metabolism favoring cytoplasm-centered "aerobic glycolysis" is an "emerging hallmark" of cancer,[38] leading to the production of metabolites necessary for continued proliferation and sufficient energy for tumor growth.[39,40] However, aerobic glycolysis and its effects can be curtailed by high levels of cytosolic citrate.[39−41] Elevated citrate levels in cancer cells may lead to cell cycle arrest, metabolic changes favoring pro-apoptotic over anti-apoptotic proteins, and increased cytosolic- or mitochondrial-induced caspase activity leading to cell death[39−42] in a threshold-dependent manner. The increased importance of citric acid derivatives in the high-dose model (Table 3 and Table S4 in the Supporting Information) perhaps reflects this concentration threshold dependency.

The ^{1}H NMR-based model that was developed here has made a significant contribution to our understanding of the impact of the crude BR extracts in controlling HT-29 cell proliferation and provides insights as to the chemopreventive nature of BR fruits. The nonanthocyanin components of the fruit that affect cell proliferation represent a very small percentage of the total phenolic and organic acid derivatives found in the BR extracts, but both the low- and high-dose models indicated their importance in curtailing cancer cell growth. Among the model-identified nonanthocyanin components, Q 3-glc, Q 3-rut, *p*-coumaric acid, and various ellagic acid derivatives have been previously considered as bioactive

constituents of BR.[4−8,30,43,44] However, the bioactivity of MEAAP specifically, BR-derived salicylates, flavan-3-ols (e.g., epicatechin), citric acid derivatives, and/or esters of benzoic acid in controlling colon cancer cell proliferation have not been cited to our knowledge in previous work. Recognition, by the model, of the contributions of these low-concentration constituents on the impact of the extracts on cell growth clearly provides paths for new lines of research into the mechanisms of BR constituents. The data will lead to studies on the interactive effects of the extracts on the chemoprotective nature of berry fruits in general and have demonstrated the utility of using this type of approach to the study of the bioactivity of natural products.

Further advanced NMR analysis with unassigned bins (Tables S3 and S4 in the Supporting Information) may lead to the identification of additional important compounds. As this study was focused on model development and viewed as a proof of concept, recognition by the model of all of the important BR bioactive compounds was limited by the use of acidic methanol extracts and the in vitro HT-29 cell proliferation assay. However, our overall approach is readily adaptable to modeling the effects of a series of extracts including those containing compounds that differ substantially in solubility from that of phenols (e.g., carotenoids, steroids)[5] and can be adapted to accommodate other continuous *Y*-variables such as control of tumor development, enzymatic activity, or biomarker levels, which would lead to a richer understanding of the complex mechanisms by which BR compounds may affect carcinogenesis. Likewise, our approach can also be applied to assess the activity of other natural products with complex NMR spectra, not only against cancer but also for any complex interaction that can be evaluated using a biological assay.

■ ASSOCIATED CONTENT

Supporting Information

Table S1, variability in HT-29 colon cancer cell % inhibition following exposure to 73 BR extracts at two concentrations; Table S2, ^{1}H NMR-determined concentrations of cyanidin glycosides in BR extracts; Tables S3 and S4, regression vector values, bin rankings, compounds, associated protons (number and type), δ^1H range (ppm), and bin numbers for low- and high-dose PLS models; Figures S1−S11, structure data resulting from compound analysis using additional 1D selective TOCSY and 2D NMR techniques; Figure S12, selection criteria for the 100 bin model of the high-dose bioassay. This material is available free of charge via the Internet at http://pubs.acs.org.

■ AUTHOR INFORMATION

Corresponding Authors

*(F.J.W.) Phone: +01 (419) 755-4342. E-mail: wyzgoski.1@osu.edu).
*(R.N.R.) Phone: +01 (605) 688-4568. E-mail: Neil.Reese@SDState.edu.

Funding

Salaries and research support were provided in part by state and federal funds appropriated by The Ohio State University, Ohio Agricultural Research and Development Center, U.S. Department of Agriculture Special Research Grants for Dietary Intervention 2005-38903-02313, 2006-38903-03560, 2007-38903-03560, 2008-38903-19245, 2009-38903-19901, and 2010-38903-20977. Salaries and supports were also provided in part by the South Dakota Agricultural Experiment Station. The NMR equipment used is this work was purchased with funds from the Kresge Foundation and the donors to the Kresge Challenge program at The University of Akron.

Notes

The authors declare no competing financial interest.

■ ACKNOWLEDGMENTS

We acknowledge Deborah A. Miller for preparing the black raspberry extracts.

■ REFERENCES

(1) Carlsen, M.; Halvorsen, B.; Holte, K.; Bohn, S.; Dragland, S.; Sampson, L.; Willey, C.; Senoo, H.; Umezono, Y.; Sanada, C.; Barikmo, I.; Berhe, N.; Willett, W.; Phillips, K.; Jacobs, D.; Blomhoff, R. The total antioxidant content of more than 3100 foods, beverages, spices, herbs and supplements used worldwide. *Nutr. J.* **2010**, *9*, 3.
(2) Stoner, G. D.; Seeram, N. P. *Berries and Cancer Prevention*; Springer: New York, 2011.
(3) Kale, A.; Gwasnde, S.; Kotwal, S. Cancer phytotherapeutics: role for flavonoids at the cellular level. *Phytother. Res.* **2008**, *22*, 567−577.
(4) Seeram, N. P. Berry fruits: compositional elements, biochemical activities and the impact of their intake on human health, performance and disease. *J. Agric. Food Chem.* **2008**, *56*, 627−629.
(5) Stoner, G. D. Foodstuffs for preventing cancer: the preclinical and clinical development of berries. *Cancer Prev. Res.* **2009**, *2*, 187−194.
(6) Stoner, G. D.; Wang, L.-S.; Casto, B. C. Laboratory and clinical studies of cancer chemoprevention by antioxidants in berries. *Carcinogenesis* **2008**, *29*, 1665−1674.
(7) Wang, L-S; Hecht, S. S.; Carmella, S. G.; Yu, N.; Larue, B.; Henry, C.; McIntyre, C.; Rocha, C.; Lechner, J. F.; Stoner, G. D. Anthocyanins in black raspberries prevent esophageal tumors in rats. *Cancer Prevention Res.* **2009**, *2*, 84−93.
(8) Wang, L.-S.; Stoner, G. D. Anthocyanins and their role in cancer prevention. *Cancer Lett.* **2008**, *269*, 281−290.
(9) Wagner, H.; Ulrich-Merzenich, G. Synergy research: approaching a new generation of phytopharmaceuticals. *Phytomedicine* **2009**, *16*, 97−110.
(10) Manach, C.; Hubert, J.; Llorach, R.; Scalbert, A. The complex links between dietary phytochemicals and human health deciphered by metabolomics. *Mol. Nutr. Food Res.* **2009**, *53*, 1302−1315.
(11) Gomez-Casati, D. F.; Zanor, M. I.; Busi, M. V. Metabolomics in plants and humans: applications in the prevention and diagnosis of diseases. *Biomed. Res. Int.* **2013**, *2013*, 1−11.
(12) Blekherman, G.; Laubenbacher, R.; Cortes, D. F.; Mendes, P.; Torti, F. M.; Akman, S.; Torti, S. V.; Shulaev, V. Bioinformatics tools for cancer metabolomics. *Metabolomics* **2011**, *7*, 329−343.
(13) Ravoori, S.; Vadhanam, M. V.; Aqil, F.; Gupta, R. C. Inhibition of estrogen-mediated mammary tumorigenesis by blueberry and black raspberry. *J. Agric. Food Chem.* **2012**, *60*, 5547−5555.
(14) Zhang, Z.; Knobloch, T. J.; Seamon, L. G.; Stoner, G. D.; Cohn, D. E.; Paskett, E. D.; Fowler, J. M.; Weghorst, C. M. A black raspberry extract inhibits proliferation and regulates apoptosis in cervical cancer cells. *Gynecol. Oncol.* **2011**, *123*, 401−406.
(15) Liu, Z.; Schwimer, J.; Liu, D.; Greenway, F. L.; Anthony, C. T.; Woltering, E. A. Black raspberry extract and fractions contain angiogenesis inhibitors. *J. Agric. Food Chem.* **2005**, *53*, 3909−3915.
(16) Bodenhausen, G.; Ruben, D. J. Natural abundance nitrogen-15 NMR by enhanced heteronuclear spectroscopy. *J. Chem. Phys. Lett.* **1980**, *69*, 185−189.
(17) Bax, A.; Summers, M. F. Proton and carbon-13 assignments from sensitivity-enhanced detection of heteronuclear multiple-bond connectivity by 2D multiple quantum NMR. *J. Am. Chem. Soc.* **1986**, *108*, 2093−2094.
(18) Ozgen, M.; Wyzgoski, F. J.; Tulio, A. Z., Jr.; Gazula, A.; Miller, A. R.; Scheerens, J. C.; Reese, R. N.; Wright, S. R. Antioxidant capacity and phenolic antioxidants of Midwestern black raspberries grown for direct markets are influenced by production site. *HortScience* **2008**, *43* (7), 2039−2047.

(19) Tulio, A. Z., Jr.; Reese, R. N.; Wyzgoski, F. J.; Rinaldi, P. L.; Fu, R.; Scheerens, J. C.; Miller, A. R. Cyanidin 3-rutinoside and cyanidin 3-xylosylrutinoside as primary phenolic antioxidants in black raspberry. *J. Agric. Food Chem.* **2008**, *56*, 1880−1888.
(20) Wyzgoski, F. J.; Paudel, L.; Rinaldi, P. L.; Reese, R. N.; Ozgen, M.; Tulio, A. Z., Jr.; Miller, A. R.; Scheerens, J. C.; Hardy, J. K. Modeling relationships among active components in black raspberry (*Rubus occidentalis* L.) fruit extracts using high-resolution ^{1}H nuclear magnetic resonance (NMR) spectroscopy and multivariate statistical analysis. *J. Agric. Food Chem.* **2010**, *58*, 3407−3414.
(21) Johnson, J. L.; Bomser, J. A.; Scheerens, J. C.; Giusti, M. M. Effect of black raspberry (*Rubus occidentalis* L.) extract variation conditioned by cultivar, production site, and fruit maturity stage on colon cancer cell proliferation. *J. Agric. Food Chem.* **2011**, *59*, 1638−1645.
(22) Paudel, L.; Wyzgoski, F. J.; Scheerens, J. C.; Chanon, A. M.; Reese, R. N.; Smiljanic, D.; Wesdemiotis, C.; Blakeslee, J. J.; Riedl, K. M.; Rinaldi, P. L. Nonanthocyanin secondary metabolites of black raspberry (*Rubus occidentalis* L.) fruits: identification by HPLC-DAD, NMR, HPLC-ESI-MS, and ESI-MS/MS analysis. *J. Agric. Food Chem.* **2013**, *61*, 12032−12043.
(23) Skoog, D. A.; Holler, F. J.; Nieman, T. A. Introduction. In *Principles of Instrumental Analysis*; Saunders College Publishing: Philadelphia, PA, USA, 1998; pp 1−19.
(24) Westerhuis, J. A.; de Jong, S.; Smilde, A. K. Direct orthogonal signal correction. *Chemom. Intell. Lab. Syst.* **2001**, *56*, 13−25.
(25) Leiss, K. A.; Choi, Y. H.; Verpoorte, R.; Klinkhamer, P. G. L. An overview of NMR-based metabolomics to identify secondary plant compounds involved in host plant resistance. *Phytochem. Rev.* **2011**, *10*, 205−216.
(26) Gavaghan, C. L.; Li, J. V.; Hadfield, S. T.; Hole, S.; Nicholson, J. K.; Wilson, I. D.; Howe, P. W. A.; Stanley, P. D.; Holmes, E. Application of NMR-based metabolomics to the investigation of salt stress in maize. *Phytochem. Anal.* **2010**, *22*, 214−224.
(27) Eriksson, L.; Johansson, E.; Kettaneh-Wold, N.; Wold, S. Scaling. In *Introduction to Multi- and Megavariate Data Analysis Using Projection Methods (PCA & PLS)*; Umetrics Inc.: Umea, Sweden, 1999; pp 213−225.
(28) Wu, X.; Beecher, G. R.; Holden, J. M.; Haytowitz, D. B.; Gehardt, S. E.; Prior, R. L. Concentrations of anthocyanins in common foods in the United States and estimation of normal consumption. *J. Agric. Food Chem.* **2006**, *54*, 4069−4075.
(29) Seguin, C. M.; Wang, L.-S.; Stoner, G. D. Chemopreventive effects of berries and berry components in the rodent esophagus. In *Berries and Cancer Prevention*; Stoner, G. D., Seeram, N. P., Eds.; Springer: New York, 2011; pp 143−161.
(30) Landete, J. M. Ellagitannins, ellagic acid and their derived metabolites: a review about source, metabolism, functions and health. *Food Res. Int.* **2011**, *44*, 1150−1160.
(31) Butt, M. S.; Sultan, M. T. Green tea: nature's defense against malignancies. *Crit. Rev. Food Sci. Nutr.* **2009**, *49*, 463−473.
(32) Elwood, P. C.; Gallagher, A. M.; Duthie, G. G.; Mur, L. A. J.; Morgan, G. Aspirin, salicylates, and cancer. *Lancet* **2009**, *373*, 1301−1309.
(33) Warren, C. A.; Paulhill, K. J.; Davidson, L. A.; Lupton, J. R.; Taddeo, S. S.; Hong, M. Y.; Carroll, R. J.; Chapkin, R. S.; Turner, N. D. Quercetin may suppress rat aberrant crypt foci formation by suppressing inflammatory mediators that influence proliferation and apoptosis. *J. Nutr.* **2008**, *139*, 101−105.
(34) Zhang, Y.; Seeram, N. P.; Lee, R.; Feng, L.; Heber, D. Isolation and identification of strawberry phenolics with antioxidant and human cancer cell antiproliferative properties. *J. Agric. Food Chem.* **2008**, *56*, 670−675.
(35) Hsu, A.; Bruno, R. S.; Lohr, C. V.; Taylor, A. W.; Dashwood, R. H.; Bray, T. M.; Ho, E. Dietary soy and tea mitigate chronic inflammation and prostate cancer via NFκB pathway in the Noble rat model. *J. Nutr. Biochem.* **2011**, *22*, 502−510.
(36) Zhao, C.; Giusti, M. M.; Malik, M.; Moyer, M. P.; Magnuson, B. A. Effects of commercial anthocyanin-rich extracts on colonic cancer and nontumorigenic colonic cell growth. *J. Agric. Food Chem.* **2004**, *52*, 6122−6128.
(37) Masella, R.; Santangelo, C.; D'Archivio, M.; Li Volti, G.; Giovannini, C.; Galvano, F. Protocatechuic acid and human disease prevention: biological activities and molecular mechanisms. *Curr. Med. Chem.* **2012**, *19*, 2901−2917.
(38) Hanahan, D.; Weinberg, R. A. Hallmarks of cancer: the next generation. *Cell* **2011**, *144*, 657−674.
(39) Icard, P.; Lincet, H. A global view of the biochemical pathways involved in the regulation of the metabolism of cancer cells. *Biochim. Biophys. Acta* **2012**, *1826*, 423−433.
(40) Zaidi, N.; Swinnen, J. V.; Smans, K. ATP-citrate lyase: a key player in cancer metabolism. *Cancer Res.* **2012**, *72*, 3709−3714.
(41) Zhang, X.; Varin, E.; Allouche, S.; Poulain, L.; Icard, P. Effect of citrate on malignant pleural mesothelioma cells: a synergistic effect with cisplatin. *Anticancer Res.* **2009**, *29*, 1249−1254.
(42) Kruspig, B.; Nilchian, A.; Orrenius, S.; Zhivotovsky, B.; Gogvadze, V. Citrate kills tumor cells through activation of apical caspases. *Cell. Mol. Life Sci.* **2012**, *69*, 4229−4237.
(43) Jo, J.-Y.; de Mejia, E. G.; Lila, M. A. Catalytic inhibition of human DNA topoisomerase II by interactions of grape cell culture polyphenols. *J. Agric. Food Chem.* **2006**, *54*, 2083−2087.
(44) Wang, L.-S.; Arnold, M.; Huang, Y.; Sardo, C.; Seguin, C.; Martin, E.; Huang, T. H.-M.; Riedl, K.; Schwartz, S.; Frankel, W.; Pearl, D.; Xu, Y.; Winston, J., III; Yang, G.-Y.; Stoner, G. Modulation of genetic and epigenetic biomarkers of colorectal cancer in humans by black raspberries: a phase I pilot study. *Clin. Cancer Res.* **2011**, *17*, 598−610.

units/mL, including ≥7500 units/mL sulfatase), S9 mix, NADP, UDP-glucuronic acid (UDPGA), Tris-dithiothreitol, $MgCl_2$, and bovine serum albumin from Sigma-Aldrich, Inc. (St. Louis, MO, USA). Isorhapontigenin was purchased from TCI (Tokyo, Japan). The compound *cis*-resveratrol (≥98%) was obtained from Cayman Chemical Co., Inc. (Ann Arbor, MI, USA). Dihydroresveratrol (≥98%) was purchased from LKT Laboratories, Inc. (St. Paul, MN, USA). The compounds *t*RV 4′-*O*-glucuronide, *t*RV 3-*O*-glucuronide, and *t*RV 3-sulfate sodium salt were purchased from Wako Pure Chemical Industries, Ltd. (Osaka, Japan). *β*-Glucosidase from almonds (≥2000 units/g) was obtained from Shin Nihon Chemical Industries, Inc. (Aichi, Japan).

*t*RV powder, 720 mg (3.2 mmol) *t*RV/g, was obtained by extracting *t*RV from capsules of dietary supplements of resveratrol (Douglas Laboratories, Pittsburgh, PA, USA) with a 10-fold amount of ethanol three times (25 mL × 3). The MSE powder (YMP-M-100109) containing 91% MSE and 9% dextrin was obtained from Yamada Bee Co., Inc. (Kagamino, Japan).

The preparation of solutions and all experiments using resveratrol derivatives were performed in dim LED light to avoid the photochemical isomerization of the *trans* form to the *cis* form.

Contents of Resveratrol Derivatives in *t*RV and MSE Powder. Analysis of resveratrol derivatives in *t*RV and MSE powder with and without hydrolysis was performed by the Prominence high-performance liquid chromatography (HPLC) system (Shimadzu) with a Cosmosil 5C18-ARII column (Nacalai Tesque, 4.6 × 250 mm), following the analysis conditions reported by Mark et al.[16] with minor modifications. A gradient solvent system of MeOH (20%, 5 min hold; 20−70%, 45 min linear gradient; 100%, 10 min hold; and 20%, 10 min hold) in 0.1% trifluoroacetic acid was used at a flow rate of 1.0 mL/min, and detection was at 320 nm.

Enzymatic Hydrolysis of Glucosides in MSE Powder. Hydrolysis of glucosides of resveratrol derivatives in MSE powder was performed following the method reported by La Torre et al.[17] with minor modifications. Briefly, a total of 100 mg of *β*-glucosidase in 1 mL of 100 mM acetic acid was added to MSE powder (10 mg) in 1 mL of 100 mM acetic acid and incubated at 55 °C for 2 h. A volume of 3 mL of acetonitrile was added to the reaction mixture, and after stirring, was centrifuged at 13000*g* for 15 min at 4 °C. The residue was washed twice with 1 mL of acetonitrile and centrifuged at 13000*g* for 15 min at 4 °C. The supernatant was collected and evaporated with nitrogen gas and dissolved in 10 mL of 30% aqueous acetonitrile containing 1% acetic acid for HPLC analysis.

Extraction and Isolation. The extraction of melinjo was performed as previously described by Kato et al.[1] with slight modifications. In brief, the dried endosperms (250 g) were powdered and soaked in 55% ethanol (750 mL) at room temperature for 3 days. The filtrate was evaporated in vacuo to obtain the MSE (23 g). The extract was then purified as previously described[1] to obtain gnetin C (≥99%), gnemonoside A (≥99%), gnemonoside C (≥99%), gnemonoside D (≥99%), and gnetin L (≥99%).

Gnetin C monoglucuronide was obtained by following the method reported by Otake et al.[18] with minor modifications. First, gnetin C (24 mg) was incubated with incubation mixtures containing 250 μL of S9 mix (5 μg of protein), 72 mg of UDPGA, 95 mg of NADP, 570 mg of $MgCl_2$, 185 mg of dithiothreitol, and 480 mg of bovine serum albumin in 480 mL of 50 mM Tris buffer (pH 7.4). After incubation at 37 °C for 24 h, the reactions were terminated by the addition of 480 mL of acetonitrile. The samples were centrifuged at 13000*g* for 15 min at 4 °C, and supernatants were evaporated. After 6.7 g of residue was dissolved in 36 mL of water, 3 mL of the solution was loaded onto the column (Strata C18-E 55 μm, 70A, 100 mg/3 mL, Shimadzu GLC Ltd., Tokyo, Japan), which was preconditioned with 3 mL of methanol and 3 mL of water. After a washing with 9 mL of methanol, all of the eluates were collected and evaporated. The crude glucuronides (71 mg) were dissolved in 470 mL of methanol and loaded onto a preparative C18 column (Cosmosil 5C-18-AR-II, 20 × 250 mm). The semipreparative HPLC Waters 600E multisolvent delivery system was used with a 200 μL loop (Waters, Milford, MA, USA). The mobile phase consisting of water/trifluoroacetic acid (0.1%) and methanol in the ratio of (45:55, v/v) was delivered at 7.5 mL/min. The injection volume was 40 μL. The eluent was monitored at 320 nm and the fraction at 23 min was collected. The methanol was evaporated, and the aqueous layer was lyophilized to obtain the glucuronide as a white solid (2.9 mg ≥96%). The structure was confirmed by liquid chromatography−tandem mass spectrometry (LC-MS/MS).

Subjects and Study Design. The study design was approved by the Yamada Bee Co. Ethics Committee. All of the subjects gave their written informed consent.

Single-Dose Study. Ten healthy volunteers (23−34 years; six men and four women) were divided into two groups: a *t*RV dose group and an MSE dose group. Two days before the study and during the study, the volunteers were given a diet that was low in polyphenols. Grape and peanut products were excluded. Subjects in the *t*RV dose group were provided a capsule containing 1.36 mg of *t*RV powder, 149 mg of dextrin, 29 mg of cellulose, 9 mg of sucrose esters of fatty acids, and 64 mg of gelatin. Subjects in the *t*RV dose group consumed five capsules after breakfast. Subjects in the MSE dose group were provided a capsule containing 250 mg of MSE powder, 29 mg of cellulose, 9 mg of sucrose esters of fatty acids, and 64 mg of gelatin. Subjects in the MSE dose group consumed four capsules after breakfast. Blood samples were collected at 1, 2, 4, 6, 8, 12, 24, 48, 72, and 96 h after intake of the capsules. The collected blood samples were centrifuged at 1200*g* for 10 min at ambient temperature. The obtained plasma samples were stored at −80 °C until UPLC-MS/MS analysis.

Repeated-Dose Study. In a placebo-controlled study, 44 healthy volunteers (32−49 years; 22 men and 22 women) were divided into four groups: placebo and 1000, 2000, or 5000 mg of MSE powder. In the placebo capsule, 250 mg of dextrin was used instead of 250 mg of MSE powder. All subjects consumed 20 capsules every morning for 28 days in the proportion of placebo and melinjo capsule, 20:0 (placebo group), 16:4 (1000 mg MSE dose group), 12:8 (2000 mg MSE dose group), and 0:20 (5000 mg MSE dose group). During the study, the volunteers were given a diet low in polyphenols. Grape and peanut products were excluded. The portion of plasma samples obtained at 14 and 28 days after the intake of 1000 mg of MSE powder was used for measuring blood levels of resveratrol derivatives. In addition, before and 28 days after the intake of placebo, 1000, 2000, or 5000 mg of MSE powder, clinical laboratory tests, including blood pressure, pulse, body mass index, and blood and urine biochemical parameters, were performed for the volunteers.

Sample Preparation for Plasma. For UPLC-MS/MS analysis, 250 μL of human plasma was mixed with 750 μL of cold acetonitrile and centrifuged at 13000*g* for 15 min at 4 °C. The supernatant was evaporated with nitrogen gas and dissolved in 750 μL of 0.5% citric acid/acetonitrile (1:3) solution. The solution was loaded onto an SPE column (Superco HybridSPE PPT/30 mg, Sigma-Aldrich, St. Louis, MO, USA), preconditioned with 400 μL of 0.5% citric acid/acetonitrile (1:3) solution. After washing with 0.5% citric acid/acetonitrile solution, the eluate was combined and concentrated by evaporation with nitrogen gas. The pellet was resuspended in 250 μL of 30% aqueous acetonitrile before filtering with a 0.2 μm filter (DISMIC-13HP, Advantec, Tokyo, Japan), and 4 μL of the filtrate was injected onto UPLC-MS/MS.

Enzymatic Hydrolysis of Glucuronate and Sulfate Conjugates. The enzymatic cleavage of glucuronate and sulfate conjugate of plasma metabolites was performed as follows. A volume of 250 μL of human plasma was mixed with 750 μL of cold acetonitrile and centrifuged at 13000*g* for 15 min at 4 °C. The supernatant was evaporated with nitrogen gas and dissolved in 250 μL of water. The solution was mixed with 100 μL of sulfatase type H-1 from *H. pomatia* (≥10000 units/g, including ≥30000 units/g *β*-glucuronidase) solution in 0.1 M sodium acetate buffer (pH 4.7). The mixture was incubated at 37 °C in a heating block for 2 h. The reaction was terminated by adding 750 μL of 0.5% citric acid/acetonitrile (1:3) solution. The reaction mixture was centrifuged at 2000*g* for 5 min at ambient temperature. The supernatant was treated in the same way as that for samples with no hydrolysis, and UPLC-MS/MS analysis was performed.

UPLC-MS/MS Analysis. UPLC analysis was performed using an Acquity UPLC (Waters) system. Separation of metabolites was performed at 40 °C using a reversed-phase column (Acquity UPLC

Table 1. Mass Parameters for Melinjo Constituents and Their Metabolites

compound	mode	precursor (m/z)	cone (V)	product (m/z)	collision (eV)	RT (min)	LOD/LOQ (nM)
*t*RV	ES^-	227.3	36.0	143.0	25.0	7.7	7.9/26
				159.0	19.0		
				185.2	18.0		
cis-resveratrol	ES^-	227.3	36.0	143.0	25.0	9.2	26/88
				159.0	19.0		
				185.2	18.0		
dihydroresveratrol	ES^-	229.2	30.0	81.0	28.0	8.1	26/87
				106.0	18.0		
				123.0	16.0		
piceid	ES^-	389.0	20.0	143.0	45.0	6.2	3.6/12
				185.0	40.0		
				227.0	22.0		
isorhapontigenin	ES^-	257.0	30.0	224.0	20.0	8.2	19/65
				241.3	20.0		
gnetin C	ES^+	455.1	42.0	329.1	329.1	12.4	1.7/5.7
				361.2	361.2		
				437.2	437.2		
cis-gnetin C	ES^+	455.1	42.0	329.1	329.1	14.5	
				361.2	361.2		
				437.2	437.2		
gnetin C monoglucuronide	ES^+	455.1	42.0	329.1	329.1	10.1	1.4/16
				361.2	361.2		
				437.2	437.2		
gnetin L	ES^+	485.7	30.0	257.2	24.0	13.2	0.50/1.7
				361.2	20.0		
				467.4	20.0		
gnemonoside A	ES^-	777.5	50.0	411.3	44.0	6.3	4.2/14
				452.7	36.0		
				615.2	24.0		
gnemonoside D	ES^-	615.5	50.0	315.5	46.0	7.9	19/65
				241.3	20.0		
				453.3	24.0		

BEH C18, 2.1 × 100 mm, 1.7 μm). Injections were carried out with an autosampler maintained at 20 °C. The mobile phase consisted of water and acetonitrile and was pumped at a flow rate of 0.3 mL/min. The gradient system was as follows: 5% acetonitrile (0−2 min), 5−15% acetonitrile (2−7 min), 15−50% acetonitrile (7−27 min), 50−100% acetonitrile (27−31 min), and linear gradient, 100% acetonitrile (31−35 min). There was a 5 min reequilibration period with the initial solvent mixture between analyses. MS/MS was performed on a Q-Premier XE triple-quadrupole mass spectrometer (Waters) equipped with a turbo electrospray ion source (ESI) in the positive and negative modes and a heated curtain gas interface to the high-vacuum region of the mass analyzer. Mass detection and quantification of analytes were accomplished in the multiple reaction monitoring (MRM) mode, and spectra were analyzed by MassLynx Software (Waters). The ESI source was operated in the positive/negative ionization mode at 120 °C, with a desolvation temperature of 400 °C, an 800 L/h desolvation gas flow rate, and a capillary voltage set at 3.34 kV. The extractor and radiofrequency voltage were fixed to 3.0 and 0.1 V, respectively. The cone voltage varied from 20 to 50 V depending on the compound investigated. Argon was used as the collision gas at a flow rate of 0.25 mL/min, with collision energies of 16−46 eV. Quantification of *t*RV, *cis*-resveratrol, dihydroresveratrol, piceid, isorhapontigenin, gnetin C, gnetin C monoglucuronide, gnetin L, and gnemonosides A, C, and D was performed using the plasma matrix standard curve. The limits of detection (LOD) and limits of quantitation (LOQ) were determined as the analyte concentration that gave a signal-to-noise ratio of 3 and 10, respectively. Optimal conditions, LOD, and LOQ for each compound are shown in Table 1. The retention time of *cis*-gnetin C was confirmed using gnetin C solutions irradiated with artificial UV light for 0.5 h.

Pharmacokinetic Analysis. Maximum plasma concentration (C_{max}) and the time to reach C_{max} (t_{max}) were taken directly from observed plasma concentration−time profiles. The area under the plasma concentration time curve (AUC_{0-96}, nM·h) and the area under the first moment curve ($AUMC_{0-96}$, nM·h^2) were calculated by the trapezoidal rule to the last time point, 96 h.[19] The mean residence time (MRT, h) was calculated from the following formula:[19]

$$MRT = AUMC/AUC$$

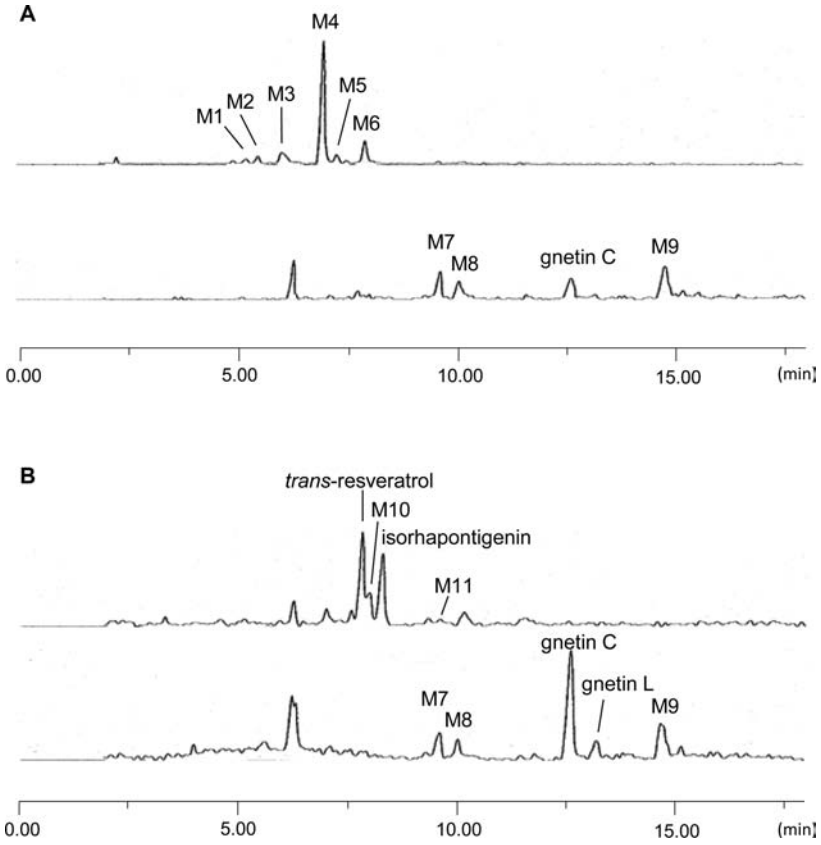

Figure 1. Liquid chromatography−mass spectrometry chromatogram of resveratrol derivatives and their major metabolites in plasma: *t*RV 4′-*O*-glucuronide (M1), isorhapontigenin monoglucuronide (M2), *t*RV 3-*O*-glucuronide (M3), *t*RV 3-sulfate (M4), isorhapontigenin monosulfate (M5), resveratrol monosulfate (M6), gnetin C monoglucuronides (M7, M8), *cis*-gnetin C (M9), dihydroresveratrol (M10), and *cis*-resveratrol (M11) without hydrolysis (A) and with hydrolysis (B) in a subject 8 h after a single oral administration of MSE powder (1000 mg).

Plasma concentration (C_p) time profiles of *t*RV and gnetin C with hydrolysis after a single dose of MSE were analyzed by a one-compartment model with first-order absorption. A curve-fitting study was performed with the least-squares regression program MULTI[20] by using the equation[19]

$$C_p = \frac{k_a FD}{V_d(k_a - k_{el})}(e^{-k_{el}t} - e^{-k_a t})$$

where k_a, k_{el}, F, D, and V_d are the absorption rate constant, elimination rate constant, bioavailability, dose, and distribution volume, respectively. Plasma concentrations after multiple doses of MSE were simulated by using the parameters obtained with the fitting study for the single dose of MSE.

Statistical Analysis. Statistical analyses were carried out using JMP for Windows 5 (SAS Institute Japan, Tokyo, Japan). In all of the tests, the criterion for statistical significance was $p < 0.05$.

RESULTS AND DISCUSSION

Identification of Metabolites for Resveratrol Monomer and Dimer Derivatives from MSE Powder. The contents of resveratrol monomer and dimer derivatives in MSE powder were as follows: resveratrol monomers, 1.2 mg/g (5.26 μmol/g) *t*RV, 5 mg/g (12.8 μmol/g) *trans*-piceid, 2.0 mg/g (7.75 μmol/g) isorhapontigenin; and dimers, 28 mg/g (61.7 μmol/g) gnetin C, 102 mg/g (131 μmol/g) gnemonoside A, 18 mg/g (29.2 μmol/g) gnemonoside C, 47 mg/g (76.3 μmol/g) gnemonoside D, 2.4 mg/L (4.95 μmol/g) gnetin L. After enzymatic hydrolysis of glucosides, the content of *t*RV was 5.4 mg/g (23.7 μmol/g) and those of isorhapontigenin, gnetin C, and gnetin L were 5.6, 150, and 12 mg/g (21.7, 350, and 24.8 μmol/g), respectively.

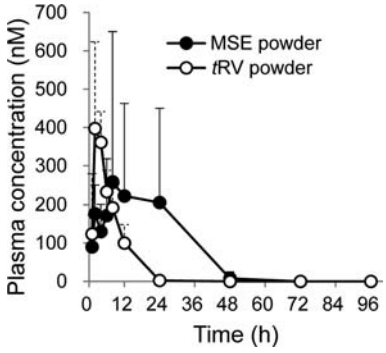

Figure 2. Plasma concentration−time curves of *t*RV with enzymatic hydrolysis in healthy human subjects who received a single dose of MSE powder (1000 mg) or *t*RV powder ($n = 5$). Results are expressed as the mean, and the bars indicate the SD.

Blood collected up to 96 h from volunteers who received 1000 mg of MSE powder was used for identification of metabolites of resveratrol monomer and dimer derivatives. Samples were prepared from plasma with and without enzymatic hydrolysis of glucuronide and sulfate. Samples were analyzed by UPLC-MS/MS.

Figure 1A shows the representative metabolites in plasma after intake of MSE powder. Five conjugates of resveratrol were found as two monoglucuronides (403/227) and two monosulfates (307/227) by MRM. The conjugate pattern of *t*RV was the same as that after intake of *t*RV powder intake (data not shown), which was also in good agreement with previous studies.[21,22] Two

dx.doi.org/10.1021/jf4048435 | J. Agric. Food Chem. 2014, 62, 1999−2007

Table 2. C_{max}, t_{max}, AUC, and MRT of Resveratrol Derivatives after Hydrolysis in Plasma Volunteers after a Single Oral Dose of MSE Powder[a]

sample	conjugated metabolite	C_{max} (nM)	t_{max} (h)	AUC_{1-96h} (nM h^{-1})	MRT (h)
*t*RV	*t*RV	473 ± 117	2.4 ± 0.9	3326 ± 470	6.6 ± 1.4
MSE	*t*RV	462 ± 314	11.6 ± 7.3*	7401 ± 5774	13.7 ± 7.7
	dihydroresveratrol	124 ± 228	18.0 ± 10.4	1371 ± 1770	6.7 ± 1.2
	isorhapontigenin	262 ± 155	6.7 ± 1.2	2962 ± 2010	11.3 ± 7.0
	gnetin C	143 ± 84	16.6 ± 7.5	6977 ± 4097	36.3 ± 8.1
	gnetin C monoglucuronide	77.9 ± 44.4	10.4 ± 8.3	2511 ± 990	36.5 ± 5.8
	gnetin L	13.1 ± 8.7	6.8 ± 5.0	372 ± 412	6.6 ± 1.4

[a]Results are expressed as the mean ± SD of experiments (n = 5). *, P < 0.05, Welch's test.

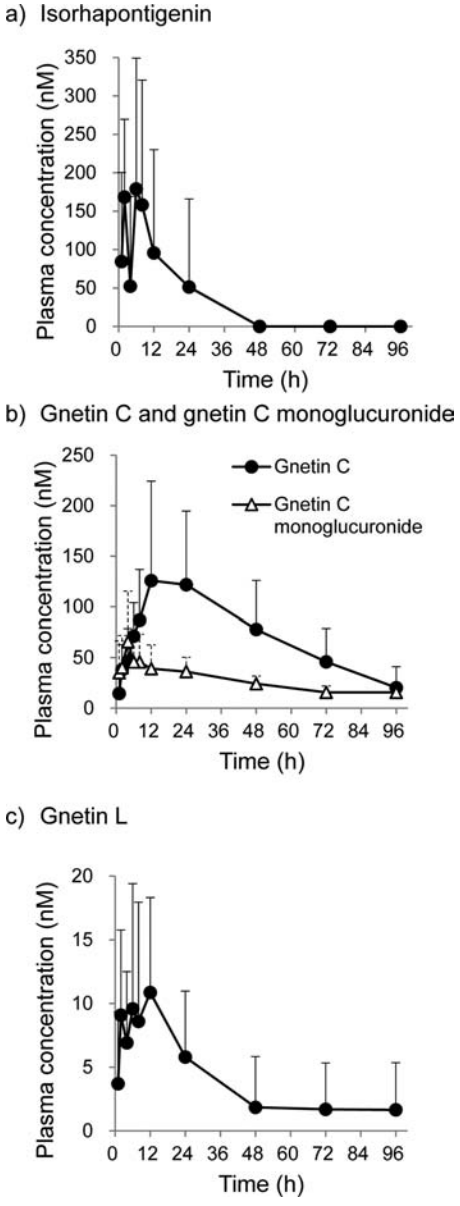

Figure 3. Plasma concentration−time curves of isorhapontigenin (a), gnetin C and gnetin C monoglucuronide (b), and gnetin L (c) with enzymatic hydrolysis in healthy human subjects (n = 5) who received a single dose of MSE powder (1000 mg). Results are expressed as the mean, and the bars indicate the SD.

conjugates of isorhapontigenin were also found as one monoglucronide and one monosulfate of isorhapontigenin by the following MRM transitions: 433.0 → 257.0 (loss of a glucuronide from isorhapontigenin) and 337.0 → 257.0 (loss of a sulfate from isorhapontigenin). Moreover, two monoglucuronides of gnetin C were found by the following MRM transitions: 631.0 → 455.1 (loss of glucuronic acid from gnetin C). In this research, the glucosides of gnetin C, such as gnemonosides A, C, and D, were not detected in plasma, suggesting that resveratrol dimers are absorbed after deglucosylation, as is the case in the intake of piceid.[15]

After enzymatic hydrolysis, most of these conjugates disappeared and *t*RV, *cis*-resveratrol, dihydroresveratrol, isorhapontigenin, and gnetin C were released (Figure 1B). However, two peaks of gnetin C glucuronides were not hydrolyzed, but the peak area of gnetin C was increased (Figure 1B). This finding indicated that several metabolites of gnetin C, other than monoglucuronide, remain to be identified.

Among the detected conjugates, two monoglucuronides and one sulfate of resveratrol were identified as *t*RV 4′-*O*-glucuronide, *t*RV 3-*O*-glucuronide, and *t*RV 3-sulfate by comparing them with their authentic samples. The conjugates of isorhapontigenin and gnetin C were characteristic metabolites of MSE, and their structures need to be elucidated in the future. On the other hand, the dihydro derivatives of gnetin C were not observed after enzymatic hydrolysis, suggesting that gnetin C is not susceptible to hydrogenation by colonic bacteria.

Pharmacokinetics of *t*RV and Its Derivative after Oral Dosing of MSE Powder. Without enzymatic hydrolysis, *t*RV, piceid, isorhapontigenin, and gnemonosides A, C, and D were not detectable in any of the plasma samples. Among *t*RV dimer derivatives, gnetin C was only detected (<25 nM) in some plasma samples after intake of MSE, but in most samples, the concentration was below the limit of quantification (data not shown).

Figure 2 and Table 2 show the plasma concentration−time profiles of *t*RV and dihydroresveratrol with hydrolysis and pharmacokinetic parameters after a single intake of MSE powder or *t*RV powder containing 4.9 mg of *t*RV only.

After intake of MSE powder, the plasma concentration of *t*RV reached 462 ± 314 nM (mean ± SD) at 12 h (Figure 2). Plasma *t*RV concentrations then declined within 48 h (Figure 2). The t_{max} of *t*RV after intake of MSE powder was significantly delayed by 9 h compared with that after *t*RV powder intake (p = 0.01) by Welch's test for parametric data, and the MRT also showed an increasing tendency compared with that after the intake of *t*RV powder (Table 2). After the intake of *t*RV powder, the plasma concentration of *t*RV with hydrolysis treatment reached C_{max}, 473 ± 117 nM, at 2 h and declined within 24 h (Figure 2), indicating that *t*RV was rapidly absorbed and mainly circulated as conjugates in plasma and then rapidly eliminated from plasma,

dx.doi.org/10.1021/jf4048435 | J. Agric. Food Chem. 2014, 62, 1999−2007

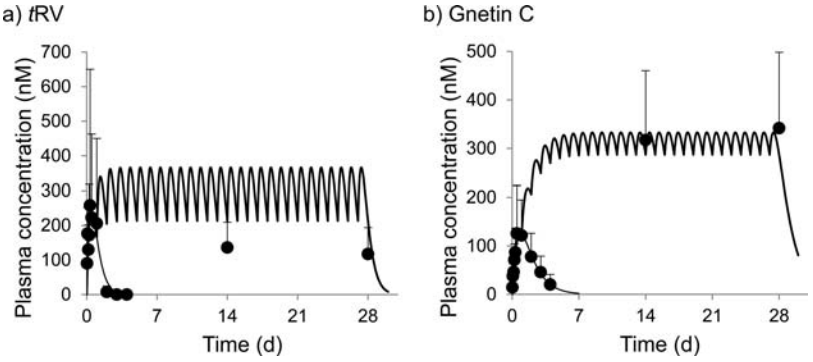

Figure 4. Effect of multiple dosing of MSE on plasma concentrations of *t*RV and gnetin C after hydrolysis. Plasma concentrations after a single dose of MSE (1000 mg, at 1−24 h) are shown together with those after multiple doses (1000 mg, 14 and 28 days) for *t*RV (a) and gnetin C (b) with hydrolysis. Thick solid lines show the fitting lines of plasma concentrations of *t*RV (a) and gnetin C (b) with hydrolysis after a single dose of MSE powder. Thin solid lines show the simulated concentrations of *t*RV (a) and gnetin C (b) with hydrolysis after multiple doses of MSE. Pharmacokinetic analysis was performed on the basis of the one-compartment model with first-order absorption as described under Materials and Methods. The parameters obtained by a fitting study, which were used for the simulation, were as follows: (a) *t*RV with hydrolysis, D = 23700 nmol as *t*RV after hydrolysis, V_d/F = 37.3 L, k_a = 0.093 h^{-1}, k_{el} = 0.086 h^{-1}; (b) gnetin C with hydrolysis, D 350000 nmol as gnetin C after hydrolysis, V_d/F = 1387.0 L, k_a = 0.064 h^{-1}, and k_{el} = 0.033 h^{-1}.

which are similar to many results.[23] With a single oral administration of MSE powder, *t*RV and its conjugates were efficiently absorbed and persisted in plasma as conjugates with a t_{max} of 12 h and a MRT of 14 h and then eliminated from plasma within 48 h (Figure 2). This delay in absorption could be because glucosides are absorbed as aglycone, which is released from glucosides by bacterial microflora in the large intestine. Indeed, after a single dose of 85.5 mg of piceid (*t*RV 3-*O*-D-glucoside) in humans, t_{max} of resveratrol conjugates in plasma was reported to be 6−8 h.[15] Furthermore, it has been reported that *t*RV is absorbed by simple diffusion and conjugated inside enterocytes to glucuronides and sulfates, which are then secreted in part to the intestinal lumen via MRP2 and BCRP.[24] The conjugates of *t*RV that avoid excretion toward the intestinal lumen are transported to the bloodstream through MRP3.[25] Therefore, several conjugates of *t*RV and its metabolites could inhibit each other in terms of elimination via transporters, leading to a long residence of *t*RV conjugates in plasma.

On the other hand, in these experiments, *cis*-resveratrol and dihydroresveratrol were also detected in some plasma samples, but in most samples, their concentrations were below the limit of quantification (data not shown).

Figure 3a shows that the concentration of isorhapontigenin reached 262 ± 155 nM at 7 h and then declined 48 h after the intake of MSE powder. In the case of tRV dimer derivatives, isorhapontigenin and gnetin L were detectable (Figure 3a,c), but gnetin C and its monoglucuronides were found to be much higher than gnetin L in plasma concentration. Because gnetin C monoglucuronides were not hydrolyzed by enzyme treatment, we isolated a monoglucuronide of gnetin C (Figure 1, M8) and quantified it separately from cleaved gnetin C. Monoglucuronides of gnetin C (Figure 1, M7) and *cis*-gnetin C could not be quantified because the authentic samples were not available. Gnetin C and gnetin C monoglucuronide had peaks of 143 ± 84.0 nM at 17 h and 77.9 ± 44.4 nM at 10 h, respectively (Figure 3b). Plasma concentrations of gnetin C and gnetin C monoglucuronide gradually declined over 96 h. Gnetin L also had a small peak of 13.1 ± 8.7 nM at 7 h, and its concentration declined over 48 h (Figure 3c). The persistence of gnetin C conjugates in plasma for >96 h might be due to slow absorption of their glucosides, because they would be absorbed as aglycone after release from glucosides by bacterial microflora as is the case of *t*RV. Furthermore, their elimination from plasma might also be mediated via several transporters as described above, and a possible inhibition by metabolites and conjugates of gnetin C and its glucoside might be responsible for their long residence in plasma. However, further studies are required to clarify the reason for this finding.

Plasma Persistence of Metabolites and Safety Assessment. In the repeated-dose administration experiment, 1000 mg of MSE powder was administered to subjects once daily after breakfast for 28 days. On days 14 and 28, blood samples were collected at 24 h after taking the dose. In this study, we focused on *t*RV and gnetin C, because gnetin C was found to be the most abundant dimer in plasma after enzymatic hydrolysis (Figure 3b,c).

Plasma concentrations of *t*RV and gnetin C that were determined after enzymatic hydrolysis are shown with those after a single administration in Figure 4a,b. Following the repeated dosing of MSE powder, a cumulative increase in plasma concentrations of *t*RV with hydrolysis was not observed (Figure 4a). Although the ratios of plasma *t*RV concentrations on days 14 and 28 to those at 24 h after the first dose were under unity, the *t*RV value at 24 h had a large variability, and observed concentrations on days 14 and 28 were not contradictory to the simulation curve calculated on the basis of a one-compartment model with first-order absorption (Figure 4a). The theoretical accumulation ratio calculated with k_a and k_{el} values was 1.28, suggesting that during multiple doses of MSE powder, *t*RV with hydrolysis follows pharmacokinetics similar to those after a single oral administration. We observed that plasma gnetin C concentrations after hydrolysis were increased by multiple dosing of MSE powder, which were in good agreement with the theoretically calculated simulation curve (Figure 4b). However, the accumulation ratio was moderate (2.8), which is also consistent with the theoretical value of 2.33 calculated by k_a and k_{el} values. This suggests that plasma gnetin C with hydrolysis during multiple doses follows similar pharmacokinetics to that after a single dose of MSE powder.

After intake of MSE powder, the variability in plasma concentrations of *t*RV and its derivatives with hydrolysis was considerably high in subjects (Figures 2 and 3; Table 2). This finding could be due to the interindividual differences of metabolism and pharmacokinetics of resveratrol derivatives.

Table 3. Blood Biochemistry Parameters in Healthy Subjects (n = 11) before and after Repeated Oral Administration of Melinjo for 28 Days[a]

		dose of MSE powder			
	days	placebo	1000 mg	2000 mg	5000 mg
ALT (U/L)	0	19.3 ± 11	22.8 ± 12.4	15.5 ± 4.6	13.9 ± 6.0
	28	19.7 ± 10.5	19.3 ± 10.6	17.4 ± 6.7	15.0 ± 5.3
γ-GTP (U/L)	0	26.9 ± 19.4	31.5 ± 17.8	17.4 ± 4.9	15.5 ± 4.2
	28	26.8 ± 20.1	27.8 ± 14.4	19.5 ± 8.8	14.6 ± 3.5
blood glucose	0	89.8 ± 7.9	91.9 ± 8.23	92.2 ± 7.9	91.9 ± 9.2
(mg/dL)	28	93.8 ± 6.3	93.4 ± 8.2	93.3 ± 8.3	91.2 ± 8.5
total protein	0	7.42 ± 0.35	7.35 ± 0.56	7.38 ± 0.28	7.37 ± 0.43
(g/dL)	28	7.23 ± 0.34	7.35 ± 0.52	7.28 ± 0.3	7.05 ± 0.42
albumin	0	4.52 ± 0.17	4.41 ± 0.37	4.56 ± 0.16	4.45 ± 0.25
(g/dL)	28	4.36 ± 0.17	4.37 ± 0.38	4.45 ± 0.14	4.2 ± 0.28
A/G ratio	0	1.56	1.54	1.64	1.54
	28	1.53	1.49	1.49	1.58
LDH (U/L)	0	153 ± 27	148 ± 27	164 ± 30	157 ± 22
	28	148 ± 24	155 ± 26	158 ± 25	154 ± 19
total bilirubin	0	0.79 ± 0.36	0.77 ± 0.31	0.68 ± 0.31	0.53 ± 0.19
(mg/dL)	28	0.66 ± 0.18	0.82 ± 0.34	0.78 ± 0.35	0.59 ± 0.27
creatinine (g/L)	0	1.51 ± 0.82	1.28 ± 0.65	1.42 ± 0.83	1.68 ± 1.30
	28	1.34 ± 0.66	1.85 ± 1.09	1.88 ± 1.04	1.50 ± 1.09
sodium	0	2.96 ± 1.18	3.15 ± 1.48	3.28 ± 1.21	2.27 ± 1.06
(g/L)	28	3.22 ± 1.45	2.68 ± 1.01	3.09 ± 0.91	2.72 ± 1.32
potassium	0	2.66 ± 1.63	2.00 ± 1.13	2.59 ± 0.96	2.15 ± 1.36
(g/L)	28	1.97 ± 0.75	2.97 ± 1.51	3.33 ± 1.36	2.28 ± 1.15
HS-CRP	0	0.052 ± 0.088	0.10 ± 0.28	0.022 ± 0.034	0.061 ± 0.155
(mg/dL)	28	0.044 ± 0.086	0.13 ± 0.37	0.098 ± 0.17	0.021 ± 0.019
chloride	0	6.14 ± 2.58	5.58 ± 2.31	6.49 ± 2.14	4.42 ± 2.66
(g/L)	28	5.86 ± 2.65	5.48 ± 1.67	7.18 ± 1.96	5.07 ± 1.99

[a]Results are expressed as the mean ± SD. ALT, alanine aminotransferase; γ-GTP, γ-glutamyl transpeptidase; AG ratio, albumin/globulin ratio; LDH, lactate dehydrogenase; HS-CRP, high-sensitivity C-reactive protein.

For the safety assessment of MSE powder, in addition to the 1000 mg dosing study, repeated-dose administration experiments were also performed at 0 (placebo), 2000, and 5000 mg for 28 days. Before and after 28 day multiple dosings, subjects were monitored by a physician and evaluated for body weight, heart rate, and blood pressure. Throughout the single and repeated administration experiments, no clinically noteworthy abnormalities were observed. Additionally, blood biochemistry parameters were not significantly different ($p > 0.05$) by Dunnet's test for parametric parameters, between before and after each oral administration of 1000, 2000, and 5000 mg of MSE powder (Table 3). This finding suggests that MSE is safe, at least in the short term, such as 1 month, and in an amount consumed in a usual manner.

Most studies have focused on *t*RV in the in vitro experiments, but it has been reported that *cis*-resveratrol, dihydroresveratrol, resveratrol conjugates, and other metabolites, such as piceatannol, a hydroxylated metabolite of resveratrol, have some biological activity.[26−31] Furthermore, pterostilbene, a methoxy derivative of resveratrol, is better absorbed and more bioactive once it is absorbed than *t*RV in the rat.[32] Recently, we reported that gnetin C reduces cell viability of tube-forming human umbilical vein epithelial cells more potently than *t*RV.[3] We also found that a monoglucuronide of gnetin C did not lose xanthine oxidase inhibitory activity.[6]

In animal experiments, it has been reported that resveratrol metabolites and conjugated resveratrol metabolites were distributed into several tissues and that these metabolites might provide a pool for local or systemic regulation of resveratrol metabolites.[33,34] Therefore, the metabolism and distribution of resveratrol derivatives from MSE in several tissues need to be clarified. Further studies are now in progress to elucidate the details of metabolism of resveratrol derivatives from MSE.

dx.doi.org/10.1021/jf4048435 | J. Agric. Food Chem. 2014, 62, 1999−2007

In conclusion, the repeated oral administration of a daily dose of MSE powder was well-tolerated up to 5000 mg/day. Clinical usefulness of MSE powder is likely because of the persistence of resveratrol monomer and dimer conjugates in plasma. However, the relationships between plasma concentrations of these conjugates and biological activity remain unclear.

AUTHOR INFORMATION

Corresponding Author

*(H.T.) E-mail: ht0807@yamada-bee.com. Phone: +81-868-54-3825. Fax: +81-868-54-3211.

Notes

The authors declare no competing financial interest.

ACKNOWLEDGMENTS

We express gratitude to Dr. E. Kato in Hosoda SHC Co. Ltd. and the Institute of World Health Development of Mukogawa Women's University for helpful discussions.

REFERENCES

(1) Kato, E.; Tokunaga, Y.; Sakan, F. Stilbenoids isolated from the seeds of melinjo (*Gnetum gnemon* L.) and their biological activity. *J. Agric. Food Chem.* **2009**, *57*, 2544−2549.

(2) Kato, H.; Samizo, M.; Kawabata, R.; Takano, F.; Ohta, T. Stilbenoids from the melinjo (*Gnetum gnemon* L.) fruit modulate cytokine production in murine Peyer's patch cells ex vivo. *Planta Med.* **2011**, *77*, 1027−1034.

(3) Kunimasa, K.; Ohta, T.; Tani, H.; Kato, E.; Eguchi, R.; Kaji, K.; Ikeda, K.; Mori, H.; Mori, M.; Tatefuji, T.; Yamori, Y. Resveratrol derivative-rich melinjo (*Gnetum gnemon* L.) seed extract suppresses multiple angiogenesis-related endothelial cell functions and tumor angiogenesis. *Mol. Nutr. Food Res.* **2011**, *55*, 1730−1734.

(4) Matsuura, D. The anti-metabolic syndrome activity of melinjo (*Gnetum gnemon* L.) seed extract. *Food Style 21* **2012**, *16*, 20−22.

(5) Ota, H.; Akishita, M.; Tani, H.; Tatefuji, T.; Ogawa, S.; Iijima, K.; Eto, M.; Shirasawa, T.; Ouchi, Y. *trans*-Resveratrol in *Gnetum gnemon* protects against oxidative-stress-induced endothelial senescence. *J. Nat. Prod.* **2013**, *76*, 1242−1247.

(6) Konno, H.; Kanai, Y.; Katagiri, M.; Watanabe, T.; Mori, A.; Ikuta, T.; Tani, H.; Fukushima, S.; Tatefuji, T.; Shirasawa, T. Melinjo (*Gnetum gnemon* L.) seed extract decreases serum uric acid levels in nonobese Japanese males: a randomized controlled study. *Evidence-Based Complement. Alternat. Med.* **2013**, *2013*, 9.

(7) Iliya, I.; Ali, Z.; Tanaka, T.; Iinuma, M.; Furusawa, M.; Nakaya, K.; Murata, J.; Darnaedi, D.; Matsuura, N.; Ubukata, M. Stilbene derivatives from *Gnetum gnemon* Linn. *Phytochemistry* **2003**, *62*, 601−606.

(8) Yanagihara, M.; Yoshimatsu, M.; Inoue, A.; Kanno, T.; Tatefuji, T.; Hashimoto, K. Inhibitory effect of gnetin C, a resveratrol dimer from melinjo (*Gnetum gnemon*), on tyrosinase activity and melanin biosynthesis. *Biol. Pharm. Bull.* **2012**, *35*, 993−996.

(9) Kaldas, M. I.; Walle, U. K.; Walle, T. Resveratrol transport and metabolism by human intestinal Caco-2 cells. *J. Pharm. Pharmacol.* **2003**, *55*, 307−312.

(10) De Santi, C.; Pietrabissa, A.; Spisni, R.; Mosca, F.; Pacifici, G. M. Sulphation of resveratrol, a natural product present in grapes and wine, in the human liver and duodenum. *Xenobiotica* **2000**, *30*, 609−617.

(11) Walle, T.; Hsieh, F.; DeLegge, M.; Oatis, J.; Walle, U. High absorption but very low bioavailability of oral resveratrol in humans. *Drug Metab. Dispos.* **2004**, *32*, 1377−1382.

(12) Boocock, D. J.; Faust, G. E.; Patel, K. R.; Schinas, A. M.; Brown, V. A.; Ducharme, M. P.; Booth, T. D.; Crowell, J. A.; Perloff, M.; Gescher, A. J.; Steward, W. P.; Brenner, D. E. Phase I dose escalation pharmacokinetic study in healthy volunteers of resveratrol, a potential cancer chemopreventive agent. *Cancer Epidemiol. Biomarkers Prev.* **2007**, *16*, 1246−1252.

(13) Shankar, S.; Singh, G.; Srivastava, R. K. Chemoprevention by resveratrol: molecular mechanisms and therapeutic potential. *Front. Biosci.* **2007**, *12*, 4839−4854.

(14) Bode, L. M.; Bunzel, D.; Huch, M.; Cho, G. S.; Ruhland, D.; Bunzel, M.; Bub, A.; Franz, C. M.; Kulling, S. E. In vivo and in vitro metabolism of *trans*-resveratrol by human gut microbiota. *Am. J. Clin. Nutr.* **2013**, *97*, 295−309.

(15) Burkon, A.; Somoza, V. Quantification of free and protein-bound *trans*-resveratrol metabolites and identification of *trans*-resveratrol-C/O-conjugated diglucuronides − two novel resveratrol metabolites in human plasma. *Mol. Nutr. Food Res.* **2008**, *52*, 549−557.

(16) Mark, L.; Nikfardjam, M. S.; Avar, P.; Ohmacht, R. A validated HPLC method for the quantitative analysis of *trans*-resveratrol and *trans*-piceid in Hungarian wines. *J. Chromatogr. Sci.* **2005**, *43*, 445−449.

(17) La Torre, G. L.; Laganà, G.; Bellocco, E.; Vilasi, F.; Salvo, F.; Dugo, G. Improvement on enzymatic hydrolysis of resveratrol glucosides in wine. *Food Chem.* **2004**, *85*, 259−266.

(18) Otake, Y.; Hsieh, F.; Walle, T. Glucuronidation versus oxidation of the flavonoid galangin by human liver microsomes and hepatocytes. *Drug Metab. Dispos.* **2002**, *30*, 576−581.

(19) Higaki, K. Pharmacokinetics. In *Pharmaceutics*, 5th ed.; Sezaki, H., Kimura, T., Hashida, M., Eds.; Hirokawa Publishing: Tokyo, Japan, 2011; pp 343−434.

(20) Yamaoka, K.; Tanigawara, Y.; Nakagawa, T.; Uno, T. A pharmacokinetic analysis program (multi) for microcomputer. *J. Pharmacobiodyn.* **1981**, *4*, 879−885.

(21) Boocock, D. J.; Patel, K. R.; Faust, G. E.; Normolle, D. P.; Marczylo, T. H.; Crowell, J. A.; Brenner, D. E.; Booth, T. D.; Gescher, A.; Steward, W. P. Quantitation of *trans*-resveratrol and detection of its metabolites in human plasma and urine by high performance liquid chromatography. *J. Chromatogr., B: Anal. Technol. Biomed. Life Sci.* **2007**, *848*, 182−187.

(22) Urpi-Sarda, M.; Zamora-Ros, R.; Lamuela-Raventos, R.; Cherubini, A.; Jauregui, O.; de la Torre, R.; Covas, M. I.; Estruch, R.; Jaeger, W.; Andres-Lacueva, C. HPLC-tandem mass spectrometric method to characterize resveratrol metabolism in humans. *Clin. Chem.* **2007**, *53*, 292−299.

(23) Rocha-Gonzalez, H. I.; Ambriz-Tututi, M.; Granados-Soto, V. Resveratrol: a natural compound with pharmacological potential in neurodegenerative diseases. *CNS Neurosci. Ther.* **2008**, *14*, 234−247.

(24) Juan, M. E.; Gonzalez-Pons, E.; Planas, J. M. Multidrug resistance proteins restrain the intestinal absorption of *trans*-resveratrol in rats. *J. Nutr.* **2010**, *140*, 489−495.

(25) van de Wetering, K.; Burkon, A.; Feddema, W.; Bot, A.; de Jonge, H.; Somoza, V.; Borst, P. Intestinal breast cancer resistance protein (BCRP)/Bcrp1 and multidrug resistance protein 3 (MRP3)/Mrp3 are involved in the pharmacokinetics of resveratrol. *Mol. Pharmacol.* **2009**, *75*, 876−885.

(26) Delmas, D.; Aires, V.; Limagne, E.; Dutartre, P.; Mazué, F.; Ghiringhelli, F.; Latruffe, N. Transport, stability, and biological activity of resveratrol. *Ann. N.Y. Acad. Sci.* **2011**, *1215*, 48−59.

(27) Gakh, A. A.; Anisimova, N. Y.; Kiselevsky, M. V.; Sadovnikov, S. V.; Stankov, I. N.; Yudin, M. V.; Rufanov, K. A.; Krasavin, M. Y.; Sosnov, A. V. Dihydroresveratrol − a potent dietary polyphenol. *Bioorg. Med. Chem. Lett.* **2010**, *20*, 6149−6151.

(28) Wang, L.-X.; Heredia, A.; Song, H.; Zhang, Z.; Yu, B.; Davis, C.; Redfield, R. Resveratrol glucuronides as the metabolites of resveratrol in humans: characterization, synthesis, and anti-HIV activity. *J. Pharm. Sci.* **2004**, *93*, 2448−2457.

(29) Hoshino, J.; Park, E. J.; Kondratyuk, T. P.; Marler, L.; Pezzuto, J. M.; van Breemen, R. B.; Mo, S.; Li, Y.; Cushman, M. Selective synthesis and biological evaluation of sulfate-conjugated resveratrol metabolites. *J. Med. Chem.* **2010**, *53*, 5033−5043.

(30) Calamini, B.; Ratia, K.; Malkowski, M. G.; Cuendet, M.; Pezzuto, J. M.; Santarsiero, B. D.; Mesecar, A. D. Pleiotropic mechanisms facilitated by resveratrol and its metabolites. *Biochem. J.* **2010**, *429*, 273−282.

(31) Kim, D. H.; Ahn, T.; Jung, H. C.; Pan, J. G.; Yun, C. H. Generation of the human metabolite piceatannol from the anticancer-preventive

agent resveratrol by bacterial cytochrome P450 BM3. *Drug Metab. Dispos.* **2009**, *37*, 932−936.
(32) Kapetanovic, I. M.; Muzzio, M.; Huang, Z.; Thompson, T. N.; McCormick, D. L. Pharmacokinetics, oral bioavailability, and metabolic profile of resveratrol and its dimethylether analog, pterostilbene, in rats. *Cancer Chemother. Pharmacol.* **2011**, *68*, 593−601.
(33) Abd El-Mohsen, M.; Bayele, H.; Kuhnle, G.; Gibson, G.; Debnam, E.; Kaila Srai, S.; Rice-Evans, C.; Spencer, J. P. Distribution of [^{3}H]*trans*-resveratrol in rat tissues following oral administration. *Br. J. Nutr.* **2006**, *96*, 62−70.
(34) Andres-Lacueva, C.; Macarulla, M. T.; Rotches-Ribalta, M.; Boto-Ordonez, M.; Urpi-Sarda, M.; Rodriguez, V. M.; Portillo, M. P. Distribution of resveratrol metabolites in liver, adipose tissue, and skeletal muscle in rats fed different doses of this polyphenol. *J. Agric. Food Chem.* **2012**, *60*, 4833−4840.

NOTE ADDED AFTER ASAP PUBLICATION

There was an error in the fifth paragraph of the Pharmacokinetics of *t*RV and Its Derivative after Oral Dosing of MSE Powder section in the version of this paper published February 12, 2014. The correct version published February 13, 2014.

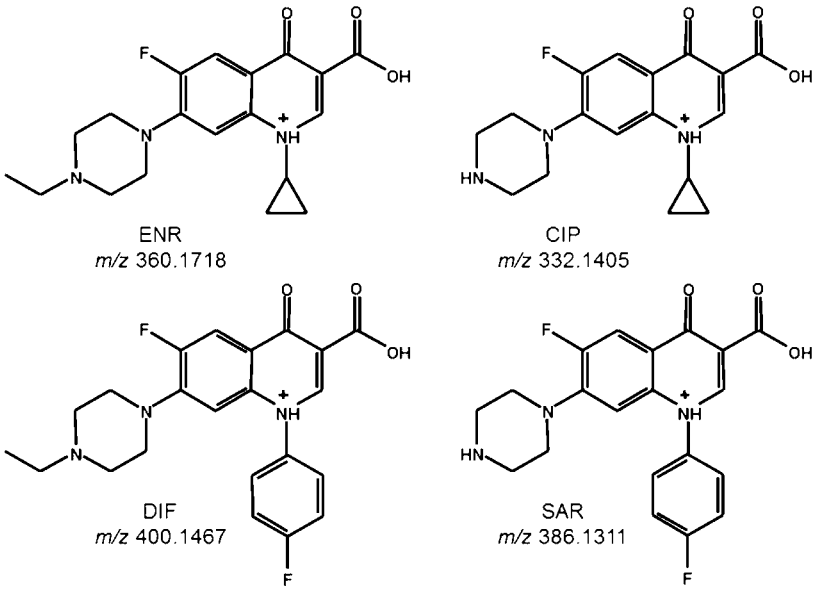

Figure 1. Structures of the four quinolones studied (ENR, CIP, DIF, and SAR).

chromatography (LC) coupled to high-resolution mass spectrometry (ToF and LTQ-Orbitrap).

EXPERIMENTAL PROCEDURES

Chemicals and Apparatus. The standards were purchased from several pharmaceutical firms: ENR from Cenavisa (Reus, Spain), CIP from Ipsen Pharma (Barcelona, Spain), DIF from Abbott (Madrid, Spain), and SAR from AK Scientific Inc. (CA,USA).

All reagents were of analytical grade unless indicated. Formic acid (HOCHO), acetic acid (HOAc), acetonitrile (MeCN), methanol (MeOH), sodium dihydrogenphosphate, and sodium hydroxide (NaOH) were supplied by Merck (Darmstadt, Germany). Water was ultrapurified by a Milli-Q system (Millipore, Bedford, MA, USA).

The quinolone individual stock solutions (ENR, CIP, DIF, and SAR) were prepared at a concentration of 500 μg mL^{-1} in 50 mM HOAc aqueous solution. The individual working solutions that were used to spike the milk samples were prepared by dilution of the individual stock solution at a concentration of 20 μg mL^{-1} in water.

Sodium dihydrogenphosphate solution 0.1 M adjusted with NaOH 5 M to pH 10 was added to milk samples prior to the cleanup step.

The SPE cartridges used in this study were Oasis HLB (3 cm^3/60 mg), obtained from Waters (Milford, MA, USA).

To simulate the thermal treatment of milk, a laboratory oven (Memmert) was used to warm the samples. A Rotanta 460RS (Hettich Zentrifuguen, Germany) centrifuge was used to separate precipitated proteins and fat of supernatant after the extraction. The SPE step was carried out in a Supelco vacuum manifold with disposable liners for 24 cartridges (Bellefonte, PA, USA), connected to a Supelco vacuum tank. Evaporation to dryness was performed in a TurboVap LV (Caliper Life Science, Hopkinton, MA, USA). A Crison 2002 potentiometer (±0.1 mV) (Crison, Barcelona, Spain) with a Crison 5203 combined pH electrode from Orion Research (Boston, MA, USA) was used to measure the pH of the phosphate solution and the mobile phase.

Milk Samples. Milk samples used in the work have been supplied by the Laboratori Interprofessional Lleter de Catalunya (ALLIC), control laboratory of milk in Catalonia. The samples were analyzed previously by ALLIC using a screening method to determine if the milk contained residues of antibiotics. The milk samples that were negative in antibiotics were used as blank samples in this work. Four positive samples in ENR were used to study the metabolites.

LC-MS Instrumentation and Working Conditions. *LC Conditions.* Quinolones, their metabolites, and degradation products were separated in a Zorbax Eclipse XDB-C8 column (5 μm, 4.6 × 150 mm) from Agilent Technologies (Santa Clara, CA, USA), using a Kromasil C8 (5 μm, 4.6 × 15 mm) precolumn supplied by Akady (Barcelona, Spain) when samples were analyzed by LC-ToF. A Pursuit UPS C18 column (2.4 μm, 2 × 50 mm) from Varian (Harbor City, CA, USA) was used when samples were injected into the LC-LTQ-Orbitrap.

For both columns, the mobile phase was composed of an aqueous solution of 0.1% HOCHO (solvent A) and MeCN with 0.1% HOCHO (solvent B) at a constant flow rate of 1 or 0.3 mL min^{-1}, respectively. The injection volume was 20 μL in LC-ToF and 10 μL in LC-LTQ-Orbitrap. Separations were carried out in a Zorbax Eclipse XDB-C8 column for 11 min under the following gradients: from 0 to 1 min, 15% B; 4 min, 45% B; 7 min, 56% B; 8.5 min, 15% B; and 11 min, 15% B. Separations were carried out in a Pursuit UPS C18 column under the following conditions: from 0 to 3.5 min, 1% B; 4.5 min, 25% B; 5 min, 50% B; 6.5 min, 50% B; 7.5 min, 25% B; 8.5 min, 10% B; and 11 min, 1% B.

LC-MS (ToF). A HP Agilent Technologies 1100 LC system was equipped with an autosampler and coupled to a 6220 oa-ToF LC/MS mass spectrometer with an electrospray ionization source (ESI) (Agilent Technologies, Santa Clara, CA, USA). The system was controlled by Mass Hunter workstation software (Agilent Technologies) for the acquisition and processing of data from the ToF mass spectrometer.

The optimum parameters of ToF in positive mode were as follows: capillary voltage, 4000 V; drying gas (N_2) temperature, 300 °C; drying gas (N_2) flow rate, 9 L min^{-1}; nebulizer gas (N_2), 40 psi; fragmentor voltage, 150 V; skimmer voltage, 60 V; and OCT 1 RF voltage, 250 V. The ToF-MS mass resolving power was approximately 10000 full width at half-maximum (fwhm) at m/z 922. Spectra were acquired over the m/z 50−1100 range. Data storage was in profile and centroid modes.

LC-MS (LTQ-Orbitrap). An Accela LC system (Thermo Scientific, Hemel Hempstead, UK) was equipped with a thermostatic autosampler and coupled to an LTQ Orbitrap Velos mass spectrometer (Thermo Scientific), with an ESI source. XCalibur software was used for the data analyses.

The operation parameters used were as follows: source voltage, 3.5 kV; sheath gas (N_2), 40 (arbitrary units); auxiliary gas (N_2), 10 (arbitrary units); sweep gas (N_2), 10 (arbitrary units); and capillary temperature, 275 °C. Default values were used for most other acquisition parameters (Fourier transform (FT) automatic gain control (AGC) target 1 × 10^6 for MS mode and 5 × 10^4 for MS^n mode). Milk samples were first analyzed in full MS mode with the Orbitrap mass resolving power set at 30000 fwhm at m/z 400. The

Table 1. Accurate Masses of Ions Observed in Spiked Milk Samples but Not in Blank Milk Samples by LC-ToF[a]

m/z				m/z			
exptl	theor	structure	error (ppm)	exptl	theor	structure	error (ppm)
		ENR				**CIP**	
157.5685	157.5686	$[CIP + 2H - H_2O]^{2+}$	0.6	157.5690	157.5686	$[CIP + 2H - H_2O]^{2+}$	2.5
166.5740	166.5739	$[CIP + 2H]^{2+}$	0.6	166.5742	166.5739	$[CIP + 2H]^{2+}$	1.8
167.5820	na[b]	$[334.1569]^{2+}$		274.0989	na	na	
171.5845	171.5843	$[ENR + 2H - H_2O]^{2+}$	1.2	288.1511	288.1507	$[CIP + H - CO_2]^{+}$	1.4
180.5897	180.5897	$[ENR + 2H]^{2+}$	0.1	314.1293	314.1288	$[CIP + H - H_2O]^{+}$	1.6
316.1817	316.1820	$[ENR + H - CO_2]^{+}$	0.9	332.1400	332.1405	$[CIP + H]^{+}$	1.5
332.1402	332.1405	$[CIP + H]^{+}$	0.9	348.1334	na	na	
334.1569	na	na		362.1148[d]	na	na	
342.1603	342.1612	$[ENR + H - H_2O]^{+}$	2.6	374.1509	na	na	
360.1719	360.1718	$[ENR + H]^{+}$	0.3	375.1563	na	na	
376.1656[c]	na	na		573.1431	na	na	
390.1461[d]	na	na		656.2477	na	na	
719.3349	719.3363	$[2ENR + H]^{+}$	1.9				
		DIF				**SAR**	
191.5714	191.5717	$[DIF + 2H - H_2O]^{2+}$	0.5	184.5637	184.5639	$[SAR + 2H - H_2O]^{2+}$	1.1
200.5761	200.5770	$[DIF + 2H]^{2+}$	3.0	193.5692	193.5692	$[SAR + 2H]^{2+}$	0.1
299.0980	na	na		342.1422	342.1412	$[SAR + H - CO_2]^{+}$	2.9
374.1284	na	na		360.1181	na	na	
382.1367	382.1362	$[DIF + H - H_2O]^{+}$	1.3	368.1193	368.1205	$[SAR + H - H_2O]^{+}$	3.3
386.2209	386.1311	$[SAR + H]^{+}$	0.3	386.1311	386.1311	$[SAR + H]^{+}$	0.1
400.1446	400.1467	$[DIF + H]^{+}$	2.0	402.1241	na	na	
416.1396[c]	na	na		416.1069	na	na	
430.1185[d]	na	na		428.1410	na	na	
				429.1395	na	na	

[a]The errors (ppm) are calculated from the theoretical and proposed structures. [b]na, nonassigned. [c]Two chromatographic peaks with the same m/z (at different retention times). [d]Three chromatographic peaks with the same m/z (at different retention times).

following analyses were carried out in MS^n mode with the Orbitrap mass resolving power set at 15000 fwhm at m/z 400. The maximum injection time was set to 100 ms with one micro scan for MS mode and to 500 ms with one micro scan for MS^n mode. TPs were fragmented in the HCD collision cell because some metabolites were not fragmented in the trap. The selected HCD voltage was 45 V, although in some cases it was raised to 50 and 60 V. The mass range was from m/z 100 to 1000.

Procedures. *Thermal Study.* In this study, individual standards of quinolones (ENR, CIP, DIF, and SAR) at 1 $\mu g\ mL^{-1}$ in water were warmed to degrade the antibiotics. All quinolones were heat-treated under conditions of temperature and time corresponding to three thermal processes of milk: pasteurization at 60 °C for 30 min (T1) or 72 °C for 15 s (T2) and sterilization at 120 °C for 20 min (T3). Subsequently, individual milk samples spiked with ENR, CIP, DIF, and SAR were warmed at 120 °C for 20 and 60 min (T3.20 and T3.60). The samples heated at different temperatures were compared with spiked nonheated samples (T0) and with blank milk samples at same thermal condition; for example, samples at T3.20 were compared with blank at T3.20. Milk samples from animals medicated with ENR were also thermally treated at T3.20 and T3.60 and compared with the same sample but nonheated. All experiments were made in triplicate.

Sample Treatment and Cleanup (SPE). The method for analyzing the milk sample was used previously to determine the antibiotics in the milk.[9−12] The extraction method consisted of the addition of 0.5 mL of 0.1 M phosphate solution at pH 10 and 2 mL of water to 2 g of milk, centrifugation of samples, and an SPE process. The SPE cartridges used were Oasis HLB, and these were preconditioned with 1 mL of MeOH, 1 mL of water, and 1 mL of 0.1 M phosphate solution at pH 10. After sample loading, the cartridge was washed with 3 mL of water and the analytes were eluted with 2 mL of MeOH.

The methanolic fraction eluted from the SPE was evaporated to dryness under a nitrogen stream by TurboVap LV and a water temperature of 35 °C. The extract was then reconstituted with 200 μL of water and filtered through membrane filters (Ultra free Durapore PVDF 0.22 μm from Millipore) before injection into the LC-LTQ-Orbitrap.

Data Treatment. The LC-ToF data were treated using two procedures to find metabolites and TPs in milk samples from medicated cows with ENR. The first corresponds to the manual comparison of mass spectra of blanks and samples. This procedure was used initially to detect the TPs in standards and spiked cow's milk. The other option consists of the use of MZmine2[42,43] free software, which provides a list of all m/z on mass spectra. The list can be shortened by removing all of the ions that appear only in the blank spectra and those that have a similar or higher intensity in the blanks than in the samples. Only the ions that appeared between 1 and 9 min and from 150 to 800 Da were considered. Also, a mass defect filter (MDF) of 120 mDa was applied.

RESULTS AND DISCUSSION

Determination of Thermal TPs by LC-ToF-MS. Blank and spiked water samples were subjected to the thermal conditions explained under LC Conditions and analyzed by LC-ToF-MS. The total ion current chromatograms (TIC) of spiked water samples were compared with the TIC of blank water samples to examine possible TPs. The two chromatograms were nearly identical except for the spiked antibiotic peak.

The mass spectra of blank and spiked water samples were compared by overlapping. The only difference between the spiked sample and the blanks was the peak of the parent compound. However, a decrease in the area of the protonated molecule of quinolones was noted when the temperature rose.

dx.doi.org/10.1021/jf405554z | J. Agric. Food Chem. 2014, 62, 2008−2021

Table 2. Accurate Masses of Parent Quinolones, Given Reactions, All TPs Observed, and Fragments Obtained by LC-LTQ-Orbitrap[a]

	t_R[b] (min)	m/z	gain or loss	reaction[c]	m/z TPs	fragmentation	mol formula	DBE	theor mass	error (ppm)
Common Reactions of 4 Quinolones										
ENR	4.7	360.1718	+15.9949	HX	376.1666	358.1560, 340.1121, 286.1018, 244.0912, 243.0877	$C_{19}H_{23}FN_3O_4$	10	376.1667	−0.3
ENR	5.8	360.1718	+15.9949	N-O	376.1665	359.1639, 330,1611, 315.1741, 300.1506, 257.1085, 231.0928, 84.0807	$C_{19}H_{23}FN_3O_4$	10	376.1667	−0.5
CIP	3.6	332.1405	+15.9949	HX	348.1355	330.1248, 310.1184, 136.0617	$C_{17}H_{19}FN_3O_4$	10	348.1354	0.3
DIF	6.0	400.1467	+15.9949	HX	416.1416	398.1307, 343.0880, 329.0725, 316.0647, 256.0801	$C_{21}H_{20}F_2N_3O_4$	13	416.1416	0.0
DIF	6.3	400.1467	+15.9949	N-O	416.1418	399.1388, 370.1359, 355.1489, 299.09899	$C_{21}H_{20}F_2N_3O_4$	13	416.1416	0.5
SAR	5.8	386.1311	+15.9949	HX	402.1261	384.1156, 382.1197, 364.1089, 343.0882, 316.0653, 136.0758	$C_{20}H_{18}F_2N_3O_4$	13	402.1260	0.2
ENR	5.8	360.1718	+29.9740	HX + K	390.1458	372.1353, 362.1509, 346.1560, 318.1246, 301.0982, 289.09813, 245.1083, 128.0706, 100.0756, 72.0808	$C_{19}H_{21}FN_3O_5$	11	390.1460	−0.5
ENR	6.7	360.1718	+29.9740	HX + K	390.1462	372.1356, 362.1510, 291.07754, 273.0670, 259.0514, 100.0757, 72.0808	$C_{19}H_{21}FN_3O_5$	11	390.1460	0.5
ENR	6.8	360.1718	+29.9740	HX + K	390.1461	372.1355, 362.1509, 291.0774, 273.0669, 259.0513, 100.0756, 72.0809	$C_{19}H_{21}FN_3O_5$	11	390.1460	0.3
CIP	6.1	332.1405	+29.9740	HX + K	362.1141[d]		$C_{17}H_{17}FN_3O_5$	11	362.1147	−1.7
DIF	6.0	400.1467	+29.9740	HX + K	430.1209	412.1102, 402.1259, 386.1309, 368.1204, 329,0730, 299.0988, 197.1029, 114.0549, 70.0650	$C_{21}H_{18}F_2N_3O_5$	14	430.1209	0.0
DIF	6.9	400.1467	+29.9740	HX + K	430.1207	412.1101, 402.1258, 384.1151, 345.0678, 327.0572, 86.0599	$C_{21}H_{18}F_2N_3O_5$	14	430.1209	−0.5
DIF	7.1	400.1467	+29.9740	HX + K	430.1207	412.1101, 402.1258, 384.1151, 345.0678, 327.0572, 86.0599	$C_{21}H_{18}F_2N_3O_5$	14	430.1209	−0.5
SAR	6.7	386.1311	+29.9740	HX + K	416.1053[d]		$C_{20}H_{16}F_2N_3O_5$	14	416.1053	0.0
ENR	4.4	360.1718	−26.0146	DE + H	334.1560	316.1464, 311.3906, 296.1393, 289.098, 263.0825, 219.0927, 164.1069, 86.0600, 72.0807	$C_{17}H_{21}FN_3O_3$	9	334.1561	−0.3
CIP	3.6	332.1405	−26.0146	DE + H	306.1246	288.1141, 268.108, 263.0824, 245.1084	$C_{15}H_{17}FN_3O_3$	9	306.1248	−0.7
DIF	5.8	400.1467	−26.0146	DE + H	374.1307	354.1246, 343.0884, 336.1138, 317.0728, 299.0988, 280.1242, 273.0830	$C_{19}H_{18}F_2N_3O_3$	12	374.1311	−1.1
SAR	5.9	386.1311	−26.0146	DE + H	360.1156	343.0883, 342.1048, 340.1089, 322.0986, 317.07310, 299.0991	$C_{18}H_{16}F_2N_3O_3$	12	360.1154	0.6
Other Reactions										
ENR	5.0	360.1718	−28.0303	DE	332.1404		$C_{17}H_{19}FN_3O_3$	10	332.1405	−0.3
DIF	6.0	400.1467	−14.0157	DM	386.1309		$C_{20}H_{18}F_2N_3O_3$	13	386.1311	−0.5
CIP	7.0	332.1405	+42.0103	A	374.1509	356.1402, 314.1297, 300.0777, 272.0827, 249.0669, 243.0563, 231.0562, 215.0249	$C_{19}H_{21}FN_3O_4$	11	374.1511	−0.5
SAR	8.0	386.1311	+42.0103	A	428.1416	410.1310, 382.1361, 368.1203	$C_{22}H_{20}F_2N_3O_4$	14	428.1416	0.0
CIP	6.6	332.1405	+43.0056	F	375.1463	357.1356, 340.1096, 332.1402, 314.1297, 270.0671, 243.0563, 231.0563, 216.0692	$C_{18}H_{20}FN_4O_4$	11	375.1463	0.0
SAR	7.2	386.1311	+43.0056	F	429.1369	411.1264, 386.1312, 368.1205, 348.1141	$C_{21}H_{19}F_2N_4O_4$	14	429.1369	0.0
CIP	5.0	332.1405	−58.0419	DY + DCP	274.0986[e]	231.0562,[e] 217.0404,[e] 203.0611, 187.0663, 175.0664, 163.0665, 148.0556, 136.557[e]	$C_{14}H_{13}FN_3O_2$	10	274.0986	0.0
CIP	5.0	332.1405	+241.0024		573.1429[d]					
CIP	4.0	332.1405	+324.1056	LC	656.2457	638.2450, 620.2246, 494.1929, 476.1825, 404.1616, 344.1400, 332.1401	$C_{29}H_{39}FN_3O_{13}$	12	656.2461	−0.6

[a]The DBE calculated with the deprotonated molecular formula and the calculated error (ppm) of the assignation of structure. [b]Retention time when LC-ToF is used. [c]HX, hydroxylation; N-O, *N*-oxide; K, ketone formation; DE, deethylation; H, hydrogenation; CC, cysteine conjugation; DC, decarboxylation; DF, reductive defluorination; DM, demethylation; A, acetylation; F, formamidation; DY, dehydration; DCP, decyclopropylation; LC, lactose conjugation. [d]Concentration too low to be fragmented. [e]These masses were also observed with a molecule of water (+18.0105) but at low concentration.

The highest decrease was seen when the samples were heated at 120 °C for 20 min (T3.20), in some cases up to 20%. A new condition of 120 °C for 60 min (T3.60) was also applied to ensure that TPs were obtained in sufficiently high concentrations to be detected.

Raw cow's milk samples free of quinolones were spiked and heated under the selected conditions. To assess whether any TPs had formed, the same procedure as that used for the water standards was followed. In this case, some ions were identified in the mass spectra of the spiked milk samples that were not observed in the blank milk samples. Some ions were identified as doubly charged protonated molecules, with characteristic losses of water and carbon dioxide. These ions were also detected in the water samples. The doubly protonated identity was confirmed by the isotopic pattern. The difference between $[M + 2H]^{2+}$ and $[M + 1 + 2H]^{2+}$ was m/z 0.5. In addition, the same retention time (t_R) of the compounds in the extracted ion chromatogram (EIC) was observed.[44] The losses of H_2O (18.0105) and CO_2 (43.9898) are not considered as TPs because these were also observed in the source by CID-in-

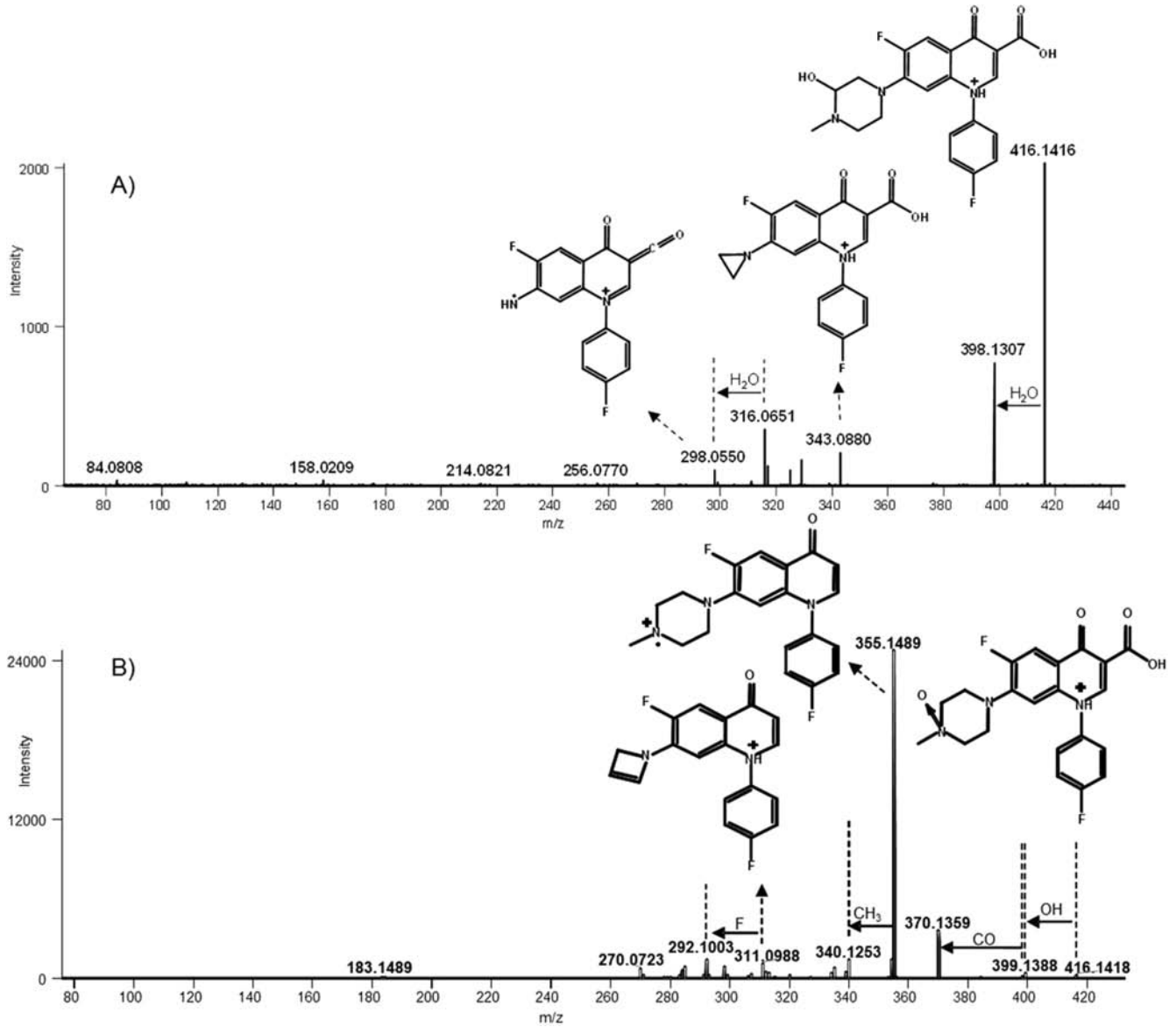

Figure 2. (A) MS^2 spectrum for the hydroxylated TP of DIF; (B) MS^2 spectrum for the *N*-oxide TP of DIF.

source fragmentation.[40,45−48] The ions m/z 332.1405 and 386.1311 were detected in samples that were spiked with ENR and DIF, respectively. These m/z values are consistent with the m/z of CIP and SAR. The EIC were obtained for blank and spiked samples to check the presence of TPs. Table 1 shows all of the ions found in milk and their identification, sorted by the original antibiotic. As can be observed, the errors between experimental mass and assigned structure were <3.0 ppm.

To assign a structure to the remaining ions that were observed, an in-house database was created using a list of 106 metabolic reactions[49] that can take place in milk and another list of milk components (including carbohydrates, amino acids, vitamins, and lipids; a total of 188 components).[50] The exact mass of the starting antibiotic or a known fragment is introduced into the database, and a series of combinations of reactions and/or possible additions are obtained that give rise to a molecule with an exact mass similar to that observed in the mass spectra of ToF.

Identification of Thermal TPs by LC-LTQ-Orbitrap-MS. As a ToF spectrometer cannot fragment molecules, we used an LTQ-Orbitrap to elucidate the TPs, as it has a higher mass resolving power than ToF and can fragment the compound to obtain structural information.

For each quinolone, Table 2 shows the retention time (t_R), m/z values, gains and losses of mass compared to the parent quinolone, m/z of the TPs observed, and fragments observed in mass spectra. Table 2 also shows the proposed reactions, with the assigned molecular formula, the double-bond equivalents (DBE) of neutral molecules, the theoretical mass, and the error (in ppm) calculated for the formula. The information is provided as common reactions that occurred in all of the studied quinolones and other reactions that were observed in only some quinolones.

Common Reactions of the Four Quinolones. Several gains and losses of mass were common among the four quinolones studied. Our database shows that the gain of m/z 15.9949 (Table 2) could correspond to two different reactions: hydroxylation and *N*-oxide formation. An evaluation of MS/MS spectra could be used to differentiate between both structures. As an example, Figure 2A shows the MS/MS

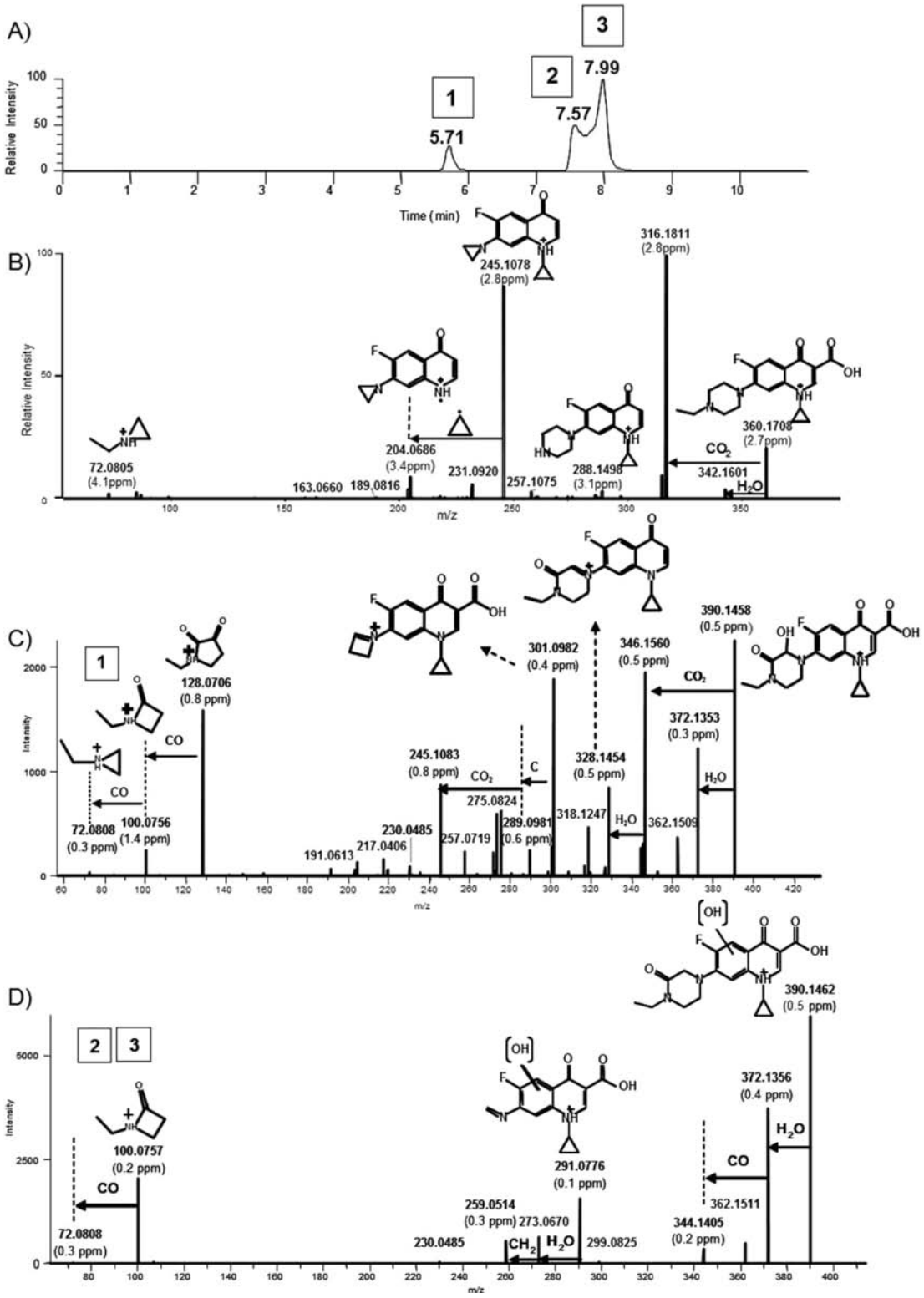

Figure 3. (A) EIC of ion m/z 390.1460 in the milk sample spiked with ENR; (B) MS^2 spectrum for ENR; (C) MS^2 spectrum for the first peak (t_R 5.71 min); (D) MS^2 spectrum for the remaining peaks (t_R 7.57 and 7.99 min).

spectrum of ions m/z 416.1416 in samples of DIF and discussion about elucidation is given in the Supporting Information. The position of OH could not be assigned with certainty, but our proposal is hydroxylation in position 3 of the piperazine ring, as in oxo-ciprofloxacin, the metabolite described in the bibliography.[36,37,40] For the four quinolones, the hydroxylated TPs were observed, but the concentrations of TPs from ENR and DIF were higher than from CIP and SAR. *N*-Oxide formation occurred only in ENR and DIF in N^4-alkylpiperazinyl. This metabolite has been described previously.[38,51] For this structure, a loss of OH is characteristic in fragmentation and was experimentally observed in Figure 2B of

dx.doi.org/10.1021/jf405554z | J. Agric. Food Chem. 2014, 62, 2008−2021

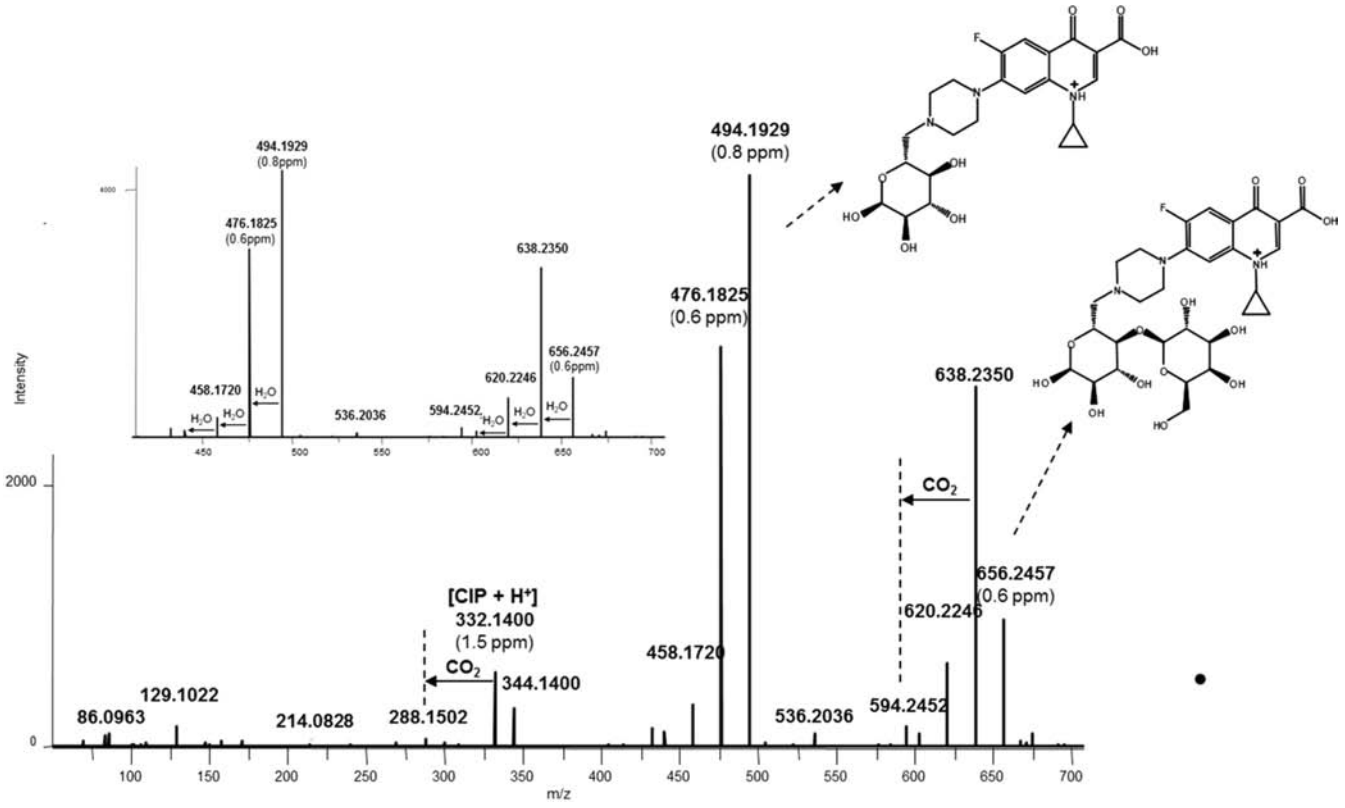

Figure 4. Product ion scan (MS^2) of CIP lactose conjugate (precursor ion m/z 656.2457): (top left) extended mass spectrum showing losses of water molecules.

the MS/MS spectrum of ions m/z 416.1416 for DIF. In this case, the DBEs of TPs undergo no alteration of values in comparison with the DBE of parent quinolones. Different fragmentation patterns were observed for the hydroxylated and *N*-oxide compounds that were found, as can be observed in Figure 2. In Figure 2B, corresponding to the *N*-oxide TP, the peak of the precursor ion disappeared almost completely when the same voltage was applied (HCD: 45). This finding suggests that hydroxylated compounds are more stable than *N*-oxide TP. The structures assigned to the rest of the ions are shown in Figure 2. Table 2 shows the fragmentation ions, the molecular formula, the DBE, and the calculated error in the assignation of the different structures.

A gain of m/z 29.9740 was also observed for the four quinolones, as shown in Table 2. Three peaks were found for ENR and DIF, whereas only one peak was observed for their main metabolites (CIP and SAR), at a concentration too low to be isolated and fragmented. The mass spectra of all peaks of ENR and DIF were studied. Figure 3 shows the mass spectra of ions with m/z 390.1460 of ENR. In Figure 3A, the separation by LC-LTQ-Orbitrap is shown with peaks at 5.71, 7.57, and 7.99 min. Although the retention time of ENR matches peak 1, the mass spectra are different, as can be observed in Figure 3B,C. A comparison of both mass spectra revealed only two ions (m/z 245.1077 and 72.0805) in common. The m/z 245.1077 indicates that the differences between the TP of peak 1 and ENR are in the loss fragment (part of the piperazinyl ring). The accurate mass of the fragment m/z 128.0706 corresponds to the molecular formula $C_6H_{10}NO_2$ with a DBE value of 3 and is the key to the elucidation as is shown in Figure 3C and in the Supporting Information.[52]

Unlike the first molecule, the other two ions of m/z 390.1460 (peaks 2 and 3) had low fragmentation as can be observed in Figure 3. Nevertheless, their structures were elucidated. The retention time of these peaks are different, but their mass spectra are identical, which indicates that they are isomers (Figure 3D). The m/z 245.1085 observed in the mass spectrum of ENR (Figure 3B) could not be found in the spectra of peaks 2 and 3. The molecules were broken up from the piperazinyl ring, resulting in the ions 100.0756 and 291.0774. The fragment 100.0756 is the same as that observed in Figure 3C, which indicates that there was only a ketone in the ring. The fragmentation of 291.0774 leads us to conclude that OH is on the aromatic ring. Two different vacant positions in the aromatic ring led to the two different isomers. For DIF, the fragmentations were similar to those shown in ENR, as can be observed in Table 2.

TPs corresponding to a net loss of 26.0146 were observed for all compounds (ENR, CIP, DIF, and SAR). For the TPs of ENR and DIF losses of N^4-alkylamine from the piperazinyl ring were observed. However, as CIP and SAR do not have an alkyl group in N^4, losses of ammonia (17.0275) were seen. Moreover, the TPs had DBE 1 unit lower than the parent compound, due to the break in the piperazinyl ring. Therefore, the peaks at m/z 334.1560, 306.1246, 374.1307, and 360.1156 have been assigned to desethylenequinolone TPs.[34−37] As Table 2 shows, when Orbitrap was used to elucidate the structures, the calculation errors (ppm) were <2 ppm. Slightly higher error values were obtained when ToF was used.

Other Reactions. The major metabolites, CIP and SAR, underwent other transformations, as can be observed in Table 2. Due to the absence of the alkyl chain in the N^4-piperazinyl ring, two reactions, acetylation (acetyl-CIP (m/z 374.1509) and

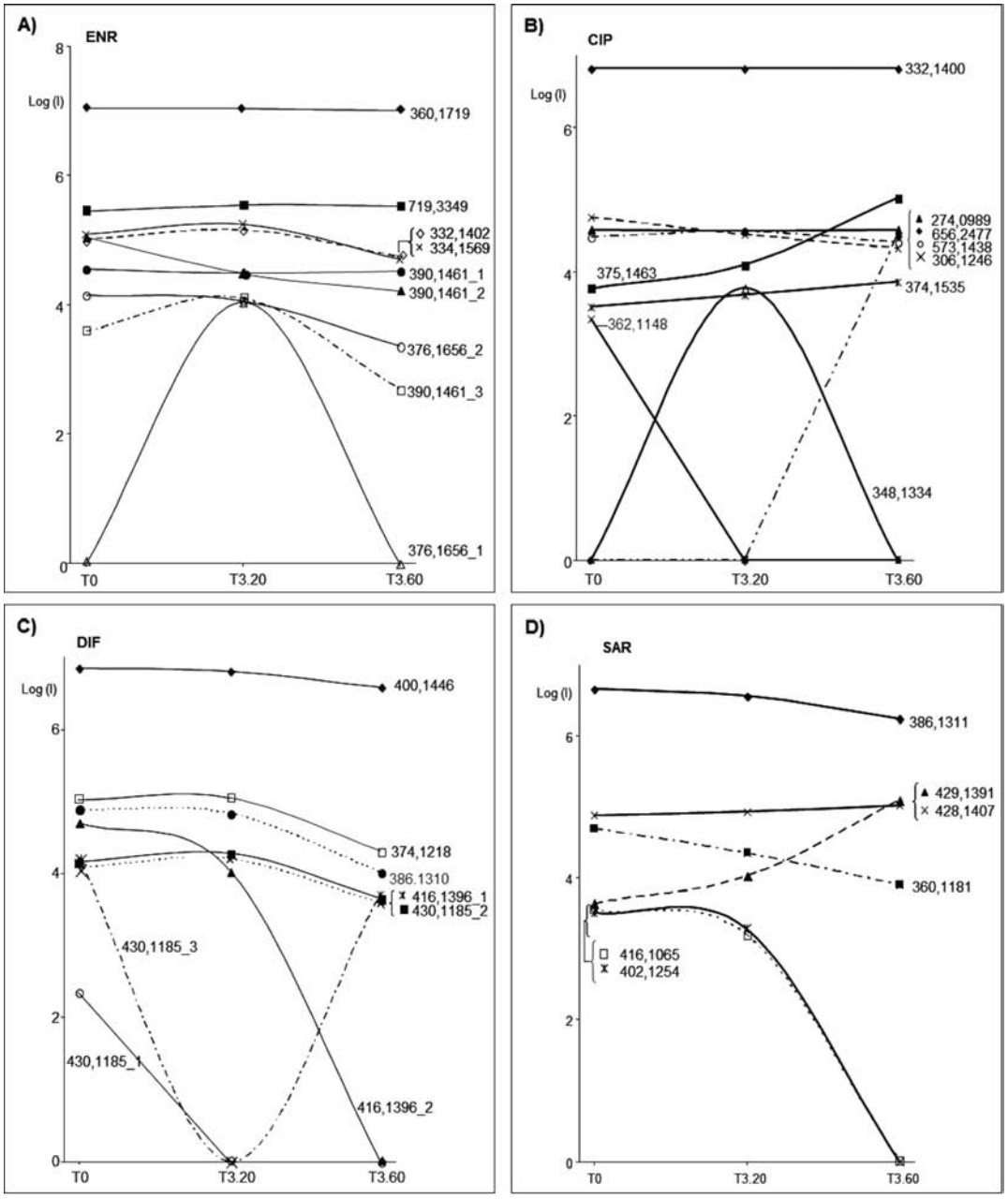

Figure 5. Influence of the different warming conditions in areas of different TPs of ENR, CIP, DIF, and SAR.

acetyl-SAR (m/z 428.1416)) and formamidation (formamide-CIP (m/z 375.1463) and formamide-SAR (m/z 429.1416)), took place. The corresponding explanation of elucidation is in the Supporting Information.

In addition to the above-mentioned reactions, CIP gave three more TPs (m/z 274.0986, 573.1429, and 656.2457). The ion 573.1429 was observed at a very low concentration and could not be fragmented. For the mass 274.0986, the ion 292.1091 could also be observed, at less intensity, corresponding to the gain of a water molecule. The main ion obtained by MS^2 of the ion 274.0986 was 231.0564, and this was isolated and fragmented again. In the MS^3 spectrum, the ion m/z 249.0668 was also observed with m/z 231.0564, which corresponds to the gain of a water molecule. This gain of water was observed only in the ions that kept the carbonyl group of acid, which is capable of hydrating the initial carboxylic acid again. The rest of the ions were mainly due to fragmentation of the piperazine ring. The structure assigned to m/z 292.1091 was CIP, with loss of the cyclopropyl group.

The last TP (656.2457) was obtained by heating the spiked milk sample with CIP at T3.60. When a HCD voltage of 45 V was used, only fragments with low m/z were found. To obtain structural information, the voltage was reduced to 35 V. The CIP ion (m/z 332.1400) could be identified among all of the fragments as can be seen in Figure 4. As can be followed in the Supporting Information, the molecule CIP (332.1405) is combined with the lactose (galactose + glucose) present in milk at high concentration. This new product was favored when samples were heated at a high temperature for a long time (60 min).

Effect of Temperature on the Stability of TPs. For each TP ion, the areas obtained from milk samples were plotted versus the heating conditions (T0, T3.20, and T3.60) (Figure 5). For ENR and CIP (Figure 5A,B), all of the TPs were

dx.doi.org/10.1021/jf405554z | J. Agric. Food Chem. 2014, 62, 2008−2021

Table 3. Metabolites and TPs Found in Medicated Cow's Milk with ENR Sorted by Accurate Mass[a]

m/z (ToF)	*m/z* (Orbitrap)	*m/z* theorical	t_R [a] (min)	Molecular formula [b]	Error (ppm) (ToF)	Error (ppm) (Orbitrap)	Suggested Structure	DBE	
263.0828	263.0834	263.0826	6.85	$C_{13}H_{12}FN_2O_3^+$	0.8	3.0	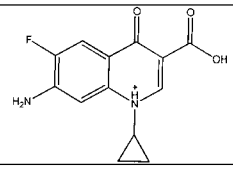	9	ENR-1
288.1349	288.1345	288.1343	2.9	$C_{15}H_{18}O_3N_3^+$	2.1	0.7	na		
291.0770	291.0783	291.0776	6.7	$C_{14}H_{12}FN_2O_4^+$	-2.1	2.4	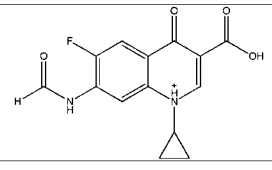	10	ENR-2
302.1501	302.1506	302.1499	5.7	$C_{16}H_{20}N_3O_3^+$	0.7	2.3	na		
306.1239	306.1256	306.1248	3.6	$C_{15}H_{17F}N_3O_3^+$	-2.9	2.6	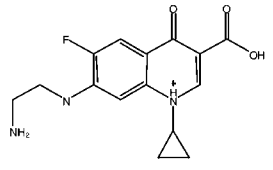	9	ENR-3
307.1083	307.1097	307.1089	6.5	$C_{15}H_{16}FN_2O_4^+$	-1.9	1.9	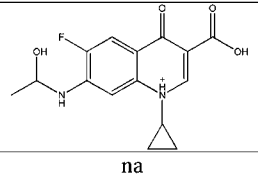	9	ENR-4
329.1485	329.1498	329.1496	3.4	$C_{18}H_{21}N_2O_4^+$	-3.3	0.6	na		
329.1485	329.1498	329.1496	4.9	$C_{18}H_{21}N_2O_4^+$	-3.3	0.6	na		
332.1408	332.1405	332.1405	5.0	$C_{17}H_{19}FN_3O_3^+$	0.9	0	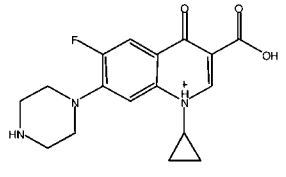	10	CIP
334.1189	334.1207	334.1198	6.4	$C_{16}H_{17}FN_3O_4^+$	-2.7	2.7	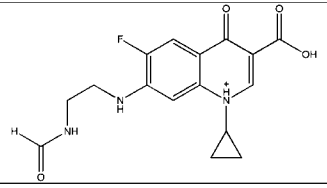	10	ENR-5
334.1539	334.1566	334.1561	4.35	$C_{17}H_{21}FN_3O_3^+$	-6.5	1.5	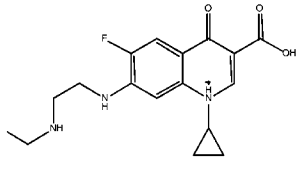	9	ENR-6
346.1190	346.1204	346.1198	6.5	$C_{17}H_{17}FN_3O_4^+$	-2.3	1.7	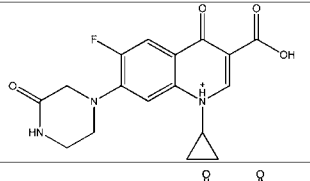	11	ENR-7
348.1343	348.1350	348.1354	3.6	$C_{17}H_{19}FN_3O_4^+$	-3.1	-1.1	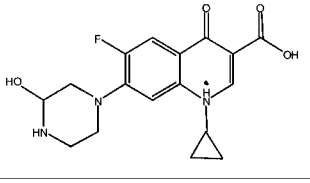	10	ENR-8

dx.doi.org/10.1021/jf405554z | J. Agric. Food Chem. 2014, 62, 2008−2021

Table 3. continued

m/z (ToF)	*m/z* (Orbitrap)	*m/z* theorical	t_R [a] (min)	Molecular formula [b]	Error (ppm) (ToF)	Error (ppm) (Orbitrap)	Suggested Structure	DBE	
360.1357	360.1360	360.1354	6.9	$C_{18}H_{19}FN_3O_4^+$	0.8	1.7	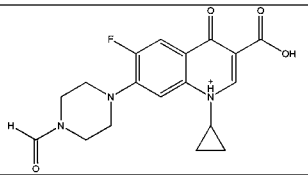	11	ENR-10
362.1137	362.1152	362.1147	6.1	$C_{17}H_{17}FN_3O_5^+$	-2.8	1.4	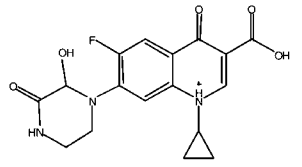	11	ENR-11
362.1137	362.1152	362.1147	6.8	$C_{17}H_{17}FN_3O_5^+$	-2.8	1.4	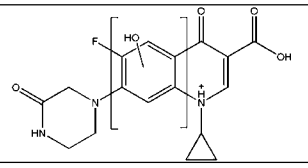	11	ENR-12
362.1137	362.1152	362.1147	7.1	$C_{17}H_{17}FN_3O_5^+$	-2.8	1.4		11	ENR-13
374.1510	374.1523	374.1511	7.0	$C_{19}H_{21}FN_3O_4^+$	-0.3	2.7	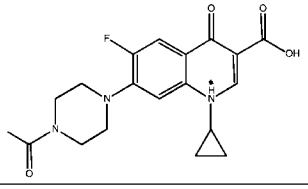	11	ENR-14
375.1462	375.1464	375.1463	6.6	$C_{18}H_{20}FN_4O_4^+$	-0.3	0.3	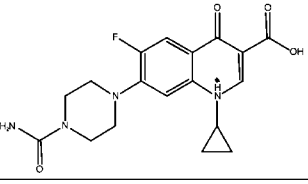	11	ENR-15
376.1656	376.1671	376.1667	4.6	$C_{19}H_{23}FN_3O_3^+$	-2.9	1.1	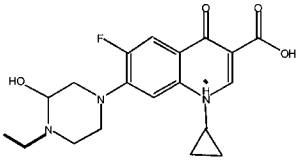	10	ENR-16
376.1656	376.1673	376.1667	5.8	$C_{19}H_{23}FN_3O_3^+$	-2.9	1.6	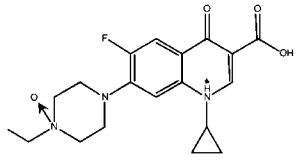	10	ENR-17
390.1459	390.1461	390.1460	6.65	$C_{19}H_{21}FN_3O_5^+$	-0.3	0.3	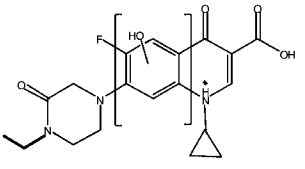	11	ENR-18
390.1459	390.1461	390.1460	6.85	$C_{19}H_{21}FN_3O_5^+$	-0.3	0.3		11	ENR-19

[a]Accurate masses analyzed by ToF and Orbitrap and their theorical mass assigned to molecular formula are given with calculated error (ppm) for the assignation of suggested structure for the two analysers. [a]Retention time when LC-ToF is used. [b]These molecular formulas are hypothetical in cases of metabolites without assigned structure. na, nonassigned.

observed at T0 except for hydroxylated quinolones (*m/z* 376.1656_1 and 348.1334, respectively). The concentration of these ions was raised by heating at T3.20 and disappeared at T3.60. In the case of ENR (Figure 5A), the concentration of some TPs, including CIP (332.1402), desethylene-ENR (334.1569), and two isomers of hydroxylation and ketone formation (390.1461_1 and 390.1461_3), increased slightly by warming at T3.20 and decreased at T3.60. For CIP, T3.60 was required for conjugation with lactose (656.2477) to occur (Figure 5B). The acetylated (374.1535) and formamidated (375.1463) compounds were present at T0 and their concentrations increased by heating. The 362.1148 ion

dx.doi.org/10.1021/jf405554z | J. Agric. Food Chem. 2014, 62, 2008−2021

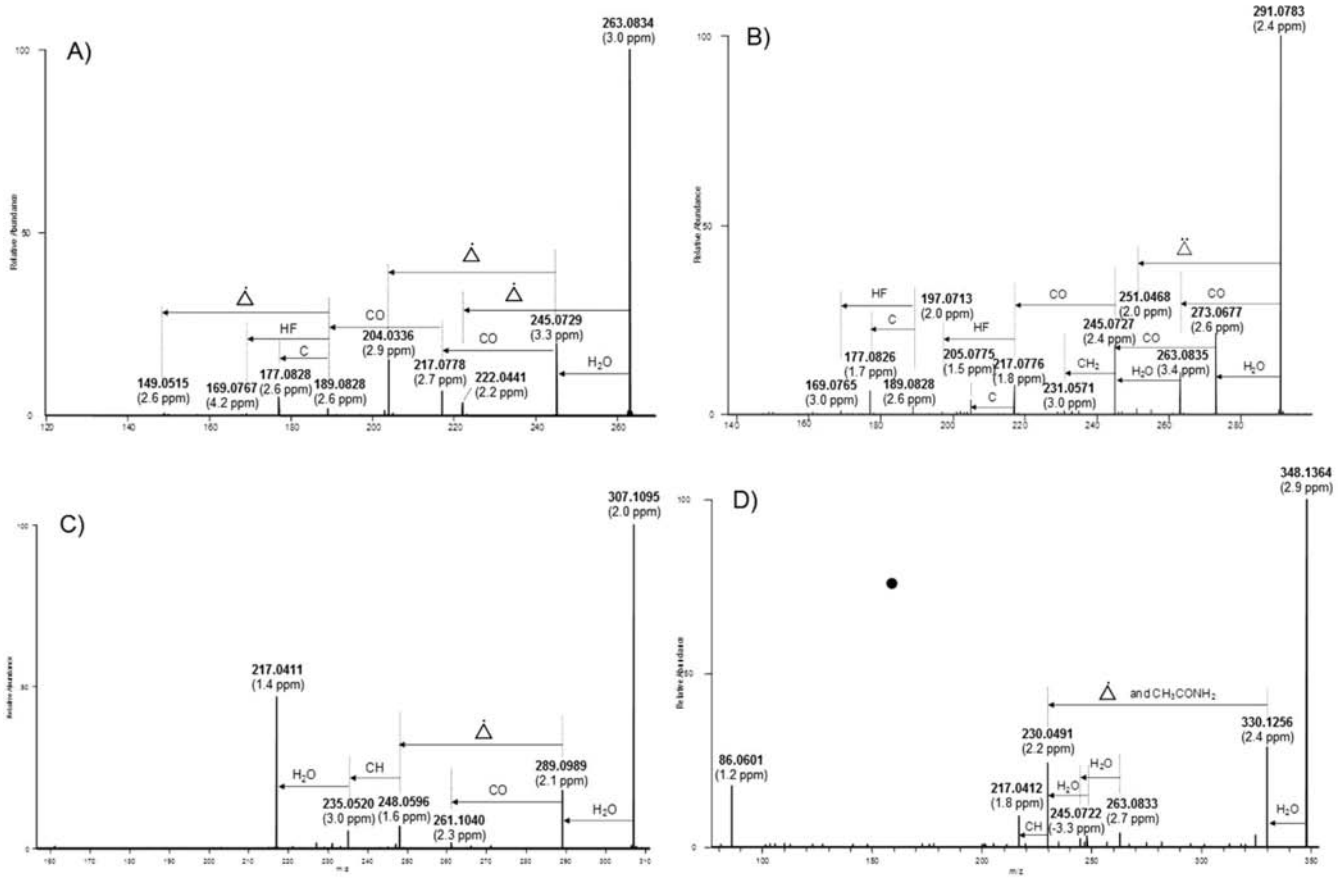

Figure 6. MS^2 spectra for the metabolites of ENR: (A) m/z 263.0828 (ENR-1); (B) m/z 291.0776 (ENR-2); (C) m/z 307.1089 (ENR-4); (D) m/z 348.1354 (ENR-9).

(corresponding to gain $[M + H + 29.974]^+$) was initially present (T0), but was destroyed by heating.

In contrast, the concentration of most of the ions in DIF samples increased slightly when the temperature was increased (Figure 5C). A general downward trend of DIF ions was seen at T3.60. Completely different behavior was observed for the 430.1185_3 ion, which underwent a sharp decrease at T3.20 and a sharp rise in formation when the warming time was increased, possibly due to the ion coming from different sources, and for the 430.1185_1 ion, which disappeared completely at T3.20. The acetylated (428.1407) and formamidated (429.1391) TPs of SAR (Figure 5D) behaved in the same way as those of CIP; that is, their concentration increased with temperature.

Determination of Metabolites and TPs in Medicated Cow's Milk. Four raw milk samples from cows medicated with ENR were submitted to the same thermal treatments as the spiked milk samples. The extracts were analyzed by LC-ToF, and the metabolites and TPs were fragmented by LC-LTQ-Orbitrap.

In this case, metabolites and TPs were found using the two data treatments (LC-MS (LTQ-Orbitrap)). When exact mass, retention time, and MS/MS spectra were compared, some of the compounds in milk spiked with ENR and CIP were also present in medicated cow's milk.

Table 3 shows the retention time (t_R) of metabolites in samples analyzed by LC-ToF, the accurate m/z of metabolites determined by ToF and LTQ-Orbitrap, the assigned molecular formula, the theoretical mass, the error (in ppm) calculated for the assigned formula, the proposed structures, and the double-bond equivalents (DBE) of the neutral molecule.

CIP (m/z 332.1405), the main metabolite of ENR, was one of the common compounds. In addition, desethylene metabolites of ENR (m/z 334.1561) (ENR-6) and CIP (m/z 306.1248) (ENR-3) were observed. The TPs of ENR corresponded to hydroxylation (ENR-16) and *N*-oxide formation (ENR-17) (m/z 376.1667), and two isomers of compound m/z 390.1460 (ENR-18 and ENR-19) (hydroxylation and ketone formation, Figure 3D) were also found. Four TPs of CIP were observed in medicated cow's milk. At 3.6 min was found the hydroxy-CIP (m/z 348.1354) (ENR-8) and at 6.1 min the m/z 362.1147 (ENR-11), although this time the MS^2 spectrum could not be obtained due to its low concentration. The other metabolites were from acetylation (m/z 374.1511) (ENR-14) and formamidation (m/z 375.1463) (ENR-15) of CIP.

Other compounds were found in milk from medicated cows, but not in spiked milk. These compounds were produced by metabolism of the antibiotic in the cow, and some of them were identified for the first time.

The metabolite with the highest intensity after CIP (332.1405) and desethylene-ENR (334.1561)(ENR-6) had m/z 263.0834 (ENR-1). The m/z of the metabolite was lower than the m/z of ENR. Therefore, the MS/MS spectrum was analyzed to find which part of the parent compound had been modified. Figure 6A shows the MS/MS spectrum of ENR-1. It was concluded that the metabolite structure corresponded to

dx.doi.org/10.1021/jf405554z | J. Agric. Food Chem. 2014, 62, 2008−2021

CIP without a piperazine ring (Supporting Information). Only the amino group was maintained, as shown in Table 3.

In the MS/MS spectrum of metabolite ENR-2 with m/z 291.0783 (Figure 6B), the ion m/z 263.0834 (ENR-1), discussed in the Supporting Information and in Figure 6A, was observed. The difference between both ions corresponded to a carbonyl group (27.9949). The assigned structure for this metabolite is given in Table 3.

Another metabolite elucidated was m/z 307.1095 (ENR-4). Some explanations of the fragments are shown in Figure 6C and the Supporting Information. Its structure can be observed in Table 3.

The ion m/z 334.1189 (ENR-5) was identified as formyldesethylene-CIP.[25] Its structure was checked by its mass spectrum. The molecule was broken up from the piperazinyl ring, resulting in the ions m/z 72.0445 and 263.0834 cited before. Other important fragments were m/z 245.0730 [263.0834 − H_2O], 230.0489 [334.1189 − H_2O − cyclopropyl − formamide], and 217.0411 [230.0489 − CH].

A compound (ENR-9) with the same m/z as hydroxy-CIP (m/z 348.1354) (ENR-8) was also studied, because the retention time differed by about 4 min from the peak observed in spiked samples. The MS/MS spectrum (Figure 6D) was very similar to the spectrum of formyldesethylene-CIP (m/z 334.1189) (ENR-5). The most striking difference between both spectra was that instead of fragment m/z 72.0444 was observed a fragment of m/z 86.0601. This fragment corresponds to the addition of a methyl group to fragment m/z 72.0444. In conclusion, a structure of acetyldesethylene-CIP (ENR-9) is suggested, which could be formed from the oxidation of the side chain of desethylene-ENR (m/z 334.1561) (ENR-6).

The EIC of ion m/z 362.1137 (ENR-12 and ENR-13) from a full-scan of ToF was very similar to that obtained for the m/z 390.1460 (ENR-18 and ENR-19) in spiked samples with ENR (Figure 3). Three peaks were observed in the EIC. The first one was at 6.1 min, which coincides with the peak observed in samples fortified with CIP. Also were seen two peaks at 6.8 and 7.1 min, with the same shape as the two peaks at 7.6 and 7.99 in Figure 3. Unfortunately, when the sample was analyzed by LC-LTQ-Orbitrap, it was degraded and only one peak was observed and fragmented. In the MS/MS spectrum, the ions m/z 291.0776 and 259.0820 were present, as elucidated previously in Figure 3D. Another fragment that helped to determine the structure corresponded to m/z 72.0444, which is like fragment 100.0757 of metabolite 390.1460 without the alkyl chain of ENR. Due to the resemblances between the EICs and mass spectra of ions m/z 362.1137 (ENR-12 and ENR-13) and 390.1460 (ENR-18 and ENR-19), it can be assumed that these compounds are the same, but one is from CIP and the other from ENR, respectively.

The last two elucidated metabolites corresponded to oxo-CIP (m/z 346.1198) (ENR-7) and formyl-CIP (360.1354) (ENR-10), which have been described previously in the literature.[36,40] Their structures were confirmed by their MS/MS spectra.

The rest of the metabolites found in medicated cow's milk could not be elucidated. In any case, Table 3 shows their m/z, retention time (t_R), hypothetical molecular formula, DBE, and errors.

■ ASSOCIATED CONTENT

Supporting Information

Explanation of MS elucidation of some TPs and metabolites of quinolones (ENR, CIP, DIF, and SAR). This material is available free of charge via the Internet at http://pubs.acs.org.

■ AUTHOR INFORMATION

Corresponding Author

*(D.B.) Phone: +34-934033797. E-mail: dolores.barron@ub.edu.

Funding

We are grateful to the Ministerio de Ciencia e Innovación (MICINN) (Project CTQ2010-19044/BQU) for financial support. A.J. received support from MICINN (BES-2011-045849) for the training of researchers.

Notes

The authors declare no competing financial interest.

■ REFERENCES

(1) Council Regulation No. 1831/2003 of the European Parliament and of the Council of 22 September 2003 on additives for use in animal nutrition.

(2) Hammerum, A. M.; Heuer, O. E.; Lester, C. H.; Agers, Y.; Seyfarth, A. M.; Emborg, H. D.; Frimodt-Moller, N.; Monnet, D. L. Comment on: Withdrawal of growth-promoting antibiotics in Europe and its effects in relation to human health. *Int. J. Antimicrob. Agents* **2007**, *30*, 466−468.

(3) Fábrega, A.; Sánchez-Céspedes, J.; Soto, S.; Vila, J. Quinolone resistance in the food chain. *Int. J. Antimicrob. Agents* **2008**, *31*, 307−315.

(4) Commission of the European Communities. *Off. J. Eur. Communities* **2009**, *L15/1*, No. 37/2010, Dec 22.

(5) Zorraquino, M. A.; Althaus, R. L.; Roca, M.; Molina, M. P. Effect of heat treatments on aminoglycosides in milk. *J. Food Prot.* **2009**, *72*, 1338−1341.

(6) Early, R. *The Technology of Dairy Products*, 2nd ed.; Aspen Publishers; Gaithersburg, MD, USA, 1998.

(7) Picó, Y.; Barceló, D. The expanding role of LC/MS in analyzing metabolites and degradation products of food contaminants. *Trends Anal. Chem.* **2008**, *27*, 821−835.

(8) Becker, M.; Zittlan, E.; Petz, M. Residue analysis of 15 penicillins and cephalosporins in bovine muscle, kidney and milk by liquid chromatography−tandem mass spectrometry. *Anal. Chim. Acta* **2004**, *520*, 19−32.

(9) Junza, A.; Amatya, R.; Barrón, D.; Barbosa, J. Comparative study of the LC−MS/MS and UPLC−MS/MS for the multi-residue analysis of quinolones, penicillins and cephalosporins in cow milk, and validation according to the regulation 2002/657/EC. *J. Chromatogr., B* **2011**, *879*, 2601−2610.

(10) Reyns, T.; Cherlet, M.; De Baere, S.; De Backer, P.; Croubels, S. Rapid method for the quantification of amoxicillin and its major metabolites in pig tissues by liquid chromatography-tandem mass spectrometry with emphasis on stability issues. *J. Chromatogr., B* **2008**, *861*, 108−116.

(11) Granelli, K.; Elgerud, C.; Lundström, A.; Ohlsson, A.; Sjöberg, P. Rapid multi-residue analysis of antibiotics in muscle by liquid chromatography−tandem mass spectrometry. *Anal. Chim. Acta* **2009**, *637*, 87−91.

(12) Martínez-Huélamo, M.; Jiménez-Gámez, E.; Hermo, M. P.; Barrón, D.; Barbosa, J. Determination of penicillins in milk using LC-UV, LC-MS and LC-MS/MS. *J. Chromatogr., A* **2009**, *32*, 2385−2393.

(13) Nemutlu, E.; Kir, S.; Katlan, D.; Beksaç, M. S. Simultaneous multiresponse optimization of an HPLC method to separate seven cephalosporins in plasma and amniotic fluid: application to validation and quantification of cefepime, cefixime and cefoperazone. *Talanta* **2009**, *80*, 117−126.

(14) Mol, H. G. J.; Plaza-Bolaños, P.; Zomer, P.; de Rijk, T. C.; Stolker, A. A. M.; Mulder, P. P. J. Toward a generic extraction method for simultaneous determination of pesticides, mycotoxins, plant toxins, and veterinary drugs in feed and food matrixes. *Anal. Chem.* **2008**, *80*, 9450−9459.
(15) Marazuela, M. D.; Bogialli, S. A review of novel strategies of sample preparation for the determination of antibacterial residues in foodstuffs using liquid chromatography-based analytical methods. *Anal. Chim. Acta* **2009**, *645*, 5−17.
(16) Moreno-Bondi, M. C.; Marazuela, M. D.; Herranz, S.; Rodríguez, E. An overview of sample preparation procedures for LC-MS multiclass antibiotic determination in environmental and food samples. *Anal. Bioanal. Chem.* **2009**, *395*, 921−946.
(17) Blasco, C.; Torres, C. M.; Picó, Y. Progress in analysis of residual antibacterials in food. *Trends Anal. Chem.* **2007**, *26*, 895−913.
(18) Andreu, V.; Blasco, C.; Picó, Y. Analytical strategies to determine quinolone residues in food and the environment. *Trends Anal. Chem.* **2007**, *26*, 534−556.
(19) Bogialli, S.; Di Corcia, A. Recent applications of liquid chromatography−mass spectrometry to residue analysis of antimicrobials in food of animal origin. *Anal. Bioanal. Chem.* **2009**, *395*, 947−966.
(20) Tang, Q.; Yang, T.; Tan, X.; Luo, J. Simultaneous determination of fluoroquinolone antibiotic residues in milk sample by solid-phase extraction−liquid chromatography−tandem mass spectrometry. *J. Agric. Food Chem.* **2009**, *57*, 4535−4539.
(21) Romero-González, R.; Aguilera-Luiz, M. M.; Plaza-Bolaños, P.; Garrido Frenich, A.; Martínez Vidal, J. L. Food contaminant analysis at high resolution mass spectrometry: application for the determination of veterinary drugs in milk. *J. Chromatogr., A* **2011**, *1218*, 9353−9365.
(22) Kaufmann, A. Strategy for the elucidation of elemental compositions of trace analytes based on a mass resolution of 100 000 full width at half maximum. *Rapid Commun. Mass Spectrom.* **2010**, *24*, 2035−2045.
(23) Zhu, M.; Ma, L.; Zhang, D.; Ray, K.; Zhao, W.; Humphreys, W. G.; Skiles, G.; Sanders, M.; Zhang, H. Detection and characterization of metabolites in biological matrices using mass defect filtering of liquid chromatography/high resolution mass spectrometry data. *Drug Metab. Dispos.* **2006**, *34*, 1722−1733.
(24) Nägele, E.; Moritz, R. Structure elucidation of degradation products of the antibiotic amoxicillin with ion trap MS*n* and accurate mass determination by ESI TOF. *J. Am. Soc. Mass Spectrom.* **2005**, *16*, 1670−1676.
(25) Calza, P.; Medana, C.; Carbone, F.; Giancotti, V.; Baiocchi, C. Characterization of intermediate compounds formed upon photo-induced degradation of quinolones by high-performance liquid chromatography/high-resolution multiple-stage mass spectrometry. *Rapid Commun. Mass Spectrom.* **2008**, *22*, 1533−1552.
(26) Gómez, M. J.; Gómez-Ramos, M. M.; Malato, O.; Mezcua, M.; Fernández-Alba, A. R. Rapid automated screening, identification and quantification of organic micro-contaminants and their main transformation products in wastewater and river waters using liquid chromatography−quadrupole-time-of-flight mass spectrometry with an accurate-mass database. *J. Chromatogr., A* **2010**, *1217*, 7038−7054.
(27) Kaufmann, A. Determination of the elemental composition of trace analytes in complex matrices using exact masses of product ions and corresponding neutral losses. *Rapid Commun. Mass Spectrom.* **2007**, *21*, 2003−2013.
(28) Berendsen, B. J. A.; Essers, M. L.; Mulder, P. P. J.; van Bruchem Lommen, A.; van Overbeek, W. M.; Stolker, L. A. M. Newly identified degradation products of ceftiofur and cephapirin impact the analytical approach for quantitative analysis of kidney. *J. Chromatogr., A* **2009**, *1216*, 8177−8186.
(29) Krauss, M.; Singer, H.; Hollonder, J. LC−high resolution MS in environmental analysis: from target screening to the identification of unknowns. *Anal. Bioanal. Chem.* **2010**, *397*, 943−951.
(30) Prasad, B.; Garg, A.; Takwani, H.; Singh, S. Metabolite identification by liquid chromatography-mass spectrometry. *Trends Anal. Chem.* **2011**, *30*, 360−387.
(31) Lacorte, S.; Fernández-Alba, A. R. Time of flight mass spectrometry applied to the liquid chromatography analysis of pesticides in water and food. *Mass Spectrom. Rev.* **2006**, *25*, 866−880.
(32) Malik, A. K.; Blasco, C.; Picó, Y. Liquid chromatography−mass spectrometry in food safety. *J. Chromatogr., A* **2010**, *1217*, 4018−4040.
(33) Koulman, A.; Lane, G. A.; Harrison, S. J.; Volmer, D. A. From differentiating metabolites to biomarkers. *Anal. Bioanal. Chem.* **2009**, *394*, 663−670.
(34) Jacobs, D. M.; Spiesser, L.; Garnier, M.; de Roo, N.; van Dorsten Hollebrands, B.; van Velzen, E.; Draijer, R.; van Duynhoven, J. SPE−NMR metabolite sub-profiling of urine. *Anal. Bioanal. Chem.* **2012**, *404*, 2349−2361.
(35) Sturini, M.; Speltini, A.; Maraschi, F.; Profumo, A.; Pretali, L.; Fasani, E.; Albini, A. Photochemical degradation of marbofloxacin and enrofloxacin in natural waters. *Environ. Sci. Technol.* **2010**, *l44*, 4564−4569.
(36) Anadón, A.; Martínez-Larrañaga, M. R.; Iturbe, J.; Martínez, M. A.; Díaz, M. J.; Frejo, M. T.; Martínez, M. Pharmacokinetics and residues of ciprofloxacin and its metabolites in broiler chickens. *Res. Vet. Sci.* **2001**, *71*, 101−109.
(37) Turnipseed, S. B.; Storey, J. M.; Clark, S. B.; Miller, K. E. Analysis of veterinary drugs and metabolites in milk using quadrupole time-of-flight liquid chromatography−mass spectrometry. *J. Agric. Food Chem.* **2011**, *59*, 7569−7581.
(38) Sukul, P.; Lamshöft, M.; Kusari, S.; Zühlke, S.; Spiteller, M. Metabolism and excretion kinetics of ^{14}C-labeled and non-labeled difloxacin in pigs after oral administration, and antimicrobial activity of manure containing difloxacin and its metabolites. *Environ. Res.* **2009**, *109*, 225−231.
(39) Turiel, E.; Bordin, G.; Rodríguez, A. R. Study of the evolution and degradation products of ciprofloxacin and oxolinic acid in river water samples by HPLC-UV/MS/MS-MS. *J. Environ. Monit.* **2005**, *7*, 189−195.
(40) Volmer, D. A.; Mansoori, B.; Locke, S. J. Study of 4-quinolone antibiotics in biological samples by short-column liquid chromatography coupled with electrospray ionization tandem mass spectrometry. *Anal. Chem.* **1997**, *69*, 4143−4155.
(41) Terzic, S.; Senta, I.; Matosic, M.; Ahel, M. Identification of biotransformation products of macrolide and fluoroquinolone antimicrobials in membrane bioreactor treatment by ultrahigh-performance liquid chromatography/quadrupole time-of-flight mass spectrometry.). *Anal. Bioanal. Chem.* **2011**, *401*, 353−363.
(42) http://mzmine.sourceforge.net (accessed Jan 17, 2014).
(43) Pluskal, T.; Castillo, S.; Villar-Briones, A.; Oresic, M. MZmine 2: Modular framework for processing, visualizing, and analyzing mass spectrometry-based molecular profile data. *Bioinformatics* **2010**, *11*, 395−405.
(44) Wu, L.; Liu, D. Q. Data-dependent tandem mass spectrometry of doubly protonated molecules in pharmaceutical analysis. *Rapid Commun. Mass Spectrom.* **2007**, *21*, 455−458.
(45) Clemente, M.; Hermo, M. P.; Barrón, D.; Barbosa, J. Confirmatory and quantitative analysis using experimental design for the extraction and liquid chromatography−UV, liquid chromatography−mass spectrometry and liquid chromatography−mass spectrometry/mass spectrometry determination of quinolones in turkey muscle. *J. Chromatogr., A* **2006**, *1135*, 170−178.
(46) Picó, Y.; Andreu, V. Fluoroquinolones in soil − risks and challenges. *Anal. Bioanal. Chem.* **2007**, *387*, 1287−1299.
(47) Hermo, M. P.; Barrón, D.; Barbosa, J. Multiresidue determination of quinolones regulated by the European Union in bovine and porcine plasma. Application of chromatographic and capillary electrophoretic methodologies. *J. Chromatogr., A* **2008**, *1201*, 1−14.
(48) Kaufmann, A.; Butcher, P.; Maden, K.; Widmer, M.; Giles, K.; Uría, D. Are liquid chromatography/electrospray tandem quadrupole fragmentation ratios unequivocal confirmation criteria? *Rapid Commun. Mass Spectrom.* **2009**, *23*, 985−998.
(49) Thermo Scientific Analytical Tools for Metabolism. Biotransformation Reference Guide, 2009.

(50) http://foodbs.org/examples/milk (accessed Jan 17, 2014).
(51) Rust, H.; Scheer, M.; Hallenbach, W. BAYER AG, Preparation of quinolone and naphthylidinone *N*-oxides as antibacterials. Patent ES 2 161 361 T3, January 12, 2001.
(52) Badertscher, M.; Bischofberger, K.; Munk, M. E.; Pretsch, E. A novel formalism to characterize the degree of unsaturation of organic molecules. *J. Chem. Inf. Comput. Sci.* **2001**, *41*, 889−893.

JOURNAL OF AGRICULTURAL AND FOOD CHEMISTRY

Addition/Correction

pubs.acs.org/JAFC

Correction to Induction of Phenolsulfotransferase Expression by Phenolic Acids in Human Hepatoma $HepG_2$ Cells

Chi-Tai Yeh, Shang-Ming Huang, and Gow-Chin Yen*

J. Agric. Food Chem. **2005**, *53* (12), 4766−4773. DOI: 10.1021/jf050388n

Due to an inadvertent error noted in Figure 5B, the GAPDH data have been corrected and updated, which does not affect the findings reported in our paper.

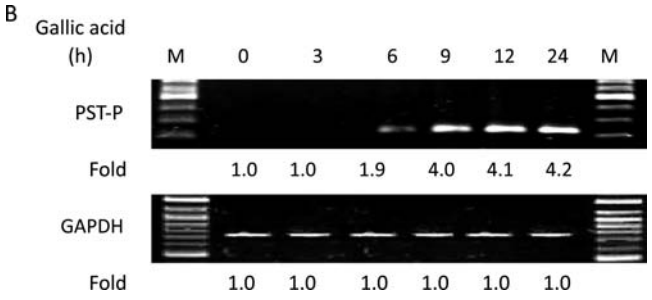

Figure 5. Induction of PST-P mRNA expression in $HepG_2$ cells by gallic acid. $HepG_2$ cells were exposed to the indicated concentrations of gallic acid for 24 h in a dose−response experiment (A) or to 50 μM gallic acid for 3−24 h in a time course experiment (B). Cellular RNA was extracted with an Invitrogen RNA isolation kit, and RT-PCR was performed as described under Materials and Methods. The RT-PCR products were separated on 1.8% agarose gel and digitally imaged after staining with ethidium bromide. GAPDH, the housekeeping gene, was used as an internal control. The results are presented as the ratios of PST-P mRNA in treated cells to those of control.

Published: February 14, 2014

ACS Publications © 2014 American Chemical Society

dx.doi.org/10.1021/jf500736h | *J. Agric. Food Chem.* 2014, 62, 2022−2022

Experiments were conducted using a wetted-wall column to examine the partitioning of the nearly pure endosulfan isomers from water into air. When starting with β-endosulfan, α-endosulfan was virtually the only isomer observed in air phase.[14,15] In regional and long-range transport studies of endosulfan isomers in air, β-endosulfan was infrequently observed relative to α-endosulfan, so much so that it was disregarded in the data analyses.[16,17] The isomerization of β-endosulfan to α-endosulfan has been suggested as a possible reason for the observed overabundance of α-endosulfan in the atmosphere.[6,18] Finally, this isomerization has also been observed directly on surfaces.[19]

A mechanism for β-endosulfan conversion to α-endosulfan and its irreversibility have been proposed and has been supported with data from differential scanning calorimetry (DSC) and NMR experiments and from computational chemistry calculations.[18] DCS scans of pure α-endosulfan, pure β-endosulfan, and mixtures were acquired; temperatures ranged from 25 to 280 °C. Scans of mixtures showed a large phase transition not observed in either of the pure isomer scans, suggesting a new transition which we assigned to the isomerization process. Furthermore, analysis of the remaining material after the scans revealed a eutectic mixture of an approximately 60:40 mixture of the α:β isomers, again demonstrating conversion. No degradation other than isomeric conversion was observed. Using computational chemistry, a mechanism was proposed whereby movement of the S═O moiety followed pseudorotation of the seven-membered ring of β-endosulfan resulted in formation of α-endosulfan. Furthermore, we concluded that the increase in entropy caused by the asymmetry in α-endosulfan precluded the reverse process of α-endosulfan conversion to β-endosulfan.

The three mixtures of endosulfan (nearly pure α-endosulfan, nearly pure β-endosulfan, and mixtures) have identical chemical compositions, i.e., they differ only in spatial arrangement of the atoms, yet the phase transitions observed using DSC were markedly different in all three mixtures.[18,20] This indicates that the thermal energy is absorbed by different sets of atoms. In addition, DSC does not identify which part of the molecule or bond(s) absorb the thermal energy. Raman spectroscopy provides spectral evidence (frequency signals) identifying the sets of atoms or bonds which are affected by energy absorption. Using the technique of temperature-dependent Raman (TDR) spectroscopy recently developed in our laboratory, molecular sites which respond most strongly to the thermal temperature gradient can be identified. Frequencies which covary with intensity and/or wavenumber shift starting at a specific temperature can indicate the individual molecular site or molecular movement that triggers a reversible or irreversible transition event. From these data, the sequence of molecular movements absorbing a threshold amount of thermal energy can be organized to explain the mechanism of a transition event. The purpose of this article is to provide such evidence that, in concert with previous work, demonstrates the molecular level pathway through which phase transition events occur, particularly, the irreversible process of β-endosulfan converting to α-endosulfan.

MATERIALS AND METHODS

Materials. Certified analytical grade Thiodan (α:β-endosulfan 60:40), β-endosulfan (nearly 100%), and α-endosulfan (99.8% α; 0.2% β) were each obtained commercially from ChemServices (West Chester, PA) and used as is.

Temperature Dependent Raman Measurement System. A Raman spectroscopy system was assembled to collect temperature dependent Raman (TDR) spectra from the samples. A 16-bit CCD camera with 1024 × 256 pixels (Newton DU920N-BR-DD, Andor Technology, South Windsor, CT) was used to acquire Raman scattering signals. A Raman spectrometer (Raman Explorer 785, Headwall Photonics, Fitchburg, MA) was mounted to the camera. The spectrometer accepts light through an input slit (5 mm long × 100 μm wide) and detects a Raman shift range of 102.2−2538.1 cm^{-1} with a spectral resolution of 3.7 cm^{-1}. A 785 nm laser module (I0785MM0350MF-NL, Innovative Photonic Solutions, Monmouth Junction, NJ) served as the excitation source. A fiber optic Raman probe (RPB, InPhotonics, Norwood, MA) was used to focus the laser and acquire the Raman signals. A bifurcated fiber bundle was used to deliver the laser light to the probe and transfer the collected Raman signals to the spectrometer.

A hot plate with a ceramic top surface (Isotemp, Fisher Scientific, Hampton, NH) was used to heat the samples. The powder samples were put in a copper sample holder. Two thermocouple probes (type K) were attached to two sides of the sample area, and they were connected to a dual-input thermometer (EasyView EA15, Extech Instruments, Nashua, NH) to measure the temperature of the samples. Average values of the two probes were used as the sample temperature, and the data were transferred to a computer via a RS-232 port. A copper heat sink was placed between the ceramic heat surface and the sample holder to slow down the speed of the temperature increase. A relatively high temperature resolution was consequently achieved for the temperature-dependent Raman data. The Raman probe, the hot plate, and the sample materials were placed in a closed black box to avoid the influence of ambient light. System software was developed using LabVIEW (National Instruments, Austin, TX) to fulfill functions such as camera control, data acquisition, temperature measurement, and synchronization.[21] Each experiment was conducted in triplicate. Over 200 spectra of 1600 data points were collected for each experiment, resulting in a data set of approximately 10^6 data points.

RESULTS AND DISCUSSION

Raman Spectra Mode Assignments for Each Isomer. Endosulfan consists of two structural parts, a hexachlorinated norboryl moiety and a seven-membered, dioxathiepine-3-oxide ring system. The norbene portion is rigid, which is reflected in the absence of C−Cl Raman vibrational modes except for one signal at 374 cm^{-1}.[22] Vibrational frequencies characteristic of seven-membered ring structures, including cycloheptane and 1,3-dioxepane, have been identified.[21] The seven atoms of these simpler ring systems gave rise to eight ring-bending frequencies, four symmetrical and four asymmetrical. The seven-membered ring in the endosulfan isomers is a structural analogue of 1,3-dioxepane and, correspondingly, the same eight frequencies apply. For brevity, the same numbering of ring atoms in 1,3-dioxepane are used here: the ring oxygen atoms are atoms 1 and 3, sulfur is atom 2, the methylene carbons are C4 and C7, and the methine carbons are C5 and C6 (Figure 1).

The difference in the relative orientation of the axial hydrogens on the methylene carbons, C4 and C7, is responsible for the three discrete forms of endosulfan. In β-endosulfan, one hydrogen atom on each of the methylene carbons is axial above the seven-membered ring system, affording a symmetrical molecule in which $CHCH_2O$ on the right half of the ring is in the same conformation as the left half. This contrasts with the two α-endosulfans, where only one hydrogen atom is axial above the ring, not both, i.e., the axial hydrogen on the other methylene carbon is axial below the ring system. The right half of the ring system is not identical to the left half, giving rise to two asymmetrical enantiomers. As molecules which are direct

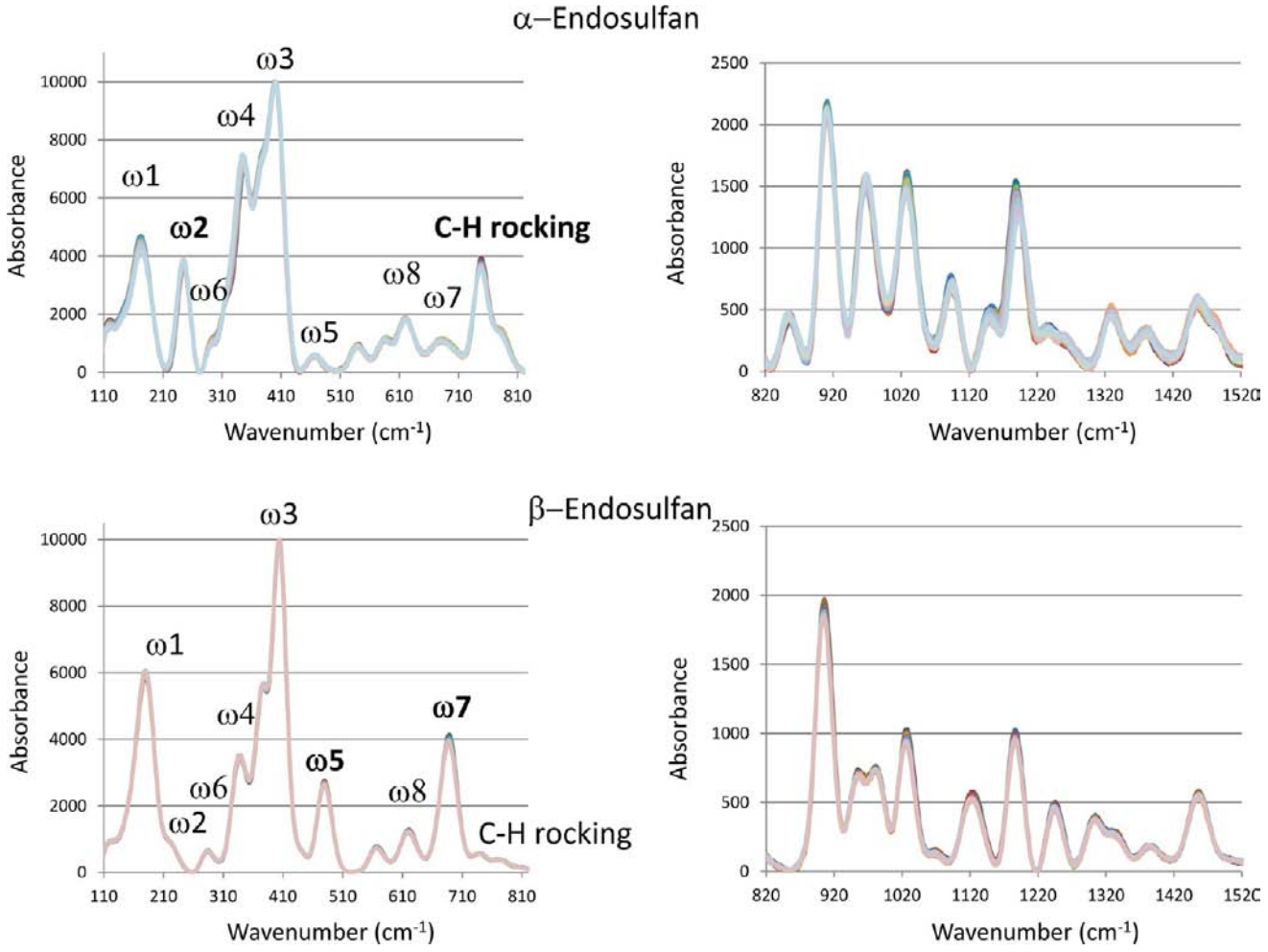

Figure 2. Raman spectra from 110 to 820 cm^{-1} and 820 to 1520 cm^{-1} acquired at 1 °C intervals from 50 to 102 °C for nearly pure α-endosulfan and for essentially pure β-endosulfan. Vibrational modes, ω1 through ω8 (Table 1), and C−H rocking, in the 110−820 cm^{-1} range are indentified. Relative intensities of each vibrational mode in the individual isomers were essentially temperature independent.

mirror images of each other, the two α-endosulfans will have identical Raman spectra.

Raman spectra were acquired at 1 °C intervals from 50 to 102 °C for nearly pure α-endosulfan and for essentially pure β-endosulfan; four major differences in the 110−810 cm^{-1} region were observed (Figure 2). Two major peaks were found in the α-endosulfan spectra at 229 cm^{-1} (ω2) and 748 cm^{-1} but were very weak in the spectra of β-endosulfan, whereas peaks seen in the β-endosulfan spectra at 460 cm^{-1} (ω5) and 686 cm^{-1} (ω7) were weak in the α-endosulfan spectra. Differences were also observed in the Raman fingerprint region, 820−1520 cm^{-1}. None of the peaks in the spectra of each nearly pure isomer showed a major change in intensity as a function of temperature.

From the work of Bocian and Strauss,[23] eight modes in the ring frequency region, 110−700 cm^{-1}, were assigned corresponding to the four symmetrical vibrational modes (ω1, ω3, ω5, and ω7) and to four asymmetrical vibrational modes (ω2, ω4, ω6, and ω8) (Table 1). Ring frequencies involve only the atoms in the ring, not the hydrogens bound to the carbons in the ring or the oxygen not part of the ring. Four of these vibrational modes represent changes in dipolar moment within the ring, that is, ω1, ω2, ω3, and ω4 correspond to changes in electron density among the ring atoms. Modes ω1 and ω3 represent symmetrical dipolar changes with respect to O−S−O, whereas modes ω2 and ω4 are asymmetrical. The asymmetrical dipolar moment ω2 is extremely weak in β-endosulfan. The other four vibrational modes correspond to ring-bending, ω5, ω6, ω7, and ω8. Modes ω5 and ω7 are symmetrical movements of the ring, and because α-endosulfan is asymmetrical, these modes are extremely weak. Asymmetrical ring-bending is depicted modes ω6 and ω8 and are weak peaks in the symmetrical β-endosulfan.

The modes observed in the fingerprint region of 720−1520 cm^{-1} correspond to the molecular vibrations of C−H. These movements include asymmetrical and symmetrical stretching, rocking, twisting, scissoring, and wagging. A peak at 748 cm^{-1} was observed in only α-endosulfan and corresponds to an asymmetrical C−H rocking movement. The remaining modes observed in the spectra of the pure isomers were difficult to assign unambiguously to specific atom vibrations.

Raman Spectra Mode Assignments for a 60:40 Mixture of α-Endosulfan:β-Endosulfan. Under similar gradient conditions for the individual isomers, Raman spectra were acquired at 1 °C intervals from 50 to 102 °C for a 60:40 mixture of α-endosulfan:β-endosulfan. The same eight ring vibrational modes, ω1−ω8, were observed in the 110−710 cm^{-1} range (Table 1; Figure 3). The peak which was only seen in the α-endosulfan spectra, 748 cm^{-1}, was also present in the

dx.doi.org/10.1021/jf404404w | J. Agric. Food Chem. 2014, 62, 2023−2030

Table 1. Assigned Vibrational Modes Observed in α-Endosulfan, β-Endosulfan, and a 60:40 Mixture α:β[a]

Vibrational Modes	Symmetry [1]	α-Endosulfan [2] (cm^{-1})	β-Endosulfan [2] (cm^{-1})	Mixture [2,3] (cm^{-1})
Dipolar Moment				
ω1	S	169 s	177 s	174 - 180 s
ω3	S	396 vs	401 vs	401 s
ω2	A	240 s	223 vw	234 - 249 s
ω4	A	339 vs	337 s	342 - 345 s
Ring Movement				
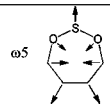 ω5	S	460 w	476 s	476 s
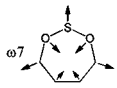 ω7	S	678 vw	686 s	683-689 s
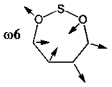 ω6	A	289 w	281 w	289 w
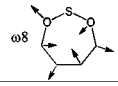 ω8	A	616 w	619 w	619 s

[a]Assignments were made using the vibrational modes observed in the structural analogue, 1,3-dioxepane.[23]. [1]A = asymmetrical, S = symmetrical. [2]vs = very strong, s = strong, w = weak, vw = very weak. [3]60:40 mixture of α-endosulfan:β-endosulfan.

mixture, as well as the peak corresponding to C−Cl vibration at 378 cm^{-1}. The intensity of these modes remained essentially unchanged as a function of temperature until 88 °C, after which some temperature dependence in some peaks was observed. Peaks corresponding to ω2 and ω8 increased by approximately 10%, while the peak intensity of ω1 decreased by 26%. Two additional small peaks which displayed some temperature dependence were observed at 542 and 590 cm^{-1} but were not assigned.

In the more flexible fingerprint of 720−1520 cm^{-1}, temperature dependency was much more dramatic (Figure 3). Below 97 °C, temperature had little effect on peak intensity, however, above 97 °C, intensity of several modes increased substantially, indicating that these sites in the molecules of one or both isomers were more flexible and therefore absorbed the increased thermal energy. Using the assignments of Bocian and Strauss,[23] Anconi et al.,[24] and Artur et al.,[25] the vibrational modes were identified, however, these peaks cannot be assigned definitively to one or both isomers. The intensity of the peaks at 907 cm^{-1} (C−H rocking) increased by 12%, at 968 cm^{-1} (ring expansion and C−H rocking) increased by 70%, and at 1028 cm^{-1} (ring expansion and bending) increased by 35%. Larger peak intensity increases of 140% and 200% were observed at 1092 cm^{-1} (ring expansion and mixed C−H motions) and 1350 cm^{-1} (C−H wagging and twisting), respectively.

These observations indicate that the nonuniform molecular surroundings of the mixture allow for temperature dependent changes in the intensity of vibrational movements which are not observed in the pure isomers. Furthermore, the nonuniform molecular surroundings allow for the intensity of asymmetrical ring frequencies to increase and, correspondingly, the symmetrical ring frequencies to decrease in intensity. At temperatures at 150 °C and above, pure β-endosulfan begins to exhibit isomerization as a result of formation of a nonuniform molecular environment caused by the changes in the lattice structure (phase change) of the pure compound.[18]

Contour Plots of TDR Spectra. Contour plots of temperature as a function of frequency (wavenumber) and spectral density were developed for the Raman spectral data of the 60:40 mixture and are shown over the temperature range of 88−102 °C and for the wavenumbers of 110−1500 cm^{-1} (Figure 4). These plots provide a more facile visualization of the data and enable identification of concurrent changes in frequency and intensity within the temperature gradient. If the frequency of a specific peak changes with increasing temperature, the slope of the line band will change, and if no changes occur in the frequency, the band will appear vertical in the plot. Spectral density (peak intensity) is represented by color change moving from cool colors (blue to green) to warmer colors (yellow to orange to red) as intensity increases. Over this temperature range, several vibrational modes were essentially temperature independent, ω3, ω4, ω7, and C−H rocking at 748 cm^{-1}.

For all the remaining modes, discrete temperature dependent changes occurred above 97 °C. Slight intensity increases, peak broadening, and peak shifting were observed for ω2, ω8, and C−H rocking at 907 cm^{-1}, while the peak at ω1 narrowed and decreased in intensity somewhat. The most dramatic changes occurred at 970, 1027, 1092, and 1350 cm^{-1}, where spectral density increased, peaks shifted, and peaks broaden substantially as the temperature increased. The response of these four vibrational modes indicate that these molecular sites are the most sensitive to the temperature (i.e., absorption of thermal energy) and are, therefore, the most flexible.

Correlating TDR Observations with Phase Transition Data. DSC is used to measure thermal absorption based upon aggregates of molecules, or macroscopic properties, such as melting, boiling, and sublimation, changes in crystal lattice structure, or isomerization. In contrast, Raman spectroscopic data provide information about molecular changes that take place at specific molecular sites and may or may not be involved in molecular aggregation/macroscopic changes. While TDR and DSC do not necessarily measure the same physical phenomenon, when the temperature dependence over a specific temperature gradient between the two does correlate, the macroscopic and molecular properties presumably overlap.

DSC data were collected over a temperature range of 50.0−110 °C and have been presented elsewhere.[20] A phase transition for α-endosulfan was observed at 90−96 °C with a maximum at 93 °C, whereas, for β-endosulfan, a phase transition was seen at 97−102 °C. A much broader range in the phase transition temperature occurred in a 60:40 mixture of α-endosulfan:β-endosulfan beginning at 80 °C and ending at 104 °C, with a maximum at 94 °C. The DSC results identify the discretely different temperature ranges over which thermal absorption of the individual endosulfan isomers occurs. The phase transition seen at 97−102 °C for β-endosulfan corresponds to the largest spectral differences in the TDR spectra. Therefore, the observed temperature-dependent

dx.doi.org/10.1021/jf404404w | J. Agric. Food Chem. 2014, 62, 2023−2030

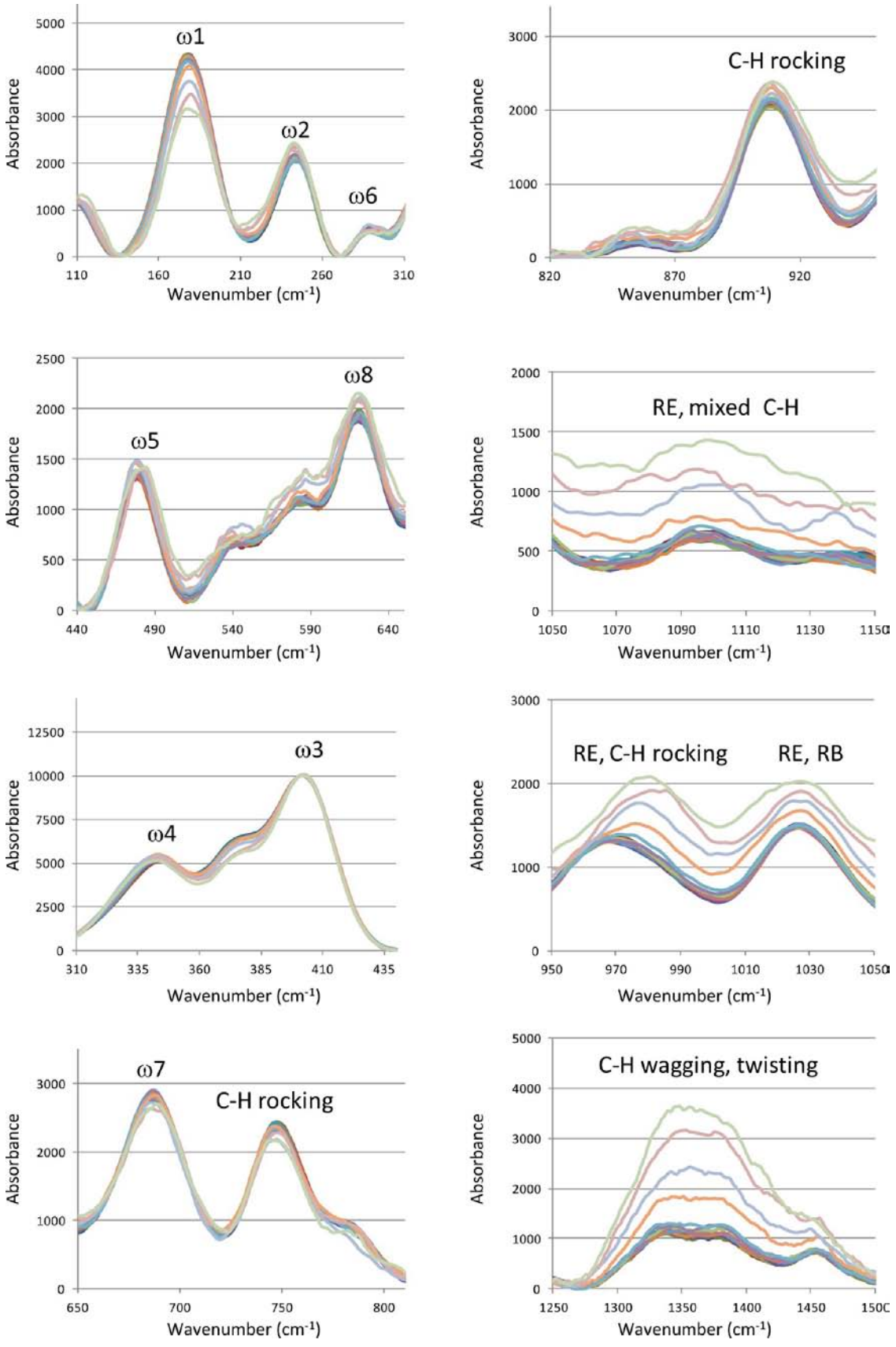

Figure 3. Raman spectra from 110 to 1520 cm^{-1} acquired at 1 °C intervals from 50 to 102 °C for a mixture of 60:40 α-endosulfan:β-endosulfan; each line represents a spectrum at an individual temperature. Vibrational modes are identified: ω1 through ω8 (Table 1), C−H rocking, wagging, and twisting, ring expansion (RE), and ring bending (RB). Relative intensities of each vibrational mode were essentially temperature independent until 97 °C. Noticeable temperature dependence was observed for vibrational modes at 177, 970, 1027, 1092, and 1350 cm^{-1}.

dx.doi.org/10.1021/jf404404w | J. Agric. Food Chem. 2014, 62, 2023−2030

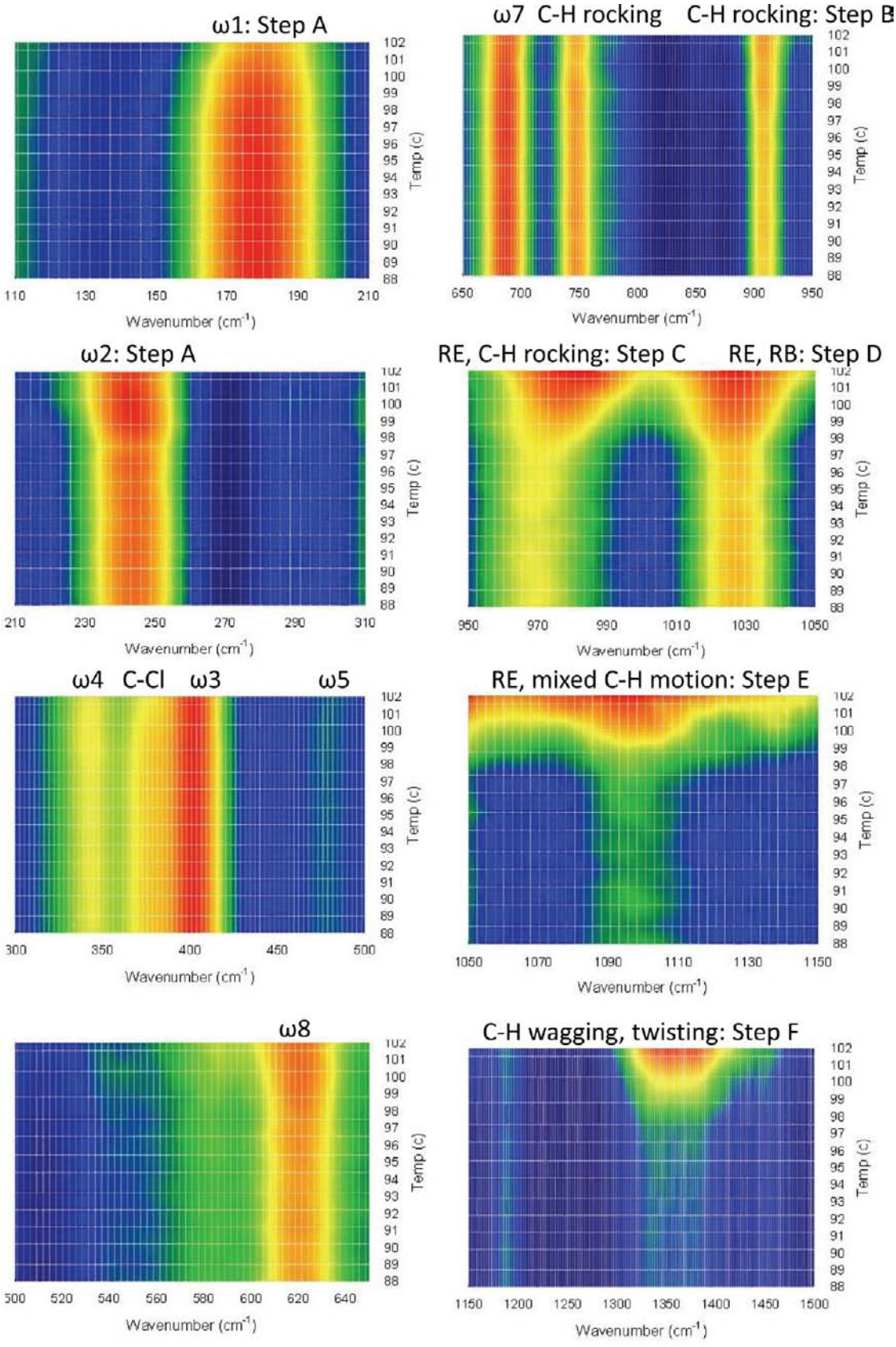

Figure 4. Contour plot of temperature as a function of frequency (wavenumber) and spectral density for the Raman spectral data of a 60:40 mixture of α-endosulfan:β-endosulfan over the temperature range of 88−102 °C and for the wavenumbers of 110−1500 cm^{-1}. Spectral density (peak intensity) is represented by color change moving from cool colors (blue to green) to warmer colors (yellow to orange to red) as intensity increases. Vibrational modes are identified as well as the mechanistic steps A−F of β-endosulfan isomerization to α-endosulfan.

dx.doi.org/10.1021/jf404404w | J. Agric. Food Chem. 2014, 62, 2023−2030

Raman spectral changes are due to changes in β-endosulfan not α-endosulfan.

Mechanism for Isomerization of β-Endosulfan to α-Endosulfan. Using the identified vibrational modes and the temperature dependence data, the mechanism for β-endosulfan isomerization to α-endosulfan becomes readily apparent (Figure 5). At 97 °C, the asymmetrical electron density

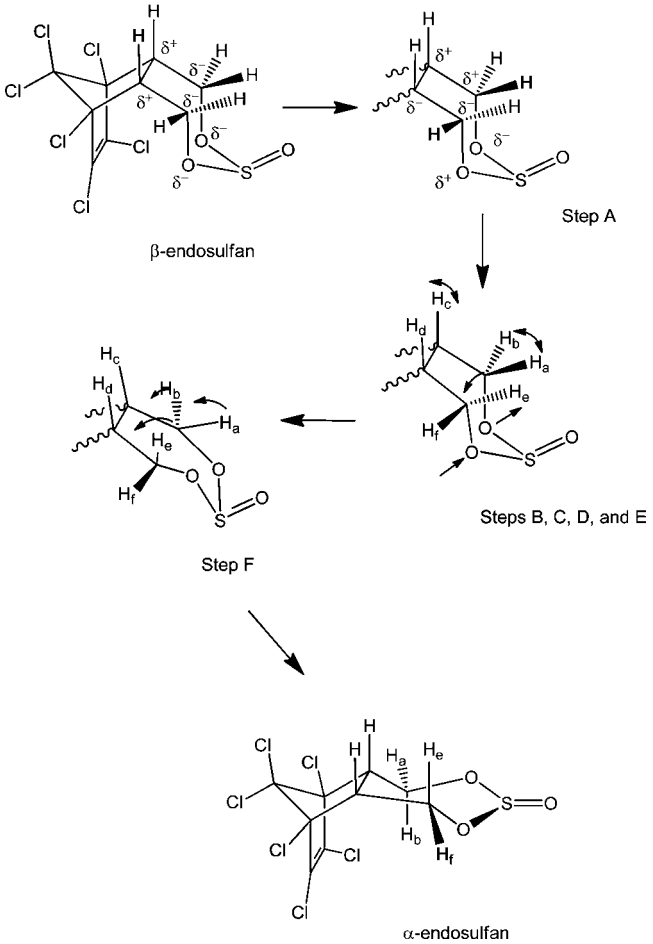

Figure 5. Mechanism steps A–F of β-endosulfan isomerization to α-endosulfan.

distribution in the seven-membered ring, ω2, begins to increase, and a corresponding decrease in the symmetrical electron density distribution, ω1, is observed (step A). Concurrently, the C–H rocking of the methylene carbons at 908 cm^{-1} increases (step B), followed by additional increases vibrational modes in C–H rocking and ring expansion at 970 cm^{-1} (step C) and ring expansion and ring bending at 1028 cm^{-1} (step D). At 99 °C, ring expansion and mixed C–H motions vibrational modes at 1092 cm^{-1} broaden substantially (step E). The final C–H wagging and twisting at 1350 cm^{-1} causes the methylene carbon to "flip", affording α-endosulfan (step F). From these data, we conclude that the reverse process of α-endosulfan isomerization to β-endosulfan is precluded.

This mechanism provides a rationale for the lack of changes in the TDR of nearly pure β-endosulfan. In the symmetrical crystal lattice of solid β-endosulfan, the symmetrical vibrational modes ω1 and ω3 are most dominant, while the asymmetrical vibrational mode ω2 is very weak (Table 1). An asymmetrical molecular surrounding appears to be critical to isomerization of β-endosulfan, as is the case in the mixture of α-endosulfan and β-endosulfan.

Relevance to the Environmental Fate of Endosulfan. In the environment, α- and β-endosulfan do not exist as pure compounds and β-endosulfan is not bound by the crystal lattice structure which inhibits isomerization. Therefore, with sufficient energy applied, isomerization of β- to α-endosulfan can occur in environmental matrices. Results presented here including the combination of DSC and TDR indicate that isomerization from α- to β-endosulfan does not occur and this process should not be observed in the environment. However, two publications have provided evidence of isomerization from α- to β-endosulfan under environmentally relevant conditions.[26,27]

The first publication describes application of individual isomers to field plots of a chickpead crop (three plots per isomer).[26] Leaf samples were collected just after application and periodically over a 15 day period. The specific purity of the solution was not reported, only that "pure" β-endosulfan was used. In the α-endosulfan-applied plots, after 7 days, 83% dissipation of α-endosulfan was observed and 2% β-endosulfan and 17% endosulfan sulfate was detected. In the β-endosulfan-applied plots, after 7 days 52% dissipation of β-endosulfan was observed and 8% α-endosulfan and 42% endosulfan sulfate was detected. The small contribution from β-endosulfan in the α-endosulfan applied plots was likely due to impurities in the original solution. Commercially available standards of endosulfan isomers are rarely 100% pure and typically contain traces of the other isomer. Because the specific purities of the starting solutions were not reported and a complete mass balance was not obtained, conclusions regarding isomerization cannot be confirmed.

The second publication[27] examined the fate of endosulfan and the formation of degradation products in estuarine mesocosms. Mesocosms were spiked separately with α-endosulfan, β-endosulfan, or the technical mixture of 70:30 α- to β-endosulfan. The purity of the single isomer standards is listed as 99.99% as determined by gas chromatography electron capture detection. Water samples were collected over a 100 h period and analyzed for both isomers and degradation products. For the β-endosulfan applied mesocosm, loss was listed as 96.9 ± 0.3%, with approximately 84% mass recovered. The authors list 2.1 ± 0.1% α-endosulfan detected. In the α-endosulfan applied mesocosm, the loss of α-endosulfan was listed as 93.6 ± 0.4%, with approximately 60% mass recovered. The percentage of β-endosulfan detected was 0.7 ± 0.1%. The percentage of β-endosulfan detected in the α-endosulfan-applied mesocosm was less than 1% and could be attributed to contamination in the original spiking material when taking into account the typical level of variability in gas chromatography–mass spectrometry analysis.

The only other published paper that has reported isomerization of α- to β-endosulfan is Guerrini et al.[28] The authors utilized surface-enhanced Raman scattering (SERS) to analyze the two isomers in their pure form as solids and then α-endosulfan as complexed with charged Ag nanoparticles coated with an organic compound (bis-acridinium lucigenin). Isomerization of α- to β-endosulfan was reported based on comparison of SERS spectral data. The SERS spectral data for the complexed α-endosulfan is reported to indicate weakening of bands associated with α-endosulfan and intensification of bands associated with β-endosulfan. However, background interferences from the bis-acridinium lucigenin coating were subtracted

from the spectra of the nanoparticle complexes, leading to a negative peak in a critical region of the spectra. No other confirmatory data concerning presence of β-endosulfan were discussed. Therefore, α- to β-endosulfan isomerization cannot be conclusively identified.

AUTHOR INFORMATION

Corresponding Author

*E-mail: cathleen.hapeman@ars.usda.gov.

Funding

This work was supported financially by U.S. Department of Agriculture, Agricultural Research Service intramural projects: 1265-42000-018-00 and 1265-12610-001-00.

Notes

Mention of specific products is for identification and does not imply endorsement by the U.S. Department of Agriculture to the exclusion of other suitable products or suppliers.
The authors declare no competing financial interest.

ABBREVIATIONS USED

DSC, differential scanning calorimetry; POP, persistent organic pollutants; RE, ring expansion; RB, ring bending; TDR, temperature-dependent Raman; UNEP, United Nations Environmental Programme

REFERENCES

(1) Maier-Bode, H. Properties, effect, residues and analytics of the insecticide endosulfan. *Residue Rev.* **1968**, *22*, 1−44.

(2) *EPA Action to Terminate Endosulfan*; United States Environmental Protection Agency: Washington, DC, June 2010; http://www.epa.gov/pesticides/reregistration/endosulfan/endosulfan-cancl-fs.html#decision (Accessed September 20, 2013).

(3) Lubick, N. Endosulfan's exit: U.S. EPA pesticide review leads to a ban. *Science* **2010**, *328*, 1466.

(4) *Endosulfan Phase-Out*; United States Environmental Protection Agency: Washington, DC, November, 2010; http://www.epa.gov/pesticides/reregistration/endosulfan/endosulfan-agreement.html (Accessed September 20, 2013).

(5) *United Nations Targets Widely-Used Pesticide Endosulfan for Phase Out*; United Nations Environment Programme: Geneva, May 3, 2011; http://chm.pops.int/TheConvention/Media/PressReleases/COP5Geneva,3May2011Endosulfanphaseout/tabid/2216/Default.aspx (Accessed September 20, 2013).

(6) Weber, J.; Halsall, C. J.; Muir, D.; Teixeira, C.; Small, J.; Solomon, K.; Hermanson, M.; Hung, H.; Bidleman, T. Endosulfan, a global pesticide: a review of its fate in the environment and occurrence in the Arctic. *Sci. Total Environ.* **2010**, *408*, 2966−2984.

(7) Becker, L.; Scheringer, M.; Schenker, U.; Hungerbühler, K. Assessment of the environmental persistence and long-range transport of endosulfan. *Environ. Pollut.* **2011**, *159*, 1737−1743.

(8) Janssen, M. P. M. *Endosulfan. A Closer Look at the Arguments against a Worldwide Phase Out*; RIVM Letter Report 601356002/2011; National Institute for Public Health and the Environment: Bilthoven, Netherlands, 2011; 92 pp, http://www.rivm.nl/bibliotheek/rapporten/601356002.pdf (Accessed September 20, 2013).

(9) Riemschneider, R.; Hilscher, J. C. Thiodan und analoge Verbindungen IV: Zur Kenntnis der Thiodan-Isomerie. *Z. Naturforsch., B: Chem. Sci.* **1960**, *15*, 809−810.

(10) Riemschneider, R.; Wuscherpfennig, V. Über den räumlichen Bau der Thiodan-Isomeren. *Naturwissenschaften* **1961**, *48* (5), 130−131.

(11) Riemschneider, R.; Wucherpfennig, V. Thiodan und analoge Verbindungen, 7. Konstellationen und Dipolmomente isomerer Thiodane. *Z. Naturforsch., B: Chem. Sci.* **1962**, *17*, 723.

(12) Forman, S. E.; Durbetaki, A. J.; Cohen, M. V.; Olofson, R. A. Conformational equilibria in cyclic sulfites and sulfates. The configurations and conformations of the two isomeric thiodans. *J. Org. Chem.* **1965**, *30*, 169−175.

(13) Schmidt, W. F.; Hapeman, C. J.; Fettinger, J. C.; Rice, C. P.; Bilboulian, S. Structure and asymmetry in the isomeric conversion of β- to α-endosulfan. *J. Agric. Food Chem.* **1997**, *45*, 1023−1026.

(14) Rice, C. P.; Chernyak, S. M.; Hapeman, C. J.; Bilboulian, S. Air−water distribution of the endosulfan isomers. *J. Environ. Qual.* **1997**, *26*, 1101−1106.

(15) Rice, C. P.; Chernyak, S. M.; McConnell, L. L. Henry's law constants for pesticides measured as a function of temperature and salinity. *J. Agric. Food Chem.* **1997**, *45*, 2291−2298.

(16) Simonich, S. L.; Hites, R. A. Global distribution of persistent organochlorine compounds. *Science* **1995**, *269*, 1851−1854.

(17) Burgoyne, T. W.; Hites, R. A. Effects of temperature and wind direction on the atmospheric concentrations of α-endosulfan. *Environ. Sci. Technol.* **1993**, *27*, 910−914.

(18) Schmidt, W. F.; Bilboulian, S.; Rice, C. P.; McConnell, L. L.; Fettinger, J. C.; Hapeman, C. J. Thermodynamic, spectroscopic, and computational evidence for the irreversible conversion of β- to α-endosulfan. *J. Agric. Food Chem.* **2001**, *49*, 5372−5376.

(19) Walse, S. S.; Shimizu, K. D.; Ferry, J. L. Surface-catalyzed transformations of aqueous endosulfan. *Environ. Sci. Technol.* **2002**, *36*, 4846−4853.

(20) Schmidt, W. F., Nguyen, J. K., Qin, J., Kim, M. S., Mookherji, S., McConnell, L. L., Hapeman, C. J. DSC and Raman spectra of α- and β-endosulfan plus 60/40 mixture. In *SPIE Defense, Security, and Sensing*; International Society for Optics and Photonics: Bellingham, WA, May 2013; pp 87210R-1−87210R-7.

(21) Qin, J.; Chao, K.; Kim, M. S. Raman chemical imaging system for food safety and quality inspection. *Trans. ASABE* **2010**, *53*, 1873−1882.

(22) Moore, W. H.; Ching, J. H. C.; Warrier, A. V. R.; Krimm, S. Assignment of torsion and low frequency bending vibrations of secondary chlorides. *Spectrochim. Acta, Part A* **1973**, *29*, 1847−1858.

(23) Bocian, D. F.; Strauss, H. L. Vibrational spectra, conformations, and potential functions of cycloheptane and related oxepanes. *J. Am. Chem. Soc.* **1977**, *99*, 2866−2878.

(24) Anconi, C. P. A.; Nascimento, C. S., Jr.; Dos Santos, H. F.; DeAlmeida, W. B. A highly correlated ab initio investigation of the temperature dependent conformational analysis of cycloheptane. *Chem. Phys. Lett.* **2006**, *418*, 459−466.

(25) Artur, C.; Le Ru, R. C.; Etchegoin, P. G. Temperature dependence of the homogeneous broadening of resonant Raman peaks measured by single-molecule surface-enhanced Raman spectroscopy. *J. Phys. Chem. Lett.* **2011**, *2*, 3002−3005.

(26) Gopal, M.; Mukherjee, I. Determination of residues of endosulfan and endosulfan sulfate on eggplant, mustard and chickpea. *Pestic. Sci.* **1994**, *37*, 67−72.

(27) Walse, S. S.; Scott, G. I.; Ferry, J. L. Stereoselective degradation of aqueous endosulfan in modular estuarine mesocosms: formation of endosulfan γ-hydroxycarboxylate. *J. Environ. Monit.* **2003**, *5*, 373−379.

(28) Guerrini, L.; Aliaga, A. E.; Carcamo, J.; Gomez-Jeria, J. S.; Sanchez-Cortes, S.; Campo-Vallette, M. M.; Garcia-Ramos, J. V. Functionalization of Ag nano-particles with the bis-acridinium lucigenin as a chemical assembler in the detection of persistent organic pollutants by surface-enhanced Raman scattering. *Anal. Chim. Acta* **2008**, *624*, 286−293.

Table 1. Source, Cultivar Name, and Species Designation for Table Beet and Related Subspecies Cultivars[a]

source	cultivar	cultigroup[b]
Alf Christianson Seed Co. (Mount Vernon, WA, USA)	'Beagle' Swiss chard	leaf beet group
	'Touchstone Gold'	garden beet group
	'Merlin'	garden beet group
	'Cylindra'	garden beet group
Bejo (Warmenhuizen, The Netherlands)	carrot, Ankara F1	na
Johnny's Selected Seeds (Winslow, ME, USA)	'Chioggia'	garden beet group
	'Blankoma'	garden beet group
Johnny's Selected Seeds, W. Atlee Burpee and Co. (Winslow, ME, and Warminster, PA, USA, respectively)[c]	'Bull's Blood'	garden beet group
J. W. Jung Seed Co. (Randolph, WI, USA)	'Golden Eckendorf' mangel	fodder beet group
	'Detroit Supreme'	garden beet group
Michigan State University USDA Sugar beet and Bean Research Unit (East Lansing, MI, USA)	sugar beet, line EL-A015028	sugar beet group
Seedway (Hall, NY, USA)	'Ruby Queen'	garden beet group

[a]Included are table beet (garden beet group), mangel (fodder beet group), or Swiss chard (leaf beet group) cultivars of *Beta vulgaris* ssp. *vulgaris* and one carrot cultivar (*Dacus carota* ssp. *sativus*) grown in three environments for geosmin screening, 2011−2012. [b]Reference 21. [c]Equal mixture of seed from both sources.

market. However, knowledge of geosmin variation among cultivars grown in a single environment does not provide a full picture of how geosmin levels may be influenced by environment. Eleven commercial table beet cultivars and related species were evaluated, including sugar beet [*B. vulgaris* ssp. *vulgaris* (sugar beet group)], Swiss chard [*B. vulgaris* ssp. *vulgaris* (leaf beet group)], and mangel [*B. vulgaris* ssp. *vulgaris* (fodder beet group)], as well as a carrot (*Dacus carota* ssp. *sativus*), which does not contain measurable geosmin, in three different environments over two years for geosmin levels. Environments included a field trial, a greenhouse trial with nonautoclaved soil, and a greenhouse trial with autoclaved soil. The aim of this study was to measure geosmin levels in a collection of *B. vulgaris* cultivars grown in replicated field trials and in nonautoclaved and autoclaved soils. If soil microorganisms contribute to or are responsible for the geosmin content of beets, plants grown in autoclaved soil may have altered geosmin profiles.

MATERIALS AND METHODS

Standards and Reagents. All laboratory chemicals used were of analytical grade. Menthone [(1*R*,4*S*)-*p*-menthan-3-one] and geosmin (2*β*,6*α*-dimethylbicyclo[4.4.0]decan-1*β*-ol)) were purchased from Sigma-Aldrich (St. Louis, MO, USA). Water for analytical analyses was deionized using a Milli-Q water purification system (Millipore, Bedford, MA, USA). Weed control in experimental plots was accomplished using the herbicides Ro-Neet (Stauffer Chemical Co., Westport, CT, USA) and chloridazon (Pyramin) (Nufarm Australia, Victoria, Australia).

Plant Material. Twelve different cultivars, including 11 from the Chenopodiaceae and one from *Daucus*, were analyzed for geosmin levels in this experiment. Seeds used came from six different companies (Table 1). Table beet [*B. vulgaris* ssp. *vulgaris* (garden beet group)], Swiss chard [*B. vulgaris* ssp. *vulgaris* (leaf beet group)], and mangel [*B. vulgaris* ssp. *vulgaris* (fodder beet group)] varieties were used as known geosmin producers, whereas carrot does not produce measurable geosmin and was used as an internal control.

Field Design. The field experiment was conducted at the Arlington Research Farm (University of Wisconsin Arlington Research Farm, Arlington, WI, USA) using a randomized complete block design with three replications. Cultivar was considered the experimental unit. Plant material was direct seeded into 3.7 m long rows spaced 46 cm apart using a cone seeder. This experiment was conducted over two years. The 2011 planting occurred on June 13 and the 2012 planting on June 4. Pre-emergent herbicides cycloate (Ro-Neet; Stauffer Chemical Co.) and chloridazon (Pyramin; Nufarm Australia) were applied to the field at recommended rates before planting. Routine maintenance including hand weeding was conducted. Irrigation was used in 2012 due to drought conditions at the beginning of the season. Experimental plant material was bordered by guard rows of the table beet cultivar Merlin.

Plants were harvested after 72 days on August 23, 2011, and August 14, 2012. Roots from all cultivars were harvested. Ten plants per cultivar per replication were harvested. Roots were bulked. Roots were stored at 5 °C until sampled. Root cores were sampled using a core-borer to remove a cylinder 1 cm in diameter and 2 cm deep. Root samples included skin tissue and were removed from the thickest part of the root. Cylinders were frozen at −20 °C.

Ten roots from a guard row were harvested to conduct an experiment measuring the root-to-root geosmin variation. In 2011, roots were stored at 3−5 °C for 3 weeks until sampled, ground, and frozen at −20 °C, whereas in 2012, roots were at 5 °C for 1 day before they were sampled and frozen at −20 °C until ground and frozen. Samples consisted of half of each root.

Greenhouse Design. The greenhouse experiment was conducted at King Hall Greenhouse, University of Wisconsin, Madison, WI, USA. A randomized complete block design was used and consisted of three replications per treatment, randomized by cultivar. Each cultivar was assigned to a row of six pots, 13.97 cm diameter × 15.24 cm tall. Field soil was removed from the same field where the field experiment was conducted and transported to Madison. Field soil was divided into two treatments, autoclaved and nonautoclaved. Autoclaved soil was autoclaved for 3 h at 103.42 kPa and 220−225 °C. The 2011 planting date occurred on June 2, 2011, and the 2012 planting date on May 31, 2012. Multiple seeds were sown per pot and thinned to the most vigorous seedling per pot. All cultivars were planted in both treatments. Plants were watered daily.

Harvest occurred on August 11, 2011, after 71 days and on August 10, 2012, after 72 days. Roots (minus leaves) were cleaned of all field soil and bulked. Because roots were generally much smaller sized than field-grown roots, whole beets were bulked rather than removing a cylinder of tissue. Samples were kept on ice until frozen at −20 °C.

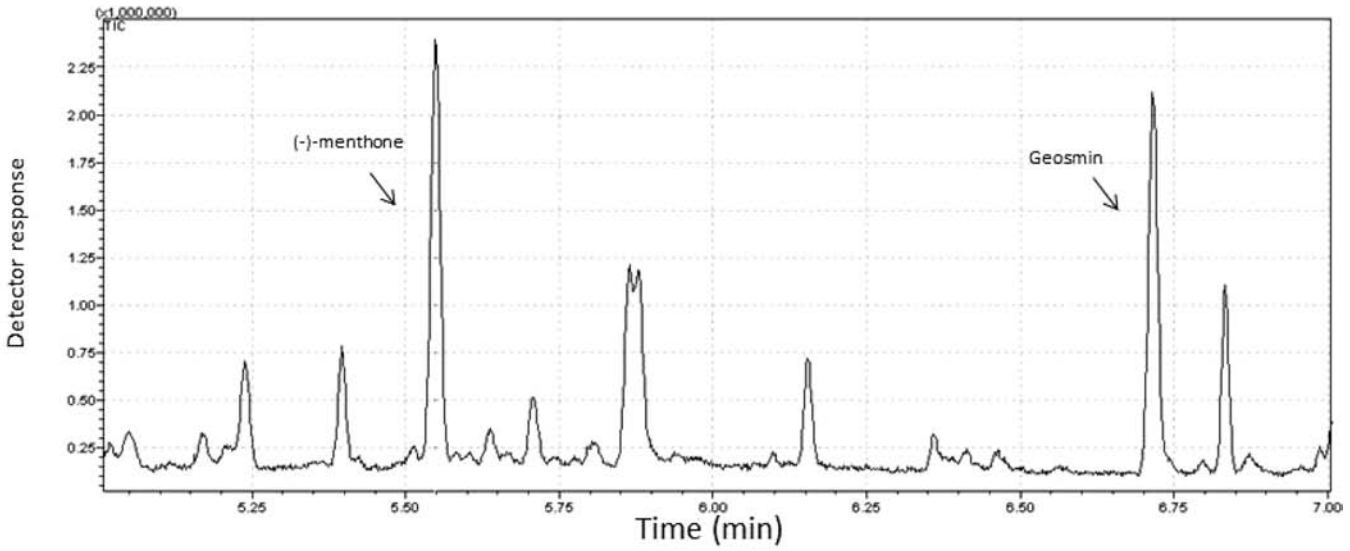

Figure 1. Sample chromatogram of geosmin and internal standard (−)-menthone from table beet. (−)-Geosmin was detected using headspace solid-phase microextraction and gas chromatography−mass spectrometry. Geosmin peak retention time, 6.670 min; (−)-menthone peak retention time, 5.596 min.

Sample Preparation. Samples were removed and thawed at room temperature for 5−10 min. All cores, roots, and leaves were cut into small chunks and blended at a 1:1 ratio of fresh weight grams of tissue/grams of Milli-Q water in an industrial blender for 2 min. All data were expressed on a fresh weight basis. All water used was stored in glass to avoid phthalate contamination. Homogenate was frozen at −20 °C until analyzed.

HSPME Preparation. Preparation occurred similarly to the methods of Lu et al.[15] Frozen samples were thawed in a 28 °C water bath for no longer than 10 min. Samples were stirred, and a 5 g sample was put into a sample glass vial containing 1 g of NaCl. Vials were capped immediately with screwcaps containing a PTFE/silicone septum. Water standards were prepared using 5 g of Milli-Q water. A (−)-menthone internal standard was added to water standards and samples at a concentration of 5.64 μg kg^{-1} (Sigma-Aldrich). Geosmin standard addition to water blanks occurred at concentrations of 21.6, 10, and 5 μg geosmin (kg water)$^{-1}$. Relative recovery rates were assessed using ground beet root samples of cultivar 'Merlin' and additions of geosmin standard at 5, 10, 15, and 21.6 μg geosmin (kg root tissue)$^{-1}$ sample concentrations. Recovery rates were based on the calculation of Lu et al.:[15]

$$\text{relative recovery} = \frac{(\mu\text{g geosmin total} - \mu\text{g geosmin originally in beet})}{\mu\text{g geosmin spiked}} \times 100\%$$

HSPME and GC-MS Analyses. Samples were loaded onto a Shimadzu GC-MS model QP2010SE with an AOC-5000 Shimadzu autoinjector (Shimadzu, Kyoto, Japan). Samples were incubated and agitated for 3 min at 60 °C and 500 rpm, followed by extraction for 10 min in the same conditions using PDMS/DVB fibers conditioned according to manufacturer specifications (Supelco: Sigma-Aldrich, St. Louis, MO, USA). The fiber was thermally desorbed into the GC system at 250 °C for 1 min. Injection mode was split, and a splitless liner was used. The split ratio was 10. The column used was a 30 m SHRXI-SMS with 0.25 mm i.d. and 0.25 mm df (Shimadzu). The temperature program was as follows: 40 °C for 1 min, increase at 35 °C min^{-1} to 300 °C, and hold for 2 min. Total program time was 10.43 min. Between samples, fibers were conditioned at 250 °C for 10 min.

Statistical Analysis. Data were log transformed to meet assumptions of constant variance and were analyzed as a mixed-effects ANOVA using the PROC MIXED procedure of SAS (SAS Institute Inc., Cary, NC, USA). Log-transformed data were used for all statistical analyses. Fixed effects included growth environment (referred to as "environment" in previous sections), cultivar, and the interaction of cultivar and environment. Replicate and replicate within year were considered random effects. Individual cultivars or treatments were compared following significant F tests using pairwise t tests. Values of $P \leq 0.05$ were considered significant.

RESULTS AND DISCUSSION

Relative Recovery. Relative recovery experiments were conducted each year field and greenhouse samples were evaluated to quantitate extraction efficiency. The relative recovery rates averaged over all spiked geosmin levels were 66.86% in 2011 and 47.81% in 2012. Values for field- and greenhouse-grown samples were corrected using each respective year's average relative recovery rate under the assumption that a complete extraction would produce a 100% relative recovery rate.

Root Geosmin Content of Cultivars Grown in Three Environments. *Year Effects.* Table beet and related subspecies cultivar roots were analyzed for geosmin levels using GC-MS over two years (Figure 1). We observed significant effects of both cultivar and environment as well as for the interaction of cultivar × environment (Table 2). A negligible amount of variance was estimated for the effect of year and a very small amount for replicate within year. Data were therefore averaged over year and replicate.

Table 2. Analysis of Variance for Geosmin Levels (Micrograms of Geosmin per Kilogram of Root Tissue) in Table Beet and Related Subspecies Cultivars

source of variation	df numerator	df denominator	P	significance[a]
environment	2	150	0.0141	*
cultivar	10	150	<0.0001	***
cultivar × environment	20	150	<0.0001	***

[a]*, ***, significant at $P \leq 0.05$ or 0.001, respectively.

dx.doi.org/10.1021/jf4047336 | J. Agric. Food Chem. 2014, 62, 2031−2036

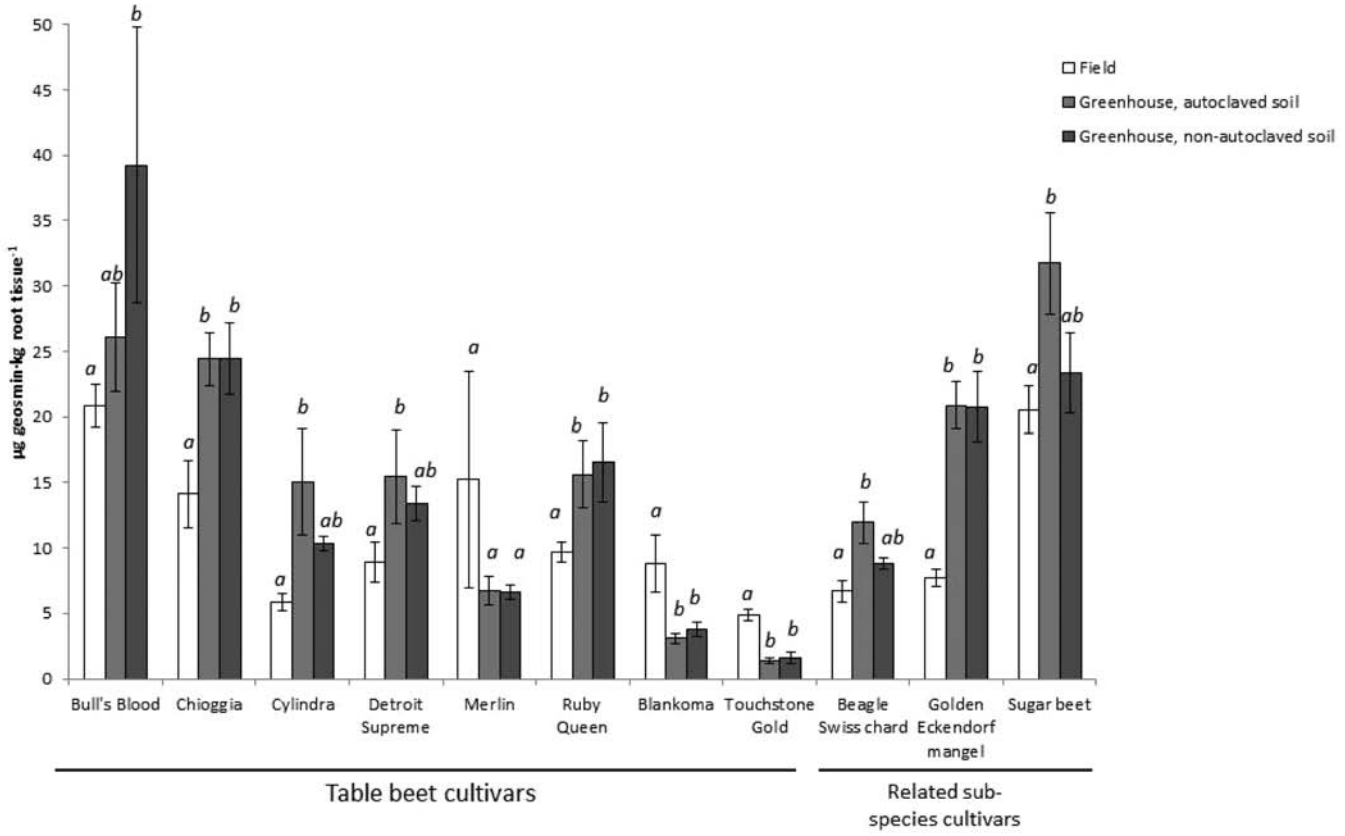

Figure 2. Mean geosmin concentrations of table beet and related subspecies cultivars. Cultivars were grown in field soil (Arlington, WI, USA), in the greenhouse with autoclaved soil, and in the greenhouse with nonautoclaved soil (Madison, WI, USA), 2011−2012. Pairwise comparisons within cultivar use log-transformed data. Means with different letters show significant differences at $P \leq 0.05$.

The lack of variation from year to year raises the possibility that geosmin production in table beet and related subspecies cultivars is endogenously produced. This suggests that a cultivar's geosmin content is a highly characteristic trait of each individual cultivar that may be under genetic control. This is interesting given that field environmental conditions varied from 2011 to 2012. In 2012, average temperatures for June and July were, on average, 2.3 and 1.3 °C higher, respectively, and the area experienced a severe drought. However, the limited irrigation the field environment received in 2012 and the drought tolerance of beet may have helped mitigate the effects of drought and higher temperatures.

Environmental Effects. Mean geosmin concentrations of each cultivar grown in each growth environment are presented in Figure 2. Geosmin concentrations in the field ranged from 4.84 to 20.82 μg geosmin (kg root tissue)$^{-1}$, whereas those in the greenhouse ranged from 1.36 to 31.74 μg geosmin (kg root tissue)$^{-1}$ and from 1.59 to 39.24 μg geosmin (kg root tissue)$^{-1}$ for autoclaved and nonautoclaved soil environments, respectively.

The significant interaction of cultivar × environment was not due to large changes in cultivar rank across environments. Because of this highly significant interaction, additional comparisons between growth environments were performed within a single cultivar (Figure 2). No cultivars exhibited a significant difference between roots grown in the greenhouse in autoclaved soil and those grown in nonautoclaved soil. This is of interest because of the potential for microorganisms to contribute to root geosmin content.[3] A significantly higher geosmin content of roots grown in nonautoclaved soil where the field microbial community has not been subjected to autoclaving might point to a significant association between roots and geosmin-producing microorganisms, such as *Streptomyces* soil bacteria. A consistent pattern of higher geosmin levels was not observed across cultivars tested in nonautoclaved soil, although some cultivars did have higher levels in this environment compared to those grown in autoclaved soil. Geosmin levels from greenhouse-grown plants were in some cases higher than those in field-grown plants. One of the possible explanations for this finding is the smaller size of greenhouse-grown roots, which would possess a higher ratio of root surface tissue to root interior tissue and consequently could be higher in geosmin than an identical genotype with a larger root volume.

Our results are more consistent with the scenario whereby table beet and related subspecies cultivars produce geosmin endogenously. In this instance, a significant difference between roots grown in autoclaved and nonautoclaved soil would not be expected because the microbial community differences would not affect endogenous production. The microbial community was not identified or measured in this study. Assessing the extent that autoclaving affects the soil microbial community over the duration of the growth period could help identify if geosmin-producing soil bacteria and fungi are present. Finding a lack of geosmin-producing microorganisms and no significant difference in geosmin content between roots grown in that environment and nonautoclaved soil with native microorganisms would strengthen the conclusion of endogenous geosmin production.

dx.doi.org/10.1021/jf4047336 | J. Agric. Food Chem. 2014, 62, 2031−2036

Another source of geosmin-producing microorganisms is endophytic bacteria, such as the actinomycetes, which have been observed in beet.[20] However, the geosmin contributions of these bacteria would have to be very substantial to account for the high geosmin content of certain cultivars.

Cultivar Effects. Despite the highly significant interaction of cultivar × environment, some general patterns exist on the cultivar level. Yellow table beet cultivar 'Touchstone Gold' produced the least amount of geosmin in any growth environment. The red table beet 'Bull's Blood' grown in nonautoclaved soil in the greenhouse produced the highest geosmin level measured across all environments, 39.24 μg geosmin (kg root tissue)$^{-1}$. 'Bull's Blood', 'Chioggia' (a table beet containing concentric circles of red pigment), and sugar beet contained the three highest levels of geosmin across all three environments as compared to the remaining cultivars. Besides 'Touchstone Gold', pigmentless table beet 'Blankoma' produced lesser amounts of geosmin in both greenhouse growth environments. In the field, however, 'Blankoma' contained the fifth lowest level. Carrot, used as a vegetable control, had no detectable geosmin for roots grown in any environment.

Mean geosmin concentrations are comparable to those obtained by Lu et al.[15] Cultivar 'Chioggia' has a reported value of 26.7 μg geosmin (kg root tissue)$^{-1}$, which is 12.6 μg geosmin (kg root tissue^{-1}) higher from our measured value of field-grown 'Chioggia', but only 2.3 μg geosmin (kg root tissue)$^{-1}$ higher than greenhouse-grown roots (either soil environment). This similarity is especially interesting given that there was no difference between years in our experiment. It again suggests that on a cultivar level, geosmin production is characteristic and under genetic control. Tyler et al. found levels ranging from 0.6 to 3.7 μg geosmin (kg root tissue)$^{-1}$ for various field-grown beet and related subspecies cultivars, which are considerably lower than our results.[17] However, a different extraction method was used. In their study, Swiss chard had the highest geosmin content, followed by sugar beet, with the lowest measured being beet cultivar 'Nero'. We also found sugar beet to have a high-geosmin-producing cultivar relative to all cultivars studied.

It is interesting that two table beet cultivars, 'Touchstone Gold' and 'Blankoma', that do not contain red pigment have lower geosmin levels, whereas two of the higher producing cultivars ('Bull's Blood' and 'Chioggia') both contain red pigment. Perhaps when these cultivars were developed, plant breeders associated the traditional red pigmentation of table beet cultivars with its traditional earthy flavors. When lighter colored table beets were developed, they may have been selected for different, and perhaps milder, flavors. Regardless of the cause, this information may be of interest to consumers looking for greater or lesser flavor characteristics in this vegetable. Sugar beet produces higher levels of geosmin as well but has not been selected specifically for fresh market palatability, nor has the mangel cultivar 'Golden Eckendorf', which contains midrange geosmin levels. Other red table beets all produce more geosmin than the yellow or white table beet (with the exception of 'Blankoma' grown in the field environment). Beagle Swiss chard produces more than white- or yellow-rooted cultivars tested but is a leaf crop, so root flavor is not an important trait.

Breeding and Interroot Variation. On a cultivar level, geosmin content variation has been identified that could be exploited in breeding for a higher or lower geosmin-containing table beet. Once we established cultivar differences, we began to question what would be the most effective experimental unit on which to base breeding decisions: a cultivar mean or individual root value? If a root with higher geosmin levels was selected and intermated with roots that also contained higher geosmin levels, the mean could increase at a faster rate from generation to generation. If assessing geosmin levels on a cultivar level, the geosmin content for an individual root entering the breeding population is unknown. For example, this could lead to lower geosmin individuals within a higher geosmin-containing cultivar being intermated, which would presumably slow movement of the mean geosmin content if breeding for increased geosmin. If significant interroot variation for geosmin concentration exists in table beet, selecting roots to intermate in a population on a cultivar basis may be less efficient for moving a quantitative trait mean.

To address some of these questions, the magnitude of interroot variation was assessed for a single F1 cultivar, 'Merlin', grown in 2011 and 2102. Two different methods were used to examine geosmin levels in this assessment, and 10 individual roots were examined from this cultivar in each of the two years. Our data revealed that a small but significant amount of variation existed between individual roots from the cultivar 'Merlin' in 2011 and a larger and significant amount of variation existed among individual roots from this cultivar in 2012 (data not shown). More substantial investigation of this point may be useful in establishing a breeding program in which geosmin concentration is a target trait. Although unknown if interroot variation exists within all cultivars, the possibility that interroot variation exists has been demonstrated. When cultivars or lines are evaluted for geosmin content, a decision must be made whether or not it is feasible to select parents on an individual root basis. A trade-off may exist between workload/resource availability and the rate the mean geosmin content of a population is moved up or down.

Geosmin production may be largely endogenous and cultivar specific but not entirely without influence from the growing environment. Further indication of the genetic control of geosmin production was suggested by the lack of significant difference in geosmin levels between roots grown in autoclaved and nonautoclaved field soils in the greenhouse and in the lack of variation between years. For breeding purposes, it is probably most useful to evaluate potential parents on the basis of evaluations of field-grown beets. Beets are grown for market in this way, and despite a significant cultivar × environment interaction, cultivar ranks did not vary widely across growth environments. However, an assessment of feasibility should be performed to determine if selection of breeding parents on an individual root basis is possible or if cultivar means will suffice. Selection of cultivars to assemble a breeding population to begin breeding for beets with higher and lower geosmin levels would be an area for further research. As selection for divergence in geosmin level occurs, perhaps a genetic or pleiotropic relationship will be reveled between genes influencing geosmin production and root pigmentation.

■ ASSOCIATED CONTENT

Ⓢ Supporting Information

Structure of the geosmin molecule and biosynthetic pathway for geosmin. This material is available free of charge via the Internet at http://pubs.acs.org.

AUTHOR INFORMATION

Corresponding Author

*(I.L.G.) Phone: (608) 262-1624. Fax: (608) 262-4743. E-mail: ilgoldma@wisc.edu.

Notes

The authors declare no competing financial interest.

ACKNOWLEDGMENTS

We thank the Michigan State University USDA Sugarbeet and Bean Research Unit for providing sugar beet seed. We also thank Al Seier and Nicholas Keuler for their respective assistance with technical aspects of the work and statistical analysis.

REFERENCES

(1) Marshall, J.; Hochstetler, A. The synthesis of (±)-geosmin and other 1,10-dimethyl-9-decalol isomers. *J. Org. Chem.* **1968**, *33*, 2593−2595.

(2) Gerber, N. Geosmin, an earthy-smelling substance isolated from actinomycetes. *Biotechnol. Bioeng.* **1967**, *9*, 321−327.

(3) Paterson, R.; Venancio, A.; Lima, N. Why do food and drink smell like earth? In *Communicating Current Research and Educational Topics and Trends in Applied Microbiology*; Mendez-Vilas, A., Ed.; Formatex: Badajoz, Spain, 2007; pp 120−128.

(4) Tyler, L.; Acree, T.; Smith, N. Sensory evaluation of geosmin in juice made from cooked beets. *J. Food Sci.* **1979**, *44*, 79−81.

(5) Buttery, R.; Guadagni, D.; Ling, L. Geosmin, a musty off-flavor of dry beans. *J. Agric. Food Chem.* **1976**, *24*, 419−420.

(6) Darriet, P.; Pons, M.; Lamy, S.; Dubourdieu, D. Identification and quantification of geosmin, an earthy odorant contaminating wines. *J. Agric. Food Chem.* **2000**, *48*, 4835−4838.

(7) Frisvad, J.; Samson, R.; Rassing, B.; van der Horst, M.; van Rijn, F.; Stark, J. Penicillium discolor, a new species from cheese, nuts and vegetables. *Antonie van Leeuwenhoek* **1997**, *72*, 119−126.

(8) Izaguirre, G.; Taylor, W. A guide to geosmin- and MIB-producing cyanobacteria in the United States. *Water Sci. Technol.* **2004**, *49*, 19−24.

(9) La Guerche, S.; Garcia, C.; Darriet, P.; Dubourdieu, D.; Labarére, J. Characterization of *Penicillium* species isolated from grape berries by their internal transcribed spacer (ITS1) sequences and by gas chromatography-mass spectrometry analysis of geosmin production. *Curr. Microbiol.* **2004**, *48*, 405−411.

(10) Lloyd, S.; Grimm, C. Analysis of 2-methylisoborneol and geosmin in catfish by microwave distillation-solid phase micro-extraction. *J. Agric. Food Chem.* **1999**, *47*, 164−169.

(11) Cane, D.; Watt, R. Expression and mechanistic analysis of a germacradienol synthase from *Streptomyces coelicolor* implicated in geosmin biosynthesis. *Proc. Natl. Acad. Sci. U.S.A.* **2003**, *100*, 1547−1551.

(12) Jiang, J.; He, X.; Cane, D. Geosmin biosynthesis. *Streptomyces coelicolor* germacradienol/germacrene D synthase converts farnesyl diphosphate to geosmin. *J. Am. Chem. Soc.* **2006**, *128*, 8128−8129.

(13) Mattheis, J.; Roberts, R. Identification of geosmin as a volatile metabolite of *Penicillium expansum*. *Appl. Environ. Microbiol.* **1992**, *58*, 3170−3172.

(14) Parliament, T.; Kolor, M.; Maing, I. Identification of the major volatile components of cooked beets. *J. Food Sci.* **1977**, *42*, 1592−1593.

(15) Lu, G.; Fellman, J.; Edwards, C.; Mattinson, D.; Navazio, J. Quantitative determination of geosmin in red beets (*Beta vulgaris* L.) using headspace solid-phase microextraction. *J. Agric. Food Chem.* **2003**, *51*, 1021−1025.

(16) Morales-Valle, H.; Silva, L.; Paterson, R.; Oliveira, J.; Venâncio, A.; Lima, N. Microextraction and gas chromatography/mass spectrometry for improved analysis of geosmin and other fungal "off" volatiles in grape juice. *J. Microbiol. Methods* **2010**, *83*, 48−52.

(17) Tyler, L.; Acree, T.; Becker, R.; Nelson, R.; Butts, R. Effect of maturity, cultivar, field history, and the operations of peeling and coring on the geosmin content of *Beta vulgaris*. *J. Agric. Food Chem.* **1978**, *26*, 1466−1469.

(18) Lu, G.; Edwards, C.; Fellman, J.; Mattinson, D.; Navazio, J. Biosynthetic origin of geosmin in red beets (*Beta vulgaris* L.). *J. Agric. Food Chem.* **2003**, *51*, 1026−1029.

(19) Buttery, R.; Seifert, R.; Guadagni, D.; Black, D.; Ling, L. Characterization of some volatile constituents of carrot. *J. Agric. Food Chem.* **1968**, *16*, 1009−1015.

(20) Lutman, B. *Actinomycetes in Various Parts of the Potato and Other Plants*; Agricultural Experiment Station, University of Vermont State Agricultural College; Burlington, VT, USA, 1945.

(21) Lange, W.; Brandenburg, W.; De Bock, T. Taxonomy and cultonomy of beet (*Beta vulgaris* L.). *Bot. J. Linnean Soc.* **1999**, *130*, 81−96.

for the conditioning of the column prior to the injection, and (c) a gradient of falling concentrations of acetate and NaOH.

The novel HPAEC-PAD method was to be validated in terms of specificity, repeatability, range, peak resolution, linearity, and the limits of detection (LOD), identification (LOI) and quantification (LOQ). Its accuracy was to be evaluated by comparison with the conventional methods[17] of pectin analysis based on gas chromatography, titrimetry, and colorimetry.

2. MATERIALS AND METHODS

2.1. Chemicals and Sample Material Used. The sodium hydroxide solution (50% w/w; Baker Analyzed reagent) for the eluents was from J.T. Baker (Avantor Performance Materials, Griesheim, Germany). The reference standards, comprising the neutral sugars L-(+)-arabinose (Ara), L-(−)-fucose (Fuc), D-(+)-galactose (Gal), D-(+)-mannose (Man), L-(+)-rhamnose (Rha), and D-(+)-xylose (Xyl), and the uronic acids D-(+)-galacturonic acid (GalUA) and D-(+)-glucuronic acid (GlcUA), were purchased from Sigma-Aldrich (Steinheim, Germany). Unstandardized citrus and apple pectins were made available by Herbstreith & Fox KG (Neuenbürg, Germany). Bovine serum albumin was from Serva Electrophoresis (Heidelberg, Germany), *m*-hydroxydiphenyl (MHDP) from Eastman Kodak (Rochester, NY, USA). All other reagents or solvents (analytical or HPLC grade) were obtained from VWR International (Darmstadt, Germany) or Sigma-Aldrich (Steinheim, Germany).

Hydrochloric acid (HCl) was used to prepare acidic methanol.[18] While ∼150 mL HCl (37% w/w) was heated in a round-bottom flask on a low heat, the gas was slowly flushed for ∼20 min through 100 mL of methanol in a gas-washing bottle, using an uncooled distillation apparatus with gas inlet tube. Subsequently, the molarity of the acidic methanol was determined by titration of an aliquot with 0.25 N NaOH to pH 7.0 (Titrino 716 DMS; Metrohm, Filderstadt, Germany) and then adjusted to 2.0 ± 0.1 M HCl.

2.2. HPAEC-PAD Analyses. The developed HPAEC-PAD method comprised two variants (M_{Dx1}, M_{Dx2}) differing in both the amount of hydrolyzed pectin (section 2.2.1) and the injection volume (section 2.2.2). The first variant (M_{Dx1}) was based on an initial sample weight of 20 μg for hydrolysis at sample/acid ratios of 40 μg mL^{-1}, as recommended by De Ruiter et al.[19] A 5-fold initial amount (100 μg) was used in the second variant M_{Dx2}, where the sample/acid ratios were increased 2.5-fold to ensure an adequate time for the subsequent removal of the acidic solvents by evaporation. In M_{Dx2}, a 5-fold amount of dried hydrolysate was dissolved in a double amount of water to inject only two-fifths (10 μL) of the volume applied in M_{Dx1} (25 μL). Thus, the theoretical absolute amounts of hydrolyzed sample that were injected in both variants were identical.

2.2.1. Hydrolysis of Pectins. According to De Ruiter et al.,[19] the neutral sugar and uronic acid residues were released by methanolysis and subsequent hydrolysis with trifluoroacetic acid (TFA). Each run comprised 6 pectin samples and 3 recovery standards (cf. section 2.2.2) that were treated in parallel. Approximately 20 mg of pectin was exactly weighed into a 20 mL volumetric flask and dissolved in 10 mL of ultrapure water overnight under automatic shaking. After adjusting the volumes, the pectin solution (method variant M_{Dx1}, 20 μL; M_{Dx2}, 100 μL) and the recovery standard (100 μL) were transferred into separate Pyrex tubes (16 × 100 mm). The screw-cap tubes were placed in a Pierce Reacti Therm heating module (30 °C) (Thermo Fisher Scientific, Waltham, MA, USA). The solutions were dried by an airstream that was provided by a Reacti Vap evaporation unit (Thermo Fisher Scientific) comprising nine single-use needles with Luer-Lock hub (⌀ 0.6 × 80 mm; Stericon, B. Braun, Melsungen, Germany). After adding anhydrous 2 M HCl in methanol (M_{Dx1}, 0.5 mL; M_{Dx2}, 1 mL), the tubes were closed and placed on a vortex mixer for stirring and then into a Thermochem CH 2 C heating device (Liebisch, Bielefeld, Germany) for heating (80 °C, 18 h), followed by cooling (5 min) in an ice−water bath. To each tube was added 100 μL of 2-methylpropan-2-ol to improve coevaporation of HCl,[20] when the recooled samples were dried again at 30 °C (heating module) by an airstream. For acidic hydrolysis, 0.5 mL (M_{Dx1}) or 1 mL (M_{Dx2}) of 2 M TFA was added. The tubes were closed and placed into the heating device (121 °C) after stirring on the vortex mixer. After 60 min of heating, the tubes were recooled in the ice−water bath (10 min), and the hydrolyzed samples were dried at 30 °C (heating module) by an airstream. Subsequently, the dry residues were dissolved by adding 0.5 mL (M_{Dx1}) or 1 mL (M_{Dx2}) of ultrapure water into each screw-cap tube. By analogy, 1 mL of ultrapure water was used for the recovery standard that had undergone the hydrolysis procedure (RS_h). The solutions were thoroughly stirred on a vortex mixer and filtered into vials through polyamide membrane filters (0.45 μm).

2.2.2. HPAEC-PAD. An ICS 3000 Dionex System (Thermo Fisher Scientific) with an AS50 Dionex autosampler was used for HPAEC. A 3 × 30 mm AminoTrap column, a 3 × 30 mm CarboPac PA20 guard column, and a 3 × 150 mm CarboPac PA20 column (Thermo Fisher Scientific) were connected in series. For saccharide detection without postcolumn base addition, an ED pulsed-amperometric detector (Thermo Fisher Scientific) with a nondisposable gold working electrode and an Ag/AgCl reference electrode was used, applying the standard carbohydrate quadrupole−potential waveform (Chromeleon software version 6.80). Eluent *A* was ultrapure water (0.055 μS cm^{-1} at 25 °C). According to Garna et al.,[21] eluent *B* contained 170 mM sodium acetate (NaOAc) in 100 mM NaOH, while eluent *C* consisted of 500 mM NaOH. Eluent *B* was prepared by dissolving NaOAc in ultrapure water and subsequent filtration through a Whatman 0.2 μm nylon filter (⌀ 50 mm). The required volumes of ultrapure water and NaOAc solution, respectively, were degassed by flushing them with nitrogen before and during the addition of a 50% (w/w) solution of NaOH. All eluents were kept under nitrogen. After injection (M_{Dx1}, 25 μL; M_{Dx2}, 10 μL), the neutral sugars and the uronic acids were separated in a single run (28 °C), using the eluent gradient profile shown in Table 1 at a flow rate of 0.2 mL min^{-1}.

Table 1. Eluent Composition and Gradient Profile for the Simultaneous Quantitation of Neutral Sugars and Uronic Acids by HPAEC-PAD[a] (28 °C, 0.2 mL min^{-1}) without Postcolumn Base Addition on a CarboPac PA20 Column with Upstream AminoTrap and PA20 Guard Columns

				eluent dosage [%]		
stage	step		time [min]	eluent *A* water	eluent *B* 100 mM NaOH + 170 mM NaOAc	eluent *C* 500 mM NaOH
regeneration	*a*	onset isocratic 1	−14.0	60	0	40
		end isocratic 1	−12.0	60	0	40
equilibration injection[b]	*b*	onset isocratic 2	−11.9	98	2	0
		end isocratic 2	0.0			
elution	*c*	onset falling linear gradient	+0.001	98	2	0
	d	onset isocratic 3	+0.5	99	1	0
		end isocratic 3	+30.0	99	1	0
	e	onset isocratic 4	+30.1	0	100	0
		end isocratic 4	+40.0	0	100	0
elution plus regeneration	*f*	restart isocratic 1	+40.1	60	0	40
		run end	+46.0	60	0	40

[a]For pulsed amperometric detection (PAD), a nondisposable gold working electrode and the standard carbohydrate quadrupole−potential waveform (Chromeleon version 6.80) were applied. [b]Injection volume: 25 μL (method variant M_{Dx1}); 10 μL (method variant M_{Dx2}).

For each analyte, calibration lines through 6 standard concentrations and the origin were produced by simple linear regression. For method variant M_{Dx1}, the standard solutions covered a range of 1.7−128 μmol L^{-1} for GalUA and 0.28−30.3 μmol L^{-1} for the other

analytes. Standard solutions having the 2.5-fold concentrations were used for M_{Dx2}.

A mixed recovery standard (RS) containing the neutral sugars (100−123 μmol L^{-1}), GlcUA (92 μmol L^{-1}), and GalUA (202 μmol L^{-1}) was used to calculate the relative recovery factors (RRF) according to De Ruiter et al.[19] for each run of method variant M_{Dx1}. The RS used in M_{Dx2} contained the respective 2.5-fold concentrations. The RRF of each analyte was the ratio of the concentration $c(RS_h)$, which was found for the RS after the two-stage hydrolysis procedure according to the respective calibration line, to its initial concentration $c(RS_0)$: RRF = $c(RS_h)/c(RS_0)$. The analyte concentrations of the samples were corrected by multiplying them by the inverse mean RRF of the 3 recovery standards that had undergone the same hydrolysis run like the samples in question. Time-dependent changes in the detector response were minimized by consecutive injection series consisting of the 6 calibration standards, the water blank, 3 samples, the 3 RS_h, and 3 further samples. In this way, each of the pectins was hydrolyzed and analyzed 6 times. The analyte contents of the pectins (in g kg^{-1}) were calculated for the bound monomer units, using the molecular weights of the respective anhydro-monosaccharides. The summated contents of the GalUA and GlcUA anhydro-monomers were considered as the total anhydro-uronic acid content (AUA_{Dx1}, AUA_{Dx2}) of the pectin according to the HPAEC-PAD method variant used, while the sum of the other anhydro-monomer contents represented the total neutral anhydro-sugar content (ANS_{Dx1}, ANS_{Dx2}).

2.3. Validation Experiments. *2.3.1. Determination of the Peak Resolution.* The resolution ($R_{P1,P2}$; eq 1) between two adjacent peaks (P1, P2) was deduced from the retention times of the two analytes (RT_{P1}, RT_{P2}) and the baseline widths (W_{P1}, W_{P2}) resulting from the tangents of the inflection points of each peak[22] by means of the Chromeleon 6.80 software (Thermo Fisher Scientific).

$$R_{P1,P2} = 2(RT_{P2} - RT_{P1})/(W_{P2} + W_{P1}) \quad (1)$$

2.3.2. Evaluation of Repeatability, Range, and Linearity. For the retention times (RT) and the response factors (RF), the day-to-day repeatability was deduced from ten consecutive calibration series to evaluate the stabilities of the separation and the detection systems, respectively, for the method variant M_{Dx1}. These data were also used to determine the ranges and the linearity of M_{Dx1}. For this purpose, mixed standard solutions covering six concentration levels (cf. section 2.2.2) were injected within four days (60 injections). The RF, being the quotient of the response (peak area, nC min) and the respective standard concentration (μmol L^{-1}), was calculated as the mean of 60 single measurements. Linearity was evaluated according to Mandel's fitting test,[23] which involved the comparison of the variances for a linear and a quadratic calibration equation.

To study the precision of the method variants M_{Dx1} and M_{Dx2}, respectively, each of four pectin samples was hydrolyzed and analyzed by HPAEC-PAD (n = 6) based on 2−4 runs that were performed by the same person within 5 days, using the same equipment, chemicals, and standards.

2.3.3. Determination of the Limits of Detection, Identification, and Quantification. The LOD, LOI, and LOQ were identified according to the calibration method of DIN 32645,[24] involving ten consecutive calibration runs (method variant M_{Dx1}) and 7 concentration levels (0.43−17 μmol L^{-1} for GalUA, otherwise 0.06−3.78 μmol L^{-1}) near the bottom end of the ranges. As detailed by Hirsch et al.,[25] the LOD was calculated as the lowest analyte concentration producing the critical minimum response. The latter was deduced from the ordinate intercept of the regression line and the width of its one-sided prediction interval based on the quantile of the one-sided Student's t-distribution (P = 0.05; $f = n - 2$ degrees of freedom). As explained elsewhere,[25] multiplication of the LOD by the factor 2 yielded the LOI, while the LOQ was iteratively calculated for a relative uncertainty of 33.3%, using the standard deviation of the procedure of the regression line and the quantile of the two-sided Student's distribution (P = 0.05; $f = n - 2$).

2.3.4. Evaluation of Accuracy. Being defined as the closeness of the measured value to the true value,[26] the accuracy of the analytical procedure was directly indicated by the RRF of the recovery standards (cf. section 2.2.2). Additionally, significant differences ($P \leq 0.05$) between the carbohydrate contents that different methods yielded for the pectins were identified by multiple pairwise comparisons of means (Duncan's test) with SAS 9.1 (SAS Institute, Cary, NC, USA).

2.4. Reference Methods for the Evaluation of Accuracy. By analogy with the HPAEC-PAD analyses (cf. section 2.2.2), the contents of the neutral sugar and uronic acid residues of the pectins were always calculated for the anhydro-monomers.

The neutral sugars released by two-stage hydrolysis with sulfuric acid (H_2SO_4) were derivatized into the alditol acetates and quantified by gas chromatography with flame ionization detection (GC-FID) (method M_{GC}).[17] Each sample was prepared and injected twice (n = 4). The total contents of neutral anhydro-sugars (ANS_{GC}) were calculated by summing up the individual contents.

The total anhydro-uronic acid (AUA) contents of the pectins (AUA_{MHDP}) were quantified, using the *m*-hydroxydiphenyl assay (method M_{MHDP}) as described by Sirisakulwat et al.[17] Hydrolysis of the pectin with H_2SO_4 (72% w/w) at ambient temperature (60 min) was carried out in duplicate for this purpose. Colorimetric analysis in triplicate followed two times per pectin hydrolysate.

As detailed by Sirisakulwat et al.,[17] the AUA content was also determined titrimetrically (AUA_{titr}) according to the JECFA standard method (M_{titr}), which yielded the degree of esterification (DE) simultaneously.[27] One-fold purification of the pectin was followed by titration in duplicate.

Furthermore, the methyl and acetyl residues were released by saponification of the pectin in duplicate to quantify their contents by HPLC, separating each saponified sample twice (n = 4) on an Aminex HPX-87H column (Bio-Rad Laboratories, Hercules, CA, USA).[17] The degrees of methylation (DMe) and acetylation (DAc) were calculated as the molar ratios of methanol ($MeOH_{HPLC}$) and acetic acid (HAc_{HPLC}), respectively, to the AUA content, which resulted from the HPAEC-PAD method variant M_{Dx2} (AUA_{Dx2}).

2.5. Quantification of Non-Carbohydrate Compounds in Pectin. The total protein contents of the pectins were determined photometrically according to the Bradford assay protocol of Sigma Aldrich for 2 mL.[28] The Bradford reagent was prepared as described elsewhere[29] and used after stirring in an amber bottle overnight and subsequent filtration through a Macherey-Nagel MN 617 ¼ filter. The pectin (~75 mg) was dissolved in ultrapure water overnight under automatic shaking. After the volume had been made up to 20 mL, an aliquot (200−500 μL) was transferred into a cuvette. Ultrapure water was added to complete 1 mL before adding the Bradford reagent (1 mL) and mixing (vortex). After exactly 10 min, the absorbance at 595 nm was measured with a Cary 100 spectrometer (Varian, Mulgrave, VIC, Australia). Each pectin solution was analyzed 6 times versus the water blank. Calibration using bovine serum albumin covered a linear range of 4−10 mg L^{-1}.

The moisture and ash contents of the pectins were determined gravimetrically in duplicate, as described earlier.[17] Their starch contents were quantitated enzymatically in duplicate, using a commercial test kit (R-Biopharm, Darmstadt, Germany).

3. RESULTS AND DISCUSSION

3.1. Specificity and Stability of the Column Performance. All compounds were eluted within 46 min after injection (Figure 1). The total run time was 60 min, including regeneration of the column with 200 mM NaOH and equilibration at 3.4 mM NaOAc in 2 mM NaOH before each injection (Table 1). Directly after the injection, the NaOAc and NaOH concentrations used for equilibration were reduced to 1.7 and 1 mM, respectively, within 30 s by applying a declining linear gradient to induce the predominantly isocratic elution of the neutral sugars (**1**−**7**) at the latter eluent composition (Figure 1). The uronic acids (**8**−**9**) were eluted, after the eluent concentration had sharply been raised to 170 mM NaOAc in 100 mM NaOH[21] and then to 200 mM NaOH (Table 1).

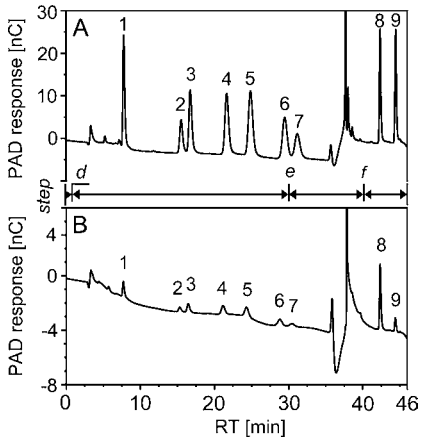

Figure 1. HPAEC-PAD chromatograms of (A) the recovery standard (RS_h) after methanolysis and TFA hydrolysis and (B) the calibration standard at the lowest concentration level (GalUA, 1.7 μmol L^{-1}; GlcUA, neutral sugars, 0.28−0.38 μmol L^{-1}) according to method variant M_{Dx1} (injection volume: 25 μL). For the gradient steps *d*−*f*, cf. Table 1. Peak assignment: **1**, fucose (Fuc); **2**, rhamnose (Rha); **3**, arabinose (Ara); **4**, galactose (Gal); **5**, glucose (Glc); **6**, xylose (Xyl); **7**, mannose (Man); **8**, galacturonic acid (GalUA); **9**, glucuronic acid (GlcUA).

As required for a highly specific method,[26] the gradient profile shown in Table 1 enabled baseline separation of Fuc, Gal, Glc, GalUA, and GlcUA over the calibrated concentration range (**1**, **4**−**5**, **8**−**9** in Figure 1). The resolutions of the adjacent peaks of Rha (**2**) and Ara (**3**) ranged from 1.45 ± 0.15 for the highest standard concentration (Rha, 27.4 μmol L^{-1}; Ara, 30.3 μmol L^{-1}) to 1.67 ± 0.06 for the lowest one (Figure 1B; Rha, Ara: 0.34−0.38 μmol L^{-1}). The peaks of Xyl (**6**) and Man (**7**) showed the poorest, but still satisfactory separation with resolutions between 1.21 ± 0.02 and 1.43 ± 0.05. The time-saving and peak-sharpening effect of the acetate loading before injection, as recommended by Davis[14] for the CarboPac PA1 column, was also observed for the present column generation (CarboPac PA20; data not shown). The peak-sharpening effect was especially of interest regarding the late-eluting neutral sugars Xyl and Man (**6**−**7**), which tended to peak broadening. For PAD detection without the need for postcolumn pH adjustment, the pH was kept above pH 11.5 at 28 °C for the elution of the neutral sugars at minimal alkaline pH and ionic strength. In this way, the response was sufficient, although the pH was sporadically below the recommended value.[30]

Subsequent elution of the uronic acids (**8**−**9**) required a sharp increase of the NaOAc and NaOH concentrations to levels of 170 and 100 mM, respectively, which were chosen according to Garna et al.[21] For this purpose, an appropriate step gradient was started (*e* in Table 1) parallel to the elution of Man (**7**) to bridge the void time, since the resulting acetate signal occurred at retention times of 36−39 min (phase *e*−*f* in Figure 1). However, the high acetate load had to be removed by strongly alkaline rinsing (200 mM NaOH) to ensure proper, reproducible, and time-saving equilibration of the column at a lower acetate concentration before the next injection.

The gradient profile in Table 1 resulted from the optimization of column temperature and acetate loading regarding maximal resolution for each of the critical sugar pairs **2**−**3** and **6**−**7**. Reduction of the column temperature increased the retention times of the neutral sugars and improved the separation of Xyl and Man (**6**−**7**), but the resolution of Rha and Ara (**2**−**3**) got worse. Equilibration (phase *b*−*c* in Table 1) at a higher acetate load and for a longer time, respectively, had the opposite effects. Exemplarily, Figure S1 of the Supporting Information shows the separation of a mixed standard solution for both the gradient profile in Table 1 at 28 °C (chromatogram A) and a modified one at only 16 °C, but with a longer equilibration phase at the 3-fold concentrations of NaOAc and NaOH (chromatogram B). These modifications increased the intervals between the elution of the individual neutral sugars, but induced peak broadening. Consistently, the resolution of Rha (**2**) and Ara (**3**) was higher for chromatogram B (1.88 ± 0.03; n = 3) than for chromatogram A (1.67 ± 0.04, n = 3). Peak overlapping of Xyl (**6**) and Man (**7**) was less pronounced, but the reduced response and peak broadening at the lower column temperature caused a poorer resolution of **6** and **7** (1.29 ± 0.04) compared to the optimized separation conditions (1.41 ± 0.03). Consequently, lower column temperatures may be appropriate for systems that include postcolumn base addition to increase the otherwise lower detector response. The detector sensitivity provided by the brand-new nondisposable electrode (chromatogram C in Figure S1 in the Supporting Information) was not fully restored by manual polishing of this electrode for the first time (chromatogram B), but the latter level was recovered by further manual polishing procedures. According to Schädel et al.,[7] 20 °C was optimal for separating Rha from Ara and Xyl from Man on the CarboPac PA20 column by isocratic elution with water and postcolumn base addition. Also higher temperatures of 40−50 °C were reported to improve the separation of Xyl and Man on the CarboPac 20 column, since an increase in temperature had a stronger retarding effect on Man than on Xyl.[31]

Additional involvement of an AminoTrap column was recommended for protein-rich glycoproteins.[32] However, this precolumn was reported to affect the separation of Rha from Ara and to cause a slight loss in sensitivity.[33] Although interferences of free amino acids may be marginal in view of the low protein contents of citrus (CP1, CP2) and apple (AP1, AP2) pectins (cf. section 3.6), the AminoTrap column was included, since the protein contents of pectic polysaccharides may vary due to the presence of arabinogalactan proteins.[34] A protein content of 5.2 g hg^{-1} was described for sugar beet pectin.[35] Apart from an unknown peak (IP_2, Figure 2D), which was not completely baseline-separated from GlcUA (**9**), all unidentified impurities of hydrolyzed pectin solutions were eluted either prior to 7.6 min (IP_1, Figure 2A) or between 35 and 41.5 min (Figure 2) and were thus baseline-separated from the analytes. Elution of the latter impurities occurred, after the NaOAc and NaOH concentrations had been raised (Table 1).

The separating performance of the column proved to be stable. Irrespective of the standard concentration, the retention times were perfectly repeatable (RT, Table 2), with the relative standard deviations (RSD) being <1%. This was in line with an earlier study[32] comprising 220 consecutive injections of a mixture of six monosaccharides on a CarboPac PA20 column.

Unlike the retention times, the response factors (RF, Table 2) varied more clearly (n = 60), especially those for Glc, Fuc, and Man (5% < RSD < 10%). However, the RSD of the RF for Rha, Ara, Gal, Xyl, GalUA, and GlcUA were below 5% (Table 2). According to the RF−concentration plot of each analyte (not shown), the RF only marginally declined with increasing concentration in the calibration range (by −0.00007 and −0.0046 nC min μmol^{-2} L^2 on average for GalUA and Glc, respectively). However, since incomplete separation of Man from

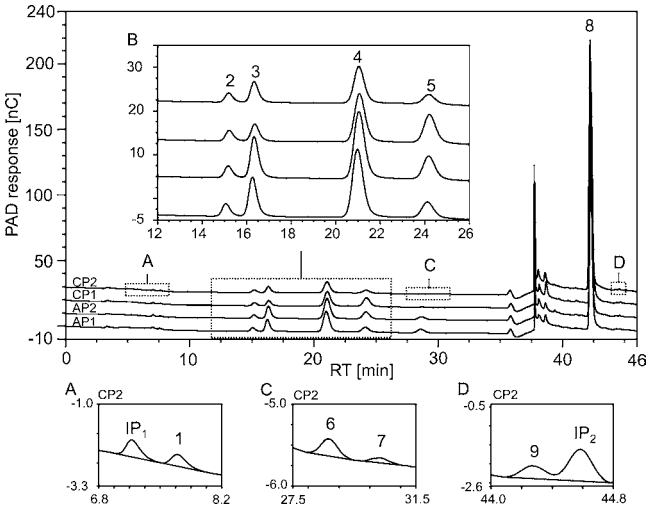

Figure 2. HPAEC-PAD chromatograms obtained for hydrolyzed apple (AP1, AP2) and citrus pectins (CP1, CP2), using method variant M_{Dx2}. For the peak assignment, cf. Figure 1. IP_1, IP_2, impurity peaks.

Xyl was associated with a slightly lower RF at low Man concentrations, the average concentration dependence of the RF was 0.0048 nC min μmol^{-2} L^2 for Man. Degradation of the sugars and changes in the detector response stability may influence the RF repeatability as well. Besides, the response factors of 8 calibration standard solutions, which were stored in the autosampler at 20 °C to compare the RF of each before and after 228 injections of samples, decreased by 1.2 ± 3.6% (GalUA) and 14.7 ± 4.3% (Man) on average within this period. Hence, unknown instabilities of the analytes and the detector response, respectively, were compensated by consecutive injection of hydrolyzed samples and recovery standards (RS_h) of the same hydrolysis series.

3.2. Limits, Range, and Linearity of the Analytical Procedure. As deduced from regression lines for a standard dilution series to infinitesimal levels (Figure S2 of the Supporting Information) according to DIN 32645,[24] the LOD ranged at 179 nmol L^{-1} for GalUA and 30−81 nmol L^{-1} for the other analytes (Table 2). This corresponded to detector loads of 0.8−4.5 pmol. The mixed standard solution representing the bottom end of this series yielded peaks being ∼32 and 7−32 times above the noise level for GalUA (0.43 μmol L^{-1}) and the other analytes (0.06−0.08 μmol L^{-1}), respectively. The RSD of the concentrations that were analytically determined for this solution (n = 10) were 2.5−15.5%, except for glucose (35.8%). The LOQ suggested by the regression approach was ∼3.8 times higher than the LOD and was thus 675 nmol L^{-1} for GalUA and 114−304 nmol L^{-1} for the other analytes (Tables 2), consistent with detector loads of 2.8−16.9 pmol. The recovery rates of the standard levels next to LOQ were 95% for GalUA (0.85 μmol L^{-1}) and 85−102% for the other analytes (0.14−0.38 μmol L^{-1}). For another method on a CarboPac PA20 without postcolumn base addition,[33] estimation according to DIN 32645[24] had indicated slightly lower levels for the LOD (13−54 nmol L^{-1}) and LOQ (35−131 nmol L^{-1}) based on injections of 50 μL, but separation of Rha from Ara and Xyl from Man by 2 mM NaOH without NaOAc had been incomplete.

For the calibration prior to HPAEC-PAD analyses, both linear and quadratic functions had been reported.[5,36] Consistently, large ranges exceeding 30 μmol L^{-1} rather

Table 2. Validation Characteristics of the HPAEC-PAD Method for the Simultaneous Quantitation of Neutral Sugars and Uronic Acids: Repeatability of the Retention Times (RT), Response Factors (RF), and the Relative Recovery Factors (RRF) of the Two-Stage Hydrolysis Procedure, Respectively, plus the Limits of Detection (LOD), Identification (LOI), and Quantification (LOQ)[a]

	method variant	**1**, Fuc	**2**, Rha	**3**, Ara	**4**, Gal	**5**, Glc	**6**, Xyl	**7**, Man	**8**, GalUA	**9**, GlcUA
RT [min][b]	M_{Dx1}	7.66 ± 0.03	15.21 ± 0.10	16.36 ± 0.07	21.08 ± 0.07	24.22 ± 0.09	28.68 ± 0.12	30.31 ± 0.14	42.21 ± 0.07	44.25 ± 0.07
RSD [%]		0.5	0.7	0.4	0.4	0.4	0.4	0.5	0.2	0.2
RF [nC min L μmol^{-1}][c]	M_{Dx1}	0.82 ± 0.06	0.37 ± 0.02	0.67 ± 0.03	1.02 ± 0.04	1.12 ± 0.06	0.76 ± 0.03	0.54 ± 0.05	0.66 ± 0.02	1.03 ± 0.03
RSD [%]		6.9	4.4	4.2	3.9	5.3	4.3	9.2	2.6	3.3
RRF[d]	M_{Dx1}	0.91 ± 0.05	0.93 ± 0.02	0.90 ± 0.01	0.90 ± 0.02	0.98 ± 0.04	0.80 ± 0.02	0.83 ± 0.05	0.50 ± 0.02	0.73 ± 0.03
	M_{Dx2}	0.95 ± 0.07	0.91 ± 0.06	0.88 ± 0.05	0.87 ± 0.06	0.92 ± 0.07	0.75 ± 0.05	0.82 ± 0.06	0.52 ± 0.04	0.73 ± 0.05
LOD [nmol L^{-1}][e]	M_{Dx1}	81	43	50	65	71	75	30	179	47
LOI [nmol L^{-1}][e]	M_{Dx1}	163	85	99	131	141	151	60	357	94
LOQ [nmol L^{-1}][e]	M_{Dx1}	304	161	187	245	264	283	114	675	177

[a] Analytes **1**−**9** (cf. Figure 1): Fuc, fucose; Rha, rhamnose; Ara, arabinose; Gal, galactose; Man, mannose; Xyl, xylose; GalUA, galacturonic acid; GlcUA, glucuronic acid. RSD, relative standard deviation; M_{Dx1} and M_{Dx2}, method variants designed for injection volumes of 25 and 10 μL, respectively (cf. section 2.2). [b] RT mean ± standard deviation (SD), as deduced from 10 runs of a mixed calibration standard (neutral sugars, glucuronic acid: 11.4−13.7 μmol L^{-1}; galacturonic acid: 71.0 μmol L^{-1}) that was injected every ninth time within the same test series. [c] RF mean ± SD (n = 60), as defined by the average area/concentration ratio of 60 injections within 10 consecutive calibration series covering a range of 1.7−128 μmol L^{-1} for galacturonic acid and 0.28−30.3 μmol L^{-1} for the other analytes. [d] RRF mean ± SD (n = 24), with the RRF = $c(RS_h)/c(RS_0)$ being the concentration ratio of the recovery standard RS after ($c(RS_h)$) and before ($c(RS_0)$) the two-step hydrolysis procedure (cf. section 2.2.2). [e] LOD, LOI, and LOQ as estimated according to the calibration method of DIN 32645[24] (cf. section 2.3.3) on the basis of the means of ten 25 μL-injections per standard solution (m = 1) for 7 concentration levels (n = 7) in a range of 0.43−17 μmol L^{-1} for galacturonic acid and 0.06−3.78 μmol L^{-1} for each of the other analytes.

dx.doi.org/10.1021/jf404626d | J. Agric. Food Chem. 2014, 62, 2037−2048

suggested a second-order function than a linear calibration line for the neutral sugars to cover the whole range by a single equation for injection volumes of 25 μL (data not shown). However, the concentration dependence of GlcUA and GalUA was linear up to 57 and 319 μmol L^{-1}, respectively. Consequently, linearity was evaluated for ranges that were relevant for pectin analysis, but limited by the tolerable upper levels of neutral sugars. The calibration lines (Figure S3 of the Supporting Information) deduced from ten consecutive 6-point calibration series above the LOQ for ranges ≤128 μmol L^{-1} for GalUA and ≤30.3 μmol L^{-1} for Fuc, Rha, Ara, Gal, Glc, Xyl, and GlcUA, respectively, had correlation coefficients >0.999, which are generally considered acceptable.[26] According to Mandel's fitting test,[23] second-order equations did not yield significantly better fits for these analytes. The only exception was Man, for which the correlation coefficient of the calibration line was lower (0.9987), presumably due to the lower peak resolution occurring especially at higher concentrations.

3.3. Accuracy of the Analytical Procedure as Deduced from Recovery Standards. All kinds of hydrolytic processes prior to the glycosyl composition analyses of polysaccharides are known to be compromises between the complete cleavage of differently stable glycosidic linkages and minimal degradation of already released monomers that are also differently acid-resistant.[6,19,37] As suggested earlier,[19] inevitable losses caused by the two-stage hydrolysis were assessed by external recovery standards (RS, cf. section 2.2.2) yielding the relative recovery factors (RRF, Table 2). Methanolysis with HCl followed by TFA hydrolysis had been recommended especially for HPAEC-PAD.[19] Advantages are the evaporability of the acids after each step and the intermediary conversion of monomers into more acid-stable methyl glycosides, including methyl esterification of the carboxyl groups of uronic acid residues. The methyl glycosides are demethylated in the second step.[19,38] The use of TFA had been shown to damage neutral sugars and uronic acids to a smaller extent compared to hydrolysis with H_2SO_4 or HCl under otherwise identical conditions.[6] Due to the marked degradation of free uronic acids with irreproducible lactone formation,[39] hydrolysis with H_2SO_4, being common prior to GC-FID analyses of neutral sugars,[17,40] has been deemed inapplicable for quantitating both neutral and acidic carbohydrate monomers by HPAEC-PAD.[41,42] The selective removal of sulfate ions prior to HPAEC runs is known to be difficult in the presence of uronic acids,[19] but had turned out to be feasible by means of an additional guard column.[42] Methanolysis with subsequent TFA hydrolysis was thus preferred, considering two sample weights by adjusting the procedure to different sample/acid ratios (variants M_{Dx1} and M_{Dx2}).

The acid treatment of the recovery standards caused a loss of neutral sugars by 2−25%, both at the original (M_{Dx1}) and the 2.5-fold (M_{Dx2}) analyte/acid ratio. Consistent with the findings of De Ruiter et al.,[19] the RRF were maximal for Glc and Fuc, but the least stable neutral sugar was Xyl (Table 2). Monosaccharides had been reported to be stable in methanolic HCl (2 M, 85 °C, 24 h), besides a loss of hexuronic acids by 3%.[38] To minimize monosaccharide losses that are known to be large for rotary evaporation of methanolic HCl,[38] the small volumes used in M_{Dx1} (0.5 mL) and M_{Dx2} (1 mL), respectively, were evaporated by an airstream[18] within 20 min at 30 °C, while the removal of HCl was facilitated by adding 2-methylpropan-2-ol.[20]

In contrast, complete removal of aqueous 2 M TFA by an airstream required up to ∼2 h at 30 °C. This long time may lead to additional degradation of monomers, especially for uronic acids that are known to be more sensitive to TFA hydrolysis than hexoses.[19,36] Accordingly, poor but reproducible RRF for GlcUA and GalUA after the two-stage hydrolysis process (Table 2) were the result of losses by 27 and ≥48%, respectively. As expected,[19] corrections based on the RRF of recovery standards that had undergone the same hydrolysis run proved to be indispensable for the analysis of samples.

3.4. Precision and Accuracy as Deduced from Comparative Neutral Sugar Analyses. In addition to the accuracy revealed by the mean RRF of the recovery standards (Table 2, cf. section 3.3) for each HPAEC-PAD method variant (M_{Dx1}, M_{Dx2}), the accuracy of both procedures was also evaluated for 4 unstandardized pectins in terms of the closeness of the measured contents to those yielded by a well-established reference method to include the effectiveness of pectin hydrolysis. As regards the neutral sugar residues, the findings are summarized in Table 3. Determination of neutral sugars by GC-FID of their alditol acetates[43,44] and the trimethylsilyl ethers of methyl glycosides,[4] respectively, is still common due to high sensitivity and resolution, but derivatization[18,40] requires additional time and excludes direct evaluation of the hydrolysis process regarding its effectiveness. Due to less complex chromatograms,[18] GC-FID of alditol acetates has often been preferred and combined with various hydrolysis techniques.[6,19,45] Together with H_2SO_4 hydrolysis,[44,46] it thus served as the reference method M_{GC},[17] despite its inapplicability for uronic acids.

For each of the 4 pectins, the HPAEC-PAD chromatograms indicated good resolution for all neutral sugars (Figure 2). Also the minor compounds (**1**, **6**−**7**), mostly occurring at levels < LOQ (Fuc, Xyl, Man; Table 3), were detected without interference of background noise or impurities. Compared with M_{GC}, M_{Dx1} and M_{Dx2} always yielded the 1.2−1.4-fold Rha contents (Table 3). This significant difference was ascribed to the different hydrolysis modes prior to GC-FID (M_{GC}) and HPAEC-PAD (M_{Dx1}, M_{Dx2}).[6,19] Due to the greater resistance of glycosiduronic acid linkages, hydrolysis of the rhamnogalacturonan I backbone by the treatment with H_2SO_4 might have been incomplete,[6,19,37] while the released rhamnose is more sensitive to H_2SO_4 (M_{GC}) than to TFA (M_{Dx1}, M_{Dx2}).[6] By contrast, 1.02−1.23 times higher Gal contents were obtained by GC-FID (M_{GC}, Table 3). The Xyl and Glc contents were 1.04−2.0 times higher, when M_{Dx1} had been used instead of M_{Dx2}, which involved the 2.5-fold sample/acid ratio but the lower injection volume. As regards the total neutral sugar content (ANS, Table 3), M_{Dx1} yielded the maximal levels (103−112% relative to M_{GC}), but M_{Dx2} came quite close to the reference method (97−105%). Thus, M_{Dx1} resulted either in slight overestimation or in the improved release of neutral sugars due to the lower sample/acid ratio relative to M_{Dx2}. The latter case would consequently imply slight underestimation by the reference method M_{GC} due to incomplete hydrolysis and/or derivatization.

The RSD of mean contents >2 g kg^{-1} were usually ≤2.9% for the GC-FID analyses (n = 4) and ≤4.8% and ≤4.2% for the HPAEC-PAD method variants M_{Dx1} and M_{Dx2} (n = 6), respectively (Table 3). Contents between 0.1 and 2 g kg^{-1} might show greater variation (RSD ≤11.5%, ≤25.4%, and ≤12.6% for M_{GC}, M_{Dx1}, and M_{Dx2}, respectively). Especially the minor sugars, such as Fuc and Man, were determined more precisely by means of M_{Dx2} instead of M_{Dx1}.

3.5. Precision and Accuracy as Deduced from Comparative Uronic Acid Analyses. As expected, analysis

Table 3. Day-to-Day Repeatability and Accuracy of the Neutral Sugar Contents[a] Resulting from Each of the Two HPAEC-PAD Method Variants with Combined Methanolysis and TFA Hydrolysis (M_{Dx1}, M_{Dx2}) and from GC-FID after Hydrolysis with Sulfuric Acid (M_{GC}), Respectively, for Unstandardized Apple (AP) and Citrus (CP) Pectins[b]

			Fuc [g kg^{-1}]					Rha [g kg^{-1}]					Ara [g kg^{-1}]					Gal [g kg^{-1}]				
sample	method	n[c]	mean	SD	RSD [%]	SE	$CI_{P=0.05}$	mean	SD	RSD [%]	SE	$CI_{P=0.05}$	mean	SD	RSD [%]	SE	$CI_{P=0.05}$	mean	SD	RSD [%]	SE	$CI_{P=0.05}$
AP1	M_{GC}	4	1.06^{A} (100)[d]	0.01	1.3	0.01	0.02	16.0^{C} (100)	0.4	2.7	0.2	0.7	34.3^{A} (100)	0.4	1.2	0.2	0.6	66.9^{A} (100)	0.8	1.1	0.4	1.2
	M_{Dx1}	6	1.08^{A} (101)[e]	0.05	4.6	0.02	0.05	21.6^{A} (135)	0.3	1.3	0.1	0.3	33.8^{AB} (99)	0.4	1.0	0.1	0.4	63.4^{B} (95)	1.3	2.0	0.5	1.4
	M_{Dx2}	6	1.03^{A} (96)[e]	0.03	3.0	0.01	0.03	20.5^{B} (128)	0.5	2.4	0.2	0.5	33.3^{B} (97)	0.9	2.6	0.3	0.9	62.0^{C} (93)	0.7	1.2	0.3	0.8
AP2	M_{GC}	4	1.07^{B} (100)[d]	0.03	2.5	0.01	0.04	15.9^{C} (100)	0.4	2.8	0.2	0.7	32.6^{B} (100)	0.6	2.0	0.3	1.0	66.1^{A} (100)	1.3	2.0	0.7	2.1
	M_{Dx1}	6	1.17^{A} (109)	0.09	8.0	0.04	0.10	20.3^{A} (128)	0.3	1.5	0.1	0.3	35.0^{A} (107)	0.4	1.1	0.2	0.4	63.2^{B} (96)	0.8	1.2	0.3	0.8
	M_{Dx2}	6	1.04^{B} (98)	0.02	2.0	0.01	0.02	18.8^{B} (118)	0.5	2.8	0.2	0.5	32.7^{B} (100)	0.7	2.0	0.3	0.7	59.5^{C} (90)	0.8	1.3	0.3	0.8
CP1	M_{GC}	4	0.67^{B} (100)[d]	0.01	0.8	0.003	0.01	13.4^{B} (100)	0.1	1.0	0.1	0.2	12.6^{C} (100)	0.1	1.0	0.1	0.2	42.2^{A} (100)	0.4	1.0	0.2	0.7
	M_{Dx1}	6	0.73^{A} (110)[e]	0.05	7.2	0.02	0.06	16.9^{A} (126)	0.5	2.7	0.2	0.5	14.1^{A} (112)	0.3	2.0	0.1	0.3	39.9^{B} (95)	0.6	1.4	0.2	0.6
	M_{Dx2}	6	0.76^{A} (114)[e]	0.03	3.7	0.01	0.03	16.8^{A} (125)	0.3	1.6	0.1	0.3	13.7^{B} (109)	0.3	2.1	0.1	0.3	40.2^{B} (95)	0.6	1.5	0.2	0.6
CP2	M_{GC}	4	0.56^{B} (100)[d]	0.01	2.4	0.01	0.02	9.79^{C} (100)	0.03	0.34	0.02	0.05	14.1^{C} (100)	0.2	1.2	0.1	0.3	31.3^{A} (100)	0.3	1.0	0.2	0.5
	M_{Dx1}	6	0.64^{A} (114)[e]	0.04	6.8	0.02	0.05	13.3^{A} (136)	0.3	2.0	0.1	0.3	15.3^{A} (108)	0.3	1.9	0.1	0.3	30.7^{A} (98)	0.7	2.1	0.3	0.7
	M_{Dx2}	6	0.66^{A} (117)[e]	0.02	3.0	0.01	0.02	12.6^{B} (129)	0.3	2.3	0.1	0.3	14.7^{B} (104)	0.4	2.6	0.2	0.4	29.3^{B} (94)	0.8	2.9	0.3	0.9

			Glc [g kg^{-1}]					Xyl [g kg^{-1}]					Man [g kg^{-1}]					ANS [g kg^{-1}]				
sample	method	n[c]	mean	SD	RSD [%]	SE	$CI_{P=0.05}$	mean	SD	RSD [%]	SE	$CI_{P=0.05}$	mean	SD	RSD [%]	SE	$CI_{P=0.05}$	mean	SD	RSD [%]	SE	$CI_{P=0.05}$
AP1	M_{GC}	4	13.2^{A} (100)	0.2	1.2	0.1	0.3	14.7^{B} (100)	0.1	1.0	0.1	0.2	1.82^{A} (100)[d]	0.15	8.01	0.07	0.23	147.9 (100)	1.8	1.2	0.9	2.9
	M_{Dx1}	6	13.5^{A} (102)	0.6	4.1	0.2	0.6	17.0^{A} (116)	0.4	2.5	0.2	0.4	1.86^{A} (103)	0.26	14.08	0.11	0.28	152.2 (103)	2.3	1.5	0.9	2.4
	M_{Dx2}	6	12.0^{B} (90)	0.4	3.3	0.2	0.4	15.2^{B} (104)	0.6	3.9	0.2	0.6	0.79^{B} (43)[e]	0.04	5.03	0.02	0.04	144.8 (98)	2.8	1.9	1.1	2.9
AP2	M_{GC}	4	19.1^{B} (100)	0.3	1.5	0.1	0.5	11.9^{B} (100)	0.2	1.7	0.1	0.3	1.30^{B} (100)[d]	0.08	6.05	0.04	0.13	148.1 (100)	3.0	2.0	1.5	4.8
	M_{Dx1}	6	22.2^{A} (116)	0.6	2.6	0.2	0.6	15.1^{A} (126)	0.5	3.5	0.2	0.6	2.22^{A} (170)	0.56	25.43	0.23	0.59	159.2 (108)	2.1	1.3	0.9	2.2
	M_{Dx2}	6	18.7^{B} (98)	0.5	2.7	0.2	0.5	12.6^{B} (105)	0.5	3.8	0.2	0.5	0.80^{C} (61)[e]	0.10	12.63	0.04	0.11	144.1 (97)	2.5	1.7	1.0	2.6
CP1	M_{GC}	4	20.2^{C} (100)	0.6	2.9	0.3	0.9	1.39^{B} (100)[d]	0.02	1.3	0.01	0.03	0.55^{B} (100)[d]	0.03	6.16	0.02	0.05	91.0 (100)	1.2	1.4	0.6	2.0
	M_{Dx1}	6	23.7^{A} (117)	0.9	3.8	0.4	0.9	2.38^{A} (171)	0.11	4.8	0.05	0.12	0.98^{A} (177)[e]	0.12	12.40	0.05	0.13	98.7 (108)	1.6	1.6	0.7	1.7
	M_{Dx2}	6	22.7^{B} (112)	0.3	1.3	0.1	0.3	1.32^{B} (94)	0.09	6.9	0.04	0.09	0.45^{C} (82)[e]	0.05	10.65	0.02	0.05	96.0 (105)	1.1	1.2	0.5	1.2
CP2	M_{GC}	4	5.11^{C} (100)	0.06	1.2	0.03	0.10	1.07^{B} (100)[d]	0.12	11.5	0.06	0.20	0.70^{B} (100)[d]	0.07	9.61	0.03	0.11	62.6 (100)	0.5	0.8	0.2	0.8
	M_{Dx1}	6	7.30^{A} (143)	0.35	4.8	0.14	0.37	2.02^{A} (188)	0.21	10.2	0.08	0.22	0.85^{A} (120)[e]	0.08	9.83	0.03	0.09	70.1 (112)	1.7	2.4	0.7	1.7
	M_{Dx2}	6	6.72^{B} (131)	0.28	4.2	0.11	0.29	1.03^{B} (96)	0.07	6.4	0.03	0.07	0.57^{C} (80)[e]	0.05	8.88	0.02	0.05	65.5 (105)	1.5	2.2	0.6	1.5

[a]Mean contents of the analytes based on the molecular weights of the respective anhydro-monosaccharides. Different superscript letters (A–C) vertically refer to significant differences ($P \leq 0.05$) between the mean analyte contents that were found for the same pectin sample using different methods. Values in parentheses indicate the analyte amount relative to the respective content that was yielded by the reference method M_{GC}. [b]SD, standard deviation; RSD, relative standard deviation; SE, standard error; CI confidence interval ($t_{0.05;n-1}$ SD/$\sqrt{n}$); Fuc, fucose; Rha, rhamnose; Ara, arabinose; Gal, galactose; Glc, glucose; Xyl, xylose; Man, mannose; ANS, total content of the 7 neutral sugars (neutral anhydro-sugars). [c]n, number of HPAEC injections (1 for each of n hydrolysis runs per pectin) for M_{Dx1} and M_{Dx2}, respectively, and number of GC injections (2 for each of 2 hydrolysis runs) for M_{GC}. [d]Peak area below the area of the lowest standard. [e]Below the limit of quantification.

dx.doi.org/10.1021/jf404626d | J. Agric. Food Chem. 2014, 62, 2037–2048

Table 4. Day-to-Day Repeatability and Accuracy of the Uronic Acid Contents[a] Resulting from Each of the Two HPAEC-PAD Method Variants with Combined Methanolysis and TFA Hydrolysis (M_{Dx1}, M_{Dx2}), the Colorimetric *m*-Hydroxydiphenyl Method (M_{MHDP}), and the Titrimetric Method of the JECFA[27] (M_{titr}), Respectively, for Unstandardized Apple (AP) and Citrus (CP) Pectins[b]

			GalUA [g kg^{-1}]					GlcUA [g kg^{-1}]					AUA [g kg^{-1}]				
sample	method	n[c]	mean	SD	RSD [%]	SE	$CI_{P=0.05}$	mean	SD	RSD [%]	SE	$CI_{P=0.05}$	mean	SD	RSD [%]	SE	$CI_{P=0.05}$
AP1	M_{MHDP}	12	708^{Ad}	45	6.4	13.0	33						708^{A} (110)	45	6.4	13.0	33
	M_{titr}	2	645^{Bd}	0.8	0.1	0.6	7.4						645^{B} (100)	0.8	0.1	0.6	7.4
	M_{Dx1}	6	633^{B}	22	3.5	9.0	23	1.25^{Ae}	0.08	6.4	0.03	0.08	634^{B} (98)	22	3.5	9.0	23
	M_{Dx2}	6	621^{B}	24	3.9	9.8	25	0.97^{Be}	0.03	3.4	0.01	0.03	622^{B} (97)	24	3.9	9.8	25
AP2	M_{MHDP}	12	717^{Ad}	21	3.0	6.2	16						717^{A} (108)	21	3.0	6.2	16
	M_{titr}	2	662^{Bd}	10	1.5	7.0	89						662^{B} (100)	10	1.5	7.0	89
	M_{Dx1}	6	649^{BC}	8.0	1.2	3.3	8.4	1.25^{Ae}	0.07	5.6	0.03	0.07	651^{BC} (98)	8.0	1.2	3.3	8.4
	M_{Dx2}	6	631^{C}	15	2.4	6.2	16	1.03^{Be}	0.06	6.2	0.03	0.07	632^{C} (95)	15	2.4	6.2	16
CP1	M_{MHDP}	12	825^{Ad}	26	3.2	7.6	19						825^{A} (116)	26	3.2	7.6	19
	M_{titr}	2	713^{Bd}	6.0	0.8	4.2	54						713^{B} (100)	6.0	0.8	4.2	54
	M_{Dx1}	6	712^{B}	30	4.2	12.3	32	0.93^{Ae}	0.05	5.8	0.02	0.06	713^{B} (100)	30	4.2	12.3	32
	M_{Dx2}	6	727^{B}	23	3.1	9.3	24	0.62^{Be}	0.03	4.6	0.01	0.03	727^{B} (102)	23	3.1	9.3	24
CP2	M_{MHDP}	12	776^{Ad}	40	5.2	11.7	30						776^{A} (103)	40	5.2	11.7	30
	M_{titr}	2	753^{Bd}	14	1.8	9.8	125						753^{B} (100)	14	1.8	9.8	125
	M_{Dx1}	6	760^{B}	24	3.1	9.6	25	0.65^{Ae}	0.02	3.8	0.01	0.03	760^{B} (101)	24	3.1	9.6	25
	M_{Dx2}	6	743^{B}	22	2.9	8.9	23	0.47^{Be}	0.03	6.2	0.01	0.03	743^{B} (99)	22	2.9	8.9	23

[a]Mean contents of the analytes based on the molecular weights of the respective anhydro-monosaccharides. Different superscript letters (A−C) vertically refer to significant differences ($P \leq 0.05$) between the mean analyte contents that were found for the same pectin sample using different methods. Values in parentheses indicate the analyte amount relative to the respective content that was yielded by the reference method M_{titr}. [b]SD, standard deviation; RSD, relative standard deviation; SE, standard error; CI confidence interval ($t_{0.05;n-1}$ SD/$\sqrt{n}$); GalUA, galacturonic acid; GlcUA, glucuronic acid; AUA, total content of the two uronic acids (anhydro-uronic acids). [c]n, number of replications: number of HPAEC injections (1 for each of n hydrolysis runs per pectin) for M_{Dx1} and M_{Dx2}, respectively; number of colorimetric measurements for M_{MHDP}; number of titrations per pectin after one-fold purification for M_{titr}. [d]The content of anhydro-galacturonic acid yielded by these methods actually represents the AUA content. [e]Below the limit of quantification.

of the pectins AP1−CP2 by HPAEC-PAD (M_{Dx1}, M_{Dx2}) confirmed GalUA to be the major carbohydrate residue (621−760 g kg^{-1}, Table 4). Due to the broad linear range for GalUA (Figure S3D in the Supporting Information), all analytes, including those having much lower contents (**1**−**7**, **9**), could be quantitated, using either M_{Dx1} or M_{Dx2} (Figure 2). Minor GlcUA contents < LOQ were also found (Table 4). GC-FID of the trimethylsilyl ethers of methyl glycosides also allows quantitation of both neutral and acidic carbohydrates in a single run.[4,18] Alternatively, the more common acetylation of the reduced monomers may be modified to include the methyl ester alditol acetates or *N*-propylaldonamide acetates of the uronic acids,[47,48] depending on the prior hydrolysis method. However, as regards pectins, the analysis of neutral sugar residues by GC-FID of the alditol acetates has usually been accompanied by separate spectrophotometric quantitation of the total uronic acid residues (AUA) with MHDP relative to GalUA standards,[43,44,46] preferably using an automated assay[49] to ensure fully standardized procedures.[50] HPAEC-PAD analyses of neutral sugars have also been combined with the MHDP assay for AUA.[10,51] Hence, the colorimetric method was included in the comparative pectin analyses as regards the uronic acid residues (M_{MHDP},[17] Table 4). However, since commercial pectins for food applications require a minimum galacturonic acid content of 65% (w/w) on a dried and ash-free basis according to the official titrimetric method of the JECFA (AP1−CP2: 81.2−90.9% w/w),[27] this industrially relevant method not needing pectin hydrolysis served as the reference method for the acidic carbohydrates, but the results were expressed relative to the unpurified pectin samples (M_{titr}, Table 4), by analogy with the other methods.[17] Being unspecific for the type of uronic acid, M_{MHDP} and M_{titr} actually yielded the total AUA contents, but in good approximation of the GalUA contents of pectins (Table 4).

Irrespective of the disparity in the specificity, the reference method M_{titr} and the HPAEC-PAD method variants resulted in almost identical total AUA contents (M_{Dx1}, 98−101%; M_{Dx2}, 95−102%; Table 4), with the differences being mostly insignificant ($P \leq 0.05$). This conformity suggested good accuracy of M_{Dx1} and M_{Dx2} and complete hydrolytic release of the uronic acids prior to HPAEC-PAD. In contrast, AUA contents being significantly higher by the factor 1.03−1.16 indicated overestimation by the method M_{MHDP} compared to M_{titr}, similarly to an earlier report.[17] Both HPAEC-PAD method variants yielded identical GalUA contents for each pectin, but the minor GlcUA contents that were found by means of M_{Dx1} always exceeded those from M_{Dx2} significantly ($P \leq 0.05$; Table 4), as analogously shown above (cf. section 3.4) for various neutral sugars (Table 3).

In conformity with the precision of the HPAEC-PAD results for most of the neutral sugars (cf. section 3.4), the RSD was ≤4.2% for the contents of GalUA and total AUA, respectively, according to M_{Dx1} or M_{Dx2} (n = 6; Table 4). The apparently lower RSD (≤2%) of AUA values resulting from M_{titr} only reflected the precision of the titration procedure (n = 2), without considering the repeatability of the obligatory acidic purification of the pectin prior to titration. Among the methods used to determine the uronic acids, M_{MHDP} comprising nonautomated serial analyses showed the poorest precision (RSD ≤ 6%, n = 12).

3.6. Accuracy of Carbohydrate Analyses as Deduced from Pectin Composition. Although the carbohydrate

Table 5. Composition and Esterification Indices of Unstandardized Apple (AP) and Citrus (CP) Pectins, Including the Mass Balances

	AP1	AP2	CP1	CP2
compound [g hg^{-1}][a]				
moisture	6.67 ± 0.32	7.01 ± 0.01	9.59 ± 0.18	8.65 ± 0.08
ash	3.67 ± 0.18	3.86 ± 0.22	2.23 ± 0.06	3.29 ± 0.06
protein	0.27 ± 0.02	0.28 ± 0.01	0.73 ± 0.04	0.38 ± 0.02
starch	0.14 ± 0.03	0.74 ± 0.02	0.15 ± 0.01	0.23 ± 0.01
∑non-pectin compounds	10.7	11.9	12.7	12.6
ANS_{Dx2} (starch-corrected)[b]	14.3 ± 0.3	13.7 ± 0.3	9.45 ± 0.11	6.32 ± 0.15
AUA_{Dx2}[b]	62.2 ± 2.4	63.2 ± 1.5	72.8 ± 2.3	74.3 ± 2.2
$MeOH_{HPLC}$	7.48 ± 0.17	7.76 ± 0.12	8.06 ± 0.13	9.23 ± 0.11
HAc_{HPLC}	0.99 ± 0.01	1.02 ± 0.01	0.41 ± 0.01	0.39 ± 0.005
total TM_1	95.8	97.5	103.4	102.8
ANS_{GC} (starch-corrected)[b]	14.7 ± 0.2	14.1 ± 0.3	8.96 ± 0.12	6.03 ± 0.05
AUA_{titr}[b]	64.5 ± 0.1	66.2 ± 1.0	71.3 ± 0.6	75.3 ± 1.4
$MeOH_{titr}$	8.17 ± 0.03	8.61 ± 0.18	8.51 ± 0.10	9.26 ± 0.26
total TM_2	98.1	100.8	101.5	103.2
esterification indices [mol hmol^{-1}][a]				
DE[c]	72.0 ± 0.2	73.8 ± 0.4	67.8 ± 0.2	69.8 ± 0.7
DMe[d]	66.0 ± 0.9	67.6 ± 0.6	60.9 ± 0.6	68.3 ± 0.6
DAc[d]	4.69 ± 0.04	4.69 ± 0.03	1.65 ± 0.02	1.52 ± 0.02

[a]Mean ± standard deviation. ANS_{Dx2}, total neutral sugars without the glucose of starch (HPAEC-PAD method variant M_{Dx2}); AUA_{Dx2}, total uronic acids (HPAEC-PAD method variant M_{Dx2}); $MeOH_{HPLC}$, methyl residues (as methanol quantified by HPLC); HAc_{HPLC}, acetyl residues (as acetic acid quantified by HPLC); TM_1, mass balance comprising the totaled non-pectin compounds, ANS_{Dx2}, AUA_{Dx2}, $MeOH_{HPLC}$, and HAc_{HPLC}. ANS_{GC}, total neutral sugars without the glucose of starch (GC-FID method M_{GC}); AUA_{titr}, total uronic acids (titrimetric method M_{titr}); $MeOH_{titr}$, ester residues (as the tritrimetric methanol content, method M_{titr}); TM_2, mass balance comprising the totaled non-pectin compounds, ANS_{GC}, AUA_{titr}, and $MeOH_{titr}$. DE, degree of esterification; DMe, degree of methylation; DAc, degree of acetylation. [b]Contents of the carbohydrate residues based on the molecular weights of the respective anhydro-monosaccharides. [c]Determined titrimetrically (method M_{titr}). [d]Ester residues (as determined by HPLC) relative to AUA_{Dx2}.

composition of the four pectins was largely confirmed by the different approaches used for the comparative pectin analyses (Tables 3 and 4), slight over- or underestimation due to known methodological flaws could not be excluded for individual methods (cf. sections 3.4 and 3.5). Therefore, the carbohydrate results from those methods that yielded the most consistent data were used to calculate the mass balances (TM_1, TM_2) of the pectins for two analytical basic approaches (Table 5). Accordingly, TM_1 was the total based on M_{Dx2}, while TM_2 rested upon M_{GC} and M_{titr}. For this purpose, the ester groups of the pectins and the non-pectin compounds of the four samples were also considered (Table 5). Ranges of 96−103% (w/w) for TM_1 and 98−103% (w/w) for TM_2 indicated successful identification and quantification of all major compounds, irrespective of using the HPAEC-PAD method variant M_{Dx2} or the gas chromatographic/titrimetric approach for carbohydrate analysis. Within these ranges, the mass balances for the two citrus pectins (CP1, CP2) were always higher than those for the apple pectins (AP1, AP2). Due to ∼7−16% lower GalUA levels (Table 4), the two apple pectins displayed lower contents of uronic acids (AUA, Table 5), but were ∼1.8 times richer in neutral sugars (ANS, Table 5), chiefly in Xyl besides Ara and others (Table 3). The notable Xyl and Ara portions of AP1 and AP2 can be ascribed to the presence of xylogalacturonans and arabinans in apple tissue.[34] From an analytical point of view, the relative differences between both sample classes were thus mainly related to the major and one of the minor constituents. However, apart from the Xyl contents of CP1 and CP2, the RSD covered similar ranges for Xyl, Ara, and GalUA (Tables 3 and 4).

Being a key property regarding the gelling behavior and applicability of pectin,[52] the titrimetrically determined degree of esterification (DE, Table 5) should actually be equivalent to the totaled molar percentages of methyl and acetyl ester groups relative to AUA. Unlike the DE values on basis of the titrimetric AUA levels, the chromatographically quantified degrees of methylation and acetylation were expressed relative to the AUA levels resulting from method variant M_{Dx2} (DMe and DAc, respectively; Table 5). Despite different methods, the sum of DMe and DAc came quite close (92−100%) to the DE. Altogether, the four pectins displayed the composition expected for highly esterified apple and citrus pectins,[52,53] as independently confirmed by applying various analytical methods. Hence, acceptable accuracy of the HPAEC-PAD method (M_{Dx2}) was proven.

3.7. Applicability of the Analytical Procedure. Irrespective of the initial sample weight, both HPAEC-PAD method variants could be used for pectin analysis. As deduced from the LOQ and the relative recovery factors (RRF, Table 2) for the variant M_{Dx1}, the sample material should contain GalUA and each of the other 8 analytes at theoretical levels of at least 5.9 and 0.6−1.2 g kg^{-1}, respectively, to yield analyte concentrations ≥LOQ after injection. If necessary, determination of minor compounds might be improved by adding an appropriate solvent volume to the dried hydrolysate in order to adjust the analyte concentrations for HPAEC-PAD. However, the analysis of more concentrated hydrolysates might be hindered by exceeding the upper calibration limits of the major compounds such as Gal (**4**, Figure 2). This may then necessitate two injections at different concentration levels. For this purpose, the variant M_{Dx2}, involving the 5-fold initial sample amount, was introduced to make sufficient amount of hydrolyzed material available for a broader range of optional hydrolysate dilution levels. Besides, M_{Dx2} proved superior to M_{Dx1} because of a more representative sample amount and the

lower RSD observed for the minor compounds in the comparative pectin analyses.

M_{Dx2} was thus recommended for the glycosyl composition analysis of pectins. In terms of accuracy, it proved to be equivalent to the gas chromatographic/titrimetric reference methods, but allowed quantitation of all neutral and acidic analytes in a single run without tedious derivatization. All major carbohydrate constituents ($\geq$1.5 g kg^{-1}) were quantifiable with good day-to-day repeatability (RSD $\leq$ 4.2%). However, hydrolytic losses of 5−27% depending on the analyte (48% for GalUA) required correction by considering concomitantly analyzed recovery standards. According to the effectiveness of methanolysis with subsequent TFA hydrolysis,[19] M_{Dx2} was deemed applicable to pectins, but also to other noncrystalline polysaccharides. By contrast, depolymerization of highly ordered or crystalline polysaccharides requires either treatment with sulfuric acid[4] or methanolysis after enzymatic prehydrolysis of cellulose.[54]

The reproducible and simultaneous separation of Xyl from Man and Rha from Ara proved to be the greatest asset of the suggested HPAEC-PAD method. Elution from the CarboPac PA20 column by means of the suggested NaOAc/NaOH gradient profile ensured their otherwise difficult separation almost to the baseline and detection without postcolumn pH adjustment. Besides the chosen temperature, two factors turned out to be crucial for this purpose: (1) equilibration of the column at an appropriate NaOAc/NaOH level prior to injection; (2) the subsequent short-term linear gradient to the low NaOAc/NaOH level needed for the elution of neutral monosaccharides.

In conclusion, reproducible and accurate determination of 9 neutral and acidic monosaccharides of pectin hydrolysates by HPAEC-PAD in a single run without postcolumn pH adjustment proved to be feasible due to the suggested NaOAc/NaOH gradient. As regards the neutral sugars, the method was deemed equivalent to GC-FID of alditol acetates in terms of repeatability and accuracy. Like HPAEC-PAD, hydrophilic interaction liquid chromatography with evaporative light scattering detection (HILIC-ELSD) also requires no derivatization. Coupled with mass spectrometry, HILIC-ELSD has chiefly been preferred for the analysis of acidic oligosaccharides, because saponification of the methyl esters and acetyl groups is avoided.[55] However, compared with published HILIC-ELSD methods for the analysis of monosaccharides,[56,57] the resolution of the validated HPAEC-PAD method was clearly superior.

■ ASSOCIATED CONTENT

Supporting Information

Figure S1 shows the effects of various factors on the separation performance. Figure S2, displaying regression lines at the bottom end of the range, refers to the sensitivity of the HPAEC-PAD method variant M_{Dx1}. Figure S3 comprises the calibration lines, indicating the range and linearity. This material is available free of charge via the Internet at http://pubs.acs.org.

■ AUTHOR INFORMATION

Corresponding Author

*Phone: +49(0)711 459 22317. Fax: +49(0)711 459 24110. E-mail: Sybille.Neidhart@uni-hohenheim.de.

Funding

This research was funded by Deutsche Forschungsgemeinschaft (DFG), Bonn, Germany: Project SFB 564-T3. It is part of the Special Research Program "Research for Sustainable Land Use and Rural Development in Mountainous Regions of Southeast Asia" (The Uplands Program).

Notes

The authors declare no competing financial interest.

■ ACKNOWLEDGMENTS

Herbstreith & Fox KG, Neuenbürg, Germany is gratefully acknowledged for providing the unstandardized pectins.

■ ABBREVIATIONS USED

ANS, total neutral anhydro-sugars; Ara, arabinose; AUA, total anhydro-uronic acids; CI, confidence interval; DAc, degree of acetylation; DE, degree of esterification; DMe, degree of methylation; Fuc, fucose; Gal, galactose; GalUA, galacturonic acid; Glc, glucose; GlcUA, glucuronic acid; HAc, acetic acid; HPAEC, high-performance anion exchange chromatography; LOD, limit of detection; LOI, limit of identification; LOQ, limit of quantification; MeOH, methanol; Man, mannose; MHDP, *m*-hydroxydiphenyl; NaOAc, sodium acetate; PAD, pulsed amperometric detection; R^2, coefficient of determination; RF, response factor; Rha, rhamnose; RRF, relative recovery factor; RS, recovery standard; RS_h, RS after the hydrolysis process; RT, retention time; TFA, trifluoroacetic acid; TM, total mass (mass balance); Xyl, xylose; indices *i* of abbreviations for methods (M_i) and sample properties therefrom, $_{Dx1}$, $_{Dx2}$, by means of HPAEC-PAD method variant 1 or 2; $_{GC}$, gas chromatographically; $_{HPLC}$, by HPLC; $_{MHDP}$, by means of the MHDP assay; $_{titr}$, titrimetrically

■ REFERENCES

(1) Rocklin, R. D.; Pohl, C. A. Determination of carbohydrates by anion exchange chromatography with pulsed amperometric detection. *J. Liq. Chromatogr.* **1983**, *6*, 1577−1590.

(2) Schols, H. A.; Voragen, A. G. J. Pectic polysaccharides. In *Handbook of Food Enzymology*; Whitaker, J. R., Voragen, A. G. J., Wong, D. W. S., Eds.; Marcel Dekker: New York, NY, USA, 2003; pp 829−843.

(3) Cataldi, T. R. I.; Campa, C.; De Benedetto, G. E. Carbohydrate analysis by high-performance anion-exchange chromatography with pulsed amperometric detection: The potential is still growing. *Fresenius J. Anal. Chem.* **2000**, *368*, 739−758.

(4) Willför, S.; Pranovich, A.; Tamminen, T.; Puls, J.; Laine, A.; Suurnäkki, C.; Saake, B.; Uotila, K.; Simolin, H.; Hemming, J.; Holmbom, B. Carbohydrate analysis of plant materials with uronic acid-containing polysaccharides − A comparison between different hydrolysis and subsequent chromatographic analytical techniques. *Ind. Crops Prod.* **2009**, *29*, 571−580.

(5) Currie, H. A.; Perry, C. C. Resolution of complex monosaccharide mixtures from plant cell wall isolates by high pH anion exchange chromatography. *J. Chromatogr., A* **2006**, *1128*, 90−96.

(6) Garna, H.; Mabon, N.; Wathelet, B.; Paquot, M. New method for a two-step hydrolysis and chromatographic analysis of pectin neutral sugar chains. *J. Agric. Food Chem.* **2004**, *52*, 4652−4659.

(7) Schädel, C.; Blöchl, A.; Richter, A.; Hoch, G. Quantification and monosaccharide composition of hemicelluloses from different plant functional types. *Plant Physiol. Biochem.* **2010**, *48*, 1−8.

(8) Øbro, J.; Harholt, J.; Scheller, H. V.; Orfila, C. Rhamnogalacturonan I in *Solanum tuberosum* tubers contains complex arabinogalactan structures. *Phytochemistry* **2004**, *65*, 1429−1438.

(9) Eder, M.; Tenhaken, R.; Driouich, A.; Lütz-Meindl, U. Occurrence and characterization of arabinogalactan-like proteins and hemicelluloses in *Micrasterias* (Streptophyta). *J. Phycol.* **2008**, *44*, 1221−1234.

(10) Liaotrakoon, W.; Van Buggenhout, S.; Christiaens, S.; Houben, K.; De Clercq, N.; Dewettinck, K.; Hendrickx, M. E. An explorative

study on the cell wall polysaccharides in the pulp and peel of dragon fruits (*Hylocereus* spp.). *Eur. Food. Res. Technol.* **2013**, *237*, 341−351.
(11) Lebet, V.; Arrigoni, E.; Amadò, R. Neutral-sugar determination by HPAEC-PAD to characterise polysaccharide degradation by colonic bacteria. *Z. Lebensm.-Unters. -Forsch. A* **1997**, *205*, 257−261.
(12) Campbell, J. M.; Flickinger, E. A.; Fahey, G. C., Jr. A comparative study of dietary fiber methodologies using pulsed electrochemical detection of monosaccharide constituents. *Semin. Food Anal.* **1997**, *2*, 43−53.
(13) Schütz, K.; Muks, E.; Carle, R.; Schieber, A. Separation and quantification of inulin in selected artichoke (*Cynara scolymus* L.) cultivars and dandelion (*Taraxacum officinale* WEB. ex. WIGG.) roots by high-performance anion exchange chromatography with pulsed amperometric detection. *Biomed. Chromatogr.* **2006**, *20*, 1295−1303.
(14) Davis, M. W. A rapid modified method for compositional carbohydrate analysis of lignocellulosics by high pH anion-exchange chromatography with pulsed amperometric detection (HPAEC/PAD). *J. Wood Chem. Technol.* **1998**, *18*, 235−252.
(15) Lee, Y. C. High-performance anion-exchange chromatography for carbohydrate analysis. *Anal. Biochem.* **1990**, *189*, 151−162.
(16) Yang, X.; Baskin, C. C.; Baskin, J. M.; Zhang, W.; Huang, Z. Degradation of seed mucilage by soil microflora promotes early seedling growth of a dessert sand dune plant. *Plant Cell Environ.* **2012**, *35*, 872−883.
(17) Sirisakulwat, S.; Nagel, A.; Sruamsiri, P.; Carle, R.; Neidhart, S. Yield and quality of pectins extractable from the peels of Thai mango cultivars depending on fruit ripeness. *J. Agric. Food Chem.* **2008**, *56*, 10727−10738.
(18) York, W. S.; Darvill, A. G.; McNeil, M.; Stevenson, T. T.; Albersheim, P. Isolation and characterization of plant cell walls and cell wall components. In *Plant Molecular Biology. Methods in Enzymology*; Weissbach, A., Weissbach, H., Eds.; Academic Press: Orlando, FL, USA, 1986; Vol. *118*, pp 3−40.
(19) De Ruiter, G. A.; Schols, H. A.; Voragen, A. G. J.; Rombouts, F. M. Carbohydrate analysis of water-soluble uronic acid-containing polysaccharides with high-performance anion-exchange chromatography using methanolysis combined with TFA hydrolysis is superior to four other methods. *Anal. Biochem.* **1992**, *207*, 176−185.
(20) Chaplin, M. F. A rapid and sensitive method for the analysis of carbohydrate components in glycoproteins using gas-liquid chromatography. *Anal. Biochem.* **1982**, *123*, 336−341.
(21) Garna, H.; Mabon, N.; Wathelet, B.; Paquot, M. Combined enzymatic hydrolysis and HPAEC method for simultaneous analysis of galacturonic acid and neutral sugars of pectin. *Commun. Agric. Appl. Biol. Sci.* **2003**, *68*, 297−300.
(22) Shah, R. D.; Maryanoff, C. A. Reversed phase HPLC. In *HPLC: Practical and Industrial Applications*, 2nd ed.; Swadesh, J. K., Ed.; CRC Press: Boca Raton, FL, USA, 2001; pp 141−200.
(23) Funk, W.; Dammann, V.; Donnevert, G. Anpassungstest nach Mandel. In *Qualitätssicherung in der analytischen Chemie*; VCH: Weinheim, Germany, 1992; pp 17.
(24) DIN Deutsches Institut für Normung e.V. Chemische Analytik. Nachweis-, Erfassungs- und Bestimmungsgrenze. *DIN 32645*; Beuth: Berlin, Germany, 1994.
(25) Hirsch, A. R.; Carle, R.; Neidhart, S. Validation and applicability of a standardized procedure for evaluating freshness of *Citrus* juices based on pectin methylesterase activity quantitation. *J. Appl. Bot. Food Qual.* **2012**, *85*, 6−16.
(26) Green, J. M. A practical guide to analytical method validation. *Anal. Chem. News Features* **1996**, *68*, 305A−309A.
(27) Joint FAO/WHO Expert Committee on Food Additives (JECFA) Compendium of food additive specifications. *FAO JECFA Monographs 7*; Food and Agriculture Organization of the United Nations: Rome, Italy, 2009. http://www.fao.org/ag/agn/jecfa-additives/specs/monograph7/additive-306-m7.pdf (accessed Apr 17, 2013).
(28) Product information − Bradford reagent (product No. B 6916); Technical Bulletin; Sigma-Aldrich: Saint Louis, MO, USA, 2004. http://www.sigmaaldrich.com/etc/medialib/docs/Sigma/Bulletin/b6916bul.Par.0001.File.tmp/b6916bul.pdf (accessed Sep 05, 2013).
(29) Bradford, M. M. A rapid and sensitive method for the quantitation of microgram quantities of protein utilizing the principle of protein-dye binding. *Anal. Biochem.* **1976**, *72*, 248−254.
(30) Thermo Scientific. Analysis of carbohydrates by high-performance anion-exchange chromatography with pulsed amperometric detection (HPAE-PAD). *Technical Note 20*; Dionex: Sunnyvale, CA, USA, 2004.
(31) Sevcik, R. S.; Mowery, R. A.; Becker, C.; Chambliss, C. K. Rapid analysis of carbohydrates in aqueous extracts and hydrolysates of biomass using a carbonate-modified anion-exchange column. *J. Chromatogr., A* **2011**, *1218*, 1236−1243.
(32) Weitzhandler, M.; Barreto, V.; Pohl, C.; Jandik, P.; Cheng, J.; Avdalovic, N. CarboPac^{TM} PA20: a new monosaccharide separator column with electrochemical detection with disposable gold electrodes. *J. Biochem. Biophys. Methods* **2004**, *60*, 309−317.
(33) Meyer, A.; Fischer, H.; Kuzyakov, Y.; Fischer, K. Improved RP-HPLC and anion-exchange cromatography methods for the determination of amino acids and carbohydrates in soil solutions. *J. Plant Nutr. Soil Sci.* **2008**, *171*, 917−926.
(34) Voragen, F.; Beldman, G.; Schols, H. Chemistry and enzymology of pectins. In *Advanced Dietary Fibre Technology*; McCleary, B. V., Prosky, L., Eds.; Blackwell Science: Oxford, U.K., 2001; pp 379−398.
(35) Mesbahi, G.; Jamalian, J.; Farahnaky, A. A comparative study on functional properties of beet and citrus pectins in food systems. *Food Hydrocolloids* **2005**, *19*, 731−738.
(36) Arnous, A.; Meyer, A. S. Comparison of methods for compositional characterization of grape (*Vitis vinifera* L.) and apple (*Malus domestica*) skins. *Food Bioprod. Process.* **2008**, *86*, 79−86.
(37) Carpita, N. C.; Shea, E. M. Linkage structure of carbohydrates by gas chromatography-mass spectrometry (GC-MS) of partially methylated alditol acetates. In *Analysis of Carbohydrates by GLC and MS*; Biermann, C. J., McGinnis, G. D., Eds.; CRC Press: Boca Raton, FL, USA, 1989; pp 157−216.
(38) Chambers, R. E.; Clamp, J. R. An assessment of methanolysis and other factors used in the analysis of carbohydrate-containing materials. *Biochem. J.* **1971**, *125*, 1009−1018.
(39) Blake, J. D.; Richards, G. N. Problems of lactonisation in the analysis of uronic acids. *Carbohydr. Res.* **1968**, *8*, 275−281.
(40) Blakeney, A. B.; Harris, P. J.; Henry, R. J.; Stone, B. A. A simple and rapid preparation of alditol acetates for monosaccharide analysis. *Carbohydr. Res.* **1983**, *113*, 291−299.
(41) Garna, H.; Mabon, N.; Nott, K.; Wathelet, B.; Paquot, M. Kinetic of the hydrolysis of pectin galacturonic acid chains and quantification by ionic chromatography. *Food Chem.* **2006**, *96*, 477−484.
(42) Quigley, M. E.; Englyst, H. N. Determination of the uronic acid constituents of non-starch polysaccharides by high-performance liquid chromatography with pulsed amperometric detection. *Analyst* **1994**, *119*, 1511−1518.
(43) Tanhatan-Nasseri, A.; Crépeau, M.-J.; Thibault, J.-F.; Ralet, M.-C. Isolation and characterization of model homogalacturonans of tailored methylesterification patterns. *Carbohydr. Polym.* **2011**, *86*, 1236−1243.
(44) Ramasamy, U. S.; Gruppen, H.; Schols, H. A. Structural and water-holding characteristics of untreated and ensiled chicory root pulp. *J. Agric. Food Chem.* **2013**, *61*, 6077−6085.
(45) Trad, M.; Le Bourvellec, C.; Gaaliche, B.; Ginies, C.; Renard, C. M. G. C.; Mars, M. Caprification modifies polyphenols but not cell wall concentrations in ripe figs. *Sci. Hortic.* **2013**, *160*, 115−122.
(46) Agoda-Tandjawa, G.; Durand, S.; Gaillard, C.; Garnier, C.; Doublier, J. L. Properties of cellulose/pectins composites: Implication for structural and mechanical properties of cell wall. *Carbohydr. Polym.* **2012**, *90*, 1081−1091.
(47) Sassaki, G. L.; Souza, L. M.; Serrato, R. V.; Cipriani, T. R.; Gorin, P. A. J.; Iacomini, M. Application of acetate derivatives for gas

chromatography−mass spectrometry: novel approaches on carbohydrates, lipids and amino acids analysis. *J. Chromatogr., A* **2008**, *1208*, 215−222.
(48) Lehrfeld, J. Simultaneous gas-liquid chromatographic determination of aldoses and alduronic acids. *J. Chromatogr.* **1987**, *408*, 245−253.
(49) Thibault, J.-F. Automatisation du dosage des substances pectiques par la méthode au méta-hydroxydiphényl. *LWT* **1979**, *12*, 247−251.
(50) Yapo, B. M. On the colorimetric-sulfuric acid analysis of uronic acids in food materials: potential sources of discrepancies in data and how to circumvent them. *Food Anal. Methods* **2012**, *5*, 195−215.
(51) Yoo, S.-H.; Lee, B.-H.; Lee, H.; Lee, S.; Bae, I. Y; Lee, H. G.; Fishman, M.; Chau, H. K.; Savary, B. J.; Hotchkiss, A. T., Jr. Structural characteristics of pumpkin pectin extracted by microwave heating. *J. Food Sci.* **2012**, *77*, C1169−C1173.
(52) Endress, H.-U.; Mattes, F.; Norz, K. Pectins. In *Handbook of Food Science, Technology, and Engineering*; Hui, Y. H., Ed.; CRC Press, Taylor & Francis Group: Boca Raton, FL, USA, 2006; Vol. 3, pp 140/1−140/35.
(53) Neidhart, S.; Hannak, C.; Gierschner, K. Sol-gel transitions of high-esterified pectins and their molecular structure. In *Advances in Pectin and Pectinase Research*; Voragen, F., Schols, H., Visser, R., Eds.; Kluwer Academic Publishers, Dordrecht, The Netherlands, 2003; pp 431−448.
(54) Quemener, B.; Lahaye, M.; Thibault, J.-F. Studies on the simultaneous determination of acidic and neutral sugars of plant cell wall materials by HPLC of their methyl glycosides after combined methanolysis and enzymatic prehydrolysis. *Carbohydr. Polym.* **1993**, *20*, 87−94.
(55) Remoroza, C.; Cord-Landwehr, S.; Leijdekkers, A. G. M.; Moerschbacher, B. M.; Schols, H. A.; Gruppen, H. Combined HILIC-ELSD/ESI-MS^n enables the separation, identification and quantification of sugar beet pectin derived oligomers. *Carbohydr. Polym.* **2012**, *90*, 41−48.
(56) Karlsson, G.; Winge, S.; Sandberg, H. Separation of monosaccharides by hydrophilic interaction chromatography with evaporative light scattering detection. *J. Chromatogr., A* **2005**, *1092*, 246−249.
(57) Filson, P. B.; Dawson-Andoh, B. E. Characterization of sugars from model and enzyme-mediated pulp hydrolyzates using high-performance liquid chromatography coupled to evaporative light scattering detection. *Bioresour. Technol.* **2009**, *100*, 6661−6664.

dilution of phosphine in nitrogen (74.1 mL/m^3, corresponding to 102.97 μg/L) was used as reference gas (Linde, Unterschleissheim, Germany). Its shelf life is 1 year as stated by the provider. *Caution:* PH_3 is toxic and its gas preparation has to be handled with care and appropriate equipment in a fume hood.

Sample Preparation. Samples with incurred residues were obtained from different supermarkets and companies. They were raw and untreated, except of storage, milling, filling. Samples (about 250 g) were ground using standard laboratory mills, for example, a Grindomix (Retsch, Basel, Switzerland), and homogenized for 1 min using a Turbula-mixer (Willy A. Bachofen AG Maschinenfabrik, Muttenz, Switzerland). Twenty milliliter headspace vials were used for calibration and extraction of samples (BGB Analytik, Böckten, Switzerland). One gram of sample (standard amount) was weighed as such or ground into a headspace vial, and 5% sulfuric acid was added to reach the same level as in the calibration vials. Samples were analyzed in duplicates, and per vial only one injection was made. Powdery samples have to be briefly mixed with a plastic stirrer to avoid enclosure of bubbles and to facilitate mixing. The vials were immediately closed (caps with Teflon septum, Wicom Int., Maienfeld, Switzerland) and vigorously shaken by hand for 5 s to achieve good mixing and wetting before incubation in a heated agitator. If samples foam, 3−4 drops of silicon oil (Merck) can be added.

Calibration. Reference gas was filled into a gastight bag with a septum (Tedlar gas sampling bag, SKC, Dorset, UK). For calibration, appropriate aliquots were taken through this septum using gastight syringes (Hamilton, Bonaduz, Switzerland) and directly added to the headspace of the closed vials containing 15 mL of 5% sulfuric acid. Afterward, the vials were immediately shaken by hand. For screening purposes an external calibration of 0.1, 0.3, 0.5, and 1.0 μg/kg may be used whereby 1, 3, 5, and 10 μL of reference gas are added (on the basis of 1 g of sample). Quantitation is done by standard addition to compensate for the different partitioning of PH_3 over the solvent if sample matrix is present (see below). Thereto, the aliquots of reference gas were added to the headspace of the closed vials containing sample and 5% sulfuric acid prior to incubation. Additions should be approximately 50, 100, and 150−200% of the signal from the unspiked sample, which may be analyzed in duplicate. The content of phosphine is calculated via the regression equation, and the coefficient of determination (R^2) must be ≥0.95. This criterion is somewhat loose but is a compromise between practical feasibility and accuracy and reflects the substantial variation of this analysis (see also Interlaboratory Comparisons).

Instrumentation. Partitioning of phosphine was carried out under acidic conditions with heating and shaking to reach a stable equilibrium. Headspace sampling was followed by gas chromatography (GC) with either pulsed flame photometric detection (PFPD) or MS detection. Incubation of all vials (samples and calibration) was done using an MPS2-Sampler (Gerstel, Sursee, Switzerland) at the following conditions: heating at 65 °C for 20 min with shaking in intervals, 60 s at 750 rpm followed by 90 s without shaking. After incubation, 1000 μL of headspace was injected splitless (1 min) onto a PLOT column (PLOT fused silica, 25 m × 0.53 mm; Coating Poraplot Q, Agilent, Basel, Switzerland) in 2 s using a heated syringe (70 °C, Gerstel). Alternatively, only 500 μL can be injected if sensitivity allows, and headspace or splitless liners (i.d. 2 mm, Agilent) may be used. The syringe was flushed with nitrogen after each injection for 30 s. A GC system (Varian 3800, Zug, Switzerland) with FPD was used. The injector was held at 220 °C, and chromatography was performed isothermally at 50 °C for 15 min with a column head pressure of 10 kPa and hydrogen as carrier gas. A PFPD was used in the P-mode at 300 °C. For system maintenance regular change of the injector septum (about every 30 injections) and regular baking out of the column at its maximum temperature (250 °C) are recommended. For detection by MS (DSQII, Thermo Electron Corp., Austin, TX, USA) helium was used as carrier gas (3 mL/min), and a deactivated fused silica column (BGB, Boeckten, Switzerland) was installed after the PLOT column (2 m, 0.25 mm i.d.) ending in the transfer line (200 °C). To prevent particles from the PLOT column entering the ion source, a press-fit connection with an inner diameter of about 0.1 mm was used. Ionization was done in positive EI mode at 70 eV and 200 °C, and the masses m/z 34 and 33 were monitored. As an alternative injection technique, an automated balanced pressure system (Perkin-Elmer, Boston, MA, USA) was used with the following conditions: pressurization at 190 kPa (helium, 1 min); injection time, 0.2 min; transfer line at 80 °C (deactivated capillary, 2.0 m × 0.32 mm).

Data Interpretation. All calculations were done using Microsoft Excel 2010. For interpretation of the interlaboratory comparison (round 2) the mean of all submitted results except the outlier was chosen as assigned value. The standard deviation for proficiency (σ_p) was derived by the Horwitz equation[15] from the mean.

RESULTS AND DISCUSSION

Method Optimization. The method was optimized for sensitivity, precision, and reliable quantitation. For signal optimization, the sample amount, the volume of 5% sulfuric acid, and the conditions to establish equilibrium (temperature, time, shaking) were investigated using samples with incurred residues only. Signals increased for larger sample amounts for a given volume of acid (Figure 1). However, doubling the sample

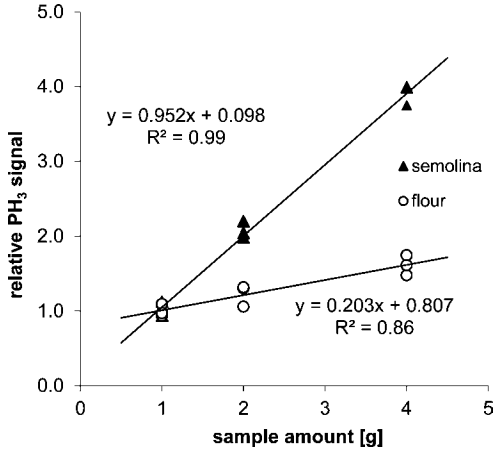

Figure 1. Influence of sample amount on PH_3 signal for wheat flour and semolina. Basis: average peak area for 1 g (n = 3, 15 mL of 5% sulfuric acid).

amount did not result in doubled signals, especially for the flour. Higher sample amounts increased the solubility of phosphine in the sample phase due to stronger interaction with matrix components and changed the viscosity of the sample phase. These effects changed the activity coefficient of PH_3, whereby its concentration in the gas phase did not increase to the same extent as the sample amount. The effect depended on the sample type (see slopes in Figure 1): whereas the signal for semolina almost doubled for doubled sample amounts, the increase was 4.6 times lower for flour. This is explained by their different compositions and interactions with the analyte and by their different viscosities. For larger sample amounts the partitioning strongly changed as compared to pure solvent; that is, the signal per weight decreased. Thus, the sample amount is a critical factor and needs to be carefully controlled and quantitation with external calibration is pointless, especially for more than 1 g of sample (see also below). The two samples were not related to each other and, thus, no direct conclusion can be drawn. However, the effect on viscosity and matrix in solution is expectedly smaller for semolina, which is in line with the usually larger signals in whole compared to ground samples. Small sample amounts such as 1 g are easier to mix and suspend during shaking (see below), and the difference in partitioning as

compared to pure solvent is smaller (see Figures 1 and 4). This allows to draw indicative values from external calibration and facilitates estimating appropriate amounts for standard additions.

Figure 2 shows that the signal of phosphine increased with higher volumes of acid. This can be explained by a smaller

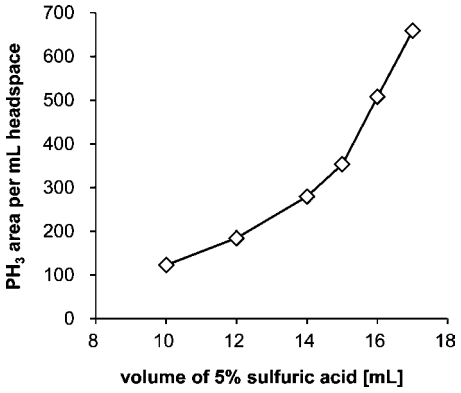

Figure 2. Influence of volume of 5% sulfuric acid on PH_3 signal (wheat flour, 1 g; injection volume = 1 mL).

phase ratio and a lower retention of PH_3 in the more diluted sample phase (i.e., increased activity coefficient).[16] Both effects may have contributed to the increase of signal. Although a small headspace volume has the advantage of larger signals, an intermediate volume of 15 mL acid was chosen as a compromise. Thereby, shaking and suspending were more effective (see below), enough solvent was provided to establish equilibrium faster, and enough headspace was available for needle intrusion and sampling.

Increasing temperature during incubation in the heated agitator gave larger signals (Figure 3) because the partition

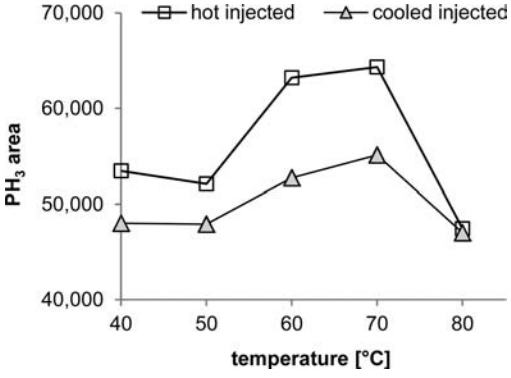

Figure 3. Influence of incubation temperature on PH_3 signal: injection of hot and cooled samples (2 g of wheat flour, n = 2, 15 mL of 5% sulfuric acid).

coefficient depends exponentially on the inverse temperature.[16] At about 70 °C a maximum was observed for both hot and cool injected samples. The influence of temperature was less pronounced for samples cooled before injection, and their signals were generally lower compared to immediate, hot injection. This is because partitioning toward the liquid phase is favored at lower temperatures. Nevertheless, injection after cooling has the advantage of reducing solvent load on the analytical column. Incubation at 80 °C decreased the signal in both hot and cool injected samples, and clumping was more frequent. This decrease may be due to oxidation or other reactions with matrix components. Therefore, an incubation temperature of 65 °C was chosen as a compromise. In the literature, boiling for 20 min in 10% sulfuric acid was described as release condition,[17,18] whereas other methods use longer times.[7] In contrast, Ren et al. found a maximum signal in the headspace after heating wheat at 45 °C for 20 min.[19]

Extraction and partitioning were also checked for the present method as follows: A sample of wheat flour (1 g, 15 mL of 5% sulfuric acid) was analyzed in duplicate. After cooling to room temperature, the vials were opened, flushed with a gentle stream of air for 10 s to remove PH_3 from the headspace, capped again, and reanalyzed including incubation in the heated agitator. The same was done with a calibration standard (0.3 μg/kg, n = 3). The PH_3 signal in the sample reached 23% of the first analysis, whereas in the calibration standard 16% was found. This shows that equilibrium is on the side of the gas phase and that partitioning is the key factor after extraction. Also, it again demonstrates the different partitioning if sample matrix is present (see Figure 4).

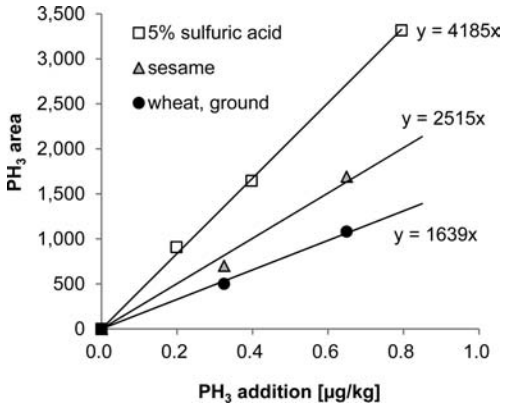

Figure 4. Calibration functions obtained in different matrices. Signal from sample was subtracted (1.5 g of sample, 15 mL of 5% sulfuric acid).

In addition, the influence of shaking on the signal was checked. Samples need to be intensively shaken by hand to achieve good mixing and wetting before incubation in a heated agitator. Thereto, an appropriate ratio of sample and solvent is important, for example, 1 g and 15 mL. Small sample amounts are easier to suspend and swell during shaking and are less prone to form viscous doughs. An intensive (750 rpm on the agitator) and prolonged shaking (20 min) gave best results for a given combination of sample amount, temperature, and volume of acid. Equilibrium was reached for 1 g of wheat flour in 15 mL of solvent after incubation for 20 min, whereas for solvent standards it was established already after 5 min (no data shown). The effect of a more intensive shaking becomes particularly evident for larger sample amounts and for matrices with pronounced swelling. Samples may also be incubated in a GC oven, for example, for 20 min at 65 °C and manual shaking in regular intervals (e.g., every 5 min for 1 min) if a heated agitator is not available. If a classical convection oven is used, a higher temperature (about 80 °C) is recommended because the temperature of the vials is substantially lower due to less efficient heat transfer as compared to a heated agitator or a GC oven. Nevertheless, the use of a heated agitator combined with an autosampler is recommended for practical and reproduci-

Table 1. Characterization of Samples and Results of the Interlaboratory Comparison Tests[a]

	characterization of samples			results of interlaboratory comparison				
	1	2	3	COOP[b]	State Lab[c]			
	(n = 10)	(n = 10)	(n = 3)	(n = 2)	(n = 2)	mean	n	σ_p
Round 1								
wheat flour	23 (11%)	27 (4%)	21	22.9	18.5	9.9 (79%)	9	
wheat semolina	0.18 (6%)	0.23 (5%)	0.20	0.21	0.26	0.18 (51%)	3	
rice	1.03 (7%)	0.9 (10%)	0.4	1.2	0.9	0.9 (26%)	6	
Round 2								
wheat flour	3.0 (13%)	3.7 (14%)	4.8	5.1	4.3	2.9 (56%)	12	1.1
red lentils	2.5 (18%)	2.9 (13%)	3.1	3.5	3.5	2.5 (55%)	11	1.0
jasmine rice	15.4 (20%)	15.9 (10%)	17.2	13.7	15.7	13.1 (47%)	12	4.0

[a]RSD, relative standard deviation (in parentheses); σ_p, standard deviation for proficiency, Horwitz (only round 2); outlier excluded. [b]Injection with syringe (1 mL), detection by PFPD. [c]Injection with pressure system, detection by FPD.

bility reasons. Heating and shaking of all vials prior to injection presents an improvement for quantitation as compared to other methods relying on external calibration where partition of phosphine between headspace and liquid phase is not taken into account.[17,18]

Linearity was checked using five concentration levels (n = 1) in 5% sulfuric acid in the range of 0.19−1.95 μg/kg plus a blank. Mandel's test confirmed a linear calibration function (R^2 = 0.98). Linearity was also checked in the range from 0.1 to 10 μg/kg (total of 10 levels, n = 1), and again a linear function was found (R^2 = 0.99). On the basis of 1 g of sample and 15 mL of acid, a limit of quantitation of 0.1 μg/kg was easily achieved without matrix, which corresponds to 0.1 to about 0.4 μg/kg in real samples. This is sufficient to check samples for compliance to residue limits, especially organic samples. In cereal samples, concentrations as low as 0.2 μg/kg were determined by standard addition in our laboratory. The precision, that is, RSD, of results obtained by standard addition accounted for 16% (wheat flour, n = 4, mean = 3.5 μg/kg). This is similar for results obtained with all types of samples analyzed by the two authors' laboratories (COOP and State Lab) in the interlaboratory comparison studies (Table 1). Thus, the method is well reproducible provided that some experience and appropriate equipment are present.

Figure 4 shows that the signal for a given amount of PH_3 was largest in the absence of any sample matrix (5% sulfuric acid only). The effect of sample type (Figure 4) and sample amount (Figures 1 and 5) can vary considerably. Similar effects were also reported in the literature.[9,17] As a consequence, quantitation by external calibration in 5% sulfuric acid mostly leads to an underestimation of phosphine contents and comparability of results may be limited. External calibration using a generic matrix devoid of residues only partially overcomes this problem because of varying effects in different matrices. Therefore, results obtained by external calibration are indicative and not quantitative, especially when large sample amounts are used. Furthermore, recovery experiments and partly also standard additions suffer from the fact that added PH_3 remains largely in the gas phase and poorly sorbs to the matrix.[7] In contrast, incurred residues need to be extracted from the matrix into the liquid phase (diffusion controlled) from where they partition to the gas phase. Standard additions compensate at least for part of these effects, for example, partition between liquid and gas phase, as can be seen from the lower signals from matrices as compared to solvent (Figure 4). Therefore, recoveries in the classical analytical sense cannot be truly determined for incurred residues of phosphine. The key

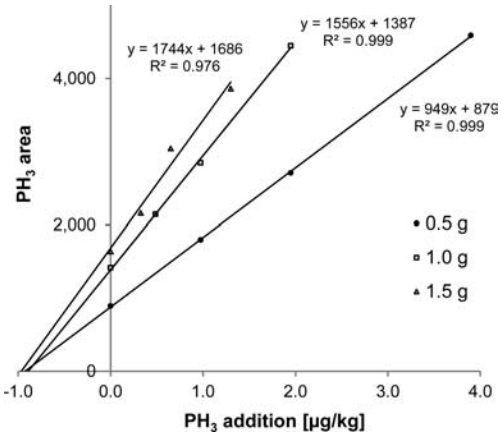

Figure 5. Standard addition experiments with ground cereal risotto using different sample amounts (15 mL of 5% sulfuric acid). Results for different sample amounts: 0.5 g, 0.93 μg/kg; 1.0 g, 0.89 μg/kg; 1.5 g, 0.97 μg/kg.

point is to reach equilibrium under reproducible conditions. A reasonably good correlation in standard addition serves as an indicator for reproducible equilibrium. Recoveries from 50 to 90% were reported, and sample type and amount both affected recovery.[17,20] In this study recoveries from as low as 20 to 140% were found, depending on matrix and sample amount, showing the limited significance of recoveries.

Time is another factor affecting results obtained in screening with external calibration. This was checked with two sets of samples of ground rice (1 g, 15 mL of acid, n = 10 each), of which the first set was directly incubated and analyzed and the other set was left to stand for 2 h before incubation. A significant decrease of 17% of the signal (t test: $p < 0.0001$) was observed for samples left to stand for >2 h. Therefore, long series of samples should be avoided or samples should be prepared batchwise to prevent standing times of >2 h before incubation. The only feasible way to obtain reliable quantitative data is to analyze samples using the standard addition approach. This is preferably done after screening the samples against an external calibration in 5% sulfuric acid to check for the presence of PH_3. In the performance of standard addition experiments, the sample amount is not critical as long as it is within a low range (0.5−1.5 g) as can be seen in Figure 5: very similar results were obtained for the different sample amounts analyzed because the matrix effect was compensated (see slopes in Figure 5).

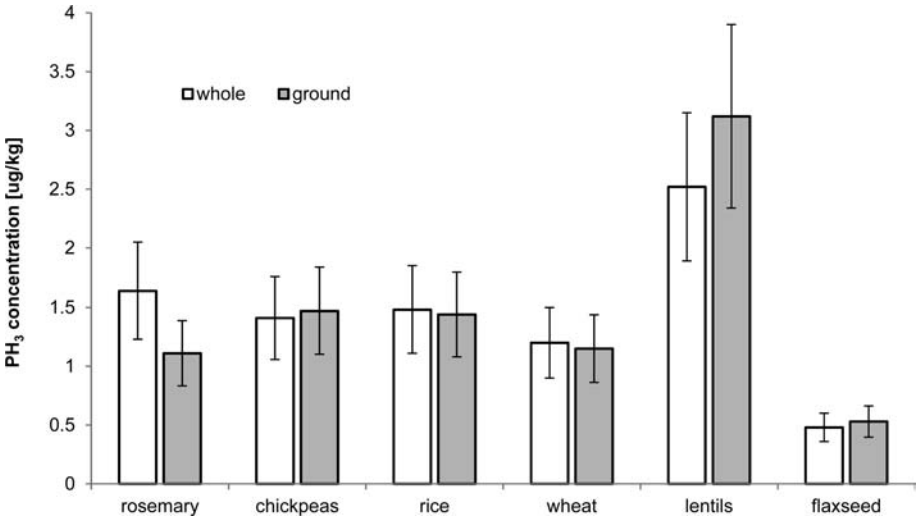

Figure 6. Concentrations of phosphine in whole and ground samples, determined by standard addition. Error bars are ±25% (n = 2, 1 g of sample, 15 mL of 5% sulfuric acid).

Sample homogeneity is critical for standard addition experiments: For heterogeneous samples (e.g., cereal mixtures or Muesli) and for large particles (e.g., cereal grains) the variation of residue per "unit" makes it sometimes impossible to obtain a standard addition with an acceptable R^2. The limited sample amount (usually <2 g) is another factor that contributes to this problem. To overcome this, grinding and mixing of the samples are inevitable. Variation of peak area was substantial for rice as grain (RSD = 28%, n = 10), whereas it was 3 times lower after grinding (RSD = 9%, n = 10). However, grinding is questioned for the analysis of volatile analytes such as PH_3 because losses via evaporation during grinding and mixing have to be considered. Nevertheless, the effect of grinding was tested for different matrices (Figure 6). For all six matrices no significant difference was found between the concentrations of whole and ground samples. Shown error bars present a generic variation of 25%, which is easily achievable with standard addition. Quantitation was done in all cases by standard addition. Thereby, matrix effects were compensated for, which otherwise impair quantitation by external calibration. For example, almost the same result was obtained in the wheat sample of Figure 6: 1.20 μg/kg for whole grain (regression: y = 1962x + 2349) and 1.15 μg/kg for ground wheat (regression: y = 1621x + 1856), but the intercepts and slopes differed because of the different partition. However, sometimes three to four attempts are needed to obtain a standard addition with an $R^2 \geq$ 0.95 for whole wheat kernels or other coarse samples, whereas it usually works straight for ground samples. For many samples it is hard to obtain an acceptable standard addition experiment without grinding. Furthermore, it can be concluded from the data shown in Figure 6 that phosphine is not present in a free gaseous form, which would be readily lost. It is rather sorbed to the sample and may be present in the form of (partially reacted) phosphides or reaction products[21] being released only during incubation in acid. Similar findings are discussed in the literature.[7,8] Some negligible losses during grinding are compensated by a better release of the analyte from the ground matrix. An explanation of previously reported "losses" after grinding or mixing[9] may be due to different partitioning. Ground samples are more easily extracted, and smaller particles have lower resistance to diffusion, whereby equilibrium is established earlier as compared to whole grains.[9,13]

The optimized method differs from the method of Amstutz et al.[6] in several important aspects: Less sample is used (1 vs 5 g), more solvent is added (15 vs 10 mL), quantitation is based on standard additions and not on external calibration without matrix, coarse samples are ground rather than analyzed as such, and longer incubation is performed (10 vs 20 min) to reach equilibrium. Critical points causing variation may be establishing reproducible equilibrium for all sample types and maintaining the same filling levels in the vials.

Interlaboratory Comparisons. To gain data on the variation of PH_3 determination in different laboratories and to characterize and validate the present method, two rounds of an international interlaboratory comparison test were organized in 2011 and 2012. For both tests only samples with incurred, aged residues were used. They were selected from the monitoring samples taken from the market and characterized for stability and homogeneity before sending (Table 1). Analysis 2 took place 15 days after analysis 1 and 1 week before distribution of samples. Analysis 3 was performed after the last results were submitted (about 3 months later). The samples were reasonably homogeneous and stable over the whole test period with the exception of the rice in the first round, where some losses may have occurred after distribution.

In Table 1 the means of results from the two rounds are presented and compared to the results of the two authors' laboratories (COOP and State Lab). In the first round three samples were sent to 10 laboratories without giving detailed advice on the method. Nine of the 10 laboratories returned results. The values reported for the wheat flour ranged from 2.3 to 22.9 μg/kg (factor of 10). Variation of results was considerable and much larger than observed during characterization or between the authors' laboratories (Table 1). Feedback from participants revealed that calibration without any matrix and high sample amounts (3−5 g) were used. This led to some low results, whereas in the authors' laboratories some 20 μg/kg was found. Values varied to a lesser extent for the rice sample (range = 0.48−1.20 μg/kg) but only six participants were able to determine a residue around 1 μg/kg. For semolina merely three results were submitted (range = 0.08−0.26 μg/kg). This shows that for most laboratories a limit of quantitation below 1 μg/kg is not achievable and enforcement of such residues lacks analytical practicability.

z scores for these data set are of limited meaning due to the small number of results and the strong variation, especially for the flour sample. This round simply highlighted the difficulties encountered with this analysis.

For the second round all participants were provided a revised method (as described in the present paper) and were invited to submit results obtained by their own, in-house method (set of "own methods") as well as by this proposed method. Three samples (wheat flour, red lentils, jasmine rice) were sent to 14 laboratories in four European countries, and 13 participants returned results. The participants were asked to analyze the lentils as such and after grinding. Results obtained by a photometric method (e.g., wheat flour, 15.3 μg/kg) were identified as outlier by Grubbs' test and dismissed for all samples. Problems with blanks, as stated by the participant, are a probable explanation of too high values, which were also reported for a similar method.[13]

The mean of all results was 2.9 μg/kg (median = 2.8 μg/kg) for wheat flour, which is slightly below the values obtained during characterization and by the authors' laboratories (Table 1). Figure 7 shows results for wheat flour as a function of the applied method. No significant difference was observed between proposed and the set of own methods. A trend toward lower results is observed for the set of own methods. This may be due to large sample amounts and/or external calibration, which both lead to an underestimation (see Figures 1 and 4). Variation was considerable in all categories for wheat flour, independent of the method and detection (RSD = 45−61%, error bars in Figure 7) but lower as compared to the first round. Providing a method with analytical details to all participants may have contributed to this improvement. Because the majority of participants submitted results based on only external calibration (with or without generic matrix) or standard addition, the interpretation regarding the method of quantitation is limited because of effects mentioned above and the low number of results. Therefore, this aspect cannot be discussed in detail: No significant difference between quantitation types was found (overall and within sets of methods). If only results from laboratories using both types of quantitation were compared, then the mean from standard additions was slightly but not significantly larger than from external calibration (3.6 vs 3.4 μg/kg). Overall, for residues at low μg/kg levels in flour results may vary by some 50% (round 2), irrespective of the method used. Among the 23 results for this sample, 3 were assigned a z score outside the range of $-2 \leq z \leq 2$. The results from MS detectors and (P)FPD detectors were grouped and compared to each other (Figure 7). No significant difference was found between the two different types of detection, which is in line with our own tests (no data shown). Thus, both detectors give equal results and are capable of determining PH_3 residues in the low μg/kg range. The strong overall variation of the methods are rather explained by differences in sample amount, incubation, and method of quantitation than by the applied detector.

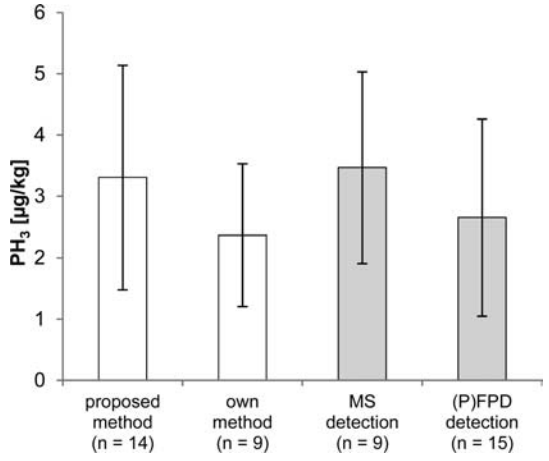

Figure 7. Results of the interlaboratory comparison test for wheat flour, categorized for applied method and used detector (mean values, error bars are ± standard deviation). Outlier was excluded.

For the lentils the sets of proposed and own methods gave similar mean values of 2.4 μg/kg (RSD = 57%) and 2.7 μg/kg (RSD = 48%), respectively. As expected from grinding experiments (Figure 6) no significant difference was found between mean residues of whole (2.5 μg/kg, RSD = 55%, n = 22) and ground lentils (3.0 μg/kg, RSD = 65%, n = 21). This confirms our experimental results and demonstrates that grinding has no discrimination effect. Among the 23 different results obtained for the whole lentils, 3 were assigned a z score outside the range of $-2 \leq z \leq 2$.

Also for the rice sample no significant differences were observed between both types of methods. On average, 13.0 μg/kg was found in the set of own methods (RSD = 54%) and 14.1 μg/kg (RSD = 45%) for the proposed method. Among the 23 results, 5 were assigned a z score outside the range of $-2 \leq z \leq 2$.

Generally, the proposed method gave similar results compared to other methods being used, except the photometric one. Headspace sampling with GC-(P)FPD or GC-MS detection presents a selective and sensitive approach that enables monitoring organic samples for compliance. Because of the mentioned effects of high sample amounts, not more than 2 g should be used and standard addition is necessary for quantitation. Following exactly the proposed protocol gave z scores within the range of $-2 \leq z \leq 2$ for all samples. The variation within a laboratory may account for some 20%, whereas interlaboratory variation is about 50%. Therefore, an extended uncertainty of measurement of roughly 50% is proposed, not including a coverage factor of 2 as is the case in pesticide residue analysis.[22] This value presents a rough estimate derived from RSDs in the comparison test, and it is rather a description of the reality than a precisely calculated value. It is slightly higher than the Horwitz value for concentrations of ≥1 μg/kg. Experiences in pesticide residue analysis are similar, especially at low μg/kg levels. Thus, the determination of phosphine at low concentrations is challenging in practice, and difficulties are revealed only by such interlaboratory comparisons. This substantial variation has to be taken into account when results are compared and checked against maximum residue levels, and it also demands further harmonization and proficiency testing between methods and laboratories. The results from the authors' laboratories differ by no more than 25% from each other (16% on average, Table 1), which demonstrates that the method is robust and delivers results with acceptable variation providing that the proposed protocol is exactly followed. Residues below 1 μg/kg are below the detection limit of many laboratories and can therefore hardly be monitored. However, the present method allows for the detection of residues of about 0.1 μg/kg providing appropriate equipment. Grinding of samples does not lead to lower results and is an important measure to cope with sample

homogeneity. It allows for acceptable standard addition experiments, which are needed to obtain reliable results and which compensate for different partitioning. Screening with calibration in a generic matrix may be an option but suffers from considerably different behavior of seemingly similar samples, which can easily differ by a factor 2 or 3 (Figure 1). This is even more problematic if many different samples have to be analyzed. Therefore, we rather suggest to screen without matrix calibration for the presence of PH_3 whereby only indicative or merely "yes" or "no" results are obtained. Thereafter, any relevant detection of PH_3 is quantified by standard addition. The method was also successfully applied to other matrices such as raw coffee beans, dried mushrooms, spices, chickpeas, tea, dried fruits, and nuts. Because of differences in partitioning between different matrices, sample amounts and also incubation parameters (e.g., time, temperature) may need to be checked individually to ensure equilibrium.

AUTHOR INFORMATION

Corresponding Author

*(T.M.A.) E-mail: thomas.amrein@coop.ch. Phone: +41 61 825 46 80.

Notes

The authors declare no competing financial interest.

REFERENCES

(1) Fields, P. G.; White, N. D. G Alternatives to methyl bromide treatments for stored-product and quarantine insects. *Annu. Rev. Entomol.* **2002**, *47*, 331−359.

(2) Association of Organic Processors, Wholesalers and Retailers (BNN). *BNN Orientation Value for Pesticides − A Guideline to Evaluate Pesticide Residues in Organic Product*; Berlin, Germany, 2012.

(3) Imhof, D. *Stock Preservation for Organic Food* (in German); VKCS, Association of Swiss Food Control Authorities: Brunnen, Switzerland, 2011.

(4) Andrey, D. *Stock Preservation for Organic Food* (in German); VKCS, Association of Swiss Food Control Authorities: Brunnen, Switzerland, 2007.

(5) Scherbaum, E.; Perz, R.; Caspart, E.; Barth, A.; Wolheim, A.; Köhl, D. Residues of the fumigant phosphine in arid vegetable foods, www.cvuas.de/pub/beitrag.asp?subid=1&ID=1616&Thema_ID=5&lang=EN (accessed Sept 16, 2013).

(6) Amstutz, R.; Knecht, A.; Andrey, D. Detection of phosphine residues in organic cereals. *Mitt. Lebensm. Hyg.* **2003**, *94*, 603−608.

(7) Desmarchelier, J. M.; Ren, Y. L. Analysis of fumigant residues − a critical review. *J. Assoc. Off. Anal. Chem. Int.* **1999**, *82*, 1261−1280.

(8) Allen, S. E.; Ren, Y. L.; Desmarchelier, J. M. Comparison of six methods for determining aged phosphine residues in wheat. *J. Assoc. Off. Anal. Chem. Int.* **1998**, *81*, 633−637.

(9) Desmarchelier, J. M.; Allen, S. E.; Ren, Y. L. Modifications of a method for determining multifumigant residues. *J. Assoc. Off. Anal. Chem. Int.* **1998**, *81*, 638−644.

(10) Brockwell, C. A. Determination of phosphine in wheat by headspace gas-liquid-chromatography. *J. Agric. Food Chem.* **1978**, *26*, 962−964.

(11) Norman, K. N. T.; Leonard, K. Gas chromatography-mass spectrometry determination of phosphine residues in stored products and processed foods. *J. Agric. Food Chem.* **2000**, *48*, 4066−4070.

(12) Longobardi, F.; Pascale, M.; Silvestri, M.; Visconti, A. Rapid method for the determination of phosphine residues in wheat. *Food Anal. Methods* **2008**, *1*, 220−225.

(13) Bruce, R. B.; Robbins, A. J.; Tuft, T. O. Phosphine residues from Phostoxin-treated grain. *J. Agric. Food Chem.* **1962**, *10*, 18−21.

(14) Federal Office of Public Health. *Swiss Food Manual*, Berne, http://www.slmb.bag.admin.ch/slmb/index.html (accessed Sept 18, 2013).

(15) Horwitz, W. Evaluation of analytical methods used for regulation for food and drugs. *Anal. Chem.* **1982**, *54*, 67A−76A.

(16) Kolb, B.; Ettre, L. S. *Static Headspace-Gas Chromatography: Theory and Pactice*, 2nd ed.; Wiley-VCH: New York, 2006.

(17) Nowicki, T. W. Gas-liquid chromatography and flame photometric detection of phosphine in wheat. *J. Assoc. Off. Anal. Chem.* **1978**, *61*, 829−836.

(18) Scudamore, K. A.; Goodship, G. Determination of phosphine residues in fumigated cereals and other foodstuffs. *Pestic. Sci.* **1986**, *17*, 385−395.

(19) Ren, Y. L.; Padovan, B.; Desmarchelier, J. M. Evaluation of headspace solid-phase microextraction for analysis of phosphine residues in wheat. *J. Assoc. Off. Anal. Chem. Int.* **2012**, *95*, 549−553.

(20) Corley, J.; Kahl, J.; Burkhart, D.; Diaz, E.; Möller, G. Rapid zinc phosphide trace analysis in agricultural commodities by phosphine generation, toluene trapping, and gas chromatography. *J. Agric. Food Chem.* **1998**, *46*, 999−1004.

(21) Tkachuk, R. Phosphorous residues in wheat due to phosphine fumigation. *Cereal Chem.* **1972**, *49*, 258−267.

(22) Alder, L.; Korth, W.; Patey, A. L.; van der Schee, H. A.; Schoeneweiss, S. Estimation of measurement uncertainty in pesticide residue analysis. *J. Assoc. Off. Anal. Chem. Int.* **2001**, *84*, 1569−1578.

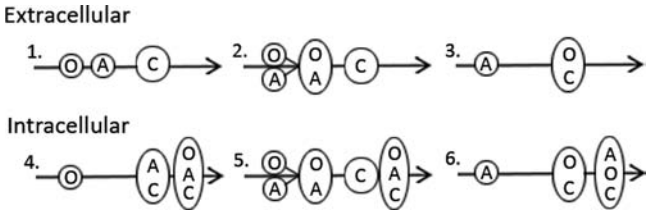

Figure 1. Potential acting position of antioxidants on a cell and possible reaction pathways. A denotes antioxidant, C denotes cell, and O denotes oxidant.

(A denotes antioxidant, C denotes cell, and O denotes oxidant). Extracellular antioxidants that cannot enter cells such as glutathione or ascorbic acid supplement[15,16] have a blocking role against extracellular oxidants (as shown in Figure 1), but their oxidized products can exert some side effects on cells. These potential responses have been reflected in 2, 5, and 6 of Figure 1. Others that can enter the cytoplasm[17] and remain in the cell membrane also must be considered (as shown in 4 of Figure 1). Therefore, this study would reveal the different effects of three sequences for adding antioxidants in the processes of the oxidative hemolysis test on antioxidant evaluation.

MATERIALS AND METHODS

Materials. Hb was purchased from Sigma (USA), L-carosine (L-c) was obtained from Beijing Biotop Technology Co., Ltd. (Beijing, China), reduced glutathione (GSH) was purchased from Shanghai Sangon Biological Engineering (Shanghai, China), L-cysteine (Cys) was purchased from Sinopharm Chemical Reagent Co., Ltd. (Shanghai, China), and the synthesized peptide IWHDC was designed by our laboratory and prepared from ChinaPeptides Co., Ltd. (Shanghai, China). Hydrogen peroxide (H_2O_2), trichloroacetic acid (TCA), nitric acid (HNO_3), and perchloric acid ($HClO_4$) were all of analytical grade and were procured from Sinopharm Chemical Reagent Co., Ltd.

Oxidation Test of Erythrocytes. *Preparation of Human Erythrocytes.* Fresh human venous blood was obtained from healthy donors, which was authorized by Yangzhou Blood Center. Blood anticoagulated with citric acid solution (anticoagulant, 4.8 g of $C_6H_8O_7 \cdot H_2O$, 13.2 g of $C_6H_5Na_3O_7 \cdot 2H_2O$, and 14.7 g of $C_6H_{12}O_6 \cdot H_2O$ in each 1000 mL of water) was centrifuged at 625*g* for 3 min and washed three times with 6 mL of cold phosphate-buffered saline (PBS; 145 mmol/L, NaCl, 8.1 mmol/L Na_2HPO_4, and 1.9 mmol/L NaH_2PO_4, pH 7.4) to separate erythrocytes from the white cell layer, plasma, and free Hb released from injured erythrocytes. The packed erythrocytes were diluted with cold Alsever's stock solution (31 mmol/L $C_6H_5Na_3O_7$, 2.9 mmol/L $C_6H_8O_7$, 113.8 mmol/L $C_6H_{12}O_6$, and 71.8 mmol/L NaCl, pH 6.1) to a cell density of 2×10^8 cells/mL. During every trial, erythrocyte solution was saved in a sterile penicillin bottle and stored at 4 °C for not more than 48 h to ensure cell viability and cellular antioxidative level.

Cell Oxidation Induced by H_2O_2. The above erythrocyte solution was treated with different concentrations of H_2O_2 solution at 37 °C for 30 min, and the final concentrations of H_2O_2 were 1.665, 4.995, 16.65, and 166.5 μmol/L, respectively. After centrifuging in 625*g* for 10 min, the hemolytic supernatant was transferred to 96-well plates (NUNC, Thermo Scientific, USA), and the absorbance at 405 nm (hereafter denoted Abs) was detected with the plate reader (Multiskan FC, Thermo Scientific, USA).

Hb Oxidation Induced by H_2O_2. Hb solution was prepared in PBS at a concentration of 20 mg/mL and then reacted with different concentrations of H_2O_2 at room temperature until no bubbles were generated. The reaction solution was transferred to 96-well plates and read at 405 nm with a Multiskan FC plate reader (Thermo Scientific, USA). The same reaction mixture was transferred to a 96-well black plate, and its fluorescent intensity (FI) was read at the excitation wavelength of 355 nm and the emission wavelength of 460 nm with a Fluoroskan Ascent FL plate reader (Thermo Scientific, USA).

Quantitation of Ferric Ions Released from Hb Oxidation by Inductively Coupled Plasma Spectrometry. *Ferric Ion Extraction.* The extraction method was as follows. The Hb reaction mixture was separated through an ultrafiltration membrane (5000 Da) at 4 °C (Vivaflow 200, Sartorius, Goettingen, Germany), and the filtrate was collected. A 10% (v/v) TCA solution was mixed with the Hb reaction solution at 4 °C for 30 min, and then the supernatant was collected. Finally, the Hb reaction mixture was heated in a water bath at 100 °C for 1 h, and the supernatant was collected.

Ferric Ion Detection. Extracted ferric ions were added to a solution of $HNO_3/HClO_4$ (v/v, 4:1). The digestion lasted for 2 h at 140 °C, and the solution was heated again at 190 °C to remove acid. The digested ferric ion solution was diluted with ultrapure water, and then the ferric ions were detected by Elan DRC-e inductively coupled plasma spectrometry (Perkin-Elmer, USA).

Multiple Assessment of Antioxidant Activity with Hemolysis Tests. A 100 μL solution of erythrocytes was treated with H_2O_2 of 166.5 μmol/mL of the final concentration and one antioxidant liquor in each test group. The selected antioxidants were GSH of 1.67 mmol/L, L-c of 1.67 mmol/L, Cys of 1.67 mmol/L, and IWHDC of 0.167 mg/mL, respectively. Both the H_2O_2 and antioxidant were dissolved in PBS and cultured with erythrocytes at 37 °C for several hours. Three different sequences of antioxidant addition were examined in this work. The first kind of reaction consisted of two steps and was denoted R1. The erythrocytes were preincubated with antioxidant for 15 min and then combined with H_2O_2 for 4 h to accomplish hemolysis. The second kind of reaction also included two steps and was denoted R2. Antioxidant and H_2O_2 were fully blended for 15 min prior to dispensing the erythrocytes solution, and the mixture obtained was allowed to sit for 4 h. The third kind of reaction, denoted R3, was slightly different from R1 when H_2O_2 was added. Briefly, H_2O_2 was mixed with the erythrocyte solution to initiate the oxidative stress of cells, and after 5 min, antioxidant was injected immediately to inhibit the oxidative hemolysis, and the mixture was allowed to sit for 4 h. Additionally, H_2O_2-induced hemolysis in the absence of all antioxidants was performed as the injury control group, and the solution was also maintained for 4 h, during which an equal volume of PBS or other solvent was added instead of the antioxidant liquor. All solutions were freshly prepared and used immediately.

Statistical Analysis. Statistical analysis was performed with Microsoft Excel. Statistical significance was tested using the paired-samples *t* test. Significant difference between data sets was assessed by a *p* value of <0.05. Each value shown in this paper represented typical responses from three trials.

RESULTS AND DISCUSSION

Comparison of Hemolysis Tests under Various Concentrations of H_2O_2. Optimization of measurement condition, including cell count, culture time, and temperature, is the first step during the process for evaluating antioxidant activity. In this work, we focused on the effect of H_2O_2 dose on hemolysis to screen a cell model with high sensitivity to oxidative damage.

Erythrocytes were incubated with various final concentrations of H_2O_2 solution (0, 1.665, 4.995, 16.65, and 166.5 μmol/mL; Figure 2). Hemolysis curves were obtained on the basis of the absorbance of Hb in the supernatant. According to the theory that oxidants can induce cell membrane breakage, the absorbance of the hemolysis supernatant should increase as the H_2O_2 dose increases. Hemolysis induced by 1.665 μmol/mL of H_2O_2 appeared to be inhibited, as represented in curves D1 and D2 in Figure 2. This decrease of absorbance suggested that the erythrocytes were not damaged by H_2O_2. These results were unexpected. The decline deserved further research

dx.doi.org/10.1021/jf4049935 | J. Agric. Food Chem. 2014, 62, 2056−2061

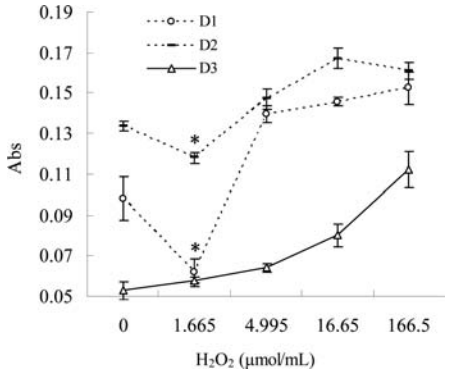

Figure 2. Hemolysis responses to H_2O_2 doses in three donor cell samples (D1, D2, and D3). Erythrocytes were incubated with H_2O_2 at 37 °C for 30 min. Each value is the mean ± SD of three experiments. A line chart is used instead of a scatter graph to more clearly display the trend of each data point. The dashed lines indicate abnormal values at 1.665 μmol/mL of H_2O_2 that are lower than those at 0 μmol/L of H_2O_2. Significant differences are marked by asterisks (∗).

because it generated a negative inference on traditional hemolysis measurements.

Interfering Effect of Free Hb on the Evaluation of Oxidative Hemolysis. MetHb formation occurs during cellular oxidative stress and then promotes membrane leakage through the cross-linking of membrane proteins, leading to intracellular Hb release.[18] However, Figure 3 shows that there

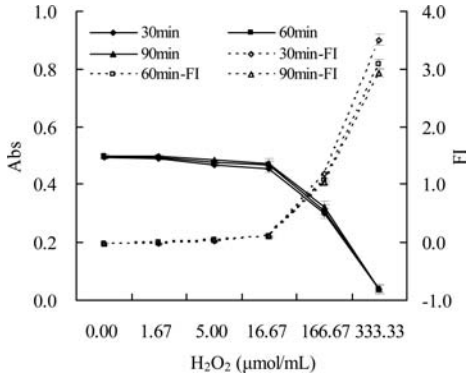

Figure 3. Oxidation of free Hb measured with spectrophotometry (solid line) and fluorometry (dashed line). Hb was incubated with various doses of H_2O_2 for 30, 60, and 90 min.

were other reactions during the oxidation of Hb, for example, color fading. The reducing Abs suggested Hb loss at higher doses of H_2O_2. The decrease of Abs in Figure 2 probably resulted from the further oxidative destruction of MetHb into hemichrome or other degradation products.[14]

Curves D1 and D2 in Figure 2 showed that the Abs values at 0 μmol/L of H_2O_2 were both above 0.1, whereas the Abs at the same abscissa on curve D3 was 0.052 (the supernatant was nearly colorless). This indicated that there was a little free Hb at the beginning of the hemolysis test, and this part of Hb might be attacked first and then degraded by H_2O_2.

To prove whether the initial free Hb presents interferences with the determination of hemolysis, we attempted to add Hb solution to the erythrocyte suspension (the supernatant of this suspension with Abs_{405} of 0.07 was also nearly colorless) before the hemolysis test. The results coincided with the assumption, showing that in the suspension with extra Hb added, Abs at 1.665 μmol/mL of H_2O_2 was lower than that at 0 μmol/L of H_2O_2 (Figure 4). These results suggested that H_2O_2 had

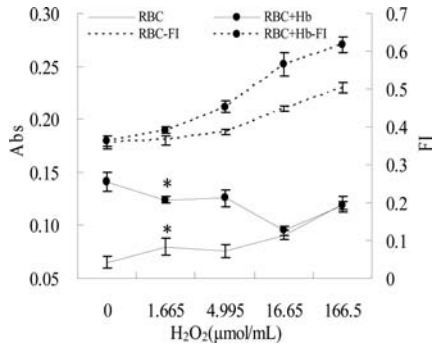

Figure 4. Hemolysis curves for the normal suspension and the suspension with added Hb obtained by absorbance assay (solid line) and fluorescence assay (dashed line). Each hemolysis suspension was cultured at 37 °C for 30 min. Data are the mean ± SD of three experiments. Values with significant difference compared to 0 μmol/L H_2O_2 under addition of Hb are marked by asterisk (∗).

reacted quickly with the extracellular Hb before its entry to cells. Moreover, the trend of the FI data was contrary to the Abs. FI was increasing with the dose of H_2O_2 damage, and all values of FI in the group with Hb added were higher than those without extra Hb (Figure 4). These results suggested that the extra-added Hb had suffered H_2O_2-oxidative damage and the degradation of Hb was along with the hemolysis as well. Therefore, when the degree of hemolysis is determined by spectrophotometry, the degraded Hb by oxidation would be a novel interference in hemolysis evaluation, which could reduce the measurement accuracy.

Degradation of Hb Oxidized by H_2O_2. As shown in Figure 3, the Abs of the Hb solution changed little with the extension of oxidation time, whereas the FI at 333.3 μmol/mL of H_2O_2 decreased clearly, especially at 90 min. This indicated that the initial degraded Hb with fluorescence might be further turned into some nonfluorescing substances during oxidation.

According to previous papers, the reaction time was usually >1 h, and the Hb concentration was at a higher level. Thus, we compared the results of the following tests, one in which the Hb of 0.138 mg was oxidized for 15 min, and the other in which the Hb of 8 mg (H_2O_2 doses were the same as in the first test) was oxidized for 90 min (Figure 5). In Figure 5B, the value of FI declined when the dose of H_2O_2 was higher. However, when the reaction time was extended from 90 min to 24 h, the fluorescent products were found to be stable with no significant variation in the FI value. This revealed that many kinds of fluorescent products were generated during Hb oxidized degradation; some of the products could be further degraded, and some were stable, which would be useful for correcting the Hb absorbance. As shown in Figure 5A, the FI value did not decrease at any dose of H_2O_2, whereas in Figure 5B, a significant decrease of FI was observed at higher doses of H_2O_2. This difference might result from two situations. One was that no sufficient fluorescent products could be further decomposed during Hb degradation so that there was little effect on the FI value, as shown in Figure 5A. The other was that there was not enough time for Hb to completely degrade. Therefore, to better imitate in vivo reaction, the process in Figure 5B would be implemented in the following study.

dx.doi.org/10.1021/jf4049935 | J. Agric. Food Chem. 2014, 62, 2056−2061

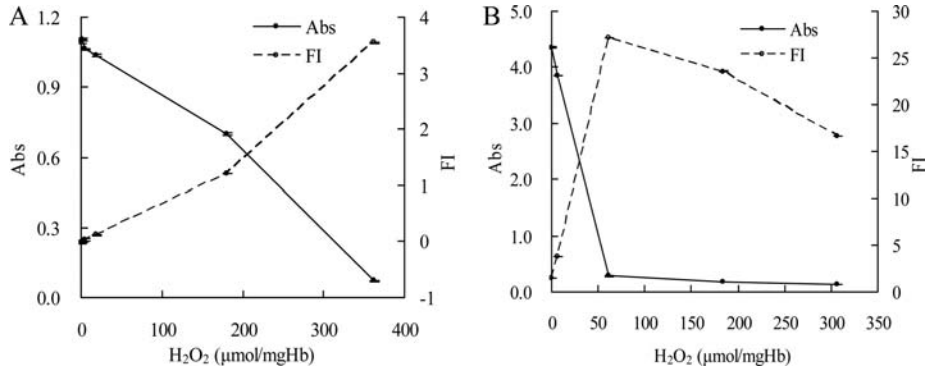

Figure 5. Oxidation curves of free Hb measured with spectrophotometry (solid line) and fluorometry (dashed line). (A) Hb (0.138 mg) was incubated with H_2O_2 for 15 min, and the relative doses of H_2O_2 were 0, 1.81, 5.43, 18.10, 180.98, and 361.96 μmol/mgHb. (B) Hb (8 mg) was incubated with H_2O_2 for 15 min, and the relative doses of H_2O_2 were 0, 6.12, 61.2, 183.64, and 306.07 μmol/mgHb.

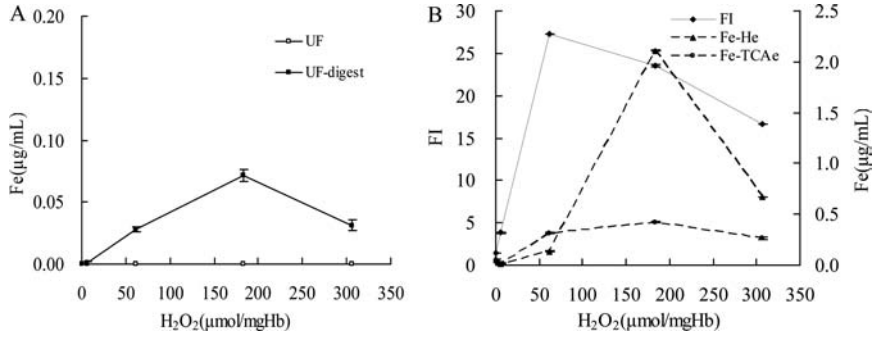

Figure 6. Different assays to extract the ferric ions released from Hb. Hb (8 mg) was incubated with different concentrations of H_2O_2 for 90 min. The ferric ions were extracted by ultrafiltration membrane (A), boiled water bath, and TCA precipitation (B), respectively.

It was found that Hb degradation not only generated fluorescent products but also induced ferric ion release from heme. We studied this release in three different ways (Figure 6). In the ultrafiltration test, the number of ferric ions after digestion was significantly higher compared with nondigestion (Figure 6A), which could indicate that the released ferric ions were binding with other protein substances. The number of released ferric ions extracted by the TCA and heating assays was significantly higher than that extracted by the ultrafiltration assay (Figure 6B). It was possible that some ferric ion conjugates were trapped by the 5000 Da ultrafiltration membrane due to the decrease in flux or that the ferric ions binding to other substances could not be extracted in this way. At the same time, all three assays showed that the highest ferric ion content was obtained when the H_2O_2 concentration was 183.6 μmol/mgHb, which was different from the FI values. This explained coincidentally why the decrease of FI values happened at a higher dose of H_2O_2 (183.6 μmol/mgHb), because there was further degradation.

Correction of Abs in Hemolysis. The above discussion indicated that the oxidative degradation of Hb was the key interfering factor in hemolysis evaluation. The following description was about establishing the model of Hb oxidation and correcting the lost Hb detection beyond the visible spectrum.

Normal erythrocytes contain 95% Hb, so in either in vivo or in vitro hemolysis, the dose of H_2O_2 is relatively little and can be calculated in units of micromoles per milligram of Hb. As shown in Figure 7, the H_2O_2 dose range was between 0 and 61 μmol/mg Hb. Abs and FI showed a good complementary linear relationship. We found that the actual concentration of Hb

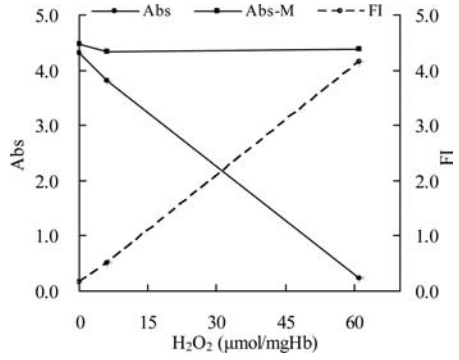

Figure 7. Relationship between Abs and FI in the H_2O_2-induced degradation of Hb.

could be expressed as Hb_{actual} = FI/CC + Abs if FI values divided a constant value (noted as the correction coefficient (CC)). According to the law of conservation of mass, the total Hb content must remain constant before and after degradation. The Abs-M curve in Figure 7 is the calibration curve of Hb with the CC value of 6.436. It can be seen that the Abs of Hb after modification by FI remained close to the initial level with increasing doses of H_2O_2. This confirmed that the correction of absorbance was effective in hemolysis on the basis of the stable fluorescent products.

Effect of the Sequence of Adding Antioxidants on the Assessment of Antioxidant Activity. The previous sections had modified hemolysis measurement, but here we wondered how to improve the protocol of the cell model to imitate the physical oxidation and antioxidation. The widely applied

dx.doi.org/10.1021/jf4049935 | J. Agric. Food Chem. 2014, 62, 2056−2061

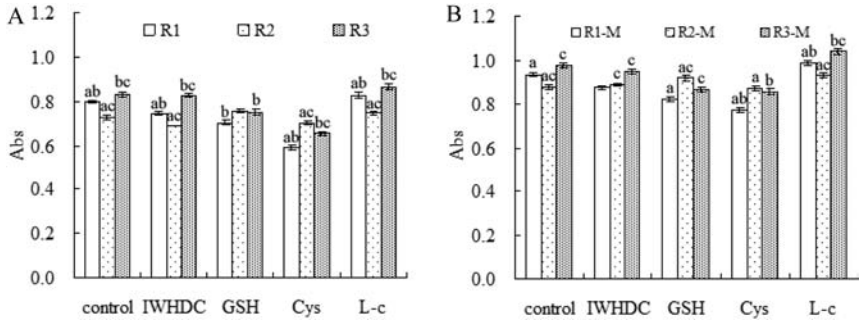

Figure 8. Antioxidant activity of IWHDC, GSH, Cys, and L-c under hemolysis induced by 166.5 μmol/L of H_2O_2: (A) results without modification; (B) results modified by correction factor for FI. Hemolysis reaction was conducted using three different sequences of adding antioxidants (R1, R2, R3), and the control group contained no antioxidant. Each value is the mean ± SD of three experiments. Significant differences are indicated by a, b, and c: a, compared with R1 and R2, $p < 0.05$; b, compared with R1 and R3, $p < 0.05$; c, compared with R2 and R3, $p < 0.05$.

sequence R1, preincubation with antioxidant and erythrocytes,[19,20] reflects the comprehensive activity of exogenous antioxidants because redundant antioxidants can also work outside the cells. Sequence R2, simulating the role of antioxidants on extracellular free radical scavenging, is actually a part of sequence R1 when antioxidants enter the cells.[21] Sequence R3 is also a part of R1[22] and reflects the ability to inhibit free radical chain reaction and repair injury when erythrocytes are in a state of unremitting oxidative stress. These three sequences were tested separately here, but in human blood, they always exist simultaneously and synergistically. Therefore, multidimensional analysis may be better for evaluating antioxidant capacity based on erythrocyte models. Three recognized antioxidants (GSH, Cys, and L-c) and a synthetic peptide (the amino acid sequence IWHDC designed by our laboratory) were evaluated on the basis of their order of addition in this study. First, we compared the difference between the results of unmodified hemolysis (Figure 8A) and those modified by FI (Figure 8B). The antihemolysis activities changed when Abs was modified by FI; therefore, we chose Abs modified by FI for antioxidant activity evaluation.

The three sequences (R1, R2, and R3) showed different hemolysis results not only in the antioxidant groups but also in the control group. The difference observed in the control group may be related to the tolerance of erythrocytes to oxidative stress, whereas the differences observed in antioxidant groups may also be related to the antioxidant mechanism and membrane transfer ability in the samples. As an amino acid antioxidant, Cys showed the highest activity in each of the three evaluation sequences, mainly because the rich disulfide bond provided protection from oxidation. The results of the R3 sequence showed that Cys may have entered the cell and controlled intracellular oxidative damage; the R2 sequence showed no activity, which could be directly related to the lack of scavenging H_2O_2 (data not shown). GSSH generated in the R2 sequence may disrupt the extracellular GSSH/GSH ratio such that the red blood cells exhibit abnormalities of metabolism. The poor performance of L-c in this study may be due to an inappropriate dose. Pentapeptide IWHDC had H_2O_2-scavenging capacity (data not shown) and showed antioxidative capability in the R1 and R3 groups, but not in the R2 group, suggesting that the oxidation products of IWHDC may disrupt cellular metabolism and reduce antihemolytic activity.

On the basis of the modified hemolysis measurement, we investigated how variation in activity assessment if antioxidants were added in three different sequences. The results showed differences in both the control group and the antioxidant groups for all three sequences may be related to cell resistance to oxidation, membrane transport capacity, and the other effect on cellular metabolism. According to the R1, R2, and R3 groups, more activity pathways can be analyzed, and results from them would have considerable value in the initial stage of antioxidant development. In future studies to find the intracellular oxidation level and explain the membrane roles, we will describe the detail mechanisms observed via fluorescent tracer, Western blot, and Fourier transform infrared spectroscopy techniques.

AUTHOR INFORMATION

Corresponding Author

*(X.X.) Phone: +86-1895-2731677. Fax: +86-0514-87313372. E-mail: xuxin@yzu.edu.cn.

Author Contributions

‖X.X. and J.H. contributed equally to this study and share first authorship.

Notes

The authors declare no competing financial interest.

ACKNOWLEDGMENTS

We are grateful to our volunteers, Mao WD, Guo ML, and Zhang JY, and to all of the students in the food safety major of the class of 2010 who provided their blood samples for hemolysis testing. This work was supported by Yangzhou University Science and Technology Innovation Fund (2013CXJ085).

REFERENCES

(1) Honzel, D.; Carter, S. G.; Redman, K. A.; Schauss, A. G.; Endres, J. R.; Jensen, G. S. Comparison of chemical and cell-based antioxidant methods for evaluation of foods and natural products: generating multifaceted data by parallel testing using erythrocytes and polymorphonuclear cells. *J. Agric. Food Chem.* **2008**, *56*, 8319−8325.

(2) Buehler, P. W.; Alayash, A. I. Redox biology of blood revisited: the role of red blood cells in maintaining circulatory reductive capacity. *Antioxid. Redox Signal.* **2005**, *7*, 1755−1760.

(3) Frankel, E. N.; Meyer, A. S. The problems of using one-dimensional methods to evaluate multifunctional food and biological antioxidants. *J. Sci. Food Agric.* **2000**, *80*, 1925−1941.

(4) Stocks, J.; Dormandy, T. L. The autoxidation of human red cell lipids induced by hydrogen peroxide. *Br. J. Hamaetol.* **1971**, *20*, 95−111.

(5) Landi, L.; Cipollone, M.; Cabrini, L.; Fiorentini, D.; Farruggia, G.; Galli, M. C. Injury of rat thymocytes caused by exogenous peroxyl radicals in vitro. *Biochim. Biophys. Acta* **1995**, *1239*, 207−212.
(6) Vissers, M. C. M.; Stern, A.; Kuypers, F.; Berg, J. V. D.; Winterbourn, C. C. Membrane changes associated with lysis of red blood cells by hypochlorous acid. *Free Radical Biol. Med.* **1994**, *16*, 703−712.
(7) Wrobel, A.; Lukaszynska, B.; Kedzierska, J. The effect of peroxynitrite and some antioxidants on the rate of osmotic hemolysis of bovine erythrocytes. *Cell. Mol. Biol. Lett.* **2003**, *8*, 445−460.
(8) Wolfe, K. L.; Liu, R. H. Cellular antioxidant activity (CAA) assay for assessing antioxidants, foods, and dietary supplements. *J. Agric. Food Chem.* **2007**, *55*, 8896−8907.
(9) Blasa, M.; Angelino, D.; Gennari, L.; Ninfali, P. The cellular antioxidant activity in red blood cells (CAA-RBC): Aa new approach to bioavailability and synergy of phytochemicals and botanical extracts. *Food Chem.* **2011**, *125*, 685−691.
(10) Arbos, K. A.; Claro, L. M.; Borges, L.; Santos, C. A. M.; Weffort-Santos, A. M. Human erythrocytes as a system for evaluating the antioxidant capacity of vegetable extracts. *Nutr. Res. (N.Y.)* **2008**, *28*, 457−463.
(11) Takebayashi, J.; Iwahashi, N.; Ishimi, Y.; Tai, A. Development of a simple 96-well plate method for evaluation of antioxidant activity based on the oxidative haemolysis inhibition assay (OxHLIA). *Food Chem.* **2012**, *134*, 606−610.
(12) Tunsaringkarn, T.; Soogarun, S.; Rungsiyothin, A.; Palasuwan, A. Inhibitory activity of Heinz body induction in vitro antioxidant model and tannin concentration of Thai mimosaceous plant extracts. *J. Med. Plants Res.* **2012**, *6*, 4096−4101.
(13) Guitton, J.; Servanin, S.; Francina, A. Hexose monophosphate shunt activities in human erythrocytes during oxidative damage induced by hydrogen peroxide. *Mol. Toxicol.* **2003**, *77*, 410−417.
(14) Nagababu, E.; Rifkind, J. M. Formation of fluorescent heme degradation products during the oxidation of hemoglobin by hydrogen peroxide. *Biochem. Biophys. Res. Commun.* **1998**, *247*, 592−596.
(15) Hani, A.; Hagai, G. Heme degradation in the presence of glutathione. *J. Biol. Chem.* **1995**, *270*, 24876−24883.
(16) May, J. M.; Qua, Z. C.; Qiao, H.; Koury, M. J. Maturational loss of the vitamin C transporter in erythrocytes. *Biochem. Biophys. Res. Commun.* **2007**, *360*, 295−298.
(17) Lochs, H.; Morse, E. L.; Adibi, S. A. Uptake and metabolism of dipeptides by human red blood cells. *Biochem. J.* **1990**, *271*, 133−137.
(18) Jarolim, P.; Lahav, M.; Liu, S. C.; Palek, J. Effect of hemoglobin oxidation products on the stability of red cell membrane skeletons and the associations of skeletal proteins: correlation with a release of hemin. *Blood* **1990**, *76*, 2125−2131.
(19) Paiva-Martins, F.; Fernandes, J.; Santos, V.; Silva, L.; Borges, F.; Rocha, S.; et al. Powerful protective role of 3,4-dihydroxyphenylethanol−elenolic acid dialdehyde against erythrocyte oxidative-induced hemolysis. *J. Agric. Food Chem.* **2012**, *28*, 135−140.
(20) Serem, J. C.; Bester, M. J. Physicochemical properties, antioxidant activity and cellular protective effects of honeys from southern Africa. *Food Chem.* **2012**, *133*, 1544−1550.
(21) Manna, C.; Galletti, P.; Cucciolla, V.; Montedoro, G.; Zappia, V. Olive oil hydroxytyrosol protects human erythrocytes against oxidative damages. *J. Nutr. Biochem.* **1999**, *10*, 159−165.
(22) Okoko, T.; Ere, D. Reduction of hydrogen peroxide−induced erythrocyte damage by Carica papaya leaf extract. *Asian Pac. J. Trop. Biomed.* **2012**, *2*, 449−453.

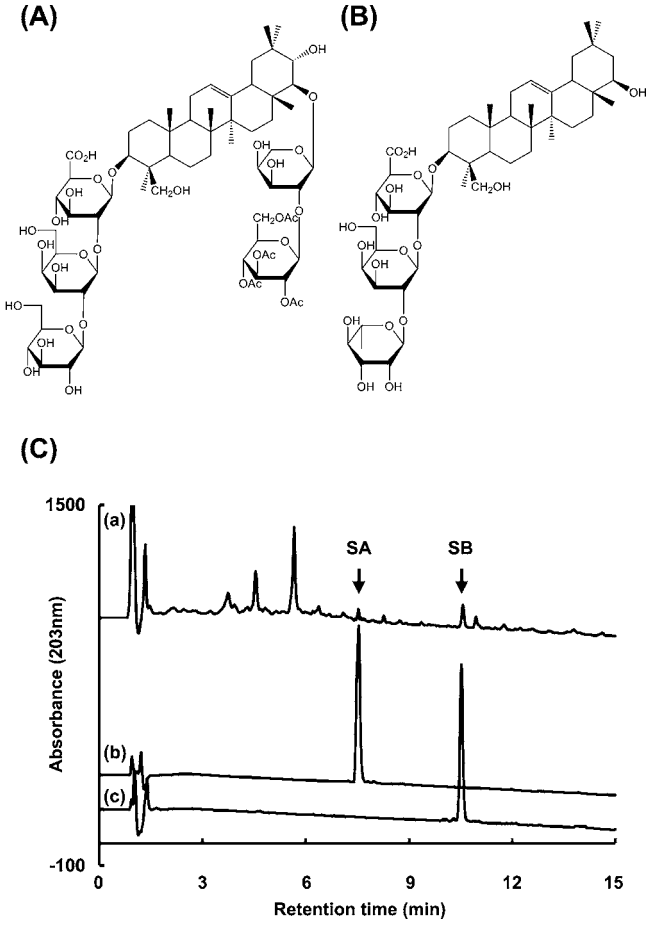

Figure 1. Structures of soyasaponins Ab (A) and Bb (B) Isolated from *Glycine max* Merr and HPLC chromatogram (C) of soybean ethanol extract (a) and isolated SA (b) and SB (c).

^{13}C NMR) analysis, similar to as reported previously.[18−21] The purities of the isolated soyasaponins were assayed by HPLC (Hewlett-Packard 1100 series, Ramsey, MN, U.S.) equipped with Zorbax Eclipse Plus C18 column (4.6 × 100 mm, 5 μm, Agilent Technologies, Santa Clara, CA, U.S.), a HP 1100 series binary pump, a HP 1100 series autosampler, and UV detector (203 nm). The HPLC was done by eluting with a linear gradient of 10% CH_3CN to 60% CH_3CN (flow rate, 1 mL/min) for 15 min. The retention times of soyasaponin Ab and Bb were 9.92 and 12.03 min, respectively.

Soyasaponin Ab. White amorphous powder. FAB-MS: *m*/*z* 1436 $[M - H]^-$.

Soyasaponin Bb. White amorphous powder. FAB-MS: *m*/*z* 941 $[M + H]^+$.

AChE Activity Assay. AChE activity was measured according to the method described by Lee et al.[22] Briefly, a reaction mixture (225 μL) containing 15 mM ATCh (25 μL), 3 mM DTNB (125 μL), 50 mM Tris-HCl (50 μL, pH 8.0), and test agents (25 μL) in a microplate was preincubated for 10 min. AChE (0.226 U/mL, 25 μL) was then added in the mixture, and scanned for 10 min at 405 nm in a microplate reader (Model Biotek μQuant MQX200, Winooski, VT, U.S.). Enzyme activity was indicated as a percentage of the activity when treated with vehicle instead of inhibitors.

Animals. All animal experiment protocols were performed according to the National Institute of Health (U.S.) and Kyung Hee University guidelines for Laboratory Animals Care and Usage and approved by the University Animal Care and Usage Committee of Laboratory Animals in the College of Pharmacy, Kyung Hee University.

Male ICR mice (18−22 g, 5 weeks) were obtained from the Orient Animal Breeding Center, a branch of Charles River Laboratories (Sungnam, Korea). All animals were housed in wire cages under a 12 h light/dark cycle (light on 07:30−19:30) at 20−22 °C and 50 ± 10% humidity and fed standard laboratory chow and water ad libitum.

Passive Avoidance Task. Acquisition and retention of the passive avoidance task was assessed using a two-compartment acrylic box wherein a lighted compartment (20 × 20 × 20 cm^3) was connected to a dark compartment (20 × 20 × 20 cm^3) by an entrance door (5 × 5 cm^2), according to the method of Lee et al.[22] Briefly, the mice underwent acquisition and retention trials. In the acquisition trial, a mouse was initially placed in the lighted chamber, and the entrance door was opened after 10 s. When the mouse entered the dark chamber, the door automatically closed, and a 0.3 mA electrical shock for 2 s was delivered through the grid floor. One hour before the retention trial, the mice were orally administered with soy ethanol extract (SE, 100 and 200 mg/kg), SA or SB (5, 10, 20, and 40 mg/kg), tacrine (10 mg/kg) as a positive control,[23] and vehicle (2% Tween 80, the scopolamine group) as a negative control. Memory impairment was induced by intraperitoneal injection of scopolamine (0.9 mg/kg) 30 min after oral administrations of test agents. The passive avoidance maze task was carried out 30 min after scopolamine treatment. A retention trial was carried out 24 h after the acquisition trial. Thereafter, the mice were placed in the light compartment again and the latency time taken to enter the dark compartment was recorded for each mouse. If the mouse did not enter the dark compartment within 300 s, then we concluded that the mouse remembered the foot shock from the acquisition trial.

Y-Maze Task. Y-maze was used to measure the immediate spatial working memory, which is a form of short-term memory, and was carried out as previously described.[22] A Y-maze is a three-arm horizontal maze symmetrically separated by 120° angles from each other (length, 40 cm; width, 3 cm; and height, 12 cm). The floor and wall of the maze were constructed using dark polyvinyl plastic, as previously reported.[22] During the maze task, the mice were placed inside one arm, and the sequence (i.e., ACCABC, etc.) of arm entries were manually recorded for each mouse for 8 min. An actual alternation was defined as consecutive entries into all three arms (i.e., ABC, CAB, or BAC, but not BAB). Memory impairment was induced by intraperitoneal injection of scopolamine (0.9 mg/kg). To remove mouse odors, maze arms were cleaned between two consecutive tasks. Test agents. i.e., SE (100 and 200 mg/kg), SA or SB (10 mg/kg, p.o.), tacrine (10 mg/kg, p.o.), or vehicle (p.o.) were orally administered 1 h before the maze task. The maze task was carried out 30 min after treatment with scopolamine. The alternation percentage was calculated: alternation percentage = [(number of alternations)/(total arm entries −2)] × 100. The number of arm entries was served as the indicator of locomotor activity.

Morris Water Maze Task. Spatial memory and learning was studied with the Morris water maze task by using a circular pool (diameter, 90 cm; height, 45 cm), according to the method described by Lee et al.[22] First, the pool was filled with water (20 ± 1 °C) up to 30 cm depth, and nonfat milk (500 mL) was mixed with water. A white platform (diameter, 6 cm; height, 29 cm) was centered in one of four quadrants of the milk-filled pool (southwest area) and hidden 1 cm below the water surface. On the first day of the maze task, the mice were given swimming training for 60 s in the platform-free pool. Starting from the second day, the mice were given four swimming training trial sessions per day for four consecutive days. Escape latencies for each mouse were measured and recorded. For each mouse, this parameter was averaged for each trial session. Once the mouse located the platform, the mouse stayed on the platform for 10 s. If the mouse could not search the platform within 60 s, then the mouse was then placed on the platform for 10 s. During this period, a fixed platform was used. After each trial, the animals were taken to the cage and were dried under an infrared lamp. The trial time interval was 30 s. On the last day of training, the mice were underwent a probe trial session after the platform was removed, wherein they were allowed to swim for 60 s. The swimming time spent in platform quadrant section of the pool was recorded. SA or SB (10 mg/kg, *p.o.*), tacrine (10 mg/kg, *p.o.*), or vehicle (*p.o.*) was administered 1 h before the maze task was conducted at every consecutive day. Scopolamine (0.9 mg/kg)

was intraperitoneally administered 30 min after oral administrations of test agents.

Immunoblotting. Mice were sacrificed 30 min after the acquisition trial of the passive avoidance task (2 h after scopolamine treatment). The hippocampi were promptly excised and homogenized in 200 μL of ice-cold RIPA buffer containing a protease inhibitor cocktail. The homogenates were centrifuged for 15 min at 13 000*g*. The resulting supernatants were aliquoted into Eppendorf tubes and stored at −80 °C until required. The expression levels of BDNF, CREB, p-CREB, and β-actin were measured by immunoblotting according to the method of Lee et al.[22] The protein assay was performed using Bradford protein assay kit.

Ex vivo AChE Activity Assay. The mice were randomly divided into 4 groups (n = 4) and were orally administered vehicle (2% tween), SA (10 mg/kg), SB (10 mg/kg), and tacrine (10 mg/kg). The mice were sacrificed 60 min after each administration, and their brains were removed. Their hippocampi were dissected and homogenized in cold RIPA buffer. The homogenates were centrifuged at 10 000*g* for 10 min at 4 °C, and the resulting supernatants were used as enzyme sources. Their AChE activities were measured as triplicates. The protein amount was determined using Bradford protein assay kits (Bio-Rad, Hercules, CA, U.S.). AChE activity per protein amount of the homogenate supernatant (mg) was calculated.

Statistics. All experimental data are expressed as mean ± standard error of mean (SEM).

Distributions in the passive avoidance and Y-maze tasks were depicted by box-plots. A box-plot consists of a box and tails for each group. The horizontal line through the box depicts the median, and the top and bottom of the box mark the upper and lower quartiles, respectively. For passive avoidance task, the significance among data was analyzed by a Kruskal−Wallis nonparametric one-way analysis of variance (ANOVA) test. For the Y-maze, and Morris water maze tasks, the significance was analyzed by ANOVA followed by Student−Newman−Keuls test for multiple comparisons. Statistical significance was set at $p < 0.05$.

RESULTS

SE Protected Scopolamine-Induced Memory Impairment. Preliminary experiment indicated that SE potently prevented scopolamine-induced memory impairment in passive avoidance and Y-maze tasks. The performance of mice treated with SE (200 mg/kg, p.o.) and scopolamine in passive avoidance and Y-maze tasks was 43% (F = 11.97, $P < 0.05$) and 98% (F = 4.84, $P < 0.05$), respectively, of vehicle-treated normal control mice (Figure 2).

Therefore, to understand the possible role of soyasaponins in memory impairment, we isolated the two main soyasaponins SA and SB and identified them by FAB-MS and ^{1}H- and ^{13}C NMR. Isolated SA and SB exhibited soyasponin-specific seven angular methyl singlet signals [δ 0.70 (25-CH_3), 0.86 (26-CH_3), 0.96 (29-CH_3), 0.99 (28-CH_3), 1.23 (27-CH_3), 1.30 (30-CH_3), 1.45 (23-CH_3)] and [δ 0.67 (25-CH_3), 0.90 (26-CH_3), 1.23 (29-CH_3), 1.26 (28-CH_3), 1.33 (27-CH_3), 1.35 (30-CH_3), and 1.41 (23-CH_3)], respectively, in ^{1}H NMR and m/z 1436 $[M - H]^-$ and m/z 941 $[M + H]^+$, respectively, in FAB-MS.

SA and SB Prevented Scopolamine-Induced Memory Impairment. We investigated the preventive effects of SA and SB against scopolamine-induced memory impairment in mice in the passive avoidance task (Figure 3A,B). Both SA and SB significantly prevented scopolamine-induced memory impairment. SB protected memory impairment; however, the effect was more with SB than with SA. SA and SB at a dose of 10 mg/kg (p.o.) restored memory impairment to 86% (F = 85.33, $P <$ 0.05) and 97% (F = 68.10, $P < 0.05$) of untreated normal control mice, respectively. These effects are comparable to that of tacrine (10 mg/kg), a positive control, which restored the step-through latency to 91% of untreated normal control mice. However, no significant differences among the groups treated with SA (10 mg/kg), SB (10 mg/kg), and tacrine (10 mg/kg) were observed. During the acquisition trial, no latency differences were observed among test groups (Figure 3A,B). On the Y-maze task, SA and SB (10 mg/kg) restored spontaneous alteration, which was lowered by scopolamine (Figure 3C). Compared to SA, SB restored memory impairment more potently. SB (10 mg/kg, p.o.) significantly restored the lowered spontaneous alteration induced by scopolamine to 78% of that of untreated normal control mice (F = 35.57, $P <$ 0.05). However, no significant differences between those of SA and SB were observed.

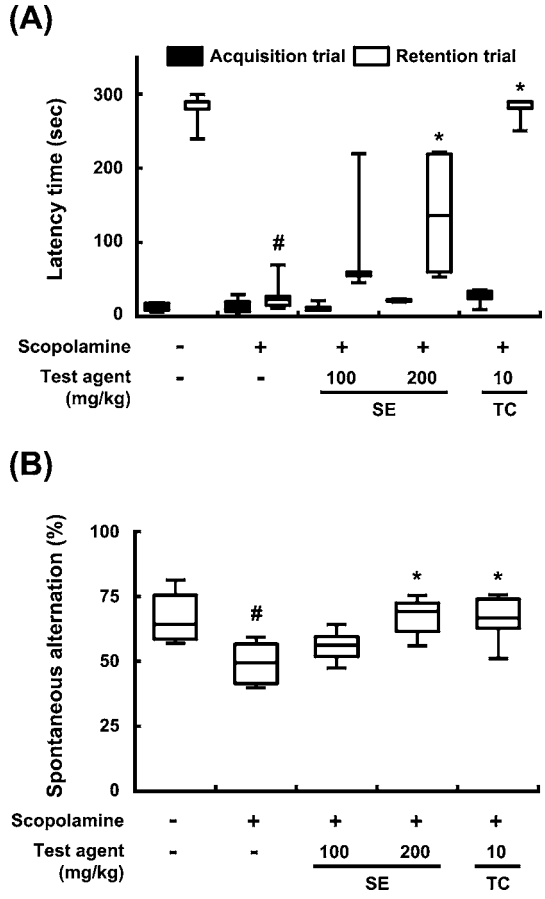

Figure 2. The protecting effect of SE against scopolamine-induced memory impairment in mice. (A) Effect of SE in passive avoidance task. (B) Effect of SE in Y-maze task. SE (100 or 200 mg/kg, p.o.), tacrine (TC, 10 mg/kg, p.o.) or vehicle (the same volume of 2% Tween 80) was administered to mice 1 h before treatment with scopolamine. Memory impairment was induced by scopolamine treatment (0.9 mg/kg i.p.). Normal control mice were treated with vehicle instead of scopolamine. Six different animals were used in each treatment group. Acquisition trials were carried out 30 min after a single scopolamine treatment. Test agents (NOR, none; SCO, scopolamine alone; SE100, 100 mg/kg SE with scopolamine; SE200, 200 mg/kg of SE with scopolamine; closed triangle, 10 mg/kg tacrine with scopolamine) was orally treated 1 h before maze task. Box-plots—To depict a distribution, a box-plot consists of a box and tails for each group. The horizontal line through the box depicts the median, and the top and bottom of the box mark the upper and lower quartiles. #Significantly different from normal mice ($P < 0.05$). *Significantly different from scopolamine-treated control ($P < 0.05$).

dx.doi.org/10.1021/jf4046528 | J. Agric. Food Chem. 2014, 62, 2062−2068

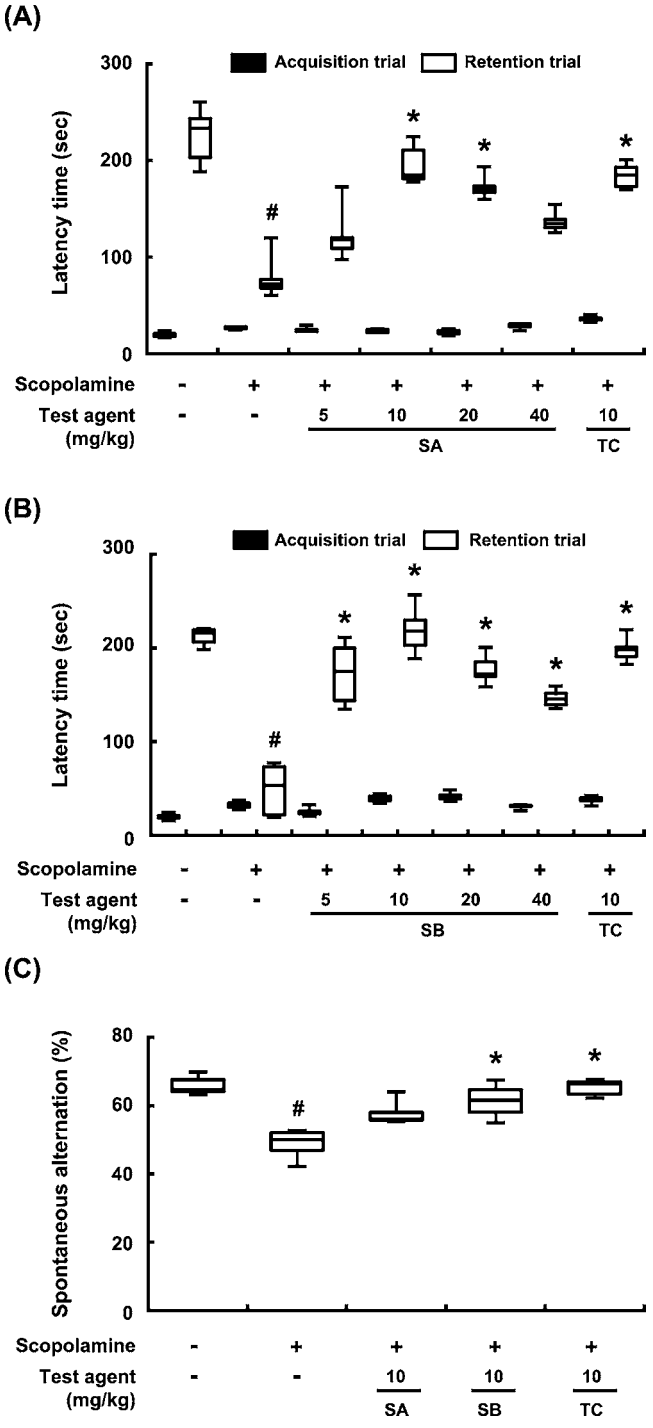

Figure 3. Effects of soyasaponins Ab (SA) and Bb (SB) on scopolamine-induced memory impairment in mice in the passive avoidance and Y-maze tasks. (A) Effect of SA in passive avoidance task. (B) Effect of SB in passive avoidance task. (C) Effects of SA and SB in Y-maze task. Soyasaponins (5, 10, 20, or 40 mg/kg, p.o.), tacrine (TC, 10 mg/kg, p.o.) or vehicle (the same volume of 2% Tween 80) was administered to mice 1 h before treatment with scopolamine. Memory impairment was induced by scopolamine treatment (0.9 mg/kg i.p.). Normal control mice were treated with vehicle instead of scopolamine. Six different animals were used in each treatment group. Acquisition trials were carried out 30 min after a single scopolamine treatment. The retention trials were carried out for 5 min, 24 h after the acquisition trials. Box plot details see Figure 2. #Significantly different from normal mice ($P < 0.05$). *Significantly different from scopolamine-treated control ($P < 0.05$).

We also investigated the effect of SA and SB (10 mg/kg, p.o.) on escape latencies in the Morris water maze task (Figure 4A). Escape latencies were prolonged by scopolamine treatment. SA significantly shortened the escape latencies on the fifth day ($F = 14.51$, $P < 0.05$). However, SB-treated mice showed

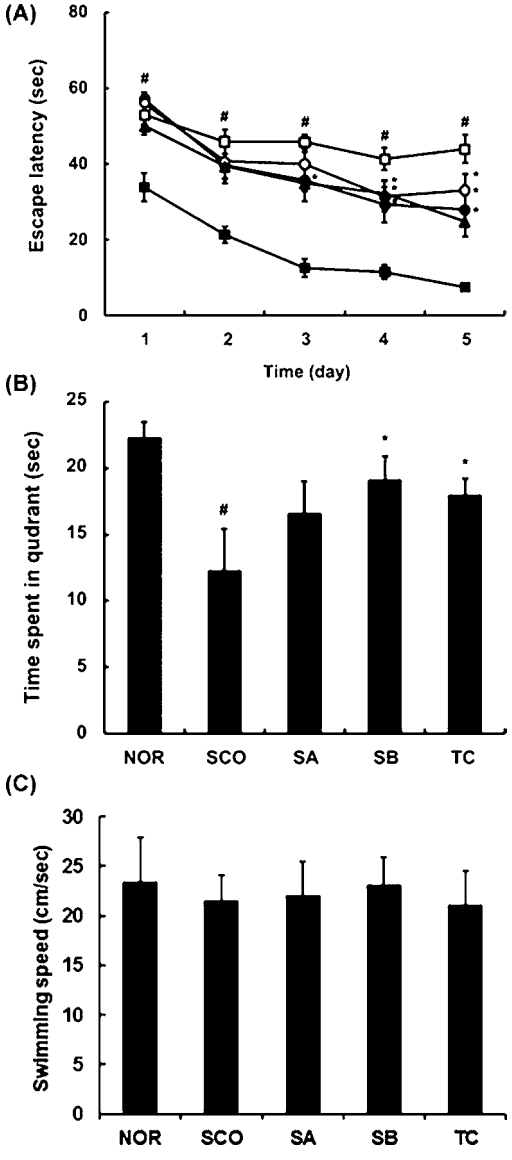

Figure 4. Effects of soyasaponins Ab (SA) and Bb (SB) on scopolamine-induced memory impairment in morris water maze tasks. (A) Effects in escape latencies during training trial sessions. (B) Effects in swimming times spent in target quadrant. (C) Effects in swimming speed. Soyasaponins (10 mg/kg, p.o.) or tacrine (TC, 10 mg/kg, p.o.) was given 1 h before the first trial session at every consecutive day. Memory impairment was induced with scopolamine (0.9 mg/kg, i.p.) at 30 min after treatment with each test agent. Normal group was treated with vehicle instead of scopolamine and test agents. The training trials for 5 days and the probe trial sessions in the last day were performed as described in the Materials and Methods. Open square, group treated with scopolamine; closed square, normal control group; open circle, group treated with scopolamine in the presence of SA; closed circle, group treated with scopolamine in the presence of SB; closed triangle, group treated with scopolamine in the presence of tacrine. Values are expressed as mean ± SEM ($n = 6$). #Significantly different from normal mice ($P < 0.05$). *Significantly different from scopolamine-treated control ($P < 0.05$).

dx.doi.org/10.1021/jf4046528 | J. Agric. Food Chem. 2014, 62, 2062−2068

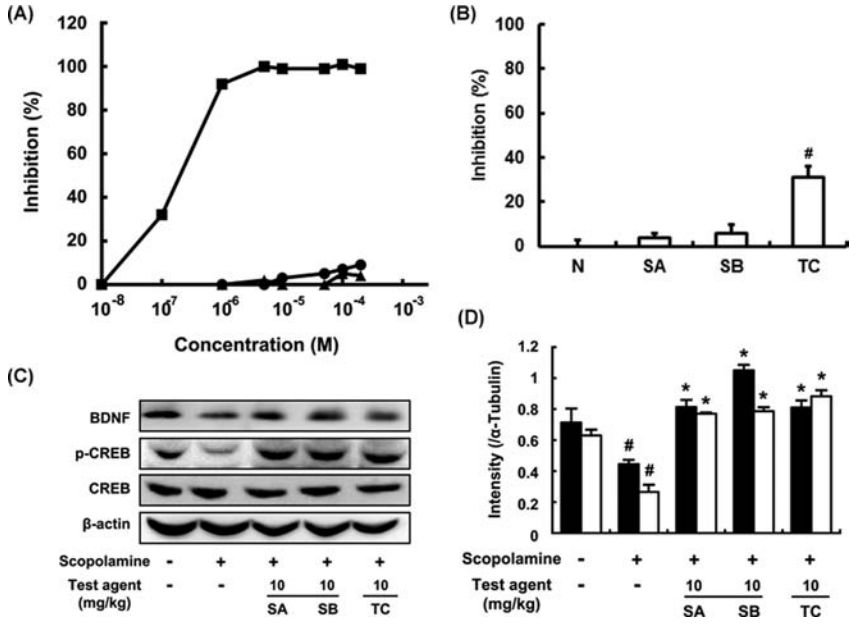

Figure 5. Effects of soyasaponins Ab (SA) and Bb (SB) on aceytlcholinesterase (AChE) activity in vitro and on BDNF expression and CREB phosphorylation in the hippocampus of scopolamine-treated mice. (A) Effect on AChE activity. The inhibitory potencies of SA (closed circle), SB (closed triangle), and tacrine (closed square) against AChE activity were measured in vitro by using electric eel type VI−S AChE. (B) Effect in hippocampal acetylcholinesterase activity. SA (10 mg/kg, p.o.), SB (10 mg/kg, p.o.) or tacrine (TC, 10 mg/kg, p.o.) was orally administered to mice only once and sacrificed 60 min after treatment with test agents and measured hippocampal AChE activity (n = 4). Each sample was measured as triplicates. (C) Effect on BDNF expression. SA (10 mg/kg, p.o.), SB (10 mg/kg, p.o.) or tacrine (TC, 10 mg/kg, p.o.) was orally administered to mice for once. Control group received an equal volume of vehicle for the same period. Memory impairment was induced by scopolamine treatment (0.9 mg/kg, i.p.) 1 h after the administration of each test agent. The normal control group was treated with vehicle instead of scopolamine and test agents. The expression levels of BDNF, CREB, and p-CREB were measured by immunoblotting. (D) Intensity graph showing the quantification of BDNF/β-actin and p-CREB/CREB expression levels measured by densitometry. β-actin was used as an internal control. Values are expressed as mean ± SEM (n = 3). #Significantly different from normal mice (P < 0.05). *Significantly different from scopolamine-treated control (P < 0.05).

significantly shorter latencies from the third day (F = 6.70, P < 0.05) to the fifth day (F = 14.51, P < 0.05). On the day after the last training session, the mean swimming time within the platform quadrant was significantly lower in mice treated with scopolamine alone than in those untreated normal control mice. Soyasaponins increased the swimming time within the platform quadrant (F = 21.52, P < 0.05) (Figure 4B). SB increased the target quadrant swim time more than SA. The effect of SB is comparable to that of tacrine in Morris water maze task. No significant differences in swimming speed within the target quadrant were observed between the groups treated with vehicle alone, scopolamine, and/or test agents (Figure 4C). This demonstrates that scopolamine and soyasaponins have no effect on general locomotor behavior.

Next, we measured the inhibitory effects of these soyasaponins on AChE activity in vitro. These soyasaponins did not inhibit AChE activity (IC_{50}, > 0.2 mM), however, tacrine potently inhibited it (IC_{50} = 0.12 μM) (Figure 5A). We also measured AChE activity in hippocampi of mice orally treated with SA, SB, or tacrine (10 mg/kg). Treatment with SA or SB did not inhibit hippocampal AChE activity, whereas treatment with tacrine inhibited it by 31% (Figure 5B). Next, we investigated the effect of SB on BDNF expression and CREB phosphorylation in the hippocampi of scopolamine-treated memory-impaired mice (Figure 5C,D). Scopolamine significantly reduced BDNF expressions and CREB phosphorylation. However, when SA or SB was administered in these mice, BDNF expression (F = 33.69; P < 0.05) and CREB phosphorylation (F = 91.62; P < 0.05) were significantly increased, as previously reported.[7,12] No significant difference in β-actin level was observed.

DISCUSSION

A decrease in cholinergic function, particularly within the basal forebrain, can decline memory and cognitive function with age.[5] A commercial anticholinergic drug, scopolamine, causes memory impairment in healthy young people, which is the equivalent of memory impairment observed in nondemented drug-free elderly people. Furthermore, several studies have reported that scopolamine is increasingly disruptive with age and declines cognitive function.[7] This is consistent with the previously reported hypothesis that the function of cholinergic neurons decreases with increasing age and dementia.[5,7] In the present study, SE and its constituents SA and SB significantly prevented scopolamine-induced memory impairment in mice in the passive avoidance, Y-maze and Morris water maze tasks. SB rescued memory impairment more potently than SA. However, both SA and SB did not inhibit AChE activity in vitro and ex vivo. Orally administered SA and SB are metabolized to their aglycones by intestinal microbiota of mouse and human feces.[19,24] Therefore, to elucidate the ability of SA, SB, and their metabolites soyasapogenols A and B, their AChE-inhibitory activities were measured. Soyasaponins and their metabolites did not inhibit AChE activity. These results suggest that the amelioration of memory impairment by SA and SB may not be dependent on AChE inhibition. When soyasaponins were orally administered to mice, these compounds might be metabolized to their aglycones soyasapogenols A and B, which are possibly the active

dx.doi.org/10.1021/jf4046528 | J. Agric. Food Chem. 2014, 62, 2062−2068

candidates responsible for preventing memory impairment. However, these metabolisms may not be quickly catalyzed by intestinal microbiota. These results suggest that the effect of SA and SB may be due to parental compounds rather than their metabolites by intestinal microbiota. Nevertheless, both SA and SB prevented scopolamine-induced memory impairment. The memory impairment-ameliorating effect of SB was more potent than that of SA in passive avoidance (5 mg/kg, p.o.) and Y-maze tasks (10 mg/kg, p.o.). However, the effects of SA and SB were not significantly different. Although the AChE-inhibitory effects of SA and SB may be different between in vitro and in vivo studies, these soyasaponins may ameliorate scopolamine-induced memory impairment in mice without the inhibiton of acetylcholinesterase. Furthermore, in the mouse hippocampus, SA and SB potently restored scopolamine-mediated reduced expression of BDNF. BDNF influences neuronal synaptic plasticity by depolarizing neurons as rapidly as glutamate does by activating tyrosine kinase receptors,[25] enhancing glutamatergic synaptic transmission,[26] increasing the *N*-methyl-D-aspartate receptor subunit phosphorylation in the hippocampus, and facilitating hippocampal LTP.[27] Notably, the expression of BDNF in the entorhinal cortex and hippocampus is lower in patients with AD than in healthy male.[8,28] CREB may be the most important transcription factor regulating BDNF expression.[29] Being a cellular transcription factor, CREB regulates the expression of BDNF, tyrosine hydroxylase, and many neuropeptides.[29−31] Several studies have suggested that BDNF and CREB may possess therapeutic potential in patients with AD.[22,32,33] In the present study, we demonstrated that scopolamine inhibited CREB phosphorylation, as previously reported.[22,33] Orally administered SA and SB potently restored scopolamine-mediated reduction of CREB phosphorylation. Overall, compared to SA, SB prevented scopolamine-induced memory impairment more potently. These studies suggest that soyasaponins restore the reduction of BDNF expression and CREB phosphorylation caused by scopolamine and reverse neuronal synaptic plasticity mediated by BDNF, which binds cell surface receptors such as TrkB and low-affinity nerve growth factor receptor. On the basis of these findings, we suggest that soybean, particularly soyasaponins, ameliorates scopolamine-induced memory impairment by increasing BDNF expression and CREB activation.

AUTHOR INFORMATION

Corresponding Author

*Tel: +82-2-961-0374; fax: +82-2-957-5030; e-mail: dhkim@khu.ac.kr.

Notes

The authors declare no competing financial interest.

ABBREVIATIONS USED

AChE,acetylcholinesterase; AD,Alzheimer's disease; ATCh,acetylthiocholine; BDNF,brain-derived neurotrophic factor; CREB,cAMP response element-binding protein; LTP,long-term potentiation; RIPA,radioimmuno-precipitation assay; SA,soyasaponin Ab; SB,soyasaponin Bb; SE,soy ethanol extract

REFERENCES

(1) Everitt, B. J.; Robbins, T. W. Central Cholinergic Systems and Cognition. *Annu. Rev. Psychol.* **1997**, *48*, 649−684.

(2) Whitehouse, P. J.; Price, D. L.; Clark, A. W.; Coyle, J. T.; DeLong, M. R. Alzheimer Disease: Evidence for Selective Loss of Cholinergic Neurons in the Nucleus Basalis. *Ann. Neurol.* **1981**, *10*, 122−126.

(3) Hardy, J.; Selkoe, D. J. The Amyloid Hypothesis of Alzheimer'S Disease: Progress and Problems on the Road to Therapeutics. *Science* **2002**, *297*, 353−356.

(4) Goedert, M.; Spillantini, M. G.; Crowther, R. A. Tau Proteins and Neurofibrillary Degeneration. *Brain Pathol.* **1991**, *1*, 279−286.

(5) Araujo, J. A.; Studzinski, C. M.; Milgram, N. W. Further Evidence for the Cholinergic Hypothesis of Aging and Dementia from the Canine Model of Aging. *Prog. Neuropsychopharmacol. Biol. Psych.* **2005**, *29*, 411−422.

(6) Kotani, S.; Yamauchi, T.; Teramoto, T.; Ogura, H. Pharmacological Evidence of Cholinergic Involvement in Adult Hippocampal Neurogenesis in Rats. *Neuroscience* **2006**, *142*, 505−514.

(7) Tariot, P. N.; Patel, S. V.; Cox, C.; Henderson, R. E. Age-Related Decline in Central Cholinergic Function Demonstrated with Scopolamine. *Psychopharmacology* **1996**, *125*, 50−56.

(8) Hock, C.; Heese, K.; Hulette, C.; Rosenberg, C.; Otten, U. Region-Specific Neurotrophin Imbalances in Alzheimer Disease: Decreased Levels of Brain-Derived Neurotrophic Factor and Increased Levels of Nerve Growth Factor in Hippocampus and Cortical Areas. *Arch. Neurol.* **2000**, *57*, 846−851.

(9) Lu, B.; Pang, P. T.; Woo, N. H. The Yin and Yang of Neurotrophin Action. *Nat. Rev. Neurosci.* **2005**, *6*, 603−614.

(10) Lu, Y.; Christian, K.; Lu, B. BDNF: a Key Regulator for Protein Synthesis-Dependent LTP and Long-Term Memory? *Neurobiol. Learn. Mem.* **2008**, *89*, 312−323.

(11) Kim, D. H.; Jeon, S. J.; Son, K. H.; Jung, J. W.; Lee, S.; Yoon, B. H.; Lee, J. J.; Cho, Y. W.; Cheong, J. H.; Ko, K. H.; Ryu, J. H. The Ameliorating Effect of Oroxylin a on Scopolamine-Induced Memory Impairment in Mice. *Neurobiol. Learn. Mem.* **2007**, *87*, 536−546.

(12) Joh, E. H.; Yang, J. W.; Kim, D. H. Gypenoside LXXIV Ameliorates Scopolamine-Induced Learning Impairment in Mice. *Planta Med.* **2010**, *76*, 793−795.

(13) Kim, S. L.; Berhow, M. A.; Kim, J. T.; Chi, H. Y.; Lee, S. J.; Chung, I. M. Evaluation of Soyasaponin, Isoflavone, Protein, Lipid, And Free Sugar Accumulation in Developing Soybean Seeds. *J. Agric. Food Chem.* **2006**, *54*, 10003−10010.

(14) Liu, Y. Q.; Xin, T. R.; Lü, X. Y.; Ji, Q.; Jin, Y.; Yang, H. D. Memory Performance of Hypercholesterolemic Mice in Response to Treatment with Soy Isoflavones. *Neurosci. Res.* **2007**, *57*, 544−549.

(15) Kato-Kataoka, A.; Sakai, M.; Ebina, R.; Nonaka, C.; Asano, T.; Miyamori, T. Soybean-Derived Phosphatidylserine Improves Memory Function of the Elderly Japanese Subjects with Memory Complaints. *J. Clin. Biochem. Nutr.* **2010**, *47*, 246−255.

(16) File, S. E.; Jarrett, N.; Fluck, E.; Duffy, R.; Casey, K.; Wiseman, H. Eating Soya Improves Human Memory. *Psychopharmacology* **2001**, *157*, 430−436.

(17) Pan, M.; Li, Z.; Yeung, V.; Xu, R. J. Dietary Supplementation of Soy Germ Phytoestrogens or Estradiol Improves Spatial Memory Performance and Increases Gene Expression of BDNF, TrkB Receptor and Synaptic Factors in Ovariectomized Rats. *Nutr. Metab.* **2010**, *7*, 75.

(18) Lee, I. A.; Park, Y. J.; Yeo, H. K.; Han, M. J.; Kim, D. H. Soyasaponin I Attenuates TNBS-Induced Colitis in Mice by Inhibiting NF-kappaB Pathway. *J. Agric. Food Chem.* **2011**, *58*, 10929−10934.

(19) Chang, S. Y.; Han, M. J.; Joh, E. H.; Kim, D. H. Liquid Chromatography/Mass Spectrometry-Based Structural Analysis of Soyasaponin Ab Metabolites by Human Fecal Microflora. *J. Pharm. Biomed. Anal.* **2010**, *52*, 752−756.

(20) Kitagawa, I.; Taniyama, T.; Nagahama, Y.; Okubo, K.; Yamauchi, F.; Yoshikawa, M. Structure of Acetyl-Soyasaponin A_1, A_2 and A_3, Astringent Partially Acetylated Bisdesmoside of Soyasapogenol a Form American Soybean, The Seed of Glycine Max MERRILL. *Chem. Pharm. Bull.* **1988**, *36*, 2819−2828.

(21) Kitagawa, I.; Yoshikawa, M.; Yosioka, I. Saponin and Sapogenol. XIII. Structures of Three Soybean Saponins: Soyasaponin I, Soyasaponin II, and Soyasaponin III. *Chem. Pharm. Bull.* **1976**, *24*, 121−129.

(22) Lee, B.; Jung, K.; Kim, D. H. Timosaponin AIII, a Saponin Isolated from *Anemarrhena asphodeloides*, Ameliorates Learning and Memory Impairments in Mice. *Pharmacol., Biochem. Behav.* **2009**, *93*, 121−127.
(23) Nielsen, J. A.; Mena, E. E.; Williams, I. H.; Nocerini, M. R.; Liston, D. Correlation of Brain Levels of 9-Amino-1,2,3,4-tetrahydroacridine (THA) with Neurochemical and Behavioral Changes. *Eur. J. Pharmacol.* **1989**, *173*, 53−64.
(24) Chang, S. Y.; Han, M. J.; Joh, E. H.; Kim, D. H. Metabolism of Soyasaponin I by Human Intestinal Microflora and Its Estrogenic and Cytotoxic Effects. *Biomol. Therap.* **2009**, *17*, 430−437.
(25) Kafitz, K. W.; Rose, C. R.; Thoenen, H.; Konnerth, A. Neurotrophin-Evoked Rapid Excitation through TrkB Receptors. *Nature* **1999**, *401*, 918−921.
(26) Figurov, A.; Pozzo-Miller, L. D.; Olafsson, P.; Wang, T.; Lu, B. Regulation of Synaptic Responses to High-Frequency Stimulation and LTP by Neurotrophins in the Hippocampus. *Nature* **1996**, *381*, 706−709.
(27) Connor, B.; Young, D.; Yan, Q.; Faull, R. L.; Synek, B.; Dragunow, M. Brain-Derived Neurotrophic Factor Is Reduced in Alzheimer'S Disease. *Brain Res. Mol. Brain Res.* **1997**, *49*, 71−81.
(28) Levine, E. S.; Dreyfus, C. F.; Black, I. B.; Plummer, M. R. Brain-Derived Neurotrophic Factor Rapidly Enhances Synaptic Transmission in Hippocampal Neurons via Postsynaptic Tyrosine Kinase Receptors. *Proc. Natl. Acad. Sci. U.S.A.* **1995**, *92*, 8074−8077.
(29) Bourtchuladze, R.; Frenguelli, B.; Blendy, J.; Cioffi, D.; Schutz, G.; Silva, A. J. Deficient Long-Term Memory in Mice with a Targeted Mutation of the cAMP-Responsive Element-Binding Protein. *Cell* **1994**, *79*, 59−68.
(30) Pugazhenthi, S.; Wang, M.; Pham, S.; Sze, C. I.; Eckman, C. B. Downregulation of CREB Expression in Alzheimer'S Brain and in Aβ-Treated Rat Hippocampal Neurons. *Mol. Neurodegener.* **2011**, *6*, 60.
(31) Jeon, S. J.; Rhee, S. Y.; Seo, J. E.; Bak, H. R.; Lee, S. H.; Ryu, J. H.; Cheong, J. H.; Shin, C. Y.; Kim, G. H.; Lee, Y. S.; Ko, K. H. Oroxylin A Increases BDNF Production by Activation of MAPK-CREB Pathway in Rat Primary Cortical Neuronal Culture. *Neurosci. Res.* **2011**, *69*, 214−222.
(32) Nagahara, A. H.; Merrill, D. A.; Coppola, G.; Tsukada, S.; Schroeder, B. E.; Shaked, G. M.; Wang, L.; Blesch, A.; Kim, A.; Conner, J. M.; Rockenstein, E.; Chao, M. V.; Koo, E. H.; Geschwind, D.; Masliah, E.; Chiba, A. A.; Tuszynski, M. H. Neuroprotective Effects of Brain-Derived Neurotrophic Factor in Rodent and Primate Models of Alzheimer'S Disease. *Nat. Med.* **2000**, *15*, 331−337.
(33) Bejar, C.; Wang, R. H.; Weinstock, M. Effect of Rivastigmine on Scopolamine-Induced Memory Impairment in Rats. *Eur. J. Pharmacol.* **1999**, *383*, 231−240.

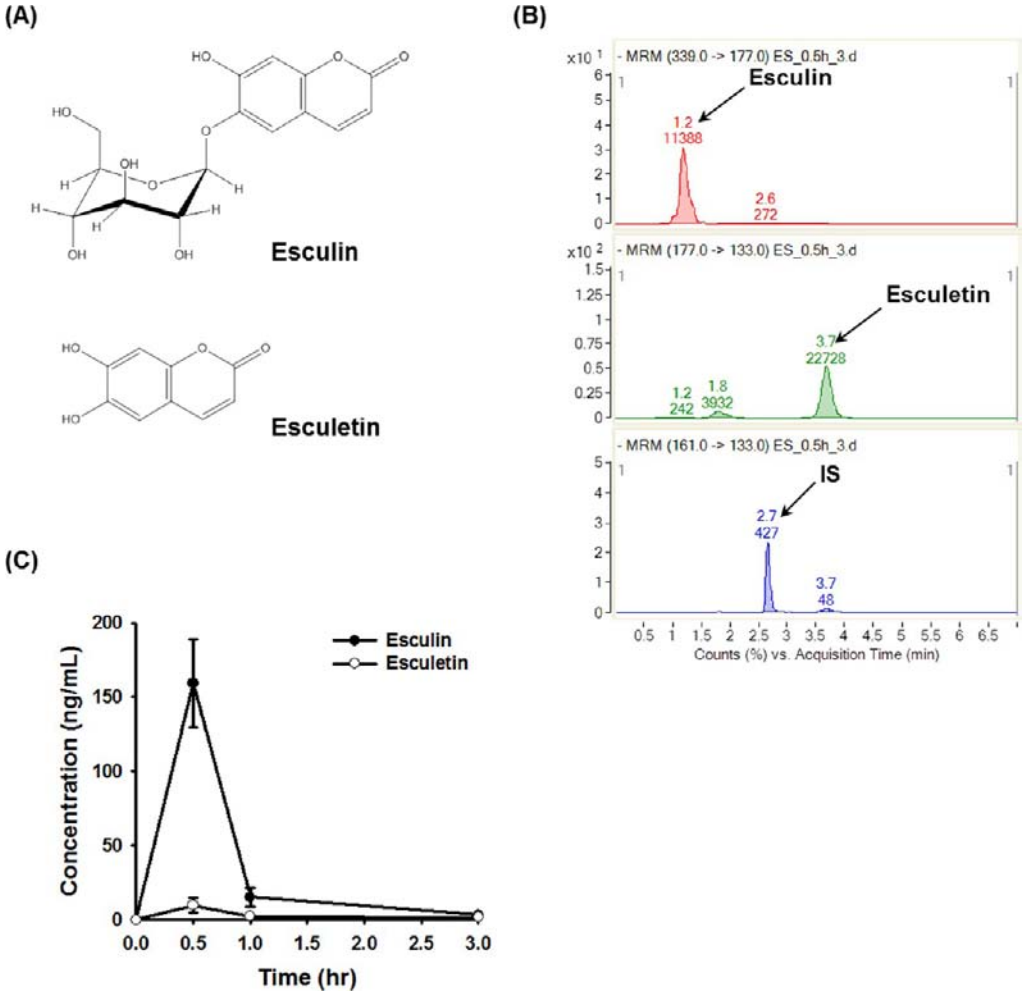

Figure 1. Blood levels of esculin and esculetin after oral administration of esculin in mice. (A) Structures of esculin and esculetin. (B) Representative MRM chromatograms for plasma samples collected after administration of esculin. (C) Blood concentrations of esculin and esculetin in mice.

renal damage are limited. To address this shortcoming, we investigated the effect of esculin, a major active component of ash bark, on glucose metabolism, oxidative stress, and inflammation in diabetic-damaged kidney to identify its effects and mechanism of action in diabetes. Furthermore, the pharmacokinetics of esculin and its metabolite esculetin were simultaneously examined in plasma samples from mice by liquid chromatography-electrospray ionization-tandem mass spectrometry.

MATERIALS AND METHODS

Chemicals. Streptozotocin (STZ), esculin, and esculetin (purity 98−100%) were purchased from Sigma Aldrich (Seoul, South Korea). Antibodies for Akt, phosphor-Ser473 Akt (pS473-Akt), insulin receptor β (IRβ), phosphor-IRβ at Tyr1150/1151 (pY1150/51-IR), glycogen synthase kinase 3β (Gsk3β), phosphor-Ser9-Gsk3β (pS9-Gsk3β), glyceraldehyde 3-phosphate dehydrogenase (GAPDH), cleaved caspase-3, β-actin, and horseradish peroxidase (HRP) conjugated antirabbit antibodies were purchased from Cell Signaling (Boston, MA, USA). Other chemicals and reagents used were of high quality and obtained from commercial sources.

Cell Culture. C2C12 mouse myoblast cell line was obtained from ATCC and cultured in Dulbecco's modified Eagle's medium (DMEM; Invitrogen, Carlsbad, CA, USA) supplemented with 10% fetal bovine serum (FBS; HyClone Laboratories, Logan, UT, USA) and 1% penicillin/streptomycin (Invitrogen) at 37 °C with 5% CO_2 in air.

Myotube Formation and Immunoblotting. C2C12 myoblast were cultured in DMEM until 90% of confluence. Cells were differentiated into myotubes with DMEM containing 2% horse serum for 4 days and then incubated for 16 h in DMEM containing 2% BSA and 10% FBS in the absence or presence of esculin. Subsequently, the esculin-treated cells were stimulated with 100 nM insulin for 10 min. After stimulation, cells were washed twice with PBS and harvested. For Western blotting, antibodies for Akt, phosphor-Ser473 Akt (pS473-Akt), insulin receptor β (IRβ), phosphor- IRβ Tyr1135/1136 IGF-1 Rβ /Tyr1150/1151, Gsk3β phosphor-Ser9-Gsk3β, and GAPDH were used.

2-[*N*-(7-Nitrobenz-2-oxa-1,3-diazol-4-yl)amino]-2-deoxy-D-glucose (2-NBDG) Glucose Uptake Assay. The myotubes, which were obtained from the above procedures, were stimulated with 100 nM insulin for 1 h. After insulin stimulation, the myotubes were incubated with 50 μM 2-NBDG (Invitrogen) for 15 min and then washed with PBS three times to remove free 2-NBDG. The fluorescence intensity of cells containing 2-NBDG was measured on the Infinite M1000 microplate reader (TECKAN) with excitation at 485 nm and emission at 535 nm.

Animal Experiments. The Guidelines for Animal Experimentation, approved by the Korea Institute of Science and Technology, were followed in these experiments. Male ICR mice weighing 30−35 g were used for evaluating the protection of the esculin against STZ-induced diabetic renal damage. The mice were housed under temperature (23 ± 2 °C) and humidity (55 ± 5%) conditions with a standard light (12 h light/dark). The mice were given free access to water and a normal diet (38057, Agribrands Purina Korea, Seongnam, Gyeonggi, Korea)

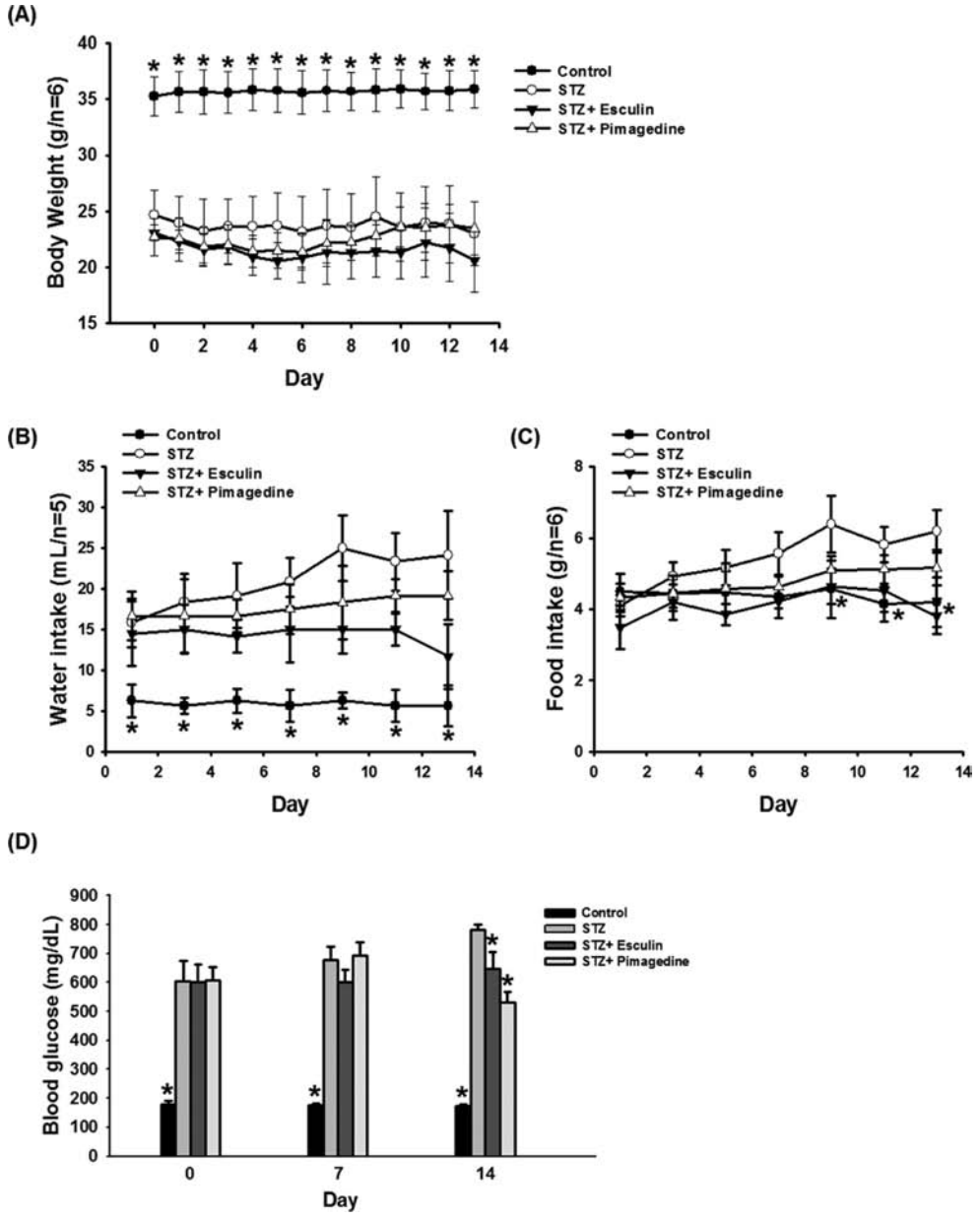

Figure 2. Effects of esculin on physiological parameters in the STZ-induced diabetes model. (A) Changes in body weight. (B) Changes in water intake. (C) Changes in food intake. (D) Changes in blood glucose levels. $p < 0.05$ compared to the STZ-treated control value.

containing 10 kcal % fat for a period of 1 week after arrival. After several days of adaptation, STZ dissolved in citrate buffer (10 mM, pH 4.5) was injected intraperitoneally at a dose of 200 mg/kg body weight following overnight fasting. The mice underwent a sham injection of citrate buffer without STZ and were also used as normal group ($n = 5$). The blood glucose level was determined, and the body weight was measured after 7 days of STZ injection, and to avoid any intergroup differences in these indices, the diabetic mice were divided into three experimental groups: group 1, diabetic mice received water (diabetic control, $n = 6$); groups 2, diabetic mice received 20 mg/kg body weight/day of esculin orally via gavage once a day (diabetic + esculin, $n = 6$); and group 3, diabetic mice received 20 mg/kg body weight/day of pimagedine orally via gavage once a day (diabetic + pimagedine, $n = 6$). The 20 mg/kg of esculin dosage was chosen according to the literature[18] and preliminary experiments. The mice were sacrificed 14 days after sample administration under light ether anesthesia. Blood samples were collected from abdominal aorta, and the serum was separated immediately from the blood samples by centrifugation. Kidneys and livers were removed, quickly frozen, and kept at −80 °C until analysis. All preparations and analyses of various parameters were performed simultaneously under similar experimental conditions to avoid any day to day variations.

Another abbreviated experiment to compare the blood levels of esculin and esculetin at three selected time points (0.5, 1, and 3 h) in mice ($n = 4$) was also conducted. Blood samples were collected from abdominal aorta under light ether anesthesia at 0.5, 1, and 3 h after esculin oral administration (20 mg/kg). The mice were sacrificed in each time point. About 500 μL blood was drawn and collected in a heparin-coated tube, and plasma was obtained following rapid centrifugation and immediately frozen at −80 °C until analysis.

LC/MS/MS Analyses for Esculin and Esculetin in Blood. Plasma samples were analyzed for esculin and esculetin using the LC/MS/MS method reported previously.[19] The LC/MS/MS system consisted of an Agilent 1260 Infinity high-performance liquid chromatography (HPLC) system with an Agilent 6460 triple-quadrupole mass spectrometer (Agilent Technologies, Palo Alto, CA) equipped with a turbo ion spray source. Chromatographic separation was achieved with a BDS Hypersil C_{18} column (50 mm

dx.doi.org/10.1021/jf403840c | J. Agric. Food Chem. 2014, 62, 2069−2076

×2.1 mm ID, 5 μL, Thermo Fisher Scientific Inc., Waltham, MA), and oven temperature was maintained at 40 °C. The mobile phase consisted of 0.1% formic acid (solvent A) and 90% acetonitrile with 0.1% formic acid (solvent B). A gradient program was used for HPLC separation, with a flow rate of 0.25 mL/min the gradient program began with 10% B, which was increased to 90% in 1 min, was maintained to 4 min, and followed by 4 min re-equilibration. Electrospray ionization was performed in negative ion mode. The precursor−product ion pairs monitored in multiple reaction monitoring (MRM) detection were 339→177 for esculin, 177→133 for esculetin, and 161→133 for 7-OH-coumarin (IS). The representative MRM chromatograms are shown in Figure 1B. Calibration curves for analytes were obtained using 9 points in the range 1−500 ng/mL. Calibration curves were generated by plotting the peak area ratio for esculin or esculetin to IS versus the concentration of esculin or esculetin in the standard-spiked plasma by least-squares linear regression. The calibration curve equations are $y = 0.1215x - 0.0368$ ($r^2 = 0.999$) for esculin and $y = 0.0747x - 0.0058$ ($r^2 = 0.999$) for esculetin.

Histological Examination. After fixation of the kidneys with 10% formalin, renal tissues were sectioned and stained with hematoxylin and eosin (HE) reagents for histological examination. Tubular damage in HE-stained sections was examined under the microscope and scored based on the percentage of cortical tubules showing epithelial necrosis: 0, normal; 1, <10%; 2, 10−25%; 3, 26−75%; 4, >75%. Tubular necrosis was defined as tubular epithelial degeneration, interstitial inflammation, and archiectural abnormality as described previously.[20] The morphometric examination was performed in a blinded manner by two independent investigators.

Western Blot Analysis. Frozen kidney tissues were homogenized with a lysis buffer (contents of 1% NP-40, 20 mM Tris-HCl, 150 mM NaCl, 1 mM Na_2EDTA, 1 mM EGTA, 1% sodium deoxycholate, and 100 mM PMSF) and centrifuged at 13 000 rpm at 4 °C for 20 min to obtain the cellular proteins in the supernatant. Differential protein expression patterns were assessed by Western blot following protein quantification by the Lowry and Bradford methods. Equal amounts of proteins from each sample were resolved by SDS-PAGE, transferred to polyvinylidene fluoride (PVDF) membranes for 1 h at semidry, and blocked in blocking buffer for 1 h at room temperature. PVDF membranes were incubated with primary antibody against cleaved caspase-3 (1:1000 dilution), β-actin (1:1000 dilution) overnight at 4 °C, washed three times for 5 min to wash buffer, incubated with HRP-conjugated secondary antibody (1:2000 dilution, antirabbit) for 1 h at room temperature, washed three times, and then detected with ECL solution.

Gene Expression Analysis. Total RNA was isolated from tissue using the TRIzol reagent (Invitrogen, Carlsbad, CA) according to the manufacturer's instructions. The RNA concentration of each sample was determined by spectrophotometry at 260 nm; the integrity of each RNA sample was evaluated using the Agilent 2100 BioAnalyzer (Agilent Technologies, SantaClara, CA). cDNA synthesis was performed using 1 μg of total RNA in 20 μL with random primers and Superscript II reverse transcriptase. Quantitative real-time PCR (Q-PCR) analyses were performed with SYBR green fluorescent dye using the 7500 Real-Time PCR System (Applied Biosystem, Foster City, CA). Data analyses were performed using 7500 System SDS software version 1.3.1 (Applied Biosystem). Primer sets used in this study were as follows: glucose 6-phosphatase (G6 Pase), forward 5′-ATGACTTTGGGATCCAGTCG-3′ and reverse 5′- TGGAACCA-GATGGGAAAGAG-3′ and glyceraldehyde-3-phosphate dehydrogenase (GAPDH), forward 5′-TTGTTGCCATCAACGACCCC-3′ and reverse 5′- GCCGTTGAATTTGCCGTGAG-3′.

Statistical Analysis. Statistical significance was determined through analysis of variance (ANOVA) followed by a multiple comparison test with a Bonferroni adjustment. *P* values of less than 0.05 were considered statistically significant.

RESULTS

Blood Levels of Esculin and Esculetin after Oral Administration of Esculin in Mice. After oral administration of esculin to mice (20 mg/kg body weight), there was a rapid and short-lasting increase in plasma esculin and esculetin levels. The concentrations of esculin and esculetin in blood were 159.5 ± 29.8 and 9.7 ± 4.9 ng/mL at 30 min, respectively (Figure 1C). Although a large portion of esculin was detected in the blood, esculetin, which is a deglycosylated metabolite of esculin, was also detected (Figure 1C).

Antidiabetic Effect and Mechanism of Esculin Against STZ-Induced Type 1 Diabetes in Mice. Figure 2 shows the effects of esculin on the changes in physico-metabolic symptoms with diabetes over the 14-day experimental period. The body weight of mice after STZ and STZ + esculin or pimagedine was markedly reduced compared to that of control mice (Figure 2A). In comparison, the intake of water and food were significantly increased in the STZ-treated mice (Figure 2B and 2C). Although no significant amelioration was evident, oral administration of esculin or pimagedine at a dose of 20 mg/kg for 14 days attenuated the diabetes-induced physiological abnormalities. The blood glucose level of diabetic mice was markedly higher than that of normal mice, and it was continuously increased during the experimental period. The elevated glucose level was significantly reduced in diabetic mice given 20 mg/kg esculin or pimagedine (Figure 2D).

As shown in Figure 3A, the plasma alanine aminotransferase (ALT) levels of diabetic mice were significantly increased more than those of normal control mice. However, treatment with esculin led to a significant decrease in plasma ALT levels (Figure 3A). The expression level of G6 Pase gene expression in the liver was significantly increased in diabetic animals. The elevated expression level of G6 Pase was markedly reduced in esculin-treated diabetic mice (Figure 3B), supporting the antidiabetic effects of esculin; however, the effect of esculin was weaker than that of pimagedine (Figure 3B).

Effect of Esculin on Insulin Sensitivity. To ascertain the positive effects of esculin on insulin sensitivity, we first examined glucose uptake in C2C12 myotubes under normal conditions. As shown in Figure 4A, glucose uptake in C2C12 myotubes in the absence or presence of insulin was significantly enhanced by esculin treatment under normal conditions. Correspondingly, esculin (50 μM) application also enhanced the insulin-evoked phosphorylation of IR, Akt, and GSK-3β under normal conditions, indicating a potential for improvement of insulin sensitivity (Figure 4B).

Renoprotective Effect of Esculin Against STZ-Induced Diabetic Renal Damage in Mice. The elevated serum creatinine level of STZ-treated mice was significantly reduced by esculin (Figure 5A). HE staining was performed on renal sections to measure tubular damage. As shown in the representative pictures of renal sections, severe tubulointerstitial injuries including tubular epithelial cell detachments, cystic dilatation of tubules, and inflammatory cell infiltration occurred in kidneys of STZ-treated diabetic mice (Figure 5B). However, the increased tubular damage in STZ-treated mice was reduced by treatment with esculin (Figure 5B). Figure 6A shows the effect of esculin on the cleaved caspase-3 protein expression in STZ-treated mice kidneys. The cleaved caspase-3 protein expression was significantly increased after STZ injection, and cotreatment with esculin afforded significant renoprotection (Figure 6B).

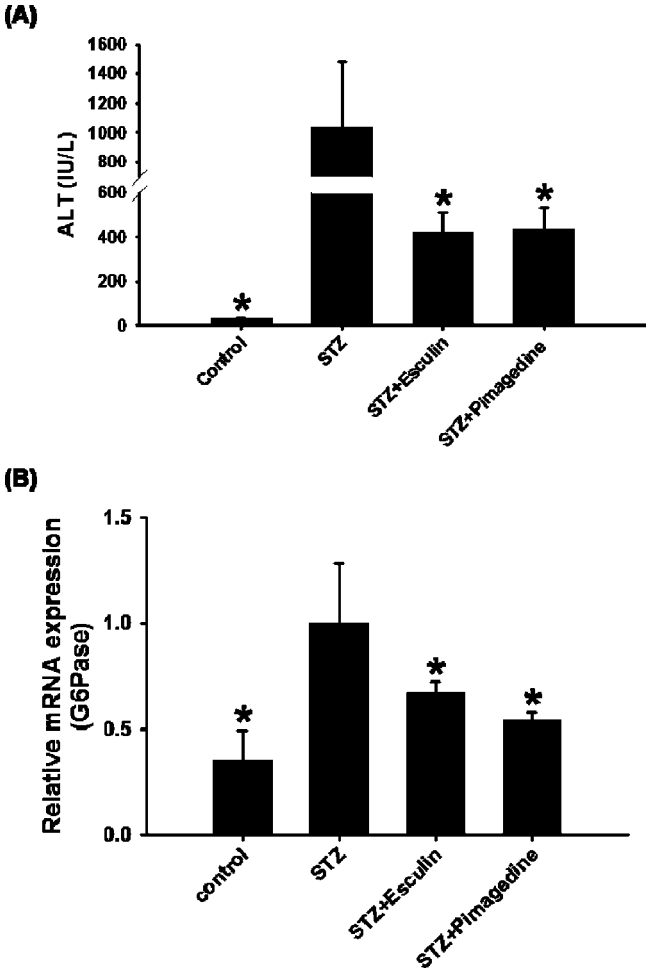

Figure 3. Effects of esculin on serum ALT and hepatic glucose 6-phosphatase levels in the STZ-induced diabetes model. (A) Serum ALT levels. (B) Hepatic glucose 6-phosphatase levels. $p < 0.05$ compared to the STZ-treated control value.

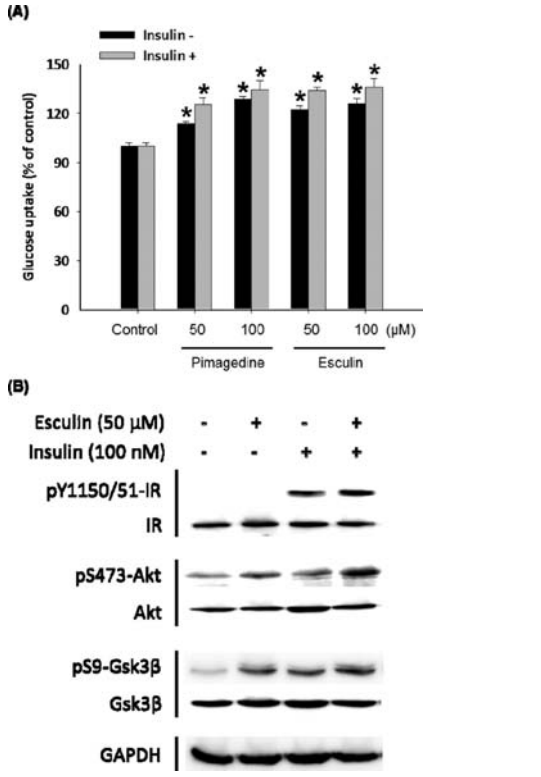

Figure 4. Effects of esculin on glucose uptake and insulin sensitivity in C2C12 myotubes. (A) Basal and insulin-stimulated glucose uptake in pimagedine and esculin-treated C2C12 myotubes under normal conditions. (B) Level of phosphorylation of IR, Akt, and GSK-3β in esculin-treated C2C12 myotubes under normal conditions. Protein levels were analyzed by Western blot. $p < 0.05$ compared to the control value.

DISCUSSION

Many diabetic patients choose complementary and alternative therapies along with mainstream antidiabetic drugs, which has increased demand for alternative therapies for diabetes.[21] In the present study, we investigated the antidiabetic effect and mechanism of esculin, an active ingredient of ash bark, on kidney damage caused by hyperglycemia, oxidative stress, and inflammation to evaluate its possible use in treatment of diabetic renal damage.

To evaluate the effect of esculin on diabetic renal damage, we administered esculin to STZ-induced diabetic mice and monitored plasma glucose levels in each animals. After oral administration of esculin to mice, there was a rapid and short-lasting increase in plasma esculin and esculetin levels. Over the experimental period, the levels of water and food intake were significantly elevated in diabetic mice, indicating the changes in physiological changes that result from the increased blood glucose levels. STZ enters the β cell via a glucose transporter (GLUT2) and liberates toxic amounts of free radicals that cause damage to the DNA. Oxidative inflammation is implicated in pancreatic β-cell injury, leading to development of diabetes mellitus.[22] The pancreatic islet size and blood insulin levels of diabetic mice was markedly lowered than those of normal control mice, but there were no significant ameliorations in islet size or blood insulin levels after esculin treatments (Supplemental Figure 1, Supporting Information). Therefore, the beneficial effect of esculin on blood glucose might be related to other factors than pancreatic damage by STZ. Because hepatic gluconeogenesis gene expression is markedly increased in diabetic animals and contributes to hyperglycemia, expression of G6 Pase, one of the key enzymes in gluconeogenesis,[23] was measured in the liver tissue of diabetic mice. The expression level of G6 Pase was significantly reduced in esculin-treated mice, supporting the antidiabetic effect of esculin.

The tyrosine phosphorylation of IRβ subunit is necessary for insulin signal transduction into the cells. In particular, phosphorylation of tyrosine 1146, 1150, and 1151 is crucial for activation of the IR which initiates further downstream signaling events.[24] Akt regulates glycogen synthesis through phosphorylation within the carboxy terminus at Ser473 and inactivation of GSK-3α and β, which was initially identified as an enzyme that regulates glycogen synthesis in response to insulin.[25] In the present study, esculin increased the uptake of glucose and induced the insulin-evoked phosphorylation of IRβ, Akt, and glycogen synthase kinase 3β in C2C12 myotubes, indicating a potential for improvement of insulin sensitivity.

Hyperglycemia-induced abnormal production of ROS has been implicated in the etiology of diabetic nephropathy, with ROS having critical roles in the development and progression of kidney damage.[26−28] In patients with diabetes and/or renal failure, the level of blood creatinine, which is an effective index for expressing the glomerular filtration rate, increases

dx.doi.org/10.1021/jf403840c | J. Agric. Food Chem. 2014, 62, 2069−2076

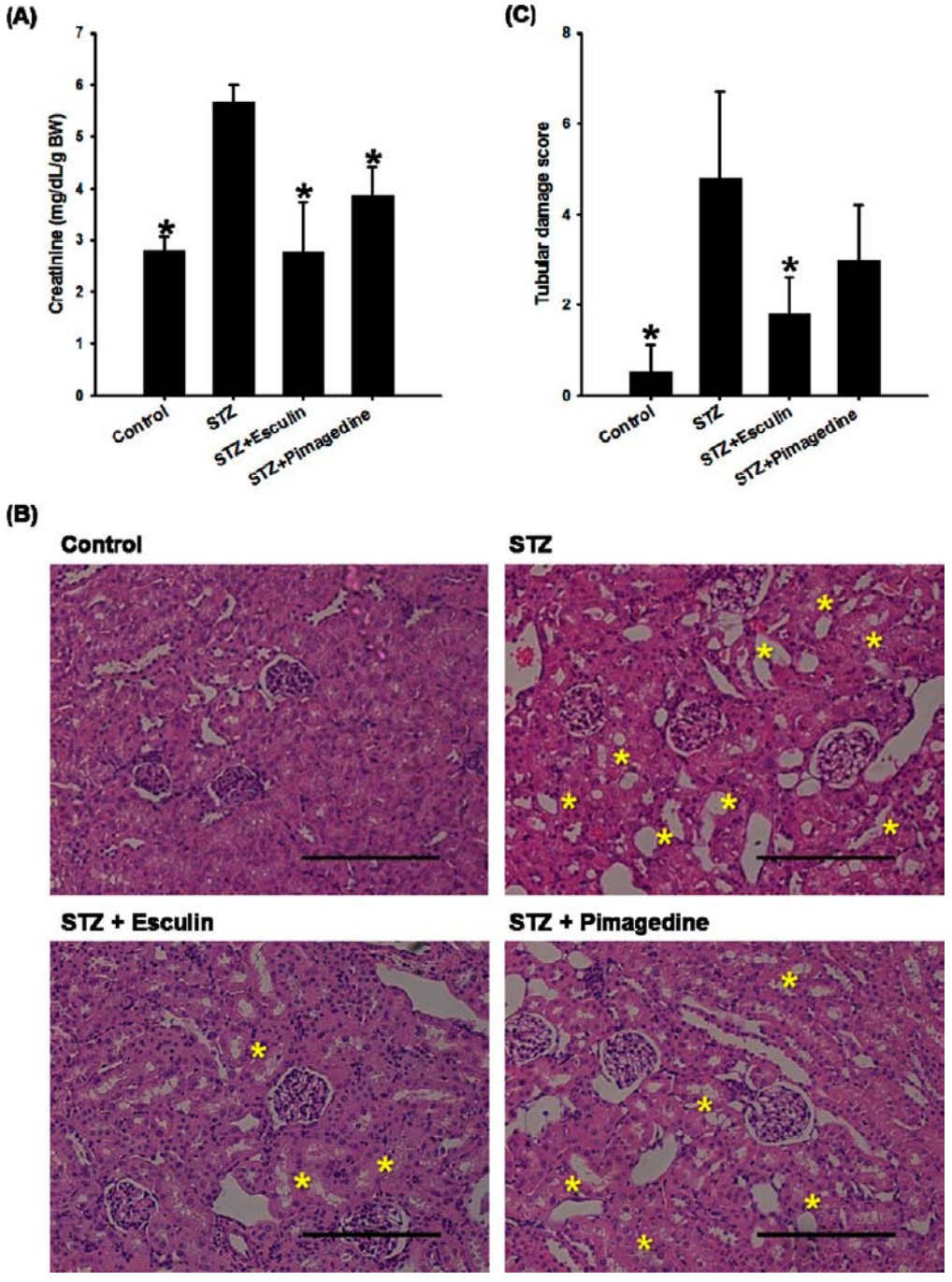

Figure 5. Effects of esculin on renal function and histopathological changes in the STZ-induced diabetes model. (A) Serum creatinine levels. (B) HE staining of representative renal section. (C) Tubular damage score. Yellow asterisks indicate tubular damage. $p < 0.05$ compared to the STZ-treated control value.

exponentially and eventually causes nephritic syndrome.[29] However, the present investigation showed that administration of esculin or pimagedine for 14 days significantly reduced the levels of blood creatinine. Therefore, the diabetic renal dysfunctions of diabetic mice were improved by the administration of esculin.

STZ activates various pro-inflammatory and apoptotic molecules including the caspase-3 and Bax systems.[30−32] Synthetic or naturally occurring caspase inhibitors have the potential to minimize uncontrolled apoptosis in STZ-induced nephropathy.[31,33] For example, the antioxidant compound alpha-lipoic acid can abrogate the oxidative stress induced in mesangial cells and rat kidney by elevated glucose levels.[30] Our results also showed significant increases in cleaved caspase-3 in the kidneys of diabetic mice; the elevated level was significantly reduced after esculin administration. These results imply that esculin may alleviate oxidative stress by preventing caspase-3 activation and related inflammation in the kidney.

Clinical evidence has suggested that the appropriate use of nutraceuticals or herbal medicines can prevent or ameliorate development of diabetic complications.[34,35] However, these medicines usually have an insufficient scientific basis and the exact mechanisms behind their beneficial effects are unknown. This study demonstrates that esculin ameliorates diabetes-

dx.doi.org/10.1021/jf403840c | J. Agric. Food Chem. 2014, 62, 2069−2076

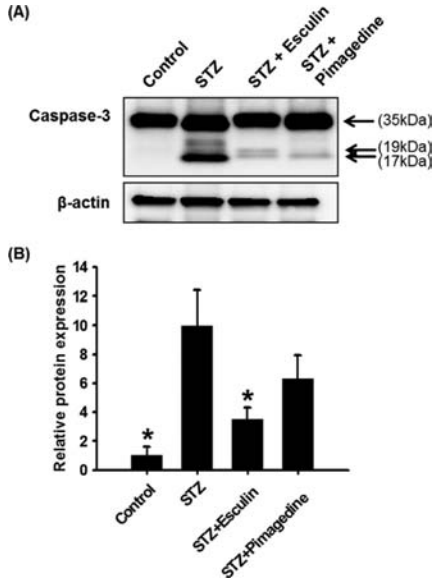

Figure 6. Effects of esculin on renal caspase-3 activation in the STZ-induced diabetes model. (A) Cleaved caspase-3 protein expression and (B) its quantitative data for Western blot analysis of renal cortex tissues. $p < 0.05$ compared to the STZ-treated control value.

induced renal dysfunction by reducing the activation of caspase-3 in the kidney. The current experimental results provide therapeutic evidence of the renoprotective effects of esculin both in vitro and in vivo.

■ ASSOCIATED CONTENT

Supporting Information

This material is available free of charge via the Internet at http://pubs.acs.org.

■ AUTHOR INFORMATION

Corresponding Authors

*Phone: 82-33-650-3512. Fax: 82-33-650-3028. E-mail: kkang@kist.re.kr.

*Phone: 82-33-650-3503. Fax: 82-33-650-3028. E-mail: snkim@kist.re.kr.

Funding

This work was funded by the Korea Institute of Science and Technology institutional program (2Z04210).

Notes

The authors declare no competing financial interest.

■ REFERENCES

(1) Ahmed, N. Advanced glycation endproducts-role in pathology of diabetic complications. *Diabetes Res. Clin. Pract.* **2005**, *67*, 3−21.

(2) Baynes, J. W. Role of oxidative stress in development of complications in diabetes. *Diabetes* **1991**, *40*, 405−412.

(3) Selby, J. V.; FitzSimmons, S. C.; Newman, J. M.; Katz, P. P.; Sepe, S.; Showstack, J. The natural history and epidemiology of diabetic nephropathy. Implications for prevention and control. *JAMA* **1990**, *263*, 1954−1960.

(4) The Diabetes Control and Complications Trial Research Group.. The effect of intensive treatment of diabetes on the development and progression of long-term complications in insulin-dependent diabetes mellitus. *N. Engl. J. Med.* **1993**, *329*, 977−986.

(5) Yamabe, N.; Yokozawa, T.; Oya, T.; Kim, M. Therapeutic potential of (-)-epigallocatechin 3-O-gallate on renal damage in diabetic nephropathy model mice. *J. Pharmacol. Exp. Ther.* **2006**, *319*, 228−236.

(6) Kim, H. Y.; Kang, K. S.; Yamabe, N.; Nagai, R.; Yokozawa, T. Protective effect of heat-processed American ginseng against diabetic renal damage in rats. *J. Agric. Food Chem.* **2007**, *55*, 8491−8497.

(7) Rao, A. V.; Snyder, D. M. Raspberries and human health: a review. *J. Agric. Food Chem.* **2010**, *58*, 3871−3883.

(8) Paya, M.; Halliwell, B.; Hoult, J. R. S. Interactions of a series of coumarins with reactive oxygen species. Scavenging of superoxide, hypochlorous acid and hydroxyl radicals. *Biochem. Pharmacol.* **1999**, *44*, 205−214.

(9) Lin, W. L.; Wang, C. J.; Tsai, Y. Y.; Liu, C. L.; Hwang, J. M.; Tseng, T. H. Inhibitory effect of esculetin on oxidative damage induced by t-butyl hydroperoxide in rat liver. *Arch. Toxicol.* **2000**, *74*, 467−472.

(10) Kostova, I. Synthetic and natural coumarins as cytotoxic agents. *Curr. Med. Chem.* **2005**, *5*, 29−46.

(11) Riveiro, M. E.; Moglioni, A.; Vazquez, R.; Gomez, N.; Facorro, G.; Piehl, L.; de Celis, E. R.; Shayo, C.; Davio, C. Structural insights into hydroxycoumarin-induced apoptosis in U-937 cells. *Bioorg. Med. Chem.* **2008**, *16*, 2665−2675.

(12) Witaicenis, A.; Seito, L. N.; Stasi, L. C. Intestinal anti-inflammatory activity of esculetin and 4-methylesculetin in the trinitrobenzenesulphonic acid model of rat colitis. *Chem. Biol. Interact.* **2010**, *186*, 211−218.

(13) Lee, B. C.; Lee, S. Y.; Lee, H. J.; Sim, G. S.; Kim, J. H.; Kim, J. H.; Cho, Y. H.; Lee, D. H.; Pyo, H. B.; Choe, T. B.; Moon, D. C.; Yun, Y. P.; Hong, J. T. Anti-oxidative and photo-protective effects of coumarins isolated from Fraxinus chinensis. *Arch. Pharm. Res.* **2007**, *30*, 1293−1301.

(14) Park, C.; Jin, C. Y.; Kim, G. Y.; Choi, I. W.; Kwon, T. K.; Choi, B. T.; Lee, S. J.; Lee, W. H.; Choi, Y. H. Induction of apoptosis by esculetin in human leukemia U937 cells through activation of JNK and ERK. *Toxicol. Appl. Pharmacol.* **2008**, *227*, 219−228.

(15) Wang, C. J.; Hsieh, Y. J.; Chu, C. Y.; Lin, Y. L.; Tseng, T. H. Inhibition of cell cycle progression in human leukemia HL-60 cells by esculetin. *Cancer Lett.* **2002**, *183*, 163−168.

(16) Jung, H. A.; Park, J. J.; Islam, M. N.; Jin, S. E.; Min, B. S.; Lee, J. H.; Sohn, H. S.; Choi, J. S. Inhibitory activity of coumarins from Artemisia capillaris against advanced glycation endproduct formation. *Arch. Pharm. Res.* **2012**, *35*, 1021−1035.

(17) Nurul Islam, M.; Jung, H. A.; Sohn, H. S.; Kim, H. M.; Choi, J. S. Potent α-glucosidase and protein tyrosine phosphatase 1B inhibitors from Artemisia capillaris. *Arch. Pharm. Res.* **2013**, *36*, 542−552.

(18) Li, J. M.; Zhang, X.; Wang, X.; Xie, Y. C.; Kong, L. D. Protective effects of cortex fraxini coumarines against oxonate-induced hyperuricemia and renal dysfunction in mice. *Eur. J. Pharmacol.* **2011**, *666*, 196−204.

(19) Li, Y. Y.; Song, Y. Y.; Liu, C. H.; Huang, X. T.; Zheng, X.; Li, N.; Xu, M. L.; Mi, S. Q.; Wang, N. S. Simultaneous determination of esculin and its metabolite esculetin in rat plasma by LC-ESI-MS/MS and its application in pharmacokinetic study. *J. Chromatogr., B: Anal. Technol. Biomed. Life Sci.* **2012**, *907*, 27−33.

(20) Mukhopadhyay, P.; Rajesh, M.; Pan, H.; Patel, V.; Mukhopadhyay, B.; Bátkai, S.; Gao, B.; Haskó, G.; Pacher, P. Cannabinoid-2 receptor limits inflammation, oxidative/nitrosative stress, and cell death in nephropathy. *Free Radical Biol. Med.* **2010**, *48*, 457−467.

(21) Ceylan-Isik, A. F.; Fliethman, R. M.; Wold, L. E.; Ren, J. Herbal and traditional Chinese medicine for the treatment of cardiovascular complications in diabetes mellitus. *Curr. Diabetes Rev.* **2008**, *4*, 320−328.

(22) Yabaluri, N.; Bashyam, M. D. Hormonal regulation of gluconeogenic gene transcription in the liver. *J. Biosci.* **2010**, *35*, 473−484.

(23) Szkudelski, T. The mechanism of alloxan and streptozotocin action in B cells of the rat pancreas. *Physiol, Res.* **2001**, *50*, 537−546.

(24) González-Sánchez, J. L.; Serrano-Ríos, M. Molecular basis of insulin action. *Drug News Perspect.* **2007**, *20*, 527−531.

(25) Kaidanovich, O.; Eldar-Finkelman, H. The role of glycogen synthase kinase-3 in insulin resistance and type 2 diabetes. *Expert Opin. Ther. Targets* **2002**, *6*, 555−561.
(26) Li, J. M.; Shah, A. M. ROS generation by nonphagocytic NADPH oxidase: potential relevance in diabetic nephropathy. *J. Am. Soc. Nephrol.* **2003**, *14*, S221−S226.
(27) Forbes, J. M.; Coughlan, M. T.; Cooper, M. E. Oxidative stress as a major culprit in kidney disease in diabetes. *Diabetes* **2008**, *57*, 1446−1454.
(28) Heyman, S. N.; Rosen, S.; Rosenberger, C. A role for oxidative stress. *Contrib. Nephrol.* **2011**, *174*, 138−148.
(29) Bell, D. S. Diabetic nephropathy: changing concepts of pathogenesis and treatment. *Am. J. Med. Sci.* **1991**, *301*, 195−200.
(30) Singh, L. P.; Cheng, D. W.; Kowluru, R.; Levi, E.; Jiang, Y. Hexosamine induction of oxidative stress, hypertrophy and laminin expression in renal mesangial cells: effect of the anti-oxidant alpha-lipoic acid. *Cell Biochem. Funct.* **2007**, *25*, 537−550.
(31) Kuhad, A.; Sachdeva, A. K.; Chopra, K. Attenuation of renoinflammatory cascade in experimental model of diabetic nephropathy by sesamol. *J. Agric. Food Chem.* **2009**, *57*, 6123−6128.
(32) Jung, D. S.; Lee, S. H.; Kwak, S. J.; Li, J. J.; Kim, D. H.; Nam, B. Y.; Kang, H. Y.; Chang, T. I.; Park, J. T.; Han, S. H.; Yoo, T. H.; Kang, S. W. Apoptosis occurs differentially according to glomerular size in diabetic kidney disease. *Nephrol. Dial. Transplant.* **2012**, *27*, 259−266.
(33) Nakano, M.; Matsumoto, I.; Sawada, T.; Ansite, J.; Oberbroeckling, J.; Zhang, H. J.; Kirchhof, N.; Shearer, J.; Sutherland, D. E.; Hering, B. J. Caspase-3 inhibitor prevents apoptosis of human islets immediately after isolation and improves islet graft function. *Pancreas* **2004**, *29*, 104−109.
(34) Chao, M.; Zou, D.; Zhang, Y.; Chen, Y.; Wang, M.; Wu, H.; Ning, G.; Wang, W. Improving insulin resistance with traditional Chinese medicine in type 2 diabetic patients. *Endocrine* **2009**, *36*, 268−274.
(35) Omar, E. A.; Kam, A.; Alqahtani, A.; Li, K. M.; Razmovski-Naumovski, V.; Nammi, S.; Chan, K.; Roufogalis, B. D.; Li, G. Q. Herbal medicines and nutraceuticals for diabetic vascular complications: mechanisms of action and bioactive phytochemicals. *Curr. Pharm. Des.* **2010**, *16*, 3776−3807.

underutilized palm heart species and support the claims of locals with regard to their health potential in treating diabetes, these two vegetables were investigated using related in vitro assays.

MATERIALS AND METHODS

Preparation of Samples. Lalis (*P. geminiflora*) and pantu (*E. insignis*) were purchased at Satok market in Kuching, Sarawak, Malaysia. About 15 kg of each sample was collected and stored in a freezer (−20 °C) and then brought back to the laboratory by flight within 3 days. Voucher specimens of the samples, lalis (SK2276/13) and pantu (SK2277/13), were deposited at the Biodiversity Unit, Bioscience Institute, Universiti Putra Malaysia, Malaysia. The peels of sample were removed, and edible parts were cleaned and chopped into small pieces. Samples were subjected to lyophilization for 72 h using a benchtop freeze-dryer (Virtis, Gardiner, NY, USA). Subsequently, the dried vegetables were ground into fine particles and stored at −40 °C.

Proximate Analyses. The moisture content of the studied vegetables was evaluated through a direct drying method (AOAC method 964.22) using a convection oven (Memmert Universal, Schwabach, Germany). Ash content was measured using a dry ashing method (AOAC method 923.03) whereby the samples were incinerated at 550 °C in a furnace (Furnace 62700, Barnstead/Thermolyne, Dubuque, IA, USA). Lipid content was determined using the Soxhlet method (AOAC method 920.39C), and protein content (N × 6.25) was measured according to the Kjeldahl method (AOAC method 955.04) by Kjeltec instrument (Kjeltec 2200, Foss, Höganäs, Sweden). The above analyses followed AOAC methods.[9] Total carbohydrate was determined using a Clegg anthrone method.[10]

Total (TDF) and insoluble dietary fiber (IDF) contents were measured using a gravimetric method.[11] Dietary fiber analyses were carried out using a Fibertec system (Fibertec System E 1023 filtration module, Sweden). Result was obtained after subtracting the protein and ash contents of residue. Soluble dietary fiber (SDF) was calculated as TDF − IDF value.

Mineral Analysis. The resulting ash sample obtained from the dry-ashing method was dissolved in 100 mL of 1 N hydrochloric acid solution. Subsequently, the ash solution was used in determination of the mineral contents. Minerals (sodium, potassium, calcium, magnesium, iron, zinc, phosphorus, manganese, and copper) were determined using an inductively coupled plasma optical emission spectrometry (ICP-OES) (ICP-OES, PerkinElmer DV2000, Boston, MA, USA) method.[12]

Sample Extraction. The extraction method was according to Liu et al.[13] with slight modification. Four grams of powder extract was mixed with 100 mL of 70% ethanol containing 1.2 M HCl (ratio of 1:25, g/v) and gently shaken at room temperature using an incubator shaker (Heidolph Instruments Incubator1000, Schwabach, Germany) set at 200 rpm for 5 h. After that, sample extracts were filtered through Whatman paper no. 1, and the filtrate was used for total phenolic and flavonoid content determination. The remaining extract was evaporated using a rotary evaporator (Buchi Rotavapor R-200, Essen, Germany) to remove the solvent and then lyophilized. The yield of extracts was subjected to antioxidant and antidiabetic in vitro assays.

Total Phenolic and Flavonoid Contents. Total phenolic content (TPC) of studied samples was determined according to method of Velioglu et al.[14] Results were generated from the standard calibration curve of gallic acid (20−100 μg/mL). Total flavonoid content (TFC) of studied samples was evaluated by an aluminum chloride colorimetric assay[15] with a slight modification. A standard calibration curve was generated using rutin (0.01−0.08 μg/mL).

Phenolic Compounds Analysis. Sample extract was prepared according to a method described by Liu et al.[16] with modifications. Quantification of phenolics in the studied vegetable extracts was performed using a HPLC system consisting of an Agilent 1100 series liquid chromatographic system equipped with an Agilent 1100 series diode array detector (DAD) (Agilent Technologies, Santa Clara, CA, USA) as described by He and Xia.[17] Separation of compounds was implemented using an eclipse XDB-C18 column (250 mm × 4.6 mm i.d.) (Hewlett-Packard, Palo Alto, CA, USA). The mobile phases consisted of 0.5% acetic acid (v/v) (A) and methanol (B). The applied gradient elution composition was a linear increase to 90% B in 20 min, then isocratic for 5 min, and returned to the initial condition in 5 min. Run time and column temperature were set at 30 min and 30 °C, respectively. Flow rate was 0.6 mL/min, and injection volume was 20 μL. The wavelength was set at 280 nm. The compounds in extracts were identified by comparison of their retention times and UV−vis absorption spectra with authentic standards and further confirmed by spiking of extract with authentic standards. External standards with different concentrations (20−100 μg/mL) diluted in ethanol were performed to determine the quantity of identified compounds. This linearity of detector response was assessed using five different concentrations, with three injections for all concentrations. A linear relationship was found between peak area and concentration (20−100 μg/mL). The correlation coefficient ranges from $r = 0.985$ to $r = 0.998$.

After completion of HPLC analysis, the liquid chromatography electrospray ionization mass spectrometry (LC-ESI-MS) analysis was conducted using an Applied TSQ Quantum Ultra-LCMS (Thermo Fisher, San Diego, CA, USA) to check the molecular mass of detected compounds in the HPLC chromatogram. A reversed-phase Lichrospher C18 column (250 mm × 4 mm, i.d., 5 μm; Merck, Damstadt, Germany) was used. Both positive and negative ion modes were used, and optimum resolution used was 3000 Da. The spray voltage was maintained at 3.5 kV. The sheath/auxiliary/sweep gas was 99% pure. The sheath and auxiliary gas pressures were set at 30 and 5 psi, respectively. The capillary temperature was 270 °C. The flush speed was 100 μL/s, and the injection volume was 10 μL. Samples were run using a gradient elution system as described by Hassan et al.[18] Continuous full mass spectral data were achieved by scanning from m/z 100 to 800. Determination of phenolic compounds was carried out by comparing the retention times, UV−vis absorption spectra, and reference standards available.

In Vitro Antioxidant Capacities. *Ferric Reducing Antioxidant Power (FRAP) Assay.* The ability of extract to convert Fe^{3+}/ferricyanide complex to Fe^{2+} ions was assessed on the basis of the method of Benzie and Strain,[19] with some modifications. Concentration of samples was at 0.2 mg/mL. A preliminary test had been carried out to determine the concentration of samples that gave readings within the standard curve range.

Oxygen Radical Absorbance Capacity (ORAC) Assay. The ORAC assay[20] was based on the inhibition of peroxyl radical-induced oxidation initiated by thermal decomposition of 2,2′-azobis(2-methylpropionamidine) dihydrochloride (AAPH). Different dilutions of Trolox (12.5−200 μM) and sample extracts were prepared in phosphate buffer (10 mM, pH 7.4). A concentration of samples was at 0.5 mg/mL. A preliminary test was carried out to determine the concentration of samples that gave readings within the range of Trolox standard curve. Briefly, 10 nM fluorescein (150 μL) was added into a black 96-well plate (Nunc, Roskilde, Denmark) and followed by 25 μL of Trolox, sample, or blank (phosphate buffer). The plate was covered and incubated for 10 min at 37 °C. After incubation, fluorescence measurements (excitation wavelength, 485 nm; emission wavelength, 520 nm) were taken every 90 s to determine the background signal. The fluorescence measurement was performed using microplate reader FLUOstar Omega (BMG LABTECH, Offenburg, Germany). After four cycles, 25 μL of 240 mM AAPH was injected via onboard injector. The test was continued, and fluorescence intensity measurements were taken up to 120 min. ORAC values were calculated on the basis of the difference in area under the fluorescence decay curve between the blank and sample. The antioxidant capacity (ORAC) was calculated according to the following equation:

$$\text{ORAC value} = [(\text{AUC}_{\text{sample}} - \text{AUC}_{\text{blank}})/(\text{AUC}_{\text{Trolox}} - \text{AUC}_{\text{blank}}) \times [\text{Trolox}]\ \text{dilution factor}$$

Inhibition of Lipid Membrane Erythrocytes Oxidation Assay. This assay was done according to the method described by Rodriguez et

al.[21] with some modifications. The blood sample (10 mL) was obtained from a volunteer and collected into EDTA tubes. Then, the tube was immediately centrifuged at 3000 rpm and 4 °C for 10 min. After removal of plasma, the packed red blood cells (RBC) were directly washed three times with 0.9% NaCl (2 mL). After the third wash, packed RBC were gently resuspended in phosphate buffer saline (PBS) (pH 7.4) to obtain a 5% hematocrit in the presence of 1 mM NaN_3 and preincubated at 37 °C for 10 min. Then, the mixture was divided into aliquots (1.6 mL) for each experimental treatment. Concentrations of samples and standard were 0.05 and 0.2 mg/mL, respectively. All treatment groups and BHT (0.2 mL) were challenged with 0.01 M H_2O_2 (0.2 mL). Meanwhile, negative and positive controls were made with solvent and H_2O_2 alone, respectively. After 60 min of incubation at 37 °C, the tube was kept in an ice bath for 1 min.

Malondialdehyde (MDA) produced from membrane lipid oxidation of erythrocyte oxidation was measured using the TBARS method of Buege and Aust,[22] with some modifications. One milliliter of erythrocyte solution was vortexed with 1 mL of TCA/TBA/HCl reagent (15% TCA/0.375% TBA/0.25 mol of HCl) (1:1:1, v/v/v) for 10 s. Then, the mixture was heated in a boiling water for 15 min. Subsequently, the mixture was cooled at room temperature for 10 min and centrifuged at 3000 rpm for 10 min. The absorbance of supernatant was read at 535 nm against a blank of 15% TCA/0.375% TBA/0.25 mol of HCl reagent. The results were expressed as micromolar MDA. The MDA level was calculated using the equation

$$\text{concentration (M)} = \text{absorbance}/(\text{molar extinction} \times \text{length of cuvette used})$$

where molar extinction was $1.56 \times 10^5\ M^{-1}\ cm^{-1}$.

Inhibition of Erythrocyte Hemolysis. Erythrocyte hemolysis was performed on the basis of method of Huang et al.[23] The packed RBC or erythrocytes obtained from previous analysis were diluted in PBS. The suspension of 2% erythrocytes in PBS (1 mL) was mixed with 0.5 mL of the extract. Concentrations of samples and standard were 0.05 and 0.2 mg/mL, respectively. Subsequently, 50 μL of H_2O_2 (100 mmol/L) was added to the mixture. The reaction mixture was incubated at 37 °C for 1 h and then diluted with 8 mL of PBS. The diluted reaction mixture was centrifuged at 1000*g* for 10 min. The absorbance of supernatant was measured at 415 nm. Erythrocytes were treated with 100 mmol/L H_2O_2 and without extract to obtain a complete hemolysis (control). The percentage of inhibition was calculated by using the following equation:

$$\text{inhibition of hemolysis (\%)} = (\text{absorbance of } H_2O_2\text{-induced hemolysis} - \text{absorbance of sample}/\text{absorbance of } H_2O_2\text{-induced hemolysis}) \times 100$$

In Vitro Antidiabetic Properties. *α-Amylase Inhibition Assay.* This assay was performed according to the method of Apostolidis et al.[24] Acarbose (62.5−1000 μg/mL) was used as positive control. The percentage of inhibition was calculated by using the equation

$$\text{inhibition (\%)} = (A_c - A_e)/A_c \times 100$$

where A_c is absorbance of control and A_e is absorbance of sample extracts or standard. Control was using phosphate buffer to replace extracts.

α-Glucosidase Inhibition Assay. The α-glucosidase inhibition assay was carried out according to the method of Kim et al.[25] The α-glucosidase inhibitory activity was expressed as percent inhibition and was calculated as

$$\text{inhibition (\%)} = (\Delta A_c - \Delta A_e)/\Delta A_c \times 100$$

where ΔA_c and ΔA_e are the difference of absorbance before and after incubation of control and sample extracts, respectively. Acarbose (0.125−2 mg/mL) dissolved in phosphate buffer was used as a positive control.

Cell Viability Assay. The viability of the BRIN BD11 cell line in the presence of sample extracts was determined using an MTT (3-(4,5-dimethylthiazol-2yl)-2,5-diphenyltetrazolium bromide) assay.[26] BRIN BD11 cell line was obtained from the Malaysian Institute Nuclear Technology (MINT). Cells were cultivated in T-25 cm^2 culture flasks using Roswell Park Memorial Institute (RPMI)-1640 medium (Gibco BRL Products, Rockville, MD, USA) with 2.0 g/L sodium bicarbonate, antibiotics (100 units of penicillin/mL and 100 μg of streptomycin/mL), and 10% fetal bovine serum (FBS). Cells were maintained in a humidified atmosphere of 5% CO_2 at 37 °C and were harvested at 80−90% confluence to maintain exponential growth. The extracts were dissolved in water and filtered through a sterile 0.22 μm syringe filter.

Insulin Secretion Assay. Insulin secretion activity was evaluated according to the method of Hamid et al.[27] The BRIN BD11 cell line was seeded at a density of 1.0×10^5 cells per well in a 24-well plate cultured in 1 mL of RPMI-1640 culture medium containing 11.1 mM glucose supplemented with 10% (v/v) of fetal bovine serum (FBS) and antibiotics (100 IU mL^{-1} penicillin and 0.1 g L^{-1} streptomycin) to allow attachment overnight prior to the test. Cells were washed three times with Krebs−Ringer bicarbonate buffer (KRBB, pH 7.4) supplemented with 0.5% (w/v) bovine serum albumin (BSA) and 1.1 mM glucose and preincubated for 40 min at 37 °C. The buffer was removed, and cells were then incubated for 30 min with 1 mL of KRBB test buffer supplemented with 0.5% (w/v) BSA and 1.1 mM glucose in the presence of sample extract (0.625−5 mg/mL). Insulin concentration was measured using rat insulin ELISA kit (Mercodia AB, Uppsala, Sweden).

Statistical Analysis. All results were expressed as the mean ± standard deviation (SD) for three replicates unless specified. The data were analyzed by statistical software, SPSS version 20.0 for windows (SPSS Inc., Chicago, IL, USA). One-way analysis of variance (ANOVA) and Tukey's test were performed to determine differences of means among groups. Statistical significance was set at $p < 0.05$.

RESULTS AND DISCUSSION

Nutritional Values of Underutilized Vegetables. The nutritional compositions of the studied vegetables are presented in Table 1. These vegetables were high in moisture content (>87%). The moisture content in the studied vegetables is

Table 1. Nutrient Compositions of Underutilized Vegetables[a]

nutrient composition	lalis	pantu
Macronutrients (g/100 g fw)		
moisture	87.97 ± 0.13b	90.70 ± 0.07a
ash	1.09 ± 0.27a	0.36 ± 0.03b
protein	3.86 ± 0.04a	1.67 ± 0.03b
lipid	0.56 ± 0.04a	0.33 ± 0.02b
total carbohydrate	1.56 ± 0.01b	2.43 ± 0.00a
total dietary fiber (TDF)	4.54 ± 0.01a	3.32 ± 0.26b
soluble dietary fiber (SDF)	0.48 ± 0.01a	0.22 ± 0.25a
insoluble dietary fiber (IDF)	4.06 ± 0.00a	3.10 ± 0.01b
Micronutrients (mg/100 g fw)		
calcium	47.07 ± 2.78a	27.75 ± 4.52b
magnesium	30.62 ± 0.47a	33.57 ± 4.98a
sodium	1.74 ± 0.10a	1.62 ± 0.83a
potassium	343.03 ± 2.19a	236.94 ± 32.09a
iron	0.32 ± 0.01a	0.22 ± 0.03a
copper	0.18 ± 0.00a	0.22 ± 0.01a
zinc	1.76 ± 0.05a	1.08 ± 0.15b
phosphorus	41.18 ± 0.29a	34.96 ± 5.53a
manganese	13.16 ± 0.20a	1.63 ± 0.24b

[a]Values are the mean ± SD ($n = 3$), except for dietary fiber ($n = 2$). Values with different letters are significantly different at $p < 0.05$ within the same row.

Table 2. Antioxidant Contents and Capacities of Underutilized Vegetables[a]

sample	TPC (mg GAE/100 g dw)	TFC (mg RE/100 g dw)	FRAP (μmol Fe^{2+}/100 g dw)	ORAC (μM TE/100 g dw)
lalis	2504.88 ± 61.15a	6.85 ± 0.27b	226.83 ± 14.43b	159.21 ± 19.88b
pantu	1959.70 ± 122.32b	10.63 ± 0.35a	396.83 ± 38.19a	203.58 ± 8.63a

[a]Values are the mean ± SD (n = 3). Values with different letters are significantly different at $p < 0.05$ within the same column.

similar to those of some other Malaysian vegetables such as *Etlingera elatior* (Jack), *Kaempferia galangal* L., and *Apium graveolons* L.[28] Additionally, comparable findings also have been demonstrated in three *Caulerpa* species (82−92%).[29] Lalis contained significantly higher ash, protein, lipid, and dietary fiber compared to pantu, except for total carbohydrate. However, a lower carbohydrate content was found for the studied vegetables compared with the nutrient databank value for raw palm hearts (25.6 g/100 fw).[30]

It was observed that dietary fiber (DF) content was an abundant nutrient in both vegetables, followed by protein value in lalis and total carbohydrate in pantu. A predominant portion of dietary fiber in the vegetables was insoluble DF compared to soluble DF. It was observed that total dietary fiber (TDF) in the samples was higher than their total available carbohydrate content. This may due to a high content of total indigestible carbohydrates in these samples.[18] It was noted that TDF contents of the studied vegetables exceeded the content in common Malaysian vegetables such as bamboo shoot, celery, and *kantan*.[31] The TDF of studied vegetables was considerably higher compared to other nutrients examined in this study, with the ratio of soluble to insoluble within 8.5−14.1. The ratio was higher compared to other vegetables such as seaweed due to more fibrous tissue.[32]

A higher level of potassium, zinc, calcium, phosphorus, and magnesium was observed in the studied vegetables as shown in Table 2. A similar pattern was observed for calcium, magnesium, and phosphorus levels with the same vegetables studied by Voon and Kueh.[33] Interestingly, higher amounts of potassium, magnesium, and phosphorus were found compared to common tomato.[34] It was found that the potassium level was higher than the sodium level, as is ordinary for plant foods. The high potassium content together with low sodium had shown a protective effect toward several diseases.[35] The studied vegetables could be a potential zinc source for daily intake as it contributes about 25% of zinc in the Recommended Nutrient Intake (RNI) of Malaysia.[36]

Antioxidant Properties of Underutilized Vegetables. The total phenolic (TPC) and flavonoid (TFC) contents of studied vegetables are depicted in Table 3. Lalis had significantly higher phenolic content (2505 mg GAE/100 g dw). In contrast, pantu exhibited a significantly higher TFC value (11 mg RE/100 g dw). The TPC values were much higher than those reported in vegetables from Indonesia (440−1143 mg GAE/100 g dw).[37] The studied vegetables showed a comparable TPC content and a lower flavonoid content compared to an ethanolic extract of *Barringtonia racemosa* stem.[38]

As total phenolic and flavonoid levels were determined, further identification and quantification of the polyphenol profile were performed using HPLC-DAD (Figure 1). To confirm the result of HPLC analysis, nine phenolic compounds were determined using LC-ESI-MS. MS data for the compounds are shown in Table 3. From the results, major compounds were detected in ESI(−) mode compared to ESI(+) mode. Seven compounds (protocatechuic acid, catechin, epigallocatechin gallate, chlorogenic acid, methyl gallate, 4-hydroxybenzoic acid, and myricetin) were present in pantu. Meanwhile, a total of five compounds (protocatechuic acid, chlorogenic acid, myricetin, morin, and genistein) were detected in lalis. Due to a lack of availability of standard phenolic compounds, certain peaks cannot be identified. Chlorogenic acid was the most abundant phenolic found in lalis (4.8 mg/g dw) and pantu (16.8 mg/g dw) (Table 4). This content was higher compared to chlorogenic content of commercial vegetables such as carrot, sprout, cauliflower, courgettes, and broccoli (0.01−0.44 mg/g dw).[39,40] The phenolic acid compounds identified in our vegetable extracts are quite similar to those of bamboo shoots.[41] The myricetin content in both of the studied vegetables was higher than the content in vegetables from Indonesia.[37] Comparable protocatechuic acid was found in wild mushroom, *Ramaria botrytis* (0.34 mg/g dw).[42] There is considerable interest as 4-hydroxybenzoic acid functions as a polyester precursor in plants and protocatechuic acid as an antioxidant.[43]

Table 3. Phenolic Compounds Detected in Lalis and Pantu by HPLC-DAD and LC-ESI-MS

compound	t_R (min)	MW	$[M + H]^+$ (m/z)	$[M - H]^-$ (m/z)
protocatechuic acid	15.4	154	nd[a]	153.1
catechin	15.9	290	291.2	nd
epigallocatechin gallate	16.1	458	nd	457.2
chlorogenic acid	16.4	354	nd	353.2
methyl gallate	16.7	184	nd	183.2
4-hydroxybenzoic acid	17.8	138	nd	137.0
myricetin	21.8	318	nd	317.2
morin	22.6	302	nd	301.0
genistein	24.2	270	nd	269.1

[a]nd, not detected above the limit of detection.

Antioxidant activity of extracts was evaluated by measuring the ability to reduce ferric ions in ferric reducing antioxidant power (FRAP) assay. Significant FRAP values of both studied vegetables were observed, as shown in Table 3. The ORAC assay determined the scavenging capacity of vegetable extracts against a peroxyl radical. The ORAC values for lalis and pantu were 159.2 and 203.6 μM TE/100 g dw, respectively (Table 3). In inhibition of lipid membrane erythrocyte oxidation assay (Table 5), the result demonstrated that both vegetables had good protective effects on membrane erythrocyte oxidation. The malondialdehyde (MDA) formation exhibited by lalis and pantu extract is comparable with that of BHT. In addition, pantu exhibited a significantly higher inhibition on erythrocyte hemolysis as compared to standard (Table 5). The inhibition activities of both samples were higher than that of gallic acid.

The FRAP value (226.8−396.8 μmol Fe^{2+}/100 g) was comparable with values reported for pumpkin leaves and butternut (104−744 mmol/L Fe[II]/g extract).[43] However, the studied vegetables showed a lower FRAP valued compared to commercial carrot (680 μmol Fe^{2+}/100 g).[44] Similar findings were found in ORAC values of some commercial vegetables

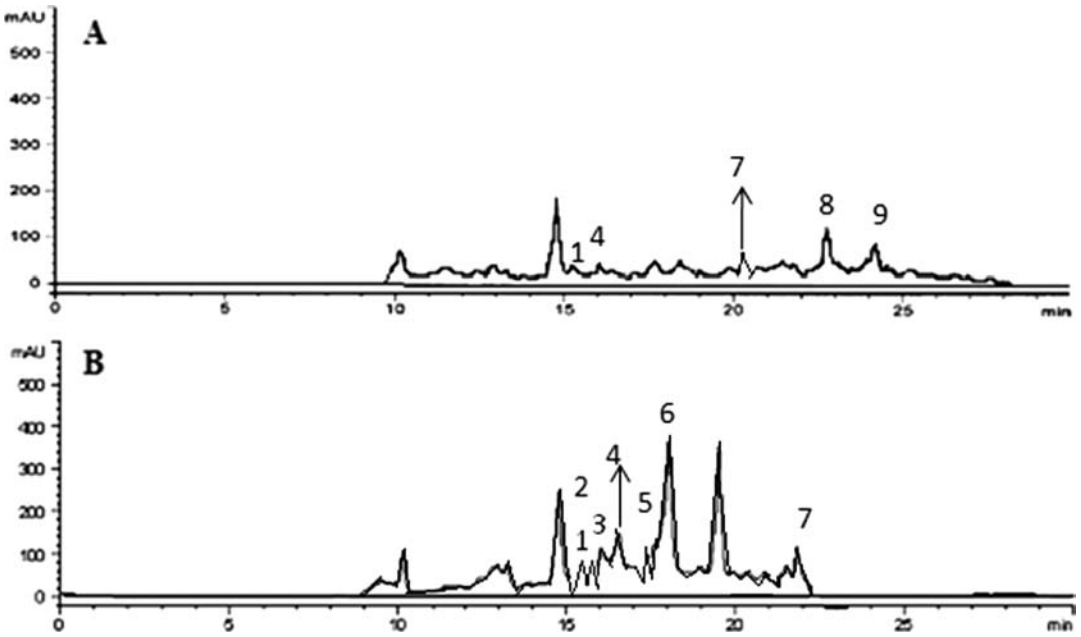

Figure 1. HPLC-DAD chromatograms of phenolic compounds in (A) lalis and (B) pantu. Detection was done at 280 nm. Peaks: (1) protocatechuic acid; (2) catechin; (3) epigallocatechin gallate; (4) chlorogenic acid; (5) methyl gallate; (6) 4-hydroxybenzoic acid; (7) myricetin; (8) morin; (9) genistein.

Table 4. Concentration of Phenolic Compounds in Lalis and Pantu Using HPLC-DAD[a]

peak	compound	lalis (mg/g dw)	pantu (mg/g dw)
1	protocatechuic acid	0.30 ± 0.08	0.79 ± 0.20
2	catechin	nd	0.60 ± 0.14
3	epigallocatechin gallate (EGCG)	nd	1.44 ± 0.27
4	chlorogenic acid	4.80 ± 3.22	16.77 ± 0.30
5	methyl gallate	nd	0.05 ± 0.01
6	4-hydroxybenzoic acid	nd	0.84 ± 0.03
7	myricetin	0.56 ± 0.02	1.45 ± 0.04
8	morin	2.04 ± 0.05	nd
9	genistein	0.17 ± 0.01	nd

[a]Values are expressed as the mean ± standard deviation (n = 3). The calibration coefficients were >0.99. nd, not detected above the limit of detection of phenolic compounds.

Table 5. Antioxidant Capacities of Underutilized Vegetables Using Inhibition Assays on RBC Cell Damage[a]

sample	inhibition of lipid membrane of erythrocyte oxidation (MDA, μM)	inhibition of erythrocyte hemolysis (%)
lalis	0.67 ± 0.02a	48.70 ± 1.47ab
pantu	0.77 ± 0.01a	53.51 ± 1.11a
standard	0.65 ± 0.19α,a	44.96 ± 0.28β,b

[a]Values are the mean ± SD (n = 3). Values with different letters are significantly different at $p < 0.05$ within the same column. α, BHT; β, gallic acid.

such as Brussels sprout, eggplant, and green beans.[45] Furthermore, no significant difference of ORAC values was found among the vegetables and standard. Due to the high hydrophilic phenolic compound content in lalis (Table 4), this may contribute to hinder MDA formation. It was noted that the more polar hydrophilic compounds present in the extract, the greater the ability the extract has to neutralize lipid peroxidation.[46]

Inhibitory Activities of Extracts against Digestive Enzymes. Consumption of foods that contain potential α-amylase and α-glucosidase inhibitors can be dietary solutions for management of type II diabetes. α-Amylase enzyme is able to catalyze the hydrolysis of glycosidic linkages in starch. The α-amylase inhibitors are considered starch blockers as they bind with the reactive sites of amylase enzyme and consequently control the blood glucose level. The studied vegetables showed high inhibition of α-amylase activity (>50%) (Figure 2a). This result was higher than that of wild legume grains (10.6−18.5%)[47] and comparable with those of finger and Proso millets (77−78%).[48]

α-Glucosidase is an enzyme situated in the epithelium of the small intestine and catalyzes the breakdown of disaccharides into glucose for subsequent absorption. An inhibitor of α-glucosidase could delay the glucose absorption rate through the intestine. The impediment of glucose absorption may give a positive effect in controlling the postprandial blood sugar level. In contrast with α-amylase inhibition, the studied vegetables exhibited low levels of α-glucosidase inihibition activity (<45%) (Figure 2b). No IC_{50} was found for either vegetable. However, the inhibition activity of pantu is comparable with wild legume grain inhibition (35.8−49.9%).[47] Low activity at higher concentrations could be due to reduced and no effects of compounds from the extract at higher doses. To our knowledge, this is the first study revealing the enzyme inhibition activity of these underutilized vegetables. On the basis of these preliminary results, the studied vegetables may indicate a potential resource as an inhibitor of α-amylase activity. However, further in vivo research is warranted to confirm its potential value in human subjects.

Effects of Extracts on Cell Viability and Insulin Secretory Activity of BRIN BD11 Cells. Results showed that no cytotoxic effects from either vegetable in BRIN BD11 cells up to a concentration of 2 mg/mL ethanolic extract (data

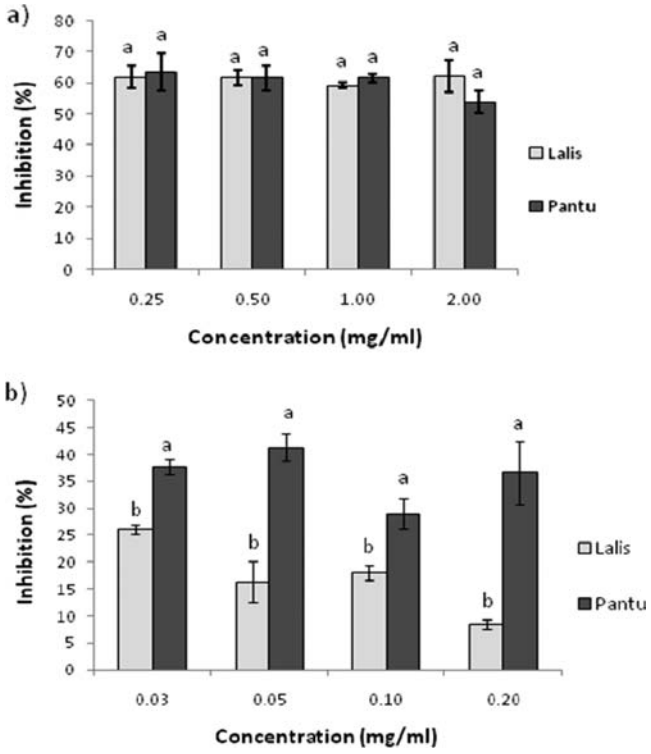

Figure 2. (a) α-Amylase and (b) α-glucosidase inhibition activity of vegetable extracts. Values represent the mean ± standard deviation (n = 3).

not shown). Lesser cell viability, as a sign of reducing blue formazan compound with increased concentrations of both extracts, was observed. In addition, no IC_{50} (inhibition of cell viability at 50%) was found for either vegetable. Hence, the assay did not exhibit toxicity to pancreatic cell line at all doses examined for lalis and pantu after 48 h of incubation.

The insulinotropic activities of vegetable extracts with different concentrations (0.625, 1.25, 2.5, and 5 mg/mL) using BRIN BD11 cells are demonstrated in Figure 3. From the results, no insulinotropic effect was found between the samples and control. This result was in agreement with Hamid et al.,[27] who found *Strobilanthus crispus* extract exhibited no insulinotrophic effect. In contrast, stem bark of *Tinaspora crispa* showed a stimulatory effect on insulin secretion.[27]

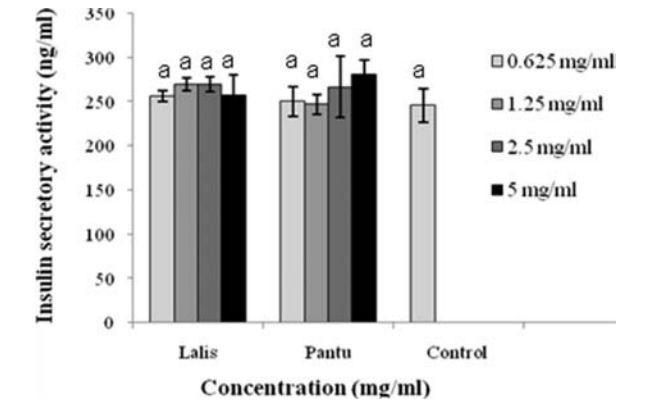

Figure 3. Insulin secretion activity of BRIN BD11 cell lines treated with vegetable extracts. Values are the mean ± SD (n = 3).

In conclusion, this research signifies the initial effort to evaluate the antioxidant and antidiabetic properties of these underutilized vegetables. It is revealed that they are providing valuable sources of dietary fiber, potassium, and zinc contents and exhibited potential antioxidant and antidiabetic properties. Different phenolic acids and flavonoid compounds were found in the studied vegetables such as chlorogenic acid and morin. High inhibition activity (>50%) was exhibited by all samples in α-amylase inihibition assay. Nevertheless, low activity (<50%) of samples was observed in α-glucosidase inhibition assay. In addition, no cytotoxicity effects were found on rat pancreatic BRIN-BD11 cells supplemented with all extracts (0.25−2 mg/mL). Moreover, no significant difference of insulinotrophic activity among the samples with different concentrations was found. It can be suggested these underutilized vegetable palm hearts are interesting indigenous resources to be embraced in local diets.

AUTHOR INFORMATION

Corresponding Author

*(A.I.) E-mail: aminis@upm.edu.my. Phone: +603 8947 2435. Fax: +603 8942 6769.

Funding

We are grateful for financial support under the Research University Grant Scheme (RUGS) (Project 04-05-11-1590RU) from Universiti Putra Malaysia, Serdang, Selangor, Malaysia.

Notes

The authors declare no competing financial interest.

ACKNOWLEDGMENTS

We thank Nur Naazira Iman Song Abdullah for helping in collection of samples in Kuching, Sarawak, Malaysia. Laboratory facilities and technical support were from the Department of Nutrition and Dietetics, Faculty of Medicine and Health Sciences, Universiti Putra Malaysia (UPM).

REFERENCES

(1) Valko, M.; Leibfritz, D.; Moncol, J.; Cronin, M. T. D.; Mazur, M.; Telser, J. Free radicals and antioxidant in normal physiological function and human disease. *Int. J. Biochem. Cell Biol.* **2007**, *39*, 44−84.

(2) Krentz, A. J.; Bailey, C. J. Oral antidiabetic agents: current role in type 2 diabetes mellitus. *Drugs* **2005**, *65*, 385−411.

(3) Rhabasa-Lhoret, R.; Chiasson, J. L. α-Glucosidase inhibitors. In *International Textbook of Diabetes Mellitus*, 3rd ed.; Defronzo, R. A., Ferrannini, E., Keen, H., Zimmet, P., Eds.; Wiley: Chichester, UK, 2004; Vol. 1.

(4) Jaenicke, H.; Höschle-Zeledon, I. *Strategic Framework for Underutilised Plant Species Research and Development, with Special Reference to Asia and the Pacific, and to Sub-Saharan Africa*; International Centre for Underutilised Crops: Colombo, Sri Lanka; and Global Facilitation Unit for Underutilised Species: Rome, Italy, 2006; pp 1−33.

(5) Raghuvanshi, R. S.; Singh, R. Nutritional Composition of uncommon foods and their role in meeting in micronutrient needs. *Int. J. Food Sci. Nutr.* **2001**, *32*, 331−335.

(6) Ikram, E. H. K.; Eng, K. H.; Jalil, A. M. M.; Ismail, A.; Idris, S.; Azlan, A.; et al. Antioxidant capacity and total phenolic content of Malaysian underutilized fruits. *J. Food Compos. Anal.* **2009**, *22* (5), 388−393.

(7) Rodas, M. A. B.; Marsiglia, D. A. P.; Rodrigues, R. S. M. Processed heart palm: sanitary aspects according the Brazilian legislation In *Proceedings of XIV Brazilian Meeting on Food Analysis*, Goiânia, Goiás, Brazil, 2005; p 173.

(8) Chew, L. Y.; Prasad, K. N.; Amin, I.; Azrina, A.; Lau, C. Y. Nutritional composition and antioxidant properties of *Canarium*

odontophyllum Miq. (dabai) fruits. *J. Food Compos. Anal.* **2011**, *24* (4–5), 670–677.
(9) Association of Official Analytical Chemistry (AOAC). *Official Methods of Analysis*, 15th ed.; Association of Official Analytical Chemists: Gaithersburg, MD, USA, 1990.
(10) Peris-Tortajada, M. Carbohydrates and starch. In *Handbook of Food Analysis. Physical Characterization and Nutrient Analysis*; Leo, M. L. N., Ed.; Dekker: New York, 2004; pp 392.
(11) Prosky, L.; Asp, N. G.; Schweizer, T. F.; De Vries, J. W.; Furda, I. Determination of insoluble, soluble and total dietary fiber in foods and food products: collaboration study. *J. Assoc. Off. Anal. Chem.* **1988**, *71* (5), 1017–1023.
(12) Ahmad; Esa, M. Penggunaan ICP-OES dalam analisis pertanian. Manual Makmal Untuk Analisis Tanah dan Tumbuhan, Unit Kimia Analisis, MARDI, Serdang, Selangor, 1993.
(13) Liu, H.; Qiu, N.; Ding, H.; Yao, R. Polyphenols contents and antioxidant capacity of 68 Chinese herbals suitable for medical or food uses. *Food Res. Int.* **2008**, *41*, 363–370.
(14) Velioglu, Y. S.; Mazza, G.; Gao, L.; Oomah, B. D. Antioxidant activity and total phenolics in selected fruits, vegetables, and grain products. *J. Agric. Food Chem.* **1998**, *46* (10), 4113–4117.
(15) Quettier-Deleu, C.; Gressier, B.; Vasseur, J.; Dine, T.; Brunet, C.; Luyckx, M.; et al. Phenolic compounds and antioxidant activities of buckwheat (*Fagopyrum esculentum* Moench) hulls and flour. *J. Ethnopharmacol.* **2000**, *72*, 35–42.
(16) Liu, H.; Qiu, N.; Ding, H.; Yao, R. Polyphenols contents and antioxidant capacity of 68 Chinese herbals suitable for medical or food uses. *Food Res. Int.* **2008**, *41*, 363–370.
(17) He, Z.; Xia, W. Analysis of phenolic compounds in Chinese olive (*Canarium album* L.) fruit by RPHPLC–DAD–ESI–MS. *Food Chem.* **2007**, *105* (3), 1307–1311.
(18) Hassan, F. A.; Ismail, A.; Hamid, A. A.; Azlan, A. Identification and quantification of phenolic compounds in bambangan (*Mangifera pajang* Kort.) peels and their free radical scavenging activity. *J. Agric. Food Chem.* **2011**, *59*, 9102–9111.
(19) Benzie, I. F. F.; Strain, J. J. The ferric reducing ability of plasma as a measure of antioxidant power, the FRAP assay. *Anal. Biochem.* **1996**, *239*, 70–76.
(20) Huang, W. Y.; Majumder, K.; Wu, J. Oxygen radical absorbance capacity of peptides from egg white protein ovotransferrin and their interactions with phytochemicals. *Food Chem.* **2010**, *123*, 635–641.
(21) Rodríguez, J.; Di Pierro, D.; Gioia, M.; Monaco, S.; Delgado, R.; Coletta, M.; Marini, S. Effects of a natural extract from *Mangifera indica* L, and its active compound, mangiferin, on energy state and lipid peroxidation of red blood cells. *Bioenergetics* **2006**, *1760*, 1333–1342.
(22) Buege, J. A.; Aust, S. D. Microsomal lipid peroxidation. *Methods Enzymol.* **1978**, *52*, 302–310.
(23) Huang, W.; Xue, A.; Niu, H.; Jia, Z.; Wanga, J. Optimised ultrasonic-assisted extraction of flavonoids from *Folium eucommiae* and evaluation of antioxidant activity in multi-test systems *in vitro*. *Food Chem.* **2009**, *114*, 1147–1154.
(24) Apostolidis, E.; Kwon, Y. I.; Shetty, K. Inhibitory potential of herb, fruit, and fungal-enriched cheese against key enzymes linked to type 2 diabetes and hypertension. *Innovative Food Sci. Emerging Technol.* **2007**, *8*, 46–54.
(25) Kim, S. J.; Kwon, C. S.; Son, K. H. Inhibition of α-glucosidase and amylase by luteolin, a flavonoid. *Biosci., Biotechnol., Biochem.* **2000**, *64*, 2458–2461.
(26) Mosmann, T. Rapid colorimetric assay for cellular growth and survival: application to proliferation and cytotoxicity assays. *J. Immunol. Methods* **1983**, *65*, 55–63.
(27) Hamid, M.; Bohari, S. P. M.; Bastami, M. S.; Ali, A. M.; Mustapha, N. M.; Shari, K. Evaluation of the insulinotropic activity of Malaysian traditional plants extracts. *J. Biol. Sci.* **2008**, *8* (1), 201–204.
(28) Sulaiman, S. F.; Sajak, A. A. B.; Ooi, K. L.; Supriatno; Seow, E. M. Effect of solvents in extracting polyphenols and antioxidants of selected raw vegetables. *J. Food Compos. Anal.* **2011**, *24* (4–5), 506–515.
(29) Kumar, M.; Gupta, V.; Kumari, P.; Reddy, C. R. K.; Jha, B. Assessment of nutrient composition and antioxidant potential of *Caulerpaceae* seaweeds. *J. Food Compos. Anal.* **2011**, *24* (2), 270–278.
(30) U.S. Department Agriculture (USDA). USDA Database for the Added Sugars Content of Selected Foods, http://www.megaheart.com/pdf/addedsugars.pdf, 2006.
(31) Tee, E. S.; Mohd Ismail, N.; Mohd Nasir, A.; Idris, K. *Nutrient Composition of Malaysian Foods*; Division of Human Nutrition, Institute for the Medical Research: Kuala Lumpur, Malaysia, 1997; p 24.
(32) Yaich, H.; Garna, H.; Besbes, S.; Paquot, M.; Blecker, C.; Attia, H. Chemical composition and functional properties of *Ulva lactuca* seaweed collected in Tunisia. *Food Chem.* **2011**, *128*, 895–901.
(33) Voon, B. H.; Kueh, H. S. The nutritional value of indigenous fruits and vegetables in Sarawak. *Asia Pac. J. Clin. Nutr.* **1999**, *8* (1), 24–31.
(34) Guil-Guerrero, J. L.; Rebolloso-Fuentes, M. M. Nutrient composition and antioxidant activity of eight tomato (*Lycopersicon esculentum*) varieties. *J. Food Compos. Anal.* **2009**, *22*, 123–129.
(35) Afolayan, A. J.; Jimoh, F. O. Nutritional quality of some wild leafy vegetables in South Africa. *Int. J. Food Sci. Nutr.* **2009**, *60* (5), 424–431.
(36) Ministry of Health (MOH). *Recommeded Nutrient Intake for Malaysia 2005: Summary Table. Recommeded Nutrient Intake for Malaysia*, 2005.
(37) Andarwulan, N.; Batari, R.; Sandrasari, D. A.; Bolling, B.; Wijaya, H. Flavonoid content and antioxidant activity of vegetables from Indonesia. *Food Chem.* **2010**, *121*, 1231–1235.
(38) Kong, K. W.; Mat-Junit, S.; Aminudin, N.; Ismail, A.; Abdul-Aziz, A. Antioxidant activities and polyphenolics from the shoots of *Barringtonia racemosa* (L.) Spreng in a polar to apolar medium system. *Food Chem.* **2012**, *134*, 324–332.
(39) Pellegrini, N.; Chiavaro, E.; Gardana, C.; Mazzeo, T.; Contino, D.; Gallo, M.; Riso, P.; Fogliano, V.; Porrini, M. Effect of different cooking methods on color, phytochemical concentration, and antioxidant capacity of raw and frozen *Brassica* vegetables. *J. Agric. Food Chem.* **2010**, *58* (7), 4310–4321.
(40) Park, E.-J.; Jhon, D.-Y. The antioxidant, angiotensin converting enzyme inhibition activity, and phenolic compounds of bamboo shoot extracts. *LWT–Food Sci Technol.* **2010**, *43* (4), 655–659.
(41) Barros, L.; Ferreira, I. C. F. R.; Baptista, P.; Santos-Buelga, C. Phenolic acids determination by HPLC–DAD–ESI/MS in sixteen different Portuguese wild mushrooms species. *Food Chem. Toxicol.* **2009**, *47* (6), 1076–1079.
(42) Dong, D.; Jiang, S.; Ni, Y.; Jiang, B. Syntheses and properties of thermotropic copolyesters of *p*-hydroxybenzoic acid. *Eur. Polym. J.* **2001**, *37*, 611–617.
(43) Kunyanga, C. N.; Imungi, J. K.; Okoth, M. W.; Biesalski, H. K.; Vadivel, V. Total phenolic content, antioxidant and antidiabetic properties of methanolic extract of raw and traditionally processed Kenyan indigenous food ingredients. *LWT–Food Sci Technol* **2012**, *45*, 269–276.
(44) Song, W.; Derito, C. M.; Liu, M. K.; He, X.; Dong, M.; Liu, R. H. Cellular antioxidant activity of common vegetables. *J. Agric. Food Chem.* **2010**, *58*, 6621–6629.
(45) Navarre, D. A.; Pillai, S. S.; Shakya, R.; Holden, M. J. HPLC profiling of phenolics in diverse potato genotypes. *Food Chem.* **2011**, *127* (1), 34–41.
(46) Pérez-Tortosa, V.; López-Orenes, A.; Martínez-Pérez, A.; Ferrer, M. A.; Calderón, A. A. Antioxidant activity and rosmarinic acid changes in salicyclic acid-treated *Thymus membranaceus* shoots. *Food Chem.* **2012**, *130*, 362–369.
(47) Vadivel, V.; Stuetz, W.; Scherbaum, V.; Biesalski, H. K. Total free phenolic content and health relevant functionality of Indian wild legume grains: Effect of indigenous processing methods. *J. Food Compos. Anal.* **2011**, *24*, 935–943.
(48) Kim, J. S.; Hyun, T. K.; Kim, M. J. The inhibitory effects of ethanol extracts from sorghum, foxtail millet and proso millet on α-

glucosidase and α-amylase activities. *Food Chem.* **2011**, *124*, 1647−1651.

targeting the intracellular signaling pathway regulating cell cycle progression is an important strategy in lung cancer treatment.[18] The comprehensive reports demonstrate that the mutation in p53 has potency to establish the novel strategies improving the lung cancer prognosis.

The cell cycle is a critical regulation mechanism of cell growth, proliferation, and survival. The dysregulation of the cell cycle leads to uncontrolled cell proliferation and has been demonstrated in many different human cell tumorigeneses.[19] The mammalian cell cycle comprises five sequential stages, quiescent phase G0, G1, S, G2, and mitotic (M) phase. G1 and G2 represent the gap intervals, where cells prepare themselves for the successful completion of S and M phases subsequently. The cells in the S phase receive a signal and faithfully replicate the genetic material, while the M phase portions out the cellular components into two daughter cells.[20] The regulatory molecules of the successive cell cycle progression consist of cyclin and cyclin-dependent kinase (CDK) complexes. Different cyclin−CDK complexes are activated to ensure that cells successfully complete the previous phase and entering the new stage.[21] Furthermore, to ensure genome integrity and chromosomal stability, cell cycle checkpoints are important mechanisms to monitor cells transmitting precise copies of their genome into the next generation. CDK inhibitors (CDKIs) play an important role in checkpoint control of cell cycle progression. CDKIs are divided into two major families, INK4 and WAF/KIP families. The WAF/KIP family, including $p21^{Waf1/Cip1}$, $p27^{Kip1}$, and $p57^{Kip2}$, intends to inhibit CDK2 and CDK4/cyclin complex activities via protein−complex association. Moreover, the members of INK4, containing $p16^{INK4A}$, $p15^{INK4B}$, $p18^{INK4C}$, and $p19^{INK4D}$, bind to either CDK4 or CDK6 and inhibit the action of the D type of cyclins.[22] Activation of p53-$p21^{Waf1/Cip1}$ signaling is an important mechanism to prevent cells from G1 entering the S phase.[23,24] It has been shown that garcinol induced G1 cell cycle arrest and apoptosis in pancreatic cancer cells.[25] However, the molecular mechanism of cell cycle progression in p53-mutated lung cancer cells modulated via $p21^{Waf1/Cip1}$ activation with garcinol treatment is still unknown.

The mitogen-activated protein kinase (MAPK) family, a member of serine/threonine protein kinases, is involved in extracellular signal-regulated kinase (ERK), c-Jun-N-terminal kinase (JNK), and p38-MAPK signaling pathways. They mediate a variety of cellular functions through different extracellular stimulations.[26] The ERK pathway has been linked to cell proliferation and growth and is primarily induced by mitogens, while p38-MAPK and JNK are generally activated by cellular stress and inflammatory cytokines.[27] p38-MAPK is also involved in senescence, differentiation, and DNA-damage response.[28] A usual fate of p38-MAPK activation through extracellular stimulation is cell cycle arrest or apoptosis.[28−30] The proliferative role of p38-MAPK has also been reported in several cancers, especially in NSCLC.[31−33] Furthermore, p38-MAPK activation has shown the requirement during some mitogen-stimulated cell proliferation.[34,35] Recently, our group reported that lipopolysaccharide (LPS)-induced COX-2 expression was inhibited by garcinol through p38 inactivation in macrophages.[6] Therefore, it is important to verify the relationship between garcinol and p38-MAPK in tumorigenesis for cancer prevention or treatment.

In this study, we examined antiproliferative effects of garcinol on p53-wild type H460 and p53-null H1299 lung cancer cells. Our data showed that garcinol significantly induced a dose-dependent apoptosis in H460 cells, although a dose-dependent G1 cell cycle arrest was observed in garcinol-treated H1299 cells. We developed an interest in the molecular mechanism of the p53-independent G1 cell cycle in garcinol-stimulated H1299 cells. We found that garcinol downregulated the expression of the D type of cyclins, CDK2, and CDK4, in contrast to upregulating cyclin E and CDK6 protein expression. Garcinol also induced $p21^{Waf1/Cip1}$ and $p27^{Kip1}$ expressions and concomitantly inhibited CDK2- and CDK4-mediated signals. In addition, ERK and p38-MAPK phosphorylations were also downregulated in a time-dependent manner by garcinol treatment. Treatment with p38-MAPK inhibitor enhanced garcinol-induced G1 arrest and cyclin E, p21 $^{Waf1/Cip1}$, and $p27^{KIP1}$ expression in H1299 cells. Our data suggested that the garcinol-induced p53-independent G1 cell cycle arrest might be through downregulation of p38-MAPK phosphorylation, resulting in accumulation of $p21^{Waf1/Cip1}$ protein in H1299 lung cancer cells.

MATERIALS AND METHODS

Reagents. Garcinol (purity = 95%) was purchased from Biomol/Enzo Life Sciences International, Inc. (Plymouth Meeting, PA). Anti-cyclin D1, D3, E, CDK2, CDK4, CDK6, anti-ERK, and anti-p38 antibodies were obtained from Cell Signaling (Beverly, MA). Anti-β-actin antibody was received from Sigma-Aldrich (St. Louis, MO). PD98059 and SB203580 were obtained from Calbiochem (La Jolla, CA). Protein A/G plus agarose was acquired from Santa Cruz Biotechnology (Santa Cruz, CA).

Cell Culture and Cytotoxicity Assay. NSCLC p53-wild type H460 and p53-null H1299 cell lines were obtained from the American Type Culture Collection (Manassas, VA). Both of the cell lines were cultured in RPMI-1640 (Hyclone Laboratories, Logan, UT) supplemented with 5% fetal bovine serum and maintained at 37 °C in a humidified atmosphere at 95% air and 5% CO_2. Cells (1×10^4/well) were cultured in 96-well plates and incubated for 24 h. After the cells were treated with various dosages of garcinol for 24, 48, and 72 h, the incubation media were changed every 2 days during the experiments. At the end of incubation, cell viability was determined by the 3-(4,5-dimethylthiazol-2-yl)-2,5-diphenyltetrazolium bromide (MTT) assay.

Cell Synchronization, Drug Treatment, and Flow Cytometric Analysis. Lung cancer cells H460 and H1299 were plating for 24 h. Cells were then synchronized for 24 h. After synchronization, the media were removed and changed to complementary media containing various dosages of garcinol for 24 h. After the treatment, cells were harvested and stained with propidium iodide (50 μg/mL) (Sigma Chemical, MO) and DNA contents were measured using a FACScan laser flow cytometer analysis system (Beckman Coulter, CA).

Western Blot Analysis. Control and garcinol-treated cells were rinsed twice with ice-cold phosphate-buffered saline (PBS) and then lysed in an appropriate RIPA extraction buffer [20 mM Tris−HCl at pH 7.5, 150 mM NaCl, 1 mM disodium salt of ethylenediaminetetraacetic acid (Na_2EDTA), 1 mM ethylene glycol bis(2-aminoethyl ether)-*N*,*N*,*N*′,*N*′-tetraacetic acid (EGTA), 1% (v/v) NP-40, 1% (v/v) sodium deoxycholate, 2.5 mM sodium pyrophosphate, 1 mM β-glycerophosphate, 1 mM Na_3VO_4, and 1 μg/mL leupeptin] on ice for 30 min. The extracts were then centrifuged at 12000*g* for 30 min. Proteins were loaded at 40 μg/lane and separated by sodium dodecyl sulfate−polyacrylamide gel electrophoresis (SDS−PAGE). Thereafter, protein was transferred to Immobilon polyvinylidene difluoride membrane (Millipore, MA). Membrane was blocked by blocking buffer (3% bovine serum albumin and 0.5% Tween 20) for 40 min and incubated with different primary antibodies at room temperature for 2 h afterward. After 2 h of incubation, membrane was washed and soaked in horseradish-peroxidase-labeled secondary antibodies at 25 °C for 1 h. The blot was revealed by chemiluminescence (ECL kits, Amersham Pharmacia Biotech, Arlington Heights, IL). Band intensities were quantitated by UVP BioSpectrum Imaging System ChemiDoc-It2

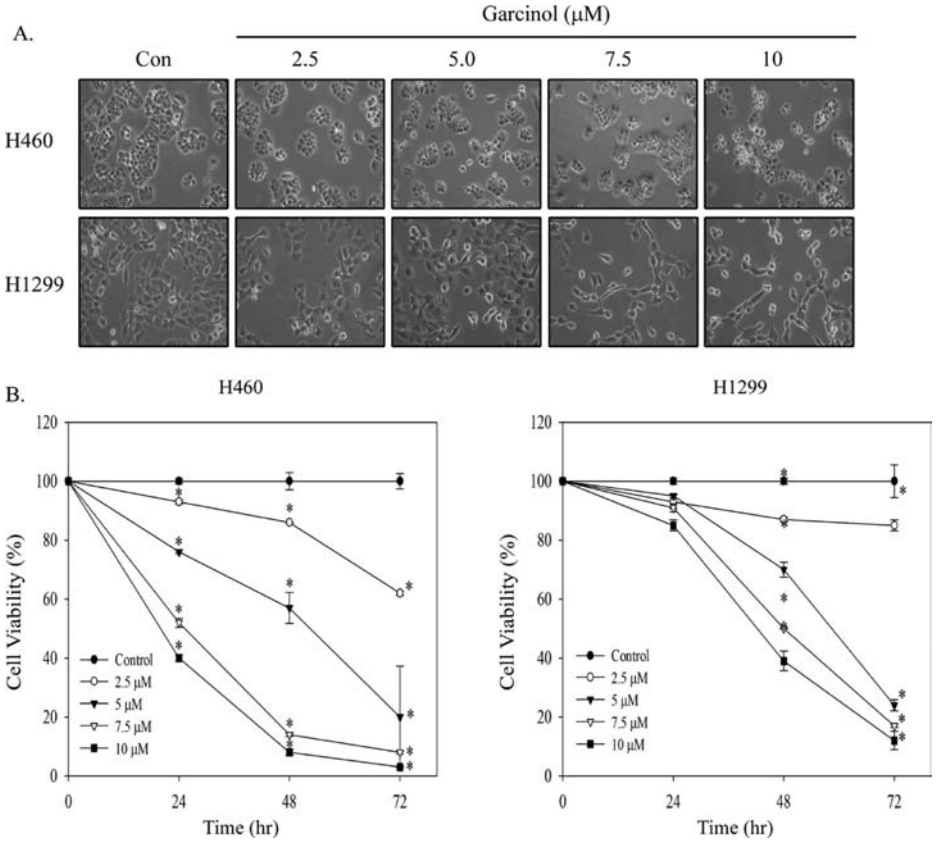

Figure 1. Growth inhibition effect of garcinol in H460 and H1299 lung cancer cells. (A) Morphological changes in garcinol-treated lung cancer cells. H460 and H1299 were treated with various concentrations of garcinol for 24 h. Morphological changes were observed by a microscope at 10 × 10 magnification. (B). Effects of garcinol on cell viability in H460 and H1299 lung cancer cells. H460 and H1299 were maintained in a 96-well plate at a density of 1×10^3/well for 24 h. Cells were then treated with various doses of garcinol for 24, 48, and 72 h. The cell viability was measured using the MTT assay. Data were the mean ± SD of triplicate samples. (*) $p < 0.05$ compared to control cells.

810 (UVP, LLC, Upland, CA). β-Actin was used as the internal control.

Immunoprecipitation. H1299 lung cancer cells were cultured in 100 mm dishes for 24 h, following synchronization. Thereafter, cells were switched to complementary media containing 10 μM garcinol for 24 h. Cells were then harvested and extracted by lysis buffer. The cell lysate was clarified by centrifugation at 12000*g* at 4 °C for 30 min. A total of 250 μg of protein was incubated with anti-CDK2 or anti-CDK4 antibody and protein A/G plus agarose at 4 °C for 18 h. The immunoprecipitate was washed twice with immunoprecipitation buffer [10 mM Tris−HCl at pH 7.4, 1 mM EDTA, 1 mM EGTA, 150 mM NaCl, 0.2 mM sodium vanadate, 0.2 mM phenylmethanesulfonyl fluoride (PMSF), 1% (v/v) Triton X-100, and 0.5% (v/v) NP-40]. CDK2 and/or CDK4 immunoprecipitates were resuspended in 25 μL of RIPA lysis buffer, mixed with protein loading buffer, and separated by SDS−PAGE. After transfer, membranes were blotted with anti-$p21^{Waf1/Cip1}$ and anti-$p27^{Kip1}$ primary antibodies. Blots were then stripped and reprobed with CDK2 and CDK4 as internal controls. The densities of the bands were then expressed as the relative densities compared to controls, which were taken as 1-fold.

Reverse Transcription Polymerase Chain Reaction (RT-PCR). After garcinol treatment, cells were washed in ice-cold PBS and total RNA was isolated by RNA mini kit (Qiagen, Taiwan). cDNAs were prepared from the total RNA (5.0 μg) with high-capacity cDNA reverse transcription kit (Invitrogen, Taiwan) at 42 °C for 60 min. PCR was performed in a final volume of 25 μL containing deoxynucleotide triphosphates (dNTPs) (each at 200 μM), 1× reaction buffer, 2 μL of RT-cDNA products, and 50 units/mL pro Taq DNA polymerase (Promega, WI). PCR primers for $p21^{Waf1/Cip1}$, $p27^{Kip1}$, and GADPH were synthesized according to the following oligonucleotide sequences: $p21^{Waf1/Cip1}$, forward primer, 5′-GGCGCCATGTCAGAACCGGCTG-3′; reverse primer, 5′-ACCCAGCGGACAAGTGGGGAGG-3′; $p27^{Kip1}$, forward primer, 5′-ACGAAGAGTTAACCCGGGACTTGG-3′; reverse primer, 5′-GGGCGTCTGCTCCACAGAACCG-3′; and GAPDH, forward primer, 5′-TGAAGGTCGGAGTCAACGGGTGAGTT-3′; reverse primer, 5′-CATGTAGACCCCTTGAAGAGG-3′.

After an initial denaturation for $p21^{Waf1/Cip1}$ PCR (851 kb) at 95 °C for 5 min, 26 cycles of amplification (95 °C for 50 s, 60 °C for 45 s, and 72 °C for 60 s) were performed and followed by an extension at 72 °C for 10 min. Similarly, for $p27^{Kip1}$ PCR (452 kb), 29 cycles of amplification (95 °C for 50 s, 57 °C for 45 s, and 72 °C for 45 s) were performed and followed by an extension at 72 °C for 10 min. In GAPDH amplification, 29 cycles of reaction (94 °C for 50 s, 60 °C for 45 s, and 72 °C for 120 s) were performed and followed by an extension at 72 °C for 10 min. The PCR products were separated by electrophoresis on 1.8% agarose gel and visualized by SYBR Safe (Life Technologies, Taiwan) staining.

Small Interfering RNA and Dominant Negative p38-MAPK (DN p38-MAPK) Transfection. H1299 cells were cultured to 70% confluence and then transfected with the siRNA duplexes at a final concentration of 10 nM using GenMute siRNA transfection reagent (SignaGen Laboratories, Ijamsville, MD) according to the instructions of the manufacturer. Cellular levels of the $p21^{Waf1/Cip1}$ proteins specific for the siRNA transfection were checked by immunoblotting, and all experiments were performed at 6 h after transfection. DN p38-MAPK plasmid was kindly obtained from Dr. Kuo-Tai Hua. H1299 cells were transfected with DN p38-MAPK using Lipofectamine 2000 transfection reagent according to the protocol of the manufacturer (Invitrogen, Carlsbad, CA).

Statistical Analysis. The results were expressed as the mean ± standard deviation (SD) calculated from the specified numbers of

determination. One-way analysis of variation (ANOVA) was used to compare individual data with the control value. A probability of $p < 0.05$ was taken as denoting a significant difference from the control data.

RESULTS

Cell Viability Inhibition by Garcinol on Human H460 and H1299 Lung Cancer Cells. The cell viability inhibition by garcinol on p53-wild type H460 and p53-null H1299 cells has been examined. Cells were treated with serial dosages of garcinol (0, 2.5, 5, 7.5, and 10 μM) at the time points of 24, 48, and 72 h, respectively. The cell viability was measured by the MTT assay. H460 and H1299 cells were treated with 10 μM garcinol for 24 h, exhibiting morphological changes (Figure 1A). As shown in Figure 1A, the cell shrunk and detachment was observed in garcinol-treated H460 and H1299 cells. In addition, the cell debris was noticed only in garcinol-treated H460 cells. Furthermore, the growth inhibition effect of garcinol was observed in dose- and time-dependent manners in these cell lines (Figure 1B). These results showed that the cell viability was significantly decreased in garcinol-treated H460 cells compared to H1299 cells.

Effects of Garcinol on Cell Cycle Distribution in Human H460 and H1299 Lung Cancer Cells. To further evaluate the hypothesis of the cytotoxic effect of garcinol mediated via alternations in cell cycle development, p53-wild type H460 and p53-null H1299 cells were used. Both H460 and H1299 cells were synchronized for 24 h and immediately treated with garcinol for another 24 h. At the end of treatment, cells were harvested and flow cytometry analysis was performed. As shown in Figure 2, the percentage of cells in the G1 phase increased from 63.7% in the control to 76.0% in garcinol-treated H1299 cells. Up to 13% of the G1 phase was boosted after garcinol treatment in H1299 cells. A sub-G1 fraction increased from 3.3% in the control to 11.2% in a dose-dependent mode in garcinol-treated H460 cells. However, garcinol significantly induced G1 cell cycle arrest in H1299 cells. The results implicated that garcinol possessed different biological activities via distinct p53 statuses.

Expression of Cell Cycle Regulatory Proteins in Garcinol-Treated H1299 Cells. In several studies, it has been demonstrated that garcinol induced apoptosis in many types of cancer cells.[8,9,11,12,25] However, further studies on the G1 arrest molecular mechanism in garcinol-induced p53-null cancer cells are still deficient. Therefore, we focused on the verification of the molecular mechanism of garcinol in H1299 cells. The cyclins and CDKs are two important cell cycle regulatory protein families. It has been well-characterized that D- and E-type cyclins are associated with CDK2 and CDK4/6, which control G1 cell cycle progression.[19,22] To investigate biological pathways of G1 arrest induced by garcinol via the regulatory protein expression, H1299 cells were synchronized and treated with garcinol for 24 h. After 24 h of treatment, the cells were harvested and changes in the expression of cyclin D1, D3, E, CDK2, CDK4, and CDK6 were inspected by western blots. Decreases in the protein levels of cyclin D1, D3, CDK2, and CDK4 were detected in a dose-dependent manner with garcinol treatment, as shown in Figure 3A, while increases in the expression of cyclin E and CDK6 were observed (Figure 3A).

Garcinol Induced G1 Cell Cycle Arrest through the Upregulation of CDK Inhibitors. Previous results showed that CDK activity was inhibited by CDK inhibitors, $p21^{Waf1/Cip1}$ and $p27^{Kip1}$. Furthermore, the activities of $p21^{Waf1/Cip1}$ and $p27^{Kip1}$ associated with the complexes of cyclin/CDK were repressed, resulting in cell cycle arrest.[22,23] The effects of garcinol on the expression of $p21^{Waf1/Cip1}$ and $p27^{Kip1}$ were characterized by western blot, as shown in Figure 3B. Obviously, the protein levels of $p21^{Waf1/Cip1}$ and $p27^{Kip1}$ were upregulated by garcinol treatment in a dose-dependent mode (Figure 3B). The verification of the activities of garcinol-inhibited CDK2 or CDK4 enhanced by $p21^{Waf1/Cip1}$ and $p27^{Kip1}$ was performed by H1299 cell synchronization treated with or without garcinol. The outcomes revealed that the bound

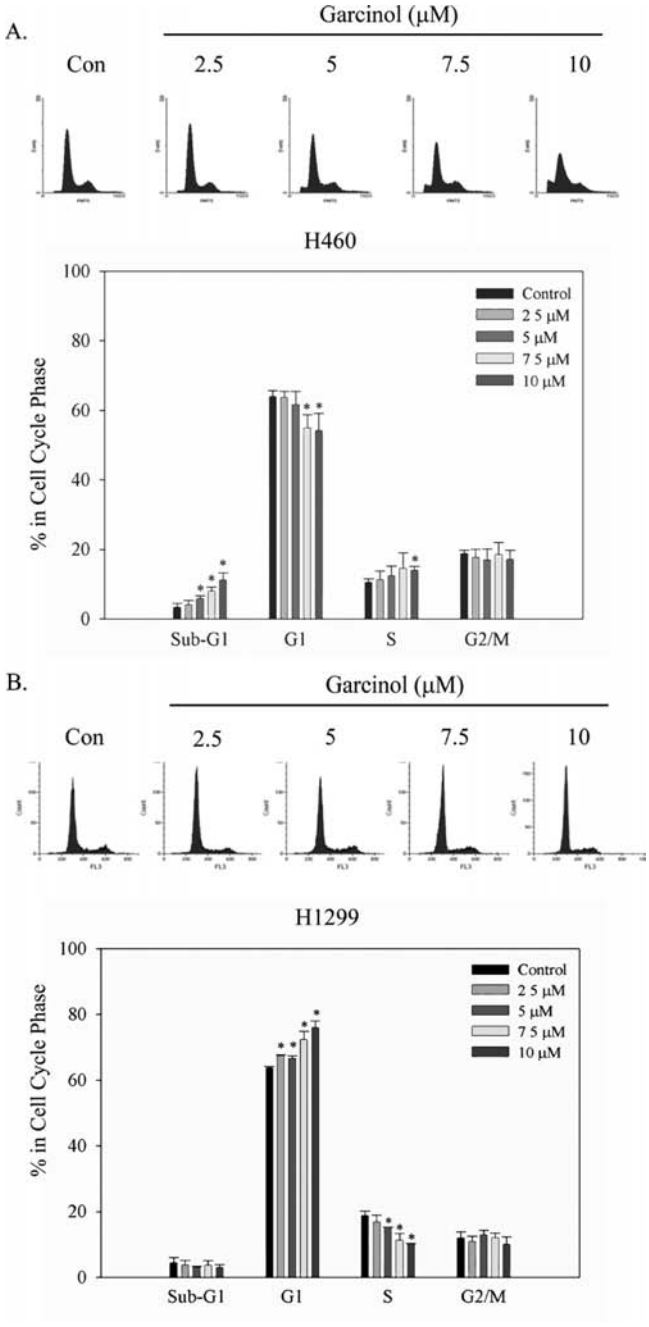

Figure 2. Effects of garcinol on cell cycle distribution in H460 and H1299 lung cancer cells. (A) H460 and (B) H1299 cells were treated with garcinol for 24 h, and then cells were harvested for cell cycle distribution analyses by flow cytometry. Three samples were analyzed in each group, and the results are presented as the mean ± SD. (*) Significant difference was observed from the control group ($p < 0.05$).

dx.doi.org/10.1021/jf4037722 | J. Agric. Food Chem. 2014, 62, 2085−2095

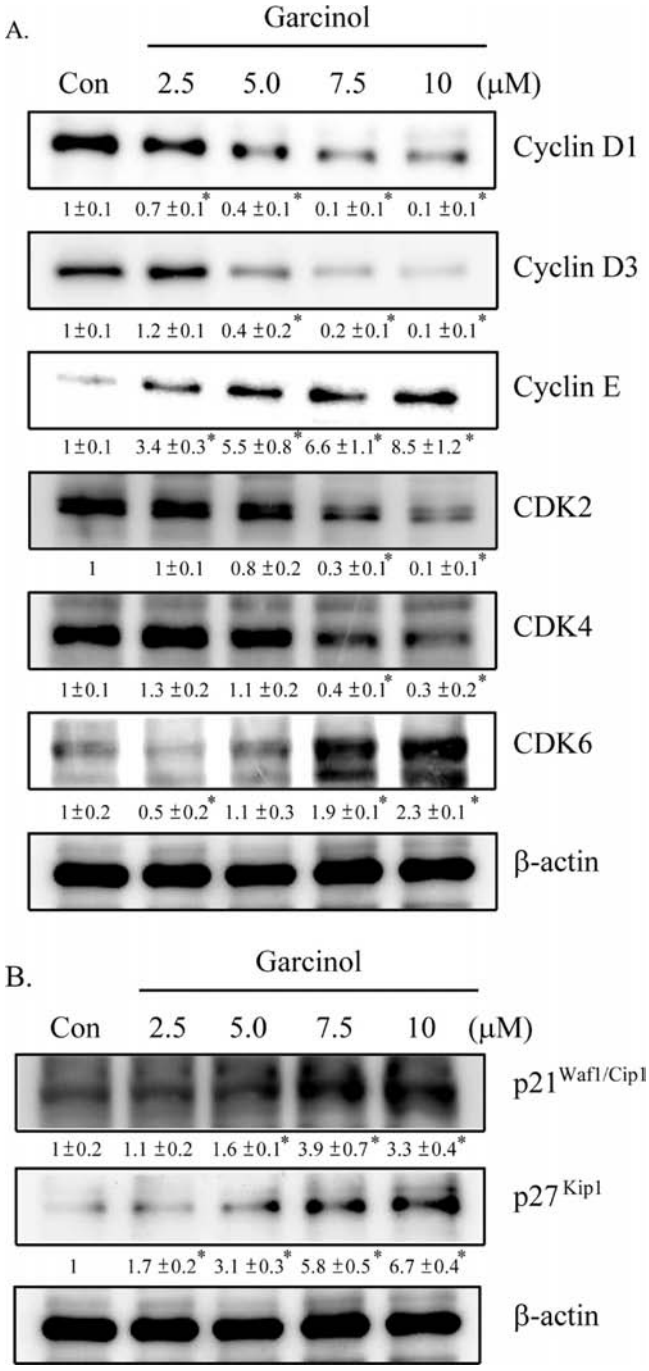

Figure 3. Effects of garcinol on the expressions of cyclins, CDKs, and CDK inhibitors. H1299 lung cancer cells were initially synchronized by serum-free medium and then serum-supplemented medium containing various doses of garcinol (0, 2.5, 5, 7.5, and 10 μM). After the cells were harvested, western blot analyses were performed with (A) anti-cyclin D1, cyclin D3, cyclin E, CDK2, CDK4, and CDK6 and (B) anti-$p21^{Waf1/Cip1}$, $p27^{Kip1}$, and β-actin antibodies. The protein levels in each treatment after normalization with the levels of β-actin are shown in parentheses. Data shown are representative of at least three independent experiments.

protein levels of $p21^{Waf1/Cip1}$ with CDK2 were increased about 3-fold in garcinol-treated cells, otherwise a 5-fold increase in bound protein levels of $p21^{Waf1/Cip1}$ with CDK4 in garcinol-treated cells (Figure 4). Nevertheless, $p27^{Kip1}$, bound with CDK2, was increased about 2-fold in garcinol-treated cells. The results implicated that the garcinol-induced G1 cell cycle arrest might be through upregulation of $p21^{Waf1/Cip1}$ and $p27^{Kip1}$ expression, resulting in downregulated CDK activities via enhancing the association.

It has been confirmed that $p21^{Cip1/Waf1}$ expression is regulated by p53-dependent and -independent transcriptional mechanisms.[23] After the cells were treated with garcinol for 12 h, total RNA was collected and RT-PCR was perform to investigate the expression of $p21^{Waf1/Cip1}$ induced by garcinol through transcriptional activation. The $p21^{Waf1/Cip1}$ mRNA expression was increased in a dose-dependent manner. Conversely, the expression of $p27^{Kip1}$ mRNA was declined (Figure 5A). To further verify whether garcinol-induced $p21^{Waf1/Cip1}$ expression in H1299 cells correlated with G1 growth arrest, we knocked down $p21^{Waf1/Cip1}$ expression by siRNA and analyzed the cell cycle distribution in garcinol-treated cells. As shown in Figure 5B, the protein level of $p21^{Waf1/Cip1}$ was dramatically downregulated after specific siRNA transfection. Furthermore, garcinol-induced G1 arrest was completely prevented by transfection with $p21^{Waf1/Cip1}$ siRNA into H1299 cells (Figure 5B). These results suggested that the garcinol-induced G1 arrest in H1299 cells was through upregulation of $p21^{Waf1/Cip1}$ protein.

Garcinol Inhibited ERK and p38-MAPK Activation. To explore the molecular mechanism of garcinol-induced G1 arrest, the phosphorylation of ERK and p38-MAPK, two important molecules in MAPK pathways involving cell cycle regulation, were analyzed in garcinol-treated H1299 cells. The outcomes exhibited that ERK phosphorylation was briefly stimulated between 0.5 and 1 h by serum significantly. Conversely, serum-stimulated ERK activation was repressed with 10 μM garcinol treatment (Figure 6). p38-MAPK was induced at 0.5 h and remained active in serum stimulation for 12 h. With garcinol treatment, the level of active p38-MAPK was diminished in a time-dependent mode (Figure 6). The results implicated that G1 arrest prompted by garcinol might be through ERK and p38-MAPK inhibition in H1299 cells.

p38-MAPK Rather than ERK Involved in Garcinol-Induced G1 Arrest. In the present study, the mechanism of garcinol-induced G1 arrest through $p21^{Waf1/Cip1}$ and $p27^{Kip1}$ activation, following the inhibition of CDK activity, via association with CDKs, was established (Figure 4). Furthermore, ERK and p38-MAPK were activated in garcinol-treated H1299 cells (Figure 6). The pharmacological inhibitors, PD98059 and SB203580, for ERK and p38-MAPK, correspondingly, were used to understand the correlation in the activated pathways between ERK and p38-MAPK and the destination of garcinol-treated cells. H1299 cells were pretreated with 10 μM PD98059 or SB203580 for 30 min before stimulated with 10 μM garcinol for 24 h. Cells were collected for flow cytometry analysis. G1 arrest was observed in H1299 cells treated with ERK and p38-MAPK inhibitors alone (Figure 7). Interestingly, the synergistic effect of the G1 arrest population was detected in combinational treatments with p38-MAPK inhibitor and garcinol unlike in the co-treatment of ERK inhibitor and garcinol. Additionally, H1299 cells were pretreated with p38-MAPK inhibitor before 10 μM garcinol stimulation to verify the cell cycle regulators participated in p38-MAPK signaling when garcinol was supplied. The results showed that the expression of CDK2 was reduced in garcinol-treated cells on western blot (Figure 8A). Moreover, the expression of CDK2 was repressed by the combinational treatment with p38-MAPK inhibitor and garcinol. The

dx.doi.org/10.1021/jf4037722 | J. Agric. Food Chem. 2014, 62, 2085−2095

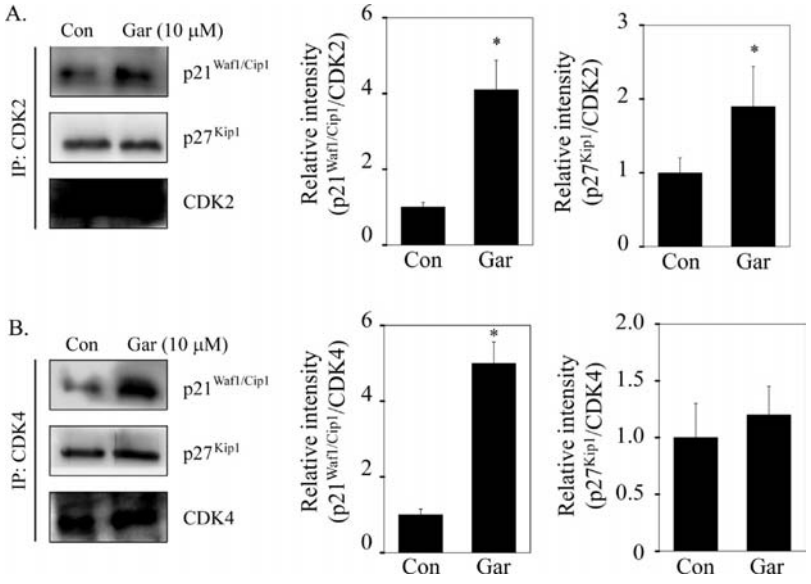

Figure 4. Effects of garcinol on the expressions of CDK−CDKI complexes in lung carcinoma H1299 cells. H1299 cells were treated with 10 μM garcinol for 24 h. Cell lysates were then incubated with protein A/G agarose beads conjugated with (A) anti-CDK2 or (B) anti-CDK4 antibody. The immunoprecipitates were electrophoresed, and the separated proteins reacted against primary antibodies, anti-$p21^{Waf1/Cip1}$, $p27^{Kip1}$, CDK2, and CDK4, to monitor protein interaction by western blot. The bound levels of $p21^{Waf1/Cip1}$ and $p27^{Kip1}$ in each treatment normalized with the levels of immunoprecipitation loading control are shown and representative of an experiment performed in triplicate. The density of the band was then expressed as the relative density compared to that in untreated cells (control), which was taken as 1-fold.

expression of cyclin E in the co-treatment of p38-MAPK inhibitor and garcinol was upregulated (Figure 8A). Similarly, the expression of $p21^{Waf1/Cip1}$ and $p27^{Kip1}$ in co-treatment with p38-MAPK inhibitor and garcinol was increased, especially in the protein level of $p21^{Waf1/Cip1}$ (Figure 8B). To further evaluate the significance of the p38-MAPK signaling in garcinol-induced $p21^{Waf1/Cip1}$ expression, H1299 cells transiently transfected the DN p38-MAPK. As shown in Figure 8C, ectopic expression of DN p38-MAPK enhanced garcinol-induced $p21^{Waf1/Cip1}$ expression. These results revealed that the garcinol-induced $p21^{Waf1/Cip1}$ expression was through inhibition of p38-MAPK activation.

DISCUSSION

Natural products represent good candidates to downregulate cancer cell growth. Major beneficial effects of these natural components as cancer-preventive agents are their comparative nontoxic effects. These non-nutritive components in a diet have been demonstrated to contribute from their pleiotropic effects, including downregulation of survival signaling and activating the death signaling pathway in cancer cells.[1,2] Garcinol has been indicated to possess numerous biological activities, such as antioxidation, anti-inflammation,[4−6,36] and upregulation of death signaling.[7,9,11,12,25] Although there is countless literature on the anticancer properties of garcinol, the effect of garcinol is still unclear regarding the molecular mechanism of diverse p53 statuses in lung cancer. Here, we have demonstrated that p38-MAPK signaling might be the essential target in p53 mutant lung cancer cell growth via garcinol treatment. Both p53-wild type H460 and p53-null H1299 lung cancer cell growth were inhibited by garcinol treatment. Garcinol significantly induced G1 cell cycle arrest in H1299 but not in H460 lung cancer cells. Furthermore, the D type of cyclin, CDK2, and CDK4 expressions were downregulated, whereas cyclin E and CDK6 expressions were upregulated in garcinol-stimulated H1299 cells. Also, the protein levels of $p21^{Waf1/Cip1}$ and $p27^{Kip1}$ were prompted in garcinol-treated cells, and the upregulation of $p21^{Waf1/Cip1}$ was associated with CDK2 and CDK4, followed by the inhibition of cyclin/CDK complex activity. Meanwhile, the upregulation of $p21^{Waf1/Cip1}$ expression via garcinol stimulation was through transcriptional regulation. The studies indicated that garcinol inhibited ERK and p38-MAPK phosphorylation and merely a combination with the p38-MAPK inhibitor resulted in the enhancement of G1 cell cycle arrest. The expressions of cyclin E, $p21^{Waf1/Cip1}$, and $p27^{Kip1}$ were also boosted after co-treatment of the p38-MAPK inhibitor and garcinol.

Tumor suppressor protein p53 has been shown to participate in numerous cellular processes.[15,24,37] The pivotal roles of p53 are involved in the cell growth arrest and cell death induction in cancer treatment. However, p53 mutations are present in almost half of NSCLC and award chemoresistance and poorer survival prognosis in lung cancer patients.[15,37] The application of disrupting the oncogenic effects is certainly important for the treatment and prevention of lung cancer. One of the advanced strategies for preventive or therapeutic p53 mutant tumors is the probing of active components to restore the p53-regulated pathway in the cells. Garcinol has evaluated its growth inhibition and apoptosis induction in a number of cancer models.[7,9−11,25] However, the role of p53 in garcinol-treated cancer cells is still unclear. We hypothesized that p53 statuses of lung cancer cells might affect the distinct molecular pathways in garcinol-treated cells. The effects of garcinol in p53-wild type and p53-null lung cancer cells were studied to further validate our hypothesis. The results revealed that garcinol induced the morphological changes and decreased the amount of lung cancer cells. Moreover, H460 cells were more active treated with garcinol (Figure 1). To further verify the cytotoxic effects in garcinol-treated cells, the cell cycle distribution was investigated. The outcomes showed that the G1 cell cycle arrest was enhanced by garcinol in H1299 cells (Figure 2). Our results revealed that garcinol induced apoptosis and G1 growth

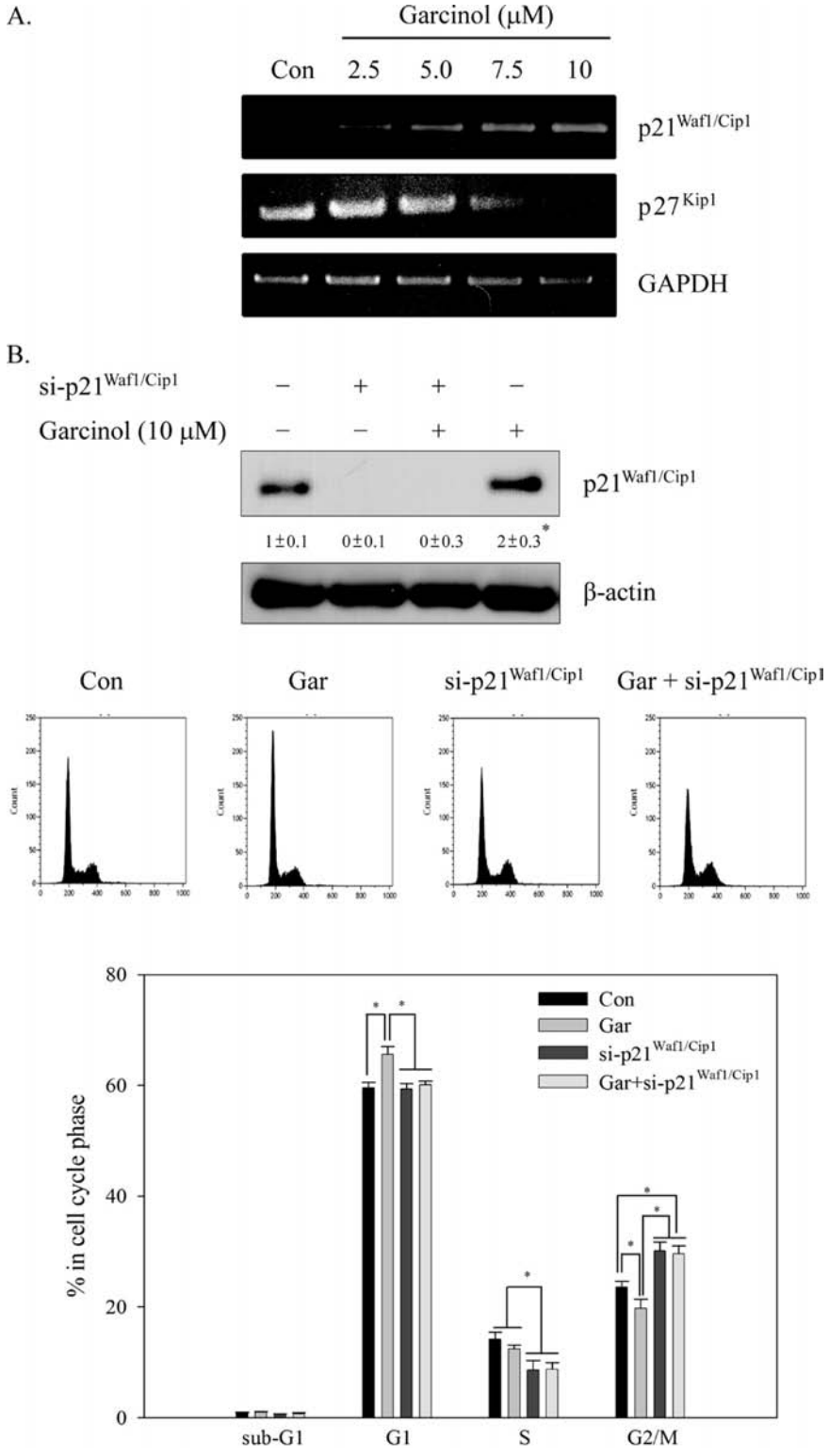

Figure 5. Role of $p21^{Waf1/Cip1}$ in the garcinol-induced G1 cell cycle arrest. (A) H1299 cells were treated with garcinol for 12 h, and total mRNA was extracted afterward. After the extraction of total mRNA, $p21^{Waf1/Cip1}$, $p27^{Kip1}$, and GAPDH RT-PCR were performed, as described in the Materials and Methods. (B) Knock-down $p21^{Waf1/Cip1}$ expression prevented garcinol-induced G1 cell cycle arrest in H1299 cells. H1299 cells were transfected with $p21^{Waf1/Cip1}$ siRNAs as described in the Materials and Methods. After transfection, H1299 cells were synchronized for 24 h and then treated with or without garcinol (10 μM) for an additional 24 h. Cells were harvested for Western blot and cell cycle progression analyses.

arrest in lung cancer cells in different p53 statuses. Tumor suppressor protein p53 might be regarded as a key factor in control cell apoptosis or G1 growth arrest in garcinol-treated lung cancer cells. However, a low concentration (4 μM) of garcinol-treated p53 wild-type A549 cells does not show apoptosis and/or G1 arrest induction.[38] In our study, garcinol-induced significant apoptotic or G1 arrest cell accumulation was observed upper 5 μM garcinol treatment in two cell lines

dx.doi.org/10.1021/jf4037722 | J. Agric. Food Chem. 2014, 62, 2085−2095

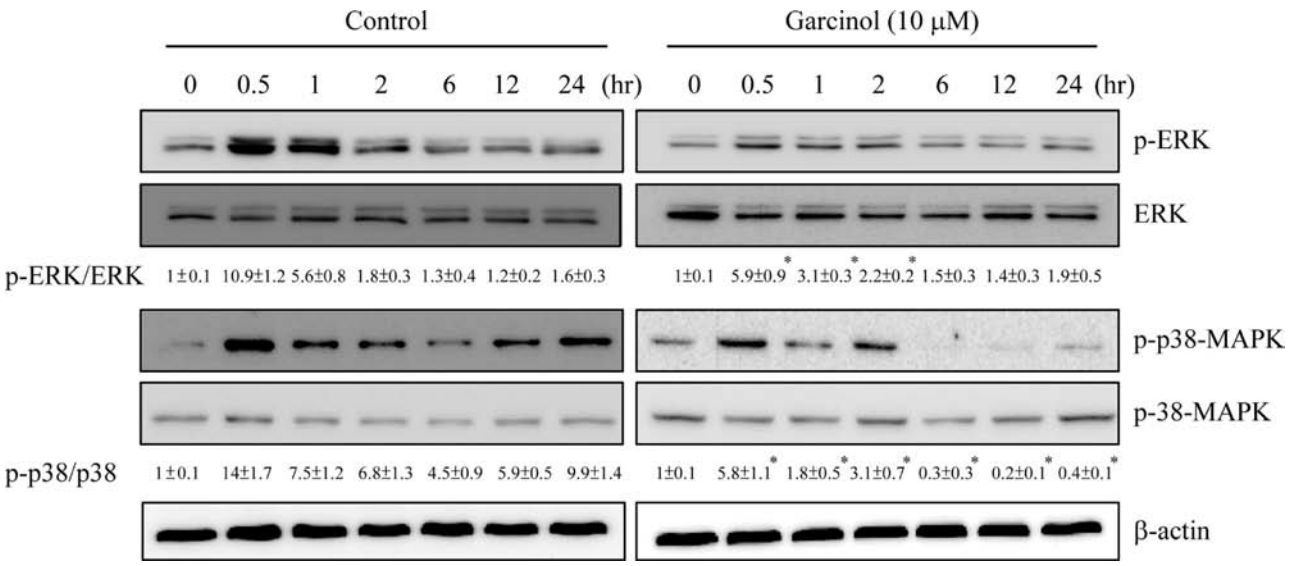

Figure 6. Effects of garcinol on ERK and p38-MAPK expressions in H1299 lung cancer cells. H1299 cells were treated with garcinol (10 μM) for indicated time intervals, and western blot analyses were performed with anti-p-ERK, ERK, p-p38-MAPK, p38-MAPK, and β-actin antibodies. The ratio of phospho-form/non-phospho-form protein in each treatment normalized with the levels of β-actin are shown in parentheses. Data shown are representative of at least three independent experiments. (*) Significant differences were compared to the control and determined by one-way ANOVA ($p < 0.05$).

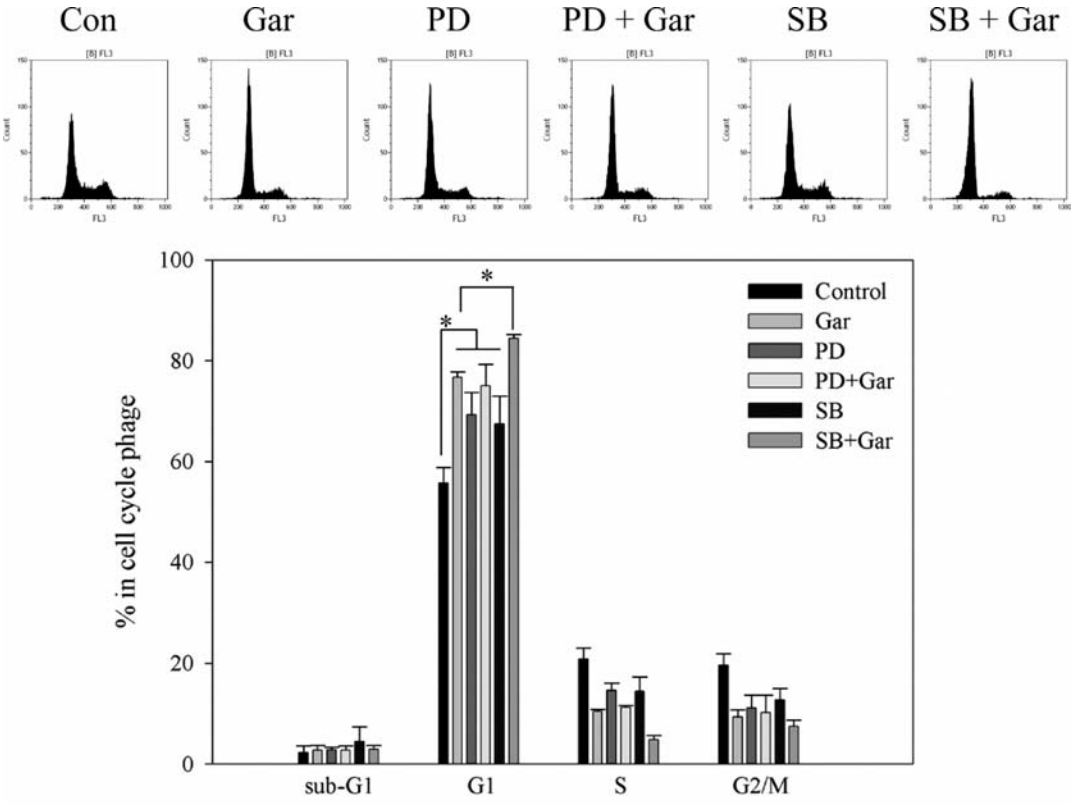

Figure 7. Effect of ERK and p38-MAPK inhibitors on cell cycle distribution in garcinol-treated H1299 cells. H1299 cells were treated with 10 μM PD98059 or SB203580 for 30 min and then stimulated with or without 10 μM garcinol for 24 h. Cells were harvested and stained with propidium iodine subsequently. Cell cycle distribution was determined by FACScan analysis. Three samples were analyzed in each group. (*) Significant differences were determined by Student's t test using the mean ± SD from the control group ($p < 0.05$).

(Figure 2). These results suggested that the effective dosage of garcinol should be carefully concerned in anticancer actions. Furthermore, treatment with a high dosage of garcinol (50 μM) has been demonstrated to induce ROS-dependent apoptosis rather than G1 arrest in p53-negative hepatocellular cancer Hep3B cells.[12] Although treatment with a high dosage of garcinol might induce p53-independnet apoptosis in cancer cells, other side effects might emerge in clinical application.

It has been well-known that garcinol induced the apoptosis of cancer cells through intrinsic and extrinsic pathways.[8,9,11,12]

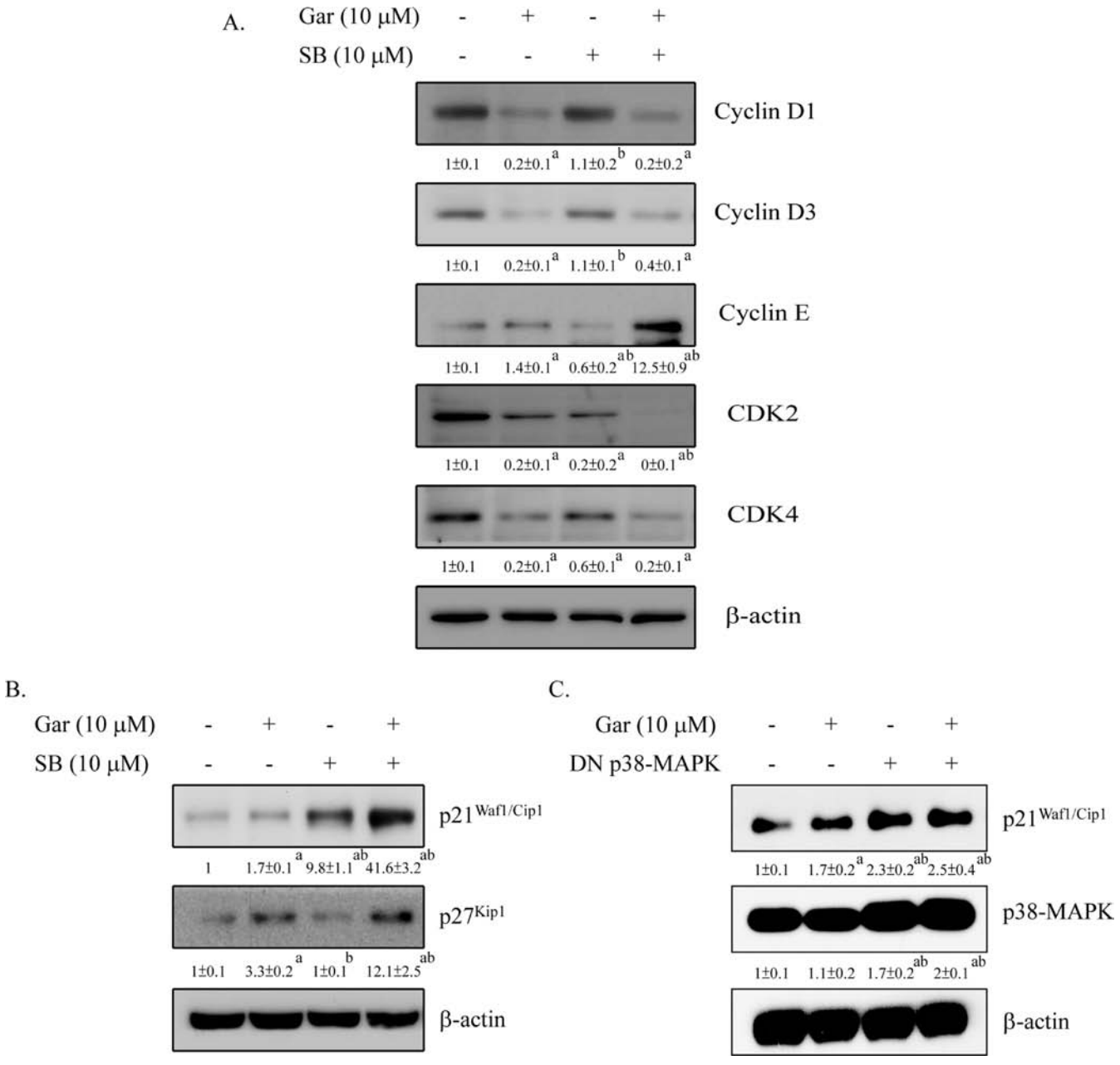

Figure 8. Effects of p38-MAPK inhibitor and garcinol co-treatment on the expressions of cyclins, CDKs, and CDKIs in H1299 cells. H1299 cells were treated with 10 μM SB203580 for 30 min and then stimulated with or without 10 μM garcinol for 24 h. Cells were harvested, and western blot was implemented with (A) anti-cyclin D1, cyclin D3, cyclin E, CDK2, and CDK4 and (B) anti-$p21^{Waf1/Cip1}$, $p27^{Kip1}$, and β-actin antibodies. (C). H1299 cells were transiently transfected with DN p38-MAPK, and then treated with 10 μM garcinol for 24 h. The protein levels of $p21^{Waf1/Cip1}$, p38-MAPK, and β-actin were determined by western blotting. The protein levels in each treatment after normalization with the levels of β-actin were shown in parentheses. Data shown were representative of at least three independent experiments. The significant differences were determined by one-way ANOVA (a) compared to the control ($p < 0.05$) and (b) compared to the garcinol-treated group ($p < 0.05$).

Besides, Collins et al. demonstrated that, with garcinol-induced p53 expression, acetylation accompanied G1 phase population accumulation in breast cancer cells.[39] Additionally, the proliferation of the nicotine-stimulated breast cancer cell is blocked by garcinol, which diminished nicotine receptor signal cascade to mediate cyclin D3 expression and induce p53-$p21^{Waf1/Cip1}$ signaling, resulting in G1 arrest.[10] The reports confirm that garcinol induced G1 cell cycle arrest through p53-related signaling pathways. However, the effects of garcinol in cell cycle regulation on p53-null cancer cells are still mysterious. The results indicated that the D type of cyclins, CDK2, and CDK4 were reduced, whereas the protein level of cyclin E was increased, in garcinol-treated H1299 cells (Figure 3A). The progression of the cell cycle is tightly regulated by the complexes of cyclins and CDKs. In the transition from the G1 to S phase, cyclin D/CDK4/6 and cyclin E/CDK2 control the cycle entry.[19] Furthermore, the activities of cyclin−CDK complexes are modulated through CDK inhibitors. The prominent CDK inhibitors are the WAF/KIP family, including $p21^{Waf1/Cip1}$, $p27^{Kip1}$, and p57 ^{Kip2}.[23] We demonstrated that CDK inhibitors, $p21^{Waf1/Cip1}$ and $p27^{Kip1}$, were enhanced in a dose-dependent manner (Figure 3B). The association between

dx.doi.org/10.1021/jf4037722 | J. Agric. Food Chem. 2014, 62, 2085−2095

$p21^{Waf1/Cip1}$ and CDK2/4 was raised in garcinol-treated cells. However, $p27^{Kip1}$ was only complexed with CDK2 (Figure 4). The data disclosed that the garcinol-induced G1 cell cycle arrest might be through p53-independent upregulation of $p21^{Waf1/Cip1}$ rather than $p27^{Kip1}$, resulting in the inhibition of cyclin−CDK activities via the strengthening binding activity.

It is well-established that $p21^{Waf1/Cip1}$ is necessary and sufficient for p53-dependent repressing of genes regulating cell cycle progression.[23] Post-translational modifications of $p21^{Waf1/Cip1}$, such as phosphorylation, increasing protein stability following cell accumulation at the G1 phase, were acknowledged.[29] In this study, the gene expression of $p21^{Waf1/Cip1}$ was further examined after the treatment with garcinol. The RNA level of $p21^{Waf1/Cip1}$ was considerably increased in a dose-dependent profile (Figure 5A). The data suggested that the garcinol-induced expression of $p21^{Waf1/Cip1}$ might be through transcriptional regulation. Furthermore, to further investigate the relationship between garcinol-induced $p21^{Waf1/Cip1}$ expression and G1 arrest, we knocked down $p21^{Waf1/Cip1}$ expression by specific siRNA before garcinol stimulation. Our results revealed that downregulation of $p21^{Waf1/Cip1}$ by siRNA transfection completely prevented the garcinol-induced G1 arrest (Figure 5B). According to our results, garcinol-induced G1 growth arrest was through $p21^{Waf1/Cip1}$ upregulaion.

MAPK pathways have been demonstrated to play an important role in cell cycle regulation, especially ERK and p38-MAPK.[26,28,30,40] ERK kinases are activated in various cell types as a survival signal through mitogenic and cytokine stimulation. Inhibition of active ERK has been investigated in blockage of cell cycle progression.[26] Moreover, p38-MAPK is generally activated by inflammatory cytokines and cellular stress and then results in G1 arrest, which mediated differentiation.[26−28] Emerging evidence points out the roles of p38-MAPK in cell cycle regulation, proliferation, and metastasis in different cells. The level of active p38-MAPK is higher in 18 analyzed primary NSCLC tumor tissues than normal lung tissue. Active p38-MAPK is discovered in the nucleus and cytoplasm of malignant and dysplastic cells.[33] p38-MAPK has been proven to promote melanoma cell proliferation through ATF-2-meidated upregulation of cyclin D1.[34] Faust et al. indicate that mitogen- and stress-induced activations of p38-MAPK have different functions. The duration of p38-MAPK activation determines the cell's destination, proliferation, or induction of cell cycle arrest.[27] Mitogen stimulation induces a weak and transient p38-MAPK phosphorylation, which is required for the G1−S transition. However, stress induces the strong and sustained p38-MAPK activation, following increasing cyclic adenosine monophosphate (cAMP) response element-binding protein (CREB) phosphorylation and cell arrest.[27] Furthermore, our recent report showed that chrysin induced sustained p38-MAPK activation and upregulation of $p21^{Waf1/Cip1}$ expression, following downregulated C6 glioma cell growth.[29] The results also revealed that p38-MAPK phosphorylation was detected at 0.5 h and persisted up to 6 h after serum stimulation. Moreover, serum-stimulated p38-MAPK activation was suppressed by garcinol (Figure 6). Inconclusively, garcinol inhibited serum-stimulated p38-MAPK activation, resulting in the disruption of p38-MAPK-mediated cell proliferation via G1 arrest.

Recent reports show that $p21^{Waf1/Cip1}$ is positively regulated via p38-MAPK phosphorylation and subsequent cell accumulation at the G1 phase.[29,30] Nevertheless, p38-MAPK also affects the cell fate to arrest the G1 phase in the survival cascade of several cancer cell types.[27,32,35] These dual roles of p38-MAPK in cell cycle regulation may depend upon the cell type and other related factors. In our studies, garcinol inhibited serum-stimulated ERK and p38-MAPK activation in a time-dependent profile (Figure 6). The co-treatment of SB203580 and not PD98059 plus garcinol revealed the substantial G1 accumulation compared to garcinol treatment alone (Figure 7). The data suggested that the garcinol-induced G1 cell cycle arrest might be partially proceeded by the means of p38-MAPK inhibition. Also, co-treatment with SB203580 and garcinol enhanced cyclin E and $p21^{Waf1/Cip1}$ expressions compared to garcinol-treatment alone in H1299 cells (Figure 8). Furthermore, transiently transfecting the DN p38-MAPK also enhanced garcinol-induced $p21^{Waf1/Cip1}$ expression (Figure 8C). Therefore, the expression of $p21^{Waf1/Cip1}$ induced by garcinol might be through downregulation of p38-MAPK activity. However, recent evidence reveals that nuclear factor-κB (NF-κB) is a transcription factor regulating cell growth, apoptosis, and inflammation[6,8,41] and also involved in the $p21^{Waf1/Cip1}$-mediated cell cycle arrest of breast and colon cancer cells.[41,42] Knock-down NF-κB expression by siRNA enhances 4-*O*-methylhonokiol, resulting in increasing $p21^{Waf1/Cip1}$ expression in colon cancer cells.[41] Accordingly, NF-κB is a key regulator in the expression of $p21^{Waf1/Cip1}$. NF-κB-mediated proliferative and inflammatory gene expressions have previously been identified through the p38-MAPK signaling pathway.[6,41] In addition, the downregulation of NF-κB via garcinol-augmented cell death has been demonstrated in breast and pancreatic cancer cells.[8,25] It was speculated that p53-independent $p21^{Waf1/Cip1}$ expression induced by garcinol might be as a consequence of the downregulation of p38-MAPK-mediated NF-κB activity. In summary, the G1 cell cycle evoked by garcinol was triggered by p53-independent $p21^{Waf1/Cip1}$ activation by means of the negative regulation of p38-MAPK activation in H1299 lung cancer cells. Our finding revealed that garcinol might become a candidate of the chemopreventive agent for p53-independent lung cancer cells in the future.

AUTHOR INFORMATION

Corresponding Author

*Telephone: 886-2-2905-3776. Fax: 886-2-2902-1215. E-mail: 078670@mail.fju.edu.tw.

Funding

This work was supported by grants from the National Science Council of Taiwan, Republic of China, NSC100-2313-B-030-003.

Notes

The authors declare no competing financial interest.

REFERENCES

(1) Lee, K. W.; Bode, A. M.; Dong, Z. Molecular targets of phytochemicals for cancer prevention. *Nat. Rev. Cancer* **2011**, *11*, 211−218.

(2) Sarkar, F. H.; Li, Y. Harnessing the fruits of nature for the development of multi-targeted cancer therapeutics. *Cancer Treat. Rev.* **2009**, *35*, 597−607.

(3) Padhye, S.; Ahmad, A.; Oswal, N.; Sarkar, F. H. Emerging role of garcinol, the antioxidant chalcone from *Garcinia indica* Choisy and its synthetic analogs. *J. Hematol. Oncol.* **2009**, *2*, 38.

(4) Liao, C. H.; Ho, C. T.; Lin, J. K. Effects of garcinol on free radical generation and NO production in embryonic rat cortical neurons and astrocytes. *Biochem. Biophys. Res. Commun.* **2005**, *329*, 1306−1314.
(5) Yamaguchi, F.; Saito, M.; Ariga, T.; Yoshimura, Y.; Nakazawa, H. Free radical scavenging activity and antiulcer activity of garcinol from *Garcinia indica* fruit rind. *J. Agric. Food Chem.* **2000**, *48*, 2320−2325.
(6) Liao, C. H.; Sang, S.; Liang, Y. C.; Ho, C. T.; Lin, J. K. Suppression of inducible nitric oxide synthase and cyclooxygenase-2 in downregulating nuclear factor-κB pathway by garcinol. *Mol. Carcinog.* **2004**, *41*, 140−149.
(7) Ahmad, A.; Sarkar, S. H.; Aboukameel, A.; Ali, S.; Biersack, B.; Seibt, S.; Li, Y.; Bao, B.; Kong, D.; Banerjee, S.; Schobert, R.; Padhye, S. B.; Sarkar, F. H. Anticancer action of garcinol in vitro and in vivo is in part mediated through inhibition of STAT-3 signaling. *Carcinogenesis* **2012**, *33*, 2450−2456.
(8) Ahmad, A.; Wang, Z.; Ali, R.; Maitah, M. Y.; Kong, D.; Banerjee, S.; Padhye, S.; Sarkar, F. H. Apoptosis-inducing effect of garcinol is mediated by NF-κB signaling in breast cancer cells. *J. Cell. Biochem.* **2010**, *109*, 1134−1141.
(9) Prasad, S.; Ravindran, J.; Sung, B.; Pandey, M. K.; Aggarwal, B. B. Garcinol potentiates TRAIL-induced apoptosis through modulation of death receptors and antiapoptotic proteins. *Mol. Cancer Ther.* **2010**, *9*, 856−868.
(10) Chen, C. S.; Lee, C. H.; Hsieh, C. D.; Ho, C. T.; Pan, M. H.; Huang, C. S.; Tu, S. H.; Wang, Y. J.; Chen, L. C.; Chang, Y. J.; Wei, P. L.; Yang, Y. Y.; Wu, C. H.; Ho, Y. S. Nicotine-induced human breast cancer cell proliferation attenuated by garcinol through down-regulation of the nicotinic receptor and cyclin D3 proteins. *Breast Cancer Res. Treat.* **2011**, *125*, 73−87.
(11) Liao, C. H.; Sang, S.; Ho, C. T.; Lin, J. K. Garcinol modulates tyrosine phosphorylation of FAK and subsequently induces apoptosis through down-regulation of Src, ERK, and Akt survival signaling in human colon cancer cells. *J. Cell. Biochem.* **2005**, *96*, 155−169.
(12) Cheng, A. C.; Tsai, M. L.; Liu, C. M.; Lee, M. F.; Nagabhushanam, K.; Ho, C. T.; Pan, M. H. Garcinol inhibits cell growth in hepatocellular carcinoma Hep3B cells through induction of ROS-dependent apoptosis. *Food Funct.* **2010**, *1*, 301−307.
(13) Tanaka, T.; Kohno, H.; Shimada, R.; Kagami, S.; Yamaguchi, F.; Kataoka, S.; Ariga, T.; Murakami, A.; Koshimizu, K.; Ohigashi, H. Prevention of colonic aberrant crypt foci by dietary feeding of garcinol in male F344 rats. *Carcinogenesis* **2000**, *21*, 1183−1189.
(14) Jemal, A.; Bray, F.; Center, M. M.; Ferlay, J.; Ward, E.; Forman, D. Global cancer statistics. *Ca-Cancer J. Clin.* **2011**, *61*, 69−90.
(15) Viktorsson, K.; De Petris, L.; Lewensohn, R. The role of p53 in treatment responses of lung cancer. *Biochem. Biophys. Res. Commun.* **2005**, *331*, 868−880.
(16) Steels, E.; Paesmans, M.; Berghmans, T.; Branle, F.; Lemaitre, F.; Mascaux, C.; Meert, A. P.; Vallot, F.; Lafitte, J. J.; Sculier, J. P. Role of p53 as a prognostic factor for survival in lung cancer: A systematic review of the literature with a meta-analysis. *Eur. Respir. J.* **2001**, *18*, 705−719.
(17) Bodner, S. M.; Minna, J. D.; Jensen, S. M.; D'Amico, D.; Carbone, D.; Mitsudomi, T.; Fedorko, J.; Buchhagen, D. L.; Nau, M. M.; Gazdar, A. F.; et al. Expression of mutant p53 proteins in lung cancer correlates with the class of p53 gene mutation. *Oncogene* **1992**, *7*, 743−749.
(18) Hodkinson, P. S.; Mackinnon, A.; Sethi, T. Targeting growth factors in lung cancer. *Chest* **2008**, *133*, 1209−1216.
(19) Malumbres, M.; Barbacid, M. Cell cycle, CDKs and cancer: A changing paradigm. *Nat. Rev. Cancer* **2009**, *9*, 153−166.
(20) Eymin, B.; Gazzeri, S. Role of cell cycle regulators in lung carcinogenesis. *Cell Adhes. Migr.* **2010**, *4*, 114−123.
(21) Hartwell, L. H.; Weinert, T. A. Checkpoints: Controls that ensure the order of cell cycle events. *Science* **1989**, *246*, 629−634.
(22) Sherr, C. J.; Roberts, J. M. CDK inhibitors: Positive and negative regulators of G1-phase progression. *Genes Dev.* **1999**, *13*, 1501−1512.
(23) Abbas, T.; Dutta, A. p21 in cancer: Intricate networks and multiple activities. *Nat. Rev. Cancer* **2009**, *9*, 400−414.
(24) Baldi, A.; De Luca, A.; Esposito, V.; Campioni, M.; Spugnini, E. P.; Citro, G. Tumor suppressors and cell-cycle proteins in lung cancer. *Pathol. Res. Int.* **2011**, *2011*, 605042.
(25) Parasramka, M. A.; Gupta, S. V. Garcinol inhibits cell proliferation and promotes apoptosis in pancreatic adenocarcinoma cells. *Nutr. Cancer* **2011**, *63*, 456−465.
(26) Plotnikov, A.; Zehorai, E.; Procaccia, S.; Seger, R. The MAPK cascades: Signaling components, nuclear roles and mechanisms of nuclear translocation. *Biochim. Biophys. Acta* **2011**, *1813*, 1619−1633.
(27) Faust, D.; Schmitt, C.; Oesch, F.; Oesch-Bartlomowicz, B.; Schreck, I.; Weiss, C.; Dietrich, C. Differential p38-dependent signalling in response to cellular stress and mitogenic stimulation in fibroblasts. *Cell Commun. Signaling* **2012**, *10*, 6.
(28) Han, J.; Sun, P. The pathways to tumor suppression via route p38. *Trends Biochem. Sci.* **2007**, *32*, 364−371.
(29) Weng, M. S.; Ho, Y. S.; Lin, J. K. Chrysin induces G1 phase cell cycle arrest in C6 glioma cells through inducing p21Waf1/Cip1 expression: Involvement of p38 mitogen-activated protein kinase. *Biochem. Pharmacol.* **2005**, *69*, 1815−1827.
(30) Kim, G. Y.; Mercer, S. E.; Ewton, D. Z.; Yan, Z.; Jin, K.; Friedman, E. The stress-activated protein kinases p38α and JNK1 stabilize $p21^{Cip1}$ by phosphorylation. *J. Biol. Chem.* **2002**, *277*, 29792−29802.
(31) Chen, L.; Mayer, J. A.; Krisko, T. I.; Speers, C. W.; Wang, T.; Hilsenbeck, S. G.; Brown, P. H. Inhibition of the p38 kinase suppresses the proliferation of human ER-negative breast cancer cells. *Cancer Res.* **2009**, *69*, 8853−8861.
(32) Halawani, D.; Mondeh, R.; Stanton, L. A.; Beier, F. p38 MAP kinase signaling is necessary for rat chondrosarcoma cell proliferation. *Oncogene* **2004**, *23*, 3726−3731.
(33) Greenberg, A. K.; Basu, S.; Hu, J.; Yie, T. A.; Tchou-Wong, K. M.; Rom, W. N.; Lee, T. C. Selective p38 activation in human non-small cell lung cancer. *Am. J. Respir. Cell Mol. Biol.* **2002**, *26*, 558−5564.
(34) Recio, J. A.; Merlino, G. Hepatocyte growth factor/scatter factor activates proliferation in melanoma cells through p38 MAPK, ATF-2 and cyclin D1. *Oncogene* **2002**, *21*, 1000−1008.
(35) Maher, P. p38 mitogen-activated protein kinase activation is required for fibroblast growth factor-2-stimulated cell proliferation but not differentiation. *J. Biol. Chem.* **1999**, *274*, 17491−17498.
(36) Yamaguchi, F.; Ariga, T.; Yoshimura, Y.; Nakazawa, H. Antioxidative and anti-glycation activity of garcinol from *Garcinia indica* fruit rind. *J. Agric. Food Chem.* **2000**, *48*, 180−185.
(37) Vogt, U.; Zaczek, A.; Klinke, F.; Granetzny, A.; Bielawski, K.; Falkiewicz, B. p53 gene status in relation to ex vivo chemosensitivity of non-small cell lung cancer. *J. Cancer Res. Clin. Oncol.* **2002**, *128*, 141−147.
(38) Oike, T.; Ogiwara, H.; Torikai, K.; Nakano, T.; Yokota, J.; Kohno, T. Garcinol, a histone acetyltransferase inhibitor, radiosensitizes cancer cells by inhibiting non-homologous end joining. *Int. J. Radiat. Oncol., Biol., Phys.* **2012**, *84*, 815−821.
(39) Collins, H. M.; Abdelghany, M. K.; Messmer, M.; Yue, B.; Deeves, S. E.; Kindle, K. B.; Mantelingu, K.; Aslam, A.; Winkler, G. S.; Kundu, T. K.; Heery, D. M. Differential effects of garcinol and curcumin on histone and p53 modifications in tumour cells. *BMC Cancer* **2013**, *13*, 37.
(40) Yang, S. H.; Sharrocks, A. D.; Whitmarsh, A. J. MAP kinase signalling cascades and transcriptional regulation. *Gene* **2013**, *513*, 1−13.
(41) Oh, J. H.; Ban, J. O.; Cho, M. C.; Jo, M.; Jung, J. K.; Ahn, B.; Yoon, D. Y.; Han, S. B.; Hong, J. T. 4-*O*-Methylhonokiol inhibits colon tumor growth via p21-mediated suppression of NF-κB activity. *J. Nutr. Biochem.* **2012**, *23*, 706−715.
(42) Hellin, A. C.; Bentires-Alj, M.; Verlaet, M.; Benoit, V.; Gielen, J.; Bours, V.; Merville, M. P. Roles of nuclear factor-κB, p53, and p21/WAF1 in daunomycin-induced cell cycle arrest and apoptosis. *J. Pharmacol. Exp. Ther.* **2000**, *295*, 870−878.

inhibition of ROS.[20] In addition, Wang et al. found that Rh2 also acted against the doxorubicin-induced cardiotoxicity.[21] Unfortunately, such good health benefits of ginsenosides including cardiovascular protection shown in vitro attenuated, to some extent, in vivo due to their poor bioavailabilities. To our best knowledge, there is no information on whether the bioactivities of ginsenosides are enhanced or decreased through synthesis of their esterified derivatives.

In this study, first, to exam whether Rh2 ester has better bioavailability than Rh2, the transepithelial transport and absorption mechanisms of Rh2 and its derivative were studied in the Caco-2 system. Caco-2 cell monolayers have been generally accepted as an in vitro model for prediction of drug absorption across the human intestine and for mechanistic studies of intestinal drug transport due to their morphologic and functional similarities to human small intestinal epithelial cells.[22−24] Subsequently, an oxidative injury model was established using human umbilical vein endothelial cells (HUVECs) exogenously exposed to hydrogen peroxide (H_2O_2). The protective effects of Rh2 and its derivative on oxidative injury were evaluated to exam whether Rh2 ester with an enhanced absorption rate had similar or even better pharmaceutical function than Rh2. The present study will provide useful information on the pharmaceutical and preclinical research of ginsenosides and their structure modification.

MATERIALS AND METHODS

Materials and Chemicals. The human colon adenocarcinoma cell line, Caco-2, was purchased from the cell bank of the Chinese Academy of Sciences (Shanghai, China). HUVECs were obtained from the College of Medicine, Nanchang University. Dulbecco's modified Eagle's medium (DMEM), nonessential amino acids (NEAA), penicillin−streptomycin (10000 IU/mL), Hank's balanced salt solution (HBSS), trypsin, and ethylenediaminetetraacetic acid (EDTA) (0.25%/0.02%) in phosphate buffer saline (PBS) were all from Invitrogen Corp. (Carlsbad, CA, USA). Fetal bovine serum (FBS) was obtained from Gibco BRL (N.V. Life Technologies, Paisley, UK). 3-(4,5-Dimethylthiazol-2-yl)-2,5-diphenyltetrazolium bromide (MTT), mannitol, verapamil, and MK-571 were purchased from Sigma-Aldrich (St. Louis, MO, USA). The Rh2 and its ester derivative Rh2-O were kindly provided by Dr. Yinan Zheng, Jilin Agricultural University China. Transwell cell culture chambers (pore size = 0.4 μM, diameter = 24 mm) and the Millicell-ERS volt-ohmmeter with Ag/AgCl electrodes were purchased from Costar Corp (Cambridge, MA, USA) and from Nihon Millipore (Tokyo, Japan), respectively. The microplate reader was purchased from Thermo Fisher (Thermo Scientific Multiskan MK3, USA).

Culture of Caco-2 Cells and HUVECs. Caco-2 cells were cultured in DMEM supplemented with FBS (10%, v/v), NEAA (1%, v/v), penicillin (100 U/mL), streptomycin (0.1 mg/mL), and glutamine (0.29 g/L). The cells were incubated in a humidified atmosphere of 5% CO_2 at 37 °C. The medium was replaced every 2 days, and the cells were passaged at about 90% confluence using a trypsin/EDTA solution (0.25%/0.02%) at a split ratio of 1:4. Caco-2 cells used in this study were between passage 40 and 60. HUVECs were grown in DMEM containing FBS (10%, v/v), penicillin (100 U/mL), streptomycin (0.1 mg/mL), and glutamine (0.29 g/L). Cultures were maintained at 37 °C in a humidified atmosphere of 5% CO_2 in air.

Cytotoxicity Assay. The cytotoxicity of Rh2 and Rh2-O to Caco-2 cells and HUVECs was quantified using MTT assays.[25,26] The Rh2 and Rh2-O were first dissolved in DMSO and then diluted to desire concentration using PBS (ensuring the concentration of DMSO was <0.5%). Briefly, 0.1 mL of cells was seeded onto 96-well plates with a density of 10000 cells per well in a 96-well plate. The cells were grown in an atmosphere with 5% CO_2 and 95% relative humidity. Following incubation for 24 h, test compounds at different concentrations were added. Thereafter, 0.2 mL of 10% MTT solution was added to each well and incubated for 4 h in the dark. The medium was then removed, and the MTT−formazan crystals were solubilized by incubating with 0.15 mL of DMSO with gentle shaking for 10 min; the absorbance was determined at 490 nm in a microplate reader. Cells incubated without the test compounds were used as controls. In each MTT assay, every sample was tested in five replicates.

Transepithelial Transport Experiments across Caco-2 Monolayer. For transport experiments, Caco-2 cells were seeded onto the 6-well transwell inserts coated with type-I collagen at a density of 4×10^5 cells/well to generate Caco-2 monolayers. Medium was replaced every 2−3 days, and the monolayers used for the experiments were cultured to differentiate for 21−27 days after postseeding. The integrity of the cell layer and the full development of the tight junctions were monitored before every experiment by measurement of transepithelial electrical resistance (TEER) of filter-grown cell monolayers with millicell-ERS equipment. Only a monolayer with a TEER value of >300 $\Omega \cdot cm^2$ was used for the transepithelial transport experiments.

The transport of Rh2 and Rh2-O across Caco-2 monolayers was investigated using the methods described previously with minor modifications.[27] Briefly, the cell monolayers were gently rinsed twice with warm HBSS (pH 7.4, 37 °C) before the experiments. Cell monolayers were then incubated at 37 °C for 30 min in the transport buffer. To measure the apical-to-basolated (AP-BL) transport, 1.5 mL of mixture containing Rh2 or Rh2-O over 10−50 μM (final concentrations) in transport buffer was added to the AP side of the transwell insert and 2.6 mL of HBSS was added to the BL chamber. The plates were then put in an incubator at 37 °C. At a designated time point (30 min interval), 0.4 mL aliquots of solution were collected from the BL side and then replaced with an equal volume of transport buffer. In the direction of BL-AP, Rh2 or Rh2-O dissolved in 2.6 mL of transport buffer over 10−50 μM (final concentrations) was added to the BL side and 1.5 mL of the HBSS to the AP side, and 0.4 mL of the samples was collected from the AP side. All experiments were performed in triplicates.

For ethylenebis(oxyethylenenitrilo)tetraacetic acid (EGTA)-modulated transport experiments, the cell monolayers were pretreated with 2.5 mM EGTA in both AP and BL sides for 15 min at 37 °C after the initial 30 min of preincubation. Cell monolayers were then washed three times with transport buffer. AP to BL transport was initiated in the same way as described above. In the present study, the inhibitory effects of MK-517 and verapamil on Rh2 and Rh2-O flux by Caco-2 monolayers were examined by addition of 100 μM of each inhibitor to the AP side, regardless of where samples were loaded. Thereafter, the transport study was performed according to the method described above.

Superoxide Radical Scavenging Capability of Rh2 and Rh2-O in a Cell-Free System. The superoxide radical scavenging capability of Rh2 and Rh2-O was assayed by a photochemical system (Analytik Jena, Berlin, Germany); the principle of this method was photochemiluminescence (PCL), which is based on the photoinduced autoxidation inhibition of luminol by antioxidants mediated from the radical anion superoxide. The PCL assay was based on the method previously described.[28] Trolox is used as reference compound to evaluate the superoxide radical scavenging capability, and all of the samples were quantified as equivalent units of trolox.

Oxidative Stress Model Induced by H_2O_2. The HUVECs were incubated under the conditions described above. Before H_2O_2 treatment, cells were seeded in 96-well microstate plates at a density of 5×10^3 cells/well and grown to approximately 80% confluence. The plates were incubated at 37 °C for 24 h before further treatments. Then H_2O_2 solutions at various concentrations were added into each well and incubated at 37 °C for 1 h. Cell survival was evaluated by the MTT assay as described above. In this study, the cell survival rate decreased significantly ($p < 0.05$, data not shown) when the H_2O_2 concentration was >100 μM. Therefore, HUVECs treated with freshly prepared 100 μM H_2O_2 for 1 h were used as the oxidative stress model.

Cytoprotective Assay. The HUVECs were seeded in 6-well microstate plates at a density of 4×10^5 cells/well and incubated as

described above before further treatments. After 90% confluence, cells were washed with fresh medium and pretreated with 20 μM ginsenoside for 2 h and then stimulated by 100 μM H_2O_2 for 1 h. The samples were collected for the following analysis. Each sample was assayed in triplicate.

Preparation of Cell Lysates. After completion of the incubation assay, the culture supernatant was collected for analysis of lactate dehydrogenase (LDH) and NO release. The cells were scraped from the plates and extracted with ice-cold lysis buffer (methanol containing 1% Triton X-100), and protein concentration was determined as mentioned above. Aliquots were stored at −80 °C until detection for malondialdehyde (MDA) content and glutathione peroxidase (GSH-Px) and catalase (CAT) activities.

Determination of NO Release. NO release amounts was measured as its oxidative product, nitrite. Briefly, at the end of incubation, 100 μL of supernatant was collected and then reacted with 100 μL of Griess reagent (1 part 1% sulfanilamide and 1 part 0.1% *N*-naphthylethyl-ethylenediamine dihydrochloride (NEDA) in 5% phosphoric acid). Absorbance at 550 nm was measured using a plate reader, and nitrite concentration was caculated using a curve calibrated on sodium nitrite standards.

Determination of LDH Activity. LDH activity released into the medium was detected with an assay kit (Sigma-Aldrich, USA) according to the manufacturer's protocol. Absorbance at 450 nm was detected using a plate reader. One unit of LDH activity is defined as the amount of enzyme that catalyzes the conversion of lactate into pyruvate to generate 1.0 mmol of NADH per minute at 37 °C, and the activity of enzyme was expressed as units per liter.

MDA Assay. Lipid peroxidation in HUVECs was assessed by the thiobarbituric acid (TBA) reaction using a commercial kit (Sigma-Aldrich, USA) following the manufacturer's protocol. Briefly, cells were collected and lysed as described above. Two hundred microliters of cell lysate or MDA standards was incubated with 600 μL of TBA solution at 95 °C for 60 min and then cooled to room temperature in an ice bath for 10 min. Two hundred microliters from each reaction mixture was pipetted into a 96-well plate, and the absorbance was read at 532 nm. Values of MDA level were expressed as nanomoles per milligram of protein.

Determination of GSH-Px Activity. The activity of GSH-Px was determined with commercial assay kits (Sigma-Aldrich, USA) according to the manufacturer's instruction. The GSH-Px activity was calculated indirectly. The assay was based on the oxidation of glutathione catalyzed by GSH-Px, which was then coupled to the recycling of oxidized glutathione back to glutathione utilizing glutathione reductase (GR) and NADPH. GSH-Px was the rate-limiting factor of the coupled reactions. The activity of GSH-Px was indicated by the decrease in NADPH absorbance measured at 340 nm during the oxidation of NADPH to NADP+. In general, 1 unit of GSH-Px was defined as the formation of 1.0 μmol of NADP+ from NADPH per minute in a coupled reaction, and the value of GSH-Px was expressed as units per milligram of protein.

Determination of CAT Activity. The activity of catalase was determined with commercial assay kits (Sigma-Aldrich, USA) according to the manufacturer's instruction. This assay is based on the measurement of the hydrogen peroxide substrate remaining after the action of catalase. The amount of hydrogen peroxide remaining was determined by a colorimetric method, of which the absorbance was measured at 520 nm. One unit of catalase was defined as 1.0 μmol of hydrogen peroxide decomposed to oxygen and water per minute at pH 7.0 at 25 °C at a substrate concentration of 50 mM hydrogen peroxide, and the activity of catalase was expressed as units per milligram of protein.

Effect of Rh2 and Rh2-O on the HUVEC Apoptosis Induced by H_2O_2. Flow cytometry analysis was run using an Annexin V−fluorescein isothiocyanate (FITC) apoptosis detection assay kit to determine H_2O_2-induced cell apoptosis. The assay was performed according to the manufacturer's instruction. Briefly, the cells were collected, centrifuged, and washed several times with PBS. Washed cell pellets were resuspended in fluorochrome solution containing propidium iodide (PI) and Annexin V−FITC for 5 min and analyzed with a BD FACS CaliburFlow Cytometry System (Becton-Dickinson, Franklin Lakes, NJ, USA).

Determination of Caspase-3 Activity. Caspase-3 activity was tested in cells pretreated with or without 20 μM ginsenoside for 2 h in 96-well plates with preseeded cells as previously described and then exposed to 100 μM H_2O_2 for 1 h. Caspase-3 activity was measured with the Promega Apo-ONE homogeneous caspase-3/7 fluorescence assay kit according to the manufacturer's instructions (Fisher, Unionville, ON, Canada). Briefly, after being washed three times with PBS, Apo-ONE homogeneous caspase-3/7 buffer was added to the cells with DMEM at a 1:1 (v/v) ratio. Cells were incubated for an additional 1 h at room temperature prior to recording of the fluorescence with emission and excitation wavelengths of 528 and 485 nm, respectively, in a multiplate reader (PLX 800, Bio-Tek Instruments Inc., Winooski, VT, USA). Values are expressed as relative fluorescence units (RLU) and normalized to untreated control cells from the same aliquot as experimental groups.

Analysis by HPLC. The analysis of ginsenoside Rh2 and Rh2-O was performed according to a previous paper with a slight modification.[29] The HPLC system consisted of an Agilent HPLC series 1100 (Agilent Technologies, Little Falls, DE, USA) with a diode array detector (DAD). The detection wavelength was set at 203 nm. A Hypersil ODS column (150 mm × 3.9 mm, 4.6 μm, Waters, Milford, MA, USA) was used for sample analysis. The mobile phase was acetonitrile/ammonium chloride (90:10, v/v), and the flow rate was 1.0 mL/min. The standard concentrations of Rh2 and Rh2-O were analyzed by HPLC, and peak area measurement was used to generate calibration curves for the quantification of samples. The corresponding standards of Rh2 and Rh2-O for quantification were prepared in methanol solution. The HPLC methods have been validated through accuracy, precision, and recovery experiments. The method had acceptable accuracy (90−110% of true values) and precision (the intraday and interday coefficient variations <15%) over the concentration range (0.10−100 μM). The recovery of samples was between 80 and 120%. The limits of quantitation (LOQ), defined as the minimum concentration that could be determined with acceptable accuracy and precision, were 0.02 and 0.01 μM for Rh2 and Rh2-O, respectively.

Data Analysis. The cumulative quantity of test compound permeated at each time interval was measured and plotted against time. The flux was defined as the amount of compound across the monolayers per square centimeter (nmol/cm^2). The apparent permeability coefficients (P_{app}, cm/s) were calculated using the equation

$$P_{app} = \left(\frac{dQ}{dt}\right)\left(\frac{1}{AC_0}\right)$$

where dQ/dt is the rate of permeability (nmol/s), A is the surface area of the insert (cm^2), and C_0 is the initial concentration (final concentration initially adding to the wells). The efflux ratio (R_e) was determined by calculating the ratio of $P_{app}(B-A)$ versus $P_{app}(A-B)$ as the following equation:

$$R_e = \frac{P_{app}(B-A)}{P_{app}(A-B)}$$

Statistical Analysis. Results are presented as the mean ± SD from three replicates. Student's t test was conducted with a P value of <0.05 as statistically significant. All statistical analysis was carried out using SPSS 13.0 software for Windows.

RESULTS AND DISCUSSION

Cytotoxicity of Rh2 and Rh2-O toward Caco-2 Cells and HUVECs. Prior to investigation of the transepithelial transport of Rh2 and Rh2-O in Caco-2 cell system and whether Rh2 and Rh2-O could protect HUVECs from H_2O_2-induced cell injury, the viability of cells was directly measured using the MTT test to evaluate the cytotoxicity of Rh2 or Rh2-O toward Caco-2 cells. Generally, a cell viability value of <50% of the

controls was considered as the reduction of mitochondrial activity, whereas a higher cell viability of >90% indicated that the compounds at the concentrations were nontoxic to the cells.[30] As shown in Figure 1A, Rh2 and Rh2-O at 50 μM or

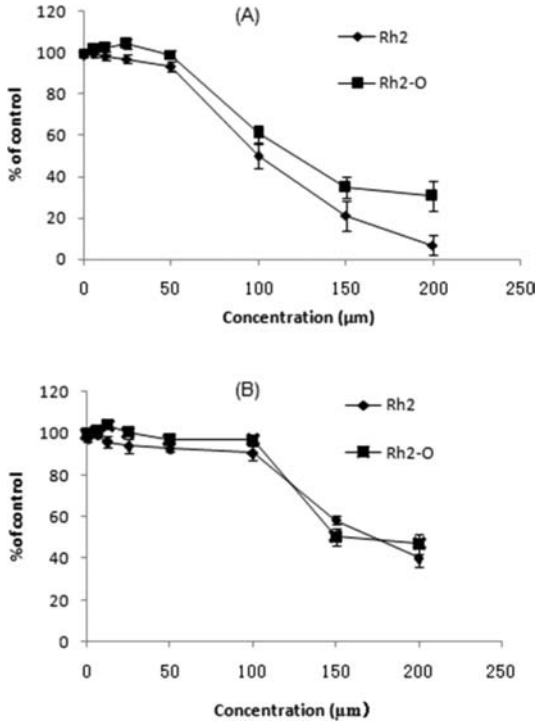

Figure 1. Cytotoxicity of Rh2 (◆) and Rh2-O (■) on (A) Caco-2 cell monolayers and (B) HUVECs using the MTT assay. Data represent the mean ± SD from five replicates.

below were nontoxic to the Caco-2 cells after 2 h of exposure. However, significant inhibition was observed with the rise of concentration to >50 μM. Figure 1B shows that Rh2 and Rh2-O were nontoxic toward HUVECs at concentrations below 100 μM. Therefore, to ensure cell viability, we chose nontoxic concentration of <50 μM Rh2 and Rh2-O in further experiments to examine the transport of Rh2 and Rh2-O across Caco-2 cell monolayer and the protective effect of Rh2 and Rh2-O on H_2O_2-induced cell apoptosis.

Enhancement Effects of Esterification on the Transport of Rh-2 across Caco-2 Cell Monolayers. The results of bidirectional transport of Rh2 and Rh2-O across Caco-2 cell monolayers at 20 μM are shown in Table 1. The apparent permeability coefficient (P_{app}) of Rh2 (20 μM) in BL to AP direction was determined as 3.26×10^{-6} cm/s over 2 h, which was much greater than that of AP to BL direction with efflux ratio (R_e) values of 15.5. This result indicated that an efflux mechanism may be involved in the transport process of Rh2. The flux amounts of Rh2-O in both directions were of similar magnitude and increased linearly over the initial 2 h. As shown in Table 1, the P_{app} value of Rh2-O (20 μM) in the direction of AP-BL was determined as 1.96×10^{-6} cm/s, which was significantly greater than that of Rh2, and $P_{app}(B - A)$ of Rh2-O (20 μM) was 2.08×10^{-6} cm/s. It was reported that there was a close correlation between the permeability across Caco-2 cell monolayers and the absorption of oral administration in vivo.[31] Generally, compounds with P_{app} values of $<1 \times 10^{-6}$ cm/s, between 1×10^{-6} and 1×10^{-5} cm/s, and $>1 \times 10^{-5}$ cm/s were considered to have low (<30%), moderate (30−0%), and high absorption (>70%).[32] According to these criteria, compounds such as Rh2 with a P_{app} value of $<1 \times 10^{-6}$ cm/s in Caco-2 cell monolayers might have poor absorption from the intestine in humans, whereas its ester derivative (Rh2-O) may have moderate absorption. Our results were consistent with a previous study which showed that Rh2 had an extremely low oral bioavailability (approximately 5%) in rats.[10]

Subsequently, the effects of Rh2 and Rh2-O concentrations (10−50 μM) on their transport flux were determined in the directions from AP to BL and from BL to AP (Figure 2A). The AP to BL flux amount of Rh2 was essentially linear up to 2 h and in a dose-dependent manner without any apparent saturation at the selected time points tested. These results indicated that the transport of Rh2 was mainly by passive diffusion in the direction of AP to BL. The corresponding $P_{app}(A - B)$ value (0.21×10^{-6} cm/s) over 10−50 μM had no significant difference and was independent of doses ($P > 0.05$). However, the BL to AP flux of Rh2 was much faster than that of the AP to BL direction and increased with increasing concentrations, with saturation at concentrations >20 μM. The determined $P_{app}(B - A)$ values of Rh2 at different concentrations were significantly greater than those from AP to BL with R_e values of 15.5, 9.7, 8.1, and 6.1 at 20, 30, 40, and 50 μM, respectively. The significant decrease in $P_{app}(B - A)$ values of Rh2 at concentrations >20 μM suggested the saturable flux amount of Rh2 from the BL to AP direction. These results indicated that the permeation mechanism of Rh2 may be passive diffusion with a BL to AP active efflux involved.

Table 1. Transcellular Transport of Rh2 and Rh2-O at 20 μM across Monolayers of Caco-2 Cells in the Absence or Presence of Inhibitors ($n = 3$)[a]

		P_{app} ($\times 10^{-6}$ cm/s)		
sample	inhibitor	AP-BL	BL-AP	efflux ratio (R_e)
Rh2		0.21 ± 0.01 a	3.26 ± 0.25 c	15.5 ± 1.2 b
Rh2	verapamil	2.38 ± 0.29 c	2.41 ± 0.28 b	1.0 ± 0.1 a
Rh2	MK571	0.22 ± 0.02 a	3.59 ± 0.34 c	16.3 ± 1.5 b
Rh2	EGTA	0.19 ± 0.01 a		
Rh2-O		1.96 ± 0.23 b	2.08 ± 0.31 a	1.1 ± 0.2 a
Rh2-O	verapamil	1.98 ± 0.14 b	2.08 ± 0.24 a	1.1 ± 0.1 a
Rh2-O	MK571	2.01 ± 0.17 b	2.11 ± 0.29 a	1.0 ± 0.1 a
Rh2-O	EGTA	1.96 ± 0.26 b		
mannitol	EGTA	2.75 ± 0.27 d		
mannitol		0.24 ± 0.03 a		

[a]Values are the mean ± SD, $n = 3$. Values followed by a different letter in the same column are significantly different ($P < 0.05$).

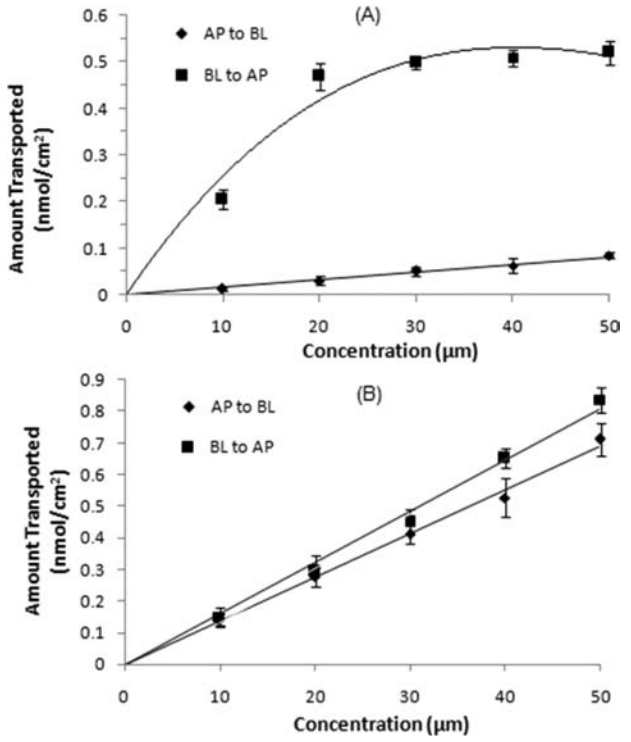

Figure 2. Effects of concentrations on the transport of (A) Rh2 and (B) Rh2-O across Caco-2 cell monolayers in both directions. Data represent the mean ± SD from three replicates.

The flux amounts of Rh2-O in both directions were similar and directly proportional to Rh2-O concentrations over 10−50 μM (Figure 2B). The P_{app} values of Rh2-O (1.96×10^{-6} cm/s for AP to BL and 2.16×10^{-6} cm/s for BL to AP) were not dependent on concentration but of similar magnitude in both directions with R_e values around 1.1. Generally, transport flux of a compound with R_e values >2 was considered as an active efflux. Therefore, the mechanism of permeation for Rh2-O in the translocation across Caco-2 cell monolayers may be passive diffusion with no active efflux involved.

Effects of Various Compounds on Rh2 and Rh2-O Transport. In the present study, EGTA, verapamil, and MK-571 were investigated for their effects on the transport flux of Rh2 and Rh2-O across the Caco-2 cells. The drug molecule can use either a transcellular (passive or active) or paracellular (passive) route to cross intestinal epithelium into systemic circulation after oral administration.[33] Generally, lipophilic molecules might have a significant transport by passive diffusion through the transcellular route, whereas hydrophilic molecules with low molecular weight cross the intestinal epithelium predominantly by paracellular passive diffusion process.[34] Because of much lower surface area available to the molecules entering the intercellular space and tight junctions in the intercellular space, the efficiency of absorption through the paracellular route is lower than that of the transcellular route. Therefore, one of the first transport mechanisms to be determined for studying the processes involved in the absorption of compounds across monolayers was the contribution of the paracellular route. Manipulating tight junction integrity of Caco-2 monolayers, which was performed by a depletion of calcium concentration in the transport medium with a calcium chelator, can be used as an approach to define absorption routes.[35] EGTA, a selective calcium chelator, is known to open the intercellular tight junctions of the Caco-2 monolayers, thus enhancing transport through the paracellular route. Compounds fluxing across Caco-2 monolayers by the paracellular pathway are very sensitive to manipulations of tight junction integrity. The Caco-2 monolayers pretreated with EGTA were employed in transport assay of Rh2 and Rh2-O to characterize the contributions of transcellular and paracellular transports of these two compounds. The $P_{app}(A - B)$ value of mannitol, a compound that is absorbed mainly via the paracellular route, acting as a positive control, was increased significantly after treatment of 2.5 mM EGTA (Table 1), indicating the opening of the tight junctions of Caco-2 monolayers in the experiment. In addition, no significant changes were observed in the P_{app} values for Rh2 and Rh2-O after treatment with 2.5 mM EGTA at 37 °C for 15 min, suggesting that the paracellular route had little contribution to their transport. These results demonstrated that the predominant transport route for both compounds was transcellular.

Verapamil and MK-571 are well-known as inhibitors of P-glycoprotein (P-gp) and multidrug resistance-related proteins (MRP1/2), respectively. Both P-gp and MRP1/2 overexpressing in Caco-2 cells and other cancer cell lines are considered as the most prevalent efflux transporters and possess a high capacity to efflux cytotoxic drugs.[36] To investigate the involvement of active efflux in transport for Rh2 and Rh2-O, the effects of verapamil and MK-571 on the transports of these two compounds were examined. Verapamil and MK-571 showed no significant effects on the P_{app} values of Rh2-O for either AP to BL or BL to AP (Table 1). Similarly, MK-571 did not significantly affect the P_{app} values of Rh2 in both transport directions. However, the treatment of verapamil alone at the apical side was able to completely inhibit the efflux transport of Rh2, and the efflux ratio was decreased to close to 1. As expected, the P_{app} value from the AP to BL was significantly increased by 11-fold and the P_{app} value from the BL to AP was significantly decreased after verapamil treatment, indicating that Rh2 may be the substrate of P-gp. Therefore, our results indicated that the major transport mechanism for Rh2 was passive transcellular diffusion with the involvement of active efflux from the BL to AP flux in Caco-2 cell monolayers. These results were similar to the report by Yang et al., which also found that the permeation mechanism of Rh2 was passive diffusion with an efflux pump (P-gp) involved in the Caco-2 cell monolayers.[37] On the other hand, however, it was reported that Rh2 was not a substrate of P-gp because 10 μM verapamil did not affect the transport of Rh2 in the Caco-2 cell model, which is contradictory to our conclusion.[38] The discrepancy may be due to the difference of P-gp expression levels in Caco-2 cells or inhibitor concentrations used among laboratories. Meanwhile, the mechanism of transport of Rh2-O was determined as passive diffusion with no active efflux involved because there was a lack of effect caused by transporter inhibitors, such as verapamil and MK-571.

Superoxide Radical Scavenging Capability of Rh2 and Rh2-O. PCL assay results showed that the superoxide radical scavenging capabilities of Rh2 and Rh2-O (1 nmol) were equivalent to 0.76 and 0.69 nmol of Trolox (data not shown), respectively. These results indicated that ginsenoside Rh2 and Rh2-O exhibited a relatively higher antioxidant capacity scavenging the superoxide radical in the cell-free systems, and the impact of esterification on superoxide radical scavenging capability of Rh2 was limited.

Effects of Rh2 and Rh2-O on H_2O_2-Induced Apoptosis of HUVECs. Endothelial cell injury caused by ROS plays a critical role in the pathogenesis of AS, and a previous study

reported that AS is characterized by the excessive apoptosis of vascular endothelial cells.[39] Oxidative stress in the vascular wall is closely related to the excessive apoptosis of HUVECs.[40] Therefore, inhibition of the excessive apoptosis of HUVECs may be considered as an efficient route in the prevention and control of AS. In the present study, HUVEC apoptosis was stimulated by H_2O_2, a commonly used oxidant. HUVECs control and pretreated cells were stained with Annexin V−FITC/PI and gated into four quadrants. The cells in the lower right (LR) and upper right (UR) were considered early apoptotic (Annexin+/PI−) and late apoptotic (Annexin+/PI+), respectively, whereas the cells in the lower left and upper left quadrants were considered live and necrotic, respectively. Extent of apoptosis was expressed as the total percentages in LR and UR quadrants. As shown in Figure 3, the apoptosis rate in untreated controls was 2.6 ± 1.1%, whereas the apoptosis rate elevated to 84.9 ± 4.3% after pretreatment with 100 μM H_2O_2-treated cells. In contrast, the apoptosis rates of HUVECs pretreated with 20 μM Rh2 markedly decreased to 63.5 ± 2.2%, and the apoptosis rates of HUVECs pretreated with Rh2-O (69.7 ± 3.9%) have no significant difference from that of pretreated with Rh2. These results demonstrated that both Rh2 and Rh2-O possess similar protective effects against oxidative stress-related cellular apoptosis.

Effects of Rh2 and Rh2-O on the NO, LDH, MDA, GSH-Px, and CAT of HUVECs. The results of effect of Rh2 and Rh2-O on the NO, LDH, MDA, GSH-Px and CAT levels of oxidative injury HUVECs are shown in Table 2. NO has gained recognition as a crucial modulator in vascular disease. It is derived from the action of eNOS and is usually regarded as an endothelial cell survival factor inhibiting cell apoptosis.[41] As shown in Table 2, compared to control group, NO levels in the medium were markedly decreased by exposure to H_2O_2, whereas pretreatment of HUVECs cells with Rh2 or Rh2-O significantly inhibited H_2O_2-induced NO level decrease.

LDH is an oxidoreductase enzyme that catalyzes the interconversion of pyruvate and lactate and is widely used as an indicator for cell damage. As shown in Table 2, LDH release in HUVECs was minimal in the control group (41.39 ± 3.97 U/L), and addition of 100 μM H_2O_2 caused a significant increase (95.25 ± 8.13 U/L). However, pretreatment of Rh2 and Rh2-O significantly attenuated the increase in LDH release induced by H_2O_2. Lipid peroxidation is the degradation of lipids that occurs as a result of oxidative damage and is a useful marker for oxidative stress. Generally, polyunsaturated lipids are susceptible to attack by ROS, resulting in the formation of MDA. Therefore, MDA can be employed as an indicator of lipid peroxidation or oxidative damage in cells.[42] The MDA concentration was 4.58 ± 0.61 nmol/mg protein in the control group (Table 2) and markedly increased to 10.32 ± 1.13 nmol/mg protein after 1 h of exposure to 100 μM H_2O_2. In contrast, the MDA concentration significantly decreased to 7.92 ± 0.69 and 6.11 ± 0.74 nmol/mg protein, respectively, after pretreatment with 20 μM Rh2 and Rh2-O, respectively.

To protect cells from the oxidative damage caused by ROS, organisms have developed several defense mechanisms to remove ROS including antioxidant enzymes GSH-PX and CAT. Both GSH-PX and CAT represent the most important H_2O_2 detoxification system in endothelial cells. GSH-Px enzymes reduce peroxides to alcohols using glutathione, thus preventing the formation of free radical damaging cells, whereas CAT directly catalyzes the decomposition of hydrogen peroxide (H_2O_2) to water and oxygen. As shown in Table 2, the activities

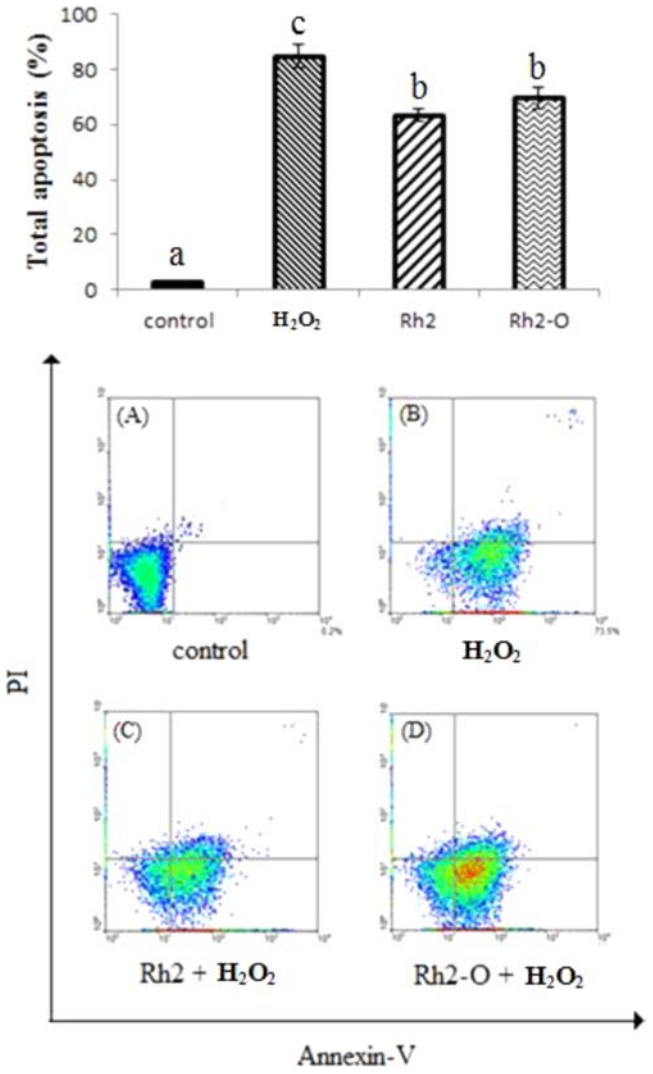

Figure 3. Analysis of HUVEC apoptosis by flow cytometry using Annexin V−FITC and PI. Quadrant analysis of fluorescence intensity of gated cells in Annexin V−FITC and PI channels was from 20000 events. Different letters above the bars present significant difference ($P < 0.05$). (A) Control; (B) H_2O_2 group (100 μM); (C) Rh2 group (20 μM); (D) Rh2-O group (20 μM).

of GSH-Px and CAT significantly decreased in the H_2O_2 group compared to the control, whereas pretreating with Rh2 and Rh2-O significantly increased the GSH-PX and CAT activities in the HUVECs. These results jointly indicated that enhancement of endogenous antioxidant preservation and attenuation of lipid peroxidation may represent major mechanisms of cellular protection against oxidative damage by ginsenoside Rh2 and its derivative Rh2-O. In addition, as depicted in Table 2, no significant difference was observed in the NO, LDH, MDA, GSH-Px, and CAT levels between the Rh2 and Rh2-O groups. These results further indicated that the synthesis of esterified derivative of Rh2 caused little impact on its bioactive protection against HUVEC oxidative damage.

Effects of Rh2 and Rh2-O on Caspase-3 Activation of HUVECs. Cell apoptosis is induced mainly via two pathways, the mitochondrial apoptotic pathway and the death receptor pathway. Both pathways converge at caspase-3 activation. Caspase-3 is one of the downstream effectors of the caspase family and regarded as a major executor caspase that leads to

Table 2. Effect of Rh2 and Rh2-O on the Nitrite, LDH, MDA, GSH-Px, and CAT Activities in HUVECs[a]

group	NO (μmol/L)	LDH (U/L)	MDA (nmol/mg protein)	GSH-PX (U/mg protein)	CAT (U/mg protein)
control	32.58 ± 3.15	41.39 ± 3.97	4.58 ± 0.61	167.92 ± 18.25	40.38 ± 2.68
DMSO	30.36 ± 3.21	42.86 ± 3.52	4.03 ± 0.55	171.35 ± 20.12	46.25 ± 3.14
H_2O_2	12.83 ± 1.54*	95.25 ± 8.13*	10.32 ± 1.13*	108.63 ± 9.65*	15.97 ± 1.06*
Rh_2 + H_2O_2	23.24 ± 2.12#	70.84 ± 5.99#	7.92 ± 0.69#	253.75 ± 21.84	57.28 ± 1.98#
Rh_2-O + H_2O_2	20.69 ± 2.36#	75.28 ± 5.45#	6.11 ± 0.74#	246.28 ± 18.33#	50.19 ± 3.83#

[a]Values are the mean ± SD, n = 3. *, statistically significant differences between the untreated and the H_2O_2 group ($p < 0.05$); #, statistically significant differences between the H_2O_2- and the drug-treated group ($p < 0.05$).

apoptosis.[16] Caspase-3 activity was expressed as the fold of control group in this study; a lower value means better inhibitory activity. As depicted in Figure S1 (Supporting Information), an increase in caspase-3 activity was obvious in cells incubated with 100 μM H_2O_2 for 1 h. However, when the cells were pretreated with 20 μM Rh2 or Rh2-O for 2 h prior to the addition of 100 μM H_2O_2, the caspase-3 activation was significantly inhibited, which was consistent with the above results that Rh2 and Rh2-O protected HUVECs from oxidative damage and markedly decreased the HUVEC apoptosis. Furthermore, the inhibitory effects on caspase-3 activation had no significant difference between Rh2 and its esterified derivative as well. These studies demonstrated that Rh2 or Rh2-O can effectively restrain cell apoptosis by preventing caspase-3 activation.

In conclusion, the transport of the ginsenoside Rh2 across the intestinal epithelium was evidenced as very poor, whereas its esterified derivative Rh2-O was verified to possess a better absorption in vitro. Because verapamil had a significant effect on the P_{app} values of Rh2 and a negligible effect on that of Rh2-O, the transport mechanisms for both Rh2 and Rh2-O across Caco-2 monolayers were speculated to be transcellular passive diffusion, with an active efflux pump (P-gp) involved for Rh2 and without an active efflux involved for Rh2-O. In addition, both Rh2 and Rh2-O exhibited protective effects against HUVEC oxidative damage stimulated by H_2O_2 and effectively suppressed the activation of caspase-3 and HUVEC apoptosis. Meanwhile, we found that the synthesis of esterified derivative of Rh2 caused an ignorable impact on its bioactivities against HUVEC oxidative injury. Therefore, it is noteworthy that the findings of the present study may provide useful strategy for molecular structure modification of ginsenosides to improve oral absorption of compounds in vitro without affecting their bioactivities against the oxidative injury of HUVECs. Our further work will examine whether the intestinal absorption of Rh2 and its oral bioavailabilities are enhanced in vitro through esterification of Rh2, as well as the effects of structure modification on its bioactivities in vivo.

■ ASSOCIATED CONTENT

Supporting Information

Effect of Rh2 and Rh2-O on H_2O_2-induced caspase-3 activation in HUVECs. This material is available free of charge via the Internet at http://pubs.acs.org.

■ AUTHOR INFORMATION

Corresponding Authors

*(J.-N.H.) Phone: +86 791 88304449-8230. E-mail: hujiangning2005@hotmail.com.
*(Z.-Y.D.) Phone/fax: +86 791 88304402. E-mail: zeyuandeng@hotmail.com.

Funding

This work was supported by the National Natural Science Foundation of China (Grant 31360370), the Youth Foundation of Jiangxi Educational Committee (Grant GJJ13023), the Open Project Program of State Key Laboratory of Food Science and Technology, Nanchang University (Grants SKLF-KF-201211, SKLF-QN-201109); and the Young Teachers Development Programs of Jiangxi Province and Graduate Innovation Special Fund of Jiangxi Province (Grant YC2012-B007).

Notes

The authors declare no competing financial interest.

■ REFERENCES

(1) Yuan, C. S.; Wang, C. Z.; Wicks, S. M.; Qi, L. W. Chemical and pharmacological studies of saponins with a focus on American ginseng. *J. Ginseng Res.* **2010**, *34*, 160.
(2) Christensen, L. P. Ginsenosides: chemistry, biosynthesis, analysis, and potential health effects. *Adv. Food Nutr. Res.* **2008**, *55*, 1−99.
(3) Li, Q. Y.; Chen, L.; Fu, W. H.; Li, Z. D.; Wang, B.; Shi, X. J.; Zhong, M. K. Ginsenoside Rb1 inhibits proliferation and inflammatory responses in rat aortic smooth muscle cells. *J. Agric. Food Chem.* **2011**, *59*, 6312−6318.
(4) Yoon, S. R.; Lee, G. D.; Park, J. H.; Lee, I. S.; Kwon, J. H. Ginsenoside composition and antiproliferative activities of explosively puffed ginseng (*Panax* ginseng C.A. Meyer). *J. Food Sci.* **2010**, *75*, 378−382.
(5) Yun, T. K. *Panax ginseng* − a non-organ-specific cancer preventive? *Lancet Oncol.* **2001**, *2*, 49−55.
(6) Buettner, C.; Yeh, G. Y.; Phillips, R. S.; Mittleman, M. A.; Kaptchuk, T. J. Systematic review of the effects of ginseng on cardiovascular risk factors. *Ann. Pharmacother.* **2006**, *40*, 83−95.
(7) Coleman, C. I.; Hebert, J. H.; Reddy, P. The effects of *Panax* ginseng on quality of life. *J. Clin. Pharm. Ther.* **2003**, *28*, 5−15.
(8) Jia, L.; Zhao, Y.; Liang, X. J. Current evaluation of the millennium phytomedicine−ginseng (II): collected chemical entities, modern pharmacology, and clinical applications emanated from traditional Chinese medicine. *Curr. Med. Chem.* **2009**, *16*, 2924.
(9) Kitagawa, I.; Yoshikawa, M.; Yoshihara, M.; Hayashi, T.; Taniyama, T. Chemical studies of crude drugs (1). Constituents of Ginseng radix rubra. *Yakugaku Zasshi* **1983**, *103*, 612−622.
(10) Gu, Y.; Wang, G. J.; Sun, J. G.; Jia, Y. W.; Wang, W.; Xu, M. J.; Lv, T.; Zheng, Y. T.; Sai, Y. Pharmacokinetic characterization of ginsenoside Rh2, an anticancer nutrient from ginseng, in rats and dogs. *Food Chem. Toxicol.* **2009**, *47*, 2257−2268.
(11) Liu, H.; Yang, J.; Du, F.; Gao, X.; Ma, X.; Huang, Y.; Xu, F.; Niu, W.; Wang, F.; Mao, Y. Absorption and disposition of ginsenosides after oral administration of *Panax* notoginseng extract to rats. *Drug Metab. Dispos.* **2009**, *37*, 2290−2298.
(12) Cao, F.; Guo, J. X.; Ping, Q. N.; Liao, Z. G. Prodrugs of scutellarin: ethyl, benzyl and *N*,*N*-diethylglycolamide ester synthesis, physicochemical properties, intestinal metabolism and oral bioavailability in the rats. *Eur. J. Pharm. Sci.* **2006**, *29*, 385−393.
(13) Dhaneshwar, S.; Tewari, K.; Joshi, S.; Godbole, D.; Ghosh, P. Diglyceride prodrug strategy for enhancing the bioavailability of norfloxacin. *Chem. Phys. Lipids* **2011**, *164*, 307−313.

(14) Taylor, M. D. Improved passive oral drug delivery via prodrugs. *Adv. Drug Delivery Rev.* **1996**, *19*, 131−148.
(15) Melzig, M. F.; Bader, G.; Loose, R. Investigations of the mechanism of membrane activity of selected triterpenoid saponins. *Planta Med.* **2001**, *67*, 43−48.
(16) Wang, Y. K.; Hong, Y. J.; Wei, M.; Wu, Y.; Huang, Z. Q.; Chen, R. Z.; Chen, H. Z. Curculigoside attenuates human umbilical vein endothelial cell injury induced by H_2O_2. *J. Ethnopharmacol.* **2010**, *132*, 233−239.
(17) Wang, B. C.; Peng, L.; Zhu, L. C.; Ren, P. Protective effect of total flavonoids from *Spirodela polyrrhiza* Schleid on human umbilical vein endothelial cell damage induced by hydrogen peroxide. *Colloids Surf. B: Biointerfaces* **2007**, *60*, 36−40.
(18) Torres De Pinedo, A.; Penalver, P.; Morales, J. C. Synthesis and evaluation of new phenolic-based antioxidants: structure−activity relationship. *Food Chem.* **2007**, *103*, 55−61.
(19) Zhu, D.; Wu, L.; Li, C. R.; Wang, X. W.; Ma, Y. J.; Zhong, Z. Y.; Zhao, H. B.; Cui, J.; Xun, S. F.; Huang, X. L. Ginsenoside Rg1 protects rat cardiomyocyte from hypoxia/reoxygenation oxidative injury via antioxidant and intracellular calcium homeostasis. *J. Cell. Biochem.* **2009**, *108*, 117−124.
(20) Cuong, T. T.; Yang, C. S.; Yuk, J. M.; Lee, H. M.; Ko, S. R.; Cho, B. G.; Jo, E. K. Glucocorticoid receptor agonist compound K regulates dectin-1-dependent inflammatory signaling through inhibition of reactive oxygen species. *Life Sci.* **2009**, *85*, 625−633.
(21) Wang, H. B.; Yu, P. F.; Gou, H. T.; Zhang, J. Q.; Zhu, M.; Wang, Z. H.; Tian, J. W.; Jiang, Y. T.; Fu, F. H. Cardioprotective effects of 20(*S*)-ginsenoside Rh2 against doxorubicin-induced cardiotoxicity in vitro and in vivo. *Evidence-Based Complement. Altern. Med.* **2012**, *2012*.
(22) Borlak, J.; Zwadlo, C. Expression of drug-metabolizing enzymes, nuclear transcription factors and ABC transporters in Caco-2 cells. *Xenobiotica* **2003**, *33*, 927−943.
(23) Grasset, E.; Pinto, M.; Dussaulx, E.; Zweibaum, A.; Desjeux, J. F. Epithelial properties of human colonic carcinoma cell line Caco-2: electrical parameters. *Am. J. Physiol.* **1984**, *247*, C260−C267.
(24) Pinto, M. Enterocyte-like differentiation and polarization of the human colon carcinoma cell line Caco-2 in culture. *Biol. Cell.* **1983**, *47*, 323−330.
(25) Fischer, D.; Li, Y. X.; Ahlemeyer, B.; Krieglstein, J.; Kissel, T. In vitro cytotoxicity testing of polycations: influence of polymer structure on cell viability and hemolysis. *Biomaterials* **2003**, *24*, 1121−1131.
(26) Sgouras, D.; Duncan, R. Methods for the evaluation of biocompatibility of soluble synthetic polymers which have potential for biomedical use: 1 − Use of the tetrazolium-based colorimetric assay (MTT) as a preliminary screen for evaluation ofin vitro cytotoxicity. *J. Mater. Sci: Mater. Med.* **1990**, *1*, 61−68.
(27) Li, H.; Chung, S. J.; Kim, D. C.; Kim, H. S.; Lee, J. W.; Shim, C. K. The transport of a reversible proton pump antagonist, 5,6-dimethyl-2-(4-fluorophenylamino)-4-(1-methyl-1,2,3,4-tetrahydroisoquinoline-2-yl) pyrimidine hydrochloride (YH1885), across Caco-2 cell monolayers. *Drug Metab. Dispos.* **2001**, *29*, 54−59.
(28) Li, H.; Deng, Z.; Liu, R.; Loewen, S.; Tsao, R. Ultra-performance liquid chromatographic separation of geometric isomers of carotenoids and antioxidant activities of 20 tomato cultivars and breeding lines. *Food Chem.* **2012**, *132*, 508−517.
(29) Xie, H. T.; Wang, G. J.; Lv, H.; Sun, R. W. J. G.; Jiang, X. L.; Li, H.; Wang, W.; Huang, C. R.; Xu, M. J. Development of a HPLC-MS assay for ginsenoside Rh2, a new anti-tumor substance from natural product and its pharacokinetic study in dogs. *Eur. J. Drug Metab. Pharmacokinet.* **2005**, *30*, 63−67.
(30) Wahlang, B.; Pawar, Y. B.; Bansal, A. K. Identification of permeability-related hurdles in oral delivery of curcumin using the Caco-2 cell model. *Eur. J. Pharm. Biopharm.* **2011**, *77*, 275−282.
(31) Artursson, P.; Karlsson, J. Correlation between oral drug absorption in humans and apparent drug permeability coefficients in human intestinal epithelial (Caco-2) cells. *Biochem. Biophys. Res. Commun.* **1991**, *175*, 880−885.
(32) Yee, S. In vitro permeability across Caco-2 cells (colonic) can predict in vivo (small intestinal) absorption in man − fact or myth. *Pharm. Res.* **1997**, *14*, 763−766.
(33) Gan, L. S. L.; Thakker, D. R. Applications of the Caco-2 model in the design and development of orally active drugs: Elucidation of biochemical and physical barriers posed by the intestinal epithelium. *Adv. Drug Delivery Rev.* **1997**, *23*, 77−98.
(34) Zhou, L.; Lee, K.; Thakker, D. R.; Boykin, D. W.; Tidwell, R. R.; Hall, J. E. Enhanced permeability of the antimicrobial agent 2,5-bis(4-amidinophenyl) furan across Caco-2 cell monolayers via its methylamidoxime prodrug. *Pharm. Res.* **2002**, *19*, 1689−1695.
(35) Artursson, P.; Magnusson, C. Epithelial transport of drugs in cell culture. II: Effect of extracellular calcium concentration on the paracellular transport of drugs of different lipophilicities across monolayers of intestinal epithelial (Caco-2) cells. *J. Pharm. Sci.* **1990**, *79*, 595−600.
(36) Bromberg, L.; Alakhov, V. Effects of polyether-modified poly (acrylic acid) microgels on doxorubicin transport in human intestinal epithelial Caco-2 cell layers. *J. Controlled Release* **2003**, *88*, 11−22.
(37) Yang, Z.; Gao, S.; Wang, J.; Yin, T.; Teng, Y.; Wu, B.; You, M.; Jiang, Z.; Hu, M. Enhancement of oral bioavailability of 20(*S*)-ginsenoside Rh2 through improved understanding of its absorption and efflux mechanisms. *Drug Metab. Dispos.* **2011**, *39*, 1866−1872.
(38) Zhang, J. W.; Zhou, F.; Wu, X. L.; Gu, Y.; Ai, H.; Zheng, Y. T.; Li, Y. N.; Zhang, X. X.; Hao, G.; Sun, J. G. 20(*S*)-Ginsenoside Rh2 noncompetitively inhibits P-glycoprotein in vitro and in vivo: a case for herb-drug interactions. *Drug Metab. Dispos.* **2010**, *38*, 2179−2187.
(39) González-Navarro, H.; Nabah, Y. N. A.; Vinué, Á.; Andrés-Manzano, M. J.; Collado, M.; Serrano, M.; Andrés, V. p19ARF deficiency reduces macrophage and vascular smooth muscle cell apoptosis and aggravates atherosclerosis. *J. Am. Coll. Cardiol.* **2010**, *55*, 2258−2268.
(40) Park, S.; Kim, J. A.; Choi, S.; Suh, S. H. Superoxide is a potential culprit of caspase-3 dependent endothelial cell death induced by lysophosphatidylcholine. *J. Physiol. Pharmacol.* **2010**, *61*, 375.
(41) Dimmeler, S.; Zeiher, A. M. Nitric oxide − an endothelial cell survival factor. *Cell Death Differ.* **1999**, *6*, 964.
(42) Roebuck, K. A. Oxidant stress regulation of IL-8 and ICAM-1 gene expression: differential activation and binding of the transcription factors AP-1 and NF-kappaB (review). *Int. J. Mol. Med.* **1999**, *4*, 223−253.

concentration of charged surface-active components present.[6,21,22] Several studies have shown that lipid oxidation rates in O/W emulsions stabilized with anionic surfactants are much higher due to the electrostatic attraction of cationic transition metals, whereas O/W emulsions stabilized with cationic surfactants oxidize more slowly because of electrostatic repulsion of metals away from the lipids.[23−26] The role of droplet charge has also been demonstrated in the studies of lipid oxidation in protein-stabilized O/W emulsions. In this case, lipid oxidation occurs more rapidly when the pH is above the isoelectric point (p*I*) of proteins and the emulsion droplet is negatively charged.[27−30]

Although a great deal of research has focused on the influence of different emulsifiers on lipid oxidation in O/W emulsions, there are fewer studies on the effects of emulsifiers on lipid oxidation in W/O emulsions. For example, little is known about how emulsifier type (e.g., biopolymers, anionic and cationic small molecular surfactants), concentrations, and aqueous phase pH influence lipid oxidation in W/O emulsions. Preliminary experiments showed that among such lipophilic emulsifiers as polyglycerol polyricinoleate (PGPR), lecithin, and span 60, 65, 80, and 85, PGPR was the only one tested capable of forming a stable W/O. Therefore, in the present work, PGPR was used to form stable W/O emulsions. Dodecyltrimethylammonium bromide (DTAB), sodium dodecyl sulfate (SDS), and polyoxyethylene sorbitan monolaurate (Tween 20) were added as small molecular surfactants that are cationic, anionic, and nonionic, respectively. WPI was used as an example of a biopolymer emulsifier. Experiments were then conducted to determine if these emulsifiers influenced lipid oxidation in PGPR-stabilized W/O emulsions. The knowledge gained from these studies could provide fundamental knowledge that could be used to improve the oxidative stability of oils in W/O emulsions by using different emulsifiers.

MATERIALS AND METHODS

Materials. Walnut oil was purchased from Hain Celestial Group Inc. (Melville, NY, USA) ($C_{16:0}$ = 7.13%; $C_{16:1}$ = 0.11%; $C_{18:0}$ = 3.58%; $C_{18:1}$ = 17.72%; $C_{18:2}$ = 61.91%; $C_{18:3}$ = 9.27%; $C_{20:0}$ = 0.12%; $C_{20:1}$ = 0.24%). Ferrous sulfate, cumene hydroperoxide, hexadecane, $BaCl_2$, SDS, Tween 20, DTAB, and sodium phosphate mono- and dibasic were obtained from Sigma-Aldrich Co. (St. Louis, MO, USA). Methanol, *n*-hexane, and 1-butanol were purchased from Fisher Scientific (Fair Lawn, NJ, USA). Polyglycerol polyricinoleate (PGPR, 4175) was gifted by Palsgaard (Morristown, NJ, USA). WPI was obtained from Davisco Food International, Inc. (Eden Praire, MN, USA), and used without further purification. The protein content of WPI was 97.6 wt %. The major protein components of WPI were 55−61% β-lactoglobulin, 19−22% α-lactoalbumin, and 6−8% bovine serum albumin. All of the chemicals used in these experiments were of analytical grade or better. Glassware was placed in 2 M HCl overnight to remove transition metals followed by rinsing with double-distilled water and then drying before use. Double-distilled, deionized water was used for the preparation of all solutions.

Methods. *Emulsion Preparation and Storage Condition.* PGPR-stabilized W/O emulsions were prepared by mixing 0.5 g of PGPR into 100 g of walnut oil. Aqueous phase (2% of a 20 mM phosphate buffer solution at pH 3.0 or 7.0) with different emulsifiers was added to the PGPR−walnut oil blend, and a coarse emulsion was made by homogenization with a hand-held mixer (M133/1281-0, Biospec Products, Inc., Bartlesville, OK, USA) for 2 min. The coarse emulsion was then homogenized with a microfluidizer (Microfluidics, Newton, MA, USA) at a pressure of 12 kbar for three passes. After emulsion preparation, samples were transferred into 10 mL GC vials and sealed with aluminum caps with PTFE/silicone septa and stored at 45 °C in the dark. Three vials of each treatment were taken every day to determine lipid hydroperoxides and hexanal formation. Raw walnut oil also underwent the same emulsification process as the W/O emulsion in the experiment conducted to compare the effect of the existence of water droplet interface on the lipid oxidation.

Measurement of Physical Properties of Emulsions. The particle size of the emulsions was measured at 25 °C using a dynamic light scattering instrument (Zetasizer Nano-ZS, Malvern Instruments, Worcestershire, UK). This instrument measures the rate of electrophoretic diffusion of particles. Samples were appropriately diluted with hexadecane (refractive index = 1.434, viscosity = 3.13 mPa s at 25 °C) according to the method of Choi et al., [20] mixed, and immediately measured by transferring the diluted emulsions into 3 mL plastic curvettes. Particle size was reported as the scattering intensity−weighted mean diameter, *z*-average. The emulsion droplet size ranged from 0.2 to 0.4 μm, and there was no significant change in the droplet size of each emulsion over the course of study (data not shown). Visual observation also showed that there was no phase separation during storage in all treatments. This indicated that the emulsions were stable to droplet coalescence, sedimentation, and phase separation.

Measurement of Lipid Hydroperoxides. Lipid hydroperoxides were measured as the primary oxidation products using a method described by Shantha et al.[31] with some modifications. Emulsions (0.2 mL) were accurately weighed before they were added to a mixture of methanol/butanol (2.8 mL, 2:1, v/v) followed by addition of 15 μL of 3.94 M ammonium thiocyanate and 15 μL of ferrous iron solution (prepared by adding equal amounts of 0.132 M $BaCl_2$ and 0.144 M $FeSO_4$). The solution was vortexed, and after 20 min, the absorbance was measured at 510 nm using a Genesys 20 spectrophotometer (ThermoSpectronic, Waltham, MA, USA). The concentration of hydroperoxides was calculated from a cumene hydroperoxide standard curve.

Measurement of Hexanal. The secondary oxidation product, headspace hexanal, was monitored using a GC-17A Shimadzu gas chromatograph equipped with an AOC-5000 autosampler (Shimadzu, Kyoto, Japan) according to the method described by Panya et al.[32] with some modifications. Samples (1 mL) in 10 mL glass vials capped with aluminum caps with PTFE/silicone septa were heated at 55 °C for 8 min in an autosampler heating block before measurement. A 50/30 μm DVB/Carboxen/PDMS solid-phase microextraction (SPME) fiber needle from Supelco (Bellefonte, PA, USA) was injected into the vial for 2 min to absorb volatiles and was then transferred to the injector port (250 °C) for 3 min. The injection port was operated in split mode, and the split ratio was set at 1:7. Volatiles were separated on a 30 m × 0.32 mm Equity DB-1 column from Supelco with a 1 μm film thickness at 65 °C for 10 min. The carrier gas was helium at 15.0 mL/min. A flame ionization detector was used at a temperature of 250 °C. Hexanal concentrations were determined from peak areas using a standard curve prepared from an authentic standard.

Measurement of Iron-Binding Capacity of WPI. The ability of WPI to bind iron was determined using a modified method of Bincan et al.[33] Dialysis bags (molecular mass cutoff 8 kDa, Shengya Co., Xi'an, China) were cleaned by heating them twice at 80 °C for 30 min in a 2% sodium bicarbonate and 1 mM EDTA solution. The bag was then thoroughly rinsed with deionized water and stored at 5 °C in a 0.1% sodium azide solution. WPI solutions (10% w/v) were prepared with 20 mM phosphate buffer solution at pH 3.0 and 7.0, respectively, using 1.0 M NaOH and HCl to adjust the pH. Two aliquots of 1 mL of WPI solution at pH 3.0 or 7.0 were pipetted into the dialysis bag, equilibrated for 30 min at room temperature in 98 mL of 20 mM phosphate buffer solution at pH 3.0 or 7.0, respectively, and constantly stirred. One milliliter of an 80 μg/mL Fe^{2+} solution (prepared from Fe_2SO_4 in 20 mM phosphate buffer solution at pH 3.0 or 7.0) was then added to the flask so that the final concentration of ferrous outside the dialysis bag was 8 μg/mL. After equilibrium for 24 h, the concentrations of Fe^{2+} outside the dialysis bag were measured by flame atomic absorption spectrophotometer (Sollar-3500, USA).

Statistical Analysis. All analyses were performed on triplicate samples. Oxidation lag phases were defined as the first data point significantly greater than the 0 time value. In all cases, comparisons of the means were performed using Duncan's multiple-range tests. A significance level of $p < 0.05$ was defined as being statistically different.

All calculations were performed using the statistical analysis software SPSS 17 (Statistical Package for the Social Sciences).

RESULTS AND DISCUSSION

Effects of Type and Concentration of Surfactants on the Oxidative Stability of Water-in-Walnut Oil Emulsions. As far as O/W emulsions are concerned, Boon et al.[26] and Haahr et al.[34] have proposed that the oxidative stability of oil-in-water emulsions is determined by the ability of the droplet to attract or repel cationic metals. Emulsion droplet charge is dependent on the type of surfactants (cationic, anionic, or neutral) and the emulsion pH that affects surfactant charge.[7,17] Many studies have confirmed that lipid oxidation was promoted when positively charged transition metals were electrostatically attracted to the surface of the negatively charged emulsion droplets due to close interaction between the lipid substrate and prooxidative transition metals, whereas lipid oxidation was retarded by cationic surfactants that electrostatically repelled metals away from the lipids.[23−30]

In the case of W/O emulsions, to obtain a better understanding of the influence of the type of surfactants on the lipid oxidation, a comparison of oxidation rates as determined by lipid hydroperoxide and headspace hexanal was conducted in walnut oil and 2% water-in-walnut oil emulsions stabilized by PGPR alone or with SDS, DTAB, or Tween 20. Emulsions were incubated at 45 °C for up to 25 days, and the results are shown in Figure 1.

Interestingly, regardless of the type of emulsifier used, all of the emulsions containing 2% water had higher lipid hydroperoxide and hexanal formation rates than the walnut oil alone. The results were different from the observation by Fritsch, who stated that the rates of lipid oxidation in W/O emulsions would be similar to that in bulk oils if the same amount of surface lipid was exposed to air.[35] As stated earlier, the decomposition of lipid hydroperoxides into highly reactive radicals by prooxidants such as transition metals is the main pathway for the promotion of lipid oxidation. Lipid hydroperoxides are surface-active compounds and are thus able to accumulate at the water−lipid interface of emulsion droplets.[19,36] In this way, the higher rates of lipid oxidation in W/O emulsions were possibly due to the large surface area that facilitated interactions between the lipid hydroperoxides and water-soluble prooxidants. Similar phenomena have been observed in O/W emulsions.[16] The results indicated that the presence of a large interface between oil and water in W/O emulsions might also affect the lipid oxidation.

With regard to the type of surfactants, significant differences in oxidation rates were observed among the samples containing different surfactants, suggesting that the type of surfactants in emulsions was an important factor influencing the lipid oxidation in W/O emulsions. However, surprisingly, it could be seen that lipid hydroperoxides increased rapidly in W/O emulsions containing PGPR + DTAB compared to PGPR alone (lag phase 2 and 7 days, respectively), whereas lipid hydroperoxide concentrations were lowest in emulsions containing PGPR + SDS (lag phase 10 days). No differences in lipid hydroperoxide formation were found between the PGPR and PGPR + Tween 20 emulsions (lag phase 7 days). When the secondary lipid oxidation product, hexanal, was measured to monitor lipid oxidation in emulsions containing different surfactants, a similar trend in lipid oxidation rates was observed with PGPR + DTAB > PGPR ≈ PGPR + Tween 20 > PGPR + SDS, indicating that the anionic surfactant again inhibited lipid oxidation, whereas the cationic surfactant promoted lipid oxidation in W/O emulsions.

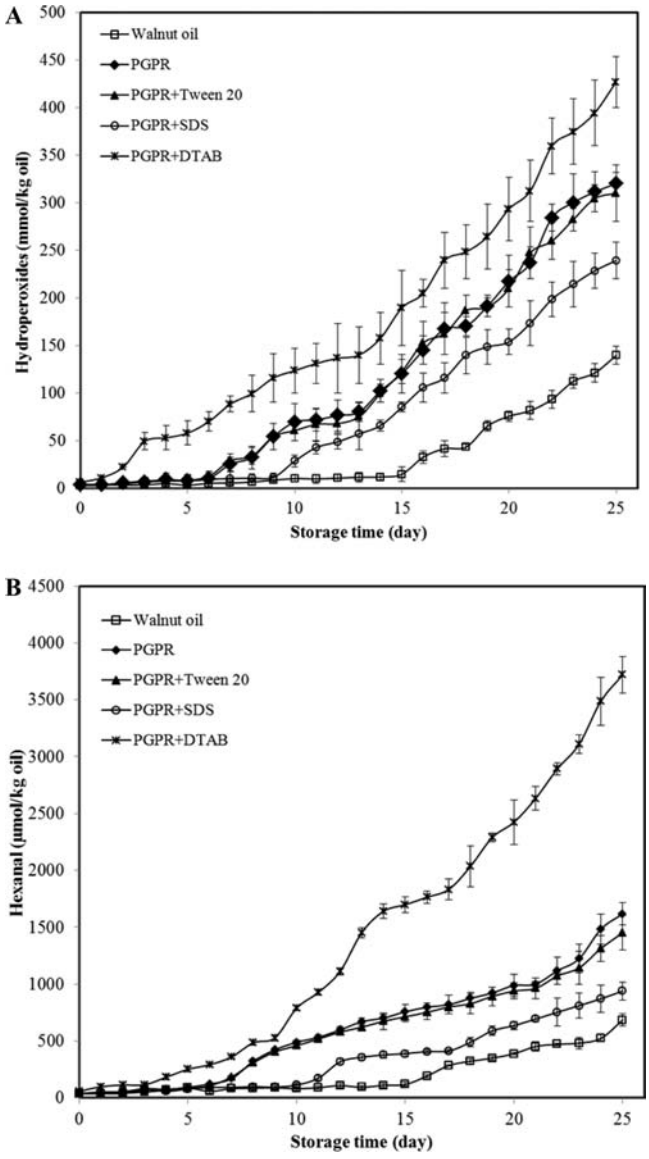

Figure 1. Effects of different surfactants in the aqueous phase (0.1 wt % of emulsions) on the oxidative stability of 2% water-in-walnut oil at aqueous phase pH 7.0 during storage at 45 °C in the dark for 25 days. Lipid oxidation was monitored by measuring hydroperoxides (A) and hexanal (B). Data points and error bars represent means (n = 3) ± standard deviations.

Figures 2 and 3 clearly show that the oxidative stability of emulsions with increasing SDS concentrations did not further increase oxidative stability but increasing DTAB did cause additional promotion of oxidation. These results were completely opposite to the studies in O/W systems by Mei et al.,[23,24] Silvestre et al.,[25] Boon et al.,[26] Hu et al.,[27,28] and Mancuso et al.,[29,30] who found that lipid oxidation was retarded by cationic surfactants and promoted by anionic surfactants, presumably because the surface of the positively charged emulsion droplets containing cationic surfactants repelled metals away from the water−oil interface where lipid oxidation usually occurs, whereas the surface of the negatively charged emulsion droplets containing anionic surfactants attracted metals to the interface.

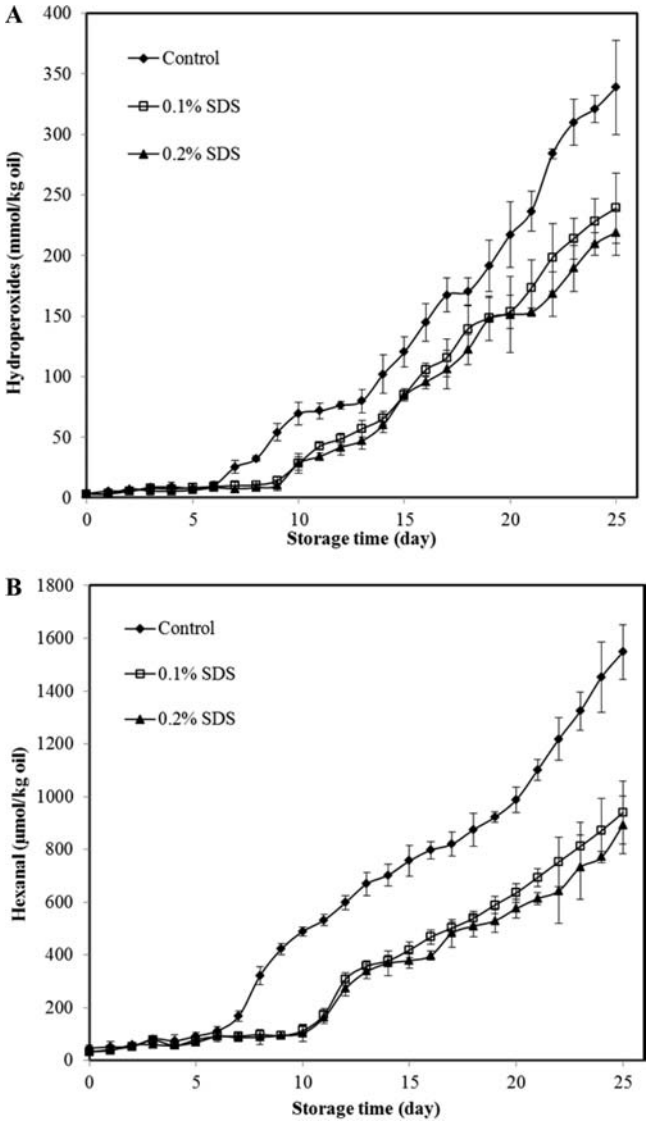

Figure 2. Effects of concentration of SDS in the aqueous phase on the oxidative stability of 2% water-in-walnut oil at aqueous phase pH 7.0 during storage at 45 °C in the dark for 25 days. Lipid oxidation was monitored by measuring hydroperoxides (A) and hexanal (B). Data points and error bars represent means (n = 3) ± standard deviations.

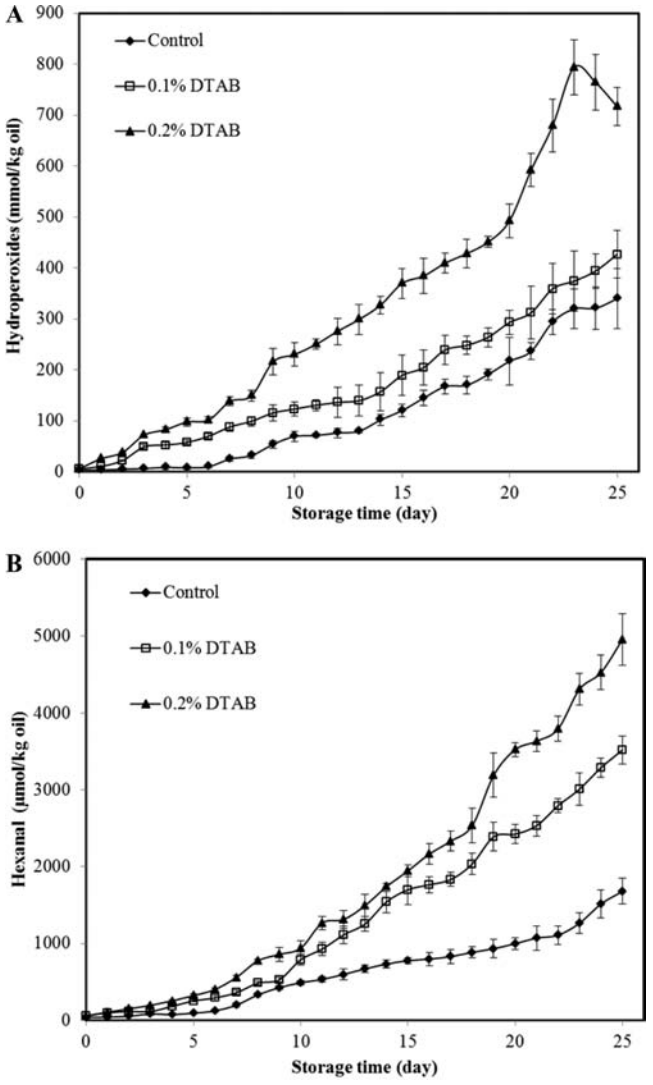

Figure 3. Effects of concentration of DTAB in the aqueous phase on the oxidative stability of 2% water-in-walnut oil at aqueous phase pH 7.0 during storage at 45 °C in the dark for 25 days. Lipid oxidation was monitored by measuring hydroperoxide (A) and hexanal (B). Data points and error bars represent means (n = 3) ± standard deviations.

The reason W/O emulsions containing SDS had higher oxidative stability seemed likely due to the fact that aqueous phase SDS formed negative micelles that were able to electrostatically attract transition metals, thereby reducing the concentration of prooxidants (e.g., transition metals) at the oil−water surface, a location where lipid oxidation reactions primarily occurs (seen in Figure 4). Similar results were found for the hemoglobin-catalyzed oxidation of a safflower oil-in-water emulsion, where the presence of excess anionic surfactant in the aqueous phase of the emulsion increased the oxidative stability.[37] Tween 20 is weakly anionic and thus might not be able to remove metals away from the lipid−water interface. It is unclear why a cationic surfactant such as DTAB would promote oxidation in the W/O emulsion.

Effects of WPI on the Oxidative Stability of Water-in-Walnut Oil Emulsions. Whey protein products such as WPI are commonly used as emulsifiers in O/W emulsions because they have good emulsifying and stabilizing properties.[38,39]

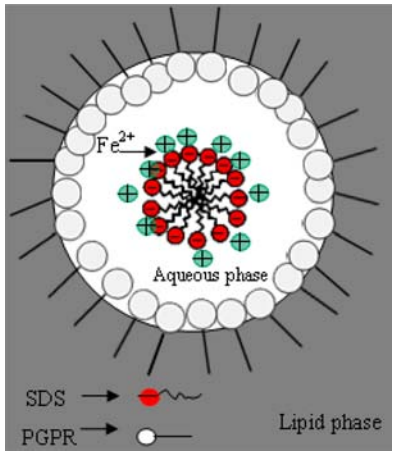

Figure 4. Schematic demonstration of the ability of SDS in the aqueous phase of W/O emulsions to interact with transition metals such as iron and inhibit lipid oxidation.

dx.doi.org/10.1021/jf404593f | J. Agric. Food Chem. 2014, 62, 2104−2111

Moreover, WPI has been shown to possess antioxidative properties in O/W emulsions when they are either at the emulsion droplet surface or in the aqueous phase.[28,40,41] Tong et al.[42] reported that the origin of the antioxidant activity of whey proteins was due to free radical scavenging by sulfhydryl and aromatic amino acids and transition metal chelation. To determine if WPI influenced the oxidative stability of W/O emulsions, the oxidative rates were analyzed by monitoring the formation of lipid hydroperoxides and hexanal. Figure 5 shows

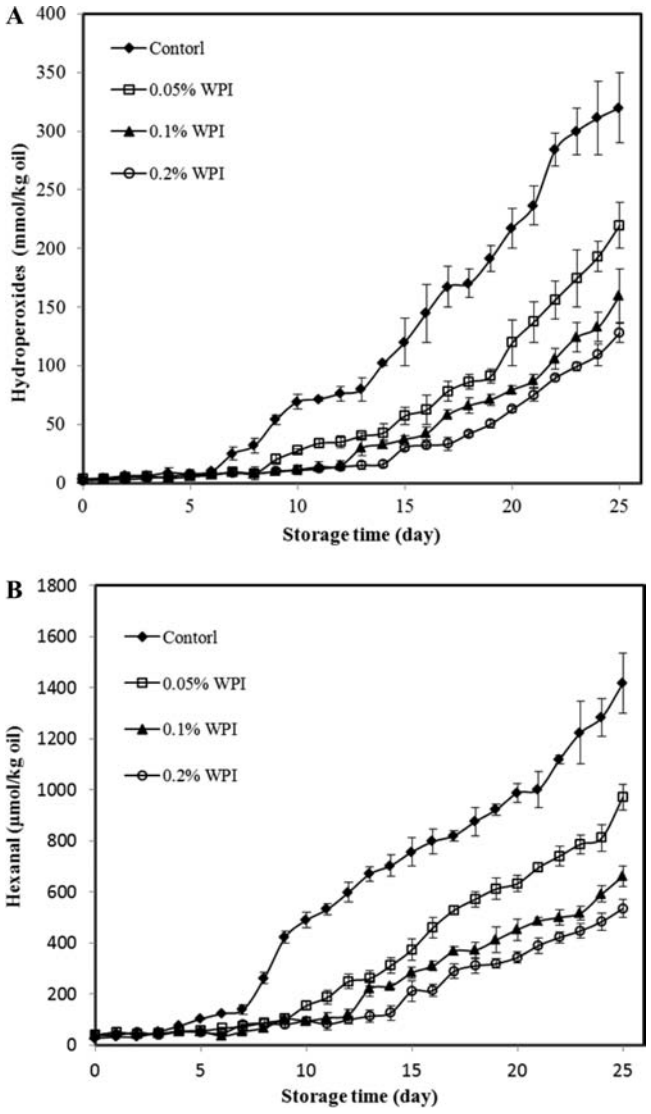

Figure 5. Effects of the concentration of WPI in the aqueous phase on the oxidative stability of 2% water-in-walnut oil at aqueous phase pH 7.0 during storage at 45 °C in the dark for 25 days. Lipid oxidation was monitored by measuring hydroperoxide (A) and hexanal (B). Data points and error bars represent means (n = 3) ± standard deviations.

that increasing concentration of WPI in W/O emulsions at pH 7.0 could decrease lipid oxidation rates. The lag phases of lipid hydroperoxide and hexanal formation in the control (without WPI) were 7 and 8 days, respectively. In the presence of 0.05, 0.1, or 0.2 wt % WPI (of emulsions), the lag phase increased to 9, 13, and 15 days for lipid hydroperoxides, respectively, and 10, 13, and 15 days for hexanal, respectively, suggesting that a higher concentration of WPI in the aqueous phase of W/O emulsions might have contributed to the better oxidative stability.

Hu et al.[27] and Kulmyrzaev et al.[43] have reported that the isoelectric point (pI) of WPI is 5.1, and pH values below or above the pI can dramatically affect the antioxidant activity of WPI. Therefore, further comparisons of oxidation rates as a function of aqueous phase pH were also determined. Figure 6

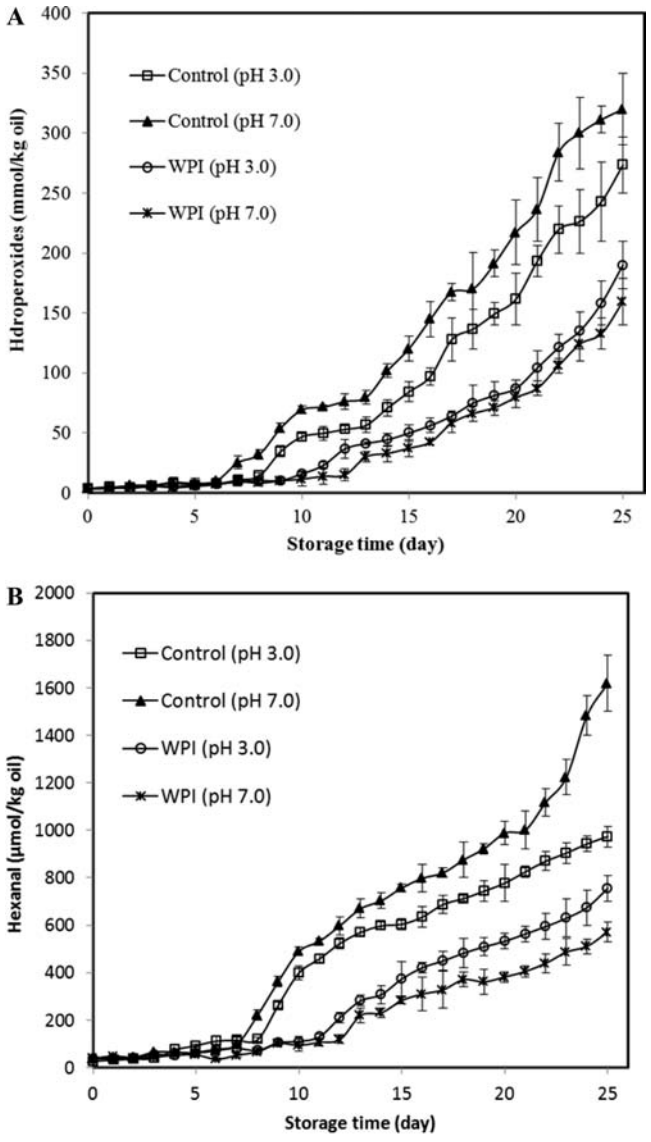

Figure 6. Effects of WPI (0.1 wt % of emulsions) as a function of different aqueous phase pH on the oxidative stability of 2% water-in-walnut oil during storage at 45 °C in the dark for 25 days. Lipid oxidation was monitored by measuring hydroperoxides (A) and hexanal (B). Data points and error bars represent means (n = 3) ± standard deviations.

shows that lipid oxidation of the controls was more rapid when the aqueous phase was pH 7.0 than when it was pH 3.0. At aqueous phase pH 7.0, lipid oxidation of the emulsions occurred slowly with the lag phases of both lipid hydroperoxide and hexanal formation being 7 and 8 days, respectively. The lag phases of lipid hydroperoxide and hexanal formation in the control at aqueous phase pH 3.0 were the same at 9 days of storage. Mancusco et al.[44] also observed that oxidation rates increased with increasing pH in Tween 20-stabilized salmon

dx.doi.org/10.1021/jf404593f | J. Agric. Food Chem. 2014, 62, 2104−2111

oil-in-water emulsion. The same authors proposed that at pH 7.0, low iron solubility resulted in precipitation of metal onto the lipid droplet surface, thereby bringing iron in closer contact with the lipid compared to pH 3.0, where the water solubility of iron is dramatically higher. If the same was true in the W/O emulsions, where iron could precipitate onto the lipid surface, it was not surprising that high pH in the aqueous phase microenvironment promoted lipid oxidation in W/O emulsions. In addition, it was reported that at pH 7.0, free fatty acids in the oil are negatively charged and thus can attract transition metals and increase lipid oxidation rates.[45,46] At pH 3.0 the free fatty acids lose their charge and are less prooxidative. Because all refined oils contain some free fatty acids, it is possible that the decrease in lipid oxidation rates with decreasing pH observed in this study could be due to the presence of free fatty acids.

The ability of WPI to inhibit lipid oxidation in W/O emulsions was greater at pH 7.0 than at pH 3.0 (Figure 6). For example, the lag phase of hexanal formation increased from 8 days (control) to 13 days in the presence of 0.1 wt % WPI at pH 7.0. This compares to an increase the lag phase of hexanal formation from 9 days (control) to 12 days in the presence of 0.1 wt % WPI at pH 3.0. The antioxidant activity of proteins in the continuous phase of O/W emulsions has also been found to be greater at pH values above the p*I* of the protein.[47] The reason for increased antioxidant activity of proteins at pH values above the p*I* is thought to be the increased ability of proteins to bind transition metals when they are negatively charged. For example, WPI bound over 3 times more iron at aqueous phase pH 7.0 than at aqueous phase pH 3.0 (Figure 7).

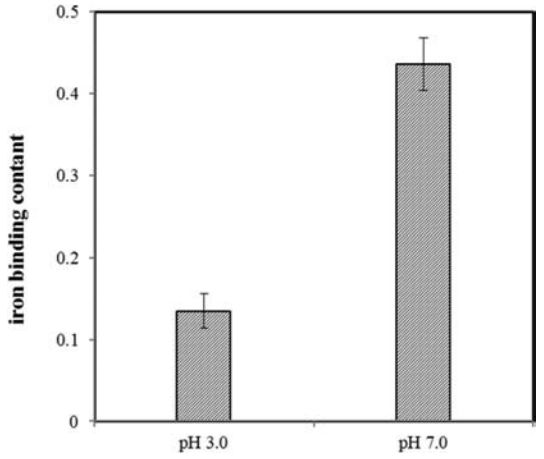

Figure 7. Iron bonding constant per gram WPI during incubation of ferrous ion (8 mg/L) in WPI solution at different pH values for 24 h. Data points and error bars represent means (n = 3) ± standard deviations.

Thus, it was possible that in the microenvironment of the aqueous phase in the W/O emulsions, WPI exhibited better antioxidant activity at pH 7.0 than at pH 3.0 due to binding more transition metals. However, it should be noted that WPI did inhibit lipid oxidation at pH 3.0 when the protein was cationic. This could still be due to its weak chelating activity but also could be due to its free radical scavenging activity.

Effects of WPI and Surfactants Combinations on the Oxidative Stability of Water-in-Walnut Oil Emulsions. Combinations of molecules in emulsion can often interact and synergistically or antagonistically impact lipid oxidation rates.[48] The impact of combinations of between WPI and DTAB or SDS on lipid oxidation rates in the W/O emulsion were tested at both pH 3.0 and 7.0 because the antioxidant activity of WPI was strongly influenced by pH.

The oxidative stability of the controls was observed to be pH dependent, with higher pH increasing lipid oxidation rates in the W/O emulsions as also observed in Figure 6. WPI was again found to be a stronger antioxidant at pH 7.0 than at pH 3.0 as first reported in Figure 6. Table 1 shows that emulsions

Table 1. Effects of the Interaction of WPI with SDS on Lag Phases of Lipid Hydroperoxide and Hexanal Formation in 2% Water-in-Walnut Oil Emulsions during Storage at 45 °C in the Dark for 25 Days

	lag phases[a] (days)	
treatment	hydroperoxide formation	hexanal formation
WPI (pH 3.0)	11	12
WPI (pH 7.0)	13	13
SDS (pH 3.0)	10	10
SDS (pH 7.0)	10	10
WPI + SDS (pH 3.0)	12	13
WPI + SDS (pH 7.0)	15	15
control (pH 3.0)	9	9
control (pH 7.0)	7	7

[a]Oxidation lag phases were defined as the first data point significantly greater than the 0 time value at the level of $p < 0.05$. All concentrations of emulsifiers were 0.1 wt % of emulsions.

containing WPI alone oxidized significantly more slowly than emulsions containing SDS alone, indicating that WPI had stronger antioxidant activity than SDS. From Table 1, it can also be seen that pH had no significant influence on the lag phases of both lipid hydroperoxide and hexanal formation in emulsions containing SDS ($p > 0.05$). The combination of WPI and SDS increased the lag phases of both lipid hydroperoxide and hexanal formation greater than either WPI or SDS alone at both pH 3.0 and 7.0. This increase in antioxidant activity by the WPI/SDS combination could simply due to an increase in the total metal chelating capacity in the emulsion. However, it is also well-known that SDS can induce denaturation of proteins and that exposing amino acids in the core of proteins can increase the ability of proteins to inhibit lipid oxidation.[49,50] The greater inhibition of lipid oxidation by the combination of WPI/SDS at pH 7.0 than at pH 3.0 could be due to WPI's greater antioxidant activity when it is negatively charged.

The influence of interactions between WPI and DTAB on lag phases of lipid hydroperoxide and hexanal formation in W/O emulsions was also investigated (Table 2). DTAB alone consistently promoted lipid oxidation, whereas WPI alone consistently inhibited lipid oxidation in W/O emulsions, similar to the results above (Figures 3 and 6). The combination of WPI and DTAB resulted in lag phases for 5 and 6 days for hydroperoxides and hexanal formation, respectively, at pH 3.0 (Table 2). At pH 7.0, lag phases for hydroperoxides and hexanal formation were 7 and 8 days, respectively, for the DTAB/WPI combination (Table 2). These lag phases are greater than those for DTAB alone but less than for WPI. This is likely because the antioxidant capability of WPI was able to counteract some of the prooxidant activity of DTAB but not to the extent that the lag phases were equal to WPI alone. The lag phases for hydroperoxides and hexanal formation for the WPI/DTAB combination were greater at pH 7.0 than at pH 3.0,

dx.doi.org/10.1021/jf404593f | J. Agric. Food Chem. 2014, 62, 2104−2111

Table 2. Effects of the Interaction of WPI with DTAB on Lag Phases of Lipid Hydroperoxide and Hexanal Formation in 2% Water-in-Walnut Oil Emulsions during Storage at 45 °C in the Dark for 25 Days

	lag phases[a] (days)	
treatment	hydroperoxide formation	hexanal formation
WPI (pH 3.0)	11	12
WPI (pH 7.0)	13	13
DTAB (pH 3.0)	2	4
DTAB (pH 7.0)	2	4
WPI + DTAB (pH 3.0)	5	6
WPI + DTAB (pH 7.0)	7	8
control (pH 3.0)	9	9
control (pH 7.0)	7	7

[a]Oxidation lag phases were defined as the first data point significantly greater than the 0 time value at the level of $p < 0.05$. All concentrations of emulsifiers were 0.1 wt % of emulsions.

which again could be attributed to the increase antioxidant activity of WPI when it is anionic and better able to chelate metals.

In conclusion, the current study shows that formation of a W/O emulsion increased oxidation rates compared to bulk oil. This acceleration of oxidation could be due to the increase in surface area that could facilitate interactions between lipids and water-soluble transition metals. The present work also indicates that Tween 20 had no impact on lipid oxidation rates, whereas DTAB increased oxidation in an unknown manner. SDS and WPI inhibited lipid oxidation in the W/O emulsions, which could be due to metal chelation by these anionic surfactants. WPI was a better antioxidant at pH 7.0 than at pH 3.0 presumably due to its higher transition metal-binding capacity at pH values above the p*I* of the proteins, where the proteins would be anionic. However, WPI was also able to inhibit oxidation at pH 3.0 when it would be cationic, suggesting that it may also be able to inhibit oxidation by scavenging free radicals. Only the combination of WPI and SDS resulted in increased antioxidant activity compared to the individual compounds, which could be due to increased metal chelating capacity or combining both metal chelating and free radical scavenging activities. These results suggest that compounds that chelate transition metal could be used to increase the oxidative stability of W/O emulsions. The ability of WPI to inhibit lipid oxidation in W/O emulsions suggests that it could be used as a natural antioxidant in foods such as spreads.

AUTHOR INFORMATION

Corresponding Author

*(J.Y.) E-mail: yijianhua@sust.edu.cn.

Funding

This study was supported by the Cultivation of Academic Program of Shaanxi University of Science and Technology (XS11-07).

Notes

The authors declare no competing financial interest.

ACKNOWLEDGMENTS

We thank Yuhua Chang, Jean Alamed, and Leann Barden for assistance.

REFERENCES

(1) Laguerre, M.; Lecomte, J.; Villeneuve, P. Evaluation of the ability of antioxidants to counteract lipid oxidation: existing methods, new trends and challenges. *Prog. Lipid Res.* **2007**, *46* (5), 244−282.

(2) Poyato, C.; Navarro-Blasco, I.; Calvo, M. I.; Cavero, R. Y.; Astiasarán, I.; Ansorena, D. Oxidative stability of O/W and W/O/W emulsions: effect of lipid composition and antioxidant polarity. *Food Res. Int.* **2013**, *51*, 132−142.

(3) Barriuso, B.; Astiasarán, I.; Ansorena, D. A review of analytical methods measuring lipid oxidation status in foods: a challenging task. *Eur. Food Res. Technol.* **2013**, *236*, 1−15.

(4) Chen, B. C.; McClements, D. J.; Decker, E. A. Minor components in food oils: a critical review of their roles on lipid oxidation chemistry in bulk oils and emulsions. *Crit. Rev. Food Sci. Nutr.* **2011**, *51*, 901−916.

(5) McClements, D. J. *Food Emulsions Principles, Practice and Techniques*, 2nd ed.; CRC Press: Boca Raton, FL, USA, 2005.

(6) McClements, D. J.; Decker, E. A. Lipid oxidation in oil-in-water emulsions: impact of molecular environment on chemical reactions in heterogeneous food systems. *J. Food Sci.* **2000**, *65*, 1270−1282.

(7) Coupland, J. N.; McClements, D. J. Lipid oxidation in food emulsions. *Trends Food Sci. Technol.* **1996**, *7*, 83−91.

(8) Mosca, M.; Ceglie, A.; Ambrosone, L. Lipid oxidation in water-in-olive oil emulsions initiated by a lipophilic radical source. *J. Phys. Chem. B* **2010**, *114*, 3550−3558.

(9) Velasco, J.; Dobarganes, M. C.; Márquez-Ruiz, G. Antioxidant activity of phenolic compounds in sunflower oil-in-water emulsions containing sodium caseinate and lactose. *Eur. J. Lipid Sci. Technol.* **2004**, *106*, 325−333.

(10) McClements, D. J. In *Food Emulsions: Principles, Practice and Techniques*; CRC Press: Boca Raton, FL, USA, 1999; 392 pp.

(11) Walstra, P. Principles of emulsion formation. *Chem. Eng. Sci.* **1993**, *48*, 333−350.

(12) Ogawa, S.; Decker, E. A.; McClements, D. J. Production and characterization of O/W emulsions containing cationic droplets stabilized by lecithin−chitosan membranes. *J. Agric. Food Chem.* **2003**, *51*, 2806−2812.

(13) Mosca, M.; Cuomo, F.; Lopez, F.; Ceglie, A. Role of emulsifier layer, antioxidants and radical intiators in the oxidation of olive oil-in-water emulsions. *Food Res. Int.* **2013**, *50*, 377−383.

(14) Yuji, H.; Weiss, J.; Villeneuve, P.; Giraldo, L. J. L.; Figueroa-Espinoza, M.; Decker, E. A. Ability of surface-active antioxidants to inhibit lipid oxidation in oil-in-water emulsion. *J. Agric. Food Chem.* **2007**, *55*, 11052−11056.

(15) Krog, N. J. Food emulsifiers. In *Food Emulsions*, 3rd ed.; Friberg, S., Larsson, K., Eds.; Dekker: New York, 1997; 141 pp.

(16) Waraho, T.; McClements, D. J.; Decker, E. A. Mechanism of lipid oxidation in food dispersions. *Trends Food Sci. Technol.* **2011**, *22*, 3−13.

(17) Mancuso, J. R.; McClements, D. J.; Decker, E. A. Iron-accelerated cumene hydroperoxide decomposition in hexadecane and trilaurin emulsions. *J. Agric. Food Chem.* **2000**, *48*, 213−219.

(18) Decker, E. A. Strategies for manipulating the prooxidative/antioxidative balance of food to maximize oxidative stability. *Trends Food Sci. Technol.* **1998**, *9*, 241−248.

(19) Mosca, M.; Ceglie, A.; Ambrosone, L. Antioxidant dispersions in emulsified olive oils. *Food Res. Int.* **2008**, 201−207.

(20) Choi, S. J.; Decker, E. A.; McClements, D. J. Impact of iron encapsulation within the interior aqueous phase of water-in-water emulsions on lipid oxidation. *Food Chem.* **2009**, *116*, 271−276.

(21) Shaw, L.; McClements, D. J.; Decker, E. A. Spray-dried multilayered emulsions as a delivery method for ω-3 fatty acids into food systems. *J. Agric. Food Chem.* **2007**, *55*, 3112−3119.

(22) Djordjevic, D.; Cercaci, L.; Alamed, J.; McClements, D. J.; Decker, E. A. Chemical and physical stability of citral and limonene in sodium dodecyl sulfate chitosan and gum arabic-stabilized oil-in-water emulsions. *J. Agric. Food Chem.* **2007**, *55*, 3585−3591.

(23) Mei, L.; McClements, D. J.; Wu, J.; Decker, E. A. Iron-catalyzed lipid oxidation in emulsions as affected by surfactant, pH and NaCl. *Food Chem.* **1998**, *61*, 307−312.
(24) Mei, L.; Decker, E.; McClements, D. J. Evidence of iron association with emulsion droplets and its impact on lipid oxidation. *J. Agric. Food Chem.* **1998**, *46*, 5072−5077.
(25) Silvestre, M.; Chaiyasit, W.; Brannan, R. E.; McClements, D. J.; Decker, E. A. Ability of surfactant head group size to alter lipid and antioxidant oxidation in oil-in-water emulsions. *J. Agric. Food Chem.* **2000**, *48*, 2057−2061.
(26) Boon, C.; Xu, Z.; Yue, X.; McClements, D. J.; Weiss, J.; Decker, E. A. Factors affecting lycopene oxidation in oil-in-water emulsions. *J. Agric. Food Chem.* **2008**, *56*, 1408−1414.
(27) Hu, M.; McClements, D. J.; Decker, E. A. Lipid oxidation in corn oil-in-water emulsions stabilized by casein, whey protein isolate, and soy protein isolate. *J. Agric. Food Chem.* **2002**, *51*, 1696−1700.
(28) Hu, M.; McClements, D. J.; Decker, E. A. Impact of whey protein emulsifiers on the oxidative stability of salmon oil-in-water emulsions. *J. Agric. Food Chem.* **2003**, *51*, 1435−1439.
(29) Mancuso, J. R.; McClements, D. J.; Decker, E. A. The effects of surfactant type, pH, and chelators on the oxidant of salmon oil-in-water emulsions. *J. Agric. Food Chem.* **1999**, *47*, 4112−4116.
(30) Mancuso, J. R.; McClements, D. J.; Decker, E. A. Iron accelerated cumene hydroperoxide decomposition in hexadecane and trilaurin emulsions. *J. Agric. Food Chem.* **2000**, *48*, 213−219.
(31) Shantha, N. C.; Decker, E. A. Rapid, sensitive, iron-based spectrophotometric methods for determination of peroxide values of food lipids. *J. AOAC Int.* **1994**, *77*, 421−424.
(32) Panya, A.; Laguerre, M.; Lecomte; J. Villeneuve, P. Effects of chitosan and rosmarinate esters on the physical and oxidative stability of liposomes. *J. Agric. Food Chem.* **2010**, *58*, 5679−5684.
(33) Chen, B. C.; McClements, D. J.; Decker, E. A. Role of continuous phase anionic polysaccharides on the oxidative stability of menhaden oil-in-water emulsions. *J. Agric. Food Chem.* **2010**, *58*, 3779−3784.
(34) Haahr, A.; Jacobsen, C. Emulsifier type, metal chelation and pH affect oxidative stability of n-3-enriched emulsions. *Eur. J. Lipid Sci. Technol.* **2008**, *110* (10), 949−961.
(35) Fritsch, C. W. Lipid oxidation − the other dimensions. *INFORM* **1994**, *5*, 23−436.
(36) Ambrosone, L.; Mosca, M.; Ceglie, A. Impact of edible surfactants on the oxidation of olive oil in water-in-oil emulsions. *Food Hydrocolloids* **2007**, *21*, 1163−1171.
(37) Sims, R. J.; Fioriti, J. A.; Trumbetas, J. Effect of sugars and sugar alcohols on autoxidation of safflower oil in emulsions. *J Am. Oil Chem. Soc.* **1979**, *56*, 742−745.
(38) Horn, A. F.; Wulff, T.; Nielsen, N. S.; Jacobsen, C. Effect of α-lactalbumin and β-lactoglobulin on the oxidative stability of 10% fish oil-in-water emulsions depends on pH. *Food Chem.* **2013**, 574−581.
(39) Xu, D.; Yuan, F.; Gao, Y.; McClements, D. J.; Decker, E. A. Influence of pH, metal chelator, free radical scavenger and interfacial characteristics of the oxidative stability of β-carotene in conjugated whey protein-pectin stabilized emulsion. *Food Chem.* **2013**, *139*, 1098−1104.
(40) Lesmes, U.; Sandra, S.; McClements, D. J.; Decker, E. A. Impact of surface deposition of lactoferrin on physical and chemical stability of omega-3 rich lipid droplets stabilized by caseinate. *Food Chem.* **2010**, *123*, 99−106.
(41) Elias, R. J.; McClements, D. J.; Decker, E. A. Antioxidant activity of cysteine, tryptophan, and methionine residues in continuous phase β-lactoglobulin in oil-in-water emulsions. *J. Agric. Food Chem.* **2005**, *53*, 10248−10253.
(42) Tong, L. J.; Sasaki, S.; McClements, D. J.; Decker, E. A. Mechanisms of the antioxidant activity of a high molecular weight fraction of whey. *J. Agric. Food Chem.* **2000**, *48*, 1473−1478.
(43) Kulmyrzaev, A.; Chanamai, R.; McClements, D. J. Influence of pH and $CaCl_2$ on the stability of dilute whey protein stabilized emulsions. *Food Res. Int.* **2000**, *33*, 15−20.
(44) Mancusco, J. R.; McClements, D. J.; Decker, E. A. The effects of surfactant type, pH, and chelators on the oxidation of salmon oil-in-water emulsions. *J. Agric. Food Chem.* **1999**, *47*, 4112−4116.
(45) Waraho, T.; Cardenia, V.; Rodriguez-Estrada, M. T.; McClements, D. J.; Decker, E. A. Prooxidant mechanisms of free fatty acids in stripped soybean oil-in-water emulsions. *J. Agric. Food Chem.* **2009**, *57*, 7112−7117.
(46) Yi, J. H.; Zhu, Z. B.; Dong, W. B.; McClements, D. J.; Decker, E. A. Influence of free fatty acids on oxidative stability in water-in-walnut oil emulsions. *Eur. J. Lipid Sci. Technol.* **2013**, *115* (9), 1013−1020.
(47) Faraji, H.; McClements, D. J.; Decker, E. A. Role of continuous phase protein on the oxidative stabilityof fish oil-in-water emulsions. *J. Agric. Food Chem.* **2004**, *52*, 4558−4564.
(48) Panya, A.; Kittipongpittaya, K.; Laguerre, M.; Bayrasy, C.; Lecomte, J.; Villeneuve, P.; McClements, D. J.; Decker, E. A. Interactions between α-tocopherol and rosmarinic acid and its alkyl esters in emulsions: synergistic, additive, or antagonistic effect? *J. Agric. Food Chem.* **2012**, *60*, 10320−10330.
(49) Elias, R. J.; McClements, D. J.; Decker, E. A. Impact of thermal processing on the antioxidant mechanisms of continuous phase β-lactoglobulin in oil-in-water emulsions. *Food Chem.* **2007**, *104*, 1402−1409.
(50) Elias, R. J.; Bridgewater, J. D.; Vachet, R. W.; Waraho, T.; McClements, D. J.; Decker, E. A. Antioxidant mechanisms of enzymatic hydrolysates of β-lactoglobulin in food lipid dispersions. *J. Agric. Food Chem.* **2006**, *54*, 9565−9572.

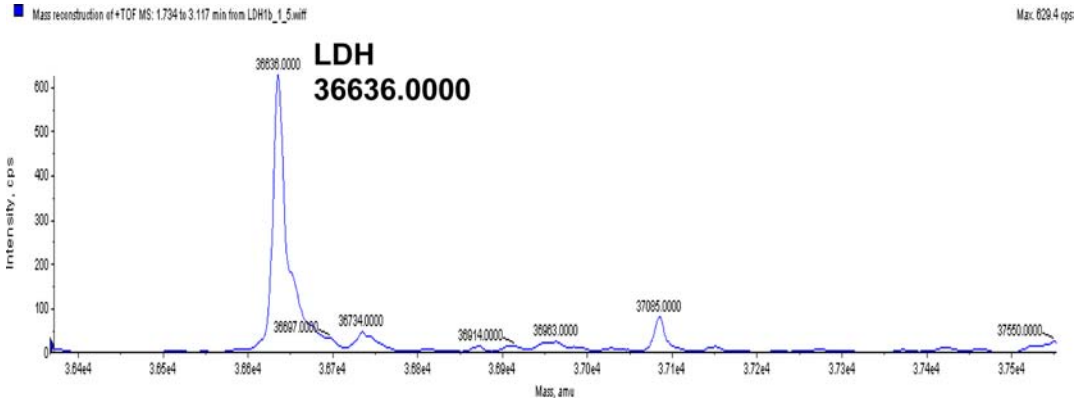

Figure 1. ESI-MS spectrum of bovine LDH control (0.2 mM) at pH 7.4. The *X*-axis indicates mass measured as atomic mass unit (amu) and *Y*-axis indicates intensity measured as counts per second (cps).

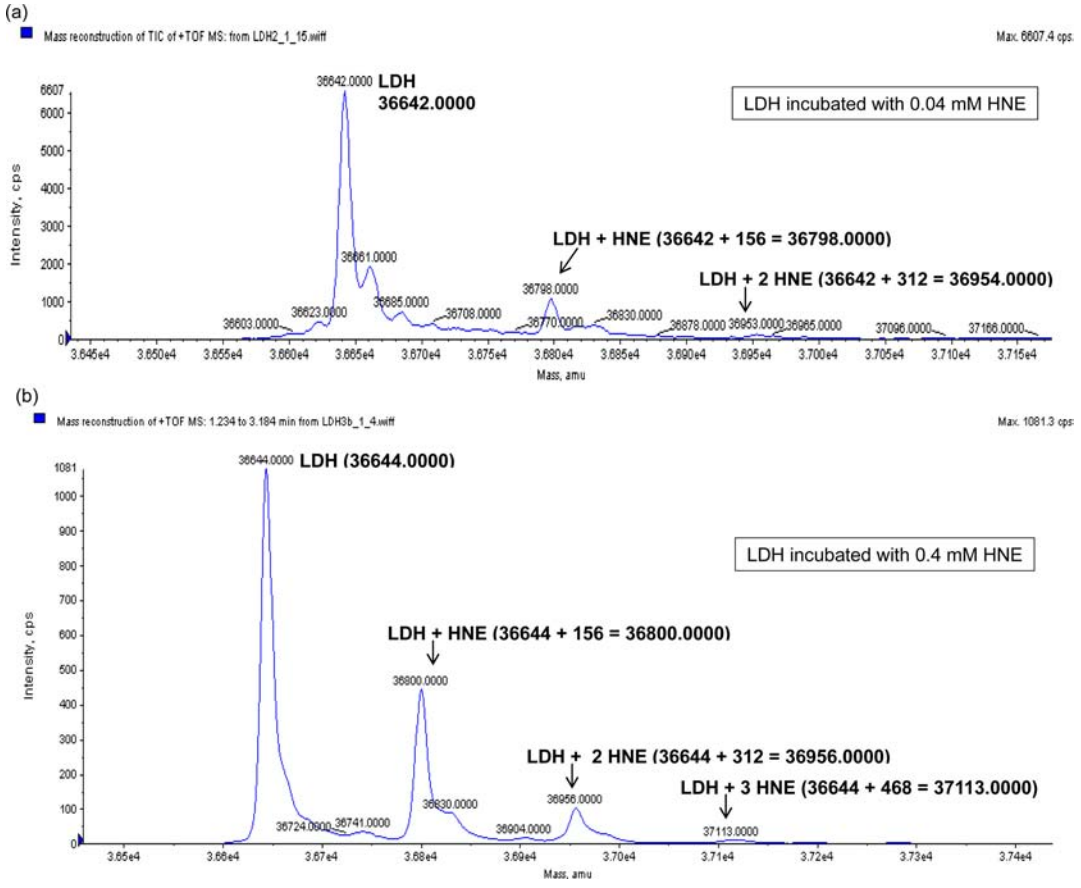

Figure 2. ESI-MS spectrum of bovine LDH (0.2 mM) incubated with (a) HNE 0.04 mM and (b) 0.4 mM at pH 7.4. The *X*-axis indicates mass measured as atomic mass unit (amu) and *Y*-axis indicates intensity measured as counts per second (cps).

Louis, MO). 4-Hydroxy-2-nonenal was obtained from Cayman Chemical Co. (Ann Arbor, MI). PD-10 columns, CM and DEAE cellulose ion exchange chromatography columns were obtained from Pharmacia (Piscataway, NJ). All chemicals were of reagent grade or greater purity.

Myoglobin Isolation and Preparation of Metmyoglobin. Beef myoglobin was purified via ammonium sulfate precipitation and gel filtration chromatography according to Faustman and Phillips.[17] The isolated myoglobin was a mixture of oxy-, deoxy-, and metmyoglobin. To limit the interference with metmyoglobin reduction in the current study, oxidizing agents were not used to convert oxy- or deoxymyoglobin to metmyoglobin. Hence, metmyoglobin was prepared by incubating myoglobin at 37 °C for 24 h. Columns precalibrated with either 50 mM phosphate buffer (pH 7.4) or 50 mM phosphate buffer (pH 5.6) were used to adjust the pH of metmyoglobin solutions. The initial metmyoglobin content was 98.9%, determined according to Tang et al.[18]

Isolation of NADH-Dependent Cytochrome b5 Reductase. Metmyoglobin reductase was isolated according to Hagler et al.[19] and Faustman et al.[20] Aliquots (1 mL) were stored at −80 °C until use.

Effects of HNE on Lactate Dehydrogenase Activity. Commercially purchased purified bovine heart LDH (0.2 mM) was incubated with HNE (0, 0.04, or 0.4 mM dissolved in ethanol) for 5 h at pH 7.4 or for 72 h at pH 5.6 (normal meat pH) in a glass test tube. Lactate dehydrogenase activity was measured as the formation of NADH at 0, 1, 3, and 5 h at pH 7.4 and 0, 24, 48, and 72 h at pH 5.6. Briefly, lactate (50 mM), LDH (0.2 mM), and NAD (0.2 mM) were reacted in incubation buffer (50 mM phosphate buffer) at both pH

dx.doi.org/10.1021/jf404900y | J. Agric. Food Chem. 2014, 62, 2112−2117

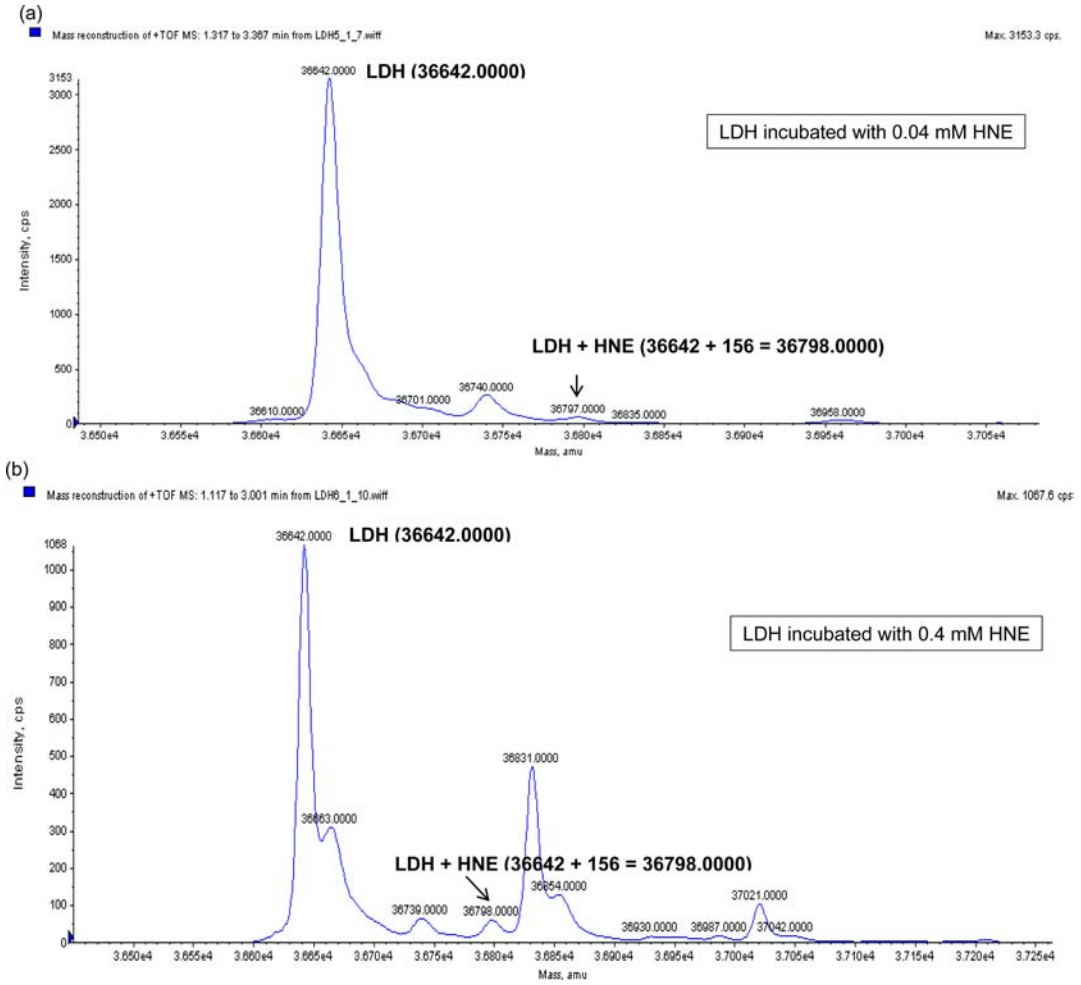

Figure 3. ESI-MS spectrum of bovine LDH (0.2 mM) incubated with (a) HNE 0.04 mM and (b) 0.4 mM at pH 5.6. The *X*-axis indicates mass measured as atomic mass unit (amu) and *Y*-axis indicates intensity measured as counts per second (cps).

Table 1. Summary of MS/MS Analysis Used to Determine HNE Adduction to LDH at pH 5.6 and 7.4

pH	treatment (mM)	enzyme used for peptide digestion	peptide	peptide sequence	HNE modification	precursor peptide *m*/*z*
5.6	HNE 0.04	trypsin	280−299	GMYGIENEVFLSLP**C**ILNAR	C294	2395
	HNE 0.4	trypsin	159−170	VIGSG**C**NLDSAR	C164	1347
		trypsin	280−299	GMYGIENEVFLSLP**C**ILNAR	C294	2395
7.4	HNE 0.04	trypsin	159−170	VIGSG**C**NLDSAR	C164	1347
	HNE 0.4	trypsin	159−170	VIGSG**C**NLDSAR	C164	1347
		trypsin	280−299	GMYGIENEVFLSLP**C**ILNAR	C294	2395
		trypsin/Asp-N	65−77	DLQ**H**GSLFLQTPK	H68	1640
		trypsin/Asp-N	179−195	LGIHPSS**C**HGWILGEHG	C186	1956

values in a quartz cuvette for 3 min. The formation of NADH was measured according to Bergmeyer[21] and Ramanathan et al.,[22] where an increase in absorbance at 340 nm indicates NADH formation. Following determination of LDH activity, a PD column was used to remove unbound HNE and LDH was stored at −80 °C until use.

NADH-Dependent Cytochrome b5 Metmyoglobin Reduction. The methodology according to Reddy and Carpenter[2] was modified to determine NADH-dependent cytochrome b5 metmyoglobin reduction. The assay mixture contained 0.15 mM metmyoglobin in either 50 mM phosphate buffer at pH 5.6 or 7.4, 0.05 mL of 0.2 mM NAD, 0.05 mL of 1 M lactate, 0.1 mL of 5 mM EDTA, 0.1 mL of 3.0 mM potassium ferrocyanide, and 0.03 mL of purified NADH-dependent cytochrome b5 reductase. The reaction was initiated by the addition of LDH at 25 °C according to Ramanathan et al.[15] (0.02 mM LDH in the final reaction mixture; LDH preincubation with HNE or ethanol described in the previous section). Metmyoglobin reduction (nanomoles of metmyoglobin reduced per minute per milligram of reductase) was calculated according to Faustman et al.[20] using the change in absorbance at 580 nm. The protein concentration of reductase was determined using a bicinchoninic acid protein assay.

Mass Spectrometry. Protein masses of native and HNE-treated LDH, including LDH peptide preparation and analysis (Trypsin digestion), were measured according to the method described by Nair et al.[23] For Asp-N and double digestion, 10 μL of LDH solution was dried and digested in 10 μL of 40 mM ammonium bicarbonate +9% acetonitrile containing 0.02 μg (Sigma, St. Louis, MO) proteomics grade endoproteinase Asp-N at room temperature for 4 h.

Statistical Analysis. The experimental design was a completely randomized design with repeated measures, and each experiment was replicated five times (n = 5). Fixed effects for both NADH-dependent

cytochrome b5 reductase and LDH activity include HNE concentration, incubation time, and their interaction. Data was analyzed using the MIXED Procedure of SAS (version 9.1, SAS Institute Inc. Cary, NC), and the Repeated option was used for both NADH-dependent cytochrome b5 reductase and LDH activity measurements. The diff option (LSD at $P < 0.05$ for significance) was used to separate least-squares means from protected F-tests ($P < 0.05$).

RESULTS AND DISCUSSION

Effects of HNE on Covalent Binding on LDH. Characterization of LDH using MS revealed that the mass of protein samples used in the current study matched that of LDH B (isoform predominantly present in cardiac muscle; Figure 1). Mass spectrometric examination revealed that HNE adducted to LDH. Mono-, di-, and triadducts were detected at pH 7.4, whereas only monoadducts were identified at pH 5.6 (Figures 2 and 3). More specifically, MS/MS results indicate that HNE can bind with cysteine residues of LDH at pH 5.6 and 7.4 (Table 1).

Table 2. Active Site Residues in Bovine Heart Lactate Dehydrogenase

active site	position in the sequence	amino acid
NAD binding	100	arginine
substrate binding	106	arginine
NAD/substrate binding	139	asparagine
substrate binding	170	arginine
proton acceptor	194	histidine
substrate binding	249	threonine

Carbon 3 within HNE can covalently bind via Michael addition to histidine residues within myoglobin from all livestock and poultry species and result in increased oxymyoglobin oxidation.[24−27] In addition, HNE adduction makes myoglobin a poor substrate for enzymatic metmyoglobin reduction.[28] Furthermore, covalent binding of HNE to myoglobin can increase heme release.[29]

The active site residues involved in LDH enzymatic activity are summarized in Table 2. Although HNE did not bind to residues within the active sites, the current study suggests that binding to other amino acids can influence enzyme activity. For example, the amino acid sequence of LDH has 7 histidine, 5 cysteine, and 26 lysine residues (Figure 4; www.expasy.org).

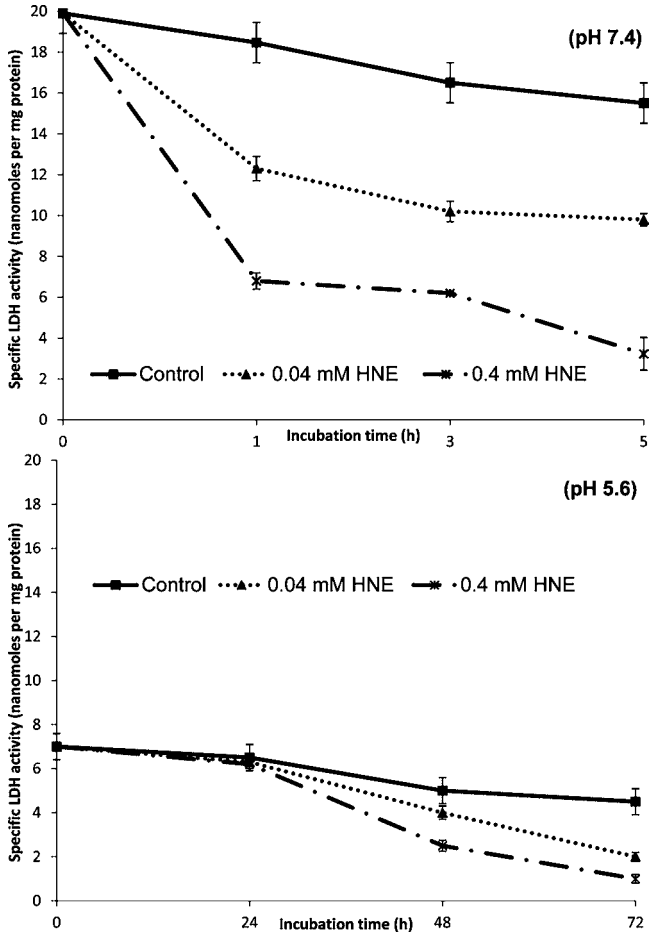

Figure 5. Effect of HNE on LDH activity at pH 5.6 and 7.4. Standard error bars are indicated.

The MS/MS analysis in the current research indicates that HNE binds to cysteine and histidine residues (Table 1). More specifically, at 0.4 mM HNE, four sites of HNE adduction were identified at His-68, Cys-164, Cys-186, and Cys-294 at pH 7.4. However, no histidine adducts were identified at pH 5.6, likely because histidine residues would be expected to have a greater positive charge at pH 5.6 than 7.4, which would reduce reactivity with HNE.[30] The current study is the first to report

```
0     MATLKEKLIAPVAEEETRIP NNKITVVGVG QVGMACAISI LGKSLTDELA LVDVLEDKLK

60    GEMMDLQHGS LFLQTPKIVA DKDYSVTANS KIVVVTAGVR QQEGESRLNL VQRNVNVFKF

120   IIPQIVKYSP DCIIIVVSNP VDILTYVTWK LSGLPKHRVI GSGCNLDSAR FRYLMAEKLG

180   IHPSSCHGWI LGEHGDSSVA VWSGVNVAGV SLQELNPEMG TDNDSENWKE VHKMVVESAY

240   EVIKLKGYTN WAIGLSVADL IESMLKNLSR IHPVSTMVKG MYGIENEVFL SLPCILNARG

300   LTSVINQKLK DEEVAQLKKS ADTLWGIQKD LKDL
```

Number of histidines = 7; cysteines = 5; lysines = 26

Figure 4. Primary structure of bovine LDH.

dx.doi.org/10.1021/jf404900y | J. Agric. Food Chem. 2014, 62, 2112−2117

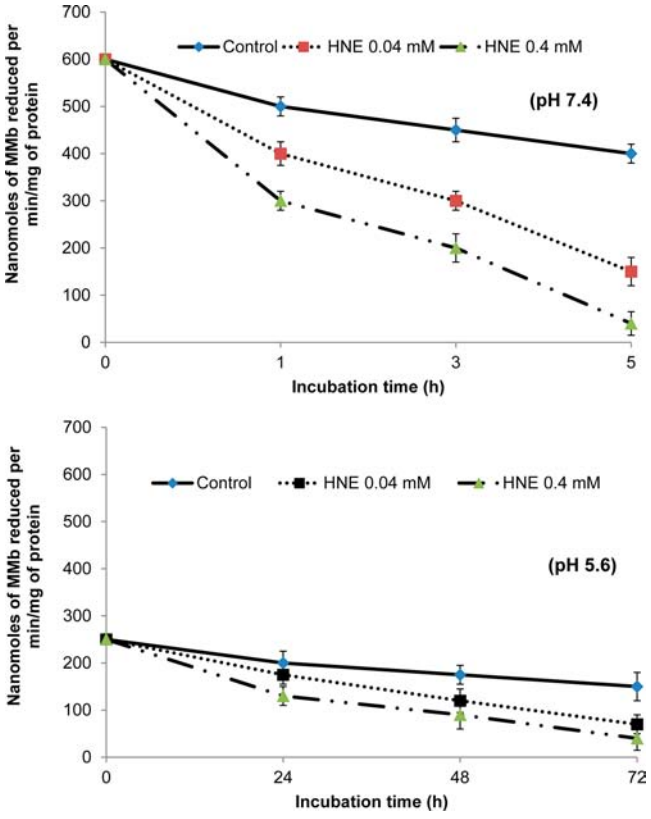

Figure 6. Effect of HNE on LDH-mediated enzymatic metmyoglobin reduction at pH 5.6 and 7.4. Standard error bars are indicated.

that HNE can influence enzymes involved in metmyoglobin reduction.

Previous studies have shown that HNE can covalently bind to enzymes and decrease activity. For example, Hussain et al.[31] reported that HNE decreased rabbit muscle enolase activity in vitro. Covalent binding of HNE to cysteines, histidine, and lysine residues of glyceraldehyde 3-phosphate dehydrogenase and subsequent enzyme inactivation was reported by Uchida and Stadtman.[32] In support, the current study indicates that HNE can bind to cysteine and histidine residues in LDH.

Effects of HNE on LDH Activity and Metmyoglobin Reduction. There was a significant HNE × incubation time interaction for LDH activity (Figure 5). Decreased NADH formation in samples treated with HNE was supported by limited enzymatic metmyoglobin reduction (Figure 6). The effect of HNE on LDH activity was concentration dependent, and HNE had a greater effect on enzyme activity at pH 7.4 than at pH 5.6. Several studies have reported that lipid oxidation and myoglobin oxidation are interrelated. In addition to direct interaction between myoglobin and HNE, the current study indicates that lipid oxidation products decrease meat color stability by influencing enzymes involved in NADH production and metmyoglobin reduction.

In conclusion, HNE can covalently bind to histidine and cysteine residues in LDH and will decrease NADH formation. The results indicate that secondary lipid oxidation products will inactivate enzymes involved in metmyoglobin reduction and, as a result, increase beef discoloration.

AUTHOR INFORMATION

Corresponding Author

*Phone: +1 860 486 1775. Fax: +1 860 486 4375. E-mail: richard.mancini@uconn.edu.

Notes

The authors declare no competing financial interest.

ACKNOWLEDGMENTS

Mass spectrometric analysis was performed at the University of Kentucky's Proteomics Core Facility, supported in part by funds from the Office of the Vice President for Research.

ABBREVIATIONS USED

LHD, L-lactic dehydrogenase; NAD, nicotinamide adenine dinucleotide; NADH, reduced form, nicotinamide adenine dinucleotide; HNE, 4- hydroxy-2-nonenal; MS, mass spectrometry; amu, atomic mass unit; cps, counts per second

REFERENCES

(1) Ledward, D. A. Post-slaughter influences on the formation of metmyoglobin in beef muscles. *Meat Sci.* **1985**, *15*, 149−171.

(2) Reddy, I. M.; Carpenter, C. E. Determination of metmyoglobin reductase activity in bovine skeletal muscles. *J. Food Sci.* **1991**, *56*, 1161−1164.

(3) Sakai, T.; Kuwazuru, S.; Yamauchi, K.; Uchida, K. A. Lipid oxidation-derived aldehyde, 4-hydroxy-2-nonenal and omega-6 fatty acid contents in meats. *Bio. Biotechnol. Biochem.* **1995**, *59*, 1379−1380.

(4) Lynch, M. P.; Faustman, C.; Silbart, L. K.; Rood, D.; Furr, H. C. Detection of lipid-derived aldehydes and aldehyde:protein adducts in vitro and in beef. *J. Food Sci.* **2001**, *66*, 1093−1099.

(5) Szweda, L. I.; Uchida, K.; Tsai, L.; Stadtman, E. R. Inactivation of glucose-6-phosphate dehydrogenase by 4-hydroxy-2-nonenal. *J. Biol. Chem.* **1993**, *268*, 3342−3347.

(6) Patel, M. S.; Korotchkina, L. G. Pyruvate dehydrogenase complex as a marker of mitochondrial metabolism. Inhibition by 4-hydroxy-2-nonenal. *Methods Mol. Biol.* **2002**, *186*, 255−263.

(7) Jagt, D. L. V.; Hunsaker, L. A.; Jagt, T. J. V.; Gomeg, M. S.; Gonzales, D. M.; Deck, L. M. Inactivation of glutathione reductase by hydroxynonenal and other endogenous aldehydes. *Biochem. Pharmacol.* **1997**, *53*, 1133−1140.

(8) Drake, J.; Petroze, R.; Castegna, A.; Ding, Q.; Keller, J. N.; Markesbery, W. R. 4-Hydroxynonenal oxidatively modifies histones: implications for Alzheimer's disease. *Neurosci. Lett.* **2004**, *356*, 155−158.

(9) Chen, J.; Schenker, S.; Frosto, T. A.; Henderson, G. I. Inhibition of cytochrome c oxidase activity by 4-hydroxynonenal (HNE). Role of HNE adduct formation with the enzyme subunits. *Biochim. Biophys. Acta* **1998**, *1380*, 336−344.

(10) Esterbauer, H.; Schaur, R. J.; Zollner, H. Chemistry and biochemistry of 4-hydroxynonenal, malonaldehyde and related aldehydes. *Free Radical Biol. Med.* **1991**, *11*, 81−128.

(11) Watts, B. M.; Kendrick, J.; Zipser, M. W.; Hutchins, B.; Saleh, B. Enzymatic reducing pathways inmeat. *J. Food Sci.* **1966**, *31*, 855−862.

(12) Saleh, B.; Watts, B. M. Substrates and intermediates in the enzymatic reduction of metmyoglobin in ground beef. *J. Food Sci.* **1968**, *33*, 353−358.

(13) Stewart, M. R.; Hutchins, B. K.; Zipser, M. W.; Watts, B. M. Enzymatic reduction of metmyoglobin by ground beef. *J. Food Sci.* **1965**, *30*, 487−491.

(14) Kim, Y. H.; Hunt, M. C.; Mancini, R. A.; Seyfert, M.; Loughin, T. M.; Kropf, D. H. Mechanism for lactate−color stabilization in injection-enhanced beef. *J. Agric. Food Chem.* **2006**, *54*, 7856−7862.

(15) Ramanathan, R.; Mancini, R. A.; Naveena, B. M. Effects of lactate on bovine heart mitochondria-mediated metmyoglobin reduction. *J. Agric. Food Chem.* **2010**, *58*, 5724−5729.

(16) Ramanathan, R.; Mancini, R. A.; Suman, S. P.; Cantino, M. E. Effects of 4-hydroxy-2-nonenal on beef heart mitochondrial ultrastructure, oxygen consumption, and metmyoglobin reduction. *Meat Sci.* **2012**, *90*, 564−571.
(17) Faustman, C.; Phillips, A. L. Measurement of discoloration in fresh meat. *Current Protocols in Food Analytical Chemistry*; Wiley: New York, 2001; Chapter F3, p F3.3.
(18) Tang, J.; Faustman, C.; Hoagland, T. A. Krzywicki revisited: equations for spectrophotometric determination of myoglobin redox forms in aqueous meat extracts. *J. Food Sci.* **2004**, *69*, C717−C720.
(19) Hagler, L.; Coppes, R. I., Jr.; Herman, R. H. Metmyoglobin reductase. Identification and purification of a reduced NADH dependent enzyme from bovine heart which reduces metmyoglobin. *J. Biol. Chem.* **1979**, *254*, 6505−6514.
(20) Faustman, C.; Cassens, R. G.; Greaser, M. L. Reduction of metmyoglobinby extracts of bovine liver and cardiac muscle. *J. Food Sci.* **1988**, *53*, 1065−1067.
(21) Bergmeyer, H. U. *Methods of Enzymatic Analysis*; Academic Press: New York, 1974; pp 545−546.
(22) Ramanathan, R.; Mancini, R. A; Joseph, P.; Suman, S. P. Bovine mitochondrial oxygen consumption effects on oxymyoglobin in the presence of lactate as a substrate for respiration. *Meat Sci.* **2013**, *93*, 893−897.
(23) Nair, M. N.; Suman, S. P.; Li, S.; Joseph, P.; Beach, C. M. Lipid oxidation-induced oxidation in emu and ostrich myoglobins. *Meat Sci* **2014**, *96*, 984−993.
(24) Alderton, A. L.; Faustman, C.; Liebler, D. C.; Hill, D. W. Induction of redox instability of bovine myoglobin by adduction with 4-hydroxy-2-nonenal. *Biochemistry* **2003**, *42*, 4398−4405.
(25) Suman, S. P.; Faustman, C.; Stamer, S. L.; Liebler, D. C. Proteomics of lipid oxidation-induced oxidation of porcine and bovine oxymyoglobins. *Proteomics* **2007**, *7*, 628−640.
(26) Naveena, B. M.; Faustman, C.; Tatiyaborworntham, N.; Yin, S.; Ramanathan, R.; Mancini, R. A. Mass spectrometric characterization and redox instability of turkey and chicken myoglobins as induced by unsaturated aldehydes. *J. Agric. Food Chem.* **2010**, *57*, 8668−8676.
(27) Yin, S.; Faustman, C.; Tatiyaborworntham, N.; Ramanathan, R.; Maheswarappa, N. B.; Mancini, R. A.; Joseph, P.; Suman, S. P.; Sun, Q. Species-specific myoglobin oxidation. *J. Agric. Food Chem.* **2011**, *59*, 12198−12203.
(28) Lynch, M. P.; Faustman, C. Effect of aldehyde lipid oxidation products on myoglobin. *J. Agric. Food Chem.* **2000**, *48*, 600−604.
(29) Faustman, C.; Richards, M. P.; Naveena, B. M.; Grunwald, E. M. Effect of HNE on bovine and porcine myoglobin redox stability and heme release. Institute of Food Technologists Annual Meeting, Anaheim, CA, June 6−9, 2009, .
(30) Barrick, D.; Hughson, F. M.; Baldwin, R. L. Molecular mechanisms of acid denaturation. The role of histidine residues in the partial unfolding of apomyoglobin. *J. Mol. Biol.* **1994**, *237*, 588−601.
(31) Hussain, S. N. A.; Ghassan Matar, G.; Barreiro, E.; Florian, M.; Divangahi, M.; Theodoros Vassilakopoulos, T. Modifications of proteins by 4-hydroxy-2-nonenal in the ventilator muscles of rats. *Am. J. Physiol.: Lung Cell Mol. Phys.* **2006**, *290*, L996−L1003.
(32) Uchida, K.; Stadtman, E. R. Covalent attachment of 4-hydroxynonenal to glyceraldehyde-3-phosphate dehydrogenase. A possible involvement of intra- and intermolecular cross-linking reaction. *J. Biol. Chem.* **1993**, *268*, 6388−6393.

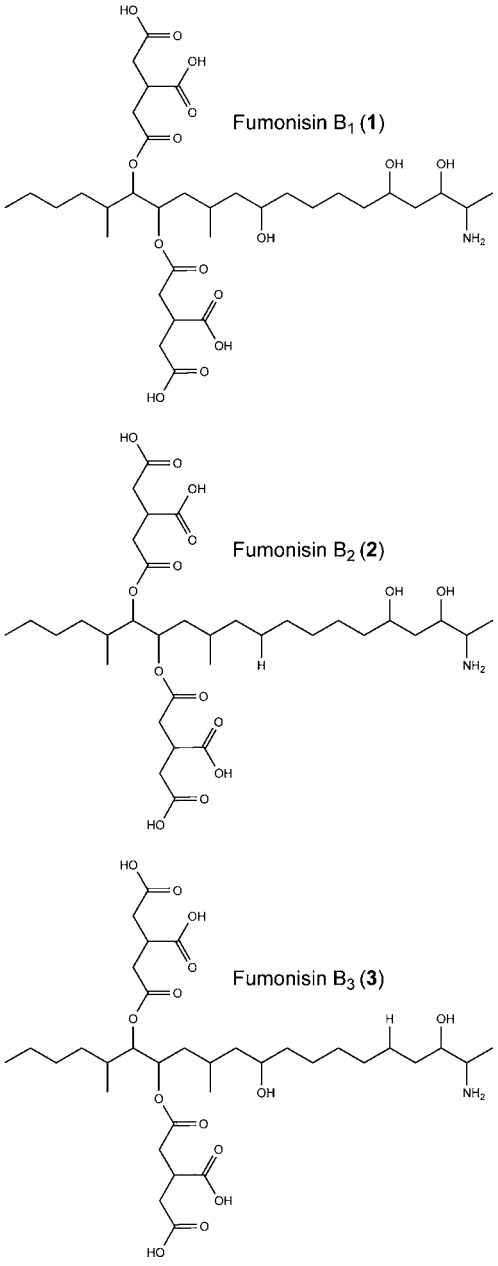

Figure 1. Chemical structures of the B-series fumonisins, FB_1 (**1**), FB_2 (**2**), and FB_3 (**3**).

aerial tissues did analyze the first, second, and third leaves and determined the highest fumonisin accumulation occurred in the first leaf of maize seedlings grown from seed inoculated with *F. verticillioides*.[24] Accumulation of fumonisins in these tissues was noted as containing a significantly higher ratio of FB_1 to FB_2 and FB_3 compared to the observed accumulations in the roots,[24] suggesting a mechanism of greater accumulation of FB_1 over the other analogues by either selective transport or selective production of FB_1 by the fungus colonizing the leaf. Further questions arose about the mechanism of fumonisin accumulation when uninoculated seedlings were watered with FB_1 and FB_2 without detectable accumulation in the leaf tissues,[25] thus suggesting the fungus is essential for accumulation of FB_1 in the leaves. In the current study we address the colonization and fumonisin accumulation discrepancies of why FB_1 does accumulate in leaves infected with *F. verticillioides*, yet does not accumulate in leaves when uninfected seedlings are watered with an aqueous FB_1 solution. Additionally, we also address the potential necessity of conidia for colonization of the seedlings. A holistic sampling strategy was utilized to address the following questions: (i) What is the extent of colonization in maize seedlings when seeds are inoculated with fumonisin-producing and nonproducing strains in combination with wild-type conidiation versus aconidial phenotypes? (ii) What is the resulting fumonisin accumulation in those seedlings? (iii) Are the patterns of fumonisin accumulation and *F. verticillioides* colonization different in fumonisin-insensitive compared to fumonisin-sensitive maize lines? (iv) Does transpiration have a possible role in the movement and accumulation of FB_1?

MATERIALS AND METHODS

Chemicals. Acetonitrile (MeCN) (Burdick & Jackson, Muskegon, MI, USA) and water (J. T. Baker, Phillipsburg, NJ, USA) were of HPLC grade, and formic acid (>95%) (Sigma-Aldrich, St. Louis, MO, USA) was of reagent grade. Fumonisin B_1 (FB_1), fumonisin B_2 (FB_2), and fumonisin B_3 (FB_3) for standard preparation were provided as a gift from Ronald Plattner, National Center for Agricultural Utilization Research, USDA-ARS, Peoria, IL, USA. D-*erythro*-C_{17}-Sphingosine-1-phosphate, D-*ribo*-phytosphingosine-1-phosphate, D-*erythro*-sphingosine 1-phosphate, and D-*erythro*-dihydrosphingosine-1-phosphate were purchased from Avanti Polar Lipids (Alabaster, AL, USA). Phytosphingosine, DL-*erythro*-dihydrosphingosine, and D-*erythro*-sphingosine were purchased from Sigma-Aldrich. D-*erythro*-C_{16}-Sphingosine was from Matreya (Pleasant Gap, PA, USA). Stock solutions, working standards, and internal standards were prepared as previously described.[22] Sucrose (Sigma-Aldrich), Murashige and Skoog basal medium macrosalts and microsalts (Sigma-Aldrich) and Bacto Agar (Difco Laboratories, Inc., Sparks, MD, USA) were utilized for the plant nutrient agar.[26]

Extraction and Analysis of Fumonisins. The procedures for extraction of fumonisins from soil and plant tissues have been reported previously.[24,27] Briefly, lyophilized maize leaf tissues were ground to a powder, spiked with D-*erythro*-C_{16}-sphingosine and D-*erythro*-C_{17}-sphingosine-1-phosphate internal standards (10 μL each at 100 ng/μL) and then extracted with an aliquot of 1:1 MeCN/water + 5% formic acid (1 mL per 10 mg tissue). The filtered extracts (100 μL aliquots) were diluted into the initial mobile phase (900 μL) used for reverse phase high-performance liquid chromatography (RP-HPLC). Air-dried soils were extracted in a similar manner in 1:1 MeCN/water + 5% formic acid (25 mL per 2 g).

All analyses were performed as described previously.[24] Analyses were conducted using a Finnigan Micro AS autosampler coupled to a Surveyor MS pump (Thermo-Fisher, Woodstock, GA, USA). Separation was accomplished using a Cadenza 150 × 2 mm i.d., 3 μm, CW-C18 column (Imtakt, Philadelphia, PA, USA). Column effluent was coupled to a Finnigan LTQ linear ion trap mass spectrometer (MS). The fumonisins, sphingoid bases, and sphingoid base 1-phosphates were analyzed, but only the fumonisin data are reported.

Fungal Strains. The four strains of *F. verticillioides* used in this study were JFL-A04516 (JFL = John F. Leslie, Department of Plant Pathology, Kansas State University, Manhattan, KS, USA), AEG 3-A3-2 (AEG = Anthony E. Glenn, Russell Research Center, USDA-ARS, Athens, GA, USA), AEG 3-A3-5, and MRC826 (Medical Research Council, Tygerberg, South Africa). Both AEG strains are unable to produce conidia.[28] AEG 3-A3-5 produces fumonisins, whereas AEG 3-A3-2 lacks the FUM gene cluster and does not produce fumonisins. Strain JFL-A04516 also does not produce fumonisins due to a point mutation in *FUM1*, a polyketide synthase necessary for fumonisin production.[20] MRC826, as our positive control, is wild type for fumonisin production and conidiation.

Maize Seedling Assay. The maize lines used were Silver Queen (SQ) (Gurney's Seed & Nursery Co., Yankton, SD, USA), a sweet

corn line that is susceptible to *F. verticillioides*-induced maize seedling disease;[23] W23 (The Germplasm Resources Information Network (GRIN), accession no. NSL 30060), a resistant field corn inbred; and B73 (GRIN, accession no. Bc5S4), a moderately resistant field corn inbred. Maize kernels were treated as described previously.[23] Briefly, kernels were surface-disinfected for 10 min in 100% commercial bleach (5.25% hypochlorite), rinsed with sterile water, and allowed to imbibe for 4 h in sterile water. The seeds were then heat shocked by placing them in a 60 °C water bath for 5 min for internal sterilization.[29] Seeds were inoculated with a 10^4 spores/mL suspension and incubated overnight at 27 °C. Three replicates of 10 seeds each were planted in sterile 10 cm plastic azalea pots (Hummert International, Earth City, MO, USA) containing twice-autoclaved commercial potting soil mix (Conrad Faford Inc., Agawam, MA, USA).

The treatments were as follows: SQ/control, SQ/MRC 826, SQ/AEG 3-A3-2, SQ/AEG 3-A3-5, SQ/JFL-A04516, W23/control, W23/MRC826, B73/control, and B73/MRC826. Pots were watered as needed throughout the duration of the assay. Assays were performed under aseptic conditions in a plant growth chamber at 30 °C under a 14 h light (cool-white, high-output fluorescent tubes at an average of 254 μmol/m^2/s) and 10 h dark regimen at 20 °C. Plant tissues were collected for analysis 14 days after planting. During harvest, the shoot portions of the seedlings were separated into first, second, and third leaves (numbered in order of their emergence and expansion) for each replicate pot. Leaves were excised approximately 5 mm from the ligule, such that all portions of the sheath were excluded from the analyses. After removal, a 2−3 cm section of the leaf was sampled and stored for culturing. An approximate 3−4 cm section of the stem between the soil surface and the first leaf was also excised and stored for culturing. Root tissues were also collected and processed as described previously.[23] During root harvest, a section of the mesocotyl (as large as possible) was also sampled and stored for culturing. All tissues removed for culturing were stored briefly at 4 °C. The root and leaf tissues to be analyzed for fumonisins, sphingoid bases, and sphingoid base 1-phosphates were immediately frozen at −20 °C.

In Planta Colonization. Plant tissues reserved for culturing were surface sterilized according to tissue type. Leaves were sterilized in s 10% bleach solution for 10 min followed by a 95% ethanol wash for 5 min. Stems and mesocotyls were sterilized in 20% bleach for 15 min followed by a 95% ethanol wash for 10 min. Tissues were rinsed five times with sterile distilled water (dH_2O) and then plated on potato dextrose agar (PDA) (Sigma, St. Louis, MO, USA) and incubated at 27 °C to assess internally colonizing fungal strains. Tissue infection was observed after 6 days and checked again after 10 days to allow for emergence of any slow-growing fungi. Fungal isolates were identified to genus on the basis of morphological features, including microscopic examination for production of conidia.

Soil Colonization. In the first trial, soil was collected from each individual pot and air-dried for 2 weeks in open plastic bags. After 2 weeks, 1 g of soil was added to 100 mL of autoclaved dH_2O and placed on a 250 rpm rotary shaker for 10 min. A 100,000-fold dilution was made of each soil sample, and 100 μL each of this dilution was plated in triplicate on PDA. Plates were incubated at 27 °C for 4 days. After 4 days, colony-forming units (CFU) were identified as *Fusarium* or other genera. The second trial was quantitated in the same manner, but was performed using wet soil and sampled immediately at the end of the trial to detect fungi that may have been sensitive to desiccation in the first trial. After sampling, the soils from the second trial was air-dried as before.

In Vitro Test Tube Exposure of FB_1. Maize kernels were sterilized and imbibed as described previously.[23] Lines utilized were Silver Queen, W23, and Tama Flint (GRIN, accession no. NSL 217411), a landrace previously noted to be highly insensitive to FB_1.[30] Individual kernels were placed in 25 × 150 mm culture test tubes (Kimble Chase LLC, Rockwood, TN, USA) with 4 mL of plant agar media.[26] Maize seedlings were grown for 7 days under the same growth chamber conditions noted above and culled for fungal contamination. Using a syringe, FB_1 (10 μM), abscisic acid (ABA) (200 μM), or FB_1 and ABA (10 and 200 μM) were injected into the media. Plants were harvested after 24 and 48 h by separating the leaves and stems from the roots. Care was taken not to allow the leaves or stems to have contact with the FB_1-containing agar media. Samples were lyophilized and extracted as mentioned above to assess FB_1 accumulation in the plant.

Statistical Analysis. Statistical analysis was performed using SigmaStat software (Jandel Scientific, San Rafael, CA, USA). For most data sets comparing many groups, one-way analysis of variance was used and ordered by Student−Newman−Keuls test. The maize seedling tissue colonization data were evaluated using the Kruskal−Wallis one-way analysis of variance to determine significant differences between treatments within each tissue type. Except where indicated otherwise, all data were expressed as the mean ± standard deviation, and differences among means were considered to be significant if the probability (P) was $\leq$0.05. All results for plant tissues are expressed as dry weight.

RESULTS AND DISCUSSION

On the basis of our previous work, we hypothesized fumonisin is mobile in planta, accumulates in the leaves, and requires the presence of the fungus in the roots but does not require direct fungal colonization of the leaves. Thus, it should follow that fumonisin accumulation in the leaves is likely via a plant-derived mechanism affected by the fungus in a manner other than direct colonization of the leaves. To assess colonization and colocalization of fumonisin accumulation during seedling infection, the sweet corn cultivar Silver Queen was inoculated with *F. verticillioides* strain MRC826, JFL-A04516, AEG 3-A3-2, or AEG 3-A3-5. Silver Queen is highly susceptible to fumonisin-related seedling blight.[17,23,27] Results are presented separately for the two biological replicates, noted as trial 1 and trial 2, because these data could not be grouped statistically because of significant differences in colonization rates and fumonisin accumulation. Both trials independently show patterns that support the same conclusions despite the significant biological variation. Silver Queen seedlings demonstrated a clear correlation between seed inoculation with fumonisin-producing strains and development of disease symptoms (Table 1). We also assessed the fumonisin-insensitive inbreds W23 and B73 in trial 1 only. These seeds were contaminated with several naturally occurring fungi, such as species of *Acremonium*, *Aspergillus*, *Penicillium*, and *Fusarium*, despite our attempts to sterilize the seed. When inoculated with

Table 1. Characteristics of *Fusarium verticillioides* Strains and Resulting Disease Incidence on Silver Queen (SQ), B73, and W23

			disease incidence[a] (%)		
			sensitive	insensitive	
strain	conidia production	fumonisin production	SQ[b]	B73[c]	W23[c]
water control			0/0	0	0
MRC826	yes	yes	59/92	0	4
JFL-AO4516	yes	no	0/0	ND	ND
AEG 3-A3-5	no	yes	76/87	ND	ND
AEG 3-A3-2	no	no	0/0	ND	ND

[a]Disease incidence is defined as the average percentage of seedlings that exhibit the symptoms associated with disease, such as stunting, leaf lesions, and leaf abnormalities. [b]Disease incidence for trials 1 and 2 of the experiment is reported separately for SQ (trial 1/trial2). [c]B73 and W23 were included only in trial 1 and were inoculated only with MRC826. Disease incidence was not determined (ND) for other strains on B73 and W23.

MRC826, B73 showed no symptoms of seedling blight. Similarly, W23 had very few seedlings with disease symptoms.

Soil analysis was performed to evaluate the ability of the *F. verticillioides* strains to colonize the soil during seedling assays. Colonization of the dried soil from trial 1 was significant for MRC826 and JFL-A04516. In contrast, no colonization was observed for AEG 3-A3-2 and AEG 3-A3-5 (Figure 2A) even at

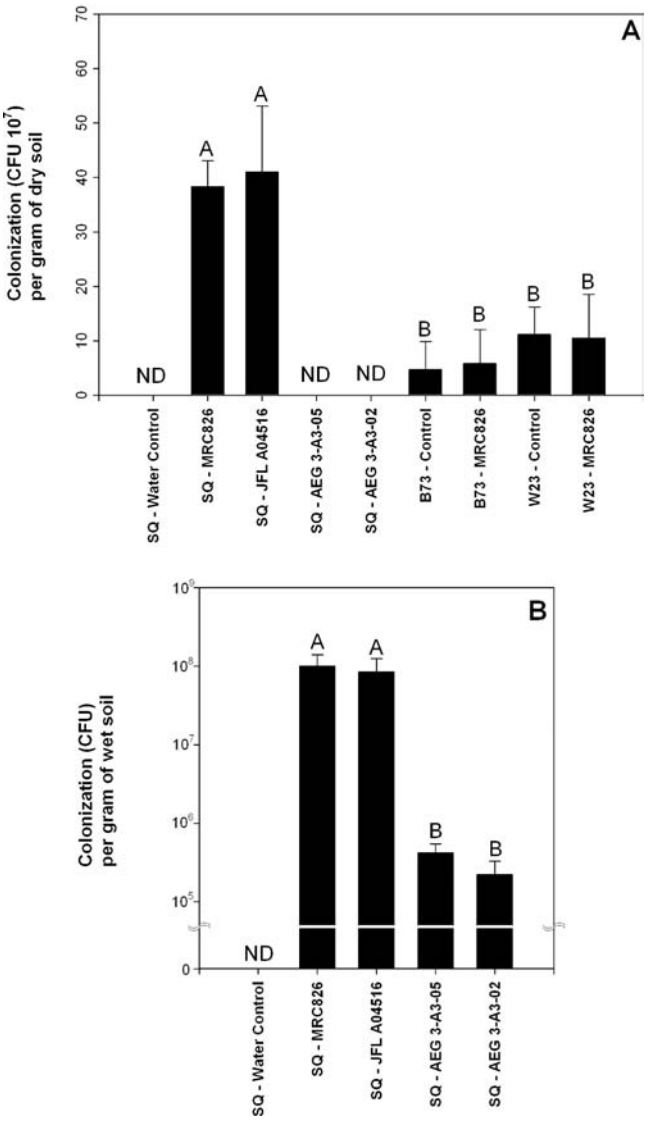

Figure 2. Soil colonization by strains of *Fusarium verticillioides*. Values are the mean ± standard deviation, and letters indicate a statistically significant difference ($P \leq 0.05$, $n = 3$ pots per trial). Trial 1 (A) shows quantification of *F. verticillioides* strains in dried soil at the end of the 14 day experiment involving Silver Queen (SQ) grown from seed inoculated with the strains. Also shown are B73 and W23 water controls and MRC826 inoculations. Trial 2 (B) was similar but based on wet weight of soil. Trial 2 did not include B73 and W23 treatments. ND indicates no *Fusarium* colonies detected.

low serial dilutions. For B73 and W23, soil colonization was observed in both control and MRC826 treatments, which was not surprising given the seed contamination noted above. When performing the second trial, wet soil was sampled to determine if the viability of aconidial strains AEG 3-A3-2 and AEG 3-A3-5 was more susceptible to desiccation effects (Figure 2B). Soil colonization was noted for AEG 3-A3-2 and AEG 3-A3-5, even though the CFU calculations were 250−500-fold less compared to the conidia-producing wild-type MRC826 (Figure 2B). The drying procedure in the first trial apparently did affect the viability of these aconidial strains, likely due to the lack of drought-resistant structures (i.e., spores). Other than this difference in how the soils were sampled for colonization (dry versus wet), all other experimental protocols were identical between trials 1 and 2.

Figure 3 shows fumonisin accumulation in the soil and Figure 4, in the roots. Trials 1 and 2 provided similar results,

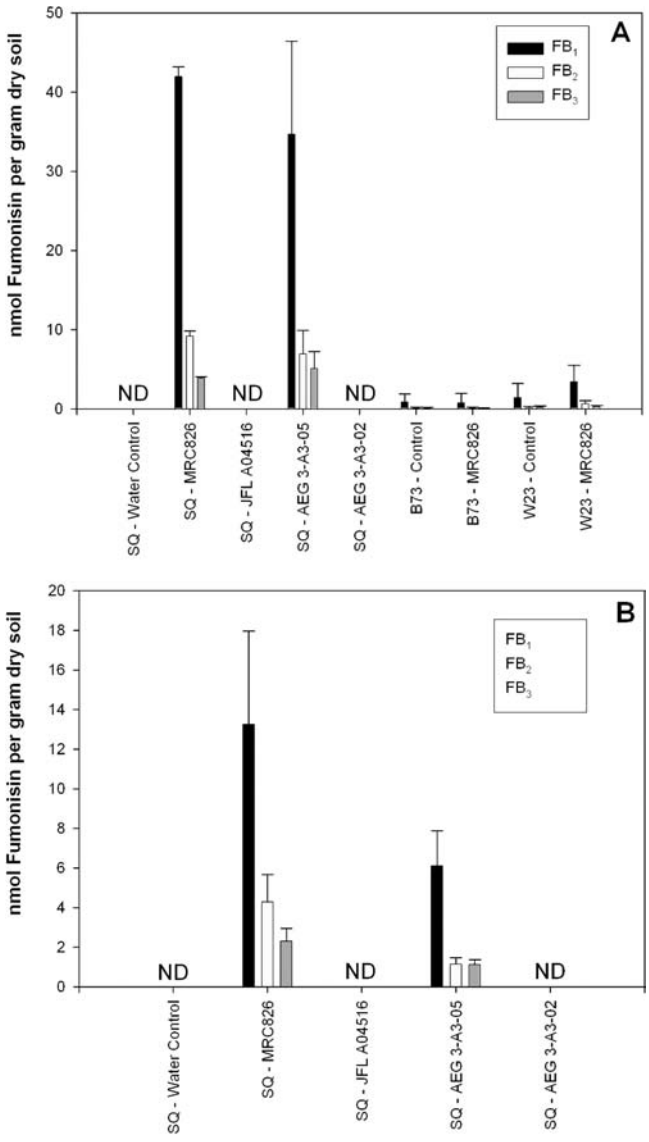

Figure 3. Fumonisin accumulation in soil. Values are the mean ± standard deviation of fumonisin B_1, B_2, and B_3 (respectively, FB_1, FB_2, and FB_3) accumulation in the soil for trial 1 (A) and trial 2 (B) ($n = 3$ pots per trial). ND indicates none detected.

where only fumonisin-producing strains resulted in fumonisin accumulation in the soil or the root tissues. Relatively small amounts of fumonisins were detected in soils from inbreds B73 and W23. Only a small amount of FB_1 (0.34 ± 0.2 nmol/g) was detected in the roots of W23 inoculated with MRC826. Despite the lower soil colonization detected for AEG 3-A3-5, the levels of fumonisin contamination in the soil were not statistically different from MRC826 (Figure 3). A similar trend was noted

dx.doi.org/10.1021/jf5001106 | J. Agric. Food Chem. 2014, 62, 2118−2125

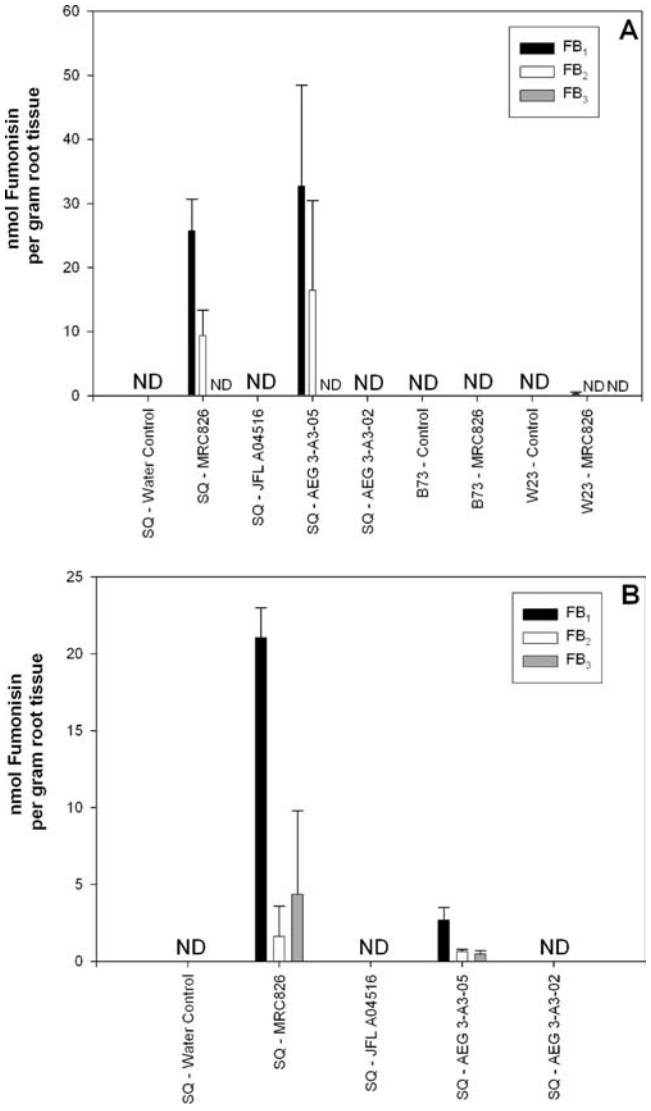

Figure 4. Fumonisin accumulation in root tissue. Values are the mean ± standard deviation of fumonisin B_1, B_2, and B_3 (respectively, FB_1, FB_2, and FB_3) accumulation in the root tissue for trial 1 (A) and trial 2 (B) (n = 3 pots per trial). ND indicates none detected.

for fumonisin in roots (Figure 4). Statistical differences were noted for fumonisin accumulation in roots of MRC826 and AEG 3-A3-5 in trial 2 (Figure 4B).

Tissue colonization by the different strains of *F. verticillioides* is summarized in Table 2. Differences were noted between trials 1 and 2 for frequency of colonization, which suggested that colonization of the plant tissue can be highly variable. Such variability also may explain the differences in fumonisin accumulation in roots noted above. Despite the variability, the Kruskal–Wallis one-way analysis of variance determined that significant differences (P = 0.004) existed between treatments within each tissue type for each trail. Minor colonization of the mesocotyl and stem was observed in Silver Queen uninoculated controls in both trials and may reflect the sensitivity of the test and the difficulties of preventing cross-contamination despite precautionary efforts. It should be noted that despite colonization of the Silver Queen control roots, fumonisins were not detected in the soil or roots, suggesting the background colonization had minimal effects on the parameters we assessed during the course of this study. The AEG 3-A3-2 and AEG 3-A3-5 strains had minimal colonization of the mesocotyl and no colonization of the stem in trial 1, but showed higher colonization rates in trial 2 (Table 2). Neither AEG 3-A3-2 nor AEG 3-A3-5 colonized the leaf tissues in trials 1 and 2. Interestingly, fumonisin accumulation in the leaves (Figure 5) was clearly evident for AEG 3-A3-5 despite the inability to colonize the leaves. In trial 1, only MRC826 colonized the first leaf. In trial 2, colonization was noted for MRC826 and JFL-A04516 in all three leaves at varying rates. Although the trials indicate that leaf colonization is variable, it is clear that the aconidial strains AEG 3-A3-2 and AEG 3-A3-5 are greatly attenuated in their ability to infect the leaves of seedlings.

Only FB_1 was detected in the leaves, FB_2 and FB_3 were not, which supports the observations of Williams et al.[23] and Zitomer et al.[24] Trial 1 (Figure 5A) and trial 2 (Figure 5B) had similar accumulations of FB_1 in the first and second leaves for MRC826 and AEG 3-A3-5 inoculated Silver Queen despite the fact that AEG 3-A3-5 did not colonize leaf tissue (Table 2). B73 and W23 had no detectable FB_1 in the leaves despite higher rates of colonization than in Silver Queen (Table 2). Colonization was counterintuitively higher in the uninoculated control leaf tissues for B73 and W23 compared to the MRC826 inoculated plants. Perhaps inoculation triggered plant defenses, thus lowering colonization frequency. This observation requires further experimentation.

Our data suggest *F. verticillioides* is necessary for accumulation of FB_1 in leaves but that leaf colonization is not required for FB_1 accumulation in these tissues. Further investigations are necessary to understand what mechanism may be responsible for such distal accumulation and how it preferentially targets FB_1. Furthermore, is this mechanism an important component of colonization of the leaves and progression of seedling blight symptom development? Perhaps of most interest is how the resistant inbreds seem to suppress growth of *F. verticillioides* and its capacity for fumonisin production and tissue colonization.

To refine our observations with W23 and eliminate any influence of the fungi contaminating the seed, an experiment was performed on plant nutrient agar in test tubes to quantitate the uptake of FB_1 (10 μM) into the roots and aerial tissues when the FB_1 is added to the agar (Figure 6). Silver Queen and Tama Flint were included as well. The high insensitivity of Tama Flint to FB_1 was noted previously.[30] Germinated seeds were screened to eliminate any samples having fungal contamination.

Analysis of the FB_1 accumulation in the roots revealed a significant difference in root uptake of FB_1 for W23 and Tama Flint compared to Silver Queen. No FB_1 was noted in the aerial tissues in all three maize lines (data not shown). As suggested by the seedling blight assays, the test tube assay indicated the FB_1-insensitive maize lines W23 and Tama Flint absorb less bioavailable fumonisin than does Silver Queen. The mechanism for absorption of fumonisin into the roots may explain differences in the FB_1-sensitive and -insensitive phenotypes. One possibility is that uptake of FB_1 may be driven by transpiration and bulk flow. The hormone abscisic acid (ABA) is known for triggering stomatal closure, thus limiting transpiration.[31] We hypothesized that if FB_1 uptake is dependent on transpiration and bulk flow, then the addition of ABA should limit uptake by closing stomata. To investigate this possibility, Silver Queen was coexposed to ABA and FB_1 in test tube assays. FB_1 absorption was significantly less in ABA coexposed roots after 48 h, suggesting transpiration may have a

Table 2. Percent Tissue Colonization by *Fusarium verticillioides* in Trials 1 and 2[a]

	mesocotyl	stem	leaf 1	leaf 2	leaf 3
			Trial 1		
SQ, water control	38 ± 2	30 ± 44	0	0	0
SQ, MRC826	100	100	26 ± 25	0	0
SQ, JFL-A04516	100	100	0	0	0
SQ, AEG 3-A3-5	49 ± 29	0	0	0	0
SQ, AEG 3-A3-2	47 ± 45	0	0	0	0
B73, water control	95 ± 8	86 ± 15	33 ± 58	26 ± 45	15 ± 26
B73, MRC826	51 ± 17	75 ± 7	0	0	0
W23, water control	59 ± 18	41 ± 37	31 ± 34	17 ± 29	19 ± 33
W23, MRC826	100	95 ± 8	6 ± 11	0	0
			Trial 2		
SQ, water control	51 ± 38	43 ± 32	0	0	0
SQ, MRC826	100	100	17 ± 41	15 ± 24	36 ± 44
SQ, JFL-A04516	100	100	8 ± 20	11 ± 20	33 ± 52
SQ, AEG 3-A3-5	100	20 ± 18	0	0	0
SQ, AEG 3-A3-2	100	20 ± 13	0	0	0

[a]Values are presented as the mean ± standard deviation of percent tissue from each treatment per pot (n = 3 pots per trial).

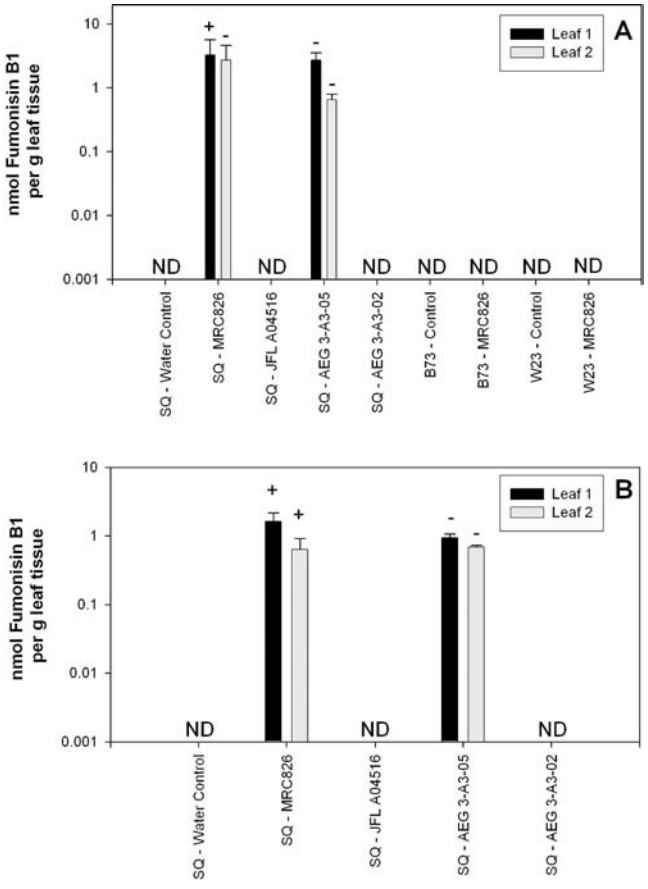

Figure 5. Fumonisin B_1 accumulation in leaves. Values are the mean ± standard deviation of fumonisin B_1 detected in leaves 1 and 2 in trials 1 (A) and 2 (B) (n = 3 pots per trial). Fumonisin B_2 and B_3 were not detected in the leaves. ND indicates not detected, and ± indicates colonization status of the leaf.

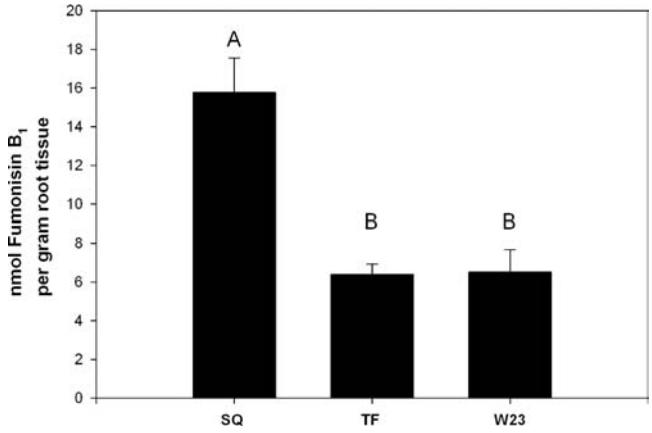

Figure 6. Fumonisin B_1 (FB_1) root accumulation in Silver Queen (SQ), Tama Flint (TF), and W23. FB_1 was spiked into the agar of the test tubes containing the seedling for a final concentration of 10 μM and harvested 48 h after exposure. Accumulation of FB_1 is reported as the mean ± standard deviation from two biological replicates (n = 3 per replicate), and letters indicate a statistically significant difference ($P \leq 0.05$).

role in FB_1 absorption into the roots (Figure 7). Future experiments will evaluate transpiration differences between Silver Queen, W23, and Tama Flint.

In summary, on the basis of our Silver Queen model, local colonization of maize seedling leaf tissue is not necessary for accumulation of FB_1 in those leaves. However, the mechanism for shootward movement of FB_1 into the leaf tissues does require the presence of the fungus in the roots. Such distal movement has been elucidated for other mycotoxins. For example, wheat spikes infected with *Fusarium culmorum* were shown to have trichothecenes migrating beyond the infection hyphae into the xylem and phloem sieve tubes where no fungal colonization was apparent.[32] Our experiments would suggest a similar fate of FB_1 moving ahead of colonization, at least in Silver Queen. Absorption of FB_1 was markedly decreased in the insensitive maize genotypes. The mechanism of FB_1 uptake into the roots is unknown; however, our study suggests ABA might modulate FB_1 uptake and alludes to a possible connection to bulk flow and transpiration. More research on the mechanism for FB_1 accumulation in the roots and how the fungus facilitates movement of FB_1 into the leaves will give us a better understanding of seedling blight disease progression and associated virulence of *F. verticillioides* and perhaps whether such movement contributes to any food safety or exposure concerns. Also, B73 and W23 seem to have inhibitory

dx.doi.org/10.1021/jf5001106 | J. Agric. Food Chem. 2014, 62, 2118−2125

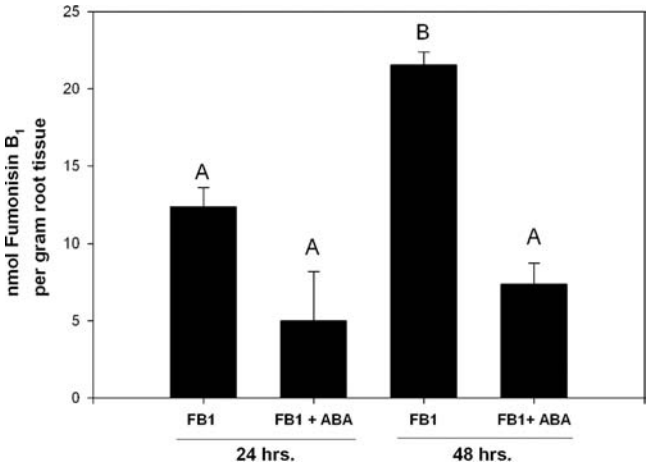

Figure 7. Fumonisin B_1 (FB_1) accumulation in seedlings coexposed with abscisic acid (ABA). Seedlings were assessed after 24 and 48 h of exposure to FB_1 (10 μM final concentration) or FB_1 plus ABA (200 μM). Accumulation of FB_1 is reported as the mean ± standard deviation from two biological replicates (n = 3 per replicate), and letters indicate a statistically significant difference ($P \leq 0.05$).

properties that decrease the growth and fumonisin production by *F. verticillioides* in the soil. This could be due to a range of defense mechanisms expressed by the plant, such as fortifying the cell wall with callose deposits, activation of a hypersensitive response, expression of chitinases and β-1,3-glucanases, and release of phytoprotective compounds such as the cyclic hydroxamic acids (DIMBOA and DIBOA).[33−37] Another possibility is that the fungi naturally inhabiting the seed of B73 and W23, such as *Acremonium zeae*, may be antagonists suppressing the growth of *F. verticillioides*.[38] Future research will investigate the role of plant defense mechanisms and competitive inhibition strategies for the control of *F. verticillioides*.

AUTHOR INFORMATION

Corresponding Author

*(A.E.G.) Phone: (706) 546-3119. Fax: (706) 546-3116. E-mail: anthony.glenn@ars.usda.gov.

Notes

The authors declare no competing financial interest.

ACKNOWLEDGMENTS

We thank Jency Showker and Britton Davis for their outstanding technical assistance. We give special thanks to John F. Leslie, Manhatten, KS, for his gift of the *F. verticillioides* strain.

REFERENCES

(1) Kommedahl, T.; Windels, C. E. Root-, stalk-, and ear infection *Fusarium* species on corn in the USA. *Fusarium: Diseases, Biology, and Taxonomy*; Pennsylvania State University: University Park, PA, USA, 1981; pp 94−103.

(2) Bacon, C. W.; Hinton, D. M. Symptomless endophytic colonization of maize by *Fusarium moniliforme*. *Can. J. Bot.* **1996**, *74*, 1195−1202.

(3) Fotso, J.; Leslie, J. F.; Smith, J. S. Production of beauvericin, moniliformin, fusaproliferin, and fumonisins B1, B2, and B3 by fifteen ex-type strains of *Fusarium* species. *Appl. Environ. Microbiol.* **2002**, *68*, 5195−5197.

(4) Giesbert, S.; Schuerg, T.; Scheele, S.; Tudzynski, P. The NADPH oxidase Cpnox1 is required for full pathogenicity of the ergot fungus *Claviceps purpurea*. *Mol. Plant Pathol.* **2008**, *9*, 317−327.

(5) Marasas, W. F. O.; Thiel, P. G.; Rabie, C. J.; Nelson, P. E.; Toussoun, T. A. Moniliformin production in *Fusarium* section *Liseola*. *Mycologia* **1986**, *78*, 242−247.

(6) Wiebe, L. A.; Bjeldanes, L. F.; Fusarin, C. A mutagen from *Fusarium moniliforme* grown on corn. *J. Food Sci.* **1981**, *46*, 1424−1426.

(7) Marasas, W. F. O. Fumonisins: their implications for human and animal health. *Nat. Toxins* **1995**, *3*, 193−198.

(8) Bartok, T.; Tolgyesi, L.; Szekeres, A.; Varga, M.; Bartha, R.; Szecsi, A.; Bartok, M.; Mesterhazy, A. Detection and characterization of twenty-eight isomers of fumonisin B1 (FB1) mycotoxin in a solid ice culture infected with *Fusarium verticillioides* by reversed-phase high-performance liquid chromatography/electrospray ionization time-of-flight and ion trap mass spectrometry. *Rapid Commun. Mass Spectrom.* **2010**, *24*, 35−42.

(9) Marasas, W. F.; Kellerman, T. S.; Gelderblom, W. C.; Coetzer, J. A.; Thiel, P. G.; Van der Lugt, J. J. Leukoencephalomalacia in a horse induced by fumonisin B1 isolated from *Fusarium moniliforme*. *Onderstepoort J. Vet. Res* **1988**, *55*, 197−203.

(10) Colvin, B. M.; Harrison, L. R. Fumonisin-induced pulmonary edema and hydrothorax in swine. *Mycopathologia* **1992**, *117*, 79−82.

(11) IARC. Fumonisin B1. In *IARC Monographs on the Evaluation of Carcinogenic Risks to Humans: Some Traditional Medicines, Some Mycotoxins, Napththalene and Styrene*: IARC Press: Lyon, France, 2002; Vol. 82, pp 301−366.

(12) Marasas, W. F. O.; Riley, R. T.; Hendricks, K. A.; Stevens, V. L.; Sadler, T. W.; Gelineau-van Waes, J.; Missmer, S. A.; Cabrera, J.; Torres, O.; Gelderblom, W. C. A.; Allegood, J.; Martinez, C.; Maddox, J.; Miller, J. D.; Starr, L.; Sullards, M. C.; Roman, A. V.; Voss, K. A.; Wang, E.; Merrill, A. H. Fumonisins disrupt sphingolipid metabolism, folate transport, and neural tube development in embryo Culture and *in vivo*: a potential risk factor for human neural tube defects among populations consuming fumonisin-contaminated maize. *J. Nutr.* **2004**, *134*, 711−716.

(13) Wang, E.; Norred, W. P.; Bacon, C. W.; Riley, R. T.; Merrill, A. H. Inhibition of sphingolipid biosynthesis by fumonisins. Implications for diseases associated with *Fusarium moniliforme*. *J. Biol. Chem.* **1991**, *266*, 14486−14490.

(14) Abbas, H. K.; Tanaka, T.; Duke, S. O.; Porter, J. K.; Wray, E. M.; Hodges, L.; Sessions, A. E.; Wang, E.; Merrill, A. H.; Riley, R. T. Fumonisin-and AAL-toxin-induced disruption of sphingolipid metabolism with accumulation of free sphingoid bases. *Plant Physiol.* **1994**, *106*, 1085−1093.

(15) Brandwagt, B. F.; Mesbah, L. A.; Takken, F. W.; Laurent, P. L.; Kneppers, T. J.; Hille, J.; Nijkamp, H. J. A longevity assurance gene homolog of tomato mediates resistance to *Alternaria alternata* f. sp *Lycopersici* toxins and fumonisin B1. *Proc. Natl. Acad. Sci. U.S.A.* **2000**, *97*, 4961−4966.

(16) Spassieva, S. D.; Markham, J. E.; Hille, J. The plant disease resistance gene Asc-1 prevents disruption of sphingolipid metabolism during AAL-toxin-induced programmed cell death. *Plant J.* **2002**, *32*, 561−572.

(17) Glenn, A. E.; Zitomer, N. C.; Zimeri, A. M.; Williams, L. D.; Riley, R. T.; Proctor, R. H. Transformation-mediated complementation of a fum gene cluster deletion in *Fusarium verticillioides* restores both fumonisin production and pathogenicity on maize seedlings. *Mol. Plant−Microbe Interact.* **2008**, *21*, 87−97.

(18) Sanchez-Rangel, D.; Sanchez-Nieto, S.; Plasencia, J. Fumonisin B1, a toxin produced by *Fusarium verticillioides*, modulates maize β-1,3-glucanase activities involved in defense response. *Planta* **2012**, *235*, 965−978.

(19) Vicente, M.; Larios-Zarate, G.; Plasencia, J. Disruption of sphingolipid biosynthesis in *Nicotiana benthamiana* activates salicylic acid-dependent responses and compromises resistance to *Alternaria alternata* f. sp. *lycopersici*. *Planta* **2013**, *237*, 121−136.

(20) Desjardins, A. E.; Munkvold, G. P.; Plattner, R. D.; Proctor, R. H. FUM1 − a gene required for fumonisin biosynthesis but not for maize ear rot and ear infection by *Gibberella moniliformis* in field tests. *Mol. Plant−Microbe Interact.* **2002**, *15*, 1157−1164.
(21) Desjardins, A. E.; Plattner, R. D.; Lu, M.; Claflin, L. E. Distribution of fumonisins in maize ears infected with strains of *Fusarium moniliforme* that differ in fumonisin production. *Plant Dis.* **1998**, *82*, 953−958.
(22) Desjardins, A. E.; Busman, M.; Muhitch, M.; Proctor, R. H. Complementary host−pathogen genetic analyses of the role of gumonisins in the *Zea mays−Gibberella moniliformis* interaction. *Physiol. Mol. Plant Pathol.* **2007**, *70*, 149−160.
(23) Williams, L. D.; Glenn, A. E.; Zimeri, A. M.; Bacon, C. W.; Smith, M. A.; Riley, R. T. Fumonisin disruption of ceramide biosynthesis in maize roots and the effects on plant development and *Fusarium verticillioides* induced seedling disease. *J. Agric. Food Chem.* **2007**, *55*, 2937−2946.
(24) Zitomer, N. C.; Glenn, A. E.; Bacon, C. W.; Riley, R. T. A single extraction method for the analysis by liquid chromatography/tandem mass spectrometry of fumonisins and biomarkers of disrupted sphingolipid metabolism in tissues of maize seedlings. *Anal. Bioanal. Chem.* **2008**, *391*, 2257−2263.
(25) Zitomer, N. C.; Jones, S.; Bacon, C. W.; Glenn, A. E.; Baldwin, T. T.; Riley, R. T. Translocation of sphingoid bases and their 1-phosphates, but not fumonisins, from roots to aerial tissues of maize seedlings watered with fumonisins. *J. Agric. Food Chem.* **2010**, *58*, 7476−7481.
(26) Bohorova, N.; Fenell, S.; McLean, S.; Pellegrineschi, A.; Hoisington, D. Laboratory protocols: CIMMYT applied genetic engineering lab. *Mexico D.F.: CIMMYT*; 1999, http://repository.cimmyt.org/xmlui/handle/10883/628.
(27) Williams, L. D.; Glenn, A. E.; Bacon, C. W.; Smith, M. A.; Riley, R. T. Fumonisin production and bioavailability to maize seedlings grown from seeds inoculated with *Fusarium verticillioides* and grown in natural soils. *J. Agric. Food Chem.* **2006**, *54*, 5694−5700.
(28) Glenn, A. E.; Richardson, E. A.; Bacon, C. W. Genetic and morphological characterization of a *Fusarium verticillioides* conidiation mutant. *Mycologia* **2004**, *96*, 968−980.
(29) Bacon, C. W.; Hinton, D. M.; Richardson, M. D. A corn seedling assay for resistance to *Fusarium moniliforme*. *Plant Dis.* **1994**, *78*, 302−305.
(30) Desjardins, A. E.; Plattner, R. D.; Stessman, R. J.; McCormick, S. P.; Millard, M. J. Identification and heritability of fumonisin insensitivity in *Zea mays*. *Phytochemistry* **2005**, *66*, 2474−2480.
(31) Schroeder, J. I.; Allen, G. J.; Hugouvieux, V.; Kwak, J. M.; Waner, D. Guard cell signal transduction. *Annu. Rev. Plant Physiol. Plant Mol. Biol.* **2001**, *52*, 627−658.
(32) Kang, Z.; Buchenauer, H. Studies on the infection process of *Fusarium culmorum* in wheat spikes: degradation of host cell wall components and localization of trichothecene toxins in infected tissue. *Eur. J. Plant Pathol.* **2002**, *108*, 653−660.
(33) Balasubramanian, V.; Vashisht, D.; Cletus, J.; Sakthivel, N. Plant β-1,3-glucanases: their biological functions and transgenic expression against phytopathogenic fungi. *Biotechnol. Lett.* **2012**, *34*, 1983−1990.
(34) Gupta, P.; Ravi, I.; Sharma, V. Induction of β-1,3-glucanase and chitinase activity in the defense response of *Eruca sativa* plants against the fungal pathogen *Alternaria brassicicola*. *J. Plant Interact.* **2013**, *8*, 155−161.
(35) Østergaard, L.; Petersen, M.; Mattsson, O.; Mundy, J. An *Arabidopsis* callose synthase. *Plant Mol. Biol.* **2002**, *49*, 559−566.
(36) Greenberg, J. T.; Guo, A. L.; Klessig, D. F.; Ausubel, F. M. Programmed cell death in plants: a pathogen-triggered response activated coordinately with multiple defense functions. *Cell* **1994**, *77*, 551−563.
(37) Frey, M.; Chomet, P.; Glawischnig, E.; Stettner, C.; Grun, S.; Winklmair, A.; Eisenreich, W.; Bacher, A.; Meeley, R. B.; Briggs, S. P.; Simcox, K.; Gierl, A. Analysis of a chemical plant defense mechanism in grasses. *Science* **1997**, *277*, 696−699.
(38) Wicklow, D. T.; Roth, S.; Deyrup, S. T.; Gloer, J. B. A protective endophyte of maize: *Acremonium zeae* antibiotics inhibitory to *Aspergillus flavus* and *Fusarium verticillioides*. *Mycol. Res.* **2005**, *109*, 610−618.

Plant Materials. Three blueberry species, *V. bracteatum* Thunb. (VB), *V. oldhamii* Miquel. (VO), and *V. corymbosum* L. (VC), were investigated in this study. VB and VO samples were collected from Sanghyo-dong, Seogwipo-si, Jeju Island, South Korea; annual precipitation in this area is approximately 2000 mm, and they are approximately 300 and 500 m above sea level, respectively. VC, which is a common highbush blueberry, was harvested from Sagye-ri, Andeok-myeon, Seogwipo-si, Jeju Island, South Korea. This region is 100 m above sea level and receives 1400 mm of rainfall annually. The blueberry samples were freeze-dried for 5 days and stored at below −70 °C before extraction.

Sample Preparation. Dried samples were homogenized using a mortar and pestle. Each powdered sample (50 mg) was extracted with 1 mL of solvent mixture (methanol/water/chloroform = 2.5:1:1) by using a Retsch MM400 mixer mill (Retsch GmbH & Co, Haan, Germany) at 30 Hz/s for 10 min and centrifuged at 4 °C and 1200 rpm for 5 min. The supernatant (100 μL) was completely dried using a speed vacuum concentrator (Biotron, Seoul, Korea). For gas chromatography−time-of-flight-mass spectrometry (GC-TOF-MS) analysis, two derivatization steps were performed. First, oximation was conducted by dissolving the dried extracts in 50 μL of methoxyamine hydrochloride (20 mg/mL in pyridine) and reacting at 30 °C for 90 min. The samples were then silylated with 50 μL of MSTFA at 37 °C for 30 min. For ultraperformance liquid chromatography−quadrupole-time-of-flight-mass spectrometry (UPLC-Q-TOF-MS) analysis, dried extracts of supernatant (100 μL) were resolved with methanol and filtered through a 0.2 μm PTFE filter. Five biological and two analytical replications were performed using both GC-TOF-MS and UPLC-Q-TOF-MS analyses.

GC-TOF-MS Analysis. An Agilent 7890A GC system (Palo Alto, CA) equipped with an Agilent 7693 autosampler was attached to a TOF Pegasus III mass spectrometer (Leco, St. Joseph, MI, USA), operating in electron ionization (EI) mode (70 eV). A DB-5MS column (30 m length × 0.25 mm i.d. × 0.25 m film thickness, J & W Scientific, Folsom, CA, USA) was used with helium as a carrier gas at a constant flow of 1.5 mL/min. Then, 1 μL of the derivatized sample was injected in a splitless mode. The oven temperature was maintained at 75 °C for 2 min, increased to 300 °C at the rate of 15 °C/min, and then held at 300 °C for 3 min. The acquisition rate was set to 20 scans/s with a mass scan range of m/z 45−1000. The injector and ion source temperatures were 250 and 230 °C, respectively.

UPLC-Q-TOF-MS Analysis. A Waters ACQUITY UPLC system (Waters Corp., Milford, MA, USA) equipped with a binary solvent delivery system, an autosampler, and a UV detector was combined with a Waters Q-TOF Premier MS (Micromass MS Technologies, Manchester, UK) system. Aliquots (5 μL) of each sample were then injected into an ACQUITY BEH C_{18} column (100 mm × 2.1 mm i.d. × 1.7 μm particle size) at a flow rate of 0.3 mL/min. The elution was performed with an acetonitrile/water gradient containing 0.1% formic acid. The gradient was linearly increased from 5% to 100% acetonitrile over 10 min and then decreased to 5% over 2 min. The total run time, including re-equilibration of the column to the initial conditions, was 12 min. The mass spectrometer was operated in both negative and positive ion modes with an m/z range 100−1000. The desolvation gas (nitrogen) was set to 650 L/h at a temperature of 300 °C. The cone gas (nitrogen) was set to 50 L/h, and the source temperature was 80 °C. The capillary and cone voltages were set to 2.3 kV and 30 V, respectively. Data were collected in the centroid mode, with a scan accumulation time of 0.2 s. All analyses were performed using an independent reference spray via the LockSpray interference to ensure accuracy and reproducibility; leucine enkephalin ions were used as the lock mass (m/z 554.2615 [−] and 556.2771 [+]) at a flow rate of 10 μL/min. Accurate mass and elemental composition were calculated using the MassLynx software (Waters Corp.) incorporated in the instrument.

The LC-IT-MS/MS analysis was performed using a 212-LC binary solvent delivery system equipped with a Prostar 410 autosampler and a Prostar 335 photodiode array detector (PDA), which was coupled with a Varian 500-MS ion-trap mass spectrometer equipped with an electrospray interface (Varian Tech., Palo Alto, CA, USA). Aliquots (10 μL) of each sample were then injected into a PurSuit XRs C18 column (100 mm × 2.0 mm i.d., 3 μm; Varian, Lake Forest, CA, USA) with a MetaGuard 2.0 PurSuit XRs C18 guard column (Varian, Lake Forest, CA, USA). The column temperature was set at 40 °C, and the flow rate was 0.2 mL/min. The mobile phase consisted of 0.1% v/v formic acid in water (solvent A) and 0.1% v/v formic acid in acetonitrile (solvent B). The gradient applied was as follows: 10% B from 0 to 2 min, 40% B from 2 to 10 min, 70% B from 10 to 20 min, 90% B from 20 to 30 min, 10% B from 30 to 40 min, and held at 10% B before the next sample injection. Mass spectra were performed in both negative and positive modes through a range of m/z 100−1000. The parameters were as follows: drying temperature, 300 °C; capillary voltage, 70 V; needle voltage, 5 kV; drying gas pressure (nitrogen), 20 psi; and nebulizer gas pressure (air), 40 psi. MS^n analysis was performed using Turbo data-dependent scanning (DDS) under the same conditions used for full scanning. The PDA was set at an absorbance from 200 to 600 nm and managed by Polyview 2000 (version 6.9) (Varian, Walnut Creek, CA).

Data Processing and Statistical Analysis. GC-TOF-MS raw data were converted to netCDF format with ChromaTOF software (LECO). UPLC-Q-TOF-MS raw data were acquired with MassLynx software and converted into netCDF format with Waters DataBridge version 2.1 software. After conversion, the MS data were processed using the Metalign software package (http://www.metalign.nl). The resulting data were exported to Excel (Microsoft, Redmond, WA, USA), and a statistical analysis was performed using SIMCA-P+ 12.0 software (Umetrics, Umea, Sweden). Principal component analysis (PCA) and partial least-squares discriminant analysis (PLS-DA) were used to compare the three blueberry species and to identify the major metabolites in each. The data sets were unit variance scaled in a column-wise manner prior to PCA and PLS-DA modeling. Metabolites with a variable importance projection (VIP) value greater than 0.7 and a p value less than 0.05 were selected as potential metabolites related to different species. Differences in total phenolic content (TP), total flavonoid content (TF), total anthocyanin content (TA), DPPH, and ABTS radical scavenging activities were tested by analysis of variance and Duncan's multiple range test using SPSS version 12.0 software (SPSS Inc., Chicago, IL, USA). Relative contents of significantly different metabolites and antioxidant activities were represented by Pearson's correlation coefficient.

Metabolite Identification and Visualization. After the multivariate statistical analysis, major metabolites were positively identified using standard compounds by comparing both the mass spectra and retention times. When standard compounds were not available, a tentative identification was made based on databases from the NIST05 MS Library (NIST, 2005), published references, and an in-house library. In UPLC-Q-TOF-MS analysis, accurate masses and elemental compositions were calculated using MassLynx software (Waters Corp.). MS^n fragmentation patterns and UV spectra were also used to identify major metabolites with MS workstation software (version 6.9, Varian, USA) in LC-IT-MS/MS. Metabolites were quantified by their m/z peak areas calculated using the software provided with the instrument and by data processing. This quantification aided in making relative comparisons of the metabolites in the three blueberry species. To visualize metabolite profiles, heatmaps were generated using MultiExperiment Viewer software version 4.8 (http://www.tm4.org/), and correlation networks between metabolites and antioxidant activities were constructed with Cytoscape software (http://www.cytoscape.org/).

Determination of Antioxidant Activities by ABTS and DPPH Free Radical Scavenging Activity. For the ABTS assay, we followed the method of Re et al.[21] with some modifications. The stock solutions included 7 mM ABTS solution and 2.45 mM potassium persulfate solution. The working solution was prepared by mixing the two stock solutions in equal quantities and allowing them to react for 1 day at room temperature in the dark. The solution was then diluted until the absorbance reached 0.7 ± 0.02 at 734 nm by using a spectrophotometer (Spectronic Genesys 6, Thermo Electron, Madison, WI, USA). The dried extracts of supernatant were resolved in a solvent mixture and diluted in the ratio of 1:4. Each diluted sample

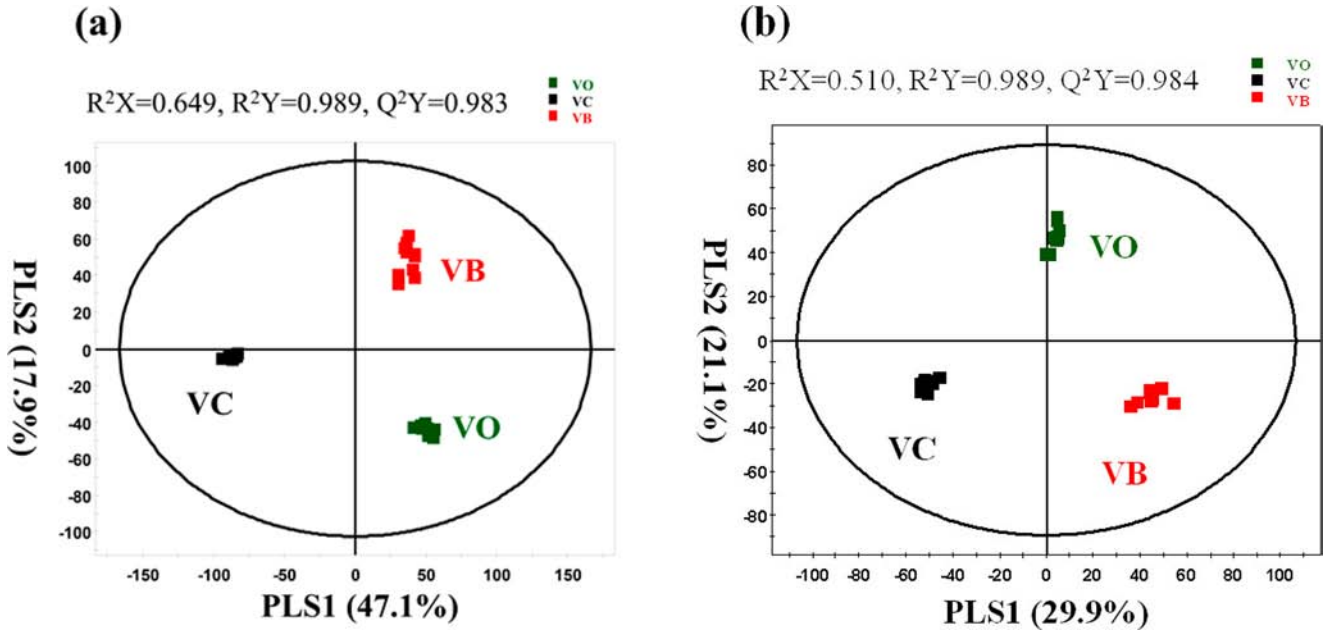

Figure 1. PLS-DA score plots of metabolite profiles in three blueberry species (*Vaccinium bracteatum* Thunb., VB; *V. oldhamii* Miquel., VO; and *V. corymbosum* L., VC). The data sets were obtained using (a) GC-TOF-MS and (b) UPLC-Q-TOF-MS.

of blueberry extract (10 μL) was reacted with 190 μL of the diluted ABTS solution for 7 min in the dark. Absorbance was then measured at 734 nm using a spectrophotometer. The standard curve was linear between 0.0625 and 1 mM Trolox equivalents (TE). Results are expressed in millimolar TE per milligram of dry weight of extract (ext). The DPPH assay was conducted according to the method described by Dietz et al.[22] with some modifications. Diluted samples of blueberry extracts (20 μL) were reacted with 180 μM DPPH solution for 20 min at room temperature. Absorbance was then measured at 515 nm. The standard curve was linear between 0.0625 and 1 mM TE. Experiments were conducted in triplicate.

Total Phenolic Content and Total Flavonoid Content. Total phenolic content (TP) in blueberry samples was determined according to the Folin−Ciocalteu colorimetric method, as modified by Yildirim et al.[23] Briefly, 100 μL of 0.2 N Folin−Ciocalteu's phenol reagent was added to 20 μL of each sample placed in 96-well plates, followed by incubation in the dark for 5 min. After that, 80 μL of 7.5% sodium carbonate solution was added to the mixture and measured at 750 nm using a microplate reader (Thermo Electron, Spectronic Genesys 6, Madison, WI, USA). TP was calculated on the basis of a standard curve with gallic acid (GA) equivalent concentration (ppm). The standard solution concentration curve ranged from 31.25 to 500 ppm. All experiments were conducted in triplicate.

Total flavonoid content (TF) was measured, and 180 μL of 90% diethylene glycol, 20 μL of 1 N NaOH, and 20 μL of each sample were then mixed and incubated for 60 min at room temperature in the dark. Absorbance was measured at 405 nm using a microplate reader (Thermo Electron, Spectronic Genesys 6, Madison, WI, USA). The results are presented as naringin (NG) equivalent concentration (ppm). The standard solution concentration curve ranged from 15.625 to 2000 ppm. All experiments were conducted in triplicate.

Total Anthocyanin Content. Total anthocyanin content (TA) of the blueberry samples was estimated using a microplate reader (Thermo Electron, Spectronic Genesys 6, Madison, WI, USA) by the pH-differential method using two buffer systems, potassium chloride buffer, pH 1.0, and sodium acetate buffer, pH 4.5, as modified by Khanal et al.[24] A diluted sample of 20 μL was mixed with 180 μL of corresponding buffer and read against a blank at 515 and 750 nm. Absorbance was calculated by the following formula: $A = (A_{515\ nm} - A_{750\ nm})_{pH1.0} - (A_{515\ nm} - A_{750\ nm})_{pH4.5}$. Monomeric anthocyanin pigment concentration was expressed as milligrams of cyanidin-3-glucoside: monomeric anthocyanin pigment (mg/L) = $A \times M_r \times DF \times 1000/(\varepsilon \times 1)$, where A is the absorbance, M_r is the molecular weight (449.2), DF is the dilution factor, and ε is the molar absorptivity (26 900). The final concentration of anthocyanins (mg/100 g) was calculated based on the total volume of extract and the weight of the sample.

RESULTS AND DISCUSSION

Multivariate Analysis of *Vaccinium* spp. Using GC-TOF-MS and UPLC-Q-TOF-MS Data. Species-specific metabolite profiling of blueberries (*Vaccinium* spp.) was performed using GC-TOF-MS and UPLC-Q-TOF-MS combined multivariate analysis. Multivariate analysis was used to separate species and to identify species-specific metabolites in three blueberry species. The analysis was performed by both unsupervised PCA and by supervised PLS-DA to identify differences among the three species. Species-specific separation can be observed in the PLS-DA score plots (Figure 1). Similar patterns were found in the PCA analysis (Supporting Information, Figure 1S). As shown in Figure 1a, metabolite profiles of the three species (VO, VB, and VC) were clearly separated by PLS1 and PLS2, and the score plot of GC-TOF-MS data explained 65.0% of the total variability (PLS1: 47.1%; PLS2: 17.9%). VC was separated from VB and VO along PLS1, whereas VB was separated from VO and VC along PLS2. The satisfaction values of X and Y variables were 0.649 (R^2X) and 0.989 (R^2Y), respectively, and prediction accuracy was 0.984 (Q^2Y). PCA and PLS-DA models of metabolites analyzed by UPLC-Q-TOF-MS showed similar patterns as those obtained by GC-TOF-MS analysis (Figure 1b, Supporting Information, Figure 1S). In the score plot of PLS-DA (using positive ion mode data), VC was clearly discriminated by PLS1 (29.9%), and VO was separated by PLS2 (21.1%), with quality parameters of 0.510 (R^2X), 0.989 (R^2Y), and 0.984 (Q^2Y). By using negative ion mode data, VB was separated from VC by PLS1 (27.7%), and VO was separated by PLS2 (15.5%) (Supporting Information, Figure 2S).

Species-Specific Metabolite Profiling of *Vaccinium* spp. Using GC-TOF-MS and UPLC-Q-TOF-MS Analyses.

dx.doi.org/10.1021/jf405272b | J. Agric. Food Chem. 2014, 62, 2126−2133

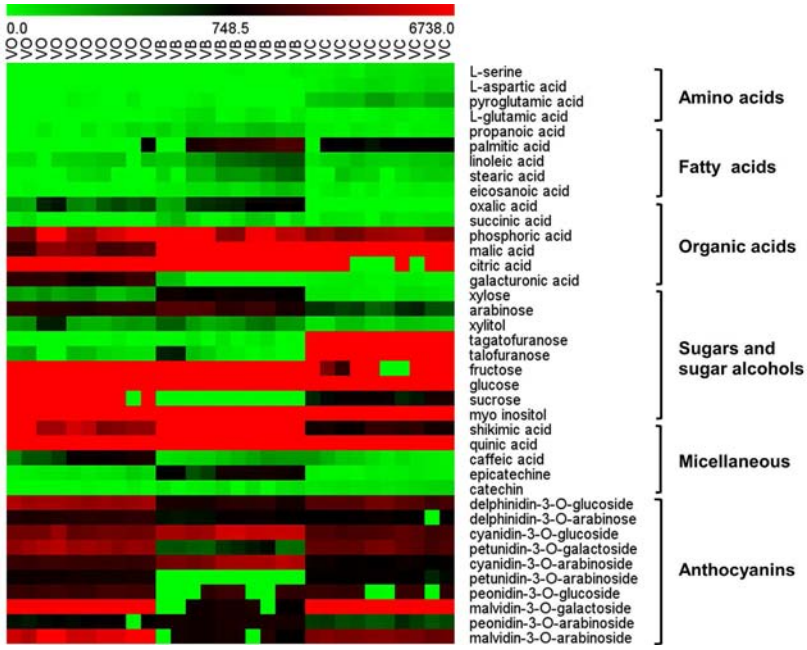

Figure 2. Key metabolites identified using PLS-DA showed a differential pattern in different blueberry species (*Vaccinium bracteatum* Thunb., VB; *V. oldhamii* Miquel., VO; and *V. corymbosum* L., VC). Metabolites (n = 39) that show statistically significant changes among samples (VIP > 0.7 and p < 0.05) are represented using a heatmap, with relative intensities indicated by the heat scale.

Table 1. Differential Metabolites Analyzed Using GC-TOF-MS in Three Species of Blueberry (*Vaccinium* spp.)

VarID	t_R (min)[a]	identified ion (m/z)[b]	VIP value	derivatized[c]	tentative metabolite[d]	ID[e]
4139	5.65	147	1.18	$(TMS)_2$	oxalic acid	MS/STD
7296	7.05	299	0.72	$(TMS)_3$	phosphoric acid	MS/STD
4142	7.39	147	0.92	$(TMS)_2$	succinic acid	MS/STD
5607	7.86	204	1.12	$(TMS)_2$	L-serine	MS/STD
4147	8.98	147	0.82	$(TMS)_3$	malic acid	MS/STD
6369	9.25	232	1.32	$(TMS)_3$	L-aspartic acid	MS/STD
4517	9.30	156	1.39	$(TMS)_2$	pyroglutamic acid	MS/STD
6609	10.03	246	1.01	$(TMS)_3$	L-glutamic acid	MS/STD
7406	10.39	307	0.75	$(TMS)_4$	xylose	MS/STD
7407	10.44	307	1.01	$(TMS)_4$	arabinose	MS/STD
4165	10.87	147	1.01	$(TMS)_5$	xylitol	MS/STD
5613	11.44	204	0.99	$(TMS)_4$	shikimic acid	MS/STD
5970	11.50	217	1.44	$(TMS)_4$	tagatofuranose	MS
6987	11.56	273	1.21	$(TMS)_4$	citric acid	MS/STD
5973	11.75	217	1.42	$(TMS)_4$	talofuranose	MS
7862	11.90	345	1.39	$(TMS)_5$	quinic acid	MS/STD
7414	11.99	307	1.36	MeOX $(TMS)_5$	fructose	MS/STD
7569	12.18	319	1.32	MeOX $(TMS)_5$	glucose	MS/STD
7759	12.48	333	0.81	$(TMS)_4$	galacturonic acid	MS/STD
3173	12.95	117	1.26	TMS	palmitic acid	MS/STD
7384	13.41	305	1.63	$(TMS)_6$	*myo*-inositol	MS/STD
6119	13.57	219	0.79	$(TMS)_4$	caffeic acid	MS/STD
3520	13.98	129	1.30	TMS	linoleic acid	MS/STD
3190	14.13	117	1.25	TMS	stearic acid	MS/STD
3196	15.22	117	1.34	TMS	eicosanoic acid	MS
8018	16.47	361	1.22	$(TMS)_8$	sucrose	MS/STD
8106	17.43	368	1.48	$(TMS)_5$	epicatechine	MS/STD
8107	17.54	368	0.96	$(TMS)_5$	catechin	MS/STD

[a] t_R is the retention time. [b] m/z are the selected ion(s) for identification and quantification of individual derivatized metabolites. [c] MEOX, methyloxime; TMS, trimethylsilyl. [d] Identified metabolites based on variable importance projection (VIP) analysis with a cutoff value of 0.7 and a p value < 0.05. [e] Identification: MS mass spectrum was consistent with those of NIST and in-house libraries; STD mass spectrum was consistent with those of standard compounds.

dx.doi.org/10.1021/jf405272b | J. Agric. Food Chem. 2014, 62, 2126−2133

Table 2. Differential Metabolites Identified Using UPLC-Q-TOF-MS in Three Species of Blueberry (*Vaccinium* spp.)

			UPLC-Q-TOF-MS				LC-IT-MS/MS				
no.	t_R[a]	VIP value	Experimental mass $[M + H]^+$	formula	Δppm	iFit[b]	$[M + H]^+$	MS^n fragment ions (m/z)	UV (nm)	tentative metabolite[c]	ID[d]
1	2.86	1.48	465.1031	$C_{21}H_{21}O_{12}$	−0.4	0.9	465	465 > 303 > 257	275, 524	delphinidin-3-*O*-glucoside	ref
2	3.00	1.39	435.0901	$C_{20}H_{19}O_{11}$	−0.6	0.3	435	435 > 303	300, 522	delphinidin-3-*O*-arabinose	ref
3	3.04	1.24	449.1088	$C_{21}H_{21}O_{11}$	0.9	0.0	449	449 > 287 > 213	297, 523	cyanidin-3-*O*-glucoside	std
4	3.11	1.45	479.1195	$C_{22}H_{23}O_{12}$	1.0	0.0	479	479 > 317 > 302	299, 521	petunidin-3-*O*-galactoside	ref
5	3.20	1.27	419.0982	$C_{20}H_{19}O_{10}$	1.0	0.0	419	419 > 287 > 213	299, 520	cyanidin-3-*O*-arabinoside	ref
6	3.23	1.44	449.1057	$C_{21}H_{21}O_{11}$	−6.0	0.0	449	449 > 317 > 302	302, 527	petunidin-3-*O*-arabinoside	ref
7	3.29	0.79	463.1132	$C_{22}H_{23}O_{11}$	−1.5	0.0	463	463 > 301	307, 522	peonidin-3-*O*-glucoside	std
8	3.31	1.36	493.1337	$C_{23}H_{25}O_{12}$	−1.8	0.0	493	493 > 331 > 299	313, 527	malvidin-3-*O*-galactoside	std
9	3.45	1.2	433.1105	$C_{21}H_{21}O_{10}$	−6.9	0.0	433	433 > 301	307, 522	peonidin-3-*O*-arabinoside	ref
10	3.47	1.46	463.1225	$C_{22}H_{23}O_{11}$	3.2	0.1	463	463 > 331 > 299	312, 534	malvidin-3-*O*-arabinoside	ref

[a] t_R is the retention time. [b] iFit is a measure of how well the observed isotope pattern matches the predicted isotope pattern for the formula on that line. A lower score indicates a better fit. [c] Identified metabolites based on variable importance projection (VIP) analysis with a cutoff value of 0.7 and a p value < 0.05. [d] Identification: std, standard compound; ref, references.

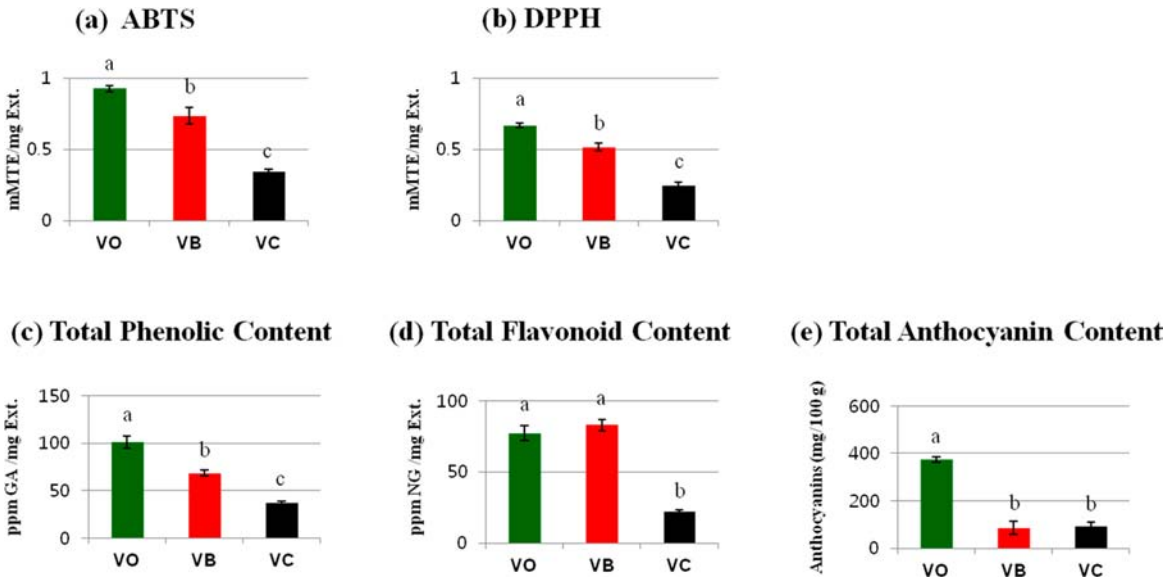

Figure 3. Antioxidant activity tests (a) ABTS and (b) DPPH and (c) total phenolic content, (d) total flavonoid content, and (e) total anthocyanin content of blueberries (*Vaccinium* spp.). Values are the averages of triplicates (n = 3). The same letters are not significantly different by Duncan's multiple range test at the 5% level.

Species-specific separation of *Vaccinium* spp. was observed in the PLS-DA score plots (Figure 1), and their related metabolites were selected based on VIP values (VIP > 0.7) and p values (p < 0.05). The relative differential distribution of selected metabolites is represented by a heatmap (Figure 2). In the GC-TOF-MS analysis, metabolite profiles of the three species were clearly separated by PLS1 and PLS2. In Table 1, 28 metabolites, including amino acids, organic acids, fatty acids, sugar and sugar alcohols, and phenolic acids, were selected as differential variables using VIP values and p values. On the basis of the separation of the three species according to PLS1, we identified oxalic acid, phosphoric acid, xylose, arabinose, xylitol, shikimic acid, citric acid, quinic acid, fructose, and glucose as major metabolites in both VO and VB, while serine, aspartic acid, tagatofuranose, talofuranose, and catechin were associated with VC. In particular, VB contained much higher levels of fatty acids, that is, palmitic acid, linoleic acid, stearic acid, and eicosanoic acid (Figure 2 and Supporting Information, Table 1S). In contrast, citric acid, quinic acid, fructose, glucose, galacturonic acid, caffeic acid, and sucrose were the main metabolites in VO. Organic acids such as oxalic acid, phosphoric acid, and citric acid were associated with both VO and VB, while succinic acid was associated with VB. Malic acid and citric acid are the predominant organic acids related to fruit ripening, and citric acid is the major compound that contributes to the acidity of fruits.[25] Citric acid was most abundant in VO (Figure 2 and Supporting Information, Table 1S). Levels of amino acids such as serine, aspartic acid, and

dx.doi.org/10.1021/jf405272b | J. Agric. Food Chem. 2014, 62, 2126−2133

pyroglutamic acid were higher in VC, while phenolic acids such as quinic acid and caffeic acid, which are related to antioxidant activity, were main components of VO.

In the UPLC-Q-TOF-MS positive ion mode analysis, the three species were separated by PLS-DA, and their related metabolites are listed in Table 2. In total, 10 metabolites were identified as highly differential metabolites contributing to species-specific separation based on VIP values (VIP > 0.7) and p values ($p < 0.05$). Anthocyanins were identified as major metabolites separating the three species. Anthocyanins and their derivatives were identified based on specific MS fragments and UV−vis absorbance (Table 2). Anthocyanins were represented by their specific aglycone cations and showed particular UV absorbance at 520−534 nm. The MS^n fragments of these compounds had characteristic ions at m/z 303, 287, 317, 301, and 331, corresponding to the $[M - \text{sugar}]^+$ product ions of delphinidin, cyanidin, petunidin, peonidin, and malvidin, respectively. The 3-glucoside(s) and 3-galactoside(s) of delphinidin, malvidin, petunidin, cyanidin, and peonidin are the primary anthocyanins that have been identified in blueberries,[1,26] and they were confirmed in this study. Glucoside and galactoside of delphinidin, petunidin, peonidin, and malvidin were mainly detected in VO and VC; in particular, the levels of delphinidin derivatives (delphinidin-3-*O*-glucoside and delphinidin-3-*O*-arabinoside) were high in VO (Figure 2 and Supporting Information, Table 2S). Cyanidin derivatives (cyanidin-3-*O*-glucoside and cyanidin-3-*O*-arabinoside) were mostly identified in VB, and their relative contents were high in this species. In the UPLC-Q-TOF-MS negative ion mode analysis, 11 metabolites, including chlorogenic acid, quercetin-3-*O*-glucoside, and quercetin-3-*O*-rutinoside, were identified as the major metabolites separating the three species (Supporting Information, Figure 2S and Table 3S). Chlorogenic acid is considered a prominent compound in highbush blueberry (*Vaccinium corymbosum* L.),[5] and levels of this compound were also high in VO as well as VC in our study (Supporting Information, Table 3S). Quercetin-3-*O*-glucoside and quercetin-3-*O*-rutinoside are also known compounds in berries.[27] These metabolites showed high levels in VO and VC, respectively.

Correlations between Metabolites and Antioxidant Activities in Different Blueberries. Antioxidant activities (ABTS and DPPH), TP, TF, and TA were measured in the three species. As shown in Figure 3, the wild species (VO and VB) demonstrated significantly higher scavenging activities than VC, which is a commonly cultivated species. TP and TF of VO and VB were also higher than those of VC. In particular, VO showed the highest TP (100.69 ppm GA/mg ext), TA (374.06 mg/100 g ext), and antioxidant activities (ABTS, 0.93 mM TE/mg ext; DPPH, 0.67 mM TE/mg ext) among the three species.

Correlation networks between metabolites and antioxidant activities are illustrated in Figure 4. Pearson's correlation coefficients among all metabolites identified in GC/LC-MS, TP, TF, TA, and antioxidant activity tests (ABTS and DPPH) were calculated (Supporting Information, Table 3S). Selected metabolites, TP, TF, and TA showed positive or negative correlations with antioxidant activities. Correlation coefficients of TP and TF with antioxidant activities were higher than that of TA. In particular, TP was much more strongly correlated with antioxidant activities (DPPH, 0.986; ABTS, 0.978) than was TA (DPPH, 0.766; ABTS, 0.737). Similar results were reported by Koca et al., who found a high correlation between

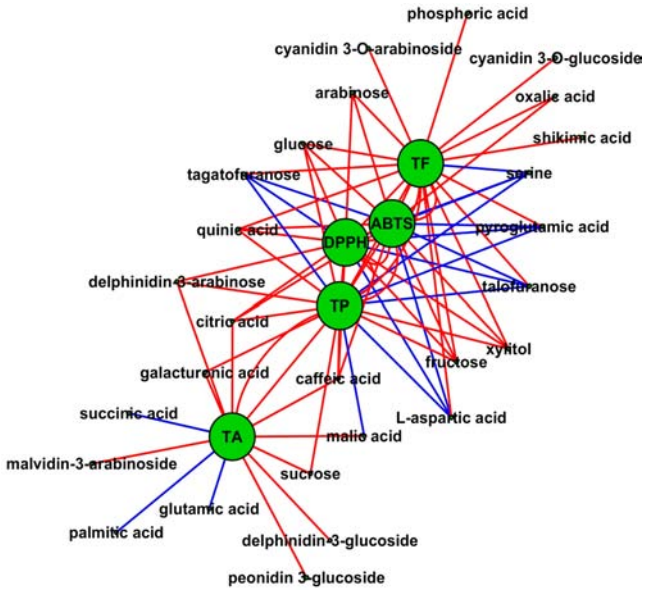

Figure 4. Visualization of the correlation network among metabolite total phenolic content (TP), total flavonoid content (TF), total anthocyanin content (TA), and antioxidant activities (ABTS, DPPH) of blueberries (*Vaccinium* spp.), according to Pearson's correlation coefficient (> ± 0.8). Positive or negative correlations are indicated by connecting red and blue lines, respectively.

total polyphenol content and antioxidant activity in *V. arctostaphylos* (a lowbush species) and *V. coymbosum*.[28]

To construct a correlation network, Pearson's correlation coefficients greater than ±0.8 were selected. TP, TF, and TA were significantly positively correlated with antioxidant activities (ABTS and DPPH). Previous research on antioxidant activity in blueberries has indicated that antioxidant activities are influenced by TP, TF, and TA.[7,29] In Figure 4, nine metabolites (oxalic acid, citric acid, arabinose, xylitol, fructose, glucose, quinic acid, caffeic acid, and delphinidin-3-*O*-arabinose) were highly positively correlated with antioxidant activities, whereas five metabolites (serine, aspartic acid, pyroglutamic acid, tagatofuranose, and talofuranose) showed a negative correlation with antioxidant activities. Some phenolic compounds may be associated with antioxidant activities, and their relative amounts in different blueberry species affect different antioxidant activities. In this study, VO and VB demonstrated significantly higher scavenging activities than VC and had higher levels of quinic acid, caffeic acid, delphinidin-3-*O*-arabinoside, cyanidin-3-*O*-glucoside, and cyanidin-3-*O*-arabinoside. In particular, VO, which showed the highest antioxidant activities, exhibited high contents of quinic acid, caffeic acid, delphinidin-3-*O*-glucoside, and delphinidin-3-*O*-arabinoside. Phenolic acids such as caffeic acid, quinic acid, gallic acid, hydroxybenzoic acid, and chlorogenic acid are the important antioxidants rich in blueberries.[9,30] The antioxidant activities of these phenolic acids are associated to some extent with the number of hydroxyl groups in their molecular structure.[31] In particular, caffeic acid, which exhibited high levels in VO in our study, is an antioxidant found in all plants as a key intermediate in the biosynthesis of lignin.[32] Anthocyanins are a major class of flavonoid phenolics that cause fruit pigmentation, and they are strong antioxidants that contribute to the health-beneficial properties of blueberries.[33] Monoglucosides of delphinidin, malvidin, petunidin, cyanidin, and peonidin are the primary

anthocyanins that have been identified in blueberries.[5−8] Among these, delphinidin and cyanidin, which have more hydroxyl groups, are more active as antioxidants than those with only one hydroxyl substitute, such as pelargonidin, malvidin, and peonidin.[34,35] In particular, VO contained high levels of delphinidin-3-*O*-arabinose, which had a high positive correlation coefficient in the antioxidant activity test results. Although they are not represented in our correlation network (Figure 4), chlorogenic acid and flavonol glycoside were also related to antioxidant activities. Chlorogenic acid, the major nonflavonoid phenolic acid in blueberry,[5] was abundant in both VO and VC. Quercetin derivatives are also well-known antioxidants in plants.[36] Quercetin-3-*O*-glucoside and quercetin-3-*O*-rutinoside levels were high in VO and VC, respectively.

Overall, our results suggest that antioxidant activities are correlated not only with various antioxidants such as phenolic compounds but also with the relative contents of these compounds. *Vaccinium* species rich in phenolic compounds, including phenolic acids, flavonol glycosides, and anthocyanins, represent antioxidant sources that may have potential beneficial effects on human health.

■ ASSOCIATED CONTENT

Supporting Information

Score plots; tables of significantly different metabolites and their relative contents analyzed by GC-TOF-MS and UPLC-Q-TOF-MS; and Pearson's correlation coefficients between identified metabolites and antioxidant activities of different blueberry species. This material is available free of charge via the Internet at http://pubs.acs.org.

■ AUTHOR INFORMATION

Corresponding Author

*Phone: +82-2-2049-6177; fax: +82-2-455-4291; e-mail: chlee123@konkuk.ac.kr.

Funding

This research was supported by a grant from the Eco-Innovation project of the Ministry of Environment (grant no. 416-111-006), Republic of Korea.

Notes

The authors declare no competing financial interest.

■ REFERENCES

(1) Mazza, G.; Miniati, E. *Anthocyanins in Fruits, Vegetables, and Grain*; CRC Press: Boca Raton, FL, 1993; p 362.

(2) Johns, L.; Stevenson, V. *Fruit for the Home and Garden*; Angus & Robertson: Sydney, Australia, 1990; p 252.

(3) Kotecha, P. M.; Madhavi, D. L. *Handbook of Fruit Science and Technology: Production, Composition, Storage, and Processing*. Marcel Dekker, Inc.: New York, 1995; p 315.

(4) Ayaz, F. A.; Hayirlioglu-Ayaz, S.; Gruz, J.; Novak, O.; Strnad, M. Separation, characterization, and quantitation of phenolic acids in a little-known blueberry (*Vaccinium arctostaphylos* L.) fruit by HPLC-MS. *J. Agric. Food Chem.* **2005**, *53*, 8116−8122.

(5) Kalt, W.; Lawand, C.; Ryan, D. A. J.; McDonald, J. E.; Donner, H.; Forney, C. F. Oxygen radical absorbing capacity, anthocyanin and phenolic content of highbush blueberries (*Vaccinium corymbosum* L.) during ripening and storage. *J. Am. Soc. Hortic. Sci.* **2003**, *128*, 917−923.

(6) Kalt, W.; McDonald, J. E.; Donner, H. Anthocyanins, phenolics, and antioxidant capacity of processed lowbush blueberry products. *J. Food Sci.* **2000**, *65*, 390−393.

(7) Prior, R. L.; Cao, G.; Martin, A.; Sofic, E.; McEwen, J.; O'Brien, C.; Lischner, N.; Ehlenfeldt, M.; Kalt, W.; Krewer, G.; Mainland, C. M. Antioxidant capacity as influenced by total phenolic and anthocyanin content, maturity, and variety of *Vaccinium* species. *J. Agric. Food Chem.* **1998**, *46*, 2686−2693.

(8) Prior, R. L.; Lazarus, S. A.; Cao, G.; Muccitelli, H.; Hammerstone, J. F. Identification of procyanidins and anthocyanins in blueberries and cranberries (*Vaccinium* spp.) using high-performance liquid chromatography/mass spectrometry. *J. Agric. Food Chem.* **2001**, *49*, 1270−1276.

(9) Sellappan, S.; Akoh, C. C.; Krewer, G. Phenolic compounds and antioxidant capacity of Georgia-grown blueberries and blackberries. *J. Agric. Food Chem.* **2002**, *50*, 2432−2438.

(10) Smith, J. L.; Marley, K. A.; Seigler, D.; Singletary, K. W.; Meline, B. Bioactive properties of wild blueberry fruits. *J. Food Sci.* **2000**, *65*, 352−356.

(11) Song, J. T. *The Sauras of Korean Resources Plants II*; II-heung: Seoul, South Korea, 1989; pp 48−49.

(12) Kim, T. J. *Korean Resources Plants III*; Seoul National University: Seoul, South Korea, 1996; p 230.

(13) Cho, H.-S.; Cho, Y.-S.; Cho, J.-A. Eco-physiological and horticultural characteristics of two Korean wild Vacciniums. *Acta Hortic.* **2012**, *926*, 149−156.

(14) Schauer, N.; Fernie, A. R. Plant metabolomics: Towards biological function and mechanism. *Trends Plant Sci.* **2006**, *11*, 508−516.

(15) Kim, J. K.; Bamba, T.; Harada, K.; Fukusaki, E.; Kobayashi, A. Time-course metabolic processing in *Arabidopsis thaliana* cell cultures after salt stress treatment. *J. Exp. Bot.* **2007**, *58*, 415−424.

(16) Zhang, J.; Wang, X.; Yu, O.; Tang, J.; Gu, X.; Wan, X.; Fang, C. Metabolic profiling of strawberry (*Fragaria*×*ananassa* Duch.) during fruit development and maturation. *J. Exp. Bot.* **2011**, *62*, 1103−1118.

(17) Ma, C.; Dastmalchi, K.; Flores, G.; Wu, S. B.; Pedraza-Peñalosa, P.; Long, C.; Kennelly, E. J. Antioxidant and metabolite profiling of North American and neotropical blueberries using LC-TOF-MS and multivariate analyses. *J. Agric. Food Chem.* **2013**, *61*, 3548−3559.

(18) t'Kindt, R.; Morreel, K.; Deforce, D.; Boerjan, W.; Bocxlaer, J. V. Joint GC−MS and LC−MS platforms for comprehensive plant metabolomics: Repeatability and sample pre-treatment. *J. Chromatogr. A.* **2009**, *877*, 3572−3580.

(19) Arbona, V.; Iglesias, D. J.; Talón, M.; Gómez-Cadenas, A. Plant phenotype demarcation using nontargeted LC-MS and GC-MS metabolite profiling. *J. Agric. Food Chem.* **2009**, *57*, 7338−7347.

(20) Wahyuni, Y.; Ballester, A.-R.; Tikunov, Y.; de Vos, R. C. H.; Pelgrom, K.T. B.; Maharijaya, A.; Sudarmonowati, E.; Bino, R. J.; Bovy, A. G. Metabolomics and molecular marker analysis to explore pepper (*Capsicum* sp.) biodiversity. *Metabolomics* **2013**, *9*, 130−144.

(21) Re, R.; Pellegrini, N.; Proteggente, A.; Pannala, A.; Yang, M.; Rice-Evans, C. Antioxidant activity applying an improved ABTS radical cation decolorization assay. *Free Radical Biol. Med.* **1999**, *26*, 1231−1237.

(22) Dietz, B. M.; Kang, Y. H.; Liu, G.; Eggler, A. L.; Yao, P.; Chadwick, L. R.; Pauli, G. F.; Farnsworth, N. R.; Mesecar, A. D.; van Breemen, R. B.; Bolton, J. L. Xanthohumol isolated from *Humulus lupulus* inhibits menadione-induced DNA damage through induction of quinone reductase. *Chem. Res. Toxicol.* **2005**, *18*, 1296−1305.

(23) Yildirim, A.; Mavi, A.; Kara, A. A. Determination of antioxidant and antimicrobial activities of *Rumex crispus* L. extracts. *J. Agric. Food Chem.* **2001**, *9*, 4083−4089.

(24) Khanal, R. C.; Howard, L. R.; Brownmiller, C. R.; Prior, R. L. Influence of extrusion processing on procyanidin composition and total anthocyanin contents of blueberry pomace. *J. Food Sci.* **2009**, *74*, H52−H58.

(25) Kafkas, E.; Kosar, M.; Turemis, N.; Baser, K. H. C. Analysis of sugars, organic acids and vitamin C contents of blackberry genotypes from Turkey. *Food Chem.* **2006**, *97*, 732−736.

(26) Gao, L.; Mazza, G. Quantitation and distribution of simple and acylated anthocyanins and other phenolics in blueberries. *J. Food Sci.* **1994**, *59*, 1057−1059.

(27) Häkkinen, S.; Auriola, S. High-performance liquid chromatography with electrospray ionization mass spectrometry and diode array

ultra violet detection in the identification of flavonol aglycones and glycosides in berries. *J. Chromatogr. A* **1998**, *829*, 91−100.
(28) Koca, I.; Karadeniz, B. Antioxidant properties of blackberry and blueberry fruits grown in the Black Sea Region of Turkey. *Sci. Hortic.* **2009**, *121*, 447−450.
(29) Howard, L. R.; Clark, J. R.; Brownmiller, C. Antioxidant capacity and phenolic content in blueberries as affected by genotype and growing season. *J. Sci. Food Agric.* **2003**, *83*, 1238−1247.
(30) Castrejón, A. D. R.; Eichholz, I.; Rohn, S.; Kroh, L. W.; Huyskens-Keil, S. Phenolic profile and antioxidant activity of highbush blueberry (*Vaccinium corymbosum* L.) during fruit maturation and ripening. *Food Chem.* **2008**, *109*, 564−572.
(31) Rice-Evans, C. A.; Miller, N. J. Structure-antioxidant activity relationships of flavonoids and isoflavonoids. In *Flavonoids in Health and Disease*; Rice-Evans, C. A., Packer, C., Eds.; Marcel Dekker: New York, 1998; pp 199−219.
(32) Boerjan, W.; Ralph, J.; Baucher, M. Lignin biosynthesis. *Annu. Rev. Plant Biol.* **2003**, *54*, 519−546.
(33) Santos-Buelga, C.; Scalbert, A. Proanthocyanidins and tannin-like compounds − Nature, occurrence, dietary intake and effects on nutrition and health. *J. Sci. Food Agric.* **2000**, *80*, 1094−1117.
(34) Wang, H.; Cao, G.; Prior, R. L. Oxygen radical absorbing capacity of anthocyanins. *J. Agric. Food Chem.* **1997**, *45*, 304−309.
(35) Rahman, M. M.; Ichiyanagi, T.; Komiyama, T.; Hatano, Y.; Konishi, T. Superoxide radical- and peroxynitrite-scavenging activity of anthocyanins; structure-activity relationship and their synergism. *Free Radical Res.* **2006**, *40*, 993−1002.
(36) Rice-Evans, C. A.; Miller, N. J.; Bolwell, P. G.; Pridham, J. B. The relative antioxidant activities of plant-derived polyphenolic flavonoids. *Free Radical Res.* **1995**, *22*, 375−383.

dealing with the grapefruit furanocoumarin metabolites has been conducted in humans.[13] Authors reported that the consumption of 900 mL of commercial GFJ led to urinary excretion of BT and its conjugated forms, which were evaluated by enzymatic hydrolysis. Although this procedure allowed for the quantification of metabolites as BT equivalents, information about structures, concentration profiles, and overall distribution of metabolites was lost.

Thus, the main objective of the present study was to provide a further qualitative and quantitative characterization of furanocoumarin metabolites in urine after GFJ consumption. Identities of main metabolites of GFJ furanocoumarins were elucidated by accurate-mass measurements and multi-stage mass experiments (MS^n) using high-resolution/accurate-mass (HR/AM) hybrid linear trap quadrupole-Orbitrap mass spectrometry (LTQ-Orbitrap). To improve the detection limits for the determination of the identified metabolites, a rapid and sensitive methodology based on solid-phase extraction (SPE) and ultraperformance liquid chromatography coupled to triple quadrupole-tandem mass spectrometry (UPLC−QqQ-MS/MS) was developed. Finally, to demonstrate the applicability of the proposed method and the potential of furanocoumarin metabolites as specific biomarkers of GFJ consumption, urine samples of five volunteers were analyzed after intakes of moderate doses of different citrus fruit juices: grapefruit, lemon, and orange juices.

MATERIALS AND METHODS

Reagents and Materials. BT, BMT, and bergapten were purchased from Extrasynthese (Genay, France), whereas DHBMT was supplied by Cayman Europe (Tallinn, Estonia). The internal standard 4-methylumbelliferone (4-MU) was obtained from Sigma (Madrid, Spain). Formic acid (∼98%) and sodium hydroxide (≥98%) were purchased from Panreac (Barcelona, Spain). Ammonium hydroxide (32%, w/w), acetic acid glacial (100%), hydrochloric acid (37%, w/v), sodium acetate anhydrous, acetonitrile, acetone, and methanol were obtained from Merck (Barcelona, Spain). Solvents were high-performance liquid chromatography (HPLC)-grade, and all other chemicals were analytical-reagent-grade. Ultrapure water was obtained from a Milli-Q gradient water purification system (Millipore, Bedford, MA). Individual stock solutions of each analyte and a mixture of them were prepared in methanol. Working standard solutions were made by appropriate dilution in 80% methanol in water acidified with 0.1% formic acid and then stored in amber glass vials at −20 °C.

Sweet orange (*Citrus sinensis* L. Osbeck, cv. Navelate), lemon (*Citrus limon* L., cv. Fino), and grapefruit (*C. paradisi* Macfad., cv. Star Ruby) of different Spanish cultivars were purchased from a local market at maturity.

Subjects and Study Design. Five healthy Caucasian male volunteers, ranging between 20 and 35 years old, were recruited for this study. The participants had no history of cardiovascular, hepatic, or renal disease and had stable alimentary habits. They had not adhered to any special diet for at least 4 weeks prior to the consumption; therefore, the obtained results can be attributed to a normal dietary pattern. The study protocol was approved by the Ethics Committee of Clinical Investigation of the University of Barcelona (IRB00003099). The study was explained to subjects through verbal and written instructions, and written informed consent was obtained from all participants.

Before each intervention, participants followed a 7-day wash-out period, in which they were requested not to consume citrus fruit or their processed products. After this period, subjects collected their blank urines. The feeding study consisted of three interventions, involving the consumption at dinner of a glass of juice (250 mL) of orange, lemon, and grapefruit. Fresh juices were prepared on the day of each intervention using a home juicer machine. Participants were asked to collect the first morning urine, 10 h after juice intake. All samples were collected in 100 mL random coded sterile specimen containers and immediately stored at 4 °C. Upon receipt of each sample, four aliquots of 1.0 mL were transferred to individual 1.5 mL capped Eppendorf tubes and stored at −80 °C until the analyses.

Because of the lack of commercial standards of furanocoumarin metabolites, a pooled urine sample, prepared by mixing equal volumes of urine from two volunteers after GFJ consumption, was employed for the method development. To ensure concentration levels high enough to allow for the determination of major and minor metabolites, the two volunteers drank a rather large volume (1 L) of freshly prepared GFJ.

Sample Preparation. On the day of the analysis, the urine samples were thawed on ice, vortexed for 1 min, and centrifuged at 15000*g* for 5 min at 4 °C. Supernatants (990 μL) were then spiked with 10 μL of the internal standard solution (4-MU, 30 μg/mL in methanol) and 175 μL of 2 M sodium acetate buffer (pH 4.80) and vortexed for 30 s.

Sample cleanup was carried out by SPE using Oasis WAX 96-well plates (30 mg, 30 μm). The optimized protocol involved conditioning the cartridges with 1 mL of methanol, equilibrating with 1 mL of 300 mM sodium acetate buffer (pH 4.80), loading 1 mL of urine sample, washing with 1 mL of 300 mM sodium acetate buffer (pH 4.80) followed by 1 mL of 15% methanol in 300 mM sodium acetate buffer (pH 4.80), and then eluting the analytes with 1.5 mL of 2.5% (v/v) ammonium hydroxide in methanol. The eluate was brought to dryness under a nitrogen flow and then reconstituted with 200 μL of 0.1% formic acid in water. The extract was passed through a 0.20 μm polytetrafluoroethylene (PTFE) syringe filter and analyzed by UPLC−QqQ-MS/MS. All samples were analyzed in triplicate.

UPLC−MS Analysis. Sample analyses were performed on a Waters Acquity ultraperformance liquid chromatography (UPLC) system (Waters, Milford, MA) consisting of a binary pump, a vacuum degasser, an autosampler, and a thermostatted column compartment. Chromatographic separation was performed on a reversed-phase column Acquity UPLC BEH C18 (50 × 2.1 mm, 1.7 μm) also from Waters, maintained at 25 °C. Mobile phases A and B were 0.1% formic acid in water and 0.1% formic acid in acetonitrile, respectively. The following linear gradient was used: 0 min, 25% B; 0.20 min, 25% B; 3.5 min, 65% B; 4.0 min, 100% B; 4.20 min, 100% B; 4.80 min, 25% B, and 6.0 min, 25% B. The flow rate was set to 550 μL/min, and the injection volume was 10 μL.

For qualitative characterization of the GFJ furanocoumarin metabolites, the UPLC system was coupled to a linear trap quadrupole-Orbitrap mass spectrometer LTQ-Orbitrap Velos from Thermo Fisher Scientific (San Jose, CA) equipped with an electrospray ionization (ESI) source. The ESI was operated in both polarity modes under the following specific conditions: spray voltage, −3.5 kV for negative mode and +3.8 kV for positive mode; sheath gas, 40 arbitrary units; auxiliary gas, 10 arbitrary units; sweep gas, 10 arbitrary units; and capillary temperature, 320 °C. Nitrogen (>99.98%) was employed as sheath, auxiliary, and sweep gas. The scan cycle used a full-scan event at a resolution of 60 000 (at m/z 400) and three data-dependent MS/MS events acquired at a resolving power of 30 000. The most intense ions detected in the full-scan spectrum were selected for data-dependent scan. Parent ions were fragmented by high-energy C-trap dissociation (HCD) with a normalized collision energy of 45% and an activation time of 100 ms. Additionally, MS^3 experiments were performed on the most intense MS/MS fragments of each metabolite using collision-induced dissociation (CID) with a normalized collision energy of 35%. Instrument control and data acquisition were performed with Xcalibur 2.0.7 software (Thermo Fisher Scientific). An external calibration for mass accuracy was carried out the day before the analysis according to the guidelines of the manufacturer.

Quantification was carried out on a triple quadrupole mass spectrometer API 3000 (Applied Biosystems, Foster City, CA) equipped with a TurboIonspray ionization source. The mass spectrometer was operated in the negative ESI mode under the following specific conditions: ion spray voltage (IS), −4.5 kV; source temperature (TEM), 350 °C; curtain gas (CUR), 12 arbitrary units; nebulizer gas (NEB), 10 arbitrary units; entrance potential (EP), −10 V; cell exit potential (CXP), −15 V; focusing potential (FP), −200 V; and collisionally activated dissociation (CAD) gas, 4 arbitrary units. Nitrogen (>99.98%) was employed as curtain, nebulizer, and collision gas. The detection was performed in the multiple reaction monitoring (MRM) mode. Analyst v1.4 software (Applied Biosystems) was used for data acquisition and control of all system components.

Statistical Analysis. Statistical calculations were made using the software package GraphPad Prism, version 5.0 (GraphPad Software,

Table 1. Identification of GFJ Metabolites in Human Urine

compound	t_R (min)	formula	measured mass (Da)	Δm (ppm)[a]	$[M-H]^-$ (m/z)	MS/MS fragments (m/z)	MS/MS/MS fragments (m/z)
NAR-diglcU 1	0.84	$C_{27}H_{28}O_{17}$	624.1324	−0.35	623.1254	447.093, 271.061, 227.071, 151.002, 119.049	447 > 429, 271, 175
NAR-glcU-SO_3 1	0.87	$C_{21}H_{20}O_{14}S$	528.0567	−1.21	527.0497	447.093, 351.018, 331.122, 271.061, 151.002,	351 > 271, 151
NAR-SO_3 1	0.97	$C_{15}H_{12}O_8S$	352.0249	−0.99	351.0179	271.061, 177.018, 151.002, 119.049, 107.012	271 > 151, 177, 119
NAR-diglcU 2	1.00	$C_{27}H_{28}O_{17}$	624.1326	−0.06	623.1256	447.093, 271.061, 227.071, 151.002, 119.049	447 > 429, 271, 175
BT-glcU	1.10	$C_{17}H_{14}O_{10}$	378.0583	−1.14	377.0513	201.018, 173.023, 145.028, 117.033	201 > 191, 173, 163, 147, 145, 119, 117
BT-SO_3	1.27	$C_{11}H_6O_7S$	281.9833	−0.57	280.9763	201.018, 173.023, 145.028, 117.033	201 > 191, 173, 163, 147, 145, 119, 117
NAR-glcU	1.44	$C_{21}H_{20}O_{11}$	448.1002	−0.85	447.0932	271.061, 177.018, 151.002, 113.023, 119.049	271 > 151, 177, 119
NAR-glcU-SO_3 2	1.47	$C_{21}H_{20}O_{14}S$	528.0572	−0.28	527.0502	271.061, 254.981, 175.024, 96.959	271 > 151, 177, 119
NAR-SO_3 2	1.62	$C_{15}H_{12}O_8S$	352.0250	−0.91	351.0180	271.061, 177.018, 151.002, 119.049, 107.012	271 > 151, 177, 119
BT[b]	2.10	$C_{11}H_6O_4$	202.0257	−4.45	201.0187	191.034, 173.023, 163.039, 145.028, 117.033	173 > 163, 145, 117
DHBMT-glcU	2.32	$C_{27}H_{32}O_{12}$	548.1890	−0.78	547.1820	371.148, 345.154, 201.018, 173.023	201 > 191, 173, 163, 147, 145, 119, 117
NAR[b]	2.38	$C_{15}H_{12}O_5$	272.0683	−0.74	271.0613	177.018, 151.003, 119.049, 107.012	151 > 107, 83, 64
HBMT-glcU 1	2.66	$C_{27}H_{30}O_{11}$	530.1787	−0.21	529.1717	353.138, 201.018, 173.023	201 > 191, 173, 163, 147, 145, 119, 117
HBMT-glcU 2	2.79	$C_{27}H_{30}O_{11}$	530.1783	−1.02	529.1713	353.138, 201.018, 173.023	201 > 191, 173, 163, 147, 145, 119, 117

[a] Δm = mass measurement error. [b] Positively identified.

San Diego, CA). Unless otherwise specified, data are presented as the mean ± standard deviation (SD). Statistical significance was determined by one-way analysis of variation (ANOVA) followed by Dunnett's multiple comparison tests when comparing more than two groups and two-way ANOVA followed by Bonferroni's test when comparing two factors.

RESULTS AND DISCUSSION

Characterization of GFJ Metabolites by HR/AM Mass Spectrometry. To elucidate the chemical structures of the main GFJ metabolites, a pooled urine sample was collected 10 h after the intake of 1 L of freshly prepared GFJ and analyzed by UPLC coupled to a LTQ-Orbitrap mass spectrometer. Taking advantage of the HR/AM of this MS instrument, main GFJ metabolites could be tentatively identified with mass measurement errors below 4.5 ppm (Table 1). Combining HR/AM measurement and MS^n increased the confidence of the proposed metabolites. Thus, the availability of chemical formulas for the precursor and product ions generated from high-resolution data-dependent accurate-mass analysis allowed for the speed up of structural elucidation of metabolites.

After the intake of GFJ, a major metabolite was found at 1.10 min, showing a $[M-H]^-$ ion at m/z 377.0513. Its MS/MS fragmentation produced a base ion at m/z 201.018 (M − H − 176, loss of glucuronic acid moiety), which corresponds to the deprotonated molecule of BT (Figure 1a). Thus, this compound was tentatively identified as a glucuronide metabolite of BT (BT-glcU). Another main metabolite with $[M-H]^-$ ion at m/z 280.9763 eluted at 1.27 min, yielding again a MS/MS base ion at m/z 201.018 produced by the loss of 80 Da (Figure 1b). This characteristic loss of a sulfate group indicated that this metabolite might be the sulfoconjugate of BT (BT-SO_3). On the basis of data obtained by enzymatic hydrolysis, Messer et al. [13] proposed BT glucuronide and sulfate as main GFJ furanocoumarin metabolites in humans. To the best of our knowledge, these metabolites have been identified for the first time in the present work using a mass spectrometry approach. Free BT could also be positively identified in urine after GFJ consumption, which is in agreement with the results previously reported.[13] As shown in Figure 1c, the fragmentation by HCD of the $[M-H]^-$ ion at m/z 201.0187 produced characteristic ions at m/z 173.023, 145.028, and 117.033. Glucuronide metabolite of DHBMT (DHBMT-glcU) was also tentatively identified (Δm = −0.78 ppm) at 2.32 min with a $[M-H]^-$ ion at m/z 547.1820. Its MS/MS spectrum (Figure 1d) showed fragment ions at m/z 371.148 (M − H − 176, loss of glucuronic acid), which corresponds to the deprotonated molecule of DHBMT, m/z 345.154 (M − H − BT), and also m/z 201.018. In the study conducted by Messer et al.,[13] no DHBMT could be detected after enzymatic hydrolysis of urine, which authors mainly attributed to the possible transformation into free BT during its metabolism. An explanation to this disagreement might rely on the hydrolysis step used by the authors, because enzymatic efficiency greatly depends upon the structure of the metabolites.[18] Two isomeric forms of another metabolite could also be detected at 2.66 and 2.79 min with a $[M-H]^-$ ion at m/z 530.1787. Its fragmentation yielded an ion at m/z 353.138, corresponding to the loss of a glucuronic acid moiety, and also the characteristic ion of BT at m/z 201.018. This pattern suggested that these metabolites might be glucuronides of a hydroxybergamottin-like compound (HBMT-glcU) (Figure 1e). To the best of our knowledge, this study provides for the first time evidence of the existence in urine of glucuronides of DHBMT and HBMT as GFJ furanocoumarin metabolites. No free furanocoumarins, other than BT, could be detected (in both polarity ESI modes) in urine after the GFJ consumption, which indicated that they are mainly metabolized to the reported forms.

In addition to these furanocoumarin metabolites, naringenin (NAR) and its glucuronide and sulfate conjugates were also identified in urine (Table 1), which is in agreement with previous studies dealing with the metabolism of GFJ flavonoids.[19,20]

SPE Optimization. Once the main furanocoumarin metabolites present in urine were identified, the research was focused on the development of an analytical method sensitive enough to allow for their detection after the consumption of a low regular dose of GFJ. To this end, an approach based on the use of SPE and UPLC coupled to triple quadrupole mass spectrometry was performed. The specific MRM conditions for quantification and confirmation are detailed in Table 2.

As known, the sorbent type and solvent composition for washing and elution steps are crucial parameters for the

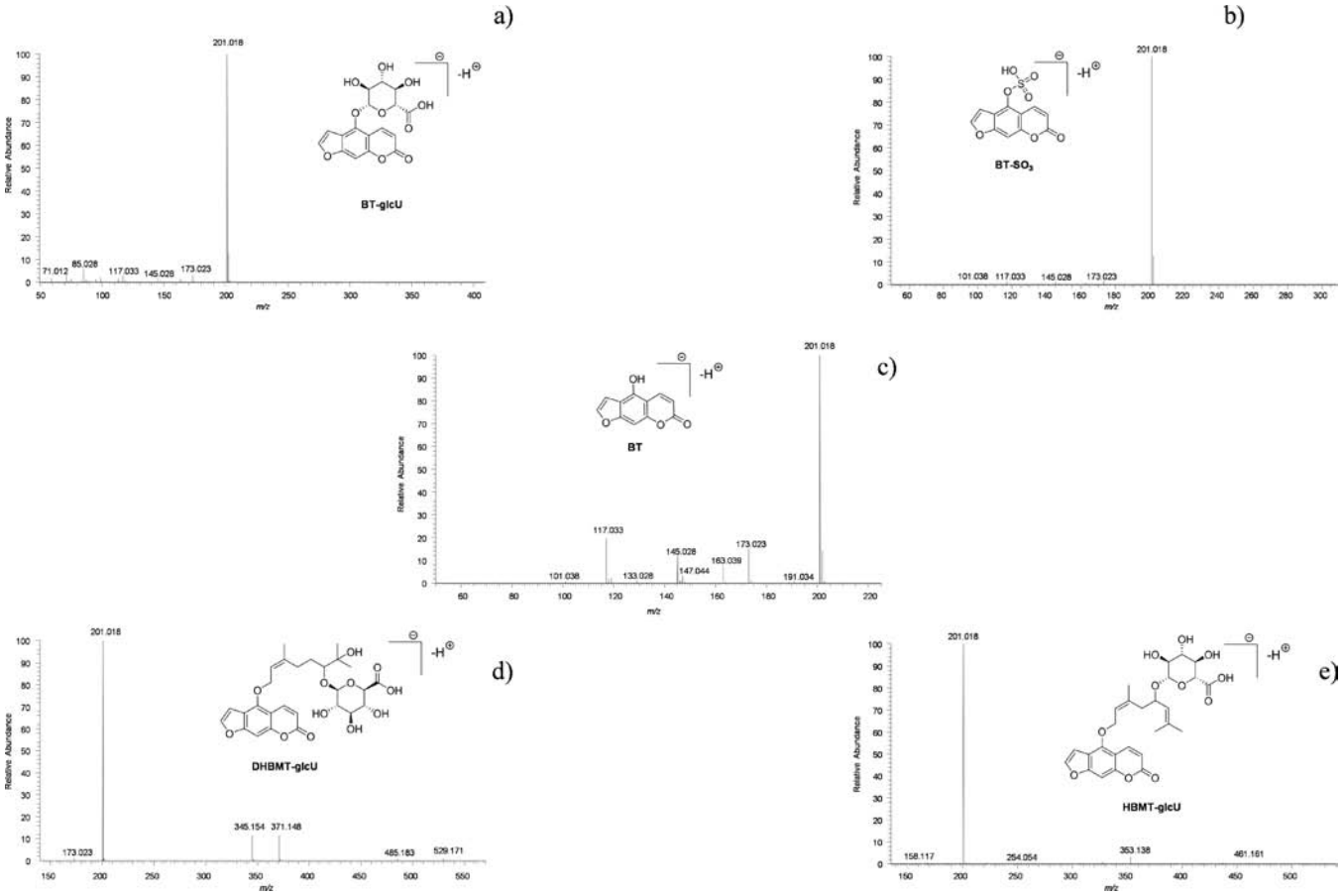

Figure 1. MS/MS spectra obtained for the identified furanocoumarin metabolites: (a) BT-glcU, (b) BT-SO_3, (c) BT, (d) DHBMT-glcU, and (e) HBMT-glcU.

Table 2. Specific MRM Conditions for the Determination of GFJ Furanocoumarin Metabolites

compound	t_R (min)	parent ion	MRM1 (m/z, quantifier)	CE1 (eV)[a]	MRM2 (m/z, qualifier)	CE2 (eV)[a]
BT-glcU	1.10	$[M-H]^-$	377 > 201	−25	377 > 173	−28
BT-SO_3	1.27	$[M-H]^-$	281 > 201	−22	281 > 173	−34
4-MU (IS)[b]	1.71	$[M-H]^-$	175 > 133	−30	175 > 119	−35
BT	2.10	$[M-H]^-$	201 > 117	−40	201 > 145	−35
DHBMT-glcU	2.32	$[M-H]^-$	547 > 201	−35	547 > 345	−32
HBMT-glcU 1	2.66	$[M-H]^-$	529 > 201	−25	529 > 353	−23
HBMT-glcU 2	2.79	$[M-H]^-$	529 > 201	−25	529 > 353	−23

[a]CE = collision energy. [b]IS = internal standard.

optimization of any SPE procedure. Taking into account the ionizable nature of major furanocoumarin metabolites, mainly glucuronide and sulfate derivatives, it was hypothesized with the use of an ionic-exchange mechanism. Glucuronide metabolites can be easily ionized because of the presence of the carboxylic group on the glucuronic acid moiety, which usually shows pK_a values around 3,[21] whereas sulfate conjugates carry a permanent negative charge (pK_a < 1). Therefore, a mixed-mode weak anion-exchange (WAX)/reversed-phase polymeric sorbent was evaluated for the extraction and preconcentration of furanocoumarin metabolites from urine. As a result of their dual properties, this kind of sorbent has been used to efficiently retain both neutral and acidic metabolites from biological samples.[22] Stramm et al.[23] were able to selectively retain glucuronides and sulfate conjugates of steroids using Oasis WAX SPE cartridges.

To obtain maximal retention, it is necessary to deprotonate glucuronides while maintaining the piperazine anion-exchange groups of sorbent positively charged (pK_a ∼ 6). Thus, urine was buffered to pH 4.8 prior to the loading step, which guarantees a deprotonation rate of glucuronides higher than 98%. Working under these pH conditions, different percentages of methanol (0−15%) were tested, aiming to improve the cleanup step (Figure 2). This study may be especially critical for the neutral compounds, such as the BT, because they are only retained by a reversed-phase mechanism. No reduction in the amounts of any of target metabolites was observed in the studied range; therefore, 15% methanol was finally selected.

Another critical step is the selection of a suitable phase for the quantitative elution of the retained compounds. When dealing with weak anion-exchange mechanisms, two different approaches are usually possible to achieve the elution. The most common one consists of the protonation of the acidic compounds by using an elution solvent with a pH low enough. Nevertheless, sulfoconjugates are no able to elute under these

dx.doi.org/10.1021/jf405701a | J. Agric. Food Chem. 2014, 62, 2134−2140

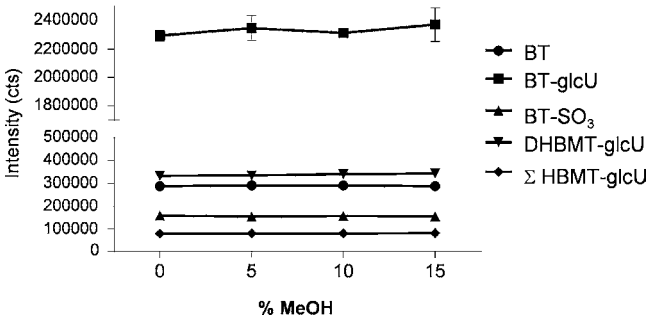

Figure 2. Effect of the proportion of methanol during the SPE washing step.

conditions, because they are not prone to neutralization. Therefore, elution could only be carried out by neutralizing the piperazine anion-exchange function of the sorbent. Three different proportions of NH_4OH in methanol were evaluated for the elution of furanocoumarin metabolites (Figure 3). Whereas no differences were observed between the use of 2.5 and 5% NH_4OH, the amounts of metabolites eluted were statistically lower when using 1% NH_4OH. The only exception to this behavior was found for BT, which is the only metabolite retained exclusively by the reversed-phased mechanism. Consequently, its elution should not be pH-dependent. Therefore, 2.5% NH_4OH in methanol was chosen for the elution of furanocoumarin metabolites from the WAX sorbent.

Because of the lack of commercial standards for the furanocoumarin metabolites, the recovery of the SPE procedure could only be evaluated for BT. A blank urine sample was spiked at concentrations of 50, 500, and 5000 ng/mL, and the recovery was calculated by dividing the difference between the measured concentrations for spiked and non-spiked samples by the added concentrations. Quantitative recoveries, in the range of 94−102%, were obtained for all concentration levels. The precision of the method was evaluated by calculating the relative standard deviation (RSD) at the same three concentration levels. Satisfactory results were obtained with RSD values below 7% in all cases. Limits of detection (LODs), calculated for a signal-to-noise ratio (S/N) of 3 using the less sensitive MS/MS transition, were in the range of 0.9−1.5 ng/mL.

Feeding Study. The proposed method was applied to the analysis of urine samples from five volunteers (U1−U5) after the consumption at dinner of a glass (250 mL) of freshly prepared juice of orange, lemon, and grapefruit. Because no standards were available, only BT could be accurately quantified in the urine samples. For the rest of the metabolites, concentrations were estimated as equivalents of BT, which provide semi-quantitative information about their levels in urine.

The subjects were requested not to consume citrus fruits or derivatives during the 7 days previous to each intervention. First morning urines were collected the day before the intake and in the morning following the intervention, 10 h after juice consumption. No furanocoumarin metabolites were detected in the urine samples after the wash-out periods or after the consumption of orange and lemon juices. Nevertheless, important concentrations of metabolites were found in the urine samples of all of the volunteers after the intake of a glass of GFJ (Table 3). Figure 4 shows the MRM chromatograms for the quantification MS/MS transitions obtained for U2 after the intake of 250 mL of GFJ.

The concentration of BT showed considerable variation among the five volunteers, ranging from 382 to 2670 ng/mL (median of 595 ng/mL). Messer et al.[13] found BT in free and conjugated forms, as the only furanocoumarin excreted in urine within 6 h after consumption of 900 mL of GFJ. On the basis of results of enzymatic hydrolysis, they suggested that the majority of BT was excreted as conjugate forms. Our data suggest a similar pattern with estimated concentrations for the total BT in conjugate forms between 30- and 130-fold higher than those of free BT. Among the furanocoumarin metabolites, BT-glcU was in all cases the major urinary metabolite, showing a median concentration around 33 μg/mL (Figure 5). BT-SO_3 and DHBMT-glcU were also found at concentrations in the microgram per milliliter level. As shown, the glucuronides of HBMT were the least abundant conjugates, with a median concentration of 621 ng/mL.

Our findings suggest that GFJ furanocoumarins are mainly excreted as glucuronide and sulfate conjugates, whereas a lower

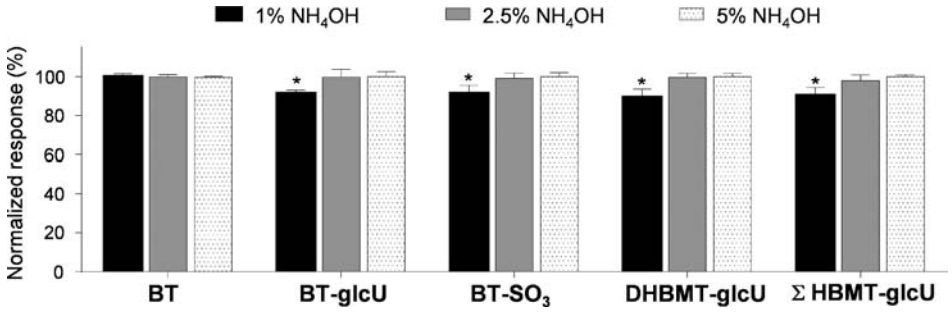

Figure 3. Influence of the percentage of ammonia solution during the SPE elution step. (*) $p < 0.05$ compared to 2.5% NH_4OH and 5% NH_4OH.

Table 3. Urinary Concentrations of Furanocoumarin Metabolites after Consumption of 250 mL of GFJ

	concentration ± SD (ng/mL, n = 3)				
volunteer	BT	BT-glcU	BT-SO_3	DHBMT-glcU	∑HBMT-glcU
U1	382 ± 17	32649 ± 1210	11294 ± 540	4037 ± 251	461 ± 14
U2	334 ± 20	32913 ± 1954	9833 ± 428	3826 ± 263	1045 ± 46
U3	595 ± 22	38702 ± 2326	24551 ± 456	4780 ± 298	1091 ± 36
U4	2679 ± 136	69229 ± 3815	8524 ± 475	6353 ± 344	562 ± 43

dx.doi.org/10.1021/jf405701a | J. Agric. Food Chem. 2014, 62, 2134−2140

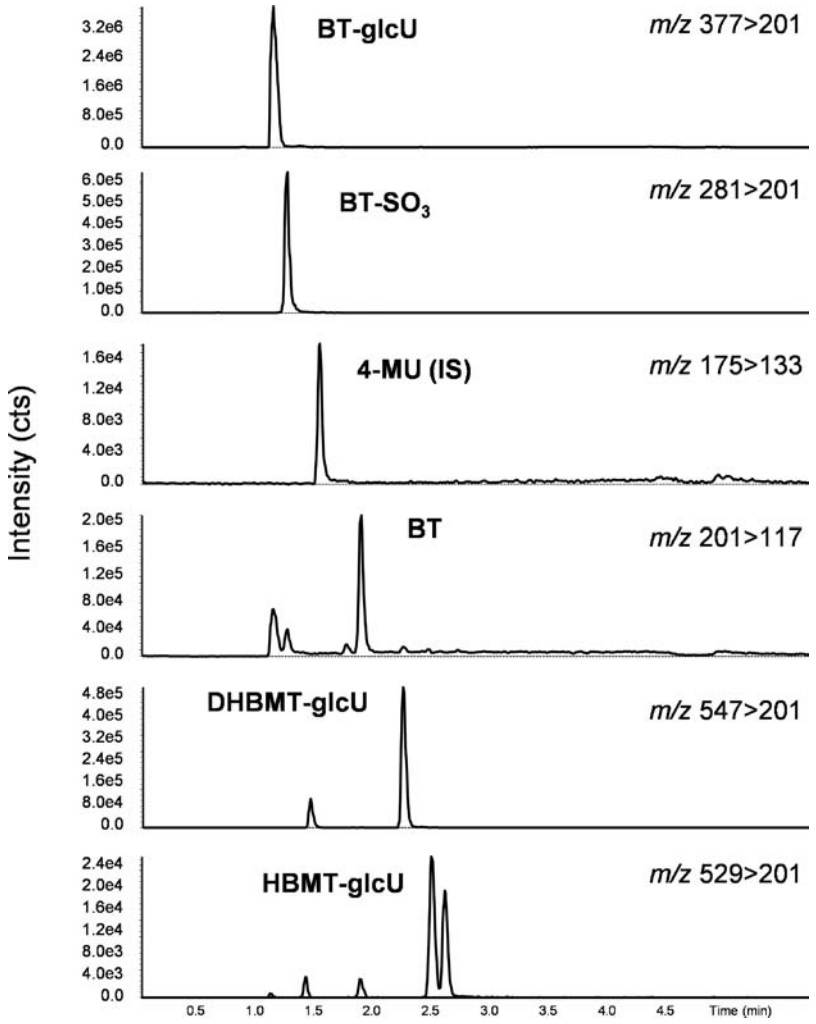

Figure 4. MRM chromatograms obtained for a real urine sample (U2 in Table 3) after the intake of 250 mL of GFJ.

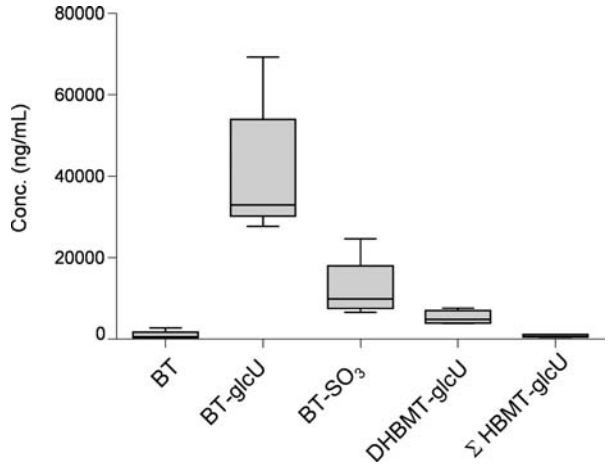

Figure 5. Box plots of the metabolite concentration in urine from five volunteers after the intake of 250 mL of GFJ.

amount is excreted as free BT. The proposed method for the determination of these metabolites might be useful for studying the grapefruit–drug interactions in dietary studies. In addition, these results demonstrate that these metabolites can be selective enough to be considered as potential biomarkers of GFJ consumption, because they were not detected in urine after the wash-out periods or after consumption of orange and lemon juices.

AUTHOR INFORMATION

Corresponding Author

*Telephone: +34934034843. Fax: +34934035931. E-mail: lamuela@ub.edu.

Funding

The authors express their gratitude for financial support from the Interdepartmental Committee of Science and Technology (CICYT) (AGL2010-22319-C03) from the Spanish Ministry of Science and Innovation (MICINN) and from CIBERobn, an initiative of the ISCIII, Spain. Jorge Regueiro acknowledges MICINN for his Juan de la Cierva contract.

Notes

The authors declare no competing financial interest.

REFERENCES

(1) Chaudhary, P. R.; Jayaprakasha, G. K.; Patil, B. S.; Porat, R. Grapefruit degreening influence on health promoting limonoids and flavonoids. *Acta Hortic.* **2012**, *939*, 113–120.

(2) Chebrolu, K. K.; Jayaprakasha, G. K.; Jifon, J.; Patil, B. S. Production system and storage temperature influence grapefruit vitamin C, limonoids, and carotenoids. *J. Agric. Food Chem.* **2012**, *60*, 7096–7103.

(3) Miller, E. G.; Peacock, J. J.; Bourland, T. C.; Taylor, S. E.; Wright, J. M.; Patil, B. S.; Miller, E. G. Inhibition of oral carcinogenesis by citrus flavonoids. *Nutr. Cancer* **2008**, *60*, 69−74.
(4) Vanamala, J.; Leonardi, T.; Patil, B. S.; Taddeo, S. S.; Murphy, M. E.; Pike, L. M.; Chapkin, R. S.; Lupton, J. R.; Turner, N. D. Suppression of colon carcinogenesis by bioactive compounds in grapefruit. *Carcinogenesis* **2006**, *27*, 1257−1265.
(5) Keevil, J. G.; Osman, H. E.; Reed, J. D.; Folts, J. D. Grape juice, but not orange juice or grapefruit juice, inhibits human platelet aggregation. *J. Nutr.* **2000**, *130*, 53−56.
(6) Gorinstein, S.; Caspi, A.; Libman, I.; Lerner, H. T.; Huang, D.; Leontowicz, H.; Leontowicz, M.; Tashma, Z.; Katrich, E.; Feng, S.; Trakhtenberg, S. Red grapefruit positively influences serum triglyceride level in patients suffering from coronary atherosclerosis: Studies in vitro and in humans. *J. Agric. Food Chem.* **2006**, *54*, 1887−1892.
(7) Lian-Qing, G.; Fukuda, K.; Ohta, T.; Yamazoe, Y. Role of furanocoumarin derivatives on grapefruit juice-mediated inhibition of human CYP3A activity. *Drug Metab. Dispos.* **2000**, *28*, 766−771.
(8) Schmiedlin-Ren, P.; Edwards, D. J.; Fitzsimmons, M. E.; He, K.; Lown, K. S.; Woster, P. M.; Rahman, A.; Thummel, K. E.; Fisher, J. M.; Hollenberg, P. F.; Watkins, P. B. Mechanisms of enhanced oral availability of CYP3A4 substrates by grapefruit constituents: Decreased enterocyte CYP3A4 concentration and mechanism-based inactivation by furanocoumarins. *Drug Metab. Dispos.* **1997**, *25*, 1228−1233.
(9) Seden, K.; Dickinson, L.; Khoo, S.; Back, D. Grapefruit−drug interactions. *Drugs* **2010**, *70*, 2373−2407.
(10) Edwards, D. J.; Bellevue, F. H.; Woster, P. M. Identification of 6′,7′-dihydroxybergamottin, a cytochrome P450 inhibitor, in grapefruit juice. *Drug Metab. Dispos.* **1996**, *24*, 1287−1290.
(11) Ohta, T.; Miyamoto, Y.; Maruyama, T.; Kiuchi, F.; Tsukamoto, S. Localization and contents of paradisins, the most potent CYP3A4 inhibitors, in grapefruit *Citrus paradisii* and grapefruit juice. *Nat. Med.* **2002**, *56*, 264−267.
(12) Girennavar, B.; Poulose, S. M.; Jayaprakasha, G. K.; Bhat, N. G.; Patil, B. S. Furocoumarins from grapefruit juice and their effect on human CYP 3A4 and CYP 1B1 isoenzymes. *Bioorg. Med. Chem.* **2006**, *14*, 2606−2612.
(13) Messer, A.; Nieborowski, A.; Strasser, C.; Lohr, C.; Schrenk, D. Major furocoumarins in grapefruit juice I: Levels and urinary metabolite(s). *Food Chem. Toxicol.* **2011**, *49*, 3224−3231.
(14) Manthey, J. A.; Buslig, B. S. Distribution of furanocoumarins in grapefruit juice fractions. *J. Agric. Food Chem.* **2005**, *53*, 5158−5163.
(15) De Castro, W. V.; Mertens-Talcott, S.; Rubner, A.; Butterweck, V.; Derendorf, H. Variation of flavonoids and furanocoumarins in grapefruit juices: A potential source of variability in grapefruit juice−drug interaction studies. *J. Agric. Food Chem.* **2006**, *54*, 249−255.
(16) Girennavar, B.; Jayaprakasha, G. K.; Jifon, J. L.; Patil, B. S. Variation of bioactive furocoumarins and flavonoids in different varieties of grapefruits and pummelo. *Eur. Food Res. Technol.* **2008**, *226*, 1269−1275.
(17) Girennavar, B.; Jayaprakasha, G. K.; Patil, B. S. Influence of pre- and post-harvest factors and processing on the levels of furocoumarins in grapefruits (*Citrus paradisi* Macfed.). *Food Chem.* **2008**, *111*, 387−392.
(18) Trontelj, J. Quantification of glucuronide metabolites in biological matrices by LC−MS/MS. In *Tandem Mass Spectrometry—Applications and Principles*; Prasain, D. J., Ed.; InTech: Rijeka, Croatia, 2012.
(19) Zhang, J.; Brodbelt, J. S. Screening flavonoid metabolites of naringin and narirutin in urine after human consumption of grapefruit juice by LC−MS and LC−MS/MS. *Analyst* **2004**, *129*, 1227−1233.
(20) Erlund, I.; Meririnne, E.; Alfthan, G.; Aro, A. Plasma kinetics and urinary excretion of the flavanones naringenin and hesperetin in humans after ingestion of orange juice and grapefruit juice. *J. Nutr.* **2001**, *131*, 235−241.
(21) Farrell, T.; Poquet, L.; Dionisi, F.; Barron, D.; Williamson, G. Characterization of hydroxycinnamic acid glucuronide and sulfate conjugates by HPLC−DAD−MS^2: Enhancing chromatographic quantification and application in Caco-2 cell metabolism. *J. Pharm. Biomed. Anal.* **2011**, *55*, 1245−1254.
(22) Fontanals, N.; Marcé, R. M.; Borrull, F.; Cormack, P. A. G. Mixed-mode ion-exchange polymeric sorbents: Dual-phase materials that improve selectivity and capacity. *TrAC, Trends Anal. Chem.* **2010**, *29*, 765−779.
(23) Strahm, E.; Rudaz, S.; Veuthey, J.-L.; Saugy, M.; Saudan, C. Profiling of 19-norsteroid sulfoconjugates in human urine by liquid chromatography mass spectrometry. *Anal. Chim. Acta* **2008**, *613*, 228−223.

Pyraclostrobin is used to control a wide range of plant pathogens. For example, pyraclostrobin applications limited the growth and disease severity of *Rhizoctonia* species related to rice (*Oryza sativa*).[10] Reported plant dissipation rates are rapid, with pyraclostrobin DT_{50} of <2 days in corn (*Zea mays*) plants[11] and 11 days in peanut (*Arachus hypogaea*) plants.[12] However, pyraclostrobin is reported to dissipate relatively slowly in soil, with an average half-life (DT_{50}) of 32 days.[13] Slightly more rapid soil dissipation has been reported as well in a sandy loam (DT_{50} = 29 days) and a sandy clay (DT_{50} = 22 days).[14] Dissipation of pyraclostrobin in sterilized soil was 47 days, indicating that biotic processes, while dominant, may not be the only loss mechanism.[14] Photodegradation of pyraclostrobin [by ultraviolet (UV) lamp irradiation] was rapid, with reported DT_{50} values as low as 39 min and as high as 128 min for a 5.9 μmol L^{-1} solution.[15] Thus, multiple loss mechanisms are possible. The high *n*-octanol/water coefficient (log K_{ow} = 3.99)[16] and very high adsorption coefficient (log K_{oc} = 3.96) [16] further suggest that, although it is somewhat immobilized in soil, it still has potential for runoff into surface water.

Characterization of pyraclostrobin in sugarcane and the soil in which it is grown is not reported in the literature because of its recent U.S. EPA Emergency Use Label addition for sugarcane. Degradation rates of active substances in crop protection products are important parameters for assessing environmental exposure. Therefore, the purpose of this study is to investigate the dissipation rate of pyraclostrobin in sugarcane soil and the retention of the fungicide to sugarcane leaves when subjected to wash-off conditions.

MATERIALS AND METHODS

Pyraclostrobin Stock Solution Preparation. The pyraclostrobin stock solution used for amending soil samples was prepared from commercial Headline SC [BASF, 250 g of active ingredient (a.i.) L^{-1}] by adding 1 mL of Headline SC to 10 mL of 18 MΩ deionized (DI) water that was acidified with 0.3 mL of 12 M HCl. Pyraclostrobin was then extracted by liquid−liquid extraction with 3 × 10 mL of ethyl acetate in a separatory funnel. The extracts were filtered and concentrated to a final volume of 10 mL and analyzed by high-performance liquid chromatography (HPLC), as outlined below under the Instrumental Analysis section. The resulting concentration was determined to be 1250 μg mL^{-1} based on calibration with standards made from a 100 μg/mL pyraclostrobin standard solution.

Soil Sample Preparation. Cancienne silt loam (fine silty, mixed, superactive, non-acid, hyperthermic Fluvaquentic Epiaquepts) was collected from the United States Department of Agriculture (USDA)−Agricultural Research Service (ARS) Sugarcane Research Unit's Ardoyne Farm in Schriever, LA (29° 38′ 09.37″ N, 90° 56′ 25.79″ W). The soil was collected from a depth of 0−15 cm, transported to the laboratory, sieved to pass a 2 mm screen, and stored at 4 °C until the experiment commenced. The soil was collected from a field with no history of pyraclostrobin application. The water content was estimated by oven-drying at 90 °C for 1 h. An air-dried sample was characterized by Brookside Laboratories in New Bremen, OH. The cation-exchange capacity (CEC) was 18.10 cmol kg^{-1} of soil; the soil pH (1:1 soil/water) was 6.10; and the organic matter (by loss on ignition) was 1.61%. The estimated nitrogen release (calculated by loss on ignition) was 58 kg ha^{-1}. Mehlich III extractable nutrients in the soil were 8 mg kg^{-1} of sulfur, 32 mg kg^{-1} of phosphorus, 2087 mg kg^{-1} of calcium, 467 mg kg^{-1} of magnesium, 121 mg kg^{-1} of potassium, 25 mg kg^{-1} of sodium, 0.56 mg kg^{-1} of boron, 286 mg kg^{-1} of iron, 122 mg kg^{-1} of manganese, 5.97 mg kg^{-1} of copper, 4.33 mg kg^{-1} of zinc, and 501 mg kg^{-1} of aluminum. The total carbon (C) and nitrogen (N) by dry combustion were 1.01 and 0.11%, respectively, with a C/N ratio of 9.2.

For the laboratory incubation, the soil moisture was adjusted to 0.20 g of water g^{-1} of soil using distilled water. A total of 50 g (dry weight equivalent) of soil was placed each into a series of 28 Erlenmeyer flasks (250 mL) along with 0.2 g of pyraclostrobin-spiked sand. The spiked sand was prepared by the addition of pyraclostrobin stock solution (1250 μg mL^{-1}) to sterilized fine-grain sand, followed by evaporation of the ethyl acetate solvent, giving a calculated concentration of 1000 μg g^{-1}. The pyraclostrobin-spiked sand was added to each flask, and the contents were mixed and sealed with a rubber stopper. The initial concentration of pyraclostrobin was calculated to be 3.3 μg g^{-1}. Flasks were incubated in the dark at 22 °C and sampled in triplicate at 0, 4, 11, 14, 28, 42, and 63 days. Four control flasks containing only 0.2 g of spiked sand were stored and sampled in duplicate at 0 and 63 days. Flasks were removed from incubation and stored in a freezer at −20 °C.

Extraction Method Optimization. Two extraction methods were adapted and compared for this experiment: a method designed by BASF and provided by the U.S. EPA[17] and a method using dispersive solid-phase extraction (dSPE) quick, easy, cheap, effective, rugged, and safe (QuEChERS).[18] Both adapted methods assayed pyraclostrobin levels using HPLC with ultraviolet−visible (UV−vis) detection (HPLC−UV). Briefly, 50 g of soil sample along with 50 mL of acetonitrile was shaken for 30 min at 200 rpm. The sample was then vacuum-filtered through a medium-porosity filter, and the supernatant was collected and evaporated to dryness. The residue was redissolved in 1.0 mL of acetonitrile and analyzed by HPLC. For the QuEChERS method, 15 g of soil was placed into a 50 mL polytetrafluoroethylene (PTFE) centrifuge tube with 15 mL of acetonitrile and vortexed for 1 min. The sample was then centrifuged for 5 min at 5000 rpm, after which 1.0 mL of the resulting supernatant was added to a 2.0 mL QuEChERS tube containing 150 mg of $MgSO_4$, 50 mg of primary−secondary amine sorbent (PSA), and 50 mg of C18 material. This tube was vortexed and centrifuged as above. The supernatant was removed and filtered through a 0.22 μm nylon filter and analyzed by HPLC.

Wash-off Studies. Commercial Headline SC fungicide was applied according to the label instructions (14 g of a.i. ha^{-1}) to three rows of variety "HoCP 96-540" commercial sugarcane using a three-row spray boom calibrated to deliver 280 L ha^{-1}. At the time of application, the plant-cane crop was infected with brown rust. Five plants were randomly selected and harvested at 0.5, 6, 24, 48, and 72 h after application of the fungicide. Replicates (n = 3) were obtained by harvesting one five-plant sample from each of the front, middle, and back of the field. Upon harvesting, the whole green leaves of all five plants were removed at the dewlap, submerged in 2 L of room-temperature tap water, and agitated on a shaker at 100 rpm for 30 min. The leaves were removed from the water, dried for 1 week at 60 °C, and weighed, and the aqueous extract was filtered through a filter under vacuum, collected in 1 L polypropylene bottles, and frozen at −20 °C. The contents in the bottles were later thawed and concentrated by passing through a methanol-conditioned (10 mL) Oasis hydrophilic−lipophilic balanced (HLB) 6 mL (200 mg, 30 μm particle size) cartridge (Waters, Taunton, MA) under vacuum until dry. The cartridges were immediately stored at −20 °C until the recovery for analysis by HPLC. The pyraclostrobin extracted from the wash water was then recovered from each cartridge by eluting with 10.0 mL of HPLC-grade acetonitrile (EMD Millipore, Billerica, MA). A total of 1 mL of each sample was filtered through a 0.22 μm nylon filter and assayed for pyraclostrobin by HPLC, as outlined below.

Instrumental Analysis. The method developed for the analysis of strobilurins in tomato residues[19] and the method D9812/1 submitted to the U.S. EPA by BASF for product registration were adapted into this study.[17] Analysis was performed using a Hitachi HPLC system (Hitachi LaChrome Elite L-2310, Dallas, TX) with a UV−vis detector L-2420 and a column oven (Hitachi model L-2350) and a manual injector from Rheodyne model 7725 (Rohnert Park, CA). A 20 μL sample was injected onto a C18 ZORBAX Eclipse PAH, 5 μm, 4.6 × 150 mm (Agilent, Santa Clara CA), and eluted isocratically [70:30 acetonitrile (ACN)/0.1% formic acid solution] at a flow rate of 1.0 mL min^{-1} at 40 °C. The pesticide was detected at 275 nm. Standards ranging from 1 to 10 μg mL^{-1} were prepared in ACN using a 100 μg

mL^{-1} stock solution from AccuStandard (New Haven, CT). The resulting calibration line had a R^2 of 0.9989, and the detection limit for the analysis was 0.01 $\mu g\ mL^{-1}$.

The recoveries of the extraction method were determined by spiking three unamended soil samples and two control flasks with pyraclostrobin stock solution to a final concentration of 3.17 $\mu g\ g^{-1}$ and performing the extraction procedure as described above. The spike recoveries were calculated to be 97% (±6%), comparable to soil recoveries using QuEChERS by Zhang et al.[12]

Data Analysis. The major goal of this study is to investigate the dissipation rate of pyraclostrobin and predict its persistence in sugarcane soil. On the basis of different dissipation pathways, various kinetic models can be derived, which can subsequently be used to model the pesticide and estimate the DT_{50} and DT_{90} end points. For the selection of the kinetic model that best describes the dissipation results, FOCUS work group guidance recommendations were followed.[20]

Dissipation data were fitted to four models: simple first-order (SFO) kinetics model ($C = C_0e^{-kt}$), Gustafson−Holden[21] or first-order multi-compartment (FOMC) model ($C = C_0/((t/\beta) + 1)^{\alpha}$), hockey-stick (HS) model ($C = C_0e^{-k_1t_b}e^{-k_2(t - t_b)}$ for $t > t_b$ and $C = C_0e^{-k_1t}$ for $t \leq t_b$), and bi-exponential or double-first-order in parallel (DFOP) model ($C = C_0(ge^{-k_1t} + [1 - g]e^{-k_2t})$),[20] where C is the fungicide soil concentration in $\mu g\ g^{-1}$ at time t, C_0 is the initial concentration of fungicide, k_x values are degradation rate constants, α and β are shape and location parameters (FOMC model), respectively, t_b is the point where the rate constant changes (HS model), and g is the fraction of C_0 applied to compartment 1 (DFOP model). DT_{50} and DT_{90} values were determined using analytical equations described by the FOCUS work group; however, for the DFOP model, an analytical solution for the DT_{50} and DT_{90} values does not exist. Instead, the values must be determined graphically by finding the time at which only 50 and 10% of the initial amount of pesticide remains.

For each model, the goodness of fit was determined through visual observation of the residual plot and the χ^2 significance test using Microsoft Excel with the solver add in package.[20] Because the coefficient of determination (R^2) applies to linear data, model efficiency (EF) was determined to assess agreement of measured and calculated data. Pyraclostrobin levels in each soil sample at each time point were calculated on a $\mu g\ g^{-1}$ soil basis. Wash-off data were normalized to the gram of dry leaf biomass for each sample. Data for both pyraclostrobin levels in soil and on leaves were analyzed for analysis of variation (ANOVA) using Proc Mixed in SAS,[22] with time after fungicide treatment as the fixed effect and replicate as the random variable. Means were separated at the $p < 0.05$ level using the Saxton Macro.[23]

RESULTS AND DISCUSSION

The BASF extraction method resulted in interfering peaks possibly because of polar molecules from the extraction matrix, which introduce error in the integration of peak areas; however, interfering peaks were reduced, and integration of pyraclostrobin peak area was significantly improved using the adapted QuEChERS method[18] (Figure 2). The QuEChERS data were used for subsequent analysis and modeling. Pyraclostrobin percent recovery from soil was determined to average 97% (±6%) by comparing the day 0 samples to non-treated controls from the same period. Data were not corrected for this minor amount. Similar recoveries from soil were reported previously.[12] The purity of the pyraclostrobin peak was checked by analyzing an extracted soil sample and pyraclostrobin standards using two different HPLC methods that employed columns of different polarity.

Pyraclostrobin degraded under laboratory-controlled soil conditions over the duration of the experiment (63 days) to levels that were about 50% of the initial amended level (Table 1). Initial pyraclostrobin levels measured in soil (3.17 $\mu g\ g^{-1}$) were significantly lower by 4 days (2.45 $\mu g\ g^{-1}$) and continued to decrease, with significant differences detected at 28 days (2.10 $\mu g\ g^{-1}$), 42 days (1.70 $\mu g\ g^{-1}$), and 63 days (1.55 $\mu g\ g^{-1}$).

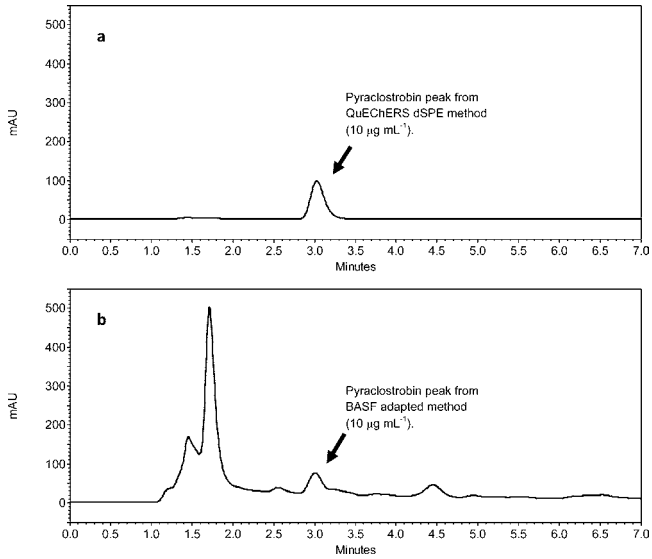

Figure 2. Chromatograms of pyraclostrobin in soil extract using (a) QuEChERS method or (b) BASF adapted method. The retention time for pyraclostrobin is 2.95 min. Note the decrease in intensity of the interfering peaks at 1.0−2.5 min using the QuEChERS method.

Table 1. Amount of Pyraclostrobin Extracted from Exposed Soil as a Function of the Exposure Time[a]

time (day)	concentration ($\mu g\ g^{-1}$ of soil)	total pyraclostrobin (μg)	fraction remaining
0	3.17 a[b]	190	1.00
4	2.45 b	147	0.77
11	2.20 b	133	0.70
14	2.22 bc	133	0.70
28	2.10 cd	123	0.65
42	1.70 de	105	0.55
63	1.55 e	93	0.49

[a]Each value is the mean of three replicates. [b]Means with the same letter are not different at the $p < 0.05$ level.

The results showed an initial rapid degradation, followed by a slower dissipation rate after several days (Figure 3). The results were fit to each of the four different models (Table 2). Although the SFO model does an adequate job of approximating the DT_{50} value at 65 days (similar to the experimentally determined value), the goodness of fit as measured by inspection of the residual plot is poor (Figure 4) and the model efficiency (EF) (0.8139) is unsatisfactory (Table 3). The dissipation kinetics appears to be biphasic, which is commonly characterized by a rapid decrease in the concentration, followed by a slower rate of decrease. This may be due to a reduction in substrate availability because of adsorption onto soil organic matter. In addition to the SFO model, three biphasic models (FOMC, HS, and DFOP) were used to model the data.[20] The HS and DFOP models have the best fit graphically, with acceptable residual plots (Figure 4). The χ^2 values are lowest for these two models (7.815 for both), and the model EFs are 0.9946 and 0.9945, respectively (Table 3), suggesting that they have the best agreement with the data. However, it should be noted that the HS model is not commonly used for modeling soil degradation kinetics because

dx.doi.org/10.1021/jf405506p | J. Agric. Food Chem. 2014, 62, 2141−2146

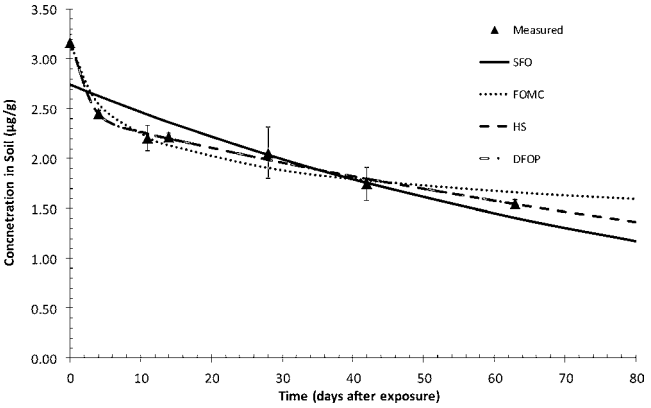

Figure 3. Degradation of pyraclsotrobin in amended soil under controlled conditions at an initial concentration of 3.17 μg mL^{-1}. Measured values are the mean (n = 3) ± standard deviation. The best-fit data for the models: (a) simple first-order kinetics model (SFO), (b) Gustafson−Holden multi-compartment model (FOMC), (c) hockey-stick model (HS), and (d) bi-exponential model (DFOP).

Table 2. Calculated Parameters for the Four Models: (1) Simple First-Order Kinetics Model (SFO), (2) Gustafson−Holden Multi-compartment Model (FOMC), (3) Hockey-Stick Model (HS), and (4) Bi-exponential Model (DFOP)

parameter	SFO	FOMC	HS	DFOP
C_0[a] (μg g^{-1})	2.74	3.15	3.17	3.17
k_1[b] (day^{-1})	0.0106		0.0640	0.5421
k_2[c] (day^{-1})			0.0072	0.0072
g[d]				0.2310
a[e]		0.1765		
b[f] (day^{-1})		1.7233		
t_b[g] (day)			4.6300	

[a]C_0 = concentration at t = 0. [b]k_1 = rate constant until $t = t_b$. [c]k_2 = rate constant from $t = t_b$. [d]g = fraction of C_0 applied to compartment 1. [e]a = shape parameter. [f]b = location parameter. [g]t_b = breakpoint (time at which the rate constant changes).

Table 3. Comparison of the Calculated End Points, DT_{50} and DT_{90}, Model Efficiency (EF), and the χ^2 Test with the Four Models: (1) Simple First-Order Kinetics Model (SFO), (2) Gustafson−Holden Multi-compartment Model (FOMC), (3) Hockey-Stick Model (HS), and (4) Bi-exponential Model (DFOP)[a]

	SFO	FOMC	HS	DFOP
DT_{50} (day)	65	86	59	60
DT_{90} (day)	217	797030	282	282
m (degree of freedom)	5	4	3	3
visual (residual plot)	not good	fair	good	good
χ^2 calculated (0.05, m)	11.07	9.488	7.815	7.815
model efficiency (EF)	0.8139	0.9676	0.9946	0.9945

[a]Models 1, 3, and 4 are similar in their predictions.

it offers no advantage over the other two biphasic models.[20] Calculated DT_{50} and DT_{90} values were 59 and 282 days, respectively, using the HS model and 60 and 282 days, respectively, using the DFOP model. The DT_{50} values are in agreement with the experimentally determined DT_{50} value of 63 days. The FOMC has an appreciable model efficiency of 0.9676, but visual inspection of the fit shows that the model is not appropriate for pyraclostrobin dissipation modeling. While the residual plot is fair, it is not as accurate as the HS and DFOP models.

The value obtained for DT_{50} here (63 days) was higher than other reported values. Reddy et al.[14] found DT_{50} range from a low of 9.2 days (sludge-amended soil) to 47 days (sterilized soil), with an average of 28 days. Zhang et al.[12] found DT_{50} in peanut field soil to be 13−17 days. Footprint[13] lists "typical" DT_{50} of 32 days. The slower dissipation of pyraclostrobin observed in the present study was similar to dissipation of another strobilurin, axozystrobin, in soil amended with compost (DT_{50} = 73 days).[24] However, varied rates of azoxystrobin dissipation are also common. Wang et al.[25] reported a range of azoxystrobin DT_{50} in soil used to cultivate bananas of 8.8−13 days. The rate of pyraclostrobin should minimally impact dissipation, as Reddy et al.[14] showed similar DT_{50} (28 days) for soil amended with either 1 or 10 μg g^{-1}. The slow dissipation may be related to the field not having a prior history of pyraclostrobin application. Additional applications may lead to enhanced dissipation, as reported for the fungicide tebuconazole in agricultural soil.[26] Repeated applications during one growing season resulted in DT_{50} decreases from 43 to 5 days.[26] The recommended split applications of pyraclostrobin may result in a similar scenario. Indeed, in a field trial, only low levels of pyraclostrobin were detected (≤0.20 μg g^{-1}) in soil following four applications at higher than label rates (112.5 g of a.i. ha^{-1}).[12] Organic components of the soil are also likely to affect the dissipation rate in soil. The log K_{oc} for pyraclostrobin is 3.96,[16] which is moderately high, indicating strong adsorption to the soil. However, the low organic matter content of the soil (1.61%) most likely significantly reduces this effect.

Because pyraclostrobin is primarily applied to leaves to control brown rust, a wash-off study was conducted to determine if a time period existed after application when precipitation would most likely result in pyraclostrobin wash-off onto the soil surface. By taking 57 000 stalks ha^{-1},[28] a rainfall event of 2.28 mm would need to occur to obtain the equivalent of 2 L of wash-off water per 5 stalks sampled. Daily rainfall amounts of at least 2.28 mm were recorded on May 1, 2, 10, 11, 22, and 23, 2013, and June 2, 8, 9, 11, 14, 23, and 29, 2013 at the Ardoyne Farm. The timing of these rains coincided with the highest incidence of brown rust.[1] However, yearly weather patterns will dictate brown rust severity. Additionally, rainfall events exceeded 2.28 mm at 75 and 47% of the time for May and June 2013 at the study site, respectively. Thus, wash-off of pyraclostrobin onto the soil surface is a legitimate environmental fate for pyraclostrobin in Louisiana sugarcane fields. Initial measurements prior to pyraclostrobin application indicated no presence of the chemical (Figure 5). Significant pyraclostrobin in the wash was observed at 30 min after application, with a value of over 35 μg g^{-1} dry leaf tissue. Significant decreases in pyraclostrobin wash-off were observed at each subsequent sample time, with a 38, 32, 57, and 52% reduction at 6, 24, 48, and 72 h, respectively (Figure 5). The amount recovered at 72 h was not statistically different from the control. The data are in good agreement with the product label that lists a rain fastness of 48 h for Headline SC.[27]

The QuEChERS method allowed for better baseline chromatogram linearity as well as shortened analysis time per sample. The DT_{50} for pyraclostrobin in this study was 63 days. The value is higher than previously reported DT_{50} and indicates that pyraclostrobin is moderately persistent to persistent in Louisiana sugarcane soil. Modeling suggests that the degradation of the pesticide follows biphasic kinetics. Wash-off studies

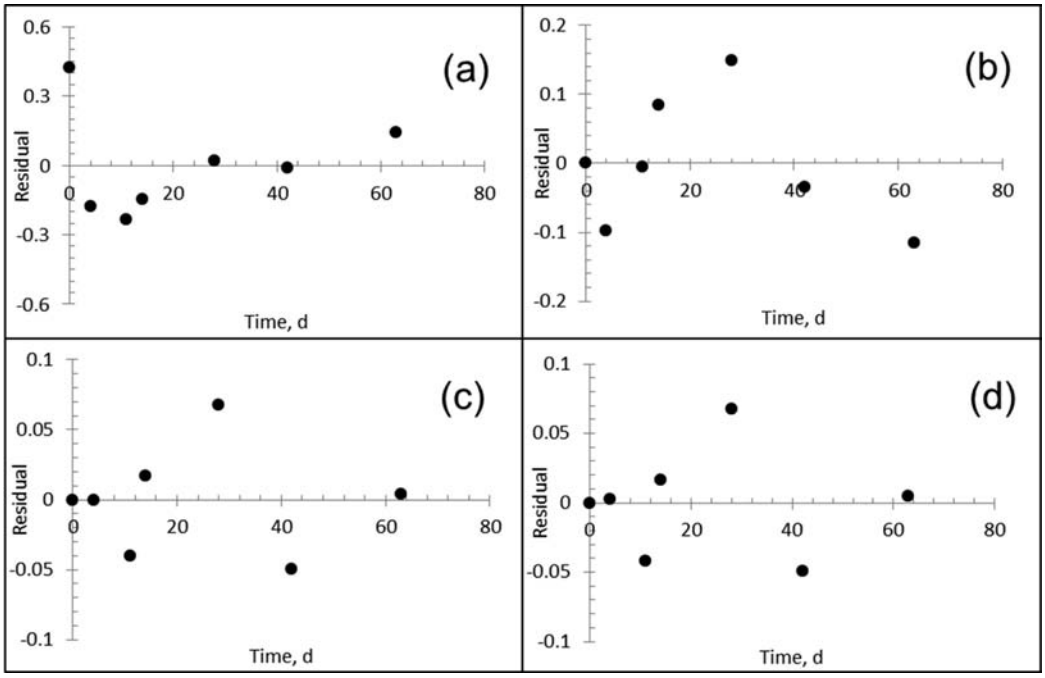

Figure 4. Residual plots for the best-fit data for the models: (a) simple first-order kinetics model (SFO), (b) Gustafson−Holden multi-compartment model (FOMC), (c) hockey-stick model (HS), and (d) bi-exponential model (DFOP).

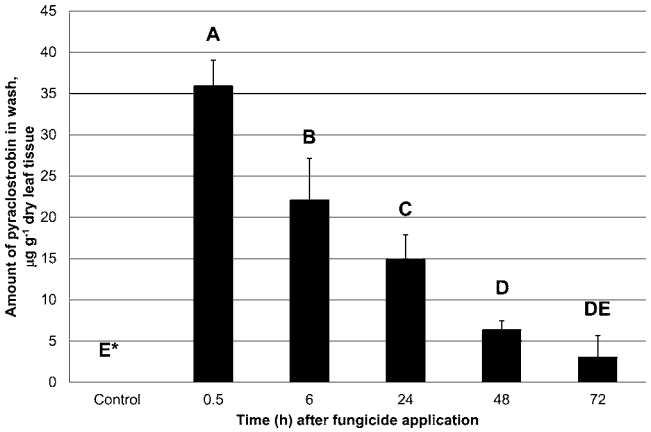

Figure 5. Appearance of pyraclostrobin in the wash-off after application to sugarcane leaves. No rainfall occurred during the period of the study. (∗) Bars with the same letter are not different at the $p < 0.05$ level.

indicate that application of Headline SC within 48 h of a rainfall event may result in significant transport of pyraclostrobin off of leaf surfaces. With the resurgence of brown rust and discovery of orange rust, applications of pyraclostrobin and other strobilurin and triazole fungicides will remain a necessity. Prudent spray timing designed to miss rainfall events will improve chemical effectiveness and sugarcane yields.

AUTHOR INFORMATION

Corresponding Author

*Telephone: 985-448-4502. Fax: 985-448-4641. E-mail: darcey.wayment@nicholls.edu.

Funding

Funding was provided by Nicholls State University and the USDA−ARS Sugarcane Research Unit in Houma, LA. Mention of trade names or commercial products is solely for the purpose of providing specific information and does not imply recommendation or endorsement by the USDA.

Notes

The authors declare no competing financial interest.

ACKNOWLEDGMENTS

The laboratory assistance of Catherine Danos was greatly appreciated.

REFERENCES

(1) Hoy, J.; Hollier, C. Effect of brown rust on yield of sugarcane in Louisiana. *Plant Dis.* **2009**, *93*, 1171−1174.

(2) Legendre, B.; Gravois, K. The 2005 Louisiana sugarcane variety survey. *Sugar Bull.* **2005**, *83*, 15−21.

(3) Legendre, B.; Gravois, K. The 2009 Louisiana sugarcane variety survey. *Sugar Bull.* **2009**, *87*, 17−22.

(4) Hoy, J. Impact of rust on LCP 85-384. *Sugar Bull.* **2005**, *84*, 12−13.

(5) Orgeron, A. Personal communication, 2013.

(6) Bogren, R. *New Disease Reaches Louisiana Sugarcane*; LSUAgCenter: Baton Rouge, LA, 2012; http://www.lsuagcenter.com/news_archive/2012/july/headline_news/New-disease-reaches-Louisiana-sugarcane.htm (accessed July 16, 2013).

(7) Mossler, M. *Crop Profile for Sugarcane in Florida*; IPM Center: Raleigh, NC, 2008; http://www.ipmcenters.org/cropprofiles/docs/FLsugarcane.pdf (accessed July 16, 2013).

(8) United States Environmental Protection Agency (U.S. EPA). *Pyraclostrobin; Pesticide Tolerances for Emergency Exemptions*; U.S. EPA: Washington, D.C., 2009; Federal Register Publication EPA-HQ-OPP-2008-0936, p 74.

(9) United States Environmental Protection Agency (U.S. EPA). *Extension of Tolerances for Emergency Exemptions (Multiple Chemicals)*; U.S. EPA: Washington, D.C., 2011; Federal Register Publication EPA-HQ-OPP-2011-0972, p 76.

(10) Lanoiselet, V.; Cother, E.; Ash, G.; Harper, J. Yield loss in rice caused by *Rhizoctonia oryzae* and *R. oryzae-sativae* in Australia. *Australas. Plant Pathol.* **2005**, *34*, 175−179.

(11) You, X.; Liu, C.; Liu, F.; Liu, Y.; Dong, J. Dissipation of pyraclostrobin and its metabolite BF-500-3 in maize under field conditions. *Ecotoxicol. Environ. Saf.* **2012**, *80*, 252−257.
(12) Zhang, F.; Wang, L.; Zhou, L.; Wu, D.; Pan, H.; Pan, C. Residue dynamics of pyraclostrobin in peanut and field soil by QuEChERS and LC−MS/MS. *Ecotoxicol. Environ. Saf.* **2012**, *78*, 116−122.
(13) Footprint. *Pesticide Properties Database (PPDB)*; http://sitem.herts.ac.uk/aeru/footprint/en/index.htm (accessed July 16, 2013).
(14) Reddy, S.; Gupta, S.; Gajbhiye, V. Effect of moisture, organic matter, microbial population and fortification on dissipation of pyraclostrobin in soils. *Bull. Environ. Contam. Toxicol.* **2013**, *91*, 356−361.
(15) Lagunas-Allué, L.; Martínez-Soria, M.; Sanz-Asensio, J.; Salvador, A.; Ferronato, C.; Chovelon, J. Degradation intermediates and reaction pathway of pyraclostrobin with TiO_2 photocatalysis. *Appl. Catal., B* **2012**, *115−116*, 285−293.
(16) Health Canada Pest Management Regulatory Agency. *Regulatory Note: Pyraclostrobin*; Health Canada Pest Management Regulatory Agency: Ottawa, Ontario, Canada, 2003; Publication REG2003-06, p 7.
(17) Collins, L.; Gooding, R. *Pyraclostrobin, U.S. Environmental Protection Agency Index of Environmental Chemistry Methods (ECM), An LC−MS Method for the Analysis of Pyraclostrobin in Soil. Provided by BASF to the EPA. MRID 451187-07, The Determination of BAS 500F and Its Metabolites, BF 500-3, BF 500-4, BF 500-5, BF 500-6, and BF 500-7 in Soil Using LC/MS*; BASF Corporation: Research Triangle Park, NC, 1999; Tech. No. 1999/5087, http://www.epa.gov/pesticides/methods/ecmmethods/451187-07-S.pdf (accessed Nov 12, 2013).
(18) Payá, P.; Anastassiades, M.; Mack, D.; Sigalova, I.; Tasdelen, B.; Oliva, J.; Barba, A. Analysis of pesticide residues using the quick easy cheap effective rugged and safe (QuEChERS) pesticide multiresidue method in combination with gas and liquid chromatography and tandem mass spectrometric detection. *Anal. Bioanal. Chem.* **2007**, *389*, 1697−1714.
(19) Nageswara, R.; Ramesh, A.; Parvathamma, T.; Suresh, G. Development and validation of a HPLC−UV method for simultaneous determination of strobilurin fungicide residues in tomato fruits followed by matrix solid-phase dispersion (MSPD). *Indian J. Sci. Res.* **2012**, *3*, 113−118.
(20) Forum for the Coordination of Pesticide Fate Models and Their Use (FOCUS). *Guidance Document on Estimating Persistence and Degradation Kinetics from Environmental Fate Studies on Pesticides in EU Registration*; Report of the FOCUS Work Group on Degradation Kinetics, EC Document Reference Sanco/10058/2005, version 2.0, 2005; http://focus.jrc.ec.europa.eu/dk/docs/finalreportFOCDegKin04June06linked.pdf (accessed July 17, 2013).
(21) Gustafson, D.; Holden, L. Nonlinear pesticide dissipation in soil: A new model based on spatial variability. *Environ. Sci. Technol.* **1990**, *24*, 1032−1038.
(22) SAS Institute. *SAS for Windows, Version 9.2*; SAS Institute: Cary, NC, 2008.
(23) Saxton, A. M. A macro for converting mean separation output to letter groupings in PROC MIXED. *Proceedings of the 23rd SAS Users Group International Conference*; April 11−14, 1999; pp 1243−1246.
(24) Ghosh, R.; Singh, N. Effect of organic manure on sorption and degradation of azoxystrobin in soil. *J. Agric. Food Chem.* **2009**, *57*, 632−636.
(25) Wang, S.; Sun, H.; Liu, Y. Dissipation and residue of azoxystrobin in banana under field condition. *Environ. Monit. Assess.* **2013**, *185*, 7757−7761.
(26) Potter, T.; Strickland, T.; Joo, H.; Culbreath, A. Accelerated soil dissipation of tebuconazole following multiple applications to peanut. *J. Environ. Qual.* **2005**, *34*, 1205−1213.
(27) BASF Corporation. *Headline SC Specimen Label. EPA Reg. No. 7969-186*; BASF Corporation: Research Triangle Park, NC, 2012; http://agproducts.basf.us/app/cdms?manuf=16&pd=6223&ms=2274 (accessed July 17, 2013).
(28) Viator, R. P. Personal communication, 2013.

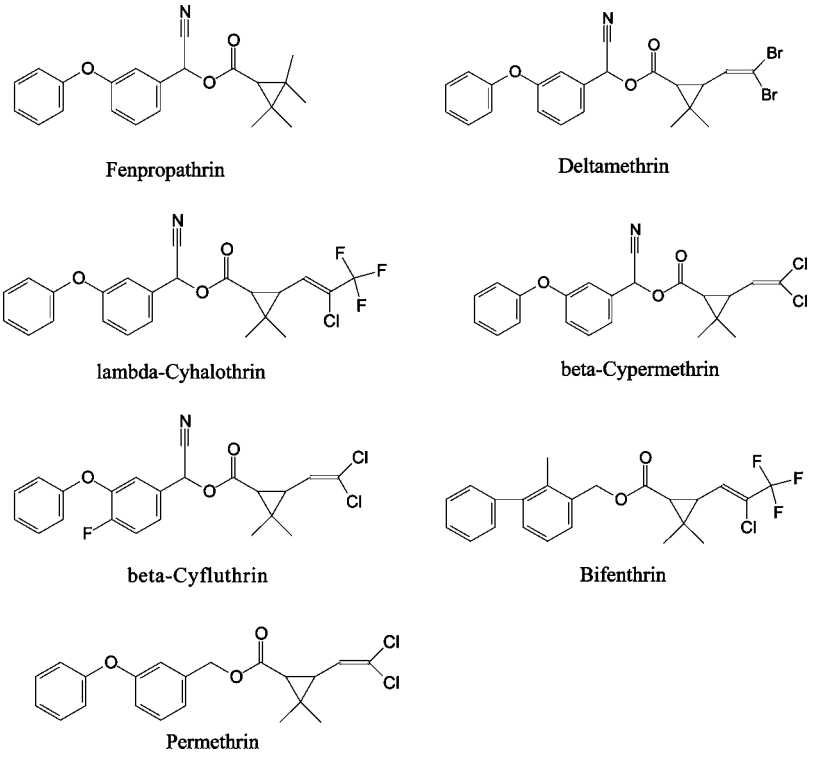

Figure 1. Molecular structures of SPs.

xenobiotic compounds can be successfully eliminated by diverse microorganisms belonging to different taxonomic groups.[25−29] Recently, Cycoń et al.[24] reported that *Bacillus* sp. TDS-2 isolated from sandy soil successfully removed thiophanate-methyl (100 mg kg^{-1}) from soils within 24 days. Chen et al.[26] reported that about 80% of the initial dose of *β*-cypermethrin (50 mg kg^{-1}) was removed from the sterilized soils by *Streptomyces aureus* HP-S-01 within 10 days. A few bacterial species, including *Sphingobium* sp. JZ-2,[30] *Sphingobium* sp. JQL4-5,[31] *Clostridium* sp. ZP3,[32] and *Ochrobactrum trtici* pyd-1,[33] have been reported for the degradation of fenpropathrin. However, these isolates commonly degraded only a couple of pyrethroid insecticides, which may limit their use in bioremediation as various regions are usually contaminated by multiple pyrethroid compounds.[3,4,9−11] Furthermore, little is known about the biodegradation pathway and catalytic mechanisms of fenpropathrin.

In our previous study, *Bacillus* sp. DG-02 was isolated from the pyrethroid-manufacturing wastewater treatment system.[34] In the present study, we demonstrated that strain DG-02 was capable of degrading not only fenpropathrin but also other related SPs. The aims of this study were to investigate the biodegradation kinetics and to determine the bacterial metabolic products of fenpropathrin. Finally, our findings highlight the promising potentials and advantages of *Bacillus* sp. DG-02 for bioremediation of pyrethroid-contaminated environments.

MATERIALS AND METHODS

Chemicals. Deltamethrin (98%), fenpropathrin (93%), *λ*-cyhalothrin (95%), *β*-cypermethrin (94.8%), *β*-cyfluthrin (95%), bifenthrin (98%), and permethrin (95%) were obtained from Zhongshan Aestar Fine Chemical Inc., Ltd., China. The chromatographic grade acetonitrile were purchased from Sigma-Aldrich, USA. The chemicals were dissolved in dimethyl sulfoxide (DMSO) or acetone at a stock concentration of 10 g L^{-1}, and stored in dark bottles at 4 °C prior to use. The stock solutions were sterilized by membrane filtration and rationed into medium to get the desired concentrations. At high concentrations, polysorbate 80 was used as emulsifier to disperse the possible precipitate in the liquid medium. All other chemicals and solvents used in this study were of analytical grade.

Bacterium Used in This Study. The mineral salt medium (MSM) containing (g L^{-1}) $(NH_4)_2SO_4$, 2; $MgSO_4{\cdot}7H_2O$, 0.2; $CaCl_2{\cdot}2H_2O$, 0.01; $FeSO_4{\cdot}7H_2O$, 0.001, $Na_2HPO_4{\cdot}12H_2O$, 1.5; and KH_2PO_4, 1.5, was used for the isolation of potential degrading strains. The final pH was adjusted to 7.5. The bacterial strain DG-02, which was deposited in the China Center for Type Culture Collection (collection no. CCTCC M 20111382), was isolated from a pyrethroid-manufacturing wastewater treatment system using an enrichment culture technique.[34] In this study, the bacterium was further identified by API 50 CHB systems (bioMérieux Inc., France) according to the instructions of the manufacturer.

Inoculum Preparation. The bacterial strain was stored in 15% glycerol at −80 °C. Before each experiment the strain was thawed and grown in 250 mL Erlenmeyer flasks containing 50 mL of sterile Luria−Bertani (LB) medium (containing tryptone, 10 g L^{-1}; yeast extract, 5 g L^{-1}; NaCl, 10 g L^{-1}). At 30 °C, the flasks were placed on a platform shaker at 180*g*. The bacterial cells in the late-exponential growth phase were harvested by centrifugation (5 min, 4000*g*) at 4 °C and washed twice in 0.9% normal saline (N-saline) before inoculation. Unless otherwise stated, the densities of strain DG-02 were adjusted with sterile N-saline to approximately 1.0×10^8 colony-forming units (CFU) mL^{-1}. One percent of this suspension was used as the inocula for the subsequent studies.

Growth and Degradation Experiments. For the growth and degradation experiments, triplicate cultures were grown in MSM supplemented with 50 mg L^{-1} of fenpropathrin as the sole carbon source at 30 °C and 180*g* on a rotary shaker. A noninoculated culture served as a control. Samples were collected periodically from the cultures. The bacterial growth was monitored by counting the CFU per liter of serial dilutions, and the amount of residual fenpropathrin was determined by high-performance liquid chromatography (HPLC) as described below.

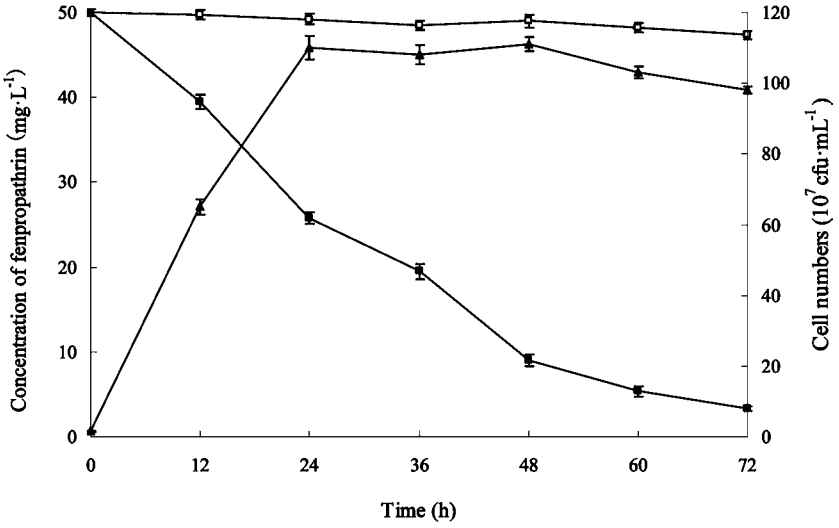

Figure 2. Degradation and utilization of fenpropathrin (50 mg L^{-1}) during growth of strain DG-02: (□) fenpropathrin control; (■) fenpropathrin degradation by strain DG-02; (▲) cell growth. Error bars indicate the standard deviation of three replicates.

The mineral salt media containing different final concentrations of fenpropathrin (25, 50, 100, 200, 400, 600, 800, 1000, and 1200 mg L^{-1}) were inoculated respectively with strain DG-02 and incubated at 30 °C and 180*g* on a rotary shaker. Each treatment was performed in triplicate, and fenpropathrin residues were measured at an interval of 12 h.

Identification of Metabolites during Fenpropathrin Degradation. The metabolic products of fenpropathrin in cell-free filtrates of strain DG-02 cultures containing different concentrations of fenpropathrin (50, 100, and 200 mg L^{-1}) were extracted and identified by gas chromatopraphy−mass spectrometry (GC-MS) (Agilent 6890N/5975, USA). The cell-free filtrates were taken at an interval of 12 h. The same bacterial culture supernatants lacking fenpropathrin were used as a negative control, and noninoculated control containing the same amount of fenpropathrin was included as well. The metabolites were extracted with ethyl acetate from the cell-free filtrates after acidification to pH 2 with 2 M HCl. The organic layer was dehydrated, dried, and redissolved in methanol.[30,35] After filtration with a 0.45 μm membrane (Millipore, USA), the samples were subjected to GC-MS as described below. The metabolites identified by mass spectrometry analysis were matched with authentic standard compounds from the National Institute of Standards and Technology (NIST, USA) library database.

Degradation Kinetics of Various SPs. To determine its ability to degrade various SPs, strain DG-02 was inoculated into fresh MSM supplemented with 50 mg L^{-1} deltamethrin, λ-cyhalothrin, β-cypermethrin, β-cyfluthrin, bifenthrin, and permethrin, respectively. Triplicate cultures were grown in MSM at 30 °C. Degradation measurements were carried out periodically as described above.

Biodegradation of Fenpropathrin in Soils. The soil samples were collected from the top 0−20 cm from a farm in South China Agricultural University, Guangzhou, southern China, that had never been treated with fenpropathrin or organic and inorganic fertilizers. The detailed physicochemical properties of the soils were (g kg^{-1} of dry weight): organic matter, 10.5; total N, 0.5; total P, 0.4; total K, 18.2; and pH, 6.9. The soils have a sandy loam texture (sand, 65.0%; silt, 28.0%; clay, 7.0%).[34] In the laboratory, the soils were gently air-dried to the point of soil moisture suitable for sieving. After sieving to a maximum particle size of <2 mm, the soils were used in the bioremediation experiments.

The bioremediation experiment with strain DG-02 was performed in sterile and nonsterile soils. In the first case, soils were sterilized by autoclaving for 1 h at 121 °C. The stock solution of fenpropathrin was sprayed on the surface of 200 g of sterile and nonsterile soils.[24] The applied dose of insecticide corresponded to a soil concentration of 50 mg kg^{-1}. After thorough mixing, the bacterial suspension was introduced in triplicate into the soils by drip irrigation to give a final bacterial count of approximately 1.0×10^8 CFU g^{-1} of soil. The triplicate samples of sterile and nonsterile soils without strain DG-02 were kept as controls, respectively. The same amount of pesticide was applied to these soils. The water contents were adjusted to approximately 40% of water-holding capacity by the addition of sterile deionized water.[24] All of the soil samples were incubated in a darkened thermostatic chamber maintained at 30 °C for 15 days. Soil treatments (20 g) were removed aseptically at 0, 3, 6, 9, 12, and 15 days for the determination of fenpropathrin concentrations.

Chemical Analyses. Pyrethroid quantification was performed on an Agilent 1100 HPLC equipped with a ternary gradient pump, programmable variable-wavelength UV detector, column oven, electric sample valve, and C_{18} reversed-phase column (Hypersil ODS2 5 μm × 4.6 mm × 250 mm) with array detection from 190 to 400 nm (total scan) based on retention time and peak area of the pure standard. The samples were performed using a mobile phase of 90:10 acetonitrile/water. Sample injection volume was 10 μL, and mobile phase was programmed at a flow rate of 1 mL min^{-1}.[36,37]

The metabolites of fenpropathrin were confirmed on an Agilent 6890N/5975 GC-MS system equipped with an autosampler and on-column, split/splitless capillary injection system, with a HP-5MS capillary column (30.0 m × 250 μm × 0.25 μm) with array detection from 30 to 500 nm (total scan). The operating conditions were as follows: the column was held initially at a temperature of 90 °C for 2 min, then raised at 6 °C min^{-1} to 150 °C for 1 min, at 10 °C min^{-1} to 180 °C for 4 min, and finally at 20 °C min^{-1} to 260 °C for 10 min. The temperatures corresponding to the transfer line and the ion trap were 280 and 230 °C, respectively, and the ionization energy was 70 eV. The injection volume was 1.0 μL with splitless sampling at 250 °C. Helium was used as a carrier gas at a flow rate of 1.5 mL min^{-1}.[38]

Kinetics Analyses. The substrate inhibition model (eq 1) was used to fit the specific degradation rate (q) at different initial concentrations of fenpropathrin.

$$q = \frac{q_{max} S}{S + K_s + (S^2/K_i)} \quad (1)$$

q_{max} is the maximum specific fenpropathrin degradation rate (h^{-1}), K_i is the substrate inhibition constant (mg L^{-1}), K_s is the half-saturation constant (mg L^{-1}), and S is the inhibitor concentration (mg L^{-1}).

The disappearance of fenpropathrin and other pyrethroids in MSM or soils was fitted to the first-order kinetic model (eq 2).

$$C_t = C_0 \times e^{-kt} \quad (2)$$

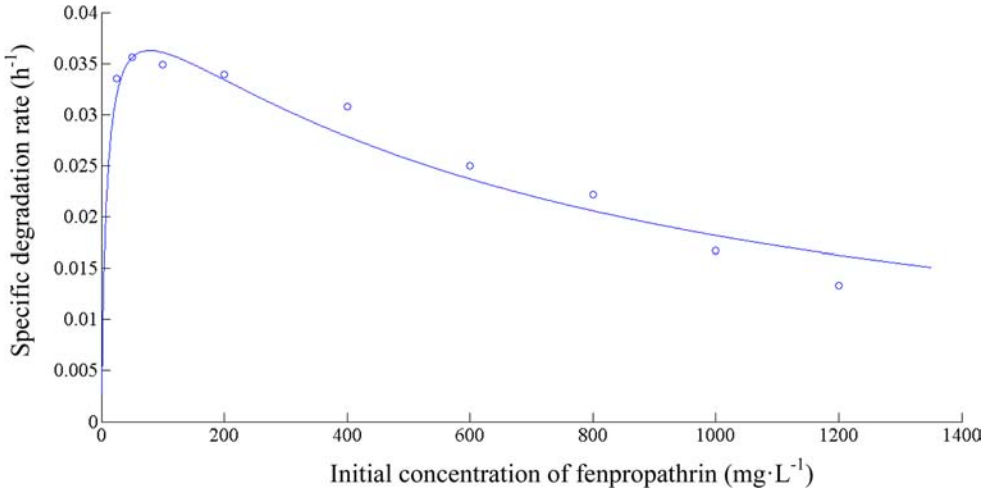

Figure 3. Relationship between initial fenpropathrin concentration and specific degradation rate by strain DG-02.

C_0 is the amount of substrate at time zero, C_t is the amount of substrate at time t, and k and t are the degradation rate constant (h^{-1}) and degradation period in hours, respectively.

The algorithm as expressed in eq 3 was used to determine the theoretical half-life ($t_{1/2}$) values of fenpropathrin and other pyrethroids.

$$t_{1/2} = \frac{\ln(2)}{k} \tag{3}$$

ln 2 is the natural logarithm of 2, and k is the rate constant (h^{-1}).

RESULTS AND DISCUSSION

Identification of Strain DG-02 Using API Systems. In our previous studies, stain DG-02 was tentatively identified as *Bacillus* sp. based on the morphology and 16S rDNA gene analysis.[34] In this study, the bacterium was further classified as *Bacillus cereus* by API 50 CHB systems (bioMérieux Inc., France) according to the instructions of the manufacturer, with good identification (95.3%). It was positive in tests such as glycerol, maltose, ribose, trehalose, adonitol, cellobiose, gluconate, and *N*-acetylglucosamine. It was negative in tests such as erythritol, sannose, sorbose, rhamnose, melibiose, 5-keto-D-gluconate, and methyl α-D-mannoside. Detailed biochemical properties of strain DG-02 are presented in Table S1 in the Supporting Information.

Utilization of Fenpropathrin as a Growth Substrate by Strain DG-02. The growth of strain DG-02 on fenpropathrin and the ability of this bacterium to degrade fenpropathrin are shown in Figure 2. Strain DG-02 degraded fenpropathrin rapidly with about 82% of the initial dose being eliminated within 48 h. During this time, the number of strain DG-02 cells was increased to its maximum level. After incubation for 72 h, approximately 93.3% of the added fenpropathrin was degraded by strain DG-02 when fenpropathrin was used as the growth substrate. It is worth mentioning that partial bacterial strain DG-02 perhaps utilize their dead cells for growth. Finally, the residual amount of the pesticide was not detectable by HPLC at 120 h post incubation (data not shown). In contrast with previous studies, the current study showed that the strain DG-02 could efficiently degrade fenpropathrin, suggesting this isolate may be an ideal candidate for bioremediation of a fenpropathrin-contaminated environment. In the control test, no significant change in fenpropathrin concentration was observed in the uninoculated medium.

Biodegradation of Fenpropathrin with Different Initial Concentrations. To test the effect of fenpropathrin concentration on its degradation, strain DG-02 was inoculated to the media containing various initial fenpropathrin concentrations ranging from 25 to 1200 mg L^{-1} (Figure S1 in the Supporting Information). Strain DG-02 rapidly degraded and utilized the added fenpropathrin up to the concentration of 1200 mg L^{-1}, and a lag period was observed at higher fenpropathrin concentrations. At a concentration of 25 mg L^{-1}, the residual level of fenpropathrin could not be detected in just over 72 h. Further loading of the organic compound in subsequent experiments demonstrated that strain DG-02 was capable of degrading about 93.3 and 90.4% of fenpropathrin at a dose of 50 and 100 mg L^{-1} in 72 h, respectively, and the strain completely degraded the added doses in approximately 120 h. When the concentration was increased to 200, 400, and 600 mg L^{-1}, respectively, about 87.6, 84.7, and 80.5% degradations of this compound were observed in 72 h, respectively, and complete degradation occurred after a prolonged culture. Over this time period the cells could utilize only 75.8, 67.2, and 61.2% of fenpropathrin when it was given 800, 1000, and 1200 mg L^{-1}, respectively. These findings suggest that increased concentration of fenpropathrin has a slight effect on biodegradation performance of strain DG-02 with a modest increase in the duration of lag phase, but did not lead to complete inhibition or cell death. Previous studies showed that the pyrethroid-degrading strains usually transform the added pesticides with a concentration lower than 200 mg L^{-1}.[39,40] At higher concentrations, however, the metabolic activity of the reported pyrethroid-degrading strains was subject to complete catabolite repression.[41] Noticeably, our results suggest this particular isolate could tolerate and degrade fenpropathrin up to a concentration as high as 1200 mg L^{-1}. This feature gives the pesticide degrader a competitive advantage in variable environments, as they could survive and utilize the pollutants even exposed to a high concentration.[42]

The decrease in fenpropathrin degradation rate following an increase in the initial fenpropathrin concentration implies that fenpropathrin may act as a partial inhibitor to strain DG-02. To address this possibility, the substrate inhibition model (eq 1) adapted from Luong was used to fit the specific degradation rate (q) at different initial concentrations.[43] The relationship between q and S is shown in Figure 3. The kinetic parameters of strain DG-02 determined from nonlinear regression using

Table 1. Chromatographic Properties of Metabolites of Fenpropathrin during Degradation by Strain DG-02

Compound	RT (min)	*m/z*	Chemical structural formula in NIST library	Name
A	17.293	349	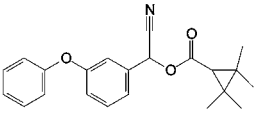	Fenpropathrin
B	15.919	218	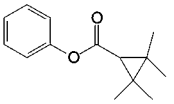	2,2,3,3-Tetramethyl cyclopropanecarboxylic acid phenyl ester
C	11.034	154	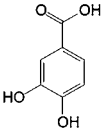	3,4-Dihydroxy benzoic acid
D	9.744	228	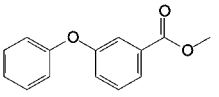	3-Phenoxybenzoate
E	9.576	154	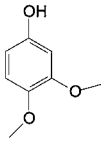	3,4-Dimethoxy phenol
F	8.025	198	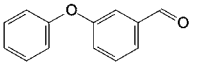	3-Phenoxybenzaldehyde
G	7.907	225	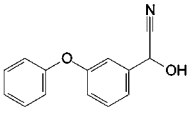	α-Hydroxy-3-phenoxy-benzeneacetonitrile
H	4.392	94	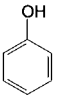	Phenol

matrix laboratory (MATLAB) software package (version 7.8) were q_{max} = 0.05 h^{-1} and K_s = 9.0 mg L^{-1}. The inhibitory effect of fenpropathrin was considered to occur in a linear manner at K_i = 694.8 mg L^{-1}. The critical inhibitor concentration (S_m) was established to be 78.9 mg L^{-1} by calculating the square root of $K_i \times K_s$. The coefficient of determination (R^2) was 0.9549, which indicates that the experimental data were well correlated with the model. As shown in Figure 3, when the initial concentration of fenpropathrin was <78.9 mg L^{-1}, the q value was gradually increased. At higher concentrations, inhibition by fenpropathrin became substantial and the q value was proportionally decreased in a dosage-dependent manner. This reveals that the fenpropathrin degradation activity of strain DG-02 could be partially inhibited at a high concentration of fenpropathrin but may not lead to a complete repression.

Degradation Products and Degradation Pathway of Fenpropathrin. The predicted chemical structures, retention times (RT), and characteristic ions of the mass spectra (m/z) are summarized in Table 1. Compound **A**, with a RT of 17.293 min, showed a prominent protonated molecular ion at m/z 349, which is similar to the characteristic parental ion of fenpropathrin (Figure 4a). Additionally, compound **A** also has the same RT as the authentic fenpropathrin. Therefore, compound **A** was identified as fenpropathrin. Along with the degradation process, compound **A** disappeared concomitantly with formation of seven new compounds (Figure 4b–h). The changes in fenpropathrin peak area over time are shown in Figure S2 in the Supporting Information. The seven compounds were characterized as 2,2,3,3-tetramethylcyclopropanecarboxylic acid phenyl ester, 3,4-dihydroxybenzoic acid, 3-phenoxybenzoate, 3,4-dimethoxyphenol, 3-phenoxybenzaldehyde, α-hydroxy-3-phenoxybenzeneacetonitrile, and phenol, respectively, on the basis of the similarity of their fragment retention times and molecular ions to those of corresponding authentic compounds in the NIST library database (Figure S3 in the Supporting Information). Among these products, 3-phenoxybenzaldehyde, 3-phenoxybenzoate, and 3,4-dimethoxybenzoic acid were also reported during the degradation of fenpropathrin in previous studies,[30,33] but the other four metabolic products of fenpropathrin were detected for the first time in this study. These metabolite concentrations were very low. We also noted that these metabolites were transient, suggesting that fenpropathrin was completely degraded by the strain DG-02 without any noncleavable metabolites at the end of the experiment. In the negative control lacking fenpropathrin, none of these metabolites was detected. In the noninoculated control containing the same amount of fenpropathrin, only fenpropathrin was detected (Figure S4 in the Supporting Information).

dx.doi.org/10.1021/jf404908j | J. Agric. Food Chem. 2014, 62, 2147–2157

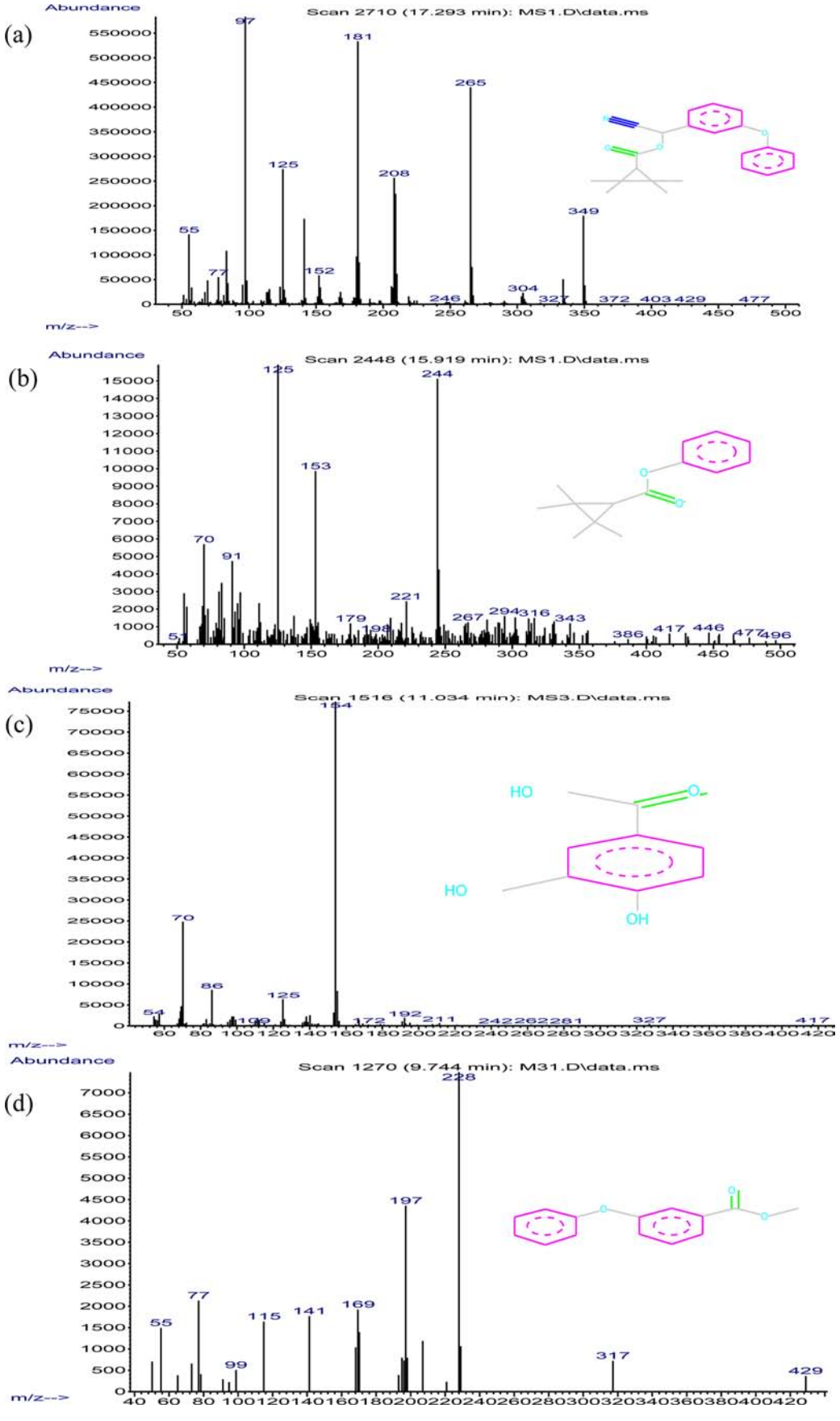

Figure 4. continued

dx.doi.org/10.1021/jf404908j | J. Agric. Food Chem. 2014, 62, 2147−2157

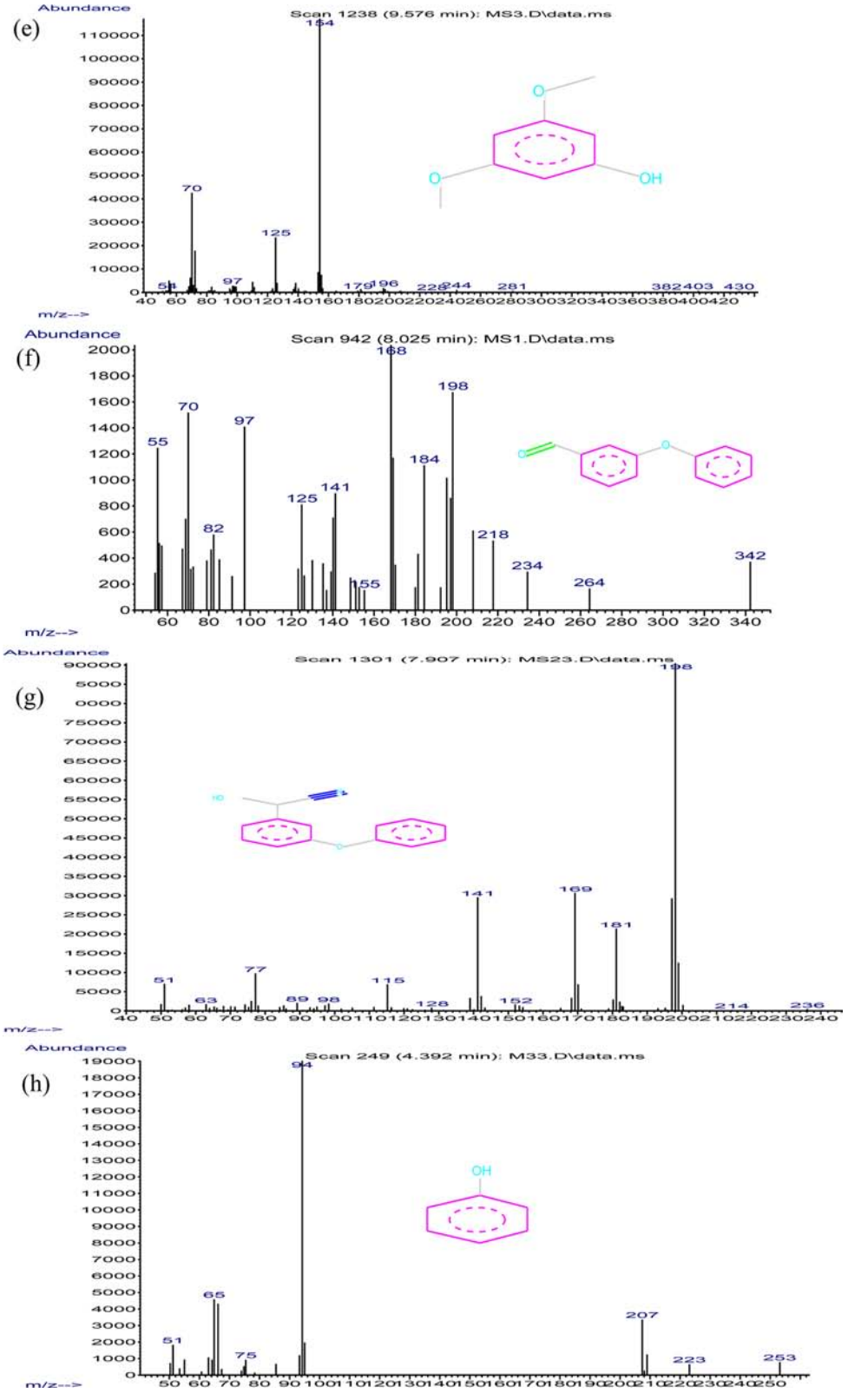

Figure 4. GC-MS analysis of the metabolites produced from fenpropathrin degradation by strain DG-02. (a–h) Characteristic ions of compounds **A–H** in GC-MS. The retention times of the compounds were 17.293, 15.919, 11.034, 9.744, 9.576, 8.025, 7.907, and 4.392 min, respectively, which were identified as fenpropathrin, 2,2,3,3-tetramethylcyclopropanecarboxylic acid phenyl ester, 3,4-dihydroxybenzoic acid, 3-phenoxybenzoate, 3,4-dimethoxyphenol, 3-phenoxybenzaldehyde, α-hydroxy-3-phenoxybenzeneacetonitrile, and phenol, respectively.

On the basis of the chemical structures of fenpropathrin and the metabolic products formed during fermentation, we propose a degradation pathway of fenpropathrin in strain DG-02 (Figure 5). According to this pathway, fenpropathrin was initially hydrolyzed by cleavage of the carboxylester linkage to produce α-hydroxy-3-phenoxybenzeneacetonitrile and

dx.doi.org/10.1021/jf404908j | J. Agric. Food Chem. 2014, 62, 2147–2157

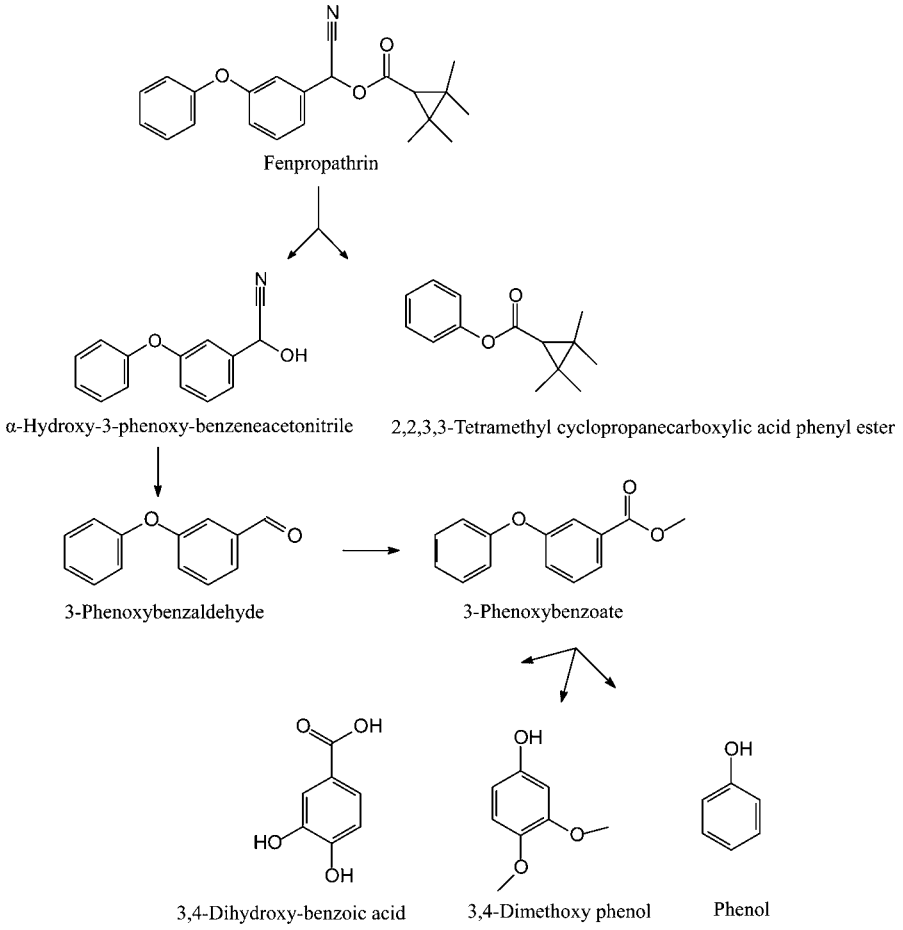

Figure 5. Proposed pathway for degradation of fenpropathrin in strain DG-02.

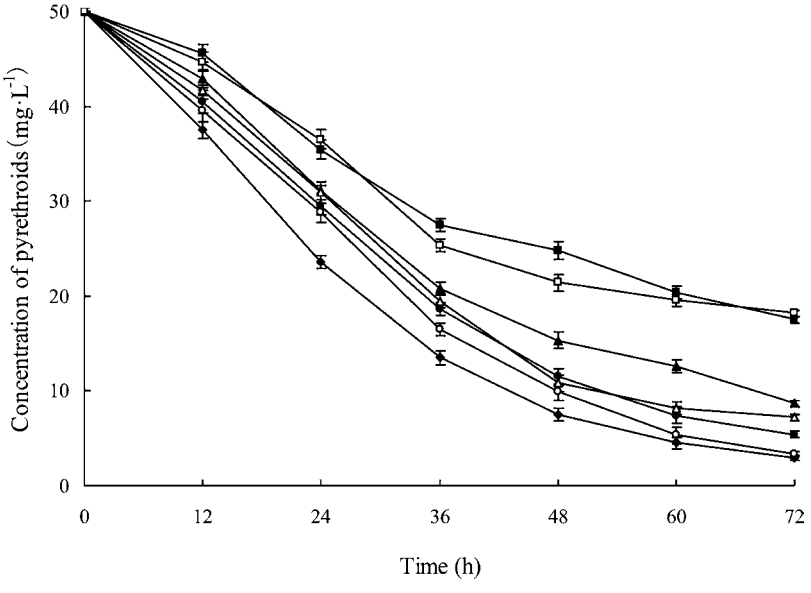

Figure 6. Degradation kinetics of various SPs by strain DG-02: (◆) deltamethrin; (◇) fenpropathrin; (●) *β*-cypermethrin; (△) *β*-cyfluthrin; (▲) *λ*-cyhalothrin; (□) permethrin; (■) bifenthrin. Error bars indicate the standard deviation of three replicates.

2,2,3,3-tetramethylcyclopropanecarboxylic acid phenyl ester. The intermediate product *α*-hydroxy-3-phenoxybenzeneacetonitrile was unstable in the environment, which was spontaneously converted to 3-phenoxybenzaldehyde. Subsequent oxidization of 3-phenoxybenzaldehyde yielded 3-phenoxybenzoate, which was then subject to diaryl cleavage, resulting in the formation of 3,4-dihydroxybenzoic acid, 3,4-dimethoxyphenol, and phenol. However, these compounds were transient. Eventually, no persistent accumulative product was detected by GC-MS analysis, indicating that these compounds under-

dx.doi.org/10.1021/jf404908j | J. Agric. Food Chem. 2014, 62, 2147−2157

went aromatic ring cleavage and further metabolism. Very interestingly, in our previous studies we demonstrated that strain DG-02 also degraded 3-phenoxybenzoic acid to give 3,4-dihydroxybenzoic acid, 3,4-dimethoxyphenol, and phenol.[34] Clearly, the bacterial strain appears to harbor a complete metabolic pathway for degradation and metabolism of fenpropathrin, indicating that the isolate could be an ideal candidate for bioremediation of the environments contaminated by fenpropathrin and the related pyrethroid insecticides.

It was evident from the results that strain DG-02 degrades fenpropathrin by first cleavage of the carboxylester linkage and diaryl bond of fenpropathrin. Similar findings were also observed in biodegradation of other pyrethroid insecticides such as cyfluthrin and cypermethrin.[38,42] However, our results were very different from the previous findings of Zhang et al.,[32] who reported that *Clostridium* sp. ZP3 degraded fenpropathrin with an oxidization process to yield 3,5-dimethylamphetamine, benzenemethanol, and benzyl alcohol. It was generally regarded that ester hydrolysis via carboxylesterases was the primary degradation pathway of various pyrethroids in a multitude of species, from mammals to insects to microorganisms.[30,40,44,45] The fenpropathrin degradation pathway in strain DG-02 appears to be similar to the initial steps of most environmental isolates in pyrethroid biodegradation processes, in which pyrethroids were converted to 2,2,3,3-tetramethylcyclopropanecarboxylic acid and 3-phenoxybenzoic acid through hydrolysis of the carboxylester linkage.[30,35,39] Unfortunately, however, it is not clear whether these microorganisms are capable of further metabolism of pyrethroids. In this study, we showed that strain DG-02 could further metabolize the intermediate 3-phenoxybenzoate by cleavage of the diaryl bond (Figure 5), leading to complete degradation of the pesticide, which is rarely seen in other pyrethroid-degrading strains.

Degradation Kinetics of Various SPs. The abilities of strain DG-02 to degrade various pyrethroids are shown in Figure 6. The strain was capable of utilizing all of the pyrethroids tested. As shown in Figure 6, degradation of all tested compounds started rapidly at the beginning of incubation with no apparent lag period. Deltamethrin and fenpropathrin were the most preferred substrates, with degradation rates of 94.1 and 93.3% within 72 h of incubation, respectively. β-Cypermethrin, β-cyfluthrin, and λ-cyhalothrin were degraded relatively more slowly than deltamethrin and fenpropathrin, with degradation rates of 89.2, 85.6, and 82.7%, respectively. Bifenthrin and permethrin were the most persistent; only 65.1 and 63.6% of the added substrates were degraded under the same experimental conditions, suggesting that absence of the cyano group may cause a substantial reduction in the hydrolysis rate. These results contrast with the previous findings that degradation reduction in pyrethroid compounds with a cyano group is due to its toxic effect.[33] Our results provide a strong endorsement to the previous view that different capacities of various microorganisms to utilize pyrethroid compounds could be attributed to a number of factors, including the differences in substrate transportation, enzyme specificity, and molecular structures of these compounds.[34]

Several papers on the microbial degradation of fenpropathrin have been published. *Sphingobium* sp. JZ-2 could use fenpropathrin as the sole carbon source in MSM and could degrade >80% of the added pesticide at a concentration of 50 mg L^{-1} after 4 days of incubation.[30] A genetically engineered microorganism named JQL4-5-*mpd* was also able to simultaneously degrade methyl parathion and fenpropathrin in MSM.[31] *Clostridium* sp. ZP3 was reported to be capable of degrading fenpropathrin in liquid medium with the presence of an extra carbon source (glucose).[32] One recently isolated fenpropathrin-degrading strain, *O. trtici* pyd-1, could also utilize fenpropathrin as a growth substrate and degrade approximately 90% of 100 mg L^{-1} of the pesticide in 72 h in liquid culture.[33] However, these strains either could degrade only a limited number of pyrethroids or showed a low degradation efficiency, which limits their use in bioremediation of environments contaminated with multiple pyrethroids. It is noteworthy that strain DG-02 could degrade not only fenpropathrin but also other pyrethroids, which is rarely seen in other microorganisms.

Previous papers suggest that the bacterial isolates from *Bacillus* genus could be the most metabolically active microorganisms, as they are capable of degrading a wide variety of xenobiotic aromatic compounds, including thiophanate-methyl,[24] chlorpyrifos,[29] and 4-chloro-2-nitrophenol.[46] The results from this study further expand the metabolic list of the *Bacillus* species. In our previous studies, strain DG-02 was found to be highly efficient in degrading 3-phenoxybenzoic acid.[34] 3-Phenoxybenzoic acid is a major product common to most of the pyrethroids.[47] Degradation of this compound by the same strain that degrades pyrethroids is very important because 3-phenoxybenzoic acid is generally antimicrobial, and it would be accumulated if not degradable, which prevents further degradation and may cause growth arrest.[37] Importantly, the ability of strain DG-02 in degrading a wide range of pyrethroids suggests that this particular isolate has promising potentials and advantages as a bioremediation organism in removing pyrethroid residues from various environments as most contaminated regions were affected by multiple pyrethroid compounds.[3,4,9−11]

To predict the ability of strain DG-02 in biodegradation of various substrates in environment, the degradation process was fitted to the first-order kinetic model (eq 2). The kinetic parameters for all runs calculated from the equations are presented in Table 2. In these studies, the degradation rate and the substrate concentration were in direct proportion, and the degradation process corresponded to the first-order kinetic model, with an R^2 ranging from 0.9564 to 0.9826, indicating that the experimental data were well-correlated with the model. The degradation process was characterized by a k ranging from 0.0160 to 0.0355 h^{-1} and a $t_{1/2}$ varying from 19.5 to 43.3 h (Table 3). Given that the reported $t_{1/2}$ values for various pyrethroids in water or soil are usually between 17 and 600 days,[1] addition of strain DG-02 significantly shortened the $t_{1/2}$ for pyrethroids, suggesting that this strain is suitable for the efficient and rapid degradation of pyrethroid residues and cleanup of contaminated environments.

Table 2. Kinetic Parameters of Degradation of Various SPs by Strain DG-02

treatment	regression eq	k (h^{-1})	$t_{1/2}$ (h)	R^2
deltamethrin	$C_t = 52.0e^{-0.0355t}$	0.0355	19.5	0.9826
fenpropathrin	$C_t = 52.3e^{-0.0315t}$	0.0315	22.0	0.9735
β-cypermethrin	$C_t = 54.8e^{-0.0286t}$	0.0286	24.2	0.9657
β-cyfluthrin	$C_t = 53.2e^{-0.0277t}$	0.0277	25.0	0.9688
λ-cyhalothrin	$C_t = 51.9e^{-0.0234t}$	0.0234	29.6	0.9564
bifenthrin	$C_t = 52.0e^{-0.0155t}$	0.0155	44.7	0.9574
permethrin	$C_t = 50.7e^{-0.0160t}$	0.0160	43.3	0.9718

Table 3. Kinetic Parameters of Degradation of Fenpropathrin in Sterile and Nonsterile Soils Inoculated with Strain DG-02

treatment	regression eq	k (day^{-1})	$t_{1/2}$ (days)	R^2
sterile soils + fenpropathrin	$C_t = 49.8e^{-0.0098t}$	0.0098	70.7	0.9791
nonsterile soils + fenpropathrin	$C_t = 49.9e^{-0.00187t}$	0.0187	37.1	0.9913
sterile soils + fenpropathrin + DG-02	$C_t = 51.6e^{-0.0981t}$	0.0981	7.1	0.9849
nonsterile soils + fenpropathrin + DG-02	$C_t = 51.0e^{-0.1281t}$	0.1281	5.4	0.9916

Biodegradation of Fenpropathrin in Soils. The abilities of strain DG-02 to degrade fenpropathrin in sterile and nonsterile soils were investigated, respectively. The kinetic parameters for all treatments are presented in Table 3. Kinetic data showed that the degradation process corresponded to the first-order model and was characterized by k ranging from 0.0098 to 0.1281 day^{-1}. The coefficient of determination R^2 was determined to be 0.9791−0.9916, showing that the experimental data are well-correlated with the model. Without strain DG-02, the $t_{1/2}$ values were 70.7 and 37.1 days for fenpropathrin in sterile and nonsterile soils, respectively. In contrast, the $t_{1/2}$ values for fenpropathrin in sterile and nonsterile soils inoculated with strain DG-02 were shortened, giving $t_{1/2}$ values of 7.1 and 5.4 days, respectively. Our results confirmed previous observation made by Khan et al.[48] indicating that biodegradation is the main mechanism of SP dissipation in soils, whereas its abiotic breakdown is less important. Studies on other SPs have shown that microorganisms which can degrade them in culture conditions also perform their degradation in soils.[26,49] In our bioremediation experiment, strain DG-02 efficiently degraded fenpropathrin in soils, suggesting that strain DG-02 may be ideal for bioremediation of soils contaminated with fenpropathrin.

In conclusion, *Bacillus* sp. DG-02 was found to be highly efficient in degrading fenpropathrin in different contaminated soils and water resources. This strain was able to utilize fenpropathrin as the growth substrate and rapidly degraded the pesticide in a concentration as high as 1200 mg L^{-1}. This is an important feature of a microorganism to be employed for bioremediation of variable environments. Moreover, we presented evidence that the bacterium harbors the metabolic pathway for complete degradation and metabolism of fenpropathrin. The strain could degrade both the carboxylester linkage and the diaryl bond of fenpropathrin, which plays a key role in the fenpropathrin biogeocycle. Another important feature which is worth mentioning is that this particular strain was capable of degrading a wide range of synthetic pyrethroids, suggesting that the isolate has promising potentials and advantages as a bioremediation organism in removing pyrethroid residues from water, soils, or crops.

■ ASSOCIATED CONTENT

Supporting Information

Table S1 and Figures S1−S4. This material is available free of charge via the Internet at http://pubs.acs.org.

■ AUTHOR INFORMATION

Corresponding Authors

*(G.Z.) E-mail: guohuazhong@scau.edu.cn

*(L.-H.Z.) Phone: +86-20-85288229. Fax: +86-20-85280292. E-mail: lianhui@imcb.a-star.edu.sg.

Funding

Financial support for some of this research was received from the Guangdong Hopson-Pearl River Education Development Foundation (HPEDF).

Notes

The authors declare no competing financial interest.

■ REFERENCES

(1) Laskowski, D. A. Physical and chemical properties of pyrethroids. *Rev. Environ. Contam. Toxicol.* **2002**, *174*, 49−170.

(2) Kuivila, K. M.; Hladik, M. L.; Ingersoll, C. G.; Kemble, N. E.; Moran, P. W.; Calhoun, D. L.; Nowell, L. H.; Gilliom, R. J. Occurrence and potential sources of pyrethroid insecticides in stream sediments from seven U.S. metropolitan areas. *Environ. Sci. Technol.* **2012**, *46*, 4297−4303.

(3) Hintzen, E. P.; Lydy, M. J.; Belden, J. B. Occurrence and potential toxicity of pyrethroids and other insecticides in bed sediments of urban streams in central Texas. *Environ. Pollut.* **2009**, *157*, 110−116.

(4) Weston, D. P.; Holmes, R. W.; Lydy, M. J. Residential runoff as a source of pyrethroid pesticides to urban creeks. *Environ. Pollut.* **2009**, *157*, 287−294.

(5) Zhang, C.; Jia, L.; Wang, S. H.; Qu, J.; Xu, L. L.; Shi, H. H.; Yan, Y. C. Biodegradation of β-cypermethrin by two *Serratia* spp. with different cell surface hydrophobicity. *Bioresour. Technol.* **2010**, *101*, 3423−3429.

(6) Spurlock, F.; Lee, M. Synthetic pyrethroid use patterns, properties, and environmental effects. In *Synthetic Pyrethroids: Occurrence and Behavior in Aquatic Environments*; Gan, J., Spurlock, F., Hendley, P., Weston, D., Eds.; American Chemical Society: Washington, DC, 2008; pp 3−25.

(7) Nieradko-Iwanicka, B.; Borzecki, A. Influence of fenpropathrin on memory and movement in mice after transient incomplete cerebral ischemia. *J. Toxicol. Environ. Health A* **2010**, *73*, 1166−1172.

(8) Bu, N.; Wang, S. H.; Yu, C. M.; Zhang, Y.; Ma, C. Y.; Li, X. M.; Ma, L. J. Genotoxicity of fenpropathrin and fenitrothion on root tip cells of *Vicia faba*. *Bull. Environ. Contam. Toxicol.* **2011**, *87*, 517−521.

(9) Weston, D. P.; Lydy, M. J. Urban and agricultural sources of pyrethroid insecticides to the Sacramento-San Joaquin Delta of California. *Environ. Sci. Technol.* **2010**, *44*, 1833−1840.

(10) Delgado-Moreno, L.; Lin, K.; Veiga-Nascimento, R.; Gan, J. Occurrence and toxicity of three classes of insecticides in water and sediment in two southern California coastal watersheds. *J. Agric. Food Chem.* **2011**, *59*, 9448−9456.

(11) Weston, D. P.; Ding, Y.; Zhang, M.; Lydy, M. J. Identifying the cause of sediment toxicity in agricultural sediments: the role of pyrethroids and nine seldom-measured hydrophobic pesticides. *Chemosphere* **2013**, *90*, 958−964.

(12) Barr, D. B.; Olsson, A. O.; Wong, L. Y.; Udunka, S.; Baker, S. E.; Whitehead, R. D.; Magsumbol, M. S.; Williams, B. L.; Needham, L. L. Urinary concentrations of metabolites of pyrethroid insecticides in the general U.S. population: national health and nutrition examination survey 1999−2002. *Environ. Health Perspect.* **2010**, *118*, 742−748.

(13) Ahn, K. C.; Kim, H. J.; McCoy, M. R.; Gee, S. J.; Hammock, B. D. Immunoassays and biosensors for monitoring environmental and human exposure to pyrethroid insecticides. *J. Agric. Food Chem.* **2011**, *59*, 2792−2802.

(14) Babina, K.; Dollard, M.; Pilotto, L.; Edwards, J. W. Environmental exposure to organophosphorus and pyrethroid pesticides in South Australian preschool children: a cross sectional study. *Environ. Int.* **2012**, *48*, 109−120.

(15) Corcellas, C.; Feo, M. L.; Torres, J. P.; Malm, O.; Ocampo-Duque, W.; Eljarrat, E.; Barceló, D. Pyrethroids in human breast milk:

occurrence and nursing daily intake estimation. *Environ. Int.* **2012**, *47*, 17−22.
(16) Morgan, M. K. Children's exposures to pyrethroid insecticides at home: a review of data collected in published exposure measurement studies conducted in the United States. *Int. J. Environ. Res. Public Health* **2012**, *9*, 2964−2985.
(17) Wolansky, M. J.; Harrill, J. A. Neurobehavioral toxicology of pyrethroid insecticides in adult animals: a critical review. *Neurotoxicol. Teratol.* **2008**, *30*, 55−78.
(18) Meeker, J. D.; Barr, D. B.; Hauser, R. Pyrethroid insecticide metabolites are associated with sperm hormone levels in adult men. *Reprod. Toxicol.* **2009**, *27*, 155−160.
(19) Kaneko, H. Pyrethroids: mammalian metabolism and toxicity. *J. Agric. Food Chem.* **2011**, *59*, 2786−2791.
(20) Alonso, M. B.; Feo, M. L.; Corcellas, C.; Vidal, L. G.; Bertozzi, C. P.; Marigo, J.; Secchi, E. R.; Bassoi, M.; Azevedo, A. F.; Dorneles, P. R.; Torres, J. P.; Lailson-Brito, J.; Malm, O.; Eljarrat, E.; Barceló, D. Pyrethroids: a new threat to marine mammals. *Environ Int.* **2012**, *47*, 99−106.
(21) Luo, Y.; Zhang, M. Environmental modeling and exposure assessment of sediment-associated pyrethroids in an agricultural watershed. *PLoS One* **2011**, *6*, e15794.
(22) Arora, P. K.; Sasikala, C.; Ramana, C. V. Degradation of chlorinated nitroaromatic compounds. *Appl. Microbiol. Biotechnol.* **2012**, *93*, 2265−2277.
(23) Gao, Y.; Chen, S.; Hu, M.; Hu, Q.; Luo, J.; Li, Y. Purification and characterization of a novel chlorpyrifos hydrolase from *Cladosporium cladosporioides* Hu-01. *PLoS One* **2012**, *7*, e38137.
(24) Cycoń, M.; Wojcik, M.; Piotrowska-Seget, Z. Biodegradation kinetics of the benzimidazole fungicide thiophanate-methyl by bacteria isolated from loamy sand soil. *Biodegradation* **2011**, *22*, 573−583.
(25) Zhang, J.; Zheng, J. W.; Liang, B.; Wang, C. H.; Cai, S.; Ni, Y. Y.; He, J.; Li, S. P. Biodegradation of chloroacetamide herbicides by *Paracoccus* sp. FLY-8 in vitro. *J. Agric. Food Chem.* **2011**, *59*, 4614−4621.
(26) Chen, S.; Geng, P.; Xiao, Y.; Hu, M. Bioremediation of β-cypermethrin and 3-phenoxybenzaldehyde contaminated soils using *Streptomyces aureus* HP-S-01. *Appl. Microbiol. Biotechnol.* **2012**, *94*, 505−515.
(27) Feng, Z. Z.; Li, Q. F.; Zhang, J.; Zhang, J.; Huang, X.; Lu, P.; Li, S. P. Microbial degradation of fomesafen by a newly isolated strain *Pseudomonas zeshuii* BY-1 and the biochemical degradation pathway. *J. Agric. Food Chem.* **2012**, *60*, 7104−7110.
(28) Li, C.; Zhang, J.; Wu, Z. G.; Cao, L.; Yan, X.; Li, S. P. Biodegradation of buprofezin by *Rhodococcus* sp. strain YL-1 isolated from rice field soil. *J. Agric. Food Chem.* **2012**, *60*, 2531−2537.
(29) Zhang, Q.; Wang, B. C.; Cao, Z. Y.; Yu, Y. L. Plasmid-mediated bioaugmentation for the degradation of chlorpyrifos in soil. *J. Hazard. Mater.* **2012**, *221*−*222*, 178−184.
(30) Guo, P.; Wang, B. Z.; Hang, B. J.; Li, L.; Ali, S. W.; He, J.; Li, S. P. Pyrethroid-degrading *Sphingobium* sp. JZ-2 and the purification and characterization of a novel pyrethroid hydrolase. *Int. Biodeterior. Biodegrad.* **2009**, *63*, 1107−1112.
(31) Hong, Y.; Zhou, J.; Hong, Q.; Wang, Q.; Jiang, J.; Li, S. P. Characterization of a fenpropathrin-degrading strain and construction of a genetically engineered microorganism for simultaneous degradation of methyl parathion and fenpropathrin. *J. Environ. Manage.* **2010**, *91*, 2295−2300.
(32) Zhang, S. B.; Yin, L. B.; Liu, Y.; Zhang, D. Y.; Luo, X. W.; Cheng, J. E.; Cheng, F. X.; Dai, J. P. Cometabolic biotransformation of fenpropathrin by *Clostridium* species strain ZP3. *Biodegradation* **2011**, *22*, 869−875.
(33) Wang, B. Z.; Ma, Y.; Zhou, W. Y.; Zheng, J. W.; He, J.; Li, S. P. Biodegradation of synthetic pyrethroids by *Ochrobactrum tritici* strain pyd-1. *World J. Microbiol. Biotechnol.* **2011**, *27*, 2315−2324.
(34) Chen, S. H.; Hu, W.; Xiao, Y.; Deng, Y. Y.; Jia, J. W.; Hu, M. Y. Degradation of 3-phenoxybenzoic acid by a *Bacillus* sp. *PLoS One* **2012**, *7*, e50456.
(35) Tallur, P. N.; Megadi, V. B.; Ninnekar, H. Z. Biodegradation of cypermethrin by *Micrococcus* sp. strain CPN 1. *Biodegradation* **2008**, *28*, 77−82.
(36) Chen, S. H.; Hu, Q. B.; Hu, M. Y.; Luo, J. J.; Weng, Q. F.; Lai, K. P. Isolation and characterization of a fungus able to degrade pyrethroids and 3-phenoxybenzaldehyde. *Bioresour. Technol.* **2011**, *102*, 8110−8116.
(37) Chen, S. H.; Hu, M. Y.; Liu, J. J.; Zhong, G. H.; Yang, L.; Rizwan-ul-Haq, M.; Han, H. T. Biodegradation of β-cypermethrin and 3-phenoxybenzoic acid by a novel *Ochrobactrum lupini* DG-S-01. *J. Hazard. Mater.* **2011**, *187*, 433−440.
(38) Chen, S. H.; Luo, J. J.; Hu, M. Y.; Lai, K. P.; Geng, P.; Huang, H. S. Enhancement of cypermethrin degradation by a coculture of *Bacillus cereus* ZH-3 and *Streptomyces aureus* HP-S-01. *Bioresour. Technol.* **2012**, *110*, 97−104.
(39) Lin, Q. S.; Chen, S. H.; Hu, M. Y.; Rizwan-ul-Haq, M.; Yang, L.; Li, H. Biodegradation of cypermethrin by a newly isolated actinomycetes HU-S-01 from wastewater sludge. *Int. J. Environ. Sci. Technol.* **2011**, *8*, 45−56.
(40) Zhang, C.; Wang, S. H.; Yan, Y. C. Isomerization and biodegradation of β-cypermethrin by *Pseudomonas aeruginosa* CH7 with biosurfactant production. *Bioresour. Technol.* **2011**, *102*, 7139−7146.
(41) Jilani, S.; Khan, M. A. Biodegradation of cypermethrin by *Pseudomonas* in a batch activated sludge process. *Int. J. Environ. Sci. Technol.* **2006**, *3*, 371−380.
(42) Chen, S. H.; Dong, Y. H.; Chang, C. Q.; Deng, Y. Y.; Zhang, X. F.; Zhong, G. H.; Song, H. W.; Hu, M. Y.; Zhang, L. H. Characterization of a novel cyfluthrin-degrading bacterial strain *Brevibacterium aureum* and its biochemical degradation pathway. *Bioresour. Technol.* **2013**, *132*, 16−23.
(43) Luong, J. H. T. Generalization of Monod kinetics for analyses of growth data with substrate inhibition. *Biotechnol. Bioeng.* **1988**, *29*, 242−248.
(44) Wang, B. Z.; Guo, P.; Hang, B. J.; Li, L.; He, J.; Li, S. P. Cloning of a novel pyrethroid-hadrolyzing carboxylesterase gene from *Sphingobium* sp. strain JZ-1 and characteization of the gene product. *Appl. Environ. Microbiol.* **2009**, *75*, 5496−5500.
(45) Zhai, Y.; Li, K.; Song, J.; Shi, Y.; Yan, Y. Molecular cloning, purification and biochemical characterization of a novel pyrethroid-hydrolyzing carboxylesterase gene from *Ochrobactrum anthropi* YZ-1. *J. Hazard. Mater.* **2012**, *221*−*222*, 206−212.
(46) Arora, P. K. Decolourization of 4-chloro-2-nitrophenol by a soil bacterium, *Bacillus subtilis* RKJ 700. *PLoS One* **2012**, *7*, e52012.
(47) McCoy, M. R.; Yang, Z.; Fu, X.; Ahn, K. C.; Gee, S. J.; Bom, D. C.; Zhong, P.; Chang, D.; Hammock, B. D. Monitoring of total type II pyrethroid pesticides in citrus oils and water by converting to a common product 3-phenoxybenzoic acid. *J. Agric. Food Chem.* **2012**, *60*, 5065−5070.
(48) Khan, S. U.; Bekhi, R. M.; Tapping, R. I.; Akhbar, M. H. Deltamethrin residues in an organic soil under laboratory conditions and its degradation by bacterial strain. *J. Agric. Food Chem.* **1988**, *36*, 636−638.
(49) Cycoń, M.; Zmijowska, A.; Piotrowska-Seget, Z. Enhancement of deltamethrin degradation by soil bioaugmentation with two different strains of *Serratia marcescens*. *Int. J. Environ. Sci. Technol.* **2013**, DOI: 10.1007-s13762-013-0322-0.

(3NT).[13] Skibsted[1] recently postulated the potential facile conversion among ROS and RNS in cured meat systems assisted by other additives, such as ascorbate. However, the connection between oxidative and nitrosative reactions and the impact of protein nitration on the quality of cured muscle foods are poorly understood. Already 35 years ago, Cassens et al.[14] reported that almost half of the inorganic nitrite added to a meat product is bound to proteins, while only 10% corresponds to the addition of nitrite to myoglobin to form nitrosylmyoglobin. A full comprehension of the fate of reactive nitrite and its implication in the formation of specific protein oxidation and nitration products requires a second look to the chemistry of curing agents using innovative methodologies. The understanding of the redox chemistry of nitrite and ascorbate will enable, in turn, the identification of the real impact of these reactions on meat proteins and cured muscle foods.

This study was planned to elucidate the impact of nitrite and ascorbate on the chemical changes suffered by myofibrillar proteins in a pro-oxidative environment.

MATERIALS AND METHODS

Chemicals and Raw Material. All chemicals, reagents, and high-performance liquid chromatography (HPLC)-grade solvents were purchased from Panreac (Panreac Química S.A., Barcelona, Spain), Merck (Merk, Darmstadt, Germany), and Sigma Chemicals (Sigma-Aldrich, Steinheim, Germany). The water used was purified by passage through a Milli-Q system (Millipore Corporation, Bedford, MA). Porcine meat (muscle longissimus dorsi) was obtained from a local slaughterhouse.

Synthesis of α-Aminoadipic Semialdehyde (AAS) Standard Compound. *N*-Acetyl-L-AAS was synthesized from *Nα*-acetyl-L-lysine using lysyl oxidase activity from an egg shell membrane following the procedure described by Akagawa et al.[15] Briefly, 10 mM *Nα*-acetyl-L-lysine was incubated with constant stirring with 5 g of egg shell membrane in 50 mL of 20 mM sodium phosphate buffer at pH 9.0 at 37 °C for 24 h. The egg shell membrane then was removed by centrifugation, and the pH of the solution was adjusted to 6.0 using 1 M HCl. The resulting aldehydes were reductively aminated with 3 mmol of *p*-aminobenzoic acid (ABA) in the presence of 4.5 mmol sodium cyanoborohydride ($NaBH_3CN$) at 37 °C for 2 h with stirring. Then, ABA derivatives were hydrolyzed by 50 mL of 12 M HCl at 110 °C for 10 h. The hydrolysates were evaporated at 40 °C *in vacuo* to dryness. The resulting AAS−ABA was purified using silica gel column chromatography and ethyl acetate/acetic acid/water (20:2:1, v/v/v) as the elution solvent. The purity of the resulting solution and authenticity of the standard compounds obtained following the aforementioned procedures have been checked using mass spectrometry (MS) and proton nuclear magnetic resonance (^{1}H NMR).[15,16]

Extraction of Myofibrillar Proteins (MPs). MPs were extracted from 10 g of porcine meat according to the method described by Utrera and Estévez,[8] with slight modifications. Meat was weighed, chopped finely with a knife, and treated with 4 volumes of 10 mM potassium phosphate buffer at pH 7. The mixture was homogenized in the ULTRA-TURRAX for 30 s and then centrifuged at 670*g* for 15 min. Then, the supernatant was carefully removed, and 4 volumes of 10 mM potassium phosphate buffer at pH 7 was added again. The vials were shaken vigorously and centrifuged under the aforementioned conditions, and the supernatant was removed. A total of 4 volumes of 0.1 M NaCl was added, and the samples were stirred and centrifuged as in the previous steps. This procedure was repeated 3 times. Before the last centrifugation, the solution was filtered by passing through a gauze. The pH of this solution was adjusted to 6 with 0.1 N HCl, and the vials were centrifuged. Finally, the supernatant was carefully withdrawn and added to 200 mL of 100 mM sodium phosphate buffer at pH 7 with 0.6 M NaCl and 8 M urea to obtain a concentration of MP of 4 mg/mL.

Experimental Setting. MP suspensions (4 mg/mL) were oxidized for 4 days in screw-capped vials using a hydroxyl radical generating system [25 μM Fe(III) and 2.5 mM H_2O_2, final concentrations]. A previous kinetic study was undertaken to set the concentration of pro-oxidants and the length of the assay. The headspace of the vials was generously flushed with nitrogen and immediately transferred to an oven to induce oxidation at 37 °C and constant stirring. Dependent upon the addition of sodium nitrite (N; 0, 75, and 150 mg/L) and sodium ascorbate (A; 0, 250, and 500 mg/L), nine different reaction units were prepared in triplicate (n = 3) according to a total factorial design. Upon completion of the oxidation assay, samples were analyzed for the concentration of tryptophan, AAS, SBs, and 3NT.

Analysis of AAS. A total of 400 μL of protein suspension were dispensed in Eppendorf tubes and treated with a cold 10% trichloroacetic acid (TCA) solution. Each Eppendorf tube was vortexed and then subjected to centrifugation at 2000*g* for 30 min at 4 °C. The supernatant was removed, and the pellet was treated with a cold 5% TCA solution. A new centrifugation was performed at 5000*g* for 5 min at 4 °C. The supernatant was removed, and the pellets were incubated with the following freshly prepared solutions: 0.5 mL of 250 mM 2-(*N*-morpholino)ethanesulfonic acid (MES) buffer at pH 6.0 containing 1% sodium dodecyl sulfate (SDS) and 1 mM diethylenetriaminepentaacetic acid (DTPA), 0.5 mL of 50 mM ABA in 250 mM MES buffer at pH 6.0, and 0.25 mL of 100 mM $NaBH_3CN$ in 250 mM MES buffer at pH 6.0. The tubes were vortexed and then incubated in an oven at 37 °C for 90 min. The samples were stirred every 15 min. After derivatization, samples were treated with a cold 50% TCA solution and centrifuged at 5000*g* for 10 min. The pellet was then washed twice with 10% TCA and diethyl ether/ethanol (1:1). Finally, the pellet was treated with 6 N HCl and kept in an oven at 110 °C for 18 h until completion of hydrolysis. The hydrolysates were dried *in vacuo* in a centrifugal evaporator. The generated residue was reconstituted with 200 μL of Milli-Q water and then filtered through hydrophilic polypropylene GH Polypro (GHP) syringe filters (0.45 μm pore size, Pall Corporation, Port Washington, NY) for HPLC analysis.

A Shimadzu "Prominence" HPLC apparatus (Shimadzu Corporation, Kyoto, Japan), equipped with a quaternary solvent delivery system (LC-20AD), a DGU-20AS online degasser, a SIL-20A autosampler, a RF-10A XL fluorescence detector, and a CBM-20A system controller, was used. An aliquot (1 μL) from the reconstituted protein hydrolysates was injected and analyzed in the above-mentioned HPLC equipment. AAS−ABA was eluted in a Cosmosil 5C18-AR-II RP-HPLC column (5 μm, 150 × 4.6 mm) equipped with a guard column (10 × 4.6 mm) packed with the same material. The flow rate was kept at 1 mL/min, and the temperature of the column was maintained constant at 30 °C. The eluate was monitored with excitation and emission wavelengths set at 283 and 350 nm, respectively. Standards (0.1 μL) were run and analyzed under the same conditions. Identification of both derivatized semialdehydes in the fluorescence detection (FLD) chromatograms was carried out by comparing their retention times to those from the standard compounds. The peak corresponding to AAS−ABA was manually integrated from FLD chromatograms, and the resulting areas were plotted against an ABA standard curve with known concentrations that ranged from 0.1 to 0.5 mM. Results are expressed as nanomoles of carbonyl compound per milligram of protein.

Analysis of TRP. The decrease of TRP fluorescence in MP suspensions was measured on a Perkin-Elmer LS 55 luminescence spectrometer (PerkinElmer, Beaconsfield, U.K.). The emission spectra were recorded from 300 to 400 nm with the excitation wavelength established at 283 nm. Emission spectra of the buffer were recorded under the same conditions and used as background spectra. Excitation and emission slit widths were set at 10 nm, and the speed of data collection while scanning was of 500 nm/min. The TRP content was calculated from a standard curve of the analogous *N*-acetyl-L-tryptophanamide (NATA). The linearity (R^2 = 0.9955; $p < 0.05$) between the NATA concentration (ranging from 0.1 to 0.5 μM) and fluorescence intensity was statistically significant. Results were expressed as milligrams of NATA equivalents per gram of protein. The percent loss of TRP was calculated as $[(T_0 - T_4)/T_0] \times 100$, where T_0 is the concentration of TRP in samples at day 0 and T_4 is the remaining concentration at the end of the oxidation assay (4 days). The effect of nitrite and ascorbate against TRP oxidation was calculated as $[(T_C -$

$T_T)/T_C] \times 100$, where T_C is the concentration of TRP in the control sample and T_T is the percent of TRP loss for each treated sample.

Analysis of SBs. The formation of SBs was assessed in myofibrillar protein isolates (MPIs) using a LS-55 Perkin-Elmer fluorescence spectrometer (PerkinElmer, Beaconsfield, U.K.). Prior to the analysis, reaction mixtures were diluted (1:20) with 8 M urea in 100 mM sodium phosphate buffer at pH 7. SBs were excited at 350 nm, and the emitted fluorescence was recorded at 450 nm. The excitation and emission slit widths were set at 10 nm, and the speed of data collection while scanning was of 500 nm/min. The height of the peaks corresponding to SB spectra was recorded. After the applied dilutions were taken into consideration, the results were expressed as fluorescence units.

Analysis of 3NT. The extent of protein nitration was evaluated by calculating the nitrosation degree (ND), which is defined as the average number of 3NT residues divided by the total number of tyrosine residues in a protein molecule. 3NT was quantified by spectrophotometry according to the procedure recently described by Yang et al.[17] Briefly, 5 mL of MP suspension was treated with 10% cold TCA and then centrifuged at 670*g* for 5 min. Protein pellets were reconstituted with 1 mL of 8 M urea in 100 mM sodium phosphate buffer at pH 3.5. Tyrosine and 3NT were assessed at 280 and 357 nm, respectively.

Statistical Analysis. Data from the analysis ($n = 3$) were collected and subjected to statistical analyses. To assess the effect of the different concentrations of nitrite and ascorbate, an analysis of variance (ANOVA) was applied (SPSS, version 15.5). A Tukey test was applied when ANOVA found significant differences between treatments. The statistical significance was set at $p < 0.05$. Response surface analysis was also carried out using the Unscrambler program (version 10.1).

RESULTS AND DISCUSSION

Effect of Nitrite and Ascorbate against TRP Oxidation. Table 1 shows the residual amounts of TRP in the suspensions of MP treated with curing agents after the *in vitro* oxidation assay. The initial concentration of TRP in the protein suspensions (~13 mg/g of protein; no significant differences between experimental units) significantly decreased as a result of the pro-oxidant action of the hydroxyl-radical-generating system. The loss of TRP ranged from 51 to 80% depending upon the treatment applied to the MP suspensions. These results are consistent with previous studies aimed to assess the oxidation of TRP by systems emulating the Fenton chemistry.[18,19] A decrease of the TRP fluorescence denotes chemical changes on the TRP residue typically attributed to oxidative deterioration.[5] Simat and Steinhart,[20] Salminen and Heinonen,[21] and Utrera and Estévez[19] attributed the oxidative degradation of TRP to the action of hydroxyl radicals and the subsequent reaction between these radicals and the pyrrole ring or the phenyl moiety of the TRP residue. The depletion of TRP in processed muscle foods has also been ascribed to oxidative stress and regarded as a relevant nutritional loss.[22,23]

Table 1. Concentration of TRP (mg of NATA/g of Protein) in MPIs with Added Nitrite (N) and Ascorbate (A) (Mean ± Standard Deviation)[a]

	0 mg/L N	75 mg/L N	150 mg/L N	p^b
0 mg/L A	3.32 y ± 0.37	2.63 y ± 0.70	2.59 y ± 0.22	0.369
250 mg/L A	4.01 y ± 0.49	4.45 x ± 0.58	4.47 x ± 0.44	0.500
500 mg/L A	6.35 x ± 1.46	4.85 x ± 0.71	5.58 x ± 0.99	0.986
p^c	0.013	0.004	0.003	

[a]Means with different letters (x and y) within a column were significantly different ($p < 0.05$) in a Tukey's test subsequent to ANOVA. [b]Significance value of ANOVA for the effect of added nitrite. [c]Significance value of ANOVA for the effect of added ascorbate.

The addition of nitrite had no influence on the residual amount of TRP in the experimental units. In opposition to our initial hypothesis, nitrite displayed neither antioxidant nor pro-oxidant actions on TRP residues. Among the antioxidant properties attributed to nitrite, authors have reported the ability of nitrite to sequester oxygen and to chelate metals and, hence, block their pro-oxidant actions.[1,2] Oxygen was removed from the headspace of the experimental units, and its role in the oxidation events described in the present study may have been negligible. On the other hand, the chelation of iron, given its role in the Fenton chemistry and the metal-catalyzed oxidation of proteins,[6] would have been a hypothetical mechanism for nitrite to inhibit TRP oxidation. In fact, the chelation of transition metals by phenolic compounds has been reported to be behind the antioxidant action of various phytochemicals on TRP residues.[19,21,24] Whereas the ability of nitrite to chelate iron in the conditions of the present experiment remains indefinite, it is obvious that this mechanism was not effective to inhibit TRP oxidation. The potential pro-oxidant effect of nitrite on TRP residues was not found, even though RNS, such as peroxynitrite, were actually found in the present samples (data not shown). TRP residues are known to be sensitive to both ROS[20] and RNS.[25] Because TRP depletion was independent of the nitrite concentration, it is reasonable to conclude that RNS contributed to neither the oxidation nor the nitration of TRP, because both nitrite-mediated modifications would have led to the loss of TRP fluorescence. Consistently, Ito et al.[26] reported that, even at the most favorable conditions of acidic pH and protein conformation, nitrite weakly reacts with TRP in myosin to form nitrosated species. Additional insight on the nitration of protein residues will be provided in the 3NT section.

Ascorbate had a significant effect on the residual amounts of TRP (Table 1). Regardless of the concentration of nitrite, MP suspensions treated with 500 mg/L of ascorbate had significantly higher concentrations of TRP than the control counterparts. The effect of the combination of both curing agents as displayed in the response surface (Figure 1A) is similar to that of the ascorbate alone. The potential pro-oxidant effect of ascorbate in the presence of transition metals via the Fenton reaction (reaction 2) was obviously not observed in the present study. On the contrary, these results reflect an antioxidant effect of ascorbate against the oxidation of TRP residues. Ascorbate has been highlighted as an efficient scavenger of hydroxyl radicals,[27] and this ability may explain the present results. The ascorbyl radical formed as a result of the electron donation finds stability in the form of the dehydroascorbic acid, which does not yield further reaction species.[27] In medical research, Frei et al.[28] already described as "outstanding" the antioxidant activity of ascorbate in human plasma. Unfortunately, the authors reported the antioxidant effect on plasma lipids, while the effect on other plasma components, such as proteins, was not assessed. While the food science literature on this topic is scarce, studies on medical research often varied and, at times, provided contradictory results on the effect of ascorbate on TRP. Some authors highlight the pro-oxidant action of ascorbate under physiological conditions,[29,30] while others described the ability of ascorbate to inhibit and even revert oxidation and nitrosation of TRP residues.[31] The present results show that ascorbate offers antioxidant protection to TRP in MP as a likely consequence of scavenging hydroxyl radicals.

Effect of Nitrite and Ascorbate on AAS Formation. As expected, the hydroxyl-radical-generating system induced efficiently the formation of AAS in MP (Table 2). The

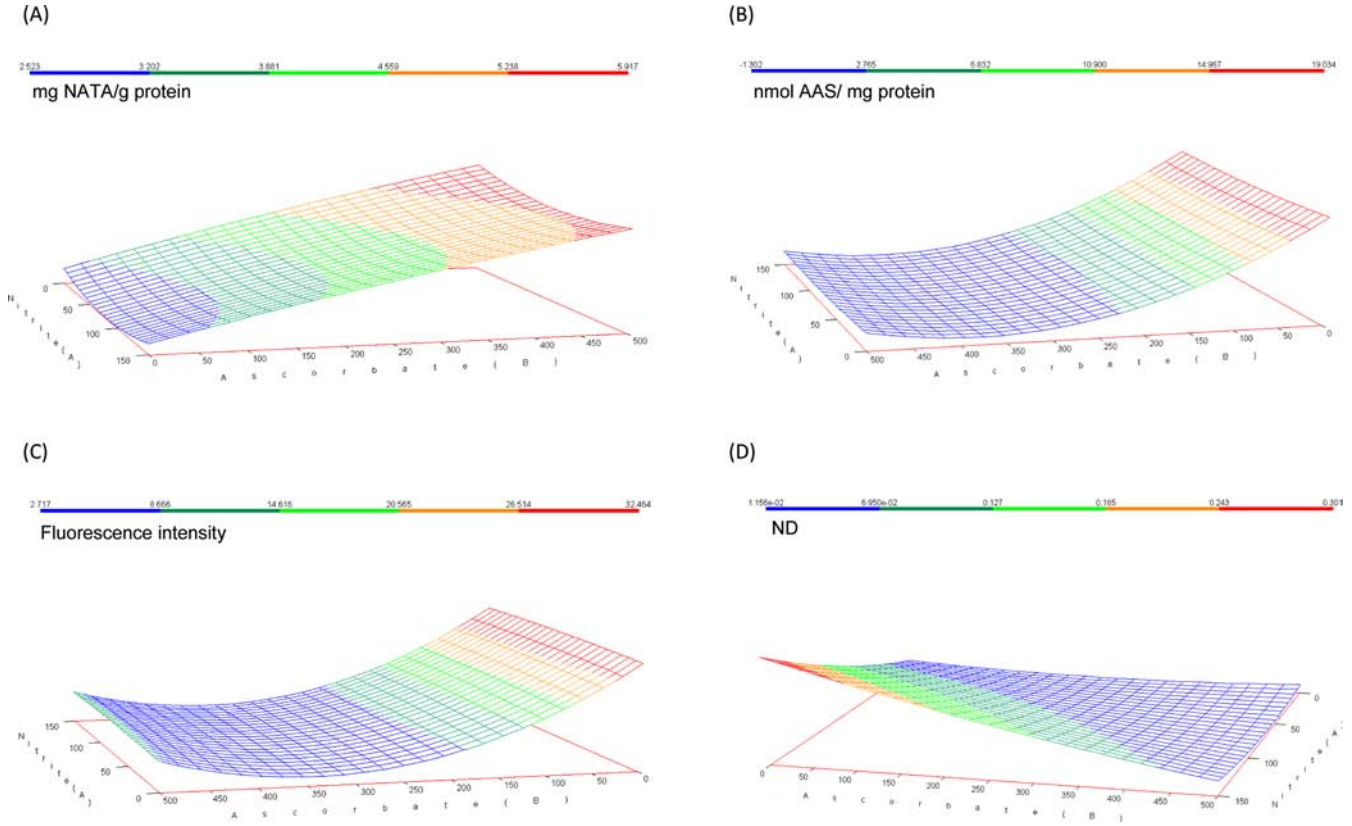

Figure 1. Response surfaces corresponding to the effects of "ascorbate concentration" and "nitrite concentration" on the concentration of (A) TRP, (B) AAS, (C) SBs, and (D) ND in MP suspensions subjected to a hydroxyl radical generation system.

Table 2. Concentration of AAS (nmol of AAS/mg of Protein) in MPIs with Added Nitrite (N) and Ascorbate (A) (Mean ± Standard Deviation)[a]

	0 mg/L N	75 mg/L N	150 mg/L N	p^b
0 mg/L A	19.29 x ± 0.67	17.86 x ± 0.31	19.18 x ± 1.07	0.105
250 mg/L A	1.56 y ± 0.34	1.48 y ± 0.48	1.26 y ± 0.26	0.620
500 mg/L A	1.52 a,y ± 0.25	0.71 b,y ± 0.18	0.97 b,y ± 0.06	0.004
p^c	<0.001	<0.001	<0.001	

[a]Means with different letters within a row (a and b) and column (x and y) were significantly different ($p < 0.05$) in a Tukey's test subsequent to ANOVA. [b]Significance value of ANOVA for the effect of added nitrite. [c]Significance value of ANOVA for the effect of added ascorbate.

abstraction of an electron from a susceptible protein-bound lysine residue by radical species leads to the formation of a carbon-centered radical, which is followed by the formation of a carbonyl compound upon the catalytic action of a transition metal, such as iron.[16] The concentration of AAS in this study is consistent with previous studies, in which MPs were oxidized *in vitro* using a combination of hydrogen peroxide, iron, copper, and myoglobin.[8,16,31] The addition of nitrite, alone, had no significant effect on the formation of AAS (Table 2). As aforementioned for TRP oxidation, the mechanisms ascribed to the antioxidant properties of nitrite (oxygen sequestering and metal chelation) may not be applicable to protein carbonylation. The formation of protein carbonyls takes place in the absence of oxygen,[7] which was, furthermore, removed from the headspace of the present reaction mixtures. Iron catalyzes the oxidative deamination of lysine residues to yield AAS,[7] and therefore, the chelation of this metal has been reported to be a likely mechanism to control protein carbonylation in muscle proteins.[31,32] Once again, either nitrite was unable to chelate iron or this mechanism was not efficient to inhibit protein carbonylation. Considering the present results, the antioxidant properties of nitrite, usually reported on lipids, may involve specific mechanisms that may not be applicable to proteins, such as the physicochemical stabilization of unsaturated fatty acids proposed by Igene et al.[33]

As for TRP oxidation, nitrite and its reactive derivatives were not able to promote protein carbonylation. Similar results were found by Bian et al.[34] in bovine serum albumin and biological samples oxidized by a combination of nitrite, hydrogen peroxide, and heme/non-heme iron. According to these authors, carbonylation of BSA had no relationship with the nitrite concentration. Apparently, RNS may not be able to initiate the carbonylation pathway from lysine residues in the conditions of the present experiment. The same conclusions came from Vossen et al.,[4] who found no effect of nitrite on the formation of protein carbonyls in cured liver pâté. The present experiment do not allow for the statement of whether the reason for the lack of pro-oxidant action of RNS is qualitative (the type of RNS did not react with lysine residues) or quantitative (the amount of RNS was insufficient to produce a significant effect).

Table 3. Fluorescence Intensity Emitted by SBs (Fluorescence Intensity Units) in MPIs with Added Nitrite (N) and Ascorbate (A) (Mean ± Standard Deviation)[a]

	0 mg/L N	75 mg/L N	150 mg/L N	p^b
0 mg/L A	30.70 x ± 3.27	33.47 x ± 3.03	31.47 x ± 1.90	0.354
250 mg/L A	5.58 y ± 0.95	5.74 y ± 1.08	6.85 y ± 1.88	0.257
500 mg/L A	9.33 y ± 1.91	9.48 y ± 1.11	9.32 y ± 1.75	0.277
p^c	<0.001	<0.001	<0.001	

[a]Means with different letters (x and y) within a column were significantly different ($p < 0.05$) in a Tukey's test subsequent to ANOVA. [b]Significance value of ANOVA for the effect of added nitrite. [c]Significance value of ANOVA for the effect of added ascorbate.

Table 4. ND in MPIs with Added Nitrite (N) and Ascorbate (A) (Mean ± Standard Deviation)[a]

	0 mg/L N	75 mg/L N	150 mg/L N	p^b
0 mg/L A	0.04 c ± 0.01	0.13 b,x ± 0.02	0.31 a,x ± 0.05	<0.001
250 mg/L A	0.02 c ± 0.01	0.07 b,y ± 0.02	0.15 a,y ± 0.02	<0.001
500 mg/L A	0.02 ± 0.01	0.03 z ± 0.01	0.04 z ± 0.01	0.054
p^c	0.055	0.001	<0.001	

[a]Means with different letters within a row (a–c) and column (x–z) were significantly different ($p < 0.05$) in a Tukey's test subsequent to ANOVA. [b]Significance value of ANOVA for the effect of added nitrite. [c]Significance value of ANOVA for the effect of added ascorbate.

In contrast to nitrite, ascorbate had a significantly and quantitatively remarkable effect on the formation of AAS (Table 2). The protection of ascorbate against protein carbonylation was already significant at 250 mg/L. Increasing its concentration to 500 mg/L did not lead to a significant improvement. As aforementioned, ascorbate is known to be an efficient scavenger of the hydroxyl radical, which was the likely initiator of protein carbonylation in the present experiment. In agreement with the TRP results, the present study confirms that ascorbate also protects proteins against protein carbonylation induced by a hydroxyl-radical-generating system. In line with the enthusiastic description made by Frei et al.[28] on the antioxidant capabilities of ascorbate in plasma, the protective effect of ascorbate against AAS formation in MP is considerably higher than that displayed by plant phenolics and other phytochemicals in previous studies.[24,31,32]

Measured as percent inhibition, the effect of ascorbate against carbonylation was more intense than that against TRP oxidation (~90 versus ~50%). Consistent with the present results, the rate constants for the reaction of the hydroxyl radical with TRP and ascorbate are comparable (~1×10^{10} L mol^{-1} s^{-1}) and notably higher than that between the hydroxyl radical and lysine (~3.4×10^8 L mol^{-1} s^{-1}).[35] Additionally, TRP residues are typically buried in the hydrophobic protein core, while hydrophilic lysine residues are usually exposed on the surface. The accessibility of the oxidation promoters and the curing agents to the protein residues may also have had an influence on the present results.

The response surface in Figure 1B shows the combined effect of nitrite and ascorbate on AAS formation. Interestingly, the lowest concentration of AAS was found in reaction mixtures with 500 mg/L ascorbate and 75 and 150 mg/L nitrite. The present results suggest that the presence of ascorbate enabled an antioxidant action of nitrite. This antioxidant effect may be attributed to the nitric oxide likely formed as a result of the reaction already described between nitrite and ascorbate (reaction 3). This finding is of great technological interest because nitrite and ascorbate are commonly combined at these concentrations in cured meat products to guarantee color stability and inhibit microbial growth.[2] The present results confirm that this arrangement is also successful to control protein carbonylation. Given that carbonylation is considered to be responsible for an impaired functionality of MPs and loss of nutritional value,[7,8] the combination of curing agents in the aforementioned proportions may be recommended to improve the quality of muscle foods.

Effect of Nitrite and Ascorbate on SB Formation. Table 3 shows the SBs found in protein suspensions treated with curing agents after 4 days of *in vitro* oxidation. The formation of SBs, already described in oxidized protein isolates, is attributed to the reaction between protein carbonyls and lysine residues.[7] AAS is the most reactive of the protein carbonyls,[7] and therefore, the formation of SBs is interpreted as an advanced oxidation product of lysine through the carbonylation pathway.[8,22,32] This advanced expression of the oxidative damage to proteins is independent of hydrogen peroxide and only requires the timely proximity between AAS and lysine residues.[7] Consistently, the SB results are comparable to those reported above for the AAS, reflecting the connection between both oxidation products. Nitrite had no influence on the concentration of SBs, while ascorbate significantly inhibited the formation of these structures in MPs. Once again, no significant differences were found between 250 and 500 mg/L ascorbate. As reflected in the corresponding response surface (Figure 1C), no interaction between both curing agents was found. The effect of ascorbate against the formation of SBs may be a reflection of the protective role of this compound on lysine residues. A reduced concentration of AAS in experimental units treated with ascorbate may reasonably lead to a lower formation of SBs in these samples compared to the control counterparts. SBs have been described to be responsible for an impaired functionality of MPs because SBs compromise the solubility and worsen the aggregation and the gelling capacity of MPs.[8] Therefore, the positive effect of ascorbate against the formation of SBs may be regarded as a beneficial outcome of its antioxidant properties in muscle foods, where the functionality of MPs plays a major role (i.e., meat emulsions).

Effect of Nitrite and Ascorbate on 3NT Formation. As shown in Table 4, 3NT was found in MPs incubated in the absence of nitrite, which is consistent with the basal levels usually reported for proteins in living systems derived from the physiological nitrosative stress.[13] The present study confirms that the ND increases in the presence of nitrite in a highly oxidative environment. The reaction between RNS, including peroxynitrite and nitrogen dioxide, and tyrosyl residues in proteins results in a number of tyrosine modifications, of which

the formation of 3NT is one of the most investigated.[34] The formation of 3NT is usually linked to the formation of peroxynitrite via reaction between nitric oxide and superoxide radical[36] (reaction 5).

$$NO^{\bullet} + O_2^{\bullet -} \rightarrow {}^{-}ONOO \quad (5)$$

Peroxynitrite reacts with CO_2 to produce metastable nitrating, nitrosating, and oxidizing species as intermediates, including the 3NT.[36] Considering the oxidizing conditions of the present experiment, the most plausible pathway for the formation of 3NT in MPs may involve the reaction between the hydroxyl radical and nitrite to yield the nitrogen dioxide radical (reaction 6), which is eventually able to bind to tyrosyl residues in proteins.[37]

$$OH^{\bullet} + NO_2^{-} \rightarrow NO_2^{\bullet} + OH^{-} \quad (6)$$

Among biotargets that can react directly with peroxynitrite and other RNS, heme-containing proteins, such as hemoglobin, seem to react particularly rapidly.[12,36] This also applies to heme-containing muscle proteins, such as myoglobin.[2] Because Woolford et al.[38] reported the formation of 3NT in non-heme muscle proteins, few studies have aimed to describe the occurrence and impact of protein nitration in muscle foods.[39,40] According to the present results, other major muscle proteins, such as MPs, may also be susceptible to nitrosative stress. Whether ROS and RNS may be formed simultaneously, the different behaviors of nitrite on the oxidative and nitrosative damage to meat proteins suggest that protein oxidation and protein nitration seem to be two independent and distinguishable processes. The same conclusion came from Bian et al.,[34] who studied the heme-iron-mediated nitration of tyrosyl residues in proteins.

The addition of ascorbate inhibited efficiently the nitrosation of MPs. A dose-dependent anti-nitrosation effect was observed at 75 and 150 mg/L nitrite. The ND in MP suspensions treated with 150 mg/L nitrite and 500 mg/L ascorbate was similar to the basal level (Figure 1D), which means that ascorbate completely inhibited the nitrosation damage to MPs. The anti-nitrosative effect of ascorbate could also be ascribed to the radical scavenging activity of ascorbate on the hydroxyl radical and, in this case, also RNS, such as the nitric dioxide radical. As far as the authors know, this study originally provides scientific evidence of the ability of ascorbate to inhibit the nitrosation of MPs.

The present paper provides novel insight into the interaction between curing agents and meat proteins. These chemistry fundamentals may be helpful to fully understand the role of nitrite and ascorbate on cured muscle foods and optimize formulation to design muscle foods with enhanced quality traits. However, the occurrence of these reactions in cured muscle foods and their consequences on food quality and human nutrition and health require further investigations.

AUTHOR INFORMATION

Corresponding Author

*Telephone: +34927257100, ext. 51390. Fax: +34927257110. E-mail: mariovet@unex.es.

Funding

Mario Estévez received support from the Spanish Ministry of Economics and Competitiveness (SMEC) through Contract RYC-2009-03901 and Project AGL2010-15134 and the Executive Research Agency from the European Community through the Marie Curie Reintegration Fellowship (PERG05-GA-2009-248959, Pox-MEAT). Adriana Villaverde is supported by a predoctoral Formación de Personal Investigador (FPI) grant from SMEC.

Notes

The authors declare no competing financial interest.

REFERENCES

(1) Skibsted, L. H. Nitric oxide and quality and safety of muscle based foods. *Nitric Oxide* **2011**, *24*, 176−183.

(2) Honikel, K.-O. The use and control of nitrate and nitrite for the processing of meat products. *Meat Sci.* **2008**, *78*, 68−76.

(3) Doolaege, E. H. A.; Vossen, E.; Raes, K.; De Meulenaer, B.; Verhé, R.; Paelinck, H.; De Smet, S. Effect of rosemary extract dose on lipid oxidation, colour stability and antioxidant concentrations, in reduced nitrite liver pâtés. *Meat Sci.* **2012**, *90*, 925−931.

(4) Vossen, E.; Doolaege, E. H. A.; Moges, H. D.; de Meulenaer, B.; Szczepaniak, S.; Raes, K.; de Smet, S. Effect of sodium ascorbate dose on the shelf life stability of reduced nitrite liver pâtés. *Meat Sci.* **2012**, *91*, 29−35.

(5) Lund, M. N.; Heinonen, M.; Baron, C. P.; Estévez, M. Protein oxidation in muscle foods: A review. *Mol. Nutr. Food Res.* **2011**, *55*, 83−95.

(6) Requena, J. R.; Chao, C. C.; Levine, R. L.; Stadtman, E. R. Glutamic and aminoadipic semialdehydes are the main carbonyl products of metal-catalyzed oxidation of proteins. *Proc. Natl. Acad. Sci. U. S. A.* **2001**, *98*, 69−74.

(7) Estévez, M. Protein carbonyls in meat systems: A review. *Meat Sci.* **2011**, *89*, 259−279.

(8) Utrera, M.; Estévez, M. Oxidation of myofibrillar proteins and impaired functionality: Underlying mechanisms of the carbonylation pathway. *J. Agric. Food Chem.* **2012**, *60*, 8002−8011.

(9) Santé-Lhoutellier, V.; Aubry, L.; Gatellier, P. Effect of oxidation on *in vitro* digestibility of skeletal muscle myofibrillar proteins. *J. Agric. Food Chem.* **2007**, *55*, 5343−5348.

(10) Utrera, M.; Parra, V.; Estévez, M. Protein oxidation during frozen storage and subsequent processing of different beef muscles. *Meat Sci.* **2014**, *96*, 812−820.

(11) Lund, M. N.; Lametsch, R.; Hviid, M. S.; Jensen, O. N.; Skibsted, L. H. High-oxygen packaging atmosphere influences protein oxidation and tenderness of porcine longissimus dorsi during chill storage. *Meat Sci.* **2007**, *77*, 295−303.

(12) Pacher, P.; Beckman, J. S.; Liaudet, L. Nitric oxide and peroxynitrite: In health and disease. *Physiol. Rev.* **2007**, *87*, 315−424.

(13) Ohshima, H.; Friesen, M.; Brouet, I.; Bartsch, H. Nitrotyrosine as a new marker for endogenous nitrosation and nitration of proteins. *Food Chem. Toxicol.* **1990**, *28*, 647−52.

(14) Cassens, R. G.; Ito, I.; Lee, M.; Buege, D. The use of nitrite in meat. *Bioscience* **1978**, *28*, 633−637.

(15) Akagawa, M.; Sasaki, T.; Suyama, K. Oxidative deamination of lysine residue in plasma protein of diabetic rats. Novel mechanism via the Maillard reaction. *Eur. J. Biochem.* **2002**, *269*, 5451−5458.

(16) Estévez, M.; Ollilainen, V.; Heinonen, M. Analysis of protein oxidation markers α-aminoadipic and γ-glutamic semialdehydes in food proteins using liquid chromatography (LC)−electrospray ionization (ESI)−multistage tandem mass spectrometry (MS). *J. Agric. Food Chem.* **2009**, *57*, 3901−3910.

(17) Yang, H.; Zhang, Y.; Pöschl, U. Quantification of nitrotyrosine in nitrated proteins. *Anal. Bioanal. Chem.* **2010**, *397*, 879−886.

(18) Dubinina, E. E.; Gavrovskaya, S. V.; Kuzmich, E. V.; Leonova, N. V.; Morozova, M. G.; Kovrugina, S. V.; Smirnova, T. A. Oxidative modification of proteins: Oxidation of tryptophan and production of dityrosine in purified proteins using Fenton's system. *Biochemistry* **2002**, *67* (3), 343−350.

(19) Utrera, M.; Estévez, M. Analysis of tryptophan oxidation by fluorescence spectroscopy: Effect of metal-catalyzed oxidation and selected phenolic compounds. *Food Chem.* **2012**, *135*, 88−93.

(20) Simat, T. J.; Steinhart, H. Oxidation of free tryptophan and tryptophan residues in peptides and proteins. *J. Agric. Food Chem.* **1998**, *46*, 490−498.

(21) Salminen, H.; Heinonen, M. Plant phenolics affect oxidation of tryptophan. *J. Agric. Food Chem.* **2008**, *56*, 7472−7481.
(22) Utrera, M.; Rodríguez-Carpena, J. G.; Morcuende, D.; Estévez, M. Formation of lysine-derived oxidation products and loss of tryptophan during processing of porcine patties with added avocado by products. *J. Agric. Food Chem.* **2012**, *60*, 3917−3926.
(23) Ganhão, R.; Morcuende, D.; Estévez, M. Tryptophan depletion and formation of α-aminoadipic and γ-glutamic semialdehydes in porcine burger patties with added phenolic-rich fruit extracts. *J. Agric. Food Chem.* **2010**, *58*, 3541−3548.
(24) Estévez, M.; Kylli, P.; Puolanne, E.; Kivikari, R.; Heinonen, M. Oxidation of skeletal muscle myofibrillar proteins in oil-in-water emulsions: Interaction with lipids and effect of selected phenolic compounds. *J. Agric. Food Chem.* **2008**, *56*, 10933−10940.
(25) Yamakura, F.; Ikeda, K. Modification of tryptophan and tryptophan residues in proteins by reactive nitrogen species. *Nitric Oxide* **2006**, *14*, 152−161.
(26) Ito, I.; Cassens, R. G.; Greaser, M. L. Reaction of nitrite with tryptophyl residues of proteins. *J. Food Sci.* **1979**, *44* (4), 1144−1146.
(27) Buettner, G. R. The pecking order of free radicals and antioxidants: Lipid peroxidation, α-tocopherol, and ascorbate. *Arch. Biochem. Biophys.* **1993**, *300*, 535−543.
(28) Frei, B.; England, L.; Ames, B. N. Ascorbate is an outstanding antioxidant in human blood plasma. *Proc. Natl. Acad. Sci. U. S. A.* **1989**, *86*, 6377−6381.
(29) Moreaux, V.; Birlouez-Aragon, I.; Ducauze, C. Copper chelation by tryptophan inhibits the copper−ascorbate oxidation of tryptophan. *Redox Rep.* **1996**, *2*, 191−197.
(30) Kytzia, A.; Korth, H.-G.; Sustmann, R.; De Groot, H.; Kirsch, M. On the mechanism of the ascorbic acid-induced release of nitric oxide from N-nitrosated tryptophan derivatives: Scavenging of NO by ascorbyl radicals. *Chem.—Eur. J.* **2006**, *12*, 8786−8797.
(31) Estévez, M.; Heinonen, M. Effect of phenolic compounds on the formation of α-aminoadipic and γ-glutamic semialdehydes from myofibrillar proteins oxidized by copper, iron, and myoglobin. *J. Agric. Food Chem.* **2010**, *58*, 4448−4455.
(32) Utrera, M.; Estevez, M. Impact of trolox, quercetin, genistein and gallic acid on the oxidative damage to myofibrillar proteins: The carbonylation pathway. *Food Chem.* **2013**, *141*, 400−409.
(33) Igene, J. O.; Yamauchi, K.; Pearson, A. M.; Gray, J. I.; Aust, S. D. Mechanisms by which nitrite inhibits the development of warmed-over flavour (WOF) in cured meat. *Food Chem.* **1985**, *18*, 1−18.
(34) Bian, K.; Gao, Z.; Weisbrodt, N.; Murad, F. The nature of heme/iron-induced protein tyrosine nitration. *Proc. Natl. Acad. Sci. U. S. A.* **2003**, *100*, 5712−5717.
(35) Cadenas, E.; Davies, K. J. A. Mitochondrial free radical generation, oxidative stress, and aging. *Free Radical Biol. Med.* **2000**, *29*, 222−230.
(36) Squadrito, G. L.; Pryor, W. A. Oxidative chemistry of nitric oxide: The roles of superoxide, peroxynitrite, and carbon dioxide. *Free Radical Biol. Med.* **1998**, *25*, 392−403.
(37) Augusto, O.; Bonini, M. G.; Amanso, A. M.; Linares, E.; Santos, C. C. X.; De Menezes, S. L. Nitrogen dioxide and carbonate radical anion: Two emerging radicals in biology. *Free Radical Biol. Med.* **2002**, *32*, 841−859.
(38) Woolford, G.; Cassens, R. G.; Greaser, M. L.; Sebranek, J. G. The fate of nitrite: Reaction with protein. *J. Food Sci.* **1976**, *41*, 585−588.
(39) Stagsted, J.; Bendixen, E.; Andersen, H. J. Identification of specific oxidatively modified proteins in chicken muscles using a combined immunologic and proteomic approach. *J. Agric. Food Chem.* **2004**, *52*, 3967−3974.
(40) Sullivan, G. A.; Sebranek, J. G. Nitrosylation of myoglobin and nitrosation of cysteine by nitrite in a model system simulating meat curing. *J. Agric. Food Chem.* **2012**, *60*, 1748−1754.

data generated.[19−22] Additionally, in modern GC-TOF MS methods using the recently revived atmospheric pressure chemical ionization source (APCI), the investigation of target compounds is easier and more efficient. This is due to the soft ionization that takes place under APCI in comparison with the high fragmentation observed in the widely used electron ionization (EI) source. Thus, working with APCI, the molecular ion ($M^{+\bullet}$) or the protonated molecule ($[M + H]^+$) is commonly presented in the mass spectrum (in most cases as base peak), which improves both selectivity and sensitivity of the screening detection.[23] Also, the availability of a QTOF instrument allows MS/MS and/or MS^E experiments to go further in the identification of compounds detected due to the structure information given by the fragmentation pathways.

The aim of the present work is to complement a previously developed screening based on liquid chromatography coupled to high-resolution mass spectrometry (LC-HRMS).[22] By combination of GC-HRMS and LC-HRMS we pursue one of the main challenges in food safety and toxicology: advancing toward the ideal "universal" screening whereby all types of analytes, independently of their polarity and volatility, would be detected in the analysis. A QuEChERS-based sample treatment has been applied, with some modifications. A critical stage was to validate the GC-QTOF MS method for both pesticides and PAHs, establishing the screening detection limit (SDL) in complex aquaculture samples. The validated method has been applied for screening pesticides and PAHs in commercially and experimentally available real samples.

MATERIALS AND METHODS

Reagents and Chemicals. Individual pesticide reference standards were purchased from Dr. Ehrenstorfer (Scharlab, Barcelona, Spain) with purity between 93 and 99%. Stock standard solutions (around 500 mg/L) were prepared in acetone and were stored in a freezer at −20 °C. Nineteen mixtures of pesticide standards (individual concentration of each pesticide around 50 mg/L) were prepared by dilution of stock individual solutions in acetone. A working standard solution containing all pesticides at 1 mg/L was prepared by dilution of mixtures with acetone. In our target list, ethoxyquin is included as a preservative. It is mainly considered as a synthetic preservative, but it is also used as a pesticide (under the commercial name as "Stop-Scald") to prevent oxidation in vegetable and fruit samples.

Benzo[*j*]fluoranthene, 5-methylchrysene, benzo[*c*]fluorene, dibenzo[*a,e*]pyrene, dibenzo[*a,h*]pyrene, dibenzo[*a,i*]pyrene, dibenzo-[*a,l*]pyrene, and cyclopenta[*c,d*]pyrene individual standard solutions and mixture PAH MIX 9 containing naphthalene, acenaphthylene, acenaphthene, fluorene, phenanthrene, anthracene, fluoranthene, pyrene, benzo[*a*]anthracene, chrysene, benzo[*b*]fluoranthene, benzo-[*k*]fluoranthene, benzo[*a*]pyrene, indeno[1,2,3-*cd*]pyrene, dibenzo-[*a,h*]anthracene, and benzo[*g,h,i*]perylene at10 mg/L were purchased from Dr. Ehrenstorfer. A working standard solution containing all compounds at 1 mg/L except for cyclopenta[*c,d*]pyrene, which was at 0.5 mg/L, was prepared by combining the standard mixtures and diluting in *n*-hexane.

Acetone (pesticide residue analysis quality), *n*-hexane (ultratrace quality), acetonitrile (reagent grade), toluene (for GC residue analysis), and glacial acetic acid were purchased from Scharlab. Anhydrous magnesium sulfate (extra pure) and anhydrous sodium acetate (reagent grade) were purchased from Scharlab. The QuEChERS commercial products composed by 2 mL microcentrifuge tubes for d-SPE containing 50 mg of primary−secondary amine (PSA), 150 mg of anhydrous $MgSO_4$, and 50 mg of C18 were purchased from Teknokroma (Barcelona, Spain). This was the kit selected in our recommended procedure. Moreover, another QuEChERS kit with the same composition together graphitized carbon black (GCB, 50 mg) was also purchased from Teknokroma. It was also studied in the optimization of the method (Scharlab).

Samples. Feed ingredients that are either used or tested and aquafeeds were directly purchased or provided from manufacturers. Protein feed ingredients were pea protein (2 samples), pea (1), wheat (3), wheat gluten (4), corn gluten (3), soy protein (4), sunflower meal (1), rapeseed cake (1), fish meal (2), krill meal (1), and fish protein (1). Oil ingredients such as rapeseed oil (5), palm oil (2), linseed oil (1), and fish oil (2) were also studied. With regard to feed, five different aquafeeds were analyzed that had different compositions of marine ingredients and plant ingredients. Three fish species (Atlantic salmon (*Salmo salar*), sea bass (*Dicentrarchus labrax*), and sea bream (*Sparus aurata*)) were directly purchased from supermarkets. Sea bream fillets (3) and one fish liver from other growing experiments were also collected from IATS facilities.

GC-QTOF MS Instrumentation. The GC system (Agilent 7890A, Palo Alto, CA, USA) was equipped with an autosampler (Agilent 7693) and coupled to a hybrid quadrupole-orthogonal acceleration-TOF mass spectrometer (XEVO G2 QTOF, Waters Micromass, Manchester, UK), using an APCI source (APGC by Waters Corp.). A fused silica DB-5MS capillary column (30 m long × 0.25 mm i.d. × 0.25 μm df) (J&W Scientific, Folsom, CA, USA) was used for GC separation. The injector was operated in splitless mode, injecting 1 μL at 280 °C. The oven temperature was programmed as follows: 90 °C (1 min), raised at 5 °C/min to 315 °C (5 min). Helium was used as carrier gas at 2 mL/min. The interface temperature was set to 280 °C using N_2 (from liquid N_2) as auxiliary gas at 150 L/h and as cone gas at 16 L/h and N_2 (from gas cylinder quality 99.9990%) as makeup gas at 320 mL/min. The APCI corona pin was operated at 1.8 μA, and the cone voltage was set to 20 V. The ionization process occurred within a closed ion volume, which enabled control over the protonation/charge transfer processes. The water, used as modifier when working under proton-transfer conditions, was placed in an uncapped vial, which was located within a specially designed holder placed in the source door. In these conditions, the most critical separation was between benzo[*b*]-fluoranthene, benzo[*j*]fluoranthene, and benzo[*k*]fluoranthene, by one side, and between dibenzo[*a,i*]pyrene and dibenzo[*a,h*]pyrene, by the other side, the results of which should be treated as primary data.

For MS^E experiments, two acquisition functions with different collision energies were generated. The low-energy (LE) function, selecting a collision energy of 4 eV, and the high-energy (HE) function, with a collision energy ramp ranging from 10 to 40 eV to obtain a greater range of fragment ions.[23] It should be noted that all of the exact masses shown in this work have a deviation of 0.55 mDa from the "true" value, as the calculation performed by the MassLynx software uses the mass of hydrogen instead of a proton when calculating $[M + H]^+$ exact mass. However, as this deviation is also applied during mass axis calibration, there is no negative impact on the mass errors presented in this paper. MS data were acquired in centroid mode and were processed by the ChromaLynx XS application manager (within MassLynx v4.1; Waters Corp.).

Recommended Analytical Procedure. Before analysis, ingredients and feed samples were thawed at room temperature and ground using a Super JS mill from Moulinex (Bagnolet Cedex, France). Fish tissues were also thawed at room temperature and processed in a crushing machine (Thermomix, Vorwerk España M.S.L., S.C., Madrid, Spain). As a result, homogenized samples were obtained in both cases. Five grams of sample was accurately weighed (precision = 0.1 mg) into centrifuge tubes (50 mL) and mixed in a vortex with 10 mL of acetonitrile (Figure 1). Then, 4 g of $MgSO_4$ was added, and the tube was again shaken in a vortex during 30 s. The extract was centrifuged at 4500 rpm for 5 min (Consul centrifuge, Orto-Alresa, Madrid, Spain), and the upper layer of the extract was transferred to a new centrifuge tube (15 mL) and stored overnight in a freezer to precipitate proteins and fix lipids to the tube walls (freezing cleanup). Afterward, 1 mL of the extract was carefully transferred to the cleanup QuEChERS vial (50 mg of PSA + 150 mg of $MgSO_4$ + 50 mg of C18), and it was shaken for 30 s and centrifuged at 12000 rpm for 5 min. After this cleanup, 0.5 mL was transferred to a new Eppendorf vial with the addition of 0.1 mL of hexane. The extract was concentrated to

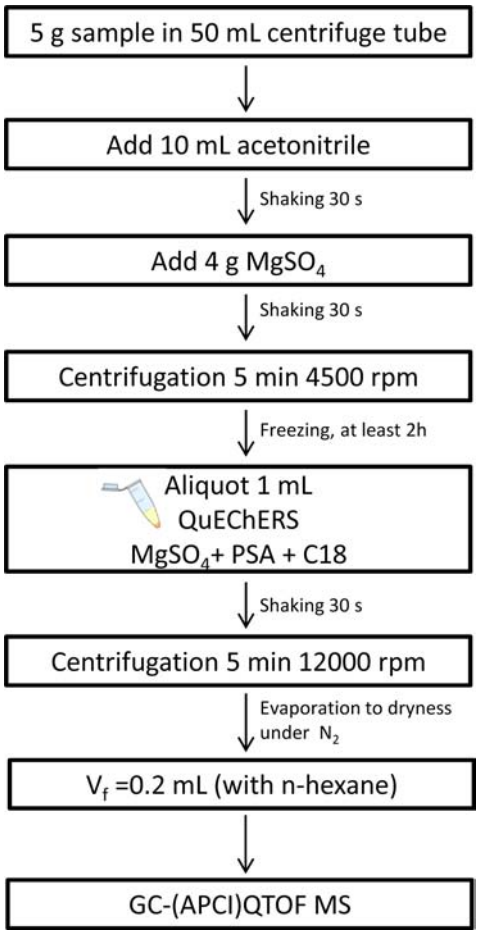

Figure 1. Sample treatment applied in the GC-(APCI) QTOF MS screening method.

dryness at 30 °C (to remove acetonitrile) under a gentle stream of nitrogen, reconstituted with 0.2 mL of *n*-hexane, and finally transferred to a vial for GC injection. The samples were run twice, using water as modifier to favor in-source protonation and without the addition of water for those compounds for which no protonation was observed.

Method Validation. Validation of the screening method was performed for qualitative purposes on the basis of European analytical guidelines.[24,25] Twenty different samples (details under Samples) were spiked with over 133 pesticides and 24 PAHs at two levels, 0.01 and 0.05 mg/kg (0.005 and 0.025 mg/kg for cyclopenta[*c*,*d*]pyrene), and analyzed together with their nonspiked samples ("blanks"). Additionally, two method blanks were analyzed to ensure that no laboratory contamination was introduced during the procedure. The SDL was set up as the main validation parameter to estimate the threshold concentration at which detection becomes reliable. SDL was established as the lowest concentration tested at which a compound was detected in at least 95% of 20 spiked samples under study (i.e., detected in at least 19 samples at each concentration level) independent of its recovery and precision. The detection was made by using the most abundant ion measured at its accurate mass (typically the protonated molecule). This means that, at least, one peak (SDL) had to be observed in the respective narrow-window extracted ion chromatogram (nw-XIC) at the same retention time (tolerance of ±0.5% with respect to standard) and measured at accurate mass (mass error < 5 ppm). Tables 1 and 2 show the results obtained at each spiked level.

RESULTS AND DISCUSSION

Feed ingredients, feed compositions, and fish tissues are complex matrices that contain a large number of interferences that may hamper detection and identification of undesirable compounds. To investigate the presence of any GC-amenable organic contaminant in this kind of sample, cleanup steps are normally applied to improve sensitivity and selectivity.[4,7,12−15,18] However, when the screening is focused on different chemical families of compounds, the situation is more problematic because analytes have rather different chemical and physical properties, and the analytical strategy should be suitable for all of them.[22,26] In this work, the screening was focused on many different pesticides and PAHs in a single analysis. As the objective was the detection and subsequent identification of the compounds detected in samples, no recoveries and precisions were calculated in this work.

Sample Treatment Optimization. One of the goals of a wide screening method is to minimize the possible analyte losses along sample treatment, so any restrictive step should be carefully studied. Acetonitrile solvent was selected because it is not highly amenable with lipid content and offers good recoveries for many GC-amenable compounds. In addition, to reduce the amount of extracted interferences, different conditions were tested, such as (1) the addition of water, (2) the addition of toluene and/or hexane together with acetonitrile for the extraction, and (3) the addition of sodium acetate.

1. The addition of water did not offer better results than the use of only acetonitrile. Thus, many compounds could not be detected at the lowest spiked level. Although some authors reported that water incorporation to fatty samples improves the determination of many pesticides,[27] in the samples under study the addition of water did not represent a relevant improvement for pesticides.

2. The use of organic solvents such as hexane or toluene reduced the coextractives in the acetonitrile layer but also the presence of several nonpolar compounds, such as DDTs, heptachlors, and HCH isomers, in the sample extract, as they have more affinity to the hexane or toluene layer.[27,28]

3. The addition of sodium acetate seemed not much favorable because it generated a turbid extract. Although this situation does not represent a great disadvantage as reported by other authors,[29] in our case, better results were obtained without using sodium acetate.

One of the easiest ways to reduce the amount of matrix interferences is to store the organic extract in a freezer. Thus, the solution obtained is rather clean as most proteins and lipids are fixed on the bottom and walls of the tube, respectively. As previously reported, the application of low temperature before d-SPE cleanup substantially reduces the amount of coextractives.[13,14] Moreover, improved chromatographic peak shapes, reduced signal suppression, and minimized retention time shifts were observed for some compounds, as supported by the bibliography.[13,14] After the freezing, an aliquot can be easily taken and centrifuged to improve the solid−liquid separation.

The d-SPE cleanup step was also studied by using two commercially available QuEChERS kits (d-SPE with 150 mg of Mg_2SO_4, 50 mg of PSA, and 50 mg of C18; and d-SPE with 150 mg of Mg_2SO_4, 50 mg of PSA, 50 mg of C18, and 50 mg of GCB). The kit containing GCB was tested to try to improve the removal of matrix that hampers the detection.[12,27] After using these cleanup cartridges, several pesticides, such as HCB and DDTs, were not detected at the spiked levels. GCB seems to properly remove additional matrix components from vegetable extracts, but it also tends to retain certain pesticides,

Table 1. Validation Results for Pesticides

compound[a]	m/z	positive/negative results (n = 20) 0.01 mg/kg +/−	0.05 mg/kg +/−	SDL[b] (mg/kg)	compound[a]	m/z	positive/negative results (n = 20) 0.01 mg/kg+/−	0.05 mg/kg+/−	SDL[b] (mg/kg)
2-phenylphenol	171.0810	20/0	20/0	0.01	fipronil	436.9465	20/0	20/0	0.01
4,4′-dichlorobenzophenone	251.0030	20/0	20/0	0.01	flucythrinate[c]	412.1549	11/9	20/0	0.05
alachlor[c]	238.0999	19/1	20/0	0.01	**fludioxonil**	248.0397	17/3	19/1	0.05
aldrin	362.8835	4/16	14/6	–	folpet[c]	259.9340	19/1	20/0	0.01
α-endosulfan	404.8247	14/6	20/0	0.05	**γ-HCH**[c]	180.9379	13/7	19/1	0.05
α-HCH[c]	180.9379	14/6	19/1	0.05	**HCB**	281.8131	13/7	19/1	0.05
atrazine	216.1016	20/0	20/0	0.01	**heptachlor**[c]	335.8601	18/2	20/0	0.05
atrazine desethyl	188.0703	20/0	20/0	0.01	heptachlor epoxide A	386.8238	5/15	20/0	0.05
atrazine desisopropyl	174.0546	20/0	20/0	0.01	heptachlor epoxide B	386.8238	5/15	20/0	0.05
azinphos methyl	318.0136	5/15	11/9	–	**hexachlorobutadiene**	257.8131	10/10	16/4	–
azoxystrobin	404.1246	20/0	20/0	0.01	imazalil	297.0561	5/15	10/10	–
β-endosulfan	404.8247	12/8	20/0	0.05	iprodione	330.0412	20/0	20/0	0.01
β-HCH[c]	180.9379	13/7	19/1	0.05	isodrin	362.8835	4/16	14/6	–
bifenthrin[c]	181.1017	20/0	20/0	0.01	λ-cyhalothrin	450.1084	7/13	20/0	0.05
bromophos	392.8883	20/0	20/0	0.01	leptophos	410.8778	19/1	20/0	0.01
bromophos ethyl	364.8570	19/1	20/0	0.01	malathion	331.0439	20/0	20/0	0.01
bromopropilate[c]	156.9864	19/1	20/0	0.01	metalaxyl	280.1549	20/0	20/0	0.01
buprofezin	306.1640	19/1	20/0	0.01	methamidophos	142.0092	15/5	19/1	0.05
cadusafos	271.0955	18/2	20/0	0.05	methidathion	302.9697	12/8	15/5	–
captafol	347.9186	1/19	3/17	–	methiocarb[c]	169.0687	20/0	20/0	0.01
captan[c]	263.9653	4/16	4/16	–	methoxychlor[c]	236.9641	20/0	20/0	0.01
carbaryl[c]	145.0646	7/13	20/0	0.05	metolachlor	284.1417	20/0	20/0	0.01
carbofuran[c]	165.0916	8/12	20/0	0.05	metribuzin	215.0967	20/0	20/0	0.01
carbophenothion	342.9817	1/19	12/8	–	**mirex**[c]	269.8131	10/10	18/2	–
carfentrazone ethyl	412.0443	19/1	20/0	0.01	molinate	188.1109	20/0	20/0	0.01
chinomethionat	235.0000	20/0	20/0	0.01	oxadixyl	279.1345	13/7	19/1	0.05
chlorfenapyr	406.9774	20/0	20/0	0.01	oxyfluorfen	362.0407	20/0	20/0	0.01
chlorfenson	302.9649	13/7	15/5	–	**p,p′-DDD**[c]	235.0081	16/4	20/0	0.05
chlorfenvinphos	358.9774	20/0	20/0	0.01	**p,p′-DDE**	315.9380	14/6	20/0	0.05
chlorothalonil	264.8894	3/17	19/1	0.05	**p,p′-DDT**[c]	235.0081	14/6	19/1	0.05
chlorpropham[c]	172.0165	20/0	20/0	0.01	parathion ethyl	292.0409	20/0	20/0	0.01
chlorpyrifos ethyl	349.9341	20/0	20/0	0.01	parathionmethyl	264.0096	20/0	20/0	0.01
chlorpyrifos methyl	321.9028	20/0	20/0	0.01	pendimethalin	282.1454	9/11	14/6	–
coumaphos	363.0223	20/0	20/0	0.01	**pentachlorobenzene**	247.8521	14/6	20/0	0.05
cyanazine	241.0968	18/2	20/0	0.05	permethrin[c]	355.1101	2/18	20/0	0.05
cyanophos	244.0197	20/0	20/0	0.01	phorate	261.0207	12/8	19/1	0.05
cyfluthrin	434.0726	1/19	3/17	–	phosmet	318.0024	12/8	20/0	0.05
cypermethrin	416.0820	0/20	3/17	–	pirimicarb	239.1508	20/0	20/0	0.01
cyprodinil	226.1344	20/0	20/0	0.01	pirimiphos methyl	306.1041	20/0	20/0	0.01
δ-HCH[c]	180.9379	13/7	19/1	0.05	procymidone	284.0245	20/0	20/0	0.01
deltamethrin	503.9810	0/20	4/16	–	propetamphos	282.0929	1/19	9/11	–
diazinon	305.1089	20/0	20/0	0.01	propham[c]	138.0550	20/0	20/0	0.01
dichlofenthion	314.9778	20/0	20/0	0.01	propiconazole	342.0776	20/0	20/0	0.01
dichloran	206.9728	20/0	20/0	0.01	propoxur	210.1130	10/10	20/0	0.05
dichlorvos	220.9537	20/0	20/0	0.01	propyzamide	256.0296	20/0	20/0	0.01
dieldrin	378.8785	14/6	20/0	0.05	pyriproxyfen	322.1443	20/0	20/0	0.01
diflufenican	395.0819	20/0	20/0	0.01	quinalphos	299.0619	20/0	20/0	0.01
dimethoate	230.0074	15/5	19/1	0.05	resmethrin	339.1960	20/0	20/0	0.01
dioxathion[c]	271.0228	16/4	20/0	0.05	simazine	202.0859	20/0	20/0	0.01
diphenylamine	170.0970	20/0	20/0	0.01	τ-fluvalinate	503.1349	1/19	12/8	–
endosulfan ether	340.8628	20/0	20/0	0.01	tefluthrin	419.0649	14/6	20/0	0.05
endosulfan sulfate	420.8196	4/16	12/8	–	terbacil[c]	161.0118	20/0	20/0	0.01
endrin	378.8785	12/8	20/0	0.05	terbumeton	226.1668	20/0	20/0	0.01
EPN	324.0459	20/0	20/0	0.01	terbumeton desethyl	198.1355	19/1	20/0	0.01
ethalfluralin	334.1015	20/0	20/0	0.01	terbuthylazine	230.1172	18/2	20/0	0.05
ethion	384.9954	12/8	20/0	0.05	terbuthylazine desethyl	202.0859	20/0	20/0	0.01
ethoxyquin	218.1545	20/0	20/0	–[d]	terbutryn	242.1439	20/0	20/0	0.01
etofenprox[c]	359.2011	19/1	20/0	0.01	tetradifon	354.8921	19/1	19/1	0.01
famphur	326.0286	20/0	20/0	0.01	thiabendazole	202.0439	4/16	20/0	0.05
fenamiphos	304.1136	17/3	20/0	0.05	tolclofos methyl	300.9622	19/1	20/0	0.01
fenarimol	331.0405	20/0	20/0	0.01	tolyfluanid[c]	237.9660	10/10	12/8	–

dx.doi.org/10.1021/jf405366n | J. Agric. Food Chem. 2014, 62, 2165−2174

Table 1. continued

compound[a]	m/z	positive/negative results (n = 20) 0.01 mg/kg +/−	0.05 mg/kg +/−	SDL[b] (mg/kg)	compound[a]	m/z	positive/negative results (n = 20) 0.01 mg/kg+/−	0.05 mg/kg+/−	SDL[b] (mg/kg)
fenhexamid	302.0715	20/0	20/0	0.01	***trans*-chlordane**[c]	370.8289	16/4	19/1	0.05
fenitrothion	278.0252	20/0	20/0	0.01	triadimefon	294.1009	20/0	20/0	0.01
fenoxycarb	302.1392	19/1	20/0	0.01	triflumizole	346.0934	18/2	20/0	0.05
fenthion	279.0278	20/0	20/0	0.01	trifluralin	336.1171	20/0	20/0	0.01
fenvalerate	420.1366	0/20	5/15	−	vinclozolin	286.0038	19/1	20/0	0.01

[a]All compounds were measured as $[M + H]^+$ after the addition of water in the APCI source, except for those marked in bold that were measured as $M^{+\bullet}$ without water added as modifier. [b]SDL, screening detection limit. [c]These compounds were measured as fragment ions. [d](−) The evaluation of the SDL was not feasible due to the presence of the analyte in several samples used for validation.

Table 2. Validation Results for PAHs

compound[a]	m/z	positive/negative results (n = 20) 0.01 mg/kg +/−	0.05 mg/kg +/−	SDL[b]
naphthalene	129.0704	20/0	20/0	−[c]
acenaphthylene	153.0704	20/0	20/0	−[c]
acenaphthene	155.0861	20/0	20/0	−[c]
fluorene	167.0861	20/0	20/0	−[c]
phenanthrene	179.0861	20/0	20/0	−[c]
anthracene	179.0861	20/0	20/0	−[c]
fluoranthene	203.0861	20/0	20/0	−[c]
pyrene	203.0861	20/0	20/0	−[c]
benzo[*c*]fluorene	217.1017	20/0	20/0	0.01
cyclopenta[*c*,*d*]pyrene[d]	227.0861	20/0	20/0	0.005
benzo[*a*]anthracene	229.1017	20/0	20/0	0.01
chrysene	229.1017	20/0	20/0	0.01
5-methylchrysene	243.1174	19/1	20/0	0.01
benzo[*j*]fluoranthene	253.1017	19/1	20/0	0.01
benzo[*b*]fluoranthene	253.1017	19/1	20/0	0.01
benzo[*k*]fluoranthene	253.1017	19/1	20/0	0.01
benzo[*a*]pyrene	253.1017	19/1	20/0	0.01
indeno[1,2,3,*cd*]pyrene	277.1017	19/1	20/0	0.01
dibenzo[*a*,*h*]anthracene	279.1174	19/1	20/0	0.01
benzo[*g*,*h*,*i*]perylene	277.1017	19/1	20/0	0.01
dibenzo[*a*,*l*]pyrene	303.1174	9/11	20/0	0.05
dibenzo[*a*,*e*]pyrene	303.1174	9/11	20/0	0.05
dibenzo[*a*,*i*]pyrene	303.1174	9/11	20/0	0.05
dibenzo[*a*,*h*]pyrene	303.1174	9/11	20/0	0.05

[a]PAHs were measured as $[M + H]^+$ after the addition of water in the APCI source. [b]SDL, screening detection limit. [c](−) The evaluation of the SDL was not feasible due to the presence of the analyte in the samples used for validation. [d]Cyclopenta[*c*,*d*]pyrene was spiked at 0.005 and 0.025 mg/kg, respectively.

such as terbufos, thiabendazole, HCB, and other planar-ring analytes.[12] Finally, the QuEChERS kit without GCB was selected for sample cleanup.

APCI. Ionization in GC-(APCI) MS occurs by charge transfer and/or proton transfer, resulting in the formation of the molecular ion, protonated molecule, or both. By deliberately introducing water in the source, this protonation can be promoted (details on this issue can be found in recent publications).[23,30] Thus, many compounds, including most pesticides and PAHs, gave higher response when water was used as modifier and the protonated molecule was measured. On the contrary, halogenated hydrocarbons without any other heteroatoms, such as some organochlorine pesticides, showed better response under charge-transfer conditions, the molecular ion being the diagnostic ion. In the latter case, better response was obtained without the addition of water in the source. However, in some cases, this behavior was observed to show some irreproducibility over time. This might be due to the fact that humidity present in the atmosphere is an uncontrolled parameter that may affect differently those compounds ionized under charge-transfer conditions. Also, for those compounds that show a tendency to protonation, ambient humidity might be even better than the saturation conditions reached after the deliberate introduction of water in the source. Under these circumstances, the fact of adding or not adding water would affect mainly the sensitivity, particularly for a few selected compounds. Consequently, samples were run twice (with and without intentional use of water as modifier), which allowed the optimum conditions to be reached for each compound.

QTOF MS Data Processing. The acquired data files from the GC-QTOF MS were processed by using ChromaLynx software. A *txt* file with the list of the molecular formulas for representative ions was collected together with the retention time per compound. This information was available when the reference standard was injected and was used to search the recorded masses for each file. The software searches for $[M + H]^+$, $M^{+\bullet}$, and/or fragment ions at a prefixed retention time (target approach).

When the reference standard was not available, the only information was that either the molecular ion or the protonated molecule would be expected upon GC-(APCI) QTOF MS analysis. In this case, both ions were included in the processing screening method, as the behavior in the APCI source could not be previously evaluated for these compounds. Any detection being made in this way would indicate the potential presence of the compound, and more information would be required for further identification (e.g., MS/MS experiments). Obviously, as no reference standard was injected, no experimental data on the behavior of the compound during sample preparation and GC-MS sensitivity were available. The acquisition of reference standard and injection in the GC-QTOF MS system would be needed for unequivocal confirmation of the tentative identification.

Qualitative Validation of the Screening Method. First, different samples of each matrix were injected to find the lowest contaminated matrix for spiking. In this previous analysis, we found some matrices positive for several target compounds. It is noteworthy that ethoxyquin and light PAHs were present in the wide majority of samples analyzed. The lowest contaminated samples for each type of matrix were then spiked with a mixture of pesticides and PAHs at concentrations of 0.01 and 0.05 mg/kg for each analyte (0.005 and 0.025 mg/kg for cyclopenta-[*c*,*d*]pyrene). One hundred and thirty-three pesticides and 24

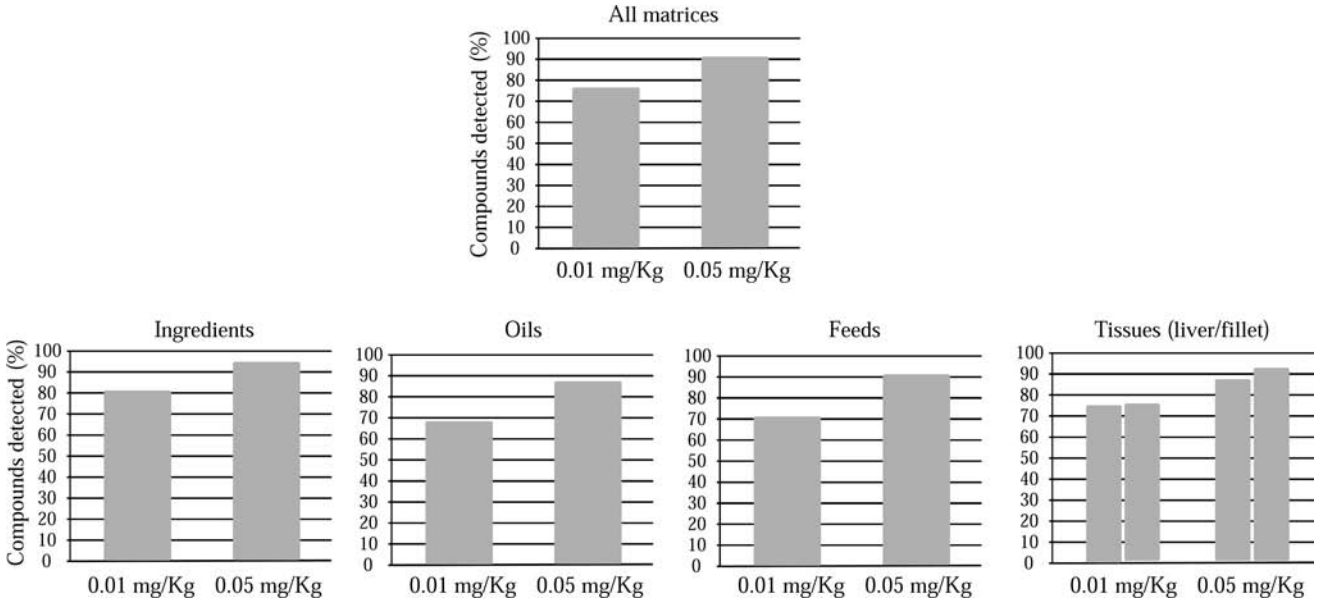

Figure 2. Validation results: number of pesticides detected at 0.01 and 0.05 mg/kg in different types of samples.

PAHs were selected to qualitatively validate the screening by GC-QTOF MS. Twenty different samples of interest for marine seafood were used for validation experiments. Tables 1 and 2 show the number of positive/negative findings for pesticides and PAHs, respectively, at each spiked level in the samples studied. At 0.01 mg/kg, 76% of pesticides and 83% of PAHs were detected. At the highest level validated (0.05 mg/kg), these values improved to 91% of detected pesticides and to 100% of PAHs. Figure 2 shows the percentage of detections for the different matrices studied. As can be seen, oils were the most problematic matrices followed by feeds and tissues, whereas feed ingredients represented lower difficulty for detections. With regard to fish tissues, liver was trickier than fish fillets.

Figure 3 shows different examples of the qualitative validation at the 0.01 mg/kg level. Four groups are illustrated, attending at the samples studied: (A) ingredients, (B) oils, (C) feeds, and (D) fish tissues. The bottom of each figure shows the nw-XIC for the nonspiked sample, and the top shows the nw-XIC for the spiked sample at 0.01 mg/kg with the most abundant ion used for detection, measured at accurate mass (mass error in ppm is also given). In the case of ingredients (Figure 3A), HCH isomers were properly detected at 0.01 mg/kg in fish meal. These compounds were satisfactorily validated in all samples at 0.01 mg/kg except for oils, so a SDL at 0.05 mg/kg was finally proposed (Table 1). Dibenzo[*a*,*l*]pyrene, dibenzo[*a*,*e*]pyrene, dibenzo[*a*,*i*]pyrene, and dibenzo[*a*,*h*]-pyrene were validated at 0.05 mg/kg because they could not be detected in at least 95% of samples at the lowest level, despite that in corn gluten these isomers were detected at 0.01 mg/kg. The figure for oils (Figure 3B) illustrates the validation for benzo[*a*]pyrene, a toxicity reference, at 0.01 mg/kg. The validation of chlorpyrifos methyl was of relevance because it is widely used as an insecticide. In both cases, the detection at 0.01 mg/kg was feasible in oils within low mass errors below 5 ppm. In the case of feeds (Figure 3C), the widely known DDTs, included in the target list due to their common presence in marine resources as part of the larger group of fat-soluble POPs that readily accumulate along the marine food chain, were satisfactorily validated at 0.01 mg/kg for ingredients, feeds, and tissues but not for oils, so a SDL at 0.05 mg/kg was finally proposed. The herbicide carfentrazone ethyl is used in many crops such as wheat, corn, or soy. Therefore, it was included in the target list and also because subproducts from these crops are commonly incorporated in feed compositions (wheat gluten, corn gluten, soy protein). A SDL at 0.01 mg/kg was achieved in all samples studied for this compound. Finally, in fish tissues (Figure 3D), the nw-XICs illustrate the presence of phenanthrene and anthracene in the nonspiked samples, a fact that was also observed in other types of samples, supporting the ubiquity of light PAHs in many environmental and food samples. The same occurred for ethoxyquin, a synthetic preservative widely used in fatty compositions to prevent lipid oxidation. The presence of at least two representative ions for each compound at the expected retention time with accepted mass errors (<5 ppm) allowed the reliable identification in positive samples.

Screening of Real Samples. The validated screening was applied to different types of samples, searching for the target list of validated compounds. After the detection of any compound in the samples, the reliable identification was required to avoid reporting false positives. Although the presence of a m/z ion (commonly $[M + H]^+$), measured at accurate mass with low mass error, and the agreement in retention time, gives confidence to the analysis, we followed strict criteria for confirmation, which was based on the presence of, at least, another representative m/z ion (commonly fragment ion) with low mass error.[23] This is feasible working in the QTOF MS instrument that allows the use of MS^E mode (details in GC-QTOF MS instrumentation).

Figure 4 shows different positive findings in oils, proteins, and feeds commonly used in animal farming. As shown, at least two representative m/z ions were necessary to unequivocally identify the presence of the compound in the sample, at the expected retention time (deviation $\leq \pm 0.5\%$, in comparison to standards) and measured at accurate mass within acceptable mass deviation ($\leq$5 ppm). The main pesticides found were chlorpyrifos methyl and pirimiphos methyl, which were detected in several vegetable samples. Ethoxyquin, the use of which is currently authorized in feed ingredients, was also

dx.doi.org/10.1021/jf405366n | J. Agric. Food Chem. 2014, 62, 2165−2174

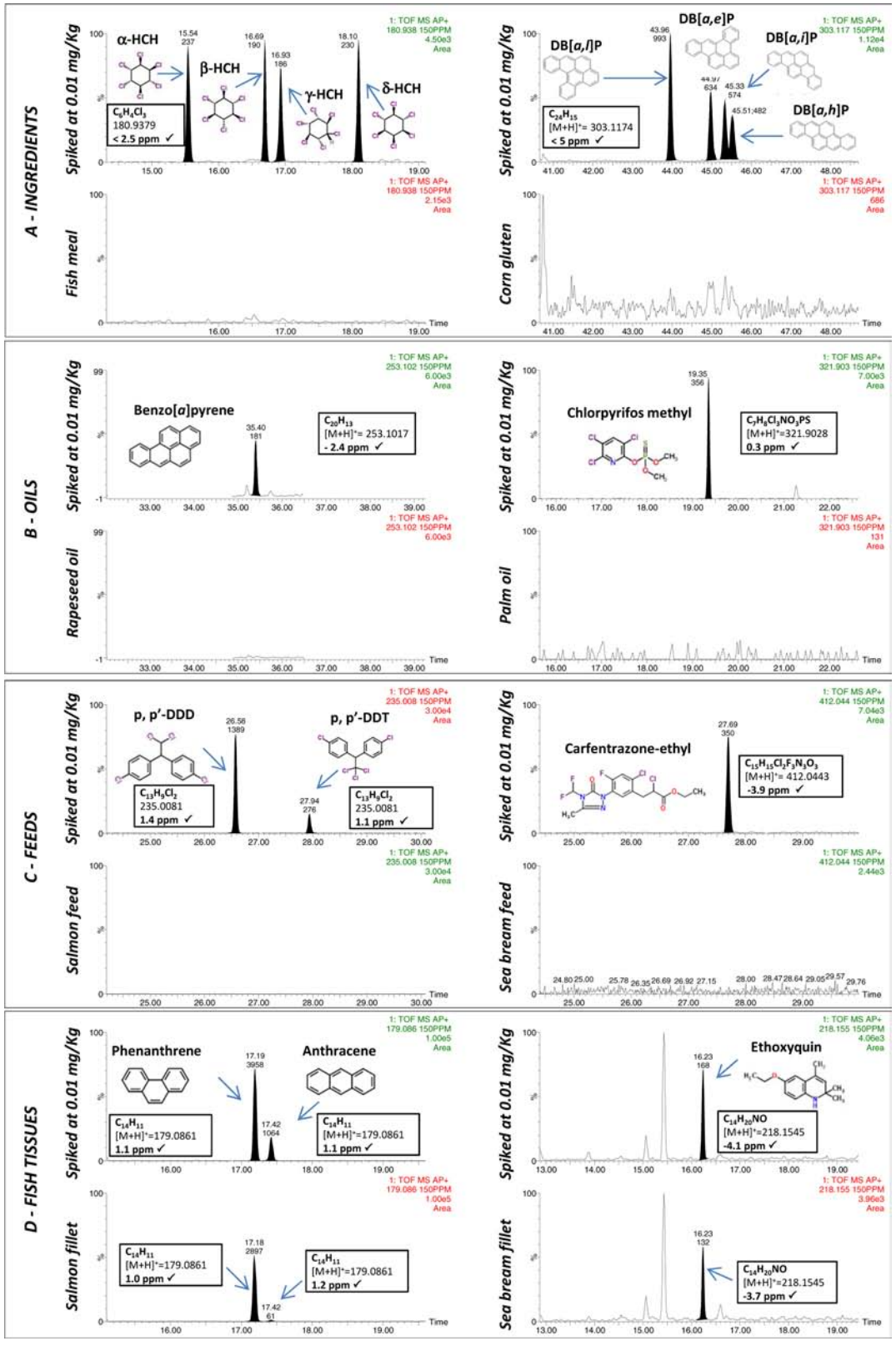

Figure 3. Validation: nw-XICs for the diagnostic m/z ion in samples spiked at 0.01 mg/kg (top) and nonspiked samples (bottom). Diagnostic ion corresponds to $[M + H]^+$ except for HCH isomers and DDTs, for which it corresponds to a fragment ion: (A) α-, β-, γ-, and δ-HCH isomers and dibenzo[*a*,*l*]pyrene, dibenzo[*a*,*e*]pyrene, dibenzo[*a*,*i*]pyrene, and dibenzo[*a*,*h*]pyrene in feed ingredients; (B) benzo[*a*]pyrene and chlorpyrifos methyl in oils; (C) *p*,*p*′-DDD, *p*,*p*′-DDT, and carfentrazone-ethyl in feeds; (D) phenanthrene, anthracene, and ethoxyquin in fish tissues. (Check mark) Accurate mass deviations within tolerance limits.

found in feeds but, additionally, it was identified in the edible part of several commercial fish samples. It seems that this synthetic preservative (and possibly its transformation products) can reach consumers. Earlier studies also reported the

dx.doi.org/10.1021/jf405366n | J. Agric. Food Chem. 2014, 62, 2165−2174

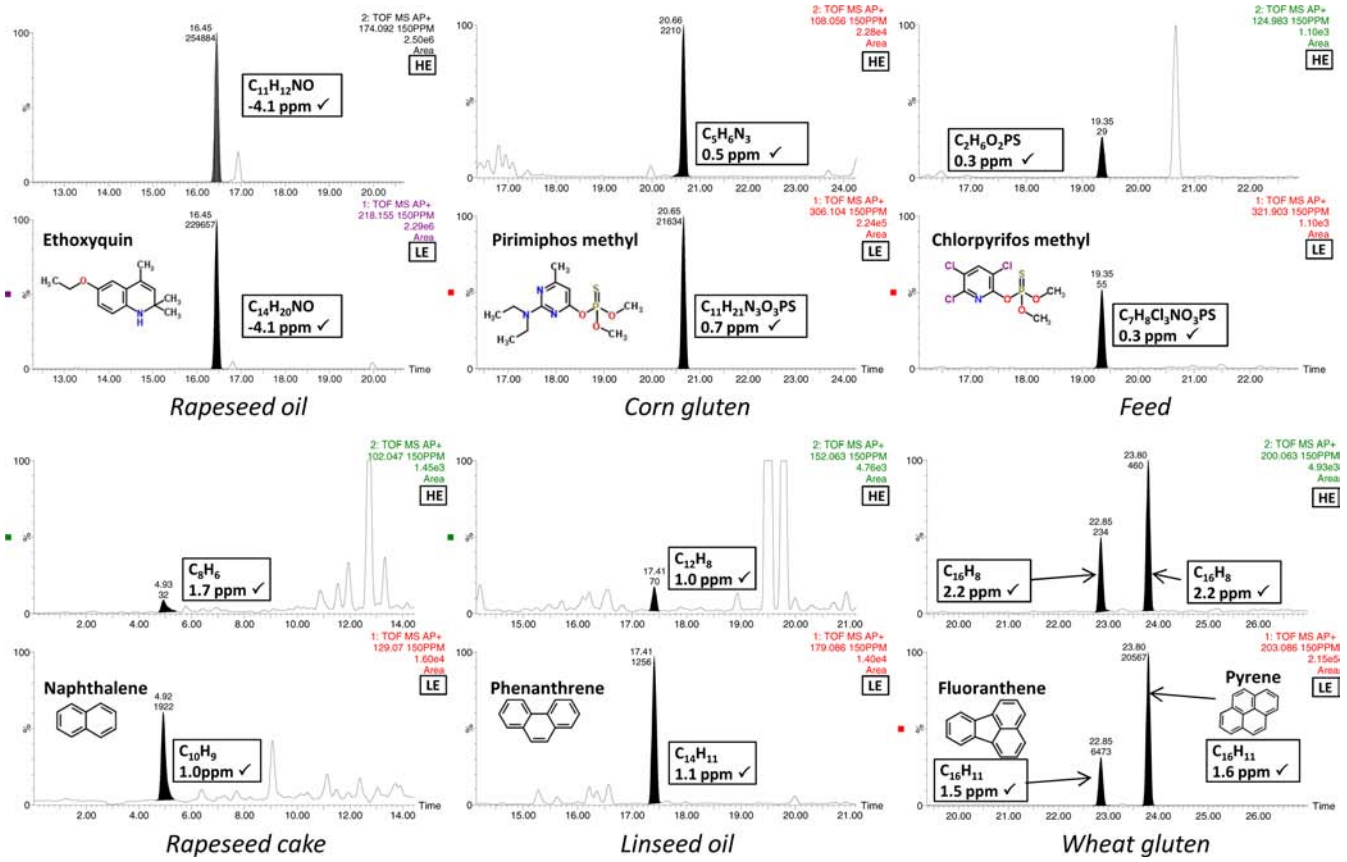

Figure 4. Real-world samples: nw-XICs for identified compounds in oils, proteins, and feeds. For each matrix, the LE function (bottom) and HE (top) are shown to illustrate the presence of the protonated molecule (LE) and fragment ions (HE). (Check mark) Accurate mass deviations within tolerance limits.

overall presence of synthetic antioxidants, such as ethoxyquin, in several commercially important species of farmed fish, namely Atlantic salmon, halibut, cod, and rainbow trout, and their aquafeeds,[31] as well as the carry-over from feed to fillet.[32] Therefore, quantitative methods directed toward this compound and its derivatives will surely be necessary in the near future.

With regard to PAHs, "light" PAHs (e.g., phenanthrene, pyrene) were in nearly all samples analyzed. Although they are not carcinogenic PAHs according to EFSA, they are contaminants that can give (noncarcinogenic) toxic reactions in fish.[33] PAHs present poor MS fragmentation, a fact that makes their identification troublesome. In this work, after evaluation of the presence of the protonated molecule in the LE function, collision-induced dissociation (CID) fragments, or characteristic isotopic ions, were also evaluated for positive samples to achieve a proper identification. As illustrative examples, at the bottom of Figure 4, positive findings for light PAHs are presented for samples of rapeseed, linseed, and wheat.

After the first screening for which reference standards were available, we focused our screening to find any other pesticides for which reference standards were not available in our laboratory. Although tentative detection for some of these pesticides occurred, based on the presence of $[M + H]^+$ and/or $M^{+\bullet}$ in the LE function, further investigation of fragment ions, from the LE and/or HE function, did not allow us to confirm their identity, so they could not be reported as positive identifications.

With this work, we pursued the achievement of an essential tool in food safety and toxicology: the use of wide-scope screening for the detection and identification of a large number of compounds. The combination of GC-HRMS and LC-HRMS is nowadays the closest approach to the ideal "universal" screening. The GC-QTOF MS screening developed has been qualitatively validated for a notable number of pesticides and PAHs in complex samples from aquaculture activities, allowing the detection of these compounds in a rapid and efficient way at the low SDL established. This method in combination with the LC-QTOF MS screening previously developed allows searching for many undesirables of different polarities and volatilities in distinct sample matrices.[22,34,35]

AUTHOR INFORMATION

Corresponding Author

*(F.H.) Phone: +34-964-387366. E-mail: felix.hernandez@qfa.uji.es.

Funding

This work has been (partly) funded under the EU Seventh Framework Programme by ARRAINA Project 288925: Advanced Research Initiatives for Nutrition and Aquaculture. The views expressed in this work are the sole responsibility of the authors and do not necessarily reflect the views of the European Commission. This work has been developed within the framework of the Research Unit of Marine Ecotoxicology (IATS (CSIC)-IUPA (UJI)). We also acknowledge the financial support of Generalitat Valenciana (research group of excellence PROMETEO/2009/054; ISIC 2012/016).

Notes

The authors declare no competing financial interest.

REFERENCES

(1) Nácher-Mestre, J.; Serrano, R.; Benedito-Palos, L.; Navarro, J. C.; López, F. J.; Pérez-Sánchez, J. Effects of fish oil replacement and re-feeding on the bioaccumulation of organochlorine compounds in gilthead sea bream (*Sparus aurata* L.) of market size. *Chemosphere* **2009**, *76*, 811−817.

(2) Berntssen, M. H. G.; Maage, A.; Julshamn, K.; Oeye, B. E.; Lundebye, A.-K. Carry-over of dietary organochlorine pesticides, PCDD/Fs, PCBs, and brominated flame retardants to Atlantic salmon (*Salmo salar* L.) fillets. *Chemosphere* **2011**, *83*, 95−103.

(3) Nácher-Mestre, J.; Serrano, R.; Benedito-Palos, L.; Navarro, J. C.; López, F. J.; Kaushik, S.; Pérez-Sánchez, J. Bioaccumulation of polycyclic aromatic hydrocarbons in gilthead sea bream (*Sparus aurata* L.) exposed to long term feeding trials with different experimental diets. *Arch. Environ. Contam. Toxicol.* **2010**, *59*, 137−146.

(4) Nácher-Mestre, J.; Serrano, R.; Portolés-Nicolau, T.; Hernández, F.; Benedito-Palos, L.; Pérez-Sánchez, J. A reliable analytical approach based on gas chromatography coupled to triple quadrupole and time-of-flight mass analyzers for the determination and confirmation of polycyclic aromatic hydrocarbons in complex matrices from aquaculture activities. *Rapid Commun. Mass Spectrom.* **2009**, *23*, 2075−2086.

(5) Kalachova, K.; Pulkrabova, J.; Cajka, T.; Drabova, L.; Stupak, M.; Hajslova, J. Gas chromatography-triple quadrupole tandem mass spectrometry: a powerful tool for the (ultra)trace analysis of multiclass environmental contaminants in fish and fish feed. *Anal. Bioanal. Chem.* **2013**, *405*, 7803−7815.

(6) Hernández, F.; Portolés, T.; Pitarch, E.; López, F. J. Gas chromatography coupled to high-resolution time-of-flight mass spectrometry to analyze trace-level organic compounds in the environment, food safety and toxicology. *TrAC−Trends Anal. Chem.* **2011**, *30*, 388−400.

(7) Fajar, N. M.; Carro, A. M.; Lorenzo, R. A.; Fernandez, F.; Cela, R. Optimization of microwave-assisted extraction with saponification (MAES) for the determination of polybrominated flame retardants in aquaculture samples. *Food Addit. Contam. A* **2008**, *25*, 1015−1023.

(8) García-Rodríguez, D.; Cela-Torrijos, R.; Lorenzo-Ferreira, R. A.; Carro-Díaz, A. M. Analysis of pesticide residues in seaweeds using matrix solid-phase dispersion and gas chromatography-mass spectrometry detection. *Food Chem.* **2012**, *135*, 259−267.

(9) Nácher-Mestre, J.; Serrano, R.; Hernández, F.; Benedito-Palos, L.; Pérez-Sánchez, J. Gas chromatography-mass spectrometric determination of polybrominated diphenyl ethers in complex fatty matrices from aquaculture activities. *Anal. Chim. Acta* **2010**, *664*, 190−198.

(10) Anastassiades, M.; Lehotay, S. J.; Štajnbaher, D.; Schenck, F. J. Fast and easy multiresidue method employing acetonitrile extraction/partitioning and "dispersive solid-phase extraction" for the determination of pesticide residues in produce. *J. AOAC Int.* **2003**, *86*, 412−431.

(11) Lehotay, S. J.; de Kok, A.; Hiemstra, M.; van Bodegraven, P. Validation of a fast and easy method for the determination of residues from 229 pesticides in fruits and vegetables using gas and liquid chromatography and mass spectrometric detection. *J. AOAC Int.* **2005**, *88*, 595−614.

(12) Lehotay, S. J.; Mastovská, K.; Yun, S. J. Evaluation of two fast and easy methods for pesticide residue analysis in fatty food matrixes. *J. AOAC Int.* **2005**, *88*, 630−638.

(13) Walorczyk, S. Development of a multi-residue method for the determination of pesticides in cereals and dry animal feed using gas chromatography−tandem quadrupole mass spectrometry II. Improvement and extension to new analytes. *J. Chromatogr., A* **2008**, *1208*, 202−214.

(14) Walorczyk, S.; Drozdzynski, D. Improvement and extension to new analytes of a multi-residue method for the determination of pesticides in cereals and dry animal feed using gas chromatography−tandem quadrupole mass spectrometry revisited. *J. Chromatogr., A* **2012**, *1251*, 219−231.

(15) Norman, D. F.; Glenn, R. W.; Anderson, K. A. Determination of parent and substituted polycyclic aromatic hydrocarbons in high-fat salmon using a modified QuEChERS extraction, dispersive SPE and GC-MS. *J. Agric. Food Chem.* **2011**, *59*, 8108−8116.

(16) Norli, H. R.; Christiansen, A.; Deribe, E. Application of QuEChERS method for extraction of selected persistent organic pollutants in fish tissue and analysis by gas chromatography mass spectrometry. *J. Chromatogr., A* **2011**, *1218*, 7234−7241.

(17) Ariel, R. F.; Camargo, A.; Martinez, L. D.; Altamirano, J. C. Dispersive solid-phase extraction as a simplified clean-up technique for biological sample extracts. Determination of polybrominated diphenyl ethers by gas chromatography−tandem mass spectrometry. *J. Chromatogr., A* **2011**, *1218*, 2490−2496.

(18) Castillo, M.; González, C.; Miralles, A. An evaluation method for determination of non-polar pesticide residues in animal fat samples by using dispersive solid-phase extraction clean-up and GC-MS. *Anal. Bioanal. Chem.* **2011**, *400*, 1315−1328.

(19) Hernández, F.; Sancho, J. V.; Ibáñez, M.; Abad, E.; Portolés, T.; Mattioli, L. Current use of high-resolution mass spectrometry in the environmental sciences. *Anal. Bioanal. Chem.* **2012**, *403*, 1251−1264.

(20) Serrano, R.; Nácher-Mestre, J.; Portolés, T.; Amat, F.; Hernández, F. Non-target screening of organic contaminants in marine salts by gas chromatography coupled to high-resolution time-of-flight mass spectrometry. *Talanta* **2011**, *85*, 877−884.

(21) Nácher-Mestre, J.; Serrano, R.; Portolés, T.; Hernández, F. Investigation of organophosphate esters in fresh water, salt and brine samples by GC-TOF MS. *Anal. Methods* **2011**, *3*, 1779−1785.

(22) Nácher-Mestre, J.; Ibáñez, M.; Serrano, R.; Pérez-Sánchez, J.; Hernández, F. Qualitative screening of undesirable compounds from feeds to fish by liquid chromatography coupled to mass spectrometry. *J. Agric. Food Chem.* **2013**, *61*, 2077−2087.

(23) Portolés, T.; Mol J. G. J.; Sancho, J. V.; Hernández, F. Use of electron ionization and atmospheric pressure chemical ionization in gas chromatography coupled to time-of-flight mass spectrometry for screening of organic pollutants in waters. *J. Chromatogr., A* **2014**, in press.

(24) Method validation and quality control procedures for pesticide residues analysis in food and feed, Document SANCO/12495/2011.

(25) European Commission, Decision 2002/657/EC, implementing Council Directive 96/23/EC concerning the performance of analytical methods and the interpretation of results.

(26) Aguilera-Luiz, M. M.; Romero-González, R.; Plaza-Bolaños, P.; Martínez Vidal, J. L.; Garrido Frenich, A. Wide-scope analysis of veterinary drug and pesticide residues in animal feed by liquid chromatography coupled to quadrupole-time-of-flight mass spectrometry. *Anal. Bioanal. Chem.* **2013**, *405*, 6543−6553.

(27) Wiest, L.; Buleté, A.; Giroud, B.; Fratta, C.; Amic, S.; Lambert, O.; Pouliquen, H.; Arnaudguilhem, C. Multi-residue analysis of 80 environmental contaminants in honeys, honeybees and pollens by one extraction procedure followed by liquid and gas chromatography coupled with mass spectrometric detection. *J. Chromatogr., A* **2011**, *1218*, 5743−5756.

(28) Przybylski, C.; Segard, C. Method for routine screening of pesticides and metabolites in meat based baby-food using extraction and gas chromatography-mass spectrometry. *J. Sep. Sci.* **2009**, *32*, 1858−1867.

(29) Lehotay, S. J.; Son, K. A.; Kwon, H.; Koesukwiwat, U.; Fu, W.; Mastovska, K.; Hoh, E.; Leepipatpiboon, N. Comparison of QuEChERS sample preparation methods for the analysis of pesticide residues in fruits and vegetables. *J. Chromatogr., A* **2010**, *1217*, 2548−2560.

(30) Portolés, T.; Sancho, J. V.; Hernández, F.; Newton, A.; Hancock, P. Potential of atmospheric pressure chemical ionization source in GC-QTOF MS for pesticide residue analysis. *J. Mass Spectrom.* **2010**, *45*, 926−936.

(31) Lundebye, A. K.; Hove, H.; Mage, A.; Bohne, V. J. B.; Hamre, K. Levels of synthetic antioxidants (ethoxyquin, butylated hydroxytoluene

and butylated hydroxyanisole) in fish feed and commercially farmed fish. *Food Addit. Contam. Part A—Chem.* **2010**, *27*, 1652—1657.
(32) Bohne, V. J. B.; Lundebye, A. K.; Harare, K. Accumulation and depuration of the synthetic antioxidant ethoxyquin in the muscle of Atlantic salmon (*Salmo salar* L.). *Food Chem. Toxicol.* **2008**, *46*, 1834—1843.
(33) Monteiro, P. R. R.; Reis-Henriques, M. A.; Coimbra, J. Plasma steroid levels in female flounder (*Platichthys flesus*) after chronic dietary exposure to single polycyclic aromatic hydrocarbons. *Mar. Environ. Res.* **2000**, *49*, 453—467.
(34) Díaz, R.; Ibáñez, M.; Sancho, J. V.; Hernández, F. Target and non-target screening strategies for organic contaminants, residues and illicit substances in food, environmental and human biological samples by UHPLC-QTOF-MS. *Anal. Methods* **2012**, *4*, 196—209.
(35) Ibáñez, M.; Portolés, T.; Rúbies, A.; Muñoz, E.; Muñoz, G.; Pineda, L.; Serrahima, E.; Sancho, J. V.; Centrich, F.; Hernández, F. The power of hyphenated chromatography/time-of-flight mass spectrometry in public health laboratories. *J. Agric. Food Chem.* **2012**, *60*, 5311—5323.

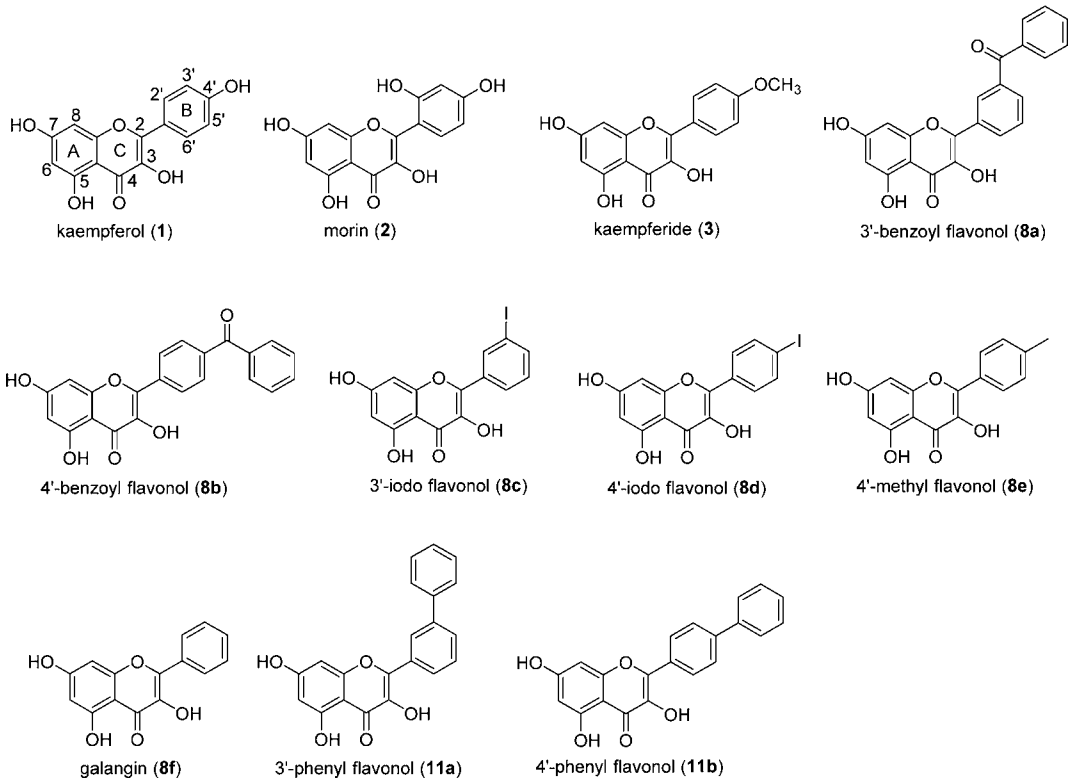

Figure 1. Structures of natural and synthetic flavonols.

General Procedure for the Synthesis of the Flavonol Analogues. Synthesis of the Flavonol Methyl Ethers. Methoxyphloroacetophenone (50 mg, 2.53 mmol) was placed into a round-bottom flask and dissolved in 1,2-dichloroethane (5 mL), and 4 mL was distilled to remove water. The carboxylic acid (3.54 mmol) and the acid chloride (8.33 mmol) were then added, followed by triethylamine (5 mL) and dimethylformamide (DMF) (15 mL). The solution was stirred at room temperature under argon for 3 h before being heated to reflux for an additional 12 h. The triethylamine and DMF were then removed under vacuum. The residue was dissolved in 3.8 mL of ethanol and heated to reflux. A solution of KOH (1.0 g) in H_2O (1.4 mL) was then added, and the mixture was refluxed for an additional 60 min. The solvents were removed under vacuum. The solid was dissolved in water (30 mL) and the crude product was precipitated out of solution by the addition of 10% HCl until the solution reached pH 5. The crude precipitate was extracted into chloroform (5 mL) and rinsed with saturated aqueous sodium bicarbonate (10 mL × 2). Because the desired product was only partially soluble in chloroform, these last two steps must be repeated several times (6−10 times until the chloroform extractions are no longer yellow). The chloroform was removed under vacuum. The crude product was then dissolved in a minimal amount of acetone (~0.5 mL/10 mg of flavonol). The solution becomes cloudy upon the addition of hexanes (10 mL) and was filtered through a pipet packed with glass wool. The filtrate contains the desired yellow product. The filtrate was evaporated under vacuum and set aside. Because some of the product remained in the precipitate, the precipitate on the glass wool in the pipet was dissolved in acetone, the acetone was evaporated, and trituration with acetone (~0.5 mL)/hexanes (10 mL) was repeated (2−4 times until the filtrate is no longer yellow). The NMR spectrum confirmed that all of the product was removed from the crude precipitate.

Deprotection. The methyl ether flavonol (20 mg, 0.06 mmol) was placed into a round-bottom flask and dissolved in acetic acid (16 mL). HBr (48% aqueous solution, 2 mL) was added via a syringe. The solution was heated to reflux for 24 h. Water (150 mL) was then added, resulting in a cloudy solution. The precipitate was isolated by filtration. This crude product was dissolved in chloroform (10 mL) and rinsed with saturated aqueous sodium bicarbonate (3 × 10 mL). The chloroform was evaporated under vacuum. The crude product was dissolved in a minimal amount of acetone (0.5 mL), and an excess of hexanes (10 mL) was added. The filtrate was collected, and the process was repeated several times. The filtrate was dried under vacuum to give a yellow precipitate.

*2-(3-Benzoylphenyl)-3,5,7-trihydroxy-4H-chromen-4-one (**8a**):* data was consistent with previous papers.[24]

*2-(4-Benzoylphenyl)-5,7-dihydroxy-3-methoxy-4H-chromen-4-one (**7b**).* 62% yield (121 mg, 0.312 mmol); ^{1}H NMR (300 MHz, acetone) δ 12.10 (s, 1H), 8.28 (ddd, 2H, J = 1.8, 3.6, 8.4 Hz), 7.96 (ddd, 2H, J = 1.8, 3.6, 8.7 Hz), 7.85 (m, 2H), 7.71 (dddd, 1H, J = 1.7, 3.4, 7.4, 14.7 Hz), 7.60 (dddd, 2H, J = 1.6, 3.2, 7.4, 14.7 Hz), 6.56 (d, 1H, J = 1.8 Hz), 6.31 (d, 1H, J = 1.8 Hz), 3.96 (s, 3H); ^{13}C NMR (75 MHz, acetone) δ 195.09 (C), 178.84 (C), 164.77 (C), 162. 46 (C), 157.29 (C), 154.27 (C), 140.27 (C), 139.30 (C), 137.38 (C), 134.31 (C), 132.95 (CH), 129.98 (CH), 129.95 (CH), 128.72 (CH), 128.52 (CH), 105.47 (C), 99.03 (CH), 94.04 (CH), 60.14 (CH_3).

*2-(4-Benzoylphenyl)-3,5,7-trihydroxy-4H-chromen-4-one (**8b**):* 84% yield (98 mg, 0.262 mmol), dec 221 °C; IR (KBr, cm^{-1}) 3283.9 (b), 1655.3 (s), 1636.8 (s), 1598.1 (s), 1501.2 (m), 1376.7 (m), 1319.5 (s), 1169.0 (s); ^{1}H NMR (500 MHz, acetone) δ 12.02 (s), 8.43 (d, 2H, J = 8.5 Hz), 7.95 (d, 2H, J = 8.5 Hz), 7.85 (m, 2H), 7.69 (m, 2H), 7.59 (ddd, 1H, J = 1.5, 7.5, 13.5 Hz), 6.61 (d, 1H, J = 2.5 Hz), 6.30 (d, 1H, J = 2.0 Hz); ^{13}C NMR (125 MHz, acetone) δ 195.90 (C), 176.94 (C), 165.53 (C), 162.32 (C), 158.06 (C), 144.66 (C), 139.11 (C), 138.96 (C), 138.26 (C), 135.64 (C), 133.51 (CH), 130.67 (CH), 130.65 (CH), 129.36 (CH), 128.30 (CH), 104.38 (C), 99.32 (CH), 94.67 (CH); HRMS (TOF) m/z calcd for $C_{22}H_{14}O_6$ (M^+) 375.0868, found 375.0803. Anal. Calcd for $C_{22}H_{14}O_6 \cdot H_2O$: C, 67.35%; H, 4.11%. Found: C, 65.55; H, 4.10%.

*5,7-Dihydroxy-2-(3-iodophenyl)-3-methoxy-4H-chromen-4-one (**7c**):* 64% yield (34 mg, 0.083 mmol); ^{1}H NMR (500 MHz, MeOH) δ 8.39 (dd, 1H, J = 2.0, 3.5 Hz), 8.07 (ddd, 1H, J = 1.0, 1.5, 8.0 Hz), 7.9 (ddd, 1H, J = 1.0, 2.0, 8.0 Hz), 7.32 (t, 1H, J = 7.8, 15.5 Hz), 6.44 (d, 1H, J = 2.0 Hz), 6.23 (d, 1H, J = 2.0 Hz), 3.81 (s, 3H); ^{13}C NMR (125 MHz, MeOH) δ 180.06 (C), 166.38 (C), 163.27 (C), 158.59 (C), 155.46 (C), 140.97 (CH), 138.05 (CH), 133.78 (C), 131.50 (CH),

128.74 (CH), 106.21 (C), 100.03 (CH), 94.90 (CH), 94.68 (C), 60.93 (CH_3).

*3,5,7-Trihydroxy-2-(3-iodophenyl)-4H-chromen-4-one (**8c**):* 90% yield (18 mg, 0.045 mmol), dec 143 °C; IR (KBr, cm^{-1}) 3318.5 (b), 1690.8 (w), 1654.7 (s), 1601.9 (s), 1517.2 (m), 1375.6 (m), 1317.5 (m), 1168.3 (s); ^{1}H NMR (300 MHz, acetone) δ 12.10 (s, 1H), 8.62 (dd, 1H, J = 1.7, 3.3 Hz), 8.27 (ddd, 1H, J = 1.2, 1.7, 8.1 Hz), 7.88 (ddd, 1H, J = 1.2, 1.7, 8.1 Hz), 7.40 (t, 1H, J = 8.1, 15.9 Hz), 6.59 (d, 1H, J = 2.1 Hz), 6.30 (d, 1H, J = 2.1 Hz); ^{13}C NMR (125 MHz, MeOH) δ 177.65 (C), 166.22 (C), 162.67 (C), 158.42 (C), 144.80 (C), 139.70 (CH), 139.09 (C), 137.31 (CH), 134.71 (C), 131.27 (CH), 127.79 (CH), 104.71 (C), 99.54 (CH), 94.66 (C), 94.59 (CH); HRMS (TOF) m/z calcd for $C_{15}H_9IO_5$ (M^+) 396.9573, found 396.9591. Anal. Calcd for $C_{15}H_9IO_5 \cdot H_2O$: C, 43.50%; H, 2.68%. Found: C, 44.39%; H, 2.60%

*3,5,7-Trihydroxy-2-(4-iodophenyl)-4H-chromen-4-one (**8d**):* data was consistent with previous papers.[25]

*5,7-Dihydroxy-3-methoxy-2-(p-tolyl)-4H-chromen-4-one (**7e**):* 20% yield (15 mg, 0.050 mmol); ^{1}H NMR (500 MHz, MeOH) δ 7.96 (d, 2H, J = 8.5 Hz), 7.36 (d, 2H, J = 8.0 Hz), 6.41 (d, 1H, J = 2.0 Hz), 6.20 (d, 1H, J = 2.0 Hz), 3.78 (s, 3H), 2.43 (s, 3H); ^{13}C NMR (125 MHz, MeOH) δ 180.12 (C), 166.32 (C), 163.19 (C), 158.60 (C), 157.67 (C), 142.96 (C), 140.30 (C), 130.40 (CH), 129.40 (CH), 128.91 (C), 106.01 (C), 99.92 (CH), 94.84 (CH), 60.73 (CH_3), 21.52 (CH_3).

*3,5,7-Trihydroxy-2-(p-tolyl)-4H-chromen-4-one (**8e**):* 80% yield (4 mg, 0.014 mmol), dec 139 °C; IR (KBr, cm^{-1}) 3299.7 (b), 1700.9 (w), 1654.2 (s), 1598.1 (s), 1500.0 (m), 1371.6 (m), 1313.5 (m), 1166.6 (s); ^{1}H NMR (500 MHz, acetone) δ 12.20 (s, 1H), 8.17 (d, 2H, J = 8.5 Hz), 7.40 (d, 2H, J = 8.0 Hz), 6.58 (d, 1H, J = 2.0 Hz), 6.30 (d, 1H, J = 2.0 Hz), 2.43 (s, 3H); ^{13}C NMR (125 MHz, acetone) 176.13 (C), 164.41 (C), 161.51 (C), 157.31 (C), 145.77 (C), 140.59 (C), 136.87 (C), 129.42 (CH), 128.64 (C), 127.82 (CH), 103.60 (C), 98.47 (CH), 93.91 (CH), 20.78 (CH_3); HRMS (TOF) m/z calcd for $C_{16}H_{12}O_5$ (M^+) 285.0763, found 285.0783. Anal. Calcd for $C_{16}H_{12}O_5 \cdot H_2O$: C, 63.57%; H, 4.67%. Found: C, 65.60%; H, 4.91%.

*Galangin (**8f**):* data was consistent with previous papers.[26−29]

General Procedure for the Synthesis of Aryl Flavonol Ethers through Suzuki−Miyaura Cross-Coupling Reactions. The procedure developed by Molander and Biolatto[30] was used with minor modifications. The organotrifluoroborate (0.073 mmol), the iodo flavonol methyl ether (20 mg, 0.049 mmol), potassium carbonate (20 mg, 0.146 mmol), and $Pd(OAc)_2$ (1 mg, 0.004 mmol) were placed in a round-bottom flask. These compounds were dissolved in 4 mL of methanol and heated to 65 °C overnight (16 h) with stirring. The solution was cooled to room temperature, and 10% HCl was added until the solution reached pH 5. The resulting precipitate was isolated by filtration. The precipitate was extracted with acetone until the extracts were no longer yellow and then the acetone was removed under vacuum. The crude product was dissolved in a minimal amount of acetone (0.5 mL), and excess hexanes (10 mL) were added. The precipitate was isolated by filtration, and this process was repeated several times. The filtrate was dried under vacuum to give a yellow precipitate. Deprotection of the flavonol ethers was achieved as described earlier.

*2-([1,1′-Biphenyl]-3-yl)-5,7-dihydroxy-3-methoxy-4H-chromen-4-one (**10a**):* 68% yield (30 mg, 0.083 mmol); ^{1}H NMR (500 MHz, MeOH) δ 8.28 (dd, 1H, J = 1.5, 3.0 Hz), 8.02 (ddd, 1H, J = 1.0, 1.5, 7.5 Hz), 7.79 (ddd, 1H, J = 1.0, 2.3, 7.5 Hz), 7.67 (m, 2H), 7.63 (t, 1H, J = 8.0, 16.0 Hz), 7.49 (m, 2H), 7.39 (ddd, 1H, J = 1.5, 3.5, 7.5 Hz), 6.43 (d, 1H, J = 2.5 Hz), 6.21 (d, 1H, J = 2.0 Hz), 3.83 (s, 3H); ^{13}C NMR (125 MHz, MeOH) δ 180.10 (C), 163.20 (C), 158.78 (C), 157.35 (C), 143.07 (C), 141.67 (C), 140.73 (C), 137.50 (C), 132.39 (C), 130.69 (CH), 130.34 (CH), 130.10 (CH), 128.91 (CH), 128.28 (CH), 128.13 (CH), 127.99 (CH), 105.97 (C), 100.26 (CH), 95.12 (CH), 60.97 (CH_3).

*2-([1,1′-Biphenyl]-3-yl)-3,5,7-trihydroxy-4H-chromen-4-one (**11a**):* 93% yield (18 mg, 0.051 mmol), dec 138 °C; IR (KBr, cm^{-1}) 3331.1 (b), 1686.1 (w), 1654.4 (s), 1603.6 (s), 1508.3 (m), 1375.4 (m), 1319.9 (m), 1169.0 (s); ^{1}H NMR (500 MHz, acetone) δ 8.54 (s, 1H), 8.25 (d, 1H, J = 8.0 Hz), 7.80 (d, 1H, J = 7.5 Hz), 7.75 (d, 2H, J = 7.5 Hz), 7.68 (t, 1H, J = 7.5, 15.0 Hz), 7.53 (m, 2H), 7.43 (t, 2H, J = 7.5, 15.0 Hz), 6.61 (d, 1H, J = 2.0 Hz), 6.30 (d, 1H, J = 2.0 Hz); ^{13}C NMR (125 MHz, acetone) δ 176.32 (C), 164.75 (C), 161.78 (C), 157.41 (C), 145.41 (C), 141.61 (C), 140.74 (C), 132.09 (C), 129.39 (CH), 129.22 (CH), 128.77 (CH), 127.95 (CH), 127.28 (CH), 126.81 (CH), 126.38 (CH), 103.75 (C), 98.66 (CH), 94.08 (CH); HRMS (TOF) m/z calcd for $C_{21}H_{14}O_5$ (M^+) 347.0919, found 347.0967. Anal. Calcd for $C_{21}H_{14}O_5 \cdot H_2O$: C, 69.23%; H, 4.43%. Found: C, 69.09%; H, 4.30%.

*2-([1,1′-Biphenyl]-4-yl)-5,7-dihydroxy-3-methoxy-4H-chromen-4-one (**10b**):* 67% yield (6.0 mg, 0.017 mmol); ^{1}H NMR (500 MHz, acetone) δ 12.70 (s, 1H), 8.21 (ddd, 2H, J = 2.0, 3.9, 4.0, 8.5 Hz), 7.87 (ddd, 2H, J = 2.0, 3.0, 9.0 Hz), 7.77 (m, 2H), 7.52 (m, 2H), 7.43 (dddd, 1H, J = 1.5, 2.5, 7.5, 15.0 Hz), 6.55 (d, 1H, J = 2.0 Hz), 6.28 (d, 1H, J = 2.0 Hz), 3.93 (s, 3H); ^{13}C NMR (125 MHz, acetone) δ 179.62 (C), 165.04 (C), 163.25 (C), 158.01 (C), 156.04 (C), 144.07 (C), 140.60 (C), 130.44 (C), 129.90 (CH), 129.77 (CH), 128.97 (CH), 127.84 (CH), 127.83 (CH), 106.11 (C), 99.47 (CH), 94.56 (CH), 60.49 (CH_3).

*2-([1,1′-Biphenyl]-4-yl)-3,5,7-trihydroxy-4H-chromen-4-one (**11b**):* 98% yield (6 mg, 0.016 mmol), dec 148 °C; IR (KBr, cm^{-1}) 3299.7 (b), 1702.1 (w), 1654.3 (s), 1625.1 (s), 1603.4 (s), 1508.0 (m), 1384.0 (m), 1314.4 (m), 1166.2 (s) 1H NMR (500 MHz, acetone) δ 12.10 (s, 1H), 8.36 (ddd, 2H, J = 2.0, 4.3, 8.5 Hz), 7.87 (ddd, 2H, J = 2.0, 3.5, 9.0 Hz), 7.77 (m, 2H), 7.51 (dddd, 2H, J = 1.5, 4.0, 8.0, 15.0 Hz), 7.41 (dddd, 1H, J = 1.3, 2.6, 7.5, 15.0 Hz), 6.59 (d, 1H, J = 2.0 Hz), 6.29 (d, 1H, J = 2.0 Hz); ^{13}C NMR (125 MHz, acetone) δ 176.82 (C), 165.26 (C), 162.41 (C), 157.99 (C), 145.87 (C), 143.15 (C), 140.76 (C), 138.05 (C), 131.04 (C), 129.86 (CH), 129.01 (CH), 128.82 (CH), 127.79 (CH), 127.76 (CH), 104.33 (C), 99.24 (CH), 94.61 (CH); HRMS (TOF) m/z calcd for $C_{21}H_{14}O_5$ (M^+) 347.0919, found 347.0995. Anal. Calcd for $C_{21}H_{14}O_5 \cdot H_2O$: C, 69.23%; H, 4.43%. Found: C, 68.21%; H, 4.27%.

Biological Reagents and Plant Material. Kaempferide, kaempferol, and morin were purchased from Indofine (Hillsborough, NJ, USA). Pollen germination assays were conducted using flavonol-deficient transgenic petunia plants. The procedure for growing and collecting the flavonol-deficient petunia pollen has been previously described.[12,31] Conditionally male fertile (CMF) transgenic V26 petunias were grown on a 16/8 h photoperiod, newly dehiscent anthers of flowers lacking pigmentation were collected, and the pollen from these anthers was suspended in germination media (GM).

Pollen-Rescue Assay. These assays were performed using the method developed by Mo et al.[12] in which PEG 4000 GM was used in the suspension of petunia pollen grains at a density of (1−2) × 10^4 grains/mL. Stock solutions were prepared by dissolving the flavonols (0.001−4000 nM) in dimethyl sulfoxide (DMSO) and then adding them to the GM for a final concentration of 0.2% DMSO per well. Unreported results from our laboratory show that 0.5% v/v DMSO and below are not toxic to pollen and did not activate the pollination sequence. The assays were performed in triplicate by adding flavonols, at various concentrations, to the pollen in GM in 96-well plates. Control samples were incubated without flavonols, but in the presence of DMSO. The plates were incubated at 25 °C and gently rotated (150 rpm) for 4 h at room temperature before germination was assessed. A pollen grain was scored as germinated when the length of the pollen grain tubes was greater than one diameter. The EC_{50} values were calculated by finding the maximum and minimum for each flavonol and determining the midpoint between these two concentrations. A minimum of seven concentrations were selected for each experiment.

Competition Assay. The stock solutions were prepared identically to those in the pollen-rescue assay. The competition assays were run under two sets of conditions. The first assay studied the effects of keeping the concentration of kaempferol constant (500 nM) and varying the concentrations of flavonol analogues (0−4000 nM). The second assay compared the reverse conditions, varying the concentration of kaempferol (0−4000 nM) and keeping the concentrations of the flavonol analogues (500 nM) constant. Pollen germination was assessed as described for the pollen-rescue assay.

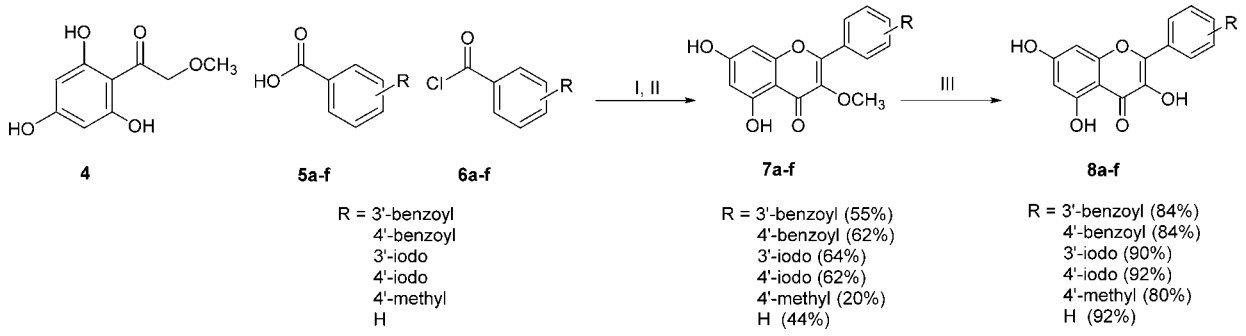

Figure 2. Synthesis of flavonol analogues. Reagents and conditions: (I) Et_3N, DMF, **5**, **6**, reflux; (II) KOH/H_2O, ethanol, reflux; (III) HBr, acetic acid, reflux.

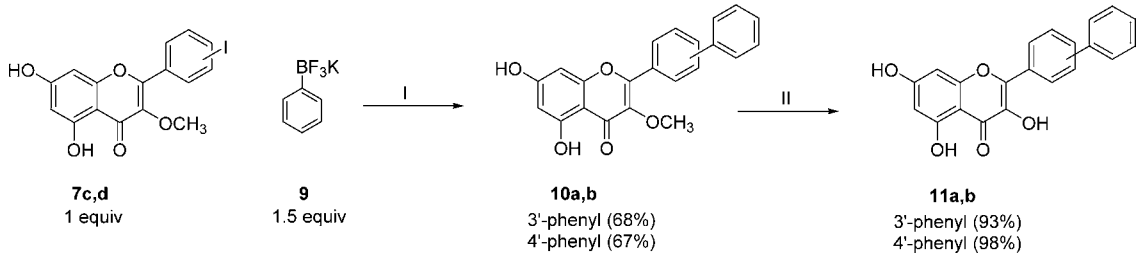

Figure 3. Synthesis of biaryl flavonol analogues. Reagents and conditions: (I) $Pd(OAc)_2$, K_2CO_3 (3 equiv), MeOH, 65 °C; (II) HBr, acetic acid, reflux.

Table 1. Potency and Efficacy of Natural and Synthetic Flavonols on Pollen Germination[a]

	pollen-rescue assay		
flavonols[b]	potency EC_{50} values (nM)	flavonols[b]	efficacy maximal response (% G[c])
3′-phenyl flavonol (**11a**)	0.849 ± 1.32 a	kaempferol (**1**)	60.51 ± 2.18 A
kaempferol (**1**)	161.54 ± 0.81 b	galangin (**8f**)	52.71 ± 0.93 B
galangin (**8f**)	181.04 ± 14.97 b	morin (**2**)	46.00 ± 1.33 B
kaempferide (**3**)	333.74 ± 85.96 c	4′-methyl flavonol (**8e**)	35.40 ± 1.61 C
morin (**2**)	1152.89 ± 60.66 d	kaempferide (**3**)	30.58 ± 0.50 C
4′-methyl flavonol (**8e**)	1840.76 ± 79.51 e	3′-phenyl flavonol (**11a**)	12.39 ± 1.48 D
3′-iodo flavonol (**8c**)	N/A	3′-benzoyl flavonol (**8a**)	4.84 ± 0.39 E
4′-iodo flavonol (**8d**)	N/A	3′-iodo flavonol (**8c**)	4.10 ± 0.09 E
4′-phenyl flavonol (**11b**)	N/A	4′-benzoyl flavonol (**8b**)	3.43 ± 1.37 E
3′-benzoyl flavonol (**8a**)	N/A	4′-iodo flavonol (**8d**)	3.27 ± 0.20 E
4′-benzoyl flavonol (**8b**)	N/A	4′-phenyl flavonol (**11b**)	2.48 ± 0.405 E
DMSO (control)	N/A	DMSO (control)	1.98 ± 1.24 E

[a]Values are the mean ± SEM of two independent experiments, done in triplicate, except for 4′-methyl flavonol and kaempferide in which the mean reflects three independent experiments. Tukey's multiple-comparison tests determined statistical differences between the EC_{50} values (lower case letters) and the maximal responses (upper case letters) of each flavonol after ANOVA ($P < 0.05$). N/A, not statistically different from the control. Statistical analysis was performed using the software Origin. [b]Concentration ranges: 0.001−4000 nM. [c]Percent germination.

Statistical Analysis. The EC_{50} values and maximal responses of the flavonols in each cell line were analyzed by Tukey's multiple-comparison tests after one-way analysis of variance (ANOVA). Differences were considered significant at $P < 0.05$.

RESULTS AND DISCUSSION

Chemistry. Flavonol analogues were synthesized through a "one pot" procedure described by Ichikawa et al.[32] in which the ω-methoxyphloroacetophenone **4** was esterified by the acid chloride **6a−f** to produce a triester intermediate, which then proceeded to cyclize (Figure 2). Ester hydrolysis of this intermediate resulted in the synthesis of the flavonol methyl ethers, compounds **7a−f** ((3′-benzoyl (55%), 4′-benzoyl (62%), 3′-iodo (64%), 4′-iodo (62%), galangin (44%), and 4′-methyl (20%) flavonol methyl ethers). Demethylation of the flavonol methyl ethers **7a−f** was attempted using BBr_3 in chloroform[33] or sodium sulfide in DMF.[34] Only partial demethylation occurred with BBr_3, and no demethylation was observed with sodium sulfide. A disadvantage to the first method is that BBr_3 is water sensitive and thus difficult on a small scale. In the second method, it is believed that deprotection of **7a−f** did not occur because the phenolic hydrogen atoms were deprotonated, making the ring more electron rich, causing the methoxy group to become unreactive. Complete deprotection and high yields were achieved using HBr in acetic acid to give the desired flavonols, compounds **8a−f** (3′-benzoyl (84%), 4′-benzoyl (84%), 3′-iodo (90%), 4′-iodo (92%), galangin (92%), and 4′-methyl (80%) flavonols).[35]

The 3′- and 4′-phenyl flavonols were synthesized via an organotrifluoroborate chemistry developed by Molander et al.

dx.doi.org/10.1021/jf405688d | J. Agric. Food Chem. 2014, 62, 2175−2181

(Figure 3).[30] This method utilized a palladium-catalyzed Suzuki−Miyaura cross-coupling reaction. Good yields were achieved in the synthesis of both the 3′-phenyl **10a** (68%) and 4′-phenyl **10b** (67%) flavonol methyl ethers. These yields are noteworthy for the lack of reactivity of the cross-coupling reaction to the redox active flavonols. High yields were achieved in the demethylation of these intermediates to the 3′-phenyl **11a** (93%) and 4′-phenyl **11b** (98%) flavonols. All synthetic flavonols (galangin, 3′- and 4′-benzoyl, 3′- and 4′-iodo, 3′- and 4′-phenyl, and 4′-methyl flavonols) were identified through spectroscopic and spectrometric data (NMR and IR spectroscopy and high-resolution MS).

Pollen-Rescue Assays. In vitro pollen-rescue assays were conducted to explore which naturally occurring flavonols (kaempferol, kaempferide, galangin, and morin) and flavonol analogues (3′- and 4′-benzoyl, 3′- and 4′-phenyl, 3′- and 4′-iodo, and 4′-methyl flavonols) were the most effective at activating the pollination sequence and, thus, were the most efficient agonists (Table 1 and Figure 4). DMSO has been shown to have no significant effect in activating the pollination sequence at concentrations of <0.6% and was used as a vehicle control at concentrations of 0.2%.[12] The use of a DMSO blank served as the negative control. The effectiveness of these agonists was determined on the basis of two criteria, potency (EC_{50}) and efficacy (maximal response). An ideal agonist has high potency (low EC_{50}) and high efficacy. The natural products kaempferol, galangin, and kaempferide had the highest potencies. Morin, as well as the flavonol analogue 4′-methyl flavonol, were somewhat less potent. A different trend was observed in the efficacy of the flavonols. The natural product, kaempferol, had the highest efficacy, whereas galangin and morin were partial agonists. Kaempferide and the flavonol analogue 4′-methyl flavonol had the lowest efficacy, achieving half the maximal response. The remaining hydrophobic flavonol analogues (3′- and 4′-benzoyl, 3′- and 4′-phenyl, and 3′- and 4′-iodo flavonols) gave minimal or no response when tested in concentrations up to 4 μM when compared to the negative control. These results show that kaempferol is the best agonist among the flavonols tested and that the hydrophobic analogues (3′- and 4′-benzoyl, 4′-phenyl, and 3′- and 4′-iodo flavonols) do not act as agonists.

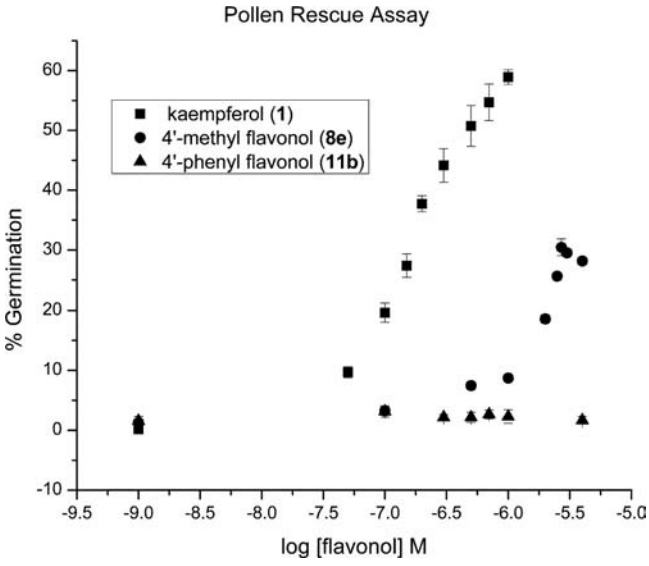

Figure 4. Comparison of a fully (kaempferol, 4′-OH), partially (4′-methyl flavonol), and minimally (4′-phenyl flavonol) active flavonol to induce pollen germination.

Competition Assays. Possible antagonists were identified by comparing the potency and efficacy of kaempferol in the presence and absence of the flavonol analogues (Table 2 and Figure 5). Thus, in vitro competition assays were run between

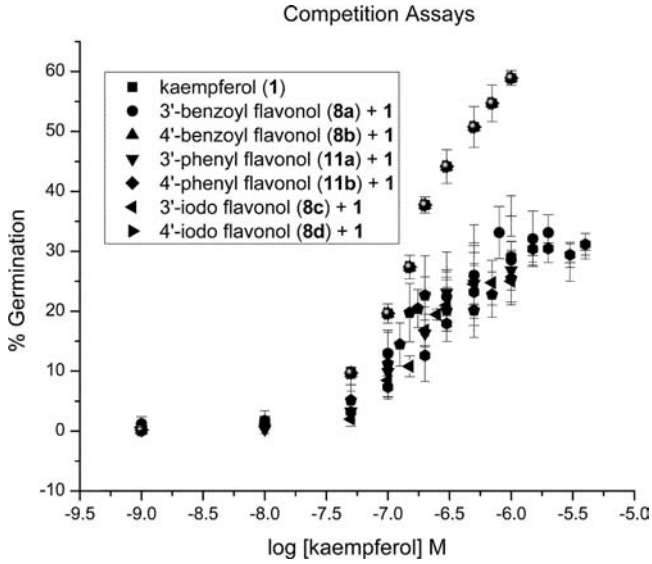

Figure 5. Comparison of kaempferol (**1**) in the presence and absence of flavonol analogues to activate the pollination sequence.

Table 2. Potency and Efficacy of Kaempferol in the Presence and Absence of Flavonol Analogues on Pollen Germination[a]

	competition assay		
flavonols[b]	potency EC_{50} values (nM)	flavonols[b]	efficacy maximal response (% G[c])
kaempferol (**1**), control	162 ± 1 a	kaempferol (**1**), control	61 ± 2 A
3′-iodo flavonol (**8c**) + **1**	103 ± 2 a	3′-benzoyl flavonol (**8a**) + **1**	33 ± 2 B
4′-iodo flavonol (**8d**) + **1**	114 ± 26 a	4′-phenyl flavonol (**11b**) + **1**	32 ± 0 B
3′-phenyl flavonol (**11a**) + **1**	156 ± 31 a	4′-iodo flavonol (**8d**) + **1**	30 ± 1 B
3′-phenyl flavonol (**11a**) + **1**	157 ± 31 a	4′-benzoyl flavonol (**8b**) + **1**	29 ± 2 B
3′-benzoyl flavonol (**8a**) + **1**	169 ± 26 a	3′-phenyl flavonol (**11a**) + **1**	26 ± 3 B
4′-phenyl flavonol (**11b**) + **1**	250 ± 59 a	3′-iodo flavonol (**8c**) + **1**	25 ± 3 B

[a]Values are the mean ± SEM of two independent experiments done in triplicate. Tukey's multiple-comparison tests determined statistical differences between the relative EC_{50} values (lower case letters) and maximal responses (upper case letters) of each flavonol after ANOVA ($P < 0.05$). [b]Concentration ranges: flavonol analogues (**8a−d** and **11a,b**), 0−4000 nM; kaempferol (**1**), 500 nM. [c]Percent germination.

dx.doi.org/10.1021/jf405688d | J. Agric. Food Chem. 2014, 62, 2175−2181

the model agonist, kaempferol, and the minimally activating flavonols (3′- and 4′-benzoyl, 3′- and 4′-phenyl, and 3′- and 4′-iodo flavonols). A classical antagonist decreases the potency (increased EC_{50}) and efficacy of a full agonist such as kaempferol. From these assays, we found no difference between the potency of kaempferol in the presence or absence of these minimally activating flavonols; however, the efficacy of kaempferol was diminished by half. Kaempferol was unable to increase the percent germination above half its maximal response in the presence of these flavonols, even at high concentrations (>1 mM). In other words, the flavonols caused kaempferol to act as a partial agonist. On the basis of this information, all of the hydrophobic flavonol analogues (3′- and 4′-benzoyl, 3′- and 4′-phenyl, and 3′- and 4′-iodo flavonols) inhibited kaempferol action in a noncompetitive manner. Additional studies are needed to determine the mechanism by which flavonols are acting as noncompetitive inhibitors in pollen germination.

Structure–Activity Relationship Comparisons. The effects of hydrophilicity, hydrophobicity, steric bulk, hydrogen bonding, and planarity in the B ring of flavonols were studied to determine which characteristics activated (agonist) or inhibited (antagonist) the pollen germination sequence. Previous research has shown that the best flavonol agonists were flavonols with a more hydrophobic, less hydroxylated B ring.[11,12] For example, flavonols with one (kaempferol) B-ring hydroxyl group were 10 times more potent than flavonols with two (quercetin) and 100 times more potent than flavonols with three (myricetin) B-ring hydroxyl groups. We observed this trend between kaempferol and the 2′,4′-dihydroxy flavonol, morin.

Flavonols with a B-ring substituent capable of hydrogen bonding also appear to make better agonists. Substituting a 4′-hydroxyl group (kaempferol, 162 nM and 61% G) with a methoxy group (kaempferide, 334 nM and 31% G) decreased both its potency and efficacy by 50%. Substituting the 4′-hydroxyl group (kaempferol, 162 nM and 61% G) with a methyl group (4′-methyl flavonol, 1841 nM and 35% G) lowered the potency 11-fold and decreased the efficacy by 50%.

Another interesting, but not completely understood, observation was that the more hydrophobic 3′-phenyl flavonol (0.849 nM and 12% G) was the only flavonol analogue that appeared to act as an agonist. All other hydrophobic flavonol analogues (3′- and 4′-benzoyl, 3′- and 4′-iodo flavonols), including the isomeric 4′-phenyl flavonol, acted as apparent antagonists. A plausible explanation is that there is a size restriction on the flavonol binding site and only smaller less sterically hindered compounds, such as kaempferol and galangin, and/or compounds with small planar groups at the C3 position of ring B (3′-phenyl flavonol) are able to fit into the binding site. Flavonols with bulky groups (4′-phenyl, 3′- and 4′-benzoyl, 3′- and 4′-iodo flavonols) likely bind to a different site, an idea supported by the fact that the flavonol analogues appear to be inhibiting the action of kaempferol in a noncompetitive manner. Additionally, steric bulk could explain why the more hydroxylated flavonols (quercetin, morin, and myricetin) were not as efficient at activating the pollination sequence as kaempferol. The decrease in efficiency might be a consequence of more hydrophobic, less hydroxylated flavonols' inability to fit into the flavonol binding site rather than a preference for more hydrophobic flavonols or a combination of both characteristics.

Structure–activity relationship studies have shown that efficacy is not as simple as the previously proposed idea that more hydrophobic, less hydroxylated flavonols make the best agonists.[11,12] Of the flavonols tested, only the smaller, less sterically hindered compounds (kaempferol, galangin, kaempferide, morin, and 4′-methyl flavonol) were found to act as agonists, whereas the larger more hydrophobic flavonols (4′-phenyl, 3′- and 4′-benzoyl, 3′- and 4′-iodo flavonols) had no agonist activity, but interfered with the action of kaempferol. This action could involve receptor-mediated events such as noncompetitive antagonism or could represent a form of functional antagonism. Our results suggest that the most important factor in determining if a flavonol will function as an agonist is its size, with hydrogen bonding and/or planarity appearing to improve the potency and efficacy of the agonist as long as it is not sterically hindered. Further studies are needed to identify the biologically relevant receptor of flavonols in plants to better understand the biological mechanism(s) by which flavonols activate pollen germination, possibly through the use of benzoyl flavonols as photoaffinity reagents.[36] Irreversible binding of benzoyl flavonols to the receptor could allow isolation of the complex. These findings also provide important information for the exploitation and use of flavonoids in the development of new agrichemicals.

■ ASSOCIATED CONTENT

Ⓢ Supporting Information

Spectroscopic and spectrometric data for **7a,d,f** and **8a,d,f** is available free of charge via the Internet at http://pubs.acs.org.

■ AUTHOR INFORMATION

Corresponding Author

*(A.M.F.) Phone: (206) 523-9867. Fax: (509) 335-8867. E-mail: alforbes@wsu.edu.

Funding

We acknowledge that this research was supported in part by a grant from the College of Science at Washington State University.

Notes

The authors declare no competing financial interest.

■ REFERENCES

(1) Middleton, E., Jr.; Kandaswami, C.; Theoharides, T. C. The effects of plant flavonoids on mammalian cells: implications for inflammation, heart disease, and cancer. *Pharmacol. Rev.* **2000**, *52*, 673–751.

(2) Taylor, L. P.; Grotewold, E. Flavonoids as developmental regulators. *Curr. Opin. Plant Biol.* **2005**, *8*, 317–323.

(3) Solovchenko, A.; Merzlyak, M. Optical properties and contribution of cuticle to UV protection in plants: experiments with apple fruit. *Photochem. Photobiol. Sci.* **2003**, *2*, 861–866.

(4) Smith, G. J.; Markham, R. K. Tautomerism of flavonol glucosides: relevance to plant UV protection and flower color. *J. Photochem. Photobiol.* **1998**, *118*, 99–105.

(5) Vogt, T.; Pollak, P.; Tarlyn, N.; Taylor, L. P. Pollination- or wound-induced kaempferol accumulation in petunia stigmas enhances seed production. *Plant Cell* **1994**, *6*, 11–23.

(6) Pollak, P. E.; Vogt, T.; Mo, Y.; Taylor, L. P. Chalcone synthase and flavonol accumulation in stigmas and anthers of petunia hybrida. *Plant Physiol.* **1993**, *102*, 925–932.

(7) Taylor, L. P.; Hepler, P. K. Pollen germination and tube growth. *Annu. Rev. Plant Physiol. Plant Mol. Biol.* **1997**, *48*, 461–491.

(8) Neera Garg, G. Symbiotic nitrogen fixation in legume nodules: process and signaling. *Agron. Sustain. Dev.* **2007**, *27*, 59–68.

(9) Shaw, L. J.; Morris, P.; Hooker, J. E. Perception and modification of plant flavonoid signals by rhizosphere microorganisms. *Environ. Microbiol.* **2006**, *8*, 1867−1880.
(10) Harborne, J. B. *The Flavonoids: Advances in Research since 1980*; Chapman and Hall: New York, 1988.
(11) Vogt, T.; Wollenweber, E.; Taylor, L. P. The structural requirements of flavonols that induce pollen germination of conditionally male fertile petunia. *Phytochemistry* **1995**, *38*, 589−592.
(12) Mo, Y.; Nagel, C.; Taylor, L. P. Biochemical complementation of chalcone synthase mutants defines a role of flavonols in functional pollen. *Proc. Natl. Acad. Sci. U.S.A.* **1992**, *89*, 7213−7217.
(13) Schijlen, E. G.; de Vos, C. H.; Martens, S.; Jonker, H. H.; Rosin, F. M.; Molthoff, J. W.; Tikunov, Y. M.; Angenent, G. C.; van Tunen, A. J.; Bovy, A. G. RNA interference silencing of chalcone synthase, the first step in the flavonoid biosynthesis pathway, leads to parthenocarpic tomato fruits. *Plant Physiol.* **2007**, *144*, 1520−1530.
(14) Dumont-BeBoux, N.; von Aderkas, P. In vitro pollen tube growth in Douglas-fir. *Can. J. For. Res.* **1997**, *27*, 674−678.
(15) Ylstra, B.; Touraev, A.; Moreno, R. M.; Stoger, E.; van Tunen, A. J.; Vicente, O.; Mol, J. N.; Heberle-Bors, E. Flavonols stimulate development, germination, and tube growth of tobacco pollen. *Plant Physiol.* **1992**, *100*, 902−907.
(16) Mahajan, M.; Ahuja, P. S.; Yadav, S. K. Post-transcriptional silencing of flavonol synthase mRNA in tobacco leads to fruits with arrested seed set. *PLoS One* **2011**, *6*, e28315.
(17) Yin, R.; Messner, B.; Faus-Kessler, T.; Hoffmann, T.; Schwab, W.; Hajirezaei, M. R.; von Saint Paul, V.; Heller, W.; Schaffner, A. R. Feedback inhibition of general phenylpropanoid and flavonol biosynthesis pathways upon a compromised flavonol-3-O-glycosylation. *J. Exp. Bot.* **2012**, *63*, 2465−2478.
(18) Thompson, E. P.; Wilkins, C.; Demidchik, V.; Davies, J. M.; Glover, B. J. An *Arabidopsis* flavonoid transporter is required for anther dehiscence and pollen development. *J. Exp. Bot.* **2010**, *61*, 439−451.
(19) Jia, L.; Wu, Q.; Ye, N.; Liu, R.; Shi, L.; Xu, W.; Zhi, H.; Rahman, A. N.; Xia, Y.; Zhang, J. Proanthocyanidins inhibits seed germination by maintaining a high level of abscisic acid in *Arabidopsis thaliana*. *J. Integr. Plant Biol.* **2012**, *54*, 663−673.
(20) Muir, S. R.; Collins, G. J.; Robinson, S.; Hughes, S.; Bovy, A.; Ric De Vos, C. H.; van Tunen, A. J.; Verhoeyen, M. E. Overexpression of petunia chalcone isomerase in tomato results in fruit containing increased levels of flavonols. *Nat. Biotechnol.* **2001**, *19*, 470−474.
(21) Charkraborty, K.; Devakumar, C. Ethyloxanilates as specific male gametocides for wheat (*Triticum aestivum* L.). *Plant Breed.* **2006**, *125*, 441−447.
(22) Charkraborty, K.; Devakumar, C. *N*-Acylanilines, herbicide-CHA chimera, and amino acid analogues as novel chemical hybridizing agents for wheat (*Triticum aestivum* L.). *J. Agric. Food Chem.* **2005**, *53*, 7899−7907.
(23) Cheng, S. H.; Zhuang, J. Y.; Fan, Y. Y.; Du, J. H.; Cao, L. Y. Progress in research and development on hybrid rice: a super-domesticate in China. *Ann. Bot.* **2007**, *100*, 959−966.
(24) Tanaka, H.; Stohlmeyer, M. M.; Wandless, T. J.; Taylor, L. P. Synthesis of flavonol derivatives as probes of biological processes. *Tetrahedron Lett.* **2000**, *41*, 9735−9739.
(25) Boumendjel, A.; Bois, F.; Beney, C.; Mariotte, A. M.; Conseil, G.; Di Pietro, A. B-ring substituted 5,7-dihydroxyflavonols with high-affinity binding to P-glycoprotein responsible for cell multidrug resistance. *Bioorg. Med. Chem. Lett.* **2001**, *11*, 75−77.
(26) Azimova, S. S.; Vinogradova, V. I. G. *Natural Compounds: Flavonoids: Plant Sources, Structure and Properties*; Springer: New York, 2013; pp 96.
(27) Batirov, E. K.; Kiyamitdinova, F.; Malikov, V. M. Flavonoids of the epigeal part of *Glycyrrhiza glabra*. *Chem. Nat. Compd.* **1986**, *22*, 107−108.
(28) Yuldashev, M. P. Flavonoids of the epigeal part of *Glycyrrhiza uralensis*. *Chem. Nat. Compd.* **1998**, *34*, 508−509.
(29) Agrawal, P. K.; Rastogi, R. P. ^{13}C NMR spectroscopy of flavonoids. *Heterocycles* **1981**, *16*, 2181.
(30) Molander, G. A.; Biolatto, B. Palladium-catalyzed Suzuki-Miyaura cross-coupling reactions of potassium aryl- and heteroaryltrifluoroborates. *J. Org. Chem.* **2003**, *68*, 4302−4314.
(31) Taylor, L. P.; Jorgenson, R. Conditional male fertility in chalcone synthase-deficient petunia. *J. Hered.* **1992**, *83*, 11−17.
(32) Ichikawa, M.; Pamukcu, A. M.; Bryan, G. T. A convenient method for the synthesis of kaempferol. *Org. Prep. Proc. Int.* **1982**, *14*, 183−187.
(33) Mais, D. E.; Bowling, N. L.; True, T. A.; Naka, M.; Morinelli, T. A.; Oatis, J. E.; Hamanaka, N.; Halushka, P. V. Novel synthesis and biochemical properties of an [^{125}I]-labeled photoaffinity probe for thromboxane A_2/prostagladin H_2 receptors. *J. Med. Chem.* **1991**, *34*, 1511−1514.
(34) Newman, M. S.; Sankaran, V.; Olson, D. R. Phenolic and ketonic tautomers in polycyclic aromatic hydrocarbons. *J. Am. Chem. Soc.* **1976**, *98*, 3237−3242.
(35) Landini, D.; Montanari, F.; Rolla, F. Cleavage of dialkyl and aryl alkyl ethers with hydrobromic acid in the presence of phase-transfer catalysts. *Synthesis* **1978**, *10*, 771−773.
(36) Taylor, L. P.; Miller, K. D. The use of a photoactivatable kaempferol analogue to probe the role of flavonol 3-*O*-galactosyltransferase in pollen germination. *Adv. Exp. Med. Biol.* **2002**, *505*, 41−50.

although its effectiveness remains controversial.[15,16] Therefore, new drugs for RSV treatment and prevention are urgently needed.

Natural products serve as an important source of potential antiviral agents based on their traditional uses.[17] In the present study, we reported the supercritical fluid extract of "Guangchenpi" possessing *in vitro* antiviral activity against RSV. Therefore, the objectives of the present study were to investigate the anti-RSV constituents of the supercritical fluid extract of "Guangchenpi" and to probe the possible mechanism of the most active constituent in the extract.

MATERIALS AND METHODS

Plant Material. The mature pericarps of *Citrus reticulata* 'Chachi' were collected in Xinhui city, Guangdong Province, China, and then were oven-dried at 80 °C for 4 h. The plant was authenticated by Prof. Guang-Xiong Zhou, College of Pharmacy, Jinan University. A voucher specimen with accession No. 20090226 was deposited in the Herbarium of the College of Pharmacy, Jinan University.

General Apparatus and Chemicals. Supercritical CO_2 fluid extraction was performed in a HA-121-50-02 supercritical fluid CO_2 extraction apparatus (Jiangsu Nantong Huaan Supercritical Fluid Extraction Inc., Jiangsu, China). Optical rotations were measured in a JASCO P-1030 automatic digital polarimeter. IR spectra were determined using a JASCO FT/IR-480 plus infrared spectrometer with KBr pellets. NMR spectra were performed on a Bruker Avance 400 MHz spectrometer with TMS as the internal standard. Chemical shifts were expressed in δ values (ppm) with reference to the solvent signals. ESI-MS data were recorded on a Finnigan LCQ Advantage Max ion trap mass spectrometer. Silica gel (200−300 mesh, Qingdao Marine Chemical Inc., China) and Sephadex LH-20 (Pharmacia, Sweden) were used for column chromatography (CC). Thin-layer chromatography (TLC) was performed on precoated silica gel plates (GF254, Yantai, China). Analytical high-performance liquid chromatography (HPLC) was performed on a Dionex chromatograph equipped with a P680 pump, a PDA-100 photodiode array detector, and an Agilent Zorbax SB-C_{18} reversed-phase column (4.6 mm × 250 mm, 5 μm). Preparative high performance liquid chromatography (HPLC) was carried out on a Varian Postar 210 chromatograph equipped with a Varian-306 pump and a Varian UV/vis-152 detector with a C_{18} reversed-phase column (Cosmosil, 10 mm × 250 mm, 5 μm). All reagents were purchased from Tianjin Damao Chemical Company (Tianjin, P. R. China).

Extraction and Isolation. The supercritical fluid extract of "Guangchenpi" was prepared with the method described in a previous report.[14] Briefly, supercritical fluid extraction was conducted at a pressure of 25 MPa and a temperature of 35 °C for 2 h, and the flow rate of CO_2 was 20 L/h. Supercritical fluid extract (46.2 g) passed through a normal-phase silica gel column chromatography (10 cm × 40 cm, 300 mesh, 1 kg) eluted with petroleum ether, petroleum ether−acetone gradients (99:1, 98:2, 97:3, 95:5, 93:7, 90:10, 85:15, 80:20, 70:30, and 60:40, v/v) and finally pure methnol to obtain 12 fractions (A−L) based on TLC analysis. Fractions D−G were subjected to further isolation due to their anti-RSV activity. Fraction D (3.5 g) was purified by repeated silica gel column chromatography (4 cm × 30 cm, 300 mesh, 100 g) eluted with cyclohexane−ethyl acetate (300:1 → 1:1, v/v), and recrystallized from cyclohexane to yield compound **3** (218.5 mg). Compound **2** (517.8 mg) was isolated from fraction E (3.3 g) by a silica gel column (4 cm × 20 cm, 300 mesh, 85 g) eluted with cyclohexane−ethyl acetate (200:1 → 1:1, v/v), and recrystallization from cyclohexane. Compounds **4** (9.4 mg) and **5** (11.7 mg) were obtained from fraction F (1.3 g) by repeated silica gel column chromatography (3 cm × 12 cm, 300 mesh, 30 g) eluted with cyclohexane−ethyl acetate (200:1 → 1:1, v/v) and then sephadex LH-20 column chromatography (2.5 cm × 75 cm, 50 g) using chlorofrom−methanol (2:1, v/v) as eluent. Fraction G (3.2 g) was separated by silica gel column chromatography (4 cm × 30 cm, 300 mesh, 100 g), eluted with chloroform−methanol (100:1 → 1:1, v/v), and further purified by preparative HPLC column [RP-18 (10 × 250 mm, 5 μm)], using methanol−water (85:15, v/v) as the mobile phase to obtain compound **1** (82.5 mg).

HPLC Analysis. The contents of the active compounds **2** (tangeretin) and **3** (nobiletin) in the supercritical fluid extract of "Guangchenpi" were analyzed by a Dionex chromatograph equipped with a P680 pump and a PDA-100 photodiode array detector using an Agilent Zorbax SB-C_{18} reversed-phase column (4.6 mm × 250 mm, 5 μm). Compounds **2** and **3**, obtained from the isolation, were well separated from other peaks with relative abundance in the supercritical fliud extract as displayed in their HPLC profiles (Figure 2). In the experiment, compounds **2**, **3**, and the supercritical fluid extract of "Guangchenpi" were dissolved in methanol and filtered through a 0.22 μm PTFE syringe filter before injection into the HPLC. The column temperature was set to 25 °C. The mobile phase consisted of A (water with 0.5% acetic acid) and B (acetonitrile). Gradient elution conditions were 0−15 min, isocratic 49% B, and 16−25 min, 100% B. The flow rate was 1.0 mL/min. The injection volume was 10 μL. The analytes were monitored at 330 nm.

Cell and Virus. Human larynx epidermoid carcinoma (HEp-2, ATCC CCL-23) cells and RSV A2 (ATCC VR-1540), Long (ATCC VR-26), and B (ATCC VR-955) strains were purchased from Medicinal Virology Institute, Wuhan University, China. The RSV strains were grown and titered in HEp-2 cells. The HEp-2 cells were cultured in Dulbecco's modified Eagle's medium (DMEM; Gibco, USA) plus 100 U/mL penicillin and streptomycin solution, 2 mM L-glutamine, and 10% fetal bovine serum (FBS; Sijiqing Biological Engineering Company, China), which is designated as growth medium (GM). Virus-infected cells were maintained in DMEM with 100 U/mL penicillin and streptomycin solution, 2 mM L-glutamine, and 2% FBS (Maintenance Medium, MM). Virus titers were determined by the 50% tissue culture-infective dose ($TCID_{50}$) method and plaque reduction assay. Ribavirin (Sigma, USA) was used as a positive control in the anti-RSV tests. All of the cells were cultured at 37 °C in a 95% humidified atmosphere supplied with 5% CO_2. The RSV strains were stored at −80 °C until use.

3-(4,5-Dimethylthiazol-2-yl)-2,5-diphenyl Tetrazolium Bromide (MTT) Assay. The cytotoxicity of the supercritical fluid extract and the compounds on HEp-2 cells was detected by MTT assay in 96-well plates (Corning, USA).[18] In brief, sample was added to confluent HEp-2 cell monolayers, and MM without the sample was used as cell control. The cells were incubated for 72 h, then MTT solution (Sigma, USA) was added. The plate was further incubated for 4 h to form formazan crystals. The optical density (OD) values were measured with an enzyme immunoassay (EIA) reader (Thermo Labsystems Multiskan MK3) at 570 nm. The 50% cytotoxic concentration (CC_{50}) of the sample was calculated by regression analysis of the dose−response curve generated from the OD values. The maximal noncytotoxic concentration (MNCC) of the sample on the cells was also calculated through the OD values.

Cytopathic Effect (CPE) Reduction Assay. CPE reduction assay was adopted to evaluate the anti-RSV activity of the supercritical fluid extract and compounds against A2, Long, and B strains.[19] The anti-RSV activity of each sample was tested using MNCC as the beginning concentration. Briefly, HEp-2 cells were seeded in 96-well plate. Cell monolayers were inoculated with the mixture of a serial 2-fold dilution of sample and virus suspension (100 $TCID_{50}$). Virus suspension and MM without sample were added as virus and cell controls, respectively. The plate was incubated for about 3−4 days. The virus-induced CPE was observed under light microscopy. The concentration that reduced 50% of CPE with respect to virus control was estimated from the plots of the data and was defined as the 50% inhibitory concentration (IC_{50}) of the tested sample. The selective index (SI) value was calculated from the ratio CC_{50}/IC_{50}.

Plaque Reduction Assay. The anti-RSV activity of tangeretin (compound **2**, the most active compound in the extract) was further determined by plaque reduction assay.[20] HEp-2 cells were seeded in 24-well plates for 24 h. The virus suspension with 60−80 plaque forming units (PFUs) and a serial 2-fold dilution of tested sample were added to the confluent cell monolayer. Virus suspension and the MM

Table 1. Primers Used for the Real-Time PCR Analysis of RSV Amplicons and GAPDH

genes	forward primer (5′−3′)	reverse primer (5′−3′)
RSV N	ACACGCTAGTGTGCAAGCAG	TGATGCTTTTGGGTTGTTCA
RSV P	TCAAAGAAGACCCTACGCCAAGTGA	ACCATCCCGAGCAGATGTAGGTCC
RSV L	AAAGGTTACGGCAGAGCCAAA	GTTAACAACCCAAGGGCAAA
RSV NS1	GGGCAGCAATTCGTTGAGTA	AGCACTGGCATTGTTGTGAA
RSV NS2	TTGATGAAAGACAGGCCACA	TATCGGCATAGGGAAAGTGC
RSV M2-1	GTTGCCATGAGCAAACTCCT	ACGTCTGCTGGCAATCTTTT
RSV M2-2	TGACCATGCCAAAAATAATGA	TCAAGTCTTGTGAGGTCCAATG
GAPDH	CCCACTCCTCCACCTTTGAC	TCTTCCTCTTGTGCTCTTGC

without sample were added as the virus and cell controls, respectively. The plate was incubated in 5% CO_2 at 37 °C with intermittent shaking at 15 min intervals for 2 h, and the medium was aspirated. The cell monolayers were washed with PBS twice and then overlaid with agarose overlay medium. After the agarose solidified, samples with different concentrations and MM were added to the corresponding and virus control wells, respectively. The plates were then incubated for 4−5 days to allow the formation of RSV plaques. The cells were fixed with 10% formalin and stained with 1% crystal violet, and the number of plaques was counted. Half of the maximal concentration inhibiting the RSV-induced plaque formation by the sample was defined as the IC_{50} value in the assay.

Plaque reduction assay was also adopted to investigate the inhibitory effects of tangeretin on the RSV extracellular and intracellular replication as described in the previous report.[21] In conventional RSV assays, the time allowed for virus attachment and penetration (extracellular replication phase) is about 2 h. In this experiment, the sample was added to the confluent HEp-2 cells at three different infection phases: (1) during the extracellular replication phase (sample present first 2 h of infection) only, (2) during the whole infection phase (sample present throughout the experiment), or (3) during the intracellular replication phase (sample present after 2 h postinfection) only. The plate was incubated for 4−5 days to allow for the formation of plaques. After fixation and coloration, the number of plaques was counted. The plaque inhibition (%) was calculated as follows: [(mean number of plaques in virus control) − (mean number of plaques in sample)/(mean number of plaques in virus control)] × 100%.

Attachment Inhibitory Assay. The attachment inhibitory effect of tangeretin against RSV Long strain was also determined with plaque reduction assay.[22] HEp-2 cell monolayers in a 6-well plate were prechilled at 4 °C for 1 h, and then the medium was aspirated. Cell monolayers were infected with 60−80 PFU RSV Long strain in the absence (as virus control) or presence of a serial dilution of the tested sample at 4 °C for 2 h. Afterward, the unabsorbed virus was removed, and the cell monolayer was washed with ice-cold PBS twice, covered with overlay medium, and incubated for further 4−5 days at 37 °C under 5% CO_2 to allow the formation of RSV plaques.

Penetration Inhibitory Assay. Penetration inhibitory effect of tangeretin against RSV Long strain was also tested with plaque reduction assay.[23] HEp-2 cell monolayers grown in 24-well plate were prechilled at 4 °C, and infected by 60−80 PFU RSV Long virus (diluted in cool MM) for another 2 h at 4 °C to allow virus attachment to the cells. The unabsorbed viruses were aspirated, and cells were washed with PBS twice. The plate was then covered with a serially diluted sample or only MM (as virus control) and shifted to 37 °C to allow time for virus penetration into the cells. After 2 h of incubation, the cells were treated with PBS at pH 3 for 1 min to inactive the unpenetrated RSV and then treated with an equal volume of PBS at pH 11 for neutralization. The cells were overlaid and incubated for 4−5 days. After fixation and coloration, the number of plaques was counted.

Quantitative Real-Time PCR Assay. Quantitative real-time PCR assay was conducted to determine how tangeretin regulated mRNA expression of RSV proteins relating to RSV intracellular replication.[24] HEp-2 cell monolayers in a 6-well plate were infected with RSV Long strain (MOI = 1) at 37 °C for 2 h, followed by adding tangeretin. After incubated for another 14 h, the plate was washed with PBS twice, replenished with MM, and further incubated until 24 h postinfection. Total RNA was extracted using TRIzol reagent (Invitrogen, USA), purified by calculating OD_{260}/OD_{280}, which was between 1.8 and 2.2, quantified according to the dilution ratio and the value of OD_{260}, and stored at −80 °C until use. Relative quantitation of the expression of selected genes was performed by the Light Cycler 480 (Roche, USA) system. The primer pairs for PCR are shown in Table 1. The cycling conditions were 95 °C for 5 min, followed by 40 cycles of 95 °C for 10 s, 57 °C for 10 s, and 72 °C for 10 s. A dissociation curve was generated by a cycle of 95 °C for 5 s, 67 °C for 1 min, and 97 °C for 15 s. Results were normalized using GAPDH as a reference gene.

Confocal Assay. HEp-2 cells were infected with RSV Long strain (MOI = 1) for virus absorption. After removing the free virus, the infected cells were overlaid with tangeretin, and then incubated at 37 °C for 24 h. The cells were fixed, permeabilized, and immunostained with the anti-RSV phosphoprotein antibody (Abcam, UK) and then the secondary goat antibody. The cell nuclei were visualized with DAPI (Sigma, USA). Fluorescence was recorded in a confocal laser scanning microscope LSM 510 (Zeiss, Germany).

Western Blot Assay. HEp-2 cells were seeded in 100 mm culture dishes (Corning, USA) and cultured for 24 h at 37 °C. RSV Long strain (MOI = 1) was added to confluent cell monolayers. After 2 h postinfection, the cells were washed with PBS twice and treated with tangeretin until 24 h postinfection. Cells were detached from culture dishes by trypsinization with 0.25% Trypsin−EDTA and then transferred to centrifuge tubes, followed by centrifugation at 800*g* for 3 min. Cell pellets were washed three times with ice-cold PBS, lysed in RIPA buffer containing 0.5 M DTT, 0.1 M PMSF, and 20 × phosphatase inhibitor for 30 min on ice, and then centrifuged at 12000*g* at 4 °C for 15 min. The supernatant containing total cellular proteins was collected and stored at −80 °C until use. Protein concentration was determined by the BCA protein assay kit (Thermo, USA). Protein was subjected to SDS−polyacrylamide gel electrophoresis (SDS−PAGE), after SDS−PAGE proteins were blotted onto a PVDF membrane. The membranes were probed with the anti-RSV phosphoprotein antibody (Abcam, UK) and the secondary goat anti-mouse IgG antibody labeled with horseradish peroxidase (HRP; CST, USA). With the ECL plus Western Blotting reagent pack (Thermo, USA), specific bands were detected.

Statistical Analysis. Data were reported as the mean ± SD for triplicate determinations. The IC_{50} values were estimated from the graphic plots of the data by Origin 8.0. Statistical analysis was performed using Graphpad Prism 5.0 by one-way ANOVA and Tukey post hoc test.

RESULTS AND DISCUSSION

Anti-RSV Activity and Constituents of the Supercritical Fluid Extract of "Guangchenpi". CPE reduction assay showed that the supercritical fluid extract of "Guangchenpi" possessed *in vitro* anti-RSV activity against RSV A2, Long, and B strains with IC_{50} values of 12.5−25.0 μg/mL, whereas its aqueous extract was not active against these RSV strains even at the concentration of 100.0 μg/mL. Based on the observation, polymethoxylated flavonoids found in "Guang-

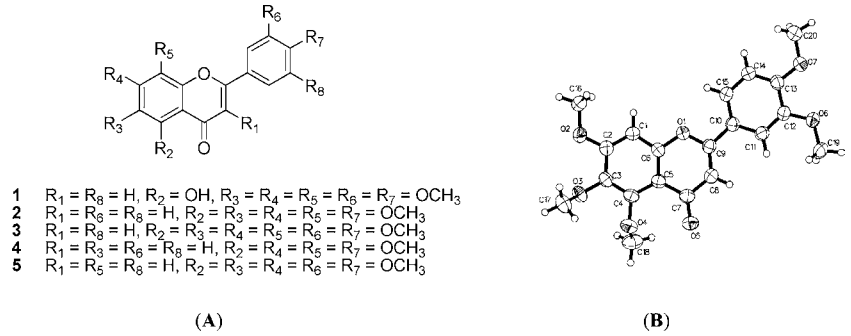

Figure 1. Structures of the polymethoxylated flavones (A) and X-ray structure of **5** with atom labeling scheme (B).

Table 2. Cytotoxicity, Anti-RSV Activity, and Selective Index of Compounds 1−5 (n = 3)

	cytotoxicity	anti-RSV A2 strain		anti-RSV Long strain		anti-RSV B strain	
compounds	CC_{50}[a] (μM)	IC_{50}[b] (μM)	SI[c]	IC_{50}[b] (μM)	SI[c]	IC_{50}[b] (μM)	SI[c]
1	233.2 ± 2.5	64.4 ± 0.7	3.6	70.4 ± 0.9	3.3	68.7 ± 1.3	3.4
2	417.2 ± 1.3	8.3 ± 1.1	50.3	6.7 ± 1.6	62.3	6.7 ± 1.2	62.3
3	252.1 ± 1.9	15.4 ± 0.8	16.4	10.9 ± 1.2	23.1	11.2 ± 0.9	15.6
4	>500.0	73.1 ± 0.9	>6.8	73.1 ± 1.1	>6.8	75.4 ± 1.6	>6.6
5	>500.0	134.4 ± 1.2	>3.7	134.4 ± 0.9	>3.7	132.9 ± 0.9	>3.8
ribavirin	255.9 ± 1.8	10.2 ± 1.1	25.1	10.2 ± 0.9	25.1	12.3 ± 1.1	20.8

[a]CC_{50} was evaluated by MTT assay; data were expressed as mean ± SD. [b]IC_{50} was detected by CPE reduction assay with RSV strains at 100 $TCID_{50}$; data are expressed as mean ± SD. [c]SI value equals CC_{50}/IC_{50}.

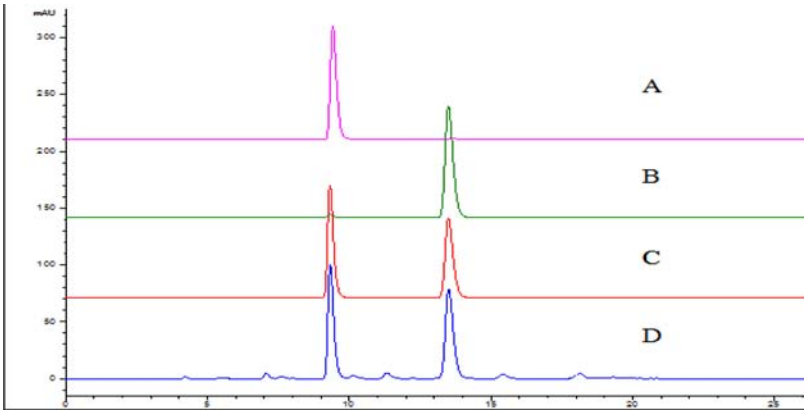

Figure 2. HPLC chromatograms of (A) compound **3**, (B) compound **2**, (C) a mixture of compounds **3** and **2**, and (D) the supercritical fluid extract of "Guangchenpi". The chromatograms were generated using a HPLC column (Agilent Zorbax SB-C_{18}, 4.6 mm × 250 mm × 5 μm) at 330 nm. The mobile phase consisted of A (water with 0.5% acetic acid) and B (acetonitrile). The elution programs were 0−15 min, 49% B, and then 16−25 min, 100% B. The flow rate was 1.0 mL/min. The injection volume was 10 μL.

chenpi" were speculated to be the major anti-RSV constituents.[14] Bioassay-guided isolation of the supercritical fluid extract and spectroscopic identification with published literature comparison found five polymethoxylated flavones, namely, 5-*O*-demethylnobiletin (**1**),[25] tangeretin (**2**),[25] nobiletin (**3**),[25] 6-demethoxytangeretin (**4**),[25] and sinensetin (**5**)[25] (Figure 1A). Moreover, the structure of compound **5** was further confirmed by X-ray diffraction analysis (Figure 1B) of yellow block crystals, $C_{20}H_{20}O_7$, M_r = 372.36, monoclinic, space group $P2_1/n$, a = 14.9739(4) Å, b = 8.2788(2) Å, c = 15.1899(4) Å, β = 110.994(3)°, V = 1758.03(9) Å^3, Z = 4, d_x = 1.407 Mg/m^3, $F(000)$ = 784.0, μ(Cu Kα) = 0.896 mm^{-1}. Data collection was performed on a Gemini S Ultra using graphite-monochromated radiation (λ = 1.54184 Å) with 2799 unique reflections collected to θ_{max} = 62.70°, where 2468 reflections were observed [$F^2 > 2\sigma(F^2)$]. The structure was solved by direct methods (SHELXS 97) and refined by full-matrix least-squares on F^2. The final R = 0.0366, R_w = 0.0985, and S = 1.035. Crystallographic data of this structure is first reported in this paper and has been deposited at the Cambridge Crystallographic Data Centre under the reference number CCDC 950510.

These five polymethoxylated flavones (**1**−**5**) were screened for their *in vitro* anti-RSV activity with CPE reduction assay. All of them were active against RSV A2, Long, and B strains to different extents (Table 2). Both tangeretin (**2**) and nobiletin (**3**) displayed better activity compared with the positive control ribavirin. It is noteworthy that only two compounds (**2** and **3**) out of the five have four methoxyl groups in the A ring of flavone, which may be important to their anti-RSV activity. Polymethoxylated flavonoids (PMFs) are an interesting group of bioactive compounds in *Citrus* plants. Although PMFs have

been reported to possess antiviral activity against influenza virus[26] and HIV,[27] their anti-RSV activity was reported in the present study for the first time.

Contents of Tangeretin and Nobiletin in the Supercritical Fluid Extract. The HPLC chromatograms (Figure 2) recorded the areas of the active compounds **2** and **3** in the supercritical fluid extract. The HPLC method showed a good baseline resolution of compounds **2** and **3** with sharp symmetrical peaks. The calibration curves of the two compounds have a good linearity over the full range tested. As shown in Figure 2, both compounds **2** and **3** were two major polymethoxylated flavones in the supercritical fluid extract. Their contents (w/w %) in the supercritical fluid extract were calculated to be 11.28% and 11.12%, respectively (Table 3).

Table 3. Linearity Studies of Compounds Tangeretin and Nobiletin

compounds	contents (%)	regression equation[a]	R^2	injection amount (μg)
tangeritin (**2**)	11.28	$y = 3.6691 \times 10^3 x - 4.0437 \times 10$	0.9998	1.2−6.6 μg
nobiletin (**3**)	11.12	$y = 3.4918 \times 10^3 x + 3.9858 \times 10$	0.9999	1.36−7.48 μg

[a] y, peak area count; x, injection amount (μg).

In our previous study, UV method with tangeretin as a standard was used to test for the total contents of PMFs in both the supercritical fluid extract and the aqueous extract of "Guangchenpi". Results showed that the total PMF content in the supercritical fluid extract was much higher than that in the aqueous one.[14] The present study demonstrated that both tangeretin (**2**) and nobiletin (**3**), the two more active polymethoxylated flavones, have higher content in the supercritical fluid extract. Overall, supercritical CO_2 fluid extraction can effectively enrich the anti-RSV constituents in "Guangchenpi".

Anti-RSV Activity of Tangeretin with Plaque Reduction Assay. As a most active constituent in the supercritical fluid extract of "Guangchenpi", tangeretin was further investigated for its anti-RSV activity with plaque reduction assay. In Figure 3, tangeretin could dose-dependently inhibit the RSV-induced plaque formation on HEp-2 cells. Its IC_{50} and SI values against RSV A2, Long, and B strains were 7.0 ± 1.5, 5.6 ± 1.5, and 5.4 ± 0.9 μM and 59.6, 73.8, and 75.5, respectively. Meanwhile, the corresponding values for ribavirin were 10.6 ± 1.2, 10.2 ± 1.5, and 10.2 ± 1.2 μM and 24.1, 25.1, and 25.1, respectively.

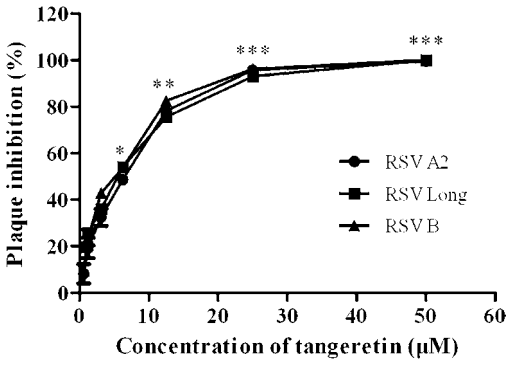

Figure 3. Results of different concentrations of tangeretin against different RSV strains (A2, Long, and B) with plaque reduction assay. Results were expressed as plaque inhibition of control (mean ± SD) from three independent experiments. Significant differences between tangeretin and virus control at $P < 0.05$ (*), $P < 0.01$ (**), $P < 0.001$ (***).

Subsequently, the inhibitory effects of tangeretin on the RSV extracellular and intracellular replication using plaque reduction assay were assessed. At the concentration of 12.5 μM, tangeretin inhibited both extracellular and intracellular replication of RSV by 15.9% and 68.8%, respectively (Figure 4). Ribavirin inhibited intracellular replication of RSV by 56.2%.

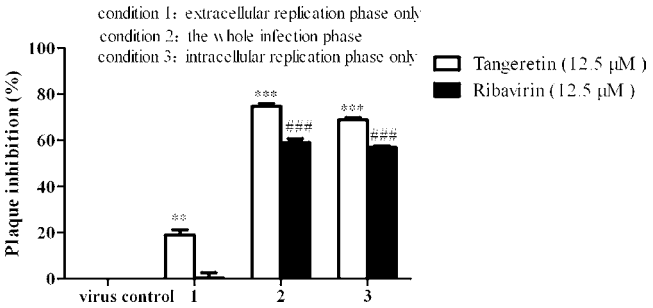

Figure 4. Antiviral activity of tangeretin and ribavirin (positive control) under different virus phases. Results were expressed as plaque inhibition of control (mean ± SD) from three independent experiments. Significant difference between tangeretin and virus control at $P < 0.05$ (*), $P < 0.01$ (**), and $P < 0.001$ (***); significant difference between ribavirin and virus control at $P < 0.05$ (#), $P < 0.01$ (##), and $P < 0.001$ (###).

However, no significant plaque inhibition (%) was observed when ribavirin was present only in the extracellular replication phase (Figure 4), and this result was the same as reported previously.[21]

Effects of Tangeretin on RSV Attachment and Penetration. Generally, attachment and penetration are two important stages in the extracellular replication of virus. In the attachment inhibitory experiment, tangeretin did not show any effect on the RSV absorption to the HEp-2 cells even at the concentration of 100.0 μM, similar to ribavirin (data was not shown). On the other hand, it inhibited 50% RSV entry into HEp-2 cells at the concentration of 43.5 μM, while its plaque inhibition (%) on RSV penetration was 67.9% at the concentration of 100.0 μM (Figure 5), which is much higher than that of the control, ribavirin. These results suggested that the efficacy of tangeretin to interfere with the RSV extracellular

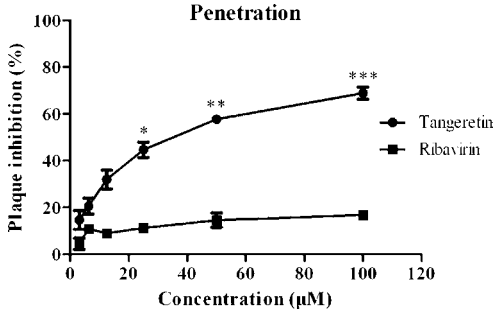

Figure 5. Results of penetration inhibitory assay. Results were expressed as plaque inhibition of control (mean ± SD) from three independent experiments. Significant difference between tangeretin and virus control at $P < 0.05$ (*), $P < 0.01$ (**), and $P < 0.001$ (***).

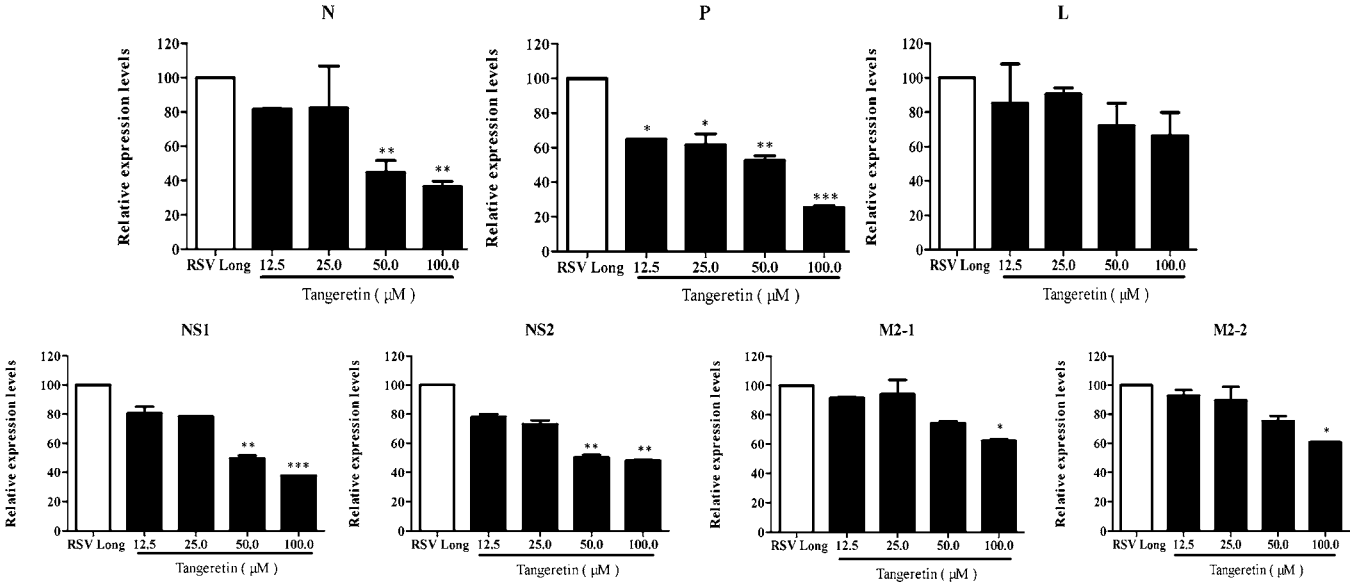

Figure 6. The effects of tangeretin on the mRNA expression levels of RSV proteins (N, P, L, NS1, NS2, M2-1, and M2-2). Results were expressed as relative expression levels (mean ± SD) by three independent experiments. Significant difference between tangeretin and virus control at $P < 0.05$ (*), $P < 0.01$ (**), and $P < 0.001$ (***).

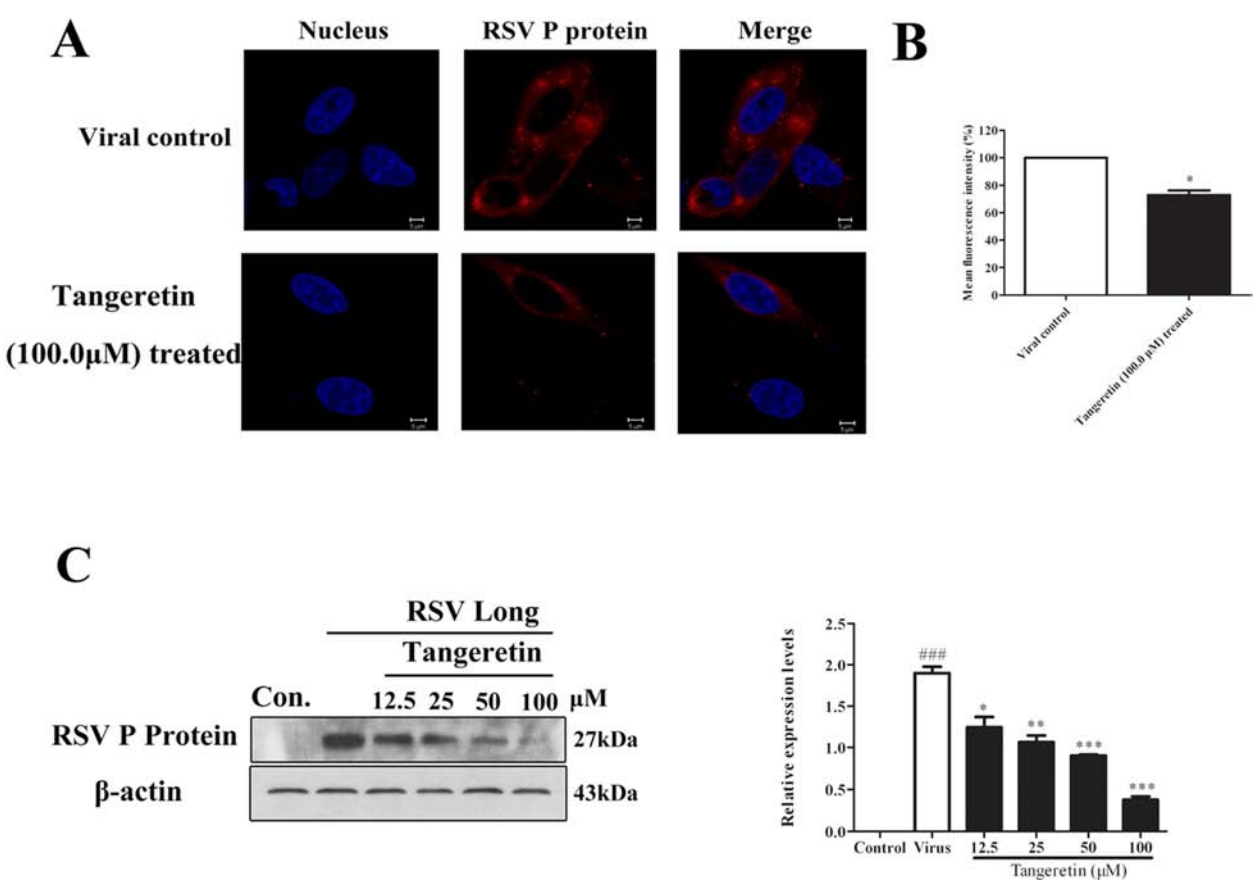

Figure 7. Results from the confocal and Western blot assays: (A) representative images (scale bar, 5 μm) and (B) densitometric analysis for the confocal assay and (C) representative images and densitometric analysis for the Western bloat assay. Results were expressed as relative expression levels (mean ± SD) by three independent experiments. Significant difference between tangeretin and virus control at $P < 0.05$ (*), $P < 0.01$ (**), and $P < 0.001$ (***); significant difference between control and virus group at $P < 0.05$ (#), $P < 0.01$ (##), and $P < 0.001$ (###).

replication was likely contributed by the inhibition of RSV penetration. RSV fusion (F) protein is a glycoprotein that is associated with the RSV penetration.[28] This protein interacts with toll-like receptor 4 (TLR4), and triggers the nuclear factor-κB (NF-κB) signaling pathway.[29] NF-κB is a critical regulator of the immediate early pathogen response, playing an important role in the RSV infection.[30] It has been reported that tangeretin inhibited the activation of the NF-κB pathway.[31]

dx.doi.org/10.1021/jf404310y | J. Agric. Food Chem. 2014, 62, 2182−2189

Therefore, we speculate that tangeretin may directly or indirectly inhibit the NF-κB pathway and interfere with RSV entry into the host cells.

Effect of Tangeretin on the mRNA Expression Levels of RSV. Quantitative real-time PCR analysis was carried out to evaluate the effect of tangeretin on the mRNA expression levels of proteins related to RSV intracellular replication. HEp-2 cell monolayers were first infected with RSV Long strain (MOI = 1), then treated with different concentrations of tangeretin. Total RNA was extracted from the infected cells, and the changes in mRNA expressions of RSV amplicons nonstructural (NS1, NS2), regulatory (M2-1, M2-2), nucleocapsid (N), phosphoprotein (P), and polymerase (L) proteins were analyzed. As shown in Figure 6, tangeretin significantly inhibited the mRNA expression of RSV nonstructural proteins NS1 and NS2 at the concentration of 50.0 μM. It also reduced the RSV regulatory proteins M2-1 and M2-2 at the concentration of 100.0 μM. Interestingly, tangeretin decreased the mRNA expression levels of RSV nucleocapsid-associated proteins N, P, and L to different extents. This compound downregulated the mRNA expression level of RSV P protein with inhibition rates of 49.3% and 74.5% at the concentrations of 50.0 and 100.0 μM, respectively.

Effect of Tangeretin on RSV P Protein. In the present study, confocal assay was used to investigate the influence of tangeretin on RSV P protein. All cells in each group (about 5000 cells) were calculated for the mean fluorescence intensity by the Array Scan Infinity (Thermo, USA). As shown in Figure 7A, almost all the infected cells (control) were observed to emit the red fluorescence from P protein under confocal laser scanning microscopy, whereas fewer cells with tangeretin treatment showed red fluorescence. Apparently, tangeretin significantly decreased the expression of RSV P protein (Figure 7B).

Furthermore, the influence of tangeretin on RSV P protein expression was evaluated by Western blot assay. RSV P protein expression was significantly decreased by tangeretin in a dose-dependent manner (Figure 7C). These results further confirmed the inhibition effect of tangeretin on the expression of RSV P protein.

Based on the results of the present study, tangeretin mainly affected the intracellular replication of RSV. Quantitative real-time PCR results showed that tangeretin mainly down-regulated mRNA expression of RSV P protein, while both confocal and Western blot assays exhibited that tangeretin could attenuate the expression of RSV P protein, suggesting that RSV P protein might be one of the anti-RSV targets of this compound. RSV P protein in combination with RSV L, N, M2-1, and M2-2 proteins (ribonucleoproteins) has been reported to be involved in viral transcription and replication processes.[32,33] Therefore, tangeretin may influence RSV transcription and replication through inhibiting the expression of RSV P protein. Further study on the anti-RSV mechanism of tangeretin is currently in progress in our group.

As a broad-spectrum antiviral agent, ribavirin can potentially act via inhibiting various stages of the virus replication cycle, including viral translation, genome or transcript capping, RNA synthesis, and progeny virus spread, which belong to the intracellular replication of virus.[34,35] Apparently, the anti-RSV mechanism of tangeretin is different from that of ribavirin.

In summary, our work demonstrated that the supercritical fluid extract of "Guangchenpi" possessed *in vitro* anti-RSV activity and that its active constituents were polymethoxylated flavones. Tangeretin and nobiletin were two major polymethoxylated flavones found in the supercritical fluid extract of "Guangchenpi", and they had potent anti-RSV activity comparable to the positive control ribavirin. The anti-RSV mechanism of tangeretin was different from that of ribavirin. Tangeretin mainly affected the intracellular replication of RSV and could inhibit RSV entry into HEp-2 cells. RSV P protein might be one of the anti-RSV targets of this compound. These results suggest that the supercritical fluid extract of "Guangchenpi" and tangeretin may have good potential to be used in the treatment and the prevention of RSV infection.

■ ASSOCIATED CONTENT

Supporting Information

The ^{1}H and ^{13}C NMR spectra of compounds **1**−**5**. This material is available free of charge via the Internet at http://pubs.acs.org.

■ AUTHOR INFORMATION

Corresponding Authors

*Phone: +86 20 85221728. Fax: +86 20 85221559. E-mail address: tliyl@jnu.edu.cn (Y. L. Li).

*E-mail wang_guocai@hotmail.com (G. C. Wang).

Author Contributions

§J.-J.X., X.W., and M.-M.L. contributed equally to this study.

Funding

This work was supported financially by the Natural Science Foundations of China (Grants 81202429, 81072535, and 81273390), the Science and Technology Planning Project of Guangzhou (Grant No. 2011Y1-00017-2), the Fundamental Research Funds for the Central Universities (Grant 21612417), and the China Postdoctoral Science Foundation (Grant 2012M521656).

Notes

The authors declare no competing financial interest.

■ REFERENCES

(1) Zheng, G. D.; Jiang, L.; Yang, D. P.; Zhou, F.; Yang, X.; Lin, L. W. Determination of five flavonoids in Pericarpium Citri Reticulate collected from different regions by HPLC. *Chin. Tradit. Herb. Drugs* **2010**, *41*, 652−655.

(2) Xia, J.; Kotani, A.; Hakamata, H.; Kusu, F. Determination of hesperidin in *Pericarpium Citri Reticulatae* by semi-micro HPLC with electrochemical detection. *J. Pharm. Biomed. Anal.* **2006**, *41*, 1401−1405.

(3) Xu, G. H.; Chen, J. C.; Liu, D. H.; Zhang, Y. H.; Jiang, P. P.; Ye, X. Q. Minerals, phenolic compounds, and antioxidant capacity of *Citrus* peel extract by hot water. *J. Food Sci.* **2008**, *73* (1), C11−C18.

(4) Tripoli, E.; Guardia, M. L.; Giammanco, S.; Majo, D. D.; Giammanco, M. *Citrus* flavonoids: Molecular structure, biological activity and nutritional properties: A review. *Food Chem.* **2007**, *104*, 466−479.

(5) Barreca, D.; Bisignano, C.; Ginestra, G.; Bisignano, G.; Bellocco, E.; Leuzzi, U.; Gattuso, G. Polymethoxylated, *C*- and *O*-glycosyl flavonoids in tangelo juice and their influence on antioxidant properties. *Food Chem.* **2013**, *141*, 1481−1488.

(6) Chen, J.; Montanari, A. M.; Widmer, W. W. Two new polymethoxylated flavones, a class of compounds with potential anticancer activity, isolated from cold pressed dancy tangerine peel oil solids. *J. Agric. Food Chem.* **1997**, *45*, 364−368.

(7) Attaway, J. A. *Citrus* juice flavonoids with anticarcinogenic and antitumor properties. *ACS Symp. Ser.* **1994**, *546*, 240−248.

(8) Ho, C.; Li, S.; Pan, M.; Lo, C. Polymethoxyflavonoids and hydroxylated polymethoxyflavonoids in *Citrus* peels and their potential health beneficial properties. *Pacifichem* **2010**, No. AGRO-253.
(9) Liu, L.; Xu, X. Y.; Cheng, D.; Yao, X. L.; Pan, S. Y. Structure-activity relationship of *Citrus* polymethoxylated flavones and their inhibitory effects on *Aspergillus niger*. *J. Agric. Food Chem.* **2012**, *60*, 4336−4341.
(10) Lam, I. K.; Alex, D.; Wang, Y. H.; Liu, P.; Liu, A. L.; Du, G. H.; Yuen, L.; Simon, M. *In vitro* and *in vivo* structure and activity relationship analysis of polymethoxylated flavonoids: Identifying sinensetin as a novel antiangiogenesis agent. *Mol. Nutr. Food Res.* **2012**, *56*, 945−956.
(11) Johann, S.; Lopes, O. V.; Pizzolatti, M. G.; Schripsema, J.; Braz-Filho, R.; Branco, A.; Smania, A. J. Antimicrobial activity of wax and hexane extracts from *Citrus spp*. peels. *Mem. Inst. Oswaldo Cruz* **2007**, *102*, 681−685.
(12) Li, S. M.; Lo, C. Y.; Dushenkov, S.; Ho, C. T. Polymethoxyflavones: Chemistry, biological activity, and occurrence in orange peel. *ACS Symp. Ser.* **2008**, *987*, 191−210.
(13) Tominari, T.; Hirata, M.; Matsumoto, C.; Inada, M.; Miyaura, C. Polymethoxy flavonoids, nobiletin and tangeretin, prevent lipopolysaccharide-induced inflammatory bone loss in an experimental model for periodontitis. *J. Pharmacol. Sci.* **2012**, *119*, 390−394.
(14) Yang, Y. T.; Luo, H. J.; Ye, Y. S.; Liao, J. H.; Li, Y. L. Study on the extraction of polymethoxylated flavones from *Citrus reticulata* 'Chachi' of different storage years. *Sci. Tech. Food Ind.* **2011**, *9*, 258−260 (In Chinese).
(15) Meyer, G.; Deplanche, M.; Schelcher, F. Human and bovine respiratory syncytial virus vaccine research and development. *Comp. Immunol. Microbiol. Infect. Dis.* **2008**, *31*, 191−225.
(16) Antonelli, G.; Turriziani, O. Antiviral therapy: Old and current issues. *Int. J. Antimicrob. Agents* **2012**, *40*, 95−102.
(17) Glatthaar Saalmüller, B.; Rauchhaus, U.; Rode, S.; Haunschild, J.; Saaalmuller, A. Antiviral activity *in vitro* of two preparations of the herbal medicinal product Sinupret against viruses causing respiratory infections. *Phytomedicine* **2011**, *19*, 1−7.
(18) Li, Y. L.; Leung, K. T.; Yao, F. H.; Ooi, L. S.; Ooi, V. E. C. Antiviral flavans from the leaves of *Pithecellobium cylpearia*. *J. Nat. Prod.* **2006**, *69* (5), 833−835.
(19) Cos, P.; Vlietinck, A. J.; Berghe, D. V.; Maes, L. Anti-infective potential of natural products: How to develop a stronger *in vitro* 'proof-of-concept'. *J. Ethnopharmacol.* **2006**, *106*, 290−302.
(20) Shigeta, S.; Mori, S.; Baba, M.; Ito, M.; Honzumi, K.; Nakamara, K.; Oshitani, H.; Numazaki, Y.; Matsuda, A.; Obara, T.; Shuto, S.; De Clercq, E. Antiviral activities of ribavirin, 5-ethynyl-1-D-ribofuranosylimidazole-4-carboxamide, and 6′-(*R*)-6′-*C*-methylneplanocin against several ortho-and paramyxoviruses. *Antimicrob. Agents Chemother.* **1992**, *36*, 435−439.
(21) Ho, W. S.; Xue, J. Y.; Sun, S. S. M.; Ooi, V. E. C.; Li, Y. L. Antiviral activity of Daphnoretin isolated from *Wikstroemia indica*. *Phytother. Res.* **2010**, *24*, 657−660.
(22) Li, Y. L.; But, P. P. H.; Ooi, V. E. C. Antiviral activity and mode of action of caffeoylquinic acids from *Schefflera heptaphylla* (L.) Frodin. *Antivir. Res.* **2005**, *68*, 1−9.
(23) Kimura, K.; Mori, S.; Tomita, K.; Takahashi, K.; Shigeta, S.; Terada, M. Antiviral activity of $NMSO_3$ against respiratory syncytial virus infection *in vitro* and *in vivo*. *Antivir. Res.* **2000**, *47*, 41−51.
(24) Trasino, S. E.; Kim, Y. S.; Wang, T. T. Y. Ligand, receptor, and cell type-dependent regulation of ABCA1 and ABCG1 mRNA in prostate cancer epithelial cells. *Mol. Cancer Ther.* **2009**, *8*, 1934−1945.
(25) Nagase, H.; Omae, N.; Omori, A.; Nakagawasai, Osamu.; Tadano, T.; Yokosuka, A.; Sashida, Y.; Mimaki, Y.; Yamakuni, T.; Ohizumi, Y. Nobiletin and its related flavonoids with CRE-dependent transcription-stimulating and neuritegenic activities. *Biochem. Biophys. Res. Commun.* **2005**, *337*, 1330−1336.
(26) Sharma, A.; Tendulkar, A. V.; Wangikar, P. P. Drug discovery against H1N1 virus (influenza A virus) via computational virtual screening approach. *Med. Chem. Res.* **2011**, *20*, 1445−1449.
(27) Jiang, Y.; Wong, J. H.; Fu, M.; Ng, T. B.; Liu, Z. K.; Wang, C. R.; Li, N.; Qiao, W. T.; Wen, T. Y.; Liu, F. Isolation of adenosine, isosinensetin and dimethylguanosine with antioxidant and HIV-1 protease inhibiting activities from fruiting bodies of *Cordyceps militaris*. *Phytomedicine* **2011**, *18*, 189−193.
(28) Sun, Z. W.; Pan, Y. B.; Lu, L. Respiratory syncytial virus entry inhibitors targeting the F protein. *Viruses* **2013**, *5*, 211−225.
(29) Remer, K. A.; Brcic, M.; Jungi, T. W. Toll-like receptor-4 is involved in eliciting an LPS-induced oxidative burst in neutrophils. *Immunol. Lett.* **2003**, *85*, 75−80.
(30) Santoro, M. G.; Rossi, A.; Amici, C. NF-kappaB and virus infection: Who controls whom. *EMBO J.* **2003**, *22*, 2552−2560.
(31) Jiang, S. E.; Ryu, K. R.; Park, S. H.; Chuang, S.; Teruya, Y.; Han, M. J.; Woo, J. T.; Kim, D. Y. Nobiletin and tangeretin ameliorate scratching behavior in mice by inhibiting the action of histamine and the activation of NF-κB, AP-1 and p38. *Int. Immonopharmocol.* **2013**, 1705−1878.
(32) Asenjo, A.; Mendieta, J.; Gonmez-Puertas, P.; Villanueva, N. Residues in human respiratory syncytial virus P protein that are essential for its activity on RNA viral synthesis. *Virus Res.* **2008**, *132*, 160−173.
(33) Lay, M. K.; Gonzalez, P. A.; Leon, M. A.; Cespedes, P. F.; Bueno, S. M.; Riedel, C. A.; Kalergis, A. M. Advances in understanding respiratory syncytial virus infection in airway epithelial cells and consequential effects on the immune response. *Microbes Infect.* **2013**, *15*, 230−242.
(34) Kim, Y.; Lee, C. Ribavirin efficiently suppresses porcine nidovirous replication. *Virus Res.* **2013**, *171*, 44−53.
(35) Keck, M.; Mindru, C.; Kalil, A. C.; Mercer, D. F.; Florescu, D. F. Respiratory syncytial virus lower respiratory tract infection in a pediatric liver transplant recipient treated with oral ribavirin. *Pediatr. Transplant.* **2012**, *16*, E348−E351.

NOTE ADDED AFTER ASAP PUBLICATION

There was an error in the Quantitative Real-Time PCR Assay section in the version of this paper published February 28, 2014. The correct version published March 12, 2014.

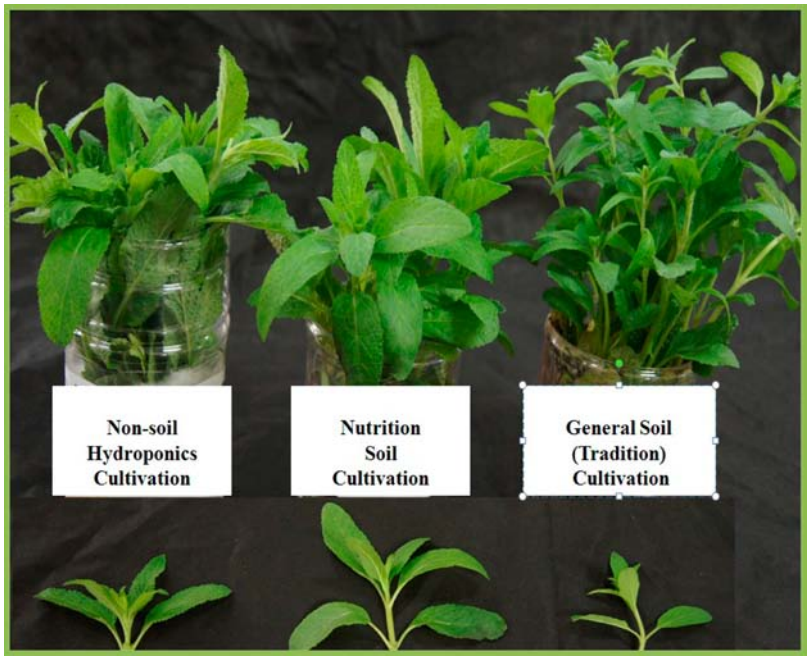

Figure 1. Plebeian herba cultivated in three different conditions.

Kyungpook National University (Daegu, Korea). Soil fertility was enhanced with 15.2 ± 0.2 g/kg organic matter, 1.0 ± 0.1 g/kg total N, 0.25 ± 0.03 g/kg total P, and 100.9 ± 1.8 g kg total K. In this study, Plebeian herba cultured in nutrition hydroponics, nutrition plus soil, and general soil (non-nutritive solution) are referred to as NHC, NSC, and GSC, respectively (Figure 1).

Measurement of Leaf Chlorophyll Content. Fresh leaves were sampled for determining the chlorophyll content. Plebeian herba leaves (0.8 g) were homogenized in 5 mL of 80% acetone. The absorbance of the leaf extract was determined spectrophotometrically at 663, 645, 505, and 453 nm.[17] The concentrations of the pigments were calculated using the following formulas and were expressed per leaf fresh weight (mg/g FW):

$$\text{chlorophyll } a = 0.999 \times \text{Abs}_{663} - 0.0989 \times \text{Abs}_{645}$$

$$\text{chlorophyll } b = -0.328 \times \text{Abs}_{663} + 1.77 \times \text{Abs}_{645}$$

$$\beta\text{-carotene} = 0.216 \times \text{Abs}_{663} - 1.22 \times \text{Abs}_{645} - 0.304 \times \text{Abs}_{505} + 0.452 \times \text{Abs}_{453}$$

Preparation of Extract. Leaves were pulverized with a grinder after drying at 40 °C. Extraction was carried out using 1 g of plant mixed with 20 mL of 100% ethanol and extracted at 50 °C for 3 h. The extraction was repeated twice until the extracts became colorless. The extract was filtrated through Whatman no. 2 paper and then evaporated in a vacuum at 45 °C by using a rotary evaporator (JP/N 1000S-W; Eyela, Japan) and water bath (Digital Water Bath SB-651; Rikakikai, Tokyo, Japan) to remove the ethanol. The final samples were dissolved in dimethyl sulfoxide (DMSO) for analysis of antioxidant and enzyme inhibitory effects. On the other hand, the evaporated extract was dissolved in methanol (HPLC grade) and filtered through a 0.45 μM membrane filter prior to HPLC analysis.

Extraction of Soluble Free and Bound Phenolics. For the extraction of soluble free phenols, the prepared methanol extract was homogenized further using a Polytron homogenizer for an additional 3 min to obtain a thoroughly homogenized sample. After centrifugation, the supernatant was saved. The remaining precipitate was rehomogenized and centrifuged as above. The two supernatants were combined.[18] To determine bound phenolics in the methanol extract, the residues from the above soluble free extraction were drained off and hydrolyzed directly with 20 mL of 4 M NaOH at room temperature for 1 h with shaking. The mixture was acidified to pH 1 with concentrated hydrochloric acid and extracted five times with ethyl acetate. The ethyl acetate fraction was finally evaporated to dryness at 45 °C. The residues were dispersed in 50 mL of 4 M NaOH and stirred for 4 h under nitrogen. The solution was then acidified to pH 1 and centrifuged, and the bound phenolics were extracted with diethyl ether/ethyl acetate (1:1, v/v) as described for esterified phenolics. Free and bound phenolic extracts were dried to a powder and stored at −70 °C until use.

Analysis of Total Phenolics and Flavonoid Content. Total free phenolics were estimated using the Folin−Ciocalteu reagent,[19] and the absorbance was recorded at 725 nm with a UV−vis spectrometer (Power Wave XS, Bio-Tek Instrument, Winooski, VT, USA). On the basis of the standard curve prepared with gallic acid (0−40 μg/mL), the amount of total phenolics in the extract was calculated and expressed in milligrams of gallic acid equivalents (GE) per gram of sample on a dry weight basis (mg GE/g DW). The content of total flavonoids was determined using the previous method.[18] Briefly, 100 μL of tested sample solution was mixed with 7.5 μL of 10% aluminum trichloride ($AlCl_3$) and 7.5 μL of 5% sodium nitrate solution (in DW). After 6 min, 100 μL of 1 N sodium hydroxide and 25 μL of distilled water were added. The total flavonoid content was determined using a standard curve with quercetin (Sigma-Aldrich Chemie, Steinheim, Germany) (0−40 μg/mL) as the standard. The mean of three readings at 415 nm was used and expressed as milligrams of naringin equivalents (NE) per gram of dry weight (mg NE/g DW).

HPLC Analysis of Ascorbic Acid and Phenolic Compounds. The phenolic compounds were determined by using HPLC (Waters, Milford, MA, USA) on a Zorbax Eclipse XDB-C18 (4.6 cm × 250 mm, 5 μm, Agilent, Santa Clara, CA, USA) column, associated with a UV−visible detector (Jasco, Tokyo, Japan) . The column was operated at a temperature of 25 °C.

For determination of ascorbic acid, the mobile phase consisted of methanol/distilled water (50:50, v/v) with 0.5% of phosphoric acid (A) and methanol (100%) with 0.25% of phosphoric acid (B). The gradient program was as follows: 0−6 min, 50% A; 6−10 min, 20% A; 10−20 min, 0% A; 20−22 min, 10% A; 22−25 min, 40% A; 25−40 min, 50% A. The UV detection was carried out at 230 nm.[19] The phenolic compounds were determined using methanol/water (50:50, v/v, pH 2.5 with trifluoroacetic acid) as mobile phase and UV detection of 345 nm.[20]

The flow rate of the mobile phase was 0.7 mL/min, and the injection volumes were 10 μL of the standards and sample extracts. All phenolic compounds and capsaicins were quantified using the external standard method. Quantification was based on peak area. Calibration curves of the standards were made by diluting stock standards in methanol.

DPPH Scavenging Activity. The DPPH radical scavenging activity of ethanolic extract was analyzed by following our previous method.[21] The ethanolic extract (10 μL) was added to 190 μL (0.025 mg/mL) of DPPH solution. After 30 min of standing in darkness, the absorbance was recorded at 517 nm. Gallic acid solution (50 μg/mL) was used as a positive control.

ABTS Scavenging Activity. The total antioxidant activity was measured by the $ABTS^+$ radical cation decolorization assay.[22] Distilled water was used to dissolve ABTS to 7 mM concentration, and the ABTS radical cation ($ABTS^+$) was produced by reaction with 2.45 mM potassium persulfate; the mixture was left in darkness at room temperature. After 12 h, the absorbance was adjusted to 0.70 ± 0.05 at 734 nm by adding absolute ethanol. To determine the scavenging activity, 190 μL of ABTS reagent was mixed with 10 μL of extracts, and absorbance was measured after 6 min of reaction at room temperature, using trolox as a control.

Nitric Oxide Radical Scavenging Activity. NO generated from sodium nitroferricyanide dihydrate (SNP) was measured by the Griess reagent, as described previously.[18] Each 25 μL of sample or quercetin was mixed with 25 μL of 10 mM SNP in PBS (pH 7.4) and incubated at 25 °C for 150 min, and then 50 μL of Griess reagent (2% sulfanilamide in distilled water and 0.2% naphthylethylenediamine dihydrochloride in 4% phosphoric acid) was added. DMSO was used instead of test samples as a control. The absorbance of the chromophore formed during the diazotization of nitrite with sulfanilamide and subsequent coupling with naphthylethylenediamine was read at 540 nm and referred to the absorbance of standard solutions of sodium nitrite treated in the same way with Griess reagent. The plot between the concentration of nitrite and incubation time exhibited the best incubation time for nitrite production from SNP.

Superoxide Dismutase (SOD) Activity. The SOD activity was determined according to our previous study.[18] Extract samples were mixed with tris(hydrochloric acid) buffers and 7.2 mM pyrogallol solution. The reaction was stopped by the addition of 30 μL of 1 N hydrochloric acid. Absorbance of the mixture was determined at 420 nm against a blank. This assay was replicated three times. The inhibition was calculated as

$$\%\ \text{inhibition} = 100 - [\{(A - B)/C\} \times 100]$$

where A is absorbance of sample with reagent, B is absorbance of sample without reagent, and C is absorbance of the control

α-Glucosidase Inhibition Assay. This assay was performed according to our previous study.[23] In brief, 50 μL samples were diluted with 100 μL of 100 mM phosphate buffer (pH 6.9) in a 96-well microplate and incubated with 50 μL of α-glucosidase (0.76 U/mL in same buffer) at 25 °C for 5 min. Fifty microliters of 5 mM *p*-nitrophenyl-α-D-glucopyranoside (prepared in the same buffer) was added to each well in time intervals after pre-incubation. In both cases before and after incubation, absorbance was recorded at 405 nm and compared to a control that had 50 μL of buffer solution in place of the extract.

Statistical Analysis. All results were obtained with means ± SD of three parallel measurements. Data were subjected to an analysis of variance (ANOVA), followed by mean comparisons by Duncan's multiple-range test at $p < 0.05$.

RESULTS AND DISCUSSION

As shown in Table 1, chlorophyll *a*, chlorophyll *b*, water content, and extraction yield were similar in NHC, NSC, and GSC of Plebeian herba. The highest levels of β-carotene and ascorbic acid were found in NSC. Kimura and Rodriguez[24] showed that the hydroponic leafy vegetables had significantly

Table 1. Nutritional Constituents and Enolic Content of Plebeian Herba Grown in Hydroponics and Soil[a]

	chlorophyll content (mg/g FW)			phenolic content (GE^b)				flavonoids content (NE^c)						
sample	chlorophyll *a*	chlorophyll *b*	β-carotene	free	bound	esterified	total	free	bound	esterified	total	AA^d	WC^e (%)	EY^f (%)
NHC	0.25 ± 0.02a	0.08 ± 0.01a	0.04 ± 0.02c	10.2 ± 0.6	2.4 ± 0.2	0.8 ± 0.0	13.4 ± 0.9	5.2 ± 0.4	0.8 ± 0.1	0.1 ± 0.0	6.1 ± 1.0	7.5a	12.2	29.6
NSC	0.28 ± 0.08a	0.09 ± 0.03a	0.09 ± 0.01a	16. 5 ±2.3	2.8 ± 0.5	1.2 ± 0.2	20.5 ± 2.1	8.0 ± 0.3	1.6 ± 0.1	0.9 ± 0.0	10.5 ± 1.5	7.9a	12.1	27.6
GSC	0.30 ± 0.01a	0.07 ± 0.00a	0.07 ± 0.01a	10.5 ± 1.2	2.8 ± 0.5	1.1 ± 0.0	14.4 ± 0.5	3.4 ± 0.6	1.8 ± 0.1	0.4 ± 0.1	5.6 ± 1.3	4.5b	10.9	28.6

[a]Values represent the mean ± SE from three independent repeats. Different letters indicate a significant difference by Duncan's multiple ranges at $p < 0.05$. [b]Phenols content is express as gallic acid equivalents (GE) mg/g DW. [c]Flavonoids content is expressed as naringin equivalents (NE) mg/g DW. [d]Ascorbic acid content is expressed as mg pure compound of ascorbic acid (mg/g DW). [e]Water content (moisture content in fresh leaf). [f]Extract yield (extract ratio of dry leaf).

dx.doi.org/10.1021/jf404570s | J. Agric. Food Chem. 2014, 62, 2190−2197

lower lutein and β-carotene contents than the conventionally produced plants. A significant difference ($p < 0.05$) in β-carotene content was observed between hydroponic and soil cultivation, whereas for ascorbic acid content, a significant difference ($p < 0.01$) between the two treatments was observed for products cultivated in nutrition (NHC and NSC) and non-nutrition (GSC). In comparison to field studies, Plebeian herba plant grown in the nutrition cultured systems had a higher amount of ascorbic acid than previously reported in the literature for wild-harvested salvia plant.[25,26]

Content of Total Phenolics and Flavonoids. The free, esterified, and insoluble-bound phenolics in the extracts of Plebeian herba are shown in Table 1. The results revealed that the free phenolic contents were significantly higher than the bound and esterified phenolics content in each sample. It can be observed that the NSC extract contained the highest amount of phenolics (20.5 mg GE/g DW) among all of the extracts analyzed. The NHC and GSC had a comparatively lower presence of phenolics content at 13.4 and 14.4 mg GE/g DW, respectively. Free phenolics contributed approximately 76, 80, and 72% in NHC, NSC, and GSC extracts, respectively. The bound phenolics ranged from 13 to 19%, whereas esterified phenolics contributed 6−8% to the total.

Phenolics Content. Phenolic compounds are known as high-level antioxidants because of their ability to scavenge free radicals and active oxygen species such as singlet oxygen, superoxide anion radical, and hydroxyl radicals.[21] The highest flavonoid content was also found in NSC extract, contributing 10.5 mg/g DW. Free flavonoids content ranged from 3.4 mg/g DW (GSC) to 8.0 mg/g DW (NSC), whereas bound flavonoids ranged from 0.8 mg/g DW (NHC) to 1.8 mg/g DW (GSC). The contribution of bound flavonoids to NSC was <16%, whereas the contribution of esterified flavonoids was much higher as compared to that of NHC and GCS. Bound flavonoids in the GSC contributed 2.5 and 2.1 times more to the NHC and NSC, respectively. In the study of Grinder-Pedersen et al.[27] the growing conditions of fruits and vegetables (conventional vs nutritional) affect the content of flavonoids, resulting in differences in the urinary excretion of major dietary flavonoids, such as quercetin. It is well-known that variable agronomic and environmental factors such as climate, soil type, light intensity, irrigation, nutrient supply, pest control, weather, growing location, cultivation methods, and time of harvest can affect the phytochemical profile.[28,29] The effects of organic and conventional cultures on total phenolics and antioxidant activity in blueberry fruit were studied,[30] and the results showed that fruit produced following nutrition procedure showed a higher content of phytochemicals with respect to conventionally grown plants. The contents of flavonoids and ascorbic acid in these extracts were in the order NSC > NHC > GSC extracts; moreover, phenolics contents (mg/g DW) were in the order NSC > GSC > NHC extracts.

Antioxidant Activity. Plebeian herba containing high levels of phytochemicals can contribute to antioxidant activity, which is a promising component in decreasing the risk of degenerative diseases.[5] DPPH is a stable free radical that accepts the hydrogen radical to become a stable diamagnetic molecule: yellow-colored diphenylpicrylhydrazine.[31] The scavenging activities of Plebeian herba leaf extracts on the DPPH radical are shown in Figure 2A. All of the tested extracts reacted directly with DPPH radicals and quenched them to different degrees, with increasing activities at higher concentrations. Overall, the extract of NSC showed the highest scavenging

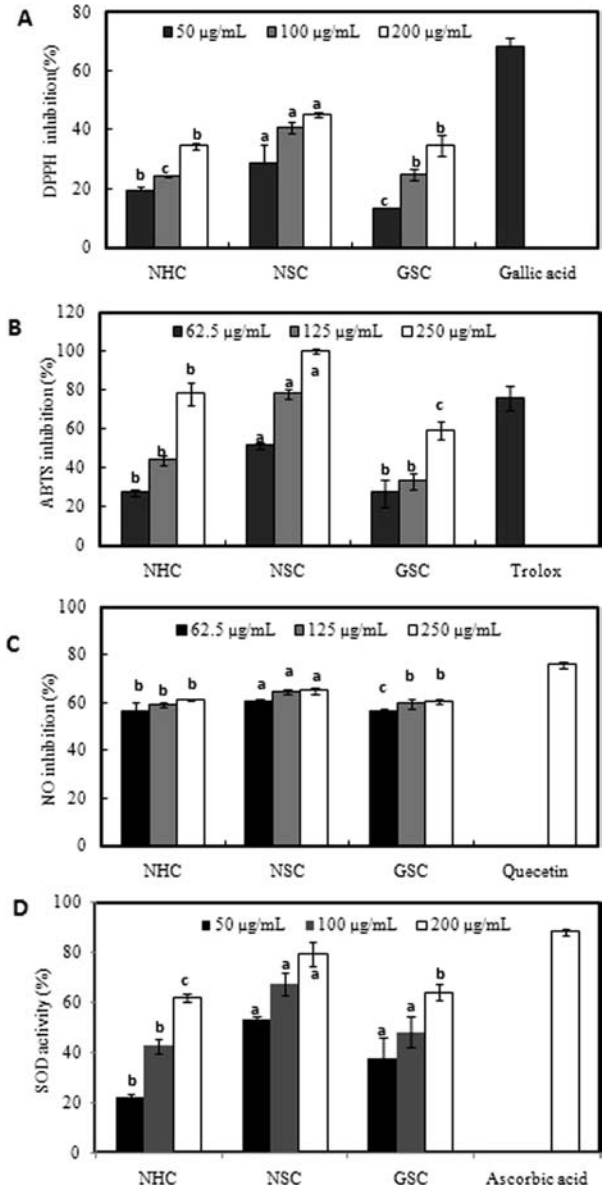

Figure 2. Antioxidant activities of Plebeian herba leaf extracts at different concentrations: (A) DPPH radical inhibition; (B) ABTS radical inhibition; (C) NO inhibition; (D) SOD activity. Different letters indicate a significant difference by Duncan's multiple ranges at $p < 0.05$.

activity. At 200 μg/mL, the scavenging activity of NSC extract reached a plateau of 45.2%. There was no significant variation between NHC (34.6%) and GSC (34.8%) extract, at the same concentration. Scavenging of DPPH radical allows evaluation of the hydrogen-donating potency of phenolic compounds. Plants of the *Salvia* genus mainly contain essential oil and phenolic compounds such as flavonoids, phenolic acids, and phenolic diterpenes.[4] As previously observed on *S. plebeia* extracts,[32] 6-methoxyluteolin-7-glucoside, β-sitosterol, and 2′-hydroxy-5′-methoxybiochanin were demonstrated to be responsible for their strong antioxidant activities. Earlier studies on the antioxidant activity of *Salvia officinalis* reported it to be attributed mainly to the presence of phenolic compounds, such as carsonic acid, rosmarinic acid, and salvianolic acid.[32,4] Therefore, these phenolic compounds in the extracts could be

dx.doi.org/10.1021/jf404570s | J. Agric. Food Chem. 2014, 62, 2190−2197

Table 2. Scavenging Capacity of Free, Bound, Esterified, and Total Phenolics of Plebeian Herba Grown in Hydroponics and Soil[a]

		scavenging capacity (μg/mL)		
	distribution	NHC	NSC	GCS
DPPH[b]	free	1695.6 ±33.7	1298.9 ± 11.9	1037.8 ± 31.1
	bound	123.9 ± 31.4	113.2 ± 9.5	127.3 ± 17.4
	esterified	880.5 ± 6.5	700.9 ± 8.9	910.1 ± 6.6
	total	342.9 ± 3.7	233.7 ± 9.6	345.3 ± 4.7
ABTS[b]	free	712.5 ± 83.9	678.6 ± 18.5	723.8 ± 9.3
	bound	122.0 ± 12.9	120.9 ± 9.1	102.4 ± 4.1
	esterified	525.9 ± 7.4	546.1 ± 8.8	544.2 ± 6.9
	total	159.5 ± 4.0	125.2 ± 7.4	210.8 ± 7.6
NO[b]	free	952.2 ± 12.5	900.8 ± 32.5	886.9 ± 12.2
	bound	188.6 ± 13.6	167.4 ± 2.9	190.8 ± 23.4
	esterified	752 ± 23.6	685.6 ± 14.8	708.8 ± 16.5
	total	206.5 ± 4.8	188.2 ± 11.2	216.0 ± 2.9
SOD[c]	free	769.6 ± 10.0	708.6 ± 23.5	798.5 ± 5.6
	bound	145.6 ± 8.9	108.8 ± 14.4	127.6 ± 26.0
	esterified	600.5 ± 12.	528.6 ± 24.8	602.6 ± 12.6
	total	168.0 ± 3.4	126.0 ± 18.4	166.2 ± 5.4

[a]Mean values ± standard deviations (n = 3). [b]Amount of sample required to decrease by 50% the initial DPPH, ABTS, and NO concentrations, respectively. [c]IC_{50} of SOD.

Table 3. Major Phenolic Compounds of Plebeian Herba Grown in Hydroponics and Soil[a]

	NHC			NSC			GSC		
phenolic compound	mg/g DW	recovery (%)	RSD (%)	mg/g DW	recovery (%)	RSD (%)	mg/g DW	recovery (%)	RSD (%)
caffeic acid	3.88 ± 0.06	95.6	1.5	4.17 ± 0.09	96.3	1.8	0.23 ± 0.01	93.8	2.1
luteolin-7-glucoside	1.35 ± 0.04	99.8	1.7	2.35 ± 0.13	98.2	2.0	0.34 ± 0.02	102.4	2.9
homoplantaginin	4.16 ± 0.20	101.6	1.8	5.08 ± 0.22	100.5	2.3	2.98 ± 0.05	101.8	2.4
hispidulin	2.28 ± 0.17	95.8	1.6	2.29 ± 0.08	97.6	1.6	2.10 ± 0.23	99.6	1.5
eupatorin	0.92 ± 0.11	97.3	1.3	1.72 ± 0.15	102.8	2.1	0.30 ± 0.01	99.6	3.1

[a]The data represent the average of three determinations. Recovery (%) = 100 × (amount found − original amount)/amount spiked.

responsible for the antioxidant activity found in the present study.

The ABTS radical scavenging activities of extracts were measured at three concentrations, ranging from 62.5 to 250 μg/mL. Of all the tested samples, NSC showed an outstanding scavenging activity with an inhibition value of 99.8% at 250 μg/mL concentration; NHC (78.4%) and GSC (59.3%) were found to have significantly weaker activity, at the same dose (Figure 2B). Determination of the antioxidant capacity by ABTS assay of nutrition cultured *S. plebeia* R. Br. plant was the first approach in this study. The term "antioxidant capacity" used in this assay corresponds to the measure of the moles of a given free radical scavenged by a test solution, independent of the antioxidant activity of any antioxidant present in the mixture.[33]

Because of the complex nature of plants, extracts cannot be evaluated by single methods. In this study, we additionally adopted in vitro NO inhibitory methods to determine the ability to inhibit free radicals. Figure 2C shows the NO radical scavenging activity of Plebeian herba leaf extract. All of the tested extracts inhibited the degradation of NO efficiently. A similar plateau to scavenge NO radical at 250 μg/mL is reached for NSC extract already at a concentration of 125 μg/mL. No significant difference between NHC (61.4%) and GSC (60.7%) extract was found at the same concentration. To the best of our knowledge, the antioxidant activity of NO free radical scavenging activity of nutrition hydroponics and soil cultured Plebeian herba has not been investigated.

SOD is a class of enzymes that catalyze the dismutation of superoxide into oxygen and hydrogen peroxide. The results of this study showed a concentration dependency in the SOD activity in the extracts of NHC, NSC, and GSC (Figure 2D). At a concentration of 200 μg/mL, the NSC extract showed the strongest SOD activity (79.4%), followed by GSC (64.0%) and NHC (62.1%) extracts.

To shed light on the contribution of phenolics to antioxidant activity, the antioxidant capacities of the free, esterified, and bound phenolics were analyzed (Table 2). The concentration of NSC to inhibit 50% of DPPH was 233.7 μg/mL. To obtain the same IC_{50} scavenging activity of NHC and GSC, the concentrations needed for NHC and GSC were 342.9 and 345.3 μg/mL, respectively. In the DPPH assay, bound phenolics exhibited the strongest scavenging capacity with IC_{50} values ranging from 113 to 127 μg/mL. Again, the IC_{50} values of ABTS in the bound phenolics were much lower than those exhibited by free and esterified phenolics. The highest inhibition of NO was exhibited by bound phenolics, whereas free phenolics exhibited the weakest antioxidant effect. The IC_{50} inhibition of NO of bound phenolics varied from 170.4 to 190.8 μg/mL. Consistent with the results obtained from these

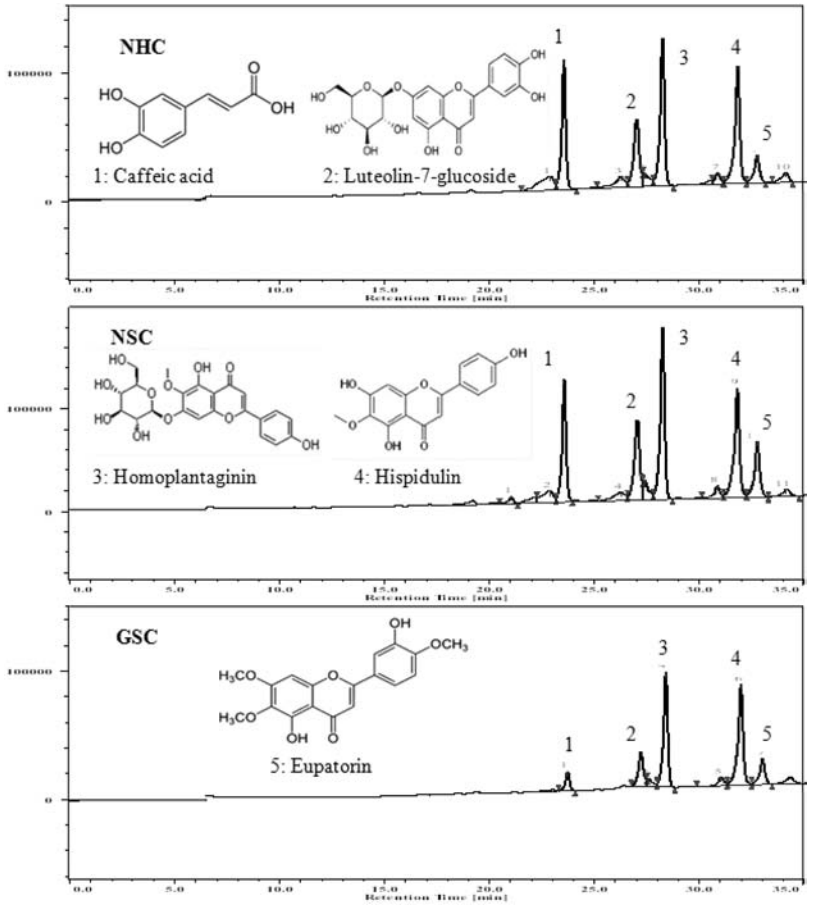

Figure 3. HPLC profiles of methanolic extracts from Plebeian herba. Peaks: caffeic acid (1); luteolin-7-glucoside (2); homoplantaginin (3); hispidulin (4); and eupatorin (5).

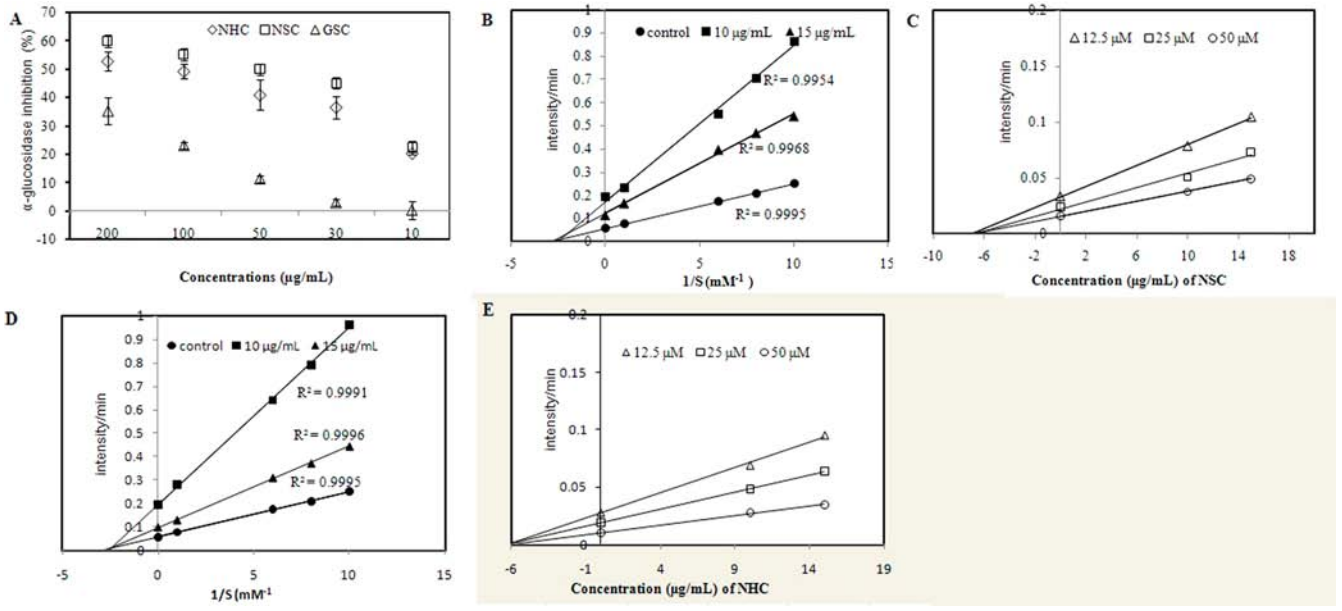

Figure 4. α-Glucosidase inhibition (A) by extracts of Plebeian herba at different concentrations. Data represent the mean of three independent experiments, each performed in duplicated samples. Lineweaver−Burk plot of kinetic analysis of α-glucosidas inhibition by NSC (B). α-Glucosidase was treated with various concentrations of PNP-glycoside (0.125−0.5 mM) in the absence or presence (C) of NSC at two different concentrations (10 and 15 μg/mL). (D) α-Glucosidase was treated with various concentrations of PNP-glycoside (0.125−0.5 mM) in the absence or presence (E) of NHC at two different concentrations (10 and 15 μg/ML) The enzyme reaction was performed by incubating the mixture at 37 °C for 15 min.

dx.doi.org/10.1021/jf404570s | J. Agric. Food Chem. 2014, 62, 2190−2197

assays employed in this study, the same trend of the phenolic-dependent SOD activity values was observed. The extract from NHC, NSC, and GSC, which had the highest content of free phenolics among all varieties tested, exhibited the highest antioxidant activity.

Phenolic Constituents. Different phenolic compounds normally possess specific chromatographic behavior and UV−visible spectral characteristics. Major phenolic compounds in Plebeian herba tested in this study were preliminarily and systematically identified using RP-HPLC with UV by comparison with authentic phenolic standards and relative literature data.[10,34] Major chemical classes and representative constituents of phenolic compounds identified in this study are summarized in Table 3. Figure 3 shows the HPLC profiles of the phenolic standards and leaf extracts of Plebeian herba. Peaks 1−5 in Figure 3 was identified as caffeic acid (1), luteolin-7-glucoside (2), homoplantaginin (3), hispidulin (4), and eupatorin (5). Although some peaks were not completely identified by the relative authentic standards, they could be other phenolic diterpenes, flavonoids, and aromatic volatile compounds, which were confirmed by our chromatographic and UV spectral data and by the analytical characteristics of phenolics reported by Jin et al.[10] Table 3 shows that caffeic acid, homoplantaginin, and hispidulin were the most common phenolics in the analyzed samples, whereas the contents of these three compounds remained low in the GSC. Very high levels of homoplantaginin (5.08 mg/g DW) and caffeic acid (4.17 mg/g DW) were found in the NSC. A previous study also reported the presence in Plebeian herba of hispidulin, homoplantaginin, luteolin-7-glucoside, and caffeic acid.[9] The precision for the 10 analyses was described as the relative standard deviation (RSD), and the test results are given in Table 3. The overall precision in Plebeian herba ranged from 1.3 to 3.1%. The recovery test was determined by standard addition method. Phenolic compounds were spiked into the samples and then extracted, processed, and quantified in accordance with the previous procedures (preparation of extract). The average recoveries of the five phenolic compounds were 93.8−102.4%. This indicated that the method was precise, accurate, and sensitive enough for simultaneous quantitative evaluation of these phenolic compounds in Plebeian herba.

α-Glucosidase Inhibition. As shown in Figure 4A, all of the extracts of Plebeiaen herba had the ability to inhibit α-glucosidase. The inhibitory activities of α-glucosidase increased proportionally to the concentration of the extracts. At a concentration of 200 μg/mL, NSC had the highest inhibitory activity (60.4%) followed by NHC (53.0%) and GSC (35.4%). The extracts of NHC had low phenolic content and had a relatively lower α-glucosidase inhibition. A recent study indicated that a polyphenolic extract of black cumin containing a mixture of phenolic compounds[35] showed significant inhibition of intestinal α-glucosidase activity. The inhibition mode against α-glucosidase activity was analyzed using Lineweaver−Burk plots ($1/V$ vs $1/S$). NSC showed the most significant inhibition; α-glucosidase was treated with NSC (10, 15 μg/mL) using PNP-glycoside (0.125−2 mM) as the substrate to determine the inhibition type. Double-reciprocal plots of enzyme kinetics demonstrated a noncompetitive inhibition of α-glucosidase activity (intersected at a nonzero point on the x-axis ($-K_i$)) (Figure 4B). The data revealed that NSC as the inhibitor is only bound to the enzyme−substrate complex in this model. The inhibition kinetics was also analyzed by Dixon plots, ($1/V$ vs [I] with various concentrations of substrate) (Figure 4C). The K_m value of PNP-glycoside for α-glucosidase was 1.21 mM (data not shown), and a higher V_{max} (0.05 M/min) in the presence of NSC was obtained, as compared to the control. Paneld D and E of Figure 4 show Lineweaver−Burk plots of α-glucosidase inhibitory activities in the presence of NHC at the same dose with NSC and in the absence of the inhibitor with different substrate concentrations of PNP-glycoside. With increasing NHC concentration, the vertical axis intercept ($1/V_m$) increased; however, the horizontal axis intercept ($\lfloor 1/K_m$) remained the same. These results indicate that the velocity of the reaction catalyzed by α-glucosidase was slowed with increasing NHC concentration, and the K_m value of α-glucosidase was not affected, which was correlated with the classical pattern of noncompetitive inhibition and indicated that NHC and the substrate did not bind to α-glucosidase at the same site.

The results presented here show that phenolics, flavonoids, and ascorbic acid highly existed in extracts of Plebeian herba. This investigation provides a strong rationale for further studies on Plebeian herba as a strategy to prevent type 2 diabetes. Furthermore, horticultural production is increasingly oriented toward high-quality products, in particular for the contents of antioxidants including ascorbic acid and phenolics. Thus, the production of high-quality plant tissues requires optimization of the growth environment for consistent production of specific metabolites, such as phenolics and flavonoids.

AUTHOR INFORMATION

Corresponding Author

*(Y.-H.K.) Phone: +82-10-4120-7594. Fax: +82-53-950-7752. E-mail: youngh@knu.ac.kr.

Notes

The authors declare no competing financial interest.

ABBREVIATIONS USED

NHC, nonsoil hydroponics cultivation; NSC, nutrition soil cultivation; GSC, general soil cultivation (traditional condition)

REFERENCES

(1) Jensen, M. H.; Collins, W. L. Hydroponic vegetable production. *Hortic. Rev.* **1985**, *7*, 483−558.

(2) Montanari, M.; Degl'Innocenti, E.; Maggini, R.; Pacifici, S.; Pardossi, A.; Guidi, L. Effect of nitrate fertilization and saline stress on the contents of active constituents of *Echinacea angustifolia* DC. *Food Chem.* **2008**, *107*, 1461−1466.

(3) Zheng, Y.; Dixon, M.; Saxena, P. K. Growing environment and nutrient availability affect the content of some phenolic compounds in *Echinacea purpurea* and *Echinacea angustifolia*. *Planta Med.* **2006**, *72*, 1407−1414.

(4) Lu, Y.; Foo, Y. Salvianolic acid, a potent phenolic antioxidant from *Salvia officinalis*. *Tetrahedron Lett.* **2001**, *42*, 8223−8225.

(5) Weng, X. C.; Cao, G. F.; Dong, X. W. Study on the antioxidant of *Salvia plebeia*. *J. Chin. Cereal Oil Assoc.* **1997**, *13*, 32−35.

(6) Xiang, L.; Chen, H. N.; Xu, C. M.; Zhang, S. S.; Wang, H. Y. Study on flavanoids from *Salvia plebeian*. *Chin. Pharm. J.* **2008**, *43*, 813−815.

(7) Gupta, H. C.; Ayengar, K. N.; Rangaswami, S. Structure and synthesis of salvitin, a new flavone isolated from *Salvia plebeian*. *Indian J. Chem.* **1975**, *15*, 215−217.

(8) Plattner, R. D.; Powell, R. G. A secoisolariciresinol branched fatty diester from *Salvia plebeia* seed. *Phytochemistry* **1978**, *17*, 149−150.

(9) Jin, Q.; Han, X. H.; Hwang, J. H.; Hong, S. S.; Park, M.; Lee, C.; Lee, C. H.; Lee, D.; Lee, M. K.; Hwang, B. Y. A new phenylbutanone glucoside from *Salvia plebeian*. *Nat. Prod. Sci.* **2009**, *15*, 106−109.
(10) Jin, X. F.; Lu, Y. H.; Wei, D. Z.; Wang, Z. T. Chemical fingerprint and quantitative analysis of *Salvia plebeian R. Br.* by high-performance liquid chromatography. *J. Pharm. Biomed. Anal.* **2008**, *48*, 100−104.
(11) Kim, S. J.; Heo, M. Y.; Son, K. H.; Kim, H. P. Tyrosinase inhibitory activity of 80 plant extracts (II). *J. Appl. Pharmacol.* **2003**, *11*, 5−7.
(12) Lim, J. A.; Yun, B. W.; Baek, S. H. Antioxidative activity and nitrite scavenging ability of methanol extract from *Salvia plebeia R. Br. Kor. J. Med. Crop Sci.* **2007**, *15*, 183−188.
(13) Jeong, H. J.; Hong, S. H.; Kim, H. M. Oriental medicines with anti-anaphylactic effect. *Oriental Pharm. Exp. Med.* **2004**, *4*, 125−136.
(14) Kwon, Y. I.; Vattem, D. V.; Shetty, K. Evaluation of clonal herb of *Lamiaceae* species for management of diabetes and hypertension. *Asia Pac. J. Clin. Nutr.* **2006**, *15*, 107−118.
(15) Ali, H.; Houghton, P. J.; Soumyanath, A. α-Amylase inhibitory activity of some Malaysian plants used to treat diabetes with particular reference to *Phyllanthus amarus*. *J. Ethnopharmacol.* **2006**, *107*, 449−455.
(16) Sgherri, C.; Cecconami, S.; Pinzino, C.; Navari-Izzo, F.; Lzzo, R. Levels of antioxidants and nutraceuticals in basil grown in hydroponics and soil. *Food Chem.* **2010**, *123*, 416−422.
(17) Nagata, M.; Yamashita, I. Simple method for simultaneous determination of chlorophyll and carotenoids in tomato fruit. *J. Jpn. Soc. Food Sci. Technol.* **1992**, *39*, 925−928.
(18) Chen, L.; Kang, Y. H. Anti-inflammatory and antioxidant activities of red pepper (*Capsicum annuum* L) stalk extracts: comparison of pericarp and placenta extracts. *J. Funct. Foods* **2013**, DOI: 10.1016/j.jff.2013.07.018.
(19) Tounekti, T.; Hernández, I.; Müller, M.; Khemira, H.; Munné-Bosch, S. Kinetin applications alleviate salt stress and improve the antioxidant composition of leaf extracts in *Salvia officinalis*. *Plant Physiol. Biochem.* **2011**, *49*, 1165−1176.
(20) Miean, K. H.; Mohamed, S. Flavonoid (myricetin, quercetin, kaempferol, luteolin, and apigenin) content of edible tropical plants. *J. Agric. Food Chem.* **2001**, *49*, 3106−3112.
(21) Chen, L.; Hwang, J. E.; Gu, K. M.; Kim, J. H.; Choi, B.; Song, K. S.; Park, Y.; Kang, Y. H. Comparative study of antioxidant effects of five Korean varieties red pepper (*Capsicum annuum* L) extracts from various parts including placenta, stalk, and pericarp. *Food Sci. Biotechnol.* **2012**, *21*, 715−721.
(22) Re, R.; Pellegrini, N.; Proteggente, A.; Pannala, A.; Yang, M. Antioxidant activity applying an improved ABTS radical cation decolorization assay. *Free Radical Biol. Med.* **1999**, *26*, 1231−1237.
(23) Chen, L.; Kang, Y. H. In vitro inhibitory potential against key enzymes relevant for hyperglycemia and hypertension of red pepper (*Capsicum annuum* L.) including pericarp, placenta, and stalk. *J. Food Biochem.* **2013**, DOI: 10.1111/jfbc.12048.
(24) Kimura, M.; Rodriguez-Amaya, D. B.; Godoy, H. T. Assessment of the saponification step in the quantitative determination of carotenoids and provitamins A. *Food Chem.* **1990**, *35*, 187−195.
(25) Nickavar, B.; Kamalinejad, M.; Izadpanah, H. In vitro free radical scavenging activity of five salvia species. *Pak. J. Pharm. Sci.* **2007**, *20*, 291−294.
(26) Miliauskas, G.; Venskutonis, P. R.; van Beek, T. A. Screening of radical scavenging activity of some medicinal and aromatic plant extracts. *Food Chem.* **2004**, *85*, 231−237.
(27) Grinder-Pedersen, L.; Rasmussen, S. E.; Bugel, S.; Jérgensen, L. V.; Dragsted, L. O.; Gundersen, V.; Sandstrom, B. Effect of diets based on foods from conventional versus organic production on intake and excretion of flavonoids and markers of antioxidative defense in humans. *J. Agric. Food Chem.* **2003**, *51*, 5671−5676.
(28) Fallovo, C.; Rouphael, Y.; Rea, E.; Battistelli, A.; Colla, G. Nutrient solution concentration and growing season affect yield and quality of *Lactuca sativa* L. var. acephala in floating raft culture. *J. Sci. Food Agric.* **2009**, *89*, 1682−1689.
(29) Lima, G. P. P.; Vianello, F. Review on the main differences between organic and conventional plant-based foods. *Int. J. Food Sci. Technol.* **2011**, *46*, 1−13.
(30) Wang, S. Y.; Chen, C. T.; Sciarappa, W.; Wang, C. Y.; Camp, M. J. Fruit quality, antioxidant capacity, and flavonoid content of organically and conventionally grown blueberries. *J. Agric. Food Chem.* **2008**, *56*, 5788−5794.
(31) Soares, J. R.; Dinis, T. C.; Cunhua, A. P.; Ameida, L. M. Antioxidant activities of some extracts of *Thymus*. *Free Radical Res.* **1997**, *26*, 469−478.
(32) Weng, X. C.; Wang, W. Antioxidant activity of compounds isolated from *Salvia plebeian*. *Food Chem.* **2000**, *71*, 489−493.
(33) Ghiselli, A.; Serafini, M.; Natella, F.; Scaccini, C. Total antioxidant capacity as a tool to assess redox status: critical view and experimental data. *Free Radical Biol. Med.* **2000**, *29*, 1106−1114.
(34) Ghang, T. L.; Chao, H. D.; Jung, N. L.; Kwang, S. L.; Jin, T. H.; Kun, K. L. Phytochemical constituents from *Salvia plebeian*. *Nat. Prod. Sci.* **2010**, *16*, 207−210.
(35) Ani, V.; Naidu, K. A. Antihyperglycemic activity of polyphenolic components of black/bitter cumin *Centratherum anthelminticum* (L.) Kuntze seeds. *Eur. Food Res. Technol.* **2008**, *226*, 897−903.

MATERIALS AND METHODS

Apparatus. ^{1}H nuclear magnetic resonance (NMR, 600 MHz), ^{13}C NMR (150 MHz), ^{1}H−^{1}H correlation spectroscopy (^{1}H−^{1}H COSY), heteronuclear single quantum coherence, heteronuclear multiple bond correlation (HMBC), and rotating-frame overhauser enhancement (ROE) spectroscopy spectra were recorded on a Bruker AV600 instrument (Bruker Biospin GmbH, Rheinstetten, Germany); chemical shifts are given in δ (ppm) relative to the solvent signal (CD_3OD, δ_H 3.31; δ_C 49.01, 300, or 243 K). Electrospray ionization (ESI) time-of-flight mass spectrometry (TOFMS) was carried out on a QSTAR Elite system (AB Sciex, Tokyo, Japan). All chromatographic experiments were carried out on an high performance liquid chromatography (HPLC) system (Hitachi, Tokyo, Japan), which consisted of an L-7150 pump, a 7161 injector (Rheodyne, loop capacity: 10 mL), an L-7455 diode-array detector (DAD, optical path length of a flow cell: 0.2 mm), and an SF-2120 fraction collector (Advantec, Tokyo, Japan). Chromatograms were recorded on a personal computer using D-7000 chromatography data station software (Hitachi). HSCCC experiments were carried out using an HPLC system (Hitachi) equipped with a type-J coil-planet centrifuge (J-CPC) (Easy-PREP 320, Kutsuwa Sangyo, Hiroshima, Japan) between the 7161 injector and L-7455 DAD. The J-CPC apparatus contains three multilayer-coil separation columns placed symmetrically at a distance of 7 cm from the central axis of the centrifuge. Each separation column was fabricated by directly winding a single piece of polytetrafluoroethylene (PTFE) tubing (1.6 mm i.d. × 50 m length) onto each column holder. The total capacity of the three columns is about 320 mL. Optical rotations were measured with a P-2200 polarimeter (JASCO, Tokyo, Japan). UV data were measured with a U-2900 spectrophotometer (Hitachi). All solvents (high or HPLC grade) for extraction and chromatographic separation were purchased from Wako Pure Chemical Industries, Ltd. (Osaka, Japan).

Plant Material and Sample Preparation. In this study, the spray-dried powder of the polyphenol-rich extract from hop bracts (HBP; food additive grade in Japan) was used as a raw material. The factory-scale preparation method for HBP is described in previous papers.[2,4] To describe it briefly, HBP was prepared from the crude hop bract extract supplied by Simon H. Steiner Hopfen GmbH (Germany). The extract was produced by extracting 101 t of the female inflorescence of hop bracts with 50% aqueous ethanol (100 kL, 50 °C, 10 h), centrifuging the material to remove solids, and evaporating ethanol. The bracts were obtained to crush hop cones (cropped in Hallertau, Germany, in 2003) and to remove the lupulin glands by sifting. Next, the crude extract from the 101 t of hop bracts was dissolved in distilled water and passed through a SEPABEADS SP-850 column (150 cm i.d. × 230 cm, Mitsubishi Chemical Corporation, Tokyo, Japan). The column was washed with distilled water (12 kL) and eluted with 50% aqueous ethanol (12 kL). After concentrating the eluting fraction, the concentrated fraction was spray-dried to obtain 2 t of HBP powder (yield: 2.0%). In this study, a small portion of HBP powder (25 g) was used for the following HSCCC separation.

HSCCC Conditions. The HSCCC separation of HBP was carried out using a two-phase solvent system composed of methyl *t*-butyl ether (MTBE)−acetonitrile−0.1% aqueous trifluoroacetic acid (TFA) (2:2:3) in the NP partition mode (initial mobile phase: organic upper-phase (UP) solvent; stationary phase: aqueous lower-phase (LP) solvent). First, the three-coil PTFE columns (capacity: 320 mL) of J-CPC were entirely filled with the LP solvent as a stationary phase. Then, the columns were rotated at 1000 rpm (112*g*), while the UP mobile phase was pumped into the columns in the tail-to-head direction at a flow rate of 4.0 mL/min. After hydrodynamic mixing between the two phases in the columns reached equilibrium, 10 mL of sample solution (5 g of HBP dissolved with 5 mL each of the UP and LP solvents) was injected, and the hydrophobic constituents of the HBP sample were separated using the UP mobile phase. Following elution using UP for 120 min, the mobile phase was switched to LP, which completely eluted the polar constituents retained on the column, and elution was performed using LP for 100 min. During HSCCC separation, the UV absorbance of the eluate was monitored by a DAD. The eluate (12 mL) was collected every 3 min by a fraction collector, and each collected fraction was evaporated and lyophilized. For treatment of 25 g of HBP, HSCCC separation was repeated five times.

HILIC Conditions. The lyophilized HSCCC fractions were further separated by HILIC using an amide column under the following conditions. HILIC separation was carried on a TSKgel Amide-80 column (21.5 mm i.d. × 300 mm, 10 μm, Tosoh, Tokyo, Japan) protected with a guard column (21.5 mm i.d. × 75 mm). The mobile phase consisted of eluent A (90% aqueous acetonitrile) and eluent B (50% aqueous acetonitrile). A multilinear gradient was applied from 100:0 (A:B) to 80:20 over 20 min, and then it was changed to 50:50 over 60 min. The flow rate was maintained at 13 mL/min, and the sample solution (a maximum of 200 mg of a lyophilized HSCCC fraction dissolved in a maximum of 10 mL of eluent A) was injected through a sample loop. During HILIC separation, the UV absorbance of the eluate was monitored by a DAD. The eluate (13 mL) was collected every 1 min by a fraction collector, and each collected fraction was evaporated and lyophilized.

RP-HPLC Conditions Using ODS Column. The lyophilized HILIC fractions were further separated by RP-HPLC using an ODS column under the following conditions. The RP-HPLC separation was carried out on a Mightysil RP-18 GP column (10 mm i.d. × 250 mm, 5 μm, Kanto Chemical, Tokyo, Japan) protected with a guard column (10 mm i.d. × 10 mm). The mobile phase consisted of eluent A (10% aqueous acetonitrile) and eluent B (50% aqueous acetonitrile). An isocratic elution of 100:0 (A:B) was started for 20 min, and then a linear gradient was applied from 100:0 to 50:50 over 40 min. The flow rate was maintained at 13 mL/min, and the sample solution (a maximum of 100 mg of a lyophilized HILIC fraction dissolved in a maximum of 5 mL of eluent A) was injected through a sample loop. During RP-HPLC separation, the UV absorbance of the eluate was monitored by a DAD. The eluate (13 mL) was collected every 1 min by a fraction collector, and each collected peak fraction was evaporated and lyophilized.

RP-HPLC Conditions Using Phenyl Column. When the isolation of a pure compound by the above RP-HPLC method was unsuccessful, a further RP-HPLC separation step using a phenyl column was performed under the following conditions. The RP-HPLC separation was carried out on an Inertsil Ph-3 column (10 mm i.d. × 250 mm, 5 μm, GL Science, Tokyo, Japan) protected with a guard column (10 mm i.d. × 10 mm). The isocratic elution of a mobile phase with aqueous acetonitrile (an appropriate volume ratio was applied on a case-by-case basis) was performed at a flow rate of 13 mL/min. The sample solution (a maximum of 100 mg of a lyophilized RP-HPLC fraction obtained from step 3 dissolved in a maximum of 5 mL of the mobile phase) was injected through a sample loop. During RP-HPLC separation, the UV absorbance of the eluate was monitored by a DAD. The eluate (13 mL) was collected every 1 min by a fraction collector, and each collected peak fraction was evaporated and lyophilized.

Ultrafiltration. For the purification of high-molecular-weight compounds (proanthocyanidins) in HSCCC fraction J, ultrafiltration was performed under the following conditions. A portion of the lyophilized powder of fraction J dissolved in 50% methanol was applied to an Amicon ultra filter device (exclusion molecular weight limit: 3000 Da, Millipore) and centrifuged (14000*g*, 30 min). The concentrated solution containing highly oligomeric proanthocyanidins (over 20-mers) was washed with the dissolving solvent twice and was evaporated and lyophilized for further NMR analysis.

RESULTS AND DISCUSSION

HSCCC Separation and Fractionation of Hop Bract Extract. In this study, the spray-dried powder of HBP was used as raw material. HBP contains various types of polyphenolic compounds,[4] but the phenolic composition of HBP has yet to be fully elucidated. First, the constituents of HBP were fractionated by HSCCC using a two-phase solvent system composed of MTBE−acetonitrile−0.1% aqueous TFA (2:2:3) in the NP partition mode (initial mobile-phase: organic UP

solvent; stationary phase: aqueous LP solvent). Ten milliliters of sample solution (5 g of HBP dissolved with 5 mL each of the UP and LP solvents) was injected into the HSCCC column (capacity: 330 mL). To treat 25 g of HBP, HSCCC separation was repeated 5 times. Figure 1 shows the NP-HSCCC

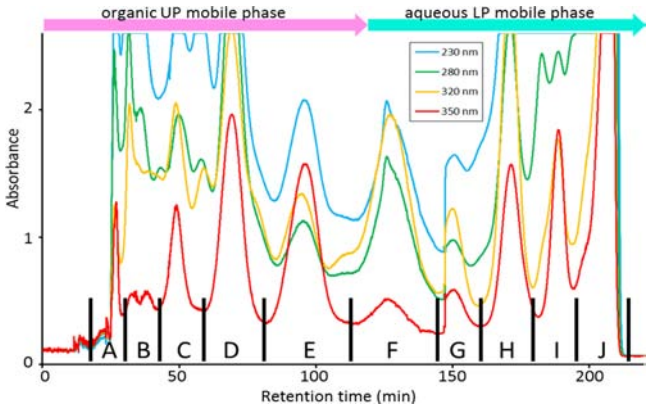

Figure 1. HSCCC separation and fractionation profile of HBP (5 g). Separation was carried out using a two-phase solvent system composed of MTBE–acetonitrile–0.1% aqueous TFA (2:2:3) and NP partition mode (initial mobile phase: organic UP; stationary phase: aqueous LP). Flow rate: 4 mL/min. Retention % of stationary phase: 65%. Other chromatographic conditions: see Materials and Methods. All eluates were collected and divided into 10 fractions (fractions A–J).

chromatogram of HBP (5 g) separation. In the separation profile, hydrophobic constituents of HBP were quickly eluted with the organic UP mobile-phase solvent within 145 min, whereas the polar/hydrophilic constituents were strongly retained on the aqueous LP stationary phase in the HSCCC column. Then, the mobile-phase solvent was switched from UP to LP at 120 min after HBP injection, and then the remaining polar/hydrophilic constituents eluted through the column by 215 min. As shown in Figure 1, all eluates were collected and divided into 10 fractions (fractions A–J). The weights and yields of the fractions are listed in Table 1. The total yield of HBP from the HSCCC method (5 g × 5 times) was calculated to be 90.4%. The yield reveals that almost all of the constituents of HBP are recovered with no loss due to HSCCC treatment because the moisture content of the spray-dried HBP powder is about 5–10%. Among all the HSCCC fractions, the weight and yield of fraction J were the highest—13.5 g, 54.0%. Fraction J was the most hydrophilic fraction, and it contained a wide variety of oligomeric proanthocyanidins (details of the characterization of the fraction J constituents are described below). Furthermore, the moderate hydrophobic polyphenols of the above HSCCC fractions (except for hydrophilic fraction J and hydrophobic fractions A and B) were sequentially separated by conventional HPLC. Unfortunately, the sequential separation for the fractions A and B were incomplete in the present study because the constituents in the both fractions were too hydrophobic for next HILIC separation.

Sequential Chromatographic Isolation of Polyphenolic Constituents of the HSCCC Fractions of HBP. The phenolic constituents of the HSCCC fractions C–I were further separated by HILIC using an amide column followed by RP-HPLC using ODS and phenyl columns. The schemes for sequential HPLC separation of HSCCC fractions C–I are shown in Figure 2. As a result of comprehensive HPLC separation, 102 types of single-peak compounds were isolated and recovered with amounts ranging from 0.1 mg to 40 mg. Furthermore, the structures of the compounds were elucidated on the basis of their spectroscopic data including ESI-TOFMS and 1D/2D NMR.

Structural Analyses of the Isolated Compounds. Among the isolated compounds described above, 35 known compounds, 1 known compound identified for the first time in plants, and 3 new compounds were found. As shown in Table 2, the structures of the 35 known compounds (**5**–**39**) were identified by comparing their LC retention times, MS, NMR, and other spectroscopic data with those of experimental and literature values of standard compounds. They included 2-(2-methylbutyryl)phloroglucinol-1-*O*-*β*-glucopyranoside (**5**);[16] 2-isobutyrylphloroglucinol-1-*O*-*β*-glucopyranoside (**6**);[16] 3-*O*-caffeoylquinic acid (**7**);[17] 4-*O*-caffeoylquinic acid (**8**);[17] 5-*O*-caffeoylquinic acid (**9**);[17] 4-*O*-*β*-glucopyranosyl-*p*-coumaric acid (**10**);[18] *trans*-3-*O*-*p*-coumaroylquinic acid (**11**);[19] *cis*-3-*O*-*p*-coumaroylquinic acid (**12**);[19] 4-*O*-*p*-coumaroylquinic acid (**13**);[20] 3-*O*-feruloylquinic acid (**14**);[21] 4-*O*-feruloylquinic acid (**15**);[21] kaempferol-3-*O*-*β*-glucopyranoside (**16**);[22] quercetin-3-*O*-*β*-glucopyranoside (**17**);[22] kaempferol-3-*O*-*β*-rutinoside (**18**);[22] kaempferol-3-*O*-*β*-neohesperidoside (**19**);[22] quercetin-3-*O*-*β*-neohesperidoside (**20**);[22] quercetin-3-*O*-(2″-*O*-*α*-rhamnosyl-6″-*O*-malonyl)-*β*-glucopyranoside (**21**);[22] myricetin-3-*O*-*β*-glucopyranoside (**22**);[22] kaempferol-3-*O*-*β*-(6-*O*-malonyl)-glucopyranoside (**23**);[23] quercetin-3-*O*-*β*-(6-*O*-malonyl)-glucopyranoside (**24**);[23] procyanidin B1 (**25**);[24] epicatechin-(4*β*-8)-epicatechin-(4*β*-8)-catechin (**26**);[25] epicatechin-(4*β*-6)-epicatechin-(4*β*-8)-catechin (**27**);[25] tryptophan (**28**); 2-(3-hydroxy-2-oxoindolin-3-yl)acetic acid (**29**);[26] 1,2,3,4-tetrahydro-*β*-carboline-3-carboxylic acid (**30**);[27] 1-methyl-1,2,3,4-tetrahydro-*β*-carboline-3-carboxylic acid (**31**);[28] pinoresinol-4″-*O*-*β*-glucopyranoside (**32**);[29] isolariciresinol-3*α*-*O*-*β*-glucopyranoside (**33**);[30] lariciresinol-4-*O*-*β*-glucopyranoside (**34**);[31] (3*S*)-*O*-*β*-glucopyranosyl-6-[3-oxo-(2*R*)-butenylidenyl]-1,1,5-trimethylcyclohexane-(5*R*)-ol (**35**);[32] dihydrovomifoliol-3′-*O*-*β*-glucopyranoside (**36**);[33] 5-*O*-*β*-xylopyranosylgentisic acid (**37**);[34] 4-*O*-*β*-glucopyranosyl-*p*-hydroxybenzoic acid (**38**);[35] and (2*E*,4*E*)-8-*β*-glucopyranosyloxy-2,7-dimethyl-2,4-decadiene-1,10-dioic acid (**39**).[36] The 20 compounds (**10**–**15**, **21**, **22**, **27**, **29**–**39**) have not been reported from hops.

The spectroscopic data of compounds (**1**–**4**) are also shown in Tables 2–4. Compound **1** was obtained as a yellow amorphous powder. Its TOFMS signal (*m*/*z* 431.2273 [M + H]$^+$) confirmed that its molecular formula was $C_{21}H_{34}O_9$. The ^{1}H NMR spectrum of **1** showed two *trans*-coupled olefinic signals ($^3J_{H\text{-}4,H\text{-}5}$ = 15.6), a singlet olefinic signal, an oxygen-

Table 1. Weights and Yields of Fractions A–J Obtained from HBP (25 g) by NP-HSCCC Separation

	HSCCC fractions										
	A	B	C	D	E	F	G	H	I	J	total
weights (g)	0.2	0.5	0.7	1.5	0.8	0.9	0.8	1.7	2.0	13.5	22.6
yields (%)	0.8	2.0	2.8	6.0	3.2	3.6	3.2	6.8	8.0	54.0	90.4

dx.doi.org/10.1021/jf405544n | J. Agric. Food Chem. 2014, 62, 2198–2206

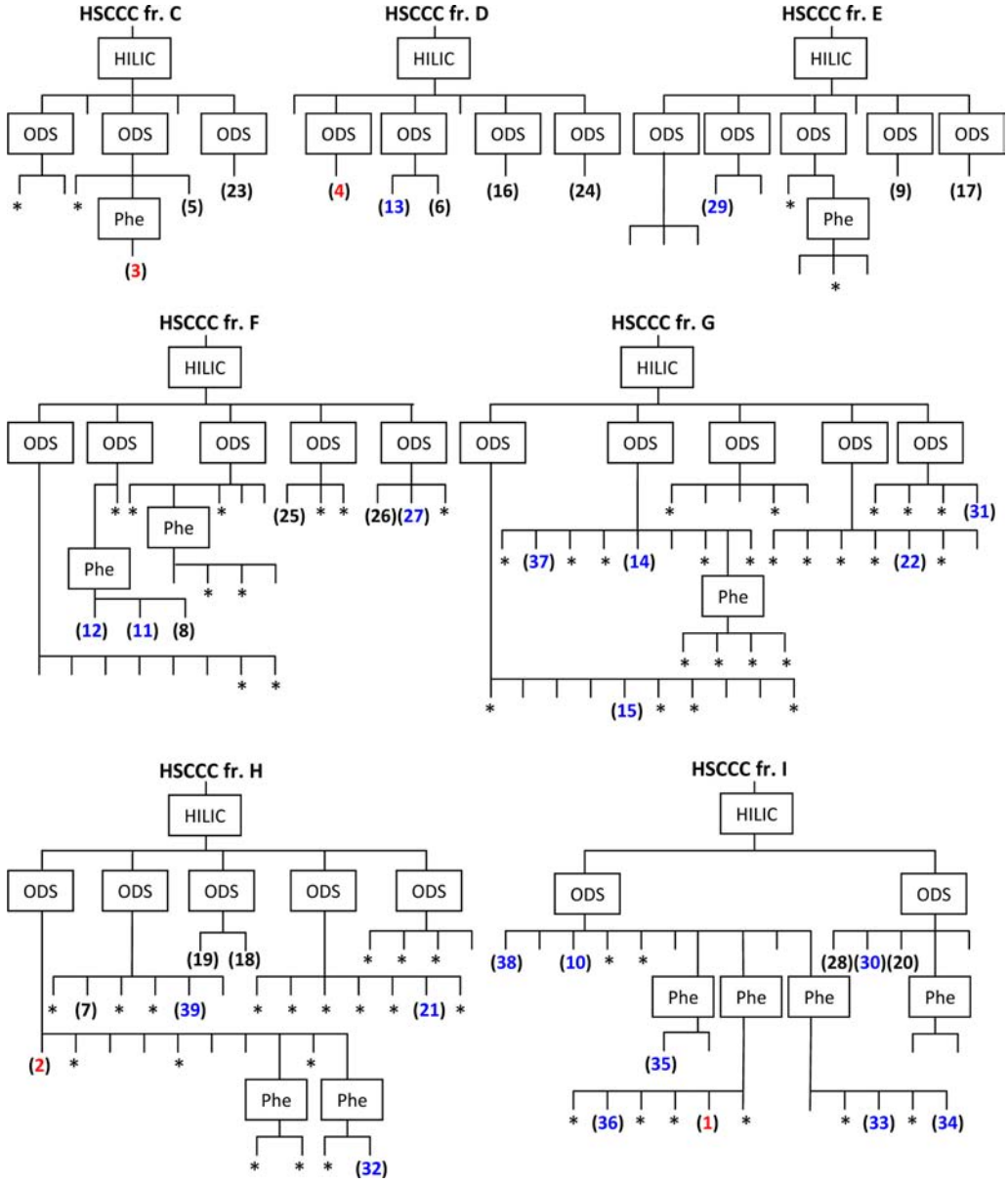

Figure 2. Schemes of sequential HPLC separations of HSCCC fractions C–I. Numbers in red indicate new compounds and a known one, which has been identified for the first time in plants. Numbers in blue indicate known compounds that have not been reported from hops. Asterisk (*) indicates isolated compounds whose structures could not be determined in this study.

bearing methine signal, a sugar moiety, four methylene signals, a methine signal, a secondary methyl group, two tertiary methyl groups, and an olefinic methyl group (Table 3). The $^{1}H-^{1}H$ COSY correlation from H-4 to H-5 and the HMBC correlations from H-2 to C-1 and from H-6 to C-2, C-3, and C-4 indicated the presence of the 3-methyl-2,4-pentadienoyl group (Figure 3). The proton connectivities of H-7′, H-2′, H-3′, H-4′, and H-5′ assigned by $^{1}H-^{1}H$ COSY and the HMBC correlations from H-2′ax, H-3′eq, H-5′eq, H-8′, and H-9′ to C-1′ and from H-5′ax, H-5′eq, H-8′, and H-9′ to C-6′ supported the presence of the 1,4-dihydroxy-2,6,6-trimethylcyclohexane moiety (Figure 3). The HMBC correlation between H-5 and C-1′ indicated that the acyl group was attached at C-1′, suggesting that **1** has 2′,3′,4′,4′-tetrahydroabscisic acid as the aglycon portion (Figure 3).[37] The ROE correlations from H-2′ax to H-4′ax and H-8′ and from H-5 to H-3′ax and H-5′ax supported the chair conformation. The ROE between H-2 and H-6 indicated the *cis* orientation of H-2 with respect to H-6 (Table 3). Coupling constants in ^{1}H NMR and chemical shifts in ^{13}C NMR supported the presence of the *O*-*β*-glucopyranosyl moiety (Table 3). The HMBC correlation between H-Glc1 and C-1 confirmed that the sugar moiety was attached at C-1. Therefore, the structure of **1** was confirmed to be 1-*O*-(2′,3′,4′,4′-tetrahydroabscisoyl)-*β*-glucopyranose (Figure 4).

Compound **2** was obtained as a yellow amorphous powder. Its TOFMS signal (*m*/*z* 142.0497 $[M + H]^{+}$) confirmed that the molecular formula was $C_6H_7NO_3$. The ^{1}H and ^{13}C NMR spectra of **2** were consistent with those of a known chemical synthetic intermediate, (*R*)-4-methylene-5-oxopyrrolidine-2-carboxylic acid.[38] The absolute configuration of the structure was expected to have the 2*S*-form because of positive optical rotation, the sign of which was reversed compared to the literature value of the above compound, and this was consistent with L-pyroglutamic acid in methanol. On the basis of these

dx.doi.org/10.1021/jf405544n | J. Agric. Food Chem. 2014, 62, 2198–2206

Table 2. Yields, Maximum Absorption Wavelengths, and Mass Spectral Data of Purified Compounds

no.	yield (%)	λ_{max} (nm)	$[M - H]^-$	$[M + H]^+$	attribution
1	0.01	270	429.2	431.2	1-*O*-(2′,3′,4′,4′-tetrahydroabscisoyl)-*β*-glucopyranose
2	0.02	206	140.1	142.0	(*S*)-4-methylene-5-oxopyrrolidine-2-carboxylic acid
3	0.02	312	323.1	325.1	6-*O*-*p*-coumaroyl-L-galactono-1,4-lactone
4	0.05	324	353.1	355.1	6-*O*-feruloyl-L-galactono-1,4-lactone
5	0.04	222, 285	371.1	373.1	2-(2-methylbutyryl)phloroglucinol-1-*O*-*β*-glucopyranside
6	0.07	222, 284	357.1	359.1	2-isobutyrylphloroglucinol-1-*O*-*β*-glucopyranoside
7	0.39	320	353.1	355.1	3-*O*-caffeoylquinic acid
8	0.04	322	353.1	355.1	4-*O*-caffeoylquinic acid
9	0.09	322	353.1	355.1	5-*O*-caffeoylquinic acid
10	0.04	223, 293	325.1	327.1	4-*O*-*β*-glucopyranosyl-*p*-coumaric acid
11	0.18	308	337.1	339.1	*trans*-3-*O*-*p*-coumaroylquinic acid
12	0.01	304	337.1	339.1	*cis*-3-*O*-*p*-coumaroylquinic acid
13	0.32	226, 310	337.1	339.1	4-*O*-*p*-coumaroylquinic acid
14	0.13	322	367.1	369.1	3-*O*-feruloylquinic acid
15	0.07	324	367.1	369.1	4-*O*-feruloylquinic acid
16	0.42	264, 345	447.1	449.1	kaempferol-3-*O*-*β*-glucopyranoside
17	0.40	254, 352	463.1	465.1	quercetin-3-*O*-*β*-glucopyranoside
18	0.12	265, 346	593.2	595.2	kaempferol-3-*O*-*β*-rutinoside
19	0.05	265, 344	593.2	595.2	kaempferol-3-*O*-*β*-neohesperidoside
20	0.08	255, 352	609.2	611.2	quercetin-3-*O*-*β*-neohesperidoside
21	0.03	257, 355	695.2	697.2	quercetin-3-*O*-(2″-*O*-*α*-rhamnosyl-6″-*O*-malonyl)-*β*-glucopyranoside
22	0.02	254, 378	479.1	481.1	myricetin-3-*O*-*β*-glucopyranoside
23	0.12	262, 345	533.1	535.1	kaempferol-3-*O*-*β*-(6-*O*-malonyl)- -glucopyranoside
24	0.51	254, 351	549.1	551.1	quercetin-3-*O*-*β*-(6-*O*-malonyl)-glucopyranoside
25	0.02	278	577.1	579.1	procyanidin B1
26	0.01	280	865.3	867.2	epicatechin-(4*β*-8)-epicatechin-(4*β*-8)-catechin
27	0.01	280	865.3	867.2	epicatechin-(4*β*-6)-epicatechin-(4*β*-8)-catechin
28	0.10	219, 278	203.1	205.1	tryptophan
29	0.05	253	206.0	208.1	2-(3-hydroxy-2-oxoindolin-3-yl)-acetic acid
30	0.07	219, 278	215.1	217.1	1,2,3,4-tetrahydro-*β*-carboline-3-carboxylic acid
31	0.02	278	229.1	231.1	1-methyl-1,2,3,4-tetrahydro-*β*-carboline-3-carboxylic acid
32	0.01	228, 278	519.2	521.2	pinoresinol-4″-*O*-*β*-glucopyranoside
33	0.01	283	521.2	523.2	isolariciresinol-3*α*-*O*-*β*-glucopyranoside
34	0.01	226, 278	521.2	n.d.[a]	lariciresinol-4-*O*-*β*-glucopyranoside
35	0.04	234	n.d.[a]	431.2	(3*S*)-*O*-*β*-glucopyranosyl-6-[3-oxo-(2*R*)-butenylidenyl]-1,1,5-trimethylcyclohexane-(5*R*)-ol
36	0.01	248	387.2	389.2	dihydrovomifoliol-3′-*O*-*β*-glucopyranoside
37	0.04	314	285.1	287.1	5-*O*-*β*-xylopyranosylgentisic acid
38	0.02	248	299.1	301.1	4-*O*-*β*-glucopyranosyl-*p*-hydroxybenzoic acid
39	0.03	267	403.2	405.2	(2*E*,4*E*)-8-*β*-glucopyranosyloxy-2,7-dimethyl-2,4-decadiene-1,10-dioic acid

[a]Not detected.

data, **2** was determined to be (*S*)-4-methylene-5-oxopyrrolidine-2-carboxylic acid, which was identified for the first time in plants (Figure 4).

Compounds **3** and **4** were obtained as yellow amorphous powders. Their molecular formulas were determined to be $C_{15}H_{16}O_8$ and $C_{16}H_{18}O_9$ (*m*/*z* 325.0912 $[M + H]^+$ and 355.1007 $[M + H]^+$), respectively, by TOFMS analyses. The ^{1}H NMR spectrum of **4** was similar to that of **3**, except for the presence of a methoxy signal and the integral values of the olefinic signals. The ^{13}C NMR spectra of **3** and **4** supported the presence of the *p*-coumaroyl group (*δ* 127.1, 131.2, 116.8, 161.4, 116.8, 131.2, 147.0, 114.8, and 168.9) in **3** and the feruloyl group (*δ* 127.7, 111.8, 149.4, 150.7, 116.5, 124.2, 147.3, 115.1, 168.8, and 56.4) in **4** (Table 4). The ^{1}H and ^{13}C NMR spectra of **3** and **4** indicated that they contain the same sugar moiety; it was identified to be galactono-1,4-lactone[39] by coupling constants ($^3J_{H\text{-}2,H\text{-}3}$ = 8.7, $^3J_{H\text{-}3,H\text{-}4}$ = 8.7, $^3J_{H\text{-}4,H\text{-}5}$ = 2.4, $^3J_{H\text{-}5,H\text{-}6}$ = 6.0, 6.9, and $^3J_{H\text{-}6,H\text{-}6}$ = 11.1 in **3** and $^3J_{H\text{-}2,H\text{-}3}$ = 8.1, $^3J_{H\text{-}3,H\text{-}4}$ = 8.1, $^3J_{H\text{-}4,H\text{-}5}$ = 2.4, $^3J_{H\text{-}5,H\text{-}6}$ =5.7, 7.5, and $^3J_{H\text{-}6,H\text{-}6}$ = 11.1 in **4**), the HMBC correlation between H-2 and C-1, and the isotopic shifts of C-2, C-3, and C-5 in the H−D exchange experiments (CD_3OH and CD_3OD); the moiety was confirmed by a comparison of experimental values with a standard compound (Table 4). The HMBC correlation between H-6 and C-9′ confirmed that the sugar moiety was attached at C-9′. The absolute configuration of the sugar moiety in **4** was expected to have the L-form because of positive optical rotation, which was consistent with L-galactono-1,4-lactone in methanol. The absolute configuration of **3** was expected to have the same form, although the optical rotation of **3** could not be observed because of its small amount. Therefore, the structures of **3** and **4** were determined to be 6-*O*-*p*-coumaroyl-L-galactono-1,4-lactone and 6-*O*-feruloyl-L-galactono-1,4-lactone, respectively (Figure 4). To our knowledge, compounds **1**−**4** have been identified for the first time in plants.

Structural Characterization of Hydrophilic Proanthocyanidins in HBP. As shown in Figure 1 and Table 1, the constituents of HSCCC fraction J were a mixture of the most

Table 3. ^{1}H and ^{13}C NMR Spectroscopic Data (δ_H, 600 MHz; δ_C, 150 MHz, CD_3OD) for 1

position	δ_H[a]	δ_C	ROE correlations
1		166.1	
2	5.77 s	116.6	6
3		154.3	
4	7.80 d (15.6)	129.1	
5	6.52 d (15.6)	140.1	3′ax, 5′ax, 9′
6	2.09 d (1.2)	21.5	2
1′		80.1	
2′ax	2.06 m	37.0	4′ax, 7′, 8′
3′eq	1.83 m	42.5	3′ax, 4′ax, 7′
3′ax	1.20 dt (13.2, 11.7)		5, 3′eq
4′ax	3.92 m	67.1	2′ax, 3′eq, 5′eq, 8′
5′eq	1.68 ddd (12.6, 4.8, 1.8)	47.9	4′ax, 8′, 9′
5′ax	1.51 t (12.6)		5, 9′
6′		40.6	
7′	0.81 d (6.6)	27.0	2′ax, 3′eq
8′	1.08 s	23.5	2′ax, 4′ax, 5′eq
9′	0.83 s	16.6	5, 5′eq, 5′ax
Glc1	5.51 d (8.4)	95.4	
Glc2	3.36 t (8.4)	74.0	
Glc3	3.43 t (8.4)	78.1	
Glc4	3.35 t (8.4)	71.1	
Glc5	3.39 m	78.8	
Glc6	3.84 dd (12.0, 2.4)	62.4	
	3.68 dd (12.0, 4.8)		

[a]Coupling constants (J in Hz) in parentheses.

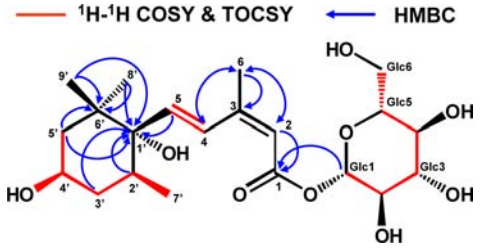

Figure 3. Key HMBC and ^{1}H−^{1}H COSY correlations of 1.

abundant and hydrophilic compounds in HBP. Further LC separations (HILIC and ODS) of the fraction J constituents were incomplete because both chromatograms showed an unresolved broad peak (data not shown). It was noted that hops contain an abundance of proanthocyanidins with different degrees of polymerization (DP),[40] and the hydrophobicity of oligomeric proanthocyanidin significantly decreases as its DP value increases.[41] Furthermore, in our preliminary examinations, the acid hydrolysis of the fraction J constituents resulted in the production of a large amount of red pigments (anthocyanidins), and the gel-permeation chromatogram of fraction J showed a broad and large peak, which was attributed

Table 4. ^{1}H and ^{13}C NMR Spectroscopic Data (δ_H, 600 MHz; δ_C, 150 MHz, CD_3OD) for 3 and 4

	3		4	
position	δ_H[a]	δ_C	δ_H[a]	δ_C
1		176.0		176.0
2	4.38 d (8.7)	75.6	4.39 d (8.1)	75.6
3	4.33 t (8.7)	74.4	4.33 t (8.1)	74.4
4	4.19 dd (8.7, 2.4)	81.4	4.20 dd (8.1, 2.4)	81.4
5	4.07 m	67.8	4.07 m	67.8
6	4.29 dd (11.1, 6.0)	65.9	4.29 dd (11.1, 5.7)	65.9
	4.33 dd (11.1, 6.9)		4.33 dd (11.1, 7.5)	
1′		127.1		127.7
2′	7.47 d (9.0)	131.2	7.2 d (1.8)	111.8
3′	6.81 d (9.0)	116.8		149.4
4′		161.4		150.7
5′	6.81 d (9.0)[b]	116.8[b]	6.82 d (8.1)	116.5
6′	7.47 d (9.0)[c]	131.2[c]	7.09 dd (8.1, 1.8)	124.2
7′	7.67 d (15.9)	147.0	7.67 d (15.9)	147.3
8′	6.37 d (15.9)	114.8	6.40 d (15.9)	115.1
9′		168.9		168.8
3′-OMe			3.90 s	56.4

[a]Coupling constants (J in Hz) in parentheses. [b]Equivalent to 3′ because of symmetrical structure. [c]Equivalent to 2′ because of symmetrical structure.

to the existence of high-molecular-weight compounds (over 3000 Da). These results revealed that the main constituents of fraction J are highly oligomeric proanthocyanidins. Then, for the further purification of the high-molecular-weight compounds (proanthocyanidins) in fraction J, ultrafiltration was performed. In our previous study,[3] highly oligomeric proanthocyanidins (over 20-mer) were purified and concentrated by this treatment. As shown in Figure 5, the ^{1}H NMR spectrum of the highly purified oligomeric proanthocyanidins from fraction J showed broad peaks at δ 6.3−7.2 (H-2′, H-5′, and H-6′), 5.7−6.2 (H-6 and H-8), 5.1 (H-2), 4.2−4.8 (H-4 in interflavan linkages), 3.5−4.0 (H-3), and 2.3−2.7 (H-4) that matched catechin or epicatechin units (Figure 5). The ^{13}C NMR spectrum also showed broad peaks at δ 156 (C-5, C-7, and C-8a), 146 (C-3′ and C-4′), 132 (C-1′), 119 (C-6′), 115 (C-2′ and C-5′), 107 (C-6 or C-8 in interflavan linkages), 97 (C-4a, C-6, and C-8 that are not used in interflavan linkages), 77 (C-2), 73 (C-3), 38 (C-4 in interflavan linkages), and 30 (C-4), indicating that the proanthocyanidins in the hop bract extract are B-type procyanidins, with flavan-3-ol units that are linked through C-4 to C-8 (or C-6) interflavan bonds (Figure 5).[25]

In the present LC separation scheme of the hop bract extract, HSCCC using a two-phase solvent system was highly effective, resulting in high-recovery separation and in the considerable reduction of the amount of extract utilized. The comprehensive

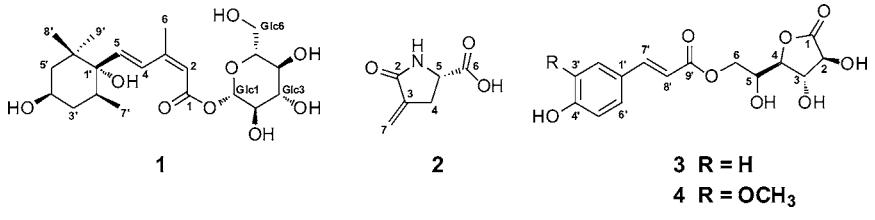

Figure 4. Structures of 1−4.

dx.doi.org/10.1021/jf405544n | J. Agric. Food Chem. 2014, 62, 2198−2206

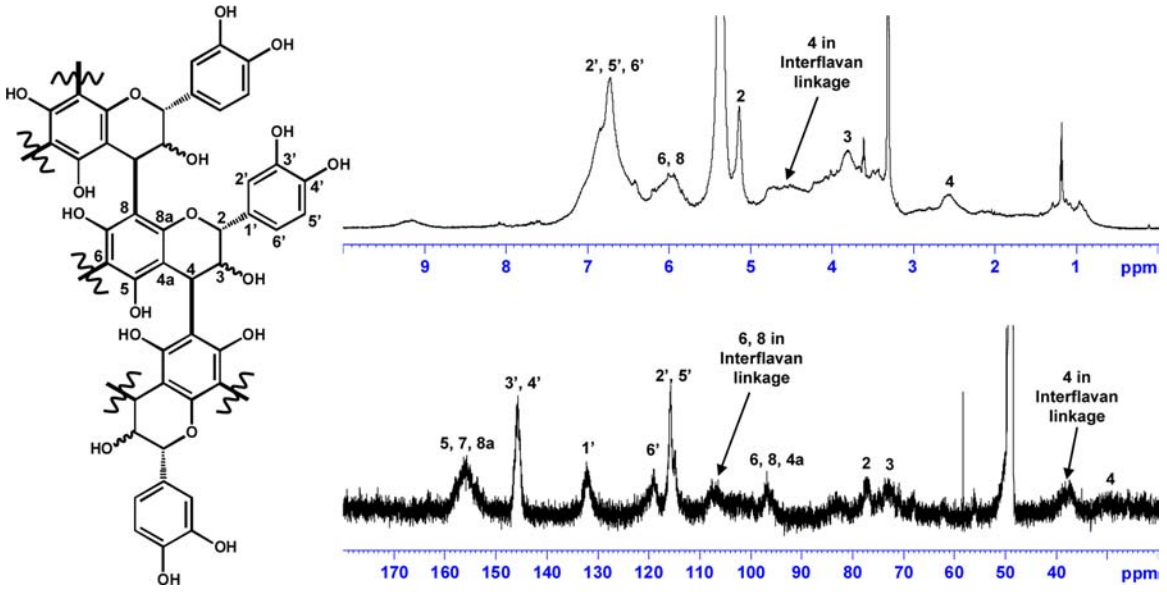

Figure 5. ^{1}H and ^{13}C NMR spectra of high-molecular-weight proanthocyanidins in HBP.

separation and structural analyses resulted in four compounds that have been identified for the first time in plants, and 20 compounds that have not been reported from hops were also identified. Most of the compounds were hydrophilic glycosylated and/or esterified analogues of abscisic acids, hydroxycinnamic acids, flavonols, lignans, hydroxybenzoic acids, or carotenoid. In addition, large amounts of highly oligomeric proanthocyanidins were found in the hop bract extract. They were easily separated from the hydrophilic fraction (fraction J) by the first HSCCC fractionation following ultrafiltration. Furthermore, the ^{1}H and ^{13}C NMR spectra revealed that hop proanthocyanidins have B-type procyanidin structures, which is in agreement with previous studies.[24,42] Hereafter, biological studies of all isolated compounds are needed for the elucidation of the various physiological activities of hop compounds and the industrial uses of hop bracts.

1-*O*-(2′,3′,4′,4′-Tetrahydroabscisoyl)-*β*-glucopyranose (1). Yellow amorphous powder; $[\alpha]_D^{20}$ + 23° (c 0.2, methanol); UV (methanol) λ_{max} (log ε) 270 (4.42) nm; for ^{1}H and ^{13}C NMR spectroscopic data, see Table 2; TOFMS *m*/*z* 431.2273 $[M + H]^+$ (calcd for $C_{21}H_{35}O_9$, 431.2275).

(*S*)-4-Methylene-5-oxopyrrolidine-2-carboxylic acid (2). Yellow amorphous powder; $[\alpha]_D^{20}$ +6° (c 0.3, methanol); UV (methanol) λ_{max} (log ε) 206 (3.56), shoulder at 230 (3.35) nm; TOFMS 142.0497 $[M + H]^+$ (calcd for $C_6H_8NO_3$, 142.0498).

6-*O*-*p*-Coumaroyl-L-galactono-1,4-lactone (3). Yellow amorphous powder; UV (methanol) λ_{max} (log ε) 211 (4.45), 225 (4.45), 312 (4.73) nm; for ^{1}H and ^{13}C NMR spectroscopic data, see Table 4; TOFMS *m*/*z* 325.0912 $[M + H]^+$ (calcd for $C_{15}H_{17}O_8$, 325.0917).

6-*O*-Feruloyl-L-galactono-1,4-lactone (4). Yellow amorphous powder; $[\alpha]_D^{20}$ +8° (c 0.2, methanol); UV (methanol) λ_{max} (log ε) 216 (4.08), 235 (4.01), shoulder at 295 (4.09), 324 (4.25) nm; for ^{1}H and ^{13}C NMR spectroscopic data, see Table 4; TOFMS *m*/*z* 355.1007 $[M + H]^+$ (calcd for $C_{16}H_{19}O_9$, 355.1023).

AUTHOR INFORMATION

Corresponding Author

*Phone: +81-297-46-9551. Fax: +81-297-46-1507. E-mail: yoshihisa.tanaka@asahigroup-holdings.com.

Notes

The authors declare no competing financial interest.

ABBREVIATIONS USED

LC, liquid chromatography; HSCCC, high-speed countercurrent chromatography; HILIC, hydrophilic interaction chromatography; RP, reversed-phase; ODS, octadecylsilyl; NP, normal-phase; COSY, correlation spectroscopy; HMBC, heteronuclear multiple bond correlation; ROE, rotating-frame overhauser enhancement; ESI, electrospray ionization; TOFMS, time-of-flight mass spectrometry; HPLC, high performance liquid chromatography; J-CPC, type-J coil-planet centrifuge; PTFE, polytetrafluoroethylene; HBP, polyphenol-rich extract from hop bracts; MTBE, methyl *t*-butyl ether; TFA, trifluoroacetic acid; UP, upper-phase; LP, lower-phase; DP, degrees of polymerization

REFERENCES

(1) De Keukeleire, J.; Ooms, G.; Heyerick, A.; Roldan-Ruiz, I.; Van Bockstaele, E.; De Keukeleire, D. Formation and accumulation of *α*-acids, *β*-acids, desmethylxanthohumol, and xanthohumol during flowering of hops (*Humulus lupulus* L.). *J. Agric. Food Chem.* **2003**, *51*, 4436−4441.

(2) Tagashira, M.; Uchiyama, K.; Yoshimura, T.; Shirota, M.; Uemitsu, N. Inhibition by hop bract polyphenols of cellular adherence and water-insoluble glucan synthesis of mutans streptococci. *Biosci. Biotechnol. Biochem.* **1997**, *61*, 332−335.

(3) Kurumatani, M.; Fujita, R.; Tagashira, M.; Shoji, T.; Kanda, T.; Ikeda, M.; Shoji, A.; Yanagida, A.; Shibusawa, Y.; Shindo, H.; Ito, Y. Analysis of polyphenols from hop bract region using CCC. *J. Liq. Chromatogr. Relat. Technol.* **2005**, *28*, 1971−1983.

(4) Tanaka, Y.; Honma, D.; Tamura, M.; Yanagida, A.; Zhao, P.; Shoji, T.; Tagashira, M.; Shibusawa, Y.; Kanda, T. New chromanone and acylphloroglucinol glycosides from the bracts of hops. *Phytochem. Lett.* **2012**, *5*, 514−518.

(5) Shinada, K.; Tagashira, M.; Watanabe, H.; Sopapornamorn, P.; Kanayama, A.; Kanda, T.; Ikeda, M.; Kawaguchi, Y. Hop bract

polyphenols reduced three-day dental plaque regrowth. *J. Dent. Res.* **2007**, *86*, 848−851.
(6) Yaegaki, K.; Tanaka, T.; Sato, T.; Murata, T.; Imai, T.; Tagashira, M.; Akazome, Y.; Hirai, N.; Ohtake, Y. Hop polyphenols suppress production of water-insoluble glucan by *Streptococcus mutans* and dental plaque growth *in vivo*. *J. Clin. Dent.* **2008**, *19*, 74−78.
(7) Inaba, H.; Tagashira, M.; Kanda, T.; Ohno, T.; Kawai, S.; Amano, A. Apple- and hop-polyphenols protect periodontal ligament cells stimulated with enamel matrix derivative from *Porphyromonas gingivalis*. *J. Periodontol.* **2005**, *76*, 2223−2229.
(8) Inaba, H.; Tagashira, M.; Honma, D.; Kanda, T.; Kou, Y.; Ohtake, Y.; Amano, A. Identification of hop polyphenolic components which inhibit prostaglandin E2 production by gingival epithelial cells stimulated with periodontal pathogen. *Biol. Pharm. Bull.* **2008**, *31*, 527−530.
(9) Kou, Y.; Inaba, H.; Kato, T.; Tagashira, M.; Honma, D.; Kanda, T.; Ohtake, Y.; Amano, A. Inflammatory responses of gingival epithelial cells stimulated with porphyromonas gingivalis vesicles are inhibited by hop-associated polyphenols. *J. Periodontol.* **2008**, *79*, 174−180.
(10) Morinaga, N.; Iwamaru, Y.; Yahiro, K.; Tagashira, M.; Moss, J.; Noda, M. Differential activities of plant polyphenols on the binding and internalization of cholera toxin in Vero cells. *J. Biol. Chem.* **2005**, *280*, 23303−23309.
(11) Yahiro, K.; Shirasaka, D.; Tagashira, M.; Wada, A.; Morinaga, N.; Kuroda, F.; Choi, O.; Inoue, M.; Aoyama, N.; Ikeda, M.; Hirayama, T.; Moss, J.; Noda, M. Inhibitory effects of polyphenols on gastric injury by *Helicobacter pylori* VacA toxin. *Helicobacter* **2005**, *10*, 231−239.
(12) Choi, O.; Yahiro, K.; Morinaga, N.; Miyazaki, M.; Noda, M. Inhibitory effects of various plant polyphenols on the toxicity of Staphylococcal α-toxin. *Microb. Pathog.* **2007**, *42*, 215−224.
(13) Ito, Y.; Bowman, R. L. Countercurrent chromatography: Liquid-liquid partition chromatography without solid support. *Science* **1970**, *167*, 281−283.
(14) Ito, Y. Golden rules and pitfalls in selecting optimum conditions for high-speed counter-current chromatography. *J. Chromatogr., A* **2005**, *1065*, 145−168.
(15) Alpert, A. J. Hydrophilic-interaction chromatography for the separation of peptides, nucleic acids and other polar compounds. *J. Chromatogr.* **1990**, *499*, 177−196.
(16) Bohr, G.; Gerhaüser, C.; Knauft, J.; Zapp, J.; Becker, H. Anti-inflammatory acylphloroglucinol derivatives from hops (*Humulus lupulus*). *J. Nat. Prod.* **2005**, *68*, 1545−1548.
(17) Fuchs, C.; Spiteller, G. Rapid and easy identification of isomers of coumaroyl and caffeoyl-D-quinic acid by gas chromatography/mass spectrometry. *J. Mass Spectrom.* **1996**, *31*, 602−608.
(18) Struijs, K.; Vincken, J.-P.; Verhoef, R.; van Oostveen-van Casteren, W. H. M.; Voragen, A. G. J.; Gruppen, H. The flavonoid herbacetin diglucoside as a constituent of the lignan macromolecule from flaxseed hulls. *Phytochemistry* **2007**, *68*, 1227−1235.
(19) Ossipov, V.; Nurmi, K.; Loponen, J.; Haukioja, E.; Pihlaja, K. High-performance liquid chromatographic separation and identification of phenolic compounds from leaves of *Betula pubescens* and *Betula pendula*. *J. Chromatogr., A* **1996**, *721*, 59−68.
(20) Nakamura, K.; Ogasawara, Y.; Endou, K.; Fujimori, S.; Koyama, M.; Akano, H. Phenolic compounds responsible for the superoxide dismutase-like activity in high-brix apple vinegar. *J. Agric. Food Chem.* **2010**, *58*, 10124−10132.
(21) Ge, F.; Ke, C.; Tang, W.; Yang, X.; Tang, C.; Qin, G.; Xu, R.; Li, T.; Chen, X.; Zuo, J.; Ye, Y. Isolation of chlorogenic acids and their derivatives from *Stemona japonica* by preparative HPLC and evaluation of their anti-AIV (H5N1) activity *in vitro*. *Phytochem. Anal.* **2007**, *18*, 213−218.
(22) Kazuma, K.; Noda, N.; Suzuki, M. Malonylated flavonol glycosides from the petals of *Clitoria ternatea*. *Phytochemistry* **2003**, *62*, 229−237.
(23) Wald, B.; Wray, V.; Galensa, R.; Herrmann, K. Malonated flavonol glycosides and 3,5-dicaffeoylquinic acid from pears. *Phytochemistry* **1989**, *28*, 663−664.
(24) Stevens, J. F.; Miranda, C. L.; Wolthers, K. R.; Schimerlik, M.; Deinzer, M. L.; Buhler, D. R. Identification and *in vitro* biological activities of hop proanthocyanidins: inhibition of nNOS activity and scavenging of reactive nitrogen species. *J. Agric. Food Chem.* **2002**, *50*, 3435−3443.
(25) Shoji, T.; Mutsuga, M.; Nakamura, T.; Kanda, T.; Akiyama, H.; Goda, Y. Isolation and structural elucidation of some procyanidins from apple by low-temperature nuclear magnetic resonance. *J. Agric. Food Chem.* **2003**, *51*, 3806−3813.
(26) Kato, T.; Tomita, N.; Hoshikawa, M.; Ehara, K.; Shima, J.; Takahashi, N.; Sugiyama, H. *In vitro* oxidation of indoleacetic acid by crude enzyme from rice husk - An aspect of preharvest sprouting. *Heterocycles* **1998**, *47*, 497−500.
(27) Tilstra, L.; Sattler, M. C.; Cherry, W. R.; Barkley, M. D. Fluorescence of a rotationally constrained tryptophan derivative, 3-carboxy-1,2,3,4-tetrahydro-2-carboline. *J. Am. Chem. Soc.* **1990**, *112*, 9176−9182.
(28) Simat, T.; Meyer, K.; Steinhart, H. Synthesis and analysis of oxidation and carbonyl condensation compounds of tryptophan. *J. Chromatogr., A* **1994**, *661*, 93−99.
(29) Chiba, M.; Hisada, S.; Nishibe, S.; Thieme, H. ^{13}C NMR analysis of symplocosin and (+)-epipinoresinol glucoside. *Phytochemistry* **1980**, *19*, 335−336.
(30) Ono, M.; Oda, E.; Tanaka, T.; Iida, Y.; Yamasaki, T.; Masuoka, C.; Ikeda, T.; Nohara, T. DPPH radical-scavenging effect on some constituents from the aerial parts of *Lippia triphylla*. *J. Nat. Med.* **2008**, *62*, 101−106.
(31) Park, J.-H.; Yeon, S.-W.; Cho, J.-G.; Lee, D.-Y.; Kim, Y.-S.; Baek, N.-I. Lignans from silkworm droppings and their promotional activities on heme oxygenase-1 (HO-1). *J. Appl. Biol. Chem.* **2010**, *53*, 734−739.
(32) Hisamoto, M.; Kikuzaki, H.; Nakatani, N. Constituents of the leaves of *Peucedanum japonicum* Thunb. and their biological activity. *J. Agric. Food Chem.* **2004**, *52*, 445−450.
(33) Andersson, R.; Lundgren, L. N. Monoaryl and cyclohexenone glycosides from needles of *Pinus sylvestris*. *Phytochemistry* **1988**, *27*, 559−562.
(34) Fayos, J.; Bellés, J. M.; López-Gresa, M. P.; Primo, J.; Conejero, V. Induction of gentisic acid 5-*O*-β-D-xylopyranoside in tomato and cucumber plants infected by different pathogens. *Phytochemistry* **2006**, *67*, 142−148.
(35) Strack, D.; Heilemann, J.; Wray, V.; Dirks, H. Structures and accumulation patterns of soluble and insoluble phenolics from norway spruce needles. *Phytochemistry* **1989**, *28*, 2071−2078.
(36) Hegde, V. R.; Pu, H.; Patel, M.; Jachens, A.; Gullo, V. P.; Chan, T.-M. A new antitumor compound from the plant *Oryctanthus* sp. as a VEGF receptor binding inhibitor. *Bioorg. Med. Chem. Lett.* **2005**, *15*, 4907−4909.
(37) Lamb, N.; Shaw, A. C.; Abrams, S. R.; Reaney, M. J. T.; Ewan, B.; Robertson, A. J.; Gusta, L. V. Oxidation of the 8′-position of a biologically active abscisic acid analogue. *Phytochemistry* **1993**, *34*, 905−917.
(38) Bertoli, A.; Fanfoni, L.; Felluga, F.; Pitacco, G.; Valentin, E. Chemoenzymatic synthesis of optically active α-methylene-γ-carboxy-γ-lactams and γ-lactones. *Tetrahedron Asymmetry* **2009**, *20*, 2305−2310.
(39) Walaszek, Z.; Horton, D. Conformational studies on aldonolactones by N.M.R. spectroscopy. conformations of D-glucono-, D-mannono-, D-gulono- and D-galactono-1,4-lactone in solution. *Carbohydr. Res.* **1982**, *105*, 131−143.
(40) Taylor, A. W.; Barofsky, E.; Kennedy, J. A.; Deinzer, M. L. Hop (*Humulus lupulus* L.) proanthocyanidins characterized by mass spectrometry, acid catalysis, and gel permeation chromatography. *J. Agric. Food Chem.* **2003**, *51*, 4101−4110.
(41) Yanagida, A.; Murao, H.; Ohnishi-Kameyama, M.; Yamakawa, Y.; Shoji, A.; Tagashira, M.; Kanda, T.; Shindo, H.; Shibusawa, Y.

Retention behavior of oligomeric proanthocyanidins in hydrophilic interaction chromatography. *J. Chromatogr., A* **2007**, *1143*, 153−161.
(42) Li, H.-J.; Deinzer, M. L. Structural identification and distribution of proanthocyanidins in 13 different hops. *J. Agric. Food Chem.* **2006**, *54*, 4048−4056.

NOTE ADDED AFTER ASAP PUBLICATION

This paper was published ASAP on February 26, 2014, with Figures 3 and 4 incorrectly cited, and an error to Figure 5. The corrected version was reposted on February 28, 2014.

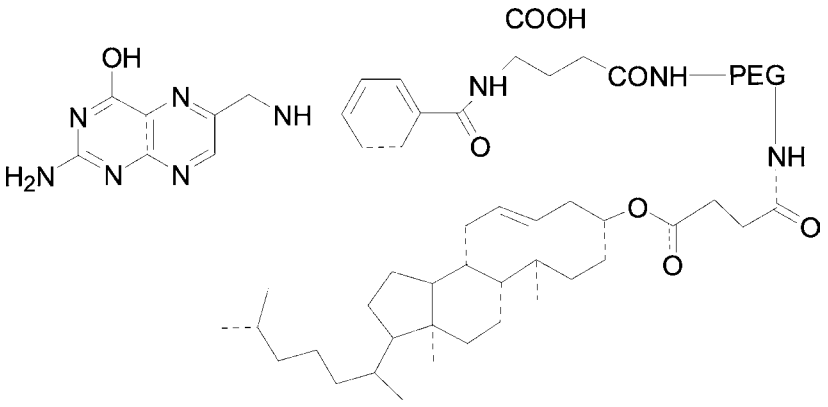

Figure 2. Molecular structure of folate-PEG-CHEMS.

novel lipophilic folate derivative; its amide and ester linkages are certainly more resistant to hydrolysis than other lipophilic derivatives, such as folate-PEG-DSPE and folate-PEG-cholesterol.[31] We examined tumor cell uptake performance of this folate conjugate. Then, we used the thin-film dispersion method to prepare folate-targeted liposomal UA (FTL-UA) and determined its mean diameter, zeta potential, entrapment efficiency, and stability. We investigated in vitro cellular cytotoxicity, apoptosis, cell cycle analysis, in vivo pharmacokinetic studies, and antitumor efficiency on KB xenografts.

MATERIALS AND METHODS

Materials. UA and folate-PEG-CHEMS were obtained from the pharmacy school of Tongji Medical College, Huazhong University of Science and Technology, Wuhan, China (purity > 95%). Hydrogenated soybean phosphatidylcholine (HSPC) was purchased from Avanti Polar Lipids Inc. (Alabaster, AL, USA). Monomethoxy polyethylene glycol 2000-distearoyl phosphatidylethanolamine (mPEG-DSPE2000) was obtained from Lipoid GmbH (Germany). Cholesterol (CHOL) was purchased from Acros Organics. Calcein was obtained from Aladdin Chemistry Co. Ltd. Folic acid was purchased from Sinopharm Chemical Regent Co., Ltd. All solvents and reagents were of analytical or HPLC grade and used without further purification.

RPMI 1640 media and Hoechst 33258 (product B 2883) were purchased from Sigma-Aldrich Corp. (St. Louis, MO, USA). Annexin V/PI apoptosis kits were purchased from MultiSciences Biotech, Hangzhou, China. Methylthiazolyl-diphenyl-tetrazolium bromide (MTT), cell cycle and apoptosis analysis kit, penicillin−streptomycin solution, and trypsin solution were purchased from Beyotime Institute of Biotechnology, Jiangsu, China. Fetal bovine serum (FBS) was purchased from Zhejiang Tianhang Biological Technology Co., Ltd., Hangzhou, China. Human oral cancer KB cell line has been identified as being derived from the human oral epidermoid carcinoma cancer and obtained from a cell bank (Wuhan University, Hubei, China).

Female Kunming mice (25 g, 6−8 weeks old) and female Balb/c nu/nu mice (20 g, 6−8 weeks old) were obtained from Beijing Huafukang Bioscience Technology Co. (Beijing, China; license SCXK (jing) 2009-0004).

Preparation of Liposomes. The thin-film dispersed hydration method was used to prepare liposomes encapsulating UA.[32] The lipid compositions of the nontargeted PEGylated liposome (PL-UA) and the FR-targeted liposome (FTL-UA) were HSPC/CHOL/mPEG-DSPE2000 at a molar ratio of 63:32:5 (at weights of 48, 12, and 16.7 mg) and HSPC/CHOL/mPEG-DSPE2000/F-PEG-CHEMS at a molar ratio of 63:32:4.5:0.5 (at weights of 48, 12, 13.4, and 5 mg), respectively. UA to lipid ratio is 1:20 (w/w). Liposome colloidal suspensions were prepared by dissolving the lipid mixture (about 78 mg) in chloroform and dried to form a thin lipid film in a pear-shaped glass flask on a rotary evaporator under reduced pressure at 40 °C. Traces of residual solvent were eliminated overnight at room temperature by using a glass drying oven connected to a vacuum pump. The resulting lipid film was hydrated in 4 mL of phosphate-buffered saline (PBS, pH 6.8) and incubated at 60 °C for 30 min. The suspension of lipids was then extruded five times through a 0.2 μm pore size polycarbonate membrane to produce unilamellar vesicles distributed more uniformly with a Lipex Extruder (Northern Lipids Inc., Vancouver, BC, Canada) driven by pressurized nitrogen (0.5−1.0 MPa) at 60 °C.

Determination of Entrapment Efficiency. The entrapment efficiency of the liposome was evaluated after removal of the free UA (low-speed centrifugation at 3000*g* for 10 min at room temperature to separate the free UA; liposome was dispersed in the supernatant liquid). UA concentration in the liposome was determined by HPLC measuring absorption at 210 nm following liposome lysis in methanol. The amount of UA entrapped in liposome was determined as a difference between the amount of UA initially added during liposome preparation and the amount of the entrapped UA present in the supernatant liquid following lysis. The drug loading efficiency was calculated using the following equation:[33]

$$\text{entrapment efficiency (\%)} = \frac{\text{amount of encapsulated UA in liposome}}{\text{amount of UA initially added}} \times 100$$

Characterization of Liposome. The size distribution of the liposomes was determined by dynamic light scattering on a DelsaNano series (Beckman Coulter, Inc., Fullerton, CA, USA). All particle size data refer to volume-weighted distributions, and liposomes were diluted to appropriate concentrations and measured at 25 °C. The zeta potential of the liposome indicates the charge on the surface of liposome, which was measured by Zeta PALS (Zeta Potential Analyzer, Brookhaven Instruments Corp., Holtsville, NY, USA) at 25 °C.

Cell Culture. Human oral cancer KB cell line was cultured in folate-free RPMI 1640 media supplemented with 100 U/mL penicillin, 0.1 mg/mL streptomycin, and 10% fetal bovine serum (FBS). Cells were maintained in a humidified atmosphere containing 5% CO_2 at 37 °C.

Uptake of FR-Targeted Liposome Assay. KB cells in logarithmic phase were suspended with trypsin and collected in Eppendorf tubes. The cell suspension was centrifuged at 1000*g* for 5 min. The supernates were discarded, the precipitants were resuspended with folate-free RPMI-1640 media, and KB cells treated with various drugs were incubated for 1 h at 37 °C. The various drugs were nontargeted liposomal calcein (L-calcein) and FR-targeted liposomal calcein (F-L-calcein). To determine the role of FR binding, 0.1 mL of folate (10 mM) was added to the media in the FR blocking group. After incubation, the cells were washed three times with cold PBS to remove unbound liposomes. Then, for quantification analysis, resuspended cells in PBS were analyzed by flow cytometry using a BD-LSRFortessa flow cytometer (BD Biosciences, USA), with an

Table 1. Characterization of PL-UA and FTL-UA[a]

	0 months				3 months			
	diameter (nm)	zeta (mV)	PDI	EE (%)	diameter (nm)	zeta (mV)	PDI	EE (%)
PL-UA	151.4 ± 16.1	−23.15 ± 6.7	0.167 ± 0.066	86.7 ± 12.1	173.8 ± 14.9	−17.23 ± 4.8	0.146 ± 0.024	80.2 ± 10.7
FTL-UA	160.1 ± 12.5	−21.24 ± 4.2	0.196 ± 0.052	88.9 ± 7.9	180.3 ± 7.9	−15.17 ± 5.3	0.172 ± 0.045	81.7 ± 7.4

[a]PL-UA, nontargeted PEGylated liposome of UA; FTL-UA, FR-targeted liposome of UA; PDI, polydispersity index; EE, entrapment efficiency. (Liposomes were stored in PBS buffer solution at 4 °C.)

excitation wavelength of 488 nm, with results expressed as mean fluorescence intensity.

Cytotoxicity Assay. The cytotoxic effects of free UA or UA liposomal formulations were evaluated by the 3-(4,5-dimethylthiazol-2-yl)-2,5-diphenyltetrazolium bromide (MTT) assay. KB cells grown in folate-free RPMI 1640 medium were placed in 96-well tissue culture dishes at 6×10^4 cells/mL, cultured for 24 h, and then incubated with various concentrations (6, 12.5, 25, 50, 100, and 200 μM) of the UA sample including free UA, PL-UA, FTL-UA, and FR blocking group for an additional 48 or 72 h. Then, 20 μL of MTT (5 mg/mL) was added to each well, and the 96-well plate was incubated for 4 h at 37 °C. Medium was removed and replaced with 150 μL of DMSO to dissolve the blue formazan crystals produced by live cells. The plates were then read on an ELISA reader (Thermo Labsystems, Shanghai Co. Ltd., Vantaa, Finland), and the cell viability ratio was determined from the absorbance measured at 492 nm.

Nuclear Staining with Hoechst 33258. The nuclear morphology of cells was evaluated using the cell-permeable DNA dye, Hoechst 33258, which is a DNA-specific fluorescent dye. It is an apporpriate fluorochrome for chromosome analysis, because it penetrates cell membranes significantly. The KB cells were seeded in 24-well plates and were divided into four groups at the concentration of 1.0×10^5 cells/mL. Twenty-four hours after seeding, the cells were treated with PBS, 50 μM PL-UA, 50 μM FTL-UA, and 50 μM FR blocking group, repectively, and further incubated for 24 h at 37 °C. The cells were fixed for 10 min in 1 mL of 4% paraformaldehyde at 4 °C and washed with ice-cold PBS (2 × 1 mL). Hoechst 33258 (1 mL) was added at a final concentration (5 μg/mL) and incubated for 10−20 min at 37 °C. Hoechst 33258, which was not ingested by KB cells, was removed by ice-cold PBS (2 × 1 mL washes). To examine the degree of cell apoptosis, the stained cells were observed under the inverted fluorescence microscope equipped with an Olympus color digital camera (exposure factor was 30).

Cell Cycle Analysis. To determine the proportion of apoptotic sub-G1 hypodiploid cells, we conducted cell cycle assay by flow cytometry. The KB cells were placed in 6-well plates, divided into four groups at the concentration of 4.7×10^5 cells/mL, and, 24 h after plating, the cells were treated with PBS, 50 μM PL-UA, 50 μM FTL-UA, and 50 μM FR blocking group, respectively. Then, after 24 h, the cells were digested by trypsin, washed with ice-cold PBS (1 × 1 mL), and fixed for 24 h in 1 mL of 70% ethanol at 4 °C. The KB cells were washed with ice-cold PBS (2 × 1 mL) and were treated in 0.5 mL of propidium iodide (PI) staining buffer from the 3 mL staining buffer containing 150 μL of PI and 60 μL of RNaseA for 30 min in the dark at 37 °C. Flow cytometric analysis was conducted using flow cytometry. The effects on cell cycle assay were demonstrated by differences in the percentage of cell distribution at each phase of the cell cycle.

Cell Apoptosis Assay. The KB cells were divided into four groups at a concentration of 4.7×10^5 cells/mL in 6-well plates and cultured for 24 h. After treatment with PBS, 50 μM PL-UA, 50 μM FTL-UA, and 50 μM FR blocking group for 24 h at 37 °C, KB cells were harvested and washed with ice-cold PBS (1 × 1 mL). The harvested cells were incubated for 5 min in the binding buffer containing 5 μL of Annexin V-FITC and 10 μL of PI at room temperature in the dark and then were washed twice with ice-cold PBS. Afterward, the stained cells were analyzed by flow cytometer, and then were defined as follows: upper left quadrant (Q_1), primary necrotic cells (Annexin V−/PI+); upper right quadrant (Q_2), late apoptotic cells (Annexin V+/PI+); lower left quadrant (Q_3), living cells (Annexin V−/PI−); lower right quadrant (Q_4), early apoptotic cells (Annexin V+/PI−) .

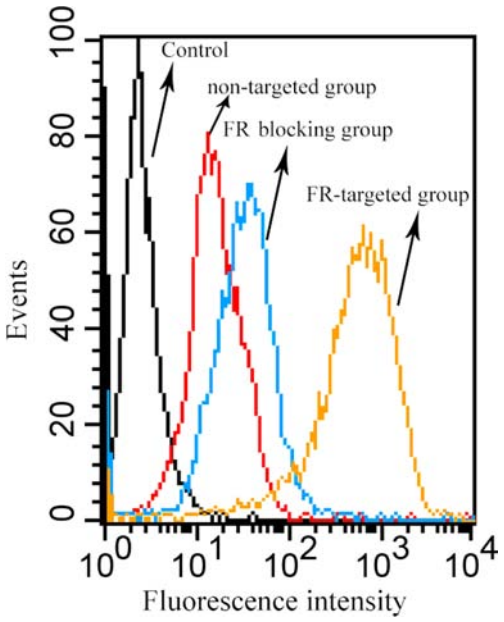

Figure 3. Uptake of calcein-loaded liposome by KB cells measured by flow cytometry. KB cells were treated with PBS (control), L-calcein (nontargeted group), F-L-calcein (FR-targeted group), and F-L-calcein plus 1 mM folate (FR blocking group) for 1 h at 37 °C.

Pharmacokinetic Studies. Animal experiments were carried out in agreement with the principles and procedures outlined by the ethics committee of Huazhong University of Science and Technology (IACUC no. 303). Female Kunming mice (25 g, 6−8 weeks old) were used for pharmacokinetic studies. Free UA, PL-UA, and FTL-UA (20 mg/kg, respectively) were injected (300 μL) through the tail vein (each group of four animals). Blood samples (100 μL) were taken from the mouse eyeball at various times (10 min and 0.5, 1, 2, 4, 8, 12, and 24 h) and placed in Eppendorf tubes containing 20 U of heparin sodium. The samples were centrifuged (5000*g*, 5 min) at room temperature and supernatants collected. Methanol (200 μL) was added to plasma samples to precipitate plasma proteins. Ethyl acetate (400 μL) was added to plasma samples, which were vortex-mixed and then centrifuged (12000*g*, 10 min) at 4 °C. The supernates were collected in Eppendorf tubes, and the ethyl acetate (400 μL) extraction, vortexing, and centrifugation were repeated. The supernates were combined and evaporated to dryness under nitrogen flux at 60 °C (thermostated water bath) and stored at −20 °C. Before the HPLC analysis, the residue was resuspended in methanol (100 μL, HPLC grade) and then centrifuged at 12000*g* for 10 min at 20 °C. The supernate from each sample was collected and placed in HPLC glass vials for the analytical determination. Analysis was performed by using an HPLC system (Waters, Milford, MA, USA) consisting of a 600 binary pump, a 717 plus autosampler, a thermostated column compartment, and a Waters 2487 dual-absorbance detector. Data were acquired and processed with Empower chromatography manager software (Waters). Chromatographic separation was carried out at 20 °C using a Sapphire RP C_{18} column (4.6 × 250 mm, 5 μm particle size, Sepax, USA). The mobile phase consisted of methanol (HPLC grade), ultrapure water, and triethylamine hydrochloride (90:10:0.03 v/v/v) and with glacial acetic acid to adjust the pH to 7.2. The flow rate

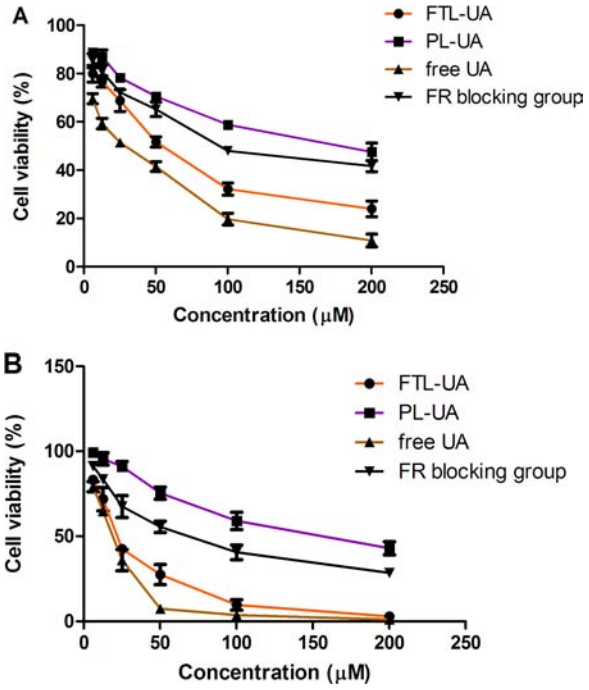

Figure 4. In vitro concentration and time-dependent antitumor effects induced by free UA, PL-UA (nontargeted group), FTL-UA (FR-targeted group), and FR blocking group: (A) 48 h; (B) 72 h. Cytotoxic analysis was performed by MTT assay. $P < 0.05$.

was 1.2 mL/min, and UV detection was performed at 210 nm. The sample and the standards were injected at a volume of 20 μL. The UA quantification was carried out by using an external standard curve in the linear concentration range between 0.4 and 200 μg mL^{-1}. UA was identified by comparison of concentrations (μg mL^{-1}) and peak areas from the chromatograms.

In Vivo Antitumor Assay. KB cells (3.6×10^6), resuspended in 150 μL of 0.9% physiological saline, were inoculated subcutaneously in the right hind flank of each female Balb/c nu/nu mouse (20 g, 6−8 weeks old). On day 7 after tumor implantation, the mice were raised on a folate-free diet for 1 week and maintained on the special feed throughout the study. Mice were randomly distributed into four treatment groups (control, free UA, PL-UA, and FTL-UA) of 6 mice per group. On day 7 after feeding folate-free diet, the tumors were about 60−150 mm^3. Mice (six per group) were given an intravenous injection via the tail vein of different UA formulations at the dose of 4.5 mg/kg every other day for five doses. We chose this total dosage (23 mg/kg) on the basis of the multiple-dose PK study in which 98 mg/m^2 was administered.[14] Then the dosage was calcuated (human body surface area A (m^2) = 0.0061 × height (cm) + 0.0128 × weight (kg) − 0.1529; and animal body surface area formula A (m^2) = $K \times (W^{2/3})/10000$, mice (K value) = 9.1). During the administration, the weight of nude mice and the size of xenografts were measured regularly. Tumor volume was determined by measuring the tumor in three dimensions with calipers and calculated using the formula tumor volume = (width^2 × length)/2. At the end, animals were killed when their tumors reached 2 cm in diameter. Survival cycle was calculated from the first day of treatment until the day of killing. All data analysis was performed using GraphPad Prism version 5.01.

RESULTS AND DISCUSSION

Characterization of Liposomes. In a typical preparation, liposomes were prepared by thin-film dispersion followed by high-pressure extrusion. Mean size distributions of PL-UA and FTL-UA were 150−160 nm. The mean entrapment efficiency of UA was about 87% at the drug/lipid ratio of 1:20 (w/w). The size distribution of the colloidal dispersion (dispersity index) indicates the formation of a colloidal system with a suitable homogeneity (Table 1). The zeta potentials of PL-UA and FTL-UA were −23.15 and −21.24 mV, respectively. The negative zeta potential of the formulations was due to the presence of the negatively charged lipid mPEG-DSPE;[31,34] the

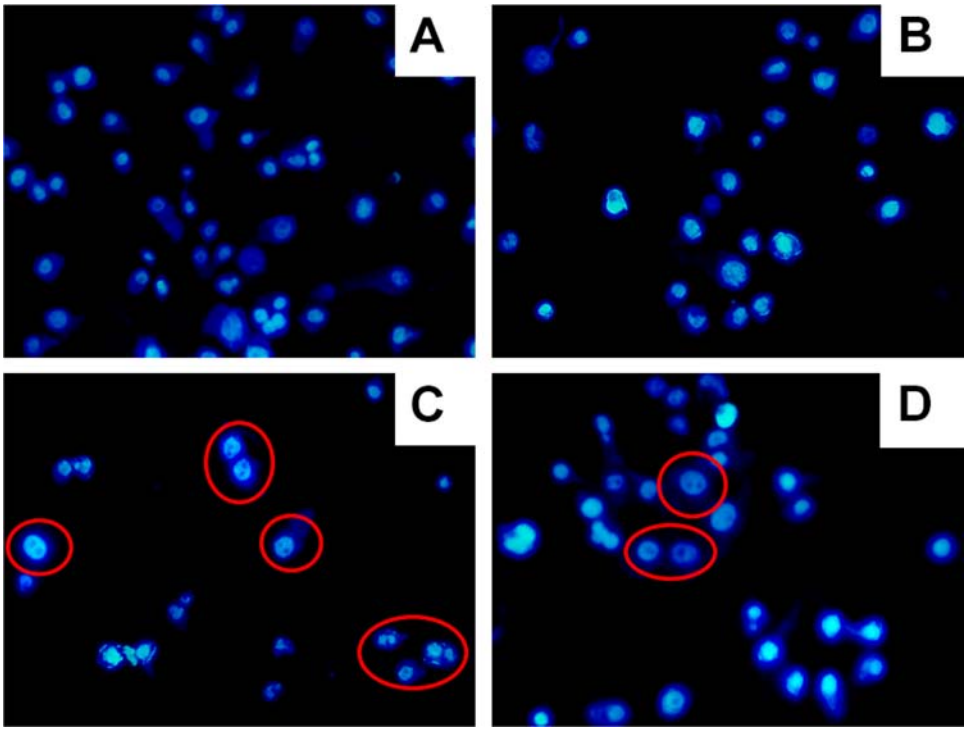

Figure 5. Induction of UA loaded liposome on apoptotic body formation in KB cells: (A) control; (B) nontargeted group (PL-UA); (C) FR-targeted group (FTL-UA); (D) FR blocking group (FTL-UA plus 1 mM folate), containing 50 μM UA, respectively. KB cells stained with Hoechst 33258 were visualized for apoptotic bodies (circled in red) under inverted fluorescent microscope (40×, exposure factor was 30).

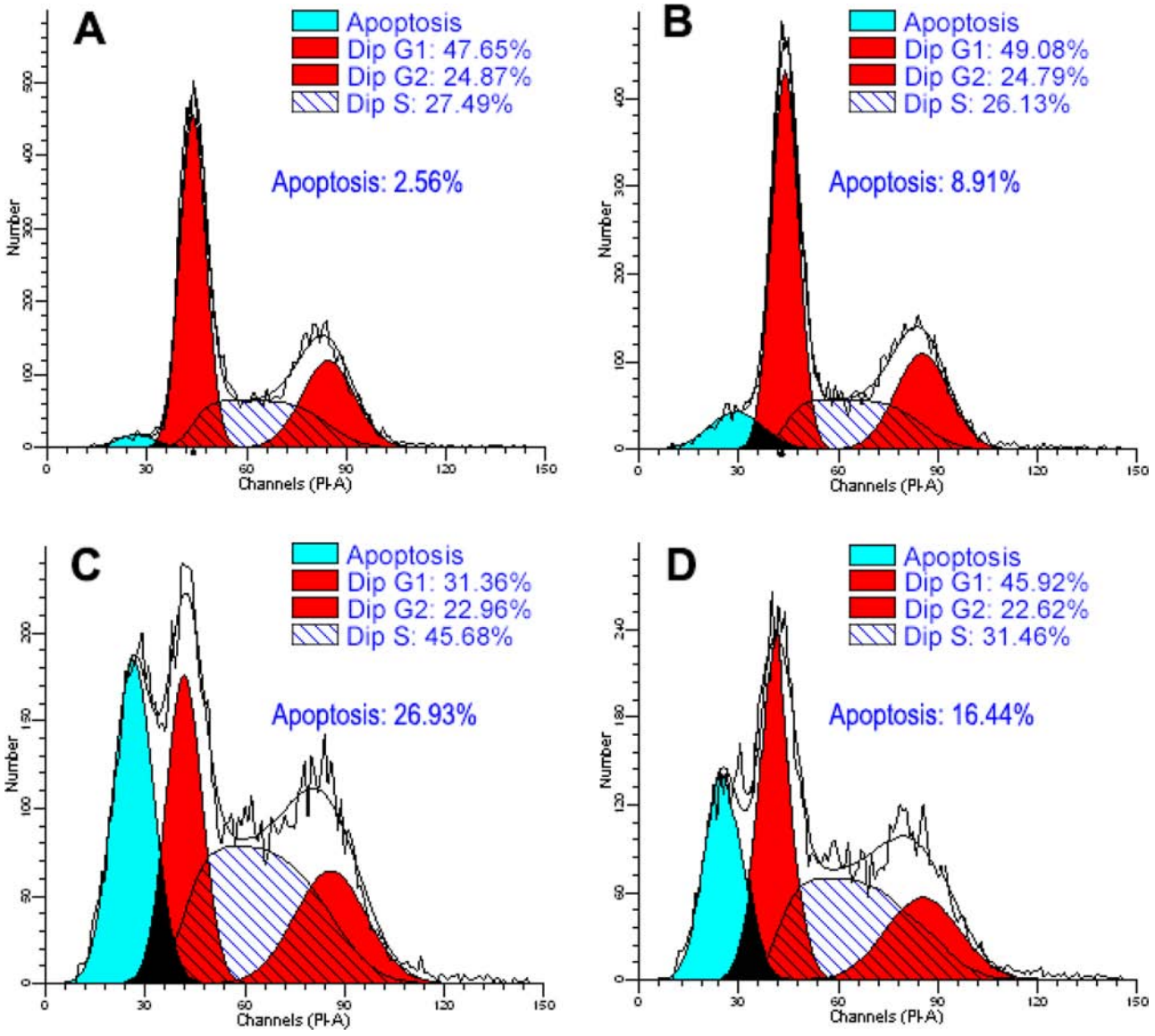

Figure 6. Effect of UA loaded liposome on cell cycle pattern and apoptotic cell proportion in KB cells: (A) control; (B) nontargeted group (PL-UA); (C) FR-targeted group (FTL-UA); (D) FR blocking group (FTL-UA plus 1 mM folate), containing 50 μM UA, respectively. Apoptotic sub-G1 DNA content was detected by flow cytometry after propidium iodide staining.

high negative potential made the particles repel each other. Thus, interparticle aggregation can be avoided, and stability can be maintained for a long period of time.[35] The liposomes showed good stability when stored in PBS at 4 °C. After 3 months in storage, the mean particle size increased from 156 to 177 nm and UA release from the liposomes was <10% (Table 1).

Cellular Uptake Assay. Uptake of FR-targeted liposome by KB cells was analyzed by flow cytometry. Calcein as the fluorescent indicator was entrapped into the liposome aqueous phase. As shown in Figure 3, the fluorescence intensity of F-L-calcein was about 31 times higher than that of L-calcein, and the intensity decreased when 1 mM free folic acid was added. (The mean fluorescence intensities of L-calcein, F-L-calcein, and FR blocking groups were 20.09, 628.14, and 36.28, respectively.) The results indicated that more folate-linked particles were actively taken up by FR-positive cells than the nontargeted particles, and the uptake could be blocked by 1 mM folic acid. These data show that FR-targeted liposomes could effectively target KB cells through the FR-mediated pathway.

In Vitro Evaluation of Cell Viability. Cell viability of free UA and UA loaded liposomes was assayed on KB cells and was compared with the untreated cells. This was carried out to evaluate both the concentration response and the incubation time effect. We first analyzed the effect of different concentrations of free UA, PL-UA, FTL-UA, and FR blocking groups on the inhibition of KB cancer cells. As shown in Figure 4, the cytotoxic effect was observed after 48 and 72 h of incubation of different groups. FTL-UA induced significant time- and dose-dependent effects, and a lower IC_{50} value of FTL-UA versus PL-UA was achieved at 72 h (22.05 vs 146.3 μM). The IC_{50} value of FTL-UA was lower than that of the FR blocking group for KB cell lines (22.05 vs 65.66 μM). These data were consistent with the results from the above-described cellular uptake assay and showed that FTL-UA is potentially useful as a therapeutic agent.

Free UA exerted great efficacy with IC_{50} of 16.49 μM (72 h). Lower IC_{50} values of the free UA in comparison with PL-UA and FTL-UA can be explained by the fact that the conjugates

dx.doi.org/10.1021/jf405675g | J. Agric. Food Chem. 2014, 62, 2207−2215

on the surface of the liposome enter the cells via the slower endocytosis pathways. Therefore, the higher IC_{50} observed for PL-UA and FTL-UA is likely explained by their slower drug release rate and hindered structure, the cytotoxic activity being present only after the drug is released from the liposome.[36]

Nuclear Morphological Analysis. In the qualitative study of inducing cell apoptosis, KB cells were stained with the cell-permeable DNA dye Hoechst 33258 and visualized by inverted fluorescent microscopy (Olympus Corp., Japan). Apoptosis is characterized by typical cellular morphology changes and biochemical features including cell shrinkage, chromatin condensation, cytoplasm vacuolization, mitochondrial degradation, DNA fragmentation, and cellular breakdown into apoptotic bodies.[37] As shown in Figure 5A, an image of untreated cells featuring round intact nuclei was observed. In contrast, the PL-UA-treated cells showed bright staining, however, there is no evidence of apoptotic bodies (Figure 5B). The typical morphological changes mentioned above were apparent in FTL-UA and FR blocking group samples. Apoptotic bodies and DNA fragmentation in FTL-UA group were readily visible (Figure 5C). There were some brighter stained cells in the FR-blocking group, but the number of cells did not decrease (Figure 5D). On the basis of morphologic observation, it is suggested that FTL-UA induced KB cell death via a mechanism involving apoptosis.

Analysis of Cell Cycle and Quantitative Percentage of Apoptotic Cells. The cell cycle distributions of KB cells were investigated by flow cytometry. As shown in Figure 6A, the sub-G1 hypodiploid cells number percentage was 2.56% in the controlled group. However, as demonstrated in Figure 6B–D, PL-UA, FTL-UA, and FR blocking group treatments of the KB cells induced significant differences in the proportions of apoptotic cells, which were reflected by the subdiploid peak (8.91, 26.93, and 16.44%). These results demonstrate that FTL-UA-induced cell death was caused principally by apoptosis induction, which mainly caused S cell cycle arrest. This result was consistent with the assessment of apoptosis induction by UA on human ACC-83 tumor cells, by cell cycle arrest in S phase.[38]

Apoptosis Analysis. Annexin V-FITC/PI double staining was carried out to determine whether FTL-UA demonstrated greater apoptotic effects than PL-UA. The KB cells were treated with various drugs at the same concentration of 50 μM UA for 24 h, subjected to simultaneous staining with Annexin V-FITC and PI, and then analyzed by flow cytometry. As shown in Figure 7, compared to the control group, the percentage of viable cells decreased significantly and apoptotic cells increased markedly when KB cells were exposed to FTL-UA. The results suggest that FTL-UA in activation of apoptosis (the percentage of late-apoptotic cells was 36.2%) was more effective than PL-UA (the percentage of late-apoptotic cells was 8.8%). Moreover, FTL-UA enhanced activation of apoptosis of KB cells, especially in the late stage of apoptosis. The number of apoptotic cells at the early and late stages increased in a dose-dependent manner. The percentage of apoptotic cells at late stage of apoptosis increased from 12.7 to 36.2% when the dose was changed from 20 to 50 μM. The activation of apoptosis of the blocking group (21.4%) was not better than that of FTL-UA group; it is demonstrated once again that the apoptosis-promoting activity of FTL-UA can be blocked by folic acid and that it induces apoptosis of KB cells through the FR-mediated pathway.

Pharmacokinetic Studies. Pharmacokinetic parameters were determined using the software DAS 2.1.1 (Drug and Statistics, China), and noncompartment open model was used to fit data.

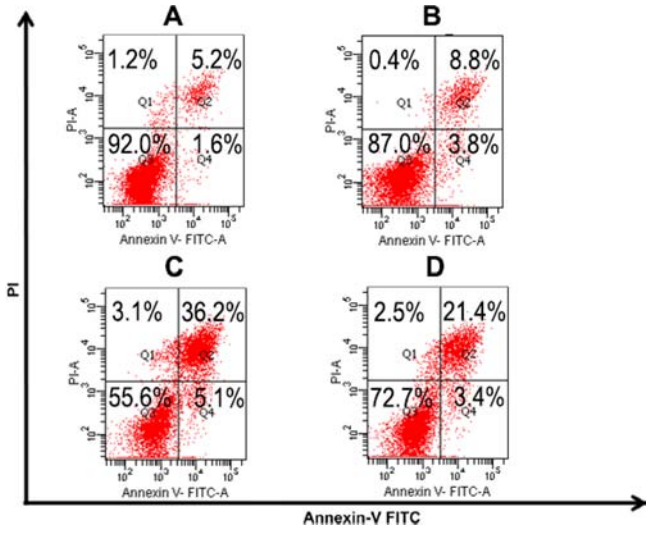

Figure 7. Effect of apoptosis of Annexin-V FITC and PI double staining assay: (A) control; (B) nontargeted group (PL-UA); (C) FR-targeted group (FTL-UA); (D) FR blocking group (FTL-UA plus 1 mM free folate), containing 50 μM UA, respectively.

The chromatographic method provided a suitable separation of the peaks of UA and other plasma components. Plasma concentration profiles of free UA, PL-UA, and FTL-UA and a summary of the major pharmacokinetic parameters are compared in Figure 8 and Table 2, respectively. As expected,

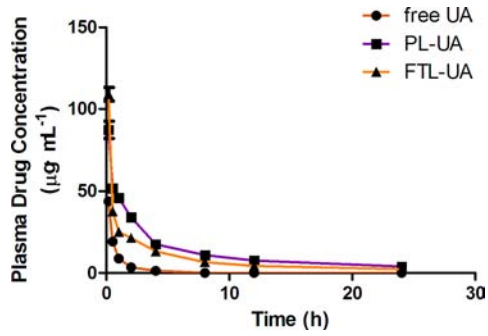

Figure 8. Pharmacokinetic profiles of free UA, PL-UA, and FTL-UA in Kunming mice (6–8 weeks old) following iv administration (20 mg/kg per mice). Data represent the mean ± standard deviation (n = 4). The UA loaded liposome profile was significantly different from that of free UA. $P < 0.005$.

free UA disappeared rapidly from plasma probably due to metabolic conversion or distribution to other organs. However, when free UA was entrapped in liposomes, significant differences in the pharmacokinetic profile and parameters were observed. UA liposome was slowly removed from blood circulation following intravenous administration. The AUC value of FTL-UA (218.32 mg/L·h) was 6-fold higher than that of free UA (36.88 mg/L·h). The MRT and $t_{1/2z}$ value of FTL-UA (MRT = 5.54 h, $t_{1/2z}$ = 7.61 h) showed improvements of 7.2- and 9.8-fold with respect to free UA (MRT = 0.77 h, $t_{1/2z}$ = 0.78 h). Meanwhile, PL-UA formulations showed much longer circulation times. FTL-UA was observed to be cleared from circulation more rapidly than PL-UA, and this result is consistent with a previous study on liposomes containing folate–polyethyleneglycol–distearoylphosphatidylethanolamine (F-PEG-DSPE).[39] It might be due to increased uptake of the liposomes

Table 2. In Vivo Pharmacokinetic Parameters of UA and Its Liposome after a Single Intravenous Administration at a Dose of 20 mg/kg in Kunming Mice[a]

	units	free UA	PL-UA	FTL-UA
AUC	mg/L·h	36.88 ± 2.16	316.11 ± 3.48	218.32 ± 12.73
AUMC	mg/L·h^2	28.23 ± 1.00	1987.11 ± 82.99	1210.01 ± 85.41
MRT	h	0.77 ± 0.04	6.29 ± 0.27	5.54 ± 0.14
Clz	L/h/kg	0.531 ± 0.037	0.056 ± 0.003	0.084 ± 0.009
Vz	L/kg	0.591 ± 0.228	0.737 ± 0.133	0.9 ± 0.237
$t_{1/2z}$	h	0.78 ± 0.33	9.25 ± 2.05	7.61 ± 2.41
C_{max}	mg/L	43.82 ± 4.49	87.15 ± 10.48	109.03 ± 8.30

[a]AUC, area under curve; AUMC, area under mean curve; CLz, clearance; $t_{1/2z}$, plasma half-life; MRT, mean residence time; Vz, distribution volume during elimination phase; C_{max}, maximum plasma drug concentration (n = 4 animals for each group).

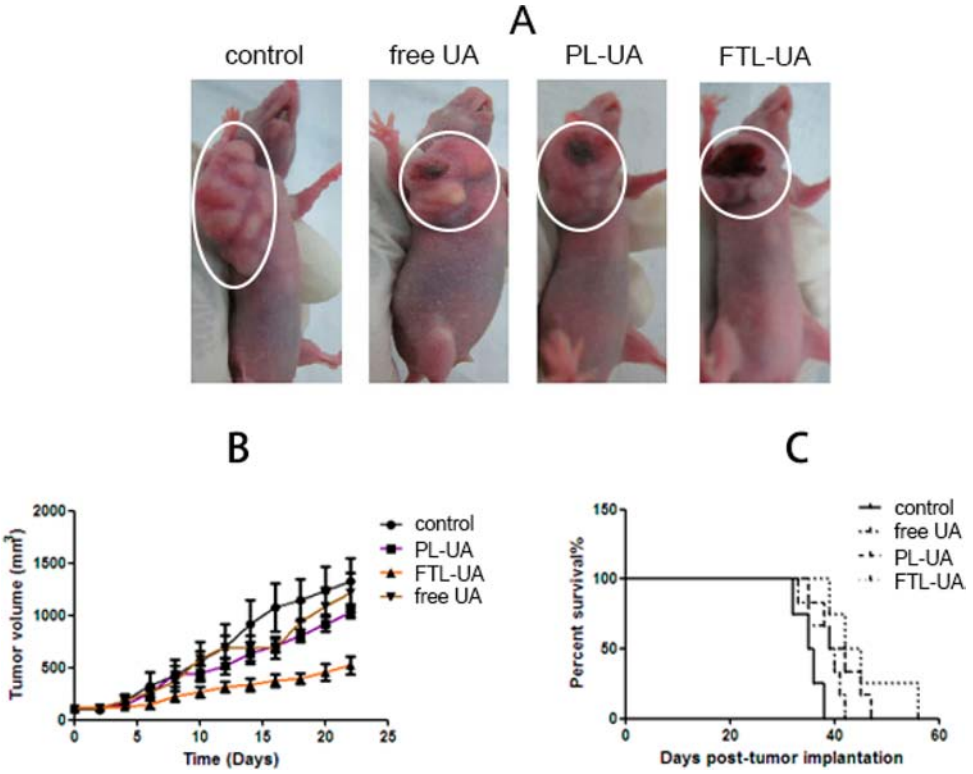

Figure 9. In vivo antitumor efficacy of KB tumor-bearing female Balb/c nu/nu mice treated with PBS, free UA, PL-UA, and FTL-UA (n = 6): (A) representative photographs of each group's female Balb/c nu/nu mice; (B) tumor growth curve ($P < 0.001$); (C) survival curves. $P < 0.02$.

by the phagocytic cells of the reticuloendothelial system (RES), which express a low level of FR-β.[40] The explanation is supported by the finding that the accelerated clearance of FR-targeted liposomes was blocked by free folic acid.[41] Pharmacokinetic and plasma stability studies clearly show that FTL-UA offers optimal conditions to treat KB tumor: (1) it is stable in plasma; (2) it remains in plasma with a long half-life and high AUC without rapidly diffusing into the tissues.

Pharmacodynamic Studies. PL-UA and FTL-UA were tested for antitumor efficacy using the human KB tumor xenograft model in female Balb/c nude mice. During our experiment, each group of nude mice was in good spirits and had freedom of movement. They had good appetite for food and water, and excretion was normal. It is obvious from Figure 9A that there were necrosis voids on the surface of the KB tumor xenograft in each mouse of the FTL-UA group. There was just a little necrosis in the surface of KB tumor xenograft in other groups. From the beginning of the administration, the tumor volume was measured once every 2 days for 24 days. The tumor growth curve was plotted. The data of tumor growth curves are shown in Figure 9B, which demonstrates very significant tumor growth inhibition in response to treatment with FTL-UA compared to other groups. One-way analysis of variance (ANOVA) was performed to demonstrate the difference among the volumes. Tumor-bearing mice treated with FTL-UA had about 55% reduction in tumor volume compared with PBS-treated mice ($P < 0.05$). For the negative control (PBS-treated) group, tumor growth is most evident and maintained a level of rapid growth. In contrast, free UA did not decrease tumor growth compared with the control group. The survival curves of each group were estimated by using the Kaplan−Meier method, and the difference of the median survival times was assessed by the log-rank test.[42] All of the untreated mice (control group) were killed because their tumors reached about 2 cm in diameter within 39 days following implantation, and free UA- or PL-UA-treated mice died within 42 and 47 days, respectively. However, the tumor-bearing mice treated with FTL-UA were alive for

dx.doi.org/10.1021/jf405675g | J. Agric. Food Chem. 2014, 62, 2207−2215

56 days (Figure 9C). Pharmacodynamic experimental results confirmed that FTL-UA slows tumor growth and that tumor volume was smaller compared to other groups. This demonstrates that FTL-UA has played a significant role in the efficacy of anti-KB tumor activity.

In recent years, plant-derived compound UA has attracted public attention because of its beneficial effects in the treatment of diseases. However, UA is poorly bioavailable and has suboptimal phamacokinetics that largely confine its broad application. Some researchers entrapped it in different formulations to curtail its limitations. Both et al. synthesized UA liposome to maintain ceramide and collagen content in human skin cells.[43] Most liposomes including liposome-anchored PEG molecules are for passive targeting. In view of this, we synthesized FR-targeted liposomal UA, the active-targeting formulation, to improve the poor availability that limits the utility of free UA. In 1995, Lee et al. first prepared folate-targeted liposomes, which were incorporated by a folate-PEG-DSPE construct into the lipid bilayer and were loaded with doxorubicin (DOX), an anticancer drug. Uptake of folate-PEG-liposomal DOX by KB cells was 45-fold higher than that of nontargeted liposomal DOX.[44] Folate-targeted liposomes as a mature preparation technology developed rapidly for nearly 20 years. So far, there is no literature reporting the synthesis of FR-targeted liposomal UA.

In this study, we encapsulated UA in FR-targeted liposomes. This formulation largely enhanced the solubility and bioavailability of UA. The cytotoxicity, apoptosis assay, pharmacokinetic, and plasma stability studies clearly show that FTL-UA offers the possibility to treat KB tumor cells. In the pharmacodynamic study, FTL-UA showed obvious antitumor advantage over the other treatment groups. These results provide the experimental basis for preclinical research and clinical development for the treatment of KB patients. Future work will be needed to evaluate the antitumor efficacy of our UA-loaded liposome in other tumor xenografts or in combination therapy to provide an effective basis for wide clinical applications in the treatment of cancers.

AUTHOR INFORMATION

Corresponding Author

*(G.X.) Phone: 86-27-83692793. E-mail: gyxiang1968@hotmail.com.

*(X.M.) Phone: 86-13986032181. E-mail: xiangma@hust.edu.cn.

Funding

This research was supported by the National Natural Science Foundation of China (NSFC) (no. 81072596, no. 81301235).

Notes

The authors declare no competing financial interest.

REFERENCES

(1) Frighetto, R. T. S.; Welendorf, R. M.; Nigro, E. N.; Frighetto, N.; Siani, A. C. Isolation of ursolic acid from apple peels by high speed counter-current chromatography. *Food Chem.* **2008**, *106*, 767−771.

(2) Kim, E.; Sy-Cordero, A.; Graf, T. N.; Brantley, S. J.; Paine, M. F.; Oberlies, N. H. Isolation and identification of intestinal CYP3A inhibitors from cranberry (*Vaccinium macrocarpon*) using human intestinal microsomes. *Planta Med.* **2011**, *77* (3), 265−270.

(3) Hsu, C.; Hong, B.; Yu, Y.; Yen, G. Antioxidant and anti-inflammatory effects of *Orthosiphon aristatus* and its bioactive compounds. *J. Agric. Food Chem.* **2010**, *58*, 2150−2156.

(4) Abe, F.; Yamauchi, T.; Nagao, T.; Kinjo, J.; Okabe, H.; Higo, H.; Akahane, H. Ursolic acid as a trypanocidal constituent in rosemary. *Biol. Pharm. Bull.* **2002**, *25*, 1485−1487.

(5) Liu, J. Oleanolic acid and ursolic acid: research perspectives. *J. Ethnopharmacol.* **2005**, *100*, 92−94.

(6) Liu, X. S.; Jiang, J. Induction of apoptosis and regulation of the MAPK pathway by ursolic acid in human leukemia K562 cells. *Planta Med.* **2007**, *73* (11), 1192−1194.

(7) He, X.; Wang, Y.; Hu, H.; Zhang, Z. In vitro and in vivo antimammary tumor activities and mechanisms of the apple total triterpenoids. *J. Agric. Food Chem.* **2012**, *60*, 9430−9436.

(8) Wang, J.; Ren, T. N.; Xi, T. Ursolic acid induces apoptosis by suppressing the expression of FoxM1 in MCF-7 human breast cancer cells. *Med Oncol.* **2012**, *29*, 10−15.

(9) Hsu, Y. L.; Kuo, P. L.; Lin, C. C. Proliferative inhibition, cell-cycle dysregulation, and induction of apoptosis by ursolic acid in human non-small cell lung cancer A549 cells. *Life Sci.* **2004**, *75* (19), 2303−2316.

(10) Manu, K. A.; Kuttan, G. Ursolic acid induces apoptosis by activating p53 and caspase-3 gene expressions and suppressing NF-kappaB mediated activation of bcl-2 in B16F-10 melanoma cells. *Int. Immunopharmacol.* **2008**, *8* (7), 974−981.

(11) Achiwa, Y.; Hasegawa, K.; Komiya, T.; Udagawa, Y. Ursolic acid induces Bax-dependent apoptosis through the caspase-3 pathway in endometrial cancer SNG-II cells. *Oncol. Rep.* **2005**, *13* (1), 51−57.

(12) Cuicu, Z.; Xishan, H.; et al. A phase I clinical trial of ursolic acid nanoliposome for evaluating its single-dose tolerance and safety. *Chinese J. New Drugs* **2011**, *20* (2), 148−151.

(13) Cerga, O.; Borcan, F. Syntheses of new cyclodextrin complexes with oleanolic and ursolic acids. *J. Agroaliment. Processes Technol.* **2011**, *17* (4), 405−409.

(14) Zhu, Z.; Qian, Z.; et al. A phase I pharmacokinetic study of ursolic acid nanoliposomes in healthy volunteers and patients with advanced solid tumors. *Int. J. Nanomed.* **2013**, *8*, 129−136.

(15) Chen, C.; Han, D.; Cai, C.; Tang, X. An overview of liposome lyophilization and its future potential. *J. Controlled Release* **2010**, *142*, 299−311.

(16) Torchilin, V. P. Recent advances with liposomes as pharmaceutical carriers. *Nat. Rev. Drug Discovery* **2005**, *4*, 145−160.

(17) Mamot, C.; Drummond, D. C.; Hong, K.; Kirpotin, D. B.; Park, J. W. Liposome-based approaches to overcome anticancer drug resistance. *Drug Resist. Updates* **2003**, *6*, 271−279.

(18) Immordino, M. L.; Dosio, F.; Cattel, L. Stealth liposomes: review of the basic science, rationale, and clinical applications, existing and potential. *Int. J. Nanomed.* **2006**, *1*, 297−315.

(19) Li, S. D.; Huang, L. Stealth nanoparticles: high density but sheddable PEG is a key for tumor targeting. *J. Controlled Release* **2010**, *145*, 178−181.

(20) Song, C. K.; Jung, S. H.; Kim, D. D.; Jeong, K. S.; Shin, B. C.; Seong, H. Disaccharide-modified liposomes and their in vitro intracellular uptake. *Int. J. Pharm.* **2009**, *380* (1−2), 161−169.

(21) Takara, K.; Hatakeyama, H.; Ohga, N.; Hida, K.; Harashima, H. Design of a dual-ligand system using a specific ligand and cell penetrating peptide, resulting in a synergistic effect on selectivity and cellular uptake. *Int. J. Pharm.* **2010**, *396* (1−2), 143−148.

(22) Torchilin, V. P. Tat peptide-mediated intracellular delivery of pharmaceutical nanocarriers. *Adv. Drug Delivery Rev.* **2008**, *60* (4−5), 548−558.

(23) Li, X.; Ding, L.; Xu, Y.; Wang, Y.; Ping, Q. Targeted delivery of doxorubicin using stealth liposomes modified with transferrin. *Int. J. Pharm.* **2009**, *373* (1−2), 116−123.

(24) Ying, X.; Wen, H. E.; Lu, W. L.; et al. Dual-targeting daunorubicin liposomes improve the therapeutic efficacy of brain glioma in animals. *J. Controlled Release* **2010**, *141* (2), 183−192.

(25) Hattori, Y.; Maitani, Y. Enhanced in vitro DNA Transfection efficiency by novel folate-linked nanoparticles in human prostate cancer and oral cancer. *J. Controlled Release* **2004**, *97*, 173−183.

(26) Riviere, K.; Huang, Z.; Jerger, K. Antitumor effect of folate-targeted liposomal doxorubicin in KB tumor-bearing mice after intravenous administration. *J. Drug Target.* **2011**, *19* (1), 14−24.

(27) Tyagi, N.; Ghosh, P. C. Folate receptor mediated targeted delivery of ricin entrapped into sterically stabilized liposomes to human epidermoid carcinoma (KB) cells: effect of monensin

intercalated into folate-tagged liposomes. *Eur. J. Pharm. Sci.* **2011**, *43* (4), 343−353.
(28) Pan, X. Q.; Lee, R. J. In vivo antitumor activity of folate receptor-targeted liposomal daunorubicin in a murine leukemia model. *Anticancer Res.* **2005**, *25* (1A), 343−346.
(29) Xie, M.; Zhang, H.; Xu, Y.; Liu, T.; Chen, S.; Wang, J.; Zhang, T. Expression of folate receptors in nasopharyngeal and laryngeal carcinoma and folate receptor-mediated endocytosis by molecular targeted nanomedicine. *Int. J. Nanomed.* **2013**, *8*, 2443−2451.
(30) Sega, E. I.; Low, P. S. Tumor detection using folate receptor-targeted imaging agents. *Cancer Metastasis Rev.* **2008**, *27*, 655−664.
(31) Xiang, G.; Wu, J.; Lu, Y.; Liu, Z.; Lee, R. J. Synthesis and evaluation of a novel ligand for folate-mediated targeting liposomes. *Int. J. Pharm.* **2008**, *356*, 29−36.
(32) Dua, J. S.; Rana, A. C.; Bhandari, A. K. Liposome: methods of preparation and applications. *Int. J. Pharm. Stud. Res.* **2012**, *47*, 14−20.
(33) Liu, J. B.; Lee, H. L.; Huesca, M.; Young, A. P.; Allen, C. Liposome formulation of a novel hydrophobic aryl-imidazole compound for anti-cancer therapy. *Cancer Chemother. Pharmacol.* **2006**, *58*, 306−318.
(34) Hinrichs, W. L.; Mancěnido, F. A.; Sanders, N. N.; Braeckmans, K.; De Smedt, S. C.; Demeester, J.; Frijlink, H. W. The choice of a suitable oligosaccharide to prevent aggregation of PEGylated nanoparticles during freeze thawing and freeze drying. *Int. J. Pharm.* **2006**, *311*, 237−244.
(35) Mohanty, C.; Sahoc, S. K. The in vitro stability and in vivo pharmacokinetics of curcumin prepared as aqueous nanoparticulate formulation. *Biomaterials* **2010**, *31*, 6597−6611.
(36) Pasut, G.; Canala, F.; Schiavon, O.; et al. Antitumoral activity of PEG−gemcitabine prodrugs targeted by folic acid. *J. Controlled Release* **2008**, *127*, 239−248.
(37) Heo, S. J.; Kim, K. N.; Yoon, W. J.; Oh, C.; Choi, Y. U.; Affan, A.; et al. Chromene induces apoptosis via caspase-3 activation in human leukemia HL-60 cells. *Food Chem. Toxicol.* **2011**, *49*, 1998−2004.
(38) Lei, M.; Ni, J.; et al. In vitro study on the anti-proliferation and apoptosis of ursolic acid in human ACC-83 cells. *J. Oral Maxillofacial Surg.* **2010**, *20*, 389−393.
(39) Lu, Y.; Wu, J.; Lee, R. J. Role of formulation composition in folate receptor-targeted liposomal doxorubicin delivery to acute myelogenous leukemia cells. *Mol. Pharmaceutics* **2007**, *4*, 707−712.
(40) Gabizon, A.; Shmeeda, H.; Horowitz, A. T.; Zalipsky, S. Tumor cell targeting of liposome-entrapped drugs with phospholipids-anchored folic-PEG conjugates. *Adv. Drug Delivery Rev.* **2004**, *56*, 1177−1192.
(41) Gabizon, A.; Shmeeda, H.; Zalipsky, S. Pros and cons of the liposome platform in cancer drug targeting. *J. Liposome Res.* **2006**, *16*, 175−183.
(42) Soukaina Réjiba, L.; Reddy, H.; Hajri, A. Squalenoyl gemcitabine nanomedicine overcomes the low efficacy of gemcitabine therapy in pancreatic cancer. *Nanomedicine* **2011**, *7* (6), 841−849.
(43) Both, D. M.; Goodtzova, K.; Yarosh, D. B.; Brown, D. A. Liposome-encapsulated ursolic acid increases ceramides and collagen in human skin cells. *Arch. Dermatol. Res.* **2002**, *293*, 569−575.
(44) Lee, R. J.; Low, P. S. Folate-mediated tumor cell targeting of liposome-entrapped doxorubicin in vitro. *Biochim. Biophys. Acta* **1995**, *1233*, 134−144.

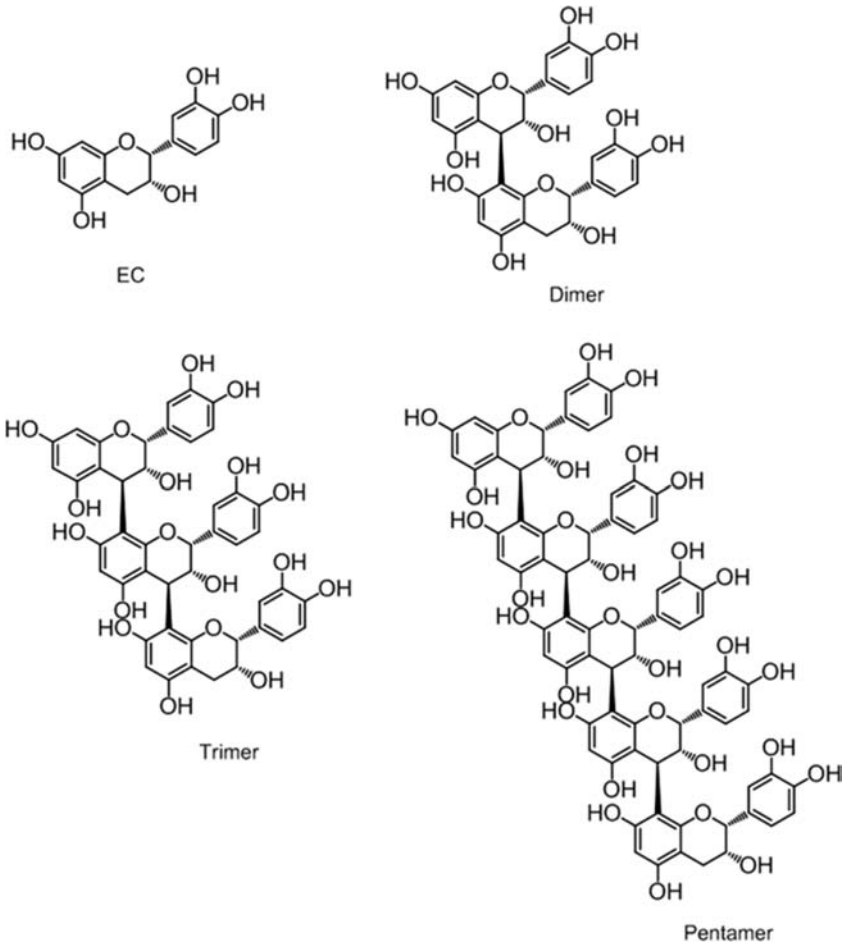

Figure 1. Structures of representative cocoa flavan-3-ols: EC and select oligomers.

between the catechin monomers (C, EC) and the PCs (oligomers and polymers), all of which are present in cocoa. EC and cocoa procyanidins have been shown to possess antiobesity and antidiabetic properties.[25−27] Emerging data suggest that these bioactivities may be highly correlated to flavanol DP.[28−30] Recently, Yamashita et al.[31] demonstrated that a tetrameric cocoa flavanol significantly improved insulin secretion in mice compared to monomeric, dimeric, and trimeric flavanols (EC, PC B_2, and PC C_1, respectively).[31] Furthermore, cinnamtannin A_2 significantly increased glucagon-like peptide-1 (GLP-1) secretion. These results suggest that insulin secretion and glucose homeostasis could be dependent on flavanol DP. Aside from this study, data on the antiobesity and antidiabetic activities of cocoa flavanols with distinct DPs in vivo are notably lacking. To our knowledge there has not been a long-term feeding study to examine the impact of chronic exposure to cocoa flavanols of distinct sizes on the onset of obesity and impaired glucose tolerance.

The objective of this study was to compare the effects of long-term dietary exposure to cocoa flavanol monomers, oligomers, and polymers on obesity and impaired glucose tolerance. This was done by fractionating cocoa flavanols into matrices with different mDP values and then evaluating the ability of each fraction to prevent obesity, insulin resistance, and impaired glucose tolerance after chronic administration in mice fed a high-fat (HF) diet. We hypothesized that the ability of cocoa flavanols to inhibit weight gain and the onset of insulin resistance and impaired glucose tolerance during an animal model of HF feeding was dependent upon flavanol DP.

MATERIALS AND METHODS

Chemicals and Standards. (±)-C, (−)-EC, epigallocatechin [(−)-(EGC)], epicatechin gallate [(−)-ECG], and epigallocatechin gallate [(−)-(EGCG)] were obtained from Sigma (St. Louis, MO, USA). PC dimer B_2 and trimer C_1 were obtained from ChromaDex (Irvine, CA, USA). Purified PC dimer B_1, dimer B_2-gallate, dimer B_5, trimer T_2, tetramer A_2, and pentamers (DP5) through decamers (DP10) were obtained from Planta Analytica (Danbury, CT, USA). Solvents for extraction, fractionation, and normal-phase HPLC were of ACS grade or better (Fisher, Pittsburgh, PA, USA; or VWR, Radnor, PA, USA). Solvents for UPLC-MS/MS were of LC-MS grade (VWR).

Cocoa Flavanol Extraction and Fractionation. A flavanol-rich cocoa extract (CE) was produced following the methods of Adamson et al.[32] and Robbins et al.[1] with modifications. For methodological details, see the Supporting Information. CE was fractionated by solid phase extraction to produce three fractions with different mDP values (monomers, oligomers, and polymers) according to the method used by Sun et al.[33] with modifications. The total polyphenol composition of the fractions was quantified by the Folin−Ciocalteu assay. For methodological details, see the Supporting Information.

Estimation of mDP by Thiolysis. Thiolysis was employed to determine the mDP of the flavan-3-ols that comprised each fraction on the basis of the methods described by Guyot et al.[34] and Gu et al.[35] with modifications. For methodological details, see the Supporting Information.

Normal-Phase HPLC and UPLC-MS/MS of Cocoa Procyanidins. Cocoa fractionation was further evaluated by normal-phase HPLC profiling (n = 1)[36] and UPLC-MS/MS (n = 3) to quantify

individual monomer and PC species up to decamers. For methodological details, see the Supporting Information.

Animals. Animal experiments were approved by the Institutional Animal Care and Use Committee at Virginia Polytechnic Institute and State University (protocol 13-099-FST). Male C57BL/6J mice (N = 54, ~25 g) were obtained from Jackson (Bar Harbor, ME, USA). Following arrival, mice were maintained on standard rodent chow for 2 weeks under standard housing conditions (3 mice/cage, 12 h light/dark cycle, 30−70% relative humidity, 20−26 °C) to acclimatize to the vivarium environment. To reduce coprophagy, bedding was changed twice per week throughout the study. Mice were provided food and water ad libitum unless otherwise specified.

Diets. Mice were assigned to one of six diet/treatment combinations (n = 9/group) (Table 1). Animals were fed one of two diets from the diet-induced obesity model series (Research Diets, Inc., New Brunswick, NJ, USA): a low-fat diet (LF, D12450J) with 10% kcal from fat or a high-fat diet (HF, D12492) with 60% kcal from fat (diets were sucrose-matched). LF and HF diet formulas are displayed in Table 2. The HF diet was provided alone or supplemented with one of the four cocoa fractions. The diets containing CE or cocoa fractions provided doses of 25 mg/kg body weight (BW)/day (262.53 mg/kg diet) based on an estimated daily food consumption of 95.23 g food/kg BW/day for male C57BL/6J mice from previous studies in our laboratory (data not shown). Diets were maintained at −20 °C throughout the study to prevent degradation of lipids or cocoa compounds. To maintain freshness and prevent degradation of fat or cocoa compounds, food was replaced twice per week for all cages. Animals were maintained on diets for 12 weeks.

Table 1. Description of Mouse Diet and Treatment Groups

abbreviation	basal diet	cocoa treatment	n
LF	LF	LF control	9
HF	HF	HF control	9
HF+CE	HF	cocoa extract	9
HF+M	HF	monomers	9
HF+O	HF	oligomers	9
HF+P	HF	polymers	9

Food intake for each cage was measured twice per week by weighing the food provided to the cage and then weighing the leftover food prior to its replacement with fresh food. Food intake for each cage was calculated as the difference between fresh food and leftover food weights and then divided by the number of animals per cage. To minimize food waste and inherent inaccuracies in food intake measurements for powdered diets, food was placed in metal feeding cups with a small opening at the top. Additionally, food inside the cups was covered with a metal grate. These measures reduced, but did not completely eliminate, food waste.

Body Weight and Body Composition. Mice were weighed weekly throughout the study. Mouse body composition was measured during weeks 1, 5, 8, and 11 in duplicate using a Bruker LF90 NMR analyzer (Billerica, MA, USA) as described in the manufacturer's instructions.

Glucose Tolerance and Insulin Tolerance Tests. Glucose tolerance tests (GTTs) were performed during week 10. Mice were fasted for 12 h and administered glucose (USP-grade, Hospira, Inc., Lake Forest, IL, USA) via intraperitoneal (ip) injection (1 g glucose/kg BW in saline). Blood was collected from the tail at 0 min (baseline) and 30, 60, 90, and 120 min following glucose administration. The tail tip was removed with surgical scissors, and a droplet of blood was obtained for glucose measurement. Glucose was measured using One Touch Ultra Blue test strips (LifeScan, Inc., Milpitas, CA, USA) and a glucometer. During week 11, mice underwent insulin tolerance test (ITTs). Mice were fasted for 4 h and injected with insulin ip (Humulin R, Cardinal Health, Dublin, OH, USA; 0.65 U insulin/kg BW in saline), and a droplet of blood was expressed from the tail at 0 min (baseline) and after 15, 30, 45, and 60 min. Blood collection and glucose measurement were performed as described for GTT.

Table 2. Composition of Basal Mouse Diets from the Research Diets Diet-Induced Obesity (DIO) Model Series

	LF diet[a]		HF diet[b,c]	
component	g %	kcal %	g %	kcal %
protein	19.2	20.0	26.2	20.0
carbohydrate	67.3	70.0	26.3	20.0
fat	4.3	10.0	34.0	60.0
total		100.0		100.0
kcal/g	3.9		5.2	
ingredient	g	kcal	g	kcal
casein, 80 mesh	200.0	800.0	200.0	800.0
L-cystine	3.0	12.0	3.0	12.0
corn starch	506.2	2024.8	0.0	0.0
maltodextrin 10	125.0	500.0	125.0	500.0
sucrose	68.8	275.2	68.8	275.2
cellulose, BW200	50.0	0.0	50.0	0.0
soybean oil	25.0	225.0	25.0	225.0
lard[d]	20.0	180.0	245.0	2205.0
mineral mix s10026	10.0	0.0	10.0	0.0
dicalcium phosphate	13.0	0.0	13.0	0.0
calcium carbonate	5.5	0.0	5.5	0.0
potassium citrate·1H_2O	16.5	0.0	16.5	0.0
vitamin mix v10001	10.0	40.0	10.0	40.0
choline bitartrate	2.0	0.0	2.0	0.0
FD&C yellow dye no. 5	0.0	0.0	0.0	0.0
FD&C blue dye no. 1	0.0	0.0	0.1	0.0
total	1055.1	4057.0	773.9	4057.0

[a]Research Diets D12450J. [b]Research Diets D12492. [c]Cocoa extract or the monomer-, oligomer-, or polymer-rich fractions were added to the HF diet at 262.53 mg/kg. [d]Lard contributed 72 mg cholesterol/100 g lard. The cholesterol contents of the LF and HF diets were 51.6 and 279.6 mg/kg, respectively.

Euthanasia and Necropsy. At the end of week 12, mice were fasted overnight and euthanized by CO_2 (following AVMA Guidelines on Euthanasia) followed by bilateral pneumothorax. Blood was immediately collected by cardiac puncture (with 1 cm^3 tuberculin syringes and $^1/_2$ in. 26 gauge needles) and clotted for 30 min at room temperature in BD Vacutainer serum separation tubes with Clot Activator. Clotted blood was centrifuged (15 min, 4 °C, 1500g), and the resulting serum was stored at −80 °C.

Fasting Serum Insulin and Endotoxin. Insulin in serum was measured using a murine insulin ELISA assay kit (Millipore, Billerica, MA, USA) in duplicate. Endotoxin in serum was determined using PyroGene Recombinant Factor C Endotoxin Detection assay kits (Lonza Walkersville, Inc., Walkersville, MD, USA).[37] Limulus Amebocyte Lysate assay plates and reagent water and pyrogen-free tubes (all from Lonza) were employed to minimize exogenous endotoxin contamination. Assays were performed in triplicate on 100 μL of diluted serum (50 μL of serum + 50 μL of LAL water). Fluorescence was quantified using a BioTek Synergy 2 plate reader (Winooski, VT, USA), and data were processed using Gen 5 software (v1.08, BioTek).

Data and Statistical Analysis. Outliers were identified and removed using Dixon's Q test at the α = 0.05 level if necessary. Data were analyzed by one-way ANOVA to determine the overall significance of treatment. If significance was detected, a Fisher's LSD post hoc test was then performed to compare all treatment means. Significance was defined as $P < 0.05$.

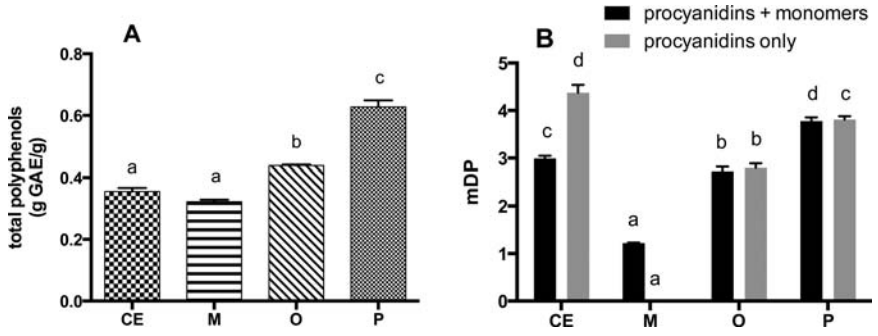

Figure 2. (A) Total polyphenols content [expressed as g gallic acid equivalents (GAE)/g of material] of CE and individual cocoa fractions as quantified by the Folin−Ciocalteu assay. Values are the mean ± SEM of $n = 3$ replicate analyses. Statistical comparisons were performed using one-way ANOVA with Fisher's LSD post hoc test ($P < 0.05$). Treatments with different letters are significantly different. (B) Actual mDP values of CE and individual cocoa fractions as determined by thiolysis. Values are presented on the basis of including procyanidins only (DP ≥ 2, i.e., the thiolysis value) or procyanidins + monomers (all flavanols) in the calculation. Values are the mean ± SEM of $n = 5$ replicate analyses. Statistical comparisons between fractions were performed separately for procyanidin values and values including both procyanidins + monomers values using one-way ANOVA with Fisher's LSD post hoc test ($P < 0.05$). Treatments with different letters are significantly different within each value type. Note that for the monomer (M) fraction, the procyanidin-only value is presented as 0 as the thiolysis value for this fraction was negative due to the poor suitability of thiolysis for characterizing monomer-rich matrices. CE, cocoa extract; M, monomer-rich fraction; O, oligomer-rich fraction; P, polymer-rich fraction.

Table 3. Levels of Native Monomers and Procyanidins in Cocoa Extract and Individual Cocoa Fractions

	composition[a,b] (mg compound/g dried fraction)			
compound	CE[c]	monomer	oligomer	polymer
(±)-catechin	1.67 ± 0.0183 b	9.52 ± 0.180 c	0.119 ± 0.00183 a	0.0129 ± 0.00328 a
(−)-epicatechin	5.90 ± 0.0635 b	30.6 ± 0.530 c	0.667 ± 0.0152 a	0.0726 ± 0.00914 a
(−)-epigallocatechin	0.0151 ± 0.000498 b	0.0237 ± 0.00322 b	0.0199 ± 0.00102 b	0.0132 ± 0.00440 a
procyanidin dimer B_1	0.356 ± 0.0126 b	0.476 ± 0.0103 c	1.12 ± 0.00765 d	0.0135 ± 0.00100 a
procyanidin dimer B_2	4.88 ± 0.149 b	6.12 ± 0.125 c	15.4 ± 0.201 d	0.250 ± 0.00346 a
procyanidin dimer B_5	3.10 ± 0.0298 b	7.52 ± 0.246 c	7.32 ± 0.206 c	0.0838 ± 0.0419 a
unknown procyanidin dimer 1[d]	0.0360 ± 0.00645 b	0.0474 ± 0.0109 b	0.114 ± 0.00897 c	0 a
unknown procyanidin dimer 2[d]	0.116 ± 0.00989 b	0.157 ± 0.0140 b	0.433 ± 0.0222 c	0 a
unknown procyanidin dimer 3[d]	0 a	0.678 ± 0.0118 c	0.311 ± 0.156 b	0 a
procyanidin trimer C_1	8.12 ± 0.197 c	6.31 ± 0.276 b	26.3 ± 0.427 d	0.932 ± 0.0330 a
cinnamtannin tetramer A_2	3.52 ± 0.296 c	2.29 ± 0.290 b	10.6 ± 0.209 d	0.534 ± 0.0493 a
procyanidin pentamers	3.69 ± 0.261 b	1.73 ± 0.0943a	9.77 ± 0.438 c	1.40 ± 0.0732 a
procyanidin hexamers	2.70 ± 0.164 b	0 a	3.65 ± 0.193 c	2.18 ± 0.216 b
procyanidin heptamers	2.14 ± 0.116 b	0 a	1.93 ± 0.187 b	2.72 ± 0.255 c
procyanidin octamers	0.736 ± 0.0757 c	0.196 ± 0.0122 b	1.88 ± 0.0598 d	0 a
procyanidin nonamers	1.78 ± 0.292 b	0.142 ± 0.142 a	3.03 ± 0.186 c	1.87 ± 0.123 b
procyanidin decamers	0 a	0 a	0 a	3.68 ± 1.228 a
total monomers	7.59 ± 0.0806 b	40.2 ± 0.682 c	0.806 ± 0.0129 a	0.0899 ± 0.0146 a
total dimers	8.48 ± 0.155 b	15.0 ± 0.394 c	24.7 ± 0.267 d	0.347 ± 0.0408 a
total procyanidins DP 3−6	18.0 ± 0.763 c	10.3 ± 0.422 b	50.4 ± 1.08 d	5.04 ± 0.231 a
total procyanidins DP 7−10	4.65 ± 0.208 b	0.338 ± 0.153 a	6.83 ± 0.141 b	5.82 ± 1.45 b

[a]Treatments with different letters for the same compound (or sum of compounds) are significantly different. [b]Data are reported as the mean ± SEM from $n = 3$ replicate analyses. [c]Cocoa extract. [d]Likely procyanidin dimers B_3, B_4, and either B_6, B_7, or B_8.

RESULTS AND DISCUSSION

Cocoa Fractions. The total amounts and yields of CE and the cocoa fractions produced for this study are displayed in the Supporting Information (Table S3). As shown in Figure 2A, the total polyphenol contents (on a w/w basis) of the CE and the fractions were P > O > M = CE. As shown in Figure 2B, the mean mDP values of the PCs for each fraction were significantly different (CE > polymer > oligomer > monomer). As thiolysis measures the mDP of only dimers and above, an additional calculation was required to factor in the monomer content (see the Supporting Information). The mDP values accounting for both monomers and PCs were also significantly different (polymer > CE > oligomer > monomer). It should be noted that thiolysis is a qualitative procedure likely approximates relative differences between fractions as opposed to representing absolute mDP values. This measure indicates that the four fractions had significantly different average flavanol sizes. The polymer fraction was enriched for the larger species and therefore had a larger mDP than CE, whereas the monomer and oligomer fractions were enriched for distinct subsets of the smaller species and had smaller mDP values than CE.

Reverse-Phase UPLC-MS/MS Analysis. The levels of native monomers and specific PCs that were detected in the CE

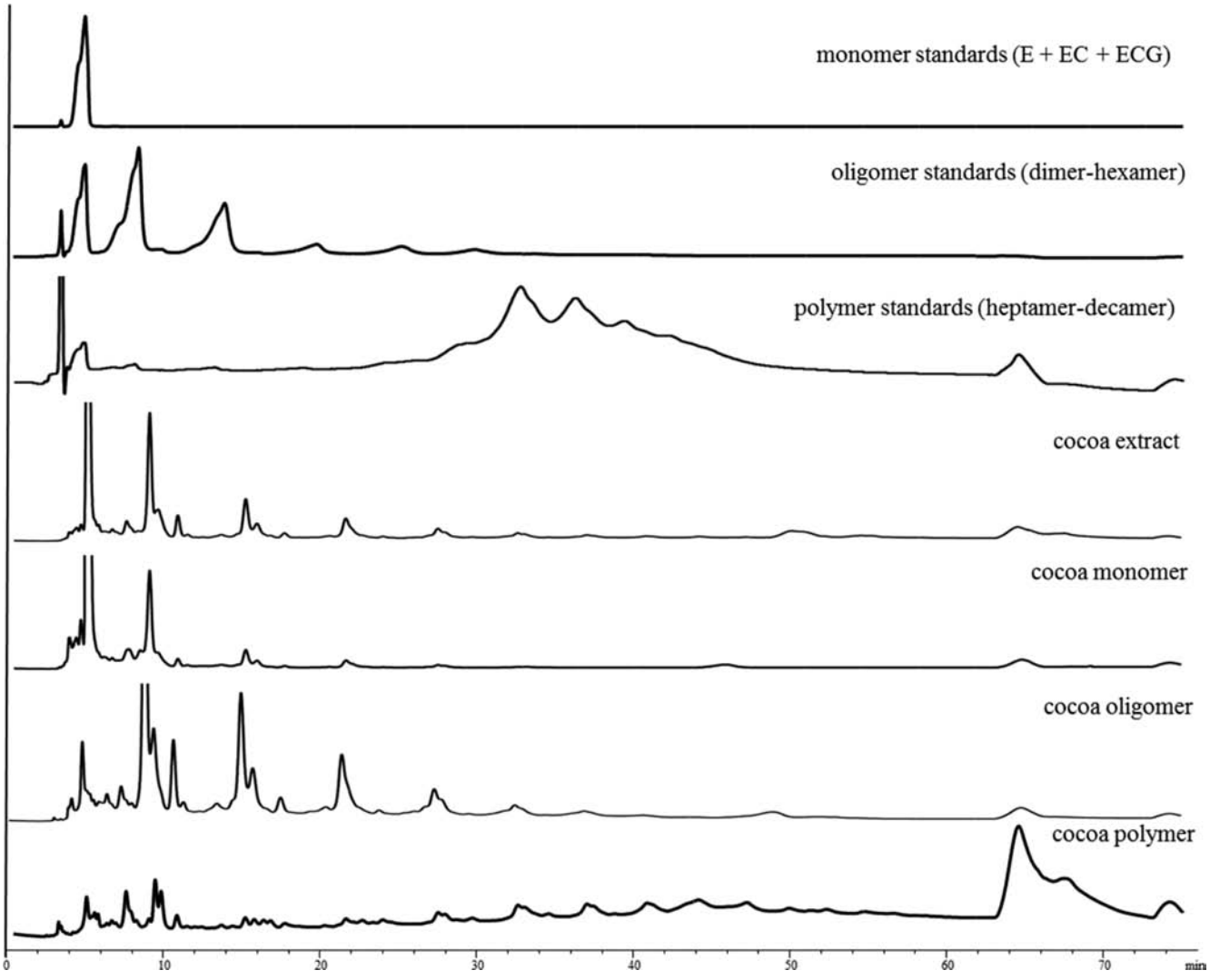

Figure 3. Fluorescence profiles of normal-phase HPLC chromatograms of authentic standards [monomers, oligomers (DP 2−6), and polymers (DP 7−10)] and the profiles of the cocoa extract, monomer, oligomer, and polymer fractions used in the mouse diets. Note that the scale is different for each chromatogram (chromatograms were scaled/cropped to emphasize relative peak heights within each trace). The scale for each chromatogram in fluorescence units (LU) is as follows: monomer standards, 740 LU; oligomer standards, 72 LU; polymer standards, 46 LU; CE, 230 LU; monomer-rich fraction, 160 LU; oligomer-rich fraction, 150 LU; polymer-rich fraction, 40 LU.

and cocoa monomer, oligomer, and polymer fractions are presented in Table 3. CE was composed of large amounts of monomers, dimers, and PCs with DP 3−6 and 7−10. It should be noted that CE had roughly the same amount of PC C1 as the six dimers combined, whereas dimers typically predominate over trimers in cocoa by a factor of 1.5−3 times. The reasons for this could include variations in the extraction conditions, the sensitivity of our instrument, or variations in the cocoa raw material. The monomer fraction was highly enriched for monomer species compared to CE and was slightly enriched for dimers compared to CE, but was somewhat reduced in PCs of DP 3−6 and depleted of PCs DP 7−10 compared to CE. The oligomer fraction was highly depleted of monomers compared to CE, but was greatly enriched for dimers and PCs DP 3−6 compared to CE and was slightly enriched for DP 7−10 compared to CE. Finally, the polymer fraction was highly depleted for monomers, dimers, and PCs DP 3−6 compared to CE and was slightly enriched for PCs DP 7−10 compared to CE. As the reverse-phase UPLC analysis quantified PCs only up to DP 10, the composition of larger PCs that make up a large portion of CE and the majority of the polymer fraction (see Figure 3) is not reflected in the total composition values in Table 3.

Normal-Phase HPLC Analysis. Normal-phase HPLC flavanol profiles of CE and cocoa PC fractions are shown in Figure 3. Analysis of standards showed that retention time roughly correlated to DP (larger species eluted later, top three chromatograms in Figure 3). CE appeared to have a wide range of early- and late-eluting flavanol species. By comparing relative peak heights within each chromatogram (bottom four chromatograms in Figure 3), the monomer, oligomer, and polymer fractions appeared to be enriched for early-, mid-, and late-eluting flavanol species, respectively. Figure 3 shows that the polymer fraction was relatively enriched for late-eluting large polymers compared to CE and the monomer- and oligomer-rich fractions, although these were not quantifiable by UPLC-MS/MS (see Table 3). It should be noted that fluorescence chromatograms do not accurately represent relative PC composition, as relative response factors for fluorescence detection decrease rapidly with increasing DP.[1]

Taken together, four separate measures of PC composition provide evidence to support that fractions designated "monomer", "oligomer", and "polymer" were indeed relatively enriched for flavanol monomers, oligomers, and polymers, respectively, compared to CE and each other. It should be noted that Table 3 reflects quantities of flavanol compounds only for which authentic standards were available. The Folin data (Figure 2A) show that the CE and the fractions were predominantly composed of polyphenols, as the gallic acid equivalents (GAE) were >30%. Although there were differences in the total polyphenols as measured by GAE between the fractions, structural differences may account for some of these differences.

Food Intake. Food intakes at weeks 3, 6, and 9 of the feeding study are presented in Figure 4. The average weekly food intake per animal was consistent across all groups in the HF diet (one-way ANOVA indicated no overall effect of treatment on food intake within the HF diet). This supports the conclusion that supplementation of the HF diet with CE or cocoa fractions did not affect food intake, which excludes reduced food intake as the mechanism by which cocoa fractions modulated weight gain, obesity, or glucose homeostasis in this experiment. The differences in measured food intake between the LF and HF diets may be due to differences in caloric density[38] (Table 2) and/or differences in consistency (LF was a powder, whereas HF was mealy/doughy), which may have affected diet wasting due to the ability of the mice to remove feed from the feed cups without eating it. Lack of apparent increases in food intake with weight gain may be due to the inherent difficulties in accurately measuring intake of powdered diets.

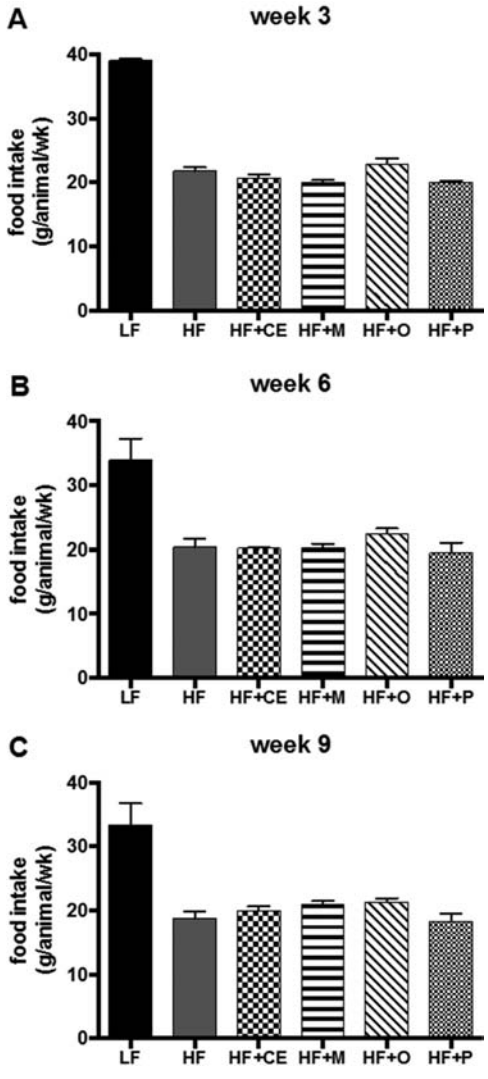

Figure 4. Calculated food intake values at weeks 3 (A), 6 (B), and 9 (C) of the feeding study. Data shown are the mean ± SEM of $n = 3$ replicate cages/treatment ($n = 3$ mice/cage). One-way ANOVA indicated no overall effect of dietary treatment on food intake ($P = 0.1439$, 0.0792, and 0.0541 for overall diet effect at 3, 6, and 9 weeks, respectively). Therefore, post hoc test for significance between treatment means was not performed. LF, low-fat control diet; HF, high-fat control diet; HF+M, high-fat control diet + monomer-rich fraction; HF+O, high-fat control diet + oligomer-rich fraction; HF+P, high-fat control diet + polymer-rich fraction.

Weight Gain and Body Composition. Weight gains during the feeding study are displayed in Figure 5A. HF feeding caused a significantly greater weight gain compared to the LF control group. Mice fed HF diets supplemented with cocoa monomers and oligomers did not gain a significantly different amount of weight compared to mice fed a LF control diet. However, within the HF diet, only the HF+O group was significantly different from the HF control. Changes in fat mass during the feeding study are displayed in Figure 5B. Mice from the HF control group gained significantly more fat mass than did mice in the LF control group. Supplementation of the HF diet with cocoa oligomers inhibited a significant increase in fat mass compared to the LF control, whereas supplementation of

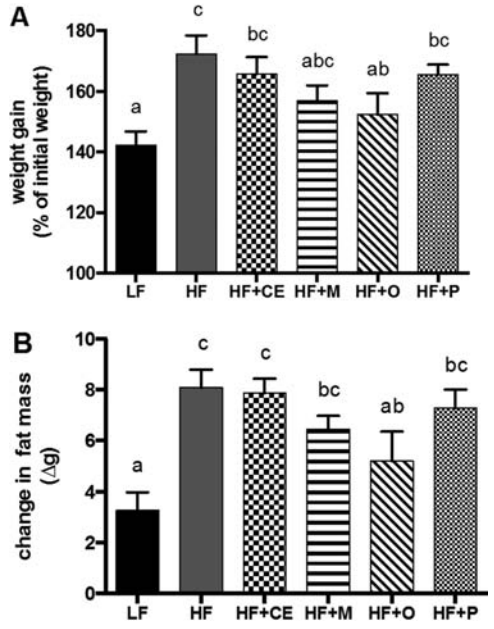

Figure 5. (A) Weight gains (final weights expressed as a percentage of initial weight) after 12 weeks of feeding; (B) changes in total body fat mass (difference between final and initial fat masses) after 11 weeks of feeding. Data shown are the mean ± SEM of $n = 9$ animals/treatment ($n = 8$ for the HF+M group due to loss of one mouse from this group during the feeding study). Significance between treatments was determined with a one-way ANOVA and Fisher's LSD post hoc test ($P < 0.05$). Treatments with different letters are significantly different. LF, low-fat control diet; HF, high-fat control diet; HF+M, high-fat control diet + monomer-rich fraction; HF+O, high-fat control diet + oligomer-rich fraction; HF+P, high-fat control diet + polymer-rich fraction.

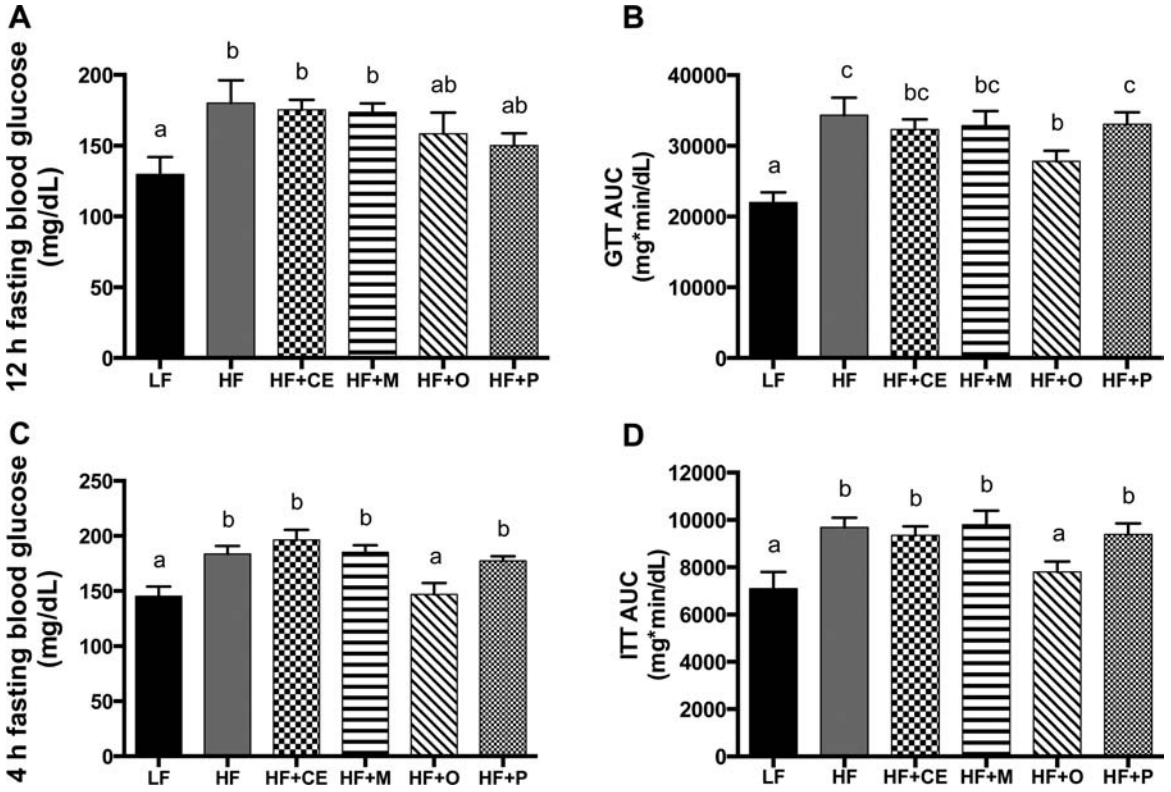

Figure 6. (A) Fasting (12 h) blood glucose levels at week 10; (B) glucose tolerance test (GTT) area under the blood glucose concentration curve (AUC) at week 10; (C) fasting (4 h) blood glucose levels at week 11; (D) insulin tolerance test (ITT) AUC at week 11. Data shown are the mean ± SEM of $n = 9$ animals/treatment ($n = 8$ for the HF+M group due to loss of one mouse from this group during the feeding study). Significance between treatments was determined with a one-way ANOVA and Fisher's LSD post hoc test ($P < 0.05$). Treatments with different letters are significantly different. LF, low-fat control diet; HF, high-fat control diet; HF+M, high-fat control diet + monomer-rich fraction; HF+O, high-fat control diet + oligomer-rich fraction; HF+P, high-fat control diet + polymer-rich fraction.

the HF diet with CE, monomers, and polymers did not significantly inhibit increases in fat mass compared to the LF control. Within the HF diet, supplementation with cocoa oligomers significantly inhibited increases in fat mass compared to CE but not compared to monomers or polymers.

Glucose and Insulin Tolerance. Fasting (12 h) blood glucose levels at week 10 are displayed in Figure 6A. Mice fed a HF control diet had significantly elevated fasting glucose levels compared to the LF control group. Fasting glucose levels of the HF + CE and HF + monomer groups were also significantly elevated compared to the LF control. Supplementation of the HF diets with cocoa oligomers and polymers resulted in intermediate fasting glucose levels that were not statistically different from those of either the LF or HF control groups. Figure 6B displays the GTT data as measured by the area under the curve (AUC) of the blood glucose levels over time following glucose administration. The HF control exhibited significantly higher AUC (i.e., impaired glucose tolerance) compared to a LF diet. Supplementation of the HF diet with oligomers resulted in an intermediate GTT AUC that was significantly lower than that of the HF control but also significantly higher than that of the LF control. Supplementation of the HF diet with CE, monomers, and polymers did not lower GTT AUC compared to the HF control.

Fasting (4 h) blood glucose levels at week 11 are shown in Figure 6C. Mice fed the HF control diet had significantly elevated 4 h fasting blood glucose levels compared to mice fed the LF control diet. Supplementation of the HF diet with cocoa oligomers inhibited increased fasting blood glucose compared to LF control. Supplementation of the HF diet with CE, cocoa monomers, or polymers did not inhibit increased 4 h fasting blood glucose levels, as these treatments had levels significantly higher than the LF control and not significantly different from the HF control. Figure 6D displays the ITT data as measured by the blood glucose AUC over time following insulin administration. The ITT data closely mirrored the 4 h fasting glucose data. Mice fed the HF control diet had significantly elevated ITT AUC values compared to mice fed the LF control diet. Supplementation of the HF diet with cocoa oligomers inhibited increased ITT AUC compared to LF control. Supplementation of the HF diet with CE, cocoa monomers, or polymers did not inhibit increased ITT AUC values, as these treatments had values significantly higher than the LF control and not significantly different from the HF control.

Fasting Insulin. Fasting serum insulin levels are presented in Figure 7. The HF diet significantly elevated fasting serum insulin levels compared to the LF control. Supplementation of the HF diet with CE did not significantly inhibit increases in fasting serum insulin, as this treatment was not significantly different compared to the HF diet alone but was significantly higher than the control LF diet. Supplementation of the HF diet with monomers, oligomers, and polymers resulted in fasting insulin levels that were significantly lower than those with the HF diet and not significantly different from those of the control LF diet.

Endotoxin. Fasting serum endotoxin levels are presented in Figure 8. HF feeding did not significantly increase fasting serum endotoxin concentrations compared to the LF diet. Supple-

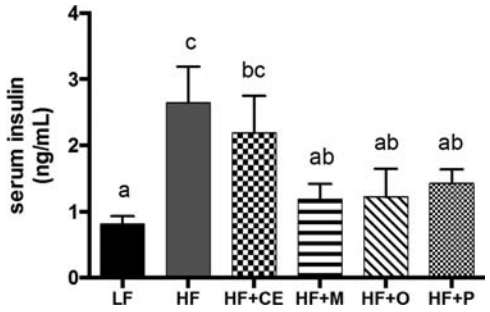

Figure 7. Fasting serum insulin levels following the 12 week feeding study. Data shown are the mean ± SEM of $n = 9$ animals/treatment ($n = 8$ for the HF+M group due to loss of one mouse from this group during the feeding study; $n = 6$ for the HF+M group and $n = 7$ for the HF+P group due to loss of samples during preparation for the ELISA assay). Significance between treatments was determined with a one-way ANOVA and Fisher's LSD post hoc test ($P < 0.05$). Treatments with different letters are significantly different. LF, low-fat control diet; HF, high-fat control diet; HF+M, high-fat control diet + monomer-rich fraction; HF+O, high-fat control diet + oligomer-rich fraction; HF +P, high-fat control diet + polymer-rich fraction.

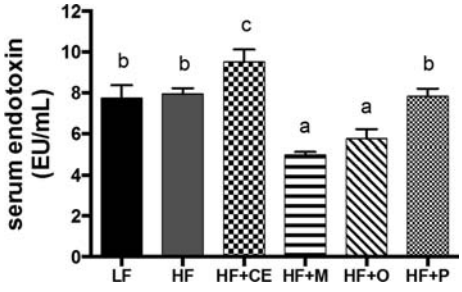

Figure 8. Fasting serum endotoxin levels following the 12 week feeding study. Data shown are the mean ± SEM of $n = 9$ animals/treatment ($n = 8$ for the HF+M group due to loss of one mouse from this group during the feeding study). Significance between treatments was determined with a one-way ANOVA and Fisher's LSD post hoc test ($P < 0.05$). Treatments with different letters are significantly different. LF, low-fat control diet; HF, high-fat control diet; HF+M, high-fat control diet + monomer-rich fraction; HF+O, high-fat control diet + oligomer-rich fraction; HF+P, high-fat control diet + polymer-rich fraction.

mentation of the HF diet with CE significantly increased endotoxin compared to the LF and HF controls. Conversely, supplementation of the HF diet with monomers and oligomers significantly decreased endotoxin compared to LF and HF controls. Supplementation of the HF diet with polymers did not significantly affect endotoxin levels compared to LF and HF controls.

Discussion. We believe this to be the first long-term feeding study to examine the correlation between flavanol PC size (individual species DP and overall mDP of the matrix) and the ability to inhibit the deleterious effects of a HF diet. Our results indicate that a cocoa fraction enriched in oligomeric PCs likely possess enhanced bioactivity compared to other flavanols as well as the composite CE itself. It should be noted that the oligomer-rich fraction had significantly greater total polyphenol content (GAE, w/w) than both CE and the monomer-rich fraction (Figure 2A). However, it also had significantly less total polyphenol content than the polymer-rich fraction. The fact that bioactivity was not correlated with total polyphenol content supports our observations that structure and mDP contribute to flavanol biological activity.

Our results generally agree with the few previous studies of the impact of flavanol DP on obesity and glucose homeostasis. Gu et al.[39] demonstrated that PC DP was generally proportional to inhibitory activity against digestive enzymes, suggesting that larger PCs may more effectively control glucose release. Yamashita et al.[40] showed that larger PCs (DP ≥ 4) more effectively inhibited intestinal α-glucosidase than smaller PCs (DP ≤ 3), although smaller PCs more effectively stimulated glucose uptake and AMP-activated protein kinase phosphorylation in rat skeletal muscle cells. Yamashita et al.[31] further demonstrated that PC oligomer cinnamtannin A_2 more effectively stimulates insulin secretion and activation of insulin signaling in skeletal muscle than smaller PCs and EC. Montagut et al.[41] also demonstrated that PC oligomers can activate insulin signaling and stimulate glucose uptake.[41] Whereas these studies suggested various relationships between PC size and specific bioactivities, our data suggest that the overall effect on diet-induced obesity and impaired glucose tolerance is optimal for intermediate size values.

It should also be noted that, although all three flavanol fractions effectively inhibited hyperinsulinemia (Figure 7), only the oligomer-rich fraction effectively improved glucose tolerance compared to the HF diet (Figure 6B), inhibited increases in 4 h fasting glucose compared to the LF control (Figure 6C), and inhibited the development of insulin resistance (Figure 6D). Therefore, only the oligomer-rich fraction effectively prevented development of a prediabetic phenotype. Studies[42,43] suggest that flavanols decrease lipid accumulation in β-cells and subsequent glucose-stimulated insulin production under hyperlipidemic conditions. However, studies in healthy animals suggest that flavanols may actually increase insulin secretion by increasing levels of glucagon-like peptide-1 (GLP-1), which is a hormone secreted from gut L-cells in response to carbohydrate ingestion that stimulates insulin secretion.[31] In vitro and animal studies also suggest that PCs improve insulin sensitivity in skeletal muscle and adipocytes, thus decreasing the need for insulin secretion.[40,44] These studies and our data highlight the fact that the effects of flavanols on mechanisms related to glucose homeostasis are highly context dependent. Distinct mechanisms of action may be involved in the prevention of obesity and insulin resistance versus the amelioration of existing obesity and insulin resistance.[45] Furthermore, flavanols may improve insulin and blood glucose levels by distinct mechanisms in the acute postprandial state (gut mechanisms such as inhibiting macronutrient digestion/absorption, increased GLP-1 and insulin secretion)[31,39] versus chronic effects in the fasted state (peripheral tissue mechanisms such as decreased insulin secretion and improved insulin sensitivity).

Our finding that an oligomer-rich fraction was generally more effective than a monomer-rich fraction is intriguing, as the absorption and systemic bioavailability of PCs are generally regarded to be inversely proportional to size.[46−48] This suggests that oligomers, which are largely unabsorbed in their native form, may act primarily through a mechanism located in the gut. This hypothesis is supported by the fact that PCs appear to improve glucose tolerance and increase insulin secretion when glucose is administered orally but not by ip injection.[49] Potential mechanisms by which unabsorbed PCs may act in the gut to inhibit the onset of obesity and impaired glucose tolerance include inhibition of macronutrient digestion and

absorption,[39,40] stimulation of GLP-1 secretion and GLP-1 driven insulin secretion,[31] and inhibition of GLP-1 degradation by dipeptidyl peptidase-IV.[49] In the present study, cocoa oligomers appear to more effectively control 4 h fasting glucose levels versus 12 h fasting glucose levels (Figure 6A,C). These data indicate that oligomers more effectively modulate postprandial blood glucose control as opposed to blood glucose levels after longer periods of fasting, suggesting that oligomers may primarily exert acute postmeal effects while the compounds are still in the upper gastrointestinal tract, as opposed to chronic systemic effects.

Another possible mechanism for cocoa PC action in the gut is the inhibition of metabolic endotoxemia. Low-grade inflammation has been shown to impair insulin signaling and induce metabolic derangements in skeletal muscle.[50,51] A key mediator of this inflammatory state is endotoxin, the major glycolipid component of the outer membrane of Gram-negative commensal bacteria in the gut. Circulating endotoxin activates the Toll-like family of pathogen-associated molecular pattern recognition receptors that initiate an inflammatory signaling response via NF-κB activation.[52] HF feeding induces a chronically elevated endotoxin state.[53] Research in mice and humans has linked chronically elevated endotoxin to the development of obesity and insulin resistance via activation of Toll-like receptor (TLR) 4 in skeletal muscle. PCs are well-known to reduce inflammation,[54] and control of the chronic low-grade inflammatory state resulting from high-fat feeding may represent a mechanism by which dietary PCs prevent and/or ameliorate metabolic syndrome. PCs may inhibit metabolic endotoxemia and the resulting metabolic derangements (including insulin resistance) by reducing epithelial permeability to endotoxin,[55,56] or by blunting TLR4 stimulation[57] and induction of inflammation by circulating endotoxin.[58,59] Gu et al.[60] demonstrated that cocoa reduces circulating endotoxin, improves gut barrier function, and reduces systemic inflammation induced by HF feeding. Although these activities have all been demonstrated separately for PCs, inhibition of endotoxemia has yet to be shown as the mechanism by which cocoa PCs improve skeletal muscle insulin signaling and systemic glucose tolerance. Data definitively linking improved regulation of inflammatory tone to prevention of insulin resistance would represent a novel mechanism by which PCs prevent metabolic syndrome. The present data indicated that HF feeding did not significantly elevate fasting serum endotoxin compared to the LF diet (Figure 8). However, this lack of difference may be due to the prolonged (12 h) fast, as increases in circulating endotoxin are generally observed in the postprandial (fed) state.[53] Circulating endotoxin was measured in the 12 h fasting state in recently euthanized animals, as opposed to the postprandial state, as this was a post hoc assay. Nevertheless, supplementation of the HF diet with both monomers and oligomers significantly reduced fasting endotoxin concentrations. This suggests that these fractions warrant further consideration for prevention of metabolic endotoxemia. The potential mechanisms by which monomers and oligomers reduce serum endotoxin concentrations include reduced endotoxin production in the gut (by gut microflora) and/or reduced paracellular permeability of the gut to endotoxin (by increased gut junction protein expression). Additional studies are required to determine the impact of cocoa flavanols on postprandial serum endotoxin profiles.

Potential antiobesity and antidiabetic activities of cocoa flavanols that require absorption and distribution of PCs to target tissues, such as direct stimulation of pancreatic β-cell function[43,61] and insulin signaling in skeletal muscle,[41] likely play a complementary role to the gut-mediated activities that we have identified due to the poor bioavailability of PCs. Further research is required to determine the relative importance of the gut activities of unabsorbed PCs versus the systemic activities (in the pancreas, liver, adipose tissue, skeletal muscle, etc.) of absorbed PCs. Additionally, the microbial metabolites of these compounds may play a role in systemic activities of poorly absorbed native compounds.

It is important to note the low doses employed in the present study. We employed CE and cocoa fractions at 25 mg/kg BW/day [0.02625% (w/w) in the diet]. This is considerably lower than doses used in the majority of previous feeding studies of cocoa or cocoa extracts (Supporting Information). Previous studies have employed doses of 600 mg/kg body weight/day or 0.5−12.5% (w/w) in the diet (although the higher percentage compositions in the diet were cocoa powder, which is ∼2−5% flavan-3-ols by weight).[17−23] The doses employed in previous studies may be on the extreme end of what is feasible for translation to human dietary dosing. However, we have demonstrated here that cocoa extracts or fractions can be effective at lower doses, which translate to more reasonable human doses [25 mg cocoa flavanols/kg BW/day in a 20 g mouse is equivalent to 2.03 mg/kg cocoa flavanols in a human[62]]. Therefore, our data suggest that moderate doses of cocoa flavanols or cocoa powder have the potential to be more effective in human clinical trials than previously thought. This concept was proposed previously by Castell-Auvi et al.,[42] who demonstrated that high doses had no effect on hyperinsulinemia and lower doses (5−15 mg/kg BW) actually worsened hyperinsulinemia, whereas 25 mg/kg BW improved hyperinsulinemia. It is also important to note that this dose did not alter food intake in our model, whereas the higher doses in previous studies may have inhibited the onset of diet-induced obesity and insulin resistance by significantly altering food intake (and, hence, macronutrient intake) due to poor palatability or other factors (however, this is unknown as food intake is rarely reported).

One factor in our study design that warrants mention was that mice were fed equivalent doses of the CE and cocoa fractions on a mg/kg BW basis. Due to differences in average molecular weight (MW) of the species in each treatment, mice were therefore fed different concentrations on a mol/kg BW basis. However, the oligomer fraction was still the most effective treatment despite the fact that the mice on the monomer treatment received significantly greater doses than mice on the oligomer treatment, on a mol/kg BW basis. This further reinforces the conclusion that oligomers possess enhanced bioactivities. Furthermore, attempting to formulate the diets on an equivalent mol/kg BW basis would have been problematic due to the fact that thiolysis is only an estimation of MW, and there may be components not accounted for by the assays used to characterize CE and cocoa fractions (normal-phase HPLC, which was qualitative, and UPLC, which measured only up to DP 10). Therefore, formulation on a mg/kg BW basis was determined to be the preferred approach.

Oligomeric PCs appear to possess the greatest antiobesity and antidiabetic bioactivities of the flavanols in cocoa, particularly at the low doses employed for the present study. The extraction and fractionation methods employed here are capable of producing gram quantities of flavanol fractions from complex matrices for long-term feeding studies, thus over-

coming a major limitation in experimental design. Additional studies of prolonged feeding of flavanol fractions in vivo are needed to further identify the fractions with the highest bioactivities and therefore the greatest potential for translation to human clinical applications at reasonable doses.

The results of this study suggest several future directions. First, isolation of individual compounds in the oligomer fraction for long-term feeding studies are needed to further refine our understanding of which cocoa flavanols possess the greatest potential for activity in humans. Second, additional studies are needed to determine the relative importance of the gut activities of unabsorbed PCs versus the systemic activities of absorbed PCs (or absorbed microbial metabolites) in the oligomer fraction. Identification and localization of the mechanistic target will guide design of the most effective delivery strategies for human interventions. Third, mechanistic studies are needed to identify the primary mechanism(s) by which PC oligomers inhibit the onset of obesity and impaired glucose tolerance during HF feeding. The majority of studies (including the present study) simply observe biomarkers that are improved during supplementation with PCs. Although useful for hypothesis generation, mechanistic experiments are needed that specifically inhibit and/or stimulate putative mechanistic targets to isolate and definitively identify the specific mechanisms of action. Identification of specific mechanisms essential for PC bioactivities will facilitate the design of human interventions with appropriate mechanistic targets. The most promising mechanisms appear to be located in the gut: inhibition of macronutrient digestion/absorption, GLP-1/DPP4 activity, and inhibition of endotoxin production and/or uptake. Finally, studies are required to determine whether the antiobesity and antidiabetic effects of PC oligomers are primarily acute postprandial activities due to oligomers in the upper gastrointestinal tract or systemic effects due to circulating PCs and colonic metabolites.

■ ASSOCIATED CONTENT

Supporting Information

Detailed methodologies for extraction and fractionation of flavanols, normal-phase HPLC and UPLC-MS/MS analysis, Folin−Ciocalteu assay, and thiolysis analysis of cocoa extract and cocoa fractions, summary of current literature exploring the antiobesity and antidiabetic effects of cocoa flavanols in animal models, and amounts of cocoa extract and fractions produced. This material is available free of charge via the Internet at http://pubs.acs.org.

■ AUTHOR INFORMATION

Corresponding Author

*(A.P.N.) Phone: 1 (540) 231-8391. Fax: 1 (540) 231-9293. E-mail: andrewn@vt.edu.

Funding

Start-up research funding for A.P.N. from the Department of Food Science and Technology and the College of Agriculture and Life Sciences at the Virginia Polytechnic Institute and State University was used to support this research.

Notes

The authors declare no competing financial interest.

■ ACKNOWLEDGMENTS

We acknowledge the contributions of Karen Strat, Pamela Suroski, Charles Nwaihesie, Benjamin Furrow, and Julie Holdridge for assistance with the animal experiments and Dr. Hengjian Wang for assistance with the Folin assay.

■ ABBREVIATIONS USED

C, catechin; EC, epicatechin; ECG, epicatechin gallate; EGC, epigallocatechin; EGCG, epigallocatechin gallate; PC, procyanidin; DP, degree of polymerization; mDP, mean degree of polymerization; GLP-1, glucagon-like peptide; CE, cocoa extract; MeOH, methanol; ddH_2O, distilled deionized water; ACN, acetonitrile; ESI, electrospray ionization; TQD, triple quadrupole; MRM, multireaction monitoring; LF, low fat; HF, high fat; BW, body weight; GSE, grape seed extract; GTT, glucose tolerance test; ip, intraperitoneal; ITT, insulin tolerance test; AUC, area under the curve; EU, endotoxin units; TLR, Toll-like receptors; MW, molecular weight

■ REFERENCES

(1) Robbins, R. J.; Leonczak, J.; Li, J.; Johnson, J. C.; Collins, T.; Kwik-Uribe, C.; Schmitz, H. H. Determination of flavanol and procyanidin (by degree of polymerization 1−10) content of chocolate, cocoa liquors, powder(s), and cocoa flavanol extracts by normal phase high-performance liquid chromatography: collaborative study. *J. AOAC Int.* **2012**, *95*, 1153−1160.

(2) Hammerstone, J. F. Procyanidin content and variation in some commonly consumed foods. *J. Nutr.* **2000**, *130*, 2086S−2092S.

(3) Lee, K. W. Cocoa has more phenolic phytochemicals and a higher antioxidant capacity than teas and red wine. *J. Agric. Food Chem.* **2003**, *51*, 7292−7295.

(4) Crozier, S. J.; Preston, A. G.; Hurst, J. W.; Payne, M. J.; Mann, J.; Hainly, L.; Miller, D. L. Cacao seeds are a "Super Fruit": a comparative analysis of various fruit powders and products. *Chem. Cent. J.* **2011**, *5*, 5.

(5) Belščak, A.; Komes, D.; Horžić, D.; Ganić, K. K. Comparative study of commercially available cocoa products in terms of their bioactive composition. *Food Res. Int.* **2009**, *42*, 707−716.

(6) Andres-Lacueva, C.; Monagas, M.; Khan, N.; Izquierdo-Pulido, M.; Urpi-Sarda, M.; Permanyer, J.; Lamuela-Raventos, R. M. Flavanol and flavonol contents of cocoa powder products: influence of the manufacturing process. *J. Agric. Food Chem.* **2008**, *56*, 3111−3117.

(7) Langer, S. Flavanols and methylxanthines in commercially available dark chocolate: a study of the correlation with nonfat cocoa solids. *J. Agric. Food Chem.* **2011**, *59*, 8435−8441.

(8) Wollgast, J.; Anklam, E. Review on polyphenols in Theobroma cacao: changes in composition during the manufacture of chocolate and methodology for identification and quantification. *Food Res. Int.* **2000**, *33*, 423−447.

(9) Gu, L. W.; House, S. E.; Wu, X. L.; Ou, B. X.; Prior, R. L. Procyanidin and catechin contents and antioxidant capacity of cocoa and chocolate products. *J. Agric. Food Chem.* **2006**, *54*, 4057−4061.

(10) Cooper, K. A.; Campos-Gimenez, E.; Alvarez, D. J.; Nagy, K.; Donovan, J. L.; Williamson, G. Rapid reversed phase ultra-performance liquid chromatography analysis of the major cocoa polyphenols and inter-relationships of their concentrations in chocolate. *J. Agric. Food Chem.* **2007**, *55*, 2841−2847.

(11) Payne, M. J.; Hurst, W. J.; Miller, K. B.; Rank, C.; Stuart, D. A. Impact of fermentation, drying, roasting, and Dutch processing on epicatechin and catechin content of cacao beans and cocoa ingredients. *J. Agric. Food Chem.* **2010**, *58*, 10518−10527.

(12) Vinson, J. A. Phenol antioxidant quantity and quality in foods: cocoa, dark chocolate, and milk chocolate. *J. Agric. Food Chem.* **1999**, *47*, 4821−4824.

(13) Gu, L. Procyanidin and catechin contents and antioxidant capacity of cocoa and chocolate products. *J. Agric. Food Chem.* **2006**, *54*, 4057−4061.

(14) Grassi, D. Short-term administration of dark chocolate is followed by a significant increase in insulin sensitivity and a decrease in

blood pressure in healthy persons. *Am. J. Clin. Nutr.* **2005**, *81*, 611−614.
(15) Grassi, D. Cocoa reduces blood pressure and insulin resistance and improves endothelium-dependent vasodilation in hypertensives. *Hypertension* **2005**, *46*, 398−405.
(16) Taub, P. R.; Ramirez-Sanchez, I.; Ciaraldi, T. P.; Perkins, G.; Murphy, A. N.; Naviaux, R.; Hogan, M.; Maisel, A. S.; Henry, R. R.; Ceballos, G.; Villarreal, F. Alterations in skeletal muscle indicators of mitochondrial structure and biogenesis in patients with type 2 diabetes and heart failure: effects of epicatechin rich cocoa. *Clin. Transl. Sci.* **2012**, *5*, 43−47.
(17) Tomaru, M.; Takano, H.; Osakabe, N.; Yasuda, A.; Inoue, K.; Yanagisawa, R.; Ohwatari, T.; Uematsu, H. Dietary supplementation with cacao liquor proanthocyanidins prevents elevation of blood glucose levels in diabetic obese mice. *Nutrition* **2007**, *23*, 351−355.
(18) Yamashita, Y. Prevention mechanisms of glucose intolerance and obesity by cacao liquor procyanidin extract in high-fat diet-fed C57BL/6 mice. *Arch. Biochem. Biophys.* **2012**, *527*, 95−104.
(19) Ruzaidi, A.; Amin, I.; Nawalyah, A. G.; Hamid, M. The effect of Malaysian cocoa extract on glucose levels and lipid profiles in diabetic rats. *J. Ethnopharmacol.* **2005**, *98*, 55−60.
(20) Jalil, A. M. M.; Ismail, A.; Pei, C. P.; Hamid, M.; Kamaruddin, S. H. S. Effects of cocoa extract on glucometabolism, oxidative stress, and antioxidant enzymes in obese-diabetic (Ob-db) rats. *J. Agric. Food Chem.* **2008**, *56*, 7877−7884.
(21) Jalil, A. M. M.; Ismail, A.; Chong, P. P.; Hamid, M.; Kamaruddin, S. H. S. Effects of cocoa extract containing polyphenols and methylxanthines on biochemical parameters of obese-diabetic rats. *J. Sci. Food Agric.* **2009**, *89*, 130−137.
(22) Sanchez, D.; Moulay, L.; Muguerza, B.; Quinones, M.; Miguel, M.; Aleixandre, A. Effect of a soluble cocoa fiber-enriched diet in Zucker fatty rats. *J. Med. Food* **2010**, *13*, 621−628.
(23) Matsui, N.; Ito, R.; Nishimura, E.; Yoshikawa, M.; Kato, M.; Kamei, M.; Shibata, H.; Matsumoto, I.; Abe, K.; Hashizume, S. Ingested cocoa can prevent high-fat diet-induced obesity by regulating the expression of genes for fatty acid metabolism. *Nutrition* **2005**, *21*, 594−601.
(24) Eteng, M. U.; Ibekwe, H. A.; Umoh, U. I.; Ebong, P. E.; Umoh, I. B.; Eyong, E. U. Theobromine rich cocoa powder induces weight loss and changes in lipid profile of obese Wistar rats. *Discov. Innovat.* **2006**, *18*, 191−196.
(25) Cordero-Herrera, I.; Martín, M. Á.; Goya, L.; Ramos, S. Cocoa flavonoids attenuate high glucose-induced insulin signalling blockade and modulate glucose uptake and production in human HepG2 cells. *Food Chem. Toxicol.* **2014**, *64*, 10−19.
(26) Cordero-Herrera, I.; Martín, M. A.; Bravo, L.; Goya, L.; Ramos, S. Cocoa flavonoids improve insulin signalling and modulate glucose production via AKT and AMPK in HepG2 cells. *Mol. Nutr. Food Res.* **2013**, *57*, 974−985.
(27) Martín, M. Á.; Fernández-Millán, E.; Ramos, S.; Bravo, L.; Goya, L. Cocoa flavonoid epicatechin protects pancreatic beta cell viability and function against oxidative stress. *Mol. Nutr. Food Res.* **2014**, DOI: 10.1002/mnfr.201300291.
(28) Karim, M. Effects of cocoa extracts on endothelium-dependent relaxation. *J. Nutr.* **2000**, *130*, 2105S−2108S.
(29) Kim, Y. Protective effects of oligomeric and polymeric procyanidin fractions from defatted grape seeds on *tert*-butyl hydroperoxide-induced oxidative damage in HepG2 cells. *Food Chem.* **2013**, *137*, 136−141.
(30) Gentile, C.; Allegra, M.; Angileri, F.; Pintaudi, A. M.; Livrea, M. A.; Tesoriere, L. Polymeric proanthocyanidins from Sicilian pistachio (*Pistacia vera* L.) nut extract inhibit lipopolysaccharide-induced inflammatory response in RAW 264.7 cells. *Eur. J. Nutr.* **2012**, *51*, 353−363.
(31) Yamashita, Y.; Okabe, M.; Natsume, M.; Ashida, H. Cinnamtannin A2, a tetrameric procyanidin, increases GLP-1 and insulin secretion in mice. *Biosci., Biotechnol., Biochem.* **2013**, *77*, 888−891.
(32) Adamson, G. E. HPLC method for the quantification of procyanidins in cocoa and chocolate samples and correlation to total antioxidant capacity. *J. Agric. Food Chem.* **1999**, *47*, 4184−4188.
(33) Sun, B. Separation of grape and wine proanthocyanidins according to their degree of polymerization. *J. Agric. Food Chem.* **1998**, *46*, 1390−1396.
(34) Guyot, S. Reversed-phase HPLC following thiolysis for quantitative estimation and characterization of the four main classes of phenolic compounds in different tissue zones of a french cider apple variety (var. Kermerrien). *J. Agric. Food Chem.* **1998**, *46*, 1698−1705.
(35) Gu, L. Fractionation of polymeric procyanidins from lowbush blueberry and quantification of procyanidins in selected foods with an optimized normal-phase HPLC−MS fluorescent detection method. *J. Agric. Food Chem.* **2002**, *50*, 4852−4860.
(36) Robbins, R. J. Method performance and multi-laboratory assessment of a normal phase high pressure liquid chromatography−fluorescence detection method for the quantitation of flavanols and procyanidins in cocoa and chocolate containing samples. *J. Chromatogr.* **2009**, *1216*, 4831−4840.
(37) Reheman, A.; Tasneem, S.; Ni, H.; Hayward, C. P. Mice with deleted multimerin 1 and alpha-synuclein genes have impaired platelet adhesion and impaired thrombus formation that is corrected by multimerin 1. *Thromb. Res.* **2010**, *125*, e177−e183.
(38) Lin, S. Development of high fat diet-induced obesity and leptin resistance in C57Bl/6J mice. *Int. J. Obes. Relat. Metab. Disord.* **2000**, *24*, 639−646.
(39) Gu, Y. Y.; Hurst, W. J.; Stuart, D. A.; Lambert, J. D. Inhibition of key digestive enzymes by cocoa extracts and procyanidins. *J. Agric. Food Chem.* **2011**, *59*, 5305−5311.
(40) Yamashita, Y.; Okabe, M.; Natsume, M.; Ashida, H. Comparison of anti-hyperglycemic activities between low- and high-degree of polymerization procyanidin fractions from cacao liquor extract. *J. Food Drug Anal.* **2012**, *20*, 283−287.
(41) Montagut, G.; Onnockx, S.; Vaque, M.; Blade, C.; Blay, M.; Fernandez-Larrea, J.; Pujadas, G.; Salvado, M. J.; Arola, L.; Pirson, I.; Ardevol, A.; Pinent, M. Oligomers of grape-seed procyanidin extract activate the insulin receptor and key targets of the insulin signaling pathway differently from insulin. *J. Nutr. Biochem.* **2010**, *21*, 476−481.
(42) Castell-Auvi, A.; Cedo, L.; Pallares, V.; Blay, M. T.; Pinent, M.; Motilva, M. J.; Garcia-Vallve, S.; Pujadas, G.; Maechler, P.; Ardevol, A. Procyanidins modify insulinemia by affecting insulin production and degradation. *J. Nutr. Biochem.* **2012**, *23*, 1565−1572.
(43) Castell-Auvi, A.; Cedo, L.; Pallares, V.; Blay, M.; Pinent, M.; Ardevol, A. Grape seed procyanidins improve beta-cell functionality under lipotoxic conditions due to their lipid-lowering effect. *J. Nutr. Biochem.* **2013**, *24*, 948−953.
(44) Montagut, G.; Blade, C.; Blay, M.; Fernandez-Larrea, J.; Pujadas, G.; Salvado, M. J.; Arola, L.; Pinent, M.; Ardevol, A. Effects of a grapeseed procyanidin extract (GSPE) on insulin resistance. *J. Nutr. Biochem.* **2010**, *21*, 961−967.
(45) Pinent, M.; Cedo, L.; Montagut, G.; Blay, M.; Ardevol, A. Procyanidins improve some disrupted glucose homoeostatic situations: an analysis of doses and treatments according to different animal models. *CRC Crit. Rev. Food Sci.* **2012**, *52*, 569−584.
(46) Zumdick, S.; Deters, A.; Hensel, A. In vitro intestinal transport of oligomeric procyanidins (DP 2 to 4) across monolayers of Caco-2 cells. *Fitoterapia* **2012**, *83*, 1210−1217.
(47) Deprez, S.; Mila, I.; Huneau, J. F.; Tome, D.; Scalbert, A. Transport of proanthocyanidin dimer, trimer, and polymer across monolayers of human intestinal epithelial Caco-2 cells. *Antioxid. Redox Signal.* **2001**, *3*, 957−967.
(48) Prasain, J. K.; Peng, N.; Dai, Y. Y.; Moore, R.; Arabshahi, A.; Wilson, L.; Barnes, S.; Wyss, J. M.; Kim, H.; Watts, R. L. Liquid chromatography tandem mass spectrometry identification of proanthocyanidins in rat plasma after oral administration of grape seed extract. *Phytomedicine* **2009**, *16*, 233−243.
(49) Gonzalez-Abuin, N.; Martinez-Micaelo, N.; Blay, M.; Pujadas, G.; Garcia-Vallve, S.; Pinent, M.; Ardevol, A. Grape seed-derived

procyanidins decrease dipeptidyl-peptidase 4 activity and expression. *J. Agric. Food Chem.* **2012**, *60*, 9055−9061.
(50) Creely, S. J.; McTernan, P. G.; Kusminski, C. M.; Fisher, F. M.; Da Silva, N. F.; Khanolkar, M.; Evans, M.; Harte, A. L.; Kumar, S. Lipopolysaccharide activates an innate immune system response in human adipose tissue in obesity and type 2 diabetes. *Am. J. Physiol.: Endocrinol. Metab.* **2007**, *292*, E740−E747.
(51) Shi, H.; Kokoeva, M. V.; Inouye, K.; Tzameli, I.; Yin, H.; Flier, J. S. TLR4 links innate immunity and fatty acid-induced insulin resistance. *J. Clin. Invest.* **2006**, *116*, 3015−3025.
(52) Frisard, M. I.; McMillan, R. P.; Marchand, J.; Wahlberg, K. A.; Wu, Y.; Voelker, K. A.; Heilbronn, L.; Haynie, K.; Muoio, B.; Li, L.; Hulver, M. W. Toll-like receptor 4 modulates skeletal muscle substrate metabolism. *Am. J. Physiol.: Endocrinol. Metab.* **2010**, *298*, E988−E998.
(53) Cani, P. D.; Amar, J.; Iglesias, M. A.; Poggi, M.; Knauf, C.; Bastelica, D.; Neyrinck, A. M.; Fava, F.; Tuohy, K. M.; Chabo, C.; Waget, A.; Delmee, E.; Cousin, B.; Sulpice, T.; Chamontin, B.; Ferrieres, J.; Tanti, J. F.; Gibson, G. R.; Casteilla, L.; Delzenne, N. M.; Alessi, M. C.; Burcelin, R. Metabolic endotoxemia initiates obesity and insulin resistance. *Diabetes* **2007**, *56*, 1761−1772.
(54) Terra, X.; Montagut, G.; Bustos, M.; Llopiz, N.; Ardevol, A.; Blade, C.; Fernandez-Larrea, J.; Pujadas, G.; Salvado, J.; Arola, L.; Blay, M. Grape-seed procyanidins prevent low-grade inflammation by modulating cytokine expression in rats fed a high-fat diet. *J. Nutr. Biochem.* **2009**, *20*, 210−218.
(55) Song, P.; Zhang, R.; Wang, X.; He, P.; Tan, L.; Ma, X. Dietary grape-seed procyanidins decreased postweaning diarrhea by modulating intestinal permeability and suppressing oxidative stress in rats. *J. Agric. Food Chem.* **2011**, *59*, 6227−6232.
(56) Goodrich, K. M.; Fundaro, G.; Griffin, L. E.; Grant, A.; Hulver, M. W.; Ponder, M. A.; Neilson, A. P. Chronic administration of dietary grape seed extract increases colonic expression of gut tight junction protein occludin and reduces fecal calprotectin in a secondary analysis of healthy Wistar Furth rats. *Nutr. Res. (N.Y.)* **2012**, *32*, 787−794.
(57) Sung, N. Y.; Yang, M. S.; Song, D. S.; Kim, J. K.; Park, J. H.; Song, B. S.; Park, S. H.; Lee, J. W.; Park, H. J.; Kim, J. H.; Byun, E. B.; Byun, E. H. Procyanidin dimer B2-mediated IRAK-M induction negatively regulates TLR4 signaling in macrophages. *Biochem. Biophys. Res. Commun.* **2013**, *438*, 122−128.
(58) Terra, X.; Valls, J.; Vitrac, X.; Mérrillon, J.-M.; Arola, L.; Ardèvol, A.; Bladé, C.; Fernández-Larrea, J.; Pujadas, G.; Salvadó, J.; Blay, M. Grape-seed procyanidins act as antiinflammatory agents in endotoxin-stimulated RAW 264.7 macrophages by inhibiting NFκB signaling pathway. *J. Agric. Food Chem.* **2007**, *55*, 4357−4365.
(59) Pallares, V.; Fernandez-Iglesias, A.; Cedo, L.; Castell-Auvi, A.; Pinent, M.; Ardevol, A.; Salvado, M. J.; Garcia-Vallve, S.; Blay, M. Grape seed procyanidin extract reduces the endotoxic effects induced by lipopolysaccharide in rats. *Free Radical Biol. Med.* **2013**, *60*, 107−114.
(60) Gu, Y.; Yu, S.; Park, J. Y.; Harvatine, K.; Lambert, J. D. Dietary cocoa reduces metabolic endotoxemia and adipose tissue inflammation in high-fat fed mice. *J. Nutr. Biochem.* **2014**, DOI: 10.1016/j.jnutbio.2013.12.004.
(61) Ding, Y.; Zhang, Z. F.; Dai, X. Q.; Jiang, Y. F.; Bao, L.; Li, Y. J.; Li, Y. Grape seed proanthocyanidins ameliorate pancreatic beta-cell dysfunction and death in low-dose streptozotocin- and high-carbohydrate/high-fat diet-induced diabetic rats partially by regulating endoplasmic reticulum stress. *Nutr. Metabolism* **2013**, *10*, 51.
(62) Reagan-Shaw, S.; Nihal, M.; Ahmad, N. Dose translation from animal to human studies revisited. *FASEB J.* **2008**, *22*, 659−661.

serum (FBS) was from Invitrogen. The microsomal triglyceride inhibitor BMS212122 was a kind gift from Bristol-Meyers Squibb; a 200 μmol/L stock solution of it was prepared in DMSO. The antibody against SR-BI was purchased from Novus Europe (UK). The ELISA kit ab46044 for determining IL-6 was from Abcam (UK). Red wine and dealcoholized red wine were kind gifts of Bodegas Torres (Barcelona, Spain), and their phenolic composition can be found in Chiva-Blanch et al.[14] Green tea (a kind gift of Bonomelli s.p.a., Bologna, Italy) was fully characterized[15] and was freshly prepared on the day of the experiment by brewing loose-leaf tea (2 g/100 mL) for 3 min in just-boiled water. A fully characterized (Supplementary Table 1) cocoa extract was a kind gift from Kraft Foods.

Methods. Caco-2 cells were grown on 100 mm plates and were subcultured onto microporous membranes inserted into Transwells. Cells were grown with DMEM supplemented with 10% FBS, penicillin, and streptomycin. Media in the Transwell cultures was replaced every other day, and cultures were used for experimentation at least 10 days postconfluence, to ensure differentiation. Only the apical compartment contained phenol red, and monolayer integrity was assessed by measuring the appearance of phenol red in the basolateral compartment. This method was shown to be equivalent to measuring TEER[16] with the added benefit that the phenol red analysis is done once the experiment is ended and, therefore, there is no risk of puncturing the monolayer with electrodes. The concentration of phenol red was determined spectrophotometrically at 560 nm, in aliquots of basolateral media containing 5% 1 N NaOH as previously reported.[16]

The different sources of polyphenols (red wine, green tea, or cocoa extracts) or ethanol were administered to Caco-2 monolayers to the apical compartment containing DMEM + 10% FBS. The amounts added to each well corresponded to a final concentration of 50 μM total polyphenols (calculated as gallic acid equivalents), which approximates the intestinal concentrations that can be attained after ingestion.[1] The final concentration of ethanol in all samples was 0.2%, corresponding to the same amount contained in red wine.

Cholesterol Efflux and HDL Functionality. For experiments in which basolateral cholesterol efflux and HDL functionality were measured, the basolateral compartments of the Transwells were incubated with DMEM without phenol red and the apical compartments with BMS212122 (0.05 μmol/L) in DMEM + 10% FBS for 3 h prior to the apical addition of polyphenols (DMSO did not exceed 0.05%). BMS212122 is an inhibitor of the microsomal triglyceride transfer protein (MTP), which completely inhibits the assembly and secretion of apolipoprotein B-containing lipoproteins, that is, chylomicrons;[17] therefore, all of the cholesterol secreted basolaterally from the Caco-2 monolayers was HDL-associated. Polyphenols from red wine, dealcoholized red wine, green tea, or cocoa were added apically to a final concentration of 50 μM (gallic acid equivalents) total polyphenol. The antibody against SR-BI (aSR-BI) was added to the basolateral compartment (1:1000 dilution) for experiments in which HDL functionality was determined.

Determination of Free and Total Cholesterol. Free cholesterol and esterified cholesterol were determined as previously described.[16] Briefly, 2 mL of basolateral medium was collected after 24 h, and 5 μL of the internal standard ergosterol (1 mg/mL in EtOH) and 4 mL of EtOH were added. The mixture was thoroughly vortexed. Lipids were then extracted with 2 mL of methyl *tert*-butyl ether (MTBE) and 6 mL of hexane. After vigorous shaking, the lower aqueous phase was discarded and the upper organic phase was separated in two glass tubes (approximately 4 mL each); the first tube was evaporated under nitrogen, and the residue was silylated using pyridine and BSTFA + 1% TMCS (1:1) to measure free cholesterol. The second tube was evaporated under nitrogen, and the residue was suspended in 1 mL of methanolic KOH (1 mL of 3 N KOH + 9 mL of MeOH) and incubated at 80 °C for 1 h to allow for saponification. Samples were then neutralized with 50 μL of 6 N HCl, and 3 mL of hexane was added to extract the lipids: the lower aqueous phase was discarded, the upper organic phase was evaporated, and the residue was silylated using pyridine and BSTFA + 1% TMCS (1:1) to measure total cholesterol. Esterified cholesterol was determined by subtracting the amount of free cholesterol to the amount of total cholesterol. Cholesterol and ergosterol were quantified by GC-MS using selective ion monitoring, as described previously.[16]

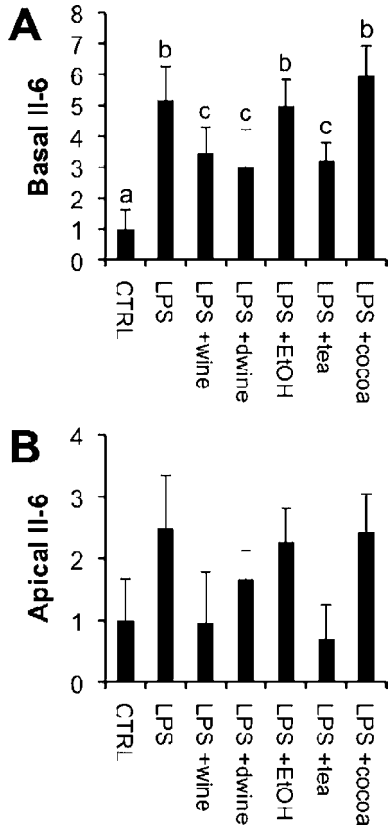

Figure 1. Red wine and green tea polyphenols reduce IL-6 secretion by Caco-2 cells. Cells were treated apically with the indicated polyphenolic extracts from red wine, green tea, or cocoa for 4 h. Freshly dissolved LPS was then added where indicated at a concentration of 10 μg/mL. After 2 h, IL-6 was determined in apical and basolateral media. Basal, basolateral; Ctrl, controls; LPS, lipopolysaccharide; dwine, dealcoholized wine. Treatments without a common letter differ, $p < 0.05$.

IL-6 Determination, RNA Extraction, and Quantitative PCR. The IL-6 high-sensitivity human ELISA kit (ab46044) was used according to the manufacturer's instructions to determine IL-6 in apical and basolateral compartments.

For gene assays, cells were washed twice with cold 0.9% NaCl and were scraped off the microporous membrane. RNA was extracted with Qiazol according to the manufacturer's instructions. cDNA synthesis was performed with Superscript III following the manufacturer's instructions. Primers (available upon request) were designed and, for each primer set, the melting curves were verified to make sure that a single product was amplified. PCR amplification was performed with a 7900 real-time PCR system (Applied Biosystems) in 384-well plates. SYBR Green was used in 10 μL reactions with 30 ng of total RNA input and 500 μM of each primer. GAPDH was used as reference gene, and fold change in expression levels was determined as $2^{-\Delta\Delta Ct}$. Results were normalized to control treatments.

Statistical Analyses. For every experiment each treatment was performed at least in triplicate, and the same experiment was performed at least twice. Results are expressed as the mean ± standard deviation of at least two separate experiments. Statistical analysis was performed using the SAS Statistical Analysis Systems (version 9.2, SAS Institute Inc., Cary, NC, USA). One-way ANOVA with the Bonferroni post hoc analysis was performed to determine the effect of the different treatments. A $p < 0.05$ was considered significant.

RESULTS AND DISCUSSION

Wine and Tea Polyphenols Reduce IL-6 Secretion by Caco-2 Cells. The secretion of IL-6 by controls was greater

dx.doi.org/10.1021/jf500348u | J. Agric. Food Chem. 2014, 62, 2228−2232

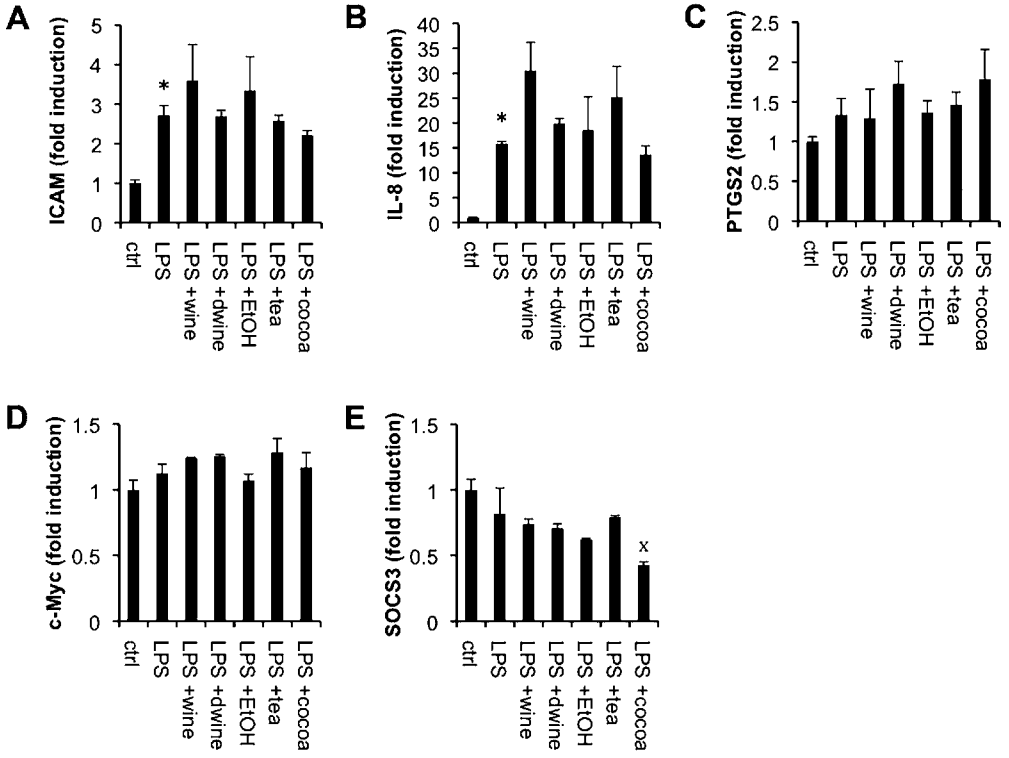

Figure 2. Effects of polyphenols on intestinal inflammatory gene expression. Caco-2 monolayers grown in Transwells were treated apically with the indicated polyphenolic extracts from red wine, green tea, or cocoa for 4 h. LPS was then added where indicated at a concentration of 10 μg/mL. After 2 h, cells were collected and gene expression was determined by qPCR. Ctrl, controls; LPS, lipopolysaccharide; dwine, dealcoholized wine. (*) $p < 0.001$ as compared with control cells, $x < 0.03$ as compared with LPS treatment.

basolaterally (0.16 ± 0.08 pg/mL) than apically (0.09 ± 0.08 pg/mL). IL-6 secretion by LPS-treated cells was significantly ($p < 0.03$) greater basolaterally (0.48 ± 0.02 pg/mL) than apically (0.29 ± 0.07 pg/mL), suggesting that intestinal inflammation leads to the release of inflammatory cytokines into the circulation. Polyphenols from red wine and green tea, but not those from cocoa, significantly reduced basolateral IL-6 secretion from Caco-2 monolayers grown on Transwells and challenged with LPS (Figure 1A). A similar effect was seen on apical secretion, although it was not significant, perhaps due to the very small quantities of IL-6 secreted apically (Figure 1B). Even though red wine and green tea polyphenols significantly inhibited IL-6 production, the absolute effect was moderate and we observed a high variability between experiments.

To further investigate the effect of polyphenols on induced inflammation, we determined, by qPCR, the expression of selected inflammation genes. *IL-8*, *ICAM*, and *PTGS2* (*COX-2*) mRNA expressions were significantly increased by LPS by approximately 15-, 3-, and 1.3-fold, respectively (Figure 2). Unfortunately, IL-6 quantification by qPCR was not feasible due to an elevated Ct. However, polyphenols from either source did not decrease the expression of *IL-8*, *ICAM*, or *PTGS2* in LPS-treated cells (Figure 2), casting some doubt on the factual anti-inflammatory actions of polyphenols at the intestinal level and at dietary concentrations. Indeed, emerging evidence suggests that, rather than direct anti-inflammatory actions, polyphenols affect the intestine by modulating the microbiota.[1]

As the IL-6 signaling pathway involves STAT3 activation, we measured the expressions of c-MYC and SOCS3, which are induced by STAT3. c-MYC was increased by LPS and even more so by red wine and green tea polyphenol supplementation (Figure 2). Conversely, SOCS3 (which acts as a feedback inhibitor of the JAK/STAT signaling pathway) expression was reduced by LPS treatment. Wine and tea polyphenols had no effect, but the cocoa extract significantly reduced SOCS3 expression relative to LPS treatment ($p < 0.03$, Figure 2), confirming that polyphenols have limited intestinal anti-inflammatory activities when used in concentrations that approximate dietary intakes. Nutraceuticals and supplements provide pharmanutritional[19] doses that might, conversely, produce beneficial effects.[20]

HDL Secretion and Functionality. As mentioned in the Introduction, several human studies report an association between polyphenol intake and circulating HDL-c concentrations. Therefore, much research is concentrating on investigating the mechanism(s) behind this arguably positive piece of evidence. In addition to the putative protective role of HDL in cardiovascular disease, cholesterol efflux from macrophages is predictive of cardiovascular risk,[21,22] even though this notion needs further confirmation.[23] HDL functionality is generally assessed by its capacity to efflux cholesterol from macrophages. Indeed, some polyphenols have been shown to increase macrophage cholesterol efflux ex vivo.[24−26] However, we believe that HDL functionality should be assessed not only by its capacity to efflux cholesterol from macrophages but also by its capacity to deliver cholesterol via SR-BI because this is the last step in reverse cholesterol transport.[13,27] Therefore, both aspects must be considered to determine HDL functionality. If the HDL particle can induce efflux from macrophages, but cannot deliver cholesterol properly via SR-BI, then cholesterol will accumulate in plasma as associated with HDL. We treated Caco-2 monolayers with different polyphenols and measured HDL functionality determined as the capacity of HDL to deliver cholesterol to cells via SR-BI (measured as the percent cholesterol

dx.doi.org/10.1021/jf500348u | J. Agric. Food Chem. 2014, 62, 2228−2232

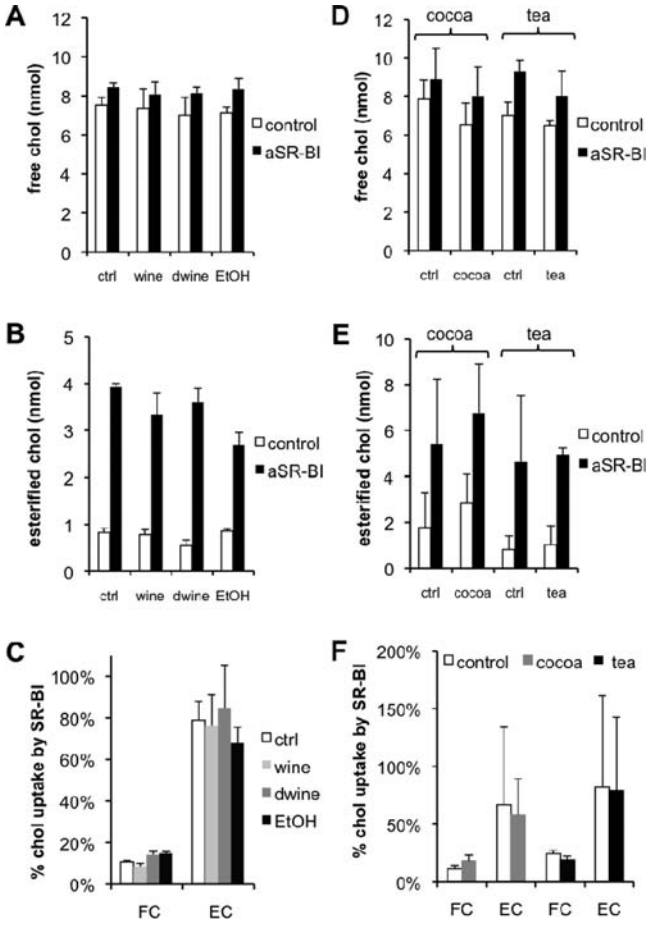

Figure 3. Red wine, green tea, or cocoa polyphenols do no alter intestinal cholesterol efflux or HDL functionality. Caco-2 monolayers were pretreated apically with the microsomial trygliceride transfer protein inhibitor BMS212122 for 3 h. At time 0, basolateral medium was replaced with fresh DMEM without phenol red in the presence or absence of aSR-BI, and polyphenols or EtOH was administered apically. At 24 h, free (A, D) and esterified cholesterol (B, E) were measured and HDL functionality (C, F) was determined. Chol, cholesterol; FC, free cholesterol; EC, esterified cholesterol; aSR-BI, antibody against SR-BI; dwine, dealcoholized wine.

taken up by SR-BI: (1 − cholesterol in the absence of aSR-BI/cholesterol in the presence of aSR-BI) × 100%.[16] Cholesterol can be secreted basolaterally by Caco-2 monolayers associated with HDL or to chylomicrons. Because we were interested only in looking at cholesterol secretion associated with HDL and HDL functionality, we used the microsomal triglyceride transfer protein inhibitor BMS212122 to inhibit chylomicron secretion. We did not record an effect on cholesterol secretion or cholesterol uptake by SR-BI when cells were treated for 24 h with polyphenols from red wine (Figure 3A−C), cocoa (Figure 3D,F), or green tea (Figure 3E,F). We then assessed HDL functionality in an inflamed state by LPS induction: similarly, we did not see a difference in cholesterol secretion (results not shown) or cholesterol uptake by SR-BI (Supplemental Figure 1). Taken together, these data suggest that polyphenols (at least those from red wine, cocoa, and green tea) administered at a dietary dose neither increase cholesterol secretion by intestinal cells nor enhance HDL functionality. It should be noted that Yasuda et al. explored a different pathway of HDL synthesis as influenced by cocoa polyphenols in Caco-2 cells[28] by measuring apolipoprotein A1 (apoA1) secretion. They report increased apoA1 production as a result of up-regulation of mature form SREBPs and increased LDL receptor activity induced by cocoa polyphenols. However, it should be noted that these authors used undifferentiated Caco-2 cells instead of confluent monolayers as we did, and metabolism is very different in these cells. Lipoproteins are secreted only by differentiated Caco-2 monolayers and not by undifferentiated cells. Therefore, issues of concentrations and pathways of HDL production should be further addressed to elucidate this matter. Further studies are also warranted to ascertain whether the positive associations between polyphenol consumption and HDL-c concentrations are the result of confounding factors or are, indeed, due to these secondary metabolites.

Another cautionary note concerns the ApoE effects on cholesterol secretion. In this respect, Caco-2 cells possess the most commonly found ApoE3/E3 genotype[29] and, therefore, our results should be applied to the general population. However, the intestines of genotypically different individuals might react differently to polyphenol exposure. Finally, cell cultures are very useful to study mechanisms, but in vivo conditions such as pH, osmolarity, microbiota, and mucus might evidently differentially modulate the effects we report.

In conclusion, by using human intestinal cells supplemented with physiological concentrations of polyphenols from three different sources, we confirm their limited anti-inflammatory visceral actions and report that they do not directly affect cholesterol secretion or HDL functionality.

■ ASSOCIATED CONTENT

Ⓢ Supporting Information

Supplemental Figure 1. In an inflamed state, red wine polyphenols do no alter cholesterol efflux or HDL functionality. Caco-2 monolayers were pretreated apically with BMS212122 for 3 h in DMEM. 10% FBS and DMEM without phenol red were added basolaterally. At time 0 basolateral medium was replaced with fresh DMEM without phenol red in the presence or absence of aSR-BI, and red wine, dealcoholized wine, or EtOH was administered apically. At 4 h LPS was added at a final concentration of 10 μg/mL. At 24 h FC and EC were measured and HDL functionality was determined. FC, free cholesterol; EC, esterified cholesterol; aSR-BI, antibody against SR-BI. This material is available free of charge via the Internet at http://pubs.acs.org.

■ AUTHOR INFORMATION

Corresponding Author

*(F.V.) Mailing address: IMDEA-Food, Edificio CLAID, Calle Faraday 7, 28049 Madrid, Spain. E-mail: francesco.visioli@imdea.org. Phone: +34912786983.

Funding

G.C.-B. is grateful for a fellowship from the Fundació Universitària Agustı Pedro i Pons, University of Barcelona, Spain. Funded by a "Proactive" grant of IMDEA-Food.

Notes

The authors declare no competing financial interest.

■ REFERENCES

(1) Visioli, F.; De La Lastra, C. A.; Andres-Lacueva, C.; Aviram, M.; Calhau, C.; Cassano, A.; D'Archivio, M.; Faria, A.; Fave, G.; Fogliano, V.; Llorach, R.; Vitaglione, P.; Zoratti, M.; Edeas, M. Polyphenols and human health: a prospectus. *Crit. Rev. Food Sci. Nutr.* **2011**, *51*, 524−546.

(2) Ruiz, P. A.; Haller, D. Functional diversity of flavonoids in the inhibition of the proinflammatory NF-κB, IRF, and Akt signaling pathways in murine intestinal epithelial cells. *J. Nutr.* **2006**, *136*, 664−671.
(3) Camacho-Barquero, L.; Villegas, I.; Sanchez-Calvo, J. M.; Talero, E.; Sanchez-Fidalgo, S.; Motilva, V.; Alarcon de la Lastra, C. Curcumin, a *Curcuma longa* constituent, acts on MAPK p38 pathway modulating COX-2 and iNOS expression in chronic experimental colitis. *Int. Immunopharmacol.* **2007**, *7*, 333−342.
(4) Romier-Crouzet, B.; Van De Walle, J.; During, A.; Joly, A.; Rousseau, C.; Henry, O.; Larondelle, Y.; Schneider, Y. J. Inhibition of inflammatory mediators by polyphenolic plant extracts in human intestinal Caco-2 cells. *Food Chem. Toxicol.* **2009**, *47*, 1221−1230.
(5) Mellor, D. D.; Sathyapalan, T.; Kilpatrick, E. S.; Beckett, S.; Atkin, S. L. High-cocoa polyphenol-rich chocolate improves HDL cholesterol in type 2 diabetes patients. *Diabetic Med.* **2010**, *27*, 1318−1321.
(6) Baba, S.; Natsume, M.; Yasuda, A.; Nakamura, Y.; Tamura, T.; Osakabe, N.; Kanegae, M.; Kondo, K. Plasma LDL and HDL cholesterol and oxidized LDL concentrations are altered in normo- and hypercholesterolemic humans after intake of different levels of cocoa powder. *J. Nutr.* **2007**, *137*, 1436−1441.
(7) Wan, Y.; Vinson, J. A.; Etherton, T. D.; Proch, J.; Lazarus, S. A.; Kris-Etherton, P. M. Effects of cocoa powder and dark chocolate on LDL oxidative susceptibility and prostaglandin concentrations in humans. *Am. J. Clin. Nutr.* **2001**, *74*, 596−602.
(8) Maron, D. J.; Lu, G. P.; Cai, N. S.; Wu, Z. G.; Li, Y. H.; Chen, H.; Zhu, J. Q.; Jin, X. J.; Wouters, B. C.; Zhao, J. Cholesterol-lowering effect of a theaflavin-enriched green tea extract: a randomized controlled trial. *Arch. Intern. Med.* **2003**, *163*, 1448−1453.
(9) Covas, M. I.; Nyyssonen, K.; Poulsen, H. E.; Kaikkonen, J.; Zunft, H. J.; Kiesewetter, H.; Gaddi, A.; de la Torre, R.; Mursu, J.; Baumler, H.; Nascetti, S.; Salonen, J. T.; Fito, M.; Virtanen, J.; Marrugat, J. The effect of polyphenols in olive oil on heart disease risk factors: a randomized trial. *Ann. Intern. Med.* **2006**, *145*, 333−341.
(10) Brunham, L. R.; Kruit, J. K.; Iqbal, J.; Fievet, C.; Timmins, J. M.; Pape, T. D.; Coburn, B. A.; Bissada, N.; Staels, B.; Groen, A. K.; Hussain, M. M.; Parks, J. S.; Kuipers, F.; Hayden, M. R. Intestinal ABCA1 directly contributes to HDL biogenesis in vivo. *J. Clin. Invest.* **2006**, *116*, 1052−1062.
(11) Jakulj, L.; Besseling, J.; Stroes, E. S.; Groen, A. K. Intestinal cholesterol secretion: future clinical implications. *Neth. J. Med.* **2013**, *71*, 459−465.
(12) Lee-Rueckert, M.; Blanco-Vaca, F.; Kovanen, P. T.; Escola-Gil, J. C. The role of the gut in reverse cholesterol transport–focus on the enterocyte. *Prog. Lipid Res.* **2013**, *52*, 317−328.
(13) Davalos, A.; Fernandez-Hernando, C. From evolution to revolution: miRNAs as pharmacological targets for modulating cholesterol efflux and reverse cholesterol transport. *Pharmacol. Res.* **2013**, *75*, 60−72.
(14) Chiva-Blanch, G.; Urpi-Sarda, M.; Llorach, R.; Rotches-Ribalta, M.; Guillen, M.; Casas, R.; Arranz, S.; Valderas-Martinez, P.; Portoles, O.; Corella, D.; Tinahones, F.; Lamuela-Raventos, R. M.; Andres-Lacueva, C.; Estruch, R. Differential effects of polyphenols and alcohol of red wine on the expression of adhesion molecules and inflammatory cytokines related to atherosclerosis: a randomized clinical trial. *Am. J. Clin. Nutr.* **2012**, *95*, 326−334.
(15) Richard, D.; Kefi, K.; Barbe, U.; Poli, A.; Bausero, P.; Visioli, F. Weight and plasma lipid control by decaffeinated green tea. *Pharmacol. Res.* **2009**, *59*, 351−354.
(16) Nicod, N.; Parker, R. S. Vitamin E secretion by Caco-2 monolayers to APOA1, but not to HDL, is vitamer selective. *J. Nutr.* **2013**, *143*, 1565−1572.
(17) Rizzo, M.; Wierzbicki, A. S. New lipid modulating drugs: the role of microsomal transport protein inhibitors. *Curr. Pharm. Des.* **2011**, *17*, 943−949.
(18) Hewing, B.; Parathath, S.; Mai, C. K.; Fiel, M. I.; Guo, L.; Fisher, E. A. Rapid regression of atherosclerosis with MTP inhibitor treatment. *Atherosclerosis* **2013**, *227*, 125−129.
(19) Visioli, F. Pharma and nutrition: crossing the Rubicon. *PharmaNutrition* **2013**, *1*, 9.
(20) Magrone, T.; Perez de Heredia, F.; Jirillo, E.; Morabito, G.; Marcos, A.; Serafini, M. Functional foods and nutraceuticals as therapeutic tools for the treatment of diet-related diseases. *Can. J. Physiol. Pharmacol.* **2013**, *91*, 387−396.
(21) Feig, J. E.; Hewing, B.; Smith, J. D.; Hazen, S. L.; Fisher, E. A. High-density lipoprotein and atherosclerosis regression: evidence from preclinical and clinical studies. *Circ. Res.* **2014**, *114*, 205−213.
(22) Khera, A. V.; Cuchel, M.; de la Llera-Moya, M.; Rodrigues, A.; Burke, M. F.; Jafri, K.; French, B. C.; Phillips, J. A.; Mucksavage, M. L.; Wilensky, R. L.; Mohler, E. R.; Rothblat, G. H.; Rader, D. J. Cholesterol efflux capacity, high-density lipoprotein function, and atherosclerosis. *N. Engl. J. Med.* **2011**, *364*, 127−135.
(23) Li, X. M.; Tang, W. H.; Mosior, M. K.; Huang, Y.; Wu, Y.; Matter, W.; Gao, V.; Schmitt, D.; Didonato, J. A.; Fisher, E. A.; Smith, J. D.; Hazen, S. L. Paradoxical association of enhanced cholesterol efflux with increased incident cardiovascular risks. *Arterioscler. Thromb. Vasc. Biol.* **2013**, *33*, 1696−1705.
(24) Berrougui, H.; Grenier, G.; Loued, S.; Drouin, G.; Khalil, A. A new insight into resveratrol as an atheroprotective compound: inhibition of lipid peroxidation and enhancement of cholesterol efflux. *Atherosclerosis* **2009**, *207*, 420−427.
(25) Xia, M.; Hou, M.; Zhu, H.; Ma, J.; Tang, Z.; Wang, Q.; Li, Y.; Chi, D.; Yu, X.; Zhao, T.; Han, P.; Xia, X.; Ling, W. Anthocyanins induce cholesterol efflux from mouse peritoneal macrophages: the role of the peroxisome proliferator-activated receptor γ-liver X receptor α-ABCA1 pathway. *J. Biol. Chem.* **2005**, *280*, 36792−36801.
(26) Uto-Kondo, H.; Ayaori, M.; Ogura, M.; Nakaya, K.; Ito, M.; Suzuki, A.; Takiguchi, S.; Yakushiji, E.; Terao, Y.; Ozasa, H.; Hisada, T.; Sasaki, M.; Ohsuzu, F.; Ikewaki, K. Coffee consumption enhances high-density lipoprotein-mediated cholesterol efflux in macrophages. *Circ. Res.* **2010**, *106*, 779−787.
(27) Nicod, N.; Visioli, F.; Ramirez de Molina, A. Quality control of HDL: nutrition and not numbers may determine HDL functionality. *J. Pharm. Nutr. Sci.* **2011**, *1*, 130−133.
(28) Yasuda, A.; Natsume, M.; Osakabe, N.; Kawahata, K.; Koga, J. Cacao polyphenols influence the regulation of apolipoprotein in HepG2 and Caco2 cells. *J. Agric. Food Chem.* **2011**, *59*, 1470−1476.
(29) Schaffer, S.; Lam, V. Y.; Ernst, I. M.; Huebbe, P.; Rimbach, G.; Halliwell, B. Variability in APOE genotype status in human-derived cell lines: a cause for concern in cell culture studies? *Genes Nutr.* **2014**, *9*, 364.

dients allows vegetable oils to perform as base oil and as additive(s). The additive function depends on the chemical nature of the group introduced into their structure. For example, introduction of branching through synthetic conversion will allow the vegetable oil to also take on the role of a pour point depressant additive because it will result in lowered pour point and cloud point properties.[12,16] Thus, such multifunctional characteristics make it unnecessary to incorporate, analyze, and control pour point depressant in the formulation, which is a big cost savings for the lubricant user. This study was designed to enzymatically synthesize, purify, identify, and characterize crude and purified lipoyl glyceride product mixtures for extreme pressure and other tribological properties.

MATERIALS AND METHODS

Materials. α-Lipoic acid (D/L racemic mixture, **1**) and 2-methyl-2-butanol were purchased from Sigma-Aldrich (St. Louis, MO, USA). Novozym 435 (*Candida antarctica* lipase B immobilized on acrylic beads) was purchased from Novozymes North America (Franklinton, NC, USA). High-oleic sunflower oil (81% oleic acid, **2**) was purchased from Columbus Foods (Des Plaines, IL, USA). Refined, bleached, and deodorized soybean oil, **3**, was obtained from Pioneer Hi-Breed International (Des Moines, IA, USA). Polyalphaolefin with a viscosity of 6 cSt at 100 °C (PAO6), known under the trade name Durasyn 166, **4**, was a free sample from Ineos Oligomers (League City, TX, USA). Di-*tert*-dodecyl polysulfide, $(t\text{-}C_{12}H_{25})_2S_5$, known under the trade name TPS-32, was a free sample supplied by Arkema Canada Inc. (Burlington, ON, Canada).

Synthesis of Lipoyl Glycerides. Lipoic acid, **1** (20.6 g; 0.10 mol), high-oleic sunflower oil, **2** (133 g; 0.15 mol), and 2-methyl-2-butanol (46 g) were treated with Novozym 435 (15.4 g; 10:1 substrate to enzyme ratio) for 24 h at 60 °C in an orbital shaker. The reaction mixture was then placed under partial vacuum (250 mbar) for 6 h at 60 °C using a rotary evaporator, which served to slightly increase the generation of lipoyl glycerides. The enzyme was separated from the product by filtration through a 20 μm nylon Spectra/Mesh (Cole-Parmer, Vernon Hills, IL, USA) and washed with acetone (200 mL) to increase product recovery. Solvent was removed under reduced pressure at 60 °C, and 133 g (89% yield) of the crude lipoyl glyceride product was obtained.

Solvent Fractionation of Lipoyl Glycerides. The reaction product was extracted with methanol (2 × 300 mL) to remove lipoic acid and free fatty acids. The oil phase was freed of residual solvent under reduced pressure at 60 °C to give 93 g, 61% isolated yield, of purified lipoyl glyceride product.

HPLC Analysis. Analyses were performed using a Thermo Separation Products (San Jose, CA, USA) HPLC system consisting of a Spectra System AS3000 autosampler, a Spectra System P4000 pump, a Spectra System UV6000LP detector, an Alltech (Deerfield, IL, USA) 500 evaporative light-scattering detector, and a 250 mm × 4.6 mm i.d., 5 μm, Luna Phenyl-Hexyl column (Phenomenex, Torrance, CA, USA). The column was eluted isocratically with 95% acetonitrile/5% acetone/0.05% acetic acid (v/v/v) at a flow rate of 1.5 mL/min, with UV detection at 340 nm. Injection volumes were 10 μL.

LC High-Resolution Mass Spectroscopy Analysis. Structural confirmation of derivative structures was obtained by high-resolution mass spectrometry using a Thermo Scientific Accela UHPLC system (autoinjector, PDA detector, and a 1250 quaternary pump) coupled with an LTQ Orbitrap Discovery mass spectrometer (MS), with an Ion Max electrospray ionization (ESI) source, all running under Thermo Scientific Xcalibur LC-MS software. The MS was run with the ESI probe in the positive mode. The source inlet temperature was 350 °C; the sheath gas rate was set at 10 arbitrary units; the auxiliary gas rate was set at 2 arbitrary units; and the sweep gas rate was set at 2 arbitrary units. The maximal mass resolution was set at 30000, the spray voltage was set at 3.0 kV, and the tube lens was set at −100 V. Other parameters were determined and set by the calibration and tuning process. The column (Luna Phenyl-Hexyl; 5 μm, 250 mm × 4.6 mm) was eluted isocratically with 95% acetonitrile/5% acetone containing 0.1% formic acid at a flow rate of 1.0 mL/min, with UV detection at 340 nm.

Solubility in Petroleum-Based Oils. The solubility of lipoyl glyceride product mixtures in **4** at room temperature was determined gravimetrically, using visual inspection for any changes in oil transparency, and is expressed as a percentage of the total weight.

Surface Tension. Equilibrium surface tension at room temperature (23 ± 2 °C) was measured using the axisymmetric drop shape analysis method[17] on the FTA 200 automated goniometer (First Ten Angstroms, Portsmouth, VA, USA), using previously reported procedure.[18]

Density, Viscosity, and Viscosity Index. Density and dynamic and kinematic viscosity as a function of temperature were measured on a Stabinger SVM3000/G2 viscometer (Anton Paar GmbH, Graz, Austria). Viscosity index was calculated from kinematic viscosity data at 40 and 100 °C following the procedure outlined in ASTM D 2270-93.[19]

Pressurized Differential Scanning Calorimetry (PDSC). PDSC tests were conducted on a Q20P pressure differential scanning calorimeter (TA Instruments−Waters LLC, New Castle, DE, USA) fitted with a computer and appropriate software to allow for data acquisition and analysis. All tests were conducted with the cell pressurized with pure oxygen to 500 ± 25 psig in dynamic mode, that is, with a positive oxygen flow rate of 100 ± 10 mL/min. In a typical experiment, an oil sample of 1.2−2.0 mg was placed onto an aluminum pan, which was then hermetically sealed; a small pinhole was punched on the top cover, and the pan was placed in the instrument cell. The cell was then pressurized to 500 ± 25 psig and the temperature allowed to equilibrate to 50 °C. Oxygen was then allowed to flow at 100 ± 10 mL/min. Once the desired oxygen pressure, flow rate, and initial cell temperature were attained, the cell temperature was ramped up to 250 °C at a rate of 10 °C/min. The resulting heat flow versus temperature data were plotted and analyzed using the instrument computer and software to determine onset temperature and peak temperature. Duplicate runs were conducted, and average values are reported.

Four-Ball (4-Ball) Instrument and Test Specimen. The 4-ball tests were conducted on a model KTR-30L 4-ball tribometer equipped with TriboDATA software (Koehler Instruments, Bohemia, NY, USA). The specification and detailed description of the instrument hardware and software have been given before.[6] Test balls used in 4-ball experiments were obtained from Falex Corp. (Aurora, IL, USA), and their specifications have also been given before.[6]

4-Ball Antiwear Test. The 4-ball antiwear tests were conducted according to the procedure outlined in ASTM D 4172-94.[20] The coefficient of friction for each test was calculated from the corresponding torque and load data using the procedure outlined in ASTM D 5183-95.[21] The wear scar diameters of the balls used in the test were measured using a wear scar measurement system comprising hardware and ScarView software (Koehler Instruments). The wear scar diameters along and across the wear direction of the three balls were used to calculate the average wear scar diameters for the test. Each test lubricant was used in at least two antiwear measurements, and average coefficient of friction and wear scar diameters values were reported.

4-Ball Extreme Pressure Test. The 4-ball extreme pressure test was conducted according to the procedure outlined in ASTM D 2783-88.[22] The test comprises a series of 10 s tests at increasing loads until welding of the four balls is observed. The load at which welding is observed is the weld point and is a characteristic extreme pressure property of the lubricant tested. For tests below the weld point, the average wear scar diameter of the three balls, measured in accordance with ASTM D 4172-94,[27] is recorded as a function of the test load.

RESULTS AND DISCUSSION

Lipoic Acid Basics. Lipoic acid, **1**, is a naturally occurring cellular cofactor that has a cyclic disulfide moiety.[23] Sulfur is

one of several elements known to provide extreme pressure properties to lubricants.[24] This makes derivatives of lipoic acid potential candidates for application in extreme pressure lubrication. Lipoic acid is an ingredient in dietary supplements and cosmetics.[25,26] In addition, lipoic acid exhibits beneficial effects in the therapy of many diseases. In the past few years, several papers have described its chemical modifications to improve pharmacological properties.[27] The solubility of lipoic acid in lubricating oils is very low but can be significantly improved with appropriate modifications. Novel conjugates of 1,3-dioleoyl-glycerol and lipoic acid have been already described in the literature.[28] The enzymatic route described in this paper is a green synthesis approach that is readily scalable to high production volumes through proven continuous packed-column technology[29] and does not rely on single-use catalysts described in the literature[28] procedure.

Synthesis and Characterization of Lipoyl Glycerides. A schematic for the enzymatic synthesis of lipoyl glycerides is given in Figure 1. A detailed description of the synthesis, purification, and characterization of lipoyl glycerides has been given previously.[30]

Various glycerides of lipoic acid (**1**) were obtained by a lipase-catalyzed transesterification reaction between high-oleic sunflower oil (**2**) and **1** (Figure 1). A 1:1.5 molar ratio of **1** to **2** was used. Application of excess **2** in the reaction helped ensure that a large proportion of **1** was incorporated into the glyceride species. The reaction product was a complex mixture of unreacted starting materials (**1** and **2**) as well as various structures of lipoyl glycerides and free fatty acids (**9**). Some of the structures in the reaction product mixture are depicted in Figure 1.

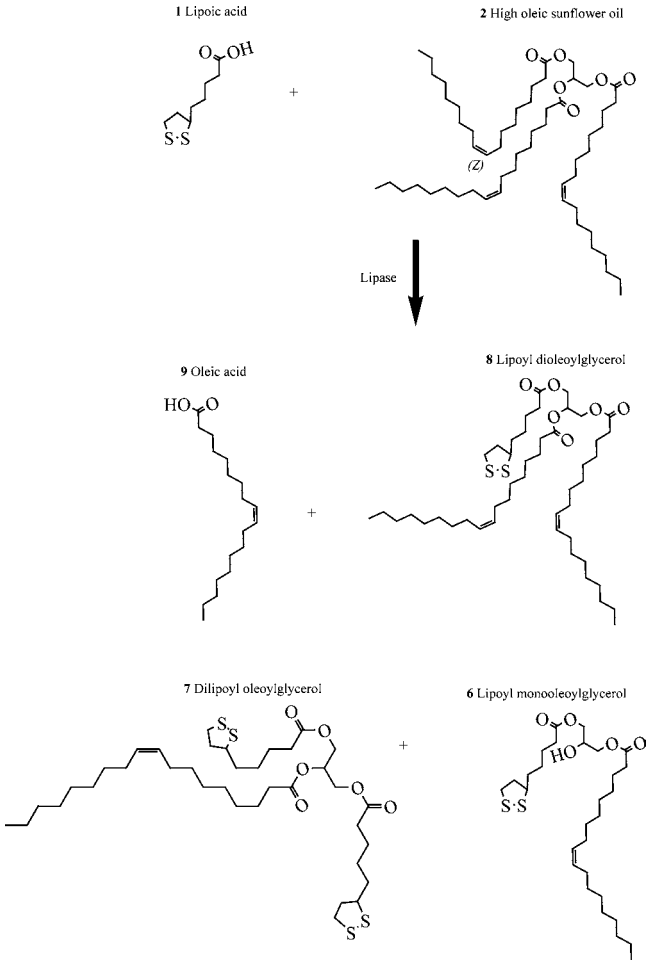

Figure 1. Schematic of the transesterification reaction of lipoic acid with high-oleic sunflower oil.

HPLC and LC-MS analyses were used to identify and quantitate **1** and the various lipoyl products in the product mixture. The following principal lipoyl reaction products were observed: lipoyl glycerol (**5**), lipoyl monooleoylglycerol (**6**), dilipoyl oleoylglycerol (**7**), and lipoyl dioleoylglycerol (**8**). The mass spectra of these entities are shown in Figure 2. In all cases, the parent compound was identified in a complex with a metal ion (K^+ or Na^+) or formate resulting from the MS ionization process. Multiple complexes were observed, including dimers. The fact that the principal products are oleoylglycerides is consistent with the fatty acid composition of **2**, which is mainly (81%) oleic acid (Table 1).[31] As expected, small quantities of similar lipoyl derivatives of other fatty acids of **2** were also observed.

The analysis of the lipoyl product mixture showed that 72 mol % of the original **1** participated in the transesterification reaction to produce a variety of lipoyl products, whereas 28 mol % did not react at all (Table 2). The relative molar composition of reacted **1** in the crude product mixture decreased in the order **8** > **7** > **6** > **5** (Table 2).

The crude product mixture containing lipoyl glycerides was extracted with a polar solvent, methanol. The resulting purified mixture was analyzed using the same procedures used to analyze the crude product mixture. Table 3 compares the composition (% w/w and mol/mol) of the major species in the crude versus purified product mixtures. As expected, extraction with methanol completely removed the more polar species from the crude product. As a result, the purified product was free of unreacted **1** and **9** generated by the transesterification reaction. These two species are the most polar components in the crude product mixture. Their removal resulted in an increase in the relative proportion of the less polar components **2**, **8**, and **7** in the purified product mixture (Table 3). Thus, the crude and purified product mixtures represented two different compositions and were evaluated for their physical and tribological properties.

Density. The densities of neat soybean oil (**3**), **2**, crude and purified product mixtures, and blends at 40, 75, and 100 °C are compared in Table 4. As expected, the densities of all the oils investigated decreased with increasing temperature. The data in Table 4 show that the crude and purified product mixtures had higher densities than the starting **2**, which had lower density than **3**. The higher density of the product mixtures over **2** can be attributed to the insertion of the heavier sulfur atoms during transesterification. The density results also show a slightly higher value for the crude than for the purified product mixture. However, for all practical purposes, the two product mixtures can be considered to have similar densities. The data in Table 4 also show that the blends have higher densities than the neat vegetable oils (**2**, **3**), and the density increases proportionately with increasing concentrations of the product mixtures in **2** and **3**. An important observation in Table 4 is the relative density of the crude product mixture blend in **2** versus that in **3**. The density of the blend in **3** is greater than that in **2** at 40 and 75 °C but is reversed (**2** > **3**) at 100 °C. This could be due to a higher propensity of crude product mixture to decompose in **3** than in **2** at 100 °C, which is close to the melting point of sulfur.

dx.doi.org/10.1021/jf404289r | J. Agric. Food Chem. 2014, 62, 2233−2243

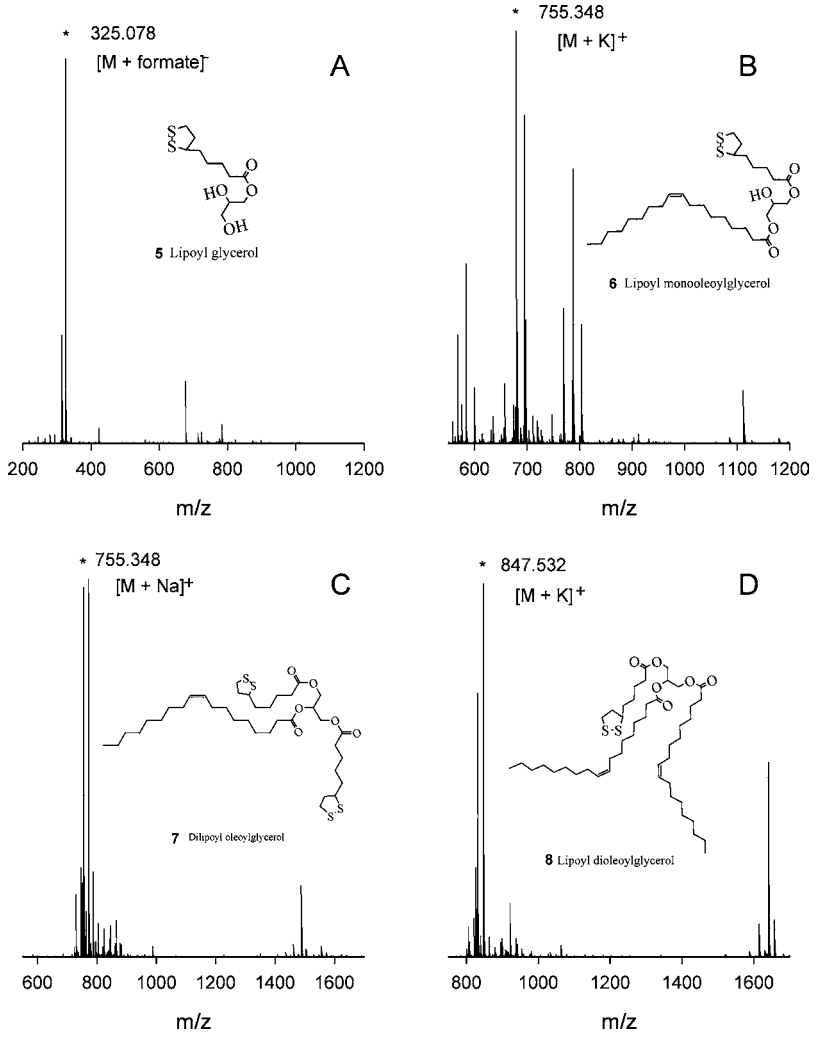

Figure 2. Mass spectra of (A) lipoyl glycerol, (B) lipoyl monooleoylglycerol, (C) dilipoyl oleoylglycerol, and (D) lipoyl dioleoylglycerol. The asterisk in each panel marks the identifying peak for the illustrated compound.

Table 1. Fatty Acid Composition of High-Oleic Sunflower (2) and Soybean (3) Oils

fatty acid name	fatty acid structure	**2**, % w/w[31]	**3**, % w/w[5]
palmitic	C16:0	5	10.6
stearic	C18:0	4	4.0
oleic	C18:1	81	23.2
linoleic	C18:2	9	53.7
linolenic	C18:3	0.5	7.6

Viscosity and Viscosity Index. The kinematic and dynamic viscosities of neat **2**, **3**, crude and purified product mixtures, and blends are compared in Table 4. As with density, the viscosities of the transesterification products were higher than that of the starting **2**, which was more viscous than **3** (Table 4). The increased viscosity of the two product mixtures relative to **2** can be attributed to the increased polarity of the molecules after transesterification. The increased polarity will increase the intermolecular interactions between the molecules and thereby retard oil flow. Table 4 also shows that the purified product mixture is more viscous than the crude, which is the reverse of the relative densities between these two product mixtures. This could be due to the higher average molecular weight of the purified product mixture relative to the crude. The data in Table 4 also show that the kinematic and dynamic viscosity of blends in **2** or **3** increased with increasing concentrations of product mixtures in the blend.

The viscosity indices of neat **2**, **3**, crude and purified product mixtures, and blends are also given in Table 4. Transesterification resulted in slightly lowering the viscosity index of **2** from about 200 to 178−185. Despite this lowering, the viscosity index range for the neat product mixtures was much higher than the best petroleum-based and polyalphaolefin (**4**) oils. Blending of lipoyl glyceride product mixtures in **2** and **3** caused a slight reduction in the viscosity index of these two vegetable oils. As shown in Table 4, the viscosity index decreased with increasing concentration of the two product mixtures in the vegetable oils.

Surface Tension. The surface tensions of the neat oils and blends are compared in Table 5. As shown in Table 5, within one standard deviation, transesterification did not cause any change in the surface tension of **2**. The surface tension of **2**, which is slightly higher than that of **3**, remained more or less the same. However, as shown in Table 5, blending of the crude product mixtures into **3** increased the surface tension of **3** by almost 1 dyn/cm to the value of the neat product mixtures.

Solubility in Polyalphaolefin Oil (4). Application of lipoyl glycerides as lubricant additives requires that they be soluble

dx.doi.org/10.1021/jf404289r | J. Agric. Food Chem. 2014, 62, 2233−2243

Table 2. Relative Molar Distribution of Lipoyl Species in the Crude Lipoyl Glyceride Product Obtained from the Transesterification Reaction between Lipoic Acid and High-Oleic Sunflower Oil

lipoic species	lipoic moiety distribution,[a] mol %	*m/z* (calcd)	*m/z* (found)[b]
1, lipoic acid	28 ± 1[c]	ND[d]	ND[d]
5, lipoyl glycerol	6 ± 1	325.078 $C_{12}H_{21}O_6S_2$	325.078 $[M + formate]^-$
6, lipoyl monooleoylglycerol	12 ± 2	583.289 $C_{29}H_{52}O_5S_2K$	583.306 $[M + K]^+$
7, dilipoyl oleoylglycerol	15 ± 1	755.348 $C_{37}H_{64}O_6S_4Na$	755.348 $[M + Na]^+$
8, lipoyl dioleoylglycerol	39 ± 2	847.535 $C_{47}H_{84}O_6S_2K$	847.532 $[M + K]^+$

[a]Mean and standard deviation (n = 3) of the lipoic species (relative to the initial moles of lipoic acid) concentration based on detected UV absorbance (340 nm) during HPLC. Includes oleic and other fatty acid species. [b]Determined by LC-MS. [c]28 mol % of the starting lipoic acid did not participate in the transesterification reaction. [d]Not determined.

Table 3. Composition of Crude (LGc) and Purified (LGp) Lipoyl Glyceride Product Mixture Obtained from Transesterification of Lipoic Acid with High-Oleic Sunflower Oil

		%, mol/mol		%, w/w		[S] % in	
component	mol wt, g/mol[a]	LGc	LGp[b]	LGc	LGp[b]	LGc	LGp
1, lipoic acid	206	10.2	0.0	4.0	0.0	1.2	0.0
9, free fatty acids	282	35.4	0.0	18.0	0.0	0.0	0.0
5, lipoyl glycerol	280	2.4	2.9	1.3	1.0	0.3	0.2
6, lipoyl monooleoylglycerol	544	5.1	3.0	5.0	2.0	0.6	0.2
7, dilipoyl oleoylglycerol[c]	733	3.0	6.7	4.0	6.0	0.7	1.1
8, lipoyl dioleoylglycerol	809	15.6	41.3	22.8	41.0	1.8	3.2
2, high-oleic sunflower oil	885	28.2	46.1	45.0	50.0	0.0	0.0
LGc (wt av)	701						
LGp (wt av)	831						
total [S], % w/w						4.6	4.7

[a]Molecular weight calculations are based on oleic acid as the fatty acid in the component. [b]Reaction product after solvent fractionation. [c]Taking into account that dilipoyl oleoylglycerol has two lipoyl groups, its molecular species portion was considered to be half of its proportion measured by HPLC at 340 nm.

Table 4. Density (d), Kinematic Viscosity (kVis), Dynamic Viscosity (dVis), and Viscosity Index (VI) of Neat Oils (2, 3, and Crude (LGc) and Purified (LGp) Lipoyl Glyceride Product Mixtures) and Blends[a]

		neat oils				blends of LGc in **3**		blends of LGc in **2**	
	T (°C)	**3**	**2**	LGc	LGp	5% w/w	10% w/w	5% w/w	10% w/w
d, g/mL	40	0.9068	0.8994	0.9284	0.9274	0.9080	0.9087	0.9006	0.9021
	75	0.8838	0.8763	0.9045	0.9040	0.8847	0.8854	0.8775	0.8790
	100	0.8671	0.8683	0.8902	0.8875	0.8684	0.8690	0.8711	0.8761
kVis, mm^2/s	40	31.88	40.77	42.18	45.96	33.15	33.26	40.85	40.03
	75	12.57	14.69	14.44	15.74	12.72	12.69	14.635	14.36
	100	7.68	8.72	8.35	9.12	7.80	7.74	8.67	8.50
dVis, mPa-s	40	28.91	36.67	39.25	42.62	30.10	30.22	36.42	36.67
	75	11.11	12.87	13.09	14.23	11.26	11.24	12.75	12.78
	100	6.66	7.5	7.44	8.1	6.78	6.73	7.43	7.43
VI		224	200	178.5	185.0	218.5	215.0	199	197.5

[a]Standard deviations: d, ±0.0000−0.0199 g/mL; kVis, ±0.00−0.58 mm^2/s; dVis, ±0.00−0.81 mPa-s; VI, ±0.00−2.1

not only in biobased base oils such as **2** and **3** but also in petroleum-based oils such as **4**. Solubility investigation showed that both product mixtures are highly soluble in **2** and **3**. The results of the solubility study in **4**, which has a viscosity close to that of **3**, are also summarized in Table 5. As shown in Table 5, the crude product mixture was found to be insoluble in **4**,

dx.doi.org/10.1021/jf404289r | J. Agric. Food Chem. 2014, 62, 2233−2243

Table 5. Solubility, Surface Tension, Cloud Point, and Pour Point of Neat Oils (2, 3, and Crude (LGc) and Purified (LGp) Lipoyl Glyceride Product Mixtures) and Some Blends

	solubility in polyalphaolefin oil, % w/w	surface tension, dyn/cm	cloud point, °C	pour point, °C
neat oils				
3		31.8 ± 0.5		−9[5]
2		32.7 ± 0.2		−12[9]
LGc	<0.4	32.8 ± 0.3	−3.5 ± 0.3	−17.7 ± 0.6
LGp	>11.0	33.0 ± 0.3	−1.4 ± 0.2	−16.3 ± 0.6
blends				
5% LGc in **3**		32.6 ± 0.1		
10% LGc in **3**		32.7 ± 0.1		

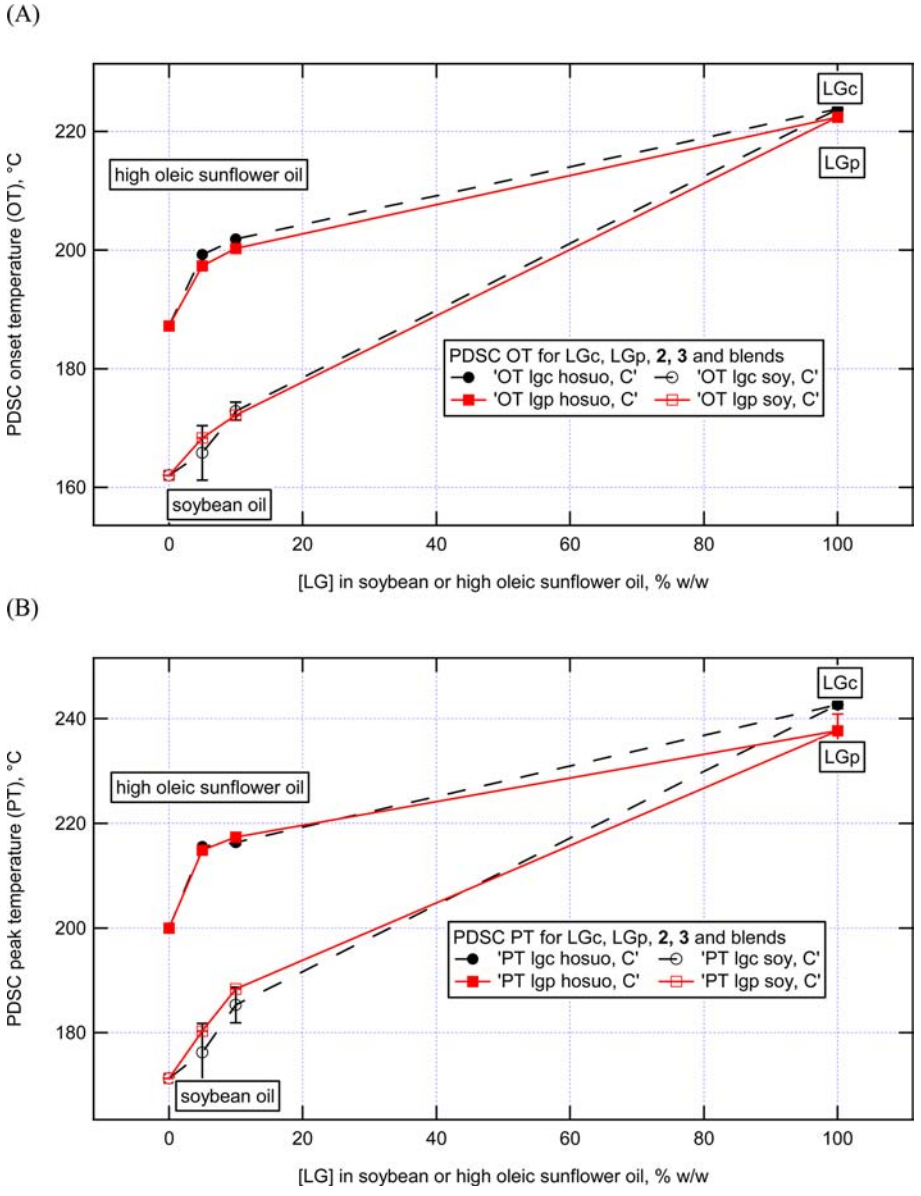

Figure 3. PDSC: (A) onset temperature (OT) and (B) peak temperature (PT) of **2**, **3**, crude (LGc) and purified (LGp) lipoyl glyceride product mixtures, and blends (°C).

whereas the purified product mixture was highly soluble. The difference in the solubility of these two product mixtures is a reflection of the difference in their compositions. As shown in Table 3, the crude contains almost 48% mol/mol of polar or hydrophilic components (**1**, **5**, **9**), whereas the purified contained a mere 2.9% mol/mol. As a result, the crude mixture is hydrophilic and insoluble in the lipophilic **4**, whereas the purified mixture is lipophilic and highly soluble in **4**, as shown in Table 5.

dx.doi.org/10.1021/jf404289r | J. Agric. Food Chem. 2014, 62, 2233−2243

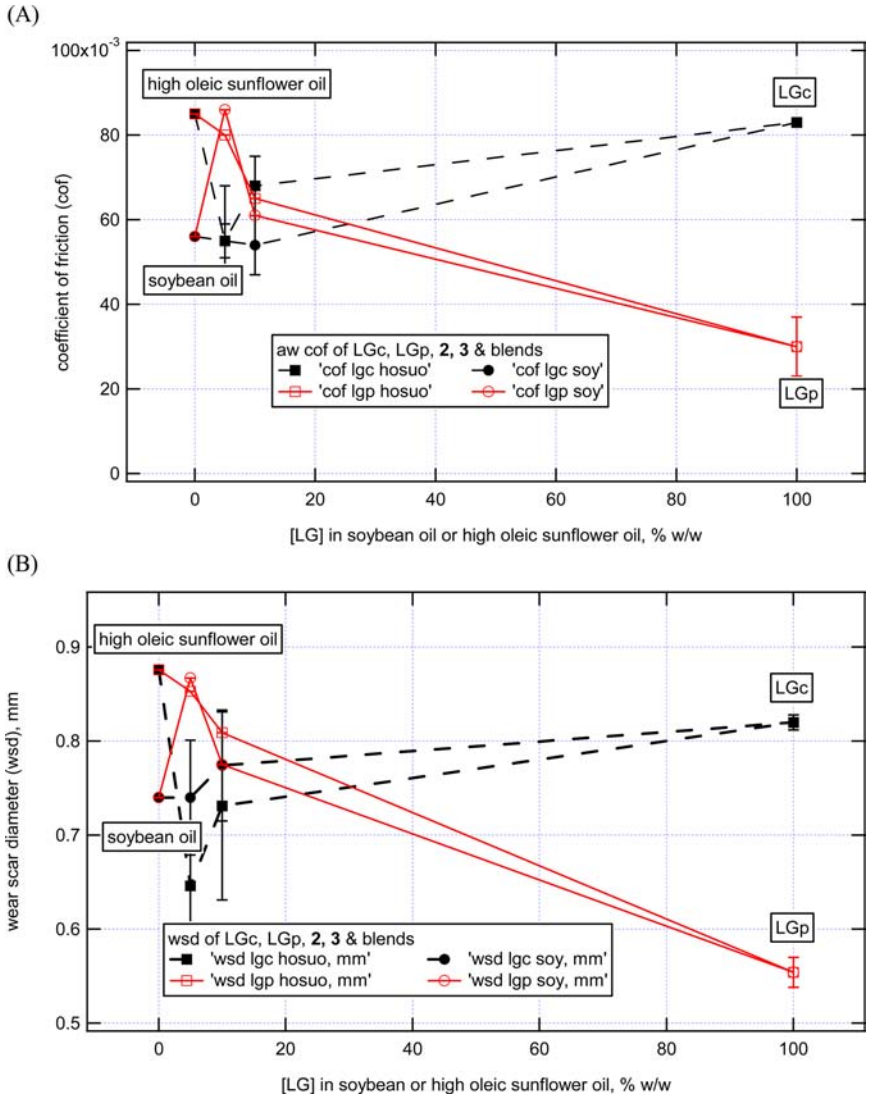

Figure 4. Antiwear properties of **2**, **3**, crude (LGc) and purified (LGp) lipoyl glyceride product mixtures, and blends: (A) coefficient of friction (COF); (B) wear scar diameter (WSD, mm).

Oxidation Stability. Oxidation stability was investigated using PDSC. In this procedure, the oils are heated at a fixed rate (°C/min) under a pressurized oxygen atmosphere until oxidation is detected due to changes in heat flow. The temperatures at which the oxidation begins, called the onset temperature, and maximum oxidation occur, called the peak temperature, are used to compare the oxidation stability properties of oils. Onset and peak temperatures correlate very well, and either or both values can be used to compare the oxidation stability of vegetable oils. The higher the onset and peak temperatures, the more stable the oil is toward oxidation.

The oxidation of vegetable oils has been attributed to the presence of allylic and bis-allylic protons in their structures.[2,15] Thus, the relative abundance of mono- and polyunsaturated fatty acids in the respective triglycerides of the vegetable oils has a strong influence on oxidation stability properties. The higher the degree of unsaturation, the less oxidatively stable the oil.

Table 1 compares the fatty acid compositions of **2** and **3** and provides data about the structure of the fatty acid as it relates to the number of double bonds as well as the relative fraction of each fatty acid in the triglyceride mixture in the oil. The data in Table 1 can be used to estimate the degree of unsaturation or unsaturation index (UI) for the vegetable oils as[32]

$$\mathrm{UI} = 100 \times [\Sigma(d_i \times w_i)] \quad (1)$$

where d_i is the number of double bonds on a fatty acid and w_i is the weight fraction of the fatty acid in the vegetable oil.

According to eq 1, the larger the number of double bonds in the fatty acid and the larger its weight fraction among the fatty acids in the triglyceride, the higher the UI value and the less oxidatively stable the oil will be. Application of eq 1 to the data in Table 1 gave UI values of 100.5 and 153.4 for **2** and **3**, respectively. Thus, eq 1 predicts that **2** will have a lower UI and, hence, will be more oxidatively stable than **3**.

Figure 3 compares the PDSC results for neat **2**, **3**, crude and purified product mixtures, and their blends. The data for the neat vegetable oils shows higher onset and peak temperatures for **2** than for **3**, as was predicted by eq 1. The data in Figure 3 also show that the neat crude and purified product mixtures have significantly higher oxidation stability than either vegetable oil. It also shows that the addition of small amounts of the crude or purified product mixture to the vegetable oils resulted in significant improvement in their oxidation stability. The

dx.doi.org/10.1021/jf404289r | J. Agric. Food Chem. 2014, 62, 2233−2243

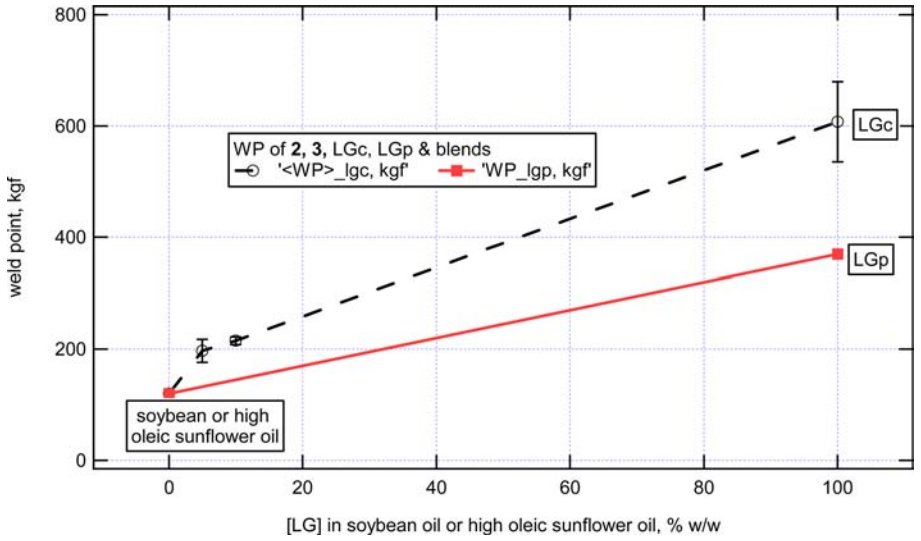

Figure 5. Weld points (WP) of **2**, **3**, crude (LGc) and purified (LGp) lipoyl glyceride product mixtures, and blends (kgf).

onset and peak temperatures of the vegetable increased with increasing concentration of crude and purified product mixtures in the blend.

There are two possible reasons for the improvements in the oxidation stability of **2** after the transesterification reaction with **1**. The most obvious reason is the replacement of fatty acids with mono- or polyunsaturation by **1**, which has zero unsaturation. A second possible reason is the antioxidant property of the sulfur moiety in the crude and purified product mixtures. Improvements in the oxidation stability properties of oils with sulfur moieties have been reported previously and have been attributed to the antioxidation property of the sulfur group.[16,33,34]

Examination of Figure 3 shows slightly higher onset and peak temperatures for the crude than for the purified product mixture, which corresponds to a slightly better oxidation stability for the crude product mixture. This difference cannot be attributed to differences in sulfur content between the two products, because they are about equal (Table 3). However, it might be due to other properties related to compositional differences. As discussed before, two types of lipoyl glyceride species were generated after transesterification: hydrophilic (polar) and lipophilic (nonpolar). As shown in Tables 2 and 3, almost 50% of the species in the crude mixture are hydrophilic, whereas the corresponding value in the purified mixture is <3%. The improved oxidation stability of the crude product might be an indication of a better antioxidant characteristic for the hydrophilic than for the lipophilic lipoyl glyceride species.

Cold-Flow Properties. Cold-flow properties correspond to temperatures below which the oils cease to flow. It is an important property of lubricating oils that dictates the seasons and geographic locations where the oils can be applied. Pour point and cloud point are used to quantify cold-flow properties. Table 5 compares the pour points and cloud points of crude and purified product mixtures, along with those of **2** and **3**. As shown in Table 5, improvements in pour point and cloud point have been observed as a result of the transesterification reaction. Both the crude and purified product mixtures displayed improved cold-flow properties over those reported for the parent **2**[9] or for **3**.[5] Improvements in cold-flow properties are usually associated with the introduction of branching to the triglyceride chains, which is not the case here. Two possible reasons are replacement of long-chain fatty acids (C_{16} and higher) in the starting triglycerides, which causes crystallization and solidification at lower temperature, by the shorter chain (C_8) **1** during transesterification (see Figure 1 and Table 1), and production of a much more complex product mixture after transesterification than that of the starting **2**, which will result in depressed melting temperatures.

Antiwear Properties. 4-Ball friction and wear properties under antiwear conditions (40 kgf, 1200 rpm, 75 °C, 60 min) are compared in Figure 4. The test provides two parameters: coefficient of friction and wear scar diameter. Neat **2** showed a higher coefficient of friction and higher wear scar diameter than neat **3**. This result is contrary to expectation based on the relative viscosities of these two vegetable oils (Table 4). Antiwear tests are conducted under mixed film conditions where both the viscosity and chemical properties of the oils will have an effect. In oils with similar chemical properties, viscosity becomes the dominant predictor of antiwear results. In this particular case, however, viscosity effects were overwhelmed by chemical effects. This indicates major differences in chemical properties between these two vegetable oils, far beyond what is quantified by the fatty acid composition shown in Table 1.

Comparison of the antiwear results for the two product mixtures showed a different result from that between **2** and **3**. Here, the two product mixtures have similar chemical origins. Both are transesterification products of **1** and **2**, which means they have similar chemical species in their mixture. However, because of the differences in purification procedures, they comprise different proportions of the same species. The consequence of this, as discussed previously, was differences in lipophilicity and viscosity. The crude mixture was found to be less viscous and less lipophilic than the purified (Tables 3 and 4). As a result, the crude mixture, because of its hydrophilic properties, was found to be insoluble in the lipophilic base oil **4** (Table 5). The consequence of viscosity is illustrated in Figure 4, where the lower viscous crude product displayed a poorer coefficient of friction and wear scar diameter. Such a result is expected in mixed film test conditions of oils with similar chemical properties but different viscosities.[24]

Extreme Pressure (EP) Properties. Extreme pressure tests are conducted to determine if the oils are capable of providing lubrication at very high pressures and/or temperature

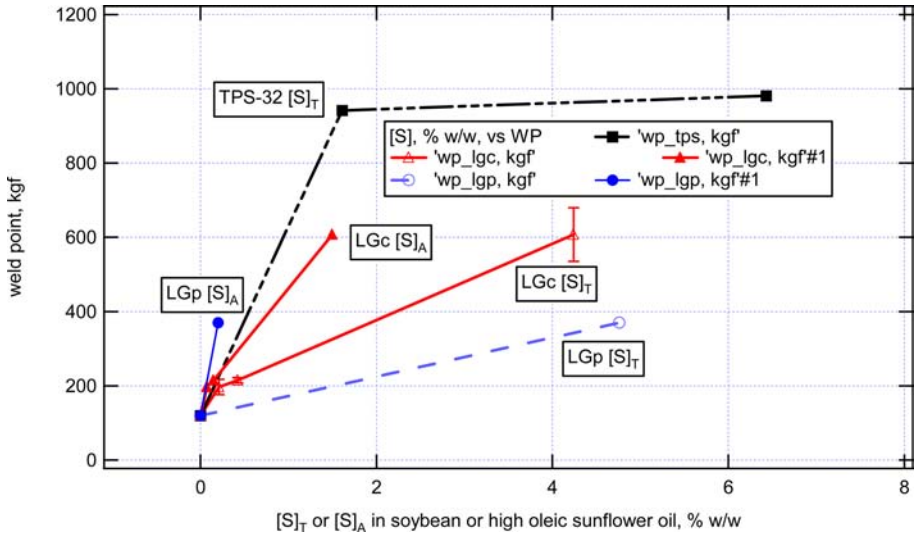

Figure 6. Effect of total versus active sulfur concentration on weld point (WP) for the commercial additive TPS-32 and crude (LGc) and purified (LGp) lipoyl glyceride product mixtures in the vegetable oil **2** or **3** (kgf).

conditions. To do so, the oils must be capable, under the lubrication conditions, of participating in a tribochemical reaction with the friction surfaces and in situ generating tribofilms that[24] reduce friction and separate the friction surfaces so they do not damage each other. Such properties have been observed in oils that contain certain elements including sulfur, phosphorus, and halogens. Therefore, it was of interest to investigate if the lipoyl glyceride mixtures, which contain disulfide moieties in their structures, could undergo tribochemical reactions under EP conditions and in situ produce tribofilms with beneficial properties. In the 4-ball extreme pressure test, a series of 10 s tests are conducted at 1760 rpm and room temperature, with the load progressively increasing until lubricant failure is observed due to the welding of the four balls. The load at which welding occurs is called the weld point and is the characteristic EP property of the oil. The higher the weld point, the better the extreme pressure property of the oil.

Neat vegetable and mineral base oils have weld point values of around 100 kgf and are considered not to have beneficial EP properties. Improving the EP properties of such oils is accomplished with the blending of additives that have one or more of the elements listed above.

The 4-ball extreme pressure test results on **2**, **3**, crude and purified product mixtures, and their blends are summarized in Figure 5. Similar weld point values of about 120 kgf were observed for **2** and **3**. As mentioned before, this value is expected and not high enough to be considered a beneficial extreme pressure characteristic. On the other hand, the crude and purified product mixtures displayed weld point values that were 4−6-fold higher (Figure 5). These results are considered a substantial improvement over the value of the neat vegetable oils and an indication of beneficial extreme pressure characteristic. The improved extreme pressure results of neat product mixtures indicates that the disulfide moieties in these products did participate in tribochemical reactions with the metal surfaces in situ during the test. The result of such tribochemical reaction is the generation of tribofilms that lower friction, prevent surface damage, and allow the lubrication process to proceed under the extreme conditions. In fact, small additions of the crude mixture to **2** or **3** resulted in increased weld point for the blends (Figure 5). This observation indicates that lipoyl glyceride product mixtures can also be used as extreme pressure additives to improve the EP pressure properties of vegetable oils.

Close examination of the data in Figure 5 shows big differences in the extreme pressure performance of neat crude product relative to neat purified product mixture. As it turns out, the hydrophilic crude product mixture was significantly more effective than the lipophilic purified product mixture in improving the EP properties of transesterified **2**. As mentioned previously, these two products are mixtures of species of similar chemical structures. However, they differ in the proportion of the chemical species. The crude mixture contains about equal molar quantities (% mol/mol) of hydrophilic and lipophic species, whereas purified mixture contains very little hydrophilic and almost all lipophilic species (Table 3). As a result, the crude mixture is soluble in polar vegetable oils but insoluble in lipophilic petroleum-based base oils. The purified product, on the other hand, is soluble in both polar and nonpolar base oils. It is also more viscous than the crude product, but viscosity has no contribution to EP properties.[24] Thus, understanding the difference in the extreme pressure performance of these two product mixtures will require closer examination of the relative composition of the species in their product mixture and of their solubility.

Effect of Chemical Structure. To better understand the difference in the EP properties of the crude and purified product mixtures, we compared the results with that of a commercial polysulfide extreme pressure additive, TPS-32, which has been described as di-*tert*-dodecyl polysulfide, $(t\text{-}C_{12}H_{25})_2S_5$, with five sulfur atoms per molecule.[35] In conducting the comparison, we assumed that TPS-32 has the single structure shown above and that all five sulfur atoms are active and participate in tribochemical reactions under EP conditions. On the other hand, crude and purified products comprise mixtures of lipophilic and hydrophilic structures with sulfur atoms for which relative tribochemical activity under extreme pressure conditions is unknown.

The weld points of the crude and purified products from this work were compared with the published weld point of TPS-32[35] as a function of the concentration of sulfur (% w/w) in

dx.doi.org/10.1021/jf404289r | J. Agric. Food Chem. 2014, 62, 2233−2243

each mixture. The concentrations of sulfur in the crude and purified product mixtures were estimated and are given in Table 3. The concentration of sulfur in TPS-32 was estimated by assuming that the material contains a single structure, $(t\text{-}C_{12}H_{25})_2S_5$. Two types of sulfur concentrations were used in the comparisons: total sulfur or $[S]_T$, the weight fraction of sulfur in all components in the material; and active sulfur or $[S]_A$, the weight fraction of sulfur in all of the components that participate in the tribochemical reaction. For TPS-32, because it is assumed that there is only one component in the mixture, $[S]_T = [S]_A$. However, for crude and purified product mixtures, $[S]_T$ is different from $[S]_A$. The value of $[S]_T$ was calculated from the contributions of all sulfur-containing components in each mixture, which is detailed in Table 3. However, $[S]_A$ values for the crude and purified mixtures were obtained from the contributions of the sulfur-containing hydrophilic components in the mixture, namely, **1**and **5** in Table 3.

This type of analysis was selected to test the hypothesis that the better extreme pressure performance of the crude product was an indication of preferential tribochemical reaction by the sulfur atoms of the hydrophilic species in the mixture. According to this hypothesis, the hydrophilic species will have lower solubility in the lipophilic **2** and will preferentially adsorb onto the hydrophilic metal surface rather than stay in solution in the lipophilic oil. In other words, the equilibrium between surface versus solution concentration is different for the hydrophilic and lipophilic species. The hydrophilic species will preferentially concentrate on the surface, whereas the lipophilic species will preferentially stay in solution. As a result, in the case of the crude product, there will be a higher concentration of sulfur atoms on the surface to participate in the tribochemical reactions with the metal surface and produce in situ the tribofilms responsible for the favorable extreme pressure outcome.

Figure 6 compares the weld points of TPS-32 and crude and purified products as a function of $[S]_T$ and $[S]_A$. Weld point values as a function of $[S]_T$ increased in the order purified $\ll$ crude $\ll$ TPS-32. On the other hand, weld point values as a function of $[S]_A$ displayed the following order: purified $\approx$ TPS-32 $\approx$ crude. Of course, this analysis is not proof of the mechanism for the extreme pressure performance of the crude and purified product mixtures. It is one of the many possible explanations for the observed differences in the EP properties between the two products. Further work is needed to verify the validity of this and alternative mechanisms.

Farm-based products provide a sustainable, abundant, safe, and environmentally friendly raw material base for many consumer and industrial products currently manufactured from petroleum. However, successful replacement of petroleum with farm-based raw materials will require solving a number of inherent weaknesses in natural products. In this work, enzymatic transesterification was applied to improve the lubrication properties of high-oleic sunflower oil. The enzymatically modified oil displayed improved oxidation stability and cold-flow properties relative to the unmodified oil. It also displayed highly improved extreme pressure properties that were comparable to those of a commercial extreme pressure additive widely used in various lubricant formulations currently on the market.

AUTHOR INFORMATION

Corresponding Author

*(G.B.) Phone: (309) 681-6479. Fax: (309) 681-6524. E-mail: girma.biresaw@ars.usda.gov.

Notes

Disclosure. Mention of trade names or commercial products in this publication is solely for the purpose of providing specific information and does not imply recommendation or endorsement by the U.S. Department of Agriculture.

The authors declare no competing financial interest.

ACKNOWLEDGMENTS

We gratefully acknowledge Linda Cao, Benetria Banks, and Leslie Smith for their technical help in this investigation.

REFERENCES

(1) Bremmer, B. J.; Plonsker, L. *Bio-Based Lubricants: A Market Opportunity Study Update*; Omni-Tech International: Midland, MI, USA, 2008.

(2) Schneider, M. P. Plant-oil-based lubricants and hydraulic fluids. *J. Sci. Food Agric.* **2004**, *86*, 1769−1780.

(3) Miller, M. EPA to require green lubes for vessels. *Lubes-n-Greases* **2013**, *19*, 22−26.

(4) Hope, K. Balancing lubricant properties with vegetable oil and PAO blends. *Proceedings of the Lubricants and Fluids Technical Advisory Panel*; United Soybean Board: Chicago, IL, USA, 2006.

(5) Lawate, S. S.; Lal, K.; Huang, C. Vegetable oils − structure and performance. In *Tribology Data Handbook*; Booser, E. R., Ed.; CRC Press: New York, 1997; pp 103−116.

(6) Asadauskas, S. J.; Biresaw, G.; McClure, T. G. Effects of chlorinated paraffin and ZDDP concentrations on boundary lubrication properties of mineral and soybean oils. *Tribol. Lett.* **2010**, *37*, 111−121.

(7) Rudnick, L. R.; Abdellatif, M. A.; Gül, O.; Biresaw, G. Vaporization and carbonization tendency of vegetable oils as a function of chemical composition: morphology of carbon deposits on steel surfaces at elevated temperature. In *Surfactants in Tribology*; Biresaw, G., Mittal, K. L., Eds.; Taylor & Francis: Boca Raton, FL, USA, 2011; Vol. 2, pp 409−433.

(8) Biresaw, G.; Bantchev, G. Elastohydrodynamic (EHD) traction properties of seed oils. *Tribol. Trans.* **2010**, *53*, 573−583.

(9) Asadauskas, S.; Erhan, S. Z. Depression of pour points of vegetable oils by blending with diluents used for biodegradable lubricants. *J. Am. Oil Chem. Soc.* **1999**, *76*, 313−316.

(10) Govindapillai, A.; Jayadas, N. H.; Bhasi, M. Analysis of the pour point of coconut oil as a lubricant base stock using differential scanning calorimetry. *Lubr. Sci.* **2009**, *21*, 13−26.

(11) Harry-O'kuru, R. E.; Holser, R. A.; Abbott, T. P.; Weisleder, D. Synthesis and characteristics of polyhydroxy triglycerides from milkweed oil. *Ind. Crops Prod.* **2002**, *15*, 51−58.

(12) Salimon, J.; Saliha, N.; Yousif, E. Triester derivatives of oleic acid: the effect of chemical structure on low temperature, thermo-oxidation and tribological properties. *Ind. Crops Prod.* **2012**, *38*, 107−114.

(13) Adhvaryu, A.; Erhan, S. Z.; Perez, J. M. Tribological studies of thermally and chemically modified vegetable oils for use as environmentally friendly lubricants. *Wear* **2004**, *257*, 359−367.

(14) Bantchev, G. B.; Kenar, J. A.; Biresaw, G.; Han, M. G. Free radical addition of butanethiol to vegetable oil double bonds. *J. Agric. Food Chem.* **2009**, *57*, 1282−1290.

(15) Knothe, G. Structure indices in FA chemistry. How relevant is the iodine value? *J. Am. Oil Chem. Soc.* **2002**, *79*, 847−854.

(16) Biresaw, G.; Bantchev, G. B.; Cermak, S. C. Tribological properties of sulfur modified vegetable oils. *Tribol. Lett.* **2011**, *43*, 17−32.

(17) Rotenberg, Y.; Boruvka, L.; Neumann, A. W. Determination of surface tension and contact angle from the shapes of axisymmetric fluid interfaces. *J. Colloid Interface Sci.* **1983**, *3*, 169−183.
(18) Biresaw, G. Adsorption of amphiphies at an oil-water vs. an oil-metal interface. *J. Am. Oil Chem. Soc.* **2005**, *82*, 285−292.
(19) ASTM D 2270-93. Standard practice for calculating viscosity index from kinematic viscosity at 40 and 100 °C. *Annual Book of ASTM Standards*; ASTM: West Conshohocken, PA, USA, 2002; Vol. 05.01, pp 769−774
(20) ASTM D 4172-94. Standard test method for wear preventive characteristics of lubricating fluid (four-ball method). *Annual Book of ASTM Standards*; ASTM: West Conshohocken, PA, USA, 2002; Vol. 05.02, pp 752−756
(21) ASTM D 5183-95. Standard test method for determination of the coefficient of friction of lubricants using the four-ball wear test machine. *Annual Book of ASTM Standards*; ASTM: West Conshohocken, PA, USA, 2002, Vol. 05.03, pp 165−169
(22) ASTM D 2783-88. Standard test method for measurement of extreme-pressure properties of lubricating fluids (four-ball method). *Annual Book of ASTM Standards*; ASTM: West Conshohocken, PA, USA, 2002; Vol. 05.02, pp 130−137
(23) Packer, L.; Cadenas, E. Lipoic acid: energy metabolism and redox regulation of transcription and cell signaling. *J. Clin. Biochem. Nutr.* **2011**, *48*, 26−32.
(24) Schey, J. A. *Tribology in Metalworking Friction, Lubrication and Wear*; American Society of Metals: Metals Park, OH, USA, 1983.
(25) Segall, A.; Sosa, M.; Alami, A.; Enero, C.; Hormaechea, F.; Pizzorno, M. T.; Bregni, C.; Serrao, R. Stability study of lipoc acid in the presence of vitamins A and E in o/w emulsions for cosmetic application. *J. Cosmet. Sci.* **2004**, *55*, 449−461.
(26) Smith, A. R.; Shenvi, S. V.; Widlansky, M.; Suh, J. H.; Hagen, T. M. Lipoic acid as a potential therapy for chronic diseases associated with oxidative stress. *Curr. Med. Chem.* **2004**, *11*, 1135−1146.
(27) Bernini, R.; Crisante, F.; Merendino, N.; Molinari, R.; Soldatelli, M. C. *Eur. J. Mol. Chem.* **2011**, *46*, 439−446.
(28) Madawala, S. R. P.; Andersson, R. E.; Jastrebova, J. A.; Almeida, M.; Dutta, P. C. Novel conjugates of 1,3-diacylglycerol and lipoic acid: synthesis, DPPH assay, and RP-LC-MS-APCI analysis *J. Lipids* **2011**, DOI: 10.1155/2011/419809.
(29) Laszlo, J. A.; Compton, D. L.; DeFilippi, L. J.; Grall, S. Methods of making compositions comprising a UV-absorbing chromophore. U.S. Patent 7,572,610 B2, Aug 11, 2009
(30) Laszlo, J. A.; Evans, K. O.; Vermillion, K. E.; Appell, M. Feruloyl dioleoylglycerol antioxidant capacity in phospholipid vesicles. *J. Agric. Food Chem.* **2010**, *58*, 5842−5850.
(31) National Sunflower Association. Sunflower oil fatty acid profile; http://www.sunflowernsa.com/oil/four-types-of-sunflower-oil/ (accessed Feb 6, 2014).
(32) Biresaw, G.; Bantchev, G. B. Effect of chemical structure on film-forming properties of seed oils. *J. Synth. Lubr.* **2008**, *25*, 159−183.
(33) Bala, V.; Hartley, R. J.; Hughes, L. J. The influence of chemical structure on the oxidative stability of organic sulfides. *Lubr. Eng.* **1996**, *52*, 868−873.
(34) Qiu, C.; Han, S.; Cheng, X.; Ren, T. Determining the antioxidant activities of organic sulfides by rotary bomb oxidation test and pressurized differential scanning calorimetry. *Thermochim. Acta* **2006**, *447*, 36−40.
(35) Biresaw, G.; Asadauskas, S. J.; McClure, T. G. Polysulfide and biobased extreme pressure additive performance in vegetable vs. paraffinic base oils. *Ind. Eng. Chem. Res.* **2012**, *51*, 262−273.

based on the release of specific compounds present in the polymer formulation with controlled kinetics in particular environments.[16] It is known that the addition of active agents to polymer matrices avoids food degradation processes improving the quality, safety, and health properties of foodstuff.[17] In this sense, the combination of active technologies, such as the addition of antioxidant and/or antimicrobial agents to packaging materials, with the use of nanocomposites can synergistically lead to formulations with balanced properties and functionalities.[8,18] Regarding the development of active films based on PCL, Salmieri et al.[19] incorporated oregano, savory, and cinnamon essential oils (EOs) at 1% (w/w) as natural antioxidants to alginate/PCL-based films. Their results confirmed the plasticizing effect of EOs in addition to their bioactive role, with the oregano-based films demonstrating the most effective antiradical systems. β-carotene is another widely available natural antioxidant, and it has been reported that the addition of low amounts of this compound to PCL resulted in a significant plasticization of the matrix improving its ductile properties.[20] In this sense, the use of hydroxytyrosol (3,4-dihydroxyphenylethanol, HT), a compound with the highest antioxidant effect among the various polyphenols present in olives,[21] could be a promising approach from an economical point of view, because it would turn agricultural residues into higher added-value active food packaging additives. In previous studies, certain decrease in thermal properties of natural antioxidants has been observed for compression molded packaging materials at high temperatures.[22] However, hydroxytyrosol showed a good performance in polypropylene materials acting as antioxidant, and it might be considered as a promising alternative to use in active packaging formulations.

The novelty of this work lies on the use of HT as natural antioxidant combined with a commercial nanoclay to develop films for active packaging based on PCL. The addition of the nanoclay could help to improve the intrinsically poor PCL barrier properties. Also, the use of HT is justified to improve shelf life of foodstuff by the antioxidant performance of this compound. At the best of our knowledge, there is no evidence in scientific literature of PCL-based packaging systems where the poor thermal resistance and barrier properties of PCL are overcome. In this way, this study is focused on the development and full characterization of new nanocomposites based on PCL, HT, and a commercial MMT (Cloisite30B, C30B), with high potential to improve thermal and barrier properties in biopolymers.[23] Active nanobiocomposite films were obtained by melt-blending followed by compression molding, which were further characterized on their thermal, structural, mechanical, and functional properties. In addition, the release of HT from these nanobiocomposites at different times was also evaluated.

MATERIALS AND METHODS

Materials. Poly(ε-caprolactone) (PCL, CAPA6800) commercial grade (pellets) was kindly supplied by Perstorp Holding AB (Sweden). Hydroxytyrosol (98% purity) (HT) was kindly supplied by Fine & Performance Chemicals Ltd. (Middlesbrough, U.K.). The commercial organo-modified montmorillonite used in this study was Cloisite30B (C30B), and it was supplied by Southern Clay Products (Austin, TX). This nanoclay was synthesized by replacing sodium ions in different silicate layers by methyl bis(2-hydroxyethyl) tallow alkyl ammonium cations by ion exchange.

Nanobiocomposites Preparation. PCL nanocomposites were processed by melt blending in a Haake Polylab QC mixer (ThermoFischer Scientific, Waltham, MA) at 80 °C for 5 min at 100 rpm. Before processing, PCL and C30B were left in an oven at 50 °C for 20 h and 100 °C for 24 h, respectively, to eliminate moisture. Both additives were introduced in the mixer once the polymer was in the melt state in order to avoid unnecessary losses. The 50 cm^3 mixing chamber was filled with 50 g of total mass. Eight different formulations were obtained by adding different amounts of HT and C30B in concentrations ranges of 5−10 wt % and 2.5−5 wt %, respectively (Table 1). An additional sample without any additive was also prepared and used as control (PCL0).

Table 1. PCL Nanobiocomposites and Thickness (Mean ± SD, n = 5)

formulation	HT (wt %)	C30B (wt %)	thickness (μm)
PCL0			204 ± 3
PCL/HT5	5		202 ± 6
PCL/HT10	10		206 ± 6
PCL/C30B2.5		2.5	191 ± 4
PCL/C30B5		5	198 ± 3
PCL/HT5/C30B2.5	5	2.5	196 ± 5
PCL/HT10/C30B2.5	10	2.5	201 ± 3
PCL/HT5/C30B5	5	5	191 ± 2
PCL/HT10/C30B5	10	5	198 ± 4

Films were obtained by compression-molding at 120 °C in a hot-plate hydraulic press from Carver, Inc., model 3850 (Wabash, IN). Materials were kept between the plates at atmospheric pressure for 5 min until melting, and then they were successively pressed under 2 MPa (1 min), 3 MPa (1 min), and lastly 5 MPa (5 min) to liberate the trapped air bubbles. The average thickness of the obtained films was around 200 μm, as measured with a 293 MDC-Lite Digimatic Micrometer (Mitutoyo, Japan) at five random positions (Table 1), after 48 h of conditioning at 50% relative humidity (RH) and 23 °C. The final appearance of the films was completely homogeneous.

Nanobiocomposites Characterization. *Differential Scanning Calorimetry (DSC).* Tests were conducted in triplicate by using a TA DSC Q-2000 instrument (New Castle, DE) under inert N_2 atmosphere. Samples (3 mg) were introduced in aluminum pans (40 μL) and were submitted to the following thermal program: heating from −90 to 160 °C (3 min hold), cooling to −90 °C (3 min hold), and heating to 160 °C, all steps at 10 °C min^{-1}. The crystallization and melting parameters were determined from the second heating scan. The crystallinity at room temperature (χ_c) of each material was evaluated by using eq 1:

$$\chi_c = \left(\frac{\Delta H_m}{\Delta H_m^0 \left(1 - \frac{\%\,wt_{clay}}{100}\right)} \right) \times 100 \quad (1)$$

where ΔH_m is the specific melting enthalpy of the sample, and ΔH_m° is the melting enthalpy of the 100% crystalline PCL matrix (142.0 J g^{-1}).[10]

Thermogravimetric Analysis (TGA). Thermogravimetric analysis was performed in a TGA/SDTA 851e Mettler Toledo thermal analyzer (Schwarzenbach, Switzerland). Samples (5 mg) were weighed in alumina pans (70 μL) and were heated

Table 2. DSC Results Obtained for All Formulations in Nitrogen Atmosphere (Mean ± SD, n = 3)[a]

sample	T_C (°C)	T_m (°C)	ΔH_C (J g^{-1})	ΔH_m (J g^{-1})	χ (%)
PCL0	28 ± 2^a	51 ± 2^a	48 ± 1^a	66 ± 4^a	46 ± 1^a
PCL/HT5	32 ± 2^{ab}	56 ± 1^b	53 ± 3^b	70 ± 2^a	49 ± 1^b
PCL/HT10	27 ± 3^a	55 ± 2^{ab}	55 ± 1^b	72 ± 2^a	51 ± 2^b
PCL/C30B2.5	35 ± 1^b	59 ± 2^b	58 ± 3^b	72 ± 1^a	52 ± 2^b
PCL/C30B5	34 ± 4^{ab}	58 ± 1^b	53 ± 2^b	69 ± 2^a	51 ± 1^b
PCL/HT5/C30B2.5	31 ± 1^a	57 ± 3^b	52 ± 1^b	69 ± 3^a	50 ± 1^b
PCL/HT10/C30B2.5	28 ± 2^a	56 ± 1^b	49 ± 2^{ab}	71 ± 2^a	51 ± 2^b
PCL/HT5/C30B5	28 ± 2^a	56 ± 2^b	51 ± 2^{ab}	63 ± 2^a	47 ± 2^b
PCL/HT10/C30B5	27 ± 3^a	55 ± 1^a	49 ± 1^{ab}	60 ± 4^a	48 ± 1^b

[a]Different superscripts within the same column indicate statistically significant different values ($p < 0.05$).

from 30 to 700 °C at 10 °C min^{-1} under N_2 atmosphere (flow rate of 50 mL min^{-1}). Analyses were repeated three times for each sample.

Tensile Tests. Tensile tests were carried out by using a 3340 Series Single Column System Instron Instrument, LR30K model (Fareham Hants, U.K.) equipped with a 2 kN load cell. Tests were performed in rectangular probes (100 × 10 mm^2), an initial grip separation of 60 mm, and a crosshead speed of 25 mm min^{-1}. Before testing, all samples were equilibrated for 48 h at 50 RH %. Tensile strength, elongation at break, and elastic modulus were calculated from the resulting stress−strain curves by following the ASTM D882-09 standard.[24] Tests were carried out at room temperature. Five repetitions were performed for each film composition, and mean values were reported.

Oxygen Transmission Rate (OTR). Oxygen transmission rate was determined with an oxygen permeation analyzer (8500 model Systech, Metrotec S.A, Spain). Tests were carried out by introducing O_2 (99.9% purity) into the upper half of the diffusion chamber while N_2 was injected into the lower half, where an oxygen sensor was located. Films were cut into 14 cm diameter circles for each formulation, and they were clamped in the diffusion chamber at 25 °C. Tests were performed in triplicate and were expressed as oxygen transmission rate per film thickness (OTR·e).

Scanning Electronic Microscopy (SEM). Micrographs were obtained for surfaces and cross sections of cryo-fractured films with a JEOL JSM-840 microscope (Peabody, MA) running at 12 kV. Samples were coated with gold layers prior to analysis to increase their electrical conductivity. Images were registered at magnifications of 100× and 500×.

Transmission Electron Microscopy (TEM). Transmission electron microscopy tests were performed by using a JEOL JEM-2010 microscope (Tokyo, Japan) operated at 100 kV. Films were previously ultramicrotomed to obtain slices of 100 nm thickness (RMC, model MTXL).

X-ray Diffraction (XRD). X-ray diffraction patterns were recorded at room temperature in the 2.1−40° (2θ) range (step size = 0.01°, scanning rate = 8 s step^{-1}) by using filtered Cu Kα radiation (λ = 1.54 Å). A Bruker D8-Advance diffractometer (Billerica, MA) was used to determine the interlayer spacing of clay platelets.

Color. Color changes on the films' surfaces due to the additives were analyzed with a KONICA CM-3600d COLOR-FLEX-DIFF2 colorimeter, HunterLab (Reston, VA). The L^*, a^*, b^* system (CIELab) was employed; the L^* axis represents the lightness from black ($L^* = 0$) to absolute white ($L^* = 100$), the a^* axis varies from green (−) to red (+), and the b^* axis varies from blue (−) to yellow (+). These parameters were measured at five different locations on each specimen, and average values were calculated. The total color difference, ΔE^*, between the control PCL film and nanocomposite films was calculated by using eq 2:

$$\Delta E* = [(\Delta L*)^2 + (\Delta a*)^2 + (\Delta b*)^2]^{1/2} \quad (2)$$

where ΔL^*, Δa^*, and Δb^* are the difference between initial and final values (before and after the additives addition) of L^*, a^*, and b^*, respectively.

HT Release from Films. The evaluation of the release rate of HT from each film at different times was carried out for 4 cm^2 samples immersed in 100 mL of methanol. The extracts were periodically taken and further analyzed by UV−vis spectroscopy with a Shimadzu Spectrophotometer 2450 (Kyoto, Japan). Spectra were obtained on extracts directly inserted in the cell compartment, and they were studied over the 200−300 nm wavelength range, which includes the maximum absorption wavelength of HT at 281 nm. Spectra were acquired each minute for 1 h to ensure that the release of the active agent to the methanol solution had reached a maximum value. In order to quantify the amount of HT released, the specific extinction coefficient, ε (mg^{-1} L cm^{-1}), for HT in methanol was calculated to be 0.0124 mg^{-1} L cm^{-1}, through the measurement of the absorbance A at 281 nm of a set of HT standard solutions with concentration, c (mg L^{-1}), and by using the Lambert−Beer law equation:

$$A = cl\varepsilon \quad (3)$$

where l = 1 cm. In all experiments, temperature was kept constant at 25.0 °C with a Multistirrer 6 thermostatic bath from Velp Scientifica (Usmate, Italy). During HT release experiments, composite-containing solutions were stirred at ∼220 rpm.

Statistical Analysis. Statistical analysis of results was performed with SPSS commercial software (Chicago, IL). A one-way analysis of variance (ANOVA) was carried out. Differences between average values were assessed on the basis of confidence intervals by using the Tukey test at a $p \leq 0.05$ significance level.

RESULTS AND DISCUSSION

Thermal Characterization. DSC tests were performed to elucidate the effect of the nanoclay and HT addition on the thermal properties of the PCL matrix. Four parameters were determined: crystallization temperature, T_c; melting temperature, T_m; crystallization enthalpy, ΔH_c; and melting enthalpy, ΔH_m. These results are summarized in Table 2. It should be highlighted that the melting temperature of neat PCL was lower than that obtained for the rest of the materials formulated in this study. This result gives an indication of the lower

dx.doi.org/10.1021/jf405111a | J. Agric. Food Chem. 2014, 62, 2244−2252

Table 3. Thermal (Mean ± SD, n = 3) and Mechanical Properties (Mean ± SD, n = 5) of the Studied Films[a]

sample	$T_{ini\ 5wt\%}$ (°C)	T_{max} (°C)	ε_B (%)	E (MPa)	TS (MPa)
PCL0	348 ± 2^{a}	415 ± 3^{a}	20 ± 1^{a}	507 ± 21^{a}	12 ± 2^{a}
PCL/HT5	350 ± 2^{a}	412 ± 4^{a}	29 ± 2^{b}	453 ± 25^{b}	10 ± 2^{ab}
PCL/HT10	330 ± 3^{b}	416 ± 1^{a}	38 ± 2^{c}	413 ± 25^{b}	10 ± 1^{a}
PCL/C30B2.5	300 ± 5^{c}	409 ± 4^{a}	40 ± 2^{c}	687 ± 31^{c}	9 ± 1^{a}
PCL/C30B5	280 ± 3^{d}	390 ± 2^{b}	49 ± 1^{d}	794 ± 24^{d}	7 ± 1^{b}
PCL/HT5/C30B2.5	330 ± 1^{b}	405 ± 4^{a}	36 ± 3^{c}	491 ± 33^{a}	9 ± 1^{ab}
PCL/HT10/C30B2.5	330 ± 3^{b}	411 ± 1^{a}	41 ± 2^{cef}	463 ± 18^{b}	8 ± 2^{ab}
PCL/HT5/C30B5	328 ± 3^{b}	403 ± 3^{a}	43 ± 2^{e}	622 ± 29^{c}	9 ± 2^{ab}
PCL/HT10/C30B5	327 ± 4^{b}	407 ± 3^{a}	46 ± 1^{ef}	732 ± 45^{d}	7 ± 3^{ab}

[a]Different superscripts within the same column indicate statistically significant different values ($p < 0.05$).

crystallinity of neat PCL when compared to nanobiocomposites, as it has been reported by other authors.[11]

Regarding crystallinity values, this parameter increased with the addition of HT ($p < 0.05$) due to the interaction between the polymer matrix and the additive molecules, which can show some plasticizing effects. On the other hand, the addition of the polar C30B to the polyester matrix also resulted in a significant increase ($p < 0.05$) of the crystallization rate and could modify the PCL crystalline structure due to the ability of the nanoclay particles to heterogeneously nucleate the crystallization of the polymer matrix, as it has been well-documented for a wide range of nanocomposites.[25] Similar results were obtained by Persico et al. in LDPE nanocomposite films containing carvacrol, where differences in crystallinity values were considered a consequence of two main factors: the presence of heterogeneous nucleation sites and changes in chain mobility. In this sense, they reported that clay platelets could act as nuclei for the initial heterogeneous nucleation and subsequent growth of crystallites. Furthermore, they hypothesized that the increase in chain mobility promoted by carvacrol enhanced the ability of the polymer to crystallize.[26]

However, no significant differences ($p > 0.05$) were observed in crystallinity values for films containing 2.5 and 5 wt % of nanoclay (Table 2). Similar results were found for the ternary nanobiocomposites containing the same amount of C30B ($p > 0.05$), and a decrease was noted for those with 5 wt % of nanoclay, although without significant differences ($p > 0.05$). In this sense, it was reported that the variations in the crystallinity by the addition of nanoclays can be accounted for by two factors: nucleation that increases crystallinity and reduction in the flexibility of polymer macromolecular chains that impedes their rearrangement into ordered crystalline structures, reducing crystallinity. Both factors are related to nanoclay dispersion and content, and different results should be obtained depending on the prevailing effect.[11] Furthermore, the addition of HT enhanced polymer chain mobility, promoting its self-nucleation and crystallinity. In conclusion, the neat crystallinity observed for materials with both additives (HT and C30B) can be attributed to the superposition of all these contributions. The reduction in chain mobility as the result of the nanoclay addition can be considered an important factor in controlling the final properties and structure developed by the material.

TGA results indicated that the thermal degradation of PCL in inert atmosphere took place through the rupture of the polyester chains via ester pyrolysis reaction with the release of CO_2, H_2O, and carboxylic acids. In the case of polyesters, such as PCL, pyrolysis results in chain cleavages randomly distributed along the macromolecular chains. It was reported that when two pyrolysis reactions occur with neighboring ester functions, 5-hexenoic acid is one of the reaction products.[13] TGA curves obtained for all the studied PCL nanobiocomposites just showed one main degradation step. The initial degradation temperatures (T_{ini}) determined at 5% weight loss and maximum degradation temperatures (T_{max}) obtained for all formulations are shown in Table 3. The incorporation of the active compound and the nanoclay brings about a significant effect on the thermal stability of the obtained nanobiocomposites ($p < 0.05$). In this sense, the addition of 10 wt % HT to PCL resulted in a 18 °C reduction in T_{ini}. This result could be explained by the plasticizing effect of HT to PCL, as already stated in the DSC study. In this sense, it was reported that the addition of plasticizers to biopolyesters, such as PLA, results in some decrease in the polymer thermal stability.[27] On the other hand, the addition of the nanoclay also produced some significant decrease ($p < 0.05$) in the PCL thermal stability, but this decrease was not enough to result in PCL degradation at processing temperatures. It was reported that layered silicates could catalyze PCL pyrolysis by a catalytic action played by the nanoclay due to the presence of Lewis acidic sites, created upon organic modifier degradation.[13]

Mechanical Properties. The addition of low nanoclay content (less than 10 wt %) to polymers is expected to improve mechanical properties, particularly when effective nanoclay exfoliation occurs.[22,1] The enhancement in mechanical properties of polymer nanocomposites can be attributed to the high rigidity and aspect ratio of nanoclays together with the good affinity through interfacial interaction between polymer matrix and dispersed nanoclay.[28]

In this study, tensile tests were performed to evaluate the influence of the addition of the nanoclay and/or the active additive on the mechanical properties of PCL-based nanobiocomposites. Results are shown in Table 3, where the elastic modulus E (MPa), elongation at break ε_B (%), and tensile strength TS (MPa) were determined in all materials. The addition of HT to PCL resulted in some modification in E and ε values ($p < 0.05$), whereas no significant differences were observed in TS ($p > 0.05$). In this sense, an increase in the HT concentration caused an increase in ε and a decrease in E values compared to the neat polymer. This behavior could be explained by the plasticizing effect of HT resulting in the increase in ductility of the polymer, and it is consistent with results obtained by other authors with the addition of similar additives to biopolymer matrices.[20,29] In this sense, it should be noted that the physical state of HT is a viscous liquid, with the consequence of the intimate mixture of HT molecules within the macromolecular chains, permitting the enhancement on the internal movement and consequently on ductile properties.

On the other hand, the addition of the nanoclay caused a significant increase in both the elastic modulus and elongation at the break of nanobiocomposites ($p < 0.05$). Concomitantly, a decrease (~40%) of tensile strength ($p < 0.05$) was observed when the amount of the nanoclay in the film increased from zero to 5 wt %. The constrained polymer model developed by Beall can be used to explain some of the general phenomena observed in polymer/clay nanocomposites, including changes in mechanical properties, such as modulus improvement and increased elongation at break. In this sense, the constrained polymer region could be viewed as temporary cross-links, which certainly contribute to increase moduli but when strained can break and reform as the stress and strain increase. In examining the crazes formed in composites that exhibit this increase in elongation at break, it has been observed that fibrils form where the clay plate align along the direction of the fibril length. This gives a convenient platform for the polymer to break the temporary cross-links and then reattach along the clay platelets.[30] For the ternary nanobiocomposites and regarding the *E* values, it was observed that the effect of the nanoclay was predominant for C30B5 ternary composites, resulting in a clear increase in *E* values ($p < 0.05$), although a superposition of the influence of both additives (i.e., nanoclay and HT) should be taken into account to explain results obtained for C30B2.5 materials. In fact, the ultimate behavior observed in mechanical properties can be considered as the result of several factors, such as crystallinity, polymer plasticization, filler−matrix interface, all of which affect the stress−strain properties in a complex way.[26] Although there are difficulties in considering antagonist effects by HT and C30B in ternary composites, it could be concluded that the addition of the nanoclay induced reinforcement effects provided by the high aspect ratio and surface area of silicate layers. The improvement in these properties could be considered a clear indication of the high dispersion of the nanoclay through the polymer matrix and their high compatibility.[31]

Morphological Study. SEM micrographs of films (not shown) showed a featureless and nonporous morphology, indicating a good dispersion of C30B and HT in the PCL matrix; that is, no phase separation was observed.

The morphological characterization of these materials was completed by transmission electron microscopy (TEM), allowing a qualitative evaluation of the dispersion degree of the nanoclay in the PCL matrix. TEM micrographs of PCL nanocomposites containing C30B showed partial exfoliation, because swollen and single dispersed clay layers were observed (Figure 1). Complete exfoliation of nanoclays into individual platelets is not often achieved in nanocomposites, and consequently, a mixed morphology consisting of intercalated and exfoliated structures is usually obtained.[1]

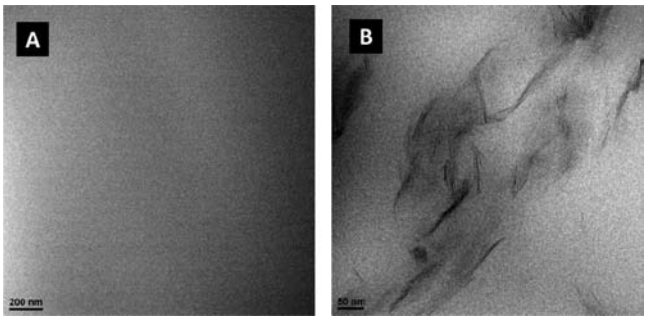

Figure 1. TEM images of neat PCL (A) and PCL/HT5/C30B2.5 (B) nanobiocomposite.

In general terms, TEM tests suggested the good dispersion of C30B in the PCL matrix, because no aggregates were observed. These results could be attributed to the strong interactions between polymer and nanoclay, which are caused by the hydrogen bonding between the carbonyl group in the polymer structure and the hydroxyl groups of the organo-modified nanoclay.[1]

XRD Analysis. The dispersion of clays in nanocomposite films was studied by using X-ray diffraction (XRD). The XRD pattern of PCL was characterized by the presence of two distinct peaks at $2\theta = 24.9°$ and 27.5° corresponding to the (110) and (200) planes, respectively, suggesting a semicrystalline structure.[14] No noticeable differences were found from the XRD patterns for all formulations in this angle range, suggesting that the polymer matrix structure was not influenced by the presence of the filler and/or HT.

The most important variations in XRD patterns of these PCL-based nanobiocomposites were found in the low angle range (below 10°), which gives an indication of the clay dispersion into the polymer matrix (Figure 2). C30B was characterized by a single diffraction peak at $2\theta = 4.8°$, corresponding to the (001) basal reflection,[14] accounting for the 18.6 Å interlayer distance. A shift of the clay diffraction peak to lower angles in these nanobiocomposites was observed, indicating a good interaction of the nanoclay with the polymer matrix, showing an increase in the interlayer distance up to 32.7 Å for PCL/C30B5 due to the intercalation of PCL macromolecular chains into the clay galleries. Ludueña et al. reported similar results for PCL/C30B nanocomposites showing a final d_{001} spacing value increased to 33.1 Å (79% from the initial value).[32] These results could be correlated as well with those obtained for oxygen barrier properties, because an inverse correlation between *d*-spacing and oxygen transmission rate was apparent.[28] However, there was no shift in the interlayer distance in nanobiocomposites with different clay content, suggesting that clay load did not affect the clay platelets' intercalation. Similar results were found by Ahmed et al. for PCL/C30B films with nanoclay compositions ranging from 2.5 to 10 wt %.[12]

In addition, some decrease in the C30B peak intensity was observed, in particular when the active additive was introduced in the formulation. Because C30B is characterized by the presence of free hydroxyl groups, the short alkyl chains of the C30B organic modifier would make these groups available for interactions with the polymer macromolecules and HT reactive functional groups, resulting in higher dispersion degree of the nanoclay in the polymer matrix.[14] On the other hand, the basal diffraction around 5.2° in nanobiocomposites' XRD patterns may correspond to a fraction characterized by a different alkylammonium chain arrangement in the interlayer space or to a small amount of unmodified C30B.[26]

Barrier Properties. Barrier to oxygen is one of the main issues in the design of materials for food packaging applications. The high sensitivity of many food products to oxygen degradation, microbial growth stimulated by moisture, and aroma retention needed for keeping the food quality requires the improvement in biopolymers barrier properties to gases, vapors, and aromas.[1] In general, permeability of a polymer to oxygen or water vapor is dependent on some inter-related factors, including polarity, hydrogen bonding between side

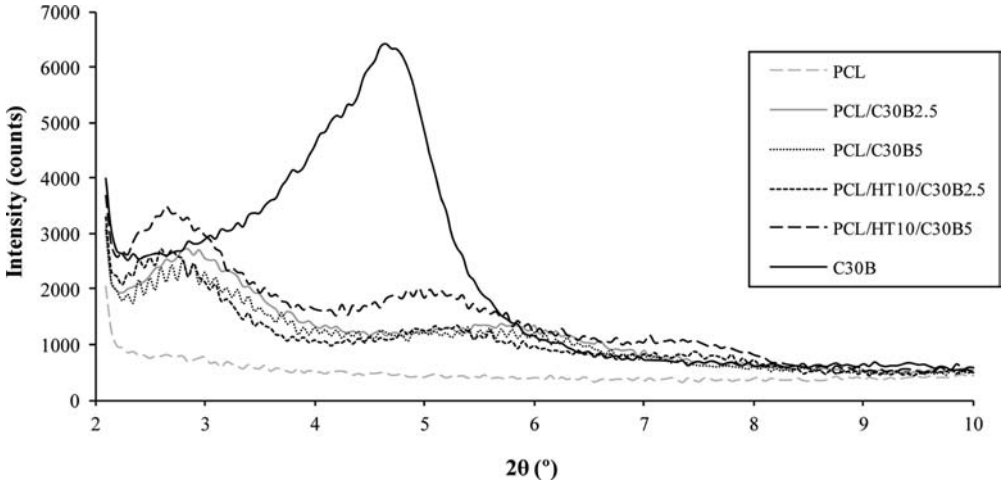

Figure 2. XRD patterns of C30B, PCL, and the obtained PCL bionanocomposites in the (2−10°) angle range.

Table 4. Color Coordinates (Mean ± SD, n = 5) and OTR·e Values from Active Films (e: Thickness, mm; Mean ± SD, n = 3)[a]

		colorimetric parameters			
sample	OTR·e (cm^3 mm m^{-2} day)	L^*	a^*	b^*	ΔE
PCL0	51 ± 2[a]	83.6 ± 0.6[a]	−0.9 ± 0.4[a]	2.4 ± 0.6[a]	
PCL/HT5	54 ± 1[a]	79.1 ± 1.2[b]	−0.6 ± 0.6[a]	6.1 ± 0.3[b]	2.5 ± 0.2[a]
PCL/HT10	56 ± 3[a]	75.5 ± 1.7[c]	−0.7 ± 0.2[a]	9.8 ± 0.3[c]	3.1 ± 0.1[b]
PCL/C30B2.5	49 ± 4[a]	76.0 ± 2.2[c]	−0.9 ± 0.2[a]	4.1 ± 0.2[d]	2.1 ± 0.2[a]
PCL/C30B5	49 ± 5[a]	75.4 ± 1.2[c]	−1.3 ± 0.5[a]	6.9 ± 0.4[b]	2.6 ± 0.2[a]
PCL/HT5/C30B2.5	50 ± 4[a]	52.9 ± 0.8[d]	2.3 ± 0.2[b]	10.4 ± 0.4[c]	3.2 ± 0.2[bc]
PCL/HT10/C30B2.5	31 ± 1[b]	51.6 ± 2.9[d]	3.6 ± 0.8[c]	12.9 ± 04[e]	3.6 ± 0.3[c]
PCL/HT5/C30B5	40 ± 3[c]	47.5 ± 0.9[e]	3.1 ± 0.6[c]	11.9 ± 0.6[e]	3.4 ± 0.2[bc]
PCL/HT10/C30B5	32 ± 2[b]	40.6 ± 2.8[f]	2.9 ± 0.5[c]	10.1 ± 0.3[c]	3.2 ± 0.2[bc]

[a]Different superscripts within the same column indicate statistically significant different values (p < 0.05).

chains, molar mass and polydispersity, cross-linking, processing methodology, and crystallinity.[33]

Results obtained for the oxygen transmission rate per film thickness (e), OTR·e, for all the studied materials are shown in Table 4. Films containing nanoclay showed a slight decrease in OTR·e (p > 0.05) due to the nanoclay intercalation into the PCL structure. On the other hand, some increase in OTR·e was observed for samples with HT (p > 0.05). This effect could be due to the plasticizing effect of HT resulting in the increase in the mobility of PCL chains.[34] A significant improvement in oxygen barrier (p < 0.05) was achieved for ternary nanobiocomposites containing C30B and 10 wt % HT, rendering more competitive materials for oxygen-sensitive products. This result also suggests that the incorporation of the active additive could promote the intercalation of the nanofiller into the PCL matrix by improving the dispersion of the nanoclay in the PCL matrix and finally improving oxygen barrier properties. A similar effect was observed in nanobiocomposites based on plasticized PLA containing C30B.[23] This improvement in barrier properties may be explained by the theory developed by Nielsen,[35] based on the tortuous pathway that gas molecules should follow to diffuse through the polymer. This tortuosity is produced by the good dispersion in the matrix of the layered silicates platelets and the consequent longer diffusion pathway increasing the diffusion time and decreasing permeability.[33−36] According to Duncan,[35] barrier properties are not only influenced by tortuosity but also by changes in the polymer matrix at the interfacial regions. In the case of favorable interactions between polymer and nanofiller, polymer strands close to each nanoparticle can be partially immobilized, working against the gases' diffusion. In this sense, the Beall[30] model states that the polymer region around the clay affecting diffusion is the constrained region, characterized by lower free volume and diffusion coefficient.

Regarding the nanofiller content, no significant differences were observed by comparing OTR·e results for films containing 2.5 and 5 wt % of nanoclay (p > 0.05), suggesting a possible filler agglomeration in films with higher amounts of C30B. In this sense, Sánchez et al. found that composites containing 5 wt % of different nanofillers exhibited the highest oxygen barrier performance, and that the addition of larger amounts of nanoclays (10 wt %) to various biopolyesters did not result in further oxygen barrier improvements.[1] These results suggest that there should be a balance between the filler content, the nanocomposite morphology, and the possibility of permeability deterioration caused by filler agglomeration.[22]

Colorimetric Analysis. Color is an important factor to be considered for some industrial applications. Colorimetric analysis of films was carried out to evaluate the effect of the presence of the studied additives (Table 4) in this important property. Significant differences in color were observed as the result of the HT and/or C30B addition to PCL (p < 0.05). In this sense, neat PCL showed the highest L^* value, with a significant decrease in the presence of additives, especially for the ternary nanobiocomposites, indicating a significant darkening of these films. ΔE^* values increased in ternary nanobiocomposites. A significant improvement in a^* and b^* values was also found for these films (p < 0.05), resulting in a

slightly amber color. Similar color changes were reported for polypropylene stabilized with hydroxytyrosol,[22] contributing to strengthen the color of the obtained films. Rhim[37] also reported a decrease in L^* values and an increase in b^* and ΔE^* values in films produced by blending agar with C20A and C30B, suggesting that differences in color might be attributed to the dispersion of the nanoclays in the polymer matrix.

Release of HT from PCL Nanobiocomposites. The combination of active additives and nanocomposites can synergistically lead to materials with balanced properties and functionalities for food packaging applications. The formulation of novel antioxidant nanobiocomposites based on PCL and HT can be considered as a way to control solubility and release of the antioxidant agent to foodstuff. In this sense, phenolic compounds from virgin olive oil, such as HT, are known to play an antioxidant role in preventing damage to biomolecules. One of the most abundant components of olive oil is an oleuropein derivative named oleacein (dialdehydic form of decarboxymethyl elenolic acid linked to HT).[38] The evaluation of equilibrium and kinetic properties of hydroxytirosol in these nanobiocomposite films was carried out with methanol as release media. It is known that the tendency of HT (and other phenols) to be solubilized, transferred, or diffused into a given solvent is governed by thermodynamics. One of the primary thermodynamic factors describing this tendency is the activity coefficient,[39] which increases as solubility decreases. Although methanol is not commonly used as food simulant, the activity coefficient of HT at 25 °C in this solvent (0.20) is between those shown in ethanol (0.027) and water (0.91),[40] thereby allowing the exploration of broader applications of these nanobiocomposites.

Figure 3a shows the HT release for the three obtained nanobiocomposite films containing HT 10 wt %. As indicated,

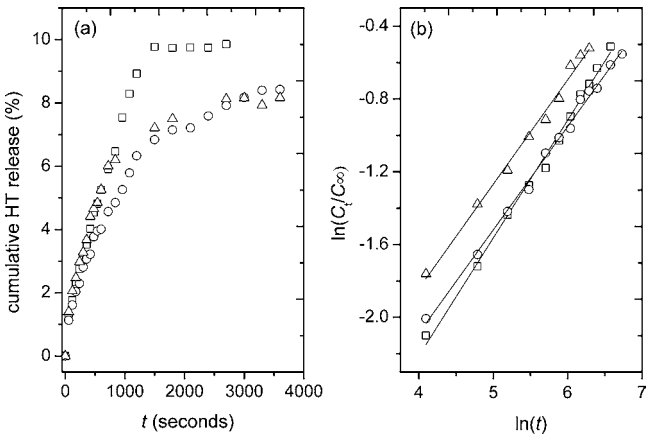

Figure 3. (a) Desorption release profiles (a) and short-time range ($C_t/C_\infty < 0.6$) desorption kinetics (b) of HT from PCL/HT10 (□), PCL/HT10/C30B2.5 (○), and PCL/HT10/C30B5 (△) films; solid lines (b) represent the fitting of eq 4 to desorption kinetic experimental data.

desorption equilibrium was reached after ∼1 h from the beginning of the process. It is important to note that the release experiment was very aggressive, because materials were completely immersed in methanol. The presence of the nanoclay leads to the decrease in the HT release, with cumulative release values of 7.9 and 7.7% for C30B2.5 and C30B5, respectively (Table 5). This behavior could be probably related to interactions between C30B and HT. In this sense, Sánchez et al. found an enhancement in thymol solubility in PCL nanocomposites due to the presence of nanoplatelets, possibly due to the retention of the active agent over their surface.[1] They also found a decrease in the thymol diffusion coefficient with the addition of nanoclays, as the result of the tortuous path imposed to the diffusion of the active agent through the nanocomposite bulk. These results suggest that it is possible to control the release of natural agents with interest in the design of novel active films and coatings through incorporation of laminar nanoclays into bioplastics, such as PCL. A similar behavior was found for Pereira et al. for urea−montmorillonite nanocomposites, showing slower release when compared to pure urea.[41] This profile was probably related to the fact that, as a consequence of some interaction between montmorillonite and urea, this compound would need to adsorb in montmorillonite platelets after its dissolution; this also shows the importance of exfoliation in the controlled release.

The assessment on the release mechanism was performed by using the power law Korsemeyer−Peppas equation[42]

$$C_t/C_\infty = kt^n \tag{4}$$

where C_t and C_∞ are the cumulative concentrations of HT released at time t and at infinite time, respectively, and k and n are fitting parameters, giving the later useful information on the release mechanism. The validity of eq 4 is restricted to $C_t/C_\infty < 0.60$.[43]

Figure 3b shows the fitting of eq 4 to the experimental data, and the computed fitting parameters are summarized in Table 5. It was observed that the desorption mechanism of HT in PCL/HT10 is non-Fickian ($0.5 < n < 1$), which is indicative of coupling diffusion and relaxation mechanisms. However, for nanobiocomposites, n values were approximately 0.5, showing that HT desorption is diffusion-controlled (so-called Fickian). In this case, the apparent diffusion coefficients, D_{ap}, can be computed directly from k, by using the following equation

$$k = (4/l)*(D_{ap}/\pi)^{0.5} \tag{5}$$

where l is the film thickness (cm). The calculated diffusion coefficients for HT desorption from PCL/HT10/C30B2.5 and PCL/HT10/C30B5 were 2.9 (±0.5) × 10^{-10} cm^2 s^{-1} and 4.5 (±0.6) × 10^{-10} cm^2 s^{-1}, respectively. These values show that the release of HT under these conditions is very slow and also suggests that the diffusion follows the trend of the O_2 permeation; that is, an increase in the nanoclay content leads to an increase in O_2 permeation and HT diffusion. Taking into account these data, it is evident that the transport mechanism is rather complex and the reasons behind that are not yet well understood.

In conclusion, the effect of the addition of HT and C30B on properties of PCL-based nanobiocomposites was evaluated by using several analytical techniques. In this sense, some decrease in elastic modulus was observed for films containing HT, suggesting some plasticizing effect in the polymer matrix. On the other hand, the incorporation of C30B resulted in some decrease in thermal stability and a significant enhancement in oxygen barrier and tensile properties, due to the successful intercalation of the nanofiller into the matrix. Slight differences in color with the addition of the additives for all films were also observed. Nanobiocomposites showed slow release for HT, which is an important result for its potential application as PCL-based active films and coating systems, with eventual

Table 5. Concentration of HT Released in the HT 10 wt % Formulations

		eq 4		
sample	HT released (%)	n	k / s^{-n}	R^2
PCL/HT10	9.2	0.65 (±0.02)	0.008 (±0.001)	0.9942
PCL/HT10/C30B2.5	7.9	0.56 (±0.01)	0.013 (±0.001)	0.9952
PCL/HT10/C30B5	7.7	0.57 (±0.02)	0.016 (±0.002)	0.9914

R^2: correlation coefficient.

substitution of common synthetic antioxidants used in packaging materials. The obtained PCL-based nanocomposites have shown improved functional properties and can be regarded as potentially interesting materials for active packaging applications within the food manufacturing and agricultural sectors. To complete these investigations, further tests are to be carried out in order to evaluate the migration and antioxidant performance of these nanobiocomposites by contact with food.

AUTHOR INFORMATION

Corresponding Author

*E-mail: mc.garrigos@ua.es. Fax: +34 965903527. Tel.: +34 965903400, Ext 1242.

Funding

Financial support by the Spanish Ministry of Economy and Competitiveness (no. MAT2011-28468-C02-01) and University of Alicante (UAUSTI12-04) is also acknowledged.

Notes

The authors declare no competing financial interest.

ACKNOWLEDGMENTS

Authors would like to thank Fine & Performance Chemicals Ltd. and Perstorp for kindly providing hydroxytyrosol and PCL, respectively.

REFERENCES

(1) Sánchez, M. D.; Lagaron, J. M. Novel clay-based nanobiocomposites of biopolyesters with synergistic barrier to UV light, gas and vapour. *J. Appl. Polym. Sci.* **2010**, *118*, 188−199.

(2) Ludueña, L.; Vázquez, A.; Álvarez, A. Effect of lignocellulosic filler type and content on the behavior of polycaprolactone based ecocomposites for packaging applications. *Carbohydr. Polym.* **2012**, *87*, 411−421.

(3) Woodruff, M. A.; Hutmacher, D. W. The return of a forgotten polymer: Polycaprolactone in the 21st century. *Prog. Polym. Sci.* **2010**, *35*, 1217−1256.

(4) Labet, M.; Thielemans, W. Synthesis of polycaprolactone: A review. *Chem. Soc. Rev.* **2009**, *38*, 3484−3504.

(5) Lee, J. E.; Kim, K. M. Characteristics of soy protein isolate−montmorillonite composite films. *J. Appl. Polym. Sci.* **2010**, *118*, 2257−2263.

(6) Khan, R.; Beck, S.; Dussault, D.; Salmieri, S.; Bouchard, J.; Lacroix, M. Mechanical and barrier properties of nanocrystalline cellulose reinforced poly(caprolactone) composites: Effect of gamma radiation. *J. Appl. Polym. Sci.* **2013**, *129*, 3038−3046.

(7) Martínez-Abad, A.; Sánchez, G.; Fuster, V.; Lagarón, J. M.; Ocio, M. J. Antibacterial performance of solvent cast polycaprolactone (PCL) films containing essential oils. *Food Control* **2013**, *34*, 214−220.

(8) Sánchez-García, M. D.; Ocio, M. J.; Giménez, E.; Lagaron, J. M. Novel polycaprolactone nanocomposites containing thymol of interest in antimicrobial film and coating applications. *J. Plast. Film Sheeting* **2008**, *24*, 239−251.

(9) Pérez-Masiá, R.; López-Rubio, A.; Fabra, M. J.; Lagarón, J. M. Biodegradable polyester-based heat management materials of interest in refrigeration and smart packaging coatings. *J. Appl. Polym. Sci.* **2013**, *130*, 3251−3262.

(10) Swapna, J. C.; Prashanth, H.; Rastogi, N. K.; Indiramma, A. R.; Reddy, Y.; Raghavarao, K. S. M. S. Optimum blend of chitosan and poly-(ε-caprolactone) for fabrication of films for food packaging applications. *Food Bioprocess Tech.* **2011**, *4*, 1179−1185.

(11) Azeredo, H. Nanocomposites for food packaging applications. *Food Res. Int.* **2009**, *42*, 1240−1253.

(12) Ahmed, J.; Auras, R.; Kijchavengkul, T.; Varshney, S. K. Rheological, thermal and structural behavior of poly(ε-caprolactone) and nanoclay blended films. *J. Food Eng.* **2012**, *111*, 580−589.

(13) Oana, M. I.; Biqiong, C. Porous exfoliated poly(ε-caprolactone)/clay nanocomposites: Preparation, structure, and properties. *J. Appl. Polym. Sci.* **2012**, *125*, 102−112.

(14) Pantoustier, N.; Lepoittevin, B.; Alexandre, M.; Dubois, P.; Kubies, D.; Calberg, C.; Jérôme, R. Biodegradable polyester layered silicate nanocomposites based on poly(ε-caprolactone). *Polym. Eng. Sci.* **2002**, *42*, 1928−1937.

(15) Fukushima, K.; Tabuani, D.; Camino, G. Nanocomposites of PLA and PCL based on montmorillonite and sepiolite. *Mater. Sci. Eng.* **2009**, *29*, 1433−1441.

(16) Costantino, U.; Bugatti, V.; Gorrasi, G.; Montanari, F.; Nocchetti, M.; Tammaro, L.; Vittoria, V. New polymeric composites based on poly(ε-caprolactone) and layered double hydroxides containing antimicrobial species. *ACS Appl. Mater. Interfaces* **2009**, *1*, 668−677.

(17) Fabra, M. J.; Hambleton, A.; Talens, P.; Debeaufort, F.; Chiralt, A. Effect of ferulic acid and α-tocopherol antioxidants on properties of sodium caseinate edible films. *Food Hydrocolloids* **2011**, *25*, 1441−1447.

(18) Abdollahi, M.; Rezaei, M.; Farzi, G. A novel active bionanocomposite film incorporating rosemary essential oil and nanoclay into chitosan. *J. Food Eng.* **2012**, *111*, 343−350.

(19) Salmieri, S.; Lacroix, M. Physicochemical properties of alginate/polycaprolactone-based films containing essential oils. *J. Agric. Food Chem.* **2006**, *54*, 10205−10214.

(20) López, A.; Lagaron, J. M. Improvement of UV stability and mechanical properties of biopolyesters through the addition of β-carotene. *Polym. Degrad. Stab.* **2010**, *95*, 2162−2168.

(21) Bubonja, M.; Giacometti, J.; Abram, J. Antioxidant and antilisterial activity of olive oil, cocoa and rosemary extract polyphenols. *Food Chem.* **2011**, *127*, 1821−1827.

(22) Peltzer, M.; Jiménez, A. Determination of oxidation parameters by DSC for polypropylene stabilized with hydroxytyrosol (3,4-dihydroxy-phenylethanol). *J Therm. Anal. Calorim.* **2009**, *96*, 243−248.

(23) Martino, V. P.; Jiménez, A.; Ruseckaite, R. A.; Averous, L. Structure and properties of clay nano-biocomposites based on poly(lactic acid) plasticized with polyadipates. *Polym. Adv. Technol.* **2011**, *22*, 2206−2213.

(24) ASTM D882-09. Standard test method for tensile properties of thin plastic sheeting. 468 Annual Book of ASTM Standards. American Society for Testing and Materials: Philadelphia, PA, 2009.

(25) Miltner, H. E.; Watzeels, N.; Gotzen, N. A.; Goffin, A. L.; Duquesne, E.; Benali, S.; Ruelle, B.; Peeterbroeck, S.; Dubois, P.; Goderis, B.; Assche, G.; Rahier, H.; Van Mele, B. The effect of nano-sized filler particles on the crystalline-amorphous interphase and thermal properties in polyester nanocomposites. *Polymer* **2012**, *53*, 1494−1506.

(26) Persico, P.; Ambrogi, V.; Carfagna, C.; Cerruti, P.; Ferrocino, I.; Mauriello, G. Nanocomposite polymer films containing carvacrol for antimicrobial active packaging. *Polym. Eng. Sci.* **2009**, *49*, 1447−1455.

(27) Martino, V. P.; Jiménez, A.; Ruseckaite, R. A. Processing and characterization of poly(lactic acid) films plasticized with commercial polyadipates. *J. Appl. Polym. Sci.* **2009**, *112*, 2010−2018.
(28) Rhim, J. W.; Park, H. M.; Ha, C. S. Bio-nanocomposites for food packaging applications. *Prog. Polym. Sci.* **2013**, *38*, 1629−1652.
(29) Jamshidian, M.; Tehrany, E. A.; Imran, M.; Akhtar, M. J.; Cleymand, F.; Desobry, S. Structural, mechanical and barrier properties of active PLA−antioxidant films. *J. Food Eng.* **2012**, *110*, 380−389.
(30) Beall, G. W. New conceptual model for interpreting nanocomposite behavior. In *Polymer-Clay Nanocomposites*; Pinnavaia, T. J., Beall, G. W., Eds.; John Wiley & Sons, Inc.: New York, 2000; pp 267−279.
(31) Quilaqueo-Gutiérrez, M.; Echeverría, I.; Ihl, M.; Bifani, V.; Mauri, A. N. Carboxymethylcellulose−montmorillonite nanocomposite films activated with murta (Ugni molinae Turcz) leaves extract. *Carbohydr. Polym.* **2012**, *87*, 1495−1502.
(32) Ludueña, L. N.; Kenny, J. M.; Vázquez, A.; Álvarez, V. A. Effect of clay organic modifier on the final performance of PCL/clay nanocomposites. *Mater. Sci. Eng. A.* **2011**, *529*, 215−223.
(33) Duncan, T. V. Applications of nanotechnology in food packaging and food safety: barrier materials, antimicrobials and sensors. *J. Colloid Interface Sci.* **2011**, *363*, 1−24.
(34) Sothornvit, R.; Krochta, J. M. Oxygen permeability and mechanical properties of films from hydrolyzed whey protein. *J. Agric. Food Chem.* **2000**, *48*, 3913−3916.
(35) Nielsen, L. E. Models for the permeability of filled polymer systems. *J. Macromol. Sci. A.* **1967**, *1*, 929−942.
(36) Molinaro, S.; Romero, M. C.; Boaro, M.; Sensidoni, A.; Lagazio, C.; Morris, M.; Kerry, J. Effect of nanoclay-type and PLA optical purity on the characteristics of PLA-based nanocomposite films. *J. Food Eng.* **2013**, *117*, 113−123.
(37) Rhim, J. W.; Lee, S. B.; Hong, S. I. Preparation and characterization of agar/clay nanocomposite films: The effect of clay type. *J. Food Sci.* **2011**, *76*, 40−48.
(38) Czerwinska, M.; Kiss, A. K.; Naruszewicz, M. A comparison of antioxidant activities of oleuropein and its dialdehydic derivative from olive oil, oleacein. *Food Chem.* **2012**, *131*, 940−947.
(39) Queimada, A. J.; Mota, F. L.; Pinho, S. P.; Macedo, E. A. Solubility of biologically active phenolic compounds: Measurements and modelling. *J. Phys. Chem. B* **2009**, *113*, 3469−3476.
(40) Galanakis, C. M.; Goulas, V.; Tsakona, S.; Manganaris, G. A.; Gekas, V. A knowledge base for the recovery of natural phenols with different solvents. *Int. J. Food Prop.* **2013**, *16*, 382−396.
(41) Pereira, E. I.; Minussi, F. B.; Da Cruz, C. C. T.; Bernardi, A. C. C.; Ribeiro, C. Urea-montmorillonite-extruded nanocomposites: A novel slow-release material. *J. Agric. Food Chem.* **2012**, *60*, 5267−5272.
(42) Korsmeyer, R. W.; Gurny, R.; Docler, E.; Buri, P.; Peppas, N. A. Mechanisms of solute release from porous hydrophilic polymers. *Int. J. Pharm.* **1983**, *15*, 25−35.
(43) Crank, J. *The Mathematics of Diffusion*, 2nd ed.; Oxford University Press, Inc.: New York, 1975.

Table 1. Fatty Acid Composition of Emulsifiers, Coconut Oil, Palm Olein, and Their Mixtures with the Two Commercial Emulsifiers[a]

	fatty acids[b] (g/100 g)							
	8:0	10:0	12:0	14:0	16:0	18:0	18:1	18:2
EM1	ND	ND	ND	ND	22.8 ± 0.2	2.2 ± 0.1	16.2 ± 0.1	58.8 ± 0.1
EM2	ND	ND	ND	ND	10.5 ± 0.1	89.2 ± 0.1		0.3 ± 0.1
CO	2.4 ± 0.0a	3.3 ± 0.0a	42.6 ± 0.2a	21.0 ± 0.5a	12.2 ± 0.1a	1.7 ± 0.0a	11.6 ± 0.0a	5.1 ± 0.1a
CO + 1% EM1	2.3 ± 0.0a	3.3 ± 0.0a	42.2 ± 0.2a	20.8 ± 0.0a	12.3 ± 0.1a	1.7 ± 0.0a	11.7 ± 0.1a	6.6 ± 0.1a
CO + 3% EM1	2.3 ± 0.0a	3.2 ± 0.0a	41.4 ± 0.2a	20.4 ± 0.0a	12.5 ± 0.1a	1.7 ± 0.0a	11.7 ± 0.1a	6.7 ± 0.1a
CO + 1% EM2	2.3 ± 0.0a	3.3 ± 0.0a	42.2 ± 0.2a	20.8 ± 0.0a	12.1 ± 0.1a	1.6 ± 0.0a	11.5 ± 0.1a	6.4 ± 2.7a
CO + 3% EM2	2.3 ± 0.0a	3.2 ± 0.0a	41.4 ± 0.2a	20.4 ± 0.0a	12.1 ± 0.1a	1.4 ± 0.0a	11.3 ± 0.1a	6.9 ± 0.1a
PO	ND	ND	0.5 ± 0.0b	0.7 ± 0.0b	36.9 ± 0.5b	4.7 ± 0.0b	47.6 ± 0.2b	10.6 ± 0.3b
PO + 1% EM1	ND	ND	0.5 ± 0.0b	0.7 ± 0.0b	36.7 ± 0.5b	4.7 ± 0.0b	47.3 ± 0.2b	10.0 ± 0.3b
PO + 3% EM1	ND	ND	0.5 ± 0.0b	0.7 ± 0.0b	36.4 ± 0.4b	4.6 ± 0.0b	46.6 ± 0.2b	10.0 ± 0.3b
PO + 1% EM2	ND	ND	0.5 ± 0.0b	0.7 ± 0.0b	36.6 ± 0.5b	4.5 ± 0.0b	47.1 ± 0.2b	10.5 ± 0.3b
PO + 3% EM2	ND	ND	0.5 ± 0.0b	0.7 ± 0.0b	36.1 ± 0.4b	4.2 ± 0.0b	46.2 ± 0.2b	10.3 ± 0.3b

	fatty acids[c] (g/100 g)						
	SFA	MCSFAC	LCSFA	UNSFA	MUFA	PUFA	IV
EM1	24.9 ± 0.2	ND	24.9 ± 0.2	75.0 ± 0.2	16.2 ± 0.1	58.8 ± 0.1	115.8 ± 0.2
EM2	99.7 ± 0.1	ND	99.7 ± 0.1	0.3 ± 0.1		0.3 ± 0.1	0.5 ± 0.1
CO	83.3 ± 0.2a	48.4 ± 0.3a	13.9 ± 0.1a	16.7 ± 0.1a	11.6 ± 0.1a	5.1 ± 0.0a	18.8 ± 0.3a
CO + 1% EM1	82.7 ± 0.1a	47.9 ± 0.0a	34.8 ± 0.1a	17.3 ± 0.1a	11.6 ± 0.1a	5.6 ± 0.0a	19.8 ± 0.1a
CO + 3% EM1	81.5 ± 1.8a	46.9 ± 2.7a	35.6 ± 0.9a	18.4 ± 1.8a	11.7 ± 1.2a	6.7 ± 0.6a	21.7 ± 2.1a
CO + 1% EM2	83.5 ± 1.4a	47.9 ± 2.5a	35.6 ± 1.1a	14.9 ± 1.4a	11.5 ± 1.0a	3.4 ± 0.4a	15.8 ± 1.6a
CO + 3% EM2	83.8 ± 0.3a	46.9 ± 0.1a	36.9 ± 0.3a	16.2 ± 0.3a	11.3 ± 0.1a	4.9 ± 0.2a	18.2 ± 0.4a
PO	42.8 ± 0.5b	0.5 ± 0.0b	42.3 ± 0.5b	57.1 ± 0.5b	47.6 ± 0.2b	10.6 ± 0.3b	57.5 ± 0.7b
PO+1%EM1	42.7 ± 0.2b	0.5 ± 0.0b	42.1 ± 0.2b	57.3 ± 02b	47.3 ± 0.2b	10.0 ± 0.1b	58.1 ± 0.2b
PO + 3% EM1	42.3 ± 0.1b	0.5 ± 0.0b	41.8 ± 0.3b	57.7 ± 0.1b	46.6 ± 0.2b	11.0 ± 0.1b	59.2 ± 0.2b
PO + 1% EM2	43.4 ± 0.1b	0.5 ± 0.0b	42.9 ± 0.1b	56.6 ± 0.1b	47.1 ± 0.2b	10.5 ± 0.1b	56.9 ± 0.1b
PO + 3% EM2	44.6 ± 0.7b	0.5 ± 0.7b	44.0 ± 0.7b	55.4 ± 0.7b	46.2 ± 0.7b	10.3 ± 0.0b	55.8 ± 1.2b

[a]Values are shown as means ± SD of three replications. Means (n = 3) with different lower case letters in the same column are significantly different (p < 0.05). ND, undetected; EM1, emulsifier 1; EM2, emulsifier 2; CO, coconut oil; PO, palm olein. [b]8:0, caprylic acid; 10:0, capric acid; 12:0, lauric acid; 14:0, myristic acid; 16:0, palmitic acid; 18:0, stearic acid; 18:1, oleic acid; 18:2, linoleic acid; 18:3 linolenic acid. [c]SFA, saturated fatty acids; MCSFA, medium-chain saturated fatty acids; LCSFA, long-chain saturated fatty acids; UNSFA, unsaturated fatty acids; MUFA, monounsaturated fatty acids; PUFA, polyunsaturated fatty acids; IV, iodine value (g iodine/100 g).

diacylglycerols on fat crystallization in oil-in-water emulsions.[16,17] Herrera's group studied the effect of different additives on the crystallization behavior of bulk lipids.[18−22] Radujko et al. studied the influence of different emulsifiers on the physical and crystallization characteristics of edible fats.[14] Basso et al. studied the effect of monoacylglycerols as modifiers in the crystallization of palm oil.[24] The main effects of these additives in the crystallization of fats occur during the stages of nucleation and growth of the crystalline network, changing physical properties such as crystal size, solid fat content, and microstructure. The issue of promoting or inhibiting crystallization, however, is still debatable. In general, studies indicate that emulsifiers with acyl groups similar to those of the crystallized fat accelerate this process.[23]

For the above reasons, two semisolid fats were selected (palm olein and coconut oil), which have great potential for use as fat ingredients in the food industry. This paper aims to study of changes in the crystallization behavior of palm olein and coconut oil after the addition of commercial emulsifiers containing predominantly MAGs.

MATERIALS AND METHODS

Materials. Palm olein was obtained from Agropalma S/A (Pará, Brazil) and coconut oil from Copra Alimentos Ltd.a. (Alagoas, Brazil). The emulsifiers were provided by DuPont Nutrition & Health (São Paulo, Brazil) and are constituted mainly by monoacylglycerols (EM1 >90.0% MAGs produced from edible vegetable oil; EM2 >52.0% MAGs produced from refined fully hydrogenated vegetable fats). The fatty acid compositions of these fats, emulsifiers, and their blends were determined by gas chromatography and are presented in Table 1. The fats were stored at 0 °C prior to use. All other reagents and solvents were of analytical or chromatographical grade.

Sample Preparation. Commercial emulsifiers (1.0 and 3.0% w/w) were dispersed in the melted coconut oil and palm olein and stirred with a magnetic stirrer at 70 ± 0.5 °C until a homogeneous sample was obtained.

Fatty Acid Composition. The fatty acid composition was determined after conversion of fatty acids into their corresponding methyl esters (FAMES) using the method described by ISO method 5509.[25] Analyses of FAMES were carried out in a Varian gas chromatograph (model 430 GC, Varian Chromatograph Systems, Walnut Creek, CA, USA), equipped with a CP 8412 autoinjector. Galaxie software was used for quantification and identification of peaks. Injections were performed into a 100 m fused silica capillary column (i.d. = 0.25 mm) coated with 0.2 μm of polyethylene glycol (SP-2560, Supelco, Bellefonte, PA, USA) using helium as the carrier gas at an isobaric pressure of 37 psi; linear velocity of 20 cm/s; makeup gas, helium at 29 mL/min at a split ratio of 1:50; and volume injected, 1.0 μL. The injector temperature was set at 250 °C, and the detector temperature was set at 280 °C. The oven temperature was initially held at 140 °C for 5 min, then stepped to 240 °C at a rate of 4 °C/min, and held isothermally for 30 min. Pure oils and theirs blends were analyzed in triplicate, and reported values represent the average of the three runs.

Medium-chain saturated fatty acids (MCSFAs) are expressed as the sum of the amounts of caprylic, capric, and lauric acids. Long-chain saturated fatty acids (LCSFAs) are expressed as the sum of the amounts of myristic, palmitic, and stearic acids. Saturated fatty acids (SFAs) are expressed as the sum of the amounts of caprylic, capric, lauric, myristic, palmitic, and stearic fatty acids. Unsaturated fatty acids (USFAs) content is expressed as the sum of the amounts of oleic, linoleic, and linolenic acids. Monounsaturated fatty acids (MUFAs) content is expressed as the amount of oleic acid. Polyunsaturated fatty acids (PUFAs) content is expressed as the sum of the amounts of linoleic and linolenic acids.

Triacylglycerol Composition. Triacylglycerol composition was analyzed in a Varian gas chromatograph (model 3400CX, Varian Ind. Com. Ltd.a., São Paulo, Brazil). A DB-17HT Agilent (catalog no. 122-1811) capillary column (50% phenyl-methylpolysiloxane, 15 m in length × 0.25 mm bore and containing 0.15 μm film). The conditions were as follows: split injection, ratio, 1:100; column temperature, 250 °C; programmed to 350 °C at 5 °C/min; carrier gas, helium, at 1.0 mL/min flow rate; injector temperature, 360 °C; detector temperature, 375 °C; injection volume, 1.0 μL; sample concentration, 100 mg/5 mL of hexane.[26] All samples were analyzed in triplicate, and the reported values are the average of three runs. TAG profiles were followed throughout the reactions by plotting the percents of the areas of carbon number peaks groups.

Regiospecific Distribution of Fatty Acids. A proton-decoupled ^{13}C NMR was used to analyze the positional distribution of fatty acids on the triacylglycerol backbone. Lipid samples (250 mg) were dissolved in $CDCl_3$ (0.5 mL) in 5 mm NMR tubes, and NMR spectra were recorded on a Bruker Advance DPX spectrometer operating at 300 MHz. The ^{13}C spectra of the lipid samples were acquired with a spectral width of 2332.090 Hz, pulse of 10.2 μs, and a relaxation delay of 30s. Determination of ^{13}C was performed at a frequency of 75.8 MHz with a multinuclear probe of 5 mm operating at 30 °C, using the method described by Vlahov.[27] The results showed the compositions of saturated fatty acids, oleic acid, and linoleic plus linolenic acids in *sn*-2 and *sn*-1,3 positions. All samples were analyzed in triplicate, and the reported values are the average of three analyses.

Polarized Light Microscopy. Samples were melted at the temperature of 70 °C in an oven and, with a capillary tube a drop of sample was placed on a glass slide preheated at a controlled temperature (70 °C) and covered with a cover glass. Samples were kept in the stove at the analysis temperatures (10, 15, and 20 °C) for 24 h. Crystal morphology was evaluated by means of the polarized light microscope (Olympus, model BX 50) coupled to the digital video camera (Media Cybernetics). Glass slides were placed on a hot plate LTS 32; heating and freezing stages were operated by a TP93 temperature programmer (Linkam Scientific Instruments Ltd., Surrey, UK). The images were captured using Image Pro-Plus software version 7.0 for Windows (Media Cybernetics) using polarized light and amplified up to 100 times.

For each glass slide, three visual fields were focused, of which only one was chosen to represent the observed crystals. The evaluation parameter selected for quantitative image analysis was the mean diameter of crystals and was measured by the Image Pro-Plus software, version 7.0 for Windows (Media Cybernetics).[28]

Differential Scanning Calorimetry (DSC). DSC curves were obtained by DSC (DSC 4000, Perkin-Elmer Corp., Norwalk, CT, USA), under a dynamic atmosphere of He (20 mL/min) and a cooling rate of −10 °C/min and heating at 5 °C/min, at temperatures ranging from 80 to −60 °C for cooling with isothermal time of 10 min at 80 °C with an isothermal of 10 min at −60 °C (AOCS Cj 1-94, 2009), using sealed aluminum capsules containing sample mass between 5 and 10 mg. The temperature and heat of melting were calibrated with indium (initial temperature of 156.6 °C). Curves were processed in the program Pyris, and melting and crystallization curves were analyzed for the onset (T_{onset}, °C) of melting and crystallization, peak crystallization and melting temperatures (T_{pc} and T_{pm}, °C), and crystallization and melting enthalpies (ΔH_c and ΔH_m, J/g). The samples were analyzed in triplicate.[29]

Statistical Analysis. Results were expressed as the mean ± SD in triplicate. Differences between the samples (melting and crystallization behavior, diameter of crystals, and fatty acids composition) during the experimental period were statistically analyzed using one-way analysis of variance (ANOVA), followed by post hoc Tukey test, taking on $p > 0.05$. Statistical analysis was performed using Statistica 11.0 software.[30]

RESULTS AND DISCUSSION

Fatty Acid Composition. The fatty acid composition is very important because it is directly related to the properties of each fat, such as melting point and crystallization characteristics.

Table 2. Triacylglycerol Composition (Grams per 100 g) of Coconut Oil (CO) and Palm Olein (PO)

TAG group	CO	PO
CN[a] 28 (CaCC)	2.2 ± 0.1	
CN 30 (CaCLa)	8.4 ± 0.3	
CN 32(CCLa)	12.8 ± 0.5	
CN 34 (CLaLa)	16.1 ± 0.1	
CN 36 (LaLaLa)	16.5 ± 0.6	
CN 38 (LaLaM)	12.9 ± 0.2	
CN 40 (LaMM)	10.4 ± 0.5	
CN 42 (LaMP)	6.5 ± 0.4	
CN 44 (LaPP)	4.2 ± 0.2	
CN 46 (CaOO/LaPO/PPM/MMO/MML)	3.6 ± 0.6	
CN 48 (MPO/MPL/PPP)	3.1 ± 0.2	2.1 ± 0.2
CN 50 (PPL/MLO/MLL)	2.6 ± 0.2	37.7 ± 0.6
CN 52 (PLL/PLO)		48.2 ± 1.1
CN 54 (OOO/LOO/LOL)		11.8 ± 1.5

[a]CN, carbon number.

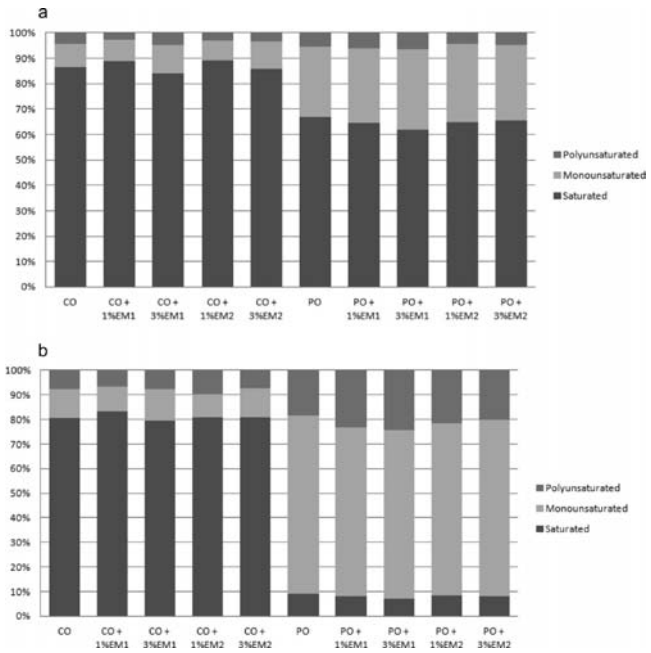

Figure 1. Regiospecific distribution of fatty acids in *sn*-1,3 positions (a) and *sn*-2 position (b) in triacylglycerols of coconut oil, palm olein, and their mixture with the two commercial emulsifiers.

Fatty acid compositions of the individual fats and their mixtures with the two commercial emulsifiers are presented in Table 1. Fatty acid compositions of palm olein and coconut oil are in accordance with the results published in the literature.[31,32] Saturated fatty acids are predominant in coconut oil ($p < 0.05$),

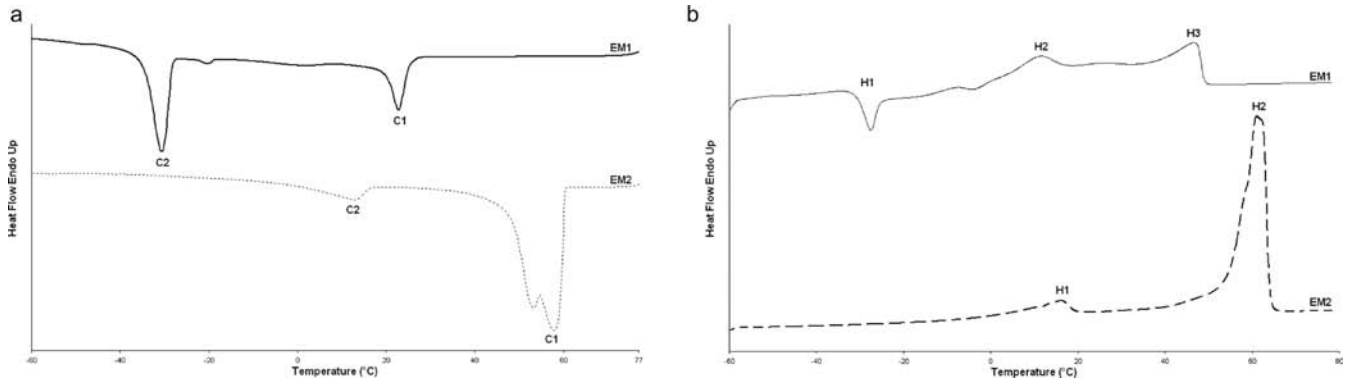

Figure 2. DSC crystallization (a, c) and melting (b, d) curves of the two commercial emulsifiers.

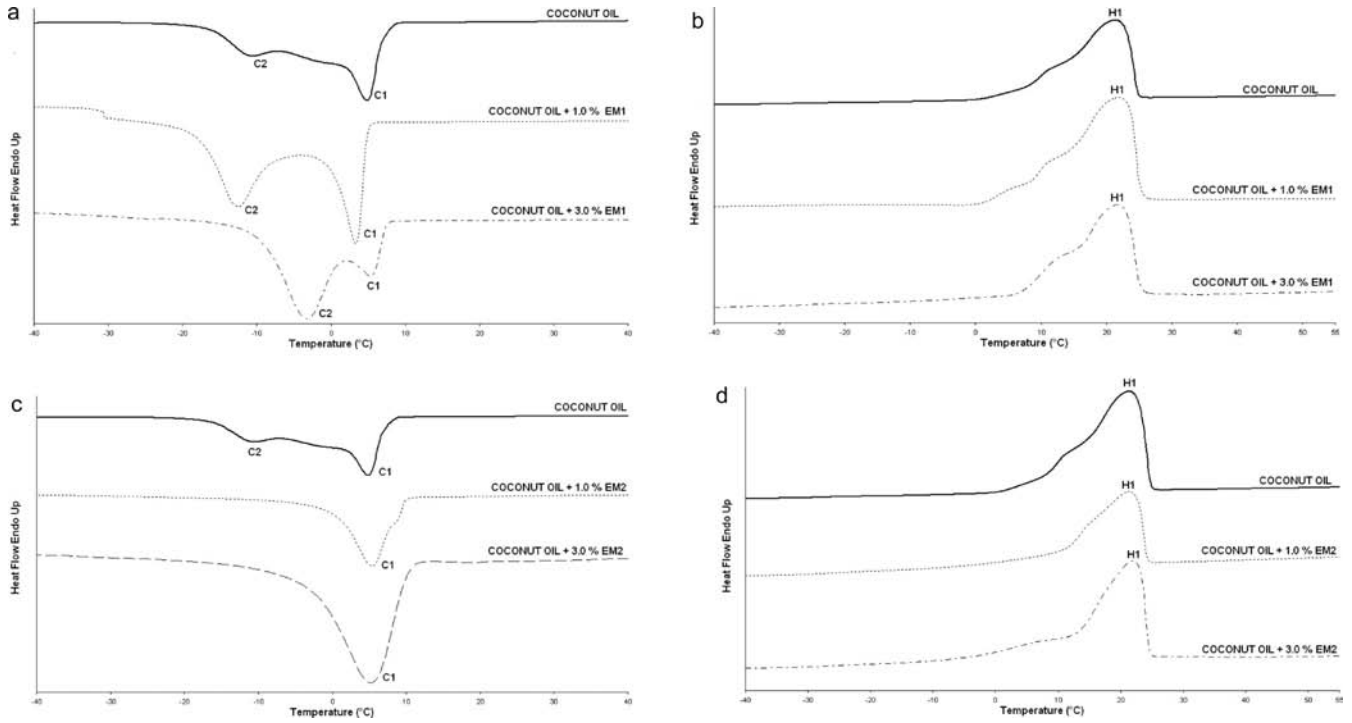

Figure 3. DSC crystallization (a, c) and melting (b, d) curves of coconut oil and its mixture with the two commercial emulsifiers.

Table 3. Onset Melting Temperature (T_{onset}), Peak Melting Temperature (T_{pm}), Melting Enthalpy (ΔH_m), Onset Crystallization Temperature (T_{onset}), Peak Crystallization Temperature (T_{pc}), and Crystallization Enthalpy (ΔH_c) with the Two Commercial Emulsifiers[a]

	H1			H2			H3		
	T_{onset} (°C)	T_{pm} (°C)	ΔH_m (J/g)	T_{onset} (°C)	T_{pm} (°C)	ΔH_m (J/g)	T_{onset} (°C)	T_{pm} (°C)	ΔH_m (J/g)
EM1	−30.5 ± 0.0	−27.5 ± 0.0	9.3 ± 0.8	1.25 ± 0.1	10.9 ± 0.1	37.0 ± 0.1	46.7 ± 0.2	78.8 ± 0.0	44.9 ± 0.6
EM2	6.4 ± 0.5	46.1 ± 0.1	13.3 ± 1.1	56.6 ± 0.0	60.9 ± 0.0	122.1 ± 0.2			

	C1			C2		
	T_{onset} (°C)	T_{pc} (°C)	ΔH_c (J/g)	T_{onset} (°C)	T_{pc} (°C)	ΔH_c (J/g)
EM1	25.0 ± 0.1	22.7 ± 0.1	28.2 ± 0.0	−30.6 ± 0.0	−30.0 ± 0.0	42.7 ± 0.3
EM2	60.4 ± 0.0	57.8 ± 0.1	117.3 ± 2.5	16.4 ± 0.1	12.2 ± 0.0	12.7 ± 0.3

[a]Values are shown as means ± SD of three replications. Means (n = 3) with different lower case letters in the same column are significantly different ($p < 0.05$).

mainly lauric, miristic, and palmitic acids, respectively. Palm olein showed predominance of unsaturated fatty acids ($p > 0.05$), mainly oleic acid, and at the same time has high amounts of palmitic acid (36.9 ± 0.5%). Unsaturated fatty acids are predominant in EM1, mainly linoleic acid, and EM2 showed the highest content of saturated fatty acids, mainly stearic acid (Table 1).

The addition of EM1 and EM2, in both proportions, showed no significant differences ($p < 0.05$) in the composition of fatty acids in coconut oil and palm olein.

dx.doi.org/10.1021/jf405221n | J. Agric. Food Chem. 2014, 62, 2253−2263

Table 4. Onset Melting Temperature (T_{onset}), Peak Melting Temperature (T_{pm}), Melting Enthalpy (ΔH_m), Onset Crystallization Temperature (T_{onset}), Peak Crystallization Temperature (T_{pc}), and Crystallization Enthalpy (ΔH_c) of Coconut Oil and Its Mixtures with the Two Commercial Emulsifiers[a]

	H1		
	T_{onset} (°C)	T_{pm} (°C)	ΔH_m (J/g)
CO	10.1 ± 0.1a	21.2 ± 0.1a	63.7 ± 0.9a
CO + 1% EM1	10.4 ± 0.3a	21.3 ± 0.7a	105.5 ± 0.5b
CO + 3% EM1	12.4 ± 0.1b	21.6 ± 0.0a	94.9 ± 0.1b
CO + 1% EM2	9.9 ± 0.1a	21.4 ± 0.0a	62.8 ± 0.9a
CO + 3% EM2	11.6 ± 0.6b	22.2 ± 0.6a	59.0 ± 0.3a

	C1			C2		
	T_{onset} (°C)	T_{pc} (°C)	ΔH_c (J/g)	T_{onset} (°C)	T_{pc} (°C)	ΔH_c (J/g)
CO	6.7 ± 0.3a	4.7 ± 0.2a	18.8 ± 1.2a	−7.1 ± 0.4a	−11.4 ± 0.1a	7.6 ± 4.8a
CO + 1.0% EM1	4.9 ± 0.1b	3.3 ± 0.0b	26.7 ± 0.1 a	−7.8 ± 0.7a	−12.6 ± 0.0b	25.8 ± 0.0b
CO + 3.0% EM1	7.1 ± 0.2a	5.6 ± 0.1a	10.2 ± 0.1 a	0.7 ± 0.0b	−3.4 ± 0.0c	38.6 ± 0.6c
CO + 1.0% EM2	9.1 ± 0.5c	5.1 ± 0.3a	58.7 ± 2.9b			
CO + 3.0% EM2	11.3 ± 0.2d	6.3 ± 0.3a	56.5 ± 0.4b			

[a]Values are shown as means ± SD of three replications. Means (n = 3) with different lower case letters in the same column are significantly different ($p < 0.05$).

Table 5. Onset Melting Temperature (T_{onset}), Peak Melting Temperature (T_{pm}), Melting Enthalpy (ΔH_m), Onset Crystallization Temperature (T_{onset}), Peak Crystallization Temperature (T_{pc}), and Crystallization Enthalpy (ΔH_c) of Palm Olein and Its Mixtures with the Two Commercial Emulsifiers[a]

	H1		
	T_{onset} (°C)	T_{pm} (°C)	ΔH_m (J/g)
PO	−1.8 ± 0.3a	2.2 ± 0.1a	38.0 ± 0.6a
PO + 1% EM1	0.7 ± 0.0b	2.4 ± 0.1ab	72.9 ± 0.6b
PO + 3% EM1	2.7 ± 0.0c	4.5 ± 0.0c	76.5 ± 1.8b
PO + 1% EM2	0.8 ± 0.0c	2.5 ± 0.0ab	71.8 ± 1.0b
PO + 3% EM2	2.9 ± 0.1c	4.8 ± 0.1c	76.7 ± 4.1b

	C1		
	T_{onset} (°C)	T_{pc} (°C)	ΔH_c (J/g)
PO	5.1 ± 0.2a	−0.4 ± 0.2a	31.3 ± 0.5a
PO + 1.0% EM1	4.2 ± 0.0b	−2.2 ± 0.0b	66.8 ± 4.8b
PO + 3.0% EM1	3.7 ± 0.0c	−2.5 ± 0.1c	72.4 ± 0.6c
PO + 1.0% EM2	4.1 ± 0.0d	−0.8 ± 0.0d	28.7 ± 0.2d
PO + 3.0% EM2	2.9 ± 0.1e	−2.0 ± 0.1e	65.0 ± 0.8e

[a]Values are shown as means ± SD of three replications. Means (n = 3) with different letters in the same column are significantly different ($p < 0.05$).

Triacylglycerol Composition. TAG composition is responsible for providing specific physical properties of lipids. In a processed food that contains significant fat content, the product's behavior may depend on the triacylglycerol composition of that fat.[28] Oils and fats are considered complex samples, because they are composed of a large number of triacylglycerols. Thus, the identification of triacylglycerols becomes a difficult process, in which the number of possible structural forms is very large compared to the number of fatty acids.[33] TAG compositions of the individual fats are presented in Table 2.

In palm olein, four triacylglycerol groups were identified and were similar to those reported by other authors.[34] Palm olein has triacylglycerols ranging from C48 to C54, mainly C52 (48.2%) and C50 (37.7%).

The high diversity of TAGs in coconut oil ranged from C28 to C54. The triacylglycerol profile of coconut oil showed 14 triacylglycerol groups; TAGs C32 (CCLa, 12.8%), C34 (CLaLa, 16.1%), C36 (LaLaLa, 16.6%), C38 (LaLaM, 12.9%), and C40 (LaMM, 10.5%), where C = capric acid, La = lauric acid, and M = myristic acid, were the major mainly saturated TAGs (84.5%). The triunsaturated triacylglycerols in coconut oil were only 0.2%. The triacylglycerol species identified in the coconut oil samples were similar to those reported by other authors.[35]

Regiospecific Distribution of Fatty Acids. Regiospecific distribution of fatty acids in triacylglycerols has implications for the nutritional quality and technology of oils and fats.

Analysis of the regiospecific distribution of fatty acids in triacylglycerols by NMR is desirable, as it does not require hydrolysis by pancreatic lipase, further separation of partial acylglycerols by thin layer chromatography, and finally analysis of fatty acids by gas chromatography.[36] The NMR technique shows that the signal of the spectra corresponding to the *sn*-2 position is always equivalent to around 33.3 g/100 g (an acyl group of three), whereas the signal corresponding to *sn*-1,3 positions is always equivalent to around 66.6 g/100 g (two acyl groups of three).

Results for fatty acid composition by NMR were similar to those obtained by gas chromatography of most samples of this study to saturated fatty acids, 18:1 cis and trans and 18:2 + 18:3.

Figure 1 shows the regiospecific distribution of fatty acids in *sn*-1,3 positions (a) and *sn*-2 position (b) in triacylglycerols of coconut oil, palm olein, and their mixture with the two commercial emulsifiers. Saturated fatty acids were found mainly in the *sn*-1,3 positions, and polyunsaturated fatty acids were found mainly in the *sn*-2 position, a typical feature of vegetable oils.[37]

Coconut oil was composed by 86.5% saturated fatty acids, 8.9% monounsaturated fatty acids, and 4.6% polyunsaturated fatty acids at the *sn*-1,3 positions, whereas 80.7% saturated fatty acids, 11.6% monounsaturated fatty acids, and 7.7% polyunsaturated fatty acids were found at the *sn*-2 position.

Palm olein was composed by 67.0% saturated fatty acids, 27.3% monounsaturated fatty acids, and 5.5% polyunsaturated fatty acids at the *sn*-1,3 positions, whereas 18.5% polyunsaturated fatty acids, 72.3% monounsaturated fatty acids, and 9.1% saturated fatty acids were found at the *sn*-2 position.

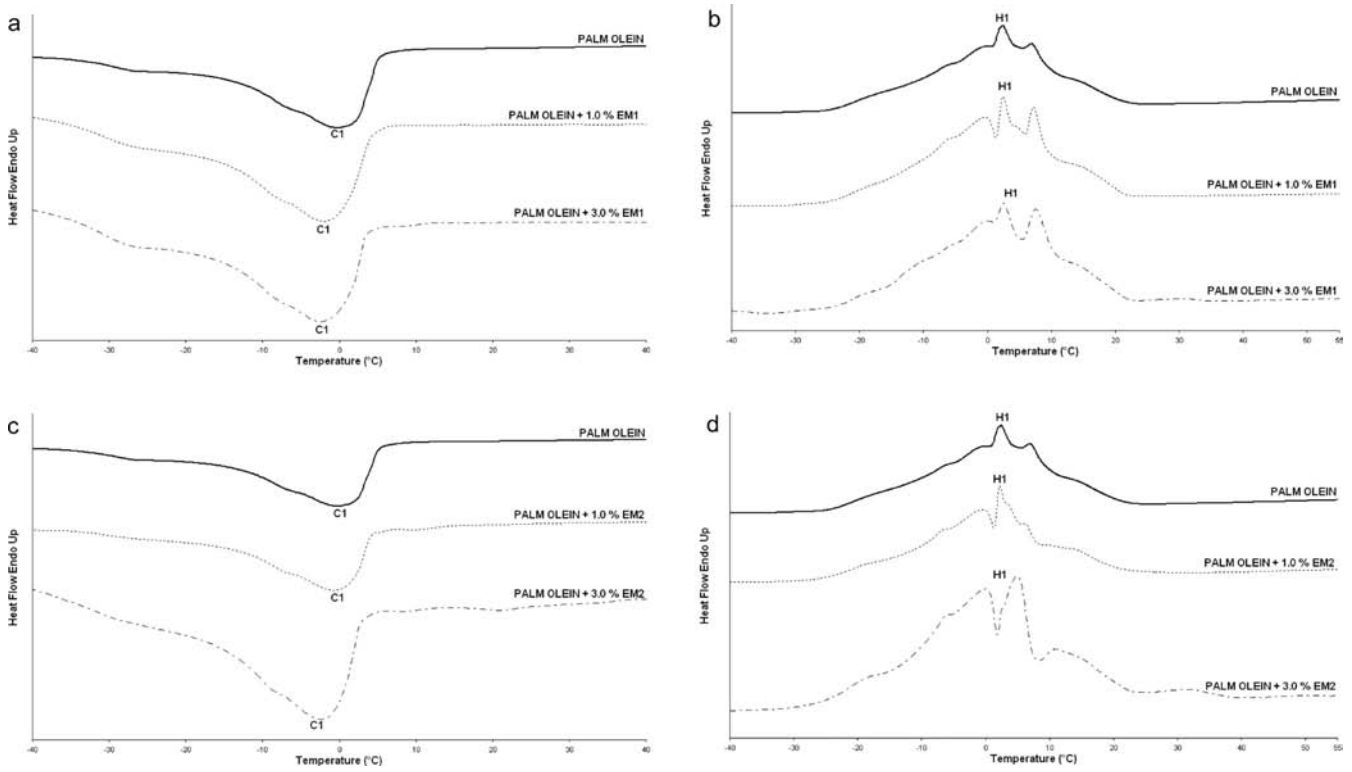

Figure 4. DSC crystallization (a, c) and melting (b, d) curves of palm olein and its mixture with the two commercial emulsifiers.

According to Hayes and Khosla,[38] palm olein is composed by 85% oleic acid and 10% palmitic acid at the *sn*-2 position. These authors also claim that saturated fatty acids are found in higher proportion at the *sn*-2 in highly saturated fats such as coconut oil.

The addition of EM1 and EM2, in both proportions (1 and 3%), to coconut oil and palm olein did not change the regiospecific distribution of fatty acids compared to pure oils.

Differential Scanning Calorimetry. Figure 2 shows the melting and crystallization curves obtained by DSC of two emulsifiers. Figure 3 shows the changes in crystallization profiles of coconut oil crystallized with and without the addition of EM1 (a) and EM2 (b).

Coconut oil showed two distinct but overlapping exothermic peaks, one minor exothermic peak at −11.0 ± 0.2 °C (C2) and a second peak at 4.7 ± 0.2 °C (C1). These slightly different temperatures from those reported by Marina et al.[39] and Mansor et al.[40] can be attributed to the different nature of preparation of the coconut oil, the growing condition of the coconut, cultivar type, and maturity of the coconut.[40] The existence of the two major exothermic peaks in coconut oil is related to crystallization to the saturated and unsaturated TAGs.

The addition of EM1 in two different ratios (1.0 and 3.0% w/w) changed the crystallization behavior of coconut oil (Figure 3). The enthalpy of crystallization of the peak related to the unsaturated TAGs (C2) was significantly increased ($p < 0.05$) with 1.0 and 3.0% (w/w) EM1; this is due to the composition of the emulsifier being predominantly unsaturated. For this reason, the first peak of coconut oil referring to saturated TAGs was reduced with the addition of 3.0% (w/w) EM1.

In many investigations, the first thermal effect during the crystallization process is considered the start of nucleation.[41] However, in DSC thermograms, for example, a minor component may affect the initial, minor peak, whereas the later crystallization peak (representing the bulk of crystallization) may not be affected.[41]

On the basis of the data plotted in Figure 3 and the values obtained for T_{onset} (°C) and T_{pc} (°C), it is possible to observe that the addition of 3% EM1 in coconut oil affected the second stage of the crystallization, the crystal growth, and this effect is probably due to the presence of the emulsifier containing 90% MAGs. Basso et al.[24] also observed this effect with the addition of 1% MAGs to palm oil. According to Fredrick,[42] MAGs accelerate the polymorphic transition to stable forms.

The addition of EM2 also accelerated the process of crystallization but, otherwise, crystallization was affected at the beginning of the first peak (T_{onset}, °C); it may be stated that the addition of this emulsifier affected the nucleation of crystallization.

The onset temperatures (T_{onset}, °C) were significantly higher ($p > 0.05$), 9.1 ± 0.5 °C for 1.0% (w/w) of addition and 11.3 ± 0.2 °C for 3.0% (w/w), compared with pure coconut oil that showed an onset temperature (T_{onset}, °C) of 6.7 ± 0.3 °C. With the addition of EM2 (1.0 and 3.0% w/w) was not observed the formation of the second crystallization peak for the coconut oil.

Tables 3, 4, and 5 show the parameters regarding the crystallization curves of coconut oil, palm olein, and their mixture with the commercial emulsifiers.

The enthalpy of crystallization was also changed, with higher values observed in total ΔH_c of crystallization for all mixtures. The greatest variation in enthalpy of coconut oil occurred with the addition EM2, which shows significant difference from coconut oil ($p > 0.05$). The enthalpy of crystallization shows a significant difference between the peaks ($p > 0.05$), indicating that more crystals are present in these samples.

The melting curves for coconut oil and mixtures with EM1 (b) and EM2 (d) are shown in Figure 3. Tables 3, 4, and 5 show the

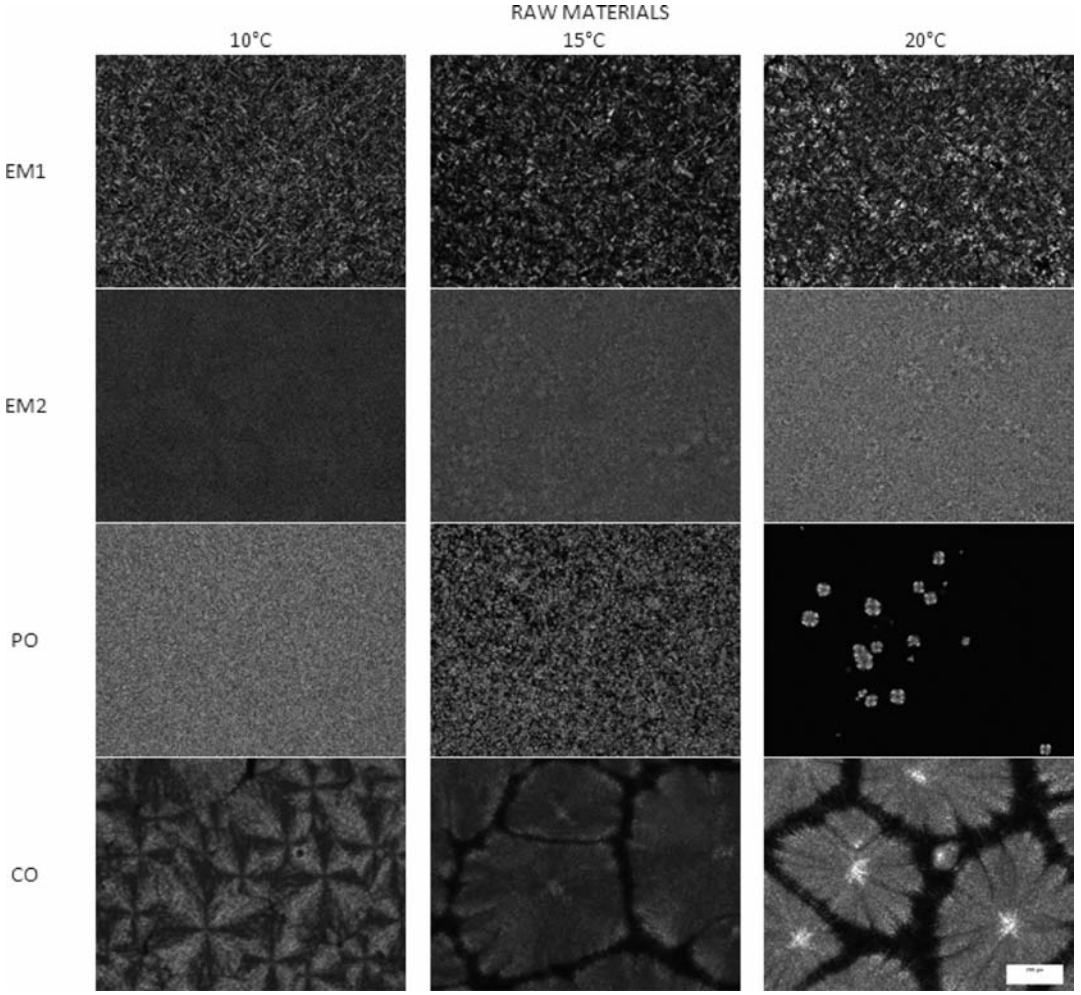

Figure 5. Images of the crystallization of individual commercial emulsifiers, pure coconut oil, and palm olein. The bar represents 200 μm.

parameters regarding the melting curves of coconut oil, palm olein, and their mixture with the commercial emulsifiers.

The addition of EM1 produced a few changes on the melting temperatures (T_{onset} °C) for coconut oil, and mixtures demonstrated close values in a range that varies from 9.9 ± 0.1 to 12.4 ± 0.2 °C with no significant difference ($p > 0.05$). On the other hand, enthalpy of melting was significantly affected ($p < 0.05$) mainly by adding the EM1, in which there was an increase of total ΔH_m in both proportions.

The crystallization curves of palm olein with added EM1 (a) and EM2 (b) are shown in Figure 4. The formation of only one peak crystallization in mixtures with the two commercial emulsifiers was observed.

The addition of emulsifiers (EM1 and EM2) changed the crystallization profile of palm olein, showing significant difference ($p > 0.05$) in the crystallization temperature (T_{onset}, °C). The addition of 1.0 and 3.0% (w/w) EM2 showed crystallization temperature (T_{onset}, °C) lower than observed in pure palm olein and EM1, indicating that the addition of EM2 delayed the crystallization of this oil.

Increasing the crystallization temperature (T_{onset}, °C) by the addition of EM2, rich in saturated MAGs, in coconut oil and palm olein is in agreement with the results of studies by Man et al.[43] and Basso et al.,[24] in which the crystallization peaks (T_{onset}, °C) of the compounds containing more saturated triacylglycerols moved to the region of higher temperatures.

The enthalpy of crystallization (ΔH_c) suffered the most relevant effects, with an increase of 35.1 ± 0.8 J/g in the energy released. Similar results were observed with the addition of 3.0% (w/w) EM1, which increased the energy delivered to the crystallization peak to 40.4 ± 0.8 J/g. This indicates that adding EM1 to the palm olein has an effect on energy released in the crystallization.

On the other hand, the addition of the emulsifier in a proportion of 1.0% (w/w) of EM2 produced no significant ($p < 0.05$) effect on the enthalpy of crystallization (ΔH_c), showing a decrease of 3.0 ± 0.2 J/g in the energy released when compared to the pure olein. A great increase in the release of heat during the crystallization process may be detrimental, because it may result in elevated temperatures that will cause the dissolution of already-formed crystals.[24]

The melting curves of mixtures showed melting peaks very close to that of palm olein, but the enthalpies of melting (ΔH_m) were significantly higher for EM1 and for EM2 added in a proportion of 3.0% (w/w) and also did not present significant differences for EM2 at 1.0% (w/w).

In summary, the emulsifiers modified the DSC melting properties of the coconut oil and palm olein that are ascribed to the influences of the emulsifiers on the crystallization properties. The melting profiles were different, indicating that interactions between TAGs changed due to emulsifier addition.

dx.doi.org/10.1021/jf405221n | J. Agric. Food Chem. 2014, 62, 2253−2263

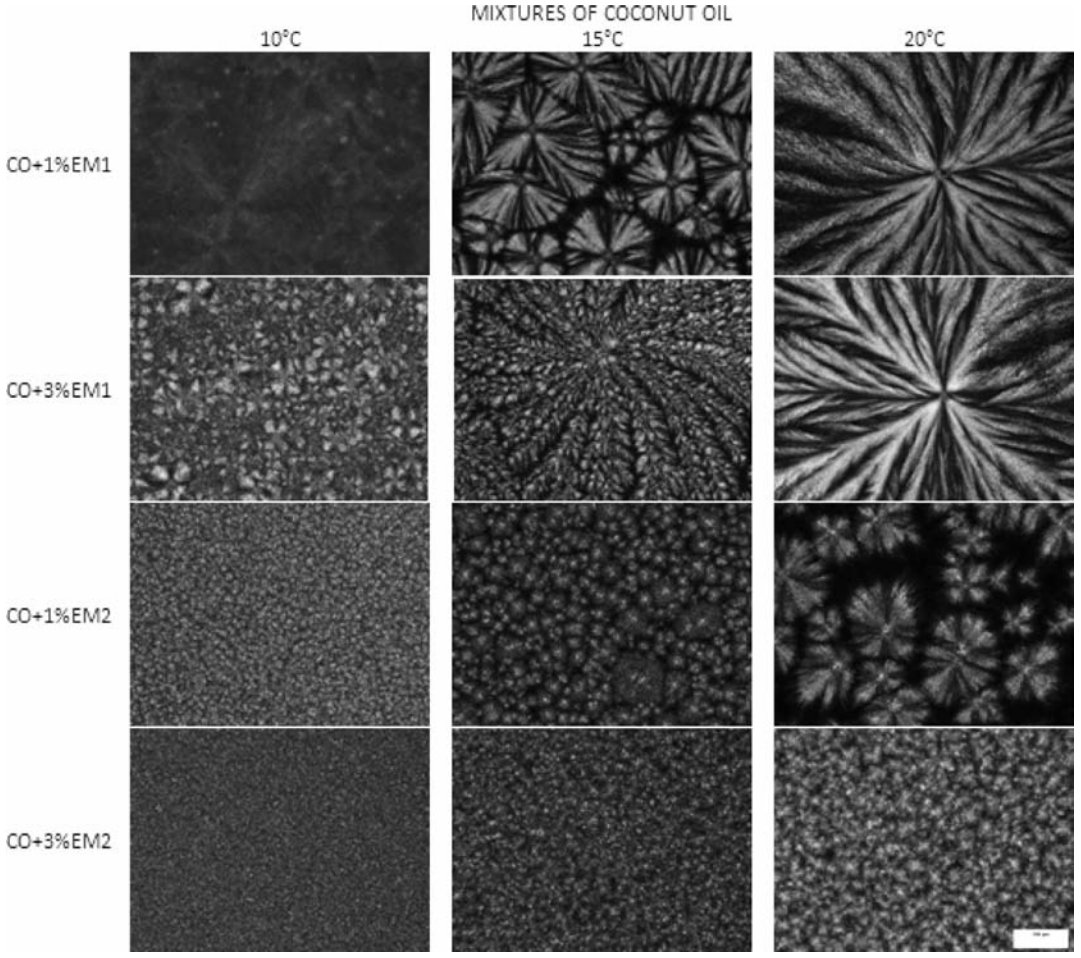

Figure 6. Images of the crystallization of coconut oil their mixture with EM1 and EM2. The bar represents 200 μm.

Polarized Light Microscopy. The study of crystalline microstructure of fat systems has become increasingly important because the functional properties of many foods depend on knowledge of their fine structure. Microstructure is dependent on the composition of a fat, as well as its crystallization behavior, including polymorphism, and the characteristics of the microstructure in turn determine the physical properties of the fat. Success in the measurements requires several stages including obtaining a truly representative image of material, analyzing that image properly, and interpreting the resulting data.[44]

The anisotropic solid phase lattice in the analysis under polarized light refracts light differently from the isotropic liquid phase. The liquid phase appears in the images in black and solid phase in white or grayscale.[45] The "crystals" seen by light microscopy in natural fats are actually clusters of many individual crystals. Fast cooling rates create smaller crystals and slow cooling rates create larger visible crystals, respectively. Thus, the conditions of process determine the size of the clusters, but not the size of the crystals.[46]

The samples were crystallized at 10, 15, and 20 °C. An image was taken directly after 24 h of formation of the fat crystal network, as can be seen in Figures 5, 6, and 7. Crystal mean diameter values of coconut oil, palm olein, and their mixture with the commercial emulsifiers are shown in Table 6.

Figure 5 shows the individual commercial emulsifiers, pure coconut oil, and palm olein. The EM1 sample, which has a composition with high unsaturated fatty acids content, gives a network of small needle-shaped and granular crystals, which can possibly be explained by the crystallization of a β'-polymorph.[47] The increasing of the temperature did not affect the microstructure of EM1.

EM2, which has a high content of saturated fatty acids, showed a dense structure of very small crystals. This is probably due to conditions of cooling that affect the crystallization of higher saturated emulsifier. Even at the highest temperature of crystallization (20 °C) the grain structure maintained crystallization.

Coconut oil at 10 °C showed a dense structure of large crystals; the image showed very compact spherulites type, with no empty space between them, and low birefringence, but with good definition. At 15 and 20 °C this oil shows extra-large spherulites, the nucleus had higher birefringence, and the edges showed little needles. In coconut oil as the temperature was increased to 15 °C the microstructure of this oil was sharply affected. Temperatures up to 20 °C increased the voids between spherulites, which consequently decrease the crystallized area.

Palm olein (Figure 7) showed a dense structure of very small crystals with instantaneous and homogeneous crystallization, which is observed in a large number of small crystals and with the increase in temperature (20 °C) had reduced the total spherulites.

From the observation of microscope images it is possible to affirm that the use of these pure fats (coconut oil and palm olein) has many limitations for applications in those foods that require higher storage temperatures because the temperature of 20 °C formed extra-large spherulites type (coconut oil) or hardly

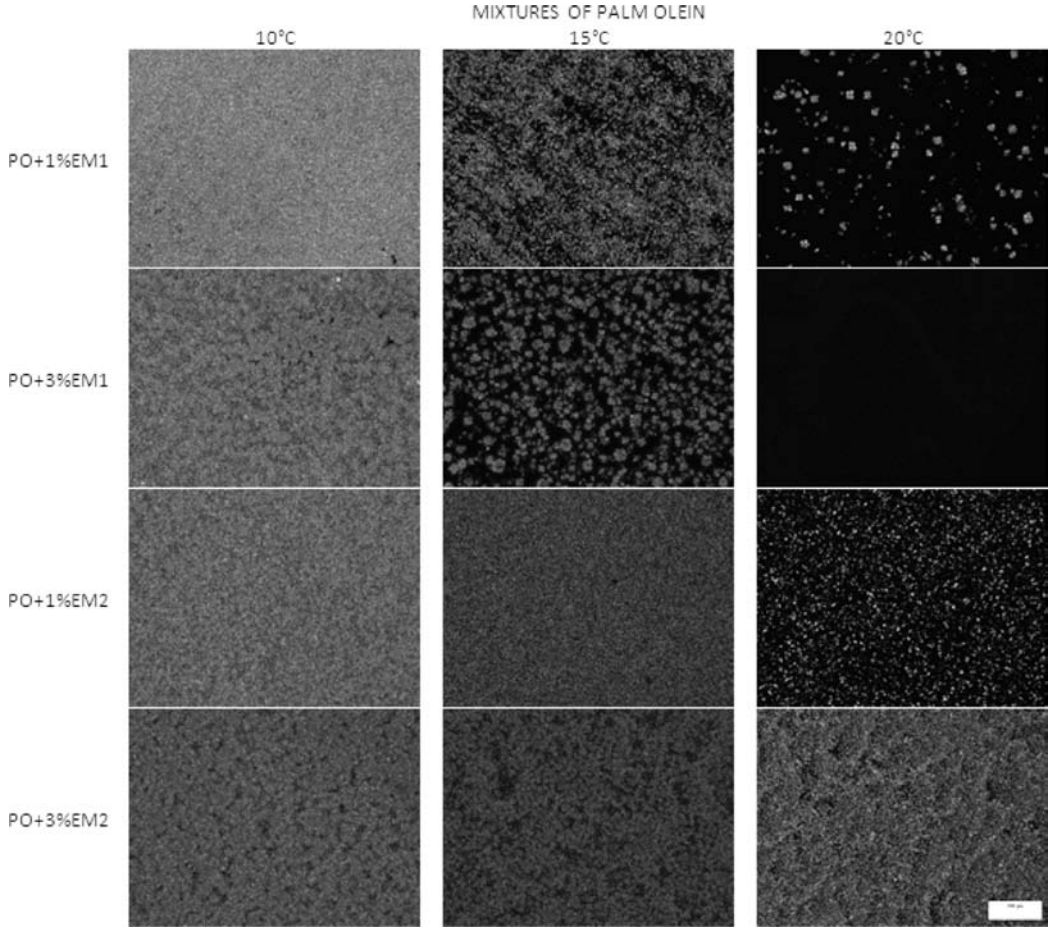

Figure 7. Images of the crystallization of palm olein and their mixture with EM1 and EM2. The bar represents 200 μm.

Table 6. Mean Crystal Diameter (Micrometers) of Coconut Oil (CO), Palm Olein (PO), and Their Mixture with the Two Commercial Emulsifiers

sample	10 °C	15 °C	20 °C
CO	302.8 ± 133.3a	490.7 ± 181.2a	584.6 ± 35.3a
CO + EM1 (1.0% w/w)	194.5 ± 86.6b	248.9 ± 111.6a	1250.0 ± 9.9b
CO + EM1 (3.0% w/w)	125.0 ± 27.0b	75.8 ± 20.7a	1250.0 ± 26.4b
CO + EM2 (1.0% w/w)	37.3 ± 6.0c	456.7 ± 127.0b	297.0 ± 0.0c
CO + EM2 (3.0% w/w)	3.2 ± 1.1c	3.7 ± 0.2c	49.4 ± 10.8d
PO	2.7 ± 0.0a	5.4 ± 2.6a	37.2 ± 15.6a
PO + EM1 (1.0% w/w)	1.5 ± 0.0a	4.6 ± 0.3a	18.2 ± 2.7b
PO + EM 1 (3.0% w/w)	1.1 ± 0.0b	14.6 ± 2.2a	0.0 ± 0.0b
PO + EM2 (1.0% w/w)	1.3 ± 0.3b	2.3 ± 0.5a	6.8 ± 0.8b
PO + EM2 (3.0% w/w)	2.5 ± 0.6a	1.8 ± 0.5a	6.6 ± 0.9b

crystallized (palm olein), and these microstructures are not suitable for application in foods.

Figure 6 shows the coconut oil addition with 1.0 and 3.0% (w/w) of EM1 and EM2.

The addition of EM1 to coconut oil changed the crystallization pattern. The spherulite size was significantly lower when added 1.0 and 3.0% (w/w) of EM1 were added at temperatures of 10 and 15 °C (Table 6). At 20 °C the addition of EM1 in coconut oil produced large spherulites that extrapolated the visual field of the slide; therefore, for statistical purposes a maximum value of the visual field has been estimated as 1250 μm.

The addition of EM2 to coconut oil considerably changed the behavior of this oil. The spherulites after the addition of 1.0 and 3.0% (w/w) were significantly smaller in size (Table 6) than the pure coconut oil and that with EM1 added. The addition of 3.0% (w/w) also maintained the large number of spherulites even at higher temperatures (20 °C), which makes this percentage addition a more interesting technological standpoint.

Figure 6 shows the palm olein addition with 1.0 and 3.0% (w/w) of EM1 and EM2.

In palm olein, the addition of 1.0% (w/w) EM1 did not alter the microstructure of this fat at any of the temperatures, but the increase in this ratio to 3.0% (w/w) of this emulsifier altered the pattern of crystallization of this fat. With the increased temperature occurred a reduction of crystallized area, and at 20 °C no crystallization occurred even after 24 h.

These results for microstructure with addition of EM2 are consistent with the findings of Basso et al.,[24] who described that the addition of saturated monoacylglycerols leads to the formation of a greater number of crystallization seeds, possibly more stable to the effect of temperature. During the crystallization process, a crystalline network is formed that allows for greater interaction between triacylglycerol molecules, between which intermolecular attractive forces such as the van der Waal's forces can act, which may promote greater intermolecular attraction, leading to a decrease in system

dx.doi.org/10.1021/jf405221n | J. Agric. Food Chem. 2014, 62, 2253−2263

solubility, more evident at high temperatures, contributing to the crystallization process.

According to Herrera et al.,[48] fats for food product applications should have crystal diameters of <30 μm to prevent grainy mouthfeel. The crystal dispersion of fats with a large number of small crystals can provide desirable properties such as good spreadability. In this study, the addition of emulsifiers with monoacylglycerols induced the formation of large numbers of small crystalline nuclei, in agreement with that described by Foubert et al.,[49] who reported an increase in the amount of crystallization seed and in the number of crystals formed and a decrease in the induction period, due to the influence of existing partial acylglycerols. The minimum diameter values, 3.2 μm for coconut oil and 1.1 μm for palm olein, were much lower than those obtained for these oils in the absence of monoacylglycerols.

From the results presented in polarized light microscopy and DSC it was possible to observe great coherence between them, the addition of emulsifiers affecting the crystallization of both oils, but this modification acts at different times of crystallization (nucleation and crystal growth). The addition of EM1 to coconut oil affects the second stage of crystallization crystal growth, and this behavior can be observed both in the DSC curve (Figure 3) and in the microscope images (Figure 6), where the addition of the emulsifier led to crystallization of fewer cores of larger diameters. Although the effects of adding EM1 were more effective in coconut oil, it also affected the crystallization of the palm olein. Furthermore, the results of the DSC crystallization curve with respect to the addition of EM2 indicated that the addition of the emulsifier affected the nucleation; this behavior can be observed in Figures 3 and 4 for the DSC curves, and also can be viewed in Figures 6 and 7, in which the nucleation density was retained even at high temperatures.

On the basis of the DSC and microstructure, the coconut oil and palm olein crystallization process was modified by adding the commercial emulsifiers. Several conclusions can be drawn from this study: (a) The crystallization behavior of fat blends strongly depends on the type of emulsifier used and the chemical composition of the sample. (b) The addition of emulsifiers affects not only the type of crystals formed (fractionation) but also the amount of crystals obtained (enthalpy), inducing or delaying the crystallization process. Higher crystallization rates decrease process costs and would make it possible to use this oil in the production of food that requires high rates of crystallization, such as candy coatings and cookie fillings, conserving the desired coconut oil and palm olein characteristics such as its plasticity.

AUTHOR INFORMATION

Corresponding Author

*(R.C.d.S.) Phone: 55 11 3091 2379. E-mail: robertaclaro@usp.br.

Funding

We gratefully acknowledge the generous support from the Brazilian agencies Conselho Nacional de Desenvolvimento Científico e Tecnológico (CNPq), Coordenação de Aperfeiçoamento de Pessoal de Nível Superior (CAPES), and Fundação de Amparo à Pesquisa do Estado de São Paulo (FAPESP) as well as Agropalma S/A, DuPont Nutrition & Health and Copra Indústria.

Notes

The authors declare no competing financial interest.

REFERENCES

(1) Foubert, I.; Dewettinck, K.; Van De Walk, D.; Dijkstra, A. J.; Quinn, P. J. Physical properties: structural and physical characteristics. In *The Lipid Handbook*; Gunstone, F. D., Harwood, J. L., Dijkstra, A. J., Eds.; CRC Press: Boca Raton, FL, USA, 2007; pp 471−508.

(2) Metin, S.; Hartel, R. W. Crystallization of fats and oils. *Bailey's Industrial Oil and Fat Products*; Shahidi, F., Ed.; Wiley Interscience: New York, 2005; pp 45−76.

(3) Karabulut, I.; Turan, S.; Ergin, G. Effects of chemical interesterification on solid fat content and slip melting point of fat/oil blends. *Eur. J. Lipid Sci. Technol.* **2004**, *218*, 224−229.

(4) Soares, F. A. S.D. M.; Da Silva, R. C.; Da Silva, K. C. G.; Lourenço, N. B.; Soares, D. F.; Gioielli, L. A. Effects of chemical interesterification on physicochemical properties of blends of palm stearin and palm olein. *Food Res. Int.* **2009**, *42*, 1287−1294.

(5) Gold, I. L.; Ukhun, M. E. Microstructure and polymorphism of blended and restructured palm olein and palm kernel oil. *Riv. Ital. Sostanze Grasse* **2008**, *85*, 45−53.

(6) Pantzaris, T. P.; Basiron, Y. The lauric (coconut and palmkernel) oils. In *Vegetable Oils in Food Technology: Composition, Properties and Uses*; Gunstone, F. D., Ed.; Blackwell Publishing: Oxford, UK, 2002; pp 157−201.

(7) Assunção, M. L.; Ferreira, H. S.; Santos, A. F.; Cabral, C. R., Jr.; Florêncio, T. M. M. T. Effects of dietary coconut oil on the biochemical and anthropometric profiles of women presenting abdominal obesity. *Lipids* **2009**, *44*, 593−601.

(8) Shin, J. A.; Akoh, C. C.; Lee, K. T. Enzymatic interesterification of anhydrous butterfat with flaxseed oil and palm stearin to produce low-trans spreadable fat. *Food Chem.* **2010**, *120*, 1−9.

(9) O'Brien, R. D. *Fats and Oils: Formulating and Processing for Applications*; CRC Press: Boca Raton, FL, USA, 2009; Chapter 1.

(10) Byers, T. Hardened fats, hardened arteries. *New Engl. J. Med.* **1997**, *327*, 1544−1545.

(11) Pietinen, P.; Ascherio, A.; Korhonen, P. Intake of fatty acids and risk of coronary heart disease in a cohort of Finnish men. The ATBCCancer Prevention Study. *Am. J. Epidemiol.* **1998**, *145*, 876−877.

(12) Marina, A. M.; Che Man, Y. B; Amin, I. Virgin coconut oil: emerging functional food oil. *Trends Food Sci. Technol.* **2009**, *20*, 481−487.

(13) Beerman, C.; Jelinek, J.; Reinecker, T.; Hauenschild, A.; Boehm, G.; Klör, H. U. Short term effects of dietary medium-chain fatty acids and n-3 long-chain polyunsaturated fatty acids on the fat metabolism of healthy volunteers. *Lipids Health Dis.* **2003**, *2*, article 10.

(14) Radujko, I.; Juric, J.; Pajin, B.; Omorjan, R.; Seres, Z.; Simovic, D. S. The influence of combined emulsifier 2 in 1 on physical and crystallization characteristics of edible fats. *Eur. Food Res. Technol.* **2011**, *232*, 899−904.

(15) Mazzanti, G.; et al. Effect of minor components and temperature profiles on polymorphism in milk fat. *Cryst. Growth Des.* **2004**, *4*, 1303−1309.

(16) Awad, T.; Sato, K. Effects of hydrophobic additives on crystallization behavior of palm mid fraction in oil-in-water emulsion. *J. Am. Oil Chem. Soc.* **2001**, *78*, 837−842.

(17) Awad, T.; Hamada, T.; Sato, K. Effects of addition of diacylglycerols on fat crystallization in oil-in-water emulsion. *Eur. J. Lipid Sci. Technol.* **2001**, *103*, 735−741.

(18) Martini, S.; Herrera, M. L.; Hartel, R. W. Effect of processing conditions on microstructure of milk fat fraction and sunflower oil blends. *J. Am. Oil Chem. Soc.* **2002**, *79*, 1063−1068.

(19) Martini, S.; Puppo, M. C.; Hartel, R. W.; Herrera, M. L. Effect of sucrose esters and sunflower oil addition on microstructure of a high-melting milk fat fraction. *J. Food Sci.* **2002**, *67*, 3412−3418.

(20) Puppo, M. C.; Martini, S.; Hartel, R. W.; Herrera, M. L. Effect of sucrose esters on isothermal crystallization and rheological behavior of blends of high-melting milk fat fraction and sunflower oil. *J. Food Sci.* **2002**, *67*, 3419−3426.

(21) Cerdeira, M.; Martini, S.; Hartel, R. W.; Herrera, M. L. Effect of sucrose ester addition on nucleation and growth behavior of milk fat-sunflower oil blends. *J. Agric. Food Chem.* **2003**, *51*, 6550−6557.

(22) Martini, S.; Herrera, M. L. Physical properties of shortenings with low-trans fatty acids as affected by emulsifiers and storage conditions. *Eur. J. Lipid Sci. Technol.* **2008**, *110*, 172−182.
(23) Aini, I. N.; Miskandar, M. S. Utilization of palm oil and palm products in shortenings and margarines. *Eur. J. Lipid Sci. Technol.* **2007**, *109*, 422−432.
(24) Basso, R. C.; Ribeiro, A. P. B.; Masuchi, M. H.; Gioielli, L. A.; Gonçalves, L. A. G.; Santos, A. O.; Cardoso, L. P.; Grimaldi, R. Tripalmitin and monoacylglycerols as modifiers in the crystallisation of palm oil. *Food Chem.* **2010**, *122*, 1185−1192.
(25) ISO. Standard 5509, *Animal and Vegetable Fats and Oils Preparation of Methyl Esters of Fatty Acids*; International Organization for Standardization: Geneva, Switzerland, 2000.
(26) Ribeiro, A. P. B.; Grimaldi, R.; Gioielli, L. A.; Gonçalves, L. A. G. Zero *trans* fats from soybean oil and fully hydrogenated soybean oil: physico-chemical properties and food applications. *Food Res. Int.* **2009**, *42*, 401−410.
(27) Vlahov, G. ^{13}C nuclear magnetic resonance spectroscopy to check 1,3-random, 2-random pattern of fatty acid distribution in olive oil triacylglycerols. *Spectroscopy* **2005**, *19*, 109−117.
(28) Díaz Gamboa, O. W.; Gioielli, L. A. Crystallization behavior of structured lipids produced from palm kernel fat and fish oil. *Quim. Nova* **2006**, 646−653.
(29) Ribeiro, A. P. B.; Basso, R. C.; Grimaldi, R.; Gioielli, L. A.; Gonçalves, L. A. G. Instrumental methods for the evaluation of interesterified fats. *Food Anal. Methods* **2009**, *2*, 282−302.
(30) *Statistica, 11.0 for Windows*; Statsoft: Tulsa, OK, USA, 2013; Vol. IV.
(31) Soares, F. A. S. M.; Silva, R. C.; Hazzan, M.; Capacla, R.; Viccola, E. R.; Maruyama, J. M.; Gioielli, L. A. Chemical interesterification of blends of palm stearin, coconut oil and canola oil: physicochemical properties. *J. Agric. Food Chem.* **2012**, *60*, 1461−1469.
(32) Gee, P. T. Analytical characteristics of crude and refined palm oil and fractions. *Eur. J. Lipid Sci. Technol.* **2007**, 373−379.
(33) Ribeiro, A. P. B.; Basso, R. C.; Grimaldi, R.; Gioielli, L. A.; Gonçalves, L. A. G. Effect of chemical interesterification on physicochemical properties and industrial applications of canola oil and fully hydrogenated cottonseed oil blends. *Lipids* **2009**, *16*, 362−384.
(34) Braipson-Danthine, S.; Gibon, V. Comparative analysis of triacylglycerol composition, melting properties and polymorphic behavior of palm oil and fractions. *Eur. J. Lipid Sci. Technol.* **2007**, *109*, 359−372.
(35) Reena, M. B.; Reddy, S. R. Y.; Lokesh, B. R. Changes in triacylglycerol molecular species and thermal properties of blended and interesterified mixtures of coconut oil or palm oil with rice bran oil or sesame oil. *Eur. J. Lipid Sci. Technol.* **2009**, *111*, 346−357.
(36) D'agostini, D.; Gioielli, L. A. Distribuição estereoespecífica de lipídios estruturados a partir de gorduras de palma, palmiste e triacilgliceróis de cadeia média. *Rev. Bras. Cienc. Farm.* **2002**, *38*, 345−354.
(37) da Silva, R. C.; Soares, D. F.; Lourenco, M. B.; Soares, F. A. S. M.; da Silva, K. G.; Goncalves, M. I. A.; Gioielli, L. A. Structured lipids obtained by chemical interesterification of olive oil and palm stearin. *Food Sci. Technol.* **2010**, *43*, 752−758.
(38) Hayes, K. C.; Khosla, P. The complex interplay of palm oil fatty acids on blood lipids. *Eur. J. Lipid Sci. Technol.* **2007**, *109*, 453−464.
(39) Marina, A. M.; Che Man, Y. B.; Nazimah, S. A. H.; Amin, I. Monitoring adulteration of virgin coconut oil by selected vegetable oils using differential scanning calorimetry. *J. Food Lipids* **2009**, *16*, 50−61.
(40) Mansor, T. S. T.; Che Man, Y. B.; Shuhaimi, M. Employment of differential scanning calorimetry in detecting lard adulteration in virgin coconut oil. *J. Am. Oil Chem. Soc.* **2012**, *89*, 485−496.
(41) Smith, K. W.; et al. Crystallization of fats: influence of minor components and additives. *J. Am. Oil Chem. Soc.* **2011**, *88*, 1085−1101.
(42) Fredrick, E.; Foubert, I.; Van De Sype, J.; Dewettinck, K. Influence of monoglycerides on the crystallization behavior of palm oil. *Cryst. Growth Des.* **2008**, *8*, 1833−1839.
(43) Man, Y. B. C.; Haryati, T.; Ghazali, H. M.; Asbi, B. A. Composition and thermal profile of crude palm oil and its products. *J. Am. Oil Chem. Soc.* **1999**, *76*, 237−242.
(44) Gioielli, L. A.; Simoes, I. S.; Rodrigues, J. N. Crystal morphology and interactions of binary and ternary mixtures of hydrogenated fats. *J. Food Eng.* **2003**, *57*, 347−355.
(45) Narine, S. S.; Marangoni, A. G. Fractal nature of fat crystal networks. *Phys. Rev.* **1999**, *59*, 1908−1920.
(46) Timms, R. E. Phase behaviour of fats and their mixtures. *Prog. Lipid Res.* **1984**, *23*, 1−38.
(47) Litwinenko, J. W.; Rojas, A. M.; Gerschenson, L. N.; Marangoni, A. G. Relationship between crystallization behavior, microstructure, and mechanical properties in a palm oil-based shortening. *J. Am. Oil Chem. Soc.* **2002**, *79*, 647−654.
(48) Herrera, M. L.; Falabella, C.; Melgarejo, M.; Anón, M. C. Isothermal crystallization of hydrogenated sunflower oil: I − Nucleation. *J. Am. Oil Chem. Soc.* **1998**, *75*, 1273−1280.
(49) Foubert, I.; Vanhoutte, B.; Dewettinck, K. Temperature and concentration dependent effect of partial glycerides on milk fat crystallization. *Eur. J. Lipid Sci. Technol.* **2004**, *106*, 531−539.

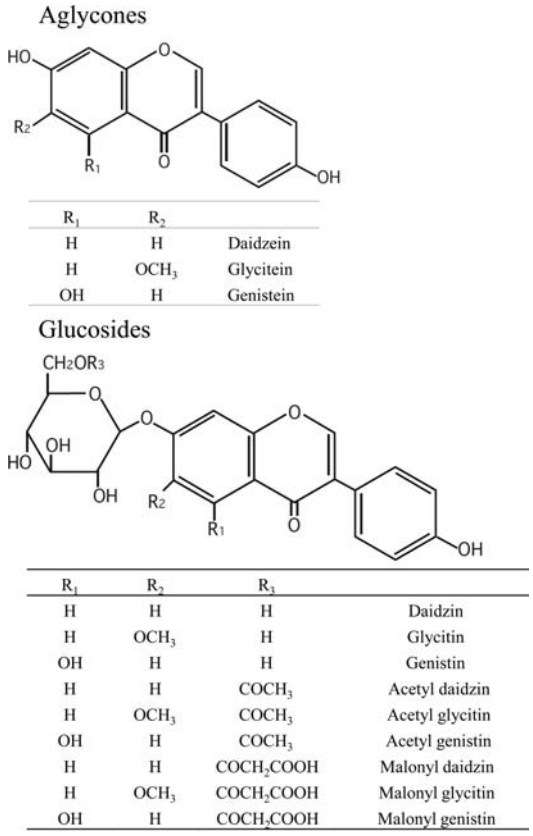

Figure 1. Chemical structures for isoflavone aglycones, isoflavone glucosides, acetyl isoflavone glucosides, and malonyl isoflavone glucosides.

information regarding the absorbability of M-Iso. The aim of the present study was to define the intestinal absorption characteristics of malonyl daidzin stratified according to the molecular structure and water solubility. First, we used soybean hypocotyls to generate isoflavone preparations rich in malonyl daidzin and then compared the absorption of M-Iso and nonmalonyl isoflavone glucosides (G-Iso) in different sections of the intestinal tract. Finally, we determined the enteric site of hydrolysis of each glucoside substance to aglycones.

MATERIALS AND METHODS

Materials. Isoflavone standards were purchased from Fujicco Co. (Hyogo, Japan), and equol was obtained from Funakoshi Co. (Tokyo, Japan). M-Iso were produced by first adding soybean hypocotyls to 70% (v/v) ethanol. After extraction for 12 h at 25 °C, the solvent was removed and dried. The concentrate was loaded onto a column (DIAION HP-20, Mitsubishi Chemical Co., Tokyo), eluted with 25% (v/v) ethanol, and the isoflavone-rich elute dried to yield a powder. G-Iso (Isomax-80) was purchased from Tokiwa Phytochemicals (Chiba, Japan). The isoflavone composition of M-Iso and G-Iso is shown in Table 1.

Measurement of Plasma Isoflavone Concentration in Rats. Female Wistar rats (9 weeks old) were purchased from Charles River Laboratories Japan Inc. (Kanagawa, Japan) and maintained under a 12−12 h light−dark cycle with free access to water and food. All rats were fed a soybean-free diet (F2PLD1; Oriental Yeast, Tokyo) for 1 week, and food was removed overnight. Because the compositions of isoflavones in M-Iso and G-Iso were different, the dosage was adjusted to 25 mg/kg of daidzein family. Therefore, 2.29% (w/w) M-Iso and 1.00% (w/w) G-Iso dissolved in distilled water were administered orally at 6.78 mL/kg. This was followed by extraction of 300 μL of blood from the tail vein at 0, 1, 3, 6, 10, 24, 34, and 48 h

Table 1. Isoflavone Composition of Each Substance and Dosages

	composition[a] (%)		dose (mg/kg body wt)	
	M-Iso[b]	G-Iso[b]	M-Iso	G-Iso
daidzin	4.2	66.6	1.7	24.6
glycitin	2.3	29.9	0.9	11.1
genistin	0.6	2.4	0.2	0.9
malonyl daidzin	55.5	0.2	22.7	0.1
malonyl glycitin	24.8	ND[c]	10.2	ND
malonyl genistin	10.9	ND	4.5	ND
acetyl daidzin	1.3	0.2	0.5	0.1
acetyl glycitin	0.3	ND	0.1	ND
acetyl genistin	0.2	ND	0.1	ND
daidzein	ND	0.7	ND	0.2
glycitein	ND	0.2	ND	0.1
genistein	ND	ND	ND	ND
total	100.0	100.0	41.0	37.0
daidzein family	61.0	67.5	25.0	25.0
glycitein family	27.4	30.1	11.2	11.1
genistein family	11.6	2.4	4.8	0.9
glucosides	7.0	98.8	2.9	36.6
malonyl glucosides	91.1	0.2	37.3	0.1
acetyl glucosides	1.8	0.2	0.7	0.1
aglycone	ND	0.8	ND	0.3

[a]aglycone equivalent. [b]M-Iso, malonyl isoflavone glucosides; G-Iso, isoflavone glucosides. [c]ND, not detectable.

postadministration. The blood samples were centrifuged at 12000 rpm for 5 min, and 150 μL of plasma was transferred into a microtube and kept at −80 °C until analysis.

Analysis of Isoflavones and Metabolites by HPLC and LC-MS/MS. Quantitative analysis of isoflavones by HPLC was performed using the method described by Kudou et al.[9] To analyze the plasma concentration of isoflavones and metabolites, β-glucuronidase (Nippon Biotest Laboratories Inc., Tokyo) diluted in 0.1 M acetate buffer (pH 4.5) was added to 200 μL of each plasma sample. After mixing, each solution was incubated overnight at 38 °C. After incubation, ethyl acetate was added and the solution vigorously shaken and then centrifuged for 5 min at 1000 rpm. The organic solvent layer was transferred to a clean tube and evaporated under a nitrogen gas stream. The dried sample was dissolved in 0.01 M NaOH, and the solution was centrifuged at 10000 rpm for 5 min. The upper layer was injected into LC-MS/MS. The samples were separated on a PEGASIL ODS column (5 μm 4.6 × 150 mm, Senshu Scientific Co., Tokyo) at 22 °C using a linear gradient consisting of methanol/water/acetonitrile/acetic acid (43:41:16:0.007; v/v/v/v) and methanol/acetonitrile/acetic acid (73:27:0.007; v/v/v) at a flow rate of 0.4 mL/min. The column elute was detected using a photodiode array detector monitoring 200−650 nm and ion trap MS (Quattro Ultima, Waters, MA, USA) fitted with an electrospray interface operating in negative ion mode.

Transport Experiments in Caco-2 Cells. We performed transport experiments using Caco-2 cells for the four isoflavone materials. M-Iso, G-Iso, and their aglycones were hydrolyzed fully with commercial almond β-glucosidase (Oriental Yeast, Tokyo, Japan). The Caco-2 cell line, from human colorectal carcinoma, was obtained from Dainippon Sumitomo Pharma Co. (Osaka, Japan). Experiments were performed using the protocol described by Steensma et al.[17] with some modifications. After determination of the integrity of the monolayers, the transport experiment was performed at 37 °C in an atmosphere of 5% CO_2 and 95% relative humidity in Hanks balanced salt solution, with the apical side at pH 6.5 and the basolateral side at pH 7.4. Transport of the test compound across cells was expressed as the amount transferred to the basolateral side.

dx.doi.org/10.1021/jf404378r | J. Agric. Food Chem. 2014, 62, 2264−2270

Hydrolysis of Glucoside Substances by Rat Intestinal Homogenates. This experiment was performed following the protocol described by Ioku et al.[18] Intestinal tissue samples were prepared from 10-week-old female Wistar rats fed a soybean-free diet (F2PLD1) for 1 week and fasted prior to the experiment. After sacrifice by cervical dislocation, duodenum, jejunum, ileum, and colon were dissected and fixed at both ends with clips. Each was rinsed with 0.1 M potassium phosphate buffer (pH 7.0) and homogenized in 3 volumes of 0.1 M maleic acid buffer (pH 6.0). Supernatants were obtained by centrifugation (20000 rpm for 30 min at 4 °C). The mean value (n = 3) of β-glucosidase in the four intestinal solutions was as follows: duodenum, 0.007 U; jejunum, 0.015 U; ileum, 0.031 U; and colon, 0.006 U. Substrates (M-Iso or G-Iso) were prepared by dissolving each in 80% methanol to a concentration of 2000 mg/L. One hundred microliters (200 μg as aglycone) of the substrate solution and 500 μL of enzyme solution were added to a tube, and 0.1 M phosphate buffer solution, pH 7.0, was added up to 1.5 mL. All tubes were incubated at 37 °C and samples removed at 0, 1, 3, 6, and 24 h. Prior to HPLC analysis, the enzyme reaction was stopped by the addition of up to 5 mL of 80% methanol.

Statistical Analysis and Ethics Approval. Results are expressed as the mean ± SEM. Two-way ANOVA was used to determine the effects of isoflavone substances (S), time course of changes (T), interactions (T × S) with respect to plasma isoflavone concentration and the amount of transported substrates from M-Iso and G-Iso. Fischer's least significant difference (LSD) test was used for post hoc analysis of comparison of means within a factor after one-way ANOVA. Dunnett's test was also used as another post hoc analysis for comparisons of baseline values (0 h) and each time point value after one-way ANOVA. The effect of isoflavone absorption calculated from the area under the curve (AUC) for the plasma concentration time course was examined by Student's unpaired t test and the equality of variance determined using Levene's test. Differences were considered significant at $P < 0.05$. Statistical analysis was performed using SPSS II (version 11) for Windows (SPSS Inc., Chicago, IL, USA).

All animals were treated in accordance with guidelines established by the Japanese Society of Nutrition and Food Science (Law 105 and Notification 6 of the Japanese government).

RESULTS

Water Solubility of Isoflavone Compounds. The water solubility of M-Iso and G-Iso was measured by a spectrophotometer set to a wavelength of 660 nm. Compounds were dissolved in distilled water at various concentrations as aglycone (5−50 mg/mL). The G-Iso solution showed a concentration-dependent increase in turbidity (0.5 mg/100 mL, 0.023; 5 mg/100 mL, 0.460; 50 mg/100 mL, 2.767), whereas the M-Iso solution remained clear throughout the test (<0.001).

Changes in Plasma Isoflavone Concentrations after Substance Administration. Figure 2 shows the serial changes in plasma isoflavone concentration after ingestion of G-Iso and M-Iso. The plasma concentration of daidzein 1 h after administration of G-Iso was significantly higher than that after administration of M-Iso. However, the concentration of daidzein 3 h after administration of M-Iso was significantly higher than that after administration of G-Iso (Figure 2A). We also evaluated isoflavone absorption by comparing AUCs spanning from 0 to 48 h (Figure 3). The AUC of daidzein using M-Iso was significantly greater than that with G-Iso. The plasma equol concentration after administration of M-Iso tended to increase after 24 h compared with G-Iso (Figure 2B). The AUCs of equol showed a trend similar to that of daidzein (Figure 3). The plasma concentration of genistein was significantly higher after administration of M-Iso compared with G-Iso (data not shown). This finding is due to the larger amount of genistein family in M-Iso relative to that in G-Iso.

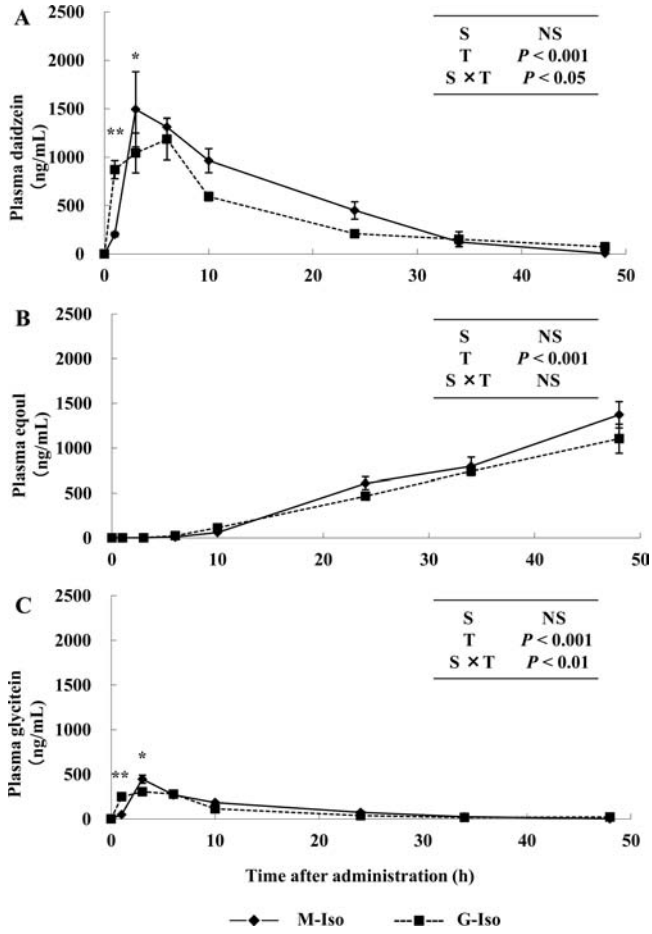

Figure 2. Plasma concentrations of daidzein (A), equol (B), and glycitein (C) after oral administration of M-Iso and G-Iso in rats. Data are expressed as the mean ± SE (n = 5). Because the compositions of isoflavones in M-Iso and G-Iso were different, the dosage was adjusted to 25 mg/kg of daidzein family. Therefore, 2.29% (w/w) M-Iso and 1.00% (w/w) G-Iso dissolved in distilled water were administered orally at 6.78 mL/kg. Plasma concentrations of isoflavones and equol were measured by HPLC and LC-MS/MS. Two-way ANOVA was used to determine the main effects of isoflavone substances (S), time course of changes (T), and interactions (S × T) with respect to isoflavonoid concentrations in plasma. LSD test was used for comparison of means within a factor. Significant difference between the M-Iso group and the G-Iso group at a particular time point; (∗) $P < 0.05$ and (∗∗) $P < 0.01$. NS, not significant. For abbreviations, see Table 1.

Similar changes were noted in plasma glycitein concentration following the administration of G-Iso and M-Iso, although the levels were small in both substrates (Figure 2C).

Transport Experiments Using Caco-2 Cells. Figure 4 shows the results of the transport experiments on M-Iso, G-Iso, and their hydrolysates (M-Iso-hydrolysate and G-Iso-hydrolysate). Negligible transportation of the two glucosides (from the apical side to the basolateral side) was observed in M-Iso and G-Iso, whereas their aglycones were transported to the basolateral side. In addition, only aglycones were detected on the basolateral side (data not shown).

Enteric Specificity of Isoflavone Glucoside Hydrolysis from Rat Intestinal Homogenates. Figure 5 shows the substrate specificity of isoflavone glucoside hydrolysis in the four intestinal segments. Malonyl daidzin in M-Iso was hydrolyzed to aglycone only after treatment with colonic

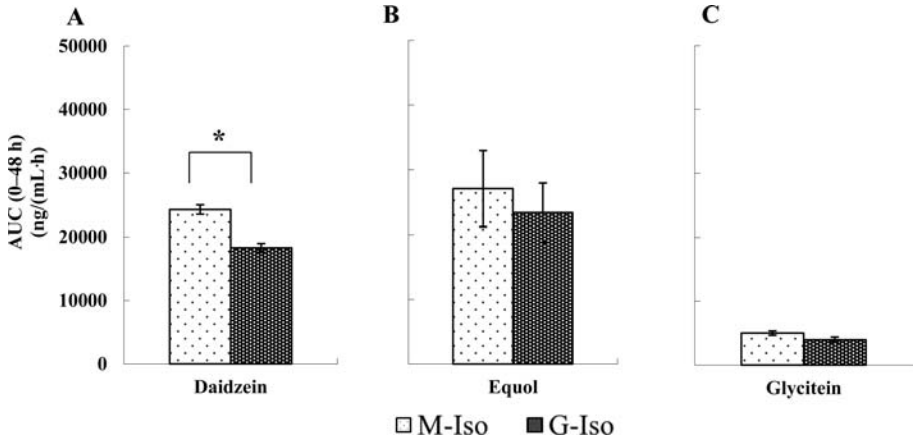

Figure 3. AUCs for daidzein (A), equol (B), and glycitein (C), calculated for each plasma isoflavone from 0 to 48 h on the basis of the initial baseline value. Data are the mean ± SEM (n = 5). Significant difference between M-Iso and G-Iso by Student's unpaired t test after Levene's test for equality; (*) $P < 0.05$. For abbreviations, see Table 1.

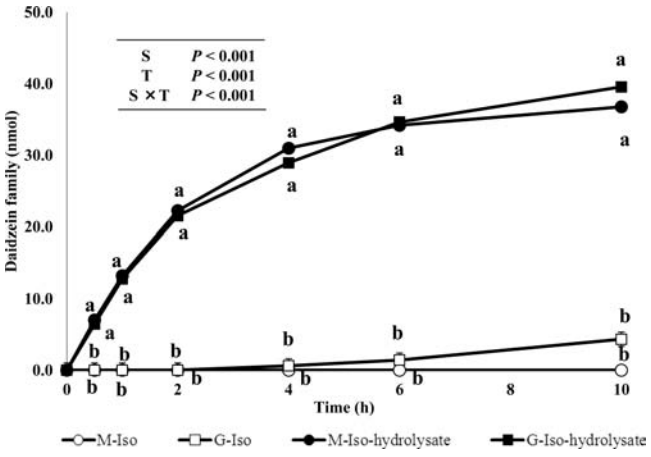

Figure 4. Transport of M-Iso, G-Iso, and their hydrolysates in Caco-2 cells. Initial substrate amounts were 65 nmol of daidzein family for M-Iso, G-Iso, M-Iso-hydrolysate, and G-Iso-hydrolysate. Hydrolyzation of M-Iso and G-Iso was performed using commercial almond β-glucosidase. Data are expressed as the mean of triplicate measurements. Two-way ANOVA was used to determine the main effects of isoflavone substances (S), time course of changes (T), and the interactions (S × T) with respect to isoflavonoid concentrations in plasma. LSD test was used for comparison of means within a factor after one-way ANOVA. Different letters denote significant differences at a particular time point; $P < 0.05$. For abbreviations, see Table 1.

homogenate (Figure 5D), and hydrolysis was barely observable following processing by duodenal, jejunal, and ileal homogenates (Figure 5A–C). Malonyl daidzin content was decreased and daidzin content increased following processing by colonic homogenates up to 6 h and then decreased until 24 h in M-Iso (Figure 5D). These findings suggest that M-Iso are hydrolyzed to aglycone via nonmalonyl glucosides from malonyl glucosides. On the other hand, daidzin in G-Iso was hydrolyzed to the aglycone by jejunal, ileal, and colonic homogenates (Figure 5F–H), but not duodenal homogenate (Figure 5E). A steady increase in daidzein was observed following treatment with colonic homogenate, and the majority of daidzin was hydrolyzed to aglycone within 24 h in G-Iso (Figure 5H). Treatment of G-Iso, however, with jejunal and ileal homogenates promoted rapid hydrolysis until 6 h, but this process slowed after 6 h (Figure 5F,G). With M-Iso treatment by colon homogenates, the amount of daidzein after 24 h was almost identical to the initial malonyl daidzin amount (Figure 5D). However, the total amount of daidzein was decreased with G-Iso (Figure 5H).

DISCUSSION

In this study, we demonstrated that M-Iso were mainly hydrolyzed and absorbed in colon and that absorption properties differed between M-Iso and G-Iso.

The transport experiment showed that M-Iso and G-Iso were barely transported across the Caco-2 monolayer, whereas their aglycones prepared by glycoside hydrolase were transported (Figure 4). These results suggest that conversion of glycosides to aglycones is necessary for intestinal absorption.

We evaluated characteristics of isoflavone hydrolysis dependent on the localization in rat intestine (Figure 5). M-Iso were hydrolyzed only in colon homogenate (Figure 5A–D), whereas aglyconization of G-Iso occurred in homogenates of jejunum, ileum, and colon (Figure 4E–H). These results indicate that the degree of isoflavone hydrolysis differed by the intestinal section. Upon M-Iso hydrolysis in the colon homogenate, the glycoside increased after 6 h and then decreased (Figure 5D). This result suggests that M-Iso were hydrolyzed to aglycone via nonmalonyl glycoside. Hydrolysis curves of G-Iso were somewhat different on the basis of intestinal localization (jejunum, ileum, or colon). In the colon, G-Iso was linearly hydrolyzed and most glucosides were aglyconized within 24 h (Figure 5H). In the jejunum and ileum, however, G-Iso was rapidly aglyconized within 6 h, with the reaction then slowing (Figure 5F,G). In accordance with these data, Ismail and Hayes[19] reported that the hydrolysis property of β-glucosidase varies on the basis of the type of isoflavone. The different hydrolysis patterns of M-Iso and G-Iso in the four intestinal segments likely reflects the substrate specificity of different β-glucosidases in the intestine. In addition, our data seem to indicate that malonyl and acetyl glucosides are hydrolyzed in the distal regions of the gut having very high bacterial concentrations.[20] The amount of daidzein after 24 h of treatment of M-Iso by colonic homogenate was almost identical to the initial amount of total daidzin (Figure 5D). However, with G-Iso, the amount of daidzein at 24 h was decreased compared to the initial daidzin (Figure 5H). G-Iso may be transformed to other metabolites, for example, O-desmethyl

dx.doi.org/10.1021/jf404378r | J. Agric. Food Chem. 2014, 62, 2264–2270

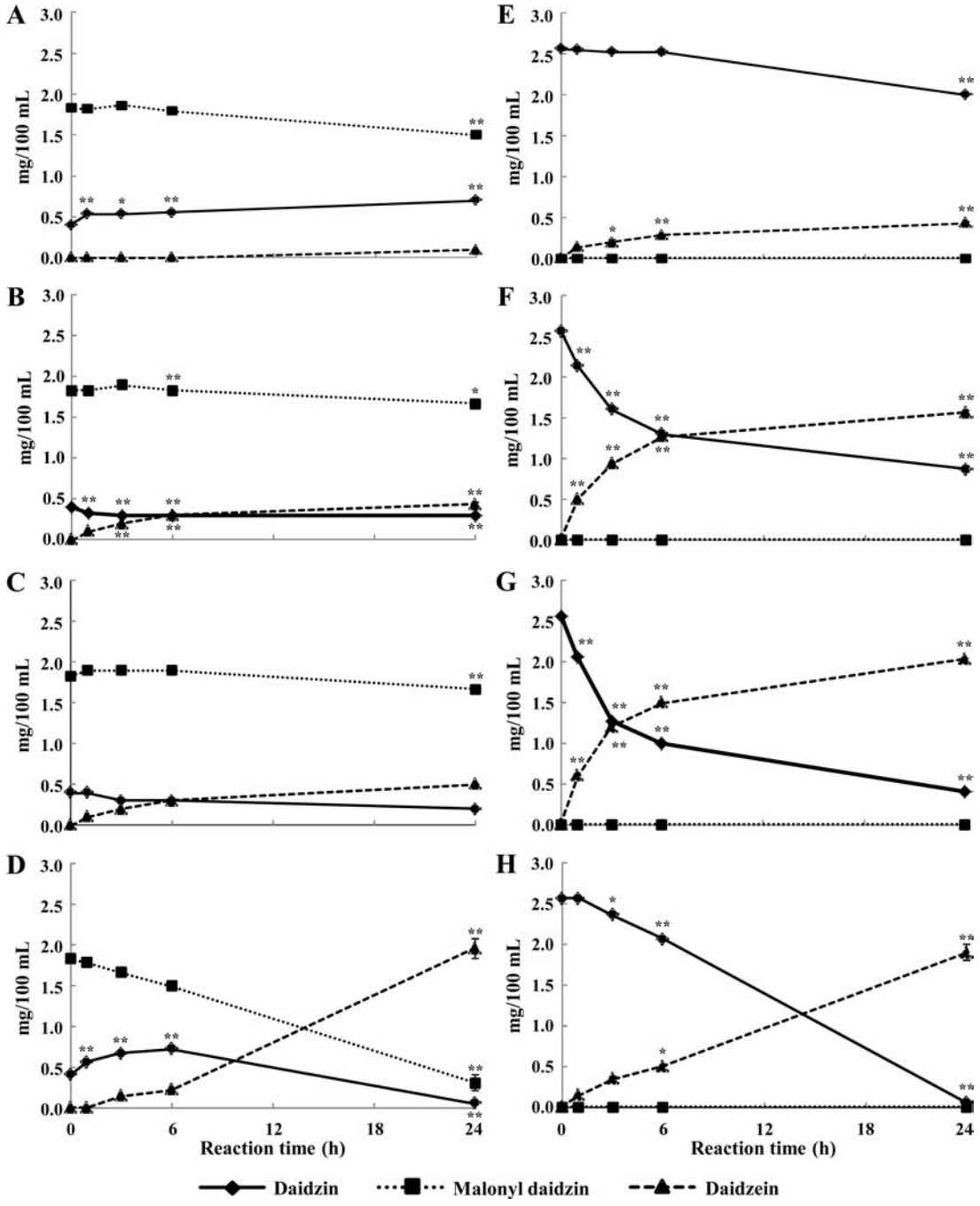

Figure 5. Hydrolysis of M-Iso and G-Iso in four intestinal homogenates: (A) M-Iso treated with duodenal homogenate; (B) M-Iso treated with jejunal homogenate; (C) M-Iso treated with ileal homogenate; (D) M-Iso treated with colonic homogenate; (E) G-Iso treated with duodenal homogenate; (F) G-Iso treated with jejunal homogenate; (G) G-Iso treated with ileal homogenate; (H) G-Iso treated with colonic homogenate. Measurements of isoflavones were performed by HPLC. Each isoflavone concentration is shown as the aglycone equivalent. Data are the mean ± SEM (n = 3). Significant difference from the baseline value (0 h) at a particular time point by Dunnett's test as a post hoc test after one-way ANOVA; (*) $P < 0.05$ and (**) $P < 0.01$. For abbreviations, see Table 1.

angolensin (*O*-DMA), or degradation products of daidzein, which were not measured in the present study.

Plasma daidzein and glycitein concentrations measured within 1 h of G-Iso administration increased more rapidly than with M-Iso; however, concentrations measured 3 h after M-Iso administration were higher than those with G-Iso (Figure 2). As well, M-Iso AUCs were greater than that of G-Iso (Figure 3). Plasma equol concentration after ingestion of M-Iso or G-Iso was also similar to plasma daidzein and glycitein; equol concentration after M-Iso tended to be lower than after G-Iso up to 10 h, but tended to increase thereafter, and it is likely that AUCs of equol would increase after 48 h. These results signified important differences between M-Iso and G-Iso in hydrolysis and absorption. Further studies are necessary to confirm these results. In addition, other metabolites, such as dihydrodaidzein and *O*-DMA, were not measured as they are minor metabolites in the blood of rats fed a diet supplemented with daidzein.[21]

Hydrolysis of isoflavone glucosides in the four intestinal segments suggests that G-Iso is hydrolyzed more quickly in the

upper small intestine than in the large intestine. The results also indicate that plasma concentration was higher in G-Iso than in M-Iso in the early stages (Figure 2). Andlauer et al.[22] investigated intestinal absorption and metabolism of isoflavones from tofu and demonstrated that the major aglycones (e.g., genistein and daidzein) in the small intestine originated from glucosides. Furthermore, aglycones that are absorbed from the intestinal tract are rereleased as glucuronides in the intestine.[22] This suggests that at least part of aglycones derived from glucosides are absorbed into the blood through the intestine, whereas the remaining components are rereleased into the intestinal tract. Wang et al.[23] investigated the effects of structural differences on isoflavone metabolism in the intestine. Using an intestinal perfusion model, they found significant differences in absorption and excretion between isoflavones and their respective glucuronides. The glucuronides were mainly excreted in the small intestine, with very little in the colon. As discussed above, non-malonyl glucoside-rich isoflavones were hydrolyzed to aglycones and absorbed from the small intestine and thus were rereleased again as glucuronide into the intestine.[24] On the other hand, isoflavones rich in malonyl forms, which are not hydrolyzed in the small intestine, would reach the colon and be absorbed effectively after hydrolysis (Figure 6).

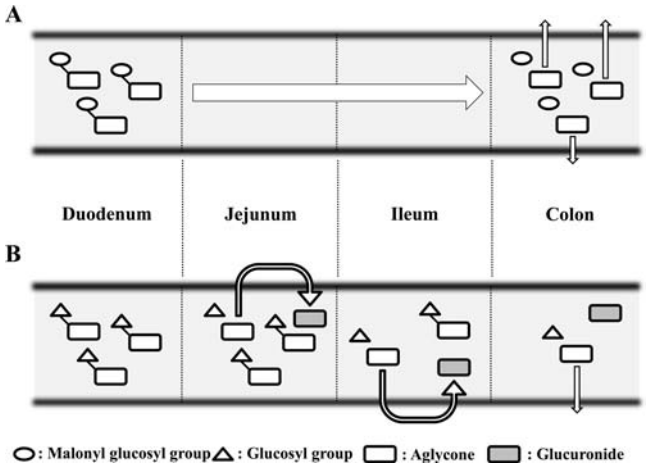

Figure 6. Schematic diagram of the hydrolysis and absorption processes of M-Iso (A) and G-Iso (B) in the intestine.

Yamada et al.[25] evaluated the absorbability and degradability of hesperidin, which is dependent on conjugation with glucosides in the intestine. Their results showed that glucosyl hesperidin is absorbed more rapidly and efficiently than hesperidin alone, due to its high water solubility. The water solubility of M-Iso in the present study may have also contributed to the absorbability.

In conclusion, our data suggest that M-Iso, which are not hydrolyzed in the small intestine, reach the colon and are hydrolyzed there. Effective absorption of malonyl-rich isoflavone aglycones in the colon likely contributes to the significant increase in plasma isoflavone levels. Furthermore, intake of malonyl isoflavone aglycones may be superior in regard to the production of equol, as they are more likely to reach the colon.

AUTHOR INFORMATION

Corresponding Author

*(H.Y.-Y.) Phone: +81-72-463-1751. Fax: +81-72-463-1117. E-mail: yonemoto.hiroko@so.fujioil.co.jp.

Notes

The authors declare no competing financial interest.

ACKNOWLEDGMENTS

We express our gratitude to Dr. Nobuhiko Tachibana and Masashi Asanoma from the Food Science Institute, Fuji Oil Co. Ltd., for their skillful technical support and expert advice.

REFERENCES

(1) Taku, K.; Melby, M. K.; Kurzer, M. S.; Mizuno, S.; Watanabe, S.; Ishimi, Y. Effects of soy isoflavone supplements on bone turnover markers in menopausal women: systematic review and meta-analysis of randomized controlled trials. *Bone* **2010**, *47*, 413−423.

(2) Uesugi, S.; Watanabe, S.; Ishiwata, N.; Uehara, M.; Ouchi, K. Effects of isoflavone supplementation on bone metabolic markers and climacteric symptoms in Japanese women. *Biofactors* **2004**, *22*, 221−228.

(3) Alekel, D. L.; Germain, A. S.; Peterson, C. T.; Hanson, K. B.; Stewart, J. W.; Toda, T. Isoflavone-rich soy protein isolate attenuates bone loss in the lumbar spine of perimenopausal women. *Am. J. Clin. Nutr.* **2000**, *72*, 844−852.

(4) Yamamoto, S.; Sobue, T.; Kobayashi, M.; Sasaki, S.; Tsugane, S. Soy, isoflavones, and breast cancer risk in Japan. *J. Natl. Cancer Inst.* **2003**, *95*, 906−913.

(5) Breinholt, V.; Larsen, J. C. Detection of weak estrogenic flavonoids using a recombinant yeast strain and a modified MCF7 cell proliferation assay. *Chem. Res. Toxicol.* **1998**, *11*, 622−629.

(6) Setchell, K. D.; Borriello, S. P.; Hulme, P.; Kirk, D. N.; Axelson, M. Nonsteroidal estrogens of dietary origin: possible roles in hormone-dependent disease. *Am. J. Clin. Nutr.* **1984**, *40*, 569−578.

(7) Yerramsetty, V.; Mathias, K.; Bunzel, M.; Ismail, B. Detection and structural characterization of thermally generated isoflavone malonyl glucoside derivatives. *J. Agric. Food Chem.* **2011**, *59*, 174−183.

(8) Franke, A. A.; Custer, L. J.; Cerna, C. M.; Narala, K. K. Quantitation of phytoestrogens in legumes by HPLC. *J. Agric. Food Chem.* **1994**, *42*, 1905−1913.

(9) Kudou, S.; Fleury, Y.; Welti, D.; Magnolato, D.; Uchida, T.; Kitamura, K.; Okubo, K. Malonyl isoflavone glycosides in soybean seeds (*Glycine max* Merrill). *Agric. Biol. Chem.* **1991**, *55*, 2227−2233.

(10) Watanabe, S.; Yamaguchi, M.; Sobue, T.; Takahashi, T.; Miura, T.; Arai, Y.; Mazur, W.; Wähälä, K.; Adlercreutz, H. Pharmacokinetics of soybean isoflavones in plasma, urine and feces of men after ingestion of 60 g baked soybean powder (kinako). *J. Nutr.* **1998**, *128*, 1710−1715.

(11) Adlercreutz, H.; Mazur, W. Phyto-oestrogens and Western diseases. *Ann. Med.* **1997**, *29*, 95−120.

(12) Setchell, K. D.; Brown, N. M.; Lydeking-Olsen, E. The clinical importance of the metabolite equol − a clue to the effectiveness of soy and its isoflavones. *J. Nutr.* **2002**, *132*, 3577−3584.

(13) Richelle, M.; Pridmore-Merten, S.; Bodenstab, S.; Enslen, M.; Offord, E. A. Hydrolysis of isoflavone glycosides to aglycones by β-glycosidase does not alter plasma and urine isoflavone pharmacokinetics in postmenopausal women. *J. Nutr.* **2002**, *132*, 2587−2592.

(14) Qiu, F.; Chen, X. Y.; Song, B.; Zhong, D. F.; Liu, C. X. Influence of dosage forms on pharmacokinetics of daidzein and its main metabolitedaidzein-7-*O*-glucuronide in rats. *Acta Pharmacol. Sin.* **2005**, *26*, 1145−1152.

(15) Lee, S. H.; Kim, Y. H.; Yu, H. J.; Cho, N. S.; Kim, T. H.; Kim, D. C.; Chung, C. B.; Hwang, Y. I.; Kim, K. H. Enhanced bioavailability of soy isoflavones by complexation with β-cyclodextrin in rats. *Biosci., Biotechnol., Biochem.* **2007**, *71*, 2927−2933.

(16) Vitale, D. C.; Piazza, C.; Melilli, B.; Drago, F.; Salomone, S. Isoflavones: estrogenic activity, biological effect and bioavailability. *Eur. J. Drug Metab. Pharmacokinet.* **2013**, *38*, 15−25.
(17) Steensma, A.; Noteborn, H. P.; Jagt, R. C.; Polman, T. H.; Mengelers, M. J.; Kuiper, H. A. Bioavailability of genistein, daidzein, and their glycosides in intestinal epithelial Caco-2 cells. *Environ. Toxicol. Pharmacol.* **1999**, *7*, 209−212.
(18) Ioku, K.; Pongpiriyadacha, Y.; Konishi, Y.; Takei, Y.; Nakatani, N.; Terao, J. β-Glucosidase activity in the rat small intestine toward quercetin monoglucosides. *Biosci., Biotechnol., Biochem.* **1998**, *62*, 1428−1431.
(19) Ismail, B.; Hayes, K. β-Glycosidase activity toward different glycosidic forms of isoflavones. *J. Agric. Food Chem.* **2005**, *53*, 4918−4924.
(20) Barnes, S.; Sfakianos, J.; Coward, L.; Kirk, M. Soy isoflavonoids and cancer prevention. Underlying biochemical and pharmacological issues. *Adv. Exp. Med. Biol.* **1996**, *401*, 87−100.
(21) Lamartiniere, C. A.; Wang, J.; Smith-Johnson, M.; Eltoum, I. E. Daidzein: bioavailability, potential for reproductive toxicity, and breast cancer chemoprevention in female rats. *Toxicol. Sci.* **2002**, *65*, 228−238.
(22) Andlauer, W.; Kolb, J.; Fürst, P. Isoflavones from tofu are absorbed and metabolized in the isolated rat small intestine. *J. Nutr.* **2000**, *130*, 3021−3027.
(23) Wang, S. W.; Chen, J.; Jia, X.; Tam, V. H.; Hu, M. Disposition of flavonoids via enteric recycling: structural effects and lack of correlations between in vitro and in situ metabolic properties. *Drug Metab. Dispos.* **2006**, *34*, 1837−1848.
(24) Barnes, S. The biochemistry, chemistry and physiology of the isoflavones in soybeans and their food products. *Lymphat. Res. Biol.* **2010**, *8*, 89−98.
(25) Yamada, M.; Tanabe, F.; Arai, N.; Mitsuzumi, H.; Miwa, Y.; Kubota, M.; Chaen, H.; Kibata, M. Bioavailability of glucosyl hesperidin in rats. *Biosci., Biotechnol., Biochem.* **2006**, *70*, 1386−1394.

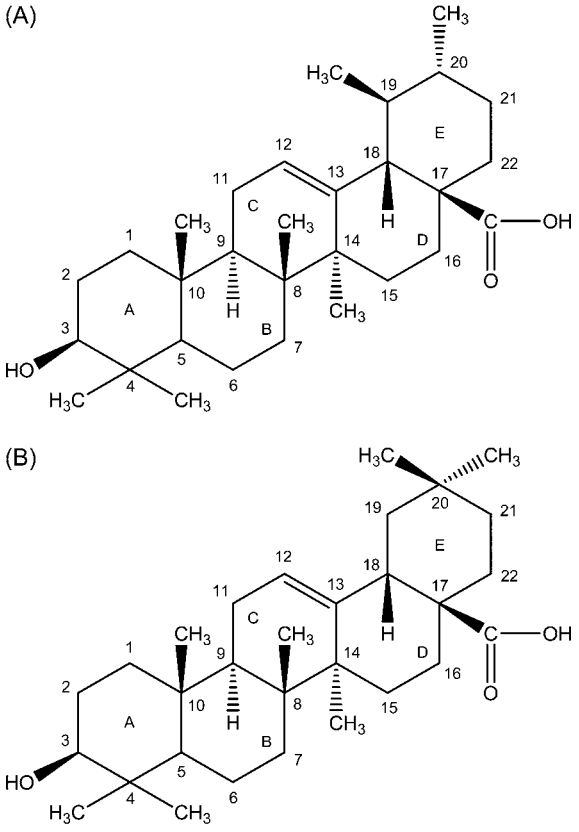

Figure 1. Molecular structure of (A) ursolic acid and (B) oleanolic acid.

production in mitochondria upon incubation with 5.0 ng mL^{-1} ursolic acid occurred. Therefore, they considered that mild mitochondrial uncoupling evoked through pharmacological concentrations (1.6−5.0 ng mL^{-1}) of ursolic acid as discovered in some herbal preparations may be helpful in cardioprotection.

In another study, oleanolic acid was found to obstruct lipopolysaccharide-intervened secretion of high-mobility group box 1 protein by endothelial cells as well as high-mobility group box 1 protein-mediated proinflammatory responses, which creates a decline in monocyte adhesion and migration.[8] Oleanolic acid also deterred high-mobility group box 1 protein-interfered nuclear factor-κB and tumor necrosis factor-α production, which are the most principal inflammatory mediators. These discoveries could offer that oleanolic acid may be utilized as an anti-inflammatory ligand for vascular inflammatory infirmity medication. Owning to its easily obtainable, low-cost material and various biological roles, humankind in many cultures, as well as animals globally, have been reliably consuming these triterpenoids, e.g., ursolic acid and oleanolic acid, in their victual, or have been utilizing them for curative objects, for numerous centuries without marked disease actions.[9,10] Accordingly, an exponential growth in the amount of information about bioactive ursolic acid and oleanolic acid or other triterpenoids over the early decade mirrors the increasing core in their concealed cosmeceutical, nutraceutical, and medicinal applications.

Unfavorably, the demerit of applying ursolic acid and oleanolic acid, indeed, is the toxicity related to their hemolytic and cytostatic character.[4] In a more recent examination, Jilani et al.[11] described that contact of leukocyte depleted erythrocytes for 48 h to Ringer's solution containing ursolic acid (0.5−10 μM) and diminished forward scatter, a result arriving statistically significantly at 5.0 μM, revealing cell shrinkage. Also, activation of Ca^{2+} entry, ceramide shaping, eliciting phospholipid scrambling and to a lesser extent hemolysis in human erythrocytes have been perceived upon addition of ursolic acid. These consequences were ascribed to frank evidence of the ursolic acid influencing erythrocytes from flowing blood and exciting the suicidal demise of erythrocytes, with a consequent generation in anemia. For all of these, the episteme of the existence and biological functions of these natural triterpenoid chemicals, in particular those derived from edible and pharmaceutical herbaceous plants, are of enormous relish.

Blood plasma includes many proteins or other substances such as enzymes that are eagerly bound with ligands especially drugs and, consequently, impress the pharmacodynamics and pharmacokinetics of many drugs, but most investigations on the binding of drugs to assorted proteins in blood have evidently displayed that likely the most significant protein is albumin.[12] Even though albumin has a net negative charge at the pH of blood, pH = 7.4, it binds both positively and negatively charged ligands, such as tetracyclines, digitoxin, salicylates, sulfonamide, phenylbutazone, barbiturates, acid dyes, vitamins C, uric acid, histamine, bilirubin, etc.[13] Pharmacologically, albumin protein recognition is a weighty factor of pharmacokinetics as it decides how much of a drug will be accessible in its free state for therapeutic utility, nontarget effectiveness (side effects), toxicity, and circulation into other human body cabins.[14] Drugs that are greatly bound to albumin protein generally have a low proportion of distribution and could be smaller promptly swept from the body as just the free section is usable for renal elimination. Depending on the expected target of a drug and the hopeful period of action, a high extent of albumin protein binding may or may not be an attractive characteristic.[15] An in vitro albumin protein recognition forecasts the degree to which an objective chemical will be recognized by albumin protein in the same species in vivo.

In arousing pharmacological and toxicological responses, drugs mostly connect either reversibly or irreversibly with target sites on intrastitial biopolymers or organelles, and therefore bring about changes of physicochemical or biochemical procedures in the living organism.[16,17] As has been shown, although drugs can bind to different proteins in blood, the chief plasma and tissue protein which is typically chargeable for the broad spectrum binding of most drugs is albumin. Despite a large quantity of literature, there is little consolidated knowledge obtainable on the kinetic and physiological dispersal of albumin−triterpenoids in the human body. It is thereby proper to contemplate the function of albumin in influencing triterpenoid binding and pharmacokinetics. The objective of the present study was to inspect the molecular recognition as well as the solution structure of the complexes fashioned between the triterpenoids ursolic acid and oleanolic acid and the protein bovine serum albumin (abbreviation: BSA, Figure 2), by means of computer-aided molecular modeling, steady state and time-resolved fluorescence, site-specific ligands, and hydrophobic 8-anilino-1-naphthalenesulfonic acid displacement. Furthermore, the conformation of BSA protein upon complexation was monitored by circular dichroism (CD) and synchronous fluorescence along with three-dimensional fluorescence measurements. These clues stated here can probably be useful when exploiting new synthesized drugs, which have analogous configuration with triterpenoids, whether the

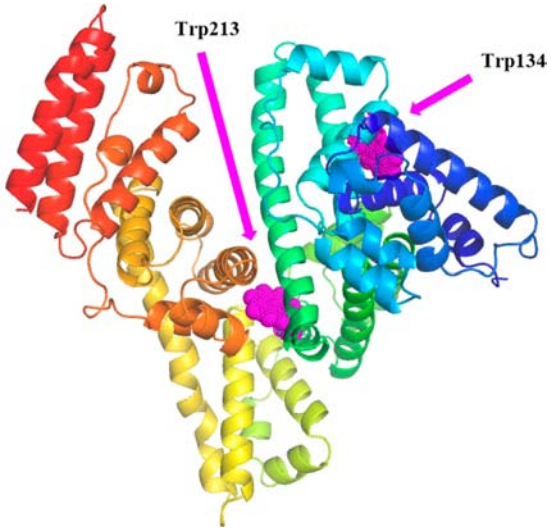

Figure 2. The ribbon model of the BSA derived from X-ray diffraction crystallography (PDB: 4JK4) and the tryptophan (Trp) residues located in domain I and II. This diagram was fabricated using PyMOL on the basis of the atomic coordinates accessible at the Brookhaven Protein Data Bank (http://www.rcsb.org/pdb).

intention is to utilize their depot role or to avoid binding to BSA.

EXPERIMENTAL SECTION

Materials. Albumin from bovine serum (A7030, lyophilized powder, fatty acid free, globulin free, ≥98%), ursolic acid (U6753, ≥90%), oleanolic acid (O5504, ≥97%), and 8-anilino-1-naphthalenesulfonic acid (A1028, ≥97%) were received from Sigma-Aldrich (St. Louis, MO) and used without further purification, and deionized water was obtained from a Milli-Q Ultrapure Water Purification System from Millipore (Billerica, MA). Tris (0.2 M)−HCl (0.1 M) buffer of pH = 7.4, with ionic strength 0.1 in the presence of NaCl, was used, and the pH was measured with an Orion Star A211 pH Benchtop Meter (Thermo Scientific, Waltham, MA). Dilutions of the BSA stock solution (10 μM) in Tris−HCl buffer were prepared immediately before use, and the concentration of BSA was checked spectrophotometrically using $E^{1\%}_{1cm}$ = 6.6.[18] All other reagents employed were of analytical grade and purchased from Sigma-Aldrich.

Molecular Modeling. Molecular modeling of the BSA−triterpenoid complexes was operated on an SGI Fuel Visual Workstation. The crystal structure of BSA (entry codes 4JK4), determined at a resolution 2.65 Å, was retrieved from the Brookhaven Protein Data Bank (http://www.rcsb.org/pdb). After being imported in the program Sybyl Version 7.3 (http://tripos.com), BSA structure was carefully checked for atom and bond type correctness assignment. Hydrogen atoms were computationally added using the Sybyl Biopolymer and Build/Edit menus. To avoid negative acid/acid interactions and repulsive steric clashes, added hydrogen atoms were energy minimized with the Powell algorithm with 0.05 kcal mol^{-1} energy gradient convergence criteria for 1500 cycles; this procedure does not change positions to heavy atoms, and the potential of the three-dimensional structure of BSA was assigned according to the AMBER force field with Kollman all-atom charges. The two-dimensional structure of triterpenoid was downloaded from PubChem (http://pubchem.ncbi.nlm.nih.gov), and the initial structure of the molecule was produced by Sybyl 7.3. The geometry of triterpenoid was subsequently optimized to minimal energy (tolerance of 0.5 kcal mol^{-1}) using the Tripos force field with Gasteiger−Hückel charges, and the lowest energy conformer was utilized for the docking analysis. The Surflex-Dock program which employs an automatic flexible docking algorithm was applied to analyze the possible conformation of the ligand that binds to BSA, and the program PyMOL (http://www.pymol.org) was finally used for visualization of the molecular docking results.

Steady State Fluorescence. Fluorescence emission spectra were obtained with a 1.0 cm path length quartz cell using a F-7000 spectrofluorimeter (Hitachi, Japan) equipped with a thermostatic bath. The excitation and emission slits were set at 5.0 nm each, intrinsic fluorescence was carried out by exciting the continuously stirred protein solution at 295 nm to favor tryptophan (Trp) excitation, and the emission spectra were read in the wavelength range of 300−450 nm at a scanning speed of 240 nm min^{-1}. The reference sample consisting of the Tris−HCl buffer of triterpenoid in corresponding concentrations was subtracted from all fluorescence measurements.

Time-Resolved Fluorescence. Time-resolved fluorescence was examined with a FLS920 spectrometer (Edinburgh Instruments, U.K.), using the time-correlated single photon counting system with a hydrogen flash lamp excitation source, in air equilibrated solution at ambient temperature. The excitation wavelength was 295 nm, and the number of counts gathered in the channel of maximum intensity was 4,000. The instrument response function (IRF) was gauged exploiting Ludox to scatter light at the excitation wavelength. The data were analyzed with a nonlinear least-squares iterative method utilizing Fluorescence Analysis Software Technology, which is a sophisticated software package designed by Edinburgh Photonics for the analysis of fluorescence and phosphorescence decay kinetics; IRF was deconvoluted from the experimental data, and the resolution limit after deconvolution was 0.2 ns. The value of χ^2 (0.9−1.2), the Durbin−Watson parameter (greater than 1.7), and a visual inspection of the residuals were used to assess how well the calculated decay fit the data. Average fluorescence lifetime (τ) for multiexponential function fittings were from the following relation:[19]

$$I(t) = \sum_i A_i \, e^{-t/\tau_i} \quad (1)$$

where τ_i are fluorescence lifetimes and A_i are their relative amplitudes, with i variable from 1 to 2.

Site-Specific Ligand. Binding location studies between BSA and triterpenoid in the presence of four typical site markers (phenylbutazone, flufenamic acid, digitoxin, and hemin) were executed using the fluorescence titration approach. The concentrations of BSA and site markers were held equimolar (1.0 μM), and then triterpenoid was added to the BSA-site marker mixtures. An excitation wavelength of 295 nm was chosen, and the fluorescence emission wavelength was acquired from 300 to 450 nm.

Hydrophobic ANS Displacement. In the first series of experiments, BSA concentration was kept fixed at 1.0 μM, triterpenoid/ANS concentration was varied from 5.0 to 45 μM, and BSA fluorescence was gained (λ_{ex} = 295 nm, λ_{em} = 341 nm). In the second series of experiments, triterpenoid was added to solutions of BSA and ANS held in equimolar concentration (1.0 μM), the concentration of triterpenoid was also varied from 5.0 to 45 μM, and the fluorescence of ANS was recorded (λ_{ex} = 370 nm, λ_{em} = 465 nm).

CD Spectra. Far-UV CD spectra were collected with a Jasco-815 spectropolarimeter (Jasco, Japan) equipped with a microcomputer; the apparatus was sufficiently purged with 99.9% dry nitrogen gas before starting the instrument, and then it was calibrated with d_{10}-camphorsulfonic acid. All the CD spectra were obtained at 298 K with a PFD-425S Peltier temperature controller attached to a water bath with an accuracy of ±0.1 °C. Each spectrum was performed with use of a precision quartz cuvette of 1.0 cm path length and taken at wavelengths between 200 and 260 nm, which provides a signal extremely sensitive to small secondary conformational distortions. Every determination was the average of five successive scans encoded with 0.1 nm step resolution and recorded at a speed of 50 nm min^{-1} and response time of 1 s. All observed CD data were baseline subtracted for buffer, and the estimation of the secondary structure elements was obtained by exploiting Jasco Spectra Manager II, which computes the different designations of secondary structures by comparison with CD spectra, determined from distinct proteins for which high-quality X-ray diffraction data are available.[20]

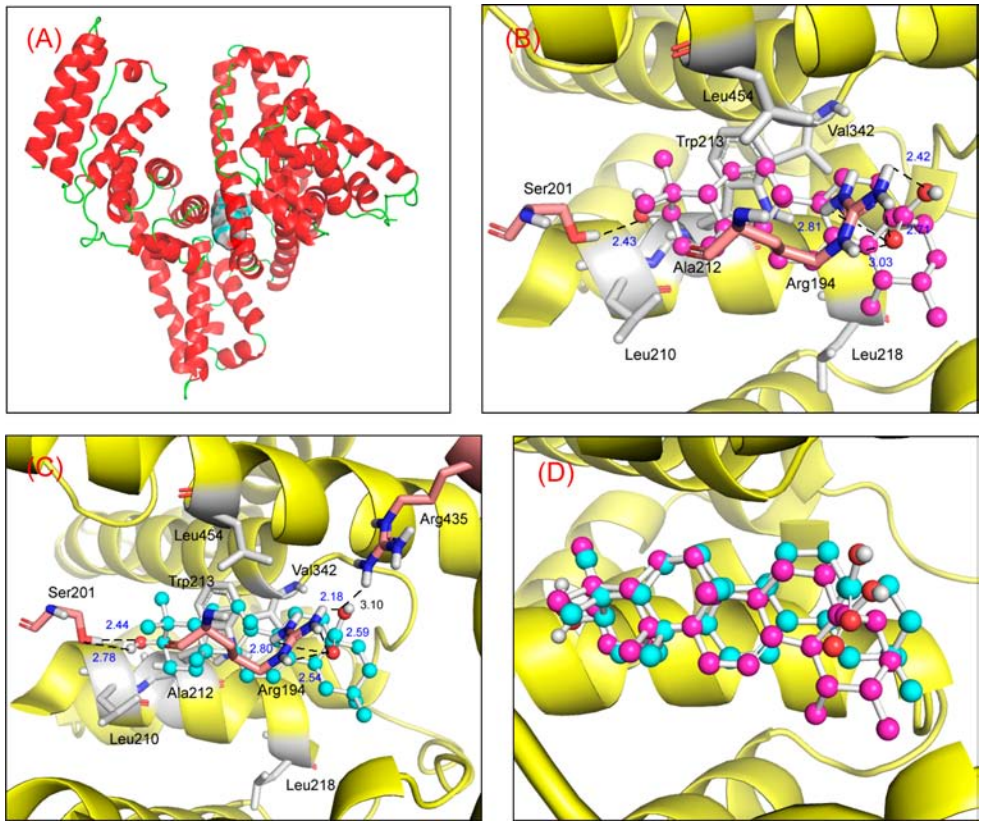

Figure 3. Molecular modeling of triterpenoids docked to BSA. Panel A shows docked triterpenoids in BSA at subdomain IIA, BSA displayed in surface colored in red, to triterpenoids, colored as per the atoms and endowed with opaque surface of electron spin density. Panels B and C indicate the amino acid residues involved in binding of triterpenoids. The ball-and-stick model represents triterpenoids, colored as per the atoms, and the pivotal amino acid residues around triterpenoids have been described in stick model; salmon stick model portrays hydrogen bonds between Arg-194, Ser-201 (B) and Arg-194, Ser-201, Arg-435 (C) residues and ursolic acid and oleanolic acid, respectively; white stick model narrates hydrophobic interactions between Leu-210, Ala-212, Trp-213, Leu-218, Val-342, Leu-454 (B) and Leu-210, Ala-212, Trp-213, Leu-218, Val-342, Leu-454 (C) residues and ursolic acid and oleanolic acid, respectively. Panel D interprets the conformational superposition of ursolic acid (magenta) and oleanolic acid (cyan) in the subdomain IIA of BSA.

Three-Dimensional Fluorescence. The emission wavelength was reaped between 200 and 500 nm, the initial excitation wavelength was set to 200 nm with increment of 10 nm, the number of scanning curves was 16, and the other scanning parameters were identical to those for the steady state fluorescence above.

Principle of Fluorescence Quenching. Fluorescence quenching refers to any process that decreases the fluorescence intensity of a sample. A variety of molecular interactions can result in quenching, such as excited state reactions, molecular rearrangements, energy transfer, ground state complex formation, and collisional quenching. Fluorescence quenching is described by the well-known Stern−Volmer equation:[21]

$$\frac{F_0}{F} = 1 + k_q\tau_0[Q] = 1 + K_{SV}[Q] \quad (2)$$

In this equation, F_0 and F are the fluorescence intensities in the absence and presence of quencher, respectively, k_q is the bimolecular quenching constant, τ_0 is the lifetime of the fluorophore in the absence of quencher, [Q] is the concentration of quencher, and K_{SV} is obtained by linear regression of a plot of F_0/F versus [Q].

Calculation of Recognition Ability. When ligand molecules bind independently to a set of equivalent sites on a macromolecule, the equilibrium between free and bound ligand molecules is given by the following relation:[22]

$$\log\frac{F_0 - F}{F} = \log K + n\log[Q] \quad (3)$$

In this equation, F_0 and F are the fluorescence intensities in the absence and presence of quencher, respectively, K and n are the association constant and the number of binding sites, respectively, and [Q] is the concentration of quencher. Thus, a plot of $\log(F_0 - F)/F$ against log [Q] can be used to calculate K and n. Moreover, the fluorescence intensities were corrected for absorption of the exciting light and reabsorption of the emitted light to decrease the inner filter effect by using the following relationship:[21]

$$F_{cor} = F_{obs} \times e^{(A_{ex}+A_{em})/2} \quad (4)$$

where F_{cor} and F_{obs} are the fluorescence intensities corrected and observed, respectively, and A_{ex} and A_{em} are the absorption of the systems at the excitation and the emission wavelength, respectively. The fluorescence intensity utilized in this work is the corrected intensity.

Statistical Analysis. All assays were executed in triplicate, and the mean values, standard deviations, and statistical differences were estimated using analysis of variance (ANOVA). The mean values were compared using Student's *t*-test, and all statistic data were treated using the OriginPro Software (OriginLab Corporation, Northampton, MA, USA).

RESULTS AND DISCUSSION

Molecular Modeling. The purpose of ligand−receptor docking is the ability to prefigure the preponderant recognition patterns of a ligand with an acceptor such as protein or nucleic acid of established three-dimensional crystal structure. We first

dx.doi.org/10.1021/jf4049512 | J. Agric. Food Chem. 2014, 62, 2271−2283

used this computational modeling technique to visually look over the binding modes between the BSA and the triterpenoids. Majorek et al.[23] and Bujacz et al.[24,25] in the first place declared a structure of albumin from bovine serum to 2.70 Å and 2.47 Å, severally, derived from tetragonal crystals obtained from defatted commercial BSA. The tertiary structure of BSA received from these X-ray diffraction measurements is a heart-shaped molecule, and it includes 583 amino acid residues and has 9 loops formed by 17 disulfides. The three-dimensional configuration is composed of three homologous domains (I, II, and III), each domain in turn is the spawn of two subdomains (A and B), which are largely helical and widely cross-linked through several disulfide bridges. Besides, the 6 subdomains partake of a joint helical motif, and the motif mainly corresponds to the amino acids surrounded within the double disulfide bonds 1, 3, 4, 6, 7, and 9. Two tryptophans (Trp), namely, Trp-134 and Trp-213, situated in domain I and domain II, respectively, and Trp-134 residue are lying in a hydrophilic circumstance, close to the protein surface, while Trp-213 residue is encircled by a hydrophobic surrounding within a protein patch.[12,26,27] The best docked energy conformation is shown in Figure 3; it was clear that both ursolic acid and oleanolic acid binding sites are located within subdomain IIA formed by six-helices (Figure 3A), but the recognition ability of subdomain IIA with the latter is higher, compared with the former.

For the BSA−ursolic acid mixture, the oxygen atoms of the carbonyl group and the oxygen atom of the hydroxyl group in ursolic acid can make hydrogen bonds (Figure 3B) with the hydrogen atoms of the amino group in Arg-194 and the hydrogen atom of the hydroxyl group in Ser-201 residues; the bond lengths are 2.42 Å, 2.71 Å, 2.81 Å, 3.03 Å, and 2.43 Å, respectively. For BSA−oleanolic acid complex, the oxygen atoms of the carbonyl group, the oxygen atom of the hydroxyl group, the hydrogen atom of the hydroxyl group, and the oxygen atom of the hydroxyl group can form hydrogen bonds with the hydrogen atoms of the amino group in Arg-194, the hydrogen atom of the hydroxyl group in Ser-201, the oxygen atom of the hydroxyl group in Ser-201, and the hydrogen atom of the amino group in Arg-435 residues; the bond lengths, respectively, are 2.18 Å, 2.54 Å, 2.59 Å, 2.80 Å, 2.44 Å, 2.78 Å, and 3.10 Å (Figure 3C). On the basis of surface modification of the amino acid residues composed of subdomain IIA, we may ascertain a hydrophobic region of subdomain IIA composed of Leu-210, Ala-212, Trp-213, Leu-218, Val-342, and Leu-454 residues, the skeleton of 22 carbon atoms organized into five rings toward the domain, which implied that hydrophobic interaction was exerting a heavy effect between them.

Apparently, ursolic acid and oleanolic acid have greatly close molecular structures but have only disparate sites of methyl group on the E-ring; if the methyl group at C_{19} of ursolic acid is shifted to C_{20}, it turns to oleanolic acid. To elaborate the divergence of binding mode between ursolic acid and oleanolic acid, the optimized conformations of ursolic acid and oleanolic acid have been overlapped in the subdomain IIA (Figure 3D). It was effortlessly seen that the dissimilarities of both locality and conformation between ursolic acid and oleanolic acid were tiny. Therefore, we could speculate that the different position of one methyl group on the E-ring might give rise to moderately disparate affinities of triterpenoids. In comparison with these noncovalent interactions, particularly hydrogen bonds residing in the BSA−triterpenoid conjugation, we may obtain some beneficial information regarding this distinction. Chemically, although hydrogen bond energies may seem small, on the order of 4.0−25.0 kJ mol^{-1}, it should be remembered that they commonly occur as a system of interconnections; thus they are additive and donate considerably to the comprehensive stability of systems such as the polypeptide polymer and protein or nucleic acid.[28,29] It was evident at first glance that the hydrogen bonds between BSA and triterpenoids look very alike to one another, for example, the carbonyl group in triterpenoids could generate a hydrogen bond network with the Arg-194 residue in BSA, but they do have at least two differences between the two systems. The first is the number of hydrogen bonds. Careful examination of Figure 3B and Figure 3C shows that oleanolic acid may form two strong hydrogen bonds with Ser-201 residue, whereas only one hydrogen bond can be yielded for ursolic acid. Furthermore, another hydrogen bond could be formed between oleanolic acid and the Arg-435 residue. A second theme is the differentiation between these hydrogen bonds. Intuitively, the lengths of hydrogen bonds between ursolic acid and the Arg-194 residue are larger than the oleanolic acid; this means that oleanolic acid has greater affinity than the ursolic acid. These distinctions mentioned above macroscopically behave in the diverse affinities between triterpenoids and BSA, i.e., $K = 1.419 \times 10^4$ M^{-1} (ursolic acid−BSA) and $K = 1.811 \times 10^4$ M^{-1} (oleanolic acid−BSA), respectively.

It is well testified that the biological activities of ursolic acid and oleanolic acid may be related to the methyl group on the E-ring. Ovesná et al.[30] conducted an in vitro study to scrutinize the protective effects of ursolic acid and oleanolic acid in leukemic cells. They lucidly revealed that in murine leukemia cells L1210 and K562 cells, the antioxidant activity of oleanolic acid measured by single cell gel electrophoresis was notably better in contrast with the antioxidant activity of ursolic acid. But for HL-60 cells, the percentage of ursolic acid protective outcome was 63.8%−61.6% at the concentration range of 2.5−10 μM, and the antioxidant effect of oleanolic acid was reasonably inferiorly collated with the activity of ursolic acid; however, the inconsistency between the protective activity of ursolic acid and oleanolic acid was not remarkable. In a recent study, ursolic acid and oleanolic acid were found to be powerful inducers of apoptosis in four human liver cancer cell lines involving mitochondrial dysfunctions.[31] Interestingly, the anticancer activities of the two triterpenoids were not uniform; ursolic acid at tantamount volume was larger than oleanolic acid in suppressing Na^+-K^+-ATPase activity in HepG2 cell; ursolic acid at 8.0 μM induced more DNA destruction than oleanolic acid in HepG2 and Hep3B cells, yet oleanolic acid at 8.0 μM stimulated more mitochondrial membrane latent decrease than ursolic acid in Huh7 and HA22T cells. The computational analyses quoted above, as a result, corresponded absolutely closely with these depictions found in the reference, i.e., the position of substituting group ($-CH_3$) on the E-ring may quite likely have an effect on the noncovalent interactions between triterpenoids and the amino acid residues in BSA, and result in different affinities between these triterpenoids. Moreover, the significant driving forces in the BSA−triterpenoid conjugation are hydrogen bonds and hydrophobic interactions; we also presume that the three-dimensional spatial structure of BSA may be perturbed due to the triterpenoids operating on the amino acid residues in a polypeptide chain by noncovalent bonds. Consequently, the information manifested in solution experiments expatiated below, as deduced from steady state and time-resolved fluorescence, competitive ligand

displacement, CD spectra, synchronous fluorescence, and three-dimensional fluorescence techniques, was applied to affirm upper molecular modeling corollaries.

Photochemical Properties of BSA−Triterpenoids. The molecular recognition of triterpenoids by BSA was evaluated by the assessment of intrinsic fluorescence of Trp residues, and Figure S1 (Supporting Information) conveys the raw data for quenching of BSA fluorescence at pH = 7.4 by addition of triterpenoids. It will be noticed that BSA arose to have a fluorescence peak at 341 nm, following an excitation at 295 nm. In BSA, the three aromatic amino acid residues Phe, Tyr, and Trp are all fluorescent, but emission of BSA is controlled by Trp residues, which absorbs at the longest wavelength and exhibits the largest extinction coefficient.[12,26,27] Clearly, a regular shortening of the Trp residues' fluorescence intensity was perceived from Figure 4 accompanied by growth in the

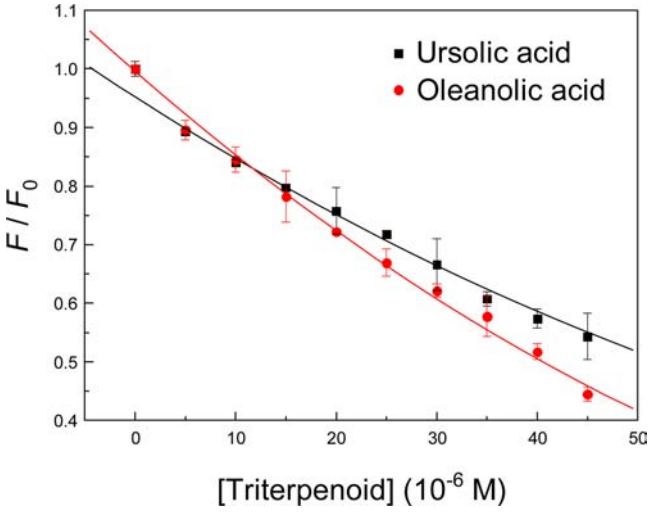

Figure 4. Trp residue fluorescence quenching of BSA (1.0 μM) at pH = 7.4 and T = 298 K, plotted as expunction of fluorescence intensity (F/F_0) *against* triterpenoid concentrations: 0, 5.0, 10, 15, 20, 25, 30, 35, 40, and 45 μM. The fluorescence intensity was read at λ_{ex} = 295 nm and the λ_{em} maximum obtained at 341 nm. All data were corrected for quencher fluorescence, and each point was the mean of three independent observations ± SD ranging from 0.38% to 4.44%.

concentration of triterpenoids. Under the present conditions triterpenoids displayed no fluorescence emission in the range 300−450 nm, which did not affect BSA intrinsic Trp residues' fluorescence. These phenomenon explained plainly that there were association reactions between BSA and triterpenoids and the ligand was localized in the region where Trp residues located within or near the fluorophores.[32] Further, the fluorescence quenching effect of oleanolic acid was better than that of ursolic acid, which denotes that oleanolic acid has a good affinity to complex with BSA, and this result is almost totally in agreement with the affinity imparity that branched from molecular modeling simulations. A similar finding has also been illustrated by Bourassa et al.[33] for the molecular recognition of antioxidant polyphenols resveratrol, genistein, and curcumin by milk α- and β-caseins.

Normally, quenching mechanism research can be employed to expose the localization of fluorophores in proteins and may also signify the dispersal of quenchers over middling large distances comparable to the dimension of proteins.[21] In order to expound the essence of fluorescence quenching of BSA by triterpenoids, the data were dissected according to the Stern−Volmer eq 2, and the corresponding results fitted from Stern−Volmer plots (Figure 5) are collected in Table 1. Usually, a

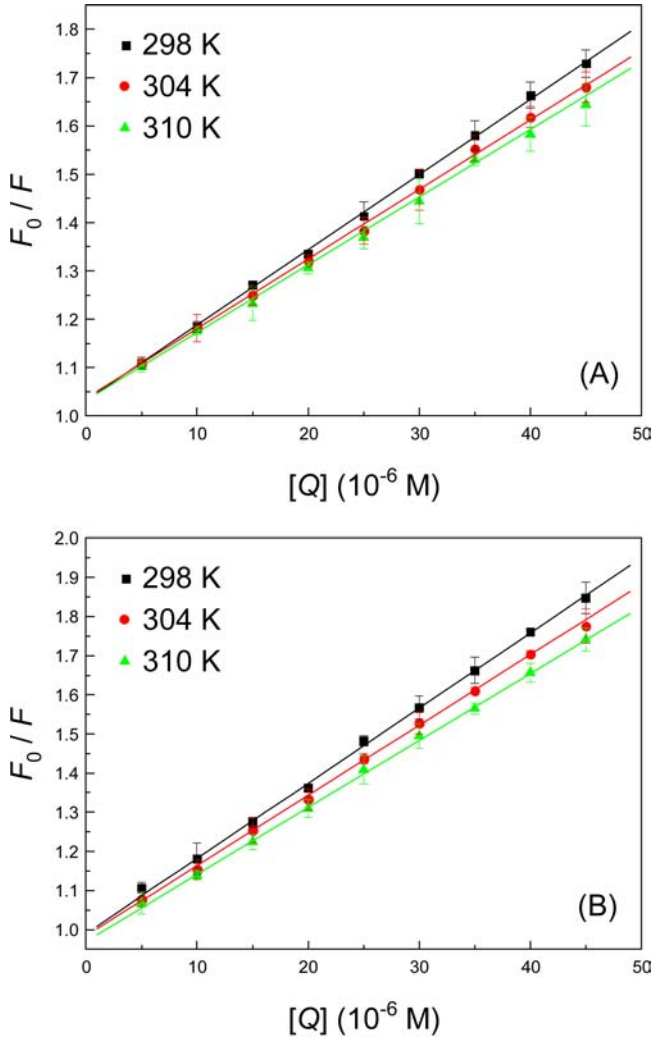

Figure 5. Stern−Volmer plot depicting Trp residue quenching of BSA (1.0 μM) at pH = 7.4 in the presence of 5.0, 10, 15, 20, 25, 30, 35, 40, and 45 μM ursolic acid (A) and oleanolic acid (B). Each data was the average of three separate determinations ± SD ranging from 0.62% to 4.64%.

linear Stern−Volmer plot is exhibitive of a single kind of fluorophore, all equivalently attainable to quencher. The Stern−Volmer plots for triterpenoids are apparently linear,

Table 1. Stern−Volmer (K_{SV}) and Bimolecular (k_q) Quenching Constants for the Molecular Recognition of BSA with Triterpenoids

system	T (K)	K_{SV} (×10^4 M^{-1})	k_q (×10^{12} M^{-1} s^{-1})	R^a
BSA + ursolic acid	298	1.568	2.732	0.9996
	304	1.449	2.524	0.9994
	310	1.374	2.394	0.9992
BSA + oleanolic acid	298	1.894	3.300	0.9994
	304	1.784	3.108	0.9995
	310	1.704	2.969	0.9996

[a] R is the correlation coefficient.

dx.doi.org/10.1021/jf4049512 | J. Agric. Food Chem. 2014, 62, 2271−2283

which hints that just one type of quenching reaction exists. Simultaneously, the Stern−Volmer quenching constant K_{SV} is contrarily connected with temperature and the value of k_q is 100-fold greater than the biggest feasible value of bimolecular quenching constant in aqueous solution (1.0×10^{10} M^{-1} s^{-1}), demonstrating that the probable quenching mechanism for BSA fluorescence emission by triterpenoids is a static type, because higher temperature will classically result in the dissociation of weakly bound complexes, and thus lesser quantities of static quenching.

One consideration to bear in mind is that static and dynamic quenching can be discerned by their differing reliance on temperature or viscosity, but preferably by fluorescence lifetime measurements, which can discriminate between static and dynamic processes straightly.[21] To further acquire direct proof of the nature of the BSA−triterpenoid recognition, the representative fluorescence decay figures of BSA at different molar ratios of triterpenoids in Tris−HCl buffer, pH = 7.4, are displayed in Figure S2 in the Supporting Information, and the fluorescence lifetime and their amplitudes are summarized in Table 2. Obviously, the decay curves fitted well to a biexponential function, and the relatively fluorescence lifetimes being exhibited are τ_1 = 3.68 ns and τ_2 = 6.95 ns of BSA, whereas in the maximum concentration of ursolic acid or oleanolic acid, the lifetimes are τ_1 = 2.89/3.03 ns and τ_2 = 6.07/5.99 ns, respectively. Considering Trp residues are known to show multiexponential decays, a transparent allotment of the observed individual fluorescence lifetime constituents to the dissimilar fluorescent Trp residues is tough for a multiple Trp residue protein such as BSA. Therefore we have not sought to assign the separate components; on the contrary, the average fluorescence lifetime has been employed in order to capture a qualitative analysis. The mean fluorescence lifetime of BSA did not change obviously, just from 5.74 ns to 5.53/5.43 ns, at different ursolic acid or oleanolic acid concentrations, indicating evidently that fluorescence quenching is truly a static mechanism. The results match our previous discussion based on molecular modeling and steady state fluorescence that quenching is static in nature, triterpenoids binds in the vicinity of Trp residues in subdomain IIA, and BSA−triterpenoid complexes are formed between fluorophore and the triterpenoids, which is nonfluorescent. Recent research by Abou-Zied et al.[22] also found similar phenomena when BSA from human serum recognizes with anticancer agents 6-hydroxyquinoline, 7-hydroxyquinoline, and 8-hydroxyquinoline.

Table 2. Fluorescence Lifetime Data of BSA as a Function of Concentrations of Triterpenoids

samples	τ_1 (ns)	τ_2 (ns)	A_1	A_2	τ (ns)	χ^2
free BSA	3.68	6.95	0.37	0.63	5.74	0.99
BSA + ursolic acid (1:1)	3.45	6.31	0.29	0.71	5.48	1.02
BSA + ursolic acid (1:2)	3.21	6.12	0.19	0.81	5.57	1.05
BSA + ursolic acid (1:4)	2.89	6.07	0.17	0.83	5.53	0.98
BSA + oleanolic acid (1:1)	3.29	6.42	0.31	0.69	5.45	1.07
BSA + oleanolic acid (1:2)	3.54	6.19	0.22	0.78	5.61	0.99
BSA + oleanolic acid (1:4)	3.03	5.99	0.19	0.81	5.43	1.03

Frequently, drugs possess some specificity for the binding site on the acceptor like target protein; if the specificity is lower, it alludes binding affinity is lower, and a bigger potion of drug will be needed, which is related with some side effects.[34,35] Therefore the efficacy of a drug depends on its binding strength for the binding site as well as its binding affinity to generate the desired effects. In order to reckon the binding strength of triterpenoids to BSA, eq 3 was applied to estimate K and n by linear regression of a plot of the $\log(F_0-F)/F$ versus $\log [Q]$ (Figure S3 in the Supporting Information), and the results are also displayed in Table 3. The affinity K reduced with rising temperature, showing the destabilization of the BSA−triterpenoid complex; likewise, the affinity of BSA with oleanolic acid is greater than that of ursolic acid, and this corroborates perfectly our preceding results found on molecular modeling that the strength of ursolic acid with BSA is lower than that of oleanolic acid. According to Dangles and Dufour[36] and united with the recent reports on the subject of protein−ligand recognition, such as piperine, bile acids, hydroxyquinoline derivatives, retinol, retinoic acid, and folic acid,[37−41] it is fairly plain that the recognition of triterpenoids by BSA belongs to intermediate affinity. In addition, the value of n is properly 1, which may infer the presence of just one sort of binding site in BSA for triterpenoids. This fact also overlaps the foregoing molecular modeling and further agrees with the following site-specific ligands and hydrophobic 8-anilino-1-naphthalenesulfonic acid displacement experiments.

It is should be mentioned that the binding intensity of circulating triterpenoids for albumin is moderately small, but the physiological concentration of albumin is in all probability roomy enough (~640 μM) to allow triterpenoids vast binding. Albumin binding may effectually prolong the in vivo half-life of triterpenoids, and the concentration of triterpenoids ordinarily accumulated in some organs such as brain, heart, kidney, liver, and plasma, which is in logical harmony with the in vivo experiments in healthy volunteers and different animals specified somewhere. For example, Song et al.[42] and Xia et al.[43] administrated healthy volunteers with single doses of oleanolic acid and ursolic acid and found that the peak plasma

Table 3. Affinity Constants (K) and Thermodynamic Parameters for the Molecular Recognition of Triterpenoids by BSA at Different Temperatures

system	T (K)	K ($\times 10^4$ M^{-1})	n	R^a	ΔH (kJ mol^{-1})	ΔG (kJ mol^{-1})	ΔS (J mol^{-1} K^{-1})
BSA + ursolic acid	298	1.507	0.99	0.9995	−37.50	−23.84	−46.07
	304	1.042	0.97	0.9996		−23.38	
	310	0.8395	0.96	0.9995		−23.29	
BSA + oleanolic acid	298	1.734	0.99	0.9993	−40.55	−24.18	−36.19
	304	1.186	0.96	0.9995		−23.71	
	310	0.9863	0.96	0.9995		−23.70	

[a] R is the correlation coefficient.

dx.doi.org/10.1021/jf4049512 | J. Agric. Food Chem. 2014, 62, 2271−2283

concentration (C_{max}) and time to peak concentration (T_{max}), respectively, are 12.12 ng mL^{-1} and 5.2 h for oleanolic acid and 3404.6 ng mL^{-1} and 4.0 h for ursolic acid. These results distinctly proved that oleanolic acid and ursolic acid were distributed to an immense degree out of the blood chamber or accumulated in some tissues. In a study with Sprague−Dawley rats, the C_{max} and T_{max} were found to be 1.10 μg mL^{-1} and 0.42 h, and the dispersion order of ursolic acid in various organs was detected as follows: lung > spleen > liver > cerebrum > heart > kidney.[44] This in vivo study hence concluded that ursolic acid was mostly distributed in ample blood furnishing tissues such as lung, spleen, and liver, and the spreading depended chiefly upon the blood flow and perfusion rate of the organ. In another very recent pharmacokinetic study, Yin et al.[45] announced that triterpenoids were assimilated, metabolized, and stored in tissues which in reverse exerted their regional and systemic activities. In this experiment, male C57BL/6 mice were fed triterpenoids for approximately 8 weeks, and it can unmistakably be heeded that the liver not only had the utmost bioavailability for triterpenoids paralleled with other tissues but also was the outstanding organ for triterpenoid reposition and metabolism. In light of the above experimental observations, we could obviously view that the bioavailability and deposit of triterpenoids such as ursolic acid and oleanolic acid in the human body relied mainly upon the blood circulation, or rather plasma protein binding. Consequently, more attention should be paid to this issue, because albumin can usually act as an important vector for nearly all endogenous and exogenous ligands in human plasma to deliver the triterpenoids to the target organs, where it brings forth its pharmacological and toxicological effect.

Thermodynamic Analysis. As noted earlier, molecular recognition commonly show a striking level of specificity and high-affinity. Basically, binding transpires only when it is linked with a negative Gibbs free energy of binding (ΔG°), which may have differing thermodynamic symbols, changing from enthalpy to entropy driven. Therefore, the apprehension of the acting forces running the recognition and interaction request a detailed recountal of the binding thermodynamics, and a relationship of the thermodynamic functions with the structures of interacting mates.[46] To attest the noncovalent interactions between BSA and triterpenoids, supposing the enthalpy ΔH° do not vary clearly over the temperature range studied, the three thermodynamic functions are related by the following equations:

$$\ln K = \frac{-\Delta H^\circ}{RT} + \frac{\Delta S^\circ}{R} \quad (5)$$

$$\Delta G^\circ = \Delta H^\circ - T\Delta S^\circ \quad (6)$$

where K is the affinity constant for a given association reaction under a definite set of experimental conditions, R is the gas constant, and T is the absolute temperature. A linear plot (Figure 6) of ln K versus $1/T$ produces ΔH° and ΔS°, and the data fitted from Figure 6 also shown in Table 3. Ross and Subramanian[47] generalized the signs and magnitudes of the thermodynamic parameters associated with different solitary kinds of interactions that might settle in protein association processes, as recounted below. For classic hydrophobic interactions, both ΔH° and ΔS° are positive, while they are negative for van der Waals forces and hydrogen bonds shaping in low dielectric medium. Furthermore, concrete electrostatic interactions between ionic species in aqueous solution were

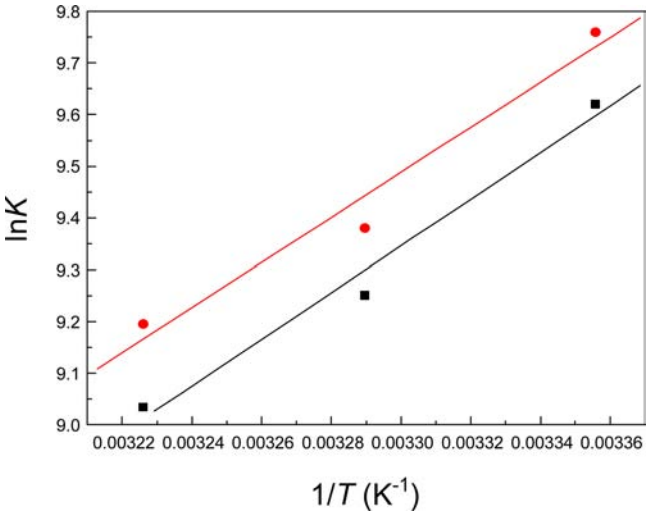

Figure 6. van't Hoff plot for the molecular recognition of ursolic acid (■) and oleanolic acid (●) by BSA in Tris-HCl buffer, pH = 7.4.

defined by a positive value of ΔS° and a negative ΔH° (almost zero). A negative ΔH° is observed whenever there is a hydrogen bond in the process. In the current instance of BSA−triterpenoid system, ursolic acid and oleanolic acid involve several hydrophobic cyclic systems (6-membered ring) and these cyclic systems dominantly function with amino acid residues of BSA to generate hydrophobic interactions; therefore, one could reasonably proclaim that hydrogen bonds, van der Waals forces, and hydrophobic interactions all weigh heavily in the molecular recognition of triterpenoids by BSA. Moreover, the BSA−triterpenoid recognition process is an unprompted exothermic reaction owing to the negative value of ΔG°; the experimental data ΔG° (298 K) is also greatly close to the theoretical data ΔG° = −23.69 kJ mol^{-1} and ΔG° = −24.29 kJ mol^{-1} for ursolic acid and oleanolic acid, respectively, confirming the reliability of the results of steady state fluorescence.

Identification of Binding Domain. As we have seen, both ursolic acid and oleanolic acid were located in subdomain IIA (Sudlow's site I) by building on the results of molecular modeling and eq 3. To further clarify this aspect, site-specific ligand experiments between the triterpenoids and the other ligands that specifically bind to a known site or domain were executed. The curious feature of albumin to bind various substances is predominantly dependent on the existence of two foremost binding sites, that is, Sudlow's site I and site II, which are situated within particular regions in subdomains IIA and IIIA,[48,49] respectively. Site I is known as the warfarin−azapropazone site and formed as a cave in subdomain IIA, the residue Trp-213 of BSA in this patch. The internal wall of the pocket is formed by hydrophobic side chains, whereas the entry to the cavity is enveloped by positively charged residues. The unusual quality of this site is the binding of the ligand which is a bulky heterocyclic anion with a negative charge localized in the middle of the molecule, such as warfarin, phenylbutazone, 3,5-diiodosalicylic acid, and azapropazone.[25,27] Site II corresponds to the hole of subdomain IIIA and is renowned as the indole−benzodiazepine site, which is almost equal in size to site I; the interior of the domain is composed of hydrophobic amino acid residues, and the external pocket existed two basic amino acid residues (Arg-410 and Tyr-411).[23−25] Ligands binding to site II are aromatic carboxylic

acids with a negatively charged acidic group at the end of the molecule, e.g., ibuprofen, flufenamic acid, diflunisal, and diazepam. Subsequently Brodersen et al.[50] proposed that digitoxin binding in albumin is autonomous from Sudlow's site I and site II, and perch on what was nominated as site III. In the present work, the competitor used involved phenylbutazone, a typical marker for site I, flufenamic acid for site II, digitoxin for site III, and hemin for domain I. According to eq 3, the affinity constants were fitted from raw fluorescence data and found to be $0.1967 \times 10^4/0.1538 \times 10^4$ M^{-1}, $1.459 \times 10^4/1.522 \times 10^4$ M^{-1}, $1.461 \times 10^4/1.653 \times 10^4$ M^{-1}, and $1.384 \times 10^4/1.619 \times 10^4$ M^{-1} for ursolic acid and oleanolic acid, respectively, in the presence of phenylbutazone, flufenamic acid, digitoxin, and hemin. The outcomes advocate triterpenoids having the same site with phenylbutazone in BSA, and authorize the simulation of molecular modeling putting the triterpenoids at subdomain IIA and is also in agreement with 8-anilino-1-naphthalenesulfonic acid displacement below.

Fluorescence dye 8-anilino-1-naphthalenesulfonic acid (ANS) is accepted to bind to hydrophobic patches of proteins and can serve as a perceptive announcer of conjugation in the vicinity of protein Trp residues; thereby it has been employed to specify all the hydrophobic sites of proteins.[51] For the purpose of further ensuring the property of the molecular recognition of triterpenoids by BSA, binding studies were carried out in the presence of ANS under unanimous conditions. Based on the protocol designed above, the relative fluorescence intensity (F/F_0) *against* ligand concentration ([Ligand]) plots is indicated in Figure 7. Vividly, at a ligand concentration of 45 μM, both triterpenoids and ANS dribble Trp-213 residue fluorescence, but the pitch of quenching by triterpenoids was to some degree lower than ANS; ANS could extinguish about 69.05%, whereas ursolic acid and oleanolic acid, respectively, could just slake 46.16% and 54.01% of Trp-213 residue fluorescence. In a much earlier report, Stryer[52] imprimis asserted that the quantum yield of ANS is approximately 0.002 in aqueous buffer, but near 0.4 when bound to protein, with almost no contribution from the unbound probe. When triterpenoids are added to the ANS−BSA mixture, it can compete with ANS for its hydrophobic domain, and the fluorescence would trim. The valid explanation for this is that ANS is virtually nonfluorescent when in aqueous solution, but it will become highly fluorescent in nonpolar solvents or when it is bound to proteins. As can be seen in Figure 7, ANS−BSA fluorescence faded about 30.87% and 35.87% in the presence of ursolic acid and oleanolic acid, respectively, pronouncing that triterpenoids may contend against ANS moderately for its binding site. Although still partially debatable, consensus prevailed today that there are five discrepant binding sites for ANS associated with BSA, but preferentially at a site close to the Trp-213 residue.[53] In this context, ANS powerfully stifles the fluorescence of BSA, which justifies that the binding position for ANS in this high-affinity site comes near to Trp-213; about 30.87% and 35.87% displacement of ANS fluorescence illustrates that triterpenoids and ANS likely participate at a conjunct site in BSA, viz., the site is located next to the residue Trp-213. An analogous consequence has also been transmitted by Sen et al.[54] for the binding of gold nanoparticle to albumin from human serum.

Structure and Stability of BSA. Conformational changes in acceptors upon binding ligands are possibly key in a number of biomedical systems, and frequently a conformation change in the receptor would noticeably be a mechanism for cooperativity.[55] In terms of molecular modeling, we deduced that the conformation of BSA has changed after the triterpenoid conjugation. To verify this point, the circular dichroism (CD) spectra of BSA in the absence and presence of triterpenoids are displayed in Figure S4 in the Supporting Information, and the secondary structure components calculated based on raw CD data are pooled in Table 4. The CD curves of BSA exhibited

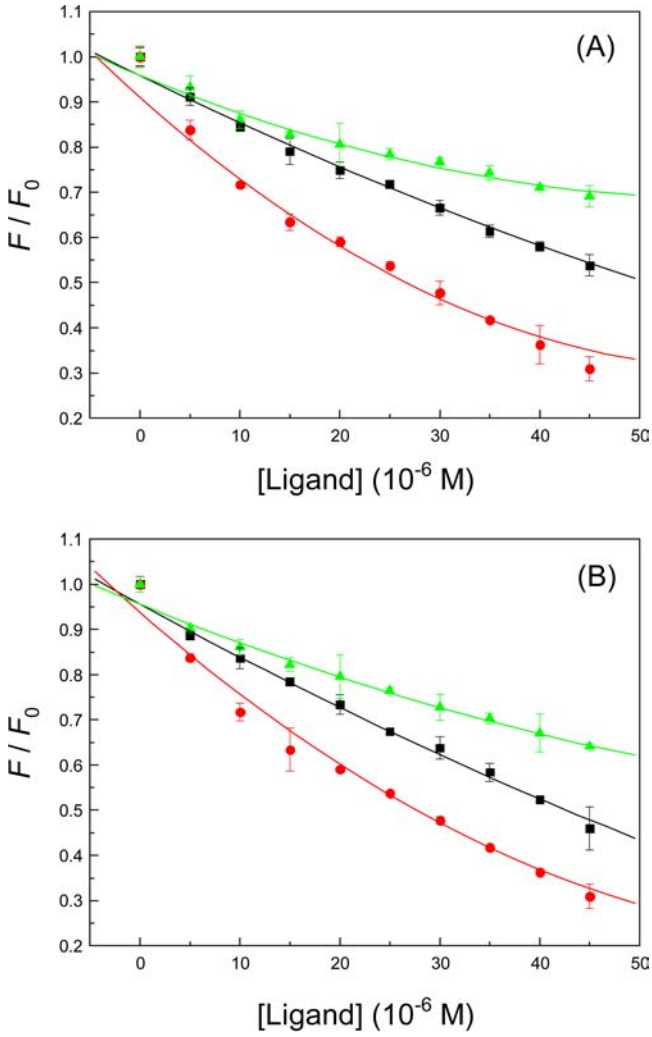

Figure 7. Fluorescence quenching silhouettes of BSA and BSA−ANS mixture; binding isotherm of (A) ursolic acid (■) and (B) oleanolic acid (■) and ANS (●) provoked quenching of BSA fluorescence and quenching of BSA−ANS complex fluorescence by (A) ursolic acid (▲) and (B) oleanolic acid (▲); pH = 7.4, T = 298 K. Each data was the mean of three individual measurements ± SD ranging from 0.23% to 4.82%.

Table 4. Secondary Structure Constituents of BSA Recognition with Triterpenoids at pH = 7.4 Appraised by Jasco Spectra Manager II Software

samples	secondary structure components (%)			
	α-helix	β-sheet	turn	random
free BSA	61.3	8.1	11.9	18.7
BSA + ursolic acid (1:2)	57.8	8.7	12.6	20.9
BSA + ursolic acid (1:4)	52.1	9.9	14.2	23.8
BSA + oleanolic acid (1:2)	56.4	8.9	12.8	21.9
BSA + oleanolic acid (1:4)	49.2	10.1	14.4	26.3

dx.doi.org/10.1021/jf4049512 | J. Agric. Food Chem. 2014, 62, 2271−2283

two negative peaks in the far-UV CD region at 208 and 222 nm, characteristic of α-helical structure of BSA. The rational elucidation is that the negative bands between 208 and 209 nm and 222 and 223 nm are both contributed by the $\pi \rightarrow \pi^*$ and the n $\rightarrow \pi^*$ transition for the peptide bond of α-helix.[56] Free BSA has 61.3% α-helix, 8.1% β-sheet, 11.9% turn, and 18.7% random coil; upon complexing with ursolic acid and oleanolic acid, a decline of α-helix was detected from 61.3% free BSA to 52.1%/49.2% BSA−triterpenoid complexes, while elevation was detected in β-sheet, turn, and random coil from 8.1%, 11.9%, and 18.7% free BSA to 9.9%, 14.2%, and 23.8% BSA−ursolic acid and 10.1%, 14.4%, and 26.3% BSA−oleanolic acid at a molar ratio of BSA to triterpenoids of 1:4. The decrease of α-helix with an increment in the β-sheet, turn, and random coil explained triterpenoids bound with amino acid residues of the polypeptide chain and giving rise to the destabilization of the BSA spatial structure,[57] i.e., some degree of BSA destabilization upon triterpenoid complexation.

Another testimony of structural changes of BSA after complexing with triterpenoids was represented by synchronous fluorescence spectra. It involves simultaneously scanning of the excitation and emission monochromators while retaining a stable wavelength interval ($\Delta\lambda$) or fixed increment of energy ($\Delta\nu$) between them.[58] Fuller and Miller[59] suggested that if the D-value ($\Delta\lambda$) between excitation and emission wavelengths was riveted at 60 nm, the synchronous fluorescence states the idiosyncratic clue of Trp residues. Figure 8 displays the synchronous fluorescence of BSA in Tris−HCl buffer in the presence of different amounts of triterpenoids. A faint red shift can be noted from Figure 8, which sustained that the hydrophobicity around the Trp residue was abated and the hydrophilicity expanded.[60] Moreover, it has been frankly shown in Figure 9 that the slope was higher for the BSA−oleanolic acid mixture, interpreting that the quenching effect of Trp-213 residue fluorescence by ursolic acid was definitely frailer than that of oleanolic acid.

To procure more exhaustive information on the conformational alterations of triterpenoid complexes with BSA, three-dimensional fluorescence of BSA and BSA−triterpenoid complex is scanned in Figure S5 in the Supporting Information, and the corresponding parameters are also filed in Table 5. Peak 1 (λ_{ex} = 280.0 nm, λ_{em} = 360.0 nm) chiefly unravels the spectral trait of Tyr and Trp residues, because when BSA is excited at 280.0 nm, it principally shows the intrinsic fluorescence of Tyr and Trp residues, and the Phe residue fluorescence can be trifling.[21] Besides peak 1, peak 2 mainly exposits the fluorescence spectral action of polypeptide chain backbone structure C═O. The fluorescence intensity of peak 2 alleviated a lot after the addition of triterpenoids, which delivered that the peptide chain structure of BSA was changed and this espouses far-UV CD spectra. Analyzing from the fluorescence intensity variations of the two peaks which decreased tangibly, but to an unequal tune: the intensity of peak 1 has been receded of 40.29% and 50.32%, while peak 2 of 18.4% and 21.16% for BSA−ursolic acid and BSA−oleanolic acid, respectively, evincing that the molecular recognition of triterpenoids with BSA begot the conspicuous destabilizing of the polypeptide chain of protein, which augmented the unwrapping of some hydrophobic patches that had been entombed before.[61] All of the above inspections and analyses verified that the conjugation of triterpenoids with BSA evoked spatial structure changes in protein, which may be associated with its physiological function. This phenomenon is also in

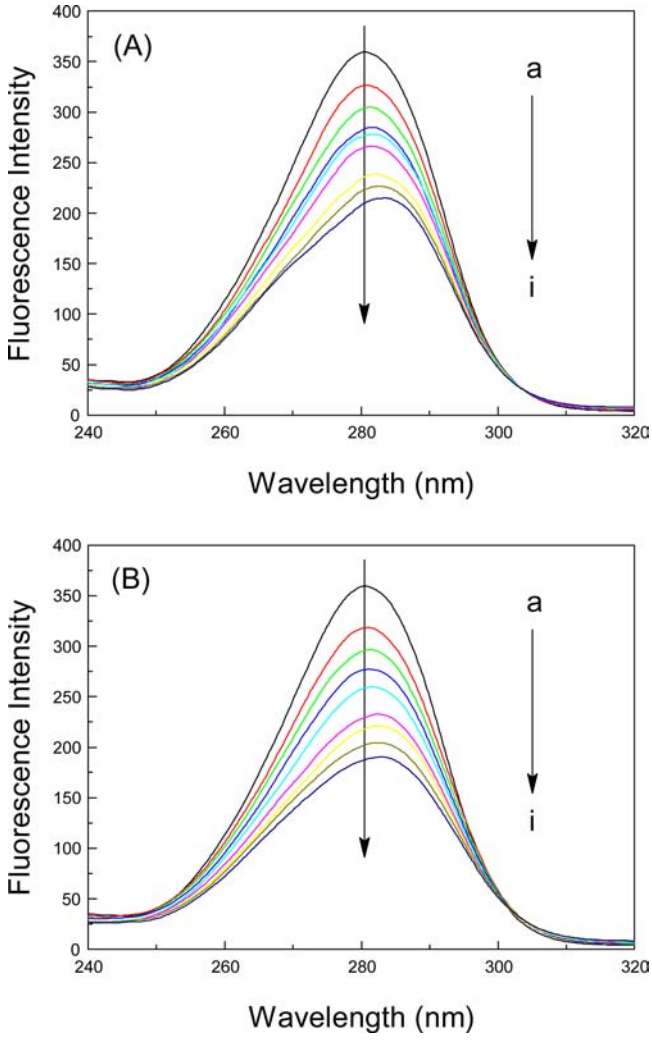

Figure 8. Synchronous fluorescence spectra ($\Delta\lambda$ = 60 nm) of BSA (1.0 μM) in the presence of 0, 5.0, 10, 15, 20, 25, 30, 35, and 40 μM ursolic acid (A) and oleanolic acid (B); pH = 7.4 and T = 298 K.

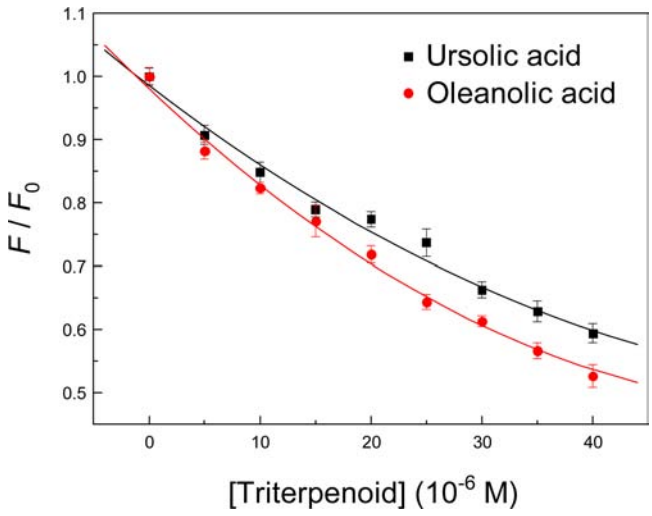

Figure 9. Synchronous fluorescence quenching ($\Delta\lambda$ = 60 nm) efficiency of BSA (1.0 μM) at pH = 7.4 and T = 298 K, plotted as elimination of fluorescence intensity (F/F_0) versus triterpenoid concentration. Each point was the average of three independent experiments ± SD ranging from 0.87% to 2.49%.

dx.doi.org/10.1021/jf4049512 | J. Agric. Food Chem. 2014, 62, 2271−2283

Table 5. Three-Dimensional Fluorescence Spectral Distinctive Parameters of BSA and BSA−Triterpenoid Complex

system	peak 1 ($\lambda_{ex}/\lambda_{em}$)	$\Delta\lambda$ (nm)	intensity F	peak 2 ($\lambda_{ex}/\lambda_{em}$)	$\Delta\lambda$ (nm)	intensity F
BSA	280.0/360.0	80.0	788.5	230.0/362.0	132.0	326.1
BSA + ursolic acid	280.0/364.0	84.0	470.8	230.0/363.0	133.0	266.1
BSA + oleanolic acid	280.0/367.0	87.0	391.7	230.0/366.0	136.0	257.1

accordance with the inference based on UV/vis absorption spectra introduced by Rada et al.,[62] and then, the extent of α-helical content changes induced by ursolic acid was smaller than that by oleanolic acid, which gave indirect proof to the affinity of human serum protein (mainly albumin) with oleanolic acid being larger than that with ursolic acid.

In a word, we have decoded the molecular recognition of two naturally bioactive triterpenoids, ursolic acid and oleanolic acid, by protein BSA under physiological conditions, which were dissected by blending with molecular modeling, steady state and time-resolved fluorescence, and CD spectra. The results explained that both ursolic acid and oleanolic acid are fastened in subdomain IIA, Sudlow's site I of albumin, substantially by the noncovalent interactions such as hydrogen bonds and van der Waals and hydrophobic interactions, but the strength of oleanolic acid with BSA is better, compared with ursolic acid, which are related to the position of methyl substituting group in the molecular structure of triterpenoids. Further assays will be performed to earn integrative information concerning the stereochemistry and different position of methyl group substitutions on the E-ring meddled with their affinity toward protein albumin by using nuclear magnetic resonance and molecular dynamics simulation, and the work is now in process. Steady state and time-resolved fluorescence endorse that the quenching of BSA Trp residue fluorescence resulted from a static mechanism, or rather the nonfluorescent BSA−triterpenoid complex formation with a comparatively modest intensity of 10^4 M^{-1}. Furthermore, the conformation of BSA was proved to be moderately disturbed upon the addition of triterpenoids with a shrinkage of α-helix accompanied by a rise in β-sheet, turn, and random coil, counseling a partial disruption of protein. All the data gathered herein fit well with the fact that the molecular recognition of triterpenoids by albumin may also be coherent with the pharmacological or toxicological style of the hugely utilized natural pentacyclic triterpenoids ursolic acid and oleanolic acid, as the biological effect of natural products is, assumedly, regulated through cellular diffusion bound to the most copious plasma protein.

■ ASSOCIATED CONTENT

Supporting Information

Figures depicting steady state fluorescence of BSA, time-resolved fluorescence decays of BSA−ursolic acid and BSA−oleanolic acid, association constant plot illustrating Trp residue quenching of BSA, far-UV CD spectra of the BSA−ursolic acid and BSA−oleanolic acid system, and three-dimensional fluorescence spectra of BSA, BSA−ursolic acid, and BSA−oleanolic acid mixture. This material is available free of charge via the Internet at http://pubs.acs.org.

■ AUTHOR INFORMATION

Corresponding Authors

*E-mail: alexf.ting@gmail.com, feiding@cau.edu.cn. Phone/fax: +86-29-87092367.

*E-mail: pyk2009@nwsuaf.edu.cn. Phone/fax: +86-29-87092367.

Author Contributions

§These authors contributed equally to this work.

Notes

The authors declare no competing financial interest.

■ ACKNOWLEDGMENTS

We are greatly indebted to Professor Ulrich Kragh-Hansen of Department of Medical Biochemistry, University of Aarhus, for the priceless gift of his doctoral dissertation. We are much obliged to Professor John W. Finley of Department of Food Science, Louisiana State University, for his warm support during the manuscript processing. Thanks also go to the reviewers of this manuscript for their valuable and constructive suggestions.

■ ABBREVIATIONS USED

Ala, alanine; ANOVA, analysis of variance; ANS, 8-anilino-1-naphthalenesulfonic acid; Arg, arginine; BSA, bovine serum albumin; CD, circular dichroism; DNA, deoxyribonucleic acid; IRF, instrument response function; Leu, leucine; Phe, phenylalanine; R, correlation coefficient; SD, standard deviation; Ser, serine; Tris, tris(hydroxymethyl)aminomethane; Trp, tryptophan; Tyr, tyrosine; UV/vis, ultraviolet−visible spectroscopy; Val, valine

■ REFERENCES

(1) Szakiel, A.; Pączkowski, C.; Koivuniemi, H.; Huttunen, S. Comparison of the triterpenoid content of berries and leaves of lingonberry *Vaccinium vitis-idaea* from Finland and Poland. *J. Agric. Food Chem.* **2012**, *60*, 4994−5002.

(2) Noller, C. R. The chemistry of the triterpenes. *Annu. Rev. Biochem.* **1945**, *14*, 383−406.

(3) Szakiel, A.; Pączkowski, C.; Pensec, F.; Bertsch, C. Fruit cuticular waxes as a source of biologically active triterpenoids. *Phytochem. Rev.* **2012**, *11*, 263−284.

(4) Dzubak, P.; Hajduch, M.; Vydra, D.; Hustova, A.; Kvasnica, M.; Biedermann, D.; Markova, L.; Urban, M.; Sarek, J. Pharmacological activities of natural triterpenoids and their therapeutic implications. *Nat. Prod. Rep.* **2006**, *23*, 394−411.

(5) Sporn, M. B.; Liby, K.; Yore, M. M.; Suh, N.; Albini, A.; Honda, T.; Sundararajan, C.; Gribble, G. W. Platforms and networks in triterpenoid pharmacology. *Drug Dev. Res.* **2007**, *68*, 174−182.

(6) Peragón, J. Time course of pentacyclic triterpenoids from fruits and leaves of olive tree (*Olea europaea* L.) cv. Picual and cv. Cornezuelo during ripening. *J. Agric. Food Chem.* **2013**, *61*, 6671−6678.

(7) Liobikas, J.; Majiene, D.; Trumbeckaite, S.; Kursvietiene, L.; Masteikova, R.; Kopustinskiene, D. M.; Savickas, A.; Bernatoniene, J. Uncoupling and antioxidant effects of ursolic acid in isolated rat heart mitochondria. *J. Nat. Prod.* **2011**, *74*, 1640−1644.

(8) Yang, E.-J.; Lee, W.; Ku, S.-K.; Song, K.-S.; Bae, J.-S. Anti-inflammatory activities of oleanolic acid on HMGB1 activated HUVECs. *Food Chem. Toxicol.* **2012**, *50*, 1288−1294.

(9) Ikeda, Y.; Murakami, A.; Ohigashi, H. Ursolic acid: An anti- and pro-inflammatory triterpenoid. *Mol. Nutr. Food Res.* **2008**, *52*, 26−42.

(10) Salvador, J. A. R.; Moreira, V. M.; Gonçalves, B. M. F.; Leal, A. S.; Jing, Y. K. Ursane-type pentacyclic triterpenoids as useful platforms to discover anticancer drugs. *Nat. Prod. Rep.* **2012**, *29*, 1463−1479.

(11) Jilani, K.; Abed, M.; Zelenak, C.; Lang, E.; Qadri, S. M.; Lang, F. Triggering of erythrocyte cell membrane scrambling by ursolic acid. *J. Nat. Prod.* **2011**, *74*, 2181−2186.
(12) Peters, T., Jr. Serum albumin. *Adv. Protein Chem.* **1985**, *37*, 161−245.
(13) Kragh-Hansen, U. Molecular aspects of ligand binding to serum albumin. *Pharmacol. Rev.* **1981**, *33*, 17−53.
(14) Carter, D. C. Crystallographic survey of albumin drug interaction and preliminary applications in cancer chemotherapy. In *Burger's Medicinal Chemistry, Drug Discovery, and Development*, 7th ed.; Abraham, D. J., Rotella, D. P., Eds.; John Wiley & Sons, Inc.: Hoboken, NJ, 2010; pp 437−467.
(15) DeGorter, M. K.; Xia, C. Q.; Yang, J. J.; Kim, R. B. Drug transporters in drug efficacy and toxicity. *Annu. Rev. Pharmacol. Toxicol.* **2012**, *52*, 249−273.
(16) Swartz, M. A.; Fleury, M. E. Interstitial flow and its effects in soft tissues. *Annu. Rev. Biomed. Eng.* **2007**, *9*, 229−256.
(17) Davies, N. A.; Garcia, R.; Proven, A.; Jalan, R. Albumin: Not just a plasma expander. In *Ascites, Hyponatremia and Hepatorenal Syndrome: Progress in Treatment*; Gerbes, A. L., Eds.; Karger Medical and Scientific Publishers: Basel, Switzerland, 2011; pp 40−51.
(18) Chignell, C. F. Optical studies of drug-protein complexes. II. Interaction of phenylbutazone and its analogues with human serum albumin. *Mol. Pharmacol.* **1969**, *5*, 244−252.
(19) Nishijima, M.; Pace, T. C. S.; Nakamura, A.; Mori, T.; Wada, T.; Bohne, C.; Inoue, Y. Supramolecular photochirogenesis with biomolecules. Mechanistic studies on the enantiodifferentiation for the photocyclodimerization of 2-anthracenecarboxylate mediated by bovine serum albumin. *J. Org. Chem.* **2007**, *72*, 2707−2715.
(20) Sreerama, N.; Woody, R. W. Computation and analysis of protein circular dichroism spectra. *Methods Enzymol.* **2004**, *383*, 318−351.
(21) Lakowicz, J. R. *Principles of Fluorescence Spectroscopy*, 3rd ed.; Springer Science+Business Media: New York, NY, 2006; pp 63−351.
(22) Abou-Zied, O. K.; Al-Lawatia, N.; Elstner, M.; Steinbrecher, T. B. Binding of hydroxyquinoline probes to human serum albumin: Combining molecular modeling and Förster's resonance energy transfer spectroscopy to understand flexible ligand binding. *J. Phys. Chem. B* **2013**, *117*, 1062−1074.
(23) Majorek, K. A.; Porebski, P. J.; Dayal, A.; Zimmerman, M. D.; Jablonska, K.; Stewart, A. J.; Chruszcz, M.; Minor, W. Structural and immunologic characterization of bovine, horse, and rabbit serum albumins. *Mol. Immunol.* **2012**, *52*, 174−182.
(24) Bujacz, A. Structures of bovine, equine and leporine serum albumin. *Acta Crystallogr., Sect. D: Biol. Crystallogr.* **2012**, *68*, 1278−1289.
(25) Sekula, B.; Zielinski, K.; Bujacz, A. Crystallographic studies of the complexes of bovine and equine serum albumin with 3,5-diiodosalicylic acid. *Int. J. Biol. Macromol.* **2013**, *60*, 316−324.
(26) Peters, T., Jr. Serum albumin. *Adv. Clin. Chem.* **1970**, *13*, 37−111.
(27) Peters, T. Jr. *All About Albumin: Biochemistry, Genetics, and Medical Applications*; Academic Press: San Diego, CA, 1995.
(28) Emsley, J. Very strong hydrogen bonding. *Chem. Soc. Rev.* **1980**, *9*, 91−124.
(29) Perrin, C. L.; Nielson, J. B. "Strong" hydrogen bonds in chemistry and biology. *Annu. Rev. Phys. Chem.* **1997**, *48*, 511−544.
(30) Ovesná, Z.; Kozics, K.; Slameňová, D. Protective effects of ursolic acid and oleanolic acid in leukemic cells. *Mutat. Res., Fundam. Mol. Mech. Mutagen.* **2006**, *600*, 131−137.
(31) Yan, S.-l.; Huang, C.-y.; Wu, S.-t.; Yin, M.-c. Oleanolic acid and ursolic acid induce apoptosis in four human liver cancer cell lines. *Toxicol. In Vitro* **2010**, *24*, 842−848.
(32) Cao, S. N.; Liu, B. S.; Li, Z. Y.; Chong, B. H. A fluorescence spectroscopic study of the interaction between Glipizide and bovine serum albumin and its analytical application. *J. Lumin.* **2014**, *145*, 94−99.
(33) Bourassa, P.; Bariyanga, J.; Tajmir-Riahi, H. A. Binding sites of resveratrol, genistein, and curcumin with milk α- and β-caseins. *J. Phys. Chem. B* **2013**, *117*, 1287−1295.
(34) Elsadek, B.; Kratz, F. Impact of albumin on drug delivery - New applications on the horizon. *J. Controlled Release* **2012**, *157*, 4−28.
(35) Kratz, F.; Elsadek, B. Clinical impact of serum proteins on drug delivery. *J. Controlled Release* **2012**, *161*, 429−445.
(36) Dufour, C.; Dangles, O. Flavonoid-serum albumin complexation: determination of binding constants and binding sites by fluorescence spectroscopy. *Biochim. Biophys. Acta, Gen. Subj.* **2005**, *1721*, 164−173.
(37) Suresh, D. V.; Mahesha, H. G.; Rao, A. G. A.; Srinivasan, K. Binding of bioactive phytochemical piperine with human serum albumin: A spectrofluorometric study. *Biopolymers* **2007**, *86*, 265−275.
(38) Rohacova, J.; Sastre, G.; Marin, M. L.; Miranda, M. A. Dansyl labeling to modulate the relative affinity of bile acids for the binding sites of human serum albumin. *J. Phys. Chem. B* **2011**, *115*, 10518−10524.
(39) Abou-Zied, O. K.; Al-Lawatia, N. Exploring the drug-binding site Sudlow I of human serum albumin: The role of water and Trp214 in molecular recognition and ligand binding. *ChemPhysChem* **2011**, *12*, 270−274.
(40) Belatik, A.; Hotchandani, S.; Bariyanga, J.; Tajmir-Riahi, H. A. Binding sites of retinol and retinoic acid with serum albumins. *Eur. J. Med. Chem.* **2012**, *48*, 114−123.
(41) Bourassa, P.; Tajmir-Riahi, H. A. Locating the binding sites of folic acid with milk α- and β-caseins. *J. Phys. Chem. B* **2012**, *116*, 513−519.
(42) Song, M.; Hang, T.-j.; Wang, Y.; Jiang, L.; Wu, X.-l. Determination of oleanolic acid in human plasma and study of its pharmacokinetics in Chinese healthy male volunteers by HPLC tandem mass spectrometry. *J. Pharm. Biomed. Anal.* **2006**, *40*, 190−196.
(43) Xia, Y. Y.; Wei, G. L.; Si, D. Y.; Liu, C. X. Quantitation of ursolic acid in human plasma by ultra performance liquid chromatography tandem mass spectrometry and its pharmacokinetic study. *J. Chromatogr. B: Biomed. Sci. Appl.* **2011**, *879*, 219−224.
(44) Chen, Q. H.; Luo, S. W.; Zhang, Y. L.; Chen, Z. L. Development of a liquid chromatography-mass spectrometry method for the determination of ursolic acid in rat plasma and tissue: Application to the pharmacokinetic and tissue distribution study. *Anal. Bioanal. Chem.* **2011**, *399*, 2877−2884.
(45) Yin, M.-C.; Lin, M.-C.; Mong, M.-C.; Lin, C.-Y. Bioavailability, distribution, and antioxidative effects of selected triterpenes in mice. *J. Agric. Food Chem.* **2012**, *60*, 7697−7701.
(46) Record, M. T., Jr.; Anderson, C. F.; Lohman, T. M. Thermodynamic analysis of ion effects on the binding and conformational equilibria of proteins and nucleic acids: the roles of ion association or release, screening, and ion effects on water activity. *Q. Rev. Biophys.* **1978**, *11*, 103−178.
(47) Ross, P. D.; Subramanian, S. Thermodynamics of protein association reactions: Forces contributing to stability. *Biochemistry* **1981**, *20*, 3096−3102.
(48) Sudlow, G.; Birkett, D. J.; Wade, D. N. The characterization of two specific drug binding sites on human serum albumin. *Mol. Pharmacol.* **1975**, *11*, 824−832.
(49) Birkett, D. J.; Myers, S. P.; Sudlow, G. Effects of fatty acids on two specific drug binding sites on human serum albumin. *Mol. Pharmacol.* **1977**, *13*, 987−992.
(50) Brodersen, R.; Sjödin, T.; Sjöholm, I. Independent binding of ligands to human serum albumin. *J. Biol. Chem.* **1977**, *252*, 5067−5072.
(51) Naik, D. V.; Paul, W. L.; Threatte, R. M.; Schulman, S. G. Fluorometric determination of drug-protein association constants: The binding of 8-anilino-1-naphthalenesulfonate by bovine serum albumin. *Anal. Chem.* **1975**, *47*, 267−270.
(52) Stryer, L. The interaction of a naphthalene dye with apomyoglobin and apohemoglobin: A fluorescent probe of non-polar binding sites. *J. Mol. Biol.* **1965**, *13*, 482−495.

(53) Togashi, D. M.; Ryder, A. G. A fluorescence analysis of ANS bound to bovine serum albumin: Binding properties revisited by using energy transfer. *J. Fluoresc.* **2008**, *18*, 519−526.
(54) Sen, T.; Mandal, S.; Haldar, S.; Chattopadhyay, K.; Patra, A. Interaction of gold nanoparticle with human serum albumin (HSA) protein using surface energy transfer. *J. Phys. Chem. C* **2011**, *115*, 24037−24044.
(55) Goodsell, D. S.; Olson, A. J. Structural symmetry and protein function. *Annu. Rev. Biophys. Biomol. Struct.* **2000**, *29*, 105−153.
(56) Woody, R. W. Circular dichroism. *Methods Enzymol.* **1995**, *246*, 34−71.
(57) Punith, R.; Seetharamappa, J. Spectral characterization of the binding and conformational changes of serum albumins upon interaction with an anticancer drug, anastrozole. *Spectrochim. Acta, Part A* **2012**, *92*, 37−41.
(58) Lloyd, J. B. F. Partly quenched, synchronously excited fluorescence emission spectra in the characterisation of complex mixtures. *Analyst* **1974**, *99*, 729−738.
(59) Fuller, C. W.; Miller, J. N. Silver Medal lectures. *Proc. Anal. Div. Chem. Soc.* **1979**, *16*, 199−208.
(60) Samari, F.; Hemmateenejad, B.; Shamsipur, M.; Rashidi, M.; Samouei, H. Affinity of two novel five-coordinated anticancer Pt(II) complexes to human and bovine serum albumins: A spectroscopic approach. *Inorg. Chem.* **2012**, *51*, 3454−3464.
(61) Sandhya, B.; Hegde, A. H.; Ramesh, K. C.; Seetharamappa, J. Exploring the binding mechanism of ondansetron hydrochloride to serum albumins: Spectroscopic approach. *Spectrochim. Acta, Part A* **2012**, *86*, 410−416.
(62) Rada, M.; Ruiz-Gutiérrez, V.; Guinda, Á. Determination of triterpenic acids in human serum by high-performance liquid chromatography: Triterpenoid interaction with serum protein. *J. Agric. Food Chem.* **2011**, *59*, 2308−2313.

$$\frac{(F_0 - F)F_\infty}{(F_0 - F_\infty)F} = \frac{[O_2]}{[O_2]_\infty} \quad (2)$$

which removes the need to know K_D;[16] the subscript "∞" means the fluorescence intensity and concentration when the material has reached oxygen equilibrium. The challenge in oxygen solubility and transfer studies is often the interference of atmospheric oxygen and the need to reliably remove oxygen prior to measurement to obtain F_0. Measuring the process of oxygen transfer across an emulsion interface is very challenging due to the need to create the initial conditions such that oxygen is saturated in the aqueous phase but the fast process of diffusion across an interface with nanometer scale thickness has not yet occurred. Considering Einstein's formula $h \approx (Dt)^{1/2}$, the time a molecule needs to leap across the distance, h = 10 nm is of the order of 1 μs if $D = 10^{-6}$ cm^2/s or 1 ms if $D = 10^{-9}$ cm^2/s. Within the oil droplet oxygen diffusivity is of the order of 10^{-5} cm^2/s. Hence, if the droplet radius is of the order of 100 nm, it reaches steady state in 10 μs.

As a result, it is improbable that the fluorescence technique is able to capture such fast kinetics, unless the diffusivity in the droplet film is extremely low, on the order of $<10^{-14}$ cm^2/s. Moreover, the collective response of an emulsion sample does not truly represent the situation in an individual droplet. We applied the fluorescence technique for various emulsions based on milk proteins and other food emulsifiers to verify our assumption described above. The detailed results are not reported within this paper, but the experimental details, the modeling applied, and the overall results are briefly presented in the Supporting Information.

After considering the fluorescence technique, we decided to approach the problem by using a planar air−water interface, which although different from the o/w emulsion interface is still considered to be a good model of such systems.[5] The aim of the present work was to investigate whether scanning electrochemical microscopy (SECM) combined with a Langmuir trough is a suitable method for measuring oxygen permeability of protein interfaces. Similar setups have been used previously for oxygen permeability studies across phospholipid and octadecanol monolayers.[17−20]

MATERIALS AND METHODS

Materials. β-Lactoglobulin (L3908) and β-casein (C6905) were obtained from Sigma (Steinheim, Germany). Twenty-five millimolar phosphate buffer (pH 7) was prepared with $NaH_2PO_4 \cdot H_2O$ and Na_2HPO_4 from J. T. Baker (Deventer, The Netherlands). All solutions were prepared with MQ water. Molar masses used in the calculation of mean molecular area were 18400 g/mol for β-lactoglobulin and 24100 g/mol for β-casein, respectively.

Procedure. In an SECM experiment, a microelectrode tip is biased at a potential where the reaction of interest is occurring, and tip current is recorded as a function of distance from the interface (Figure 1). A Langmuir trough is used for forming a protein film at the air−water interface under controlled conditions. A compressed layer was studied because a protein film at an emulsion interface is expected to consist of a compact layer. As the method is based on induced transfer beginning at equilibrium conditions, the presence of atmospheric oxygen and the short time scale of the transfer process do not have a critical impact on the measurement.

An inverted ultramicroelectrode was placed in the water subphase within the well of a Langmuir trough, and the protein film was formed on the water surface (Figure 1). The tip was biased at a potential where oxygen is reduced, resulting in a current-distance response (so-called approach curve) that provides information on the oxygen permeability of the interface. Close to a permeable interface, the current is higher than in the bulk solution as the electrode reaction drives the transfer of oxygen from the phase that has a higher concentration of oxygen. Close to an impermeable surface, the current is lower than in the bulk due to hindered diffusion of oxygen to the electrode. The response can be modeled by solving the diffusion equation for the axisymmetric cylindrical SECM geometry, taking into account the kinetics of the interfacial oxygen transfer, finally yielding the rate constant for oxygen transfer.

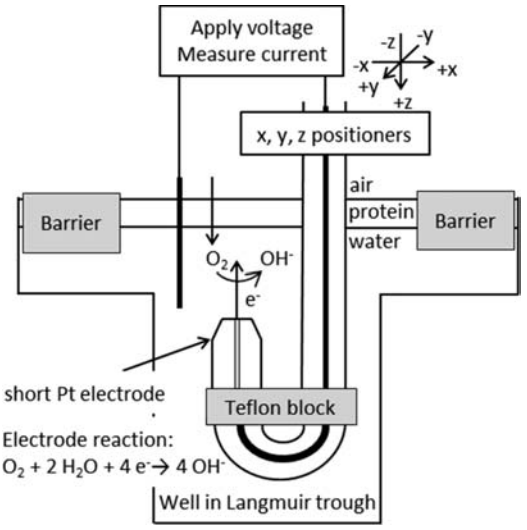

Figure 1. Schematic of the measurement setup (not to scale). An inverted ultramicroelectrode is used to measure the rate of oxygen transfer. SECM is used to control the potential and position of the electrode while recording the current.

SECM measurements were performed with a CHI900 instrument (CH Instruments, Austin, TX, USA) in a Langmuir trough with a well (195 cm^2, KSV Instruments Ltd., Helsinki, Finland). Phosphate buffer was used to counter the local shift in pH due to the formation of hydroxide ions as well as acting as the supporting electrolyte. The trough was filled with the buffer solution and thermostated to 23.5 °C. The interface was cleaned with a suction pipet with the barriers closed. Barriers were opened, and a homemade inverted Pt ultramicroelectrode with a radius a = 12.5 μm and RG = 10 (ratio of the radii of the insulating glass sheath and the electrode) was positioned in the well of the Langmuir trough. Ag wire acted as the counter and quasi-reference electrode. The current versus distance curves, or approach curves, were recorded at 0.5 μm/s with respect to the clean air−water interface to ensure that the response corresponded to a diffusion-controlled transfer with no kinetic limitations (pure positive feedback) for a clean interface. Prior to each approach curve measurement, the working electrode was activated by cycling 10 times from −0.35 to 1.2 V followed by a cyclic voltammogram (3 cycles) for oxygen reduction from 0.5 to −0.8 V.[21] This pretreatment together with the use of a buffer solution resulted in stable and reproducible voltammograms and approach curves. Approach curves for the oxygen reduction were recorded by biasing the electrode at −0.75 V, where oxygen reduction occurred at a diffusion-controlled rate.

After reproducible pure positive feedback was obtained for a clean interface, 200 μL of refrigerated protein solution (0.1 mg/mL in 25 mM, pH 7, phosphate buffer) was evenly spread on the subphase using a Hamilton syringe. The surface was stabilized for 30 min, and a surface pressure−area isotherm was recorded at a compression speed of 5 mm/min. Approach curves were then measured at the end point of the compression.

RESULTS AND DISCUSSION

Simulation of Theoretical Approach Curves. Theoretical approach curves were simulated for the system with

dx.doi.org/10.1021/jf5008715 | J. Agric. Food Chem. 2014, 62, 2284−2288

concentrations, diffusion coefficients, and dimensions as outlined in Figure 2.

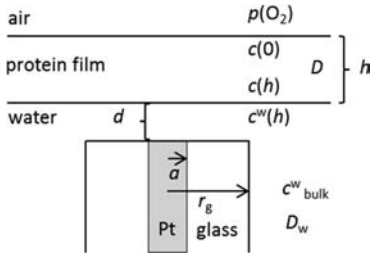

Figure 2. Outline of the system (not to scale). Film thickness = h, electrode-interface distance = d, electrode radius = a, radius of the glass sheath = r_g. D is the diffusion coefficient of oxygen in the film and D_w that in water. Oxygen concentrations: $c(0)$ at the air–film interface, $c(h)$ in the film, $c^w(h)$ in water at the film–water interface, and c^w_{bulk} in the bulk water phase.

Approach curves were simulated using the Finite Element Method in Comsol Multiphysics. The diffusion equation in axisymmetric circular cylindrical geometry using dimensionless variables is

$$\frac{\partial C}{\partial T} = \frac{\partial^2 C}{\partial R^2} + \frac{1}{R}\frac{\partial C}{\partial R} + \frac{\partial^2 C}{\partial Z^2} = 0 \quad (3)$$

The steady state solution gives the concentration profile in the system. The dimensionless variables are defined as $Z = z/a$, $R = r/a$, $L = d/a$, $C = c/c_{bulk}$, $T = D_w t/a^2$, and RG = r_g/a.

Current response is obtained from the concentration profile as the integral at the electrode surface:

$$\frac{I}{I_{bulk}} = \frac{\pi}{2}\int_0^1 \left(\frac{\partial C}{\partial Z}\right)_{Z=0} R\ dR \quad (4)$$

To calculate the concentration profile, a boundary condition to describe the kinetic limitation provided by the protein film at the interface is derived by using the oxygen flux across the interface from the concentrations in the aqueous phase. Similar situations have been considered previously,[17−20,22,23] but the theory is briefly presented below. Using the concentrations defined in Figure 2, oxygen solubility in water and in the protein film is described according to Henry's law as

$$c^w_{bulk} = \frac{p_{O_2}}{K_H},\ c(0) = \frac{p_{O_2}}{K_H^m} \quad (5)$$

where K_H is the Henry constant for oxygen solubility in water and K_H^m is that in the protein film. The partition between water and the film, P, is therefore

$$\frac{c(0)}{c^w_{bulk}} = \frac{K_H}{K_H^m} = P = \frac{c(h)}{c^w(h)} \quad (6)$$

That is, partition equilibrium naturally applies also at the water–film interface. Oxygen flux across the film is according to Fick's first law

$$j_{O_2} = \frac{D}{h}[c(0) - c(h)] = \frac{D}{h}c(0)\left[1 - \frac{c^w(h)}{c^w_{bulk}}\right] \quad (7)$$

by applying eq 6. The flux can be written in the dimensionless form as

$$J_{O_2} = K[1 - C(L)];\ K = \frac{D}{D_w}\frac{a}{h}P \quad (8)$$

The simulated approach curves for different values of the dimensionless rate constant, K, between 1000 for an ideally permeable interface and 0 for an ideally impermeable interface are presented in Figure 3. It is worth noting that the sensitivity

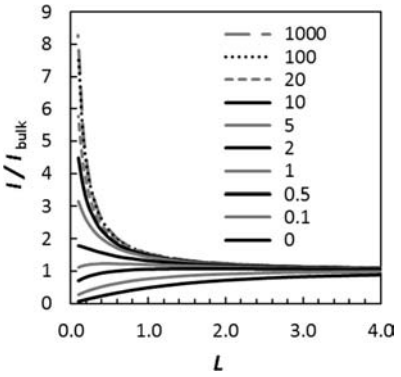

Figure 3. Simulated approach curves with the dimensionless rate constant, K, ranging from K = 1000 (highest curve, positive feedback) to K = 0 (lowest curve, negative feedback).

of the method at the limit of large K decreases and the curves for K = 1000 and K = 100 nearly overlap. When K > 5, the curves start to differ only below L = 1, whereas for lower K, the deviation from positive feedback is already evident at greater distances from the interface.

The distance of closest approach is obtained for each measurement from the approach curves to clean interface and is taken to be the point at which the current starts to level out and deviate from the ideal positive feedback. From the measurements, the criteria of $I > 5I_{bulk}$ and $L < 0.15$ were chosen as the point for an acceptable response for a clean interface. The distance of closest approach can never reach zero due to the roughness of the electrode surface, and it is assumed to remain the same for the approach to the protein-modified interface as has been previously supposed with octadecanol and phospholipids.[17,19,20,22,23] The nanoscale thickness of the interface is unlikely to have an effect on the distance of closest approach, which is on the order of micrometers.

Compression Isotherms and Experimental Approach Curves. Surface pressure–area isotherms for protein films are shown in Figure 4, and the isotherms were found to be highly reproducible for each protein. At the end point of the

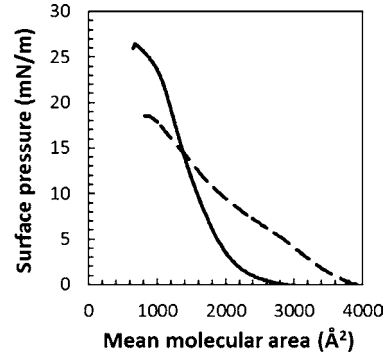

Figure 4. Langmuir compression isotherms for β-lactoglobulin (solid line) and β-casein (dotted line).

dx.doi.org/10.1021/jf5008715 | J. Agric. Food Chem. 2014, 62, 2284−2288

compression, the trough area is 40 cm^2 and the theoretical maximum surface mass concentration of the protein is therefore 5 mg/m^2. The corresponding mean molecular areas for β-casein and β-lactoglobulin are 820 and 650 $Å^2$, respectively. When β-casein was adsorbed on polystyrene beads, saturation of the layer was found to occur around this concentration,[24,25] and it is also in the same order of magnitude (1−3 mg/m^2) of the concentration at which the layer thicknesses for both proteins have been determined by neutron reflectivity.[10]

Typical experimental approach curves to an air−water interface without protein and to an interface modified with β-lactoglobulin and β-casein at surface pressures at the end point of the compression, 26.5 mN/m for β-lactoglobulin and 18.5 mN/m for β-casein, are shown in Figure 5.

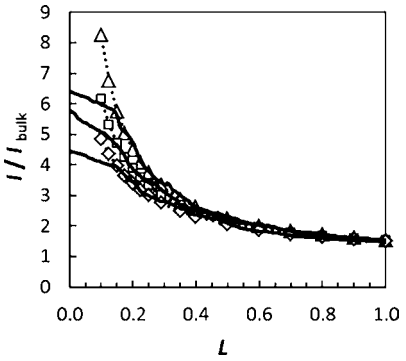

Figure 5. Experimental approach curves for the air−water interface (from top to bottom) without a protein fitted for K = 1000 (△), with β-casein film fitted for K = 25 (□), and with β-lactoglobulin film fitted for K = 12 (◇). Low K indicates low permeability to oxygen.

The response for an air−water interface without a protein fits the theoretical curve of K = 1000 corresponding to ideal positive feedback with no kinetic limitation at the interface as expected. The response for β-lactoglobulin fits the theoretical curve of K = 12 and β-casein to K = 25. Using a diffusion coefficient of oxygen in water of $D_w = 2.0 \times 10^{-5}$ cm^2/s and a film thickness of 3.1 nm for β-lactoglobulin or 5.4 nm for β-casein,[5] we obtain the product PD from eq 8 as 0.6×10^{-7} cm^2/s for β-lactoglobulin and 2.2×10^{-7} cm^2/s for β-casein, showing that β-lactoglobulin provides a better barrier to oxygen transfer. A possible explanation is the more compact structure of the β-lactoglobulin film originating from stronger intermolecular interactions as previously demonstrated by surface rheological measurements.[26] For β-lactoglobulin, 3-fold dilatational elasticity could be determined. In contrast, for β-casein, the determination of stress strain curves in surface shear measurements was not possible due to the weakness of the film.

Oxygen solubility in the protein film can be assumed to be smaller than in water due to the free volume effect. Therefore, even though the solubility in the film is not known, the *lowest limit* for the diffusion coefficient can be obtained by assuming that $c(0) = c^w_{bulk}$, that is, P = 1, and the value PD directly corresponds to the diffusion coefficient. Compared to the diffusion coefficient of oxygen in solid polymers (10^{-8} cm^2/s), the obtained values are in a reasonable range.

Even though β-lactoglobulin is known to form thinner films, it was less permeable to oxygen than β-casein under the conditions applied here and demonstrates the inhibition of oxygen transfer in β-lactoglobulin. To the best of our knowledge, this is the first study that allows independent characterization of oxygen permeability of protein interfaces. We demonstrated that oxygen permeabilities of interfacial layers of β-casein and β-lactoglobulin can be distinguished with this setup. The results of the oxidation studies by Berton et al.[27,28] comparing these proteins suggest, however, that the difference in oxygen permeability may not be enough to determine the rate of oxidation in emulsions as β-casein was shown to be more effective in protecting the lipid from oxidation. Due to the extremely thin, nanometer size, interface, oxygen permeability is unlikely to be the limiting step in controlling lipid oxidation in emulsions having the time scale of the oxidation reactions on the order of days, unless oxygen transfer is practically blocked. As the size of an oxygen molecule is on the ångstrom scale, it is unlikely that the surface coverage of any protein interface would be sufficient to completely block the oxygen transfer. Our results, however, clearly indicate that for decreased oxygen permeability, a globular structure forming a viscoelastic layer is more effective than a fluid-like structure.

Applying SECM for liquid−liquid interfaces would be an interesting step toward a more realistic model of the emulsion interface as, in contrast to air−liquid interfaces, proteins are reported to be more firmly attached to liquid−liquid interfaces.[25] For attempts to develop better interfaces with highly improved oxygen blocking efficacy, the SECM method provides an excellent tool to characterize and compare the blocking properties of different interfaces.

■ ASSOCIATED CONTENT

Ⓢ Supporting Information

Experimental details, modeling, and discussion of the fluorescence experiments. This material is available free of charge via the Internet at http://pubs.acs.org.

■ AUTHOR INFORMATION

Corresponding Author

*(O.T.) Mailing address: Department of Chemistry, Aalto University, P.O. Box 16100, FI-00076 Aalto, Finland. Phone: +358 50 3435167. Fax: +358 9 470 22580. E-mail: outi.toikkanen@iki.fi.

Funding

The Academy of Finland is acknowledged for financial support (project 259584).

Notes

The authors declare no competing financial interest.

■ ACKNOWLEDGMENTS

Dr. Benjamin P. Wilson is gratefully acknowledged for proofreading the manuscript.

■ REFERENCES

(1) Waraho, T.; McClements, D. J.; Decker, E. A. Mechanisms of lipid oxidation in food dispersions. *Trends Food Sci. Technol.* **2011**, *22*, 3−13.

(2) Orlien, V.; Risbo, J.; Rantanen, H.; Skibsted, L. H. Temperature-dependence of rate of oxidation of rapeseed oil encapsulated in a glassy food matrix. *Food Chem.* **2006**, *94*, 37−46.

(3) Silvestre, M. P. C.; Chaiyasit, W.; Brannan, R. G.; McClements, D. J.; Decker, E. A. Ability of surfactant headgroup size to alter lipid and antioxidant oxidation in oil-in-water emulsions. *J. Agric. Food Chem.* **2000**, *48*, 2057−2061.

(4) Ma, H.; Forssell, P.; Kylli, P.; Lampi, A.; Buchert, J.; Boer, H.; Partanen, R. Transglutaminase catalyzed cross-linking of sodium

caseinate improves oxidative stability of flaxseed oil emulsion. *J. Agric. Food Chem.* **2012**, *60*, 6223−6229.
(5) Berton-Carabin, C.; Genot, C.; Gaillard, C.; Guibert, D.; Ropers, M. H. Design of interfacial films to control lipid oxidation in oil-in-water emulsions. *Food Hydrocolloids* **2013**, *33*, 99−105.
(6) Clausen, M. R.; Skibsted, L. H.; Stagsted, J. Characterization of major radical scavenger species in bovine milk through size exclusion chromatography and functional assays. *J. Agric. Food Chem.* **2009**, *57*, 2912−2919.
(7) Hu, M.; McClements, D. J.; Decker, E. A. Lipid oxidation in corn oil-in-water emulsions stabilized by casein, whey protein isolate, and soy protein isolate. *J. Agric. Food Chem.* **2003**, *51*, 1696−1700.
(8) Villiere, A.; Viau, M.; Bronnec, I.; Moreau, N.; Genot, C. Oxidative stability of bovine serum albumin- and sodium caseinate-stabilized emulsions depends on metal availability. *J. Agric. Food Chem.* **2005**, *53*, 1514−1520.
(9) Faraji, H.; McClements, D. J.; Decker, E. A. Role of continuous phase protein on the oxidative stability of fish oil-in-water emulsions. *J. Agric. Food Chem.* **2004**, *52*, 4558−4564.
(10) Atkinson, P. J.; Dickinson, E.; Horne, D. S.; Richardson, R. M. Neutron reflectivity of adsorbed β-casein and β-lactoglobulin at the air/water interface. *J. Chem. Soc., Faraday Trans.* **1995**, *91*, 2847−2854.
(11) Russev, S. C.; Arguirov, T. V.; Gurkov, T. D. β-Casein adsorption kinetics on air−water and oil−water interfaces studied by ellipsometry. *Colloids Surf. B: Biointerfaces* **2000**, *19*, 89−100.
(12) Wierenga, P. A.; Egmond, M. R.; Voragen, A. G. J.; de Jongh, H. H. J. The adsorption and unfolding kinetics determines the folding state of proteins at the air−water interface and thereby the equation of state. *J. Colloid Interface Sci.* **2006**, *299*, 850−857.
(13) Platikanov, D.; Nedyalkov, M.; Nasteva, V. Line tension of Newton black films. II. Determination by the diminishing bubble method. *J. Colloid Interface Sci.* **1980**, *75*, 620−628.
(14) Bezelgues, J. B.; Serieye, S.; Crosset-Perrotin, L.; Leser, M. E. Interfacial and foaming properties of some food grade low molecular weight surfactants. *Colloids Surf. Physicochem. Eng. Aspects* **2008**, *331*, 56−62.
(15) Lakowicz, J. R. *Principles of Fluorescence Spectroscopy*; Springer: Singapore, 2006; p 278.
(16) Tikekar, R. V.; Johnson, A.; Nitin, N. Real-time measurement of oxygen transport across an oil−water emulsion interface. *J. Food Eng.* **2011**, *103*, 14−20.
(17) Slevin, C. J.; Ryley, S.; Walton, D. J.; Unwin, P. R. A new approach for measuring the effect of a monolayer on molecular transfer across an air/water interface using scanning electrochemical microscopy. *Langmuir* **1998**, *14*, 5331−5334.
(18) Strutwolf, J.; Zhang, J.; Barker, A. L.; Unwin, P. R. Effect of phospholipids on the kinetics of dioxygen transfer across a 1,2-dichloroethane/water interface. *Phys. Chem. Chem. Phys.* **2001**, *3*, 5553−5558.
(19) Zhang, J.; Strutwolf, J.; Cannan, S.; Unwin, P. R. Combined scanning electrochemical microscopy−Langmuir trough technique for investigating phase transfer kinetics across liquid/liquid interfaces modified by a molecular monolayer. *Electrochem. Commun.* **2003**, *5*, 105−110.
(20) Cannan, S.; Zhang, J.; Grunfeld, F.; Unwin, P. R. Scanning electrochemical microscopy (SECM) studies of oxygen transfer across phospholipid monolayers under surface pressure control: comparison of monolayers at air/water and oil/water interfaces. *Langmuir* **2004**, *20*, 701−707.
(21) Carano, M.; Holt, K. B.; Bard, A. J. Scanning electrochemical microscopy. 49. Gas-phase scanning electrochemical microscopy measurements with a Clark oxygen ultramicroelectrode. *Anal. Chem.* **2003**, *75*, 5071−5079.
(22) Ciani, I.; Burt, D. P.; Daniele, S.; Unwin, P. R. Effect of surface pressure on oxygen transfer across molecular monolayers at the air/water interface: Scanning electrochemical microscopy investigations using a mercury hemispherical microelectrode probe. *J. Phys. Chem. B* **2004**, *108*, 3801−3809.
(23) Barker, A. L.; Macpherson, J. V.; Slevin, C. J.; Unwin, P. R. Scanning electrochemical microscopy (SECM) as a probe of transfer processes in two-phase systems: theory and experimental applications of SECM-induced transfer with arbitrary partition coefficients, diffusion coefficients, and interfacial kinetics. *J. Phys. Chem. B* **1998**, *102*, 1586−1598.
(24) Husband, F. A.; Wilde, P. J.; Mackie, A. R.; Garrood, M. J. A comparison of the functional and interfacial properties of β-casein and dephosphorylated β-casein. *J. Colloid Interface Sci.* **1997**, *195*, 77−85.
(25) Partanen, R.; Forssell, P.; Mackie, A.; Blomberg, E. Interfacial cross-linking of β-casein changes the structure of the adsorbed layer. *Food Hydrocolloids* **2013**, *32*, 271−277.
(26) Martin, A. H.; Grolle, K.; Bos, M. A.; Stuart, M. A. C.; van Vliet, T. Network forming properties of various proteins adsorbed at the air/water interface in relation to foam stability. *J. Colloid Interface Sci.* **2002**, *254*, 175−183.
(27) Berton, C.; Ropers, M.; Viau, M.; Genot, C. Contribution of the interfacial layer to the protection of emulsified lipids against oxidation. *J. Agric. Food Chem.* **2011**, *59*, 5052−5061.
(28) Berton, C.; Ropers, M.; Bertrand, D.; Viau, M.; Genot, C. Oxidative stability of oil-in-water emulsions stabilised with protein or surfactant emulsifiers in various oxidation conditions. *Food Chem.* **2012**, *131*, 1360−1369.

granules, thus producing starch with unimodal granule size distribution.

MATERIALS AND METHODS

Plant Material. A collection of 142 barley (*Hordeum vulgare* L.) genotypes of diverse origins (Table 1) were analyzed for starch granule size distribution. Seven widely grown Canadian barley varieties CDC Dolly (Canadian Food Inspection Agency (CFIA), Ottawa, Ontario, Canada, Variety registration Office (VRO) registration certificate # 3967), CDC Clyde (CFIA registration certificate # 2103), CDC Kendall (CFIA registration certificate # 0298), CDC Copeland (CFIA registration certificate # 1100), CDC Battleford (CFIA registration certificate # 1104), CDC Meredith (CFIA registration certificate # 3942), and AC Metcalfe[26] and Harrington were also evaluated. Plants from the barley germplasm collection were grown in a growth chamber at 18 °C under 16 h photoperiod (200 μmol m^{-2} s^{-1} photosynthetic photon flux density) until maturity. Plants in the field were grown in rows or small plots at three locations on the University of Saskatchewan farm near Saskatoon, Saskatchewan, Canada (52° 8′ N/106° 38′ W). Single heads of mature plants were collected for eventual analysis of the grain.

Starch Granule Size Determination. All starch analyses were conducted on grain collected from the middle section of spikes. Starch samples for microscopic imaging were prepared and analyzed (≥5000 starch granules) as described.[27] Samples to be analyzed by laser diffraction (Mastersizer 2000, MAL 1030346, Malvern Instruments, Malvern, England) were prepared using a modified starch extraction procedure as follows: A sample of coarsely ground barley grain (1 g) was steeped overnight at 4 °C in 2 mL of 0.02 N HCl. Starch granules were separated from cell wall and protein matrix by digestion at 37 °C for 3 h with 15 units *Streptomyces griseus* type XXV proteinase (Sigma), 2 units lichenase (Megazyme), and 8 units *Thermomyces lanuginosus* β-xylanase (Sigma), as described.[28] Digested grain samples were mixed using a glass rod, filtered over 100 μm nylon filter, and centrifuged for 10 min at 3000*g*. The crude starch granule preparation was purified by cesium chloride density gradient centrifugations as described.[29] The purified starch granules were suspended in water to 40 mg/mL concentration and briefly dispersed by sonication prior to analysis. Laser diffraction analysis of starch was done using Mastersizer 2000 and initiated by adding 0.5 mL starch suspension to sample handling unit (Hydro 2000SA, Malvern Istruments, Malvern, England) held under constant mixing (pump speed 1700 rpm). During sample addition, laser obscuration was maintained between 12% and 14%, and readings were obtained using refractive indices of 1.31 for water and 1.52 as standard. A measurement time of 12 s with 12 000 measurement snaps was used for data analysis with measuring range from 0.02 to 96.86 μm. Grains from two biological replicates for each genotype were used for starch granule preparations. From each starch sample two aliquots were separately analyzed twice, and the average of the two measurements was used for statistical analysis. Volume based calculations were derived from Mie theory as described.[30]

Total Starch Concentration. Barley grain (10 g) samples were finely ground in a UDY mill (UDY Corporation, Fort Collins, CO) to pass through a 0.5 mm sieve. Total starch concentration in the meal was determined by an enzymatic hydrolysis method[31] using a commercial kit (Megazyme International Ireland, Wicklow, Ireland). In this method, 100 mg of meal was digested for 8 min in boiling water bath with 300 U α-amylase in 3 mL of 50 mM 3-(*N*-morpholino) propanesulfonic acid (MOPS) pH 7.0 buffer followed by addition of 4.0 mL of 200 mM sodium acetate buffer pH 4.5 and 20 U amyloglucosidase followed by incubation for an additional 30 min at 50 °C. Released glucose was determined using glucose oxidase/peroxidase assay by measuring absorbance at 510 nm. Starch concentration was calculated as described.[32]

Determination of Amylose Concentration. Samples of extracted starch (10 mg) were suspended in 10 mL of water, gelatinized for 5 min by boiling followed by debranching using *Pseudomonas* sp. isoamylase (Megazyme) as described.[33] Thereafter, long (amylose) and short (amylopectin) glucan chains in 1 mg of debranched starch

Table 1. Barley Genotypes Analyzed for Starch Granule Size Distribution

			av diameter (μm)	
barley genotype	number of granules analyzed	number B-type (%)[a]	B-type	A-type
96B616	9034	83.1	5.61	19.94
31-19	11 648	93.0	5.32	16.74
32-53	14 985	88.5	5.70	17.90
36-13	11 005	86.5	5.48	19.78
71II-66-22-5	11 123	92.0	5.49	20.48
970211-32	9881	70.4	5.51	20.54
Abee	7932	88.6	5.30	18.47
Abyssinian Intermediate	10 286	88.4	5.44	19.64
Alaska 46	7107	81.5	5.17	21.29
Alaska 52	10 560	86.0	5.01	20.94
Aramir	10 538	82.1	5.54	20.85
Argyle	7870	92.9	5.59	18.37
Australia	7969	79.9	5.47	20.52
Avro	6081	82.8	5.26	20.42
Berac	7425	71.6	5.29	19.52
Betzes	7811	75.2	5.56	20.28
Bido	11 487	87.4	5.85	19.10
Bomi	6788	76.8	5.55	17.59
Bonanza	11 338	95.9	4.72	20.94
Br6355-28-1-1	7867	81.5	4.98	19.66
BT459	11 448	79.2	5.63	20.50
Cambrinus	8642	85.1	5.93	17.77
Canadian Thorpe	7066	83.1	5.79	17.00
Carlsberg-2	6514	77.4	5.73	19.62
CDC Dawn	9612	73.3	5.94	19.24
Centennial	6350	87.7	5.51	20.23
Chevallier	7385	87.1	5.11	20.18
CI 10512	9048	77.9	5.17	19.29
CI 3124	9191	93.3	5.07	19.18
CI 5845	10 343	93.5	5.57	17.22
CI 9545	6988	78.8	4.98	20.81
CI 9592	10481	90.0	6.01	17.33
CI 9669	9635	91.2	5.41	17.53
CI 9819	11 509	92.8	5.54	18.19
CI 9820	15 109	93.5	5.34	18.64
CI 9825	8546	93.8	5.04	20.05
Clho 4369	8138	74.2	5.32	19.92
Clho 4969	7448	80.9	5.50	20.49
Clho 6496	8530	83.2	5.58	20.68
Conquest	5848	82.7	5.21	19.32
Diva	9725	87.5	5.48	19.42
Deuce	7800	92.1	5.43	18.21
Drake	12 400	92.7	5.46	17.47
Drossel	8692	87.0	5.80	18.88
Duke	9729	92.5	5.15	17.64
Duncan	7384	71.2	5.93	19.74
Ellice	8805	90.4	5.54	20.21
Elrose	9814	85.7	5.58	18.21
Emir	8261	90.3	5.33	19.81
English	8874	82.6	4.75	18.34
Etu	5583	53.4[b]	5.83	21.17
Fairfield	10 947	94.8	5.39	17.34
Feronia	9282	90.0	5.28	20.27
Field 5916	9328	75.9	5.33	19.39
Fjola	6160	77.5	5.58	20.28
Gateway	9777	89.4	5.05	20.44
Gerkra	10 276	86.0	5.41	19.85

dx.doi.org/10.1021/jf405424x | J. Agric. Food Chem. 2014, 62, 2289−2296

Table 1. continued

barley genotype	number of granules analyzed	number B-type (%)[a]	av diameter (μm) B-type	av diameter (μm) A-type
Glacier	7862	75.7	6.20	16.51
Golden Promise	9096	80.5	5.54	19.66
Grimmet	7303	85.3	5.56	19.59
Hankkija 673	9750	88.7	5.04	21.30
Harrington	10 429	88.8	5.83	20.73
Hassan	6556	84.6	5.27	20.86
HB 774/1/10/15	8215	90.3	5.29	19.17
HB335 (CDC McGwire)	8559	94.4	5.43	17.18
Heartland	7796	*68.2*[b]	5.64	19.49
Hector	5991	82.7	5.54	22.23
Hunter	8206	79.1	5.63	19.11
Husky	14 095	71.6	5.24	19.15
Impala	7964	89.0	5.46	18.44
Jet	6688	77.8	5.65	19.69
Jo 1095	7086	85.3	5.56	20.80
Johnston	8197	94.0	5.29	17.49
Julia	9392	88.0	5.40	17.87
Karri	12 675	79.6	6.00	20.20
Kenia	9607	82.0	5.46	20.42
Kinai-Kyoshinkai 2	9551	*69.3*[c]	5.20	21.50
Kindred	6382	72.5	5.00	18.96
Klages	7900	82.5	5.55	22.09
Larker	8789	84.2	5.42	19.09
lb6-3	11 599	86.3	5.23	19.26
Leduc	5059	90.7	5.21	17.19
Mala	9992	80.0	5.92	18.97
Malebo	8801	84.5	5.87	17.69
Malst	8288	82.7	5.74	19.32
Manley	7307	84.2	5.21	19.17
Mariout	11 846	86.1	5.95	17.08
Maris Baldric	11 382	81.3	5.72	16.93
Mazurka	11 289	86.7	5.66	20.02
Mc247	10 953	95.7	5.00	18.45
Mensury	6001	*57.8*[b]	5.23	19.93
Midas	10 773	79.7	5.95	20.62
Montcalm	10 378	91.7	5.43	18.18
Morex	8862	73.8	5.51	20.70
Ndb104	7621	84.5	5.59	19.24
Ndb124	11 119	92.8	5.77	17.74
Noname-CN2321	10 441	87.2	5.34	18.09
Noname-CN294	8665	89.8	5.22	19.31
Norbert	12 496	88.2	5.91	18.88
Nordal	8534	80.1	5.72	21.39
Nordgard 264	8064	90.2	5.67	18.12
Oac 21(66)	8735	*58.5*[b]	5.29	18.96
Oac 21(68)	8967	92.9	5.01	19.22
Ofir	9266	85.0	5.75	20.65
Old Oac 21	8074	84.9	5.33	20.58
Olli	7541	84.7	5.38	22.06
Orkoe	9068	77.4	5.29	17.70
Otra	9490	89.1	5.23	20.12
Parkland	7765	88.6	4.86	19.96
Pauline	7137	86.5	5.71	20.28
PGR 2049	9898	88.8	5.08	18.66
Piroline	8153	88.6	5.35	18.95
Plumage	9502	80.2	5.17	20.05
Plush	12 374	88.6	5.50	18.94
Pomo	6590	76.4	5.14	17.91

Table 1. continued

barley genotype	number of granules analyzed	number B-type (%)[a]	av diameter (μm) B-type	av diameter (μm) A-type
Qb20-37	7927	93.0	5.57	20.09
Riso 8	9622	90.4	5.36	18.40
Samson	8901	92.2	4.90	18.97
Sanalta	8393	89.6	5.29	19.54
Seton	9765	86.3	5.18	18.12
Seton	9765	86.3	5.18	18.12
Silja	9023	89.7	5.22	19.21
Spratt Archer	7250	84.4	4.83	19.78
Stephan	15 054	93.1	5.39	16.56
Steptoe	10 950	83.8	5.11	18.52
Tankard	9413	90.9	4.99	21.39
Tern	8530	86.7	5.54	18.56
TR117 (CDC Guardian)	6256	80.6	5.17	19.66
TR150 (CDC Copeland)	8328	91.1	5.50	20.07
TR490 Manley	7375	72.6	5.64	20.15
TR544 Bridge	8420	88.5	5.29	19.70
TR941 Prospect	9940	93.5	5.72	16.98
Traill	10 594	85.0	5.06	18.74
Tregal	9990	88.3	5.45	19.17
Tristan	9630	93.9	5.08	21.01
Triumphant	12 021	90.2	5.47	17.78
Trophy	6786	76.3	5.43	20.43
Tupper	9007	81.0	5.58	19.39
Vanguard	9429	90.5	5.61	17.74
Zephyr	9837	84.8	5.25	18.67
av	9079	84.6	5.43	19.3

[a]Italicized values are lower than 70%. [b]Low B-type granule content subject to environmental influences. [c]Stable low B-type granule content in multiple environments.

were separated by high performance size exclusion chromatography (HPSEC) employing a Waters HPLC system (Waters Corporation, Milford, MA) equipped with a Phenogel 5 μm guard column (30 mm × 4.6 mm) attached to Phenogel 300 mm × 4.6 mm i.d. column (Phenomenex, Torrance, CA) and a refractive index detector. Debranched waxy barley starch was used as amylopectin standard in the analysis.

Statistical Analysis. The analysis of variance (ANOVA) of the means and Pearson's correlation was performed with SPSS multivariate analysis (SPSS Inc. version 17). Multiple means comparisons were determined with the Duncan's multiple range test at $p < 0.05$ confidence level.[34]

RESULTS

Screening of Barley Genotypes for Altered Starch Granule Size Distribution. All starch samples prepared from 139 barley genotypes showed bimodal distribution when analyzed by light microscopy of starch granule sizes (Table 1). The average diameter for A-type starch granules among the genotypes was 19.3 (16.51−22.23) μm. The number of B-type small starch granules (≥10.0 μm in diameter) in the samples was on average 84.6% (53.4−95.9%), and their diameters were on average 5.43 (4.72−6.20) μm (Table 1). Five genotypes (Etu, Heartland, Kinai-Kyoshinkai 2 (KK-2), Mensury, and Oac21) showed B-type starch granule number that were unusually low (<70.0%; Table 1). Since reduced number of small starch granules could be caused by environmental conditions, the five genotypes were selected for additional studies. Repeated trials

with the genotypes grown under greenhouse conditions consistently confirmed reduced small granules content for genotype KK-2, but not for the remaining four genotypes, which were excluded from further analysis.

KK-2 Barley Produces Starch with Reduced Number of Small Starch Granules. To test if the starch phenotype observed for genotype KK-2 grown under green house could be repeated in the field, the genotype was grown at three different locations in Saskatoon, Canada. Included in the trial were also the Canadian cultivars CDC Battleford, CDC Dolly, and Harrington, which all produce normal starch. A microscopic image analysis of starch prepared from the three normal starch genotypes showed an average number of B-type starch granules ranging from 77.5% to 90.6%. In contrast, KK-2 produced a significantly ($p < 0.01$) lower number of small starch granules (60.2−67.5%) at all three locations (Table 2, Supporting Information Figure 1). Thus, the low number of B-type starch granules seen for KK-2 was concluded to be relatively stable across different environments.

Table 2. Microscopic Analysis of Starch Granules of Field Grown Plants[a]

barley genotype	B-type starch granules at location			
	Kernen	Preston	seed farm	av
CDC Battleford	80.9	88.6	77.5	82.3 ± 8.6[b]
CDC Dolly	86.7	90.6	81.2	86.2 ± 6.2[b]
Harrington	78.8	82.3	84.4	81.8 ± 4.5[b]
Kinai Kyoshinkai-2 (KK-2)	60.2	67.5	65.3	64.3 ± 3.1[a]

[a]Values followed by same letter are not significantly different ($p < 0.05$).

The relative starch volume contributed by the different size classes of starch granules was determined using laser diffraction analysis, which in contrast to microscope image analysis is more efficient and reliable for screening a large number of genotypes. Similar to granule size distribution by microscope image analysis (Figure 1A), the laser diffraction analysis showed a bimodal distribution of starch granule volumes (Figure 1B). The starch granule volume distributions among the Canadian barley varieties showed similar profiles with a low point around 5−6 μm separating the very small C-type starch granule volume from the larger granule population. For KK-2, the starch granule profile showed a low point around 5 μm, an increased volume for starch granules with 5−15 μm diameter range, and reduced volume for A-type starch granules (Figure 1B). The starch granule volume distribution profile suggested the increase to the 5−15 μm granule fraction in KK-2 occurred at the expense of the largest A-type starch granules. On the basis of three classes, the ratio between A-type, B-type, and C-type volume percentages for KK-2 starch was 7.5:7.1:1, and the corresponding ratio for normal starch was 7.1:3.3:1 (CDC Kendall, Table 3).

Introgression of Altered Starch Granule Size Trait into a Canadian Cultivar. To introgress the reduced number of small starch granules in a Canadian malting barley genotype, KK-2 was crossed with spring-type malting barley cultivar CDC Kendall. The F_2 population of 112 lines showed variation for starch granule size with transgressive segregation seen at both ends of the starch granule size volume distribution (Figure 2A). There were 21 lines that showed higher A-type starch granule volumes than CDC Kendall and five lines that produced lower small starch granules volumes than KK-2 (Figure 2A). None of the lines in F_2 population showed significantly reduced large

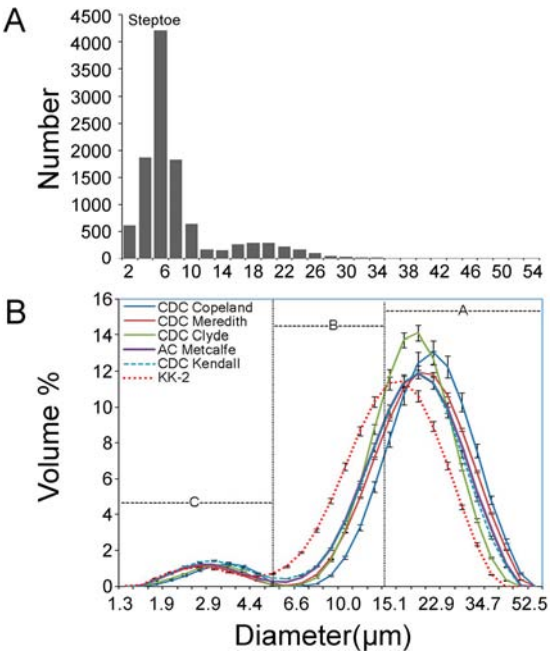

Figure 1. Starch analyses by microscope and laser diffraction particle sizing. (A) Distribution of starch granules in barley cv. Steptoe based on size and number as determined by microscope. (B) Distribution of starch granule volumes as determined by laser diffraction analyses. The granule volume profiles of five Canadian barley lines with normal granule sizes and Japanese barley line KK-2 are shown. Each data points represent mean of two replicates with SD.

A-type starch granule volume percentage than KK-2, and 80 lines produced significantly higher volume percentage of the medium size B-type starch granules than CDC-Kendall; thus, an overall increase in the average size of starch granule population was seen for the F_2 population. To study the inheritance of the starch phenotypes, the F_2 population was advanced to the F_5 generation for further starch analysis.

A total of 154 F_5 lines were selected for analysis of starch granule size distribution. As compared to the F_2 population, the F_5 lines showed on average a higher volume of A-type starch granules (54.3% versus 49.6%), similar volumes of B-type starch granules (38.1% versus 39.6%), and lower volume of C-type starch granules (7.6% versus 10.9%) (Figure 2). Five of the F_5 lines distinguished themselves as producers of 5−13% higher volume of A-type starch granules as compared to CDC Kendall (LSD = 2.74, $p < 0.05$), 24 lines showed lower C-type starch granules volume than KK-2 (LSD = 1.26, $p < 0.05$), and 10 lines had higher B-type (5−15 μm) starch granule volume than KK-2 (Figure 2B). Among the low C-type starch granule phenotype extremes were six lines with near zero concentration of C-type starch granules, and hence, a unimodal distribution curve for starch granule volume was observed for these lines (Figure 2). However, only three F_5 lines 116, 144, and 168 showed unimodal starch granule size distribution across several environments (Figure 3).

Reduction in C-Type Starch Granules Affects Grain Characteristics. The total starch concentration for barley F_5 lines 116, 144, and 168 with unimodal starch granule size ranged from 40.8% to 46.5% (Table 3) and were similar to KK-2 (48.5 ± 2.0%) but lower than normal barley starch (57.8 ± 5.0%). A normal amylose concentration was observed in starch extracted from lines 116, 144, 168 and both the parental genotypes (24−26.8%). Thousand grain weight (TGW) in the

Table 3. Starch and Grain Filling Characteristic of Selected F_5 Lines and Their Parents

				starch granule volume (%)[a]		
barley line	TGW (g)	starch (%)	amylose[b] (%)	A-type (>15 μm)	B-type (5−15 μm)	C-type (<5 μm)
CDC Kendall	45.9 ± 0.6[e]	57.8 ± 5.0 [c]	26.8 ± 0.8[a]	62.1 ± 2.6[c]	29.1 ± 2.7[e]	8.8 ± 0.9[h]
KK-2	18.3 ± 0.1[a]	48.5 ± 2.0[b]	27.4 ± 0.8[a]	48.2 ± 3.0[a]	45.4 ± 4.8[f]	6.4 ± 2.0[d-g]
F_5 line 116[c]	21.4 ± 0.4[b]	45.8 ± 0.5[b]	24.2 ± 1.4[a]	54.7 ± 1.6[b]	45.2 ± 1.0[f]	0.1 ± 0[c]
F_5 line 144[c]	27.8 ± 0.7[d]	40.8 ± 0.1[a]	26.5 ± 0.2[a]	55.1 ± 0.8[b]	44.8 ± 0.6[f]	0.07 ± 0[a]
F_5 line 168[c]	25.1 ± 0.2[c]	46.5 ± 3.4 [b]	24.0 ± 0.7[a]	56.7 ± 0.3[b]	43.2 ± 0.2[f]	0.09 ± 0[b]
F_5 line 70[d]	25.5 ± 1.1[c]	47.8 ± 0.4[b]	24.1 ± 0.4[a]	70.0 ± 0.1[e]	24.8 ± 0.1[a]	5.2 ± 0.1[d]
F_5 line 75[d]	49.3 ± 0.8[g]	63.5 ± 2.6[c]	24.7 ± 0.3[a]	65.2 ± 0.1[c]	28.5 ± 0.1[e]	6.2 ± 0.1[e]
F_5 line 78[d]	43.6 ± 0.7[e]	66.4 ± 5.1[d]	25.1 ± 0.2[a]	65.8 ± 0.1[c]	27.3 ± 0.1[c]	7.0 ± 0.1[g]
F_5 line 82[d]	47.6 ± 0.4[f]	61.1 ± 2.2[c]	24.3 ± 1.2[a]	67.2 ± 0.1[d]	26.3 ± 0.1[b]	6.5 ± 0.1[f]
F_5 line 101[d]	33.8 ± 0.6[d]	51.4 ± 0.2[c]	26.1 ± 0.1[a]	65.1 ± 0.1 [c]	28.3 ± 0.1[d]	6.5 ± 0.1[f]

[a]Determined by laser diffraction particle size. Values for starch granule volume are the mean of eight replicate samples for parental lines and four replicate samples for F_5 lines. TGW, % starch, and % amylose were determined from two replicate samples. Values followed by same letter are not significantly different ($p < 0.05$). [b]Concentration (%) in total starch. [c]F_5 lines with unimodal distribution. [d]Lines with increased A-type starch granule volume than CDC-Kendall.

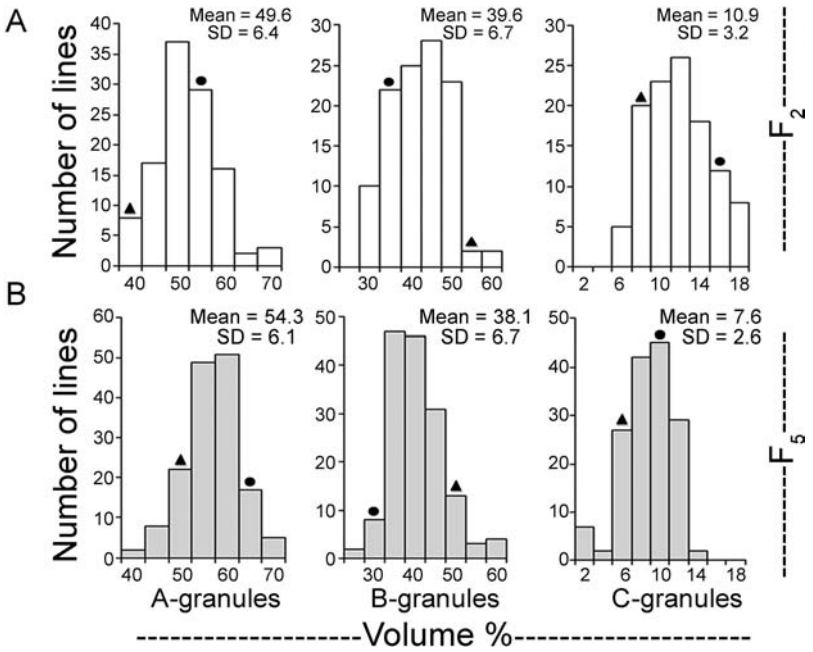

Figure 2. Distribution of starch granules volume fractions in F_2 and F_5 generation from a CDC Kendall × KK-2 cross. A total of 112 F_2 (A) and 154 F_5 (B) lines were analyzed. The volumes (%) of each granule fraction for KK-2 (▲) and CDC Kendall (●) are indicated.

three selected lines (21.4−27.8 g) was also significantly less compared to CDC Kendall (45.9 ± 0.6 g), but slightly higher than KK-2 (18.3 ± 0.1) (Table 3). Overall, the grain characteristics of barley lines with unimodal starch granule size distribution were more similar to KK-2 than CDC Kendall.

In contrast to F_5 lines 116, 144 and 168, lines 75 and 82 with larger A-type granule volumes produced grain with slightly higher TGW and total starch concentration than normal starch (Table 3). Starch granules in these lines showed granule volume distribution profiles similar to CDC Kendall. Amylose concentration in the selected F_5 lines and parent genotypes was not significantly different which indicates starch granule size distribution trait is independent of amylose concentration in CDC Kendall × KK-2 population. However, total starch concentration showed weak but significant ($r^2 = 0.226$, $p < 0.01$) interaction with amylose and thousand grain weight ($r^2 = 0.437$, $p < 0.01$) (Table 4).

Correlation among Granule Distribution Parameters. The distribution curve obtained from starch granule volume size distribution analysis obtained from Malvern mastersizer can also be analyzed by the values of d0.1, which infer 10% of volume distribution is below this value, d0.5, where 50% distribution is above and 50% below, and d0.9, where 90% of the volume distribution is below this value. The average value of d0.1 in CDC Kendall was 7.6 ± 0.2 and in KK-2 was 6.9 ± 0.5. Median value for diameter or d0.5 was 17.5 ± 0.7 in CDC Kendall and 14.8 ± 0.5 in KK-2. Maximum diameter occupied by only 10% of starch granule population shown as d0.9 was 29.9 ± 1.02 in CDC Kendall and 25.49 ± 0.99 in KK-2. Pearson two tail correlation analyses among starch granule population parameters revealed significant influence of A- and B-type starch granule volume on their ratio shown as A/B ($r^2 = 0.9$, $p < 0.01$). Small size C-type starch granules volume (%) affect distribution by significantly affecting d0.1 ($r^2 = 0.8$, $p < 0.01$) and having a minor impact on A/B %

dx.doi.org/10.1021/jf405424x | J. Agric. Food Chem. 2014, 62, 2289−2296

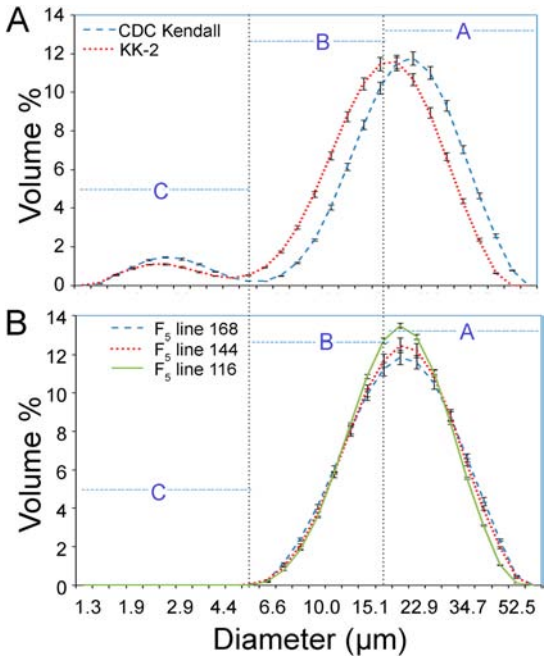

Figure 3. Unimodal starch granule size distribution in CDC Kendall × KK-2 progeny. (A) Starch granule volume distribution in parental lines and (B) three F_5 breeding lines as determined by laser diffraction particle analysis. Each data point represents a mean of three replicates with SD.

($r^2 = 0.14$, $p < 0.05$). A- and B- type starch granules volume (%) significantly ($p < 0.01$) affected d0.5 and d0.9 (Table 4). Among all parameters under study, d0.9 has strongest influence on A/B%. (Table 4). Grain filling represented as TGW is significantly ($r^2 = 0.241$, $p < 0.01$) affected by C-type starch granules volume (Table 4).

DISCUSSION

The analysis presented in this study supports division of barley grain starch granules into three types: large lenticular A-type (>15 μm), small oval B-type (5−15 μm), and very small irregularly shaped C-type (<5 μm) granules. Similar allocation of granule types is present in wheat endosperm starch.[7,8,13] In normal barley starch, the volume distribution of the three types is approximately 7:3:1, but the relative ratios can be genetically altered as shown in this study. The apparent discrepancy between Malvern mastersizer laser light scattering and microscopy analysis (shifting of peak split) could be due to differences in shape based calculation differences. The microscope image analysis observes surface view; hence, there is only one dimension. Mastersizer 2000 used in this study calculates volume distribution based on Mie theory which assumes particles to be spherical and is more realistic than the Fraunhofer approximation used in other laser light scattering based instruments.[30] In microscope image analysis, volume is calculated on the basis of the shape observed for a particle to give more accurate data, but it is based on a very small fraction of starch granule population. It is also very tedious and resource demanding to screen a large number of genotypes or breeding lines.

Initial microscopic screening of 139 barley starches suggested 10 of the 139 genotypes which produced starch with reduced number (<70%) of small starch granules (Table 1). However, repeated studies of these lines confirmed reduced number of small starch granules only in genotype KK-2. This inconsistency in starch granule size for the nine lines was likely caused by environmental effects on starch traits in one experiment. As observed earlier, the heritability for starch granule traits is low to intermediate on single plot basis, but more accurate data can be obtained if starch traits are analyzed over multiple environments.[35]

Various environmental effects on starch deposition and composition are known for wheat[36] and often affect the ratio between A-type and B-type starch granules size, A-type starch granule surface area, granule volumes, and contribution to total starch.[35] Growth conditions affecting wheat grain starch concentration are often related to stresses such as high temperature or drought.[36,37] Heat-sensitive wheat cultivars are known to produce 18−23% fewer B-type starch granules as compared to heat-tolerant wheat cultivars.[38] Similarly, the drought sensitive wheat cultivar Cappelle Desprez accumulates fewer small B-type starch granules when compared to drought tolerant cultivar Plainsman V.[37] Heat stress reduces starch accumulation in barley grain and results in a reduction in number of starch granules, but not granule size.[39] As the A-type, B-type, and C-type starch granules populations are initiated at different time points during grain development, a sudden stress during the later stages of grain filling has a larger effect on the number of small starch granules than large starch granules and may lead to abnormal ratios between large and small starch granules. These indirect effects of environment might be responsible for the inconsistency of starch granule size distribution phenotype of some of the barley genotypes initially selected in this study (Table 1).

Table 4. Correlation Analysis of Starch Granule Related Parameters[a]

	A	B	C	A/B	d0.1	d0.5	d0.9	starch (%)	amylose (%)	TGW (%)
A	1	−0.917[c]	0.061	0.905[c]	0.221[b]	0.896[c]	0.764[c]	0.069	−0.111	0.036
B		1	−0.454[c]	−0.865[c]	0.121[b]	−0.817[c]	−0.698[c]	−0.141	0.069	−0.129
C			1	0.144[b]	0.794[c]	0.046	0.042	0.198	0.076	0.241[c]
A/B				1	0.115[b]	0.956	0.910[c]	0.140	−0.130	0.150
d0.1					1	0.219[c]	0.144[c]	−0.060	−0.090	−0.161[b]
d0.5						1	0.950[c]	0.121	−0.114	0.145
d0.9							1	0.122	−0.125	0.192[b]
starch (%)								1	0.226[c]	0.437[c]
amylose (%)									1	0.129
TGW										1

[a]Data analyzed was derived from 154 F_5 derived lines from CDC Kendall × KK-2 cross. The analyses of A (>15 μm), B (5−15 μm), C (<5 μm) granules volume %, total starch, amylose %, and thousand grain weight (TGW) were determined on duplicate samples. [b]Correlation is significant at $p < 0.05$ level (2-tailed). [c]Correlation is significant at $p < 0.01$ (2-tailed).

Analysis of progeny derived from the cross between KK-2 × CDC Kendall cross showed a large diversity in starch granule size distribution. Indeed, starch granule size phenotypes not seen in the parental genotypes were obtained by the three F_5 lines lacking C-type starch granules. These lines showed more extreme skewing of C-type and A-type starch granule fractions toward the 5−15 μm starch granules population than the parent KK-2, thus giving a near unimodal starch granule size distribution (Table 3, Figure 3). The study suggests KK-2 carries more than one gene affecting primarily the production of C-type starch granules, where a certain gene combination led to lines producing unimodal starch granule size. However, the correlation analysis in this study indicated A/B-type granule volume ratio is not much influenced (r^2 = 0.14, $p < 0.05$) by C-type starch granules volume % (Table 4). Therefore, other combinations of KK-2-derived genes likely caused the higher A-type starch granule size volume observed in five F_5 lines (Table 3). Genetic mapping studies of starch granule size and volume traits in barley have identified quantitative trait loci (QTL) on chromosomes 2H, 4H, and 5H,[20] but the underlying genes are unknown. In wheat, a QTL on chromosome 4B affects the ratio of A- and B-type starch granules[40] and another QTL on 4DS affects starch granule size.[41] In the wild wheat *Aegilops*, a QTL for small starch granules has been identified on chromosome 4S, and the locus is postulated to stimulate starch granule initiation.[42] Whether any of the barley lines developed in this study carry genes corresponding to identified QTLs in wheat or barley needs to be investigated.

The barley lines with unimodal starch granule size distribution showed reduced grain weight and starch concentration as compared to CDC Kendall (Table 3); hence, they are not optimal for production of malting barley grain. However, lines with increased A-type starch granule volumes did not indicate any effect on TGW or starch production and may be better suited for development of improved malting varieties. The F_5 barley lines with variant starch granule size distribution characterized in this study will be valuable to study the relationships between grain yield, starch concentration, and starch granule size distribution. The characterized barley lines will also be valuable to understand the genetics of starch granule size initiation and growth in barley and other triticeae members. It will also enable researchers to alter starch granule size distribution in triticeae cereal members to meet the specific needs of industries.

■ ASSOCIATED CONTENT

Ⓢ Supporting Information

Additional figure showing microscopy images. This material is available free of charge via the Internet at http://pubs.acs.org.

■ AUTHOR INFORMATION

Corresponding Author

*E-mail: ravi.chibbar@usask.ca. Phone: 1-306-966-4969. Fax: 1-306-966-5015.

Notes

The authors declare no competing financial interest.

■ ACKNOWLEDGMENTS

Financial support for this project from Saskatchewan Agricultural Development Fund, Brewing and Malting Barley Research Institute, Winnipeg, Manitoba, Canada, Natural Sciences and Engineering Research Council, Canada, Discovery Grant, Canada Research Chairs program, and Canada Foundation for Innovation is gratefully acknowledged.

■ REFERENCES

(1) Banks, W.; Greenwood, T. C.; Walker, J. T. Studies on the starches of barley genotypes. A comparison of the starches from normal and high-amylose barley. *Starch/Stärke* **1971**, *23*, 12−15.

(2) Morell, M. K.; Kosar-Hashemi, B.; Cmiel, M.; Samuel, M. S.; Chandler, P.; Rahman, S.; Buleon, A.; Batey, I. L.; Li, Z. Barley sex6 mutants lack starch synthase IIa activity and contain a starch with novel properties. *Plant J.* **2003**, *34*, 173−185.

(3) Takeda, Y.; Hizkuri, S.; Takeda, C.; Suzuki, A. Structure of branched molecules of amylose of various origins, and molar fractions of branched and unbranched molecules. *Carbohydr. Res.* **1987**, *165*, 139−145.

(4) Lindeboom, N.; Chang, P. R.; Tyler, R. P. Analytical, biochemical and physicochemical aspects of starch granule size, with emphasis on small granule starches, a review. *Starch/Stärke* **2004**, *56*, 89−99.

(5) Dengate, H.; Meredith, P. Variation in size distribution of starch granules from wheat grain. *J. Cereal Sci.* **1984**, *3*, 83−90.

(6) Stoddard, F. L. Survey of starch particle-size distribution in wheat and related species. *Cereal Chem.* **1999**, *76*, 145−149.

(7) Bechtel, D.; Zayas, I.; Kaleikau, A.; Pomeranz, Y. Size-distribution of wheat starch granules during endosperm development. *Cereal Chem.* **1990**, *67*, 59−63.

(8) Raeker, M. O.; Gaines, C. S.; Finney, P. L.; Donelson, T. Granule size distribution and chemical composition of starches from 12 soft wheat cultivars. *Cereal Chem.* **1998**, *75*, 721−728.

(9) Buttrose, M. S. Submicroscopic development and structure of starch granules in cereal endosperms. *J. Ultrastruct. Res.* **1960**, *4*, 231−257.

(10) Hughes, C. E.; Briarty, L. G. Stereological analysis of the contribution made to mature wheat endosperm by large and small granules. *Starch/Stärke* **1976**, *10*, 336−337.

(11) Buttrose, M. S. Ultrastructure of the developing wheat endosperm. *Aust. J. Biol. Sci.* **1963**, *16*, 305−317.

(12) Parker, M. L. The relationship between A-type and B-type starch granules in the developing granules of wheat. *J. Cereal Sci.* **1985**, *3*, 271−278.

(13) Wei, C.; Zhang, J.; Chen, Y.; Zhou, W.; Xu, B.; Wang, Y.; Chen, J. Physicochemical properties and development of wheat large and small starch granules during endosperm development. *Acta Physiol. Plant.* **2010**, *32*, 905−916.

(14) Evers, A. D.; Blakeney, A. B.; Brien, L. O. Cereal structure and composition. *Aust. J. Agric. Res.* **1999**, *50*, 629−650.

(15) Farmakis, L.; Koliadima, A.; Karaiskakis, G.; Zattoni, A.; Reschiglian, P. Study of the influence of surfactants on the size distribution and mass ratio of wheat starch granules by sedimentation/steric field-flow fractionation. *Food Hydrocolloids* **2008**, *22*, 961−972.

(16) Peng, M.; Gao, M.; Abdel-Aal, E. S. M.; Hucl, P.; Chibbar, R. N. Separation and characterization of A and B type starch granules in wheat endosperm. *Cereal Chem.* **1999**, *76*, 375−379.

(17) Morrison, W. R. Starch lipids and how they relate to starch structure and functionality. *Cereal Foods World* **1995**, *40*, 437−446.

(18) MacGregor, A. W. The effect of barley structure and composition on malt quality. *Proc. 23rd Eur Brew Convention*; Lisbon, Portugal. IRL Press: Oxford, 1991, pp 37−50.

(19) MacGregor, A. W.; Ballance, D. L. Hydrolysis of large and small starch granules from normal and waxy barley cultivars by alpha-amylases from barley malt. *Cereal Chem.* **1980**, *57*, 397−402.

(20) Borém, A.; Mather, D. E.; Rasmusson, D. C.; Fulcher, R. G.; Hayes, P. M. Mapping quantitative trait loci for starch granule traits in barley. *J. Cereal Sci.* **1999**, *29*, 153−160.

(21) Kang, M. Y.; Sugimato, Y.; Kato, I.; Sakamato, S.; Fuwa, H. Some properties of large and small starch granules of barley endosperm. *Agric. Biol. Chem.* **1985**, *49*, 1291−1297.

(22) Brennan, C. S.; Harris, N.; Smith, D.; Shewry, P. R. Structural differences in the mature endosperms of good and poor malting barley cultivars. *J. Cereal Sci.* **1996**, *24*, 171−177.

(23) Psota, V.; Chmelík, J.; Bohaèenko, I.; Hartmann, J. Relationship between starch granule size distribution and selected malting parameters. *J. Am. Soc. Brew. Chem.* **2008**, *66*, 162−166.
(24) Tillet, I. J. L.; Bryce, J. H. The regulation of starch granule size in endosperm of developing barley grains. *Proc. 24th Eur Brew Convention*; Oslo. IRL Press: Oxford, 1993, pp 45−52.
(25) Bohačenko, I.; Chmelík, J.; Psota, V. Determination of the contents of A- and B-starches in barley using low angle laser light scattering. *Czech J. Food Sci.* 2005, *24*, 11−18.
(26) Legge, W. G.; Metcalfe, D. R.; Haber, S.; Harder, D. E.; Noll, J. S.; Tekauz, A.; Thomas, P. L. AC Metcalfe barley. *Can. J. Plant Sci.* **2003**, *83*, 381−384.
(27) Peng, M.; Gao, M.; Båga, M.; Hucl, P.; Chibbar, R. N. Starch-branching enzymes preferentially associated with A-type starch granules in wheat endosperm. *Plant Physiol.* **2000**, *124*, 265−272.
(28) You, S.; Izydorczyk, M. S. Molecular characteristics of barley starches with variable amylose content. *Carbohydr. Polym.* **2002**, *49*, 33−42.
(29) Asare, E. K.; Jaiswal, S.; Maley, J.; Båga, M.; Sammynaiken, R.; Rossnagel, B. G.; Chibbar, R. N. Barley grain constituents, starch composition, and structure affect starch in vitro enzymatic hydrolysis. *J. Agric. Food Chem.* **2011**, *59*, 4743−4754.
(30) *Mastersizer 2000 User Manual*; Malvern Instruments Limited: Worcs, U.K, 2007; Man0384 issue 1.0, March 2007.
(31) AACC International. Method 76-13 Total Starch Assay Procedure (Megazyme Amyloglucosidase/alpha-Amylase Method. *Approved Methods of American Association of Cereal Chemists,* 11th Ed.; AACC International: St. Paul, MN, 2000.
(32) McCleary, B. V.; Salah, V.; Gibson, T. S. Quantitative measurement of total starch in cereal flour and products. *J. Cereal Sci.* **1994**, *20*, 51−58.
(33) Demeke, T.; Hucl, P.; Abdel-Aal, E. S. M.; Båga, M.; Chibbar, R. N. Biochemical characterization of the wheat waxy a protein and its effect on starch properties. *Cereal Chem.* **1999**, *76*, 694−698.
(34) Duncan, D B. Multiple range and multiple F tests. *Biometrics* **1955**, *11*, 1−42.
(35) Oliveira, A. B.; Rasmusson, D. C.; Fulcher, R. G. Genetic aspects of starch granule trait in barley. *Crop Sci.* **1994**, *34*, 1176−1180.
(36) Altenbach, S. B.; Dupont, F. M.; Kothari, K. M.; Chan, R.; Johnson, E. L.; Lieu, D. Temperature, water and fertilizer influence the timing of key events during grain development in a US spring wheat. *J. Cereal Sci.* **2003**, *37*, 9−20.
(37) Fábián, A.; Jäger, K.; Rakszegi, M.; Barnabás, B. Embryo and endosperm development in wheat (*Triticum aestivum* L.) kernels subjected to drought stress. *Plant Cell Rep.* **2011**, *30*, 551−563.
(38) Blumenthal, C.; Wrigley, C. W.; Batey, I. L.; Barlow, E. W. R. The heat-shock response relevant to molecular and structural changes in wheat yield and quality. *Aust. J. Plant Physiol.* **1994**, *21*, 901−909.
(39) Savin, R.; Stone, P. J.; Nicolas, M. E. Responses of grain growth and malting quality of barley to short periods of high temperature in field studies using portable chambers. *Aust. J. Agric. Res.* **1996**, *47*, 465−477.
(40) Batey, I. L.; Hayden, M. J.; Cai, S.; Sharp, P. J.; Cornish, G. B.; Morell, M. K.; Appels, R. Genetic mapping of commercially significant starch characteristics in wheat crosses. *Aust. J. Agric. Res.* **2001**, *52*, 1287−1296.
(41) Igrejas, G.; Faucher, B.; Bertrand, D.; Guibert, D.; Leroy, P.; Branlard, G. Genetic analysis of the size of endosperm starch granules in a mapped segregating wheat population. *J. Cereal Sci.* **2002**, *35*, 103−107.
(42) Howard, T.; Rejab, N. A.; Griffiths, S.; Leigh, F.; Waite, M. L.; Simmonds, J.; Uauy, C.; Trafford, K. Identification of a major QTL controlling the content of B-type starch granules in *Aegilops*. *J. Exp. Bot.* **2011**, *62*, 2217−2228.

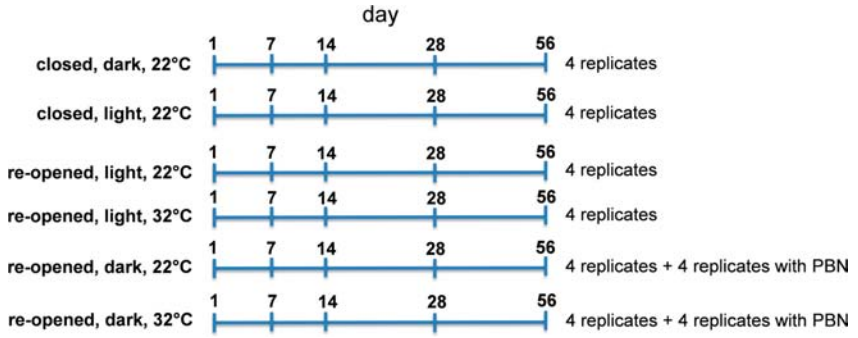

Figure 1. Study design. Soybean oil was stored under different conditions for 56 days. Samples for analyses were drawn on days 1, 7, 14, 28, and 56. Four replicates were performed for each sampling time and condition. For measurement of lipid radicals, four separate replicates were incubated with 20 mM PBN on day 1.

surface of the oil, the degree of saturation of the oil, and the presence of antioxidants, metals, and enzymes have been identified to influence the process of lipid oxidation in vegetable oils.[4,5,11,12] The environmental factors, temperature, light, and oxygen, have also been demonstrated to play a pivotal role in the deterioration of edible oils.[12−14] However, the individual contribution of each environmental factor, under mimicked household conditions, to the oxidative status of soybean oil, one of the most commonly used vegetable oils to supply developing countries with vitamin A,[15] has not been demonstrated so far. The aim of the current study was to identify the major inducer of lipid oxidation in soybean oil stored at household conditions with regard to the oxygen volume, storage temperature, and cold fluorescent light. In addition, several lipid oxidation products were analyzed to identify the most reliable method for assessing the oil quality under retail and household storage conditions.

MATERIALS AND METHODS

Chemicals. Hexanal-d_{12} (98.5 atom % D) was purchased from C/D/N Isotopes Inc., Quebec, Canada. α-Phenyl-*tert*-butylnitrone (PBN) was obtained from Enzo Life Sciences. All-Rac-Tocol was delivered by Matreya LLC, Pleasant Gap, PA, USA. All other chemicals were ordered from Sigma-Aldrich Austria or Carl Roth Germany.

Oil Samples and Study Design. The refined soybean oil was purchased from Henry Lamotte Oils GmbH (Bremen, Germany). Soybean oil was delivered in dark containers and was subjected to peroxide value (POV) analyses, which revealed a mean content of POV of 1.43 ± 0.24 meq O_2/kg. Aliquots of 460 ± 0.1 g were transferred upon arrival into 0.5 L transparent PET bottles, which were kindly provided by Rauch Fruchtsäfte GmbH (Rankweil, Austria). The oil-containing bottles were closed and stored under different conditions for 56 days (Figure 1). To study the individual effects of temperature and cold fluorescent light on the oxidative status of the oil, the bottles were shortly reopened for sampling after 7, 14, 28, and 56 days and were stored in the dark or exposed to cold fluorescent light in a cycle of 12 h light, alternating with 12 h darkness, at 22 ± 1 °C or 32 ± 1 °C. For each oil sample stored under a certain condition, 20 oil-containing bottles were needed to draw samples from four replicates on day 1, 7, 14, 28, and 56. As the light source, lamps (Philips Tornado cool daylight, 1450 lm corresponding to a 103-W incandescent light bulb, Philips, Eindhoven, The Netherlands) were used. These lamps emit cold fluorescent light designed to mimic the 5000 K blackbody spectrum of natural daylight. The distance between the light source and the head of the bottle was set up to be 34 cm, while the distance between the bottles was 15 cm. To study the effect of oxygen on the lipid oxidation of the oil, the bottles, which were kept in the dark at 22 ± 1 °C, remained closed or were shortly reopened for sampling after above-mentioned days. Before sampling, the bottles were mixed to exclude inhomogeneity. The samples were frozen at −80 °C until analyses. To detect the free lipid radicals by electron spin resonance (ESR) spectroscopy, four additional bottles were required due to the inhibiting effect of the spin trap PBN on the lipid oxidation.[16] On day one, PBN was added at a concentration of 20 mM. Bottles were stored in the dark and reopened as described above.

Calculation of Oxygen Volume in Headspace. The headspace of the bottles at the beginning of the study was calculated by the difference of the total volume of the bottle and the sample volume of 460 ± 0.1 g of soybean oil. After each withdrawal of sample, the headspace increased accordingly. As the surrounding air consists of approximately 21% O_2, the amount of O_2 in the headspace was calculated for each sampling day (Table 1).

Table 1. Calculated Oxygen Volume [mL] and Amount [mmol] in the Headspace of PET Bottles after Sampling on Specific Days

sampling day	calculated oxygen volume in headspace [mL]	calculated oxygen amount in headspace at 300 K [mmol]	headspace volume [mL]
0	14.0	0.57	67.0
1	24.8	1.01	118
7	33.7	1.37	161
14	42.6	1.73	203
21	50.3	2.04	240
28	59.2	2.40	283

Quantification of Fatty Acid Composition by GC/FID. The fatty acid composition was quantified according to Lall et al.[17] Briefly, 500 μL of heptadecanoic acid methyl ester (1%) was added as an internal standard to 100 mg oil sample. The mixture was dissolved in 2 mL of toluene. Afterward, a total of 100 mg of pyrogallol was added to protect from oxidative deterioration. To achieve derivatization of fatty acids, 4 mL of sodium methoxide in methanol (0.5 M) was added to the reaction mixture. The mixture was purged with nitrogen for 2 min and heated up to 50 °C for 10 min. After the mixture was cooled down to room temperature, 200 μL of glacial acetic acid, 5 mL of double distilled water, and 5 mL of *n*-hexane were added for extraction. The hexane extracts were dried with Na_2SO_4 and filtrated (0.45 μm) prior to GC/FID analyses. Fatty acid methyl esters (FAMEs) were separated on a ZB-WAX Zebron capillary column (30 m × 0.25 mm i.d., 0.25 μm film thickness, Phenomenex, Aschaffenburg, Germany) using the Shimadzu GC-2010 Plus (Shimadzu, Vienna, Austria) which was equipped with a flame ionization detector (FID). The hexane extracts were injected (1 μL) with a split ratio of 1:20 at 220 °C. Helium was used as a carrier gas with a column flow rate of 3 mL/min. The FID detector needed synthetic air and nitrogen as makeup gas with a flow of 30 mL/min, hydrogen gas with a flow of 40 mL/min, and synthetic air with a flow of 400 mL/min. FAMEs were separated using a temperature gradient starting at 60 °C for 2 min. The temperature was increased at 13 °C/min to 150 °C and then at 2

°C/min to finally yield 240 °C. The fatty acid composition of the study oil under different storage conditions was quantified by external calibration. The recovery was determined to be 115 ± 7.23%. Table 2 depicts the LOD and LOQ of the respective FAMEs.

Table 2. Limit of Detection and Limit of Quantification of Fatty Acid Methyl Esters

FAME	LOD [μg/mL]	LOQ [μg/mL]
methyl palmitate (C16:0)	34.8 ± 0.05	123 ± 0.18
methyl stearate (C18:0)	38.2 ± 0.04	130 ± 0.15
methyl oleate (C18:1)	36.8 ± 0.29	120 ± 0.15
methyl linoleate (C18:2)	36.4 ± 0.05	127 ± 0.18
methyl linolenate (C18:3)	39.2 ± 0.05	127 ± 0.15
methyl arachidate (C20:0)	59.4 ± 0.09	190 ± 0.28

Analyses of Fatty Acid Composition by NMR. ^{1}H NMR spectra were recorded with a Bruker Avance III 500 MHz instrument at 500.32 MHz at ambient temperature. The oil samples (0.2 g) were dissolved in deuterated chloroform. Spectra were acquired from oil samples on day 1 and after storage of 56 days under different conditions. The number of protons was determined by integration of the signals. The aliphatic-to-olefinic ratio was calculated by assigning the signals as described earlier.[18]

Soybean oil: δ (ppm) 0.87 [m, 3 H, CH], 0.96 [t, 3 H, CH], 1.27 [m, 2 H, CH], 1.60 [m, 2 H, CH], 2.02 [m, 2 H, CH], 2.29 [m, 2 H, CH], 2.77 [m, 2 H, CH], 4.13 [dd, 2 H, CH], 4.29 [dd, 2 H, CH], 5.25 [m, 1 H, CH], 5.34 [m, 1 H, CH].

UV-Spectrometric Analyses of Conjugated Dienes. The measurement of conjugated dienes was performed as described previously.[19] Briefly, 0.01 g of oil was dissolved in isooctane, and the UV-absorbance was detected at 233 nm. The concentration of conjugated dienes in oil sample was calculated using the absorption coefficient of linoleic acid hydroperoxide (2.525×10^4 M^{-1} cm^{-1}).

Determination of the Peroxide Value. The POV was determined according to AOCS official method Cd 8-53.[20] Briefly, samples of 5.0 g of soybean oil were dissolved in a mixture of 30 mL of glacial acetic acid and chloroform (3:2, v/v). A total of 0.5 mL of a saturated potassium iodide was added to the oil solution and vortexed for 1 min. After addition of 30 mL of distilled water, iodine was reduced by 0.1 N sodium thiosulfate, and few drops of a starch solution were used to indicate the end point of the titration. The peroxide value was calculated using the following equation:

$$\mathrm{POV\ (meq/kg)} = ((\mathrm{Va} - \mathrm{Vb})N \times 1000)/W$$

where Va is the volume (mL) of sodium thiosulfate needed for the reduction of iodine in the oil sample, Vb is the volume (mL) of sodium thiosulfate needed for the reduction of potential iodine in the blank sample, N is the normality of the sodium thiosulfate solution, and W is the weight of the oil sample (g). The POV was expressed as percent value, setting the results of the first day to zero.

ESR Measurements of Lipid Radicals. Oil samples (500 μL) were thawed and transferred into ESR flat cell (ER 160 FC-Q). The ESR flat cell was positioned in a rectangular TE102 microwave cavity to acquire ESR spectra at room temperature by means of a Bruker ESP300 operating at 9 GHz with 100 kHz modulation frequency. Spectra were recorded every 84 s, averaging every 5 consecutive spectra. ESR measurements were performed by applying the following settings: center field, 3490.6 G; sweep width, 70 G; sweep time, 83.9 s; modulation amplitude, 1.32 G; microwave power, 20 mW; conversion time, 81.9 ms; time constant, 81.9 ms; resolution 1024 points. The receiver gain was adjusted for each sample and considered in the calculations. The first derivative of the microwave absorption was double-integrated to calculate the area under the curve. ESR spectra were simulated to obtain the hyperfine coupling constants with the public EPR software tools from the National Institute of Environmental Health Sciences. The hyperfine coupling constants were calculated to be 14.81 and 2.00 G, which are characteristic for the coupling of the free electron with adjacent nitrogen and hydrogen nucleus. However, due to line broadening effects of the viscous oil samples, the hydrogen splitting could not be observed, resulting in a triplet rather than the expected triplet of doublets. The spin trap, PBN, was chosen to predominantly detect carbon-centered radicals.[16]

HS-GC/MS Analyses of Hexanal. The sample preparation was performed with slight modifications according to Giuffrida et al.[21] Headspace vials (20 mL) for Combi Pal were filled with 2.5 g of sample oil and 2.72 mL of water/methanol (3:1). The sample mixture was spiked with 4 μg/mL hexanal-d_{12}. The headspace vials were sealed with magnetic screw caps silicone/PTFE (La-Pha-Pack, Langerwehe, Germany) and preheated at 70 °C with an agitator speed set to 750 rpm for 15 min on a CTC Combi Pal (CTC Analytics AG, Zwingen, Switzerland). After incubation, 1000 μL of headspace was injected by a 90 °C preheated gastight syringe on a ZB-Wax Zebron capillary column (30 m × 0.25 mm i.d., 0.25 μm film thickness) using a split ratio of 1:5 at 250 °C. GC/MS analysis was performed on a Shimadzu GCMS-QP 2010 Ultra (Shimadzu, Vienna, Austria) using helium as a carrier gas at a column flow rate of 1.31 mL/min. The initial oven temperature of 35 °C was held for 2 min before it was increased at a rate of 15 °C/min to 65 °C. Then, the oven was heated up to 80 °C at 2 °C/min and finally yielded 230 °C at a rate of 30 °C/min to hold the temperature for 5 min. The temperature of the ion source was set to 200 °C, and the acquisition parameters applied were full scan mode, scan range 40−600 m/z, scan speed 3333 u/s, SIM mode for 56 m/z and 72 m/z (specific for hexanal) and 64 m/z and 80 m/z (specific for hexanal-d_{12}). Labeled and unlabeled hexanal were identified by comparing the mass spectra with the NIST 11 mass spectral library and retention times with reference standards. Hexanal-d_{12} eluted at 5.13 min, whereas hexanal eluted at 5.21 min. Stable isotope dilution analysis was performed using the fragment ions 80 m/z (hexanal-d_{12}) and 72 m/z (hexanal), as described recently.[22] The response factor was calculated to be 1.09 ± 0.08. The LOD and LOQ of hexanal were determined to be 0.03 ± 0.02 μg/mL and 0.10 ± 0.00 μg/mL, respectively.

Quantification of Tocopherols. The analyses of tocopherols in soybean oil samples were performed with slight modifications according to Gliszczynska-Swiglo and Sikorska.[23] A total of 0.05 g of soybean oil was dissolved in 1 mL of 2-propanol, and 5 μg/mL tocol was added as internal standard. After syringe filtration with a nylon filter (0.2 μm), 5 μL was injected into a Dionex Ultimate 3000 LC system (Thermo Fisher Scientific, Vienna, Austria) equipped with a diode array detector. UV chromatograms were recorded at 295 nm. The tocopherols were separated at 25 °C on a PFP Kinetex C18 column (100 × 2.10 mm, 1.7 μm, Phenomenex, Aschaffenburg, Germany) with a flow rate of 0.5 mL/min. The mobile phase consisted of bidestilled water and methanol and with an initial ratio of 25:75 (v/v) which increased to 100% methanol within 10 min. α-, β-, γ-, and δ-Tocopherols were eluted at 6.71, 6.10, 6.24, and 5.59 min, respectively. Total tocopherols were calculated by the sum of tocopherol isomers. Each tocopherol isomer was quantified by external calibration. The recovery of total tocopherols was 94 ± 12.1%. The LOD for α-tocopherol, γ-tocopherol, and δ-tocopherol was 0.24 ± 0.02 μg/mL, 0.04 ± 0.01 μg/mL, and 0.02 ± 0.01 μg/mL, respectively.

Statistical Data Assessment. Statistical analyses were conducted with SigmaPlot 11 (Systat software Inc., Chicago, Illinois). All experiments consisted of four bottles and two technical replicates. All data were subjected to the Nalimov outlier test and are presented as mean ± standard deviation. Normal distribution of the data was assessed by the Shapiro-Wilk test. ANOVA was performed to analyze statistically significant differences ($p < 0.05$) between day 1 and the other sampling days. The Dunnett's post hoc test and in case of heterogeneity of variance the Dunn's post hoc test were applied to identify the differences, which are indicated with an asterisk in the graphs. To analyze statistically significant differences between oils stored under different conditions, the area under the curve (AUC) was determined after data were normalized by the value obtained on day 1. Statistical significant differences ($p < 0.05$) between the AUCs were calculated by means of the Student's t test. In the case of heterogeneity of variance, the Mann−Whitney−Wilcoxon test was applied.

Correlation coefficients were determined to detect relationships between two variables ($p < 0.05$). The Pearson product-moment correlation coefficient was calculated for normally distributed data, whereas the Spearman's rank correlation coefficient was calculated if the data did not show a normal distribution.

RESULTS AND DISCUSSION

The purpose of the current study was to study the oxidative stability of soybean oil stored in transparent PET bottles under household conditions. Soybean oil, which belongs to the four most commonly consumed vegetable oils worldwide, with a production of 35.7 million tonnes in the year 2008/09,[24] is usually sold and stored in transparent PET bottles at ambient temperatures of 22−32 °C. Withdrawal of oil by the consumer leads to an increased headspace and oxygen availability. We aimed to identify the contribution of each of these environmental factors, such as oxygen, temperature, and cold fluorescent light under household conditions on the oxidative status in refined soybean oil. Although literature data demonstrate that each of these environmental factors is attributed to the promotion of oxidative deterioration in vegetable oils,[12−14] it has not been demonstrated so far which of these environmental factors chiefly contributes to lipid oxidation in refined soybean oil stored at household conditions.

Effects of Increasing Headspace Volume at Atmospheric Pressure on the Formation of Hydroperoxides in Soybean Oil. To study the impact of oxygen on the deterioration of soybean oil, we determined the POV in oil stored under constant and increasing oxygen volume at 22 °C and atmospheric pressure for one month. To mimic consumer handling of the oil bottles, the closed PET bottles filled with soybean oil were shortly reopened for sample drawings. The short reopening and sampling resulted in an increased headspace volume and supply with atmospheric oxygen (Table 1). As expected, increasing oxygen volume caused a rise of the POV by 91.0 ± 1.09%, whereas constant oxygen volume led only to an increase of the POV by 46.6 ± 4.65% (Table 3). Thus, the increasing headspace volume at atmospheric pressure had a significant impact on the oxidative stability of soybean oil. However, the air-exposed area-to-mass ratios have also been shown to play an essential role in lipid oxidation of olive oil.[25] When different masses of olive oil were stored in brown glass vials with 20 mm i.d. at 38 °C in the dark in the presence of air-derived oxygen, a high area-to-mass ratio with 1.25, 2.5, and 3.5 g olive oil resulted in a POV of at least 50 meq O_2/kg after 700 h of storage, whereas a low area-to-mass ratio with 7 g olive oil did not lead to a POV of greater than 30 meq O_2/kg after 1400 h of storage. The results of the current study are also in accordance with findings reported by Chung et al.,[13] showing that 5 g of soybean oil exposed to light at 55 °C for 24 h absorbed 54.6 μmol of oxygen.[13] We, therefore, conclude that enhancing the headspace oxygen volume by reopening the bottles, as a common household practice, promotes oxidative rancidity of the oil. The impact of increasing headspace oxygen introduced by intermittent bottle-opening was obvious after 28 days of storage, as demonstrated by an accelerated POV increase compared to nonopened bottles. Consecutive experiments included the more severe condition of intermittent bottle openings for 56 days, which is also of greater practical relevance for consumer handling.

Table 3. Increase of POV [%] in Soybean Oil Stored in Permanently Closed Bottles under Constant O_2 Volume or in Reopened Bottles under Increasing O_2 Volume at 22°C for 28 Days[a]

	increase of POV [%]	
time [days]	constant O_2 volume (permanently closed)	increasing O_2 volume in headspace (reopened)
1	0	0
7	36.6 ± 13.0[a]	50.1 ± 16.5[a]
14	29.0 ± 6.35[a]	63.3 ± 1.20[b]
28	46.6 ± 4.65[a]	91.0 ± 1.09[b]

[a]Data are expressed as mean ± SD ($n = 4$). All POVs were normalized to the POV on day 1. Different letters in a row indicate statistically significant difference between the POV in oil stored under constant and variable O_2 volume, as calculated by the Student's t test.

Effects of Temperature and Cold Fluorescent Light on the Formation of Primary and Secondary Lipid Oxidation Products in Soybean Oil. For studying the effect of temperature on the lipid oxidation, a storage temperature of 22 and 32 °C was chosen to imitate widely common room temperatures. To investigate the influence of cold fluorescent light, bulbs were chosen that emit electromagnetic irradiation in the cold fluorescent range thereby mimicking the storage condition in a typical household.

Autoxidation of vegetable oils rich in polyunsaturated fatty acids is known to lead to the formation of conjugated dienes, which strongly absorb UV irradiation at around 233 nm.[26] In this study, the closed PET bottles, which were filled with soybean oil and stored in the dark or exposed to cold fluorescent light, were reopened for sampling throughout the study at 22 and 32 °C. Figure 2A shows that the formation of conjugated dienes on day 1 and 56 remained unchanged in the study oil stored in the dark, independent of the storage temperature. The minimal decrease in the formation of conjugated dienes on day 7 and 14 might be explained by a higher decomposition than production rate of conjugated dienes. By exposing the soybean oil to cold fluorescent light for 56 days, the concentration of conjugated dienes increased from 19.5 ± 3.50 μM to 26.2 ± 0.15 μM, and to 29.0 ± 1.14 μM at 22 and 32 °C, respectively (Figure 2B). In the presence of cold fluorescent light, a statistically significant difference could be observed between the oils stored at the two distinct temperatures with regard to the content of conjugated dienes. At these household-mimicking conditions, cold fluorescent light was demonstrated to play a pivotal role in the oxidation of soybean oil in the presence of air-derived oxygen at atmospheric pressure, whereas temperature in the range of 22 and 32 °C did not influence the oxidation process in the absence of cold fluorescent light. Thus, the rate of photo-oxidation dominates the rate of autoxidation at household conditions. The light-induced lipid oxidation might be promoted by photosensitizers, such as chlorophylls. Natural pigments were demonstrated to be responsible for photo-oxidative deterioration of extra virgin olive oil stored at 27 ± 1 °C in the presence of cold fluorescent light for up to 72 h.[27] A POV of 153 meq/kg was obtained after a 36 h storage of extra virgin olive oil, while a POV of less than 13 meq/kg was measured after 72 h of storage, when chlorophyll and other minor components had been removed during the stripping process. Khatoon and Krishna[28] reported elevated concentrations of conjugated dienes in refined safflower oil which was subjected to static heating at 180 °C for 8 h in an open pan. Because of the high temperature and surface area, the

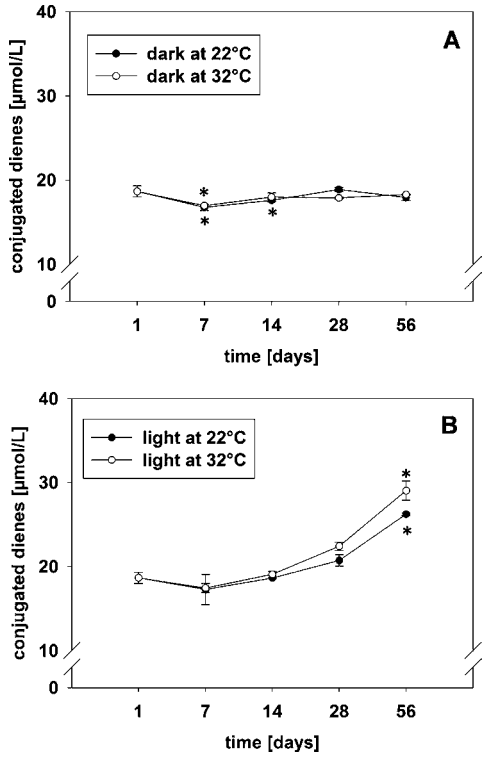

Figure 2. Changes of the formation of conjugated dienes in soybean oil stored in the absence (A) or in the presence of cold fluorescent light (B) at 22 or 32 °C in reopened bottles during storage for 56 days. Data are expressed as mean ± SD (n = 4). The concentrations of conjugated dienes on days 7, 14, 28, and 56 were normalized to the concentration of conjugated dienes on day 1. Asterisks indicate statistically significant differences compared to day 1 ($p < 0.05$).

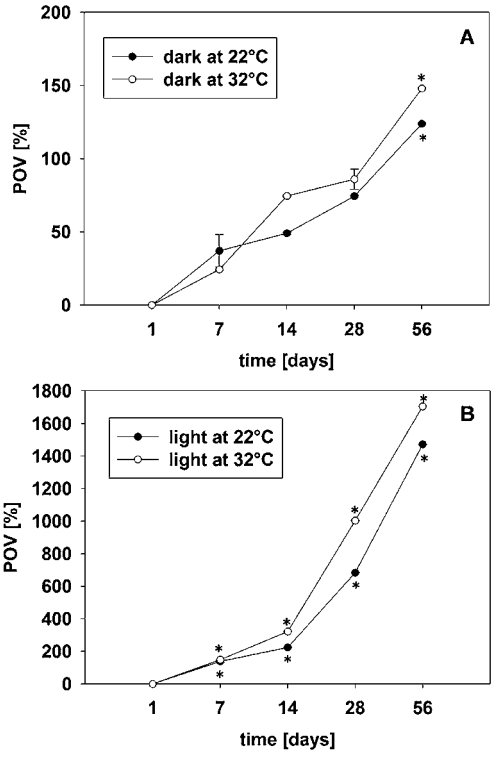

Figure 3. Changes of POVs in soybean oil stored in the absence (A) or in the presence of cold fluorescent light (B) at 22 or 32 °C in reopened bottles during storage for 56 days. Data are expressed as mean ± SD (n = 4). POVs were normalized to the individual POV on day 1. Asterisks indicate statistically significant differences compared to day 1 ($p < 0.05$).

concentrations of conjugated dienes were increased from approximately 0.5 g/L to 4.1 g/L. However, studies that investigate the effects of temperature and light at household conditions on the generation of conjugated dienes are lacking.

Because of the suitability of the POV and its wide acceptance,[26] we also analyzed the amount of peroxides formed during storage of soybean oil in reopened PET bottles at the two distinct temperatures in the presence or absence of cold fluorescent light to mimic household conditions. As expected, the POV in the soybean oil was enhanced after storage for 56 days, independent of light exposure and the temperature applied (Figure 3). Because the POV results indicated a significant increase of the lipid oxidation in oils stored in the dark, which was not demonstrated by quantitative data for conjugated dienes, the suitability of the POV analyses for assessing the early stages of lipid oxidation in vegetable oils can be confirmed. Similar to the results obtained for concentrations of conjugated dienes, exposure of the oil to cold fluorescent light had a pronounced impact on the POV. While the POV in the oil stored in the dark for 56 days increased by 124 ± 0.62% and 148 ± 0.70% at 22 and 32 °C, respectively, the POV in the oil exposed to cold fluorescent light rose by 1473 ± 1.79% and 1706 ± 0.79%, respectively. A similar effect of light on the POV in soybean oil stored in open glass bottles at 30 °C for 30 days was demonstrated by Naz et al.[29] In their study, the POV in soybean oil stored in the dark was significantly ($p < 0.01$) lower than that of oil samples exposed to daylight. However, open glass bottles filled with oil do not mimic typical household conditions. Chung et al.[13] could demonstrate a significant impact of light exposure of a 200-W tungsten lamp to soybean oil stored at 55 °C for 24 h in 45 mL serum bottles sealed with septa and caps, thereby also not mimicking household conditions. While the POV in the oil stored in the dark only reached 1.80 meq O_2/kg, the presence of light caused a marked increase of the POV to yield 12.4 meq O_2/kg. However, a traditional household incandescent light bulb is characterized by a consumption of 40−100 W, which has been considered in the current study.

Besides mimicking the household conditions by exposing oil to fluorescent light, the ambient temperatures of 22 and 32 °C were chosen to study the effects of household temperatures on the oxidative stability of soybean oil. No difference with regard to the POV was observed between the two distinct temperatures of 22 and 32 °C when the study oil was stored in the dark (Figure 3A). In contrast, a statistical significant difference was obtained when the oil was exposed to cold fluorescent light in a cycle of 12 h light alternating with 12 h darkness (Figure 3B). Abramovic and Abram[30] also investigated the effect of two different temperatures on the POV of camelina oil stored in glass bottles in the dark. It could be shown that the POV of the oil stored in the dark at room temperature for 30 days increased from 2.38 meq O_2/kg to 8.12 meq O_2/kg, while the POV of the oil stored in the dark at 8 °C for 30 days remained almost constant. As we could not determine any difference with regard to the concentration of conjugated dienes and the POV between the soybean oils stored in the dark at 22 and 32 °C, this prompted us to reinvestigate the oxidative stability of the soybean oil kept in dark at the two distinct temperatures by means of ESR, a method with higher sensitivity.[16]

dx.doi.org/10.1021/jf405736j | J. Agric. Food Chem. 2014, 62, 2297−2305

ESR is regarded as a more sensitive method to study early lipid oxidation reactions, since free radicals were detected in canola oil, sunflower oil, and fish oil stored at 40 °C in the dark in a desiccator with P_2O_5 before POV increased.[16] The current study investigated, for the first time, the effect of retail and household storage conditions of soybean oil in the dark at 22 and 32 °C on the formation of lipid radicals (Figure 4A). After storage for 28 days, the formation of lipid radicals was significantly increased at both temperatures. Albeit not detectable by iodometric measurements, applying ESR spectroscopy revealed a more pronounced increase of the formation of lipid radicals in the study oil stored in the dark at 32 °C than in the oil stored at 22 °C. Thus, ESR spin trapping technique proved to be a suitable method to detect early stages of lipid oxidation in vegetable oils. However, the signal intensity of the PBN adducts was shown to correlate well with the POV in soybean oil stored in the dark at 32 °C for 56 days with a correlation coefficient of 0.938 ($p < 0.05$) (Figure 4B), implying that ESR spectroscopy might be a reliable method to monitor the oxidative status in vegetable oils. Even a moderate increase of temperature from 22 to 32 °C induced the formation of lipid oxidation in soybean oil, independent of the exposure to light. However, if the impact of light on lipid oxidation is to be studied by ESR spectroscopy, a nonlight sensitive spin trap, such as 5,5-dimethyl-1-pyrroline-*N*-oxide (DMPO), has to be used.

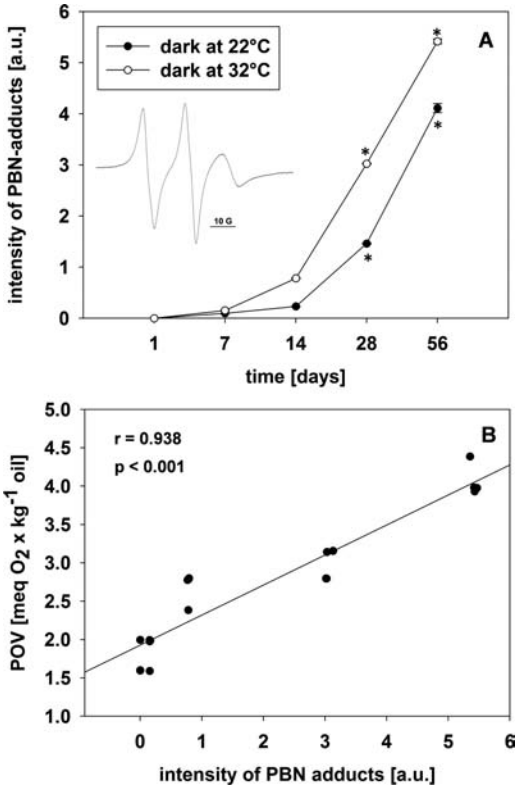

Figure 4. Changes of the formation of lipid radicals in soybean oil stored in the dark at 22 or 32 °C in reopened bottles during storage for 56 days (A). Correlation between POV and the intensity of the PBN adducts in soybean oil stored in the dark at 32 °C in reopened bottles for 56 days with a coefficient of 0.938, $p < 0.05$ (B). Data are expressed as mean ± SD ($n = 4$). All POV were normalized to the POV on day 1. Asterisks indicate statistically significant differences compared to day 1 ($p < 0.05$).

In this study, the effect of temperature and cold fluorescent light was also studied by quantifying the fatty acid composition of soybean oil stored in bottles with increasing headspace for 56 days. Although no significant changes of the fatty acid profile of the soybean oil were expected due to the moderate household storage and handling conditions, the fatty acid profile was analyzed to characterize the soybean oil. The predominant fatty acids in soybean oil, C16:0, C18:0, C18:1, C18:2, C18:3, and C20:0, were quantified on day 1 and 56 (Table 4). Linoleic acid was identified as the dominant fatty acid in soybean oil, reaching a concentration of 499 ± 29.6 mg/mL. The fatty acid profile obtained at day 1 was in accordance with results obtained by Ivanov et al.[31] However, our results did not indicate any significant changes of the fatty acid concentrations in soybean oil after storage for two months independent of the storage conditions chosen. Though a decrease of unsaturated fatty acids and a corresponding increase of saturated fatty acids might be conceivable in oil undergoing lipid oxidation, the degree of saturation remained unchanged. There is no comparable study that investigated the effects of light, temperature, and oxygen at household conditions on the fatty acid profile of soybean oil. Crapiste et al.[32] observed a marked decrease of unsaturated fatty acids in sunflower oil after storage for 55 days at a higher temperature of 67 °C. It could be shown that the oleic acid to linoleic acid ratio increased from 0.334 to 0.568 in pressed sunflower oil. However, the results presented here indicate that the fatty acid composition analyzed by GCMS might not be a reliable and sensitive method for assessing early stages of lipid oxidation of vegetable oils during household storage conditions.

Studying the changes in the proton absorption of the fatty acids in the differently stored soybean oil by NMR confirmed the GCMS results. The aliphatic-to-olefinic ratio of the oil was 10.6 ± 0.05 and 10.5 ± 0.06 on day 1 and 56, respectively, independent of the storage condition. There is no literature available showing the impact of temperature, light, and oxygen at household conditions on the aliphatic-to-olefinic ratio of

Table 4. Fatty Acid Composition in Soybean Oil Analyzed by GC/FID on Day 1 and 56 after Different Storage Conditions[a]

		dark at 22 °C		dark at 32 °C		light at 22 °C		light at 32 °C	
fatty acid	day 1 [mg/mL]	day 56 [mg/mL]	change [%]	day 56 [mg/mL]	change [%]	day 56 [mg/mL]	change [%]	day 56 [mg/mL]	change [%]
C16:0	101 ± 5.79	102 ± 4.90	+0.99	96.0 ± 2.06	−4.95	101 ± 5.44	0.00	101 ± 11.9	0.00
C18:0	31.5 ± 1.82	31.9 ± 1.57	+1.27	30.1 ± 0.59	−4.44	31.6 ± 1.72	+0.32	31.7 ± 3.70	+0.63
C18:1	236 ± 13.9	237 ± 11.0	+0.42	221 ± 4.29	−6.36	233 ± 11.8	−1.27	234 ± 27.9	−0.85
C18:2	499 ± 29.6	506 ± 23.7	+1.40	472 ± 9.90	−5.41	495 ± 25.2	−0.80	497 ± 59.3	−0.40
C18:3	49.3 ± 2.89	50.6 ± 2.38	+2.64	47.2 ± 1.01	−4.26	49.2 ± 2.53	−0.20	49.4 ± 5.94	+0.20
C20:0	4.71 ± 0.28	4.71 ± 0.24	0.00	4.41 ± 0.02	−6.37	4.70 ± 0.25	+0.21	4.65 ± 0.53	−1.27

[a]Data are expressed as mean ± SD ($n = 4$). No statistical differences were obtained.

vegetable oil. Wanasundara et al.[33] showed that the aliphatic-to-olefinic ratio of soybean oil stored at nonhousehold conditions in open flasks at high temperature of 65 °C in the dark increased from approximately 10 on day 1 to approximately 13 on day 30. NMR spectroscopy is commonly used to characterize the degree of saturation in oils treated at high temperatures.[18,34] However, the application of NMR to evaluate the oxidative status in vegetable oil stored under household conditions might not lead to noteworthy results.

Next to the primary reaction products of lipid oxidation, the decomposition products of fatty acid hydroperoxides are commonly used markers for assessing lipid oxidation in vegetable oils.[35] One of the most reliably used biomarkers for evaluating the oxidative status is hexanal. Hexanal is known to be a decomposition product from linoleic acid, which is the predominant fatty acid of soybean oil.[36] In the current study, we also determined the impact of temperature and light at household conditions on the formation of hexanal. As a result, hexanal concentration remained constant upon the storage conditions applied (Figure 5). This suggests a singlet oxygen-

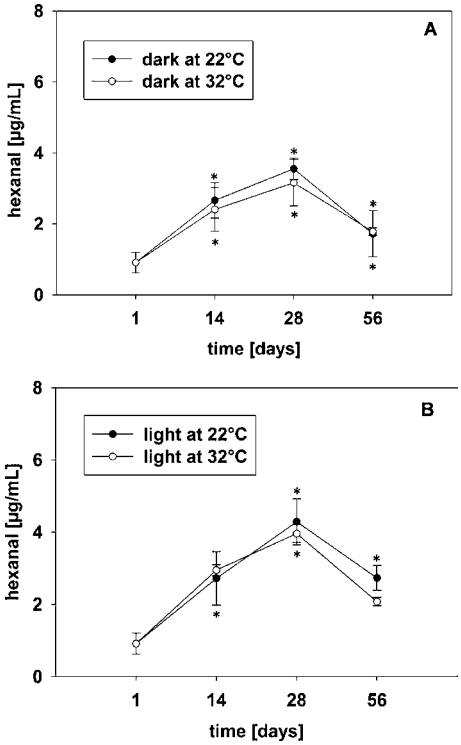

Figure 5. Changes of hexanal formation in soybean oil during storage for 56 days in reopened bottles in the absence (A) or presence (B) of cold fluorescent light at 22 and 32 °C. Data are expressed as mean ± SD (n = 4). Asterisks indicate statistically significant differences compared to day 1 (p < 0.05).

derived peroxidation of linoleic acid by a nonpropagating two-electron "ene" mechanism without the initiation of lipid peroxidation chain reactions.[37,38] Singlet oxygen has no impact on the stability of peroxides, whereas metals, which initiate radical chain reactions, lower the stability of peroxides.[5] However, there is a lack of studies investigating the effect of temperature and light at household conditions on the formation of hexanal in soybean oil. Sanches-Silva et al.[39] investigated the hexanal content in potato crisps stored in the dark and in the presence of natural light. It could be shown that the hexanal content did not change in potato crisps stored in the dark, whereas the storage in the presence of natural light led to an approximately 10-fold significant rise of the hexanal content. This high amount of hexanal might be explained by the frying conditions of the potato crisps in olive oil but also making the effect of light more prominent.

The peak concentration of hexanal analyzed on day 28 in the current study indicates higher decomposition rate than formation rate of hexanal, leading to a decrease of hexanal concentration after storage of the oil for 1 month accompanied by an increase of POVs.

Effects of Temperature and Cold Fluorescent Light on the Stability of Tocopherols in Soybean Oil. Tocopherols have been shown to exert antioxidative as well as pro-oxidative effects in different vegetable oils, by donating hydrogen to the lipid radical and by being converted to a more stabilized radical. The stabilized radical, if not regenerated by antioxidants, contributes to the propagation of lipid radicals.[40,41] Thus, the total tocopherol content of a vegetable oil is crucial for its oxidative stability. In the current study, soybean oil contained 489 ± 34.6 ppm total tocopherols, which is less than the tocopherol content of 1546 ppm found in refined soybean oil, as described elsewhere.[42] The lower amount of tocopherols detected in the beginning of the current study might be due to different processing steps during production of the soybean oil. Tocopherols also act as a marker for reflecting the oxidative deterioration of the oil. Many studies have shown an association between the decrease of the content of tocopherols of a vegetable oil and the progress of the lipid oxidation.[43−45] In this study, a decrease of all tocopherol isomers in oil stored for 56 days, independent of the storage conditions, was demonstrated (Table 5). The most pronounced loss of α-, β-,

Table 5. Percent Decrease of Tocopherol Isomers [%] in Soybean Oil Stored under Different Conditions for up to 56 Days[a]

			decrease [%]	
tocopherol isomer			day 28	day 56
α	dark	22 °C	34.3 ± 8.49[a]	48.9 ± 3.55*[a]
		32 °C	37.4 ± 0.67[a]	49.3 ± 0.33*[a]
	light	22 °C	39.6 ± 4.27[a]	58.0 ± 1.50*[b]
		32 °C	42.9 ± 4.52[a]	60.2 ± 2.40*[b]
γ	dark	22 °C	40.7 ± 2.71[a]	69.4 ± 2.10*[a]
		32 °C	40.2 ± 1.62[a]	62.1 ± 6.38*[a]
	light	22 °C	43.6 ± 14.4[a]	77.3 ± 3.52*[c]
		32 °C	41.2 ± 6.89[a]	85.4 ± 4.11*[d]
δ	dark	22 °C	−1.36 ± 12.7[a]	15.8 ± 6.85[abc]
		32 °C	1.55 ± 0.56*[a]	10.2 ± 0.91*[b]
	light	22 °C	8.50 ± 10.1[a]	23.4 ± 0.67*[abc]
		32 °C	7.51 ± 8.11[a]	24.6 ± 0.82*[c]

[a]Data are expressed as mean ± SD (n = 4). Distinct letters indicate statistically significant difference within the same column and isomeric compound (p < 0.05). The asterisk indicates statistically significant difference with regard to day 1 (p < 0.05).

and γ-tocopherol by 60.2 ± 2.40%, 85.4 ± 4.11%, and 24.6 ± 0.82%, respectively, was obtained in oil samples exposed to light and stored at 32 °C for 56 days. This high loss of total tocopherols correlated significantly with an increase in the POV (r = −0.900; p < 0.05). Thus, monitoring the decrease of tocopherols might be a reliable marker to evaluate lipid oxidation in vegetable oils. Others reported dramatic loss of α-,

β-, and γ-tocopherol by 100%, 47.1%, and 31.2%, respectively, in soybean oil heat-treated at 95 °C for 1 day.[45] In agreement with the POVs from our soybean oil study, a more pronounced decrease ($p < 0.05$) of the most abundant tocopherol isomer (128 μg/mL γ-tocopherol on day 1) was observed in the study oil exposed to cold fluorescent light (77.3 ± 3.52% at 22 °C and 85.4 ± 4.11% at 32 °C) compared to the oil stored in the dark (69.4 ± 2.10% at 22 °C and 62.1 ± 6.38% at 32 °C) (Table 5), indicating that cold fluorescent light has the most pronounced impact on lipid oxidation and tocopherol stability at the conditions chosen in this study. Khan et al.[46] also showed that the photooxidative effect of chlorophyll dominated the antioxidative effect of tocopherols as evident by a significant higher POV of 28.3 ± 0.11 meq/kg of nonstripped borage oil compared to the POV of 11.6 ± 0.03 meq/kg of stripped borage oil after storage at 27 ± 1 °C in the presence of cold fluorescent light for 48 h.

Taken together, we could demonstrate that increasing (i) the oxygen containing headspace volume from 67 to 283 mL, (ii) the ambient temperature from 22 to 32 °C, and (iii) adding the exposure to cold fluorescent light contributes to the oxidative status of soybean oil in transparent PET bottles, albeit the extent of the contribution differs. The most pronounced effect with respect to promoting lipid oxidation in soybean oil stored in transparent bottles at household conditions with increasing oxygen volumes was attributed to cold fluorescent light. The higher ambient temperature at 32 °C as well as the increasing headspace oxygen volume up to 283 mL throughout the study, mimicking consumer handling, showed only little effects on the oxidative deterioration of the study oil. For studying the lipid oxidation of vegetable oils stored in the dark, the detection of lipid radicals by ESR spin trapping technique using PBN as a spin-trap proved to be a suitable method to detect early stages of lipid oxidation in vegetable oils. Cold fluorescent light has been proven to be the predominant inducer of oxidative deterioration of soybean oil stored under household conditions, suggesting the use of nontransparent bottles accompanied by consumer education.

AUTHOR INFORMATION

Corresponding Author

*Address: Department of Nutritional and Physiological Chemistry, University of Vienna, Althanstraße 14, 1090 Vienna, Austria. Tel: +43 1 4277 70601. E-mail: veronika.somoza@univie.ac.at. Fax: +43 1 4277 9706.

Funding

The study was sponsored by Sight and Life.

Notes

The authors declare the following competing financial interest(s): The study was sponsored by Sight and Life. The author Klaus Kraemer is the head of the think tank, Sight and Life. Georg Steiger is the head of NIP Product and Technology Development at DSM.

ACKNOWLEDGMENTS

The authors thank Markus Galanski from the Department of Inorganic Chemistry, University of Vienna, Austria, for recording the NMR spectra. The study was sponsored by Sight and Life.

ABBREVIATIONS

FAME, fatty acid methyl ester; HS, headspace; PBN, α-phenyl-*tert*-butylnitrone; PET, polyethylene terephthalate; POV, peroxide value

REFERENCES

(1) Wegelin, M.; Canonica, S.; Alder, A. C.; Marazuela, D.; Suter, M. J. F.; Bucheli, T. D.; Haefliger, O. P.; Zenobi, R.; McGuigan, K. G.; Kelly, M. T.; Ibrahim, P.; Larroque, M. Does sunlight change the material and content of polyethylene terephthalate (PET) bottles? *J. Water Supply: Res. Technol.—AQUA* **2001**, *50*, 125−133.

(2) Velasco, J.; Andersen, M. L.; Skibsted, L. H. Evaluation of oxidative stability of vegetable oils by monitoring the tendency to radical formation. A comparison of electron spin resonance spectroscopy with the Rancimat method and differential scanning calorimetry. *Food Chem.* **2004**, *85*, 623−632.

(3) Hiatt, R.; Mill, T.; Irwin, K. C.; Mayo, T. R.; Gould, C. W.; Castleman, J. K. Homolytic decomposition of hydroperoxides. *J. Org. Chem.* **1968**, *33*, 1416−1441.

(4) Frankel, E. N. Lipid Oxidation - Mechanisms, Products and Biological Significance. *J. Am. Oil Chem. Soc.* **1984**, *61*, 1908−1917.

(5) Choe, E.; Min, D. B. Mechanisms and factors for edible oil oxidation. *Compr. Rev. Food Sci. Food Safety* **2006**, *5*, 169−186.

(6) Vaisey-Genser, M.; Malcomson, L. J.; Przybylski, R.; Eskin, N. A. M. Consumer acceptance of stored canola oils in canola. 12th Project report research on canola, seed, oil meal. *Canada Canola Council, Canada* **1999**, 189−202.

(7) Steenson, D. F.; Lee, J. H.; Min, D. B. Solid phase microextraction of volatile soybean oil and corn oil compounds. *J. Food Sci.* **2002**, *67*, 71−76.

(8) Tanouti, K.; Serghini-Caid, H.; Sindic, M.; Wathelet, J.; Bouseta, A.; Elamrani, A. Volatile Compounds, Profiles of Virgin Olive Oils Produced In the Eastern Morocco: Oxidative Stability and Sensory Defects. *J. Food Res.* **2012**, *1*, 194−206.

(9) Kanner, J. Dietary advanced lipid oxidation endproducts are risk factors to human health. *Mol. Nutr. Food Res.* **2007**, *51*, 1094−101.

(10) Bohm, T.; Berger, H.; Nejabat, M.; Riegler, T.; Kellner, F.; Kuttke, M.; Sagmeister, S.; Bazanella, M.; Stolze, K.; Daryabeigi, A.; Bintner, N.; Murkovic, M.; Wagner, K. H.; Schulte-Hermann, R.; Rohr-Udilova, N.; Huber, W.; Grasl-Kraupp, B. Food-derived peroxidized fatty acids may trigger hepatic inflammation: A novel hypothesis to explain steatohepatitis. *J. Hepatol.* **2013**, *59*, 563−70.

(11) Kamal-Eldin, A.; Makinen, M.; Lampi, A. M. *Lipid Oxidation Pathways*; Kamal-Eldin, A., Makinen, M., Lampi, A. M., Eds.; AOCS Press: Champaign, IL, 2003; pp 1−36.

(12) Tawfik, M. S.; Huyghebaert, A. Interaction of packaging materials and vegetable oils: oil stability. *Food Chem.* **1999**, *64*, 451−459.

(13) Chung, H. J.; Colakoglu, A. S.; Min, D. B. Relationships among headspace oxygen, peroxide value, and conjugated diene content of soybean oil oxidation. *J. Food Sci.* **2004**, *69*, C83−C88.

(14) Farhoosh, R.; Khodaparast, M. H. H.; Sharif, A.; Rafiee, S. A. Olive oil oxidation: Rejection points in terms of polar, conjugated diene, and carbonyl values. *Food Chem.* **2012**, *131*, 1385−1390.

(15) Latham, M. C. Human nutrition in the developing world. In *Food and Nutrition Series*; Latham, M. C., Ed.; Food and Agriculture Organization of the United Nations: Rome, Italy, 1997; p 29.

(16) Velasco, J.; Andersen, M. L.; Skibsted, L. H. Electron spin resonance spin trapping for analysis of lipid oxidation in oils: inhibiting effect of the spin trap alpha-phenyl-*N*-*tert*-butylnitrone on lipid oxidation. *J. Agric. Food Chem.* **2005**, *53*, 1328−1336.

(17) Lall, R. K.; Proctor, A.; Jain, V. P. A Rapid, Micro FAME Preparation Method for Vegetable Oil Fatty Acid Analysis by Gas Chromatography. *J. Am. Oil Chem. Soc.* **2009**, *86*, 309−314.

(18) Guillen, M. D.; Ruiz, A. High resolution H-1 nuclear magnetic resonance in the study of edible oils and fats. *Trends Food Sci. Technol.* **2001**, *12*, 328−338.

(19) Pegg, R. B. Measurement of Primary Lipid Oxidation Products. In *Current Protocols in Food Analytical Chemistry*; Pegg, R. B., Ed.; Wiley: New York, 2001; pp D2.2.2−D2.2.25.
(20) Firestone, D. Method Cd 8−53. In *Official Methods and Recommended Practices of the American Oil Chemists' Society*; Firestone, D.; American Oil Chemists' Society: Champaign, 1997.
(21) Giuffrida, F.; Golay, P. A.; Destaillats, F.; Hug, B.; Dionisi, F. Accurate determination of hexanal in beef bouillons by headspace solid-phase microextraction gas-chromatography mass-spectrometry. *Eur. J. Lipid Sci. Technol.* **2005**, *107*, 792−798.
(22) Panseri, S.; Soncin, S.; Chiesa, L. M.; Biondi, P. A. A headspace solid-phase microextraction gas-chromatographic mass-spectrometric method (HS-SPME-GC/MS) to quantify hexanal in butter during storage as marker of lipid oxidation. *Food Chem.* **2011**, *127*, 886−889.
(23) Gliszczynska-Swiglo, A.; Sikorska, E. Simple reversed-phase liquid chromatography method for determination of tocopherols in edible plant oils. *J. Chromatogr. A* **2004**, *1048*, 195−8.
(24) Gunstone, F. D. Production and trade of vegetable oils. In *Vegetable Oils in Food and Technology: Composition, Properties and Uses*; Gunstone, F. D., Ed.; Blackwell Publishing Ltd.: Oxford, 2011; pp 1−24.
(25) Kanavouras, A.; Cert, A.; Hernandez, R. J. Oxidation of olive oil under still air. *Food Sci. Technol. Int.* **2005**, *11*, 183−189.
(26) Pignitter, M.; Somoza, V. Critical Evaluation of Methods for the Measurement of Oxidative Rancidity in Vegetable Oils. *J. Food Drug Anal.* **2012**, *20*, 772−777.
(27) Khan, M. A.; Shahidi, F. Rapid oxidation of commercial extra virgin olive oil stored under fluorescent light. *J. Food Lipids* **1999**, *6*, 331−339.
(28) Khatoon, S.; Krishna, A. G. G. Assessment of oxidation in heated safflower oil by physical, chemical and spectroscopic methods. *J. Food Lipids* **1998**, *5*, 247−267.
(29) Naz, S.; Siddiqi, R.; Sheikh, H.; Sayeed, S. A. Deterioration of olive, corn and soybean oils due to air, light, heat and deep-frying. *Food Res. Int.* **2005**, *38*, 127−134.
(30) Abramovic, H.; Abram, V. Physico-chemical properties, composition and oxidative stability of Camelina sativa oil. *Food Technol. Biotechnol.* **2005**, *43*, 63−70.
(31) Ivanov, D. S.; Levic, L. D.; Sredanovic, S. A. Fatty acid composition of various soybean products. *Food Feed Res.* **2009**, 65−70.
(32) Crapiste, G. H.; Brevedan, M. I. V.; Carelli, A. A. Oxidation of sunflower oil during storage. *J. Am. Oil Chem. Soc.* **1999**, *76*, 1437−1443.
(33) Wanasundara, U. N.; Shahidi, F.; Jablonski, C. R. Comparison of Standard and Nmr Methodologies for Assessment of Oxidative Stability of Canola and Soybean Oils. *Food Chem.* **1995**, *52*, 249−253.
(34) Guillen, M. D.; Ruiz, A. Monitoring the oxidation of unsaturated oils and formation of oxygenated aldehydes by proton NMR. *Eur. J. Lipid Sci. Technol.* **2005**, *107*, 36−47.
(35) Shahidi, F.; Wanasundara, U. N. *Food Lipids: Chemistry, Nutrition and Biotechnology*. Shahidi, F.; Wanasundara, U. N.; Marcel Dekker, Inc.: New York, 2002; pp 465−487.
(36) Belitz, H. D.; Grosch, W.; Schieberle, P. *Food Chemistry*, 4 ed.; Springer: Berlin, 2009.
(37) Frankel, E. N. Chemistry of Free-Radical and Singlet Oxidation of Lipids. *Prog. Lipid Res.* **1984**, *23*, 197−221.
(38) Dix, T. A.; Aikens, J. Mechanisms and Biological Relevance of Lipid-Peroxidation Initiation. *Chem. Res. Toxicol.* **1993**, *6*, 2−18.
(39) Sanches-Silva, A.; de Quiros, A. R. B.; Lopez-Hernandez, J.; Paseiro-Losada, P. Determination of hexanal as indicator of the lipidic oxidation state in potato crisps using gas chromatography and high-performance liquid chromatography. *J. Chromatogr. A* **2004**, *1046*, 75−81.
(40) Kamal-Eldin, A.; Appelqvist, L. A. The chemistry and antioxidant properties of tocopherols and tocotrienols. *Lipids* **1996**, *31*, 671−701.
(41) Halliwell, B.; Gutteridge, J. M. *Free Radicals in Biology and Medicine*, 4th ed.; Oxford University Press: New York, 2007.
(42) Jung, M. Y.; Yoon, S. H.; Min, D. B. Effects of Processing Steps on the Contents of Minor Compounds and Oxidation of Soybean Oil. *J. Am. Oil Chem. Soc.* **1989**, *66*, 118−120.
(43) Jung, M. Y.; Min, D. B. Effects of Alpha-Tocopherol, Gamma-Tocopherol, and Delta-Tocopherol on Oxidative Stability of Soybean Oil. *J. Food Sci.* **1990**, *55*, 1464−1465.
(44) Player, M. E.; Kim, H. J.; Lee, H. O.; Min, D. B. Stability of alpha-, gamma-, or delta-tocopherol during soybean oil oxidation. *J. Food Sci.* **2006**, *71*, C456−C460.
(45) Elisia, I.; Young, J. W.; Yuan, Y. V.; Kitts, D. D. Association between tocopherol isoform composition and lipid oxidation in selected multiple edible oils. *Food Res. Int.* **2013**, *52*, 508−514.
(46) Khan, M. A.; Shahidi, F. Photooxidative stability of stripped and non-stripped borage and evening primrose oils and their emulsions in water. *Food Chem.* **2002**, *79*, 47−53.

present, e.g., their solubility and molecular geometry.[17] A number of low-energy approaches have been developed to form nanoemulsions, including spontaneous emulsification (SE), emulsion inversion point (EPI), phase inversion temperature (PIT), and phase inversion composition (PIC) methods.[17−20] These methods are currently not widely used in the food industry, and where they are used, there is a relatively poor understanding of their physicochemical basis and the major factors impacting their performance.[17,21] Low-energy approaches may have advantages over high-energy approaches for certain applications: they are often more effective at producing very fine droplets; they have lower equipment and energy costs; and they are simpler to implement. On the other hand, there are also some potential drawbacks of low-energy methods, including limitations on the types of oils and surfactants that can be used to form stable nanoemulsions and the fact that relatively high surfactant/oil ratios (SORs) are typically needed to produce them.[19,20,22]

In the current study, we examine the potential of using an isothermal low-energy method (spontaneous emulsification) for producing transparent orange oil nanoemulsions suitable for utilization in foods and beverages. In general, this method involves titrating an organic phase (containing oil and surfactant) into an aqueous phase with continuous mixing, which leads to the spontaneous formation of ultrafine droplets because of rapid diffusion of the surfactant from the organic phase into the aqueous phase.[18,21,23] This method allows for nanoemulsions to be fabricated at room temperature using simple stirring rather than expensive homogenization equipment. This approach may therefore be particularly suitable for utilization within certain sectors of the food and other industries.

To the best of our knowledge, the formation of orange oil nanoemulsions by spontaneous emulsification has not yet been reported. Previous studies in spontaneous emulsification have shown that the size of the droplets generated using the spontaneous emulsification process depends upon many factors, including the type and concentration of surfactant and oils used, stirring conditions, and injection conditions.[4,23−25] The purpose of the present study was to investigate the major factors influencing the formation and stability of orange oil nanoemulsions. The results of this study have important implications for the design and utilization of nanoemulsions as delivery systems in the food and other industries. In particular, they may be useful for implementation in beverage emulsions, where only low concentrations of oil and surfactant are present in the final product.[26]

MATERIALS AND METHODS

Materials. Orange oil (1× fold; lot SC020295) was obtained from International Fragrances and Flavors (Union Beach, NJ). The nonionic surfactants (Tween 20, 40, 60, 80, and 85 and Span 20) were purchased from Sigma-Aldrich Co. (St. Louis, MO). Medium-chain triglyceride (MCT) oil (Miglyol 812) was purchased from Sassol Germany GmbH (Witten, Germany). The manufacturer reported that the fatty acid composition of MCT was 50−65% caprylic acid (C8:0) and 30−45% capric acid (C10:0). The aqueous phase used to prepare the emulsions was citrate buffer solution (5 mM; pH 3.5), which was chosen to mimic the acidic conditions in certain soft drinks and other beverages. Double-distilled water was used in the preparation of all solutions and emulsions.

Emulsion Preparation. Nanoemulsion formation was carried out using a method based on a spontaneous emulsification procedure described previously, with some minor modifications.[21] In brief, spontaneous emulsification was performed by titration of an organic phase (containing different amounts of orange oil, MCT, and nonionic surfactant) into an aqueous phase (5 mM citrate buffer at pH 3.5) while continuously stirring (500 rpm) the system with a magnetic stirrer at ambient temperature (≈25 °C). Unless otherwise stated, the experiments were carried out using standardized conditions: a total oil phase (orange oil + MCT) content of 10 wt %, surfactant content of 20 wt %, and aqueous phase content of 70 wt %. In these samples, the oil (10 g) and surfactant (20 g) were first mixed together and then the mixture was titrated into 70 g of aqueous phase at a rate of 2 mL/min. In some experiments, systems with different surfactant/emulsion ratios (SERs) were prepared by varying the amount of surfactant in the overall system. For example, a system with SER = 10% contains 10 g of surfactant in 100 g total (surfactant + oil + buffer).

Particle Size Measurements. The particle size distributions and mean particle diameters (Z averages) of nanoemulsions were measured using a dynamic light scattering instrument (Zetasizer Nano ZS, Malvern Instruments, Malvern, U.K.). This instrument determines the particle size from intensity−time fluctuations of a laser beam (633 nm) scattered from a sample at an angle of 173°. Each individual measurement was an average of 13 runs. To avoid multiple scattering effects, samples were diluted before the particle size measurements using citrate buffer solution (5 mM, pH 3.5).

Nanoemulsion Thermal Stability Measurements. The thermal stability of the nanoemulsions was determined by measuring their turbidity (600 nm) during heating and cooling using a temperature-scanning spectrophotometer (Evolution Array, Thermo Scientific). The turbidity was measured as the temperature was increased from 20 to 90 °C at a rate of 1 °C/min and then decreased back to 20 °C at the same rate. A citrate buffer solution (5 mM, pH 3.5) was used as a blank.

Statistical Analysis. All experiments were carried out 2 or 3 times using freshly prepared samples, and the results are reported as the calculated mean and standard deviation of these measurements. Means were subjected to Duncan's test, and a p value of <0.05 was considered statistically significant.

RESULTS AND DISCUSSION

Effect of the Oil Composition on the Particle Size. Initially, we examined the influence of oil-phase composition on the size of the droplets formed in nanoemulsions produced using spontaneous emulsification. Oil-phase composition was varied by combining different mass ratios of orange oil and MCT prior to emulsification. Otherwise, the system composition was standardized: oil content (orange oil + MCT) = 10 wt %; surfactant content = 20 wt %; and surfactant = Tween 80.

Oil-phase composition (orange oil/MCT ratio) had a major effect on the formation of emulsions and nanoemulsions by spontaneous emulsification (Figure 1). Orange oil alone was not able to form stable nanoemulsions: the emulsions produced were extremely unstable and inhomogeneous (data not shown). Transparent nanoemulsions containing fine droplet ($d \approx 25$ nm) could only be produced if the orange oil was mixed with a certain amount of MCT carrier oil (Figure 1). When the orange oil level in the lipid phase decreased to <30 wt % or increased to >50%, there was an appreciable increase in the mean particle diameter and no transparent nanoemulsions could be formed, although the droplet sizes in most of the systems were still relatively small ($d < 100$ nm) (Figure 1). We observed a similar phenomenon when another essential oil (carvacrol) was used to spontaneously form nanoemulsions.[6] The large particle sizes observed at high orange oil contents can be attributed to emulsion instability caused by Ostwald ripening and/or coalescence. The large particle sizes observed at higher orange oil contents may be due to changes in the phase behavior of the surfactant−oil−water system at certain compositions.[20] The

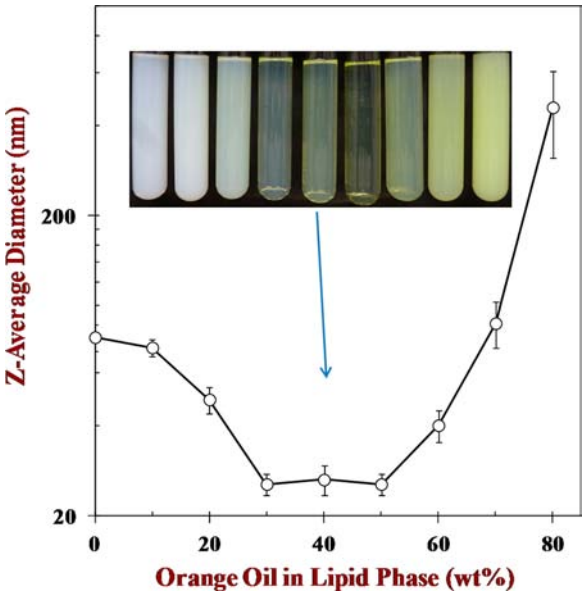

Figure 1. Effect of the oil-phase composition (wt % of orange oil in the oil phase) on the mean particle diameter of emulsions and nanoemulsions produced by spontaneous emulsification. Emulsions and nanoemulsions were prepared using 10 wt % oil (orange oil + MCT), 20 wt % surfactant (Tween 80), and 70 wt % water (pH 3.5 citrate buffer solution) at a stirring speed of 500 rpm at ambient temperature (≈25 °C). From left to right, the photograph shows orange oil concentrations in the lipid phase of 0, 10, 20, 30, 40, 50, 60, 70, and 80 wt %, respectively.

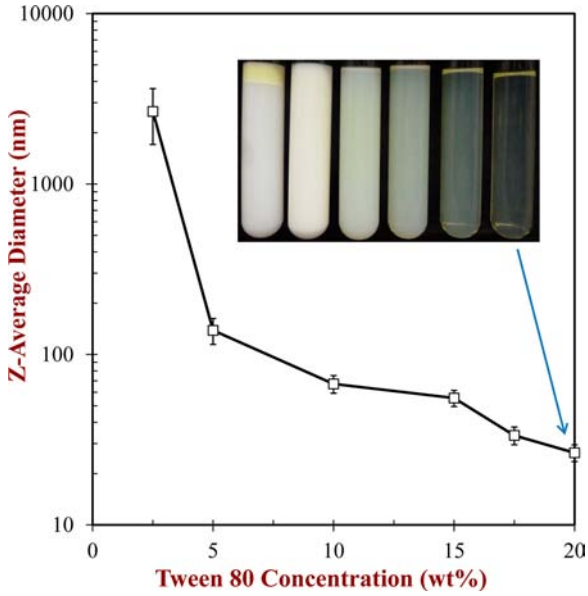

Figure 2. Effect of the surfactant concentration on the mean particle diameter and physical stability of emulsions produced by spontaneous emulsification. The surfactant (Tween 80) concentration in emulsion varied from 2.5 to 20 wt %, as indicated. Oil phase = 4% orange oil + 6% MCT.

physicochemical mechanisms governing the size of the droplets produced by spontaneous emulsification are still not clearly understood, and further research is still required in this area.

It should be noted that the type of carrier oil was also critical for the formation of ultrafine droplets by spontaneous emulsification. We could not form stable orange oil nanoemulsions at any oil-phase composition when long-chain triglycerides (e.g., corn and canola oils) were used as carrier oils rather than MCTs (data not shown). These experiments indicate that both the type and amount of carrier oil used to form nanoemulsions using the spontaneous emulsification method is critical.

Effect of the Surfactant Concentration on the Particle Size. The effect of the surfactant concentration on the particle size was investigated by preparing a series of emulsions with a fixed oil-phase composition (4% orange oil + 6% MCT) and surfactant type (Tween 80) but different SERs. Here, SER equals the mass of surfactant divided by the mass of the overall emulsion expressed as a percentage: SER = 100 × m_S/m_E. The amount of surfactant present had a pronounced influence on the size of the droplets produced, with the smallest droplets being formed at the highest surfactant concentrations, i.e., SER from 5 to 20 wt % (Figure 2). For example, at SER = 2.5 wt %, the emulsions formed contained relatively large droplets (d > 2000 nm) and phase separation occurred quickly. On the other hand, at SERs = 5, 10, 15, 17.5, and 20 wt %, the mean particle diameter decreased to 139, 67, 56, 34, and 25, respectively (Figure 2). In addition, the systems became optically transparent at the highest surfactant levels. Thus, it was possible to make clear colloidal delivery systems that contained very small droplets at high SERs.

This phenomenon is in agreement with earlier studies[21] and can be attributed to a number of physicochemical mechanisms. Higher surfactant concentrations at the oil−water boundary cause a large reduction in the interfacial tension, which may lead to a highly dynamic interface that spontaneously generates fine droplets through interfacial turbulence.[27] Second, higher surfactant concentrations mean that a larger oil−water interface can be stabilized, which means that smaller droplets can be produced.[11]

It should be noted that one of the major disadvantages of the low-energy approach of forming orange oil nanoemulsions is that a high surfactant level is required. However, in many cases, the concentration of the oil phase required in final food and beverage products is very low, and therefore, nanoemulsions will be highly diluted after formation. For example, the flavor oils used in soft drinks and waters are often appreciably less than 0.1% of the final product, and therefore, the surfactant level is also low.[26]

Effect of the Surfactant Type on the Particle Size. The impact of non-ionic surfactant type on the size of the droplets formed in the nanoemulsions was also investigated. A series of nanoemulsions with fixed oil composition (4% orange oil + 6% MCT) was prepared using the same surfactant concentration (20 wt %) but different surfactant types (Tween 20, 40, 60, 80, 85, and Span 20). The type of non-ionic surfactant had an appreciable impact on the mean particle diameter of the emulsions formed (Figure 3). Transparent nanoemulsions containing very fine droplets were formed in the systems prepared from Tween 40, 60, or 80 (d ≈ 25 nm), whereas opaque emulsions containing relatively large droplets that were unstable to gravitational separation were formed using Tween 20 or 85 or Span 80 (Figure 3). These results suggest that surfactants with too high hydrophilic−lipophilic balance HLB numbers (Tween 20, HLB = 16.7) or too low HLB numbers (Tween 85, HLB = 11; Span 80, HLB = 8.6) were unsuitable for the formation of nanoemulsions using the oil phase used in this study (Figure 3). On the contrary, surfactants with intermediate HLB numbers seemed to be more suitable for the

dx.doi.org/10.1021/jf500160y | J. Agric. Food Chem. 2014, 62, 2306−2312

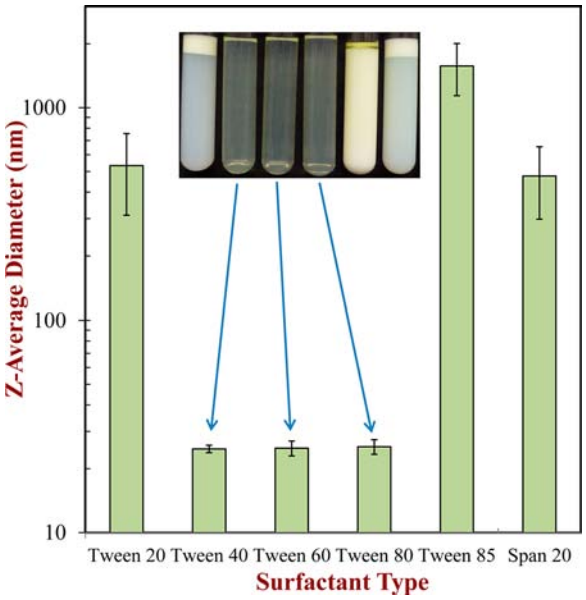

Figure 3. Effect of the surfactant type on the mean particle diameter and physical stability of emulsions produced by spontaneous emulsification. Oil phase = 4% orange oil + 6% MCT. Surfactant was 20 wt % in the system.

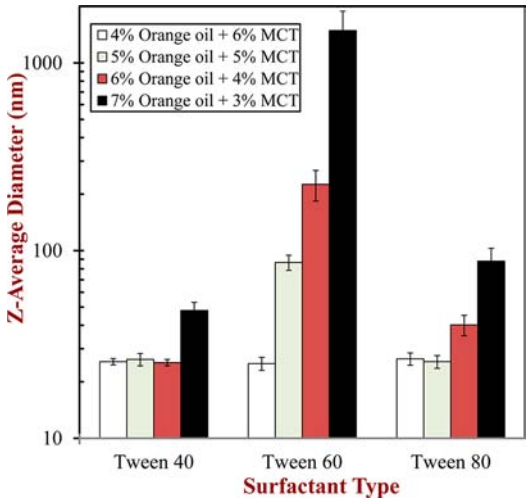

Figure 4. Effect of the surfactant type and oil-phase composition on the mean particle diameter of emulsions produced by spontaneous emulsification. The oil-phase composition (varying ratio of orange oil/MCT; total oil = 10 wt %) was indicated in the legend. The surfactant was 20 wt % in system. The results indicate that Tween 40 can load the most amount of orange oil (6%), producing transparent nanoemulsions with very small particle sizes ($d \approx 25$ nm), while Tween 60 can load the least amount of orange oil (4%), and Tween 60 is in the middle (5% orange oil). Other types of surfactants cannot produce transparent orange oil nanoemulsions, regardless of the oil phase.

formation of orange oil emulsions, because Tween 40, 60, and 80 (with HLB numbers 15.6, 14.9, and 15.0, respectively) were able to form clear nanoemulsions that were stable for separation (Figure 3). There are a number of possible reasons why surfactants with intermediate HLB values may favor the formation of ultrafine orange oil nanoemulsions. The spontaneous formation of ultrafine droplets at the oil–water boundary may require a very low interfacial tension to stimulate interfacial turbulence. Surfactants with intermediate HLB numbers might be expected to form monolayers with low interfacial tensions. If the HLB number is too low, then the surfactant will remain in the oil phase rather than moving into the water phase. If the HLB number is too high, then the interfacial tension and optimum curvature of the surfactant monolayer may be too high to form very fine oil droplets.

Effect of the Different Surfactant Types and Oil-Phase Compositions on the Particle Size. Having established that Tween 40, 60, and 80 could all form transparent orange oil nanoemulsions, we further investigated the effect of oil-phase composition on the size of the droplets produced using only these surfactants. Our aim was to establish which surfactant was most effective at producing small droplets and high orange oil loading capacities. In these experiments, the total surfactant concentration (20 wt %) and oil-phase concentration (10 wt %) were held constant, while the mass ratio of orange oil/MCT in the oil phase was varied. Our results indicated that surfactant type had a major influence on the formation of nanoemulsions with high loading capacities (Figure 4): Tween 40, 60, and 80 were capable of incorporating 6, 4, and 5% orange oil while still maintaining ultrafine droplets, i.e., $d < 30$ nm. At higher orange oil levels, there was an appreciable increase in the mean particle diameter. There are a number of possible reasons for the observed increase in the particle size at higher orange oil levels, which are associated with either emulsion formation or emulsion stability. During emulsion formation, there may be an optimum surfactant and oil-phase composition that leads to an ultralow interfacial tension and spontaneous droplet formation at the oil–water boundary. After emulsion formation, droplet growth may occur because of Ostwald ripening or coalescence processes, which depend upon surfactant type and the composition of the oil phase. In particular, Ostwald ripening has been shown to occur rapidly in oil-in-water emulsions containing flavor oils because of their relatively high water solubility.[28,29] The addition of water-insoluble oils (such as MCT or long-chain triglyceride) to flavor oils has been shown to inhibit this form of droplet growth, which has been attributed to an entropy of mixing effect that opposed Ostwald ripening.[29] Thus, there may be a minimum amount of MCT that has to be present in the emulsions to prevent rapid droplet growth from occurring after emulsion formation.

Thermal Stability of Selected Orange Oil Nanoemulsions. Emulsified flavor oils may be subject to thermal treatments (such as pasteurization) during food processing. We therefore examined the thermal stability of selected orange oil nanoemulsions (10% oil phase and 20% surfactant) by measuring the change in sample turbidity during a controlled heating–cooling cycle. Nanoemulsions with three different oil-phase compositions were examined: 4 wt % orange oil + 6 wt % MCT, 5 wt % orange oil + 5 wt % MCT, and, 6 wt % orange oil + 4 wt % MCT. The nanoemulsions were heated from 20 to 90 °C and then cooled to 20 °C at a heating/cooling rate of 1 °C/min. The turbidity of all of the samples before and after heating is summarized in Figure 5. The full turbidity–temperature profiles during heating and cooling of selected samples are shown in Figure 6.

Tween 40. The nanoemulsions with three different oil compositions were all initially transparent ($\tau \approx 0$ cm^{-1}), but they all became highly turbid ($\tau > 0.6$ cm^{-1}) after the heating–cooling cycle, which is indicative of temperature-induced droplet growth (Figure 5). A representative turbidity–temperature profile for the 5% orange oil + 5% MCT system is shown

dx.doi.org/10.1021/jf500160y | J. Agric. Food Chem. 2014, 62, 2306–2312

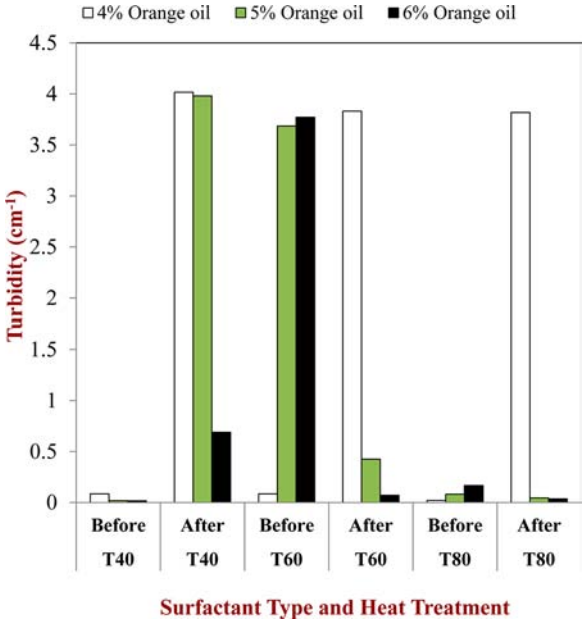

Figure 5. Turbidity of representative orange oil emulsions/nanoemulsions before and after heating. The samples were heated from 20 to 90 °C at a rate of 1 °C/min and then cooled to 20 °C at the same rate. In the figure, "before" means the turbidity (at 600 nm) of samples before the heat−cooling circle and "after" means the turbidity after the heat−cooling treatment.

in Figure 6a. This system was initially transparent. During heating, the turbidity remained close to zero from 20 to 63 °C, increased to a maximum around 77 °C, and then decreased to close to zero again around 80 °C. We postulate that the increase in turbidity observed around 75 °C was due to droplet coalescence as the system approached the PIT. The decrease in turbidity at higher temperatures is attributed to the formation of a clear microemulsion around the PIT. Upon cooling, the turbidity increased steeply around 74 °C and the system remained opaque at lower temperatures, which was attributed to rapid droplet coalescence at temperatures just below the PIT.

Tween 60. Before heating, nanoemulsions containing 4 wt % orange oil were transparent ($\tau \approx 0$ cm^{-1}), whereas those containing 5 or 6 wt % orange oil were opaque ($\tau > 3$ cm^{-1}) (Figure 5). Conversely, the nanoemulsions containing 4 wt % orange oil became opaque after heating, whereas those containing 5 or 6 wt % orange oil were much lower. A representative turbidity−temperature profile for the 5% orange oil + 5% MCT system is shown in Figure 6b. This system initially appeared optically opaque ($\tau > 3$ cm^{-1}). During heating, the turbidity remained high from 20 to 75 °C, then decreased steeply, had a value close to zero from 79 to 85 °C, and then increased steeply around 86 °C. We postulate that the decrease in turbidity observed around 75 °C was due to the formation of a clear microemulsion phase around the PIT, while the steep increase at 86 °C was due to the formation of a water-in-oil (W/O) emulsion containing relatively large water droplets at temperatures well above the PIT. Upon cooling, there was a steep decrease in turbidity around 83 °C until the system became transparent from around 77 to 66 °C, which was attributed to the formation of a clear microemulsion around the PIT. Upon further cooling, the turbidity of the system increased somewhat, which was attributed to some droplet coalescence at temperatures just below the PIT.

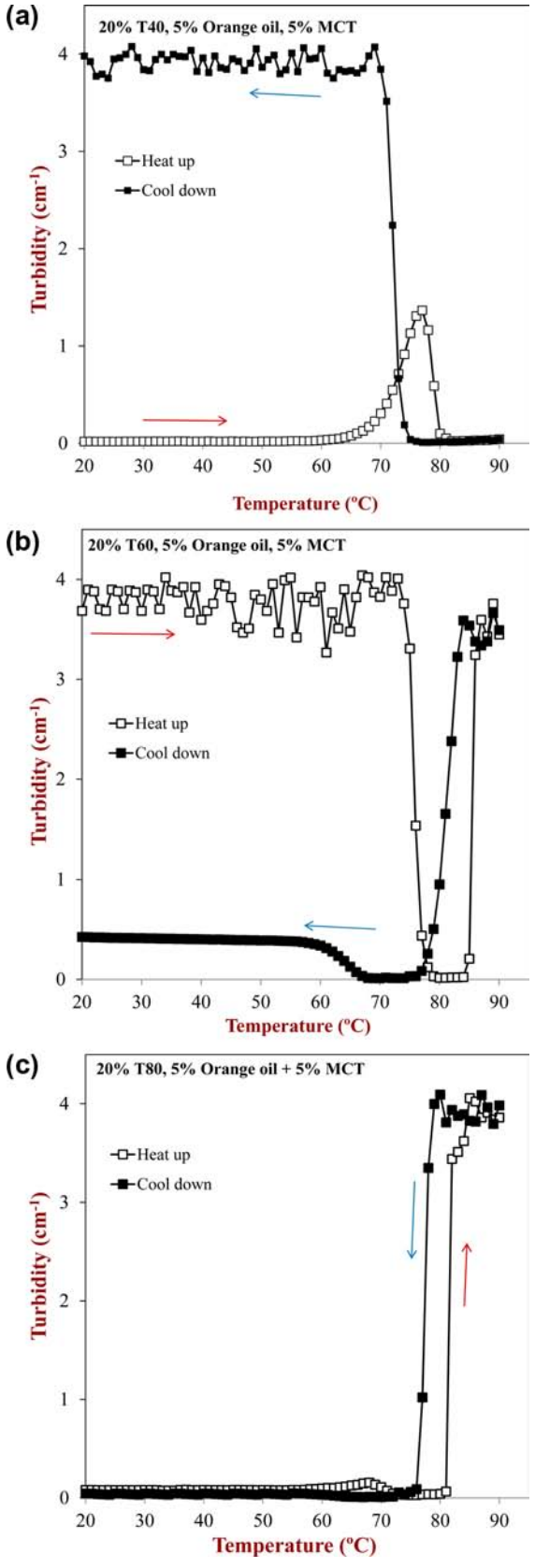

Figure 6. Turbidity−temperature profiles during heating and cooling of selected orange oil emulsion/nanoemulsion samples. Oil compositions and surfactants are shown in the legend. (c) Nanoemulsion containing 20% Tween 80, 5% orange oil, and 5% MCT was temperature-reversible (i.e., remaining transparent after heating and cooling).

dx.doi.org/10.1021/jf500160y | J. Agric. Food Chem. 2014, 62, 2306−2312

Tween 80. Prior to heating, all of the nanoemulsions had relatively low turbidities, but after heating, the systems containing 4 wt % orange oil became opaque, whereas those containing 5 or 6 wt % orange oil were clear (Figure 5). A representative turbidity–temperature profile for the 5% orange oil + 5% MCT system is shown in Figure 6c. This system initially had a relatively low turbidity. During heating, the turbidity remained close to zero from 20 to 60 °C, increased to a slight maximum around 66 °C, decreased close to zero from 72 to 80 °C, and then increased steeply around 81 °C until the system became opaque ($\tau > 3$ cm^{-1}). We postulate that the increase in turbidity observed around 66 °C was due to droplet coalescence as the system approached the PIT. We attribute the low turbidity from 72 to 80 °C to the formation of a microemulsion around the PIT and the large increase in turbidity above 81 °C to phase inversion to a W/O emulsion containing large water droplets that scatter light strongly. Upon cooling, the turbidity of the system decreased rapidly below 78 °C, which was attributed to the formation of a clear microemulsion again around the PIT and a nanoemulsion at lower temperatures.

These results clearly show that the temperature dependence of orange oil nanoemulsions is complex and depends upon the nature of the surfactant and oil phase used to fabricate them. In some cases, clear nanoemulsions formed at ambient temperatures by spontaneous emulsification remain stable after thermal treatment, whereas in other cases, they do not. In other cases, unstable opaque emulsions formed at ambient temperatures by spontaneous emulsification revert to clear nanoemulsions after thermal treatment, whereas in other cases, they remain unstable. We postulate that the most important factor determining droplet growth after heating is their coalescence stability near the PIT. Some systems underwent rapid droplet growth during cooling, whereas others did not.

Storage Stability of the Spontaneously Emulsified Orange Oil Nanoemulsions. For most commercial applications, it is important that nanoemulsion-based delivery systems remain physically stable throughout their shelf life; i.e., there is little change in their particle size during storage. We therefore examined the influence of storage time on the stability of a representative nanoemulsion: 5% orange oil + 5% MCT and 20 wt % Tween 80. This system was selected because it was the only one that formed transparent nanoemulsions at ambient temperature after spontaneous emulsification and was also stable to heating and cooling (see previous section). There was an appreciable increase in the mean droplet diameter from around 25 to 46 nm during storage for 40 days at ambient temperature (Figure 7), which suggests that some droplet growth occurred because of either coalescence or Ostwald ripening. Nevertheless, when the nanoemulsion was diluted 10 times in aqueous solution (5 mM citrate buffer at pH 3.5), the rate of droplet growth was appreciably reduced; i.e., the diameter only increased around 25–32 nm after 40 days of storage at ambient temperature (Figure 7). It should also be noted that, after a certain time, the droplet diameter remained relatively stable; e.g., after 19, 26, and 40 days, the particle size of the diluted nanoemulsions was 31, 32, and 32 nm ($p > 0.05$). Practically, the concentration of essential oil required in a final food product is usually very low, and therefore, nanoemulsions will be highly diluted after formation. Consequently, they should remain relatively stable in commercial applications.

The fact that the stabilities of the nanoemulsions improved after dilution suggests that the instability of the undiluted

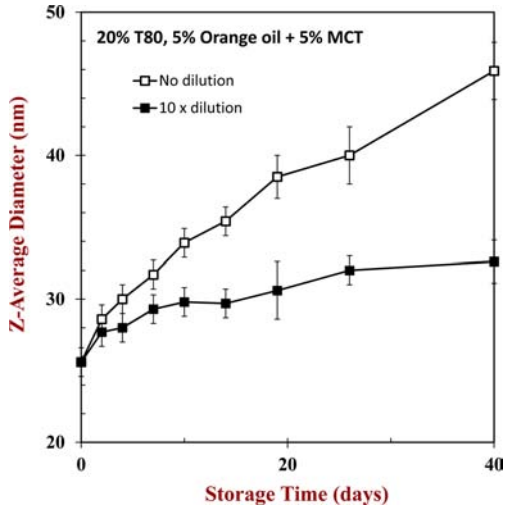

Figure 7. Increase in the mean particle diameter of selected nanoemulsions during 40 days of storage at room temperature. Nanoemulsions were prepared using 10 wt % oil (5% orange oil + 5% MCT), 20 wt % surfactant (Tween 80), and 70 wt % water (pH 3.5 citrate buffer solution) at a stirring speed of 500 rpm at ambient temperature (≈25 °C). This nanoemulsion was selected because it was transparent with very small sizes ($d \approx 25$ nm) and temperature-reversible (remaining to be transparent after heating–cooling circles). The nanoemulsion was either undiluted or diluted 10 times by citrate buffer. The results indicated that the size of the nanoemulsion increased over storage, but this effect was much reduced if the nanoemulsion was diluted.

emulsion may have been due to the relatively high amount of surfactant present (SER = 20 wt %). At relatively high surfactant levels, there may have been appreciable amounts of free surfactant micelles present that could transfer oil molecules between droplets through Ostwald ripening or promote droplet aggregation through depletion,[30,31] which is in accordance with results that we reported previously on essential oil nanoemulsions.[20]

In this paper, we have described the influence of surfactant and oil composition on the fabrication and stability of orange oil nanoemulsions formed by spontaneous emulsification. We found that oil-phase composition (orange oil/MCT ratio), surfactant type, and surfactant concentration all had an appreciable impact on the particle size and nanoemulsion stability. Clear nanoemulsions could be formed under certain system compositions: 20% Tween 40, 60 or 80 and 4–6% orange oil with 6–4% MCT). Surfactant type and oil-phase composition also affected the thermal stability of the nanoemulsions. Only nanoemulsions containing 20% Tween 80, 5% orange oil, and 5% MCT remained clear after heating and cooling. The droplet size of these nanoemulsions increased over time during storage at ambient temperature. Nevertheless, the rate of droplet growth could be retarded by dilution of the nanoemulsions in aqueous solutions prior to storage.

These nanoemulsion preparation methods described in this study could be implemented by the food and beverage industries. Under the optimized conditions established in this study, physically stable and transparent orange nanoemulsions could be formed by simple mixing. The fabrication of nanoemulsions by spontaneous emulsification has a number of potential advantages: simplicity of implementation, no expensive equipment required, and lower energy and operating costs. Additionally, in comparison to high-energy methods (e.g.,

high-pressure homogenization), spontaneous emulsification can produce nanoemulsions with smaller droplet sizes, making them particularly suitable for application in clear beverages. The major disadvantage of this method is that high amounts of synthetic surfactant are required, but this may not be a problem where the oil concentration required in a final product is relatively low, e.g., beverage emulsions.

AUTHOR INFORMATION

Corresponding Author

*Telephone: 413-545-1019. Fax: 413-545-1262. E-mail: mcclements@foodsci.umass.edu.

Funding

This material is based on work supported by United States Department of Agriculture, National Research Initiative (NRI) and Agriculture and Food Research Initiative (AFRI) Grants. The author Yuhua Chang thanks the National Natural Science Foundation of China (31101242) for support.

Notes

The authors declare no competing financial interest.

REFERENCES

(1) Perez-Cacho, P. R.; Rouseff, R. Processing and storage effects on orange juice aroma: A review. *J. Agric. Food Chem.* **2008**, *56* (21), 9785−9796.

(2) Perez-Cacho, P. R.; Rouseff, R. L. Fresh squeezed orange juice odor: A review. *Crit. Rev. Food Sci. Nutr.* **2008**, *48* (7), 681−695.

(3) Vora, J. D.; Matthews, R. F.; Crandall, P. G.; Cook, R. Preparation and chemical composition of orange oil concentrates. *J. Food Sci.* **1983**, *48* (4), 1197−1199.

(4) Chang, Y.; McLandsborough, L.; McClements, D. J. Physical properties and antimicrobial efficacy of thyme oil nanoemulsions: Influence of ripening inhibitors. *J. Agric. Food Chem.* **2012**, *60* (48), 12056−12063.

(5) Ziani, K.; Chang, Y. H.; McLandsborough, L.; McClements, D. J. Influence of surfactant charge on antimicrobial efficacy of surfactant-stabilized thyme oil nanoemulsions. *J. Agric. Food Chem.* **2011**, *59* (11), 6247−6255.

(6) Chang, Y.; McLandsborough, L.; McClements, D. J. Physicochemical properties and antimicrobial efficacy of carvacrol nanoemulsions formed by spontaneous emulsification. *J. Agric. Food Chem.* **2013**, *61* (37), 8906−8913.

(7) McClements, D. J. Nanoemulsions versus microemulsions: Terminology, differences, and similarities. *Soft Matter* **2012**, *8* (6), 1719−1729.

(8) Garti, N.; Aserin, A. Micelles and microemulsions as food ingredient and nutraceutical delivery systems. In *Encapsulation Technologies and Delivery Systems for Food Ingredients and Nutraceuticals*; Garti, N., McClements, D. J., Eds.; Woodhead Publishing: Cambridge, U.K., 2012; Woodhead Publishing Series in Food Science, Technology and Nutrition, pp 211−251.

(9) Patel, A. R.; Velikov, K. P. Colloidal delivery systems in foods: A general comparison with oral drug delivery. *LWT—Food Sci. Technol.* **2011**, *44* (9), 1958−1964.

(10) Mason, T. G.; Wilking, J. N.; Meleson, K.; Chang, C. B.; Graves, S. M. Nanoemulsions: Formation, structure, and physical properties. *J. Phys.: Condens. Matter* **2006**, *18* (41), R635−R666.

(11) McClements, D. J. Edible nanoemulsions: Fabrication, properties, and functional performance. *Soft Matter* **2011**, *7* (6), 2297−2316.

(12) McClements, D. J.; Rao, J. Food-grade nanoemulsions: Formulation, fabrication, properties, performance, biological fate, and potential toxicity. *Crit. Rev. Food Sci. Nutr.* **2011**, *51* (4), 285−330.

(13) Tadros, T.; Izquierdo, P.; Esquena, J.; Solans, C. Formation and stability of nano-emulsions. *Adv. Colloid Interface Sci.* **2004**, *108−109* (0), 303−318.

(14) Acosta, E. Bioavailability of nanoparticles in nutrient and nutraceutical delivery. *Curr. Opin. Colloid Interface Sci.* **2009**, *14* (1), 3−15.

(15) Huang, Q. R.; Yu, H. L.; Ru, Q. M. Bioavailability and delivery of nutraceuticals using nanotechnology. *J. Food Sci.* **2010**, *75* (1), R50−R57.

(16) Hatanaka, J.; Chikamori, H.; Sato, H.; Uchida, S.; Debari, K.; Onoue, S.; Yamada, S. Physicochemical and pharmacological characterization of α-tocopherol-loaded nano-emulsion system. *Int. J. Pharm.* **2010**, *396* (1−2), 188−193.

(17) Date, A. A.; Desai, N.; Dixit, R.; Nagarsenker, M. Self-nanoemulsifying drug delivery systems: Formulation insights, applications and advances. *Nanomedicine* **2010**, *5* (10), 1595−1616.

(18) Anton, N.; Benoit, J. P.; Saulnier, P. Design and production of nanoparticles formulated from nano-emulsion templates—A review. *J. Controlled Release* **2008**, *128* (3), 185−199.

(19) Ostertag, F.; Weiss, J.; McClements, D. J. Low-energy formation of edible nanoemulsions: Factors influencing droplet size produced by emulsion phase inversion. *J. Colloid Interface Sci.* **2012**, *388*, 95−102.

(20) Saberi, A. H.; Fang, Y.; McClements, D. J. Fabrication of vitamin E-enriched nanoemulsions: Factors affecting particle size using spontaneous emulsification. *J. Colloid Interface Sci.* **2013**, *391*, 95−102.

(21) Anton, N.; Vandamme, T. F. The universality of low-energy nano-emulsification. *Int. J. Pharm.* **2009**, *377* (1−2), 142−147.

(22) Yang, Y.; Marshall-Breton, C.; Leser, M. E.; Sher, A. A.; McClements, D. J. Fabrication of ultrafine edible emulsions: Comparison of high-energy and low-energy homogenization methods. *Food Hydrocolloids* **2012**, *29* (2), 398−406.

(23) Bouchemal, K.; Briancon, S.; Perrier, E.; Fessi, H. Nano-emulsion formulation using spontaneous emulsification: Solvent, oil and surfactant optimization. *Int. J. Pharm.* **2004**, *280* (1−2), 241−251.

(24) López-Montilla, J. C.; Herrera-Morales, P. E.; Pandey, S.; Shah, D. O. Spontaneous emulsification: Mechanisms, physicochemical aspects, modeling, and applications. *J. Dispersion Sci. Technol.* **2002**, *23* (1−3), 219−268.

(25) Miller, C. A. Spontaneous emulsification produced by diffusion—A review. *Colloids Surf.* **1988**, *29* (1), 89−102.

(26) Given, P. S. Encapsulation of flavors in emulsions for beverages. *Curr. Opin. Colloid Interface Sci.* **2009**, *14* (1), 43−47.

(27) Lamaallam, S.; Bataller, H.; Dicharry, C.; Lachaise, J. Formation and stability of miniemulsions produced by dispersion of water/oil/surfactants concentrates in a large amount of water. *Colloids Surf., A* **2005**, *270−271* (0), 44−51.

(28) Rao, J. J.; McClements, D. J. Impact of lemon oil composition on formation and stability of model food and beverage emulsions. *Food Chem.* **2012**, *134* (2), 749−757.

(29) McClements, D. J.; Henson, L.; Popplewell, L. M.; Decker, E. A.; Choi, S. J. Inhibition of Ostwald ripening in model beverage emulsions by addition of poorly water soluble triglyceride oils. *J. Food Sci.* **2012**, *77* (1), C33−C38.

(30) McClements, D. J.; Dungan, S. R. Factors that affect the rate of oil exchange between oil-in-water emulsion droplets stabilized by a nonionic surfactant: droplet size, surfactant concentration, and ionic-strength. *J. Phys. Chem.* **1993**, *97* (28), 7304−7308.

(31) McClements, D. J. Ultrasonic determination of depletion flocculation in oil-in-water emulsions containing a nonionic surfactant. *Colloids Surf., A* **1994**, *90* (1), 25−35.

However, the mechanisms for the hyperaccumulation of F and Al in tea leaves remain unknown. We hypothesize that the localization of F and Al in tea plants plays an important role in their detoxification. On one hand, F and Al may be immobilized by pectin and hemicellulose in the apoplasts of cell walls, limiting their movement through membranes, prohibiting them from entering symplasts, and thus reducing their toxicities to cells. On the other hand, F and Al are captured and compartmentalized by vacuoles after entering protoplasts, reducing their contacts with organelles in symplasts. However, the mechanisms controlling the subcellular localization of F and Al in tea plants are not fully understood.

To test our hypothesis that the subcellular localization contributes to the detoxification of F and Al in tea plants, different subcellular fractions such as those of the cell wall rich, pellet, and soluble fractions of tea leaves and roots were separated using the differential centrifugation and osmotic lysis methods. Then the concentrations of F and Al in these subcellular fractions were analyzed using ion chromatography and atomic absorption spectrometry, respectively. Finally, the distribution of F and Al in different subcellular fractions was examined to test our hypothesis.

MATERIALS AND METHODS

Tea Plants and Growth Conditions. Tea seeds (Shuchazao, *Camellia sinensis* L.) were collected from the High-tech Demonstration Garden (E117°38′, N31°43′) of the Anhui Agricultural University. The seeds were immersed in water for 2 days. Afterward, the healthy ones were chosen and planted in the trays containing moist quartz sand (particle size of 0.3 cm), and then the trays were placed into automatic climate chambers (50% humidity, 12 h light/dark cycle, 550 μE m^{-2} s^{-1} illumination, and day and night temperatures of 25 and 20 °C, respectively). The seeds were irrigated with 5 mM F (NaF) and 2.5 mM Al [$Al(NO_3)_3$] for 6−8 days until the first trifoliate leaves had just expanded. Finally, the roots and leaves were washed several times with deionized water, and the water on the surfaces of roots and leaves was wiped up with filter paper.

Isolation of Cell Wall, Organelle, and Cytoplasm Fractions from Tea Leaves and Roots. The fractions of the cell wall, organelle, and cytoplasm of tea roots and leaves were isolated according to the methods proposed by Weigel and Jager.[22] In brief, 100 pieces of 10 mm tea root tips or 2.0 g of tea leaves was homogenized using a mortar and pestle in a medium containing 250 mM sucrose, 50 mM Tris-HCl (pH7.5), and 1 mM dithiothreitol. All the steps were performed at 4 °C. The resulting debris was strained through eight layers of cheesecloth, and the liquid was filtered through the cheesecloth, with the residue left on the cheesecloth. The residue on the cheesecloth was washed twice with the grinding medium. The pooled washes, together with the first filtrate, were centrifuged at 300*g* for 30 s (Z36HK, Hermle). The resulting pellet combined with the residue on the cheesecloth contained mainly cell walls and cell wall debris and was designated as the cell wall rich fraction. The supernatant from the first centrifugation step was then centrifuged at 20000*g* for 45 min to sediment cell organelles. The sediment on the bottom of the centrifugal tube mainly contained organelles, and organelle debris was considered as the pellet fraction (20000*g*). The resultant supernatant solution in the centrifugal tube was termed the soluble fraction. The purity of each fraction was tested by examining activities of cytochrome *c* oxidase (the marker for mitochondria) and glucose-6-phosphate dehydrogenase (the marker for cytosol), as described in Enzyme Assays.

Preparation of Protoplasts. The protoplast fraction of tea roots and leaves was prepared following the method described by Yoo et al.[23] The surfaces of healthy fresh leaves were sterilized with 70% alcohol. The leaves were cut into 0.5−1.0 mm pieces from intercostal tissue using a sharp razor blade. Two grams of leaf pieces was quickly and gently transferred into 5 mL of a 2-morpholinoethanesulfonic acid (MES) enzyme buffer solution (20 mM, pH 5.7) containing 1.5% cellulase, 0.4% macerozyme, 0.4 M mannitol, 20 mM KCl, 10 mM $CaCl_2$, and 0.1% bovine serum albumin (BSA). The leaf pieces were incubated in a vacuum container for at least 3 h at room temperature (25 °C) in the dark. The MES enzyme solution turned green after a gentle swirling motion, indicating the release of protoplasts, which was checked under a microscope (400×, Motic B5, Motic, Shanghai, China).

Five milliliters of the enzyme/protoplast solution was diluted with 5 mL of a 2 mM MES buffer solution containing 154 mM NaCl, 125 mM $CaCl_2$, and 5 mM KCl to achieve the release of protoplasts before filtration to remove undigested leaf tissues. The enzyme solution containing protoplasts was filtered through a 75 μm mesh nylon filter. The filtrate was centrifuged at 100*g* for 2 min to sediment the protoplasts in a 50 mL round-bottom centrifugal tube. The supernatant was completely removed, and the protoplast pellet was resuspended with 10 mL of a 2 mM MES buffer solution. An aliquot of 5 mL of 0.6 M sucrose containing 20 mM MES (pH 5.7) was put on the bottom of the tube that was centrifuged at 150 rpm for 15 min. The protoplasts were suspended on the sucrose layer and collected with a 5 mL syringe. Then the collected protoplasts were suspended in 30 mL of suspension medium. An additional 5 mL of the sucrose solution (0.6 M) was injected below the suspended protoplasts, and the tube was centrifuged at 100*g* for 15 min. The washing procedure was repeated twice, and the protoplast pellet was suspended in 2.5 mL of 0.6 M mannitol. The green layer between the sucrose interfaces contained purified protoplasts.

Preparation and Identification of Vacuoles. The vacuoles of protoplasts of tea roots and leaves were separated using the osmotic lysis method.[24−26] The protoplast suspensions (2.5 mL) were lysed by being mixed with 12.5 mL of 60 mM K_2HPO_4 (pH 8.0) containing 12% (w/v) Ficoll and 1 mM dithiothreitol (DTT). The mixture was gently blended by repeatedly inverting the tube for 5 min. Then 5 mL of 0.6 M mannitol, 50 mM potassium phosphate (pH 7.0), and 1 mM (Na^+) EDTA were layered on the top of the lysate and centrifuged at 1000*g* for 15 min. During centrifugation, the vacuoles migrated toward the top and were recovered in the top 4 mL of the Ficoll layer. The concentrations of protoplasts and vacuoles were determined by using a hemocytometer.

Enzyme Assays. The α-mannosidase activities in isolated protoplast and vacuole fractions were assayed by measuring the liberation of *p*-nitrophenol from PNP-α-mannopyranoside substrates according to the method of Boller and Kende.[27] Briefly, a 0.5 mL assay mixture containing 50 μL of α-mannosidase (usually 1−5 μg of protein and 0.1−0.5 unit of activity) and 50 μM succinic acid was adjusted to pH 5.0 with NaOH, and 0.3 μmol of the PNP-α-mannopyranoside substrate was also added. The reaction was started by the addition of 0.3 μmol of the PNP-α-mannopyranoside substrate and stopped after 60 min by adding 0.8 mL of 1 M Na_2CO_3. The α-mannosidase activities were determined at 405 nm using a spectrophotometer.

Cytochrome *c* oxidase (the marker for mitochondria) was assayed at room temperature (25 °C) by following the oxidation of cytochrome *c*.[28] The 3 mL reaction mixture contained 10−50 μg of protein, 15 μM cytochrome *c* reduced with sodium dithionite, 10‰ digitonin, and 50 mM phosphate buffer (pH 7.5). The activities of cytochrome *c* oxidation were determined at 550 nm using a spectrophotometer. Glucose-6-phosphate dehydrogenase (the marker for cytosol) was determined spectrophotometrically.[29] An assay contained 800 μL of 0.1 M triethanolamine buffer (pH 7.6), 70 μL of 0.1 M $MgCl_2$, 30 μL of 35 mM glucose 6-phosphate, and 30 μL of 11 mM $NADP^+$, in a total volume of 1 mL. The reaction was started by the addition of 70 μL of different homogenized subcelluar fractions of tea leaves and roots and measured at room temperature at 340 nm using a spectrophotometer.

Isolation of Pectin and Hemicellulose from Cell Walls. The crude cell walls of tea roots obtained from the procedures described in Isolation of Cell Wall, Organelle, and Cytoplasm Fractions from Tea Leaves and Roots were washed in a 15 mL centrifugal tube with two aliquots of 3.5 mL of ice-cold 75% ethanol and kept undisturbed for 20 min in an ice−water bath. The homogenates were then centrifuged for

10 min at 1000*g* and the pellets washed three times with 5 mL of ice-cold acetone, a methanol/chloroform mixture [1:1 (v/v)], and methanol.[30] The supernatant of each wash was discarded, and the final deposits were freeze-dried overnight. The dry deposits were weighed and considered crude cell walls that were then used for further removal of pectin and hemicellulose components.

The pectin and hemicellulose were removed from the crude cell walls following the method of Mort et al.[31] In brief, an aliquot of 0.2 g of crude cell walls was transferred into a 50 mL plastic centrifuge tube with 30 mL of a 0.5 M imidazole/acetate solution (pH 7.0). To remove pectin, the cell walls were shaken for 24 h on a shaker at 400 rpm (25 °C) after the centrifugal tubes had been sealed with a stopper and aluminum foil. Afterward, the homogenates were separated by centrifugation for 15 min at 20000*g*, and the pectin in the supernatant was transferred to a 50 mL test tube for further analysis. The same procedure was performed to remove alkaline pectin with 50 mmol of $NaCO_3$ per liter. The procedures for isolating pectin fractions were repeated three times. To remove hemicellulose, the residues (cell walls without pectin) in the centrifugal tube were mixed with 5 mL of 4% KOH and then 8% KOH in sequence containing 0.1% $NaBH_4$, shaken for 8 h at 200 rpm, and centrifuged for 15 min at 20000*g*. The hemicellulose in the supernatant was transferred into the 50 mL test tube for further analysis. The final residues in the centrifugal tube were the cell walls without pectin and hemicellulose. Triplicate experiments were performed for each extraction step. All the extracts from cell walls were stored in a freezer before the determination of Al levels, digested by HNO_3, and then analyzed using atomic absorption spectrometry (ZEEnit700, Analytik Jena AG).[19] Whole cell walls, cell wall residues without pectin, and cell wall residues without pectin and hemicellulose (most were cellulose) were freeze-dried prior to adsorption experiments.

Al Adsorption in Different Fractions of Cell Walls. Batch experiments were conducted to determine the adsorption of Al on different components of cell walls in tea roots; 0.5 g of whole cell walls, cell wall residues without pectin, or cell wall residues without pectin and hemicellulose were introduced into 250 mL centrifugal tubes, and then 200 mL Al solutions in 5 mM were also added. The ionic strength in the centrifugal tubes was adjusted using 0.1 mM KNO_3, and the pH was kept at 6.0 using 0.1 M NaOH and 0.1 M HCl. The Al mixtures were shaken on a shaker at 200 rpm (25 °C) after the centrifuge tubes had been sealed with a stopper and Teflon film. At the end of the 2 h adsorption equilibrium time, the Al mixtures were subsequently centrifuged at 20 °C for 10 min at 1000*g*. The concentrations of Al in the supernatant were determined using atomic absorption spectrometry (ZEEnit700, Analytik Jena AG).[19]

The mass of Al adsorbed on the whole cell walls and their residues was obtained by the difference between the mass of Al originally added and that from the solution phase at the end of adsorption experiments. The amount of Al adsorbed was calculated by the equation

$$Qa = (C_0 - C_e) \times V/M \quad (1)$$

where Qa is the amount of Al adsorbed (milligrams per gram), C_0 is the initial concentration of Al (millimoles per liter), C_e is the equilibrium concentration of Al at the end of the adsorption experiment (millimoles per liter), V is the volume of the solution (liters), and M is the mass of the whole cell walls or their residues (grams).

Extraction and Determination of Levels of F and Al in Tea Samples. The fluoride that accumulated in tea plants was extracted according to the method optimized by Zhang et al.[32] Briefly, root or leaf samples were weighed, placed into 50 mL centrifugal tubes that contained 30 mL of redistilled water, and extracted at 100 °C for 30 min in water. The extraction mixtures were cooled to room temperature and then centrifuged at 2500*g* for 10 min at 20 °C to separate the supernatant. The F concentrations in root, leaf, protoplast, and vacuole fractions were determined by ion chromatography (ICS-1100, Dionex), equipped with an Ionpac AS23 anion-exchange column (4 mm × 50 mm) coupled with an IonPac AG23 Guard column (4 mm × 50 mm). The separation of F was performed with a mixed solutuion of 4.5 mM Na_2CO_3 and 0.8 mM $NaHCO_3$ at 30 °C. The flow rate was 1.0 mL/min, and the injection volume was 25 μL.

For Al determination, the protoplast and vacuole fractions as well as the root and leaf samples were weighed and digested with HNO_3 as described by Shen et al.[19] The Al concentrations in the protoplasts, vacuoles, roots, and leaves were determined by atomic absorption spectrometry (ZEEnit700, Analytik Jena AG).

Statistics. The contents of F and Al in different subcellular fractions (the cell wall rich, pellet, and soluble fractions) of tea roots and leaves were expressed as micrograms per gram on a fresh weight basis. The contents of F and Al in protoplasts and vacuoles were calculated as micrograms of F and Al per 10^6 protoplasts and vacuoles, respectively. The experiments were repeated in triplicate for statistical analysis. The experimental data were subjected to one-way or two-way analysis of variance (ANOVA) to analyze the contents of F and Al in the different parts of tea roots and leaves. Fisher's least significant differences (LSDs) followed by Duncan's multiple range tests were performed to compare the means of F and Al in different fractions of tea roots and leaves. The data in the tables are presented as means ± the standard deviation. For statistical analysis, SAS version 9.0 and SPSS version 13.0 for windows were employed.

RESULTS

Subcellular Localization of F and Al in Tea Roots and Leaves. The purity of subcellular fractions, including the cell wall rich, pellet, and soluble fractions of tea leaves, was tested by examining the activities of marker enzymes. Mitochondria were widely distributed in most of the plant cells and selected as the representative of the organelle fraction. Cytochrome *c* oxidase and glucose-6-phosphate dehydrogenase are primarily present in mitochondria and cytosol and therefore considered as marker enzymes of mitochondria and the soluble fraction of tea leaves, respectively. The activities of both cytochrome *c* oxidase and glucose-6-phosphate dehydrogenase were undetectable in the cell wall rich fraction, indicating no contamination of the cell wall rich fraction by the pellet and soluble fractions (Table 1). Therefore, the Al and F detected in the cell wall rich fraction derived from the retention and accumulation of Al and F, rather than from the release from the pellet and soluble fractions. The activity of glucose-6-phosphate dehydrogenase (the marker for cytosol) in the pellet fraction was 1.4 nmol/min, which was 5.2% of that in the soluble fraction (26.7 nmol/min). This revealed that the level of contamination of the pellet fraction by the soluble fraction was very low, and Al and F examined in the pellet fraction that originated from Al and F contaminated by the soluble fraction were trivial (~5%). The activities of cytochrome *c* oxidase (the marker for mitochondria) in the pellet and soluble fractions were 39.6 and 5.6 nmol/min, respectively, indicating that 12.3% of the pellet fraction may be released into the soluble fraction. Therefore, levels of Al and F measured in the soluble fraction

Table 1. Selected Enzyme Activities in Different Fractions of Tea Leaves[a]

enzyme	cell wall rich fraction (nmol/min)	pellet fraction (nmol/min)	soluble fraction (nmol/min)
glucose-6-phosphate dehydrogenase	undetectable	1.4 ± 0.3 b	26.7 ± 5.8 a
cytochrome *c* oxidase	undetectable	39.6 ± 5.3 a	5.6 ± 1.4 b

[a]The averages within the lines followed by a and b represent significant differences ($p < 0.05$) among selected enzyme activities in the cell wall rich, pellet, and soluble fractions in tea leaves.

dx.doi.org/10.1021/jf4038437 | J. Agric. Food Chem. 2014, 62, 2313−2319

Table 2. Subcellular Localization of F in Tea Roots and Leaves

	roots		leaves	
	[F] (μg/g of fresh weight)	percentage (%)	[F] (μg/g of fresh weight)	percentage (%)
cell wall rich fraction	5.2 ± 1.0 b[a]B[b]	24.6	5.6 ± 0.3 bA	18.9
pellet fraction	4.9 ± 0.2 bB	23.1	2.8 ± 0.2 cB	9.3
soluble fraction	11.1 ± 0.8 aA	52.3	21.4 ± 0.4 aA	71. 8
total/recovery[R]	22.4	94.6[R]	31.5	94.6[R]

[a]The means within the columns followed by a−c were significantly different ($p < 0.05$) among F concentrations in the cell wall rich, pellet (20000g centrifugal force), and soluble fractions of tea roots and leaves. [b]The means within the lines followed by A and B were significantly different ($p < 0.05$) among F concentrations in the cell wall rich, pellet, and soluble fractions between tea roots and leaves.

Table 3. Subcellular Localization of Al in Tea Roots and Leaves

	roots		leaves	
	[Al] (μg/g of fresh weight)	percentage (%)	[Al] (μg/g of fresh weight)	percentage (%)
cell wall rich fraction	108.1 ± 5.8 a[a]A[b]	69.8	160.2 ± 0.5 aA	75.2
pellet fraction	12.1 ± 0.4 cC	7.8	15.1 ± 0.9 cC	7.09
soluble fraction	34.6 ± 1.2 bB	22.4	37.7 ± 1.8 bB	17.7
total/recovery[R]	162.1	95.5[R]	213.0	95.7[R]

[a]The means within the columns followed by a−c were significantly different ($p < 0.05$) among Al concentrations in the cell wall rich, pellet (20000g centrifugal force), and soluble fractions in tea roots and leaves. [b]The means within the lines followed by A and B were significantly different ($p < 0.05$) among Al concentrations in the cell wall rich, pellet, and soluble fractions between tea roots and leaves.

possibly from the release from the pellet fraction during the homogenization were relatively low (approximately 12.3%), but this barely affected the results for Al and F. This result showed that the purity of the cell wall rich, pellet, and soluble fractions isolated from tea leaves was good for Al and F determination.

The total concentration of F in tea roots was 22.4 μg/g, and those in the cell wall rich, pellet, and soluble fractions of tea roots were 5.2, 4.9, and 11.1 μg/g, respectively, accounting for 24.6, 23.1, and 52.3% of that of the total fluoride that accumulated in tea roots, respectively (Table 2). The total concentration of F in leaves was 31.5 μg/g, and those in the cell wall rich, pellet, and soluble fractions of tea leaves were 5.6, 2.8, and 21.4 μg/g, respectively, which account for 18.9, 9.3, and 71.8% of that of the total fluoride that accumulated in tea leaves, respectively (Table 2). The amounts of F in the cell wall rich, pellet, and soluble fractions were 94.6% of those in intact roots and leaves.

Total Al concentrations in tea roots and leaves were 162.1 and 213.0 μg/g, respectively (Table 3). The concentration of total Al in tea leaves was 31.4% higher than that in tea roots. The concentrations of Al in the cell wall rich, soluble, and pellet fractions were 108.1, 34.6, and 12.1 μg/g, respectively, accounting for 69.8, 22.4, and 7.8% of that of the total Al that accumulated in tea roots, respectively (Table 3). In tea leaves, Al concentrations in the cell wall rich, soluble, and pellet fractions were 160.2, 37.7, and 15.1 μg/g, respectively, accounting for 75.2, 17.7, and 7.1% of that of the total Al found in tea leaves, respectively (Table 3). The sums of Al detected in the cell wall rich, pellet, and soluble fractions were 95.5 and 95.7% of that of the total Al measured in intact roots and leaves, respectively (Table 3). More than 70.0% of the total Al in tea roots and leaves was present in the cell wall rich fraction, suggesting that the cell wall rich fraction may immobilize more Al than the pellet and soluble fractions.

F and Al Concentrations in Protoplasts and Vacuoles. Vacuoles were isolated from protoplasts by the lysis of protoplasts and the subsequent purification process. α-Mannosidase is almost exclusively present in vacuoles and therefore considered as a marker enzyme of vacuoles.[27] The purity of vacuoles was examined under a light microscope and by the activity of α-mannosidase. The protoplasts separated from tea leaves were uniform in size (diameters from 15 to 30 μm), and the vacuoles were clearly observed, indicating that the vacuoles were successfully isolated from protoplasts (Figure 1).

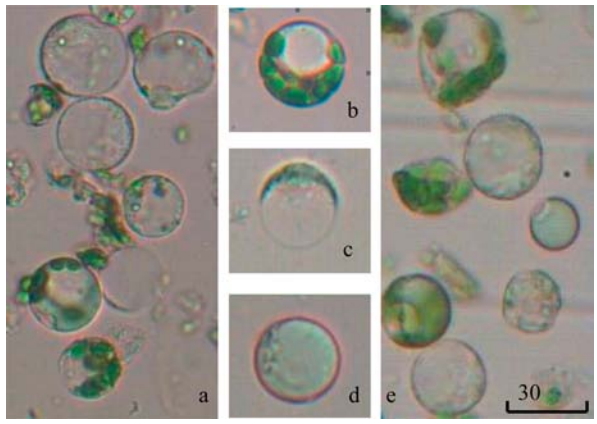

Figure 1. Light micrographs of protoplasts and vacuoles of tea leaves (400×): (a) mixture of protoplasts and vacuoles released from tea leaf pieces, (b) unvacuolated protoplasts, (c) swollen vacuoles, (d) intact vacuoles, and (e) protoplasts and vacuoles on a hemocytometer.

Assuming only one vacuole was released from each protoplast, the activities of α-mannosidase measured in 10^6 protoplasts and 10^6 vacuoles were approximately the same.[33] The activity of α-mannosidase in the vacuoles of the protoplasts of tea leaves was 7.7 nmol/min, accounting for 99.1% of that of the total α-mannosidase (7.6 nmol/min) in protoplasts (Table 4).

To detect the contamination of the vacuoles during the isolation of vacuoles from the protoplasts, extravacuolar marker enzymes, including glucose-6-phosphate dehydrogenase and cytochrome c oxidase, were measured in protoplasts and vacuoles (Table 4). The activities of glucose-6-phosphate dehydrogenase (the marker for cytosol) and cytochrome c oxidase (the marker for mitochondria) in vacuoles were 2.4 and

Table 4. Selected Enzyme Activities in Protoplasts and Vacuoles of Tea Leaves

enzyme	per 10^6 protoplasts (nmol/min)	per 10^6 vacuoles (nmol/min)	relative activity in vacuoles (%)[b]
α-mannosidase	7.7 ± 1.5 a[a]	7.6 ± 1.8 a	99.1
glucose-6-phosphate dehydrogenase	42.3 ± 3.9 a	1.0 ± 0.2 b	2.4
cytochrome *c* oxidase	65.4 ± 5.1 a	1.2 ± 0.3 b	1.8

[a]The averages within the lines followed by a and b represent significant differences ($p < 0.05$) among selected enzyme activity in 10^6 protoplasts and 10^6 vacuoles in tea leaves. [b]The ratio of activity in 10^6 vacuoles to that in 10^6 protoplasts.

1.8% of those detected in the protoplasts, respectively. This result indicated that the level of contamination of the vacuoles by cytosol and mitochondria from protoplasts was very low.

The amounts of F in 10^6 protoplasts and 10^6 vacuole rich fractions were 29.7 and 29.1 μg (fresh weigh), respectively, indicating that the vacuole rich factions contained 98.0% of the total F present in the homogenates of protoplast fractions (Table 5). The amounts of Al were 19.5 and 17.2 μg (fresh weigh) per 10^6 protoplasts and vacuole rich fractions, respectively (Table 5). Approximately 88.0% of the total Al in protoplasts was stored in the vacuole rich fractions. This result indicated that most of the F and Al was localized in the vacuole rich fractions of protoplasts after entering the cytoplasm.

Table 5. Amounts of F and Al in the Protoplasts and Vacuoles of Tea Leaves[a]

	F (μg)	Al (μg)
per 10^6 protoplasts	29.7 ± 3.6 a	19.5 ± 2.7 a
per 10^6 vacuoles	29.1 ± 4.2 a	17.2 ± 1.9 a
% in vacuoles	98.0	88.3

[a]The same letter in each row represents no significant difference ($p > 0.05$) among F and Al concentrations in 10^6 protoplasts and 10^6 vacuoles in tea leaves.

Distributions of Aluminum in Different Fractions of Tea Roots. The total concentration of Al in the whole cell walls was 108.1 μg/g, but the Al concentrations were reduced to 52.1 and 29.0 μg/g, respectively, after the pectin fractions and pectin and hemicellulose fractions had been removed (Table 6). This indicated that pectin and hemicellulose fractions immobilized 51.8 and 21.4% of the total Al, respectively, in the whole cell walls.

The adsorption experiments revealed that the quantities of Al adsorbed on the whole cell walls, cell wall residues without pectin, and cell wall residues without pectin and hemicellulose were increased by 41.0, 6.7, and 9.4%, respectively, as the adsorption time increased from 1 to 2 h (Table 6) . At each adsorption time, the amounts of Al adsorbed on the whole cell walls were significantly larger than those on the cell wall residues without pectin and the cell wall residues without pectin and hemicellulose. The amounts of Al adsorbed on the cell wall residues without pectin were reduced by 28.0 and 54.6% compared with those on the whole cell walls after adsorption for 1 and 2 h, respectively. When both pectin and hemicellulose were removed from the cell walls, the amounts of Al adsorbed on the residual fractions were reduced by 72.5 and 82.0% compared with those on the whole cell walls after adsorption for 1 and 2 h, respectively. These results indicated that pectin and hemicellulose in cell walls may immobilize large amounts of Al in the apoplasts of tea roots.

Table 6. Concentrations and Adsorption of Al in Different Fractions of Tea Roots

		Al adsorption (mg/g)	
	[Al] (μg/g)	1 h	2 h
whole cell walls	108.1 ± 5.8 a[a]	20.4 ± 0.6 aB[b]	34.6 ± 1.2 aA
cell wall residues without pectin	52.1 ± 0.4 b	14.7 ± 0.5 bA	15.7 ± 0.9 bA
cell wall residues without pectin and hemicellulose	29.0 ± 0.8 c	5.6 ± 0.3 cA	6.2 ± 0.7 cA

[a]The means within the columns followed by a–c were significantly different ($p < 0.05$) among Al concentrations or quantities of Al adsorbed on the whole cell walls, cell wall residues without pectin, and cell wall residues without pectin and hemicellulose of tea roots. [b]The means within the lines followed by A and B were significantly different ($p < 0.05$) among Al quantities adsorbed on the whole cell walls, cell wall residues without pectin, and cell wall residues without pectin and hemicellulose of tea roots between 1 and 2 h adsorption times.

DISCUSSION

Tea plants have been found to contain concentrations of Al and F higher than those of many other plants[34] without showing any signs of toxicity, suggesting that Al and F may be detoxified in tea plants. The detoxification by means of compartmentalization at the subcellular level is a common characteristic of hyperaccumulator plants. Sequestration in vacuoles has been suggested to be responsible for heavy metal tolerance in hyperaccumulator plants.[20] For instance, in hyperaccumulator *Thlaspi caerulescens*, Zn is primarily localized in the vacuoles.[21] More than 80% of the total Al in buckwheat leaves was present in the protoplasts, and most Al was localized in the vacuoles, demonstrating that Al was sequestered in the vacuoles of the leaves of plants in which Al accumulates.[19] This study shows that most of the F and Al were present in the soluble fractions of tea roots and leaves, and vacuoles contained 98.0% of the total F and 88.3% of the total Al measured in the protoplasts of tea leaves. This result suggested that internal detoxification of Al and F in the tea roots and leaves may be achieved by their sequestration into vacuoles.[35] In the vacuoles, Al may be chelated with citrate, oxalate, and other organic acids, because the Al–citrate and –oxalate complexes are the stable, less toxic forms of Al, reducing the toxicity of Al in vacuoles.[36] Free fluoride ion (F^-) can also be chelated with cations such as Al^{3+}, Fe^{3+}, and Ca^{2+}. Because the toxicity of AlF_n^{3-n} (such as AlF^{2+}, AlF_2^+, AlF_3, and AlF_4^-), Fe_n^{3-n} (such as FeF^{2+}, FeF_2^+, FeF_3, and FeF_4^-), and CaF_2 complexes is lower than that of F^-, the toxicity of F^- in tea plants can thus be reduced.

Compartmentalization in cell walls may be another major mechanism responsible for Al detoxicification. Root apoplastic spaces, including cell walls and intercellular spaces, are the first compartments of roots that make contact with the potentially toxic Al, and most of the Al that accumulates in roots corresponds to Al in this apoplastic space.[37] Our results demonstrate that cell walls contained 69.8 and 75.2% of the total Al detected in the tea roots and leaves, respectively. This is supported by the observations of Tolra et al.,[38] who indicated that Al was mainly localized in the cell walls of the leaf epidermal cells in tea plants. Carr et al.[39] found that Al in both

young and old tea leaves preferentially accumulated in the cell walls and that the Al concentration in this compartment increased with time. Because cell walls are regarded as a pivotal site for metal storage in plants,[40,41] the deposition of metals in cell walls is considered to be a crucial mechanism for improving heavy metal tolerance. Taylor et al.[35] pointed out that the cell wall is the major site of Al accumulation, and the immobilization of Al in cell walls was one of the crucial exclusion mechanisms for Al detoxification.[16] Wang et al.[42] revealed that more than 85% of the Al absorbed in maize roots was localized in cell walls. In plant cell walls, pectin is a polysaccharide containing galacturonic acids with high electronegativity, which can easily chelate with Al and thus immobilize the Al in cell walls. It was found that both the contents and methylation of pectin contributed to the tolerance of maize to Al toxicity.[43] These results indicate that when pectin was removed from the cell walls of tea roots, the Al concentrations were reduced by 51.8%, and the adsorption of Al in the cell wall residues also significantly declined. These findings suggested that the pectin fractions in the cell walls of tea roots may fix the Al in apoplasts and thus reduce the toxicity of Al to tea plants.

The positive correlations between F and Al concentrations in tea plants have been observed, leading to the hypothesis that the uptake of F and Al were somewhat linked.[44] Free fluoride ions (F^-) can be chelated with aluminum ions (Al^{3+}) in the forms of AlF^{2+}, AlF_2^+, AlF_3, AlF_4^-, etc.[34] F and Al in the forms of Al−F complexes were readily taken up and transported in the xylem of tea shoots.[13,45] Al−F complexes such as AlF_2^+ and AlF^{2+} were less toxic than hydroxy and Al^{3+} forms such as Al^{3+}, $Al(OH)_2^+$, and $Al(OH)^{2+}$.[46] These findings suggested that the forms of F and Al also determined their toxicity to tea plants. F and Al complexes could be in the form of AlF^{2+}, AlF_2^+, AlF_3, AlF_4^-, etc., or their combinations. However, the exact forms of F and Al complexes in the different subcellular fractions of tea plants are still unclear. Consequently, further studies are needed to understand the chemical species of Al−F complexes in different parts of tea plants to determine the mechanisms of the tolerance of tea plants to F and Al toxicity.

AUTHOR INFORMATION

Corresponding Author

*School of Resources and Environment, Anhui Agricultural University, 130 W. Changjiang Rd., Hefei 230036, People's Republic of China. E-mail: hjgao@ahau.edu.cn. Telephone: +86-551-65867447. Fax: +86-551-65786316.

Funding

This work was supported by the National Natural Science Foundation of China (41071158 and 31272254), the Science Foundation for Distinguished Young Scholars of Anhui Province (1408085J01), and the earmarked fund for Modern Agro-industry Technology Research System by the Chinese Ministry of Agriculture (nycytx-26).

Notes

The authors declare no competing financial interest.

ACKNOWLEDGMENTS

We thank Hai-sheng Cao and Xun-gang Gu at Anhui Agricultural University for analyzing Al and F in tea plants using ion chromatography.

REFERENCES

(1) Yamamoto, T.; Juneja, L. R.; Kim, M. *Chemistry and application of green tea*; CRC Press Inc.: Boca Raton, FL, 1997.

(2) Xie, Z. M.; Ye, Z. H.; Wong, M. H. Distribution characteristics of fluoride and aluminum in soil profiles of an abandoned tea plantation and their uptake by six woody species. *Environ. Int.* **2001**, *26*, 341−346.

(3) Simpson, A.; Shaw, L.; Smith, A. J. The bio-availability of fluoride from black tea. *J. Dent.* **2001**, *29*, 15−21.

(4) Guo, B. Y.; Cheng, Q. K. Chelating capability of tea components with metal ion. *J. Tea Sci.* **1991**, *11*, 139−144.

(5) Gao, H. J.; Jin, Y. Q.; Wei, J. L. Health risk assessment of fluoride in drinking water from Anhui province in China. *Environ. Monit. Assess.* **2013**, *185*, 3687−3695.

(6) Cao, J.; Zhao, Y.; Liu, J. Brick tea consumption as the cause of dental fluorosis among children from Mongol, Kazak and Yugu populations in China. *Food Chem. Toxicol.* **1997**, *35*, 827−833.

(7) McLachlan, D. R. C. Aluminum and the risk for Alzheimer's disease. *Environmetrics* **1995**, *6*, 233−275.

(8) Cao, J.; Zhao, Y.; Liu, J.; Xirao, L. D.; Danzeng, S. B.; Daji, D. W.; Yan, Y. Brick tea fluoride as a main source of adult fluorosis. *Food Chem. Toxicol.* **2003**, *41*, 535−542.

(9) Erdemoğlu, S. B.; Pyrzyniska, K.; Güçer, Ş. Speciation of aluminum in tea infusion by ion-exchange resins and flame AAS detection. *Anal. Chim. Acta* **2000**, *411*, 81−89.

(10) Gao, H. J.; Zhang, Z. Z.; Wan, X. C. Influences of charcoal and bamboo charcoal amendment on soil fluoride fractions and bioaccumulation of fluoride in tea plants. *Environ. Geochem. Health* **2012**, *34*, 551−562.

(11) Karak, T.; Bhagat, R. M. Trace elements in tea leaves, made tea and tea infusion: A review. *Food Res. Int.* **2010**, *43*, 2234−2252.

(12) Wenzel, W. W.; Blum, W. E. H. Fluorine speciation and mobility in F-contaminated soils. *Soil Sci.* **1992**, *153*, 357−364.

(13) Nagata, T.; Haytsu, M.; Kosuge, N. Aluminum kinetics in the tea plant using ^{27}Al-NMR and ^{19}F-NMR. *Phytochemsity* **1993**, *32*, 771−775.

(14) Ding, R. X.; Huang, X. Biogeochemical cycle of aluminum and fluorine in tea garden soil system and its relationship to soil acidification. *Turang Xuebao* **1991**, *28*, 229−236.

(15) Matsumoto, H.; Hirasawa, E.; Morimura, E.; Takahashi, E. Localization of aluminum in tea leaves. *Plant Cell Physiol.* **1976**, *17*, 627−631.

(16) Taylor, G. J. Current views of the aluminum stress response: The physiological basis of tolerance. *Curr. Top. Plant Biochem. Physiol.* **1991**, *10*, 57−93.

(17) Zheng, S. J.; Yang, J. L.; He, Y. F.; Yu, X. H.; Zhang, L.; You, J. F.; Shen, R. F.; Matsumoto, H. Immobilization of aluminum with phosphorus in roots is associated with high aluminum resistance in buckwheat. *Plant Physiol.* **2005**, *138*, 297−303.

(18) Morita, A.; Horie, H.; Fujii, Y.; Takatsu, S.; Watanabe, N.; Yagi, A.; Yokota, H. Chemical forms of aluminum in xylem sap of tea plants (*Camellia sinensis* L.). *Phytochemistry* **2004**, *65*, 2775−2780.

(19) Shen, R. F.; Ma, J. F.; Kyo, M.; Iwashita, T. Compartmentation of aluminum in leaves of an accumulator, *Fagopyrum esculentum* Moench. *Planta* **2002**, *215*, 394−398.

(20) Hall, J. L. Cellular mechanisms for heavy metal detoxification and tolerance. *J. Exp. Bot.* **2002**, *53*, 1−11.

(21) Küpper, H.; Zhao, F. J.; McGrath, S. P. Cellular compartmentation of zinc in leaves of the hyperaccumulator *Thlaspi caerulescens*. *Plant Physiol.* **1999**, *119*, 305−311.

(22) Weigel, H. J.; Jäger, H. J. Subcellular distribution and chemical form of cadmium in bean plants. *Plant Physiol.* **1980**, *65*, 480−482.

(23) Yoo, S. D.; Cho, Y. H.; Sheen, J. *Arabidopsis* mesophyll protoplasts: A versatile cell system for transient gene expression analysis. *Nat. Protoc.* **2007**, *2*, 1565−1572.

(24) Cooking, E. C. A method for the isolation of plant protoplasts and vacuoles. *Nature* **1960**, *4771*, 962−963.

(25) Wagner, G. J.; Siegelman, H. W. Large-scale isolation of intact vacuoles and isolation of chloroplasts from protoplasts of mature plant tissues. *Science* **1975**, *190*, 1298−1299.

(26) Granstedt, R. C.; Huffaker, R. C. Identification of the leaf vacuole as a major nitrate storage pool. *Plant Physiol.* **1982**, *70*, 410−413.
(27) Boller, T.; Kende, H. Hydrolytic enzymes in the central vacuole of plant cells. *Plant Physiol.* **1979**, *63*, 1123−1132.
(28) Leonard, R. T.; Hansen, D.; Hodges, T. K. Membrane-bound adenosine triphosphatase activities of oat roots. *Plant Physiol.* **1973**, *51*, 749−754.
(29) Hiiusler, E.; Petersen, M.; Alfermann, A. W. Isolation of protoplasts and vacuoles from cell suspension cultures of *Coleus blumei* Benth. *Plant Cell Rep.* **1993**, *12*, 510−512.
(30) Zhong, H. L.; Lauchli, A. Changes of cell wall composition and polymer size in primary roots of cotton seedlings under high salinity. *J. Exp. Bot.* **1993**, *44*, 773−778.
(31) Mort, A. J.; Moerschbacher, B. M.; Pierce, M. L.; Maness, N. O. Problems encountered during the extraction, purification and chromatography of pectin fragments, and some solution to them. *Carbohydr. Res.* **1991**, *215*, 219−277.
(32) Zhang, X. C.; Gao, H. J.; Zhang, Z. Z.; Wan, X. C. Influences of different ion channel inhibitors on the absorption of fluoride in tea plants (*Camellia sinesis* L.). *Plant Growth Regul.* **2013**, *69*, 99−106.
(33) Martinoia, E.; Heck, U.; Wiemken, A. Vacuoles as storage compartments for nitrate in barley leaves. *Nature* **1981**, *289*, 292−293.
(34) Xie, Z. L.; Chen, Z.; Sun, W. T.; Guo, X. J.; Yin, B.; Wang, J. H. Distribution of aluminum and fluoride in tea plant and soil of tea garden in central and southwest China. *Chinese Geographical Science* **2007**, *17*, 376−382.
(35) Taylor, G. J.; McDonald-Stephens, J. L.; Hunter, D. B.; Bertsch, P. M.; Elmore, D.; Rengel, Z.; Reid, R. J. Direct measurement of aluminum uptake and distribution in single cells of *Chara corallina*. *Plant Physiol.* **2000**, *123*, 987−996.
(36) Morita, A.; Yanagisawa, O.; Takatsu, S.; Maeda, S.; Hiradate, S. Mechanism for the detoxification of aluminum in roots of tea plant (*Camellia sinensis* (L.) *Kuntze*). *Phytochemistry* **2008**, *69*, 147−153.
(37) Heim, A.; Luster, J.; Brunner, I.; Frey, B.; Frossard, E. Effects of aluminum treatment on Norway spruce roots: Aluminum binding forms, element distribution, and release of organic substances. *Plant Soil* **1999**, *216*, 103−115.
(38) Tolra, R.; Vogel-Mikus, K.; Hajiboland, R.; Kump, P.; Pongrac, P.; Kaulich, B.; Gianoncelli, A.; Babin, V.; Barcelo, J.; Regvar, M.; Poschenrieder, C. Localization of aluminum in tea (*Camellia sinensis* L.) leaves using low energy X-ray fluorescence spectro-microscopy. *J. Plant Res.* **2011**, *124*, 165−172.
(39) Carr, H. P.; Lombi, E.; Kupper, H.; McGrath, S. P.; Wong, M. H. Accumulation and distribution of aluminum and other elements in tea (*Camellia sinensis* L.) leaves. *Agronomie* **2003**, *23*, 705−710.
(40) Lozano-Rodriguez, E.; Hemandz, L. E.; Bonay, P.; Carpena-rui, R. O. Distribution of cadmium in root tissues of maize and pea plants: Physiological disturbances. *J. Exp. Bot.* **1997**, *306*, 123−128.
(41) Carrier, P.; Baryla, A.; Havaux, M. Cadmium distribution and microlocalization in oilseed rape (*Brassica napus*) after long-term growth on cadmium-contaminated soil. *Planta* **2003**, *216*, 939−950.
(42) Wang, Y.; Stass, A.; Horst, W. J. Apoplastic binding of aluminum is involved in silicon-induced amelioration of aluminum toxicity in maize. *Plant Physiol.* **2004**, *136*, 3762−3770.
(43) Eticha, D.; Stass, A.; Horst, W. J. Cell wall pectin and its degree of methylation in the maize root-apex: Significance for genotypic differences in aluminum resistance. *Plant, Cell Environ.* **2005**, *28*, 1410−1420.
(44) Ruan, J. Y.; Ma, L. F.; Shi, Y. Z.; Han, W. Y. Uptake of fluoride by tea plant (*Camellia sinensis* L.) and the impact of aluminum. *J. Sci. Food Agric.* **2003**, *83*, 1342−1348.
(45) Yumata, H.; Hattori, T. Investigation of the relationship between aluminum and fluorine in plants (Part 1). Relationship between aluminum and fluorine in tea leaves. *J. Sci. Soil Manure* **1977**, *48*, 253−261.
(46) Stevens, D. P.; McLaughlin, M. J.; Alston, A. M. Phytotoxicity of aluminum-fluoride complexes and their uptake from solution culture by *Avena sativa* and *Lycopersicon esculentum*. *Plant Soil* **1997**, *192*, 81−93.

This led researchers to monitor stable isotope labeled anthocyanins in grapes cultured in vitro at high and low temperatures, demonstrating that high temperatures resulted in anthocyanin degradation.[15] Increased temperature has been shown to alter the profile of anthocyanins, resulting in an increase of trihydroxylated as well as acetylated and coumarylated moiety proportions.[16,17] At present, a clear understanding of temperature's influence on individual anthocyanin regulation and/or degradation is still lacking.

The perceived quality of red grapes for winemaking is highly dependent on the resulting pigmentation of the final wine.[18] Although color is not the only factor, red grapes grown in warm growing regions such as the central valley of California, Riverlands in Australia, or Languedoc in France have only moderate color and command prices that are significantly lower than those grown in cooler regions. With an increased understanding of how warm climates affect anthocyanin concentrations, it may be possible to improve the pigmentation of warm-region grapes. An understanding of the mechanisms that control color loss as suggested below may lead to treatments to preserve color in warmer climates.

To address the need for following the metabolic pathway of anthocyanins in grape berries, a method was recently reported that utilizes a distinct isotopic label.[19] Tracing this label can provide a means to follow the appearance and loss of substances in the phenylpropanoid pathway as well as how environmental factors may influence the pathway. Anthocyanin turnover has been shown in *Brunfelsia calycina* flowers and in mustard seedlings;[20,21] however, the prevention of anthocyanin degradation has only recently been targeted for color improvement in agricultural crops.[22] Anthocyanin degradation in grapes has been demonstrated, but only using an in vitro model on Petri dishes.[15] The current study utilizes L-phenyl-$^{13}C_6$-alanine (Phe^{13}) as a tracer to investigate flavonoid metabolism and catabolism in *V. vinifera* cv. Cabernet Sauvignon berries on the vine throughout maturation during two growing seasons to begin to address the color issue in warm-climate grapes.

MATERIALS AND METHODS

Sample Collection and Tracer Addition. This research utilizes a method that was recently developed and is briefly described below. Grape samples came from self-rooted Cabernet Sauvignon, Clone 8, vines in the Hopkins experimental vineyard at the University of California, Davis, CA, USA. Grape maturation studies were conducted during the summers of 2010 and 2011 on clusters selected from contiguous vines within a single row. Grape berry clusters were soaked in Phe^{13} for 48 h while remaining on the vine at two different stages of maturity: unripe green grapes and ripening red grapes.

In 2010, the grape clusters were treated with tracer on July 29 and August 31 for green and red treatments, respectively. In 2011, grape clusters received tracer on July 7 and August 22 for green and red treatments, respectively. For each treatment, 4 clusters received the tracer, and 3 individual grapes from each cluster were harvested for each time point, yielding 12 berries per time point. The excised berries were frozen at −80 °C and stored until extraction.

Extraction and LC-DAD-MS/MS Analysis. Individual, lyophilized grape berries without their seeds were extracted in 60% acetone for 24 h. The supernatant was then centrifugally evaporated and reconstituted in water. The resulting extract was stored at −80 °C until analysis by HPLC-DAD-MS/MS. Analysis of grape extracts was conducted using an Agilent series 1200 instrument in line with an Agilent 6430 triple-quadrupole mass spectrometer with electrospray injection (Agilent Technologies, Santa Clara, CA, USA). A binary gradient of 10% formic acid in water versus pure acetonitrile was used to separate phenolics on an Agilent Zorbax SB-C18 Rapid Resolution HT small-particle column (4.6 mm × 100 mm, 1.8 μm) with a precolumn filter. The diode array detector (DAD) monitored four wavelenths: 280, 316, 365, and 520 nm. The mass spectrometer acquired data using "dynamic MRM" mode so it was possible to measure positively and negatively ionized isotopomers during the same run. Specific retention times and MRM transitions for each isotopomer can be found in our previous publication.[19] Quantitation of total phenolic levels was achieved through external standardization by UV−vis absorbance using representative standards for each class of compounds (caffeic acid for hydroxycinnamates, rutin for flavonols, and malvidin-3-glucoside for anthocyanins). The total concentration was then multiplied by the ratio of labeled to unlabeled phenolics to determine their respective concentrations. External standards of Phe and Phe^{13} were used for quantitation by LC-MRM-MS (166.3 → 120 and 172.3 → 126, respectively). The graphical heatmaps in Figures 2 and 3 were created using the open source Excel add-in imDev.[23]

Statistical Analysis. Comparisons of each metabolite over time were analyzed using R (version 3.0.2). A one-way ANOVA with p values adjusted for multiple hypothesis testing at $q = 0.05$ was used to determine significant changes over time for each metabolite in red and green berries from 2010 and 2011.[24]

RESULTS AND DISCUSSION

Using our recently developed technique to incorporate stable isotopic label into grape flavonoids in situ, we sought to probe the evolution and turnover of grape phenolics throughout maturation.[19] Multiple classes of Phe-derived phenolics were monitored throughout the maturation process over two vintages, providing a rare glimpse of overall phenolic metabolism. Furthermore, using the Phe^{13} tracer, we hoped to shed light on several facets of grape phenolic metabolism: the disappearance of hydroxycinnamates, the different patterns of flavonol biosynthesis, and the turnover or degradation of anthocyanins. Although our tracer did not perform exactly as we had expected, the deviations from our expectations suggest there are even more mysteries in phenolic substrate regulation.

Levels of grape phenolics were monitored throughout the 2010 and 2011 growing seasons starting on July 29 and July 7, respectively. In addition, the stable isotopic tracer L-phenyl-$^{13}C_6$-alanine was introduced to berry clusters on the vine two times during each season to observe the incorporation of label at two stages of maturity: green preripened and red ripening grapes. Following each of the four treatments, the concentrations of both unlabeled and labeled phenolic metabolites were monitored throughout the ripening season. Berry variability was generally below 15, 20, or 15% (relative standard error) for unlabeled hydroxycinnamates, flavonols, and anthocyanins at concentrations above 10 nmol/berry, respectively (Supporting Information file 1).

Phenylalanine Tracer. Phenylalanine levels ranged from 7.3 to 57.2 nmol/berry in 2010 and from 12.0 to 112.2 nmol/berry in 2011 in the red and green grape trials (Figure 1b). After the treatment of the clusters, Phe^{13} was readily found in the grape berries, and its gradual decline typically followed within 2 weeks. However, in all four trials a steady, but very low, level of Phe^{13} persisted until the end of the season, in one case 89 days after the treatment was concluded (Figure 1b). In both years more Phe^{13} was absorbed into red berries, although we cannot explain why this occurred.

Phenolic Metabolites during Maturation. Hydroxycinnamate tartrate esters were already present in green grapes prior to treatment and declined precipitously after the onset of ripening. Caftaric, *cis*-coutaric, and *trans*-coutaric acids dropped to <10% of their initial values over the course of the

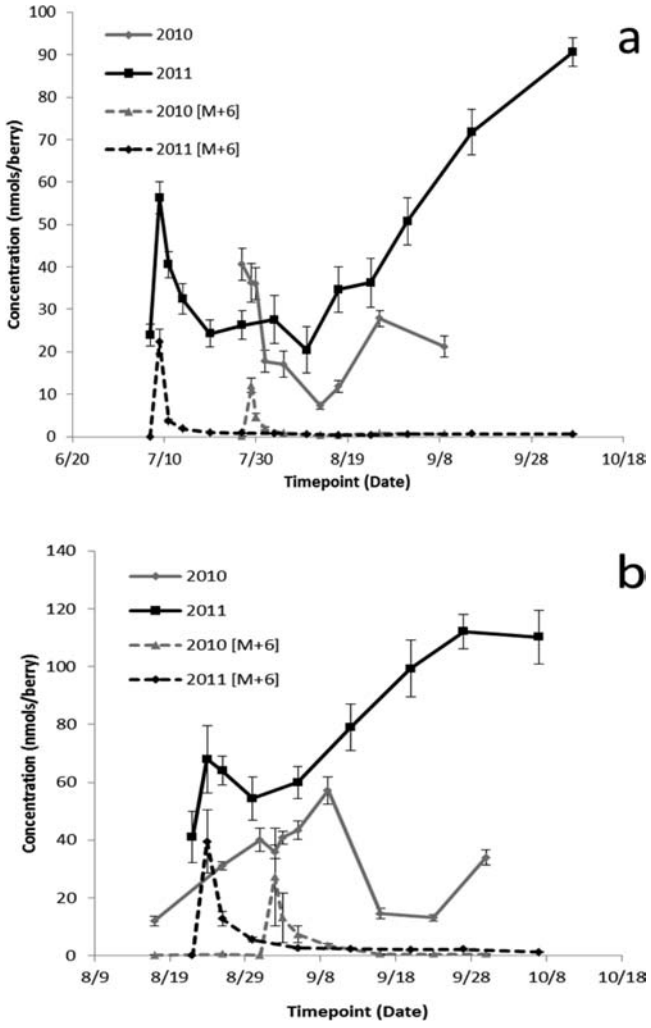

Figure 1. Average phenyalanine concentration ± standard error (nmol/berry) in labeled and unlabeled grape berries following treatment with Phe[13] in (a) green and (b) red grapes.

experiments (Supporting Information file 1), consistent with previous studies.[3−5] Although miniscule amounts of labeled *cis*-coutaric and *trans*-coutaric acids were detected at a few time points from green grapes in 2010 and 2011, their quantities were below the limit of quantitation (data not shown). Label was never found in caftaric acid or in any of the hydroxycinnamates in treated red grapes. The tiny, or nonexistent, labeling of these phenylpropanoids could be a result of the hydroxycinnamic−tartrate ester pool having already been amassed with no further biosynthesis or from the label not entering the pulp of the berry, where these compounds are synthesized and stored.

Flavonols, with the exception of quercetin-3-*O*-glucuronide, were not present in great quantity per berry prior to the onset of ripening. After the onset of ripening, levels steadily increased for 3−4 weeks until reaching a semisteady state. Quercetin-3-*O*-glucuronide, on the other hand, was present at the beginning of each experiment, and its level did not appear to be strongly influenced by maturity. Incorporation of tracer into flavonols depended on grape maturity at the time of treatment. Green grapes that were treated produced detectable levels of myricetin, quercetin, laricitran (2011 only), and kaempferol moieties, whereas quercetin was the sole flavonol found in treated red grapes. With the exception of quercetin, each of the labeled flavonols did not appear until after the onset of ripening. Ultimately, labeled flavonols were present in very minute amounts, most likely due to the dominance of anthocyanin production occurring simultaneously (Supporting Information file 1).

The entire anthocyanin data set is represented in four graphical heatmaps standardized by the relative quantities of each metabolite (Figures 2 and 3). With the exception of the malvidin moieties, anthocyanin ripening profiles generally followed a consistent pattern regardless of substitutions on the 3-*O*-glucose. Concentrations tended to peak in mid to late August but declined in 2010 and remained stagnant in 2011 during the remainder of the season. Malvidin moieties, on the other hand, climbed steadily throughout maturation and often continued to accumulate (Figure 4a), especially the acetylated and coumarylated varieties, until the end of the trial.

Although previous studies consistently indicate that comparative higher temperatures tend to increase the proportion of hydroxylated and methylated anthocyanin B rings,[16,17] many studies have not commented on the change in profile over the ripening process. Our results indicate that moieties of malvidin and, to a lesser extent, peonidin tend to increase during late-stage ripening, whereas cyanidin and dephinidin decrease (Figures 2a and 3a). A previous study also showed cyanidin to decrease during late-stage ripening; however, in the same study delphinidin continued to increase.[10] In our study, it is unclear whether the decrease of di- and trihydroxylated anthocyanins represents anthocyanin degradation or if the shift represents continued metabolism by anthocyanin *O*-methyltransferase (AOMT), which may be the dominant pathway in grapes.[25,26] Acylated anthocyanins also showed similar trends during ripening during 2010 and 2011; however, AOMT has shown no affinity for coumarylated anthocyanins,[27] and no studies to our knowledge have assessed the enzyme's activity with acetylated anthocyanins.

Overall, the total quantity of incorporated label per berry varied depending upon the time of incorporation (Supporting Information file 1). The sum of incorporated label detected in all of the labeled metabolites reached 46, 7, 16, and 13% of the maximum concentration of Phe[13] measured in 2010 and 2011 green and 2010 and 2011 red berries, respectively. The large difference between 2010 and 2011 green incorporation percentages reflects the addition of tracer at the onset of ripening in 2010 versus tracer addition 2−3 weeks prior to veraison in 2011. These data illustrate that adding tracer immediately prior to veraison resulted in the greatest recovery of label.

Labeled Anthocyanins during Maturation. Labeled anthocyanins were typically present at 0.1−1% of their unlabeled counterparts, depending on how recently the grapes were treated in green grapes or the stage of maturity in red grapes. The variability of labeled anthocyanins within 12 replicate berries was generally below 30% in red-treated grapes and below 20% (relative standard error) in green-treated grapes (Supporting Information file 1). Labeled metabolites in red grapes from 2011 tended to have higher variation and resulted in only a select few labeled metabolites varying significantly over time (Figure 3b). Labeled cyanidin and delphinidin moieties tended to increase rapidly after tracer incorporation in red grapes or after the onset of ripening in green grapes but began to decrease shortly thereafter, with the exception of red grapes labeled in 2010, which experienced a slight surge in late September. After rising rapidly, labeled petunidin tended to

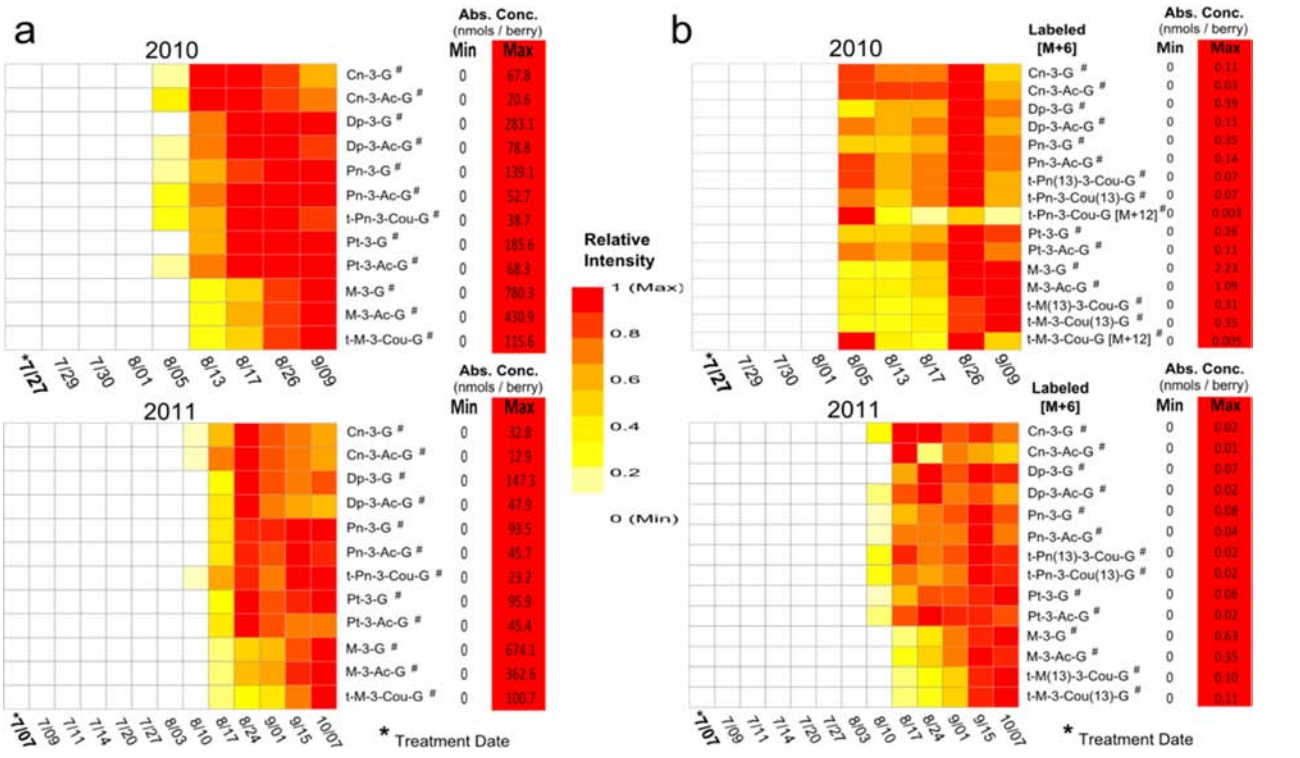

Figure 2. Relative intensities of (a) unlabeled and (b) labeled anthocyanins following treatment of green grapes with Phe[13] tracer. Cn, cyanidin; G, glucoside; Ac, acetyl; Dp, delphinidin; Pn, peonidin; Pn(13), labeled peonidin; Cou, coumaryl; Cou(13), labeled coumaryl; Pt, petunidin; M, malvidin; M(13), labeled malvidin. #, Multiple measures adjusted $p < 0.01$.

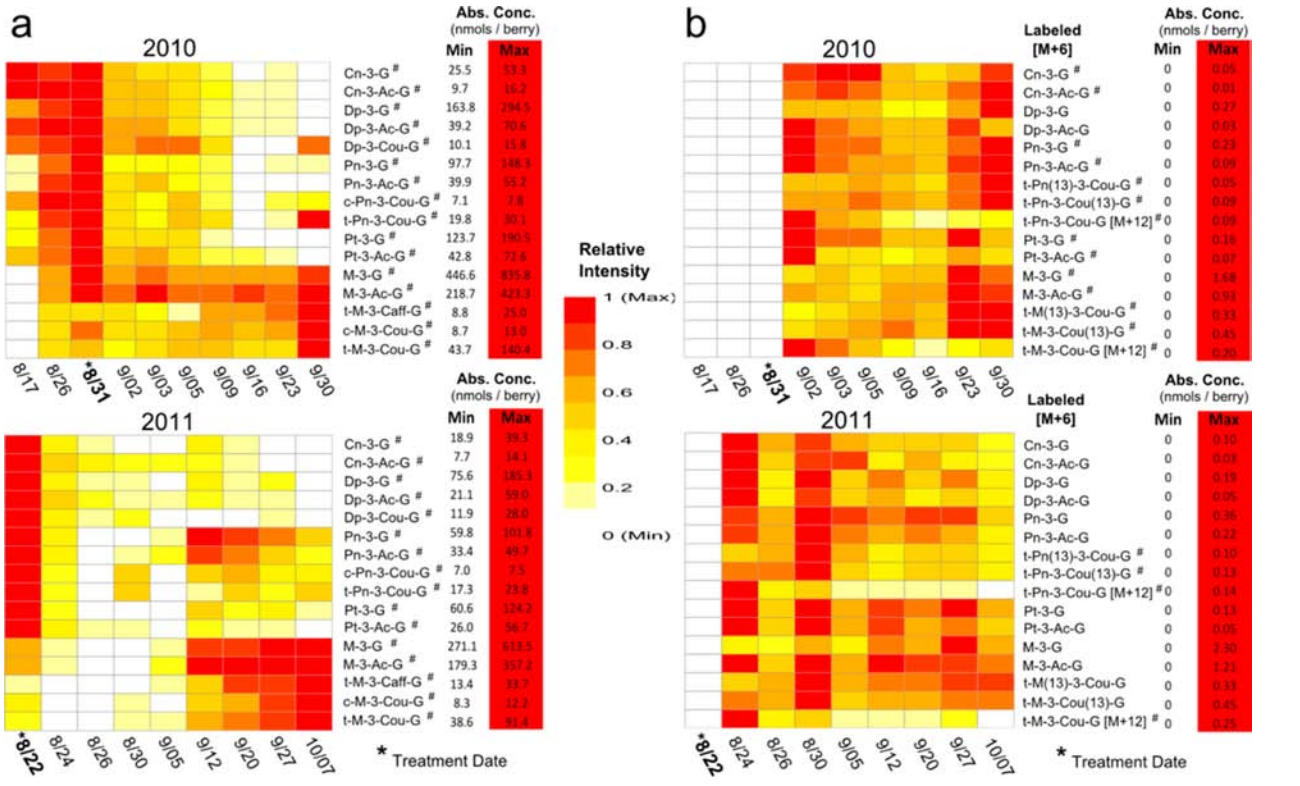

Figure 3. Relative intensities of (a) unlabeled and (b) labeled anthocyanins following treatment of red grapes with Phe[13] tracer. Cn, cyanidin; G, glucoside; Ac, acetyl; Dp, delphinidin; Pn, peonidin; Pn(13), labeled peonidin; Cou, coumaryl; Cou(13), labeled coumaryl; Pt, petunidin; M, malvidin; M(13), labeled malvidin. #, Multiple measures adjusted $p < 0.05$.

level off and remain constant during ripening. Labeled peonidin profiles appeared erratic, whereas malvidin was the only labeled anthocyanin to regularly increase in concentration throughout ripening (Figure 4b). However, both malvidin and peonidin

dx.doi.org/10.1021/jf402229u | J. Agric. Food Chem. 2014, 62, 2321−2326

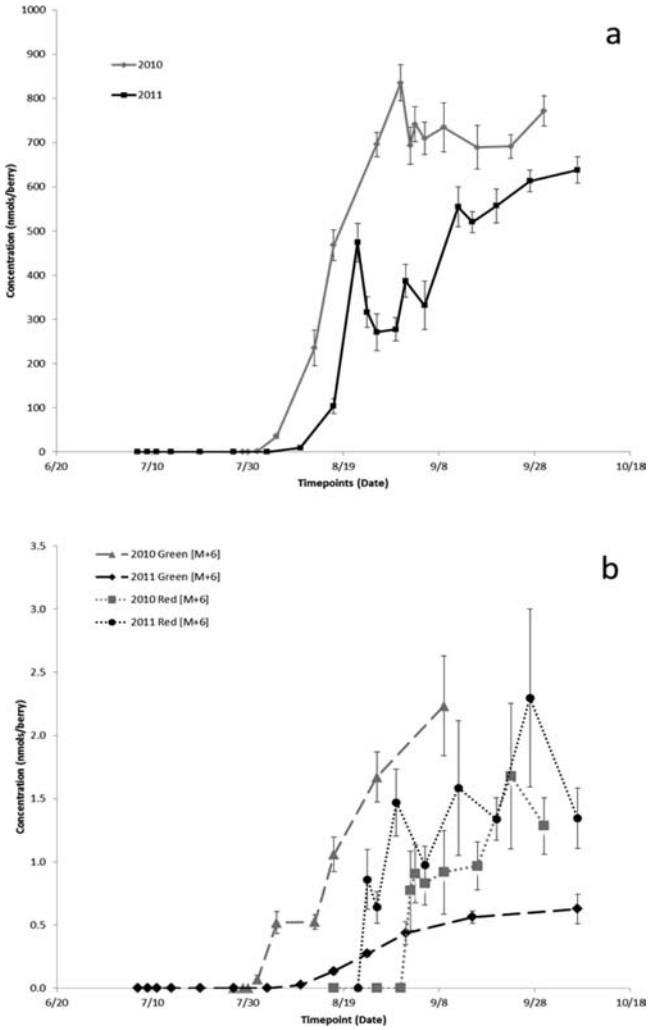

Figure 4. Average malvidin-3-glucoside (M-3-G) concentration ± standard error (nmol/berry) during the 2010 and 2011 growing seasons: (a) ripening profile of unlabeled M-3-G throughout ripening; (b) labeled M-3-G in grape berries following Phe^{13} addition to green and red grapes. Each metabolite varied significantly due to the influence of date with the exception of labeled M-3-G in red 2011 grapes.

had consistently higher percentages of label (labeled/unlabeled) as compared to delphinidin, petunidin, and cyanidin in red grape treatments. When considered alongside the development profiles, this may indicate that AOMT activity is active throughout the metabolism of anthocyanins and acts upon compounds typically considered final metabolites (i.e., delphinidin, cyanidin, petunidin), whereas flavonoid-3′,5′-hydroxylase does not.

A notable intricacy of anthocyanin metabolism in grapes is the production of coumarylated anthocyanins. When Phe^{13} is present, three labeled isotopomers become possible: a labeled anthocyanidin (antho^{13}-cou), a labeled *p*-coumaroyl group (antho-cou^{13}), and a molecule that contains both the labeled anthocyanidin and a *p*-coumaroyl group. The relative incorporation of label between these different isotopomers can provide information on pathway regulation. In our study, when red grape berries were treated with Phe^{13}, there was an increase in the proportion of antho-cou^{13} as compared to antho^{13}-cou. However, this trend was not observed when green grapes were treated; the antho-cou^{13} and antho^{13}-cou isotopomers of malvidin had the same proportions as compared to the unlabeled moiety. This trend indicates that coumarate may be esterified to anthocyanin glucosides well after their initial biosynthesis. Under this hypothesis, when label is added to red grapes, labeled coumaryl groups are conjugated to existing, unlabeled anthocyanins in addition to newly produced, labeled anthocyanins, whereas when the label was added to green grapes, the label formed a uniform pool that was distributed equitably between the two possible positions after the onset of ripening.

Persistence of Label and Implications. Perhaps the most interesting result of the study is the production of labeled anthocyanins as late as 1 month after tracer addition (Figures 1a and 2a) in green grapes incubated in 2011. Whereas the concentration of Phe^{13} dropped to, and remained less than, 1 nmol/berry by July 20, anthocyanins did not begin to be produced until August 10, 2011. Despite the apparent low levels of Phe^{13}, labeled malvidin-3-glucoside continued to accumulate until September 15, 2011. In fact, in all treatments, levels of Phe^{13} dropped to <1 nmol/berry but remained persistent throughout ripening (Supporting Information file 1). This holdover of label indicates that there may be an intermediate pool of label held sequestered in grape berries until the onset of ripening when phenylpropanoid metabolism is ramped up. We suspect that the large in-flux of Phe^{13} is readily converted into a storage form and is subsequently released as needed during maturation. The most obvious candidate for the hypothetical pool of stored label is in the form of phenolamides. Phenolamides are known to exist in grape berries[28] and have been recently suggested as serving as intermediates for phenolic metabolism.[29] Phenolic metabolism has long been assumed to occur directly from phenylalanine, but mounting evidence supports the theory that there is an intermediate substrate pool that may be accumulated and further metabolized under demand. Ultimately, further research must be completed to confirm and identify the hidden source of labeled Phe^{13} that seems apparent here.

Using the longstanding model of phenylpropanoid metabolism, our experiment was designed to follow the lifetime of individual anthocyanins after they were labeled with stable isotopic tracer. Our results demonstrated the expected accumulation of anthocyanins and the direction of label almost exclusively to those flavonoids. However, under this design, we hoped to estimate the turnover of anthocyanins in grape berries in situ. However, the unexpected persistence of labeled substrate prevented a fair assessment of turnover because we continued to see biosynthesis of labeled metabolites well after each treatment. This persistence of label presents new evidence that there may be an intermediate pool of phenolic substrate in grape berries, perhaps stored in anticipation of the onset of ripening. Future studies to uncover the intermediate pool as well as to compare tracer incorporation and turnover between warm- and cool-climate grapes are underway.

■ ASSOCIATED CONTENT

Supporting Information

Supplemental spreadsheet 1 contains the average concentrations (nmol/berry), standard deviation (Stdev), standard error (StErr) of the mean, and relative standard error of the mean (%) for phenylalanine, hydroxycinnamate tartrate esters, flavonols, and anthocyanin at each time point measured during the 2 years. Additionally, the multiple measurement adjusted *p*

dx.doi.org/10.1021/jf402229u | J. Agric. Food Chem. 2014, 62, 2321−2326

values from one-way ANOVAs are included. This material is available free of charge via the Internet at http://pubs.acs.org.

AUTHOR INFORMATION

Corresponding Author

*Phone: +1-530-752-4777. E-mail: alwaterhouse@ucdavis.edu.

Present Address

†Genome Center − Metbolomics, University of California, Davis, CA 95616, USA. NIH 1U24DK097154; PI Fiehn, Oliver.

Funding

A.W.C. was supported by graduate student fellowships including the Mario P. Tribuno Memorial Research Fellowship, Wine Spectator Scholarship, Horace O. Lanza Scholarship, Adolf L. & Richie C. Heck Research Scholarship, Leon D. Adams Research Scholarship, and Curtis J. Alley Memorial Research Scholarship.

Notes

The authors declare no competing financial interest.

ACKNOWLEDGMENTS

Anita Oberholster was incredibly kind to grant access to her LC-DAD-MS/MS instrument. Undergraduate student researchers Christopher Barberi, Monthakan Boonpermpol, Aaron Garlits, Sarah Suharwardy, Nina Vuoso, Natalie Bates, and C. Damon Roberts helped with sample extraction. Dmitry Grapov adapted his software package, ImDev, to enable the graphical heatmaps present in this paper.

REFERENCES

(1) Koukol, J.; Conn, E. E. The metabolism of aromatic compounds in higher plants: IV. Purification and properties of the phenylalanine deaminase of *Hordeum vulgare*. *J. Biol. Chem.* **1961**, *236*, 2692−2698.

(2) Neish, A. C. Biosynthetic pathways of aromatic compounds. *Annu. Rev. Plant Physiol. Plant Mol. Biol.* **1960**, *11*, 55−80.

(3) Desimon, B. F.; Hernandez, T.; Estrella, I. Phenolic composition of white grapes (var. Airen) − changes during ripening. *Food Chem.* **1993**, *47*, 47−52.

(4) Romeyer, F. M.; Macheix, J. J.; Goiffon, J. P.; Reminiac, C. C.; Sapis, J. C. The browning capacity of grapes. 3. Changes and importance of hydroxycinnamic acid tartaric acid-esters during development and maturation of the fruit. *J. Agric. Food Chem.* **1983**, *31*, 346−349.

(5) Adams, D. O. Phenolics and ripening in grape berries. *Am. J. Enol. Vitic.* **2006**, *57*, 249−256.

(6) Koyama, K.; Ikeda, H.; Poudel, P. R.; Goto-Yamamoto, N. Light quality affects flavonoid biosynthesis in young berries of Cabernet Sauvignon grape. *Phytochemistry* **2012**, *78*, 54−64.

(7) Downey, M. O.; Harvey, J. S.; Robinson, S. P. The effect of bunch shading on berry development and flavonoid accumulation in Shiraz grapes. *Aust. J. Grape Wine Res.* **2004**, *10*, 55−73.

(8) Price, S. F.; Breen, P. J.; Valladao, M.; Watson, B. T. Cluster sun exposure and quercetin in Pinot-Noir grapes and wine. *Am. J. Enol. Vitic.* **1995**, *46*, 187−194.

(9) Downey, M. O.; Harvey, J. S.; Robinson, S. P. Synthesis of flavonols and expression of flavonol synthase genes in the developing grape berries of Shiraz and Chardonnay (*Vitis vinifera* L.). *Aust. J. Grape Wine Res.* **2003**, *9*, 110−121.

(10) Brar, H. S.; Singh, Z.; Swinny, E. Dynamics of anthocyanin and flavonol profiles in the 'Crimson Seedless' grape berry skin during development and ripening. *Sci. Hortic.* **2008**, *117*, 349−356.

(11) Boss, P.; Davies, C. Molecular biology of anthocyanin accumulation in grape berries. *Grapevine Mol. Physiol. Biotechnol.* **2009**, 263−292.

(12) Fournand, D.; Vicens, A.; Sidhoum, L.; Souquet, J. M.; Moutounet, M.; Cheynier, V. Accumulation and extractability of grape skin tannins and anthocyanins at different advanced physiological stages. *J. Agric. Food Chem.* **2006**, *54*, 7331−7338.

(13) Downey, M.; Dokoozlian, N.; Krstic, M. Cultural practice and environmental impacts on the flavonoid composition of grapes and wine: a review of recent research. *Am. J. Enol. Vitic.* **2006**, *57*, 257.

(14) Winkler, A.; Cook, J.; Kliewer, W.; Lider, L. Development and composition of grapes. *General Viticulture*; University of California Press: Berkeley, CA, 1962; Vol. 4.

(15) Mori, K.; Goto-Yamamoto, N.; Kitayama, M.; Hashizume, K. Loss of anthocyanins in red-wine grape under high temperature. *J. Exp. Bot.* **2007**, *58*, 1935−1945.

(16) Cohen, S. D.; Tarara, J. M.; Kennedy, J. A. Assessing the impact of temperature on grape phenolic metabolism. *Anal. Chim. Acta* **2008**, *621*, 57−67.

(17) Tarara, J. M.; Lee, J. M.; Spayd, S. E.; Scagel, C. F. Berry temperature and solar radiation alter acylation, proportion, and concentration of anthocyanin in Merlot grapes. *Am. J. Enol. Vitic.* **2008**, *59*, 235−247.

(18) Somers, C. *The Wine Spectrum*; Hyde Park Press: Adelaide, Australia, 1998.

(19) Chassy, A. W.; Adams, D. O.; Laurie, V. F.; Waterhouse, A. L. Tracing phenolic biosynthesis in *Vitis vinifera* via in situ C-13 labeling and liquid chromatography−diode-array detector−mass spectrometer/mass spectrometer detection. *Anal. Chim. Acta* **2012**, *747*, 51−57.

(20) Vaknin, H.; Bar-Akiva, A.; Ovadia, R.; Nissim-Levi, A.; Forer, I.; Weiss, D.; Oren-Shamir, M. Active anthocyanin degradation in *Brunfelsia calycina* (yesterday−today−tomorrow) flowers. *Planta* **2005**, *222*, 19−26.

(21) Zenner, K.; Bopp, M. Anthocyanin turnover in *Sinapis alba* L. *J. Plant Physiol.* **1987**, *126*, 475−482.

(22) Oren-Shamir, M. Does anthocyanin degradation play a significant role in determining pigment concentration in plants? *Plant Sci.* **2009**, *177*, 310−316.

(23) Grapov, D.; Newman, J. W. imDEV: a graphical user interface to R multivariate analysis tools in Microsoft Excel. *Bioinformatics* **2012**, *28*, 2288−2290.

(24) Benjamini, Y.; Hochberg, Y. Controlling the false discovery rate: a practical and powerful approach to multiple testing. *J. R. Stat. Soc. Ser. B (Methodol.)* **1995**, 289−300.

(25) Fournier-Level, A.; Hugueney, P.; Verries, C.; This, P.; Ageorges, A. Genetic mechanisms underlying the methylation level of anthocyanins in grape (*Vitis vinifera* L.). *BMC Plant Biol.* **2011**, *11*, 179.

(26) Hugueney, P.; Provenzano, S.; Verries, C.; Ferrandino, A.; Meudec, E.; Batelli, G.; Merdinoglu, D.; Cheynier, V.; Schubert, A.; Ageorges, A. A novel cation-dependent *O*-methyltransferase involved in anthocyanin methylation in grapevine. *Plant Physiol.* **2009**, *150*, 2057−2070.

(27) Bailly, C.; Cormier, F.; Do, C. B. Characterization and activities of *S*-adenosyl-L-methionine:cyanidin 3-glucoside 3′-*O*-methyltransferase in relation to anthocyanin accumulation in *Vitis vinifera* cell suspension cultures. *Plant Sci.* **1997**, *122*, 81−89.

(28) Geny, L.; Colin, L.; Brezillon, I.; Broquedis, M. Hydroxycinnamic acid amines in flowers and berries of *Vitis vinifera*. *Vitis* **1999**, *38*, 157−160.

(29) Bassard, J. E.; Ullmann, P.; Bernier, F.; Werck-Reichhart, D. Phenolamides: bridging polyamines to the phenolic metabolism. *Phytochemistry* **2010**, *71*, 1808−1824.

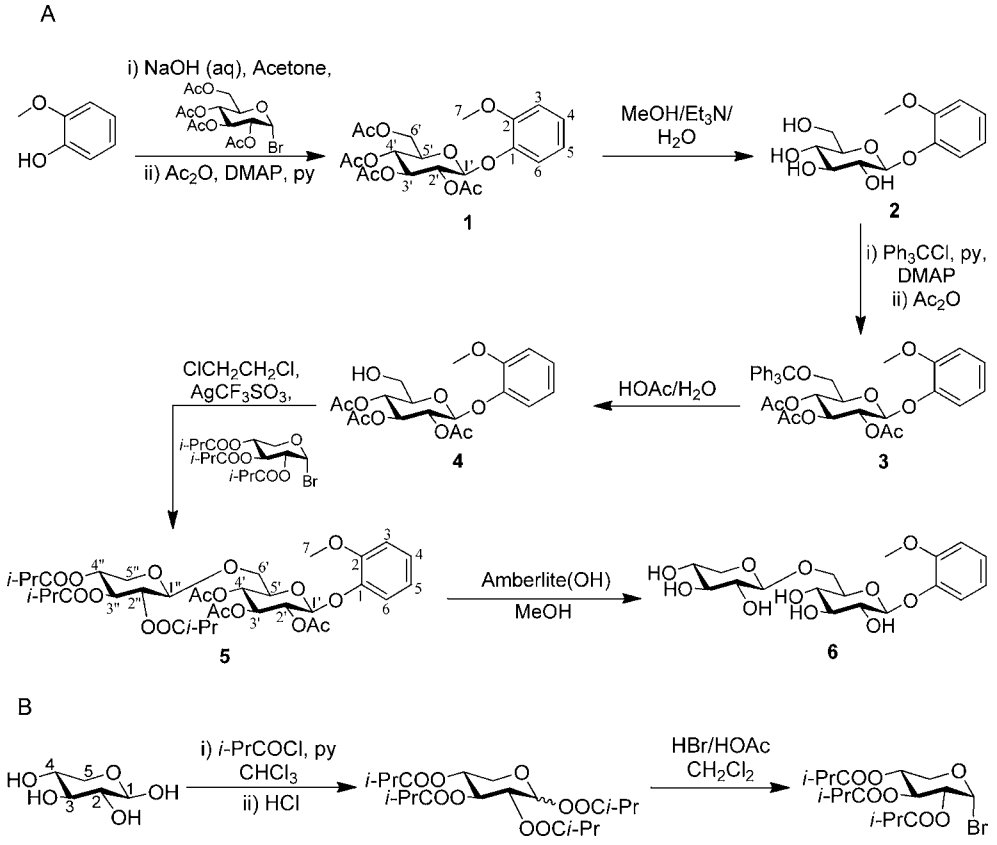

Figure 1. Synthesis of (A) guaiacyl β-D-primeveroside (6) and (B) tri-*O*-isobutyryl-α-D-xylopyranosyl bromide.

bushfires that occurred in the period 7 February−14 March 2009. These fires, particularly those in the period of 7 February, were of extremely high intensity, causing extensive loss of vineyards and winery buildings in the Yarra Valley, and can be considered one of the worst fire events in Australia's history. Smoke was present in the area for an extended period as a result. Smoke-exposed grapes and wines made from smoke-exposed grapes were obtained from producers who identified these as showing clear smoke flavor.

Materials. Guaiacol, 4-methylguaiacol, *o*-cresol, *m*-cresol, *p*-cresol, syringol and 4-methylsyringol, and d_7-*p*-cresol were purchased from Sigma-Aldrich (Castle Hill, Australia). d_3-Guaiacol and d_3-4-methylguaiacol had been previously synthesized in-house.[9,10] d_3-Syringol was prepared according to the method of Aihara et al.,[11] and syringol β-D-glucoside and syringol β-D-gentiobioside were synthesized in house, as previously reported.[7] All chemicals were analytical-reagent-grade unless otherwise stated. Water was obtained from a Milli-Q purification system (Millipore, North Ryde, Australia).

Guaiacol-β-D-Primeveroside (2-methoxyphenyl-6-*O*-(β-D-xylopyranosyl)-β-D-glucopyranoside) Synthesis. All chemicals were analytical-reagent grade. Guaiacyl β-D-primeveroside (**6**) was synthesized using a procedure (Figure 1A) based on a method employed previously by our group to prepare d_3-syringyl β-D-gentiobioside.[12] Briefly, guaiacyl-2′,3′,4′-tri-*O*-acetyl-β-D-glucopyranoside (**4**) was prepared in four steps by coupling guaiacol and tetra-*O*-acetyl-α-D-glucopyranosyl bromide, followed successively by glucose deprotection, tritylation, and acetylation, and finally detritylation. The protected disaccharide was prepared using synthesized isobutyryl-protected xylopyranosyl bromide as the glycosyl donor (Figure 1B) to avoid excessive orthoester byproduct formation during coupling. Deprotection with Amberlite(OH) resin gave the disaccharide **6**.

Instrumentation. Proton (^{1}H) and carbon (^{13}C) Nuclear Magnetic Resonance (NMR) spectra were recorded with a Bruker spectrometer operating at 400 or 600 MHz for proton and 100 or 150 MHz for carbon nuclei, respectively. Chemical shifts were recorded as δ values in parts per million (ppm). Spectra were acquired in chloroform-*d* or deuterium oxide (D_2O) at ambient temperature, and resonances were assigned by routine 2D correlation experiments. For ^{1}H NMR spectra, the peak as a result of residual $CHCl_3$ (δ 7.26) or the CH_3 peak of acetonitrile (δ 2.06), added when D_2O was the solvent, was used as the internal reference. For ^{13}C NMR spectra, the central peak of the $CDCl_3$ triplet (δ 77.16) or the CH_3 peak of acetonitrile (δ 1.47), added when D_2O was the solvent, was used as the internal reference. High-Resolution Mass Spectrometry (HRMS) spectra were obtained on a Bruker microTOF-Q II with electrospray ionization (ESI) or atmospheric-pressure chemical ionization (APCI) in positive mode. Samples dissolved in water or methanol at concentrations of approximately 1−2 mg/L were analyzed by flow injection. Specific optical rotations were recorded with a PolAAr 21 polarimeter, referenced to the sodium D line (589 nm) at 20 °C, using the spectroscopic-grade solvents specified and at the concentrations (*c*, g/100 mL) indicated. The measurements were carried out in a cell with a 1 dm path length. Melting points were measured with a Buchi Melting Point B-540 unit and were uncorrected.

Synthesis of Tri-O-isobutyryl-D-xylopyranose. Isobutyryl chloride (51 g, 480 mmol) in $CHCl_3$ (100 mL) was added dropwise to a stirred solution of D-(+)-xylose (10 g, 68 mmol) in anhydrous pyridine (49 mL, 610 mmol) at 0 °C under N_2. The yellow mixture was stirred at room temperature for 18 h. The resultant orange mixture was diluted with a further 200 mL $CHCl_3$ and washed with 2 M HCl (3 × 150 mL), saturated $NaHCO_3$ (3 × 150 mL), water (2 × 50 mL), and brine (3 × 50 mL). The organic layer was dried (Na_2SO_4), filtered, and concentrated in vacuo. The oily reaction product was purified by silica gel column chromatography eluted with 15% EtOAc/hexane to give a colorless oil as a 97:3 mixture of α/β epimers (29 g, 99%). R_f 0.33 (15% EtOAc/hexane). $[\alpha]_D$ + 65.4 (*c* 0.67, CH_2Cl_2). ^{1}H NMR for α epimer (600 MHz, $CDCl_3$): δ 6.27 (1H, d, J = 3.7 Hz, H_1); 5.52 (1H, t, J = 9.9 Hz, H_3); 5.06 (1H, dd, J = 9.9, 3.7 Hz, H_2); 5.05 (1H, dd, J = 11.1, 9.9 Hz, H_4); 3.91 (1H, dd, J = 11.0, 5.8 Hz, H_{5eq}); 3.68 (1H, app t, J = 11.0 Hz, H_{5ax}); 2.70−2.41 (4H, m, C*H*Me$_2$); 1.24−1.07 (24H, m, Me). ^{13}C NMR (150 MHz, $CDCl_3$): δ 176.10−175.10 (C═O); 89.16

dx.doi.org/10.1021/jf405327s | J. Agric. Food Chem. 2014, 62, 2327−2336

(C_1); 69.49 (C_2); 69.09 (C_3); 68.40 (C_4); 60.89 (C_5); 34.16−33.89 (4 × $CHMe_2$); 19.13−18.76 (8 × $(CH_3)_2CH$). APCI-HRMS (m/z): $[M + NH_4]^+$ Calcd for $C_{21}H_{38}NO_9^+$ 448.2541; Found, 448.2511.

Synthesis of Tri-O-isobutyryl-α-D-xylopyranosyl Bromide. Under an N_2 atmosphere with NaOH pellets in a trap, 33% HBr/HOAc (12 mL, 66 mmol) was added to a stirred solution of tetra-*O*-isobutryl-D-xylose (97:3 *α*:*β*, 6.2 g, 14 mmol) in CH_2Cl_2 (30 mL) at 0 °C. After 20 h, CH_2Cl_2 (200 mL) was added, and the reaction mixture was successively washed with sat. aq. $NaHCO_3$ solution (2 × 100 mL), H_2O (100 mL), and brine (100 mL). The organic layer was dried (Na_2SO_4) and concentrated in vacuo (5.8 g, 95%). A portion was recrystallized from EtOH for characterization purposes to afford tri-*O*-isobutyryl-*α*-D-glucopyranosyl bromide as white crystals.

R_f 0.73 (1:4:95 petroleum ether/Et_2O/CH_2Cl_2), mp 54.1−54.7 °C. $[\alpha]_D$ + 179.2 (*c* 0.94, $CHCl_3$). ^1H NMR (400 MHz, $CDCl_3$): *δ* 6.57 (1H, d, *J* = 4.1 Hz, H_1); 5.62 (1H, t, *J* = 9.8 Hz, H_3); 5.06 (1H, td, *J* = 10.3, 5.9 Hz, H_4); 4.78 (1H, dd, *J* = 9.8, 4.1 Hz, H_2); 4.03 (1H, dd, *J* = 11.2, 5.9 Hz, H_{5eq}); 3.87 (1H, app t, *J* = 11.2 Hz, H_{5ax}); 2.56 (1H, sept, *J* = 7.0 Hz, $CHMe_2$); 2.53 (1H, sept, *J* = 7.0 Hz, $CHMe_2$); 2.50 (1H, sept, *J* = 7.0 Hz, $CHMe_2$); 1.17−1.10 (18H, m, $(CH_3)_2CH$). ^{13}C NMR (100 MHz, $CDCl_3$): *δ* 176.04−175.73 (*C*=O); 87.97 (C_1); 70.81 (C_2); 69.22 (C_3); 67.84 (C_4); 62.78 (C_5); 34.04−33.93 ($CHMe_2$); 19.04−18.78 (6 × $(CH_3)_2CH$). APCI-HRMS (m/z): $[M-Br]^+$ Calcd for $C_{17}H_{27}O_7^+$ 343.1751; Found, 343.1757.

*Synthesis of Guaiacyl 2′,3′,4′,6′-tetra-O-acetyl-β-D-glucopyranoside (**1**).* Under N_2, a solution of tetra-*O*-acetyl-*α*-D-glucopyranosyl bromide (3.9 g, 9.4 mmol) in acetone (20 mL) was added via cannula into a stirred solution of guaiacol (1.2 g, 9.5 mmol) in 0.3 M NaOH (31.5 mL, 9.5 mmol). The resultant orange reaction mixture was stirred under N_2. The pH was monitored and maintained at 12 over a 5 h period using 1 M NaOH. The solution was acetylated with Ac_2O (8.5 mL, 90 mmol) and 4-dimethylaminopyridine (DMAP) (10 mg, 0.08 mmol) in pyridine (9 mL, 110 mmol) and stirred overnight at room temperature. The flask was concentrated in vacuo to give a syrup. Et_2O/CH_2Cl_2 (4:1, 150 mL) was added, and the suspension was filtered then washed successively with 0.2 M HCl (2 × 75 mL), water (3 × 50 mL), and brine (3 × 50 mL). The organic layer was dried (Na_2SO_4), filtered and concentrated in vacuo. The crude product was purified by silica gel column chromatography using 0→5% Et_2O/CH_2Cl_2 giving a white solid. This was recrystallized from EtOH to give 1.4 g (34%) of **1** as white crystals. R_f 0.33 (10% Et_2O/CH_2Cl_2). ^1H NMR data agreed with the literature.[13]

*Synthesis of Guaiacyl β-D-glucopyranoside (**2**).* A suspension of **1** (1.4 g, 3.2 mmol) was stirred in a mixture of MeOH/Et_3N/H_2O (8:1:1, 25 mL) overnight at room temperature. Additional MeOH/Et_3N/H_2O (8:1:1, 5 mL) was added, and the solution was stirred for a further 5 h. The resultant clear solution was concentrated in vacuo, H_2O was added, and the solution was concentrated again. This procedure was repeated several times until the solid reached a constant weight. This crude solid was recrystallized from EtOH to give **2** as a white crystalline solid (820 mg, 90%). ^1H NMR data agreed with the literature.[8]

*Synthesis of Guaiacyl-2′,3′,4′-tri-O-acetyl-6′-O-trityl-β-D-glucopyranoside (**3**).* Anhydrous pyridine (2.2 mL, 27 mmol) was added via syringe to **2** (0.63 g, 2.2 mmol), DMAP (8 mg, 0.07 mmol), and Ph_3CCl (1.1 g, 3.8 mmol) under a N_2 atmosphere. The mixture was stirred at 50 °C for 9 h, and then stirred overnight at room temperature. Ac_2O (2.2 mL, 23 mmol) was added, and the reaction was stirred for a further 90 min. The flask was placed on ice, MeOH (2.5 mL) was added, and the resultant mixture was stirred for 30 min. The solvent was removed in vacuo, and the crude solid was dissolved in CH_2Cl_2. This solution was washed sequentially with 0.2 M HCl, water, and brine. The organic layer was dried (Na_2SO_4), filtered, and concentrated in vacuo. The crude material was purified by silica gel column chromatography eluted with 3→10% Et_2O/CH_2Cl_2 to give a white solid (800 mg, 56%). R_f 0.24 (3% Et_2O/CH_2Cl_2). mp 90−95 °C. $[\alpha]_D$ +13.8 (*c* 0.44, $CHCl_3$). ^1H NMR (600 MHz, $CDCl_3$): *δ* 7.45 (6H, dt, *J* = 7.7, 1.6 Hz, *ortho* CPh_3); 7.36 (1H,, dd, *J* = 7.9, 1.4 Hz, H_6); 7.28 (6H, tt, *J* = 7.7, 1.6 Hz, *meta* CPh_3); 7.22 (3H, tt, *J* = 7.2, 1.6 Hz, *para* CPh_3); 7.09 (1H, td, *J* = 7.9, 1.4 Hz, H_4); 6.93 (1H, dd, *J* = 7.9, 1.4 Hz, H_3); 6.90 (1H,td, *J* = 7.9, 1.4 Hz, H_5); 5.36 (1H, dd, *J* = 9.3, 8.0 Hz, $H_{2'}$); 5.24 (1H, app t, *J* = 9.3 Hz, $H_{3'}$); 5.20 (1H, app t, *J* = 9.5 Hz, $H_{4'}$); 4.97 (1H, d, *J* = 8.0 Hz, $H_{1'}$); 3.84 (3H, s, H_7); 3.62 (1H, ddd, *J* = 9.5, 5.4, 2.2 Hz, $H_{5'}$); 3.22 (1H, dd, *J* = 10.4, 2.2 Hz, $H_{6b'}$); 3.15 (1 H, dd, *J* = 10.4, 5.4 Hz, $H_{6a'}$); 2.08 (3H, s, $COCH_3$); 2.02 (3H, s, $COCH_3$); 1.74 (3H, s, $COCH_3$). ^{13}C NMR (150 MHz, $CDCl_3$): *δ* 170.56 (C=O); 169.69 (C=O); 169.14 (C=O); 150.81 (C_2); 146.42 (C_1); 143.67 (*ipso* CPh_3); 128.78 (*ortho* CPh_3); 127.94 (*meta* CPh_3); 127.13 (*para* CPh_3); 124.68 (C_4); 121.04 (C_5); 120.49 (C_6); 112.71 (C_3); 101.07 ($C_{1'}$); 86.73 (CPh_3); 73.65 ($C_{5'}$); 73.00 ($C_{3'}$); 71.53 ($C_{2'}$); 68.82 ($C_{4'}$); 61.88 ($C_{6'}$); 56.12 (C_7); 20.86 (2 × $COCH_3$); 20.51 ($COCH_3$). APCI-HRMS (m/z): Calcd for $C_{38}H_{42}NO_{10}^+$ ($[M + NH_4]^+$), 672.2803; Found, 672.2791.

Compound **3** (390 mg, 0.59 mmol) was dissolved in HOAc/H_2O (4:1, 3.9 mL), and the solution was stirred under N_2 at 60 °C for 4 h. The reaction mixture was cooled, toluene (3 mL) was added, and the solution was concentrated in vacuo. This step was repeated twice, and the crude material was purified by silica gel column chromatography eluted with 20% Et_2O/CH_2Cl_2 to give **4** as a white solid (200 mg, 83%). R_f 0.18 (15% Et_2O/CH_2Cl_2). mp 160.6−160.8 °C. $[\alpha]_D$ = −30.8 (*c* 0.55, CH_2Cl_2). ^1H NMR (600 MHz, $CDCl_3$): *δ* 7.08 (1H, dd, *J* = 7.8, 1.2 Hz, H_6); 7.06 (1H, td, *J* = 7.8, 1.2 Hz, H_4); 6.90 (1H, dd, *J* = 7.8, 1.2 Hz, H_3); 6.87 (1H, td, *J* = 7.8, 1.2 Hz, H_5); 5.32 (1H, app t, *J* = 9.5 Hz, $H_{3'}$); 5.26 (1H, dd, *J* = 9.5, 7.8 Hz, $H_{2'}$); 5.10 (1H, app t, *J* = 9.5 Hz, $H_{4'}$); 5.02 (1H, d, *J* = 7.8 Hz, $H_{1'}$); 3.81 (3H, s, H_7); 3.74 (1H, ddd, *J* = 11.9, 8.2, 2.0 Hz, $H_{6b'}$); 3.63 (1H, dd, *J* = 11.9, 5.9 Hz, $H_{6a'}$); 3.59 (1H, ddd, *J* = 9.5, 5.0, 2.0 Hz, $H_{5'}$); 2.35 (1H, dd, *J* = 7.8, 5.9 Hz, *OH*); 2.07 (3H, s, $COCH_3$); 2.05 (3H, s, $COCH_3$); 2.03 (3H, s, $COCH_3$). ^{13}C NMR (150 MHz, $CDCl_3$): *δ* 170.45 (C=O); 170.13 (C=O); 169.54 (C=O); 150.71 (C_2); 146.12 (C_1); 124.80 (C_4); 121.02 (C_5); 119.96 (C_6); 112.82 (C_3); 100.84 ($C_{1'}$); 74.46 ($C_{5'}$); 72.63 ($C_{3'}$); 71.48 ($C_{2'}$); 68.74 ($C_{4'}$); 61.45 ($C_{6'}$); 56.07 (C_7); 20.79−20.77 (3 × $COCH_3$). APCI-HRMS (m/z): $[M + NH_4]^+$ Calcd for $C_{19}H_{28}NO_{10}^+$, 430.1708; Found, 430.1682.

*Synthesis of Guaiacyl-2′,3′,4′-tri-O-acetyl-2″,3″,4″-tri-O-isobutyryl-β Primeveroside (**5**).* Under a N_2 atmosphere at −15 °C, anhydrous 1,2-dichloroethane (2.6 mL) was added to $AgCF_3SO_3$ (0.12 g, 0.48 mmol), activated 4 Å molecular sieves (0.23 g), tri-*O*-isobutyryl-*α*-D-xylopyranosyl bromide (190 mg, 0.45 mmol) and **4**·(93 mg, 0.23 mmol). The slurry was stirred for 10 min, then 2,6-di-*tert*-butyl-4-methylpyridine (93 mg, 0.45 mmol) was added, and the mixture was stirred overnight at room temperature. The reaction mixture was diluted with CH_2Cl_2, filtered through diatomaceous earth, and concentrated to dryness. The resulting crude material was purified by silica gel column chromatography, eluting with 95:4:1 petroleum ether/Et_2O/CH_2Cl_2 to give **5** as a white gummy solid (160 mg, 91%). R_f = 0.22 (95:4:1 petroleum ether/Et_2O/CH_2Cl_2). $[\alpha]_D$ = −51.8 (*c* 0.55, $CHCl_3$). ^1H NMR (400 MHz, $CDCl_3$): *δ* 7.11 (1H, d, *J* = 7.8 Hz, H_6); 7.10 (1H, td, *J* = 7.8, 1.6 Hz, H_4); 6.98 (1H, td, *J* = 7.8, 1.6 Hz, H_5); 6.93 (1H, dd, *J* = 7.8, 1.6 Hz, H_3); 5.26 (1H, app t, *J* = 9.4 Hz, $H_{3'}$); 5.22 (1H, dd, *J* = 9.4, 7.6 Hz, $H_{2'}$); 5.13 (1H, app t, *J* = 9.0 Hz, $H_{4''}$); 4.97 (1H, d, *J* = 7.6 Hz, $H_{1'}$); 4.96 (1H, app t, *J* = 9.4 Hz, $H_{4'}$); 4.92 (1H, app t, *J* = 9.0 Hz, $H_{3''}$); 4.89 (1H, dd, *J* = 9.0, 7.2 Hz, $H_{2''}$); 4.53 (1H, d, *J* = 7.2 Hz, $H_{1''}$); 4.05 (1H, dd, *J* = 11.6, 5.4 Hz, $H_{5eq''}$); 3.83 (3H, s, H_7); 3.73 (2H, m, $H_{6'}$); 3.70 (1H, ddd, *J* = 9.3, 5.4, 2.8 Hz, $H_{5'}$); 3.22 (1H, dd, *J* = 11.6, 9.3 Hz, $H_{5ax''}$); 2.50 (1H, sept, *J* = 7.0 Hz, $CHMe_2$); 2.48 (1H, sept, *J* = 7.0 Hz, $CHMe_2$); 2.33 (1H, sept, *J* = 7.0 Hz, $CHMe_2$); 2.07 (3H, s, $COCH_3$); 2.03 (3H, s, $COCH_3$); 2.01 (3H, s, $COCH_3$); 1.12 (6H, d, *J* = 7.0 Hz, $(CH_3)_2CH$); 1.11 (6H, d, *J* = 7.0 Hz, $(CH_3)_2CH$); 1.09 (6H, d, *J* = 7.0 Hz, $(CH_3)_2CH$); 1.08 (6H, d, *J* = 7.0 Hz, $(CH_3)_2CH$); 1.01 (6H, d, *J* = 7.0 Hz, $(CH_3)_2CH$). ^{13}C NMR (150 MHz, $CDCl_3$): *δ* 175.99 (Me_2CHC=O); 175.96 (Me_2CHC=O); 175.45 (Me_2CHC=O); 170.39 (CH_3C=O); 169.73 (CH_3C=O); 169.51 (CH_3C=O); 150.81 (C_2); 146.18 (C_1); 125.02 (C_4); 121.54 (C_5); 120.41 (C_6); 113.05 (C_3); 100.83 ($C_{1'}$); 100.76 ($C_{1''}$); 74.53 ($C_{5'}$); 72.70 ($C_{3'}$); 71.43 ($C_{2'}$); 71.36 ($C_{4''}$); 70.47 ($C_{2''}$); 69.07 ($C_{4'}$); 68.84 ($C_{3''}$); 67.23 ($C_{6'}$); 62.47 ($C_{5''}$); 56.20 (C_7); 34.01 ($CHMe_2$); 33.99 ($CHMe_2$); 33.91 ($CHMe_2$); 20.77 (3 × $COCH_3$); 19.01 (2 × $((CH_3)_2CH$); 18.96 (2 × $((CH_3)_2CH$);

18.84 ($(CH_3)_2CH$), 18.81 ($(CH_3)_2CH$). ESI−HRMS (m/z): $[M + Na]^+$ Calcd for $C_{36}H_{50}NaO_{17}^+$, 777.2940; Found, 777.2934.

*Synthesis of Guaiacyl β-Primeveroside (**6**).* A solution of **5** (66 mg, 0.09 mmol) in MeOH (10 mL) containing Amberlite IRA-400(OH) resin (0.5 g) was stirred gently overnight. The reaction mixture was filtered and washed successively with MeOH and water. The combined filtrate was concentrated in vacuo to give the product as a white solid (27 mg, 73%). mp 209.9−210.9 °C. $[\alpha]_D = -63.9$ (c 0.204, H_2O). ^1H NMR (400 MHz, D_2O): δ 7.23 (1H, dd, J = 8.2, 1.3 Hz, H_3); 7.15 (1H, td, J = 8.2, 1.3 Hz, H_4); 7.12 (1H, dd, J = 8.2, 2.6 Hz, H_6); 7.02 (1H, ddd J = 8.2, 6.4, 2.6 Hz, H_5); 5.14 (1H, m, $H_{1'}$); 4.39 (1H, d, J = 7.8 Hz, $H_{1''}$); 4.12 (1H, dd, J = 12.0, 1.8 Hz $H_{6b'}$); 3.91 (1 H, dd, J = 11.6, 5.4 Hz, $H_{5eq''}$); 3.88 (3H, s, H_7); 3.86 (1H, dd, J = 12.0, 5.8 Hz, $H_{6a'}$); 3.75 (1H, ddd, J = 9.6, 5.8, 1.8 Hz, $H_{5'}$); 3.63 (1H, dd, J = 8.8, 7.6 Hz, $H_{2'}$); 3.61 (1H, dd, J = 9.6, 8.8 Hz, $H_{3'}$); 3.59−3.51 (2H, m, $H_{4'', 4'}$); 3.35 (1H, app t, J = 9.2 Hz, $H_{3''}$); 3.25 (1H, dd, J = 9.4, 7.8 Hz, $H_{2''}$); 3.18 (1H, dd, J = 11.6, 10.5 Hz, $H_{5ax''}$). ^{13}C NMR (100 MHz, D_2O): δ 149.47 (C_2); 145.85 (C_1); 124.60 (C_4); 122.19 (C_5); 117.07 (C_6); 113.71 (C_3); 103.80 ($C_{1''}$); 100.94 ($C_{1'}$); 76.15 ($C_{3''}$); 76.08 ($C_{3'}$); 76.02 ($C_{5'}$); 73.59 ($C_{2''}$); 73.44 ($C_{2'}$); 69.88 ($C_{4'}$); 69.80 ($C_{4''}$); 68.78 ($C_{6'}$); 65.68 ($C_{5''}$); 56.48 (C_7). ESI−HRMS (m/z): $[M + Na]^+$ Calcd for $C_{18}H_{26}NaO_{11}^+$, 441.1367; Found, 441.1364.

Isolation of Glycosides from Smoke Affected Grapes. Ten kg of smoke-tainted grapes were homogenized using a knife mill (Grindomix GM 200, Retsch GmbH, Germany) centrifuged at 4000 rpm for 5 min, and the supernatant was slowly (over 20 h) passed through a low-pressure column (capacity 600 mL) of an absorbent polymer resin (Amberlite FPX66, The Dow Chemical Company, Camberwell, Victoria, Australia). After removal of nonabsorbed material with water (5 L) and removal of volatiles with pentane (2.5 L), the glycosidic fraction was eluted from the column with food grade ethanol (2 L), concentrated on a rotary evaporator to dryness, then redissolved in 50 mL of ethanol, and stored at −20 °C until required. The glycosides were quantified as previously reported.[14] For the reconstitution study, an aliquot of the ethanolic solution was added directly to the base wine.

Chemical Analyses. Standard chemical analysis and quantification of free volatile phenols for all wines were conducted by Commercial Services at the Australian Wine Research Institute (AWRI, Adelaide, Australia), as reported elsewhere.[7]

Sensory Analysis. The reconstitution and the smoke affected wine sensory studies were conducted several months apart in mid-2011, with the sensory protocols being very similar. Ten panelists were used for the smoke affected wine study (six female), while 11 were used for the reconstitution study (seven female), all were part of the AWRI trained descriptive analysis panel with experience in wine descriptive analysis studies (age range, 32−60), and recruitment and training criteria as previously described.[4] All data were collected in accordance with standard institutional procedures, including risk assessment and informed consent, and all samples were expectorated. For both studies, the assessors had three training sessions: two 2 h discussion sessions to generate and define attributes by consensus though assessment of pairs of wines, followed by one practice rating session in isolated booths, where a subset of the samples was presented in duplicate and performance was assessed. For the smoke affected wine study, the assessors rated six aroma (*overall fruit*, *vanilla*, *oaky*, *earthy/dirty*, *smoky/burnt*, and *band-aid*) and 11 palate attributes (*overall fruit flavor*, *vanilla flavor*, *oaky flavor*, *burnt/charred flavor*, *bandaid flavor*, *bitterness*, *astringency*, *hotness*, *ashy aftertaste*, *acid aftertaste*, and *burning aftertaste*). For the reconstitution study, ten aroma (*overall fruit*, *red fruit*, *dark fruit*, *fresh green*, *musty/dusty*, *woody*, *earthy*, *smoky*, *medicinal*, and *alcohol*) and eight palate attributes (*overall fruit flavor*, *woody flavor*, *smoky flavor*, *burnt rubber flavor*, *medicinal flavor*, *bitterness*, *astringency*, and *burnt/ashy aftertaste*) were rated. For attribute definitions and reference standards used, see SI Tables S4 and S5.

The intensity of each attribute was rated using an unstructured 15 cm line scale from 0 to 10, with indented anchor points of "low" and "high" placed at 10% and 90%, respectively.

Samples were assessed at 22−24 °C in three or five formal sessions, lasting a maximum of 2 h, under sodium lighting in isolated ventilated tasting booths. Assessors were presented with 15 (smoke affected wines) or 16 (reconstitution study) samples per session, in sets of three or four for the two studies, respectively, with 90 s rest breaks between each sample. Assessors were instructed to rinse their mouths after each evaluation with aqueous citrus pectin solution (1 g/L, Fluka), followed by two rinses of water. There was a forced rest of at least 10 min between each of the sets of three or four samples. Samples (30 mL) were presented in a random and balanced order across the assessors, in coded, covered International Organization for Standardization tasting glasses. Two replications of each of the 20 samples for the smoke-affected wine study and three replications of the 20 reconstitution samples were assessed. FIZZ software (Version 2.46, Biosystemes, France) was used for the collection of all data.

Experimental Design of the Reconstitution Study. Different volatiles, singly and in combination; an isolated glycoside fraction from smoke-affected grapes; and synthesized glycosides were added at different concentrations to a red base wine, as specified in Table 1. The red base wine was a relatively low flavor bag-in-box commercial Shiraz wine with negligible or not detected concentrations of volatile phenols. The concentrations of the compounds added were chosen with regard to measured concentrations in a smoke-tainted wine (Wine 15, SI Table S2). Two smoke-affected wines were also included. Wine 15 was not included due to volume limitations. Stock solutions of all compounds were prepared using 96% v/v food grade ethanol (Tarac Technologies, South Australia, Australia) and stored at 4 °C during the experiment, with appropriate volumes added directly to the base red wine 1 h prior to testing.

Table 1. Samples for Sensory Analysis with Details of Concentrations of Each Compound Added to a Base Wine[a]

sample code	details
base wine[a]	no addition
all Ph	all volatile phenols[b]
Gu	guaiacol 79 μg/L
all Cr	*o*-cresol 20 μg/L, *p*-cresol 10 μg/L, *m*-cresol 16 μg/L
m-Cr	*m*-cresol 16 μg/L
o-Cr	*o*-cresol 20 μg/L
p-Cr	*p*-cresol 10 μg/L
Syr	syringol 148 μg/L
Gu+4-Me	guaiacol 79 μg/L, 4-methylguaiacol 43 μg/L
Gu+all Cr	guaiacol 79 μg/L, *o*-cresol 20 μg/L, *p*-cresol 10 μg/L, *m*-cresol 16 μg/L
low Gly[c]	low glycoside-isolate addition (equivalent to 500 μg/L SyrGG)
high Gly	high glycoside-isolate addition (equivalent to 1500 μg/L SyrGG)
high Gly + all Ph	high glycoside-isolate and all volatile phenols in combination[b]
low Gly + all Ph	low glycoside-isolate and all volatile phenols in combination[b]
Gu + Gu-Glu	guaiacol 79 μg/L and guaiacol glucoside 500 μg/L
Gu-Glu	guaiacol glucoside 500 μg/L
m-Cr-Glu	*m*-cresol glucoside 500 μg/L
Syr-Glu-Glu	syringol gentiobioside 500 μg/L
wine 18[d]	smoke-tainted wine 2007, Pinot Noir, Yarra Valley
wine 19	smoke-tainted wine 2009, Shiraz, Yarra Valley

[a]Base wine: 2010 Merlot bag-in-box wine (2L). [b]Volatile phenols matching the concentration of phenols of smoke tainted wine (Shiraz, 2007): Guaiacol 79 μg/L, 4-Methylguaiacol 43 μg/L, Syringol 148 μg/L, Methylsyringol 38 μg/L, *o*-Cresol 20 μg/L, *p*-Cresol 10 μg/L, *m*-Cresol 16 μg/L. [c]Glycoside fraction isolated from smoke affected grapes. [d]For details of wines 18 and 19, see SI Table S1.

Sample Preparation. *Saliva Collection and Incubation.* Saliva was collected from healthy nonsmoking volunteers, with normal

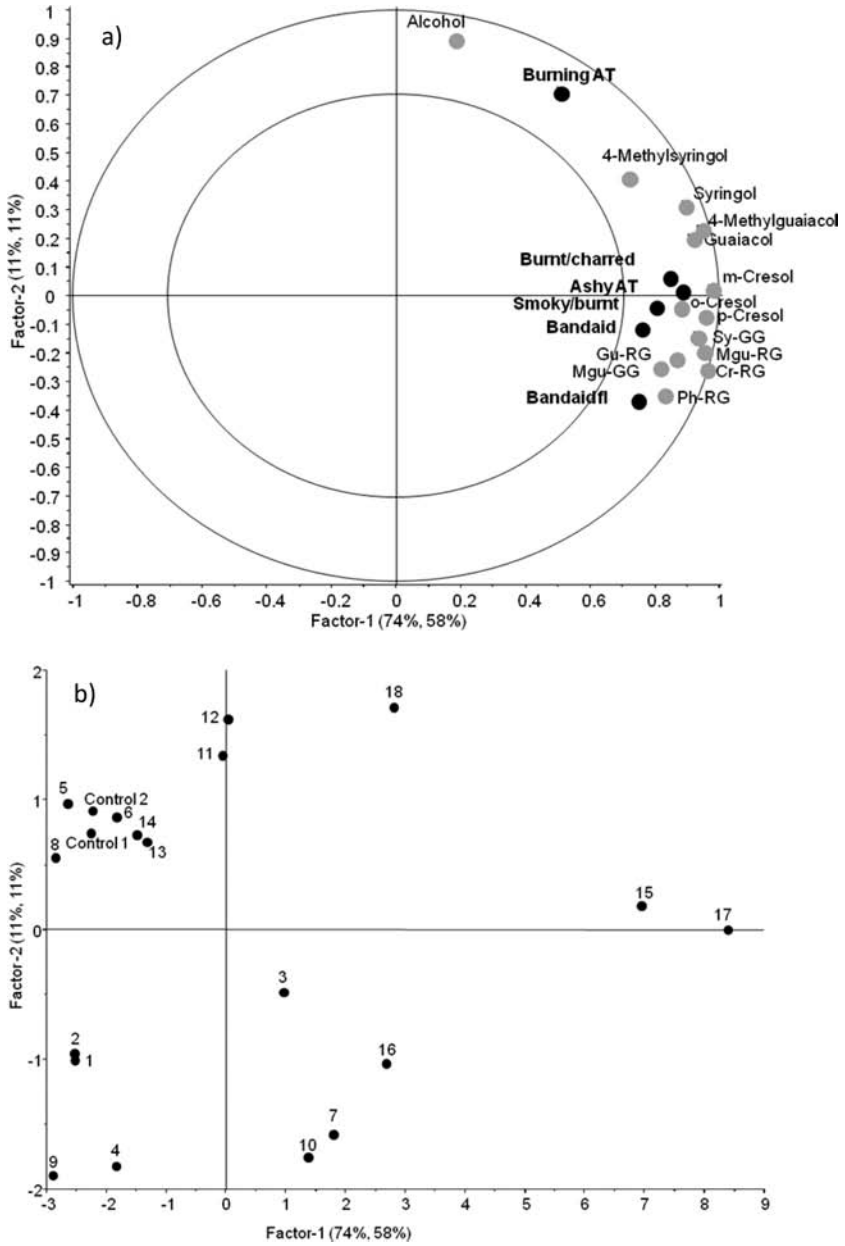

Figure 2. Partial least-squares regression analysis of volatile phenols, their glycoconjugates and sensory attributes (a) *x* and *y* loading plot; *x*-loading: chemical composition; *y*-loadings: sensory attributes; Ph: Phenol; Cr: Cresol; Gu: Guaiacol; Mg: 4-Methylguaiacol; Sy: Syringol; Msy: 4-Methylsyringol; GG: β-D-glucosyl-β-D-glucosides; PG: Pentosylglucosides; RG: α-L-rhamnosyl-β-D-glucoside (b) scores plot for the 20 wine samples, sample codes as per SI Table S1.

salivary flow and olfactory and gustatory function from within the staff of the AWRI, and selected from prior knowledge that they could consistently perceive smoke flavor from tasting glycosides. Samples were taken in duplicate at different days at different times. Note that these subjects were not members of the sensory panels.

The salivary flow was increased by chewing Parafilm (Pechiney Plastic Packaging) for approximately 10 min and collected in a test tube through expectoration. At each collection period, saliva (3.0 mL) was transferred to a 22 mL amber vial with screw cap Teflon seal. A standard condition was used with guaiacol monoglucoside added (6.32 μg in 1 mL water) incubated in a water bath (37 °C) and stirred for 30 min on a magnetic stirrer. The reaction was stopped by adding saturated aqueous $CaCl_2$ (2 mL), and the free volatiles quantified. In a single study using a single subject different conditions were examined with standard conditions involving 3 mL saliva, 6.32 μg guaiacol monoglucoside in 2 mL saturated tartaric acid pH 3.5, 0% v/v alcohol, 0 g/L glucose, and no mouthwash, with variables studied involving pH (adjusted using 2 M NaOH or 2 M tartaric acid); temperature; ethanol concentration; glucose concentration; and chlorhexidine mouthwash rinsing (0.2% w/v chlorhexidine gluconate, GlaxoSmithKline Consumer Healthcare GmbH&Co., Stuttgart, Germany). The latter was investigated following thorough rinsing for one minute with saliva collected immediately after rinsing and after five minutes.

Volatile Phenol Analysis. For analysis of the released volatiles by solid-phase microextraction (SPME), deuterated standards (d_3-guaiacol, d_3-4-methylguaiacol, d_7-*p*-cresol, and d_3-syringol) were added to the saliva samples in the 22 mL amber vials, after the reaction was stopped. A Gerstel autosampler (MPS) was fitted with a 85 μm PA (polyacrylate) fiber assembly (Supelco) to sample the headspace above the stirred wine sample for 30 min at 50 °C, immediately prior to instrumental analysis. Instrumental analyses were carried out with a Hewlett-Packard (HP) 6890 gas chromatograph and a HP 5973 mass selective detector (Agilent Technologies, Forest Hill, Australia) fitted with a Gerstel autosampler (MPS).

The gas chromatograph was fitted with a 60 m × 0.25 mm J&W fused silica capillary column DB-WAX, 0.25 μm film thickness. The carrier gas was helium, linear velocity was 33 cm/sec, and flow rate was 1.4 mL/min. The oven temperature was started at 40 °C, held at this temperature for 2 min, increased to 240 °C at a 10 °C/min rate, and held at this temperature for 10 min. The injector temperature was 220 °C, and the transfer line was held at 280 °C. For quantification, mass spectra were recorded in Selective Ion Monitoring (SIM) mode. The ions used for quantification in SIM runs were m/z 127 for d_3-guaiacol; m/z 124 for guaiacol; m/z 141 for d_3-4-methylguaiacol; m/z 138 for 4-methylguaiacol; m/z 115 for d_7-cresol; m/z 108 for cresol; m/z 157 for d_3-syringol; and m/z 154 for syringol.

In Mouth Measurements with SBSE (Stir Bar Sorptive Extraction). This method was modified from the BOSS System, developed by Buettner et al.[15,16] A SBSE bar (film thickness 1.0 mm, 20 mm length, Gerstel, Germany) was held in the mouth for 5 min, by attaching it to a very thin spatula and rotating it by the subject. The lips and velum were kept closed, and the spatula was moved carefully within the oral cavity. After equilibration, the SBSE bar was removed from the oral cavity, dipped into water, briefly dried with lint-free tissue, and placed in individually sealed glass liners in the autosampler tray for analysis. Thermodesorption of the samples was performed by inserting the glass liners in a thermodesorption unit (TDU, Gerstel GmbH) in combination with a CIS-4 PTV injector (Gerstel GmbH), which allows cryofocusing of the analytes. The sampling parameters were as follows: splitless thermal desorption was performed with the TDU set at 40 °C for 0.2 min and then heated with a rate of 100 to 240 °C for 5 min. Cryofocusing was performed with liquid nitrogen at −100 °C. Injection was performed with a ramp of 12 °C/s from −100 to 240 °C (5 min). The gas chromatographic conditions were as for the SPME analysis.

Gas Chromatography-Olfactometry (GC-O). GC-O was performed using an Agilent 6890 gas chromatograph, equipped with a Gerstel MPS2 multipurpose sampler and coupled to an Agilent 5973N mass selective detector. The GC was also fitted with a Gerstel olfactory detection port (ODP) and the flow was split between MS and ODP in a 1:1 ratio. The instrument was controlled with Agilent G1701DA ChemStation software with the Maestro software integrated version 1.3.3.51/3.3. The GC column and oven program was as described for GC-SPME analysis.

Data Analysis. Sensory descriptive data for each attribute were analyzed using an analysis of variance (ANOVA) testing for the effects of sample, judge and replicate and their two-way interactions, treating judge as a random effect. Tukey's HSD was applied as a means comparison test. Principal component analysis (PCA) and partial least-squares regression (PLS) were carried out using The Unscrambler 10.2 (CAMO Technologies Inc., Woodbridge, NJ). All PLSR analyses were carried out using standardized data, using the PLS2 algorithm with full cross-validation, with the y data set being the sensory attribute scores, and the x data being the chemical compositional data. Following ANOVA of the reconstitution study, contrast tests were performed to assess significant differences between particular pairs of samples.

RESULTS AND DISCUSSION

Sensory Investigations. The importance of nonvolatile glycoconjugates of phenols relative to volatile phenols to the in-mouth characteristics of smoke-affected wines was assessed in two ways, first with an examination of wines made from grapes affected by bushfire events, and second by a reconstitution study with volatiles and nonvolatiles added to a base wine.

An initial study was aimed at confirming the importance of volatile phenols and their glycosides on the sensory of smoke-affected wines, which was shown in an earlier investigation,[4] using wines with a wider range of phenol concentrations, and to allow selection of a wine with known composition as point of reference for the subsequent reconstitution study. While some wines made from potentially smoke-affected grapes had comparable concentrations of volatile phenols and glycosides of phenols to the control wines (see SI Tables S2 and S3), there were many wines with concentrations substantially higher, with differences much greater than the analytical error (coefficient of variation of less than 15%[7,12]). Generally, there was a high degree of correlation among the phenolic compounds, with Pearson coefficients above approximately 0.8 for almost all-pair wise correlations, and all being statistically significant ($P < 0.05$, $r > 0.44$, $n = 20$), with the exception of the gentiobioside glycoside of phenol (Ph-GG), which was only weakly and insignificantly related to the other analytes. Wine 15 was highest in almost all the compounds measured. This indicates that smoke exposure gives consistent concentrations of the range of volatile phenols.

From the ANOVA of the sensory descriptive analysis data, there were significant differences among the wines for all sensory attributes rated. Considering the fact that these were commercially produced wines with varied extent of oak treatment and of different vintages, and because it was of greatest interest to assess the relationship of the smoke related sensory attributes with the phenol compounds measured for each wine, the fruit and oak related attributes were not considered in subsequent analysis. A partial least-squares regression (PLS) analysis (Figure 2) showed that the smoke related attributes *bandaid* and *smoky burnt* aroma, and *bandaid*, *burnt/charred*, and *ashy aftertaste* (palate) were associated strongly with most of the volatile phenols and their glycosides, being rated highest in the wines 15 and 17. The *burning aftertaste* attribute was strongly associated with the alcohol concentration of the wines, and was not related to the smoke-related attributes. Three factors were considered important to the model, with the third component showing a separation of the *bandaid* attributes from the other smoke related attributes, and *bandaid* was more associated with the three cresols (data not shown). There was a good ability to model the smoke related sensory attributes with the chemical data (76% of the variance of the sensory data explained), with the coefficients of determination for predicted versus measured (calibration) being from 0.71 to 0.86 for each of the smoke-related palate attributes. The validation values were also similarly high (0.61 to 0.66), indicating the predictive ability of the model for new samples, not included in the model, was good.

Regarding the key in-mouth attribute ashy aftertaste, using a model including only the volatiles (two-factor model, 72% of the variance of the sensory data explained) gave slightly poorer R^2 values for this attribute compared to the complete model (R^2 predicted vs measured: calibration, x, validation y), while a model including glycosides only (one-factor model, 59% of the variance of the sensory data explained) also gave slightly poorer R^2 values for the ashy aftertaste (R^2 predicted vs measured: calibration, 0.63, validation 0.59), indicating that both volatile phenols and nonvolatile precursors are contributing to this attribute. While almost all volatile and glycoside conjugates of phenols were important to the model, the analytes with greatest positive contribution were 4-methyl guaiacol, guaiacol, the three volatile cresols, as well as phenol rutinoside (Ph-RG), methylguaiacol rutinoside (MGu-RG), guaiacol rutinoside (Gu-RG), and cresol rutinoside (Cr-RG). The free volatile compounds syringol and 4-methyl syringol had small negative or negligibly positive regression coefficients.

The results of this study confirmed the results of the previous work,[4] that multiple volatile phenols and nonvolatile glyco-conjugates were together associated with smoky off-flavor. The

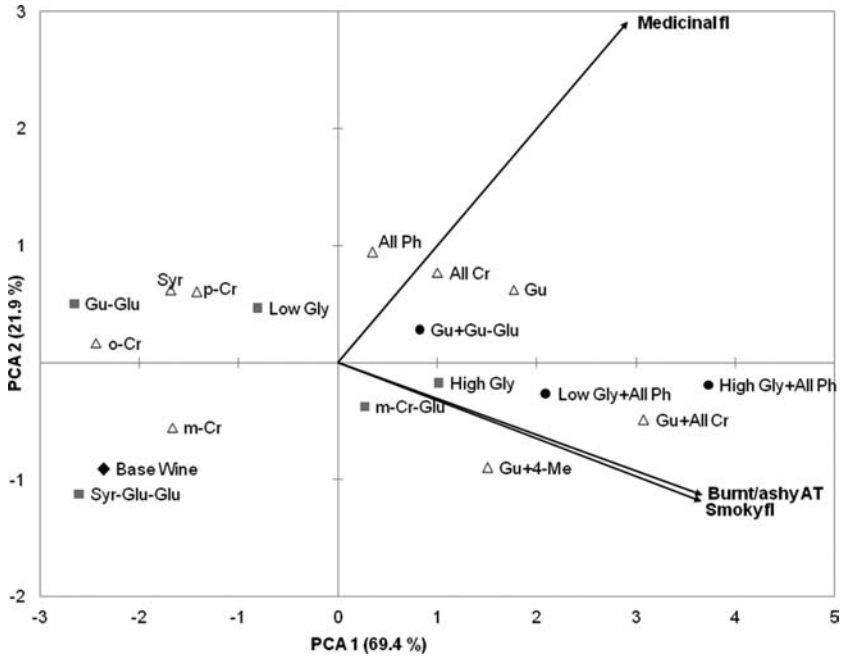

Figure 3. Principal component analysis biplot of the flavor sensory attribute mean values for wines with added volatiles (△), glycoconjugates (■), or both (●).

composition of the wine 17 was used as the basis for a confirmatory study using a reconstitution approach to further assess the sensory significance of the volatile phenols and the nonvolatile glycosides.

Reconstitution Sensory Study. Descriptive sensory analysis was used to characterize differences in the flavor attributes of a red wine, after addition of volatiles, synthetic glycoconjugates, fractions containing glycoconjugates isolated from smoke-affected grapes, or combinations thereof. The combinations used were based on hypotheses based on results of the initial sensory correlative study and a previous study,[4] so that the relative influence of individual volatile phenols and combinations, notably guaiacol, 4-methyl guaiacol and the cresols, were investigated at concentrations that were found in the smoke-affected wine 17 (see SI Table S1). Also included in the sensory descriptive analysis study were two smoke-affected wines (wines 18 and 19, see SI Table S1) as reference samples. Table 1 provides details of the 20 samples included.

From an inspection of the data for the 20 samples, it was noted that the smoke-affected wines (Wines 18 and 19) were rated highly in several attributes, including "woody" and "fresh green", which were not evident in the reconstitution samples or the base wine, and these two wines (Wines 18 and 19) were rated substantially higher for the smoke related attributes. To assess the various additions, the two wines made from smoke-affected grapes were excluded, and ANOVA was conducted for the remaining 18 samples listed in Table 1. Aroma attributes were rated for the samples as well as in-mouth attributes, and from the ANOVA there were no significant differences between any of the glycoside samples with no addition of volatiles (that is Low Gly, High Gly and *m*-Cr-Glu, and Syr-Glu-Glu and Gu-Glu) and the base wine in the *smoke* and *medicinal* aroma attributes, as determined by contrast tests. The concentration of free volatile phenols in the glycoside samples was also found to be negligible, and below the detection limit of the analytical method. Accordingly, only the palate attributes were investigated further.

From the ANOVA, the attributes *medicinal flavor*, *smoky flavor*, and *burnt ashy aftertaste* were rated significantly different across the samples. The attributes *smoky flavor* and *burnt ashy aftertaste* were highly correlated (r = 0.74, n = 18). Figure 3 shows the PCA for the significant flavor attributes. The major separation along PC1, which accounted for close to 70% of the variance in the sensory data, related to differences in ratings for *burnt ashy aftertaste* and *smoky* flavor. Separation along PC2 was related mainly to differences in *medicinal* flavor. The base wine, plotted to the lower left quadrant of the figure, was rated low in each of these attributes. The addition of syringol and the individual cresols (*o*-, *m*-, and *p*-cresol) had only a small effect on the flavor properties of the base wine, while the base wine with the three cresols added together (All Cr) was shifted strongly to the right and to the upper half of the figure, demonstrating an additive effect of the three compounds together, giving higher *medicinal* and *smoky* flavor. The samples with guaiacol alone (Gu) and guaiacol with 4-methyl guaiacol (Gu+4-Me) were rated higher again in *burnt/ashy* and *smoky* flavor, with the Gu+4-Me wine being lower in the *medicinal* flavor score. The combination of guaiacol and cresols (Gu + All Cr) had a very high rating in the *smoky* attributes. Interestingly, the All Ph sample, was rated lower in the *burnt/ashy* and *smoky flavor* attributes than the Gu and all Cr samples, indicating a suppressing effect of the other phenols in the mixture. Assessing statistical significance for these two attributes, there was a trend (P = 0.097) for the All Ph sample to be rated lower in *burnt/ashy aftertaste* than the Gu sample, while other pairwise comparisons for All Ph, Gu, and All Cr were not significant.

Regarding the glycosides, the wine with added syringol gentiobioside (Syr-Glu-Glu) was rated very similarly to the base wine, while the Gu-Glu sample was rated significantly higher only for the *medicinal* attribute. The *m*-cresol glucoside was rated substantially higher in *burnt/ashy* and *smoky*, at a similar intensity to the free guaiacol alone. Importantly, for the glycoside fraction isolated from the smoke affected grapes,

there was a perceptible flavor effect for the low Gly sample, being rated significantly higher in *medicinal* (P = 0.05) compared to the base wine, while the high Gly was rated significantly higher in *smoky* flavor compared to the base wine (P = 0.02).

As expected, the glycoside samples with volatile phenols added were rated higher in the smoky attributes than their counterparts with no volatiles added, so that the (Gu+Gu-Glu) wine was rated moderately highly in the smoke related attributes, at a concentration similar to that of the guaiacol addition alone, and the high Gly+ All Ph sample was overall rated as most different from the base wine, being situated to the far right of Figure 3, and substantially and significantly higher in scores for these attributes than the (All Ph) wine, confirming that the glycoside fraction contributed flavor.

Breakdown of Glycoconjugates with Incubation of Saliva. Results from the reconstitution study confirmed a direct sensory effect of glycosidically bound volatiles on smoke related flavor attributes. In addition, previous studies had demostrated that monoglucosidically bound volatiles in a model wine system or water could give rise to a smoky flavor in-mouth and that the respective volatiles were released.[4] These investigations from Parker et al.[4] indicated that the release of volatiles is highly variable across individuals.

A series of investigations were conducted to gain a better understanding of the variability between individuals and to assess factors responsible for differences in release of phenols through of glycoside hydrolysis.

Table 2 presents a summary of a set of experiments aiming to assess release of guaiacol from incubation with saliva from four individuals. Subject A had a mean release of guaiacol from its monoglucoside of 17% (release range of 9.7−25%). A comparison across the four different subjects showed that person D had a greater, and more consistent, activity to release guaiacol than the other subjects. The wide variation among individuals may be due to differing mouth biota and will be investigated in future studies.

Table 2. Release of Guaiacol from Guaiacol Monoglucoside Following Incubation with Saliva Obtained from Four Subjects in Vitro[a]

subject	mean release (standard deviation) %	minimum release (%)	maximum release (%)	number of replicates
A	17 (6)	9.7	25	6
B	31 (13)	21.0	52	9
C	12 (8)	3.8	20	4
D	63 (5)	57.0	68	4

[a]30 min incubation, 37 °C.

For this study, the glucosides, dissolved in water, were added directly to human saliva. When the glycosides were added to a model wine (pH 3.5, 12% v/v alcohol) and added to the saliva, the release was strongly reduced, so that there was a complete inhibition if saliva was mixed with model wine in a 3:2 ratio. A series of samples were examined to assess the influence of the model wine system on the release, in a single replicate for each condition from a single subject. Replication was not possible due to limitations in quantity of the guaiacol glucoside, but the results are comparable across treatments to provide screening data of the most important variables influencing release. As expected, the release decreased with lowering of the pH, with a total inhibition at a pH of 3.5 (Table 3). The release of guaiacol was lower when incubated at room temperature and nearly totally inhibited when incubated at 0 °C in comparison to body temperature (37 °C).

Table 3. Percentage Release of Guaiacol from Guaiacol Monoglucoside Following Incubation with Saliva in Vitro From One Subject[a] with Each Value Obtained As a Single Replicate As a Function of Temperature, pH, Alcohol Concentration, Glucose Concentration, and Time after Rinsing with Chlorhexidine Antibacterial Mouthwash[b]

condition	release (%)
temperature (°C)	
37	18
20	6
0	n.d.[c]
pH	
7.0	22
5.6	17
3.5	n.d.
ethanol (% v/v)	
0	39
10	18
15	6
glucose (g/L)	
0	55
3	5
45	4
time after chlorhexidine mouthwash (min)	
0	0.2
5	0.1

[a]Subject A from Table 1. [b]Unless otherwise stated, conditions were 30 min incubation, 3 mL saliva, 6.32 μg guaiacol monoglucoside in 2 mL saturated tartaric acid pH 3.5, 37 °C, 0% v/v alcohol, 0 g/L glucose, no mouthwash. [c]Not detected.

The alcohol concentration was found to have a strong effect on the release of guaiacol (Table 3), with the release decreasing from 39% to 6.3% with increasing ethanol concentration. However, the presence of alcohol did not lead to a complete inhibition of the guaiacol release. The same effect could be seen for a high glucose concentration, with 3 g/L of glucose leading to a strong decrease in the guaiacol release from 55% to 5%. Another inhibiting effect of the release could be seen by using antibacterial mouthwash. The use of chlorhexidine mouthwash completely inhibited the release of guaiacol from the glucoside for up to 2 h after application. These results are in agreement with the findings that bacterial microorganisms in saliva are the agents for release.[17]

Beside guaiacol, monoglucosides of syringol and *m*-cresol were also investigated. The mean release of six measurements for each glycoside was determined (Table 4). The proportion of both compounds released was high, similar to that of guaiacol glucoside.

Most volatile phenols in grapes and wine are found as disaccharide glycosides, and some in relatively high concentrations.[7] Therefore, the interaction of these glycoconjugates with saliva is of great interest. The degradation of syringol gentiobioside (2,6-dimethoxyphenyl-1-*O*-*β*-D-glucopyranosyl-(1→6)-*β*-D-glucopyranoside) and guaiacol primeveroside (2-methoxyphenyl-6-*O*-(*β*-D-xylopyranosyl)-*β*-D-glucopyranoside) was studied, and the results are shown in Table 4. The syringol gentiobioside reacted with the saliva in a similar way to its

Table 4. Release of Guaiacol, Syringol and *m*-Cresol from Mono- and Disaccharide Glycosides Following Incubation with Saliva in Vitro[a]

glycoside	release (standard deviation) %
syringol glucoside	40 (8)
m-cresol glucoside	50 (9)
syringol gentiobioside	27 (3.7)
guaiacol primeveraside	3 (2.4)

[a]30 min incubation, two subjects, 37 °C, mean of three replicates per subject.

monoglucoside, with a mean of six measurements giving 27% release. A much lower mean release of 3% resulted for the guaiacol primeveroside, indicating that the active principle in saliva, presumably bacterial enzyme activity, is able to hydrolyze both mono- and disaccharides, with evidence for variability in activity according to the nature of the sugar and the aglycone.

In addition, the release of free volatiles was confirmed in vivo, by placing SBSE bars in mouth after holding the glycoside solution in mouth. Surprisingly, free guaiacol and syringol could be detected, by means of GC-olfactometry, up to 15 min after spitting out the glycoside solution

In conclusion, monoglucosides and disaccharide glycosides can be released by the activity of saliva, with a great dependency on the glycoside and the individual. The release is greatly affected by a low pH, alcohol, and glucose concentration. Considering the buffering properties and alcohol dilution of saliva, as well as rapidly elevated temperature following ingestion, hydrolysis of glycosides is likely to continue as long as there is residual wine in the oral cavity. The decrease in release following chlorhexadine mouth wash, as observed previously in studies on flavonoid glucosides,[7] provides further evidence that it is in-mouth bacteria that play a role in the hydrolysis, with previous studies indicating the presence of gram-positive cocci in tetrads and gram-negative diplococci,[7] although oral epithelial cells may also be involved.[7] The reconstitution study clearly showed that the glycosidically bound volatiles have a direct impact on perceived smoke flavor, including aftertaste, and together with the data from the in vitro experiments, it is apparent that the breakdown of glycosides in mouth, including disaccharide glycosides, is an important mechanism of flavor perception in wine.

■ ASSOCIATED CONTENT

Ⓢ Supporting Information

Basic wine chemical composition and vintage and variety details; free volatile phenol and glycoconjugate concentration of the red wines; and sensory attributes and their definitions used in the two sensory descriptive analysis studies. This material is available free of charge via the Internet at http://pubs.acs.org.

■ AUTHOR INFORMATION

Corresponding Author

*Phone: +61 883036600; fax: +61 883036601; e-mail: leigh.francis@awri.com.au.

Notes

The authors declare no competing financial interest.

■ ACKNOWLEDGMENTS

We thank the sensory panelists, Dr. David Jeffery for advice with the synthesis, Belinda Bramley for assistance with the sensory panel, the Victorian wine industry for donating samples, and Con Simos and Adrian Coulter for arranging the samples. The Australian Wine Research Institute (AWRI), a member of the Wine Innovation Cluster on the Waite precinct in Adelaide, is supported by Australian grapegrowers and winemakers through their investment body the Grape and Wine Research and Development Corporation (GWRDC), with matching funds from the Australian Government.

■ REFERENCES

(1) Høj, P.; Pretorius, I. S.; Blair, R. *The Australian Wine Research Institute, Annual Report*, 2003, p 37.

(2) Prida, A.; Chatonnet, P. Impact of Oak-Derived Compounds on the Olfactory Perception of Barrel-Aged Wines. *Am. J. Enol. Vitic.* **2010**, *3*, 408−413.

(3) Kennison, K. R.; Wilkinson, K. L.; Williams, H. G.; Smith, J. H.; Gibberd, M. R. Smoke-Derived Taint in Wine: Effect of Postharvest Smoke Exposure of Grapes on the Chemical Composition and Sensory Characteristics of Wine. *J. Agric. Food Chem.* **2007**, *55*, 10897−10901.

(4) Parker, M.; Osidacz, P.; Baldock, G.; Hayasaka, Y.; Black, C.; Pardon, K. H.; Jeffery, D. W.; Geue, J. P.; Herderich, M. J.; Francis, I. L. Contribution of Several Volatile Phenols and Their Glycoconjugates to Smoke-Related Sensory Properties of Red Wine. *J. Agric. Food Chem.* **2012**, *60*, 2629−2637.

(5) Kennison, K. R.; Gibberd, M. R.; Pollnitz, A. P.; Wilkinson, K. L. Smoke-Derived Taint in Wine: The Release of Smoke-Derived Volatile Phenols During Fermentation of Merlot Juice Following Grapevine Exposure to Smoke. *J. Agric. Food Chem.* **2008**, *56*, 7379−7383.

(6) Singh, D. P.; Chong, H. H.; Pitt, K. M.; Cleary, M.; Dokoozlian, N. K.; Downey, M. O. Guaiacol and 4-Methylguaiacol Accumulate in Wines Made from Smoke-Affected Fruit Because of Hydrolysis of Their Conjugates. *Aust. J. Grape Wine Res.* **2011**, *17*, S13−S21.

(7) Hayasaka, Y.; Baldock, G. A.; Parker, M.; Pardon, K. H.; Black, C. A.; Herderich, M. J.; Jeffery, D. W. Glycosylation of Smoke-Derived Volatile Phenols in Grapes as a Consequence of Grapevine Exposure to Bushfire Smoke. *J. Agric. Food Chem.* **2010**, 10989−10998.

(8) Hayasaka, Y.; Dungey, K. A.; Baldock, G. A.; Kennison, K. R.; Wilkinson, K. L. Identification of a Beta-D-Glucopyranoside Precursor to Guaiacol in Grape Juice Following Grapevine Exposure to Smoke. *Anal. Chim. Acta* **2010**, *660*, 143−148.

(9) Hayasaka, Y.; Baldock, G. A.; Pardon, K. H.; Jeffery, D. W.; Herderich, M. J. Investigation into the Formation of Guaiacol Conjugates in Berries and Leaves of Grapevine *Vitis vinifera* L. Cv. Cabernet Sauvignon Using Stable Isotope Tracers Combined with HPLC-MS and MS/MS Analysis. *J. Agric. Food Chem.* **2010**, *58*, 2076−2081.

(10) Pollnitz, A. P.; Pardon, K. H.; Sykes, M.; Sefton, M. A. The Effects of Sample Preparation and Gas Chromatograph Injection Techniques on the Accuracy of Measuring Guaiacol, 4-Methylguaiacol and Other Volatile Oak Compounds in Oak Extracts by Stable Isotope Dilution Analyses. *J. Agric. Food Chem.* **2004**, *52*, 3244−3252.

(11) Aihara, K.; Urano, Y.; Higuchi, T.; Hirobe, M. Mechanistic Studies of Selective Catechol Formation from *o*-Methoxyphenols Using a Copper (II)-Ascorbic Acid-Dioxygen System. *J. Chem. Soc., Perkin Trans. 2* **1993**, 2165−2170.

(12) Hayasaka, Y.; Parker, M.; Baldock, G. A.; Pardon, K. H.; Black, C. A.; Jeffery, D. W.; Herderich, M. J. Assessing the Impact of Smoke Exposure in Grapes: Development and Validation of a HPLC-MS/MS Method for the Quantitative Analysis of Smoke-Derived Phenolic Glycosides in Grapes and Wine. *J. Agric. Food Chem.* **2013**, *61*, 25−33.

(13) Zhong, F.-Y.; Zhou, J.-H. 6-Acetoxymethyl-2-(2-Methoxyphenoxy)tetrahydropyran-3,4,5-Triyl Triacetate. *Acta Crystallogr.* **2005**, *E61*, o2701−o2703.

(14) Dungey, K. A.; Hayasaka, Y.; Wilkinson, K. L. Quantitative Analysis of Glycoconjugate Precursors of Guaiacol in Smoke-Affected Grapes Using Liquid Chromatography−Tandem Mass Spectrometry

Based Stable Isotope Dilution Analysis. *Food Chem.* **2011**, *126*, 801−806.
(15) Buettner, A. Investigation of Potent Odorants and Afterodor Development in Two Chardonnay Wines Using the Buccal Odor Screening System (BOSS). *J. Agric. Food Chem.* **2004**, *52*, 2339−2346.
(16) Buettner, A.; Otto, S.; Beer, A.; Mestres, M.; Schieberle, P.; Hummel, T. Dynamics of Retronasal Aroma Perception During Consumption: Cross-Linking On-Line Breath Analysis with Medico-Analytical Tools to Elucidate a Complex Process. *Food Chem.* **2008**, *108*, 1234−1246.
(17) Hemingway, K. M.; Alston, M. J.; Chappell, C. G.; Taylor, A. J. Carbohydrate-Flavor Conjugates in Wine. *Carbohydr. Polym.* **1999**, *38*, 283−286.

FPIAs can be performed in microtiter plates (MTPs) or cuvettes with different instrumental configurations. Generally, the assays performed in cuvettes are faster for individual sample measurements (approximately 2 min), but up to 20 or 30 samples can be measured simultaneously within 10 min in MTPs.[18] The missing (enzymatic) amplification step can lead to a lower overall sensitivity of the assay; for example, the EIA for the determination of the herbicide simazine yielded a 30 times lower detection limit than the FPIA using the same antibody.[19] Usually working ranges in the micrograms per liter to milligrams per liter range are observed for FPIAs;[20] for example, the detection limit of the herbicide chlorsulfuron was 10 μg/L.[17] FPIAs have been used for high-throughput screenings of small-molecule analytes such as the mycotoxins ochratoxin A (OTA), zearalenone, and deoxynivalenol in food-safety control within the following ranges: 5−200, 500−5000, and 100−2000 μg/L, respectively.[20]

Here, we present and compare two novel FPIAs for the fast, easy, and cost-effective determination of caffeine in beverages and cosmetics, one performed with a multimode plate reader, the other in a spectrometer especially developed for FPIA measurements. The concentrations obtained with these assays were verified with LC tandem mass spectrometry (LC−MS/MS) and ELISA using TMB as substrate. Additionally, the applicability of quality criteria from heterogeneous to homogeneous immunoassays was tested.

MATERIALS AND METHODS

Reagents and Materials. All solvents and chemicals were purchased from Sigma-Aldrich (Taufkirchen, Germany), Merck KGaA (Darmstadt, Germany), Serva (Heidelberg, Germany), and Mallinckrodt Baker (Griesheim, Germany) in the highest available quality. 5-(Aminoacetamido)fluorescein was obtained from Invitrogen (Carlsbad, CA, U. S. A.). The enzyme HRP (EIA grade) was obtained from Roche (Mannheim, Germany). The synthesis of the caffeine HRP conjugate was described before.[13] To obtain ultrapure reagent water for the preparation of buffers and solutions, a Synthesis A10 Milli-Q water purification system from Millipore (Schwalbach, Germany) was used.

All MTPs with 96 flat-bottomed wells were purchased from Greiner Bio-One (Frickenhausen, Germany). Black nonbinding MTPs were employed for fluorescence polarization measurements, whereas clear Microlon 600 MTPs were used for ELISAs. The caffeine reference standard used for the preparation of the calibrators was obtained from Sigma-Aldrich (Cat. no. C1778-1VL). The anti-mouse IgG whole molecule antibody (polyclonal, sheep, lot 21481) was purchased from Acris Antibodies (Herford, Germany). The anti-caffeine antibody (monoclonal, mouse IgG2B, clone 1.BB.877, lot L2051502M) was obtained from United States Biological (Swampscott, MA, U. S. A.). The beverages, coffees, tea, and cosmetics were purchased in a local supermarket.

Synthesis and Characterization of the Caffeine Fluorescein Conjugates. The synthesis of a caffeine spacer derivative (CafD) 7-(5-carboxypentyl)-1,3-dimethylxanthine was described elsewhere.[13] For the FPIA application in MTPs, the following protocol was used to synthesize the caffeine fluorescein conjugate: 2.42 mg of CafD were dissolved in *N*,*N*-dimethylformamide (DMF) and a small amount of *N*,*N*′-disuccinimidyl carbonate was added. *N*-Hydroxysuccinimide and *N*,*N*-dicyclohexylcarbodiimide were both dissolved in DMF, and each was added to the CafD solution in a molar excess of 1.2 compared to the amount of CafD. The mixture was shaken for 18 h at 21 °C (750 rpm). Then the reaction mixture was centrifuged for 10 min. The solution containing the activated NHS caffeine ester was mixed with the 5-(aminoacetamido)fluorescein (dissolved in 0.27 mol/L sodium dihydrogencarbonate) in a molar ratio of 1.5:1. After shaking for 18 h at room temperature, the chemical identity of the reaction product was confirmed with high-resolution mass spectrometry (Orbitrap Exactive, Thermo Scientific, Schwerte, Germany; ESI negative). A mass peak of m/z = 679.22 showed that the caffeine fluorescein conjugate had formed.

The product was cleaned by HPLC (Series 1200, Agilent Technologies, Waldbronn, Germany; column: Phen 250 × 3 mm, Sepserv, Berlin, Germany). The oven temperature was set to 40 °C, the flow rate was 0.4 mL/min, and the pressure was 170 bar. The solvents were ultrapure water (A) and methanol (B) containing 10 mmol/L ammonium acetate and 0.1% acetic acid. At the beginning, 80% solvent A was used. After 3 min, the percentage of solvent B was linearly increased to 95% within 17 min. After 28 min, the percentage of solvent B was decreased to 20% within 1 min. Then the composition was kept constant until the end of the run (40 min). The fraction containing the main peak was evaporated to dryness under a current of nitrogen and dissolved in methanol.

For the fluorescein conjugate for the application in cuvette, CafD was coupled to aminopropylamido carboxyfluorescein. This conjugate was obtained from *aokin* AG (Berlin, Germany).

Sample Preparation. The soft drink, energy drink, and caffeine-containing beer were degassed by shaking, followed by approximately 15 min in an ultrasonic bath. One bag of caffeine powder for soft drinks (2 g, containing 120 mg caffeine) was dissolved in 250 mL water. One bag of tea (Ceylon-Assam black tea, 1.75 g per bag) was brewed with 250 mL of boiling water allowing an infusion time of 10 min. The cosmetic sample (caffeine-containing shampoo) was prepared by dissolving 5.05 g in 1 L ultrapure reagent water. The espresso was prepared in a capsule espresso machine (Nespresso, Ristretto capsule). The instant coffee was prepared by dissolving 2.50 g of the instant coffee granulate in 200 mL boiling water.

A total of 7.00 ± 0.05 g of ground coffee powder per sample (three different types of 100% arabica ground coffee (1, 2, and 3 (decaffeinated), and one 100% robusta ground coffee) were brewed with 250 mL of boiling water. Different preparation methods for all coffees were employed; however, the same masses of ground coffee and water were always used. (i) A filter coffee machine was used. (ii) In a French press, an infusion time of 5 min was allowed. (iii) A Turkish coffee was prepared by pouring hot water on the ground coffee. When the coffee cooled down, it was filtered. (iv) For the preparation of the Italian espresso, an electric espresso machine (De'Longhi, Italy) was used.

For arabica 1, one other preparation method was used: the ground coffee was boiled with water and then refilled gravimetrically with water. Three different approaches were used for this preparation method: 5.00 g of coffee was boiled with 400 mL of water for 10 min, or 7.00 g of coffee was boiled with 250 mL of water for 10 or 30 min. The reference standard for decaffeinated coffee was obtained from FAPAS (Sand Hutton, Great Britain) and prepared as Turkish coffee (iii).

FPIA in Cuvettes (FPIA 1). The FPIA 1 was performed in the filter-based *aokin* spectrometer FP 470 (*aokin* AG), that was developed especially for FPIA measurements. All reagents were

pipetted with the *aokin* Liquid Handling Workstation directly into the round glass cuvette within the spectrometer. The system was controlled by the *aokin* software mycontrol v. 3.4.3.1. The excitation wavelength was set to 470 nm, and the emission was measured at 520 nm. The fluorescence intensities at perpendicular and parallel polarizer settings were measured simultaneously and constantly (kinetic measurement). First, 2.2 mL of reaction buffer (phosphate buffered saline based buffer) were pipetted into the cuvette that contained a stir bar. An ∼1 g/L methanolic stock solution of caffeine was prepared gravimetrically, and calibrators were obtained by sequential dilution with ultrapure water. A total of 200 μL of the calibrator (0−1000 μg/L) or sample dilution were added, followed by the addition of 100 μL of the caffeine fluorescein conjugate dilution (*aokin* AG). Afterward, 100 μL of the anti-caffeine antibody dilution (*aokin* AG) were added. The caffeine concentrations were determined by the software over a defined time range (40−80 s after the antibody was added). The degrees of polarization (in millipolarization units mP) for the calibration curve were determined 60 s after the antibody was added. The degrees of polarization were corrected by the background signal and G-factor (0.979). All samples and calibrators were measured in triplicate.

The degrees of polarization were subjected to a Grubbs outlier test ($\alpha = 0.01$). The mean values of the calibrators were fitted to a four-parameter logistic function with the parameters A (upper asymptote), B (slope at the test midpoint), C (concentration at test midpoint), and D (lower asymptote)[21] using the Origin 8G software (OriginLab, Northampton, U. S. A.).[22] Standard deviations of the mean signals were used to obtain the precision profile according to Ekins by calculating the relative error of each calibrator caffeine concentration.[23] The accordingly determined range with a relative error of the concentration below 30% was assigned the measurement range of the assay.

FPIA in MTPs (FPIA 2). All pipetting steps were carried out with 8-channel pipettes from Eppendorf (Hamburg, Germany). A total of 300 μL of TRIS buffer (10 mmol/L tris-(hydroxymethyl)aminomethane, 150 mmol/L sodium chloride, pH 8.5) with 0.01% Triton X-100 and 1% methanol were pipetted into each well. After adding 20 μL of the calibrators in triplicate (0−1000 μg/L) and sample dilutions (6-fold), a background measurement was performed on the monochromator-based multimode reader SpectraMax M5 (Molecular Devices, Biberach an der Riss, Germany) with the following settings: excitation at 492 nm, emission at 520 nm (at parallel and perpendicular polarizer settings), and a cutoff filter at 515 nm. A total of 10 μL of caffeine fluorescein conjugate, diluted in TRIS buffer, was added to each well, followed by 10 μL of the anti-caffeine antibody (1.37 mg/L in TRIS buffer). After shaking for 10 min on the plate shaker Titramax 101 from Heidolph (Schwabach, Germany; 750 rpm), the fluorescence was measured with the settings described above. The perpendicular and parallel intensities resulting from the background measurement were subtracted from the respective values. These background-corrected values were then used for the calculation of the degree of polarization. The values were corrected by the G-factor (0.946) of the instrument. The background corrected intensities and the degrees of polarization were subjected to a Grubbs outlier test. The assay was repeated four times, yielding a 6 × 4 determination of the caffeine concentration for each sample. The calibration curve was fitted as described above. A calibration curve with 8 calibrators was used to determine the caffeine concentrations of the samples. These calibrators were measured on each MTP. The measurement range was determined as described above with 16 calibrators in triplicate.

Reference Methods. Caffeine determination with the reference methods HRP TMB ELISA and the LC−MS/MS were performed with the same instruments and methods as described before by Grandke et al.[14]

RESULTS AND DISCUSSION

Comparison of the Caffeine FPIAs and Applicability of Quality Criteria. The FPIA in cuvettes (FPIA 1) is a kinetic assay where the degree of polarization can be measured as a function of time (Figure 1); here, no incubation step is required as it is a continuous process. One time point was chosen at which the values for the calibration curves and precision profile were determined (60 s after the antibody was added). The caffeine concentrations for real samples were determined over a time range (40−80 s). In contrast, the degrees of polarization for the FPIA in MTPs (FPIA 2) were determined after a defined time of 10 min (end point measurement). The incubation time in MTPs is prolonged compared to measurements in the cuvettes, as it takes longer to reach the equilibration because the circulation is much faster when a stir bar is used than on a plate shaker.

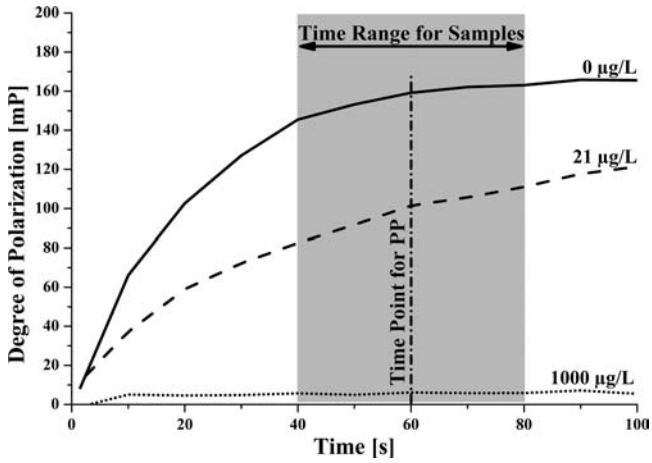

Figure 1. Kinetic measurement of the degree of polarization after antibody addition shown for three caffeine calibrators (0, 21, and 1000 μg/L) measured with the FPIA in cuvettes. The time range for the determination of caffeine concentrations in samples (40−80 s, gray background) and the time point (60 s, dash-dotted line) at which the values for the calibration curve and the precision profile (PP) were determined are highlighted.

The FPIAs were optimized in regard to the parameters buffer basis, buffer additives, anti-caffeine antibody concentration, and caffeine fluorescein conjugate concentration. Additionally, different types of MTPs (nonbinding and untreated MTPs, different manufacturers) were tested for FPIA 2. Calibration curves with precision profiles for the FPIAs were determined under optimized conditions. Quality criteria for the assessment of caffeine EIAs in respect of the calibration curves (4-PL) had been previously defined and applied to a series of heterogeneous EIAs.[14,24] The applicability of these criteria to FPIAs was to be evaluated in this study.

The sensitivity in terms of the test midpoint C of the calibration curve was determined to 27.4 μg/L for FPIA 1

(Figure 2) and is approximately three times higher than that obtained for FPIA 2 with 9.9 μg/L (Figure 3). Therefore, FPIA

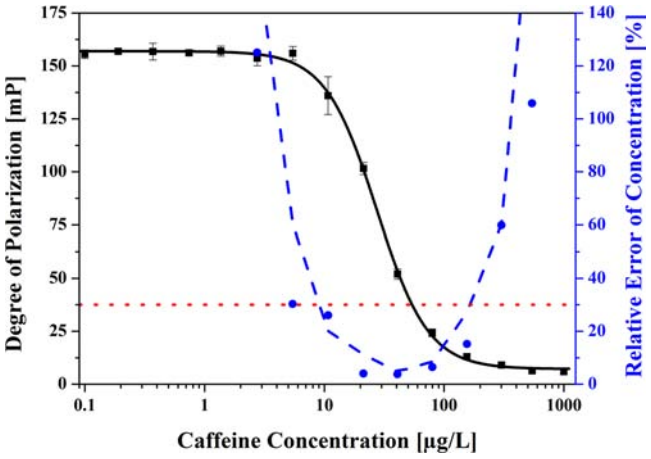

Figure 2. Calibration curve (black squares and solid line), precision profile (blue circles and dashed line), and measurement range (intersection points at 30% relative error of concentration, dotted red line; 8.94−164 μg/L) were determined for FPIA 1 in cuvettes (A = 157 mP; B = 2.02; C = 27.41 μg/L; D = 7.20 mP; R^2 = 0.999; RDR = 0.96).

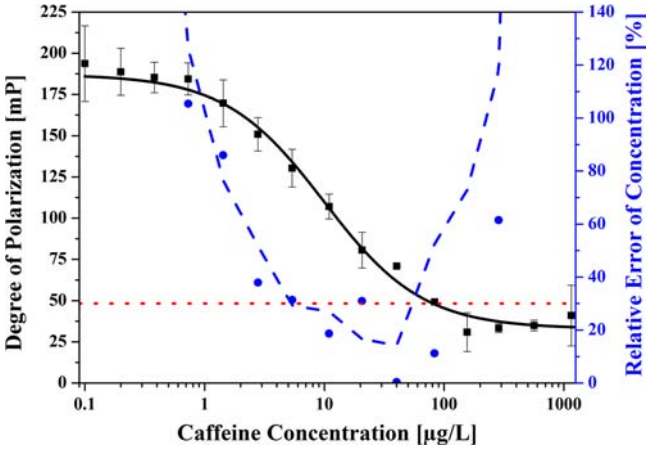

Figure 3. Calibration curve (black squares and solid line), precision profile (blue circles and dashed line), and measurement range (intersection points at 30% relative error of concentration, dotted red line; 5.19−55.5 μg/L) were determined for FPIA 2 in MTPs (A = 187 mP; B = 1.05; C = 9.93 μg/L; D = 33.0 mP; R^2 = 0.986; RDR = 0.82).

2 is more sensitive than FPIA 1. Compared to that of the ELISA (C = 95 ng/L),[14] the test midpoint of FPIA 2 is relatively high. FPIAs for other analytes showed higher test midpoints: 207 μg/L for butachlor and 165 μg/L for melamine.[25,26] Hence, the sensitivity of our caffeine FPIAs is comparatively good. Similar dynamic ranges were observed for FPIA 1 and 2 (150 mP and 154 mP, respectively). The relative dynamic ranges (RDRs) were on a normalized scale 0.96 for FPIA 1, and 0.82 for FPIA 2. Accordingly, only FPIA 1 fulfilled the predefined required threshold of 0.90. The calibration curve of FPIA 1 showed a slope B at the test midpoint of 2.02. The slope of the calibration curve for FPIA 2 was 1.05. The coefficient of determination R^2 is a measure for the goodness of fit. FPIA 1 showed a good R^2 value of 0.999, whereas FPIA 2 (R^2 = 0.986) did not reach the required value of 0.990. Additionally, the standard deviations of the measured values were analyzed. The highest standard deviation for FPIA 1 was 9.94 mP, whereas the highest standard deviation for FPIA 2 was 22.95 mP. Overall, a better goodness of fit was obtained for FPIA 1 compared to FPIA 2. Measurement ranges of 8.94−164 μg/L and 5.19−55.5 μg/L were determined for FPIA 1 and FPIA 2 according to the precision profiles. Neither of the ranges covered 3 orders of magnitude, even though the measurement range than that of FPIA 1 was three times wider than FPIA 2. Other FPIAs had shown comparable measurement ranges: 5−200 μg/L for OTA,[20] 32.0−1220 μg/L for the herbicide butachlor.[25] Therefore, a critical assessment of the requirement for this criterion should follow for homogeneous assays. In summary, FPIA 1 fulfilled all quality criteria for the calibration curve with the exception of the measurement range.

Assay Evaluation for Different Matrixes. The most common matrixes of caffeine occurrence were selected to compare the suitability of the FPIAs for caffeine determination (Figure 4). For the kinetic FPIA 1, the measurement for one

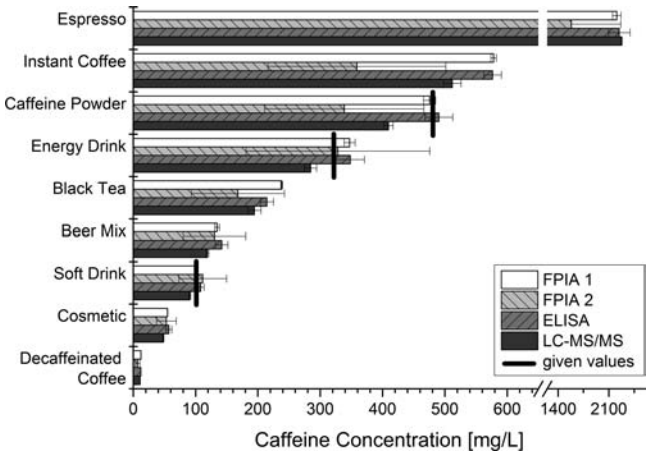

Figure 4. Caffeine concentrations of beverages and cosmetics determined with FPIA 1 and 2, ELISA, and LC−MS/MS. Furthermore, the values provided by the manufacturer are depicted for three samples (black lines). For better comparability, the caffeine concentrations are given in milligrams per liter.

sample takes approximately 2 min. This assay is automated, and eight samples can be measured in triplicate with the liquid handling workstation in one run. FPIA 2 allows a 6-fold determination of eight samples within 20 min, including all pipetting, incubation, and measurement steps. Smaller sample volumes are required for FPIA 2 than for FPIA 1. Additionally, all samples were measured by ELISA and LC−MS/MS.

Beverages with high caffeine concentrations (>150 mg/L) need to be labeled as required by Commission Directive 2002/67/EG.[27] Here, a direct comparison is possible between the values provided by the manufacturer and the determined values. The closest agreement for the energy drink was found with 328 mg/L for FPIA 2 compared to the given value of 320 mg/L. The values for ELISA and FPIA 1 were higher with 348 mg/L and 347 mg/L, respectively, whereas the concentration obtained with LC−MS/MS was lower with 285 mg/L. One bag of the caffeine powder (dissolved in 250 mL water) should contain 120 mg caffeine. The caffeine contents calculated from the results of ELISA and FPIA 1 were 122 mg and 119 mg, respectively, and were therefore very close to the value given by

dx.doi.org/10.1021/jf4053226 | J. Agric. Food Chem. 2014, 62, 2337−2343

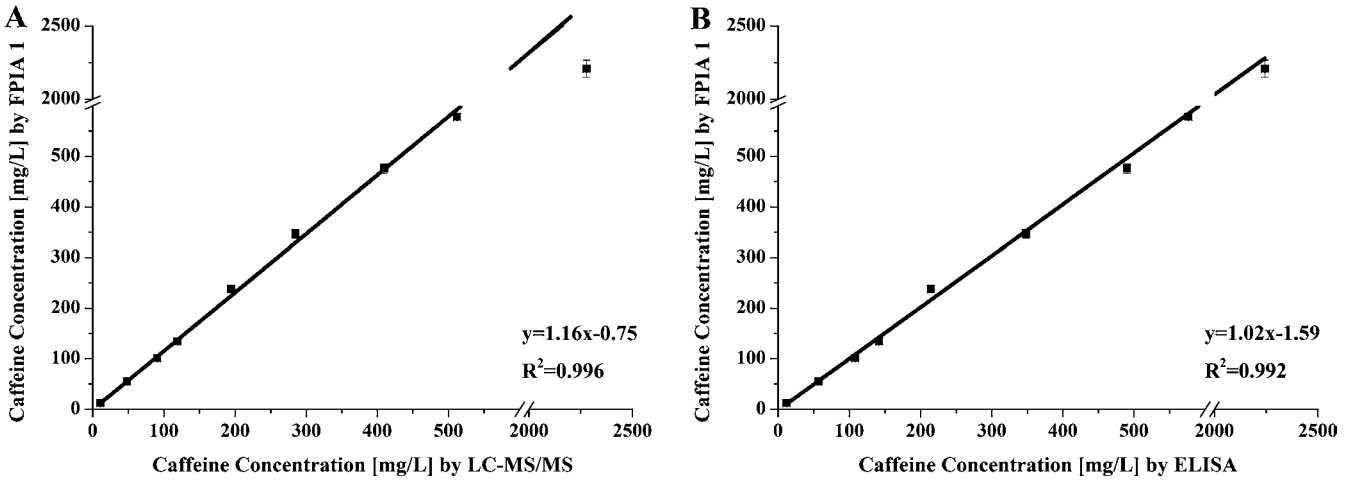

Figure 5. Correlation between FPIA 1 and LC−MS/MS (A) and ELISA (B) for caffeine-containing beverages and cosmetics.

Table 1. Caffeine Concentrations (FPIA 1) and Coefficients of Variation (CVs) for Several Preparation Methods (Filter Coffee, French Press, Turkish Coffee, Italian Espresso) Determined for Different Types of Coffee (Robusta, Arabica 1, 2, and 3 (Decaffeinated))

	filter coffee		French press		Turkish coffee		Italian espresso	
	concn [mg/L]	CV [%]	concn [mg/L]	CV [%]	concn [mg/L]	CV [%]	concn [mg/L]	CV [%]
robusta	742 ± 15	2.0	825 ± 6	0.7	761 ± 15	2.0	848 ± 17	2.1
arabica 1	487 ± 4	0.9	387 ± 4	0.9	454 ± 8	1.7	490 ± 4	0.9
arabica 2	452 ± 4	1.0	512 ± 6	1.1	471 ± 10	2.2	465 ± 4	0.9
arabica 3	16.2 ± 0.4	2.7	14.7 ± 0.1	0.9	14.6 ± 0.5	3.4	17.1 ± 0.2	0.9

the manufacturer. FPIA 2 and LC−MS/MS led to underestimations. FPIA 1 with 101 mg/L, led to the best agreement for the soft drink compared to the expected value of 100 mg/L. Slight overestimations were observed with ELISA (108 mg/L) and FPIA 2 (112 mg/L). LC−MS/MS showed lower concentrations for all three samples than the expected values. The caffeine contents of the shampoo determined with the different methods were all very similar: 9.56 (LC−MS/MS), 11.3 (ELISA), 10.9 (FPIA 1), and 10.5 mg/g (FPIA 2) based on the amount of shampoo. These data correlate well with the values obtained by Carvalho et al.[13]

A decaffeinated reference standard was investigated. All determined concentrations were within the satisfactory range of 193−606 g/kg. The closest agreement to the assigned value of 399 mg/kg was found for LC−MS/MS with 390 mg/kg. FPIA 1 (438 mg/kg) and ELISA (428 mg/kg) led to higher values, whereas FPIA 2 led to a lower caffeine concentration (246 mg/kg).

The concentrations determined with FPIA 2 for the energy drink, beer mix, soft drink, and cosmetic showed a good correlation with the data determined for ELISA and FPIA 1. For the other samples (espresso, instant coffee, caffeine powder, black tea, and decaffeinated coffee), a large underestimation was observed compared to the other immunoanalytical methods. The coefficients of variation (CVs) for the FPIA 2 were very high. The CVs for LC−MS/MS, ELISA and FPIA 1 were below 6%, 9%, and 4%, respectively. High precision corresponding to low CVs and the applicability to many different matrixes is desired. Therefore, FPIA 2 is not suitable for the quantitative determination of caffeine in these consumer products yet. This method can be used for fast semiquantitative analysis of many samples.

The intra- and interplate variations of concentrations of real samples as a measure for precision were proposed by Grandke et al. to assess the applicability of EIAs.[14] For the FPIAs performed in cuvettes, no intra- and interplate variations could be determined. The FPIAs performed in MTPs showed very high CVs for the real samples, which evidently exceed the desired values of 10% for the intraplate and 20% for the interplate variation. All in all, the parameters for intra- and interplate precision are not applicable.

Additionally, the correlation with LC−MS/MS as reference method was proposed as a measure for accuracy.[14] However, the cross-reactivity of the antibody toward other alkaloids can cause overestimations compared to instrumental methods. Therefore, the HRP TMB ELISA using the same monoclonal antibody was used as immunoanalytical reference method to render the correlation independent of cross-reactivity. For FPIA 1, the following correlation parameters were determined: slope $m = 1.16$, intercept $n = -0.75$, and coefficient of determination $R^2 = 0.996$ for LC−MS/MS and $m = 1.02$, $n = -1.59$, and $R^2 = 0.992$ for ELISA (Figure 5). The parameters n and R^2 show similar results for both linear regressions and are in agreement with the required values ($R^2 > 0.95$, n near 0). However, the crucial slope parameter m is significantly better (requirement: 1.00 ± 0.05) for the correlation with ELISA.

For FPIA 2, the parameters for the correlations with LC−MS/MS ($m = 1.90$, $n = -2.03$, $R^2 = 0.933$) and ELISA ($m = 0.80$, $n = -1.98$, $R^2 = 0.954$) did not fulfill all requirements, especially because the slope parameter differed significantly from unity. A notable underestimation was observed for the correlation with ELISA, although the same monoclonal antibody was used. Altogether, the best correlation was found for FPIA 1 and ELISA, resulting in a highly accurate assay.

dx.doi.org/10.1021/jf4053226 | J. Agric. Food Chem. 2014, 62, 2337−2343

Applicability of FPIA for Different Ground Coffees and Preparation Methods. The caffeine concentration of different types of ground coffee (arabica and robusta) and preparation methods (filter coffee, French press, Turkish coffee, and Italian espresso) were measured with the newly developed FPIA methods. On the basis of the previous findings, only the results obtained for FPIA 1 are discussed (Table 1). Generally, the coffees made of robusta beans showed higher caffeine concentrations (740−850 mg/L) than arabica beans, in agreement with Casal et al.[3] The arabica coffees 1 and 2 showed similar caffeine concentrations (390−510 mg/L), and for arabica 3, the decaffeinated coffee, caffeine concentrations in the range of 15−17 mg/L were determined. For all samples, no preconcentration steps were necessary; on the contrary, the decaffeinated coffee samples had to be diluted as well.

Comparing the various preparation methods, the French press method revealed opposing results for the different arabica coffees (arabica 1 and 2) because, here, the highest and the lowest caffeine concentrations were determined. All other preparation methods led to relatively similar results. For the robusta coffee, the highest caffeine concentrations were found for the French press and Italian espresso preparation method. No clear correlation between the preparation method and the caffeine concentration could be concluded for different ground coffees.

In addition to the four preparation methods, the influence of the boiling time and the ratio of coffee to water on the extracted caffeine amount was investigated (Table 2). A higher ratio of coffee to water yielded lower extracted caffeine amounts (based on the mass of coffee). Moreover, the extracted caffeine amount from ground coffee increased from 12.9 to 14.1 mg/kg with longer boiling times (30 min instead of 10 min). These results confirm the conclusions made by Bell et al.[28] The results obtained for the coffee samples with FPIA 1 are precise as indicated by the good CVs, which are all below 4%.

Table 2. Caffeine Contents and Coefficients of Variation (CVs) Determined for Different Ratios of Ground Coffee to Water and Different Boiling Times of Arabica 1

mass of arabica 1 [g]	volume of water [mL]	boiling time [min]	concn [mg/kg]	CV [%]
5.0	400	10	13.5 ± 0.2	1.5
7.0	250	10	12.9 ± 0.5	3.5
7.0	250	30	14.1 ± 0.5	3.8

Two caffeine FPIA formats (FPIA 1 in cuvettes and FPIA 2 in MTPs) were developed and carefully optimized. In contrast to previously developed instrumental methods, neither FPIA requires sample preparation steps, which are typically time- and cost-intensive. Also, the measurement time for each sample is much lower for homogeneous assays compared to instrumental methods; for example, the caffeine determination in one sample takes 40 min using LC−MS/MS instead of 2 min with FPIA 1 or 20 min for the measurement of up to 24 samples simultaneously using FPIA 2. Additionally, the instruments for immunoanalytical methods are usually less expensive than equipment needed for instrumental methods like LC−MS/MS. Compared to heterogeneous immunoassays (e.g., ELISA) the FPIA is a mix-and-read assay, so no time-consuming incubation or washing steps are necessary. This makes the homogeneous assay a fast and easy screening method with sufficient sensitivity (but lower than ELISA) for almost all caffeine-containing beverages.

Both FPIAs were assessed with quality criteria previously defined for heterogeneous assays.[14,24] FPIA 2 did not fulfill the requirements for the quality criteria and showed high coefficients of variation for the caffeine determination in real samples. Because of its high throughput, FPIA 2 is a good screening tool for semiquantitative caffeine determination. FPIA 1 fulfilled almost all quality criteria for the calibration curve. A variety of matrixes were analyzed and led to reliable and accurate caffeine concentrations with FPIA 1. This homogeneous assay represents an automatable method for the fast and easy quantification of caffeine in consumer products.

AUTHOR INFORMATION

Corresponding Author

*R. J. Schneider. Tel.: +49 30 8104 1151. Fax: +49 30 8104 1157. E-mail: rudolf.schneider@bam.de.

Author Contributions

¶These authors contributed equally to this work.

Funding

This work was supported by grants from the Federal Ministry of Economic Affairs and Energy (BMWi, program MNPQ, project no. 22/11) and the BAM Federal Institute for Materials Research and Testing Ph.D. program.

Notes

The authors declare no competing financial interest.

ACKNOWLEDGMENTS

We express our gratitude to A. Lehmann and M. Engel for LC−MS/MS measurements, N. Scheel for the HPLC cleanup, S. Weise for the high-resolution MS measurements, A. Stoyanova for technical assistance (all BAM), and N. Abdallah for selected FPIA measurements (*aokin* AG).

ABBREVIATIONS USED

CafD, caffeine derivative; EIA, enzyme immunoassay; ELISA, enzyme-linked immunosorbent assay; FPIA, fluorescence polarization immunoassay; FRET, fluorescence resonance energy transfer; HRP, horseradish peroxidase; MTP, microtiter plate; OTA, ochratoxin A; RDR, relative dynamic range; TMB, 3,3′,5,5′-tetramethylbenzidine

REFERENCES

(1) Fredholm, B. B.; Battig, K.; Holmen, J.; Nehlig, A.; Zvartau, E. E. Actions of caffeine in the brain with special reference to factors that contribute to its widespread use. *Pharmacol. Rev.* **1999**, *51*, 83−133.

(2) Rudolph, E.; Faerbinger, A.; Koenig, J. Determination of the caffeine contents of various food items within the Austrian market and validation of a caffeine assessment tool (CAT). *Food Addit. Contam., Part A* **2012**, *29*, 1849−1860.

(3) Casal, S.; Oliveira, M.; Alves, M. R.; Ferreira, M. A. Discriminate analysis of roasted coffee varieties for trigonelline, nicotinic acid, and caffeine content. *J. Agric. Food Chem.* **2000**, *48*, 3420−3424.

(4) Barone, J. J.; Roberts, H. R. Caffeine consumption. *Food Chem. Toxicol.* **1996**, *34*, 119−129.

(5) McCusker, R. R.; Goldberger, B. A.; Cone, E. J. Caffeine content of specialty coffees. *J. Anal. Toxicol.* **2003**, *27*, 520−522.

(6) Mandel, H. G. Update on caffeine consumption, disposition and action. *Food Chem. Toxicol.* **2002**, *40*, 1231−1234.

(7) Stefanidou, E. M.; Caramellino, L.; Patriarca, A.; Menato, G. Maternal caffeine consumption and sine causa recurrent miscarriage. *Eur. J. Obstet. Gynecol. Reprod. Biol.* **2011**, *158*, 220−224.
(8) Luisier, N.; Ruggi, A.; Steinmann, S. N.; Favre, L.; Gaeng, N.; Corminboeuf, C.; Severin, K. A ratiometric fluorescence sensor for caffeine. *Org. Biomol. Chem.* **2012**, *10*, 7487−7490.
(9) Santini, A.; Ferracane, R.; Mikusova, P.; Eged, S.; Srobarova, A.; Meca, G.; Manes, J.; Ritieni, A. Influence of different coffee drink preparations on ochratoxin A content and evaluation of the antioxidant activity and caffeine variations. *Food Control* **2011**, *22*, 1240−1245.
(10) Maeso, N.; del Castillo, C.; Cornejo, L.; Garcia-Acicollar, A.; Alguacil, L. F.; Barbas, C. Capillary electrophoresis for caffeine and pyroglutamate determination in coffees - Study of the in vivo effect on learning and locomotor activity in mice. *J. Pharm. Biomed. Anal.* **2006**, *41*, 1095−1100.
(11) Mesaros, C.; Culea, M.; Iordache, A. M.; Visovan, I.; Cozar, C.; Cosma, C. A new caffeine test for diagnosis of cirrhosis by GC/MS. *Asian J. Chem.* **2010**, *22*, 3608−3614.
(12) Gardinali, P. R.; Zhao, X. Trace determination of caffeine in surface water samples by liquid chromatography−atmospheric pressure chemical ionization−mass spectrometry (LC−APCI−MS). *Environ. Int.* **2002**, *28*, 521−528.
(13) Carvalho, J. J.; Weller, M. G.; Panne, U.; Schneider, R. J. A highly sensitive caffeine immunoassay based on a monoclonal antibody. *Anal. Bioanal. Chem.* **2010**, *396*, 2617−2628.
(14) Grandke, J.; Oberleitner, L.; Resch-Genger, U.; Garbe, L.-A.; Schneider, R. J. Quality assurance in immunoassay performance—comparison of different enzyme immunoassays for the determination of caffeine in consumer products. *Anal. Bioanal. Chem.* **2013**, *405*, 1601−1611.
(15) Tan, C.; Gajovic-Eichelmann, N.; Stöcklein, W. F. M.; Polzius, R.; Bier, F. F. Direct detection of Δ9-tetrahydrocannabinol in saliva using a novel homogeneous competitive immunoassay with fluorescence quenching. *Anal. Chim. Acta* **2010**, *658*, 187−192.
(16) Gutierrez, M. C.; Gomez-Hens, A.; Perez-Bendito, D. Immunoassay methods based on fluorescence polarization. *Talanta* **1989**, *36*, 1187−1201.
(17) Eremin, S. A.; Ryabova, I. A.; Yakovleva, J. N.; Yazynina, E. V.; Zherdev, A. V.; Dzantiev, B. B. Development of a rapid, specific fluorescence polarization immunoassay for the herbicide chlorsulfuron. *Anal. Chim. Acta* **2002**, *468*, 229−236.
(18) Chun, H. S.; Choi, E. H.; Chang, H.-J.; Choi, S.-W.; Eremin, S. A. A fluorescence polarization immunoassay for the detection of zearalenone in corn. *Anal. Chim. Acta* **2009**, *639*, 83−89.
(19) Eremin, S. A.; Samsonova, J. V. Development of polarization fluoroimmunoassay for the detection of s-triazine herbicides. *Anal. Lett.* **1994**, *27*, 3013−3025.
(20) Smith, D. S.; Eremin, S. A. Fluorescence polarization immunoassays and related methods for simple, high-throughput screening of small molecules. *Anal. Bioanal. Chem.* **2008**, *391*, 1499−1507.
(21) Grandke, J.; Resch-Genger, U.; Bremser, W.; Garbe, L.-A.; Schneider, R. J. Quality assurance in immunoassay performance-temperature effects. *Anal. Methods* **2012**, *4*, 901−905.
(22) Dudley, R. A.; Edwards, P.; Ekins, R. P.; Finney, D. J.; McKenzie, I. G. M.; Raab, G. M.; Rodbard, D.; Rodgers, R. P. C. Guidelines for Immunoassay Data-Processing. *Clin. Chem.* **1985**, *31*, 1264−1271.
(23) Ekins, R. The precision profile: its use in RIA assessment and design. *Ligand Q.* **1981**, *4*, 33−44.
(24) Grandke, J.; Oberleitner, L.; Resch-Genger, U.; Garbe, L.-A.; Schneider, R. J. Quality assurance in immunoassay performance - carbamazepine immunoassay format evaluation and application on surface and waste water. *Anal. Methods* **2013**, *5*, 3754−3760.
(25) Lei, H.; Xue, G.; Yu, C.; Haughey, S. A.; Eremin, S. A.; Sun, Y.; Wang, Z.; Xu, Z.; Wang, H.; Shen, Y.; Wu, Q. Fluorescence polarization as a tool for the detection of a widely used herbicide, butachlor, in polluted waters. *Anal. Methods* **2011**, *3*, 2334−2340.
(26) Wang, Q.; Haughey, S. A.; Sun, Y.-M.; Eremin, S. A.; Li, Z.-F.; Liu, H.; Xu, Z.-L.; Shen, Y.-D.; Lei, H.-T. Development of a fluorescence polarization immunoassay for the detection of melamine in milk and milk powder. *Anal. Bioanal. Chem.* **2011**, *399*, 2275−2284.
(27) Commission Directive 2002/67/EG on the labelling of foodstuffs containing chinine and of foodstuffs containing caffeine. http://eur-lex.europa.eu/LexUriServ/LexUriServ.do?uri=OJ:L:2002:191:0020:0021:DE:PDF (accessed Nov. 18, 2013)
(28) Bell, L. N.; Wetzel, C. R.; Grand, A. N. Caffeine content in coffee as influenced by grinding and brewing techniques. *Food Res. Int.* **1996**, *29*, 785−789.

gas chromatography mass spectrometry (GC−MS), methylation analysis, nuclear magnetic resonance (NMR) spectroscopy (^{1}H,^{13}C, H−H COSY, HSQC, TOCSY, and NOESY), and atomic force microscopy (AFM). In addition, in vitro antioxidant activity was investigated by the reducing power, superoxide anion scavenging activity, and the DPPH radical scavenging activity assays.

MATERIALS AND METHODS

Materials and Reagents. The 6-month-old *Achatina fulica* (China white jade snails) with an average shell size of 3−5 cm were supplied by the Huzhou Fenren Company (Zhejiang, China). Table 1 shows the composition of *A. fulica* soft body in this study.

Table 1. Composition of *Achatina fulica*

composition	wt % in *A. fulica* soft part
carbohydrate[b]	25.75 (0.527)[a]
protein[b]	71.58 (0.871)
lipid[b]	3.76 (0.136)
moisture[c]	78.15 (1.673)
ash[b]	5.04 (0.362)

[a]Data were shown as mean (SD), n = 3. [b]Dry weight. [c]Fresh weight.

Monosaccharide standards and disaccharide lactose were purchased from Sigma (St. Louis, MO, USA). Papain (1200 U g^{-1}) and L-cysteine hydrochloride (Cys) were purchased from Fluka (Seelze, Germany). The derivatization reagent 1-phenyl-3-methyl-5-pyrazolone (PMP) was from Sinopharm Chemical Reagents (Shanghai, China). 2,2-Diphenyl-1-picryl-hydrazyl (DPPH), ferrozine, nitroblue tetrazolium (NBT), phenazine methosulfate (PMS), reduced nicotinamide adenine dinucleotide (NADH), and vitamin C were purchased from Sigma-Aldrich Co. All the other reagents used were of analytical grade.

Composition Analysis of *Achatina fulica* Soft Body. The whole soft body of *A. fulica* was oven-dried to constant weight (102 °C for 18−24 h) to determine moisture contents. Lipids were extracted in baths of diethyl ether,[16] and protein contents were determined by the Lowry method.[17] Ash contents were determined by combusting extracted samples in a muffle furnace at 550 °C for 8 h, and carbohydrates were analyzed using the phenol sulfuric acid method of Dubois et al.[18,19]

Isolation and Purification of AFPS-IB. Polysaccharides were isolated using a previously described procedure with some modifications.[8] The shell of *A. fulica* was removed, and fresh muscle was freeze-dried and ground to a powder, which was then defatted using acetone for 24 h. Five grams of defatted powder was suspended in 50 mL of 0.1 M sodium carbonate buffer (pH 6.0). The suspension was shaken for 24 h at 200 rpm and 60 °C after the addition of papain (250 mg), EDTA (73.1 mg), and Cys (39.4 mg). The supernatant was precipitated with four volumes of ethanol at 4 °C overnight and then centrifuged (Beckman Model J-21B centrifuge, Beckman Inst, Inc., Palo Alto, CA, USA) for 30 min at 8000 × g. The precipitate was washed sequentially with alcohol and acetone and then dissolved in 10 mL of ice-cold distilled water. The digestion mixture was cooled to 4 °C, and trichloroacetic acid was added to a final concentration of 5% (w/v). The sample was mixed, allowed to stand for 1 h, and then centrifuged for 20 min at 8000 × g. The supernatant was recovered by decanting before mixing with three volumes of ethanol. The suspension was stored overnight at 4 °C and then centrifuged for 30 min at 8000 × g. The precipitate was washed with absolute ethanol, dissolved in water, and dialyzed against 100 volumes of water. The dialyzate was freeze-dried to obtain crude polysaccharide AFPS.

AFPS was dissolved in distilled water, applied to a DEAE-Sephacel column (2.6 cm ×30 cm, Whatman, Brentford, UK), and eluted with distilled water, followed by 0.1 M NaCl and 0.5 M NaCl, respectively. Each fraction of 5 mL was collected at a flow rate of 30 mL h^{-1} and monitored by the phenol-sulfuric acid method at 490 nm.[19] The collected fractions were further chromatographed on a Sephacryl S-300 HR gel filtration column (1.6 cm × 100 cm, Amersham Biosciences, Uppsala, Sweden) eluted with distilled water; fractions were collected and lyophilized to give a white powder consisting of polysaccharides designated AFPS-IA, AFPS-IB, and AFPS-IC. AFPS-IB was subjected to subsequent analyses. The whole procedure is shown in Figure S1.

Homogeneity and Molecular Weight Determination. The homogeneity and molecular weight of AFPS-IB were determined by high performance size exclusion chromatography (HPSEC) on a TSK-Gel G4000 PWXL column (300 mm × 7.5 mm, Tosoh Biosep, Japan), with a column temperature of 40 °C. The polysaccharides were eluted with 0.2 M NaCl at a flow rate of 1.0 mL min^{-1} and detected by a refractive index detector (Water 2414). Preliminary calibration of the column was performed using dextrin in a range of molecular weights measured in kDa (500, 66.9, 48, 20, 5; Showa-Denko, Japan).

Monosaccharide Composition Analysis. The monosaccharide composition was determined using a PMP-HPLC method.[20] In brief, polysaccharides (typically 1 mg) were hydrolyzed with 2 M trifluoroacetic acid (TFA) at 110 °C under nitrogen for 8 h with lactose added as an internal standard. The monosaccharide hydrolysate was dried under vacuum and then derivatized with 450 μL of 1-phenyl-3-methyl-5-pyrazolone (PMP) solution (0.5 M, in methanol) and 450 μL of 0.3 M NaOH at 70 °C for 30 min. The reaction was stopped by neutralization with 450 μL of 0.3 M HCl before extraction with chloroform (3 × 1 mL). HPLC analyses were performed on an Agilent ZORBAX Eclipse XDB-C18 column (5 μm, 4.6 mm × 150 mm) at 25 °C and UV detection at 250 nm. The mobile phase was 0.05 M KH_2PO_4 (pH 6.9) with 15% (solvent A) and 40% (solvent B) acetonitrile in water. A gradient of B from 8% to 19% in 25 min was used. Sulfate content was determined by the $BaCl_2$/gelatin method and ion-exchange chromatography.[21]

Methylation Analyses. The polysaccharide fraction (0.5 mg) was dissolved in DMSO (0.5 mL) and *O*-methylated using two consecutive cycles of NaOH−MeI.[22] The per-*O*-methylated product showed no band in the region of 3600−3300 cm^{-1}. It was then hydrolyzed with 45% (v/v) formic acid at 100 °C for 15 h. The hydrolyzed product was evaporated to dryness, and the residue was then reduced with $NaBH_4$ and acetylated with acetic anhydride to obtain a mixture of partially *O*-methylated alditol acetates. Qualitative and quantitative analyses were conducted by gas chromatography−mass spectrometry (GC-MS) (Finnigan trace, Thermo Electron Finnigan Co. Ltd., USA) with helium as the carrier gas (2 mL min^{-1}). A capillary column of OV1701 (30 m × 0.25 mm ID, 0.25 μm film thickness; Supelco) was held at 150 °C during the injection and then programmed to increase at 3 °C min^{-1} to 250 °C (constant temperature). The resulting partially *O*-methylated alditol acetates were identified by their typical retention times and electron impact spectra.

UV, IR, and NMR Analyses. The UV−vis absorption spectra were recorded using a UV-2550 spectrophotometer (Shimadzu, Japan) in the wavelength range of 200−800 nm. The FT-IR spectrum (KBr pellets) of the polysaccharide (2 mg) was recorded on a Nicolet 5700 FT-IR (Thermo Electron, Madison, WI, US) in a range of 400−4000 cm^{-1} at room temperature.

For NMR analysis, polysaccharide-containing fractions (about 50 mg) were lyophilized in D_2O (99.8%) twice and dissolved in 500 μL of high-quality D_2O (99.96%) containing 0.1 μL of acetone. ^{1}H, ^{13}C NMR experiments were carried out at 600 MHz on a Bruker Avance III 600 spectrometer (Bruker BioSpin Corporation, Fallanden, Switzerland). Spectra were recorded at 60 °C to place the HDO signals with minimal disturbance to carbohydrate protons. The observed ^{1}H chemical shifts were reported relative to the internal acetone (2.23 ppm). Standard homo- and heteronuclear correlated 2D techniques were used for general assignments of the polysaccharide (AFPS-IB): COSY, TOCSY, NOESY, and HSQC.[23] Spectra were also carried out at 60 °C.

Atomic Force Microscopy (AFM). AFPS-IB was imaged using AFM according to the method described by Sun and Zhang (2006).[24] A stock solution (10 mg mL^{-1}) was prepared by adding some AFPS-IB into double-distilled H_2O. The solution was diluted to a final

concentration of 1 μg mL^{-1}. Approximately 5 μL of diluted AFPS-IB solution was dropped on the surface of a mica sample carrier, allowed to dry, and then imaged in air at room temperature. Scanning probe microscopy images were obtained using a Nano Scope III atomic force microscope (Digital Instruments, Santa Barbara, CA, USA) and collected by tapping mode atomic force microscopy (TmAFM). All measurements were performed in air at ambient pressure and 30−40% relative humidity (RH).

Reducing Power Assay. The reducing power was determined using the method of Li, Zhou, and Li (2007), with some modifications.[25] Samples of 1 mL of different concentrations (2−12 mg mL^{-1}) in phosphate buffer (0.2 M, pH 6.6) were mixed with 1 mL of potassium ferricyanide (1%, w/v) and incubated at 50 °C for 20 min. The reaction was terminated by the addition of 1 mL of TCA (10%, w/v), the solution was then mixed with 0.2 mL of ferric chloride (0.1%, w/v), and the absorbance was measured at 700 nm. Increased absorbance of the reaction mixture indicated greater reducing power. Vitamin C was used as reference material. Reducing power was expressed as a percentage of the activity of a 1 mM solution of vitamin C.

Superoxide Radical Scavenging Capacity. The superoxide radical scavenging activity assay was performed using the photoreduction of the NBT (nitroblue tetrazolium) method as described by Li, Zhou, and Han (2006), with some modifications.[26] Superoxide radicals were generated in 3 mL of phosphate buffer (0.1 M, pH 7.4) containing 156 μM NADH (reduced form), 52 μM NBT, 20 μM phenazin methosulfate, and varying concentrations of AFPS-IB (2−12 mg mL^{-1}). The color reaction of superoxide radicals and NBT was detected by monitoring the absorbance at 560 nm. Vitamin C was used as reference material. In the essential control, NADH was substituted with phosphate buffer. The inhibition percentage was calculated using the following formula: Scavenging effect (%) = $(A_{\text{Control 560}} - A_{\text{Sample 560}})/A_{\text{Control 560}} \times 100$, where A is the absorbance.

DPPH Radical Scavenging Capacity. The DPPH radical scavenging activity was measured using the method reported by Li, Zhou, and Han (2006) with slight modifications.[26] Briefly, 0.2 mL of DPPH· solution (400 μM in dehydrated alcohol) was added to 1.0 mL of sample solution, and then 2.0 mL of water was added. The mixture was shaken vigorously for 2−3 min and allowed to stand at room temperature in the dark for 30 min. The absorbance was measured at 517 nm against a blank (water instead of sample and DPPH solution). Vitamin C was used as reference material. The scavenging percentage was calculated by the following equation: Scavenging effect (%) = $(A_{\text{Control 560}} - A_{\text{Sample 560}})/A_{\text{Control 560}} \times 100$, where A is the absorbance.

Statistical Analysis. Data were reported as the mean ± standard deviation (SD) (n = 3) and evaluated by one-way analysis of variance (ANOVA) followed by the Student's t-test. Differences were considered to be statistically significant if $P < 0.05$. All statistical analyses were carried out using SPSS for Windows, Version 16.0 (SPSS Inc., Chicago, IL, USA).

RESULTS AND DISCUSSION

Isolation, Purification, and Composition of AFPS-IB. The nutritional ingredients of *Achatina fulica* (China white jade snail) are shown in Table 1. Twenty to thirty percent of carbohydrates are included in *A. fulica*. The crude polysaccharides (AFPS) were isolated from *A. fulica* soft body with a yield of 15.54% (dry weight), which were further separated by ion exchange chromatography on a DEAE-52 column. The polysaccharide fractions (AFPS-I) were pooled and further purified by Sephacryl S-300 HR gel-permeation chromatography (Figure 1a). Three major water-soluble factions, AFPS-IA, AFPS-IB, and AFPS-IC, were collected with yields of 1.12, 5.23, and 2.76% of the dry material, respectively (Figure 2b).

Fraction AFPS-IB, which exhibited a larger peak area in the elution profile, was collected for further study. The homogeneity and average molecular weight of AFPS-IB were analyzed by the HPSEC method (Figure 2c). AFPS-IB appeared as a single peak on the HPSEC molecular weight profile, corresponding to an average molecular weight of 128 kDa.

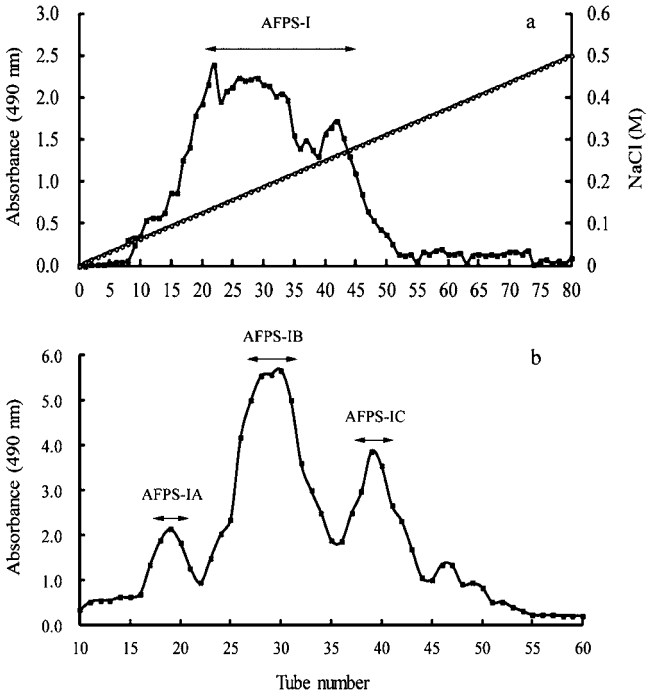

Figure 1. Purification of AFPS-IB. (a) The crude extract was fractionated on a DEAE ion-exchange column and (b) the collected fractions were further purified by gel filtration chromatography on a Sephacryl S-300 HR column.

Monosaccharide composition analysis of AFPS-IB showed that it consisted of Glc, Fuc, Rha, Man, and Gal in a molar ratio of 189:2:1:1:2, respectively. The presence of glucose as the main monosaccharide indicated that AFPS-IB was a glucan. The sulfate content of AFPS-IB was estimated at 2.7% (Table 2).

UV and IR Spectrum of AFPS-IB. The polysaccharide AFPS-IB showed negative response to the Lowry test and no absorption at 280 or 260 nm in the UV−vis spectrum, indicating the absence of protein and nucleic acids. Figure 3 shows the IR spectra of the polysaccharide fraction AFPS-IB of *A. fulica*. The bands in the region of 3428 cm^{-1} were assigned to the hydroxyl stretching vibration of the polysaccharide, and those in the region of 2929 cm^{-1} were due to C−H stretching vibration. A strong band between 950 and 1160 cm^{-1} in the FT-IR spectrum of AFPS-IB was attributed to the stretching vibrations of the pyranose ring. Absorptions at 917 cm^{-1} were typical for D-glucose in the pyranose form.[27] A characteristic absorption band at 843 cm^{-1} was also observed, indicating the α-configuration of the sugar units as described previously.[28]

Structure Data from Methylation Analysis. AFPS-IB was methylated and hydrolyzed to form alditol acetate derivatives, which were prepared and analyzed by GC−MS. As shown in Table 3, the analysis identified 1,5-di-*O*-acetyl-2,3,4,6-tetra-*O*-methyl-D-glucitol, 1,4,5-tri-*O*-acetyl-2,3,6-tri-*O*-methyl-D-glucitol, and 1,4,5,6-tri-*O*-acetyl-2,3-di-*O*-methyl-D-glucitol in a molar ratio of 1:10:1, which indicated the presence of nonreducing-end D-glucopyranosyl, (1→4)-linked D-glucopyranosyl, and (1→4,6)-linked D-glucopyranosyl. The high proportion of (1→4)-linked D-glucopyranosyl indicated AFPS-IB mainly consisted of a (1→4)-linked D-glucopyranosyl backbone. The same proportion of nonreducing-end D-glucopyranosyl and (1→4,6)-linked D-glucopyranosyl indicated the appearance of a

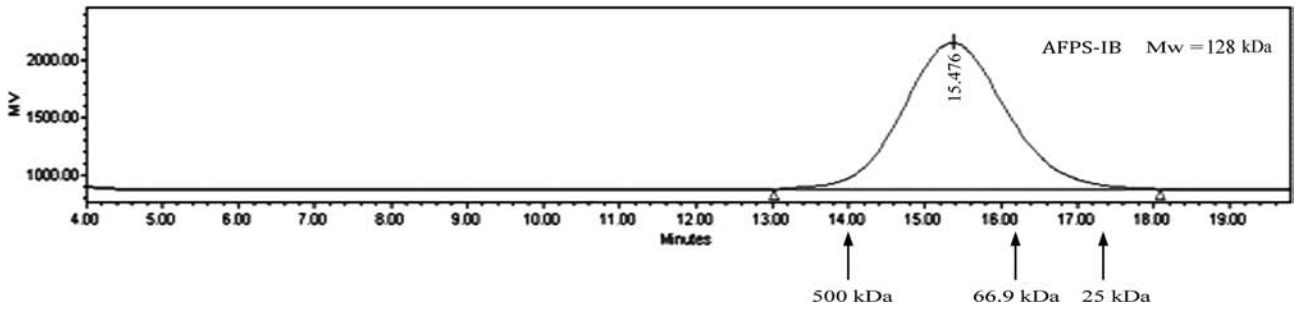

Figure 2. HPSEC profile of AFPS-IB. Molecular weight determination by HPLC on a TSK-Gel G 4000 SW_{XL} stainless steel column (300 × 7.5 mm) with 0.2 M NaCl at 1 mL/min. Range of molecular weights in kDa, 500; 66.9; 25.

Table 2. Yields, Protein Contents, Sugar Contents, Sulfate Contents, and M_w of *Achatina fulica* Polysaccharides[a]

samples	AFPS	AFPS-I	AFPS-IA	AFPS-IB	AFPS-IC
yield (%)	15.5(2.3)[b]	8.3(1.3)	1.1(0.3)	5.2(0.8)	2.2(0.5)
protein (%)	12.3(1.8)	9.3(1.9)	2.6(0.5)	ND	ND
neutral sugar (%)	80.6(3.1)	87.9(2.8)	93.7(3.5)	95.4(5.8)	94.3(1.4)
sulfate (%)	3.2(0.7)	3.6(0.2)	2.8(0.4)	2.7(0.4)	1.3(0.2)
M_w (kDa)	--[c]	--[c]	373(2.6)	128(3.8)	127(1.7)
Molar Ratio of Monosaccharides					
Rha	6.34(0.3)	5.7(1.2)	0.7(0.1)	0.2(0.04)	ND
Man	1.89(0.2)	2.12(0.4)	ND	0.1(0.03)	ND
Glc	13.8(3.5)	12.3(2.7)	1.3(0.8)	18.9(4.3)	5.4(1.8)
Gal	28.7(5.7)	25.3(4.3)	12.5(2.6)	0.2(0.06)	15.3(2.3)
Fuc	16.3(2.7)	16.4(3.4)	0.6(0.2)	0.1(0.03)	3.2(1.1)
GalN	8.95(1.7)	7.4(2.3)	1.2(0.3)	ND	ND
GlcN	25.8(5.6)	36.4(6.3)	4.1(1.2)	ND	21.7(6.2)

[a]AFPS, crude polysaccharide; AFPS-I, separated by ion exchange chromatography (DEAE-52); AFPS-IA, AFPS-IB, AFPS-IC, purified by gel-permeation chromatography (Sephacryl S-300 HR); ND, not detected; Man, mannose; Rha; rhamnose; Glc, glucose; Gal, galactose; Fuc, fucose; GalN, N-acetylgalactosamine; GlcN, N-acetylglucosamine. [b]Data were shown as mean (SD), n = 3. [c]The polysaccharide was a mixture.

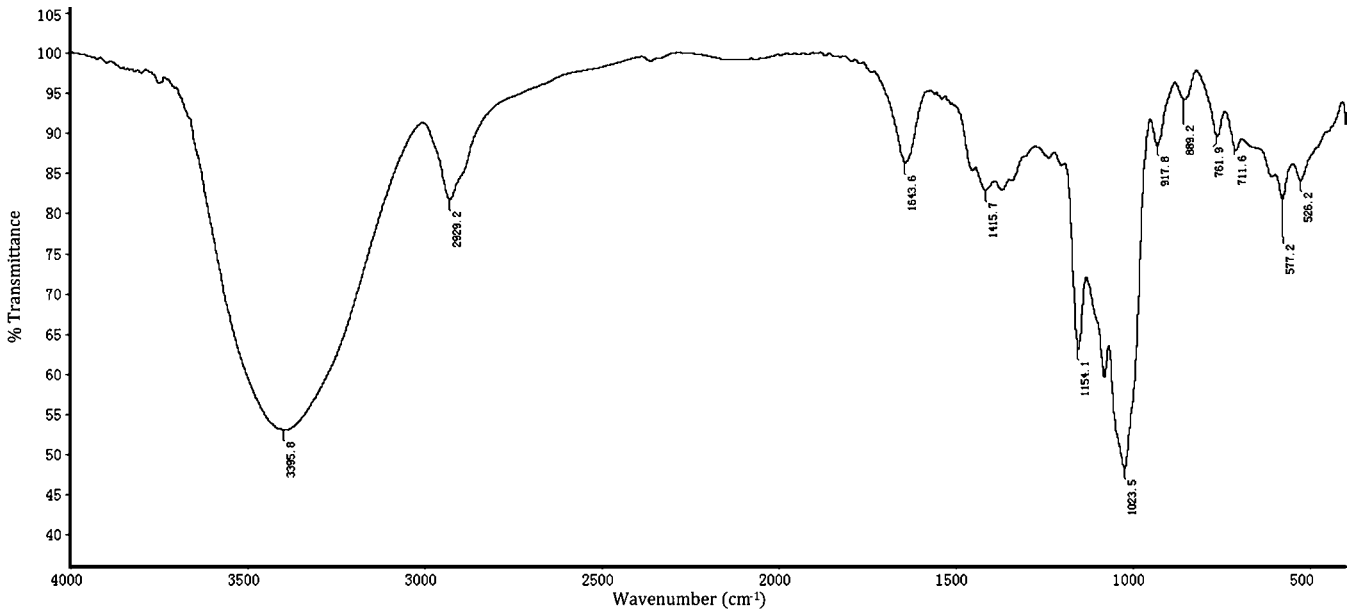

Figure 3. Infrared spectrum (IR) of the polysaccharide fraction AFPS-IB from *Achatina fulica.*

branched glucopyranosyl at the 6-position of the backbone glucose.

Structure Data from NMR and AFM. To make clear the chemical structures and chain conformations of polysaccharides is important to understand their biological activities. Combination of NMR spectroscopy and atomic force microscopy (AFM) is useful to obtain more information about the structure and properties of polysaccharides. The ^{1}H NMR spectrum of AFPS-IB in D_2O at 60 °C is shown in Figure 4a. The anomeric region (δ_H 4.3−5.6 ppm) contained three signals. The three sugar residues in AFPS-IB were arbitrarily labeled as X, Y, and Z, respectively, in a molar ratio 10:1:1. On the basis of their

dx.doi.org/10.1021/jf403896c | J. Agric. Food Chem. 2014, 62, 2344−2352

Table 3. GC-MS of Alditol Acetate Derivatives from the Methylated Product of AFPS-IB

methylated sugar[a]	R_t (min)	molar ratio	mass fragment (m/z)	type of linkage
2,3,4,6-Me4-Glc	14.82	0.97	43, 45, 59, 71, 87, 101, 117, 129, 145, 161, 205	terminal
2,3,6-Me3-Glc	16.96	10.23	43, 45, 71, 87, 99, 101, 113, 117, 129, 131, 143, 161, 173, 233	→4)-Glc*p*-(1→
2,3-Me2-Glc	19.07	1.16	43, 45, 85, 87, 101, 117, 142, 159, 201, 261	→4,6)-Glc*p*-(1→

[a]2,3,4,6-Me4-Glc, 1,5-di-*O*-acetyl-2,3,4,6-tetra-*O*-methyl-glucose, etc.

observed chemical shifts, X1 at δ_H 5.35 ($J_{H\text{-}1,H\text{-}2}$ = 4.3 Hz), Y1 at δ_H 4.98 ppm ($J_{H\text{-}1,H\text{-}2}$ = 4.7 Hz), and Z1 at δ_H 4.48 ppm ($J_{H\text{-}1,H\text{-}2}$ = 8.0 Hz), the residues X, Y, and Z were designated as α-, α-, and β-hexapyranosyl residues, respectively. The ^{13}C NMR spectra in Figure 4b show three signals in the anomeric region (δ_C 90–105 ppm); the signals were assigned to residues Z (δ_C 102.3 ppm), X (δ_C 100.8 ppm), and Y (δ_C 98.8 ppm) from the downfield to the high field, respectively, which were confirmed by cross-peaks in the $^1H,^{13}C$ HSQC spectrum (Figure 5).

The detailed proton signals (Table 4) of these three systems from H-1 to H-6 were assigned using the $^1H/^1H$ homonuclear

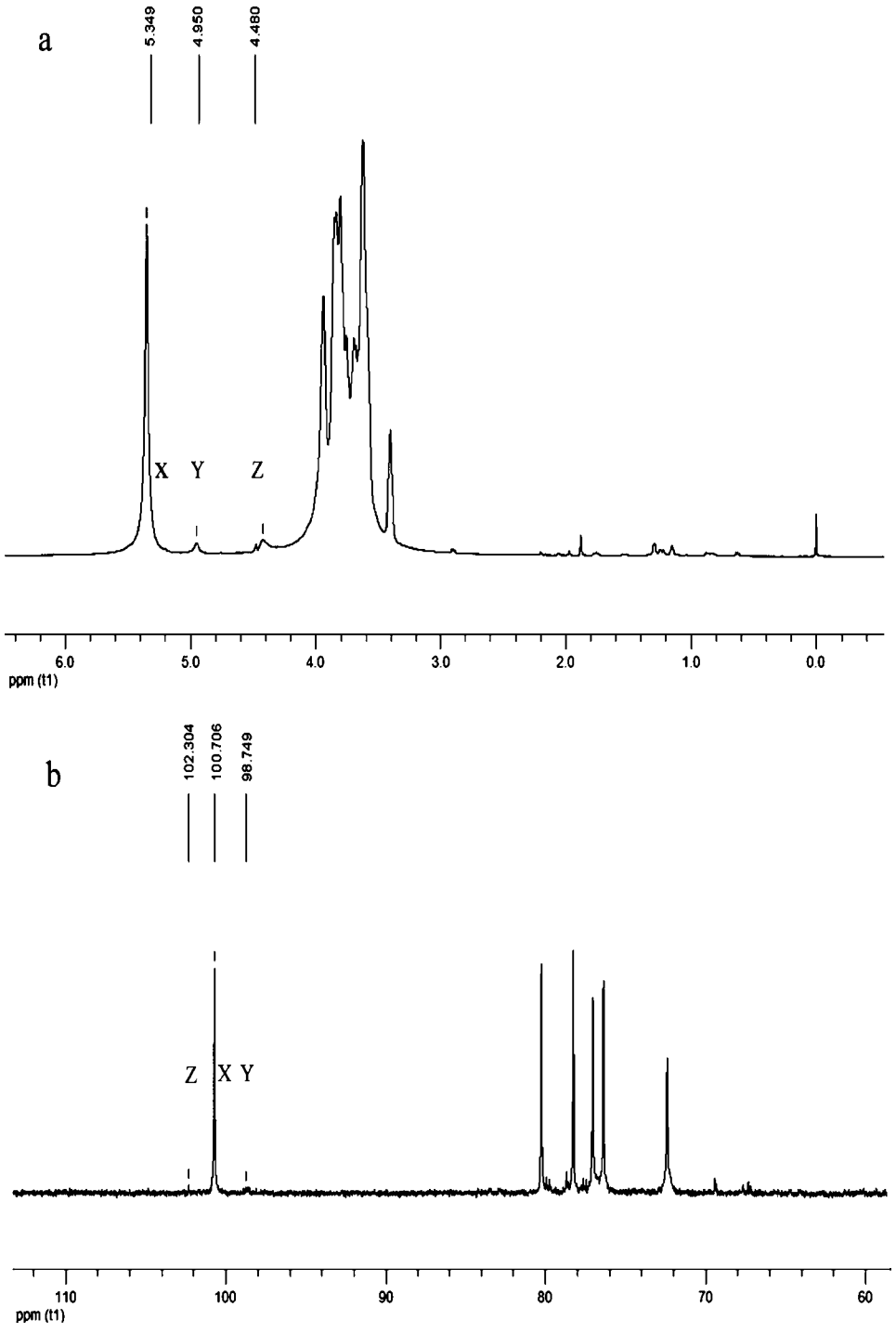

Figure 4. NMR spectrum of the polysaccharide AFPS-IB in D_2O. (a) ^1H NMR and (b) ^{13}C NMR.

dx.doi.org/10.1021/jf403896c | J. Agric. Food Chem. 2014, 62, 2344–2352

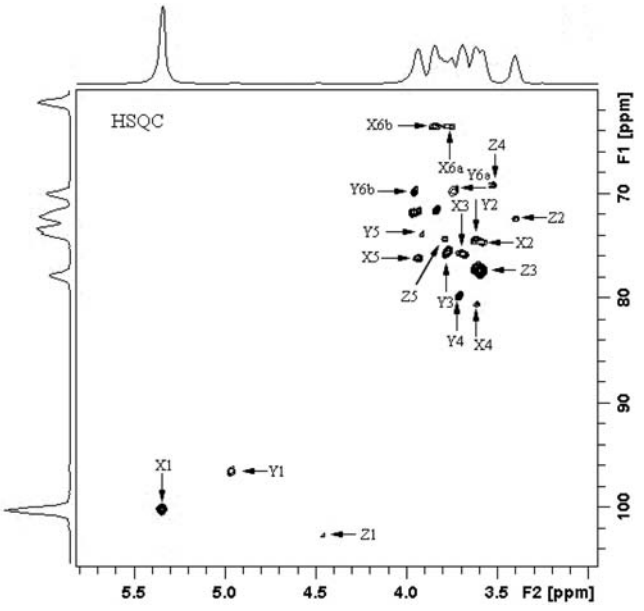

Figure 5. 600-MHz H/C-HSQC spectrum of polysaccharide AFPS-IB in D_2O at 60 °C. Relevant cross peaks have been labeled.

correlation (^{1}H−^{1}H COSY) (Figure S2) and TOCSY experiments (Figure S3). The carbon signals were assigned based on the assignment of the protons, using ^{1}H,^{13}C HSQC spectrum (Figure 5). For example, the anomeric carbon signal at δ 100.8 ppm for unit X was assigned by the correlation signal of X-H1/C1. The other signals from C2−C6 were similarly assigned as 74.5 (C-2), 75.6 (C-3), 80.1(C-4), 76.1 (C-5), and 63.4 (C-6 ppm). Similarly, the down-shift of the C-4 in unit X was a 4-linked Glc residue, whereas the down shift in the C-4 and C-6 indicated the appearance of the 4,6-linked Glc (Unit Y).

The sequence of the glycosyl residues was determined on the basis of a 2D-NOESY NMR experiment (Figure S4, Table 5). The H-1 of residue X has a strong interresidue NOE contact to H-4 of residue Y in addition to intraresidue NOE contacts to H-3, H-4, H-5, H-6a, and H-6b, it is evident that residue X is linked to the 4-position of residue Y. Similarly, residue Y has a strong interresidue NOE contact to H-4 of residue X which indicates that residue Y is linked at the 4-position of residue X. The H-1 of residue Z has a strong interresidue NOE contact to H-6a and medium to H-6b of residue Y in addition to intraresidue NOE contacts to H-2, H-3, and H-4, evidenced that residue Z is linked at the 6-position of residue Y. Based on the above results, we concluded the AFPS-IB was an association of the 4-linked α-glucan chains with (1→6)-β-linked branches. However, the NMR results do not contain information about how the chains are associated, which should be further investigated by AFM studies.

Table 5. NOE Data for the AFPS-IB Fraction Isolated from *Achatina fulica*

anomeric proton		NOE contact protons			
glycosyl residue	δ	δ	residue, atom		intensity[a,b]
→4)-α-D-Glc*p*-(1→	5.356	3.681	Y	H-4	s
X		3.812	X	H-3	s
		3.615	X	H-4	s
		3.956	X	H-5	w
		3.818	X	H-6[a]	s
		3.772	X	H-6[b]	s
→4, 6)-α-D-Glc*p*-(1→	4.955	3.615	X	H-4	s
Y		3.701	Y	H-2	w
		3.681	Y	H-4	s
		3.958	Y	H-5	s
		3.742	Y	H-6[a]	s
β-D-Glc*p*-(1→	4.482	3.973	Y	H-6[b]	w
Z		4.966	Y	H-6[b]	w
		3.391	Z	H-2	s
		3.523	Z	H-3	s
		3.614	Z	H-4	w

[a]The intensities were estimated from visual inspection of the NOESY spectra. [b]s, strong; w, weak.

Atomic force microscopy (AFM) is a powerful technique for direct observation of the conformation of individual macromolecules, including polysaccharides.[24] The persistence length can be determined from statistical analysis of the change in the tangent direction of polymer chain as a function of segment separation of the chain trajectory.[29] The AFM image of AFPS-IB is shown in Figure 6. The fiber-like structure and small branches of the AFPS-IB molecule can be observed. The chain length of the backbone was approximately 1140−1540 nm and the height was 20−40 nm. The fiber-like structure of AFPS-IB revealed by AFM was consistent with the results of NMR. NMR spectroscopy can provide useful information about the molecular conformations of polysaccharides. In some cases it is possible to directly confirm the presence of these conformations by AFM imaging of the polysaccharide.[30] Thus, the sequence of AFPS-IB was proposed below:

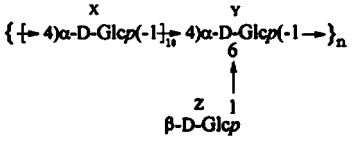

Antioxidant Activity. Figure 7 shows the antioxidant activities of AFPS-IB determined by the DPPH radical, reducing power and superoxide radicals (O_2^-) assays. Vitamin C was used as reference material. As shown in Figure 7a, AFPS-IB

Table 4. Summary of ^{1}H NMR and ^{13}C NMR Chemical Shifts for AFPS-IB

		chemical shifts (ppm)						
	glycosidic linkage	H-1/C-1	H-2/C-2	H-3/C-3	H-4/C-4	H-5/C-5	H-6/C-6	
X	→4)-α-D-Glc*p*-(1→	5.35/100.8	3.58/75.7	3.82/77.2	3.61/80.3	3.95/72.2	3.81[a] 3.77[b]	63.2
Y	→4, 6)-α-D-Glc*p*-(1→	4.95/98.8	3.70/74.1	3.73/76.6	3.68/79.5	3.95/73.6	3.74[a] 3.97[b]	69.9
Z	β-D-Glc*p*-(1→	4.48/102.3	3.39/73.1	3.52/76.2	3.61/69.1	3.69/75.3		60.4

[a,b]Interchangeable.

dx.doi.org/10.1021/jf403896c | J. Agric. Food Chem. 2014, 62, 2344−2352

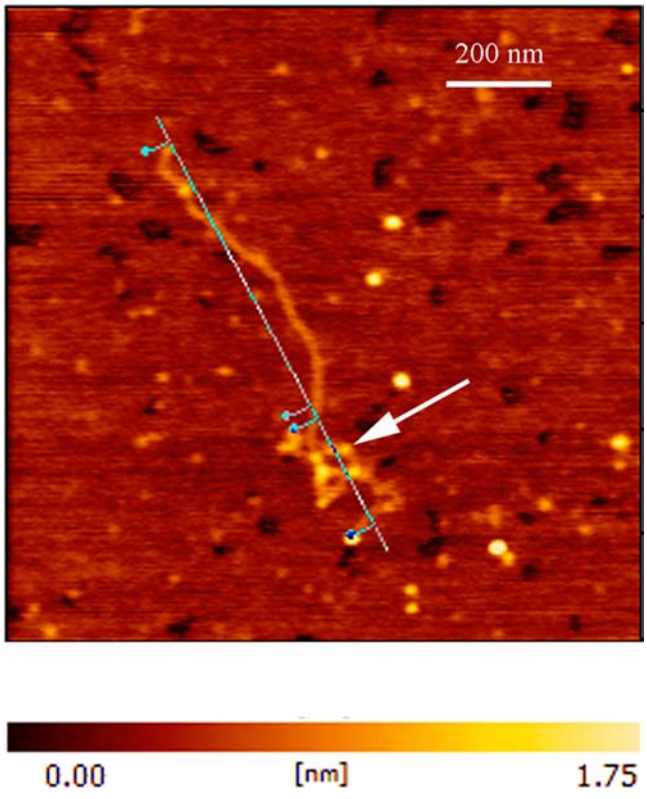

Figure 6. Atomic force microscopy (AFM) image of AFPS-IB. The AFPS-IB concentration was 1 μg mL^{-1}.

showed the ability to scavenge DPPH free radicals. The scavenging effects of the polysaccharide increased with increasing concentrations. The IC_{50} value of AFPS-IB for DPPH free radicals was 6.34 mg mL^{-1}. The maximum value of AFPS-IB reached 85.1% that of vitamin C at 12.0 mg mL^{-1}. Figure 7b depicts the reducing power of the tested sample. Reducing capacity was expressed as a percentage of the activity of a solution (1 mM) of vitamin C. In the tested sample AFPS-IB, the reducing capacity was positively correlated with sample concentration. The maximum value of AFPS-IB reached 65.6% that of vitamin C. Figure 7c shows the O_2^- scavenging ability, which indicates that the radical scavenging activity of the samples increased in a concentration dependent manner. The IC_{50} value of AFPS-IB for O_2^- radicals was 7.83 mg mL^{-1}. The maximum value of AFPS-IB reached 73.4% that of vitamin C.

Glucans, as a source of bioactive macromolecules, have diverse pharmaceutical activities which are dependent on the structural characteristics. The glycosidic linkage and configuration are two main factors determining the bioactivity. AFPS-IB, isolated from *A. fulica*, is a novel water-soluble glucan composed of (1→4)-α-D-glucose residues in the main chain with (1→6)-β-linked branches at glucose residues. The structure of AFPS-IB is similar to that of starch isolated by Baldwin et al.[31] from potato, except for the (1→6)-D-Glc*p* in AFPS-IB was β-configuration. It is also similar to a glucan characterized by Maity et al.[32] from the fruit bodies of an edible hybrid mushroom PCH9FB, except for different molar ratio of (1→4)-α-D-Glc*p* and (1→6)-β-Glc*p* residues. Antioxidation tests performed in vitro showed that AFPS-IB had higher DPPH radical and superoxide anion (O_2^-) scavenging activities than that of potato starch, which showed very poor antioxidant activity, and similar to the glucan from the fruit bodies of an edible hybrid

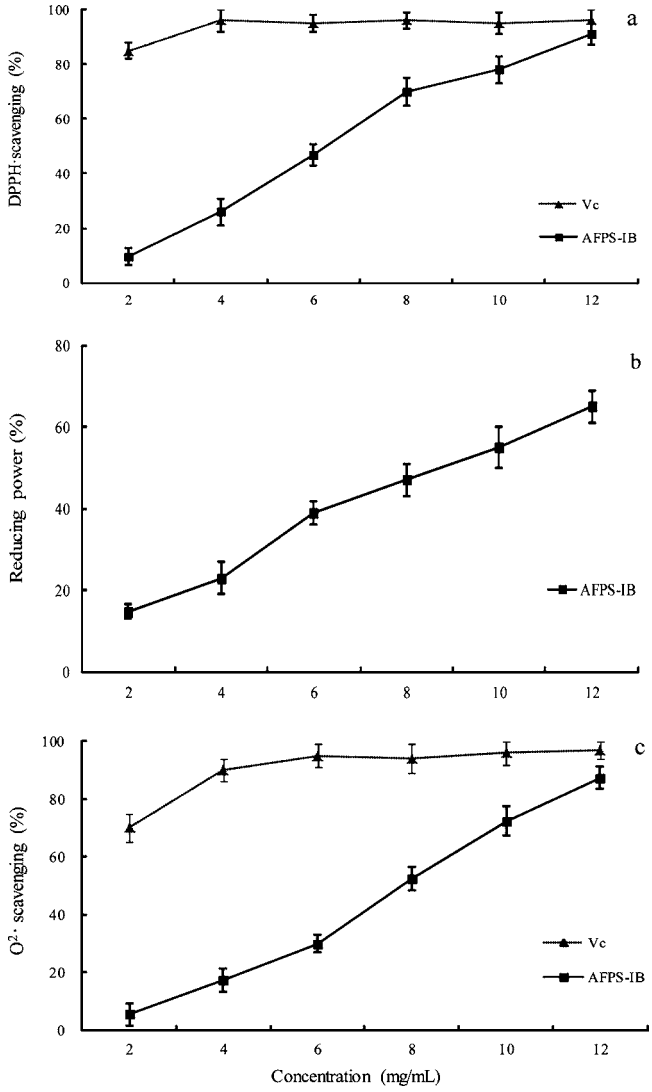

Figure 7. Antioxidant activity of the polysaccharide AFPS-IB and Vc in vitro. (a) The scavenging effect on DPPH radicals; (b) Reducing power was expressed as a percentage of the activity of vitamin C; (c) The scavenging effect on superoxide radicals. Vitamin C was used as reference material. Values are means ± SD of three separate experiments.

mushroom PCH9FB with an IC_{50} value of 5.00−7.00 mg mL^{-1}.[32] The antioxidant mechanism of glucan is not clear, nor is it clear why glucans with different glycosidic linkages and configurations have different free radical scavenging capabilities. The most pronounced hypothesis is that free radicals can abstract hydrogen atoms at all ring C−H bonds of aldoses, uronic acids, and other sites on carbohydrates. The abstraction of hydrogen atom will generate carbon-center radicals. The radicals at carbons which form glycosidic bonds will undergo a β-scission reaction resulting in the breakdown of polysaccharide chains.[33] Some free radicals have lone-pair orbitals antiperiplanar to the alkylidene C−H bond. Therefore, glycosidic linkages with different conformations can have different reaction rates with these free radicals, allowing for selectivity in cleaving β-D-linkages of polysaccharides.[34] A (1→6)-β-D-glucan and (1→4)-α-D-glucan complex isolated from mushroom has been found to have strong antioxidant activities.[35] The responses to such glucans are likely to be regulated by different conformations of glycosidic linkages. Therefore, it can be hypothesized that the

dx.doi.org/10.1021/jf403896c | J. Agric. Food Chem. 2014, 62, 2344−2352

conformation of (1→6)-β-D-Glcp residues may be responsible for its antioxidant activity.

In summary, this study isolated and characterized a novel water-soluble glucan (AFPS-IB) from the soft body of *Achatina fulica*. AFPS-IB was composed of Glc, Fuc, Rha, Man, and Gal in a molar ratio of 189:2:1:1:2, with a molecular weight of 128 kDa. The backbone of AFPS-IB was composed of (1→4)-α-D-glucose residues, which occasionally branched at O-6, and terminated with 1→)-β-glucose. Antioxidation tests performed in vitro showed that AFPS-IB had remarkable DPPH radical and superoxide anion (O_2^-) scavenging activity and high reduction potential. The information of this work and published literature have demonstrated that glucan has a key role for health functions of *Achatina fulica*. AFPS-IB could be regarded as a potential natural antioxidant. Further studies on other activities of the polysaccharide are currently in progress.

■ ASSOCIATED CONTENT

Supporting Information

Figures S1−S4. This material is available free of charge via the Internet at http://pubs.acs.org.

■ AUTHOR INFORMATION

Corresponding Authors

*Phone: 86 571 88982169. Fax: 86 571 88982154. E-mail: dhliu@zju.edu.cn (D.L.).

*Phone: 86-571-88982151. E-mail: chenshiguo210@163.com (S.C.).

Notes

The authors declare no competing financial interest.

■ ACKNOWLEDGMENTS

This research was financed by the National Natural Science Foundation of China (no. 31371872 and 31301417).

■ REFERENCES

(1) Dwek, R. A. Glycobiology: toward understanding the function of sugars. *Chem. Rev.* **1996**, *96*, 683−720.

(2) Yang, L.; Zhang, L. M. Chemical structural and chain conformational characterization of some bioactive polysaccharides isolated from natural sources. *Carbohydr. Polym.* **2009**, *76*, 349−361.

(3) Kim, M. H.; Han, S. B.; Oh, G. T.; Kim, Y. H.; Hong, D. H.; Hong, N. D.; Yoo, I. D. Stimulation of humoral and cell mediated immunity by polysaccharide from mushroom *phellinus linteus*. *Int. J. Immunopharmacol.* **1996**, *18*, 295−303.

(4) Czarnecki, R.; Grzybek, J. Antiinflammatory and vasoprotective activities of polysaccharides isolated from fruit bodies of higher Fungi P.1. polysaccharides from Trametes gibbosa (Pers.: Fr) Fr.(Polyporaceae). *Phytother. Res.* **1995**, *9*, 123−127.

(5) Li, X. M.; Ma, Y. L.; Liu, X. J. Effect of the *Lycium barbarum* polysaccharides on age-related oxidative stress in aged mice. *J. Ethnopharmacol.* **2007**, *111*, 504−511.

(6) Liu, C.; Lin, Q.; Gao, Y.; Ye, L.; Xing, Y.; Xi, T. Characterization and antitumor activity of a polysaccharide from *Strongylocentrotus nudus* eggs. *Carbohydr. Polym.* **2007**, *67*, 313−318.

(7) Zhang, D.; Wu, H.; Xia, Z.; Wang, C.; Cai, J.; Huang, Z.; Xie, J. Partial characterization, antioxidant and antitumor activities of three sulfated polysaccharides purified from *Bullacta exarata*. *J. Funct. Foods* **2012**, *4*, 784−792.

(8) Liu, D.; Liao, N.; Ye, X.; Hu, Y.; Wu, D.; Guo, X.; Chen, S. Isolation and structural characterization of a novel antioxidant mannoglucan from a marine bubble snail, Bullacta exarata (Philippi). *Mar. Drugs* **2013**, *11*, 4464−4477.

(9) Kulicke, W. M.; Lettau, A. I.; Thielking, H. Correlation between immunological activity, molar mass, and molecular structure of different (1→3)-β-D-glucans. *Carbohydr. Res.* **1997**, *297*, 135−143.

(10) Zhou, W. Analysis of nutritional compositon in *Achatina Fulica Farussac*. *Shan Di Nong Ye Sheng Wu Xue Bao* **1999**, *18*, 243−245 (in Chinese).

(11) Ku, B. S.; Kazuo, I.; Hiroshi, T. Pharmacological characteristics of four giant neurons identified in the cerebral ganglia of an african giant snail (*Achatina fulica* Férussac). *Comp. Biochem. Physiol., Part C: Pharmacol., Toxicol. Endocrinol.* **1985**, *80*, 123−128.

(12) Aboua, F. Chemical composition of *Achatina fulica*. *Tropicultura* **1990**, *8*, 121−122.

(13) Babalola, O. O.; Akinsoyinu, A. O. Proximate composition and mineral profile of snail meat from different breeds of land snail in Nigeria. *Pak. J. Nutr.* **2009**, *8*, 1842−1844.

(14) Bender, A. Meat and Meat Products in Human Nutrition in Developing Countries. *FAO Food and Nutrition Paper*; FAO: Rome, Italy, 1992; 53.

(15) Ajayi, S. S.; Tewe, O. O.; Moriarty, O.; Awesu, M. O. Observation on the biology and nutritive value of the African giant Archachatina marginata. *Afr. J. Ecol.* **1978**, *16*, 85−95.

(16) Sukhija, P. S.; Palmquist, D. L. Rapid method for determination of total fatty acid content and composition of feedstuffs and feces. *J. Agric. Food Chem.* **1988**, *36*, 1202−1206.

(17) Lowry, O. H.; Rosebrough, N. J.; Farr, A. L.; Randall, R. J. Protein measurement with the Folin phenol reagent. *J. Biol. Chem.* **1951**, *193*, 265−275.

(18) Ricklefs, R. E.; Montevecchi, M. A. Size, organic composition and energy content of north atlantic gannet Morus bassanus eggs. *Comp. Biochem. Physiol., Part A: Mol. Integr. Physiol.* **1979**, *64*, 161−165.

(19) Dubois, M.; Gilles, K. A.; Hamilton, J. K.; Rebers, P. A.; Smith, F. Colorimetric method for determination of sugars and related substances. *Anal. Chem.* **1956**, *28*, 350−356.

(20) Yang, X. B.; Zhao, Y.; Wang, Q. W.; Wang, H. F.; Mei, Q. B. Analysis of the monosaccharide components in Angelica polysaccharides by high performance liquid chromatography. *Anal. Sci.* **2005**, *21*, 1117−1180.

(21) Ohira, S. I.; Toda, K. Ion chromatographic measurement of sulfide, methanethiolate, sulfite and sulfate in aqueous and air samples. *J. Chromatogr. A* **2006**, *1121*, 280−284.

(22) Needs, P. W.; Selvendran, R. R. Avoiding oxidative degradation during sodium hydroxide/methyl oidine-mediated carbohydrate methylation in dimethyl sulfoxide. *Carbohydr. Res.* **1993**, *245*, 1−10.

(23) Chakraborty, I.; Mondal, S.; Pramanik, M.; Rout, D.; Islam, S. S. Structural investigation of a water-soluble glucan from an edible mushroom, Astraeus hygrometricus. *Carbohydr. Res.* **2004**, *339*, 2249−2254.

(24) Sun, R. G.; Zhang, J. A. Study of helical structure of glycyrrhiza polysaccharides by atomic force microscope. *Acta Chim. Sin.* **2006**, *64*, 2467−2472.

(25) Li, X. L.; Zhou, A. G.; Li, X. M. Inhibition of Lycium barbarum polysaccharides and Ganoderma lucidum polysaccharides against oxidative injury induced by c-irradiation in rat liver mitochondria. *Carbohydr. Polym.* **2007**, *69*, 172−178.

(26) Li, X.; Zhou, A.; Han, Y. Anti-oxidation and anti-microorganism activities of purification polysaccharide from Lygodium japonicum *in vitro*. *Carbohydr. Polym.* **2006**, *66*, 34−42.

(27) Ojha, A. K.; Maiti, D.; Chandra, K. Structural assignment of a heteropolysaccharide isolated from the gum of Cochlospermum religio-sum (Katira gum). *Carbohydr. Res.* **2008**, *343*, 1222−1231.

(28) Yu, R. M.; Yin, Y.; Yang, W.; Ma, W. L.; Yang, L.; Chen, X. J.; Zhang, Z.; Ye, B.; Song, L. Y. Structural elucidation and biological activity of a novel polysaccharide by alkaline extraction from cultured *Cordyceps militaris*. *Carbohydr. Polym.* **2009**, *75*, 166−171.

(29) Sletmoen, M.; Maurstad, G.; Sikorski, P.; Paulsen, B. S.; Stokke, B. T. Characterisation of bacterial polysaccharides: Steps towards singlemolecular studies. *Carbohydr. Res.* **2003**, *338*, 2459−2475.

(30) Morgan, K. R.; Roberts, C. J.; Tendler, S. J.; Davies, M. C.; Williams, P. M. A ^{13}C CP/MAS NMR spectroscopy and AFM study of the structure of Glucagel, a gelling â-glucan from barley. *Carbohydr. Res.* **1999**, *315*, 169−179.
(31) Baldwin, P. M.; Adler, J.; Davies, M. C.; Melia, C. D. High resolution imaging of starch granule surfaces by atomic force microscopy. *J. Cereal Sci.* **1998**, *27*, 255−265.
(32) Maity, K.; Maity, S.; Gantait, S. K.; Das, D.; Maiti, S.; Maiti, T. K.; Islam, S. S. Structural characterization and study of immunoenhancing and antioxidant property of a novel polysaccharide isolated from the aqueous extract of a somatic hybrid mushroom of *Pleurotus florida* and *Calocybe indica* variety APK2. *Int. J. Biol. Macromol.* **2011**, *48*, 304−310.
(33) Wang, Y.; Hollingsworth, R. I.; Kasper, D. L. Ozonolytic depolymerization of polysaccharides in aqueous solution. *Carbohydr. Res.* **1999**, *319*, 141−147.
(34) Rees, M. D.; Kennett, E. C.; Whitelock, J. M.; Davies, M. J. Oxidative damage to extracellular matrix and its role in human pathologies. *Free Radical Biol. Med.* **2008**, *44*, 1973−2001.
(35) Mizuno, M.; Morimoto, M.; Minato, K. I.; Tsuchida, H. Polysaccharides from Agaricus blazei stimulate lymphocyte T-cell subsets in mice. *Biosci., Biotechnol., Biochem.* **1998**, *62*, 434−437.

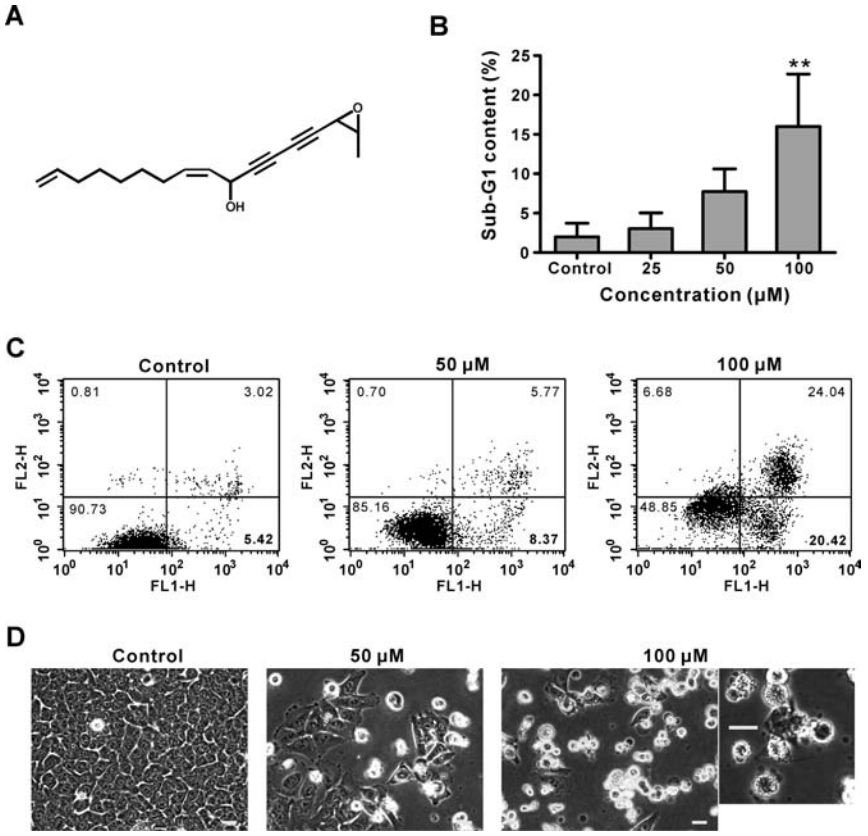

Figure 1. Induction of apoptotic cell death by GKB in HCT116 cells. HCT116 cells were treated with GKB (25−100 μM) for 24 h. (A) Chemical structure of GKB. (B) The sub-G1 content (%) was measured by flow cytometric DNA content analysis. The values represent the mean ± SD of three independent experiments. $^{**}p < 0.01$, compared with the control. (C) The externalization of phosphatidylserine was detected by flow cytometric analysis after annexin V−fluorescein and PI staining. The percentage of the cell population in each quadrant is shown. The lower right quadrant represents an early apoptotic cell population, and the percentage of cells in this quadrant is indicated in bold numbers. (D) Changes in cell morphology. The images are representative of at least three independent experiments (bar = 20 μm).

programmed cell death, including apoptosis and necroptosis, and investigated the overall cellular signaling pathway underlying the GKB-induced cancer cell death using flow cytometry, Western blot analysis, and proteomic approaches. For this task, we preferentially analyzed the secreted proteome using LC−MS/MS technology because secreted proteins play crucial roles in many of the biological processes of cancer cells. To our knowledge, this study is the first report analyzing the secreted proteome from cancer cells undergoing phytochemical-induced apoptotic cell death.

MATERIALS AND METHODS

Reagents. GKB was isolated from *G. koraiensis* as previously described.[15] Its chemical structure is shown in Figure 1A. HPLC grade LC−MS/MS solvents, including acetonitrile (ACN) and water, were purchased from Burdick and Jackson (Morristown, NJ). Trypsin was purchased from Promega (Madison, WI), and formic acid was purchased from Merck (Darmstadt, Germany). JC-1 dye was purchased from Biotium (Hayward, CA). Dithiothreitol, iodoacetamide, ammonium bicarbonate, propidium iodide (PI), z-VAD-fmk, necrostatin-1, *N*-acetylcysteine (NAC), bovine serum albumin, and all other reagents were purchased from Sigma (St. Louis, MO). Antibodies against cleaved caspase-3, cleaved caspase-8, cleaved caspase-9, PARP, Cyclin D1, AIF, BID, Bax, and Bcl-xL were purchased from Cell Signaling Biotechnology (Beverly, MA). Antibodies against Bcl-2 and β-actin were purchased from Santa Cruz Biotechnology (Santa Cruz, CA).

Cell Culture. HCT116, Caco-2, HT-29 human colorectal cancer, and HepG2 human hepatoma cells were obtained from the American Type Culture Collection (ATCC; Rockville, MD). HCT116 and HT-29 cells were cultured in minimal essential medium (MEM) supplemented with 10% fetal bovine serum (FBS), 1 g/L D-glucose, 100 units/mL penicillin, and 100 μg/mL streptomycin. Caco-2 cells were cultured in MEM supplemented with 10% heat inactivated-FBS, 1 mM sodium pyruvate, 100 units/mL penicillin, and 100 μg/mL streptomycin. HepG2 cells were cultured in DMEM supplemented with 10% FBS, 100 units/mL penicillin, and 100 μg/mL streptomycin. For the secretome analysis, HCT116 cells were cultured in conditioned media, which are described in detail below. These cells were maintained at subconfluence in a 95% air and 5% CO_2 humidified atmosphere at 37 °C.

Cell Viability Assay. HCT116, Caco-2, HT-29 cells (5000 cells per well), and HepG2 cells (1×10^4 cells per well) were seeded in a 96-well plate and incubated for 24 h. The cells were then treated with GKB for 24 or 48 h. Cell viability was determined by measuring mitochondrial dehydrogenase activity as previously described.[21,22]

Observation of Morphological Changes. The cellular morphology was observed by phase contrast microscopy as previously described.[21]

Flow Cytometric Analysis of DNA Content and Phosphatidylserine Externalization. The sub-G1 content (%), which is an indirect measure of apoptosis, was determined using flow cytometric DNA content analysis as previously described.[21,22] The externalization of phosphatidylserine, which is a precise marker of apoptotic cell death, was detected using flow cytometric analysis of cells stained with annexin V−fluorescein and PI, as previously described.[21]

Measurement of Reactive Oxygen Species. Cellular reactive oxygen species (ROS) levels were quantified using the 2′,7′-dichlorodihydrofluorescein diacetate (H_2-DCFDA) assay as previously described.[13,23]

Measurement of Mitochondrial Membrane Potential. Mitochondrial membrane potential ($\Delta\Psi_m$) was measured using flow cytometry after JC-1 dye staining. After treatment of GKB, both floating and adherent cells were harvested by trypsinization. The cells (1×10^6 cells) were washed with Dulbecco's phosphate-buffered saline (DPBS) and incubated with JC-1 (5 μM) at 37 °C for 15 min. Then, the green and red fluorescence was measured using a flow cytometer. The percentage of cells that emit the green fluorescence (JC-1 monomer) was used to quantify the alteration in mitochondrial membrane potential induced by GKB.

Evaluation of Cell Surface Expression of Fas and TNF-R1. The cell surface expression of the death receptors Fas (CD-95) and TNF-R1 was evaluated using flow cytometric immunofluorescence analysis. After treatment of GKB, both floating and adherent cells were harvested by trypsinization. The cells (1×10^6 cells) were fixed in 4% paraformaldehyde at 4 °C for 5 min and incubated in DPBS containing 0.5% bovine serum albumin (100 μL) and FITC-conjugated monoclonal antibodies (20 μL); mouse monoclonal antibody against CD95 (Becton Dickinson, San Jose, CA) and Armenian hamster monoclonal antibody against TNF-R1 (Santa Cruz Biotechnology) at 4 °C for 50 min. FITC-conjugated normal mouse and Armenian hamster isotype control antibodies (Santa Cruz Biotechnology) are used, respectively, for the check of background fluorescence. Then, fluorescence was measured using a flow cytometer. Mean values of FITC fluorescence (FL1-H) was calculated by using histogram statistics tool of CellQuest Pro software (Becton Dickinson) to quantify relative expression of Fas and TNF-R1.

Western Blot Analysis. HCT116 cells (5×10^5) were seeded on 60 mm dishes, incubated for 24 h, and then treated with GKB for 24 h. Total cell lysates were prepared and Western blot analysis was performed as previously described.[22,24]

Preparation of the Secreted Proteins. For the analysis of the secreted proteome, we used cells grown in the conditioned media for secretome analysis (CMS), which contained additional supplements instead of FBS to minimize cell death induced by serum deprivation. The CMS contained MEM supplemented with 3 g/L D-glucose, 2 mM L-glutamine, 0.1 mM L-alanine, 0.1 mM L-asparagine, 0.1 mM L-aspartic acid, 0.1 mM L-glutamic acid, 0.1 mM glycine, 0.1 mM L-proline, 0.1 mM L-serine, 100 units/mL penicillin, and 100 μg/mL streptomycin; FBS and phenol red were excluded from the media. HCT116 cells (1.5×10^7 cells) were seeded in 150 mm dishes and were incubated in normal MEM containing 10% FBS for 24 h. The cells were washed twice with DPBS and once with CMS to remove any residual FBS. Then, the cells were cultured in CMS containing GKB (0 or 50 μM) for 24 h. The media and cells were harvested by cell scraping, and the supernatant was collected twice by centrifugation at 850*g* for 5 min at 4 °C. The samples were prepared from three independent experiments. The supernatants were filtered through 0.2 μm syringe filters and concentrated using a centrifugal filter device (Vivaspin 20, GE Healthcare, Uppsala, Sweden) with a 10 kDa cutoff membrane according to the manufacturer's instructions. The protein concentrations were determined using the Bradford assay (Thermo Fisher Scientific, Rockford, IL).

One-Dimensional SDS−PAGE and In-Gel Digestion. Three replicates of freshly prepared concentrated protein samples (15 μg) were separated on a 12% SDS−PAGE gel and stained with colloidal Coomassie blue.[25] Each gel lane was excised into 11 sections, and the gel slices were washed twice with distilled water. The gels were subjected to a conventional in-gel digestion procedure with minor modifications.[26] The detailed procedures are described in the Supporting Information, Materials and Methods.

LC−MS/MS analysis. The prepared peptide samples were analyzed using a LTQ XL linear trap mass spectrometer (Thermo Scientific, San Jose, CA) equipped with a nano-HPLC system (Eksigent, Dublin, CA). The peptide sample (5 μL) was injected and loaded onto a C_{18} trap column (2.5 cm × 100 μm, Upchurch Scientific, Oak Harbor, WA) using an autosampler. The trapped samples were eluted and separated using an in-line, homemade reverse-phase C_{18} micro column, which was packed in a fused-silica nanospray tip (column dimension, 10 cm × 100 μm; particle size, 5 μm; pore size, 300 Å; Nanobaume, Wildomar, CA). The detailed elution gradients and parameters for the MS are described in the Supporting Information, Materials and Methods.

Protein Identification through Database Searching. All MS/MS samples were analyzed using Sorcerer-SEQUEST (version 3.5, Sage-N research, Milpitas, CA). SEQUEST was set to search the IPI human database (final version 3.86, 91522 entries), with up to 2 missed trypsin cleavage sites. Scaffold 3 (version 3.6.2, Proteome Software Inc., Portland, OR) was used to validate the MS/MS-based peptide and protein identifications. The detailed information concerning the parameters of the database search and the peptide/protein filtering criteria are described in the Supporting Information, Materials and Methods.

Computational Analysis of the Expression and Interaction of the Secretory Proteins. To evaluate the changes in protein expression, we exploited the spectrum counting method using the Quantification analysis tool of Scaffold 3. Because the total protein yield of the control group was less than that of the GKB-treated group but the same amount of prepared peptide samples was injected, the quantification values of the control group were corrected by multiplying by the dilution factor, 0.117. Using the corrected data, the fold-change ratio (Rsc) was calculated to compare the relative abundance of each protein. Rsc was calculated using the following formula (eq 1).

$$R_{sc} = \log_2(n_2/n_1) \quad (1)$$

where, for each protein, R_{sc} is the $\log_2$ ratio of the protein abundance between the GKB-treated and the control-treated group, and n_1 and n_2 are the normalized spectral counts of the control group and the GKB-treated group, respectively. For proteins whose spectral counts were 0 for either the control group or the GKB-treated group, the R_{sc} values were expressed as ∞ or $-\infty$, respectively. Proteins with an R_{sc} above 1.0 or below −1.0, with a minimum spectral count of 1, were selected and further analyzed for statistical significance using Student's *t*-tests.

The secretory proteins were analyzed based on their cellular compartment Gene Ontology (GO) terms using the Scaffold software and the DAVID proteomics tool.[27] Proteins were selected for further analysis if they were annotated with at least one of the following GO terms: secretory granule, extracellular matrix part, extracellular region part, extracellular matrix, proteinaceous extracellular matrix, extracellular space, external side of plasma membrane, or extracellular region.

To visualize the interactions among the identified proteins, a network was generated using the STRING tool (version 9.0).[28] The interaction network of the identified secretory proteins was exported along with the evidence score. The exported data were then imported into Cytoscape (version 3.0.1)[29] as a network file. The expression level of the identified proteins and the number of interacting partners, which were determined using the STRING tool, were also imported as 'attributes' of the interaction network.

ELISA of ADAM9, SERPINB5, and IL18. To verify the results of the LC−MS/MS analysis, we also performed ELISA to measure the actual concentration of the secreted proteins present in the media. ELISA kits were purchased from R&D Systems (Minneapolis, MN) for ADAM9, Wuhan EIAab Science (Wuhan, China) for SERPINB5, and eBioscience (Vienna, Austria) for IL18. The ELISA was performed according to the manufacturer's instructions.

Statistical Analysis. The data are expressed as the means ± SD. Statistical analyses were performed using one-way analysis of variance followed by the Dunnett's multiple comparison test or the Tukey's multiple comparison test using the GraphPad Prism 5 software (GraphPad Software, Inc., La Jolla, CA), excluding the LC−MS/MS data. $p < 0.05$ was considered statistically significant.

RESULTS

Antiproliferative Activity of GKB in Human Cancer Cells. The antiproliferative activity of GKB against mouse leukemia cells has already been reported.[11] In this study, we examined the antiproliferative activity of GKB on other human cancer cells, including human colorectal cancer. As a result, we found that GKB also inhibited the proliferation of HCT116,

Caco-2, and HT-29 human colorectal cancer cells and HepG2 human hepatoma cells (Table 1). We selected HCT116 cells, which have wild type p53, as a model cell line to study the molecular mechanisms underlying the suppression activity of GKB against human colorectal cancer.

Table 1. Antiproliferative Activity of GKB in Human Cancer Cells

	IC_{50}[a] (μM)			
	GKB		Etoposide	
cell line	24 h	48 h	24 h	48 h
HCT116	66.2 ± 14.1	53.8 ± 9.2	189.9 ± 5.3	25.6 ± 2.0
Caco-2	68.8 ± 5.7	57.2 ± 4.0	>200	32.1 ± 4.7
HT-29	58.8 ± 0.9	53.4 ± 7.6	38.1 ± 5.9	12.9 ± 1.7
HepG2	43.8 ± 4.5	43.2 ± 1.6	>200	82.8 ± 4.8

[a]The concentration that inhibits cell proliferation by 50%.

Proapoptotic Activity of GKB in Human Cancer Cells. Next, we measured the biochemical and morphological properties of HCT116 cells relating to apoptosis to examine whether this antiproliferative activity of GKB was due to apoptotic cell death. First, we measured the sub-G0/G1 content (%) using flow cytometric DNA content analysis. GKB potently induced an increase in the sub-G0/G1 content (Figure 1B). Second, we also found that GKB induced the translocation of phosphatidylserine from the cytoplasm to the cell surface using the annexin V–fluorescein and PI staining assay (Figure 1C). Third, GKB induced apoptotic morphological changes, such as the formation of apoptotic bodies (Figure 1D) and chromatin condensation (data not shown). Taken together, we concluded that GKB induced apoptotic cell death in p53-proficient HCT116 cells. GKB also induced apoptotic cell death in p53-mutated human colon cancer cells, including Caco-2, SW480, DLD-1, and HT-29 cells. In these cells, the induction of apoptotic cell death was inferred from an increase in the sub-G0/G1 content and the observation of morphological changes, such as the formation of apoptotic bodies and chromatin condensation (data not shown). Therefore, we speculated that GKB induced apoptosis in human colon cancer cells in a p53-independent manner. In addition to

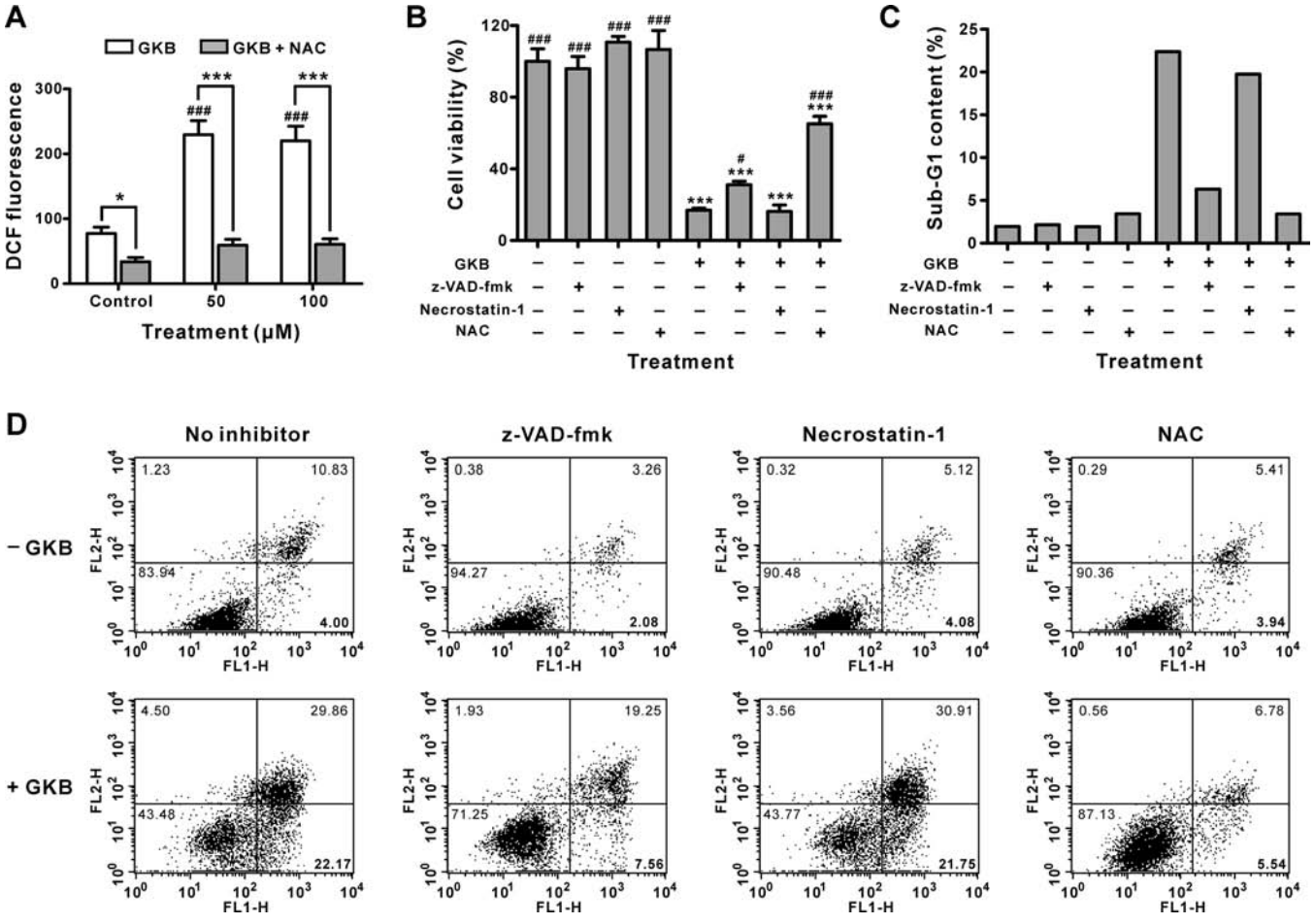

Figure 2. Effects of chemical inhibitors on the GKB-induced HCT116 cell death. (A) Effects of GKB on the intracellular accumulation of reactive oxygen species (ROS). HCT116 cells were treated with GKB (50 or 100 μM) and *N*-acetylcysteine (NAC, 10 mM) for 6 h. The values represent the mean ± SD of triplicate experiments. $^{###}p < 0.001$, compared with the control. $^{*}p < 0.05$ and $^{***}p < 0.001$, compared to the presence and absence of NAC, respectively. (B) HCT116 cells were treated with GKB (0 or 100 μM) and cell death inhibitors (20 μM z-VAD-fmk, 50 μM necrostatin-1, or 10 mM NAC) for 24 h. Then, cell viability was determined by measuring the mitochondrial dehydrogenase activity. The values represent the mean ± SD of triplicate experiments. The graph is representative of three independent experiments. $^{***}p < 0.01$, compared with the control. $^{#}p < 0.05$ and $^{###}p < 0.001$, compared with the GKB single-treatment group in the absence of cell death inhibitors. (C, D) HCT116 cells were treated with cell death inhibitors (20 μM z-VAD-fmk, 50 μM necrostatin-1, or 10 mM NAC) for 1 h and were then treated with GKB (0 or 100 μM) for 24 h. Then, (C) the sub-G1 content (%) and (D) the externalization of phosphatidylserine were measured using flow cytometry.

dx.doi.org/10.1021/jf404047z | J. Agric. Food Chem. 2014, 62, 2353−2363

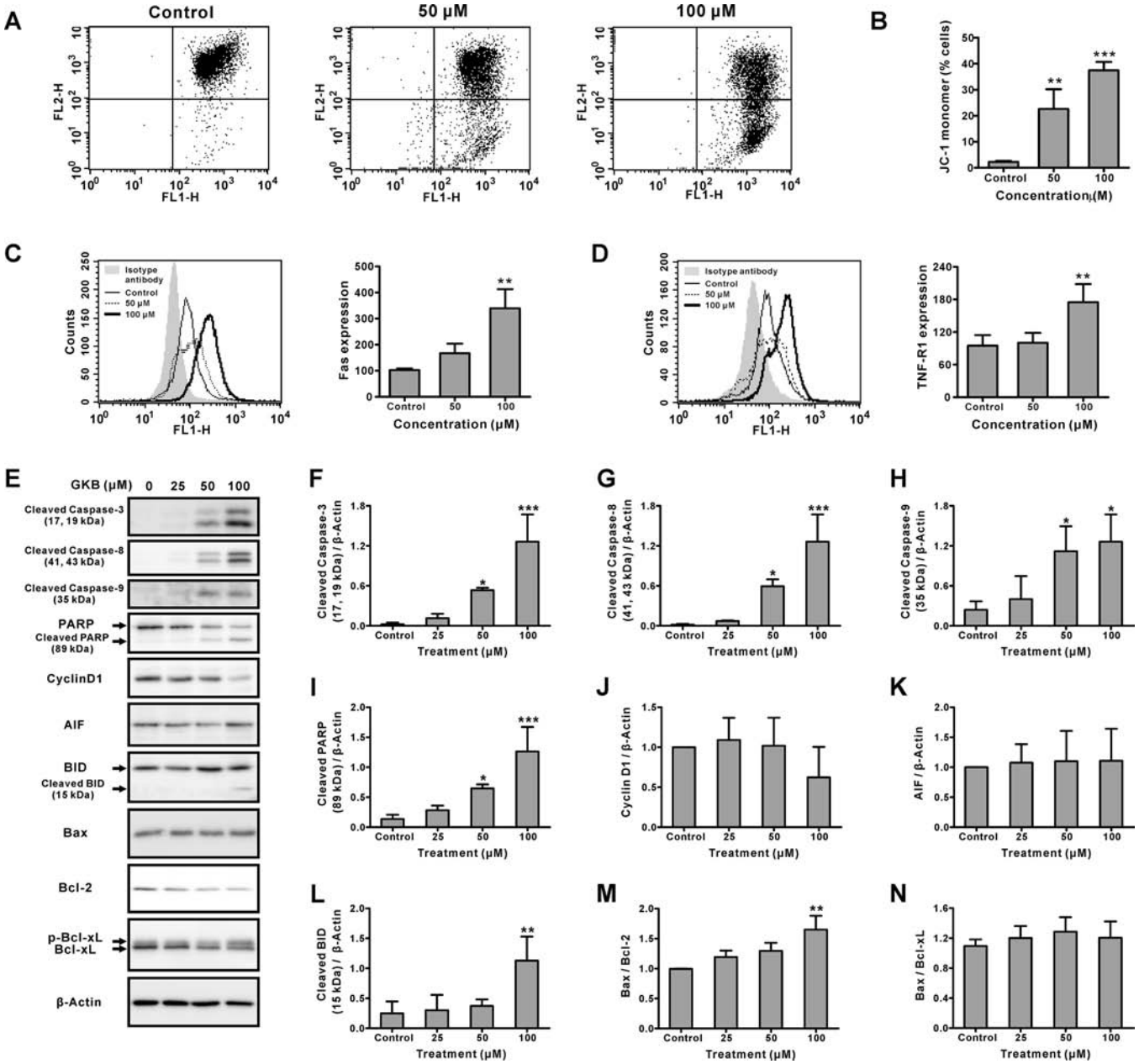

Figure 3. Effects of GKB on the intrinsic and extrinsic apoptotic signaling pathway in HCT116 cells. HCT116 cells were treated with GKB (25−100 μM) for 24 h. (A, B) Effect of GKB on the mitochondrial membrane potential, which was evaluated by flow cytometric analysis after JC-1 staining. (C, D) Effect of GKB on the cell surface expression of death receptors Fas and TNF-R1. Their expression was measured by flow cytometric immunofluorescence analysis. (E−N) The expression of apoptosis regulatory proteins was measured by Western blot analysis. (E) The Western blots shown are representative of three independent experiments. The relative expression of (F) cleaved caspase-3/β-actin, (G) cleaved caspase-8/β-actin, (H) cleaved caspase-9/β-actin, (I) cleaved PARP/β-actin, (J) Cyclin D1/β-actin, (K) AIF/β-actin, (L) cleaved BID/β-actin, (M) Bax/Bcl-2, and (N) Bax/Bcl-xL was determined by densitometry. The values represent the mean ± SD from three independent experiments. *$p < 0.05$, **$p < 0.01$, and ***$p < 0.001$, compared with the control.

colorectal cancer, GKB also induced apoptotic cell death in HepG2 (p53-proficient) human hepatoma cells (Supporting Information, Figure S1).

Effects of Chemical Inhibitors on the Programmed Cell Death Induced by GKB in HCT116 Cells. Because we hypothesized that ROS accumulation might be involved in the initiation of apoptotic cell death by GKB, we measured the accumulation of intracellular ROS using the H_2-DCFDA assay. GKB (50 or 100 μM) significantly induced an accumulation of intracellular ROS, and this accumulation was completely abrogated when the cells were cotreated with the antioxidant NAC (a precursor of glutathione) (Figure 2A).

Next, we investigated the effects of cell death inhibitors, including z-VAD-fmk (an apoptosis inhibitor), necrostatin-1 (a necroptosis inhibitor), and NAC (an antioxidant), to determine what effects necroptosis, another cell death pathway, may contribute the antiproliferative activity of GKB and to elucidate the relevance of the ROS accumulation in the GKB-induced programmed cell death. First, treating cells with z-VAD-fmk or NAC significantly recovered the cell viability that decreased following treatment with GKB; on the other hand, necrostatin-1

dx.doi.org/10.1021/jf404047z | J. Agric. Food Chem. 2014, 62, 2353−2363

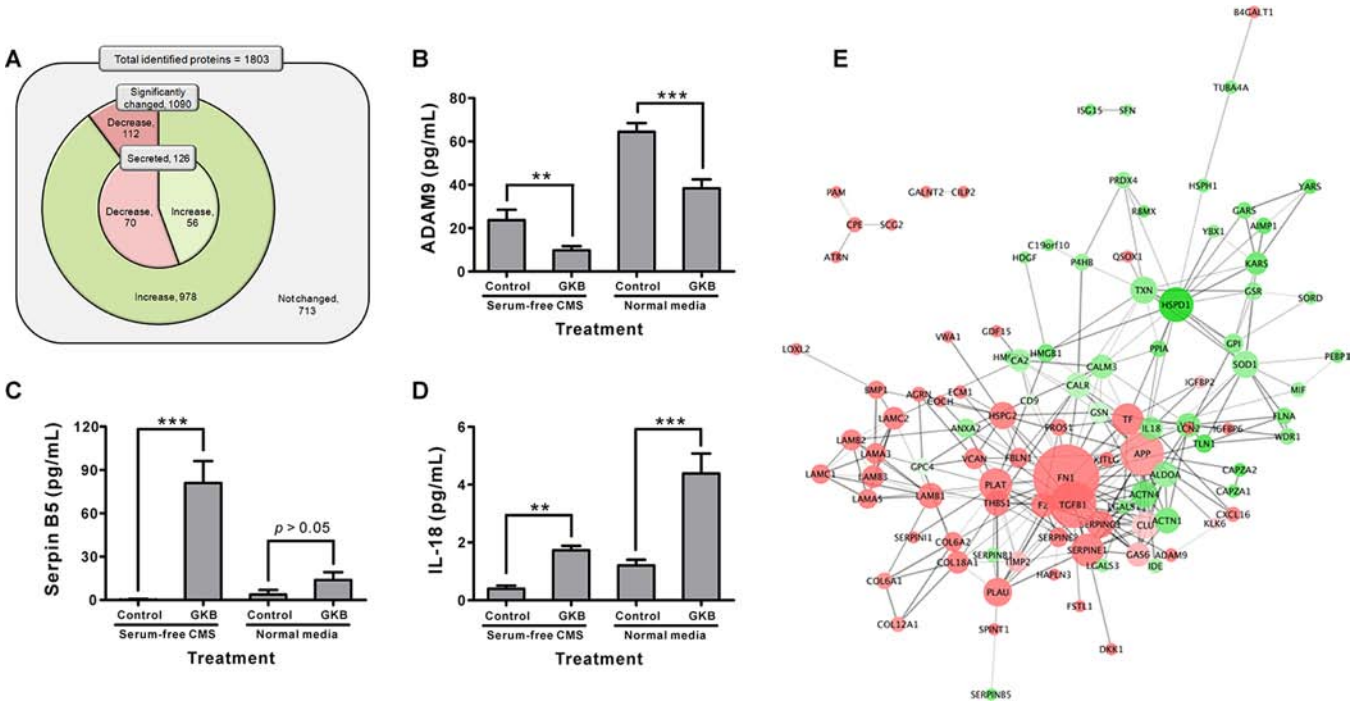

Figure 4. Effect of GKB on the expression and interaction of the secreted proteins in HCT116 cells. (A) Expression and the Venn diagram summarizing the total identified proteins and secretory proteins analyzed in this study. The relative protein expressions were analyzed using the spectrum count method, and the proteins that significantly changed following GKB treatment were determined. From these proteins, the secretory proteins were further separated based on the Gene Ontology (GO) analysis. (B–D) Confirmation of the expression levels of secreted (B) ADAM9, (C) SERPINB5, and (D) IL18 using ELISA. HCT116 cells were cultured in conditioned media for secretome analysis (CMS) supplemented with GKB (50 μM) or in normal medium supplemented with GKB (100 μM) for 24 h. The values represent the mean ± SD of three independent experiments. $^{**}p < 0.01$ and $^{***}p < 0.001$, compared with the control. (E) The protein–protein interactions of the secretory proteins that were significantly altered in response to GKB treatment. Each circular node indicates an identified protein. Proteins that were up- or downregulated are colored in green or red, respectively. The size of the protein node indicates the number of interactions; larger nodes indicate more interactions. The thickness of the connecting lines indicates the overall confidence score of the interaction, as calculated by the STRING tool; thicker lines indicate a higher degree of confidence.

did not affect the antiproliferative activity of GKB (Figure 2B). Second, z-VAD-fmk and NAC recovered the sub-G1 content (%), which was increased following treatment with GKB. The sub-G1 contents of HCT116 cells treated with GKB, GKB + z-VAD-fmk, GKB + necrostatin-1, and GKB + NAC were 22.38, 6.32, 19.75, and 3.41, respectively; while the sub-G1 content of the vehicle control cells was 1.94 (Figure 2C). Third, z-VAD-fmk and NAC also abrogated the externalization of phosphatidylserine, which was induced by treatment with GKB. The early apoptotic cell populations (%, annexin V–fluorescein positive and PI negative) of HCT116 cells treated with GKB, GKB + z-VAD-fmk, GKB + necrostatin-1, and GKB + NAC were 22.17, 7.56, 21.75, and 5.54, respectively, while that of the vehicle control cells was 4.00 (Figure 2D).

Based on these data, we speculated that apoptosis might be the main programmed cell death mechanism of the antiproliferative activity of GKB, not necroptosis. Additionally, intracellular accumulation of ROS was important in triggering apoptotic cell death in response to GKB treatment because ROS scavenging via cotreatment with NAC severely abrogated the GKB-induced apoptotic cell death observed in HCT116 cells.

Effect of GKB on Intrinsic and Extrinsic Apoptotic Signaling Pathways in HCT116 Cells. In addition to biochemical and morphological data, Western blot analysis showed that GKB induced the cleavage of caspase-3 and PARP, which are representative makers of apoptosis, in a dose-dependent manner (Figure 3E,F,I).

We further elucidated the cellular signaling pathway relating to the apoptotic cell death induced by GKB. To determine whether the intrinsic mitochondrial pathway was involved in the GKB-induced apoptotic cell death, we measured the mitochondrial membrane potential ($\Delta\Psi_m$) using the JC-1 dye staining method. As a result, we observed that GKB significantly disrupted the mitochondrial membrane potential (Figure 3A). GKB induced an increase in cell populations (%) with green fluorescence (JC-1 monomer), in a dose-dependent manner (Figure 3B). In addition, GKB also induced the cleavage of caspase-9 (Figure 3E,H) and the increase of Bax/Bcl-2 ratio (Figure 3E,M), which are representative markers of the intrinsic apoptotic pathway.

We also investigated the effect of GKB on the extrinsic death receptor pathway. For this purpose, we measured the cell surface expression of the death receptors Fas and TNF-R1 using flow cytometric analysis of immunofluorescence. As a result, we observed that GKB induced an increase in the expression of Fas and TNF-R1, in a dose-dependent manner (Figure 3C,D). In addition, GKB significantly induced the cleavage of caspase-8, which is a precise marker of extrinsic pathway (Figure 3E,G). We also discovered that the GKB induced the cleavage of BID (Figure 3E,L). BID is known to be activated via the proteolytic cleavage by caspase-8 in the Fas signaling pathway, and it induces cytochrome *c* release from mitochondria.[30] These data implied that GKB also activated the extrinsic death receptor pathway.

Taken together, we concluded that the GKB-triggered apoptotic HCT116 cell death was mediated through both intrinsic mitochondrial and extrinsic death receptor pathways.

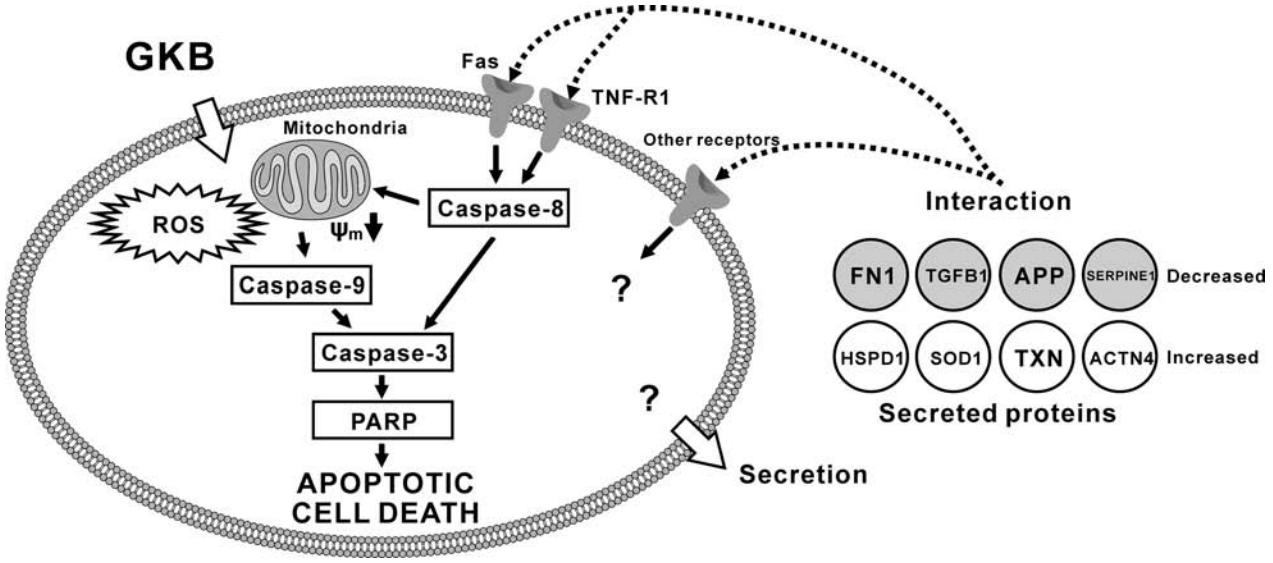

Figure 5. Schematic summary of the present study.

Comparative Analysis of the Secreted Proteome between the Control-Treated and GKB-Treated HCT116 Cells. As shown in Supporting Information, Figure S2, the conditioned media of the control-treated and GKB-treated HCT116 cells were collected for the secretome analysis. Because the IC_{50} value (29.43 ± 1.10 μM) of GKB was relatively lower when HCT116 cells were cultured in CMS, compared to normal medium, the HCT116 cells were treated with 50 μM GKB for 24 h for the LC−MS/MS analysis. As a result of the LC−MS/MS analysis, a total of 1803 proteins were identified, and all identified proteins were found in both the control and GKB-treated groups.

The fold changes in protein expression between the control-treated and GKB-treated groups and their statistical significances were analyzed using the spectral counting method. The identified proteins were further selected based on their GO term analysis. As shown in Figure 4A, among the 1803 identified proteins, 1090 proteins showed statistically significant fold changes in their expression ($p < 0.05$; Rsc >1 or Rsc < −1). Within those proteins, 126 (7.0% of the total identified proteins) proteins were annotated as secreted proteins by GO term analysis. Among those, 70 proteins were downregulated, and the other 56 proteins were upregulated based on the spectral counting method. We suggest that these 126 proteins are crucial secreted proteins related to the GKB-induced apoptotic cell death of HCT116 cells. The complete lists of proteins are shown in the Supporting Information: Table S1 (downregulated) and Table S2 (upregulated).

Validation of the Secreted Protein Expression by ELISA. The expression levels of three representative proteins, ADAM9, SERPINB5, and IL18, in the culture media were further validated using ELISA (Figure 4B−D). We selected these proteins because they have already been reported as secretory proteins that are involved in growth inhibition and the programmed cell death of various cancer cells.[19,31−33] Our results showed that the expression levels revealed by ELISA were similar to those calculated using the LC−MS/MS spectral count method. Specifically, the protein expression of IL18 and SERPINB5 was increased following GKB treatment, whereas ADAM9 expression decreased; these results were the same in both the normal and conditioned media (CMS). Therefore, based on these data, we could assume the reliability of the spectrum counting method used in this study for the relative quantitation of the secreted proteins.

Interaction among the Secreted Proteins Whose Expression Was Altered by GKB Treatment. To identify the highly interactive proteins within the secretome, the protein network was analyzed using the STRING tool (Figure 4E). Of the 126 secretory proteins, 104 proteins were found to interact with at least 1 protein. Because the size of the circle in Figure 4E indicates the number of interacting partners, we can infer that proteins such as FN1, TGFB1, APP, HSPD1, and SERPINE1 have a large number of interacting partners. For example, FN1, which had 37 interactions, was found to be the most interactive protein, followed by TGFB1 and APP, which had 24 and 22 interactions, respectively. HSPD1 (16 interactions) was the most interactive protein among the upregulated proteins. SERPINE1, PLAT, TF, and PLAU also showed relatively high degrees of interaction. A total of 15 proteins were found to interact with more than 10 partners. These highly interacting proteins are listed in Supporting Information, Table S3. We also list the 22 proteins that did not have any reported interaction partners in the STRING database (Supporting Information, Table S4).

■ DISCUSSION

Here, we present evidence that GKB, a model polyacetylene compound derived from wild vegetables, inhibited the proliferation of various human colorectal cancer cells through the intracellular accumulation of ROS and the consecutive induction of apoptotic cell death. The GKB-induced apoptotic cell death was triggered through both the intrinsic mitochondrial and extrinsic death receptor pathways. GKB induced the activation of initiator caspases, caspase-8 and caspase-9, as well as executioner caspase, caspase-3. We also elucidated the secreted proteins and the theoretical interaction network underlying the GKB-induced apoptotic HCT116 cell death using LC−MS/MS and bioinformatics analyses. The summarized schematic diagram depicting the GKB-induced apoptotic cell death in HCT116 cells and the potential secretory proteins are shown in Figure 5. To the best of our knowledge, this study is the first report describing the molecular mechanism and analyzing the secretory proteome of dietary polyacetylene-induced apoptotic cancer cells.

Secreted proteins play pivotal roles in many biological phenomena, including cancer biology, and the secreted proteome has often been analyzed using LC−MS/MS technology. However, until now, few investigations of the secreted proteome from apoptotic cancer cells induced by bioactive chemicals have been reported.[18,20] We think that this scarcity is due to several key limitations. First, serum-free medium is usually used during the analysis of the secretome to minimize the background protein signals that arise from the serum. However, serum starvation can often affect apoptotic cell death, and unwanted cell death is triggered even in the vehicle control cells.[16,34] This phenomenon can make it difficult to discriminate which secreted proteins came from the apoptotic cells. Second, as apoptotic cell death progresses, the plasma membrane integrity is gradually destroyed, and nonspecific cytosolic proteins are abundantly found along with the proteins that are actively excreted from the apoptotic cancer cells.[35,36] Until now, isotope labeling or cyanine dye staining methods have been used to compare the differential secretome profiles between the control cells and the apoptotic cells. However, these methods require expensive and cumbersome labeling procedures.

In the present study, we successfully analyzed the secreted proteome of GKB-induced apoptotic cancer cells without the use of conventional labeling methods. Our method consisted of two main strategies. First, we optimized the conditioned media for secretome analysis (CMS). To minimize unwanted cell death induced by serum deprivation, we supplemented the medium with glucose and amino acids, as glucose and amino acid deprivation are known to induce apoptosis in various cancer cells.[37−40] When HCT116 cells were cultured in CMS, the apoptotic cell population was significantly lower than the population of cells that were cultured in MEM that did not contain serum and additional nutrients, such as glucose and amino acids (data not shown). We confirmed that the changes in the protein expression of ADAM9, SERPINB5, and IL18 were well correlated between the LC−MS/MS spectral counting analysis and the ELISA both in the serum-free CMS and in the serum-containing normal medium. Although the tendencies of changes in protein expression were identical between ELISA and LC−MS/MS analysis results, the exact fold change values were somewhat different. These differences might have arisen by differences in dynamic range of the two experiments: higher sensitivity of ELISA and low dynamic range in LC−MS/MS analysis.[19] Second, we further analyzed the secretory proteins using GO term analysis to exclude the cytosolic proteins that were nonselectively excreted due to the loss of plasma membrane integrity. Before the GO term screening, most of the significantly changed proteins were classified as increased (89.7%; 112 decreased, 978 increased); on the other hand, after screening, only 44.4% of the significantly changed secretory proteins were classified as increased (70 decreased, 56 increased, Figure 4A). These data implied that many of the false positive proteins, which were thought to be the nonselectively excreted proteins due to the loss of the plasma membrane, could be excluded by the GO term analysis. We report here that the secretory proteome of chemically induced apoptotic cancer cells could be successfully analyzed without the use of the isotope or cyanine dye staining. We hope that our approaches can be used to analyze other secretomes to elucidate the molecular mechanisms underlying apoptotic cell death induced by various bioactive chemicals.

In this study, we discovered a total of 125 secretory proteins whose expression significantly changed after treatment with the dietary polyacetylene, GKB. These proteins may be involved in the apoptotic cell death of cancer cells. Therefore, their functions in the programmed cell death of cancer cells deserve to be studied. This list of candidate proteins can be narrowed down to a smaller number based on their feasibility and probability. Here, we suggest a priority list of the secretory proteins involved in the programmed cell death of human colorectal cancer cells triggered by the chemical. We analyzed the possible interactions between the secreted proteins whose expression significantly changed following treatment with the dietary polyacetylene using the STRING tool. We speculated that the highly scored or interactive proteins might have stronger influences on the apoptotic cell death of cancer cells. We suggest that the high-scored proteins, such as FN1, TGFB1, APP, HSPD1, and SERPINE1, belong in the priority group. All 15 proteins that have more than 10 interacting partners are shown in Supporting Information, Table S3. As we speculated, almost half (7 proteins) of the high-scored proteins had GO terms related to apoptosis.

We further searched the functions of these highly interactive proteins (Supporting Information, Table S3). Here we list some representative proteins. First, for decreased proteins, FN1 was reported to induce programmed cell death in human hematopoietic cell by interacting with very late antigen 5 (VLA5).[41] TGFB1 induces B lymphoid cell apoptosis by first blocking cells at the G1/S transition, followed by apoptosis.[42] APP was overexpressed during neuronal apoptosis which was induced by the treatment of *N*-methyl-D-aspartate (NMDA). [43] SERPINE1 (also known as plasminogen activator inhibitor type 1) overexpression was associated with decreased apoptosis in neoplastic cells.[44] Second, for increased proteins, HSPD1 exerted both negative and positive effect on apoptosis.[45] Proteins SOD1 and TXN were antiapoptotic in ischemic renal epithelial cells and murine skin, respectively.[46,47] ACTN4 increased rate of apoptosis by interacting with and activating DNase Y during apoptosis.[48] In some proteins, it was surveyed that the expression level and their function may not correlate with each other. However, as we could see in the case of HSPD1, proteins were found out to be both negative and positive on apoptosis. Further investigation should be needed in order to assign the accurate function of the proteins.

In addition, we believed that some proteins may be involved, but their functions and interactions may not have been reported yet, and thus they might have low scores according to the STRING analysis. These proteins may be novel because they have not yet been investigated in relation to apoptosis. For these reasons, low-scored proteins also deserve consideration. Thus, we selected 22 proteins that did not have any interacting partners among the secreted proteins found in our study (Supporting Information, Table S4). Among them, only 2 proteins had GO terms related to apoptosis. The functional study of these high- and low-scored proteins will help us understand the programmed cell death of cancer cells induced by the bioactive chemicals, and these studies should be applied to the development of novel cancer therapeutic agents. Therefore, further studies elucidating the genetic and biochemical functions of these secretory proteins are needed.

Here, we also propose that GKB, a dietary polyacetylene, is a potential cancer chemopreventive agent. In the present study, we demonstrate that the antiproliferative activity of GKB against various human cancer cells originated from the induction of apoptotic cell death, not from necroptosis. In addition to the induction of apoptotic cell death, GKB induces phase II detoxification enzymes, including quinone reductase, via the Nrf2 signaling pathway in cultured colon and liver cells.[13] A

recent animal study reported that GKB attenuated inflammation and colon carcinogenesis in the azoxymethane/dextran sodium sulfate mouse model.[12]

However, in order for GKB to be a promising chemopreventive agent, the bioavailability and stability issues have to be resolved. There are a number of studies regarding bioavailability of polyacetylenes. They include in vivo studies[49] as well as Caco-2 cell uptake assays.[50,51] In those studies, it is demonstrated that a few polyacetylenes, which appear to be hydrophobic, are bioavailable.[50] Additionally, polyacetylenes are reported to be unstable.[6,52]

To overcome these stability and bioavailability issues, various techniques may be applied. Among them, we expect that nano- or microencapsulation, a technique which is widespread throughout the food engineering and pharmaceutical industries, could be a promising solution.[53−55] Many studies have shown that the parameters of pharmacokinetics and pharmacodynamics can be improved upon nanoencapsulation of classical drugs.[53] We expect that further in-depth study including the bioavailability assessment of GKB and the application of GKB nanoencapsulation may serve as a milestone for the development of GKB as a cancer chemopreventive agent.

In summary, we demonstrated that the suppression activity of GKB against HCT116 human colorectal cancer cells was due to the induction of apoptotic cell death, which was dependent on intracellular ROS accumulation and was triggered through both mitochondrial and death receptor pathway. We also suggested possible secretory proteins that may be involved in the GKB-induced apoptotic cell death of cancer cells using LC−MS/MS and bioinformatics analyses. Our approach and data might be applied to the functional study of apoptosis-related genes, as well as to the development of novel cancer chemopreventive agents.

■ ASSOCIATED CONTENT

Supporting Information

Detailed materials and methods and additional tables and figures. This material is available free of charge via the Internet at http://pubs.acs.org.

■ AUTHOR INFORMATION

Corresponding Authors

*(C.W.N.) Tel: +82-33-650-3651. Fax: +82-33-650-3679. E-mail: cwnho@kist.re.kr.

*(C.-H.P.) Tel: +82-33-650-3652. Fax: +82-33-650-3679. E-mail: cheolpan@gmail.com.

Author Contributions

†K.K. and D.-G.S. contributed equally to this work.

Funding

This study was supported by the Korea Institute of Science and Technology Gangneung Institute intramural research grant (2Z03850).

Notes

The authors declare no competing financial interest.

■ ABBREVIATIONS USED

CMS, conditioned media for secretome analysis; FBS, fetal bovine serum; FITC, fluorescein isothiocyanate; GKB, gymnasterkoreayne B; GO, gene ontology; NAC, *N*-acetylcysteine; PI, propidium iodide

■ REFERENCES

(1) Vainio, H.; Weiderpass, E. Fruit and vegetables in cancer prevention. *Nutr. Cancer* **2006**, *54*, 111−142.

(2) Pan, M. H.; Ho, C. T. Chemopreventive effects of natural dietary compounds on cancer development. *Chem. Soc. Rev.* **2008**, *37*, 2558−2574.

(3) Liu, R. H. Potential synergy of phytochemicals in cancer prevention: mechanism of action. *J. Nutr.* **2004**, *134*, 3479S−3485S.

(4) Whelan, L. C.; Ryan, M. F. Effects of the polyacetylene capillin on human tumour cell lines. *Anticancer Res.* **2004**, *24*, 2281−2286.

(5) Dembitsky, V. M. Anticancer activity of natural and synthetic acetylenic lipids. *Lipids* **2006**, *41*, 883−924.

(6) Christensen, L. P.; Brandt, K. Bioactive polyacetylenes in food plants of the *Apiaceae* family: occurrence, bioactivity and analysis. *J. Pharm. Biomed. Anal.* **2006**, *41*, 683−693.

(7) Kobaek-Larsen, M.; Christensen, L. P.; Vach, W.; Ritskes-Hoitinga, J.; Brandt, K. Inhibitory effects of feeding with carrots or (−)-falcarinol on development of azoxymethane-induced preneoplastic lesions in the rat colon. *J. Agric. Food Chem.* **2005**, *53*, 1823−1827.

(8) Ohnuma, T.; Nakayama, S.; Anan, E.; Nishiyama, T.; Ogura, K.; Hiratsuka, A. Activation of the Nrf2/ARE pathway via S-alkylation of cysteine 151 in the chemopreventive agent-sensor Keap1 protein by falcarindiol, a conjugated diacetylene compound. *Toxicol. Appl. Pharmacol.* **2010**, *244*, 27−36.

(9) Lee, L. S.; Stephenson, K. K.; Fahey, J. W.; Parsons, T. L.; Lietman, P. S.; Andrade, A. S.; Lei, X.; Yun, H.; Soon, G. H.; Shen, P.; Danishefsky, S.; Flexner, C. Induction of chemoprotective phase 2 enzymes by ginseng and its components. *Planta Med.* **2009**, *75*, 1129−1133.

(10) Moon, J.; Yu, S. J.; Kim, H. S.; Sohn, J. Induction of G_1 cell cycle arrest and $p27^{KIP1}$ increase by panaxydol isolated from *Panax ginseng*. *Biochem. Pharmacol.* **2000**, *59*, 1109−1116.

(11) Jung, H. J.; Min, B. S.; Park, J. Y.; Kim, Y. H.; Lee, H. K.; Bae, K. H.; Gymnasterkoreaynes, A-F cytotoxic polyacetylenes from *Gymnaster koraiensis*. *J. Nat. Prod.* **2002**, *65*, 897−901.

(12) Butler, S. M.; Wallig, M. A.; Nho, C. W.; Pan, C. H.; Lee, E. H.; Jung, S. H.; Jeffery, E. H. A polyacetylene-rich extract from *Gymnaster koraiensis* strongly inhibits colitis-associated colon cancer in mice. *Food Chem. Toxicol.* **2013**, *53*, 235−239.

(13) Lee, K. M.; Kang, K.; Lee, S. B.; Nho, C. W. Nuclear factor-E2 (Nrf2) is regulated through the differential activation of ERK1/2 and PKC a/bII by Gymnasterkoreayne B. *Cancer Lett.* **2013**, *330*, 225−232.

(14) Shin, D.; Yang, J. E.; Lee, S. B.; Nho, C. W. SAR studies of gymnasterkoreayne derivatives with cancer chemopreventive activities. *Bioorg. Med. Chem. Lett.* **2010**, *20*, 7549−7552.

(15) Lee, S. B.; Kang, K.; Oidovsambuu, S.; Jho, E. H.; Yun, J. H.; Yoo, J. H.; Lee, E. H.; Pan, C. H.; Lee, J. K.; Jung, S. H.; Nho, C. W. A polyacetylene from *Gymnaster koraiensis* exerts hepatoprotective effects *in vivo* and *in vitro*. *Food Chem. Toxicol.* **2010**, *48*, 3035−3041.

(16) Eichelbaum, K.; Winter, M.; Berriel Diaz, M.; Herzig, S.; Krijgsveld, J. Selective enrichment of newly synthesized proteins for quantitative secretome analysis. *Nat. Biotechnol.* **2012**, *30*, 984−990.

(17) Zhang, Y.; Tang, X.; Yao, L.; Chen, K.; Jia, W.; Hu, X.; Xu, L. X. Lectin capture strategy for effective analysis of cell secretome. *Proteomics* **2012**, *12*, 32−36.

(18) Ji, H.; Greening, D. W.; Kapp, E. A.; Moritz, R. L.; Simpson, R. J. Secretome-based proteomics reveals sulindac-modulated proteins released from colon cancer cells. *Proteomics: Clin. Appl.* **2009**, *3*, 433−451.

(19) Yao, L.; Zhang, Y.; Chen, K.; Hu, X.; Xu, L. X. Discovery of IL-18 as a novel secreted protein contributing to doxorubicin resistance by comparative secretome analysis of MCF-7 and MCF-7/Dox. *PLoS One* **2011**, *6*, e24684.

(20) Takata, T.; Ishigaki, Y.; Shimasaki, T.; Tsuchida, H.; Motoo, Y.; Hayashi, A.; Tomosugi, N. Characterization of proteins secreted by pancreatic cancer cells with anticancer drug treatment *in vitro*. *Oncol. Rep.* **2012**, *28*, 1968−1976.

(21) Kang, K.; Lee, H. J.; Kim, C. Y.; Lee, S. B.; Tunsag, J.; Batsuren, D.; Nho, C. W. The chemopreventive effects of *Saussurea salicifolia* through

induction of apoptosis and phase II detoxification enzyme. *Biol. Pharm. Bull.* **2007**, *30*, 2352−2359.
(22) Kang, K.; Oh, S. H.; Yun, J. H.; Jho, E. H.; Kang, J. H.; Batsuren, D.; Tunsag, J.; Park, K. H.; Kim, M.; Nho, C. W. A novel topoisomerase inhibitor, daurinol, suppresses growth of HCT116 cells with low hematological toxicity compared to etoposide. *Neoplasia* **2011**, *13*, 1043−1057.
(23) Kang, K.; Jho, E. H.; Lee, H. J.; Oidovsambuu, S.; Yun, J. H.; Kim, C. Y.; Yoo, J. H.; Kim, Y. J.; Kim, J. H.; Ahn, S. Y.; Nho, C. W. *Youngia denticulata* protects against oxidative damage induced by *tert*-butylhydroperoxide in HepG2 cells. *J. Med. Food* **2011**, *14*, 1198−1207.
(24) Kang, K.; Lee, H. J.; Yoo, J. H.; Jho, E. H.; Kim, C. Y.; Kim, M.; Nho, C. W. Cell and nuclear enlargement of SW480 cells induced by a plant lignan, arctigenin: evaluation of cellular DNA content using fluorescence microscopy and flow cytometry. *DNA Cell Biol.* **2011**, *30*, 623−629.
(25) Kang, D. H.; Gho, Y. S.; Suh, M. K.; Kang, C. H. Highly sensitive and fast protein detection with coomassie brilliant blue in sodium dodecyl sulfate-polyacrylamide gel electrophoresis. *Bull. Korean Chem. Soc.* **2002**, *23*, 1511−1512.
(26) Shevchenko, A.; Tomas, H.; Havlis, J.; Olsen, J. V.; Mann, M. In-gel digestion for mass spectrometric characterization of proteins and proteomes. *Nat. Protoc.* **2006**, *1*, 2856−2860.
(27) Huang da, W.; Sherman, B. T.; Lempicki, R. A. Systematic and integrative analysis of large gene lists using DAVID bioinformatics resources. *Nat. Protoc.* **2009**, *4*, 44−57.
(28) Szklarczyk, D.; Franceschini, A.; Kuhn, M.; Simonovic, M.; Roth, A.; Minguez, P.; Doerks, T.; Stark, M.; Muller, J.; Bork, P.; Jensen, L. J.; von Mering, C. The STRING database in 2011: functional interaction networks of proteins, globally integrated and scored. *Nucleic Acids Res.* **2011**, *39*, D561−D568.
(29) Cline, M. S.; Smoot, M.; Cerami, E.; Kuchinsky, A.; Landys, N.; Workman, C.; Christmas, R.; Avila-Campilo, I.; Creech, M.; Gross, B.; Hanspers, K.; Isserlin, R.; Kelley, R.; Killcoyne, S.; Lotia, S.; Maere, S.; Morris, J.; Ono, K.; Pavlovic, V.; Pico, A. R.; Vailaya, A.; Wang, P. L.; Adler, A.; Conklin, B. R.; Hood, L.; Kuiper, M.; Sander, C.; Schmulevich, I.; Schwikowski, B.; Warner, G. J.; Ideker, T.; Bader, G. D. Integration of biological networks and gene expression data using Cytoscape. *Nat. Protoc.* **2007**, *2*, 2366−2382.
(30) Luo, X.; Budihardjo, I.; Zou, H.; Slaughter, C.; Wang, X. Bid, a Bcl2 interacting protein, mediates cytochrome c release from mitochondria in response to activation of cell surface death receptors. *Cell* **1998**, *94*, 481−490.
(31) Sung, S. Y.; Kubo, H.; Shigemura, K.; Arnold, R. S.; Logani, S.; Wang, R.; Konaka, H.; Nakagawa, M.; Mousses, S.; Amin, M.; Anderson, C.; Johnstone, P.; Petros, J. A.; Marshall, F. F.; Zhau, H. E.; Chung, L. W. Oxidative stress induces ADAM9 protein expression in human prostate cancer cells. *Cancer Res.* **2006**, *66*, 9519−9526.
(32) Toillon, R. A.; Lagadec, C.; Page, A.; Chopin, V.; Sautiere, P. E.; Ricort, J. M.; Lemoine, J.; Zhang, M.; Hondermarck, H.; Le Bourhis, X. Proteomics demonstration that normal breast epithelial cells can induce apoptosis of breast cancer cells through insulin-like growth factor-binding protein-3 and maspin. *Mol. Cell. Proteomics* **2007**, *6*, 1239−1247.
(33) Hashimoto, W.; Osaki, T.; Okamura, H.; Robbins, P. D.; Kurimoto, M.; Nagata, S.; Lotze, M. T.; Tahara, H. Differential antitumor effects of administration of recombinant IL-18 or recombinant IL-12 are mediated primarily by Fas-Fas ligand- and perforin-induced tumor apoptosis, respectively. *J. Immunol.* **1999**, *163*, 583−589.
(34) Braun, F.; Bertin-Ciftci, J.; Gallouet, A. S.; Millour, J.; Juin, P. Serum-nutrient starvation induces cell death mediated by Bax and Puma that is counteracted by p21 and unmasked by Bcl-x_L inhibition. *PLoS One* **2011**, *6*, e23577.
(35) Lai, T. C.; Chou, H. C.; Chen, Y. W.; Lee, T. R.; Chan, H. T.; Shen, H. H.; Lee, W. T.; Lin, S. T.; Lu, Y. C.; Wu, C. L.; Chan, H. L. Secretomic and proteomic analysis of potential breast cancer markers by two-dimensional differential gel electrophoresis. *J. Proteome Res.* **2010**, *9*, 1302−1322.
(36) Rieger, A. M.; Hall, B. E.; Luong le, T.; Schang, L. M.; Barreda, D. R. Conventional apoptosis assays using propidium iodide generate a significant number of false positives that prevent accurate assessment of cell death. *J. Immunol. Methods* **2010**, *358*, 81−92.
(37) Priebe, A.; Tan, L.; Wahl, H.; Kueck, A.; He, G.; Kwok, R.; Opipari, A.; Liu, J. R. Glucose deprivation activates AMPK and induces cell death through modulation of Akt in ovarian cancer cells. *Gynecol. Oncol.* **2011**, *122*, 389−395.
(38) Mendivil-Perez, M.; Jimenez-Del-Rio, M.; Velez-Pardo, C. Glucose starvation induces apoptosis in a model of acute T leukemia dependent on caspase-3 and apoptosis-inducing factor: a therapeutic strategy. *Nutr. Cancer* **2013**, *65*, 99−109.
(39) Fumarola, C.; Zerbini, A.; Guidotti, G. G. Glutamine deprivation-mediated cell shrinkage induces ligand-independent CD95 receptor signaling and apoptosis. *Cell Death Differ.* **2001**, *8*, 1004−1013.
(40) Maddocks, O. D.; Berkers, C. R.; Mason, S. M.; Zheng, L.; Blyth, K.; Gottlieb, E.; Vousden, K. H. Serine starvation induces stress and p53-dependent metabolic remodelling in cancer cells. *Nature* **2013**, *493*, 542−546.
(41) Sugahara, H.; Kanakura, Y.; Furitsu, T.; Ishihara, K.; Oritani, K.; Ikeda, H.; Kitayama, H.; Ishikawa, J.; Hashimoto, K.; Kanayama, Y. Induction of programmed cell death in human hematopoietic cell lines by fibronectin via its interaction with very late antigen 5. *J. Exp. Med.* **1994**, *179*, 1757−1766.
(42) Arsura, M.; Wu, M.; Sonenshein, G. E. TGFβ1 inhibits NF-κB/Rel activity inducing apoptosis of B cells: transcriptional activation of IκBα. *Immunity* **1996**, *5*, 31−40.
(43) Lesort, M.; Esclaire, F.; Yardin, C.; Hugon, J. NMDA induces apoptosis and necrosis in neuronal cultures. Increased APP immunoreactivity is linked to apoptotic cells. *Neurosci. Lett.* **1997**, *221*, 213−216.
(44) Chen, Y.; Kelm, R. J.; Budd, R. C.; Sobel, B. E.; Schneider, D. J. Inhibition of apoptosis and caspase-3 in vascular smooth muscle cells by plasminogen activator inhibitor type-1. *J. Cell. Biochem.* **2004**, *92*, 178−188.
(45) Kim, S.-C.; Stice, J. P.; Chen, L.; Jung, J. S.; Gupta, S.; Wang, Y.; Baumgarten, G.; Trial, J.; Knowlton, A. A. Extracellular heat shock protein 60, cardiac myocytes, and apoptosis. *Circ. Res.* **2009**, *105*, 1186−1195.
(46) Liang, H.; Arsenault, J.; Mortensen, J.; Park, F.; Johnson, C.; Nilakantan, V. Partial attenuation of cytotoxicity and apoptosis by SOD1 in ischemic renal epithelial cells. *Apoptosis* **2009**, *14*, 1176−1189.
(47) Ono, R.; Masaki, T.; Dien, S.; Yu, X.; Fukunaga, A.; Yodoi, J.; Nishigori, C. Suppressive effect of recombinant human thioredoxin on ultraviolet light-induced inflammation and apoptosis in murine skin. *J. Dermatol.* **2012**, *39*, 843−851.
(48) Liu, Q. Y.; Lei, J. X.; LeBlanc, J.; Sodja, C.; Ly, D.; Charlebois, C.; Walker, P. R.; Yamada, T.; Hirohashi, S.; Sikorska, M. Regulation of DNaseY activity by actinin-α4 during apoptosis. *Cell Death Differ.* **2004**, *11*, 645−654.
(49) Brandt, K.; Christensen, L. P.; Hansen-Møller, J.; Hansen, S. L.; Haraldsdottir, J.; Jespersen, L.; Purup, S.; Kharazmi, A.; Barkholt, V.; Frøkiær, H.; Kobæk-Larsen, M. Health promoting compounds in vegetables and fruits. *Trends Food Sci. Technol.* **2004**, *15*, 384−393.
(50) Chicca, A.; Pellati, F.; Adinolfi, B.; Matthias, A.; Massarelli, I.; Benvenuti, S.; Martinotti, E.; Bianucci, A. M.; Bone, K.; Lehmann, R.; Nieri, P. Cytotoxic activity of polyacetylenes and polyenes isolated from roots of *Echinacea pallida*. *Br. J. Pharmacol.* **2008**, *153*, 879−885.
(51) Lee, W.-C.; Peng, C.-C.; Chang, C.-H.; Huang, S.-H.; Chyau, C.-C. Extraction of antioxidant components from *Bidens pilosa* flowers and their uptake by human intestinal Caco-2 cells. *Molecules* **2013**, *18*, 1582−1601.
(52) Leonti, M.; Casu, L.; Raduner, S.; Cottiglia, F.; Floris, C.; Altmann, K.-H.; Gertsch, J. Falcarinol is a covalent cannabinoid CB1 receptor antagonist and induces pro-allergic effects in skin. *Biochem. Pharmacol.* **2010**, *79*, 1815−1826.
(53) Prados, J.; Melguizo, C.; Ortiz, R.; Perazzoli, G.; Cabeza, L.; Álvarez, P.; Rodriguez-Serrano, F.; Aranega, A. Colon cancer therapy: recent developments in nanomedicine to improve the efficacy of

conventional chemotherapeutic drugs. *Anti-Cancer Agents Med. Chem.* **2013**, *13*, 1204−1216.
(54) Yassin, A. E. B.; Anwer, M. K.; Mowafy, H. A.; El-Bagory, I. M.; Bayomi, M. A.; Alsarra, I. A. Optimization of 5-flurouracil solid-lipid nanoparticles: a preliminary study to treat colon cancer. *Int. J. Med. Sci.* **2010**, *7*, 398−408.
(55) Koo, S. Y.; Cha, K. H.; Song, D.-G.; Chung, d.; Pan, C.-H. Microencapsulation of peppermint oil in an alginate. *Int. J. Food Sci. Technol.* **2013**, *49*, 733−739.

PSPAs can scavenge oxygen free radicals, reduce lipid peroxides in blood and liver, and prevent liver damage induced by dimethylnitrosamine (DMA), *tert*-butyl hydroperoxide (T-BHP), and acetaminophen (APAP).[16−18] However, the pathological process of liver damage induced by chemicals is not the same as that induced by alcohol consumption and thus could not simulate the process of ALD. Besides, there is still no study of the preventive effect of PSPAs on acute and subacute ALD. Therefore, we carried out righting reflex loss and recovery experiments of mice under alcoholic intoxication to investigate the potential dealcoholic effect of PSPAs. In addition, to investigate the preventive effect on acute and subacute ALD of PSPAs, we tested the liver function index, lipid peroxidation degree, antioxidase activity, and liver histopathology in the body of mice treated by PSPAs by establishing acute and subacute ALD mice models.

MATERIALS AND METHODS

Plant Materials. PSP (cultivar 'YAN No. 176') was obtained from the Academy of Agricultural and Forestry Sciences in Hebei Province. They were harvested at the beginning of October 2011 and immediately kept at 10−14 °C. Within 2 weeks, the harvested PSPs were washed thoroughly, sliced, and freeze-dried. All samples were ground using a domestic grinder and stored in sealed aluminum foil bags at −20 °C prior to extraction. The proximate composition of the obtained PSP powder, which was already published by us, was as follows: moisture, 10.82 ± 0.12% (w/w); starch, 65.35 ± 1.25% (w/w); protein, 8.21 ± 0.14% (w/w); fat, 0.7 ± 0.02% (w/w); ash, 3.89 ± 0.02% (w/w); and crude fiber, 4.87 ± 0.09% (w/w).[19]

Preparation of PSPAs. Anthocyanins were extracted from PSP according to published methods.[19] Briefly, the dried PSP powder, ammonium sulfate, deionized water, and ethanol were mixed according to the quality proportion of 2:4:11:5, and the mix mentioned above was blended well and then kept still to form two phases completely. The formed aqueous two-phase system was kept in a dark place for 30 min at room temperature and then centrifuged at 4 °C and 5000*g* for 10 min. A separating funnel was used to separate the above-mentioned two phases. The upper phase was concentrated in a rotary evaporator, adsorbed by macroporous resin (AB-8), and eluted by 70% of ethanol solution at an elution flow rate of 1 mL/min. The effluent was collected, concentrated, freeze-dried, and stored at −20 °C in sealed aluminum bags.

Total Anthocyanin Quantification. A pH-differential method was used to determine the total anthocyanin content.[20] Briefly, 0.0125 g of the extract was dissolved in 1 mL of distilled water. Two water solutions were carried out on the sample. Potassium chloride (0.025 M) and sodium acetate (0.4 M) were used to set the pH values of the two solutions at 1.0 and 4.5, respectively. The two solutions were diluted to make the absorbance at 520 nm <1.2. The diluted solutions were equilibrated for 15 min, and then absorbances at 520 and 700 nm were recorded using an UV−vis spectrophotometer model UI-trospec 2000 (Amersham Pharmacia Biotech, Dubendorf, Switzerland). Absorbance was calculated as $A = (A_{510\ nm} - A_{700\ nm})_{pH1.0} - (A_{510\ nm} - A_{700\ nm})_{pH4.5}$, and total anthocyanin content was calculated using the following formula and expressed as milligrams of cyanidin 3-glucoside equivalent (CGE)/100 g PSPAs:

$$C = (A/eL) \times M \times D \times (V/W) \times 100$$

C is total anthocyanin content (mg CGE/100 g PSPAs), A is the absorbance mentioned above, e is the molar absorbance of cyanidin 3-glucoside (26900 L/cm/mol), L is cell path length (1 cm), M is the molecular weight of cyanidin 3-glucoside (432 g/mol), D is dilution multiple, V is the final volume (mL), and W is the sample weight (mg).

HPLC-ESI-MS/MS Analysis of Anthocyanins. The anthocyanins in purple sweet potato extract were analyzed using an Agilent 1200 series high-performance liquid chromatography (Agilent Technologies, Palo Alto, CA, USA) connected to an Agilent 6410 triple-quadrupole mass spectrometer. The column used was an Agilent Zorbax SB-C18 column (250 mm × 4.6 mm i.d., 5 μm). The operating conditions were as follows: flow rate, 0.5 mL/min; injection volume, 20 μL; and column temperature, 25 °C. The elution solvents were (A) 0.1% v/v trifluoroacetic acid in water and (B) acetonitrile. The gradient was as follows: from 5 to 30% B from 0 to 5 min; from 30 to 45% B from 5 to 45 min; from 45 to 90% B from 45 to 50 min. Spectra from 200 to 600 nm were scanned, and anthocyanins were detected at 254 nm. To identify PSP anthocyanins, electrospray ionization (ESI) was run in the positive ion mode in the mass range from 400 to 2000 (m/z) and under the following conditions: flow rate, 8.0 L/min; drying gas temperature, 350 °C; nebulizer pressure, 40 psi; and capillary voltage, 4500 V.[19]

Experimental Animals and Growth Conditions. Seven-week-old male inbred (C57BL/6) mice were obtained from Vital River Laboratories (VRL) (Beijing, China). The animals were kept under controlled conditions at 18−26 °C and 40−70% relative humidity with a 12 h dark−light cycle and acclimated for 2 weeks prior to use. Feed pellets and disinfected tap water were provided for cafeteria feeding. Experiments were carried out on the basis of the regulations of the Experimental Animal Welfare and Ethics Committee, Chinese Association for Laboratory Animal Sciences (CALAS).

Alcoholic Intoxication Experiments. For the righting reflex loss experiment of alcoholic intoxication, C57BL/6 mice were separated into four groups, 10 animals in each group: control group (same volume of saline), low-dose group (50 mg PSPAs/kg body weight), middle-dose group (125 mg PSPAs/kg body weight), and high-dose group (375 mg PSPAs/kg body weight). All groups were fasted for 12 h, and then PSPAs in saline were administered intragastrically. Thirty minites later, mice were treated with 50% ethanol solution (18 mL/kg body weight). Duration of the ethanol-induced loss of righting reflex was recorded. Judgment standard of lost righting reflex was as follows: the ethanol-treated mice were placed back down, and the righting reflex was judged as lost if the above pose was maintained for >30 s.

For the righting reflex recovery experiment of alcoholic intoxication, the grouping method was the same as that used in the righting reflex loss experiment of alcoholic intoxication. All groups were fasted for 12 h and then treated with 50% ethanol solution (18 mL/kg body weight). Thirty minutes later, all groups were administered intragastrically PSPAs in saline once. The duration of recovery of righting reflex was recorded.

The righting reflex for each control or treatment mouse was performed in triplicate. The duration of ethanol-induced loss of righting reflex and the duration of recovery of righting reflex for each mouse were recorded as means of three experiments.

Acute and Subacute ALD Mice Models. For the prevention experiment of PSPAs on acute ALD, C57BL/6 mice were divided into five groups of 12 animals: negative control (without anthocyanins and ethanol treatments), acute ALD mice model group (with ethanol treatment only), low-dose group (50 mg PSPAs/kg body weight), middle-dose group (125 mg PSPAs/kg body weight), and high-dose group (375 mg PSPAs/kg body weight). The same volumes of saline were administered intragastrically for the negative control and acute ALD mice model group, whereas PSPAs were administered intragastrically for low-, middle-, and high-dose groups once daily for 30 consecutive days; food and water intakes of mice were recorded once a day. Four hours after the last administration, the negative control group was fed by gavage using an equal amount of purified water, whereas the other groups were treated with a 50% ethanol solution (12 mL/kg body weight). All groups were fasted for 16 h, and then anesthesia was carried out by injecting 60 mg/kg body weight pentobarbital sodium into the abdominal cavity of the mice. Blood was sampled from the abdominal aorta to determine activities of serum aspartate aminotransferase (AST), alanine aminotransferase (ALT), triglyceride (TG), total cholesterol (TCH), low-density lipoprotein cholesterol (LDL-C), and lactate dehydrogenase (LDH). Livers were weighed and cut into slices, some of which were kept in buffered formalin for histological observation, and 10% of liver tissue homogenates was obtained from the remaining liver sections and stored at −75 °C.

For the prevention experiment of PSPAs on subacute ALD, the grouping method was the same as that used in the prevention experiment of PSPAs on acute ALD. The same volumes of saline were administered intragastrically for the negative control and acute ALD model group, whereas PSPAs were administered intragastrically for low-,

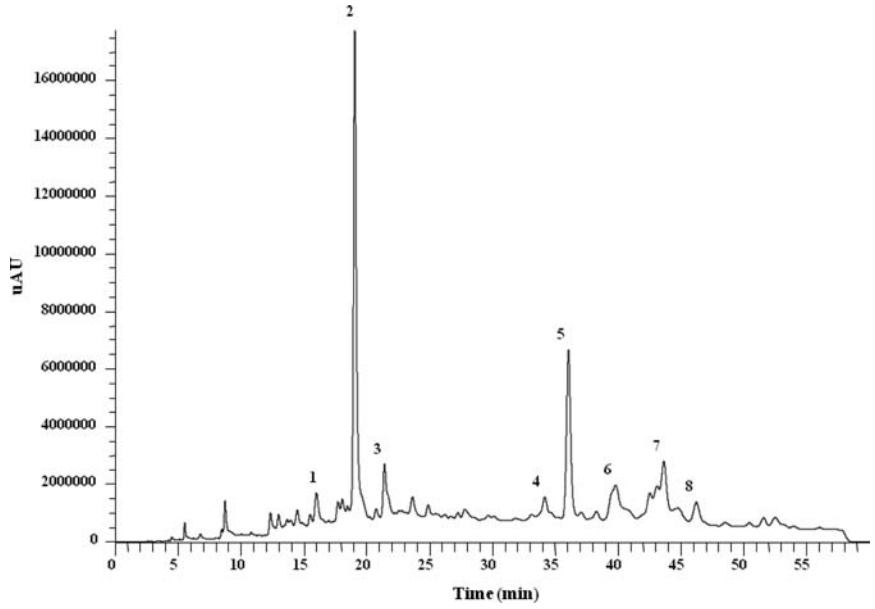

Figure 1. HPLC chromatogram of purple sweet potato anthocyanin compounds detected at 254 nm. Peak numbers refer to Table 1.

Table 1. Mass Spectrometric Data and Identification of Purple Sweet Potato Anthocyanins

peak	retention time (min)	$[M^+]$ (m/z)	major fragment ion (m/z)	identification	ref
1	16.02	471	448, 297	cyanidin-3-glucoside	22
2	19.07	730	713, 685, 377	unknown	
3	21.43	907	745	peonidin-3-*p*-hydroxybenzoylsophoroside-5-glucoside	23
4	34.19	516	499, 342, 301	peonidin-3-methoxy-glucoside	22
5	36.07	1111	949	peonidin 3-(6″,6‴-dicaffeoyl sophoroside)-5-glucoside	23
6	39.83	949	787, 463, 301	peonidin 3-caffeoyl sophoroside-5-glucoside	23
7	43.66	1069	907, 447, 301	peonidin 3-caffeoyl-*p*-hydroxybenzoylsophoroside-5-glucoside	23
8	46.26	1125	963, 463	peonidin 3-(6″-caffeoyl-6‴-feruloylsophoroside)-5- glucoside	23

middle-, and high-dose groups once daily for 30 consecutive days. A 30% ethanol solution was fed by gavage at 10 mL/kg body weight once a day to the model group and anthocyanins groups for 14 days before the finish of this experiment, and the duration between the administration of saline or anthocyanins and the administration of ethanol was >4 h. All groups were fasted for 4 h, and then anesthesia was carried out by injecting 60 mg/kg body weight pentobarbital sodium into the abdominal cavity of mice. Blood was sampled from the abdominal aorta to determine the activities of serum ALT, AST, LDH, TCH, TG, and LDL-C. Livers were weighed and cut into slices, some of which were kept in buffered formalin for histological observation, and 10% of liver tissue homogenates were obtained from the remaining liver sections and stored at −75 °C.

Determination of Liver Index. The liver index of mice was calculated according to the following equation: liver index = liver weight/body weight × 100%.

Determination of Serum ALT, AST, LDH, TCH, TG, and LDL-C Activities. Activities of serum ALT, AST, LDH, TCH, TG, and LDL-C were determined using the corresponding kits (Nanjing Jiancheng Bioengineering Institute, Nanjing, China).

Determination of Hepatic MDA, SOD, GST, and ADH Levels. Mice liver samples were blended with 30 mM cold phosphate buffer and 1% TritonX-100 and ground in a tissue grinder. The supernatant was obtained for assay of malondialdehyde (MDA), SOD, GST, and alcohol dehydrogenase (ADH) according to the instructions of corresponding kits (Nanjing Jiancheng Bioengineering Institute).

Histopathological Observation. Mice liver sections were fixed for 24 h in 10% formalin buffer, embedded in paraffin for hematoxylin and eosin staining, and then observed using a light microscope. The magnification was 100 times, and at least 10 areas of each tissue slice were observed.

Statistical Analysis. Experiments were performed in at least triplicate. The results were expressed as means ± SD (standard deviation). Statistical analysis was carried out with SAS software (version 8.1, SAS Institute Inc., Cary, NC, USA). Significant differences were decided at $p < 0.05$.

RESULTS AND DISCUSSION

Total Anthocyanins and Identification of PSPAs. On the basis of the result of the pH-differential method, the total anthocyanin content was 3.02×10^4 mg cyanidin 3-glucoside equiv/100 g PSPAs, and the yield of PSPAs corresponded to 0.93% of the PSP powder. Figure 1 shows the HPLC chromatogram of PSPAs. Eight constituents were separated. From the UV−visible spectra, LC-ESI/MS spectra, and some literature sources (Table 1 and Supporting Information Figure 1), seven constituents were identified. Peaks 1 and 4 were tentatively identified as cyanidin-3-glucoside and peonidin-3-methoxyglucoside, respectively.[21] Peaks 3, 5, 6, 7, and 8 were tentatively identified as peonidin 3-*p*-hydroxybenzoyl sophoroside-5-glucoside, peonidin 3-(6″,6‴-dicaffeoyl sophoroside)-5-glucoside, peonidin 3-caffeoyl sophoroside-5-glucoside, peonidin 3-caffeoyl-*p*-hydroxybenzoyl sophoroside-5-glucoside, and peonidin 3-(6″-caffeoyl-6‴ -feruloyl sophoroside)-5-glucoside, respectively.[22] Peak 2 was a new discovery, which will be further investigated.

Alcoholic Intoxication Experiments. The loss of righting reflex indicates that mice have become drunk, whereas the recovery of righting reflex means that mice have sobered up.[23]

Table 2 shows the effect of PSPAs on durations of ethanol-induced loss and recovery of righting reflex. Compared with control, intake of PSPAs extended the duration of ethanol-induced loss of righting reflex significantly ($p < 0.05$), especially for the high-dose PSPAs group ($p < 0.01$), where the duration of ethanol-induced loss of righting reflex was extended to 13.69 ± 2.75 min [2.29 times control (5.97 ± 2.83 min)], indicating that PSPAs may have potential prevention effect on alcoholic intoxication. Besides, in middle- and high-dose PSPA groups, the durations of the recovery of the righting reflex were both shortened significantly ($p < 0.05$), indicating that PSPAs may have a potential curative effect on alcoholic intoxication.

Table 2. Effect of PSPAs on the Durations of Ethanol-Induced Loss and Recovery of Righting Reflex[a]

treatment group	duration of loss of righting reflex (min)	duration of recovery of righting reflex (min)
control	5.97 ± 2.83	445.55 ± 24.87
low-dose PSPAs	10.22 ± 3.16#	423.51 ± 15.12
middle-dose PSPAs	11.77 ± 2.10#	383.76 ± 13.22#
high-dose PSPAs	13.69 ± 2.75##	382.73 ± 18.08#

[a]Values are the mean ± standard deviation of 10 determinations. Compared with control #, $p < 0.05$; ##, $p < 0.01$.

Growth and Liver Index of C57BL/6 Mice. The liver index can partly reflect the level of ALD.[24] Table 3a shows the effects of PSPAs on original body weight, final body weight, liver weight, and liver index of mice in the acute ALD experiment. No significant difference was found for the changes of body weight between different treatment groups, and no significant difference was found for the final body weight between the different treatment groups, either. Compared with control, acute alcohol intake resulted in a significant increase of liver weight (1.27 ± 0.12 g) and liver index (5.92 ± 0.17%) ($p < 0.01$), which were 117.59 and 123.08% of control (liver weight and liver index were 1.08 ± 0.10 g and 4.81 ± 0.22%, respectively). Compared with the model, liver weights in the low-, middle-, and high-dose groups were reduced by 3.15, 3.15, and 11.81%, respectively, and the liver indices in the low-, middle-, and high-dose groups were reduced by 6.25, 7.09, and 7.60%, respectively. However, even in the high-dose PSPA group, the liver weight (1.12 ± 0.07 g) and liver index (5.47 ± 0.12%) were still 3.70 and 13.72% higher than those of the control. Our result was in agreement with that reported by McKim et al.,[25] who found that antioxidants such as cocoa flavonoids could reduce acute ALD.

Table 3b shows the effects of PSPAs on original body weight, final body weight, liver weight, and liver index of mice in the subacute ALD experiment. Compared with control, the body weight of mice in the model group (20.82 ± 0.78 g) was reduced significantly by 6.68% ($p < 0.05$). The possible reason was that the metabolism of alcohol changed the digestive function of the stomach and intestine, resulting in changes of food consumption. The liver index can partly reflect the severity of ALD. Compared with control, subacute alcohol intake resulted in a significant increase of liver weight (1.16 ± 0.09 g) and liver index (5.57 ± 0.33%) ($p < 0.01$). Compared with model, liver weights in the middle- and high-dose PSPA groups were reduced significantly ($p < 0.01$) by 2.59 and 4.31%, respectively, and the liver indices in the middle- and high-dose PSPA groups were reduced significantly ($p < 0.01$) by 9.87 and 11.13%, respectively. Particularly, no significant difference was found between the liver index of the high-dose PSPA group and that of control.

Serum ALT, AST, and LDH Activities. The change of serum biochemical indices is an important symbol of liver damage. Serum transaminases (i.e., ALT and AST) are essential catalysts in human metabolic process. Increasing ALT is a mark of liver cell membrane damage, and increasing AST is a mark of liver cell mitochondria damage. When damages such as inflammation and necrosis happen to liver cells, ALT and AST are released into the blood, causing an increase of serum transaminase.[26] The effect of PSPAs on the activity of serum ALT and AST of the acute ALD mice is shown in Figure 2a. Compared with control, the activities of ALT and AST in the model group increased significantly ($p < 0.01$), indicating that acute alcoholism caused damages of liver cell membrane and mitochondria. Compared with the model group, the activity of ALT in low-, middle-, and high-dose groups of PSPAs decreased by 47.28, 35.15, and 45.04%, respectively, and the activity of AST decreased by 17.67, 28.39, and 30.21%, respectively, indicating that PSPAs had a preventive effect on acute ALD. Our result was similar to the effect of genistein on ALD.[27] Figure 2c shows the effect of PSPAs on the activity of serum ALT and AST of the subacute ALD mice. Compared with control, the activity of AST in the model group increased, but not

Table 3. Effect of PSPAs on Body Weight, Liver Weight, and Liver Index of Acute (a) and Subacute (b) ALD Mice[a]

	body wt			
treatment group	initial wt (g)	final wt (g)	liver wt (g)	liver index (%)
		(a) Acute ALD Mice		
control	19.15 ± 0.32	22.41 ± 0.91	1.08 ± 0.10	4.81 ± 0.22
model	18.72 ± 0.37	21.39 ± 0.78	1.27 ± 0.12**	5.92 ± 0.17**
low-dose PSPAs	19.00 ± 0.56	22.11 ± 1.12	1.23 ± 0.17**	5.55 ± 0.14**
middle-dose PSPAs	18.70 ± 0.43	22.35 ± 1.04	1.23 ± 0.08**	5.50 ± 0.19*,#
high-dose PSPAs	18.88 ± 0.46	22.17 ± 1.06	1.12 ± 0.07*	5.47 ± 0.12*,#
		(b) Subacute AL Mice		
control	19.05 ± 0.32	22.31 ± 0.91	1.08 ± 0.10	4.81 ± 0.22
model	18.82 ± 0.37	20.82 ± 0.78*	1.16 ± 0.09**	5.57 ± 0.33**
low-dose PSPAs	19.00 ± 0.56	22.01 ± 1.12	1.15 ± 0.06**	5.23 ± 0.12**
middle-dose PSPAs	18.95 ± 0.43	22.46 ± 1.04	1.13 ± 0.17*,##	5.02 ± 0.68##
high-dose PSPAs	18.88 ± 0.46	22.43 ± 1.06	1.11 ± 0.14*,##	4.95 ± 0.42##

[a]Values are the mean ± standard deviation of 10 determinations. Compared with control: *, $p < 0.05$; **, $p < 0.01$. Compared with model: #, $p < 0.05$; ##, $p < 0.01$.

dx.doi.org/10.1021/jf405032f | J. Agric. Food Chem. 2014, 62, 2364−2373

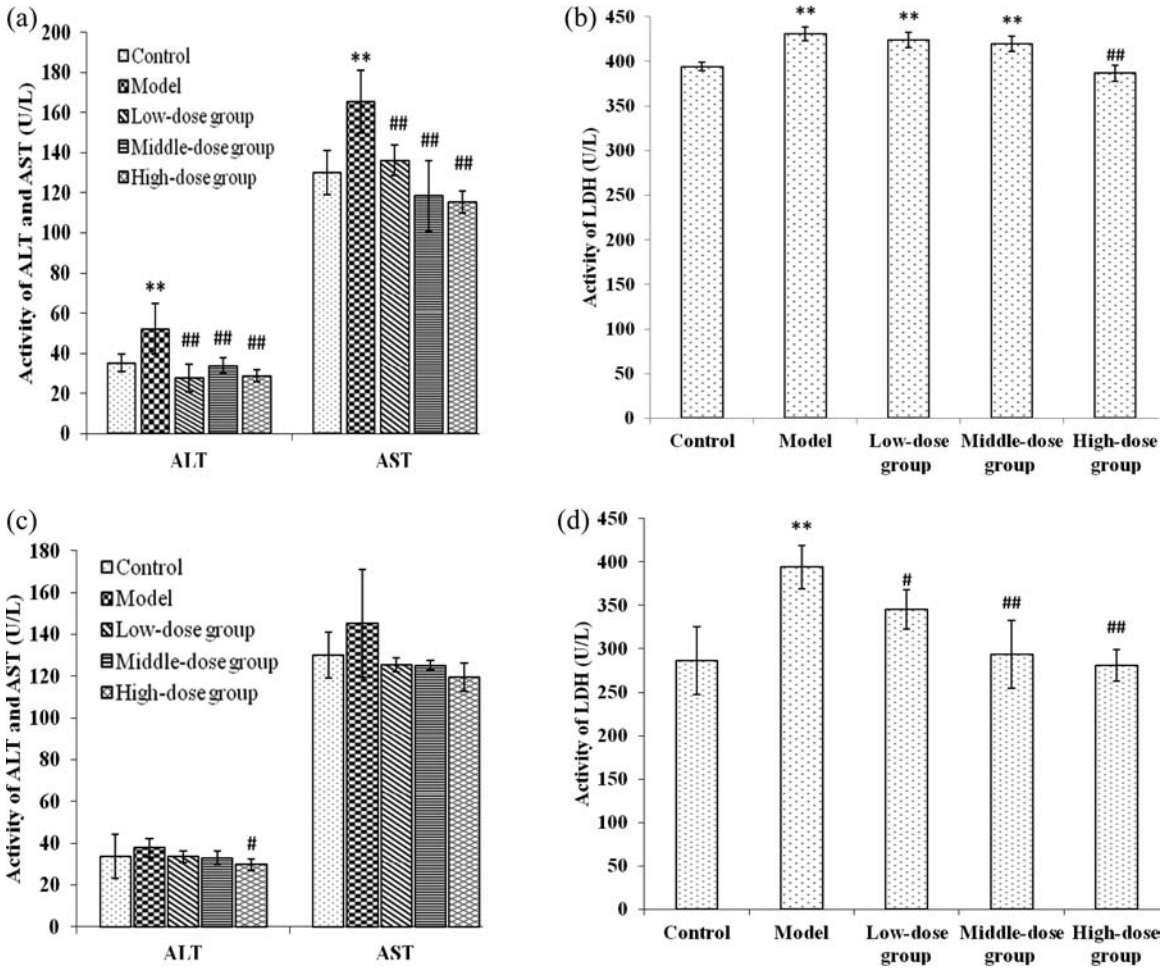

Figure 2. Effect of PSPAs on the activity of serum ALT, AST, and LDH of ALD mice: (a) effect of PSPAs on the activity of serum ALT and AST of acute ALD mice; (b) effect of PSPAs on the activity of serum LDH of acute ALD mice; (c) effect of PSPAs on the activity of serum ALT and AST of subacute ALD mice; (d) effect of PSPAs on the activity of serum LDH of subacute ALD mice. Compared with control: *, $p < 0.05$; **, $p < 0.01$. Compared with model: #, $p < 0.05$; ##, $p < 0.01$.

significantly, indicating that the intake of alcohol had caused slight damage of liver cell membrane and mitochondria. Compared with the model group, the activity of ALT in low-, middle-, and high-dose groups of PSPAs decreased by 11.11, 12.70, and 21.30%, respectively, and the activity of AST decreased by 13.60, 13.94, and 17.73%, respectively, indicating that PSPAs had a preventive effect on subacute ALD.

Besides, under normal circumstances, LDH contained in living cells could not penetrate the cell membrane; when cells were affected by outside poisonous substances, the cell membrane would be damaged, and the permeability of the cell membrane would be changed; thus, the intracellular LDH would be released into extracellular fluid, resulting in the increase of LDH activity.[28] The effect of PSPAs on the activity of serum LDH of the acute ALD mice is shown in Figure 2b. Compared with control, the LDH level of the model group showed a significant increase ($p < 0.01$). Intake of PSPAs in advance could inhibit the increase of LDH, especially in the high-dose group, for which the activity of LDH (386.80 ± 14.94 U/L) was 10.21% lower than that of model (430.80 ± 37.75 U/L), and no significant difference was found between the LDH level of the high-dose PSPAs group and that of control (394.20 ± 24.94 U/L) ($p > 0.05$). The effect of PSPAs on the activity of serum LDH of the subacute ALD mice wis shown in Figure 2d. Compared with control, the LDH level of the model group showed a significant increase ($p < 0.01$), indicating that intake of alcohol caused damage to the cell membrane. Intake of PSPAs in advance could inhibit the activity of LDH, especially in middle- and high-dose groups, as there was no significant difference between the LDH activities of the middle-dose (293.60 ± 39.29 U/L) and high-dose (281.00 ± 18.51 U/L) groups and that of control (286.40 ± 38.88 U/L) ($p > 0.05$). Our result was in agreement with that reported by Tang et al.,[29] who studied the effect of quercetin on ALD and found that quercetin could alleviate the release of liver-specific aminotransferases induced by ethanol. The possible reason is that anthocyanins and quercetin are both flavonoids, which possess strong antioxidant activity (Supporting Information Figure 2), and one of the mechanisms of alleviating ALD is inhibiting the increase of oxidative stress.

Serum TG, TCH, and LDL-C Levels. At the primary phase of alcoholic liver disease, TG and TCH will accumulate massively, which is a sensitive indicator of reflecting lipometabolism. LDL-C is endogenous TG, and excessive intake of alcohol will cause the increase of synthesis of LDL-C. The effect of PSPAs on serum TCH, TG, and LDL-C levels of acute ALD mice is shown in Figure 3a,b. Compared with control, the levels of TCH and TG in the model group increased by 4.39 and 12.96%, respectively. Compared with the model group, the levels of serum TCH in low-, middle-, and high-dose anthocyanin groups decreased by 11.34, 13.03, and 20.59%, respectively, and the levels of serum

dx.doi.org/10.1021/jf405032f | J. Agric. Food Chem. 2014, 62, 2364−2373

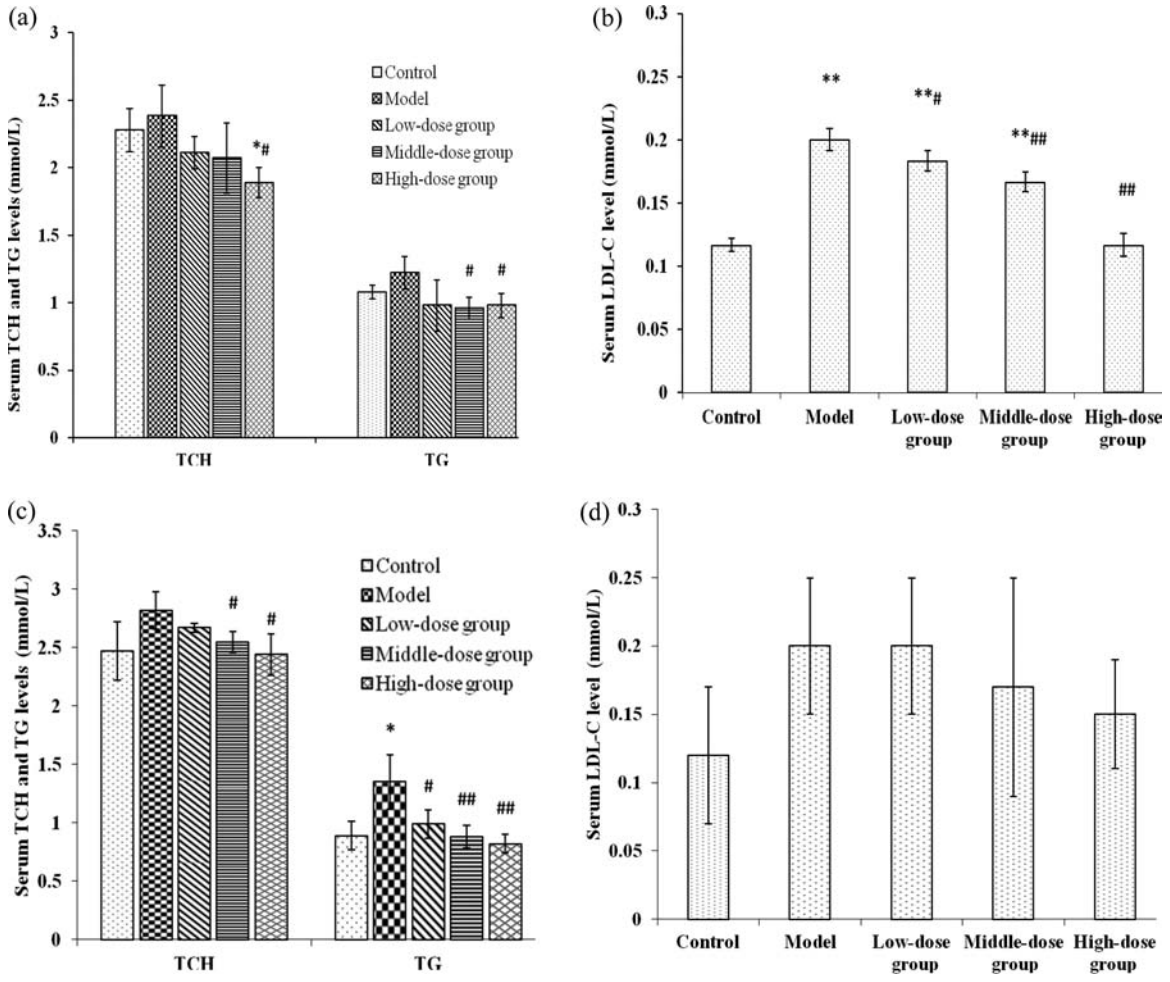

Figure 3. Effect of PSPAs on the serum TCH, TG, and LDL-C levels of ALD mice: (a) effect of PSPAs on serum TCH and TG levels of acute ALD mice; (b) effect of PSPAs on serum LDL-C level of acute ALD mice; (c) effect of PSPAs on serum TG and TCH levels of subacute ALD mice; (d) effect of PSPAs on serum LDL-C level of subacute ALD mice. Compared with control: *, $p < 0.05$; **, $p < 0.01$. Compared with model: #,$p < 0.05$; ##, $p < 0.01$.

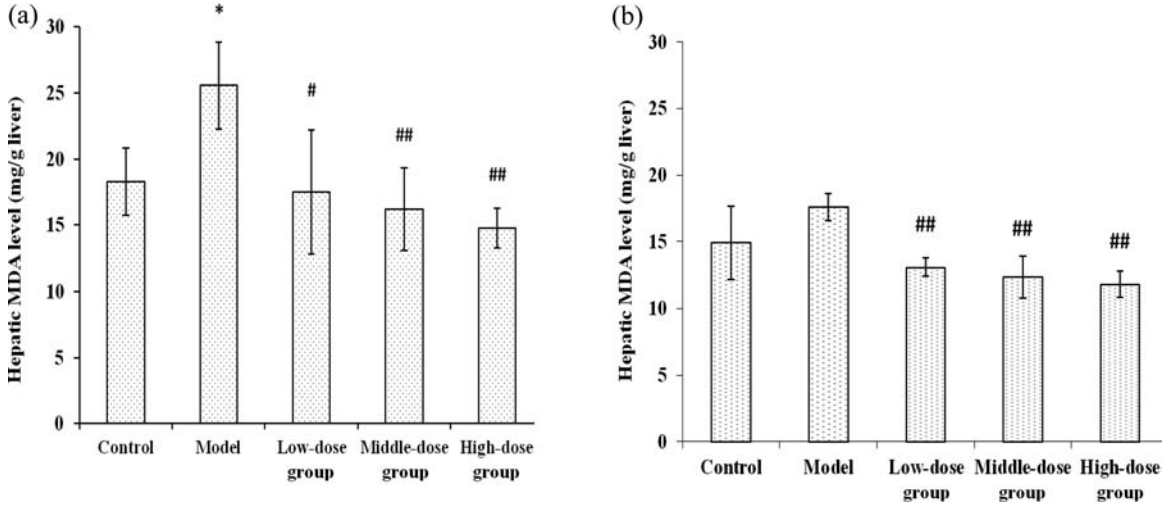

Figure 4. Effect of PSPAs on the hepatic MDA level of the ALD mice: (a) effect of PSPAs on hepatic MDA level of acute ALD mice; (b) effect of PSPAs on hepatic MDA level of subacute ALD mice. Compared with control: *, $p < 0.05$; **, $p < 0.01$. Compared with model: #, $p < 0.05$; ##, $p < 0.01$.

TG in low-, middle-, and high-dose PSPA groups decreased by 19.67, 21.31, and 19.67%, respectively. Moreover, the level of TCH in the high-dose PSPA group was 17.11% lower than control ($p < 0.05$), and no significant difference was found between the levels of TG in all PSPA groups and control. These results indicate that intake of PSPAs can alleviate alcohol-induced accumulation of TCH and TG. Our results were in accordance with those reported by Zhang et al.,[6] who found

dx.doi.org/10.1021/jf405032f | J. Agric. Food Chem. 2014, 62, 2364−2373

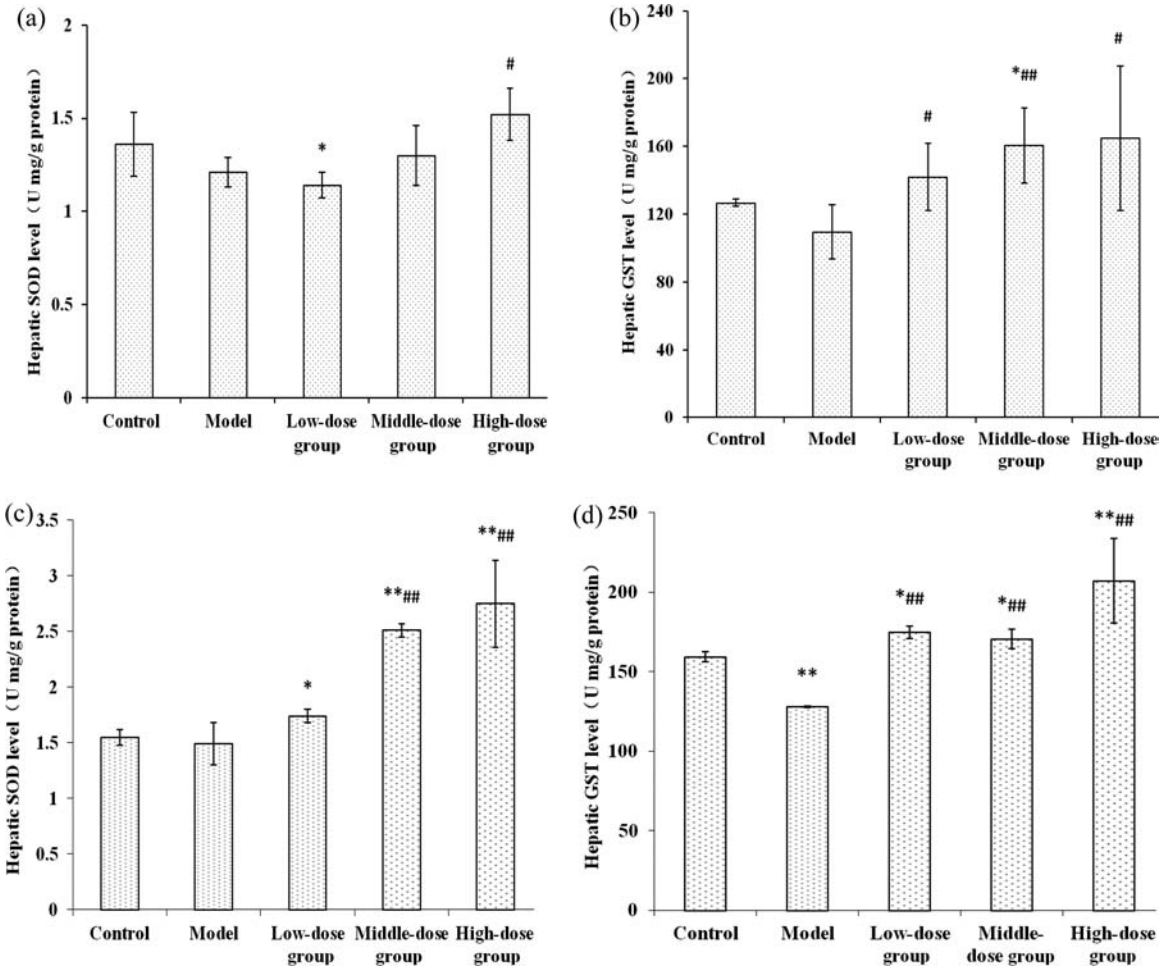

Figure 5. Effect of PSPAs on the hepatic SOD and GST levels of the ALD mice: (a) effect of PSPAs on hepatic SOD level of acute ALD mice; (b) effect of PSPAs on hepatic GST level of acute ALD mice; (c) effect of PSPAs on hepatic SOD level of the subacute ALD mice; (d) effect of PSPAs on hepatic GST level of subacute ALD mice. Compared with control: *, $p < 0.05$; **, $p < 0.01$. Compared with model: #, $p < 0.05$; ##, $p < 0.01$.

ostruthin could inhibit the increase of TCH, TG, and LDL-C induced by alcohol and alleviate acute alcohol intoxication and hepatic lipid metabolism. The possible reason was that anthocyanins and ostruthin both belong to flavonoids and possess strong antioxidant activity (Supporting Information Figure 2).

Studies showed that long-term intake of alcohol would increase the NADH/NAD^+ ratio, up-regulate lipogenesis, and down-regulate transport capacity of fatty acid, causing hepatitis.[30] Therefore, chronic intake of alcohol is often accompanied by the increase of blood lipids, but antioxidants can reduce this trend. Taurine[31] and fermented barley[32] could reduce the increase of blood lipids induced by ALD significantly because of their antioxidant activity. Our result was similar to reported results. Subacute intake of alcohol increased the levels of serum TCH and TG by 14.17 and 51.69%, respectively. Compared with the model, the levels of serum TCH in low-, middle-, and high-dose PSPA groups were decreased by 5.32, 9.57, and 13.48%, respectively, and the levels of serum TG in low-, middle-, and high-dose PSPA groups were decreased by 26.67, 34.81, and 39.26%, respectively. Furthermore, there was no significant difference between the serum TCH and TG levels of low-, middle-, high-dose PSPA groups and control (Figure 3c,d).

Hepatic MDA Level. After a lot of alcohol intake in a brief period, alcohol is metabolized in the liver, producing some aldehyde compounds, which can combine with protein, release a large amount of reactive oxide species (ROS), and increase internal oxidative stress level and lipid peroxidation. MDA is the main product of lipid peroxidation induced by ROS, and the content of MDA can reflex the oxidative stress level of liver.[33]

Figure 4a shows the effect of PSPAs on the hepatic MDA level of the acute ALD mice. Compared with control, MDA in the model group increased significantly ($p < 0.05$) by 39.69%, indicating that alcohol intake increased the oxidative stress level of liver. Compared with the model group, MDA levels in low-, middle-, and high-dose PSPA groups decreased significantly ($p < 0.05$) by 31.55, 36.56, and 42.31%, respectively, and no significant difference was found between all PSPA groups and control. The possible reason is that PSPAs possess strong antioxidant activity. Our result was similar to the result of Bharrhan et al.,[34] who found that catechin could decrease MDA in alcohol-induced damaged liver of rats.

Figure 4b shows the effect of PSPAs on the hepatic MDA of the subacute ALD mice. Compared with control, MDA in the model group increased by 17.97%. Pretreated by PSPAs, lipid peroxidation of mice was inhibited significantly, and thus MDA was decreased significantly ($p < 0.01$) by 25.47, 29.73, and 32.75% for low-, middle-, and high-dose PSPA groups,

dx.doi.org/10.1021/jf405032f | J. Agric. Food Chem. 2014, 62, 2364−2373

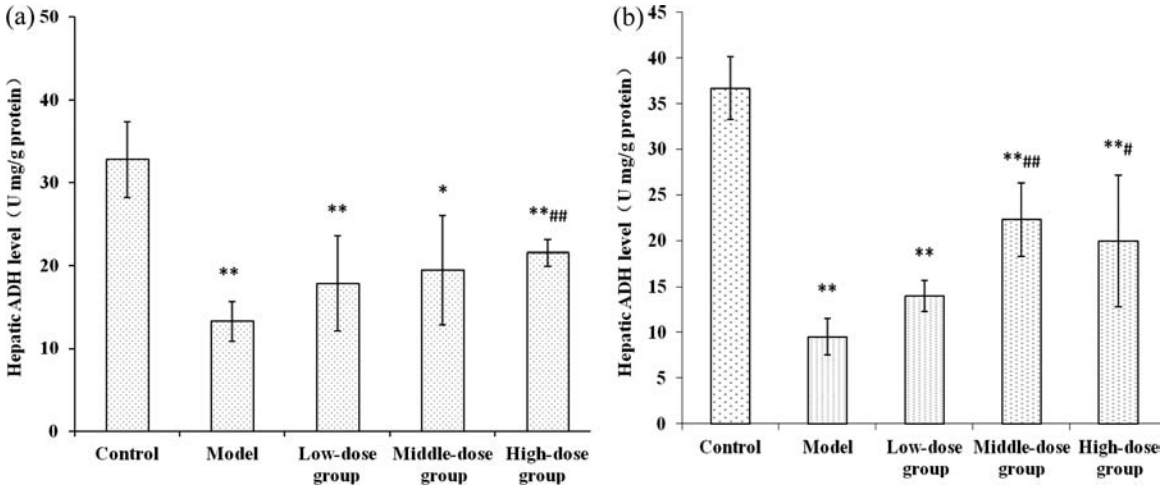

Figure 6. Effect of PSPAs on the hepatic ADH level of the ALD mice: (a) effect of PSPAs on hepatic ADH level of acute ALD mice; (b) effect of PSPAs on hepatic ADH level of the subacute ALD mice. Compared with control: *, $p < 0.05$; **, $p < 0.01$. Compared with model: #, $p < 0.05$; ##, $p < 0.01$.

Table 4. Effect of PSPAs on the Histopathology of Acute (a) and Subacute (b) ALD Mice[a]

treatment group	parallel 1	parallel 2	parallel 3
(a) Acute ALD Mice			
control	–	–	–
model	hepatocyte edema +++	hepatocyte edema ++	hepatocyte edema +++
low-dose PSPAs	hepatocyte edema ++	hepatocyte edema +	hepatocyte edema ++
middle-dose PSPAs	hepatocyte edema +	–	–
high-dose PSPAs	–	–	–
(b) Subacute ALD Mice			
control	–	–	–
model	hepatocyte edema +++	hepatocyte edema ++++	hepatocyte edema +++
low-dose PSPAs	hepatocyte edema ++	hepatocyte edema +	hepatocyte edema ++
middle-dose PSPAs	hepatocyte edema +	–	–
high-dose PSPAs	hepatocyte edema +	–	–

[a]"–" indicates no lesion; "+", minor lesion; "++", mild lesion; "+++", moderate lesion; "++++", severe lesion.

respectively. Particularly, the MDA level in the high-dose PSPA group was 20.66% lower than that in control. This can be attributed at least partly to the capacity of eliminating active oxygen radicals of anthocyanins. Our result is in agreement with the findings of You et al.[35] and López et al.,[36] who found that the antioxidants in taraxacum and amaranth had some preventive effects on ALD.

Hepatic SOD and GST Levels. In recent years, people are paying more attention to the effect of oxidative stress and lipid peroxidation on ALD. Alcohol can produce a large amount of radicals during its metabolism in the liver, for example, O_2^-, H_2O_2, and OH^-. When the radicals go beyond the elimination ability of human body, liver cells will be damaged.[37] GST and SOD are important internal antioxidases, which can alleviate oxidative stress caused by alcohol. Some studies have already showed that intake of antioxidants such as vitamin E and vitamin C in advance could alleviate alcohol-induced liver damage.[38]

The effect of PSPAs on the hepatic SOD level of the acute ALD mice is shown in Figure 5a. SOD activity in the model group (1.21 ± 0.08 U mg/g protein) was 11.03% lower than that in control, indicating that the elimination ability of mice on O_2^- was weakened by alcohol intake. Compared with the model, SOD activity in the high-dose PSPA group was increased significantly ($p < 0.05$) by 25.62% and was even 11.76% higher than normal level (control, 1.36 ± 0.17 U mg/g protein); thus, the ability to eliminate O_2^- was also improved, and the liver damage was alleviated.

Intake of alcohol will increase the internal oxidation products, and GST can eliminate oxygen free radicals effectively, prevent oxidative stress, and inhibit lipid peroxidation. Acetaldehyde is an alcohol metabolite, which can combine with GST, resulting in changes of membrane permeability and fluidity; thus, the structure and function of cells are damaged. Moreover, when the structure and function of cells are damaged, free radicals will not be eliminated; thus, liver damage will be aggravated. At present, the decrease of GST content is considered to be one of the mechanisms of ALD. Figure 5b shows the effect of PSPAs on the hepatic GST level of the acute ALD mice. Compared with control, the GST level in the model group decreased by 13.67%, indicating that the liver cell membrane was damaged. The GST content in anthocyanin groups was increased significantly in a dose-dependent relationship, and the GST contents in low-, middle-, and high-dose PSPAs groups were even 11.89, 26.62, and 30.08% higher than that in control, indicating that PSPAs could alleviate alcohol-induced oxidative stress, thus alleviating alcohol-induced liver damage. Our result is in agreement with that reported by Tang et al.,[29] who found that taurine could decrease alcohol-induced dyslipidemia and oxidative damage.

The effects of PSPAs on hepatic SOD and GST levels of the subacute ALD mice are shown in Figure 5c,d. Compared with control, the SOD and GST levels in the model group decreased.

dx.doi.org/10.1021/jf405032f | J. Agric. Food Chem. 2014, 62, 2364−2373

Intake of PSPAs in advance increased the SOD and GST activityies significantly ($p < 0.01$) to normal levels, and the SOD and GST levels in the high-dose group were 77.42 and 29.94% higher than those in the control group.

Hepatic ADH Level. ADH is a metalloenzyme existing in liver cell cytoplasm and mitochondria, which can transform ethanol into acetaldehyde and then oxidize acetaldehyde into acetic acid. In mitochondria, some acetic acid can enter into the tricarboxylic acid cycle and be oxidized into CO_2 and H_2O, which are removed from the body.[39] The effect of PSPAs on the hepatic ADH level of the acute ALD mice is shown in Figure 6a. Compared with control, the ADH level of the model group decreased significantly ($p < 0.01$) by 59.56%, indicating that a large amount of alcohol could not be metabolized into CO_2 and H_2O, causing hepatotoxicity easily. Compared with the model group, ADH activities in low-, middle-, and high-dose PSPA groups were increased by 34.31, 46.76, and 62.14%, respectively. However, the ADH activity in the high-dose PSPA group was still 34.43% lower than in the control group.

The effect of PSPAs on the hepatic ADH level of the subacute ALD mice is shown in Figure 6b. Compared with control, ADH activity in the model group decreased significantly ($p < 0.01$). Compared with the model group, ADH activity of anthocyanin groups increased significantly ($p < 0.05$). However, ADH activity of high-dose PSPA group was still 45.59% lower than that of the control group.

Histopathological Analysis. Table 4a and supplement Figure 3 showed the effect of PSPAs on the histopathology of the acute ALD mice. The liver cells of C57BL/6J mice in control group had complete structure, similar size, tight arrangement, uniform staining, and no liver pathological changes. In model group, the mice liver cells showed pathological changes, e.g. loose arrangement and cellular edema. In anthocyanins low-dose group, the pathological changes of mice liver cells were similar to that in model group, e.g. disordered arrangement of cells and cellular edema, but the degree thereof was reduced. In anthocyanins middle and high-dose groups, no pathological changes was observed, and the cellular morphology thereof was close to that of control group.

The effect of PSPAs on the histopathology of subacute ALD mice is shown in Table 4b and Supporting Information Figure 3f–i. Compared with control, pathological changes such as liver cell swelling and fatty degeneration happened to mouse liver in the model group, which included mice that were treated with alcohol continuously. After the intake of PSPAs, liver cell swelling was alleviated significantly, and the improving pathological effect showed a dose-dependent relationship. Liver tissue morphology after high-dose anthocyanin treatment was similar to that after normal treatment.

■ ASSOCIATED CONTENT

Supporting Information

Additional experimental details. This material is available free of charge via the Internet at http://pubs.acs.org.

■ AUTHOR INFORMATION

Corresponding Author

*(T.M.) Phone: (+86) 10 62815541. Fax: (+86) 10 62815541 E-mail: mutaihua@126.com.

Funding

This research was supported by Earmarked Fund for the China Agriculture Research System (CARS-11-B-19), Fundamental Research Funds for Incremental Project Budget of Chinese Academy of Agricultural Sciences (No. 2013ZL014), Crop Nutrition and Processing Characteristics Research Project of Chinese Academy of Agricultural Sciences, and Support Plan of National Science and Technology–the Suitability Evaluation and Special Varieties Screening of Sweet Potato (2012BAD29B03-03).

Notes

The authors declare no competing financial interest.

■ ACKNOWLEDGMENTS

We thank Songshu Zhang of the Academy of Agricultural and Forestry Sciences in Hebei Province for providing purple sweet potato samples for our research.

■ ABBREVIATIONS USED

ADH, alcohol dehydrogenase; ALD, alcoholic liver damage; ALT, alanine aminotransferase; AST, aspartate aminotransferase; GST, glutathione *S*-transferase; LDH, lactate dehydrogenase; LDL-C, low-density lipoprotein cholesterol; MDA, malondialdehyde; PSPAs, purple sweet potato anthocyanins; TCH, total cholesterol; TG, triglyceride

■ REFERENCES

(1) Valko, M.; Leibfritz, D.; Moncol, J.; Cronin, M. T. D.; Mazur, M.; Telser, J. Free radicals and antioxidants in normal physiological functions and human disease. *Int. J. Biochem. Cell Biol.* **2007**, *39*, 44–84.

(2) Cuevas-Rodríguez, E. O.; Dia, V. P.; Yousef, G. G.; García-Saucedo, P. A.; López-Medina, J.; Paredes-López, O.; Mejia, E. G.; Lila, M. A. Inhibition of pro-inflammatory responses and antioxidant capacity of Mexican blackberry (*Rubus* spp.) extracts. *J. Agric. Food Chem.* **2010**, *58*, 9542–9548.

(3) Nanji, A. A.; Griniuviene, B.; Hossein Sadrzadeh, S. M.; Levitsky, S.; McCully, J. D. Effect of type of dietary fat and ethanol on antioxidant enzyme mRNA induction in rat liver. *J. Lipid Res.* **1995**, *36*, 736–744.

(4) Tuma, D. J.; Sorrell, M. Alcohol and alcoholic liver disease. *Semin. Liver Dis.* **2004**, *24* (3), 215.

(5) Galligan, J. J.; Smathers, R. L.; Shearn, C. T.; Fritz, K. S.; Backos, D. S.; Jiang, H.; Franklin, C. C.; Orlicky, D. J.; MacLean, K. N.; Petersen, D. R. Oxidative stress and the ER stress response in a murine model for early-stage alcoholic liver disease. *J. Toxicol.* **2012**, 1–12.

(6) Zhang, J. J.; Xue, J.; Wang, H. B.; Zhang, Y.; Xie, M. L. Osthole improves alcohol-induced fatty liver in mice by reduction of hepatic oxidative stress. *Phytother. Res.* **2011**, *25*, 638–643.

(7) Dey, A.; Cederbaum, A. I. Alcohol and oxidative liver injury. *Hepatology* **2006**, *43* (S1), S63–S74.

(8) Lengyel, G.; Tulassay, Z. Antioxidant therapy in chronic liver diseases. *Orv. Hetil.* **2006**, *147* (24), 1113–1118.

(9) Castañeda-Ovando, A.; Pacheco-Hernández, M. L.; Páez-Hernández, M. E.; Rodríguez, J. A.; Galán-Vidal, C. A. Chemical studies of anthocyanins: a review. *Food Chem.* **2009**, *113*, 859–871.

(10) Prior, R. L.; Wu, X. Anthocyanins: structural characteristics that result in unique metabolic patterns and biological activities. *Free Radical Res.* **2006**, *40* (10), 1014–1028.

(11) Hwang, Y. P.; Choi, J. H.; Yun, H. J.; Han, E. H.; Kim, H. G.; Kim, J. Y.; Park, B. H.; Khanal, T.; Choi, J. M.; Chung, Y. C.; Jeong, H. G. Anthocyanins from purple sweet potato attenuate dimethylnitrosamine-induced liver injury in rats by inducing Nrf2-mediated antioxidant enzymes and reducing COX-2 and iNOS expression. *Food Chem. Toxicol.* **2011**, *49*, 93–99.

(12) Zhang, Z. F.; Fan, S. H.; Zheng, Y. L.; Lu, J.; Wu, D. M.; Shan, Q.; Hu, B. Purple sweet potato color attenuates oxidative stress and inflammatory response induced by D-galactose in mouse liver. *Food Chem. Toxicol.* **2009**, *47*, 496–501.

(13) Shindo, M.; Kasai, T.; Abe, A.; Kondo, Y. Effects of dietary administration of plant-derived anthocyanin-rich colors to spontaneously hypertensive rats. *J. Nutr. Sci. Vitaminol.* **2007**, *53*, 90−93.
(14) Lu, J.; Wu, D. M.; Zheng, Y. L.; Hu, B.; Cheng, W.; Zhang, Z. F. Purple sweet potato color attenuates domoic acid-induced cognitive deficits by promoting estrogen receptor-α-mediated mitochondrial biogenesis signaling in mice. *Free Radical Biol. Med.* **2012**, *52*, 646−659.
(15) Park, K. H.; Kim, J. R.; Lee, J. S.; Lee, H.; Cho, K. H. Ethanol and water extract of purple sweet potato exhibits anti-atherosclerotic activity and inhibits protein glycation. *J. Med. Food* **2010**, *13* (1), 91−98.
(16) Hwang, Y. P.; Choi, J. H.; Choi, J. M.; Chung, Y. C.; Jeong, H. G. Protective mechanisms of anthocyanins from purple sweet potato against *tert*-butyl hydroperoxide-induced hepatotoxicity. *Food Chem. Toxicol.* **2011**, *49*, 2081−2089.
(17) Choi, J. H.; Choi, C. Y.; Lee, K. J.; Hwang, Y. P.; Chung, Y. C.; Jeong, H. G. Hepatoprotective effects of an anthocyanin fraction from purple-fleshed sweet potato against acetaminophen-induced liver damage in mice. *J. Med. Food* **2009**, *12* (2), 320−326.
(18) Choi, J. H.; Hwang, Y. P.; Choi, C. Y.; Chung, Y. C.; Jeong, H. G. Anti-fibrotic effects of the anthocyanins isolated from the purple-fleshed sweet potato on hepatic fibrosis induced by dimethylnitrosamine administration in mice. *Food Chem. Toxicol.* **2010**, *48*, 3137−3143.
(19) Liu, X. L.; Mu, T. H.; Sun, H. N.; Zhang, M.; Chen, J. W. Optimisation of aqueous two-phase extraction of anthocyanins from purple sweet potatoes by response surface methodology. *Food Chem.* **2013**, *141* (3), 3034−3041.
(20) Hosseinian, F. S.; Li, W. D.; Beta, T. Measurement of anthocyanins and other phytochemicals in purple wheat. *Food Chem.* **2008**, *109* (4), 916−924.
(21) Grant, D. C.; Helleur, R. J. Rapid screening of anthocyanins in berry samples by surfactant-mediated matrix-assisted laser desorption/ionization time-of-flight mass spectrometry. *Rapid Commun Mass Spectrom.* **2008**, *22* (2), 156−164.
(22) Kim, H. W.; Kim, J. B.; Cho, S. M.; Chung, M. N.; Lee, Y. M.; Chu, S. M.; Che, J. H.; Kim, S. N.; Kim, S. Y.; Cho, Y. S.; Kim, J. H.; Park, H. J.; Lee, D. J. Anthocyanin changes in the Korean purple-fleshed sweet potato, Shinzami, as affected by steaming and baking. *Food Chem.* **2012**, *130*, 966−972.
(23) Khisti, R. T.; VanDoren, M. J.; O'Buckley, T.; Morrow, A. L. Neuroactive steroid 3α-hydroxy-5α-pregnan-20-one modulates ethanol-induced loss of righting reflex in rats. *Brain Res.* **2003**, *980* (2), 255−265.
(24) Xiang, J. L.; Zhu, W. X.; Li, Z. X.; Ling, S. B. Effect of juice and fermented vinegar from *Hovenia dulcis* peduncles on chronically alcohol-induced liver damage in mice. *Food Funct.* **2012**, *3*, 628−634.
(25) McKim, S. E.; Konno, A.; Gäbele, E.; Uesugi, T.; Froh, M.; Sies, H.; Thurman, R. G.; Arteel, G. E. Cocoa extract protects against early alcohol-induced liver injury in the rat. *Arch. Biochem. Biophys.* **2002**, *406* (1), 40−46.
(26) Rajesh, M. G.; Latha, M. S. Protective activity of *Glycyrrhiza glabra* Linn. on carbon tetrachloride-induced peroxidative damage. *Indian J. Pharmacol.* **2004**, *36* (5), 284−287.
(27) Huang, Q. F.; Huang, R. B.; Zhang, S. J.; Lin, J.; Wei, L.; He, M.; Zhuo, L.; Lin, X. Protective effect of genistein isolated from *Hydrocotyle sibthorpioides* on hepatic injury and fibrosis induced by chronic alcohol in mice. *Toxicol. Lett.* **2013**, *217* (2), 102−110.
(28) Mathew, S.; Menon, P. V.; Kurup, P. A. Effect of administration of vitamin A, ascorbic acid and nicotinamide adenine dinucleotide + flavin adenine dinucleotide on severity of myocardial infarction induced by isoproterenol in rats. *Indian J. Exp. Biol.* **1985**, *23* (9), 500−504.
(29) Tang, Y. H.; Gao, C.; Xing, M. Y.; Li, Y. Y.; Zhu, L. P.; Wang, D.; Yang, X. F.; Liu, L. G.; Yao, P. Quercetin prevents ethanol-induced dyslipidemia and mitochondrial oxidative damage. *Food Chem. Toxicol.* **2012**, *50* (5), 1194−1200.
(30) Sozio, M.; Crabb, D. W. Alcohol and lipid metabolism. *Am. J. Physiol: Endocrinol. Metab.* **2008**, *295*, E10−E16.
(31) Fang, Y. J.; Chiu, C. H.; Chang, Y. Y.; Chou, C. H.; Lin, H. W.; Chen, M. F.; Chen, Y. C. Taurine ameliorates alcoholic steatohepatitis via enhancing self-antioxidant capacity and alcohol metabolism. *Food Res. Int.* **2011**, *44*, 3105−3110.
(32) Giriwono, P. E.; Hashimoto, T.; Ohsaki, Y.; Shirakawa, H.; Hokazono, H.; Komai, M.. Extract of fermented barley attenuates chronic alcohol induced liver damage by increasing antioxidative activities. *Food Res. Int.* **2010**, *43*, 118−124.
(33) Wu, D. F.; Cederbaum, A. I. Oxidative stress and alcoholic liver disease. *Semin. Liver Dis.* **2009**, *29* (2), 141−154.
(34) Bharrhan, S.; Koul, A.; Chopra, K.; Rishi, P. Catechin suppresses an array of signalling molecules and modulates alcohol-induced endotoxin mediated liver injury in a rat model. *PLoS ONE* **2011**, *6* (6), 1−9.
(35) You, Y.; Yoo, S.; Yoon, H. G.; Park, J.; Lee, Y. H.; Kim, S.; Oh, K. T.; Lee, J.; Cho, H. Y.; Jun, W. *In vitro* and *in vivo* hepatoprotective effects of the aqueous extract from *Taraxacum officinale* (dandelion) root against alcohol-induced oxidative stress. *Food Chem. Toxicol.* **2010**, *48*, 1632−1637.
(36) López, V. R. L.; Razzeto, G. S.; Giménez, M. S.; Escudero, N. L. Antioxidant properties of *Amaranthus hypochondriacus* seeds and their effect on the liver of alcohol-treated mice. *Plant Foods Hum. Nutr.* **2011**, *66* (2), 157−162.
(37) Huang, M. C.; Chen, C. C.; Peng, F. C.; Tang, S. H.; Chen, C. H. The correlation between early alcohol withdrawal severity and oxidative stress in patients with alcohol dependence. *Prog. Neuro-Psychoph.* **2009**, *33* (1), 66−69.
(38) McDonough, K. H. Antioxidant nutrients and alcohol. *Toxicology* **2003**, *189* (1−2), 89−97.
(39) Oyama, T.; Isse, T.; Kagawa, N.; Kinaga, T.; Kim, Y. D.; Morita, M.; Sugio, K.; Weiner, H.; Yasumoto, K.; Kawamoto, T. Tissue-distribution of aldehyde dehydrogenase 2 and effects of the ALDH2 gene-disruption on the expression of enzymes involved in alcohol metabolism. *Front. Biosci.* **2005**, *10*, 951−960.

Noni (*Morinda citrifolia*) is native to lands from Southeast Asia to Australia and is also cultivated in Polynesia, India, the Caribbean, South America, and southern Taiwan.[16]

Noni can inhibit various pathogens, such as *Staphylococcus aureus*, *Pseudomonas aeruginosa*, *Proteus morgaii*, *Bacillus subtilis*, *Escherichia coli*, and different strains of *Salmonella* and *Shigella*.[17,18] Noni juice also provides an anti-inflammatory effect to relieve locally acute inflammation and selectively inhibits COX-1 and COX-2 expression.[16,19] A previous study has shown that noni fruit contains abundant polyphenols and alkaloids.[16]

Noni exhibits various biological activities, but its effect on *H. pylori* are still unknown. This study determines the effect of noni fruit extracts on the adhesion of *H. pylori* and *H. pylori*-induced inflammation.

MATERIALS AND METHODS

Preparation of Ethanol and Ethyl Acetate Extracts. One hundred grams of noni fruit powder was extracted with 1 L of 95% ethanol or 99% ethyl acetate for 24 h at room temperature. The residues were removed by filtration, and the extracts were evaporated to dryness, under vacuum, at 37 °C. The dried extracts were transferred into airtight amber bottles and stored at −80 °C. The phenolic compounds of both extracts were measured using high-performance liquid chromatography (HPLC).

HPLC Analysis of Phenolic Compounds Present in Noni Fruit Extracts. The phenolic compounds were separated using HPLC with a binary gradient intelligent pump (L6200A, Hitachi) and a UV−vis detection system (L4250, Hitachi). A Lichrospher 100 RP-18e (Merck) column (5 μm, 25 cm × 4 mm i.d.) and security guard RP-18e (5 μm, 4 × 4 mm i.d.) were used. The mobile phase consisted of 2.5% (v/v) acetic acid water solution (solvent A) and acetonitrile (solvent B). The gradient program consisted of 3% B, initially, changing to 21% B after 4 min, was maintained at 21% B until 10 min and raised to 22% B after 11 min, was maintained at 22% B until 15 min and raised to 35% B after 16 min, was maintained at 35% B until 35 min and raised to 100% B after 36 min, and was maintained at 100% B until 40 min and then reduced to 3% B after 45 min. The injection volume for all samples was 20 μL. Simultaneous monitoring was performed at 266 nm, and the flow rate was 0.8 mL/min.

Isolation and Culture of *H. pylori*. *H. pylori* was isolated from gastric ulcer patients. The gastric mucus of gastric ulcer patients was collected after executed gastroscopy. The *H. pylori*-positive tissues were detected by a urease rapid test. The gastric mucus (*H. pylori*-contained) was seeded in *H. pylori* selection medium (10 mg/mL vancomycin, 2.5 U/mL polymyxin B, 5 mg/mL trimethoprim, and 2 mg/mL amphotericin B in 22 g/L brucella broth) in an anaerobic pack at 37 °C for 72 h. The activity and purity of the *H. pylori* was determined using morphology, urease, and oxidase test (genotype belong to CagA and urease positive strains). *H. pylori* was stored in 30% glycerin-containing medium at −80 °C.

Cell Line and Culture. Human gastric cancer cell lines (AGS cells, BCRC 60102) were cultured using F12 nutrition mixture medium containing 10% FBS fetal bovine serum and 1% penicillin−streptomycin at 37 °C in a humidified incubator containing 5% CO_2.

Cell Viability Assay. The effect of extracts on cell viability was studied using 3-(4,5-dimethylthiazol-2-yl)-2,5-diphenyltetrazolium bromide (MTT). AGS cells were seeded in a 96-well plate with 200 μL (5×10^5/mL) of cells in each well and left overnight. The cells were treated with various concentrations of noni extracts (200, 400, 600, or 800 μg/mL) or *H. pylori* and 0.05 mg/mL amoxicillin at 37 °C for 24 h. The medium was replaced by fresh medium, containing 0.5 mg/mL MTT, and cultured at 37 °C for 4 h. One hundred microliters of isopropanol was added to each well to dissolve the crystals. The optical density of each sample was read at 630 nm against the blank prepared from the cell-free well.

Bacterial Drug Sensitivity Test. The *H. pylori* suspension (optical density = 0.3 at 600 nm for 1×10^8 CFUs/mL) was treated with various concentrations of noni extracts (0.05, 0.096, 0.189, 0.375, 0.75, 1.25, 2.5, 5, or 10 mg/mL) cultured in an anaerobic pack, at 37 °C for 24 h. One hundred microliters of suspension was detected using ELISA at 600 nm for the minimum inhibitory concentration (MIC) test. One hundred microliters of suspension was mixed with 100 μL of urease reagent (3 mM PBS, pH 5.8; and 2% urea and 7 μg/mL phenol red, pH 5.0) at 37 °C for 4 h, and the minimum bactericidal concentration (MBC) was measured at 560 nm.

Antiadhesion Assay. AGS cells were seeded in a 24-well plate with 5×10^5/mL cells, and 400 μL of medium was added to each well overnight. The *H. pylori* suspension (15 μL) and samples (200, 400, or 600, or 800 μg/mL) were added to each well. After 6 h, nonadherent bacteria were washed off, using PBS. The amount of adherent bacteria was estimated using urease reagent and *H. pylori* antibody−FITC (no. GTX36341, GenTex, USA). The suspension was collected to determine the amount of nonadherent bacteria at 600 nm and to measure the bacterial viability in the urease reagent at 560 nm.

Determination of IL-8 Protein. The level of IL-8 protein from the cell-cultured medium was measured using a commercial enzyme-linked immunosorbent assay kit (no. K0031216, Koma Biotech Inc., Korea).

CagA, iNOS, and COX-2 Protein Expression Assay. AGS cells were seeded in a 10 cm dish with 1×10^5/mL. *H. pylori* suspension was added and cocultured with the extracts for 6 h. All cells were collected and disintegrated by using cell lysis buffer (no. 9803, Cell Signaling, USA). Cell proteins were collected after centrifuged (6708*g*) for 10 min at 4 °C. CagA, iNOS, and COX-2 protein expression were detected by Western blot.[20]

The protein was resolved in 10% SDS−polyacrylamide gels and electroblotted on a polyvinylidene difluoride (PVDF) membrane. The membrane was blocked in 5% fatfree dried milk, dissolved in TBS buffer (25 mM Tris, pH 7.4, 150 mM NaCl, 0.3% Tween-20).

The membrane was soaked with anti-COX-2 polyclonal antibody (ab52237, Abcam, UK), anti-iNOS polyclonal antibody (ab3523, Abcam, UK), or anti-CagA monoclonal antibody (ab90490, Abcam, UK) overnight at 4 °C. The removed antibody and membrane were soaked with an appropriate HRP-conjugated secondary antibody (ab6721, Abcam, UK) for 1 h at room temperature. The reacted bands of the target proteins were revealed by enhanced chemiluminescence, using an enhanced chemiluminescence (ECL) commercial kit (Amersham Pharmacia Biotech, Piscataway, NJ, USA).

Neutrophil Isolation. Whole blood was collected from a human, mixed with 4.5% dextran, and left to subside for 40 min at 37 °C (the ratio of whole blood to 4.5% dextran was about 4:1). An upper layer was obtained, which contained neutrophils and residual red blood cells (RBCs), and this was then mixed with Ficoll hypaque and centrifuged at 400*g* for 10 min at 25 °C. The leukocytes pallet was mixed with Ficoll hypaque (the ratio of pallet to Ficoll hypaque was about 2:1) at 400*g* for 10 min at 25 °C, and the upper layer was removed. RBC lysis buffer was added for 5 min to remove erythrocyte (the ratio of pallet to RBC lysis buffer was about 1:4). After centrifuging at 250*g* for 10 min at 25 °C, the cell residue was mixed with RPMI medium (containing 15% FBS) and cultured at 37 °C for 24 h. Cell viability and morphology were determined by MTT and Giemsa stain (no. 32884, Sigma, Germany).[21]

Neutrophil Chemotaxis Assay. Neutrophil chemotaxis was determined by two-chamber techniques. Thirty microliters of supernatant of *H. pylori* cocultured with AGS cells or various concentrations of extracts were poured into the lower layer. The IL-8 protein (1000 pg/mL) was used as a positive control. Fifty microliters of neutrophils (2×10^5/mL) was added to the upper layer. A PVP-free membrane was placed between the lower and upper layers and cultured for 1 h at 37 °C. The degree of migration of neutrophil was calculated by Giemsa stain.[22]

Statistical Analysis. All results are presented as the mean ± SD (n = 6). The difference in the results for this study was assessed using a one-way ANOVA of SPSS (version 12.0; SPSS Inc.). A significant difference is identified for $p < 0.05$.

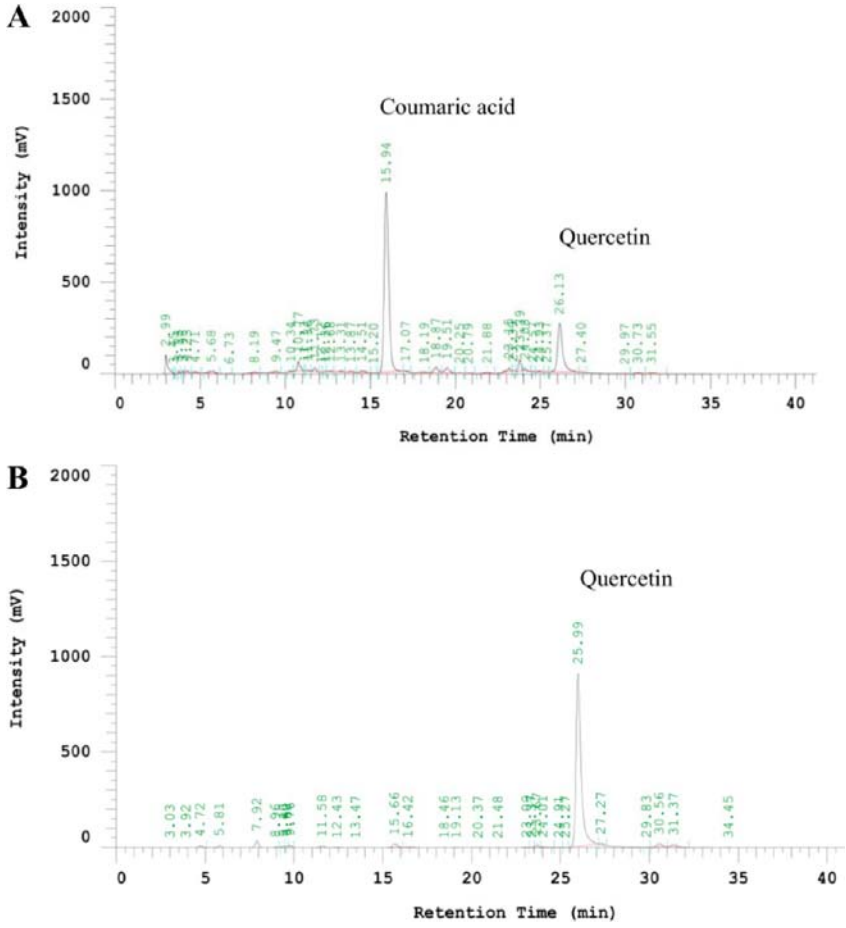

Figure 1. HPLC profiles of phenolic compounds present in ethanol (A) and ethyl acetate (B) extracts of noni fruit.

RESULTS AND DISCUSSION

Phenolic Profile of Both Extracts. Phenolics have manifold bioactive effects, such as antibacterial, antiadhesion, and anti-inflammation, in animal or cell models.[23,24] Noni fruit has been found to contain several phenolics and flavonoids.[25]

Ethanol extract contained 48.81 ± 7.06 mg/g total phenolics and 40.91 ± 1.17 mg/g total flavonoids. Ethyl acetate extract contained 68.82 ± 4.62 mg/g total phenolics and 39.38 ± 0.44 mg/g total flavonoids. Ethanol extract contained 2.8 ± 0.02 mg/g and ethyl acetate contained 6.9 ± 0.06 mg/g condensed tannins. The ethyl acetate extract was more abundant in phenolics, flavonoids ,and condensed tannins than the ethanol extract.

The phenolic profiles of ethanol and ethyl acetate extracts were measured by HPLC. Large amounts of coumaric acid and quercetin were found in the ethanol extract (23.8 and 4.4 mg/g extract), whereas the ethyl acetate extract contained abundant quercetin (28 mg/g extract) (Figure 1).

Effect of Noni Fruit Extracts on *H. pylori*. Ethanol and ethyl acetate extracts of noni fruit showed poor inhibition on the density of *H. pylori* at lower doses (0.04−2.5 mg/mL) (Figure 2A). Similar results were also found for bacterial viability (Figure 2B). The ethanol extract had a better MIC (5 mg/mL) than the ethyl acetate extract (10 mg/mL). Both extracts had the same MBC (10 mg/mL), but it was much poorer than that for amoxicillin (0.04 mg/mL). Amoxicillin is widely used to eradicate *H. pylori*; it was deemed a positive control.[26] Noni fruit extracts showed bactericidal activity at high concentrations (Figure 2B). The effects of noni fruit extracts on the growth of *H. pylori* were weak, even though both extracts contained abundant coumaric acid and quercetin (Figure 1).

Actually, *H. pylori* could resist fractional antibiotics, such as macrolides, metronidazole, tetracycline, and quinolones.[27] It is difficult to eradicate *H. pylori* from humans using antibiotics. In this study, a moderate way to prevent the colonization of *H. pylori* was demonstrated.

Antiadhesion of *H. pylori* to Gastric Epithelial Cells. *H. pylori* adhesion clearly influences local inflammation and disease formation. Thus, the adhesion of *H. pylori* on AGS cells was measured after treatment with both extracts. First, the cell viability of noni fruit extracts and appropriate ratio of *H. pylori* to AGS cells were determined. Both extracts had no effect on cell viability (200−800 μg/mL) after 24 h of culture. The appropriate ratio of *H. pylori* to cells was 300:1 (data not shown).

Panels A and B of Figure 3 show the antiadhesion activity of both extracts on *H. pylori*, which appeared to be dependent on concentration. Nonadhering *H. pylori* was detected in the cocultured suspension (Figure 3C,D). The viability of *H. pylori* in the suspension remained unchanged after treatment with both extracts except for amoxicillin (Figure 3E,F).

Noni fruit extracts showed weak inhibition of bactericidal activity on *H. pylori*, but greatly reduced its adhesion to epithelial cells. Adhesion is an important step for the growth, colonization, and transportation of bacteria pathogen-associated molecules to the host cell. The CagA protein is transported to

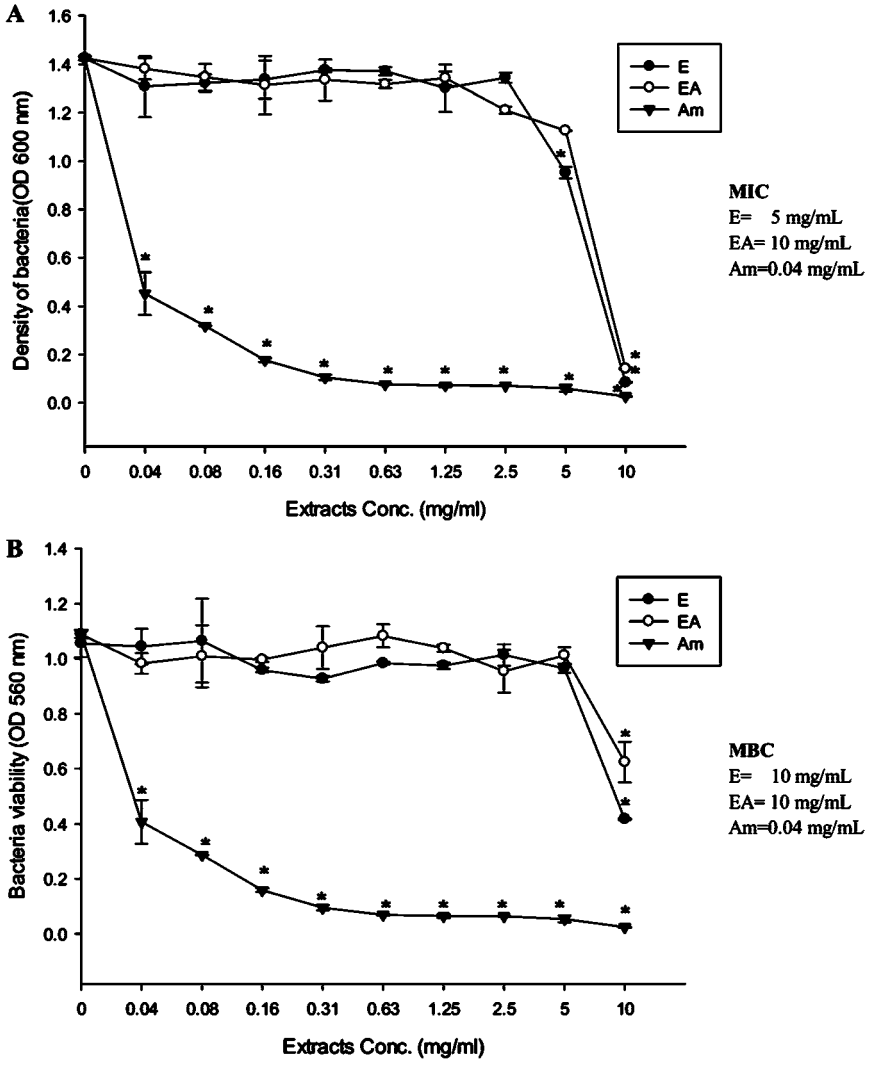

Figure 2. Density (A) and viability (B) of *H. pylori* after noni fruit extract treatment. *H. pylori* was cultured with extracts for 24 h. The MIC and MBC of treatments were measured. (∗) Significantly different as compared with 0 mg/mL. E, ethanol extract; EA, ethyl acetate extract; Am, amoxicillin.

the host cell via a T4SS after *H. pylori* adheres to the gastric epithelial cell.[28] Therefore, the inhibition of the adhesion of *H. pylori* may relieve the inflammation and decrease the risk of gastric diseases.

Inhibition on IL-8 and CagA. *H. pylori* induces inflammation and releases cytokines from host cells or immune cells. IL-8 is an important factor in the development of gastric diseases during *H. pylori* infection.[2] IL-8 protein allows neutrophil infiltration, which causes severe inflammation and tissue disruption and further leads to gastritis, gastric ulcer, and gastric cancer.[8]

CagA, iNOS, COX-2, and IL-8 proteins were induced during *H. pylori* infection. Time-dependent increases of CagA, COX-2, iNOS, and IL-8 protein production were found, and these molecules reached the maximum at 6 h (data not shown). Indeed, the production of IL-8, iNOS, and COX-2 on AGS cells was not changed during both extract treatments separately (data not shown).

Furthermore, the effects of noni fruit extracts on *H. pylori*-induced inflammatory response were determined. Ethanol extract significantly inhibited intercellular CagA protein, but there was a difference among 200, 400, 600, and 800 μg/mL (Figure 4A). Ethyl acetate extract inhibited CagA protein at concentrations >400 μg/mL (Figure 4B). Similar results also appeared on the IL-8 production; both extracts significantly inhibited IL-8 secretion (Figure 4C,D).

CagA protein is produced by *H. pylori*, which is transported into host cell via a T4SS. CagA can induce IL-8 protein secretion, and it also regulates transcription factors via CagA phosphorylation or phosphorylation-independent pathways.[5,6] The intracellular CagA protein was determined to ascertain the severity of *H. pylori* infection. These results showed the change of CagA and IL-8 resulted in antiadhesion for *H. pylori*, which prevented CagA transportation and modified IL-8 production.

Inhibition of COX-2 and iNOS. *H. pylori* induces the expressions of iNOS and COX-2 proteins, which causes tissue damage. Furthermore, iNOS and COX-2 increase the risk of gastritis, gastric ulcer, and gastric cancer. Therefore, the effect of noni fruit extracts on inflammation of *H. pylori*-induced on AGS cells was evaluated.

The expression of COX-2 protein was significantly lower for both extract treatments than with *H. pylori* infection only (Figure 5A,B). The ethanol extract did not affect the expression

dx.doi.org/10.1021/jf405199w | J. Agric. Food Chem. 2014, 62, 2374−2383

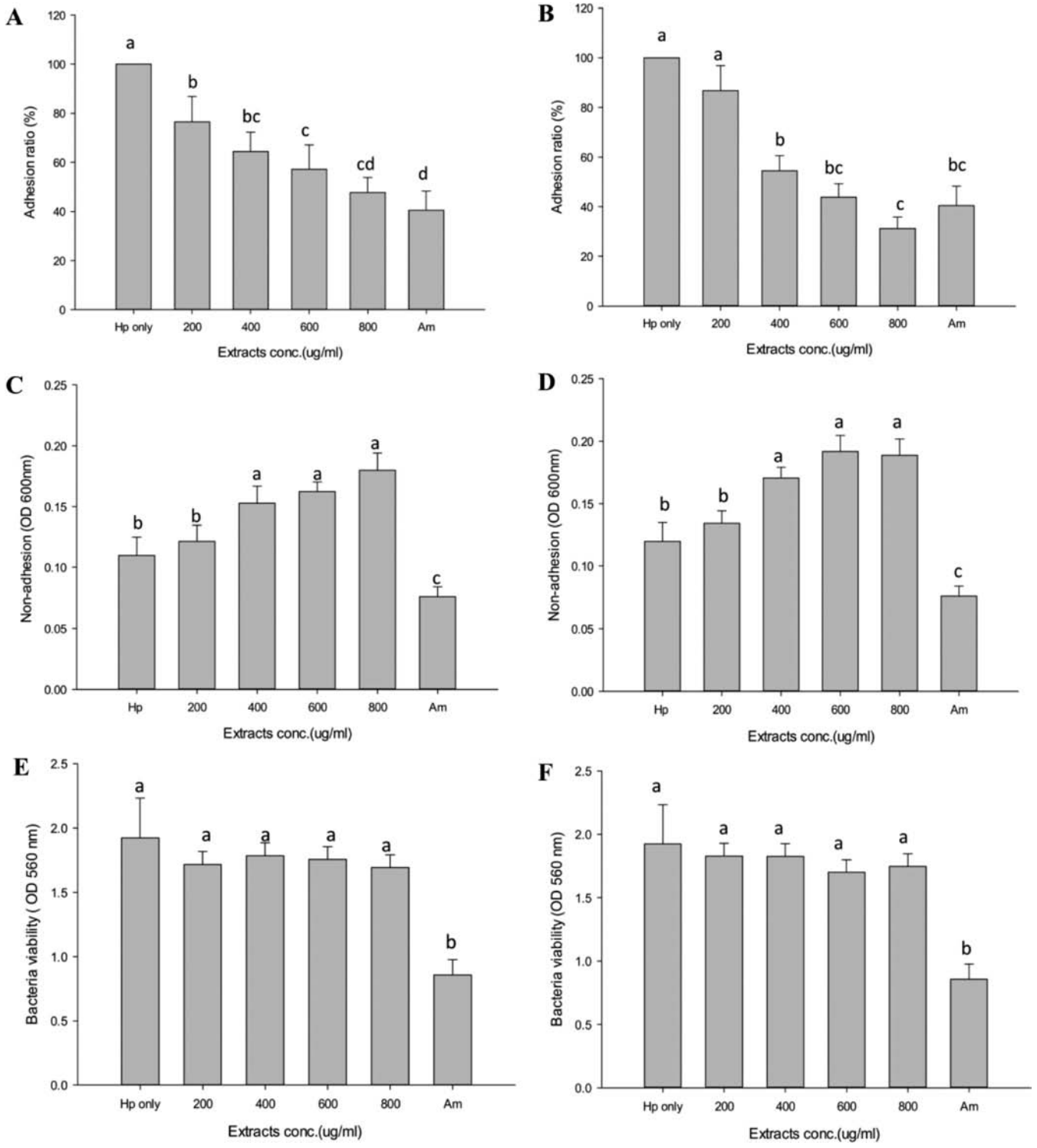

Figure 3. Adhesion of *H. pylori* to AGS cells after ethanol extract (A) and ethyl acetate extract (B) treatment, density of *H. pylori* from suspension after ethanol (C) and ethyl acetate extract (D) treatment, and viability of *H. pylori* from suspension after ethanol (E) and ethyl acetate extract (F) treatment. Different letters above bars indicate significant difference. Hp only, *H. pylori* cocultured only; Am, amoxicillin used as a positive control.

of iNOS protein. Ethyl acetate extract showed significant inhibition at concentrations >400 μg/mL (Figure 5C,D).

The expression of COX-2 and iNOS protein in gastritis, gastric ulcer, or gastric cancer patients with *H. pylori* infection is higher than in *H. pylori*-negative patients.[29] The overexpression of COX-2 protein causes host cell invasion, proliferation, and apoptosis, which increase the risk of tissue lesions.[30] The iNOS protein induces the secretion of IL-8 protein and increases tissue inflammation.[31] Interestingly, the ethanol extract demonstrated antiadhesion, but did not restrain the expression of iNOS at 200−600 μg/mL (Figures 3A and 5C). This result showed that iNOS expression may not be relevant to the adhesion of *H. pylori*.

The inhibition of COX-2 and iNOS expression by noni extracts probably proceeded via antiadhesion and regulates the inflammatory signal in the host cell during *H. pylori* infection.

dx.doi.org/10.1021/jf405199w | J. Agric. Food Chem. 2014, 62, 2374−2383

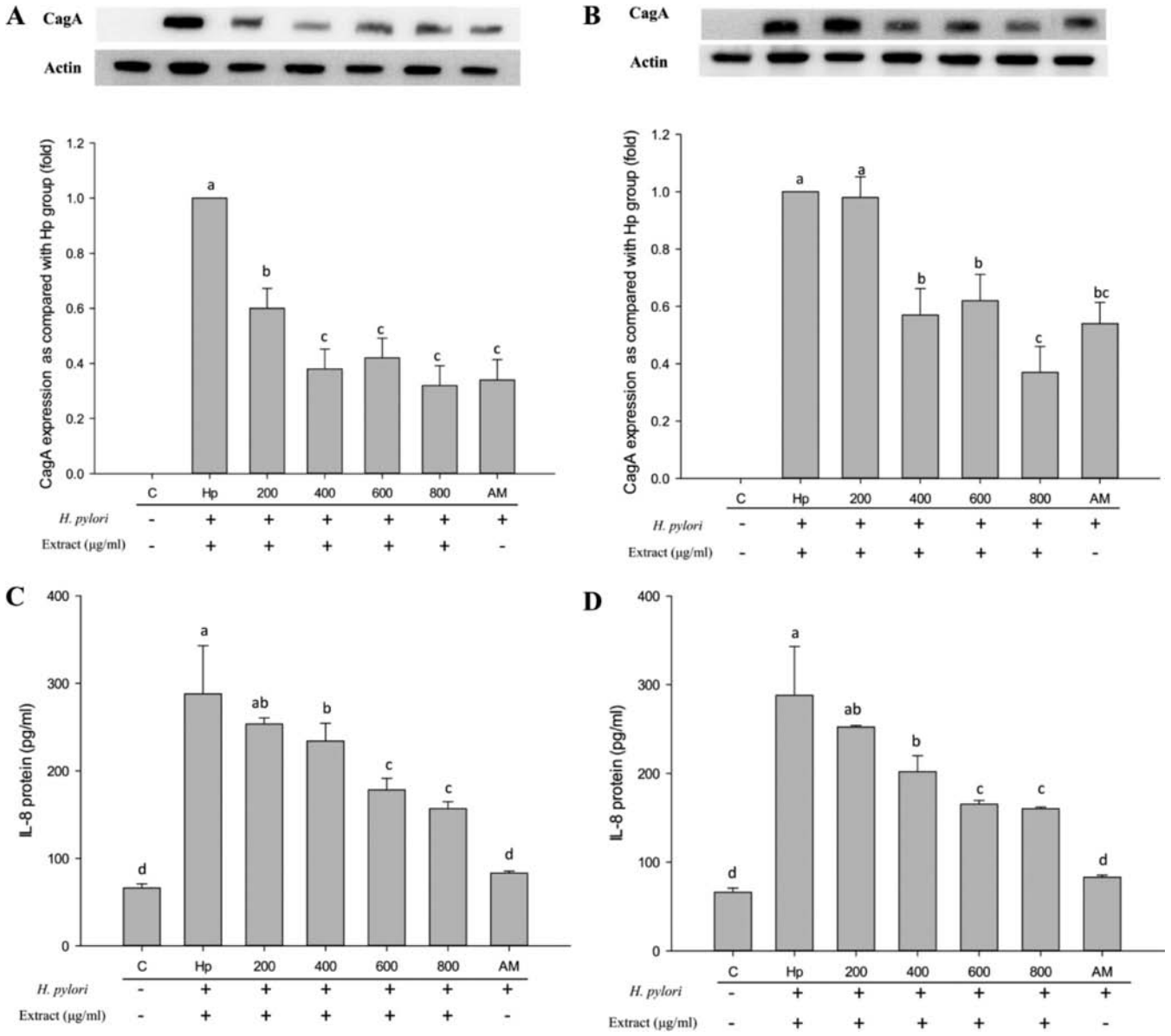

Figure 4. Transportation of CagA on AGS cells induced by *H. pylori* after ethanol (A) and ethyl acetate extract (B) treatment and expression of IL-8 induced by *H. pylori* after ethanol (C) and ethyl acetate extract (D) treatment. Extracts and *H. pylori* were cocultured with AGS cells for 6 h. Different letters above bars indicate significant difference. C, control, non-*H. pylori*; Hp, *H. pylori* cocultured only; Am, amoxicillin.

Moreover, noni root extracts are found to reduce the expression of COX-2, iNOS, and TNF-α in LPS-induced cells and animal models, and a similar composition is found in both root and fruit.[32] The ethyl acetate extract of noni fruit suppresses the expression of COX-2 and iNOS on LPS-induced macrophages.[19] The high polar extract of noni fruit also inhibits iNOS and COX-2 expression of gastric ulcer rat.[33] These results indicated that noni fruit extracts could regulate the *H. pylori*-induced inflammation.

Inhibition of Neutrophil Chemotaxis on *H. pylori* Infection. IL-8 plays a crucial role in neutrophil chemotaxis.[8] Noni fruit extracts showed inhibition on IL-8 during *H. pylori* infection (Figure 4C,D). To further demonstrate that the chemotaxis of neutrophil was relieved by noni fruit extracts, the cultured medium was collected after both extracts (800 μg/mL) and *H. pylori* (the ratio of *H. pylori* to AGS cells was the same as that for the antiadhesion assay) were cocultured with AGS cells for 6 h. The cultured medium was added to the lower layer, and the neutrophil isolated from human peripheral blood was seeded in the upper layer. Undeniably, IL-8 protein caused numerous migrations of neutrophils, and *H. pylori* groups also induced neutrophil chemotaxis (Figure 6). This result indicated that both extracts inhibited neutrophil migration (significantly different as compared with the *H. pylori* group) from a coculture medium. The ethanol extract showed powerful inhibition of neutrophil migration (significantly different to the antibiotic group) (Figure 6B).

Neutrophil is attracted during *H. pylori* infection, but the *H. pylori* cannot be eradicated. Long-term neutrophil infiltration causes tissue damage and local structural failure. The abundant infiltration of neutrophil is thought to increase the development of gastritis, gastric ulcer, or gastric cancer and to cause recurrence of gastric disease.[34] Therefore, the prevention of IL-8 secretion and neutrophil chemotaxis may decrease the risk of gastric disease.

dx.doi.org/10.1021/jf405199w | J. Agric. Food Chem. 2014, 62, 2374−2383

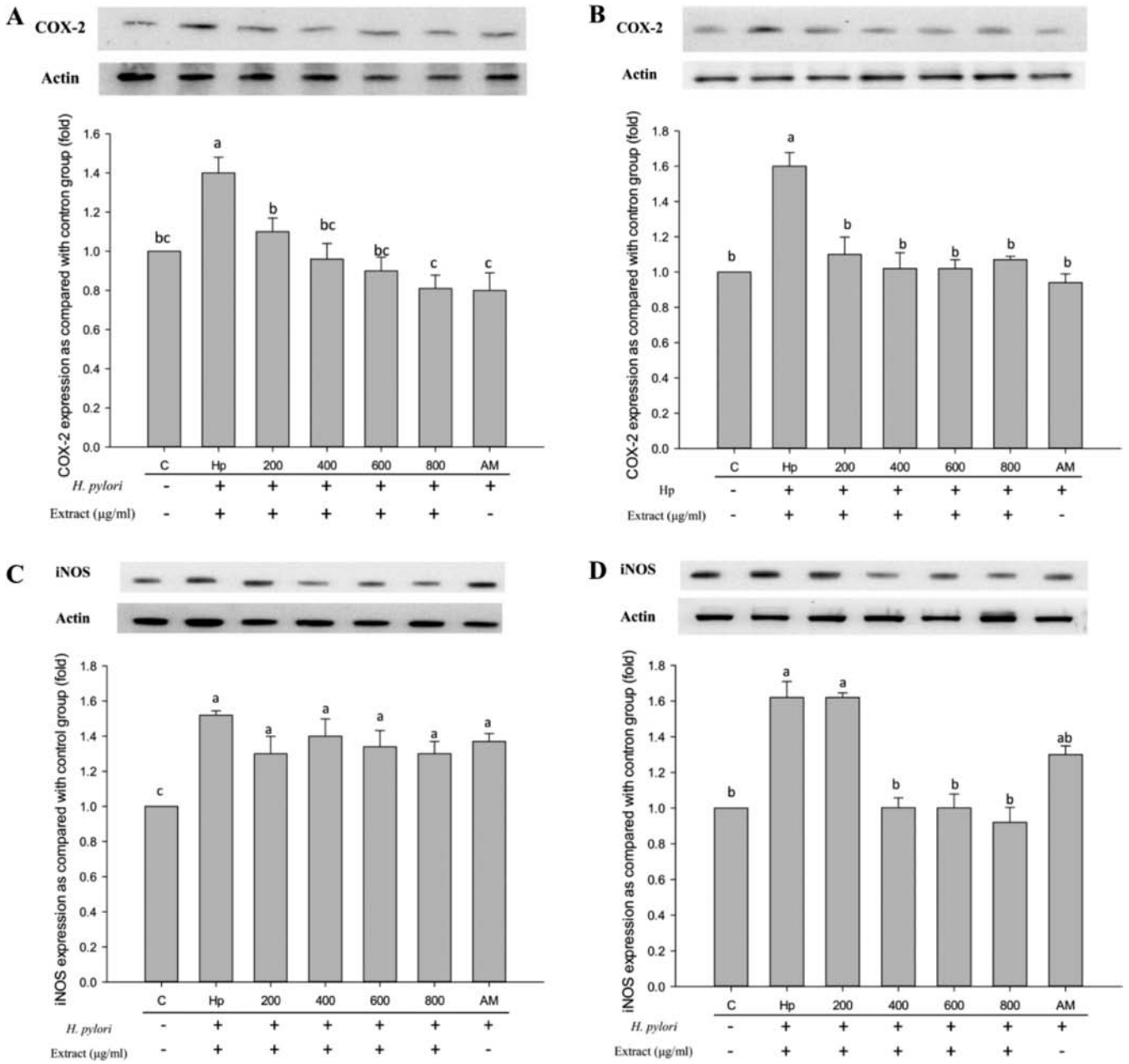

Figure 5. Expression of COX-2 on AGS cells induced by *H. pylori* after ethanol (A) and ethyl acetate extract (B) treatment and expression of iNOS induced by *H. pylori* after ethanol (C) and ethyl acetate extract (D) treatment. Noni fruit extracts and *H. pylori* were cocultured with AGS cells for 6 h. Different letters above bars indicate significant difference. C, control, non-*H. pylori*; Hp, *H. pylori* cocultured only; Am, amoxicillin.

Contribution of Phenolic Compounds to Antiadhesion. Many studies demonstrate antiadhesion on various bacteria for plants or natural products, such as cranberry, green tea, and isolates of red wine.[35−37] The active ingredients are caseinoglycopeptides, fucosylated saccharides, glycoprotein, oligosaccharides, sialylgalactosides, proanthocyanidins, and other phenolic compounds.[37,38] Previous studies indicate that condensed tannins (such as proantocyanidin) show antiadhesion of *H. pylori*.[35,36,39,40] The contents of condensed tannin were scarce in both extracts of noni fruit, and their role in antiadhesion of *H. pylori* needs to be determined.

To confirm the importance of the phenolics on antiadhesion of *H. pylori* from noni fruit extracts, polyvinylpyrrolidone (PVP) was mixed with both extracts separately to precipitate phenolics. Both extracts lost the antiadhesion of *H. pylori* when the phenolics were removed (E-PVP and EA-PVP groups) (Figure 7). Accordingly, the phenolics of noni fruit extracts may play key role on antiadhesion of *H. pylori*. However, the effects of quercetin and coumaric acid on antiadhesion of *H. pylori* remain unknown.

To replicate the extracts, pure coumaric acid and quercetin were conversed to levels of each extract and were used to evaluate the effect on the antiadhesion of *H. pylori* infection. The group of equivalent contents of coumaric acid (19.04 μg/mL) in 800 μg/mL ethanol extract (E-C) provided antiadhesion on *H. pylori* (significant difference as compared with the Hp extract group), but the effect was weaker than the ethanol extract group (Figure 7). The group of equivalent contents of coumaric acid (19.04 μg/mL) and quercetin (3.52 μg/mL) in 800 μg/mL ethanol extract (E-CQ) demonstrated

dx.doi.org/10.1021/jf405199w | J. Agric. Food Chem. 2014, 62, 2374−2383

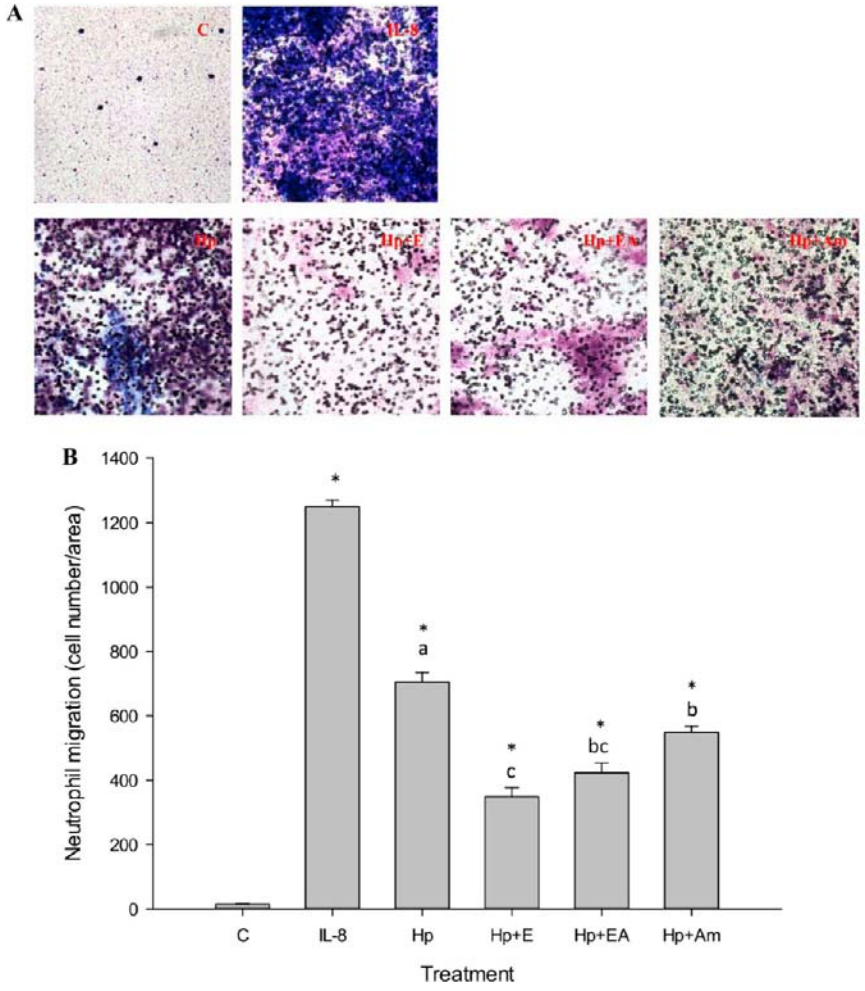

Figure 6. Effect of noni fruit extracts on neutrophil chemotaxis (A) and quantification (B). Different letters above bars indicate significant difference. (*) Significantly different as compared with the control. C, control, non-*H. pylori*; IL-8, IL-8 protein as positive control, 1000 pg/mL; Hp, *H. pylori* cocultured only; Hp+E, *H. pylori* and ethanol extract cocultured; Hp+EA, *H. pylori* and ethyl acetate extract cocultured; Hp+Am, *H. pylori* and amoxicillin cocultured.

great inhibition on adhesion (significant difference as compared with the Hp extract group) but was lower than that of the ethanol extract group (Figure 7). On other hand, the group of equivalent contents of quercetin (22.4 μg/mL) in 800 μg/mL ethyl acetate extract (EA-Q) provided inhibition on adhesion (significant difference as compared with Hp extract group) (Figure 7).

These results confirmed that quercetin and coumaric acid played key roles in the antiadhesion of *H. pylori* infection. However, the equivalent contents of coumaric acid showed weaker than ethanol or ethyl acetate extracts, respectively (Figure 7). Interestingly, the ethanol extract showed excellent inhibition on CagA transportation and antiadhesion at low dose (200 μg/mL) (Figure 4A). Thus, there are unknown components in ethanol extract of noni fruit that contribute to the antiadhesion and blocking CagA signal of *H. pylori*.

Coumaric acid can inhibit intestinal inflammation in dextran sulfate sodium (DSS)-induced rats by obstructing the COX-2 signal, but its effect on the expression of COX-2 and iNOS is weak.[41] Coumaric acid showed weak capability in prevention for *H. pylori* owing to no effect on growth of *H. pylori*.[42] In this study, the coumaric acid group (E-C) showed significant inhibition on the adhesion of *H. pylori* even though that was weaker than the ethanol extract group (Figure 7). The coumaric acid-rich ethanol extract also inhibited the expression of IL-8 and COX-2 proteins induced by *H. pylori* (Figures 4C and 5A). Coumaric acid probably interacted with other compounds to regulate inflammation during *H. pylori* infection. These results indicated that coumaric acid showed the potential to prevent formation of gastric diseases.

Undoubtedly, quercetin has a key role in the ethyl acetate extract against adhesion and inflammation during *H. pylori* infection. Quercetin is confirmed to selectively activate pro-inflammation signals, such as PGE_2 and NO production, to relieve inflammatory responses, and also to promote wound healing in animal models.[43,44] Quercetin also reduces inflammation and lipid peroxidation in *H. pylori* infection of gastric mucosa.[45]

The effect of quercetin on the adhesion of bacteria to AGS cells is still unknown. The mechanisms for the antiadhesion on bacteria are multifarious, such as target coating, adhesin inhibition, receptor inhibition, and receptor competitive inhibition.[46] The particular flavonoids, such as catechin, proanthocyanins, and anthocyanins, have been shown to change the surface modification and biofilm detachment to cause bacterial adhesion failure.[47,48] Thus, quercetin probably suppresses the adhesion of *H. pylori* via the similar pathway of catechin or proanthocyanin. The chemical structure of

dx.doi.org/10.1021/jf405199w | J. Agric. Food Chem. 2014, 62, 2374−2383

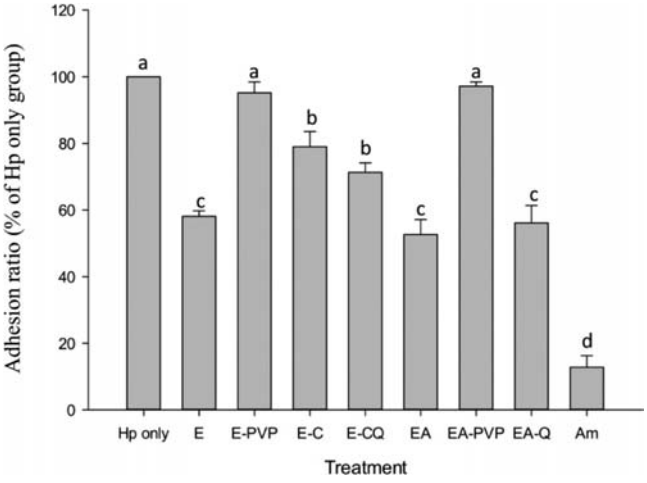

Figure 7. Contribution of phenolic compounds on antiadhesion. Different letters above bars indicate significant difference. C, control, non-*H. pylori*; Hp, *H. pylori* cocultured only; E, ethanol extract; EA, ethyl acetate extract; E-PVP, ethanol extract reacted with PVP before treated; EA-PVP, ethyl acetate extract reacted with PVP before treated; E-C, equivalent contents of ethanol extract; E-CQ, equivalent contents of coumaric acid and quercetin of ethanol extract; EA-Q, equivalent contents of quercetin of ethyl acetate extract; AM, amoxicillin.

coumaric acid is different from that of quercetin, and this could dominate the capacity of antiadhesion of bacteria.[42,43]

In this study, quercetin not only contributed to anti-inflammation but also inhibited the adhesion of *H. pylori*. It probably represented a new way to prevent or inhibit inflammation or pathogenesis that was caused by microorganisms. Indeed, the ethyl acetate fraction of noni fruit contains other phenolic compounds, such as scopoletin and rutin.[19] In this study, quercetin was found to be the major phenolic compound in ethyl acetate extract (Figure 1B). This was probably due to the variety of noni or sample extraction.

On the other hand, abundant coumaric acid and quercetin were found in the ethanol extract of noni fruit (Figure 1A). The group of equivalent contents of coumaric acid and quercetin in 800 μg/mL of ethanol extract showed weaker antiadhesion of *H. pylori* than that of ethanol extract treatment (Figure 7). This indicated that some other substances in the ethanol extract could contribute to the antiadhesion. Previous studies verify the various components in noni fruit, such as asperulosidic acid and anthraquinones, that may have the potential to affect the adhesion and inflammation for bacterial infection.[49,50] Moreover, the condensed tannin was found in ethanol extract. The antiadhesion of *H. pylori* disappeared in the E-PVP group (Figure 7). Accordingly, the high-polar condensed tannin probably played a critical role in the antiadhesion of *H. pylori*. Further studies are required.

Phenolics provide antioxidant, anti-inflammatory, or bactericidal activity and are rarely studied for their antiadhesion for bacteria. In this study, the phenolics of noni fruit were shown to regulate inflammation by impeding the attachment of *H. pylori* to the host cells. These results showed that coumaric acid and quercetin inhibited inflammation by reducing the adhesion of *H. pylori*.

Conclusion. Ethanol and ethyl acetate extracts of noni fruit showed excellent antiadhesion and anti-inflammation for AGS cells from *H. pylori* infection and decreased the risk of gastric diseases. Coumaric acid, quercetin, and unknown components probably played key roles. Further works to identify the unknown components are needed.

Noni fruit is an agent or supplement that prevents *H. pylori* adhesion or related diseases. Further work is required to confirm the actual mechanism for antiadhesion.

AUTHOR INFORMATION

Corresponding Author

*(C.-K.W.) E-mail: wckjff@gmail.com. Phone: +886424730022, ext. 11751.

Notes

The authors declare no competing financial interest.

REFERENCES

(1) Hopkins, R. J.; Girardi, L. S.; Turney, E. A. Relationship between *Helicobacter pylori* eradication and reduced duodenal and gastric ulcer recurrence: a review. *Gastroenterology* **1996**, *110*, 1244−1252.

(2) Chu, S. H.; Kim, H.; Seo, J. Y.; Lim, J. W.; Mukaida, N.; Kim, K. H. Role of NF-kappaB and AP-1 on *Helicobater pylori*-induced IL-8 expression in AGS cells. *Dig. Dis. Sci.* **2003**, *48*, 257−265.

(3) Higashi, H.; Tsutsumi, R.; Muto, S.; Sugiyama, T.; Azuma, T.; Asaka, M.; Hatakeyama, M. SHP-2 tyrosine phosphatase as an intracellular target of *Helicobacter pylori* CagA protein. *Science* **2002**, *295*, 683−686.

(4) Segal, E. D.; Cha, J.; Lo, J.; Falkow, S.; Tompkins, L. S. Altered states: involvement of phosphorylated CagA in the induction of host cellular growth changes by *Helicobacter pylori*. *Proc. Natl. Acad. Sci. U.S.A.* **1999**, *96*, 14559−14564.

(5) Lai, C.-H.; Wang, H.-J.; Chang, Y.-C.; Hsieh, W.-C.; Lin, H.-J.; Tang, C.-H.; Sheu, J. J.-C.; Lin, C.-J.; Yang, M.-S.; Tseng, S.-F.; Wang, W.-C. Helicobacter pylori CagA-mediated IL-8 induction in gastric epithelial cells is cholesterol-dependent and requires the C-terminal tyrosine phosphorylation-containing domain. *FEMS Microbiol. Lett.* **2011**, *323*, 155−163.

(6) Suzuki, M.; Mimuro, H.; Kiga, K.; Fukumatsu, M.; Ishijima, N.; Morikawa, H.; Nagai, S.; Koyasu, S.; Gilman, R. H.; Kersulyte, D.; Berg, D. E.; Sasakawa, C. *Helicobacter pylori* CagA phosphorylation-independent function in epithelial proliferation and inflammation. *Cell Host Microbe* **2009**, *5*, 23−34.

(7) Baggiolini, M.; Clark-Lewis, I. Interleukin-8, a chemotactic and inflammatory cytokine. *FEBS Lett.* **1992**, *307*, 97−101.

(8) Kukulski, F.; Ben Yebdri, F.; Lecka, J.; Kauffenstein, G.; Lévesque, S. A.; Martín-Satué, M.; Sévigny, J. Extracellular ATP and P2 receptors are required for IL-8 to induce neutrophil migration. *Cytokine* **2009**, *46*, 166−170.

(9) Rieder, G.; Hatz, R. A.; Moran, A. P.; Walz, A.; Stolte, M.; Enders, G. Role of adherence in interleukin-8 induction in *Helicobacter pylori*-associated gastritis. *Infect. Immun.* **1997**, *65*, 3622−3630.

(10) Sharma, S. A.; Tummuru, M. K.; Miller, G. G.; Blaser, M. J. Interleukin-8 response of gastric epithelial cell lines to *Helicobacter pylori* stimulation in vitro. *Infect. Immun.* **1995**, *63*, 1681−1687.

(11) Angrisano, T.; Pero, R.; Peluso, S.; Keller, S.; Sacchetti, S.; Bruni, C.; Chiariotti, L.; Lembo, F. LPS-induced IL-8 activation in human intestinal epithelial cells is accompanied by specific histone H3 acetylation and methylation changes. *BMC Microbiol.* **2010**, *10*, 172.

(12) Wambura, C.; Aoyama, N.; Shirasaka, D.; Kuroda, K.; Maekawa, S.; Ebara, S.; Watanabe, Y.; Tamura, T.; Kasuga, M. Influence of gastritis on cyclooxygenase-2 expression before and after eradication of *Helicobacter pylori* infection. *Eur. J. Gastroenterol. Hepatol.* **2004**, *16*, 969−979.

(13) Chang, Y.-J.; Wu, M.-S.; Lin, J.-T.; Chen, C.-C. *Helicobacter pylori*-induced invasion and angiogenesis of gastric cells is mediated by cyclooxygenase-2 induction through TLR2/TLR9 and promoter regulation. *J. Immunol.* **2005**, *175*, 8242−8252.

(14) van Der Hulst, R. W. M.; Keller, J. J.; Rauws, E. A. J.; Tytgat, G. N. J. Treatment of *Helicobacter pylori* infection: a review of the world literature. *Helicobacter* **1996**, *1*, 6−19.

(15) Kusters, J. G.; van Vliet, A. H.; Kuipers, E. J. Pathogenesis of *Helicobacter pylori* infection. *Clin. Microbiol. Rev.* **2006**, *19*, 449−490.
(16) Chan-Blanco, Y.; Vaillant, F.; Mercedes Perez, A.; Reynes, M.; Brillouet, J.-M.; Brat, P. The noni fruit (*Morinda citrifolia* L.): a review of agricultural research, nutritional and therapeutic properties. *J. Food Compos. Anal.* **2006**, *19*, 645−654.
(17) Atkinson, N.; Brice, H. E. Antibacterial substances produced by flowering plants. II. The antibacterial action of essential oils from some Australian plants. *Aust. J. Exp. Biol. Med. Sci.* **1955**, *33*, 547−554.
(18) Locher, C. P.; Burch, M. T.; Mower, H. F.; Berestecky, J.; Davis, H.; Van Poel, B.; Lasure, A.; Berghe, D. A. V.; Vlietinck, A. J. Antimicrobial activity and anti-complement activity of extracts obtained from selected Hawaiian medicinal plants. *J. Ethnopharmacol.* **1995**, *49*, 23−32.
(19) Nitteranon, V.; Zhang, G.; Darien, B. J.; Parkin, K. Isolation and synergism of in vitro anti-inflammatory and quinone reductase (QR) inducing agents from the fruits of *Morinda citrifolia* (noni). *Food Res. Int.* **2011**, *44*, 2271−2277.
(20) Shen, Y. C.; Chen, S. L.; Zhuang, S. R.; Wang, C. K. Contribution of tomato phenolics to suppression of COX-2 expression in KB cells. *J. Food Sci.* **2008**, *73*, C1−C10.
(21) Luo, Y.; Dorf, M. E. Isolation of mouse neutrophils. In *Current Protocols in Immunology*; Wiley: New York, 2001.
(22) Harvath, L.; Falk, W.; Leonard, E. J. Rapid quantitation of neutrophil chemotaxis: use of a polyvinylpyrrolidone-free polycarbonate membrane in a multiwell assembly. *J. Immunol. Methods* **1980**, *37*, 39−45.
(23) Konate, K.; Hilou, A.; Mavoungou, J.; Lepengue, A.; Souza, A.; Barro, N.; Datte, J.; M'Batchi, B.; Nacoulma, O. Antimicrobial activity of polyphenol-rich fractions from *Sida alba* L. (Malvaceae) against co-trimoxazol-resistant bacteria strains. *Ann. Clin. Microbiol. Antimicrob.* **2012**, *11*, 5.
(24) Löhr, G.; Beikler, T.; Podbielski, A.; Standar, K.; Redanz, S.; Hensel, A. Polyphenols from *Myrothamnus flabellifolia* Welw. inhibit in vitro adhesion of *Porphyromonas gingivalis* and exert anti-inflammatory cytoprotective effects in KB cells. *J. Clin. Periodontol.* **2011**, *38*, 457−469.
(25) Deng, S.; West, B. J.; Jensen, C. J.; Basar, S.; Westendorf, J. Development and validation of an RP-HPLC method for the analysis of anthraquinones in noni fruits and leaves. *Food Chem.* **2009**, *116*, 505−508.
(26) Malfertheiner, P.; Megraud, F.; O'Morain, C. A.; Atherton, J.; Axon, A. T. R.; Bazzoli, F.; Gensini, G. F.; Gisbert, J. P.; Graham, D. Y.; Rokkas, T.; El-Omar, E. M.; Kuipers, E. J.; The European Helicobacter Study Group. Management of *Helicobacter pylori* infection − the Maastricht IV/ Florence Consensus Report. *Gut* **2012**, *61*, 646−664.
(27) Mégraud, F. *H. pylori* antibiotic resistance: prevalence, importance, and advances in testing. *Gut* **2004**, *53*, 1374−1384.
(28) Odenbreit, S.; Püls, J.; Sedlmaier, B.; Gerland, E.; Fischer, W.; Haas, R. Translocation of *Helicobacter pylori* CagA into gastric epithelial cells by type IV secretion. *Science* **2000**, *287*, 1497−1500.
(29) Wroblewski, L. E.; Peek, R. M.; Wilson, K. T. *Helicobacter pylori* and gastric cancer: factors that modulate disease risk. *Clin. Microbiol. Rev.* **2010**, *23*, 713−739.
(30) Chang, Y. J.; Wu, M. S.; Lin, J. T.; Chen, C. C. *Helicobacter pylori*-induced invasion and angiogenesis of gastric cells is mediated by cyclooxygenase-2 induction through TLR2/TLR9 and promoter regulation. *J. Immunol.* **2005**, *175*, 8242−8252.
(31) Angrisano, T.; Lembo, F.; Peluso, S.; Keller, S.; Chiariotti, L.; Pero, R. *Helicobacter pylori* regulates iNOS promoter by histone modifications in human gastric epithelial cells. *Med. Microbiol. Immunol.* **2012**, *201*, 249−257.
(32) Kim, I.-T.; Park, H.-J.; Nam, J.-H.; Park, Y.-M.; Won, J.-H.; Choi, J.; Choe, B.-K.; Lee, K.-T. In-vitro and in-vivo anti-inflammatory and antinociceptive effects of the methanol extract of the roots of *Morinda officinalis*. *J. Pharm. Pharmacol.* **2005**, *57*, 607−615.
(33) Mahattanadul, S.; Nima, S.; Kasiwong, S.; Tewtrakul, S.; Tansakul, P. Selective iNOS and COX-2 inhibition of *Morinda citrifolia* (noni) fruit extract in rat gastric ulcerated mucosa. *Planta Med.* **2012**, *78*, PD60.
(34) Taha, A. S.; Dahill, S.; Morran, C.; Hudson, N.; Hawkey, C. J.; Lee, F. D.; Sturrock, R. D.; Russell, R. I. Neutrophils, *Helicobacter pylori*, and nonsteroidal anti-inflammatory drug ulcers. *Gastroenterology* **1999**, *116*, 254−258.
(35) Shmuely, H.; Burger, O.; Neeman, I.; Yahav, J.; Samra, Z.; Niv, Y.; Sharon, N.; Weiss, E.; Athamna, A.; Tabak, M.; Ofek, I. Susceptibility of *Helicobacter pylori* isolates to the antiadhesion activity of a high-molecular-weight constituent of cranberry. *Diagn. Microbiol. Infect. Dis.* **2004**, *50*, 231−235.
(36) Howell, A. B.; Reed, J. D.; Krueger, C. G.; Winterbottom, R.; Cunningham, D. G.; Leahy, M. A-type cranberry proanthocyanidins and uropathogenic bacterial anti-adhesion activity. *Phytochemistry* **2005**, *66*, 2281−2291.
(37) Ofek, I.; Hasty, D. L.; Sharon, N. Anti-adhesion therapy of bacterial diseases: prospects and problems. *FEMS Immunol. Med. Microbiol.* **2003**, *38*, 181−191.
(38) Daglia, M.; Stauder, M.; Papetti, A.; Signoretto, C.; Giusto, G.; Canepari, P.; Pruzzo, C.; Gazzani, G. Isolation of red wine components with anti-adhesion and anti-biofilm activity against *Streptococcus mutans*. *Food Chem.* **2010**, *119*, 1182−1188.
(39) Burger, O.; Ofek, I.; Tabak, M.; Weiss, E. I.; Sharon, N.; Neeman, I. A high molecular mass constituent of cranberry juice inhibits *Helicobacter pylori* adhesion to human gastric mucus. *FEMS Immunol. Med. Microbiol.* **2000**, *29*, 295−301.
(40) Sang, S.; He, K.; Liu, G.; Zhu, N.; Wang, M.; Jhoo, J.-w.; Zheng, Q.; Dong, Z.; Ghai, G.; Rosen, R. T.; Ho, C.-T. Citrifolinin, a new unusual iridoid with inhibition of activator protein-1 (AP-1) from the leaves of noni (*Morinda citrifolia* L.). *Tetrahedron Lett.* **2001**, *42*, 1823−1825.
(41) Yen, G.-C.; Duh, P.-D.; Huang, D.-W.; Hsu, C.-L.; Fu, T. Y.-C. Protective effect of pine (*Pinus morrisonicola* Hay.) needle on LDL oxidation and its anti-inflammatory action by modulation of iNOS and COX-2 expression in LPS-stimulated RAW 264.7 macrophages. *Food Chem. Toxicol.* **2008**, *46*, 175−185.
(42) Siddaraju, M. N.; Dharmesh, S. M. Inhibition of gastric H+,K+-ATPase and *Helicobacter pylori* growth by phenolic antioxidants of *Curcuma amada*. *J. Agric. Food Chem.* **2007**, *55*, 7377−7386.
(43) Wadsworth, T. L.; Koop, D. R. Effects of the wine polyphenolics quercetin and resveratrol on pro-inflammatory cytokine expression in RAW 264.7 macrophages. *Biochem. Pharmacol.* **1999**, *57*, 941−949.
(44) Süntar, I. P.; Akkol, E. K.; Yalçın, F. N.; Koca, U.; Keleş, H.; Yesilada, E. Wound healing potential of *Sambucus ebulus* L. leaves and isolation of an active component, quercetin 3-*O*-glucoside. *J. Ethnopharmacol.* **2010**, *129*, 106−114.
(45) González-Segovia, R.; Quintanar, J. L.; Salinas, E.; Ceballos-Salazar, R.; Aviles-Jiménez, F.; Torres-López, J. Effect of the flavonoid quercetin on inflammation and lipid peroxidation induced by *Helicobacter pylori* in gastric mucosa of guinea pig. *J. Gastroenterol.* **2008**, *43*, 441−447.
(46) Signoretto, C.; Canepari, P.; Stauder, M.; Vezzulli, L.; Pruzzo, C. Functional foods and strategies contrasting bacterial adhesion. *Curr. Opin. Biotechnol.* **2012**, *23*, 160−167.
(47) Gotteland, M.; Andrews, M.; Toledo, M.; Muñoz, L.; Caceres, P.; Anziani, A.; Wittig, E.; Speisky, H.; Salazar, G. Modulation of *Helicobacter pylori* colonization with cranberry juice and *Lactobacillus johnsonii* La1 in children. *Nutrition* **2008**, *24*, 421−426.
(48) Otake, S.; Makimura, M.; Kuroki, T.; Nishihara, Y.; Hirasawa, M. Anticaries effects of polyphenolic compounds from Japanese green tea. *Caries Res.* **1991**, *25*, 438−443.
(49) Wang, M.; Kikuzaki, H.; Csiszar, K.; Boyd, C. D.; Maunakea, A.; Fong, S. F. T.; Ghai, G.; Rosen, R. T.; Nakatani, N.; Ho, C.-T. Novel trisaccharide fatty acid ester identified from the fruits of *Morinda citrifolia* (noni). *J. Agric. Food Chem.* **1999**, *47*, 4880−4882.
(50) Xiang, W.; Song, Q.-S.; Zhang, H.-J.; Guo, S.-P. Antimicrobial anthraquinones from *Morinda angustifolia*. *Fitoterapia* **2008**, *79*, 501−504.

interferon-γ (IFN-γ) was purchased from PharMingen (San Diego, CA, USA). The AMV reverse transcriptase and dNTP mixture were obtained from Takara Bio (Kyoto, Japan). PCR primers were custom-synthesized and purified by Bioneer (Daejon, Republic of Korea). Analytical reagents were purchased from Sigma Aldrich (St. Louis, MO, USA) and used without further purification.

Preparation of Bioprocessed Polysaccharide (BPP). The isolation and characterization of BPP is described in our recent publication.[2] The amount of β-glucan in each extract was determined using a Mixed-Linkage-β-glucan Kit (Megazyme Intern Treland Ltd., Wicklow, Ireland).

Bacterial Strain and Culture Condition. *Salmonella enterica* subsp. *enterica* ser. Typhimurium (*S.* Typhimurium) ATCC 140 was obtained from the American Type Culture Collection (Manassas, VA, USA) and kept as frozen glycerol stock. Cells in frozen stock were streaked onto NA medium to produce cell colonies, from which a single colony was transferred to nutrient broth (NB) medium. For preparation of inocula, cells were grown for 20 h at 37 °C in NB. For infection, cultured bacterial cells were recovered by centrifugation at 13,000 rpm for 30 s and then washed with and resuspended in PBS. The turbidity of the cell suspensions was measured. The cell suspensions were diluted with PBS to the desired concentration of bacteria using a standard curve of optical density versus bacterial number determined as colony-forming units (CFU).

In Vitro Bactericidal Assay. *S.* Typhimurium cells were diluted with PBS to a density of 2×10^4 CFU/mL, treated with three concentrations of BPP (1, 10, and 100 μg/mL), and incubated at 37 °C for 0, 2, 4, and 8 h. After incubation, the diluted culture (100 μL) was plated onto NA medium to assess bacterial CFU.

Mammalian Cell Culture. Murine macrophage cell line RAW 264.7 from the American Type Culture Collection (Manassas, VA, USA) were cultured in RPMI 1640 medium supplemented with 10% heat-inactivated FBS containing 100 U/mL penicillin and 100 μg/mL streptomycin. The cells were cultured at 37 °C in humidified air containing 5% CO_2.

Morphologic Changes in Macrophages. RAW 264.7 cells were grown in the presence of BPP (100 μg/mL) in 24-well cell culture plates with coverslips for 8 h. The coverslips were examined under a microscope (100×) to observe morphologic changes in macrophages. Cells were selected in six blindly chosen random fields, and the morphologically changed cells were then counted and recorded. This assay was performed for at least three individual experiments.

Determination of Bacteria in Macrophages. To measure internalization and intracellular survival of bacteria in macrophages, RAW 264.7 cells were infected with *S.* Typhimurium following the method of Lu et al.[8] For analysis of macrophage bacterial uptake efficiency, inoculum (10 μL) containing 1×10^4 CFU was added to RAW 264.7 macrophage cells (1×10^4 cells) pretreated with three concentrations of the BPP (1, 10, and 100 μg/mL) and incubated for 30 or 60 min in a 5% CO_2 atmosphere. Cells were washed once with RPMI 1640 medium after incubation at 37 °C and then treated with the same medium containing 10% FBS and gentamicin (30 μg/mL) for 30 min to kill extracellular bacteria. For viable cell counting, the infected macrophage cells were washed three times and then lysed with distilled water. Aliquots of lysates were plated onto NA medium to measure bacterial CFU.

To measure intracellular survival, *S.* Typhimurium cells (1×10^4 CFU) were added to serially diluted BPP-treated macrophage sample for 4 h. The samples were incubated at 37 °C for 1 h, followed by washing once with medium and subsequent treatment with RPMI 1640 medium containing 10% FBS with gentamicin (30 μg/mL) for 2, 4, and 8 h. Cell washing, lysis, and plating procedures onto NA medium were carried out following the same protocol as for the analysis of bacterial uptake efficiency.

Mice and Treatments. The protocol for the mouse studies was approved by the Ethics Committee for Animal Care and Use, Ajou University, Republic of Korea. All experiments were performed in compliance with the relevant laws and institutional guidelines. Six- to eight-week-old female BALB/c mice were purchased from Orient Bio Inc. (Seongnam, Korea), and were hosted under a 12 h light/dark cycle at 20−22 °C and relative humidity of 50 ± 10%. The mice were fed freely a pelletized commercial chow diet obtained from Orient Bio Inc. (catalog no. 5L79) and sterile tap water during the entire period. After acclimation for 1 week, the mice were then divided into three groups (n = 10), avoiding any intergroup difference in body weight. BPP was dissolved in water, and given to mice via the dietary (oral) or the intraperitoneal (ip) route. Two groups were given BPP, whereas one was given only water. The dose of the BPP was adjusted to 10 mg/kg body weight for both routes. After administration of the BPP for 14 consecutive days, the mice were infected ip with sublethal or lethal doses of *S.* Typhimurium (1×10^4 CFU or 1×10^5 CFU). Collection of blood samples and excision of organs including liver and spleen were carried out for further experiments.

In Vivo Bactericidal Assay. After administration of BPP (10 mg/kg) for 14 consecutive days, mice were infected ip with a sublethal dose of *S.* Typhimurium (1×10^4 CFU). Two days later, the mice were sacrificed by CO_2 asphyxia, and the abdominal cavities were opened and repeatedly washed with a total PBS (10 mL) as described by Kodama et al.[9] Bacterial counts in the pooled PBS wash were determined by plating technique to measure CFU levels described above.

Serum Nitrite and Nitrate Levels. Serum nitrite and nitrate levels were measured primarily following the method of Misko et al.[10] with some modification. Blood samples collected by cardiac puncture were left at 37 °C for 20 min to obtain the serum, followed by filtration of the serum through an Ultrafree-MC microcentrifuge filter unit (Millipore, Bedford, MA, USA) for 1 h at 14,000 rpm to remove the hemoglobin released by cell lysis. The serum (50 μL) was incubated in a reaction mixture [(40 mM Tris Cl, 40 μM reduced β-nicotinamide adenine dinucleotide phosphate, 40 μM flavine adenine dinucleotide, and nitrate reductase (0.05 U/mL)] at pH 7.9 at 37 °C for 15 min. Reduced samples were incubated with an equal volume of Greiss reagent [1% sulfanilamide and 0.1% *N*-(1-naphthyl)-ethylenediamine dihydrochloride in 5% phosphoric acid] at room temperature for 15 min. The absorbance was read at 570 nm using a microplate reader (model 550, Bio-Rad, Hercules, CA, USA). Total nitrate/nitrite levels were determined by comparison with a reduced $NaNO_3$ standard curve.

Mitogen-Induced Lymphocyte Proliferation. Spleen cell suspensions were prepared by gentle pressing the spleen through a stainless steel mesh as described by Teixeira et al.[11] Thereafter, the cells were suspended in RPMI 1649 medium supplemented with 5% FBS and seeded into 24-well culture plates in the presence of concanavalin A (Con A, 2.5 μg/mL) to stimulate T cells. After stimulation for 72 h at 37 °C in 5% CO_2, cell proliferation levels were determined at 490 nm on a microplate. Cell numbers were determined using MTS [(3-(4,5-dimethylthiazol-2-yl)-5-(3-carboxymethoxyphenyl)-2-(4-sulfophenyl)-2H-tetrazolium)] assay in the form of the CellTiter 96 aqueous nonradioactive cell proliferation assay kit (Promega, Madison, WI, USA) following the manufacturer's instructions. The increase of cell growth was determined by setting as 1 the growth of spleen cells from pathogen-free mice in FBS-supplemented RPMI 1640 medium without Con A.

ELISA of Cytokines. Th1 and Th2 cytokines (IL-1, IL-2, IL-6, and IL-12 vs IL-4, IL-5, and IL-10) in the culture supernatant of spleen cells from infected or mock-infected mice without Con A were determined by ELISA kits (Life Technologies, Carlsbad, CA, USA). The ELISA kit for IFN-γ was the product of Biosource Int. (Camarillo, CA, USA). After reactions, the absorbance of the final solution at 420 nm was read in a microplate reader (model 550, Bio-Rad, Hercules, CA, USA).

Mice Salmonellosis Study. The salmonellosis assay was carried out by the method of Kim et al.,[12] with some modification. Three groups of 10 mice each (water-treated control and BPP-treated experimental groups via ip and oral routes) were used for bacterial infection. Mice were infected ip with a lethal a dose of *S.* Typhimurium (1×10^5 CFU). After infection, the mice were treated with BPP (10 mg/kg) via the ip or oral routes every 24 h during the entire experimental period. To determine the survival rate, mice were observed for an additional 28 days after bacterial infection.

Histology of Liver Tissue. For histological analysis, the liver tissue of the mice was fixed with 4% paraformaldehyde in 0.5 M phosphate buffer (pH 7.4). The tissues were rinsed with water, dehydrated with ethanol, and embedded in paraffin. The liver tissue was sectioned into 4 μm samples and mounted onto glass slides. The sections were then dewaxed using xylene and ethanol and stained with hematoxylin and eosin Y (H&E) to reveal the hemorrhagic necrosis in the liver. Histological changes were observed under a light microscope at 100× magnification.

Reverse Transcription Polymerase Chain Reaction (RT-PCR) of Cellular RNA. Total cellular RNA was prepared following acid phenol guanidium thiocyanate−chloroform extraction.[13] For reverse transcription, total RNA (1 μg) was incubated with AMV reverse transcriptase (5 U) and oligo (dT18) as primer (100 ng). DNA amplification was then primed in a reaction mixture containing dNTP mix (400 μM), *Taq* polymerase (2.5 U), and primer sets (20 μM each) representing target genes as follows: inducible nitric oxide synthase (iNOS) sense primer, 5′-ATGTCCGAAGCAAACATCAC-3′; iNOS antisense primer, 5′-TAATGTCCAGGAAGTAGGTG-3′; β-actin sense primer, GTGGGGCGCCCCAGGCACCA-3′; β-actin antisense primer, 5′-GTCCTTAATGTCACGCACGATTTC-3′. PCR was conducted using a thermocycler (model PTC-200, MJ Research Inc., Reno, NV) with one cycle for 5 min at 94 °C, followed by 30 cycles for 30 s at 94 °C, 45 s at 58 °C, and 45 s at 72 °C, and finally one cycle for 5 min at 72 °C. All amplified PCR products were subjected to 1.5% agarose gel electrophoresis and visualized with a UV illuminator. The intensity of the separated bands of DNA was quantified using a gel documentation system (model LAS-1000CH, Fuji Photo Film Co., Tokyo, Japan).

Western Blot Analysis of Cell Proteins. The BPP-treated RAW 264.7 cells were lysed and extracted using RIPA buffer (50 mM Tris Cl, 150 mM NaCl, 1% NP-40, 0.5% sodium deoxycholate, 0.1% SDS, and 1 mM EDTA, pH 7.4). Protein concentrations were determined by the Bradford method using a Bio-Rad Protein kit. Bovine serum albumin (BSA) was used as standard. The cell extract containing proteins (30 μg) was separated on 10% SDS−polyacrylamide gels and electrophoretically transferred onto nitrocellulose membrane (Millipore, Billerica, MA, USA). After blocking with 5% skim milk, the membrane was incubated with rabbit anti-mouse iNOS polyclonal antibody (Cell signaling Tech., Danvers, MA, USA) or anti-mouse β-actin monoclonal antibody (Millipore), followed by HRP-conjugated anti-IgG antibodies. Blots were developed using the ECL detection kit (Pierce, Rockford, IL, USA). The intensity of separated protein bands was quantified using a gel documentation system (model LAS-1000CH, Fuji Photo Film Co., Tokyo, Japan). At least three separate replicates were determined for each experiment.

Statistical Analysis. Results are expressed as the mean ± SD of three independent experiments. Significant differences between means were determined by ANOVA test using the Statistical Analysis Software package SAS (Cary, NC, USA). $p < 0.05$ is regarded as significant.

RESULTS AND DISCUSSION

Structure of BPP. The method we used to prepare the polysaccharide is widely used for the isolation and purification of glucans. Results from our previous study,[2] and in the present study (Table 1), suggest that BPP has a beta-glucan structure. Additional observations showed that the sharpness of the HPLC peak depends on the amount of the sample loaded on the chromatographic column. We observed sharper peaks with smaller amounts (results not shown). We cannot rule out the possibility that components other than glucan, possibly a bound protein as observed by Sanzen et al.[14] in a related study, may contribute to the observed immunostimulation described below.

Table 1. β-Glucan Content of BPPs[a]

sample	β-glucan (% of dry wt)
BPP from culture with black rice bran	0.75 ± 0.02 a
BPP from culture without black rice bran	0.40 ± 0.01 b
black rice bran only	0.03 ± 0.00 c

[a]Values expressed as means ± SD ($n = 3$) in the column with the same letters are not significantly different at $p < 0.05$.

Effect of BPP on in Vitro Growth of *Salmonella*. To find out whether BPP has antibacterial activity against *S.* Typhimurium, bacteria were incubated with serially diluted extracts in PBS (1, 10, and 100 μg/mL) at 37 °C for 0, 2, 4, and 8 h. Figure 1 shows that bacteria treated with the extracts at each concentration for different incubation times showed no significant bactericidal activities until 8 h incubation compared to that of vehicle (PBS). The data show that BPP did not kill bacteria directly. We observed similar results with *Hericium erinaceus* mushroom extracts.[5]

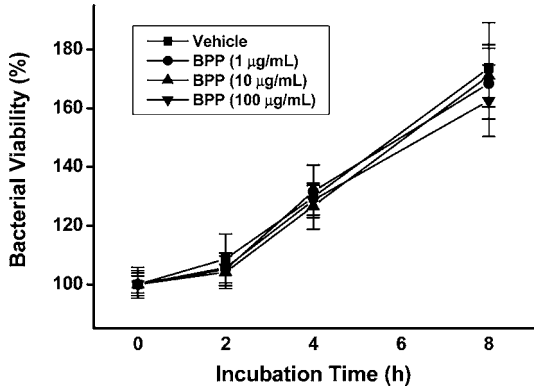

Figure 1. Effects of BPP on growth of *S.* Typhimurium. Serially diluted BPP (1, 10, and 100 μg/mL) was incubated with *S.* Typhimurium (2×10^4 CFU) for 2, 4, and 8 h. Plotted values are mean ± SD of triplicate experiments.

Induction of Morphologic Changes in Macrophages. To determine whether BPP can induce changes in the morphology in the macrophage cells, RAW 264.7 cells were cultivated in the presence of the extract (100 μg/mL) for 2, 4, and 8 h. The microscopic observation of cell morphology revealed that the cells treated with BPP changed to dendrite-like cells (Figure 2), reaching up to 3.6-, 10.3-, and 12.4-fold increases corresponding to the incubation times. Dendritic morphologic changes were not observed with PBS-treated controls regardless of incubation times.

Phagocytotic Stimulatory Effects of BPP. To examine whether BPP enhances phagocytotic activity, RAW 264.7 cells were cultivated in the presence of three concentrations (1, 10, and 100 μg/mL) for 4 h before infection. Thereafter, the *S.* Typhimurium cells were incubated for 30 and 60 min before they were lysed and contents enumerated for bacteria. Figure 3 shows that, after 60 min of incubation, the internalization of bacteria into the macrophage cells increased in a dose-dependent manner. The bacterial uptake rates of macrophages treated with 1, 10, and 100 μg/mL BPP were about 1.4-, 2.4-, and 3.5-fold greater than that of macrophages treated with the PBS control. The phagocytotic stimulatory effect of BPP was also evaluated in vivo in a mouse model. As described in Table 2, administration of the BPP via both oral and ip routes, respectively, elicited higher bactericidal effects than that of

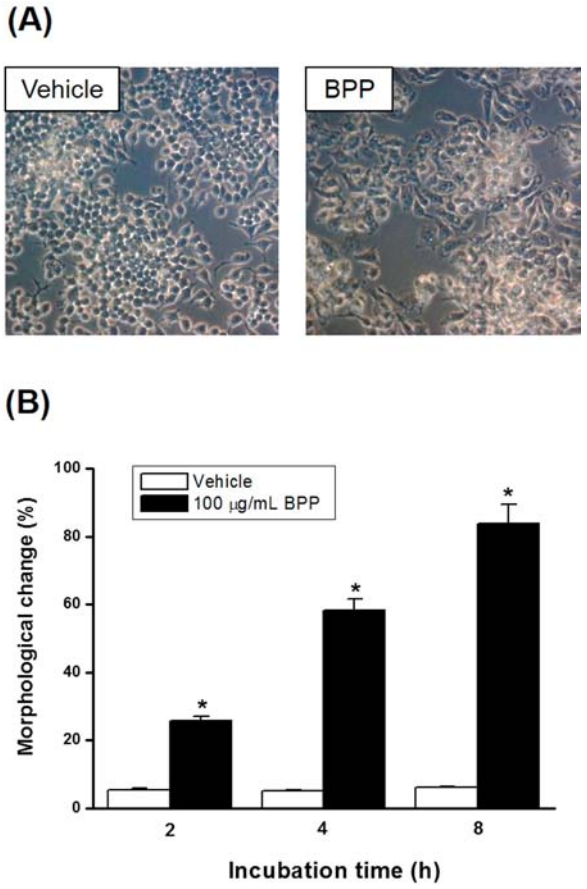

Figure 2. Effects of BPP extract on morphologic changes in macrophages. Murine macrophage cell line RAW 264.7 cells were cultured in the presence of BPP (100 μg/mL) for 2, 4, and 8 h. (A) After 8 h incubation, the morphologic changes were photographed at 100× magnification. (B) One hundred cells in five blindly chosen random fields were examined per coverslip, and the rates of morphologically changed cells were scored. Data are expressed as the mean ± SD of triplicate experiments. Asterisks indicate statistical difference at $p < 0.05$, compared to each vehicle (PBS)-treated control.

vehicle (about 48 and 44% decreases in bacterial CFU by ip and oral administration, respectively).

Effects of the BPP on Intracellular Bacterial Survival. To examine whether the BPP affects *S.* Typhimurium survival within macrophage cells, RAW 264.7 cells were treated with three concentrations of the extract (1, 10, and 100 μg/mL) for 4 h and then infected with the bacterial for 1 h. After removal of bacteria from the culture medium, infected macrophages were incubated for another 2, 4, or 8 h in the presence of gentamicin. Figure 4 shows that, 2 h after infection, the intracellular growth of *S.* Typhimurium within the cells treated with 1, 10, and 100 μg/mL BPP was about 6.9, 45.0, and 87.8% greater than that of the PBS-treated control, respectively. However, 8 h after infection, marked decreases in intracellular bacteria were observed in the cells treated with each concentration of BPP (about 12.2, 52.7, and 65.0% decreases by 1, 10, and 100 μg/mL BPP treatments, respectively) compared with the PBS-treated control.

The apparent discrepancy might be due to the fact that at 2 h after bacterial infection, the amount of bacteria in BPP-treated cells was greater than in vehicle-treated cells due to enhanced engulfment of bacteria by the BPP treatment. In contrast, at 4 h and 8 h postinfection, bacteria cell levels in BPP-treated cells were markedly reduced compared with vehicle-treated cells, probably because of time-dependent enhancement of intracellular bacteriolysis by the BPP treatment through activation of Th1 immune reaction.

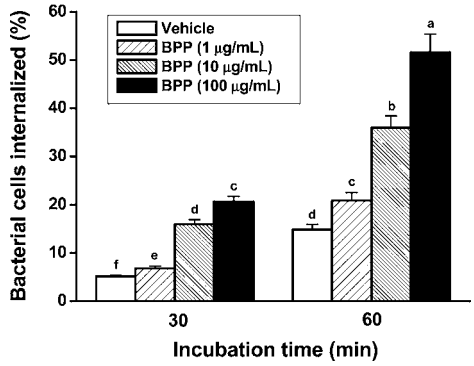

Figure 3. Changes in phagocytotic stimulatory effects of BPP on *S.* Typhimurium-infected macrophages. Murine macrophage cell line RAW 264.7 cells (1×10^4) were incubated with three concentrations of BPP (1, 10, and 100 μg/mL) for 4 h, and then infected with *S.* Typhimurium (1×10^4 CFU). Incubation continued at 37 °C for the indicated periods. After incubation, bacteria-infected macrophages were then cultured in the presence of gentamicin (30 μg/mL) for 30 min. Bacterial internalization efficiency by macrophages was determined by evaluating the protection of internalized bacteria from bactericidal action of the antibiotic gentamicin. Data are expressed as the mean ± SD of triplicate experiments. Bars sharing a common letter are not significantly different at $p < 0.05$.

Table 2. Effect of BPP on the Growth of *S.* Typhimurium Inoculated into Mouse Peritoneal Cavity[a]

treatment	colony numbers (×10^2 CFU/mL)
vehicle	5.02 ± 0.15 a
BPP ip (10 mg/kg)	2.59 ± 0.08 c
BPP oral (10 mg/kg)	2.83 ± 0.11 b

[a]Values are expressed as the mean ± SD of triplicate experiments. Values with the same letters in the column are not significantly different at $p < 0.05$.

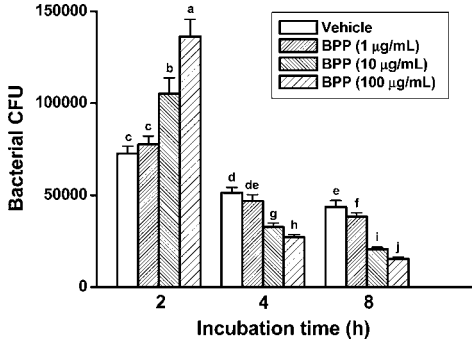

Figure 4. Survival and/or proliferation of *S.* Typhimurium within the BPP-treated macrophages. Murine macrophage cell line RAW 264.7 cells (1×10^4) were incubated with three concentrations of the BPP (1, 10, and 100 μg/mL) for 4 h and then infected with *S.* Typhimurium (1×10^4 CFU) at 37 °C for 1 h. The cells were washed and then further incubated in the presence of gentamicin (30 μg/mL) for the indicated periods. At each time point, the cells were lysed and the number of viable intracellular bacteria counted. Data are expressed as the mean ± SD of triplicate experiments. Bars sharing a common letter are not significantly different at $p < 0.05$.

dx.doi.org/10.1021/jf405223q | J. Agric. Food Chem. 2014, 62, 2384−2391

Salmonella–Immune System Relationships. To facilitate understanding the results and interpretations of the present study, we will briefly mention reported studies designed to define the role of the immune system following infection by *Salmonella* that complement our related studies with mushroom, herbal, and liquid rice hull extracts.

- The innate host defense against intracellular pathogens seems to involve signaling pathways by which macrophages inhibit replication of *Salmonella* Typhimurium by triggering the MEK kinase cascade and NADPH oxidase activity.[15]
- Dendritic cells (DCs) link innate and adaptive immunity by recognizing pathogen-associated molecular patterns (PAMPs) to specialized receptors on their surface. *Salmonella* have developed molecular mechanisms based on virulence proteins to alter DC function and suppress the immune response to cause infection in the host.[16]
- A mechanism also exists that prevents virulent *Salmonella* from evading cell uptake, thus enhancing DC immunogenicity, bacterial degradation, and induction of innate and adaptive immune pathways.[17,18]
- Feeding mice a cornstarch-based diet with added fructo-oligosaccharide (FOS) or xylo-oligosaccharide (XOS) increased the translocation of *S.* Typhimurium SL1344 to internal organs, whereas feeding 10% apple pectin increased the intestinal and fecal content of this pathogen, suggesting that the mentioned prebiotics increased the severity of the *Salmonella* infection.[19]

The results of the present study indicate that the macrophage cells associated with the immune system seem to have a strong affinity for *Salmonella* bacteria, and that the BPP treatment induced internalization of the bacteria in the cells. Our results are consistent with the above-mentioned observations in the literature on the interactions of *Salmonella* with the immune system.

Effects of BPP on Leukocyte Activation in Infected Mice. To evaluate whether BPP activates leukocytes in *S.* Typhimurium infected mice, we also determined mitogen-induced splenic lymphocyte proliferation and IFN-γ levels in sera. As shown in Table 3, administration of BPP markedly induced splenic lymphocyte proliferation by Con A stimulation (about 46.3 and 34.9% increases by the treatment by ip and oral routes, respectively). Serum IFN-γ level in *S.* Typhimurium-infected mice was also increased by the treatment with BPP (about 32.0 and 21.3% increases by ip and oral treatment, respectively). As anticipated, the treatment through the ip route was more effective than oral administration to induce IFN-γ production, most probably by more effective peritoneal macrophage stimulation.

Table 3. Effect of BPP on Spleen Lymphocyte Proliferation and Serum IFN-α Levels in *S* Typhimurium Infected Mice[a]

treatment	lymphocyte proliferation (fold-increase)	IFN-γ (pg/mL)
vehicle	1.49 ± 0.11 b	309 ± 18 b
BPP ip (10 mg/kg)	2.18 ± 0.15 a	408 ± 21 a
BPP oral (10 mg/kg)	2.01 ± 0.12 a	375 ± 15 a

[a]Values are expressed as the mean ± SD of triplicate experiments. Values with the same letters in the column are not significantly different at $p < 0.05$.

Because NO generation by iNOS is an index of macrophage activation, RT-PCR was used to examine whether the BPP treatment elicited inducible NO synthase (iNOS) gene expression in RAW264.7 murine macrophage cells. Figure 5A shows that, for 8 h, iNOS expression by BPP-treated cells was ~3.4-fold greater than in the cells infected with *S.* Typhimurium without BPP. The BPP treatment without *S.* Typhimurium infection induced iNOS expression to the same level in the bacteria-infected cells with BPP treatment (~3.5-fold increase). Western blot analysis shows that the iNOS protein expression profile was similar to that of the mRNA expression (Figure 5B).

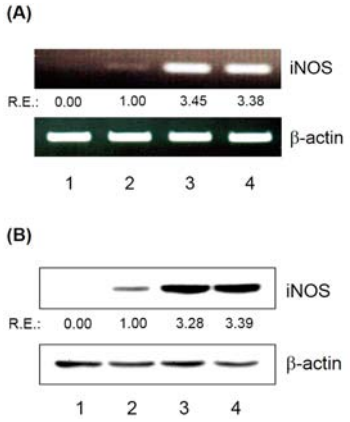

Figure 5. Effects of BPP on iNOS gene expression in *S.* Typhimurium-infected macrophages. (A) iNOS mRNA expression profiles assessed by RT-PCR. Murine macrophage cell line RAW 264.7 cells (1×10^6) were cultured with or without BPP (100 μg/mL) for 8 h. Then, *S.* Typhimurium (1×10^4 CFU) was added to RAW 264.7 cells for 8 h. After incubation, total RNA was purified and iNOS mRNA expression was determined using RT-PCR analysis. Lanes: 1, PBS-treated without bacterial infection; 2, bacterial infection alone; 3, BPP-treated without bacterial infection; 4, BPP-treated with bacterial infection. (B) iNOS polypeptide expression profiles assessed by Western blot. RAW 264.7 cells (1×10^6) treated with BPP (100 μg/mL) for 24 h and subsequent infection of *S.* Typhimurium were lysed and iNOS protein in the cell lysate was identified by Western blot using anti-mouse iNOS polyclonal antibody. Lanes: 1, PBS-treated without bacterial infection; 2, bacterial infection alone; 3, BPP-treated without bacterial infection; 4, BPP-treated with bacterial infection. The relative proportions of iNOS mRNA and polypeptide are expressed as the R.E. (relative expression) values calculated from iNOS gene/β-actin gene expression. Figures represent results from at least three individual experiments.

Effect of BPP on Th1 and Th2 Cytokine Production. To examine whether BPP has the capacity to regulate the differentiation pathway of CD4 T cells, changes in Th1 and Th2 cytokine production profiles were determined by ELISA assay. Table 4 shows that BPP administration (10 mg/kg) through both peritoneal and oral routes significantly increases Th1 cytokine production including IL-1β, IL-2, IL-6, and IL-12 from splenocyte in *S.* Typhimurium-infected mice. In contrast, BPP administration did not lead to the enhanced Th2 cytokine production including IL-4, IL-5, and IL-10 in the bacterial infected mice (Table 5).

The results imply that BPP can differentiate native CD4 T cells into Th1 cells, thereby potentiating cell-mediated immunity,[20] presumably by the above-described mechanisms.

Table 4. Effect of BPP on the Th1 Cytokine Production from Splenocytes in Mice[a]

	cytokines (pg/mL)			
treatment	IL-1β	IL-2	IL-6	IL-12
	Salmonella (−)			
vehicle	188 ± 11 c	44.6 ± 2.3 d	60.6 ± 2.9 b	252 ± 13 c
BPP ip (10 mg/kg)	205 ± 12 c	42.7 ± 3.3 d	61.0 ± 3.4 b	259 ± 10 c
BPP oral (10 mg/kg)	203 ± 15 c	45.3 ± 1.6 d	58.5 ± 2.2 b	263 ± 11 bc
	Salmonella (+)			
vehicle	235 ± 14 b	58.4 ± 2.0 c	71.2 ± 3.6 a	290 ± 18 b
BPP ip (10 mg/kg)	274 ± 16 a	75.8 ± 3.4 a	78.0 ± 3.6 a	358 ± 16 a
BPP oral (10 mg/kg)	261 ± 11 a	66.1 ± 2.9 b	75.1 ± 2.7 a	337 ± 16 a

[a]Values are expressed as the mean ± SD of triplicate experiments. Values with the same letters in the column are not significantly different at $p < 0.05$.

Table 5. Effect of BPP on the Th2 Cytokine Production from Splenocytes in Mice[a]

	cytokines (pg/mL)		
treatment	IL-4	IL-5	IL-10
	Salmonella (−)		
vehicle	56.0 ± 2.9 ab	283 ± 18 a	49.6 ± 1.1 a
BPP ip (10 mg/kg)	55.7 ± 4.9 ab	286 ± 16 a	50.0 ± 4.2 a
BPP oral (10 mg/kg)	52.6 ± 2.5 b	283 ± 12 a	48.3 ± 1.2 a
	Salmonella (+)		
vehicle	62.7 ± 3.1 a	302 ± 16 a	53.5 ± 3.1 a
BPP ip (10 mg/kg)	63.6 ± 3.9 a	304 ± 22 a	54.0 ± 4.0 a
BPP oral (10 mg/kg)	65.0 ± 4.4 a	305 ± 14 a	54.1 ± 4.4 a

[a]Values are expressed as the mean ± SD of triplicate experiments. Values with the same letters in the column are not significantly different at $p < 0.05$.

Effects of BPP on Histopathology of Mouse Livers. To examine whether BPP can ameliorate liver injury induced by salmonellosis, mice were treated ip or orally with BPP (10 mg/kg) every 24 h for 2 d after intraperitoneal infection of a sublethal dose (1×10^4 CFU) of *S.* Typhimurium. Figure 6 shows that extensive liver necrosis and hemorrhage were present in the tissues from *Salmonella*-infected control mice. However, liver tissues from bacteria-infected mice treated with BPP showed minimal damage, regardless of the administration route. These results show that BPP protected the livers against *Salmonella*-induced hepatic necrosis.

Effects of BPP on Mortality of Infected Mice. To determine possible therapeutic effects of BPP on murine salmonellosis, mice were infected with lethal doses (1×10^5 CFU) of *S.* Typhimurium and assessed for mortality. Each group of 10 mice was treated with BPP (10 mg/kg) ip or orally every 24 h during the entire experimental period. Figure 7 shows that the mortality rate in the PBS-treated control group was 100% on day 7. However, the groups treated with BPP survived until at least day 23 or longer. Ip administration of BPP was more effective in prolonging the lifespan of the mice than administration by the oral route. These observations demonstrate the potential of BPP to protect mice against the

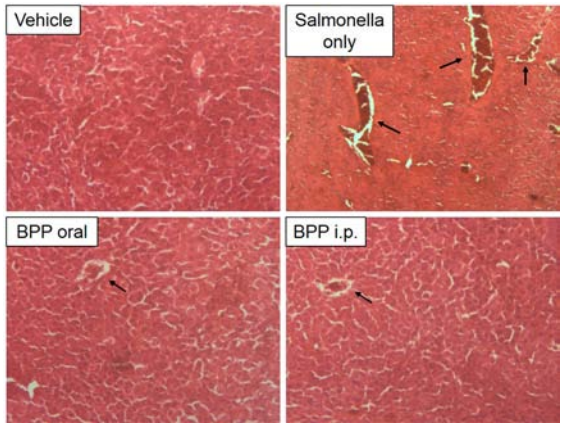

Figure 6. Effect of the BPP on the formation of pathological lesions in liver of *S.* Typhimurium-infected mice. Liver specimens from BPP-treated mice (10 mg/kg) infected with *S.* Typhimurium (1×10^4 CFU) were fixed with 4% paraformaldehyde. The sections were then stained with hematoxylin and eosin (H&E). Magnification 100×. Arrows indicate representative hemorrhagic necrosis. Figures represent results from at least three individual experiments.

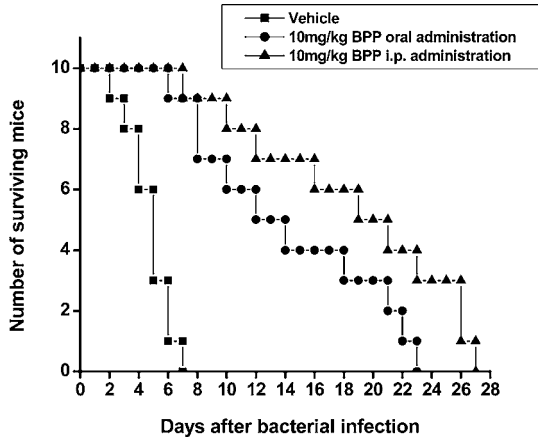

Figure 7. Histogram showing effect of BPP on *S.* Typhimurium infection-induced lethality. Balb/c mice (10 mice per group) were infected with lethal doses of *S.* Typhimurium (1×10^5 CFU) through the intraperitoneal route. Then, the extract (10 mg/kg) was intraperitoneally or orally administered every 24 h during the entire experimental period. PBS was used as the vehicle in the control group. Plotted values are mean values of triplicate determinations.

lethal effects of the bacteria, presumably via Th1 cell-mediated macrophage stimulation of the immune system.

Beta-glucan might be the active component that induces Th1 cell-mediated macrophage stimulation. This suggestion is supported by the finding that β-glucan content was highest in BPP prepared from *L. edodes* mycelial culture with black rice bran compared with that from mycelia or black rice bran only (Table 1).

Related Studies on Immunoprevention of *Salmonella* Infections. Here, we briefly mention several additional reported studies on the in vivo inhibition of *Salmonella* by natural compounds and plant extracts.

- Beta-glucan acted as an immunomodulator of the innate immune response in immature chickens that decreased organ invasion of *S. enterica*.[21]
- A safety evaluation of a mushroom β-glucan showed that the compound was not mutagenic and exhibited no

dx.doi.org/10.1021/jf405223q | J. Agric. Food Chem. 2014, 62, 2384−2391

observed adverse effect level (NOAEL) in rats at the highest dose of 2000 mg/kg/bw/day tested,[22] suggesting that BPP, which also seems to have a β-glucan structure, might also be safe.

- A study of the effect of an aqueous extract of the roots of the Indian herbal plant *Withania somnifera* on T helper (Th) immunity in mice using flow cytometry indicated selective Th1 upregulation, suggesting its use for selective Th1/Th2 modulation.[23]
- A water extract of the herb *Houttuynia cordata* extended the lifespan of mice infected with a lethal dose of *S.* Typhimurium in a dose-dependent manner, suggesting that the extract has the potential to be used in the treatment of bacterial infection.[12]
- A water extract of the roots of the Indian medicinal plant *Asparagus racemosus* containing steroidal saponins exhibited immunoadjuvant potential, as indicated by significant upregulation of Th1 (IL-2, IFN-γ, and IL-4) cytokines, suggesting its mixed Th1/Th2 adjuvant activity.[20]

It would be of interest to find out whether combinations of BPP with the above-mentioned natural compounds and plant extracts would exhibit additive or synergistic health-promoting effects.

Summary and Research Needs. We evaluated the natural biopolymer, previously shown to protect mice against *Salmonella* lipopolysaccharide-induced endotoxemia, to protect mice against *S.* Typhimurium-induced sublethal and lethal infections. Administration of BPP by ip injection or by the oral route protected the mice against both liver necrosis and lethality. BPP administered by ip was more effective than that delivered by oral feeding. The protective effect was accompanied by stimulation of innate immune cells, as demonstrated by a series of in vitro and in vivo assays. Because the previous and present studies show that BPP can protect against both endotoxemia and infection without any adverse side effects in mice, it seems that the novel biopolymer has the potential to serve as a multifunctional food.

Our observations suggest the need for additional studies that might further enhance the health-promoting characteristics of BPP. These include the following possibilities.

- Because outbreaks and exposures associated with *Salmonella enterica* occur worldwide,[24−26] it would be of interest to find out whether human consumption of BPP as part of a normal diet would protect indigenous populations and travelers against infection by *Salmonella*.
- Because *Salmonella* is a major foodborne pathogen that develops resistance to medical antibiotics,[27−29] it would be of interest to find out whether BPP would also protect against antibiotic-resistant *Salmonella* and other pathogens such as *Escherichia coli, Listeria monocytogenes, Staphylococcus aureus,* and *Vibrio cholerae*.
- It would be of interest to determine whether herbal or liquid rice hull extracts would also stimulate the production of BPP in mushroom mycelia.

Because exposure of contaminated food to natural antimicrobials might be only partly effective in inactivating virulent foodborne pathogens[30−32] and toxins[33−38] produced by the pathogens and by plants, it would also be worthwhile to determine whether adding BPP to food would protect animals and humans against residual levels of pathogens and toxins after consumption via stimulation of the immune system.

AUTHOR INFORMATION

Corresponding Authors

*S.H.N.: phone, 82-31-219-2619; fax, 82-31-219-1615; e-mail, shnam@ajou.ac.kr.

*M.F.: e-mail, Mendel.Friedman@ars.usda.gov.

Notes

The authors declare no competing financial interest.

ACKNOWLEDGMENTS

We thank Carol E. Levin for facilitating preparation of the manuscript.

ABBREVIATIONS USED

BPP, bioprocessed polymer; CD-4, helper T cells that promote adhesion to antigen-presenting cells and to B cells in response to infection; CFU, colony-forming units; Con A, concanavalin A; DCs, dendritic cells of the immune system whose main function is to present antigen material to the surface of T cells; ELISA, enzyme-linked immunosorbent assay; dNTP, deoxyribonucleotide triphosphate; FBS, fetal bovine serum; FOS, fructo-oligosaccharide; HBSS, Hanks balanced salt solution; IgG, immunoglobulin G; IL-1β, interleukin 1β; IFN-γ, interferon-γ; iNOS, inducible nitric oxide (NO) synthase; ip, intraperitoneal; LPS, lipopolysaccharide; MEK, mitogen-activated protein kinase/extracellular signal-regulated kinase; MTS, (3-[(4,5-dimethylthiazol-2-yl)-5-(3-carboxymethoxyphenyl)-2-(4-sulfophenyl)-2*H*-tetrazolium)]; NA medium, nutrient agar medium; NADPH, reduced form of nicotine adenine dinucleotide phosphate; NB medium, nutrient broth medium; NOAEL, no observed adverse effect level; *p*-NPP, *p*-nitrophenyl phosphate; PAMPs, pathogen-associated molecular patterns; PBS, phosphate-saline buffer; PDA, potato dextrose agar medium; RPMI 1640 medium, Roswell Park Memorial Institute medium; RT-PCR, reverse transcription polymerase chain reaction; Th1/Th2 cells, functionally subclasses of helper T cells that recognize the presence of microorganisms and stimulate macrophages to destroy invading pathogens; XOS, xylo-oligosaccharide

REFERENCES

(1) Centers for Disease Control and Prevention. *Salmonella: What is Salmonellosis?* http://www.cdc.gov/salmonella/general/index.html (accessed Nov 12, 2013).

(2) Kim, S. P.; Park, S. O.; Lee, S. J.; Nam, S. H.; Friedman, M. A polysaccharide isolated from the liquid culture of *Lentinus edodes* (Shiitake) mushroom mycelia containing black rice bran protects mice against a *Salmonella* lipopolysaccharide-induced endotoxemia. *J. Agric. Food Chem.* **2013**, *61*, 10987−10994.

(3) Hurley, J. C.; Guidet, B.; Offenstadt, G.; Maury, E. Endotoxemia and mortality prediction in ICU and other settings: underlying risk and co-detection of gram negative bacteremia are confounders. *Crit. Care* **2012**, DOI: 10.1186/cc11462.

(4) Hurley, J. C.; Opal, S. M. Prognostic value of endotoxemia in patients with Gram-negative bacteremia is bacterial species dependent. *J. Innate Immun.* **2013**, *5*, 555−564.

(5) Kim, S. P.; Moon, E.; Nam, S. H.; Friedman, M. *Hericium erinaceus* mushroom extracts protect infected mice against *Salmonella* Typhimurium-induced liver damage and mortality by stimulation of innate immune cells. *J. Agric. Food Chem.* **2012**, *60*, 5590−5596.

(6) Kim, S. P.; Moon, E.; Nam, S. H.; Friedman, M. Composition of Herba Pogostemonis water extract and protection of infected mice against *Salmonella* Typhimurium-induced liver damage and mortality by stimulation of innate immune cells. *J. Agric. Food Chem.* **2012**, *60*, 12122−12130.

(7) Kim, S. P.; Kang, M. Y.; Park, J. C.; Nam, S. H.; Friedman, M. Rice hull smoke extract inactivates *Salmonella* Typhimurium in laboratory media and protects infected mice against mortality. *J. Food Sci.* **2012**, *77*, M80−M85.
(8) Lu, S.; Manges, A. R.; Xu, Y.; Fang, F. C.; Riley, L. W. Analysis of virulence of clinical isolates of *Salmonella enteritidis* in vivo and in vitro. *Infect. Immun.* **1999**, *67*, 5651−5657.
(9) Kodama, N.; Yamada, N.; Nanba, H. Addition of *Maitake* D-fraction reduces the effective dosage of vancomycin for the treatment of *Listeria*-infected mice. *Jpn. J. Pharmacol.* **2001**, *87*, 327−332.
(10) Misko, T. P.; Schilling, R. J.; Salvemini, D.; Moore, W. M.; Currie, M. G. A fluorometric assay for the measurement of nitrite in biological samples. *Anal. Biochem.* **1993**, *214*, 11−16.
(11) Teixeira, S. T.; Valadares, M. C.; Gonçalves, S. A.; de Melo, A.; Queiroz, M. L. S. Prophylactic administration of *Withania somnifera* extract increases host resistance in *Listeria monocytogenes* infected mice. *Int. Immunopharmacol.* **2006**, *6*, 1535−1542.
(12) Kim, G. S.; Kim, D. H.; Lim, J. J.; Lee, J. J.; Han, D. Y.; Lee, W. M.; Jung, W. C.; Min, W. G.; Won, C. G.; Rhee, M. H.; Lee, H. J.; Kim, S. Biological and antibacterial activities of the natural herb *Houttuynia cordata* water extract against the intracellular bacterial pathogen *Salmonella* within the RAW 264.7 macrophage. *Biol. Pharm. Bull.* **2008**, *31*, 2012−2017.
(13) Chomczynski, P.; Sacchi, N. Single-step method of RNA isolation by acid guanidinium thiocyanate-phenol-chloroform extraction. *Anal. Biochem.* **1987**, *162*, 156−159.
(14) Sanzen, I.; Imanishi, N.; Takamatsu, N.; Konosu, S.; Mantani, N.; Terasawa, K.; Tazawa, K.; Odaira, Y.; Watanabe, M.; Takeyama, M.; Ochiai, H. Nitric oxide-mediated antitumor activity induced by the extract from *Grifola frondosa* (Maitake Mushroom) in a macrophage cell line, RAW264.7. *J. Exp. Clin. Cancer Res.* **2001**, *20*, 591−597.
(15) Rosenberger, C. M.; Brett Finlay, B. Macrophages inhibit *Salmonella* Typhimurium replication through MEK/ERK kinase and phagocyte NADPH oxidase activities. *J. Biol. Chem.* **2002**, *277*, 18753−18762.
(16) Bueno, S. M.; Riquelme, S.; Riedel, C. A.; Kalergis, A. M. Mechanisms used by virulent *Salmonella* to impair dendritic cell function and evade adaptive immunity. *Immunology* **2012**, *137*, 28−36.
(17) Riquelme, S. A.; Bueno, S. M.; Kalergis, A. M. IgG keeps virulent *Salmonella* from evading dendritic cell uptake. *Immunology* **2012**, *136*, 291−305.
(18) Martins, R. P.; Lorenzi, V.; Arce, C.; Lucena, C.; Carvajal, A.; Garrido, J. J. Innate and adaptive immune mechanisms are effectively induced in ileal Peyer's patches of *Salmonella* Typhimurium infected pigs. *Dev. Comp. Immunol.* **2013**, *41*, 100−104.
(19) Petersen, A.; Heegaard, P. M. H.; Pedersen, A. L.; Andersen, J. B.; Sørensen, R. B.; Frøkiær, H.; Lahtinen, S. J.; Ouwehand, A. C.; Poulsen, M.; Licht, T. R. Some putative prebiotics increase the severity of *Salmonella enterica* serovar Typhimurium infection in mice. *BMC Microbiol.* **2009**, DOI: 10.1186/1471-2180-9-245.
(20) Gautam, M.; Saha, S.; Bani, S.; Kaul, A.; Mishra, S.; Patil, D.; Satti, N. K.; Suri, K. A.; Gairola, S.; Suresh, K.; Jadhav, S.; Qazi, G. N.; Patwardhan, B. Immunomodulatory activity of *Asparagus racemosus* on systemic Th1/Th2 immunity: Implications for immunoadjuvant potential. *J. Ethnopharmacol.* **2009**, *121*, 241−247.
(21) Lowry, V. K.; Farnell, M. B.; Ferro, P. J.; Swaggerty, C. L.; Bahl, A.; Kogut, M. H. Purified β-glucan as an abiotic feed additive up-regulates the innate immune response in immature chickens against *Salmonella enterica* serovar Enteritidis. *Int. J. Food Microbiol.* **2005**, *98*, 309−318.
(22) Chen, S. N.; Nan, F. H.; Chen, S.; Wu, J. F.; Lu, C. L.; Soni, M. G. Safety assessment of mushroom β-glucan: Subchronic toxicity in rodents and mutagenicity studies. *Food Chem. Toxicol.* **2011**, *49*, 2890−2898.
(23) Bani, S.; Gautam, M.; Sheikh, F. A.; Khan, B.; Satti, N. K.; Suri, K. A.; Qazi, G. N.; Patwardhan, B. Selective Th1 up-regulating activity of *Withania somnifera* aqueous extract in an experimental system using flow cytometry. *J. Ethnopharmacol.* **2006**, *107*, 107−115.
(24) Andrews, H. L.; Bäumler, A. J. *Salmonella species*. In *Foodborne Pathogens - Microbiology and Molecular Biology*. Fratamico, P. M., Bhunia, A. K., and Smith, J. L., Eds.; Caister Academic Press: Norfolk, U.K., 2005; pp 327−339.
(25) Kim, J.; Hyeon, J. Y.; Lee, E.; Lee, D.; Kim, Y. J.; Kim, S. Molecular epidemiological analysis of five outbreaks associated with *Salmonella enterica* serovar Enteritidis between 2008 and 2010 on Jeju Island, Republic of Korea. *Foodborne Pathog. Dis.* **2014**, *11*, 38−42.
(26) Meltzer, E.; Stienlauf, S.; Leshem, E.; Sidi, Y.; Schwartz, E. A large outbreak of *Salmonella* Paratyphi A Infection among Israeli travelers to Nepal. *Clin. Infect. Dis.* **2014**, *58*, 359−364.
(27) Choudhary, A.; Gopalakrishnan, R.; Senthur Nambi, P.; Ramasubramanian, V.; Abdul Ghafur, K.; Thirunarayan, M. A. Antimicrobial susceptibility of *Salmonella enterica* serovars in a tertiary care hospital in Southern India. *Indian J. Med. Res.* **2013**, *137*, 800−802.
(28) Gupta, V.; Singla, N.; Bansal, N.; Kaistha, N.; Chander, J. Trends in the antibiotic resistance patterns of enteric fever isolates - A three year report from a tertiary care centre. *Malays. J. Med. Sci.* **2013**, *20*, 71−75.
(29) Paytubi, S.; Aznar, S.; Madrid, C.; Balsalobre, C.; Dillon, S. C.; Dorman, C. J.; Juárez, A. A novel role for antibiotic resistance plasmids in facilitating *Salmonella* adaptation to non-host environments. *Environ. Microbiol.* **2013**, DOI: 10.1111/1462-2920.12244.
(30) Todd, J.; Friedman, M.; Patel, J.; Jaroni, D.; Ravishankar, S. The antimicrobial effects of cinnamon leaf oil against multi-drug resistant *Salmonella* Newport on organic leafy greens. *Int. J. Food Microbiol.* **2013**, *166*, 193−199.
(31) Chen, C. H.; Ravishankar, S.; Marchello, J.; Friedman, M. Antimicrobial activity of plant compounds against *Salmonella* Typhimurium dt104 in ground pork and the influence of heat and storage on the antimicrobial activity. *J. Food Prot.* **2013**, *76*, 1264−1269.
(32) Juneja, V. K.; Gonzales-Barron, U.; Butler, F.; Yadav, A. S.; Friedman, M. Predictive thermal inactivation model for the combined effect of temperature, cinnamaldehyde and carvacrol on starvation-stressed multiple *Salmonella* serotypes in ground chicken. *Int. J. Food Microbiol.* **2013**, *165*, 184−199.
(33) Rasooly, R.; Do, P. M.; Griffey, S. M.; Vilches-Moure, J. G.; Friedman, M. Ingested Shiga toxin 2 (Stx2) causes histopathological changes in kidney, spleen and thymus tissues and mortality in mice. *J. Agric. Food Chem.* **2010**, *58*, 9281−9286.
(34) Rasooly, R.; Do, P. M.; Levin, C. E.; Friedman, M. Inhibition of Shiga toxin 2 (Stx2) in apple juices and its resistance to pasteurization. *J. Food Sci.* **2010**, *75*, M296−M301.
(35) Rasooly, R.; Do, P. M.; Friedman, M. Inhibition of biological activity of staphylococcal enterotoxin A (SEA) by apple juice and apple polyphenols. *J. Agric. Food Chem.* **2010**, *58*, 5421−5426.
(36) Friedman, M.; Rasooly, R.; Do, P. M.; Henika, P. R. The olive compound 4-hydroxytyrosol inactivates *Staphylococcus aureus* bacteria and staphylococcal enterotoxin A (SEA). *J. Food Sci.* **2011**, *76*, M558−M563.
(37) Rasooly, R.; He, X.; Friedman, M. Milk inhibits the biological activity of ricin. *J. Biol. Chem.* **2012**, *287*, 27924−27929.
(38) Friedman, M.; Rasooly, R. Review of the inhibition of biological activities of food-related selected toxins by natural compounds. *Toxins* **2013**, *5*, 743−775.

ampholyte-free preparative isoelectric focusing, which is referred to as autofocusing, using the method described by Hashimoto et al.,[12] using an autofocusing apparatus with 10 sample compartments (75 mm in length × 80 mm in width × 85 mm in height for each compartment). The water extract was placed in sample compartments 5 and 6. The other compartments were filled with deionized water. Autofocusing was carried out at 500 V for 18 h. The autofocusing fractions were freeze-dried.

The autofocusing fraction that exerted antihyperuricemic activity after alcalase digestion was subjected to preparative reversed-phase liquid chromatography. YFLC gel C18 (particle size of 40 μm in diameter, Yamazen, Osaka, Japan) was packed into a column (250 × 15 mm inner diameter) and equilibrated with 10% (v/v) acetonitrile in the presence of 0.1% TFA. A total of 2 g of the dried active autofocusing fraction without alcalase digestion was dissolved in 100 mL of the equilibrium solvent and loaded into the column using a MPLC system (Yamazen) at 10 mL/min. After loading of the sample, the column was washed with 100 mL of the equilibrium solvent. After elution of the non-absorbed components, the absorbed components were eluted with a linear gradient of acetonitrile from 10 to 80% in the presence of 0.1% TFA over 20 min. Fractions were collected every 1 min. Elution was monitored by absorbance at 280 nm.

Alcalase Digestion. Prior to conducting the animal experiment, an aliquot of each fraction was digested with alcalase. The sample was dissolved in water to yield 8% (w/v) and adjusted to pH 8.0 by the addition of NaOH or HCl. Alcalase (liquid form) was added at a ratio of 0.04% (v/v) to the reaction mixture and reacted at 60 °C for 4 h. The reaction was terminated by heating to 85 °C for 10 min. The reaction product was freeze-dried and stored at −20 °C until use.

Animal Experiment. Male Wistar rats were purchased from Charles River Laboratories Japan (Yokohama, Japan). All diet pellets were purchased from Oriental Yeast (Tokyo, Japan). All animals were housed (temperature, 22−24 °C; humidity, 40−60%) in the same building under a 12 h light−dark cycle and given free access to diet pellets and filtered water. The rats were allowed to adapt to the environment for 1 week before the start of the experiment. This study was conducted in accordance with the standards established by the Guide for the Care and Use of Laboratory Animals of Maruha Nichiro Holdings Central Research Institute (Tsukuba, Japan).

The test components were suspended in distilled water at an appropriate concentration and administered at a constant volume of 5 mL/kg of body weight to the rats via a stomach sonde. The doses of fractions (mg/kg of body weight) are shown in the figures. The rats in the control group were administered the same volume of distilled water (vehicle). In some cases, test components were dissolved in saline and injected into the tail vein. Before the injection, the sample was sterilized by passing through a filter (0.45 μm pore size, GL Sciences, Tokyo, Japan). At 1 h after the administration of test components, rats received a potassium oxonate solution (250 mg/2 mL of 3% gum arabic saline/kg of body weight) by intraperitoneal injection to elevate their blood uric acid level.[9,10,13] At 1 h after the oxonate injection, blood samples were collected from the caudal artery under pentobarbital anesthesia. Rats were starved for more than 12 h before their blood was drawn.

Isolation of Peptides from the Alcalase Digest of the Active Fraction. Peptides were obtained from the alcalase digest of the active fraction by preparative reversed-phase liquid chromatography and were resolved by size-exclusion chromatography (SEC) and reversed-phase high-performance liquid chromatography (RP-HPLC). A total of 1 mg of the alcalase digest of the active fraction was dissolved in 200 μL of 30% acetonitrile in the presence of 0.1% TFA and loaded into a Superdex peptide 10/30 HR (GE Healthcare, Buckinghamshire, U.K.), which had been equilibrated with 30% acetonitrile in the presence of 0.1% TFA at a flow rate of 0.5 mL/min. Fractions were collected every 1 min. The SEC fractions were dried under vacuum and dissolved in 200 μL of 10% acetonitrile in the presence of 0.1% TFA and further fractionated using a Cosmosil 5C18-MS-II (250 × 4.6 mm inner diameter, Nacalai Tesque, Kyoto, Japan). Elution was performed using a linear gradient of acetonitrile from 10 to 80% in the presence of 0.1% TFA for 30 min at a flow rate of 1 mL/min. Absorbance at 214 nm was monitored. The column was maintained at 40 °C.

Other Analytical Methods. The protein content was evaluated by amino acid analysis after HCl hydrolysis. Amino acid analysis was performed according to the method described by Bidlingmeyer et al.,[14] with slight modifications.[15] The peptide sequence was analyzed using the Edman degradation procedure using a PPSQ-21 (Shimadzu, Kyoto, Japan). Chondroitin sulfate was determined by the carbazole sulfate method using shark cartilage chondroitin sulfate C as a standard.[16]

The xanthine oxidase assay was performed according to the method by Osada et al.,[13] with slight modifications.[10] Xanthine was dissolved in 50 mM Tris−HCl buffer at pH 7.4 to give 15 mM. Xanthine oxidase was resolved in the same buffer to give 0.1 mU/mL. The sample was dissolved in the same buffer to give a suitable concentration. The substrate (40 μL), enzyme (10 μL), and sample solution (1950 μL) were mixed and incubated for 10 min at 37 °C. The reaction was terminated by the addition of 50 μL of 3.2% (v/v) perchloric acid. Absorbance at 292 nm was measured. Allopurinol and the buffer were used as positive and negative controls, respectively. Inhibitory activity is expressed as the remaining activity against the negative control (%). For the evaluation of the effect of ingestion of Tyr-Leu-Asp-Asn-Tyr on the serum xanthine oxidase inhibitory activity, 100 μL of serum from the rats that received the peptide, vehicle, or allopurinol were mixed with the buffer (1850 μL) and used as sample solution.

Statistical Analysis. Data are presented as the mean ± standard deviation. Statistical significance ($p < 0.05$ and 0.01) was analyzed by one-way analysis of variance followed by Scheffe's post-hoc test using StatView 4.11 (Abacus Concepts, Inc., Berkeley, CA).

RESULTS

As shown in Figure 1, the intact water extract did not show significant antihyperuricemic activity. However, the alcalase digest showed significant uric acid lowering activity to the oxonate-induced hyperuricemic rat by oral administration at 1 g/kg of body weight, indicating that peptides produced from the parent proteins in the water extract by alcalase digestion are responsible for the antihyperuricemic activity. The intact water-soluble components of the shark cartilage were fractionated on the basis of their isoelectric points by autofocusing. As shown in Figure 2, acidic (fraction numbers 1−5), weakly acidic (fraction numbers 6−7), and basic (fraction numbers 8−10) fractions were collected. Solid components were recovered from the acidic, weakly acidic, and basic fractions at 66, 24, and 10%, respectively. The acidic and weakly acidic fractions consisted of protein and chondroitin sulfate. In contrast, the basic fraction predominantly consisted of protein. The three fractions were digested with alcalase, and the digests were orally administered

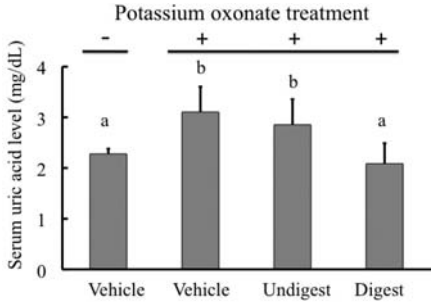

Figure 1. Effect of supplementation of the water extract of shark cartilage (undigest) and its alcalase digest (digest) on serum uric acid levels of rats treated with potassium oxonate. Data present the mean ± standard deviation ($n = 6$). Data points marked with different letters indicate significant differences ($p < 0.01$).

dx.doi.org/10.1021/jf405504u | J. Agric. Food Chem. 2014, 62, 2392−2397

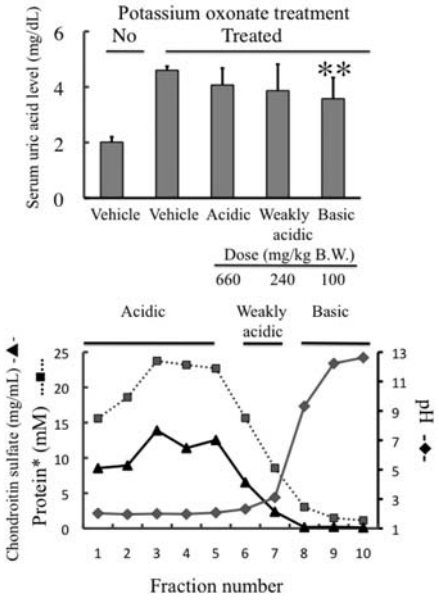

Figure 2. First purification of the protein that produces peptides with antihyperuricemic activity after alcalase digestion using ampholyte-free preparative isoelectric focusing (autofocusing). The water extract of shark cartilage without alcalase digestion was fractionated by autofocusing (lower panel). Acidic, weakly acidic, and basic fractions were collected as indicated by bars. (∗) Protein content is expressed as the sum of the constituting amino acids in the HCl hydrolysate. An aliquot of each fraction was evaluated for antihyperuricemic activity after alcalase digestion (upper panel). Dosages were determined by the following equation: (ratio of each fraction to the start material) × 1 g/kg of body weight. Data present the mean ± standard deviation (n = 6). Data marked with ∗∗ are significantly different from the cntrol group treated with potassium oxonate at $p < 0.01$.

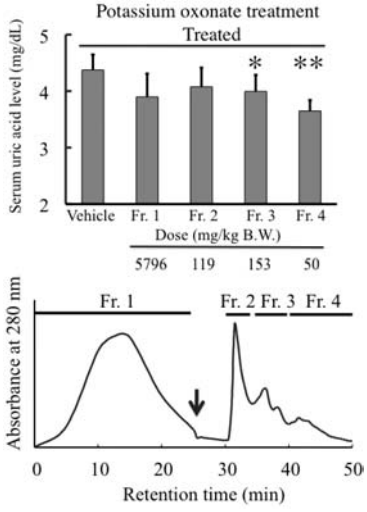

Figure 3. Second purification of the protein that produces peptides with antihyperuricemic activity after alcalase digestion by preparative reversed-phase chromatography. The basic fraction shown in Figure 2, without alcalase digestion, was used (lower). The arrow represents the start of gradient elution. Effluents were collected every minute and gathered to fractions 1−4, as shown. An aliquot of each fraction was evaluated for antihyperuricemic activity after alcalase digestion (upper). Data present the mean ± standard deviation (n = 6). (∗ and ∗∗) Significant differences from the control group (vehicle) treated with potassium oxonate at $p < 0.05$ and 0.01, respectively.

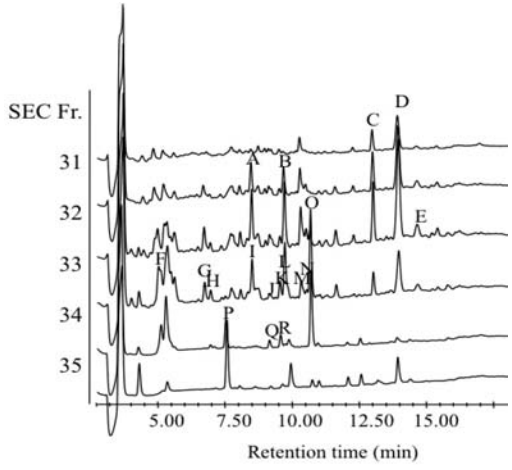

Figure 4. Isolation of peptides from the alcalase digest of the hydrophobic fraction (fraction 4 in Figure 3). The alcalase digest was first subjected to SEC. Fractions were collected every 1 min. SEC fractions (fractions 31−35) were further fractionated by RP-HPLC. Peaks marked with large characters were collected and subjected to sequence analysis. Sequences of the identified peptides are summarized in Table 1.

to the oxonate-induced hyperuricemic rats. The dose of each fraction was determined on the basis of the recovery percentage. Only the alcalase digest of the basic fraction significantly reduced the serum uric acid level at 0.1 g/kg of body weight, which is less than that of the water extract (1 g/kg of body weight) or the other fractions.

The proteins in the basic fraction were further fractionated by preparative reversed-phase liquid chromatography without alcalase digestion. As shown in Figure 3, three peaks (fractions 2−4) were eluted by gradient elution after elution of the unabsorbed components (fraction 1). These fractions were also digested with alcalase and evaluated for their antihyperuricemic activity. The dose of each fraction was determined on the basis of the recovery percentage. Only the alcalase digest of fraction 4 showed significant antihyperuricemic activity by oral administration at 50 mg/kg of body weight.

The peptides in the alcalase digest of fraction 4 were first resolved by SEC. Fractions were collected every 1 min. The SEC fractions eluted between 29 and 35 min were subjected to analytical RP-HPLC. As shown in Figure 4, the two-dimensional HPLC provided excellent resolution of the constituent peptides. The peptides marked with large characters were collected and subjected to sequence analysis. The obtained sequences are summarized in Table 1. All peptides contained aromatic amino acids: tyrosine, phenylalanine, and tryptophan. On the basis of the sequence data, all peptides were chemically synthesized and evaluated for antihyperuricemic activity. As shown in Figure 5, Tyr-Leu-Asp-Asn-Tyr (YLDNY) and Ser-Pro-Pro-Tyr-Trp-Pro-Tyr (SPPYWPY) showed significant antihyperuricemic activity by intravenous injection at 5 mg/kg ($p < 0.01$ and 0.05, respectively). However, Asp-Phe-Trp-Arg-Tyr (DFWRY) and other peptides did not show significant antihyperuricemic activity (data not shown). Oral administration of Tyr-Leu-Asp-Asn-Tyr also significantly reduced serum uric acid at 50 mg/kg of body weight (Figure 5), while Ser-Pro-Pro-Tyr-Trp-Pro-Tyr did not show significant activity by oral ingestion. Oral administration of Tyr-Leu-Asp-Asn-Tyr also significantly increased serum inhibitory activity against xanthine oxidase at the same dose (Figure 6). The

dx.doi.org/10.1021/jf405504u | J. Agric. Food Chem. 2014, 62, 2392−2397

Table 1. Summary of Sequences of Peptides from the Alcalase Digest of Fraction 4

peak[a]	sequence
A	Leu-Pro-Tyr
B	Tyr-Leu-Asp-Asn-Tyr
C	Asp-Phe-Trp-Arg-Tyr
D	Ser-Pro-Pro-Tyr-Trp-Pro-Tyr
E	Ser-Leu-Pro-Tyr-Trp-Pro-Tyr
F	Ile-Asn-Tyr
G	Val-Tyr-Gln
H	Tyr-Asn-Leu
I	Leu-Tyr
J	Ser-Ile-Tyr-Asp
K	Phe-Tyr
L	Tyr-Leu
M	Arg-Tyr-Leu
N	Gly-Tyr-Leu
O	Tyr-Phe
P	Tyr-Tyr
Q	Ser-Asn-Trp-Gln
R	Phe-Tyr

[a]Refer to Figure 4 for peak names.

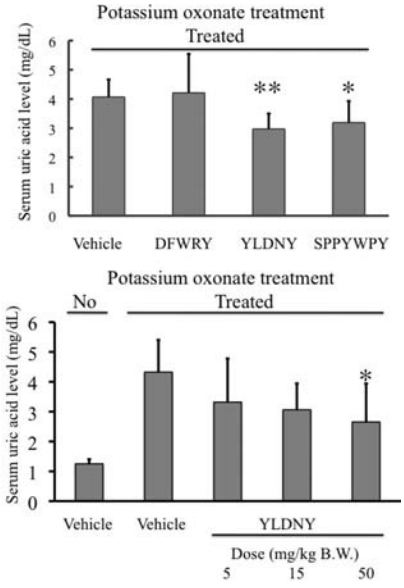

Figure 5. Antihyperuricemic activity of the synthetic peptides. Asp-Phe-Trp-Arg-Tyr (DFWRY), Tyr-Leu-Asp-Asn-Tyr (YLDNY), and Ser-Pro-Pro-Tyr-Trp-Pro-Tyr (SPPYWPY) were injected into the tail vein (5 mg/kg of body weight) (upper panel). YLDNY was also orally administered (lower panel).

xanthine oxidase inhibitory activity of Tyr-Leu-Asp-Asn-Tyr and possible fragment peptides is shown in Table 2. Asp-Asn, Leu-Asp-Asn, Asp-Asn-Tyr, and Leu-Asp-Asn-Tyr showed inhibitory activity, while Tyr-Leu-Asp-Asn-Tyr and constituting amino acids did not show the inhibitory activity. The IC_{50} values of these fragment peptides were 13−23 times higher than that of allopurinol.

DISCUSSION

Over the last few decades, numerous studies have demonstrated that ingestion of food protein hydrolysates has significant biological effects, such as moderation of hypertension, hypertriglyceridemia, hypercholesteremia, etc. The active peptides

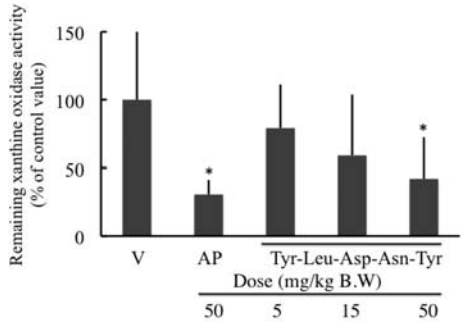

Figure 6. Inhibitory activity against xanthine oxidase by serum from the rat that had ingested vehicle (V), allopurinol (AP), and Tyr-Leu-Asp-Asn-Tyr. Data present the mean ± standard deviation ($n = 6$). (*) Significant difference from the control group (V) at $p < 0.05$.

have been identified using activity-guided fractionation based on *in vitro* assay systems using enzyme reactions and cell culture systems. Using this approach, many peptides have been apparently identified as active compounds. However, unlike other functional ingredients, proteins and peptides are further degraded into smaller peptides and constituent amino acids during digestion and absorption. As a result, the peptides in food may lose the potential biological activity detected by *in vitro* assays. Therefore, the *in vitro* activity of the peptides in the food cannot be directly linked to their biological activity after ingestion. To resolve these questions, the biological activity of potentially active peptides should be evaluated by feeding experiments using animal models. However, this approach requires relatively large amounts of peptide in comparison to the *in vitro* assays. For this approach, we have developed large-scale ampholyte-free preparative isoelectric focusing, referred to as autofocusing, which can process peptide samples up to 50−500 g.[12] Coupled with preparative reversed-phase chromatography, the parent protein, which produced antihyperuricemic peptides after alcalase digestion, was recovered from the basic and hydrophobic fractions (Figures 2 and 3). The alcalase digest of the final fraction exerted significant uric acid lowering activity at a $^1/_{20}$ dose in comparison to the crude digest. All peptides identified in the digest consisted of aromatic amino acids. Similarity research analyses using FAST and BLAST protocols revealed that these peptide sequences are similar to mammalian hypothetical proteins, of which the function is unknown. Using peptides synthesized on the basis of the sequence data, two peptides were identified, which exerted antihyperuricemic activity by intravenous injection at 5 mg/kg of body weight. Among these peptides, oral administration of Tyr-Leu-Asp-Asn-Tyr at 50 mg/kg of body weight exerted antihyperuricemic activity, which indicates that this peptide plays a significant role in the antihyperuricemic activity of shark cartilage extract. However, the dose of Tyr-Leu-Asp-Asn-Tyr necessary for the significant antihyperuricemic activity by oral ingestion was comparable to the required dose of the alcalase digest of the final fraction (fraction 4 in Figure 3). The presence of other peptides in the digest may enhance the antihyperuricemic activity of Tyr-Leu-Asp-Asn-Tyr by oral ingestion.

Our previous study demonstrated that ingestion of a protease digest of shark cartilage increases serum inhibitory activity against xanthine oxidase, a key enzyme for uric acid synthesis, whereas the digest has no *in vitro* xanthine oxidase inhibitory activity. Tyr-Leu-Asp-Asn-Tyr also had no *in vitro* xanthine

dx.doi.org/10.1021/jf405504u | J. Agric. Food Chem. 2014, 62, 2392−2397

Table 2. Xanthine Oxidase Inhibitory Activity of Possible Fragment Peptides from Tyr-Leu-Asp-Asn-Tyr[a]

	remaining activity (%)				
sample/dose (M)	1×10^{-5}	1×10^{-4}	3×10^{-4}	1×10^{-3}	IC_{50} (M)
allopurinol	73.1 ± 29.5	25.8 ± 7.2[b]	11.5 ± 10.6[b]	12.3 ± 6.7[b]	3.8×10^{-5}
Tyr-Leu	102.2 ± 2.1	106.4 ± 3.1	98.7 ± 10.2	106.9 ± 2.7	
Leu-Asp	104.7 ± 1.0	107.7 ± 5.9	88.9 ± 32.8	59.7 ± 19.7	
Asp-Asn	103.5 ± 2.0	107.8 ± 7.1	83.2 ± 17.9	16.2 ± 11.1[b]	5.0×10^{-4}
Asn-Tyr	105.2 ± 4.1	108.3 ± 6.0	101.8 ± 9.1	86.0 ± 13.1	
Try-Leu-Asp	103.5 ± 2.0	108.6 ± 5.5	103.1 ± 9.9	79.6 ± 24.1	
Leu-Asp-Asn	95.0 ± 16.9	84.4 ± 16.7	98.6 ± 12.1	35.8 ± 11.5[b]	7.6×10^{-4}
Asp-Asn-Tyr	106.6 ± 7.4	87.7 ± 28.5	86.6 ± 18.2	45.7 ± 12.7[b]	8.8×10^{-4}
Tyr-Leu-Asp-Asn	109.0 ± 10.7	108.1 ± 6.9	102.3 ± 10.9	57.1 ± 25.2[b]	
Leu-Asp-Asn-Tyr	104.2 ± 2.7	108.4 ± 6.3	99.6 ± 6.1	34.4 ± 18.9[b]	7.5×10^{-4}
Try-Leu-Asp-Asn-Tyr	100.2 ± 7.7	101.5 ± 1.3	ND[c]	101.7 ± 0.2	

[a]Allopurinol and distilled water were used as positive and negative controls, respectively. The remaining activity of xanthine oxidase is expressed as a percentage of the negative control (mean ± standard deviation; $n = 3$). [b]Significant difference versus the negative control at $p < 0.05$. [c]ND = not determined.

oxidase inhibitory activity (Table 2), whereas it increased serum xanthine oxidase inhibitory activity by ingestion (Figure 6). It has been demonstrated that most of the food-derived peptides in blood are tri- and dipeptides even after ingestion of larger peptides.[17−19] Then, Tyr-Leu-Asp-Asn-Tyr may be further degraded into smaller peptides with xanthine oxidase inhibitory activity and absorbed into the blood system. Indeed, some di- and tripeptides, which could be potentially derived from Tyr-Leu-Asp-Asn-Tyr, show xanthine oxidase inhibitory activity. The Asp-Asn motif is contained in all xanthine oxidase inhibitory peptides. These facts suggest that these fragment peptides might be absorbed in the blood and exert antihyperuricemic activity by inhibition of xanthine oxidase. Alternatively, the degradation peptides may induce endogenous xanthine oxidase inhibitors. Further studies on the metabolic fate of Tyr-Leu-Asp-Asn-Tyr and other peptides in the active fraction and on the identification of increased endogenous or food-derived xanthine oxidase inhibitors in serum after ingestion of these peptides are currently in progress to elucidate the mechanism of the antihyperuricemic activity.

The active peptide Tyr-Leu-Asp-Asn-Tyr in the alcalase digest of crude shark cartilage can be separated from chondroichin sulfate and other high-molecular-weight components by a simple selective precipitation technique using 75% ethanol, which can decrease dose to exert antihyperurecemic activity by ingestion.[17] Therefore, the peptide concentrate has potential as a functional food ingredient with antihyperuricemic activity.

AUTHOR INFORMATION

Corresponding Author

*Telephone: +81-75-703-5405. Fax: +81-75-723-3503. E-mail: k_sato@kpu.ac.jp.

Author Contributions

[†]Itsuki Murota and Satoko Taguchi contributed equally to this work.

Notes

The authors declare no competing financial interest.

REFERENCES

(1) Shipley, M. Hyperuricaemia and gout. *Publ.—R. Coll. Physicians Edinburgh* **2011**, *41*, 229−233.

(2) Robinson, P. C.; Taylor, W. J.; Merriman, T. R. Systematic review of the prevalence of gout and hyperuricaemia in Australia. *Intern. Med. J.* **2012**, *42*, 997−1007.

(3) Yu, T. F. Pharmacokinetic and clinical studies of a new uricosuric agent—Benzbromarone. *J. Rheumatol.* **1976**, *3*, 305−312.

(4) Fam, A. G. Gout in the elderly. Clinical presentation and treatment. *Drugs Aging* **1998**, *13*, 229−243.

(5) Schlesinger, N. Management of acute and chronic gouty arthritis: Present state-of-the-art. *Drugs* **2004**, *64*, 2399−2416.

(6) Fukui, N. Development of a non-alcohol-beer-taste drink. *J. Cookery Sci. Jpn.* **2011**, *44*, 257.

(7) Fukuuchi, T.; Yasuda, M.; Inazawa, K.; Ota, T.; Yamaoka, N.; Mawatari, K.; Nakagomi, K.; Kaneko, K. A simple HPLC method for determining the purine content of beer and beer-like alcoholic beverages. *Anal. Sci.* **2013**, *29*, 511−517.

(8) Shirogane, H.; Inoki, A.; Yamaguchi, Y.; Tamesada, M. Effect and safety in long-term intake of tablets containing chitosan in subjects with slight or threshold hyperuricemia. *J. Nutri. Food* **2004**, *7*, 35−47.

(9) Murota, I.; Tamai, T.; Baba, T.; Sato, R.; Hashimoto, K.; Park, E.-Y.; Nakamura, Y.; Sato, K. Uric acid lowering effect by ingestion of proteolytic digest of shark cartilage and its basic fraction. *J. Food Biochem.* **2010**, *34*, 182−194.

(10) Murota, I.; Tamai, T.; Baba, T.; Sato, N.; Park, E.-Y.; Nakamura, Y.; Sato, K. Moderation of oxonate-induced hyperuricemia in rats via the ingestion of an ethanol-soluble fraction of a shark cartilage proteolytic digest. *J. Funct. Foods* **2012**, *4*, 459−464.

(11) Kitahashi, T.; Ikawa, S.; Sakamoto, A.; Nomura, Y.; Tsujiuchi, T.; Shimizu, K.; Sasabe, S.; Park, E.-Y.; Nakamura, Y.; Tsutsumi, M.; Sato, K. Ingestion of proteoglycan fraction from shark cartilage increases serum inhibitory activity against matrix metalloproteinase-9 and suppresses development of *N*-nitrosobis 2-oxopropyl amine-induced pancreatic duct carcinogenesis in hamster. *J. Agric. Food Chem.* **2012**, *60*, 940−945.

(12) Hashimoto, K.; Sato, K.; Nakamura, Y.; Ohtsuki, K. Development of a large-scale (50 L) apparatus for ampholyte-free isoelectric focusing (autofocusing) of peptides in enzymatic hydrolysates of food proteins. *J. Agric. Food Chem.* **2005**, *53*, 3801−3806.

(13) Osada, Y.; Tsuchimoto, M.; Fukushima, H.; Takahashi, K.; Kondo, S.; Hasegawa, M.; Komoriya, K. Hypouricemic effect of the novel xanthine oxidase inhibitor, TEI-6720, in rodents. *Eur. J. Pharmacol.* **1993**, *241*, 183−188.

(14) Bidlingmeyer, B. A.; Cohen, S.; Tarvin, T. L. Rapid analysis of amino acids using precolumn derivatization. *J. Chromatogr.* **1984**, *336*, 93−104.

(15) Higaki-Sato, N.; Sato, K.; Esumi, K.; Okumura, T.; Yoshikawa, H.; Tanaka-Kuwajima, C.; Kurata, A.; Kotaru, K.; Kawabata, M.; Nakamura, Y.; Ohtsuki, K. Isolation and identification of indigestible

pyroglutamyl peptides in an enzymatic hydrolysate of wheat gluten prepared on an industrial scale. *J. Agric. Food Chem.* **2003**, *51*, 8−13.
(16) Bowness, J. M. Applicationof the carbazole reaction to the estimation of glucuronic acid and fructose in some acidic polysaccharides and in urine. *Biochem. J.* **1957**, *67*, 295−300.
(17) Iwai, K.; Hasegawa, T.; Taguchi, Y.; Morimatsu, F.; Sato, K.; Nakamura, Y.; Higashi, A.; Kido, Y.; Nakabo, Y.; Ohtsuki, K. Identification of food-derived collagen peptides in human blood after oral ingestion of gelatin hydrolysates. *J. Agric. Food Chem.* **2005**, *53*, 6531−6536.
(18) Shigemura, Y.; Akaba, S.; Kawashima, E.; Park, E.-Y.; Nakamura, Y.; Sato, K. Identification of a novel food-derived collagen peptide, hydroxyprolyl-glycine, in human peripheral blood by pre-column derivatisation with phenyl isothiocyanate. *Food Chem.* **2011**, *129*, 1019−1024.
(19) Shigemura, Y.; Nakaba, M.; Shiratsuchi, E.; Suyama, M.; Yamada, M.; Kiyono, T.; Fukamizu, K.; Park, E. Y.; Nakamura, Y.; Sato, K. Identification of food-derived elastin peptide, prolyl-glycine (Pro-Gly), in human blood after ingestion of elastin hydrolysate. *J. Agric. Food Chem.* **2012**, *60*, 5128−5133.

the process of enzymatic degradation. Negative-ion ESI-MS and CID MS/MS were employed for structural analysis and sequence of hydrolysates.

MATERIALS AND METHODS

Materials. Purified food-grade κ-carrageenan was purchased from Lubao Biochemistry Co., Ltd. (Jinjiang, China). *Pedobacter hainanensis* 13-Q^T was a strain gifted from the laboratory of Dalian Institute of Chemical Physics (Dalian, China). 3-Amino-9-ethylcarbazole (AEC), sodium cyanoborohydride ($NaBH_3CN$), and albumin of chicken egg white were purchased from Sigma-Aldrich (St. Louis, MO, USA). Bio-Gel P-2 Gel (45−90 μm wet bead size) and Bio-Gel $P\overline{4}$ Gel (90−180 μm wet bead size) were purchased from Bio-Rad Laboratories, Inc. (Hercules, USA). Molecular weight protein markers (PageRuler Unstained Protein ladder) were purchased from Fermentas Scientific Inc. (Vilnius, Lithuania). Water was purified by a Milli-Q ultrapure water purification system from Millipore (Burlington, MA, USA). All other chemicals used in the experiments were of analytical reagent grade.

Methods. *Bacterial Strains and Culture Conditions.* 50 μL of *Pedobacter hainanensis* 13-Q^T bacteria glycerol stock was inoculated into 10 mL of medium containing the following: κ-carrageenan (5 g/L), peptone (3 g/L), $NaNO_3$ (1 g/L), NaCl (20 g/L), $K_2HP_4{\cdot}3H_2O$ (1 g/L), $MgSO_4{\cdot}7H_2O$ (0.5 g/L), and $CaCl_2$ (0.1 g/L), dissolved in 1 L of distilled water, pH 7.5, and then incubated at 30 °C on a rotary shaker at a speed of 200 rpm overnight.[31] Cells were subcultured by transferring 200 μL of the cell culture into 40 mL of the above-described culture medium prior to incubation on a rotary shaker overnight (200 rpm) at 30 °C. The bacterial cells were cultured and grown to OD_{600} of 0.6−1.0 to reach the maximum output of κ-carrageenase.

Purification of κ-Carrageenase. The culture medium (100 mL) was centrifuged at 8000 rpm for 30 min. Subsequently, 80% ammonium sulfate was added to the supernatant and left overnight. The precipitates were collected by centrifugation at 8000 rpm for 50 min and then dissolved in 5 mL of 0.05 mol/L Tris-HCl buffer (pH 7.0). The clear supernatant containing κ-carrageenase was collected by centrifugation at 5000 rpm for 30 min and evaluated for enzymatic activity, where its protein content was estimated by the Bradford method.[32] Then the purified κ-carrageenase was applied to a Bio-Gel $P\overline{4}$ column (120 cm × 2 cm), equilibrated in 0.05 mol/L Tris-HCl buffer (pH 7.0), and eluted with the same buffer. Fractions were collected by continuous monitoring of the activity of κ-carrageenase. The pooled fraction was assayed for its total enzymatic activity and protein content. In order to protect the activity of κ-carrageenase, all the aforesaid steps were carried out at 4 °C.

κ-Carrageenase Assays. The determination of enzymatic activity was assayed by measuring the increase in the concentration of reducing sugar ends formed by enzymatic digestion, using the dinitrosalicylic method of Miller.[33,34] Boiled enzyme was used as a blank. 100 μL of the enzyme solution was added to 900 μL of 0.2% (w/v) κ-carrageenan in 0.05 mol/L Tris-HCl buffer (pH 7.0), and the mixture was incubated at 40 °C for 20 min. After incubation, 750 μL of modified 3,5-dinitrosalicylic acid reagent was added to the solution, and the mixture was heated for 5 min in a boiling water bath and then cooled in ice water. When the sample was cooled, 5 mL of deionized water was added and the absorption at 520 nm was measured in a (NewCentury-T6) spectrophotometer (Purkinje General Instrument Co., Ltd., Beijing, China). The amount of released sugar was estimated using a D-galactose calibration curve (0.2 to 0.8 mg/mL), and one unit of κ-carrageenase activity was defined as the amount of enzyme that produces the equivalent of 1 μmol of D-galactose from κ-carrageenan per minute under the above-described condition.

Molecular Weight Determination. The molecular weight determination of κ-carrageenase was analyzed using SDS−PAGE with a 5% (w/v) polyacrylamide for the stacking gel, a 10% (w/v) polyacrylamide for the running gel, and 0.1% (w/v) SDS. One milligram of enzyme was denatured by heating at 100 °C for 10 min in 200 μL of protein denaturation solution containing 5% SDS and 6.2% DTT. The loading amount of protein samples was 10 μg. Electrophoresis was carried out at 80 V in stacking gel and 120 V in separating gel for 4 h using an electrophoretic buffer consisting of Tris-glycine with 0.1% SDS (pH 8.3). The gels were stained with staining buffer containing 1% (w/v) Coomassie Blue-R250, 40% aqueous ethanol, and 10% aqueous acetic acid for 30 min and subsequently destained with 40% aqueous ethanol and 10% aqueous acetic acid. Visualization of the proteins was carried out using ImageQuant 350 (GE Healthcare, Piscataway, NJ, USA).

Preparation of κ-Carrageenan Oligosaccharides. κ-Carrageenan was enzymatically digested with κ-carrageenase. A 10-unit aliquot of enzyme solution was added to 100 mL of 0.2% (w/v) κ-carrageenan in 0.05 mol/L Tris-HCl buffer at pH 7.0, and the solution was incubated at 40 °C. 5 mL of the sample was taken out at intervals (i.e., 0.5 h, 1 h, 2 h, 4 h, 8 h, 12 h, 16 h, 20 h, 24 h, 28 h, 32 h, 48 h, 72 h, and 96 h) and boiled in a 100 °C water bath to stop the reactions. The products were concentrated and desalted using gel-filtration chromatography on a Bio-Gel P-2 column (40 cm × 2 cm). The column was eluted with distilled water using a pump with a flow rate of 0.8 mL/min, and fractions of 4 mL were autocollected. The elution was monitored by the phenol−sulfuric acid method.[35] Fractions containing sugar were pooled together and lyophilized for further analysis.

TLC Analysis of κ-Carrageenan Hydrolysate. Each 2 μL aliquot of 2 mg/mL reaction mixture was loaded onto a 20 cm × 20 cm plastic TLC plate precoated with 0.2 mm silica gel (Macherey-Nagel, Düren, Germany) and developed with a solvent system consisting of *n*-butanol:formic acid:water (4:7:1, v/v/v) at 25 °C. The developed plate was stained by spraying with orcinol−sulfuric acid reagent (0.2 g of orcinol, 20 mL of 98% H_2SO_4, 100 mL of methanol) and heated at 150 °C until the bands were obviously visible.[36]

3-Amino-9-ethylcarbazole (AEC) Labeling and HPLC Analysis of κ-Carrageenan Hydrolysate. Five milligrams of κ-carrageenan oligosaccharides obtained at different intervals was dissolved in 500 μL of deionized water. Two hundred microliters of 0.2 mol/L AEC in methanol, 25 μL of 0.5 mol/L aqueous sodium cyanoborohydride ($NaBH_3CN$), and 50 μL of acetic acid were added successively. The mixtures were incubated at 70 °C for 1 h.[37] These labeling reactions were then terminated by neutralization with 100 μL of 1.0 mol/L NaOH. The aqueous phase was extracted with 500 μL of dichloromethane to remove excess AEC, and then centrifuged at 8000 rpm for 3 min. The aqueous phase was taken out for chromatographic analysis. HPLC separation was performed on a Shimadzu LC-2010AHT (Tokyo, Japan). The column used was a 250 mm × 4.6 mm i.d., 5 μm, Sinochrom ODS-BP, with a 4 mm × 4 mm i.d. guard column of the same material (Elite Analytical Instruments Co., Ltd., Dalian, China). Data were collected and processed through Shimadzu Labsolutions software, version 5.51. The labeled oligosaccharides were analyzed by UV detection at 254 nm. Injection volume was 10 μL. The separation was performed at 40 °C in a linear gradient mode from 20% to 40% acetonitrile in 10 mmol/L ammonium acetate aqueous solution (pH 4.5) over 60 min. The flow rate was 0.5 mL/min.

Preparation of κ-Carrageenan Oligosaccharide Alditols. A 0.5 mL aliquot of 4% (w/v) aqueous sodium borohydride ($NaBH_4$) solution was added to 2 mg of the freeze-dried sample, and the mixture was incubated at 25 °C for 2 h.[38] The reaction was terminated by neutralization with 50 μL of acetic acid to destroy excess $NaBH_4$. Boric acid was removed by repeated coevaporation with 0.1% anhydrous methanol/HCl (v/v) three times. The oligosaccharide alditols were analyzed by CID MS/MS.

ESI-MS and CID MS/MS Analysis. The κ-carrageenan oligosaccharides were analyzed using a LTQ-XL ion-trap mass spectrometer equipped with an electrospray ion source and a HPLC system (Thermo-Fisher, Waltham, MA, USA). Data acquisition and processing were performed through the Xcalibur software. Aqueous samples (1 mg/mL) were injected via a 2 μL Rheodyne loop, and taken into the electrospray ion source by a stream of 50% aqueous methanol at a flow rate of 200 μL/min from the pump of HPLC system. For the electrospray ion source, the spray voltage was set at 4 kV, with a sheath gas (nitrogen gas) flow rate of 30 arbitrary units, an

auxiliary gas (nitrogen gas) flow rate of 5 arbitrary units, a tube lens voltage of −250 V, a capillary temperature of 350 °C, and a capillary voltage of −48 V. Scan rate was normal, and the type was full, with a microscan number of 3, searching for a mass range of m/z 200−2000. When CID MS/MS was carried out, helium (He) was used as the collision gas, and the collision energy was set at 25−30% with an isotope width of m/z 3.00.

RESULTS AND DISCUSSION

Purification of κ-Carrageenase. After incubation, the cells were removed by centrifugation and 100 mL of crude culture supernatant was obtained. The original κ-carrageenase activity was 5.72 units/mg protein, which was set as a 1-fold purification. The proteins were then precipitated by ammonium sulfate, resulting in enzymatic activity of 60.46 units/mg of protein with a 10.57-fold purification from the crude culture supernatant. Afterward, the proteins were redissolved in Tris-HCl buffer and concentrated to 5 mL of solution. The enzymatic activity reached to 107.25 units/mg protein with a 18.75-fold purification. The proteins were further purified on a Bio-Gel $P\overline{4}$ column, which separated two peaks (B and C) of proteins with κ-carrageenase activity. Peak B, containing higher κ-carrageenase activity, was combined, and peak C was omitted due to a lesser amount of protein and lower activity. Furthermore, peak B was concentrated and the solution was applied for rechromatography on Bio-Gel $P\overline{4}$. According to the rechromatographic pattern, peak B was found to have only one active peak. It was further confirmed by SDS−PAGE where only a single protein band was observed (Figure 1). Overall, after the four steps of purification, the κ-carrageenase activity increased from 5.72 units/mg of protein to 700.53 units/mg of protein, leading to a 122.47-fold purification from the crude culture supernatant. The degree of purification is shown in Table 1. With references to the reported data, it can be concluded that the purified enzyme has much higher activity than those of some enzymes from other different sources. Khambhaty et al.[24] have reported the purification of κ-carrageenase from *Pseudomonas elongate*, exhibiting maximum enzymatic activity of 426.19 units/mg of protein. Sarwar et al.[39] have reported a characterized κ-carrageenase from *Cytophaga* spp. having enzymatic activity of 5.0 units/mg of protein.

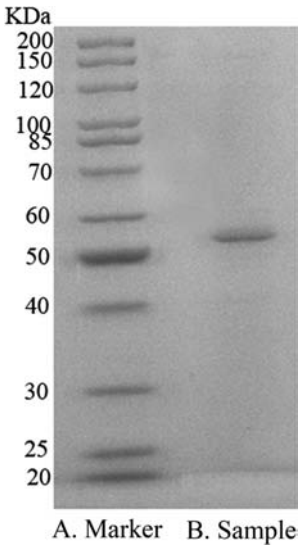

Figure 1. SDS−PAGE analysis of κ-carrageenase purified from *Pedobacter hainanensis* 13-Q^T.

Molecular Weight of κ-Carrageenase. The molecular weight of κ-carrageenase was determined by SDS−PAGE. As presented in Figure 1, the protein band of κ-carrageenase appeared as a single one between 50 kDa and 60 kDa standard molecular weight markers. The results indicated that the κ-carrageenase has an apparent molecular weight of ∼55 kDa.

TLC Analysis of κ-Carrageenan Oligosaccharides Hydrolysis by κ-Carrageenase. TLC analysis is a potent method to detect various oligosaccharides of different polymerization degrees.[40] The presence of sulfate groups in sulfate oligosaccharides has an effect on migration and resolution of these oligosaccharides on TLC plates.[41]

With molecular mass information obtained by ESI-MS analysis, the κ-carrageenan oligosaccharides were observed and monitored on TLC plates (Figure 2). Lanes a, b, c, and d,

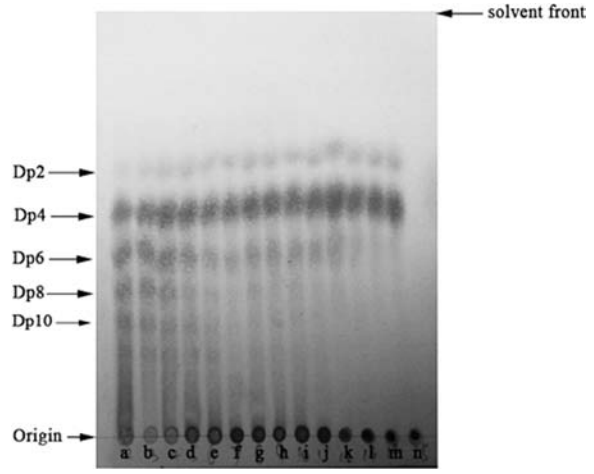

Figure 2. TLC analysis of κ-carrageenan oligosaccharides prepared through κ-carrageenase at pH 7.0 and 40 °C of a−n represented for samples of 0.5 h, 1 h, 2 h, 4 h, 8 h, 12 h, 16 h, 20 h, 24 h, 28 h, 32 h, 48 h, 72 h, and 96 h, respectively.

the product mixtures mainly containing oligosaccharides with various polymerization degrees between disaccharide (Dp 2) and decasaccharide (Dp 10), were observed as distinctive

Table 1. Purification of κ-Carrageenase from *Pedobacter hainanensis*

no.	step	total vol (mL)	total act.[a] (units)	total protein[a] (mg)	sp act.[b] (units/mg)	purifn[c] (-fold)
1	crude enzyme	100	184.30 ± 1.96	32.22 ± 0.46	5.72	1
2	$(NH_4)_2SO_4$ precipitation	40	356.11 ± 2.86	5.89 ± 0.18	60.46	10.57
3	Tris-HCl redissolution	5	14.05 ± 0.25	0.131 ± 0.0044	107.25	18.75
4	gel filtration	3	13.31 ± 0.14	0.019 ± 0.0078	700.53	122.47

[a]Values are expressed as means ± SD (n = 3). [b]Specific activity = average of total activity/average of total protein. [c]Purification fold = specific activity/5.72 (units/mg); the value of 5.72 was original specific activity, designed as a 1-fold purification.

dx.doi.org/10.1021/jf500429r | J. Agric. Food Chem. 2014, 62, 2398−2405

separated bands on the TLC plate. After hydrolysis for 12 h, the spots of oligosaccharides at Dp 10 and higher polymerization degrees became faint, indicating that κ-carrageenan was effectively degraded. The reaction mixtures loaded on lanes i, j, k, l, m, and n corresponding to 24−96 h digestion mainly contained oligosaccharides ranging from disaccharide to hexasaccharide, of which tetrasaccharide was the dominant component.

HPLC Analysis of κ-Carrageenan Oligosaccharides Hydrolysis by κ-Carrageenase. To quantitatately assess the yield of oligosaccharides of different Dps, each sample was labeled by reductive amination with AEC and analyzed by HPLC. Some chromatographic data of the reaction products of enzymatic hydrolysis for 0.5 h, 12 h, 24 h, and 96 h are depicted in Figure 3. The peaks corresponding to Dp 2, Dp 4, Dp 6, and Dp 8 were clearly detected. Over 96 h, the area of the peaks of higher molecular weight fractions gradually decreased. The quantitative data of Dp 2, Dp 4, Dp 6, and Dp 8 are summarized in Figure 4. Obviously, typical oligosaccharides were obtained at different time courses. According to the peak area of these oligosaccharides, Dp 4 was the dominant component. The content of Dp 4 was low at the beginning, higher in the middle, and lower at the end of the reaction, and the highest yield of Dp 4 was about 70% of total oligosaccharides until 24 h. The curve of Dp 6 was similar to that of Dp 4. In contrast, the area curve of Dp 8 was in a quite different trend. The content of Dp 8 reached the highest point in the beginning and then decreased continuously to the end. During the process of enzymatic hydrolysis, the content of Dp 2 gradually increased. However, Dp 2 had a relatively low yield.

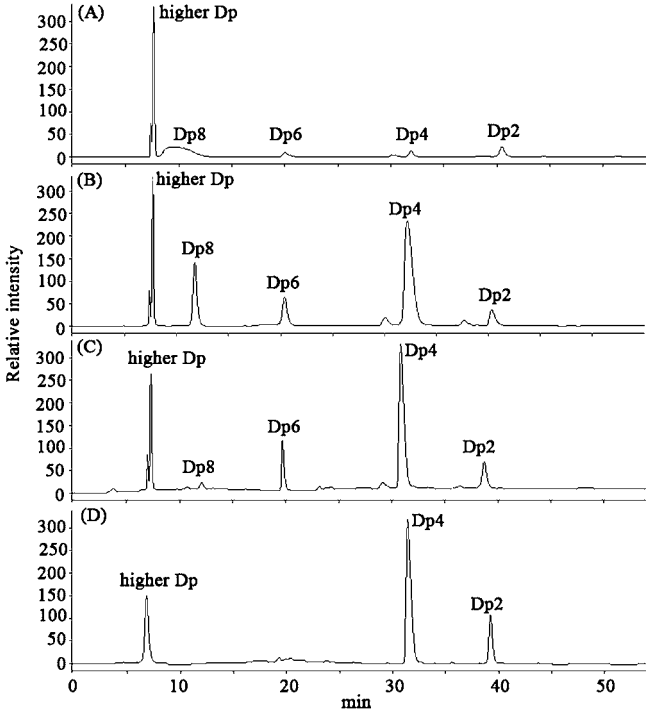

Figure 3. HPLC analysis of κ-carrageenan oligosaccharides obtained by κ-carrageenase at pH 7.0 and 40 °C (A) for 0.5 h; (B) for 12 h; (C) for 24 h; (D) for 96 h.

ESI-MS Analysis of κ-Carrageenan Oligosaccharides Hydrolysis by κ-Carrageenase. Due to the presence of sulfate groups on the oligosaccharides, all MS experiments were performed in negative-ion mode.[42] The mass spectra of the oligosaccharide mixtures obtained at 12 h, 24 h, and 96 h are depicted in Figure 5.

The mass spectra exhibited signals of multiply charged molecular anions, including singly, doubly, and triply charged

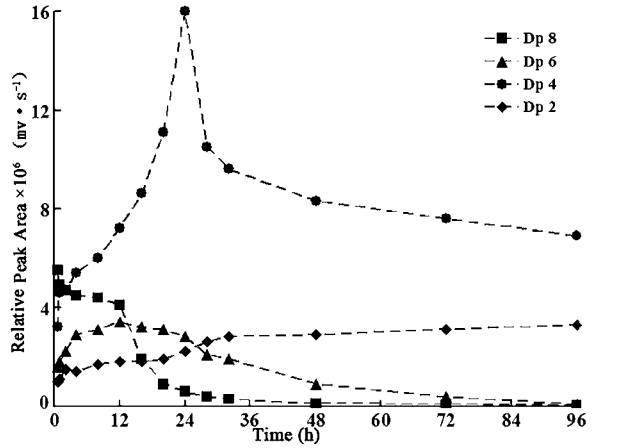

Figure 4. The yield curve of Dp 2, Dp 4, Dp 6, and Dp 8 obtained with different time courses analyzed by HPLC.

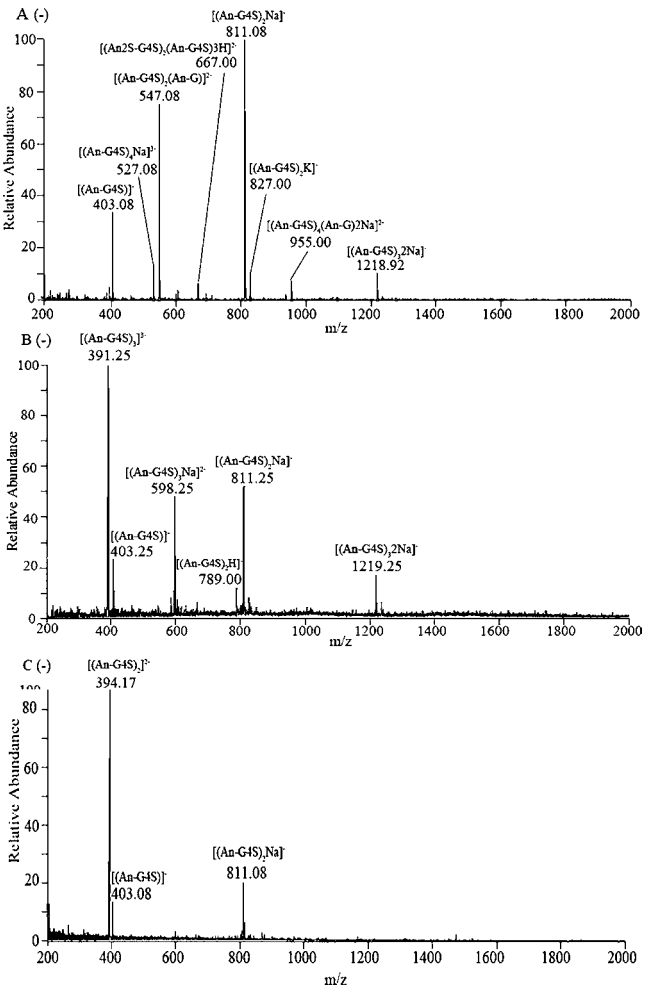

Figure 5. The ESI-MS analysis of κ-carrageenan oligosaccharides prepared by κ-carrageenase at pH 7.0 and 40 °C (A) for 12 h; (B) for 24 h; (C) for 96 h.

dx.doi.org/10.1021/jf500429r | J. Agric. Food Chem. 2014, 62, 2398−2405

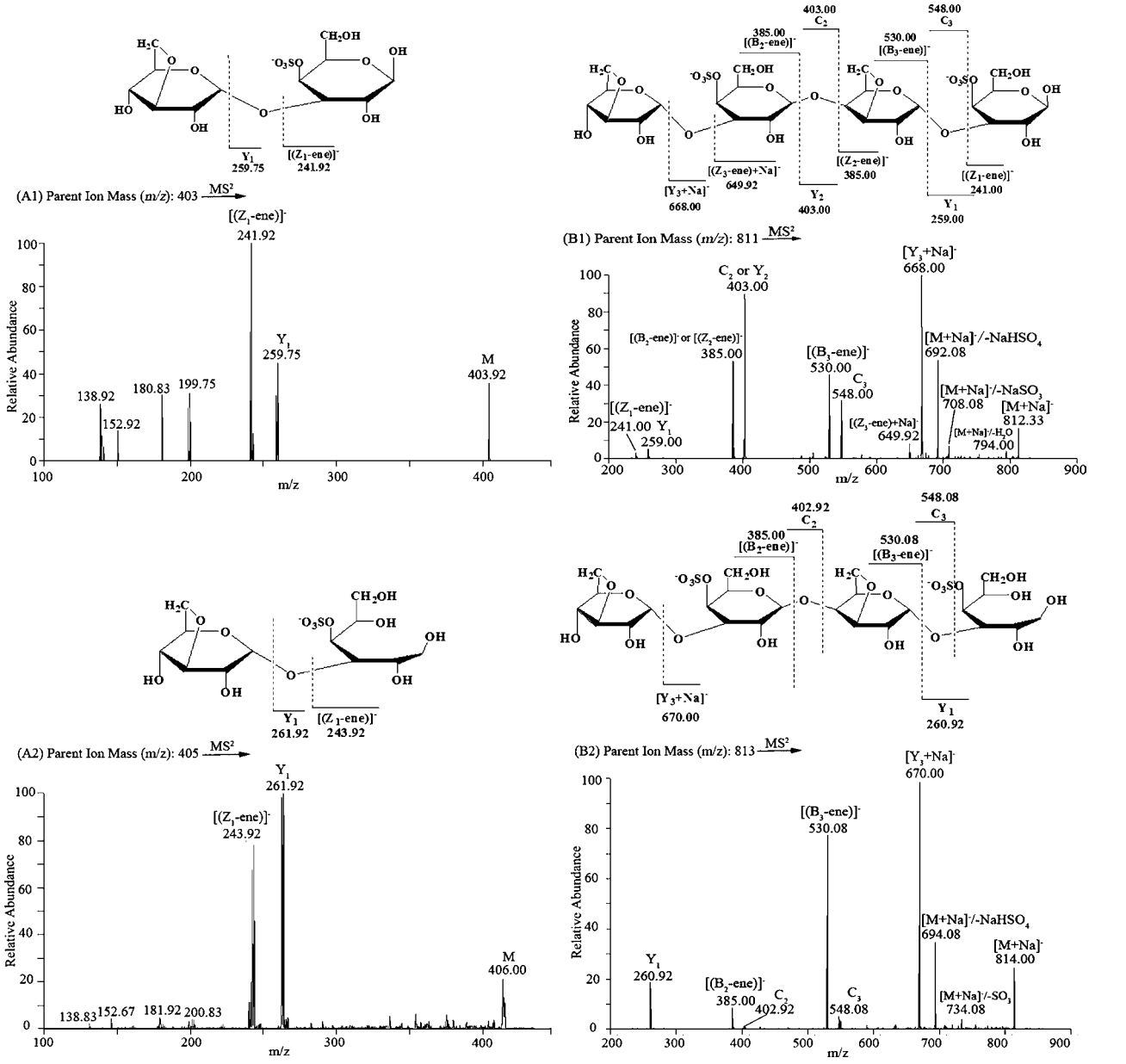

Figure 6. The CID MS/MS analysis of κ-carrageenan oligosaccharides and oligosaccharide alditols degraded by enzymatic hydrolysis. (A1) disaccharide vs (A2) disaccharide alditol, and (B1) tetrasaccharide vs (B2) tetrasaccharide alditol. Note the different fragments present in each spectrum, arising from the different linkages.

ones. As shown in Figure 5A, the sample prepared in 12 h contained a series of κ-carrageenan oligosaccharides, including disaccharide, tetrasaccharide, hexasaccharide, octasaccharide, and decasaccharide. The peak at m/z 403.08 is assigned to disaccharide $[(G4S\text{-}An)]^-$ carrying one sulfate group. The peaks corresponding to molecular anion as sodium salt $[(G4S\text{-}An)_2Na]^-$ (m/z 811.08) and potassium salt $[(G4S\text{-}An)_2K]^-$ (m/z 827.00) are assigned to tetrasaccharide carrying two sulfate groups. The base peak found at m/z 1218.92 is likely to be representative of hexasaccharide with three sulfate groups bearing two sodium ions $[(G4S\text{-}An)_3 2Na]^-$. The peak at m/z 547.08 corresponds to doubly charged desulfated hexasaccharide anions $[(An\text{-}G4S)_2(An\text{-}G)]^{2-}$ carrying two sulfate groups. This desulfation could be formed in the mass spectrometer due to high cone voltage.[42] The peak found at m/z 667.00 is assigned to the doubly charged anion $[(AnG2S\text{-}G4S)_2(An\text{-}G4S)3H]^{2-}$. The oversulfated disaccharide units of AnG2S-G4S are attributed to inclusion of ι-carrageenan, a common impurity in commercial κ-carrageenan.[42,43] The peak found at m/z 527.08 corresponds to the triply charged octasaccharide anion $[(An\text{-}G4S)_4Na]^{3-}$. The peak found at m/z 955.00 corresponds to doubly charged desulfated decasaccharide anions $[(An\text{-}G4S)_4(An\text{-}G)2Na]^{2-}$.

The κ-carrageenan oligosaccharides obtained by digestion using κ-carrageenase for 24 h are mainly between Dp 2 and Dp 6, and their MS profile is depicted in Figure 5B. We found that the peaks at m/z 811.00 and m/z 789.00 correspond to molecular anions as sodium salt $[(An\text{-}G4S)_2Na]^-$ and hydrogen salt $[(An\text{-}G4S)_2H]^-$, respectively. In the mass spectra of hexasaccharide, the base peak at m/z 1219.25 corresponds to the molecular anion with two sodium atoms ($[(An\text{-}G4S)_3 2Na]^-$); while the peaks found at m/z 391.25 and

dx.doi.org/10.1021/jf500429r | J. Agric. Food Chem. 2014, 62, 2398−2405

598.25 correspond to triply and doubly charged anions $[(An\text{-}G4S)_3]^{3-}$ and $[(An\text{-}G4S)_3Na]^{2-}$, respectively.

After enzymatic digestion for 96 h, tetrasaccharide was the major product, as shown in Figure 5C. The peak at m/z 394.17 corresponds to doubly charged tetrasaccharide anion $[(An\text{-}G4S)_2]^{2-}$.

These results showed enzymatic properties of the κ-carrageenase, for which the cleavage group was An-G4S unit, resulting in a series of neocarrabiose oligosaccharides with the code of An-G4S.

Sequencing of κ-Carrageenan Oligosaccharides by CID MS/MS. Glycosidic cleavages provide information on constituent monosaccharide sequence and branching, whereas cross-ring cleavages can be used to define linkages. The cross-ring cleavage ions are generally less abundant when compared with the glycosidic cleavage ions.[44−46] A nomenclature for describing these fragment ions was proposed by Domon and Costello[47] and widely accepted.

The detailed structures of κ-carrageenan oligosaccharides obtained by enzymatic hydrolysis were elucidated by CID MS/MS. In order to differentiate fragment ions with identical masses arising from glycosidic cleavages, the oligosaccharide mixture was reduced by $NaBH_4$ to obtain oligosaccharide alditols. Due to the reduction, the reducing terminal fragment ions showed an increase of 2 Da in CID MS/MS analysis. Therefore, the difference of reducing and nonreducing terminal fragments can be easily identified from each other.[48,49]

In the obtained MS profiles, all the oligosaccharide molecular ions showed 2 Da increase after the reduction treatment (data not shown). During the CID MS/MS analysis, disaccharide (m/z 403.25) and its alditol (m/z 405.08) form, together with tetrasaccharide (m/z 811.25) and its alditol (m/z 813.00) form, were taken as the precursors to determine the structure of κ-carrageenan oligosaccharides. The CID MS/MS spectra are depicted in Figure 6, and the assignment data are shown in Table 2.

In the MS/MS profiles of the disaccharide (Figure 6A1) and its alditol form (Figure 6A2), both glycosidic and cross-ring fragments are found. The two major glycosidic fragment ions derived from the disaccharide alditol corresponding to the peaks at m/z 243.92 and 261.92 (Figure 6A2) are 2 Da increased from the peaks at m/z 241.92 and 259.75 (Figure 6A1). In the CID MS/MS spectra of the disaccharide and its alditol, Y- and Z-type glycosidic cleavage fragments are considerably more abundant than the cross-ring cleavage fragments. The cross-ring cleavage fragment ions at m/z 152.92, 199.75, 138.92, and 180.83 are derived from the sulfated disaccharide precursor ion. The ions at m/z 152.92, 180.83, and 138.92 are assigned to $^{3,5}A_2$-, $^{2,5}A_2$-, and $^{2,4}A_2$-type fragments, respectively. The peak at m/z 199.75 is assigned to $^{1,3}X_1$-type.

In the CID MS/MS spectra of tetrasaccharide (Figure 6B1) and its alditol (Figure 6B2), mainly glycosidic cleavage fragment ions as sodium adducts are observed but no cross-ring cleavage fragments are found in the spectra. Minor desulfation occurs, as indicated by the presence of weak signals at m/z 692.08, 694.08 (−120 Da, equivalent to the loss of $NaHSO_4$), 708.08 (−103 Da, equivalent to the loss of $NaSO_3$), and 734.08 (−80 Da, equivalent to the loss of SO_3). The peaks at m/z 260.92 and 670.00 (Figure 6B2) show a 2 Da shift compared with the peaks at m/z 259.00 and 668.00 (Figure 6B1). These peaks are assigned to the reducing side fragments produced by glycosidic cleavages. The peaks at m/z 530.08 and 548.08 (Figure 6B2) observed here remain the same as the peaks at m/z 530.00 and 548.00 (Figure 6B1). These peaks are derived from cleavages at the nonreducing side of both tetrasaccharide and its alditol, determining that sulfated G4S are at the reducing terminal residue. Therefore, according to the spectral feature of glycosidic fragments from nonreducing (B- and C-type ions) and reducing sides (Y- and Z-type ions), the sequence of κ-carrageenan oligosaccharides prepared by κ-carrageenase could be readily deduced as $(An\text{-}G4S)_n$, which would give rise to oligosaccharides with terminal G4S residue.

According to ESI-MS and MS/MS analysis, the enzymatic products were a homologous series of even-numbered sulfated oligosaccharides with $(An\text{-}G4S)_n$, of which An is at the nonreducing end and G4S is at the reducing end. This result indicates that the κ-carrageenase of *Pedobacter hainanensis* cleaves at the internal β-1,4 linkages of κ-carrageenan (Figure 7).

Table 2. Fragment Ions Observed in the CID MS/MS Spectra of Disaccharide, Tetrasaccharide, and their Alditols as Precursors

	obsd fragment ion (m/z) of enzymic products $(An\text{-}G4S)_n$ and Their Alditols			
	disaccharide		tetrasaccharide	
fragment ion type	403	405	811	813
$^{2,4}A_2$	138.92	138.83		
$^{3,5}A_2$	152.92	152.67		
$^{2,5}A_2$	180.83	181.92		
$^{1,3}X_1$	199.75	200.83		
$[(Z_1\text{-ene})]^-$	241.92	243.92	241.00	
Y_1	259.75	261.92	259.00	260.92
$[(Z_2\text{-ene})]^-$ or $[(B_2\text{-ene})]^-$			385.00	385.00
C_2 or Y_2			403.00	402.92
$[(B_3\text{-ene})]^-$			530.00	530.08
C_3			548.00	548.08
$[(Z_3\text{-ene}) + Na]^-$			649.92	
$[Y_3 + Na]^-$			668.00	670.00
$[M + Na]^-/-NaHSO_4$			692.08	694.08
$[M + Na]^-/-NaSO_3$			708.08	
$[M + Na]^-/-SO_3$				734.08

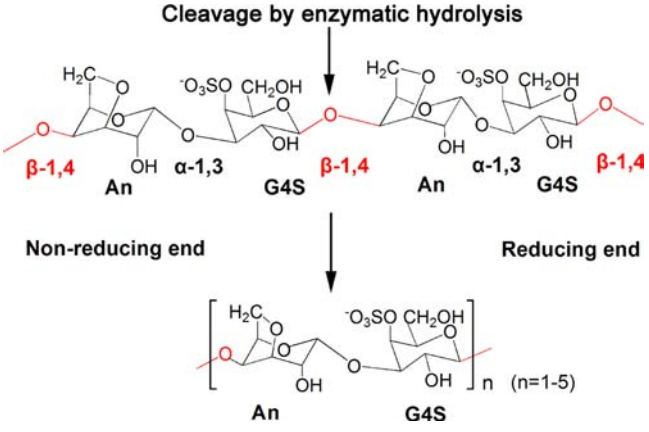

Figure 7. Schematic diagram showing two disaccharide-repeating units of κ-carrageenan. The site of enzymatic hydrolysis is specific at the internal β-1,4 linkages of κ-carrageenan.

dx.doi.org/10.1021/jf500429r | J. Agric. Food Chem. 2014, 62, 2398−2405

The purified κ-carrageenase isolated from *Pedobacter hainanensis* is a novel enzyme acting as a β-hydrolyase to produce κ-carrageenan oligosaccharides with An-G4S-type, yielding tetrasaccharide as the main end product. The action pattern of this enzyme was quite different from those of other κ-carrageenases reported earlier. Ma et al.[50] have reported a κ-carrageenase isolated from *Pseudoalteromonas* sp. They indicated that the main end products were dimers of different neocarrabioses, e.g., disaccharide, tetrasaccharide, hexasaccharide, octasaccharide, and decasaccharide. Potin et al.[26] have reported a κ-carrageenase purified and characterized from *Cytophaga* strain Dsji. They showed that tetrasaccharide and hexasaccharide were the major end products and the purified enzyme was not capable of hydrolyzing tetrasaccharide and hexasaccharide. Enzymatic activity, hydrolytic products, and various characteristics showed that the κ-carrageenase from *Pedobacter hainanensis* could be an alternative resource to produce better quality carrageenan with commercial value.

■ ASSOCIATED CONTENT

Ⓢ Supporting Information

Figure S1: Gel filtration chromatography of κ-carrageenase on Bio-Gel $P\overline{4}$ column. Figure S2: Rechromatography of the selected peak on Bio-Gel $P\overline{4}$ column. This material is available free of charge via the Internet at http://pubs.acs.org.

■ AUTHOR INFORMATION

Corresponding Author

*Tel: +86-029-88305853. Fax: +86-029-88303534. E-mail: huanglj@nwu.edu.cn.

Funding

This work was supported by the National Natural Science Foundation of China (NO. 21375103 and 31071506).

Notes

The authors declare no competing financial interest.

■ ACKNOWLEDGMENTS

The help from Prof. Yuguang Du and Dr. Yanyu Meng in Dalian Institute of Chemical Physics (Chinese Academy of Sciences) in obtaining the strain of *Pedobacter hainanensis* 13-Q^T is greatly acknowledged.

■ ABBREVIATIONS USED

Dp, degree of polymerization; CID MS/MS, electrospray tandem mass spectrometry with collision-induced dissociation; G, 1,3-linked β-D-galactopyranosyl; D, 1,4-linked α-D-galactopyranosyl; An, 3,6-anhydro-α-D-galactose; G4S, β-D-galactose-4-sulfate; SDS−PAGE, sodium dodecylsulfate polyacrylamide gel eletrophoresis; SDS, sodium dodecylsulfate; DTT, dithiothreitol; AEC, 3-amino-9-ethylcarbazole

■ REFERENCES

(1) Usov, A. I. Structural analysis of red seaweed galactans of agar and carrageenan groups. *Food Hydrocolloids* **1998**, *12*, 301−308.

(2) Ruiter, G. A. D.; Rudolph, B. Carrageenan biotechnology. *Trends Food Sci. Technol.* **1997**, *8*, 389−395.

(3) Renn, D. Biotechnology and the red seaweed polysaccharide industry: status, needs and prospects. *Trends Biotechnol.* **1997**, *15*, 9−14.

(4) Marinho-Soriano, E.; Bourret, E. Polysaccharides from the red seaweed *Gracilaria dura* (Gracilariales, Rhodophyta). *Bioresour. Technol.* **2005**, *96*, 379−382.

(5) Yuan, H.; Song, J.; Li, X.; Li, N.; Dai, J. Immunomodulation and antitumor activity of kappa-carrageenan oligosaccharides. *Cancer Lett.* **2006**, *243*, 228−234.

(6) Yuan, H.; Zhang, W.; Li, X.; Lu, X.; Li, N.; Gao, X.; Song, J. Preparation and in vitro antioxidant activity of kappa-carrageenan oligosaccharides and their oversulfated, acetylated, and phosphorylated derivatives. *Carbohydr. Res.* **2005**, *340*, 685−692.

(7) Vlieghe, P.; Clerc, T.; Pannecouque, C.; Witvrouw, M.; Clercq, E. D.; Salles, J. P.; Kraus, J. L. Synthesis of new covalently bound κ-carrageenan-AZT conjugates with improved anti-HIV activities. *J. Med. Chem.* **2002**, *45*, 1275−1283.

(8) Nardi, G. M.; Junior, J. M. S.; Monache, F. D.; Pizzolatti, M. G.; Ckless, K.; Ribeiro-do-Valle, R. M. R. Antioxidant and anti-inflammatory effects of products from *Croton celtidifolius* bailon on carrageenan-induced pleurisy in rats. *Phytomedicine* **2007**, *14*, 115−122.

(9) Abad, L. V.; Relleve, L. S.; Racadio, C. D. T.; Aranilla, C. T.; de la Rosa, A. M. Antioxidant activity potential of gamma irradiated carrageenan. *Appl. Radiat. Isot.* **2013**, *79*, 73−79.

(10) Campo, V. L.; Kawano, D. F.; da Silva, D. B.; Carvalho, I. Carrageenans: Biological properties, chemical modifications and structural analysis-A review. *Carbohydr. Polym.* **2009**, *77*, 167−180.

(11) Yuan, H.; Song, J.; Zhang, W.; Li, X.; Li, N.; Gao, X. Antioxidant activity and cytoprotective effect of κ-carrageenan oligosaccharides and their different derivatives. *Bioorg. Med. Chem. Lett.* **2006**, *16*, 1329−1334.

(12) Yuan, H.; Song, J. Preparation, structural characterization and in vitro antitumor activity of *κappa*-carrageenan oligosaccharide fraction from *Kappaphycus striatum*. *J. Appl. Phycol.* **2005**, *17*, 7−13.

(13) Jiao, G.; Yu, G.; Zhang, J.; Ewart, H. S. Chemical structure and bioactivities of sulfated polysaccharides from marine algae. *Mar. Drugs* **2011**, *9*, 196−233.

(14) Kalitnik, A. A.; Barabanova, A. O. B.; Nagorskaya, V. P.; Reunov, A. V.; Glazunov, V. P.; Solov'eva, T. F.; Yermak, I. M. Low molecular weight derivatives of different carrageenan types and their antiviral activity. *J. Appl. Phycol.* **2013**, *25*, 65−72.

(15) Michel, G.; Chantalat, L.; Duee, E.; Barbeyron, T.; Henrissat, B.; Kloareg, B.; Dideberg, O. The κ-carrageenase of *P. carrageenovora* features a tunnel-shaped active site: a novel insight in the evolution of clan-B glycoside hydrolases. *Structure* **2001**, *9*, 513−525.

(16) Knutsen, S. H.; Sletmoen, M.; Kristensen, T.; Barbeyron, T.; Kloareg, B.; Potin, P. A rapid method for the separation and analysis of carrageenan oligosaccharides released by iota- and *κappa*-carrageenanase. *Carbohydr. Res.* **2001**, *331*, 101−106.

(17) Bellion, C.; Hamer, G. K.; Yaphe, W. The degradation of *Eucheuma spinosum* and *Eucheuma cottonii* carrageenans by ι-carrageenanases and κ-carrageenanses from marine bacteria. *Can. J. Microbiol.* **1982**, *28*, 874−880.

(18) Antonopoulos, A.; Herbreteau, B.; Lafosse, M.; Helbert, W. Comparative analysis of enzymatically digested κ-carrageenans, using liquid chromatography on ion-exchange and porous graphitic carbon columns coupled to an evaporative light scattering detecter. *J. Chromatogr., A* **2004**, *1023*, 231−238.

(19) Greer, C. W.; Shomer, I.; Goldstein, M. E.; Yaphe, W. Analysis of carrageenan from *Hypnea musciformis* by using κ- and ι-carrageenanases ^{13}C NMR spectroscopy. *Carbohydr. Res.* **1984**, *129*, 189−196.

(20) Hatada, Y. J.; Mizuno, M.; Li, Z.; Ohta, Y. Hyper-production and characterization of the ι-carrageenase useful for ι-carrageenan oligosaccharide production from a deep-sea bacterium, *Microbulbifer thermotolerans* JAMB-$A94^T$, and insight into the unusual catalytic mechanism. *Mar. Biotechnol.* **2011**, *13*, 411−422.

(21) Guibet, M.; Colin, S.; Barbeyron, T.; Genicot, S.; Kloareg, B.; Michel, G.; Helbert, W. Degradation of λ-carrageenan by *Pseudoalteromonas carrageenovora* λ-carrageenase: a new family of glycoside hydrolases unrelated to κ- and ι-carrageenases. *Biochem. J.* **2007**, *404*, 105−514.

(22) Barbeyron, T.; Michel, G.; Potin, P.; Henrissat, B.; Kloareg, B. ι-Carrageenanases constitute a novel family of glycoside hydrolases,

unrelated to that of κ-carrageenases. *J. Biol. Chem.* **2000**, *275*, 35499−35505.
(23) Potin, P.; Richard, C.; Barbeyron, T.; Henrissat, B.; Gey, C.; Petillot, Y.; Forest, E.; Dideberg, O.; Rochas, C.; Kloareg, B. Processing and hydrolytic mechanism of the *cgk*A-encoded κ-carrageenanse of *Alteromonas carrageenovora*. *Eur. J. Biochem.* **1995**, *228*, 971−975.
(24) Khambhaty, Y.; Mody, K.; Jha, B. Purification and characterization of κ-carrageenanse from a novel γ-proteobacterium, *Pseudomonas elongata* (MTCC 5261) syn. *Microbulbifer elongatus* comb. nov. *Biotechnol. Bioprocess Eng.* **2007**, *12*, 668−675.
(25) Dyrset, N.; Lystad, K. Q.; Levine, D. W. Development of a fermentation process for production of a κ-carrageenanse from *Pseudomonas carrageenovora*. *Enzyme Microb. Technol.* **1997**, *20*, 418−423.
(26) Potin, P.; Sanseau, A.; Gall, Y. L.; Rochas, C.; Kloareg, B. Purification and characterization of a new κ-carrageenanse from a marine *Cytophaga*-like bacterium. *Eur. J. Biochem.* **1991**, *201*, 241−247.
(27) Weigl, J.; Yaphe, W. The enzymic hydrolysis of carrageenan by *Pseudomonas Carrageenovora*: purification of a κ-carrageenanses. *Can. J. Microbiol.* **1966**, *12*, 939−947.
(28) Guibet, M.; Kervarec, N.; Génicot, S.; Chevolot, Y.; Helbert, W. Complete assignment of ^{1}H and ^{13}C NMR spectra of *Gigartina skottsbergii* λ-carrageenan using carrabiose oligosaccharides prepared by enzymatic hydrolysis. *Carbohydr. Res.* **2006**, *341*, 1859−1869.
(29) Antonopoulos, A.; Favetta, P.; Helbert, W.; Lafosse, M. Isolation of κ-carrageenan oligosaccharides using ion-pair liquid chromatography-characterisation by electrospray ionization mass spectrometry in positive-ion mode. *Carbohydr. Res.* **2004**, *339*, 1301−1309.
(30) Meng, Y.; Fu, Y.; Wang, M.; Zhao, Y.; Liu, Q.; Du, Y. *Pedobacter hainanensis* sp. nov., isolated from seaside soil. *Curr. Microbiol.* **2013**, *66*, 487−492.
(31) Meng, Y.; Yue, M.; Zhang, J.; Wang, M.; Zhao, Y.; Yin, H.; Du, Y. Optimization of fermentation condition for κ-carrageenanse producing by *Pedobacter hainanensis* 13-Q^{T}. *China Brew.* **2013**, *32*, 20−23.
(32) Bradford, M. M. A rapid and sensitive method for the quantification of protein using the principle of protein-dye binding. *Anal. Biochem.* **1976**, *72*, 48−54.
(33) Yaphe, W.; Baxter, B. The enzymic hydrolysis of carrageenin. *Appl. Microbiol.* **1955**, *3*, 380−383.
(34) Miller, G. L. Use of dinitrosalicylic acid reagent for determination of reducing sugar. *Anal. Chem.* **1959**, *31*, 426−428.
(35) Dubois, M.; Gilles, K. A.; Hamilton, J. K.; Rebers, P. A.; Smiths, F. Colorimetric method for determination of sugars and related substances. *Anal. Chem.* **1956**, *28*, 350−356.
(36) Skipski, V. P.; Smolowe, A. F.; Barclay, M. Separation of neutral glycosphingolipids and sulfatides by thin-layer chromatography. *J. Lipid Res.* **1967**, *8*, 295−299.
(37) Zhang, Y.; Huang, L.; Wang, Z. A sensitive derivatization method for the determination of the sugar composition after pre-column reductive amination with 3-amino-9-ethylcarbazole (AEC) by high-performance liquid chromatography. *Chin. J. Chem.* **2007**, *25*, 1522−1528.
(38) Endwin, P.; Crowell, P.; Burnett, P. Determination of the carbohydrate composition of wood pulps by gas chromatography of the alditol acetates. *Anal. Chem.* **1967**, *39*, 121−124.
(39) Sarwar, G.; Matayoshi, S.; Oda, H. Purification of a κ-carrageenase from marine *Cytophaga* Species. *Microbiol. Immunol.* **1987**, *31*, 869−877.
(40) Dhalwal, K.; Shinde, V. M.; Biradar, Y. S.; Mahadik, K. R. Simultaneous quantification of bergenin, catechin, and gallic acid from *Bergenia ciliata* and *Bergenia ligulata* by using thin-layer chromatography. *J. Food Compos. Anal.* **2008**, *21*, 496−500.
(41) Zhang, Z.; Xie, J.; Zhang, F.; Linhardt, R. J. Thin-layer chromatography for the analysis of glycosaminoglycan oligosaccharides. *Anal. Biochem.* **2007**, *371*, 118−120.
(42) Ekeberg, D.; Knutsen, S. H.; Sletmoen, M. Negative-ion electrospray ionization-mass spectrometry (ESI-MS) as a tool for analysing structural heterogeneity in *κappa*-carrageenan oligosaccharides. *Carbohydr. Res.* **2001**, *334*, 49−59.
(43) Bellion, C.; Brigand, G.; Prome, J. C.; Welti, D.; Bociek, S. Identification et caractérisation des précurseurs biologiques des carraghénanes par spectroscopie de RMN-^{13}C. *Carbohydr. Res.* **1983**, *119*, 31−48.
(44) Harvey, D. J. Electrospray mass spectrometry and fragmentation of N-linked carbohydrates derivatized at the reducing terminus. *J. Am. Soc. Mass Spectrom.* **2000**, *11*, 900−915.
(45) Duffin, K. L.; Welply, J. K.; Huang, E.; Henion, J. D. Characterization of N-linked oligosaccharides by electrospray and tandem mass spectrometry. *Anal. Chem.* **1992**, *64*, 1440−1448.
(46) Gonçalves, A. G.; Ducatti, D. R. B.; Grindley, T. B.; Duarte, M. E. R.; Noseda, M. D. ESI-MS differential fragmentation of positional isomers of sulfated oligosaccharides derived from carrageenans and agarans. *J. Am. Soc. Mass Spectrom.* **2010**, *21*, 1404−1416.
(47) Domon, B.; Costello, C. E. A systematic nomenclature for carbohydrate fragmentations in FAB-MS/MS spectra of glycoconjugates. *Glycoconjugate J.* **1988**, *5*, 397−409.
(48) Yu, G.; Zhao, X.; Yang, B.; Ren, S.; Guan, H.; Zhang, Y.; Lawson, A. M.; Chai, W. G. Sequence determination of sulfated carrageenan-derived oligosaccharides by high-sensitivity negative-ion electrospray tandem mass spectrometry. *Anal. Chem.* **2006**, *78*, 8499−8505.
(49) Hantus, S.; Pauly, M.; Darvill, A. G.; Albersheim, P.; York, W. S. Structural characterization of novel L-galactose-containing oligosaccharide subunits of jojoba seed xyloglucans. *Carbohydr. Res.* **1997**, *304*, 11−20.
(50) Ma, Y. X.; Dong, S. L.; Jiang, X. L.; Li, J.; Mou, H. J. Purification and characterization of κ-carrageenase from marine bacterium mutant strain *Pseudoalteromonas* sp. AJ5−13 and its degraded products. *J. Food Biochem.* **2010**, *34*, 661−678.

carbohydrates, and the thermoplastics could therefore have better properties.

In this research, we have grafted sorghum DDG with three different types of methacrylates (methyl, ethyl, and butyl methacrylates) and the grafting conditions have been optimized. The influence of grafting conditions on the grafting parameters, properties of the grafted DDG and the thermoplastics developed from the grafted DDG have been studied.

MATERIALS AND METHODS

Materials. Sorghum DDG was obtained from an ethanol producer in Kansas, U.S.A. The three methacrylates, methyl methacrylate (99.8%, TCI America, Portland, OR), ethyl methacrylate (98%, Alfa Aesar, Ward Hill, MA), and butyl methacrylate (99%, Acros Organics, New Jersey) and the initiator (Potassium persulfate, TCI America, Portland, OR), reducing agent (sodium bisulfite, Sigma Aldrich, St. Louis, MO), and other chemicals required for the study were reagent grade and used as-received.

Grafting. Grafting was done in a four-necked flask under nitrogen atmosphere. A schematic of the grafting process is shown in Figure 1.

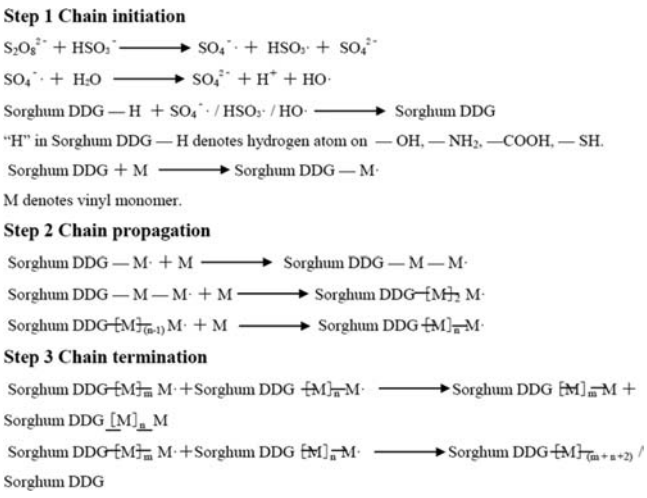

Figure 1. Schematic of the grafting process.

Sorghum DDG was dispersed in water and the monomer concentrations ranging from 20 to 180% on weight of the DDG were added into the flask, along with the required amount of initiators and reducing agents. Grafting was done by heating the flask to 70 °C for 2 h. Paradioxybenzene (2%) was added into the flask to terminate the grafting reaction and the grafted DDG was collected. Any unreacted monomers were removed by thoroughly washing the grafted DDG with water. The amount of DDG obtained after grafting was weighted and used to calculate the % grafting and other grafting parameters. The grafting parameters that were determined include % monomer conversion, molar grafting ratio, % grafting, and % homopolymers using the equations given below.[12] In this report, % grafting describes the % by weight of the monomers grafted on to the meal, grafting efficiency (%) indicated the weight % of monomers grafted to the initial weight of the monomers used and includes both the grafted polymers and the homopolymers.

$$\%\ \text{monomer conversion} = \frac{W_1 - W_2}{W_1} \times 100 \quad (1)$$

$$\%\ \text{grafting} = \frac{W_1 - W_2 - W_3}{W_0} \times 100 \quad (2)$$

$$\%\ \text{grafting efficiency} = \frac{W_1 - W_2 - W_3}{W_1 - W_2} \times 100 = \frac{\%\ \text{grafting}}{\%\ \text{monomer conversion}} \times \frac{W_0}{W_1} \times 100 \quad (3)$$

where W_b and W_a were the weight of the products before and after the extraction, respectively; W_3 and W_0 were the weight of the homopolymer and feathers, respectively, and $W_3 = W_b - W_a$.

Extracting Homopolymers. Since homopolymers affect the thermoplasticity and the properties of the products developed, the grafted samples used for compression molding were extracted with acetone to remove the homopolymers. Grafted samples were Soxhlet extracted in acetone for 24 h until all the homopolymers were removed.[12] Samples were later dried and conditioned before using for compression molding.

Characterizing Grafted DDG. *Thermal Analysis.* Grafted DDG was examined using a differential scanning calorimeter (DSC) (Mettler Toledo D822e, Columbus, OH) to observe the melting behavior. DSC studies were done by placing the samples in sealed aluminum pans and heating them up to 240 °C at a rate of 20 °C/min.

^{13}C NMR. Solid state ^{13}C NMR studies were done on a Bruker Avance 400 MHz spectrometer (Bruker Daltonics Ins, Fremont, CA) consisting of a $^1H/^{13}C/^{15}N$ triple-resonance, 3.2 mm magic angle spinning probe. Spectra were collected at room temperature using a standard cross-polarization experiment with high-power ^1H-decoupling, and spinning the samples at 20 kHz.

Developing Thermoplastic Films. Grafted DDG with and without any homopolymers was compression molded to form films. About 10 g of the grafted samples were placed between aluminum foils and compression molded in a Carver Press (Carver Inc., Wabash, IN) at 360 °F for 5 min at 40 000 PSI. After compression molding, cold water was run-in to cool the press and the samples were removed. Films obtained were conditioned under standard atmospheric conditions of 21 °C and 65% relative humidity for at least 24 h before being tested. At least 8 films were compression molded and samples were cut from the films and randomly selected for testing. Thickness of the films varied from 0.3 to 0.7 mm depending on the extent of grafting and type of monomer used.

Wet stability of the films was tested by immersing the films in 21 °C water for 30 min. After 30 min in water, the samples were immediately tested for their tensile properties according to ASTM standard D 882. Film strips measuring 15 ×1.5 cm^2 were tested on an MTS tensile tester (Model Q test 10, Eden Prairie, MN) using a gauge length of 5 cm and crosshead speed of 50 mm/min. At least 25 samples were tested for each condition and the average and ± one standard deviation are reported.

RESULTS AND DISCUSSION

Influence of Monomer Concentration on % Monomer Conversion. Figure 2 reveals that the % of monomers that were converted into polymers increased with increasing concentration of the monomers used during the reaction. Monomer conversion was considerably lower at monomer concentration of 20% but substantially increased to about 95% when the monomer concentration was increased to 60% or higher. Further increase in monomer concentration did not show any significant increase in the monomer conversion, and the monomer conversion was very similar for all three monomers studied. At low monomer concentration (20%), the molecules have a lower chance of reacting with each other and with the DDG and form polymers, and therefore had a low % conversion. Increasing monomer concentrations above 60% would result in excessive monomers that react with each other and form homopolymers. Since excessive concentration of monomers would add to the cost and does not substantially

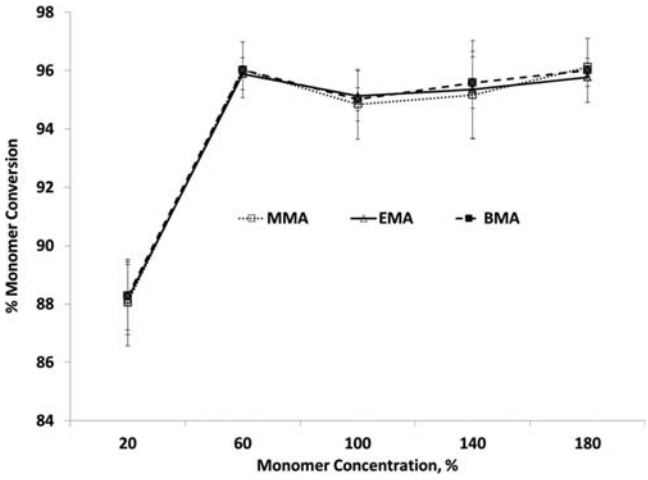

Figure 2. Influence of monomer concentration on the % monomer conversion. Grafting reaction was done at 70 °C for 120 min.

increase monomer conversion, a monomer concentration of 60% would be sufficient to get good % grafting and lower % homopolymers.

Influence of Monomer Concentration on % Grafting Efficiency. Grafting efficiency was substantially lower at high monomer concentrations as seen from Figure 3. At monomer

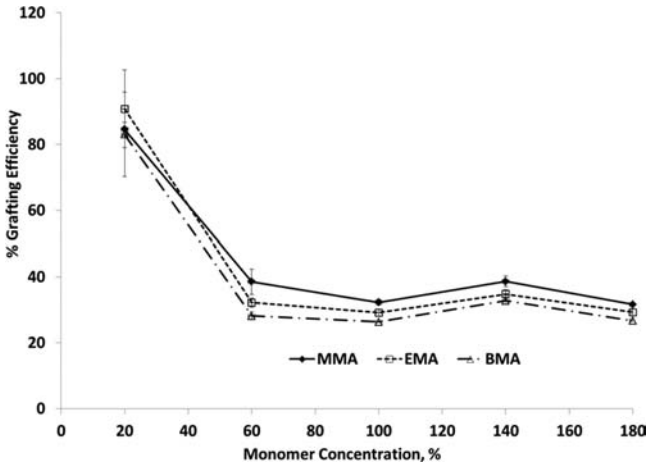

Figure 3. Influence of monomer concentration on the % grafting efficiency. Grafting reaction was done at 70 °C for 120 min.

concentrations of 20%, the grafting efficiency ranged from 66 to 91%, with the % grafting efficiency being highest for MMA, followed by EMA and BMA. Monomers containing longer side chains are more difficult to penetrate into DDG and attach onto the grafting sites. In addition, longer alkyl chains offer stearic hindrance and are more difficult to react with the DDG compared to a shorter chain monomers such as MMA. Therefore, BMA had a lower % grafting than MMA or EMA as seen from Figure 2. Changes in % grafting efficiency with increasing monomer concentration are consistent with observations made for the same monomers when grafted onto starch, soyprotein and corn DDG.

Influence of Monomer Concentration on % Grafting. Monomers (%) grafted onto DDG showed an opposite trend to the % grafting efficiency, as seen from Figure 4. Increasing monomer concentration steadily increased the % of polymers grafted onto DDG for all the monomers studied. When

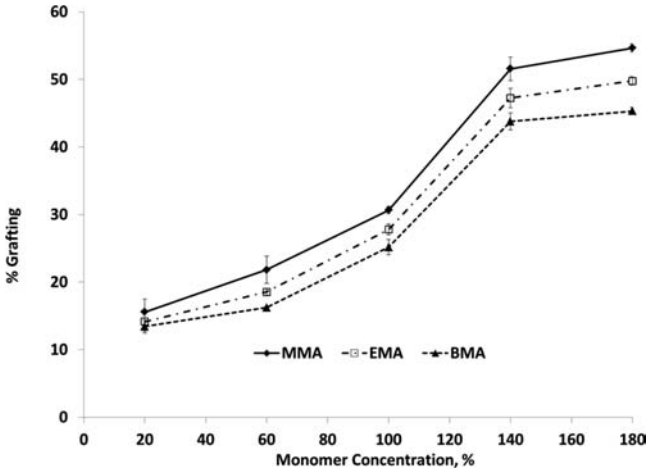

Figure 4. Increase in % grafting with increase in monomer concentration when grafted with the three monomers at 70 °C for 120 min.

monomer concentration was increased, the probability of the monomers reacting with themselves and with the DDG increased. This led to an increase in the amount of grafted chains on DDG and therefore the % grafting also increased. As seen with % grafting efficiency, MMA showed a higher % grafting than EMA and BMA because MMA are shorter polymers and readily reacted with the DDG and themselves. Longer polymer chains formed by EMA and BMA cannot penetrate easily into DDG and attach themselves to the grafting sites. Therefore, BMA had the lowest % grafting compared to the other two monomers. Molar grafting ratio data also showed that MMA had higher amounts of grafted monomers than EMA or BMA due mainly to the shorter chain length and lower stearic hindrance of MMA.

Influence of Monomer Concentration on % Homopolymers. Amount of homopolymers formed increased linearly with increasing monomer concentration as seen from Figure 5. At any particular monomer concentration, MMA had the lowest % homopolymers compared to EMA or BMA. Since MMA could react more easily with DDG, it had a lower chance to react with itself and form homopolymers. Increasing the

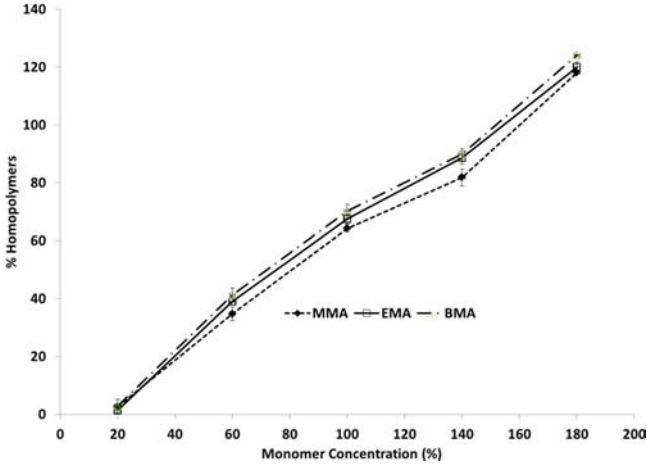

Figure 5. Changes in the amount of homopolymers formed with increasing ratio of monomers when the grafting was done at 70 °C for 120 min.

dx.doi.org/10.1021/jf405499t | J. Agric. Food Chem. 2014, 62, 2406−2411

concentration of monomers increased the reaction between the monomers and led to the formation of higher amounts of homopolymers. At monomer concentrations above 50%, the monomers predominantly form homopolymers than graft onto the DDG. Saturation of grafting sites in DDG that are accessible to the monomers decreased and that would also make the monomers to form homopolymers.

Nuclear Magnetic Resonance. NMR spectra of ungrafted and DDG grafted with EMA show distinct differences as seen from Figure 6. Since sorghum DDG contains about 25−45%

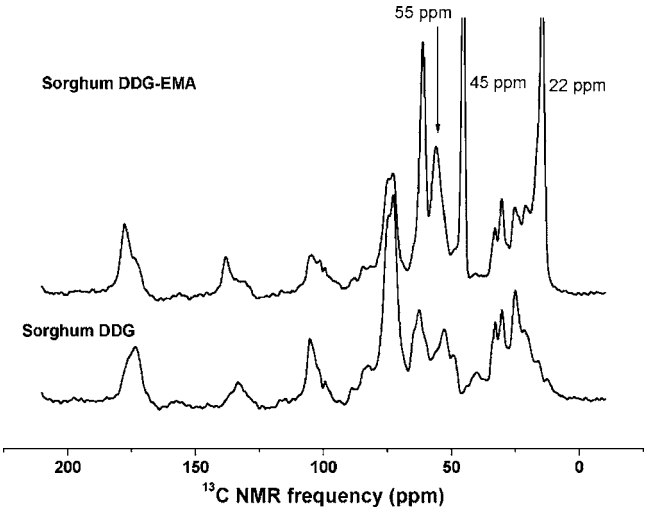

Figure 6. NMR spectrum depicting the differences between the ungrafted DDG and DDG grafted with EMA.

protein, 20% hemicellulose and 9−16% cellulose, the NMR spectra of sorghum DDG displayed major peaks belonging to the proteins, hemicellulose and cellulose. In sorghum DDG, the peak at about 175 ppm reflected amino group in protein,[13] the peak at about 75 ppm and 105 ppm represented C4 and C1 in cellulose and hemicellulose, respectively.[14,15] After EMA grafting, peaks at 22 ppm reflecting methyl groups ($-CH_3$), 45 ppm representing tertiary carbon and 55 ppm representing methoxy group ($-OCH_3$) in methacrylate are seen. The difference between the two spectra clearly indicated that EMA has been successfully grafted onto sorghum DDG.

Thermal Behavior of Grafted DDG. Figure 7 shows that the ungrafted and DDG grafted with the three monomers had distinct melting peaks. The peak at 130 °C seen in the ungrafted DDG should be due to the melting of the proteins. MMA grafted DDG had a broad melting peak suggesting poor thermoplasticity. Compared to MMA, the EMA- and BMA-grafted DDG showed considerably sharp melting peaks at 205 °C. BMA grafted DDG had an additional melting peak at about 180 °C, most likely due to the different melting behaviors of the proteins and carbohydrates in the DDG. As can be inferred from Figure 7, BMA grafted DDG had the highest melting enthalpy of 108 J/g, compared to 80 and 55 J/g for EMA and MMA, respectively. DSC curves clearly suggested that BMA imparted better thermoplasticity to DDG than MMA and EMA. Although the melting peaks for EMA and BMA were observed at 205 °C, the grafted DDG could be compression molded into films at 190 °C under pressure.

Tensile Properties of Grafted DDG films Without Homopolymers. Tensile properties of the films made from the grafted DDG after extraction of the homopolymers shown

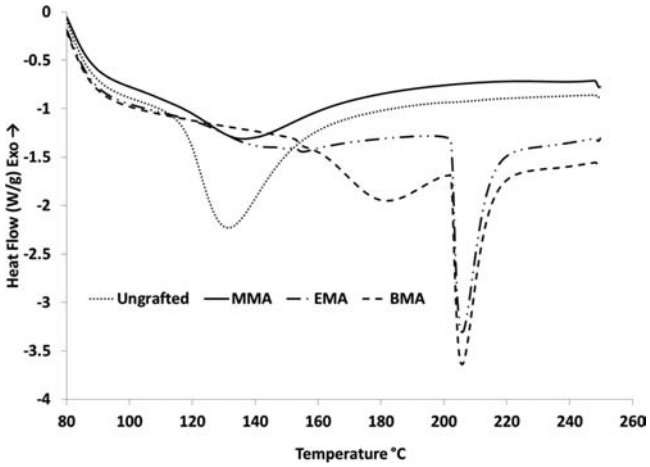

Figure 7. Differential scanning calorimetry curves for the ungrafted and DDG grafted with the three monomers shows that EMA and BMA provided better thermoplasticity compared to MMA.

in Tables 1−3 reveal some interesting features. For all three monomers, increasing the grafting ratio increased strength, except for DDG grafted with 53% BMA, where the strength decreased compared to the films obtained at 40% BMA grafting. At a grafting ratio of about 23%, films made from all three monomers had strengths between 2 and 2.3 MPa but films grafted with longer lengths of carbon chains had higher elongation. For instance, MMA-grafted films had an elongation of 0.5% compared to 1.1% for BMA grafted films. Increasing the grafting ratio from 23 to 30% more than doubled the strength and elongation of the MMA-grafted films, whereas the EMA and BMA grafted films showed a marginal increase in strength. Further increase in the grafting ratio to 40% and above led to increased strength of the films. MMA-grafted films had the highest strength but low elongation compared to EMA and BMA films, whereas BMA grafted films had higher elongation than the MMA and EMA films. The modulus of the films was highest for MMA-grafted DDG, followed by EMA- and BMA-grafted DDG. Tensile properties of the films mainly depend on the thermoplasticity of the grafted DDG. At low grafting ratios, the DDG partially melts, and the films contain considerable amounts of proteins and carbohydrates that do not melt leading to poor tensile properties. Increasing grafting ratio improves the thermoplasticity, and therefore the films have higher strength and elongation. Monomers with longer chains offer higher extensibility and better thermoplasticity. Therefore, the EMA- and BMA-grafted films had higher elongation than the MMA grafted films. Since the EMA- and BMA-grafted films are more flexible, the modulus is lower than that of the MMA films.

Wet tensile properties of the films showed a different trend than the dry properties of the films grafted with the three monomers. Films grafted with MMA showed strength retention ranging from 43 to 59% compared to 33−69% for EMA and 15−61% for BMA with increasing grafting ratio resulting in higher strength retention. Although there was no particular trend in the wet strength retention with the increasing chain length of the monomers, elongation of the films was considerably higher for BMA followed by EMA and MMA. MMA- and EMA-grafted films did not show significant change in the wet elongation but the BMA-grafted films had at least 100% increase in elongation when wet. Increasing the grafting ratio adds higher amounts of the hydrophobic polymer onto

dx.doi.org/10.1021/jf405499t | J. Agric. Food Chem. 2014, 62, 2406−2411

Table 1. Dry and Wet Tensile Properties of Thermoplastic Films Made from Sorghum DDG Grafted with Various Levels of MMA after Extraction of the Homopolymers

grafting ratio, % (mmol/g)	tensile strength, MPa		breaking elongation, %		Young's Modulus, MPa	
	dry	wet	dry	wet	dry	wet
23 (2.01)	2.3 ± 1.2	1.0 ± 0.4	0.5 ± 0.2	0.8 ± 0.2	895 ± 278	330 ± 96
30 (2.63)	4.1 ± 1.1	2.0 ± 0.6	1.1 ± 0.4	0.9 ± 0.2	984 ± 103	440 ± 121
40 (3.50)	5.2 ± 1.2	2.6 ± 0.6	1.1 ± 0.4	1.2 ± 0.3	1227 ± 175	491 ± 106
53 (4.64)	5.9 ± 1.2	3.5 ± 0.7	1.2 ± 0.3	1.2 ± 0.3	1287 ± 129	672 ± 124

Table 2. Dry and Wet Tensile Properties of Thermoplastic Films Made from Sorghum DDG Grafted with Various Levels of EMA after Extraction of the Homopolymers

grafting ratio, % (mmol/g)	tensile strength, MPa		breaking elongation, %		Young's Modulus, MPa	
	dry	wet	dry	wet	dry	wet
23 (2.01)	2.4 ± 0.7	0.8 ± 0.3	1.0 ± 0.4	1.3 ± 0.4	656 ± 94	164 ± 45
30 (2.63)	2.9 ± 0.8	0.84 ± 0.2	0.9 ± 0.3	1.6 ± 0.3	764 ± 151	158 ± 29
40 (3.50)	4.4 ± 0.8	2.3 ± 0.4	1.5 ± 0.2	1.7 ± 0.3	848 ± 86	304 ± 54
53 (4.64)	4.6 ± 0.9	3.2 ± 0.6	1.6 ± 0.1	2.0 ± 0.4	842 ± 70	388 ± 66

Table 3. Dry and Wet Tensile Properties of Thermoplastic Films Made from Sorghum DDG Grafted with Various Levels of BMA after Extraction of the Homopolymers

grafting ratio, % (mmol/g)	tensile strength, MPa		breaking elongation, %		Young's Modulus, MPa	
	dry	wet	dry	wet	dry	wet
23 (2.01)	2.0 ± 0.4	0.3 ± 0.09	1.1 ± 0.3	2.5 ± 0.5	700 ± 80	46 ± 15
30 (2.63)	2.8 ± 0.9	0.84 ± 0.2	1.6 ± 0.4	4.4 ± 0.9	427 ± 79	60 ± 20
40 (3.50)	4.3 ± 0.8	1.84 ± 0.4	2.3 ± 0.5	4.0 ± 0.9	550 ± 50	155 ± 57
53 (4.64)	3.1 ± 0.9	1.9 ± 0.8	2.3 ± 0.6	4.3 ± 1.3	580 ± 10	170 ± 91

DDG, and therefore the wet stability increased with increasing grafting ratio. Water acts as a plasticizer and allows the molecules to move more freely therby increasing the elongation. Although increasing chain length should increase hydrophobicity and improve wet tensile properties, BMA-grafted films had similar or lower strength retention than the MMA or EMA films. This should be due to the lower amounts (molar weight) of BMA on the films compared to MMA and EMA, although the % grafting ratios were similar.

Tensile Properties of Grafted DDG Films with Homopolymers. Since homopolymers are formed during the grafting reaction and the homopolymers are part of the grafted DDG, we investigated the properties of DDG films containing homopolymers. As seen from Table 4, the dry tensile properties of the films containing homopolymers were slightly different but there were considerable variations in the wet strength of the films compared to those developed from the same monomers but without the homopolymers. For instance, at 40% grafting, EMA grafted DDG without homopolymers had dry strength of 4.4 MPa compared to 6.3 MPa with homopolymers and the % elongation was 1.5% compared to 1.8%. Addition of homopolymers will increase the thermoplasticity and the hydrophobicity of the grafted DDG leading to increased strength and elongation. Also, the properties of the homopolymers will influence the properties of the DDG films. Our previous research has shown that films made from homopolymers with longer carbon chains have lower strength but higher elongations. BMA films with a dry strength of 4.8 MPa and elongation of 3.1% show excellent wet strength and elongation retention and could be useful for various applications.

Table 4. Tensile Properties of Sorghum DDG Films Grafted with MMA, EMA, and BMA under the Optimum Grafting Conditions and Including the Homopolymers[a]

	breaking strength, MPa		breaking elongation, %	
	dry	wet	dry	wet
MMA	4.5 ± 1.2	3.2 ± 1.0	1.4 ± 0.1	1.3 ± 0.4
EMA	6.3 ± 1.1	4.7 ± 1.1	1.8 ± 0.1	2.3 ± 0.2
BMA	4.8 ± 1.0	1.8 ± 0.4	3.1 ± 0.6	8.1 ± 1.2

[a]Grafting % for the three monomers was about 40% and homopolymers (%) were 54, 58 and 28% for MMA, EMA, and BMA, respectively.

Sorghum DDG grafted with methacrylates could be used to develop films with good dry and wet tensile properties. Changing the concentration of monomers resulted in higher grafting ratios and a higher percentage of homopolymers. Also, increasing grafting ratio generally increased the strength and elongation of the films. Similarly, the wet strength of the films was also higher at higher grafting ratios. Films containing homopolymers exhibited better tensile properties compared to films made from the same monomers but without the homopolymers. It was also observed that increasing the length of the alkyl chain resulted in films with lower strength but higher elongation since the monomers with longer chains are more flexible. Among the three monomers studied, BMA-grafted DDG had better thermoplasticity and also formed films with good dry and wet tensile properties. Grafting appears to be a more viable approach to develop thermoplastics from DDG compared to other common types of chemical modifications.

AUTHOR INFORMATION

Corresponding Author

*E-mail: yyang2@unl.edu.

Notes

The authors declare no competing financial interest.

■ ACKNOWLEDGMENTS

The authors wish to acknowledge the financial support from Agricultural Research Division at the University Nebraska—Lincoln and Multistate project S1054 (NEB37-037). Financial support for Zhen Shi from the Program for Changjiang Scholars and Innovative Research Team in University (No. IRT1135) at Jiangnan University, Scientific Support Program of Jiangsu Province (BE2011404), the Graduate student innovation plan of Jiangsu Province (CX10B_222Z), the Doctor Candidate Foundation of Jiangnan University (JUDCF10004) and the China Scholarship Council is also thankfully acknowledged.

■ REFERENCES

(1) Balat, M.; Balat, H. Recent Trends in Global Production and Utilization of Bio-Ethanol Fuel. *Appl. Energ.* **2009**, *86* (11), 2273−2282.

(2) Schilling, C. H.; Tomasik, P.; Karpovich, D. S.; Hart, B.; Shepardson, S.; Garcha, J.; Boettcher, P. T. Preliminary Studies on Converting Agricultural Waste into Biodegradable Plastics, Part I: Corn Distillers' Dry Grain. *J. Polym. Environ.* **2004**, *12*, 257−64.

(3) Wu, X.; Zhao, R.; Bean, S. R.; Seib, P. A.; McLaren, J. S.; Mad, R. L.; Tuinstra, M.; Lenz, M. C.; Wang, D. Factors Impacting Ethanol Production from Grain Sorghum in the Dry-Grind Process. *Cereal Chem.* **2007**, *94* (2), 130−136.

(4) Duodua, K. G.; Taylora, J. R. N.; Beltonb, P. S.; Hamaker, B. R. Factors Affecting Sorghum Protein Digestibility. *J. Cereal Sci.* **2003**, *38*, 117−131.

(5) Cheesborough, V.; Rosentrater, K.; Visser, J. Properties of Distillers Grains Composites: A Preliminary Investigation. *J. Polym. Environ.* **2008**, *16* (1), 40−50.

(6) Xu, W.; Reddy, N.; Yang, Y. An Acidic Method of Zein Extraction from DDGS. *J. Agric. Food Chem.* **2007**, *55*, 6279−6284.

(7) Xu, W.; Reddy, N.; Yang, Y. Extraction, Characterization and Potential Applications of Cellulose in Corn Kernels and Distillers' Dried Grains with Solubles (DDGS). *Carb. Polym.* **2009**, *76*, 521−27.

(8) Hu, C.; Reddy, N.; Luo, Y.; Yan, K.; Yang, Y. Thermoplastics from Acetylated Zein-and-Oil-Free Corn Distillers Dried Grains with Solubles. *Biomass Bioenerg.* **2011**, *35* (2), 884−892.

(9) Hu, C.; Reddy, N.; Yan, K.; Yang, Y. Synthesis and Characterization of Highly Flexible Thermoplastic Films from Cyanoethylated Corn Distillers Dried Grains with Solubles. *J. Agric. Food Chem.* **2011**, *59*, 1723−1728.

(10) Reddy, N.; Hu, C.; Yan, Y.; Yang, Y. Acetylation of Polysacccharides in Corn Distillers Dried Grains for Thermoplastic Applications. *Appl. Energ.* **2011**, *88* (5), 1664−1670.

(11) Reddy, N.; Jin, E.; Chen, L.; Jiang, X.; Yang, Y. Extraction, Characterization of Components, And Potential Thermoplastic Applications of Camelina Meal Grafted with Vinyl Monomers. *J. Agric. Food Chem.* **2012**, *60* (19), 4872−4879.

(12) Jin, E.; Reddy, N.; Zhu, Z..; Yang, Y. Graft Polymerization of Raw Chicken Feathers for Thermoplastic Applications. *J. Agric. Food Chem.* **2011**, *59*, 1729−1738.

(13) Luca, S.; Yau, W. M.; Leapman, R.; Tycko, R. Peptide Conformation and Supramolecular Organization in Amylin Fibrils: Constraints from Solid-State NMR. *Biochemistry* **2007**, *46*, 13505−13522.

(14) Focher, B.; Palma, M. T.; Canetti, M.; Torri, G.; Cosentino, G.; Gastaldi, G. Structural Differences between Non-Wood Plant Celluloses: Evidence from Solid State NMR, Vibrational Spectroscopy and X-ray Diffractometry. *Ind. Crops Prod.* **2001**, *13*, 193−208.

(15) Gilardi, G.; Abis, L.; Cass, A. E. G. Carbon-13 CP/MAS Solid-State NMR and FT-IR Spectroscopy of Wood Cell Wall Biodegradation. *Enzyme Microb. Technol.* **1995**, *17*, 268−275.

Table 1. Oligonucleotides Used in This Study

oligonucleotides (forward, 5′ → 3′)	usage
GGGCCGAATTCGATGACGATTTTTGATAATTATGAAGTGTGG (*EcoR* I underlined)	cloning of *araA*′ (*araA*′-up)
GGGAAGCTTTTAGCGGCGAAACCCGTA (*Hind* III underlined)	cloning of *araA*′ (*araA*′-down)
GAAGATCTCATGACCATGATTACGGAT (*Bgl* I underlined)	cloning of *lacZ* (*lacZ*-up)
CGGCTCGAGTTATTTTTGACACCAGAC (*Xho* I underlined)	cloning of *lacZ* (*lacZ*-down)

Currently, researchers are still on the lookout for some new and simpler methods of D-tagatose production. From a commercial point of view, a single-step or single-pot biosynthesis of D-tagatose from lactose is very much desired. Technically, however, it is hard to achieve because the producing strains of isomerase and hydrolase have incompatible fermentation conditions, especially the optimal pH. In the present study, we attempted to develop an efficient single-step method for the D-tagatose production from lactose. The ECAI-Q299K mutant, whose optimal conditions approached that of β-D-galactosidase, was obtained before. A recombinant strain (*E. coli*-ZY) was constructed to coexpress β-D-galactosidase and ECAI-Q299K at a fairly high level. With this *E. coli*-ZY strain, D-tagatose was successfully generated in a single step for the first time and, later, separated, purified, and crystallized to give pure powder with a high yield. The results are believed to lay down the foundation for industrialized D-tagatose production.

MATERIALS AND METHODS

Materials, Bacterial Strains, and Media. Ex-Taq DNA polymerase, restriction enzymes, T4 DNA ligase, ampicillin, and isopropyl-β-D-thiogalactopyranoside (IPTG) were purchased from Takara Biotechnology Co., Ltd. (Dalian, China). The pETDuet-01 expression vector was bought from Novagen (Darmstadt, Germany). The high-performance liquid chromatography (HPLC) and Rezex RCM-Monosaccharide Ca^{2+} columns were purchased from Agilent (Wilmington, DE) and Phenomenex (Guangzhou, China), respectively. Other reagents were of analytical grade and purchased from commercial sources. The hosts of *E. coli* BL21 (DE3) were purchased from Merck (Darmstadt, Germany). Different *E. coli* strains were cultured in Luria-Bertani (LB) medium. The *E. coli* strain and *Saccharomyces cerevisiae* NX-3 were stored at the laboratory.

Construction of the Coexpression Plasmids. As previously reported,[28] we found that alternations at Q299 of ECAI can significantly influence the optimal pH of the enzyme. Using directed evolution mutagenesis, it was found that the optimal pH of ECAI-Q299K was 6.5. The *araA*′ gene from the recombinant *E. coli* of L-arabinose isomerase Q299K and the *lacZ* gene from *E. coli* W303 were amplified using polymerase chain reaction (PCR). The up- and downstream oligonucleotide primers of the *araA*′ gene (Table 1) were *araA*′-up and *araA*′-down, respectively. The template for this PCR was the genome from recombinant *E. coli* of L-arabinose isomerase Q299K. The PCR fragment was subsequently cloned into the *EcoR* I–*Hind* III restriction sites of pETDuet-01 to generate the recombinant plasmid pETDuet-*araA*′.

The up- and downstream oligonucleotide primers of the *lacZ* gene (Table 1) were *lacZ*-up and *lacZ*-down, respectively. The template for this PCR was the genome from *E. coli* W303. The PCR fragment was subsequently cloned into the *Bgl* II–*Xho* I restriction sites of pETDuet-*araA*′ to generate the recombinant coexpression plasmid pETDuet-*araA*′-*lacZ*. The recombinant plasmid was identified by PCR and single restriction enzyme digestion (*Hind* III). The correct plasmid was sent to GenScript Biotech Co. (Nanjing, China) for DNA sequencing. The ECAI-Q299K and β-D-galactosidase coexpression plasmid were constructed successfully.

Expression of Recombinant Coexpression Plasmid in *E. coli* Strain BL21 (DE3). Expression studies were carried out using *E. coli* BL21 (DE3). Transformation was performed according to the pET system manual. The vectors of pETDuet-*araA*′-*lacZ* were transformed. A single colony from freshly transformed cells was inoculated in 5 mL of LB medium containing 50 mg/mL ampicillin and incubated for 8–10 h at 37 °C. Then, 2 mL of cell suspension was inoculated to 25 mL of LB medium supplemented with 50 mg/mL ampicillin and 1 mM isopropyl-β-D-thiogalactopyranoside (IPTG) to OD_{600} of 0.6; the culture was cultivated at 25 °C to induce protein expression; and cells were harvested by centrifugation after 22 h. The induced cells were collected by centrifugation at 5000*g* for 5 min, and the cell density was adjusted to OD_{600} = 1 using normal saline. The cells were disrupted by sonication in an ice bath. The expression of target genes was assessed by total cell protein analysis using sodium dodecyl sulfate–polyacrylamide gel electrophoresis[29] (SDS–PAGE) and Coomassie Blue staining.

Assay of Recombinant Enzymatic Activities. The preparation of crude enzyme is as follows: the *E. coli*-ZY strain liquid (1 mL) was harvested by centrifugation (10000*g* for 20 min), suspended by 1 mL of 0.1 M sodium phosphate buffer (pH 6.5), and disrupted by sonication (400 W; working time, 3 s; interval, 3 s; and cooling temperature, 4 °C). The crude enzyme supernatant was obtained by centrifugation (16000*g* for 40 s at 4 °C).

The L-arabinose isomerase activity of crude enzyme was measured by determining the amount of formed D-tagatose after a 20 min reaction with 1 mL of 100 mM D-galactose. The generated D-tagatose was determined by the cysteine–carbazol–sulfuric acid method, and the absorbance was measured at 560 nm.[30] D-Tagatose was also determined by HPLC. Lactose, D-galactose, D-glucose, and D-tagatose concentrations were determined by HPLC, using a Rezex RCM-Monosaccharide Ca^{2+} column at 80 °C with distilled water as the mobile phase at an elution rate of 0.3 mL/min. All components were analyzed with a refractive index detector RI-101. The generated D-tagatose concentration from the reaction was calibrated on the basis of the standard linear graph prepared using different D-tagatose concentrations. One unit of L-arabinose isomerase activity was defined as the amount of enzyme catalyzing the formation of 1 μmol of D-tagatose/min under optimal conditions.

The β-D-galactosidase activity of crude enzyme was measured by the *o*-nitrophenyl β-D galactopyranoside (ONPG) method. The hydrolytic activity of ONPG by β-D-galactosidase was determined by measuring the release of *o*-nitrophenol (ONP). The reaction was carried out with continuous agitation in an assay volume of 4.0 mL containing 0.5 mL of 0.1 M sodium phosphate buffer (pH 6.5), 0.5 mL of the suitably diluted crude enzyme, and 3 mL of 10 mM ONPG at 37 °C for 20 min. The reaction was stopped by adding 2.0 mL of 0.5 M sodium carbonate solution, and ONP formation was measured spectrophotometrically at 420 nm.[31] One unit of β-D-galactosidase activity was defined as the amount of enzyme catalyzing the formation of 1 μmol ONP/min under optimal conditions.

Effects of the Temperature, pH, and Metal Ions on Recombinant Enzyme Activities. To optimize the operating conditions, the effects of the temperature, pH, and metal ion were investigated. The effect of the temperature on enzyme activity was analyzed by assaying the *E. coli*-ZY cell samples over a range of 15–45 °C. The optimal pH of the recombinant enzyme was determined using the standard assay conditions with three buffer systems, namely, sodium acetate (pH 4.0–6.0), phosphate (pH 6.0–8.0), and Tris–HCl (pH 8.0–9.0). To determine the influence of metal ions on enzyme activities, 1 mL of *E. coli*-ZY liquid was used under standard conditions in the presence of several metal ions ($CoCl_2$, $MnCl_2$, $FeCl_2$, $MgCl_2$, $NiCl_2$, $CaCl_2$, $ZnCl_2$, and $CuCl_2$) at a final concentration of 1 or 10 mM. The measured activities were compared to enzyme activity without additional ions under the same conditions.

dx.doi.org/10.1021/jf4042485 | J. Agric. Food Chem. 2014, 62, 2412–2417

Effects of Cell Dosage and Substrate Concentration. The effects of cell dosage and substrate concentration were investigated to obtain the optimal conversion conditions. Preparative-scale production of D-tagatose was performed in a 1 mL reaction system containing a final concentration of 100 mM lactose, 10 mM Mn^{2+}, 1 mM Fe^{2+}, and 10 mM phosphate buffer (pH 6.5). The *E. coli*-ZY wet cells were centrifuged from 0.5, 1, 3, 5, 7, and 9 mL of fermentation broth, which was converted into wet cell weight (WCW) using the relation of 100 mL of fermentation broth = 2.4 g of WCW. To determine the influence of the substrate concentration on the conversion rate, a final concentration of 5, 10, 30, 50, 70, and 90 g/L lactose was combined with the cells centrifuged from 3 mL of fermentation broth in a 1 mL reaction system. Other investigations were performed as previously mentioned.

Biotransformation Amplification of Lactose to D-Tagatose with Borate Addition and Yeast Cell Processing. The 100 mL biotransformation system contained a final concentration of 50 g/L lactose, 10 mM $MnCl_2$, 1 mM $FeCl_2$, 100 mM phosphate buffer (pH 6.5), 235 mM borate, and the *E. coli*-ZY cells centrifuged from 300 mL of fermentation broth (6.2 g of wet cells). The reaction conditions were 34 °C and 200 rpm for 36 h. Samples (0.5 mL) were obtained at 4 h intervals for HPLC analysis. *S. cerevisiae* NX-3 was cultured at yeast extract−peptone−dextrose (YPD) medium and conditions of 30 °C and 200 rpm. The *S. cerevisiae* NX-3 cells were harvested during log phase by centrifugation at 10 000 rpm for 10 min and washed twice with sterile water. For every 100 mL of reaction syrup, 2 g of yeast cells was added. Fermentation conditions have been determined through a series of experiments; finally, fermentation was carried out in an incubator at 37 °C with shaking at 100 rpm. Samples (0.5 mL) were withdrawn at proper time intervals and analyzed.

D-Tagatose Separation, Crystallization, and Characterization. After *S. cerevisiae* NX-3 fermentation, the cells were disposed by centrifugation. Borate was separated from syrup according to DTF-01 Ca^{2+} cation-exchange chromatography, and the optimal Ca^{2+} cation-exchange chromatography conditions were investigated. D-Tagatose solution was concentrated to 20 g/L at 55 °C using rotary vacuum evaporation. Anhydrous ethanol (40 mL) was added to D-tagatose solution upon reaching room temperature; the solution became muddy and then was heated above 60 °C for dissolution. A total of 10% of total D-tagatose was added as crystal seed, while the solution was cool. The solution was refrigerated at 4 °C for 4−8 h, and 20 mL of anhydrous ethanol was added with stirring. Bulk crystallization was observed after 40 h; the crystals were harvested by centrifugation (5000 r/min for 15 min). Then, 20 mL of anhydrous ethanol was added to the resulting crystals with continuous stirring. D-Tagatose crystals were dried in a suction flask and vacuumed at 25 °C. Infrared spectroscopy and proton nuclear magnetic resonance (^{1}H NMR) were used to characterize D-tagatose production.

RESULTS

Gene Cloning and Construction of Recombinant Coexpression Plasmid pETDuet-*araA′*-*lacZ*. The successful amplification of the *araA′* gene of ECAI-Q299K and the *lacZ* gene by PCR resulted in 1.5 kbp DNA fragments (Figure 1A) and 3.07 kbp DNA fragments (Figure 1B), respectively. The *araA′* and *lacZ* genes were successively ligased with pETDuet-01 to construct the recombinant coexpression plasmid pETDuet-*araA′*-*lacZ* (Figure 2A). With the coexpression plasmid as a template, Figure 2B shows that *araA′* and *lacZ* were successfully amplified by PCR and single restriction enzyme digestion (*Hind* III). DNA sequencing results also demonstrate that a correct coexpression plasmid pETDuet-*araA′*-*lacZ* was obtained.

Coexpression of Two Enzymes and Preliminary Survey of Activities. The recombinant coexpression plasmid pETDuet-*araA′*-*lacZ* was transformed into *E. coli* BL21 (DE3). The obtained positive clones were used for the coexpression of the two enzymes. When the culture conditions were optimized,

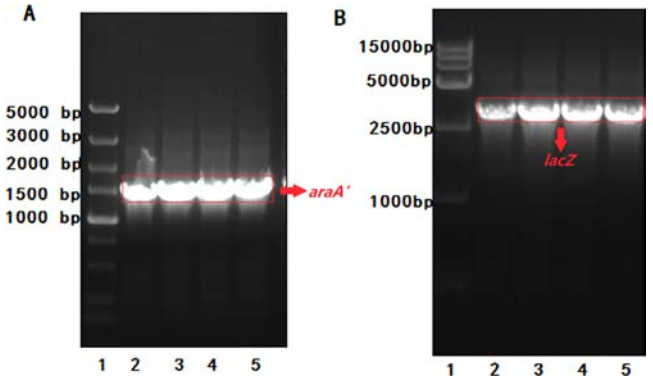

Figure 1. (A) Cloning of the *araA′* gene from the recombinant *E. coli* of L-arabinose isomerase Q299K by PCR. Lane 1, DL5000 marker; lanes 2−5, *araA′* gene. (B) Cloning of the *lacZ* gene from *E. coli* W3110 by PCR. Lane 1, DL15000 marker; lanes 2−5, *lacZ* gene.

the following conditions were obtained: 10 g/L lactose, 10 g/L NaCl, and 10 g/L yeast extract at 25 °C after 22 h. The results of SDS−PAGE analysis of recombinant protein coexpression were showed in Figure 3. It proved that the recombinant *E. coli* BL21 (DE3) strain was constructed successfully, which simultaneously expressed the *β*-D-galactosidase and ECAI-Q299K in soluble form after induction with lactose. The stripe characteristics were observed at approximately 112 and 56.2 kDa, in accordance with the previous reports for the two enzymes. This recombinant *E. coli* BL21 (DE3) strain was named *E. coli*-ZY. The enzymatic activity of ECAI-Q299K for D-galactose isomerization was 7.8 units within 1 mL of *E. coli*-ZY fermentation broth, whereas that of *β*-D-galactosidase for lactose hydrolysis was 56.3 units.

Optimal Conditions of D-Tagatose Production by the Recombinant Coexpression Cell. At an optimal pH of 6.5, the highest conversion rate for lactose to D-tagatose by the recombinant coexpression cell was 20.1%. At pH 5.0, 6.0, 7.0, and 8.0, they exhibited 27, 66, 83, and 43% of highest conversion rate, respectively (Figure 4A). The optimal temperature for D-tagatose production was 34 °C, as shown in Figure 4B. Recombinant enzyme activity was measured in the presence of 1 or 10 mM metal ions (Table 2). The enzyme activity was not stimulated by Mg^{2+} or Ni^{2+}, but Co^{2+}, Ca^{2+}, and Cu^{2+} significantly inhibited recombinant coexpression enzyme activity. However, Zn^{2+}, Fe^{2+}, and Mn^{2+} enhanced enzyme activity. Mn^{2+} (10 mM) and Fe^{2+} (1 mM) increased enzyme activity by 56.6 and 32.1%, respectively; both appeared to be required for the catalytic activity of the recombinant coexpression cell. The maximum production rate was obtained at pH 6.5 and 34 °C in the presence of 10 mM Mn^{2+} and 1 mM Fe^{2+}.

The added amount of recombinant cells was a factor in the efficient production of tagatose. Cell dosage and lactose concentration effects were investigated, and the results are shown in panels A and B of Figure 5. The optimal dosage of cells was determined to be the amount centrifuged from 3 mL fermentation broth, and the optimal lactose concentration was 50 g/L. On that condition, we obtained the highest production rate of 38.1 g L^{-1} h^{-1} and the nearly highest conversion rate of 25.4%.

Production and Purification of D-Tagatose. The time course study revealed that the conversion reached its equilibrium within 24 h (Figure 6A), the substrate lactose almost completely hydrolyzed, and the conversion rate of D-

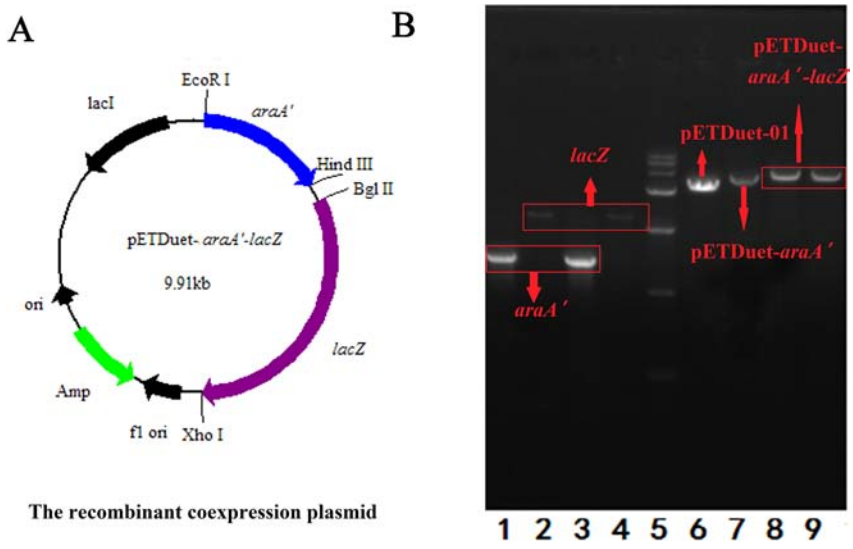

Figure 2. (A) Construction of recombinant coexpression plasmid. (B) Coexpression plasmid identification. Lanes 1 and 2, PCR for *araA′* and *lacZ* from coexpression plasmid 1; lanes 3 and 4, PCR for *araA′* and *lacZ* from coexpression plasmid 2; lane 5, DL15000 marker (15 000, 10 000, 7500, 5000, 2500, 1000 bp, etc.); lane 6, pETDuet-01 by *Hind* III digestion; lane 7, pETDuet-*araA′* by *Hind* III digestion; lanes 8 and 9, coexpression plasmid pETDuet-*araA′*-*lacZ* by *Hind* III digestion.

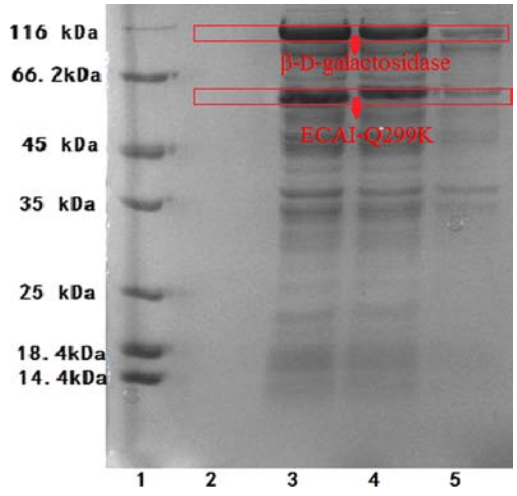

Figure 3. SDS−PAGE analysis of recombinant coexpression ECAI-Q299K and *β*-D-galactosidase. Lane 1, protein molecular weight marker; lanes 2−5, supernatant (soluble proteins) after centrifugation, whole cell, supernatant (soluble proteins) after sonication, and the residue after sonication of *E. coli* BL21 (DE3) with pETDuet-*araA′*-*lacZ*, respectively.

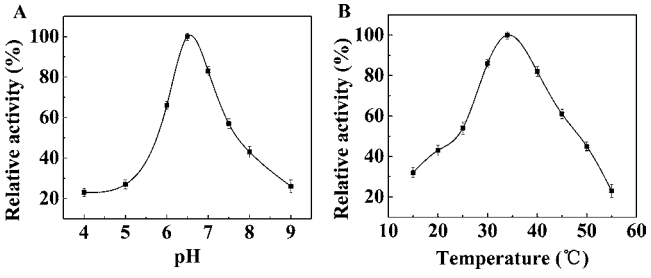

Figure 4. (A) Effect of the pH on the recombinant enzyme. (B) Effect of the temperature on the recombinant enzyme.

galactose to D-tagatose was 43%. The syrup (100 mL) containing about 10.75 g/L D-tagatose was fermented by 2 g

Table 2. Effect of Different Metal Ions on the Activity of the Recombinant Cell Enzyme

	relative activity (%)	
metal ion (1 mM)	1 mM	10 mM
none	100	100
Co^{2+}	101.3	102.1
Mn^{2+}	143.2	156.6
Fe^{2+}	132.1	128.5
Mg^{2+}	102.4	102.8
Ni^{2+}	103.2	103.6
Ca^{2+}	93.1	92.7
Zn^{2+}	105.7	106.2
Cu^{2+}	82.8	81.5

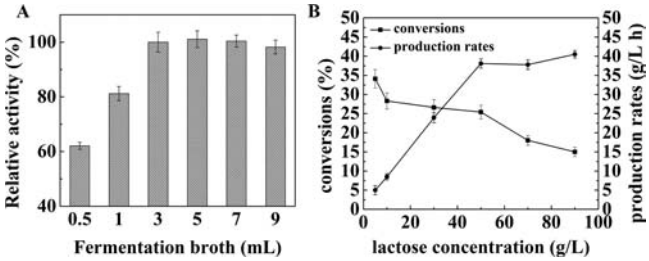

Figure 5. (A) Effect of the centrifugal cell dosage. (B) Effect of the lactose concentration.

of prepared *S. cerevisiae* NX-3 cells. Figure 6B shows that during *S. cerevisiae* NX-3 fermentation, the consumption of D-galactose and D-glucose was nearly completed at 4 h and exhausted at about 12 h, whereas no changes were observed in D-tagatose. These results indicate that D-galactose and D-glucose in the mixture were selectively used by *S. cerevisiae* NX-3. The cell pellet was disposed by centrifugation, and borate was separated from syrup by DTF-01 Ca^{2+} cation-exchange chromatography. The optimal DTF-01 Ca^{2+} cation-exchange chromatography conditions were as follows: column temperature, 70 °C; input volume, 20 mL; and flow velocity, 1.0 mL/min. The recovery of D-tagatose was 83%, and its purity reached 98%.

dx.doi.org/10.1021/jf4042485 | J. Agric. Food Chem. 2014, 62, 2412−2417

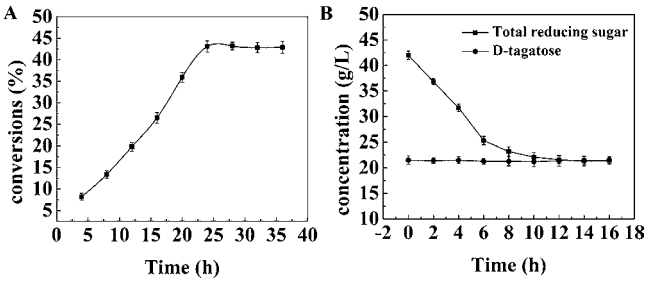

Figure 6. (A) Effect of the reaction time. (B) Time of D-tagatose syrup fermentation by yeast cells.

In short, the maximum conversion of 43% was achieved at pH 6.5 and 34 °C in the presence of 10 mM Mn^{2+}, 1 mM Fe^{2+}, and 235 mM borate. These conditions are suitable for industrial application because it would reduce byproduct formation and save energy.

D-Tagatose Crystallization and Characterization. The crystallization rate reached 58%. The crystals were confirmed to be D-tagatose by infrared spectroscopy (see Figure S1 of the Supporting Information) and ^{1}H NMR (see Figure S2 of the Supporting Information).

DISCUSSION

The aim of this work was to investigate the possibility of producing D-tagatose from lactose with the recombinant *E. coli* cells harboring β-D-galactosidase and ECAI-Q299K. As described previously, the recombinant *E. coli* BL21 (DE3) strain was successfully constructed andD-tagatose is produced in high levels by the recombinant *E. coli* with lactose as the substrate. Most previous studies reported that L-AIs are active at neutral or alkaline conditions. However, lactose is commonly hydrolyzed by β-D-galactosidase under an acidic pH. Thus, we previously modified ECAI through directed evolution to shift its optimal pH to 6.5, the same as that of β-D-galactosidase.

The D-tagatose yield of 74% was obtained in the presence of borate at 60 °C and pH 9.0 with a purified L-AI mutant from *Geobacillus thermodenitrificans* as the catalyst; this yield was 24% higher than without borate.[20] In the current work, the *E. coli*-ZY cells containing β-D-galactosidase and ECAI-Q299K were used for D-tagatose production in borate buffer. The conversion of 43% was achieved at 34 °C in the presence of approximately 235 mM borate (pH 6.5).

D-Glucose and D-galactose can be consumed by *S. cerevisiae*.[32] The paper also presents the purification and crystallization of D-tagatose. *S. cerevisiae* NX-3 was prepared by screening according to the use of D-glucose and D-galactose. Crystallization of D-tagatose was reported for the first time.

This study is the first report for developing the efficient single-step production of D-tagatose from lactose by the recombinant cells. The single-step method reduces both the time and cost in D-tagatose preparation, in comparison to the processes involving the hydrolysis of lactose and separation of D-galactose from a mixture of D-glucose and D-galactose prior to isomerization. The single-step production of D-tagatose from lactose and full-blown crystallization methods demonstrate potential for commercial applications.

The conversion rate from D-galactose to D-tagatose by the recombinant cells is lower than that by some thermophiles, such as *Thermotoga neapolitana*, *Thermotoga maritima*, *Anoxybacillus flavithermus* TC-06, etc. (Table 3). To overcome these difficulties, the following solutions were considered: (1) coexpression of β-D-galactosidase from *E. coli* and other original L-AIs and (2) modulation of the expression volume of the coexpression system to allow for the key enzyme ECAI to obtain higher activity.

ASSOCIATED CONTENT

Supporting Information

Analysis of the crystals by infrared spectroscopy (Figure S1) and ^{1}H NMR (Figure S2). This material is available free of charge via the Internet at http://pubs.acs.org.

AUTHOR INFORMATION

Corresponding Author

*Telephone/Fax: +86-25-58139433. E-mail: xuhongnjut@163.com.

Funding

This work was supported by the National Basic Research Program of China (2013CB733603), the National High-Technology Research and Development Program of China (2012AA021503), the Program for Changjiang Scholars and Innovative Research Team in University, and the National Natural Science Foundation of China (21176123 and 31371732).

Notes

The authors declare no competing financial interest.

REFERENCES

(1) Hirst, E. L.; Hough, L.; Jones, J. K. N. Composition of the gum of *Sterculia setigera*: Occurrence of D-tagatose in nature. *Nature* **1949**, *163*, 177.

(2) Troyono, E.; Martinez-Castro, I.; Olano, A. Kinetics of galactose and tagatose formation during heat-treatment of milk. *Food Chem.* **1992**, *45*, 41−43.

(3) Levin, G. V.; Zehner, L. R.; Saunders, J. P.; Beadle, J. R. Sugar substitutes: Their energy values, bulk characteristics, and potential health benefits. *Am. J. Clin. Nutr.* **1995**, *62*, 1161S−1168S.

(4) Mendoza, M. R.; Olano, A.; Villamiel, M. Chemical indicators of heat treatment in fortified and special milks. *J. Agric. Food Chem.* **2005**, *53*, 2995−2999.

Table 3. Bioconversion of D-Galactose into D-Tagatose Using L-Arabinose Isomerases from Various Microorganisms

organism	conversion yield (%)	conversion conditions	reference
Escherichia coli	43	37 °C, 24 h, and borate	this study
Geobacillus thermodenitrificans	46	65 °C and 5 h	33
Acidothermus cellulolytics ATC43068C	53	75 °C and 12 h	34
Bacillus stearothermophilus US100	48	70 °C and 7 h	35
Thermotoga neapolitana	68	80 °C and 20 h	36
Thermotoga maritima	56	80 °C and 6 h	37
Anoxybacillus flavithermus TC-06	60	95 °C, 1 h, and borate	38

(5) Kim, P. Current studies on biological tagatose production using L-arabinose isomerase, a review and future perspective. *Appl. Microbiol. Biotechnol.* **2004**, *65*, 243−249.
(6) Lu, Y.; Levin, G. V.; Donner, T. W. Tagatose, a new antidiabetic and obesity control drug. *Diabetes, Obes. Metab.* **2008**, *10*, 109−134.
(7) Zehener, L. R. D-Tagatose as a low-calorie carbohydrate sweetener and bulking agent. European Patent EP 0257626 B1, 1988.
(8) Marzur A. W. Functional sugar substitutes with reduced calories, European Patent EP 0341062 A3, 1989.
(9) Beadle, J. R.; Saunder, J. P.; Wajada, T. J., Jr. Process for manufacturing tagatose. U.S. Patent 5,078,796 A, 1991.
(10) Oh, D. K. Tagatose: Properties, applications, and biotechnological processes. *Appl. Microbiol. Biotechnol.* **2007**, *76*, 1−8.
(11) Cheetham, P. S. J.; Wootton, A. N. Bioconversion of D-galactose into D-tagatose. *Enzyme Microb. Technol.* **1993**, *15*, 105−108.
(12) Kim, H. J.; Ryu, S. A.; Kim, P.; Oh, D. K. A feasible enzymatic process for D-tagatose production by an immobilized thermostable L-arabinose isomerase in a packed-bed bioreactor. *Biotechnol. Prog.* **2003**, *19*, 400−404.
(13) Yoon, S. H.; Kim, P.; Oh, D. K. Properties of L-arabinose isomerase from *Escherichia coli* as biocatalyst for tagatose production. *World J. Microbiol. Biotechnol.* **2003**, *19*, 47−51.
(14) Chouayekh, H.; Bejar, W.; Rhimi, M.; Jelleli, K.; Mseddi, M.; Bejar, S. Characterization of an L-arabinose isomerase from the *Lactobacillus plantarum* NC8 strain showing pronounced stability at acidic pH. *FEMS Microbiol. Lett.* **2007**, *277*, 260−267.
(15) Xu, Z.; Qing, Y.; Li, S.; Feng, X.; Xu, H.; Ouyang, P. A novel L-arabinose isomerase from *Lactobacillus fermentum* CGMCC2921 for D-tagatose production: Gene cloning, purification and characterization. *J. Mol. Catal. B: Enzym.* **2011**, *70*, 1−7.
(16) Wanarska, M.; Kur, J. A method for the production of D-tagatose using a recombinant *Pichia pastoris* strain secreting β-D-galactosidase from *Arthrobacter chlorophenolicus* and a recombinant L-arabinose isomerase from *Arthrobacter* sp. 22c. *Microb. Cell Fact.* **2012**, *11*, 113.
(17) Rhimi, M.; Ilhammami, R.; Bajic, G.; Boudebbouze, S.; Maguin, E.; Haser, R.; Aghajari, N. The acid tolerant L-arabinose isomerase from the food grade *Lactobacillus sakei* 23 K is an attractive D-tagatose producer. *Bioresour. Technol.* **2010**, *101*, 9171−9177.
(18) Salonen, N.; Nyyssölä, A.; Salonen, K.; Turunen, O. *Bifidobacterium longum* L-arabinose isomerase—Overexpression in *Lactococcus lactis*, purification, and characterization. *Appl. Biochem. Biotechnol.* **2012**, *168*, 392−405.
(19) Kim, J. W.; Kim, Y. W.; Roh, H. J.; Kim, H. Y.; Cha, J. H.; Park, K. H.; Park, C. S. Production of tagatose by a recombinant thermostable L-arabinose isomerase from *Thermus* sp. IM6501. *Biotechnol. Lett.* **2003**, *25*, 963−967.
(20) Lim, B. C.; Kim, H. J.; Oh, D. K. High production of D-tagatose by the addition of boric acid. *Biotechnol. Prog.* **2007**, *23*, 824−828.
(21) Salonen, N.; Salonen, K.; Leisola, M.; Nyyssölä, A. D-Tagatose production in the presence of borate by resting *Lactococcus lactis* cells harboring *Bifidobacterium longum* L-arabinose isomerase. *Bioprocess Biosyst. Eng.* **2013**, *36*, 489−497.
(22) Bertelsen, H.; Eriknauer, K.; Bottcher, K.; Christensen, H. J. S.; Stougaard, P.; Hansen, O. C.; Jorgensen, F. Process for manufacturing of tagatose. U.S. Patent 6,991,923 B2, 2006.
(23) Ansari, S. A.; Husain, Q. Lactose hydrolysis from milk/whey in batch and continuous processes by concanavalin A-Celite 545 immobilized *Aspergillus oryzae* β-galactosidase. *Food Bioprod. Process.* **2012**, *90*, 351−359.
(24) Lederberg, J. The β-D-galactosidase of *Escherichia coli* srain K-12. *J. Bacteriol.* **1950**, *60* (4), 381.
(25) Craven, G. R.; Steers, E.; Anfcnsen, C. B. Purification, composition, and molecular weight of the β-D-galactosidase of *Escherichia coli* K12. *J. Biol. Chem.* **1964**, *240*, 2468−2477.
(26) Jacobson, R. H.; Zhang, X. J.; DuBose, R. F.; Matthews, B. W. Three-dimensional structure of β-galactosidase from *E. coli*. *Nature* **1994**, *369*, 761−766.
(27) Xu, Z.; Li, S.; Fu, F.; Li, G.; Feng, X.; Xu, H.; Ouyang, P. Production of D-tagatose, a functional sweetener, utilizing alginate immobilized *Lactobacillus fermentum* CGMCC2921 cells. *Appl. Biochem. Biotechnol.* **2012**, *166*, 961−973.
(28) Xu, Z.; Li, S.; Feng, X.; Zhan, Y.; Xu, H. Function of aspartic acid residues in optimum pH control L-arabinose isomerase from *Lactobacillus fermentum*. *Appl. Microbiol. Biotechnol.* **2013**, DOI: 10.1007/s00253-013-5342-7.
(29) Bradford, M. M. A rapid and sensitive method for the quantitation of microgram quantities of protein utilizing the principle of protein−dye binding. *Anal. Biochem.* **1976**, *72*, 248−254.
(30) Haider, T.; Husain, Q. Immobilization of β-D-galactosidase from *Aspergillus oryzae* via immunoaffinity support. *Biochem. Eng. J.* **2009**, *43*, 307−314.
(31) Dische, Z.; Borenfreund, E. A new spectrophotometric method for the detection and determination of keto sugars and trioses. *J. Biol. Chem.* **1951**, *192*, 583−58.
(32) Ibrahim, O. O.; Spradlin, J. E. Process for manufacturing D-tagatose. U.S. Patent 6,057,135 A, 2000.
(33) Kim, H. J.; Oh, D. K. Purification and characterization of an L-arabinose isomerase from an isolated strain of *Geobacillus thermodenitrificans* producing D-tagatose. *J. Biotechnol.* **2005**, *120*, 162−173.
(34) Cheng, L.; Mu, W.; Zhang, T.; Jiang, B. An L-arabinose isomerase from *Acidothermus cellulolytics* ATCC 43068: Cloning, expression, purification, and characterization. *Appl. Microbiol. Biotechnol.* **2010**, *86*, 1089−1097.
(35) Rhimi, M.; Bejar, S. Cloning, purification and biochemical characterization of metallic-ions independent and thermoactive L-arabinose isomerase from the *Bacillus stearothermophilus* US100 strain. *Biochim. Biophys. Acta* **2006**, *1760*, 191−199.
(36) Kim, B. C.; Lee, Y. H.; Lee, H. S.; Lee, D. W.; Choe, E. A.; Pyun, Y. R. Cloning, expression and characterization of L-arabinose isomerase from *Thermotoga neapolitana*: Bioconversion of D-galactose to D-tagatose using the enzyme. *FEMS Microbiol. Lett.* **2002**, *212*, 121−126.
(37) Lee, D. W.; Jang, H. J.; Choe, E. A.; Kim, B. C.; Lee, S. J.; Kim, S. B.; Hong, Y. H.; Pyun, Y. R. Characterization of a thermostable L-arabinose (D-galactose) isomerase from the hyperthermophilic eubacterium *Thermotoga maritima*. *Appl. Environ. Microbiol.* **2004**, *70*, 1397−1404.
(38) Li, Y.; Zhu, Y.; Liu, A.; Sun, Y. Identification and characterization of a novel L-arabinose isomerase from *Anoxybacillus flavithermus* useful in D-tagatose production. *Extremophiles* **2011**, *15*, 441−450.

The objective of this study was to characterize fibrillar aggregates made using pea proteins and to assemble formed fibrils into protein-based gels to study the rheological behavior of these gels. The results described in this paper include the characterization of fibrils made using pea proteins with the use of thioflavin T (Th T) assay, circular dichroism (CD), and transmission electron microscopy (TEM), and the rheological evaluation of protein-based fibrillar gels. To the best of our knowledge, this is the first report addressing the assembly of pea proteins into fibrils at low pH, the subsequent assembly of fibrils in spatial networks, and the mechanical characterization of formed gels.

MATERIALS AND METHODS

Materials. Predried dehulled commercial green pea seeds with a protein content of 22 g/100 g (dry weight basis) were purchased from a local supermarket. Whey protein isolate (WPI) Bipro was obtained from Davisco Food International, Inc. (Le Sueur, MN, USA). Soy protein isolate was extracted from defatted soy protein flour provided by Cargill BV (Amsterdam, The Netherlands). Soy protein extraction was carried out according to a previously described protocol[21] with slight modifications, in which acid precipitation was carried out at pH 4.5, instead of pH 4.8, and the final soy protein isolate was not freeze-dried. GDL, *o*-phthaldialdehyde (OPA), *N*,*N*-dimethyl-2-mercaptoethyl-ammoniumchloride (DMA), disodiumtetraborate decahydrate (Borax), sodium dodecyl sulfate (SDS), urea, dithiothreitol (DTT), trifluoroacetic acid (TFA), acetonitrile, and uranyl acetate were purchased from Sigma-Aldrich (Steinheim, Germany). Th T was obtained from Acros Organics (Geel, Belgium). All reagents were of analytical grade and used without further purification.

Pea Protein Extraction and Characterization. Pea protein isolate was extracted from commercial green peas by isoelectric precipitation. Extraction of pea protein was based on a previously described procedure,[6] with modifications. Pea protein flour was milled from dried peas in a Waring commercial blender (New Hartford, CT, USA). Milling was performed in the presence of liquid nitrogen to prevent excessive heating that may lead to heat denaturation of the proteins. Milled pea flour was dispersed in Milli-Q water in the ratio of 1:10 (g/mL) to make a protein slurry. The pH of the slurry was adjusted to pH 8.0 with 1 M NaOH and incubated at room temperature (20 ± 2 °C) for 1 h. The slurry was then centrifuged at 10000*g* (20 °C, 25 min) to remove insoluble materials. The supernatant was collected and the pH readjusted to pH 4.8 using 1 M HCl. The supernatant was then incubated at 20 °C for 2 h under continuous stirring and subsequently centrifuged at 10000*g* (20 °C, 25 min). Following this, the supernatant containing albumins and sugars was discarded. The pellet was collected and redispersed in Milli-Q water in the ratio of 1:10 (g/mL). The redispersed suspension at a pH of 4.8 was centrifuged at 10000*g* (20 °C, 25 min) and the pellet resuspended in Milli-Q water in the ratio of 1:3 (g/mL) to remove remaining sugars and albumins. The pH of the resuspended pellet was set to pH 8.0 using 2 M NaOH, and the solution was incubated at room temperature (20 ± 2 °C) for 1 h, followed by centrifugation at 10000*g* (20 °C, 25 min) to remove remaining traces of insoluble materials. The supernatant was collected and the pH measured and adjusted to a final pH of 8.0 using 2 M NaOH if necessary. The pea protein was then stored at 4 °C in the presence of 0.02% sodium azide to prevent microbial growth. The pea protein solution extracted in this way will be referred to as "native" pea protein. The protein content of native pea protein was determined using Dumas (NA 2100 Protein, CE Instruments, Milan, Italy) using a factor of 5.52[27] and was found to be about 87 ± 0.1 mg/mL. The dry matter content of native pea protein was 94 mg/mL, and the purity of pea protein extract was 92 ± 1%. Pea proteins showed a typical denaturation temperature around 77 °C as demonstrated by calorimetric measurements at a heating rate of 2 °C/min for 87 mg/mL pea protein solution (results not shown).

The protein composition of native, unheated, and heated pea protein at an approximate concentration of 10 mg/mL was analyzed using sodium dodecyl sulfate polyacrylamide gel electrophoresis (SDS-PAGE) under reducing conditions. A MOPS-SDS (20×) buffer was used as a running buffer. Electrophoresis conditions were 200 V and 10 mA throughout at 25 °C and 50 min running time. Following separation, the proteins were fixed and stained using the Simply Blue Safe stain and developed to obtain a suitable background color. The apparent molecular weights of the present proteins were determined by comparison to the molecular weight standard (Sigma wide range molecular weight markers, 6−200 kDa) applied into a separate lane. The gels were scanned, and the acquired images were analyzed by Image Master software. SDS-PAGE was also carried out on pea protein solutions heated for different periods at pH 2.0.

Pea Protein Solutions Preparation and Fibril Formation. Native pea protein solutions were diluted to 40 mg/mL in Milli-Q water adjusted to pH 2.0 using HCl. The obtained solutions were then centrifuged at 15000*g* for 30 min at 4 °C to remove any traces of insoluble material that could arise following pH readjustments. The supernatant was collected and filtered through a 1.2 μm (Millex-SV, Millipore Corp., Bedford, MA, USA) filter. The final pH of the sample was adjusted to pH 2.0 using 6 M HCl. Determined protein concentrations after centrifugation and filtration showed that negligible protein losses occurred during these processes.

Fibril preparation using pea protein was carried out according to a previously described protocol.[21] In summary, aliquots of 20 mL protein solutions prepared as described above were incubated at 85 °C for 20 h in a temperature-controlled water bath equipped with a stirring device and continuously stirred with a magnetic stirring bar at 300 rpm. After the heat treatment, samples were cooled in an ice bath and stored at 4 °C until further use, typically within 2 weeks.

Fibrils made using 40 mg/mL soy protein were prepared in a similar way as previously described[21] except for soy protein being heated in a water bath equipped with a stirring device and continuously stirred with a magnetic stirring bar at 300 rpm, instead of being heated using a shearing device, whereas fibrils made using whey protein were prepared according to a previously described protocol.[26]

Characterization of Fibrils Made Using Pea Protein. Determination of the number of primary amines present following the hydrolysis of pea proteins into peptides was carried out using the chromogenic OPA assay as previously outlined.[28] Reversed phase high-performance liquid chromatography (RP-HPLC) (Shimadzu, Kyoto, Japan) was used according to a method adapted from a previously described procedure[29] to determine how much of the protein was hydrolyzed into peptides. All samples were analyzed in aqueous solutions containing 4 M urea and 0.3% DTT. RP-HPLC was carried out using 2 M 6000A pumps in combination with a high-sensitivity accessory block (Waters), an ISS-100 injector (Perkin-Elmer, Uberlingen, Germany), a Waters model 680 gradient controller, and a Kratros 783 detector (Kratos Analytical, Ramsey, NJ, USA). A 250 × 4.6 mm Aeris wide-pore C18 column (Phenomex, The Netherlands) was used with a KrudKatcher Ultra HPLC column in-line filter (Phenomex) as a guard column. A 10 μL pea protein sample was injected onto a wide-pore C18 analytical column thermostated at 40 °C. Samples were eluted at a flow rate of 0.40 mL/min with a linear gradient of 0.10 v/v % trifluoroacetic acid (TFA) in 98 v/v % water and 2 v/v % acetonitrile to 0.10 v/v % TFA in 10 v/v % water and 90 v/v % acetonitrile. The equipment was linked to a data acquisition and processing system (Turbochrom, Perkin-Elmer). Data analysis was done with Chromeleon software version 7.1 (ThermoFisher Scientific).

Determination of the degree of conversion of peptides into fibrils was carried out on heated samples according to the previously described procedure.[21] In summary, heated pea protein solutions at pH 2.0 were diluted to 2 mg/mL. The solutions were divided into six centrifugal tubes containing filters with a molecular weight cutoff (MWCO) of 100 kDa and centrifuged in four consecutive steps (3000*g*, 30 min, 15 °C) yielding four filtrates (F1−F4). The obtained volumes were in this way sufficient to determine the protein content of each centrifugation step as determined by Dumas (NA 2100 Protein, CE Instruments) with a protein factor of 5.52.[27] The degree of conversion of monomers to fibrils was determined using eq 1

$$C = P - (F_1 + F_2 + F_3 + F_4) \times 100\% / P \quad (1)$$

where C is the conversion factor (%), P is the initial protein content (g) in the solution, F_1 is the protein content (g) in filtrate 1, F_2 is the protein content (g) in filtrate 2, F_3 is the protein content (g) in filtrate 3, and F_4 is the protein content (g) in filtrate 4.

The Th T fluorescence assay was used to evaluate the formation of β-sheet structures based on a previously described principle.[30] After fibril preparation, a volume of 48 μL of heated pea protein samples was mixed with 4 mL of filtered (0.2 μm, Schleicher and Schuell) 60 μM Th T solution in a phosphate buffer (10 mM phosphate, 150 mM NaCl at pH 7.0) and incubated for 10 min at 25 °C. Fluorescence intensity was measured using a fluorescence spectrophotometer (Perkin-Elmer LS 50 B) at an excitation wavelength of 460 nm (slit width = 2.5 nm) and an emission wavelength from 465 to 550 nm (slit width = 2.5 nm). Controls included the fluorescence intensity of Th T solution without the addition of protein solution and unheated pea protein solutions.

Spectroscopic and Microscopic Analyses. Determination of the hydrodynamic diameters of the protein aggregates was carried out using dynamic light scattering (DLS) (Zetasizer Nano ZS, Malvern Instruments, Worcestershire, UK). Changes in aggregate size during the heating of 5 mg/mL pea protein solutions at 85 °C for 20 h were recorded as a function of time at pH 2.0. Reported values are the average hydrodynamic diameters of the largest intensity peak, as found in the distribution analysis using Malvern DTS 5.03 software. The particle size distribution from DLS was derived from a deconvolution of the measured intensity autocorrelation function of the samples using a non-negatively constrained least-squares (NNLS) fitting algorithm. Duplicate measurements were performed for this analysis.

Far-UV circular dichroism (CD) was used to investigate the secondary structure of native and fibrillar pea protein solutions. Far-UV CD spectra of ∼0.2 mg/mL native and fibrillar pea protein solutions were obtained and recorded at 25 °C in the spectral range from 190 to 260 nm with a Jasco J-715 spectropolarimeter (Jasco Corp., Japan), using a quartz cuvette with an optical path of 0.1 cm. The spectral resolution was 0.5 nm, and the scan speed was 100 nm/min, with a response time of 0.125 s at a bandwidth of 1 nm. Twenty scans were accumulated and averaged, and the spectra were corrected for that of a protein-free sample.

Near-UV CD was used to investigate the tertiary and/or quaternary structure of native and pea protein fibrillar solutions. Near-UV spectra of ∼2 mg/mL native and fibrillar pea protein solutions were obtained and recorded at 25 °C in the spectral range from 250 to 350 nm with a Jasco J-715 spectropolarimeter (Jasco Corp., Japan), using a quartz cuvette with an optical path of 1 cm. The spectral resolution was 0.5 nm, and the scan speed was 100 nm/min, with a response time of 0.125 s at a bandwidth of 1 nm. Twenty scans were accumulated and averaged, and the spectra were corrected for that of a protein-free sample.

Fibrillar solutions made using pea protein were prepared for TEM by negative staining according to a previously described protocol.[26] A 10 μL aliquot of 0.25 mg/mL fibrillar solutions made using pea protein was deposited onto a carbon support film on a copper grid (Aurion-Immuno Gold Reagents and Accessories, Wageningen, The Netherlands). The excess fibrillar solution was removed after 30 s using a filter paper (Whatman no. 1, 512-1002, VWR International Europe BVBA, Leuven, Belgium). A droplet of 2% uranyl acetate at pH 3.8 was added for 30 s to improve the contrast. Excess uranyl acetate was removed by use of a filter paper. Electron micrographs were obtained using a Jeol JEM1011 transmission electron microscope (Tokyo, Japan) operating at 80 kV.

Rheological Characterization of Protein-Based Fibrillar Gels. Gelation of fibrillar aggregates made using pea protein was carried out by acid-induced cold gelation using GDL. Before gelation was initiated, the pH of the fibrillar solutions made using pea protein at pH 2 was adjusted to pH 7. The concentrations of GDL added to the samples to induce gelation were determined using the empirical relationship (% GDL (w/w) = 0.0065 × $C_{protein}$ (g/L) + 0.045).[31] GDL was added to fibrillar solutions made using pea protein with a protein concentration ranging from 40 to 160 mg/mL to induce gelation at 25 °C. For gelation at a protein concentration as high as 160 mg/mL, pea protein fibrillar solutions prepared at 40 mg/mL were concentrated by ultrafiltration using Merck Millipore Amicon stirred cell fitted with 30 kDa MWCO membrane (Darmstadt, Germany). Several trials were carried out using calculated GDL concentrations, and a final GDL concentration range of 0.3−1% was chosen to get to a final pH of about pH 5 at the end of gelation time. The pH of all samples was determined as a function of time during 15 h of incubation at 25 °C. A stress-controlled rheometer (ARG2, TA Instruments, Leatherhead, UK) with a concentric cylinder geometry (C14: cup diameter = 15.4 mm; bob diameter = 14.04 mm) was used to determine storage modulus (G') and loss modulus (G'') as a function of time (frequency, 1 Hz; temperature, 25 °C; % strain, 0.05, 15 h). After 15 h of incubation, an oscillation amplitude sweep was performed (frequency, 1 Hz; temperature, 25 °C; % strain, 0.001−100). Duplicate measurements were carried out for each protein concentration within the linear region, which was between aa strain of 0.001 and 10%.

RESULTS AND DISCUSSION

Characterization of Fibrils Prepared Using Pea Protein. *Hydrolysis of Pea Protein into Peptides.* It has been reported that the fibril formation process in β-lactoglobulin is initiated following the hydrolysis of proteins at pH 2 into peptides, some of which assemble into fibrils.[32] Heat-induced hydrolysis of protein at pH 2 has been shown to play a significant role in fibril assembly of soy 7S/11S globulin.[22] To study whether this phenomenon plays a role in fibril assembly using pea protein, the degree of hydrolysis as quantified by the number of primary amine groups available following heating of pea protein was determined by chromogenic OPA assay. The chromogenic OPA assay results showed that about 30% of primary amines could be detected after heating 40 mg/mL pea protein at pH 2.0 and 85 °C for 20 h. Assuming an average lysine content of about 8% per protein, this would correspond to an ensemble-averaged degree of hydrolysis of about three fragments generated from every protein.

SDS-PAGE was carried out on pea protein solutions to study the molecular weight degradation (Figure 1). Figure 1A (lane B) shows that the isolated pea protein used in this study

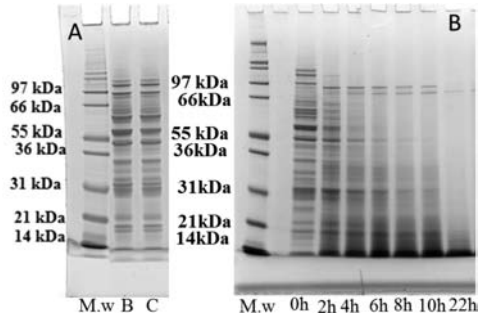

Figure 1. (A) Molecular weight degradation of pea proteins during fibril formation: SDS-PAGE electrophoretograms for standard marker (M.w), native pea protein at pH 8 (B), and pea protein at pH 2 prepared for fibril formation but not heated (C). (B) SDS-PAGE electrophoretograms for time-dependence heating of pea protein at pH 2.0 for up to 22 h. The band marked M.w is the standard marker; 0 h, 2 h, 4 h, 6 h, 8 h, 10 h, and 22 h represent heating of the samples for up to 22 h. The dominant bands at ∼70, 50, 33−14 kDa are vicilin/convicilin fraction subunits, whereas the less dominant bands at ∼40 and 20 kDa represent the legumin fraction subunits.

dx.doi.org/10.1021/jf4055215 | J. Agric. Food Chem. 2014, 62, 2418−2427

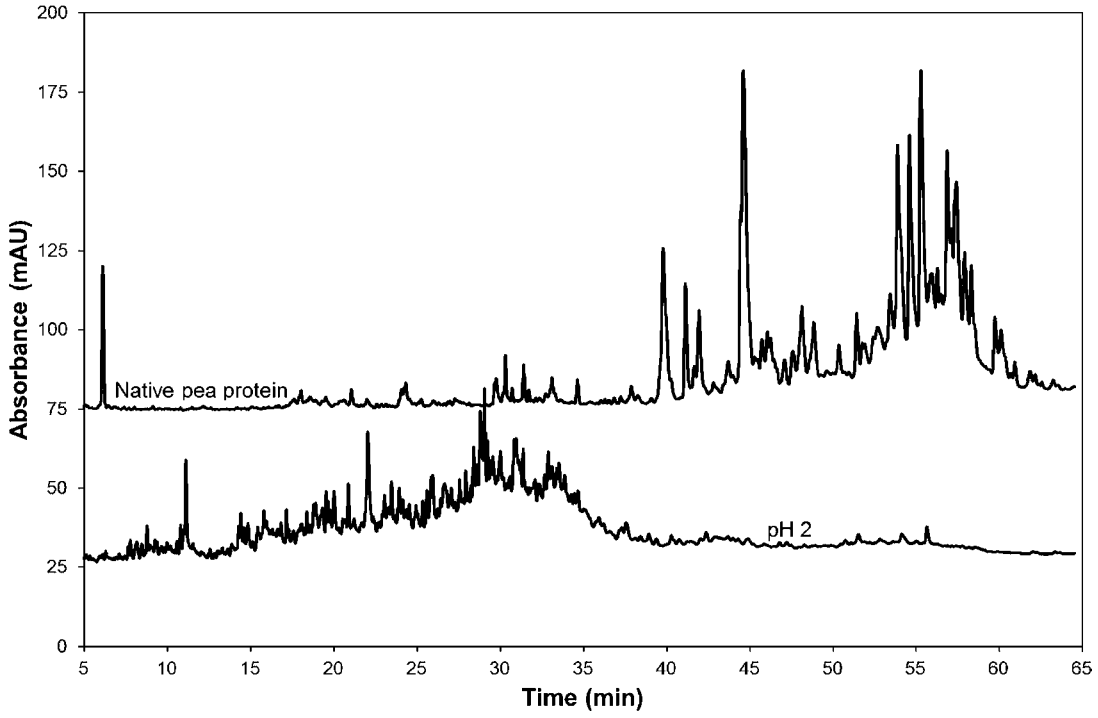

Figure 2. Hydrolysis of native pea proteins into peptides: reversed phase high-performance liquid chromatography (RP-HPLC) chromatograms for native pea protein and heated pea protein at pH 2.0.

contains both legumin (less dominant bands at ∼40 and ∼20 kDa) and vicilin/convicilin (dominant bands at ∼70, ∼50, and ∼33−14 kDa). Native pea protein at pH 8.0 (Figure 1A, lane B) showed similar bands as pea protein at pH 2.0 before heating (Figure 1A, lane C; and Figure 1B, lane 0 h). This shows that both vicillin/convicilin and legumin fractions were still present in the samples before heating. SDS-PAGE was also carried out on pH 2.0 samples as a function of heating time (h) as shown in Figure 1B. The results show that with heating of the samples for 2 h, bands of molecular weights above 97 kDa disappear. Heating the sample for longer than 10 h causes the bands above 21 kDa to disappear (Figure 1B), suggesting that progressive hydrolysis occurs during prolonged heating of pea protein at pH 2.0. There were persistent bands of between 66 and 97 kDa that remained dominant over all heating times at 85 °C (Figure 1B). The bands at around 70 kDa are convicilin polypeptides, whereas the bands around 97 kDa that seem to fade off at heating times exceeding 10 h could be traces of lipoxygenase.[4]

RP-HPLC analysis of the protein solutions following heating at pH 2.0 in comparison to native pea protein (Figure 2) showed that all proteins were degraded to different degrees from the native form. This confirms that hydrolysis of all proteins present occurs following the heating of pea proteins at pH 2.0 (Figure 2). The findings on the study of molecular weight degradation of pea protein suggest that (i) hydrolysis of pea protein into peptides which can assemble into fibrils is a process that requires prolonged heating of the samples at a pH away from the IEP, at low ionic strength, combined with heating temperatures above the denaturation temperature of the protein; (ii) gradual degradation of pea proteins occurs over incubation time (h); and (iii) hydrolysis of pea protein to peptides which assemble into fibrils follows the generic fibrillization mechanism similar to that of other globular proteins such as whey proteins,[23] soy proteins,[21] and lysozyme.[33]

Degree of Conversion of Peptides into Fibrils Made Using Pea Protein. To determine the degree of conversion of peptides into fibrils, a centrifugal filtration method was used as described before.[12] No protein was found by the Dumas method in the fourth washing step, which indicates that at this stage of the procedure, the obtained fibril solution was free from nonaggregated peptides. It was found that about 50% of the initial protein was present in the form of fibrils in pea proteins.

Th T Fluorescence Assay. Heated pea protein was checked for the presence of β-sheet aggregates as a typical characteristic for fibril assembly. Figure 3 and Table 1 show the results of Th T assay as a function of heating time (Figure 3) and pH (Table 1). The use of Th T to evaluate the formation of β-sheets in

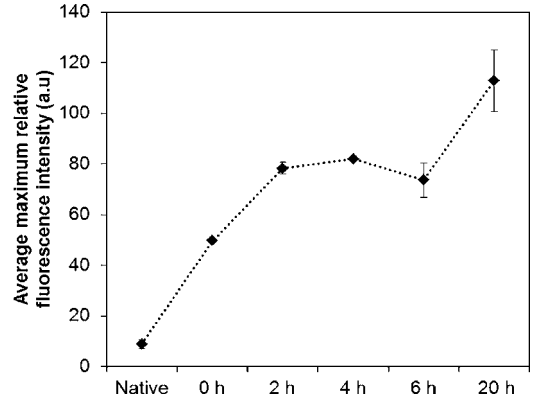

Figure 3. Formation of β-sheet aggregates as detected by Th T: average relative maximum fluorescence intensities as a function of heating time at a protein concentration of 40 mg/mL.

dx.doi.org/10.1021/jf4055215 | J. Agric. Food Chem. 2014, 62, 2418−2427

Table 1. Comparison of Maximum Relative Fluorescence Intensity for Native Pea Protein, Heated Pea Protein at pH 2.0 during the Study of Aggregate Assembly Kinetics, Heated Pea Protein at pH 2 Prepared Following Heating of 40 mg/mL of Pea Protein at 85 °C for 20 h, Heated Pea Protein at pH 7, Heated Soy Protein at pH 2, and Heated Whey Protein at pH 2.0

protein sample	pH	max rel fluorescence intensity (au) ± SD
native pea protein	8	9 ± 0.1
pea protein	2 (aggregate assembly kinetics)[a]	10 ± 0.5
pea protein	2[b]	113 ± 1
pea protein	7	62 ± 0.5
soy protein	2	121 ± 3
whey protein	2	349 ± 5

[a]Represents samples used in the study of fibril assembly kinetics that were followed over time using dynamic light scattering (aggregate size results are shown in Figure 4). [b]Represents heated pea solutions at (40 mg/mL, pH 2.0) after which the pH of the samples was adjusted to pH 7.0 for gelation to be induced using GDL.

proteins following the heating of protein solutions at low ionic strength and pH 2.0 for a prolonged time has been described in detail elsewhere.[30] Native pea protein had the lowest fluorescence intensity (Table 1). Following the incubation of pea protein solutions at pH 2.0, an increase in maximum fluorescence intensity was observed within the first 2 h of incubation (Figure 3). After 2 h of incubation, an initial gradual reduction in maximum fluorescence intensity was observed, suggesting that fibrils were formed during heating.[11] The gradual reduction in maximum fluorescence intensity after 2 h of heating coincided with the disappearance of bands of molecular weights above 66 kDa as observed in SDS-PAGE electrophoretograms (Figure 1B). A further slight decrease in maximum fluorescence intensity was observed at an incubation time of between 5 and 6 h followed by a steady increase in maximum fluorescence intensity. Such a reduction in fluorescence intensity has been attributed to the partial disruption of the highly ordered structure by further polypeptide hydrolysis.[11]

Progressive increase in fluorescence intensity was observed following heating of the samples for >6 h of incubation (Figure 3), whereas following heating of the sample for >10 h, bands of molecular weights above 21 kDa disappeared as observed in SDS-PAGE electrophoretograms (Figure 1B). An increase in the fluorescence intensity in heated samples at pH 2.0 for incubation periods above 6 h confirms the presence of β-sheets to which Th T reagent could bind. Following subsequent readjustment of the pH from 2.0 to 7.0, the fluorescence intensity of the pea protein sample was shown to decrease to almost half (Table 1). The decrease in fluorescence intensity could be as a result of partial disruption of the β-sheet fibrillar structure as previously reported for other types of fibrils.[34] The pH adjustment to pH 7.0 is essential to enable acid-induced gelation as described under rheological characterization of protein-based fibrillar gels. The findings show that thioflavin T can also bind to the β-sheets present in fibrils made using pea protein.

Changes in Structural Properties during Fibril Assembly. *Aggregate Assembly Kinetics.* Typical particle size distribution profiles of up to 12 h (by intensity) of heating of pea protein are presented in Figure 4. A concurrent increase in particle size was observed over time. This increase in particle

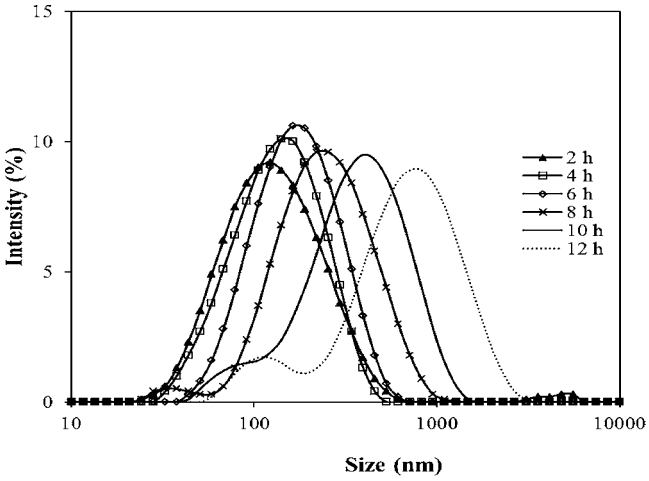

Figure 4. Hydrodynamic radius of aggregates is increased upon fibril formation: changes in aggregate size over time for 5 mg/mL pea protein heated at pH 2 and 85 °C monitored by the use of dynamic light scattering.

size is associated with thermal denaturation of the protein and subsequent aggregation. For heating periods below 6 h, predominant monomodal contributions were observed. When the heating period exceeded 6 h, the contributions became bimodal, and the distribution peaks shifted toward much higher aggregate sizes above 150 nm (Figure 4). The shift in the distribution peaks toward higher sizes coincided with a further increase in Th T binding after 6 h of incubation (see Figure 3). Bimodal contributions indicate that the fibril assembly (especially elongation of fibrils) occurred only after heating with enough incubation periods. The results show that the formation of pea protein β-sheet aggregates occurred following heating over incubation periods >6 h. The Th T assay performed on this sample following heating also showed the presence of some β-sheet aggregates (Table 1).

Secondary Structure. To probe the secondary conformational changes, far-UV CD spectra were recorded of native pea protein, heated pea protein at pH 2.0, and heated protein at pH 7.0 as shown in Figure 5A. The spectrum of native pea protein showed two minima around 222 and 208 nm and a zero crossing at 204 nm, indicative of a secondary structure that is highly predominated by α-helical and some β-sheet contributions.[35] Upon heating of pea protein at pH 2.0, a shift at the zero crossing to 197 nm was observed, illustrating a considerable loss of β-sheet strands. Substantial amounts (about 20%) of β-sheet were, however, still present in pea protein heated at pH 2.0 when the far-UV CD spectra were analyzed by the method previously described.[36] Following adjustment of the sample pH from pH 2.0 to 7.0, the CD spectrum showed a predominance of random coil elements. The predominance of random coil gives an indication of a further unfolding of the polypeptides upon adjustment of the pH of fibrillar solutions formed using pea protein at pH 2.0–7.0. Far-UV CD results were in agreement with the Th T assay as a reduction in Th T intensity occurred when the pH was adjusted from pH 2.0 to 7.0 (Table 1). Similarly, conformational changes to random coil from β-sheet structures occurred with pH adjustment (Figure 5A).

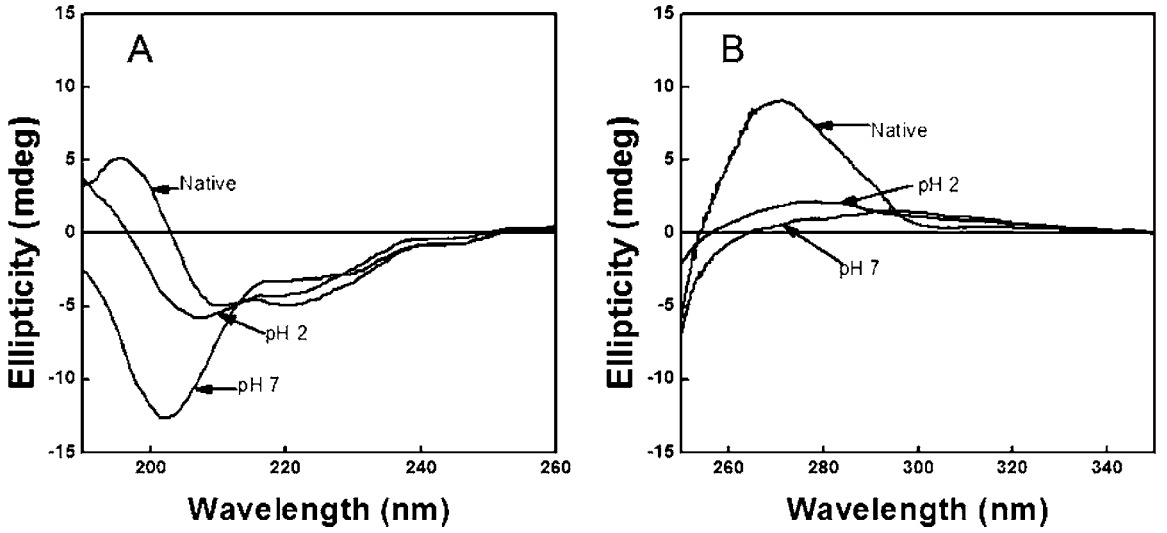

Figure 5. Changes on secondary, tertiary, and, to some extent, quaternary structural levels upon fibril formation: analysis of secondary structural elements by far UV-CD of native pea protein, heated pea protein at pH 2.0, and heated pea protein at pH 7.0 (A); near UV-CD spectra of these samples (B).

Tertiary and/or Quaternary Structure. To probe the tertiary and to some extent quaternary conformational changes, near UV-CD spectra were recorded of native pea protein, heated pea protein at pH 2.0, and heated pea protein readjusted to pH 7.0 (Figure 5B). The actual shape and magnitude of the near-UV CD spectrum of proteins depend on the number of aromatic amino acids restrained in their mobility, typically caused by spatial packing of the polypeptide.[37] Unheated native pea protein was shown to exhibit a prominent positive dichroic band at 270 nm, which is a typical contribution of tyrosine residues.[38] The magnitude of this contribution decreased substantially following heating, illustrating that the protein loses its tertiary packing constraints, resulting in the formation of a less well-defined structure. The decrease in the dichroic intensity may also reflect progressive exposure of tyrosine residue to the aqueous phase, as a result of heat-induced protein structural unfolding as well as polypeptide hydrolysis.[11] Readjustment of the pH from pH 2.0 to 7.0 did not result in major changes in tyrosine residues, implying that the protein tertiary structure remains unfolded. The results suggest that adjustment of the pH from pH 2.0 to 7.0 following heating of the protein at low pH destabilizes the secondary structure of the protein/peptides, whereas changes in tertiary structure could not be observed.

TEM. To analyze the formed pea protein fibrils on a microscopic scale, TEM pictures of the samples were taken (Figure 6). At pH 2.0 following the prolonged heating of pea protein, linear, but curly, fibrils having a worm-like appearance can be observed. The appearance of fibrils made using pea protein was comparable to that of the fibrils prepared using soy β-conglycinin at pH 2.0 and 80 °C,[11] but different from fibrils made using whey protein β-lactoglobulin.[23] Similarities between fibrils made using pea proteins and soy proteins, which are both predominantly oligomeric multidomain proteins, could be related to similarities in the thermal aggregation mechanisms of these proteins. Differences in the morphology of pea protein and whey protein fibrils could be attributed to inherent differences between plant storage and animal proteins as well as differences in the quaternary structure of the protein and its solubility, which may have a considerable influence on the aggregation behavior of the proteins.

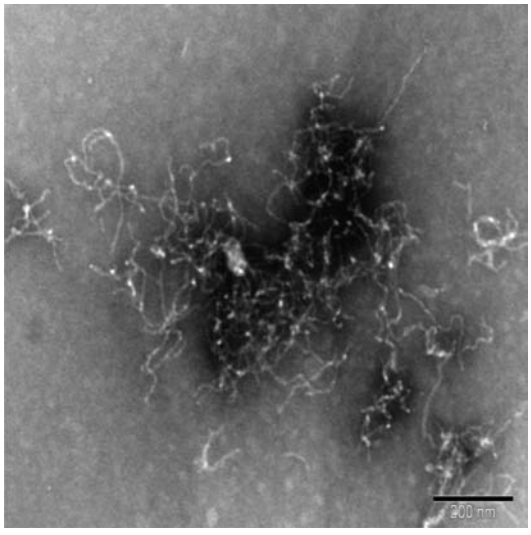

Figure 6. Morphology of pea protein fibrillar aggregates: transmission electron micrographs (TEM) of 0.25 mg/mL pea protein fibrils prepared at pH 2.0 following prolonged heating at 85 °C. Scale bars represent 200 nm.

Comparison between Fibrils Made Using Pea Proteins and Soy Proteins. Past research has shown that fibrils can be obtained using other plant storage proteins.[11,22] To compare fibrils made using pea proteins and soy proteins, characterization of fibrils prepared using soy proteins was carried out. Fibrils made using pea proteins showed a comparable ability to bind to Th T fluorescent dye as those made using soy protein (Table 1). Moreover, the characterization of fibrils assembled using pea proteins as a function of heating time also showed a similar increase in size compared to soy β-conglycinin.[11]

During the assembly of peptides from soy β-conglycinin to fibrils, an initial increase in maximum relative fluorescence intensity was observed as a function of time. A gradual decrease in the maximum fluorescence intensity following incubation periods of about 8 h was observed.[11] A similar observation was

dx.doi.org/10.1021/jf4055215 | J. Agric. Food Chem. 2014, 62, 2418−2427

recorded for fibrils made using pea protein, although the decrease in maximum fluorescence intensity occurred 2 h earlier in pea protein than in soy β-conglycinin. Fibrils formed from soy protein were found to have an approximate contour length of 1 μm, a persistence length of 2.3 μm, and a thickness of a few nanometers.[21] Fibrils made using soy protein were described as being more branched and curly than those made using whey protein,[21] which was also confirmed in our laboratory (results not shown). Comparisons of TEM micrographs of fibrils made using pea protein and soy protein showed that fibrils made using both pea proteins and soy proteins exhibited similar characteristics of being highly flexible, worm-like, and curly.

Progressive and remarkable changes in the secondary conformation as a result of fibril formation using pea proteins were observed in this study, similar to those reported for soy β-conglycinin and glycinin.[22] An increase in particle size during fibril assembly in pea proteins was also observed in this study, similar to that reported for soy proteins.[22] The results show that (i) pea proteins can be assembled into fibrils that have structural characteristics comparable to those of soy proteins and (ii) plant proteins show similar characteristics in fibril formation and, hence, pea proteins can effectively be used as a potential substitute for other plant proteins such as soy proteins.

Comparison between Fibrils Made Using Pea Proteins and Whey Proteins. The characterization of fibrils prepared using whey protein has been extensively carried out in the past[14,18,39] and also confirmed in our laboratory.[26] Considering the inherent differences in the structure and composition of pea proteins and whey proteins, it was expected that the characteristics of fibrils made using pea proteins would vary from those made using whey protein. β-Lactoglobulin (β-lg), the major fraction of WPI, has been reported to have a typical conversion factor of about 50%.[12] In this study, fibrils made using pea proteins also had a conversion factor of about 50%.

The use of Th T to compare the formation of β-sheet aggregates in pea proteins and whey proteins was also carried out. The results showed that Th T can bind to the β-sheets present in both pea proteins and whey proteins, although β-sheets in whey proteins exhibited a higher maximum relative fluorescence intensity compared to those of pea proteins (Table 1). This could give an indication of the presence of fewer β-sheet aggregates in pea proteins compared to whey proteins, with a similar incorporation in fibrillar aggregates.

Using TEM to analyze the microstructure, fibrils made using whey proteins were found to be longer and to have a thickness of a few nanometers and a length of 1 μm.[40] Fibrils prepared using whey proteins were also described as being semiflexible.[39] The characterization of fibrils made using pea protein, on the other hand, showed that the fibrils were highly flexible, more branched, and curly (Figure 6). However, depending on several conditions such as ionic strength, pH, protein concentration, and whether the protein solutions were stirred during heating or not, whey protein has been reported to be capable of forming curly fibrils that are as flexible[39] as fibrils made using pea proteins.

Rheological Characterization of Protein-based Fibrillar Gels. Fibrils have been shown to form gels at relatively low protein concentration.[41] To study the ability of fibrils made using pea protein to form gels at low protein concentrations compared to conventional cold- or heat-induced gelation of pea protein,[10] gel formation in fibril solutions made using pea protein was initiated using GDL, after fibrillar solution pH was adjusted to pH 7.0. During the adjustment of pH from 2.0 to 7.0, gelation of the fibrillar solutions did not occur, although the samples became increasingly turbid at pH 5. GDL was added to the samples at pH 7.0 to allow for slow acidification toward the isoelectric point of the sample (around pH 5). Changes in the storage modulus (G') and loss modulus (G'') were followed as a function of time after the addition of GDL (Figure 7A,B). Gelation was assumed to have occurred when the tan δ of the solution was <1 ($G' > G''$).[42]

In all gelation experiments G' values were higher than G'' at the beginning of all measurements (Figure 7A,B), whereas tan δ values were <1 at the end of all gelation experiments (Table 2). With increasing protein concentrations, G' values obtained after 15 h of gelation increased. Increasing the protein concentration to 160 mg/mL resulted in an increase in the G' with a high G' (350 Pa) being observed even at time 0 h, although self-supportive gels (gels that are firm and can retain their shape without support) could not be formed by the fibrils even at protein concentrations as high as 160 mg/mL. The inability of fibrils made using pea protein to form self-supportive gels even at relatively high protein concentrations may be related to the flexibility of the fibril rods as seen in Figure 6. The flexibility of the fibril rods could have an influence on the ability to form stronger gels at higher protein concentrations. Furthermore, an increase in protein concentration at a low ionic strength could result in a high electrostatic interaction making it difficult to form cross-links between fibrils, resulting in high percolation concentrations[43] that could influence the strength of the gels. Additionally, the analysis of steady-state birefringence by use of rheo-optic measurements as previously described[44] in fibrillar solutions made using pea protein did not show typical decay curves, and no birefringence domains were observed (results not shown). This suggests that short and/or flexible aggregates are formed using pea proteins which do not easily form strong gels.

The final pH of the samples upon the addition of GDL in this study was pH ∼5, which is close to the reported IEP of 4.8 for the legumin pea fraction but below the IEP of 5.5 for the vicillin fraction.[45] The resultant gels at pH 5 were turbid due to the final pH being close to the IEP, as opposed to the transparent gels that were prepared from pea protein isolated using ammonium sulfate at a more acidic pH using citric acid.[45]

For comparison, gels were also prepared from fibrils made using soy protein and whey protein as indicated by the dashed lines in Figure 7A (G') and Figure 7B (G''). Gels prepared from fibrils made using pea protein were comparable in strength to gels prepared from fibrils made using soy protein at the same protein concentration (Figure 7A). This may be attributed to similarities in flexibility of the rods. Pea protein-based fibrillar gels were, however, weaker than whey protein-based fibrillar gels as about 6 times more pea protein fibrils was needed to derive a G' comparable to that of whey protein-based fibrillar gels. The differences in gel strength between pea protein and whey protein may be attributed to the fact that fibrils made using whey protein may have the ability to form networks with higher efficiency compared to those made using pea protein, due to differences in the flexibility of the fibril rods.

To analyze the deformability of the gels prepared from fibrils made using pea protein, soy protein, and whey protein, an amplitude sweep was performed on protein-based fibrillar gels as a function of applied strain. Pea protein, soy protein, and whey protein-based fibrillar gels were all still within the linear

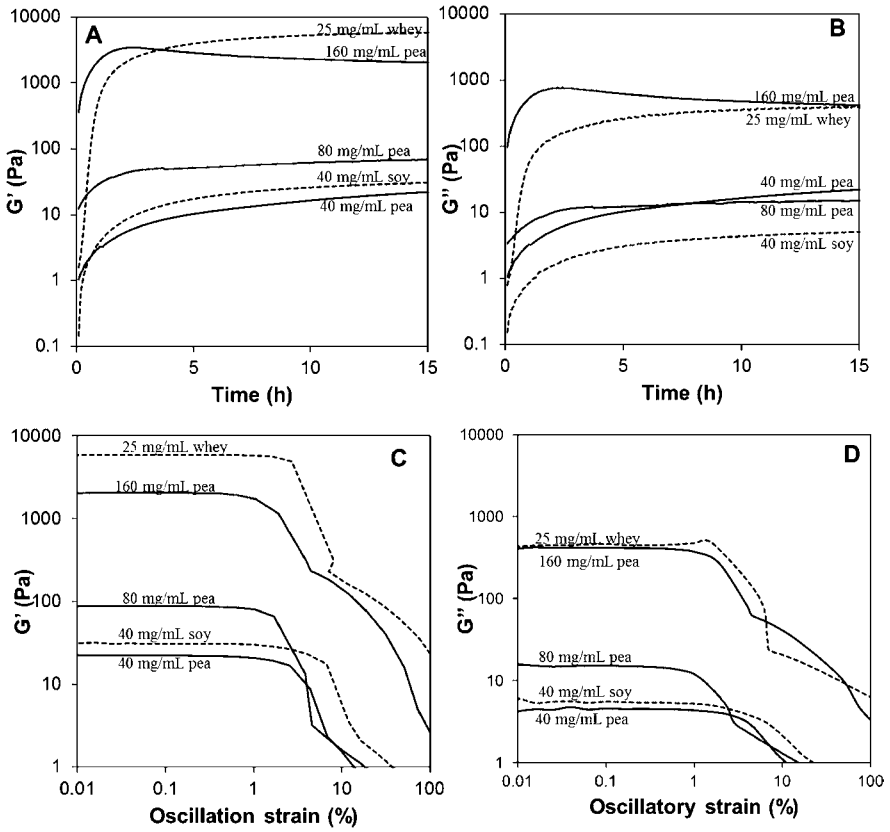

Figure 7. Changes in G' (Pa) (A) and G'' (Pa) (B) over time for 40, 80, and 160 mg/mL pea protein fibril solutions prepared at pH 2.0 and pH adjusted to pH 7.0 before initiation of gelation using GDL. The gelation was compared with 40 mg/mL of soy protein prepared at pH 2.0 and 85 °C for 20 h and 25 mg/mL of whey protein fibrils prepared at pH 2.0 and 80 °C for 20 h. Changes in oscillation strain (%) as a function of G' (Pa) (C) and G'' (Pa) (D) for 40, 80, and 160 mg/mL pea protein, 40 mg/mL soy protein, and 25 mg/mL whey protein-based fibrillar gels following slow acidification toward the isoelectric point using GDL.

region of percent strain between 0.001 and 10, at a frequency of 1 Hz, following deformation as a function of applied strain (Figure 7C,D). With an increase in oscillation strain above 10%, pea protein-based fibrillar gels prepared at a lower protein concentration (40 and 80 mg/mL) fractured earlier compared to pea protein-based fibrillar gels at a higher concentration (160 mg/mL), soy protein-based fibrillar gels (40 mg/mL), and whey protein-based fibrillar gels (25 mg/mL) (Figure 7C). The findings suggest that the fracture properties of pea protein-based fibrillar gels at a high concentration were comparable to those of soy protein and whey protein-based fibrillar gels, although pea protein- and soy protein-based fibrillar gels were generally weaker compared to whey protein-based fibrillar gels.

In conclusion, it can be stated that fibril assembly using pea protein was successfully carried out at pH 2.0. Fibrils made using pea protein were more flexible, branched, and curly compared to fibrils made using whey protein, but comparable to fibrils made using soy protein. Fibrils made using pea protein were assembled into gels that had a strength comparable to that of soy protein-based fibrillar gels but were weaker than whey protein-based fibrillar gels. The findings show that the fibril formation mechanism in plant storage proteins seems to be generic as pea protein fibrils were comparable to soy protein fibrils. Thus, pea protein can effectively be used as a possible replacement for other globular proteins such as soy protein as a structural food ingredient in protein-based fibrillar gels. These findings contribute to the existing knowledge on fibril assembly in globular protein, and the information on the rheological behavior of protein fibrils enhances the understanding of rheological behavior of pea protein-based fibrillar gels.

Table 2. Final G' and tan δ Values for Different Fibrillar Solutions Made Various Using Concentrations of Pea Protein, 40 mg/mL Soy Protein, and 25 mg/mL Whey Protein[a]

protein sample	final G' (Pa) ± SD	final tan δ ± SD
40 mg/mL pea	22 ± 2.3	0.18 ± 0.01
80 mg/mL pea	70 ± 5.01	0.22 ± 0.001
160 mg/mL pea	2058 ± 3.4	0.20 ± 0.02
40 mg/mL soy	31 ± 4.0	0.17 ± 0.01
25 mg/mL whey	5845 ± 22.0	0.07 ± 0.002

[a]The values were obtained after 15 h of gelation following addition of GDL to the fibrillar solutions at 25 °C.

AUTHOR INFORMATION

Corresponding Author

*(H.H.J.d.J.) Mail: TI Food and Nutrition, P.O. Box 557, 6700 AN, Wageningen, The Netherlands. Phone: +31 317 486160. E-mail: dejongh@tifn.nl.

Notes

The authors declare no competing financial interest.

■ ACKNOWLEDGMENTS

We acknowledge Harry Baptist for help with transmission electron microscopy, Jolan de Groot for performing HPLC analyses, and Eefjan Timmerman for assistance with pea protein extraction. We appreciate useful discussions with Laurice Pouvreau.

■ REFERENCES

(1) Pimentel, D.; Pimentel, M. Sustainability of meat-based and plant-based diets and the environment. *Am. J. Clin. Nutr.* **2003**, *78*, 660S−663S.

(2) Johnson, E. A.; Brekke, C. J. Functional properties of acylated pea protein isolates. *J. Food Sci.* **1983**, *48*, 722−725.

(3) Gharsallaoui, A.; Saurel, R.; Chambin, O.; Voilley, A. Pea (*Pisum sativum*, L.) protein isolate stabilized emulsions: a novel system for microencapsulation of lipophilic ingredients by spray drying. *Food Bioprocess Technol.* **2012**, *5*, 2211−2221.

(4) Barac, M.; Cabrilo, S.; Pesic, M.; Stanojevic, S.; Zilic, S.; Macej, O.; Ristic, N. Profile and functional properties of seed proteins from six pea (*Pisum sativum*) genotypes. *Int. J. Mol. Sci.* **2010**, *11*, 4973−4990.

(5) Croy, R.; Gatehouse, J. A.; Tyler, M.; Boulter, D. The purification and characterization of a third storage protein (convicilin) from the seeds of pea (*Pisum sativum* L.). *Biochem. J.* **1980**, *191*, 509−516.

(6) O'Kane, F. E.; Happe, R. P.; Vereijken, J. M.; Gruppen, H.; van Boekel, M. A. J. S. Characterization of pea vicilin. 1. Denoting convicilin as the α-subunit of the *Pisum* vicilin family. *J. Agric. Food Chem.* **2004**, *52*, 3141−3148.

(7) Nunes, M. C.; Raymundo, A.; Sousa, I. Rheological behaviour and microstructure of pea protein/κ-carrageenan/starch gels with different setting conditions. *Food Hydrocolloids* **2006**, *20*, 106−113.

(8) Koyoro, H. *Functional Properties of Pea Globulins*; Washington State University: Pullman, WA, USA, 1984.

(9) Bacon, J. R.; Noel, T. R.; Wright, D. J. Studies on the thermal behaviour of pea (*Pisum sativum*) vicilin. *J. Sci. Food Agric.* **1989**, *49*, 335−345.

(10) Shand, P. J.; Ya, H.; Pietrasik, Z.; Wanasundara, P. K. J. P. D. Physicochemical and textural properties of heat-induced pea protein isolate gels. *Food Chem.* **2007**, *102*, 1119−1130.

(11) Tang, C.-H.; Wang, S.-S.; Huang, Q. Improvement of heat-induced fibril assembly of soy β-conglycinin (7S globulins) at pH 2.0 through electrostatic screening. *Food Res. Int.* **2012**, *46*, 229−236.

(12) Kroes-Nijboer, A.; Sawalha, H.; Venema, P.; Bot, A.; Floter, E.; den Adel, R.; Bouwman, W. G.; van der Linden, E. Stability of aqueous food grade fibrillar systems against pH change. *Faraday Discuss.* **2012**, *158*, 125−138.

(13) Loveday, S. M.; Su, J.; Rao, M. A.; Anema, S. G.; Singh, H. Whey protein nanofibrils: kinetic, rheological and morphological effects of group IA and IIA cations. *Int. Dairy J.* **2012**, *26*, 133−140.

(14) Durand, D.; Gimel, J. C.; Nicolai, T. Aggregation, gelation and phase separation of heat denatured globular proteins. *Physica A* **2002**, *304*, 253−265.

(15) Kavanagh, G. M.; Clark, A. H.; Ross-Murphy, S. B. Heat-induced gelation of globular proteins: part 3. Molecular studies on low pH β-lactoglobulin gels. *Int. J. Biol. Macromol.* **2000**, *28*, 41−50.

(16) Veerman, C.; de Schiffart, G.; Sagis, L. M. C.; van der Linden, E. Irreversible self-assembly of ovalbumin into fibrils and the resulting network rheology. *Int. J. Biol. Macromol.* **2003**, *33*, 121−127.

(17) Veerman, C.; Sagis, L. M. C.; Heck, J.; van der Linden, E. Mesostructure of fibrillar bovine serum albumin gels. *Int. J. Biol. Macromol.* **2003**, *31*, 139−146.

(18) Bolder, S. G.; Hendrickx, H.; Sagis, L. M. C.; van der Linden, E. Fibril assemblies in aqueous whey protein mixtures. *J. Agric. Food Chem.* **2006**, *54*, 4229−4234.

(19) Tang, C.-H.; Zhang, Y.-H.; Wen, Q.-B.; Huang, Q. Formation of amyloid fibrils from kidney bean 7S globulin (phaseolin) at pH 2.0. *J. Agric. Food Chem.* **2010**, *58*, 8061−8068.

(20) Liu, J.; Tang, C.-H. Heat-induced fibril assembly of vicilin at pH 2.0: reaction kinetics, influence of ionic strength and protein concentration, and molecular mechanism. *Food Res. Int.* **2013**, *51*, 621−632.

(21) Akkermans, C.; van der Goot, A. J.; Venema, P.; Gruppen, H.; Vereijken, J. M.; van der Linden, E.; Boom, R. M. Micrometer-sized fibrillar protein aggregates from soy glycinin and soy protein isolate. *J. Agric. Food Chem.* **2007**, *55*, 9877−9882.

(22) Tang, C.-H.; Wang, C.-S. Formation and characterization of amyloid-like fibrils from soy β-conglycinin and glycinin. *J. Agric. Food Chem.* **2010**, *58*, 11058−11066.

(23) Akkermans, C.; Venema, P.; van der Goot, A. J.; Gruppen, H.; Bakx, E. J.; Boom, R. M.; van der Linden, E. Peptides are building blocks of heat-induced fibrillar protein aggregates of β-lactoglobulin formed at pH 2. *Biomacromolecules* **2008**, *9*, 1474−1479.

(24) Bolder, S. G.; Hendrickx, H.; Sagis, L. M. C.; van der Linden, E. Ca^{2+}-induced cold-set gelation of whey protein isolate fibrils. *Appl. Rheol.* **2006**, *16*, 258−264.

(25) Bolisetty, S.; Harnau, L.; Jung, J.-m.; Mezzenga, R. Gelation, phase behavior, and dynamics of β-lactoglobulin amyloid fibrils at varying concentrations and ionic strengths. *Biomacromolecules* **2012**, *13*, 3241−3252.

(26) Munialo, C. D.; de Jongh, H. H. J.; Broersen, K.; Van Der Linden, E.; Martin, A. H. Modulation of the gelation efficiency of fibrillar and spherical aggregates by means of thiolation. *J. Agric. Food Chem.* **2013**, *61*, 11628−11635.

(27) Holt, N. W.; Sosulski, F. W. Amino acid composition and protein quality of field peas. *Can. J. Plant Sci.* **1979**, *59*, 653−660.

(28) Kosters, H. A.; Broersen, K.; de Groot, J.; Simons, J. W.; Wierenga, P.; de Jongh, H. H. Chemical processing as a tool to generate ovalbumin variants with changed stability. *Biotechnol. Bioeng.* **2003**, *84*, 61−70.

(29) Visser, S.; Slangen, C. J.; Rollema, H. S. Phenotyping of bovine milk proteins by reversed-phase high-performance liquid chromatography. *J. Chromatogr., A* **1991**, *548*, 361−370.

(30) Naiki, H.; Higuchi, K.; Hosokawa, M.; Takeda, T. Fluorometric determination of amyloid fibrils invitro using the fluorescent dye, thioflavine T. *Anal. Biochem.* **1989**, *177*, 244−249.

(31) Weijers, M.; Van De Velde, F.; Stijnman, A.; Van De Pijpekamp, A.; Visschers, R. W. Structure and rheological properties of acid-induced egg white protein gels. *Food Hydrocolloids* **2006**, *20*, 146−159.

(32) Akkermans, C.; van der Goot, A. J.; Venema, P.; van der Linden, E.; Boom, R. M. Formation of fibrillar whey protein aggregates: Influence of heat and shear treatment, and resulting rheology. *Food Hydrocolloids* **2008**, *22*, 1315−1325.

(33) Mishra, R.; Sörgjerd, K.; Nyström, S.; Nordigården, A.; Yu, Y.-C.; Hammarström, P. Lysozyme amyloidogenesis is accelerated by specific nicking and fragmentation but decelerated by intact protein binding and conversion. *J. Mol. Biol.* **2007**, *366*, 1029−1044.

(34) Shammas, S. L.; Knowles, T. P. J.; Baldwin, A. J.; MacPhee, C. E.; Welland, M. E.; Dobson, C. M.; Devlin, G. L. Perturbation of the stability of amyloid fibrils through alteration of electrostatic interactions. *Biophys. J.* **2011**, *100*, 2783−2791.

(35) de Jongh, H. H. J.; Robles, C. L.; Timmerman, E.; Nordlee, J. A.; Lee, P.-W.; Baumert, J. L.; Hamilton, R. G.; Taylor, S. L.; Koppelman, S. J. Digestibility and IgE-binding of glycosylated codfish parvalbumin. *BioMed Res. Int.* **2013**, *2013*, 10.

(36) de Jongh, H. H. J.; Goormaghtigh, E.; Killian, J. A. Analysis of circular dichroism spectra of oriented protein-lipid complexes: toward a general application. *Biochemistry* **1994**, *33*, 14521−14528.

(37) Purdie, N. *Circular Dichroism and the Conformational Analysis of Biomolecules*; Fasman, G. D., Ed.; Plenum Press: New York, 1996; x + 738 pp, ISBN 0-306-45142-5; reviewed in *J. Am. Chem. Soc.* **1996**, *118*, 12871−12871.

(38) Yang, J. T.; Wu, C.-S. C.; Martinez, H. M. Calculation of protein conformation from circular dichroism. *Methods Enzymol.* **1986**, *130*, 208−269.

(39) Loveday, S. M.; Su, J.; Rao, M. A.; Anema, S. G.; Singh, H. Whey protein nanofibrils: the environment−morphology−function-

ality relationship in lyophilization, rehydration, and seeding. *J. Agric. Food Chem.* **2012**, *60*, 5229−5236.
(40) Bolder, S. G.; Sagis, L. M. C.; Venema, P.; van der Linden, E. Thioflavin T and birefringence assays to determine the conversion of proteins into fibrils. *Langmuir* **2007**, *23*, 4144−4147.
(41) Veerman, C.; Baptist, H.; Sagis, L. M. C.; van der Linden, E. A new multistep Ca^{2+}-induced cold gelation process for β-lactoglobulin. *J. Agric. Food Chem.* **2003**, *51*, 3880−3885.
(42) Ross-Murphy, S. B. Incipient behaviour of gelatin gels. *Rheol. Acta* **1991**, *30*, 401−411.
(43) Veerman, C.; Ruis, H.; Sagis, L. M. C.; van der Linden, E. Effect of electrostatic interactions on the percolation concentration of fibrillar β-lactoglobulin gels. *Biomacromolecules* **2002**, *3*, 869−873.
(44) Rogers, S. S.; Venema, P.; van der Ploeg, J. P. M.; Sagis, L. M. C.; Donald, A. M.; van der Linden, E. Electric birefringence study of an amyloid fibril system: the short end of the length distribution. *Eur. Phys. J. E* **2005**, *18*, 207−217.
(45) Bacon, J. R.; Noel, T. R.; Lambert, N. Preparation of transparent pea protein gels: a comparison of isolation procedures. *Int. J. Food Sci. Technol.* **1990**, *25*, 527−537.

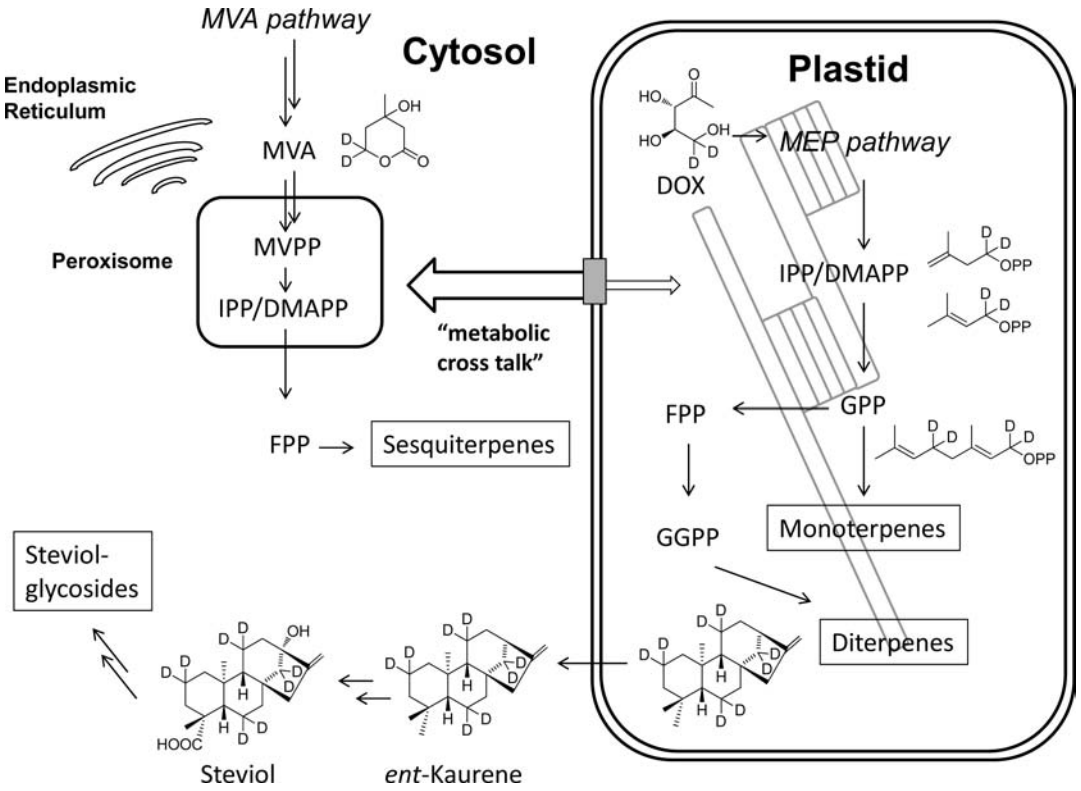

Figure 1. Proposed simplified scheme for the compartmentalization of terpene biosynthesis via MEP and MVA pathways in *Stevia rebaudiana*. Metabolic cross talk is mediated by a yet unidentified metabolite transporter, which is represented by a gray-shaded rectangle inserted into the plastid membrane. IPP, isopentenyl diphosphate; DMAPP, dimethylallyl diphosphate; FPP, farnesyl diphosphate; GGPP, geranylgeranyl diphosphate; MEP, methylerythritol phosphate; MVA, mevalonic acid; MVPP, 5-diphosphomevalonate.

rhamnose and xylose in, for example, dulcoside A and rebaudiosides C and F cannot be explained until now[10] due to lacking information about the participating enzymes.

This study aims to reinvestigate the biosynthesis of steviol glycosides by feeding experiments using the labeled precursors of the MEP and MVA pathways, namely, [5,5-$^2H_2$]-1-deoxy-D-xylulose (d_2-DOX) and [5,5-$^2H_2$]-mevalonic acid lactone (d_2-MVL), respectively. Two analytical methods were applied to detect the incorporation of the labeled intermediates: gas chromatography–mass spectrometry (GC-MS) and liquid chromatography–electrospray tandem mass spectrometry in negative ion mode (LC-(ESI)-MS/MS).[11] This experimental design is fundamentally different from the one that was chosen by Totté et al. in the aforementioned study. We chose to feed labeled precursors of the isoprenoid pathways and used the more sensitive mass spectrometry to detect the incorporation of labeled precursors. Moreover, we investigated in parallel the incorporation of the precursors into essential oil isoprenoids that were generated in glandular trichomes of *Stevia* leaves.

A comprehensive investigation of the chemical composition of leaf extracts of *S. rebaudiana* revealed that its essential oil contains numerous mono-, sesqui-, and diterpenes.[12] An appropriate technique for the analysis of such volatile organic compounds (VOC) is headspace solid phase microextraction (HS-SPME) in combination with GC-MS.[13] It has been recently employed for the study of the pathway utilization in the sesquiterpene biosynthesis of grape berries.[14] Hence, analyses of the leaf and stem volatiles of *S. rebaudiana*, including mono-, sesqui-, and diterpenes, were performed by HS-SPME-GC-MS as well to gain further insight into the pathway utilization in glandular trichomes.

MATERIALS AND METHODS

Reagents. HPLC grade acetonitrile was obtained from VWR International (Leuven, Belgium). Purified water was purchased from TKA Genopure-UV system. [5,5-$^2H_2$]-Mevalonic acid lactone (d_2-MVL) was prepared according to the method of Simpson et al.,[11] and [5,5-$^2H_2$]-1-deoxy-D-xylulose (d_2-DOX) was prepared according to the method of Meyer et al.[15] Spectral data of the labeled compounds were in all cases in good agreement with the data given in the references cited above. Stevioside, rebaudioside A, and isosteviol with purities of ≥99.0 and 98.0%, respectively, were obtained from Wako Chemicals (Neuss, Germany). Steviol with a purity of ≥98% (HPLC), α-terpineol (≥96%), β-caryophyllene (≥80%), and pyridine (anhydrous ≥99.8%) were purchased from Sigma-Aldrich (Taufkirchen, Germany). *N*-Methyl-*N*-(trimethylsilyl)trifluoroacetamide (MSTFA) in 1 mL ampules was obtained from CS-Chromatographie Service (Langerwehe, Germany), diisopropyl ether, ACS (≥99%), and linalool were obtained from Roth (Karlsruhe, Germany), anhydrous sodium sulfate EMSURE ACS and sulfuric acid (90–91%) were obtained from Merck (Darmstadt, Germany), and sulfuric acid (1 mol/L) was obtained by diluting 90–91% sulfuric acid, respectively.

Safe-lock tubes, 2.0 mL, were purchased from Eppendorf (Hamburg, Germany).

Standard Solutions. To prepare stock solutions, the steviol glycosides were dried to constant weight at 103 °C, cooled, and stored in a desiccator until use.

For LC-MS, 10 mg of dried steviol glycosides was dissolved in water (10 mL). Solutions of stevioside and rebaudioside A were prepared by diluting the respective steviol glycoside with acetonitrile/water (8:2 v/v) to obtain final concentrations of 10 μg/mL and were used for tuning the mass spectrometer.

For isosteviol identification by GC-MS, stock solutions of isosteviol (0.1 mg/mL in anhydrous pyridine) were prepared.

Plant Material and Incubation. *S. rebaudiana* plants of the genotype Gawi were obtained from the Institute of Crop Science and

dx.doi.org/10.1021/jf500270s | J. Agric. Food Chem. 2014, 62, 2428–2435

Resource Conservation (INRES), Chair of Horticultural Sciences of the University of Bonn. Shoot tip cuttings of plants with four leaves were placed in vials containing 11 mL of autoclaved half-strength MS[16] nutrient medium (solution without solidifying agar) containing each 30 mg of d_2-MVL or 30 mg of d_2-DOX or only half-strength MS medium as control. Incubation was performed in a culture cabinet at 25 °C and 80% humidity under 16 h per day reduced light conditions of 150 $\mu E \cdot m^{-2} \cdot s^{-1}$ photosynthetic active radiation. After 5 days, leaves and stems were harvested. The leaves were grouped in "old" leaves (leaves that were almost fully expanded prior to incubation) and "new" leaves (leaves that were expanding during incubation). In 2012, orienting incubations were performed with d_2-DOX, and in 2013 with d_2-DOX and d_2-MVL, respectively. In addition to the leaves, stems were sampled and analyzed separately.

Leaves and stems were ground in a mortar in the presence of some milliliters of fluid nitrogen. After the evaporation of the nitrogen, the dried leaf/stem powder was stored immediately at −20 °C prior to analysis.

Sample Extraction. *Headspace−Solid-Phase Microextraction.* The analysis of the leaf and stem volatiles was performed with the plant material of 2013. Approximately 1 cm^2 of the freshly harvested leaves or stems was placed into 10 mL headspace vials without further preparation. The subsequent measurement of the leaf and stem volatiles was performed with a polyacrylate fiber, 85 μm (Supelco, Bellefonte, PA, USA). The equilibration time of the samples was 30 min at a temperature of 45 °C; afterward, the SPME fiber was exposed to the sample headspace for a further 10 min and was subsequently thermally desorbed in the injection port of the GC.

Aqueous Extraction of Diterpene Glycosides. Freeze-dried *Stevia* leaves (25 mg) were weighed in a 2 mL Safe-lock tube and extracted three times with portions of 0.5 mL of water in a heating block set at 102 °C for 30 min. Each extract was cooled to room temperature and centrifuged (15 min, 6866*g*). The aqueous phases were transferred to a weighed tube and filled to 1.5 mL (weight correction) after the last extraction step. Recovery was 93% for rebaudioside A calculated by measuring a known sample in duplicate according to earlier investigations.[17]

Hydrolyis of Steviol Glycosides. To convert the extracted steviol glycosides to isosteviol, 100 μL of the *Stevia* extract was mixed with 4 mL of sulfuric acid (1 mol/L) and heated for 60 min at 102 °C. After cooling, the solution was extracted three times with 2 mL of diisopropyl ether each time. The combined ether phases were dried with sodium sulfate and evaporated to dryness after filtration.

Silylation. Trimethylsilyl (TMS) ethers were prepared by adding 300 μL of anhydrous pyridine and 150 μL of MSTFA to the dried samples or to an aliquot of the isosteviol stock solution, for example, 25 μL. This mixture was heated for 15 min at 60 °C. After cooling, 1 μL was injected into the GC.

Sample Preparation for LC-ESI-MS/MS Detection. *Stevia* extract was diluted with acetonitrile/water mixture (8:2 v/v) to obtain a final concentration of 0.01 mg/mL. Ten microliters was injected into the LC.

GC-MS Analysis. *HS-SPME-GC-MS Analysis.* GC-MS analysis was performed on a Varian 450 GC coupled to a Varian 240 MS ion trap spectrometer (Varian, Darmstadt, Germany). The injection port was set to 220 °C. A splitless injection was used, and the split valve was opened after 3 min. Separation was achieved on a 30 m × 0.25 mm i.d. × 0.25 μm film thickness DB5 column (Varian, Darmstadt, Germany). The carrier gas (helium 5.0) was set to 1 mL/min as constant flow. The column temperature started at 35 °C for 3 min and was increased to 230 °C at a rate of 5 °C/min. The transfer line temperature was set to 260 °C and the ion source to 150 °C. The spectrometer operated in the electronic impact (EI) mode at 70 eV scanning the m/z 50−350 range at a rate of 0.64 s/scan. Acquisition was done using Varian MS Workstation 6.9.2. The analytes were identified by comparison of the retention times and mass spectra with standard substances or were identified by their mass spectra and Kovats retention indices using the Massfinder library available from Dr. Hochmuth (Hamburg, Germany).

GC-MS Analysis of Steviol Glycosides. The GC-MS system and basic settings were the same as mentioned above. The following settings were changed for steviol glycoside analysis: The injection port was set to 250 °C, and injections were made in the split mode with a ratio of 1:20. The column temperature program started at 180 °C and was kept at this temperature for 1 min. Then it was increased to 300 °C during 10 min at a rate of 8 °C/min. Mass spectra were recorded in a range of m/z 50−450 at a scan rate of 0.82 s/scan. Isosteviol was identified by comparison of its retention time and mass spectra with the standard substance.

HPLC-(-ESI)-MS/MS Analysis. Liquid chromatography analysis was performed on a binary LC-20AD system (Shimadzu, Duisburg, Germany) equipped with an SIL-20A autosampler, a Spark Mistral column thermostat and a four-channel degasser. The HPLC system was coupled to an API2000 triple-quadrupole detector (AB Sciex, Darmstadt, Germany) equipped with an ESI source used in the tandem MS mode with multiple reaction monitoring (MRM). Analyses and data processing were performed using Analyst 1.6.1 software. The instrument operated in the negative ion mode with the following source adjustments: ion spray voltage, −4200 V; curtain gas, 20 psi; gas 1 and 2, 50 psi; capillary temperature, 400 °C. The compound-dependent parameters were for both stevioside and rebaudioside A a declustering potential of −151 V, a cell entrance potential of −42 V, a collision energy of −30 V, a focusing potential of −340 V for stevioside and of −260 V for rebaudioside A, an entrance potential of −12 V for stevioside and of −7.5 V for rebaudioside A, and a cell exit potential of −22 V for stevioside and of −26 V for rebaudioside A.

The MRM method involved the precursor/product transitions m/z 803−811 to m/z 641−649 for stevioside/d_8-stevioside and m/z 965−973 to m/z 803−811 for rebaudioside A/d_8-rebaudioside A.

For HPLC separation, a YMC-Triart Diol-HILIC column (250 × 4.6 mm, particle size = 5 μm, YMC, Dinslaken, Germany) equipped with the corresponding guard column (4 × 3.0 mm) was used. The mobile phase consisted of acetonitrile/water mixtures. The column temperature was maintained at 40 °C, and the flow was set to 0.4 mL/min. The sample injection volume was 10 μL. The solvent gradient started with 20% water for 20 min, increased linearly to 40% water over 5 min, and then decreased back to 20% water. Column reequilibration was set at 5 min.

Incorporation Rates. In all cases, incorporation rates (%) were calculated by dividing the peak area of the completely labeled compound by the peak area of the genuine compound multiplied by 100.[14]

RESULTS AND DISCUSSION

***Stevia* Plants.** Cuttings of the *S. rebaudiana* genotype Gawi were tested together with other genotypes as plant material for the feeding experiments and proven to be the most robust with the best leaf production during the investigation period. The total sweetener content is about 10%, with stevioside being the most abundant (6−7%) and rebaudioside A with a content of about 3%.[18] The feeding and incubation procedure was carried out according to the method of Totté et al.[5] but without the chloramine T supplementation. Nevertheless, no microbial infestation was observed. For a better understanding of the distribution of labeled steviol glycosides, the leaves were harvested separately and divided into "old" and "new" leaves and stems (for a description, see Plant Material and Incubation).

Analysis of Glandular Trichome Volatiles. Prior to the determination of the steviol glycosides, the plant material was analyzed by HS-SPME-GC-MS without further preparation. This method allows the selective detection of volatiles that are stored in the subcuticular space of glandular trichomes and released into the headspace.[19,20] In the foliar, 10-celled lipophilic glandular trichomes of *S. rebaudiana*, the six secretory

Table 1. Analyzed Compounds with Their Ion Traces Used for Quantitation (GC-MS, Numbers 1−8) and Transitions Used for Quantitation (LC-MS, Numbers 9 and 10), Respectively

no.	compound	molecular ion, genuine/labeled	ions and transitions for quantitation (m/z), genuine/labeled	max deuterium incorporation
1	linalool	154/158[a]	93/96[b]	d_4
2	α-terpineol	154/158[a]	136/139[b]	d_4
3	(*E*)-β-caryophyllene	204/210	161/(166[b] + 167)	d_6
4	β-farnesene[c]	204/210[a]	161/(166[b] + 167)	d_6
5	germacrene D	204/210	161/166[b]	d_6
6	13-epi-manoyloxid[c]	290/298[a]	257/265	d_8
7	*ent*-kaurene[c]	272/280	257/265	d_8
8	isosteviol	390/397	272/279	d_7
9	Stev	803/811	803→641/811→649	d_8
10	RebA	965/973	965→803/973→811	d_8

[a]Molecular ions not observed due to intense fragmentation by EI ionization. [b]Loss of deuterium due to fragmentation.[14] See Figure S4 in the Supporting Information for a detailed analysis of the fragmentation pattern and the cyclization process that gives rise to the observed labeling pattern. [c]Tentatively identified by mass spectrum and retention index.

cells form three pairs of head cells. To form the secretory sheath, the cuticular membrane detaches from the outer walls of the apical secretory cells along a line that appears to be the pectin layer.[21] For a typical HS-SPME-GC/MS chromatogram, see the Supporting Information (Figure S1). The trichome volatiles are dominated by mono-, sesqui-, and diterpenes. The identified volatiles are in agreement with those identified in previous studies on *S. rebaudiana* volatiles and also known as common headspace volatiles of other plant species.[12,22−25] The analysis of the incubated cuttings provides a comprehensive insight into the pathway utilization of the different terpene glandular trichomes. After administration of the labeled precursors, genuine terpenoid volatiles were detectable in all samples. However, contents of volatiles in old leaves were 100 times lower than those in new leaves or stems (data not shown), which can be explained by a reduced biosynthetic activity in old leaves or a reduced density of trichomes per leaf area unit.[26] Nevertheless, deuterium incorporation was detected in terpenoid volatiles in all investigated tissues. Labeled and genuine terpenes can be chromatographically separated due to the inverse isotopic effect in gas chromatography.[27] Monoterpenes are formed by two units of IPP/DMAPP, sesquiterpenes by three units, and diterpenes by four units, respectively. Because $^2H_2$-MVL and $^2H_2$-DOX are metabolized to $^2H_2$-IPP and/or $^2H_2$-DMAPP, up to four deuterium atoms can be incorporated into monoterpenes, six into sesquiterpenes, and eight into diterpenes. Deuterium incorporation, molecular ions, and ion traces used for data evaluation are given in Table 1. Results obtained in the feeding experiments for both precursors in all plant tissues are given in Table 2. d_2-DOX was incorporated into volatile mono-, sesqui-, and diterpenes and d_2-MVL mainly into sesquiterpenes with similar incorporation rates for both precursors. However, incorporation of d_2-MVL into mono- and diterpenes was barely detectable or 10−100 times lower than that obtained for d_2-DOX.

Analysis of Steviol Glycosides. Two independent analytical methods were used for determining the incorporation of deuterium into steviol glycosides. For GC-MS analysis, the steviol glycosides were hydrolyzed, yielding the aglycon steviol, which was converted to isosteviol and detected after silylation as a sum parameter. In the second method, the diterpenes were separated by LC and detected as individual steviol glycosides with (ESI)-MS/MS.

GC-MS Analysis. The hydrolysis of steviol glycosides to steviol and its conversion to isosteviol were carried out with diluted sulfuric acid in the water extract of the labeled leaves according to the method of Nowotny.[28] As the genuine steviol content in the leaves never exceeds 0.003% (w/w), its determination was omitted.[29] The detection as TMS-ester via GC-MS was performed according to the method of Ohta[9] with some modifications. The proposed derivatization reagents hexamethyldisilazane and trimethylchlorosilane tended to block the injection needle of the autosampler and were therefore substituted by MSTFA. For a typical chromatogram of isosteviol as TMS-ester, see the Supporting Information (Figure S2). In the total ion chromatogram (TIC), labeled and unlabeled isosteviol can be clearly separated due to the inverse isotope effect[27] with retention times of 12.21 min for the

Table 2. Incorporation Rates and Standard Deviations after Cut Stem Feeding Experiments of *Stevia* Cuttings with $^2H_2$-DOX and $^2H_2$-MVL (n = 2, Plant Material of 2013)[a]

sample	compound	$^2H_2$-DOX incorporation rate (%)	$^2H_2$-MVL incorporation rate (%)
new leaves	linalool	10.9 ± 4.3	nd
	α-terpineol	10.7 ± 0.9	0.5 ± 0.6
	(*E*)-β-caryophyllene	5.3 ± 2.8	49.8 ± 41.0
	β-farnesene	37.1 ± 0.8	50.8 ± 16.5
	germacrene D	25.2 ± 8.4	46.3 ± 37.3
	13-epi-manoyloxid	7.1 ± 3.1	0.3 ± 0.4
	ent-kaurene	94.5 ± 32.2	4.7 ± 6.6
old leaves	linalool	37.8 ± 3.2	nd
	α-terpineol	19.5 ± 0.7	nd
	(*E*)-β-caryophyllene	3.0 ± 0.5	14.9 ± 2.6
	β-farnesene	27.4 ± 3.0	nd
	germacrene D	10.9 ± 0.1	12.7 ± 0.4
	13-epi-manoyloxid	2.5 ± 0.5	nd
	ent-kaurene	257.7 ± 16.7	15.4 ± 9.8
stems	linalool	49.1 ± 28.8	nd
	α-terpineol	14.2 ± 2.6	0.4 ± 0.5
	(*E*)-β-caryophyllene	10.2 ± 6.0	25.2 ± 0.5
	β-farnesene	32.5 ± 5.0	31.7 ± 1.8
	germacrene D	31.1 ± 6.2	27.0 ± 2.3
	13-epi-manoyloxid	5.2 ± 1.3	0.3 ± 0.2
	ent-kaurene	107.3 ± 85.1	1.4 ± 2.0

[a]HS-SPME-GC-MS analysis of volatile terpenoids according to Table 1. nd, not detectable: signal to noise ratio <3.

dx.doi.org/10.1021/jf500270s | J. Agric. Food Chem. 2014, 62, 2428−2435

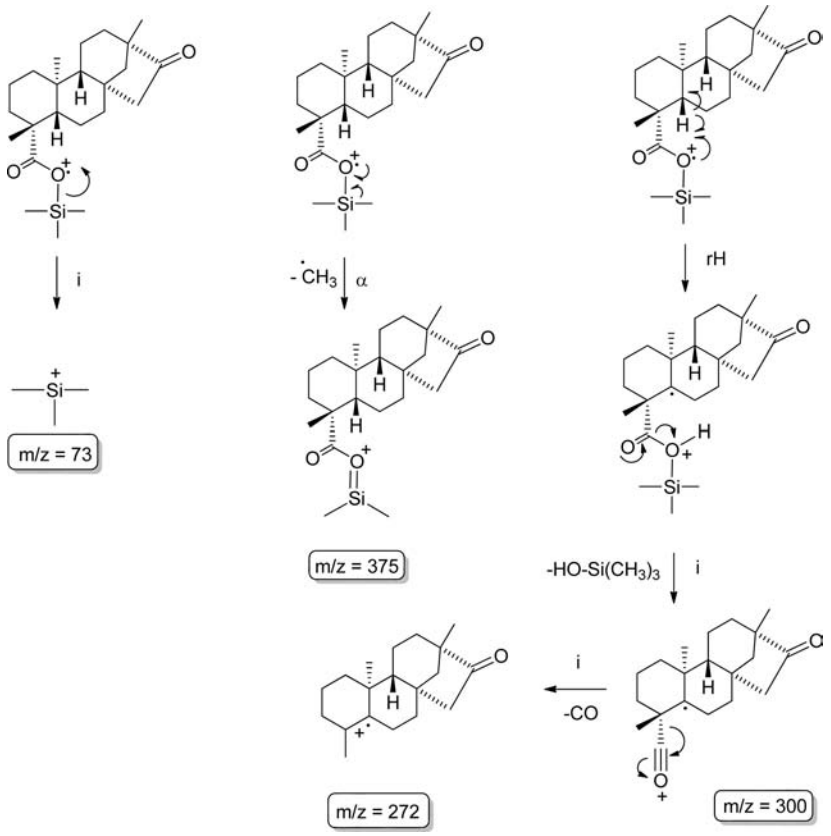

Figure 2. Proposed fragmentation scheme for isosteviol TMS-ester in EI-MS. i, charge induced scission; rH, hydrogen rearrangement; α, α scission.

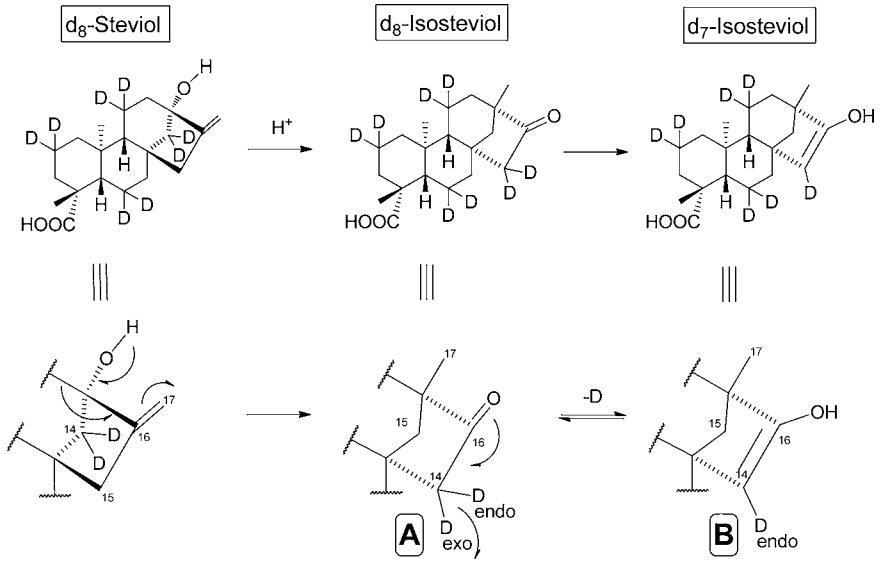

Figure 3. Wagner–Meerwein rearrangement during conversion of steviol to isosteviol and keto–enol tautomerism of isosteviol (A, B) producing an interchangeable proton at C14.

unlabeled and 12.13 min for the labeled component. The corresponding MS spectra revealed a characteristic fragmentation pattern (Figure 2) with m/z 390 (molecular ion), m/z 375 (loss of a methyl group at $COOSi(CH_3)_3$), m/z 300 (loss of $HO\text{-}Si(CH_3)_3$), and m/z 272 (subsequent loss of CO at C4) for the genuine component and mass shifts of up to seven atomic mass units for deuterium-labeled isosteviol. A retrobiosynthetic analysis predicts that a maximum of eight deuterium atoms will be incorporated into steviol because the building block of diterpenes, GGPP, is assembled by four IPP/DMAPP molecules attached to each other, each containing two deuterium atoms (Figure 1). Interestingly, we observed a maximum of seven labeled protons incorporated into isosteviol, whereas steviol glycosides, analyzed by LC-MS, exhibit eight deuterium atoms. By treatment with sulfuric acid all steviol glycosides are hydrolyzed to steviol, which undergoes rapidly a Wagner–Meerwein rearrangement to isosteviol, containing an *ent*-beyerene skeleton. After this reaction, the two labeled

dx.doi.org/10.1021/jf500270s | J. Agric. Food Chem. 2014, 62, 2428–2435

protons at C14 are at the *exo*/*endo*-position to the carbonyl group at C16 implying keto−enol tautomerism and the interchangeability of the deuterium ion preferentially at the *exo*-position (Figure 3).[30,31]

LC-(ESI)-MS/MS. The diluted water extract of the labeled leaf samples was injected into the HPLC system without further cleanup. The observed fragmentation pattern in ESI-MS/MS was the same as reported earlier.[32] As expected, a maximum of eight deuterium ions were incorporated into each steviol glycoside. No shift in retention times could be observed, and all labeled compounds had the same retention times as the unlabeled compound. For LC-MS data, see the Supporting Information (Figure S3). The incorporation rate was calculated for stevioside and rebaudioside A, respectively.

Incorporation Rates. For each terpene under study the maximum numbers of deuterium labels introduced from the respective precursors were considered. Incorporation rates were then calculated on the basis of the mass peak intensity representing the fully labeled compound in comparison to the intensity of the peak representing the unlabeled compound. However, labeled terpenes, which have not acquired the maximum number of deuterium labels, but a fraction therefrom (for example, by combination of a labeled IPP with an unlabeled DMAPP), were also detectable. These peaks were not dominant and were therefore not considered for the calculation of incorporation rates.

Tables 3 and 4 report the incorporation rates into isosteviol, stevioside, and rebaudioside A after d_2-DOX and d_2-MVL feeding using different analytical protocols.

Table 3. Incorporation Rates of Deuterium-Labeled Precursors into Isosteviol after Feeding with $^2H_2$-DOX and $^2H_2$-MVL, Respectively, Analyzed by GC-MS (n = 2)

sample	$^2H_2$-DOX incorporation rate (%)	$^2H_2$-MVL incorporation rate (%)
new leaves		
2012	23 ± 3.0	not determined
2013	11 ± 0.6	not detectable
old leaves		
2012	10 ± 0.3	not determined
2013	14 ± 2.3	not detectable
stems (2013)	not detectable	not detectable

Table 4. Incorporation Rates of Deuterium-Labeled Precursors into Steviol Glycosides after Treatment with $^2H_2$-DOX and $^2H_2$-MVL, Respectively, Analyzed by LC-(ESI)-MS/MS (n = 2)

	$^2H_2$-DOX incorporation rate (%)		$^2H_2$-MVL incorporation rate (%)	
sample	Stev	RebA	Stev	RebA
new leaves				
2012	34 ± 3.1	11 ± 0.1	not determined	not determined
2013	18 ± 1.5	7 ± 0.6	0.1	<0.1
old leaves				
2012	36 ± 0.5	14 ± 0.1	not determined	not determined
2013	20 ± 0.7	12 ± 0.4	<0.1	<0.1
stems (2013)	4.6 ± 2.3	1.0 ± 0.6	0.2	0.1

The incorporation rates for labeled DOX were high in all leaf samples, but in 2012, they were lower in old than in new leaves. This is in agreement with recent results of Kumar et al.[33] They demonstrated that gene expression of enzymes involved in the steviol glycoside biosynthesis (including enzymes of the early steps in isoprenoid biosynthesis) is at maximum in leaves at the first node (apical position). Only gene expression of 1-deoxy-D-xylulose 5-phosphate reductoisomerase (DXR) and kaurene oxidase (KO) showed highest expression at the third node. In 2013, some young leaves showed necrosis and produced less biomass. This could explain the reduced incorporation rate when compared to those in 2012. Nevertheless, no incorporation could be detected after feeding with d_2-MVL.

Table 4 gives the incorporation rates of individual steviol glycosides after LC-MS analysis. The same pattern as detected by GC-MS analysis could be observed in 2012 and 2013. In contrast to GC-MS, deuterium incorporation could be detected also in stems and even some labeling after d_2-MVL feeding. Totté et al.[5] reported after feeding experiments with [1-^{13}C]-glucose that only the plastidial methylerythritol-4-phosphate (MEP) pathway and not the cytosolic acetate-mevalonic acid (MVA) pathway is involved in the early steps of steviol biosynthesis. Glucose enters the MEP pathway by being converted to pyruvate and glyceraldehyde-3-phosphate. In contrast to Totté et al.,[5] we used an indirect intermediate of the MEP pathway, namely, d_2-DOX, which should be directly incorporated and transformed to 2-*C*-methyl-D-erythritol 4-phosphate after phosphorylation[34,46] with little diversion to other pathways. Due to remarkably high incorporation rates of about 10−30% into steviol gylcosides in leaves during the feeding period, we could confirm the results of Totté et al.[5] We verified this finding by another feeding experiment using a direct intermediate of the MVA pathway, d_2-MVL, which is transformed to mevalonate phosphate and directly incorporated.[7] No significant incorporation of deuterium using this intermediate could be detected, which confirms that the MEP pathway is the dominant route for diterpene biosynthesis in leaves. It is noteworthy that feeding glucose and feeding the specific precursors DOX and MVL yield the same results. Both approaches are not free of criticism because exogenous substrates can change the physiological conditions in the plant.[35] However, the consistent results show that at least a large part of diterpene biosynthesis is fueled by the MEP pathway, whatever the exact percentage might be under physiological conditions. For our experiments we used two different analytical methods to detect labeled precursor incorporation. We hydrolyzed all steviol glycosides to steviol/isosteviol in the gas chromatographic method and determined the incorporation rate as a sum parameter. Hence, it was not possible to report the incorporation into each steviol glycoside. In addition, we performed LC-MS-MS, which enables us to evaluate the incorporation into stevioside and rebaudioside A separately. By this approach, it could be clearly shown that the incorporation rates were significantly different for stevioside and rebaudioside A, respectively, due to successive glycosylation. This is in agreement with the reported biosynthetic sequence where stevioside is the direct precursor of rebaudioside A.[8] Three different uridine diphosphate-dependent glycosyltransferases (UGTs) contribute to the glycosylation of steviol to build steviolmonoside, steviolbioside, stevioside, and finally rebaudioside A. As expected, the incorporation rates detected by GC-MS represented the mean of the rates of the single steviol glycosides detected by using the LC-MS protocol (except for old leaves in 2012, Tables 3 and 4).

The HS-SPME-GC-MS measurements confirm the results obtained for the steviol glycosides. d_2-DOX served as the main precursor for the generation of diterpenes. d_2-MVL was incorporated into diterpenes as well, but mainly into sesquiterpenes. The labeling data provide evidence that mono- and diterpenes are almost exclusively formed by plastidial IPP/DMAPP, whereas sesquiterpene biosynthesis uses both cytosolic and plastidial IPP/DMAPP. Hence, the results indicate an export of plastidial isoprenoid intermediates into the cytosol and corroborate recent studies about the mixed biosynthetic pathway of the sesquiterpene artemisinin.[36] This model of a unidirectional pathway utilization was demonstrated by Bick and Lange with isolated chloroplasts of spinach, kale, and Indian mustard[38] and has been proposed for the first time by Arigoni and Schwarz.[37] For sesquiterpene biosynthesis it was recently confirmed in grape berries and leaves,[14,39] carrot roots and leaves,[40] snapdragon flowers,[41] and lima bean leaves.[42,43]

The relatively high incorporation rates for mono-, sesqui-, and diterpenes in glandular trichomes of *Stevia* are surprising if compared to rates obtained in other studies in which exogenous DOX was used to label trichome-derived terpenes. Monoterpenes in glandular trichomes of mint showed labeling degrees below 1%,[44] and the diterpene salvinorin A in glandular trichomes of Maria Pastora sage showed similar low labeling degrees when treated with labeled DOX.[45] Low incorporation rates of DOX have been reported to be the result of poor phosphorylation rate of exogenous DOX, partial degradation of DOX into acetate, limited active transport of DOX into plastids, and limited membrane permeability of DOX (refs 36 and 45 and references cited therein). The comparatively high incorporation rates obtained for terpenes in glandular trichomes on *Stevia* leaves and stems might be explained by their ultrastructure: Plasmodesmata, in moderate number, occur more frequently in transverse walls of the secretory head cells, as well as in those between cells of the second subapical pair and stalk cells and between the latter and basal cells. Plasmodesmata connect mesophyll cells and basal cells.[21] Thus, exogenous DOX and MVL may be easily translocated from the cut stem via mesophyll cells to the secretory cells, where the biosynthesis of terpenes is located.

The results of the feeding experiments indicate that both the MEP and the MVA pathways contribute to the biosynthesis of sesquiterpenes, whereas mono- and diterpenes, in particular, steviol glycosides, are almost exclusively formed by the MEP pathway. However, a full understanding of the interplay between the two pathways requires knowledge of the mechanisms of exchange between their respective compartments. The nature of the transporters participating and the true extent of exchange occurring in plants under natural growing conditions are still open questions.[3]

■ ASSOCIATED CONTENT

Ⓢ Supporting Information

Figures S1−S4. This material is available free of charge via the Internet at http://pubs.acs.org.

■ AUTHOR INFORMATION

Corresponding Author

*(M.W.) Phone: +49 228-732361. Fax: +49228-733499. E-mail: matthias.wuest@uni-bonn.de.

Notes

The authors declare no competing financial interest.

■ ACKNOWLEDGMENTS

We thank Andrzej Wawrzun, Stefanie Goetze, and Sarah Stanizek for technical assistance.

■ REFERENCES

(1) Kinghorn, A. Overview. In *Stevia, the Genus Stevia*; Kinghorn, A., Ed.; Taylor & Francis: London, UK, 2002; pp 1−17.

(2) Rohmer, M. Methylerythritol phosphate pathway. In *Comprehensive Natural Products II*; Mander, L., Liu, H. W., Eds.; Elsevier: Oxford, UK, 2010; pp 517−555.

(3) Opitz, S.; Nes, W. D.; Gershenzon, J. Both methylerythritol phosphate and mevalonate pathways contribute to biosynthesis of each of the major isoprenoid classes in young cotton seedlings. *Phytochemistry* **2013**, *98*, 110−119.

(4) Hanson, J.; White, A. Studies in terpenoid biosynthesis − II. *Phytochemistry* **1968**, *7*, 595−597.

(5) Totté, N.; Charon, L.; Rohmer, M.; Compernolle, F.; Baboeuf, I.; Geuns, J. M. C. Biosynthesis of the diterpenoid steviol, an ent-kaurene derivative from *Stevia rebaudiana* Bertoni, via the methylerythritol phosphate pathway. *Tetrahedron Lett.* **2000**, *41*, 6407−6410.

(6) Totté, N.; Charon, L.; Rohmer, M.; Compernolle, F.; Baboeuf, I.; Geuns, J. M. C. Corrigendum to "Biosynthesis of the diterpenoid steviol, an ent-kaurene derivative from *Stevia rebaudiana* Bertoni, via the methylerythritol phosphate pathway. *Tetrahedron Lett.* **2000**, *41*, 7595.

(7) Bouvier, F.; Rahier, A.; Camara, B. Biogenesis, molecular regulation and function of plant isoprenoids. *Prog. Lipid Res.* **2005**, *44*, 357−429.

(8) Brandle, J.; Telmer, P. Steviol glycoside biosynthesis. *Phytochemistry* **2007**, *68*, 1855−1863.

(9) Ohta, M.; Sasa, S.; Inoue, A.; Tamai, T.; Fujita, I.; Morita, K.; Matsuura, F. Characterization of novel steviol glycosides from leaves of *Stevia rebaudiana* Morita. *J. Appl. Glycosci.* **2010**, *57*, 199−209.

(10) Ceunen, S.; Geuns, J. M. C. Steviol glycosides: chemical diversity, metabolism, and function. *J. Nat. Prod.* **2013**, *76*, 1201−1228.

(11) Simpson, T. J.; Ahmed, S. A.; McIntyre, R. C.; Scott, F. E.; Sadler, I. H. Biosynthesis of polyketide-terpenoid (meroterpenoid) metabolites andibenin B and andilesin A in *Aspergillus variecolor*. *Tetrahedron.* **1997**, *53*, 4013−4034.

(12) Markovic, I.; Djarmati, Z.; Abramovic, B. Chemical composition of leaf extracts of *Stevia rebaudiana* Bertoni grown experimentally in Vojvodina. *J. Serb. Chem. Soc.* **2008**, *73*, 283−297.

(13) Pawliszyn, J. *Handbook of Solid Phase Microextraction*; Elsevier: Oxford, UK, 2011.

(14) May, B.; Lange, B. M.; Wüst, M. Biosynthesis of sesquiterpenes in grape berry exocarp of *Vitis vinifera* L.: evidence for a transport of farnesyl diphosphate precursors from plastids to the cytosol. *Phytochemistry* **2013**, *95*, 135−144.

(15) Meyer, O.; Hoeffler, J.-F.; Grosdemange-Billiard, C.; Rohmer, M. Practical synthesis of 1-deoxy-D-xylulose and 1-deoxy-D-xylulose 5-phosphate allowing deuterium labelling. *Tetrahedron* **2004**, *60*, 12153−12162.

(16) Murashige, T.; Skoog, F. A revised medium for rapid growth and bio assays with tobacco tissue cultures. *Physiol. Plant.* **1962**, *15*, 473−497.

(17) Woelwer-Rieck, U.; Lankes, C.; Wawrzun, A.; Wüst, M. Improved HPLC method for the evaluation of the major steviol glycosides in leaves of *Stevia rebaudiana*. *Eur. Food Res. Technol.* **2010**, *231*, 581−588.

(18) Lankes, C.; Zabala, U. M. Evaluation of *Stevia rebaudiana* genotypes. In *Proceedings of the 5th Stevia Symposium*, 1st ed.; Geuns, J., Ed.; Euprint: Heverlee, Belgium, 2011; pp 75−87.

(19) Wüst, M.; Beck, T.; Dietrich, A.; Mosandl, A. On the biogenesis of rose oxide in *Pelargonium graveolens* L'Heritier and *Pelargonium radens* H.E. Moore. *Enantiomer* **1996**, *1*, 167−176.

(20) Wüst, M.; Rexroth, A.; Beck, T.; Mosandl, A. Mechanistic aspects of the biogenesis of rose oxide in *Pelargonium graveolens* L'Héritier. *Chirality* **1998**, *10*, 229−237.

(21) Monteiro, W. R.; Caldeira, W.; Castro, M. D.; Mahlberg, P. G.; Cruz, M. V. Ultrastructural observations on foliar glandular trichomes of *Stevia rebaudiana*. *S. Afr. J. Bot.* **2003**, *69*, 489−499.
(22) Cioni, P. L.; Morelli, I. Qualitative and quantitative analysis of essential oils of five lines *Stevia rebaudiana* Bert. genotypes gultivated in Pisa (ltaly). *J. Essent. Oil Res.* **2006**, *18*, 76−79.
(23) Silva, C. L.; Câmara, J. S. Profiling of volatiles in the leaves of Lamiaceae species based on headspace solid phase microextraction and mass spectrometry. *Food Res. Int.* **2013**, *51*, 378−387.
(24) Rehman, S. U.; Latief, R.; Bhat, K. A.; Khuroo, M. A.; Shawl, A. S.; Chandra, S. Comparative analysis of the aroma chemicals of *Melissa officinalis* using hydrodistillation and HS-SPME techniques. *Arabian J. Chem.* **2013**, DOI: 10.1016/j.arabjc.2013.09.015.
(25) Otsuka, M. Emission of ent-kaurene, a diterpenoid hydrocarbon precursor for gibberellins, into the headspace from plants. *Plant Cell Physiol.* **2004**, *45*, 1129−1138.
(26) Turner, G. W.; Gershenzon, J.; Croteau, R. B. Distribution of peltate glandular trichomes on developing leaves of peppermint. *Plant Physiol.* **2000**, *124*, 655−664.
(27) Matucha, M.; Jockisch, W.; Verner, P.; Anders, G. Isotope effect in gas−liquid chromatography of labelled compounds. *J. Chromatogr., A* **1991**, *588*, 251−258.
(28) Nowotny, M. Entwicklung und Bewertung von Verfahren zur Gewinnung der Süßstoffe aus *Stevia rebaudiana*. Ph.D. Thesis, U. E. Grauer: Stuttgart, Germany, 1995; 73 pp.
(29) Ceunen, S.; Geuns, J. M. Spatio-temporal variation of the diterpene steviol in *Stevia rebaudiana* grown under different photoperiods. *Phytochemistry* **2013**, *89*, 32−38.
(30) Avent, A. G.; Hanson, J. R.; De Oliveira, B. H. Hydrolysis of the diterpenoid glycoside, stevioside. *Phytochemistry* **1990**, *29*, 2712−2715.
(31) Hanson, J. R.; De Oliveira, B. H. Stevioside and related sweet diterpenoid glycosides. *Nat. Prod. Rep.* **1993**, *10*, 301−309.
(32) Wölwer-Rieck, U.; Tomberg, W.; Wawrzun, A. Investigations on the stability of stevioside and rebaudioside A in soft drinks. *J. Agric. Food Chem.* **2010**, *58*, 12216−12220.
(33) Kumar, H.; Kaul, K.; Bajpai-Gupta, S.; Kaul, V. K.; Kumar, S. A comprehensive analysis of fifteen genes of steviol glycosides biosynthesis pathway in *Stevia rebaudiana* (Bertoni). *Gene* **2012**, *492*, 276−284.
(34) Wungsintaweekul, J.; Herz, S.; Hecht, S.; Eisenreich, W.; Feicht, R.; Rohdich, F.; Bacher, A.; Zenk, M. H. Phosphorylation of 1-deoxy-D-xylulose by D-xylulokinase of *Escherichia coli*. *Eur. J. Biochem.* **2001**, *268*, 310−316.
(35) Rohmer, M. The discovery of a mevalonate-independent pathway for isoprenoid biosynthesis in bacteria, algae and higher plants. *Nat. Prod. Rep.* **1999**, *16*, 565−574.
(36) Schramek, N.; Wang, H.; Römisch-Margl, W.; Keil, B.; Radykewicz, T.; Winzenhörlein, B.; Beerhues, L.; Bacher, A.; Rohdich, F.; Gershenzon, J.; Liu, B.; Eisenreich, W. Artemisinin biosynthesis in growing plants of *Artemisia annua*. A $^{13}CO_2$ study. *Phytochemistry* **2010**, *71*, 179−187.
(37) Schwarz, M. K. Terpen-Biosynthese in *Ginkgo biloba*: Eine überraschende Geschichte. Ph.D. Thesis, Zürich, Switzerland, 1994.
(38) Bick, J. A.; Lange, B. Metabolic cross talk between cytosolic and plastidial pathways of isoprenoid biosynthesis: unidirectional transport of intermediates across the chloroplast envelope membrane. *Arch. Biochem. Biophys.* **2003**, *415*, 146−154.
(39) Hampel, D.; Mosandl, A.; Wüst, M. Induction of de novo volatile terpene biosynthesis via cytosolic and plastidial pathways by methyl jasmonate in foliage of *Vitis vinifera* L. *J. Agric. Food Chem.* **2005**, *53*, 2652−2657.
(40) Hampel, D.; Mosandl, A.; Wüst, M. Biosynthesis of mono- and sesquiterpenes in carrot roots and leaves (*Daucus carota* L.): metabolic cross talk of cytosolic mevalonate and plastidial methylerythritol phosphate pathways. *Phytochemistry* **2005**, *66*, 305−311.
(41) Dudareva, N.; Andersson, S.; Orlova, I.; Gatto, N.; Reichelt, M.; Rhodes, D.; Boland, W.; Gershenzon, J. The nonmevalonate pathway supports both monoterpene and sesquiterpene formation in snapdragon flowers. *Proc. Natl. Acad. Sci. U.S.A.* **2005**, *102*, 933−938.
(42) Bartram, S.; Jux, A.; Gleixner, G.; Boland, W. Corrigendum to "Dynamic pathway allocation in early terpenoid biosynthesis of stress-induced lima bean leaves". *Phytochemistry* **2006**, *67*, 2512.
(43) Bartram, S.; Jux, A.; Gleixner, G.; Boland, W. Dynamic pathway allocation in early terpenoid biosynthesis of stress-induced lima bean leaves. *Phytochemistry* **2006**, *67*, 1661−1672.
(44) Sagner, S.; Latzel, C.; Zenk, M. H.; Eisenreich, W.; Bacher, A. Differential incorporation of 1-deoxy-D-xylulose into monoterpenes and carotenoids in higher plants. *Chem. Commun.* **1998**, 221−222.
(45) Kutrzeba, L.; Dayan, F. E.; Howell, J.; Feng, J.; Giner, J.-L.; Zjawiony, J. K. Biosynthesis of salvinorin A proceeds via the deoxyxylulose phosphate pathway. *Phytochemistry* **2007**, *68*, 1872−1881.
(46) Hemmerlin, A.; Harwood, J. L.; Bach, T. J. A raison d'être for two distinct pathways in the early steps of plant isoprenoid biosynthesis? *Prog. Lipid Res.* **2012**, *51*, 95−148.

Over the last 20 years, these concerns and the discovery of variability in the level of ODAP concentration have led to the setting up of germplasm and breeding programs which aim to select those genotypes with the lower ODAP levels.[10−12,24,25] In fact, the most common quantitative ranges for the two isomers are 0.07−7.52 and 0.05−0.79 g/dry kg for β and α isomers (Figure 1), respectively.[26−30]

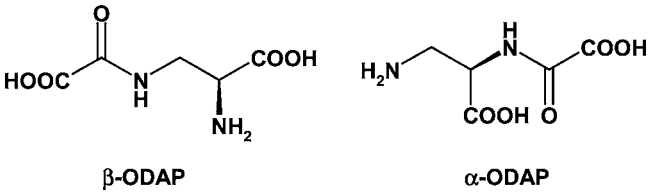

Figure 1. The two non-protein amino acids, α- and β-ODAP, of *L. sativus*.

With this in mind the present paper has the purpose of exploring agronomic, qualitative, and chemical traits of ten Sicilian accessions of grass pea in order to identify those varieties which merge high productive traits with low ODAP concentration.

MATERIALS AND METHODS

Field Trial and Plant Material. The trial was carried out in the experimental field of the University of Catania (Sicily, Southern Italy, 10 m a.s.l.) in 2006−2007 using 10 accessions of grass pea taken from farmers' collections (Table 1).

The seeds were sown on the 30th November into ploughed soil fertilized with 100 kg/ha of P_2O_5. The experiment was arranged in a complete randomized block design with plots of 4 × 3 m, replicated three times. A sowing rate of 60 plant/m^2 with rows 1.0 m far was adopted. Seeds were collected at the end of June 2007 and immediately processed for the analyses.

No irrigation was used, and weeds were managed mechanically. The soil was a clay-loam soil with pH 8.1 and medium nutrient status. During the trial rainfall and temperature were recorded. Average temperature ranged from 10 °C in January to 25 °C in June while the minimum never went below 5 °C and maximum reached 32 °C at the end of the crop cycle. Total rainfall was 495 mm, 50% of which fell in December. Temperature and rainfall data did not differ significantly from the thirty-year values.

In the field the following parameters were measured: plant height at flowering, pods per plant, seeds per pod, 1000 seed weight, seed yield, seed dimension (three-dimensional parameters: longitudinal, transversal, and thickness). Seed protein content was calculated as: (Kjeldahl nitrogen content × 6.25).

Qualitative Analyses and Isolation of α- and β-ODAP. 10 g of dried seeds was milled and extracted with water (50 mL) for 12 h at room temperature and under continuous stirring. The mixture was centrifuged (20 min, 4000 rpm) and the supernatant charged on a column filled with Dowex-50W-8% cross-linked, dry mesh 200−400 (20 mL) in acid (H^+) form. The elution was carried out using water, and the fractions were analyzed by thin layer chromatography (TLC, cellulose, acetone:butanol:water:formic acid 7:7:4:4), spraying with ninhydrin (isomer α reacts in pale rose, isomer β in pale blue). All positive fractions were pooled, and the solvent was removed at reduced pressure. The mixture was analyzed by HPLC-ELSD and NMR

HPLC Analyses. The previous mixture was analyzed by HPLC in the following conditions: HPLC model P580 (Thermo Fisher Scientific, Waltham, MA, USA), reverse phase column Luna C_{18} 250 mm × 4.6 mm i.d. × 5 μm (Phenomenex, Torrance, CA, USA), kept at 20 °C in a model TCC-100 thermostated oven (Thermo Fisher Scientific, Waltham, MA, USA). The elution was performed using a mixture of 0.13% formic acid in water; flow 0.5 mL/min; detector, model Alltech 3300 evaporative light scattering detector (ELSD) (Grace, Deerfield, IL, USA); drift tube temperature 52 °C, nebulizer gas nitrogen, gas flow 1.5 L/min. Retention times of α-ODAP and β-ODAP: 3.40 and 3.63 min, respectively.

^{1}H NMR Analyses. 5 mL of the previous mixture was evaporated to dryness and the residue dissolved in 2 mL of a 0.1 N solution of DCl in D_2O. The mixture was submitted to nuclear magnetic resonance (^{1}H NMR) in the following conditions: spectrometer model Avance 400 (Bruker Corp., Billerica, MA, USA) with 5 mm probe and Z gradient at 400.13 MHz (^{1}H), pulse power for 90°, −1.1 db; 90° pulse length, 8.0 μs; measurement temperature, 299 K; pulse angle, 90°; preacquisition delay, 6.5 μs; acquisition time, 7 min; relaxation delay, 50 s; scan number, 8; sweep width, 12 ppm; number of FID points, 32K; number of frequency points, 64K; line broadening, 0.3 Hz.

α-ODAP: ^{1}H NMR, CH_2, 3.47 H_α dd (13.4, 5.2 Hz), 3.28 H_β dd (13.4, 8.4 Hz); CH, 4.60 dd (8.4, 5.2 Hz).[31,32]

β-ODAP: ^{1}H NMR, CH_2, 3.76 H_α dd (14.8, 3.8 Hz), 3.67 H_β dd (14.8, 6.8 Hz); CH, 4.03 dd (6.8, 3.8 Hz).[31,32]

Isolation of β-ODAP. 10 mL of the previous mixture of α- and β-ODAP coming from the chromatographic separation was dried and the residue dissolved in distilled water and left at room temperature for 24 h. A white precipitate was separated by filtration and analyzed with the HPLC-ELSD and NMR procedures previously described. The resulting compound was pure β-ODAP, which was used to build the calibration curves for the quantitative analyses of the two amino acids in the HPLC analyses, and for the calibration methods in the NMR analyses.

Quantitative Analyses. *Sample Treatments.* 1 g of plant material (seeds of grass pea) of the ten samples in this study was extracted according to the procedure previously described. A 260 mL fraction coming from the Dowex column, containing the two neurotoxins, was

Table 1. Main Parameters of the Studied Grass Pea Accessions (± Standard Error)

code	provenance	altitude (m a.s.l.)	height at flowering (cm)	pod/plant (n)	seed/pod (n)	1000 seed wt (g)	seed yield (t/ha)	protein content (%)
1	Aidone 1	550	31 (±1.9)	17.1 (±2.55)	2.4 (±0.17)	242.7 (±5.44)	0.82 (±0.16)	26.0 (±0.29)
2	Aidone 2	550	31 (±2.3)	11.8 (±2.18)	2.1 (±0.11)	250.2 (±4.81)	1.48 (±0.19)	26.2 (±0.35)
3	Aidone 3	550	31 (±2.0)	13.3 (±2.64)	1.9 (±0.11)	235.5 (±5.33)	1.40 (±0.17)	25.4 (±0.31)
4	Troina	970	31 (±1.9)	8.6 (±1.59)	2.2 (±0.13)	288.5 (±5.27)	1.86 (±0.21)	27.4 (±0.45)
5	Licodia Eubea	480	31 (±1.8)	5.9 (±1.76)	2.6 (±0.15)	252.6 (±5.15)	0.86 (±0.11)	25.8 (±0.41)
6	Bronte	750	31 (±2.1)	13.1 (±2.79)	2.1 (±0.12)	220.7 (±4.94)	0.98 (±0.12)	26.8 (±0.41)
7	Corleone	530	26 (±1.6)	7.1 (±1.94)	2.3 (±0.12)	345.1 (±5.19)	0.69 (±0.10)	25.4 (±0.38)
8	Piana degli Albanesi	650	31 (±2.2)	12.2 (±2.34)	2.1 (±0.10)	181.4 (±5.86)	0.81 (±0.11)	25.7 (±0.31)
9	Maletto	1000	31 (±1.9)	13.9 (±2.13)	2.4 (±0.15)	196.6 (±5.67)	0.81 (±0.12)	26.9 (±0.33)
10	Mineo	450	26 (±1.7)	10.4 (±2.47)	2.1 (±0.13)	307.5 (±5.24)	0.96 (±0.18)	27.4 (±0.40)
M			30	10.5	2.3	247.1	1.07	26.6
CV (%)			2.22	20.93	9.44	19.83	35.69	2.92

dx.doi.org/10.1021/jf500149n | J. Agric. Food Chem. 2014, 62, 2436−2442

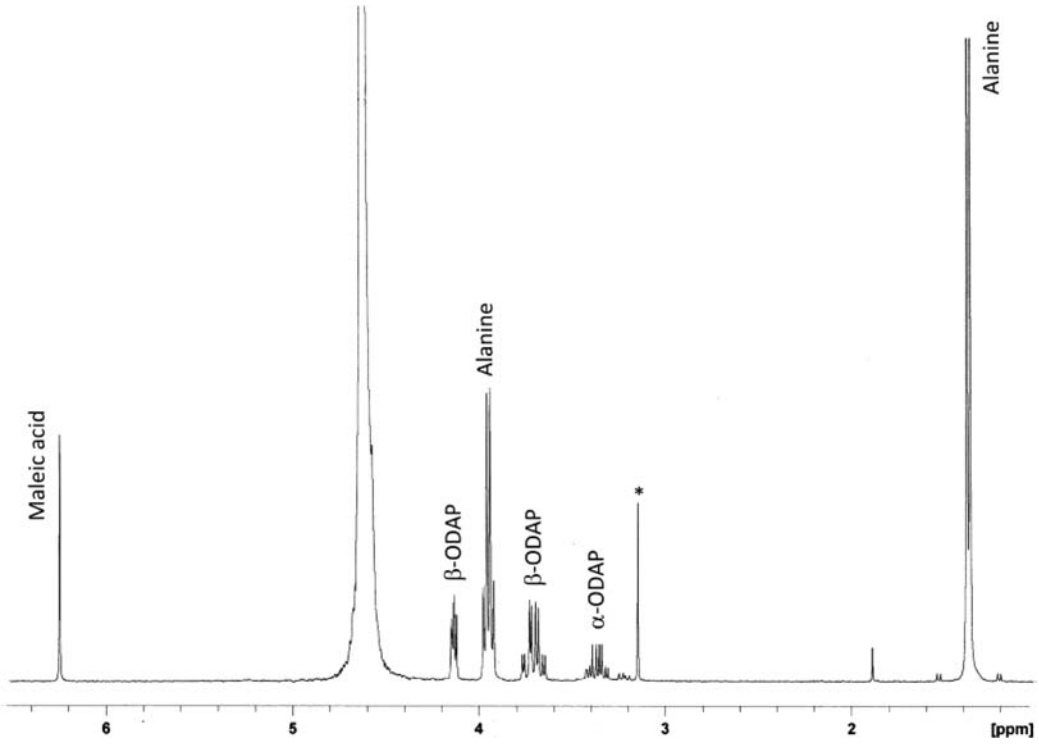

Figure 2. ^{1}H NMR quantitative determination of β- and α-ODAP, with the use of maleic acid and alanine as standards (* solvent impurity).

dried out. The final residue was dissolved in 25 mL of distilled water, and the solution was analyzed for its content of α- and β-ODAP adopting the two analytical procedures previously described, namely, HPLC-ELSD and NMR.

HPLC-ELSD Analyses. 5 mL of the previous solution was diluted (9:1) with 0.1 N HCl. 10 μL was analyzed by HPLC-ELSD in the conditions previously described. Each analysis was carried out in triplicate. For the quantitation of both amino acids the pure β-ODAP, previously purified, was used to build two calibration curves in the amount comprising between 2140 and 778 ng ($y = 0.5493x + 486.43$, $R^2 = 0.9997$) for β-ODAP and between 476 and 214 ng ($y = 0.9639x + 164.51$, $R^2 = 1$) for α-ODAP.

NMR Analyses. 20 mL of the same solution was concentrated, and each residue was dissolved in 2 mL of 0.1 N DCl in D_2O. 500 μL of the resulting solution was then submitted to nuclear magnetic resonance (^{1}H NMR) in the previously described conditions, performing four measurements every 10 min. For the calculations alanine (56 μL of a solution 0.068 M in D_2O) and maleic acid (56 μL of a solution 0.069 M in D_2O) were used as standards. Phase and baseline corrections were performed manually, as were the signal integrations. In the case of improper baseline corrections the BIAS and SLOPE functions were activated for the integral calculation. The ^{1}H NMR signals selected for the quantification of α-ODAP and β-ODAP were at 3.28 and 4.03 ppm, respectively.[31,32] The reference signals of the standard compounds were the methyl group of alanine at 1.55 ppm and the vinyl protons of maleic acid at 6.31 ppm (Figure 2).

Validation and Calibration Procedures. For the validation and intercomparisons three model mixtures were prepared gravimetrically. Mixture NMR-1 with the following molar ratio: β-ODAP (85.42 mol/mol %), alanine (8.50 mol/mol %), maleic acid (6.08 mol/mol %). Mixture NMR-2: β-ODAP (1.97 mol/mol %), alanine (95.73 mol/mol %), maleic acid (2.30 mol/mol %). Mixture NMR-3: β-ODAP (21.44 mol/mol %), alanine (7.94 mol/mol %), maleic acid (71.62 mol/mol %).

In order to check the linearity of the method, 13 model solutions containing β-ODAP were prepared in different molar ratios (from 2.02 to 99.04 mol/mol) solved in DCl/D_2O. Figure 3 shows the experimentally determined molar ratios for β-ODAP and experimental value versus estimated experimental value.

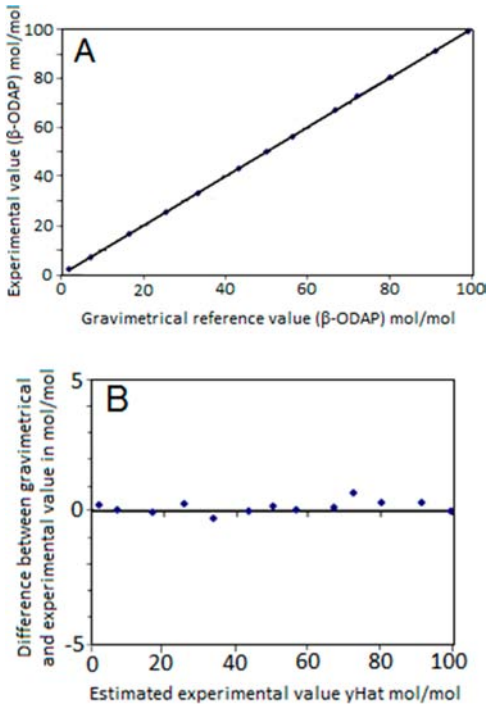

Figure 3. Tests of linearity. Theoretical and experimental molar ratios of the 13 model mixtures, calculated for β-ODAP. Correlation coefficient: 0.99996 (A). Difference between gravimetric and experimental value vs estimated experimental value yHat (with yHat =1.003x, where x represents the gravimetric value) (B).

In order to explore the relationships between the parameters, a Pearson correlation was performed.

dx.doi.org/10.1021/jf500149n | J. Agric. Food Chem. 2014, 62, 2436−2442

RESULTS AND DISCUSSION

Morphological, Productive, and Qualitative Traits. Studied accessions did not differ in relation to phenological stages. For all the accessions seed emergence occurred 24 days after sowing, flowering began in the second week of February, pod set in the second week of March, and pod maturity at the end of June, period in which seeds were harvested.

Plant height, detected at the beginning of flowering, was about 31 cm for all the studied accessions, with the exception of 'Corleone' and 'Mineo', where heights were 26 cm (Table 1). This was lower than values reported by other authors,[33,34] but it can be explained by the wide inter-row distance adopted to facilitate measurements and harvest.

Grain yield was 1.07 t/ha on average; the best results were achieved by accessions 'Troina', 'Aidone 2', and 'Aidone 3' (1.86, 1.48, and 1.40 t/ha, respectively). The lowest yield was recorded in 'Corleone' with 0.69 t/ha. The remaining accessions showed values between 0.81 and 0.98 t/ha. The production of the best accessions is in agreement with those reported previously as 1.7−2.6 t/ha,[35] 1.2−1.6 t/ha,[11] and 1.6−2.0 t/ha.[5]

As regards yield components, on average the number of pods per plant was 10.5, with a coefficient of variation of 20.9%. The highest number of pods per plant was found on 'Aidone 1' (17.1), while the lowest was recorded in 'Licodia Eubea' (5.9). The number of seeds per pod was of 2.3 on average with a limited range of variability (9.44%). On the contrary, weight of the 1000 seeds was quite variable (19.83%) with an average value of 247.1 g ranging from 181.4 to 345 g. For this parameter the accessions 'Corleone' and 'Mineo' (345.1 and 307.5 g, respectively) significantly differ from the others (Table 1).

The boxplot in Figure 4 summarizes results for seed morphological data. With regard to longitudinal section, the accession 'Aidone 3', 'Corleone', and 'Mineo' revealed the highest median values equal to 11 mm with data skewed to the right, although the skew is more prominent in the last. The accessions 'Aidone 3' and 'Mineo' showed 50% of the readings within 10 and 11 mm, whereas 'Corleone' showed the highest interquartile extent, ranging from 10 to 12 mm. When the transversal section was taken into account, accession 'Corleone', in accordance with the longitudinal data, showed the median value (11 mm) higher than the 90th percentile of all the other accessions. No valuable differences were observed in thickness.

The protein content of grass pea accessions was on average of 26.6% with a CV of 2.9. It ranged from 25.4 of genotypes 'Aidone 3' and 'Corleone' to 27.4% of genotypes 'Troina' and 'Mineo' (Table 1). These values are in agreement with those reported in the literature,[12,36] comparing several samples from eleven different accessions, which found an average value of 27.2%, and with that described by Yan et al.,[28] which reports values between 25.6 and 27.3%. It must be emphasized that this value of grass pea protein content is in general higher than those of field pea, chick pea, and fava bean, which are, instead, much more commonly consumed.

Chemical Analyses. The contents of α- and β-ODAP in the ten accessions of Sicilian grass pea were listed in Table 2. It must be emphasized that the two analytical methodologies here used were applied for the first time in the determination of α- and β-ODAP in *L. sativus*. Compared to the usual methods used for the determination of the two ODAP isomers, the instrumental tools adopted here do not require any derivatization procedure,[37−39] so they are relatively much more simple. The two procedures gave comparable results, as shown in Table 2, with some differences observed in the determination of the minor component, α-ODAP.

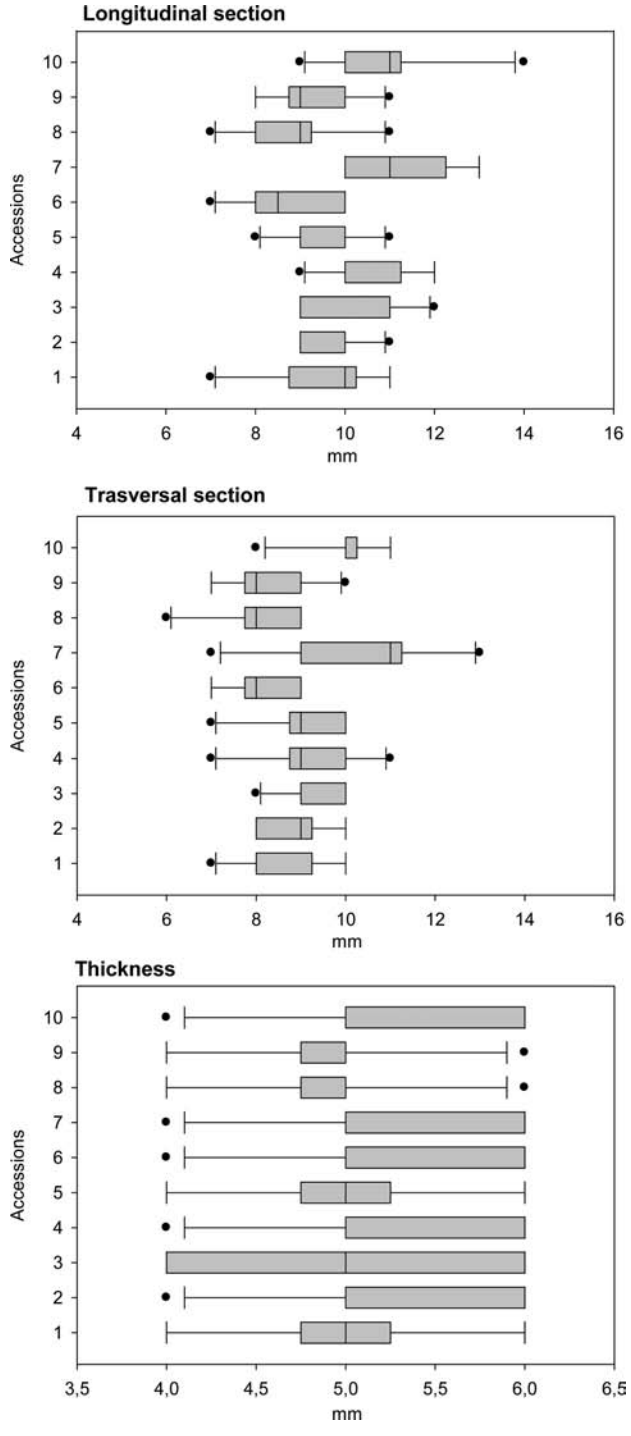

Figure 4. Distribution of the seed dimensions. In the boxes plot, each representing the distribution of 25 data, the lowest and highest boundaries indicate the 25th and 75th percentile, respectively, and the black line within the box marks the median. Whiskers on the right and left of the box indicate the 90th and 10th percentiles, respectively. Dark circles represent the 95th and the 5th percentiles.

The content of the two isomers falls in the range normally reported for these compounds.[26−30] In particular, the accessions 'Aidone 3' and 'Corleone' show the lower amount

dx.doi.org/10.1021/jf500149n | J. Agric. Food Chem. 2014, 62, 2436−2442

Table 2. Content of β- and α-ODAP (g/kg) of Ten Sicilian Accessions[a]

		NMR		HPLC-ELSD	
code	provenance	β	α	β	α
1	Aidone 1	3.05 (±0.09) d	0.51 (±0.02) b	3.12 (±0.12) de	0.60 (±0.03)
2	Aidone 2	3.69 (±0.12) b	0.48 (±0.04) b	3.68 (±0.08) b	0.72 (±0.04)
3	Aidone 3	2.96 (±0.15) d	0.42 (±0.04) b	2.93 (±0.07) e	0.52 (±0.08)
4	Troina	3.46 (±0.10) bc	0.50 (±0.12) b	3.45 (±0.07) c	0.56 (±0.12)
5	Licodia Eubea	3.21 (±0.04) cd	0.53 (±0.03) ab	3.21 (±0.08) d	0.60 (±0.03)
6	Bronte	3.47 (±0.05) bc	0.74 (±0.04) a	3.43 (±0.01) c	0.57 (±0.10)
7	Corleone	2.69 (±0.05) e	0.44 (±0.03) b	2.61 (±0.05) f	0.60 (±0.07)
8	Piana degli Albanesi	3.56 (±0.08) b	0.50 (±0.08) b	3.57 (±0.08) bc	0.60 (±0.05)
9	Maletto	4.59 (±0.05) a	0.61 (±0.19) ab	4.45 (±0.06) a	0.60 (±0.11)
10	Mineo	3.00 (±0.20) d	0.47 (±0.01) b	3.04 (±0.08) de	0.55 (±0.01)

[a]±SD reported in parentheses. Different letters in each column indicate significant difference for $p \leq 0.05$.

Table 3. Pearson Correlation Analysis of Productive and Chemical Parameters[a]

	seed/pod	1000 seed wt	seed yield	protein	β-ODAP (NMR)	α-ODAP (NMR)	β-ODAP (HPLC)	α-ODAP (HPLC)	altitude
pod/plant	−0.278	−0.586*	−0.0825	0.0361	0.297	0.252	0.33	0.00136	0.166
seed/pod		0.0692	−0.453	−0.0352	0.151	0.181	0.149	0.222	0.0564
1000 seed wt			0.111	0.0818	−0.651*	−0.468	−0.677*	−0.0919	−0.344
seed yield				0.335	0.0571	−0.209	0.0739	−0.00463	0.307
protein					0.402	0.407	0.426	−0.147	0.523
β-ODAP (NMR)						0.514	0.995***	0.328	0.733*
α-ODAP (NMR)							0.509	−0.00226	0.485
β-ODAP (HPLC)								0.344	0.709*
α-ODAP (HPLC)									−0.106

[a]*, **, and *** indicate significance for 0.05, 0.01, and 0.001, respectively.

of β isomer, whereas the samples 'Aidone 2' and 'Maletto' had a higher content of the same isomer, as shown by the NMR and HPLC-ELSD evaluations (Table 2). For the α isomer a slightly more complex situation is observed: from the NMR analyses the content of this isomer is lower in the accessions 'Aidone 3' and 'Corleone', as for the β isomer, instead the higher amount is reported for the samples 'Bronte' and 'Maletto'; by the HPLC analyses the accessions 'Aidone 3' and 'Mineo' show the lower amount, whereas six samples, namely, 'Aidone 2', 'Aidone 1', 'Licodia Eubea', 'Corleone', 'Maletto', and 'Piana degli Albanesi', show a comparable and higher amount of α isomer. These results are confirmed by the ANOVA analysis of the aforesaid quantitative results, which shows significant differences for the β isomer in the two analytical approaches (NMR and HPLC), whereas for the α isomer a less significant difference by NMR analyses and no differentiation by HPLC are observed (Table 2).

A remarkable chemical aspect of β-ODAP, which could affect the quantitative determination of this compound and its isomer in grass pea, is its spontaneous isomerization into the nontoxic isomer. This reaction is strongly influenced by the pH of the aqueous solution and, mainly, by heating, giving an equilibrium with about 40% of α-form.[28,31,40−42]

In order to verify if the aforesaid isomerization took place during the experimental procedures (extraction, analytical determinations, etc.) used in this study, pure β-ODAP was left in water at neutral pH and running ^{1}H NMR spectra at the initial time (t_0), after 24 h (t_1), four days (t_2), one week (t_3), two weeks (t_4), six weeks (t_5), and sixteen weeks (t_6). Only after one week an appreciable amount of α isomer was recorded (ca. 5% with respect to β isomer), whereas in the last experiment (t_6) a 6:4 ratio between β and α isomers was observed. It was noted that in this last experiment also an appreciable amount of 2,3-diaminopropionic acid (DAPRO) was recorded (see Supporting Information); the latter is the hydrolysis product of β- and α-ODAP, confirming that a competition between the isomerization and hydrolysis occurs in these conditions.[31] Therefore, if on one hand the β isomer isomerizes to the α isomer, on the other hand the process is very slow and cannot occur during the experimental procedures (mainly extraction step) adopted in this study, thus confirming that those detected are the real amounts of the two isomers in the Sicilian grass pea.

Pearson Correlation. Interesting relationships were found between agronomic and chemical parameters (Table 3). One expected negative correlation was found between the number of pods per plant and the 1000 seed weight (−0.586, $p < 0.045$). This is commonly measured in grain crops since increasing number of pods means that the weight of seeds decreases. Another interesting significant correlation is the one between 1000 seed weight and β-ODAP determined both with the NMR method and with the HPLC method (−0.651, $p < 0.041$, and −0.677, $p < 0.032$, respectively). In this case the β-ODAP seems negatively related with the seed weight. This observation is in agreement with Tadesse and Bekele,[43] who found negative association between seed size and ODAP content on fifty grass pea land race accessions. However, it is in contrast with the findings reported by Dahiya,[44] who, when analyzing eighteen genotypes of grass pea with a paper-chromatography technique, found that smaller seeds contain lower concentrations of ODAP.

Another valuable correlation was found between the β-ODAP content determined with HPLC and NMR and the altitude from where the seeds were collected (0.709, $p < 0.021$,

and 0.733, $p < 0.015$, respectively). From this relation, it emerges that seeds from environments with higher altitudes show a higher content of β-ODAP. On the contrary, a recent study carried out on nine grass pea genotypes in five different environments in Ethiopia showed a negative correlation between altitude and β-ODAP content;[45] therefore, the mechanism of this relation is not yet clear and needs to be fully elucidated. In agreement with Tadesse and Bekele,[43] no association was found between ODAP and protein content, indicating that ODAP is synthesized independently of protein content.

The last significant correlation refers to chemical parameters: β-ODAP HPLC is highly positively correlated to β-ODAP NMR (0.995, $p < 0.001$), testifying that the two methods are comparable and equally usable. The application of two well consolidated analytical methodologies, namely, NMR and HPLC-ELSD, gives comparable results in the quantitative determination of the two amino acids, showing at the same time some operative advantages with respect to the more complex and time-consuming analytical procedures adopted in this field up to now.

Accessions 'Aidone 2', 'Aidone 3', and 'Troina' showed a high seed yield and a valuable protein content; namely, 'Aidone 3' showed also a low β-ODAP content and so represents good material for a future breeding program. Moreover, correlations revealed that accessions with heavier seeds and those coming from low altitude environments have a lower β-ODAP content.

In conclusion, the results of this study show that the Sicilian grass pea accessions do not present very high amounts of the neurotoxic β-ODAP. In any case, taking into account the very low consumption of this species and relatively low level of the neurotoxins, its sporadic presence in the human diet does not represent a real health risk. In this view, Sicilian grass pea can be considered a niche product strongly characterizing local cultural and gastronomic traditions.

■ ASSOCIATED CONTENT

Supporting Information

Figures S1−S6 including the structures and ^{1}H NMR spectra of β-ODAP, α-ODAP, and DAPRO and the HPLC-ELSD profile of a mixture of α-ODAP and β-ODAP. This material is available free of charge via the Internet at http://pubs.acs.org.

■ AUTHOR INFORMATION

Corresponding Author

*Tel: +39 095 7338347. Fax: +39 095 7338310. E-mail: giuseppe.ruberto@icb.cnr.it.

Funding

This research work was financially supported by Consiglio Nazionale delle Ricerche (CNR—Rome).

Notes

The authors declare no competing financial interest.

■ ACKNOWLEDGMENTS

The authors thank Dr. Dario D'Angelo [SOPAT 47, Valguarnera (EN), Assessorato Risorse Agricole ed Alimentari—Regione Siciliana].

■ REFERENCES

(1) Avola, G.; Tuttobene, R. M.; Gresta, F.; Abbate, V. Weed control strategies for grain legumes. *Agron. Sustainable Dev.* **2008**, *28* (3), 389−396.

(2) Avola, G.; Gresta, F.; Abbate, V. Diversity examination based on physical, technological and chemical traits in a locally grown landrace of faba bean (*Vicia faba* L. var. *major*). *Int. J. Food Sci. Technol.* **2009**, *44*, 2568−2576.

(3) Gresta, F.; Avola, G.; Albertini, E.; Raggi, L.; Abbate, V. A study of variability in the Sicilian faba bean landrace 'Larga di Leonforte'. *Genet. Resour. Crop Evol.* **2010**, *57*, 523−531.

(4) Smartt, J. *Grain legumes: evolution and genetic resources*; Cambridge Univ. Press: Cambridge, U.K., 1990.

(5) Karadag, Y.; Iptas, S.; Yavuz, M. Agronomic potential of grass pea (*Lathyrus sativus* L.) under rainfed condition in semiarid region of Turkey. *Asian J. Plant Sci.* **2004**, *3* (2), 151−155.

(6) Chiofalo, B.; Lo Presti, V.; Chiofalo, V.; Gresta, F. The productive traits, fatty acid profile and nutritional indices of three lupin (*Lupinus* spp.) species cultivated in a Mediterranean environment for the livestock. *Anim. Feed Sci. Technol.* **2012**, *171*, 230−239.

(7) Gresta, F.; Avola, G.; Abbate, V.; Magazzù, G.; Chiofalo, B. Lupin seed for crop-livestock food chains. *Ital. J. Agron.* **2010**, *4*, 333−340.

(8) Duranti, M. Grain legume proteins and nutraceutical properties. *Fitoterapia* **2006**, *77*, 67−82.

(9) Mahler-Slasky, Y.; Kislev, M. E. Lathyrus consumption in late bronze and iron age sites in Israel: an Aegean affinity. *J. Archeol. Sci.* **2010**, *37*, 2477−2485.

(10) Hillocks, R. J.; Maruthi, M. N. Grass pea (*Lathyrus sativus*): is there a case for further crop improvement? *Euphytica* **2012**, *186* (3), 647−654.

(11) Campbell, C. G. *Grass pea. Lathyrus sativus L. Promoting the conservation and use of underutilized and neglected crops*; Publ. No. 18; Institute of Plant Genetics and Crop Plant Research, Gatersleben/International Plant Genetic Resources Institute: Rome, 1997.

(12) Hanbury, C. D.; White, C. L.; Mullan, B. P.; Siddique, K. H. M. A review of the potential of *Lathyrus sativus* L. and *L. cicera* L. grain for use as animal feed. *Anim. Feed Sci. Technol.* **2000**, *87*, 1−27.

(13) Tavoletti, S.; Iommarini, L.; Crino, P.; Granati, E. Collection and evaluation of grass pea (*Lathyrus sativus* L.) germplasm of central Italy. *Plant Breed.* **2005**, *124*, 388−391.

(14) Sillero, J. C.; Cubero, J. I.; Fernández-Aparicio, M.; Rubiales, D. Search for resistance to crenate broomrape (*Orobanche crenata*) in *Lathyrus*. *Lathyrus Lathyrism Newsl.* **2005**, *4*, 7−9.

(15) Campbell, C. G.; Mehra, R. B.; Agrawal, S. K.; Chen, Y. Z.; Abd El Moneim, A. M.; Kawaja, H. I. T.; Yadav, C. R.; Tay, J. U.; Araya, W. A. Current status and future strategy in breeding grass pea (*Lathyrus sativus*). *Euphytica* **1994**, *73*, 167−175.

(16) Grela, E. R.; Rybiński, W.; Matras, J.; Sobolewska, S. Variability of phenotypic and morphological characteristics of some *Lathyrus sativus* L. and *Lathyrus cicera* L. accessions and nutritional traits of their seeds. *Genet. Resour. Crop Evol.* **2012**, *59*, 1687−1703.

(17) Biederbeck, V. O.; Bouman, O. T.; Campbell, C. A.; Bailey, L. D.; Winkleman, G. E. Nitrogen benefits from four green-manure legumes in dryland cropping systems. *Can. J. Plant Sci.* **1996**, *76*, 307−315.

(18) Bell, E. A. Non protein amino acids of plants: significance in medicine, nutrition, and agriculture. *J. Agric. Food Chem.* **2003**, *51*, 2854−2865.

(19) Spencer, P. S.; Ludolph, A.; Dwivedi, M. P.; Roy, D. N.; Hugo, A. J.; Schaumburg, H. H. Lathyrism: evidence for role of the neuroexcitatory amino acid BOAA. *Lancet* **1986**, *2*, 1066−1067.

(20) Enneking, D. The nutritive value of grass pea (*Lathyrus sativus*) and allied species, their toxicity to animals and the role of malnutrition in neurolathyrism. *Food Chem. Toxicol.* **2011**, *49* (3), 694−709.

(21) Bradbury, J. H.; Lambein, F. Konzo and neurolathyrism: Similarities and dissimilarities between these crippling neurodegenerative diseases of the poor. *Food Chem. Toxicol.* **2011**, *49* (3), 537−538.

(22) Lambein, F.; Ngudi, D. D.; Kuo, Y.-H. *Progress in prevention of toxico-nutritional neurodegenerations*; 2009. http://www.atdforum.org/journal/html/2009-34/8 (accessed: 19 February 2014).

(23) Fikre, A.; Yami, A.; Kuo, Y. H.; Ahmed, S.; Gheysen, G.; Lambein, F. Effect of methionine supplement on physical responses

and neurological symptoms in broiler chicks fed grass pea (*Lathyrus sativus*)-based starter ration. *Food Chem. Toxicol.* **2010**, *48*, 11−17.
(24) Siddique, K. H. M.; Loss, S. P.; Herwig, S. P.; Wilson, J. M. Growth, yield and neurotoxin (ODAP) concentration of three *Lathyrus* species in Mediterranean type environments of Western Australia. *Aust. J. Exp. Agric.* **1996**, *36*, 209−218.
(25) Granati, E.; Bisignano, V.; Chiaretti, D.; Crino, P.; Polignano, G. B. Characterization of Italian and exotic *Lathyrus* germplasm for quality traits. *Genet. Resour. Crop Evol.* **2003**, *50*, 273−280.
(26) Wang, F.; Chen, X.; Chen, Q.; Qin, X.; Li, Z. Determination of neurotoxin 3-*N*-oxalyl-2,3-diaminopropionic acid and non-protein acids in *Lathyrus sativus* by pre-column derivatization with 1-fluoro-2,4-dinitrobenzene. *J. Chromatogr. A* **2000**, *883*, 113−118.
(27) Yigzaw, Y.; Larsson, N.; Gorton, L.; Ruzgas, T.; Solomon, T. Liquid chromatography determination of total 3-*N*-oxalyl-2,3-diaminopropionic acid in *Lathyrus sativus* seeds using both refractive index and bio-electrochemical detection. *J. Chromatogr. A* **2001**, *929*, 13−21.
(28) Yan, Z. Y.; Jiao, C. J.; Wang, Y. P.; Li, F. M.; Liang, Y. M.; Li, Z. X. A method for the simultaneous determination of β-ODAP, α-ODAP, homo-arginine and polyamines in *Lathyrus sativus* by liquid chromatography using a new extraction procedure. *Anal. Chim. Acta* **2005**, *534*, 199−205.
(29) Yan, Z. Y.; Spencer, P. S.; Li, Z. X.; Liang, Y. M.; Wang, Y. F.; Wang, C. Y.; Li, F. M. *Lathyrus sativus* (grass pea) and its neurotoxin ODAP. *Phytochemistry* **2006**, *67*, 107−121.
(30) Kumar, S.; Bejiga, G.; Ahmed, S.; Nakkoul, H.; Sarker, A. Genetic improvement of grass pea for low neurotoxin (β-ODAP) content. *Food Chem. Toxicol.* **2011**, *49*, 589−600.
(31) De Bruyn, A.; Becu, C.; Lambein, F.; Kebede, N.; Abegaz, B.; Nunn, P. B. The mechanism of the rearrangement of neurotoxin β-ODAP to α-ODAP. *Phytochemistry* **1994**, *36*, 85−89.
(32) Long, Y.-C.; Ye, Y.-H.; Xing, Q.-Y. Studies on the neuro-excitotoxin β-*N*-oxalo-L-α,β-diaminopropionic acid and its isomer α-*N*-oxalo-L-α,β-diaminopropionic acid from the root of *Panax* species. *Int. J. Pept. Protein Res.* **1996**, *47*, 42−46.
(33) Wuletaw, T.; Endashaw, B. Variation and association of morphological and biochemical characters in grass pea (*Lathyrus sativus* L.). *Euphytica* **2003**, *130*, 315−324.
(34) Polignano, G. B.; Bisignano, V.; Tomaselli, V.; Uggenti, P.; Alba, V.; Della Gatta, C. Genotype × environment interaction in grass pea (*Lathyrus sativus* L.) lines. *Int. J. Agron.* **2009**, DOI: 10.1155/2009/898396.
(35) De Falco, E.; Pardo, A.; Pisante, M. Possibilità di introduzione della cicerchia (*Lathyrus sativus* L.) in area collinare della Basilicata. *Riv. Agron.* **1996**, *30* (2), 181−185.
(36) Pastor-Cavada, E.; Juan, R.; Pastor, J. E.; Alaiz, M.; Vioque, J. Nutritional characteristics of seed protein in 15 *Lathyrus* species (Fabaceae) from Southern Spain. *LWT—Food Sci. Technol.* **2011**, *44*, 1059−1064.
(37) Chen, X.; Wang, F.; Chen, Q.; Qin, X. C.; Li, X. Analysis of neurotoxin 3-*N*-oxalyl-L-3,3-diaminopropionic acid and its α isomer in *Lathyrus sativus* by high-performance liquid chromatography with 6-aminoquinoyl-*N*-hydroxysuccinimidyl carbamate (AQC) derivatization. *J. Agric. Food Chem.* **2000**, *48*, 3383−3386.
(38) Thippeswamy, R.; Martin, A.; Glowda, L. R. A reverse phase high performance liquid chromatography method for analyzing of neurotoxins β-*N*-oxalyl-L-α,β-diaminopropionic acid in legume seeds. *Food Chem.* **2007**, *101*, 1290−1295.
(39) Fikre, A.; Korbu, L.; Kuo, Y.-H.; Lambein, F. The contents of the neuro-excitatory amino acid β-ODAP (β-*N*-oxalyl-L-α,β-diamino-propioninc acid), and other free and protein amino acids in the seeds of different genotypes of grass pea (*Lathyrus sativus* L.). *Food Chem.* **2008**, *110*, 422−427.
(40) Barceloux, D. G. *Medical Toxicology of Natural Substances: Foods, Fungi, Medicinal Herbs, Toxic Plants, and Venomous Animals*; John Wiley & Sons: Hoboken, NJ, 2008; pp 62−66.
(41) Lambein, F.; Kuo, Y.-H.; Kusama-Eguchi, K.; Ikegami, F. 3-*N*-oxalyl-L-2,3-diaminopropanoic acid, a multifunctional plant metabolite of toxic reputation. *ARKIVOC* **2007**, *ix*, 45−52.
(42) Moges, G.; Johansson, G. Flow injection assay for the neurotoxin β-ODAP using an immobilized glutamate oxidase reactor with prereactors to eliminate glutamate interferences. *Anal. Chem.* **1994**, *66*, 3834−3839.
(43) Tadesse, W.; Bekele, E. Variation and association of morphological and biochemical characters in grass pea (*Lathyrus sativus* L.). *Euphytica* **2003**, *130*, 315−324.
(44) Dahiya, B. S. Seed morphology as indicator of low neurotoxin in *Lathyrus sativus*. *Qual. Plant.—Plant Foods Hum. Nutr.* **1976**, *25* (3−4), 391−394.
(45) Fikre, A.; Negwo, T.; Kuo, Y. H.; Lambein, F.; Ahmed, S. Climatic, edaphic and altitudinal factors affecting yield and toxicity of *Lathyrus sativus* grown at five locations in Ethiopia. *Food Chem. Toxicol.* **2011**, *49* (3), 623−630.

Table 1. Validation Parameters of the Analytical Procedure (Milligrams per Kilogram, $n = 6$)

			GSB-7-tea		spiking recovery			
element	LOD	LOQ	certified value (mean ± U^a)	obtained value (mean ± SD^b)	added	honey samples (mean ± SD)	spiked samples (mean ± SD)	recovery (%)
Na	0.034	0.11	90 ± 10	87.0 ± 8.1	2.5	2.11 ± 0.15	4.4 ± 0.2	91.6
Mg	0.0038	0.013	1860 ± 110	1807.7 ± 116.5	25	23.05 ± 0.80	49.12 ± 0.80	104.3
P	0.051	0.17	4500 ± 300	4295.0 ± 427.5	50	24.2 ± 0.3	79.1 ± 0.5	109.8
K	0.29	0.95	16300 ± 700	16367.6 ± 531.3	500	977.6 ± 33.1	1447.22 ± 14.16	93.9
Ca	0.14	0.45	3260 ± 80	3097.1 ± 134.2	100	90.84 ± 4.02	196.8 ± 3.8	106.0
Mn	0.00020	0.00066	500 ± 20	499.7 ± 35.2	1.25	1.18 ± 0.04	2.42 ± 0.03	99.9
Fe	0.0030	0.010	242 ± 18	231.7 ± 14.2	2.5	0.23 ± 0.02	2.68 ± 0.05	98.0
Cu	0.00047	0.0016	18.6 ± 0.7	18.2 ± 0.3	0.05	0.074 ± 0.002	0.12 ± 0.05	88.3
Zn	0.0015	0.0051	51 ± 2	51.6 ± 8.7	0.5	0.36 ± 0.01	0.89 ± 0.02	107.6
Rb	0.00055	0.0018	117 ± 5	120.9 ± 2.9	1	0.94 ± 0.02	1.84 ± 0.03	90.2
Sr	0.00037	0.0012	9.1 ± 1.2	8.2 ± 0.7	0.5	0.400 ± 0.002	0.83 ± 0.01	85.9
Ba	0.00031	0.0010	9.6 ± 0.5	9.3 ± 0.9	0.5	0.35 ± 0.01	0.83 ± 0.01	95.3

$^a U$, measurement uncertainty. ^{b}SD, standard deviation.

mineral elements.[21−24] The representative studies were carried out by the team of Baralkiewicz. In 2008, Madejczyk et al.[12] determined 12 elements in 30 rape and honeydew honey samples from various locations within Poland by ICP-MS. Cluster analysis (CA) of the honey data revealed that the origins of honey samples are correlated with their chemical composition. Subsequently, Chuazinska et al.[25] studied 13 elements (Al, B, Ba, Ca, Cd, Cu, K, Mg, Mn, Na, Ni, Pb, and Zn) in 55 honeydew, buckwheat, and rape honey samples by ICP-MS. CA and PCA were applied to classify honey according to the profiles of minerals. On the basis of their previous research, Chuazinska et al.[26] studied 15 elements (Cr and Sr were added) in 140 honey samples including honeydew, buckwheat, and rape honeys from 16 areas of Poland using ICP-MS. Linear discriminant analysis (LDA) and calibration and regression tree (C&RT) were performed for the whole data set to discriminate and classify honey samples according to their botanical and geographical origins. The above studies have suggested that chemometric analysis of elemental profiles in the honeys determined by various analytical techniques may be an alternative way for evaluating the honey classes on the basis of the geographic or botanical origins of honey.

Chinese honey is very popular worldwide and holds a large proportion of the world market. Unfortunately, to the best of our knowledge, no research has been carried out to classify the botanical origins of Chinese honeys on the basis of mineral elements. At the same time, few researchers have attempted to test their developed model by reference samples.

The aim of this work is to analyze the mineral elements in Chinese honeys by ICP-MS and construct a statistical model for their botanical origin. Moreover, this study is the first to test the validation of the developed model by 42 reference samples with well-known information.

MATERIALS AND METHODS

Honey Samples. This study was carried out on 163 honey samples, including 4 kinds of honey: linden (*Tilia amurensis* Rupr.), vitex (*Vitex negundo* var. *heterophylla* Rehd.), rape (*Brassica campestris* L.), and acacia (*Robinia pseudoacacia* L.). They were collected directly from beekeepers with guaranteed origin in Heilongjiang (39 linden honey samples), Beijing (27 vitex and 25 acacia honey samples), Hebei (23 vitex and 18 acacia honey samples), and Shaanxi (19 rape and 12 acacia honey samples) regions of China from April to July 2013. All samples were unprocessed and stored in plastic containers at 4 °C until analysis.

Sample Preparation. The honey sample was liquefied at 50 °C and homogenized in an ultrasonic bath for at least 30 min prior to analysis.

Honey samples were prepared according to the following procedure: 1.0 g of honey sample was accurately weighed and placed into a PTFE digestion vessel, and 5 mL of nitric acid (65%, w/w, MOS grade) and 3 mL of hydrogen peroxide (30%, w/w, MOS grade) were added. In each set of digestion, one reagent blank solution and CRM sample were prepared in the same way. Sample was digested using a MARS 6 microwave reaction system (CEM Corp., USA) according to a previous study.[17] After the vessels were cooled, the digests were transferred to a volumetric flask and diluted to 50 mL with deionized water.

Sample Analysis. The elements standard solutions for ^{23}Na, ^{24}Mg, ^{31}P, ^{39}K, ^{43}Ca, ^{55}Mn, ^{56}Fe, ^{63}Cu, ^{66}Zn, ^{85}Rb, ^{88}Sr, and ^{137}Ba were prepared by multielement calibration standards solutions (Agilent Technologies, USA). An Agilent 7700x ICP-MS (Agilent Technologies, Japan) fitted with a standard glass concentric nebulizer, a quartz double-pass spray chamber, and nickel sampler and skimmer cones was used. The operating conditions and measurement parameters were referred to those reported in our previous study.[17]

Method Assurance. The method performance for determination of 12 mineral elements in honey samples was evaluated by limits of detection and quantification (LOD and LOQ, respectively), reference sample measurement, spiking recovery, and precision (see Table 1). Because there is no matching CRM for honey, the analytical quality control was routinely validated using a tea reference material, GSB-7-tea (GBW10016, China). As shown in Table 1, the LOQ of the major elements and trace elements are at sub parts per million and parts per billion levels, respectively. The certified and measured values of 12 mineral elements in GSB-7-tea are in good coincidence. The spiking recoveries for these 12 elements in honey samples range from 85.9 to 109.8%, with measuring precision within 10%. This suggests that the performance of the method allows accurate measurement of the levels of these elements in the honey samples.

Data Sets and Chemometric Techniques. Basic statistical and multivariate analyses were carried out using Mass Profiler Professional (MPP) software (version B. 12.05, Agilent Technologies, Santa Clara, CA, USA). Chemometric approaches such as principal component analysis (PCA), PLS-DA, and BP-ANN were performed for all of the data to discriminate and classify honey samples according to their botanical origin.

PCA is an unsupervised pattern-recognizing technique, which reduced the number of dimensions and provided a partial view and trends of the data in space.[27] It is often used to examine the relationships between the variables and the types of samples.

PLS is a well-known regression tool applied to chemometrics by Wold.[28] PLS-DA, an extension of PLS, is used to predict a set of

variables and identify them as functional classes from a large number of independent variables.

ANN has been widely used in chemometrics as a supervised pattern recognition technique, which comprises a set of interconnected processing algorithms working in parallel to mimic the processes of the human brain.[29] In this study, the neural network implementation in MPP software is the multilayer perception trained using the BP-ANN. It normally consists of three layers, the input layer, intermediate layer, and output layer; the input layer features rows to be classified that are fed into this layer, and the output layer has an output node for each class in the data set.

RESULTS AND DISCUSSION

General Features of Elements. The contents of 12 elements for all of the honey samples and each botanical origin of honey samples are listed in Table 2. According to the mean value of elements in all honeys, they were divided into three groups: abundant major elements, minor elements, and trace elements.

The first group was composed of K, Ca, P, Na, and Mg with contents of >10 mg/kg. First, it is obvious that the most abundant element in all of the honeys was K, with a mean value of 552.15 mg/kg. This finding agrees with many previous results.[12,18,24] The mean value of K in linden honey was 1426.75 mg/kg, which was 4.4−8.8 times higher than in other honeys. The highest mean value of Ca was found in linden honey, whereas the mean values of Ca in rape and acacia honeys are close to each other. The mean value of P in all honey samples was 39.55 mg/kg, and the acacia and linden honeys had the highest and lowest values of P, respectively. Na and Mg have similar mean contents in all honey samples with mean values of 12.73 and 12.87 mg/kg, respectively. Except for the linden honey, the mean values of Na in vitex, rape, and acacia honeys have similar levels. Mg was higher in linden and rape honeys than others, whereas the lowest mean value of it was found in vitex honey.

Fe and Zn displayed mean values within the range of 1−10 mg/kg (1.72 and 1.02 mg/kg, respectively) in all honey samples, and both were taken as minor elements. It was also found that Fe and Zn had similar mean values in various honeys with a difference of <0.35 mg/kg except in acacia honey samples. In addition, vitex and acacia honey samples had equal mean values of Fe, whereas linden honey had the lowest mean values of Fe and Zn.

The third group, including Mn, Cu, Rb, Sr, and Ba, had mean values lower than 1 mg/kg. In this group, the mean values of Rb were higher than those of other elements in different honey samples, whereas Cu was the lowest element. As shown in Table 2, the highest mean values of Mn, Rb, Sr, and Ba were all found in linden honey samples, especially Rb and Ba. Vitex, rape, and acacia honey samples had equal mean contents of Rb within the range of 0.41−0.43 mg/kg, and the range of Ba in them was 0.03−0.05 mg/kg. For Cu, similar mean values were found in linden and vitex honeys and rape and acacia honeys, respectively.

On the basis of the above analysis, the contents of the 12 studied elements were different in various botanical origins of honeys. Some of the honeys had their own characteristic elemental profile, especially the linden honey. However, there are variations within the same origin of the samples as demonstrated by the large difference between the minimum and maximum values in Table 2; therefore, chemometric methods are required to evaluate the tendency of sample clustering based on clustering factors such as botanical origin.

Table 2. Results of Mineral Elements in Different Types of Honeys by ICP-MS (Milligrams per Kilogram)

	all honeys			linden			vitex			rape			acacia		
element	mean	min	max	mean	min	max	mean	min	max	mean	min	max	mean	min	max
Na	12.73	1.70	56.26	3.16	1.70	10.14	14.91	3.35	29.84	12.36	8.03	21.73	17.65	5.27	56.26
Mg	12.87	3.02	78.46	17.69	9.70	35.14	7.38	3.02	15.22	17.04	13.06	20.68	13.00	4.60	78.46
P	39.55	13.02	97.01	28.04	13.02	68.12	32.18	15.68	72.02	46.25	25.28	68.51	52.09	17.61	97.01
K	552.15	87.93	1992.37	1426.75	912.93	1992.37	269.32	92.88	783.84	161.96	87.93	250.53	323.91	131.98	1241.99
Ca	47.50	12.68	157.47	86.00	55.64	157.47	28.77	13.82	56.68	42.24	30.34	56.86	39.03	12.68	94.73
Mn	0.43	0.03	2.12	1.13	0.51	2.12	0.09	0.03	0.38	0.44	0.23	1.29	0.24	0.06	1.35
Fe	1.72	0.13	38.94	0.64	0.13	2.31	2.23	0.28	38.94	1.24	0.59	2.04	2.20	0.74	10.37
Cu	0.09	<LOQ[a]	0.28	0.08	0.05	0.15	0.06	<LOQ	0.15	0.11	0.06	0.22	0.10	0.04	0.28
Zn	1.02	<LOQ	29.28	0.48	0.08	2.69	1.93	<LOQ	29.28	0.89	0.15	4.75	0.62	0.08	2.80
Rb	0.72	0.14	2.68	1.68	0.84	2.68	0.41	0.14	1.18	0.43	0.22	0.74	0.42	0.17	0.90
Sr	0.21	0.03	0.91	0.56	0.35	0.91	0.09	0.03	0.25	0.07	0.04	0.11	0.12	0.03	0.36
Ba	0.14	0.01	0.70	0.45	0.25	0.70	0.03	0.01	0.07	0.03	0.01	0.03	0.05	0.02	0.16

[a]LOQ, limit of quantification.

dx.doi.org/10.1021/jf405045q | J. Agric. Food Chem. 2014, 62, 2443−2448

Chemometric Analysis. *PCA.* PCA is widely used to find the relationships between variables and types of samples. Here the data set was first subjected to statistical analysis using ANOVA. With the p value of <0.05, 10 elements, Na, Mg, K, Ca, Mn, Fe, Cu, Rb, Sr, and Ba, displayed statistically significant values among the honey samples from different botanical origins. The levels of these significant elements in 163 honey samples were subjected to PCA algorithm in the MPP software, and 10 elements as variables were reduced to four principal components (PCs). The four PCs could explain 93.06% of the total variance. As shown in Table 3, the first PC (PC1) accounts for 62.61% of the variance and the other three PCs (PC2, PC3, and PC4) represent 19.77, 5.96, and 4.72%, respectively. Examining the loading of variables demonstrated the contribution by each element to the four PCs. As shown in Table 3, the PC1 is basically a function of Sr, Ba, K, Ca, Mn, and Rb, PC2 was associated with Na and Fe, and PC3 and PC4 were mainly related with Cu and Mg, respectively.

Table 3. Loadings of the Variables for the Four PCs

element	component 1 (62.61%)	component 2 (19.77%)	component 3 (5.96%)	component 4 (4.72%)
Na	−0.177	**0.574**	0.082	0.077
Mg	0.300	0.316	−0.215	**-0.622**
K	**0.374**	−0.045	0.241	0.330
Ca	**0.373**	0.119	0.038	−0.264
Mn	**0.364**	0.089	−0.091	−0.212
Fe	−0.095	**0.570**	0.609	0.081
Cu	0.191	0.440	**-0.644**	0.513
Rb	**0.360**	−0.138	0.088	0.319
Sr	**0.383**	0.008	0.221	0.018
Ba	**0.381**	−0.097	0.190	0.107

Obviously, PC1 and PC2 are the main components, representing 82.38% of the variables. Analysis of the loadings plot of variables for PC1 and PC2 (Figure 1) demonstrated that Na and Fe were negatively correlated with PC1, whereas Mg, K, Ca, Mn, Cu, Rb, Sr, and Ba were positively correlated with PC1. On the other hand, K, Ba, and Rb were negatively correlated with PC2, and the others were positively correlated with PC2. The loading plot of samples for PC1 and PC2 (Figure 2) shows a clear separation between linden honey and other samples. The close position of the other three types of honey samples in Figure 2 suggested that the separation of these three types of honeys did not depend on the major variables in PC1 and PC2. At the bottom right of Figure 2, the linden honey samples were positively correlated with PC1. Combined with Figure 1 and Table 3, this suggested that the linden samples have the highest values of K, Ca, Mn, Rb, Sr, and Ba, which coincides with the general feature of the data demonstrated above.

The results obtained by PCA confirmed that PCA could reduce the multivariable to four components simply and partly revealed a correlation between the elements and honey samples. The linden honey samples could be classified clearly from others with K, Ca, Mn, Rb, Sr, and Ba as their elemental markers. Although PCA could provide a visual graph on how the samples are clustered, it could not provide information on how good the clustering is and the confidence on such clustering. Hence, other chemometric tools were further explored to classify the honeys.

Classification and Prediction. To better classify the honey samples with elemental profiling, PLS-DA and BP-ANN models were built on the basis of 10 elements measured in 121 honey samples (75% of honey samples of each botanical origin randomly selected from the total samples) from different botanical origins.

PLS-DA. PLS-DA with four components was first selected for building a model to predict the botanical origins of honey samples. The model was evaluated in terms of recognition and prediction ability, which are summarized in Table 4. The recognition ability was represented by the percentage of honey samples correctly classified during the model training process, and the overall accuracy was 90.9%. Linden and rape honey samples could be classified clearly with accuracies of 100%, whereas the accuracies for vitex and acacia honey were 91.9 and 80.5%, respectively. The prediction ability was represented by the percentage of the honey samples correctly classified using a typical N-fold cross-validation procedure. The whole process was repeated 10 times with 3 folds. The overall accuracy of prediction was 88.4%, with the accuracies of vitex (89.2%) and acacia (75.6%) honey slightly lower than those in model training.

BP-ANN. To further improve the classification accuracy, a BP-ANN model was examined. In this study, a three-layer BP-ANN was built and applied to classify the honey samples on the basis of their botanical origins. Both the input and output layer have one neuron, whereas the number of neurons in each hidden layer is 15. The learning process is continued with a

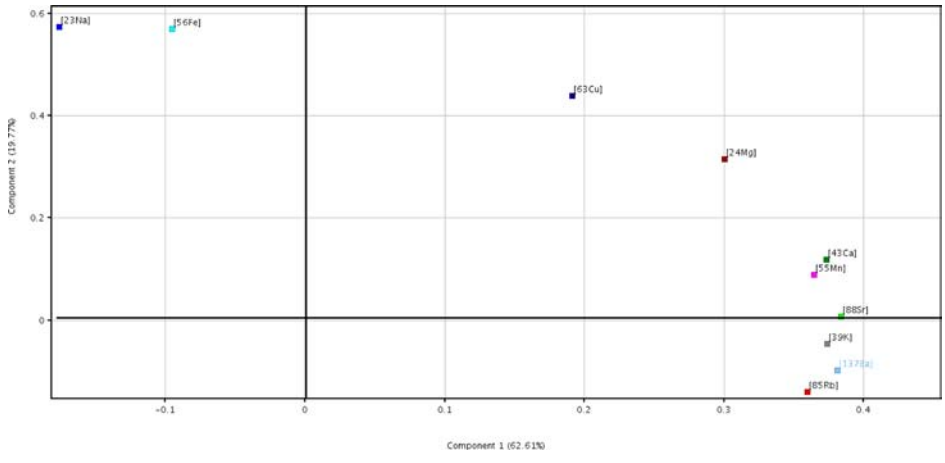

Figure 1. Two first-component loadings plot of variables.

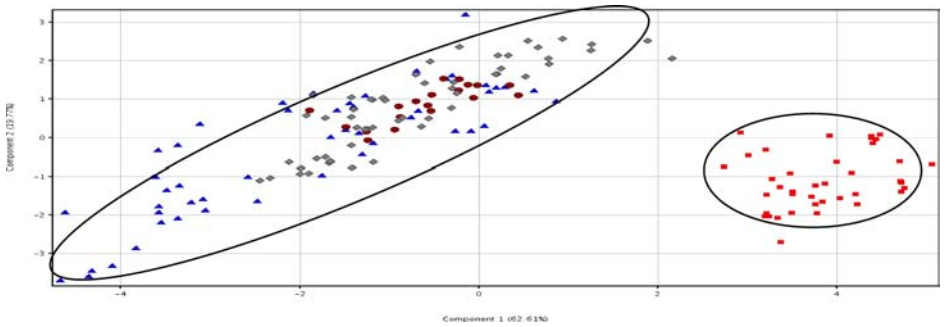

Figure 2. Two first-component scores of honeys from different botanical origins: linden (■), vitex (▲), rape (●), and acacia (◆) honey.

Table 4. Model Training and Cross-Validation Results by PLS-DA Model

	linden	vitex	rape	acacia	accuracy (%)
model training					
linden	29	0	0	0	100.0
vitex	0	34	0	3	91.9
rape	0	0	14	0	100.0
acacia	0	8	0	33	80.5
recognition ability (%)					90.9
model cross-validation					
linden	29	0	0	0	100.0
vitex	0	33	0	4	89.2
rape	0	0	14	0	100.0
acacia	0	8	2	31	75.6
prediction ability (%)					88.4

learning rate of 0.7 and the number of iterations (epochs) of 100. The model was also evaluated in terms of recognition and prediction ability. As demonstrated in Table 5, all honey samples can be successfully classified into four groups representing corresponding botanical origins during model training process. "Leave one out" was selected during the model cross-validation procedure to evaluate the robustness of the developed model. As shown in Table 5, the prediction ability of linden honey was 100% during model cross-validation. The overall accuracy of the prediction ability was slightly lower (92.6%) with the accuracies for vitex, rape, and acacia honeys of 86.5, 85.7, and 95.1%, respectively.

Table 5. Model Training and Cross-Validation Results by BP-ANN Model

	linden	vitex	rape	acacia	accuracy (%)
model training					
linden	29	0	0	0	100.0
vitex	0	37	0	0	100.0
rape	0	0	14	0	100.0
acacia	0	0	0	41	100.0
recognition ability (%)					100.0
model cross-validation					
linden	29	0	0	0	100.0
vitex	0	32	0	5	86.5
rape	0	0	12	2	85.7
acacia	0	0	2	39	95.1
prediction ability (%)					92.6

Prediction of Test Set by BP-ANN. Compared with the PLS-DA method, the performance of the BP-ANN model is more accurate. To further test the stability of the model developed for prediction, the independent test set of the remaining 42 honey samples with well-known sample information was classified using the constructed model. The results in Table 6 showed that 41 of 42 honey samples could be predicted into the four groups correctly, except that one acacia honey was wrongly classified into rape honey. The overall prediction accuracy is 97.6%, indicating the applicability of the proposed BP-ANN model.

Table 6. Model Prediction Results by BP-ANN Model

	predicted group				
test set	linden	vitex	rape	acacia	accuracy (%)
linden	10	0	0	0	100
vitex	0	13	0	0	100
rape	0	0	5	0	100
acacia	0	0	1	13	92.3
prediction ability (%)					97.6

Food source tracing has been a critical issue in recent years, especially for high-valued food products. Simply relying on anticounterfeiting labeling is insufficient to exclude faked or adulterated products from the market. However, many high-valued food products do have characteristic features depending on their chemical components. As demonstrated above, multiple elemental profiling by ICP-MS technique combined with chemometric tools can reliably classify honey samples according to their botanical origins. The developed prediction model has the advantage of high accuracy and robustness, relying little on human factors, and thus is promising for application in food classification and group assignment, especially in the field of food source tracing and adulteration studies, where elemental contents vary with food origin.

AUTHOR INFORMATION

Corresponding Authors

*(C.F.) E-mail: caiqfcl@163.com.

*(G.P.) Phone: +86 10 85783526. Fax: +86 10 85783526. E-mail: ciqpang@163.com

Funding

This study was supported by the technology plan projects of the State General Administration of Quality Supervision, Inspection and Quarantine, of the PRC (2013IK200).

Notes

The authors declare no competing financial interest.

ACKNOWLEDGMENTS

We are grateful to Dong Chen from Heilongjiang Yingchun Bee-products Corp. for help with collecting honey samples.

REFERENCES

(1) Gonzalvez, A.; Armenta, S.; De La Guardia, M. Trace-element composition and stable-isotope ratio for discrimination of foods with Protected Designation of Origin. *TrAC−Trends Anal Chem.* **2009**, *28* (11), 1295−1311.

(2) European Commission. Publication of an application for registration pursuant to Article 6(2) of Regulation (EEC) No. 2081/92 on the protection of geographical indications and designations of origin (1999/C 239/02). *Off. J. Eur. Communities* **1999**, *C 239*, 2−3.

(3) European Commission. Council Regulation (EC) No. 510/2006 of 20 March 2006 on the protection of geographical indication and designations of origin for agricultural products and foodstuffs. *Off. J. Eur. Union* **2006**, *L 93*, 12−25.

(4) Rebane, R.; Herodes, K. Evaluation of the botanical origin of Estonian uni- and polyfloral honeys by amino acid content. *J. Agric. Food Chem.* **2008**, *56* (22), 10716−10720.

(5) Baroni, M. V.; Nores, M. L.; Díaz, M. D. P.; Chiabrando, G. A.; Fassano, J. P.; Costa, C.; Wunderlin, D. A. Determination of volatile organic compound patterns characteristic of five unifloral honey by solid-phase microextraction−gas chromatography−mass spectrometry coupled to chemometrics. *J. Agric. Food Chem.* **2006**, *54* (19), 7235−7241.

(6) Dvash, L.; Afik, O.; Shafir, S.; Schaffer, A.; Yeselson, Y.; Dag, A.; Landau, S. Determination by near-infrared spectroscopy of perseitol used as a marker for the botanical origin of avocado (*Persea americana* Mill.) honey. *J. Agric. Food Chem.* **2002**, *50* (19), 5283−5287.

(7) Chen, L.; Wang, J.; Ye, Z.; Zhao, J.; Xue, X.; Heyden, Y. V.; Sun, Q. Classification of Chinese honeys according to their floral origin by near infrared spectroscopy. *Food Chem.* **2012**, *135* (2), 338−342.

(8) Ruoff, K. Authentication of the botanical origin of honey by front-face fluorescence spectroscopy. A preliminary study. *J. Agric. Food Chem.* **2005**, *53* (5), 1343−1347.

(9) Nečemer, M.; Košir, I. J.; Kump, P.; Kropf, U.; Jamnik, M.; Bertoncelj, J.; Ogrinc, N.; Golob, T. Application of total reflection X-ray spectrometry in combination with chemometric methods for determination of the botanical origin of Slovenian honey. *J. Agric. Food Chem.* **2009**, *57* (10), 4409−4414.

(10) Consonni, R.; Cagliani, L. R.; Cogliati, C. NMR characterization of saccharides in Italian honeys of different floral sources. *J. Agric. Food Chem.* **2012**, *60* (18), 4526−4534.

(11) Ankalm, E. A review of the analytical methods to determine the geographical and botanical origin of honey. *Food Chem.* **1998**, *63* (4), 549−562.

(12) Madejczyk, M.; Baralkiewicz, D. Characterization of Polish rape and honeydew honey according to their mineral contents using ICP-MS and F-AAS/AES. *Anal. Chim. Acta* **2008**, *617* (1−2), 11−17.

(13) Tuzen, M.; Silici, S.; Mendil, D.; Soylak, M. Trace element levels in honeys from different regions of Turkey. *Food Chem.* **2007**, *103* (2), 325−330.

(14) Kolayli, S.; Kongur, N.; Gundogdu, A.; Kemer, B.; Duran, C.; Aliyazicioglu, R. Mineral composition of selected honeys from Turkey. *Asian J. Chem.* **2008**, *20* (3), 2421−2425.

(15) Silici, S.; Uluozlu, O. D.; Tuzen, M.; Soylak, M. Assessment of trace element levels in *Rhododendron* honeys of Black Sea region, Turkey. *J. Hazard. Mater.* **2008**, *156* (1−3), 612−618.

(16) Chen, L. Z.; Rui, Y. K.; Zhao, J.; Ye, Z. H.; Xue, X. F.; Wang, P. Application of ICP-MS to detection of trace elements and heavy metalsin different kinds of honey. *Spectrosc. Spectral Anal.* **2008**, *28* (6), 1403−1405.

(17) Chen, H.; Fan, C. L.; Wang, Z. B.; Chang, Q. Y.; Pang, G. F. Uncertainties estimation for determination of 10 elements in northeastern China black bee honey by ICP-MS. *Anal. Methods* **2013**, *5* (13), 3291−3298.

(18) Latorre, M. J.; Peña, R.; García, S.; Herrero, C. Authentication of Galician (N.W. Spain) honeys by multivariate techniques based on metal content data. *Analyst* **2000**, *125* (2), 307−312.

(19) Terrab, A.; Hernanz, D.; Heredia, F. J. Inductively coupled plasma optical emission spectrometric determination of minerals in thyme honeys and their contribution to geographical discrimination. *J. Agric. Food Chem.* **2004**, *52* (11), 3441−3445.

(20) Baroni, M. V.; Arrua, C.; Nores, M. L.; Fayé, P.; Díaz, M. d. P.; Chiabrando, G. A.; Wunderlin, D. A. Composition of honey from Córdoba (Argentina): assessment of north/south provenance by chemometrics. *Food Chem.* **2009**, *114* (2), 727−733.

(21) Pisani, A.; Protano, G.; Riccobono, F. Minor and trace elements in different honey types produced in Siena county (Italy). *Food Chem.* **2008**, *107* (4), 1553−1560.

(22) Fernández-Torres, R.; Pérez-Bernal, J. L.; Bello-López, M. A.; Callejón-Mochón, M.; Jiménez-Sánchez, J. C.; Guiraúm-Pérez, A. Mineral content and botanical origin of Spanish honeys. *Talanta* **2005**, *65* (3), 686−691.

(23) Nozal Nalda, M. J.; Bernal Yagüe, J. L.; Diego Calva, J. C.; Martín Gómez, M. T. Classifying honeys from the Soria province of Spain via multivariate analysis. *Anal. Bioanal. Chem.* **2005**, *382* (2), 311−319.

(24) Pohl, P. Determination of metal content in honey by atomic absorption and emission spectrometries. *TrAC−Trends Anal. Chem.* **2009**, *28* (1), 117−128.

(25) Chudzinska, M.; Baralkiewicz, D. Estimation of honey authenticity by multielements characteristics using inductively coupled plasma-mass spectrometry (ICP-MS) combined with chemometrics. *Food Chem. Toxicol.* **2010**, *48* (1), 284−290.

(26) Chudzinska, M.; Baralkiewicz, D. Application of ICP-MS method of determination of 15 elements in honey with chemometric approach for the verification of their authenticity. *Food Chem. Toxicol.* **2011**, *49* (11), 2741−2749.

(27) Stanimirova, I.; Daszykowski, M.; Walczak, B. Dealing with missing values and outliers in principal component analysis. *Talanta* **2007**, *72* (1), 172−178.

(28) Wold, S.; Ruhe, A.; Wold, H.; Dunn, W. Collinearity problem in linear regression. The partial least squares (PLS) approach to generalized inverses. *J. Sci. Stat. Computations* **1984**, *5* (3), 735−743.

(29) Zupan, J.; Gasteiger, J. Neural networks: a new method for solving chemical problems or just a passing phase? *Anal. Chim. Acta* **1991**, *248* (1), 1−30.

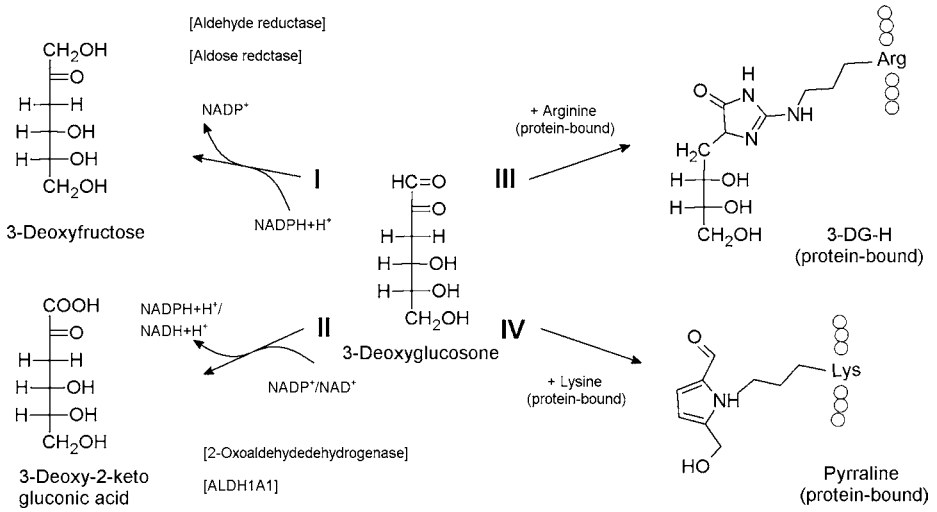

Figure 1. Degradation reactions of 3-deoxyglucosone: (I) enzymatic transformation of 3-deoxyglucosone to 3-deoxyfructose via aldehyde and aldose reductase and (II) to 3-deoxy-2-ketogluconic acid via 2-oxoaldehyde dehydrogenase and ALDH1A1; (III) nonenzymatic reaction of 3-deoxyglucosone with protein-bound arginine to the advanced glycation end product 3-DG-H (3-deoxyglucosone derived hydroimidazolone) and (IV) reaction with protein-bound lysine to form pyrraline.

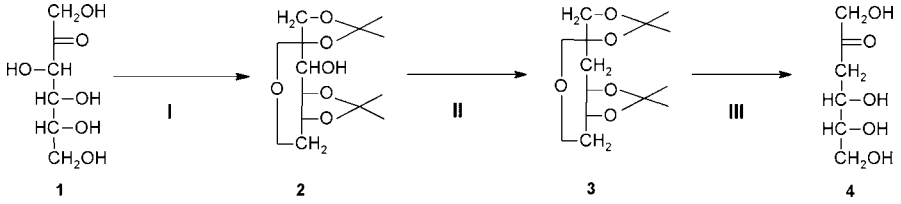

Figure 2. Synthesis of 3-deoxy-D-*erythro*-hexulose (3-DF): (I) acetone, H_2SO_4, 25 °C, 1.5 h; (II) THF, 1,1′-thiocarbonyldiimidazole, 66 °C, 3 h; (III) toluene, tributyltin hydride, 110 °C, 1 h; (IV) acetone/water (1:1, v/v), Lewatit S100, 25 °C, 24 h.

metabolic transit of 3-DG in healthy humans is available up to now.

The aim of our study, therefore, was to examine the contribution of dietary 3-DG on the "3-DG-load" of the human body. To obtain information about absorption and metabolism of 3-DG, urinary elimination of 3-DG and its major metabolite 3-DF was analyzed in healthy subjects following a diet containing 3-DG and a diet virtually free from 3-DG. During a 3 day intervention study, the influence of a single dose of honey containing a defined amount of 3-DG on the urinary elimination of 3-DG and 3-DF was observed. For this, a sensitive GC-MS for the simultaneous quantification of 3-DG and 3-DF in human urine had to be developed, and both analytes were synthesized as reference material.

MATERIALS AND METHODS

Materials. Chemicals of the highest purity available were purchased from standard suppliers: 1,1′-thiocarbonyldiimidazole (Sigma-Aldrich, Steinheim, Germany); *n*-hexane, hydroxylamine hydrochloride (Merck, Darmstadt, Germany); *N*,*O*-bis(trimethylsilyl)-trifluoroacetamide, D-fructose, methanol (Sigma-Aldrich); methyl-α-D-galactopyranoside (Acros, Geel, Belgium); pyridine (anhydrous), tributyltin hydride, urease (type C-3, 12KU) (Sigma-Aldrich). Mixed-bed ion exchanger Serdolit MB-2 was from Serva (Heidelberg, Germany), and cation exchanger (Lewatit S100) was from Bayer (Leverkusen, Germany). 3-DG was synthesized as already described[26] with some modifications.[10] [$^{13}C_6$]3-DG was prepared accordingly starting from [$^{13}C_6$]glucose (99%, Euriso-Top, Saint-Aubin Cedex, France). The water used was obtained with a Purelab plus purification system (USFilter, Ransbach-Baumbach, Germany).

Synthesis of 3-Deoxy-D-*erythro*-hexulose (3-Deoxyfructose). Protocols of synthesis were adopted with minor modifications.[27−29] Eighteen grams of D-fructose (**1**, Figure 2) was suspended in 350 mL of acetone containing 0.5% sulfuric acid and mechanically stirred at room temperature (under exclusion of moisture) until the sugar was dissolved (about 1.5 h). Termination of the reaction was carried out by adding 50 mL of ice-cold sodium hydroxide solution (c = 2.75 mmol/L) to the mixture while stirring was continued. Acetone was evaporated in vacuo, and the remaining aqueous phase (reddish brown) was extracted with methylene chloride (3 × 100 mL). The combined extracts were washed with water (2 × 50 mL) and dried over sodium sulfate. After evaporation of the organic solvent, the crude reaction product was recrystallized twice from ethanol/water 1:4 (v/v) and from ether followed by pentane. At 6 °C complete crystallization was achieved overnight. After drying, 5.1 g of long white needles of the diacetal sugar **2** (1,2:4,5-di-*O*-isopropylidene-D-fructopyranose, Figure 2) was obtained (20.2% from compound **1**). Solid 1,1′-thiocarbonyldiimidazole (2.2 g) was added to 1.5 g of the partially protected sugar, dissolved in 30 mL of tetrahydrofuran, and heated under reflux (66 °C) until complete conversion to the *O*-(imidazolylthiocarbonyl) derivative (about 3 h, monitored with thin layer chromtography).[28] The target product was isolated from the evaporated reaction mixture by flash chromatography (stationary phase: silica gel 60, mesh 0.063−0.200 mm) with ethyl acetate/hexane (1:1, v/v) as mobile phase, eluting between 80 and 260 mL.

Drying of the combined fractions yielded 1.9 g of the alkoxythiocarbony1imidazolide derivative (85% from **2**), which was completely employed for the following reduction step. The product was dissolved in 50 mL of anhydrous toluene, which was added dropwise within 30 min to a boiling tributyltin hydride/toluene solution (2.3 g in 200 mL of anhydrous toluene). After completion of reduction (about 1 h), the cooled solvent was evaporated in vacuo, and the dry residue was extracted with hot acetone (3 × 50 mL); the

dx.doi.org/10.1021/jf405546q | J. Agric. Food Chem. 2014, 62, 2449−2456

Table 1. GC-MS Parameters (SIM Mode) for the Determination of 3-Deoxyfructose (3-DF) and 3-Deoxyglucosone (3-DG)

	internal standard	quantifier ion [m/z]	qualifier ion [m/z]	internal standard quantifier ion [m/z]	internal standard qualifier ion [m/z]	dwell time (ms)
3-deoxyfructose	MGP	191	217, 524	204	217, 133	80 (for each measured ion)
3-deoxyglucosone	[$^{13}C_6$]3-DG	347	373, 537	351	379, 543	

combined extracts were washed with hexane (4 × 50 mL) to remove stannous components. Acetone was evaporated, and product isolation was performed by flash chromatography (stationary phase: silica gel 60, mesh 0.063−0.200 mm, mobile phase ethylacetate/hexane 1:1 (v/v), elution between 80 and 170 ml). After recrystallization from pentane, 0.74 g of the reduced diisopropylidene derivative **3** (Figure 2) was obtained as white needles (71% from **2**). ^{1}H nuclear magnetic resonance (NMR) analysis of this product gives a spectrum according to data published in the literature.[28] Distinct signals with chemical shifts of δ = 2.1 for the two protons at C3 indicate the successful reduction at C3 (literature δ = 2.00 and 2.06).[28]

For hydrolysis the complete yield was dissolved in 12.5 mL of acetone and 25 mL of water. Three grams of activated cation exchange resin (Lewatit S100) was added; this mixture was then stirred for 24 h at room temperature. Neutralization was achieved by stirring the solution for another 6 min with the addition of 6 g of a mixed-bed ion exchanger (Serdolit MB-2). The product was purified by flash chromatography (stationary phase as above; mobile phase: methylene chloride/ethanol/water 2:1:0.1 (v/v/v), elution between 80 and 170 mL). The combined fractions were evaporated, and the residue was taken up in water and lyophilized to yield 0.16 g of 3-DF (**4**) (Figure 2; 16% from **2**). After 6 weeks of storage at −18 °C, complete crystallization was accomplished with small, light yellow crystals. The product was characterized by ^{1}H NMR and ^{13}C NMR, and purity was examined via GC-FID. ^{1}H NMR (500 MHz, D_2O) β-pyranose: δ_H 3.43 (s, 2H, H1A/H1B), 1.78 (m, 2H, H3A/H3B), 3.95 (m, 1H, H4), 3.70 (s, 1H, H5), 3.59 (dd, 1H, H6), 3.86 (dd, 1H, H6). ^{13}C NMR (125 MHz, D_2O): δ_C 97.21 (C-2), 67.05 (C-5), 65.21 (C-1), 64.76 (C-4), 63.81 (C-6), 41.29 (C-3).

For purity control of 3-DF, the corresponding trimethylsilyl (TMS) oxime of 3-DF was subjected to GC-FID analysis. Analysis was performed on a Varian 3900 gas chromatograph with a CP-8410 automatic liquid sampler with split injector and flame ionization detection (FID). Separation was performed on a DB-5 capillary column (30 m, 0.25 mm i.d., 1.00 μm film thickness, J&W Scientific, Germany). Helium was the carrier gas with a constant flow at 1.0 mL/min, injector temperature was 250 °C, and injection mode was 1 μL at 1:20 split. The oven temperature program was adopted from the parameters of the GC-MS analysis.

Stock solutions each of 3-DF and D-fructose were prepared in water (c = 1 mM), and calibration curves (0.05−1 mM) of the TMS oximes were recorded with GC-FID. The slope of the calibration curve of 3-DF was compared to the slope of the calibration curve of D-fructose, and the ratio was assumed to indicate the purity/content of synthesized 3-DF.

Intervention Study. Nine healthy, normoglycemic volunteers (ages 24−36 years, 7 women and 2 men, nonsmoking, fasting blood sugar ≤5.5 mmol/L) collected their 24 h urine (8.00 a.m. until 8.00 a.m. the following day) on 2 consecutive days with no dietary restrictions (days 1−2). Furthermore, all nine participants took part in a 3 day intervention study consisting of one wash-out day (day 3), one intervention day (day 4), and one run-out day (day 5). From day 3 to day 5, they followed a "raw food" diet, which implies avoiding heated and fermented foods such as dairy and bakery products, coffee, juices, and beer to ensure a diet virtually free of 3-DG and Maillard reaction products. In the morning of the intervention day (day 4), the participants ingested a single dose of 50 g of honey containing a defined amount of 505 μmol of 3-DG (3-DG concentration of the honey was 1641 mg/kg). The "raw food" diet was continued on the fifth day. Twenty-four hour urine was collected every day of the study as described above. Additionally, a placebo study was performed. Two participants (ages 28 and 31 years, respectively, 1 woman and 1 man, nonsmoking, fasting blood sugar ≤5.5 mmol/L) followed the same 5 day study design as described above, but ingested 50 g of a honey analogue sugar mixture (46.5% D-fructose, 34.5% D-glucose, 1.5% saccharose, and 17.5% water)[30] instead of wild honey in the morning of the intervention day (day 4). Aliquots of collected 24 h urine samples were immediately stored at −18 °C until analysis. 3-DG and 3-DF were analyzed within 2 weeks.

Preparation of Urine Samples for GC-MS Analysis. After the urine thawed, an aliquot of 100 μL was spiked with 10 μL of internal standard solution (containing 1.0 mg/mL methyl-α-D-galactopyranoside[31] and 0.1 mg/mL [$^{13}C_6$]3-DG in water) and was then treated with 30 μL of urease (1 mg/mL in 0.2 M sodium phosphate buffer, pH 7.0) for 10 min at 37 °C in a water bath. Termination of the enzymatic reaction was realized by addition of 900 μL of ice-cold ethanol. After centrifugation (10000g, 15 min), the resulting supernatant was transferred to a new tube and evaporated to dryness under a nitrogen stream. Then the dry residue was incubated with 50 μL of hydroxylamine hydrochloride solution (10 mg/mL in anhydrous pyridine) for 30 min at 80 °C followed by evaporation to dryness. Then 50 μL of *N*,*O*-bis(trimethylsilyl)trifluoroacetamide was added to the residue and vigorously mixed by vortex for 0.5 min and incubated at room temperature for another 2 h. Subsequently, 50 μL of *n*-hexane was added; an aliquot of 80 μL was transferred to a GC vial and was then ready for GC-MS analysis.

GC-MS Analysis of 3-Deoxyglucosone and 3-Deoxyfructose. GC-MS analysis was performed using a HP6890 gas chromatograph, coupled with a HP7683 automatic liquid sampler and a HP5973 mass selective detector equipped with a HP-5MS capillary column (30 m, 0.25 mm i.d., 0.25 μm film thickness; all from Agilent, Germany) and a Zebron Z-guard column (deactivated, 5 m, 0.25 mm i.d.; Phenomenex, Germany). The carrier gas was helium with a constant flow at 1.0 mL/min, the injector temperature was 250 °C, and injection mode was 1 μL pulsed splitless. The oven temperature program started at 80 °C (hold time = 2 min) elevated to 250 °C at 10 °C/min (hold time = 3 min) and finally heated to 300 °C at 30 °C/min (hold time = 3 min), resulting in a complete run time of 25 min. Mass spectrometer was used with electron ionization (70 eV) in scan and SIM modes. In scan mode the recorded m/z area range varied from 50 to 800. For detailed SIM parameters see Table 1.

For external calibration, stock solutions of the analytes in water (0.06−0.6 mM) were pipetted (1−50 μL) to yield appropriate concentrations along with internal standards. Each calibration sample was subjected to the derivatization procedure after evaporation to dryness (see above).

Quantitative evaluation was carried out by the use of the ratio of the area of the most prominent analyte peak and the internal standard peak of the corresponding quantifier ions, despite the occurrence of peaks of *syn*- and *anti*-stereoisomers of the analytes.

The limits of detection (LOD) and quantitation (LOQ) in standard solution and urine were calculated as the concentrations of the analyte necessary to show a peak at signal-to-noise ratios of 3 and 10, respectively. For the determination of the interday repeatability, one urine sample was applied to the sample workup and derivatization procedure five times on different days. The recovery of 3-DF and 3-DG was calculated from the slope of the recovery function after urine had been spiked with three ascending concentrations of the analytes (3-DF, 6−300 μmol/L; 3-DG, 0.6−30 μmol/L) with subsequent sample workup.

NMR Spectrometry. ^{1}H and ^{13}C NMR spectra were recorded on a Bruker DRX 500 instrument (Rheinstetten, Germany) at 500 and 125 MHz, respectively. Samples were dissolved in deuterium oxide. Chemical shifts are given in parts per million (ppm), those of protons

relative to the internal HOD signal (4.70 ppm, residual proton), and those of carbon atoms relative to the external standard tetramethylsilane. Assignments of ^{1}H and ^{13}C signals are based on heteronuclear single-quantum coherence (HSQC) and distortionless enhancement by polarization transfer (DEPT) experiments.

Statistical Treatment. Comparisons of means between the daily urinary excretions of the different days were examined using Student's *t* test. *P* values ≤0.05 were considered significant (two-tailed) using OriginPro 8.6.

RESULTS AND DISCUSSION

GC-MS Analysis of Urinary 3-Deoxyglucosone and 3-Deoxyfructose: Method Evaluation. The first aim of our study was to establish a sensitive and selective method for the simultaneous determination of 3-DG and its metabolite 3-DF in urine. As 3-DF is commercially not available, it had to be synthesized as reference material. This was achieved by the preparation of the 1,2:4,5-diacetal of D-fructose, selective reduction at C3 with tri-*n*-butylstannane, and finally hydrolysis of the 3-deoxysugar, according to literature methods (compare Figure 2).[27−29] The ^{1}H NMR spectrum of the final product 3-DF showed several signals due to five tautomeric forms of the deoxysugar in aqueous solution. According to the literature, most signals of the β-pyranoide structure could be assigned, as this is the predominating form of 3-DF in aqueous solution at room temperature. Chemical shifts of the signals are in line with those reported.[29] The chemical shift of the protons at C3 (δ = 1.78) of 3-DF are characteristic for the reduction at C3 and prove the identity of 3-DF along with the other signals. Purity control of the synthesized 3-DF via GC-FID[32] indicated a purity of 99% when compared to D-fructose. The GC-FID chromatogram indicated no impurities of other sugars or sugar derivatives (data not shown).

For the GC-MS analysis of the sugar derivatives, a conversion to volatile compounds is inevitable. The first step of the derivatization is the formation of the corresponding oximes, followed by the conversion to the TMS derivatives (Figure 3).[33] With regard to the 10 isomeric forms of 3-DG[34] and the 5 tautomeric forms of 3-DF,[29] the formation of sugar oximes is advantageous because the oximes exist in open-chain form,[35] leading to only two silylated isomers per aldehyde or keto group, respectively. Compared to the published method[7] for the simultaneous determination of 3-DG and 3-DF, this optimized GC-MS method has the key advantage of higher selectivity. This is accounted for by different retention times of the two analytes and distinct *m*/*z* ratios (compare Figure 2). In the cited method[7] the retention times for both analytes are the same and the *m*/*z* ratio is only 1.

The preparation of the urine samples prior to derivatization consisted of an enzymatic removal of urea for the analysis of carbohydrates in urine.[36] The dry matter of urine contains approximately 23−49% urea,[37] which can consume large amounts of the silylating agent and therefore hamper the silylation of the analytes.[36] The adopted derivatization method[33] was slightly modified in this work, resulting in a reduction of the applied derivatization agents. The application of oxime formation in carbohydrate analysis has been already examined in detail with regard to stability, efficiency, and the number of byproducts formed.[38] The amount of *N*,*O*-bis(trimethylsilyl)trifluoroacetamide (BSTFA) was adjusted to 50 μL per derivatization assay, and derivatization was complete after 2 h at room temperature, based on time course studies. The solvent evaporation after oxime formation is time-consuming, and the silylation of the analytes in the dry residue is suboptimal compared to a silylation of the analytes in solution. The drying procedure, however, is necessary to ensure a salt concentration as low as possible in the injected sample solution to minimize contamination and signal suppression in the mass selective detector.

In Figure 4, a selected ion chromatogram of a 3-DF (at *m*/*z* 191) and 3-DG (at *m*/*z* 347) standard solution after derivatization with hydroxylamine hydrochloride and BSTFA to the corresponding TMS oximes is shown. For the TMS

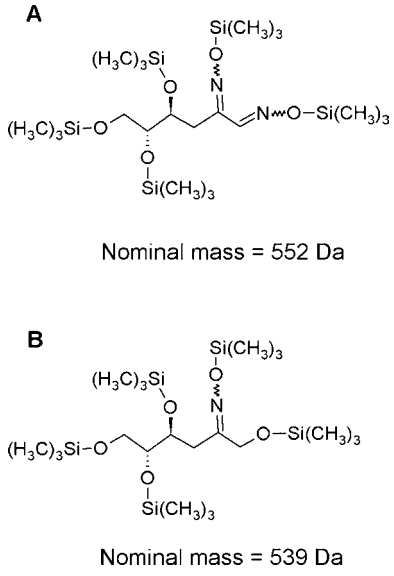

Figure 3. Structures of the trimethylsilyl oxime derivatives of (A) 3-deoxyglucosone and (B) 3-deoxyfructose with their corresponding nominal masses.

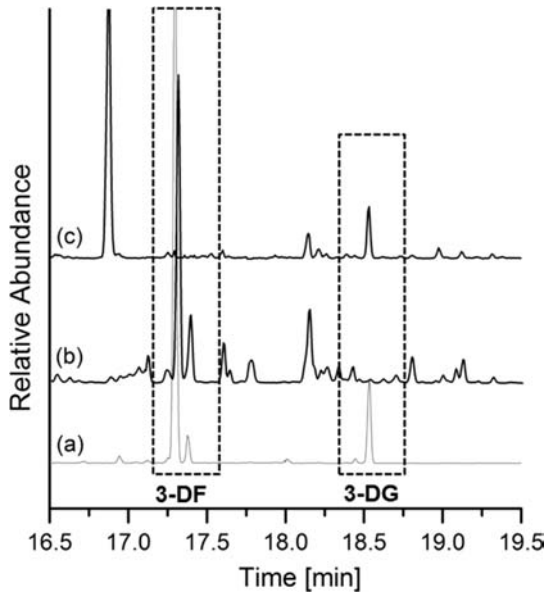

Figure 4. Selected ion monitoring chromatogram of (a) a 3-deoxyglucosone 3-DG)/3-deoxyfructose (3-DF) standard solution (*m*/*z* 347 and 191), (b) a urine sample at *m*/*z* 191, and (c) a urine sample at *m*/*z* 347. All chromatograms were acquired by GC-MS after derivatization with hydroxylamine hydrochloride and *N*,*O*-bis-(trimethylsilyl)trifluoroacetamide to the corresponding trimethylsilyl oximes.

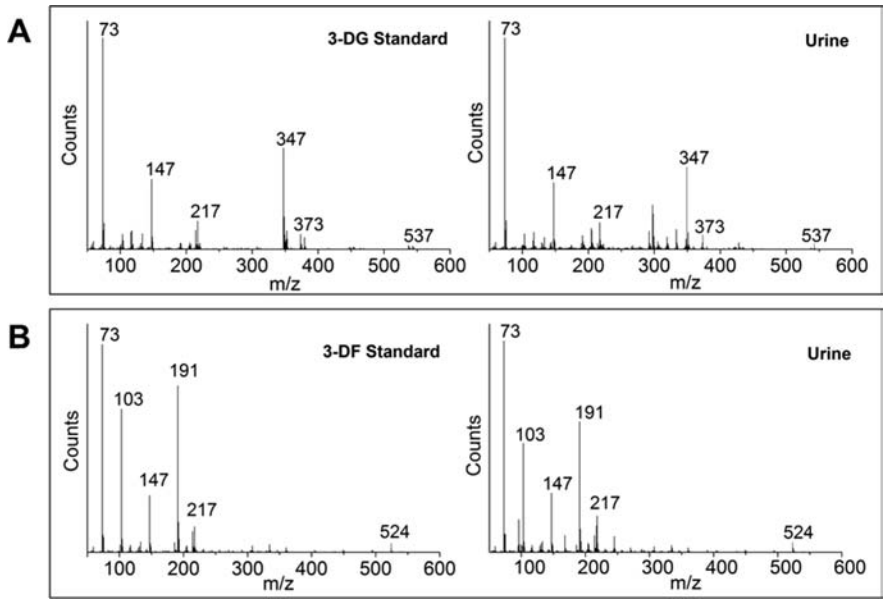

Figure 5. (A) EI-Mass spectra of the peak eluting at 18.5 min of a 3-deoxyglucosone (3-DG) standard solution and a urine sample (scan mode). (B) EI-Mass spectra of the peak eluting at 17.3 min of a 3-deoxyfructose (3-DF) standard solution and a urine sample (scan mode). All spectra were acquired by GC-MS after derivatization with hydroxylamine hydrochloride and *N*,*O*-bis(trimethylsilyl)trifluoroacetamide to the corresponding trimethylsilyl oximes.

Table 2. Performance Parameters of the GC-MS Method for the Determination of 3-Deoxyfructose (3-DF) and 3-Deoxyglucosone (3-DG) in Urine

	R^2	linear range (μmol/L)	interday repeatability[a] (%)	LOD[b] (nmol/L)	LOQ[b] (nmol/L)	recovery[c] (%)
3-deoxyfructose	0.9998	6−300	1.5	52 ± 4	155 ± 11	101.8 ± 3.8
3-deoxyglucosone	0.9980	0.6−30	1.0	20 ± 4	59 ± 13	97.4 ± 4.2

[a]Expressed as relative standard deviation. [b]LODs (limit of detection) and LOQs (limit of quantification) were calculated on the basis of signal-to-noise-ratio. [c]Recovery was determined by addition of various concentrations of 3-DF (60−300 μmol/L, $n = 3$) and 3-DG (0.6−30 μmol/L, $n = 3$) to 100 μL of urine, applying all steps of sample preparation and analysis. The value was calculated from the slope of the recovery function and is given in percent ± SE.

oxime of 3-DF, two peaks are detectable, which arise from its *syn*- and *anti*-isomers due to the derivatization reaction with hydroxylamine hydrochloride. The first peak (17.3 min) is the major peak and can presumably be assigned to the *syn*-form due to steric reasons.[35] The second minor peak (17.4 min) represents the *anti*-form and accounts for <15% of the total peak area. The stable *syn*- and *anti*-anomeric oximes are formed in constant ratio.[33,38] In the present study, the ratio between the *syn*- and *anti*-oximes was about 7:1. Therefore, the quantitation of 3-DF was performed via the ratio of the area of the major 3-DF TMS *syn*-oxime peak and the area of the peak of the silylated internal standard methyl-α-D-galactopyranoside.[31]

The TMS oxime of 3-DG theoretically exists in four different isomeric forms because of the two carbonyl groups, but in the extracted ion chromatogram of a 3-DG standard solution (at m/z 347, compare Figure 4), only one peak was observed. This may be due to steric hindrance preventing the formation of some isomers or the chromatographic system failing to resolve them. The identification of the two analytes in urine was accomplished chromatographically by comparison of the retention times of the target compounds in standard solution and urine as shown in Figure 4 together with the corresponding mass spectra (compare Figure 5).

In Figure 5A, the mass spectra (scan mode) of the peak eluting at 18.5 min in a standard solution and a urine sample are displayed. The two spectra show the same distinct signals at the mass-to-charge ratio of the quantifier ion (m/z 347) and the qualifier ion (m/z 537). The mass spectra (scan mode) of the peak eluting at 17.3 min of a 3-DF standard solution and a urine sample after derivatization to their corresponding TMS oximes are presented in Figure 5B, having consistent signals at m/z 191 (quantifier ion) and at m/z 524 (qualifier ion). Comparison of the mass spectra of the peaks of the two corresponding analytes recorded from a derivatized standard solution and a urine sample allows a doubtless and unequivocal identification of 3-DG and 3-DF in urine.

In Table 2, validation parameters of the method for the determination of 3-DG and 3-DF in urine are summarized. They indicate an accurate sample preparation, a reproducible derivatization procedure, and a reliable GC-MS analysis. On the basis of the relative interday repeatability being <1.5% for both analytes, it can be concluded that all steps from the sample preparation to the evaluation of the obtained chromatograms are precise. They also indicate that the applied internal standards ([$^{13}C_6$]3-DG for 3-DG and methyl-α-D-galactopyranoside for 3-DF) are appropriate.

Monitoring of Urinary 3-Deoxyglucosone and 3-Deoxyfructose. By comparison of the daily dietary intake of 3-DG (0.1−1.0 mmol/day)[11] with the concentrations measured for human plasma (0.04−0.16 μmol/L plasma),[6−9] questions arise concerning the impact of dietary 3-DG on the overall "3-

DG load" of the human body. To the best of our knowledge there is no information about the metabolic fate of dietary 3-DG in healthy, normoglycemic human subjects. Our work was motivated by previous results of a rat study in which orally absorbed 3-DG was eliminated as 3-DF in the urine at a percentage of about 5%.[18]

We therefore applied the developed method to monitor the 3-DG and 3-DF excretion in 24 h urine samples with nine healthy volunteers. During the first 2 days participants followed their own individual diet with no restrictions. In Figure 6 (days 1−2) the results of the urine analysis are displayed. The median 3-DG excretion in 24 h urine was 7.6 μmol on day 1 and 8.9 μmol on day 2, respectively (range = 6.4−15 μmol/day; Figure 6A). The median 3-DF excretion in 24 h urine was 146 μmol on day 1 and 165 μmol on day 2, respectively (range = 91−306 μmol/day; Figure 6B). The urinary excretion of 3-DG and 3-DF did not differ significantly between the two days ($P > 0.05$). 3-DG accounted for 4−8% (mean = 6%) of the summarized 3-DG and 3-DF amounts. This is in line with published data,[7] which show that 3-DF is the main metabolite in urine accounting for >95% of 3-DG. The daily urinary apparent 3-DF excretions are consistent with values published in the literature for healthy subjects (32−92 μmol/g creatinine),[7,26] when a daily excretion of 1.1−1.9 g creatinine is taken as a basis.[37] In the literature, urinary excretion is usually referred to the creatinine elimination for standardization purposes. The results of the urinary elimination in this work are given as the amount present in total 24 h urine. This was mainly because the creatinine excretion is dependent on internal and external factors that lead to a broad fluctuation of the excreted amount.[39]

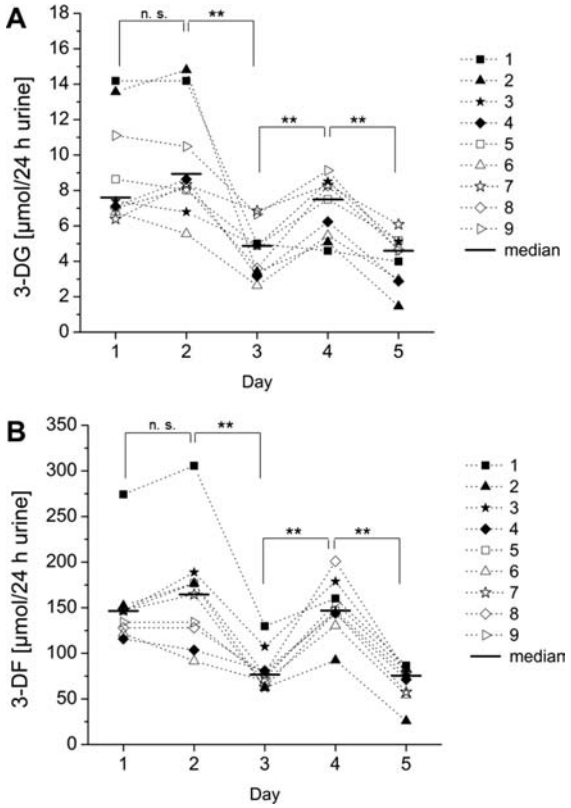

Figure 6. Urinary excretion of (A) 3-deoxyglucosone (3-DG) and (B) the metabolite 3-deoxyfructose (3-DF) in 24 h urine of nine healthy subjects. Days 1−2, participants followed their usual diet without restrictions; days 3−5 (intervention study), participants followed a "raw food" diet; day 3, wash-out day; day 4, intervention day, ingestion of 50 g of wild honey containing 505 μmol of 3-DG in the morning; day 5, run-out day. Comparisons of means were examined using Student's *t* test. n. s., not significant ($P > 0.05$); **, $P < 0.01$ (highly significant).

When the study participants followed a diet virtually free from 3-DG (wash-out day, day 3 in Figure 6), the 24 h urinary excretion of 3-DG and 3-DF significantly decreased ($P_{3\text{-DG}} < 0.001$; $P_{3\text{-DF}} < 0.002$, Figure 6). The median level of renal 3-DG excretion on the wash-out day (day 3, "raw food" diet) was 4.6 μmol/day (from 2.6 to 6.8 μmol/day), and the median level of 3-DF excretion was 77 μmol/day (from 62 to 130 μmol/day). However, the urinary excretion of 3-DG and 3-DF on day 3 can be assumed to be mostly unaffected by dietary 3-DG or other Maillard reaction products such as fructoselysine, which may form 3-DG after ingestion.[9] An important source for urinary 3-DG and 3-DF levels on this day should be endogenously formed 3-DG, which arises from the enzymatic deglycation of protein-bound Amadori compounds.[40] Varying endogenous 3-DG concentrations and, therefore, interindividual differences in the excretions of 3-DG and 3-DF are associated with differences in FN3K activity.[40,41] Because there was no wash-out phase between the days with no dietary restrictions (days 1−2) and the wash-out day (day 3), the 3-DG and 3-DF elimination could also be influenced by dietary 3-DG from the previous days, if it is slowly metabolized.

On the basis of these results it was not possible to make any statement on the bioavailability of dietary 3-DG as the exact amounts of 3-DG ingested with the diet were not quantitated. Furthermore, the influence of other compounds, for example, fructoselysine, of the consumed food could not be evaluated. A postprandial increase of plasma 3-DG in diabetic subjects was discussed to be due to the conversion of the dietary Amadori compound fructoselysine.[9] Recent findings, however, showed that dietary fructoselysine is not transported across intestinal epithelial cell monolayers in vitro and is therefore most presumably not absorbed from food in the human intestine.[42] So far, there is no information about a possible occurrence of 3-DF in foods, especially in fruits. In upcoming studies this is a crucial point to know to address an influence of possible dietary 3-DF.

Therefore, the participants took part in a further study. During a 3 day intervention study (days 3−5, Figure 6), the nine volunteers followed a "raw food" diet virtually free from 3-DG and other Maillard reaction products and consumed 50 g of honey containing 505 μmol of 3-DG on the morning of the intervention day (day 4). On day 5, the run-out day, "raw food" diet was continued. In Figure 6, the daily urinary excretions of 3-DG and 3-DF are shown. Compared to the mean urinary excretion of 3-DG and 3-DF during the two days of the dietary recall without restriction, mean values of both analytes significantly decreased on the wash-out day of the intervention study (day 3, compare Figure 6; $P_{3\text{-DG}} < 0.001$; $P_{3\text{-DF}} < 0.002$).

On the intervention day of the study (day 4), when a defined amount of 3-DG (505 μmol) via wild honey was consumed in the morning, the daily urinary excretion of 3-DG and 3-DF was significantly elevated compared to the wash-out day (day 3; $P_{3\text{-DG}} < 0.002$; $P_{3\text{-DF}} < 0.001$). Median 3-DG and 3-DF excretion increased to 7.5 μmol/day (range = 4.6−9.1 μmol/day; Figure 6A) and 147 μmol/day (range = 92−201 μmol/day; Figure 6B), respectively. With regard to the wash-out day,

the average increase of the urinary 3-DG excretion was 3.0 μmol/day (range = 0.4−3.6 μmol/day) and that of the 3-DF excretion was 70 μmol/day (range = 30−123 μmol/day). This corresponds with approximately 10−15% of the ingested amount of 3-DG being recovered in the urine. Slightly lower excretion rates into urine were observed in rats, but it is obvious that results of animal experiments could be only partly transferred to humans and the study design lasted only 2 h.[18] Median 3-DG and 3-DF excretions on the run-out day (day 5) did not differ significantly from those of day 3 ($P > 0.05$), indicating a rapid elimination of intestinally absorbed 3-DG (compare Figure 6). Despite the intake of a high amount of 3-DG on the intervention day (day 4), the median ratios of the urinary 3-DG/3-DF excretion did not vary significantly compared to the other days (see Supporting Information). In further studies it might be of interest to investigate interindividual differences of the excreted 3-DG/3-DF ratios to have further insights into possible variations of the metabolic handling, for example, during diabetes.

To rule out that the observed increase in urinary excretion of 3-DF on day 4 is due to the high sugar load and a possible formation of 3-DG from glucose or fructose in vivo, a placebo study was performed. Two volunteers consumed 50 g of a honey analogue sugar mixture virtually free of 3-DG instead of 3-DG-containing wild honey on the intervention day (data and figure shown in the Supporting Information). Urinary excretion of 3-DG and 3-DF remained constant, indicating that precursors such as fructose or glucose do not contribute to a measurable 3-DG formation in vivo or an increased urinary 3-DG and 3-DF excretion, respectively. Hence, the elevation of the urinary 3-DF excretion on the intervention day of the intervention study was exclusively due to the 3-DG consumed via the wild honey.

These experimental findings for the first time prove an influence of dietary 3-DG on urinary excretion of 3-DG and 3-DF. The results imply that dietary 3-DG is to some extent taken up from the ingested food in the intestinal tract, metabolized to 3-DF, and eliminated via urine. This allows the conclusion that detoxification systems for endogenously formed reactive aldehydes, such as aldehyde and aldose reductase,[21,22] should also be capable to degrade dietary and therewith exogenous 3-DG. In particular, the recently described small intestine aldose reductase (ALKR1B10), which is described to play a key role in detoxifying dietary and lipid-derived carbonyl compounds,[21,22] should be examined in this context. As only 10−15% of the administered 3-DG is recovered in urine as 3-DG and 3-DF, the question arises about the fate of the remaining 85−90%. Further studies will have to show whether putative 3-DG-specific metabolites such as 3-deoxy-2-keto-gluconic acid or hydroxymethylfurfural (HMF) can be found in the urine. At present, it cannot be excluded that 3-DG is to some extent transformed to HMF due to the low pH value of the stomach. 3-DG may also react with proteins to AGEs in the gastrointestinal tract or in vivo. The analysis of 3-DG and 3-DF in blood plasma plus 3-deoxy-2-keto-gluconic acid and other analytes (i.e., fructoselysine, HMF, pyrraline) of study participants after an oral load of 3-DG would unequivocally reveal if and to what extent 3-DG is absorbed into the systemic circulation and if it is metabolized. On the basis of results of animal experiments, it was concluded that orally ingested 3-DG is absorbed in the intestine to only a minor degree and that the major part remains in the content of the gastrointestinal tract.[18] This finding should be examined in a following study.

In conclusion, it was possible for the first time to reveal differences in urinary 3-DG and 3-DF elimination in healthy human subjects, dependent on the diet. These results are a prerequisite for further studies concerning metabolic pathways of 3-DG in human subjects.

■ ASSOCIATED CONTENT

Ⓢ Supporting Information

Figures I and II. This material is available free of charge via the Internet at http://pubs.acs.org.

■ AUTHOR INFORMATION

Corresponding Author

*(T.H.) Phone: +49-351-463-34647. Fax: +49-351-463-34138. E-mail: Thomas.Henle@chemie.tu-dresden.de.

Notes

The authors declare no competing financial interest.

■ ACKNOWLEDGMENTS

We thank Dr. Uwe Schwarzenbolz, Institute of Food Chemistry, Technische Universität Dresden, for his support during the LC-MS measurements. Furthermore, we thank Dr. Margit Gruner and Anett Rudolph, Institute of Organic Chemistry, Technische Universität Dresden, for recording the NMR spectra.

■ ABBREVIATIONS USED

3-DF, 3-deoxyfructose; 3-DG, 3-deoxyglucosone; 3-DG-H, 3-deoxyglucosone-derived hydroimidazolone; AGE, advanced glycation endproduct; BSTFA, *N*,*O*-bis(trimethylsilyl)-trifluoroacetamide; FID, flame ionization detector; GC-MS, gas chromatography−mass spectrometry; LOD, limit of detection; LOQ, limit of quantitation; MGP, methyl-α-D-galactopyranoside; SIM, selected ion monitoring; TMS, trimethylsilyl

■ REFERENCES

(1) Kroh, L. W. Caramelisation in food and beverages. *Food Chem.* **1994**, *51*, 373−379.

(2) Thornalley, P. J.; Langborg, A.; Minhas, H. S. Formation of glyoxal, methylglyoxal and 3-deoxyglucosone in the glycation of proteins by glucose. *Biochem. J.* **1999**, *344*, 109−116.

(3) Niwa, T. 3-Deoxyglucosone: metabolism, analysis, biological activity and clinical implication. *J. Chromatogr., B* **1999**, *731*, 23−36.

(4) Lal, S.; Szwergold, B.; Taylor, A. Metabolism of fructose-3-phosphate in the diabetic rat lens. *Arch. Biochem. Biophys.* **1995**, *318*, 191−199.

(5) Delpierre, G.; Collard, F. Fructosamine 3-kinase is involved in an intracellular deglycation pathway in human erythrocytes. *Biochem. J.* **2002**, *365*, 801−808.

(6) Lal, S.; Kappler, F.; Walker, M. A.; Orchard, T. J.; Beisswenger, P. J.; Szwergold, B. S.; Brown, T. R. Quantitation of 3-deoxyglucosone levels in human plasma. *Arch. Biochem. Biophys.* **1997**, *342*, 254−260.

(7) Knecht, K. J.; Feather, M. S.; Baynes, J. W. Detection of 3-deoxyfructose and 3-deoxyglucosone in human urine and plasma: evidence for intermediate stages of the Maillard reaction in vivo. *Arch. Biochem. Biophys.* **1992**, *294*, 130−137.

(8) Odani, H.; Shinzato, T.; Matsumoto, Y.; Usami, J.; Maeda, K. Increase in three α,β-dicarbonyl compound levels in human uremic plasma: specific in vivo determination of intermediates in advanced Maillard reaction. *Biochem. Biophys. Res. Commun.* **1999**, *256*, 89−93.

(9) Beisswenger, P. J.; Howell, S. K.; O'Dell, R. M.; Wood, M. E.; Touchette, A. D.; Szwergold, B. S. α-Dicarbonyls increase in the postprandial period and reflect the degree of hyperglycemia. *Diabetes Care* **2001**, *24*, 726−732.

(10) Hellwig, M.; Degen, J.; Henle, T. 3-Deoxygalactosone, a "new" 1,2-dicarbonyl compound in milk products. *J. Agric. Food Chem.* **2010**, *58*, 10752−10760.
(11) Degen, J.; Hellwig, M.; Henle, T. 1,2-Dicarbonyl compounds in commonly consumed foods. *J. Agric. Food Chem.* **2012**, *60*, 7071−7079.
(12) Jono, T.; Nagai, R.; Lin, X.; Ahmed, N.; Thornalley, P. J.; Takeya, M.; Horiuchi, S. N^{ε}-(Carboxymethyl)lysine and 3-DG-imidazolone are major AGE structures in protein modification by 3-deoxyglucosone. *J. Biochem.* **2004**, *136*, 351−358.
(13) Hayase, F.; Nagaraj, R. H.; Miyata, S.; Njoroge, G.; Monnier, V. M. Aging of proteins: immunological detection of a glucose-derived pyrrole formed during Maillard reaction in vivo. *J. Biol. Chem.* **1989**, *263*, 3758−3764.
(14) Miyata, S.; Liu, B. F.; Shoda, H.; Ohara, T.; Yamada, H.; Suzuki, K.; Kasuga, M. Accumulation of pyrraline-modified albumin in phagocytes due to reduced degradation by lysosomal enzymes. *J. Biol. Chem.* **1997**, *272*, 4037−4042.
(15) Ahmed, N. Advanced glycation endproducts − role in pathology of diabetic complications. *Diabetes Res. Clin. Pract.* **2005**, *67*, 3−21.
(16) Henle, T.; Miyata, T. Advanced glycation end products in uremia. *Adv. Renal Replace. Ther.* **2003**, *10*, 321−331.
(17) Miyata, T.; Ueda, Y.; Yamada, Y.; Izuhara, Y.; Wada, T.; Jadoul, M.; Saito, A.; Kuro-kawa, K.; Van Ypersele de Strihou, C. Accumulation of carbonyls an advanced stress in uremia accelerates the formation of glycation end product: carbonyl stress in uremia. *J. Am. Soc. Nephrol.* **1998**, *9*, 2349−2356.
(18) Kato, H.; van Chuyen, N.; Shinoda, T.; Sekiya, F.; Hayase, F. Metabolism of 3-deoxyglucosone, an intermediate compound in the Maillard reaction, administered orally or intravenously to rats. *Biochim. Biophys. Acta* **1990**, *1035*, 71−76.
(19) Kanazu, T.; Shinoda, M.; Nakayama, T.; Deyashiki, Y.; Hara, A.; Sawada, H. Aldehyde reductase is a major protein associated with 3-deoxyglucosone reductase activity in rat, pig and human livers. *Biochem. J.* **1991**, *279*, 903−906.
(20) Vander Jagt, D. L.; Hunsaker, L. A. Methylglyoxal metabolism and diabetic complications: roles of aldose reductase, glyoxalase-I, betaine aldehyde dehydrogenase and 2-oxoaldehyde dehydrogenase. *Chem.−Biol. Interact.* **2003**, *143/144*, 341−451.
(21) Cao, D.; Fan, S. T.; Chung, S. S. Identification and characterization of a novel human aldose reductase-like gene. *J. Biol. Chem.* **1998**, *273*, 11429−11435.
(22) Zhong, L.; Liu, Z.; Yan, R.; Johnson, S. Aldo-keto reductase family 1 B10 protein detoxifies dietary and lipid-derived α,β-unsaturated carbonyls at physiological levels. *Biochem. Biophys. Res. Commun.* **2009**, *387*, 245−250.
(23) Collard, F.; Vertommen, D.; Fortpied, J.; Duester, G.; Van Schaftingen, E. Identification of 3-deoxyglucosone dehydrogenase as aldehyde dehydrogenase 1A1 (retinaldehyde dehydrogenase 1). *Biochimie* **2007**, *89*, 369−373.
(24) Lal, S.; Szwergold, B. S.; Walker, M. A.; Randall, W. C.; Kappler, F.; Beisswenger, P. J.; Brown, T. R. Production and metabolism of 3-deoxyglucosone in humans. *The Maillard Reaction in Foods and Medicine*; Special Publication 223; Crabbe, J., Nursten, H. E., O'Brien, J., Eds.; Royal Society of Chemistry: Cambridge, UK, 1998; pp 291−297.
(25) Wells-Knecht, K. J.; Lyons, T. J.; McCance, D. R.; Thorpe, S. R.; Feather, M. S.; Baynes, J. W. 3-Deoxyfructose concentrations are increased in human plasma and urine in diabetes. *Diabetes* **1994**, *43*, 1152−1156.
(26) Henle, T.; Bachmann, A. Synthesis of pyrraline reference material. *Z. Lebensm. Unters. Forsch.* **1996**, *202*, 72−74.
(27) Brady, R. F. Cyclic acetals of ketoses. 3. Re-investigation of synthesis of isomeric di-*O*-isopropylidene-β-D-fructopyranoses. *Carbohydr. Res.* **1970**, *15*, 35−40.
(28) Rasmussen, J. R.; Slinger, C. J.; Kordish, R. J.; Newman-Evans, D. D. Synthesis of deoxy sugars. Deoxygenation by treatment with *N,N′*-thiocarbonyldiimidazole/tri-*n*-butyl-stannane. *J. Org. Chem.* **1981**, *46*, 4843−4846.
(29) Szarek, W. A.; Rafka, R. J.; Yang, T. F.; Martin, O. R. Structure-sweetness relationships for fructose analogs. Part III. 3-Deoxy-D-*erythro*-hexulose (3-deoxy-D-fructose): composition in solution and evaluation of sweetness. *Can. J. Chem.* **1995**, *73*, 1639−1644.
(30) Wahdan, H. A. L. Causes of the antimicrobial activity of honey. *Infection* **1998**, *26*, 26−31.
(31) Troyano, E.; Olano, A.; Fernaindez-Diaz, M.; Sanz, J.; Martinez-Castro, I. Gas chromatographic analysis of free monosaccharides in milk treatment of milk samples. *Chromatographia* **1991**, *32*, 379−382.
(32) Glomb, M. A.; Tschirnich, R. Detection of α-dicarbonyl compounds in Maillard reaction systems and in vivo. *J. Agric. Food Chem.* **2001**, *49*, 5543−5550.
(33) Rojas-Escudero, E.; Alarcón-Jiménez, A. L.; Elizalde-Galván, P.; Rojo-Callejas, F. Optimization of carbohydrate silylation for gas chromatography. *J. Chromatogr., A* **2004**, *1027*, 117−120.
(34) Kopper, S.; Freimund, S. The composition of keto aldoses in aqueous solution as determined by NMR spectroscopy. *Helv. Chim. Acta* **2003**, *86*, 827−843.
(35) Peterson, G. Gas-chromatographic analysis of sugars and related hydroxy acids as acyclic oxime and ester trimethylsilyl derivatives. *Carbohydr. Res.* **1974**, *33*, 47−61.
(36) Shoemaker, J. D.; Elliott, W. H. Automated screening of urine samples for carbohydrates, organic and amino acids after treatment with urease. *J. Chromatogr.* **1991**, *562*, 125−138.
(37) Lentner, C. *Units of Measurement, Body Fluids, Composition of the Body, Nutrition*; CIBA-Geigy AG: Basel, Switzerland, 1991.
(38) Molnár-Perl, I.; Horváth, K. Simultaneous quantitation of mono-, di- and trisaccharides as their TMS ether oxime derivatives by GC-MS: I. In model solutions. *Chromatographia* **1997**, *45*, 321−327.
(39) Boeniger, M. F.; Lowry, L.; Rosenberg, J. Interpretation of urine results used to assess chemical-exposure with emphasis on creatinine adjustment − a review. *Am. Ind. Hyg. Assoc. J.* **1993**, *54*, 615−627.
(40) Delpierre, G.; Veiga-da-Cunha, M.; Vertommen, D.; Buysschaert, M.; Van Schaftingen, E. Variability in erythrocyte fructosamine 3-kinase activity in humans correlates with polymorphisms in the FN3K gene and impacts on haemoglobin glycation at specific sites. *Diabetes Metab.* **2006**, *32*, 31−39.
(41) Krause, R.; Oehme, A.; Wolf, K.; Henle, T. A convenient HPLC assay for the determination of fructosamine-3-kinase activity in erythrocytes. *Anal. Bioanal. Chem.* **2006**, *386*, 2019−2025.
(42) Hellwig, M.; Geissler, S.; Matthes, R.; Peto, A.; Silow, C.; Brandsch, M.; Henle, T. Transport of free and peptide-bound glycated amino acids: synthesis, transepithelial flux at Caco-2 cell monolayers, and interaction with apical membrane transport proteins. *ChemBioChem* **2011**, *12*, 1270−1279.

JOURNAL OF AGRICULTURAL AND FOOD CHEMISTRY

Addition/Correction

pubs.acs.org/JAFC

Correction to Sulforaphane Potentiates the Efficacy of Imatinib against Chronic Leukemia Cancer Stem Cells through Enhanced Abrogation of Wnt/^{b}-Catenin Function

Li-Ching Lin, Chi-Tai Yeh, Chia-Chun Kuo, Chi-Ming Lee, Gow-Chin Yen, Liang-Shun Wang, Chih-Hsiung Wu, Wei-Chung Vivian Yang, and Alexander T. H. Wu*

J. Agric. Food Chem. **2012**, *60* (28), 7031−7039. DOI: 10.1021/jf301981n

J. Agric. Food Chem. **2013**, *61* (22), 5410−5410. DOI: 10.1021/jf402029d

In our previous correction (*J. Agric. Food Chem.* **2013**, *61* (22), 5410), we have pointed out the misplaced western strips of p-CRKL and β-catenin while compiling Figure 3. Now we note that the action controls have also been revised.

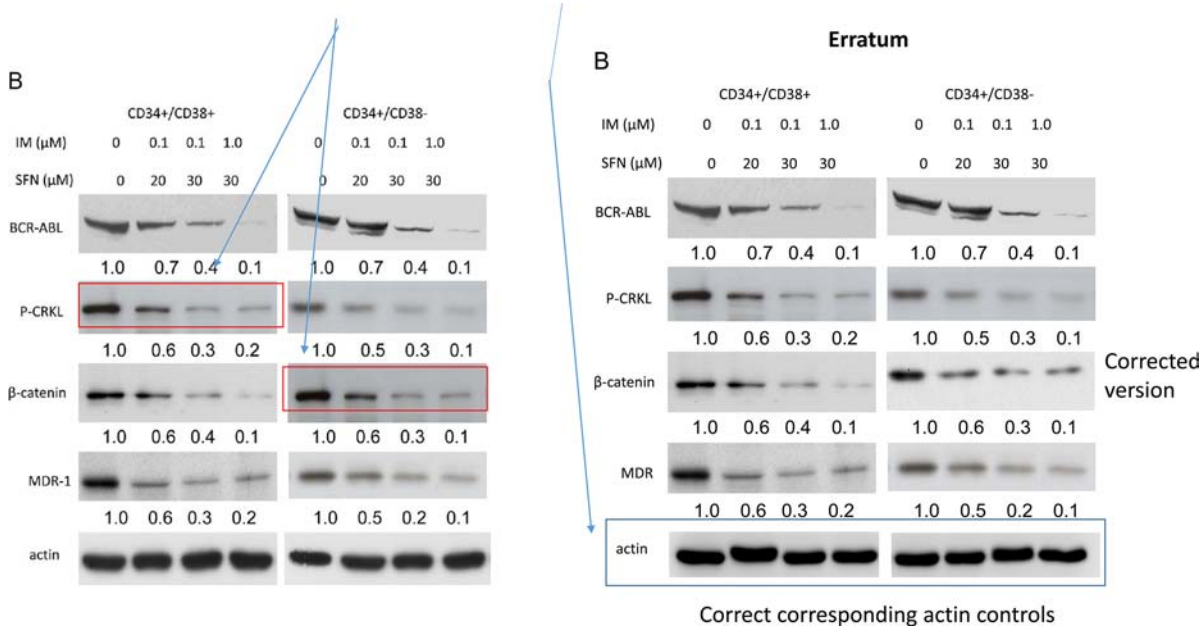

Figure 3. Corrected version of Figure 3.

Published: March 10, 2014

ACS Publications © 2014 American Chemical Society

purchased from various producers. A total of 10 samples of extra VOOs, coded F_v, F_N, F_1, Z_v, Z_1, Z_2, C_v, C_1, Cha_1, and Cha_2, were chosen among a sample collection of the laboratory. The samples were kept at −23 °C in dark glass bottles with minimum headspace flushed with N_2 until analysis.

Polar Fraction Preparation. The polar fraction was extracted from 2.5 g of VOO dissolved in 5 mL of hexane using an equal volume of methanol/water (60:40 v/v). The mixture was vortexed for 2 min and centrifuged for 10 min at 3500 rpm. The isolated polar fraction was then used for the determination of total polar phenol content (TPP) colorimetrically[10] and RP-HPLC separation of phenolic compounds prior to and after acidic hydrolysis.[8,9] A second extraction was not necessary as >95% of TPP was obtained in the first extract (n = 5). Repeatability of the process was adequate (CV% = 4.7 for TPP = 7.67 mg caffeic acid/20 g oil, n = 5).

Acidic Hydrolysis according to Mulinacci et al.[8] (Protocol 1). Briefly, an aliquot (200 μL) from the polar fraction was mixed with 200 μL of a 1 M H_2SO_4 solution. The mixture was maintained in a water bath at 80 °C for 2 h. The procedure was carried out in triplicate. Each hydrolysate was then diluted with 200 μL of acetonitrile/water 50:50, v/v. The three replicates were combined to obtain a representative hydrolysate. The latter was filtered through a 0.45 μm pore size regenerated cellulose membrane (Schleicher and Schuell, MicroScience GmbH, Dassel, Germany) before injection into the chromatograph. Method intra- and interday repeatabilities (in two different days) were examined for a VOO sample (n = 5), and the respective CV% values obtained for Htyr and Tyr were 0.9/2.4 and 1.5/2.2. Samples were then analyzed in triplicate.

Acidic Hydrolysis according to Romero and Brenes[9] (Protocol 2). Fifty milliliters of 2 M HCl was added to 2.5 g of VOO in a 100 mL glass bottle that was closed with a polypropylene cap. The mixture was vigorously agitated at 250 rpm in a shaker incubator (model MkX, Stoke Poges, UK) at 25 °C for 6 h in triplicate for each sample. Finally, 2 mL of the aqueous phase was removed by a plastic pipet from each replicate, mixed to form a representative hydrolysate, and filtered through a 0.45 μm regenerated cellulose membrane before injection into the chromatograph. Samples were analyzed in triplicate.

RP-HPLC Analysis. The elution system used for the chromatographic separation of polar phenols on a Nucleosil C_{18} (250 × 4.6 mm, 5 μm) column (Macherey-Nägel, Düren, Germany) consisted of 1% aqueous acetic acid (solvent A) and acetonitrile (solvent B). The gradient was as follows: 0−2 min, 5% B; 2−15 min, 25% B; 15−22 min, 25% B; 22−30 min, 40% B; 30−40 min, 60% B; 40−50 min, 95% B; 50−52 min, 95% B; 52−54 min, 100% B; 54−60 min, 5% B, at a flow rate of 0.5 mL/min and an injection volume of 20 μL. Diode array (UV 6000 LP model, cell volume = 10 μL, Thermo Separation Products, San Jose, CA, USA) and fluorescence (SSI 502 model, cell volume = 8 μL, Scientific Systems Inc., State College, PA, USA) detectors were used in line. Calibration curves were constructed for Htyr and Tyr at appropriate wavelengths[5] [280 nm; exc 280 nm/em 320 nm] (Supporting Information Figure S1). The limit of detection (LOD) and the limit of quantification (LOQ) were estimated for both Htyr and Tyr at 280 nm using the following equations:[11] LOD = 3.3 × σ/S' and LOQ = 10 × σ/S' (where σ is the standard error of the y intercept and S' the slope of the calibration curve). The values obtained were 0.7 and 2.0 ng/μL (Htyr) and 1.9 and 5.9 ng/μL (Tyr), respectively.

RESULTS AND DISCUSSION

First, the stability of Htyr and Tyr and the completeness of oleuropein hydrolysis claimed by Mulinacci et al.[8] were verified. Both compounds were found to be stable, and estimated losses for a solution of 250 mg/L accounted for approximately 6.1% (n = 3) for Htyr and 3% (n = 3) for Tyr using the respective calibration curves. Hydrolysis of an oleuropein solution (250 mg/L) was complete, leading to the sole formation of Htyr. Similarly, the parameter "agitation" of protocol 2 was tested for one VOO sample using two shaker types and was not found to be critical (Table 1). Nevertheless, the yields derived for Htyr and Tyr were half of those obtained using protocol 1, as shown in the same table.

Table 1. Effect of Agitation on the Yield of Htyr, Tyr, and Their Sum according to Protocol 2

hydrolysis conditions, 2 M HCl, 6 h	Htyr[a] (mg/20 g oil)	Tyr[a] (mg/20 g oil)	Htyr + Tyr (mg/20 g oil)
400 rpm[b]	0.66 a ± 0.01	0.31 a ± 0.01	0.97
200 rpm[b]	0.69 ab ± 0.02	0.33 ab ± 0.02	1.02
250 rpm[c]	0.72 b ± 0.01	0.35 b ± 0.01	1.07
isolation of polar fraction/ 1 M H_2SO_4, 2 h, 80 °C[d]	1.63 c ± 0.03	0.69 c ± 0.02	2.32

[a]Data are the mean ± standard deviation (n = 3). Different letters in the columns represent significant differences in concentration (p < 0.05). [b]Bench-top yellow-line orbital shaker (IKA-Werke GmbH & Co. KG). [c]Shaker incubator (model MkX, Stoke Poges, UK). [d]Protocol 1.

On the basis of the above findings the two protocols were applied to a series of extra VOOs varied in TPP levels (Table 2). The superiority of protocol 1 was evident in all cases (2−7-fold higher levels). The trend observed for the total content was also reflected in the ratios of individual phenol levels (data not shown). Subsequent discussion was, consequently, based on the results obtained using protocol 1. None of the extra VOO samples contained the minimum required level of total Htyr and Tyr content (5 mg/20 g oil), although some of them (Z_2, F_v, F_N, C_v) presented a rather high TPP content, unusual for commercial products. Using one standard curve for quantification of both phenols, it was evident that the use of Tyr resulted in higher levels in comparison to those using Htyr due to differences in ε values (see Figure S1A in the Supporting Information). Even so, the required limit was not achieved for any of the VOO samples. Fluorescence detection, which is more sensitive than UV absorption, gave comparable

Table 2. Effect of Acidic Hydrolysis Protocols on the Total Htyr and Tyr Content in Extra VOOs of Various TPP Levels

sample	TPP[c] (mg caffeic acid/20 g oil)	Htyr + Tyr[a,b] (mg/20 g oil) protocol 1	Htyr + Tyr[a,b] (mg/20 g oil) protocol 2	protocol 1/ protocol2
Z_v	6.42 a ± 0.3	2.34	0.88	2.7
Z_1	5.55 b ± 0.1	3.16	0.94	3.4
Z_2	8.39 c ± 0.1	3.10	1.08	2.9
C_v	7.95 cd ± 0.1	1.76	0.76	2.3
C_1	7.80 ed ± 0.1	2.92	0.70	4.2
F_v	9.07 ed ± 0.4	2.28	0.77	3.0
F_N	7.96 cd ± 0.5	2.91	0.84	3.5
F_1	2.03 f ± 0.1	3.73	0.53	7.0
Cha_1	4.20 g ± 0.3	3.11	0.51	6.1
Cha_2	7.67 h ± 0.5	2.57	1.08	2.4

[a]Quantification at 280 nm. [b]Htyr and Tyr were quantified using respective external calibration curves. Each [Htyr + Tyr] value is the sum of mean values of individual phenols measured in triplicate. [c]Data are the mean ± standard deviation (n = 3). Different letters in the same column represent significant differences in concentration (p < 0.05).

dx.doi.org/10.1021/jf5005918 | J. Agric. Food Chem. 2014, 62, 2459−2461

estimations of the total content of Htyr and Tyr (∼1.2−1.4-fold higher) by means of the two calibration curves (see Table S1 in the Supporting Information). Using one standard curve it was shown that Htyr resulted in higher levels of total phenols in comparison to those using Tyr due to differences in their fluorescence response (see Figure S1B in the Supporting Information). Some of the samples reached the required limit (see Table S1 in the Supporting Information).

From the TPP content, RP-HPLC profiles, and levels of Htyr and Tyr of the polar fraction prior to hydrolysis, it was observed that all of the oils were rich in complex forms of Htyr and Tyr. Indeed, the respective ranges prior to hydrolysis were extremely low (Htyr, 0.03−0.5 mg/20 g oil; Tyr, nd−0.43 mg/20 g oil), as expected for fresh oils. At this point we have to stress that calculation on a mass basis introduces a systematic error because the bound forms have a much higher molecular mass compared to those of simple phenols. The mean MW of the 10 most known bound forms of Htyr and Tyr[12] is ∼346 amu. If a correction factor is introduced in the quantification using both standards (Htyr, 2.2; Tyr, 2.5) to account for the differences in mass between Htyr, Tyr, and their complex forms, respectively, then 9 of 10 VOO samples satisfied the health claim using UV detection at 280 nm (5.2 −8.9 mg/20 g oil), and all of them satisfied the health claim when fluorescence was used (5.5−10.6 mg/20 g oil).

In conclusion, after many years of consultation a health claim was finally approved for VOO bioactive phenols, all of them derivatives of oleuropein and ligstroside. Addressing analytical requirements to support this health claim is imperative to ensure consumer protection and avoid unfair competition. Determination of free forms of Htyr and Tyr in the VOO polar fraction hydrolysate and introduction of a correction factor in quantification are needed to have a simple, reproducible, and undisputable analytical protocol.

Aspasia Mastralexi
Nikolaos Nenadis
Maria Z. Tsimidou*

Laboratory of Food Chemistry and Technology, School of Chemistry, Aristotle University of Thessaloniki, 541 24 Thessaloniki, Greece

■ ASSOCIATED CONTENT

Supporting Information

Table S1 and Figure S1. This material is available free of charge via the Internet at http://pubs.acs.org.

■ AUTHOR INFORMATION

Corresponding Author

*(M.Z.T.) Phone: +30 2310 997796 . Fax: +30 2310 997847. E-mail: tsimidou@chem.auth.gr.

Notes

The authors declare no competing financial interest.

■ REFERENCES

(1) European Community. Council Regulation No. 1924/2006 of 20 December 2006 on nutrition and health claims made on foods. *Off. J. Eur. Communities* **2006**, *L 404*, 9−25.

(2) European Community. Council Regulation No. 1169/2011 of 25 October 2011 on the provision of food information to consumers. *Off. J. Eur. Communities* **2011**, *L 304*, 18−63.

(3) EU Register of nutrition and health claims made on foods, http://ec.europa.eu/nuhclaims (accessed Nov 24, 2013).

(4) European Community. Council Regulation No. 432/2012 of 16 May 2012 establishing a list of permitted health claims made on foods, other than those referring to the reduction of disease risk and to children's development and health. *Off. J. Eur. Communities* **2012**, *L 136*, 1−40.

(5) Tsimidou, M. Z. Analytical methodologies: phenolic compounds related to olive oil taste issues. In *Handbook of Olive Oil: Analysis and Properties*, 2nd ed.; Aparicio, R., Harwood, J., Eds.; Springer Science + Business Media: New York, 2013; pp 311−333.

(6) EFSA Panel on Dietetic Products Nutrition and Allergens. Scientific Opinion on the substantiation of health claims related to polyphenols in olive and protection of LDL particles from oxidative damage (ID 1333, 1638 1639, 1696 2865), maintenance of normal blood HDL cholesterol concentrations (ID 1639), maintenance of normal blood pressure (ID 3781), "anti-inflammatory properties" (ID 1882), "contributes to the upper respiratory tract health" (ID 3468), "can help to maintain a normal function of gastrointestinal tract" (3779), and "contributes to body defences against external agents" (ID 3467) pursuant to Article 13(1) of Regulation (EC) No. 1924/2006. *EFSA J.* **2011**, *9*, 2033−2058.

(7) International Olive Council (IOC). Determination of biophenols in olive oil by HPLC. COI/T.20/Doc. no. 29, November 2009.

(8) Mulinacci, N.; Giaccherini, C.; Ieri, F.; Innocenti, M.; Romani, A.; Vincieri, F. F. Evaluation of lignans and free and linked hydroxy-tyrosol and tyrosol in extra virgin olive oil after hydrolysis processes. *J. Sci. Food Agric.* **2006**, *86*, 757−764.

(9) Romero, C.; Brenes, M. Analysis of total contents of hydroxytyrosol and tyrosol in olive oils. *J. Agric. Food Chem.* **2012**, *60*, 9017−9022.

(10) Blekas, G.; Psomiadou, E.; Tsimidou, M.; Boskou, D. On the importance of total polar phenols to monitor the stability of Greek virgin olive oil. *Eur. J. Lipid Sci. Technol.* **2002**, *104*, 340−346.

(11) Snyder, L. R.; Kirkland, J. J.; Dolan, J. W. *Introduction to Modern Liquid Chromatography*; Wiley: Hoboken, NJ, USA, 2010; pp 510−514.

(12) Nenadis, N.; Wang, L. F.; Tsimidou, M. Z.; Zhang, H. Y. Radical scavenging potential of phenolic compounds encountered in *O. europaea* products as indicated by calculation of bond dissociation enthalpy and ionization potential values. *J. Agric. Food Chem.* **2005**, *53*, 295−299.

Table 1. Levels of HBCD in Food, Based on Samples Collected in Catalonia (NW of Spain)[a]

	no. of samples	fat (%)	α-HBCD	γ-HBCD	α-/γ-HBCD	∑HBCDs	daily ave consumption (g)[b]
pandora	1	3.73	4.75	9.64	0.5	14.4	
sole	1	0.88	11.3	6.29	1.8	17.6	
gilthead	3	9.10	3.08	2.38	2.2	5.46	
trout	3	5.32	3.15	1.29	2.4	4.44	
mackerel	3	3.71	9.49	3.03	3.4	12.5	
anchovy	2	3.75	9.45	2.17	4.5	11.6	
sardine	1	5.06	5.81	4.88	1.2	10.7	
mussels	2	2.30	7.27	9.68	1.2	17.0	
scallops	1	1.50	11.3	6.81	1.7	18.1	
cod liver	5	71.5	2.86	1.68	4.9	4.54	
∑fish and seafood	22		6.84	4.79	2.4	11.6	94.4
chicken	3	2.42	2.03	4.53	0.6	6.56	
pork	2	9.52	0.99	1.61	0.6	2.61	
turkey	2	4.66	0.35	0.45	0.8	0.81	
veal	1	7.22	0.36	0.37	1.0	0.73	
∑meat	8		0.93	1.74	0.8	2.68	167
sausage	2	32.4	0.20	0.27	0.8	0.47	
fat	2	90.1	0.60	0.40	2.0	1.00	
∑animal fat	4		0.40	0.34	1.4	0.74	20.3
milk	3	2.88	0.27	0.34	0.9	0.61	
yoghurt	2	6.52	0.27	0.32	0.8	0.59	
cheese	2	16.8	0.53	0.59	0.9	1.12	
∑dairy products	7		0.36	0.42	0.9	0.78	351
eggs	4	9.41	0.51	1.25	0.8	1.75	31.2
vegetable oils	2	100	0.17	0.28	0.9	0.45	33.6

[a]Values are given in ng/g lw and are presented as mean concentrations. [b]Data from ref 18.

Cambridge Isotope Laboratories Inc. (WI, USA) and were of minimum 97% purity.

Sample Preparation. For meat, egg, dairy products, vegetable oil, and fat samples, the equivalent to one gram of fat was weighed. For fish samples, 20 g was weighed. Each sample aliquot was spiked with d_{18}-labeled α- and γ-HBCD as internal standards. Meat and fish samples were extracted in a Soxhlet apparatus with a mixture of hexane:dichloromethane (1:1). Dairy products were extracted in a separatory funnel with a mixture of ethanol, diethyl ether, and hexane and previous addition of an aqueous potassium oxalate solution. Egg samples were hydrolyzed with concentrated hydrochloric acid, previously extracted with hexane. The treated egg samples were extracted in a separatory funnel with a mixture of diethyl ether:hexane (1:1). Oil and fat samples were dissolved in 10 mL of hexane. After the extraction, lipid content was determined gravimetrically and the resulting extracts were redissolved in hexane. Then, fat was removed by an acid treatment: extracts were cleaned up by the addition of 10 mL of concentrated sulfuric acid. Organic fraction (containing HBCD) was evaporated to 3 mL, and the whole cleanup procedure was repeated until the acid did not turn yellow. Final purification of the extract was carried out in 5 g alumina SPE cartridges. Cartridges were conditioned with 20 mL of hexane and eluted with 30 mL of hexane:dichloromethane (1:2). Purified extracts were concentrated with a gentle nitrogen flow and spiked with d_{18}-labeled β-HBCD as injection standard, and reconstituted to a final volume of 200 μL.[4]

To avoid the presence of interfering substances, glassware was rinsed with acetone and hexane just after its use. After solvent wash, it was also cleaned with water and detergent and purified water. Finally, it was rinsed again with acetone and heated at 300 °C in an oven overnight.

Diastereosiomer Analysis. A Symbiosis Pico (Spark Holland, Emmen, The Netherlands) with a Symmetry C18 column (2.1 mm × 150 mm, 5 μm) preceded by a C18 guard column (2.1 × 10 mm) supplied by Waters (Massachusetts, USA) was used for isomeric HBCD determinations. Experiments were carried out with H_2O:methanol (3:1 v/v) as eluent A and methanol as eluent B, at a flow rate of 0.25 mL/min. The elution program started at an initial composition of 100% A and was ramped to 0% A in the first eight minutes, then eluent A increased to 10% in 17 min, and initial conditions were reached again in 3 min and returned to the starting conditions in 15 min. The injection volume was set at 10 μL.

Mass spectrometric analysis was carried out with a hybrid triple quadrupole/linear ion trap MSD Sciex 4000QTRAPTM (Applied Biosystems, Foster City, CA, USA) instrument equipped with an electrospray (ESI) Turbospray interface, working in negative ionization mode. Data acquisition was performed in selected reaction monitoring (SRM). The $[M - H]^- \rightarrow Br^-$ transitions at m/z 638.7 → 78.9 and 638.7 → 80.9 were monitored for unlabeled HBCDs. The labeled HBCDs were monitored at the 655.8 → 78.9 and 655.8 → 80.9 transitions. The MS−MS detection conditions were optimized to obtain the highest relative intensity: curtain gas at 50 psi, collision gas at 4.5×10^{-5} Torr, temperature of the turbo gas in the TurboIonSpray source at 350 °C, ion source gas 1 at 50 psi, and ion source gas 2 at 10 psi.[8]

Quality Assurance/Quality Control. Method blank samples were performed to check for interferences or contamination from solvents and glassware. No presence of analytes of interest (α-, β-, and γ-HBCDs diastereoisomers) was observed. Spiked samples with native compounds (α-, β-, and γ-HBCD) were analyzed by the described methodology to check recoveries. Recovery values ranged from 79 to 119%, with a relative standard deviation (n = 5) values between 7% and 10%.

The LC−MS−MS identification was based on three main criteria. First of all, simultaneous responses for the two monitored transitions (SRM1 and SRM2) must be obtained at the same retention time than those of available standards. Then, signal-to-noise ratios must be >3. And finally, relative peak intensity ratio must be within ±20% of the theoretical values obtained with standard solutions. Limits of detection, defined as the minimum amount of analyte which produces a peak with a signal-to-noise ratio equal to 3, were 0.03 ng/g for α-HBCD, 0.05 ng/g for β-HBCD, and 0.06 ng/g for γ-HBCD. Limits of quantification, defined as the minimum amount of analyte which produces a peak with a signal-to-noise ratio equal to 10, were 0.11, 0.18, and 0.20 ng/g for α-, γ-, and β-HBCD, respectively.

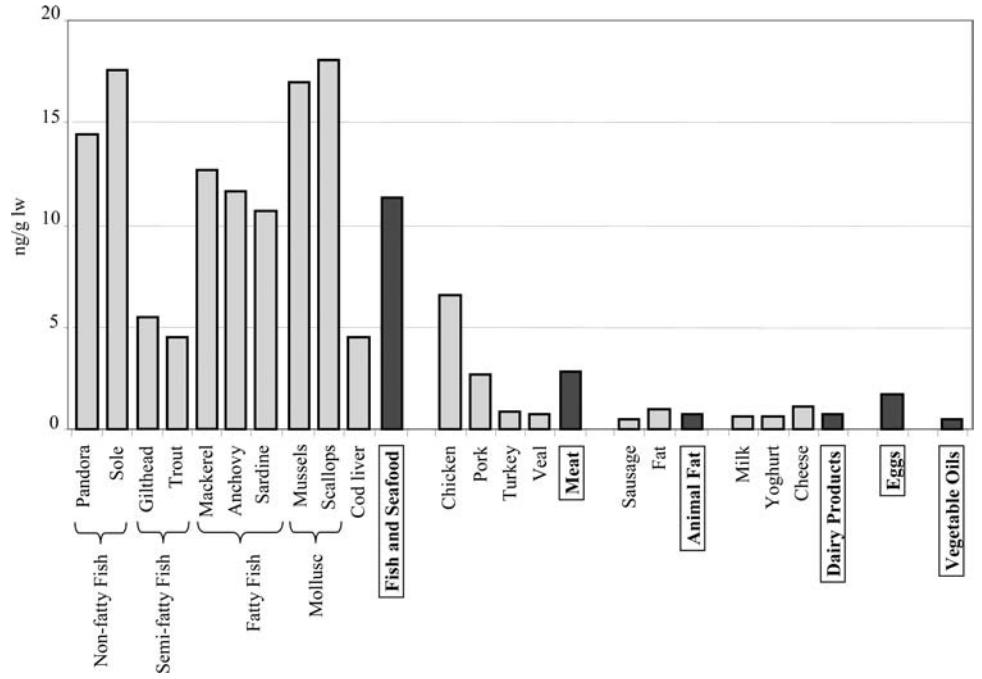

Figure 1. Occurrence of HBCD in Spanish food. Data are mean values (ng/g lw).

Enantiomeric Analysis. A Nucleodex β-PM (4.0 mm × 200 mm × 5 μm) column supplied by Macherey-Nagel (Düren, Germany) was used to perform the enantiomer-specific determination. The separation was achieved using methanol, acetonitrile, and water as mobile phase. Experiments were carried out using 70% water:30% methanol as eluent A and 70% AcN:30% methanol as eluent B, at a flow rate of 0.50 mL min^{-1}. The injection volume was set at 10 μL. The elution program started at an initial concentration of A at 50% decreased to 0% along the first 8 min, and was maintained for 17 min, and initial conditions were reached again in 5 min and maintained for additional 12 min.[9] Mass spectrometric analysis was performed using the same conditions as for diastereoisomer analysis.

Enantiomeric composition was expressed as enantiomeric fraction (EF), which is calculated by eq 1:

$$\mathrm{EF} = \frac{A_+}{(A_+ + A_-)} \quad (1)$$

where A_+ and A_- are the peak areas of eluting enantiomers. It is well-known that ESI is subjected to sample matrix effects that can cause enhancement or suppression of the target analytes' signal and can adversely affect their quantification. In order to avoid this effect that can affect EF calculations, these values are calculated according to eq 2,[10] which makes a correction based on the use of isotopic labeled standards (d_{18}-HBCDs) since d_{18}-labeled enantiomeric analogues behave in an identical manner to their native counterparts:

$$\mathrm{EF}_{\mathrm{corrected}} = \frac{([A_+]/[A_{+\mathrm{d18}}]) \times \mathrm{pg}\, A_{+\mathrm{d18}}}{([A_+]/[A_{+\mathrm{d18}}]) \times \mathrm{pg}\, A_{+\mathrm{d18}} + ([A_-]/[A_{-\mathrm{d18}}]) \times \mathrm{pg}\, A_{-\mathrm{d18}}} \quad (2)$$

where $[A_+]$ and $[A_-]$ are the peak areas of the respective (+) and (−) HBCD enantiomers, $[A_{+\mathrm{d18}}]$ and $[A_{-\mathrm{d18}}]$ are the peak areas of the respective (+) and (−) HBCD d_{18}-labeled standards, while pg $A_{+\mathrm{d18}}$ and $A_{-\mathrm{d18}}$ stand for the noncorrected determined HBCD concentrations.

RESULTS AND DISCUSSION

HBCD Occurrence in Spanish Food Samples. This study is the first to report the concentrations of α-, β-, and γ-HBCDs in different foods in Spain. HBCD levels were analyzed in fish and seafood, meat, animal fat, dairy products, eggs, and vegetable oils since HBCD is a POP and is most likely found in food with fat from animal origin. The results for the 47 products analyzed are shown in Table 1. HBCDs were detected in all analyzed foods. The highest concentrations of HBCD were found in fish and seafood (1.91−23.4 ng/g lw), followed by meat (0.73−12.9 ng/g lw), eggs (0.28−3.42 ng/g lw), dairy products (0.32−1.35 ng/g lw), animal fat (0.27−1.13 ng/g lw), and olive oils (0.18−0.72 ng/g lw). This fact would indicate a higher accumulation of HBCD in fish, similar to other POPs such as PCBs, PCDD/Fs, or PBDEs.

In samples from the meat group, HBCD levels decreased from chicken > pork > turkey > veal. As regards samples from the fish group, molluscs showed the highest levels of contamination (10.5−23.4 ng/g lw), followed by fatty fishes (10.7−14.2 ng/g lw), and then semifat fishes (3.31−7.60 ng/g lw). However, and surprisingly, HBCD levels in sole and pandora, two nonfatty fishes, are among the highest (14.4−17.6 ng/g lw) (Figure 1).

If the concentrations are expressed on fresh weight basis, the highest concentrations were those from products with high fat content: cod liver (1.37−8.44 ng/g ww) and animal fat (0.11−1.11 ng/g ww). Even in this case, fish, and seafood samples showed higher concentrations (mean value of 1.05 ng/g ww) than those detected in animal fat (mean value of 0.53 ng/g ww), vegetable oils (mean value of 0.45 ng/g ww), eggs (mean value of 0.17 ng/g ww), meat (mean value of 0.13 ng/g ww), or dairy products (mean value of 0.07 ng/g ww).

Determined HBCD concentrations were compared to those found in the literature. Most authors reported higher concentrations of HBCD in fish than in the other food categories.[11−15] Our levels in fish and seafood (mean value of 11.6 ng/g lw, or 0.63 ng/g ww) are lower than those detected by Goscinny et al.[11] in Belgium (42 ng/g lw), but higher than those reported by Törnkvist et al.[12] in Sweden (0.15 ng/g ww), Schecter et al.[15] in the US (<0.03−0.35 ng/g ww), and Shi et

dx.doi.org/10.1021/jf405007x | J. Agric. Food Chem. 2014, 62, 2462−2468

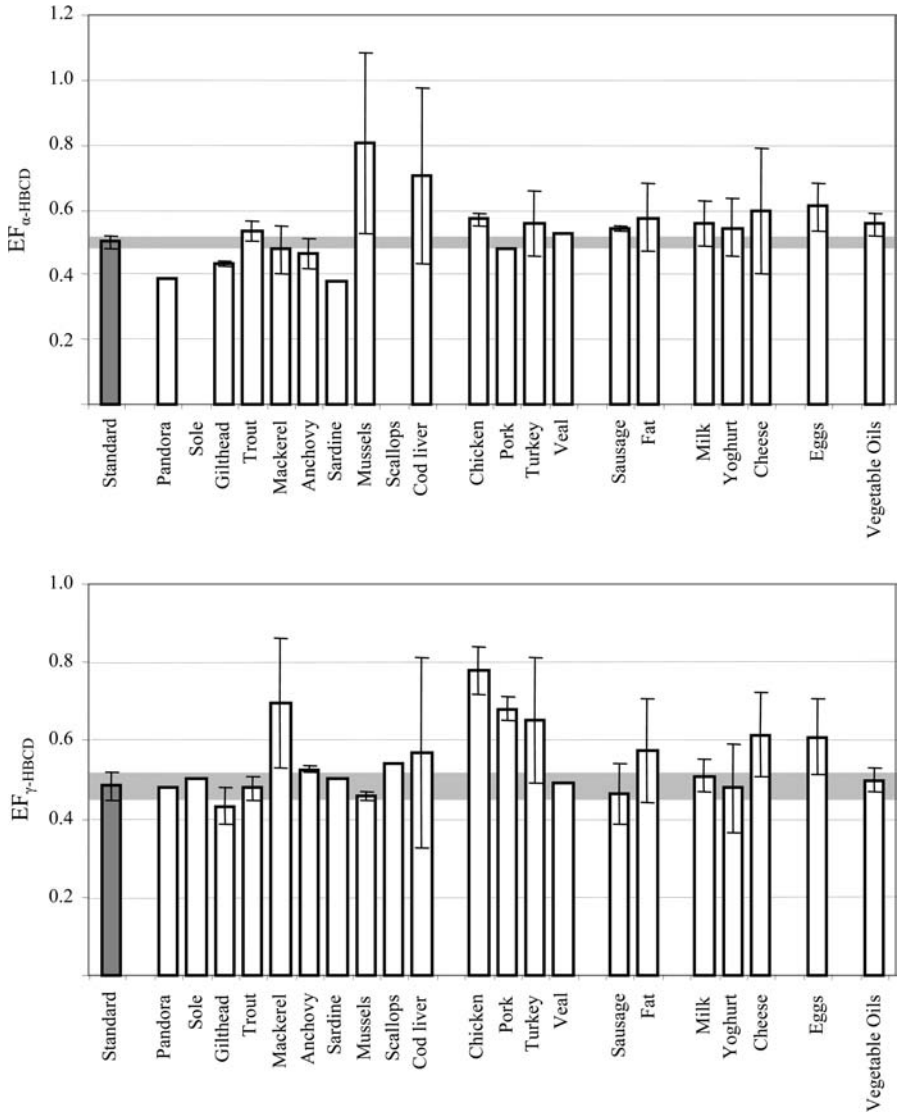

Figure 2. Enantiomeric fraction values (mean ± standard deviation) for α-HBCD and γ-HBCD in Spanish food compared to standards.

al.[13] in China (nd−2.22 ng/g lw). For some specific categories of fish and seafood (mackerel, sole, mussels), HBCD concentrations detected in our study are in the same range as those reported by Van Leeuwen and de Boer[16] in The Netherlands.

Isomeric Patterns. In all the samples, α- and γ-HBCDs were observed, whereas β-HBCD was not detected in any sample. The α- and γ-HBCD contribution was studied for the different groups of food. For fish and seafood samples, the contribution of α-HBCD was greater. In 14 out of 17 fish samples analyzed, α-HBCD concentration was higher than γ-HBCD, with α/γ ratios between 1.2 and 8.7. Similar results were found in the Belgian study, in which α-HBCD was the predominant isomer in fish samples.[11] For most of the other food samples, the trend is the inverse: γ-HBCD concentration was higher than that of α-HBCD. For meat samples, α/γ ratios ranged between 0.34 and 0.99, while for dairy products it ranged between 0.44 and 1.26. Three out of the four egg samples analyzed showed also α/γ ratios lower than 1.

Enantiomeric Fractions. EF values were calculated from the chiral column LC data, and the values were corrected according to eq 2 (Figure 2). In the case of γ-HBCD, it was observed that EF values were between 0.39 and 0.87, whereas EF for α-HBCD ranged between 0.38 and 1. If we compare these EF values with those obtained with standard solutions, in general, no significant differences were detected for γ-HBCD. The EF mean value obtained for standard solutions was 0.49 (with 7.6% of relative standard deviation (RSD)). In general, samples were between the EF value ± RSD range established with standard solutions. However, samples of mackerel (fish) (mean EF value ± SD of 0.70 ± 0.17) and chicken and pork (meat) (mean EF value ± SD of 0.78 ± 0.06 and 0.68 ± 0.03 respectively) presented an increase of EF value compared to standard value, indicating an enrichment of the (+)-γ-HBCD enantiomer in these samples.

In the case of α-HBCD, and for some fish samples (gilthead, pandora, and sardine), results showed a decrease of EF values (EF value of 0.43, 0.39, and 0.38 respectively) with respect to the standards (mean value of 0.50 with 3.6% of RSD). Thus, we can assume that an enrichment of the (−)-α-HBCD enantiomer was observed for these fish samples. Similar behavior was also detected in samples of herring muscle and falcon eggs,[17] and also significant enrichments for (−)-α-

dx.doi.org/10.1021/jf405007x | J. Agric. Food Chem. 2014, 62, 2462−2468

HBCD enantiomer was observed in human breast milk samples.[4]

Daily Intake Estimation. The estimated dietary intake (EDI) of HBCD is based on HBCD data from the present study combined with the consumption data from a Spanish diet model for determining consumer exposure to chemicals.[18] It is also important to note that we analyzed fresh foods, whereas preparation and different cooking methods can influence the levels of contaminants.[19] The Spanish dietary exposure to HBCD was 177 ng day^{-1}. Assuming the average adult body weight as 68 kg, the EDI of HBCD was 2.58 ng $(kg\ bw)^{-1}$ day^{-1}.

Our daily intake through the diet estimation was compared with other assessments in different countries around the world (Table 2). However, this comparison is not easy because there are some differences in sampling strategies, there is a lack of a standardized method for HBCD detection, and there is also a great variety in the number of analyses or different calculation methods for non detects or dietary intake. Once these parameters are taken into account, a comparison is anyway interesting.

Table 2. HBCD Daily Intake Estimation Worldwide

country	food	HBCD levels (ng/g)	daily intake (ng $(kg\ bw)^{-1}$ day^{-1})	ref
		Europe		
Sweden	fish, meat, dairy, eggs, oils	not reported	0.58−21.5	20
The Netherlands	fish, meat, dairy, eggs, oils	0.02−7.9 (ww[a])	1.5	21
The Netherlands	fish	nd[b]−230 (ww)	0.06−0.17	16
Norway	fish, meat, dairy, eggs, oils	nd−3.61 (ww)	0.3	22
Scotland, U.K.	seafood	0.03−12.1 (ww)	5.9−7.9	23
Belgium	fish, meat, dairy, egg, oils	nd−14.7 (lw[c])	0.99	11
Sweden	fish, meat, dairy, eggs, fats	nd−0.63 (ww)	0.14	12
Spain	fish, meat, dairy, eggs, oils	0.18−23.4 (lw)	2.58	this work
		Asia		
China	fish, meat, dairy, eggs	nd−9.21 (lw)	0.09−1.72	13
Japan	all market basket food	not reported	1.4−2.2	14
Japan	fish	nd−36.9 (ww)	1.3−3.7	24
Japan	seafood	12−5200 (lw)	0.45−34	25
		North America		
Canada	not reported	not reported	14	26
USA	fish, meat, dairy, eggs, vegetables	nd−0.59 (ww)	0.23	15

[a]Wet weight. [b]Not detected. [c]Lipid weight.

Some studies were carried out in different European countries. A median intake of 141 ng of HBCD per day (2.15 ng kg bw^{-1} day^{-1}) was estimated for the Swedish population, with a maximum of 1076 ng per day (21.5 ng kg bw^{-1} day^{-1}).[20] In another study,[21] the EDI was estimated at 1.5 ng kg bw^{-1} day^{-1} for the Dutch population. Later, van Leeuwen and de Boer[16] estimated the fish-related dietary exposure of HBCD for the average Dutch population. The median bound intake in that study was estimated at 8.3 ng day^{-1} for a 70 kg person (0.12 ng kg bw^{-1} day^{-1}). Dietary exposure to HBCD in the Norwegian population was established at 0.3 ng kg bw^{-1} day^{-1}.[22] The estimated adult dietary intake of HBCD arising from the United Kingdom diet resulted on higher levels than those mentioned so far, being in the range of 5.9−7.9 ng kg bw^{-1} day^{-1}.[23] This latter study only considered the intake due to seafood consumption. More recently, the intake of HBCD in Sweden was estimated by Törnkvist et al.[12] to be 0.14 ng kg bw^{-1} day^{-1} (10.2 ng day^{-1}), and Goscinny et al.[11] estimated an EDI of 0.99 ng kg bw^{-1} day^{-1} for the Belgian population. Our results were slightly higher than those reported in these studies for the European population. However, it must be taken into account that most of these studies were carried out a few years ago. It is expected that HBCD consumption has been increasing over the years due to the prohibition of PBDE use.

Few studies refer to EDI values in other continents. In Asia, Shi et al.[13] reported an EDI value in the range of 0.09−1.72 ng kg bw^{-1} day^{-1} for the Chinese population. Murata et al.[14] estimated a dietary HBCD intake of 2.2 and 1.4 ng kg bw^{-1} day^{-1} in 2002 and 2005, respectively. They analyzed 14 different food groups. However, HBCD was only detected in the fish group. In a later study, and based only on fish consumption, Nakagawa et al.[24] estimated an EDI between 1.3 and 3.7 ng kg bw^{-1} day^{-1} for the Japanese population. Higher estimation resulted from the study of Ueno et al.[25] They reported an EDI value between 0.45 and 34 ng kg bw^{-1} day^{-1}, based only on seafood consumption. These EDI values seem to be slightly higher than those reported for European citizens. Given that fish is the food group that provides the highest levels of HBCD contamination, a possible explanation could be the high consumption of fish in Asian diets.

As regards the American population, only two studies have been published dealing with HBCD EDI values. Schecter et al.[15] estimated, for the USA, an EDI value of 0.23 ng kg bw^{-1} day^{-1}, which matched reasonably well with European values. However, Environment Canada[26] established an EDI of 14 ng kg bw^{-1} day^{-1} for the Canadian population.

The calculated contributions of the different food groups to the total EDI of HBCD showed that fish and seafood was a major contributor (56%) for Spanish consumers (Figure 3). Meat (12%) and dairy products (14%) were also important

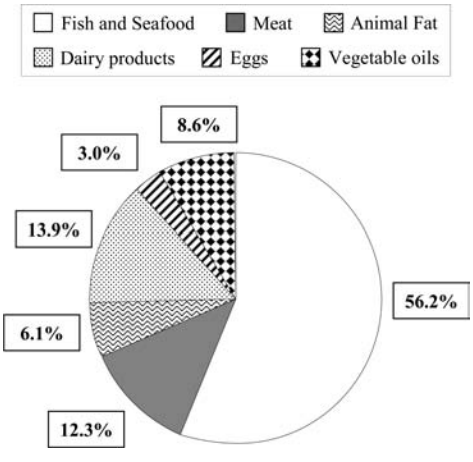

Figure 3. Relative contribution of the different food categories to the dietary intake of HBCD for Spanish consumers.

dx.doi.org/10.1021/jf405007x | J. Agric. Food Chem. 2014, 62, 2462−2468

food groups contributing to the Spanish intake of HBCD. Other studies have also reported fish as the major contributor to the HBCD intake. In the Swedish estimation[12] HBCD mainly came from fish (65%), but also dairy products (24%) and meat (10%) contributed. However, in the Belgian estimation[11] fish accounts for only 7.1% of the EDI, and the meat group was the highest contributor with 43%. This is due to the high consumption of meat and low consumption of fish in Belgium.

Previous studies have been carried out to estimate the human exposure to PBDEs through the diet in Spain. Bocio et al.[27] estimated the dietary intake of PBDEs for the general population living in Catalonia (Spain), and they found a value of 97 ng day^{-1} (1.4 ng kg bw^{-1} day^{-1}). A later study in the same area[28] showed an EDI decrease of 23%, with value of 1.1 ng kg bw^{-1} day^{-1}. An even lower value was reported by Gómara et al.[29] in a study including different locations in Spain, with an EDI value of 39 ng day^{-1} (0.6 ng kg bw^{-1} day^{-1}). However, these differences could be attributed in part to the different consumption data applied in each study, but also to other factors such as the sampling strategy, the way concentrations were given (upper, medium, and lower bound) or the number of PBDE congeners analyzed. In any case, the three values (0.6−1.4 ng kg bw^{-1} day^{-1}) obtained for the dietary intake of PBDEs in Spain were lower than the value obtained in our study for the dietary intake of HBCD (2.6 ng kg bw^{-1} day^{-1}).

Human exposure to HBCD occurs through multiple routes. For non occupationally exposed persons, the major intake of HBCD is probably from food and indoor air or dust. However, the relevance of human HBCD exposure originating from house dust versus food-based HBCD exposure is still unknown. Nondietary exposure, mainly through dust in homes, offices, schools, cars, and public environment can substantially contribute, and in some cases even dominate, the total human exposure to HBCD, especially for toddlers and other children.[30] Our study has focused on the intake of HBCD through the diet. Estimated daily intake of this contaminant for the Spanish population resulted in 2.58 ng $(kg\ bw)^{-1}$ day^{-1}. The main contributor to this intake was fish group, followed by dairy products and meat. Therefore, the exposure of frequent fish consumers could be higher than for the average consumers estimated in our study.

AUTHOR INFORMATION

Corresponding Author

*Tel: +34 934006100. E-mail: eeeqam@cid.csic.es.

Funding

This work was funded by the Spanish Ministry of Economy and Competitiveness through the project SCARCE (Consolider Ingenio 2010 CSD2009-00065). This work has also been partly funded by the Generalitat de Catalunya (Consolidated Research Group Water and Soil Quality Unit 2009-SGR-965).

Notes

The authors declare no competing financial interest.

REFERENCES

(1) EFSA. The European Food Safety Authority, 2006. Advice of the Scientific Panel on contaminants in the food chain on a request from the Commission related to relevant chemical compounds in the group of brominated flame retardants for monitoring in feed and food. EFSA J 328, 1−4. http://www.efsa.eu.int.

(2) Law, R. J.; Bersuder, P.; Allchin, C. R.; Barry, J. Levels of the flame retardants hexabromocyclododecane and tetrabromobisphenol A in the blubber of harbour porpoises (Phocoena phocoena) stranded or bycaught in the UK, with evidence for an increase in HBCD concentrations in recent years. *Environ. Sci. Technol.* **2006**, *40*, 2177−2183.

(3) Guerra, P.; de la Cal, A.; Marsh, G.; Eljarrat, E.; Barceló, D. Transfer of hexabromocyclododecane from industrial effluents to sediments and biota: Case study in Cinca river (Spain). *J. Hydrol.* **2009**, *369*, 360−367.

(4) Eljarrat, E.; Guerra, P.; Martínez, E.; Farré, M.; Alvarez, J. G.; López-Teijón, M.; Barceló, D. Hexabromocyclododecane in human breast milk: levels and enantiomeric patterns. *Environ. Sci. Technol.* **2009**, *43*, 1940−1946.

(5) Palace, V. P.; Pleskach, K.; Halldorson, T.; Danell, R.; Wautier, K.; Evans, B. Biotransformation enzymes and thyroid axis disruption in juvenile rainbow trout (*Oncorhynchus mykiss*) exposed to hexabromocyclododecane diastereoisomers. *Environ. Sci. Technol.* **2008**, *42*, 1967−72.

(6) van der Ven, L. T. M.; Slob, W.; Piersma, A. H.; Opperhuizen, A. The benchmark approach is the preferred method to describe the toxicology of tetrabromobisphenol A (TBBPA) - response to Banasik et al. (2009). *Toxicology* **2009**, *260*, 153−154.

(7) Eriksson, P.; Fischer, C.; Wallin, M.; Jakobsson, E.; Fredriksson, A. Impaired behaviour, learning and memory, in adult mice neonatally exposed to hexabromocyclododecane (HBCDD). *Environ. Toxicol. Pharmacol.* **2006**, *21*, 317−322.

(8) Guerra, P.; de la Torre, A.; Martínez, M. A.; Eljarrat, E.; Barceló, D. Identification and trace level determination of brominated flame retardants by LC-quadrupole linear ion trap (Qq-LIT) mass spectrometry. *Rapid Commun. Mass Spectrom.* **2008**, *22*, 916−924.

(9) Guerra, P.; Eljarrat, E.; Barceló, D. Enantiomeric specific determination of hexabromocyclododecane by LC-quadrupole linear ion trap (Qq-LIT) mass spectrometry in sediment samples. *J. Chromatogr.* **2008**, *1023*, 81−87.

(10) Marvin, C.; MacInnis, G.; Alahee, M.; Arsenault, G.; Tomy, G. Factors influencing enantiomeric fractions of hexabromocyclododecane measured using liquid chromatography/tandem mass spectrometry. *Rapid Commun. Mass Spectrom.* **2007**, *21*, 1925−1930.

(11) Goscinny, S.; Vandevijvere, S.; Maleki, M.; Van Overmeire, I.; Windal, I.; Hanot, V.; Blaude, M. N.; Vleminckx, C.; Van Loco, J. Dietary intake of hexabromocyclododecane diastereoisomers (α-, β-, and γ-HBCD) in the Belgian adult population. *Chemosphere* **2011**, *84*, 279−288.

(12) Törnkvist, A.; Glynn, A.; Aune, M.; Darnerud, P. O.; Ankarberg, E. H. PCDD/F, PCB, PBDE, HBCD and chlorinated pesticides in a Swedish market basket from 2005 − Levels and dietary intake estimations. *Chemosphere* **2011**, *83*, 193−199.

(13) Shi, Z. X.; Wu, Y. N.; Li, J. G.; Zhao, Y. F.; Feng, J. F. Dietary exposure assessment of Chinese adults and nursing infants to tetrabromobisphenol-A and hexabromocyclododecanes: occurrence measurements in foods and human milk. *Environ. Sci. Technol.* **2009**, *43*, 4314−4319.

(14) Murata, S.; Nakagawa, R.; Ashizuka, Y.; Hori, T.; Yasutake, D.; Tobiishi, K.; Sasaki, K. Brominated flame retardants (HBCD, TBBPA and ΣPBDEs) in market basket food samples of Northern Kyushu district in Japan. *Organohalogen Compd.* **2007**, *69*, 1985−1988.

(15) Schecter, A.; Haffner, D.; Colacino, J.; Patel, K.; Paepke, O.; Opel, M.; Birnbaum, L. S. Polybrominated Diphenyl Ethers (PBDEs) and Hexabromocyclodecane (HBCD) in Composite U.S. Food Samples. *Environ. Health Perspect.* **2010**, *118*, 357−362.

(16) van Leeuwen, S. P.; de Boer, J. Brominated flame retardants in fish and shellfish - levels and contribution of fish consumption to dietary exposure of Dutch citizens to HBCD. *Mol. Nutr. Food Res.* **2008**, *52*, 194−203.

(17) Janák, K.; Sellström, U.; Johansson, A. K.; Becher, G.; de Wit, C.; Lindberg, P.; Helander, B. Enantiomer-specific accumulation pattern of hexabromocyclododecane in eggs of predatory birds breeding in Sweden. *Organohalogen Compd.* **2005**, *67*, 204−207.

(18) AESAN, 2006. Modelo de dieta española para la determinación de la exposición del consumidor a sustancias químicas. Rev. 1. Available at http://www.aesan.msc.es/AESAN/docs/docs/notas_prensa/modelo_dieta_espanola.pdf.
(19) Perelló, G.; Martí-Cid, R.; Castell, V.; Llobet, J. M.; Domingo, J. L. Concentrations of polybromianted diphenyl ethers, hexachlorobenzene and polycyclic aromatic hydrocarbons in various foodstuffs before and after cooking. *Food Chem. Toxicol.* **2009**, *47*, 709−715.
(20) Lind, Y.; Aune, M.; Atuma, S.; Becker, W.; Bjerselius, R.; Glynn, A.; Darnerud, P. O. Food intake of the polybrominated flame retardants PBDEs and HBCD in Sweden. *Organohalogen Compd.* **2002**, *58*, 181−184.
(21) de Winter-Sorkina, R.; Bakker, M. I.; van Donkersgoed, G.; van Klaveren, M. D. Dietary intake of brominated flame retardants by the Dutch population. RIVM report n° 310305001/**2003**.
(22) Knutsen, H. K.; Kvalem, H. E.; Thomsen, C.; Froshaug, M.; Haugen, M.; Becher, G.; Alexander, J.; Meltzer, H. M. Dietary exposure to brominated flame retardants correlates with male blood levels in a selected group of Norwegians with a wide range of seafood consumption. *Mol. Nutr. Food Res.* **2008**, *52*, 217−227.
(23) Fernandes, A.; Dicks, P.; Mortimer, D.; Gem, M.; Smith, F.; Driffield, M.; White, S.; Rose, M. Brominated and chlorinated dioxins, PCBs and brominated flame retardants in Scottish shellfish: methodology, occurrence and human dietary exposure. *Mol. Nutr. Food Res.* **2008**, *52*, 238−249.
(24) Nakagawa, R.; Murata, S.; Ashizuka, Y.; Shintani, Y.; Hori, T.; Tsutsumi, T. Hexabromocyclododecane determination in seafood samples collected from Japanese coastal areas. *Chemosphere* **2010**, *81*, 445−452.
(25) Ueno, D.; Isobe, T.; Ramu, K.; Tanabe, S.; Alaee, M.; Marvin, C.; Inoue, K.; Someya, T.; Miyajima, T.; Kodama, H.; Nakata, H. Spatial distribution of hexabromocyclododecanes (HBCDs), polybrominated diphenyl ethers (PBDEs) and organochlorines in bivalves from Japanese coastal waters. *Chemosphere* **2010**, *78*, 1213−1219.
(26) Environment Canada, 2010. Draft Screening Assessment: Cyclododecane, 1,2,5,6,9,10-hexabromo. Available at http://www.ec.gc.ca/lcpe-cepa/default.asp?lang=En&n=A27E7A60-1.
(27) Bocio, A.; Llobet, J. M.; Domingo, J. L.; Corbella, J.; Teixidó, A.; Casa, C. Polybrominated diphenyl ethers (PBDEs) in foodstuffs: human exposure through the diet. *J. Agric. Food Chem.* **2003**, *51*, 3191−3195.
(28) Domingo, J. L.; Martí-Cid, R.; Castell, V.; Llobet, J. M. Human exposure to PBDEs through the diet in Catalonia, Spain: temporal trend. A review of recent literature on dietary PBDE intake. *Toxicology* **2008**, *248*, 25−32.
(29) Gómara, B.; Herrero, L.; González, M. J. Survey of polybrominated diphenyl ether levels in Spanish commercial foodstuffs. *Environ. Sci. Technol.* **2006**, *40*, 7541−7547.
(30) EFSA. Scientific opinion on hexabromocyclododecanes (HBCDDs) in food. *EFSA J.* **2011**, *9* (7), 2296.

MATERIALS AND METHODS

Chemicals and Reference Compounds. Dichloromethane (99.99%) was supplied by Fischer Scientific (Illkirch, France) and absolute ethanol (99.9%) by Merck (Semoy, France). All of the reference compounds were provided by Sigma-Aldrich (Saint-Quentin-Fallavier, France) [3-methyl-4-octanolide (98%), γ-nonalactone (98%), and eugenol (99%)].

Synthesis of 2-Nonen-4-olide. The lactone was prepared by the reaction of a stabilized vinyl Grignard reagent (isopropyl magnesium chloride, *i*PrMgCl)[20] on hexanal, as described.[21] A flame-dried 500 mL round-bottom flask, equipped with a Teflon-coated magnetic stirring bar, was loaded with 3-iodobut-2-enoic acid ethyl ester[22] (6.9 g, 32.7 mmol) under an argon atmosphere. Tetrahydrofuran (THF; 130 mL) was added and the mixture cooled to −78 °C. *i*PrMgCl solution (16.4 mL, 2 M in Et_2O) was then added dropwise. The mixture was stirred for an additional 2 h at −78 °C. This solution was added through a double-ended needle to a stirred solution of freshly distilled *n*-hexanal (1 equiv) in THF (130 mL) under argon at −78 °C. The reaction was allowed to warm slowly to 0 °C, then quenched with saturated aqueous ammonium chloride, and left to warm to room temperature. Next the reaction mixture was extracted three times with diethyl ether (Et_2O). The combined organic layers were washed with water followed by brine, dried over sodium sulfate (Na_2SO_4), filtered, and concentrated. After purification by flash chromatography over silica gel, using a PuriFlash SI Std IR-50SI (50 μm) cartridge from Interchim (Montluçon, France), 2.6 g (23%) of 2-nonen-4-olide was obtained (purity > 99%). The product exhibited the same spectral data as described by Dai:[23] ^{13}C NMR δ 13.5 (C-5′), 22.0 (C-4′), 24.2 (C-2′), 31.0 (C-3′), 32.7 (C-1′), 83.1 (C (4), 120.9 (C-2), 156.2 (C-3), 172.9 (C-1); GC-MS (EI) *m*/*z* 154 (4, M^+), 125 (72), 84 (100), 83 (19), 55 (15).

Wine Samples. All wines selected are listed in Table 1. These wines were used for various analyses, including semipreparative HPLC and GC-O/MS.

Table 1. All Wines Used in Different Essays through This Experiment, Including Vintage, Producer, Codes, and Appellation

vintage	wine	code	appellation
2001	Château Lamothe	Liq-La	Sauternes
2001	Château Malfourat	Liq-Mal	Sauternes
2002	Château Latour Blanche	Liq-Tb 2002	Sauternes
2003	Château Laville	Liq-Jcb 2003	Sauternes
2004	Castelnau de Suduiraut	Liq-Cds 2004	Sauternes
2005	Château Latour Blanche	Liq-Tb 2005	Sauternes
2005	Château Laville	Liq-Jcb 2005	Sauternes
2005	Château de Malle	Liq-Ml	Sauternes
2005	Chateau Suduiraut	Liq-Cs 2005	Sauternes
2006	Castelnau de Suduiraut	Liq-Cds 2006	Sauternes
2007	Château Laville	Liq-Jcb 2007	Sauternes
2009	Château d'Yquem	Liq-Sg 2009	Sauternes
2010	Château d'Yquem	Liq-Sg 2010	Sauternes
2006	Dauphiné Rondillon	Liq-Phd 2006	Loupiac
2007	Dauphiné Rondillon	Liq-Phd 2007	Loupiac
2008	Dauphiné Rondillon	Liq-Phd 2008	Loupiac
2010	Pavillon de Rouquette	Liq-Phd 2010	Loupiac
2006	Jean Moreau et fils	Sec-Jmf	Chablis
2007	Domaine Laroche	Sec-Lar	Chablis
2007	Billaud-Simon	Sec-Bs	Chablis
2007	Château Bonnet	Sec-Bon 2007	Bordeaux
2008	Château Moutin	Sec-Cm 2008	Graves
2008	Château Thieuley	Sec-Tey	Bordeaux
2008	Château Bonnet	Sec-Bon 2008	Entre Deux Mers
2008	Domaine Albert Mann	Sec-Ann	Alsace

Wine Extraction for HPLC Fractionation. Seven hundred and fifty milliliter wine samples were extracted at room temperature (20 °C) using 60, 60, and then 40 mL of dichloromethane with magnetic stirring (700 rpm) for 10 min each and separated in a funnel. The organic phases were collected, dried over sodium sulfate, concentrated to around 2 mL using a Buchi R-114 rotary evaporator (Buchi, Rungis, France), and then further concentrated under nitrogen flow (100 mL/min) in a graduated glass tube (Atelier Jean Prémont, Bordeaux) to obtain a 750 μL wine extract.

Semipreparative HPLC on Wine Extracts and Sensory Evaluation. Reversed-phase (RP) HPLC was performed on the raw wine extract, using a Novapak C18 column (300 × 7.8 mm internal diameter (i.d.), 6 μm, Waters, Saint Quentin, France) with a guard column of the same phase. The Ultimate 3000 semipreparative HPLC system was from Dionex (Courtaboeuf, France). The procedure was based on the method described by Ferreira et al.,[24] later adapted by Pineau et al.[16] Chromatographic conditions were as follows: flow rate, 1 mL/min; injection volume. 250 μL; gradient, eluent A, microfiltered water, eluent B, ethanol; 0−2 min, 0% B, 2−50 min, 0−100% B. Fifty effluent fractions of 1 mL were collected. Each fraction was diluted into 12% ethanol, then poured into normalized glasses from the Association Française de Normes (AFNOR), and evaluated by three experienced assessors aged 38.6 ± 9.8 [mean ± standard deviation (SD)] years old. The repeatability of the quantitation measurements for specific concentrations (65 μg/L for 3-methyl-4-octanolide, 2.5 μg/L for γ-nonalactone, 2.4 μg/L for eugenol, and 2.0 μg/L for 2-nonen-4-olide) of the considered compounds was calculated after HPLC fractionation of the same wine (i.e., 750 mL), initially extracted with dichloromethane, for 3-methyl-4-octanolide at 6%, for eugenol at 2.6%, for γ-nonalactone at 6%, and finally for 2-nonen-4-olide at 2.6%.

Extracting HPLC Fractions. Each fraction of interest (1 mL) was diluted with ultrapure water (Milli-Q, Millipore, Bedford, MA, USA) to obtain 12% ethanol (v/v) and then re-extracted three times with 1 mL of dichloromethane each time to mimic the wine extraction. The organic phases were combined and concentrated to 250 μL under nitrogen flow before GC-O analysis and heart-cut multidimensional GC-O-MS.

GC-O. GC-O analyses were carried out using a Hewlett-Packard 5890 gas chromatograph (Agilent Technologies, Palo Alto, CA, USA) equipped with a flame ionization detector (FID) and a sniffing port (ODO-1 from SGE, Ringwood, Australia). A 1 μL aliquot of concentrated wine extract was injected by a splitless injector (230 °C; purge time, 1 min; purge flow, 50 mL/min) at an oven of temperature of 45 °C into a type-HP5 capillary column (Agilent; 30 m, 0.25 mm i.d., 0.25 μm film thickness) or a type BP20 capillary column (SGE; 50 m, 0.22 mm i.d. 0.25 μm film thickness). The analysis temperature program was as follows: 45 °C for 1 min, then 3 °C/min to 230 °C, with a 20 min isotherm for both types of columns. The carrier gas was hydrogen (Air Liquide, Floirac, France) with a flow rate of 1 mL/min. Each sample was analyzed in triplicate for 30 min each time and was assessed by three well-experienced assessors. Linear retention indices (LRI) were obtained by simultaneous injection of samples and a series of alkanes (C_7−C_{23}).

Heart-Cut Multidimensional Gas Chromatography−Olfactometry−Mass Spectrometry (MDGC-O-MS). All analyses were performed using a multidimensional gas chromatograph consisting of two independent gas chromatographs (Agilent 6890), interconnected by means of a thermoregulated transfer line kept at 230 °C (West 4400, West Instruments, Gurnee, IL, USA). For chromatograph 1 (GC-1), the 6890 chromatograph (Agilent) was equipped with an FID and an olfactometric port (ODP-3, Gerstel, Mülheim an der Ruhr, Germany), both connected by a flow-splitter to the column exit for simultaneous effluent monitoring. This GC was retrofitted with a pressure-driven switching valve MCS (Multi Column Switching system, Gerstel) to transfer selected heart cuts eluted from the first column directly into the analytical column in the second chromatograph. The carrier gas helium N 60 (Air Liquide) was delivered at a constant flow of 1 mL/min. The pressure ramp program for constant flow was 224 kPa for 1 min, then increased by 1.4 kPa/min to 310 kPa, and maintained at this pressure for 42 min. The column was a 30 m ×

0.32 mm i.d. × 0.5 μm film HP5 (Agilent). An uncoated, deactivated, fused-silica column (40 cm × 0.05 mm i.d.) from Supelco (Bellefonte, PA, USA) was used as an interface between the switching valve MCS to a FID or an olfactometric port. The oven temperature program was as follows: 45 °C for 1 min, then increasing by 5 °C/min to 230 °C, and maintained at 230 °C for 43 min. The injector was maintained at 250 °C (total run time = 83.67 min). A cryotrapping unit (liquid N_2) was mounted between the two GCs for cryofocusing (−50 °C) of the heart-cut fraction at the beginning of the second column. The gas chromatograph 2 (GC-2, Agilent 6890) was coupled to an Agilent HP 5973 mass spectrometer (Agilent). Also, an olfactometric port (ODP3, Gerstel) was set up so that the 2D column exit was split between the MS and ODP3 for simultaneous mass spectrometry and sniffing detection (division 1:1). Two types of columns were used alternately in GC-2 with different polarities. The first column was a 50 m × 0.22 mm i.d. × 0.25 μm [BP20 (SGE)] and the second one a 50 m × 0.22 mm i.d. × 1 μm [BP1 (SGE)]. In GC-2, the column (BP20 or BP1) was connected to the MCS switching valve (situated in the first chromatograph) and routed via a transfer line thermostatically controlled at 230 °C. Two minutes after the heart cut, the oven temperature program (45 °C initially, then 3 °C/min increase to 230 °C) of GC-2 was activated. The pressure ramp program was 224 kPa at midpoint for the first 25 min, then increased at a rate of 1.4 kPa/min to 310 kPa, and maintained at that level for 27 min (total run time = 83.67 min). GC-O port parameters were as follows: GC effluent was combined with humidified air [reconstituted air (nitrogen 80, oxygen 20; v/v), Air Liquide] at a rate of 35 mL/min at the bottom of the glass mask (SGE) to avoid nasal dehydration. The MS parameters were as follows: transfer line at 250 °C; source at 230 °C, and quadrupole at 150 °C, in EI mode at 70 eV. The MS was used in full scan mode (m/z 40−300). MS data were recorded and processed using Chemstation software (version B04.03) from Agilent equipped with an NIST 2008 MS library (U.S. National Institute of Standards and Technology, Gaithersburg, MD, USA). For chemical ionization (CI) with methanol, a similar MDGC configuration with two Agilent 7890A GCs was coupled with a time of flight (TOF) mass spectrometer by JEOL (JEOL Europe, Croissy sur Seine, France).

Quantitation of Higher Aliphatic Lactones and Eugenol by GC-MS. The extraction protocol for quantifying aliphatic lactones and eugenol in wine or in selected HPLC fractions was applied as described by Ferreira et al.[25] Briefly, after solid phase extraction chromatography, the eluent was supplemented with external standard (100 μL of 2-octanol at 10 mg/L in CH_2Cl_2) and concentrated under nitrogen flow (approximately 100 mL/min) to 100 μL. Each extraction was repeated twice. Then, a 2 μL sample of each concentrated wine extract was injected on an Agilent 6890 gas chromatograph in splitless injector mode (injector temperature, 230 °C; purge time, 1 min; purge flow, 50 mL/min) with a Carbowax 20 M type capillary column [BP20, 50 m, 0.25 mm i.d., 0.22 μm film thickness (SGE)]. The temperature program for all analyses was as follows: 45 °C for 1 min, increased by 3 °C/min to 230 °C, followed by a 20 min isotherm. The carrier gas was helium N 60 (Air Liquide) with a constant flow rate of 1 mL/min. The detector was an Agilent HP 5973 mass spectrometer functioning in electron impact (EI) mode (70 eV) and connected to the GC with a heated transfer line at 230 °C (Agilent). The compounds were quantified using selected ion monitoring mode (SIM) on MSD Chemstation software (version B04.03) from Agilent. The external standard, 2-octanol, was detected with m/z 84 and 97 ions and quantified using m/z 84. 3-Methyl-4-octanolide was detected with m/z 99 and 42 ions and quantified with the m/z 99 ion. γ-Nonalactone was detected using the ions m/z 85 and 56 and quantified with the ion m/z 85, and eugenol was detected with ions m/z 164 and 149 and quantified with the ion m/z 164. The repeatability of the quantitation measurements was calculated by the extraction and injection of eight spiked samples (50 mL) with known concentrations of the compounds (100 μg/L for 3-methyl-4-octanolide, 25 μg/L for eugenol and γ-nonalactone). The repeatability values were for 3-methyl-4-octanolide, 5%; eugenol, 2.5%; and γ-nonalactone, 2.3%.

Quantitation of 2-Nonen-4-olide by GC-MS. The extraction protocol for quantifying 2-nonen-4-olide in wine or in selected fractions was similar to that used for 3-methyl-4-octanolide, eugenol, and γ-nonalactone. All quantitative analyses were carried out using an Agilent 6890 GC. One microliter of each concentrated extract (extraction method described by Ferreira et al.[25]) was injected in splitless mode (230 °C; purge time, 1 min; purge flow, 50 mL/min) onto a DB1 capillary column (Agilent, 30 m, 0.25 mm i.d., 0.25 μm film thickness). The temperature program was as follows: 45 °C for 1 min, increasing by 3 °C/min to 130 °C, and increasing again at 40 °C/min until 280 °C, followed by a 10 min isotherm. The carrier gas was helium N 60 (Air Liquide) with a constant flow rate of 1.5 mL/min. The detector was an Agilent HP 5973 mass spectrometer, functioning in EI mode (70 eV), with a transfer line heated to 280 °C. 2-Nonen-4-olide was detected in SIM mode by selecting the m/z 84, and 125 ions and quantified using m/z 84. The external standard, 2-octanol, was detected with m/z 84 and 97 ions and quantified using m/z 84. Measurements were linear in a range of concentrations from 0.5 to 20 μg/L [2-nonen-4-olide, μg/L) = $3.5906x - 0.0323$ (x = ratio of peak area of 2-nonen-4-olide over the peak area of the external standard); $R^2 = 0.9975$]. Repeatability of the measurement of 2-nonen-4-olide for a series of eight extractions and injection of the same wine was assessed at 1.4%. The quantitation limit (0.5 μg/L) was calculated as the minimum concentration that generated a peak signal 10-fold higher than the background noise signal. Recovery was calculated at >80%.

General Conditions for Sensory Analyses. Sensory analyses were performed as described by Martin and de Revel.[26] Samples were evaluated in individual booths, at controlled room temperature (19 ± 1 °C), using covered black Association Française des Normes (AFNOR) glasses[27] containing 50 mL of liquid, coded with random three-digit numbers. Sessions lasted approximately 10 min.

Sensory Panel. The panel consisted of 15 judges, 5 males and 10 females, aged 30.5 ± 4.6 years (mean ± SD). All panelists belong to the enology research laboratory staff at ISVV, Bordeaux University. The judges were selected for their experience in assessing fruity aromas of dessert wines.

Olfactory Thresholds. All analyses were performed in a model solution consisting of twice-distilled ethanol (12%, v/v) and tartaric acid (5 g/L) at pH 3.5 (adjusted using NaOH). For all sensory analyses, the glasses were labeled with three-digit random codes and presented to panelists in random order. All experiments were performed in duplicate.

The detection threshold of the aroma compound was determined in a model solution with an ascending procedure (0.5, 1, 2, 4, 8, 16, 32, 64, 128, and 256 μg/L), using the three-alternative forced-choice presentation method (3-AFC) (ISO 13301 2001).[27] For each concentration, subjects received a set of three glasses; two of them were blank samples (model solution), and one contained the odorant at various concentrations (positive sample). Sensory analyses covered the whole series of dilution sets: each assessor was asked to first sniff each of the three glasses in the prescribed order and then choose the spiked sample.

The detection threshold was defined as the concentration at which the probability of detection was 50%. This statistical value was determined according to an adaptation of the ASTM-E1432 method.[28] The concentration/response function fitted by a sigmoid curve [$y = 1/(1 + e^{(-\lambda x)})$] was designated by a psychometric function reflecting behavior during detection. The detection probability was corrected by the chance factor (one-third for 3-AFC): $(3p - 1)/2$. The software used for graphic resolution and nonlinear regression by ANOVA transform was Sigma Plot version 8 (SYSTAT, San Jose, CA, USA).

Reconstitution and Omission Experiments. For the reconstitution and omission tests, two different types of dessert wines were selected. One was a typical Bordeaux dessert wine (Bordeaux dessert wine 1), with a desirable odor, reminiscent of overripe fruit, particularly orange peel, whereas the other was a nontypical Bordeaux dessert wine (Bordeaux dessert wine 2), with a fresh fruity aroma. Orthonasal typicality was measured by the panel on a nonstructured scale, which was anchored by "bad example" and "good example" on the left and the right ends, respectively. The panel had to respond to the question if a presented sample was considered to be a good or a

Table 2. Concentrations (Micrograms per Liter) of Four Compounds (2-Nonen-4-olide, *trans*-3-Methyl-4-octanolide, γ-Nonalactone, and Eugenol) in Fractions 37 and 38 of Two Different Bordeaux Dessert Wines (Mean ± SD; $n = 2$)[a]

HPLC fraction	2-nonen-4-olide	*trans*-3-methyl-4-octanolide	*cis*-3-methyl-4-octanolide	γ-nonalactone	eugenol
		Bordeaux Dessert Wine 1			
F37	10.7 ± 0.9	81.1 ± 0.2	95.1 ± 0.3	tr	9.1 ± 0.1
F38	tr	1.8 ± 0.1	tr	2.9 ± 0.1	tr
		Bordeaux Dessert Wine 2			
F37	nd	tr	0.2 ± 0.1	tr	0.2 ± 0.09
F38	nd	tr	tr	0.6 ± 0.2	tr

[a]nd, not detected; tr, traces.

Table 3. Composition of Different Samples through the Reconstitution and Omission Analyses[a]

	HPLC fractions				compounds		
sample	1−36	37 + 38	39−50	3-methyl-4-octanolide	eugenol	2-nonen-4-olide	γ-nonalactone
TAR	+	+	+	−	−	−	−
37 + 38	−	+	−	−	−	−	−
PAR	+	−	+	−	−	−	−
PAR4C	+	−	+	+	+	+	+
PAR4C-WL	+	−	+	−	+	+	+
PAR4C-E	+	−	+	+	−	+	+
PAR4C-N	+	−	+	+	+	−	+
PAR4C-γN	+	−	+	+	+	+	−

[a]TAR, total aromatic reconstitution; 37 + 38, aromatic reconstitution for fractions 37 and 38; PAR, partial aromatic reconstitution; PAR4C, sample PAR plus the four compounds; +, addition; −, omission; PAR4C-W, sample PAR4C with 3-methyl-4-octanolide omission; PAR4CE, sample PAR4C with eugenol omission; PAR4C-N, sample PAR4C with 2-nonen-4-olide omission; PAR4C-γN, sample PAR4C with γ-nonalactone omission.

Table 4. Sensory Evaluation of HPLC Fractions from Various Bordeaux Dessert Wines and Dry White Wines

	dessert wines				dry white wines	
HPLC fraction	Liq-Cs 2005	Liq-Cds 2004	Liq-Cds 2006	Liq-Phd 2010	Sec-Cm 2008	Sec-Bon 2007
35	solvent	fruity	floral	floral	citrus	citrus
36	moldy	odorless	citrus	citrus	thiols	odorless
37	ripe orange	ripe orange	ripe orange	citrus	citrus	odorless
38	ripe orange/moldy	ripe orange	ripe orange	fresh fruit	floral	fruity
39	mushroom	apricot	moldy	apricot	green	cherry
40	cherry	odorless	spicy	spicy	solvent	cherry
41	banana	banana	banana	banana	banana	solvent
typicality (/10)	7.2 ± 0.8	5.6 ± 1.5	6.4 ± 1.4	0.9 ± 0.3	0.4 ± 0.2	0.6 ± 0.3

bad example for a wine of the category Bordeaux dessert wine, and no further information was asked regarding a sensory profile.[29] After fractionation of each extract by reversed-phase HPLC, the above-mentioned volatile compounds were quantified by GC-MS in selected fractions (Table 2) (experimental protocol in quantitation of higher aliphatic lactone and eugenol, 2-nonen-4-olide). Several reconstitution tests were then performed on the basis of the quantitation results. For each sensory session, samples of aromatic reconstitutions in hydroalcoholic solution (12% vol, pH 3.9) were presented. Names and compositions of the samples are presented in Table 3. The fractions of those Bordeaux dessert wines were pooled to form total aromatic reconstitution (TAR) samples, corresponding to the 50 fractions gathered together. Partial aromatic reconstitution (PAR) samples corresponded to the 50 fractions except fractions 37 + 38, PAR supplemented with the four following volatile compounds, 3-methyl-4-octanolide, eugenol, γ-nonalactone, and 2-nonen-4-olide, at concentrations assayed in specific Bordeaux dessert wine (PAR4C samples), and PAR with three of the four selected volatile compounds.

For each type of dessert wine, a specific sensory session was organized, and each session was performed in duplicate. In practical terms, during a first sensory session, the fractions corresponded to those of Bordeaux dessert wine 1, and the concentrations of the compounds added were related to those assayed in that wine. In a second sensory session, the fractions corresponded to those of Bordeaux dessert wine 2, and the concentrations of the compounds added were related to those assayed in that wine. In a third session, HPLC fractions corresponding to Bordeaux dessert wine 2 without fractions 37 + 38 were supplemented with the volatile compounds corresponding to Bordeaux dessert wine 1. Each sensory session was performed in duplicate on different days. The overripe orange aroma intensity was evaluated in a direct orthonasal way on a 0−10 point nonstructured scale. The scale used was 0 = no odor perceived and 10 = high intensity perceived. Concerning typicality experiments, the scale was 0 = bad example of Bordeaux dessert wine and 10 = good example of Bordeaux dessert wine. For aromatic reconstitutions, fractions were retained and added individually or blended together to reproduce the initial concentrations in the original wines, adding double-distilled ethanol and microfiltered water to obtain an ethanol level of 12% (v/v).

Statistical data were analyzed using R (R Foundation for Statistical Computing, Vienna, Austria, 2011) version 2.15.1 software. Analysis of variance (ANOVA) was performed, the homogeneity of variance was tested with Levene's test, and the normality of residuals was tested using the Shapiro−Wilk test. Statistical significance was set at 5% ($p < 0.05$).

RESULTS AND DISCUSSION

Characterization of Compounds Associated with Key Aromatic Fractions Reminiscent of Overripe Orange

Table 5. Distribution of Odoriferous Zones Found in Fraction 37 of a Dessert Wine Extract Analyzed by GC-O (BP20 and HP-5 Columns)

BP20 column			HP5 column		
LRI	time	odoriferous zone	LRI	time	odoriferous zone
1712	34.6	citrus	1204	28.1	plastic
1724	35	vanilla	1339	31.4	fruity
1754	37.3	warm	1346	34.7	floral
1832	39.1	citrus	1360	35.3	citrus
1912	44.3	coconut	1414−1443	38.3−38.9	overripe orange
2007	45.3	fruity	1502	41.4	plastic
2225	51.9	caramel	1690	48.8	spicy
2383	52.3	burned sugar			

Aromas. Semipreparative HPLC of wine extracts resulted in fractions containing increasing proportions of ethanol in water. It was thus possible to describe their aromatic characteristics without toxic or malodorous solvent. Selected dessert and dry white wine extracts were analyzed by HPLC to constitute fractions with different aromatic descriptors. The comparative sensory evaluation of the fractions revealed clear sensory differences between dessert wine and dry white wine extracts, particularly in the ripe fruit character, but also revealed sensory differences for the typicality appreciation (Table 4). Among others, fractions 37 and 38 in some dessert wine extracts (Liq-Cs 2005, Liq-Cds 2004, and Liq-Cds 2006) were clearly reminiscent of overripe fruits and oranges, which were not detected in the other fractions (Liq-Phd 2010) or in dry white wine extracts (Sec-Cm 2008 and Sec-Bon 2007). To characterize the compounds associated with this aroma, fraction 37, the most significant from a sensory point of view, was re-extracted with dichloromethane, and the concentrated extract was injected on both a polar (BP20) and a nonpolar capillary (HP5) to identify odoriferous zones recalling the above-mentioned descriptors. With the BP20 type capillary, it was not possible to pick out the key odoriferous zones with overripe fruit and orange aromas. However, on HP5, a typical orange aroma lasting 1 min was perceived in a chromatographic zone situated between 1414 and 1443 LRI (Table 5). At this point, MDGC-O-MS was required to analyze this complex matrix and identify the compound(s) associated with this aroma.

Identification and Quantitation of 2-Nonen-4-olide. Using MDGC technology, the odoriferous zone was targeted for its olfactory characteristics on the GC1 olfactometry port. Then, an adequate 3 min cut was performed. The separation of the extract on the analytical column (GC2, BP20 capillary), coupled with both the olfactometry port and the mass spectrometry detector, revealed several odoriferous zones potentially related to the overripe orange odor. Odoriferous zones with coconut, spicy clove, and ripe-fruit aromas corresponding to 3-methyl-4-octanolide, eugenol, and γ-nonalactone, respectively, were identified by mass spectrometry. A fourth odoriferous zone with minty and fruity aromas, corresponding to an unknown compound, was also detected. Coupling the capillary to the MS detector produced a chromatographic peak (Figure 1) with a clear mass spectrum at the retention time of this odoriferous zone, (LRI 2068, BP20 capillary, GC-2). The existence of a similar odoriferous zone associated with the same fragmentation pattern was confirmed by repeating MDGC analysis of fraction 37 extract on a nonpolar capillary BP1 (LRI 1368, GC-2). On the basis of the MS data obtained by EI and CI) which indicated a molecular mass of 154.099 ± 0.05 Da, and the associated chromatographic peak, the unknown odoriferous zone was identified as a lactone: 2-nonen-4-olide or 5-pentyl-5*H*-furan-2-one (CAS Registry No. 21963-26-8). The mass spectra of the 2-nonen-4-olide standard and the wine extract presented the same characteristics (Figure 2). To our knowledge, this was the first time that this compound had been identified in wine.

Odor Characteristics of 2-Nonen-4-olide and Assay in Wines. The perception threshold of (±)-2-nonen-4-olide was calculated at 4.3 μg/L in model solution and at 10.8 μg/L in a dessert wine (Figure 3). The 2-nonen-4-olide molecule has one asymmetrical carbon, indicating the possibility of various enantiomeric ratios between *R* and *S* forms. The perception thresholds and descriptors may change, depending on the ratio of these two isomers, as is the case for other compounds.[30−32] 2-Nonen-4-olide was then quantified in 15 dessert wines from

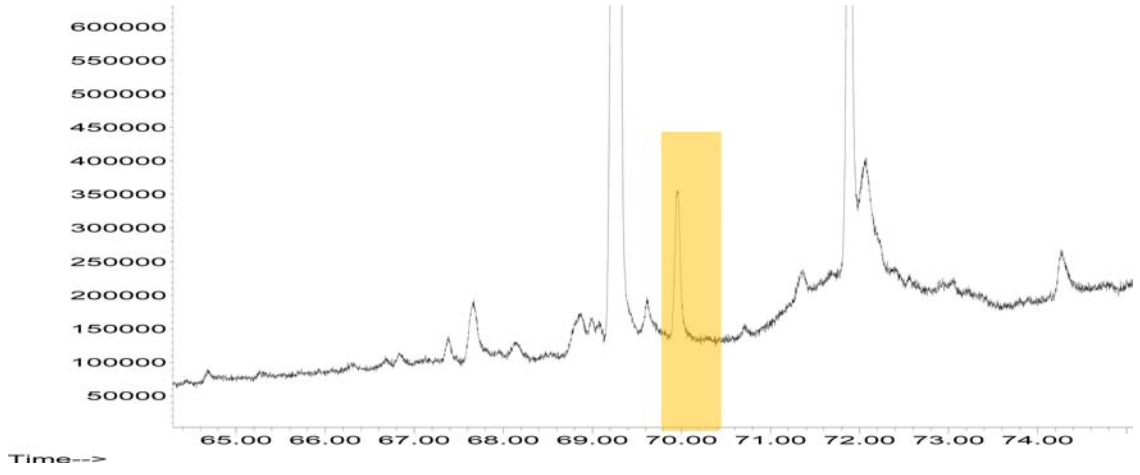

Figure 1. MDGC separation chromatogram from fraction 37 of a dessert wine on a BP1 nonpolar capillary (analysis on GC-2) indicating the peak corresponding to the odoriferous zone.

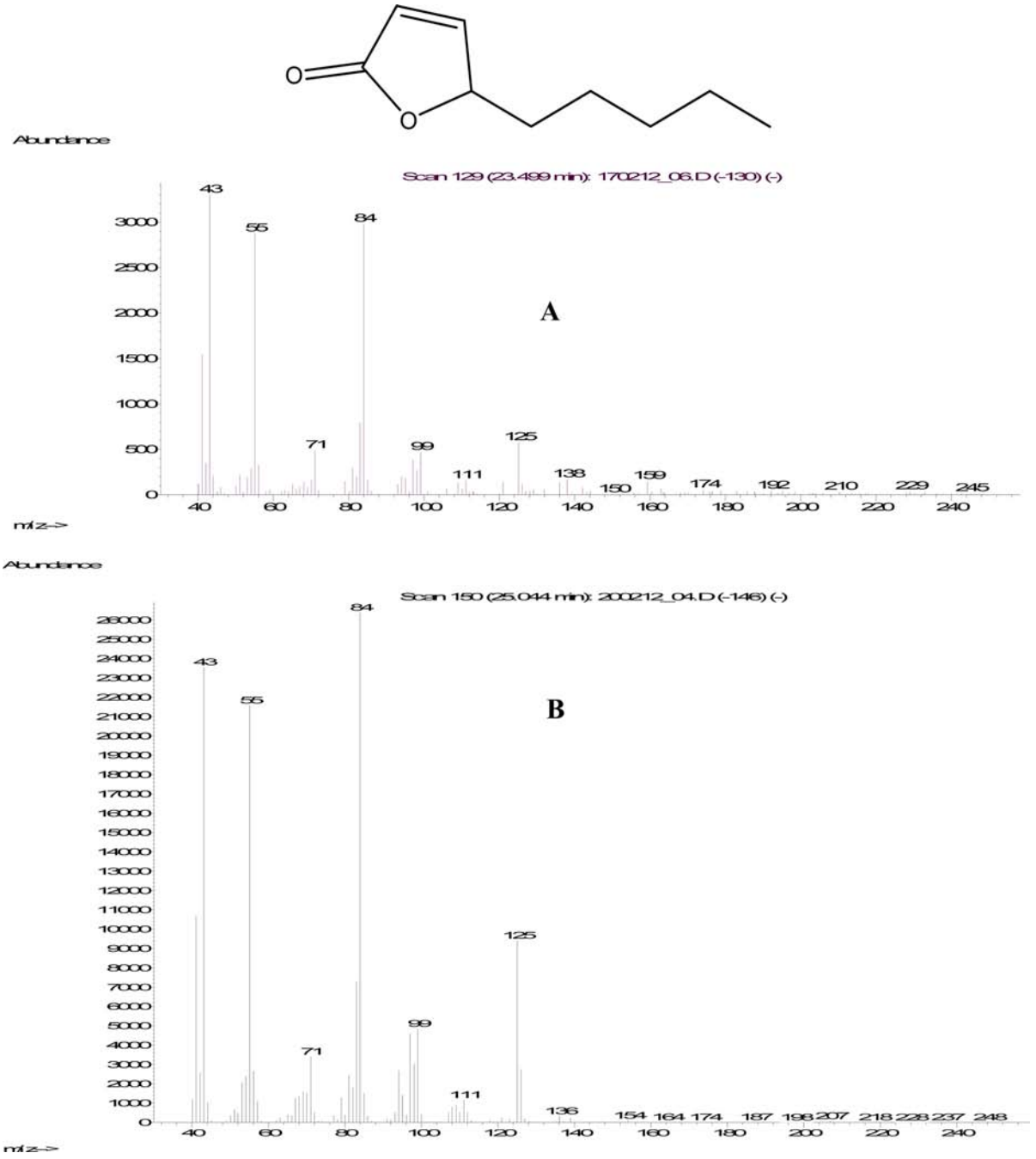

Figure 2. Chemical formula and mass spectra of 2-nonen-4-olide in wine (A) and as pure compound (B).

the Bordeaux region and 8 dry white wines from various appellations in France, including Chablis and Alsace. 2-Nonen-4-olide was not detected in dry white wines, but only in dessert wines obtained from botrytized grapes, thus indicating that this compound is perhaps specific to noble rot dessert wines. Its concentration in dessert wines apparently depends on the vintage, ranging from 2.6 to 18.2 μg/L, that is, values frequently over the olfactory detection threshold in model solution (Table 6). The absence of a specific odoriferous zone related to this overripe orange note suggested that it resulted from perceptual interactions among the above-mentioned volatile compounds (3-methyl-4-octanolide, eugenol, γ-nonalactone, and 2-nonen-4-olide), so relevant sensory analysis protocols were conducted.

Reconstitution and Omission Experiments. These experiments were conducted using two Bordeaux dessert wines presenting different levels of typicality, that is, 6.4 ± 1.4 for dessert wine 1 and 0.9 ± 0.3 for dessert wine 2 (see Materials and Methods). After fractionation of these wine extracts by HPLC, the four above-mentioned specific compounds (3-methyl-4-octanolide, eugenol, γ-nonalactone, and 2-nonen-4-olide) were assayed in HPLC fractions 37 and 38 of these two different wines (Table 2). Then, recombination and omissions tests were organized using selected HPLC fractions, and their sensory impact on the expression of the overripe fruit was studied. In particular, experiments on total aromatic reconstitution, partial aromatic reconstitution without HPLC fractions 37 + 38, or partial aromatic reconstitution

dx.doi.org/10.1021/jf405397c | J. Agric. Food Chem. 2014, 62, 2469−2478

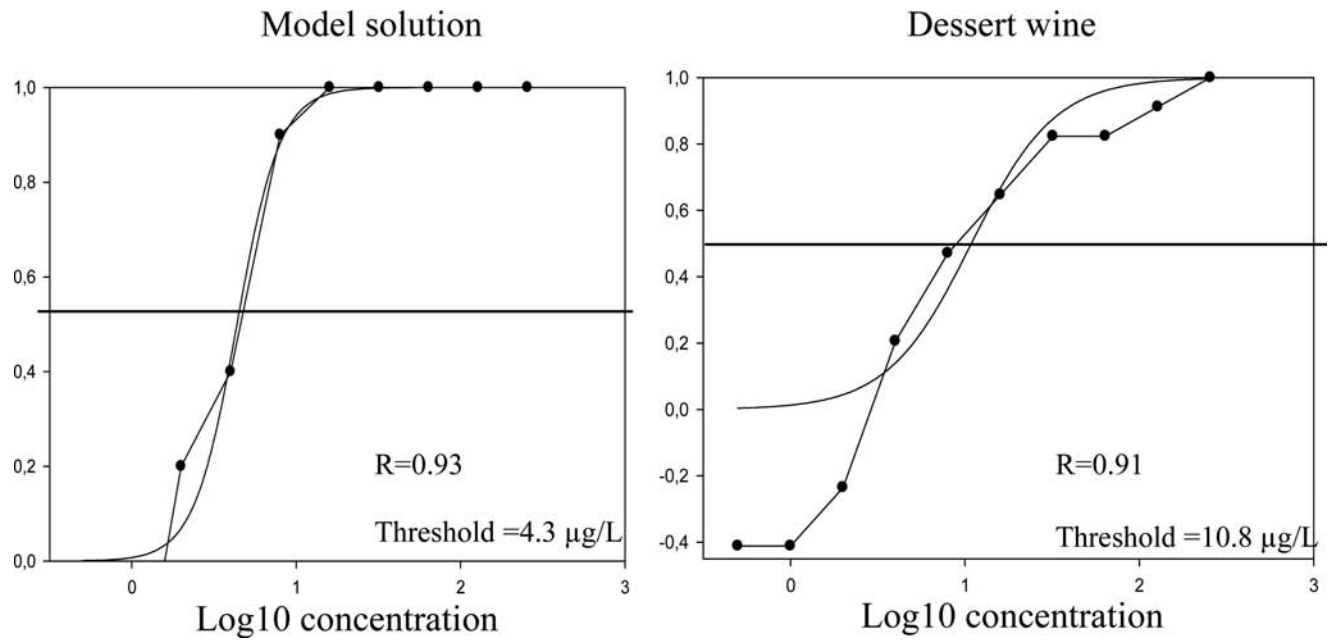

Figure 3. Detection threshold for 2-nonen-4-olide in model solution and in a dessert wine.

Table 6. 2-Nonen-4-olide Concentrations in Various Wines (Dessert Wines and Dry White Wines; Mean ± SD; n = 2)

vintage	wine	appellation	concentrations[a] (μg/L)
2001	Liq-La	Sauternes	3.7 ± 0.2
2001	Liq-Mal	Sauternes	2.6 ± 0.4
2002	Liq-Tb 2002	Sauternes	18.2 ± 0.3
2003	Liq-Jcb 2003	Sauternes	3.6 ± 0.1
2005	Liq-Tb 2005	Sauternes	5.5 ± 0.2
2005	Liq-Jcbc 2005	Sauternes	6.5 ± 0.2
2005	Liq-Ml	Sauternes	7.7 ± 0.1
2006	Liq-Cds 2006	Sauternes	11.6 ± 0.1
2007	Liq-Jcb 2007	Sauternes	7.7 ± 0.2
2009	Liq-Sg 2009	Sauternes	4.1 ± 0.3
2010	Liq-Sg 2010	Sauternes	5.0 ± 0.2
2006	Liq-Phd 2006	Loupiac	5.2 ± 0.7
2007	Liq-Phd 2007	Loupiac	4.0 ± 0.6
2008	Liq-Phd 2008	Loupiac	4.5 ± 0.1
2010	Liq-Phd 2010	Loupiac	2.0 ± 0.1
2006	Sec-Jmf	Chablis	<LOQ
2007	Sec-Lar	Chablis	<LOQ
2007	Sec-Bs	Chablis	<LOQ
2007	Sec-Bon 2007	Entre Deux Mers	<LOQ
2008	Sec-Tey	Bordeaux	<LOQ
2008	Sec-Bon 2008	Entre Deux Mers	<LOQ
2008	Sec-Cm	Graves	<LOQ
2008	Sec-Ann	Alsace	<LOQ

[a]LOQ, limit of quantitation.

without HPLC fractions 37 + 38 supplemented with the selected compounds were focused on the description of the overripe orange expression and typicality levels.

Preliminary experiments comparing the total (TAR) and partial (PAR) aromatic reconstitutions of Bordeaux dessert wine 1, with PAR supplemented with only one selected compound, revealed significant differences in the intensity of orange aroma. TAR had a mean value of 7.0 ± 0.7, whereas values for PAR and PAR with only one compound did not exceed 4.0 ± 0.7 (Supporting Information). However, a comparison between TAR and PAR supplemented with the four compounds together (PAR4C) at concentrations assayed in Bordeaux dessert wine 1 did not reveal, within two repeated sensory sessions, any significant difference in intensity of the orange descriptor (sensory sessions 1 and 1*, Table 7). The mean values for orange aroma perception in TAR sample were 6.7 ± 0.5 and 6.8 ± 0.9 with repetition, whereas PAR4C presented similar values at 6.2 ± 0.9 and 6.2 ± 0.7 with the repetition, indicating that adding all four compounds produced a sensory appreciation very close to the sample TAR. Thus, clear sensory differences were observed when PAR fractions were supplemented with only one of four selected compounds or with the four compounds together. The 37 + 38 sample presented always the highest values of 7.4 ± 0.4 and 7.5 ± 0.6 for the repetition. Then, sensory tests were conducted to study the impact of each compound omission, with Bordeaux dessert 1 wine, on the overripe aroma register. The mean values for the 37 + 38 sample were 7.6 ± 0.6 and 7.5 ± 0.7 with the repetition, whereas those of TAR were 6.7 ± 0.6 and 6.9 ± 0.6 with the repetition (sensory sessions 1 and 1*, Table 8). Under these conditions, although the mean values for PAR were 3.0 ± 0.6 and 3.3 ± 0.7, the orange aroma was always perceived as much more intense when the sample was supplemented with three of four compounds in PAR fractions. With regard to the omission of the compounds, only sample PAR4C-γN (omitting γ-nonalactone) was not significantly different from the total reconstitution. This contributes to demonstrating the direct effect of 2-nonen-4-olide, eugenol, and 3-methyl-4-octanolide on the overripe orange aroma of Bordeaux dessert wines, whereas γ-nonalactone had only a minor impact on the blend at the concentrations considered. In fact, the association of 2-nonen-4-olide with oak compounds is probably responsible for the new aromatic perception, which may be associated with perceptual blending.

When the sensory reconstitution and omission tests with Bordeaux dessert wine 2, presenting a lower typicality, on the expression of overripe orange aroma were considered, the results were much less significant. When the PAR sample was supplemented with the four above-mentioned compounds at

Table 7. Overripe Orange Odor Intensity for the Reconstitution Implicating the Four Selected Volatile Compounds (Mean ± SD)

		samples			
wine extract	sensory session	F37 + F38	TAR	PAR	PAR4C
Bordeaux dessert wine 1	1	7.4 ± 0.4 c	6.7 ± 0.5 bc	4.0 ± 0.6 a	6.2 ± 0.9 b
	1*[a]	7.5 ± 0.6 b	6.8 ± 0.9 b	3.9 ± 0.8 a	6.2 ± 0.7 b
Bordeaux dessert wine 2	2	3.3 ± 0.9 c	5.6 ± 1,0 b	4.4 ± 0.8 a	4.5 ± 0.7 a
	2*	3.5 ± 0.7 a	4.9 ± 0.7 b	3.7 ± 0.7 a	3.9 ± 0.5 ab
mixture	3	6.4 ± 0.9 b	6.7 ± 1.0 b	3.3 ± 0.9 a	6.2 ± 0.5 b
	3*	6.7 ± 0.6 b	6.7 ± 0.7 b	3.7 ± 0.6 a	6.5 ± 0.8 b

[a]The asterisk indicates a repetition.

Table 8. Overripe Orange Odor Intensity for the Omission Trails (Mean ± SD)

		samples						
wine extract	sensory session	F37 + F38	TAR	PAR	PAR4C-WL	PAR4C-γN	PAR4C-E	PAR4C-N
Bordeaux dessert wine 1	1	7.6 ± 0.6 d	6.7 ± 0.6 cd	3.0 ± 0.6 a	5.0 ± 0.5 b	6.3 ± 0.7 bc	5.4 ± 1.1b	5.2 ± 0.8 b
	1*[a]	7.5 ± 0.7 c	6.9 ± 0.6 c	3.3 ± 0.7 a	5.2 ± 0.4 b	6.4 ± 0.8 bc	5.6 ± 1.0 b	5.4 ± 0.7 b
Bordeaux dessert wine 2	2	4.5 ± 0.5 b	4.0 ± 0.6 b	2.5 ± 0.5 a	2.5 ± 0.6 a	2.8 ± 0.6 a	2.6 ± 0.6 a	2.2 ± 0.9 a
	2*	3.0 ± 1.2 a	3.7 ± 0.6 a	3.1 ± 0.7 a	2.7 ± 0.6 a	2.9 ± 0.8 a	3.4 ± 0.8 a	3.2 ± 0.7 a
mixture	3	7.6 ± 0.7 d	6.6 ± 0.4 cd	3.7 ± 0.3 a	5.4 ± 0.4 b	6.8 ± 0.4 cd	5.8 ± 0.4 bc	4.2 ± 0.3 a
	3*	7.2 ± 0.6 d	6.8 ± 0.6 d	3.9 ± 0.6 a	4.8 ± 0.6 ac	6.4 ± 0.6 bd	5.4 ± 0.8 bc	3.8 ± 0.8 a

[a]The asterisk indicates a repetition.

Table 9. Bordeaux Dessert Wines Typicality for the Reconstitution Experiments Implicating the Four Selected Volatile Compounds (Mean ± SD)

		samples			
wine extract	sensory session	F37 + F38	TAR	PAR	PAR4C
typical wine	1	6.0 ± 0.6 b	6.4 ± 0.5 b	4.5 ± 0.8 a	6.2 ± 0.5 b
	1*[a]	6.8 ± 0.6 b	6.9 ± 0.5 b	3.8 ± 0.7 a	6.5 ± 0.3 b
nontypical wine	2	2.6 ± 0.8 b	4.5 ± 1.0 a	4.3 ± 0.8 a	4.3 ± 0.5 a
	2*	3.0 ± 0.7 a	4.7 ± 0.7 b	4.0 ± 0.7 a	4.0 ± 0.5 ab
mixture	3	5.6 ± 0.8 b	7.0 ± 0.9 c	3.7 ± 1.1 a	5.4 ± 1.2 b
	3*	6.2 ± 0.5 b	7.3 ± 0.6 c	4.2 ± 0.8 a	5.9 ± 1.0 bc

[a]The asterisk indicates a repetition.

the concentrations found in the dessert wine fractions (Tables 2 and 3), no reproduction of the TAR was achieved under these conditions. PAR4C presented values at 4.5 ± 0.7 and 3.9 ± 0.5 with repetition, nonsignificantly different from PAR at 4.4 ± 0.8 and 3.7 ± 0.7 (sensory sessions 2 and 2*, Table 7). With regard to the sensory experiment with the omission of one compound of four, a significant difference was detected, with fractions from Bordeaux dessert wine 2, between samples 37 + 38 and TAR on one side, and samples PAR, PAR4C-WL, PAR4C-γN, PAR4C-E, and PAR4C-N on the other (sensory sessions 2 and 2*, Table 8). Samples 37 + 38 and TAR had the highest mean values for the overripe orange aroma, 4.5 ± 0.5 and 4.0 ± 0.6, respectively, 3 ± 1.2 and 3.7 ± 0.6 with the repetition, but at lower levels than in the sensory session with Bordeaux dessert wine 1, whereas samples PAR, PAR4C-WL, PAR4C-γN, PAR4C-E, and PAR4C-N had the lowest mean values.

Relatively to typicality appreciation, the results concerning Bordeaux dessert wine 1 indicated no significant difference between 37 + 38, TAR, and PAR4C (values situated between 6 ± 0.6 and 6.2 ± 0.5), whereas PAR presented a lower value (4.5 ± 0.8) (sensory sessions 1 and 1*, Table 9). The results expressed the same level of difference with the repetition of the session (TAR at 6.9 ± 0.5 and PAR4C at 6.5 ± 0.3, but PAR at 3.8 ± 0.7). Omitting fractions 37 + 38 clearly had a negative impact, thus confirming the contribution of the compounds involved in these fractions to wine typicality. When only one compound (3-methyl-4-octanolide, γ-nonalactone, eugenol, or 2-nonen-4-olide) was added to PAR, typicality appreciation was lower (Supporting Information). Relatively to typicality appreciation with Bordeaux dessert wine 2 samples, the addition of the four compounds to sample PAR4C had a minor impact, likely due to the low concentrations used. Whereas the results indicated a significant difference in typicality between the TAR sample and all other samples (sensory sessions 2 and 2*, Table 9), the level of Bordeaux dessert wine typicality was globally lower than with Bordeaux

dessert wine 1 sample. The highest mean values for Bordeaux dessert wine typicality was noted for sample TAR (4.5 ± 1.0 and 4.7 ± 0.7). In fact, both overripe orange aroma and typicality appreciation were limited with Bordeaux dessert wine 2, possibly due to the fact that lower concentrations of the four selected compounds were added. All of these results were confirmed during the replication of the sensory sessions.

At the end, the perception of overripe orange aroma was also studied in the Bordeaux dessert wine 2 matrix, supplemented with the targeted compounds at concentrations determined in Bordeaux dessert wine 1, as previously reported (Tables 2 and 3). Addition of the four compounds to the PAR produced a mean value almost equal to that of the TAR during the two repeated sessions, TAR and PAR4C presenting values of 6.7 ± 1.0 and 6.2 ± 0.5, respectively, much higher than that of PAR 3.3 ± 0.9 (sensory sessions 3 and 3*, Table 7). The same level of significance was confirmed with the repetition. With regard to the omission tests, samples 37 + 38, TAR, and PAR4C-γN had high mean values of 7.6 ± 0.7, 6.6 ± 0.4, and 6.8 ± 0.4, respectively, as previously noted during the sensory session with Bordeaux dessert wine 1 (sensory sessions 3 and 3*, Table 8). Unlike the previous experiment, the omission of eugenol did not significantly affect the sensory appreciation under these particular conditions. Statistical analysis revealed the TAR and PAR4C-E samples received similar intensities in terms of overripe orange fruity aroma (Table 8). In fact, throughout this experiment, when fraction 37 + 38 from Bordeaux dessert wine 1 or the targeted compounds considered at concentrations determined in this wine extract were added to the PAR fraction from Bordeaux dessert wine 2 used in session 2, the overripe orange fruit was much more intense. This emphasized the impact of 2-nonen-4-olide and 3-methyl-4-octanolide concentrations on this aroma perception. For the appreciation of Bordeaux dessert wine typicality, a significant difference was also noted between PAR, PAR4C, and TAR, once again highlighting the four compounds, on the assessment of typicality (sensory sessions 3 and 3*, Table 9).

Finally, all of these results, confirmed by replications of the sensory sessions, contribute to establish the interest of lactones, originating either from wine or oak aging, first, on the orange aroma isolated from Bordeaux dessert wines and, second, on the appreciation of typicality. Lactones are known to be active aroma compounds in many fruits.[33] The correlation between *cis*-3-methyl-4-octanolide concentrations and berry intensity in wines has been highlighted by other authors.[34] Moreover, the impact of 2-nonen-4-olide as an aroma-modifying and -intensifying compound has also been cited.[35] In our experiments, γ-nonalactone, at the concentration considered, which differs from 2-nonen-4-olide only by the absence of a double bond, does not seem to make a similar contribution to the perceptual phenomenon. In summary, through the characterization of molecular determinants for overripe aroma in dessert wines, two lactones, one originating from oak aging, 3-methyl-4-octanolide, and the second associated with noble rot development on grapes, 2-nonen-4-olide, were found to play an important role in the expression of the overripe orange aroma and typicality perceived in fractions obtained by HPLC from Bordeaux dessert wine extracts. In our experimental conditions, eugenol had a less significant effect and γ-nonalactone made a minimal contribution. The various omission and reconstitution tests demonstrated that 2-nonen-4-olide and 3-methyl-4-octanolide particularly contribute to wine aroma through perceptual blending to a synthetic perception. It was also demonstrated that this phenomenon was highly specific, because γ-nonalactone, a saturated form of 2-nonen-4-olide, made a very limited contribution to the perceptual blending. To our knowledge, this type of sensory phenomenon, involving two lactones, had never previously been demonstrated. This opens up new perspectives for interpreting the complexity and typicality of wine aroma.

■ ASSOCIATED CONTENT

Ⓢ Supporting Information

Additional tables. This material is available free of charge via the Internet at http://pubs.acs.org.

■ AUTHOR INFORMATION

Corresponding Author

*(P.D.) Phone: +33 5 57 57 58 60. Fax: +33 5 57 57 57 58 13. E-mail: philippe.darriet@u-bordeaux.fr.

Funding

We thank the Bordeaux Wine Council (Conseil Interprofessionnel du Vin de Bordeaux CIVB) and the Conseil Régional d'Aquitaine for their financial support.

Notes

The authors declare no competing financial interest.

■ ACKNOWLEDGMENTS

2-Nonen-4-olide was synthesized by Laurent Maggi and Dr. Fabrice Robvieux (Firmenich, Geneva, Switzerland).

■ REFERENCES

(1) Peynaud, E. *Le Vin et les Jours*; Dunod: Paris, France, 1985.

(2) Darriet, P.; Tominaga, T.; Lavigne, V.; Boidron, J. N.; Dubourdieu, D. Identification of a powerful aromatic component of *Vitis vinifera* L. var Sauvignon wines: 4-mercapto-4-methylpentan-2-one. *Flavour Fragrance J.* **1995**, *10*, 385−392.

(3) Tominaga, T.; Darriet, P.; Dubourdieu, D. Identification of 3-mercaptohexyl acetate in Sauvignon wine, a powerful aromatic compound exhibiting box-tree odor. *Vitis* **1996**, *35*, 207−210.

(4) Tominaga, T.; Baltenweck-Guyot, R.; Peyrot des Gachons, C.; Dubourdieu, D. Contribution of volatile thiols to the aromas of white wines made from several *Vitis vinifera* grape varieties. *Am. J. Enol. Vitic.* **2000**, *51*, 178−181.

(5) Tominaga, T.; Niclass, Y.; Frérot, E.; Dubourdieu, D. Stereoisomeric distribution of 3-mercaptohexan-1-ol and 3-mercaptohexyl acetate in dry and sweet white wines made from *Vitis vinifera* (var. Sauvignon blanc and Sémillon). *J. Agric. Food Chem.* **2006**, *54*, 7251−7255.

(6) Allen, M. S.; Lacey, M. J.; Boyd, S. J. Methoxypyrazines in red wines: occurrence of 2-methoxy-3-(1-methylethyl)pyrazine. *J. Agric. Food Chem.* **1995**, *43*, 769−772.

(7) Siebert, T. E.; Wood, C.; Elsey, G. M.; Pollnitz, A. P. Determination of rotundone, the pepper aroma impact compound, in grapes and wine. *J. Agric. Food Chem.* **2008**, *56*, 3745−3748.

(8) Pons, A.; Lavigne, V.; Frérot, E.; Darriet, P.; Dubourdieu, D. Identification of volatile compounds responsible for prune aroma in prematurely aged red wines. *J. Agric. Food Chem.* **2008**, *56*, 5285−5290.

(9) Shepherd, G. M. Smell images and the flavour system in the human brain. *Nature* **2006**, *444*, 316−321.

(10) Laing, D. G.; Jinks, A. L. Phychologival analysis of complex odor mixtures. *Chimia* **2001**, *55*, 413−420.

(11) Barkat, S.; Le Berre, E.; Coureaud, G.; Sicard, G.; Thomas-Danguin, T. Perceptual blending in odor mixtures depends on the nature of odorants and human olfactory expertise. *Chem. Senses* **2012**, *37*, 159−166.

(12) De Gelder, B.; Bertelson, P. Multisensory integration, perception and ecological validity. *Trends Cogn. Sci.* **2003**, *7*, 460−467.
(13) Wilson, D. A.; Stevenson, R. J. The fundamental role of memory in olfactory perception. *Trends Neurosci.* **2003**, *26*, 243−247.
(14) Ribéreau-Gayon, P.; Boidron, J. N.; Terrier, A. Aroma of Muscat grape varieties. *J. Agric. Food Chem.* **1975**, *23*, 1042−1047.
(15) Sarrazin, E.; Shinkaruk, S.; Tominaga, T.; Bennetau, B.; Frérot, E.; Dubourdieu, D. Odorous impact of volatile thiols on the aroma of young botrytized sweet wines: identification and quantification of new sulfanyl alcohols. *J. Agric. Food Chem.* **2007**, *55*, 1437−1444.
(16) Pineau, B.; Barbe, J. C.; van Leeuwen, C.; Dubourdieu, D. Examples of perceptive interactions involved in specific "red-" and "black-berry" aromas in red wines. *J. Agric. Food Chem.* **2009**, *57*, 3702−3708.
(17) Lytra, G.; Tempère, S.; de Revel, G.; Barbe, J. C. Impact of perceptive interactions on red wine fruity aroma. *J. Agric. Food Chem.* **2012**, *60*, 12260−12269.
(18) Sarrazin, E.; Tominaga, T.; Darriet, P. Correlation between sensory typicality and aromatic composition in Sauternes botrytised wines. *Expression of Multidisciplinary Flavor Science: Proceedings of the 12th Weurman Symposium*; Zürcher Hochschule für Angewandte Wissenschaften: Winterthur, Switzerland, 2008; pp 72−74
(19) Sarrazin, E.; Shinkaruk, S.; Pons, M.; Thibon, C.; Bennetau, B.; Darriet, P. Elucidation of the 1,3-sulfanylalcohol oxidation mechanism: an unusual identification of the disulfide of 3-sulfanylhexanol in Sauternes botrytized wines. *J. Agric. Food Chem.* **2010**, *58*, 10606−10613.
(20) Sapountzis, I.; Dohle, W.; Knochel, P. Stereoselective preparation of highly functionalized (*Z*)-3-magnesiated enoates by an iodine−magnesium exchange reaction. *Chem. Commun.* **2001**, *20*, 2068−2069.
(21) Rainka, M. P.; Milne, J. E.; Buchwald, S. L. Dynamic kinetic resolution of α,β-unsaturated lactones through asymmetric copper-catalyzed conjugate reduction: application to the total synthesis of eupomatilone-3. *Angew. Chem.* **2005**, *44*, 6177−6180.
(22) Ma, S.; Lu, X. Differentiation of the reactivities of carbon-carbon multiple bonds in one molecule. Highly chemo- and stereo-selective hydrohalogenation of allyl or propargyl propiolates. *Tetrahedron Lett.* **1990**, *31*, 7653−7656.
(23) Dai, Y. F.; Tian, H. Y.; Sun, B. G.; Chen, H. T.; Liu, X. L. Efficient synthesis of the odourant, 2-nonen-4-olide. *J. Chem. Res.* **2012**, 495−496.
(24) Ferreira, V.; Hernández-Orte, P.; Escudero, A.; López, R.; Cacho, J. Semipreparative reversed-phase liquid chromatographic fractionation of aroma extracts from wine and other alcoholic beverages. *J. Chromatogr., A* **1999**, *864*, 77−88.
(25) Ferreira, V.; Jarauta, I.; Ortega, L.; Cacho, J. Simple strategy for the optimization of solid-phase extraction procedures through the use of solid-liquid distribution coefficients: application to the determination of aliphatic lactones in wine. *J. Chromatogr., A* **2004**, *1025*, 147−156.
(26) Martin, N.; de Revel, G. Sensory evaluation: scientific bases and oenological applications. *J. Int. Sci. Vigne Vin* **1999**, *33*, 81−93.
(27) Analyse sensorielle-Méthodologie-Lignes directrices générales pour la mesure des seuils de détection d'odeur, de flaveur et de goût par une technique à choix forcé de 1 parmi 3 (3-AFC). ISO 13301. In *Analyse Sensorielle*; AFNOR: Paris, France, 2002.
(28) Cometto-Muñiz, J. E.; Abraham, M. H. Human olfactory detection of homologous *n*-alcohols measured via concentration-response functions. *Pharmacol., Biochem. Behav.* **2008**, *89*, 279−291.
(29) Ballester, J.; Dacremont, C.; Le Fur, Y.; Etiévant, P. The role of olfaction in the elaboration and use of the Chardonnay wine concept. *Food Qual. Pref.* **2005**, *16*, 351−359.
(30) Brenna, E.; Fuganti, C.; Serra, S. Enantioselective perception of chiral odorants. *Tetrahedron Asymmetry* **2003**, *14*, 1−42.
(31) Pons, A.; Lavigne, V.; Landais, Y.; Darriet, P.; Dubourdieu, D. Distribution and organoleptic impact of sotolon enantiomers in dry white wines. *J. Agric. Food Chem.* **2008**, *56*, 1606−1610.
(32) Cooke, R. C.; van Leeuwen, K. A.; Capone, D. L.; Gawel, R.; Elsey, G. M.; Sefton, M. A. Odor detection thresholds and enantiomeric distributions of several 4-alkyl substituted γ-lactones in Australian red wine. *J. Agric. Food Chem.* **2009**, *57*, 2462−2467.
(33) Gatfield, I. L.; Sommer, H. The enzymatic and fermentative production of lactones and their use in natural flavors. In *Recent Developments in Flavor and Fragrance Chemistry, 3rd International Haarman and Reimer Symposium*; Hopp, R., Mori, K., Eds.; Wiley VCH: Weinheim, Germany, 1993; pp 291−304.
(34) Spillman, P. J.; Sefton, M. A.; Gawel, R. The contribution of volatile compounds derived during oak barrel maturation to the aroma of a chardonnay and cabernet sauvignon wine. *Aust. J. Grape Wine Res.* **2004**, *10*, 227−235.
(35) Kindel, G.; Vossing, T.; Looft, J.; Wohrle, I.; Lages, R.; Loges, H. *Novel use of nonenolide*. U.S. Patent Application Publication US 2007/0297993A1.

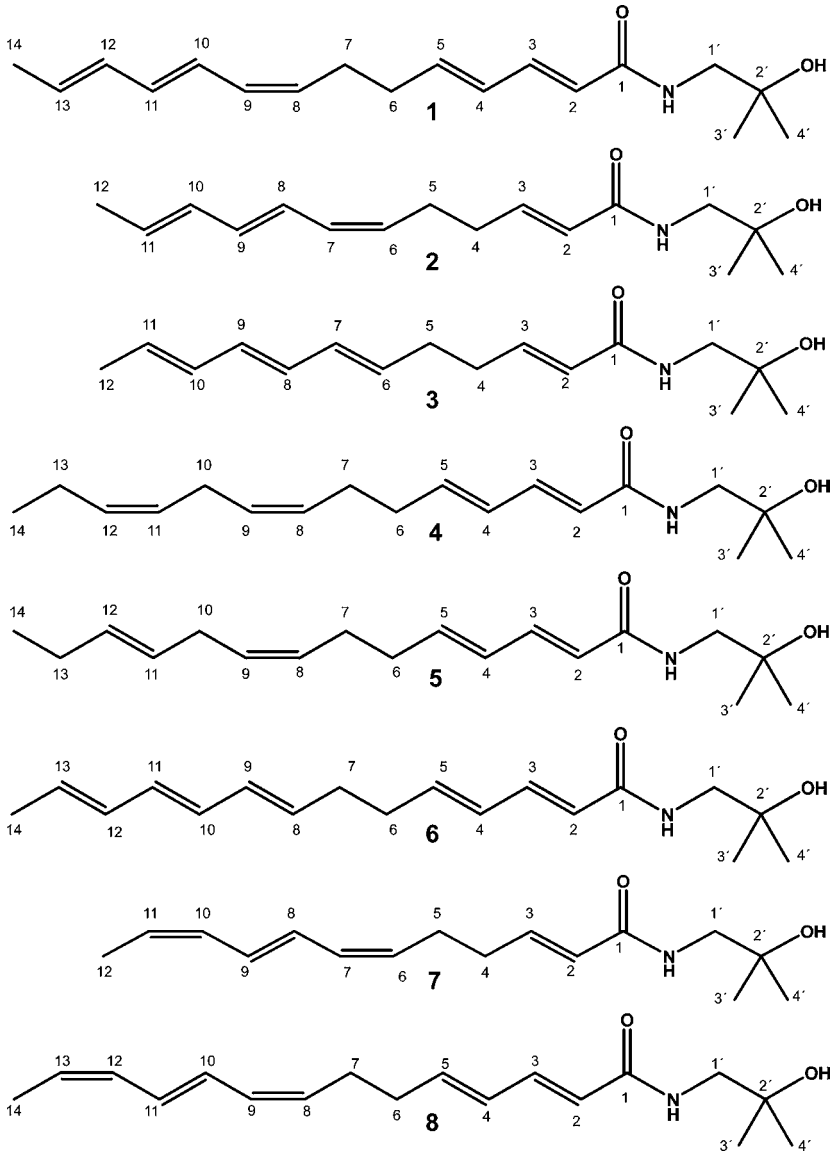

Figure 1. Chemical structures of hydroxy-γ-sanshool (**1**), hydroxy-α-sanshool (2), hydroxy-β-sanshool (**3**), bungeanool (**4**), isobungeanool (**5**), hydroxy-γ-isosanshool (**6**), hydroxy-ε-sanshool (**7**), and hydroxy-ζ-sanshool (**8**).

activate saliva,[15] but the key molecule responsible for this activity is not known yet.

Therefore, the objectives of the present study were to locate and isolate most sensory active phytochemicals from a highly tingling active supercritical fluid (SCF) extract prepared from dried pods of *Z. piperitum* by application of the taste dilution analysis (TDA),[16,17] to validate their chemical structure by means of LC-TOF-MS, LC-MS/MS, and 1D/2D NMR spectroscopy, and to determine human orosensory recognition thresholds as well as salivation-inducing activity of purified chemosensates using an ethanol-free sensory assay.[13]

MATERIALS AND METHODS

Chemicals. The following compounds were obtained commercially: Water for chromatographic separations was purified with an integral 5 system (Millipore, Schwalbach, Germany); *n*-hexane (Merck, Darmstadt, Germany) and solvents used were of HPLC grade (J. T. Baker, Deventer, The Netherlands). Deuterated solvents containing 0.03% trimethylsilane (TMS) were obtained from Eurisо-Top (Gif-Sur-Yvette, France). A supercritical fluid (SCF) extract from dried fruit pods of *Z. piperitum* was obtained from Synthite Industries (Kolenchery, Kerala, India). For sensory analysis, bottled water (Evian, low mineralization = 405 mg/L), sucrose (Sigma-Aldrich, Steinheim, Germany), piperine (Sigma-Aldrich), and capsaicine (Sigma-Aldrich) were used. Filter paper (Rundfilter classic, 94 mm; Melitta, Minden, Germany), cut into a rectangular shape (1 × 2 cm), was used as vehicle for the sensory evaluation of pungent and tingling amides.

Sensory Analyses. *General Conditions and Panel Training.* Twelve volunteers (seven women and five men, ages 25−34 years), who gave their informed consent to participate in the sensory tests of the present investigation and had no history of known taste disorders, were trained in sensory experiments with purified reference compounds at regular intervals for at least two years. The subjects were experienced in evaluating the orosensation of a tingling Szechuan pepper extract (40 μg/1 × 2 cm; Synthite, Kerala, India), isolated from *Z. piperitum* by means of supercritical carbon dioxide extraction and containing hydroxy-α-sanshool and hydroxy-β-sanshool in amounts of 9.1 and 2.5% (HPLC-UV), respectively, and the pungent compounds capsaicine (3 μg/1 × 2 cm) and piperine (20 μg/1 × 2 cm), respectively, by means of a modified half-tongue test using filter paper rectangles (1 × 2 cm) as the vehicle.[13] Panelists were instructed to rinse their mouth after each dilution step with a 3% sucrose solution (15 mL), followed by water (15 mL), and to wait for 2 min between

dx.doi.org/10.1021/jf500399w | J. Agric. Food Chem. 2014, 62, 2479−2488

each sample. Sensory analyses were performed at 19−22 °C in a sensory panel room in three different sessions.

Precaution Taken for Sensory Analysis of Food Fractions and Taste Compounds. To remove solvent traces and buffer compounds from all fractions and compounds isolated from pepper, the individual fractions were suspended in water and, after removal of the volatiles under high vacuum (<5 mPa), were freeze-dried twice. ^{1}H NMR spectroscopic, UPLC-UV-TOF-MS, and ion chromatographic analyses of an aliquot revealed that food fractions treated by that procedure were essentially free of the solvents and buffer compounds used.

Modified Half-Tongue Test. According to a literature protocol,[13] serial 1:1 dilutions of HPLC fractions or purified compounds in ethanol were applied on filter paper rectangles (1 × 2 cm) and the solvent was removed under a stream of nitrogen at 38 °C. As the control vehicle, filter paper rectangles were loaded with ethanol (blank), followed by evaporation at 38 °C. Using a 3% sucrose solution (15 mL) and water (15 mL) as cleansing solutions and an interstimulus interval length of 5 min between sample dilutions, the vehicles loaded with the stimulus in order of ascending concentration were presented to the sensory panel in three independent sessions and were randomly placed on the right or the left side of the anterior tongue together with an anonymized control vehicle (blank) on the other side. For each dilution, the subjects were asked to locate the side of the tongue on which a pungent and/or a tingling sensation was perceivable.

Taste Dilution Analysis (TDA). An aliquot (1.0 g) of the SFC extract prepared from Szechuan pepper was separated by RP-MPLC to give seven fractions, namely, F1−F7, which were freeze-dried twice and dissolved in "natural" concentration ratios, which means the fractions were used in concentrations corresponding to their yields obtained after fractionation. After each fraction had been sequentially diluted 1:1 with ethanol and applied on filter paper rectangles (1 × 2 cm), solvent traces were removed with a nitrogen stream at 38 °C, and the serial dilutions of each of these fractions were presented to the sensory panel in order of ascending concentration. Each dilution was evaluated for tingling activity by means of the half-tongue test detailed above. The dilution at which a sensory difference between the paper rectangle loaded with a Szechuan pepper fraction and a blank vehicle (control) could just be detected was defined as taste dilution (TD) factor.[13] The TD factors evaluated by six trained assessors in two different sessions were averaged. The TD factors between the trained individuals and separate sessions did not differ by more than plus/minus one dilution step.

Recognition Threshold Concentration. Threshold concentrations of the purified compounds were determined by using the half-tongue test and the filter paper rectangles as detailed above. To prevent excessive fatigue, the trials began at a concentration level two steps below the threshold concentration that had been evaluated in preliminary sensory experiments. Whenever the panelist selected incorrectly, the next trial took place at the next higher concentration step. Whenever the panelist selected correctly, the same dilution of the stimulus was evaluated again as a proof of the correctness of the data. The threshold value of the sensory group was approximated by averaging the threshold values of the individuals in three independent sessions. The geometric mean of the two lowest correctly identified concentrations was calculated and taken as the individual recognition threshold. Values between individuals and separate sessions differed by not more than plus or minus two dilution steps; that is, a threshold value of 3.0 nmol/cm^2 for the pungent reference compound piperine represents a range of 0.75−9.0 nmol/cm^2.

Salivation Experiments. Following a literature protocol[15] with some modifications, eight healthy volunteers were asked not to eat and drink for at least 1 h before the experiment started. First, the panelists rinsed the oral cavity with bottled water (8 mL) for 60 s and swallowed. To measure the nonstimulated saliva flow (control), the panelists then took bottled water (2 mL) in the mouth, simulated chewing motions for 30 s, and expectorated into preweighed cups. To measure the stimulated saliva flow, the oral cavity was rinsed again with water (8 mL) for 60 s; thereafter, the panelists took the stimulus solution (2 mL) containing the Szechuan pepper extract (100 mg/100 mL), hydroxy-α-sanshool (100 mg/100 mL), and hydroxy-β-sanshool (100 mg/100 mL), respectively, in the mouth and simulated chewing for 15 s and expectorated into preweighed vessels (stimulus sample). Without swallowing between, the subjects were asked to take water (2 mL) in the mouth, to simulate chewing for 30 s, and to expectorate again (poststimulus sample 1). This step was repeated three times (poststimulus samples 2−4). The saliva flow increase was calculated from the weight difference of the expectorated saliva/water mixture, and the aliquot (2 g) of the aqueous stimulus solution used to collect the stimulus sample and the aliquot (2 g) of water used to obtain the prestimulus sample (control) as well as poststimulus samples 1−4, respectively.

Identification of Chemosensates 1−8. A solution of the Szechuan pepper SCF extract (10 g) in methanol (400 mL) was defatted by *n*-hexane extraction (3 × 400 mL), concentrated under vacuum at 40 °C to about 30 mL, and, after dilution with water (30 mL), separated by medium-pressure liquid chromatography (MPLC) using a Sepacore system from Büchi (Flawil, Switzerland) consisting of a C-620 control unit, three C-605 type pumps, a C-660 fraction collector, a C-635 UV detector, and an injection valve (20 mL). Chromatography was performed using a 40 × 150 mm polypropylene cartridge (Büchi) filled with 25−40 μm LiChroprep RP-18 material (Merck). Monitoring the effluent (40 mL/min) at 265 nm, chromatography was performed with a mixture of aqueous formic acid (0.1% in water, pH 2.5, A) and methanol (B). A gradient was used as follows: 0 min, 65% B; 17 min, 90% B; 22 min, 90% B; 23 min, 100% B; and 28 min, 100% B. Individual fractions were collected, concentrated under vacuum at 40 °C, freeze-dried twice, and used for TDA to locate those fractions inducing a tingling and/or pungent orosensation. Fractions evaluated with high TD factors were further separated by means of preparative HPLC (Jasco, Groß-Umstadt, Germany) equipped with two PU-2087 Plus pumps, an AS-2055 Plus autosampler, a 7725i type Rheodyne injection valve (Rheodyne, Bensheim, Germany), and a MD-2010 Plus diode array detector.

By monitoring the effluent at 265 nm, isolation of amides **2**, **3**, and **7** was performed using a 21.2 × 250 mm, 5 μm, ODS-Hypersil C18 column (ThermoHypersil, Kleinostheim, Germany) using aqueous formic acid (0.1% in water, pH 2.5, A) and acetonitrile (B) as mobile phase (21 mL/min) and the following gradient: 0 min, 40% B; 18 min, 65% B; 22 min, 100% B; 24 min, 100% B; 27 min, 40% B; 30 min, 40% B.

Separation and purification of amides **1**, **4**−**6**, and **8** were achieved on a 21.2 × 250 mm, 5 μm, Varian Pursuit C18 column (Agilent, Waldbronn, Germany), equipped with a 21.2 × 50 mm guard column of the same type, and a mixture of aqueous formic acid (0.1% in water, pH 2.5, A) and acetonitrile (B) as mobile phase (18 mL/min) using the gradient as follows: 0 min, 50% B; 20 min, 70% B; 21 min, 100% B; 23 min, 100% B; 25 min, 50% B; 30 min, 50% B. After the purity of each fraction had been checked by means of analytical RP-HPLC, the isolated phytochemicals were analyzed by LC-MS and NMR spectroscopy, whereas the fractions containing mixtures of individual substances were further purified by HPLC rechromatography. The individual fractions were collected, separated from solvent under vacuum, and freeze-dried to yield the target amides **1**−**7** in a purity of >98%.

N-(2-Methyl-2-hydroxypropyl)-tetradeca-(2E,4E,8Z,10E,12E)-pentaene amide (hydroxy-γ-sanshool), **1**, Figure 1: UV−vis (acetonitrile/0.1% aqueous formic acid; 6:4, v/v), λ_{max} 240, 272, 292 nm; LC-TOF-MS (ESI$^+$), *m/z* 290.2119 (measured), *m/z* 290.2120 (calcd for $[C_{18}H_{27}NO_2 + H]^+$); MS (ESI$^+$), *m/z* (%) 290 (100, $[M + H]^+$), 272 (31, $[M + H - H_2O]^+$), 312 (28, $[M + Na]^+$), 328 (9, $[M + K]^+$); MS/MS (DP = +40 V), *m/z* (%) 272 (100), 165 (68), 72 (42), 131 (35), 173 (31), 145 (25), 201 (8); ^{1}H NMR (500 MHz, d_3-MeOD, COSY), δ 1.17 [s, 6H, H−C(3′,4′)], 1.76 [d, 3H, *J* = 6.9 Hz, H−C(14)], 2.26 [m, 2H, *J* = 6.9, 14.1 Hz, H−C(6)], 2.33 [m, 2H, *J* = 7.3, 14.5 Hz, H−C(7)], 3.26 [s, 2H, H−C(1′)], 5.37 [dt, 1H, *J* = 7.5, 10.6, H−C(8)], 5.65−5.76 [m, 1H, H−C(13)], 5.97−6.05 [m, 2H, *J* = 15.0 Hz, H−C(2, 9)], 6.07−6.19 [m, 3H, H−C(5, 11, 12)], 6.24 [dd, 1H, *J* = 10.9, 15.1 Hz, H−C(4)], 6.32−6.41 [m, 1H, H−C(10)], 7.12 [dd,

Table 1. ^{13}C NMR Chemical Shifts of Alkylamides 1−8

	compound								
carbon atom[a]	1[b,c,e,f]	2[b,c,d,f]	3[b,c,d,g]	4[b,c,e,f]	5[b,c,e,f]	6[b,c,e,f]	7[b,c,d,f]	7[b,c,e,f]	8[b,c,e,f]
C(1)	169.6	167.0	166.9	169.5	169.6	169.6	166.9	169.4	169.5
C(2)	123.3	123.7	123.6	123.3	123.2	123.3	123.7	125.1	123.3
C(3)	142.4	144.4	144.5	142.4	142.5	142.4	144.4	145.6	142.5
C(4)	130.3	32.1	31.9	130.2	130.2	130.3	32.1	33.2	130.3
C(5)	143.2	26.5	31.4	143.4	143.5	143.3	26.5	27.7	131.0
C(6)	34.0	129.5	132.0	33.9	33.9	33.9	130.3	131.5	34.0
C(7)	28.1	129.7	131.6	27.6	27.5	33.2	129.8	131.0	28.2
C(8)	130.9	125.2	130.1	129.7	129.8	133.5	127.2	128.6	131.6
C(9)	130.8	133.5	131.5	130.0	129.9	133.2	128.4	129.5	130.9
C(10)	126.7	131.8	131.6	26.5	31.4	132.7	129.5	130.9	128.7
C(11)	134.6	130.2	129.4	128.3	128.5	132.6	127.2	127.8	129.4
C(12)	133.3	18.3	18.3	132.8	133.5	131.6	13.5	13.7	131.0
C(13)	130.6			21.5	26.6	129.8			127.6
C(14)	18.5			14.7	14.4	18.4			13.7
C(1′)	51.2	50.4	50.4	51.2	51.2	51.3	50.4	51.1	51.3
C(2′)	71.7	71.1	71.1	71.7	71.7	71.5	71.0	72.0	71.8
C(3′)	27.3	27.3	27.4	27.3	27.3	27.3	27.3	27.3	27.2
C(4′)	27.3	27.3	27.4	27.3	27.3	27.3	27.3	27.3	27.2

[a]Arbitrary numbering of carbon atoms refers to chemical structures displayed in Figure 1. [b]Chemical shifts are given in relation to solvent signals. [c]Signal assignment was performed by means of *g*HSQC (^1J), *g*HMBC ($^{2,3}J$), and DEPT-135 spectroscopy. [d]$CDCl_3$ was used as solvent. [e]d_3-MeOD was used as solvent. [f]Spectrum was recorded at 125 MHz. [g]Spectrum was recorded at 100 MHz.

1H, *J* = 10.8, 15.1 Hz, H−C(3)]. The ^{13}C NMR data (125 MHz, d_3-MeOD, HSQC, HMBC) are shown in Table 1.

N-(2-Methyl-2-hydroxypropyl)-dodeca-(2E,6Z,8E,10E)-tetraene amide (hydroxy-α-sanshool), **2**, Figure 1: UV−vis (acetonitrile/0.1% aqueous formic acid; 1:1, v/v), λ_{max} 244, 272, 220 nm; LC-TOF-MS (ESI$^+$), *m/z* 286.1774 (measured), *m/z* 286.1777 (calcd for $[C_{16}H_{25}NO_2 + Na]^+$); MS (ESI$^+$), *m/z* 264 (100, $[M + H]^+$), 246 (38, $[M + H - H_2O]^+$), 286 (15, $[M + Na]^+$), 302 (15, $[M + K]^+$); MS/MS (DP = +40 V), *m/z* 246 (100), 147 (77), 107 (46), 72 (27), 133 (23), 175 (12); ^{1}H NMR (500 MHz, $CDCl_3$, COSY), *δ* 1.23 [s, 6H, H−C(3′, 4′)], 1.78 [d, 3H, *J* = 7.2 Hz, H−C(12)], 2.29 [m, 2H, *J* = 6.7, 14.44 Hz, H−C(4)], 2.34 [m, 2H, *J* = 7.6, 14.4 Hz, H−C(5)], 3.33 [d, 2H, *J* = 6.1 Hz, H−C(1′)], 5.37 [dt, 1H, *J* = 7.4, 10.6 Hz, H−C(6)], 5.73 [m, 1H, *J* = 7.0, 14.3, H−C(11)], 5.85 [dt, 1H, *J* = 1.5, 15.3 Hz, H−C(2)], 5.99 [1H, H−N], 6.02 [pt, 1H, *J* = 11.0 Hz, H−C(7)], 6.12 [m, 1H, *J* = 10.5, 14.5 Hz, H−C(10)], 6.18 [dd, 1H, *J* = 10.5, 14.4 Hz, H−C(9)], 6.33 [dd, 1H, *J* = 11.4, 14.2 Hz, H−C(8)], 6.86 [dt, 1H, *J* = 6.7, 15.3 Hz, H−C(3)]. The ^{13}C NMR data (125 MHz, d_3-MeOD, HSQC, HMBC) are shown in Table 1.

N-(2-Methyl-2-hydroxypropyl)-dodeca-(2E,6E,8E,10E)-tetraene amide (hydroxy-β-sanshool), **3**, Figure 1: UV−vis (acetonitrile/0.1% aqueous formic acid; 1:1, v/v), λ_{max} 244, 272, 220 nm; LC-TOF-MS (ESI$^+$), *m/z* 286.1774 (measured), *m/z* 286.1777 (calcd for $[C_{16}H_{25}NO_2 + Na]^+$); MS (ESI$^+$), *m/z* 264 (100%, $[M + H]^+$), 246 (66%, $[M + H - H_2O]^+$), 286 (94%, $[M + Na]^+$), 302 (36%, $[M + K]^+$); MS/MS (DP = +40 V): *m/z* (%) 107 (100), 246 (75), 79 (42), 133 (33), 139 (33), 147 (33), 175 (18); ^{1}H NMR (400 MHz, $CDCl_3$, COSY), *δ* 1.24 [s, 6H, H−C(3′, 4′)], 1.77 [d, 3H, *J* = 7.0 Hz, H−C(12)], 2.26 [m, 2H, *J* = 5.8 Hz, H−C(5)], 2.28 [m, 2H, *J* = 6.4 Hz, H−C(4)], 3.33 [d, 2H, *J* = 6.1 Hz, H−C(1′)], 5.63 [m, 1H, *J* = 7.2, 13.5 Hz, H−C(6)], 5.69 [m, 1H, *J* = 6.9, 14.3, H−C(11)], 5.82 [d, 1H, *J* = 15.3 Hz, H−C(2)], 5.84 [1H, H−N], 6.02−6.14 [m, 4H, *J* = 14.7 Hz, H−C(7−10)], 6.86 [dt, 1H, *J* = 6.5, 15.2 Hz, H−C(3)]. The ^{13}C NMR data (125 MHz, d_3-MeOD, HSQC, HMBC) are shown in Table 1.

N-(2-Methyl-2-hydroxypropyl)-tetradeca-(2E,4E,8Z,11Z)-tetraene amide (bungeanool), **4**, Figure 1: UV−vis (acetonitrile/0.1% aqueous formic acid; 7:3, v/v), λ_{max} = 272, 248 nm; LC-TOF-MS (ESI$^+$), *m/z* 292.2278 (measured), *m/z* 292.2277 (calcd for $[C_{18}H_{29}NO_2 + H]^+$); MS (ESI$^+$), *m/z* 292 (60, $[M + H]^+$), 274 (17, $[M + H - H_2O]^+$), 314 (100, $[M + Na]^+$), 330 (70, $[M + K]^+$); MS/MS (DP = +40 V), *m/z* (%) 274 (100), 119 (20), 131 (19), 72 (17), 203 (5), 175 (4); ^{1}H NMR (500 MHz, d_3-MeOD, COSY), *δ* 0.96 [t, 3H, *J* = 7.5 Hz, H−C(14)], 1.17 [s, 6H, H−C(3′,4′)], 2.03−2.11 [m, 2H, H−C(13)], 2.18−2.27 [m, 4H, H−C(6, 7)], 2.78 [dd, 2H, *J* = 5.8 Hz, H−C(10)], 3.26 [s, 2H, H−C(1′)], 5.25−5.32 [m, 1H, H−C(11)], 5.34−5.41 [m, 3H, H−C(8, 9, 12)], 6.00 [d, 1H, *J* = 15.1 Hz, H−C(2)], 6.07−6.14 [m, 1H, *J* = 6.5, 15.1 Hz, H−C(5)], 6.23 [dd, 1H, *J* = 10.8, 15.1 Hz, H−C(4)], 7.13 [dd, 1H, *J* = 10.7, 15.1 Hz, H−C(3)]. The ^{13}C NMR data (125 MHz, d_3-MeOD, HSQC, HMBC) are shown in Table 1.

N-(2-Methyl-2-hydroxypropyl)-tetradeca-(2E,4E,8Z,11E)-tetraene amide (isobungeanool), **5**, Figure 1: UV−vis (acetonitrile/0.1% aqueous formic acid; 7:3, v/v), λ_{max} = 260 nm; LC-TOF-MS (ESI$^+$), *m/z* 292.2274 (measured), *m/z* 292.2277 (calcd for $[C_{18}H_{29}NO_2 + H]^+$); MS (ESI$^+$), *m/z* 292 (100, $[M + H]^+$), 314 (52, $[M + Na]^+$), 274 (22, $[M + H - H_2O]^+$), 330 (18, $[M + K]^+$); MS/MS (DP = +20 V), *m/z* 274 (100), 72 (29), 131 (26), 119 (26), 95 (26), 203 (9), 175 (8); ^{1}H NMR (500 MHz, d_3-MeOD, COSY), *δ* 0.96 [t, 3H, *J* = 7.6, H−C(14)], 1.17 [s, 6H, H−C(3′,4′)], 1.95−2.03 [m, 2H, H−C(13)], 2.16−2.26 [m, 4H, H−C(6, 7)], 2.72 [dd, 2H, *J*=5.4 Hz, H−C(10)], 3.26 [s, 2H, H−C(1′)], 5.33−5.42 [m, 3H, H−C(8, 9, 11)], 5.42−5.51 [m, 1H, H−C(12)], 5.99 [d, 1H, *J* = 15.1 Hz, H−C(2)], 6.06−6.14 [m, 1H, *J* = 6.6, 15.1 Hz, H−C(5)], 6.22 [dd, 1H, *J* = 10.8, 15.1 Hz, H−C(4)], 7.12 [dd, 1H, *J* = 10.7, 15.1 Hz, H−C(3)]. The ^{13}C NMR data (125 MHz, d_3-MeOD, HSQC, HMBC) are shown in Table 1.

N-(2-Methyl-2-hydroxypropyl)-tetradeca-(2E,4E,8E,10E,12E)-pentaene amide (hydroxy-γ-isosanshool), **6**, Figure 1: UV−vis (acetonitrile/0.1% aqueous formic acid; 6:4, v/v), λ_{max} = 248, 272 nm; LC-TOF-MS (ESI$^+$), *m/z* 290.2122 (measured), *m/z* 290.2120 (calcd for $[C_{18}H_{27}NO_2 + H]^+$); MS (ESI$^+$), *m/z* 290 (100, $[M + H]^+$), 272 (43, $[M + H - H_2O]^+$), 312 (53, $[M + Na]^+$), 328 (16, $[M + K]^+$); MS/MS (DP = +40 V), *m/z* 272 (95), 165 (100), 107 (78), 72 (35), 173 (17), 201 (7); ^{1}H NMR (500 MHz, d_3-MeOD, COSY), *δ* 1.17 [s, 6H, H−C(3′,4′)], 1.74 [d, 3H, *J* = 7.0 Hz, H−C(14)], 2.22 [m, 2H, *J* = 6.4, 12.9 Hz, H−C(6)], 2.26 [m, 2H, *J* = 6.6, 13.0 Hz, H−C(7)], 3.26 [s, 2H, H−C(1′)], 5.60−5.70 [m, 2H, H−C(8, 13)], 5.99 [d, 1H, *J* = 15.1 Hz, H−C(2)], 6.01−6.10 [m, 4H, H−C(9, 10, 11, 12)], 6.11 [m, 1H, H−C(5)], 6.23 [dd, 1H, *J* = 10.8, 15.2 Hz, H−C(4)], 7.12 [dd, 1H, *J* = 10.7, 15.1 Hz, H−C(3)]. The ^{13}C NMR data (125 MHz, d_3-MeOD, HSQC, HMBC) are shown in Table 1.

N-(2-Methyl-2-hydroxypropyl)-dodeca-(2E,6Z,8E,10Z)-tetraene amide (hydroxy-ε-sanshool), **7**, Figure 1: UV−vis (acetonitrile/0.1% aqueous

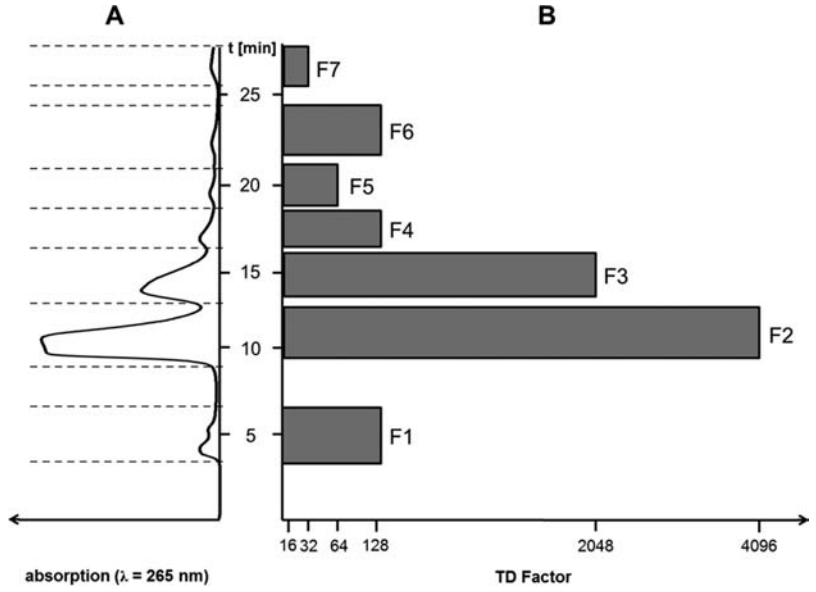

Figure 2. (A) MPLC chromatographic separation of the methanol solubles of Szechuan pepper extract and (B) taste dilution analysis (TDA) recording the tingling orosensation.

formic acid; 1:1, v/v), λ_{max} = 208, 276 nm; LC-TOF-MS (ESI^+), *m/z* 286.1774 (measured), *m/z* 286.1777 (calcd for $[C_{16}H_{25}NO_2 + Na]^+$); MS ($ESI^+$), *m/z* 264 (100, $[M + H]^+$), 246 (81, $[M + H - H_2O]^+$), 286 (70, $[M + Na]^+$), 302 (25, $[M + K]^+$); MS/MS (DP = +40 V), *m/z* 274 (100), 119 (20), 131 (19), 72 (17), 203 (5), 175 (4); ^1H NMR (500 MHz, d_3-MeOD, COSY), δ 1.19 [s, 6H, H−C(3′, 4′)], 1.77 [dd, 3H, *J* = 1.6, 7.2 Hz, H−C(12)], 2.31 [m, 2H, *J* = 6.7, 14.4 Hz, H−C(4)], 2.39 [m, 2H, *J* = 7.4, 14.5 Hz, H−C(5)], 3.27 [s, 2H, H−C(1′)], 5.44 [m, 1H, *J* = 7.6, 10.7 Hz, H−C(6)], 5.52 [m, 1H, *J* = 7.2, 10.8, H−C(11)], 6.04 [dt, 1H, *J* = 1.4, 15.4 Hz, H−C(2)], 6.07−6.11 [m, 2H, *J* = 10.4, 10.9 Hz, H−C(10, 7)], 6.48 [dd, 1H, *J* = 10.6, 14.9 Hz, H−C(8)], 6.53 [dd, 1H, *J* = 10.8, 14.9 Hz, H−C(9)], 6.81 [dt, 1H, *J* = 6.8, 15.3 Hz, H−C(3)]. ^1H NMR (500 MHz, $CDCl_3$, COSY): δ/ppm: δ 1.24 [s, 6H, H−C(3′, 4′)], 1.78 [dd, 3H, *J*=1.6, 7.2 Hz, H−C(12)], 2.29 [m, 2H, *J*=6.8, 14.4 Hz, H−C(4)], 2.37 [m, 2H, *J*=7.3, 14.4 Hz, H−C(5)], 3.32 [d, 2H, *J*=6.1 Hz, H−C(1′)], 5.43 [dt, 1H, *J*=7.4, 10.8 Hz, H−C(6)], 5.55 [m, 1H, *J*=7.2, 10.7, H−C(11)], 5.84 [dt, 1H, *J* = 1.5, 15.3 Hz, H−C(2)], 5.84 [1H, H−N], 6.08 [m, 1H, *J* = 10.8 Hz, H−C(10)], 6.10 [m, 1H, *J* = 11.1 Hz, H−C(7)], 6.43 [dd, 1H, *J* = 11.1, 14.8 Hz, H−C(8)], 6.52 [dd, 1H, *J* = 11.0, 14.8 Hz, H−C(9)], 6.87 [dt, 1H, *J* = 6.7, 15.2 Hz, H−C(3)]. The ^{13}C NMR data (125 MHz, d_3-MeOD, HSQC, HMBC) are shown in Table 1.

N-(2-Methyl-2-hydroxypropyl)-tetradeca-(2E,4E,8Z,10E,12Z)-pentaenwamide (hydroxy-ζ-sanshool), **8**, Figure 1: UV−vis (methanol/0.1% aqueous formic acid; 6:4, v/v), λ_{max} = 276, 264 nm; LC-TOF-MS (ESI^+), *m/z* 290.2114 (measured), *m/z* 290.2120 (calcd for $[C_{18}H_{27}NO_2 + H]^+$); MS (ESI^+), *m/z* 290 (100, $[M + H]^+$), 272 (22, $[M + H - H_2O]^+$), 312 (70, $[M + Na]^+$), 328 (33, $[M + K]^+$); MS/MS (DP = +40 V), *m/z* 272 (100), 165 (69), 131 (40), 72 (35), 173 (33), 107 (30), 93 (18), 201 (10); ^1H NMR (500 MHz, d_3-MeOD, COSY), δ 1.18 [s, 6H, H−C(3′,4′)], 1.76 [d, 3H, *J* = 7.1 Hz, H−C(14)], 2.27 [m, 2H, *J* = 7.3, 14.5 Hz, H−C(6)], 2.35 [m, 2H, *J* = 7.4, 14.8 Hz, H−C(7)], 3.26 [s, 2H, H−C(1′)], 5.38−5.46 [m, 1H, H−C(8)], 5.46−5.56 [m, 1H, H−C(13)], 6.00 [d, 1H, *J* = 15.2 Hz, C−H(2)], 6.03−6.17 [m, 3H, H−C(5, 9, 12)], 6.24 [dd, 1H, *J* = 10.6, 14.9 Hz, H−C(4)], 6.43−6.49 [dd, 1H, *J* = 10.2, 14.9 Hz, H−C(10)], 6.49−6.56 [dd, 1H, *J* = 10.4, 15.5 Hz, H−C(11)], 7.12 [dd, 1H, *J* = 10.8, 14.9 Hz, H−C(3)]. The ^{13}C NMR data (125 MHz, d_3-MeOD, HSQC, HMBC) are shown in Table 1.

Ultraperformance Liquid Chromatography−Time-of-Flight Mass Spectrometry (UPLC-TOF-MS). Mass spectra of the compounds were measured on a Waters Synapt G2 HDMS mass spectrometer (Waters, Manchester, UK) coupled to an Acquity UPLC core system (Waters, Milford, MA, USA) consisting of a binary solvent manager, sample manager, and column oven. Analytes were injected into the UPLC-TOF-MS system equipped with a 2.1 × 150 mm, 1.7 μm, BEH C18 column (Waters, Manchester, UK). Operated with a flow rate of 0.4 mL/min at 45 °C, the following gradient was used for chromatography: starting with a mixture (40:60, v/v) of water and acetonitrile, the acetonitrile content was increased to 100% within 4 min and, then, kept constant for 1 min. Scan time for the MS^E method (centroid) was set to 0.1 s. Analyses were performed in the positive ESI and the resolution mode using the following ion source parameters: capillary voltage, +2.0 kV; sampling cone, 30 V; extraction cone, 4.0 V; source temperature, 150 °C; desolvation temperature, 450 °C; cone gas, 30 L/h; and desolvation gas, 850 L/h. Data processing was performed by using MassLynx 4.1 SCN 779 (Waters, Manchester, UK) and the elemental composition tool for determining the accurate mass. All data were lock mass corrected on the pentapeptide leucine enkephaline (Tyr-Gly-Gly-Phe-Leu, *m/z* 556.2771, $[M + H]^+$) in a solution (2 ng/μL) of acetonitrile/0.1% formic acid (1:1, v/v). Scan time for the lock mass was set to 0.3 s, an interval of 15 and 3 scans to average with a mass window of ±0.3 Da. Calibration of the Synapt G2 in the range from *m/z* 50 to 1300 was performed using a solution of sodium formate (5 mmol/L) in 2-propanol/water (9:1, v/v). The UPLC and Synapt G2 systems were operated with MassLnyx software (Waters, Manchester, UK).

High-Performance Liquid Chromatography−Mass Spectrometry (HPLC-MS/MS). LC-MS/MS analysis was performed using an Dionex Ultimate 3000 HPLC system connected to the API 4000QTrap LC-MS/MS (AB Sciex, Darmstadt, Germany) running in the positive electrospray ionization (ESI^+) mode. Zero grade air served as nebulizer gas (45 psi) and as turbo gas (425 °C) for solvent drying (55 psi). Nitrogen served as curtain (20 psi) and collision gas (8.7×10^{-7} psi). Both quadrupoles were set at unit resolution. ESI^+ mass and product ion spectra were acquired with direct flow infusion. For ESI^+, the ion spray voltage was set at +5500 V.

Nuclear Magnetic Resonance Spectroscopy (NMR). ^1H, ^{13}C, DEPT-135, homonuclear $^1H-^1H$ correlation spectroscopy ($^1H-^1H$-*g*COSY), heteronuclear single-quantum coherence spectroscopy (*g*HSQC), heteronuclear multiple-bond correlation spectroscopy (*g*HMBC), and $^1H-^1H$ rotating frame nuclear Overhauser enhancement spectroscopy (phase-sensitive ROESY) NMR measurements were performed on an Avance III 500 MHz equipped with a CTCI probe and an Avance III 400 MHz spectrometer with a BBO probe (Bruker, Rheinstetten, Germany), respectively. Chemical shifts were referenced to the solvent signal. Data processing was performed by

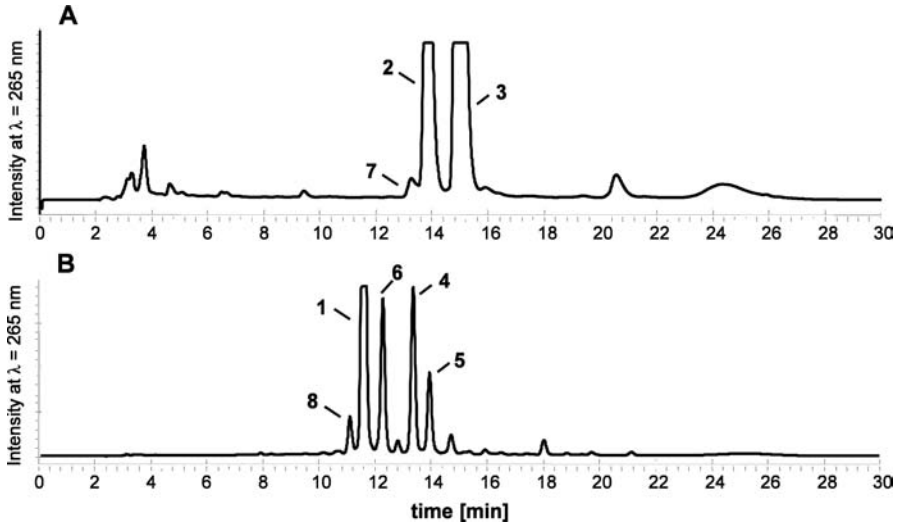

Figure 3. Preparative HPLC separation of MPLC fractions F2 (A) and F3 (B).

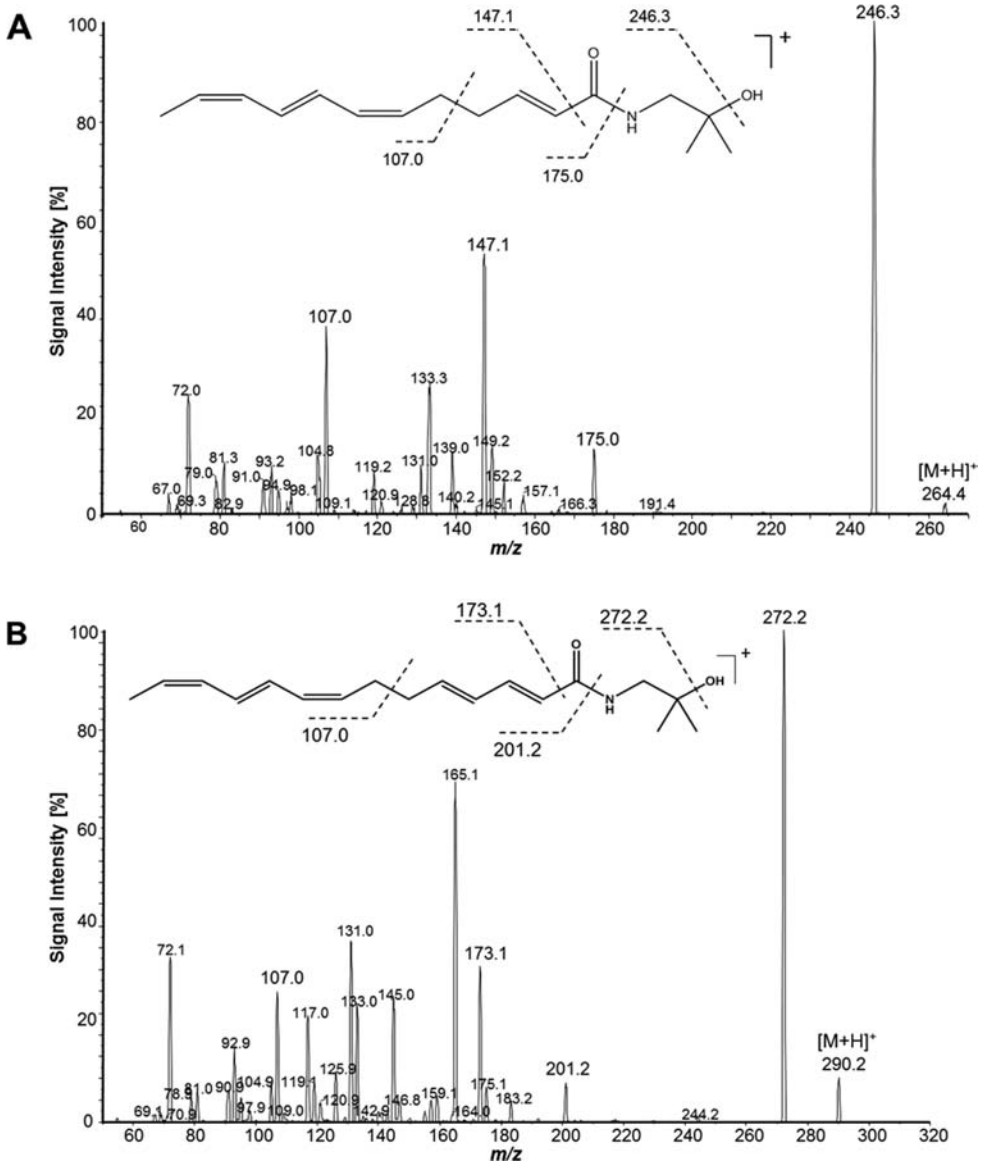

Figure 4. MS/MS spectrum (ESI$^+$, +20 V) of (A) hydroxy-ε-sanshool (**7**) and (B) hydroxy-ζ-sanshool (**8**), respectively.

dx.doi.org/10.1021/jf500399w | J. Agric. Food Chem. 2014, 62, 2479−2488

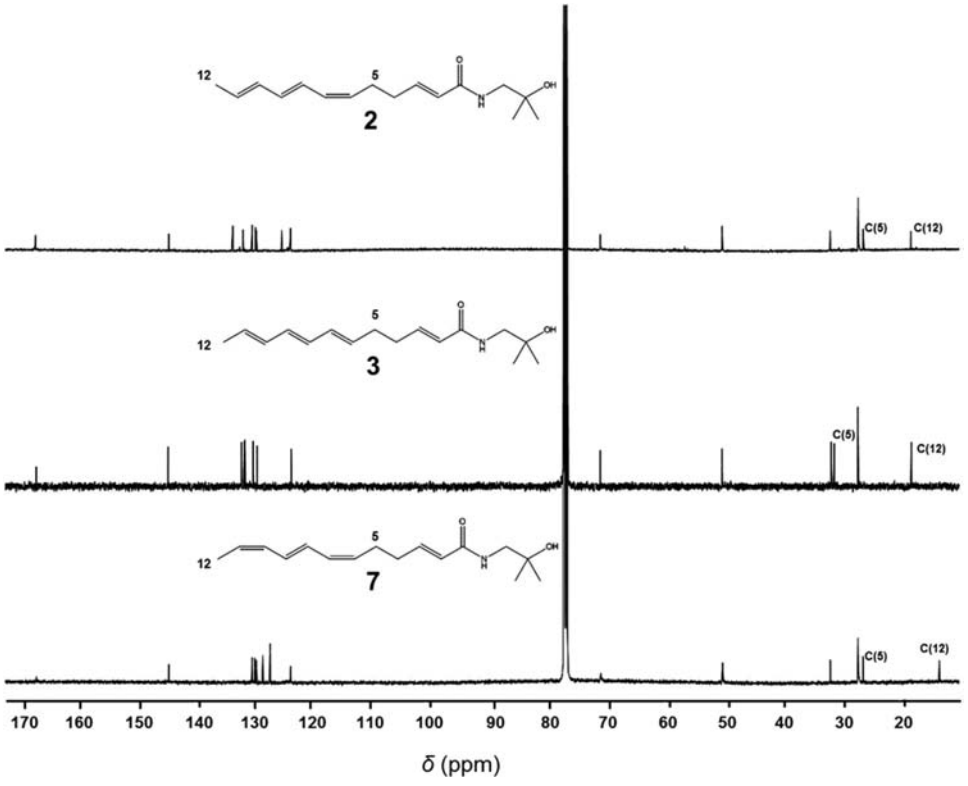

Figure 5. ^{13}C NMR spectra (125 MHz, $CDCl_3$) of alkylamides **2**, **3**, and **7**.

using Topspin version 2.1 (Bruker) and MestReNova version 6.2.1 software (Mestrelab Research, Santiago de Compostela, Spain).

RESULTS AND DISCUSSION

Using the recently developed half-mouth test,[13] orosensory evaluation of paper vehicles loaded with dilutions of the SCF extract prepared from *Z. piperitum* revealed a strong and long-lasting tingling activity in the oral cavity perceived up to a dilution of 1:16384 (data not shown). To locate the most active chemosensates in Szechuan pepper, the SFC extract was dissolved in methanol and extracted with hexane, both fractions were separated from solvent, and dilutions of the hexane extractables as well as the methanol solubles were judged in natural concentration ratios in their tingling activity by means of a TDA. The methanol solubles induced a strong tingling sensation judged with a TD factor of 8192, whereas the hexane extractables showed comparatively low activity judged with a TD factor of only 128. As a consequence, the following investigation on the primary tingling components in Szechuan pepper was focused on the methanol solubles.

Taste Dilution Analysis. To sort out the tingling compounds from the bulk of less taste-active or tasteless substances, the tingling-active methanol solubles of the SFC extract were separated by means of MPLC on RP18 material to give seven fractions, namely F1−F7, which were collected individually, separated from solvent, and used for the TDA using paper disks as vehicles.[13] Fractions F2 and F3 showed by far the highest TD factors of 4096 and 2048, respectively, whereas all other fractions showed only low tingling activity judged with TD factors of ≤128 (Figure 2). Aimed at characterizing the molecular structure of the compounds imparting the most intense tingling sensation of Szechuan pepper, further fractionation and LC-MS as well as NMR experiments were focused on MPLC fractions F2 and F3.

Isolation and Identification of Chemosensates in Fractions F2 and F3. Separation of fractions F2 and F3 by means of preparative RP-HPLC revealed nearly baseline separation of their components, which could be isolated or further purified by means of rechromatography (Figure 3).

LC-MS analysis using electrospray ionization (ESI^+) revealed m/z 264 as the pseudomolecular ion ($[M + H]^+$) and m/z 246 as the main fragment ion for the three main compounds **2**, **3**, and **7** eluting in fraction F2 (Figure 3A). Exemplified for compound **7**, the product ion scan of m/z 264 $[M + H]^+$ revealed the main fragments of m/z 246, 147, 107, and 175 (Figure 4A), indicating the loss of water as well as an alpha and an allyl cleavage, respectively. Moreover, the isobaric compounds **2**, **3**, and **7** were found by LC-TOF-MS to show identical elemental compositions of $C_{16}H_{25}NO_2$. In comparison, the early-eluting compounds **1**, **6**, and **8** in fraction F3 (Figure 3B) showed a pseudomolecular ion ($[M + H]^+$) of m/z 290 and a main fragment ion with m/z 272, well in agreement with the molecular formula of $C_{18}H_{27}NO_2$ as indicated by LC-TOF-MS analysis. The late-eluting compounds **4** and **5** in fraction F3 differed by a mass increment of 2, consistent with an elemental composition of $C_{18}H_{29}NO_2$ (LC-TOF-MS), and showed m/z 292 and 274 as the $[M + H]^+$ and the main fragment ion, respectively.

Unequivocal assignment of protons and carbon atoms could be successfully achieved by means of ^1H, ^{13}C, DEPT-135, $^1H-^1H$-*g*COSY, *g*HMBC optimized for $^2J_{C,H}$ and $^3J_{C,H}$ coupling constants, and *g*HSQC optimized for $^1J_{C,H}$ coupling constants, respectively (Table 1). Comparison of ^1H and ^{13}C NMR data with literature data[1,2] led to the identification of the amides hydroxy-γ-sanshool (**1**), hydroxy-α-sanshool (**2**), hydroxy-β-sanshool (**3**), bungeanool (**4**), isobungeanool (**5**), and hydroxy-γ-isosanshool (**6**), respectively.

dx.doi.org/10.1021/jf500399w | J. Agric. Food Chem. 2014, 62, 2479−2488

The ^{1}H NMR of compound **7** showed eight olefinic protons of the polyunsaturated fatty acid chain, namely, H−C(2), H−C(3), and H−C(6) to H−C(11), resonating in the range of 5.43−6.87 ppm, and six aliphatic protons, which could be assigned to the 2-methyl-2-hydroxypropyl moiety (H−C(1′), H−C(3′), H−C(4′)), the terminal methyl protons H−C(12), and the two methylene groups H−C(4) and H−C(5) of the fatty acid moiety. Unequivocal assignment of all protons and carbon atoms could be successfully achieved by means of 1D/2D NMR spectroscopy, which identified **7** as a geometrical isomer of amides **2** and **3** showing four double bonds at carbons C(2), C(6), C(8), and C(10), respectively. The geometry of the individual double bonds was unambiguously elucidated by comparing the $^3J_{H,H}$ coupling constants of the olefinic protons and the ^{13}C NMR chemical shifts recorded for the individual isomers, as well as by means of ROESY experiments. The protons H−C(2) and H−C(3), both resonating as double triplets, and the two double duplet protons H−C(8) and H−C(9) showed the characteristic *trans*-olefinic coupling constants of 15.2 and 14.8 Hz, respectively. In contrast, the olefinic protons H−C(10) and H−C(11) as well as H−C(6) and H−C(7) showed a $^3J_{H,H}$ coupling constant of ∼10.8 Hz, thus indicating a *cis*-configuration. By comparing the ^{13}C chemical shifts of compounds **2**, **3**, and **7**, the methylene carbon atom C(5) and the methyl carbon C(12), both adjacent to the *cis*-configured double bond, showed a clear upfield shift in **7** when compared to the all-*trans*-isomer **3** (Table 1; Figure 5). The upfield shift of the carbon C(5) from 31.4 to 26.5 ppm in **7** and **2** compared to **3** is well in agreement with a *cis*-shielding effect reported in the literature.[2,7−9] Another fingerprint carbon atom, namely C(12), showed an upfield shift of ∼5 ppm in **7** when compared to its geometric isomers **2** and **3**, respectively (Table 1; Figure 5). The configurations of the double bonds were further supported by means of a ROESY experiment; for example, a ROESY correlation was detected between the methyl protons H−C(12) and methine proton H−C(9). Taking all spectroscopic data into consideration, LC-TOF-MS, LC-MS/MS, and 1D/2D NMR experiments led to the unequivocal identification of compound **7** as *N*-(2-methyl-2-hydroxypropyl)dodeca-(2*E*,6*Z*,8*E*,10*Z*)-tetraene amide (hydroxy-ε-sanshool). which has already been mentioned in the literature,[3,5,6,10] although its chemical structure has not yet been confirmed by means of 1D/2D NMR spectroscopy.

The MS product ion scan of *m*/*z* 290 $[M + H]^+$, the pseudomolecular ion of compound **8**, revealed *m*/*z* 272, 173, 107, and 202 as the main fragment ions (Figure 4B), thus indicating the cleavage of water (*m*/*z* 272), and an alpha cleavage (*m*/*z* 173; *m*/*z* 202), as well as an allyl cleavage (*m*/*z* 107), respectively. The ^{1}H NMR of **8** showed 10 olefinic protons, namely, H−C(2) to H−C(5) and H−C(8) to H−C(13), resonating in the range of 5.38−7.12 ppm, six aliphatic protons assigned to the 2-methyl-2-hydroxypropyl moiety (H−C(1′), H−C(3′), H−C(4′)), the terminal methyl protons H−C(14), and the two methylene groups H−C(6) and H−C(7) of the fatty acid moiety. Assignment of protons and carbon atoms revealed **8** to be a geometrical isomer of the amides **1** and **6**, respectively. The $^3J_{H,H}$ coupling constants of 15.5 and 14.9 Hz of the two double duplets detected for H−C(10) and H−C(11) indicated a *trans*-configuration of this double bond (Figure 6). Moreover, carbon atoms C(7) and C(14) showed an upfield shift of ∼5 ppm in **8** when compared to its geometric isomers **1** and **6** (Table 1; Figure 1), being well in agreement with the expected *cis*-shielding effect.[2,7−9] Taking all spectroscopic data into consideration, the structure of compound **8** was determined to be *N*-(2-methyl-2-hydroxypropyl)tetradeca-(2*E*,4*E*,8*Z*,10*E*,12*Z*)-pentaene amide, coined hydroxy-ζ-sanshool, which to the best of our knowledge has not been reported before.

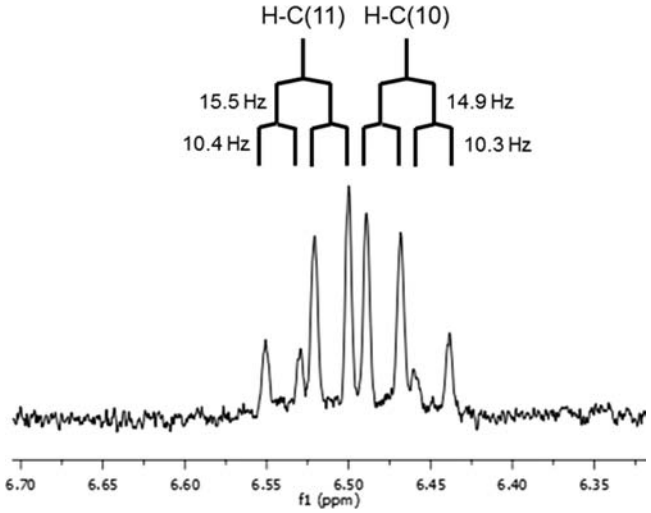

Figure 6. Excerpt (δ 6.3−6.7) of the ^{1}H NMR spectra (500 MHz, d_3-MeOD) of alkylamide **8** showing H−C(10) and H−C(11).

Sensory Evaluation of Pungent and/or Tingling Chemosensates. Prior to sensory analysis, the purity of all compounds was confirmed by LC-MS as well as ^{1}H NMR spectroscopy to be >98%. To determine the human threshold concentrations for the orosensation induced by the individual chemosensates, paper vehicles loaded with the test compounds in serial dilutions were evaluated by means of a half-tongue test.[13] Hydroxy-γ-sanshool (**1**), hydroxy-α-sanshool (**2**), bungeanool (**4**), isobungeanool (**5**), hydroxy-ε-sanshool (**7**), and the previously not reported hydroxy-ζ-sanshool (**8**) were found to elicit an oral tingling and paresthetic sensation above a rather similar threshold concentrations ranging between 3.5 and 8.3 nmol/cm^2, respectively (Table 2). It is interesting to note that the position of the *cis*-configured double bond in **1**, **2**, **4**, **5**, **7**, and **8** did not have a major impact on the tingling threshold concentration of these amides. Interestingly, the absence of a *cis*-double bond, as found for hydroxy-β-sanshool (**3**) and hydroxy-γ-isosanshool (**6**), resulted in a complete loss of the tingling activity. This is well in agreement with earlier studies

Table 2. Orosensory Recognition Thresholds of Alkylamides 1−8

compound[a]	oral sensation	threshold concn[b] (nmol/cm^2)
1	tingling, paresthetic	6.8
2	tingling, paresthetic	8.3
3	numbing, anesthetic	3.9
4	tingling, paresthetic	3.5
5	tingling, paresthetic	3.5
6	numbing, anesthetic	7.1
7	tingling, paresthetic	4.2
8	tingling, paresthetic	7.0

[a]Structures of compounds are given in Figure 1. [b]Orosensory recognition threshold concentrations were determined by means of a modified half-mouth test using paper rectangles (1 × 2 cm) as a vehicle.[13]

on synthetic polyunsaturated alkylamides[10] and those isolated from black pepper;[13] for example, saturation of the double bond in black pepper's tingling compound (2*E*,4*E*,12*Z*)-*N*-isobutyloctadeca-2,4,12-trienamide wiped out the tingling activity of (2*E*,4*E*)-*N*-isobutyloctadeca-2,4-dienamide. Although no tingling activity was detectable for the all-*trans*-configured compounds **3** and **6**, most interestingly, the sensory panelists reported an intense and long-lasting numbing and anesthetic oral impression above threshold concentrations of 3.9 nmol/cm^2 (**3**) and 7.1 nmol/cm^2 (**6**).

To answer the question of whether the tingling and numbing amides differ in their salivating activity, the major amides hydroxy-α-sanshool (**2**, tingling) and hydroxy-β-sanshool (**3**, numbing) were isolated in suitable amounts and aqueous solutions were used to orally challenge a panel of eight healthy volunteers for 15 s; the saliva flow was measured for 120 s using an assay reported recently.[15] A comparative experiment was performed with an aqueous solution of the crude Szechuan pepper extract containing 9.1% hydroxy-α-sanshool and 2.5% hydroxy-β-sanshool. All three stimuli significantly activated a long-lasting saliva flow increase (Figure 7). The tingling

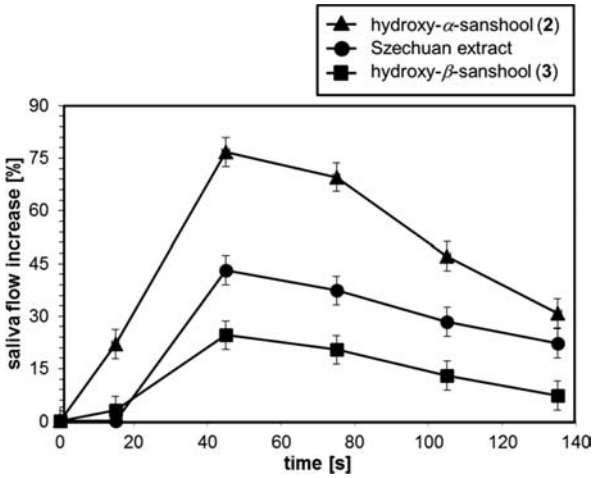

Figure 7. Time course of saliva flow increase induced by an aqueous stimulus solution (2 mL) containing (●) the Szechuan pepper extract (100 mg/100 mL), (■) hydroxy-β-sanshool (100 mg/100 mL), and (▲) hydroxy-α-sanshool (100 mg/mL). Least significant difference is visualized (LSD = 8.263).

hydroxy-α-sanshool induced a massive increase of saliva flow accounting for a maximum of ~75% after 45 s when compared to the control. Also, the Szechuan pepper extract showed a strong increase of saliva flow (~44% after 45 s), whereas the numbing hydroxy-β-sanshool showed only a marginal activity accounting for a saliva flow increase of ~25%. This demonstrates that at least one *cis*-configured double bond is needed for strong salivating activity, being well in agreement with literature data on spilanthol,[14] whereas the all-*trans*-configuration diminishes salivation. As the tingling hydroxy-α-sanshool is the quantitatively predominant amide in Szechuan pepper, this isomer is concluded to be mainly responsible for the tingling as well as the salivation enhancement activity of Szechuan pepper.

The molecular mechanisms by which hydroxy-α-sanshool (**2**) induces the tingling sensation have been a matter of debate. Although this amide is an agonist at the pain-integrating cation channels TRPV1 and TRPA1,[18] newer evidence suggests that neuron activation through a unique mechanism involving inhibition of the pH- and anesthetic-sensitive two-pore potassium channels TASK-1, TASK-3, and TRESK (previously named KCNK3, KCNK9, and KCNK18) is mediating the tingling effect of hydroxy-α-sanshool.[19] The finding that a clear tingling, paresthetic sensation is induced by amides containing at least one *cis*-configured double bond as found in **1**, **2**, **4**, **5**, **7**, and **8**, whereas an intense numbing and anesthetic impression is caused by all-*trans*-configured amides (**3** and **6**), promises the various isomers as valuable molecular probes to test candidate ion channels TASK-1, TASK-3, and TRESK for mediating the tingling effect and to challenge other receptive proteins for mediating the numbing and anesthetic effect. Such experiments will be helpful to deliver a framework for understanding the unique and complex psychophysical sensations associated with the Szechuan pepper experience.

AUTHOR INFORMATION

Corresponding Author

*(T.H.) Phone: +49-8161-71-2902. Fax: +49-8161-71-2949. E-mail: thomas.hofmann@tum.de.

Author Contributions

‖M.B. and T.D.S. contributed equally to this work.

Notes

The authors declare no competing financial interest.

REFERENCES

(1) Mizutani, K.; Fukunaga, Y.; Tanaka, O.; Takasugi, N.; Saruwatari, Y.-I.; Fuwa, T.; Yamauchi, T.; Wang, J.; Jia, M.-R.; Li, F.-Y.; Ling, Y.-K. Amides from Huajiao, pericarps of *Zanthoxylum bungeanum* Maxim. *Chem. Pharm. Bull.* **1988**, *36*, 2362−2365.

(2) Yasuda, I.; Takeya, K.; Itokawa, H. Distribution of unsaturated aliphatic acid amides in Japanese *Zanthoxylum* species. *Phytochemistry* **1982**, *21*, 1295−1298.

(3) Bryant, B. P.; Mezine, I. Alkylamides that produce tingling paresthesia activate tactile and thermal trigeminal neurons. *Brain Res.* **1999**, *842*, 452−460.

(4) Kashiwada, Y.; Ito, C.; Katagiri, H.; Mase, I.; Komatsu, K.; Namba, T.; Ikeshiro, Y. Amides of the fruit of *Zanthoxylum*. *Phytochemistry* **1997**, *44*, 1125−1127.

(5) Jang, K. H.; Chang, Y. H.; Kim, D.-D.; Oh, K.-B.; Oh, U.; Shin, J. New polyunsaturated fatty acid amides isolated from the seeds of *Zanthoxylum piperitum*. *Arch. Pharm. Res.* **2008**, *31*, 569−572.

(6) Yang, X. Aroma constituents and alkylamides of red and green Huajiao (*Zanthoxylum bungeanum* and *Zanthoxylum schinifolium*). *J. Agric. Food Chem.* **2008**, *56*, 1689−1696.

(7) Yasuda, I.; Takeya, K.; Itokawa, H. Two new pungent principles isolated from the pericarps of *Zanthoxylum ailanthoides*. *Chem. Pharm. Bull.* **1981**, *29*, 1791−1793.

(8) Yasuda, I.; Takeya, K.; Itokawa, H. Structures of amides from *Asiasarum heterotropoides* Maek. var. *mandshuricum* Maek. *Chem. Pharm. Bull.* **1981**, *29*, 564−566.

(9) Yasuda, I.; Takeya, K.; Itokawa, H. The geometric structure of spilanthol. *Chem. Pharm. Bull.* **1980**, *28*, 2251−2253.

(10) Galopin, Ch. C.; Furrer, S. M.; Goeke, A. Pungent and tingling compounds in Asian cuisine. In *Challenges in Taste Chemistry and Biology*; Hofmann, T., Ho, C. T., Pickenhagen, W., Eds.; ACS Symposium Series 876; American Chemical Sosiety: Washington, DC, USA, 2004; pp 139−152.

(11) Sugai, E.; Morimitsu, Y.; Iwasaki, Y.; Morita, A.; Watanabe, T.; Kubota, K. Pungent qualities of sanshool-related compounds evaluated by a sensory test and activation of rat TRPV1. *Biosci., Biotechnol., Biochem.* **2005**, *65*, 1951−1957.

(12) Trevisani, M.; Smart, D.; Gunthorpe, M. J.; Tognetto, M.; Barbieri, M.; Campi, B.; Amatesi, S.; Gray, J.; Jerman, J. C.; Brough, S. J.; Owen, D.; Smith, G. D.; Randall, A. D.; Harrison, S.; Bianchi, A.;

Davis, J. B.; Geppetti, P. Ethanol elicits and potentiates nociceptor responses via the vanilloid receptor-1. *Nat. Neurosci.* **2002**, *5*, 546−551.
(13) Dawid, C.; Henze, A.; Frank, O.; Glabasnia, A.; Rupp, M.; Büning, K.; Orlikowski, D.; Bader, M.; Hofmann, T. Structural and sensory characterisation of key pungent and tingling compounds from pepper (*Piper nigrum* L.). *J. Agric. Food Chem.* **2012**, *60*, 2884−2895.
(14) Ley, J. P.; Simchen, U. Quantification of the saliva-inducing properties of pellitorine and spilanthole. *Rec. Highl. Flav. Chem. Biol.* **2007**, 365−368.
(15) Lorenz, K.; Bader, M.; Klaus, A.; Weiss, W.; Görg, A.; Hofmann, T. Orosensory stimulation effects on human saliva proteome. *J. Agric. Food Chem.* **2011**, *59*, 10219−10231.
(16) Frank, O.; Ottinger, H.; Hofmann, T. Characterization of an intense bitter-tasting 1*H*,4*H*-quinolizinium-7-olate by application of the taste dilution analysis, a novel bioassay for the screening and identification of taste-active compounds in foods. *J. Agric. Food Chem.* **2001**, *49*, 231−238.
(17) Stark, T.; Hofmann, T. Application of a molecular sensory science approach on alkalized cocoa (*Theobroma cacao*): structure determination and sensory activity of non-enzymatically C-glycosylated flavan-3-ols. *J. Agric. Food Chem.* **2006**, *54*, 9510−9521.
(18) Koo, J. Y.; Jang, Y.; Cho, H.; Lee, C.-H.; Jang, K. H.; Chang, Y. H.; Shin, J.; Oh, U. Hydroxy-α-sanshool activates TRPV1 and TRPA1 in sensory neurons. *Eur. J. Neurosci.* **2007**, *26*, 1139−1147.
(19) Bautista, D. M.; Sigal, Y. M.; Milstein, A. D.; Garrison, J. L.; Zorn, J. A.; Tsuruda, P. R.; Nicoll, R. A.; Julius, D. Pungent agents from Szechuan peppers excite sensory neurons by inhibiting two-pore potassium channels. *Nat. Neurosci.* **2008**, *11* (7), 772−779.

undergo hydrolysis before absorption. Depending upon the glycoside moiety, hydrolysis and subsequent absorption can occur in either the small or the large intestine.[13] The importance of intestinal bacteria for polyphenol metabolism was highlighted by the fact that germ-free or antibiotic-treated animals no longer form the phenolic acid metabolites (ring-fission products) of (+)-catechin, apigenin, myricetin, hesperidin, naringin, rutin, and 3′,4′,5,7-tetra-*O*-*β*-hydroxyethylrutoside.[14] Moreover, the pharmacological effects of the polyphenols might be stronger after being degraded by human intestinal bacteria. For instance, the effect on platelet function of anthocyanins and their metabolites was stronger in combination.[15]

In this study, we attempted to isolate different intestinal bacteria from human feces and carry out research on their abilities and characteristics in the metabolism of isorhamnetin 3-*O*-glucoside. To further clarify the metabolic profile of isorhamnetin 3-*O*-glucoside, rapid and sensitive ultraperformance liquid chromatography/quadrupole time-of-flight mass spectrometry (UPLC/Q-TOF-MS) with automated data analysis (MetaboLynx) was used to analyze its metabolites.[16,17] As far as we know, this was the first research on the metabolites of isorhamnetin 3-*O*-glucoside by human intestinal flora which could provide a powerful analytical methodology for the identification of multiple metabolites of natural products.

EXPERIMENTAL SECTION

Materials. HPLC-grade acetonitrile was obtained from TEDIA Co. Inc. (United States), along with the anaerobic glovebox. AnaeroPack rectangular jars and AnaeroPack-Anaero were purified by Mitsubishi Gas Chemical Co. Inc. (Japan). Formic acid was purchased from Merck KGaA (Germany).

Isorhamnetin 3-*O*-glucoside was obtained from Shanghai Winherb Medical Science Co. (China). Ultrapure water was purified with an EPED superpurification system (China). Other reagents were of analytical grade.

The general anaerobic medium (GAM) used for all fermentation experiments contains 0.3 g of L-cysteine hydrochloride, 0.3 g of sodium thioglycolate, 1.2 g of beef liver extract powder, 2.2 g of beef extract, 2.5 g of KH_2PO_4, 3.0 g of glucose, 3.0 g of soya peptone, 3.0 g of NaCl, 5.0 g of soluble starch, 5.0 g of yeast extract, 10.0 g of tryptone, 10.0 g of proteose peptone, 13.5 g of digestible serum powder, and 1000 mL distilled water. The pH was adjusted to 7.3.

Bacterial Isolation and Culture Conditions. A bacterial suspension of fresh human feces was collected from a healthy female volunteer who had not taken any polyphenols before the experiment. The fecal sample was weighed and homogenized adequately with sterile physiological saline at a ratio of 1:4 (m/v), and then the mixture was centrifuged at 2000*g* for 10 min. The suspension was used as a human intestinal bacterial mixture.

After being diluted in sterile water, the bacterial mixture was spread on GAM agar plates and then incubated in anaerobic gloveboxes under anaerobic conditions at 37 °C for 2 days. As a result of the incubation, about 150 different bacteria colonies were picked up and transferred to GAM agars on an inclined plane.

Bacterial Incubation and Sample Preparation. Each bacterium was inoculated into 1.0 mL of GAM broth after being picked up from the GAM agar plate, followed by the anaerobic incubation of cultures at 37 °C for 24 h. A 0.1 mL sample of the preculture bacteria was inoculated into 0.9 mL of GAM broth with 0.1 mM isorhamnetin 3-*O*-glucoside. Then all samples which had been incubated for 48 h were extracted with ethyl acetate (1 volume of the culture) three times. Finally, the ethyl acetate layer was dried and redissolved in 0.3 mL of methanol.[18] Each supernatant of the sample was used for UPLC/MS analysis.

UPLC Analysis. The analysis of isorhamnetin 3-*O*-glucoside and its metabolites was carried out on a Waters ACQUITY UPLC system, equipped with a Syncronis C 18 column for separation. Acetonitrile (solvent system A) and ultrapure water/0.1% formic acid served as the mobile phase. HPLC was run in gradient mode (solvent system A from 10% to 40% in 0−7.5 min, from 40% to 90% in 7.5−9 min, held at 90% for 9−10 min, and back to 10% in 10−11 min for equilibration of the column) at a flow rate of 0.4 mL/min. The column temperature was set at 35 °C, while the autosampler temperature was maintained at 4 °C.

MS Analysis. Selected incubation supernatants from degradation experiments were applied for the parent and metabolit identification by electrospray ionization mass spectrometry (ESI-MS) in negative mode. Leucine-enkephalin was used as the lock mass to generate an $[M - H]^-$ ion (m/z 554.2615). The source temperature was 120 °C, while the desolvation temperature was maintained at 350 °C. The cone and capillary voltages were 40 V and 3.0 kV. Meanwhile, the gas (N_2) flows of the cone and desolvation were 50 and 600 L/h, respectively. Furthermore, the MS^E experiment was carried out to obtain fragment mass information of the parent and metabolites, which was performed in two scan functions (the mass-scan range, scan time, interscan delay, and collision energy of function 1 and function 2 were m/z 100−1000, 0.5 s, 0.02 s, and 6 V and m/z 50−1000, 0.3 s, 0.02 s, and 15−45 V, respectively). All data collected were analyzed by a Waters Metabolynx (version 4.1) program.

RESULTS

Metabolic Profile of Isorhamnetin 3-*O*-Glucoside by the Isolated Human Intestinal Bacteria. After optimization of the UPLC and MS conditions, negative ion electrospray tandem mass spectrometry and Metabolynx software were used to obtain a general survey of the isorhamnetin 3-*O*-glucoside metabolic profile. As a result of our study, the parent and five metabolites of isorhamnetin 3-*O*-glucoside (Table 1) were detected and identified in the different bacterial samples compared with the blank sample. These metabolites were probably isorhamnetin 3-*O*-glucoside (M1) catabolites: isorhamnetin (M2), kaempferol (M3), quercetin (M4), kaempferol 3-*O*-glucoside (M5), and acetylated isorhamnetin 3-*O*-glucoside (M6). The extracted ion chromatograms (XICs) from the total UPLC/MS chromatograms are shown in Figure 1. What is more, M2 and M3 were found in most of the samples of the isolated human intestinal bacteria, while M5 and M6 were obtained only in the sample of *Escherichia* sp. 12, and M4 existed only in the sample of *Escherichia* sp. 4.

Table 1. Isorhamnetin 3-*O*-Glucoside and Its Metabolites (M1−M6) Produced by Human Intestinal Bacteria Using UPLC/Q-TOF-MS

no.	t_R[a]/min	m/z, calcd	$[M - H]^-$, found	identification	formula
M1	4.75	478.1111	477.0960	isorhamnetin 3-*O*-glucoside	$C_{22}H_{22}O_{12}$
M2	8.58	316.0583	315.0415	isorhamnetin	$C_{16}H_{12}O_7$
M3	8.31	286.0477	285.0374	kaempferol	$C_{15}H_{10}O_6$
M4	6.75	302.0427	301.0359	quercetin	$C_{15}H_{10}O_7$
M5	4.56	448.1006	447.0885	kaempferol 3-*O*-glucoside	$C_{21}H_{20}O_{11}$
M6	6.03	520.1217	519.1136	acetylated isorhamnetin 3-*O*-glucoside	$C_{24}H_{24}O_{13}$

[a] t_R = retention time.

Identification of Metabolites. The characterization of metabolites in the fermentation supernatants was based on their ion fragmentation in ESI^- mode.

Parent. Isorhamnetin 3-*O*-glucoside (M1) was identified by comparing the UPLC retention time (4.75 min), accurate MS at m/z 477.0960 $[M - H]^-$, and MS/MS spectra with those of the authentic standard (Figure 2a).

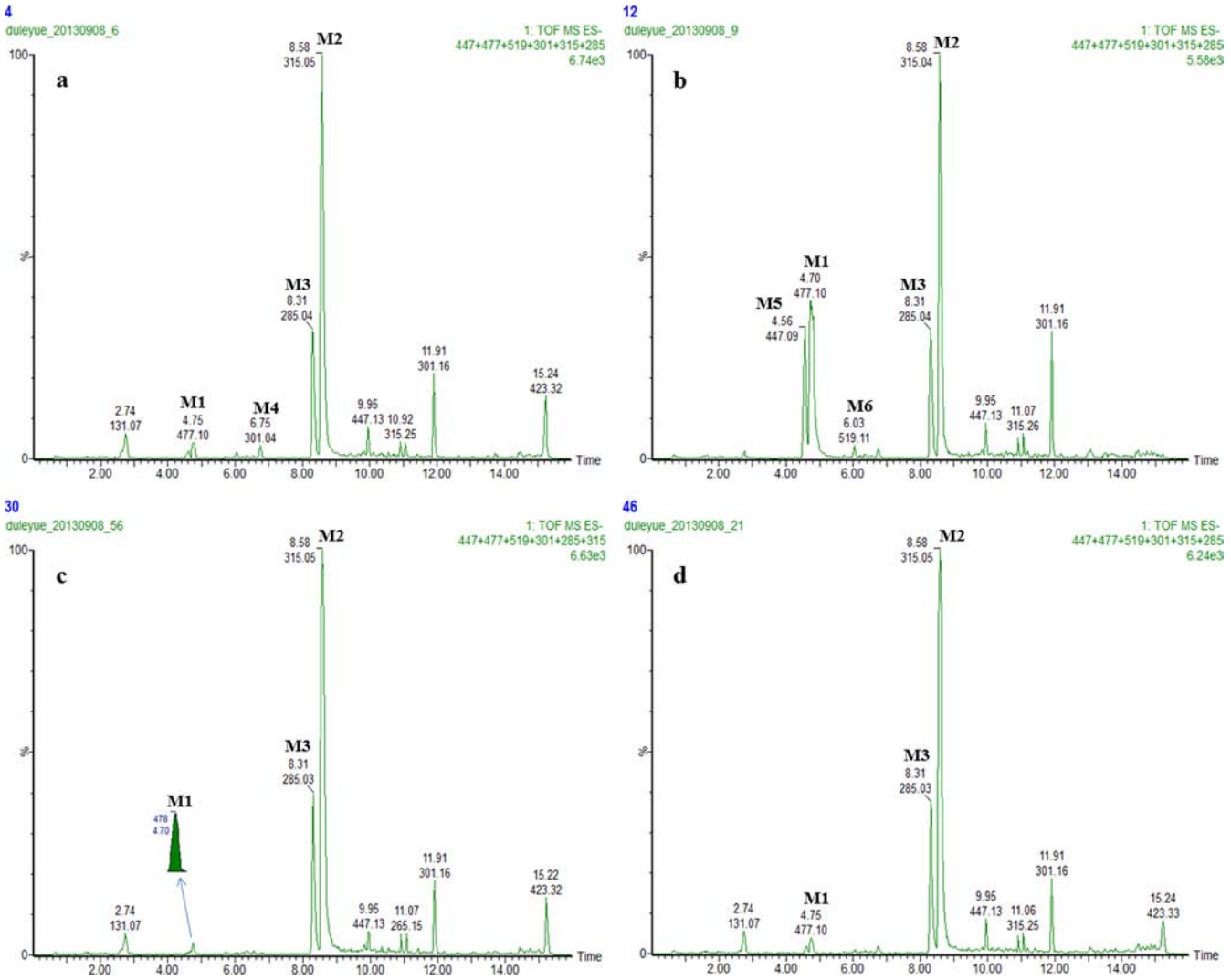

Figure 1. UPLC/MS chromatograms of isorhamnetin 3-*O*-glucoside and its metabolites: (a) strain 4 sample, (b) strain 12 sample, (c) strain 30 sample, (d) strain 46 sample.

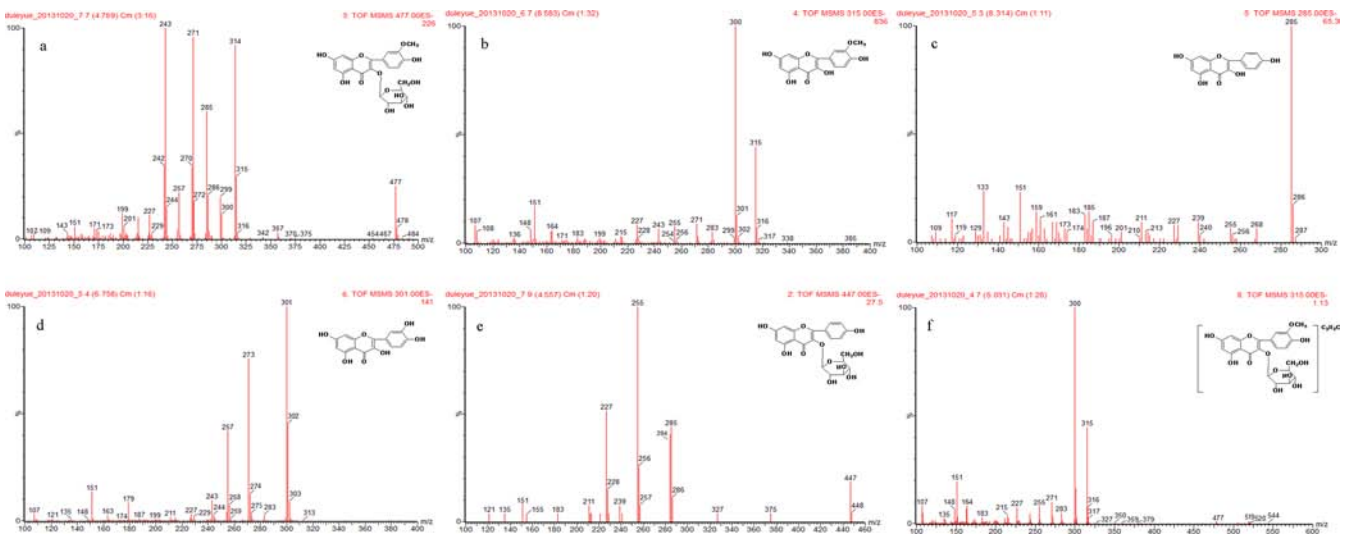

Figure 2. Representative MS/MS spectrum: (a) M1 (*m*/*z* 477), (b) M2 (*m*/*z* 315), (c) M3 (*m*/*z* 285), (d) M4 (*m*/*z* 301), (e) M5 (*m*/*z* 447), (f) M6 (*m*/*z* 519).

dx.doi.org/10.1021/jf405261a | *J. Agric. Food Chem.* 2014, 62, 2489−2495

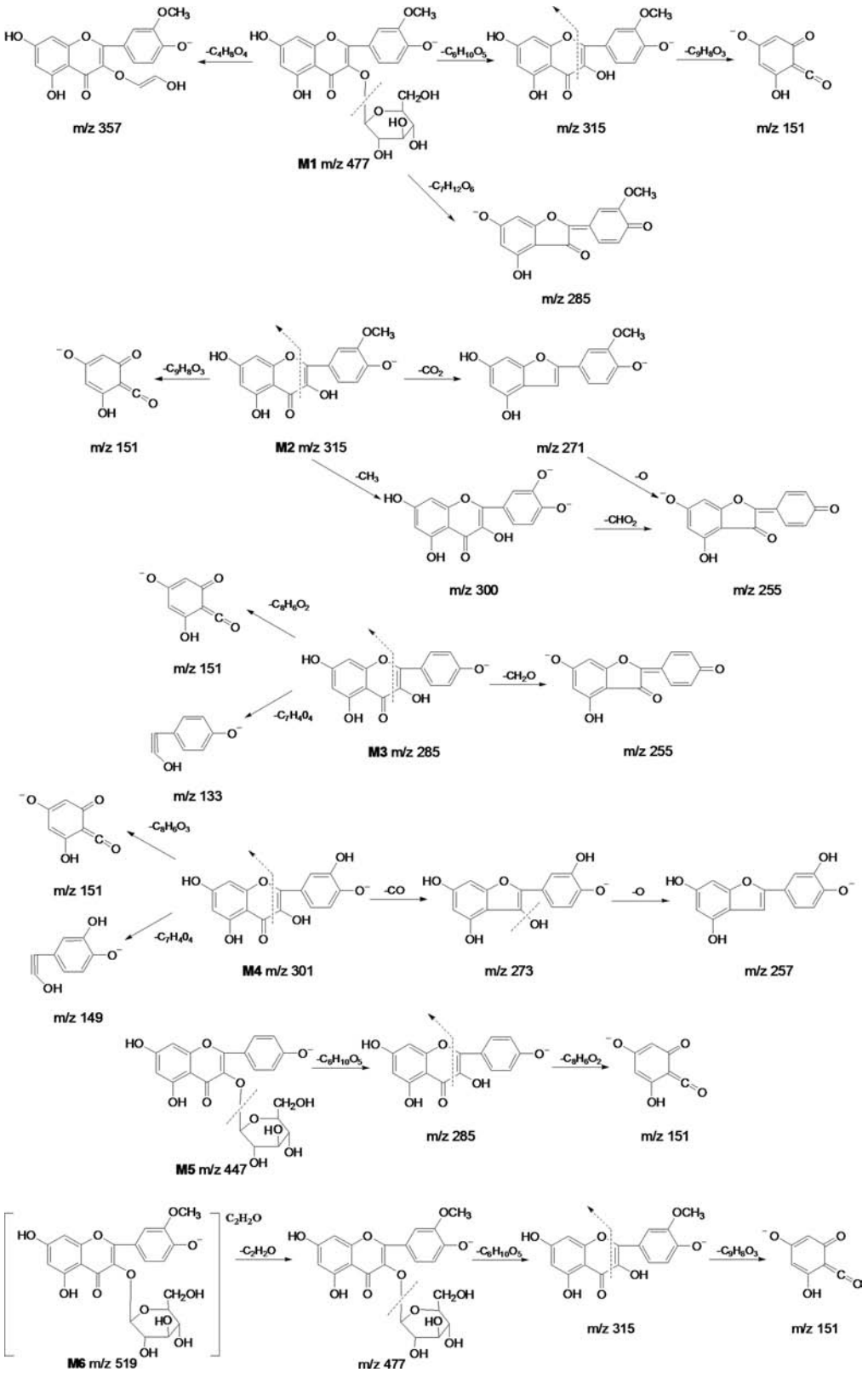

Figure 3. Proposed fragmentation pathways of isorhamnetin 3-*O*-glucoside and its metabolites.

Metabolite M2. According to Figure 2b, the $[M-H]^-$ ion of M2 was at m/z 315 with a retention time of 8.58 min, which was 162 Da lower than that of M1 isorhamnetin 3-*O*-glucoside. The MS/MS spectrum of M2 had product ions similar to those of M1. The high collision energy scan fragment ions were m/z 300, which was produced by the loss of CH_3 from m/z 315, and m/z 255, which was produced by the loss of O from m/z 271. The m/z 151 ion was produced after retro-Diels–Alder (RDA) cleavage. The product ion at m/z 271 was formed by the elimination of CO_2 from m/z 315, and then m/z 271 lost O to form m/z 255

dx.doi.org/10.1021/jf405261a | *J. Agric. Food Chem.* 2014, 62, 2489–2495

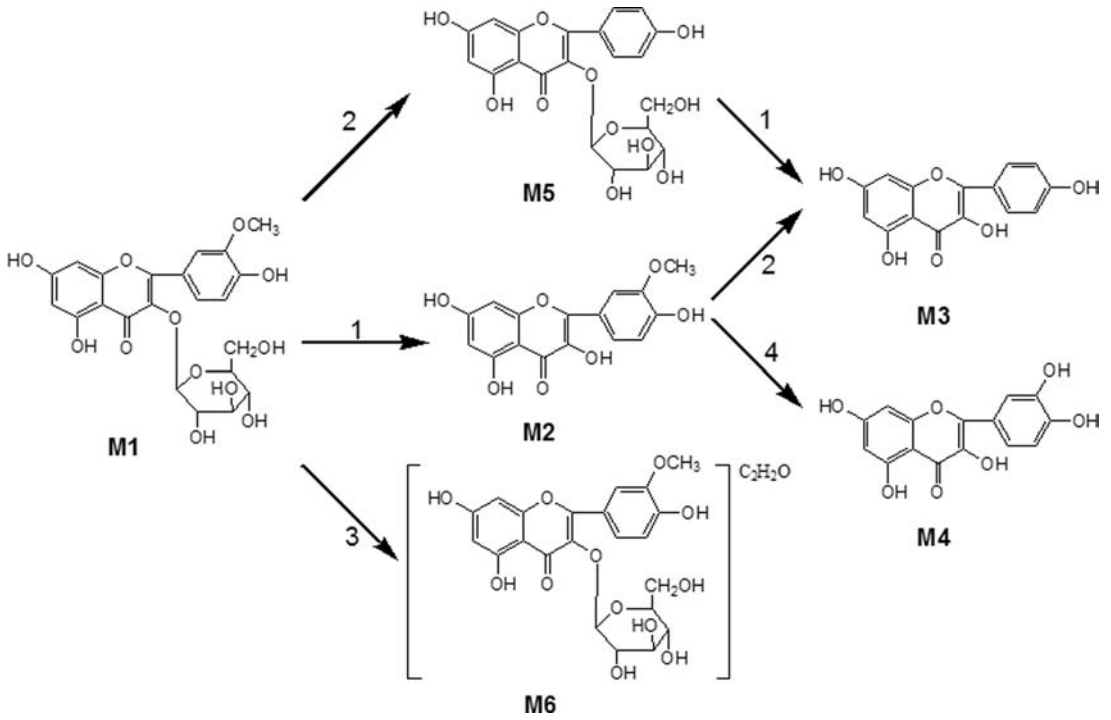

Figure 4. Possible metabolic pathways of isorhamnetin 3-*O*-glucoside by the human intestinal bacteria: 1, deglycosylation; 2, demethoxylation; 3, acetylation; 4, dehydroxylation.

(Figure 3). In view of these results, we identified M2 as isorhamnetin, the deglycosylated product of the parent by loss of a glucose.

Metabolite M3. Metabolite M3 was detected as deprotonated molecular ion $[M-H]^-$ at m/z 285 with a retention time of 8.31 min (Figure 2c). The product ion at m/z 255 was shaped by the elimination of CH_2O from m/z 285 (Figure 3). The characteristic fragment ions were m/z 133 and 151 according to RDA cleavage. On the basis of the MS/MS spectrum, we determined M3 as kaempferol.

Metabolite M4. Metabolite M4 showed a UPLC profile with a retention time of 6.75 min and an MS spectrum which gave an $[M-H]^-$ ion at m/z 301 (Figure 2d). The fragment ion m/z 151 corresponded to RDA cleavage from $[M-H]^-$ at m/z 301. The characteristic product ion at m/z 273 was formed by the elimination of CH_2O from m/z 301, and then m/z 273 lost O to form m/z 257 (Figure 3). These results indicated that M4 was quercetin, which is the demethylated product of M2 isorhamnetin.

Metabolite M5. Metabolite M5 with a retention time of 4.56 min produced a deprotonated molecular ion at m/z 447, a loss of CH_2O (30 Da) from isorhamnetin 3-*O*-glucoside (M1). On the basis of the MS/MS spectrum in Figure 2e, M5 had product ions at m/z 285, 255, and 151, which also emerged in the product ion mass spectrum of M3 kaempferol. The product ion at m/z 151 was formed from the aglycon at m/z 285 by RDA cleavage (Figure 3). Thus, metabolite M5 was tentatively identified as kaempferol 3-*O*-glucoside.

Metabolite M6. Metabolite M6 was found at 6.03 min in the UPLC system, and m/z 519 was its deprotonated molecular ion, which was 42 Da higher than that of isorhamnetin 3-*O*-glucoside. The MS/MS spectrum of M6 (Figure 2f) showed a product ion at m/z 477, which was generated from m/z 519 by loss of acetyl, and then m/z 477 lost a glucose to form the product ion at m/z 315. The other main product ions extracted from M6 were m/z 300 and m/z 151 (Figure 3). From this data analysis, M6 could be identified as acetylated isorhamnetin 3-*O*-glucoside.

Analysis of the Metabolic Pathway of Isorhamnetin 3-*O*-Glucoside by the Isolated Human Intestinal Microflora. According to our experimental results, the metabolic pathways of isorhamnetin 3-*O*-glucoside by the isolated human intestinal bacteria were proposed as displayed in Figure 4. Among all the isolated human intestinal bacteria, the majority of the strains, such as *Escherichia* sp. 12, *Enterococcus* sp. 30, and *Bacillus* sp. 46, could degrade isorhamnetin 3-*O*-glucoside (M1) to large amounts of isorhamnetin (M2) and kaempferol (M3), suggesting that this might be regarded as a common capability of intestinal bacteria. Additionally, *Escherichia* sp. 4 could also metabolize isorhamnetin 3-*O*-glucoside to isorhamnetin, which was further degraded to kaempferol and minor but detectable amounts of quercetin (M4). Isorhamnetin 3-*O*-glucoside was converted to kaempferol 3-*O*-glucoside (M5) and acetylated isorhamnetin 3-*O*-glucoside (M6) only by *Escherichia* sp. 12.

Percentage of the Isolated Human Intestinal Bacteria That Yielded Each of the Metabolites. In terms of proportion, the parent, isorhamnetin 3-*O*-glucoside (M1), was detected in 92% of the isolated human intestinal flora. All of the isolated bacteria could yield the aglycon isorhamnetin (M2), suggesting that deglycosylation was the main metabolic pathway of isorhamnetin 3-*O*-glucoside. A total of 94% of the strains metabolized isorhamnetin-3-*O*-glucoside to kaempferol (M3). The metabolite quercetin (M4) was identified in 7.4% of the strains. However, only one sample of the isolated bacteria could degrade the parent to kaempferol 3-*O*-glucoside (M5) and acetylated isorhamnetin 3-*O*-glucoside (M6). Meanwhile, on the basis of the differences in metabolic ability, 28 samples of the isolated bacteria were identified for their great vitality to metabolic isorhamnetin 3-*O*-glucoside.

dx.doi.org/10.1021/jf405261a | *J. Agric. Food Chem.* 2014, 62, 2489−2495

DISCUSSION

The metabolites of isorhamnetin 3-*O*-glucoside yielded by human intestinal bacteria and its relevant metabolic process have not been reported in advance. In this study, we established a UPLC/Q-TOF-MS technique to detect and identify the metabolites of isorhamnetin 3-*O*-glucoside produced by the isolated human intestinal microflora. After incubation with different intestinal bacteria, parent isorhamnetin 3-*O*-glucoside and its five metabolites (M1−M6) were tentatively identified in the isolated bacterial samples according to their retention times, accurate molecular masses, and fragment ions. The metabolites were converted by four main metabolic pathways, including deglycosylation, demethoxylation, dehydroxylation, and acetylation. Though the intestinal microflora is composed of massive species, it is possible that a lot of flora conduct the same metabolic steps of isorhamnetin 3-*O*-glucoside.

So far, it has been demonstrated that isorhamnetin could be rapidly absorbed and eliminated in rat plasma after oral administration of mulberry leaf extract. Additionally, double peaks were observed in the curves of mean plasma concentration for isorhamnetin. The first peak appeared at 0.19 h and the second peak at 7.25 h, which might be explained by enterohepatic recirculation.[19] In addition, numerous preclinical studies have indicated that kaempferol possesses a wide range of pharmacological activities, including antioxidant, anti-inflammatory, antimicrobial, anticancer, cardioprotective, neuroprotective, antiosteoporotic, anxiolytic, analgesic, estrogenic/antiestrogenic, and antiallergic activities.[20] Moreover, the metabolism of quercetin was claimed to exert beneficial health effects, including protection against various diseases such as osteoporosis, certain forms of cancer, and pulmonary and cardiovascular diseases, and also protection against aging. Especially the ability of quercetin to scavenge highly reactive oxygen species such as peroxynitrite and the hydroxyl radical was suggested to be involved in these possible beneficial health effects.[21] Some studies also reported that quercetin exhibits antiproliferative, antiatherosclerotic, and neuroprotective activities.[22,23] More importantly, quercetin and isorhamnetin could enhance the oral absorption of each other in rats.[24] We could arrive at a conclusion that the metabolites of isorhamnetin 3-*O*-glucoside such as isorhamnetin, kaempferol, and quercetin might have an impact on its biological effect, which would influence the clinical effects of traditional herbal medicines and medicinal plants. Additionally, these metabolites could improve the bioavailability for absorption of isorhamnetin 3-*O*-glucoside by colonic mucosa due to their lower polarity than that of the parent. It has been reported that the biological activities and bioavailability of flavonoid aglycons are usually higher than those of flavonoid glycosides.[25] Daidzein exhibited more potent antioxidant, antitumor cytotoxic, and estrogenic effects than daidzin.[26] The aglycon quercetin also had stronger anti-inflammatory activity though inhibition of inducible nitric oxide synthase expression and nitrite production and antimicrobial and antioxidant activities than its glycosides.[27−29]

On the other hand, there are massive studies on the microbial metabolism of flavonoids. Moreover, the conversion profile obtained from in vitro incubation with fecal microbiota can elucidate the conversion route. Many flavonoids undergo a ring fission in which the C-ring is degraded; hydroxylated aromatic compounds are formed from the A-ring and phenolic acids from the B-ring. The phenolic acid metabolites of flavonols reflect the hydroxylation pattern of the B-ring structure.[30] The primary metabolite of quercetin is 2-(3,4-dihydroxyphenyl)acetic acid. Further dehydroxylation results in the formation of 2-(3-hydroxyphenyl)acetic acid from both the dihydroxylated derivatives.[31] Other metabolites derived from quercetin include phloroglucinol, 3,4-dihydroxybenzaldehyde, 3,4-dihydroxytoluene, butyrate, and acetate.[32−36] What is more, *Clostridium* and *Eubacterium* genera, which are phylogenetically associated, are other common elements involved in the metabolism of many phenolics. The health benefits from phenolic consumption should be attributed to their bioactive metabolites and also to the modulation of the intestinal bacterial population.[14]

The metabolic pathway and metabolites of isorhamnetin 3-*O*-glucoside produced by isolated human intestinal bacteria shown here are very important for the evaluation of the absorption and metabolism of isorhamnetin 3-*O*-glucoside in vivo. Further research will be performed on the enzyme system which contributes to the bacterial metabolism of isorhamnetin 3-*O*-glucoside.

AUTHOR INFORMATION

Corresponding Authors

*Phone/fax: +86 25 85811516. E-mail: jiangshu2000@163.com.
*Phone/fax: +86 25 85811116 E-mail: dja@njutcm.edu.cn.

Funding

This work was fiscally supported by the National Basic Research Program of China (973 Program) (Grants 2011CB505300 and 2011CB505303), the National Natural Science Foundation of China (Grants 81072996 and 81102743), Jiangsu Province Colleges and Universities Natural Science Major Basic Research Projects (Grant 10KJA360039), and the Construction Project for Jiangsu Key Laboratory for High Technology Research of TCM Formulae (Grant BM2010576).

Notes

The authors declare no competing financial interest.

REFERENCES

(1) Bravo, L. Polyphenols: chemistry, dietary sources, metabolism, and nutritional significance. *Nutr. Rev.* **1998**, *56*, 317−333.
(2) Ravishankar, D.; Rajora, A. K.; Greco, F.; Osborn, H. M. Flavonoids as prospective compounds for anti-cancer therapy. *Int. J. Biochem. Cell Biol.* **2013**, *45*, 2821−2831.
(3) Igarashi, K.; Mikami, T.; Takahashi, Y.; Sato, H. Comparison of the preventive activity of isorhamnetin glycosides from atsumi-kabu (red turnip, *Brassica campestris* L.) leaves on carbon tetrachloride-induced liver injury in mice. *Biosci., Biotechnol., Biochem.* **2008**, *72*, 856−860.
(4) Lee, J.; Mitchell, A. E. Quercetin and isorhamnetin glycosides in onion (*Allium cepa* L.): varietal comparison, physical distribution, coproduct evaluation, and long-term storage stability. *J. Agric. Food Chem.* **2011**, *59*, 857−863.
(5) Jong, M. H.; Jong, W. C.; Jong, C. P. Effects of methanol extract of leaves of *Brassica juncea* and its major component, isorhamnetin-3-*O*-β-D-glucoside, on hepatic drug metabolizing enzymes in bromobenzene-treated rats. *Food Sci. Biotechnol.* **2007**, *6*, 439−443.
(6) Sriseadka, T.; Wongpornchai, S.; Rayanakorn, M. Quantification of flavonoids in black rice by liquid chromatography-negative electrospray ionization tandem mass spectrometry. *J. Agric. Food Chem.* **2012**, *60*, 11723−11732.
(7) Xia, X. H.; Zhang, Y.; Xi, Y. B.; Wang, G. H.; Yang, L. Q.; Xue, K. F. Advances in studies on chemical constituents and bioactivities actions of *Ginkgo biloba* L. *Chin. J. Exp. Tradit. Med. Formulae* **2009**, *15*, 100−104.
(8) Devi, V. G.; Rooban, B. N.; Sasikala, V.; Sahasranamam, V.; Abraham, A. Isorhamnetin-3-glucoside alleviates oxidative stress and opacification in selenite cataract *in vitro*. *Toxicol. Vitro* **2010**, *24*, 1662−1669.
(9) Lee, Y. S.; Lee, S.; Lee, H. S.; Kim, B. K.; Ohuchi, K.; Shin, K. H. Inhibitory effects of isorhamnetin-3-*O*-beta-D-glucoside from *Salicornia*

herbacea on rat lens aldose reductase and sorbitol accumulation in streptozotocin-induced diabetic rat tissues. *Biol. Pharm. Bull.* **2005**, *28*, 916−918.
(10) Sun, J.; Sun, G. B.; Meng, X. B.; Wang, H. M.; Luo, Y.; Qin, M.; Ma, B.; Wang, M.; Cai, D.; Guo, P.; Sun, X. B. Isorhamnetin protects against doxorubicin-induced caraitoxicity *in vivo* and *in vitro*. *PLoS One* **2013**, *8*, e64526.
(11) Purchiaroni, F.; Tortora, A.; Gabrielli, M.; Bertucci, F.; Gigante, G.; Ianiro, G.; Ojetti, V.; Scarpellini, E.; Gasbarrini, A. The role of intestinal microbiota and the immune system. *Eur. Rev. Med. Pharmacol. Sci.* **2013**, *17*, 323−333.
(12) Possemiers, S.; Bolca, S.; Verstraete, W.; Heyerick, A. The intestinal microbiome: a separate organ inside the body with the metabolic potential to influence the bioactivity of botanicals. *Fitoterapia* **2011**, *82*, 53−66.
(13) Crozier, A.; Jaganath, I. B.; Clifford, M. N. Dietary phenolics: chemistry, bioavailability and effects on health. *Nat. Prod. Rep.* **2009**, *26*, 1001−1043.
(14) Selma, M. V.; Espín, J. C.; Tomás-Barberán, F. A. Interaction between phenolics and gut microbiota: role in human health. *J. Agric. Food Chem.* **2009**, *57*, 6485−6501.
(15) Rechner, A. R.; Kroner, C. Anthocyanins and colonic metabolites of dietary polyphenols inhibit platelet function. *Thromb. Res.* **2005**, *116*, 327−334.
(16) Shen, J. Z.; Yang, C. Y.; Wu, C.; Feng, P.; Wang, Z.; Li, Y.; Li, Y. S.; Zhang, S. X. Identification of the major metabolites of quinocetone in swine urine using ultra-performance liquid chromatography/electrospray ionization quadrupole time-of-flight tandem mass spectrometry. *Rapid Commun. Mass Spectrom.* **2010**, *24*, 375−383.
(17) Han, H.; Yang, L.; Xu, Y.; Ding, Y.; Bligh, S. W.; Zhang, T.; Wang, Z. T. Identification of metabolites of geniposide in rat urine using ultra-performance liquid chromatography combined with electrospray ionization quadrupole time-of-flight tandem mass spectrometry. *Rapid Commun. Mass Spectrom.* **2011**, *25*, 3339−3350.
(18) Minamida, K.; Tanaka, M.; Abe, A.; Sone, T.; Tomita, F.; Hara, H.; Asano, K. Production of equol from daidzein by Gram-positive rod-shaped bacterium isolated from rat intestine. *J. Biosci. Bioeng.* **2006**, *102*, 247−250.
(19) He, J.; Feng, Y.; Ouyang, H. Z.; Yu, B.; Chang, Y. X.; Pan, G. X.; Dong, G. Y.; Wang, T.; Gao, X. M. A sensitive LC-MS/MS method for simultaneous determination of six flavonoids in rat plasma: application to a pharmacokinetic study of total flavonoids from mulberry leaves. *J. Pharm. Biomed. Anal.* **2013**, *84*, 189−195.
(20) Calderon-Montano, J. M.; Burgos-Moron, E.; Perez-Guerrero, C.; Lopez-Lazaro, M. A review on the dietary flavonoid kaempferol. *Mini-Rev. Med. Chem.* **2011**, *11*, 298−344.
(21) Boots, A. W.; Haenen, G. R.; Bast, A. Health effects of quercetin: from antioxidant to nutraceutical. *Eur. J. Pharmacol.* **2008**, *585*, 325−337.
(22) Kleemann, R.; Verschuren, L.; Morrison, M.; Zadelaar, S.; van Erk, M. J.; Wielinga, P. Y.; Wielinga, P. Y; Kooistra, T. Anti-inflammatory, anti-proliferative and anti-atherosclerotic effects of quercetin in human *in vitro* and *in vivo* models. *Atherosclerosis* **2011**, *218*, 44−52.
(23) Dajas, F. Life or death: neuroprotective and anticancer effects of quercetin. *J. Ethnopharmacol.* **2012**, *143*, 383−396.
(24) Lan, K.; He, J. L.; Tian, Y.; Tan, F.; Jiang, X. H.; Wang, L.; Ye, L. M. Intra-herb pharmacokinetics interaction between quercetin and isorhamnetin. *Acta Pharmacol. Sin.* **2008**, *29*, 1376−1382.
(25) Graefe, E. U.; Wittig, J.; Mueller, S.; Riethling, A. K.; Uehleke, B.; Drewelow, B.; Pforte, H.; Jacobasch, G.; Derendorf, H.; Veit, M. Pharmacokinetics and bioavailability of quercetin glycosides in humans. *J. Clin. Pharmacol.* **2001**, *41*, 492−499.
(26) Park, E. K.; Shin, J.; Bae, E. A.; Lee, Y. C.; Kim, D. H. Intestinal bacteria activate estrogenic effect of main constituents puerarin and daidzin of *Pueraria thunbergiana*. *Biol. Pharm. Bull.* **2006**, *29*, 2432−2435.
(27) Lee, S.; Park, H. S.; Notsu, Y.; Ban, H. S.; Kim, Y. P.; Ishihara, K.; Hirasawa, N.; Jung, S. H.; Lee, Y. S.; Lim, S. S.; Park, E. H.; Shin, K. H.; Seyama, T.; Hong, J.; Ohuchi, K. Effects of hyperin, isoquercitrin and quercetin onlipopolysaccharide-induced nitrite production in rat peritoneal macrophages. *Phytother. Res.* **2008**, *22*, 1552−1556.
(28) Liu, H.; Mou, Y.; Zhao, J.; Wang, J.; Zhou, L.; Wang, M.; Wang, D.; Han, J.; Yu, Z.; Yang, F. Flavonoids from *Halostachys caspica* and their antimicrobial and antioxidant activities. *Molecules* **2010**, *15*, 7933−7945.
(29) Wang, J.; Lou, J.; Luo, C.; Zhou, L.; Wang, M.; Wang, L. Phenolic compounds from *Halimodendron halodendron* (Pall.) Voss and their antimicrobial and antioxidant activities. *Int. J. Mol. Sci.* **2012**, *13*, 11349−11364.
(30) Aura, A.-M. Microbial metabolism of dietary phenolic compounds in the colon. *Phytochem. Rev.* **2008**, *7*, 407−429.
(31) Aura, A-M; O'Leary, K. A.; Williamson, G.; Ojala, M.; Bailey, M.; Puupponen-Pimia, R.; Nuutila, A. M.; Oksman-Caldentey, K.-M.; Poutanen, K. Quercetin derivatives are deconjugated and converted to hydroxyphenylacetic acids but not methylated by human fecal microflora in vitro. *J. Agric. Food Chem.* **2002**, *50*, 1725−1730.
(32) Krishnamurty, H. G.; Cheng, K. J.; Jones, G. A.; Simpson, F. J.; Watkin, J. E. Identification of products by the anaerobic degradation of rutin and related flavonoids by *Butyrovibrio* sp. C3. *Can. J. Microbiol.* **1970**, *16*, 759−767.
(33) Sawai, Y.; Kohsaka, K.; Nishiyama, Y.; Ando, K. Serum concentrations of rutoside metabolites after oral administration of a rutoside formulation to humans. *Drug Res.* **1987**, *37*, 729−732.
(34) Winter, J.; Popoff, M. R.; Grimont, P.; Bokkenhauser, V. D. *Clostridium orbiscindens* sp. nov., a human intestinal bacterium capable of cleaving the flavonoid C-ring. *Int. J. Syst. Bacteriol.* **1991**, *41*, 355−357.
(35) Schneider, H.; Schwiertz, A.; Collins, M. D.; Blaut, M. Anaerobic transformation of quercetin-3-glucoside by bacteria from the human intestinal tract. *Arch. Microbiol.* **1999**, *171*, 81−91.
(36) Rondini, L.; Peyrat-Maillard, M.-N.; Marsset-Baglieri, A.; Fromentin, G.; Durand, P.; Tome, D.; Prost, M.; Berset, C. Bound ferulic acid from bran is more bioavailable than the free compound in rat. *J. Agric. Food Chem.* **2004**, *52*, 4338−4343.

food products in which sodium has been replaced by other cations.

The effect of salting can also be determined indirectly, for example, by using low-field (LF) ^{1}H NMR to monitor changes in proton relaxation behavior as a result of salt addition. In foods, the NMR proton signals basically originate from small molecules such as water and fat. Changes in tissue microstructure due to salting will affect proton exchange with the surrounding environment. For example, tissue swelling after the addition of salt leads to a more open microstructure, causing higher water mobility. Several studies have been carried out in which LF NMR has been used to monitor changes during fish salting processes.[20−26] However, because none of these studies have dealt with low-salt tissues, it would be of interest to explore the method further as a potential tool for low-salt applications.

The objectives of the present research are to (1) evaluate the application of impedance spectroscopy to monitor physicochemical parameters in salted fish products with and without sodium replacement, (2) establish a fast and consistent method to measure sodium and potassium contents in fish products, and (3) assess the feasibility of employing LF NMR in low-salt tissues.

MATERIALS AND METHODS

Chemicals. Ammonium chloride (NH_4Cl), ammonium hydroxide (NH_4OH), ammonium hydrogen fluoride (NH_4FHF <1%, LD_{50} mg/kg not found), chloroform ($CHCl_3$), ethanol (C_2H_5OH), sulfuric acid (H_2SO_4), potassium sulfate (K_2SO_4), copper sulfate ($CuSO_4$), hydrogen peroxide (H_2O_2), and sodium hydroxide (NaOH) (Scharlau, S.A., or Thermo Fisher Scientific, USA). All chemicals were of analytical-reagent grade.

Experimental Protocol. Experiments using the impedance system were carried out in two phases. In the first phase, the system's capability to distinguish between different types and quantities of salts was evaluated. The second phase evaluated the impedance system for discriminating between fish samples salted with different salt mixtures and quantities of salt.

Phase I: Salt Solutions. Different brines were prepared by using NaCl, KCl, and a mixture of NaCl/KCl (50:50, w/w, %) at different contents. The total salt contents assessed were 0.0, 0.1, 0.5, 1.0, 1.5, 2.0, 2.5, and 3.0% (g salt/100 g distilled water). NaCl and KCl reagents (analytical-reagent grade) were obtained from Panreac Química S.A.U. (Barcelona, Spain). The brines were prepared the day before analysis to ensure that all of the salt was completely dissolved. The parameters measured in brines were a_w, pH, conductivity, and sodium and chloride contents. Sodium content in brines was determined by a Na-selective electrode. All measurements were done in triplicate. Impedance spectroscopy measurements were also carried out on the same brine solutions.

Phase II: Fish Minces. Fresh hake (*Merluccius paradoxus/capensis*) was used as raw material. The fish were caught June 13, 2012, by trawling off the coast of South Africa (FAO fishing area 47, Atlantic Southeast) and were obtained June 19, 2012, from a local supermarket in Valencia (Spain). The fish specimens were placed in styrofoam boxes with ice and transported immediately to the laboratory. Upon arrival at the laboratory, two fish were headed and gutted. Then, the fish were filleted and skinned, and the flesh was chopped with a standard food processor at low speed (Minirobot D81, Moulinex, Group SEB Iberica, Barcelona, Spain). Samples were prepared by mixing the fish mince (fish mince and salt, 200 g total) with an exact amount of salt before homogenization for 1 min in the food processor. The amount of salt added to the fish mince had been preweighed to achieve an exact salt content (NaCl or NaCl/KCl) in the final sample of 0.0, 0.5, 1.0, 2.0, or 3.0% salt (g NaCl or NaCl/KCl/100 g salted fish mince). The homogenized fish minces were divided into five plastic containers (40 g in each). Three of the plastic containers were used for the physicochemical analyses and impedance spectroscopy, whereas the remaining two containers were used for LF NMR measurements. According to the results obtained by Sánchez-Alonso,[27] the mince composition does not suffer significant alterations during the frozen storage period. The samples were stored at −18 °C and thawed to 4 °C during 18 h before analysis. Moisture, lipid, protein, ash, a_w, pH, chloride, sodium, and potassium contents were determined in the same subsamples as were subjected to impedance spectroscopy. The minces assigned for LF NMR analysis were kept frozen for 86 days before the measurements were carried out.

ANALYTICAL METHODS

Physicochemical Analyses. Moisture, lipid, protein, and ash contents were assayed according to AOAC Methods 950.46, 991.36, 928.08, and 920.153, respectively,[28] whereas pH and conductivity of brines were determined by using a multimeter MM 40 (Crison Instruments, S.A., Barcelona, Spain). The pH measurements of fish were carried out using a digital pH-meter micropH 2001 (Crison Instruments) with a puncture electrode (Crison 5231). Water activity was assessed in brines and fish minces with a fast water activity meter (GBX FAst/lab, Romans sur Isère Cedex, France).

The chloride and sodium contents in brines were measured directly in the solutions, using a chloride analyzer (Sherwood model 926, Cambridge, UK) and a Dual Star pH/ISE meter (Thermo Fisher Scientific, Waltham, MA, USA) with a Na-selective electrode (Ross Sodium Ion Selective Electrode, Thermo Fisher Scientific), respectively. Chloride, sodium (by two different analytical methods), and potassium contents of fish minces were measured in an extract of the sample. For preparing the extract, 1.5 g of the mince was homogenized in ultrapure water using an Ultraturrax T-25 (IKA, Labortechnik, Staufen, Germany) at 9000 rpm for 1 min. Then, samples were warmed to 90 °C for 30 min, cooled to room temperature, transferred to a volumetric flask, and diluted to 200 mL with ultrapure water. Finally, samples were filtered through a cellulose filter paper (Whatman no. 1, Whatman International Ltd., Maidstone, UK). For chloride and sodium determinations, an aliquot of the extract was measured at room temperature by using the chloride analyzer and the Na-selective electrode as described above. The Na-selective electrode method was a modification of the Kivikari method.[29] In this study the direct calibration method was used, contrary to the method of Kivikari, where the known addition method was used. A calibration curve was made by using three standards of analytical grade NaCl from Panreac Química S.A.U. Sodium ion strength adjustor (sodium ionic strength adjustor, Thermo Fisher Scientific) was added to all solutions to ensure that samples and standards had similar ionic strengths. Sodium and potassium contents of the samples were determined by ion chromatography (Compact IC 761, Metrohm Ltd., Herisau, Switzerland) by using an ion exchange column (Metrosep C2, 250/4.0, Metrohm Ltd.). The separation was monitored by using a regulated (20 °C) conductivity detector, and IC Net 2.3 (Methrom Ltd.) software was used for data collection and processing. Prior to analysis, samples were filtered through 0.45 μm nylon syringe filters. The isocratic elution was carried out using a solution of tartaric acid (4.0 mM)/dipicolinic acid (0.75 mM) at a flow rate of 1 mL/min. Samples were injected using a 20 μL loop injector. The content of each cation was determined by interpolation in the corresponding calibration curve. The calibration was established using a triplicate set of standard solutions of Na^+ (Fluka, Buchs, Switzerland) and K^+ (Sigma-Aldrich, St. Louis, MO, USA).

Impedance Spectroscopy. The impedance spectroscopy measurement system was developed by the Instituto de Reconocimiento Molecular y Desarrollo Tecnológico (IDM) at the Universidad Politécnica de València (UPV).[18] It consists of a software application that runs on a PC, electronic equipment, and an electrode (for more information see the Supporting Information).

Using the software application, the user chooses the frequencies and the amplitudes of the sinusoidal voltage signals. For each of the frequencies the electronic equipment generates the corresponding sinusoidal voltage waveform to the electrode. The current (I) and

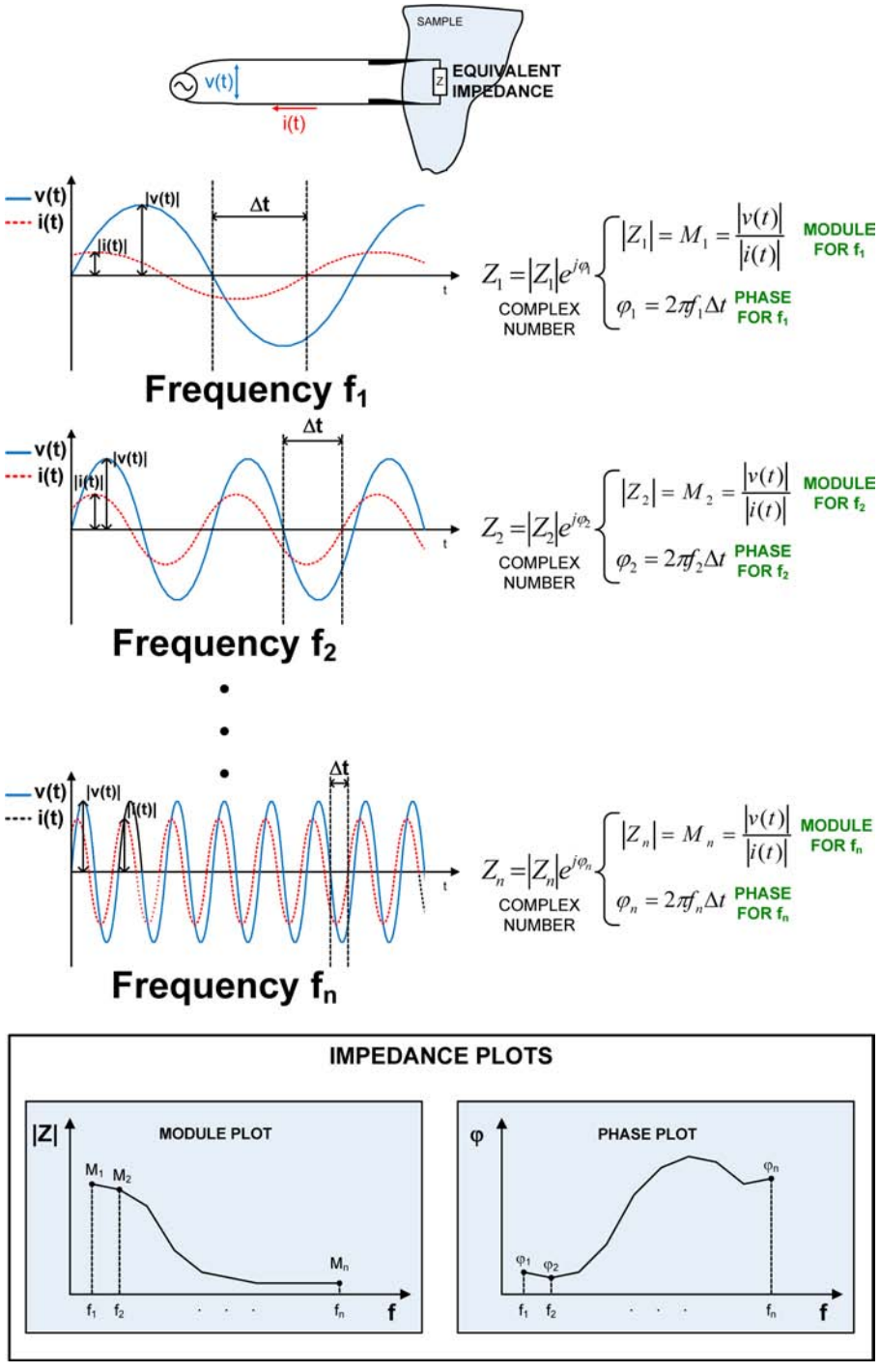

Figure 1. Scheme of impedance measurement and registered signals: module |Z|; phase (ϕ); $v(t)$, voltage signal; $i(t)$, current signal; f, frequency of the signals; Δt, time interval between the zero crossing of the voltage and current signals.

voltage (V) signals at the electrode are then sampled, and the collected data are sent to the PC, where a discrete Fourier transform analysis (DFT) is performed to determine their amplitude and phase. The module |Z| and the phase (ϕ) of the impedance are then calculated using eq 1, where $v(t)$ is the voltage signal, $i(t)$ the current signal, f the frequency of the signals, and Δt the time interval between the zero crossing of the voltage and current signals (Figure 1).

$$Z = |Z|e^{j\varphi}\begin{cases} |Z| = \dfrac{|v(t)|}{|i(t)|} & \text{module} \\ \varphi = 2\pi f \Delta t & \text{phase} \end{cases} \quad (1)$$

The electronic equipment includes a digital processing block based on two CPLDs and three random-access memories (RAM), one digital-to-analog converter, two analog-to-digital converters, and some analog signal adaption circuits.[18]

The sensor employed in this study is a double electrode designed at IDM-UPV. The sensor consists of two steel needles 1.5 cm long and 1 mm in diameter, separated by a distance of 1 cm in a nonconductive frame. This design keeps the separation between both needles constant during measurements.

The impedance measurements were taken by inserting the sensors into the middle of the plastic containers (n = 3) containing the solutions or the fish minces. Ten parallel measurements were

dx.doi.org/10.1021/jf405527t | J. Agric. Food Chem. 2014, 62, 2496−2505

Table 1. Physicochemical Parameters of Brine Solutions Prepared with Different Salts (*S*: KCl (K), NaCl:KCl (Na:K), and NaCl (Na)) and Contents (*C*)

S	*C* (g salt/100 g brine)	a_w[a]	conductivity[a] (mS/cm)	Na[a] (g/L)	Cl[a] (g/L)
K	0.1	0.999 ± 0.000aA	2.10 ± 0.11A	(0.34 ± 0.02) × 10^{-3}aA	1.03 ± 0.06aA
	0.5	0.993 ± 0.001aB	10.27 ± 1.15B	(0.76 ± 0.00) × 10^{-3}aB	3.50 ± 0.14aB
	1.0	0.996 ± 0.003aB	19.31 ± 1.24C	(0.89 ± 0.01) × 10^{-3}aC	5.78 ± 0.13aC
	1.5	0.990 ± 0.002aC	31.20 ± 0.28D	(1.26 ± 0.02) × 10^{-3}aD	8.30 ± 0.26aD
	2.0	0.985 ± 0.001aC	41.67 ± 1.21E	(1.37 ± 0.02) × 10^{-3}aE	10.54 ± 0.09aE
	2.5	0.980 ± 0.002aCD	51.23 ± 3.61F	(1.69 ± 0.04) × 10^{-3}aF	12.64 ± 0.13aF
	3.0	0.984 ± 0.002aD	63.30 ± 5.30G	(2.18 ± 0.16) × 10^{-3}aG	14.68 ± 0.33aG
Na:K	0.1	0.995 ± 0.002bA	2.07 ± 0.04A	0.26 ± 0.00bA	1.08 ± 0.08bA
	0.5	0.989 ± 0.002bB	9.90 ± 0.42B	0.77 ± 0.00bB	3.74 ± 0.21bB
	1.0	0.991 ± 0.001bB	19.33 ± 1.26C	1.67 ± 0.02bC	6.44 ± 0.17 bC
	1.5	0.985 ± 0.004bC	30.17 ± 3.06D	2.60 ± 0.01bD	9.12 ± 0.19bD
	2.0	0.985 ± 0.001bC	38.27 ± 0.81E	3.45 ± 0.01bE	11.86 ± 0.2 bE
	2.5	0.980 ± 0.002bCD	50.63 ± 3.10F	4.23 ± 0.07bF	14.72 ± 0.3 bF
	3.0	0.981 ± 0.001bD	63.10 ± 4.27G	5.17 ± 0.02bG	16.52 ± 0.15bG
Na	0.1	0.998 ± 0.002bA	2.57 ± 0.68A	0.39 ± 0.00cA	1.05 ± 0.08cA
	0.5	0.989 ± 0.001bB	10.44 ± 1.50B	1.60 ± 0.01cB	3.63 ± 0.21cB
	1.0	0.984 ± 0.004bB	19.37 ± 0.97C	3.56 ± 0.02cC	6.72 ± 0.28cC
	1.5	0.980 ± 0.002bC	28.37 ± 1.51D	5.53 ± 0.03cD	10.01 ± 0.19cD
	2.0	0.981 ± 0.002bC	39.87 ± 2.00E	7.65 ± 0.00cE	12.64 ± 0.05cE
	2.5	0.983 ± 0.001bCD	50.80 ± 3.10F	9.45 ± 0.19cF	16.20 ± 0.24cF
	3.0	0.984 ± 0.002bCD	59.10 ± 3.05G	11.07 ± 0.06cG	18.78 ± 0.26cG
			***F* Ratio**[b]		
S		22.45***	0.61ns	69815.08***	600.85***
C		80.43***	589.51***	14371.42***	10525.71***
S × *C*		7.90***	0.29ns	5104.16***	69.82***

[a]Mean values ± SD (n = 3). ANOVA F ratio for each of the two factors (S and C) and its interaction in the physicochemical parameters. Different lower case letters indicate significant differences ($p < 0.05$) for factor S (salt composition). Different capital letters indicate significant differences ($p < 0.05$) for factor C (salt content). [b]p values: ***, $p < 0.001$; **, $p < 0.01$; *, $p < 0.05$; ns, nonsignificant.

performed in each plastic container. The penetration depth of the electrodes was constant in all analyses (1.5 cm). All measurements were carried out at room temperature.

Preliminary impedance spectroscopy measurements showed that information given by low frequencies was not relevant for this study. Therefore, all of the measurements were carried out in the range of 10 kHz−1 MHz. Seventeen frequencies were chosen in this range; thus, a set of 34 values (17 module values and 17 phase values) was obtained for each sample.

Low-Field ^{1}H NMR. LF ^{1}H NMR measurements were made on all fish minces. After thawing, approximately 2 g samples were taken from each subsample of fish mince (n = 2) and placed in NMR tubes (diameter = 10 mm). There were analyzed in three parallels from each subsample with fish mince in the LF ^{1}H NMR measurements. The tubes were immediately placed in ice and kept there until the NMR measurements were carried out. The measurements were performed using a Bruker minispec mq 20 (Bruker Optik GmbH, Ettlingen, Germany) with a magnetic field strength of 0.47 T corresponding to a proton resonance frequency of 20 MHz. The instrument was equipped with a 10 mm temperature-variable probe. A built-in heating element was connected to the temperature control unit (BVT3000, Bruker Optik GmbH). The temperature in the probe was regulated to 4 °C by blowing compressed air through the sample holder. Transversal (T_2) relaxation was measured using the Carr−Purcell−Meiboom−Gill pulse sequence (CPMG).[30,31] The T_2 measurements were performed with a time delay between the 90° and 180° pulses (τ) of 150 μs. Data from 4000 echoes were acquired from 16 scan repetitions. The repetition time between two succeeding scans was set to 3 s. All even echoes were sampled. The NMR transverse relaxation data were analyzed using two different calculation methods: (1) Biexponential analysis of T_2 relaxation data was performed by fitting of the following equation to the experimental CPMG curves, similar to that reported by Erikson et al.[21] and Lambelet et al.:[32]

$$\text{signal} = A_{21}\, e^{-t/T_{21}} + A_{22}\, e^{-t/T_{22}} \quad (2)$$

T_{21} and T_{22} are the relaxation time components, and A_{21} and A_{22} are the corresponding amplitudes; 4000 data points were used, and the calculations were made using MatLab (The Mathworks Inc., Natic, MA, USA). Because the absolute relaxation amplitudes are proportional to the amount of water and fat in the sample, the relative amplitudes within samples were used. The T_{21} populations are calculated as $A_{21}/(A_{21} + A_{22})$.

For the biexponential fitting, the populations sum to 100%. Three parallel samples from each fish mince (n = 2) were averaged. (2) Multivariate data analysis was performed for all raw relaxation (CPMG) curves. These curves were normalized by setting the first sampled echo to a value of 100 and thereafter scaling the rest of the echo train. The first 600 data points were used for the principal component analysis (PCA).

Statistical Analyses. Statistical treatment of the data was performed using the Statgraphics Centurion (Statpoint Technologies, Inc., Warranton, VA, USA). A multifactor analysis of variance (ANOVA) was conducted for each evaluated parameter to test whether there were significant differences between the samples. These analyses were performed for the salt solutions and fish mince samples (phases I and II); in both cases, the physicochemical parameters were considered as dependent variables in these analyses. The type of cations and salt content, as well as its interaction, were the factors. The Tukey test (least significant difference) was used to test for differences between averages at the 5% significance level.

To evaluate the measurement techniques used in this paper, different multivariate analyses[33] were carried out using the software

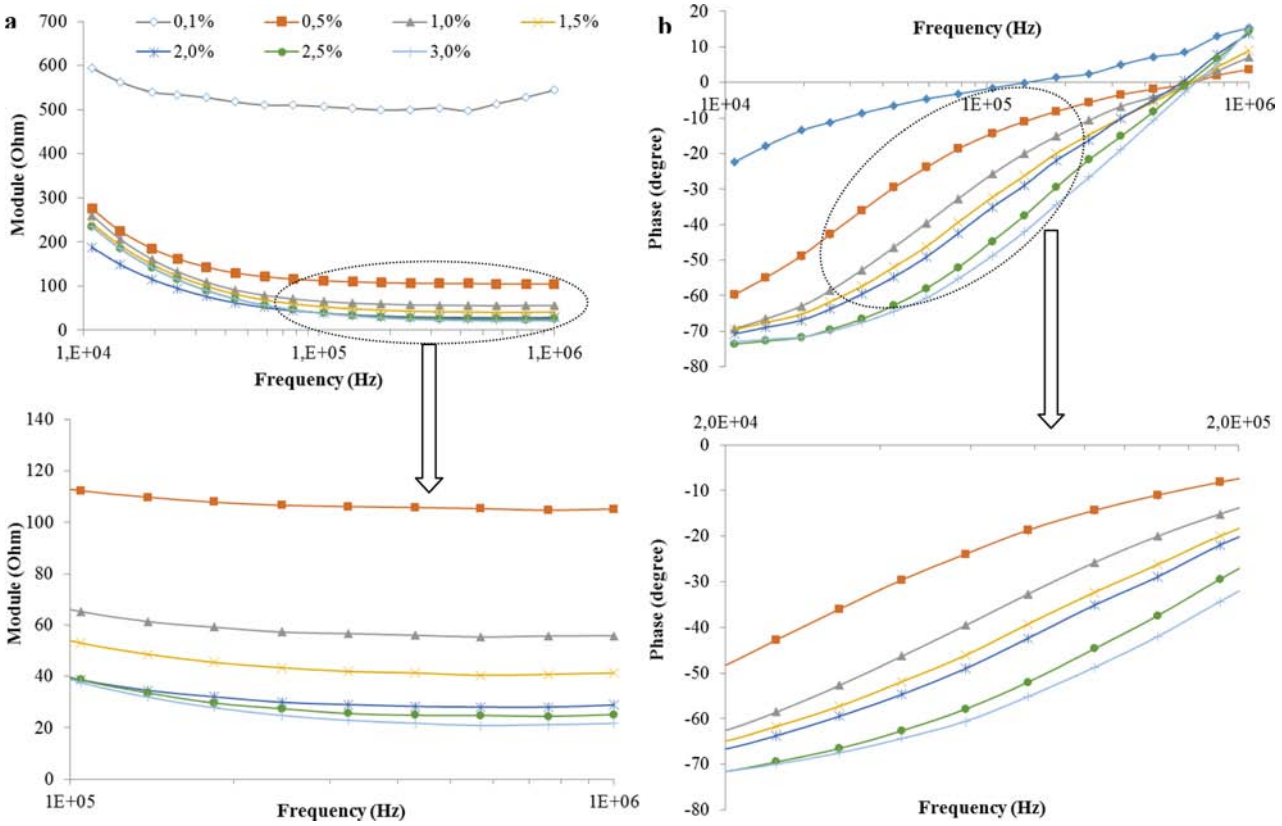

Figure 2. Mean values of modulus (a) and phase (b) of impedance spectra for the KCl solutions with different salt contents (0.1, 0.5, 1.0, 1.5, 2.0, 2.5, and 3.0 g salt/100 g distilled water, respectively).

SOLO PLS_Toolbox (eigenvector Research, Inc., Wenatchee, WA, USA).

PCA was used to discriminate the salt content level for NaCl, KCl, and mixtures. Typically, PCA projects a multidimensional data set onto a new coordinate base formed by the orthogonal directions with data maximum variance. The eigenvectors of the data matrix are called principal components (PCs), and they are uncorrelated between them. The PCs are ordered so that PC1 displays the greatest amount of variance, followed by the next greatest, PC2, and so forth. The main features of PCA are the coordinates of the data in the new base (scores plot) and the contribution to each component of the sensors (loads plot).

To create predictive models of physicochemical parameters, partial least square (PLS) regressions were applied to both impedance spectroscopy and NMR measurements. The main objective of PLS is to predict one or more parameters (dependent variables Y) from a set of measured data (independent variables X). First, the set of independent variables is projected onto a new coordinate space by maximizing the covariance between Y and X. The axes of this new space are called latent variables (LVs). The important information that correlates Y and X is contained in the first LVs. Then a prediction model is built by applying a multiple regression to a reduced number of the LVs. PLS prediction models for a_w and Na, K, NaCl, and solute contents (g/100 g) as well as solutes content in the water phase (g solutes/100 g liquid phase) were created using a set of experimental data (calibration set). First, cross-validation was used to select the number of LVs. The model was then validated with a new set of experimental data (validation set).

In the case of impedance measurements PCA and PLS regressions were performed using impedance module and phase values obtained for the 17 frequencies in the range from 10 kHz to 1 MHz. In the case of NMR measurements, the relaxation times for each defined frequency were used.

RESULTS AND DISCUSSION

Phase I: Salt Solutions. *Physicochemical Parameters.* The results of the physicochemical analyses carried out for the salt solutions are shown in Table 1. As expected, the a_w of brines decreased with increasing brine content regardless of type of salt, and the conductivity increased as salt content increased. Conductivity correlates with the total dissolved solids independent of the solute composition. In water, ions pass the electricity from one to another; therefore, the more Na^+, K^+, and Cl^- the solution contains, the more electricity is carried and the higher the conductivity. This explains the fact that the conductivity was affected by the amount of salt but not by the sodium replacement. The initial conductivity of distilled water employed for preparing the salt solutions was 0.025 ± 0.003 mS/cm. The value increased with increasing salt content, from to 2 to 60 mS/cm for the lowest and highest salt contents, respectively. Table 1 also shows the resulting contents of Na^+ and Cl^- after different salt additions to distilled water. In the solution prepared from KCl only, sodium was present in the range of 0.3−2.2 mg/L. The observed differences in chloride content depending on the type of salt are due to the different atomic masses of sodium and potassium (23 and 39 atomic mass units, respectively), owing to the fact that the salts were added equally by weight.

Impedance Spectroscopy. Module and phase impedance spectra of KCl solutions are shown in Figure 2, panels a and b, respectively. Differences in both module and phase of impedance were observed to depend on salt content.

The module of the impedance decreased as the salt content increased, and the values were much higher for the lowest content (0.1% KCl) than for the other contents. Similar

dx.doi.org/10.1021/jf405527t | J. Agric. Food Chem. 2014, 62, 2496−2505

differences between salt contents were observed for NaCl and the mixture of NaCl:KCl (data not shown). These results are in agreement with those observed for the conductivity parameters for the brine (Table 1). The results are in accordance with previous studies on impedance spectroscopy.[16−18] The correlation can be explained by the conductance of an aqueous solution as a function of the ion content of the samples, and in fact impedance measurements are related to the ions' capability of movement under the influence of an electrical field in this aqueous solution. In the present study, the behavior observed for NaCl solutions was similar to what was observed for KCl and NaCl:KCl solutions, which would indicate that impedance values were highly correlated with solute content. These results were confirmed by ANOVAs carried out for each impedance value (module and phase of impedance for each frequency), which established significant differences for solute content ($p < 0.001$) but not for the type of salt ($p > 0.05$) (ANOVA data not shown).

A PCA was performed with the data obtained in the impedance measurements (Figure 3). The statistical analysis

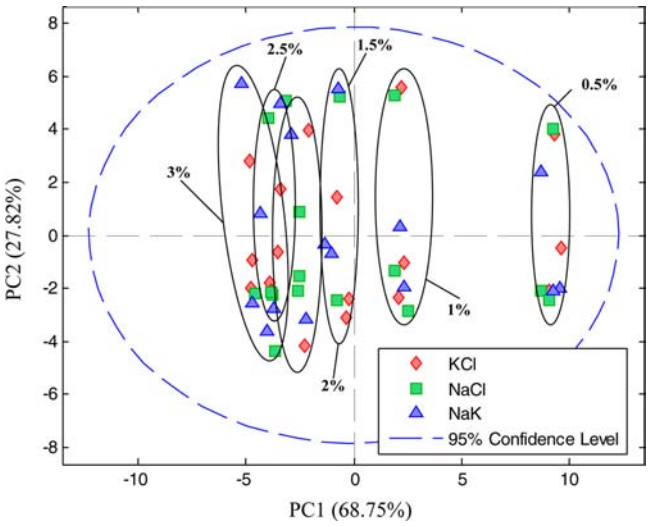

Figure 3. PCA score plot of data obtained from the impedance spectroscopy measurements in solutions with different types of salt (NaCl, KCl, and NaCl:KCl (NaK), 50:50 w/w %) and contents (0.5, 1.0, 1.5, 2.0, 2.5, and 3.0 g salt/100 g distilled water, respectively).

was able to reduce the initial variables (34 variables, 17 values of module and 17 values of phase of impedance) into a set of values of linearly uncorrelated variables called PCs, the number of principal components being less than or equal to the number of original variables. Most of the variation in the sample was explained by PC1 (68.75%) and PC2 (27.82%). According to the results obtained, the impedance spectroscopy method could distinguish between salt contents; however, it was difficult to establish a correct classification of solutions according to the type of salt (Figure 3).

Phase II: Fish Mince. *Physicochemical Analyses.* The composition of the frozen/thawed raw material was determined. Moisture, protein, lipid, and ash contents for unsalted hake were 80.2 ± 0.1 (Table 2), 15.6 ± 1.3, 0.5 ± 0.2, and 1.20 ± 0.02 g/100 g, respectively. These results are similar to those reported in other studies carried out with the same fish species.[27,34]

The results of the physicochemical analyses for salted hake mince are summarized in Table 2. As expected, adding salt to

Table 2. Physicochemical Parameters of Fish Mince Prepared with Different Salts (*S*: NaCl (Na) and NaCl:KCl (Na:K)) and Contents (*C*)

S	*C* (g salt/100 g fish mince)	moisture[a] (%)	a_w[a]	pH[a]	chloride[a] (g/100 g)	sodium[a] (g/100 g) (ISE)	sodium[a] (g/100 g) (IC)	potassium[a] (g/100 g)	ionic strength[a] (mol/kg solvent)
fish mince	0	80.15 ± 0.08	0.992 ± 0.004	6.97 ± 0.13	0.21 ± 0.01	0.05 ± 0.00	0.06 ± 0.01	0.35 ± 0.00	0.11 ± 0.00
Na:K	0.5	80.37 ± 0.24aA	0.987 ± 0.004aA	6.81 ± 0.01aA	0.43 ± 0.01aA	0.12 ± 0.01aA	0.12 ± 0.04aA	0.48 ± 0.09aA	0.18 ± 0.03aA
Na:K	1.0	79.13 ± 0.41aA	0.984 ± 0.003aAB	6.71 ± 0.04aA	0.69 ± 0.00aB	0.19 ± 0.00aB	0.19 ± 0.05aA	0.56 ± 0.12aA	0 0.26 ± 0.04aB
Na:K	2.0	79.57 ± 0.09aA	0.980 ± 0.005aB	6.83 ± 0.02aA	1.29 ±0.06aC	0.43 ± 0.04aC	0.42 ± 0.03aB	0.79 ± 0.11aB	0.47 ± 0.03aC
Na:K	3.0	78.32 ± 0.41aB	0.974 ± 0.001aC	6.69 ± 0.02aB	1.70 ± 0.03aD	0.57 ± 0.02aD	0.68 ± 0.08aC	1.17 ± 0.14aC	0.69 ± 0.05aD
Na	0.5	79.09 ± 0.94aA	0.985 ± 0.002bA	6.76 ± 0.05bA	0.50 ± 0.01bA	0.19 ± 0.00bA	0.26 ± 0.04bA	0.40 ± 0.004bA	0.22 ± 0.01bA
Na	1.0	80.47 ± 0.88aA	0.982 ± 0.001bAB	6.78 ± 0.03bA	0.82 ± 0.06bB	0.35 ± 0.01bB	0.38 ± 0.07bA	0.30 ± 0.0 6bA	0.30 ± 0.03bB
Na	2.0	78.67 ± 0.14aA	0.978 ± 0.002bB	6.67 ± 0.04bA	1.34 ± 0.11bC	0.76 ± 0.06bC	0.78 ± 0.02bB	0.40 ± 0.04bB	0.52 ± 0.03bC
Na	3.0	77.77 ± 0.06aB	0.969 ± 0.001bC	6.67 ± 0.04bB	1.90 ± 0.03bD	1.01 ± 0.00bD	1.09 ± 0.11bC	0.39 ± 0.04bC	0.71 ± 0. 03bD
					***F* Ratio**				
S		2.79ns	6.82***	6.42***	28.40***	527.67***	116.86***	112.43***	8.26***
C		15.07***	31.63***	10.26***	819.47***	720.83***	153.16***	21.40***	300.80***
S × *C*		7.80***	0.67ns	12.58***	2.71ns	60.63***	6.65***	17.82***	0.17ns

[a]Mean values ± SD ($n = 3$). Different lower case letters indicate significant differences ($p < 0.05$) for factor *S* (salt composition). Different capital letters indicate significant differences ($p < 0.05$) for factor *C* (salt content).

dx.doi.org/10.1021/jf405527t | J. Agric. Food Chem. 2014, 62, 2496−2505

the mince led to a reduction in moisture, from about 80.2% (mince without additions) to 78.3 and 77.8%, for minces containing sodium and potassium chloride (Na:K) and minces containing sodium chloride (Na), respectively. Due to the increase in mineral contents (up to 3.0 g/100 g mince) the a_w decreased from 0.992 (mince without additions) to 0.974 (Na:K) and 0.969 (Na). The moisture and a_w were significantly lower in minces containing 3.0% salt compared to minces containing less. Both the type of salt and their contents had a significant effect on the a_w, compared to the brines, where the a_w correlates only with the contents of salt. As expected, slightly higher water activities were found in the NaCl:KCl minces than in minces containing NaCl. Water activity decreases with increasing number of colligative units dissolved per volume. As K^+ is a larger ion than Na^+, replacing NaCl with an equal amount by weight of KCl will lead to a lower number of dissolved ions (colligative units) per volume and thus an increase in a_W of the product.

The pH of the unsalted mince (pH 6.97) was reduced after preparation of the mince with different salts (Na) and (Na:K) and contents (Table 2). The pH values of the raw material employed in this study are in accordance with the results obtained in other studies[34,35] for fresh hake. A decrease in pH was observed when salt was added to our minces, a little more pronounced in the case of Na than with most Na:K mixtures. Similar results have been observed in a study by Leroi and Joffraud,[36] indicating that the pH decreases in fish flesh by the addition of salt due to the increase of the ionic strength of the solution inside the cells. Another explanation might be that an increased amount of chloride ions would open the myosin filament and the more dissociable acidic groups would be water-accessible.[37] Samples containing Na exhibited lower pH than the corresponding Na:K samples: pH 6.76 vs 6.81, respectively. Similar results with fish products subjected to partial sodium replacement have also been observed.[38]

The measured contents of sodium, potassium, and chloride are shown in Table 2. The sodium (0.05−0.06 g/100 g) and potassium contents (0.35 g/100 g) of fresh fish mince (Table 2) agree with those reported in another study[39] for deboned hake. The chloride content in mince without additions was 0.21 g/100 g. When only NaCl was added to the minces, the potassium levels remained almost constant at 0.30−0.40 g/100 g, resembling the level in mince without additions.

Table 2 shows a comparison between sodium contents in the different minces as determined by the ion selective electrode and by ion chromatography. Good correlation was observed between the sodium content determined by the ion selective electrode method and ion chromatography, which was confirmed by a simple regression carried out on the data obtained by both methodologies ($y = 1.066x + 7.961$, $R^2 = 0.967$).

Impedance Spectroscopy Measurements. Impedance spectroscopy was used to detect changes in the fish mince by adding different salt contents and types of salt. A PCA was performed on the impedance spectroscopy measurements in fish mince samples with different type of salts.

The discrimination between the different salt contents observed in the PCA plot for fish minces was better than the one obtained for salt solutions (Figure 4). The percentage of variance explained by the first principal component in Figure 4 is 90.17%, whereas in Figure 3 PC1 explains only 68.75% of the total variance. This means that the correlation between impedance spectroscopy data and salt content is stronger in

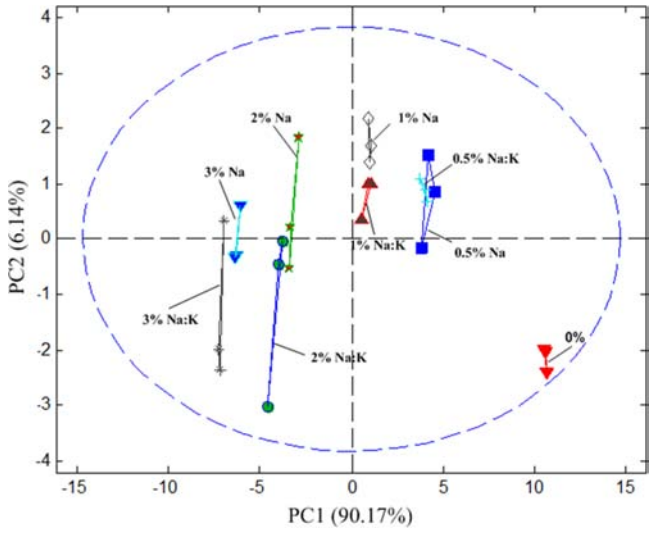

Figure 4. PCA score plot of data obtained from the impedance spectroscopy measurements in hake minces with different salt contents (NaCl (Na) or NaCl/KCl (Na:K) 0.0, 0.5, 1.0, 1.5, 2.0, and 3.0 g/100 g salted mince, respectively).

fish samples than in solutions. A possible explanation for this behavior is the salting-in effects on muscle proteins.[37] At salt contents lower than 0.5 M, the swelling of myofibrils starts and reaches a maximum at 0.8−1 M.[37] This usually causes a decrease in myofibril volume, because the myofibril tends to dissolve. However, in our study, the highest contents in the minces corresponded to 0.65 and 0.55 M for the minces with 3.0% NaCl and NaCl:KCl, respectively. The conformational changes, together with the increase in the conductivity, could be responsible for the different behavior in the IS observed among our hake minces and in the solutions. At some contents, the method also distinguished between types of cations (Na^+ or Na^+/K^+) in the fish mince, a behavior that can be explained by the different effects of sodium (kosmotrope, water-structure maker) and potassium (chaotrope, water-structure breaker) in actin and myosin.[40] Further work is needed to reveal significant differences between cations in the minces.

LF NMR. A LF NMR T_2 relaxation method was used to study the relaxation behaviors in the mince when different types of salt were added to the mince in different amounts. The two transversal relaxation times with corresponding populations obtained from fitting of NMR data are shown in Table 3. In fish muscle, typically two or three relaxation components are reported (ref 41 and references cited therein). The two major ones have relaxation times in the range of 40−60 ms (T_{21}) and 150−400 ms (T_{22}), similar to those of the present research. The mean T_{21} and T_{22} relaxation times for the unsalted hake mince were 54 and 219 ms, respectively. The interpretation of such data has been controversial, but it is now becoming more accepted that the observed changes in relaxation behavior are due primarily to chemical and diffusive proton exchange between water molecules and biopolymers (e.g., proteins).[42,43] A number of studies have nevertheless shown that these processes are linked to the morphology of the sample that in turn can be affected by, for example, processing, such as salting and mincing.[23,25,41]

After addition of 0.5% NaCl or NaCl/KCl to the mince, the proton relaxation times, found by bioexponential fitting, increased to 59−61 ms in the case of T_{21}, whereas the T_{22}

Table 3. Biexponential Fitting of LF ^{1}H NMR T_2 Relaxation Data Obtained in Fish Mince and Fish Mince Prepared with Different Salts (S: NaCl and NaCl:KCl) and Concentrations (C)

S	C (g salt100 g/ fish mince)	T_{21}[a] (ms)	T_{22}[a] (ms)	T_{21} pop[a] (%)	T_{22} pop[a] (%)
fish mince	0	54 ± 1	219 ± 7	86 ± 3	14 ± 3
NaCl/KCl	0.5	61 ± 1aA	226 ± 10aA	87 ± 2aA	13 ± 2aD
NaCl/KCl	1.0	67 ± 1aB	286 ± 46aB	96 ± 1aBD	4 ± 1aAC
NaCl/KCl	2.0	71 ± 1aD	496 ± 42aD	99 ± 0aBC	1 ± 0aBC
NaCl/KCl	3.0	68 ± 2aBC	342 ± 15aC	98 ± 0aCD	2 ± 0aAB
NaCl	0.5	59 ± 1bA	215 ± 10aA	85 ± 1bA	15 ± 1bD
NaCl	1.0	69 ± 1bC	366 ± 48bB	98 ± 1bB	2 ± 1bC
NaCl	2.0	67 ± 0bB	427 ± 34bD	99 ± 0aCD	1 ± 0aAB
NaCl	3.0	68 ± 0aBCD	423 ± 34bC	99 ± 0aD	1 ± 0aA
		F Ratio[b]			
S		9.20**	4.99*	0.30ns	0.30ns
C		214.59***	132.32***	609.87***	609.87***
$S \times C$		22.49***	17.43***	12.14***	12.14***

[a]Mean values ± SD (n = 2). Different lower case letters indicate significant differences ($p < 0.05$) for factor S (salt composition). Different capital letters indicate significant differences ($p < 0.05$) for factor C (salt concentration). [b]p values: ***, $p < 0.001$; **, $p < 0.01$; *, $p < 0.05$; ns: non significant.

value remained largely unchanged. Addition of more salt led to increases in both T_{21} and T_{22} relaxation times, with mean values of 67−71 and 286−496 ms, respectively.

By comparison, when frozen/thawed Atlantic salmon fillets were salted to 2.7% NaCl in the head part of the fillet, T_{21} increased from 47 ms (unsaltet) to 48 ms (salted), whereas the tail part of the fillet had 2.9% NaCl and T_{21} increased from 47 ms (unsalted) to 50 ms (salted), respectively. No significant changes were observed in T_{22} (140−150 ms (head part) and 140−169 ms (tail part)).[21] Similar values were obtained when fillets of the same species were salted in a 15% NaCl brine.[20] Thus, it seems that the magnitude of change in T_{21} can be similar in highly concentrated brines (whole, lean fillets) as in our lean hake mince. Notably, the mincing of cod fillets does not alter the magnitude of the T_{21} values.[44] A stronger effect of salting of cod was, however, reported,[24] where T_{21} values increased from 51 ms (raw material) to 86−94 ms after presalting by different methods (12% salt).

A PCA score plot of the relaxation time curves is presented in Figure 5. Most of the variation in the sample was explained by PC1 (76.60%) and PC2 (20.54%), and it separates minces with 0, 0.5, and 1.0−3.0% salt. Otherwise, the relaxation data did not reveal any clear trends between the magnitudes of the relaxation times at increasing salt contents above 0.5%. The increase in relaxation times when 0.5% salt was added, reflecting higher water proton mobility, suggests that a more open mince microstructure was formed. This was possibly caused by the binding of chloride ions to myosin filaments, which would induce electrostatic repulsive forces, causing an increase of filament spacing. [37]

In contrast to the increase in T_{21} as a result of the addition of 0.5% salt, the corresponding population (T_{21} pop) did not change accordingly. The T_{21} pop values remained similar to those in the mince without additions (85−87%). With further addition of salt, the values increased to 96−99%, regardless of type and amount of salt (1.0, 2.0, or 3.0% salt) with a corresponding decrease in T_{22} pop. The latter population with high mobility decreased to 1−4%. The changes in T_2 populations reflect a shift of the proton populations, increasing the amount of protons with higher mobility and decreasing the amount of protons with lower mobility. This may be explained by the changes in muscle structure due to the salting-in effect previously discussed.

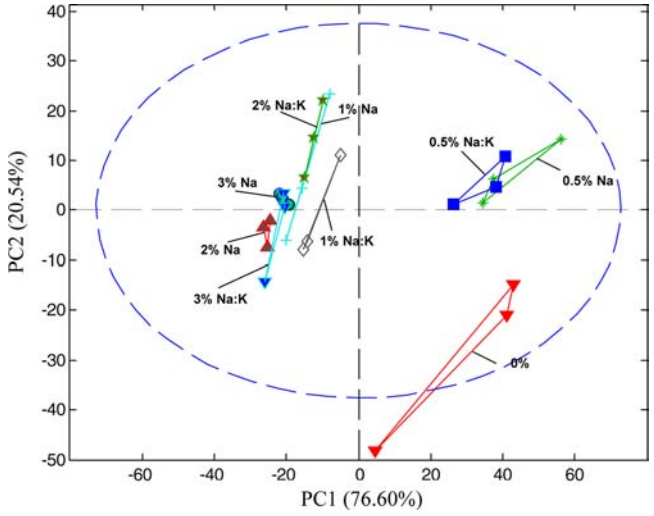

Figure 5. PCA score plot of LF ^{1}H NMR T_2 relaxation data obtained from fish mince with salt content (NaCl (Na) or NaCl/KCl (Na:K) 0.0, 0.5, 1.0, 1.5, 2.0, and 3.0 g/100 g salted mince, respectively).

On the basis of principal component analyses of the NMR T_2 relaxation data, a clear separation between samples with 0, 0.5, and 1.0−3.0% of salt was obtained. However, the LF NMR method was unable to distinguish between minces with different types of cations. In summary, the fact that the most pronounced changes in relaxation behavior occurred at low contents of salt (0−0.5%) indicates that LF ^{1}H NMR can be a suitable tool for indirect studies of structural changes in low-salt systems.[41]

PLS Results. To create predictive models of physicochemical parameters, PLS regression was applied to both impedance spectroscopy and LF NMR measurements. Table 4 shows the values of the determination coefficient (R^2), the root-mean-square error of prediction (RMSEP), and the number of LVs corresponding to the prediction models built for a_w, Na^+ (mg/

dx.doi.org/10.1021/jf405527t | J. Agric. Food Chem. 2014, 62, 2496−2505

Table 4. Parameters of the PLS Models of Physicochemical Parameters from the Impedance Measurements[a]

	LV	R^2	RMSEP
a_w	5	0.886	0.003
	1	0.812	0.003
Na (mg/100 g)	4	0.480	276.154
K (mg/100 g)	4	0.094	269.090
NaCl (g/100 g)	4	0.425	0.730
KCl (g/100 g)	3	0.393	0.628
solute content (g/100 g)	5	0.950	0.210
	1	0.953	0.203
solute content in liquid phase (g/100 g)	4	0.946	0.286

[a]LV, number of latent variables; R^2, coefficient of determination; RMSEP, root mean square error of prediction.

100 g), K^+ (mg/100 g), NaCl (g/100 g), gram salts (g/100 g), and gram solutes/100 g liquid phase using impedance spectroscopy data. Models for a_w, gram salts (g/100 g), and gram solutes/100 g liquid phase show very good behavior with R^2 values close to or higher than 0.9. However, the results obtained for Na^+ (mg/100 g), K^+ (mg/100 g), and NaCl (g/100 g) demonstrate that the proposed technique is not able to discriminate between the different types of salt. As shown in Figure 3, in the PCA plots most of the total variance corresponds to PC1. In the module and phase plots a similar discrimination between the different salt content levels could be obtained considering the module and phase values for all of the frequencies or considering just the module value for one frequency (for example, 1 MHz). On this basis, new PLS models were built for a_w and gram salts (g/100 g) using only one LV. The R^2 values for these new models are similar to those obtained using the number of LVs established by cross-validation. This opens the possibility to limit impedance measurements to the module at a single frequency so that the measurement process would be greatly shortened and the prediction could be made using a simple regression. There were no significant correlations between the LF NMR measurements and the physicochemical results. In conclusion, the PLS models of impedance spectroscopy measurements showed good correlations with R^2 values close to or higher than 0.9 for a_w, solute content, and solute content in the liquid phase. However, the results obtained for Na^+ (mg/100 g), K^+ (mg/100 g), and NaCl (g/100 g) demonstrate that the proposed technique is not able to discriminate between the different types of salt.

In conclusion, good correlations were observed between the sodium content determined by using the ion selective electrode method and ionic chromatography, which was confirmed by a simple regression, carried out using the data obtained with both methodologies. In both salt solutions and fish minces, the impedance spectroscopy measurements could separate between different salt contents down to 0.5%. However, the results obtained for cation determinations demonstrate that the proposed technique is not able to discriminate between the different types of salt. Furthermore, impedance spectroscopy measurements showed good correlations for a_w, solute content, and solute content in the liquid phase. The NMR transversal relaxation time T_2 clearly distinguishes samples with 0, 0.5, and 1.0−3.0% salt, based on PCA. We conclude that LF ^{1}H NMR can be a suitable technique for studies of low-salt products. However, the LF NMR method was unable to distinguish between minces with different types of cations.

■ ASSOCIATED CONTENT

Ⓢ Supporting Information

System block diagram. This material is available free of charge via the Internet at http://pubs.acs.org.

■ AUTHOR INFORMATION

Corresponding Author

*(K.G.) Mail: SINTEF Fisheries and Aquaculture, Brattørkaia 17C, 7465 Trondheim, Norway. Phone: +47 47 90 38 91. Fax: +47 93 27 07 01. E-mail: kirsti.greiff@sintef.no.

Funding

This research was conducted when K.G. visited Universidad Politécnica de Valencia (UPV) as a part of the project Low Salt Products, Project 185063/O10, supported by the Research Council of Norway.

Notes

The authors declare no competing financial interest.

■ ACKNOWLEDGMENTS

We thank our co-workers at UPV, Isabel Fernández-Segovia, Arantxa Rizo, and Lupis Hernandez, and Marte Schei at SINTEF Fisheries and Aquaculture for their support and valuable participation in discussions regarding planning of the experiments, production of fish mince, and guidance related to the use of the different measuring techniques.

■ REFERENCES

(1) He, F. J.; MacGregor, G. A. Effect of modest salt reduction on blood pressure: a meta-analysis of randomized trials. Implications for public health. *J. Hum. Hypertens.* **2002**, *16*, 761−70.

(2) WHO. *Reducing Salt Intake in Populations*; report of a WHO Forum and Technical Meeting; World Health Organization: Paris, France, 2006.

(3) Martínez-Alvarez, O.; Gómez-Guillén, M. C. Effect of brine salting at different pHs on the functional properties of cod muscle proteins after subsequent dry salting. *Food Chem.* **2006**, *94*, 123−129.

(4) Thorarinsdottir, K. A.; Arason, S.; Bogason, S. G.; Kristbergsson, K. The effects of various salt concentrations during brine curing of cod (*Gadus morhua*). *Int. J. Food Sci. Technol.* **2004**, *39*, 79−89.

(5) Fuentes, A.; Ferandez-Segovia, I.; Barat, J. M.; Serra, J. A. Physicochemical characterization of some smoked and marinated fish products. *J. Food Process. Preserv.* **2010**, *34*, 83−103.

(6) Aliño, M.; Fuentes, A.; Fernández-Segovia, I.; Barat, J. M. Development of a low-sodium ready-to-eat desalted cod. *J. Food Eng.* **2011**, *107*, 304−310.

(7) Fuentes, A.; Fernández-Segovia, I.; Barat, J. M.; Serra, J. A. Influence of sodium replacement and packaging on quality and shelf life of smoked sea bass (*Dicentrarchus labrax* L.). *LWT−Food Sci. Technol.* **2011**, *44*, 917−923.

(8) Toldrá, F.; Barat, J. M. Strategies for salt reduction in foods. *Recent Pat. Food Nutr. Agric.* **2012**, *4*, 19−25.

(9) Geleijnse, J. M.; Witterman, J. C. M.; Stijnen, T.; Kloos, M. W.; Hofman, A.; Grobbee, D. E. Sodium and potassium intake and risk of cardiovascular events and all-causes mortality: the Rotterdam study. *Eur. J. Epidemiol.* **2007**, *22*, 763−777.

(10) FSAI. *Salt and Health: Review of the Scientific Evidence and Recommendationsfor Public Policy in Ireland*; Dublin, Ireland, 2005.

(11) EFSA. Opinion of the Scientific Panel of Dietetic Products, Nutrition and Allergies on request from the Commission related to the tolerable upper intake level of potassium. *EFSA J.* **2005**, *193*, 1−19.

(12) Desmond, E. Reducing salt: a challenge for the meat industry. *Meat Sci.* **2006**, *74*, 188−196.

(13) Ehling, S.; Tefera, S.; Earl, R.; Cole, S. Comparison of analytical methods to determine sodium content of low-sodium foods. *J. AOAC Int.* **2010**, *93*, 628−637.

(14) AOAC. *Official Methods of Analysis of the Association of Official Analytical Chemists*, 15th ed.; AOAC: Arlington, VA, USA, 1990.
(15) Pérez-Olmos, R.; Herrero, R.; Lima, J. L. F. C.; Montenegro, M. C. B. S. M. Sequential potentiometric determination of chloride and nitrate in meat products. *Food Chem.* **1997**, *59*, 305−311.
(16) Chanet, M.; Rivière, C.; Eynard, P. Electric impedance spectrometry for the control of manufacturing process of comminuted meat products. *J. Food Eng.* **1999**, *42*, 153−159.
(17) Guerrero, L.; Gobantes, I.; Oliver, M. À.; Arnau, J.; Dolors Guàrdia, M.; Elvira, J.; Riu, P.; Grèbol, N. S.; Monfort, J. M. Green hams electrical impedance spectroscopy (EIS) measures and pastiness prediction of dry cured hams. *Meat Sci.* **2004**, *66*, 289−294.
(18) Masot, R.; Alcañiz, M.; Fuentes, A.; Schmidt, F. C.; Barat, J. M.; Gil, L.; Baigts, D.; Martínez-Máñez, R.; Soto, J. Design of a low-cost non-destructive system for punctual measurements of salt levels in food products using impedance spectroscopy. *Sensor Actuat. A−Phys.* **2010**, *158*, 217−223.
(19) Rizo, A.; Fuentes, A.; Fernández-Segovia, I.; Masot, R.; Alcañiz, M.; Barat, J. M. Development of a new salmon salting−smoking method and process monitoring by impedance spectroscopy. *LWT−Food Sci. Technol.* **2013**, *51*, 218−224.
(20) Aursand, I. G.; Gallart-Jornet, L.; Erikson, U.; Axelson, D. E.; Rustad, T. Water distribution in brine salted cod (*Gadus morhua*) and salmon (*Salmo salar*): a low-field ^{1}H NMR study. *J. Agric. Food Chem.* **2008**, *56*, 6252−6260.
(21) Aursand, I. G.; Veliyulin, E.; Böcker, U.; Ofstad, R.; Rustad, T.; Erikson, U. Water and salt distribution in Atlantic salmon (*Salmo salar*) studied by low-field ^{1}H NMR, ^{1}H and ^{23}Na MRI and light microscopy: effects of raw material quality and brine salting. *J. Agric. Food Chem.* **2008**, *57*, 46−54.
(22) Erikson, U.; Veliyulin, E.; Singstad, T. E.; Aursand, M. Salting and desalting of fresh and frozen-thawed cod (*Gadus morhua*) fillets: a comparative study using ^{23}Na NMR, ^{23}Na MRI, low-field ^{1}H NMR, and physicochemical analytical methods. *J. Food Sci.* **2004**, *69*, FEP107−FEP114.
(23) Aursand, I. G.; Erikson, U.; Veliyulin, E. Water properties and salt uptake in Atlantic salmon fillets as affected by ante-mortem stress, rigor mortis, and brine salting: a low-field ^{1}H NMR and ^{1}H/^{23}Na MRI study. *Food Chem.* **2010**, *120*, 482−489.
(24) Gudjónsdóttir, M.; Arason, S.; Rustad, T. The effects of pre-salting methods on water distribution and protein denaturation of dry salted and rehydrated cod − a low-field NMR study. *J. Food Eng.* **2011**, *104*, 23−29.
(25) Gudjonsdottir, M.; Gunnlaugsson, V. N.; Finnbogadottir, G. A.; Sveinsdottir, K.; Magnusson, H.; Arason, S.; Rustad, T. Process control of lightly salted wild and farmed Atlantic cod (*Gadus morhua*) by brine injection, brining, and freezing − a low field NMR study. *J. Food Sci.* **2010**, *75*, E527−E536.
(26) Gudjonsdottir, M.; Lauzon, H. L.; Magnusson, H.; Sveinsdottir, K.; Arason, S.; Martinsdottir, E.; Rustad, T. Low field nuclear magnetic resonance on the effect of salt and modified atmosphere packaging on cod (*Gadus morhua*) during superchilled storage. *Food Res. Int.* **2011**, *44*, 241−249.
(27) Sánchez-Alonso, I.; Martinez, I.; Sánchez-Valencia, J.; Careche, M. Estimation of freezing storage time and quality changes in hake (*Merluccius merluccius*, L.) by low field NMR. *Food Chem.* **2012**, *135*, 1626−1634.
(28) AOAC. *Official Methods of Analysis of the Association of Official Analytical Chemists*, 16th ed.; AOAC: Arlington, VA, USA, 1997.
(29) Kivikari, R. Analysis of sodium in meat products using an Na-selective electrode (in Finnish). In *Proceedings of Meat Day Seminar 536*; 1996; pp 64−66
(30) Carr, H. Y.; Purcell, E. M. Effects of diffusion on free precession in nuclear magnetic resonance experiments. *Am. J. Physiol.* **1954**, *94*, 630−638.
(31) Meiboom, S.; Gill, D. Modified spin-echo method for measuring nuclear times. *Rev. Sci. Instrum.* **1958**, *29*, 688−691.
(32) Lambelet, P.; Renevey, F.; Kaabi, C.; Raemy, A. Low-field nuclear magnetic resonance relaxation study of stored or processed cod. *J. Agric. Food Chem.* **1995**, *43*, 1462−1466.
(33) Martens, H.; Martens, M. *Multivariate Analysis of Quality. An Introduction*; Wiley: New York, 2001.
(34) Orban, E.; Nevigato, T.; Di Lena, G.; Masci, M.; Casini, I.; Caproni, R.; Rampacci, M. Total volatile basic nitrogen and trimethylamine nitrogen levels during ice storage of European hake (*Merluccius merluccius*): a seasonal and size differentiation. *Food Chem.* **2011**, *128*, 679−682.
(35) Pastoriza, L.; Sampedro, G.; Herrera, J. J.; Cabo, M. L. Influence of sodium chloride and modified atmosphere packaging on microbiological, chemical and sensorial properties in ice storage of slices of hake (*Merluccius merluccius*). *Food Chem.* **1998**, *61*, 23−28.
(36) Leroi, F.; Joffraud, J. J. Salt and smoke simultaneously affect chemical and sensory quality of cold-smoked salmon during 5 °C storage predicted using factorial design. *J. Food Prot.* **2000**, *63*, 1222−1227.
(37) Offer, G.; Trinick, J. On the mechanism of water holding in meat: the swelling and shrinking of myofibrils. *Meat Sci.* **1983**, *8*, 245−281.
(38) Fuentes, A.; Fernández-Segovia, I.; Serra, J. A.; Barat, J. M. Effect of partial sodium replacement on physicochemical parameters of smoked sea bass during storage. *Food Sci. Technol. Int.* **2012**, *18*, 207−217.
(39) Martínez-Valverde, I.; Jesús Periago, M.; Santaella, M.; Ros, G. The content and nutritional significance of minerals on fish flesh in the presence and absence of bone. *Food Chem.* **2000**, *71*, 503−509.
(40) Puolanne, E.; Halonen, M. Theoretical aspects of water-holding in meat. *Meat Sci.* **2010**, *86*, 151−165.
(41) Erikson, U.; Standal, I. B.; Aursand, I. G.; Veliyulin, E.; Aursand, M. Use of NMR in fish processing optimization: a review of recent progress. *Magn. Reson. Chem.* **2012**, *50*, 471−480.
(42) Halle, B. Molecular theory of field-dependent proton spin-lattice relaxation in tissue. *Magn. Reson. Med.* **2006**, *56*, 60−72.
(43) Belton, P. Spectroscopic approaches to the understanding of water in foods. *Food Rev. Int.* **2011**, *27*, 170−191.
(44) Andersen, C. M.; Jørgensen, B. M. On the relation between water pools and water holding capacity in cod muscle. *J. Aquat. Food Prod. Technol.* **2004**, *13*, 13−23.

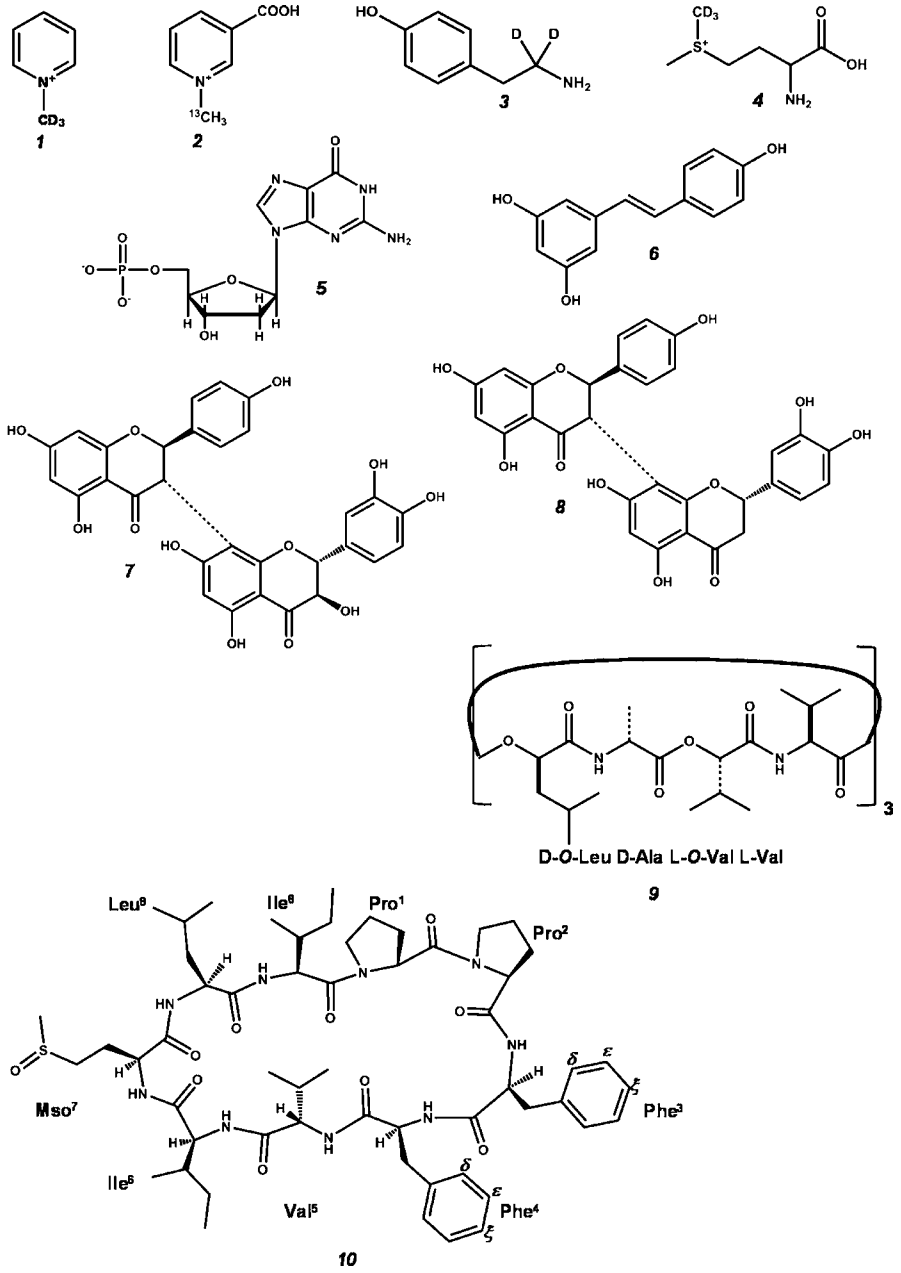

Figure 1. Synthesized and isolated compounds quantitated by qHNMR (NMP-d_3, **1**), trigonelline-$^{13}C_1$ (**2**), tyramine-d_2 (**3**), *S*-methylmethionine-d_3 (**4**), 5′-GMP (**5**), (*E*)-resveratrol (**6**), buchananiflavanone (**7**), GB-2 (**8**), cereulide (**9**), and cyclolinopeptide C (**10**).

basis of the principle of reciprocity, the NMR signal strength for a sample compound in a given coil is inversely proportional to the 90° or 360° pulse length.[19,21]

Compared to applications using internal standards for quantitative determinations, the literature on using external standards for sequential qHNMR analysis of standard and sample is rather poor. The objective of the present investigation was to develop and validate a qHNMR method using small molecules as external standards for a precise quantitation of target compounds in single-compound solutions, compound mixtures, or compounds in fractions without knowledge of their molecular weight.

■ MATERIALS AND METHODS

Chemicals. All chemicals were purchased from Sigma-Aldrich (Steinheim, Germany), solvents were obtained in HPLC grade from Merck (Darmstadt, Germany), and deuterated solvents and deuterium chloride (DCl, 7.6 mol/L in D_2O) were supplied by Euriso-top (Saarbrücken, Germany). d_3-*N*-Methylpyridinium (**1**), ^{13}C-trigonelline (**2**), d_2-tyramine (**3**), and d_3-*S*-methylmethionine (**4**) were synthesized and purified as reported in the literature (Figure 1).[23−26] The following compounds were isolated from natural sources and purified as reported in the literature: guanosine 5′-monophosphate (5′-GMP; **5**) from yeast extract, (*E*)-resveratrol (**6**) from grape berries, buchananiflavanone (**7**) and GB-2 (**8**) from *Garcinia* bark, and cereulide (**9**) from *Bacillus cereus* incubations (Figure 1).[27−30]

Fresh linseed oil was purchased from Ölmühle Solling GmbH (Boffzen, Germany).

Isolation and Structural Characterization of Cyclolinopeptide C (10), Cyclo(Pro-Pro-Phe-Phe-Val-Ile-Mso-Leu-Ile). Linseed oil (50 mL) was dissolved in *n*-hexane (50 mL) and extracted three times with methanol/water (60:40, v/v; 100 mL). The aqueous phases were combined and filtered through a wet filter paper; after removal of the solvent in a vacuum, the residue was dissolved in acetonitrile/water

dx.doi.org/10.1021/jf405529b | J. Agric. Food Chem. 2014, 62, 2506−2515

Table 1. Gravimetric and Experimental Values (qHNMR) of Commercially Available Compounds

compound	purity[a] (%)	solvent	concentration (mmol/L)		recovery[b] (%)
			gravimetric	NMR	
nicotinic acid	≥99.5	D_2O	7.84	7.75	98.9
L-tyrosine	≥99	D_2O/DCl[c]	3.05	3.03	99.3
caffeine	≥99	CD_2OD	3.12	3.12	100.0
creatinine	≥99	D_2O	5.77	5.75	99.7
inosine	≥99	DMSO-d_6	1.94	1.83	94.3
benzoic acid	≥99.99	D_2O	2.98	2.96	99.3
rutin·$3H_2O$	≥99	CD_3OD	2.68	2.71	101.1
tyramine	≥99	CD_3OD	14.65	14.78	100.8
sarsasapogenin	≥98	C_6D_6	1.37	1.35	98.5
diosgenin	≥99	C_6D_6	1.00	1.00	100.0
(−)-neomenthol	≥99	CD_3CN	27.90	27.78	99.6
(+)-menthol	≥99	CD_3CN	15.23	14.94	98.1
sucrose	≥99.5	D_2O	4.12	4.07	98.8
citric acid	≥99	D_2O	9.99	10.05	100.6
acetaldehyde[d]	≥99	C_6D_6	2.85	2.28	80.0
acetaldehyde[e]	≥99	C_6D_6	3.27	3.04	93.0
dimethyl sulfide	≥99	CD_3OD	6.20	5.79	93.4
(*E*)-resveratrol	≥98	CD_3OD	3.50	3.36	96.0

[a]Purity given by manufacturer. [b]Recovery based on the external standard caffeine (3.12 mmol/L). [c]D_2O/DCl (90:10, v/v). [d]Preparation of the stock solution at room temperature. [e]Preparation of the stock solution at room temperature with cooled C_6D_6 and acetaldehyde (4 °C).

Table 2. Quantitation and Determination of Purity of Natural Product Isolates and Synthesized Compounds

compound	solvent	concentration (mmol/L)		purity/recovery[a] (%)
		gravimetric	NMR	
(NMP-d_3)$^+$ I^-	CD_3OD	10.30	10.25	99.5
(trignonelline $^{13}C_1$)$^+$ I^-	D_2O	3.05	2.99	98.0
tyramine-d_2	D_2O	4.16	4.18	100.5
(*S*-methylmethionine-d_3)$^+$ I^-	D_2O	5.10	5.06	99.2
5′-GMP	D_2O	3.27	2.87	88.0
(*E*)-resveratrol	CD_3OD	2.65	2.36	89.1
buchananiflavanone	DMSO-d_6	2.02	1.85	91.6
GB-2	DMSO-d_6	1.73	1.34	77.5
cereulide	DMSO-d_6	1.23	0.87	71.5
cyclolinopeptide C	CD_3OD	2.50	1.75	70.0

[a]Recovery based on the external standard caffeine (3.12 mmol/L).

(70:30, v/v; 3 mL) and separated by RP-HPLC. Monitoring the effluent (5.0 mL/min) at 210/280 nm, chromatography was performed using a 250 × 10 mm, 5 μm, phenyl-hexyl column (Luna, Phenomenex, Aschaffenburg, Germany) as the stationary phase and starting with a mixture of formic acid (0.1% in water, pH 2.5) and acetonitrile (40:60, v/v). After isocratic elution for 3 min, the acetonitrile content was increased to 75% within 3 min, kept for 1 min, then raised to 100% within 3.5 min and, finally, maintained for an additional 4 min. The peak eluting at 5.30 min was collected in several runs, concentrated under reduced pressure, and freeze-dried twice to afford cyclolinopeptide C as a white amorphous powder.

*Cyclolinopeptide C, **10** (Figure 1):* (+) HRESIMS, *m/z* 1074.6063 $[M + H]^+$/1096.5879 $[M + Na]^+$ (calcd for $C_{56}H_{84}N_9O_{10}S$ 1074.6062/$C_{56}H_{84}N_9O_{10}SNa$ 1096.5881); UV−vis (acetonitrile) λ_{max} = 280 nm; ^{1}H NMR (500 MHz; DMSO-d_6; 320 K, *gs*-COSY, TOCSY, ROESY, signal assignment refers to the structure **10** in Figure 1) δ Pro^1 3.78 [bs, 1H, α], 2.06 [m, 1H, β], 1.62 [m, 1H, β], 1.91 [m, 1H, γ], 1.82 [m, 1H, γ], 3.55 [m, 2H, δ]; Pro^2 4.14 [d, 1H, *J* = 7.7 Hz, α], 1.86 [m, 1H, β], 1.60 [m, 1H, β], 1.44 [m, 1H, γ], 0.93 [m, 1H, γ], 3.24 [m, 2H, δ]; Phe^3 4.52 [m, 1H, α], 3.06 [m, 2H, β], 7.02 [m, 2H, δ], 7.21 [m, 2H, ε], 7.18 [m, 1H, ζ], 7.91 [bs, 1H, NH]; Phe^4 4.73 [m, 1H, α], 3.07 [m, 2H, β], 7.15 [m, 2H, δ], 7.20 [m, 2H, ε], 7.18 [m, 1H, ζ], 7.94 [bs, 1H, NH]; Val^5 3.87 [t, 1H, *J* = 7.2 Hz, α], 2.04 [m, 1H, β], 0.90 [m, 3H, γ], 0.87 [m, 3H, γ], 7.41 [bs, 1H, NH]; Ile^6 4.47 [m, 1H, α], 1.78 [m, 1H, β], 1.47 [m, 2H, γ], 0.87 [m, 3H, γ], 0.79 [m, 3H, δ], 7.24 [bs, 1H, NH]; Mso^7 4.40 [d, 1H, *J* = 4.0 Hz, α], 2.10 [m, 1H, β], 1.88 [m, 1H, β], 2.78 [m, H, γ], 2.62 [m, H, γ], 2.45 [s, 3H, ε]; 7.89 [bs, 1H, NH]; Leu^8 4.02 [m, 1H, α], 1.75 [m, 2H, β], 1.50 [m, 1H, γ], 0.85 [m, 3H, δ], 0.83 [m, 3H, δ], 8.14 [bs, 1H, NH]; Ile^9 3.76 [bs, 1H, α], 2.07 [m, 2H, β], 1.48 [m, 1H, γ], 1.19 [m, 1H, γ], 0.86 [m, 3H, γ], 0.78 [m, 3H, δ], 7.96 [bs, 1H, NH]; ^{13}C NMR (125 MHz; DMSO-d_6; 320 K, HSQC, HMBC) δ Pro^1 58.0 [α], 27.7 [β], 24.0 [γ], 47.1 [δ], 171.7 [C═O]; Pro^1 60.0 [α], 30.6 [β], 21.1 [γ], 46.3 [δ], 171.1 [C═O]; Phe^3 55.0 [α], 35.3 [β], 137.5 [γ], 127.7 [δ], 128.5 [ε], 125.8 [ζ], 170.6 [C═O]; Phe^4 54.2 [α], 36.3 [β], 137.8 [γ], 127.8 [δ], 128.8 [ε], 126.0 [ζ], 171.4 [C═O]; Val^5 60.2 [α], 29.5 [β], 19.0 [γ], 18.5 [γ], 171.8 [C═O]; Ile^6 54.0 [α], 36.8 [β], 23.2 [γ], 15.1 [γ], 10.3 [δ], 168.8 [C═O]; Mso^7 51.2 [α], 25.4 [β], 49.3 [γ], 37.5 [ε], 169.5 [C═O]; Leu^8 51.9 [α], 37.6 [β], 24.1 [γ], 22.6 [δ], 21.3 [δ], 170.2 [C═O]; Ile^9 60.2 [α], 34.5 [β], 24.9 [γ], 15.5 [γ], 10.7 [δ], 171.1 [C═O].

Mass Spectrometry. MS analysis was performed using an API 4000 QTrap LC-MS/MS (Applied Biosystems, Darmstadt, Germany) running in the positive electrospray ionization (ESI$^+$) mode. Zero grade air served as the nebulizer gas (45 psi) and turbo gas (425 °C) for solvent drying (55 psi); nitrogen was used as the curtain (20 psi) and collision gas (8.7×10^{-7} psi). For ESI$^+$, the ion spray voltage was set at +5500 V in the positive mode. Solutions of natural product

Table 3. Gravimetric and Experimental Values (qHNMR) Analyzing Six Samples with Different Concentrations of Benzoic Acid, Caffeine, and L-Tyrosine[a]

	concentration (mmol/L)					
	benzoic acid		caffeine		L-tyrosine	
sample	gravimetric	NMR	gravimetric	NMR	gravimetric	NMR
1	16.30	16.51	15.90	15.80	16.50	16.33
2	8.15	8.07	5.30	5.23	8.25	8.19
3	3.26	3.28	2.65	2.62	4.13	4.09
4	1.63	1.66	1.33	1.33	2.06	2.10
5	0.815	0.80	0.665	0.67	0.687	0.70
6	0.326	0.33	0.333	0.33	0.345	0.34
m		1.0108		0.9932		0.9880
b		−0.0287		−0.0018		+0.0304
R^2		0.9999		1.0000		1.0000

[a] m, slope; b, axis intercept.

isolates and synthesized compounds prepared in methanol/water (1:1, v/v) were infused using a syringe pump at a flow rate of 10 μL/min. Data processing was performed by using Analyst 1.4.1 software (AB SCIEX, Darmstadt, Germany). Mass spectra of cyclolinopetide C were measured on a Waters Synapt G2 S HDMS mass spectrometer (Waters, Manchester, UK) coupled to an Acquity UPLC core system (Waters, Milford, MA, USA). HPLC separations were performed using a semipreparative HPLC system (LC-2000 Plus Series, Jasco, Groß-Umstadt, Germany).

Preparation of Sample Solutions for qHNMR. Reference compounds and samples were prepared by weighing all compounds or fractions using three analytical balances (Shimadzu AUW120D, Ohaus DV215CD, Sartorius ED224s) randomly to minimize any potential weighing error. Solutions were prepared in volumetric flasks, providing complete dissolution in the respective solvent (Tables 1 and 2). The stock solutions for the calibration curves benzoic acid (16.30 mmol/L), caffeine (15.90 mmol/L), and L-tyrosine (16.50 mmol/L) were prepared in D_2O, CD_3OD, and D_2O/DCl (90:10, v/v), respectively, and diluted with the corresponding solvent to obtain six different concentrations for benzoic acid (16.30, 8.15, 3.26, 1.63, 0.82, 0.33 mmol/L), caffeine (15.90, 5.30, 2.65, 1.33, 0.66, 0.33 mmol/L), and L-tyrosine (16.50, 8.25, 4.13, 2.06, 0.69, 0.34 mmol/L).

Nuclear Magnetic Resonance Spectroscopy. For structure determination of the isolated materials of 5′-GMP, resveratrol, buchananiflavanone, cereulid, GB-2, and cyclolinopeptide C, H,H correlation spectroscopy (COSY) and ^{1}H, ^{13}C correlated experiments, such as heteronuclear single-quantum coherence (HSQC) as well as the heteronuclear multiple-bond correlation (HMBC), were acquired on a Bruker Avance III 500 MHz system equipped with a cryo-TCI probe (solvent cf. Table 2, 300 K). The spectra were recorded for structure assignment and to check that all chosen integral regions were free of impurities.

^{1}H qHNMR was performed at 298 K using a Bruker AV III system (Bruker, Rheinstetten, Germany) operating at a frequency of 400.13 MHz, equipped with a Z-gradient 5 mm multinuclear observe probe ($BBFO_{plus}$). The samples were dissolved in deuterated solvents (Tables 2 and 3) (Euriso-top, Gif sur Yvette Cedex, France), and aliquots (600 μL) of each sample were analyzed in 5 × 178 mm NMR tubes (USC tubes, Bruker, Faellanden, Switzerland).

To ensure high-quality spectra, the NMR probe was manually tuned and matched to 50 Ω resistive impedance to minimize radio frequency (RF) reflection, with the sample in place. After automatic optimization of the lock phase, each sample was shimmed ($z^1 - z^5$, xyz, $z^1 - z^5$), the receiver gain was set automatically with the *rga* command, and the 90° pulse width was determined individually for each sample using the AU program *pulsecal sn* (Bruker TopSpin 3.0). All spectra were acquired without spinning the sample and referenced to TMS or TMSP. The spectrum quality was verified by analyzing TMS or TMSP signal in terms of peak symmetry, peak width at half-peak height (≤0.8 Hz), and separation of the silicon satellites. All spectra were recorded in the *baseopt* mode (generates a smooth baseline at zero without offset) acquired with a maximum of 16 scans of 64 K complex data points, corresponding to an acquisition time of 3.98 s at a sweep width of 8223 Hz, and a relaxation delay of 40 s. The free induction decay (FID) was multiplied with a 0.3 Hz exponential line-broadening factor and zero-filled prior to Fourier transformation. If the automatic phase correction was not proper enough, a careful manual zero- and first-order phase correction was performed. Baseline correction was performed automatically using the command *absn*. Integration was done manually and whenever required; adjustment of the integrals was performed by the software functions SLOPE and BIAS.

For compound quantitation, defined samples of caffeine (3.55 ppm, s, 3H), benzoic acid (7.90 ppm, m, 2H), and L-tyrosine (7.10 ppm, m, 2H), respectively, were used as external standard, and the specific resonance signals (given in parentheses) were used for analysis. The concentration of each sample solution was calculated by using the ERETIC 2 function of TopSpin 3.0 (Bruker).[31] Initial calibration of the instrument for qHNMR was based on the NIST reference sample benzoic acid (2.98 mmol/L, NIST 350b, purity = 99.9978% ± 0.0044%) for verification of the direct calibrant caffeine (3.12 mmol/L). The qHNMR of the latter was calibrated by a linear response function from six calibration points. Each measurement was preceded by removing the sample from the probe and replacing it again in the spectrometer. After temperature equilibration, the probe was tuned, matched, and shimmed, and the 90° pulse was determined. Intensity of the signal was integrated manually. The T_1 relaxation times of all resonances of interest were determined by using the inversion–recovery pulse sequence, acquiring 10 recovery delays between 0.01 and 15 s, and accumulating 8 scans with an additional relaxation delay of 15 s between the scans. The T_1 time for the individual signals was determined by using TopSpin 3.0 (Bruker). The relaxation delay was set to 5 times the longest T_1 relaxation time in the molecule to ensure complete relaxation.

RESULTS AND DISCUSSION

For a robust and accurate quantitation of target compounds in natural isolates of unknown purity and/or in amounts of <1 mg, a qHNMR method was developed and validated on a 400 MHz system with external standard calibration using ERETIC 2 based on the PULCON (PULse length based CONcentration determination) methodology. The ERETIC 2 tool allows a precise concentration determination by the fact that the 90° pulse is inversely proportional to the NMR signal intensity.[21] If the concentration of a reference sample (C_{ref}) is known and the 90° pulse of all samples has been precisely calibrated, the concentration of the unknown analyte sample (C_U) can be determined using the following equation:

dx.doi.org/10.1021/jf405529b | J. Agric. Food Chem. 2014, 62, 2506−2515

$$C_U = kC_{ref}\frac{A_U T_U \theta_{90}^U n_{ref}}{A_{ref} T_{ref} \theta_{90}^{ref} n_U}$$

A indicates the integral over the resonance line(s), T the sample temperature in Kelvin, θ_{90} the 90° pulse length, and n the number of transients used for the measurement of the reference and the unknown sample. The correction factor k accounts for any experimental variations such as different receiver gains or incomplete relaxation, applied for the measurement of the reference or the unknown analyte sample. The equation is valid when the experiments are performed with the same NMR probe, which is properly tuned and matched.[21] The general working flow is given in Figure 2, and the most critical parameters and practical aspects of this qHNMR method are as follows.

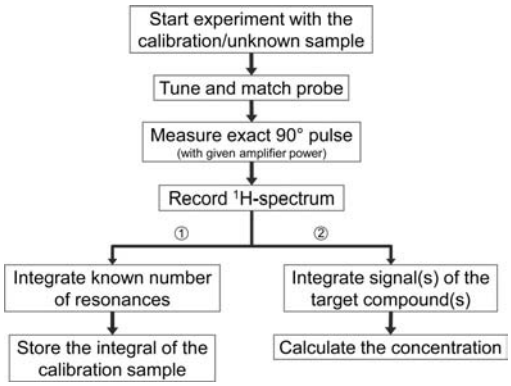

Figure 2. Working procedure for quantitation of target molecules by means of qHNMR using ERETIC 2: ①, calibration of the instrument; ②, concentration measurement according to the literature.[21,31]

Quality of the NMR Tubes. For the most reliable quantitative high-throughput analysis, the NMR tubes need to be as precise as possible to ensure a minimum difference in the active volume of the reference and the target sample. To investigate the error induced by technologically unavoidable differences between NMR tubes, five individual tubes, each containing a stock solution (600 μL) of benzoic acid (6.10 mmol/L) in a certified, highly pure form (NIST 350b, purity = 99.9978 ± 0.0044%), were analyzed using identical instrumental parameters. The experiments revealed a standard deviation of ±1.1% corresponding to the signal area, thus showing a maximum error of <2% caused by variations in the NMR tubes including the error from other sources such as deviations in integration, baseline, and phase correction, respectively.

Use of External Standard. For qHNMR, in principle, each nonvolatile and nonhygroscopic organic compound might be used as external standard if it is soluble and chemically stable in the respective solution and available in high purity. Preliminary studies demonstrated D_2O, D_2O/DCl (90:10, v/v), CD_3OD, DMSO-d_6, C_6D_6, and CD_3CN as the most suitable solvents, whereas volatile solvents such as CD_2Cl_2 and $CDCl_3$, respectively, cannot be recommended due to increasing errors caused by vaporizing effects during preparation of the stock solutions, pipetting, or spectroscopic measurement.

To check the quality of the NIST 350b reference benzoic acid stock solution in terms of precise initial balance, sample preparation, and NMR experiment, the concentrations of solutions of L-tyrosine (3.03 mmol/L, D_2O/DCl) and caffeine (3.12 mmol/L, D_2O), both with a purity >99%, were determined by using benzoic acid (2.98 mmol/L, D_2O) as the external standard. Using the working procedure given in Figure 2 excellent recovery rates of 99.8 and 99.3% were found for caffeine (3.12 mmol/L, D_2O) and L-tyrosine (3.03 mmol/L, D_2O/DCl). To check if caffeine or L-tyrosine was also an appropriate external standard, the spectrometer was calibrated with these compounds. When the spectrometer was calibrated with the caffeine solution (3.12 mmol/L), the recoveries for benzoic acid and L-tyrosine were 99.3 and 99.7% (Table 2). If L-tyrosine (3.03 mmol/L) was used for the calibration of the instrument, the concentration of the caffeine solution (3.12 mmol/L) determined by NMR was found to be 3.09 mmol/L, whereas NMR analysis of the benzoic acid stock solution (2.98 mmol/L) revealed a concentration of 2.95 mmol/L. These data clearly demonstrate each of these three compounds as a suitable calibrant for qHNMR experiments. Due to its low price, high purity, easy handling, and good solubility in a number of deuterated solvents, caffeine was selected as the most adequate candidate and used for the validation of the qHNMR method.

Pulse Sequence, Excitation Pulses, and Spin−Lattice Relaxation Time (T_1). As the qHNMR experiments were performed by using an external standard in a separate NMR tube, it is essential to use the same pulse sequence for the external standard sample as well as for the unknown analyte sample. Assuming full relaxation of all protons of interest, errors in calibration of the pulse length (τ) by an angle θ would reduce the intensity of the resonance signals by a factor of cos θ.[20] In qHNMR analysis with an internal standard, this error should affect all protons comparably, uniform excitation provided. As demonstrated in the literature, no major differences in precision and accuracy of the analytical results are expected when 30°, 45°, or 90° pulses are applied.[7,14,15] The subsequent analysis of a standard solution with a compound of known concentration and a compound to be quantitated requires a separate calibration of the pulse length for both samples, due to the influence of the solvent, concentration, salt content, etc., on the pulse length. Naturally the effect of deviations by calibration of pulses shorter than $\pi/2$ is higher compared to the 90° pulse; for example, a 1° error in a 30° pulse would result in an approximately 1% decrease of the signal intensity, whereas the same error in a 90° pulse causes only an error of <0.02%.[20] For that reason and to maximize sensitivity for all quantitative measurements, 90° pulses were used and, as a consequence, the longer interpulse delay accepted.

If the excitation is performed by a 90° pulse, all equilibrium z-magnetization is converted into detected transverse x,y-magnetization, and depending on the target molecule it is required to insert a long interpulse delay to allow the excited nuclei to re-establish their equilibrium z-magnetization prior to the application of the next pulse. This interpulse delay is generally set to 5 times the longest longitudinal or spin−lattice relaxation time (T_1) to avoid distortion of integrated signal intensity due to relaxation effects. The T_1 for protons in small molecules can range between 0.3 and >10 s and, therefore, accurate determination is fundamental for precise and reliable qHNMR results. T_1 can be determined by an inversion−recovery experiment, or at least estimated via successive prolongation of the relaxation delay until the integrated peak area remains constant compared to the fully relaxed external standard. The spin−lattice relaxation of the methine proton of caffeine resonating at 7.87 ppm via inversion recovery leads to a T_1 of 6.5 s and consequently to a relaxation delay of

approximately 35 s. Plotting the concentration determined by qHNMR against the relaxation delay revealed a constant peak area if the relaxation delay was ≈40 s and matched gravimetric value (data not shown). These data indicate that the inversion−recovery experiment and the successive prolongation of the relaxation delay revealed comparable results. If the calculation was performed by using one of the methyl groups of caffeine, an interpluse delay of 15 s was sufficient to provide fully relaxed signals, thus shortening analysis time by 50%. On the other hand, the individual determination of the T_1 relaxation for each molecule is quite time-consuming and, therefore, a relaxation delay of 40 s, suitable for most small molecules, could be set as a default value for quantitation of all compounds. This value was confirmed by the determination of spin−lattice relaxation for all protons of interest in our compounds via inversion−recovery.

Tuning and Matching. It is essential for obtaining a good signal-to-noise (S/N) ratio and, as a consequence, a high sensitivity that the probe is precisely tuned to the observe frequency and matched to 50 Ω resistive impedance to minimize RF reflection with the sample of interest. On the basis of the reciprocal relationship between excitation and observation, Mo and Raftery proposed that the relative receiving efficiency can be correlated to the 90° pulse (τ_{90}) length, if the probe is perfectly tuned and matched.[32] It is not a prerequisite that the probe is correctly tuned and matched to fulfill the principle of reciprocity, but it is a consequence of the fact that this is the only state which is reproducibly adjustable on each spectrometer. Therefore, we investigated next the influence of automatic tuning and matching versus manual tuning and matching on the precision of the observed analytical data. To achieve this, a benzoic acid solution (6.14 mmol/L in D_2O) was, therefore, measured five times with manual tuning and matching using the *atmm* function of the software and five times with the automatic tuning and matching using the *atma* command. Prior to the acquisition of the spectra, the wobble curve was randomly misadjusted and then readjusted manually (*atmm*) or automatically (*atma*), and the 90° pulse was determined by the command *pulsecal sn*. Manual tuning and matching resulted in an average concentration of 6.10 ± 0.027 mmol/L (τ_{90} = 13.06 μs ± 0.018), whereas automatic tuning and matching revealed a slightly lower average concentration of 5.94 ± 0.043 mmol/L (τ_{90} = 12.86 μs ± 0.149). Independent of the tuning/matching procedure, these results indicate a standard deviation of <2%, thus demonstrating a good precision by the use of both procedures. Comparing the gravimetric data to the averaged NMR experimental data showed a recovery of 96.7 and 99.3%, respectively, when using automatic or manual tuning and matching, thus demonstrating somewhat higher accuracy when the probe was adjusted manually.

Receiver Gain (rg) and Number of Scans (ns). The rg is used to match the amplitude of the FID to the dynamic range of the digitizer. Due to different solvents, residual water, or impurities, the rg values of the calibration and quantitation experiments could be different. Although the Avance III spectrometer is able to balance possible differences in the rg between the external standard sample and the analyte sample, the quality of its linearization was checked by analyzing an L-tyrosine solution (1.01 mmol/L in D_2O/DCl) at different rg values (4, 16, 64, 128, 203, 256, 322, 512, and 912). Plotting the value of the rg against the observed signal area showed an excellent correlation with a linear regression coefficient of r^2 = 0.9995 (Figure 3A). The calculation of the concentration by ERETIC 2 for each value of the rg and the recovery determined by comparison to the gravimetric value was within an error of ±2%.

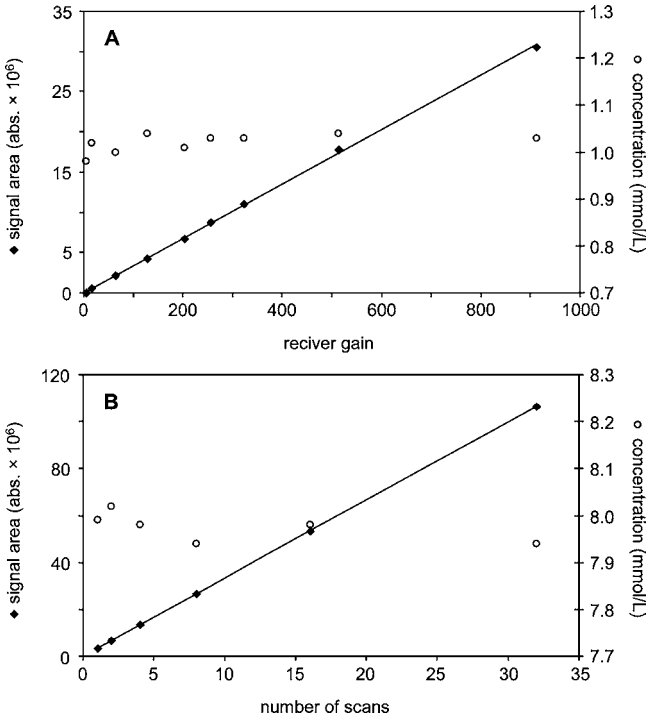

Figure 3. Quantitation of L-tyrosine samples on an Avance III spectrometer using ERETIC 2: (A) correlation between receiver gain (rg) and signal area and calculation of the concentration of L-tyrosine (1.01 mmol/L) at each rg value; (B) correlation between number of scans (ns) and signal area and calculation the concentration of L-tyrosine (8.03 mmol/L) at different ns.

Independent from the ns applied for the calibration experiment, ns applied on the analyte sample could be different. To obtain an adequate S/N ratio in low concentrated analyte samples, the ns has to be increased. In this case ERETIC 2 is able to compensate different ns used for the calibration sample and the sample of interest. To verify the quality of compensation, an L-tyrosine solution (8.03 mmol/L, D_2O) was analyzed with various ns values ranging from 1 to 32. Plotting the ns against the obtained signal area showed a regression coefficient r^2 = 1. Independent from the ns used, the calculated concentration by ERETIC 2 revealed concentrations between 7.94 and 8.02 mmol/L and, therefore, a maximum error of 1.1% (Figure 3B).

Limit of Quantitation (LOQ). As the LOQ depends on the ns, the number of nuclei generating a distinct proton signal, the shape of the signal, and its multiplicity, the LOQ was determined under predefined conditions. At a S/N ratio of 150 for the methyl group (3.55 ppm) of caffeine, obtained by using 16 scans on the 400 MHz instrument equipped with a BBFO probe, the LOQ was determined to be 0.2 mmol/L. The S/N of 150 was recommended in the literature for a target uncertainty of 1%; for an error limit of ±2% a S/N ratio of ≥40 is sufficient.[8] The LOQ can be further increased either by increasing the number of scans or by using higher field instruments equipped with a cryoprobe.

Linearity and Range of the Calibration Curve. To assess the linearity and range of the calibration curves, the

dx.doi.org/10.1021/jf405529b | J. Agric. Food Chem. 2014, 62, 2506−2515

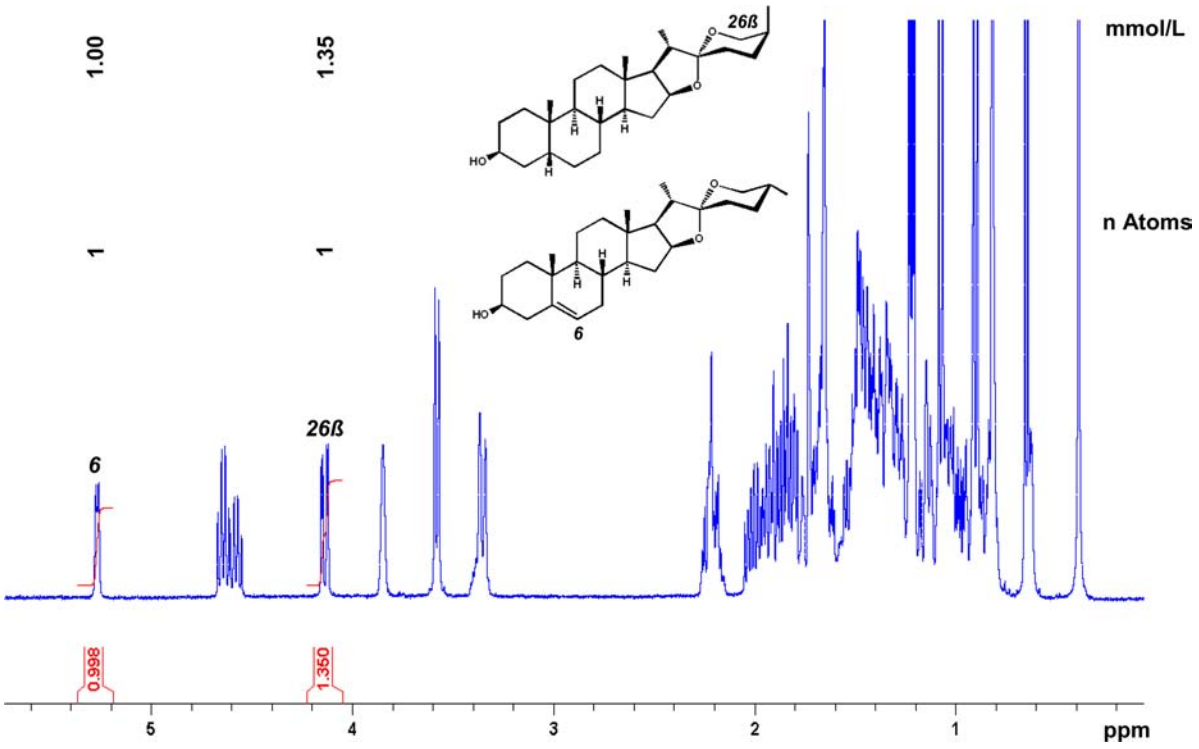

Figure 4. Quantitative ^{1}H NMR spectrum (400 MHz, benzene-d_6, 298 K) of a mixture of the steroidal sapogenins diosgenin and sarsasapogenin. Signal assignment was done according to the literature.[34,35]

reference compounds L-tyrosine (16.50, 8.25, 4.13, 2.06, 0.69, and 0.34 mmol/L), caffeine (15.90, 5.30, 2.65, 1.33, 0.66, and 0.33 mmol/L), and benzoic acid (16.30, 8.15, 3.26, 1.63, 0.82, and 0.33 mmol/L) were analyzed at the six different concentrations given in parentheses. The highest concentration was limited by the solubility of the compounds in the appropriate solvent, and the lowest concentration was somewhat above the limit of quantitation (LOQ). Plotting the experimentally determined data against the gravimetric values revealed linear regression coefficients of 1.00, 1.00, and 0.999 for L-tyrosine, benzoic acid, and caffeine, respectively (Table 3). The recovery of each individual calibration point was within an error limit of ±2%. These data clearly demonstrated an excellent linearity and recovery of the qHNMR method, independent from the compound used.

Accuracy. The accuracy of the qHNMR method was determined by analyzing solutions of benzoic acid (1.72, 6.14, and 16.21 mmol/L) and L-tyrosine (2.73, 7.33, and 9.99 mmol/L) using caffeine (3.12 mmol/L) as external standard and comparing the experimental data to those of gravimetry. The recoveries of benzoic acid were 98.8, 99.6, and 99.2%, whereas L-tyrosine revealed recoveries of 100.6, 100.7, and 100.9% (RSD < 2%).

Inter- and Intraday Precisions. The precision of the qHNMR method was determined by measuring intraday and interday variations of benzoic acid quantitation. Therefore, benzoic acid was analyzed at three different concentrations (5.91, 1.48, and 0.75 mmol/L), each in triplicates, on one day, and the same solutions were analyzed again on three subsequent days. Each measurement was preceded by removing the sample from the probe and replacing it again in the magnet. After equilibration, the probe was tuned, matched, and shimmed, and the 90° pulse was determined. When the measurements were performed at concentration levels of 5.91, 1.48, and 0.75 mmol/L, intraday precision revealed coefficients of variation (CV) of 0.6, 1.6, and 1.7%, respectively, and CVs for interday precision were 0.7, 1.6, and 1.3%.

Stability of Instrument Calibration. To study the long-term stability of the spectrometer calibration, a caffeine solution (2.65 mmol/L, CD_3OD) was used as calibrant and a 1.01 mmol/L L-tyrosine solution (D_2O/DCl) as the analyte solution. The multiplet resonating at 7.11 ppm was used for the quantitation with a S/N ratio of ≥48. Repeated analyses over a period of 6 months with periodically verified calibration prior to qHNMR analysis revealed recovery rates always >98% for the L-tyrosine solution over the entire period. These data clearly demonstrate an excellent long-term stability of the qHNMR analysis.

Influence of Operator on Analytical Robustness and Data Handling. The handling of the data by different operators is considered to be a main factor influencing the quality of qHNMR analyses.[8,11] As phase and baseline correction as well as signal integration are known as the most subjective procedures in qHNMR, three different operators (A−C) were asked to precisely follow the protocol shown in Figure 2 for data acquisition and to analyze a sample of L-tyrosine (4.94 mmol/L) without knowledge of the concentration on the calibrated spectrometer. For processing, automatic phase correction was performed by using *apk0.noe* or *apk*/*apks*. If the phase was not proper enough, a careful manual zero- and first-order phase correction was performed. Baseline correction was carried out using the command *absn*, integration was done manually, and, whenever required, the integrals were adjusted manually with the software functions SLOPE and BIAS. The concentration determined by operator A was 4.95 mmol/L (100.2%), whereas operators B and C found slightly decreased concentrations of 4.89 (99.0%) and 4.86 mmol/L (98.3%), respectively. Although these data

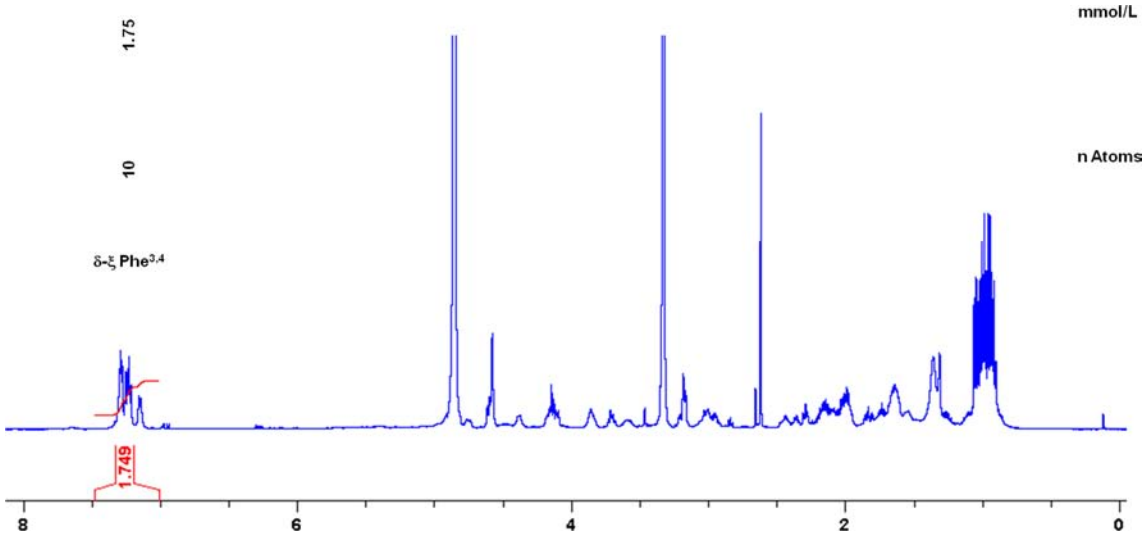

Figure 5. Quantitative ^{1}H NMR (400 MHz, methanol-d_4, 298 K) of cyclolinopeptide C, a cyclic octapeptide isolated from linseed oil. Signal assignment was done according to the literature.[36]

indicate a marginal influence of the operating individual on the qHNMR results, the protocol for acquisition and processing of the NMR data allowed an acceptable interindividual precision of ±2%.

Quantitation of Target Compounds in Reference Materials. To check the performance of the qHNMR method, solutions of a couple of chemical diverse commercial available compounds were prepared with defined concentrations ranging between 1.0 and 27.9 mmol/L in an appropriate deuterated solvent: the nitrogen-containing nicotinic acid, L-tyrosine, tyramine, caffeine, creatinine, and inosine; the polyphenols rutin and (*E*)-resveratrol; the saponins sarsasapogenin and diosgenin; the monoterpenes (−)-neomenthol and (+)-menthol; and the highly volatile odorants acetaldehyde and dimethyl sulfide, as well as the taste compounds sucrose and citric acid. The concentrations of these solutions (by gravimetry) were compared to the results obtained by qHNMR (Table 1). After data acquisition and processing, the recovery of most compounds was found to be between 98.1 and 101.1%, thus demonstrating a small error of ±2% of the method.

Moreover, a mixture of the steroidal sapogenins diosgenin and sarsasapogenin (1.00 and 1.37 mmol/L) was analyzed by qHNMR by integrating the two well-separated proton signals resonating at 5.27 and 4.14 ppm, respectively, representing proton H−C(6) of the olefinic double bond of diosgenin and H−C(26β) of the high-field shifted diastereotopic methylene proton of sarsasapogenin (Figure 4). The analysis showed excellent recovery for both compounds in the mixture (Table 1) with values of 98.5% for sarsasapogenin and 100% for diosgenin.

Compared to the nonvolatile substances, acetaldehyde and dimethyl sulfide showed somewhat lower recovery rates, most likely due to their high volatility during sample preparation. This could be partially overcome by cooling the compounds, NMR solvents, volumetric flasks, and pipets prior to the experiment; for example, the recovery rate for acetaldehyde could be increased from 80 to 93% when the equipment was cooled at 4 °C (Table 1). On the other hand, these data clearly indicate that preparing stock solutions of volatiles by using an analytical balance bears the risk of underestimating the analytical results due to the loss of compound quantity during preparation. This could be overcome by determining the concentration of such prepared solutions by qHNMR and will be helpful to improve the precision of analytical results of high volatiles such as aroma active compounds.

In another set of experiments, the qHNMR method was applied on synthesized stable isotope-labeled reference compounds, namely, *N*-methylpyridinium-d_3 (**1**), trigonelline-$^{13}C_1$ (**2**), tyramine-d_2 (**3**), and *S*-methylmethionine-d_3 (**4**) (Figure 1; Table 2) to be used for quantitative stable isotope dilution analysis (SIDA).[27,33] The purity of these stable isotope-labeled compounds was found to be between 98.0 and 100.5% (Table 2), indicating a high purity and, therefore, an excellent suitability as internal standards for SIDA. The counterion of salts such as *N*-methylpyridinum or trigonelline does not affect the concentration determination via qHNMR. In comparison, the use of an analytical balance for stock solution preparation can cause major errors when the nature of the counterion is unclear, for example, when such ionic compounds were isolated from natural sources such as foods, botanicals, or urine. Additional qHNMR experiments were performed with compounds isolated from natural sources. Solutions of the ribonucleotide 5′-GMP (**5**) isolated from yeast extract, the plant polyphenol resveratrol (**6**) purified form grape berry skins, and buchananiflavanone (**7**) and GB-2 (**8**) isolated from *Garchinia buchananii* bark, the emetic toxin cereulide (**9**) isolated from *Bacillus cereus*, and the cyclic octapeptide cyclolinopeptide C (**10**) from linseed oil were prepared after weighing and dissolving defined amounts of the isolate in NMR solvents. The concentrations of these solutions were compared to the instrumental data obtained by means of qHNMR (Table 2). Whereas the compounds **5**−**10** showed a purity of >95% by means of NMR spectroscopy, the concentrations determined by qHNMR showed in all cases significantly lower values between 70.0% (cyclolinopeptide C) and 91.6% (buchananiflavanone) compared to the concentration expected from the gravimetric preparation of the sample solutions. Although isolates **5**−**10** were freeze-dried twice after chromatographic purification, their ^{1}H NMR spectra showed considerable amounts of residual water (Figure 5) contributing to the initial sample weight and, as a consequence, leading to an under-

dx.doi.org/10.1021/jf405529b | J. Agric. Food Chem. 2014, 62, 2506−2515

estimation of the analytical results when using only the analytical balance for preparation of the stock solution of such a compound. In addition, the presence of inorganic material that is not detectable in the ^{1}H NMR spectrum could contribute to an increased sample weight and, therefore, a lower content of the target molecule in the weighted sample as expected; for example, the cyclic peptides cereulide (**9**) and cyclolinopeptide C (**10**) are known to complex monovalent inorganic cations with high affinity for potassium.

With all of these findings taken into conclusion, the presented qHNMR method is an excellent alternative to the use of previous quantitative NMR techniques using internal standards or artificial electronic signals for quantitative determination and allows a most precise and robust quantitation of organic target molecules in natural isolates and synthetic materials even in the presence of bound water or inorganic residues. As this methodology is able to deliver accurate quantitative data in <15 min per sample, it might be a valuable tool for the quantitation of natural isolates even of unknown molecular weight. This offers the advantage of directly comparing bioactivity data of individual isolates or fractions already in an early stage of bioassay-guided fractionation procedure.

■ ASSOCIATED CONTENT

Supporting Information

Table S1. This material is available free of charge via the Internet at http://pubs.acs.org.

■ AUTHOR INFORMATION

Corresponding Author

*(O.F.) Phone: +49-8161-712910. Fax: +49-8161-712949. E-mail: oliver.frank@tum.de.

Notes

The authors declare no competing financial interest.

■ REFERENCES

(1) Kaushal, R.; Kaur, N.; Upadhyay, A.; Suri, O. P.; Thakkar, A. High performance liquid chromatography detectors − a review. *Int. Res. J. Pharm.* **2011**, *2*, 1−7.

(2) Banerjee, S.; Mazumdar, S. Electrospray ionization mass spectrometry. A technique to access the information beyond the molecular weight of the analyte. *Int. J. Anal. Chem.* **2012**, *2012*, 40.

(3) Cappiello, A.; Famiglini, G.; Palma, P.; Pierini, E.; Termopoli, V.; Trufelli, H. Direct-EI in LC-MS: towards a universal detector for small molecule application. *Mass Spectrom. Rev.* **2011**, *30*, 1242−1255.

(4) Swartz, M. HPLC detectors: a brief review. *J. Liq. Chromatogr. Relat. Technol.* **2010**, *33*, 1130−1150.

(5) Pauli, G. F. qHNMR − a versatile concept for validation of natural product reference compounds. *Phytochem. Anal.* **2001**, *12*, 28−42.

(6) Berregi, I.; Santos, S. I.; del Campo, G.; Miranda, J. I.; Aizpurua, J. A. Quantitation determination of chlorogenic acid in cider apple juices by ^{1}H NMR spectrometry. *Anal. Chim. Acta* **2003**, *486*, 269−274.

(7) Pauli, G. F.; Jaki, B. U.; Lankin, D. C. Quantitative ^{1}H NMR: development and potential of a method for natural products analysis. *J. Nat. Prod.* **2005**, *68*, 133−149.

(8) Malz, F.; Jancke, H. Validation of quantitative NMR. *J. Pharm. Biomed. Anal.* **2005**, *38*, 813−823.

(9) Shao, G.; Kautz, R.; Peng, S.; Cui, G.; Giese, R. W. Calibration by NMR for quantitative analysis: *p*-toluenesulfonic acid as a reference substance. *J. Chromatogr., A* **2008**, *1138*, 305−308.

(10) Liu, S.-Y.; Hu, C.-Q. A comparative uncertainty study of the calibration of macrolide antibiotic reference standards using quantitative nuclear magnetic resonance and mass balance methods. *Anal. Chim. Acta* **2007**, *602*, 114−121.

(11) Bekiroglu, S.; Myrberg, O.; Östman, K.; Ek, M.; Arvidsson, T.; Rundlöf, T.; Hakkarainen, B. Validation of quantitative NMR method for suspected counterfeit products exemplified on determination of benzethonium chloride in grapefruit seed extracts. *J. Pharm. Biomed. Anal.* **2008**, *47*, 958−961.

(12) Sharma, R.; Gupta, P. K.; Mazumder, A.; Dubey, D. K.; Ganesan, K.; Vijayaraghavan, R. A quantitative NMR protocol for the simultaneous analysis of atropine and obidoxime in parenteral injection devices. *J. Pharm. Biomed. Anal.* **2009**, *49*, 1092−1096.

(13) Holzgrabe, U. Quantitative NMR spectroscopy in pharmaceutical applications. *Prog. Nucl. Magn. Reson. Spectrom.* **2010**, *57*, 229−240.

(14) Pieri, V.; Belancic, A.; Morales, S.; Stuppner, H. Identification and quantification of major steviol glycosides in *Stevia rebaudiana* purified extracts by ^{1}H NMR spectroscopy. *J. Agric. Food Chem.* **2011**, *59*, 4378−4384.

(15) Neumüller, K. G.; Carvalho de Souza, A.; Van Rijn, J.; Appeldoorn, M. M.; Streekstra, H.; Schols, H. A.; Gruppen, H. Fast and robust method to determine phenoyl and acetyl esters of polysaccharides by quantitative ^{1}H NMR. *J. Agric. Food Chem.* **2013**, *61*, 6282−6287.

(16) Akoka, S.; Barantin, L.; Trierweiler, M. Concentration measurement by proton NMR using the ERETIC method. *Anal. Chem.* **1999**, *71*, 2554−2557.

(17) Billault, I.; Robins, R.; Akoka, S. Determination of deuterium isotope ratios by quantitative ^{2}H NMR spectroscopy: the ERETIC method as a generic reference signal. *Anal. Chem.* **2002**, *74*, 5902−5906.

(18) Henderson, T. J. Quantitative NMR spectroscopy using coaxial inserts containing a reference standard: purity determinations for military nerve agents. *Anal. Chem.* **2002**, *74*, 191−198.

(19) Hoult, D. I.; Richards, R. E. The signal-to-noise ratio of the nuclear magnetic resonance experiment. *J. Magn. Reson.* **1976**, *24*, 71−85.

(20) Burton, I. W.; Quilliam, M. A.; Walter, J. A. Quantitative ^{1}H NMR with external standards: use in preparation of calibration solutions for algal toxins and other natural products. *Anal. Chem.* **2005**, *77*, 3123−3131.

(21) Wider, G.; Dreier, L. Measuring protein concentrations by NMR spectroscopy. *J. Am. Chem. Soc.* **2006**, *128*, 2571−2576.

(22) Korn, M.; Frank, O.; Hofmann, T.; Rychlik, M. Development of stable isotope dilution assay for ochratoxin A in blood samples. *Anal. Biochem.* **2011**, *419*, 88−94.

(23) Somoza, V.; Lindenmeier, M.; Wenzel, E.; Frank, O.; Erbersdobler, H. F.; Hofmann, T. Activity-guided identification of a chemopreventive in coffee using in vitro and in vivio techniques. *J. Agric. Food Chem.* **2003**, *51*, 6861−6869.

(24) Chiusa, W.; Nebbia, G. The preparation of salts of *N*-methylnicotinic acid. *Gaz. Chim. Ital.* **1950**, *80*, 98−99.

(25) Hothi, P.; Hay, S.; Roujeinikova, A.; Sutcliffe, M.; Lee, M.; Leys, D.; Scrutton, N. Driving force analysis of proton tunnelling across a reactivity series for an enzyme-substrate complex. *ChemBioChem* **2008**, *9*, 2839−2845.

(26) Boyle, P. H.; Davis, A. P.; Dempsey, K. J.; Hosken, G. D. Synthesis of (*S*)-2-amino-1,1-diphenylbutan-4-ol; conversion of an α-amino acid into an α-(diphenylmethyl) amine without loss of optical purity. *Tetrahedron Asymmetry* **1995**, *6*, 2819−2828.

(27) Festring, D.; Hofmann, T. Dicovery of N^2-(1-carboxyethyl)-guanosine 5′-monophosphate as an umami-enhancing Maillard-modified nucleotide in yeast extracts. *J. Agric. Food Chem.* **2010**, *58*, 10614−10622.

(28) Romero-Pérez, A. I.; Lamuela-Raventós, R. M.; Andrés-Lacueva, C.; de la Torre-Boronat, M. C. Method for the quantitative extraction of resveratrol and piceid isomers in grape berry skins. Effect of powdery mildew on the stilbene content. *J. Agric. Food Chem.* **2001**, *49*, 210−215.

(29) Stark, T. D.; Matsumoto, T.; Lösch, S.; Boakye, P. A.; Balemba, O. B.; Pasilis, S. P.; Hofmann, T. Isolation and structure elucidation of highly antioxidative 3,8″-linked biflavanones and flavanone-C-glycosides from *Garcinia buchananii* bark. *J. Agric. Food Chem.* **2012**, *60*, 2053−2062.
(30) Bauer, T.; Stark, T.; Hofmann, T.; Ehling-Schulz, M. Development of a stable isotope dilution analysis for the quantification of the *Bacillus cereus* toxin cereulide in foods. *J. Agric. Food Chem.* **2010**, *58*, 1420−1428.
(31) Bruker ERETIC 2 User's Guide − Preliminary.
(32) Mo, H.; Raftery, D. Solvent signal as an NMR concentration reference. *Anal. Chem.* **2008**, *80*, 9835−9839.
(33) Lang, R.; Yagar, E. F.; Eggers, R.; Hofmann, T. Quantitative investigation of trigonelline, nicotinic acid, and nicotinamide in foods, urine, plasma by means of LC-MS/MS and stable isotope dilution analysis. *J. Agric. Food Chem.* **2008**, *56*, 11114−11121.
(34) Puri, R.; Wong, T. C.; Puri, R. K. Solasodine and diosgenine: ^{1}H and ^{13}C assignments by two-dimensional NMR spectroscopy. *Magn. Reson. Chem.* **1993**, *31*, 278−282.
(35) Agrawal, P. K.; Bunsawansong, P.; Morris, G. A. Complete assignment of the ^{1}H and ^{13}C NMR spectra of steroidal sapogenins: smilagenin and sarsasapogenin. *Magn. Reson. Chem.* **1997**, *35*, 441−446.
(36) Morita, H.; Shishido, A.; Matsumoto, T.; Itokawa, H.; Takeya, K. Cyclolinopeptides B−E, new cyclic peptides from *Linum usitatissimum*. *Tetrahedron* **1999**, *55*, 967−976.

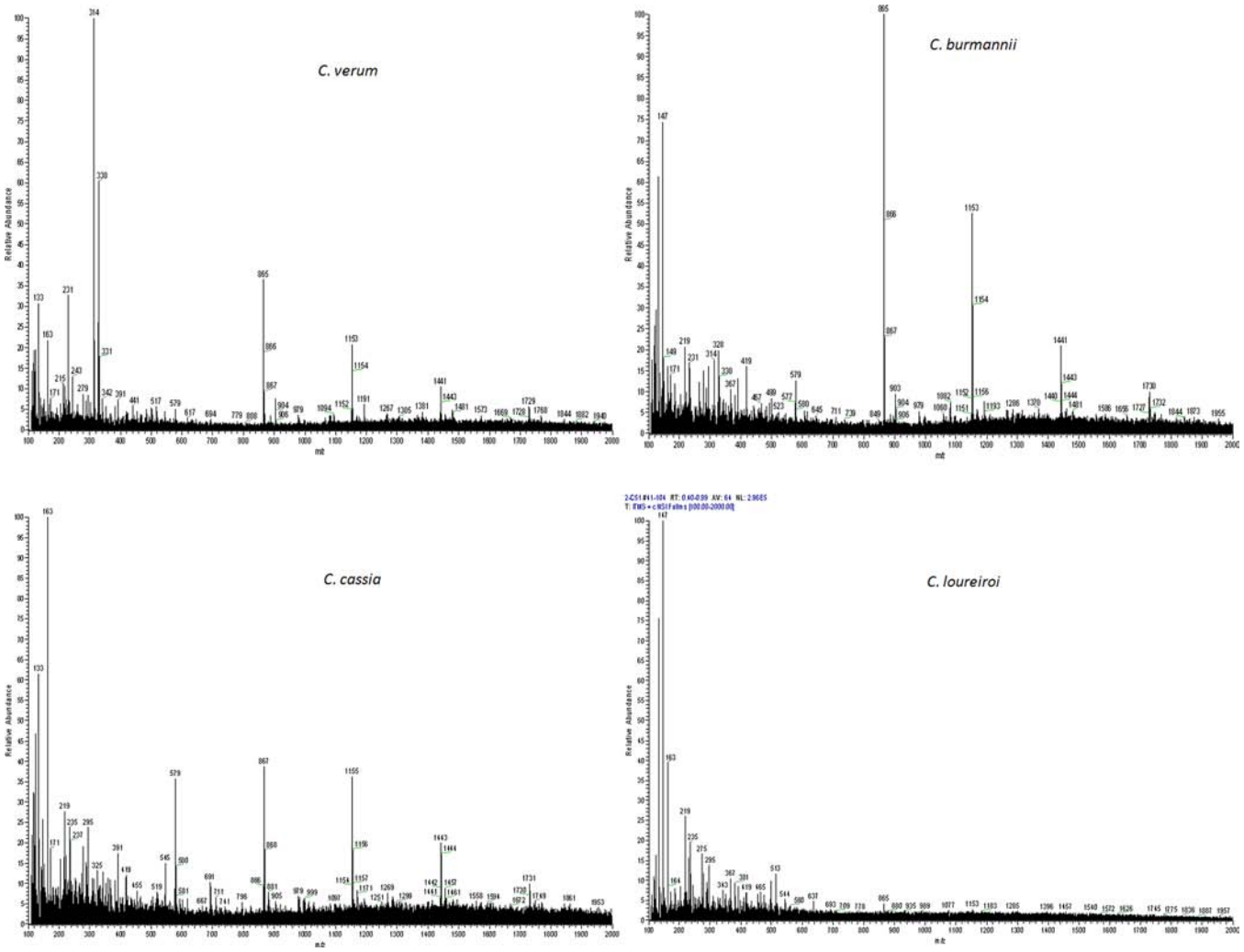

Figure 1. Typical FIMS spectra of the four species of cinnamon.

botanical materials and, consequently, place the technique on a sound statistical base. The patterns of the FIMS fingerprints (spectra with no prior separation) have been successfully used to distinguish plant genera, species, and even farming methods.[14−17] Use of the FIMS fingerprints and principal component analysis (PCA) or analysis of variance (ANOVA) prevents undue reliance on one or two marker compounds, increases the robustness of the analysis, and provides for both visual display and statistical evaluation of the data. Another advantage of the method is the fast method development time (hours) and analysis time (1 min) compared to traditional liquid chromatography−mass spectrometry (LC-MS), which can take days to weeks for method development and up to 1 h or longer for sample analysis of various natural products. A shortcoming of the FIMS technique is that it may not provide all of the information available through a full LC-MS analysis. Therefore, the combination of using both the FIMS fingerprinting technique and LC-MS on selected samples (determined by FIMS) will often be the best approach.

EXPERIMENTAL PROCEDURES

Materials. Fifty authentic cinnamon samples (3 *C. verum*, CV; 2 *C. cassia*, CC; 40 *C. burmannii*, CB; and 5 *C. loureiroi*, CL) and 3 unknown cinnamon samples (CU) were obtained from the library of McCormick & Co., Inc. (Sparks, MD, USA). At the time of the study, cinnamon, typically in the form of bark or chips, was ethylene oxide (ETO) treated and dried if necessary to constant moisture (typically 10−14%) and stored. The samples (collected in 2009−2011) were sourced and vetted through the company's global sourcing division, and the identity of each sample was confirmed by McCormick's internal chemotaxonomic methods. Samples were ground in a Schutte Hammermill (model 24-15-301) or a Brinkman Restch ZM-1 centrifugal mill and passed through a 20 mesh sieve. The ground samples were stored at room temperature in sealed glass jars until use. An additional test cinnamon sample (label claim CL) was purchased in a local supermarket in Maryland.

Water, acetonitrile, and methanol were of Optima grade (Fisher Scientific, Pittsburgh, PA, USA). Formic acid was of mass spectrometry grade (Sigma-Aldrich, St. Louis, MO, USA).

Sample Preparation. All samples were first passed through a 20 mesh sieve. Next, 10 mg of each dried ground sample was mixed with 5 mL of methanol/water (6:4 by volume) in a 15 mL centrifuge tube. All samples were sonicated for 20 min at room temperature. The sample extract was centrifuged at 5000*g* for 15 min (IEC Clinical Centrifuge, Danon/IEC Division, Needham Heights, MA, USA). The supernatant was filtered through a 17 mm (0.45 μm) PVDF syringe filter (VWR Scientific, Seattle, WA, USA). The cinnamon samples were labeled CV01−CV04 for *C. verum*, CC01 and CC02 for *C. cassia*, CB01−CB 40 for *C. burmannii*, CL01−CL05 for *C. loureiroi*, and CU01−04 for unknown and test cinnamon samples.

To avoid errors arising from unexpected degradation of some phenolic compounds, the sample analysis was completed within 24 h of the extraction. The injection volume for all samples was 5 μL. Each

sample was analyzed three times for the FIMS experiment. Representative samples from each species were analyzed one time for the UHPLC-HRMS experiment. Samples were run in randomized order.

Flow Injection Mass Spectrometry. The FIMS system consisted of a LCQ DecaXP ion-trap mass spectrometer (Thermo Fisher Scientific Inc., Waltham, MA, USA) with an Agilent 1200 HPLC system (a quaternary pump with a vacuum degasser, a thermostated column compartment, an autosampler, and a diode array detector (DAD) (Agilent Technologies, Palo Alto, CA, USA). The flow injection was passed through a guard column (Adsorbosphere All-Guard Cartridge, C18, 5 μm, 4.6 × 7.5 mm, Alltech Associates, Inc., Deerfield, IL, USA) to minimize potential contamination for the MS system. Mobile phases consisted of 0.1% formic acid in H_2O (A) and 0.1% formic acid in acetonitrile (B) with isocratic elution at 60:40 (v/v) at a flow rate of 0.5 mL/min for 1.5 min. Electrospray ionization (ESI) was performed in positive ion mode from m/z 100 to 2000 to obtain the FIMS fingerprints. The acquisition mode was centroid. The following conditions were used for the DecaXP mass spectrometer: sheath gas flow rate, 80 (arbitrary units); auxiliary gas flow rate, 10 (arbitrary units); spray voltage, 4.50 kV; heated capillary temperature, 220 °C; capillary voltage, 4.0 V; tube lens offset, 25 V. Spectra were summed from 0.4 to 1.0 min interval required for the sample bolus to enter the MS. Three repeat analyses of the 54 different samples provided 162 spectra.

Data Processing for FIMS Fingerprint. The mass spectrum for each sample consisted of a one-dimensional matrix (ion counts versus mass for m/z 100−2000). The spectra were exported to Excel (Microsoft, Inc., Belleview, WA, USA) from Xcalibur for data preprocessing and then to SOLO (eigenvector Research, Inc., Wenatchee, WA, USA) for PCA. The preprocessing in Microsoft Excel involved combining the 162 spectra, sorting the data by sample names, deleting unnecessary and redundant information (headers, sample information, instrument information, etc.), and aligning the masses (each spectrum was a different length because not all masses appeared in each spectra) using a MS Excel macro written in house. The resulting two-dimensional 162 × 1901 matrix (162 samples versus 1901 masses) was then exported to SOLO for PCA. Preprocessing in SOLO, prior to PCA, consisted of normalization (sum of squares of the counts for a spectra was set to 1) and mean centering.

Ultrahigh-Performance Liquid Chromatography−High-Resolution Mass Spectrometry (UHPLC-HRMS). The UHPLC-HRMS system consists of a Thermo LTQ Orbitrap XL mass spectrometer with an Accela 1250 binary pump, a PAL-HTC-Accela1 autosampler, an Accela 1250 PDA detector, and an Agilent column compartment (G1316A). The separation was carried out on a Thermo Hypersil Gold C18 column (200 μm × 2.1 mm, 1.9 μm) with a flow rate of 0.35 mL/min. The column heater was kept at 50 °C. Mobile phase A consisted of 0.1% formic acid in water, and mobile phase B consisted of 0.1% formic acid in acetonitrile. The elution gradient ranged from 10 to 25% mobile phase B over 0−7 min, from 25 to 40% B over 7−10 min, from 40 to 95% B over 10−12 min, and was held at 95% B for an additional 6 min with subsequent return to initial conditions. Electrospray ionization (ESI) was performed in the positive ion mode to obtain the HRMS data. The HRMS conditions were as follows: sheath gas, 70 arbitrary units; auxiliary and sweep gas, 15 arbitrary units; spray voltage, 4.0 kV; capillary temperature, 300 °C; capillary voltage, 15 V; and tube lens offset voltage, −70 V. The mass range was from m/z 100 to 2000 with a resolution of 15000, isolation width of 1.5 amu, and maximum ion injection time of 500 ms. The most intense ion was selected for the data-dependent scan with a normalization collision energy at 35%.

■ RESULTS AND DISCUSSION

FIMS Fingerprints of the Cinnamon Samples. The first goal of this study was to differentiate the four different species of cinnamon samples without chromatography. No analytical column was used, only a C_{18} reverse-phase guard column as an online filter to protect the MS. The FIMS fingerprint for each sample was obtained as the average of all spectra between 0.4 and 1.0 min. Typical FIMS fingerprints of the four species of cinnamon samples are shown in Figure 1. The differences among the four species of cinnamon are quite obvious visually even though no chromatographic separation was performed. The most notable ions for CV are at m/z 314, 330, 865, and 1153; those for CB are at m/z 133, 147, 865, and 1153; those for CC are at m/z 163, 579, 867, and 1155; and those for CL are at m/z 133, 147, and 163. Some observations from inspection of the spectra are as follows: (1) the ions at m/z 314 and 320 dominate the CV spectrum; (2) the ions at m/z 147 and 865 dominate the CB spectrum; (3) the ion at m/z 163 dominates the CC spectrum; and (4) the CL spectrum has relatively low ion counts for the high atomic mass unit molecular ions.

PCA of the FIMS Fingerprints. The advantage of using PCA to process the MS fingerprints is automation and simplification. It is easy to visually compare the mass spectra of a few samples, but the comparison of hundreds of samples quickly overwhelms our ability to discriminate useful patterns. PCA provides visual patterns that are math-based but still aesthetically and statistically useful, avoiding subjective interpretations of the data.

The PCA score plot showed the 54 cinnamon samples in four different groups (Figure 2). The three CV samples (in triplicate) did not cluster very tightly, occupying a larger area from the right to the middle of the plot, but were still separated from the other groups. The PCA score plot also successfully categorized the unknown samples. For example, three samples were categorized as *C. cassia* (CC) and the remaining sample was identified as *C. loureiroi* (CL), confirming the label claim.

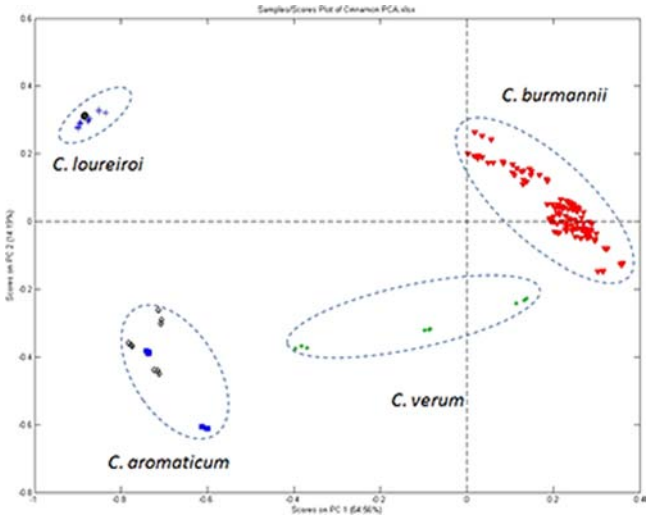

Figure 2. PCA score plot (for FIMS fingerprints) of the four species of cinnamon (▽, CB; ∗, CV; ■, CC; +, CL; ◇, unknown from McCormick; ●, unknown commercial, labeled CL).

PCA Loadings and UHPLC-HRMS Studies. The loading plot of a variable on a PCA reflects how much each of the variables contributed to that PC. The PC1 loading plot of the samples is shown in Figure 3. The plot indicates samples with higher ion counts at m/z 865, 903, 1154, and 1442 would yield a higher PC1 score, leading to positions toward the right of the PCA score plot. The important ions contributing to negative PC1 scores were m/z 133, 147, 275, 381, 465, and 513. This suggests the high molecular weight ions (m/z 865, 904, 1192,

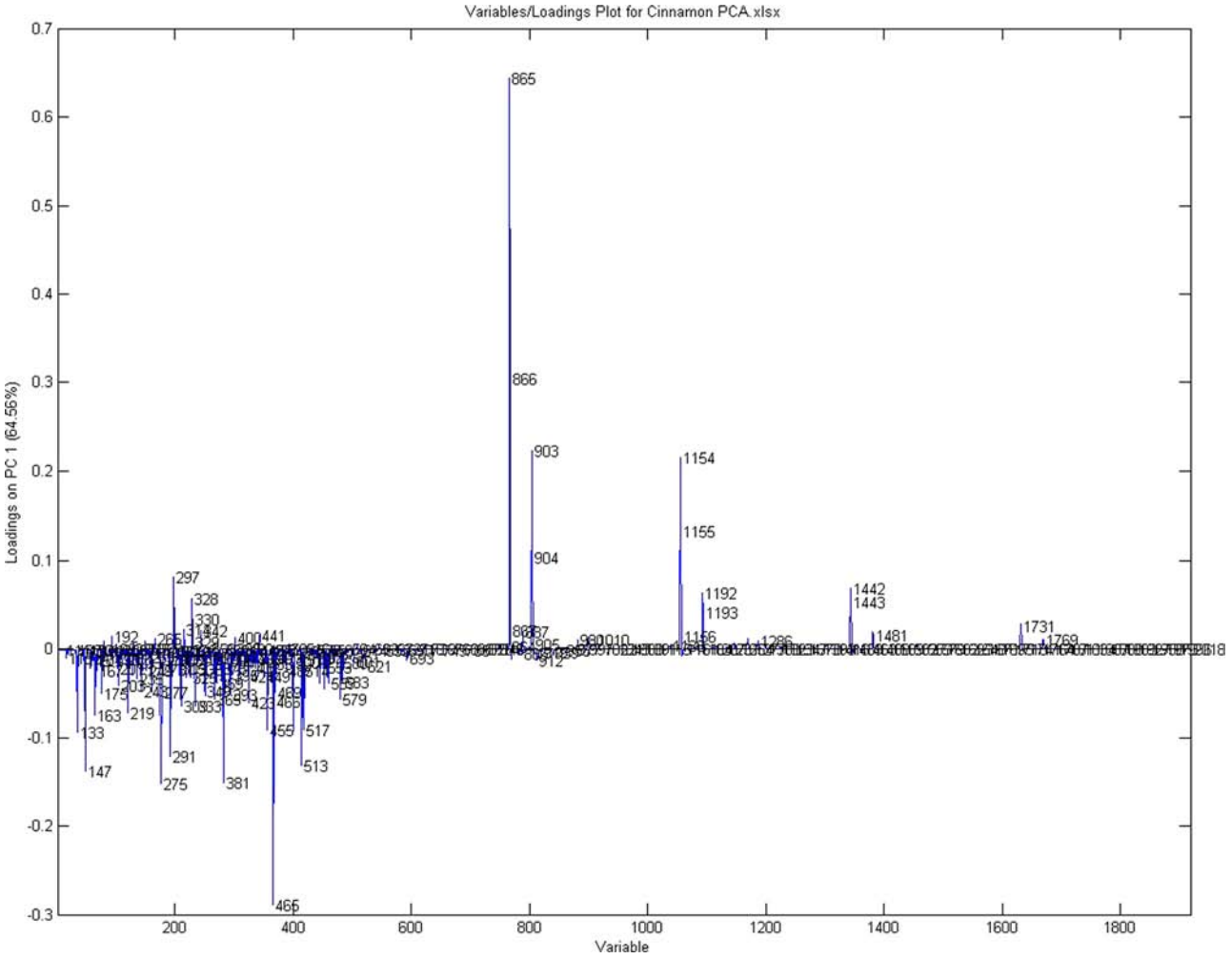

Figure 3. PCA loading plot of PC1 for FIMS fingerprints.

and 1442) tend to position the samples to the right of the PCA score plot, whereas the low molecular weight ions shifted sample positions more to the left side of the plots.

The above-mentioned ions from the PCA loading plot were further studied using UHPLC-HRMS. The HRMS measurements of the ion at *m/z* 865, 1154, and 1442 gave accurate masses of 865.1981 ($C_{45}H_{37}O_{18}$, 0.785 ppm), 1153.2629 ($C_{60}H_{49}O_{24}$, 1.796 ppm), and 1441.3259 ($C_{75}H_{61}O_{30}$, 0.785 ppm). MS^2 and MS^3 experiments were performed on these ions (spectra shown in the Supporting Information). The occurrence of an ion at *m/z* 287 in the MS^2 or MS^3 spectrum is an indication of the doubly linked A-type catechin/epicatechin oligomers, which contain $C_4 \rightarrow C_8$ carbon and $C_2 \rightarrow O \rightarrow C_7$ ether bonds. For example, the ion at *m/z* 865 had MS^2 fragments at *m/z* 533, 713, 453, and 287, in addition to the neutral losses of 286, 288, and 290, indicating it is an A-type trimer proanthocyanin, which has been previously reported.[18,19] Similarly, ions at *m/z* 1153.2629 and 1441.3259 were identified as A-type tetramers and pentamers, respectively. The HRMS measurements of the ions at *m/z* 133 and 147 gave accurate masses of 133.0646 (C_9H_9O, −1.061 ppm) and 147.0439 ($C_9H_7O_2$, −1.061 ppm). A literature paper[20] and our own data from the MS^2 studies (Supporting Information) confirmed these two ions represent the cinnamon components cinnamaldehyde and coumarin.

The PC2 loading plot of the samples is shown in Figure 4. The plot indicates samples with high ion counts at*m/z* 147, 465, 499, 513, and 865 yield a higher PC2 score, which would lead to positioning at the top of the PCA score plot. The ions contributing the most to the negative PC1 score were at *m/z* 579, 867, and 1156. The HRMS measurements of these ions indicate the formulas $C_{30}H_{27}O_{12}$ (*m/z* 579.1501, 0.447 ppm), $C_{45}H_{39}O_{18}$ (*m/z* 867.2134, 0.349 ppm), and $C_{60}H_{51}O_{24}$ (*m/z*1155.2782, 1.721 ppm). Using the *m/z* 579.1501 ion as an example, it fragmented into *m/z* 451, 427, 409, and 291 (17−26%), consistent with the report of procyanidins B_1. Similarly, ions *m/z* 867.2134 and 1155.2782 were identified as a B-type trimer and tetramer, respectively (Figure S2 in the Supporting Information).

These ions were ultimately identified as the dimer, trimer, and tetramers of B-type proanthocyanidins in cinnamon.[13]

To summarize, the coumarin and A-type proanthocyanidins give higher PC2 scores, whereas the B-type proanthocyanidins give lower PC2 scores, thus demonstrating different PCA groupings for the samples containing these profiles.

The ions at *m/z* 465, 499, and 513 are all very small peaks in the UHPLC-HRMS chromatograms. They are only visible using extracted ion mode. Regardless, it is not unusual for a relatively minor component that plays a significant role in PCA to be more visible in the FIMS spectrum than in an UHPLC-HRMS chromatogram.[17]

dx.doi.org/10.1021/jf405580c | *J. Agric. Food Chem.* 2014, 62, 2516−2521

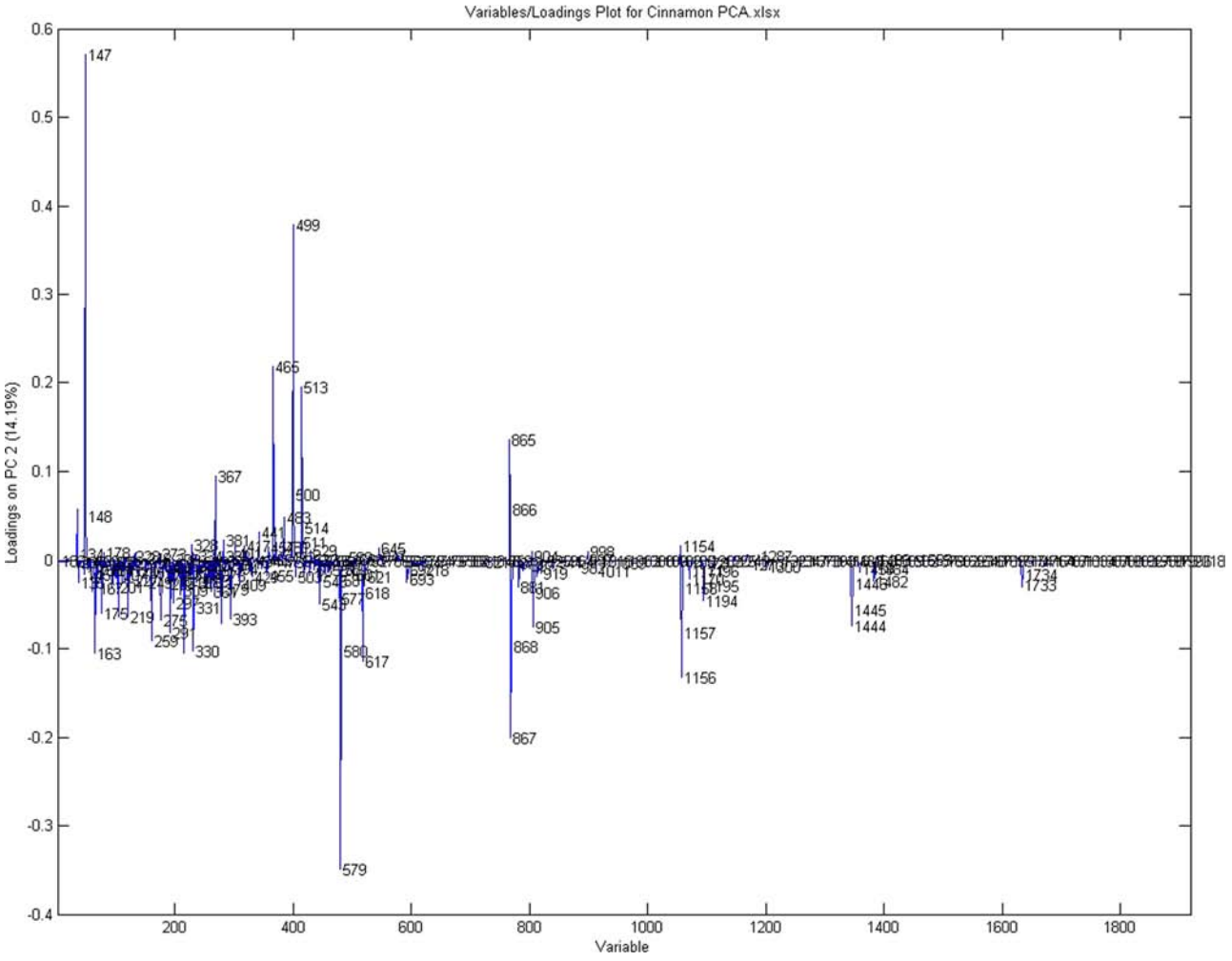

Figure 4. PCA loading plot of PC2 for FIMS fingerprints.

On a further note, it is common to observe that feeding studies and clinical trials involving natural products and their extracts give different or inconsistent test results. Cinnamon studies are no exception. Khan et al. found that cinnamon improves glucose and lipid levels of people with type 2 diabetes.[10] However, Loon's group did not reach this same conclusion.[21] Both groups claimed to use CC in their studies, but neither group attempted to identify the cinnamon samples by source or characterize the composition of the cinnamon samples before administering their respective studies. Thus, it is impossible to tell how different their respective samples are chemically and if the cinnamon used was actually CC or not. Another interesting observation is that the type-A proanthocyanidins isolated from CB were speculated to have insulin-like biological activity.[11] Yet both of the human feeding studies used CC, which contained more type-B than type-A proanthocyanidins. There was no explanation of why CC was chosen for both studies instead of CB or CV, nor were there any reports on the comparison of different cinnamon samples in human studies. The results from the present study clearly show the chemical composition differences between the four species of cinnamon samples. If the assumption is type-A proanthocyanidins have more insulin-like activity, then clearly CB or CV should be expected to perform better in human studies or biological assays, and CL would be the least effective. The results from this study show the importance of analytically determining the chemical composition of the samples when feeding studies are designed.

This study demonstrates a simple, fast, and reliable analytical method that can be used to differentiate four different species of cinnamons. Not only can the method be used for botanical authentication in food supply chains, it also can be used to help design better, more meaningful, and insightful feeding studies or assays, especially when combined with the UHPLC-HRMS method. The data suggested a model system in which the FIMS fingerprinting method is used to screen many samples quickly, whereas representative samples from a group and outlier samples are analyzed using the UHPLC-HRMS method to provide detailed information about a sample's unique chemical composition.

■ ASSOCIATED CONTENT

Ⓢ Supporting Information

Figures S1−S9. This material is available free of charge via the Internet at http://pubs.acs.org.

■ AUTHOR INFORMATION

Corresponding Author

*(P.C.) E-mail: pei.chen@ars.usda.gov.

Funding

This research is supported by the Agricultural Research Service of the U.S. Department of Agriculture and an Interagency

Agreement with the Office of Dietary Supplements of the National Institutes of Health (Grant Y01 OD001298-01).

Notes

The authors declare no competing financial interest.

REFERENCES

(1) Killday, K. B.; Davey, M. H.; Glinski, J. A.; Duan, P.; Veluri, R.; Proni, G.; Daugherty, F. J.; Tempesta, M. S. Bioactive A-type proanthocyanidins from *Cinnamomum cassia*. *J. Nat. Prod.* **2011**, *74* (9), 1833−1841.

(2) Mancini-Filho, J.; Van-Koiij, A.; Mancini, D. A.; Cozzolino, F. F.; Torres, R. P. Antioxidant activity of cinnamon (*Cinnamomum zeylanicum*, Breyne) extracts. *Boll. Chim. Farm.* **1998**, *137* (11), 443−447.

(3) Mathew, S.; Abraham, T. E. Studies on the antioxidant activities of cinnamon (*Cinnamomum verum*) bark extracts, through various in vitro models. *Food Chem.* **2006**, *94* (4), 520−528.

(4) Shan, B.; Cai, Y. Z.; Brooks, J. D.; Corke, H. Antibacterial properties and major bioactive components of cinnamon stick (*Cinnamomum burmannii*): activity against foodborne pathogenic bacteria. *J. Agric. Food Chem.* **2007**, *55* (14), 5484−5490.

(5) Ooi, L. S.; Li, Y.; Kam, S. L.; Wang, H.; Wong, E. Y.; Ooi, V. E. Antimicrobial activities of cinnamon oil and cinnamaldehyde from the Chinese medicinal herb *Cinnamomum cassia* Blume. *Am. J. Chin. Med.* **2006**, *34* (3), 511−522.

(6) Baker, W. L.; Kluger, J.; Gutierrez-Williams, G.; Coleman, C. I.; White, C. M. Effect of cinnamon on glucose control and lipid parameters. *Diabetes Care* **2008**, *31* (1), 41−43.

(7) Anderson, R. A. Chromium and polyphenols from cinnamon improve insulin sensitivity. *Proc. Nutr. Soc.* **2008**, *67* (1), 48−53.

(8) Khan, A.; Bryden, N. A.; Polansky, M. M.; Anderson, R. A. Insulin potentiating factor and chromium content of selected foods and spices. *Biol. Trace Elem. Res.* **1990**, *24* (3), 183−188.

(9) Anderson, R. A. Nutritional factors influencing the glucose/insulin system: chromium. *J. Am. Coll. Nutr.* **1997**, *16* (5), 404−410.

(10) Khan, A.; Safdar, M.; Khan, M. M. A.; Khattak, K. N.; Anderson, R. A. Cinnamon improves glucose and lipids of people with type 2 diabetes. *Diabetes Care* **2003**, *26* (12), 3215−3218.

(11) Anderson, R. A.; Broadhurst, C. L.; Polansky, M. M.; Schmidt, W. F.; Khan, A.; Flanagan, V. P.; Schoene, N. W.; Graves, D. J. Isolation and characterization of polyphenol type-A polymers from cinnamon with insulin-like biological activity. *J. Agric. Food Chem.* **2004**, *52* (1), 65−70.

(12) Corder, R.; Mullen, W.; Khan, N. Q.; Marks, S. C.; Wood, E. G.; Carrier, M. J.; Crozier, A. Oenology: red wine procyanidins and vascular health. *Nature* **2006**, *444* (7119), 566.

(13) Lu, Z. L.; Jia, Q.; Wang, R.; Wu, X. M.; Wu, Y. C.; Huang, C. G.; Li, Y. M. Hypoglycemic activities of A- and B-type procyanidin oligomer-rich extracts from different cinnamon barks. *Phytomedicine* **2011**, *18* (4), 298−302.

(14) Chen, P.; Harnly, J. M.; Lester, G. E. Flow injection mass spectral fingerprints demonstrate chemical differences in Rio Red grapefruit with respect to year, harvest time, and conventional versus organic farming. *J. Agric. Food Chem.* **2010**, *58* (8), 4545−4553.

(15) Chen, P.; Lin, L. Z.; Harnly, J. M. Mass spectroscopic fingerprinting method for differentiation between *Scutellaria lateriflora* and the germander (*Teucrium canadense* and *T. chamaedrys*) species. *J. AOAC Int.* **2010**, *93* (4), 1148−1154.

(16) Chen, P.; Harnly, J. M.; Harrington Pde, B. Flow injection mass spectroscopic fingerprinting and multivariate analysis for differentiation of three *Panax* species. *J. AOAC Int.* **2011**, *94* (1), 90−99.

(17) Sun, J.; Chen, P. A flow-injection mass spectrometry fingerprinting method for authentication and quality assessment of *Scutellaria lateriflora*-based dietary supplements. *Anal. Bioanal. Chem.* **2011**, *401* (5), 1577−1584.

(18) Jayaprakasha, G. K.; Ohnishi-Kameyama, M.; Ono, H.; Yoshida, M.; Jaganmohan Rao, L. Phenolic constituents in the fruits of *Cinnamomum zeylanicum* and their antioxidant activity. *J. Agric. Food Chem.* **2006**, *54* (5), 1672−1679.

(19) Gu, L.; Kelm, M. A.; Hammerstone, J. F.; Zhang, Z.; Beecher, G.; Holden, J.; Haytowitz, D.; Prior, R. L. Liquid chromatographic/electrospray ionization mass spectrometric studies of proanthocyanidins in foods. *J. Mass Spectrom.* **2003**, *38* (12), 1272−1280.

(20) Ding, Y.; Wu, E. Q.; Liang, C.; Chen, J.; Tran, M. N.; Hong, C. H.; Jang, Y.; Park, K. L.; Bae, K.; Kim, Y. H.; Kang, J. S. Discrimination of cinnamon bark and cinnamon twig samples sourced from various countries using HPLC-based fingerprint analysis. *Food Chem.* **2011**, *127* (2), 755−760.

(21) Vanschoonbeek, K.; Thomassen, B. J.; Senden, J. M.; Wodzig, W. K.; van Loon, L. J. Cinnamon supplementation does not improve glycemic control in postmenopausal type 2 diabetes patients. *J. Nutr.* **2006**, *136*, 977−980.

level, without knowing the glycation site(s) and glycation extent per site in the protein. Mass spectrometry, both electrospray ionization mass spectrometry (ESI-MS) and matrix-assisted laser desorption ionization−mass spectrometry (MALDI-MS), allow a detailed analysis of the nature and extent of protein modification at the molecular level.[18−20] The recent technical innovations in mass spectrometry, particularly with the advent of high-energy C-trap dissociation (HCD) and electron transfer dissociation (ETD), have enabled unambiguous characterization of peptides with various modifications.[21,22] HCD allows the detection of the fragments with low mass, which is often not detectable due to the low mass cutoff in ion trap collision-induced dissociation (CID). ETD produces sufficient c and z ions, particularly for those peptides with relatively high mass carrying multiple charges. In addition, ETD can preserve the modification on the amino acid residue, therefore enabling accurate site localization.[23,24]

The purpose of this study was to evaluate the ultrasonic pretreatment effect on the galactose glycation of BSA. We compared the galactose glycation progress of BSA with and without ultrasonic pretreatment in the dry state. The glycation sites of the native BSA and ultrasound-BSA were characterized by the combined HCD and ETD fragmentation approach. The ultrasonic pretreatment on BSA resulted in many more glycation sites and a stronger glycation degree. Our investigation clearly revealed the critical role of ultrasonication in improving the extent of protein glycation.

MATERIALS AND METHODS

Materials. BSA, galactose, trypsin, and iodoacetamide were purchased from Sigma Chemical Co. (St. Louis, MO, USA); DTT was purchased from Thermo Fisher Scientific Inc. (Waltham, MA, USA). All other reagents used were of analytical grade.

Sample Preparation. BSA (0.2 g) was dissolved in 20 mL of 50 mM sodium phosphate buffer at pH 7.4. The solution was split into two aliquots. One aliquot of BSA was used as the control. The other aliquot was treated by probe sonicator (model 550 Sonic Dismembrator, Fisher Scientific, Pittsburgh, PA, USA; 20 kHz) equipped with a microtip probe (1/8 in. = 3.2 mm). In this sonicator setup, the actual minimum ultrasonic intensity was 75 W/cm^2 and the maximum intensity was 150 W/cm^2. The sample tube was kept in the ice bath, and the solution was treated by ultrasound with a 5 s on and 5 s off pulsation at an actual ultrasound intensity of 150 W/cm^2 for 10 min to ensure the temperature of the sample solution is not elevated (lower than 15 °C). One aliquot under ultrasonic treatment was used as the second control without added galactose. To the other aliquot was added the same mass of galactose followed by ultrasonication treatment after mixing.

The equal mass of galactose (10 mg) was added to 1 mL of the native BSA and ultrasonicated BSA solution, separately. After lyophilization, the powders of the native BSA−galactose and ultrasonicated BSA−galactose complex were incubated at 65% relative humidity (saturated potassium iodide solution) and 55 °C for 1 h. The reaction was stopped by transferring the sample tubes into an ice bath. After glycation, the powders were dissolved in cold distilled water, and the free galactose and salts were filtered by a Centricon centrifugal filter unit (10000 Da cutoffs, Millipore, Bedford, MA, USA). The concentration of protein was adjusted to 15 mg/mL and stored at −20 °C for further use. Three replicates were carried out for each sample.

MALDI-TOF Analysis. Mass spectrometry analysis was carried out using a MALDI TOF-TOF mass spectrometer (AB Science, ABI 4800 Proteomics TOF/TOF Analyzer, Foster City, CA, USA) in the positive ion mode. Sinapic acid (5 mg/mL) in 50% acetonitrile with 0.1% TFA was used as the matrix. The proteins were diluted 1:100 by distilled water and mixed 1:1 with the matrix. Mixtures (1.5 μL) were spotted onto the MALDI target and air-dried before analysis. Each sample was spotted on at least three individual target positions, and 80 individual spectra of each spot were averaged to produce a mass spectrum.

The incorporation ratio (IR), that is, the average number of galactose molecules attached to each albumin molecule, was used to evaluate the degree of protein glycation.[25] On the basis of the molecular weight (MW) shift from native BSA to glycated BSA, the IR of galactose to BSA could be deduced as

$$\mathrm{IR} = (\mathrm{MW_{GA}} - \mathrm{MW_{NGA}})/162.0528 \quad (1)$$

where 162.0528 is the MW of galactose attached to albumin, $\mathrm{MW_{GA}}$ is the molecular weight of glycated BSA, and $\mathrm{MW_{NGA}}$ is the molecular weight of nonglycated BSA.

Sample Digestion. Four microliters of the protein and complex solution was added to a 500 μL centrifuge tube containing 90 μL of 50 mM ammonium bicarbonate solution and 9 μL of 100 mM DTT. The sample was incubated at 95 °C for 5 min and then cooled in the ice bath. Eighteen microliters of the alkylation buffer (100 mM iodoacetamide) was added to the tube and incubated in the dark at room temperature for 20 min. Six microliters of 0.1 μg/μL trypsin was added to hydrolyze the protein samples at 37 °C for 4 h. The reaction was then quenched by adding 2 μL of 5% trifluoroacetic acid.

Analysis by HPLC-HCD/ETD-MS/MS. A Shimadzu HPLC (Shimadzu, Kyoto Japan), with two LC-10AD pumps, was used to generate a gradient with a 100 μL/min flow rate. Solvent A was 5% acetonitrile in H_2O, 0.1% formic acid (FA), whereas solvent B consisted of 95% acetonitrile in H_2O, 0.1% FA. For analysis of proteolytic peptides, 40 μL of digested sample was injected onto a 2.0 mm i.d. × 100 mm C18 column (Phenomenex Inc., Torrance, CA, USA). After desalting for 5 min with 5% B, the peptides were eluted at 100 μL/min with a 5−10% gradient for 1 min, 10−40% for 20 min, and 40−95% for 2 min. The effluent was infused into an LTQ-Qrbitrap Velos mass spectrometry (Thermo Fisher Scientific, Waltham, MA, USA) for MS/MS analysis to identify protein glycation. The decision tree methods were enabled for data acquisition. The settings for the decision tree were as follows: ETD was performed instead of HCD if the charge state was 3 and m/z was <650, or if the charge state was 4 and the m/z was <900, or if the charge state was 5 and the m/z was <950. ETD was performed for all precursor ions with charge states >5. The normalized collision energy was set to 28% for HCD. Supplemental activation was enabled for ETD. The signal threshold for triggering an MS/MS event was set to 500 counts. Charge state screening was enabled, and precursors with unknown charge state or a charge state of 1 were excluded. Dynamic exclusion was enabled with an exclusion duration of 90 s.

To further compare the glycation extent of each peptide, the average degree of substitution per peptide molecule of BSA (DSP) was calculated according to the formulation[7,26]

$$\mathrm{DSP} = \frac{\sum_{i-0}^{n} i \times I_{(\mathrm{peptide}+i\times\mathrm{galactose})}}{\sum_{i=0}^{n} I_{(\mathrm{peptide}+i\times\mathrm{galactose})}} \quad (2)$$

where I is the sum of the intensities of glycated peptide and i is the number of galactose units attached to the peptide in each glycated form.

Database Search. Thermo proteome discoverer (ver. 1.4.0.288) was used to generate the mgf. file from mass spectrometric data, and then Mascot Daemon (ver. 2.4.0, Matrix Science, Boston, MA, USA) was used to perform the searches against the NCBInr database. Search parameters were as follows: carbamidomethyl (C) was set as a fixed modification, and glycation (K and R) and oxidation (M) were set as variable modifications. Additional search settings included a maximum of 5five missed cleavages, peptide tolerance of ±10 ppm, and MS/MS tolerance of ±0.2 Da. Peptides with a Mascot ion score >40 were considered to be positive identification or extensive similarity (p < 0.05). Peptides identified with scores between 20 and 40 were considered to be potential positive identifications and were manually validated using the criteria suggested by Chen et al.[27] and Rombouts et al.[28] Only a, b, c, or y and z ions, or associated peaks arising due to water or amine loss, were considered as daughter ions of a parent

peptide. At least five isotopically resolved independent fragment peaks were required to match the theoretical peptide fragments. At least three consecutive fragment ions in the peptide sequence were required for positive identifications. These fragment ions could be either the b or y ion series for HCD fragmentation or the c and z ion series for ETD fragmentation. In addition, for doubly or triply charged ions, only one fragment ion with an intensity higher than one-third of the maximum intensity, an m/z value larger than that of the parent ion while not matching a theoretical peptide fragment, was allowed. For single charged ions, both the b ion or y ion series were required to confirm at least three consecutive amino acid residues in the peptide sequence if the peptide ended with an arginine or lysine residue; either b ion or y ion series were required to confirm at least three consecutive amino acid residues in the peptide sequence for the C-terminal peptide without arginine or lysine residues.

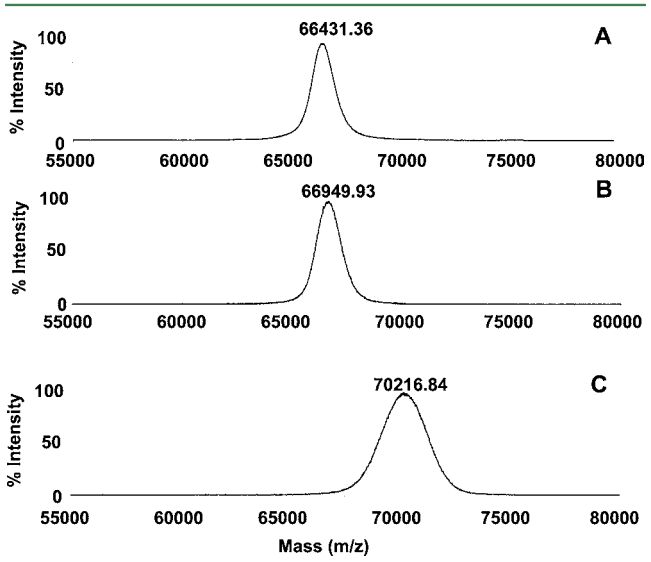

Figure 1. MALDI-TOF-MS analysis of ultrasonicated BSA (A); BSA-galactose before ultrasound (B) and after ultrasound pretreatment (C).

RESULTS AND DISCUSSION

Average Molecular Weight and Incorporation Ratio of Galactose to BSA. Figure 1 shows the MALDI-TOF-MS spectra of BSA−galactose with and without ultrasound pretreatment. The molecular weights of the native BSA and ultrasonicated BSA shifted to 66949.93 and 70216.84 Da (Figure 1B,C), respectively, much higher than the original MW of the native BSA, 66431.36 Da (Figure 1A). The IR of native BSA was calculated as 3.2, whereas that of the ultrasonicated BSA was 23.4. Ultrasonication improved the glycation extent significantly by >7 times. In addition, compared to the native BSA−galactose, the peak width of ultrasonicated BSA was much broader due to the greater incorporation of galactose. With the changes of molecular weight and peak width taken together, MALDI-TOF mass spectra clearly demonstrated that ultrasound pretreatment significantly improved the glycation

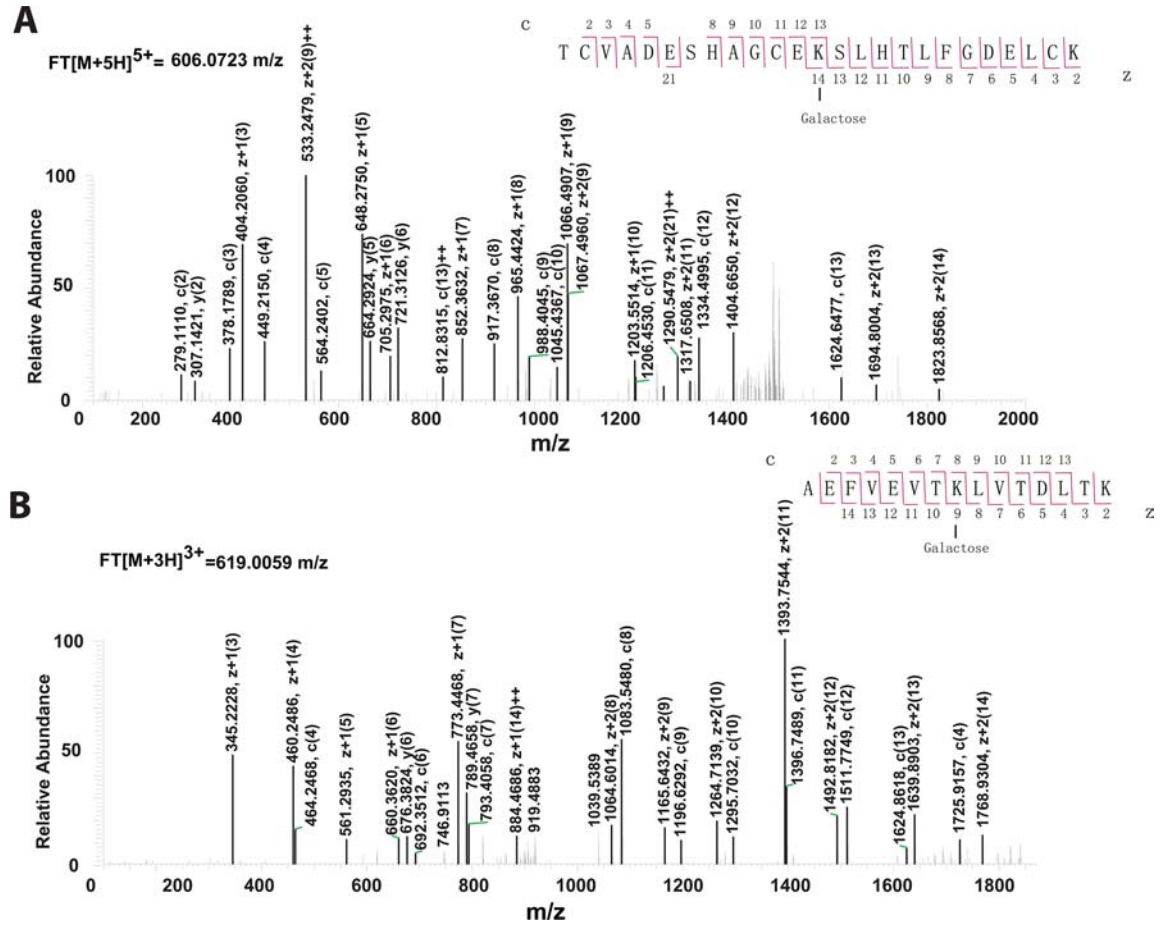

Figure 2. ETD MS/MS spectra of the glycated peptide 52−76 with m/z of 606.0723^{5+} (A) and the glycated peptide 225−239 at m/z of 619.0059^{3+} (B). The sequence of each peptide is shown on top of the peptide. The determined glycation sites are indicated by a line with galactose. The c and z ions are indicated by the numbers and lines.

dx.doi.org/10.1021/jf5002765 | J. Agric. Food Chem. 2014, 62, 2522−2530

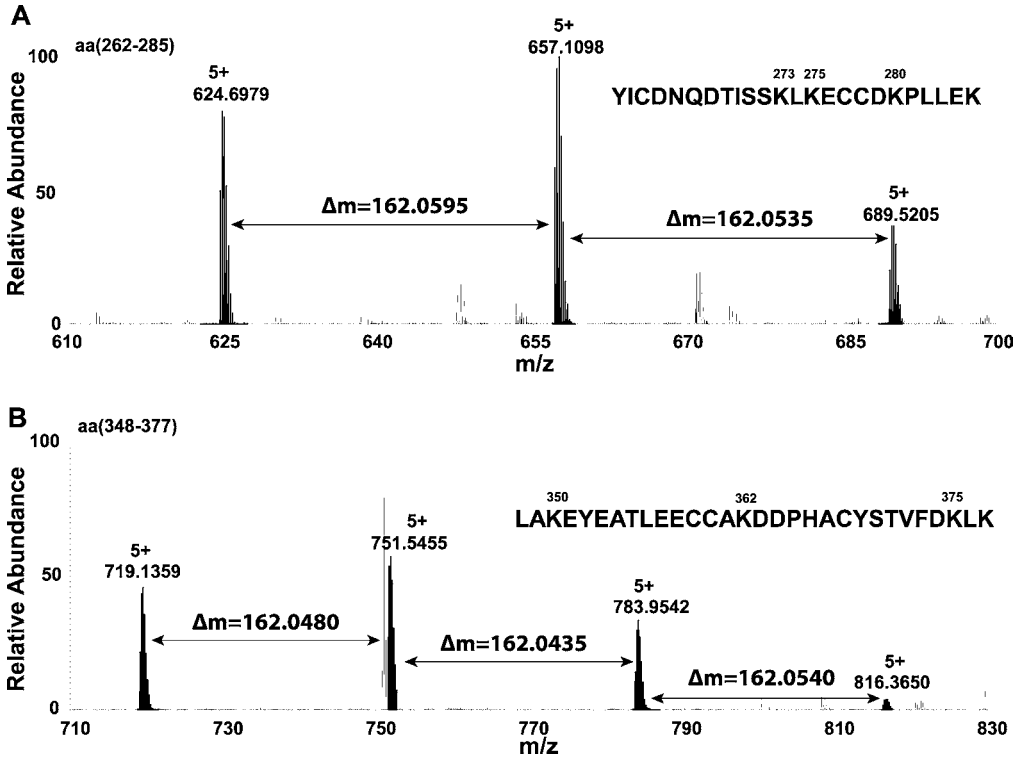

Figure 3. Mass spectra of the peptides with multiple glycation sites: (A) peptide 262−285; (B) peptide 348−377. The determined glycation sites are indicated by residue numbers. The mass differences are indicated with numbers and arrows.

extent of BSA. To fully understand the effect of ultrasound effect on the glycation extent of BSA, it is essential to obtain a detailed map of the glycation sites of BSA with and without ultrasound pretreatment. Such detailed changes in glycation could not be revealed by MALDI-TOF measurement of the intact molecular weight. To determine glycation sites and glycation extent per peptide, we performed tandem mass spectrometry including HCD and ETD after trypsin digestion.

Glycation Site Determination. Figure 2 shows the determination of glycation sites Lys64 and Lys232 by MS/MS. Both sites were found to be glycated in the native and ultrasonicated BSA. Lys64 is identified in peptide ^{52}TCVADESHAGCEKSLHTLFGDELCK^{76}. The mass of the peptide (3025.3256) matched very well with that of the glycated form (2863.2575 + 162.0528 = 3025.3103), with only a 5 ppm difference. The ETD MS/MS of the peptide generated a series of c and z ions (c1−c13 and z2−z14), unambiguously confirming the sequence of the peptide (Figure 2A). The location of the glycation (Lys64) was obtained by the mass difference between c12 and c13 ions, which is the combined mass of lysine and galactose. It is also confirmed by the mass difference between z12 and z13. Similarly, Lys232 was identified as the glycation site from the ETD fragments of the glycated peptide with m/z of 619.0059^{3+} (Figure 2B). The consecutive c and z ions ensure the positive identification of the peptide sequence and glycation site.

It should be noted that when an arginine or lysine is modified by glycation, trypsin will not be able to cleave at this particular residue, generating a peptide with a miss-cleavage. Therefore, it is common to observe dually and triply glycated peptides, especially when the glycation degree is high. Figure 3A shows the peptide 262−285, which contains three possible glycation sites at lysine 273, 275, and 280, respectively. The m/z before glycation at charge state 5 was calculated as 592.2848; after glycation, three additional ions were found at m/z 624.1098^{5+}, 657.1098^{5+}, and 689.5205^{5+}, representing one, two, and three glycated forms of this peptide, respectively. Similarly, all three potential glycation sites in the peptide 348−377 were also found to be glycated at their respective sites 350, 362, and 375 (Figure 3B).

It is possible for a certain peptide, although exhibiting the mass shift corresponding to monoglycation, to actually contain two (or more) glycated sites. The same modification occurring at different sites generated a mixture of peptides with the same molecular weight. Figure 4 shows one such example. The ion peak with m/z 638.3483^{3+} was found to elute between 4.5 and 5.4 min. The mass of this peptide is calculated as 1912.0201, which is very close to that of the singly glycated peptide ^{218}LSQKFPKAEFVEVTK^{232} (Δm = 0.93 ppm). This peptide contains two possible glycation sites, Lys221 and Lys224. The ETD fragmentation of the ion peak at an elution time of 4.92 min suggests that the glycation occurred on Lys221 with the Mascot score of 55 (Figure 4A). At a little earlier elution time of 4.87 min, an ion peak with m/z 479.0122^{4+} appeared and was selected for ETD fragmentation. The mass of the peptide is 1912.0157, also matching the peptide 218−232 with monoglycation (Δm = −1.34 ppm). The tandem mass spectrum of this ion peak indicates that the glycation mostly occurred on Lys224, instead of Lys221, with the Mascot score of 58 (Figure 4B). The results highlight the importance of the efficient ETD fragmentation on the determination of the modification sites. Due to the high similarity between these two peptides, the two mass spectra are almost indistinguishable except for a few fragment ions. The key fragment ions to distinguish the Lys221 modified peptide from the Lys224 modified peptide are c4 (m/z 636.3538) and z9 (m/z1197.6163). The appearance of a c4 ion in the former peptide

dx.doi.org/10.1021/jf5002765 | J. Agric. Food Chem. 2014, 62, 2522−2530

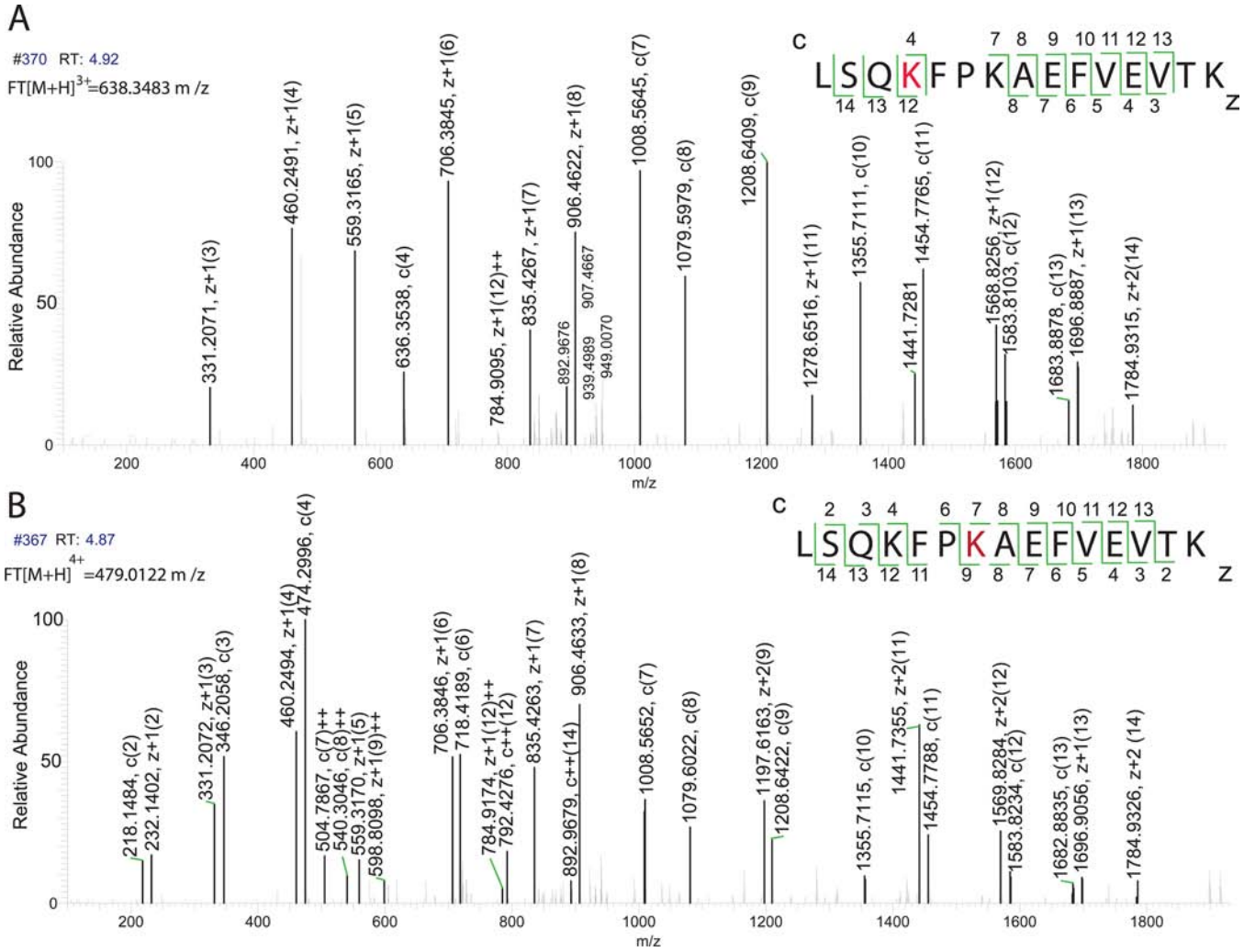

Figure 4. ETD MS/MS spectra of the singly glycated peptide 218−232 at different elution times and charge states: (A) RT = 4.92 min, charge state of 3 with m/z 638.3483^{3+}; (B) RT = 4.87 min, charge state of 4 with m/z 479.0122^{4+}. The MS/MS results indicated these two peptides are not identical, although they showed the same mass. The former is glycated at the position of 221 and the latter at the position of 224 as indicated by the colored lysine residues. The c and z ions are indicated by numbers and lines.

and a z9 ion in the latter provides unambiguous identification of the location of the glycation.

Table 1 shows the sequence and glycation sites of all glycated peptides under both conditions, determined by combined accurate mass and tandem mass spectrometry. BSA contains a total of 82 potential glycation sites including 59 lysines and 23 arginines. Before ultrasonic pretreatment, BSA was found to be glycated at only 12 sites (11K + R), including Lys64, Lys127, K173, Lys204, Lys232, Arg256, Lys280, Lys316, Lys396, Lys439, Lys524, and Lys544. After ultrasonic pretreatment, 42 sites including 39 lysines and 3 arginines were glycated. In addition to the 12 sites in untreated BSA, Lys20, Lys51, Lys76, Lys93, Lys131, Lys136, Lys211, Lys221, Lys224, Lys239, Lys261, Lys273, Lys275, Lys312, Lys322, Lys350, Lys362, Lys375, Lys388, Lys413, Lys465, Lys471, Lys474, Lys499, Lys504, Lys520, Lys523, Lys563, Arg81, and Arg444 were found to be glycated after the ultrasonic pretreatment. The majority of the glycated sites occurred on lysines, as represented by 11 of 59 (19%) and 39 of 59 (66%) lysines in untreated and treated BSA, respectively. In contrast, only 1 of 23 arginines was glycated in native BSA, and only 2 more were found to be glycated after ultrasonication. Given the reduced freedom of the amine group by steric effects from neighboring atoms, it is not surprising to see the much reduced glycation on arginine relative to lysine. Our glycation results are consistent with previous studies in which the glycation predominantly occurred on lysine but not on arginine.[7,8,29] It is worth emphasizing that arginine glycation has not been observed either in our previous study or in the other group's dry-heating of BSA.[8,29] The high-resolution mass accuracy and the versatile fragmentation methods (HCD + ETD) offered by LTQ-Orbitrap are the major contributions for finding the glycation on arginines because it enables unambiguous identification of the glycation sites, especially for those peptides containing multiple glycation sites.

Ultrasonication on the Glycation Extent of BSA. The glycation extent of a protein can be evaluated by (1) the number of the sites that are glycated and (2) the glycation extent per glycation site. When the number of glycation sites is not adequate to assess the glycation extent of the protein, the glycation extent described by DSP can be applied for additional information. In our case, we aim to compare the difference in glycation before and after ultrasonic pretreatment. The effect of this treatment has been clearly demonstrated by the drastically

Table 1. Summary of Amino Acid Residues Modified by Galactose in both Native and Ultrasonicated BSA

peptide location	m/z (glycated)	$[M + H]^+$ obsd	$[M + H]^+$ theor	Δ	sequence[a]	glycated site[b]
11−41	777.7950^{5+}	3883.9388	3883.9131	0.0257	(R)FKDLGEEHFKGLVLIAFSQYLQQC*PFDEHVK(L)	**K20**
42−64	693.3221^{4+}	2769.2595	2769.2473	0.0121	(K)LVNELTEFAKTC*VADESHAGC*EK(S)	**K51**
52−76	606.0723^{5+}	3025.3253	3025.3103	0.0149	(K)TC*VADESHAGC*EKSLHTLFGDELC*K(V)	K64
65−81	527.7740^{4+}	2107.0671	2107.0620	0.0051	(K)SLHTLFGDELC*KVASLR(E)	**K76**
77−144	782.3488^{6+}	4688.0493	4688.0411	0.0082	(K) VASLRETYGDMADC*C*EKQEPERNEC*FLSHKDDSPDLPK(L)	**K93/R98**
115−136	707.8546^{4+}	2827.3891	2827.3738	0.0153	(K)LKPDPNTLC*DEFKADEKKFWGK(Y)	K127/**K131**
132−143	579.3093^{3+}	1734.9062	1734.8981	0.0027	(K)KFWGKYLYEIAR(R)	**K136**
144−180	780.0371^{6+}	4674.1786	4674.1657	0.0129	(R)RHPYFYAPELLYYANKYNGVFQEC*C*QAEDKGAC*LLPK(I)	K173
199−208	453.2192^{3+}	1356.6357	1356.6344	0.0014	(R)C*ASIQKFGER(A)	K204
209−217	388.5526^{3+}	1162.6360	1162.6346	0.0014	(R)ALKAWSVAR(L)	**K211**
218−232	479.0138^{4+}	1912.0263	1912.0193	0.0070	(R)LSQKFPKAEFVEVTK(L)	**K221/K224**
225−239	619.0059^{3+}	1853.9959	1853.9874	0.0086	(K)AEFVEVTKLVTDLTK(V)	K232
233−261	591.6188^{6+}	3543.6694	3543.6644	0.0050	(K)LVTDLTKVHKEC*C*HGDLLEC*ADDRADLAK(Y)	**K239**
240−273	840.5726^{5+}	4197.8265	4197.8347	−0.0083	(K)VHKEC*C*HGDLLEC*ADDRADLAKYIC*DNQDTISSK(L)	R256/**K261**
262−285	689.5211^{5+}	3442.5692	3442.5565	0.0037	(K)YIC*DNQDTISSKLKEC*C*DKPLLEK(S)	**K273**, K280
274−285	565.6167^{3+}	1693.8283	1693.8266	0.0016	(K)LKEC*C*DKPLLEK(S)	**K275**/K280
286−322	882.2224^{5+}	4406.0757	4406.0570	0.0187	(K)SHC*IAEVEKDAIPENLPPLTADFAEDKDVC*KNYQEAK(D)	**K312**/K316
317−335	821.7200^{3+}	2462.1381	2462.1277	0.0103	(K)NYQEAKDAFLGSFLYEYSR(R)	**K322**
348−377	816.3695^{5+}	4076.8109	4076.7952	0.0157	(R)LAKEYEATLEEC*C*AKDDPHAC*YSTVFDKLK(H)	**K350 + K362 + K375**
378−409	995.2509^{4+}	3976.9746	3976.9629	0.0029	(K)HLVDEPQNLIKQNC*DQFEK(L)	**K388**
389−409	897.7640^{3+}	2690.2701	2690.2646	0.0055	(K)QNC*DQFEKLGEYGFQNALIVR(Y)	K396
413−427	601.3340^{3+}	1800.9801	1800.9833	−0.0032	(R)KVPQVSTPTLVEVSR(S)	**K413**
436−458	759.3470^{4+}	3033.3591	3033.3551	0.0039	(R)C*C*TKPESERMPC*TEDYLSLILNR(L)	K439/ **R444**
459−474	508.2768^{4+}	2029.0782	2029.0765	0.0016	(R)LC*VLHEKTPVSEKVTK(C)	**K465/K471**
472−499	873.4252^{4+}	3489.6718	3489.6578	0.0140	(K)VTKC*C*TESLVNRRPC*FSALTPDETYVPK(A)	**K474**
484−504	659.0692^{4+}	2632.2475	2632.2367	0.0108	(R)RPC*FSALTPDETYVPKAFDEK(L)	**K499**
500−523	606.7028^{5+}	3028.4774	3028.4740	0.0035	(K)AFDEKLFTFHADIC*TLPDTEKQIK(K)	**K504**
505−523	610.5613^{4+}	2438.2160	2438.2039	0.0121	(K)LFTFHADIC*TLPDTEKQIK(K)	**K520/K523**
524−533	435.5950^{3+}	1303.7632	1303.7599	0.0033	(K)KQTALVELLK(H)	K524
538−556	787.7276^{3+}	2360.1610	2360.1457	0.0152	(K)ATEEQLKTVMENFVAFVDK(C)	K544
545−573	868.3918^{4+}	3469.5383	3469.5186	0.0197	(K)TVMENFVAFVDKC*C*AADDKEAC*FAVEGPK(L)	**K563**

[a]C* means the cystine residue alkylated by carbamidomethyl. [b]The additional glycation sites after ultrasonic pretreatment are indicated in bold.

increased glycation sites. However, for those sites modified under both conditions, it is necessary to calculate DSP to evaluate the degree of the glycation.

Figure 5 shows mass spectra of the peptides and their corresponding glycated forms before and after ultrasonic pretreatments. The glycated forms of the peptides can be easily determined from the mass difference induced by glycation. Theoretically, if a peptide was monoglycated by galactose, the corresponding m/z peaks with one, two, three, four, or five charges will display a mass increase of 162.0528 Da, with m/z changes of 162.0528, 81.0264, 54.0176, 40.5132, and 32.4106, respectively. For example, the mass spectra of a peptide with a mass of 1356.6357 (m/z 399.2015^{+3}) shown in Figure 5B, the accurate mass and MS/MS determined that it was peptide ^{199}C(carbamidomethyl)ASIQKFGER^{208}. The peak with m/z shift of 54.0178 (m/z 453.2193^{+3}) indicated that one galactose molecule was added to the peptide 199−208, which was again confirmed by MS/MS. The relative abundance of the unglycated form of this peptide was 33.03% before ultrasonication after normalization against the glycated peptide peak. After ultrasonication, the relative abundance decreased to 4.87%, suggesting that the ultrasonication increased the degree of glycation of this peptide. Figure 5C displays another example of this type of ultrasonication effect on the glycation. The accurate mass and MS/MS determined the ion peak with m/z 564.9879^{3+} is the peptide 225−239. An ion peak appeared at the same elution time with the mass addition of 162.0528 Da, indicating one galactose molecule was added to the peptide. The relative abundance of the glycated form of this peptide increased from 25.57 to 100% after ultrasonication, whereas the relative abundance of the unglycated form of this peptide decreased from 100 to 45.99% after ultrasonication. This indicates that the ultrasonication increased the glycation degree of this peptide. Some other peptides containing glycation site(s) without ultrasonic pretreatment are also shown Figure 5, including 115−136 and 538−556 (Figure 5A,D). The mass spectra of these peptides after ultrasonication are shown underneath (purple trace). Comparison of each mass spectral pair depicted the changes of the degree of glycation of each peptide, with all of the peptides showing improved glycation after ultrasonication.

Figure 6 shows the DSP for all of the glycated peptides with and without ultrasonic pretreatment. On the basis of the DSP value, K64 and K204 are the most reactive galactose glycation sites in native BSA with DSP close to 0.8. The ultrasonic pretreatment further increased their DSP to almost full extent at 1.0. For other peptides, most of the DSP values are significantly improved by the ultrasonic pretreatment. It should be

dx.doi.org/10.1021/jf5002765 | J. Agric. Food Chem. 2014, 62, 2522−2530

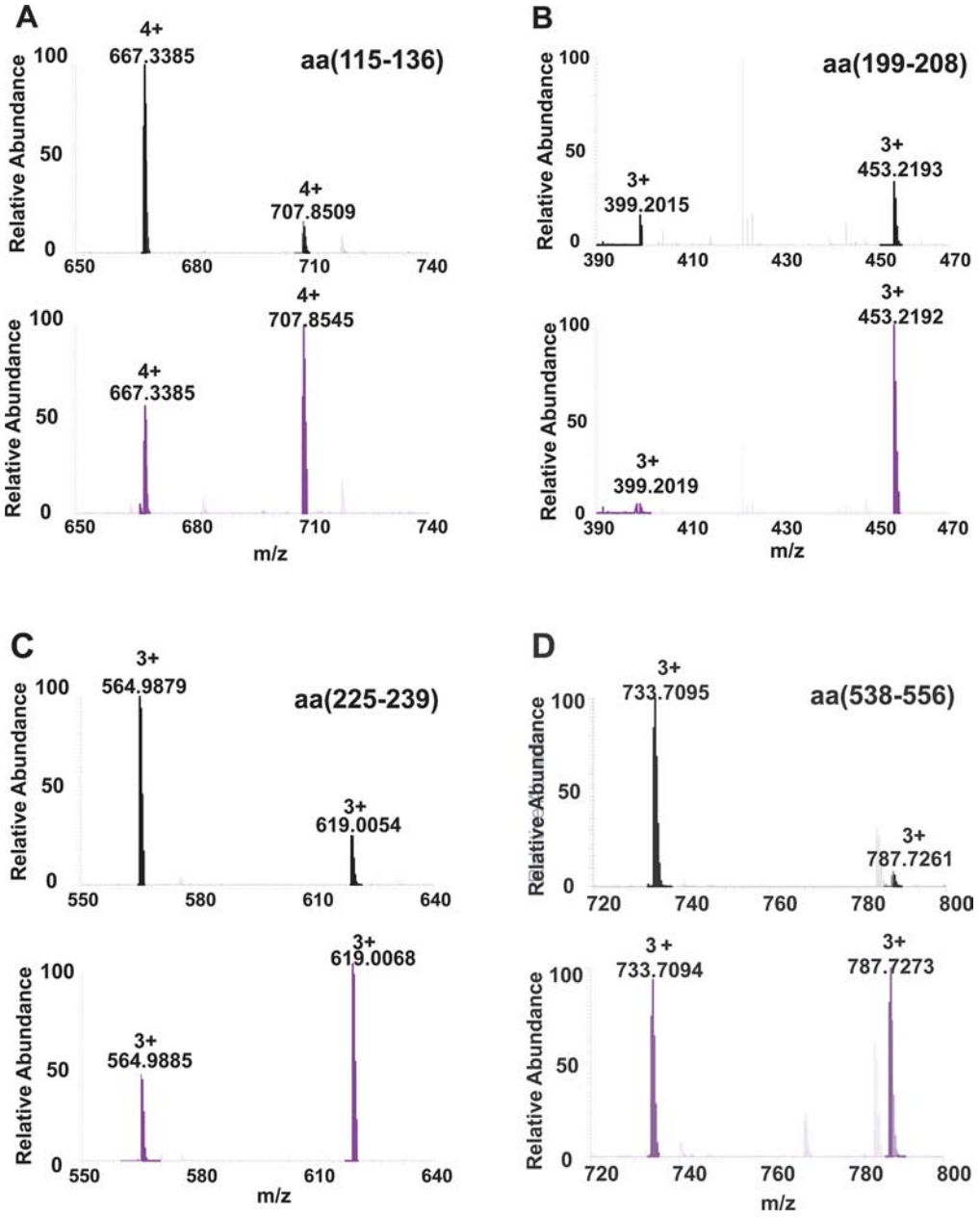

Figure 5. Mass spectra of presentative glycated peptides of BSA after trypsin digestion in both the native and ultrasonicated BSA: peptides 115−136 (A), 199−208 (B), 225−239 (C), and 538−556 (D). Black spectra are the native BSA, and purple spectra are the ultrasonicated BSA.

noted that some peptides, K136 and K474, reached the full glycation with DSP value of 1.0 even though they were not glycated in the native form. This suggests that the protein underwent a structural change under the influence of ultrasonication, exposing some regions of the protein to the solvent and, therefore, gaining more accessibility to the glycation. Because the increased DSP values are distributed all over the protein, this structural perturbation occurred throughout the protein (Figure 6). BSA can be divided into three domains, including domain I comprising residues 1−184, domain II comprising residues 185−377, and domain III comprising residues 378−583.[2] The additional glycation sites induced by ultrasonication occurred in all three domains, including 7 sites in domain I (K20, K51, K76, R81, K93, K131, K136), 12 glycation sites in domain II (K211, K221, K224, K239, K261, K273, K275, K312, K322, K350, K362, K375), and 11 sites in domain III (K388, K413, K465, K471, K474, K499, K504, K520, K523, K563, R444). Taken together, both the increased DSP values and increased glycation sites throughout all three domains suggest that the protein underwent a prevalent structural change in response to ultrasonication. This has been confirmed in a separate conformational study by hydrogen/deuterium exchange and mass spectrometry (data not shown). We have previously performed a similar study on BSA glycation under the influence of DHPM.[29] Under both of these two pretreatments, the glycation sites and glycation extent per glycation site are all significantly improved. Despite the similarity, the conformational changes in response to ultrasonication are actually different from those occurring under the influence of DHPM. The conformational changes induced by DHPM are mainly in domains II and III, but not domain I. In contrast, the ultrasonication-triggered conformational changes are distributed throughout all three

dx.doi.org/10.1021/jf5002765 | J. Agric. Food Chem. 2014, 62, 2522−2530

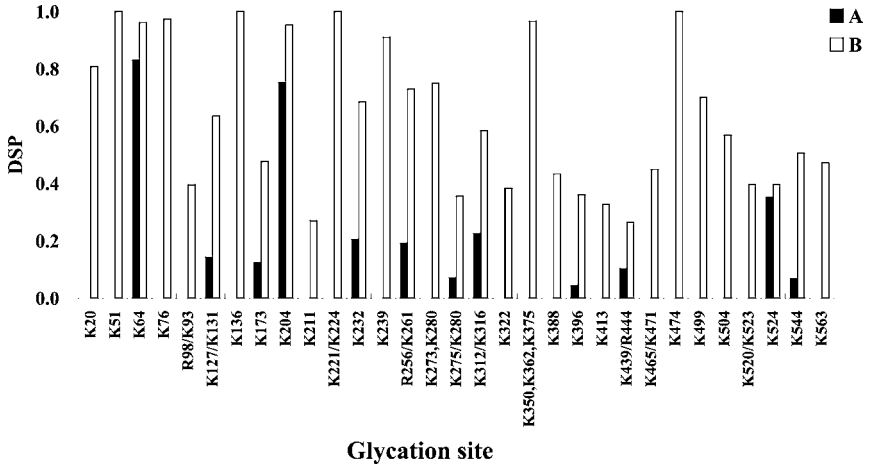

Figure 6. DSP values of glycated sites of native BSA (A) and BSA pretreated by ultrasound (B).

domains. The applications of these two pretreatments are quite similar; both are used in industry to make emulsions and to produce homogenized liquid.[30] The principle of DHPM resides in dividing a pressure stream into two parts, passing each part through a fine orifice, and directing the flows at each other in the microfluidizer interaction chamber. DHPM uses high pressure to guide the flow stream through microchannels in which it generates powerful shear, turbulence, impaction, and cavitation forces that reduce emulsion droplet size.[31,32] The major force responsible for ultrasonically induced effects is cavitation, which is the formation and collapse of vapor cavities in a flowing liquid. It is the collapse of these cavities that causes powerful shock waves to radiate throughout the solution, thereby breaking the dispersed liquid. The major difference between these two methods is that ultrasonication is a high-energy and long process, whereas DHPM is a high-energy but short process. In this work, we applied ultrasound with intensity as high as 150 W/cm^2 on the BSA for 10 min. The calculated energy density (E_v, J/m^3) was 1033 MJ/m^3, much higher than the one applied by DHPM at 100 MPa (~100 MJ/m^3).[26] It is likely that under the higher energy density of ultrasonication, the protein conformation was perturbed to a much higher extent, causing a structural distortion throughout the whole molecule. Consistent with our results, Guzey et al.[33] reported that ultrasound can change the tertiary structure of BSA solution. Ultrasonic pretreatment with temperature control has also been shown to modify the structure of proteins, leading to an increase in surface hydrophobicity.[15,34] It should be noted that in this work, the protein was pretreated with ultrasonication in the absence of sugars. The cavitation effect including the intense heat and pressure generated from ultrasonication will be only applied on the protein, but not directly on the glycation process. The improved glycation after ultrasonic pretreatment was therefore solely contributed from the conformational changes of the protein.

In conclusion, we employed high-resolution Orbitrap mass spectrometry to investigate the ultrasonication effect on the protein glycation. The results demonstrated that ultrasonication altered the protein structure, favoring glycation, indicating ultrasonication is a promising technology for improving protein functionality in the food industry. This approach opens new routes to modify the functionality of proteins in a positive way, providing a way for a better understanding of the structure–function relationship of the glycated proteins.

AUTHOR INFORMATION

Corresponding Authors

*(H.X.) Phone:1 (718) 430-3469. Fax: 1 (718) 430-8939. E-mail: hui.xiao@einstein.yu.edu.

*(Z.T.) Phone: +86791 88305938. Fax: +86791 88305938. E-mail: Tuzc_mail@aliyun.com.

Funding

This study was supported by the National High Technology Research and Development Program of China (863 Program, No. 2013AA102205), the freedom explore Program of State Key Laboratory of Food Science and Technology of Nanchang University (No. SKLF-ZZB-201310), and the Key Project for Science and Technology Innovation of Jiangxi Province (20124ACB00600).

Notes

The authors declare no competing financial interest.

ABBREVIATIONS USED

BSA, bovine serum albumin; HCD, high-energy C-trap dissociation; ETD, electron transfer dissociation; DHPM, dynamic high-pressure microfluidization; MALDI, matrix-assisted laser desorption ionization; ESI, electrospray ionization; DSP, average degree of substitution per peptide molecule; IR, incorporation ratio

REFERENCES

(1) Martins, S. I.; Jongen, W. M.; Van Boekel, M. A. A review of Maillard reaction in food and implications to kinetic modelling. *Trends Food Sci. Technol.* **2000**, *11*, 364–373.

(2) Carter, D. C.; Ho, J. X. Structure of serum-albumin. *Adv. Protein Chem.* **1994**, *45*, 153–203.

(3) Yaylayan, V. A. Classification of the Maillard reaction: a conceptual approach. *Trends Food Sci. Technol.* **1997**, *8*, 13–18.

(4) Chevalier, F.; Chobert, J.-M.; Popineau, Y.; Nicolas, M. G.; Haertlé, T. Improvement of functional properties of *β*-lactoglobulin glycated through the Maillard reaction is related to the nature of the sugar. *Int. Dairy J.* **2001**, *11*, 145–152.

(5) Liu, J.; Ru, Q.; Ding, Y. Glycation a promising method for food protein modification: physicochemical properties and structure, a review. *Food Res. Int.* **2012**, *49*, 170–183.

(6) Chobert, J.-M.; Gaudin, J.-C.; Dalgalarrondo, M.; Haertlé, T. Impact of Maillard type glycation on properties of *β*-lactoglobulin. *Biotechnol. Adv.* **2006**, *24*, 629–632.

(7) Huang, X.; Tu, Z.; Wang, H.; Zhang, Q.; Shi, Y.; Xiao, H. Increase of ovalbumin glycation by the Maillard reaction after

disruption of the disulfide bridge evaluated by liquid chromatography and high resolution mass spectrometry. *J. Agric. Food Chem.* **2013**, *61*, 2253−2262.
(8) Ledesma-Osuna, A. I.; Ramos-Clamont, G.; Vázquez-Moreno, L. Characterization of bovine serum albumin glycated with glucose, galactose and lactose. *Acta Biochim. Pol.* **2008**, *55*, 491−497.
(9) Wang, H.; Tu, Z.-C.; Liu, G.-X.; Liu, C.-M.; Huang, X.-Q.; Xiao, H. Comparison of glycation in conventionally and microwave-heated ovalbumin by high resolution mass spectrometry. *Food Chem.* **2013**, *141*, 985−991.
(10) Guan, Y.-G.; Lin, H.; Han, Z.; Wang, J.; Yu, S.-J.; Zeng, X.-A.; Liu, Y.-Y.; Xu, C.-H.; Sun, W.-W. Effects of pulsed electric field treatment on a bovine serum albumin−dextran model system, a means of promoting the Maillard reaction. *Food Chem.* **2010**, *123*, 275−280.
(11) Stanic-Vucinic, D.; Prodic, I.; Apostolovic, D.; Nikolic, M.; Velickovic, T. C. Structure and antioxidant activity of beta-lactoglobulin-glycoconjugates obtained by high-intensity-ultrasound-induced Maillard reaction in aqueous model systems under neutral conditions. *Food Chem.* **2013**, *138*, 590−599.
(12) Shi, W.-H.; Sun, W.-W.; Yu, S.-J.; Zhao, M.-M. Study on the characteristic of bovine serum albumin-glucose model system, treated by ultrasonic. *Food Res. Int.* **2010**, *43*, 2115−2118.
(13) Zhang, B.; Chi, Y. J. J.; Li, B. Effect of ultrasound treatment on the wet heating Maillard reaction between β-conglycinin and maltodextrin and on the emulsifying properties of conjugates. *Eur. Food Res. Technol.* **2014**, *238*, 129−138.
(14) Suslick, K. S.; Didenko, Y.; Fang, M. M.; Hyeon, T.; Kolbeck, K. J.; McNamara, W. B.; Mdleleni, M. M.; Wong, M. Acoustic cavitation and its chemical consequences. *Philos. Trans. R. Soc. London Ser. A: Math., Phys. Eng. Sci.* **1999**, *357*, 335−353.
(15) Gulseren, I.; Guzey, D.; Bruce, B. D.; Weiss, J. Structural and functional changes in ultrasonicated bovine serum albumin solutions. *Ultrason. Sonochem.* **2007**, *14*, 173−183.
(16) Murakami, K.; Akamatsu, M.; Sano, T. A structure-activity relationship in the binding of multicharged anionic azo and pyrene dyes to serum-albumin. *Bull. Chem. Soc. Jpn.* **1994**, *67*, 2647−2653.
(17) Guan, Y.-G.; Zhang, B.-S.; Yu, S.-J.; Wang, X.-R.; Xu, X.-B.; Wang, J.; Han, Z.; Zhang, P.-J.; Lin, H. Effects of ultrasound on a glycin−glucose model system—a means of promoting Maillard reaction. *Food Bioprocess Technol.* **2009**, *4*, 1391−1398.
(18) Oliver, C. M. Insight into the glycation of milk proteins: an ESI- and MALDI-MS perspective (review). *Crit. Rev. Food Sci. Nutr.* **2011**, *51*, 410−431.
(19) Zhang, Y.; Ficarro, S. B.; Li, S.; Marto, J. A. Optimized Orbitrap HCD for quantitative analysis of phosphopeptides. *J. Am. Soc. Mass Spectrom.* **2009**, *20*, 1425−1434.
(20) Michalski, A.; Damoc, E.; Lange, O.; Denisov, E.; Nolting, D.; Müller, M.; Viner, R.; Schwartz, J.; Remes, P.; Belford, M. Ultra high resolution linear ion trap Orbitrap mass spectrometer (Orbitrap Elite) facilitates top down LC MS/MS and versatile peptide fragmentation modes. *Mol. Cell. Proteomics* **2012**, *11*, O111.013698−1.
(21) Zhao, P.; Viner, R.; Teo, C. F.; Boons, G. J.; Horn, D.; Wells, L. Combining high-energy C-trap dissociation and electron transfer dissociation for protein O-GlcNAc modification site assignment. *J. Proteome Res.* **2011**, *10*, 4088−4104.
(22) Kaltsa, O.; Michon, C.; Yanniotis, S.; Mandala, I. Ultrasonic energy input influence on the production of sub-micron o/w emulsions containing whey protein and common stabilizers. *Ultrason. Sonochem.* **2013**, *20*, 881−891.
(23) Mikesh, L. M.; Ueberheide, B.; Chi, A.; Coon, J. J.; Syka, J. E.; Shabanowitz, J.; Hunt, D. F. The utility of ETD mass spectrometry in proteomic analysis. *Biochim. Biophys. Acta* **2006**, *1764*, 1811−1822.
(24) Singh, C.; Zampronio, C. G.; Creese, A. J.; Cooper, H. J. Higher energy collision dissociation (HCD) product ion-triggered electron transfer dissociation (ETD) mass spectrometry for the analysis of N-linked glycoproteins. *J. Proteome Res.* **2012**, *11*, 4517−4525.
(25) Bai, X.; Wang, Z.; Huang, C.; Wang, Z.; Chi, L. Investigation of non-enzymatic glycosylation of human serum albumin using ion trap-time of flight mass spectrometry. *Molecules* **2012**, *17*, 8782−8794.
(26) Jafari, S. M.; He, Y. H.; Bhandari, B. Production of sub-micron emulsions by ultrasound and microfluidization techniques. *J. Food Eng.* **2007**, *82*, 478−488.
(27) Chen, Y.; Kwon, S. W.; Kim, S. C.; Zhao, Y. Integrated approach for manual evaluation of peptides identified by searching protein sequence databases with tandem mass spectra. *J. Proteome Res.* **2005**, *4*, 998−1005.
(28) Rombouts, I.; Lagrain, B.; Brunnbauer, M.; Delcour, J. A.; Koehler, P. Improved identification of wheat gluten proteins through alkylation of cysteine residues and peptide-based mass spectrometry. *Sci. Rep.−UK* **2013**, DOI: 10.1038/srep02279.
(29) Huang, X.; Tu, Z.; Wang, H.; Zhang, Q.; Hu, Y.; Zhang, L.; Niu, P.; Shi, Y.; Xiao, H. Glycation promoted by dynamic high pressure microfluidisation pretreatment revealed by high resolution mass spectrometry. *Food Chem.* **2013**, *141*, 3250−3259.
(30) Tang, S. Y.; Shridharan, P.; Sivakumar, M. Impact of process parameters in the generation of novel aspirin nanoemulsions − comparative studies between ultrasound cavitation and microfluidizer. *Ultrason. Sonochem.* **2013**, *20*, 485−497.
(31) Silvestri, S.; Gabrielson, G. Degradation of tragacanth by high shear and turbulent forces during microfluidization. *Int. J. Pharm.* **1991**, *73*, 163−169.
(32) Magenheim, B.; Levy, M.; Benita, S. A new in vitro technique for the evaluation of drug release profile from colloidal carriers-ultrafiltration technique at low pressure. *Int. J. Pharm.* **1993**, *94*, 115−123.
(33) Guzey, D.; Gulseren, I.; Bruce, B.; Weiss, J. Interfacial properties and structural conformation of thermosonicated bovine serum albumin. *Food Hydrocolloids* **2006**, *20*, 669−677.
(34) Stanic-Vucinic, D.; Stojadinovic, M.; Atanaskovic-Markovic, M.; Ognjenovic, J.; Gronlund, H.; van Hage, M.; Lantto, R.; Sancho, A. I.; Velickovic, T. C. Structural changes and allergenic properties of β-lactoglobulin upon exposure to high-intensity ultrasound. *Mol. Nutr. Food Res.* **2012**, *56*, 1894−1905.

egg white proteins is rather nonselective. These included ovalbumin, ovalbumin-related protein Y, clusterin, PG D2 synthase, ovotransferrin, lysozyme, and an uncharacterized protein.[15] More recently, ovoinhibitor, extracellular fatty acid-binding protein precursor, and apolipoprotein D precursor were also shown to change in abundance in egg white between day 0 and day 7 of incubation.[18] Additionally, proteomic approaches applied to eggshell membranes from day 1 to day 21 of incubation revealed many proteins exhibiting fluctuation during embryonic development, suggesting a possible specific role according to the embryonic stage.[19] In contrast, there was no similar comprehensive study on yolk protein modification during incubation, although physicochemical properties of yolk are known to change during embryonic development.[20−23]

To investigate the dynamics of egg yolk components in relation to their primary role as a nutritional and physiological support for the embryo during development, we analyzed the proteomic profiles of egg yolk plasma soluble proteins isolated from fertilized and unfertilized eggs at the day of lay and after the first 12 days of incubation (at the end of embryo completion). From the proteomics studies published previously,[7] it seems that the proteins identified in the water-soluble fraction of egg yolk are representative of most of the proteins identified in egg yolk. Indeed the granular fraction is mostly composed of apovitellin, apolipoprotein, and vitellogenin (cleavage products) in high quantities, proteins which are also found in the water-soluble fraction. We believe that the analysis of the water-soluble fraction is more informative than the analysis of the granular fraction. Unfertilized eggs were used as controls to exclude proteins which undergo changes due to storage, such as temperature and automatic reversal, independently of the presence of an embryo. Therefore, this study examines proteomic changes occurring after incubation of fertilized eggs but also as a result of storage/incubation of unfertilized eggs. The results provide a general view on the utilization of egg yolk components by the embryo during incubation but also indicate how storage at high temperature (accelerated aging) can alter the protein profile of egg yolk of unfertilized eggs.

MATERIAL AND METHODS

Preparation of Egg Yolk Plasmas. Nonfertilized eggs (ISA Brown, Hendrix Genetics, St Brieuc, France) and eggs fertilized by artificial insemination (INRA, UE1295 Pôle d'Expérimentation Avicole de Tours, F-37380 Nouzilly, France) were collected at the day of lay and 12 days after incubation (45% hygrometry, 37.8 °C, automatic reversal every hour, INRA, UE1295 Pôle d'Expérimentation Avicole de Tours, F-37380 Nouzilly, France). At day 0 (day of lay) and day 12, egg yolks from eight eggs were independently collected, diluted 1:10 (w/v) in demineralized water, acidified to pH 5 with HCl according to Mann et al., [24] and centrifuged 1 h at 10 000*g*, 4 °C, to pellet the granular fraction of egg yolk. The resulting supernatants were dialyzed against 50 mM Tris-HCl, 50 mM NaCl, pH 7.4 for 24 h at 4 °C. Clarified egg yolks (egg yolk plasmas) were obtained after centrifugation at 4 °C for 1 h at 10 000*g*. All experiments were conducted according to the European legislation on the "Protection of Animals Used for Experimental and Other Scientific Purposes" (2010/63/UE) and under the supervision of an authorized scientist (S. Réhault-Godbert, Authorization no. 37-144).

The protein concentrations of each sample were determined using the Protein Dc Assay (Bio-Rad, Marnes-la-Coquette, France) and bovine serum albumin (Sigma-Aldrich, Saint-Quentin-Fallavier, France) as the standard. All samples were lyophilized and further analyzed by SDS-PAGE under denaturing, but nonreducing, conditions using 12.5% acrylamide-bisacrylamide gels and Coomassie Blue staining.

Preparation of Peptides. Reduction, carbamidomethylation, and enzymatic cleavage of yolk proteins were performed using a modified FASP (filter-aided sample preparation) method.[25] Fifty microgram aliquots of egg yolk proteins were dissolved in 100 μL of 0.1 M Tris, pH 8, containing 6 M guanidine hydrochloride and 0.01 M dithiothreitol (DTT). This mixture was heated to 56 °C for 60 min, cooled to room temperature, and loaded into a Microcon YM-30 centrifugal filter device (Millipore). DTT was removed by centrifugation at 13 000 rpm in an Eppendorf benchtop centrifuge model 5415D for 10 min and washing with 2 × 1 vol of the same buffer. Carbamidomethylation was done in the device using 0.1 M Tris buffer, pH 8, containing 6 M guanidine hydrochloride and 0.05 mM iodoacetamide and incubation for 45 min in the dark. Carbamidomethylated proteins were washed with 0.05 M ammonium hydrogen carbonate buffer, pH 8, containing 2 M urea, and centrifugation as before. Trypsin (1 μg, sequencing grade, modified; Promega, Madison, WI) was added in 40 μL of the same buffer, and the devices were incubated at 37 °C for 16 h. Peptides were collected by centrifugation, and the filters were washed twice with 40 μL of buffer. The peptide solution was acidified to pH 1−2 with trifluoroacetic acid, and peptides were cleaned and concentrated using five successive C18 Stage Tips.[26] The eluate of all five StageTips was combined for mass spectrometric analysis.

Mass Spectrometric Analysis and Evaluation. Peptide mixtures were analyzed by LC_MS/MS using an LTQ Orbitrap Velos mass spectrometer (Thermo Fisher Scientific, Bremen, Germany)[27] as described before.[28] Raw files were processed with MaxQuant (http://maxquant.org/)[29−31] version 1.3.8.1. The initial peptide mass tolerance was set to 20 ppm, and the main search tolerance was set to 6 ppm. The false discovery rate (FDR) for both peptides and proteins was set to 0.01. The maximal posterior error probability (PEP, the probability of each peptide to be a false hit considering identification score and peptide length) was set to 0.01. Carbamidomethylation was set as fixed modification. Variable modifications were oxidation (M), *N*-acetyl (protein), pyro-Glu/Gln (N-terminus), and deamidation (N,Q). The required minimal peptide length was seven amino acids, and two miss-cleavages were allowed. The Requantify and the Label-Free Quantitation (LFQ) option [32] were enabled, together with the Match between runs option using a time window of 2 min. The minimal ratio count for LFQ was set to 2. The database was a *Gallus gallus* subset of UniProt release 20012_8, containing 27 027 entries (http://www.uniprot.org/) combined with the reverse sequences and sequences of common contaminants. In general, only protein identifications with more than two sequence-unique peptides distributed in at least two replicates were accepted. Exceptions were proteins sharing peptides with similar proteins or fragments of the same protein. Label-free quantitation required the presence of 12 (of 16 possible) valid LFQ intensity values in at least one group of replicates belonging together, and the presence of at least two peptides in the razor + unique peptides column. The results of label-free quantitation were analyzed using an ANOVA multiple-sample test and hierarchical clustering provided by Perseus (http://maxquant.org/)[29−31] version 1.3.8.1. Because not all proteins yielded peptides in all replicates, missing intensity values were imputed using values from a suitable Gaussian distribution for minor proteins. One-way ANOVA was done with a permutation-based false discovery rate of 0.01 for truncation. Hierarchical clustering was done after *Z*-scoring to analyze the enrichment among all four samples (Perseus (http://maxquant.org/)).

RESULTS AND DISCUSSION

As a preliminary study, we collected samples of egg yolks at day 0, 4, 8, and 12 of incubation. The first analysis by SDS-PAGE of all our samples, collected and treated under identical conditions, indicated either a high heterogeneity between samples collected at day 4 or 8 and/or no dramatic change as compared with day 0 and day 12, respectively (Figure 1). The

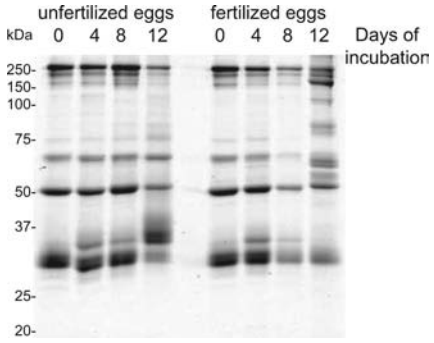

Figure 1. SDS-PAGE analysis of egg yolks from unfertilized and fertilized eggs at 0, 4, 8, and 12 days of incubation. Samples (10 μg) were prepared as described in Material and Methods.

most dramatic changes in protein band pattern were observed between day 0 and day 12 of incubation (Figure 1). From this preliminary study, we decided to compare the proteomes of egg yolk samples from fertilized and unfertilized eggs (as a negative control reflecting the absence of an embryo) at the day of lay and after 12 days of incubation. Of each of the four conditions, eight eggs were used for yolk plasma preparation, and each sample was independently analyzed twice. The resulting 64 raw files were combined for protein identification with MaxQuant. This resulted in the identification of 127 proteins that were distributed into 143 groups by MaxQuant (Supplementary Table S1). The reason for the discrepancy between protein groups and proteins was the occurrence in the database of fragments of the same protein in different entries and entries containing almost identical sequences. These latter may represent variants or isoforms containing possible micro-heterogeneities or may be due to sequencing errors. For these same reasons, the number of identified proteins may not be absolutely correct. Additional information about the protein groups, such as number of proteins in a group, additional accession numbers, peptide counts in different replicates, sequence coverage, and LTQ intensities, is provided in Supplementary Table 2. Peptide sequences and relevant data about peptides, such as distribution among replicates, scores, and posterior error probability (PEP), are contained in Supplementary Table 3. Both files also contain protein identifications not accepted because they did not meet the quality criteria, for instance, identifications with only one unique peptide. Contaminant entries and reverse hits were removed, except for contaminant peptides shared with chicken proteins.

Twenty-one of the protein groups were not identified in yolk in previous proteomic studies (Supplementary Table 1). Ten of these were immunoglobulins, a well-known fraction of the yolk proteome that varies in composition depending on hen environment. Chicken immunoglobulins (IgY) are transferred from the blood of the hen to the yolk by oocyte membrane receptors.[10] During incubation, IgY molecules are exported from the embryomic yolk sac into the blood of the embryo after binding to the chicken yolk sac IgY receptor by a pH-dependent mechanism.[33] This passive immunity is of major importance for the developing embryo because its immune system matures only after hatching. Presence and concentration of IgY molecules depend on the exposure of the mother to pathogenic and nonpathogenic microbes. Because the laying hens used in this study were not bred under controlled or sterile conditions, IgY profiles were not considered as relevant in the following sections. Other proteins, ADP-ribosyl cyclase CD157, gamma-glutamyl hydrolase, apolipoprotein A-IV, 14−3−3 zeta protein and chondrogenesis-associated lipocalin, ovosecretoglobulin, and mucin 5B, were previously identified in other egg compartments[4,5,7,11,16,28,34−37] but were identified for the first time as yolk components in the present study. Only three minor proteins were apparently identified in the chicken egg for the first time. These were α-fetoprotein, a major plasma protein produced by the yolk sac and the liver during fetal life,[38] an uncharacterized peptidase belonging to the C1 family (F1NHB8), and an uncharacterized protein with predicted Chitinase activity (F1NMM2), which is highly expressed in the stomach and the liver of chickens.[39] The presence of this latter protein in the yolk is consistent with the hepatic origin of yolk constituents. Figure 2 shows a typical annotated MS/MS spectrum for each of these new egg proteins.

For label-free quantitation, the protein distribution was analyzed with ANOVA to detect significant differences among the four sets of biological replicates, FE_D0 (fertilized, day 0), FE_D12 (fertilized, day 12), UFE_D0 (unfertilized, day 0), UFE_D12 (unfertilized, day 12). The thresholds defined in section 2.3 left 81 protein groups for quantitation. Seventy-three of these protein groups, likely representing a maximum of 69 individual proteins, showed significant differences among the sets of replicates (Supplementary Table 4).

Hierarchical clustering (Figure 3) of the data was performed to group proteins with similar change in relative abundance according to the nature of the sample (unfertilized or fertilized) and the length of incubation (D0 and D12). Four clusters, C1 to C4, were defined (Figure.3) and will be described in the following sections.

Cluster 1: Proteins with Increased Relative Abundance in Fertilized Eggs after 12 Days of Incubation. Hierarchical clustering revealed five proteins that were significantly enriched in the proteome of yolks of fertilized eggs after 12 days of incubation as compared to other conditions (Cluster 1, Table 1, Figure 3). These were vitronectin, α-fetoprotein, F2/thrombin, apolipoprotein B (distributed over several entries), and apovitellenin-1. One of these proteins, α-fetoprotein (GeneID: 422652, Table 1, bold), was a previously unidentified component of the unfertilized/table egg. α-Fetoprotein may play a role in the development of the avian immune system.[40] It is present in a wide range of chicken embryonic tissues, especially in yolk sac, liver, and connective tissues.[38] The significant increase of α-fetoprotein in yolk plasma of 12 day-old eggs is in accordance to previous evidence of a gradual increase in the yolk sac that is then followed by a decline in its synthesis starting at day 14.[41] Apolipoprotein B and apovitellenin-1 are major proteins of the granular fraction of the yolk and the cell adhesion and cell spreading protein vitronectin is a relatively minor protein of this fraction.[7] Vitronectin is a glycosaminoglycan-binding protein found in serum and tissues, which acts as a cell adhesion and spreading factor. This protein was reported to be a major cell adhesion factor in early chicken embryogenesis.[42] The higher relative abundance of these proteins in yolk plasma after incubation may result from solubilization of these proteins from the granules along with the decrease of yolk pH observed during incubation.[43] Apolipoprotein B fragments and apovitellenin-1 are major components of very low-density lipoprotein (VLDL) particles, and their enhanced appearance in the soluble fraction may reflect degradation of LDL in the course of lipid recruitment by the growing embryo.

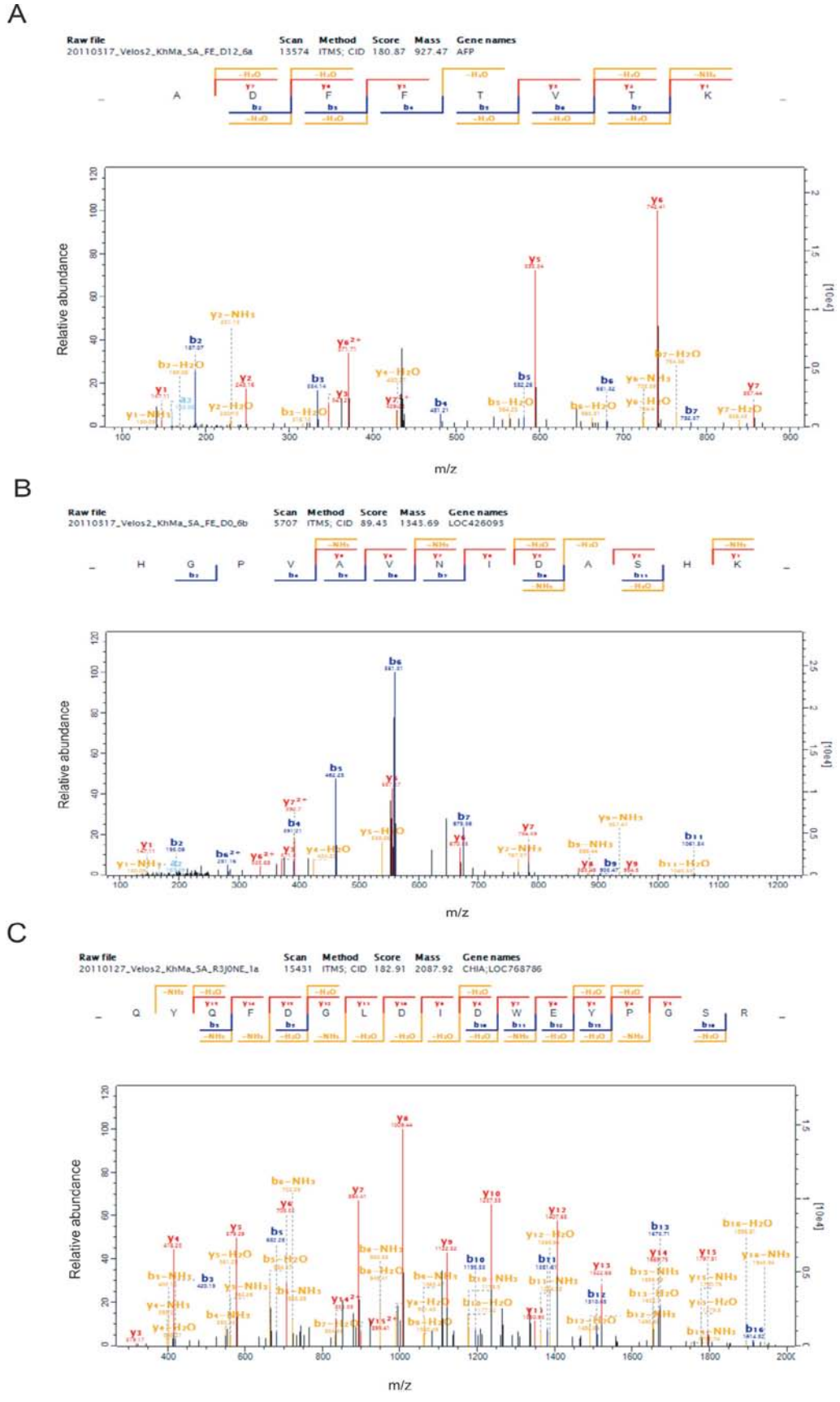

Figure 2. Typical MS/MS spectra of peptides instrumental in the identification of three new minor egg proteins. (A) Spectrum of an α-fetoprotein peptide. This doubly charged peptide was identified with a PEP of 0.0003 and a mass error of −0.75 ppm. (B) Spectrum of a triply charged peptide from F1NHB8_CHICK with a PEP of 0.005 and a mass error of −0.2 ppm. (C) Rather complex spectrum of a long doubly charged peptide of F1NMM2_CHICK with a PEP of 4.9×10^{-31} and a mass error of −2 ppm.

dx.doi.org/10.1021/jf404512x | J. Agric. Food Chem. 2014, 62, 2531−2540

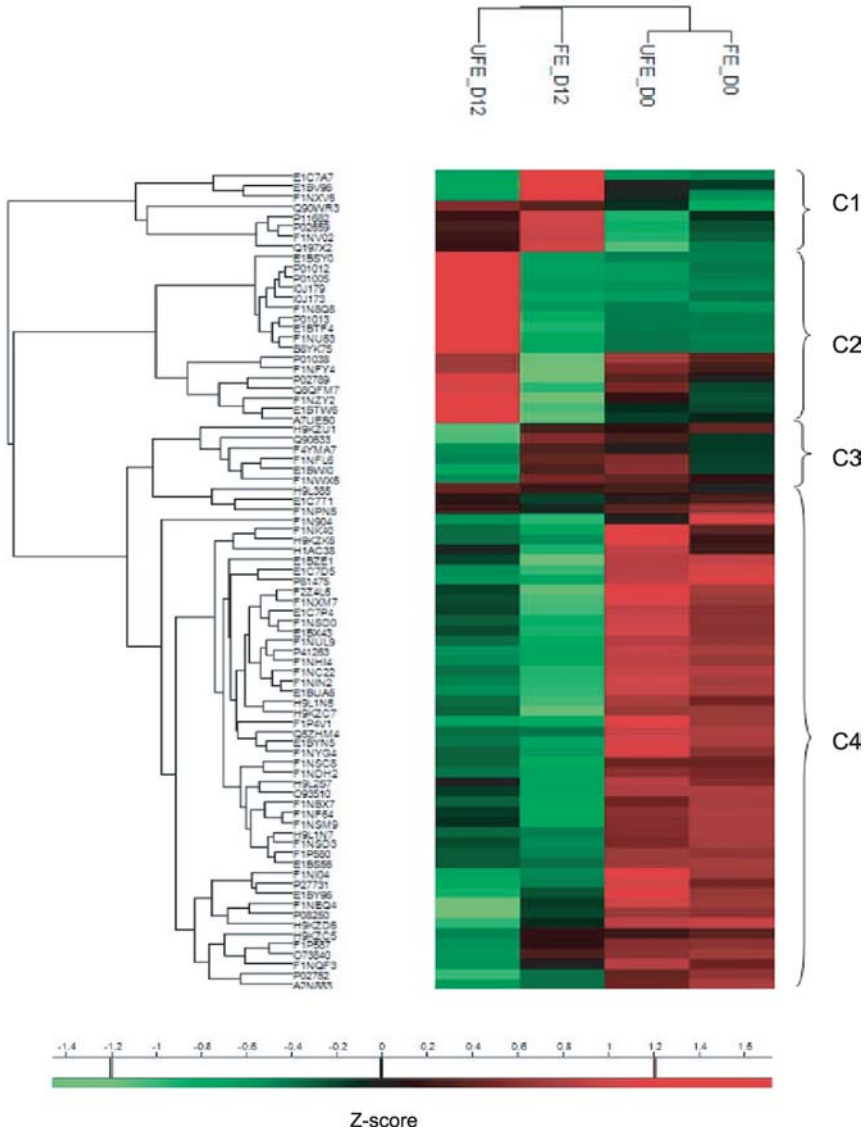

Figure 3. Hierarchical clustering of egg yolk plasma proteins. Clusters C1 to C4 are indicated.

Table 1. Proteins with Increased Abundance in 12 Day-Old Yolks from Fertilized Eggs (Cluster 1; *Z*-Scoring, Figure 3)

protein IDs	gene ID	protein description	localization
E1C7A7;F1NER8;O12945	395935	vitronectin	ES, VM, EY
E1BV96;E1C1G2;P84407	**422652**	***α*-fetoprotein**	
F1NXV6;Q91001	395306	uncharacterized/thrombin	ES, EY
Q90WR3	419076	hemopexin (fragment)	ES, EW, VM, EY
P11682	396535	apolipoprotein B (fragment)	ES, EW, VM, EY
F1NV02;F1NRG7		apolipoprotein B (fragment)	
Q197 × 2;Q7LZ77		apolipoprotein B	
P02659	396476	apovitellenin-1	ES, EW, VM, EY

ES, eggshell; EW, egg white; VM, vitelline membrane; EY, egg yolk. Protein that was identified in egg yolk for the first time is shown in bold.

Cluster 2: Proteins with Increased Relative Abundance in Unfertilized Eggs after 12 Days of Incubation. Seventeen proteins of cluster 2 (C2) showed a significant increase in relative abundance in yolks of unfertilized eggs as compared to fertilized eggs after 12 days of incubation (Table 2, Figure 3). Most of these proteins were previously described as major proteins of the egg white and the vitelline membrane,[16,36] but three of them, uncharacterized/ovosecretoglobulin, prostaglandin H2-D isomerase precursor, and mucin 5B, were identified in egg yolk for the first time (Table 2, bold). Several of these proteins were shown to decrease concomitantly in yolk of fertilized eggs upon incubation and may therefore be assimilated by the embryo during its development. These include the two protease inhibitors cystatin and ovoinhibitor, which are likely to regulate the overall proteolytic activity within the yolk compartment, but also ovotransferrin, mucin 5B, and ovoglycoprotein (Figure 3). This group also contains extracellular fatty acid-binding protein (Ex-FABP) and

dx.doi.org/10.1021/jf404512x | J. Agric. Food Chem. 2014, 62, 2531−2540

Table 2. Proteins with Increased Abundance in 12 Day-Old Yolks from Unfertilized Eggs (Cluster 2; *Z*-Scoring, Figure 3)

protein ID	gene ID	protein description	localization
E1BSY0	**ENSGALG00000024467**	**uncharacterized/ovosecretoglobin**	**EW**
P01012	396058	ovalbumin	ES, EW, VM, EY
P01005;B6 V1G0;P52267;Q6LDY9	416236	ovomucoid	ES, EW, VM, EY
I0J179	420897	ovalbumin-related Y	ES, EW, VM, EY
I0J173	395882	ovoglobulin G2/TENP	ES, EW, VM, EY
F1N8Q8;F1NGP2;Q9YGP0	395722	clusterin	ES, EW, VM, EY
P01013 ; E1BTF4	420898	ovalbumin-related protein X	ES, EW, VM, EY
F1NU63;F1NJA6;F1NJA7;E1C546; F1NJA5;P20740;F1NJB1;Q9PSS0	396151	ovostatin	ES, EW, VM, EY
B8YK75;B8YK77;B8YK79;P00698; B8YJN9;B8YJP1;B8YJT7;B8YK73;Q6LEL2	396218	lysozyme C	ES, EW, VM, EY
P01038	396497	cystatin	ES, EW, VM, EY
F1NFY4;F1NMN2;F1NUT1;Q6XLT0	416235	ovoinhibitor	ES, EW, VM, EY
P02789	396241	ovotransferrin	ES, EW, VM, EY
Q8QFM7\;E1BTX1	**374110**	**prostaglandin-h2 D-isomerase precursor**	**ES, EW, VM**
F1NZY2	**395381**	**mucin 5B**	**ES, EW, VM**
E1BTW6;E1C0K3;E1C0K0;E1C0K1; P21760;F6JXX0;F6JXW5;F6JXX6	396393	extracellular fatty acid-binding protein	ES, EW, VM, EY
A7UEB0;Q8JIG5;F1P2P7;E1BZ67	395220	alpha1-acidic glycoprotein/ovoglycoprotein	ES, EW, VM, EY

ES, eggshell; EW, egg white; VM, vitelline membrane; EY, egg yolk. Proteins that were identified in egg yolk for the first time are shown in bold.

Table 3. Proteins with Decreased Abundance in 12day-Old Yolks from Unfertilized Eggs (Cluster 3, *Z*-Scoring, Figure 3)

protein ID	gene ID	protein description	localization
H9KZU1	ENSGALG00000011667	uncharacterized/similar to natterin	EY
Q90633;A6N9E0;Q2MV09;H9L2W3	396370	complement C3	ES, EW, VM, EY
F4YMA7;F1NHT7;O42486;F1NJV8;E1C1 V3;E1C2U5;Q6PVZ8	429710	plakoglobin	EW, EY
F1NFL6;E1BYN6;F1NV01	424533	vitellogenin-2	ES, EW, VM, EY
E1BWI0	420869	uncharacterized/desmoplakin	ES, EW, VM, EY
F1NWX6;F1NTX4	421580	uncharacterized/plasminogen	EY

ES, eggshell; EW, egg white; VM, vitelline membrane; EY, egg yolk.

prostaglandin H2-D isomerase precursor, which belong to the lipocalin protein family and are encoded in genes located within the same genomic locus. Both proteins have been shown to be expressed ubiquitously by embryo tissues with especially high levels of mRNA transcripts in liver and brain.[44,45] Ex-FABP is also associated with heart (GO:0007507) and muscle development (GO:0010831, GO:0045663, GO:0048747), as suggested by Gene Ontology or GO terms (www.geneontology.org). The decreased relative abundance of both proteins in yolks of fertilized eggs after 12 days of incubation may be related to organ development in the embryo.

The observed increase in relative abundance of most of these proteins as compared to proteomes of nonincubated eggs may be due to storage at relatively high temperature (37.8 °C). Deterioration of the perivitelline membrane[46,47] and thinning of egg white upon aging [48] may facilitate the migration of egg white proteins into yolk and thus contribute to the observed increase in relative abundance. To date, the mechanism by which these proteins accumulate in the egg yolk of unfertilized eggs during incubation remains unexplained. No significant relationship between the physicochemical properties of these proteins (molecular mass/pI) and their increased relative abundance in the egg yolk could be found. Approximately 70% of these proteins exhibit an isoelectric point of 5−7 and a molecular weight of 10−50 kDa. However, lysozyme has a pI of about 9, and ovostatin has a molecular weight above 150 kDa (data not shown).

Cluster 3: Proteins with Decreased Relative Abundance in Unfertilized Eggs after 12 Days of Incubation. Cluster 3 contained four proteins exhibiting significant change that were present in both fertilized and unfertilized yolks but decrease in relative abundance specifically in egg yolks of unfertilized eggs during incubation (Table 3, Figure 3). These were a protein similar to the poison toadfish protease natterin, complement factor C3, the junction plaque component plakoglobin, and an uncharacterized protein similar to the desmosomal protein desmoplakin. All four proteins were previously identified as minor yolk components, and their role in egg yolk remains unexplored. Their distribution in yolk replicate groups indicated a loss in unfertilized eggs due to aging.

Cluster 4: Proteins with Decreased Relative Abundance after 12 Days of Incubation of Fertilized and Unfertilized Eggs. Cluster 4 (C4) comprised 43 proteins with a significant decrease in relative abundance after 12 days of incubation in both fertilized and unfertilized eggs (Figure 3, Table 4), including several immunoglobulin chains identified in the egg yolk for the first time. We suspect that the mechanism by which these proteins are decreasing in fertilized versus unfertilized eggs might be different because the presence of an embryo is likely to affect yolk proteins.

If we focus on fertilized eggs, this cluster contained several proteins known to play a role in embryonic development, such as the vitamin-A-binding retinol-binding protein 4.[44,45] Retinol-binding protein 4 has been associated with many biological processes related to embryonic development, [49] including morphogenesis (GO:0048562) and development of heart (GO:0001555; GO:0060347, GO:0007507; GO:0048738,

Table 4. Proteins with Decreased Abundance in Egg Yolks after 12 Days of Incubation (Cluster 4, Z-Scoring, Figure 3)

protein IDs	gene ID	protein description	localization
F1N904	769327	IGv fragment	
F1NK40 ; H1AC38	427942	uncharacterized/similar to alpha2-macroglobulin	EY
H9KZK6;Q98TD1	395364	uncharacterized/PIT54	ES, EY
E1BZE1	424956	alpha2-HS-glycoprotein	ES, EY
E1C7D5	421091	uncharacterized/similar to transthyretin	ES, EY
P81475		complement factor B-like protease	EY
F2Z4L6;P19121	396197	serum albumin	ES, EW, VM, EY
F1NXM7	420302	uncharacterized/similar to prostate stem cell antigen	ES, EY
E1C7P4	429057	uncharacterized/complement factor H	EY
F1NSD0;P20763;P04210	416928	Ig lambda chain C region	EW, VM, EY
E1BX43	424957	uncharacterized/kininogen-1	EY
F1NUL9;Q02020;F1P5F9;B4ZCM0;CON__P02676	373926	fibrinogen beta-chain;fibrinopeptide B;fibrinogen beta chain	ES, EY
P41263	396166	retinol-binding protein 4	ES, EY
F1NHI4	422810	superoxide dismutase [Cu−Zn]	EY
F1NC22	ENSGALG00000005937	IGv fragment	ES, EW, VM, EY
F1NIN2;Q5ZIJ5	428163	uncharacterized/cathepsin A	ES, EY
E1BUA6	421702	uncharacterized/vanin-1	EY
H9L1N5\;H9KZF6	ENSGALG00000022049	IGv fragment	
H9KZC7\;H9KZC6	ENSGALG00000005880	IGv fragment	
F1P4 V1;P14448	396307	fibrinogen alpha-chain;fibrinopeptide A;fibrinogen alpha chain	EY
Q5ZHM4;F1P4I7;E1BUA7	421702	uncharacterized/similar to vanin-2	EY
E1BYN5;E1BZD1	424534	vitellogenin-3	ES, EY
F1NYG4;E1BSE0	417431	uncharacterized/apolipoprotein H	ES, EY
F1NDH2	421543	sngiotensinogen	ES, EY
H9L2S7	ENSGALG00000022419	IGv fragment	EY
O93510;F1NKF3	395774	Gelsolin	ES, EY
F1NBX7	ENSGALG00000005946	IGv fragment	EW, EY
F1NF64	428773	uncharacterized/complement factor I	EY
F1NSM9;O93568;E1BV78	395837	fibrinogen gamma-chain	EY
H9L1N7	**ENSGALG00000022053**	**IGv fragment**	
F1NSD3	**769305**	**IGv fragment**	
F1P580	423629	uncharacterized/LOC423629	ES, EY
E1BS56	423433	uncharacterized/alpha-1-antiproteinase 2	EY
F1NI04	417829	uncharacterized/*N*-acetylglucosamine-6-sulfatase	ES, EY
P27731;F1NMT4	396277	transthyretin	ES, EY
E1BY96;F1P350	424547	uncharacterized/vitellogenin-1	ES, EW, VM, EY
F1NEQ4	427942	uncharacterized/similar to alpha2-macroglobulin	EY
P08250;F1N8F3;H9KZR3	396536	apolipoprotein A-I	ES, EW, VM, EY
H9KZD6	ENSGALG00000022501	IGv fragment	ES, VM, EY
H9KZC5;H9KZT0	ENSGALG00000022031	IGv fragment	EY
F1P587	418892	uncharacterized/similar to complement C4−1	ES, EW, EY
O73840;F1NJ16	395877	heparin cofactor II	ES, EW, EY
F1NQF3;F1N9N4;Q5ZJS7	423353	uncharacterized/epididymal secretory protein E1 precursor	ES, EW, EY
P02752;Q9PWK0;F1NX08;Q7SX70	396449	riboflavin-binding protein	ES, EW, VM, EY
A2N883\;A2N881\;A2N884\;A2N885	**776783**	**IGv fragment**	

ES, eggshell; EW, egg white; VM, vitelline membrane; EY, egg yolk. Proteins that were identified in egg yolk for the first time are shown in bold.

GO:006004 [50]), lung (GO:0030324), eye (GO:0001654, GO:0060041, GO:0060059), the skeletal system (GO:0048706), the urinary system (GO:0060157), and gonads (GO: 0008584; GO:0048807; GO:0060065; GO:0060068; GO:0060068). Its decrease in yolk of fertilized eggs during incubation suggests that it might be selectively used to for embryonic development. Similarly, we observed a marked reduction in transthyretin abundance in yolk of fertilized egg as compared to other conditions. This protein is known to interact with retinol-binding protein. Our data are consistent with previous observations suggesting a role for transthyretin (previously called prealbumin) in the transport and distribution of thyroid hormone from yolk to embryo prior to establishment of the circulatory system.[50] Yolk riboflavin-binding protein is synthesized by the liver in response to estrogen,[51] secreted into the blood and further transferred to the growing follicles.[52] During incubation, this protein is removed from yolk and egg white and accumulates in embryonic tissues in a complex with riboflavin up to the fourteenth day of incubation.[53] This accumulation in tissues coincides with the disappearance of riboflavin-binding protein from the white and the yolk compartments, [53] which is consistent with the decrease in relative abundance we observed in egg yolk after 12 days of incubation. Superoxide dismutases [Cu-Zn] are known to destroy radicals that are normally produced within the cells and are toxic to biological systems. This antioxidant has been shown to regulate angiogenesis using the model of the chicken embryo chorioallantoic membrane.[54]

Proteins which are decreasing in unfertilized eggs in egg yolk plasma during incubation are mostly "egg-yolk-specific"

dx.doi.org/10.1021/jf404512x | J. Agric. Food Chem. 2014, 62, 2531−2540

proteins (Table 4). The decrease of these proteins in yolk plasma after 12 days of incubation can be explained by at least three hypotheses: (1) endogenous degradation, (2) interaction with lipoproteins and their further relocalization to the granular fraction of the yolk, and (3) diffusion toward the egg white or other compartments. With regard to the first hypothesis, we know that several proteases are present in egg yolk, including aspartic proteases such as "similar to nothepsin",[5,7,55] many proteases involved in inflammatory cascades including thrombin and coagulation factors,[11] and matrix metalloproteinase 2.[56] These various proteases could regulate the activity of some egg yolk proteins and their subsequent degradation. Alternatively, we cannot exclude that the proteins identified in the plasma fraction at the day of lay are not recovered in this plasma fraction after incubation. Indeed, the texture and the chemical modification during incubation might affect the solubility of these proteins, which could then associate with the granular fraction of the egg yolk rather than with the plasma. Another explanation is related to the possible exchange of material between egg yolk and egg white during incubation at 37.8 °C. No significant increase in egg yolk proteins has been reported in the egg white of table eggs (unfertilized eggs) stored at ambient temperature up to 40 days.[48] However, the conditions of incubation used in our assay, a higher temperature together with the control of relative humidity and automatic egg turning, might slightly modify the dynamics of protein exchange and the physicochemical nature of egg proteins.

To our knowledge, this study is the most detailed work available at present on the change of egg yolk protein content occurring during early embryogenesis. In the present study, we have analyzed the effect of fertilization on the yolk plasma proteome after 12 days of incubation and tried to discern changes due to embryonic development from changes due to the aging processes by comparing yolks of fertilized to yolks of unfertilized eggs incubated under the same conditions. The latter results may also be applicable to the storage of table eggs although the conditions used (37.8 °C, constant relative humidity, automatic turning) were not the same as commonly used in supermarkets or homes. We suggest that these conditions may reflect some kind of accelerated aging. It turned out that in many instances, the influence of embryo development and aging overlapped to some degree with most of the identified proteins (Cluster 4). Although the decrease in relative abundance of many proteins in yolks of fertilized eggs may preferentially be attributed to their use by the developing embryo, especially if the decrease is more pronounced in fertilized eggs than nonfertilized eggs, decreases in relative abundance more pronounced in unfertilized eggs (Cluster 3) or increases under certain conditions (Clusters 1 and 2) are more difficult to explain. This analysis performed on the water-soluble fraction of egg yolk (plasma) revealed a likely interaction between yolk plasma and granules, as some proteins might be gradually solubilized from granules during incubation. We also found several proteins, including antiproteases and chelators, that were significantly less abundant after 12 days of incubation as compared to other conditions, providing some clues to study more precisely the kinetics of absorption of some specific egg proteins by the embryo and the regulation of absorption in relation to embryonic stages. Additionally, the study on unfertilized eggs may help to understand possible connections between egg compartments during storage of table eggs and how egg quality can be affected when using inappropriate storage conditions. This work has shown that many proteins initially identified in the egg white and the vitelline membrane increase in relative abundance in the egg yolk after 12 days (Cluster 2). In contrast, decreases in relative abundance could be due either to endogenous degradation by proteases or diffusion of yolk plasma proteins to egg white or the yolk granular fraction upon aging. It is known that the perivitelline membrane not only deteriorates during embryonic development in fertilized eggs but also in stored unfertilized eggs. At the same time, the egg white of unfertilized eggs show the well-known thinning that may be the consequence of reorganization of egg white protein interactions and which could enhance diffusion of proteins to the other compartments. The relatively high temperature used in this study may enhance such processes. Furthermore, the loss of certain proteins may apparently increase the relative abundance of others.

■ ASSOCIATED CONTENT

Ⓢ Supporting Information

Supplementary Table 1: identified and accepted proteins (protein groups). Supplementary Table 2: MaxQuant protein groups. Supplementary Table 3: MaxQuant peptides. Supplementary Table 4: quantified proteins (ANOVA). This material is available free of charge via the Internet at http://pubs.acs.org.

■ AUTHOR INFORMATION

Corresponding Author

*E-mail: srehault@tours.inra.fr.

Present Address

[§]Institut Technique de l'aviculture, UR83 Recherches Avicoles, F-37380 Nouzilly, France

Author Contributions

[#]These authors contributed equally.

Funding

This research was supported by the French National Research Agency (OVO-mining, ANR-09-BLAN-0136), Region Centre and INRA, Physiologie Animale et Système d'Elevage division, for the financial support of M. Bourin's PhD.

Notes

The authors declare no competing financial interest.

■ ACKNOWLEDGMENTS

The authors acknowledge the experimental unit PEAT (INRA, UE1295 Pôle d'Expérimentation Avicole de Tours, F-37380 Nouzilly, France) and more particularly, Joël Delaveau, for incubating unfertilized and fertilized eggs.

■ REFERENCES

(1) Schneider, W. J. Receptor-mediated mechanisms in ovarian follicle and oocyte development. *Gen. Comp. Endrocrinol.* **2009**, *163*, 18−23.

(2) Griffin, H. D.; Perry, M. M.; Gilbert, A. B. Yolk formation. *Physiol. Biochem. Domest. Fowl* **1984**, *5*, 345−380.

(3) Retzek, H.; Steyrer, E.; Sanders, E. J.; Nimpf, J.; Schneider, W. J. Molecular cloning and functional characterization of chicken cathepsin D, a key enzyme for yolk formation. *DNA Cell. Biol.* **1992**, *11*, 661−672.

(4) Nilsson, E.; Hanrieder, J.; Bergquist, J.; Larsson, A. Proteomic characterization of IgY preparations purified with a water dilution method. *J. Agric. Food Chem.* **2008**, *56*, 11638−11642.

(5) Farinazzo, A.; Restuccia, U.; Bachi, A.; Guerrier, L.; Fortis, F.; Boschetti, E.; Fasoli, E.; Citterio, A.; Righetti, P. G. Chicken egg yolk

cytoplasmic proteome, mined via combinatorial peptide ligand libraries. *J. Chromatogr. A* **2009**, *1216*, 1241−1252.
(6) Gautron, J.; Réhault-Godbert, S.; Nys, Y., Use of high-throughput technology to identify new egg components. In *Improving the Safety and Quality of Egg and Egg Products*; Nys, Y., Bain, M., Van Immerseel, F., Eds.; Woodhead Publishing Ltd: Cambridge, United Kingdom, 2011; Vol. *1*, pp 133−150.
(7) Mann, K.; Mann, M. The chicken egg yolk plasma and granule proteomes. *Proteomics* **2008**, *8*, 178−191.
(8) Deeley, R. G.; Mullinix, D. P.; Wetekam, W.; Kronenberg, H. M.; Meyers, M.; Eldridge, J. D.; Goldberger, R. F. Vitellogenin synthesis in the avian liver. Vitellogenin is the precursor of the egg yolk phosphoproteins. *J. Biol. Chem.* **1975**, *250*, 9060−9066.
(9) Schneider, W. J.; Carroll, R.; Severson, D. L.; Nimpf, J. Apolipoprotein VLDL-II inhibits lipolysis of triglyceride-rich lipoproteins in the laying hen. *J. Lipid Res.* **1990**, *31*, 507−513.
(10) Hamal, K. R.; Burgess, S. C.; Pevzner, I. Y.; Erf, G. F. Maternal antibody transfer from dams to their egg yolks, egg whites, and chicks in meat lines of chickens. *Poult. Sci.* **2006**, *85*, 1364−1372.
(11) D'Alessandro, A.; Righetti, P. G.; Fasoli, E.; Zolla, L. The egg white and yolk interactomes as gleaned from extensive proteomic data. *J. Proteomics* **2010**, *73*, 1028−1042.
(12) Moran, E. T., Jr. Nutrition of the developing embryo and hatchling. *Poult. Sci.* **2007**, *86*, 1043−1049.
(13) Romanoff, A. L. *The Avian Embryo*; The Macmillan Company: New York, 1960.
(14) Marshall, M. E.; Deutsch, H. F. Some protein changes in fluids of the developing chicken embryo. *J. Biol. Chem.* **1950**, *185*, 155−161.
(15) Qiu, N.; Ma, M. H.; Cai, Z. X.; Jin, Y. G.; Huang, X.; Huang, Q.; Sun, S. G. Proteomic analysis of egg white proteins during the early phase of embryonic development. *J. Proteomics* **2011**, *75*, 1895−1905.
(16) Mann, K. Proteomic analysis of the chicken egg vitelline membrane. *Proteomics* **2008**, *8*, 2322−2332.
(17) Cunningham, F. E. Changes in egg white during incubation of the fertile egg. *Poult. Sci.* **1974**, *53*, 1561−1565.
(18) Liu, Y.; Qiu, N.; Ma, M. Comparative proteomic analysis of hen egg white proteins during early phase of embryonic development by combinatorial peptide ligand library and matrix-assisted laser desorption ionization-time of flight. *Poult. Sci.* **2013**, *92*, 1897−1904.
(19) Kaweewong, K.; Garnjanagoonchorn, W.; Jirapakkul, W.; Roytrakul, S. Solubilization and identification of hen eggshell membrane proteins during different times of chicken embryo development using the proteomic approach. *Protein J.* **2013**, *32*, 297−308.
(20) Saito, Z.; Martin, W. G. Ovalbumin and other water-soluble proteins in avian yolk during embryogenesis. *Can. J. Biochem.* **1966**, *44*, 293−301.
(21) Saito, Z.; Martin, W. G.; Cook, W. H. Changes in the major macromolecular fractions of egg yolk during embryogenesis. *Can. J. Biochem.* **1965**, *43*, 1755−1770.
(22) Yadgary, L.; Cahaner, A.; Kedar, O.; Uni, Z. Yolk sac nutrient composition and fat uptake in late-term embryos in eggs from young and old broiler breeder hens. *Poult. Sci.* **2010**, *89*, 2441−2452.
(23) Sugimoto, Y.; Yamada, M. Changes in proteins from yolk and in the activity of benzoyl-L-tyrosine ethyl ester hydrolase from the yolk sac membrane during embryonic development of the chicken. *Poult. Sci.* **1986**, *65*, 789−794.
(24) Mann, K.; Mann, M. The chicken egg yolk plasma and granule proteomes. *Proteomics* **2007**, *8*, 178−191.
(25) Wisniewski, J. R.; Zougman, A.; Nagaraj, N.; Mann, M. Universal sample preparation method for proteome analysis. *Nat. Methods* **2009**, *6*, 359−362.
(26) Rappsilber, J.; Mann, M.; Ishihama, Y. Protocol for micro-purification, enrichment, pre-fractionation and storage of peptides for proteomics using StageTips. *Nat. Protoc.* **2007**, *2*, 1896−1906.
(27) Olsen, J. V.; Schwartz, J. C.; Griep-Raming, J.; Nielsen, M. L.; Damoc, E.; Denisov, E.; Lange, O.; Remes, P.; Taylor, D.; Splendore, M.; Wouters, E. R.; Senko, M.; Makarov, A.; Mann, M.; Horning, S. A dual pressure linear ion trap Orbitrap instrument with very high sequencing speed. *Mol. Cell. Proteomics* **2009**, *8*, 2759−2769.
(28) Mann, K.; Mann, M. In-depth analysis of the chicken egg white proteome using an LTQ Orbitrap Velos. *Proteome Sci.* **2011**, *9*, 7.
(29) Cox, J.; Mann, M. MaxQuant enables high peptide identification rates, individualized p.p.b.-range mass accuracies and proteome-wide protein quantification. *Nat. Biotechnol.* **2008**, *26*, 1367−1372.
(30) Cox, J.; Matic, I.; Hilger, M.; Nagaraj, N.; Selbach, M.; Olsen, J. V.; Mann, M. A practical guide to the MaxQuant computational platform for SILAC-based quantitative proteomics. *Nat. Protoc.* **2009**, *4*, 698−705.
(31) Cox, J.; Neuhauser, N.; Michalski, A.; Scheltema, R. A.; Olsen, J. V.; Mann, M. Andromeda: a peptide search engine integrated into the MaxQuant environment. *J. Proteome Res.* **2011**, *10*, 1794−1805.
(32) Luber, C. A.; Cox, J.; Lauterbach, H.; Fancke, B.; Selbach, M.; Tschopp, J.; Akira, S.; Wiegand, M.; Hochrein, H.; O'Keeffe, M.; Mann, M. Quantitative proteomics reveals subset-specific viral recognition in dendritic cells. *Immunity* **2010**, *32*, 279−289.
(33) West, A. P., Jr.; Herr, A. B.; Bjorkman, P. J. The chicken yolk sac IgY receptor, a functional equivalent of the mammalian MHC-related Fc receptor, is a phospholipase A2 receptor homolog. *Immunity* **2004**, *20*, 601−610.
(34) D'Ambrosio, C.; Arena, S.; Scaloni, A.; Guerrier, L.; Boschetti, E.; Mendieta, M. E.; Citterio, A.; Righetti, P. G. Exploring the chicken egg white proteome with combinatorial peptide ligand libraries. *J. Proteome Res.* **2008**, *7*, 3461−3474.
(35) Guerin-Dubiard, C.; Pasco, M.; Molle, D.; Desert, C.; Croguennec, T.; Nau, F. Proteomic analysis of hen egg white. *J. Agric. Food Chem.* **2006**, *54*, 3901−3910.
(36) Mann, K. The chicken egg white proteome. *Proteomics* **2007**, *7*, 3558−3568.
(37) Mann, K.; Mann, M. In-depth analysis of the chicken egg white proteome using an LTQ Orbitrap Velos. *Proteome Sci.* **2011**, *9*, No. 10.1186/1477-5956-9-7.
(38) Slade, B.; Milne, J. Localization and synthesis of alpha-fetoprotein in the chicken. *Cell Tissue Res.* **1977**, *180*, 411−9.
(39) Suzuki, M.; Fujimoto, W.; Goto, M.; Morimatsu, M.; Syuto, B.; Iwanaga, T. Cellular expression of gut Chitinase mRNA in the gastrointestinal tract of mice and chickens. *J. Histochem. Cytochem.* **2002**, *50*, 1081−1089.
(40) Neumann, U. Inhibition of in vitro lymphocyte blastogenesis by chicken alpha-fetoprotein. *Comp. Immunol. Microbiol. Infect. Dis.* **1984**, *7*, 43−52.
(41) Slade, B.; Milne, J. Ontogeny of alpha-fetoprotein in chicken. *Experientia* **1978**, *34*, 520−522.
(42) Nagano, Y.; Hamano, T.; Nakashima, N.; Ishikawa, M.; Miyazaki, K.; Hayashi, M. Yolk vitronectin. Purification and differences from its blood homologue in molecular size, heparin binding, collagen binding, and bound carbohydrate. *J. Biol. Chem.* **1992**, *267*, 24863−24870.
(43) van den Brand, H.; Reijrink, I. A. M.; Hoekstra, L. A.; Kemp, B. Storage of eggs in water affects internal egg quality, embryonic development, and hatchling quality. *Poult. Sci.* **2008**, *87*, 2350−2357.
(44) Barron, M.; McAllister, D.; Smith, S. M.; Lough, J. Expression of retinol binding protein and transthyretin during early embryogenesis. *Dev. Dyn.* **1998**, *212*, 413−422.
(45) Johansson, S.; Gustafson, A. L.; Donovan, M.; Romert, A.; Eriksson, U.; Dencker, L. Retinoid binding proteins in mouse yolk sac and chorio-allantoic placentas. *Anat. Embryol.* **1997**, *195*, 483−490.
(46) Jones, D. R.; Musgrove, M. T. Effects of extended storage on egg quality factors. *Poult. Sci.* **2005**, *84*, 1774−1777.
(47) Kido, S.; Janado, M.; Nunoura, H. Macromolecular components of the vitelline membrane of hen's egg. I. Membrane structure and its deterioration with age. *J. Biochem.* **1975**, *78*, 261−268.
(48) Omana, D. A.; Liang, Y.; Kav, N. N. V.; Wu, J. P. Proteomic analysis of egg white proteins during storage. *Proteomics* **2011**, *11*, 144−153.

(49) Johansson, S.; Gustafson, A. L.; Donovan, M.; Romert, A.; Eriksson, U.; Dencker, L. Retinoid binding proteins in mouse yolk sac and chorio-allantoic placentas. *Anat. Embryol.* **1997**, *195*, 483−490.
(50) Tragardh, L.; Anundi, H.; Rask, L.; Sege, K.; Peterson, P. A. On the stoichiometry of the interaction between prealbumin and retinol-binding protein. *J. Biol. Chem.* **1980**, *255*, 9243−9248.
(51) Vasudevan, N.; Bahadur, U.; Kondaiah, P. Characterization of chicken riboflavin carrier protein gene structure and promoter regulation by estrogen. *J. Biosci.* **2001**, *26*, 39−46.
(52) Maclachlan, I.; Nimpf, J.; Schneider, W. J. Avian riboflavin-binding-protein binds to lipoprotein receptors in association with vitellogenin. *J. Biol. Chem.* **1994**, *269*, 24127−24132.
(53) Tarhay, S. L.; Buss, E. G.; Clagett, C. O. Avian riboflavinuria 0.10. Quantitative changes of riboflavin-binding protein in individual egg tissues during incubation. *Poult. Sci.* **1975**, *54*, 562−571.
(54) Polytarchou, C.; Papadimitriou, E. Antioxidants inhibit angiogenesis in vivo through down-regulation of nitric oxide synthase expression and activity. *Free Radic. Res.* **2004**, *38*, 501−508.
(55) Bourin, M.; Gautron, J.; Berges, M.; Nys, Y.; Rehault-Godbert, S. Sex- and tissue-specific expression of "similar to nothepsin" and cathepsin D in relation to egg yolk formation in *Gallus gallus*. *Poult. Sci.* **2012**, *91*, 2288−2293.
(56) Rehault-Godbert, S.; Gautron, J. L.; Labas, V.; Belghazi, M.; Nys, Y. Identification and characterization of the precursor of chicken matrix metalloprotease 2 (pro-MMP-2) in hen egg. *J. Agric. Food Chem.* **2008**, *56*, 6294−6303.

the glucuronidation of resveratrol. Hence, it is important to evaluate the first-pass effect for stilbenes.

In this study, we investigated the absorption and metabolism of piceatannol in rats. We then determined the plasma concentration of piceatannol and identified its metabolites following intragastric administration. Furthermore, the AUC values for intact compounds and their respective metabolites were determined following administration of piceatannol and resveratrol, and the metabolic pathways were compared.

MATERIALS AND METHODS

Chemicals. Piceatannol (>98.0% purity), isorhapontigenin (>95.0% purity), and rhapontigenin (>98.0% purity) were obtained from Tokyo Chemical Industry (Tokyo, Japan). Resveratrol (>98.0% purity) was obtained from Cayman Chemical (Ann Arbor, MI). Sulfatase Type VIII from abalone entrails (EC 3.1.6.1) and β-glucuronidase Type X-A from *Escherichia coli* (EC 3.2.1.31) were obtained from Sigma (St. Louis, MO). All other reagents were purchased from Wako (Osaka, Japan) and Kanto Chemical (Tokyo, Japan), and were used without any other purification.

Animals and Treatments. Eight-week-old male Sprague−Dawley rats (Japan SLC, Shizuoka, Japan) were used in the study. The rats were housed individually in plastic cages in a room with controlled temperature (21−25 °C) and humidity (40−60%). The rats were maintained on a 12 h dark/light cycle with artificial lighting and received AIN-93G (Oriental Yeast, Tokyo, Japan) and water ad libitum. Following a conditioning period that lasted two or three days, the rats were anesthetized with pentobarbital and the right jugular vein was catheterized with silicone tubing (0.5 mm inner diameter (i.d.), 1.0 mm outer diameter). After the catheterization procedure, the rats were allowed a 1 week postoperative recovery period during which they were fed AIN-93G. Following the recovery period, the rats were fasted overnight and were then administered stilbenes. Thereafter, blood samples were collected from the rats. All animal experiments were carried out with strict compliance with the Guidelines for Proper Conduct of Animal Experiments by the Science Council of Japan. The experimental protocols and procedures were approved by the Animal Experimental Committee of Morinaga & CO., Ltd.

Experimental Design. Thirty-six cannulated rats were randomly assigned to six equal groups (n = 6) and transferred to plastic cages with stainless wire mesh floor mats. Each group was administered a different dose of piceatannol or resveratrol to evaluate the dose dependency of their absorption. Stilbene doses were based on the previous study by Marier et al.,[15] which examined resveratrol bioavailability and estimated a maximum concentration (C_{max}) of 6.57 ± 1.55 μmol/L and AUC of 7.1 ± 2.0 μmol·h/L following oral administration of 50 mg/kg (219 μmol/kg). The rats received piceatannol or resveratrol prepared with 50% (v/v) polyethylene glycol 400/saline through direct stomach intubation at doses of 90, 180, or 360 μmol/kg (22.0, 44.0, or 87.9 mg/kg for piceatannol and 20.5, 41.1, or 82.2 mg/kg for resveratrol; 2 mL/kg). Blood samples (0.4 mL) were collected from each rat before piceatannol or resveratrol administration, and at 0.25, 0.5, 1, 2, 4, 8, and 24 h after administration. The samples were collected into heparinized tubes directly from the jugular vein catheter. The rats were transferred to metabolic cages after the 8 h blood collection, where they received AIN-93G. The samples were centrifuged (4 °C, 10 min, 5000*g*), and 1/10 volume of a stabilizer (0.4% ascorbic acid/0.02% EDTA disodium/80 mmol/L sodium phosphate buffer, pH 3.6) was added to the plasma samples. Urine samples were collected using pipettes when urination was observed during the 8 h blood collection period, and 1/10 volume of the same stabilizer used for plasma samples was added to the urine samples. The urine samples were combined every four hours. After blood collection for 8 h, the rats were placed in metabolic cages and urine samples were collected in plastic tubes containing the stabilizer once between 8 and 12 h, once between 12 and 24 h, and once between 24 and 48 h following stilbene administration. Plasma and urine samples were stored at −30 °C until analysis.

In the coadministration study, 6 cannulated rats were given a mixture of piceatannol and resveratrol (each at 180 μmol/kg, 44.0 mg/kg for piceatannol and 41.1 mg/kg for resveratrol) through intragastric administration. Blood samples were collected and plasma samples were stored as described above.

Enzymatic Hydrolysis of Conjugated Metabolites in Biological Samples. We hydrolyzed the plasma samples to determine the total amount of piceatannol and resveratrol. The samples were hydrolyzed according to the method of Maeda-Yamamoto et al.,[21] but with slight modification. Briefly, 5 μL of β-glucuronidase (15.6 units) and 5 μL of sulfatase (1.3 units) were added to 50 μL of plasma samples diluted with 90 μL of sodium phosphate buffer (final concentration of 27 mmol/L; pH 6.5) and incubated at 37 °C for 45 min. The reaction was stopped with 300 μL of ice-cold acetonitrile (ACN) as described below.

Plasma Preparation for High-Performance Liquid Chromatography (HPLC) Analysis. Plasma aliquot samples (50 μL) were extracted with 100 μL of ice-cold ACN and centrifuged at 10000*g* for 10 min at 4 °C. The supernatant was transferred to another microcentrifuge tube, and the precipitate was washed with 100 μL of ice-cold ACN and then centrifuged. Thereafter, the supernatant was combined with the previous supernatant and evaporated to dryness in vacuo. The residue was redissolved in 50 μL of the initial mobile phase and used for HPLC analysis. Appropriate dilutions were performed when concentrations fell outside the analytical range (0.2−10 μmol/L). The mean recovery (at 0.2, 0.5, 1, 5, 10, and 50 μmol/L; n = 3) for piceatannol and resveratrol was 95.9% and 95.0%, respectively.

HPLC Analysis of Stilbenes. The stilbenes were analyzed using a Shimadzu (Kyoto, Japan) Prominence HPLC system equipped with an SPD-M20A photodiode array detector. The data were processed using LabSolutions chromatography workstation software (version 1.21; Shimadzu). Chromatographic separations were performed on a Mightysil RP-18 GP ODS column (150 × 4.6 mm i.d., 5 μm; Kanto Chemical) equipped with a Mightysil RP-18 GP guard column (5 × 4.6 mm i.d., 5 μm; Kanto Chemical) at 40 °C, with 0.1% (v/v) phosphoric acid/water as mobile phase A, and 0.1% (v/v) phosphoric acid/ACN as mobile phase B at a flow rate of 1 mL/min. Sample aliquots (10 μL) were injected into the HPLC system and were eluted with the following gradient conditions: 0−2 min, 14% B; 2−30 min, 14−30% B. The eluate was monitored at 320 nm by the detector. Calibration curves were prepared by supplementation with known concentrations (0.2, 0.5, 1, 2, 5, and 10 μmol/L) of piceatannol, resveratrol, isorhapontigenin, and rhapontigenin in the initial mobile phase. The correlation coefficients evaluated by linear regression analysis were 0.999 or above. The limit of detection (LOD) and the limit of quantitation (LOQ) were defined as the concentrations of the stilbenes spiked into blank plasma and prepared according to the method described in the previous section that produced a signal-to-noise ratio of at least 3 and 10, respectively. The LOD and LOQ for stilbenes were 0.1 μmol/L and 0.2 μmol/L, respectively. The intraday and interday precision of assay were assessed with two concentrations as quality control samples (0.5 and 10 μmol/L stilbenes in blank plasma) in triplicate, with precision estimates ranging from 1.0 to 9.4%.

Identification of Stilbene Metabolites. Major metabolites of piceatannol and resveratrol were fractionated from the rat urine samples using the same HPLC system and column described above. Urine aliquot samples (5 μL) were prepared according to the method used for the plasma samples injected into the HPLC system. Elution was carried out with a mixture of 0.1 mmol/L acetic acid/water and ACN at a flow rate of 1 mL/min at 40 °C. The gradient conditions were as follows: (a) 0−2 min, 10% ACN, and (b) 2−50 min, 10−30% ACN. Each peak was monitored at 320 nm and collected individually. The collected peaks were evaporated to dryness in vacuo and dissolved in 50 μL of 0.1% (v/v) formic acid/10% ACN/water.

The fractionated peak aliquots (10 μL) were injected into a Shimadzu Prominence ultrafast liquid chromatography (UFLC) system equipped with a Kinetex 2.6 μm C18 100 Å ODS column

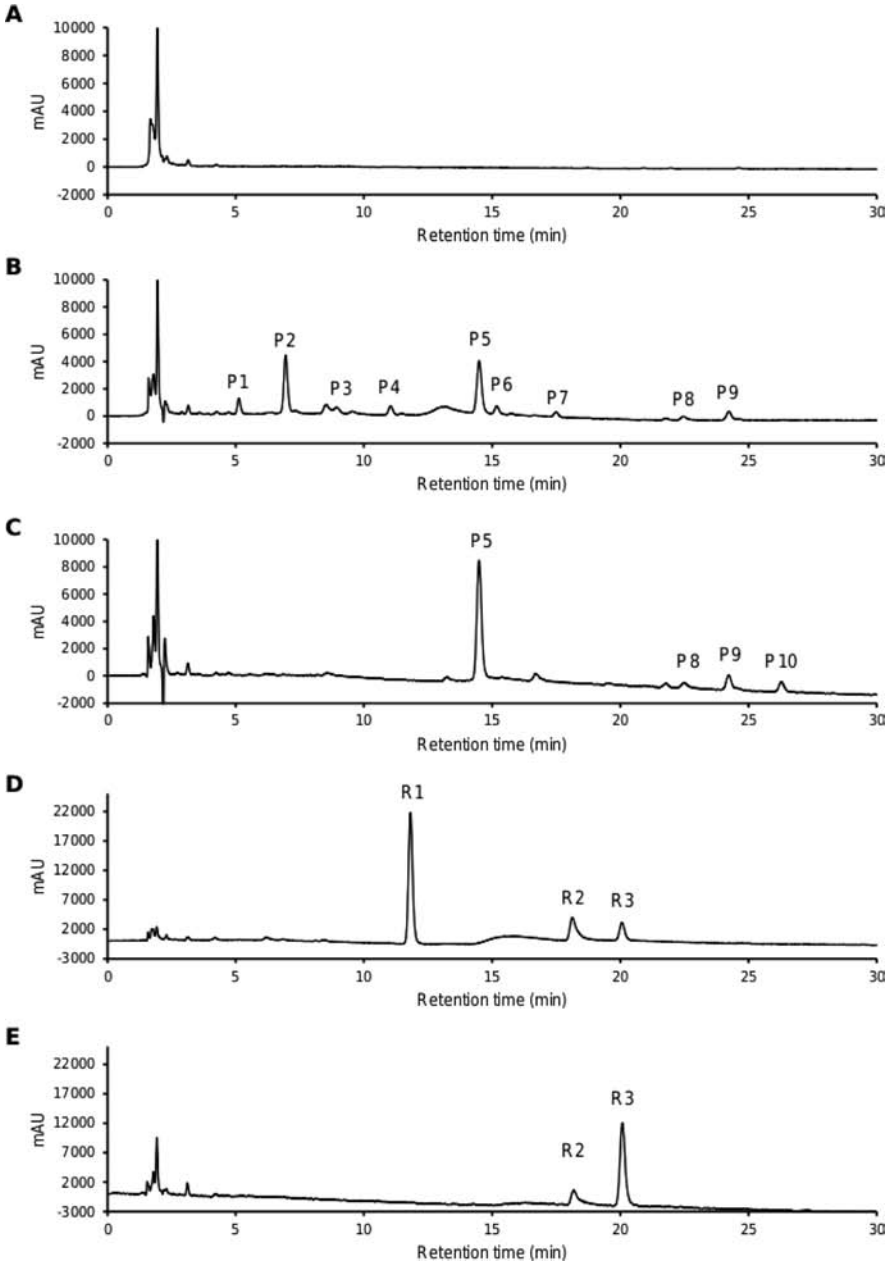

Figure 2. Representative high-performance liquid chromatography (HPLC) chromatograms of rat plasma samples before and 0.5 h after intragastric administration of 360 μmol of stilbene per kg of body weight: (A) before administration; (B) administration of piceatannol; (C) administration of piceatannol, hydrolyzed with enzymes; (D) administration of resveratrol; (E) administration of resveratrol, hydrolyzed with enzymes.

(100 × 2.1 mm i.d.; Phenomenex, Torrance, CA). Elution was carried out at 40 °C, with 0.1% (v/v) formic acid/water as mobile phase A, and 0.1% (v/v) formic acid/ACN as mobile phase B; both were carried out with a flow rate of 0.2 mL/min. The gradient conditions were as follows: (a) 0−2 min, 10% B, and (b) 2−40 min, 10−25% B. The eluate was monitored at 320 nm by using a Shimadzu SPD-M20A. Mass spectrometry analysis was performed using a 3200 QTRAP system (AB SCIEX, Framingham, MA) with an electrospray ionization source. Electrospray ionization tandem mass spectrometry was performed in negative polarity mode with the following settings: curtain gas, 40 psi; nebulizer gas, 50 psi; turbo gas, 80 psi; capillary temperature, 600 °C; ion spray voltage, −4.5 kV; declustering potential, −40 V; and collision energy, −30 V. The full-scan mass spectrum to obtain product ion of the metabolite was collected in the mass range from m/z 100 to 1000.

Data Analysis. Experimental values are expressed as the mean ± SEM. The AUC was calculated using the linear trapezoidal method. The ratio of intact (unmetabolized) compound to total detected signal was calculated by dividing the AUC corresponding to the peak of the intact compound by the total AUC (sum of intact and all metabolites). Linear regression analysis was used to assess the association between the dose and plasma AUC. Statistical significance of differences in mean values between AUC values for piceatannol and resveratrol was evaluated using 2-way analysis of variance (ANOVA) in the individual administration study, and was evaluated by paired sample t-test in the coadministration study. Repeated-measures ANOVA was used to evaluate the time-dependent variation in plasma concentrations between piceatannol and resveratrol for the coadministration study. Student's t-test was used to evaluate the differences in mean AUC values between individual administration and coadministration. Differences were considered statistically significant when $p < 0.05$. All statistical analyses were performed using SPSS version 13.0 J for Windows (SPSS, Tokyo, Japan).

RESULTS

Identification of Piceatannol Metabolites. Figure 2 shows representative HPLC chromatograms of rat plasma samples before and after intragastric administration of piceatannol or resveratrol. No remarkable peak was observed in the plasma before administration (Figure 2A), whereas piceatannol (P5) and several metabolite peaks were detected following piceatannol administration (Figure 2B). Piceatannol and P9 markedly increased together, whereas several peaks (P1, P2, P3, P4, P6, and P7) disappeared when the plasma was hydrolyzed with enzymes (Figure 2C). Moreover, P10 was newly produced after plasma hydrolysis. Resveratrol was undetected in the plasma of any rat that received piceatannol. Following resveratrol administration, a resveratrol peak (R3) was detected in rat plasma with two remarkable hydrophilic peaks (R1 and R2; Figure 2D). When the plasma was hydrolyzed with enzymes, R1 disappeared and R2 only slightly decreased, but resveratrol increased dramatically (Figure 2E). Piceatannol, isorhapontigenin, and rhapontigenin were undetected in the plasma of rats that received resveratrol.

The peaks indicating the metabolites found in rat plasma (P1−P10, R1−R3) were also observed in rat urine (Figure S1 in the Supporting Information); thus, we fractionated the metabolites from urine and identified their mass spectra (Figure S2 in the Supporting Information). Table 1 summarizes the mass spectra for the piceatannol and resveratrol metabolites fractionated from rat urine. As the table indicates, various piceatannol conjugate metabolites were identified. Based on the mass spectra and the disappearance of the peaks after hydrolysis, P1 (m/z 595/419/243) was identified as a diglucuronide metabolite of piceatannol, and both P2 (m/z 419/243) and P4 (m/z 419/243) were identified as monoglucuronide metabolites of piceatannol. Likewise, P3 (m/z 433/257), P6 (m/z 433/257), and P7 (m/z 433/257) were identified as *O*-methyl piceatannol-monoglucuronide metabolites. Although P8 was not hydrolyzed by sulfatase, P8 was considered an *O*-methyl piceatannol-monosulfate metabolite based on the mass spectrum (m/z 337/257). The mass spectra for P9 and P10 were similar to that for *O*-methyl piceatannol. Based on the retention time and the mass spectrum, P9 was identified as isorhapontigenin (3,4′,5-trihydroxy-3′-methoxystilbene; Figure 1) and P10 was identified as rhapontigenin (3,3′,5-trihydroxy-4′-methoxystilbene). In addition to the nine metabolites, other peaks speculated to be piceatannol metabolites were observed in small amounts, but the mass spectra were unidentified. The mass spectra of R1 and R2 fractionated from rat urine after resveratrol administration confirmed that R1 and R2 were conjugate metabolites of resveratrol.

Table 1. Mass Spectra of Metabolites of Piceatannol and Resveratrol

peak	t_R[a]	compound	parent and product ion pairs (m/z)
P1	5.1	piceatannol-diglucuronide	595/419/243
P2	6.9	piceatannol-monoglucuronide	419/243
P3	8.9	*O*-methyl piceatannol-monoglucuronide	433/257
P4	11.0	piceatannol-monoglucuronide	419/243
P5	14.5	piceatannol	243
P6	15.2	*O*-methyl piceatannol-monoglucuronide	433/257
P7	17.5	*O*-methyl piceatannol-monoglucuronide	433/257
P8	22.5	*O*-methyl piceatannol-monosulfate	337/257
P9	24.2	isorhapontigenin	257
P10	26.3	rhapontigenin	257
R1	11.8	resveratrol-monoglucuronide	403/227
R2	18.1	resveratrol-monosulfate	307/227
R3	20.1	resveratrol	227

[a]HPLC retention time.

Plasma Concentration Profiles of Stilbenes. Figure 3 shows the time-dependent plasma concentration profiles for piceatannol and its metabolites following piceatannol administration. Piceatannol and isorhapontigenin were detected in rat plasma, whereas rhapontigenin was undetected at any dose (Figure 3A). Piceatannol reached the C_{max} within 15 min of administration, with the measured C_{max} of 3.3 μmol/L following the 90 μmol/kg dose, 7.5 μmol/L following 180 μmol/kg, and 8.1 μmol/L following 360 μmol/kg. Piceatannol concentration for any dose subsequently declined over time to an undetectable level at 24 h. Isorhapontigenin showed a profile similar to that of piceatannol until 1 h after administration, but at lower concentrations. Isorhapontigenin concentration was almost constant between 1 and 8 h, and trace amounts of isorhapontigenin were detected at 24 h only following 360 μmol/kg administration. The plasma concentration of piceatannol and isorhapontigenin were increased with elevating doses, except the C_{max} of piceatannol between the doses of 180 and 360 μmol/kg.

Conjugate metabolites of intact and *O*-methyl piceatannol were detected in rat plasma after piceatannol administration (Figure 3B). Since P8 was not hydrolyzed, its levels were quantified using the calibration curve for piceatannol and are shown as *O*-methyl piceatannol-monosulfate in Figure 3B. Piceatannol conjugates were the dominant metabolites in plasma up to 2 h after 90 and 180 μmol/kg administration and up to 4 h after 360 μmol/kg administration, but could not be detected at 24 h. Conversely, *O*-methyl piceatannol conjugates were still detectable at 24 h, except for isorhapontigenin conjugates following 90 μmol/kg administration, and *O*-methyl piceatannol-monosulfate following 90 and 180 μmol/kg administration. The plasma concentration of conjugates of intact and *O*-methyl piceatannol was increased with elevating doses.

Plasma concentration reached the C_{max} within 15 min of resveratrol administration, with the C_{max} determined to be 3.8, 3.5, and 5.0 μmol/L following administration of 90, 180, and 360 μmol/kg, respectively (Figure S3 in the Supporting Information). Although the concentration of resveratrol declined within 2 h, secondary peaks appeared at 4 h and were notable following 360 μmol/kg administration, and very small following 180 μmol/kg administration. The plasma concentrations of resveratrol conjugates, including that of R2 quantified using the calibration curve for resveratrol, were much higher than the concentrations of the intact resveratrol. In the analysis of conjugates, notable secondary peaks appeared following 360 μmol/kg resveratrol administration, and, with lower peak AUC, following 180 μmol/kg administration. The concentration of resveratrol and its conjugates tended to increase with higher doses of resveratrol.

The AUC for piceatannol and resveratrol increased in a dose-dependent manner (Table 2). The correlation between AUC and the administered dose was well described by a linear

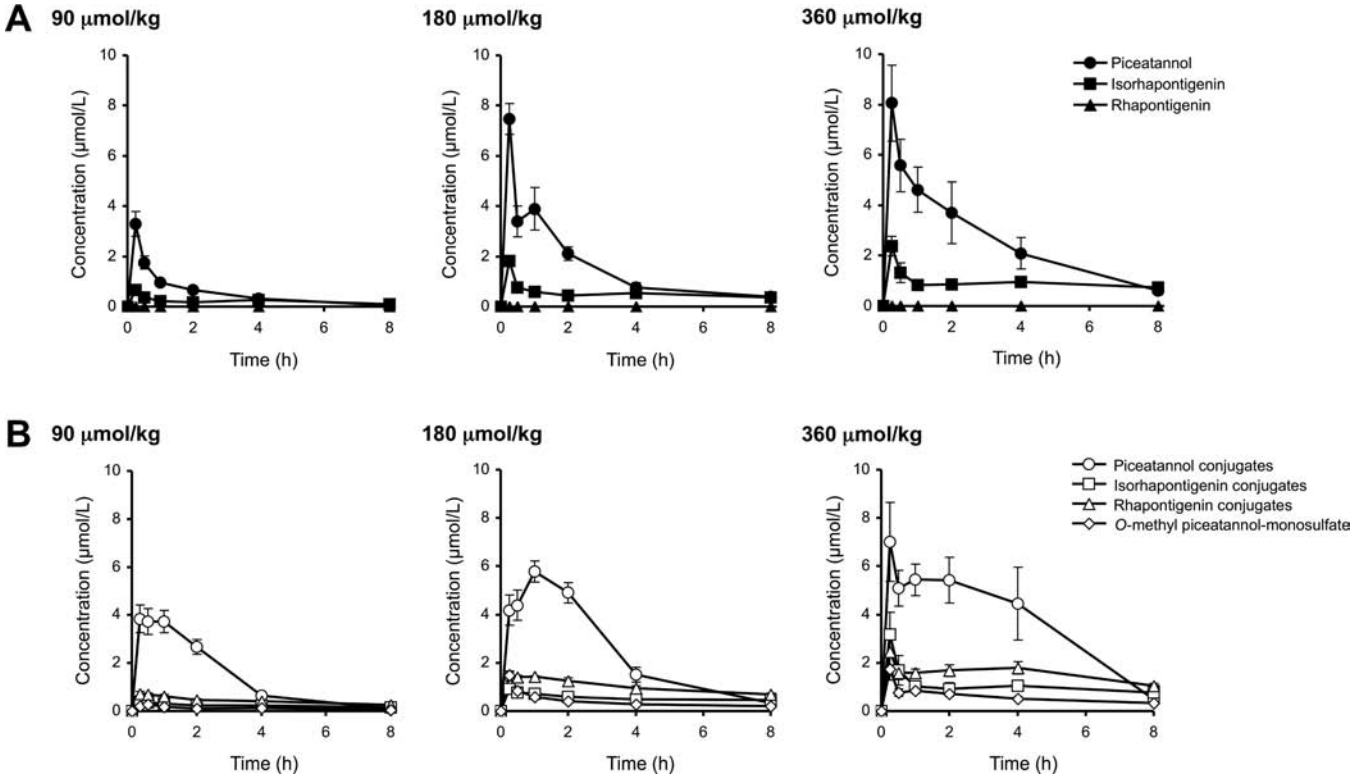

Figure 3. Plasma concentration profiles for piceatannol and its metabolites after intragastric administration of 90−360 μmol of piceatannol per kg of body weight: (A) aglycon and (B) conjugates. Values are expressed as mean ± SEM (n = 6).

regression model, with the coefficients of determination (R^2) for piceatannol and resveratrol estimated as 0.770 and 0.907, respectively. Some correlation between the administered dose and AUC of piceatannol conjugates was detected (R^2 = 0.486), with the AUC increasing with higher doses. The relationship of the AUC with dose for *O*-methyl piceatannol metabolites, resveratrol conjugates, and total piceatannol and resveratrol was good, with R^2 ranging from 0.688 to 0.945. The AUC values for piceatannol were 2.1- to 2.6-fold higher than those for resveratrol, with statistically significant differences found in all comparisons, except for administration of 90 μmol/kg. The total AUC calculated following piceatannol administration was significantly lesser than the AUC calculated for resveratrol. The ratio of intact compound to the total AUC for piceatannol was 3.7- to 4.3-fold higher than the ratio for resveratrol (p < 0.05).

Comparison between Piceatannol and Resveratrol Plasma Concentrations after Coadministration. Plasma concentration was compared between piceatannol and resveratrol after administering a mixture of these two stilbenes (each at 180 μmol/kg). The C_{max} of piceatannol was 4.2 μmol/L at 15 min, whereas the C_{max} of resveratrol was 1.6 μmol/L at 30 min (Figure 4A). Piceatannol concentration was maintained at a level higher than that of resveratrol for up to 8 h following administration. Furthermore, the AUC for piceatannol was 2.1-fold greater than that for resveratrol (p < 0.05; Table 3). In contrast, the total concentration corresponding to piceatannol was less than that associated with resveratrol administration, with statistically significant differences detected at 0.25, 0.5, and 2 h after administration (Figure 4B). Furthermore, the AUC for total piceatannol was significantly less than that for resveratrol. The intact ratio for piceatannol was 3.0-fold higher than that for resveratrol (p < 0.05). The statistically significant differences in AUC values between individual administration and coadministration were detected only for conjugates of isorhapontigenin and rhapontigenin, whereas no significant differences in AUC values of intact compounds or of other metabolites of piceatannol and resveratrol were observed.

DISCUSSION

The focus of our research was to evaluate absorption and metabolism of piceatannol following intragastric administration in rats. Roupe et al. described that only a glucuronide metabolite was evident in rat plasma after intravenous administration of piceatannol.[8] In our study, a monoglucuronide metabolite (P2) was the most abundant metabolite following intragastric administration of piceatannol. However, a number of additional metabolites were also observed in plasma. The difference in the diversity of metabolites identified between the study of Roupe et al. and the current study may be due to differences in the administration routes or, more likely, due to different analytical methods used. In addition to three conjugate metabolites (P1, P2, and P4), four *O*-methyl piceatannol conjugates (P3, P6, P7, and P8) and isorhapontigenin (P9) were identified by liquid chromatography−tandem mass spectrometry (Table 1). In contrast to piceatannol, methylated metabolites were not found with resveratrol. The occurrence of methylation only in piceatannol indicates that the catechol ring of piceatannol was metabolized by catechol-*O*-methyltransferase, as in the case of flavonoids.[22−24] The disappearance of *O*-methyl piceatannol conjugates with plasma hydrolysis was accompanied by an increase in isorhapontigenin and the appearance of rhapontigenin. Therefore, the *O*-methyl piceatannol conjugates (P3, P6, P7, and P8) were considered conjugates of isorhapontigenin and rhapontigenin. The nine piceatannol metabolites shown in Table 1 indicate the major metabolic pathway for piceatannol, involving glucuronidation,

dx.doi.org/10.1021/jf404694y | J. Agric. Food Chem. 2014, 62, 2541−2548

Table 2. Cumulative Plasma AUCs after Intragastric Administration of Piceatannol and Resveratrol to Rats

		AUC_{0-8h}[b] (μmol·h/L)		coefficient of determination[d]		statistical significance between stilbenes[e]	
	dose (μmol/kg)	piceatannol	resveratrol	piceatannol	resveratrol	main effect	simple main effect
intact	90	4.3 ± 0.3	2.0 ± 0.2	0.770	0.907		−
	180	12.3 ± 1.8	4.7 ± 0.4				+
	360	20.6 ± 2.2	8.6 ± 0.4				+
conjugates	90	11.3 ± 1.1	37.6 ± 1.6	0.486	0.938		+
	180	19.5 ± 1.7	79.6 ± 4.9				+
	360	30.2 ± 5.8	118.8 ± 4.1				+
isorhapontigenin	90	1.7 ± 0.2	nd[c]	0.858			
	180	4.2 ± 0.3	nd				
	360	7.4 ± 0.6	nd				
isorhapontigenin conjugates	90	1.9 ± 0.2	nd	0.688			
	180	4.3 ± 0.3	nd				
	360	8.3 ± 1.3	nd				
rhapontigenin	90	nd	nd				
	180	nd	nd				
	360	nd	nd				
rhapontigenin conjugates	90	3.3 ± 0.3	nd	0.796			
	180	8.1 ± 0.6	nd				
	360	12.4 ± 1.3	nd				
O-methyl piceatannol-monosulfate	90	1.0 ± 0.1	nd	0.885			
	180	3.0 ± 0.1	nd				
	360	4.7 ± 0.4	nd				
total	90	23.5 ± 1.6	39.6 ± 1.7	0.788	0.945		+
	180	51.4 ± 1.4	84.3 ± 5.0				+
	360	83.5 ± 9.6	127.4 ± 4.1				+
intact ratio[a] (%)	90	18.6 ± 1.3	5.1 ± 0.5			+	
	180	23.9 ± 3.3	5.6 ± 0.5				
	360	25.1 ± 1.4	6.8 ± 0.4				

[a]Intact ratio was calculated by dividing the AUC corresponding to the peak of the intact compound by the total AUC, and expressed as a percentage. [b]Values are expressed as mean ± SEM (n = 6). [c]Not detected. [d]Linear regression analysis was used to assess the association between the stilbene dose and plasma AUC. The analysis demonstrated a statistically significant correlation between the dose and AUC for all compounds ($p < 0.05$). [e]Statistical significance of differences in mean values between AUC values for stilbenes was assessed using 2-way ANOVA. When a significant interaction was detected ($p < 0.05$), simple main effect was analyzed for each dose. +, significant difference; −, no significant difference.

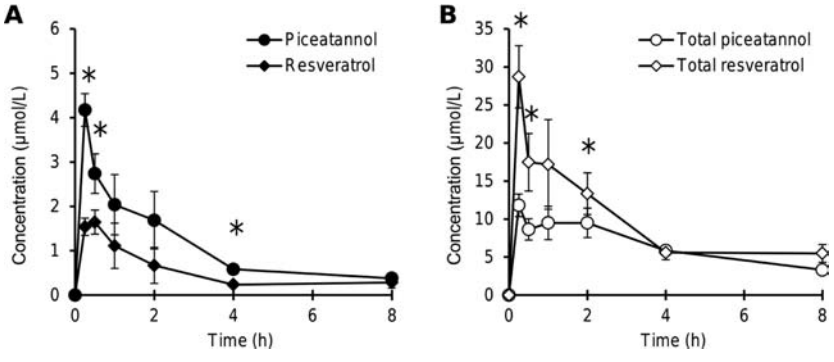

Figure 4. Plasma concentration profiles of piceatannol and resveratrol after intragastric coadministration at 180 μmol per kg of body weight: (A) intact stilbene and (B) total stilbene. Values are expressed as mean ± SEM (n = 6). *Statistically significant differences ($p < 0.05$) between stilbenes were evaluated by using repeated-measures ANOVA.

dx.doi.org/10.1021/jf404694y | J. Agric. Food Chem. 2014, 62, 2541−2548

Table 3. Cumulative Plasma AUCs after Intragastric Co-administration of Piceatannol and Resveratrol to Rats

	AUC_{0-8h}[b] (μmol h/L)	
	piceatannol	resveratrol
intact	8.6 ± 1.3 a	4.1 ± 1.0 b
conjugates	18.8 ± 1.8 a	70.2 ± 5.8 b
isorhapontigenin	4.7 ± 0.6	nd[c]
isorhapontigenin conjugates	6.4 ± 0.8	nd
rhapontigenin	nd	nd
rhapontigenin conjugates	10.2 ± 0.7	nd
O-methyl piceatannol-monosulfate	3.0 ± 0.4	nd
total	51.7 ± 4.4 a	74.3 ± 6.0 b
intact ratio[a] (%)	16.3 ± 1.7 a	5.5 ± 1.3 b

[a]Intact ratio was calculated by dividing the AUC corresponding to the peak of the intact compound by the total AUC, and expressed as a percentage. [b]Values are expressed as mean ± SEM (n = 6). Different letters (a, b) in the same row indicate significant differences ($p < 0.05$) determined using paired sample t-test. [c]Not detected.

sulfation, and methylation. Compared to piceatannol, only two conjugate metabolites (R1 and R2) were detected in the plasma of the rats that received resveratrol. In recent studies, dihydroresveratrol and its conjugates, which are microbiota-derived metabolites, were detected in rat liver, adipose tissue, skeletal muscle, and the colon content following repeated oral administration of 30 and 60 mg/kg resveratrol,[18,20] but not in the plasma.[20] We acquired HPLC chromatograms at 276 nm, the maximal absorbance for quantification of dihydroresveratrol, but no noticeable peak corresponded to a dihydro metabolite of resveratrol. It was not possible at this point to explore the possible presence or absence of the dihydroresveratrol metabolite in rat plasma, because dihydroresveratrol standard was not available. Even though unidentified metabolites of resveratrol were present in the plasma in our study, piceatannol could conceivably have a more complicated metabolic pathway due to the presence of a catechol ring, which enables methylation and increases the number of pathways available for its metabolism. Further studies are required to elucidate piceatannol metabolism.

A remarkable finding was that isorhapontigenin was detected in the intact form as a piceatannol metabolite in rat plasma, whereas, similar to flavonoids,[22,23] rhapontigenin was found only in conjugated forms. Isorhapontigenin has antioxidant, antiarteriosclerosis, and anticancer effects.[25−27] In particular, isorhapontigenin promotes inhibition of cyclooxygenase-1 and cyclooxygenase-2, whereas piceatannol does not.[27] Therefore, piceatannol can exhibit additional biological functions when it is metabolized to isorhapontigenin.

The AUCs for piceatannol and resveratrol increased in a dose-dependent manner after their intragastric administration (Table 2). These results indicate that stilbene absorption was not saturated with doses that ranged between 90 and 360 μmol/kg. Therefore, piceatannol and resveratrol were simultaneously administered at 180 μmol/kg. We had two concerns with the coadministration study. First, previous studies that examined resveratrol metabolism in vitro or in athymic mice found that resveratrol was metabolized to piceatannol.[28−30] In the present study, we did not detect piceatannol in rat plasma or urine after resveratrol administration. The reasons for the disagreement between our results and those of the previous study are unclear. We suspect the disparity might result from the differences between rats and athymic mice, or between in vivo and in vitro conditions. Similar disparities were observed with apigenin metabolism between in vivo and in vitro studies.[31] Therefore, we conclude that the piceatannol measured in rat plasma in the present study was from the administered dose, and not a resveratrol metabolite. Our second concern was that, in some cases, the bioavailability of polyphenols was affected by other compounds ingested simultaneously, and the AUCs for these polyphenols were higher than expected.[32−34] However, in our study, the AUC values for intact and total piceatannol or resveratrol in the coadministration study were similar to those in the individual administration study, and no statistically significant difference was observed between the administration methods. These results indicate that coadministration of piceatannol and resveratrol did not affect the absorption and metabolism of either stilbene. Hence, piceatannol was absorbed at levels that were 2-fold higher than those for resveratrol in the intact form. This finding predicts strong biological activity for piceatannol. In contrast, the total amount of piceatannol absorbed through the gastrointestinal tract into blood circulation (AUC for total) was significantly lower than that for resveratrol. Therefore, these findings indicate that piceatannol is more stable than resveratrol in metabolism.

In conclusion, we determined that the metabolic pathway for piceatannol is more complicated than that for resveratrol; piceatannol metabolism involves conjugation, methylation, or both. Furthermore, we showed that the AUC for intact piceatannol was higher than that of intact resveratrol. A greater AUC for intact piceatannol likely contributes to its important biological functions. Further studies examining the biological fate of piceatannol are required to determine its efficacy, and to determine its biological activity following administration.

■ ASSOCIATED CONTENT

Supporting Information

Figure S1: Representative HPLC chromatograms of rat urine samples after intragastric administration of 360 μmol/kg stilbene. Figure S2: Representative liquid chromatography−tandem mass spectrometry chromatograms and full scan product ion mass spectra of fractionated rat urine samples after intragastric administration of 360 μmol/kg stilbene. Figure S3: Plasma concentration profiles for resveratrol and its metabolites after intragastric administration of 90−360 μmol/kg resveratrol. This material is available free of charge via the Internet at http://pubs.acs.org.

■ AUTHOR INFORMATION

Corresponding Author

*Tel: +81-45-791-7670. Fax: +81-45-791-7675. E-mail: y-setoguchi-ia@morinaga.co.jp.

Notes

The authors declare no competing financial interest.

■ ACKNOWLEDGMENTS

The authors thank Professor Yukihiro Nakabou of Kawasaki University of Medical Welfare and Professor Yasuhiro Kido of Kyoto Prefectural University for their technical guidance with catheterization, and Dr. Eisaku Nishimura and Masahiko Sai of Morinaga CO., Ltd., for comments on this paper.

ABBREVIATIONS USED

AUC, area under the plasma concentration curve; i.d., inner diameter; C_{max}, maximum concentration; ACN, acetonitrile; ANOVA, analysis of variance; HPLC, high-performance liquid chromatography; LOD, limit of detection; LOQ, limit of quantitation; R^2, coefficient of determination; UFLC, ultrafast liquid chromatography

REFERENCES

(1) Piotrowska, H.; Kucinska, M.; Murias, M. Biological activity of piceatannol: Leaving the shadow of resveratrol. *Mutat. Res.* **2012**, *750*, 60−82.

(2) Matsui, Y.; Sugiyama, K.; Kamei, M.; Takahashi, T.; Suzuki, T.; Katagata, Y.; Ito, T. Extract of passion fruit (*Passiflora edulis*) seed containing high amounts of piceatannol inhibits melanogenesis and promotes collagen synthesis. *J. Agric. Food Chem.* **2010**, *58*, 11112−11118.

(3) Smoliga, J. M.; Baur, J. A.; Hausenblas, H. A. Resveratrol and health—A comprehensive review of human clinical trials. *Mol. Nutr. Food Res.* **2011**, *55*, 1129−1141.

(4) Howitz, K. T.; Bitterman, K. J.; Cohen, H. Y.; Lamming, D. W.; Lavu, S.; Wood, J. G.; Zipkin, R. E.; Chung, P.; Kisielewski, A.; Zhang, L. L.; Scherer, B.; Sinclair, D. A. Small molecule activators of sirtuins extend *Saccharomyces cerevisiae* lifespan. *Nature* **2003**, *425*, 191−196.

(5) Kinoshita, Y.; Kawakami, S.; Yanae, K.; Sano, S.; Uchida, H.; Inagaki, H.; Ito, T. Effect of long-term piceatannol treatment on eNOS levels in cultured endothelial cells. *Biochem. Biophys. Res. Commun.* **2013**, *430*, 1164−1168.

(6) Sano, S.; Sugiyama, K.; Ito, T.; Katano, Y.; Ishihata, A. Identification of the strong vasorelaxing substance scirpusin B, a dimer of piceatannol, from passion fruit (*Passiflora edulis*) seeds. *J. Agric. Food Chem.* **2011**, *59*, 6209−6213.

(7) Maruki-Uchida, H.; Kurita, I.; Sugiyama, K.; Sai, M.; Maeda, K.; Ito, T. The protective effects of piceatannol from passion fruit (*Passiflora edulis*) seeds in UVB-irradiated keratinocytes. *Biol. Pharm. Bull.* **2013**, *36*, 845−849.

(8) Roupe, K. A.; Yáñez, J. A.; Teng, X. W.; Davies, N. M. Pharmacokinetics of selected stilbenes: rhapontigenin, piceatannol and pinosylvin in rats. *J. Pharm. Pharmacol.* **2006**, *58*, 1443−1450.

(9) Miksits, M.; Maier-Salamon, A.; Vo, T. P. N.; Sulyok, M.; Schuhmacher, R.; Szekeres, T.; Jäger, W. Glucuronidation of piceatannol by human liver microsomes: major role of UGT1A1, UGT1A8 and UGT1A10. *J. Pharm. Pharmacol.* **2010**, *62*, 47−54.

(10) Miksits, M.; Sulyok, M.; Schuhmacher, R.; Szekeres, T.; Jäger, W. In-vitro sulfation of piceatannol by human liver cytosol and recombinant sulfotransferases. *J. Pharm. Pharmacol.* **2009**, *61*, 185−191.

(11) Wenzel, E.; Somoza, V. Metabolism and bioavailability of *trans*-resveratrol. *Mol. Nutr. Food Res.* **2005**, *49*, 472−481.

(12) Cottart, C. H.; Nivet-Antoine, V.; Laguillier-Morizot, C.; Beaudeux, J. L. Resveratrol bioavailability and toxicity in humans. *Mol. Nutr. Food Res.* **2010**, *54*, 7−16.

(13) Walle, T. Bioavailability of resveratrol. *Ann. N.Y. Acad. Sci.* **2011**, *1215*, 9−15.

(14) Amri, A.; Chaumeil, J. C.; Sfar, S.; Charrueau, C. Administration of resveratrol: What formulation solutions to bioavailability limitations? *J. Controlled Release* **2012**, *158*, 182−193.

(15) Marier, J. F.; Vachon, P.; Gritsas, A.; Zhang, J.; Moreau, J. P.; Ducharme, M. P. Metabolism and disposition of resveratrol in rats: Extent of absorption, glucuronidation, and enterohepatic recirculation evidenced by a linked-rat model. *J. Pharmacol. Exp. Ther.* **2002**, *302*, 369−373.

(16) Cottart, C. H.; Nivet-Antoine, V.; Beaudeux, J. L. Review of recent data on the metabolism, biological effects, and toxicity of resveratrol in humans. *Mol. Nutr. Food Res.* **2014**, *58*, 7−21.

(17) Azorín-Ortuño, M.; Yáñez-Gascón, M. J.; Vallejo, F.; Pallarés, F. J.; Larrosa, M.; Lucas, R.; Morales, J. C.; Tomás-Barberán, F. A.; García-Conesa, M. T.; Espín, J. C. Metabolites and tissue distribution of resveratrol in the pig. *Mol. Nutr. Food Res.* **2011**, *55*, 1154−1168.

(18) Andres-Lacueva, C.; Macarulla, M. T.; Rotches-Ribalta, M.; Boto-Ordóñez, M.; Urpi-Sarda, M.; Rodríguez, V. M.; Portillo, M. P. Distribution of resveratrol metabolites in liver, adipose tissue, and skeletal muscle in rats fed different doses of this polyphenol. *J. Agric. Food Chem.* **2012**, *60*, 4833−4840.

(19) Wenzel, E.; Soldo, T.; Erbersdobler, H.; Somoza, V. Bioactivity and metabolism of *trans*-resveratrol orally administered to Wistar rats. *Mol. Nutr. Food Res.* **2005**, *49*, 482−494.

(20) Alfaras, I.; Juan, M. E.; Planas, J. M. *trans*-Resveratrol reduces precancerous colonic lesions in dimethylhydrazine-treated rats. *J. Agric. Food Chem.* **2010**, *58*, 8104−8110.

(21) Maeda-Yamamoto, M.; Ema, K.; Tokuda, Y.; Monobe, M.; Tachibana, H.; Sameshima, Y.; Kuriyama, S. Effect of green tea powder (*Camellia sinensis* L. cv. Benifuuki) particle size on *O*-methylated EGCG absorption in rats; The Kakegawa Study. *Cytotechnology* **2011**, *63*, 171−179.

(22) Piskula, M. K.; Terao, J. Accumulation of (-)-epicatechin metabolites in rat plasma after oral administration and distribution of conjugation enzymes in rat tissues. *J. Nutr.* **1998**, *128*, 1172−1178.

(23) Graf, B. A.; Mullen, W.; Caldwell, S. T.; Hartley, R. C.; Duthie, G. G.; Lean, M. E. J.; Crozier, A.; Edwards, C. A. Disposition and metabolism of [2−14C]quercetin-4′-glucoside in rats. *Drug Metab. Dispos.* **2005**, *33*, 1036−1043.

(24) Chen, Z.; Chen, M.; Pan, H.; Sun, S.; Li, L.; Zeng, S.; Jiang, H. Role of catechol-*O*-methyltransferase in the disposition of luteolin in rats. *Drug Metab. Dispos.* **2011**, *39*, 667−674.

(25) Wang, Q. L.; Lin, M.; Liu, G. T. Antioxidative activity of natural isorhapontigenin. *Jpn. J. Pharmacol.* **2001**, *87*, 61−66.

(26) Liu, Y.; Liu, G. Isorhapontigenin and resveratrol suppress oxLDL-induced proliferation and activation of ERK1/2 mitogen-activated protein kinases of bovine aortic smooth muscle cells. *Biochem. Pharmacol.* **2004**, *67*, 777−785.

(27) Lee, D.; Cuender, M.; Vigo, J. S.; Graham, J. G.; Cabieses, F.; Fong, H. H. S.; Pezzuto, J. M.; Kinghorn, A. D. A novel cyclooxygenase-inhibitory stilbenolignan from the seeds of *Aiphanes aculeata*. *Org. Lett.* **2001**, *3*, 2169−2171.

(28) Niles, R. M.; Cook, C. P.; Meadows, G. G.; Fu, Y. M.; McLaughlin, J. L.; Rankin, G. O. Resveratrol is rapidly metabolized in athymic (Nu/Nu) mice and does not inhibit human melanoma xenograft tumor growth. *J. Nutr.* **2006**, *136*, 2542−2546.

(29) Potter, G. A.; Patterson, L. H.; Wanogho, E.; Perry, P. J.; Butler, P. C.; Ijaz, T.; Ruparelia, K. C.; Lamb, J. H.; Farmer, P. B.; Stanley, L. A.; Burke, M. D. The cancer preventative agent resveratrol is converted to the anticancer agent piceatannol by the cytochrome P450 enzyme CYP1B1. *Br. J. Cancer* **2002**, *86*, 774−778.

(30) Zhu, Y.; Chiang, H.; Zhou, J.; Xie, F.; Kissinger, P. T. *In vitro* metabolism study of resveratrol and identification and determination of its main metabolite piceatannol by LC/EC and LC/MS/MS. *Asian J. Drug Metab. Pharmacokinet.* **2005**, *5*, 49−54.

(31) Gradolatto, A.; Basly, J. P.; Berges, R.; Teyssier, C.; Chagnon, M. C.; Siess, M. H.; Canivenc-Lavier, M. C. Pharmacokinetics and metabolism of apigenin in female and male rats after a single oral administration. *Drug Metab. Dispos.* **2005**, *33*, 49−54.

(32) Johnson, J. J.; Nihal, M.; Siddiqui, I. A.; Scarlett, C. O.; Bailey, H. H.; Mukhtar, H.; Ahmad, N. Enhancing the bioavailability of resveratrol by combining it with piperine. *Mol. Nutr. Food Res.* **2011**, *55*, 1−8.

(33) Matsumoto, H.; Ito, K.; Yonekura, K.; Tsuda, T.; Ichiyanagi, T.; Hirayama, M.; Konishi, T. Enhanced absorption of anthocyanins after oral administration of phytic acid in rats and humans. *J. Agric. Food Chem.* **2007**, *55*, 2489−2496.

(34) Chen, L.; Lee, M. J.; Li, H.; Yang, C. S. Absorption, distribution, and elimination of tea polyphenols in rats. *Drug Metab. Dispos.* **1997**, *25*, 1045−1050.

MATERIALS AND METHODS

Reagents and Standards. Ethanol, methanol, hexane, chloroform, ethyl acetate, formic acid, hydrochloric acid, acetic acid, sodium carbonate, sodium acetate trihydrate, and anhydrous sodium sulfate were purchased from Merck (Darmstadt, Germany). All chemicals used in the study were of analytical or HPLC grade. Folin−Ciocalteu reagent, 2,2-diphenyl-1-picrylhydrazyl radical (DPPH), 2,2′-azinobis-(3-ethylbenzothiazoline-6-sulfonic acid) diammonium salt (ABTS), 2,4,6-tris(2-pyridyl)-*s*-triazine (TPTZ), 6-hydroxy-2,5,7,8-tetramethylchroman-2-carboxylic acid (Trolox), potassium persulfate, iron(III) chloride hexahydrate, iron(II) sulfate heptahydrate, gallic acid, and ellagic acid were purchased from Sigma-Aldrich (St. Louis, MO, USA). The solvents were filtered using a Phenomenex solvent filtration apparatus (Torrance, CA, USA). The water used in this experiment was purified in a Millipore Milli-Q apparatus (Purelab UHQ-PS, Elga).

Material. Geopropolis produced by *Melipona fasciculata* Smith (Figure 1) was collected in November 2008 from the internal parts of

Figure 1. Geopropolis of *Melipona fasciculata* Smith collected in Maranhao state, Brazil.

a beehive located in the municipality of Fernando Falcao, Alto Mearim and Grajau microregion (6°7′30″ S, 44°52′30″ W) (Brazilian savannah), southeastern state of Maranhao, Brazil.

Extraction and Fractionation of Crude Geopropolis Extract. The in natura geopropolis was triturated using a knife mill, and the geopropolis powder (500 g) obtained was extracted by maceration with 1000 mL of 70% ethanol/water (70:30, v/v) for 48 h at a solid to solvent ratio of 1:2 (w/v). The extract was filtered through Whatman no. 1 filter paper (Whatman, Durham, UK) in a Buchner funnel and concentrated to a small volume at 40 °C in a rotary evaporator under vacuum, obtaining the hydroalcoholic extract of geopropolis (HEG).

The geopropolis extract (HEG, 20 g) was dissolved in 100 mL of methanol/water (1:1, v/v) by stirring, and the solution was subjected to fractionation by liquid−liquid partition chromatography using hexane, chloroform, and ethyl acetate. The solutions were filtered (anhydrous Na_2SO_4) and concentrated to a small volume at 40 °C in a rotary evaporator under vacuum, obtaining the hexane fraction (HF), chloroform fraction (CF), ethyl acetate fraction (EAF), and hydroalcoholic fraction (HAF).

Determination of Total Phenolic Content (TPC). The TPC of all samples was determined with the Folin−Ciocalteu reagent and 20% sodium carbonate. The reaction mixture was kept in the dark for 2 h at room temperature, and absorbance was then measured at 760 nm in a Lambda 35 UV−vis spectrophotometer (Perkin-Elmer, Inc., Waltham, MA, USA).[5,7] TPC was calculated from the calibration curve constructed with standard solutions of gallic acid (1.0−30.0 μg/mL) and is expressed as gallic acid equivalent (%). The analyses were carried using three aliquots of each sample, measured in triplicate, and the average value was calculated for each sample.

Determination of Antioxidant Activity. *DPPH Radical Scavenging Activity.* The antioxidant activity of the sample of geopropolis was evaluated by using the DPPH free radical scavenging assay as described by Brand-Williams et al.[16] with modifications. The samples were diluted in methanol at different concentrations (1.0−100.0 μg/mL) and added to a methanol solution of DPPH (40.0 μg/mL). After 30 min of reaction at room temperature in the dark, the absorbance of each solution was read at 517 nm in a Lambda 35 UV−vis spectrophotometer (Perkin-Elmer, Inc.). Methanol was used as the control, and DPPH solution was used as the blank. Standards of gallic acid, ellagic acid, and Trolox were treated under the same conditions as the samples. The percent inhibition was calculated using the formula

$$\text{DPPH scavenging activity (\%)} = 100 - [(A_{\text{sample}} - A_{\text{blank}}) \times 100/A_{\text{control}}]$$

where A_{sample} = absorbance of the sample after 30 min of reaction, A_{blank} = absorbance of the blank, and A_{control} = absorbance of the control.

The percentage of scavenging activity was plotted against the sample concentration to obtain the IC_{50}, defined as the concentration of sample necessary to cause 50% inhibition. All experiments were done in triplicate.

$ABTS^{\bullet+}$ Assay. Antioxidant activity was evaluated by using the $ABTS^{\bullet+}$ method (2,2′-azinobis-3-ethylbenzotiazoline-6-sulfonic acid) as described by Re et al.[17] with modifications. For formation of the ABTS radical, 7 mM $ABTS^{\bullet+}$ solution was mixed with 2.45 mM potassium persulfate solution, and the mixture was stored in the dark for 16 h. The radical was diluted with ethanol PA to an absorbance of 0.700 ± 0.020 at 734 nm. Three different dilutions of the samples (1−20.0 μg/mL) were then added to 3.0 mL of ABTS radical in the dark. Absorbance was read in a Lambda 35 UV−vis spectrophotometer (Perkin-Elmer, Inc.) after 6 min of the reaction using ethanol as a blank. Standards of gallic acid, ellagic acid, and Trolox were treated under the same conditions as the samples. The percent inhibition was calculated using the formula

$$ABTS^{\bullet+}\text{ scavenging activity (\%)} = 100 - [(A_{\text{sample}} - A_{\text{blank}}) \times 100/A_{\text{control}}]$$

where A_{sample} = absorbance of the sample after 6 min of reaction, A_{blank} = absorbance of the blank, and A_{control} = absorbance of the control.

The percentage of scavenging activity was plotted against the sample concentration to obtain the IC_{50}, defined as the concentration of sample necessary to cause 50% inhibition. All experiments were done in triplicate.

Ferric Reducing Antioxidant Power Assay (FRAP). The method described by Benzie and Strain,[18] with some modifications, was used to determine the antioxidant activity based on iron reduction using the FRAP assay. FRAP measures the ferric-reducing ability of a sample in acid medium (pH 3.6), forming an intense blue color as the ferric tripyridyltriazine (Fe^{3+}−TPTZ) complex is reduced to the ferrous (Fe^{2+}) form. FRAP reagent was prepared immediately before analysis by mixing 25 mL of acetate buffer (300 mM, pH 3.6), 2.5 mL of TPTZ solution (10 mM TPTZ in 40 mM HCl), and 2.5 mL of $FeCl_3 \cdot 6H_2O$ (20 mM) in aqueous solution. Different concentrations of 100 μL of the samples (1−100.0 μg/mL) were added to 300 μL of distilled water and 3.0 mL of FRAP reagent, and the mixtures were incubated in a water bath at 37 °C for 30 min. The absorbance of the reaction mixture was read at 593 nm in a Lambda 35 UV−vis spectrophotometer (Perkin-Elmer, Inc.) using FRAP solution as a blank. The calibration curve was constructed using different concentrations of $FeSO_4 \cdot 7H_2O$ (0−2000 μM) (r^2 = 0.9987), and the results are expressed as millimoles of Fe^{2+} per gram of sample. Standards of gallic acid, ellagic acid, and Trolox were treated under the same conditions as the samples.

HPLC/UV−Vis Analysis. HPLC analysis was carried out in a Thermo Finnigan Surveyor Autosampler liquid chromatograph (San Jose, CA, USA) equipped with an injector with a 25 μL loop and a UV detector. A Hypersil BDS C-18 column (250 × 4.6 mm, 5 μm; Thermo Electron Corp., Waltham, MA, USA), protected by a C-18 precolumn (4 × 3 mm, 5 μm, Gemini; Phenomenex), was used. The compounds of the geopropolis extract and fractions were separated at room temperature using a gradient elution program at a flow rate of 1.0 mL/min. The mobile phases consisted of Milli-Q water containing 0.1% formic acid (A) and methanol (B). The following linear gradient was applied: 0−1 min, 5% B; 1−60 min, 5−30% B; 60−90 min, 30−100% B. The column was reequilibrated for 10 min before the next run. The injection volume into the HPLC system was 25 μL, and UV−

Table 1. Total Phenolic Content and Antioxidant Activity of the Extract and Fractions of Geopropolis[a]

sample	TPC (%)	DPPH IC_{50} (μg/mL)	ABTS IC_{50} (μg/mL)	FRAP (mmol Fe^{2+}/g)
HEG	47.78 ± 0.04 a	5.24 ± 0.12 a	2.56 ± 0.17 a	14.70 ± 0.43 a
HF	6.32 ± 0.02 b	nd	nd	nd
CF	20.53 ± 0.01 c	17.86 ± 0.05 b	16.29 ± 0.02 b	2.52 ± 0.01 b
EAF	57.90 ± 0.02 d	3.75 ± 0.10 c	1.44 ± 0.03 c	17.87 ± 0.28 c
HAF	36.0 ± 0.04 e	8.81 ± 0.15 d	4.41 ± 0.04 d	15.06 ± 0.98 a
gallic acid		1.83 ± 0.03 e	0.73 ± 0.04 e	25.87 ± 0.28 d
ellagic acid		1.20 ± 0.01 f	1.20 ± 0.08 c	51.32 ± 1.98 e
Trolox		5.11 ± 0.04 a	2.36 ± 0.04 a	9.09 ± 0.10 f

[a]Values represent the mean of triplicate measurements ± standard deviation. Different letters in the same column indicate a significant difference (Tukey test, $p < 0.05$). TPC, total phenolic content; HEG, hydroalcoholic extract of geopropolis; HF, hexane fraction; CF, chloroform fraction; EAF, ethyl acetate fraction; HAF, hydroalcoholic fraction; nd, not detected.

vis detection was performed at 254 nm. Before injection into the HPLC system, each extract was dissolved in the same solvent used for extraction (HPLC grade) to obtain a final concentration of about 5 mg/mL and then filtered through a 0.22 μm nylon syringe filter obtained from Allcrom (São Paulo, SP, Brazil).

HPLC-DAD-ESI-MS Analysis. The HEG and EAF fraction were analyzed with an HPLC system (LC-10AD, Shimadzu) equipped with a photodiode array detector, which was coupled to an Esquire 3000 Plus ion-trap mass spectrometer (Bruker Daltonics, Bremen, Germany) using electrospray ionization (ESI). The conditions for dilution of the samples and the mobile phase composition were the same as described above. The ionization conditions were adjusted as follows: electrospray voltage of the ion source of 40 V, capillary voltage of 4.0 kV, and capillary temperature of 320 °C. Ultrahigh-purity helium (He) was used as the collision gas and high-purity nitrogen (N_2) as the nebulizing gas. Nebulization was aided with a coaxial nitrogen sheath gas provided at a pressure of 27 psi. Desolvation was facilitated using a counter current nitrogen flow set at a rate of 7.0 L/min. Analyses were carried out using full-scan mass spectra in the negative ionization mode and data-dependent MS^2 scans from m/z 100 to 3000. The compounds were identified on the basis of the molecular ion mass, fragmentation, UV−visible spectra, or co-injection with standards.

Statistical Analysis. All analyses were performed in triplicate. The results are expressed as the mean ± standard deviation and were analyzed using the GraphPad Prism 5.0 program. One-way analysis of variance (ANOVA) and Tukey's multiple-comparisons test were used to determine significant differences between means. A level of significance of $p < 0.05$ was adopted. Pearson's correlation test was used to evaluate the correlation between TPC (%), DPPH free radical-scavenging activity (IC_{50}), ABTS free radical-scavenging activity (IC_{50}), and ferric-reducing ability (mmol Fe^{2+}/g sample).

RESULTS AND DISCUSSION

Extraction Yields, Total Phenolic Content, and Antioxidant Activity. The HEG yielded 8.80% (44 g) of a black, bitter-tasting, and resin-smelling substance. Fractionation of the HEG yielded the following fractions: HF (0.22 g), CF (2.30 g), EAF (7.44 g), and HAF (9.30 g).

TPC and antioxidant activity of the fractions and extract are shown in Table 1. EAF (57.89%) and HEG (47.78%) had the highest total phenolic content, whereas total phenolic content ranged from 6.32 to 36.0% in the remaining fractions. Abreu et al.,[5] analyzing geopropolis from *Melipona fasciculata* collected in the savannah of Maranhao state, found a TPC ranging from 14.14 to 67.46%. In contrast, Cunha et al.[7] reported total polyphenol levels ranging from 7.36 to 36.95% in hydroalcoholic extracts of geopropolis collected in the Western Lowland of Maranhao.

In the analysis of DPPH and ABTS, a lower IC_{50} value indicates higher antioxidant activity. The EAF exhibited the highest activity among the samples analyzed by the DPPH radical-scaveninging assay, with an IC_{50} value of 3.75 μg/mL. The HEG extract also exhibited antioxidant activity, with an IC_{50} value of 5.24 μg/mL. HAF and CF provided IC_{50} values of 8.81 and 17.86 μg/mL, respectively. The phenolic compounds gallic and ellagic acids, which are strong antioxidants, exhibited the highest DPPH-scavenging activity. The highest antioxidant activity was observed for EAF, which contained the highest levels of total phenols and presented the lowest IC_{50} value and its radical-scavenging activity exceeded that of Trolox (Table 1).

In the ABTS assay, the EAF, which contained the highest levels of phenolic compounds, exhibited the lowest IC_{50} value (1.44 μg/mL), similar to that of ellagic acid, followed by HEG (IC_{50} = 2.56 μg/mL), which presented antioxidant activity similar to that of Trolox. HAF and CF also exhibited antioxidant activity, with IC_{50} values of 4.41 and 16.29 μg/mL, respectively. In the FRAP assay, EAF, HEG, and HAF presented the best ferric-reducing abilities (17.87, 14.70, and 15.06 mmol Fe^{2+}/g, respectively) which were superior to the antioxidant activity of Trolox. No antioxidant activity was observed for HF in any of the antioxidant assays (Table 1). The differences in antioxidant activity between the same samples demonstrated by the different assays, even when the same standard compound was used, can be explained by the reaction mechanisms of the methods.

Correlation between Antioxidant Activity and Total Phenolics Content. The correlations between the results of the DPPH, ABTS, and FRAP methods and TPC are shown in Table 2. A negative correlation was observed for DPPH−TPC (−0.9649), ABTS−TPC (−0.9154), DPPH−FRAP (−0.9670), and ABTS−FRAP (−0.9891), with a low IC_{50} value in the DPPH and ABTS assays being correlated with a high TPC and a high FRAP value and vice versa. The correlation between TPC and FRAP was positive (0.9034) as was that between DPPH and ABTS (0.9866), indicating that a high reducing

Table 2. Pearson Correlation Coefficient between the DPPH, FRAP, and ABTS Methods and Total Phenolic Content[a]

	DPPH	ABTS	FRAP
TPC	−0.9649	−0.9154	0.9034
DPPH		0.9866	−0.9670
ABTS			−0.9891

[a]TPC, total phenolic content; DPPH, 2,2-diphenyl-1-picrylhydrazyl radical; ABTS, 2,2′-azinobis(3-ethylbenzothiazoline-6-sulfonic acid) diammonium salt; FRAP, ferric reducing antioxidant power.

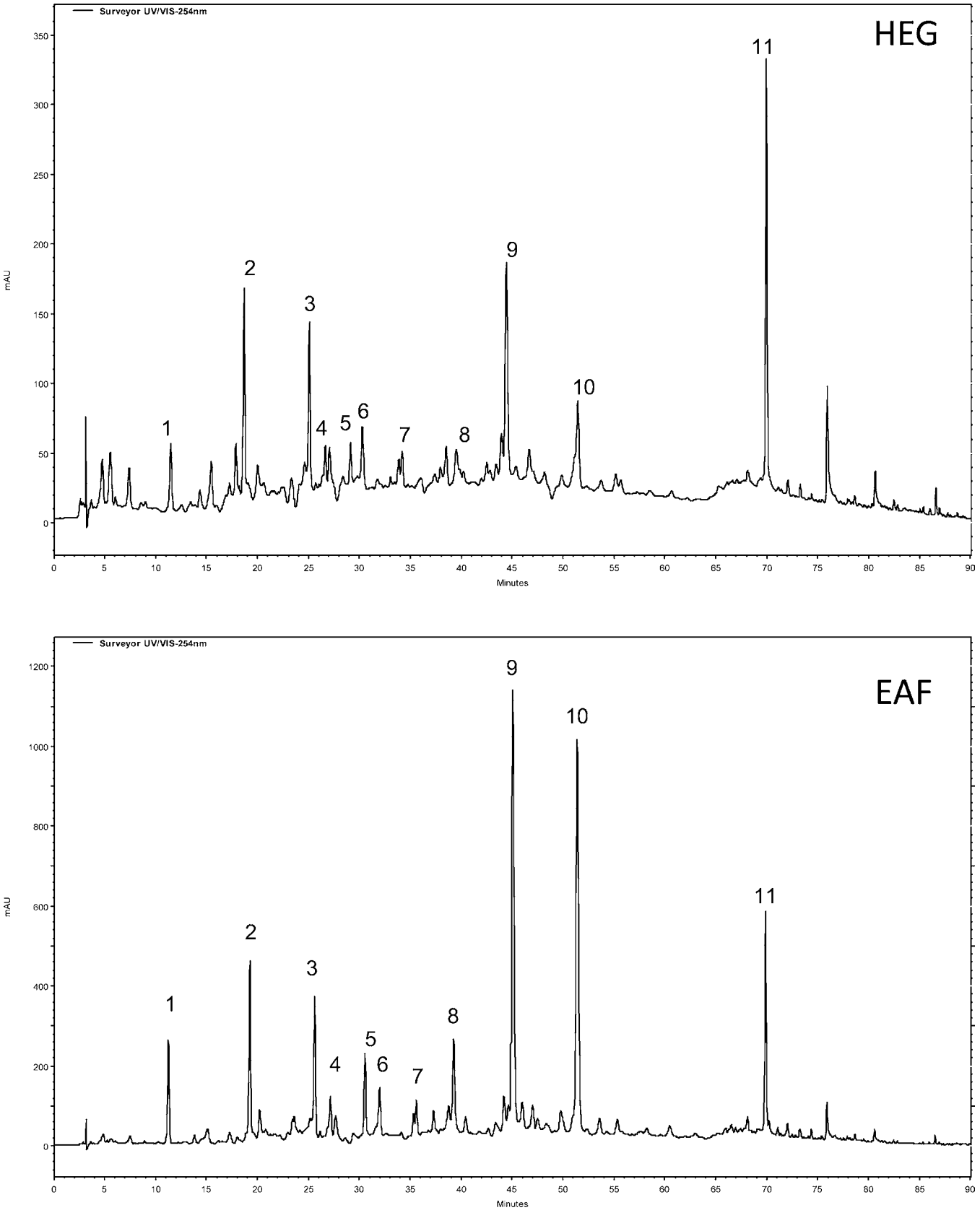

Figure 2. HLPC chromatograms of phenolic compounds detected at 254 nm in the hydroalcoholic extract (HEG) and ethyl acetate fraction (EAF) of geopropolis. Peak numbers correspond to the compounds shown in Table 3.

ability in the FRAP assay is related to the presence of phenolic compounds in the extracts.

The strongest free radical-scavenging activity and reducing ability were observed for the EAF fraction, which presented the

dx.doi.org/10.1021/jf404875v | J. Agric. Food Chem. 2014, 62, 2549−2557

highest TPC. These results suggest that total phenols, particularly hydrolyzable tannins, present in geopropolis were mainly responsible for the antioxidant activity and reducing ability of geopropolis. Other authors also reported important antioxidant activity of geopropolis obtained from the stingless bees *Melipona interrupta* and *Melipona seminigra*[19] and from *Melipona subnitida*,[20] which was correlated with the content of phenolic compounds.

TPC has been shown to be closely correlated with antioxidant activity.[21] Polyphenols have been identified as the most abundant and effective antioxidants in samples of Brazilian propolis produced by *Apis mellifera*.[22−24] In addition, Moreira et al.[25] demonstrated that propolis extracts with the highest concentrations of total polyphenols also exhibit the highest antioxidant activity. In the study of Sawaya et al.,[26] propolis produced by *Scaptotrigona* species, a stingless bee found in the Brazilian states of Maranhao and Sao Paulo, suggested that TPC and antioxidant activity are affected by the chemical composition of propolis, season of collection, and geographic origin.[26]

Identification of Phenolic Compounds. Because EAF and HEG had higher TPC and were more effective against the DPPH radical, the chemical composition of these samples was analyzed by HPLC/UV−vis and HPLC-DAD-MS/MS.

The chromatogram obtained by HPLC/UV−vis (254 nm) for HEG and EAF (Figure 2) revealed similar chemical compositions, with various peaks corresponding to phenolic acids, gallotannins, and ellagitannins on the basis of the analysis of the three-dimensional DAD-HPLC chromatogram of EAF, which established the absorption maxima at 254−363 nm (Figure 3; Figure S1 in the Supporting Information). Gallic acid

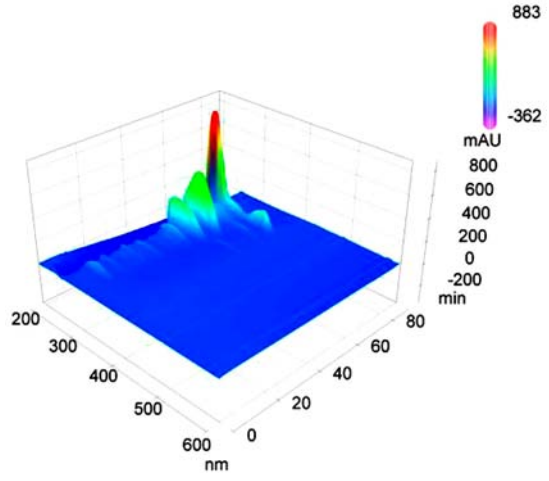

Figure 3. Three-dimensional DAD-HPLC chromatogram of the ethyl acetate fraction of geopropolis. (See also the Supporting Information.)

derivatives exhibit an absorption maximum at 254 nm, whereas ellagitannins show UV spectra similar to that of ellagic acid, with two absorption maxima at λ_{max} 254 and 365 nm. In contrast, gallotannins have only one absorption maximum at 275 nm due to the presence of galloyl and hexahydroxydiphenoyl groups.[27,28]

The compounds **1**−**11** were identified by HPLC-MS/MS as phenolic acids and hydrolyzable tannins (gallotannins and ellagitannins) as indicated by the presence of molecular ions corresponding to gallic acid, ellagic acid, trigallic acid, hexahydroxydiphenic acid (HHDP), and hexahydroxydiphenoyl-glucose (HHDP-glucose). The chemical structures of these compounds are shown in Figure 4.

Table 3 summarizes the tentatively identified phenolic compounds, their retention time, maximum UV−vis absorbance (λ_{max}), molecular weight, molecular ion $[M - H]^-$, and main product ions obtained by HPLC-MS/MS for the 11 fragmentation peaks of HEG and EAF. The compounds were identified by comparing their fragmentation profiles with reference compounds run under the same experimental conditions. When no standards were available, the compounds were identified on the basis of literature data.

The characterization of phenolic compounds is important because these compounds are associated with a variety of health benefits. HPLC with diode array and mass spectrometry detection has proven to be useful for the characterization of individual phenolic compounds, particularly gallotannins and ellagitannins. The results showed losses of 152 and 170 Da from the ion molecule, indicating the presence of galloyl groups, and a loss of 302 Da from the ion molecule, which is characteristic of HHDP groups. Loss of the carboxyl group (44 Da) and water (18 Da) from the ion molecule indicates the presence of a trigalloyl group and C-glucosidic ellagitannins, respectively.[29,30] The presence of ellagitannins was confirmed by the data indicating spontaneous lactonization of HHDP forming ellagic acid, whereas the partial lactonization of HHDP yields a product ion at m/z 319, and subsequent decarboxylation yields an ion at m/z 275 $[M - H - 44]^-$. Furthermore, tannins with molecular masses different by 2 units were observed, which are due to differences in one HHDP group or two galloyl groups.[31]

Phenolic Acids. Compounds **1** and **11** were identified as gallic acid and ellagic acid, respectively, by comparing their retention times, UV−vis spectra, fragmentation pathways observed in MS/MS spectra, and $[M - H]^-$ ions at m/z 169 and 301 with literature data. These peaks were confirmed using an authentic standard.[32,33]

Galloyl Glucose Derivatives and Ellagitannins. Compound **2** was tentatively identified as HHDP-galloylglucose (corilagin). Fragmentation of the molecular ion at m/z 633 $[M - H]^-$ produced ion fragments at m/z 481 (HHDP-glucose), due to the loss of the galloyl group, and at m/z 301, corresponding to the HHDP unit after lactonization to ellagic acid.[33]

Compound **3** showed an $[M - H]^-$ ion at m/z 481 $[M - H]^-$, followed by an ion fragment m/z 301 (ellagic acid), and was tentatively identified as HHDP-glucose after the loss of one unit of glucose.[34]

Ellagitannins with $[M - H]^-$ ions at m/z 783 and 785 were at m/z 481 $[M - H]^-$, followed by an ion fragment m/z 301 (ellagic acid), and were tentatively identified in the samples analyzed. Compound **4**, a parental $[M - H]^-$ ion at m/z 783 is present, producing ion fragments at m/z 765 (M − 18, loss of water), m/z 481, which correspond to deprotonated HHDP-glucose (M − 302 Da, loss of HHDP), and m/z 301, which corresponds to ellagic acid. These fragments were tentatively identified as di-HHDP-glucose (pedunculagin/casuariin).[28,33]

Compound **5** showed an $[M - H]^-$ ion at m/z 635 and fragments at m/z 483 $[M - H - 152]^-$, m/z 465 $[M - H - 170]$, and m/z 313 $[M - H - 152 - 152 - 18]^-$, indicating the loss of a galloyl group, the loss of gallic acid, and the loss of another galloyl group, water along with cross-ring fragmentation of glucose, and at m/z 301, corresponding to the HHDP unit after lactonization to ellagic acid. This compound was at

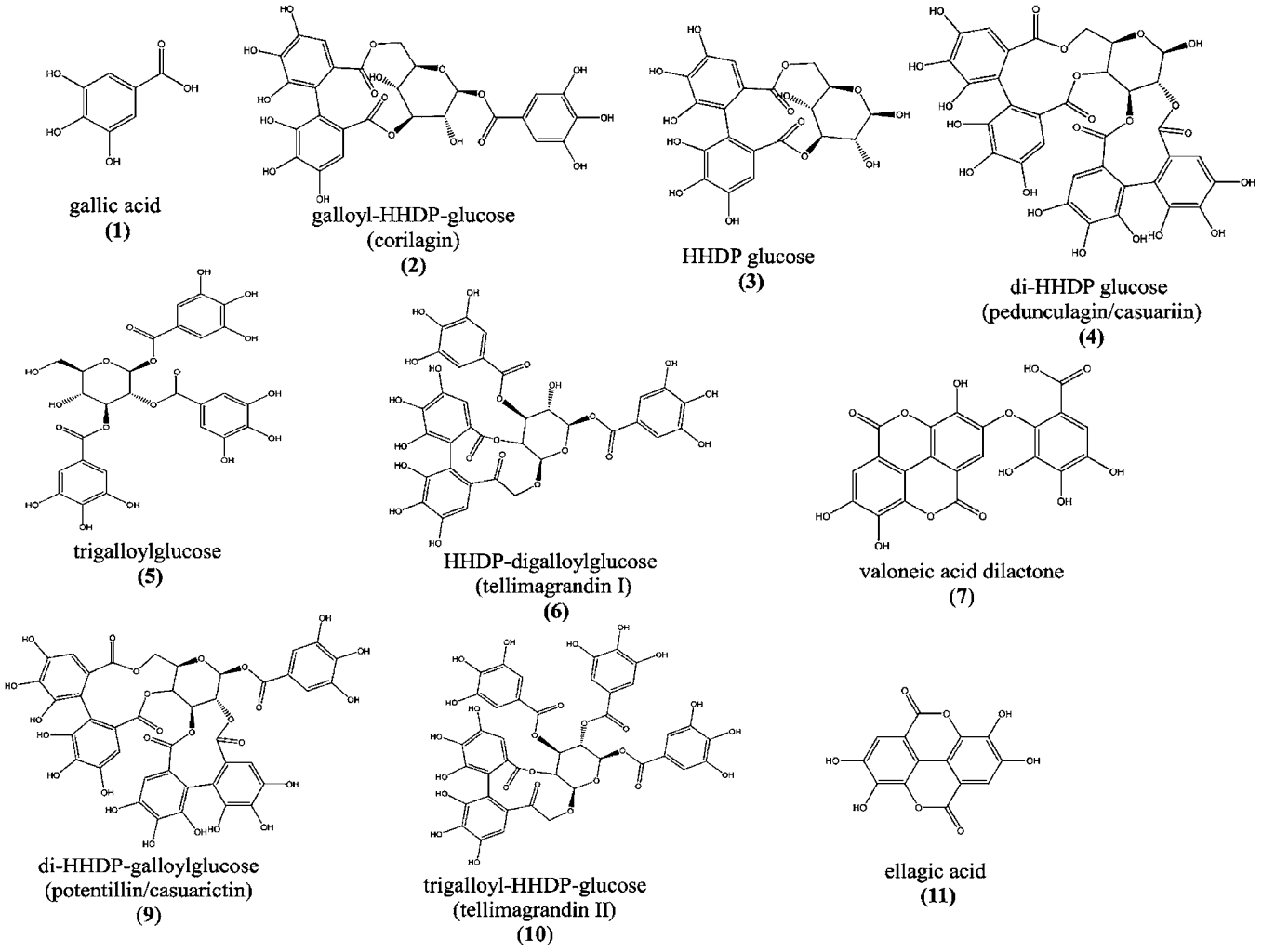

Figure 4. Chemical structures of phenolic compounds detected in geopropolis of *Melipona fasciculata* Smith.

Table 3. Tentative Identification of Phenolic Compounds in *Melipona fasciculata* Geopropolis by HPLC-DAD-ESI-MS/MS[a]

compd	RT (min)	tentative identification	HPLC-DAD λ_{max} (nm)	MW	$[M - H]^-$ (m/z)	MS/MS fragments (m/z)
1	11.23	gallic acid[b]	272	170	169	125
2	19.26	HHDP-galloylglucose[c]	262	634	633	481, 301, 275
3	25.60	HHDP-glucose[c]	267	482	481	301, 275, 169
4	27.16	di-HHDP-glucose[c]	265	784	783	764, 481, 301, 275
5	30.53	trigalloyl glucose[c]	277	636	635	483, 465, 313, 301
6	31.98	HHDP-digalloylglucose isomer[c]	274	786	785	783, 709, 633, 463, 301, 275
7	35.62	valoneic acid dilactone[c]	254, 370	470	469	425, 301
8	39.25	trisgalloyl-HHDP-glucose isomer[c]	263	952	951	907, 783, 301
9	45.08	di-HHDP-galloylglucose[c]	271	936	935	933, 633, 451, 301, 275
10	51.39	trigalloyl-HHDP-glucose[c]	277	938	937	785, 767, 635, 465, 301, 275
11	69.88	ellagic acid[b,c]	254, 363	302	301	301

[a]RT, retention time; λ_{max}, UV−vis absorption maxima; MW, molecular weight; $[M - H]^-$ molecular ion; HHDP, hexahydroxydiphenic acid. [b]Co-injection of the authentic standard. [c]Compounds identified for the first time in geopropolis.

m/z 481 $[M - H]^-$, followed by an ion fragment m/z 301 (ellagic acid), and was tentatively identified as trigalloyl-glucose.[28,33,34]

Compound **6** with m/z 785 $[M - H]^-$ was at m/z 481 $[M - H]^-$, followed by an ion fragment m/z 301 (ellagic acid), and was tentatively identified as an HHDP-digalloylglucose isomer (tellimagrandin I) because it contained ions at m/z 633 (loss of a galloyl group), m/z 483 (loss of HHDP), and m/z 313 after the loss of one unit of HHDP, one galloyl group, and water. These two compounds differ from one another by 2 atomic mass units, suggesting that compound **4** could be formed by binding of two adjacent galloyl groups in HHDP-digalloyl-glucose by means of intramolecular oxidation.[30,33,34]

Compound **7** produced $[M - H]^-$ ions at m/z 469 and two main fragments at m/z 425 and 301 due to the loss of CO_2 from the deprotonated molecule and ellagic acid fragment, suggesting the presence of valoneic acid dilactone.[30,35]

Compound **8** showed an $[M - H]^-$ ion at m/z 951, which fragmented to m/z 907, 783, and 301. On the basis of the fragmentation patterns, the peak was at m/z 481 $[M - H]^-$, followed by an ion fragment m/z 301 (ellagic acid), and was tentatively identified as the trisgalloyl-HHDP-glucose isomer. UV spectral data and the fragment ion at m/z 783 $[M - H - 168]$ indicate the presence of di-HHDP-glucose. The fragment corresponds to the presence of an additional galloyl residue, but only with a C−C bond to one of the HHDP molecules. The fragment ion at m/z 907 ($[M - H]^- - CO_2$) agrees with the presence of a free unesterified carboxyl group, and ion m/z 301 corresponds to 1 unit of HHDP after the lactonization process to ellagic acid.[28,29,33,36]

Compound **9** showed an $[M - H]^-$ ion at m/z 935, which fragmented to m/z 633 (−302 Da, loss of HHDP), m/z 481 (loss of a galloyl group), and m/z 301, and subsequent decarboxylation yields an ion at m/z 275. This compound was at m/z 481 $[M - H]^-$, followed by an ion fragment m/z 301 (ellagic acid), and was tentatively identified as di-HHDP-galloylglucose (potentillin/casuarictin).[30,32,33]

Compound **10** was tentatively identified as trigalloyl-HHDP-glucose (tellimagrandin II) on the basis of an $[M - H]^-$ ion at m/z 937, followed by ions m/z 785 and 767 (loss of water and a galloyl group, respectively), in addition to the ion fragments m/z 635 (minus one HHDP group), m/z 465 (loss of HHDP and gallic acid groups), and m/z 301, which corresponds to one unit of HHDP after the lactonization process to ellagic acid, followed by decarboxylation producing ion m/z 275. This compound differs from tellimagrandin I by the presence of an additional galloyl unit in the anomeric center of the glucopyranosyl core. Tellimagrandin II is produced by enzymatic transformation of pentagalloylglucose.[30,33]

Bankova et al.[37] demonstrated the presence of gallic acid in geopropolis produced by *Melipona compressipes* collected in the state of Piaui, Brazil. Gallic acid is one of the main compounds found in propolis samples from stingless bees collected in the Brazilian states of Pernambuco, Parana, and Sao Paulo.[38] However, there are no studies in the literature reporting the presence of ellagic acid and hydrolyzable tannins in samples of geopropolis or propolis produced by stinging or stingless bees.

Ellagitannins were the main compounds identified in the HEG and in EAF. These phenolic compounds are esters of HHDP with a polyol, usually glucose, have a high molecular weight, and are soluble in water.[39]

Ellagic acid is a phenolic compound that can occur in free form, glycosylated, or in bound form like ellagitannins. This compound is found in strawberries (*Fragaria ananassa* D.), raspberries (*Rubus idaeus* L.), pomegranates (*Punica granatum* L.), blackberries (*Morus nigra* L.), and eucalyptus (*Eucalyptus globules* L.). Ellagic acid and its derivatives (ellagitannin) have been shown to have antiviral, antioxidant, anticarcinogenic, anti-inflammatory, antifibrotic, and chemopreventive properties,[11] as well as antileishmanial activity.[40]

Antioxidants have attracted much interest because of their protective effect against free radical damage, which is the cause of many diseases, including cancer. In the present study, HEG and its EAF exhibited the highest antioxidant activity. This finding is probably due to the high content of polyphenols, such as gallic acid, ellagic acid, and hydrolyzable tannins. A similar correlation between antioxidant activity and phenolic content has been demonstrated in other studies.[21]

Zahin et al.,[41] studying the antioxidant activity of pomegranate (*Punica granatum*) peel extracts by DPPH free radical scavenging, identified gallic acid, ellagic acid, HHDP-glucose, corilagin, and pedunculagin by HPLC-MS. All of these compounds were detected for the first time in stingless bee products in the present study.

The strong correlation observed between antioxidant activity measurements and ellagitannins indicates that high molecular weight polyphenols were the main contributors of antioxidant activity. This can be attributed to the structure of ellagitannins, which is characterized by the presence of several ortho-hydroxy functions that exhibit a greater ability to donate a hydrogen atom and support the unpaired electron when compared to low molecular weight polyphenols. The antioxidant efficiency of ellagitannins and ellagic acid is directly correlated with their degree of hydroxylation and decreases in the presence of a sugar moiety.[11]

The present results provide further evidence that geopropolis is a rich source of bioactive compounds with potential health benefits, including antioxidant activity, which is related to the presence of phenolic compounds such as phenolic acids, gallotannins, and ellagitannins. Identification of the chemical composition and antioxidant substances is important for the understanding of the biological activity of geopropolis and for the standardization of extracts.

■ ASSOCIATED CONTENT

Ⓢ Supporting Information

Figure S1. This material is available free of charge via the Internet at http://pubs.acs.org.

■ AUTHOR INFORMATION

Corresponding Author

*(M.N.S.R.) E-mail: mnribeiro@ufma.br. Phone: (+55) 98 32728592.

Funding

This work was supported by Conselho Nacional de Desenvolvimento Científico e Tecnológico (CNPq) and Fundação de Amparo a Pesquisa e ao Desenvolvimento Científico e Tecnológico do Maranhão (FAPEMA).

Notes

The authors declare no competing financial interest.

■ ACKNOWLEDGMENTS

We are grateful to Ozimar Cavalcante Araújo for providing the geopropolis samples.

■ ABBREVIATIONS USED

HEG, hydroalcoholic extract of geopropolis; HF, hexane fraction; CF, chloroform fraction; EAF, ethyl acetate fraction; HAF, hydroalcoholic fraction; DPPH, 2,2-diphenyl-1-picrylhydrazyl; ABTS, 2,2′-azinobis(3-ethylbenzothiazoline-6-sulfonic acid) diammonium salt; FRAP, ferric reducing antioxidant power; HHDP, hexahydroxydiphenic acid; HPLC, high-performance liquid chromatography; ESI, electrospray ionization; MS, mass spectrometry; DAD, diode array detection; MS/MS, tandem mass spectrometry; TPC, total phenolic content

■ REFERENCES

(1) Barth, O. M. Palynological analysis of geopropolis samples obtained from six species of Meliponinae in the Campus of the Universidade de Ribeirão Preto, USP, Brazil. *Apiacta* **2006**, *41*, 71−85.

(2) Franchin, M.; Cunha, M. G.; Denny, C.; Napimoga, M. H.; Cunha, T. M.; Koo, H.; Alencar, S. M.; Ikegaki, M.; Rosalen, P. L.

Geopropolis from *Melipona scutellaris* decreases the mechanical inflammatory hypernociception by inhibiting the production of IL-1β and TNF-α. *J. Ethnopharmacol.* **2012**, *143*, 709−715.
(3) Cunha, M. G.; Franchin, M.; Galvão, L. C. C.; Ruiz, A. L. T. G.; Carvalho, J. E.; Ikegaki, M.; Alencar, S. M.; Koo, H.; Rosalen, P. L. Antimicrobial and antiproliferative activities of stingless bee *Melipona scutellaris* geopropolis. *BMC Complement. Altern. Med.* **2013**, *13*, 23.
(4) Tomas-Barberan, F. A.; García-Viguera, C.; Vit-Olivier, P.; Ferreres, F.; Tomas-Lorente, F. Phytochemical evidence for the botanical origin of tropical propolis from Venezuela. *Phytochemistry* **1993**, *34*, 191−196.
(5) Abreu, B. V. B.; Dutra, R. P.; Batista, M. C. A.; Azevedo, C. C.; Nogueira, A. M. C.; Costa, M. C. P.; Ribeiro, M. N. S. Quantificação de polifenóis de geoprópolis de *Melipona fasciculata* Smith coletado no Cerrado maranhense. *Rev. Cienc. Saude* **2006**, *8*, 18−24.
(6) Dutra, R. P.; Nogueira, A. M. C.; Marques, R. R. O.; Costa, M. C. P.; Ribeiro, M. N. S. Avaliação farmacognóstica de geoprópolis de *Melipona fasciculata* Smith da Baixada maranhense, Brasil. *Rev. Bras. Farmacogn.* **2008**, *18*, 557−562.
(7) Cunha, M. S.; Dutra, R. P.; Batista, M. C. A.; Abreu, B. V. B.; Santos, J. R.; Neiva, V. A. N.; Amaral, F. M. M.; Ribeiro, M. N. S. Padronização de extrativos de geoprópolis de *Melipona fasciculata* Smith (tiúba). *Cad. Pesq.* **2009**, *16*, 31−38.
(8) Libério, S. A.; Pereira, A. L. A.; Dutra, R. P.; Reis, A. S.; Araújo, M. J. A. M.; Mattar, N. S.; Silva, L. A.; Ribeiro, M. N. S.; Nascimento, F. R. F.; Guerra, R. N. M.; Monteiro-Neto, V. Antimicrobial activity against oral pathogens and immunomodulatory effects and toxicity of geopropolis produced by the stingless bee *Melipona fasciculata* Smith. *BMC Complement. Altern. Med.* **2011**, *11*, 108.
(9) Duailibe, S. A. C.; Gonçalves, A. G.; Ahid, F. J. M. Effect of a propolis extract on *Streptococcus mutans* counts *in vivo*. *J. Appl. Oral Sci.* **2007**, *15*, 420−423.
(10) Balasundram, N.; Sundram, K.; Samman, S. Phenolic compounds in plants and agri-industrial by-products: antioxidant activity, occurrence and potential uses. *Food Chem.* **2006**, *99*, 191−203.
(11) Landete, J. M. Ellagitannins, ellagic acid and their derived metabolites: a review about source metabolism, functions and health. *Food Res. Int.* **2011**, *44*, 1150−1160.
(12) Gregoris, E.; Stevanato, R. Correlations between polyphenolic composition and antioxidant activity of Venetian propolis. *Food Chem. Toxicol.* **2010**, *48*, 76−82.
(13) Fracassetti, D.; Costa, C.; Moulay, L.; Tomás-Barberán, F. A. Ellagic acid derivatives, ellagitannins, proanthocyanidins and other phenolics, vitamin C and antioxidant capacity of two powder products from camu-camu fruit (*Myrciaria dubia*). *Food Chem.* **2013**, *139*, 578−588.
(14) Aher, V.; Wahi, A.; Pawdey, A. M.; Sonawane, A. Antioxidants as immunomodulator: an expanding research avenue. *Int. J. Curr. Pharm. Res.* **2011**, *3*, 8−10.
(15) Carocho, M.; Ferreira, I. C. F. R. A review on antioxidants, prooxidants and related controversy: natural and synthetic compounds, screening and analysis methodologies and future perspectives. *Food Chem. Toxicol.* **2013**, *51*, 15−25.
(16) Brand-Williams, W.; Cuvelier, M. E.; Berst, C. Use of a free radical method to evaluate antioxidant activity. *Lebensm. Wiss. Technol.* **1995**, *28*, 25−30.
(17) Re, R.; Pellegrini, N.; Proteggente, A.; Pannala, A.; Yang, M.; Rice-Evans, C. Antioxidant activity applying an improved ABTS radical cation decolorization assay. *Free Radical Biol. Med.* **1999**, *26*, 1231−1237.
(18) Benzie, I. F.; Strain, J. The ferric reducing ability of plasma (FRAP) as a measure of "antioxidant power": the FRAP assay. *Anal. Biochem.* **1996**, *239*, 70−76.
(19) Da Silva, E. C. C.; Muniz, M. P.; Nunomura, R. C. S.; Nunomura, S. M.; Zilse, G. A. C. Phenolic constituents and antioxidant activity of geopropolis from two species of amazonian stingless bees. *Quim. Nova* **2013**, *36*, 628−633.
(20) Souza, S. A.; Camara, C. A.; Silva, E. M. S.; Silva, T. M. S. Composition and antioxidant activity of geopropolis collected by *Melipona subnitida* (jandaíra) bees. *Evidence-Based Complement. Altern. Med.* **2013**, *2013*.
(21) Apak, R.; Guclu, K.; Demirata, B.; Ozyurek, M.; Celik, S. E.; Bektasolu, B.; Berker, K. I.; Ozyurt, D. Comparative evaluation of various total antioxidant capacity assays applied to phenolic compounds with the CUPRAC assay. *Molecules* **2007**, *12*, 1496−1547.
(22) Baskota, A. H.; Tezuka, Y.; Prasain, J. K.; Matshuige, K.; Saiki, I.; Kadota, S. Chemical constituents of Brazilian propolis and their cytotoxic activities. *J. Nat. Prod.* **1998**, *61*, 896−900.
(23) Silva, J. F. M.; Souza, M. C.; Matta, S. R.; Andrade, M. R.; Vidal, F. V. N. Correlation analysis between phenolic levels of Brazilian propolis extracts and their antimicrobial and antioxidant activities. *J. Agric. Food Chem.* **2006**, *99*, 431−435.
(24) Cabral, I. S. R.; Oldoni, T. L. C.; Prado, A.; Bezerra, R. M. N.; Alencar, S. M. Composição fenólica, atividade antibacteriana e antioxidante da própolis vermelha brasileira. *Quim. Nova* **2009**, *32*, 1523−1527.
(25) Moreira, L.; Dias, L. G.; Pereira, J. A.; Estevinho, L. Antioxidant properties, total phenols and pollens analysis of propolis from Portugal. *Food Chem. Toxicol.* **2008**, *46*, 3482−3485.
(26) Sawaya, A. C. H. F.; Calado, J. C. P.; Santos, L. C.; Marcucci, M. C.; Akatsu, I. P.; Soares, A. E.; Abdelnur, P. V.; Cunha, I. B. S.; Eberlin, M. N. Composition and antioxidant activity of propolis from three species of *Scaptotrigona* stingless bees. *J. ApiProd. ApiMed. Sci.* **2009**, *1*, 37−42.
(27) Romani, A.; Campo, M.; Pinelli, P. HPLC/DAD/ESI-MS analyses and anti-radical activity of hydrolyzable tannins from different vegetal species. *Food Chem.* **2012**, *130*, 214−221.
(28) Gordon, A.; Jungfer, E.; Silva, B. A.; Maia, J. G. S.; Marx, F. Phenolic constituents and antioxidant capacity of four underutilized fruits from the Amazon region. *J. Agric. Food Chem.* **2011**, *59*, 7688−7699.
(29) Barry, K. M.; Davies, N. W.; Mohammed, C. L. Identification of hydrolysable tannins in the reaction zone of *Eucalyptus nitens* wood by high performance liquid chromatography-electrospray ionisation mass spectrometry. *Phytochem. Anal.* **2001**, *12*, 120−127.
(30) Fernandes, A.; Sousa, A.; Mateus, N.; Cabral, M.; Freitas, V. Analysis of phenolic compounds in cork from *Quercus suber* L. by HPLC−DAD/ESI−MS. *Food Chem.* **2011**, *125*, 1398−1405.
(31) Tan, H. P.; Ling, S. K.; Chuah, C. H. Characterisation of galloylated cyanogenic glucosides and hydrolysable tannins from leaves of *Phyllagathis rotundifolia* by LC-ESI-MS/MS. *Phytochem. Anal.* **2011**, *22*, 516−525.
(32) Santos, S. A. O.; Freire, C. S. R.; Domingues, M. R. M.; Silvestre, A. J. D.; Neto, C. P. Characterization of phenolic components in polar extracts of *Eucalyptus globulus* Labill. bark by high-performance liquid chromatography mass spectrometry. *J. Agric. Food Chem.* **2011**, *59*, 9386−9393.
(33) Boulekbache-Makhlouf, L.; Meudec, E.; Chibane, M.; Mazauric, J. P.; Slimani, S.; Henry, M.; Cheynier, V.; Madani, K. Analysis by high-performance liquid chromatography diode array detection mass spectrometry of phenolic compounds in fruit of *Eucalyptus globulus* cultivated in Algeria. *J. Agric. Food Chem.* **2010**, *58*, 12615−12624.
(34) Sandhu, A. K.; Gu, L. Antioxidant capacity, phenolic content, and profiling of phenolic compounds in the seeds, skin, and pulp of *Vitis rotundifolia* (Muscadine grapes) as determined by HPLC-DAD-ESI-MS. *J. Agric. Food Chem.* **2010**, *58*, 4681−4692.
(35) Sanz, M.; Cadahía, E.; Esteruelas, E.; Muñoz, A. M.; Fernandez de Simon, B. F.; Hernandez, T.; Estrella, I. Phenolic compounds in chestnut (*Castanea sativa* Mill.) heartwood. Effect of toasting at cooperage. *J. Agric. Food Chem.* **2010**, *56*, 9631−9640.
(36) Kähkönen, M.; Kylli, P.; Ollilainen, V.; Salminen, J. P.; Heinonen, M. Antioxidant activity of isolated ellagitannins from red raspberries and cloudberries. *J. Agric. Food. Chem.* **2012**, *60*, 1167−1174.

(37) Bankova, V.; Boudourova-Krasteva, G.; Popov, S.; Sforcin, J. M.; Funari, S. R. C. Seasonal variations of the chemical composition of Brazilian propolis. *Apidologie* **1998**, *29*, 361−367.
(38) Velikova, M.; Bankova, V.; Marcucci, M. C.; Tsvetkova, I.; Kujumgiev, A. Chemical composition and biological activity of propolis from Brazilian meliponinae. *Z. Naturforsch.* **2000**, *55C*, 785−789.
(39) Okuda, T.; Yoshida, T.; Hatano, T. Correlation of oxidative transformations of hydrolysable tannins and plant evolution. *Phytochemistry* **2000**, *55*, 513−529.
(40) Kolodziej, H.; Kayser, O.; Kiderlen, A. F.; Ito, H.; Hatano, T.; Yoshida, T.; Foo, L. Y. Antileishmanial activity of hydrolyzable tannins and their modulatory effects on nitric oxide and tumour necrosis factor-α release in macrophages *in vitro*. *Planta Med.* **2001**, *6*, 825−832.
(41) Zahin, M.; Aqil, F.; Ahmad, I. Broad spectrum antimutagenic activity of antioxidant active fraction of *Punica granatum* L. peel extracts. *Mutat. Res.* **2010**, *703*, 99−107.

largely degraded by either acids,[12−14] enzymes, or human intestinal bacteria before reaching the circulation system,[15−22] resulting in very low bioavailability of intact ginsenosides (Rb_1, 0.1−4.4%; Rb_2, 3.7%; Rg_1, 1.9−18.4%).[23,24] The degraded ginsenosides have been further proven to traverse membrane more efficiently than the intact ginsenosides.[25,26] Our previous study has shown increased anticancer activity of ginseng extract and total ginsenosides after acidic hydrolysis.[27] All these lead to a transition of study from intact ginsenosides to secondary ginsenosides.

Metabolism of ginsenosides in the large intestine, where ginsenosides are deglycosylated by colonic bacteria, was found to mediate the in vivo activity of ginsenosides and thereby was suggested to be a key step for activation of primary ginsenosides which themselves were regarded as a "pro-drug".[28,29] For example, one of the major intestinal bacterial metabolite compound K (C−K) also called M1 in some papers), which is derived from PPD-type ginsenosides, has been demonstrated to exhibit in vivo and in vitro anticancer activities.[28−30] A metabolic pathway via stepwise cleavage of sugar moieties of ginsenosides with the preference of terminal sugar > inner sugar in intestinal bacteria has been well established, and more than 10 kinds of deglycosylated metabolites have been identified.[31,32] Many kinds of bacteria were suggested to integratively metabolize ginsenosides.[31] However, among the deglycosylated ginsenosides formed in intestine bacteria, only C−K, Rh_1, F_1, Rg_3, and Rh_2 were identified in plasma and urine after oral administration of ginseng,[15,20,33,34] while many other gastrointestinal deglycosylated products were only found in feces.[35] However, as a colonic deglycosylated product produced by gut microflora, C−K appeared in plasma very late (usually 7−10 h after administration) and its plasma level varied greatly in different studies.[20,36] Our previous investigation revealed that P-gP mediated efflux was responsible for the poor absorption of C−K.[37] Because of the delayed and low absorption, the plasma level of C−K is very likely to be out of the range where a significant physiological effect can be expected.

Unlike the metabolism in gut microflora, transformation of ginsenosides in gastric juice occurred early in stomach. The resultant metabolites have great potential to be absorbed within the long transit time in intestine (2−8 h), which is usually a time span during which pharmacological activities were observed.[38] However, although previous study demonstrated the absorption of gastric juice derived metabolites, e.g., Rh_1, into the circulation of human,[33] little information on the extent and time course of this procedure was available. This greatly hindered understanding of the role of gastric juice-catalyzed biotransformation in the holistic metabolism of ginsenosides after oral uptake. Moreover, recent studies have shown that molecular diversity of ginsenosides can be generated under mild acidic condition (AcOH/EtOH 1:1),[39] suggesting that ginsenosides can be metabolized through multiple pathways in addition to the well-known deglycosylation pathway. But there is still no systematic investigation on the identification of metabolites of ginsenosides formed in gastric juice. Because transformation of ginsenosides in gastric juice is the first barrier after being taken orally, and the resulting metabolites then undergo absorption and further metabolism in the gut or liver, it is of paramount importance to investigate the metabolism profile of ginsenosides in gastric juice qualitatively and quantitatively. With this aim, we carried out an in-depth analysis of the metabolites of ginsenosides formed in artificial gastric juice by using ultraperformance liquid chromatography coupled with quadrupole time-of-flight mass spectrometry (UPLC-Q-TOF-MS) and chemical synthesis of speculated metabolites.

MATERIALS AND METHODS

Chemicals and Materials. Ginsenosides R_1, Rb_1, Rg_1, and Re (each purity >98%) were purchased from National Institute for the Control of Pharmaceutical and Biological Products (Beijing, China); 20(*S*)-Rg_3, 20(*R*)-Rg_3, 20(*S*)-Rh_2, and 20(*R*)-Rh_2 (Each purity >98%) were purchased from Scholar Bio-Tech (Chendu, China). 20(*S*)-Rg_2, 20(*R*)-Rg_2 (purity >98%), Rk_1/Rg_5, and Rg_6/F_4 were isolated in our lab and identified by HR-MS and NMR spectroscopies, and the ratio of Rk_1:Rg_5 and Rg_6/F_4 was determined to be 2.1:1.0 and 1.9:1.0, respectively, based on ^{1}H NMR. Total ginsenosides of notoginseng (NS-TG), subtotal ginsenosides of protopanaxadiol-type (NS-PPD), and subtotal ginsenosides of protopanaxatriol-type (NS-PPT) were prepared from MeOH extract of notoginseng in our lab by using column chromatography. All chemicals were of analytical grade purity.

Preparation of Hydrolysis Sample of NS-TG, NS-PPD and NS-PPT. Each of NS-TG, NS-PPD, and NS-PPT (30 mg) were accurately weighed into a 50 mL centrifuge tube and 20 mL of 0.1N HCl were added. The solutions were then incubated under 37 ± 0.5 °C with a shaking speed of 100 rpm. At the time points of 0, 0.25, 0.5, 1.0, 2.0, 3.0, 4.0, 5.0, 6.0, 7.0, and 8.0 h, a 500 μL aliquot of each sample was taken out and neutralized with 10N NaOH, and then diluted 20-fold with 50% MeOH for quantitative analysis.

UPLC-Q-TOF-MS Analysis. UPLC was performed using a Waters ACQUITY UPLC system (Waters Corp., MA, USA) which was equipped with a binary solvent delivery system and a sample manager coupled to Bruker MicroTOF mass spectrometer with an ESI source. All the operations, acquisition, and analysis of data were operated by Hystar software (Bruker).

The chromatography was performed on an Acquity BEH C_{18} column (2.1 mm × 100 mm, 1.7 μm). The mobile phase consisted of 0.1% formic acid in Milli-Q water (A) and acetonitrile containing 0.1% formic acid (B). Two optimized UPLC elution conditions as follows were employed: method I, linear gradient from 15% to 25% B at 0−8 min, 25% to 47.5% B at 8−22 min, 47.5 to 85% B at 22−27 min, and finally 85 to 100% B at 27−29 min; method II, linear gradient from 20 to 40% B within 20 min, then from 40 to 100% B at 20−29 min, and maintained at 100% B for 3 min at a flow rate of 0.35 mL/min. The injection volume was 1 μL for quantitative analysis and 10 μL for metabolites identification.

The ESI-MS data was acquired in negative mode and the conditions of MS analysis were as follows: end plate offset, −500 V; capillary voltage, 4500 V; nebulizing gas (N_2) pressure, 1.5 bar; drying gas (N_2) flow rate, 8.0L/min; drying gas temperature, 200 °C; mass range, *m*/*z* 300−1500. For accurate mass measurement, the TOF mass spectrometer was calibrated routinely using sodium formate solution (0.05 mM NaOH solution with 0.05% formic acid in 90:10 proportion of 2-propanol/distilled water) infused at a flow rate of 2.5 mL/h.

For quantitative analysis, the sample solutions were analyzed by enhanced MS scan. Ginsenosides and its metabolites were quantitatively analyzed by using extracted ion chromatogram (EIC) of the $[M - H]^-$ or $[M + HCOO]^-$ ions. The selected ion for EIC of each ginsenoside was as below: Rb_1, *m*/*z* 1107.5 ($[M - H]^-$); Rc, *m*/*z* 1077.5 ($[M - H]^-$); Rb_2, *m*/*z* 1077.5 ($[M - H]^-$); Rd, *m*/*z* 991.5 ($[M + HCOO]^-$); R_1, *m*/*z* 977.5 ($[M + HCOO]^-$); Rg_1, *m*/*z* 845.5 ($[M + HCOO]^-$); Re, *m*/*z* 991.5 ($[M + HCOO]^-$); 20(*S*)- and 20(*R*)-Rg_3, *m*/*z* 783.5 ($[M - H]^-$); 20(*S*)- and 20 (*R*)-Rh_2, *m*/*z* 667.4 ($[M + HCOO]^-$); Rk_1 and Rg_5, *m*/*z* 765.5 ($[M - H]^-$); 20(*S*)- and 20(*R*)-Rg_2, *m*/*z* 829.5 ($[M + HCOO]^-$); 20(*S*)- and 20(*R*)-Rh_2, *m*/*z* 683.5 ($[M + HCOO]^-$); Rg_6 and F_4, *m*/*z* 811.4 ($[M + HCOO]^-$). Typical calibration curve for quantitation of each ginsenoside in 50% MeOH were shown in Table 1.

Chemical Synthesis of Oxygenated Metabolites. Photosensitized oxygenation products of 20(*S*)-Rg_3, 20(*R*)-Rg_3, 20(*S*)-Rg_2, and 20(*R*)-Rg_2 were synthesized following our protocol described

Table 1. Typical Calibration Curve for Quantitation of Ginsenosides in Incubated Samples of NS-TG, NS-PPT, and NS-PPD

ginsenosides/ notoginsenoside	regression equation	linearity (mg/L)	r^2
R_1	$y = 22754x + 6905.5$	0.035−33.4	0.9976
Rg_1	$y = 37258x + 26583$	0.040−44.3	0.9924
Re	$y = 31852x + 56358$	0.042−76.5	0.9920
20(*S*)-Rg_2	$y = 21623x + 12199$	0.35−50.3	0.9954
20(*S*)-Rh_1	$y = 69284x + 44700$	0.5−24.4	0.9954
20(*R*)-Rg_2	$y = 23808x + 2114.9$	0.35−50.3	0.9997
20(*R*)-Rh_1	$y = 30436x + 20330$	1.3−196	0.9989
Rg_6	$y = 2901.1x + 642.87$	1.5−237.6	0.9997
F_4	$y = 3192.6x - 462.66$	1.5−237.6	0.9992
Rb_1	$y = 18687x + 9683.6$	0.591−151	0.9955
Rd	$y = 23118x + 31313$	0.05−58.3	0.9908
20(*S*)-Rg_3	$y = 29880x + 14483$	0.55−28.1	0.9934
20(*R*)-Rg_3	$y = 22808x + 20843$	0.35−52	0.9952
Rk_1	$y = 18966x + 25526$	0.8−121.3	0.9935
Rg_5	$y = 19458x + 20165$	0.8−121.3	0.9955
20(*S*)-Rh_2	$y = 48494x + 5778.5$	0.11−21.3	0.9991
20(*R*)-Rh_2	$y = 51129x + 3367.3$	0.13−20.0	0.9993

previously.[40] Briefly, a solution of the parent compound (200 mg) and Rose-Bengal (20 mg) in MeOH was stirred and irradiated with 400 W lamp under an oxygen atmosphere at room temperature for 10 h. After filtration, triphenylphosphine (40 mg) was added to the filtrate and the solution was stirred at room temperature for another 4 h. The solution was evaporated to dryness in vacuum, then subjected to combinative column chromatographies over silica gel eluted with $CHCl_3$−MeOH (10:0−8:2), MCI-gel CHP 20P, and Bondpack ODS (eluted with 40−100% MeOH) to give individual oxygenated products.

Epoxidation of 20(*R*)-Rg_3 and 20(*R*)-Rg_2 were performed following the procedure described in the literature with minor modifications.[41] Briefly, solution of the selected ginsenosides (100 mg) in acetonitrile (10 mL) was mixed with an aqueous EDTA-Na solution (0.4 μM, 10 mL). The mixed solution was cooled to 0 °C, and then an epoxidation dibetal catalyst solution (ketone, 60 μM in acetonitrile) and the mixture of sodium bicarbonate (155 μM) and oxone (100 μM) were added. The homogeneous solution was stirred overnight and then extracted with *n*-BuOH. The resultant *n*-BuOH layer was applied to column chromatographies over SiO_2 and ODS to afford 20(*R*)-Rg_3 epoxide (compounds **64** and **66**, 21.6 mg) and 20(*R*)-Rg_2 epoxide (compounds **35** and **36**, 15.02 mg) .

Chemical structures of the synthesized metabolites were characterized based on the elucidation of NMR data. ^{1}H- and ^{13}C NMR data were recorded on a Varian Mercury-Plus 300 MHz NMR spectrometer (300 MHz for ^{1}H and 75 MHz for ^{13}C), Varian 400 MHz FT-NMR spectrometer (400 MHz for ^{1}H and 100 MHz for ^{13}C) and Bruker NMR spectrometer (CyroFIT, 600 MHz for ^{1}H and 150 MHz for ^{13}C). Coupling constants were given in Hz and chemical shifts are represented in δ (ppm) relative to Me_4Si as internal standard. HR-ESI-MS was performed on a Q-TOF mass spectrometer (Bruker Daltonics, MA, USA).

Compound **11** [20(*S*)-Rg_2-mo] White powder. ^{1}H NMR (pyridine-d_5, 400 MHz) δ: 0.96, 1.01, 1.29, 1.30, 1.41, 1.56, 1.58, 2.16 (3H each, all s), 1.82 (3H, d, J = 6.2 Hz, Me-6″), 3.51 (1H, dd, J = 11.2, 4.6 Hz, H-3), 5.30 (1H, d, J = 6.9 Hz, H-1′), 6.08 (1H, d, J = 15.6 Hz, H-24), 6.37 (1H, ddd, J = 15.6, 9.2, 5.5 Hz, H-23), 6.55 (1H, brs, H-1″). ^{13}C NMR data was given in Table 2.

Compound **12** [20(*R*)-Rg_2-mo]: White powder. ^{1}H NMR (pyridine-d_5, 400 MHz) δ: 0.95, 1.01, 1.28, 1.37, 1.39, 1.54, 1.56, 2.10 (3H each, all s), 1.78 (3H, d, J = 6.0 Hz, Me-6″), 3.48 (1H, dd, J = 11.2, 4.8 Hz, H-3), 4.35 (1H, m, H-6), 5.25 (1H, d, J = 6.8 Hz, H-1′), 6.05 (1H, d, J = 15.6 Hz, H-24), 6.32 (1H, ddd, J = 15.6, 9.4, 5.6 Hz, H-23), 6.47 (1H, brs, H-1″). ^{13}C NMR data are given in Table 2.

Compounds **16** and **17** [20(*S*)-Rg_2-mo]: White powder. ^{1}H NMR (pyridine-d_5, 400 MHz) δ: 0.93, 0.95, 1.18, 1.34, 1.41, 1.52, 1.53, 1.89, 2.13 (3H each, all s), 1.80 (3H, d, J = 6.2 Hz, Me-6″), 3.49 (1H, dd, J = 11.3, 4.8 Hz, H-3), 4.42 (1H, dd, J = 11.6, 6.7 Hz, H-24), 4.92 (1H, s, H_a-26), 5.27, (1H, s, H_b-26), 5.28 (1H, d, J = 6.8 Hz, H-1′), 6.52 (1H, s, H-1″). ^{13}C NMR data are given in Table 2.

Compounds **21** and **24** [20(*R*)-Rg_2-mo]: White powder. ^{1}H NMR (pyridine-d_5, 400 MHz) δ: 0.94, 0.99, 1.24, 1.37, 1.41, 2.15 (3H each, all s), 1.53 (6H, s), 1.82 (3H, d, J = 5.4 Hz, CH_3-6″), 3.49 (1H, dd, J = 11.7, 6.3 Hz, H-3), 4.41 (1H, dd, J = 12.0, 7.0 Hz, H-24), 4.97 (1H, s, H_a-26), 5.30 (1H, d, J = 6.7 Hz, H-1′), 5.31 (1H, s, H_b-26), 6.51 (1H, s, H-1″). ^{13}C NMR data are given in Table 2.

Compounds **35** and **36** [20(*R*)-Rg_2 epoxides]: White powder. ^{1}H NMR (pyridine-d_5, 400 MHz) δ:0.80, 1.00, 1.20, 1.30, 1.32, 1.40, 1.42, 2.20 (3H each, all s), 1.80 (3H, d, J = 5.4 Hz, CH_3-6″), 4.02 (1H, dd, J = 9.0, 4.0 Hz), 5.10 (1H, d, J = 6.7 Hz, H-1′), 6.50 (1H, s, H-1″). ^{13}C NMR data are given in Table 2.

Compounds **44** and **52** [20(*S*)-Rg_3-mo]: White powder. ^{1}H NMR (pyridine-d_5, 300 MHz) δ: 0.80, 0.95, 0.98, 1.10, 1.29, 1.46 (3H each, all s), 1.89, 1.93 [1.5 H each, s, H-27 of 24(*S*) and 24(*R*)], 3.30 (1H, dd, J = 11.4, 3.9 Hz, H-3), 3.92 (1H, m, H-12), 4.44 (1H, dd, J = 12.0, 4.2 Hz, H-24), 4.91 (1H, d, J = 7.5 Hz, H-1′), 4.93 (1H, s, H-26), 5.25 (1H, s, H-26), 5.37 (1H, d, J = 7.5 Hz, H-1″). ^{13}C NMR data are given in Table 2.

Compound **45** [20(*S*)-Rg_3-mo]: White powder. ^{1}H NMR (pyridine-d_5, 300 MHz) δ: 0.82, 0.95, 1.02, 1.11, 1.29, 1.42 (3H each, all s), 1.56 (6H, s, CH_3-26, 27), 3.26 (1H, dd, J = 11.7, 4.5 Hz, H-3), 3.93 (1H, m, H-12), 4.92 (1H, d, J = 7.2 Hz, H-1′), 5.39 (1H, d, J = 7.5 Hz, H-1″), 6.03 (1H, d, J = 16.4 Hz, H-24), 6.50 (1H, ddd, J = 15.0, 7.2, 5.4 Hz, H-23). ^{13}C NMR data are given in Table 2.

Compounds **46** and **49** [20(*R*)-Rg_3-mo]: White powder. ^{1}H NMR (pyridine-d_5, 300 MHz) δ: 0.83, 0.97, 1.02, 1.14, 1.32, 1.44 (3H each, all s, CH_3-30, 19, 18, 29, 26, 28), 1.95, 1.97 [1.5 H each, s, CH_3-27 of 24(*S*) and 24(*R*)], 3.30 (1H, dd, J = 11.4, 3.9 Hz, H-3), 3.98 (1H, m, H-12), 4.31 (1H, dd, J = 12.6, 4.5 Hz, H-24), 4.97 (1H, d, J = 7.8 Hz, H-1′), 4.98 (1H, s, H_b-26), 5.33 (1H, s, H_a −26), 5.42 (1H, d, J = 7.8 Hz, H-1″). ^{13}C NMR data are given in Table 2.

Compound **50** [20(*R*)-Rg_3-mo]: White powder. ^{1}H NMR (pyridine-d_5, 300 MHz) δ: 0.85, 0.97, 1.06, 1.13, 1.31, 1.45, 1.56, 1.57 (3H each, all s, CH_3-30, 19, 18, 29, 28, 26, 27), 3.30 (1H, dd, J = 11.4, 4.2 Hz, H-3), 3.93 (1H, m, H-12), 4.93 (1H, d, J = 7.2 Hz, H-1′), 5.39 (1H, d, J = 7.5 Hz, H-1″), 6.03 (1H, d, J = 15.6 Hz, H-24), 6.31 (1H, ddd, J = 15.0, 8.4, 5.4 Hz, H-23). ^{13}C NMR data are given in Table 2.

Compounds **64** and **66** [20(*R*)-Rg_3 epoxides]: White powder. ^{1}H NMR (pyridine-d_5, 400 MHz) δ: 0.79, 1.01, 1.22, 1.29, 1.33, 1.45, 1.46, 2.04 (3H each, s), 3.51 (1H, dd, J = 11.0, 5.0 Hz, H-3), 3.74 (1H, m, H-12), 4.09 (1H, dd, J = 9.7, 3.8 Hz, H-24), 4.94 (1H, d, J = 7.2 Hz, H-1′), 5.40 (1H, d, J = 7.5 Hz, H-1″). ^{13}C NMR data are given in Table 2.

Cell Culture and Cytotoxicity Assay of NS-TG, NS-PPD, NS-PPT, and Their Metabolites at Different Time Points. Exponentially growing cells were plated in 96-well microplate (Becton, Dickinson and Company) at a density of 1.5 × 10^4 cells (S_{180}) and 5000 cells (Caco-2 and A_{549}) per well in 100 μL of culture medium and were allowed to adhere for 16 h before treatment (for Caco-2 and A_{549} cells). Serial concentrations of each compound in DMSO (Sigma-Aldrich) were then added (100 μL per well), and the cells were incubated for 48 h (S_{180} and A_{549}) or 72 h (Caco-2) at humidified atmosphere containing 5% CO_2 at 37 °C. The final concentration of DMSO in the culture medium was maintained at 0.3% (v/v) to avoid solvent toxicity. Cell viability was determined using 3-[4,5-dimethylthiazol-2-yl]-2,5-diphenyl- tetrazolium bromide (MTT) reduction assay. Briefly, MTT solution (10 μL per well, 5 mg/mL solution) were added to each well and incubated for 4 h at 37 °C, and 100 μL of lysing sodium dodecyl sulfate (SDS) were added and kept overnight at room temperature. The optical densities of the resulting solutions were colorimetrically determined at 570 nm using a microplate reader. Dose−response curves were obtained, and the results were expressed

Table 2. ^{13}C-NMR Data of the Chemically Synthesized New Metabolites (in Pyridine-d_5)

C	11[a]	12[a]	16 and 27[a]	21 and 24[a]	35 and 36[a]	44 and 52[a]	45[b]	46 and 49[a]	50[b]	64 and 66[a]
1	39.1	39.7	39.6	39.1	38.6	39.4	39.6	39.4	39.3	39.5
2	27.4	26.7	28.0	27.5	27.4	27.7	26.8	27.0	26.9	28.4
3	78.3	78.9	78.8	78.3	79.0	89.2	89.2	89.2	89	89.2
4	39.8	40.3	40.3	39.8	40.5	40.0	40.1	40.0	39.8	40.0
5	60.6	61.1	61.1	60.6	61.3	56.6	56.7	56.6	56.5	56.6
6	74.0	74.5	74.4	74.0	74.6	18.4	18.9	18.6	18.6	18.7
7	45.8	46.3	46.3	45.8	46.5	35.4	35.6	35.4	35.3	35.5
8	41.0	41.4	41.4	40.9	41.7	40.3	40.4	40.3	40.1	40.3
9	49.6	50.0	50.1	49.5	50.1	50.3	50.6	50.6	50.5	50.5
10	39.5	39.9	39.9	39.4	40.2	37.2	37.5	37.2	37	37.2
11	32.0	32.5	31.6	31.1	32.7	30.2	32.5	31.6	32.2	31.4
12	70.8	71.3	71.3	70.6	71.5	71.3	70.2	71.2	71.1	71.0
13	48.3	49.3	48.5	48.6	49.8	48.8	49.8	49.5	49	49.9
14	51.5	51.0	52.0	51.5	51.2	52.0	51.2	52.0	51.8	52.0
15	31.0	31.6	30.9	29.6	32.7	30.2	31.8	30.1	31.4	51.8
16	26.5	26.7	27.1	26.4	26.4	27.0	26.8	26.9	26.8	26.2
17	53.9	52.0	55.1 (54.8)	50.3 (50.1)	52.1 (52.0)	55.1 (54.9)	52.3	51.0	54.2	51.2 (51.1)
18	17.4	17.9	18.5	17.9	19.4	16.8	16.3	16.9	16.6	16.9
19	17.4	17.5	17.9	17.4	19.2	16.6	16	16.7	16	16.0
20	73.1	74.1	73.4 (73.3)	72.8	86.7(86.6)	73.4(73.3)	74.2	73.3	73.4	86.5 (86.4)
21	26.5	22.9	24.3	22.7	21.8(21.2)	27.2	23	23.2	27.7	21.6(19.3)
22	39.4	46.4	32.5	39.1	39.9 (39.6)	31.6	46.6	39.6	39.8	39.4(38.4)
23	122.9	123.1	31.6	32.0	27.9 (27.5)	30.9	121.5	32.4	123.3	27.7 (27.3)
24	141.8	142.7	76.6 (76.3)	75.9 (75.8)	87.5 (86.3)	76.6 (76.3)	142.6	76.3 (76.4)	141.8	87.4 (86.2)
25	69.6	70.2	149.7	149.6	70.9 (71.2)	150.5	70.2	150.5	69.9	70.9 (70.5)
26	30.5	31.1	110.4 (110.1)	110.0 (109.8)	26.6 (26.9)	110.4 (110.1)	31.2	110.6 (110.4)	30.8	26.4 (26.8)
27	30.5	31.1	18.8	18.1	27.2 (28.2)	18.7	31.2	18.4	30.8	30.3 (27.0)
28	27.5	28.0	29.4	27.5	31.9	28.4	28.6	28.4	28.3	31.7
29	17.0	17.4	17.2	17.0	18.1	16.1	16.8	16.1	17.1	16.7
30	16.7	17.5	17.4	17.4	18.0	17.3	17.6	17.6	16.7	17.4
1′	101.6	102.0	102.1	101.5	102.4	105.4	105.4	105.4	105.1	105.4
2′	79.2	79.7	79.7	79.2	79.9	83.6	83.7	83.7	83.3	83.6
3′	78.2	78.7	78.7	78.2	78.9	78.2	78.5	78.6	78	78.4
4′	72.1	72.6	72.5	72.1	72.8	71.9	71.8	71.9	71.7	71.8
5′	78.1	78.6	78.6	78.1	78.8	78.4	78.6	78.4	78.3	78.3
6′	62.9	63.4	63.3	62.9	63.6	62.8	63.2	63.0	62.9	63.1
1″	101.7	102.3	102.3	101.8	102.4	106.3	106.3	106.3	106	106.3
2″	72.4	72.9	72.8	72.3	73.1	77.4	77.4	77.5	77.1	77.4
3″	72.2	72.7	72.7	72.2	72.9	78.6	78.7	78.6	78.4	78.6
4″	74.2	74.5	74.6	74.1	75.0	71.9	71.2	71.9	71.7	71.9
5″	69.2	69.8	69.7	69.2	69.9	78.6	78.3	78.2	78.1	78.6
6″	18.5	19.1	19.0	18.5	20.0	62.1	63.1	63.1	62.7	63.0

[a]150 MHz for ^{13}C NMR; [b]75 MHz for ^{13}C NMR. The signals were assigned by comparing with those of reference compounds reported previously.[7,40,46,48,66]

as IC_{50} values in μg/mL. Each experiment was carried out for three times. IC_{50} results were expressed as means ± standard deviation.

RESULTS

Identification of Metabolites Formed in Artificial Gastric Juice. A primary study of NS-TG incubated in 0.1 N HCl and artificial gastric juice prepared following "Chinese Pharmacopoeia" give quiet similar profile in both metabolism pathway and metabolism time course. Further examination of NS-TG incubated in pepsin alone revealed that pepsin does not have any effect on the metabolism of NS-TG (Supporting Information). Therefore, 0.1N HCl was employed for simulating gastric condition in the current study to avoid steps for protein removal. To survey the metabolites formed in artificial gastric juice, subtotal ginsenosides of protopanaxadiol-type (NS-PPD), subtotal ginsenosides of protopanaxatriol-type (NS-PPT), and total ginsenosides (NS-TG) incubated for 3 h, the time point when most of the primary ginsenosides were transformed, were analyzed by using UPLC-Q-TOF-MS. In the incubated sample of NS-PPT, four groups of peaks can be easily observed as the major metabolites in the total ion chromatogram (TIC). These major metabolites were easily identified as deglycosylated ginsenosides, corresponding dehydration products, hydration products of primary, and secondary ginsenosides, as well as hydration products of dehydrated ginsenosides (Supporting Information). For NS-PPD (Figure 1B), similarly, the above four groups of metabolites were observed and characterized based on the retention time, quasimolecular ion, and accurate mass. Notably, the metabolites profile of NS-PPD was somewhat different from that of NS-PPT. The relative

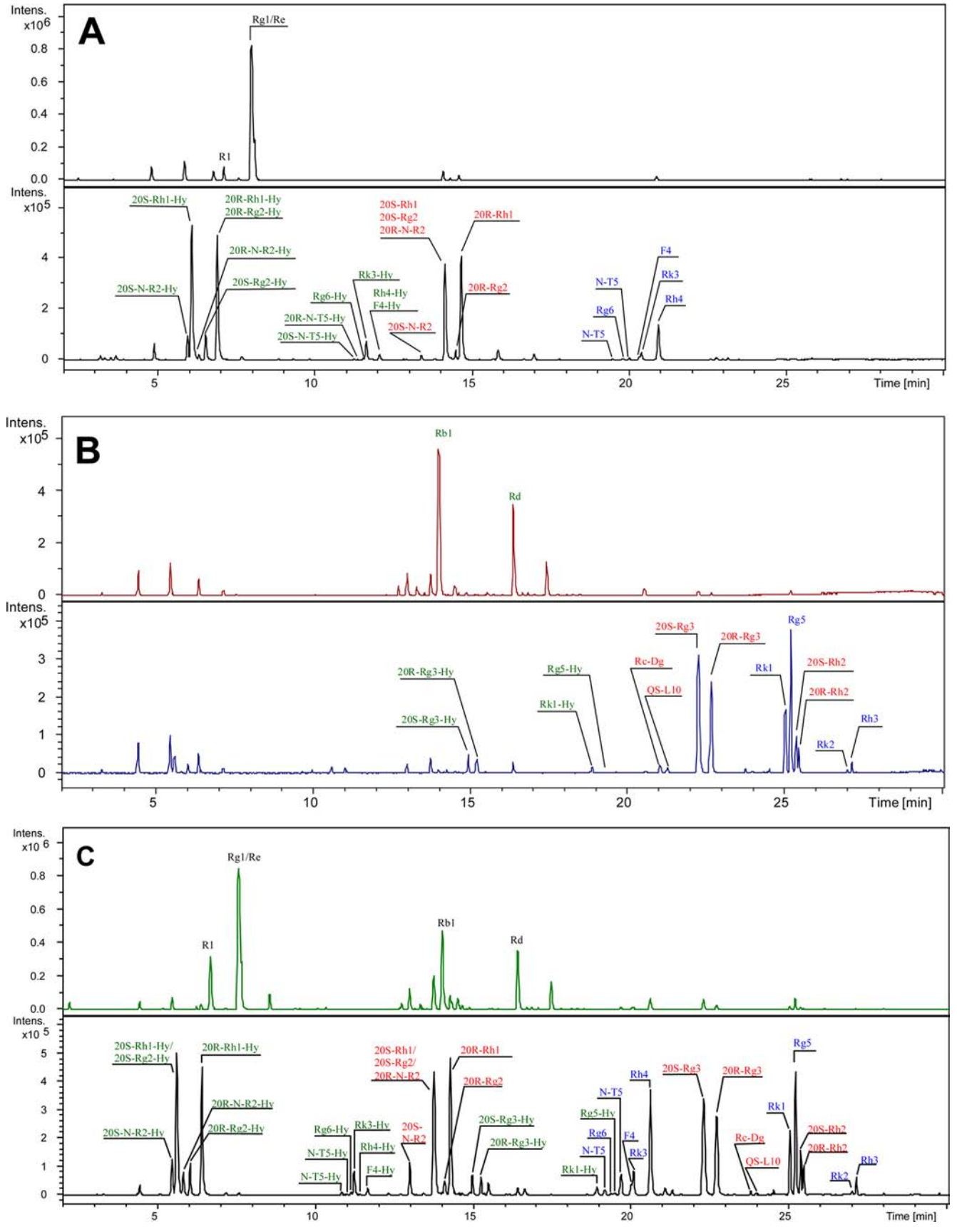

Figure 1. Total ion chromatogram (TIC) of NS-PPT (A), NS-PPD (B), and NS-TG (C) before (upper panel) and after incubation (lower panel) in artificial gastric juice for 3 h.

dx.doi.org/10.1021/jf405482s | J. Agric. Food Chem. 2014, 62, 2558−2573

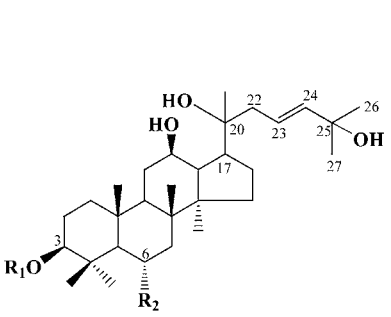

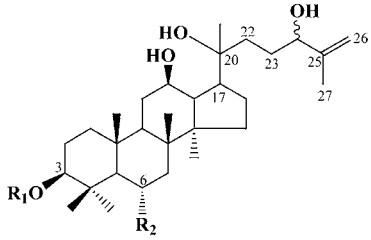

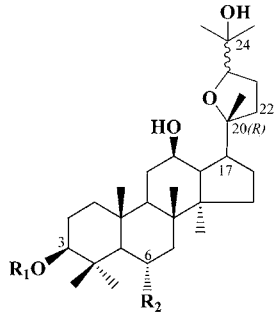

	R_1	R_2		R_1	R_2		R_1	R_2
11: 20*(S)*	H	-O-Glc^2-Rha	**16&27:** 20*(S)*	H	O-Glc^2-Rha	**35&36:** 24*(S&R)*	H	-O-Glc^2-Rha
12: 20*(R)*	H	-O-Glc^2-Rha	**21&24:** 20*(R)*	H	O-Glc^2-Rha	**64&66:** 24*(S&R)*	-Glc^2-Glc	H
45: 20*(S)*	-Glc^2-Glc	H	**44&52:** 20*(S)*	-Glc^2-Glc	H			
50: 20*(R)*	-Glc^2-Glc	H	**46&49:** 20*(R)*	-Glc^2-Glc	H			

Figure 2. Structures of the oxygenated ginsenosides identified by comparing with synthesized authentic compounds.

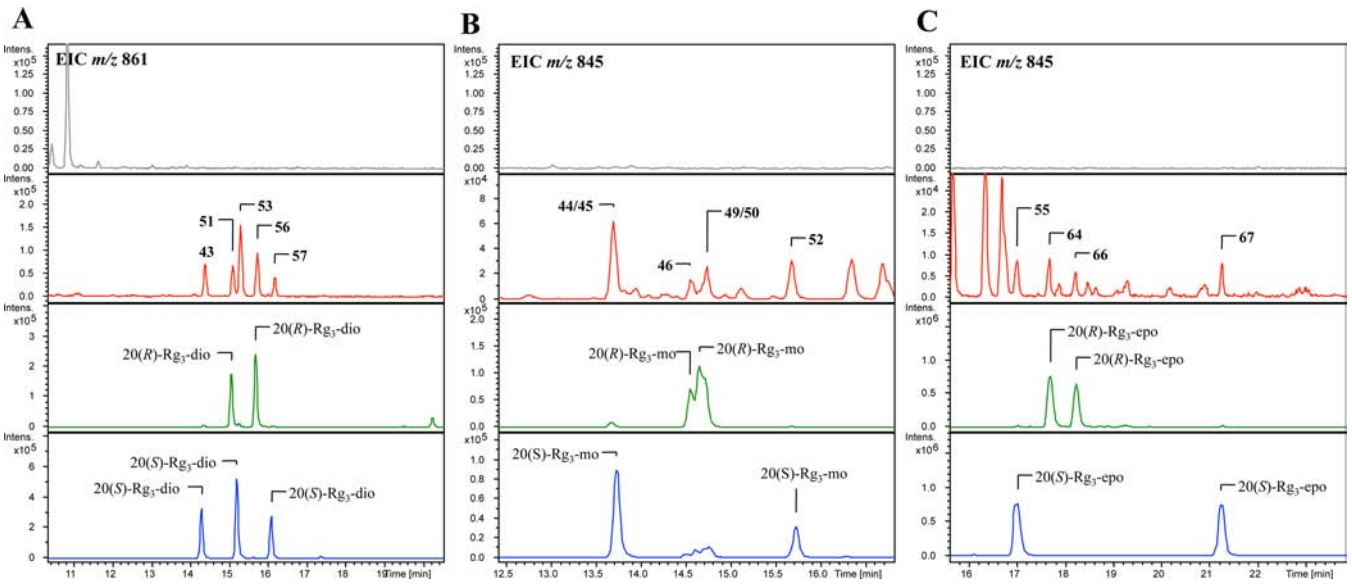

Figure 3. Identification of dioxygenated (A), mono-oxygenated (B), and epoxide metabolites (C) of Rg_3 in NS-TG incubated for 3 h in artificial gastric juice by comparing with synthesized authentic compounds. From top to bottom: NS-TG before incubation, NS-TG incubated for 3 h, and synthesized authentic metabolites of 20(*S*)- and 20(*R*)-Rg_3.

abundance of hydrated metabolites in NS-PPD was much lower than that in NS-PPT, while the intensity of dehydrated metabolites was just the opposite. Takino has reported that PPT-type ginsenosides is easily hydrated in both 0.1 N HCl and rat stomach, whereas PPD-type ginsenosides did not undergo hydration in either medium.[13,14] Our result showed that hydration of PPD-type ginsenosides also occurs in artificial gastric acid, but to much less an extent than that of PPT-type ginsenosides. On the basis of the identification of metabolites of NS-PPT and NS-PPD incubated with artificial gastric juice, metabolites derived from the primary ginsenosides R_1, Rg_1, Re, Rb_1, and Rd in the incubated sample of NS-TG through the above metabolic pathways were characterized or assigned by using the similar approach (Figure 1C).

Because oxygenated ginsenosides were also reported to form in rat stomach (in vivo) or under mild acidic condition except for the above major metabolic pathways.[42] We further screened oxygenated ginsenosides in NS-TG metabolites by using EIC mode in LC-MS. As a result, mono- and dioxygenated Rg_3 and Rg_2 were detected to be the major oxygenated metabolites of ginsenosides in artificial gastric juice. To identify the oxygenated metabolites, we synthesized speculated authentic compounds through photosensitized oxygenation and epoxidation. Chemical structures of the synthesized compounds were confirmed based on spectroscopic evidence. 20(*S*)-Rg_2-mo-I (**11**), a metabolite synthesized by using 20(*S*)-Rg_2 as the starting material, was taken as an example to show the structure elucidation of photosensitized ginsenosides. The proton and carbon signals of aglycone part in the ^{1}H NMR and ^{13}C NMR

dx.doi.org/10.1021/jf405482s | J. Agric. Food Chem. 2014, 62, 2558−2573

Table 3. Characterization of Metabolites of NS-TG in Artificial Gastric Juice by Using UPLC-Q-TOF-MS[b]

No.	t_R (min)		Measured Mass (*m/z*)	Molecular Formula ([M-H]⁻/[M+HCOO]⁻)	Theoretical mass	Mass error (ppm)	Structure		Identification
	M-I	M-II					Skeleton	Side chain	
1	1.9	1	949.5326	$C_{48}H_{81}O_{19}$	949.5378	-5.5		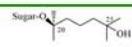	R_1-Hy
2	2.5	1.1	963.5460	$C_{48}H_{83}O_{19}$	963.5534	-7.7		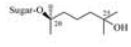	Re-Hy
3	4.3	1.1	817.4935	$C_{42}H_{73}O_{15}$	817.4955	-2.4		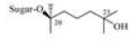	Rg_1-Hy
4	5.1	1.1	817.4885	$C_{42}H_{73}O_{15}$	817.4955	-8.6		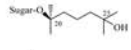	R_f-Hy
5	5.4	2.7	787.4824	$C_{41}H_{71}O_{14}$	787.4849	-3.2		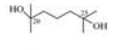	N-R_2-Hy
6	5.5	2.6	785.4638	$C_{41}H_{69}O_{14}$	785.4693	-7.0		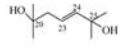	N-R_2-mo
7	5.6	2.9	655.447	$C_{36}H_{63}O_{10}$	655.4427	6.6		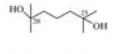	Rh_1-Hy
8	5.6	2.9	785.4689	$C_{41}H_{69}O_{14}$	785.4693	-0.5		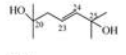	N-R_2-mo
9	5.8	2.9	787.4795	$C_{41}H_{71}O_{14}$	787.4849	-6.9		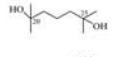	N-R_2-Hy
10	5.8	3.0	785.4635	$C_{41}H_{69}O_{14}$	785.4693	-7.4		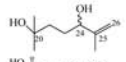	N-R_2-mo
11*	5.8	3.0	845.4906	$C_{43}H_{73}O_{16}$	845.4904	0.2		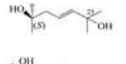	20(*S*)-Rg_2-mo
12*	5.8	3.1	845.4836	$C_{43}H_{73}O_{16}$	845.4904	8.0		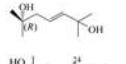	20(*R*)-Rg_2-mo
13	5.9	3.1	653.4239	$C_{36}H_{61}O_{10}$	653.4270	-4.7		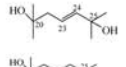	Rh_1-mo
14	6.0	3.1	801.5004	$C_{42}H_{73}O_{14}$	801.5006	-0.2		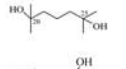	Rg_2-Hy
15	6.0	3.2	785.4703	$C_{41}H_{69}O_{14}$	785.4693	1.3		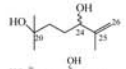	N-R_2-mo
16*	6.0	3.3	845.4896	$C_{43}H_{73}O_{16}$	845.4904	1.0		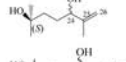	20(*S*)-Rg_2-mo
17	6.2	3.4	785.4666	$C_{41}H_{69}O_{14}$	785.4693	-3.4		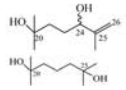	N-R_2-mo
18	6.4	3.3	801.4987	$C_{42}H_{73}O_{14}$	801.5006	-2.4		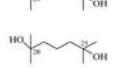	Rg_2-Hy
19	6.4	3.4	655.4449	$C_{36}H_{63}O_{10}$	655.4427	3.4		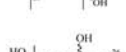	Rh_1-Hy
20	6.5	3.5	785.4666	$C_{41}H_{69}O_{14}$	785.4693	-3.4		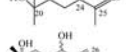	N-R_2-mo
21*	6.6	3.7	799.4839	$C_{42}H_{71}O_{14}$	799.4849	-1.3		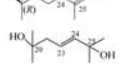	20(*R*)-Rg_2-mo
22	6.6	3.3	653.4288	$C_{36}H_{61}O_{10}$	653.4270	2.8		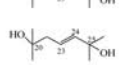	Rh_1-mo
23	6.8	3.6	653.4216	$C_{36}H_{61}O_{10}$	653.4270	-8.3		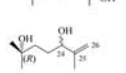	Rh_1-mo
24*	6.9	3.8	845.4890	$C_{43}H_{73}O_{16}$	845.4904	-1.7		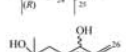	20(*R*)-Rg_2-mo
25	7.1	3.9	653.4186	$C_{36}H_{61}O_{10}$	653.4270	-12.9		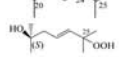	Rh_1-mo
26	7.4	4.2	815.4749	$C_{42}H_{71}O_{15}$	815.4798	-6.0		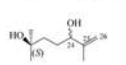	20(*S*)-Rg_2-dio
27*	7.7	4.3	845.4896	$C_{43}H_{73}O_{16}$	845.4904	-0.9		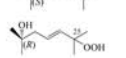	20(*S*)-Rg_2-mo
28	8.1	4.7	861.4838	$C_{43}H_{73}O_{17}$	861.4853	-1.7			20(*R*)-Rg_2-dio
29	9.9	5.4	799.4856	$C_{42}H_{71}O_{14}$	799.4849	0.9		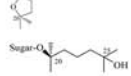	20(*S*)-Rg_2-epo (gynoside D)
30	10.0	7.3	1125.6011	$C_{54}H_{93}O_{24}$	1125.6062	-4.5		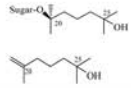	Rb_1-Hy
31	11.1	8.4	829.4955	$C_{42}H_{73}O_{15}$	829.4931	2.9			Rg_6-Hy

dx.doi.org/10.1021/jf405482s | J. Agric. Food Chem. 2014, 62, 2558−2573

Table 3. continued

No.	t_R (min)		Measured Mass (*m/z*)	Formula ([M-H]⁻/ [M+HCOO]⁻)	Theoretical mass	Mass error (ppm)	Structure		Identification
	M-I	M-II					Skeleton	Side chain	
32	11.5	9.3	963.546	$C_{48}H_{83}O_{19}$	963.5534	-7.7		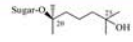	Rd-Hy
33	11.7	9.1	783.4900	$C_{42}H_{71}O_{13}$	783.4890	1.3			F_4-Hy
34	11.9	6.1	799.4812	$C_{42}H_{71}O_{14}$	799.4849	-4.6			20(*S*)-Rg_2-epo (gynoside A)
35*	12.2	6.3	845.4939	$C_{43}H_{73}O_{16}$	845.4904	4.1			20(*R*)-Rg_2-epo
36*	12.7	10.1	799.4810	$C_{42}H_{71}O_{14}$	799.4849	-4.9			20(*R*)-Rg_2-epo
37	13.2	11	769.4747	$C_{41}H_{69}O_{13}$	769.4744	0.40			20(*S*)-N-R_2
38	13.7	11.9	637.4306	$C_{36}H_{61}O_9$	637.4321	-2.4		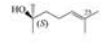	20(*S*)-Rh_1
39	13.7	12	783.4906	$C_{42}H_{71}O_{13}$	783.4900	0.80		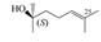	20(*S*)-Rg_2
40	13.9	12.1	769.471	$C_{41}H_{69}O_{13}$	769.4744	-4.4			20(*R*)-N-R_2
41	14.1	12.5	783.4891	$C_{42}H_{71}O_{13}$	783.4900	-1.1			20(*R*)-Rg_2
42	14.3	12.7	637.4306	$C_{36}H_{61}O_9$	637.4321	-2.4			20(*R*)-Rh_1
43	14.7	14.4	815.4787	$C_{43}H_{73}O_{17}$	815.4798	-1.3		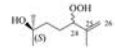	20(*S*)-Rg_3-dio
44*/45*	14.8	13.4	845.4871	$C_{43}H_{73}O_{16}$	845.4904	-3.9		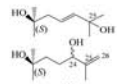	20(*S*)-Rg_3-mo
46*	14.9	14.3	799.4801	$C_{42}H_{71}O_{14}$	799.4849	-6.0		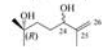	20(*R*)-Rg_3-mo
47	14.9	14	801.4984	$C_{42}H_{73}O_{14}$	801.5006	-2.7			Rg_3-Hy
48	15.2	14.4	801.4963	$C_{42}H_{73}O_{14}$	801.5006	-5.4			Rg_3-Hy
49*/50*[a]	15.4	14.5	845.4837	$C_{43}H_{73}O_{16}$	845.4904	-7.9		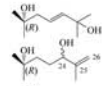	20(*R*)-Rg_3-mo
51	15.5	15.1	815.4837	$C_{43}H_{73}O_{17}$	815.4798	4.8		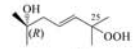	20(*R*)-Rg3-dio
52*[a]	15.5	15.4	799.4838	$C_{42}H_{71}O_{14}$	799.4849	-1.4		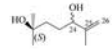	20(*S*)-Rg_3-mo
53	15.7	15.3	815.4814	$C_{43}H_{73}O_{17}$	815.4798	2.0		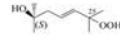	20(*S*)-Rg_3-dio
54	16.3	15.8	793.4365	$C_{42}H_{65}O_{14}$	793.4380	-1.9	-	-	R_0-Degly
55	16.9	16.7	799.4854	$C_{42}H_{71}O_{14}$	799.4849	0.6			20(*S*)-Rg_3-epo (pseudoginsenoside F11)
56	16.9	15.7	815.4806	$C_{43}H_{73}O_{17}$	815.4798	1.0		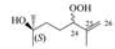	20(*R*)-Rg_3-dio
57	17.6	16.2	815.4798	$C_{43}H_{73}O_{17}$	815.4798	0.0		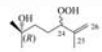	20(*S*)-Rg_3-dio
58	18.9	19.9	783.4884	$C_{42}H_{71}O_{13}$	783.4900	-2.0		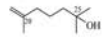	Rk_1-Hy
59	18.9	19.3	637.4298	$C_{36}H_{61}O_9$	637.4321	-3.6		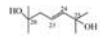	Rh_2-mo

dx.doi.org/10.1021/jf405482s | J. Agric. Food Chem. 2014, 62, 2558−2573

Table 3. continued

No.	t_R (min) M-I	t_R (min) M-II	Measured Mass (*m/z*)	Formula ([M-H]$^-$/ [M+HCOO]$^-$)	Theoretical mass	Mass error (ppm)	Structure Skeleton	Structure Side chain	Identification
60	19.3	20.1	751.4613	$C_{41}H_{67}O_{12}$	751.4638	-3.3			$N\text{-}T_5$
61	19.3	18.9	637.4305	$C_{36}H_{61}O_9$	637.4321	-2.5			Rh_2-mo
62	19.4	20.6	783.4883	$C_{42}H_{71}O_{13}$	783.4900	-2.2			Rg_5-Hy
63	19.4	20.5	765.4785	$C_{42}H_{69}O_{12}$	765.4795	-1.3			Rg_6
64*	19.5	17.4	799.4809	$C_{42}H_{71}O_{14}$	799.4849	-5.0			20(*R*)-Rg_3-epo
65	19.8	20.8	751.4628	$C_{41}H_{67}O_{12}$	751.4638	-1.3			$N\text{-}T_5$
66*	19.9	18.2	799.4882	$C_{42}H_{71}O_{14}$	799.4849	4.1			20(*R*)-Rg_3-epo
67	19.9	21.1	799.4826	$C_{42}H_{71}O_{14}$	799.4849	-2.9			20(*S*)-Rg_3-epo (pseudoginsenoside F11)
68	20.0	21.2	619.4203	$C_{36}H_{59}O_8$	619.4215	-1.9			Rk_3
69	20.0	21.3	765.4777	$C_{42}H_{69}O_{12}$	765.4795	-2.4			F_4
70	20.1	19.7	639.452	$C_{36}H_{63}O_9$	639.4478	6.6		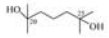	Rh_2-Hy
71	20.5	20.5	637.4289	$C_{36}H_{61}O_9$	637.4321	-5.0		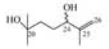	Rh_2-mo
72	20.6	21.7	619.4203	$C_{36}H_{59}O_8$	619.4215	-1.9			Rh_4
73	20.6	20.4	639.4451	$C_{36}H_{63}O_9$	639.4478	-4.2		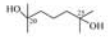	Rh_2-Hy
74	20.7	20.7	637.4289	$C_{36}H_{61}O_9$	637.4321	-5.0		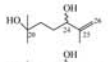	Rh_2-mo
75	21.2	21.2	637.4296	$C_{36}H_{61}O_9$	637.4321	-3.9		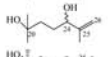	Rh_2-mo
76	22.3	22.8	783.4903	$C_{42}H_{71}O_{13}$	783.4900	0.4			20(*S*)-Rg_3
77	22.7	22.9	783.4908	$C_{42}H_{71}O_{13}$	783.4900	1.0			20(*R*)-Rg_3
78	25.0	24.6	765.4782	$C_{42}H_{69}O_{12}$	765.4795	-1.7			Rk_1
79	25.2	24.7	765.4800	$C_{42}H_{69}O_{12}$	765.4795	0.7			Rg_5
80	25.3	25	621.4315	$C_{36}H_{61}O_8$	621.4372	-9.2			20(*S*)-Rh_2
81	25.4	25	621.4324	$C_{36}H_{61}O_8$	621.4372	-7.7			20(*R*)-Rh_2
82	27.0	26.6	603.4178	$C_{36}H_{59}O_7$	603.4266	-14.6			RK_2
83	27.1	26.8	603.4166	$C_{36}H_{59}O_7$	603.4266	-16.6			Rh_3

PPT-type ginsenoside PPD-type ginsenoside ■ β-D-glucose ● α-L-rhamnose ● β-D-xylose

[a]The peak contained two metabolites which can be separated under optimized condition; Abbreviations: $N\text{-}R_2$ = notoginsenoside R_2; $N\text{-}T_5$ = notoginsenoside T_5; Hy = hydration products; Degly = deglycosylation products; dio = dioxygenated derivatives, i.e., 24- or 25-hydroperoxides; mo = mono-oxygenated derivatives, i.e., 24- or 25-hydroxides derived from photosensitization followed by reduction; epo = 20,24-epoxide. [b]*New compounds which were confirmed by comparison with chemically synthesized authentic compounds.

spectrum of **11** were found to be very similar to that of 20(*S*)-Rg_2 except for some signals arising from the side chain.[43,44] A disubstituted olefin as evidenced by the signals at δ_H 6.08 (1H, d, *J* = 15.6 Hz, H-24), 6.37 (1H, ddd, *J* = 15.6, 9.2, 5.5 Hz, H-

dx.doi.org/10.1021/jf405482s | J. Agric. Food Chem. 2014, 62, 2558−2573

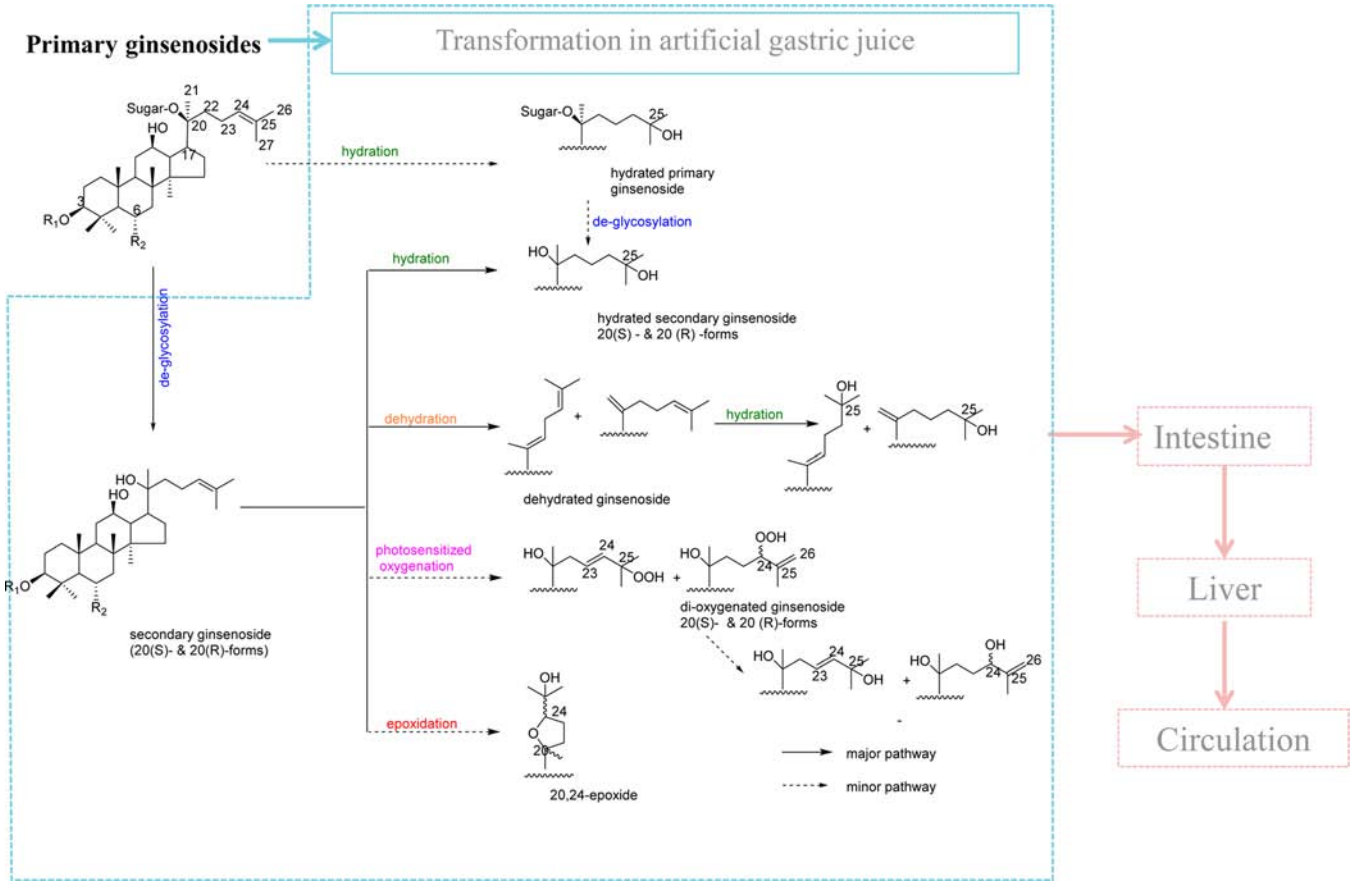

Figure 4. Proposed metabolic pathways of ginsenosides in artificial gastric juice.

23), and δ_C 122.9 (C-23), 141.8 (C-24). The downfield shift of C-22 ($\Delta\delta_C$ = 3.5 ppm), compared to that of 20(*S*)-Rg_2, clearly suggested a translocation of the double bond to C-23 and 24. The oxygenated carbon (δ_C 69.9) assigned to the remaining carbon (C-25) of the side chain indicated the presence of a hydroxyl group at C-25. These evidence revealed the structure of the side chain with a hydroxyl group at C-25 and a double bond at C-23 and C-24, which was supported by the chemical shift comparing with those of related hydroxylated ginsenosides.[7] Thus the structure of **11** was assigned as shown (Figure 2).

Structure characterization of epoxides was shown in example of 20(*R*)-Rg_2-Epo (**35** and **36**). This mixture was synthesized from 20(*R*)-Rg_2 by using epoxidation dibetal catalyst solution which could oxidize 24,25-double bond into 24,25-epoxide. The resulting 24,25-epoxy compounds are quite unstable in the existence of a 20-hydroxy group and immediately changed into 20,24-epoxides.[45] The formation of 20,24-epoxides in **35** and **36** was evidenced by the large downfield shift of C-20 ($\Delta\delta_C$ = 13.3) and C-23 ($\Delta\delta_C$ = 5.3), as well as the displacement of olefinic carbon signals with oxygenated carbon signals [δ_C 87.5(C-24), δ_C 70.9(C-25)] in comparison with that of 20(*R*)-type secondary ginsenosides,[14] and was further supported by comparing the chemical shifts to those of 20(*S*)-epoxides.[46] **35** and **36** were found to be an equivalent mixture of 24(*R*) and 24(*S*)-epimers based on the fact that the signals of C-17,20−27 appeared in pairs in the ^{13}C NMR spectrum (Table 2). On the basis of above evidence, the structure of **35** and **36** was assigned as shown (Figure 2).

By comparing with the synthesized metabolites, the dioxygenated metabolites were identified to be hydroperoxides derivatives of Rg_2 and Rg_3, while the mono-oxygenated metabolites were characterized to be corresponding hydroxides and 20,24-epoxides (Figure 3) of Rg_2 and Rg_3. Hydroperoxides and corresponding hydroxides of Rg_2 and Rg_3, as well as epoxides of 20(*R*)-Rg_2 and 20(*R*)-Rg_3, are new dammarane glycosides which were not reported before. To confirm formation pathway of the oxygenated metabolites, ginsenoside Rg_3 was incubated in artificial gastric juice, resulting in the production of above oxygenated metabolites (data not show), indicating these oxygenated metabolites can be derived from Rg_3 via oxygenation rather than from hydrolysis of hydroperoxides and corresponding hydroxides of primary ginsenosides that have been reported to exist naturally in notoginseng.[47,48]

In summary, totally 83 metabolites were identified in the incubated sample of NS-TG (Table 3). Characterization of these metabolites suggested deglycosylation, dehydration, hydration, and oxygenation as the metabolic pathways of ginsenosides in artificial gastric juice (Figure 4).

Time Course of Transformation of Ginsenosides in Artificial Gastric Juice. The time courses of degradation of primary ginsenosides, as well as the formation of deglycosylation and dehydration metabolites, were plotted by quantitatively determining the content of both parent compounds and metabolites at different time point of incubation (Figure 5). It can be seen that the three primary ginsenosides, N-R_1, Rg_1, and Re, disappeared rapidly. N-R_1 and Re were exhausted at 2 h, while Rg_1 was metabolized thoroughly at 3 h (Figure 5A,B).

dx.doi.org/10.1021/jf405482s | J. Agric. Food Chem. 2014, 62, 2558−2573

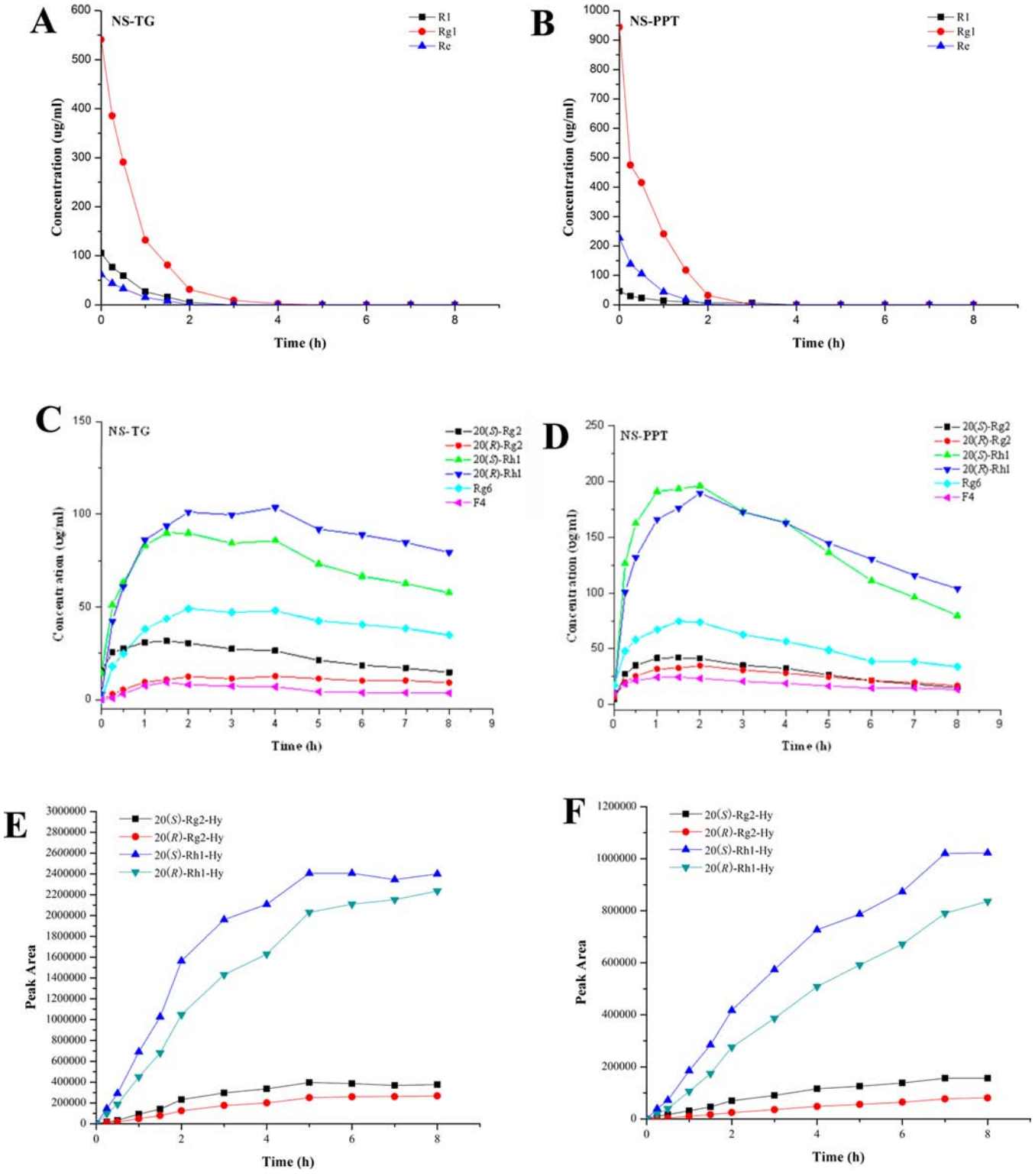

Figure 5. Time course of degradation of primary PPT-type ginsenosides (A,B), formation of deglycosylation, dehydration (C,D), and hydration metabolites (E,F) in incubated NS-TG and NS-PPT. Each sample was analyzed in duplicate, and the average value was employed for plotting.

20(*R*)- and 20(*S*)-Rh_1 were the most dominant metabolites, followed by 20(*S*)- and 20(*R*)-Rg_2 and their dehydration products Rg_6 and F_4. Production of the metabolites peaked at 2 h, and decreased stepwise after 2 h (Figure 5C,D). Decrease of the deglycosylated and dehydrated metabolites might be due to subsequent hydration, which was supported by the increased formation of hydration products after 2 h (Figure 5E,F). Formation of the dehydration products, e.g., Rg_6 and F_4, showed almost identical time course with that of corresponding secondary ginsenosides, and the ratio between them kept the same during 8 h incubation, suggesting that dehydration occurred very quickly after deglycosylation and reached equilibration rapidly. PPD-type ginsenosides showed quite similar time course to that of NS-PPT (Figure 6A–D), but

dx.doi.org/10.1021/jf405482s | J. Agric. Food Chem. 2014, 62, 2558–2573

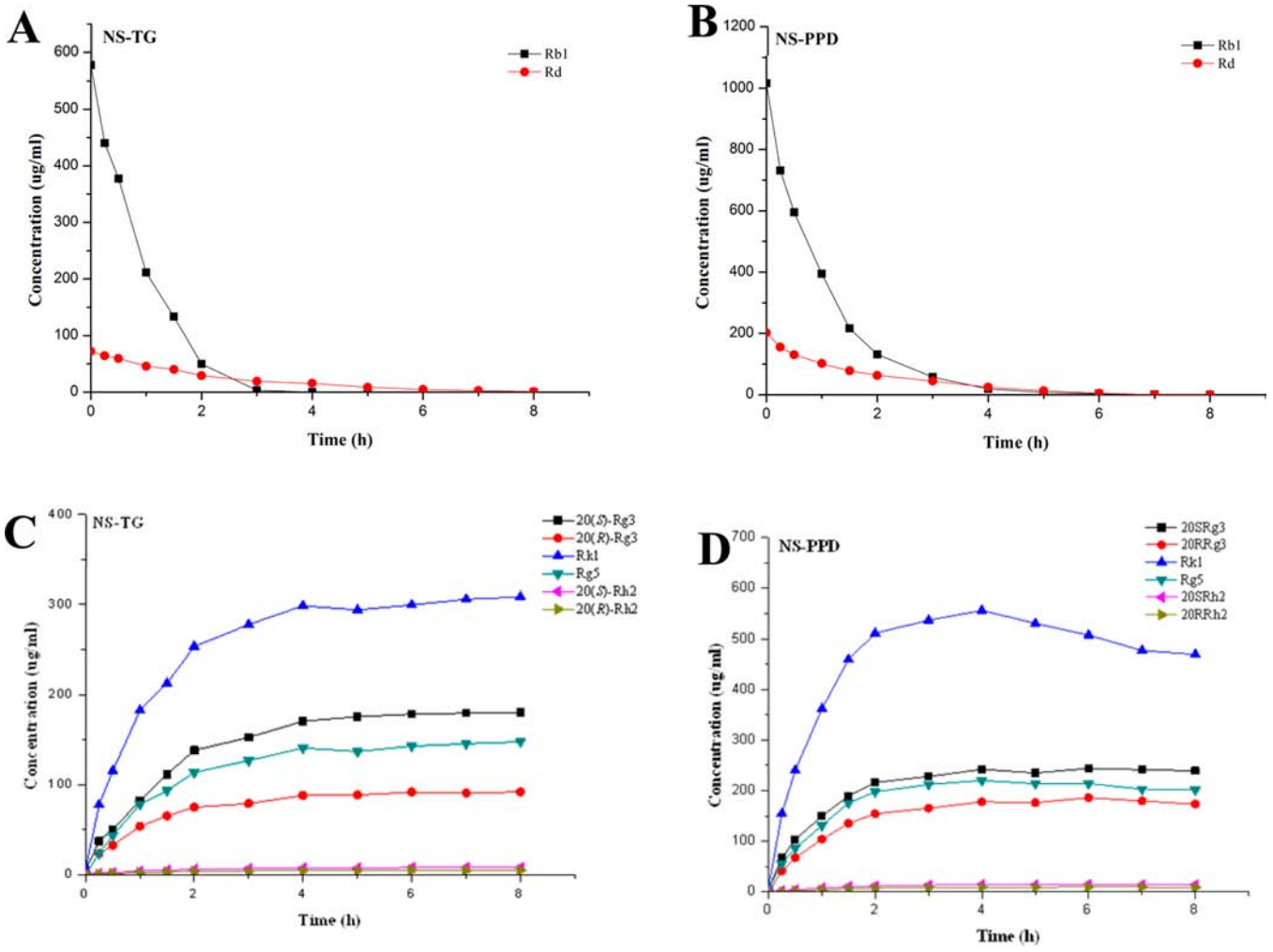

Figure 6. Time course of degradation of primary PPD-type ginsenosides (A,B) and formation of deglycosylation and dehydration metabolites (C,D) in artificial gastric juice. Each sample was analyzed in duplicate, and the average value was employed for plotting.

Table 4. Cytotoxicity of NS-TG, NS-PPT, NS-PPD, and Their Metabolites Formed at Different Time Point of Incubation in Artificial Gastric Juice Towards S_{180}, Caco-2, and A_{549}[a]

	content (μg/mg)			ratio of different types of ginsenosides			IC_{50} (μg/mL)		
sample	PG	SG	DG	SG/PG	DG/PG	(SG + DG)/PG	S_{180}	Caco-2	A_{549}
TG_0 h	905.66	25.31	3.75	0.03	0.00	0.03	>2000	>2000	>2000
TG_0.25 h	673.74	123.00	80.31	0.18	0.12	0.30	449.8 ± 13.2	776.6 ± 114.1	317.0 ± 49.5
TG_0.5 h	547.06	161.96	124.66	0.30	0.23	0.52	264.2 ± 5.2	302.6 ± 62.0	181.8 ± 47.6
TG_1 h	287.44	234.66	204.10	0.82	0.71	1.53	175.9 ± 37.2	393.7 ± 92.0	183.3 ± 46.7
TG_3 h	21.00	309.71	305.91	14.75	14.57	29.32	133.2 ± 16.5	144.5 ± 12.8	57.2 ± 12.6
PPT_0 h	812.09	21.84	17.89	0.03	0.02	0.05	>2000	>2000	>2000
PPT_0.25 h	428.56	182.77	44.11	0.43	0.10	0.53	377.2 ± 99.5	624.9 ± 282.0	286.7 ± 44.7
PPT_0.5 h	362.54	236.50	52.87	0.65	0.15	0.80	248.8 ± 5.3	337.2 ± 36.0	148.2 ± 15.7
PPT_1 h	199.08	287.17	60.87	1.44	0.31	1.75	229.9 ± 17.5	408.3 ± 49.9	153.8 ± 14.2
PPT_3 h	4.00	274.52	55.42	68.63	13.86	82.49	348.6 ± 10.5	620.5 ± 45.6	190.2 ± 5.5
PPD_0 h	812.13	3.86	9.51	0.00	0.01	0.02	>2000	>2000	>2000
PPD_0.25 h	591.08	74.25	140.01	0.13	0.24	0.36	467.1 ± 43.2	1932.7 ± 38.0	487.9 ± 10.3
PPD_0.5 h	483.66	117.45	217.36	0.24	0.45	0.69	242.5 ± 5.9	441.7 ± 82.1	228.8 ± 40.3
PPD_1 h	330.93	176.51	328.62	0.53	0.99	1.53	305.4 ± 42.3	665.1 ± 152.6	115.6 ± 1.3
PPD_3 h	67.90	276.37	499.56	4.07	7.36	11.43	121.3 ± 7.4	246.9 ± 0.6	30.5 ± 0.6

[a]Abbreviations: PG = sum of primary ginsenosides (N-R_1, Rg_1 Re, Rb_1, Rd); SG = sum of secondary ginsenosides (Rg_2, Rh_1, Rg_3, Rh_2); DH = sum of dehydration products (Rg_6, F_4, Rk_1 and Rg_5).

different from PPT-type ginsenosides, concentration of the metabolites did not decrease at the later period of incubation.

Cytotoxicity of Metabolites of Ginsenosides at Different Time Point to Cancer Cells. Cytotoxicity of ginsenosides

dx.doi.org/10.1021/jf405482s | J. Agric. Food Chem. 2014, 62, 2558−2573

toward a broad spectrum of cancer cell lines have been demonstrated, hence the most widely used cancer cell lines in our lab, S_{180}, A_{549}, and Caco-2 cells, were selected for the assaying cytotoxicity. Among these three cell lines, A_{549} and Caco-2 have been reported for evaluating cytotoxicity of ginsenosides.[49−51] As shown in Table 4, all the ginsenoside samples before incubation exhibited no cytotoxicity (IC_{50} > 2000 μg/mL) or very low cytotoxic activities. With the increase of incubation time in artificial gastric juice, cytotoxicity of all three samples enhanced gradually. Cytotoxicity potential of the ginsenosides were found to be closely related to the ratio between metabolites and primary ginsenosides, indicating that secondary and dehydrated ginsenosides are the major active principles responsible for the cytotoxicity toward cancer cells. However, MTT is a colorimetric assay based on tetrazolium dye reduction catalized by NAD(P)H-dependent oxidoreductase. Therefore, viable but metabolically quiet resting cells like thymocytes and splenocytes reduce very little MTT, leading to a false conclusion. More importantly, although MTT assay is widely used for assaying cell viability, it could not distinguish the effects of cell death or cell growth inhibition, which are important component of biological research. Further studies need to be carried out to evaluate the subtle influence of metabolism on the bioactivity of ginsenosides.

DISCUSSION

Our study revealed multiple metabolic pathways of ginsenosides in gastric juice, including deglycosylation, dehydration, hydration, and oxygenation. The hydration of PPT-type ginsenosides was much more extensive than that of PPD-type ginsenosides, indicating that this pathway is compound type-dependent. Oxygenation, which occurs through both epoxidation and photosensitization, was shown to be a minor metabolic pathway of ginsenosides in gastric juice. These results indicated that molecular diversity of ginsenosides can be generated through transformation in gastric juice, thus creating new chemomes which are more biologically associated with the activity of the herb.

In a previous study, the hydrolytic reaction of ginsenosides under mild acidic condition (AcOH/EtOH 1:1) led to the formation of deglycosylation product, dehydration product, 20-O-alkylated derivatives, 25-OH derivatives, as well as methylation product.[39] In our study, deglycosylation, dehydration and hydration product (25-OH derivatives) were found to be the major metabolic pathway of ginsenosides, suggesting that these pathways are common reaction under acidic condition.

Time course investigation suggested that the primary ginsenosides were decomposed quickly within 2 h, a period required for exclusion of stomach, implying that ginsenosides undergo extensive metabolism in gastric juice before they get into the intestine in vivo. Deglycosylation products, e.g., Rg_3, Rh_2, Rg_2, and Rh_1, were demonstrated to be the major metabolites formed in artificial gastric juice, accounting for 30−40% of the total amount of metabolites. Previous studies have shown that after oral administration significant amount of C−K can be detected in plasma while the primary ginsenosides were poorly absorbed or undetectable.[52,53] Rh_2, a deglycosylated ginsenoside derived from artificial gastric acid, was reported to have an improved intestinal absorption as evidenced by much higher bioavailability (~5% in rat, 15−25% in dog) than its parent ginsenosides Rb_1 and Rb_2 (with bioavailability of 0.78 and 0.08%, respectively), implying an improved absorption with the removal of sugar moiety.[54−56] Moreover, it has been reported that deglycosylated ginsenosides, i.e., F_2, C−K, Rh_2, Rh_1, and F_1 possessed slightly increased membrane permeability than primary ginsenosides, while aglycone, PPD and PPT further showed 1-fold higher permeability than that of deglycosylated ginsenosides in Caco-2 cells.[57] Therefore, deglycosylated metabolites might have great potential to be absorbed into circulation system. This can be exampled by previous report which showed the absorption of gastric juice-derived metabolites of ginsenosides (e.g., Rh_1 and hydrated Rh_1) at early stage (0−4 h) in urine and plasma of human after oral administration of ginseng extract.[33]

Even though, absorption of the deglycosylated ginsenosides into the circulation system could be extremely complicated because of the efflux and stereoselectivity as well as further metabolism. Actually most of the deglycosylated ginsenosides formed in gastric juice were not reported to exist in plasma or only detected in nanomolar levels.[36] A major reason might be the involvement of efflux transport. For example, 20(S)-Rh_2, a major deglycosylated PPD-type ginsenosides formed in gastric juice, was demonstrated to be a substrate of P-gP. Its transport was involved by P-gP and thus resulting in poor absorption.[58] As C-20 epimers of the deglycosylated ginsenosides formed almost simultaneously, stereoselective absorption as well as stereoselective regulation of P-glycoprotein by Rh_2 epimers will result in quite complicated interaction of these two epimers,[59,60] making it difficult to predict their absorption.

An additional issue potentiate the complexity in absorption of the metabolites is the subsequent metabolism in liver after absorption. Recent studies suggested that C-20 hydroxyl group was a determinant for hepatic disposition of ginsenosides,[61] implying that biotransformation of ginsenosides in gastric juice through hydrolysis of C-20 sugar moiety would be a key step for "activating" the subsequent P450-mediated metabolism. Except for the deglycosylated ginsenosides, the corresponding dehydrated and hydrated ginsenosides may also be metabolized in liver to form bulky metabolites. The metabolites resulting from the coupling of gastric juice and hepatic enzyme might be responsible for the unidentified circulating metabolites proposed in previous radioisotope assay, which revealed three times higher serum radioactivity of Rb_2 and its derivatives than Rb_2 level determined by HPLC.[23] It has been proved that intact ginsenosides and deglycosylated ginsenosides exhibited distinct activity on CYP enzymes.[62,63] Therefore, systemic exposure of the deglycosylated and related ginsenosides was quite valuable for evaluating the herb−drug interaction caused by the inhibition of ginsenosides on the CYP's activity.

Although substantial studies have demonstrated in vivo anticancer effect of primary ginsenosides,[64−66] no in vitro evidence of cytotoxicity of primary ginsenosides was available. Our studies showed that primary ginsenosides themselves seems to be "inactive" toward cancer cells but can gain potent cytotoxicity after biotransformation in artificial gastric juice, suggesting that this step may contribute to the observed in vivo anticancer activity of notoginseng. Moreover, both PPD- and PPT-type ginsenosides exhibited increased cytotoxicity after biotransformation and may cooperatively contribute to the activity of NS-TG metabolites. The cytotoxicity of metabolites enhanced along with the increased incubation time and showed good correlation with the ratio of both deglycosylated and dehydrated products to primary ginsenosides. This evidence indicated a major contribution of deglycosylation and dehydration products to the cytotoxicity. However, other

minor metabolites derived from hydration and oxygenation may also have potential activity that needs to be further explored.

■ ASSOCIATED CONTENT

Supporting Information

Characterization of the four groups of major metabolites. This material is available free of charge via the Internet at http://pubs.acs.org.

■ AUTHOR INFORMATION

Corresponding Authors

*For Z.-H.J.: phone, +853-8897 2777; fax, +853-2882 5886; E-mail, zhjiang@must.edu.mo; address, State Key Laboratory of Quality Research in Chinese Medicine, Macau Institute for Applied Research in Medicine and Health, Macau University of Science and Technology Taipa, Macau 00853, China.

*For L.L.: phone, +853-8897 2077; fax, +853-2882 7222; E-mail, lliu@must.edu.mo.

Funding

This project is sponsored by Macao Science and Technology Development Fund (066/2011/A3 to W.J.R.).

Notes

The authors declare no competing financial interest.

■ REFERENCES

(1) Ng, T. B. Pharmacological activity of sanchi ginseng (*Panax notoginseng*). *J. Pharm. Pharmacol.* **2006**, *58* (8), 1007−1019.

(2) Konoshima, T.; Takasaki, M.; Tokuda, H. Anti-carcinogenic activity of the roots of *Panax notoginseng*. II. *Biol. Pharm. Bull.* **1999**, *22* (10), 1150−1152.

(3) Wang, C. Z.; Yuan, C. S. Potential role of ginseng in the treatment of colorectal cancer. *Am. J. Chin. Med.* **2008**, *36* (6), 1019−1028.

(4) Yang, J. M.; Lu, F. H.; Jin, S. K.; Sun, S. W.; Zhao, Y. X.; Wang, S. J.; Zhou, X. H. A cohort study on the predictive value of factors influencing cardio-cerebro vascular death among people over 40 years of age. *Zhonghua Liuxingbingxue Zazhi* **2007**, *28* (2), 119−122.

(5) Ruan, J. Q.; Leong, W. I.; Yan, R.; Wang, Y. T. Characterization of metabolism and in vitro permeability study of notoginsenoside R1 from *Radix notoginseng*. *J. Agric. Food Chem.* **2010**, *58* (9), 5770−5776.

(6) He, N. W.; Zhao, Y.; Guo, L.; Shang, J.; Yang, X. B. Antioxidant, antiproliferative, and pro-apoptotic activities of a saponin extract derived from the roots of *Panax notoginseng* (Burk.) F.H. Chen. *J. Med. Food* **2012**, *15* (4), 350−359.

(7) Yoshikawa, M.; Murakami, T.; Ueno, T.; Hirokawa, N.; Yashiro, K.; Murakami, N.; Yamahara, J.; Matsuda, H.; Saijoh, R.; Tanaka, O. Bioactive saponins and glycosides. IX. Notoginseng (2): structures of five new dammarane-type triterpene oligoglycosides, notoginsenosides-E, -G, -H, -I, and -J, and a novel acetylenic fatty acid glycoside, notoginsenic acid β-sophoroside, from the dried root of *Panax notoginseng* (Burk.) F. H. Chen. *Chem. Pharm. Bull.* **1997**, *45*, 1056−1062.

(8) Wang, X.-Y.; Wang, D.; Ma, X.-X.; Zhang, Y.-J.; Yang, C.-R. Two new dammarane-type bisdesmosides from the fruit pedicels of *Panax notoginseng*. *Helv. Chim. Acta* **2008**, *91*, 60−66.

(9) Christensen, L. P. Ginsenosides: chemistry, biosynthesis, analysis, and potential health effects. *Adv. Food Nutr. Res.* **2009**, *55*, 1−99.

(10) Wan, J. B.; Li, S. P.; Chen, J. M.; Wang, Y. T. Chemical characteristics of three medicinal plants of the Panax genus determined by HPLC-ELSD. *J. Sep. Sci.* **2007**, *30* (6), 825−832.

(11) Wang, J. R.; Leung, C. Y.; Ho, H. M.; Chai, S.; Yau, L. F.; Zhao, Z. Z.; Jiang, Z. H. Quantitative comparison of ginsenosides and polyacetylenes in wild and cultivated American ginseng. *Chem. Biodiversity* **2010**, *7* (4), 975−983.

(12) Karikura, M.; Miyase, T.; Tanizawa, H.; Taniyama, T.; Takino, Y. Studies on absorption, distribution, excretion and metabolism of ginseng saponins. VI. The decomposition products of ginsenoside Rb2 in the stomach of rats. *Chem. Pharm. Bull. (Tokyo)* **1991**, *39* (2), 400−404.

(13) Karikura, M.; Miyase, T.; Tanizawa, H.; Taniyama, T.; Takino, Y. Studies on absorption, distribution, excretion and metabolism of ginseng saponins. VII. Comparison of the decomposition modes of ginsenoside-Rb1 and -Rb2 in the digestive tract of rats. *Chem. Pharm. Bull. (Tokyo)* **1991**, *39* (9), 2357−2361.

(14) Odani, T.; Tanizawa, H.; Takino, Y. Studies on the absorption, distribution, excretion and metabolism of ginseng saponins. IV. Decomposition of ginsenoside-Rg1 and -Rb1 in the digestive tract of rats. *Chem. Pharm. Bull. (Tokyo)* **1983**, *31* (10), 3691−3697.

(15) Wang, Y.; Wang, B. X.; Liu, T. H.; Minami, M.; Nagata, T.; Ikejima, T. Metabolism of ginsenoside Rg1 by intestinal bacteria. II. Immunological activity of ginsenoside Rg1 and Rh1. *Acta Pharmacol. Sin.* **2000**, *21*, 792−796.

(16) Bae, E.-A.; Han, M. J.; Kim, E.-J.; Kim, D.-H. Transformation of ginseng saponins to ginsenoside Rh2 by acids and human intestinal bacteria and biological activities of their transformants. *Arch. Pharm. Res.* **2004**, *27*, 61−67.

(17) Bae, E.-A.; Choo, M.-K.; Park, E.-K.; Park, S.-Y.; Shin, H.-Y.; Kim, D.-H. Metabolism of ginsenoside R(c) by human intestinal bacteria and its related antiallergic activity. *Biol. Pharm. Bull.* **2002**, *25*, 743−747.

(18) Bae, E.-A.; Shin, J.-E.; Kim, D.-H. Metabolism of ginsenoside Re by human intestinal microflora and its estrogenic effect. *Biol. Pharm. Bull.* **2005**, *28*, 1903−1908.

(19) Hasegawa, H.; Lee, K. S.; Nagaoka, T.; Tezuka, Y.; Uchiyama, M.; Kadota, S.; Saiki, I. Pharmacokinetics of ginsenoside deglycosylated by intestinal bacteria and its transformation to biologically active fatty acid esters. *Biol. Pharm. Bull.* **2000**, *23*, 298−304.

(20) Akao, T.; Kida, H.; Kanaoka, M.; Hattori, M.; Kobashi, K. Intestinal bacterial hydrolysis is required for the appearance of compound K in rat plasma after oral administration of ginsenoside Rb1 from *Panax ginseng*. *J. Pharm. Pharmacol.* **1998**, *50*, 1155.

(21) Hasegawa, H.; Sung, J. H.; Benno, Y. Role of human intestinal *Prevotella oris* in hydrolyzing ginseng saponins. *Planta Med.* **1997**, *63*, 436−440.

(22) Takino, Y. Studies on the pharmacodynamics of ginsenoside-Rg1, -Rb1 and -Rb2 in rats. *Yakugaku Zasshi* **1994**, *114*, 550−564.

(23) Hasegawa, H. Proof of the mysterious efficacy of ginseng. Basic and clinical trials: Metabolic activation of ginsenoside: Deglycosylation by intestinal bacteria and esterification with fatty acid. *J. Pharmacol. Sci. (Tokyo)* **2004**, *95*, 153−157.

(24) Joo, K. M.; Lee, J. H.; Jeon, H. Y.; Park, C. W.; Hong, D. K.; Jeong, H. J.; Lee, S. J.; Lee, S. Y.; Lim, K. M. Pharmacokinetic study of ginsenoside Re with pure ginsenoside Re and ginseng berry extracts in mouse using ultra performance liquid chromatography/mass spectrometric method. *J. Pharm. Biomed. Anal.* **2010**, *51* (1), 278−283.

(25) Xie, H. T.; Wang, G. J.; Lv, H.; Sun, R. W.; Jiang, X. L.; Li, H.; Wang, W.; Huang, C. R.; Xu, M. J. Development of a HPLC-MS assay for ginsenoside Rh2, a new anti-tumor substance from natural product and its pharacokinetic study in dogs. *Eur. J. Drug Metab. Pharmacokinet.* **2005**, *30* (1−2), 63−67.

(26) Xie, H. T.; Wang, G. J.; Sun, J. G.; Tucker, I.; Zhao, X. C.; Xie, Y. Y.; Li, H.; Jiang, X. L.; Wang, R.; Xu, M. J.; Wang, W. High performance liquid chromatographic−mass spectrometric determination of ginsenoside Rg3 and its metabolites in rat plasma using solid-phase extraction for pharmacokinetic studies. *J Chromatogr., B: Anal. Technol. Biomed. Life Sci.* **2005**, *818* (2), 167−173.

(27) Dong, H.; Bai, L. P.; Wong, V. K.; Zhou, H.; Wang, J. R.; Liu, Y.; Jiang, Z. H.; Liu, L. The in vitro structure-related anti-cancer activity of ginsenosides and their derivatives. *Molecules (Basel, Switzerland)* **2011**, *16* (12), 10619−10630.

(28) Wakabayashi, C.; Hasegawa, H.; Murata, J.; Saiki, I. In vivo antimetastatic action of ginseng protopanaxadiol saponins is based on

their intestinal bacterial metabolites after oral administration. *Oncol. Res.* **1997**, *9* (8), 411−417.
(29) Kaneko, H.; Nakanishi, K. Proof of the mysterious efficacy of ginseng. Basic and clinical trials: clinical effects of medical ginseng, korean red ginseng: specifically, its anti-stress action for prevention of disease. *J. Pharmacol. Sci.* **2004**, *95* (2), 158−162.
(30) Zhang, Z.; Du, G. J.; Wang, C. Z.; Wen, X. D.; Calway, T.; Li, Z.; He, T. C.; Du, W.; Bissonnette, M.; Musch, M. W.; Chang, E. B.; Yuan, C. S. Compound K, a Ginsenoside Metabolite, Inhibits Colon Cancer Growth via Multiple Pathways Including p53-p21 Interactions. *Int. J. Mol. Sci.* **2013**, *14* (2), 2980−2995.
(31) Hu, C.; Song, G.; Zhang, B.; Liu, Z.; Chen, R.; Zhang, H.; Hu, T. Intestinal metabolite compound K of panaxoside inhibits the growth of gastric carcinoma by augmenting apoptosis via Bid-mediated mitochondrial pathway. *J. Cell. Mol. Med.* **2012**, *16* (1), 96−106.
(32) Yang, Z.; Wang, J. R.; Niu, T.; Gao, S.; Yin, T.; You, M.; Jiang, Z. H.; Hu, M. Inhibition of P-glycoprotein leads to improved oral bioavailability of compound K, an anticancer metabolite of red ginseng extract produced by gut microflora. *Drug Metab. Dispos.* **2012**, *40* (8), 1538−1544.
(33) Tawab, M. A.; Bahr, U.; Karas, M.; Wurglics, M.; Schubert-Zsilavecz, M. Degradation of ginsenosides in humans after oral administration. *Drug Metab. Dispos.* **2003**, *31* (8), 1065−1071.
(34) Hu, Z.; Yang, J.; Cheng, C.; Huang, Y.; Du, F.; Wang, F.; Niu, W.; Xu, F.; Jiang, R.; Gao, X.; Li, C. Combinatorial metabolism notably affects human systemic exposure to ginsenosides from orally administered extract of *Panax notoginseng* roots (Sanqi). *Drug Metab. Dispos.* **2013**, *41* (7), 1457−1469.
(35) Qian, T.; Jiang, Z. H.; Cai, Z. High-performance liquid chromatography coupled with tandem mass spectrometry applied for metabolic study of ginsenoside Rb1 on rat. *Anal. Biochem.* **2006**, *352* (1), 87−96.
(36) Liu, H.; Yang, J.; Du, F.; Gao, X.; Ma, X.; Huang, Y.; Xu, F.; Niu, W.; Wang, F.; Mao, Y.; Sun, Y.; Lu, T.; Liu, C.; Zhang, B.; Li, C. Absorption and disposition of ginsenosides after oral administration of *Panax notoginseng* extract to rats. *Drug Metab. Dispos.* **2009**, *37* (12), 2290−2298.
(37) Yang, Z.; Wang, J. R.; Niu, T.; Gao, S.; Yin, T.; You, M.; Jiang, Z. H.; Hu, M. Inhibition of P-glycoprotein leads to improved oral bioavailability of compound K, an anticancer metabolite of red ginseng extract produced by gut microflora. *Drug Metabolism and Dispos.* **2012**, *40* (8), 1538−1544.
(38) Zhou, H.; Hou, S. Z.; Luo, P.; Zeng, B.; Wang, J. R.; Wong, Y. F.; Jiang, Z. H.; Liu, L. Ginseng protects rodent hearts from acute myocardial ischemia-reperfusion injury through GR/ER-activated RISK pathway in an endothelial NOS-dependent mechanism. *J. Ethnopharmacol.* **2011**, *135* (2), 287−298.
(39) Teng, R.-W.; Li, H.-Z.; Wang, D.-Z.; Yang, C.-R. Hydrolytic Reaction of Plant Extracts to Generate Molecular Diversity: New Dammarane Glycosides from the Mild Acid Hydrolysate of Root Saponins of *Panax notoginseng*. *Helv. Chim. Acta* **2004**, *87* (5), 1270−1278.
(40) Jiang, Z.-H.; Fukuoka, R.; Aoki, F.; Tanaka, T.; Kouno, I. Dammarane-type triterpene glycosides from the leaves of *Rhoiptelea chiliantha*. *Chem. Pharm. Bull.* **1999**, *47*, 257−262.
(41) Tu, Y.; Wang, Z.-X.; Shi, Y. An Efficient Asymmetric Epoxidation Method for *trans*-Olefins Mediated by a Fructose-Derived Ketone. *J. Am. Chem. Soc.* **1996**, *118*, 9806−9807.
(42) Teng, R.-W.; Li, H.-Z.; Wang, D.-Z.; Yang, C.-R. Hydrolytic reaction of plant extracts to generate molecular diversity: new dammarane glycosides from the mild acid hydrolysate of root saponins of *Panax notoginseng*. *Helv. Chim. Acta* **2004**, *87*, 1270−1278.
(43) Ko, S. R.; Suzuki, Y.; Kim, Y. H.; Choi, K. J. Enzymatic synthesis of two ginsenoside Re-beta-xylosides. *Biosci. Biotechnol. Biochem.* **2001**, *65* (5), 1223−1226.
(44) Ko, S. R.; Choi, K. J.; Suzuki, K.; Suzuki, Y. Enzymatic preparation of ginsenosides Rg2, Rh1, and F1. *Chem. Pharm. Bull. (Tokyo)* **2003**, *51* (4), 404−408.
(45) Kasai, R.; Hara, K.; Dokan, R.; Suzuki, N.; Mizutare, T.; Yoshihara, S.; Yamasaki, K. Major metabolites of ginseng sapogenins formed by rat liver microsomes. *Chem. Pharm. Bull. (Tokyo)* **2000**, *48* (8), 1226−127.
(46) Duc, N. M.; Kasai, R.; Ohtani, K.; Ito, A.; Nham, N. T.; Yamasaki, K.; Tanaka, O. Saponins from Vietnamese ginseng, *Panax vietnamensis* Ha et Grushv. collected in central Vietnam. III. *Chem. Pharm. Bull. (Tokyo)* **1994**, *42* (3), 634−640.
(47) Wang, J. R.; Yamasaki, Y.; Tanaka, T.; Kouno, I.; Jiang, Z. H. Dammarane-type triterpene saponins from the flowers of *Panax notoginseng*. *Molecules* **2009**, *14* (6), 2087−2094.
(48) Yoshikawa, M.; Murakami, T.; Ueno, T.; Yashiro, K.; Hirokawa, N.; Murakami, N.; Yamahara, J.; Matsuda, H.; Saijoh, R.; Tanaka, O. Bioactive saponins and glycosides. VIII. Notoginseng (1): new dammarane-type triterpene oligoglycosides, notoginsenosides-A, -B, -C, and -D, from the dried root of *Panax notoginseng* (Burk.) F.H. Chen. *Chem. Pharm. Bull. (Tokyo)* **1997**, *45* (6), 1039−1045.
(49) Cheng, C. C.; Yang, S. M.; Huang, C. Y.; Chen, J. C.; Chang, W. M.; Hsu, S. L. Molecular mechanisms of ginsenoside Rh2-mediated G1 growth arrest and apoptosis in human lung adenocarcinoma A549 cells. *Cancer Chemother. Pharmacol.* **2005**, *55* (6), 531−540.
(50) Popovich, D. G.; Kitts, D. D. Mechanistic studies on protopanaxadiol, Rh2, and ginseng (*Panax quinquefolius*) extract induced cytotoxicity in intestinal Caco-2 cells. *J. Biochem. Mol. Toxicol.* **2004**, *18* (3), 143−149.
(51) Popovich, D. G.; Kitts, D. D. Ginsenosides 20(*S*)-protopanaxadiol and Rh2 reduce cell proliferation and increase sub-G1 cells in two cultured intestinal cell lines, Int-407 and Caco-2. *Can. J. Physiol. Pharmacol.* **2004**, *82* (3), 183−190.
(52) Hasegawa, H.; Sung, J. H.; Benno, Y. Role of human intestinal *Prevotella oris* in hydrolyzing ginseng saponins. *Planta Med.* **1997**, *63* (5), 436−440.
(53) Akao, T.; Kida, H.; Kanaoka, M.; Hattori, M.; Kobashi, K. Intestinal bacterial hydrolysis is required for the appearance of compound K in rat plasma after oral administration of ginsenoside Rb1 from *Panax ginseng*. *J. Pharm. Pharmacol.* **1998**, *50* (10), 1155−1160.
(54) Gu, Y.; Wang, G. J.; Sun, J. G.; Jia, Y. W.; Wang, W.; Xu, M. J.; Lv, T.; Zheng, Y. T.; Sai, Y. Pharmacokinetic characterization of ginsenoside Rh2, an anticancer nutrient from ginseng, in rats and dogs. *Food Chem. Toxicol.* **2009**, *47* (9), 2257−2268.
(55) Xie, H. T.; Wang, G. J.; Lv, H.; Sun, R. W.; Jiang, X. L.; Li, H.; Wang, W.; Huang, C. R.; Xu, M. J. Development of a HPLC-MS assay for ginsenoside Rh2, a new anti-tumor substance from natural product and its pharacokinetic study in dogs. *Eur. J. Drug Metab. Pharmacokinet.* **2005**, *30* (1−2), 63−67.
(56) Zhao, J.; Su, C.; Yang, C.; Liu, M.; Tang, L.; Su, W.; Liu, Z. Determination of ginsenosides Rb1, Rb2, and Rb3 in rat plasma by a rapid and sensitive liquid chromatography tandem mass spectrometry method: application in a pharmacokinetic study. *J. Pharm. Biomed. Anal.* **2012**, *64*−*65*, 94−97.
(57) Liu, H.; Yang, J.; Du, F.; Gao, X.; Ma, X.; Huang, Y.; Xu, F.; Niu, W.; Wang, F.; Mao, Y.; Sun, Y.; Lu, T.; Liu, C.; Zhang, B.; Li, C. Absorption and Disposition of Ginsenosides after Oral Administration of *Panax notoginseng* Extract to Rats. *Drug Metab. Dispos.* **2009**, *37* (12), 2290−2298.
(58) Yang, Z.; Gao, S.; Wang, J.; Yin, T.; Teng, Y.; Wu, B.; You, M.; Jiang, Z.; Hu, M. Enhancement of oral bioavailability of 20(*S*)-ginsenoside Rh2 through improved understanding of its absorption and efflux mechanisms. *Drug Metab. Dispos.* **2011**, *39* (10), 1866−1872.
(59) Gu, Y.; Wang, G. J.; Wu, X. L.; Zheng, Y. T.; Zhang, J. W.; Ai, H.; Sun, J. G.; Jia, Y. W. Intestinal absorption mechanisms of ginsenoside Rh2: stereoselectivity and involvement of ABC transporters. *Xenobiotica* **2010**, *40* (9), 602−612.
(60) Zhang, J.; Zhou, F.; Niu, F.; Lu, M.; Wu, X.; Sun, J.; Wang, G. Stereoselective regulations of P-glycoprotein by ginsenoside Rh2 epimers and the potential mechanisms from the view of pharmacokinetics. *PloS One* **2012**, *7* (4), e35768.

(61) Hao, H.; Lai, L.; Zheng, C.; Wang, Q.; Yu, G.; Zhou, X.; Wu, L.; Gong, P.; Wang, G. Microsomal cytochrome p450-mediated metabolism of protopanaxatriol ginsenosides: metabolite profile, reaction phenotyping, and structure−metabolism relationship. *Drug Metab. Dispos.* **2010**, *38* (10), 1731−1739.
(62) Liu, Y.; Ma, H.; Zhang, J. W.; Deng, M. C.; Yang, L. Influence of ginsenoside Rh1 and F1 on human cytochrome p450 enzymes. *Planta Med.* **2006**, *72* (2), 126−131.
(63) Chang, T. K.; Chen, J.; Benetton, S. A. In vitro effect of standardized ginseng extracts and individual ginsenosides on the catalytic activity of human CYP1A1, CYP1A2, and CYP1B1. *Drug Metab. Dispos.* **2002**, *30* (4), 378−384.
(64) Nag, S. A.; Qin, J. J.; Wang, W.; Wang, M. H.; Wang, H.; Zhang, R. Ginsenosides as Anticancer Agents: In Vitro and in Vivo Activities, Structure−Activity Relationships, and Molecular Mechanisms of Action. *Front. Pharmacol.* **2012**, *3*, 25.
(65) Wong, V. K.; Cheung, S. S.; Li, T.; Jiang, Z. H.; Wang, J. R.; Dong, H.; Yi, X. Q.; Zhou, H.; Liu, L. Asian ginseng extract inhibits in vitro and in vivo growth of mouse lewis lung carcinoma via modulation of ERK-p53 and NF-kappaB signaling. *J. Cell. Biochem.* **2010**, *111* (4), 899−910.
(66) Nguyen, M. D.; Kasai, R.; Ohtani, K.; Ito, A.; Nguyen, T. N.; Yamasaki, K.; Tanaka, O. Saponins from Vietnamese Ginseng, *Panax vietnamensis* HA et Grushv. Collected in central Vietnam. II. *Chem. Pharm. Bull. (Tokyo)* **1994**, *42* (1), 115−122.

visualized by exposure to UV radiation (254 nm), or by spraying first with 10% H_2SO_4 in MeOH and then with 5% phosphomolybdic acid in EtOH, followed by heating at 110 °C for 10 min, or by exposure to iodine vapors. The HPLC system (Shimadzu, Tokyo, Japan) consisted of a series LC-10AdVP pump, FCV-10AlVP valves, SPD-10AVVP spectrophotometric detector, and DGU-14A degasser. The HPLC column used was 250 mm × 4.6 mm i.d., 5 μm, high-density Nucleosil 100-5 RP18 (Macherey-Nagel, Duren, Germany) with a 7.5 mm × 4 mm i.d. guard column of the same material (Alltech, Sedriano, Italy). Water was HPLC quality, purified in a Milli-Q system (Millipore, Bedford, MA, USA). Disposable syringe filters, Anotop 0.2 μm, were purchased from Whatman (Maidstone, U.K.). Fusaric acid was purchased from Sigma (St. Louis, MO, USA).

The methyl esters of **1** and **2** were prepared by diazotization of the corresponding acids as previously reported.[16]

Purification of 9,10-Dehydrofusaric Acid. 9,10-Dehydrofusaric acid, **2** (Figure 1), was purified from fungal culture filtrates of *Fusarium nygamai* as previously described by Capasso et al., 1996.[15] Briefly, culture filtrates were acidified up to pH 2 and exhaustively extracted with EtOAc. The organic extract was purified by combination of column and TLC on silica gel and reverse phase yielding **2** as a homogeneous amorphous solid (121.6 mg/L).

Fungal Strains, Culture Medium, and Growth Conditions. The *Fusarium oxysporum* f. sp. *pisi* race 2 isolates F42 and F69 were kindly provided by Dr. W. Chen (USDA-ARS, Pullman, WA, USA). The *F. oxysporum* f. sp. *pisi* strain CBS 127.73 NRRL36628 (*Fop*1) was provided by CBS-KNAW Fungal Biodiversity Center (Utrecht, The Netherlands). In addition, the strains Pt1 and Arg3 were isolated from wilted pea plants collected at Alvaiázere, Portugal, and Setif, Algeria, respectively. Isolation of fungal colonies on surface-sterilized wilted pea fragments was performed as described previously[3] and maintained as a single-spore colony. They have been deposited in the collection of Institute for Sustainable Agriculture, IAS-CSIC (Córdoba, Spain). The fungal strains were stored as microconidial suspensions at −80 °C in 30% glycerol. For microconidia production, cultures were grown in potato dextrose broth (PDB) (Difco, Detroit, MI) at 28 °C in a shake culture set at 170 rpm.[17] For toxin production, Erlenmeyer flasks (500 mL) containing 200 mL of Czapek−Dox medium (5% glucose, 0.1% yeast extract, 0.05% K_2HPO_4, 0.2% $NaNO_3$, 0.05% $MgSO_4{\cdot}7H_2O$, and 0.001% $FeSO_4{\cdot}7H_2O$), were inoculated with 200 μL of fresh *Fop* microconidia at 10^9 conidia/mL and incubated under shaking at 28 °C for 7 days. The content of the flask was filtered on cheesecloth and centrifuged at 7,000 rpm for 10 min. The supernatant containing the secreted *Fop* toxins was then frozen at −80 °C and lyophilized before further analysis. Morphological characterization of each strain was performed at X40 and X63 magnification with a bright light microscope with Nomarsky filter.

DNA Extraction, PCR Amplifications, and Sequencing. Genomic DNA was extracted from *F. oxysporum* mycelium following a previously reported protocol.[18] Molecular characterization of each *Fop* strain was performed by analysis of the internal transcribed spacers (ITS) and the 5′ intron-rich portion of the elongation factor alpha (EF-alpha). ITS and EF-alpha sequences were obtained by PCR amplification with primers ITS-1/ITS-4[19] and EF-1/EF-2[20] respectively. Each 50 μL reaction mixture contained 50 ng of template DNA, 2 units of BioTaq DNA polymerase (Bioline, London, U.K.), 1× PCR buffer, 2 mM $MgCl_2$, 200 μM dNTPs, and 0.3 μM of each primer. The PCR amplifications were performed on a MyCycler (Biorad, Hercules, CA) thermocycler as follows: (i) for ITS, 94 °C for 2 min, 40 cycles at 94 °C for 1 min, 55 °C for 2 min, and 72 °C for 2.5 min followed by a final step at 72 °C for 10 min; (ii) for EF-alpha, 94 °C for 5 min, 30 cycles at 94 °C for 35 s, 52 °C for 35 s, and 72 °C for 1 min followed by a final step at 72 °C for 10 min. All amplifications were purified with the PCR cleanup kit of QIAgen and cloned in pGEMT vector (Promega, Madison, WI). Two positive clones per amplicon were sequenced by STABVida (Setubal, Portugal) using the pGEMT vector specific primers SP6 and T7.

Sequence Data Analysis. Reads of each sequence were assembled and manually corrected with Chromaspro 1.7.5 (Technelysium Pty Ltd., South Brisbane, Australia). Sequences were used in BLAST[21] searches against the GenBank[22] and Mycobank[23] databases to identify the most similar sequences available in the databases. Pairwise alignments were performed with the Neddleman−Wunsh algorithm (Needle method) implemented at EMBL-EBI webserver.[24] All DNA sequences have been deposited in GenBank (Table S1 in the Supporting Information).

Plant Materials. Assignment of the different strains to a specific race of *F. oxysporum* f. sp. *pisi* was performed by testing the pathogenicity profile of these isolates on a set of differential pea lines (Table 1).[1,3] The comparison of the aggressiveness of each strain was performed on *P. sativum* cv. 'Messire'. To determine the effect of fungal culture filtrates or their corresponding organic extracts, seven pea accessions with a wide range of response to *Fop* race 2 were used including the susceptible accessions JI1213, 'Messire', and P629, the partially resistant accessions JI2480 and P615, and the resistant accessions P42 and P633.

Table 1. List of the Pea Differential Lines for *F. oxysporum* f. sp. *pisi* and Their Susceptibility Response to the New *Fop* Isolates

	expected[a]				observed[b]		
accessions	R1	R2	R5	R6	F42	Arg3	Pt1
'Dark Skin Perfection'	R	S	S	S	S	S	S
'Mini'	S	R	S	S	PR	PR	R
'New Era'	R	R	S	S	nd	R	R
'New Season'	R	R	S	R	R	R	R
'74SN5'	R	R	R	R	R	R	R
P629	R	S	nd	nd	S	S	S
JI1412	R	R	nd	nd	R	R	R
'Messire'	R	S	nd	nd	S	S	S

[a]Accessions' response to each *Fop* race as described in Kraft and Pfleger[1] and Bani et al.[3] R stand for resistant reaction and S susceptible. [b]Accessions' response to the inoculation with the reference R2 strain F42 and the isolates from Algeria and Portugal obtained in the present study.

For all experiments, germinated pea seedlings were sown in vermiculite and grown in a controlled environment under a 16/8 h light−dark photoperiod at 26 ± 2 °C with 200 μmol/m^2/s of illumination. Plants were watered every three days with tap water.

Pathogenicity Test. To determine the pathogenicity of each *Fop* isolate, seven day old pea seedlings were inoculated with the dip root technique as described previously[3] and maintained in the same growth conditions as above. Disease was then evaluated every three days by estimating the percentage of leaves with symptoms and the area under the disease progression curve (AUDPC).[3] Five plants were used per accession, and each experiment was repeated twice independently.

Extraction and Purification of Fusaric and 9,10-Dehydrofusaric Acids from Fungal Culture Filtrates. Lyophilized *Fop* culture filtrates (200 mL) were redissolved in 1/10 of the initial volume with distilled water. The pH of solutions were adjusted to 2.5 with 1N HCl and extracted with EtOAc (3 × 20 mL). The acidic organic extracts were combined, dried (Na_2SO_4), and evaporated under reduced pressure, yielding brown oily residues (38.9, 101.7, 36.4, 42.7, and 29.5 mg for F42, F69, *Fop1*, Arg3, and Pt1 respectively). The five acidic organic extracts were analyzed by TLC on silica gel [eluent EtOAc−MeOH−H_2O (8.5:2:1, v/v/v)] and on reverse phase [eluent CH_3CN−H_2O (1:1, v/v)], in comparison with authentic standard samples of **1**, **2**, and their methyl esters. To confirm the presence of **1** and **2**, the residue of organic extract of F42 was purified by TLC eluted with CH_3CN−H_2O (1:1, v/v), yielding two pure solid compounds: **1**, R_f 0.50, eluent EtOAc−MeOH−H_2O (8.5:2:1, v/v/v), R_f 0.51 eluent CH_3CN−H_2O (1:1, v/v), and **2**, R_f 0.40, eluent EtOAc−MeOH−H_2O (8.5:2:1, v/v/v), R_f 0.58, eluent CH_3CN−H_2O (1:1, v/v), which were identified as fusaric acid and 9,10-dehydrofusaric acid as described below.

Fusaric acid (1). IR, UV, and ^{1}H NMR spectra were very similar to data reported.[15] ESIMS (+) *m/z*: 381 $[2M + Na]^+$, 202 $[M + Na]^+$. ESIMS (−) *m/z*: 178 $[M - H]^-$. APCIMS (+) *m/z*: 180 $[M + H]^+$.

9,10-Dehydrofusaric acid (2). IR, UV, and ^{1}H NMR spectra were very similar to data reported.[15] ESIMS (+) *m/z*: 200 $[M + Na]^+$. ESIMS (−) *m/z*: 176 $[M - H]^-$.

HPLC Analysis of Acidic Organic Extracts. A method previously reported[16] was optimized and used for analysis. The mobile phases employed were MeOH (eluent A) and 1% K_2HPO_4 adjusted to pH 7.35 with concentrated H_3PO_4 (eluent B). Elution was initially with A:B (50:50), which was transformed using a linear gradient over 20 min to A:B (75:25); the initial conditions were restored using a linear gradient over 5 min, and the column was re-equilibrated under these conditions for 10 min before the next run was initiated. The flow rate was 1 mL/min, and 20 μL aliquots of the samples were injected for analysis. Detection was performed at 268 nm, corresponding to the maximum of absorption of **1** and **2**. The HPLC calibration curves for quantitative determination of **1** and **2** were performed with absolute amounts of standards dissolved in MeOH in the range between 0.2 and 20 μg for each compound, in triplicate for each concentration. HPLC linear regression curves (absolute amount against chromatographic peak area) for **1** and **2** were obtained based on weighted values calculated from seven amounts of the standards in the above range. The samples were dissolved in MeOH and passed through disposable filters, and aliquots (20 μL) were injected into the HPLC instrument. Each sample was assayed in triplicate. The quantitative determination of **1** and **2** was calculated by interpolating the mean area of their chromatographic peaks with the data from the calibration curves.

Recovery Studies. Recovery studies were performed using the best producer isolate F69. Pure fusaric and 9,10-dehydrofusaric acids were added to the culture filtrate from 0.3 to 2.0 mg/L. The samples were prepared as described above and the extracts analyzed by HPLC to determine recovery. Three replicate injections were performed for each concentration. The recovery throughout the range of concentration was higher than 96 ± 2%.

Biological Assays. *Leaf Absorption Assay.* The toxicity of the culture filtrate of *Fop* race 2 isolate F42 was assayed by incubating fully expanded leaves in an F42 culture filtrate. For this, the leaf petiole was immersed into an Eppendorf tube containing 1 mL of one week old fungal culture filtrate before or after autoclaving at 121 °C for 20 min and incubated at room temperature for 24 and 48 h. Four fully developed leaves were used for each pea accession.

Leaf Puncture Assay. A leaf puncture bioassay on pea leaves was performed to evaluate the toxic effect of culture filtrates from all *Fop* race 2 isolates tested. Fully expanded leaves from pea plants were placed on Petri dishes containing water−agar medium and punctured by a sterile needle on the upper surface. Droplets (10 μL) of the culture filtrate or corresponding organic extract in 1% MeOH were applied on the wounded leaves at 2 mg/mL. Plates were then incubated at room temperature under darkness. After 3 days of incubation, the area (mm^2) of the necrotic lesions was measured. Droplets of a pure standard of **1** and **2** at 2 mg/mL were used as positive control reactions while droplets of sterile water, Czapek−Dox medium, or 1% MeOH were used as negative control. The experiments were performed with four replicates for each treatment.

Statistical Analysis. Analyses of variance (ANOVA) were carried out for phytotoxicity records, with the different tested solutions and metabolites as fixed factors of their respective bioassays. One way ANOVA was also performed to test the significance of aggressiveness differences between each strain. Phytotoxicity and percentage of symptoms values were transformed using the square root transformation in order to increase the normality of their distribution. Whenever the ANOVA test was statistically significant ($p \leq 0.05$), a Duncan multiple range test assessing the differences of the means between each treatment was performed. All statistical analyses were performed using Genstat release 11.1 software (VSN International Ltd., Hemel Hempstead, U.K.).

RESULTS AND DISCUSSION

F. oxysporum species complex is composed of many species very closely related morphologically, which makes them difficult to identify. To ensure that all fungal strains corresponded to isolates of the race 2 of *F. oxysporum* f. sp. *pisi*, these isolates were characterized at morphological and molecular levels before further analysis. As expected, all fungal strains showed morphological characteristics of *F. oxysporum* complex species. Amplification of ITS and EF-alpha gave sequences ranging from 544 to 545 bp and 710 to 714 bp long respectively according to the isolate (Table S1 in the Supporting Information). These sequences showed between 99 and 100% identity to *F. oxysporum* sequences from different formae speciales including ff. spp. *pisi*, *ciceri*, *medicaginis*, and *lycopersici* according to the BLAST comparison performed. In addition they share 99.8−100% and 98.6−100% identity to the reference *Fop* race 2 strain F42 respectively (Table S1 in the Supporting Information). This clearly identified them as *F. oxysporum* although it was not possible to identify the ff. spp. to which they belong by these methods, hampered by the potential polyphyletic origin of the isolates and potential horizontal transfer of host-specificity genes.[20] Nevertheless, the in planta pathogenicity test indicated that they corresponded to *F. oxysoprum* f. sp. *pisi*. Indeed, all these strains were pathogenic on the susceptible pea cultivar 'Messire' (Figure 2). Slight differences in aggressiveness were observed between isolates as determined by their AUDPC value ($p < 0.001$). The strain F69 was the most aggressive, reaching AUDPC values of 2388, while the isolates *Fop1* and Arg3 were the least aggressive, reaching AUDPC of only 1678 and 1778.5 respectively (Figure 2A). This difference was rooted to a faster disease development induced by strain F69, which led to complete plant death as early as 12 days post inoculation (dpi) while the Arg3 and *Fop 1* strains required 25 days to induce a similar effect (Figure 2B). This was confirmed by the ANOVA, which revealed significant differences between isolates only up to 15 days post inoculation ($p < 0.001$) while at later stages the differences were not significant ($p > 0.5$). In addition, the inoculation of a set of differential lines[1,3] allowed assigning the new isolates Arg3 and Pt1 to race 2 of *Fop* since accession's response to these isolates followed a similar pattern as for the reference race 2 strain F42. Indeed, no or only mild symptoms were detected on the race 2 resistant accessions while the susceptible accessions 'Dark Skin perfection', P629, and 'Messire' developed characteristic wilt symptoms (Table 1). By contrast, *Fop*1 showed *near wilt* (leaf yellowing) symptoms on most accessions, which impeded a clear classification of this strain to a specific race (data not shown). However, the very close molecular relationship between this isolate and the Algerian (Arg3) isolate as shown by the analysis of EF-alpha sequence (Table S1 in the Supporting Information) together with the *near wilt* symptoms detected would suggest that this isolate also belongs to race 2 of *Fop*.

To characterize further the mechanisms of pathogenicity of *Fop* race 2 isolates that remain largely unknown, the effect of one week old *Fop* culture filtrates was evaluated on pea leaves. Incubation of pea leaves in F42 culture filtrate for 24 h induced leaf withering followed by leaf discoloration that initiated at the central vein and progressed to cover the whole leaf and petiole as early as 48 h of incubation (Figure 3A). Similar effects were detected on all pea accessions tested including on resistant accessions (Figure 3B). The leaf puncture assay also showed a

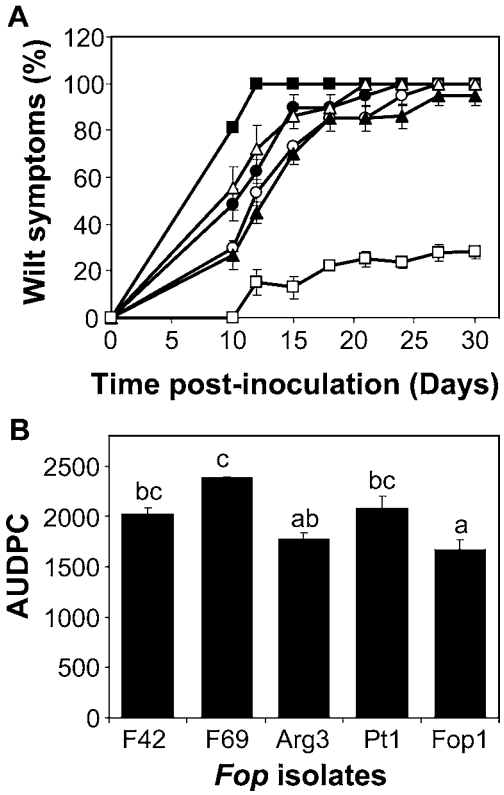

Figure 2. Pathogenicity of the *F. oxysporum* f. sp. *pisi* race 2 isolates on the susceptible pea cultivar 'Messire'. (A) Evolution of *Fusarium* wilt symptoms on the susceptible pea cultivar 'Messire' induced by the *Fop* race 2 isolates F42 (●), F69 (■), Arg3 (○), Pt1 (△), and *Fop1* (▲) respectively, compared to control plants treated with water (□). Disease progression was estimated as percentage of leaf with symptoms over time. (B) Comparison of AUDPC values calculated from the periodic assessment of development of *Fusarium* wilt symptoms. Different letters between each histogram indicate significant difference between the values according to the Duncan multiple range test at $\alpha = 0.05$. Vertical bars are standard error for $n = 5$.

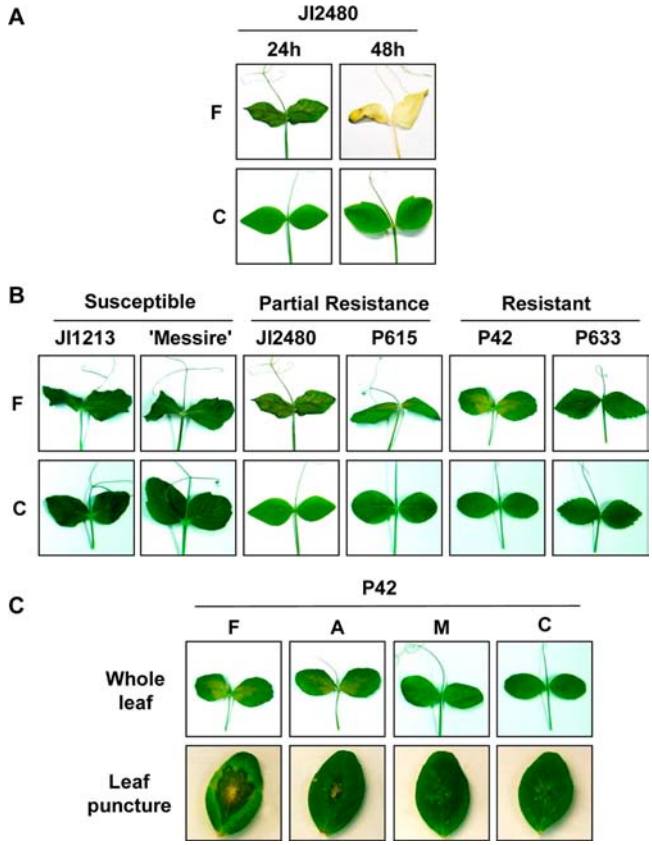

Figure 3. Effect of the culture filtrates of *F. oxysporum* f. sp. *pisi* race 2 isolate F42 on pea leaves. (A) Progression of wilting symptoms induced on the partially resistant accession JI2480 by the culture filtrates after 24 and 48 h of treatment (F) compared to control with sterile water (C). (B) Effect of the culture filtrates after 24 h of treatment on leaves of seven pea accessions differing in their susceptibility to *Fop* race 2. (C) Comparison of the leaf response of the resistant pea accession P42 to culture filtrates (F), autoclaved culture filtrates (A), sterile Czapek–Dox medium (M), and sterile water (C) evaluated with the leaf absorption and the leaf puncture assays.

progressive spreading of necrosis and leaf discoloration after treatment with the fungal culture filtrates while control remained symptomless (Figure 3C). A broad effect of *F. oxysporum* culture filtrates was previously detected for *F. oxysporum* f. sp. *orthoceras* and *F. oxysporum* f. sp. *albedinis*, which extract induced wilting on both host and nonhost species.[25,26] This supports the presence of a nonspecific toxin within these filtrates. In addition it indicated that resistance of the pea accessions tested was not based on toxin detoxification. This was also detected in *F. oxysporum* ff. spp. *melonis*[27] and *cubense*.[28] However, in the present study, only three resistant *Pisum* spp. accessions have been tested. Thus, it may still be possible that the resistance mechanisms of other resistant pea accessions are based on toxin detoxification as detected previously in near-isogenic lines of tomato differing in their susceptibility to *F. oxysporum* f. sp. *lycopersici*.[29] Interestingly, organic extracts of the culture filtrates from all *Fop* race 2 isolates tested were able to induce leaf necrosis on 'Messire' leaves when evaluated with the leaf puncture assay after 3 days of incubation (Figure 4A). However, difference in lesion size could be detected between the strains ($p < 0.001$), in agreement with the difference in aggressiveness of these strains on this pea cultivar (Figure 4B). The lesion size ranged from 16.8 mm^2 for Arg3 to 42.4 and 58.4 mm^2 for F42 and F69 culture filtrate respectively (Figure 4B).

Various pathogenicity factors including cell-wall degrading enzymes, phytoalexin-detoxifying enzymes, and toxins have been shown to mediate *F. oxysporum* virulence.[4] In contrast to a previous study that showed the complete loss of toxic activity after autoclaving culture filtrates,[29] autoclaving only slightly attenuated the toxicity of the filtrate on leaf absorption and puncture assays (Figure 3C). This ruled out that the toxicity is due to proteins and suggested the presence of heat-stable metabolites as found for other isolates of *Fop*[30] and human pathogenic strains of *F. oxysporum*.[31]

To identify the heat-stable metabolite(s) responsible for the toxicity of *Fop* race 2 culture filtrates, the organic extract of culture filtrates obtained from the isolate F42 was fractionated and further analyzed. TLC analysis of these fractions showed that this strain produced two toxins, identified as fusaric acid, **1**, and dehydrofusaric acid, **2**, by comparison with standard samples. Their corresponding methyl esters were not detected. These results were confirmed by purification of **1** and **2** from this organic extract. The ^{1}H NMR spectrum was very similar to those previously reported.[15] The data obtained from ESI MS

dx.doi.org/10.1021/jf405530g | J. Agric. Food Chem. 2014, 62, 2574−2580

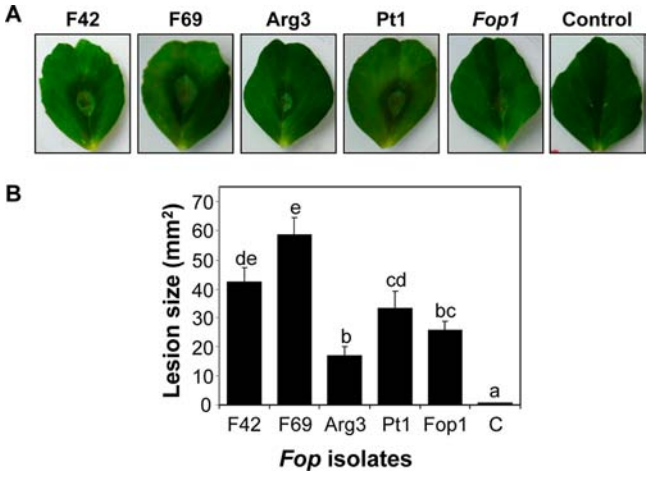

Figure 4. Effect of culture filtrates of the different *F. oxysporum* f. sp. *pisi* race 2 isolates on leaves of the susceptible pea cultivar 'Messire'. (A) Comparison of 'Messire' leaf response to culture filtrates of each *Fop* race 2 isolate or sterile Czapek–Dox medium (Control). (B) Comparison of the lesion size induced by each isolate or by sterile Czapek–Dox medium (C). Different letters between each histogram indicate significant difference between the values according to the Duncan multiple range test at $\alpha = 0.05$. Vertical bars represent standard errors for $n = 4$.

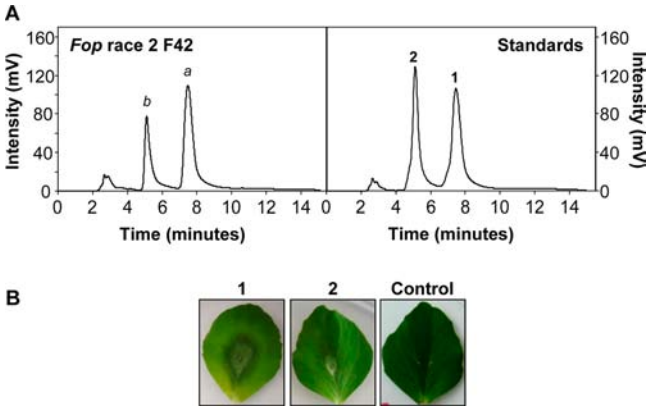

Figure 5. Characteristics of the main toxins produced by the *F. oxysporum* f. sp. *pisi* race 2 isolates. (A) HPLC profile of the organic extract of the *Fop* race 2 isolate F42 (left) and fusaric and 9,10-dehydrofusaric acids (**1** and **2**) standards (right). (B) Comparison of the leaf response of the susceptible pea cultivar 'Messire' to droplets of pure **1** and **2**.

spectra further supported the isolation of **1** and **2**. The ESI MS recorded in positive ion mode showed the sodiated dimeric form $[2M + Na]^+$ and the sodium cluster $[M + Na]^+$ at m/z 381 and 202, respectively. In APCI MS it showed the pseudomolecular ion $[M + H]^+$ at m/z 180. When the ESI MS was recorded in negative ion mode, it showed the pseudomolecular ion $[M - H]^-$ at 178. The ESI MS spectrum of **2** recorded in positive and negative ion mode showed the sodium cluster $[M + Na]^+$ and the pseudomolecular ion $[M - H]^-$ at m/z 200 and 176, respectively. Further studies indicated that all *Fop* race 2 isolates investigated produced **1** and **2** but not their related methyl esters. Both toxins have been already identified from cultures of *F. oxysporum* pathogenic to the parasitic plants *Striga hermonthica*.[16,32,33] However, it is the first time that **2** is reported from *F. oxysporum* isolates pathogenic to crops. Other toxins were not found in any of these isolates. Production of toxins showed large qualitative and quantitative variation according to growth conditions including growth medium, temperature, and ambient pH among others.[16,25,34] Thus, it could not be ruled out that these strains may produce additional toxins as described for other *F. oxysporum* strains.[11−14]

Testing these acids with the leaf puncture assay indicated that both **1** and **2** possessed phytotoxic activity and induced necrotic lesion similar to that induced by the F42 culture filtrates (Figure 5B). Comparison of lesion size indicated that **1** (55.8 mm^2) was 2.5 time more phytotoxic than **2** (22.6 mm^2). Many studies demonstrated the function of **1** in pathogenicity, although in several instance no correlation was detected between the concentration of **1** and fungal virulence.[5,7,35] **1** has been shown to alter membrane permeability, inhibit O_2 uptake and ATP synthesis, decrease mitochondrial activity, transpiration rate, and stomatal conductance, and induce cell depolarization,[7,10] suggesting that **1** participates in *F. oxysporum* pathogenicity by decreasing plant cell viability.[7] By contrast, nearly nothing is known about the action of **2**.[15] This compound was previously shown to induce tomato leaf chlorosis and inhibit root elongation to a similar extent as **1**.[15] Here we demonstrated that dehydrofusaric acid was also phytotoxic on pea leaves (Figure 4), indicating that it may also contribute to the pathogenicity of *F. oxysporum*.

To confirm the function of **1** and **2** in *Fop* race 2 pathogenicity, we quantitated the production of both acids by all *Fop* race 2 isolates tested and related it to their level of aggressiveness. For the quantitation, we slightly modified a previously reported HPLC method.[16] The characteristics of the calibration curves, the absolute range, and the detection limits (LOD) of **1** and **2** are summarized in Table S2 in the Supporting Information. Regression analysis suggests that the calibration curves are linear. A representative HPLC chromatogram of the ethyl acetate extract of the culture filtrates of *Fop* F42 is presented in Figure 5A. The metabolite chromatographic peaks (*a* and *b*) in the sample were coincident with the 7.80 and 5.20 min retention times of **1** and **2** standards (Figure 5A). The retention times were highly reproducible, varying less than 0.50 min. For all strains matrix substances absorbing at 268 nm were eluted within the first 20 min. **1** could be quantitatively and reproducibly detected from 0.5 μg, and **2** from 0.2 μg, with lower amounts having poor reproducibility.

Although **1** and **2** were secreted by all isolates of *Fop* race 2 tested, this method allowed detecting quantitative differences between these isolates ($p < 0.001$) for both toxins. Of the strain tested, F69 produced the highest amount of **1** and **2** (258.49 and 243.36 mg/L, respectively) whereas strains Arg 3 and *Fop1* produced the least **1** (9.94 mg/L) and **2** (21.44 mg/L) respectively (Figure 6). The capacity to produce and secrete **1** was significantly and positively correlated with the leaf lesion size ($r^2 = 0.83$; Figure 7A) and slightly correlated with in planta pathogenicity ($r^2 = 0.66$; Figure 7B). Production of **2** was significantly correlated with in planta pathogenicity ($r^2 = 0.8$; Figure 7D) and to a lesser extent with lesion size ($r^2 = 0.66$; Figure 7C). Interestingly, the total toxin production was significantly correlated with both virulence parameters ($r^2 = 0.78$ and 0.76 for leaf lesion size and in planta pathogenicity respectively) (Figures 7E and 7F). This reinforced the important role of **1** in *F. oxysporum* pathogenicity as it was already demonstrated for *F. oxysporum* ff. spp. *carthami*,[36] *lycopersici*,[37,38] *melonis*,[39] and *gladioli*,[40] among others. It also demonstrated that **2** is an important pathogenicity factor acting

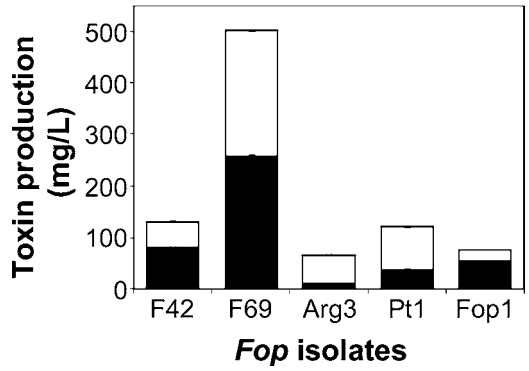

Figure 6. Quantitation of the amount of **1** and **2** produced by the different isolates of *F. oxysporum* f. sp. *pisi* race 2. The histograms show the cumulative production of **1** (black column) and **2** (white column) for each *Fop* race 2 isolate. Vertical bars are standard error for $n = 3$.

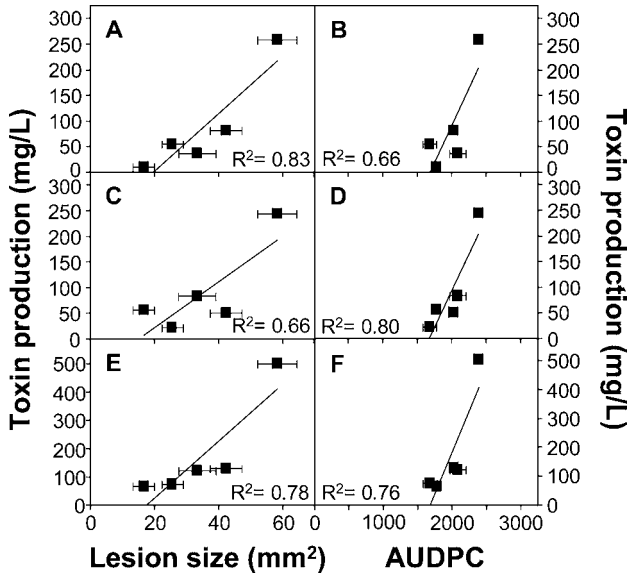

Figure 7. Relationship between toxin production and phytotoxicity. The graphics represent the linear correlation calculated for **1** (A, B), **2** (C, D), and the sum of both toxins (E, F) production by each *Fop* race 2 isolate with the lesion size induced by their corresponding culture filtrate (A, C, E) or their overal aggressiveness on the susceptible pea cultivar 'Messire' estimated by their AUDPC values (B, D, F). Horizontal bars are standard errors for lesion size area or AUDPC values with $n = 4$ and $n = 5$ respectively while vertical bars are standard error bars of toxin content calculated with $n = 3$.

in synergy with **1**, which was not described before for *F. oxysporum* (Figure 7).

In conclusion, it has been demonstrated that *Fop* race 2 isolates produced mainly two toxins that were identified as fusaric and 9,10-dehydrofusaric acids. Both toxins showed high phytotoxic activity on pea when tested on whole leaves and leaf puncture assay. In addition, the amount of both toxins within culture filtrates correlated with strain aggressiveness, which indicates a role of these toxins during *Fop* pathogenicity. Although the importance of fusaric acid in the pathogenicity of *F. oxysporum* is still under debate, the results obtained in the present study strongly indicate that toxin production is an important determinant of *Fop* race 2 pathogenicity.

■ ASSOCIATED CONTENT

Supporting Information

Table S1, comparison of ITS and EF-alpha sequence of the *Fop* isolates with the race 2 reference strain of *Fop* F42, and Table S2, analytical characteristics of calibration curves for **1** and **2**. This material is available free of charge via the Internet at http://pubs.acs.org.

■ AUTHOR INFORMATION

Corresponding Author

*Tel: +39 081 2532126. Fax: +39 081 674330. E-mail: alessio.cimmino@unina.it.

Funding

This work was supported by Spanish project AGL2011-22524/AGR from the Spanish Ministry of Economy and Competitiveness (MINECO) confinanced by FEDER and the ARIMNET subprogram MEDILEG from the European Union. N.R. is holder of a Ramón y Cajal grant from MINECO. A.E. is associated with the Istituto di Chimica Biomolecolare, CNR, Pozzuoli, Italy.

Notes

The authors declare no competing financial interest.

■ ACKNOWLEDGMENTS

The NMR spectra were recorded at the Istituto di Chimica Biomolecolare del CNR, Pozzuoli, Italy. We thank Prof. C. Steinberg (INRA-Dijon, France) and Dr. W. Chen (USDA-ARS, Pullman, WA, USA), who kindly provided the strain *Fop1* and the reference strains F42 and F69 of *F. oxysporum* respectively.

■ REFERENCES

(1) Kraft, J. M.; Pfleger, F. L. *Compendium of pea diseases and pests*, 2nd ed.; APS Press: St. Paul, MN, 2001.

(2) Infantino, A.; Kharrat, M.; Riccioni, L.; Coyne, C. J.; Mcphee, K. E.; Grunwald, N. J. Screening techniques and sources of resistance to root diseases in cool season food legumes. *Euphytica* **2006**, *147*, 201−221.

(3) Bani, M.; Rubiales, D.; Rispail, N. A detailed evaluation method to identify sources of quantitative resistance to *Fusarium oxysporum* f. sp. *pisi* race 2 within a *Pisum* spp. germplasm collection. *Plant Pathol.* **2012**, *61*, 532−542.

(4) Roncero, M. I. G.; Hera, C.; Ruiz-Rubio, M.; García Maceira, F. I.; Madrid, M. P.; Caracuel, Z.; Calero, F.; Delgado-Jarana, J.; Roldán-Rodríguez, R.; Martínez-Rocha, A. L.; Velasco, C.; Roa, J.; Martín-Urdiroz, M.; Córdoba, D.; Di Pietro, A. *Fusarium* as a model for studying virulence in soilborne plant pathogens. *Physiol. Mol. Plant Pathol.* **2003**, *62*, 87−98.

(5) Bacon, C. W.; Porter, J. K.; Norred, W. P.; Leslie, J. F. Production of fusaric acid by *Fusarium* species. *Appl. Environ. Microbiol.* **1996**, *62*, 4039−4043.

(6) Abouzeid, M. A.; Boari, A.; Zonno, M. C.; Vurro, M.; Evidente, A. Toxicity profiles of potential biocontrol agents of *Orobanche ramosa*. *Weed Sci.* **2004**, *52*, 326−332.

(7) Bouizgarne, B.; El-Maarouf-Bouteau, H.; Frankart, C.; Reboutier, D.; Madiona, K.; Pennarun, A. M.; Monesteiz, M.; Trouviere, J.; Amiar, Z.; Briand, J.; Brault, M.; Rona, J. P.; Ouhdoch, Y.; El Hadrami, I.; Bouteau, F. Early physiological responses of *Arabidopsis thaliana* cells to fusaric acid: toxic and signalling effects. *New Phytol.* **2006**, *169*, 209−218.

(8) Jiao, J.; Zhou, B.; Zhu, X.; Gao, Z.; Liang, Y. Fusaric acid induction of programmed cell death modulated through nitric oxide signalling in tobacco suspension cells. *Planta* **2013**, *238*, 727−737.

(9) Sarhan, A. R. T.; Hegazi, A. M. A. Effect of nitrogen, phosphorus and potassium on sensitivity of pepper plants to *Fusarium* wilt toxin. *Acta Phytopathol. Entomol. Hung.* **1988**, *23*, 57−60.
(10) Wang, M.; Xiong, Y.; Ling, N.; Feng, X.; Zhong, Z.; Shen, Q.; Guo, S. Detection of the dynamic response of cucumber leaves to fusaric acid using thermal imaging. *Plant Physiol. Biochem.* **2012**, *66*, 68−76.
(11) Mirocha, C. J.; Abbas, H. K.; Kommedahl, T.; Jarvis, B. B. Mycotoxin production by *Fusarium oxysporum* and *Fusarium sporotrichioides* isolated from *Baccharis* spp. from Brazil. *Appl. Environ. Microbiol.* **1989**, *55*, 254−255.
(12) Moretti, A.; Belisario, A.; Tafuri, A.; Ritieni, A.; Corazza, L.; Logrieco, A. Production of beauvericin by different races of *Fusarium oxysporum* f. sp. *melonis*, the *Fusarium* wilt agent of muskmelon. *Eur. J. Plant Pathol.* **2002**, *108*, 661−666.
(13) Son, S. W.; Kim, H. Y.; Choi, G. J.; Lim, H. K.; Jang, K. S.; Lee, S. O.; Lee, S.; Sung, N. D.; Kim, J.-C. Bikaverin and fusaric acid from *Fusarium oxysporum* show antioomycete activity against *Phytophthora infestans*. *J. Appl. Microbiol.* **2008**, *104*, 692−698.
(14) Irzykowska, L.; Bocianowski, J.; Waskiewicz, A.; Weber, Z.; Karolewski, Z.; Golinski, P.; Kostecki, M.; Irzykowski, W. Genetic variation of *Fusarium oxysporum* isolates forming fumonisin B-1 and moniliformin. *J. Appl. Genet.* **2012**, *53*, 237−247.
(15) Capasso, R.; Evidente, A.; Cutignano, A.; Vurro, M.; Zonno, M. C.; Bottalico, A. Fusaric and 9,10-dehydrofusaric acids and their methyl esters from *Fusarium nygamai*. *Phytochemistry* **1996**, *41*, 1035−1039.
(16) Amalfitano, C.; Pengue, R.; Andolfi, A.; Vurro, M.; Zonno, M. C.; Evidente, A. HPLC analysis of fusaric acid, 9,10-dehydrofusaric acid and their methyl esters, toxic metabolites from weed pathogenic *Fusarium* species. *Phytochem. Anal.* **2002**, *13*, 277−282.
(17) Di Pietro, A.; Roncero, M. I. G. Cloning, expression, and role in pathogenicity of *pg1* encoding the major extracellular endopolygalacturonase of the vascular wilt pathogen *Fusarium oxysporum*. *Mol. Plant—Microbe Interact.* **1998**, *11*, 91−98.
(18) Raeder, U.; Broda, P. Rapid preparation of DNA from filamentous fungi. *Lett. Appl. Microbiol.* **1985**, *1*, 17−20.
(19) Waalwijk, C.; Dekoning, J. R. A.; Baayen, R. P.; Gams, W. Discordant groupings of *Fusarium* spp. from sections *Elegans*, *Liseola* and *Dlaminia* based on ribosomal ITS1 and ITS2 sequences. *Mycologia* **1996**, *88*, 361−368.
(20) O'donnell, K.; Gueidan, C.; Sink, S.; Johnston, P. R.; Crous, P. W.; Glenn, A.; Riley, R.; Zitomer, N. C.; Colyer, P.; Waalwijk, C.; van der Lee, T.; Moretti, A.; Kang, S.; Kim, H.-S.; Geiser, D. M.; Juba, J. H.; Baayen, R. P.; Cromey, M. G.; Bithel, S.; Sutton, D. A.; Skovgaard, K.; Ploetz, R.; Kistler, H. C.; Elliott, M.; Davis, M.; Sarver, B. A. J. A two-locus DNA sequence database for typing plant and human pathogens within the *Fusarium oxysporum* species complex. *Fungal Genet. Biol.* **2009**, *46*, 936−948.
(21) Altschul, S. F.; Gish, W.; Miller, W.; Myers, E. W.; Lipman, D. J. Basic local alignment search tool. *J. Mol. Biol.* **1990**, *215*, 403−410.
(22) NCBI BLAST; http://www.ncbi.nlm.nih.gov/BLAST; 22 October 2013.
(23) MycoBank; http://www.mycobank.org/BioloMICSSequences.aspx?expandparm=f&file=all; 22 October 2013.
(24) EMBOSS pairwise sequence alignment tool; http://www.ebi.ac.uk/Tools/psa/emboss_needle/nucleotide.html; 22 October 2013.
(25) Dor, E.; Evidente, A.; Amalfitano, C.; Agrelli, D.; Hershenhorn, J. The influence of growth conditions on biomass, toxins and pathogenicity of *Fusarium oxysporum* f. sp. *orthoceras*, a potential agent for broomrape biocontrol. *Weed Res.* **2007**, *47*, 345−352.
(26) Sedra, M. H.; Lazrek, B. H. *Fusarium oxysporum* f. sp. *albedinis* toxin characterization and use for selection of resistant date palm to bayoud disease. In *Date Palm Biotechnology*, 18th ed.; Jain, S. M., Al-Khayri, J. M., Johnson, D. V., Eds.; Springer: Netherlands, 2011; Chapter 13, pp 253−270.
(27) Megnegneau, B.; Branchard, M. Effects of fungal culture filtrates on tissue from susceptible and resistant genotypes of muskmelon to *Fusarium oxysporum* f. sp. *melonis*. *Plant Sci.* **1991**, *79*, 105−110.
(28) Morpurgo, R.; Lopato, S. V.; Afza, R.; Novak, F. J. Selection parameters for resistance to *Fusarium oxysporum* f. sp. *cubense* race 1 and race 4 on diploid banana (*Musa acuminata* Colla). *Euphytica* **1994**, *75*, 121−129.
(29) Sutherland, M. L.; Pegg, G. F. Purification of a toxin from *Fusarium oxysporum* f. sp. *lycopersici* race 1. *Physiol. Mol. Plant Pathol.* **1995**, *46*, 243−254.
(30) Sharma, A.; Rathour, R.; Plaha, P.; Katoch, V.; Khalsa, G. S.; Patial, V.; Singh, Y.; Pathania, N. K. Induction of Fusarium wilt (*Fusarium oxysporum* f. sp. *pisi*) resistance in garden pea using induced mutagenesis and in vitro selection techniques. *Euphytica* **2010**, *173*, 345−356.
(31) Hernandes, L.; Marangon, A. V.; Salci, T.; Svidzinski, T. I. E. Toxic thermoresistant metabolites of *Fusarium oxysporum* are capable of inducing histopathological alterations in Wistar rats. *J. Venomous Anim. Toxins Incl. Trop. Dis.* **2012**, *18*, 144−149.
(32) Abraham, W. R.; Hanssen, H. P. Fusoxysporone—a new type of diterpene from *Fusarium oxysporum*. *Tetrahedron* **1992**, *48*, 10559−10562.
(33) Savard, M. E.; Miller, J. D.; Ciotola, M.; Watson, A. K. Secondary metabolites produced by a strain of *Fusarium oxysporum* used for *Striga* control in West Africa. *Biocontrol Sci. Technol.* **1997**, *7*, 61−64.
(34) Loffler, H. J. M.; Mouris, J. R. Fusaric acid: phytotoxicity and in vitro production by *Fusarium oxysporum* f. sp. *lilii*, the causal agent of basal rot in lilies. *Neth. J. Plant Pathol.* **1992**, *98*, 107−115.
(35) Gapillout, I.; Milat, M. L.; Blein, J. P. Effects of fusaric acid on cells from tomato cultivars resistant or susceptible to *Fusarium oxysporum* f. sp. *lycopersici*. *Eur. J. Plant Pathol.* **1996**, *102*, 127−132.
(36) Chakrabarti, D. K.; Chaudhary, K. C. B. Correlation between virulence and fusaric acid production in *Fusarium oxysporum* f. sp. *carthami*. *J. Phytopathol.* **1980**, *99*, 43−46.
(37) Barna, B.; Sarhan, A. R. T.; Kiraly, Z. The influence of nitrogen nutrition on the sensitivity of tomato plants to culture filtrates of *Fusarium* and to fusaric acid. *Physiol. Plant Pathol.* **1983**, *23*, 257−263.
(38) Toyoda, H.; Hashimoto, H.; Utsumi, R.; Kobayashi, H.; Ouchi, S. Detoxification of fusaric acid by a fusaric acid-resistant mutant of *Pseudomonas solanacearum* and its application to biological-control of fusarium-wilt of tomato. *Phytopathology* **1988**, *78*, 1307−1311.
(39) Megnegneau, B.; Branchard, M. Toxicity of fusaric acid observed on callus-cultures of various *Cucumis melo* genotypes. *Plant Physiol. Biochem.* **1988**, *26*, 585−588.
(40) Remotti, P. C.; Loffler, H. J. M. The involvement of fusaric acid in the bulb-rot of *Gladiolus*. *J. Phytopathol.* **1996**, *144*, 405−411.

addition, the binding mechanism of polyphenols with proteins has not been clarified yet, nor has the conjugation site of amino acids of proteins been elucidated.

Therefore, we studied the interaction of catechin and OTF in order to investigate the antioxidant activity of modified protein. Two different conjugating reactions between OTF and catechin were conducted. The identification of catechin was performed by liquid chromatography coupled online to a tandem mass spectrometer (LC−MS−MS). The possibility to graft antioxidant moieties like catechin into a proteic structure represents an interesting innovation that significantly improves the performance of the biomacromolecules, opening up new applications in the nutraceutical and functional food ingredient fields.

2. METHODS AND MATERIALS

2.1. Chemicals and Reagents. Ovotransferrin was provided by Neova Technologies Inc. (Abbotsford BC, Canada), and the purity was >89%. (+)-Catechin was purchased from Sigma (Oakville, ON, Canada), and the purity was >98%, HPLC grade. Asorbic acid, 6-hydroxy-2,5,7,8-tetramethylchromate-2-carboxylicacid (Trolox), ethylenediaminetetraacetic acid (EDTA) were also purchased from Sigma (Oakville, ON, Canada). Fluorescein disodium salt and 2,20-azobis(2-methylpropionamide) dihydrochloride (AAPH) were obtained from Fisher Scientific (Ottawa, ON, Canada). All other chemicals and reagents used in this study were obtained from Sigma and were of the analytical grade.

2.2. Conjugation of OTF and Catechin. Conjugates were prepared either by free radical[16] or alkaline method.[14] To prepare conjugates by the free radical method, in a 100 mL glass flask, 0.5 g of ovotransferrin was dispersed in 50 mL of distilled H_2O, then 1.0 mL of 5.0 M H_2O_2 (5.0 mmol) and 0.25 g of ascorbic acid (1.4 mmol) were added, and the mixture was maintained at 25 °C under atmospheric air. After 2 h, 0.35 mmol of catechin were added to solution to react for 24 h; unreacted catechin was removed by dialysis (dialysis tube with 1000 molecular weight cutoffs) at 4 °C for 48 h with Milli-Q water with eight changes. Conjugate was also prepared by the alkaline method. In the presence of alkaline, catechin is oxidized to its respective quinone. The reaction of this quinone with the nucleophilic side chains of proteins such as lysine, cysteine, methionine and tryptophan leads to a protein-phenol derivative.[14] The alkaline conjugate was prepared in a 100 mL glass flask; 0.5 g of ovotransferrin was dispersed in 50 mL of distilled H_2O, the pH was adjusted to 9.0, and the mixture was maintained at 25 °C under atmospheric air. After 2 h, 0.35 mmol of catechin were added to solution for 24 h with continuous stirring; unreacted catechin was removed by dialysis as above. The resulting solutions were frozen and freeze-dried.

2.3. Determination of Antioxidant Activities. *2.3.1. Oxygen Radical Absorbance Capacity (ORAC) Assay.* The ORAC assay using fluorescein as the fluorescent probe was performed according to Huang et al.[24] The reaction was carried out in 96-well black microplates (96F nontreated, Nunc, Roskilde, Denmark). Samples at different concentrations were mixed with 75 mM phosphate buffer (pH 7.4; 80 μL) and 200 nM fluorescein (50 μL) and incubated at 37 °C for 15 min. Then, 80 mM AAPH solution (50 μL) was added to each well using a dispenser. The fluorescence was recorded every min for 100 min by a microplate reader (Fluoroskan Ascent; Thermo Electron Corp., Vantaa, Finland). The excitation and emission wavelengths were 485 and 538 nm, respectively. Phosphate buffer was used instead of sample solution as blank. The area under curve was calculated by integrating the relative fluorescence curve. The ORAC value was calculated by dividing the slope of sample regression curve by the slope of Trolox regression curve. Final ORAC values were expressed as Trolox equivalents (TE) per mol. All the tests were performed at least in triplicates.

2.3.2. $ABTS^{\bullet+}$ Radical Scavenging Assay. ABTS was performed according to You et al.[25] $ABTS^{\bullet+}$ was produced by mixing 7 mM $ABTS^{\bullet+}$ stock solution with 2.45 mM potassium persulfate. Then the mixture was placed at room temperature in darkness for 17 h to generate radical before use. The $ABTS^{\bullet+}$ working solution was diluted with 5 mM phosphate buffered saline (pH 7.4) to an absorbance of 0.70 ± 0.02 at 734 nm. Radical scavenging activity of samples was measured by mixing 100 μL of the samples with 100 μL of diluted $ABTS^{\bullet+}$. The decline in absorbance was measured at 1 min interval for a total of 10 min. A standard curve was prepared by reacting 100 μL of a series of concentrations of Trolox (0, 2, 4, 8, 12, 16, and 20 μM) with 100 μL of diluted $ABTS^{\bullet+}$ solution. The degree of radical scavenging activity of the samples was calculated on the basis of the Trolox standard curve and was expressed as TEAC (μmol/mg sample).

2.3.3. Reducing Power Assay. The ability of samples to reduce iron(III) was determined by the method of Yildirim, Mavi, and Kara.[26] An aliquot of 1 mL of sample (5 mg/mL) was mixed with 2.5 mL of 0.2 M phosphate buffer (pH 6.6) and 2.5 mL of 1% (w/v) potassium ferricyanide. The mixtures were incubated at 50 °C for 30 min. After incubation, 2.5 mL of 10% (w/v) trichloroacetic acid was added and the reaction mixtures were centrifuged for 10 min at 3000*g*. Finally, 2.5 mL of the supernatant solution was mixed with 2.5 mL of distilled water and 0.5 mL of 0.1% (w/v) ferric chloride solution. After a 10 min reaction time, the absorbance of the resultant solution was measured at 700 nm. Higher absorbance of the reaction mixture indicated higher reducing power.

2.4. Sodium Dodecyl Sulfate Polyacrylamide Gel Electrophoresis (SDS-PAGE). SDS-PAGE was performed in a Mini-PROTEAN tetra cell with a Power Pac Basic electrophoresis apparatus (Bio-Rad Laboratories, Inc., Hercules, CA, U.S.A.) at a constant voltage of 200 V according to Offengenden et al.[27] OTF and OTF-catechin conjugates solutions (2 mg/mL) were diluted in a ratio of 1:1 with Laemmli sample buffer containing 5% β-mercaptoethanol and loaded on 12% Mini-PROTEAN TGX precast gel (Bio-Rad Laboratories, Inc., Hercules, CA, U.S.A.). Loading volume of samples and protein marker "Precision Plus Standards Dual Xtra Protein" (Bio-Rad Laboratories, Inc., Hercules, CA, U.S.A.) was 15 μL. The gel was stained with Coomassie brilliant blue R250 and scanned in an Alpha Innotech gel scanner (Alpha Innotech Corp., San Leandro, CA, U.S.A.) with Fluor Chem SP software.

2.5. Matrix-Assisted Laser Desorption/Ionization Time-of-Flight Mass Spectrometry (MALDI-TOF−MS). MALDI-TOF−MS was used to determine the molecular weights of OTF and OTF-catechin conjugates. Lyophilized OTF and OTF conjugates were dissolved in 20 μL of distilled H_2O. A 0.8 μL aliquot of sample solution was spotted to an 800 μm Bruker's anchor Chip MALDI target (Bruker Daltonics, Billerica, MA, U.S.A.). A 0.8 μL aliquot of matrix solution was then spotted on top of the sample and left to dry. 2,5-dihydroxybenzoic acid (DHB) was used as the matrix compound. Matrix solution was prepared in 50% acetonitrile at a final concentration of 3.5 mg/mL. MALDI MS was performed on an ultraflex Xtreme TM MALDI-TOF/TOF (Bruker Daltonics, Billerica, MA, U.S.A.) mass spectrometer in positive MS or lift mode.

2.6. Fluorescence. The fluorescence of samples was tested according to Roy et al.[28] with slight modification. The steady-state fluorescence spectra of samples were recorded at an excitation wavelength of 280 nm in a SepctraMax M3 spectrometer (Molecular Devices, Inc., U.S.A.), with 10 nm excitation and 5 nm emission bandwidth, in a 96 well plate. Samples were dissolved in distilled water to make a protein concentration of 10^{-5} M.

2.7. Ultra Performance Liquid Chromatography (UPLC). The hydrophilic/hydrophobic characteristics of OTF, catechin, and OTF-catechin conjugates were studied by reverse-phase chromatography using a UPLC (Waters, Miliford, MA, U.S.A.). In brief, samples were dissolved in double distilled water and filtered through a 0.2 μm nylon syringe filter prior to analyze with a Waters BEH 300 C_{18} column (2.1 × 100 mm). The column was eluted (0.5 mL/min) with a two solvent system: (A) 0.1% Trifluoroacetic acid (TFA) in water and (B) 0.1% TFA in acetonitrile, with a gradient from 0% solvent B to 75% solvent B over 30 min, and then decreased to 0% solvent B in 10 min.

2.8. LC−MS−MS. The identification of the sites of protein-catechin conjugates was performed by LC−MS−MS. Excised gel pieces from above SDS-PAGE containing the samples of interest were digested by

trypsin following the protocol of Offengenden et al.[27] OTF-catechin conjugates were analyzed by a Waters (Micro mass) Q-TOF Premier (Milford, MA, U.S.A.) according to Gu and Wu.[29] Mass was detected through quadrupole time-of-flight (Q-TOF) analyzer operated in a positive ion MS/MS mode. A MS/MS full-scan was performed for each sample. The peptides' sequences were identified from respective monoisotopic mass. Instrumental control and data analysis were performed using Mass Lynx software (Micromass U.K. Ltd.). Peaks Viewer 4.5 (Bioinformatics Solutions Inc., Waterloo, ON, Canada) in combination with manual de novo sequencing was used to process the MS/MS data.

2.9. Statistical Analysis. All sample determinations were performed in triplicate and the results were expressed as mean value ± standard deviation (SD) in this study. The fluorescence decay curves and data figures were prepared using GraphPad Prism Version 5.02 (GraphPad Software, Inc., CA, U.S.A.). Analysis of variance (ANOVA) with Tukey's post hoc test was used to determine statistical differences. Differences were considered significant with p value <0.05.

3. RESULTS AND DISCUSSION

3.1. Antioxidant Activities. Effect of conjugation on the antioxidant activities were evaluated by oxygen radical absorbance capacity assay (ORAC), $ABTS^{\bullet+}$ radical scavenging activity and reducing power as shown in Table 1. The ORAC

Table 1. Antioxidant Activities of Ovotransferrin and Ovotransferrin-Catechin Conjugates

	ORAC (mol Trolox/mol sample)	$ABTS^{\bullet+}$ scavenging activity (μmol Trolox/mg sample)	reducing power (Abs)
ovotransferrin	3.95 ± 0.08d	0.18 ± 0.01d	0.22 ± 0.01d
alkaline conjugates[a]	17.14 ± 1.01b	0.27 ± 0.01c	0.75 ± 0.04c
radical conjugates[a]	22.80 ± 0.63a	0.86 ± 0.04b	1.17 ± 0.06b
catechin	8.03 ± 0.47c	1.67 ± 0.05a	2.48 ± 0.13a

[a]Alkaline conjugates: ovotransferrin grafted with catechin by alkaline method. Radical conjugates: ovotransferrin grafted with catechin by radical method.

method based on a classic hydrogen atom transfer mechanism, and it primarily measured the oxidative degradation of the fluorescent molecule after being mixed with peroxyl radical generator.[30] The ORAC value of OTF was 3.95 mol Trolox/mol sample; after conjugation, these values were increased 4−5 times compared to OTF control. The radical conjugate showed higher ORAC value than the alkaline one. $ABTS^{\bullet+}$ radical scavenging assay and reducing power have been widely used to determine the antioxidant capacities as they require relatively standard equipment and deliver fast and reproducible results.[31] Similar to the ORAC data, the radical conjugates showed stronger $ABTS^{\bullet+}$ radical scavenging activity as well as reducing power than the alkaline one. This is due to the different methods of conjugation. For the radical method, the hydroxyl radicals, generated by the interaction between redox pair components, attack the reactive residues in the side chains of protein chain, producing protein radical. Then the catechin reacted with the radical species on the protein.[16] For the alkaline method, catechin oxidized to its respective quinone and then reacted with protein chain.[14]

Spizzirri et al.[16] also reported the improvement of antioxidant activities of antioxidant-gelatin conjugates. Generally, it is considered that a higher number of hydroxyl group substituents in a phenol structure like catechin results in a superior antioxidant activity.[32,33] The introduction of hydroxyl groups into ovotransferrin was responsible for the improved antioxidant activities of ovotransferrin-catechin conjugates.

3.2. SDS-PAGE. The effect of conjugation on the molecular weight of OTF was carried out by SDS-PAGE (Figure 1). The

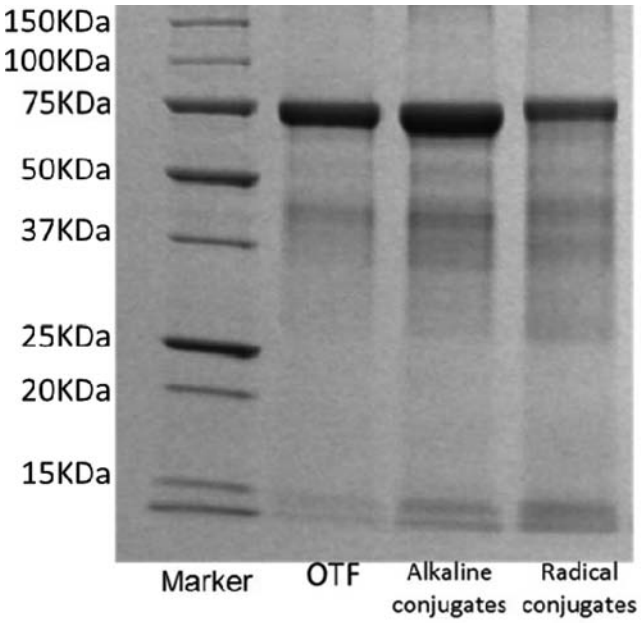

Figure 1. SDS-PAGE of ovotransferrin (OTF) and conjugates of OTF and catechin. Alkaline conjugates: conjugates formed by alkaline method. Radical conjugates: conjugates formed by radical method.

main band in OTF was around 76 kDa.[34] The band of radical conjugates slightly migrated up comparing to the band of OTF, suggesting that the molecular weight of radical conjugates increased resulting from the conjugation. An increase in molecular weight of conjugates after introduction of flavonoid compounds was also reported.[20] However, there was no obvious change in alkaline conjugate. It was reported that phenol-protein complexes could be broken in the presence of SDS,[35] whereas Brunet et al.[11] reported that SDS does not totally break the phenol-protein complex. As the molecular weight of catechin is 290 Da, a lack of change in molecular weight in alkaline conjugate may also be due to a low degree of conjugation.

3.3. MALDI-TOF−MS. Molecular weight change of conjugates was further studied by MALDI-TOF−MS. As shown in Figure 2, the molecular weight of OTF determined by this method was near 76 KDa, agreeing with molecular weight reported by Wu and Acero-Lopez.[7] The molecular weights of both conjugates were increased as shown in the peaks of both alkaline conjugates and radical conjugates. The difference of molecular weight (~400 Da) between OTF and radical conjugates might correspond to the conjugated catechin molecular into OTF monomers. Kim and Cavaco-Paulo[20] pointed out the increase of molecular weight of α-casein-flavonoid conjugates was due to the Michael addition reaction. Similar to results of SDS-PAGE, the difference of molecular weight between OTF and its alkaline conjugates was not obvious. Our MALDI-TOF−MS result further confirmed the possible conjugation of OTF with catechin.

3.4. Fluorescence. A fluorescence study was performed to evaluate changes in structure, as illustrated by the conjugation of OTF with catechin in Figure 3. The maximum emission

dx.doi.org/10.1021/jf405635q | J. Agric. Food Chem. 2014, 62, 2581−2587

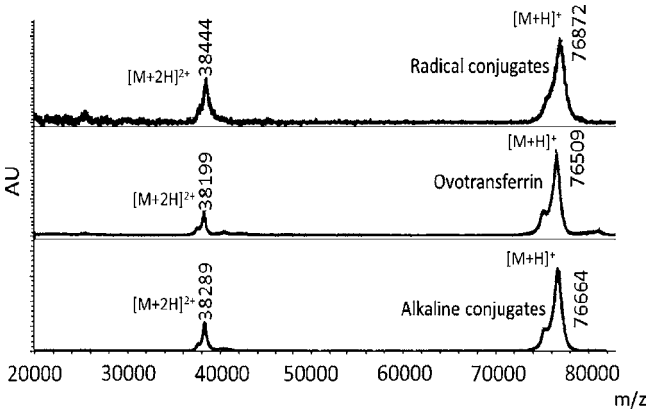

Figure 2. Matrix-assisted laser desorption/ionization time-of-flight mass spectrometry of ovotransferrin and ovotransferrin-catechin conjugates. Radical conjugates: ovotransferrin conjugated with catechin by radical method. Alkaline conjugates: ovotransferrin conjugated with catechin by alkaline method.

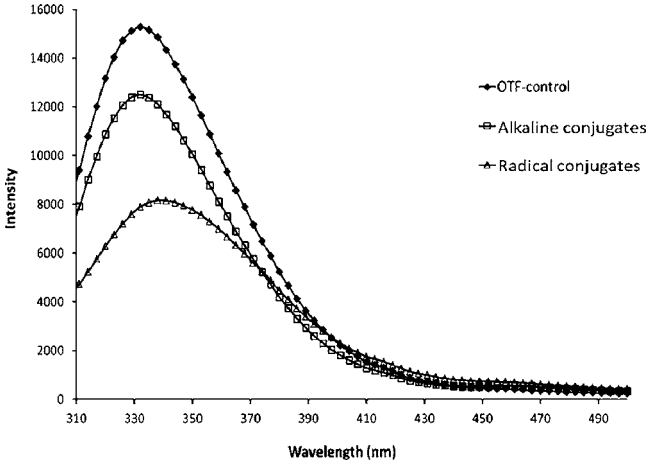

Figure 3. Fluorescence of ovotransferrin (OTF) and conjugates of OTF and catechin. Alkaline conjugates: conjugates formed by alkaline method. Radical conjugates: conjugates formed by radical method.

wavelength for the control OTF was 331 nm (Figure 3), the same as previously reported.[36] There was a red shift of 9 nm after grafted with catechin by radical method, but not the alkaline method. Spizzirri et al.[16] explained that the spectral red shift was due to the covalent conjugation of antioxidants and gelatin. Thus, from the fluorescence result confirmed that catechin was covalently conjugated to OTF by hydrogen peroxide-ascorbic acid pair as radical initiator system. In Figure 3, the fluorescence intensity of OTF-catechin conjugates decreased. Similar results were also observed when grafting flavonoids to soy protein.[37] The interaction of the aromatic ring of the phenolic with aromatic residues such as tyrosine and tryptophan of the protein may be responsible for quenching of fluorescence intensity.

3.5. Ultraperformance Liquid Chromatograph (UPLC). Catechin possesses four −OH phenolic groups located in two benzene rings connected via a nonaromatic ring in which oxygen atom and one more −OH group are present. Therefore, catechin is a well-known hydrophilic antioxidant.[38] A further molecular property of OTF that can be affected by the conjugation of catechin is its hydrophilic/hydrophobic characteristics, which can be illustrated by reversed-phase chromatography. In Figure 4, single peak in each chromatogram of alkaline and radical conjugates were observed, which

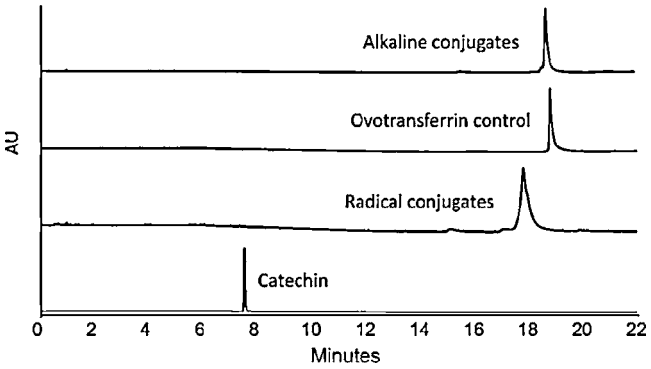

Figure 4. Ultra performance liquid chromatography (UPLC) of ovotransferrin (OTF) and OTF-catechin conjugates. Alkaline conjugates: conjugates formed by alkaline method. Radical conjugates: conjugates formed by radical method, wavelength at 280 nm.

means all the OTF were reacted with catechin. Because alkaline and radical conjugates were dialyzed prior to analysis, the free catechin in OTF-catechin conjugates was completely removed because no peak observed at retention time 7.5 min in the chromatograms of alkaline and radical conjugates (Figure 4). The retention times of OTF and catechin were 19.5 min and 7.5 min, respectively. The retention time of radical conjugate was reduced to 18.4 min, whereas the alkaline conjugate was not changed. In reverse phase chromatography, a decreased retention time indicated reduced hydrophobicity or increased hydrophilicity.[39] The increase of hydrophilicity is related to the introduction of catechin to OTF protein. The interactions between phenolic compounds and proteins would change the net charge in the protein molecules, which in turn affect the hydrophilicity/hydrophobicity of the modified protein.[37] The secondary and tertiary structures of the proteins change as a result of these interactions, influencing the surface properties of the molecules making them hydrophilic in nature.[37] Yuksel et al.[40] also reported that the hydrophobicity of milk proteins was decreased in the presence of low molecular weight phenolics. They explained the decrease in protein hydrophobicity was due to the hydrophobic binding between milk proteins and phenolics.

3.6. LC−MS/MS. LC−MS−MS was conducted in order to identify the possible binding sites of catechin with ovotransferrin. After in gel digestion by trypsin, ovotransferrin and its radical conjugates were analyzed by LC−MS/MS. Figure 5a were the MS spectrum of OTF control and OTF-catechin conjugates, respectively. A high intensity peak in radical conjugate (Figure 5a) was MS ion 597.3. MS/MS data of this doubly charged ion at m/z 597.3 was identified as FMMFESQNK (residues 644−652), which was the same as a triply charged ion at m/z 604.0. Both were part of OTF sequence. Two new MS peaks were identified at 829.5 and 830.5 in Figure 5a as a radical conjugate. Therefore, the MS ions 829.5 and 830.5 were the new ions, which could be the conjugation location. The MS/MS spectrum of these two ions listed in Figure 5b and Figure 5c. The m/z 829.5 was identified as FFSASCVPGATIE-catechin (residues 174−186), and m/z 830.5 was identified as DLLFKDSAIMLK-catechin (residues 316−327). That means catechin was possibly conjugated with the amino acids lysine (residues 327) and glutamic acid

dx.doi.org/10.1021/jf405635q | J. Agric. Food Chem. 2014, 62, 2581−2587

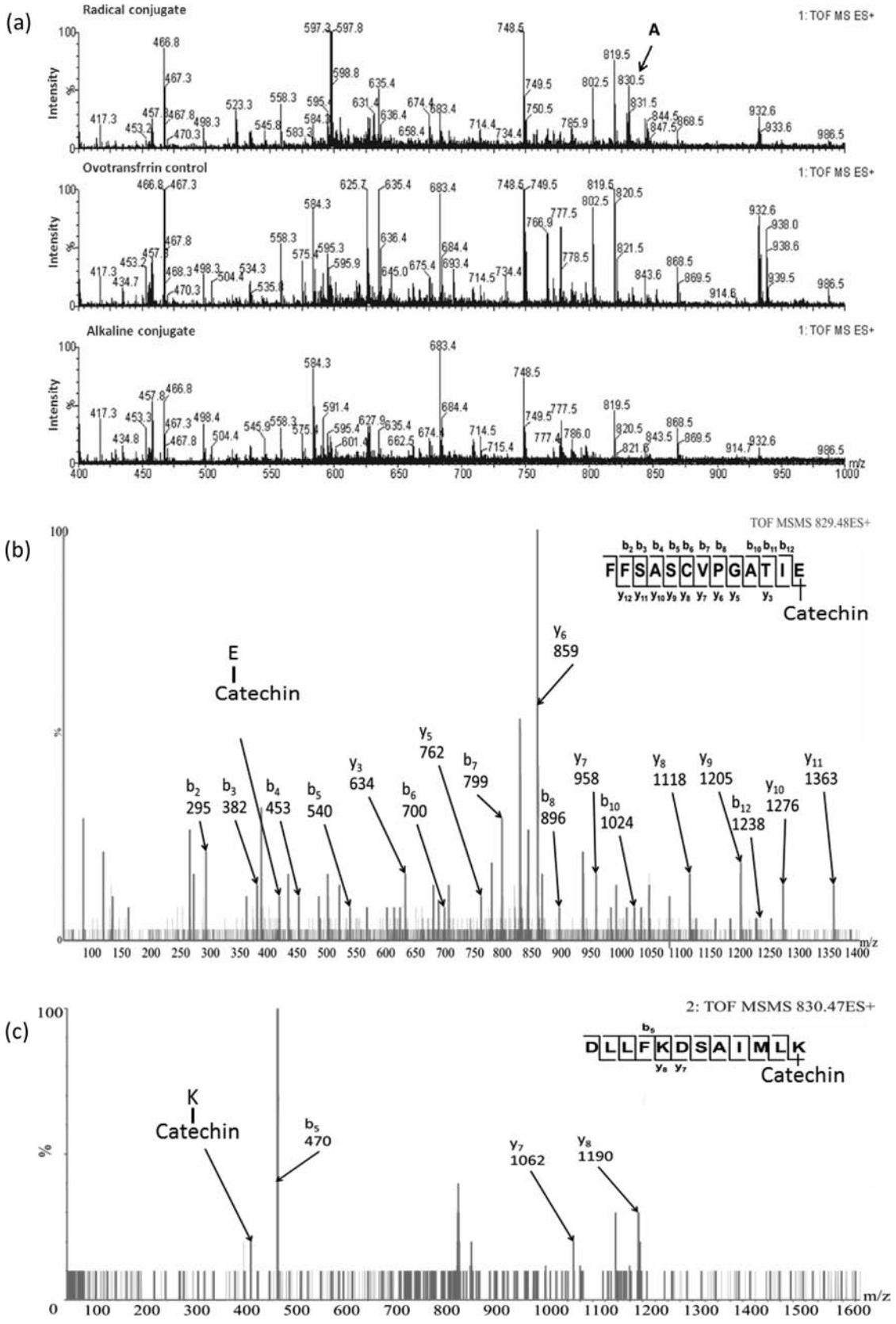

Figure 5. LC-MS-spectra of ovotransferrin (OTF) and OTF-catechin conjugates by radical method and alkaline method; Interpretation of LC−MS/MS spectra of the peak A in (a). Ions at m/z 829.5 (b) and 830.5 (c).

(residues 186) in OTF protein. Catechin is easily oxidized to form a semiquinone that rearranges to an *o*-quinone in the phenolic ring.[41] Several studies on the quinone modifications of various proteins indicate that lysine, histidine, and cysteine residues in the chains are easy to react with quinones.[20] While preparing conjugates using the radical method, as proposed by

dx.doi.org/10.1021/jf405635q | J. Agric. Food Chem. 2014, 62, 2581−2587

Spizzirri et al.,[16] the hydroxyl radicals, generated by the reaction between redox pair components, attack the amino acid in the side chains of ovotransferrin like lysine and glutamic acid, producing radical species on these amino acids. These radical species react with the catechin inducing a catechin-OTF covalent bond. Therefore, by this method, the lysine (residues 327) and glutamic acid (residues 186) in OTF first changed to radical species and then reacted with catechin.

The 3-D structure of ovotransferrin was analyzed by a molecular visualization program, RasMol (Herbert J. Bernstein, NY, U.S.A.), to identify the specific position and the structure of the peptides. RasMol competent Protein Data Bank (PDB Accession code: 1OVT) file was chosen for the analysis.[42] Within the structure of ovotransferrin, we visualized the locations of the covalent bonds (Figure 6). Both peptide DLLFKDSAIMLK and peptide FFSASCVPGATIE belong to the N-lobe.

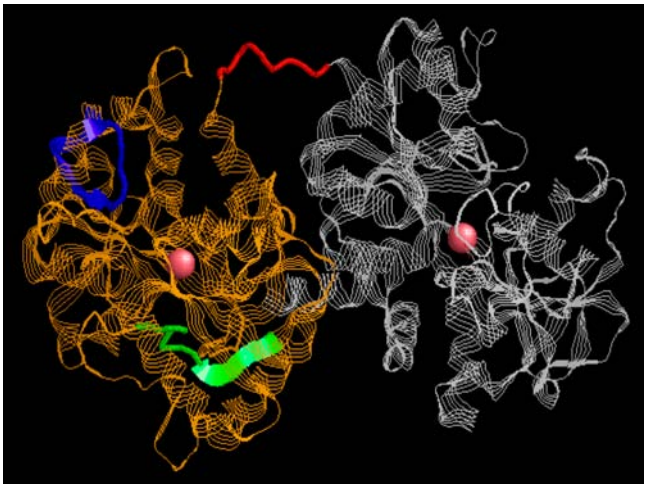

Figure 6. 3-D structure of ovotransferrin was constructed using RasMol molecular graphics software from a protein data bank (PDB) file, accession code: 1OVT. Golden part represents the N-lobe and white part represents C-lobe. Positions of two conjugated peptides FFSASCVPGATIE and DLLFKDSAIMLK were marked by blue and green, respectively.

In conclusion, ovotransferrin-catechin conjuates were successfully prepared using a hydrogen peroxide−ascorbic acid pair as radical initiator system and alkaline method. The data clearly showed that the grafting of ovotrasferrin with catechin is an effective method to improve the oxygen radical absorbance capacity of the protein. Conjugation of catechin with ovotransferrin was studied by fluorescence analyses, UPLC, MALDI-TOF and LC−MS−MS. Catechin was bonded to lysine (residues 327) of DLLFKDSAIMLK (residues 316−327) and glutamic acid (residues 186) of FFSASCVPGATIE (residues 174−186) in ovotransferrin N-lobe. The conjugates can be used as novel protein antioxidants for functional food and food applications.

AUTHOR INFORMATION

Corresponding Author

*J. Wu. Phone: (780) 492-6885. Fax: (780) 492-4265. E-mail: jianping.wu@ualberta.ca.

Funding

The work was supported by a grant from Natural Sciences and Engineering Research Council of Canada (NSERC). J.Y. was supported by China Scholarship Council.

Notes

The authors declare no competing financial interest.

REFERENCES

(1) ButterField, D. A.; Castegna, A.; Pocernich, C. B.; Drake, J.; Scapagnini, G.; Calabrese, V. Nutritional approaches to combat oxidative stress in Alzheimer's disease. *J. Nutr. Biochem.* **2002**, *13*, 444−461.

(2) Athukorala, Y.; Kim, K. N.; Jeon, Y. J. Antiproliferative and antioxidant properties of an enzymatic hydrolysate from brown alga, Ecklonia cava. *Food Chem. Toxicol.* **2006**, *44*, 1065−1074.

(3) Manso, M. A.; Miguel, M.; Even, J.; Hernández, R.; Aleixandre, A.; López-Fandiño, R. Effect of the long-term intake of an egg white hydrolysate on the oxidative status and blood lipid profile of spontaneously hypertensive rats. *Food Chem.* **2008**, *109*, 361−367.

(4) Shahidi, F. Antioxidants in food and food antioxidants. *Nahrung* **2000**, *44*, 158−163.

(5) Kunwar, A.; Priyadarsini, K. I. Free radicals, oxidative stress and importance of antioxidants in human health. *J. Med. Allied Sci.* **2011**, *1*, 53−60.

(6) Mine, Y. Egg proteins and peptides in human health-chemistry, bioactivity and production. *Curr. Pharm. Des.* **2007**, *13*, 875−884.

(7) Wu, J.; Acero-Lopez, A. Ovotransferrin: Structure, bioactivities, and preparation. *Food Res. Int.* **2012**, *46*, 480−487.

(8) Ibrahim, H. R.; Hoq, M. I.; Aoki, T. Ovotransferrin possesses SOD-like superoxide anion scavenging activity that is promoted by copper and manganese binding. *Int. J. Biol. Macromol.* **2007**, *41*, 631−640.

(9) Hernández-Ledesma, B.; Amigo, L.; Recio, I.; Bartolomé, B. ACE-inhibitory and radical−scavenging activity of peptides derived from b-lactoglobulin f (19−25) interactions with ascorbic acid. *J. Agr. Food Chem.* **2007**, *55*, 3392−3397.

(10) Yang, C. S.; Landau, J. M. Effects of tea consumption on nutrition and health. *J. Nutr.* **2000**, *130*, 2409−2412.

(11) Brunet, M. J.; Bladea, C.; Salvadoa, M. J.; Arola, L. Human apo a-I and rat transferrin are the principal plasma proteins that bind wine catechins. *J. Agr. Food Chem.* **2002**, *50*, 2708−2712.

(12) Ozdal, T.; Capanoglu, E.; Altay, F. A review on protein−phenolic interactions and associated changes. *Food Res. Int.* **2013**, *51*, 954−970.

(13) Kroll, J.; Rawel, H. M. Reactions of plant phenols with myoglobin: influence of chemical structure of the phenolic compounds. *J. Food Sci.* **2001**, *66*, 48−58.

(14) Rohn, S.; Rawel, H. M.; Kroll, J. Antioxidant activity of protein-bound quercetin. *J. Agr. Food Chem.* **2004**, *52*, 4725−4729.

(15) Xiao, J.; Kai, G. A review of dietary polyphenol-plasma protein interactions: characterization, influence on the bioactivity, and structure-affinity relationship. *Crit. Rev. Food Sci. Nutr.* **2012**, *52*, 85−101.

(16) Spizzirri, U. G.; Iemma, F.; Puoci, F.; Cirillo, G.; Curcio, M.; Parisi, O. I.; Picci, N. Synthesis of antioxidant polymers by grafting of gallic acid and catechin on gelatin. *Biomacromolecules* **2009**, *10*, 1923−1930.

(17) Cirillo, G.; Vittorioc, O.; Hampel, S.; Spizzirri, U. G.; Piccia, N.; Iemma, F. Incorporation of carbon nanotubes into a gelatin-catechin conjugate: Innovative approach for the preparation of anticancer materials. *Int. J. Pharm.* **2013**, *446*, 176−182.

(18) Trombley, J. D.; Loegel, T. N.; Danielson, N. D.; Hagerman, A. E. Capillary electrophoresis methods for the determination of covalent polyphenol-protein complexes. *Anal. Bioanal. Chem.* **2011**, *401*, 1523−1529.

(19) Jongberg, S.; Gislason, N. E.; Lund, M. N.; Skibsted, L. H.; Waterhouse, A. L. Thiol-quinone adduct formation in myofibrillar proteins detected by LC-MS. *J. Agr. Food Chem.* **2011**, *59*, 6900−6905.

(20) Kim, S.; Cavaco-Paulo, A. Laccase-catalysed protein−flavonoid conjugates for flax fibre modification. *Appl. Microbiol. Biotechnol.* **2012**, *93*, 585−600.
(21) Arts, M. J. T. L.; Haenen, G. R. M. M.; Wilms, L. C.; Beetstra, S. A. J. N.; Heijnen, C. G. M.; Voss, H. P.; Bast, A. Interactions between flavonoids and proteins: Effect on the total antioxidant capacity. *J. Agr. Food Chem.* **2002**, *50*, 1184−1187.
(22) Ryan, L.; Petit, S. Addition of whole, semiskimmed, and skimmed bovine milk reduces the total antioxidant capacity of black tea. *Nutr. Res. (N.Y.)* **2010**, *30*, 14−20.
(23) Dubeau, S.; Samson, G.; Tajmir-Riahi, H. A. Dual effect of milk on the antioxidant capacity of green, Darjeeling and English breakfast teas. *Food Chem.* **2010**, *122*, 539−545.
(24) Huang, W.; Majumder, K.; Wu, J. Oxygen radical absorbance capacity of peptides from egg white protein ovotransferrin and their interaction with phytochemicals. *Food Chem.* **2010**, *123*, 635−641.
(25) You, S.; Udenigwe, C. C.; Aluko, R. E.; Wu, J. Multifunctional peptides from egg white lysozyme. *Food Res. Int.* **2010**, *43*, 848−855.
(26) Yildirim, A.; Mavi, A.; Kara, A. A. Determination of antioxidant and antimicrobial activities of *Rumex crispus* L. extracts. *J. Agr. Food Chem.* **2001**, *49*, 4083−4089.
(27) Offengenden, M.; Fentabil, M. A.; Wu, J. N-glycosylation of ovomucin from hen egg white. *Glycoconjugate J.* **2011**, *28*, 113−123.
(28) Roy, D.; Dutta, S.; Maity, S. S.; Ghosh, S.; Roy, A. S.; Ghosh, K. S.; Dasgupta, S. Spectroscopic and docking studies of the binding of two stereoisomeric antioxidant catechins to serum albumins. *J. Lumin.* **2012**, *132*, 1364−1375.
(29) Gu, Y.; Wu, J. LC−MS/MS coupled with QSAR modeling in characterising of angiotensin I-converting enzyme inhibitory peptides from soybean proteins. *Food Chem.* **2013**, *141*, 2682−2690.
(30) Ou, B.; Hampsch-Woodill, M.; Prior, R. L. Development and validation of an improved oxygen radical absorbance capacity assay using fluorescein as the fluorescent probe. *J. Agr. Food Chem.* **2001**, *49*, 4619−4626.
(31) Dudonné, S.; Vitrac, X.; Coutière, P.; Woillez, M.; Mérillon, J.-M. Comparative study of antioxidant properties and total phenolic content of 30 plant extracts of industrial interest using DPPH, ABTS, FRAP, SOD, and ORAC assays. *J. Agr. Food Chem.* **2009**, *57*, 1768−1774.
(32) Amić, D.; Davidović-Amić, D.; Bešlo, D.; Trinajstić, N. Structure radical scavenging activity relationships of flavonoids. *Croat. Chem. Acta* **2003**, *76*, 51−61.
(33) Heijnen, C. G.M.; Haene, G. R. M. M.; van Acker, F. A. A.; van der Vijgh, W. J. F.; Bast, A. Flavonoids as peroxynitrite scavengers: the role of the hydroxyl group. *Toxicol. In Vitro* **2001**, *15*, 3−6.
(34) Giansanti, F.; Leboffe, L.; Pitari, G.; Ippoliti, R.; Antonini, G. Physiological roles of ovotransferrin. *Biochim. Biophys. Acta* **2012**, *1820*, 218−225.
(35) Hagerman, A. E.; Butler, L. G. Condensed tannin purification and characterization of tannin-associated proteins. *J. Agr. Food Chem.* **1980**, *28*, 947−952.
(36) Rabbani, G.; Ahmad, E.; Zaidi, N.; Khan, R. H. pH-dependent conformational transitions in conalbumin (Ovotransferrin), a metalloproteinase from hen egg white. *Cell Biochem. Biophys.* **2011**, *61*, 551−560.
(37) Rawel, H. M.; Czajka, D.; Rohn, S.; Kroll, J. Interactions of different phenolic acids and flavonoids with soy proteins. *Int. J. Biol. Macromol.* **2002**, *30*, 137−150.
(38) Huang, S. -W.; Frankel, E. N. Antioxidant activity of tea catechins in different lipid systems. *J. Agr. Food Chem.* **1997**, *45*, 3033−3038.
(39) Guo, D.; Mant, C. T.; Taneja, A. K.; Parker, J. M. R.; Hodges, R. S. Prediction of peptide retention times in reversed-phase high-performance liquid chromatography I. Determination of retention coefficients of amino acid residues of model synthetic peptides. *J. Chromatogr. A* **1986**, *359*, 499−517.
(40) Yuksel, Z.; Avci, E.; Erdem, Y. K. Characterization of binding interactions between green tea flavanoids and milk proteins. *Food Chem.* **2010**, *121*, 450−456.
(41) Ishii, T.; Mori, T.; Tanaka, T.; Mizuno, D.; Yamaji, R.; Kumazawa, S.; Nakayama, T.; Akagawa, M. Covalent modification of proteins by green tea polyphenol (−)-epigallocatechin-3-gallate through autoxidation. *Free Radical Biol. Med.* **2008**, *45*, 1384−1394.
(42) Majumder, K.; Wu, J. A new approach for identification of novel antihypertensive peptides from egg proteins by QSAR and bioinformatics, Food Research Research International. *Food Res. Int.* **2010**, *43*, 1371−1378.

MATERIALS AND METHODS

Chemicals. All of the flavonoid standards were obtained from Sigma-Aldrich. The purities of the reference substances were determined by gas chromatography (GC) and gas chromatography–mass spectrometry (GC–MS).

Bacterial Strain. *Agrobacterium rhizogenes* A4 strain was taken from the Central Institute of Medicinal and Aromatic Plants, Lucknow, India. The bacterial culture was maintained at 25 ± 2 °C on yeast mannitol broth (YMB) medium (Himedia).

Plant Material and *in Vitro* Culture Establishment. Tomato (*Lycopersicon esculentum*, variety Pusa Early Dwarf) seeds were purchased from the Indian Agricultural Research Institute (IARI), New Delhi, India. Seeds were washed thoroughly with Teepol (10%, w/v), followed by several washings with distilled water. Seeds were kept for 3 h in water prior to being inoculated onto solid Murashige and Skoog (MS) medium with Gamborg's B5 vitamins containing 100 mg/L myoinositol, 30.0 g/L sucrose, and 8.0 g/L agar–agar, which was used for the induction and maintenance of plant cultures through the seeds. All of the cultures were incubated under continuous light of 300 lux at 25 ± 2 °C. The young leaves of 8-week-old plants were used for genetic transformation.

***Agrobacterium*-Mediated Genetic Transformation.** *A. rhizogenes* A4 strain was cultivated at 25 ± 2 °C on YMB. The second and third leaves of *in vitro* grown tomato plants were used to transform, as described previously by Verma et al.[17] Transgenic hairy roots were excised from each wound site and maintained further at 24 ± 2 °C. Transgenic hairy roots were micropropagated on MS medium,[18] supplemented with 100 mg/L Augmentin and 250 mg/L Cefotaxime (Figure 1).

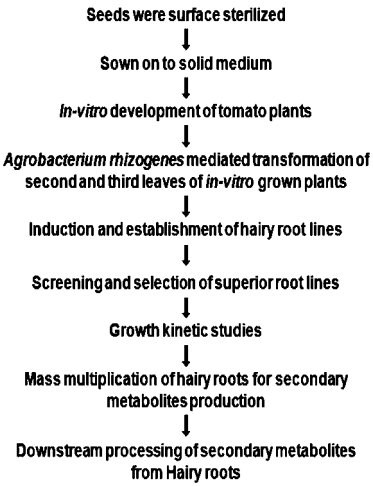

Figure 1. Flowchart of hairy root development in tomato.

Screening of Putative Transformed THRs. DNA was isolated from hairy roots using DNeasy Mini Kit (Qiagen, Valencia, CA). Polymerase chain reaction (PCR) was performed to detect Ri plasmid genes (*rolB*) in putative hairy root lines. Further, any possibility of *Agrobacterium* contamination in THR was ruled out by the amplification of the *virC* gene.

Growth Kinetics of THR. Growth of THR was regularly monitored. The fresh weight of THR was determined every 7 days until 35 days of culture to calculate the growth index (GI) at different time points. At each time interval, samples were harvested, dried on blotting paper to remove unwanted liquid medium, and dried further at 35 ± 2 °C for 7 days, followed by vacuum drying in desiccators until a constant dry weight was obtained. Samples were weighed and stored at −80 °C for further studies.

Extraction of Phenolics. Phenolics were extracted from THRs, and their level was compared to the roots of field grown and *in vitro* grown plants. To extract the phenolics, hairy roots (4 g) were finely powdered in liquid nitrogen, kept overnight in 20 mL of methanol/water (25:75, v/v) at room temperature on a rocking platform, and filtered. The filtrate was collected, and the residue was extracted twice more at 4 h intervals with the same volume of extractant. The filtrate were pooled and extracted with *n*-hexane (3 × 60 mL). The *n*-hexane fraction was discarded, and the methanol–water fraction was further extracted with chloroform (3 × 60 mL). The chloroform fractions were pooled and concentrated on a rotary evaporator.

Further, any residues were removed by freeze-drying. Dry powder (5 mg) was dissolved in high-performance liquid chromatography (HPLC)-grade methanol (1 mL), filtered through a Millipore Sample Clarification Kit (Millx GV, 13 mm, 0.22 N μm), and subjected to HPLC analysis.

Qualitative and Quantitative Analyses of Phenolics. Separation for qualitative and quantitative analyses of phenolics was performed by HPLC–photodiode array (PDA) with a LC-10 (Shimadzu, Japan). Phenolics were separated on a 250 × 4.6 mm (inner diameter), 5 mm pore size RP-C18 column (Merck) protected by a guard column packed with the same matrix. The gradient was prepared from 0.5% (v/v) phosphoric acid in HPLC-grade water (component A) and methanol (component B) in mobile phase. Nylon filters (0.45 μm) were used for filtration of all components and deaerated in an ultrasonic bath. The gradient from 25 to 50% B in 0–3 min, from 50 to 80% B in 3–18 min, from 80 to 25% B in 25 min, and 25% B in 30 min was used for conditioning of the column with a flow rate of 0.8 mL/min. Shimadzu class VP series software was used for data integration, and quantification was carried out by comparison to standard curves, which was constructed according to a previously reported method.[19] All samples and solutions were filtered through 0.45 μm nylon filters (Millipore, Billerica, MA) before analysis by HPLC. A simple mobile phase was used as a control for identification of blank peaks.

Extraction and Quantification of Antioxidant Enzymes. *Extraction of Enzymes from THRs.* Fresh tissue (200 mg) was weighed and ground to a fine powder in liquid nitrogen, allowed to thaw, and then homogenized in 1.5 mL of 0.2 M potassium phosphate buffer (pH 7.8) with 0.1 mM ethylenediaminetetraacetic acid (EDTA). Samples were centrifuged at 15000*g* at 4 °C. The supernatant was collected in a fresh tube and stored at 4 °C for further experiments.

Quantification of Enzymatic Activity. Enzymatic activity of three enzymes, i.e., ascorbate peroxidase (APX), catalase (CAT), and superoxide dismutase (SOD), which play a vital role in the reactive oxygen species (ROS) detoxification pathway, was determined spectrophotometrically, as previously described by Elavarthi and Martin.[20]

Antifeeding Activity of Hairy Root Extract against Chewing Insects. The phenolic compound extract from THRs was tested against two polyphagous insects *Helicoverpa armigera* and *Spodoptera litura*. The insect bioassay was performed as described earlier.[21] The extract of the phenolic compound was mixed with an artificial diet at different concentrations in Petri dishes. The ethanol-mixed diet and only artificial diet were taken as the control and blank, respectively. Petri dishes were kept open overnight at room temperature to let the solvent evaporate. Mortality data were recorded after 6 days. Experiment was performed in triplicate, and data were analyzed by one-way analysis of variation (ANOVA) ($p < 0.05$). Means were compared using Duncan's multiple range test (DMRT) using SPSS software.

RESULTS AND DISCUSSION

Genetic Transformation and Screening of Putative THRs. The second and third leaves of *in vitro* grown tomato plants were infected with *A. rhizogenes* A4 strain, and hairy roots were propagated on MS medium. Hairy roots that did not show necrosis and proliferated well in media were taken for further study. Seven different THRs that showed maximum elongation and branching potentials were selected and screened using PCR. Genomic DNA was isolated from all selected THRs individually, and PCR was performed with a gene-specific primer of the *rolB* gene. An amplicon of ~650 bp was obtained

dx.doi.org/10.1021/jf405695y | J. Agric. Food Chem. 2014, 62, 2588–2594

in THRs that were absent in field grown and *in vitro* grown roots. This confirmed the transformation of THR (Figure 2). *A.*

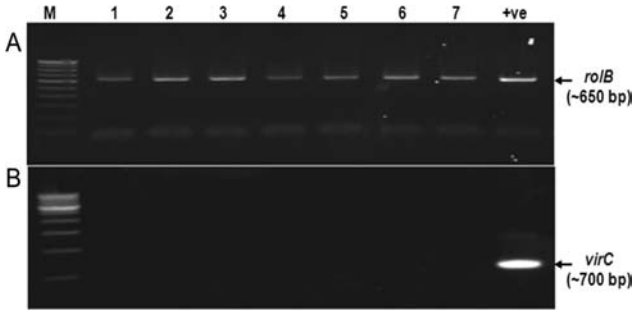

Figure 2. PCR amplification of *rolB* and *virC* genes for confirmation of transformants: (gel A) lane M, 100 bp molecular weight marker; lanes 1−7, different clones of THRs; and lane +ve, positive control and (gel B) lane M, 500 bp molecular weight marker; lanes 1−7, different clones of THRs; and lane +ve, positive control.

rhizogenes-mediated induction of hairy roots has already been reported in a large number of dicotyledonous plants, such as *Atropa, Beta, Brugmansia, Catharanthus, Glycyrrhiza, Hyoscamus, Solanum, Trachelium*, and many others.[22,23] A variety of *A. rhizogenes* strains are available for induction of hairy roots. Different groups have used strain LBA 9402 to initiate hairy roots from tomato to see the response of salt on endogenous levels of jasmonate and octadecanoid,[24] effect of salt on peroxidase activity[25] and for bioremediation of phenol using THRs[26] but we selected A4, which is very commonly used (approximately 22% used worldwide) for biotransformation.[27] *Agrobacterium* contamination in THRs was ruled out by the amplification of the *virC* gene because it was not present between the left and right borders of the Ri plasmid. PCR of THRs with the *virC* primer did not amplify any PCR product. All further studies were restricted to these seven selected THR lines.

Growth Kinetics of Selected THRs. The fact that different root clones differ distinctly, owing to each and every transformation event, has made it mandatory to screen and select the best performing hairy root line to obtain a maximum biomass in a minimum time period. Various independent hairy root clones have been studied in medicinal plants, and variations in the growth level during different growth phases have been noted among hairy root clones of the same origin.[28] Growth of all THRs was regularly monitored during different growth phases, i.e., 7, 14, 21, and 35 days (Figure 3). All THRs showed healthy appearance and lateral branching in liquid media. A gradual increase in the fresh weight up to 28 days of culture could be observed with all of the hairy root clones, which further declined in all lines, except THR-4 (slightly increased after 35 days) and THR-5 (unchanged after 35 days; Figure 4). After 28 days, maximum elongation and branching

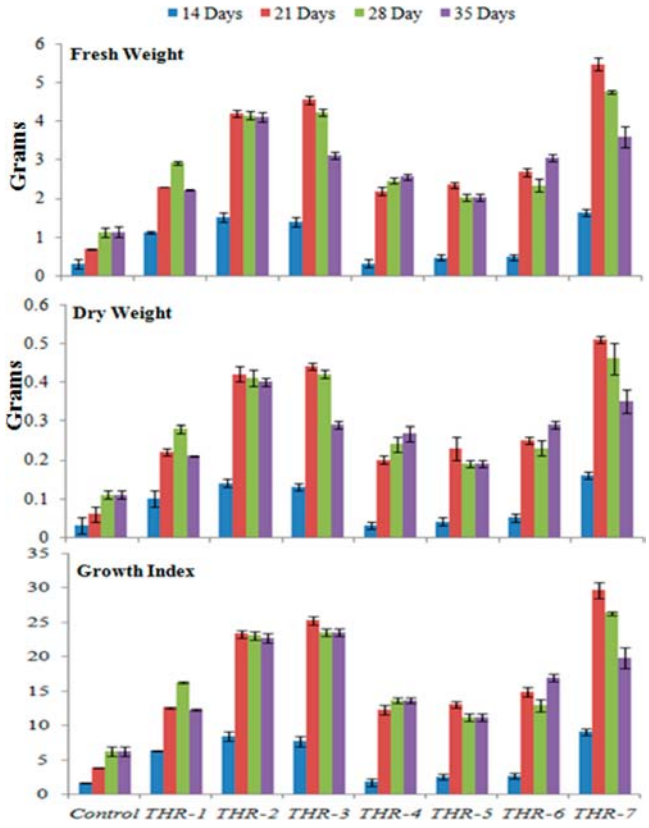

Figure 4. Graph showing growth kinetics of different THR clones.

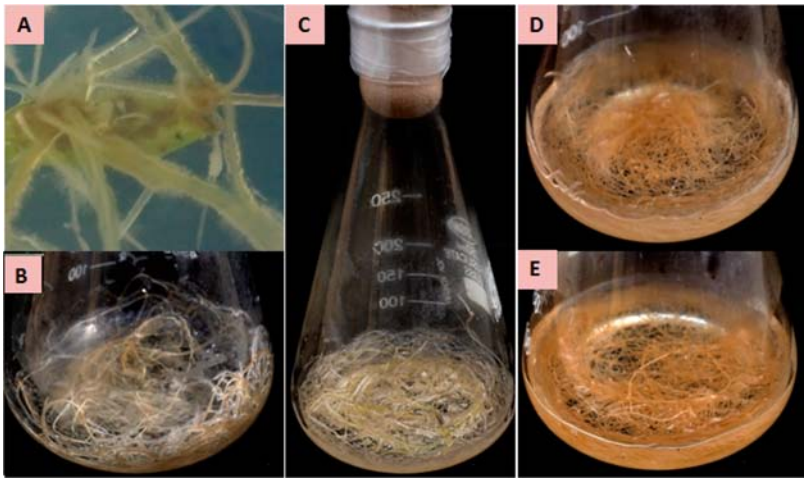

Figure 3. Different stages of development of the THR culture: (A) induction of hairy root by *A. rhizogenes* A4 and (B−E) growth of THR at different time intervals, i.e., (B) 14 days, (C) 21 days, (D) 28 days, and (E) 35 days.

dx.doi.org/10.1021/jf405695y | *J. Agric. Food Chem.* 2014, 62, 2588−2594

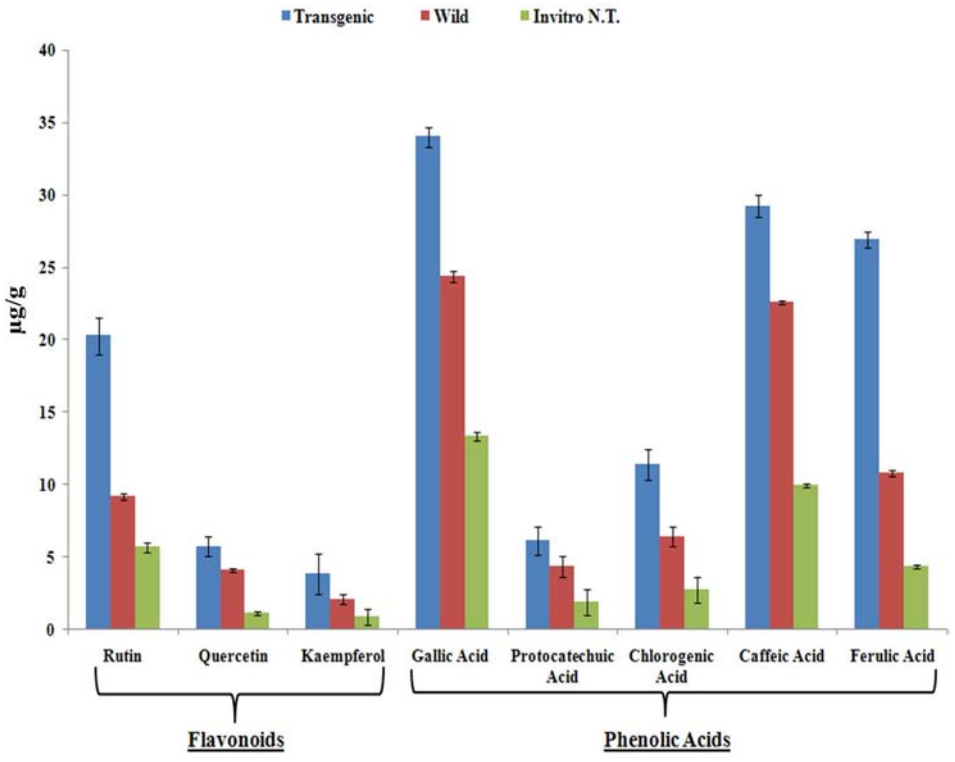

Figure 5. Graph representing the level of different phenolic compounds in THR culture.

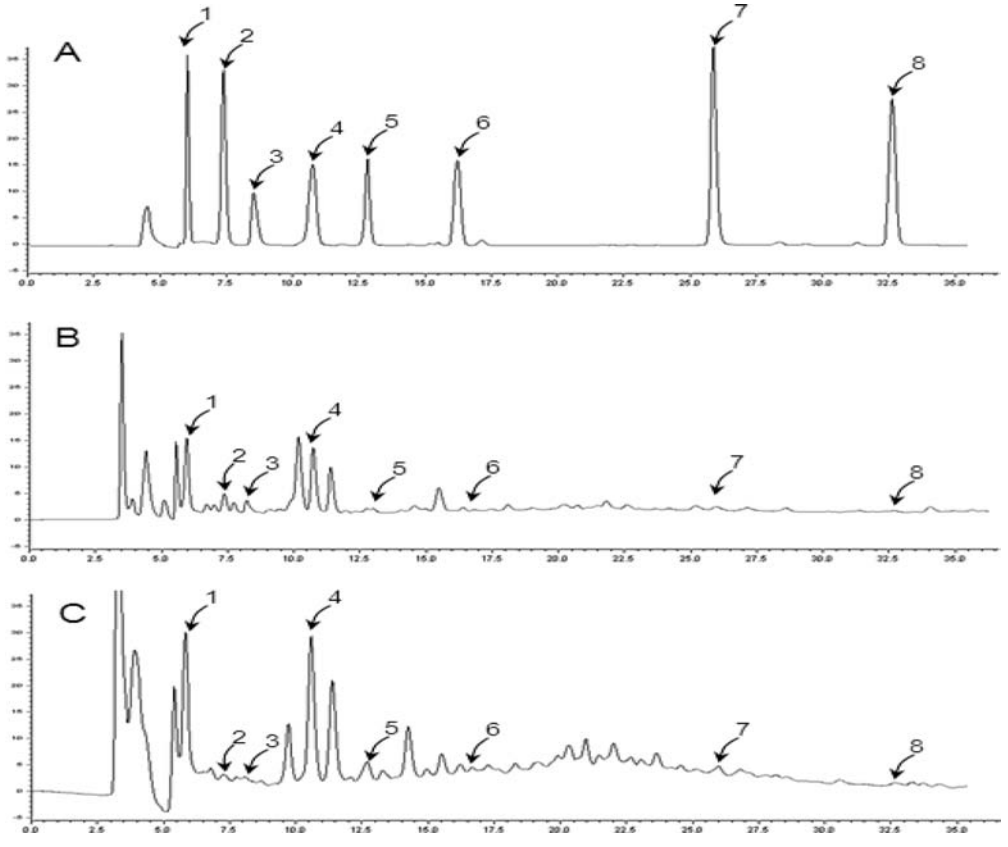

Figure 6. HPLC chromatograms of extract of different root samples: (A) standard peaks, (B) *in vitro* grown roots, and (C) hairy roots. HPLC chromatogram of standards: (1) gallic acid, (2) protocatechuic acid, (3) chlorogenic acid, (4) caffeic acid, (5) rutin, (6) ferulic acid, (7) quercetin, and (8) kaempferol.

dx.doi.org/10.1021/jf405695y | *J. Agric. Food Chem.* 2014, 62, 2588−2594

Table 1. Activity of ROS Detoxifying Enzymes in THRs

enzyme	field grown roots	*in vitro* grown roots	hairy root
ascorbate peroxidase (mM ascorbate min^{-1} g^{-1})	5.01 ± 0.24	4.50 ± 0.19	7.41 ± 0.30
catalase (mM H_2O_2 min^{-1} g^{-1})	0.79 ± 0.09	0.61 ± 0.06	0.97 ± 0.03
superoxide dismutase (units mg^{-1})	0.87 ± 0.05	0.71 ± 0.03	1.45 ± 0.05

Table 2. Insect Bioassay on an Artificial Diet with *H. armigera* and *S. litura* at Different Concentrations of THR Extract

insect bioassay on an artificial diet with different concentrations of THR extract after 6 days				
	H. armigera		*S. litura*	
extract concentration (μL/g of diet)	percent mortality (%)	percent weight reduction (%) (average weight of larvae, mg)	percent mortality (%)	percent weight reduction (%) (average weight of larvae, mg)
100 μL/g	53.34	85.43 (0.50 ± 0.17)	40.00	86.90 (0.36 ± 0.15)
50 μL/g	30.00	68.93 (1.06 ± 0.15)	26.67	52.38 (1.34 ± 0.15)
10 μL/g	16.67	23.30 (2.63 ± 0.15)	6.67	28.57 (2.00 ± 0.26)
control	3.34	0.97 (3.40 ± 0.20)	0.00	1.19 (2.76 ± 0.15)
blank	0.00	NA (3.43 ± 0.30)	0.00	NA (2.80 ± 0.3)

was observed in THR-7, followed by THR-3 and THR-2. Fresh weight of THR-7 (4.75 ± 0.05 g), THR-3 (4.22 ± 0.09 g), and THR-2 (4.14 ± 0.11 g) was 4.2-, 3.76-, and 3.69-fold higher than non-transformed root (1.12 ± 0.13 g), respectively (Figure 4). The clonal nature of the individually selected hairy root lines resulting from site-specific insertion of Ri T-DNA, and the difference in the incorporated copy numbers might finally be responsible for the interclonal variation in terms of growth.[29] Profuse adventitious root growth was attained after 21 days of growth in various medicinal plants and reached its maximum up to 35 days of culture.[30] Similar observations of decline in growth were observed in *Plumbago zeylanica*, *Plumbago kurroa*, and *Gossypium hirsutum*.[17,30,31] The decline in growth is attributed to the secretion of secondary metabolites and other phenolics in the medium, which hamper the adventitious growth of root hairs.

Qualitative and Quantitative Analyses of Phenolics. Potential of flavonoid production in hairy root cultures of tomato is not yet reported. Most of the studies are on either flavonoid production through tomato fruits or peels.[32] However, some other systems have been explored for flavonoid production through hairy roots. Hairy root cultures of *Psoralea* sp. in different stages displayed more concentrations of daidzein and coumestrol compared to callus cultures from the same plant.[33]

The hairy root line THR-7 showed distinct superiority over other lines in terms of growth indices (after 21 days) and was used to quantify the level of different phenolics. HPLC analysis confirmed the presence of several flavonoid and phenolic acids in hairy roots after 21 days of culture (Figures 5 and 6). Many flavonoids, such as rutin, quercetin, and kaempferol, were present in considerable quantity, along with the number of phenolic acids, such as gallic, protocatechuic, ferulic, colorogenic, and caffeic acids.

AtMYB12 transformed hairy roots of *Fagopyrum esculentum*-produced rutin up to 0.9 mg/g of dry weight, but in the present study, THRs produce up to 20.26 μg/g of rutin.[34] The content of gallic, protocatechuic, chlorogenic, caffeic, and ferulic acids in THR-7 was 34.02 μg/g, 6.11 μg/g, 11.35 μg/g, 29.24 μg/g, and 26.89 μg/g after 21 days. It was 1.4-fold (24.3 μg/g), 1.4-fold (4.32 μg/g), 1.7-fold (6.37 μg/g), 1.3-fold (22.5 μg/g), and 2.49-fold (10.78 μg/g) higher than field grown roots, while 2.5-fold (13.34 μg/g), 3.28-fold (1.86 μg/g), 4.15-fold (2.73 μg/g), 2.94-fold (9.94 μg/g), and 6.22-fold (4.32 μg/g) higher when compared to *in vitro* grown roots (Figures 5 and 6).

Hairy root development has been reported in various plant species. They have a very high growth rate, low maintenance cost, capablity of producing a number of products in a single step, easy recovery and purification of these compounds in biologically active form, and many other benefits. Therefore, it always offers a very good system for producing biological compounds for commercial purposes.

Enzymatic Activity. It was well-established that, when plants were exposed to stress, either biotic or abiotic, the production of ROS increases and can cause significant damage to the cells; therefore, the plant cell produces a number of enzymes, i.e., catalase and ascorbate peroxidase, which can maintain the ROS level.[35,36] Thus, the activities of enzymes involved in the ROS detoxification pathway were analyzed in THR and control samples. The activities of catalase, ascorbate peroxidase, and superoxide dismutase were quantified. The activity of catalase in THRs was 0.97 ± 0.03 mM H_2O_2 min^{-1} g^{-1}, which was 1.22-fold (0.79 ± 0.09 mM H_2O_2 min^{-1} g^{-1}) and 1.59-fold (0.61 ± 0.06 mM H_2O_2 min^{-1} g^{-1}) higher than field grown and *in vitro* grown roots, respectively (Table 1). The activities of ascorbate peroxidase and superoxide dismutase in THRs were 7.41 ± 0.30 mM ascorbate min^{-1} g^{-1} and 1.45 ± 0.05 units mg^{-1}, respectively. These were also 1.47-fold (5.01 ± 0.24 mM ascorbate min^{-1} g^{-1}) and 1.66-fold (0.87 ± 0.05 units mg^{-1}) higher than field grown roots, while 1.64-fold (4.50 ± 0.19 mM ascorbate min^{-1} g^{-1}) and 2.04-fold (0.71 ± 0.03 units mg^{-1}) higher when compared to *in vitro* grown roots (Table 1). The Ri-plasmid-transformed calli of *Rubia cordifolia* showed enhanced expression of catalase, ascorbate peroxidase, and superoxide dismutase genes encoding ROS-detoxifying enzymes.[37] The reason for enhanced activity of catalase, ascorbate peroxidase, and superoxide dismutase was due to bacterial (*A. rhizogenes*) infection. Many hairy root systems, i.e., *Brassica napus*, *Daucus carota*, *Ipomoea batatas*, and *Solanum aviculare*, were available for peroxidase production.[38,39] Peroxidase production was further increased by adding elicitors, such as yeast extract, V_2O_5, and Hg_2Cl_2, which increase phenylalanine ammonia lyase synthesis.[40]

Antifeeding Activity of Hairy Root Extract against Chewing Insects. Many reports suggested that flavonoids in their biological form were toxic to insects. The extract of *Nothofagus dombeyi* and *Nothofagus pumilio* leaves consisted of

triterpenes and flavonoids and showed antifeeding activity against the fifth instar larvae of *Ctenopsteustis obliquana*.[41] The insect-resistant genotype of soybean (*Glycine max* PI 227687) accumulated a high amount of rutin.[42] On the basis of previous findings, we tested the phenolic compounds extracted (PCE) from THR against *H. armigera* and *S. litura*. PCE showed significant mortality against both of the insects, while the surviving larvae showed significant growth retardation and have a very low average weight. At 100 μL/g concentration, PCE caused 53.34 and 40.00% mortality against *H. armigera* and *S. litura*, respectively, after 6 days, whereas no toxicity was observed in a blank diet (Table 2). Surviving larvae of *H. armigera* and *S. litura* on PCE after 6 days showed 85.43 and 86.90% growth retardation, respectively (Table 2). Our HPLC data clearly showed the presence of numerous flavonoids and phenolic acids in PCE; this might be a reason for insect toxicity. Insect mortality also revealed that extracted phenolic compounds were in their biologically active form.

AUTHOR INFORMATION

Corresponding Author

*Telephone: +91-0522-2297922. Fax: +91-0522-2205836 and +91-0522-2205839. E-mail: praveencverma@nbri.res.in.

Funding

Harpal Singh is thankful to CSIR, India, for a Senior Research Fellowship.

Notes

The authors declare no competing financial interest.

ACKNOWLEDGMENTS

The authors are thankful to Dr. Abhishek Niranjan, CIF CSIR–NBRI, for the HPLC experiments.

REFERENCES

(1) Jochum, G. M.; Mudge, K. W.; Thomas, R. B. Elevated temperatures increase leaf senescence and root secondary metabolite concentrations in the understory herb *Panax quinquefolius* (Araliaceae). *Am. J. Bot.* **2006**, *94*, 819–826.

(2) Pang, J.; Cuin, T.; Shabala, L.; Zhou, M.; Mendham, N.; Shabala, S. Effect of secondary metabolites associated with anaerobic soil conditions on ion fluxes and electrophysiology in barley roots. *Plant Physiol.* **2007**, *145*, 266–276.

(3) Stafford, H. A. Flavone and flavonone pathway. In *Flavonoids Metabolism*; CRC Press: Boca Raton, FL, 1990.

(4) Balasundram, N.; Sundram, K.; Samman, S. Phenolic compounds in plants and agri industrial by-products: Antioxidant activity, occurrence, and potential uses. *Food Chem.* **2006**, *99*, 191–203.

(5) Ferrer, J. L.; Austin, M. B.; Stewart, C. J.; Noel, J. P. Structure and function of enzymes involved in the biosynthesis of phenylpropanoids. *Plant Physiol. Biochem.* **2008**, *46*, 356–370.

(6) Benavente-García, O.; Castillo, J.; Marin, F. R.; Ortuño, A.; Río, J. A. D. Uses and properties of citrus flavonoids. *J. Agric. Food Chem.* **1997**, *45*, 4505–4515.

(7) Samman, S.; Naghii, M. R.; Lyons, W. P. M.; Verus, A. P. The nutritional and metabolic effects of boron in humans and animals. *Biol. Trace Elem. Res.* **1998**, *66*, 227–235.

(8) Middleton, E. J.; Kandaswami, C.; Theoharides, T. C. The effects of plant flavonoids on mammalian cells: Implications for inflammation, heart disease, and cancer. *Pharmacol. Rev.* **2000**, *52*, 673–751.

(9) Puupponen-Pimiä, R.; Nohynek, L.; Meier, C.; Kähkönen, M.; Heinonen, M.; Hopia, A.; Oksman-Caldentey, K. M. Antimicrobial properties of phenolic compounds from berries. *J. Appl. Microbiol.* **2001**, *90*, 494–507.

(10) Manach, C.; Mazur, A.; Scalbert, A. Polyphenols and prevention of cardiovascular diseases. *Curr. Opin. Lipidol.* **2005**, *16*, 77–84.

(11) Peng, Y.; Zhang, Y.; Ye, J. Determination of phenolic compounds and ascorbic acid in different fractions of tomato by capillary electrophoresis with electrochemical detection. *J. Agric. Food Chem.* **2008**, *56*, 1838–1844.

(12) Slimestad, R.; Fossen, T.; Verheul, M. J. The flavonoids of tomatoes. *J. Agric. Food Chem.* **2008**, *56*, 2436–2441.

(13) Moco, S.; Bino, R. J.; Vorst, O.; Verhoeven, H. A.; de Groot, J.; van Beek, T. A.; Vervoort, J.; de Vos, C. H. A liquid chromatography–mass spectrometry-based metabolome database for tomato. *Plant Physiol.* **2006**, *141*, 1205–1218.

(14) Ma, Y.; Ye, X.; Hao, Y.; Xu, G.; Xu, G.; Liu, D. Ultrasound-assisted extraction of hesperidin from Penggan (*Citrus reticulata*) peel. *Ultrason. Sonochem.* **2008**, *15*, 227–232.

(15) Adato, A.; Mandel, T.; Mintz-Oron, S.; Venger, I.; Levy, D.; Yativ, M.; Domínguez, E.; Wang, Z.; De Vos, R. C.; Jetter, R.; Schreiber, L.; Heredia, A.; Rogachev, I.; Aharoni, A. Fruit-surface flavonoid accumulation in tomato is controlled by a slmyb12-regulated transcriptional network. *PLoS Genet.* **2009**, *5* (12), No. e1000777.

(16) Wu, S. B.; Meyer, R. S.; Whitaker, B. D.; Litt, A.; Kennelly, E. J. A new liquid chromatography–mass spectrometry-based strategy to integrate chemistry, morphology, and evolution of eggplant (*Solanum*) species. *J. Chromatogr., A* **2013**, *1314*, 154–172.

(17) Verma, P. C.; Rahman, L.; Negi, A. S.; Jain, D. C.; Khanuja, S. P. S.; Banerjee, S. *Agrobacterium rhizogenes*-mediated transformation of *Picrorhiza kurroa* Royle ex Benth.: Establishment and selection of superior hairy root clone. *Plant Biotechnol. Rep.* **2007**, *1*, 169–174.

(18) Medina-Bolivar, F.; Condori, J.; Rimando, A. M.; Hubstenberger, J.; Shelton, K.; O'Keefe, S. F.; Bennett, S.; Dolan, M. C. Production and secretion of resveratrol in hairy root cultures of peanut. *Phytochemistry* **2007**, *68*, 1992–2003.

(19) Pandey, A.; Niranjan, A.; Misra, P.; Lehri, A.; Tewari, S. K.; Trivedi, P. K. Simultaneous separation and quantification of targeted group of compounds in *Psoralea corylifolia* L. using HPLC–PDA–MS–MS. *J. Liq. Chromatogr. Relat. Technol.* **2012**, *35* (18), 2567–2583.

(20) Elavarthi, S.; Martin, B. Spectrophotometric assays for antioxidant enzymes in plants. *Methods Mol. Biol.* **2010**, *639*, 273–281.

(21) Mishra, P.; Pandey, A.; Tiwari, M.; Chandrashekar, K.; Sidhu, O. P.; Asif, M. H.; Chakrabarty, D.; Singh, P. K.; Trivedi, P. K.; Nath, P.; Tuli, R. Modulation of transcriptome and metabolome of tobacco by *Arabidopsis* transcription factor, AtMYB12, leads to insect resistance. *Plant Physiol.* **2010**, *152*, 2258–2268.

(22) Shanks, J. V.; Morgan, J. Plant 'hairy root' culture. *Curr. Opin. Biotechnol.* **1999**, *10*, 151–155.

(23) Guillon, S.; Trémouillaux-Guiller, J.; Pati, P. K.; Rideau, M.; Gantet, P. Hairy root research: Recent scenario and exciting prospects. *Curr. Opin. Plant Biol.* **2006**, *9*, 341–346.

(24) Abdala, G.; Miersch, O.; Kramell, R.; Vigliocco, A.; Agostini, E.; Forchetti, G.; Alemano, S. Jasmonate and octadecanoid occurrence in tomato hairy roots. Endogenous level changes in response to NaCl. *Plant Growth Regul.* **2003**, *40*, 21–27.

(25) Talano, M. A.; Agostini, E.; Medina, M. I.; Forchetti, S. M. D.; Tigier, H. A. Tomato (*Lycopersicon esculentum* cv. Pera) hairy root cultures: Characterization and changes in peroxidase activity under NaCl treatment. *In Vitro Cell. Dev. Biol.: Plant* **2003**, *39*, 354–359.

(26) Oller, A. L. W.; Agostini, E.; Talano, M. A.; Capozucca, C.; Milrad, S. R.; Tigier, H. A.; Medina, M. I. Overexpression of a basic peroxidase in transgenic tomato (*Lycopersicon esculentum* Mill. cv. Pera) hairy roots increases phytoremediation of phenol. *Plant Sci.* **2005**, *169*, 1102–1111.

(27) Banerjee, S.; Singh, S.; Rahman, L. U. Biotransformation studies using hairy root cultures—A review. *Biotechnol. Adv.* **2012**, *30*, 461–468.

(28) Ono, N. N.; Tian, L. The multiplicity of hairy root cultures: Prolific possibilities. *Plant Sci.* **2011**, *180*, 439–444.

(29) Zehra, M.; Banerjee, S.; Sharma, S.; Kumar, S. Influence of *Agrobacterium rhizogenes* strains on biomass and alkaloid productivity in hairy root lines of *Hyoscyamus muticus* and *H. albus*. *Planta Med.* **1999**, *65*, 60–63.

(30) Verma, P. C.; Trivedi, I.; Singh, H.; Shukla, A. K.; Kumar, M.; Upadhyay, S. K.; Pandey, P.; Hans, A. L.; Singh, P. K. Efficient production of gossypol from hairy root cultures of cotton (*Gossypium hirsutum* L.). *Curr. Pharm. Biotechnol.* **2009**, *10*, 691−700.
(31) Verma, P. C.; Singh, D.; Rahman, L.; Gupta, M. M.; Banerjee, S. *In vitro* studies in *Plumbago zeylanica*: Rapid micropropagation and establishment of higher plumbagin yielding hairy root cultures. *J. Plant Physiol.* **2002**, *159*, 547−552.
(32) Slimestada, R.; Verheulb, M. Review of flavonoids and other phenolics from fruits of different tomato (*Lycopersicon esculentum* Mill.) cultivars. *J. Sci. Food Agric.* **2009**, *89*, 1255−1270.
(33) Bourgaud, F.; Bouque, V.; Guckert, A. Production of flavonoids by *Psoralea* hairy root cultures. *Plant Cell, Tissue Organ Cult.* **1999**, *56*, 97−104.
(34) Park, N. I. L.; Li, X.; Thwe, A. A.; Lee, S. Y.; Kim, S. G.; Wu, Q.; Park, S. U. Enhancement of rutin in *Fagopyrum esculentum* hairy root cultures by the *Arabidopsis* transcription factor AtMYB12. *Biotechnol. Lett.* **2012**, *34*, 577−583.
(35) Gulen, H.; Eris, A. Effect of heat stress on peroxidase activity and total protein content in strawberry plants. *Plant Sci.* **2004**, *166*, 739−744.
(36) Caverzan, A.; Passaia, G.; Rosa, S. B.; Ribeiro, C. W.; Lazzarotto, F.; Margis-Pinheiro, M. Plant responses to stresses: Role of ascorbate peroxidase in the antioxidant protection. *Genet. Mol. Biol.* **2012**, *35*, 1011−1019.
(37) Shkryl, Y. N.; Veremeichik, G. N.; Bulgakov, V. P.; Gorpenchenko, T. Y.; Aminin, D. L.; Zhuravlev, Y. N. Decreased ROS level and activation of antioxidant gene expression in *Agrobacterium rhizogenes* pRIA4-transformed calli of *Rubia cardifolia*. *Planta* **2010**, *232*, 1023−1032.
(38) Agostini, E.; de Forchetti, S. M.; Tigier, H. A. Production of peroxidases by hairy roots of *Brassica napus*. *Plant Cell* **1997**, *47*, 177−182.
(39) de Araujo, B. S.; de Oliveira, J. O.; Machado, S. S.; Pletsch, M. Comparative studies of the peroxidases from hairy roots of *Daucus carota*, *Ipomoea batatas* and *Solanum aviculare*. *Plant Sci.* **2004**, *167*, 1151−1157.
(40) Kim, Y. H.; Yoo, Y. J. Peroxidase production from carrot hairy root cell culture. *Enzyme Microb. Technol.* **1996**, *18*, 531−535.
(41) Thoison, O.; Sevenet, T.; Niemeyer, H. M.; Russell, G. B. Insect antifeedant compounds from *Nothofagus dombeyi* and *N. pumilio*. *Phytochemistry* **2004**, *65*, 2173−2176.
(42) Hoffmann-Campo, C. B.; Neto, J. A. R.; de Oliveira, M. C. N.; Oliveira, L. J. Detrimental effect of rutin on *Anticarsia gemmatalis*. *Pesqui. Agropecu. Bras.* **2006**, *41*, 1453−1459.

living organisms, this resulted in a lag time in growth, which can be overcome experimentally for some species such as algae and bacteria by adaptation to increasing amounts of D_2O.[6,7] Higher plants have been reported to tolerate 30−70% D_2O, with adverse effects increasing with D_2O concentration. Metabolic responses of plants to higher concentrations of D_2O vary among species. Abnormal morphology and delayed development are noted at concentrations of D_2O above 50% for many species.[7,11] Seed germination and root elongation are adversely affected as D_2O concentrations are increased with wheat,[12] rye,[13] and *Arabidopsis*.[11] To avoid the problems observed at 50% and higher concentrations of D_2O, plants can be cultivated at lower concentrations if sufficient deuterium incorporation can be attained for the intended use such as characterization using neutron scattering studies. Partially deuterated carrots, kale, and spinach were grown hydroponically in solutions of 15−30% D_2O to obtain isotopically labeled vegetables for nutritional studies.[8,9] Despite numerous studies being performed on the effect of deuteration on plant metabolic pathways, the impact of deuteration on individual biomass components for neutron scattering studies has not so far been investigated. In such a scenario, it is important to corroborate the methods for production of deuterated biomass and the chemical characterization of partially deuterated biomass components for progress of biofuel through neutron scattering technologies.

Annual or Italian ryegrass, *Lolium multiflorum*, is a C3 grass widely used across the world as a forage and cover crop. In the southeastern United States, the land area planted in *L. multiflorum* has increased from 1.1 million ha in 2005[14] to 1.3 million ha in 2010.[15] Due to its importance in agriculture, the composition and genetics of annual ryegrass have been extensively studied. In addition to its widespread agricultural use, *Lolium* ryegrass is frequently used for both field and laboratory research to investigate endophytes[16] phytoremediation,[17] pollutant uptake and toxicity,[18−22] morphological responses,[23] herbicide resistance[24] and studies of plasma membranes and associated enzymes such as glucan synthases.[25,26]

In this study, we investigated the effects of D_2O and high levels of deuterium enrichment on the growth and morphology of annual ryegrass (*Lolium multiflorum*), an important and intensively studied forage and cover crop, for future structural studies with SANS applications. The laboratory grown deuterium-labeled annual rye was analyzed for its deuterium incorporation levels by an NMR method.

MATERIALS AND METHODS

Substrate. Annual rye (*Lolium multiflorum*) seeds were obtained from a local gardening supply store. Identification of the species as *Lolium multiflorum*, an amenity and forage grass commonly cultivated in the southeastern United States, was confirmed based on the following characteristics exhibited by plants grown both in open pots in soil and in enclosed hydroponic conditions: plant height 70−80 cm at 60−100 days growth; absence of tillering; inflorescence head formation after 60 days; influorescence stems bare at base; shape of spikelets on influorescence stems; and presence of awns on seeds. The growth medium used for plant cultivation was Schenk and Hildebrandt's basal salts (Phytotechnology Laboratories, Shawnee Mission, KN) dissolved in Milli-Q (Millipore) water. The composition of the Schenk and Hildebrandt's basal salts for plants when prepared at 3.2 g/L in distilled water is given by the manufacturer (Phytotechnology Laboratories) as: 300 mg/L ammonium phosphate monobasic, 5 mg/L boric acid, 151 mg/L anhydrous calcium chloride, 0.1 mg/L cobalt chloride hexahdrate, 0.2 cupric sulfate penthydrate, 20 mg/L Na_2EDTA dihydrate, 15 ferrous sulfate heptahydrate, 195.4 mg/L anhydrous magnesium sulfate, 10 mg/L managanese sulfate monohydrate, 0.1 mg/L sodium molybdate dehydrate, 1 mg/L potassium iodide, 2500 mg/L potassium nitrate, 1 mg/L zinc sulfate heptahydrate, pH 4.2. Before seeding, the seeds were surface-sterilized with 70% ethanol for 2 min and then soaked in Schenk and Hildebrandt's basal salts for plants (S&H salts) in H_2O for 15 min. Initial determination of optimal D_2O concentration was established by germination and growth of seeds in a concentration range of 0 to 99.8% D_2O in jars for 26 days. The Mettler AE200 analytical balance used for weighing the deuterated plants and for weighing reagents has an accuracy of ±0.0001 g. The Ohaus CentOGram triple beam balance that was used to weigh the control ryegrass has an accuracy of ±0.01 g.

Concentration Dependence of Deuteration. The effect of D_2O concentration on growth of annual ryegrass and deuterium incorporation in biomass was initially determined using sealed glass jars with 3-mm glass beads as supports. Growth solutions were Schenk and Hildebrandt's salts (Phytotechnology Laboratories, Shawnee Mission, KS) prepared in 0, 20, 40, 60, 80, and 99.8% D_2O. Ten seeds were used per jar. Germination was scored at 14 days and plants were harvested at 26 days for analysis.

Hydroponic Cultivation in Perfusion Chambers. Deuterium enrichment of plants requires enclosure and perfusion with dried air to limit exchange with ambient water vapor as well as to limit D_2O usage and avoid microbial contamination. Since it was desirable to obtain multiple biomass samples grown at different concentrations of D_2O, a system that allows simultaneous cultivation of several plants in individual isolated chambers was devised. Suitable chambers for long-term cultivation of grasses in D_2O mixtures were constructed from graduated glass cylinders (Figure 1). Standard 1 and 3 L graduated glass cylinders were modified by the in-house glass shop at ORNL by cutting off the top 2 cm to remove the pouring lips followed by glass polishing to enable a tight fit with the rubber stoppers used as closures. The 1 and 3 L chambers were fitted with size 12 two-hole rubber stopper and three-hole size rubber stoppers respectively. Two 20.0 cm

Figure 1. Assembled growth chamber with the labeled component parts.

lengths of 0.6 cm diameter glass tubing with 90-degree bends at 7.6 cm were inserted into the stoppers. Heat-resistant silicone rubber tubing was used to connect the glass tubing to sterile 0.22 μm pore size, 33 mm diameter syringe filters (Millipore Ireland Ltd., Tullagreen, Carrigtwohill, Cork, Ireland) and to connect the tubing to PE drying tubes containing Eagle silica gel desiccant with color indicator. Glass Y-connectors were used to connect multiple chambers using the silicone tubing. Plants were perfused with ambient air from the growth room using Marina 50 and Marina 75 aquarium pumps (Rolf Hagen (USA) Corp., Mansfield, MA) that were connected to the chambers by sterile syringe filters connected to Elite aquarium tubing, with in-line valves for flow rate adjustment. The CO_2 concentration of the ambient air filtered through the silica gel desiccant ranged from 385 to 465 ppm as determined by measurement with an LI-6252 CO_2 analyzer (LI-COR, Lincoln, NE) that was calibrated with analyzed compressed air mixtures (Air Liquide, Oak Ridge, TN). Airflow into each chamber was maintained at 50−100 mL/min as measured with an Alltech Digital Flowcheck HR meter. Due to the small volumes of growth medium used per chamber and to limit evaporation losses, the chambers were perfused from the top and the growth solutions were not aerated. Two types of growth lamps were used: a metal halide lamp mounted on a stand and fluorescent Sylvania Gro-Lamps on a plant cart (Carolina Biological Supply Company, Burlington, NC). The metal halide lamp was mounted in a SunSystem 2 lamp holder (Future Garden, North Lindenhurst, NY) that was suspended from an in-house built lamp stand. Average incident light intensity was 150 μmol photons/m^2/s as measured with a LICOR-250 Light Meter equipped with a quantum sensor (LI-COR, Lincoln, NE) and 8930 lx as measured with a Traceable Light Meter (International LLC, Radnor, PA). Diurnal cycles were 12 h light, 12 h dark. Growth medium was Schenk and Hildebrandt's basal salts (Phytotechnology Laboratories, Shawnee Mission, KN) dissolved in Milli-Q (Millipore) water. Deuterium oxide (99.8%) was purchased from Cambridge Isotope Laboratories (Cambridge, MS). Hydroponic baskets with 5 cm diameter were used to support the rye seeds on 47-mm analytical glass fiber filters during growth and germination. Ambient temperature in the plant growth area was 27 °C during illumination and 21 °C during the diurnal dark period.

Cultivation of Annual Ryegrass in 50% D_2O for Production of Deuterated Biomass. Initial determination of optimal D_2O concentration was established by germination and growth of seeds in a concentration range of 0−99.8% D_2O in jars for 26 days. Deuterium incorporation did not increase above 60% D_2O, while seed germination decreased above 60% (Figure 2). Based on the preliminary tests, a concentration of 50% D_2O was used for scale-up of biomass production in the perfusion chambers. Seeds were germinated and seedling primary roots were established before transfer to the perfusion chambers. The treated seeds (thirty per dish) were germinated in 6-cm diameter polystyrene culture dishes on 47-mm glass filter disks containing 5% acrylic binder (Gelman Sciences/Pall Life Sciences, Ann Arbor, MI) moistened with 4 mL of S&H salts in H_2O. The seeded dishes were incubated in the dark for 24 h, followed by illumination with a metal halide growth lamp on a 12 h diurnal cycle. Dark temperature range was 21 to 22 °C, and light temperature range was 25 to 28 °C. The seeds began germinating at 5 days. The lids were removed from the culture dishes and the dishes holding the seedling plants were transferred to 1 L glass plant jars 6−7 days after seeding. Another 2 mL of S&H salts were added to each dish after transfer to the jars. At eleven days after seeding, the glass filters holding the seedling plant samples #1, #2, and #3 were carefully placed in 5 cm hydroponic plant baskets. Each basket was placed into a 1L perfusion chamber and 12 mL of S&H salts in 50% D_2O, 50% H_2O were added to each cylinder. These plants were watered with S&H salts in 50% D_2O, 50% H_2O once or twice weekly by injection through the perfusion tubing using sterile syringes and syringe filters to ensure that the roots remained covered with solution. Plants appeared to grow normally, with the H_2O-grown rye growing taller and faster than the plants growing in 50% D_2O as expected, yielding several grams of biomass at harvest (Figure 3 and Table 1).

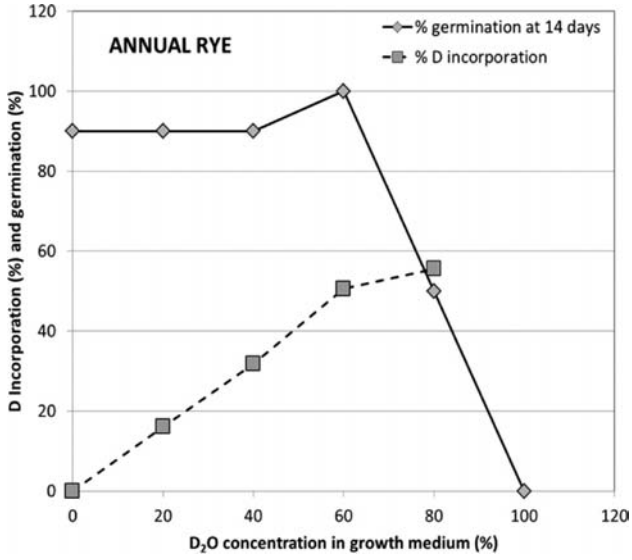

Figure 2. Germination and deuterium incorporation determined for annual ryegrass grown in increasing concentrations of D_2O to establish the optimal cultivation conditions for deuterated biomass production.

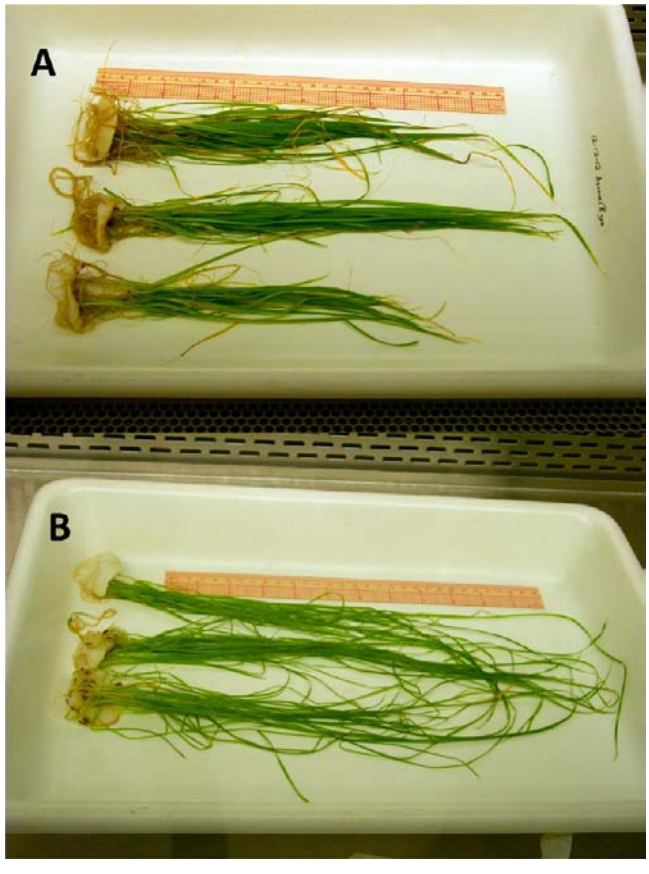

Figure 3. Annual ryegrass plants grown in (A) 50% D_2O under continuous air perfusion and (B) H_2O-grown controls.

The perfusion chamber design reduced evaporation and enabled cultivation for two months with cumulative usage of less than 100 mL solution per chamber. The total amount of hydroponic solution used for the cultivation of the protiated plants was 82 mL per plant, while the total amount of 50% D_2O solution used for the deuterated plants was 88 mL/plant. The total amount of D_2O used per plant for 50 days of growth in the 50% D_2O solution was 44.3 ± 17.5 mL. The seedling

dx.doi.org/10.1021/jf4055566 | J. Agric. Food Chem. 2014, 62, 2595−2604

Table 1. Net Biomass Yields from Annual Ryegrass Plants Grown Hydroponically with Perfusion (30 Seeds/Basket)

sample	growth solution	plant stems	wet weight total (g)
#1	start in H_2O, then at 11 days start in 50% D_2O	9	3.55
#2	start in H_2O, then at 11 days start in 50% D_2O	15	6.18
#3	start in H_2O, then at 11 days start in 50% D_2O	13	6.35
#4	H_2O	4	1.18
#5	H_2O	6	1.45
#6	H_2O	4	2.59

samples #4, #5, and #6 were transferred to hydroponic baskets on the twelfth day after seeding, and all three baskets were placed in a 3L perfusion chamber to which 150 mL of S&H salts in H_2O were added. Growth rates of the plants grown in H_2O was observed to double following transfer to the perfusion chambers, while the growth rates of the plants transferred to 50% D_2O in perfusion chambers did not change significantly compared to the initial growth rate in H_2O before perfusion (Tables 2 and 3). At harvest, plants in their baskets were

Table 2. Growth Rates of Annual Ryegrass Plants Comparing Effects of 50% D_2O and Perfusion Determined by Averaging the Slopes of the Linear Regression Lines from Tracking Growth of Seedlings as Shown in Figure 4[a]

	before perfusion		during perfusion	
sample sets	growth rate (cm d^{-1})	growth solution	growth rate (cm d^{-1})	growth solution
50% D_2O	0.399 ± 0.103 (ns)	S&H in H_2O	0.381 ± 0.065*	S&H in 50% D_2O
H_2O controls	0.396 ± 0.114	S&H in H_2O	0.907 ± 0.096	S&H in H_2O

[a]Errors are reported in term of standard deviation; ns = not significant, * = $P \leq 0.05$ calculated by student t test.

Table 3. Plant Growth and Biomass Production was Averaged for the Three Sets of Protiated Plants and the Three Sets of Deuterated Plants[a]

growth solution	growth time (days)	tallest height at harvest (cm)	total biomass yield (mg $stem^{-1}$ day^{-1})
50% D_2O	61	33.0 ± 4.5 (ns)	7.07
H_2O	47	50.3 ± 8.8	8.40

[a]Errors are reported in term of standard deviation; ns=not significant.

removed from the chambers, excess hydroponic solution was allowed to drain from the plants in a tray and then the roots and glass fiber supports were blotted with several Kim-Wipe tissues. The protiated control plants (#4, #5, and #6) were harvested at 47 days from seeding and stored at −20 °C until characterization and further use. The plants grown in 50% D_2O (#1, #2, and #3) were harvested at 61 days and used fresh. Plant growth and biomass production of protiated plants and deuterated plants after 47 and 61 days respectively are presented in Tables 1, 2, and 3.

Preparation of NMR Solution for Deuterium Incorporation Studies. Dimethyl sulfoxide (anhydrous, 99.9%), pyridinium chloride (98%), and TFA (reagent grade, 99.0%) were purchased from Sigma Aldrich. Dimethyl sulfoxide (DMSO)-d_6 (99.9% D) and trifluoroacetic acid (TFA)-d (99.5% D) were purchased from Cambridge Isotope Laboratories, Inc. (Andover, MS). Deuterated pyridinium chloride was synthesized according to a literature procedure.[27] Ionic liquid solvent mixture was prepared by mixing vacuum-dried protio pyridinium chloride or deuterated pyridinium chloride with DMSO or DMSO-d_6, respectively in 1:4 ratios in an inert atmosphere. Deuterated ryegrass (10 mg) was then dissolved in a pyridinium chloride−DMSO solvent mixture as described previously.[28] The NMR spectra of homogeneous biomass solution were recorded on a Bruker Avance 400 MHz spectrometer operated at 61.4 MHz for deuterium and 400.1 MHz for proton. ^{1}H NMR spectra were measured at 55 °C with 64 k data points, a 10 s recycle delay, and 16 scans. Deuterium (^{2}H) NMR spectra was recorded at 55 °C with 32 k data points, 10 s recycle delay, and 4000 scans.

Carbohydrates and Klason Lignin Analysis. Samples for carbohydrate and acid-insoluble lignin analysis were prepared using a two-stage acid hydrolysis protocol based on Tappi method T-222 om-88. The sugar solution was analyzed for carbohydrate components by high-performance anion-exchange chromatography with pulsed amperometric detection (HPAEC-PAD) using Dionex ICS-3000 (Dionex Corp., USA).[29] The standard deviation associated with lignin and carbohydrate analysis was 0.3 to 0.6 and 0.02 to 0.9, respectively.

Cellulose and Hemicellulose Isolation. The extractive-free annual ryegrass samples were delignified using peracetic acid as described previously.[30] Cellulose was isolated from the delignified sample (0.10 g) by extraction with a 17.5% NaOH solution (5.00 mL) at 25 °C for 2 h. The mixture was diluted to 8.75% NaOH solution by addition of 5 mL of deionized water and repeated stirring at 25 °C for an additional 2 h. The isolated α-cellulose samples were then collected by centrifugation, washed with an excess of deionized water and air-dried. For hemicellulose isolation, the filtrate obtained above, was poured into a mixture of ethanol: acetic acid (70:30, v:v). The supernatant was removed by centrifugation and the precipitated hemicellulose was again washed with a mixture of ethanol: acetic acid (70:30, v:v) and air-dried for analysis.

GPC Analysis of Cellulose. The number-average molecular weight (M_n) and weight-average molecular weight (M_w) were determined by GPC after tricarbanilation of cellulose as described previously.[31] The derivatized cellulose was dissolved in tetrahydrofuran (1 mg/mL), filtered through a 0.45 mm filter and placed in a 2-mL autosampler vial. The molecular weight distributions of the cellulose tricarbanilate samples were analyzed on an Agilent GPC Security 1200 system equipped with four Waters Styragel columns (HR1, HR2, HR4, and HR5), Agilent refractive index (RI) detector and Agilent UV detector (270 nm) using THF as the mobile phase (1 mL/min) with injection volumes of 0.02 mL. A calibration curve was constructed based on eight narrow polystyrene standards ranging in molecular weight from 1.5×10^3 to 3.6×10^6 g/mol. Data collection and processing were performed using Polymer Standards Service WinGPC Unity software (Build 6807). Molecular weights (M_n and M_w) were calculated by the software relative to the universal polystyrene calibration curve. Polydispersity index (PDI) was calculated by dividing M_w by M_n.

GPC Analysis of Hemicellulose. The GPC analyses of hemicellulose samples were carried out using an Agilent 1200 series HPLC system consisting of an online degasser and an autosampler, a RI detector and three columns of Ultrahydrogel 120, 250, and 500 (Waters Inc., USA) linked in series. The RI detector was set at 35 °C. The mobile phase was an alkaline sodium hydroxide/acetate solution (0.20 M sodium hydroxide, 0.1 M sodium acetate, pH 12−13) and the flow rate was 0.5 mL/min. The hemicellulose samples were dissolved in mobile phase (~1 mg/mL) and the solution was then filtered with a 0.2 μm filter. The filtered sample (25 μL) was injected into the GPC column system for analysis. Pullulan standard samples were used for the calibration.[32]

Sample Preparation for Solid-State Nuclear Magnetic Resonance for Crystallinity Measurement. The cellulose samples for NMR were prepared from the control protiated and deuterated annual ryegrass from the holocellulose sample (1.00 g) by mild acid 2.5 M HCl hydrolysis as described previously.[33] The isolated α-cellulose samples were then collected by filtration rinsed with an excess of deionized water and dried in a fume hood. For NMR analysis, 4-mm cylindrical ceramic MAS rotors were filled with the isolated α-cellulose. Solid-state NMR measurements were carried out on a Bruker Avance-400 spectrometer operating at a frequency of 100.55 MHz for ^{13}C in a Bruker double-resonance MAS probe at spinning speeds of 10 kHz.

CP/MAS experiments utilizing a 5 ms (90°) proton pulse, 1.5 ms contact pulse, 4 s recycle delay and 4−8 K scans. All spectra were recorded on equilibrated moisture samples (~35% water content).

FTIR Spectroscopy. Annual ryegrass samples were vacuum-dried for 24 h. Infrared (FTIR) spectra were obtained using a Perkin-Elmer 100 Series Fourier transform infrared spectrometer in an attenuated total reflectance (ATR) mode. The spectra were recorded with the accumulation of 128 scans, a resolution of 4 cm^{-1} in the range from 4000 to 500 cm^{-1}. After the baseline correction, the two spectra were scaled with respect to one another, using the C−O stretching of the glucopyranose ring at ~1053 cm^{-1}.

Scanning Electron Microscopy (SEM). Scanning electron microscope images of solvent extracted and holopulps from protiated and deuterated annual rye samples were obtained with a LEO 1530 TFE-SEM microscope operated at 5 kV. The samples were freeze-dried and fixed on carriers with conductive carbon tape. The samples were coated with gold using an ion sputter coater and observed with a thermally assisted field emission (TFE) scanning electron microscope.

Statistical Analysis. Student *t* tests were performed to determine significance between experimental values, where $p \leq 0.05$ is 95% significance (*), and $p \leq 0.01$ is 99% significance (**).

RESULTS AND DISCUSSION

Annual Ryegrass Cultivation in D_2O. From previously reported studies,[34−37] it was apparent that the effects of D_2O on higher plant growth were dependent on species, concentration, and growth stage. The typically observed concentration dependence found little effect at concentrations up to 0.5%, delayed germination and slower growth at 50%, and complete inhibition, or very stunted and abnormal, germination and growth at concentrations higher than 80%. [38] As a result, deuterium enrichment of plants is usually carried out at concentrations less than 50% D_2O using seedlings that have been sprouted and established in H_2O.[9,39] The annual ryegrass (*Lolium multiflorum*) for production of deuterated biomass were grown in enclosed chambers continually perfused with dry air to limit exchange with ambient water vapor while providing a constant supply of CO_2 for photosynthesis and O_2 for photorespiration. Initial screening found that plant germination was severely inhibited in 80% D_2O while deuterium incorporation was not substantially improved (Figure 2). Annual ryegrass germinated in 70% D_2O, but with very low germination rates and a growth rate of 21% of H_2O-grown controls. Germination reached control levels in 50% D_2O, but subsequent growth rates were 45% of H_2O-grown controls (Figure 4). Vernalization, cold treatment of seeds, has been reported to improve growth of winter rye and brome grass at low temperatures.[40] To examine whether vernalization would improve growth under deuterating conditions, seeds were incubated for 24 h at 4 °C followed by 10 days at 10 °C. Germination increased 4-fold in 70% D_2O following vernalization, but growth rate and low biomass yield (less than 10% of controls grown in H_2O) were not improved, so this approach was not further investigated. Growth rates of the plants grown in H_2O were observed to double following transfer to the perfusion chambers, while the growth rates of the plants transferred to 50% D_2O in perfusion chambers did not change significantly compared to the initial growth rate in H_2O before perfusion (Figure 4). The annual ryegrass grown in 50% D_2O was shorter and thicker in appearance than matched protiated controls, but did not appear abnormal in coloration or leaf shape (Figure 3). Possible internal changes in leaf and stem vascularization were not examined. The differences in morphology may correspond to the normal range of adaptations of *Lolium* ryegrass species and related fescue (*Festuca*) grasses to drought, cold, and light conditions,[15,23] but this will need to be confirmed by comparative studies.

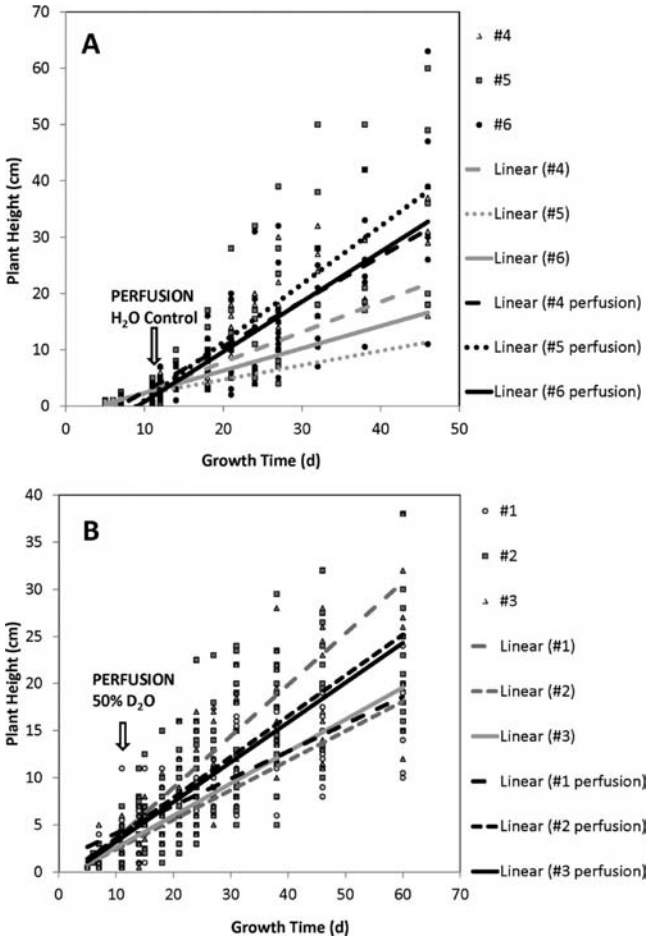

Figure 4. Growth rates determined by linear regression of individual plant heights of (A) three sets of H_2O control seedlings and (B) three sets of seedlings transferred to 50% D_2O.

NMR Analysis. The deuterium incorporation in annual ryegrass samples was examined using the methodology as described previously.[28,41] NMR analysis of annual ryegrass samples grown in increasing D_2O concentrations showed that the deuterium incorporation increased linearly with increasing D_2O concentration up to 60% D_2O, but was not improved significantly for annual rye grown in 80% D_2O, while germination was also inhibited at 80% (Figure 2). Ultimately, based on the effect of D_2O concentration on growth and biomass deuterium incorporation in the preliminary trials, annual rye grown in 50% D_2O was selected for detail structural analysis. ^1H and ^2H NMR experiments were performed in order to determine the deuterium incorporation level in rye grown in 50% D_2O. A standard inversion recovery pulse sequence was used to measure the longitudinal relaxation time for all the resonances and to determine the appropriate recycle delay. Figure 5 illustrates the ^1H and ^2H NMR spectra of annual ryegrass grown in 50% D_2O. The ^2H NMR spectrum of deuterated annual ryegrass shows the poorly resolved group of signals from 3.0 to 5.5 ppm, which is attributable to the cellulosic and other polysaccharides protons in the biomass. The protons from lignin side chain are also present in the described chemical shift range. The signals from 0.5 to 2.0 ppm are due to presence of side chain acetates and some residual

dx.doi.org/10.1021/jf4055566 | J. Agric. Food Chem. 2014, 62, 2595−2604

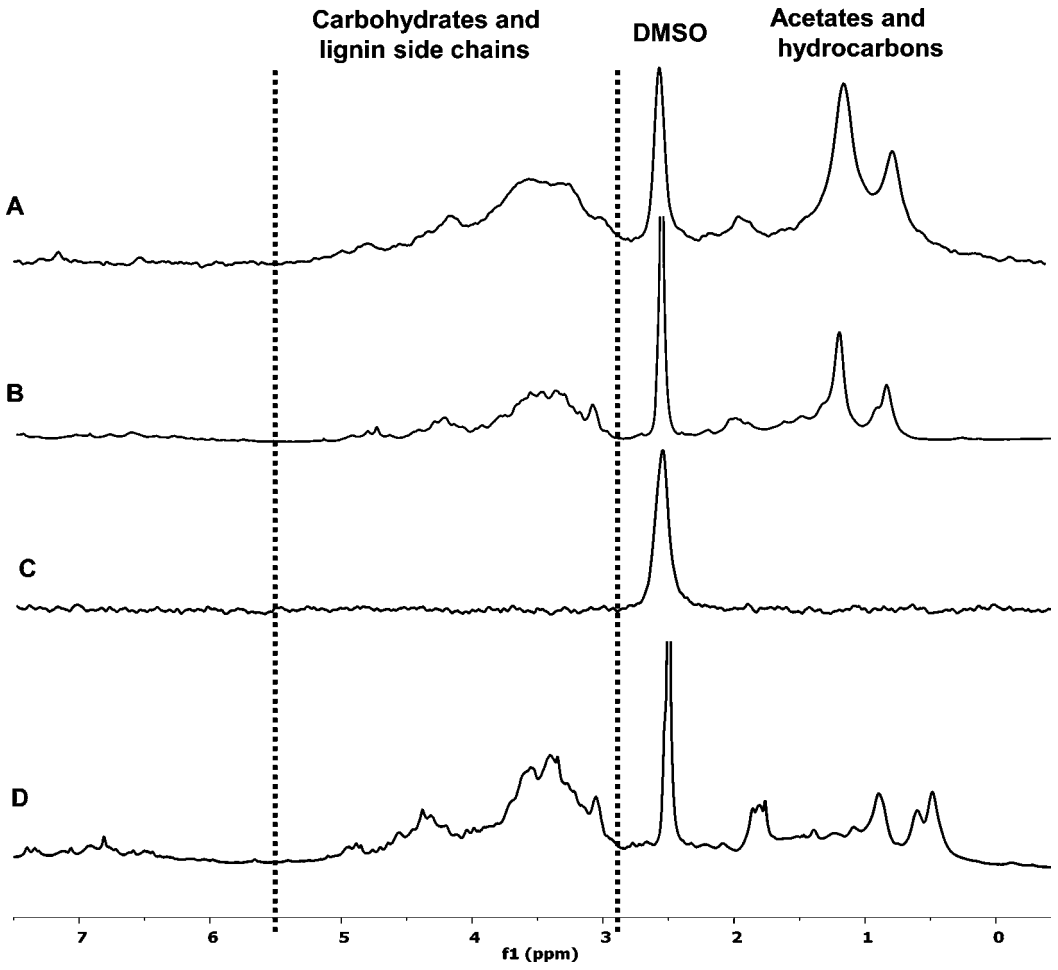

Figure 5. (A) ^{2}H NMR and (B) ^{1}H NMR spectra of deuterated annual ryegrass grown in 50% D_2O; (C) ^{2}H NMR and (D) ^{1}H NMR spectra of control annual ryegrass. The region between two dotted lines represents protons/deuterium mostly from cellulose and some lignin side chains.

Table 4. Compositional Analysis of Annual Ryegrass (Based on Dried Biomass)[a]

	Klason lignin (%)	arabinose (%)	galactose (%)	glucose (%)	xylose (%)	mannose (%)
deuterated ryegrass	10.2 ± 0.6*	5.6 ± 0.02*	3.8 ± 0.03*	66.7 ± 0.9	13.6 ± 0.5	0.0 ± 0.0
protiated ryegrass	12.8 ± 0.3	6.4 ± 0.02	4.4 ± 0.04	58.7 ± 0.7	17.6 ± 0.2	0.0 ± 0.0

[a]Errors are reported in term of standard deviation, * = $P \leq 0.05$.

fatty acids in the biomass. Further, ^{1}H spectrum of deuterated annual ryegrass exhibited the similar group of signals in the region from 3.0−5.5 ppm, while the signals corresponding to lignin aromatic protons were also observed in the ^{1}H spectrum of deuterated annual ryegrass. ^{1}H and ^{2}H NMR spectra of control protiated ryegrass were also obtained to compare and ensure the deuteration (Figure 5C,D). The ^{1}H spectrum of control protiated ryegrass exhibited all of the characteristic signals of biomass in the range of 3.0−5.5 ppm as well as also exhibited the aromatic proton signals corresponding to lignin component while the ^{2}H NMR did not show any corresponding detectable deuterium signals in that range, which confirmed the substantial deuterium incorporation in the rye grown in 50% D_2O. Further, for the quantitative analysis, the concentration of proton nuclei in deuterated ryegrass in deuterated solvent was determined from the ^{1}H NMR spectrum, with respect to an internal standard (TFA/*d*-TFA), while ^{2}H NMR spectrum of the deuterated ryegrass dissolved in a protiated solvent indicated deuteron nuclei concentration with respect to the same internal standard (TFA/*d*-TFA). After normalizing the concentration of deuterated rye in both solutions, the ratio of deuterons to protons ($^{2}H/^{1}H$) was calculated. The $^{2}H/^{1}H$ ratio indicated a deuterium incorporation of 36.9% in annual rye germinated and grown in 50% D_2O. Growth rates of protiated ryegrass plants were doubled following transfer to the perfusion chambers while the growth rates of the plants transferred to 50% D_2O did not change significantly from their growth in H_2O before perfusion. A significant increase in the deuterium incorporation to ∼60% was achieved in the ryegrass that was germinated in H_2O, then transferred to 50% D_2O and grown inside the perfusion chambers. The seedlings started in H_2O before transfer to 50% D_2O appear to better tolerate high D_2O concentrations than the plants grown from germination in 50% D_2O, which could explain the substantially higher ^{2}H incorporation. The current procedure thus offers a method to cultivate annual rye and similar plants to produced deuterated biomass with controlled deuterium incorporation for use in neutron scattering experiments.

dx.doi.org/10.1021/jf4055566 | J. Agric. Food Chem. 2014, 62, 2595−2604

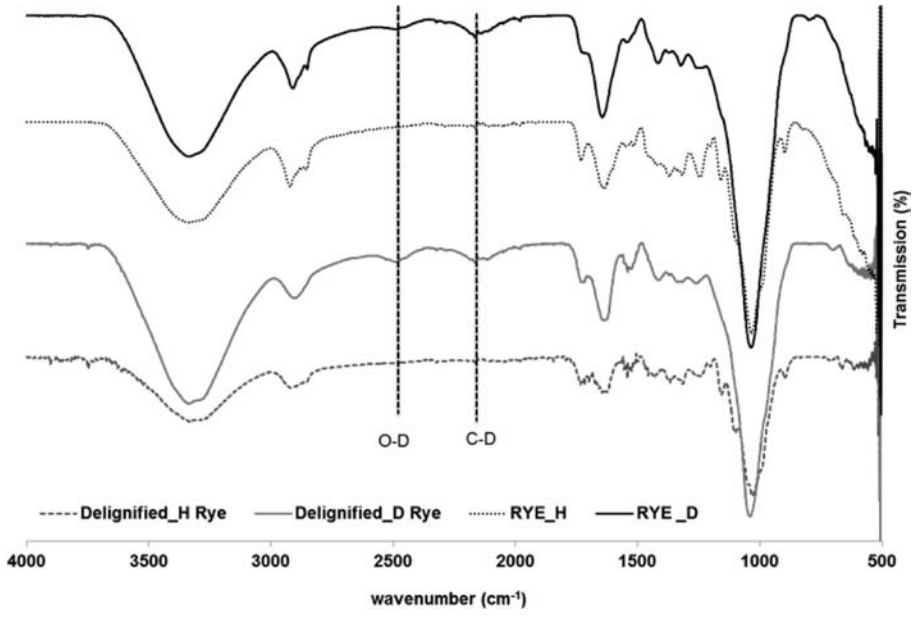

Figure 6. FTIR spectra of deuterated ryegrass, protiated ryegrass and their delignified samples.

Carbohydrate and Klason Lignin Analysis. Table 4 shows the compositional analysis of deuterated and control protiated annual ryegrass samples and is comparable with the literature values.[42] The data presented here are on an oven-dry (105 °C) basis and extractives were removed prior to each measurement. As Table 4 indicates, glucan and xylan were the predominant carbohydrates found in *Lolium* rye. The glucan content was slightly higher in deuterated annual ryegrass compared to that for control protiated annual ryegrass. The major hemicellulose found in ryegrass was xylan; however, small amounts of arabinan and galactan were also present. The total hemicellulose content of the deuterated ryegrass was slightly lower in comparison to that for control ryegrass. The relative klason lignin content was also lesser in the deuterated sample. However, there was not significant variation realized in the overall carbohydrates composition for both samples.

FTIR Analysis. The FTIR spectra of deuterated annual ryegrass, protiated annual ryegrass and their delignified samples are presented in Figure 6. The C−D stretching in deuterated samples at 2139−2251 cm^{-1} indicated nonexchangeable deuterium incorporation in the carbohydrates components of annual ryegrass. The O−D stretching at 2486 cm^{-1} attributed to the proton-deuteron exchange on the biomass surface. The broad and strong peak at ∼3334 cm^{-1} is attributed to the hydroxyl group indicating strong hydrogen bonding. All of the samples exhibited vibrations at 2917−2854 cm^{-1}, attributed to the C−H stretching and at 1378 and 1249 cm^{-1} corresponded to the C−H bending modes. IR bands centered at 1453 and 1118 cm^{-1} can be assigned as C−H symmetrical bending and C−O stretching of cellulose respectively. A nominal isotopic effect was observed in all of the C−D bands in the FTIR of deuterated samples (Table 5). For example, bands at 1375 cm^{-1}, which is characteristic of symmetric C−H deformation of cellulose[43,44] showed a slight shift toward 1326 cm^{-1} in deuterated annual rye sample. Similarly, IR band at 1460 cm^{-1} corresponding to C═C stretching vibration of the aromatic ring[44] also showed an isotopic shift in deuterated annual ryegrass (Table 5). Vibrations at 1053 and 1249 cm^{-1} are mainly attributed to the structural features related to carbohydrates and indicated isotopic shifts in deuterated samples.

Table 5. Bands Assignments[43,44] of FT-IR Spectra of Annual Ryegrass Samples

IR vibrations (ν) cm^{-1}	deuterated rye	protiated rye	deuterated rye (delignified)	protiated rye (delignified)
νO−H (stretch)	3331(b,s)	3328(b,s)	3334(b,s)	3328(b,s)
νCH_2 (stretch)	2921(s)	2946(s)	2912(s)	2917(s)
νC−H (OMe)	2854(w)	2986(w)		
νO−D (stretch)	2486(w)		2486(w)	
νC−D (stretch)	2168(m)		2168(m)	
νC═O (acid/ether)	1727(m)	1735(s)	1727(m)	1734(m)
νC═O (ketonic)	1648(s)	1647(s)	1647(s)	1648(m)
νC═C (stretch)	1548(w)	1548(m)	1543(m)	1544(w)
νCH_2 (sym.def.)	1418(m)	1460(s)	1418(m)	1457(w)
νCH_2 (bend)/ νO−D (def)	1326(w)	1375(s)	1340(m)	1370(m)
νC−O	1261(w)	1249(s)	1267(w)	1243(m)
νC−O−C (strectching)	1036(s)	1053(s)	1018(s)	1044(s)
νC−H (out-of plane def)	802(w)	827(m)	701(w)	720(w)

Molecular and Morphological Properties. In an effort to determine the effect of growing annual rye in D_2O on the biomass key characteristics related to enzymatic hydrolysis,[45,46] the important molecular properties of deuterated and control protiated ryegrass were compared. The molecular weight of cellulose and hemicellulose and cellulose crystallinity of annual ryegrass grown in 50% D_2O and its protiated control are presented in Table 6. Deuterated rye cellulose had a higher weight average and number average molecular weight compared to its protiated control. Also, it displayed higher polydispersity index than protiated rye cellulose. The difference observed here is clearly attributed to the major deuterium

dx.doi.org/10.1021/jf4055566 | J. Agric. Food Chem. 2014, 62, 2595−2604

Table 6. Molecular Weight and Crystallinity of Annual Ryegrass Cellulose

	cellulose				hemicellulose		
sample	$M_n \times 10^5$ (g/mol)	$M_w \times 10^6$ (g/mol)	PDI[b]	crystallinity index (%)	$M_n \times 10^4$ (g/mol)	$M_w \times 10^4$ (g/mol)	PDI[b]
protiated ryegrass	1.4 ± 0.03	1.8 ± 0.03	1.3	46.0 ± 2.0	2.2 ± 0.01	7.3 ± 0.01	3.3
deuterated ryegrass	1.7 ± 0.04(ns)	2.7 ± 0.03[a]	1.5	43.0 ± 2.0	2.3 ± 0.02	7.6 ± 0.01	3.3

[a] $P \leq 0.01$, ns = not significant. [b] PDI = polydispersity index.

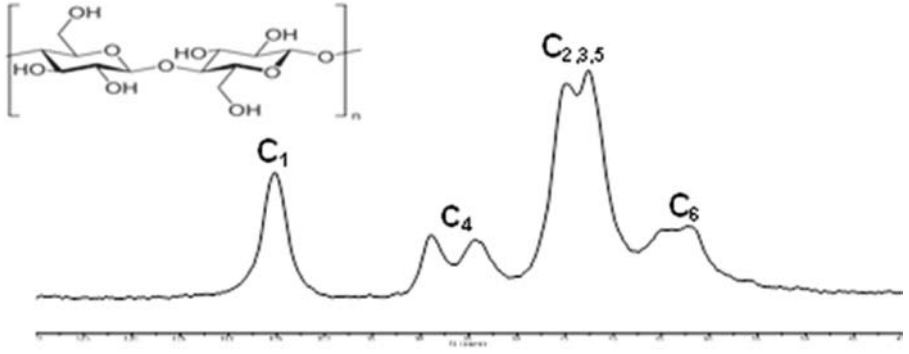

Figure 7. $^{13}C-CPMAS$ spectra of cellulose I isolated from annual ryegrass sample crystallinity index = $\delta_{86-92}/\ \delta_{80-92} \times 100$.

incorporation in the cellulose component of the biomass as also shown by the ^2H NMR spectrum. In contrast, there was no change in the weight and number average molecular weight of hemicellulose isolated from 50% D_2O annual ryegrass. Possibly the ryegrass grown in D_2O may preferentially incorporate deuterium into cellulose compared to other polysaccharides. The crystallinity of cellulose isolated from deuterated ryegrass, as determined by $^{13}CP/MAS$ (Figure 7) was ∼43% which is lower than the cellulose crystallinity of protiated ryegrass. The ^{13}C NMR spectrum of cellulose I isolated from deuterated ryegrass was similar, to that of control; however, at optimal signal-to-noise lower resolution was achieved for cellulose isolated from deuterated ryegrass (not shown). This is probably due to fewer protons available in deuterated ryegrass cellulose in comparison to protiated controls and consequently, the ^{13}C CP/MAS NMR, which is the technique based on the magnetization transfer from protons to carbons, is expected to be less efficient for deuterated substrates than for protonated substrates due to the differences in bond energy between protons and deuterons. Therefore, the subsequent enhancement of the ^{13}C signal will be lessened in 50% D_2O grown rye. Nonetheless, deuteration did not appear to cause any noticeable or significant difference in the cellulose crystallinity.

Morphology of Deuterated Annual Ryegrass. The present paper attempts to study the surface morphology of D_2O grown rye and demonstrates that no major disruption of micro fibrils was observed in the native surface of the rye grown in 50% D_2O compared to its protiated counterpart. The SEM images of control protiated and deuterated annual ryegrass before and after the peracetic acid delignification process are shown in Figure 8A–D. Both the protiated and deuterated rye samples exhibited an elongated and well-ordered surface (Figure 8A,B). The texture was compact and shielded in a thin wax layer commonly found in herbaceous biomass.[47] However, several subtle differences were observed in the deuterated rye leaf such as the deuterated rye leaf exhibited a surface layer with more debris and some noticeable granular structures on the individual fibers. Furthermore, the delignified surface of both samples was examined in an effort to find the effect of deuteration more closely on the morphological

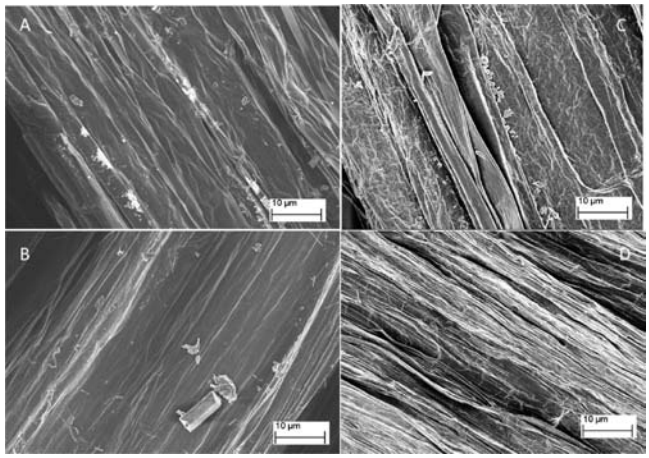

Figure 8. SEM images of (A) deuterated ryegrass, (B) control protiated ryegrass, (C) deuterated ryegrass after delignification, and (D) protiated ryegrass after delignification.

structures in both rye samples. Surface morphology of both samples changed significantly during the delignification process. In both delignified samples the overall structure was disrupted (Figure 8C,D) and the individual fibers were partially separated and dispersed. Peracetic pulping removed most of the surface layer deposits, which were noticed in the native samples and consequently exposed intact cellulose microfibrils. In a delignified deuterated ryegrass, most of the leaf surface was degraded although it showed the cellulose micro fibrils partly embedded in the noncellulosic polymers as revealed by the rough and uneven surface (Figure 8C). The study demonstrates that the leaf morphology appeared to be basically similar for the two annual ryegrass samples, but with certain differences apparent, particularly following delignification. The biomass characterization results indicated some significant changes in the biomass structure with deuteration. There was an increase in the molecular weights of cellulose, whereas hemicellulose molecular weights and cellulose crystallinity remain unaffected with the deuteration. Nevertheless, the results support the development and use of deuterated plant biomass to provide

dx.doi.org/10.1021/jf4055566 | J. Agric. Food Chem. 2014, 62, 2595–2604

crucial supporting characterization for visualization of lignocellulose structure by neutron scattering techniques and computational simulation.

AUTHOR INFORMATION

Corresponding Author

*Tel. 404-894-9701. Fax 404-894-4778. E-mail: arthur.ragauskas@chemistry.gatech.edu; arthur.ragauskas@ipst.gatech.edu.

Present Address

[‖]University of Massachusetts, Amherst, Massachusetts.

Funding

This research was supported by the Genomic Science Program, Office of Biological and Environmental Research, U.S. Department of Energy, under Contract FWP ERKP752. The research at Oak Ridge National Laboratory's Center for Structural Molecular Biology (CSMB) was supported by the Office of Biological and Environmental Research under Contract FWP ERKP291, using facilities supported by the Office of Basic Energy Sciences, U.S. Department of Energy. Oak Ridge National Laboratory is managed by UT-Battelle, LLC, for the U.S. Department of Energy under Contract DE-AC05-00OR22725. D.R. was supported by a U.S. Department of Energy Higher Education Research Experience internship managed by Oak Ridge Institute of Science and Education.

Notes

The authors declare the following competing financial interest(s): The author receives research funding in this field of study.

REFERENCES

(1) Wyman, C. E., Aqueous Pretreatment of Plant Biomass for Biological and Chemical Conversion to Fuels and Chemicals. Wiley: New York, 2013.

(2) Pingali, S. V.; Urban, V. S.; Heller, W. T.; McGaughey, J.; O'Neill, H. M.; Foston, M.; Myles, D. A.; Ragauskas, A. J.; Evans, B. R. SANS study of cellulose extracted from switchgrass. *Acta Crystallogr. Sect. D* **2010**, *66* (11), 1189−1193.

(3) Nishiyama, Y.; Okano, T.; Langan, P.; Chanzy, H. High resolution neutron fibre diffraction data on hydrogenated and deuterated cellulose. *Int. J. Biol. Macromol.* **1999**, *26* (4), 279−283.

(4) Foster, L. J.; Russell, R. A.; Sanguanchaipaiwong, V.; Stone, D. J.; Hook, J. M.; Holden, P. J. Biosynthesis and characterization of deuterated polyhydroxyoctanoate. *Biomacromolecules* **2006**, *7* (4), 1344−1349.

(5) Russell, R. A.; Holden, P. J.; Garvey, C. J.; Wilde, K. L.; Hammerton, K. M.; Foster, L. J. Investigation of the phase morphology of bacterial PHA inclusion bodies by contrast variation SANS. *Phys. B: Condensed Matter* **2006**, *385*−*386*, 859−861.

(6) Katz, J. J. Chemical and biological studies with deuterium. *Am. Sci.* **1960**, *48*, 544−580.

(7) Katz, J. J.; Crespi, H. Deuterated organisms: Cultivation and uses. *Science* **1966**, *151*, 1187−1194.

(8) Putzbach, K.; Krucker, M.; Albert, K.; Grusak, M. A.; Tang, G.; Dolnikowski, G. G. Structure Determination of partially deuterated carotenoids from intrinsically labeled vegetables by HPLC-MS and 1H NMR. *J. Agric. Food Chem.* **2005**, *53* (3), 671−677.

(9) Grusak, M. A. Intrinsic stable isotope labeling of plants for nutritional investigations in humans. *J. Nutr. Biochem.* **1997**, *8*, 164−171.

(10) Sternberg, L.; Deniro, M. J. Isotopic composition of cellulose from C3, C4, and CAM plants growing near one another. *Science* **1983**, *220* (4600), 947−949.

(11) Bhatia, C. R.; Smith, H. H. Adaptation and growth response of *Arabidopsis thaliana* to deuterium. *Planta* **1968**, *80* (2), 176−184.

(12) Burgess, J.; Northcote, D. H. Action of colchicine and heavy water on the polymerization of microtubules in wheat root meristem. *J. Cell Sci.* **1969**, *5* (2), 433−451.

(13) Waber, J.; Sakai, W. S. The effect of growth in 99.8 deuterium oxide on the ultrastructure of winter rye. *Plant Physiol.* **1974**, *53* (1), 128−130.

(14) Redfearn, D. D.; Venuto, B. C.; Pitman, W. D.; Blouin, D. C.; Alison, M. W. Multilocation annual ryegrass cultivar performance over a twelve-year period. *Crop Sci.* **2005**, *45* (6), 2388−2393.

(15) Humphreys, M.; Feuerstein, U.; Vandewalle, M.; Baert, J. *Ryegrasses. Fodder Crops and Amenity Grasses*; Boller, B., Posselt, U. K., Veronesi, F., Eds.; Springer: New York: 2010; Vol. *5*, pp 211−260.

(16) Gundel, P. E.; Martinez-Ghersa, M. A.; Omacini, M.; Cuyeu, R.; Pagano, E.; Rios, R.; Ghersa, C. M. Mutualism effectiveness and vertical transmission of symbiotic fungal endophytes in response to host genetic background. *Evol. Appl.* **2012**, *5* (8), 838−849.

(17) Rossmann, M.; Matos, A. T.; Abreu, E. C.; Silva, F. F.; Borges, A. C. Effect of influent aeration on removal of organic matter from coffee processing wastewater in constructed wetlands. *J. Environ. Manage* **2013**, *128*, 912−919.

(18) King-Díaz, B.; Montes-Ayala, J.; Escartín-Guzmán, C.; Castillo-Blum, S. E.; Iglesias-Prieto, T. Lotina-Hennsen; Barba-Behrens, N. Cobalt (II) coordination compounds of ethyl 4-methyl-5-imidazole-carboxylate: chemical and biochemical characterization on photosynthesis and seed germination. *Bioinorg. Chem. Appl.* **2005**, *3*, 93−108.

(19) Yin, L.; Colman, B. P.; McGill, B. M.; Wright, J. P.; Bernhardt, E. S. Effects of silver nanoparticle exposure on germination and early growth of eleven wetland plants. *PLoS One* **2012**, *7* (10), e47674.

(20) Houben, D.; Evrard, L. Sonnet, P. Mobility, bioavailability and pH-dependent leaching of cadmium, zinc and lead in a contaminated soil amended with biochar. *Chemosphere* **2013**, *92* (11), 1450−1457.

(21) Liu, Z.; He, X.; Chen, W.; Zhao, M. Ecotoxicological responses of three ornamental herb species to cadmium. *Environ. Toxicol. Chem.* **2013**, *32* (8), 1746−1751.

(22) Sandrin, C. Z.; Figueiredo-Ribeiro Rde, C.; Delitti, W. B.; Domingos, M. Short-term changes of fructans in ryegrass (*Lolium multiflorum 'Lema'*) in response to urban air pollutants and meteorological conditions. *Ecotoxicol. Environ. Saf.* **2013**, *96*, 80−85.

(23) Alban, V.; Didier, C.; Escobar-Gutiérrez, A. Programmable and self-organised processes in plant morphogenesis: The architectural development of ryegrass. In *Morphogenetic Engineering*; Doursat, R., Sayama, H., Michel, O., Eds. Springer: Berlin, 2012.

(24) Ge, X.; d'Avignon, D. A.; Ackerman, J. J. H.; Collavo, A.; Sattin, M.; Ostrander, E. L.; Hall, E. L.; Sammons, R. D.; Preston, C. Vacuolar glyphosate-sequestration correlates with glyphosate resistance in ryegrass (*Lolium* spp.) from Australia, South America, and Europe: A 31P NMR investigation. *J. Agric. Food Chem.* **2012**, *60* (5), 1243−1250.

(25) Schibeci, A.; Fincher, G. B.; Stone, B. A.; Wardrop, A. B. Isolation of plasma membrane from protoplasts of *Lolium multiflorum* (ryegrass) endosperm cells. *Biochem. J.* **1982**, *205* (3), 511−519.

(26) Schibeci, A.; Pnjak, A.; Fincher, G. B. Biosynthesis of arabinogalactan-protein in *Lolium multiflorum* (Italian ryegrass) endosperm cells. subcellular distribution of galactosyltransferases. *Biochem. J.* **1984**, *218* (2), 633−636.

(27) Jiang, N.; Pu, Y.; Samuel, R.; Ragauskas, A. J. Perdeuterated pyridinium molten salt (ionic liquid) for direct dissolution and NMR analysis of plant cell walls. *Green Chem.* **2009**, *11* (11), 1762−1766.

(28) Bali, G.; Foston, M. B.; O'Neill, H. M.; Evans, B. R.; He, J.; Ragauskas, A. J. The effect of deuteration on the structure of bacterial cellulose. *Carbohydr. Res.* **2013**, *374*, 82−88.

(29) Davis, M. W. A Rapid modified method for compositional carbohydrate analysis of lignocellulosics by high pH anion-exchange chromatography with pulsed amperometric detection (HPAEC/PAD). *J. Wood Chem. Technol.* **1998**, *18* (2), 235−252.

(30) Kumar, R.; Hu, F.; Hubbell, C. A.; Ragauskas, A. J.; Wyman, C. E. Comparison of laboratory delignification methods, their selectivity, and impacts on physiochemical characteristics of cellulosic biomass. *Bioresour. Technol.* **2013**, *130*, 372−81.

(31) Wood, B. F.; Conner, A. H.; Hill, C. G. The effect of precipitation on the molecular weight distribution of cellulose tricarbanilate. *J. Appl. Polym. Sci.* **1986**, *32* (2), 3703−3712.
(32) Xue, B. L.; Wen, J. L.; Xu, F.; Sun, R. C. Structural characterization of hemicelluloses fractionated by graded ethanol precipitation from *Pinus yunnanensis*. *Carbohydr. Res.* **2012**, *352*, 159−165.
(33) Foston, M. B.; Hubbell, C. A.; Ragauskas, A. J. Cellulose isolation methodology for NMR Analysis of cellulose ultrastructure. *Materials* **2011**, *4* (11), 1985−2002.
(34) Uphaus, R. A.; Crane, F. A.; Blake, M. I.; Katz, J. J. Effects of heavy water on *Atropa belladonna*. *J. Pharmaceut. Sci.* **1965**, *54* (2), 202−205.
(35) Sacchi, G. A.; Cocucci, M. Effects of deuterium oxide on growth, proton extrusion, potassium influx, and in vitro plasma membrane activities in maize root segments. *Plant Physiol.* **1992**, *100* (4), 1962−7.
(36) Siegel, S. M.; Halpern, L. A.; Giumarro, C. Germination and seedling growth of winter rye in deuterium oxide. *Nature* **1964**, *201* (4925), 1244−1245.
(37) Cope, B. T.; Bose, S.; Crespi, H. L.; Katz, J. J. Growth of *Lemna* in H2O-D2O mixtures: Enhancement by kinetin. *Bot. Gaz.* **1965**, *126* (3), 214−221.
(38) Pratt, R.; Curry, J. Growth of roots in deuterium oxide. *Am. J. Bot.* **1967**, *24* (7), 412−416.
(39) Tang, G.; Qin, J.; Dolnikowski, G. G.; Russell, R. M.; Grusak, M. A. Golden Rice is an effective source of vitamin A. *Am. J. Clin. Nutr.* **2009**, *89* (6), 1776−1783.
(40) Robertson, A. J.; Weninger, A.; Wilen, R. W.; Fu, P.; Gusta, L. V. Comparison of dehydrin gene expression and freezing tolerance in *Bromus inermis* and *Secale cereale* grown in controlled environments, hydroponics, and the field. *Plant Physiol.* **1994**, *106* (3), 1213−1216.
(41) Foston, M. B.; McGaughey, J.; O'Neill, H.; Evans, B. R.; Ragauskas, A. Deuterium incorporation in biomass cell wall components by NMR analysis. *Analyst* **2012**, *137* (5), 1090−1093.
(42) Morrison, I. M. Isolation and analysis of lignin-carbohydrate complexes from *Lolium multiflorum*. *Phytochemistry* **1973**, *12* (12), 2979−2984.
(43) K..Theerarattananoon; Wu, X.; Staggenborg, S.; Propheter, R.; Madl, R.; Wang, D. Evaluation and characterization of sorghum biomass as feedstock for sugar production. *Trans. ASAB* **2010**, *53* (2).
(44) Rumyantseva, Y. I.; Zhbankov, R. G.; Marhevka, R.; Rataiczak, H. IR spectra and structure of alkaline lignin and thiolignin. *J. Appl. Spectrosc.* **1994**, *61* (5−6), 699−703.
(45) Chang, V. S.; Holtzapple, M. T. Fundamental factors affecting biomass enzymatic reactivity. *Appl. Biochem. Biotechnol.* **2000**, *84−86*, 5−37.
(46) Zhang, Y. H.; Lynd, L. R. Toward an aggregated understanding of enzymatic hydrolysis of cellulose: noncomplexed cellulase systems. *Biotechnolgy Bioeng.* **2004**, *88* (7), 797−824.
(47) Yan, L. F.; Li, W.; Yang, J. L.; Zhu, Q. S. Direct visualization of straw cell walls by AFM. *Macromol. Biosci.* **2004**, *4* (2), 112−118.

honey − δ^{13}C protein) value, which should be ≤1 in unadulterated samples. However, a recent international laboratory ring test undertaken to assess this potential modification[11] found that filtering and/or centrifuging of honey prior to flocculation to remove insoluble material reduced the apparent C-4 sugar content not only of unadulterated honey but also of intentionally adulterated honeys (up to 15% C-4 sugar) to within acceptable limits, so the proposed filtration modification was not recommended.

More recently, instances have also arisen when pollen filtration did not resolve the anomalously high apparent C-4 sugar content of honey (up to 15%), yet the honey was not derived from hives that had undergone sugar feeding, supporting the theory that some other mechanism was also contributing to more negative δ^{13}C protein values and generating false-positive AOAC 998.12 results.[11]

This study was undertaken to investigate the cause of apparent C-4 sugar fails in New Zealand honey to address increasing concerns raised by border testing agencies in importing countries such as China, the United States of America, Hong Kong, and Europe. The stable carbon isotopes of 1023 New Zealand honeys and their corresponding proteins were analyzed, and apparent C-4 sugars were quantified. Honey floral types prone to AOAC 998.12 failure were investigated to understand which types of fails were real (where the honey is adulterated or contaminated by C-4 sugar) or false positive (contaminated via some mechanism other than sugar), and the mechanisms that may cause false-positive results were explored.

BACKGROUND

Pure and authentic honey derived solely from unique nectar sources should theoretically have similar δ^{13}C honey and δ^{13}C protein values as bees do not substantially fractionate or alter the carbon isotopes of nectar. Previous research has raised the possibility of false-positive AOAC 998.12 C-4 sugar results[9,10,12] via pollen and other insoluble material coextracted with the protein. However, there are several different mechanisms to explain the failure of honey tested under the AOAC 998.12 method.

Excess Cane Sugar Contamination (Genuine Fail). Sugar syrups are fed to bees as a supplementary carbohydrate source in times of winter nectar dearth or to prevent starvation during poor weather. Sugar syrups are also used to retain bees in specific areas such as orchards or fields to provide pollination services or to boost hives into breeding mode several weeks prior to nectar flow. However, supplementary syrup feeding also risks overuse, resulting in bees storing excess sugar syrups into brood boxes, which can later be uncapped and redistributed into collection boxes by the bees as they make more room for brood. Cane sugar (a C-4 plant, with a more positive carbon isotope value than C-3 plants) is the sole bulk sugar product available in New Zealand for commercial beekeepers. Addition or mixing of C-4 sugar syrups (which has a stable carbon isotope or δ^{13}C value of ∼−10‰) with plant nectar will shift the δ^{13}C honey isotope values to more positive isotope values than the δ^{13}C values of available C-3 plant nectar sources, which range from −24 to −27‰.

After-harvest additions of noninverted cane sugar can be readily detected using sugar chemical profiles that measure sucrose content, as there is no opportunity for the sucrose to undergo a reaction with invertase (a bee digestive enzyme), which breaks the sucrose molecule into monosaccharides of fructose and glucose. Codex[13] prescriptively sets limits whereby sucrose should not be present above 5 g/100 g of honey and in some exceptional cases 10 or 15 g/100g of honey (such as ling and lavender).

Pollen Contamination (False-Positive Fail). Protein is extracted from honey as an internal standard; AOAC criteria require $\Delta(\delta^{13}\text{C honey} - \delta^{13}\text{C protein}) \leq 1$. The δ^{13}C protein value may be contaminated by insoluble material (i.e., excess pollen from diverse sources, dust particles, or other hydrophobic components). However, when using the repetitive wash method, the AOAC 998.12 method does not remove this material and it is coextracted with the protein during flocculation. This anthropogenic pollen or dust has been shown to have a different carbon isotope value (ca. −28‰), shifting the final δ^{13}C protein value by up to 1‰ and affecting the calculation of apparent C-4 sugars.[10] In New Zealand honey, significant levels of pollen can occur in honey (in excess of 14,000,000 grains/10 g; personal observation by Rogers). At levels where pollen is >500,000 grains/10 g honey, contamination of protein by concurrently extracted pollen can result in false-positive results.[10] High pollen levels can be introduced into honey due to the robust extraction methods used to dislodge thixotropic honey (such as manuka). Frames often need manual scraping followed by high-speed centrifuging to remove honey. This procedure may dislodge large pockets of pollen stored in the frames, in contrast to gentle "prick and drain" methods employed for runnier honeys, which generally retain the comb structure and associated pollen within the frame.

Supplementary Protein Feeding (False-Positive and Genuine Fails). Supplementary protein feeding can affect δ^{13}C protein values[10] and contaminate nectar-derived protein sources. Common protein supplements include yeast (−24‰), soy flour (−25 to −27.5‰), and pea flour (−28‰),[14−17] which have a range of isotopic values and are similar to the range of honey protein values found in this study (−24.3 to −28.2‰). Although the protein supplements are usually consumed by bees, it is possible small amounts are regurgitated and stored in collections boxes, similar to bee bread and pollen pockets, contributing foreign protein to the honey. Fed at inappropriate times, supplementary feeds might also cause genuine fails due to the practice of mixing sugar syrups with the protein feed to increase palatability and consumption by bees. Issues with using yeast as a protein source were also observed in this study, where honey was more prone to fermentation over time, especially with higher moisture content honey (19−21%) and higher storage temperatures (>22 °C). Hives fed either yeast or sugar syrup inverted with yeast had a tendency to show δ^{13}C honey values that were more positive (−23 to −24.5‰), even if sugar feeding had occurred sparingly (personal observation by Rogers).

Brood Box Contribution (Genuine Fails). C-4 sugar fails may also arise if honey extraction occurs from the brood box. The brood box is where bees store pollen and/or bee bread (key protein sources) as well as nectar and/or sugar syrup, which are converted to honey (key carbohydrate sources) to provide stored sustenance and ensure survival of the colony during food shortages or bad weather. In spring, if bees have filled brood box frames with unconsumed honey, and there is no further room for brood expansion, beekeepers may exchange filled frames for empty frames to allow continued brood expansion. The extraction of honey from brood box frames is generally unacceptable in good beekeeping practices due to the

risk of contamination from winter or prenectar flow hive treatments (i.e., for varroa and other common diseases) and supplementary feeding of sugar or protein.

Unknown (Non C-4 Sugar) Mechanism (False-Positive Fail). New Zealand honey samples exceeding 7% apparent C-4 sugars continue to occur; however, in most instances none of the above causes were cited by participating beekeepers as being possible. Until this study, an unknown mechanism (which is unrelated to C-4 sugar adulteration) has been suspected as being responsible for these failed tests.[10,11] This research aims to investigate and understand false-positive results that were not caused by protein feeding or excess pollen levels in the honey.

MATERIALS AND METHODS

AOAC 998.12 Method and "Apparent" C-4 Sugar Determination. Carbon isotopes (δ^{13}C honey and δ^{13}C protein) and apparent C-4 sugar contents of 1023 New Zealand honey samples (mainly manuka but 14 multifloral and other monofloral varieties also included) were analyzed at the Stable Isotope Laboratory at GNS Science, Lower Hutt, New Zealand, between January 2011 and December 2012. The honeys were harvested between December 2007 and March 2012 and were submitted by honey companies and beekeepers as part of quality assurance requirements to test for apparent C-4 sugars before export.

Honey was submitted blind for testing, and further information was supplied after analysis based on organoleptic (i.e., flavor, odor, and color), physicochemical (i.e., conductivity and thixotropy), and/or pollen count as well as from observations by the beekeepers who target specific nectar flows. Antibacterial activity was also reported if available, including total peroxide activity (PA, caused by hydrogen peroxide which originates from the activity of the enzyme glucose oxidase in honey) or nonperoxide activity (NPA, related to a further amount of antibacterial activity attributed to other bioactive compounds such as methylglyoxal in the product).[18,19] Activity analyses were carried out in commercial testing laboratories by Hills Laboratories, Hamilton, New Zealand, or Eurofins, Hamilton, New Zealand.

Protein Extraction. Protein was extracted from honey using the AOAC 998.12 repetitive wash method whereby 4 mL of distilled H_2O was added to 10−12 g of honey in a clear 50 mL centrifuge tube. The solution was mixed well and heated gently in a water bath to aid dissolution. Two milliliters of 10% sodium tungstate and 2 mL of 0.67 N H_2SO_4 (Sigma-Aldrich) were mixed together and immediately added to the honey solution. The mix was heated at 80 °C in a water bath until a visible protein flocculent formed with clear supernatant, with further 2 mL increments of 0.67 N H_2SO_4 added if no visible flocculent formed after 5 min. The centrifuge tube was filled with water and centrifuged for 5 min at 3500 rpm The supernatant was discarded and the pellet rinsed and centrifuged five times with 50 mL portions of water, thoroughly dispersing the pellet each time. Precipitated protein was dried in an oven overnight at 60 °C. Two manuka honey samples (stored at 4 °C) were routinely analyzed as standards with each batch (18 samples or less) of samples to ensure protein preparation consistency.

Stable Isotope analysis. Approximately 0.5 mg of honey or protein was transferred into 6 × 4 mm tin capsules (IVA-Analysentechnik, Germany) and analyzed for stable carbon isotopes using a Eurovector elemental analyzer coupled to an Isoprime mass spectrometer in continuous flow mode (EA-IRMS). International and working reference standards (IAEA-CH_6, leucine, EDTA, cane and beet sugars), the two honey standards (honey and protein), and blanks were included during each run for calibration.

Isotopic ratios ($^{13}C/^{12}C$) are expressed as isotopic deviations δ defined as

$$\delta\ (‰) = \frac{R_s - R_{ref}}{R_{ref}} \times 1000$$

where R_s is the isotopic ratio measured for the sample and R_{ref} that of the international standards. The δ^{13}C value is relative to the international Vienna Pee Dee Belemnite (VPDB) standard. Results are expressed in δ (‰) versus the specific reference, and analytical precision is within ±0.2‰ for carbon.

Carbon isotopes of the whole honey were compared with their extracted protein and assessed for apparent C-4 cane sugar content using eq 1:

$$\text{apparent C-4 sugar (\%)} = 100 \times [\delta^{13}\text{C(protein)} - \delta^{13}\text{C(whole honey)}] / [\delta^{13}\text{C(protein)} - (-9.7)] \quad (1)$$

The acceptance criteria state that pure honey generally yields a value of apparent C-4 sugars of ≤7%. Some unusual varieties may slightly exceed the range, but will have δ^{13}C values for honey that are in the normal range (more negative than −24.0‰).[7]

Other Analyses. Methylglyoxal (MGO) or NPA and hydroxymethylfurfural (HMF) measurements were supplied by some honey submitters whose honey had already been tested at Hills Laboratories or Eurofins according to their in-house commercial procedures. To complete data sets where MGO and NPA data were not available and perform checks on supplied values, samples were sent to Hills Laboratories for further testing. Due to several bioactive honey measurement systems within New Zealand,[18] the NPA, UMF, and MGO bioactivity values were standardized and reported as NPA according to the UMF Honey Association conversion tool Web site (http://www.umf.org.nz/umf-trademark/methylglyoxal-npa-honey-conversion-calculator).

RESULTS AND DISCUSSION

Which New Zealand Honey Varieties Are Prone to Exceeding 7% "Apparent" C-4 Sugars? Apparent C-4 sugar analysis of 1023 New Zealand honey samples showed that 690 samples had apparent C-4 sugars ≤7% (67% pass rate) and 333 samples had apparent C-4 sugars >7% (33% fail rate) (Figure 1). The apparent C-4 sugar content found in these honeys

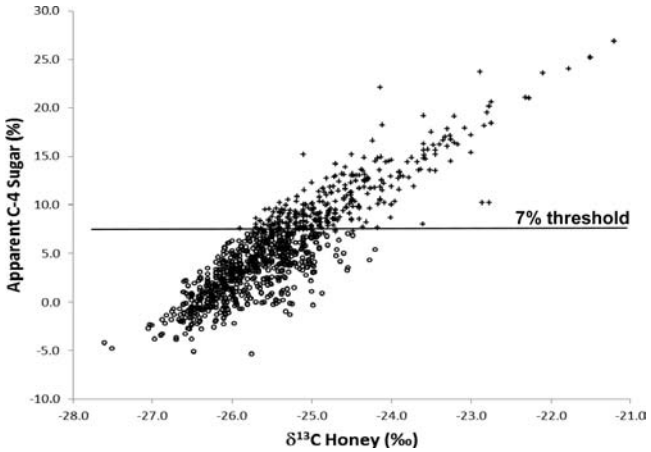

Figure 1. Distribution of δ^{13}C honey isotope values and apparent C-4 sugars for 1023 New Zealand honeys. Circles represent ≤7% apparent C-4 sugars, and crosses represent >7% apparent C-4 sugars. $R^2 = 0.81$, $y = 5.1585x + 136.55$.

ranged between −5.4 and 26.9%; δ^{13}C honey values ranged from −18.5 to −27.6‰, and δ^{13}C protein values ranged from −24.3 to −28.2‰. The average δ^{13}C honey and protein values of the 1023 New Zealand samples were −25.4 ± 0.8 and −26.3 ± 0.4‰, respectively (Table 1). The average δ^{13}C honey and protein values of honeys with apparent C-4 sugars ≤7% were

dx.doi.org/10.1021/jf404766f | J. Agric. Food Chem. 2014, 62, 2605−2614

Table 1. Carbon Isotope Values of Honey and Protein, and Percent C-4 Sugar of 1023 New Zealand Multi- and Monofloral Honeys (Standard Deviations of Average Values Reported in Parentheses)

honey type (no. of samples)	av δ^{13}C honey (‰)	range δ^{13}C honey (‰)	av δ^{13}C protein (‰)	range δ^{13}C protein (‰)	av apparent %C-4 sugar	range apparent %C sugar	apparent %C-4 sugar failure rate per floral type
blue borage and vipers bugloss (5)	−26.4 (0.4)	−26.0 to −27.0	−25.9 (0.3)	−25.6 to −26.3	−3.2 (1.3)	−5.1 to −1.9	0
clover (67)	−26.0 (0.5)	−24.5 to −27.0	−26.2 (0.4)	−25.3 to −27.1	1.1 (2.4)	−2.6 to 6.1	0
dandelion (2)	−26.9 (0.2)	−26.7 to −27.0	−26.4 (0.4)	−26.1 to −26.6	−3.1 (0.9)	−3.7 to −2.4	0
honeydew (15)	−26.2 (0.4)	−25.5 to −26.8	−26.4 (0.4)	−25.7 to −27.0	1.5 (2.6)	−4.4 to 4.1	0
kamahi (18)	−25.6 (0.6)	−24.5 to −26.6	−25.9 (0.4)	−25.1 to −26.7	1.9 (3.8)	−3.3 to 13.2	6 (1 fail)
kanuka (19)	−26.1 (0.3)	−25.5 to −26.5	−26.4 (0.2)	−26.1 to −26.8	2.1 (1.9)	−1.2 to 4.6	0
ling (4)	−25.2 (0.7)	−24.1 to −25.7	−27.3 (0.6)	−26.9 to −28.2	12.1 (6.7)	8.3 to 22.1	100 (4 fails)
manuka (757)[a]	−25.1 (0.8)	−21.0 to −27.6	−26.3 (0.5)	−24.6 to −27.9	6.9 (4.7)	−3.9 to 26.9	43 (324 fails)
manuka blend (6)	−25.9 (0.6)	−25.1 to −26.6	−26.3 (0.1)	−26.0 to −26.4	2.3 (3.1)	−1.3 to 5.8	0
multifloral (93)	−26.1 (0.5)	−24.6 to −26.9	−26.1 (0.4)	−24.5 to −27.0	0.4 (1.8)	−4.4 to 6.3	0
pohutukawa (3)	−25.8 (0.6)	−25.3 to −26.4	−26.4 (0.4)	−25.9 to −26.8	3.5 (1.2)	2.2 to 4.6	0%
rata (5)	−26.1 (0.2)	−26.0 to −26.3	−26.4 (0.1)	−26.0 to −27.0	1.11 (1.8)	−0.7 to 3.7	0
rewarewa (13)	−26.0 (0.5)	−25.3 to −26.5	−26.4 (0.3)	−26.0 to −26.8	1.6 (2.6)	−2.4 to 5.8	0
tawari (6)	−24.0 (1.3)	−21.8 to −25.0	−25.9 (0.4)	−25.4 to −26.3	11.1 (7.5)	5.0 to 24.0	80 (4 fails)
thyme (10)	−26.6 (0.7)	−25.6 to −27.6	−26.2 (0.4)	−25.9 to −26.9	−2.1 (2.0)	−4.8 to 2.0	0%
total honey (1023)	**−25.4 (0.8)**	**−18.5 to −27.6**	**−26.3 (0.4)**	**−24.3 to −28.2**	**5.5 (5.2)**	**−5.4 to 26.9**	**33 (333 fails)**
manuka nectar (25)	−26.2 (0.5)	−25.7 to −26.7	na	na	na	na	
tawari nectar (6)	−24.5 (0.5)	−23.9 to −24.9					
honey with C-4 sugars <7% (690)	−25.8 (0.5)	−24.2 to −27.6	−26.3 (0.4)	−24.9 to −27.1	2.7 (2.6)	−5.4 to 6.9	
honey with C-4 sugars ≥7% (333)	−24.6 (0.9)	−18.5 to −25.9	−26.4 (0.5)	−24.3 to −28.2	10.9 (4.4)	7 to 26.9	

[a]The range of manuka honey covers both NPA manuka honey and non-NPA manuka honey. It is possible that the floral type of some non-NPA manuka honeys has been misidentified by the beekeeper, resulting in a larger isotopic range than would be expected. However, the overall sample size (n = 757) is sufficient to provide a statistically robust isotopic average for manuka honey. Manuka blend is indicated when manuka components are present but not in sufficient quantities to dominate the floral type (being wholly or mainly as required in Codex).[13]

−25.8 ± 0.5 and −26.3 ± 0.4‰, respectively, whereas honeys with apparent C-4 sugars >7% had average δ^{13}C honey and protein values of −24.6 ± 0.9 and −26.4 ± 0.5‰, respectively. Most samples readily flocculated protein, with some manuka honey samples flocculating on warming, even before addition of the chemicals. It was noted that it was often difficult to flocculate protein from tawari and rata honey, suggesting they may contain lower levels of extractable protein.

Due to the high overall failure rate (33%), honey samples were classified into 15 floral types to investigate how prone each floral type was to failure (Table 1). Four monofloral honey types (manuka, tawari, ling, and kamahi) had samples that exceeded 7% apparent C-4 sugars and failed acceptance criteria, whereas none of the other 11 New Zealand honey varieties exceeded 7% apparent C-4 sugars (Table 1).

Comparison of the carbon isotope values of 690 honeys and their frequency of passes (apparent C-4 sugars ≤7%) to the 333 honeys and their frequency of fails (apparent C-4 sugars >7%) identifies three main regions of interest (Figure 2). In region 1, all honey samples passed and δ^{13}C honey values ranged between −27.6 and −25.9‰; 250 samples were classed as genuine passes with no apparent C-4 sugar adulteration. In region 2, all samples failed the test (apart from a few tawari and multifloral samples) and δ^{13}C honey values ranged between −24.7 and −18.5‰; 59 samples were classed as genuine fails which were attributed to apparent C-4 sugar contamination. In region 3, honey samples could either pass or fail the test and δ^{13}C honey values were between −25.9 and −24.7‰; 440 samples passed, and 274 samples failed. Of interest are the mechanisms that allowed honey samples of similar florality (and hence nectar source) and bulk isotope composition to either pass or fail in region 3 and whether they were genuine fails or false-positive fails. The delineation of region 3 is made specifically for manuka honey, where all manuka honey samples with δ^{13}C honey values more negative than −25.9‰ passed and all manuka honey samples with δ^{13}C honey values more positive than −24.7‰ failed. All samples that failed in region 3 were manuka honey.

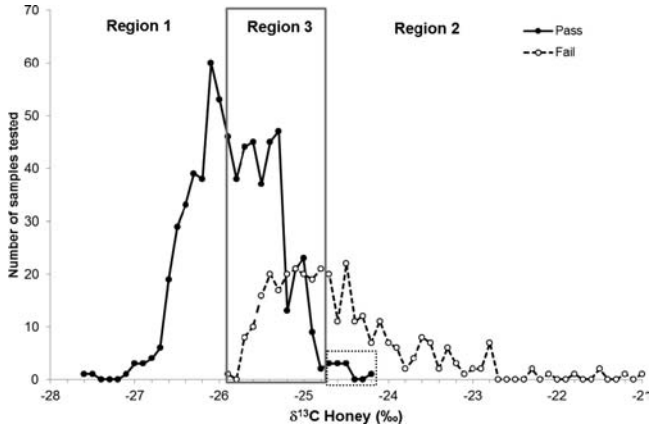

Figure 2. Frequency distribution of 1023 New Zealand δ^{13}C honey values. Region 3 represents honey samples that pass and those resulting in false positives. Several samples encompassed in the dashed box (more positive δ^{13}C honey samples than those in region 3) are tawari, clover, and multifloral samples that had C-4 sugars ≤7%.

In the past, honeys were not considered adulterated with C-4 sugars if their bulk isotope analysis (δ^{13}C honey values) was more negative than −23.5 to −24.0‰.[3,5] Even though 274

New Zealand honeys from region 3 (Figure 2) had δ^{13}C honey values more negative than −24.7‰ (and could therefore be considered as unadulterated on the basis of traditional analyses), these honeys exceeded 7% apparent C-4 sugars and failed the original AOAC 998.12 acceptance criteria.[1] As their δ^{13}C honey values were well within the acceptable range, this suggested that a shift in the δ^{13}C protein values might be affecting the outcome, rather than C-4 sugar adulteration.

An assessment of the δ^{13}C protein values of these 1023 honeys showed that the range of δ^{13}C protein values of honey samples which passed the test (apparent C-4 sugars ≤7%, −24.9 to −27.1‰) is considerably narrower than the range of δ^{13}C protein values that failed the test (apparent C-4 sugars >7%, −24.3 to −28.2‰) (Figure 3). The wide range of δ^{13}C protein values found in these 1023 New Zealand honeys (up to 4‰) may suggest that there is either a diverse isotopic range of pollen (protein source) within New Zealand's honey-producing flora or a distinctive isotope fractionation process occurring in the protein.

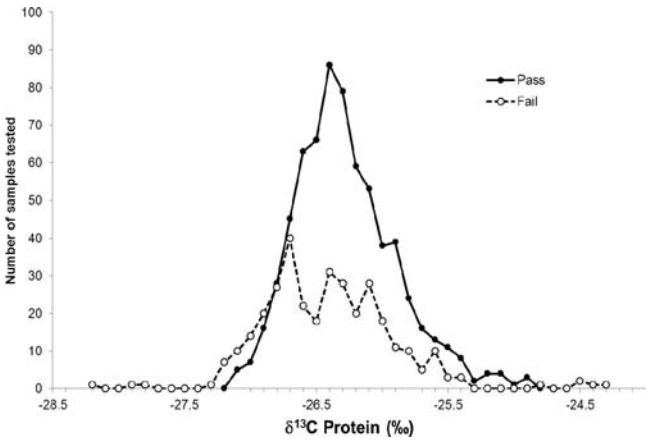

Figure 3. Frequency distribution of 1023 New Zealand δ^{13}C protein values.

Characterization of New Zealand Monofloral Honey Using Carbon Isotopes and "Apparent" C-4 Sugar Content. *Ling.* Ling (or heather) honey has traditionally been identified by Codex[13] as having "special properties" and is allowed higher sucrose contents than other honey (up to 10% w/v). All four ling samples in this study (Figure 4a) failed the AOAC 998.12 method, with apparent C-4 sugars ranging from 8.3 to 22.1%. Three samples (with apparent C-4 sugars between 8.3 and 9.0%) did not originate from hives that were sugar fed by the beekeepers, suggesting that these samples may be false-positive fails. Ling honey δ^{13}C protein values (average δ^{13}C ling protein value of −27.3‰) were up to 1.0‰ more negative than those of other honey proteins in this study (average δ^{13}C total protein value of −26.3‰), whereas the average ling δ^{13}C honey value was −25.2‰ and comparable with the average δ^{13}C total honey value of −25.4‰. One ling sample (circled in Figure 4a) had δ^{13}C honey and protein values of −24.1 and −28.2‰, respectively, which suggested a positive shift in the δ^{13}C honey value, usually associated with C-4 sugar contamination, but also indicated a significant negative shift of δ^{13}C protein values.

Kamahi. One kamahi honey (n = 18) failed the AOAC 998.12 method with an apparent C-4 sugar content of 13.2% (Figure 4b). This sample had a δ^{13}C honey value of −24.5‰ and a δ^{13}C protein value of −26.6‰. The $\Delta(\delta^{13}$C honey-protein) value of this sample was 2.2‰, which is much higher than those of the other kamahi samples in this study (−0.5 to 0.8‰), suggesting the fail was caused by either a significant honey or protein shift or both. This sample was the only sample to fail of 18 samples and was considered to be a genuine fail (most likely due to C-4 sugar) as its δ^{13}C honey value (−24.5‰) was considerably more positive than the average

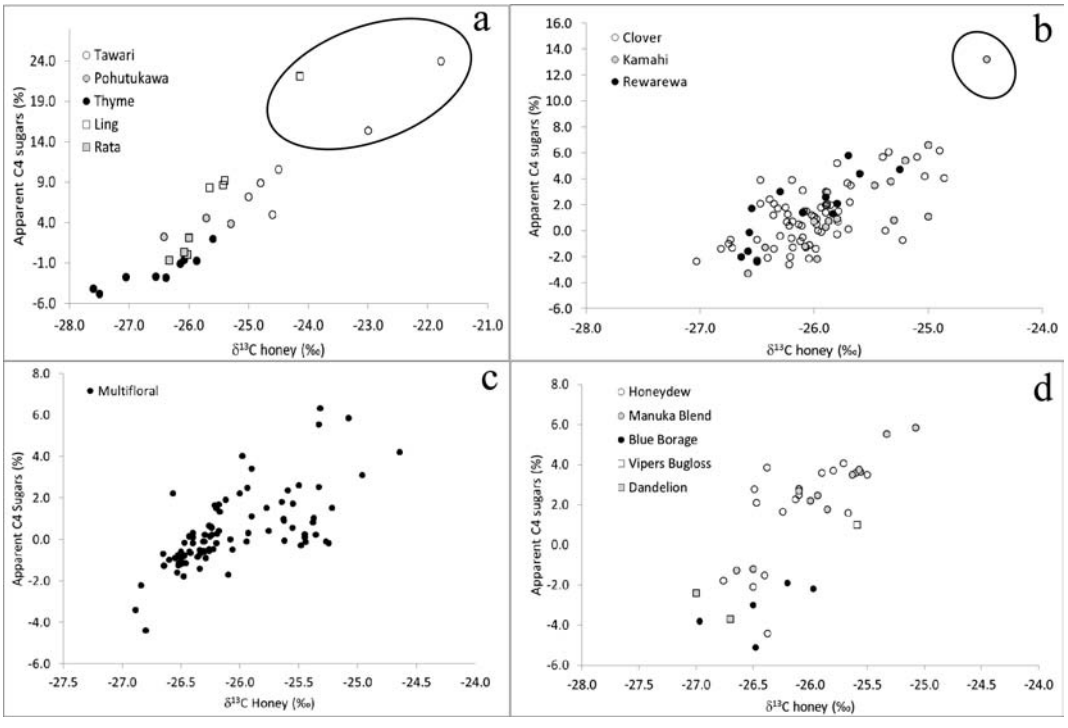

Figure 4. Carbon isotope and C-4 sugar contents of 13 New Zealand mono- and multifloral honeys using AOAC 998.12 method.

dx.doi.org/10.1021/jf404766f | J. Agric. Food Chem. 2014, 62, 2605−2614

Table 2. Breakdown of 757 Manuka Honey Samples Tested for Apparent C-4 Sugars into Pass (Region 1), Fail (Region 2), and Those That Have Pass or False-Positive Results (Region 3)

region	no. of samples (n)	av δ^{13}C honey (‰)	SD	range δ^{13}C honey (‰)	av δ^{13}C protein (‰)	SD	range δ^{13}C protein (‰)	range apparent C-4 sugars (%)
1 (pass)	161	−26.2	0.3	−25.9 to −27.6	−26.3	0.3	−24.7 to −27.1	−3.9 to 6.8
2 (fail)	113	−24.0	0.5	−21.0 to −24.7	−26.0	0.4	−24.6 to −27.9	10 to 26.9
3 (false positive)	211	−25.1	0.3	−24.7 to −25.9	−26.7	0.4	−25.8 to −27.7	7.0 to 16.7
3 (pass)	272	−25.5	0.3	−24.7 to −25.9	−26.2	0.4	−24.7 to −27.0	−3.9 to 7.0
3 (pass and false positive)	483	−25.3	0.5	−24.7 to −25.9	−26.5	0.5	−24.7 to −27.7	0 to 16.7
1 and 3 (genuine manuka honey)	644	−25.4	0.5	−24.7 to −27.6	−26.5	0.4	−24.7 to −27.27	−3.9 to 16.7
manuka nectar	25	−26.2	0.5	−25.7 to −26.7	na		na	na
total manuka	757	−25.1	0.5	−21.0 to −27.6	−26.3	0.5	−24.6 to −27.39	−3.9 to 26.9

δ^{13}C kamahi honey value (−25.6 ± 0.6‰). It was not possible to discount that some other non C-4 sugar contribution may have also occurred due to the more negative δ^{13}C protein value.

Tawari. Four of six tawari honey samples failed the AOAC 998.12 method with apparent C-4 sugars ranging from 7.2 to 24.0% (Figure 4a). Two of these samples (circled in Figure 4a) were reported to have been sampled from hives where some C-4 sugar feeding occurred prior to nectar collection (δ^{13}C honey values of −21.8 and −23.0‰, respectively) and were considered to be genuine fails. The other two tawari honey samples, which had apparent C-4 sugars >7%, had no reported association with C-4 sugar feeding and may represent false-positive results. Although only six samples of tawari honey were studied, the average δ^{13}C tawari honey value (genuine samples) was −24.6‰ (0.8‰ more positive than the average δ^{13}C honey values in this study), even though these four samples were reported by beekeepers to be genuine with no previous sugar feeding history. Six samples of tawari nectar originating from Gisborne (East Coast) were also collected and analyzed for their carbon isotopes. The average δ^{13}C tawari nectar value was found to be −24.5 ± 0.5‰, corresponding to similar δ^{13}C honey values found in tawari honey. Tawari honey was found to have more positive carbon isotope values than any other New Zealand honey floral variety in this study. These positive δ^{13}C honey values are similar to other specialty honeys containing more positive isotope values found elsewhere globally such as citrus and mesquite honeys, which have δ^{13}C honey values averaging −23.8‰.[20]

Clover and Multifloral. A large number of clover (n = 67) and multifloral (n = 93) honeys (sometimes called bush honey due to their mixed nectar source) (Figure 4b,c) were identified and analyzed. In New Zealand, these honeys are the next most popular export honeys after manuka honey. All clover and multifloral honey samples tested in this study had apparent C-4 sugars <7% and passed the AOAC 998.12 C-4 sugar method. The average δ^{13}C clover and multifloral honey values (−26.0 and −26.1‰) were more negative than the average δ^{13}C total honey value (−25.4‰). The average δ^{13}C protein values of clover and multifloral honey (−26.2 and −26.1‰) were similar to the average δ^{13}C total protein values (−26.3‰). Clover and multifloral honeys analyzed in this study had some of the lowest apparent C-4 sugars of all floral types (average 1.1 and 0.4%, respectively). The small isotopic differences between paired δ^{13}C honey and protein values suggested that these honeys were very pure and that both honey and its protein were derived from the corresponding nectar without interference from sugar or other contaminants that may affect their honey or protein isotopes.

Other Monofloral Varieties (Except Manuka and Kanuka). Eight floral varieties (blue borage and vipers bugloss, dandelion, honeydew, manuka blend, pohutukawa, rata, rewarewa, and thyme, n = 58) had average δ^{13}C honey values ≤ −26.0‰ (Figure 4a,b,d) and δ^{13}C protein values between −25.9 and −26.4‰ (Table 1). These honeys all passed the AOAC 998.12 method. Some floral types had negative apparent C-4 sugar contents, which occur when the corresponding δ^{13}C protein value of each honey is more positive than its δ^{13}C honey value. These eight floral types all had apparent C-4 sugars ≤5.8%, although it was recognized that the sample numbers for blue borage and vipers bugloss, dandelion, manuka blend, and rata were not statistically robust (as $n \leq 6$). The floral type with the most negative average δ^{13}C honey value was dandelion (−26.9‰). The floral type with the most negative δ^{13}C honey value in this study was thyme (−27.6‰).

Manuka. The largest group of honeys evaluated in the study comprised manuka honey (757 samples) primarily because these are most frequently tested prior to export. Only 433 of these manuka honeys had apparent C-4 sugars <7% (AOAC 998.12 pass criteria), whereas 324 samples (42.8% of manuka honeys tested) had apparent C-4 sugars exceeding the 7% acceptance criteria. The range of δ^{13}C manuka honey values found in this study was between −21.0 and −27.6‰, with an average honey value of −25.1 ± 0.8‰. δ^{13}C manuka protein values were between −24.6 and −27.3‰, with an average δ^{13}C manuka protein value of −26.3 ± 0.5‰. Apparent C-4 sugars ranged from −3.9 to 26.9%. Manuka honey (161 samples) was found to have apparent C-4 sugars *always* <7% as long as its corresponding δ^{13}C honey value was ≤ −25.9‰ (region 1, Figure 2; Table 1). These samples were considered to be uncontaminated by C-4 sugar and genuine passes. Manuka honey (113 samples) was found to have apparent C-4 sugars *always* >7% as long as its corresponding δ^{13}C honey value was ≥ −24.7‰ (region 2, Figure 2). These samples most likely failed because they contained some C-4 sugar contamination (genuine fail). However, it may be possible these samples are not true fails if they contained honey derived from nectar sources with more positive δ^{13}C values such as tawari or were fractionated (loss of ^{12}C) in some way by yeasts or some further (as yet unknown) mechanism. Manuka honey (483 samples) found in region 3 had δ^{13}C honey values ranging between −24.7 and −25.9 ‰, and had contained apparent C-4 sugars both below and above 7%, although none exceeded 15% apparent C-4 sugar. Of this group from region 3, 272 manuka

Table 3. NPA Rating of 376 Manuka Honey Compared to Carbon Isotopes of Honey and Apparent C-4 Sugars

NPA rating	no. of samples with NPA rating	no. of samples with C-4 sugars >7%	% fail[1a]	no. of samples with δ^{13}C honey ≥ −24.7‰	% fail[2b]
low (4−9.9)	156	17	11	4	3
medium (10−16.9)	129	79	61	44	34
high (17−30)	91	74	81	26	29
total	376	170	45	74	20

[a]% Fail[1] refers to existing criteria where 7% is the fail criteria for apparent C-4 sugars. [b]% Fail[2] refers to new proposed criteria where manuka honey with δ^{13}C honey ≤ −24.7‰ is considered genuine.

honey samples with apparent C-4 sugars below 7% were considered to be genuine passes, whereas 211 manuka honey samples with apparent C-4 sugars exceeding 7% were considered to be false-positive fails.

The lower limit of δ^{13}C honey values for manuka honey (region 3, −24.7‰) is determined by the analysis of pure manuka nectar sampled directly from *Leptospermum* (sp) flowers, which was found to have an average δ^{13}C value of −26.2 ± 0.5‰ (n = 25) (Table 2). It is expected that δ^{13}C protein and δ^{13}C honey of authentic (non-C-4 sugar contaminated) manuka honeys would have similar honey isotope values as the nectar, because the bees do not alter the isotopic values. The average manuka nectar isotope value correlates well with the δ^{13}C honey values of manuka honey, which passed the AOAC 998.12 method in region 1 and false-positive samples from region 3, but may suggest that in some of the samples which are more variable (outliers) that other nectar sources (which contain more negative or positive carbon isotopes) may have a more significant contribution. Alternatively, there may be a small change in the δ^{13}C honey value of some honeys with ripening and maturation. To ensure a statistical safety interval of 3 times the SD (i.e., a confidence level 99.7%), the lowest acceptable value (cutoff) for genuine (unadulterated) manuka δ^{13}C honey value would be −24.7‰ (−26.2‰ − (−1.5‰) = −24.7‰) as suggested by the data in Figure 2. Moreover, of 757 manuka samples analyzed in this study, no manuka samples with δ^{13}C honey value ≤ −24.7‰ (region 2) passed the AOAC 998.12 C-4 sugar method.

False-positive samples from region 3 are also found to have more negative δ^{13}C protein values (average −26.7 ‰) than those from region 2 (average −26.0 ‰, where none of the 757 screened manuka samples passed the AOAC 998.12 and C-4 sugar contamination is known to occur).

Kanuka. Kanuka (*Kunzea ecroides*) honey (19 samples) were analyzed for carbon isotopes and apparent C-4 sugars (Table 1). Flowering concurrently with manuka, examples of pure kanuka honey are not frequently found, as most kanuka honey is collected with, and identified as, manuka honey. It is not possible to distinguish between the two species using pollen identification as they have identical pollen shape and size. In the few identified cases where kanuka nectar sources predominate, the honey is reported to be lighter in color, less intense in flavor, and lower in conductivity and to have little or no thixotrophy compared to manuka honey. Unlike manuka honey, kanuka honey is not reported to have a nonperoxide activity. Kanuka honey exhibits more negative δ^{13}C honey values (average −26.1‰) than manuka (average −25.1‰), although δ^{13}C protein values are similar (average −26.4 and −26.3‰, respectively). All 19 kanuka honeys had apparent C-4 sugars <4.6%, suggesting these honeys are not prone to high apparent C-4 sugar contents, typical of excess C-4 sugar feeding or false-positive fails. As kanuka flowers at a similar time to manuka, this honey would be just as susceptible to excess C-4 sugar fails as manuka honey if sugar syrup feeding was the key reason for high apparent C-4 sugar content in manuka honey.

Could False-Positive Fails Exist for Honey with δ^{13}C Honey Values > −24.7‰? Although some samples with δ^{13}C honey values > −24.7‰ and apparent C-4 sugars >7% (considered to be C-4 sugar contaminated) were confirmed by beekeepers as originating from hives that had been fed some C-4 sugar syrup, other beekeepers stated that some samples included in this group originated from hives which had minimal C-4 sugar syrup feeding. There are several mechanisms other than C-4 sugar that can increase δ^{13}C honey values to become more positive, such as a nectar contribution from another more positive floral source or supplementary protein feeding, which may artificially shift the δ^{13}C honey values toward more positive values if the bee feed has more positive δ^{13}C values and is incorporated into the honey instead of being completely consumed.

The only floral type found in this study with substantially more positive isotope values than the average δ^{13}C honey (−25.4‰) is tawari honey (average δ^{13}C honey −24.0‰), although other types of honey with similar positive δ^{13}C honey values are known.[20] Tawari often flowers just prior to the manuka nectar flow, and brood can build up on this nectar before going directly onto manuka flowers. Tawari nectar has an average δ^{13}C nectar value of −24.5 ± 0.5‰, and if combined with manuka nectar, it may be possible to isotopically shift the overall δ^{13}C honey value to > −24.7‰, without the influence of any C-4 sugars. Other floral sources commonly used in spring built up before the manuka nectar flow are pollination crops such as apple and kiwifruit (minimal nectar) or nectar sources from willows and spring weeds. Analysis of a few commonly available pollen sources that may be consumed by bees prior to manuka nectar flow were undertaken during this study. Kiwifruit pollen had a δ^{13}C pollen value of −24.2 ± 0.3‰, and willow and buttercup (a common weed) had δ^{13}C pollen values of −23.0 ± 0.5‰. Other unknown mechanisms may occur if beekeepers feed sugar syrups or supplements that contain yeast. Further research on the consequential associated fractionation of sugars by yeast may explain more positive apparent C-4 sugar fails, although this study was not aimed at resolving how δ^{13}C honey values could become more positive other than via C-4 sugar contamination. However, it will be an important area to consider in future years for New Zealand's manuka industry if it wishes to eliminate sugar adulteration concerns completely.

Why Does Manuka Honey Have False-Positive Fails Using the AOAC 998.12 C-4 Sugar Method? False-positive manuka honey (211 samples) from region 3 (where δ^{13}C honey values were between −24.7 and −25.9‰ and δ^{13}C protein values were between −25.8 and −27.2‰) had apparent C-4 sugars ranging from 7 to 15.0% with an average apparent C-4

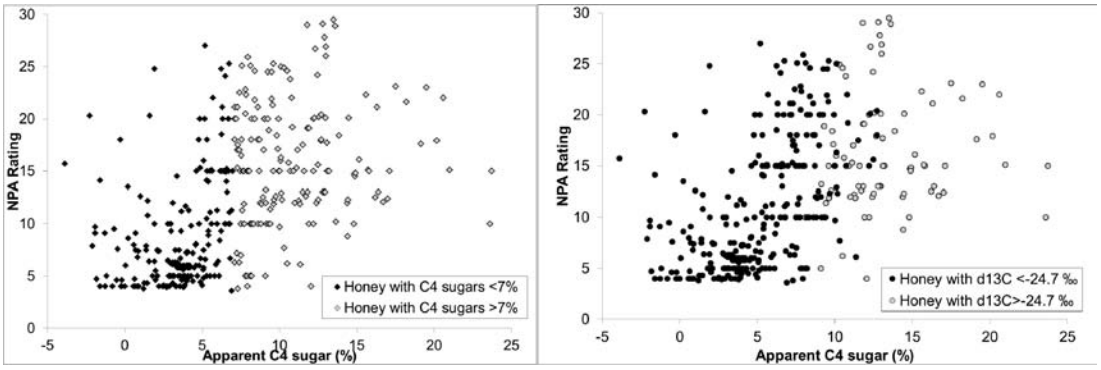

Figure 5. (a, left) Apparent C-4 sugar content versus NPA rating of 376 manuka honeys which fail and pass using (a) the AOAC 998.12 criteria of 7% apparent C-4 sugars and (b, right) the proposed acceptance threshold (from this study) where manuka δ^{13}C honey values < −24.7‰.

sugar content of 8.6 ± 1.3%, although only three samples had apparent C-4 sugars >12%. These samples are all classed as false positives because of a negative shift in δ^{13}C protein values, which artifically increases the $\Delta(\delta^{13}\text{C honey} - \delta^{13}\text{C protein})$ values to >1, whereas the δ^{13}C honey isotope value are < −24.7‰ and traditionally considered unadulterated by C-4 sugars. An assessment of protein isotope values of each region (Figure 2) showed that region 2 (failed samples) had average δ^{13}C protein values of −26.0 ± 0.4‰, region 1 (passed samples) had average δ^{13}C protein values of −26.3 ± 0.3‰, and region 3 (false-positive samples) had the most negative average δ^{13}C protein values of −26.7 ± 0.5‰. A Δ(honey-protein) shift of 0.4‰ (the difference between average δ^{13}C protein values of passed and false-positive samples) equates to an extra 2.8% of C-4 sugar.

A subset of 376 bioactive manuka honeys (Table 3) was selected from the 757 manuka samples, with NPA levels ranging from 4+ to 29.5+ to ensure a minimum level of floral purity (NPA content is considered to be unique to manuka honey and not yet reported in other honey types). From this group, 205 samples had apparent C-4 sugars ≤7% (55%), and 171 samples had apparent C-4 sugars >7% (45%), similar to the overall manuka population screened in this study. These 376 bioactive manuka honeys had δ^{13}C honey values between −21.0 and −26.8‰, δ^{13}C protein values between −24.5 and −27.9‰, and apparent C-4 sugars ranged from −3.9 to 24.5%.

NPA was plotted against apparent C-4 sugar content, and the rate of failure (where apparent C-4 sugars exceed 7%) for high, medium, and low NPA samples was documented in Table 3. Higher NPA honey (17+ to 30+) had the highest apparent C-4 sugar fail rate at 81%, and medium NPA rated honey (10+ to 17+) failed at 61%, whereas only 11% of low NPA rated honey (4+ to 10+) had apparent C-4 sugars >7% (Figure 5a). High rates of failure for high NPA manuka honey were not consistent with excess sugar syrup feeding. High NPA manuka honeys were expected to have the highest nectar purity due to their higher concentrations of methylglyoxal (key active component in NPA manuka honey), which would become diluted if C-4 syrups were fed to bees. The predisposition of high NPA manuka honey to fail and have high apparent C-4 sugar content gives a strong indication toward the cause for false-positive results.

Although the production of methylglyoxal (the compound responsible for high NPA) in manuka honey has been shown to be formed via a conversion pathway of dihydroxyacetone (DHA),[18] the mechanisms and interactions with other compounds that may catalyze the reaction are poorly understood. However, current knowledge suggests that temperature, pressure, humidity, and storage time also have critical effects on manuka honey quality and bioactivity.[21] The issue now becomes one of understanding the effects chemical reactions, which may induce fractionation effects on honey or protein such as the conversion of DHA to methylglyoxal (the chemical reaction that increases NPA) resulting in an increase of the apparent C-4 sugars in higher NPA manuka honey.

These same samples were compared again on the basis of a proposed δ^{13}C manuka honey acceptance threshold of −24.7‰ (suggested by the upper limit of region 3 in this study), where all New Zealand manuka honey with δ^{13}C honey values that are more negative than −24.7‰ are considered genuine, even if they pass or fail (Figure 5b). Of these samples, only manuka honey with apparent C-4 sugars <13% are used (Figure 5b). This value is determined from the range of apparent C-4 sugar values when the proposed δ^{13}C honey value threshold of −24.7 ‰ is applied. Using this carbon isotope threshold, the failure rate of high NPA manuka honeys (17+ to 30+) was significantly reduced with only 29% of these honeys having δ^{13}C honey values > −24.7‰. Medium (10+ to 17+) and low (4+ to 10+) NPA manuka honeys also had significantly reduced failure rates (34 and 3%, respectively) when the proposed carbon isotope threshold was used (Table 3). The failure rate of the entire subset of NPA manuka honey samples was reduced to 20% (where these failed samples had δ^{13}C honey values ≥ −24.7‰). These remaining failed samples may have some C-4 sugar contamination, but currently there is insufficient evidence to provide a robust explanation for some other mechanism contributing toward more positive carbon isotope values. In the future, more research should be conducted to understand mixing of unusual New Zealand nectar sources (tawari with its average nectar values of −24.5‰ is a key example), and/or fractionation effects via some synergistic/reactive mechanism occurring within the honey, which can alter the carbon isotopes to become more positive.

Why Do Some Other (Nonmanuka) Honey Varieties Fail? In this study, ling honey was found to have the most negative δ^{13}C protein values (average −27.3‰). It is likely this thixotropic honey has a chemical reaction or mechanism occurring within the honey that affects its protein isotopic composition similar to manuka honey. Thixotropic honeys such as manuka and ling contain a higher protein content, primarily derived from plant proteins, rather than from bee enzymes typical of many nonthixotropic honeys,[22] suggesting that there may be other thixotropic honey types from elsewhere around

the globe that also behave in a similar fashion and will have a higher tendency to fail the AOAC 998.12 method.

Tawari honey has also been found to have more positive carbon isotope values than all other New Zealand honey floral sources, where the average δ^{13}C honey value was −24.5‰, and also prone to fail C-4 sugar tests. The consequence of a tawari nectar contribution to honey derived from other floral nectars may increase their failure rate, as the resulting δ^{13}C honey values would shift to more positive values. Contamination of manuka honey by tawari nectar may be responsible for some manuka honey fails, especially when δ^{13}C manuka honey values are > −25.1‰ (average manuka δ^{13}C honey value), as concurrent flowering of the two species often takes place in the North Island of New Zealand, where much of the bioactive manuka honey is produced.

Laboratory observations during AOAC 998.12 analysis have shown that tawari honey often contains relatively low levels of extractable protein, so the corresponding protein of a manuka/tawari blend would not exhibit a similar positive shift, and it would appear that the sample contains excess C-4 sugars. An indication of this possible effect has also been observed by the presence of tawari pollen in some failed manuka honeys (personal observation by Rogers). Further studies using tawari and manuka plant-specific chemical markers would also confirm this interaction. Rewarewa and kamahi also have similar flowering times as manuka and kanuka, and it is possible that bees could collect these nectars concurrently with bioactive manuka and/or tawari nectar in sufficient quantities to cause a false-positive fail. In the future, examination of these honey varieties using specific chemical biomarkers, sugar profiles, or pollen counts may clarify mixing.

In conclusion, specific New Zealand floral varieties (blue borage, clover, dandelion, honeydew, kanuka, manuka blend, multifloral, pohutukawa, rata, thyme, and vipers bugloss honeys) do not exceed 7% apparent C-4 sugar when tested using the AOAC 998.12 method. These honeys are not prone to false-positive results, nor would they show apparent C-4 sugar contamination unless excess C-4 sugar feeding has occurred. However, in some cases, sample numbers are not statistically significant, and further isotope characterization of some monofloral varieties would be complementary. It is expected that if beekeepers continue feeding minimal sugar and bees do not rob sugar from other nearby sources (up to a flight radius of 6 km, which is the effective foraging distance for a bee)[23] and if nectar flows are strong and hive management practices are not significantly changed from one season to the next, then these specific floral types will continue to meet current AOAC 998.12 C-4 sugar method criteria.

This study highlights that higher apparent C-4 sugar contents not only occur when the δ^{13}C honey value becomes more positive (by addition of C-4 sugars or another undocumented effect) but also when the δ^{13}C protein value becomes more negative. In the absence of C-4 sugar addition, false-positive results occur where the δ^{13}C protein value becomes more negative during the honey ripening process and artificially elevates the apparent C-4 sugar content of honey. This research shows a strong tendency for manuka honey, particularly higher NPA rated manuka honey (NPA > 10+), which has undergone ripening, to have apparent C-4 sugars that exceed 7% and hence fail acceptance criteria for the AOAC 998.12 C-4 sugar method. Lesser studied honeys such as kamahi, tawari, and ling have also shown a tendency to fail the AOAC 998.12 method. In a subsequent paper, the relationship of apparent C-4 sugar content of manuka honey with NPA > 10+ is discussed. Specifically, the ripening effects of heating and/or storage of higher bioactive manuka honey on apparent C4 sugars are investigated.[21]

To improve the interpretation of the AOAC 998.12 acceptance criteria for New Zealand manuka honey and avoid false-positive fails, the following amendment to the AOAC 998.12 method is suggested:

> *Pure honey (free of corn or cane sugars) yields a value of "apparent" C-4 sugars of ≤7%. New Zealand's manuka honey may exceed this value, but will have honey δ^{13}C values which are in the normal range (more negative than −24.7‰) and an apparent C-4 sugar content no greater than 13.0% (this study and ref 20).*

AUTHOR INFORMATION

Corresponding Author

*(K.M.R.) Phone: +644 5704636. Fax: + 644 5704657. E-mail: k.rogers@gns.cri.nz.

Funding

We are grateful to AGMARDT, Ministry for Primary Industries and New Zealand honey industry cofunders for financial support of this project. Research has also been supported by GNS Science Direct Core Funding (DCF).

Notes

The authors declare no competing financial interest.

ACKNOWLEDGMENTS

We thank numerous New Zealand beekeepers who contributed honey samples and generously shared information about their samples and production practices, with particular thanks to NZ Manuka Ltd. for NPA data. We also thank. Jonathan Stephens (Comvita New Zealand Ltd), Linda Newstrom-Lloyd (Trees for Bees), and Barry Foster (Beekeeper and National Beekeeping Association President 2012−2013) for supplying nectar and pollen samples.

REFERENCES

(1) AOAC Official Method 998.12: C-4 plant sugars in honey. In *Official Methods of Analysis of AOAC International*, 16th ed.; Cunniff, P., Ed.; AOAC International: Gaithersburg, MD, USA, 1999; Vol. 2, pp 27−30.

(2) White, J. W.; Doner, L. W. Mass spectrometric detection of high-fructose corn syrup in honey by use of ^{13}C/^{12}C ratio: collaborative study. *J. Assoc. Off. Anal. Chem.* **1978**, *61*, 746−750.

(3) White, J. W.; Winters, K. Honey protein as internal standard for stable carbon isotope ratio detection of adulteration honey. *J. Assoc. Off. Anal. Chem* **1989**, *72*, 907−911.

(4) Elflein, L.; Raezke, K. P. Improved detection of honey adulteration by measuring differences between ^{13}C/^{12}C stable carbon isotope ratios of protein and sugar compounds with a combination of elemental analyzer−isotope ratio mass spectrometry and liquid chromatography−isotope ratio mass spectrometry (δ^{13}C-EA/LC-IRMS). *Apidologie* **2008**, *39*, 574−587.

(5) Padovan, G. J.; De Jong, D.; Rodrigues, L. P.; Marchini, J. S. Detection of adulteration of commercial honey samples by the ^{13}C/^{12}C isotopic ratio. *Food Chem.* **2003**, *82*, 633.

(6) Kropf, U.; Golob, T.; Necemer, M.; Kump, P.; Korosec, M.; Bertoncelj, J.; Ogrinc, N. Carbon and nitrogen natural stable isotopes in Slovene honey: adulteration and botanical and geographical aspects. *J. Agric. Food Chem.* **2010**, *58*, 12794−12803.

(7) AOAC Official Method 998.12. C-4 plant sugars in honey, first revision; AOAC International: Gaithersburg, MD, USA, 2013; 44.4.18A.

(8) Cotte, J. F.; Casabianca, H.; Chardon, S.; Lheritier, J.; Grenier-Loustalot, M. F. Application of carbohydrate analysis to verify honey authenticity. *J. Chromatogr., A* **2003**, *1021*, 145−155.
(9) Cabanero, A. I.; Recio, J. L.; Ruperez, M. Liquid chromatography coupled to isotope ratio mass spectrometry: a new perspective on honey adulteration detection. *J. Agric. Food Chem.* **2006**, *54*, 9719−9727.
(10) Rogers, K. M.; Somerton, K.; Rogers, P.; Cox, J. Eliminating false positive C-4 sugar tests on New Zealand manuka honey. *Rapid Commun. Mass Spectrom.* **2010**, *24*, 2370−2374.
(11) Rogers, K. M.; Cook, J.; Krueger, D.; Beckmann, K. Report of an inter laboratory comparison exercise: modification of AOAC Official Method 998.12 to add filtration and/or centrifugation. *J. AOAC Int.* **2013**, *96*, 607−614, DOI: 10.5740/jaoacint.12-386.
(12) Cotte, J. F.; Casabianca, H.; Lhéritier, J.; Perrucchietti, C.; Sanglar, C.; Waton, H.; Grenier-Loustalot, M. F. Study and validity of ^{13}C stable carbon isotopic ratio analysis by mass spectrometry and ^{2}H site-specific natural isotopic fractionation by nuclear magnetic resonance isotopic measurements to characterize and control the authenticity of honey. *Anal. Chim. Acta* **2007**, *582*, 125−136.
(13) Codex Alimentarius, Revised Codex Standard for Honey (rev. 2, 2001). AOAC Official Method 998.12. C-4 plant sugars in honey. In *Official Methods of Analysis of AOAC International*, 16th ed.; Cunniff, P., Ed.; AOAC International: Gaithersburg, MD, 1999; Vol. 2, pp 27−30.
(14) Brooks, J. R.; Buchmann, N.; Phillips, S.; Ehleringer, B.; Evans, R. D.; Lott, M.; Martinelli, L. A.; Pockman, W. T.; Sandquist, D.; Sparks, J. P.; Sperry, L.; Williams, D.; Ehleringer, J. R. Heavy and light beer: a carbon isotope approach to detect C(4) carbon in beers of different origins, styles, and prices. *J. Agric. Food Chem.* **2002**, *50*, 6413−6418.
(15) Jahren, A. H.; Saudek, C.; Yeung, E. H.; Kao, W. H.; Kraft, R. A.; Caballero, B. An isotopic method for quantifying sweeteners derived from corn and sugar cane. *Am. J. Clin. Nutr.* **2006**, *84*, 1380−1384.
(16) Rogers, K. M. Nitrogen isotopes as a screening tool to determine the growing regimen of some organic and nonorganic supermarket produce from New Zealand. *J. Agric. Food Chem.* **2008**, *56*, 4078−4083.
(17) Rogers, K. M. Stable isotopes as a tool to differentiate eggs laid by caged, barn, free range, and organic hens. *J. Agric. Food Chem.* **2009**, *57*, 4236−4242.
(18) Adams, C. J.; Manley-Harris, M.; Molan, P. C. The origin of methylglyoxal in New Zealand Manuka (*Leptospermum scoparium*) honey. *Carbohydr. Res.* **2009**, *344*, 1050−1053.
(19) Kato, Y.; Umeda, N.; Maeda, A.; Matsumoto, D.; Kitamoto, N.; Kikuzaki, H. Identification of a novel glycoside, leptosin, as a chemical marker of manuka honey. *J. Agric. Food Chem.* **2012**, *60*, 3418−3423.
(20) White, J. W.; Bryant, W. M.; Jones, J. G. Adulteration testing of southwestern desert honeys. *Am. Bee J.* **1991**, *131*, 123−126.
(21) Rogers, K. M.; Grainger, M.; Manley-Harris, M. The unique manuka effect: why New Zealand manuka honey fails the AOAC 998.12 C-4 sugar method. *J. Agric. Food Chem.* **2014**, DOI: 10.1021/jf404767b.
(22) White, J. W. Honey protein as internal standard for stable carbon isotope ratio detection of adulteration of honey. *J. Assoc. Off. Anal. Chem.* **1989**, *72*, 907−911.
(23) Hagler, J. R.; Mueller, S.; Teuber, L. R.; Machtley, S. A.; Van Deynze, A. Foraging range of honey bees, *Apis mellifera*, in alfalfa seed production fields. *J. Insect Sci.* **2011**, *11*, 144 (available online: insectscience.org/11.144).

Table 1. Honey and Protein Carbon Isotopes, Apparent C-4 Sugar Content, DHA Remaining, MGO and HMF Contents, and DHA/MGO Ratio of Honey Inoculated with Various Levels of DHA Incubated at 37 °C for 83 Days[a]

DHA dosage (mg kg^{-1})	δ^{13}C honey (‰)	δ^{13}C protein (‰)	apparent C-4 sugars (%)	DHA (mg kg^{-1})	MGO (mg kg^{-1})	HMF (mg kg^{-1})	DHA/MGO
0 (t = 0)	−26.3	−26.8	2.8	0.0	35.9	64.0	0
0 (t = 83)	−26.3	−26.8	2.8	0.0	39.1	86.0	0
250	−26.4	−26.9	2.8	105.9	87.4	94.6	1.2
500	−26.3	−26.9	3.0	290.4	140.9	86.7	2.1
1000	−26.4	−27.0	3.3	544.0	249.2	95.1	2.2
2000	−26.4	−27.1	3.6	1119.4	477.6	92.9	2.3
4000	−26.4	−27.2	3.9	2196.5	893.4	98.5	2.5
8000	−26.3	−27.3	5.0	4127.3	1649.3	102.2	2.5

[a]Values are reported as an average of three replicates. SDs are within 0.1‰ for isotopes and percentage relative SD of DHA, MGO, and HMF is <5%.

Clover Trial Samples. A 48000 mg kg^{-1} stock solution of DHA, supplied by Sigma-Aldrich, in type I water was prepared and diluted to give final concentrations of 8000, 4000, 2000, 1000, 500, 250, and 0 mg kg^{-1} DHA in honey. HappyBee clover blend honey (60 g) was weighed out, 1 mL of the corresponding DHA stock solution was added, and samples were thoroughly mixed. The control sample (0 mg kg^{-1} DHA) had 1 mL of type 1 water added. Replicate samples were incubated at 37 °C and tested after 83 days.

Manuka Trial Samples. Pure manuka honey samples were selected from four different regions in the southern North Island of New Zealand to see if common patterns existed during the aging of manuka honey. Samples were harvested from December 2011 to January 2012. Samples were held at 20 °C until the study began in October 2012. Replicate splits of each sample were taken in October 2012, with two sample splits (control) being frozen immediately to arrest any chemical transformations and the other paired splits being incubated at 27, 32, and 37 °C; samples withdrawn periodically (t = 21, 63, 151, and 241 days) and immediately frozen. Samples were analyzed for methylglyoxal, dihydroxyacetone, and hydroxymethylfurfural contents and carbon isotope ratios (δ^{13}C) of the honey and extracted protein.[14]

Analysis of DHA, MGO, and HMF. HA (3.34 mg mL^{-1}) was used as the internal standard solution. The PFBHA derivatizing solution (20 mg mL^{-1}) was made up in citrate buffer (0.1M) and adjusted to pH 4 with NaOH (4 M).

A six-point calibration curve was made up for each compound (DHA, MGO, and HMF) using a multicompound standard solution. Standards were made up in an artificial honey matrix (0.20 ± 0.02 g). The artificial honey comprised fructose (41%), glucose (37.5%), sucrose (2.9%), and water (18.6%), and the pH ranged from 3.13 to 3.76, reflecting the pH of honey[12] and so did not need to be adjusted. HA (internal standard, 250 μL), DHA stock (100 μL), and MGO + HMF stock (40 μL) were added, mixed, and left for 1 h. PFBHA derivatization solution (1200 μL) was added and mixed. Samples were left for 1 h to complete derivatization. Acetonitrile (6 mL) was added and the sample mixed until all crystals dissolved; water (2 mL) was added, and the standards were mixed before being transferred to autosampler vials and analyzed. A linear calibration curve was constructed using the HPLC peak area ratios of DHA/HA, MGO peak 1 + MGO peak 2/HA, and HMF peak 1/HA against the mass of the compounds.

Variability of the PFBHA method was determined by analyzing triplicate samples of each manuka honey over 4 days. This introduced real-world variability (such as sample preparation and instrumentation). The percentage relative standard deviation is <5% for all three compounds, and values are reported as averages.

Sample Preparation. Honey samples (0.20 ± 0.02 g) were weighed into test tubes, HA (internal standard, 250 μL) was added, and the sample was mixed and left for 1 h, at which time PFBHA derivatizing solution (1,200 μL) was added, mixed, and left for a further hour. ACN (6 mL) was added and mixed until all crystals were dissolved; water (2 mL) was added and mixed before analysis.

HPLC Method. HPLC to determine DHA, MGO and HMF was performed at the University of Waikato on an HPLC system fitted with two Waters 515 pumps, a 996 photodiode array (PDA) detector (240−400 nm), an autosampler (set at 20 °C), and an Alltech Elite degassing system. A Symmetry shield RP18 column (5 μm, 3.0 × 250 cm) was used for separation of compounds; a 20 μL injection was used. The system was controlled using Waters Empower 2 chromatography software. The system was operated with gradient elution using 30:70 (v/v) ACN/H_2O as mobile phase A and 100% ACN as mobile phase B. The gradient elution was run at a constant combined flow rate of 0.8 mL min^{-1}. Gradient steps were (%B) 0 (10), 2.5 (10), 10.5 (50), 18 (100), 25 (10), and 35 (10). DHA and HA were quantified at 260 nm; HMF and MGO were quantified at 279 and 244 nm, respectively.

C-4 Sugar Determination. δ^{13}C values of honey and corresponding extracted protein were measured using stable isotope analyses according to the internationally used AOAC 998.12 method.[7] Honey and extracted protein (~0.5 mg) were transferred into 6 × 4 mm tin capsules. Samples were analyzed at the Stable Isotope Laboratory at GNS Science, using a Eurovector elemental analyzer coupled to an Isoprime mass spectrometer, for isotopic abundance in continuous flow mode (EA-IRMS). International and working reference standards (IAEA-CH_6, leucine, EDTA, and cane and beet sugars), two honey standards (honey and protein), and blanks were included during each run for calibration. Isotopic ratios (^{13}C/^{12}C) are expressed as isotopic deviations δ defined as

$$\delta\ (\%) = \frac{R_s - R_{ref}}{R_{ref}} \times 1000$$

where R_s is the isotopic ratio measured for the sample and R_{ref} that of the international standards. The δ^{13}C value is relative to the international Vienna Pee Dee Belemnite (VPDB) standard. Results are expressed in δ (‰) versus the specific reference, and analytical precision is within ±0.2‰ for carbon. Apparent C-4 sugar content is calculated by

$$\text{apparent C-4 sugars (\%)} = [\delta^{13}\text{C(protein)} - \delta^{13}\text{C(honey)}]/[\delta^{13}\text{C(protein)} - (-9.7)] \times 100$$

where AOAC 998.12 method interprets pure honey as generally yielding a value of C-4 sugars of ≤7%. Some unusual varieties may slightly exceed the range, but will have δ^{13}C values for honey that are in the normal range (more negative than −24.0‰).[7] It is noted that apparent C-4 sugar is not a direct measurement of actual C-4 sugar levels but an estimation based on the positive δ^{13}C shift that occurs when C-4 sugars (which range from δ^{13}C ~9.7 to 11‰) are added to honey (typically ranging from δ^{13}C ~−24 to −27‰ in New Zealand).[8]

RESULTS AND DISCUSSION

Addition of Synthetic DHA to Clover Honey. Clover honey (which neither displays nonperoxide antibacterial activity nor contains measurable DHA) was used as matrix to investigate the effect of higher levels of DHA and MGO on the apparent C-4 sugar assay. Prior to any addition of DHA, the baseline DHA and MGO contents of the clover honey were tested and were 0 and 35.9 mg kg^{-1}, respectively (Table 1); the MGO result for clover honey is higher than would be expected but may be due to some analytical background interference. Clover honey samples were inoculated with DHA at various concentrations from 0 to 8000 mg kg^{-1} and incubated (37 °C, 83 days) with testing for DHA, MGO, and HMF at 0, 35, and 83 days and for apparent C-4 sugars at 0 and 83 days. At 35 and 83 days clover honeys to which DHA had been added were assayed for MGO content (Figure 1). Results showed

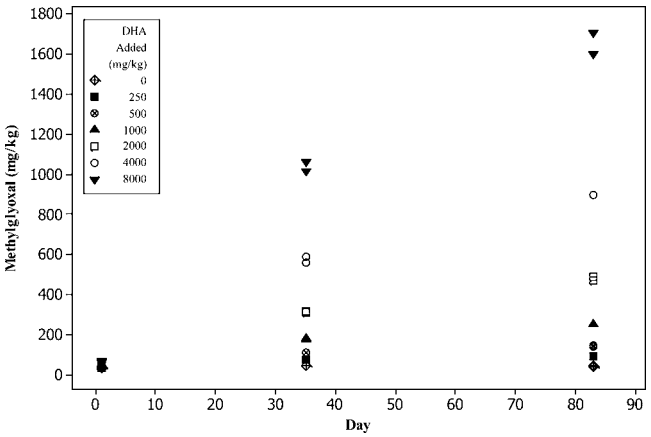

Figure 1. MGO levels (mg kg^{-1}) in replicate clover honey samples after 0, 35, and 83 days of incubation at 37 °C with different additions of DHA (mg kg^{-1}) at 0 days. (Some replicates have excellent repeatability and lie on top of the first point.)

decreased levels of DHA, increased levels of MGO (Table 1), as has been observed previously,[4] and increased levels of HMF. The highest levels of MGO and HMF observed in this trial were 1649 and 102.2 mg kg^{-1}, respectively.

At 0 and 83 days, apparent C-4 sugars were assayed (Table 1; Figure 2). At 0 days, apparent C-4 sugars were 2.8% and were comparable with an average clover honey.[8] After 83 days of incubation, the control sample still measured 2.8% apparent C-4 sugars, but the apparent C-4 sugar content of clover honey with the highest DHA addition (8000 mg kg^{-1}) was 5.0% (a 78.6% increase), the DHA content had decreased (4127 mg kg^{-1}), and the MGO content had increased (1649 mg kg^{-1}) (Figure 2). The ratio of DHA/MGO observed after 83 days was 2.0, similar to that usually observed in mature manuka honey.[15,16]

The HMF level of the clover honey before the trial (at t = 0 days) was 64 mg kg^{-1}, which exceeded recommended Codex limits at the time of purchase. After maturation at 37 °C for 83 days, the clover honey had darkened from a light brown color (at t = 0 days) to a rich caramel color and attained a maximum HMF level (in the DHA, 8000 mg kg^{-1} sample) of 102 mg kg^{-1}. The color and HMF changes are expected given the high temperature and length of incubation. A similar conversion of DHA to MGO might be achieved by using a lower temperature and a longer storage time without the formation of the high

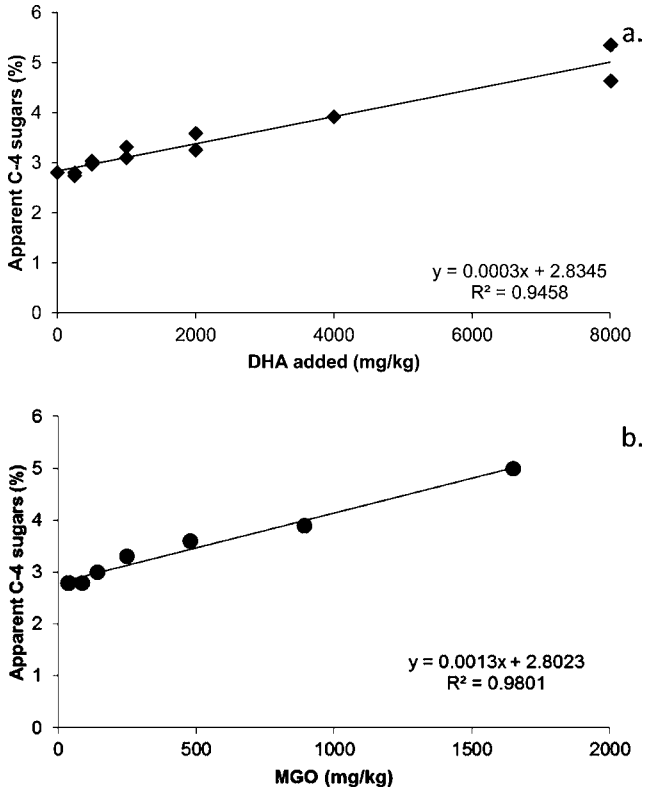

Figure 2. (a) Evolution of apparent C-4 sugars in clover honey after 83 days of incubation at 37 °C after different additions of DHA (mg kg^{-1}) at 0 days; (b) apparent C-4 sugars and corresponding MGO (mg kg^{-1}) evolved in clover honey after 83 days.

levels of HMF because the two reactions, although occurring simultaneously, are not chemically related.

All DHA inoculated clover samples and the clover honey control sample had the same δ^{13}C honey value of −26.4 ± 0.1‰, and these were not found to vary during the trial (Table 1). In contrast, the δ^{13}C protein values, which were unchanged in the control sample between 0 and 83 days, showed an increasing negative trend with increasing initial DHA content; this caused a progressive increase in $\Delta(\delta^{13}$C honey-protein) and apparent C-4 sugars (Table 1). This suggests that freshly harvested honey with a higher initial DHA content would be more likely to fail the AOAC 998.12 C-4 test once maturation had occurred because the chemical reaction converting DHA to MGO was in some way affecting the protein in the honey, causing a false-positive fail. Adams et al.[4] demonstrated that conversion of DHA to MGO was not stoichiometric; that is, not all DHA lost had been converted to MGO, suggesting that DHA and possibly MGO were reacting with other honey components. Other possible reactions that DHA or MGO might undergo include Maillard-type reactions with proteins and/or amino acids. It has been reported that DHA was more reactive with amino acids than glucose; more specifically, basic amino acids (proline, lysine, etc.) were the most reactive with DHA.[17] High concentrations of sugar relative to amino acid and low water activity, both being conditions that pertain in honey, might accelerate the reaction.

MGO is well-known for its capacity to react with and cross-link protein chains.[18] The effect of these Maillard-type reactions would be to reduce the apparent content of amino acids; further cross-linking may also change the solubility and cause

Table 2. Incubation Time, Incubation Temperature, Average DHA, HMF, and MG Contents, and Apparent C-4 Sugar Content of Four Manuka Honeys (Samples 1−4)[a]

sample	time (days)	temp (°C)	DHA (mg kg^{-1})	DHA remaining (%)	HMF (mg kg^{-1})	MGO (mg kg^{-1})	δ^{13}C honey (‰)	δ^{13}C protein (‰)	C-4 sugars (%)	DHA/ MGO
1	0	27	1612.4	100	7.3	178.5	−25.9	−26.6	4.2	9.0
1	63	27	1414.4	87.8	9.8	289.1	−25.9	−26.7	4.9	4.9
1	151	27	1051.6	65.2	15.5	386.1	−25.9	−26.8	5.4	2.7
1	241	27	746.4	46.3	48.7	500.9	−26.0	−27.0	6.1	1.5
1	0	32	1612.4	100	7.3	178.5	−25.9	−26.6	4.2	9.0
1	63	32	1242.0	77.0	13.3	337.7	−25.9	−26.8	5.6	3.7
1	151	32	816.0	50.6	27.0	419.5	−26.0	−27.0	6.6	1.9
1	241	32	557.9	34.6	68.7	459.7	−25.9	−27.2	8.0	1.2
1	0	37	1612.4	100	7.3	178.5	−25.9	−26.6	4.2	9.0
1	21	37	1350.6	83.8	12.7	282.9	−25.9	−27.0	5.0	4.8
1	63	37	950.1	58.9	28.3	369.6	−25.9	−26.9	6.3	2.6
1	151	37	468.4	29.0	75.9	393.3	−25.9	−27.2	7.9	1.2
1	241	37	294.4	18.3	213.1	364.6	−25.9	−27.7	11.1	0.8
2	0	27	2376.6	100	7.9	283.6	−25.3	−26.6	8.3	8.4
2	63	27	2005.9	84.4	10.0	404.0	−25.3	−26.7	9.0	5.0
2	151	27	1677.5	70.6	15.6	565.5	−25.3	−26.9	10.3	3.0
2	241	27	1116.3	47.0	46.9	734.3	−25.3	−27.0	10.9	1.5
2	0	32	2376.6	100	7.9	283.6	−25.3	−26.6	8.3	8.4
2	63	32	1705.8	71.8	12.8	485.5	−25.3	−26.8	9.8	3.5
2	151	32	1302.1	54.8	27.6	625.7	−25.3	−27.1	11.5	2.1
2	241	32	782.7	32.9	71.0	706.4	−25.2	−27.2	12.9	1.1
2	0	37	2376.6	100	7.9	283.6	−25.3	−26.6	8.3	8.4
2	21	37	1916.0	80.6	11.0	389.4	−25.2	−26.6	8.9	4.9
2	63	37	1332.1	56.1	25.3	559.2	−25.3	−27.1	11.9	2.4
2	151	37	780.4	32.8	83.3	627.8	−25.3	−27.2	12.4	1.2
2	241	37	444.4	18.7	200.7	641.5	−25.6	−27.6	12.6	0.7
3	0	27	2367.0	100	6.7	313.8	−25.2	−26.0	4.8	7.5
3	63	27	2204.5	93.1	11.5	468.7	−25.2	−26.1	5.7	4.7
3	151	27	1733.3	73.2	14.3	592.9	−25.2	−26.2	6.4	2.9
3	241	27	1154.3	48.8	51.5	805.4	−25.2	−26.6	9.0	1.4
3	0	32	2367.0	100	6.7	313.8	−25.2	−26.0	4.8	7.5
3	63	32	1964.6	83.0	15.5	538.6	−25.2	−26.2	6.4	3.6
3	151	32	1367.4	57.8	25.6	658.1	−25.2	−26.4	7.1	2.1
3	241	32	824.7	34.8	73.9	755.4	−25.2	−26.7	9.7	1.1
3	0	37	2367.0	100	6.7	313.8	−25.2	−26.0	4.8	7.5
3	21	37	2104.7	88.9	12.5	385.0	−25.2	−26.0	5.4	5.5
3	63	37	1525.2	64.4	29.6	467.4	−25.2	−26.4	7.7	3.3
3	151	37	814.3	34.4	73.7	652.1	−25.2	−26.7	9.5	1.2
3	241	37	460.5	19.4	199.7	669.8	−25.2	−26.9	11.0	0.7
4	0	27	3242.6	100	9.2	315.7	−26.1	−26.7	3.9	10.3
4	63	27	2964.6	91.4	11.9	459.2	−26.0	−27.1	6.7	6.5
4	151	27	2526.7	77.9	15.2	692.1	−26.0	−27.3	7.7	3.7
4	241	27	1811.0	55.9	33.1	950.0	−26.0	−27.5	9.2	1.9
4	0	32	3242.6	100	9.2	315.7	−26.1	−26.7	3.9	10.3
4	63	32	2579.2	79.5	14.7	538.1	−26.0	−27.1	6.7	4.8
4	151	32	2035.7	62.8	26.6	753.9	−26.0	−27.2	9.0	2.7
4	241	32	1375.5	42.4	47.3	964.0	−26.0	−27.7	10.4	1.4
4	0	37	3242.6	100	9.2	315.7	−26.1	−26.7	3.9	10.3
4	21	37	2849.0	87.9	14.7	473.3	−26.0	−27.0	5.9	6.0
4	63	37	2149.9	66.3	26.5	665.3	−26.0	−27.2	7.3	3.2
4	151	37	1378.7	42.5	73.2	883.2	−26.0	−27.5	9.3	1.6
4	241	37	832.5	25.7	164.8	972.1	−26.0	−28.1	12.9	0.9

[a]Values are reported as an average of three replicates. SDs are within 0.1‰ for isotopes, and percentage relative SD of DHA, MGO, and HMF is <5%.

dx.doi.org/10.1021/jf404767b | J. Agric. Food Chem. 2014, 62, 2615−2622

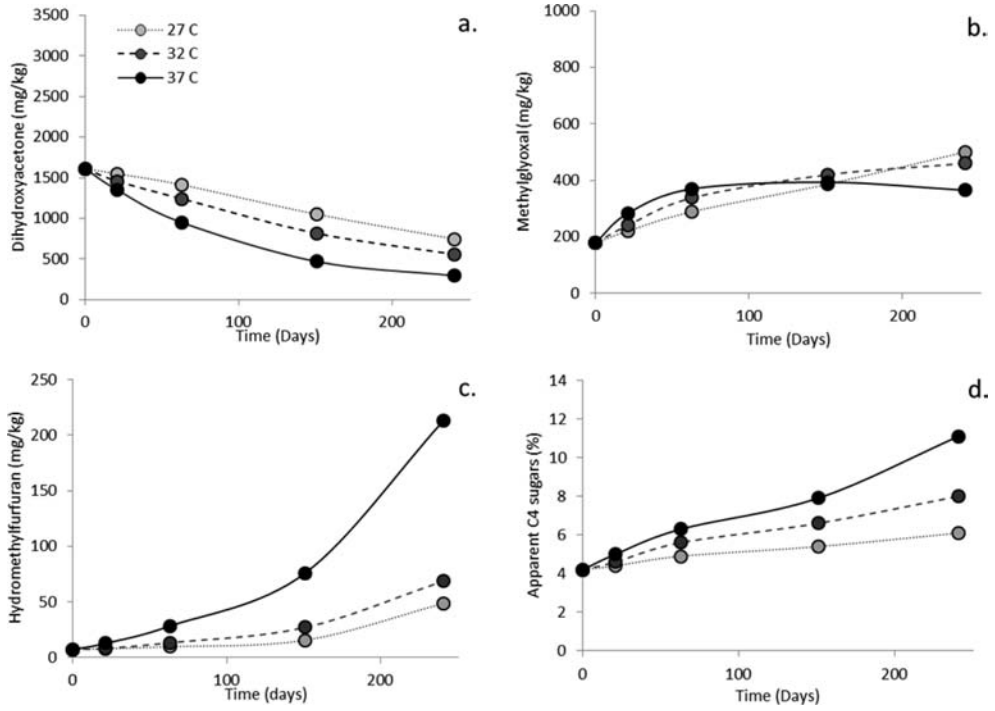

Figure 3. (a) DHA, (b) MGO, (c) HMF (mg kg^{-1}), and (d) apparent C-4 sugar contents (%) of manuka honey sample 1.

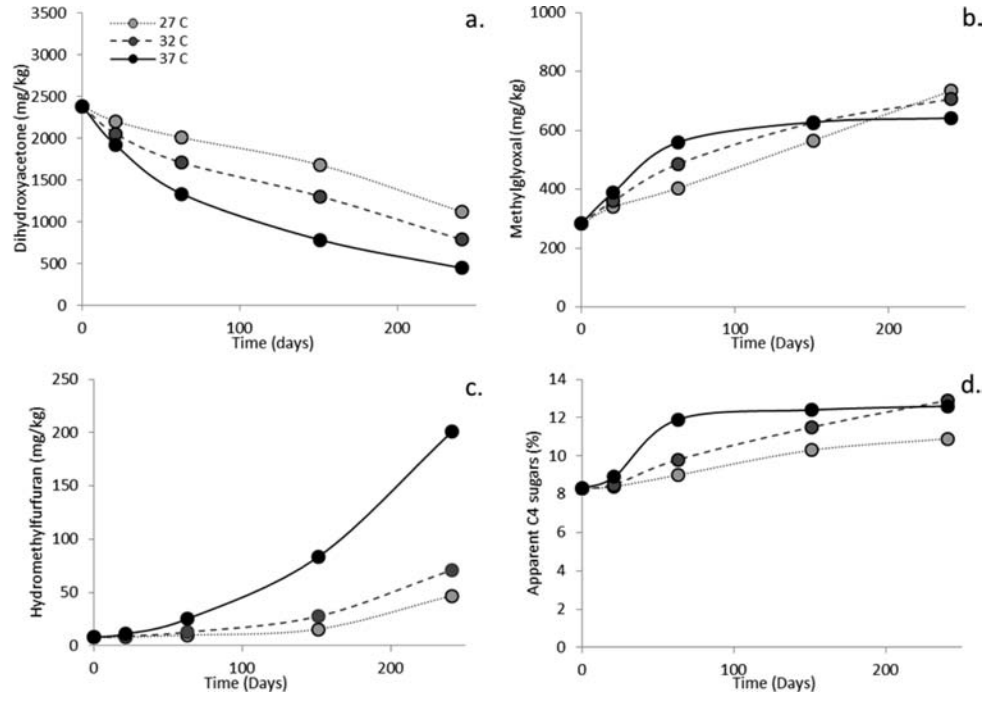

Figure 4. (a) DHA, (b) MGO, (c) HMF (mg kg^{-1}), and (d) apparent C-4 sugar contents (%) of manuka honey sample 2.

aggregation of protein. Such phenomena have been well reported in the production of milk powder.[19−21]

Isotopic enrichment of amino acids in plant seeds and leaves has been studied using LC-IRMS[22] over a range of plant types; the mean $\Delta^{13}C$ values (difference from mean $\delta^{13}C$ for all amino acids) for lysine for leaf and seed were 1.9 and 1.3, respectively. The difference between leaf and seed for lysine was significant, and it might be expected that nectar and hence honey may differ somewhat from these figures. However, it is clear that the loss of an amino acid that makes a positive contribution to the mean would render the mean more negative, similar to the more negative shift seen in clover honey $\delta^{13}C$ protein values (Table 1). A similar positive contribution by lysine was observed in plants in an earlier study.[23] Furthermore, following the demonstrated transfer of essential amino acids including lysine from pollen to eggs of the butterfly *Heliconius charitonia*,[24] it can be assumed that lysine originating from the plant might be transferred to larval bees and hence that contributions from the bee to the honey would have similar

dx.doi.org/10.1021/jf404767b | J. Agric. Food Chem. 2014, 62, 2615−2622

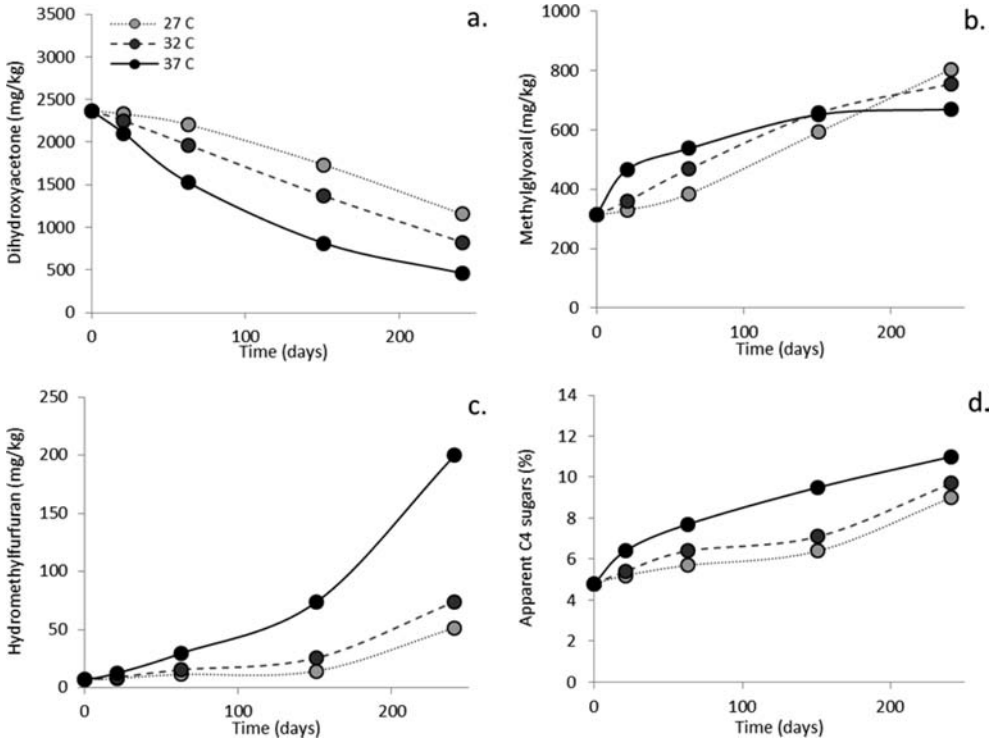

Figure 5. (a) DHA, (b) MGO, (c) HMF (mg kg^{-1}), and (d) apparent C-4 sugar contents (%) of manuka honey sample 3.

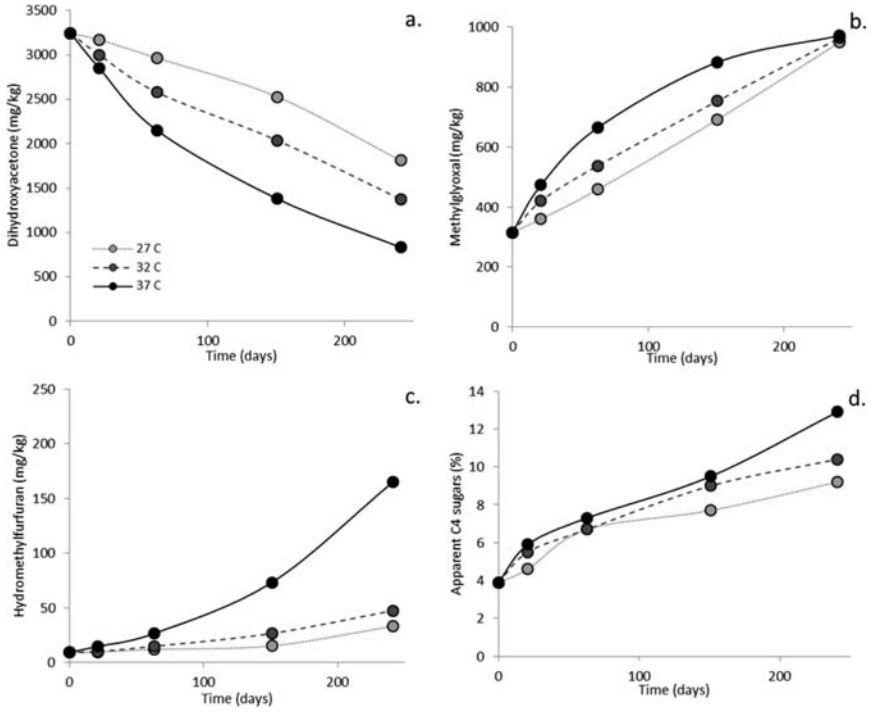

Figure 6. (a) DHA, (b) MGO, (c) HMF (mg kg^{-1}), and (d) apparent C-4 sugar contents (%) of manuka honey sample 4.

stable isotope values as the plants from which the bee derives pollen.

Manuka Honey. Four manuka honeys with different DHA and MGO contents were selected for storage trials to assess apparent C-4 sugar evolution as DHA, MGO, and HMF evolve at 27, 32, and 37 °C over 241 days (Table 2; Figures 3–6). Initial DHA levels ranged from 1612.4 to 3242.6 mg kg^{-1}. At t = 0, all samples had some MGO content ranging from 178.5 to 315.7 mg kg^{-1} (NPA 7.9+ to 11.2+) as they had been harvested and stored at 20 °C for 10 months prior to the trial.

During the course of incubation, DHA content decreased and MGO content increased (Table 2), as previously demonstrated by Adams et al.[4] The highest MGO contents attained in the study were 459.7 mg kg^{-1} in sample 1, 734.3 mg kg^{-1} in sample 2, 805.4 mg kg^{-1} in sample 3, and 972.1 mg kg^{-1} in sample 4 (which equates to NPA values between 14+ and

dx.doi.org/10.1021/jf404767b | J. Agric. Food Chem. 2014, 62, 2615–2622

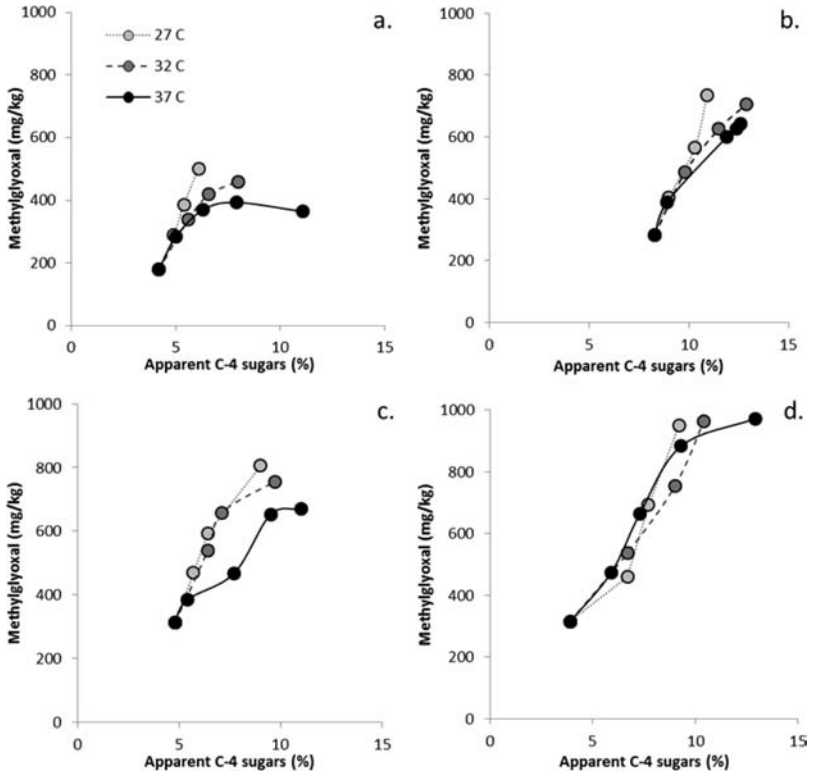

Figure 7. MGO content (mg kg^{-1}) of the four manuka honeys [(a) sample 1; (b) sample 2; (c) sample 3; (d) sample 4] and their corresponding apparent C-4 sugars (%) at 27, 32, and 37 °C.

22+). The highest MGO growth did not always occur in those samples that lost the most DHA (i.e., samples stored at 37 °C for 241 days). After heating at 37 °C, the MGO usually attained a maximum value around 150 days and began to decrease, apart from sample 4, which had a higher initial DHA content than the other samples, so its MGO growth was just attaining its maximum at t = 241 days. At 32 °C, it appeared that all samples except sample 4 were beginning to plateau at a maximum at t = 241 days, whereas sample 4 still had increasing MGO content. At 27 °C, MGO content was still increasing in all samples at t = 241 days, which suggested that at lower storage temperature, MGO content is slower to develop; however, given sufficient time, the MGO content will grow to higher levels than if stored at higher temperatures to accelerate the reaction.

The MGO growth was also accompanied by a similar increasing growth in HMF and apparent C-4 sugars. All four manuka honey samples had initial HMF levels <10 mg kg^{-1}, and by day 241 all but one replicate had exceeded 40 mg kg^{-1} (the Codex recommended threshold), with some in excess of 200 mg kg^{-1}. HMF continued to grow at a much faster rate when the honey was incubated at 37 °C than at 27 or 32 °C.

Apparent C-4 sugars increased with both increasing storage temperature and increasing time. In samples 1, 3, and 4, the apparent C-4 sugars were 4.2, 4.8, and 3.9%, respectively, before incubation, which were well below the permissible AOAC 998.12 C-4 sugar threshold of 7%. Sample 2 had apparent C-4 sugars of 8.3% at 0 days, suggesting a possible apparent C-4 sugar contamination prior to incubation. However, none of these samples were from hives that had undergone sugar feeding prior to nectar collection by bees. Apart from sample 2 at 37 °C, in which apparent C-4 sugars had rapid growth and then remained fairly constant from 63 days onward, all other samples showed steady growth of apparent C-4 sugars over the entire incubation period, and by 151 days, the average apparent C-4 sugars exceeded 7% in all cases regardless of the temperature, suggesting that storage temperatures considerably lower than 27 °C may be a critical factor in retarding the growth of apparent C-4 sugars. A plot of MGO levels and corresponding apparent C-4 sugars of the four manuka honey samples in this study showed that even though MGO growth began to peak and stabilize after t = 150 days, C-4 sugars continued to grow. This phenomenon would explain higher C-4 sugar contents found in older, low NPA or MGO honey (Figure 7). Because DHA and MGO continue to evolve in the jar, even after packaging of honey, the evolution of apparent C-4 sugars would also continue (similar to HMF content) and would be exacerbated when honey is stored at higher ambient temperatures, even for as little as 3 weeks. It is likely that temperatures exceeding 37 °C would increase apparent C-4 sugars at a faster rate.

In this study, the average apparent C-4 sugars of the four manuka honeys after 241 days of storage were 11.1, 12.9, 11.0, and 12.9%, respectively. This research strongly supports the conclusions drawn by Rogers et al.[8] that excess C-4 sugar feeding to bees is not the main cause for C-4 sugars exceeding 7% in New Zealand manuka honey. The key cause is a protein effect, which is activated in the presence of higher levels of DHA and/or MGO found in bioactive manuka honey, which react and cause isotopic fractionation and may also be responsible for other chemical changes.[25] This reaction most likely consumes acidic (^{13}C enriched) amino acids, causing the δ^{13}C protein value to become more negative and thereby generating a bigger Δ (δ^{13}C honey-protein), which artificially enhances the apparent C-4 sugar value as seen after the aging and heating of NPA honey in this study.

dx.doi.org/10.1021/jf404767b | J. Agric. Food Chem. 2014, 62, 2615−2622

When honey is analyzed using the AOAC 998.12 method, unadulterated New Zealand manuka honeys with higher NPA levels (>MGO 260 mg kg^{-1} or > NPA 10+) may have apparent C-4 sugars up to 12.9% (highest C-4 sugar content found in this study), and further increases will occur if the honey is stored for a longer duration at ambient temperature.

We therefore recommend that an exception to the AOAC method 998.12 be considered for all New Zealand manuka honey that has demonstrated DHA and/or MGO levels with the potential to grow beyond MGO > 250 mg kg^{-1}; on the basis of this study and past research,[8] allowable C-4 sugar levels should be at least 13% in manuka honey.

AUTHOR INFORMATION

Corresponding Author

*(K.M.R.) Phone: +644 5704636. Fax: + 644 5704657. E-mail: k.rogers@gns.cri.nz.

Notes

The authors declare no competing financial interest.

ACKNOWLEDGMENTS

We thank Kevin Gibbs for providing honey samples for the trials. We also thank the Stable isotope Laboratory, GNS Science, for stable isotope analyses, and AGMARDT, Ministry for Primary Industry, and New Zealand bee industry members who contributed to this research.

REFERENCES

(1) Allen, K. L.; Molan, P. C.; Reid, G. M. A survey of the antibacterial activity of some New Zealand honeys. *J. Pharm. Pharmacol.* **1991**, *43*, 817−822.

(2) Adams, C. J.; Boult, C. H.; Deadman, B. J.; Farr, J. M.; Grainger, M. N. C.; Manley-Harris, M.; Snow, M. J. Isolation by HPLC and characterization of the bioactive fraction of New Zealand manuka (*Leptospermum scoparium*) honey. *Carbohydr. Res.* **2008**, *343*, 651−659.

(3) Mavric, E.; Wittmann, S.; Barth, G.; Henle, T. Identification and quantification of methylglyoxal as the dominant antibacterial constituent of manuka (*Leptospermum scoparium*) honeys from New Zealand. *Mol. Nutr. Food Res.* **2008**, *52*, 483−489.

(4) Adams, C. J.; Manley-Harris, M.; Molan, P. C. The origin of methylglyoxal in New Zealand manuka (*Leptospermum scoparium*) honey. *Carbohydr. Res.* **2009**, *344*, 1050−1053.

(5) Codex Alimentarius, Revised Codex Standard for Honey (rev. 2, 2001). AOAC Official Method 998.12. C-4 plant sugars in honey.

(6) Fallico, B.; Zappalà, M.; Arena, E.; Verzera, A. Effects of conditioning on HMF content in unifloral honeys. *Food Chem.* **2005**, *85*, 305−313.

(7) AOAC Official Method 998.12. C-4 plant sugars in honey. In *Official Methods of Analysis of AOAC International*, 16th ed.; Cunniff, P., Ed.; AOAC International: Gaithersburg, MD, USA, 1999; Vol. 2, pp 27−30.

(8) Rogers, K. M.; Stewart, S.; Pyne, R.; Douance, C.; Cooper, J.; Phillips, A.; Sim, M.; Rogers, P. Investigating AOAC 998.12 C-4 sugar fails in New Zealand honey. *J. Agric. Food Chem.* **2014**, DOI: 10.1021/jf40766f.

(9) Rogers, K. M.; Cook, J.; Krueger, D.; Beckmann, K. Report of an inter laboratory comparison exercise: modification of AOAC Official Method 998.12 to add filtration and/or centrifugation. *J. AOAC Int.* **2013**, *96*, 607−614.

(10) Padovan, G. J.; De Jong, D.; Rodrigues, L. P.; Marchini, J. S. Detection of adulteration of commercial honey samples by the $^{13}C/^{12}C$ isotopic ratio. *Food Chem.* **2003**, *82*, 633−636.

(11) Padovan, G. J.; Rodrigues, L. P.; Leme, I. A.; De Jong, D.; Marchini, J. S. Presence of C4 sugars in honey samples detected by the carbon isotope ratio measured by IRMS. *Eurasian J. Anal. Chem.* **2007**, *2*, 134−141.

(12) White, J. W.; Doner, L. W. Mass spectrometric detection of high-fructose corn syrup in honey by use of $^{13}C/^{12}C$ ratio: collaborative study. *J. Assoc. Off. Anal. Chem.* **1978**, *61*, 746−750.

(13) Rogers, K. M.; Somerton, K.; Rogers, P.; Cox, J. Eliminating false positive C_4 sugar tests on New Zealand manuka honey. *Rapid Commun. Mass Spectrom.* **2010**, *24*, 2370−2374.

(14) White, J. W.; Winters, K. Honey protein as internal standard for stable carbon isotope ratio detection of adulteration honey. *J. Assoc. Off. Anal. Chem.* **1989**, *72*, 907−911.

(15) Atrott, J.; Haberlau, S.; Henle, T. Studies on the formation of methylglyoxal from dihydroxyacetone in manuka (*Leptospermum scoparium*) honey. *Carbohydr. Res.* **2012**, *361*, 7−11.

(16) Windsor, S.; Pappalardo, M.; Brooks, P.; Williams, S.; Manley-Harris, M. A Convenient new analysis of dihydroxyacetone and methylglyoxal applied to Australian *Leptospermum* honeys. *J. Pharmacogn. Phytother.* **2012**, *4*, 6−11.

(17) Kawashima, K.; Itoh, H.; Chibata, I. Non-enzymatic browning reactions of dihydroxyacetone with amino acids or their esters. *Agric. Biol. Chem.* **1998**, *44*, 1595−1599.

(18) De Genhardt, T. P.; Thorpe, S. R.; Baynes, J. W. Chemical modification of proteins by methylglyoxal. *Cell. Mol. Biol.* **1991**, *44*, 1139−1145.

(19) Erbersdobler, H. Loss of lysine during manufacture and storage of milk powder. *Milchwissenschaft* **1970**, *25*, 280−284.

(20) El, S. N.; Kavas, A. Available lysine in dried milk after processing. *Int. J. Food Sci. Nutr.* **1997**, *48*, 109−111.

(21) Thomas, M. E. C.; Scher, J.; Desobry-Banon, S.; Desobry, S. Milk powders ageing: effect on physical and functional properties. *Crit. Rev. Food Sci. Nutr.* **2004**, *44*, 297−322.

(22) Lynch, A. H.; McCullagh, J. S.; Hedges, R. E. Liquid chromatography/isotope ratio mass spectrometer measurement of $\delta^{13}C$ amino acids in plant proteins. *Rapid Commun. Mass Spectrom.* **2011**, *25*, 2981−2988.

(23) Larsen, T.; Taylor, D. L.; Leigh, M. B.; O'Brien, D. M. Stable isotope fingerprinting: a novel method for identifying plant, fungal or bacterial origins of amino acids. *Ecology* **2009**, *90*, 3526−3535.

(24) O'Brien, D. M.; Boggs, C. L.; Fogel, M. L. Pollen feeding in the butterfly *Heliconius charitonia*: isotopic evidence for essential amino acid transfer from pollen to eggs. *Proc. R. Soc. B* **2003**, *270*, 2631−2636.

(25) Majtan, J.; Klaudiny, J.; Bohova, J.; Kohutova, L.; Dzurova, M.; Sediva, M.; Bartosova, M.; Majtan, V. Methylglyoxal-induced modifications of significant honeybee proteinous components in manuka honey: possible therapeutic implications. *Fitoterapia* **2012**, *83*, 671−677.

Approved Method 44-15.02.[18] The protein (N × 5.7) content was measured using a Dumas combustion method, adapted from the AOAC Official Method[19] to an automated Dumas protein analysis system (EAS, VarioMax N/CN, Elt, Gouda, The Netherlands).

Gluten Hydrolysis. Gluten was hydrolyzed with porcine pancreatic Try (EC no. 3.4.21.4, Sigma-Aldrich) or Alc 2.4 L FG (EC no. 3.4.21.62, Novozymes, Bagsvaerd, Denmark). An aqueous protein dispersion was prepared by dispersing 6.0 wt % commercial gluten (protein content on dry basis of 83.3%, Syral Belgium, Aalst, Belgium) in water. The dispersion was then heated to 50 °C (Try) or 60 °C (Alc) in a water bath under continuous stirring prior to manual adjustment of the pH by addition of NaOH (1.0 M) to pH 8.0 (Try) or 10.0 (Alc). After the desired temperature and pH conditions were obtained, the peptidase was added and gluten hydrolysis was monitored using the pH-stat method.[20] The degree of hydrolysis [DH, defined as the number of peptide bonds hydrolyzed (h) over the total number of peptide bonds per unit weight present in gluten (h_{tot})] was controlled by varying the hydrolysis time. It was calculated from the amount of base needed during hydrolysis to maintain a constant pH in the hydrolysis reaction medium:

$$\mathrm{DH}\ (\%) = h \times h_{\mathrm{total}}^{-1} \times 100 = (B \times N_{\mathrm{b}} \times 100) \times (\alpha \times M_{\mathrm{p}} \times h_{\mathrm{total}})^{-1}$$

B is base consumption (mL), N_b is the molarity of the base used (1.000 M), α is the average degree of dissociation of the α-NH_2 groups (1.0 and 1.13 for the conditions used for the Alc and Try treatment, respectively), M_p is the mass of the gluten proteins used (in g), h represents hydrolysis equivalents (mequiv/g protein), and h_{total} is the theoretical overall number of peptide bonds per weight unit in gluten protein, that is, 8.3 mequiv/g protein.[20]

At appropriate DH values, the enzyme was inactivated by adjusting the pH to 6.0 using 2.0 M citric acid and subsequent heating to 95 °C for at least 10 min. After cooling to room temperature, the mixture was centrifuged (10000*g*, 20 min, 4 °C) and the supernatant freeze-dried and ground to produce a powder. The gluten hydrolysates produced were coded according to the peptidase used to form them, followed by the DH. For example "Alc3" refers to a gluten sample that was hydrolyzed with Alc to a DH of 3.

Emulsion Preparation. Oil-in-water emulsions were prepared by homogenizing 10 g of corn oil with 90 g of aqueous phase, which was prepared by dispersing powdered gluten hydrolysate (0.11−5.56 wt %) in Tris-HCl buffer (10 mM, pH 9.0, containing 0.02 wt % sodium azide to prevent microbial growth) at room temperature. After stirring for 60 min, the hydrolysate solutions were filtered (grade 4 Whatman filter paper, GE Healthcare, Uppsala, Sweden), and the filtrate was used immediately to produce emulsions. Measurement of the absorbance at 280 nm of the protein solutions before and after filtration indicated that little protein (<5.5% of the total) was lost due to this procedure for all hydrolysates tested. Prior to addition of the oil phase, the aqueous phase of the emulsion, hence, contained hydrolysate levels varying between 0.1 and 5.0 wt % on emulsion weight. A high-speed mixer (Bamix, Biospec Products, Bartlesville, OK, USA) was used to prepare a coarse emulsion, which was then fed into an air-driven microfluidizer (Microfluidics, Newton, MA, USA). The coarse emulsion was passed five times through the microfluidizer at a homogenization pressure of 83×10^6 Pa.

Protein Characterization of Hydrolysate Solutions and Aqueous Phase of Emulsions. Freshly prepared emulsions (2.00 mL) were centrifuged for 20 min in plastic filter units (Centrifugal Amicon Ultra Filter Units, molecular cutoff 100 kDa, Millipore, Cork, Ireland) at 930*g* (CL10 Centrifuge, ThermoScientific, Waltham, MA, USA). The flow-through phase was collected, and the protein content was determined and compared to the protein content of the initial hydrolysate solutions used to prepare the emulsions. Both protein contents were determined using the colorimetric Lowry protein concentration protocol,[21] calibrated with a β-lactoglobulin standard curve (0.0−0.5 mg/mL protein).

Emulsion Characterization. The particle size distribution (area-volume mean diameter d_{32}) of the freshly prepared emulsions was measured by static light scattering (Mastersizer 2000, Malvern Instruments, Malvern, UK). The droplet charge (ζ-potential) was determined by particle electrophoresis (Zetasizer Nano ZS series, Malvern Instruments, Worcestershire, UK). Prior to droplet charge analysis, samples were diluted 100-fold with 10 mM Tris-HCl buffer to avoid multiple scattering effects.

Emulsion Microstructure. The microstructure of the emulsions was visualized using optical and/or confocal scanning laser microscopy with a 60× objective and a 10× eyepiece (Nikon Eclipse 80i, Nikon Instruments Inc., Melville, NY, USA). A small aliquot (about 8 μL) was placed on a microscope slide and covered with a coverslip prior to analysis. Prior to emulsification, the oil and the aqueous phase of the emulsion samples used for confocal microscopy were stained with Nile Red [400 μL of Nile red (0.1% (w/v) solution in ethanol) on 7.5 g of oil] and fluorescein isothiocyanate [FITC, 800 μL of FITC (0.1% (w/v) solution in dimethyl sulfoxide) on 67.5 g of aqueous phase] to visualize lipids and proteins, respectively. The emissions of Nile Red and FITC were detected in the 605 and 515 nm channels, respectively, equipped with long pass filters (HQ 605LP/75 m and HQ 515/30). The microstructure images were analyzed using image analysis software (Nikon).

Emulsion Stability. *Stability to Thermal Processing.* Freshly prepared emulsions were distributed over different glass test tubes and incubated for 30 min in water baths set at different temperatures (30−90 °C). The samples were subsequently allowed to cool to 20 °C, and the particle size distribution was analyzed as described above 24 h and 9 days after the heat treatment.

Stability to Isothermal Storage. Freshly prepared emulsions were distributed over different glass test tubes and immediately incubated for 9 days in temperature-controlled chambers set at different temperatures (4, 20, 37, and 55 °C). Simultaneously, parallel samples containing 150 mM NaCl were stored under the same conditions. The ionic strength was adjusted by the addition of highly concentrated NaCl solution (6.0 M). The final concentration of oil in all of the emulsions was kept constant by adjusting the total volume of the emulsions using water. The particle size distribution of the samples was analyzed as described above 1, 2, 3, 6, and 9 days after preparation.

Stability to Different pH Conditions. Freshly prepared emulsions were distributed over different glass test tubes, and their pH values were immediately adjusted by adding NaOH (1.0 M) or HCl (1.0 M) to obtain values ranging from pH 3.0 to 9.0. The particle size distribution of these samples was determined 24 h and 9 days after adjustment of the pH.

Stability to Different Ionic Strength Conditions. The ionic strength of freshly prepared emulsions was altered by adding a highly concentrated NaCl solution (6.0 M) to produce samples containing 0.0−0.5 M NaCl. The final concentration of oil in all of the emulsions was kept constant by adding water to adjust their total volume. The particle size distribution of these samples was determined 24 h and 9 days after adjustment of the ionic strength.

Statistical Analysis. All measurements were performed on at least three freshly prepared samples (except for the preliminary experiments in which the best-performing hydrolysates were determined) and were reported as means and standard deviations, analyzed using a spreadsheet statistical package (Microsoft Excel 2011). The data were analyzed with Tukey's tests (P value <0.05) using XLStat software (Addinsoft, Brooklyn, NY, USA).

RESULTS

Gluten Hydrolysate Characterization. Gluten was hydrolyzed using Try and Alc to different DH values (DH = 1, 2, and 3 for Try; DH = 3, 6, and 10 for Alc). Alc produced hydrolysates with a higher DH due to its broader specificity relative to Try. The yield (expressed as wt % of the gluten starting material) and moisture and protein contents of the solubilized gluten peptides are listed in Table 1. The hydrolysate yield increased with increasing DH.

Table 1. Characteristics of the Produced Gluten Hydrolysates

sample	yield[a] (%)	moisture content (%)	protein content (% db)
trypsin, DH 1	30.00	4.9 (±0.2)[b]	71.9 (±0.9)[b]
trypsin, DH 2	38.66	3.4 (±0.1)	77.3 (±1.3)
trypsin, DH 3	43.27	4.1 (±0.0)	86.9 (±0.0)
alcalase, DH 3	80.67	3.5 (±0.3)	81.0 (±0.4)
alcalase, DH 6	82.87	4.6 (±0.0)	82.8 (±0.3)
alcalase, DH 10	84.01	2.5 (±0.1)	79.2 (±2.5)

[a]Calculated as the ratio of the weight of the freeze-dried soluble fraction over the total weight of the freeze-dried soluble and insoluble fraction after hydrolysis. [b]The standard deviation values presented here are based on duplicate measurements (n = 2).

Comparison of Emulsifier Properties of Different Gluten Hydrolysate Samples. Preliminary experiments (data not shown) showed that emulsion production at pH 6.5 using gluten hydrolysates did not yield (stable) emulsions with submicrometer droplet diameters. The powdered gluten hydrolysates were then dispersed in an alkaline buffer solution (Tris-HCl buffer, pH 9.0). The actual pH of the emulsion produced, however, was considerably lower (pH ≈7.5) due to citric acid remaining in the freeze-dried hydrolysates. Droplet sizes were determined after 3 h and 7 days to test how the hydrolysates performed as emulsion-forming and -stabilizing agents, respectively. Measurements after 3 h give an indication on how effective a hydrolysate is at forming emulsions with small droplets, whereas measurements after 7 days indicate how effective a hydrolysate is at stabilizing emulsions during storage. Figure 1 shows the mean droplet diameters of emulsions containing 1.0 and 2.5 wt % of the different gluten hydrolysates (i.e., Try1, Try2, Try3, Alc3, Alc6, and Alc10). At the lower hydrolysate concentration (1.0 wt %), Try hydrolysates were significantly better emulsion-forming agents than the Alc hydrolysates. However, at the higher hydrolysate concentration (2.5 wt %), the Try hydrolysates surprisingly displayed significantly worse emulsifying properties than the Alc hydrolysates. A lower concentration of hydrolysate was needed to produce emulsions with similar droplet sizes for Try than for Alc hydrolysates. After 7 days of storage, emulsions prepared using hydrolysates with a DH of 3, that is, 2.5 wt % Alc3 and 1.0 wt % Try3, had significantly smaller droplet sizes as compared to the other hydrolysates, indicating that these were best suited for stabilizing the emulsions (Figure 1). In all other cases, the droplet size drastically increased upon storage. For this reason, the Try3 and Alc3 hydrolysates were focused upon in the following experiments.

Emulsion Formation. Different concentrations of Alc3 (Figure 2a) and Try3 (Figure 2b) hydrolysates were tested for their emulsion-forming properties. All emulsions produced displayed a bimodal size distribution (results not shown), except at the higher hydrolysate concentrations (>3.0 wt %). These higher concentrations, however, did not result in the formation of stable emulsions, and the droplet size increased considerably upon 7 days of storage (>3.0 wt % for Alc3 and >1.0 wt % for Try3). In most cases, the droplet size decreased with increasing hydrolysate concentration until a minimum value was reached (Figure 2a,b), which is in agreement with the behavior expected for emulsifiers during high-pressure homogenization.[22] However, anomalous behavior was observed for the emulsions prepared with high levels of Try3 hydrolysates,

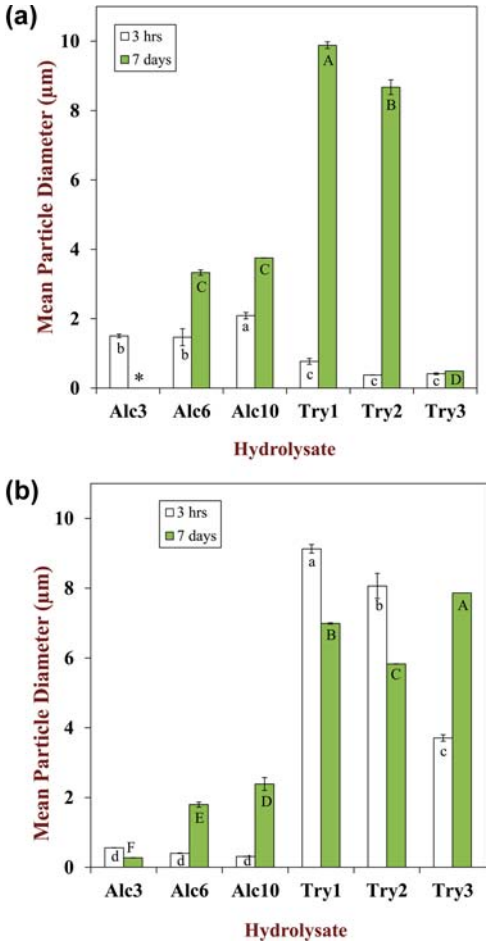

Figure 1. Influence of degree of hydrolysis (DH) on mean particle diameter of emulsions (d_{32}) made with 1.0 wt % (a) and 2.5 wt % (b) of gluten hydrolysates produced with alcalase (Alc) and trypsin (Try). The degrees of hydrolysis of the gluten hydrolysates produced with Alc were 3 (Alc3), 6 (Alc6), and 10 (Alc10), whereas those of the hydrolysates produced with Try were 1 (Try1), 2 (Try2), and 3 (Try3). All emulsions contained 10 wt % corn oil. The reported values were recorded 3 h and 7 days after emulsion production. a–d and A–F represent Tukey groups with $p < 0.05$ for comparison of the particle diameter as a function of peptidase/DH of 3-h- and 7-day-old emulsions, respectively. ∗Upon 7 days of storage, the emulsion produced with 1.0% Alc3 hydrolysate displayed extensive creaming, which hindered droplet diameter measurements.

where a steep increase in particle size was observed at hydrolysate concentrations >2.0 wt %. On the basis of particle size distribution measurements of the fresh and 7-day-old emulsions (Figure 2a,b), 1.0% Try3 and 2.0% Alc3 were selected as the best-performing hydrolysate concentrations in terms of both emulsion formation and stabilization. Microscopic analyses confirmed the bimodal droplet size distribution, as well as flocculation of emulsion droplets produced with higher hydrolysate concentrations (Figure 2c).

To obtain an estimation of the saturation concentration of the hydrolysates at the droplet interface, the protein content in the aqueous phase of the emulsions was determined and compared to the protein content in the aqueous phase prior to emulsification. This ratio was plotted as a function of increasing hydrolysate concentration (Figure 3). It was expected that for the lowest hydrolysate concentrations, no residual protein or very low protein concentrations would be found in the aqueous

dx.doi.org/10.1021/jf5001343 | J. Agric. Food Chem. 2014, 62, 2623–2630

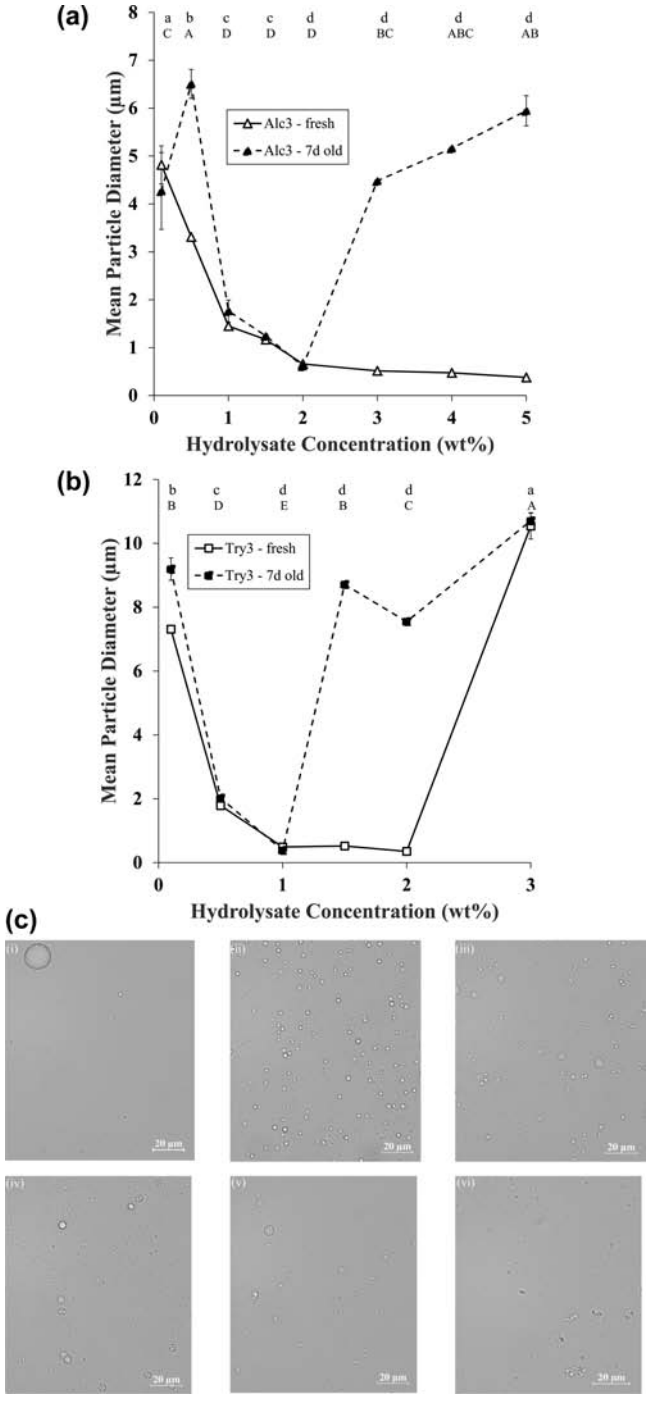

Figure 2. (a, b) Influence of gluten hydrolysate concentration on the mean particle diameter (d_{32}) of 10 wt % corn oil emulsions, freshly prepared and 7 days old. Emulsions were made using gluten hydrolysates with a degree of hydrolysis of 3 produced with alcalase [Alc3 (a)] and trypsin [Try3 (b)]. All emulsions contained 10 wt % corn oil. a–d and A–E represent Tukey groups with $p < 0.05$ for comparison of the particle diameter as a function of hydrolysate concentration of freshly made and 7-day-old emulsions, respectively. (c) Optical microscopic images of emulsions produced with increasing concentrations [i.e., 0.1 (i), 0.5 (ii), 1.0 (iii), 1.5 (iv), 2.0 (v), and 3.0 (vi) wt %] of gluten hydrolysates. The hydrolysates had a degree of hydrolysis of 3 and were produced with Try. All emulsions contained 10 wt % corn oil. The scale bars represent 20 μm.

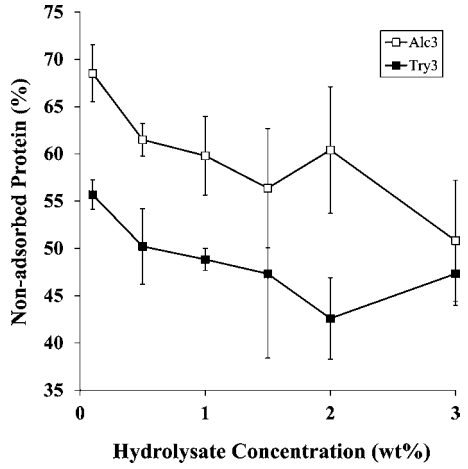

Figure 3. Influence of gluten hydrolysate concentration on the percentage of nonadsorbed proteins found in the aqueous continuous phase of 10 wt % corn oil emulsions. Emulsions were produced using gluten hydrolysates with a degree of hydrolysis of 3 made with alcalase (Alc3) and trypsin (Try3).

phase, and from a critical hydrolysate concentration on the free protein concentration would increase as a function of increasing hydrolysate addition level.[22] However, no such result was obtained (Figure 3). When the protein contents of the continuous aqueous phase of the emulsions were compared to those of the original aqueous phase prior to emulsification, it was clear that about 50 or 60% of the hydrolysates produced with Try or Alc, respectively, were not adsorbed at the droplet interface. This was largely independent of the initial protein concentration (Figure 3). The heterogeneity of the hydrolysate samples in terms of surface activity certainly contributes to this behavior. It is possible that a fraction of the hydrolysates was hydrophobic or surface-active (and therefore became associated with the oil droplets or were even solubilized in the oil phase), whereas another fraction was hydrophilic (and therefore remained in the aqueous phase). Nevertheless, further research using isolated fractions of the hydrolysates would be needed to establish this.

The surface loads of the hydrolysates (i.e., the amount adsorbed per unit surface area) at saturation were estimated to be about 9 and 13 mg/m^2 for Try3 and Alc3 hydrolystates, respectively. These values are on the high end of values typically reported for food proteins (around 1–10 mg/m^2). However, these values should be interpreted carefully for a number of reasons. First, the hydrolysates were a mixture of different types of molecules, rather than a single type, which biases the determination of the exact protein concentration Furthermore, the transfer of part of the hydrolysates to the oil phase cannot be excluded. Second, the mean droplet diameter (d_{32}) used in the calculations assumes that the droplets are not flocculated, although in reality some droplet flocculation may have occurred. For this reason, the surface load for the Try3 hydrolysate was calculated on the basis of the droplet size data at 2.0% of hydrolysate, before extensive flocculation occurred (Figure 2c). Third, there may have been some problems in making reliable protein concentration measurements in the samples due to light scattering by small emulsion droplets or protein aggregates.

Emulsion Stability. Upon 24 h of storage of the original Alc3 and Try3 emulsions, some tendency toward creaming could already be observed. Emulsions containing oil droplets coated by either Try3 or Alc3 hydrolysates were highly sensitive to changes in ionic strength and pH (Figure 4). The electrical

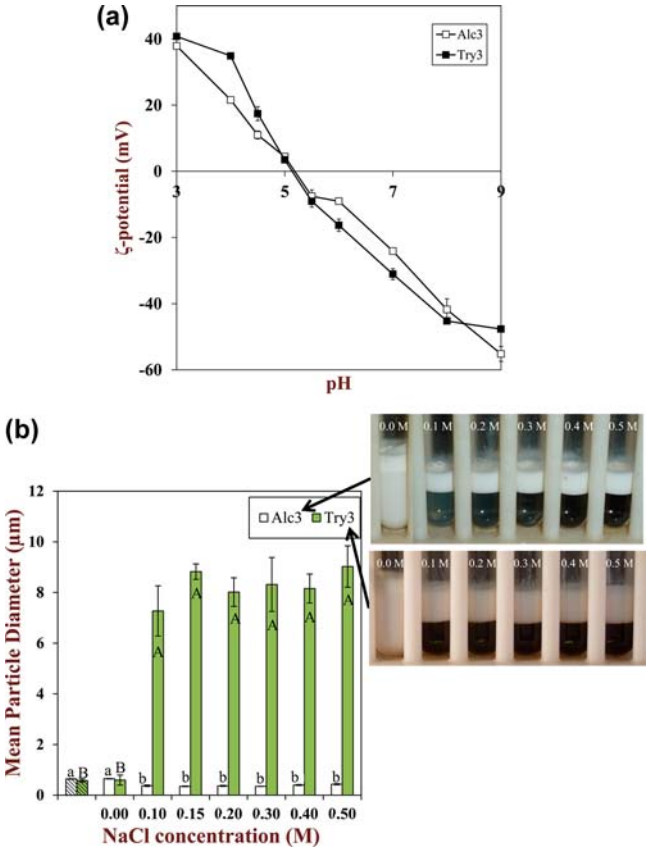

Figure 4. Emulsion characteristics in different pH and ionic strength conditions: (a) influence of pH on the ζ-potential of droplets of emulsions produced with gluten hydrolysates with a degree of hydrolysis of 3 made with alcalase (Alc3) and trypsin (Try3) (reported values were recorded 24 h after pH adjustment); (b) influence of ionic strength on mean particle diameter (d_{32}) (reported values were recorded 24 h after ionic strength adjustment). The shaded bars represent the particle diameter of the freshly made emulsions prior to ionic strength adjustment. The influence of ionic strength on the appearance of the emulsions is shown in the pictures. Extensive creaming occurred at concentrations ≥0.1 M NaCl for the Alc3 and Try3 emulsions. a and b and A and B represent Tukey groups with $p < 0.05$ for comparison of the evolution of the particle diameter in function of ionic strength of Alc3 and Try3 emulsions, respectively.

charge on the hydrolysate-coated oil droplets went from highly positive at low pH to highly negative at high pH, with a point of zero charge just above pH 5 (Figure 4a). At pH values around the isoelectric point of the droplets (pH ≈5), there was a large increase in mean particle size and extensive creaming was observed. At relatively high pH values (pH 8.0 and 9.0), the emulsions were relatively stable to droplet aggregation, maintaining relatively small droplet sizes (d_{32} < 1000 nm) after 9 days of storage (results not shown). At pH 3.0, the particle diameter of the Try3 emulsions remained relatively small, whereas Alc3 emulsions were much less stable and were prone to creaming. All emulsions produced were destabilized by salt addition and displayed extensive creaming behavior. The mean particle diameter of the emulsions produced with Try3 determined by light scattering significantly increased for NaCl ≥ 100 mM, indicating that salt addition promoted droplet aggregation. On the other hand, the particle size measured by light scattering appeared to be relatively small (d_{32} < 1000 nm) for the Alc3 emulsions at all salt concentrations (Figure 4c). However, extensive flocculation was observed in both types of emulsions using optical microscopy analysis. Thus, it is possible that the flocs in the Alc3 emulsions were disrupted during the dilution and mixing stages of the particle size analysis, which highlights the importance of using more than one method for analyzing aggregated systems.

The Alc3 emulsions were relatively stable to droplet aggregation when stored at low temperatures (4 and 20 °C), but they exhibited considerable droplet aggregation behavior when stored at more elevated temperatures (i.e., 37 and 55 °C) (Figure 5a). Conversely, the Try3 emulsions appeared to be stable during isothermal long-term storage at all storage temperatures as no significant changes in particle diameter were observed (Figure 5b). Furthermore, in contrast to Alc3 hydrolysates, Try3 hydrolysates proved to be effective at stabilizing emulsions against droplet aggregation during short-time thermal processing (30 min) (Figure 5c).

Microstructure Analysis. Microscopic analysis of the emulsions not only confirmed the bimodal size distribution of the oil droplets but also showed the presence of intriguing structures within the larger emulsion droplets. We observed smaller droplets enclosed within the larger oil droplets (Figures 2b and 6a). To explore the nature of these smaller subdroplets, the oil and water phases were stained prior to emulsification. The fact that the internal droplets were not stained by either dye suggests that they did not contain lipid or protein and may therefore have been trapped air bubbles (Figure 6b). These air-in-oil-in-water systems could be detected in all emulsions made with hydrolysate concentrations below 3.0 wt %. Above this concentration, no separate oil droplets could be observed. The strong creaming tendency of the emulsions after production is probably partially caused by the more pronounced density difference between the continuous and disperged phase due to the presence of air.

DISCUSSION

Gluten can be divided into the two main storage protein types found in wheat kernels, that is, gliadin and glutenin. In an earlier study, Takeda and co-workers[23] found that unhydrolyzed gliadin and glutenin have different emulsifying behaviors at low pH. Walstra[22] found that peptides formed by hydrolyzing native proteins are more effective emulsifiers than the native proteins themselves, provided that they are not too small, they are water-soluble, and they are amphiphilic. Previous studies have shown the emulsifying capacity of gluten protein hydrolysates using relatively simple homogenization techniques.[3,4,12,14] In most of these studies, however, no information on the droplet size distribution was reported. Linares and co-workers[13] reported oil droplet sizes of about 20 μm for emulsions produced using a high-speed blender, which could be decreased about 10-fold when they were passed through a high-pressure valve homogenizer.[15] In the current study, the average droplet diameter could be decreased into the submicrometer range using a high-pressure homogenizer (microfluidizer) provided the emulsions were prepared at pH conditions sufficiently distinct from the point of zero charge. This is in accordance with what is observed for other proteins.[24−26] The obtained particle diameters are comparable to or larger than those of emulsions made with whey protein isolate (0.27%), β-lactoglobulin (0.05%), or sodium caseinate (0.27%) using similar production parameters.[25−27] The gluten peptides formed by hydrolysis produced electrically charged droplets. The most likely stabilization mechanism preventing droplet

dx.doi.org/10.1021/jf5001343 | J. Agric. Food Chem. 2014, 62, 2623−2630

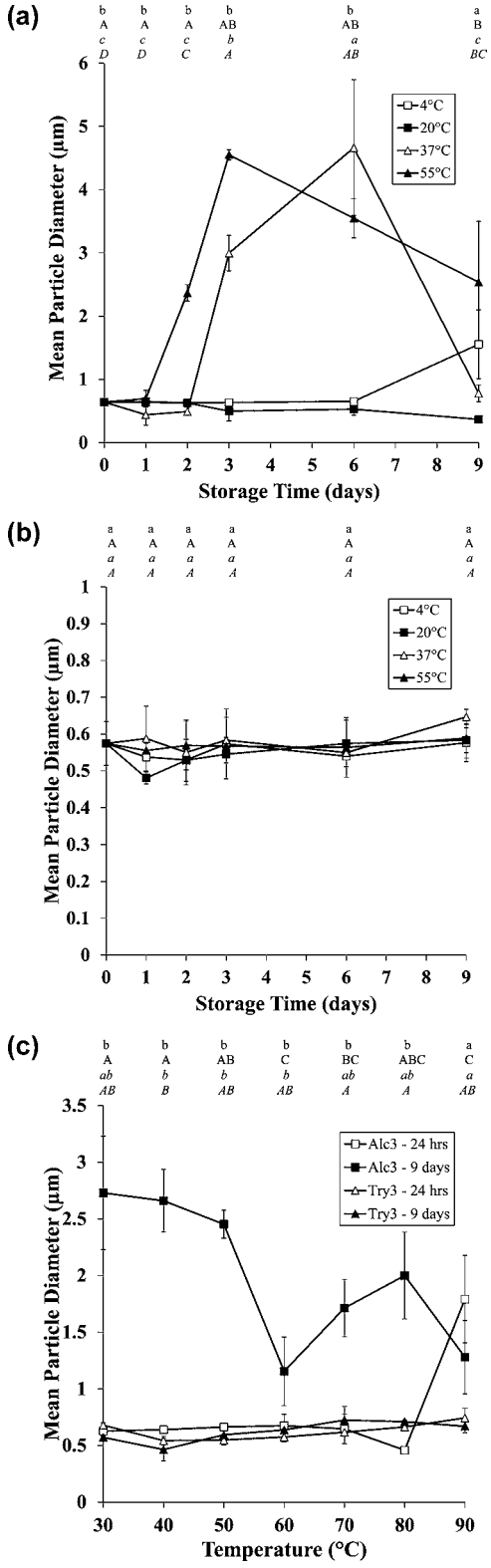

Figure 5. Emulsion stability to isothermal storage and heat processing. (a, b) Influence of isothermal storage on mean particle diameter (d_{32}) of emulsions produced with gluten hydrolysates with a degree of hydrolysis of 3 made with alcalase (a) and trypsin (b). Emulsions were stored for up to 9 days. a, b; A, B; *a*−*c*; and *A*−*D* represent Tukey groups with $p < 0.05$ for comparison of the evolution of the particle diameter in function of storage time of emulsions stored at 4, 20, 37, and 55 °C, respectively. (c) Influence of heat processing on mean particle diameter (d_{32}) of emulsions produced with gluten hydrolysates with a degree of hydrolysis of 3 made with alcalase (Alc3) and trypsin (Try3). Emulsions were heated for 30 min at the indicated temperatures before they were cooled and stored at 20 °C. Droplet sizes shown were recorded 24 h and 9 days after heat processing. a, b and A−C represent Tukey groups with $p < 0.05$ for comparison of the evolution of the particle diameter as a function of treatment temperature of freshly produced and 9-day-old Alc3 emulsions, respectively. *a*, *b* and *A*, B represent Tukey groups with $p < 0.05$ for comparison of the evolution of the particle diameter as a function of treatment temperature of freshly produced and 9-day-old Try3 emulsions, respectively.

aggregation is, hence, electrostatic repulsion.[28−30] For example, at pH 8 and 9, the oil droplets had a strong negative charge (Figure 4a), which would generate a strong electrostatic repulsion that prevents droplet flocculation (Figure 4b). By increasing the ionic strength or decreasing the pH, the net negative charge on the droplets is shielded or decreased and the emulsion is destabilized by flocculation. This is a common phenomenon observed when using proteins as emulsifiers.[31,32] The increase in net particle size due to droplet flocculation then leads to accelerated creaming. At present, a number of nutritional beverages or shakes exist that have a pH value near neutral in which the here-produced emulsion droplets coated by the hydrolysates could be used.

Upon hydrolysis of gluten proteins, a whole range of peptides with largely varying molecular weight, hydrophobicity, and surface activity are created. Previous studies[12,14] indicate that too extensive hydrolysis has an adverse effect on the hydrolysates' emulsifying capacity. Conversely, Linares and colleagues[13] did not find a correlation between degree of hydrolysis and emulsifying properties of solubilized gluten peptides. Previous research on the emulsifying properties of peptides produced from other protein sources, however, showed that there is indeed a minimum size, that is, about 2000 Da (∼20 amino acid residues), required for peptides to display emulsifying potential.[33] However, the molecular weight is not the only factor determining the surface-active properties of peptides. Turgeon and co-workers[33] described that the amphiphilicity of peptides also plays a key role and suggested that the hydrophobic residues should be grouped in discrete patches of at least three to five residues, which are separated by regions containing at least two to three polar residues.

When evaluating the peptides that could possibly be formed by Try and Alc starting from randomly selected gluten protein sequences [i.e., a HMW glutenin subunit (GenBank accession no. ABQ14770.1), a LMW glutenin subunit (GenBank accession no. AAS10192.1), a ω-gliadin (GenBank accession no. AAT01617.1), and a γ-gliadin (GenBank accession no. AAQ63860)] and assuming that Try exclusively hydrolyzes the C-terminal peptide bonds of Arg and Lys[16] and Alc displays a similar specificity on gluten proteins as has been described on casein,[17] it was found that in all cases Try produces more peptides which meet the above listed requirements to be good emulsifiers. Indeed, Alc has a preference to hydrolyze peptide bonds that are N-terminal to hydrophobic residues and C-terminal to, among other residues, Leu and Tyr. As a result, only a small number of peptides containing the above-described hydrophobic patches will be formed from gluten proteins, as these patches, if present in the original protein, are largely cut into pieces during the hydrolysis process by Alc.

dx.doi.org/10.1021/jf5001343 | J. Agric. Food Chem. 2014, 62, 2623−2630

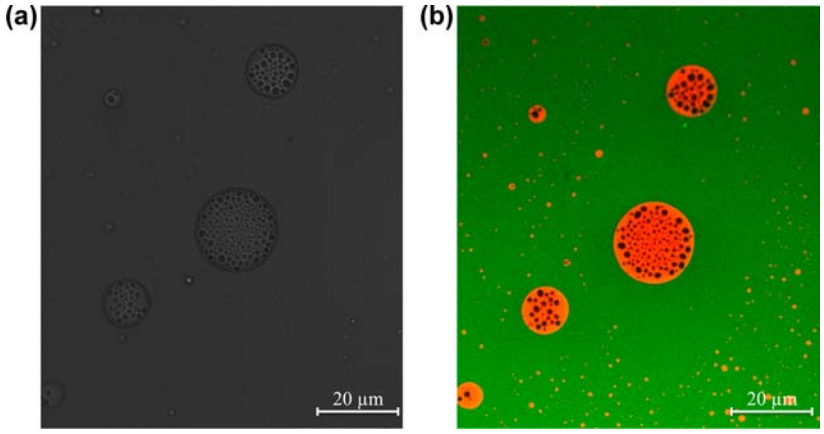

Figure 6. Optical and confocal micrographs of an emulsion made with 0.1 wt % gluten hydrolysate with a degree of hydrolysis of 3 produced with trypsin. The oil phase (red) was stained with Nile Red, whereas the aqueous phase containing the gluten hydrolysates (green) was stained with fluorescein isothiocyanate. The black bubbles inside the oil droplets are assumed to be air. All emulsions contained 10 wt % corn oil.

When the protein contents of the continuous aqueous phase of the emulsions are compared to those of the original aqueous phase prior to emulsification, it is clear that about 50 or 60% of the hydrolysates produced with Try or Alc, respectively, are not adsorbed at the droplet interface. This seems to be largely independent of the initial protein concentration and indeed reflects the above-described difference between the two peptidases and confirms the production of peptides with largely varying surface-active properties. In addition, the higher nonadsorbed protein level for Alc3 emulsions partially explains the higher level of Alc3 hydrolysates relative to the level of Try3 hydrolysates needed to produce emulsions with similar droplet diameters. Furthermore, the high level of nonadsorbed peptides probably induces depletion flocculation at higher hydrolysate concentrations, that is, >1.0 and >2.0% for Try3 and Alc3, respectively. The steep increase in droplet size and creaming tendency as well as microscopic analysis of the emulsions produced with higher hydrolysate concentrations supports this hypothesis.

Regardless of the hydrolysate concentration, all emulsions were relatively sensitive to creaming, which can be partially attributed to the presence of larger air-filled oil droplets (Figure 6). Previous studies already showed that gluten peptides are effective foaming agents.[3,13,34] Furthermore, Takeda and co-workers[23] showed that gluten, similar to one of its functions in dough, also stabilizes the air/water interface. We believe that during the production of the emulsions, air is incorporated into the liquid phase and that the gluten proteins stabilize these air bubbles in the aqueous phase. During homogenization in the microfluidizer, (part of) the air bubbles are forced into the oil droplets. As the interfacial corn oil/air tension (i.e., about 32 mN/m[35]) is lower than the interfacial hydrolysate solution/air tension (i.e., about 45 mN/m[34]), a system that is kinetically stable (but thermodynamically unstable) on the mesoscale (i.e., on the scale of emulsion droplets) is produced. Macroscale stability, however, is reasonably low as the increased density difference promotes creaming of the air-filled oil droplets.

The Try hydrolysates displayed good heat stability, which is not commonly observed with many food proteins. Try and Alc hydrolysates underwent a heat treatment while inactivating the peptidase during their production. Consequently, they were already partially thermally denatured prior to homogenization. This first heat treatment is believed to minimize extensive denaturation of the peptides when adsorbed at the oil droplet surfaces and thus provided better protection against thermal destabilization and creaming of the emulsions upon heating. Furthermore, the heat treatment had probably already converted any free thiol groups on the gluten proteins to disulfide bridges, thereby limiting any additional protein cross-linking at high temperatures.

This study has shown that gluten hydrolysates that display different emulsifying properties can be produced by careful selection of peptidase type and hydrolysis conditions. Of the two peptidases used, Try produced the most promising peptides with a DH of 3. The stability of the emulsions to environmental stresses (such as pH, ionic strength, and thermal processing) also depended on the peptidase type with which the hydrolysates were produced. Gluten hydrolysis may provide a valuable new source of emulsifiers for utilization in the food industry and could add value to byproducts created during starch isolation. The emulsifying properties of these hydrolysates may be further improved by fractionation of the complex peptide mixture. Furthermore, the capacity of the gluten peptides to produce air-filled emulsions holds promise for the production of reduced-fat products and food products with new functionalities. Further research is needed to optimize the conditions in which the latter can be produced.

AUTHOR INFORMATION

Corresponding Author

*(I.J.J.) Phone: +1 (413) 545-7157. Fax: +1 (413) 545-1262. E-mail: ijoye@foodsci.umass.edu.

Funding

We thank the U.S. Department of Agriculture, CREES, NRI, and AFRI Grants and the Massachusetts Department of Agricultural Resources for financial support of this work. I.J.J. gratefully acknowledges financial support from the Fonds voor Wetenschappelijk Onderzoek − Vlaanderen (FWO, Brussels, Belgium) and from the European Commission 7th Framework Program (FP7-People-2011-IOF-300408).

Notes

The authors declare no competing financial interest.

ACKNOWLEDGMENTS

We thank the Laboratory of Food Chemistry and Biochemistry (KU Leuven, Belgium) for assistance with the production of gluten hydrolysates.

ABBREVIATIONS USED

Alc, alcalase; DH, degree of hydrolysis; FITC, fluorescein isothiocyanate; GH, gluten hydrolysate; Try, trypsin

REFERENCES

(1) Delcour, J. A.; Joye, I. J.; Pareyt, B.; Wilderjans, E.; Brijs, K.; Lagrain, B. Wheat gluten functionality as a quality determinant in cereal-based food products. *Annu. Rev. Food Sci. Technol.* **2012**, *3*, 469−492.

(2) Krull, L. H.; Wall, J. S. Synthetic polypeptides containing side-chain amide groups − water-soluble polymers. *Biochemistry−U.S.* **1966**, *5*, 1521−1527.

(3) Popineau, Y.; Huchet, B.; Larre, C.; Berot, S. Foaming and emulsifying properties of fractions of gluten peptides obtained by limited enzymatic hydrolysis and ultrafiltration. *J. Cereal Sci.* **2002**, *35*, 327−335.

(4) Saberi, A. H.; Kadivar, M.; Keramat, J. Improvement of functional properties of glutens extracted from two Iranian wheat varieties (Sardari and Mahdavi) employing chemical and enzymatic modifications. *J. Agric. Sci. Technol.* **2008**, *10*, 243−252.

(5) Olanca, B.; Ozay, D. S. Preparation and functional properties of gluten hydrolysates with wheat-bug (*Eurygaster* spp.) protease. *Cereal Chem.* **2010**, *87*, 518−523.

(6) Mimouni, B.; Azanza, J. L.; Raymond, J. Influence of double enzymic hydrolyses on gluten functionality. *J. Sci. Food Agric.* **1999**, *79*, 1048−1053.

(7) Park, E. Y. Antioxidant activity of some protein hydrolysates and their fractions with different isoelectric points. *J. Agric. Food Chem.* **2008**, *56*, 9246−9251.

(8) Zioudrou, C.; Streaty, R. A.; Klee, W. A. Opioid peptides derived from food proteins. The exorphins. *J. Biol. Chem.* **1979**, *254*, 2446−2449.

(9) Thewissen, B. G.; Pauly, A.; Celus, I.; Brijs, K.; Delcour, J. A. Inhibition of angiotensin I-converting enzyme by wheat gliadin hydrolysates. *Food Chem.* **2011**, *127*, 1653−1658.

(10) Bengoechea, C.; Cordobes, F.; Guerrero, A. Rheology and microstructure of gluten and soya-based o/w emulsions. *Rheol. Acta* **2006**, *46*, 13−21.

(11) Agyare, K. K.; Addo, K.; Xiong, Y. L. L. Emulsifying and foaming properties of transglutaminase-treated wheat gluten hydrolysate as influenced by pH, temperature and salt. *Food Hydrocolloids* **2009**, *23*, 72−81.

(12) Kong, X. Z.; Zhou, H. M.; Qian, H. F. Enzymatic preparation and functional properties of wheat gluten hydrolysates. *Food Chem.* **2007**, *101*, 615−620.

(13) Linares, E.; Larre, C.; Lemeste, M.; Popineau, Y. Emulsifying and foaming properties of gluten hydrolysates with an increasing degree of hydrolysis: role of soluble and insoluble fractions. *Cereal Chem.* **2000**, *77*, 414−420.

(14) Wang, J.; Zhao, M.; Yang, X.; Jiang, Y. Improvement on functional properties of wheat gluten by enzymatic hydrolysis and ultrafiltration. *J. Cereal Sci.* **2006**, *44*, 93−100.

(15) Linares, E.; Larre, C.; Popineau, Y. Freeze- or spray-dried gluten hydrolysates. 2. Effect of emulsification process on droplet size and emulsion stability. *J. Food Eng.* **2001**, *48*, 137−146.

(16) Olsen, J. V.; Ong, S. E.; Mann, M. Trypsin cleaves exclusively C-terminal to arginine and lysine residues. *Mol. Cell. Proteomics* **2004**, *3*, 608−614.

(17) Adamson, N. J.; Reynolds, E. C. Characterization of casein phosphopeptides prepared using alcalase: determination of enzyme specificity. *Enzyme Microb. Technol.* **1996**, *19*, 202−207.

(18) AACC. *Approved Methods of the American Association of Cereal Chemists*; American Association of Cereal Chemists: St. Paul, MN, USA, 2000.

(19) AOAC. *Official Methods of Analysis*, 16th ed.; Association of Official Analytical Chemists: Washington, DC, 1995; Method 990.03.

(20) Adler-Nissen, J. *Enzymatic hydrolysis of Food Proteins*; Elsevier Applied Science Publishers: New York, 1985; p 427.

(21) Lowry, O. H.; Rosebrough, N. J.; Farr, L. A.; Randall, R. J. Protein measurement with the Folin phenol reagent. *J. Biol. Chem.* **1951**, *193*, 265−275.

(22) Walstra, P. The roles of proteins and peptides in formation and stabilisation of emulsions. In *Gums and Stabilisers for the Food Industry 11*; Williams, P. A., Phillips, G. O., Eds.; Royal Society of Chemistry: London, UK, 2002; Vol. 11, pp 237−244.

(23) Takeda, T.; Matsumura, Y.; Shimizu, M. Emulsifying and surface properties of wheat gluten under acidic conditions. *J. Food Sci.* **2001**, *66*, 393−399.

(24) Ruiz-Henestrosa, V. P.; Sanchez, C. C.; Yust, M. d. M.; Pedroche, J.; Millan, F.; Patino, J. M. R. Limited enzymatic hydrolysis can improve the interfacial and foaming characteristics of β-conglycinin. *J. Agric. Food Chem.* **2007**, *55*, 1536−1545.

(25) Ma, H.; Forsell, P.; Partanen, R.; Seppanen, R.; Buchert, J.; Boer, H. Sodium caseinates with an altered isoelectric point as emulsifiers in oil/water systems. *J. Agric. Food Chem.* **2009**, *57*, 3800−3807.

(26) Ma, H.; Forssell, P.; Partanen, R.; Buchert, J.; Boer, H. Charge modifications to improve the emulsifying properties of whey protein isolate. *J. Agric. Food Chem.* **2011**, *59*, 13246−13253.

(27) Katsuda, M. S.; McClements, D. J.; Miglioranza, L. H. S.; Decker, E. A. Physical and oxidative stability of fish oil-in-water emulsions stabilized with β-lactoglobulin and pectin. *J. Agric. Food Chem.* **2008**, *56*, 5926−5931.

(28) Chanamai, R.; McClements, D. J. Comparison of gum arabic, modified starch, and whey protein isolate as emulsifiers: influence of pH, $CaCl_2$ and temperature. *J. Food Sci.* **2002**, *67*, 120−125.

(29) Demetriades, K.; Coupland, J. N.; McClements, D. J. Physicochemical properties of whey protein-stabilized emulsions as affected by heating and ionic strength. *J. Food Sci.* **1997**, *62*, 462−467.

(30) Tang, L.; Sun, J.; Zhang, H. C.; Zhang, C. S.; Yu, L. N.; Bi, J.; Zhu, F.; Liu, S. F.; Yang, Q. L. Evaluation of physicochemical and antioxidant properties of peanut protein hydrolysate. *PLoS One* **2012**, *7*, 1−7.

(31) Ma, H.; Forssell, P.; Partanen, R.; Buchert, J.; Boer, H. Improving laccase catalyzed cross-linking of whey protein isolate and their application as emulsifiers. *J. Agric. Food Chem.* **2011**, *59*, 1406−1414.

(32) Onsaard, E.; Vittayanont, M.; Srigam, S.; McClements, D. J. Properties and stability of oil-in-water emulsions stabilized by coconut skim milk proteins. *J. Agric. Food Chem.* **2005**, *53*, 5747−5753.

(33) Turgeon, S. L.; Gauthier, S. F.; Molle, D.; Leonil, J. Interfacial properties of tryptic peptides of β-lactoglobulin. *J. Agric. Food Chem.* **1992**, *40*, 669−675.

(34) Thewissen, B. G.; Celus, I.; Brijs, K.; Delcour, J. A. Foaming properties of tryptic gliadin hydrolysate peptide fractions. *Food Chem.* **2011**, *128*, 606−612.

(35) O'Meara, M. *Determination of the interfacial tension between oil-steam and oil-air at elevated temperatures*. North Carolina State University, Raleigh, NC, USA, 2012.

Table 1. ^{1}H NMR Data of Compounds 1−5[a]

position	1[b]	2[b]	3[c]	4[c]	5[c]
1	2.42 (d, 11.6)	2.45 (m, 9.6)	1.20 (s)	1.22 (d, 9.6)	1.31 (d, 11.4)
	2.75 (d, 11.2)	2.67 (m, 15.2)	1.88 (d, 11.4)	1.61 (s)	1.38 (d, 10.2)
2			1.49 (m, 10.8)	1.31 (d, 15.6)	1.47 (m, 9.6)
			2.16 (m, 12.0)	1.75 (m, 14.4)	1.78 (m, 10.8)
3			0.96 (m, 9.6)	0.87 (m, 8.4)	0.98 (m, 13.2)
			2.37 (br d, 13.2)	1.34 (s)	2.36 (br d, 10.8)
5	2.86 (m, 7.6)	2.87 (m, 12.0)		1.48 (m, 13.2)	2.27 (m, 12.0)
6	1.62 (s)	1.60 (m, 11.2)	5.16 (s)	1.48 (m, 12.0)	2.36 (d, 11.4)
	2.04 (m, 12.0)	2.00 (s)		1.60 (m, 11.4)	3.04 (td, 18.0)
7	2.15 (s)	1.59 (m, 9.2)	1.65 (m, 17.4)	1.08 (d, 12.6)	5.50 (d, 6.6)
	1.56 (m, 7.6)	1.78 (m, 13.2)	2.16 (s)	1.60 (m, 9.6)	
9	1.62 (br s)	2.00 (br s)	1.73 (m, 19.2)		
11	3.89 (m, 10.8)	3.60 (m, 12)	1.29 (s)	0.93 (s)	1.59 (s)
			1.52 (m, 12.0)	1.66 (d, 13.8)	1.69 (m, 14.4)
12	1.77 (m, 12.4)	1.94 (m, 11.6)	1.98 (d, 10.2)	0.87 (m, 6.0)	2.28 (s)
	2.16 (br d, 8.8)	2.12 (d, 8.8)	2.71 (m, 12.0)	1.41 (d, 12.6)	
13	2.15 (m, 7.2)	2.60 (m, 12.0)	2.54 (m, 6.0)	1.63 (br s)	
14	1.80 (m, 11.2)	1.37 (m, 16.4)	1.49 (d, 9.6)	1.41 (s)	2.17 (d, 12.0)
	2.16 (m, 12.0)	2.12 (d, 7.2)	2.37 (m, 17.4)	1.95(d, 11.2)	2.94 (d, 8.4)
15	1.40 (d, 12.4)	1.59 (m, 9.6)	2.21 (m, 11.4)	0.87 (m, 6.0)	1.35 (m, 14.4)
	2.14 (m, 8.0)	1.78 (m, 11.2)	1.98 (d, 9.6)	2.06 (d, 12.0)	1.60 (m, 12.0)
16					1.60 (m, 12.0)
					1.87 (m, 13.8)
17	3.57 (m, 7.2)	3.63 (m, 8.4)	3.60 (m, 12.0)	3.39 (td, 6.6)	3.89 (d, 12.6)
	4.77 (d, 7.6)	4.09 (d, 7.2)	3.99 (d, 6.0)	3.49 (s)	3.99 (d, 9.6)
18	6.61 (s)	6.56 (s)	1.22 (s)	1.01 (s)	1.23 (s)
19	7.80 (s)	7.75 (s)			
20	0.85 (s)	1.05 (s)	1.21(s)	0.59 (s)	1.08 (s)
1′	4.28 (m, 7.2)	4.28 (m, 7.2)	6.44 (d, 6.6)	5.79 (d, 6.6)	6.40 (d, 12.0)
2′	3.24 (m, 8.0)	3.24 (m, 8.0)	5.97 (td, 17.6)	3.55 (td, 12.6)	4.20 (td, 11.4)
3′	3.28 (m, 8.4)	3.28 (m, 8.0)	4.47 (m, 11.4)	3.36 (m, 11.4)	4.04 (m, 10.2)
4′	3.26 (m, 8.0)	3.26 (m, 8.0)	4.49 (d, 12.6)	3.44 (s)	4.39 (m, 9.6)
5′	3.37 (m, 8.0)	3.37 (m, 8.4)	4.14 (m, 6.0)	3.59 (s)	4,29 (td, 6.6)
6′	3.65 (m, 15.6)	3.65 (m, 15.6)	4.42 (m, 13.2)	3.65 (d, 6.0)	4.42 (d, 12.0)
	3.87 (br d, 12.0)	3.87 (br d, 12.0)	4.49 (m, 12.0)	3.76 (br d, 11.2)	4.47 (br d, 12.0)
2″			5.67 (d, 18.0)		
3″			8.05 (d, 18.0)	7.81 (d, 6.6)	
4″				6.71 (d, 12.0)	
5″			7.61 (s)		
6″			7.18 (s)	6.71 (d, 12.0)	
7″				7.81 (d, 6.6)	
8″			7.18 (s)		
9″			7.61 (s)		

[a] δ in parts per million, J in hertz. NMR solvent was MeOD.([b]Obtained at 400 MHz. [c]Obtained at 600 MHz.

Plant Material. The green coffee beans of *C. arabica* var. *yunnanensis* were harvested in June 2012 by Tao Zhang and then roasted at 180 °C for 20 min to yield roasted coffee beans. The plant material was identified by Ming-hua Qiu, Kunming Institute of Botany, Chinese Academy of Sciences.

Extraction and Isolation. The powder of roasted coffee beans (200−300 mesh, 23 kg) was extracted with 80% acetone (3 × 50 L) three times (two days each times). The combined acetone extracts were evaporated under reduced pressure; then the 1.8 kg residue was suspended in H_2O and extracted with petroleum ether (PE), ethyl acetate (EtOAc), and *n*-butanol, respectively. The EtOAc layer (500 g) was subjected to silica gel column chromatography (25 × 180 cm) and eluted in a step gradient manner with PE/acetone (20:1, 10:1, 5:1, 1:1, v/v) to yield four fractions: fraction 1 (22 g), fraction 2 (67 g), fraction 3 (310 g), and fraction 4 (60 g). Fraction 4 was decolorized on an MCI gel column (5.0 × 60 cm) eluting with the step gradient of MeOH/H_2O (30−80%, v/v). The 50% MeOH/H_2O fraction (8.2 g) was chromatographed over a second silica gel column (5.0 × 100 cm, eluted with the step gradient manner of $CHCl_3$/MeOH, 15:1 to 3:1, v/v) to yield five fractions (fractions 4-1−4-5). Then fraction 4-1 (600 mg) was chromatographed on a silica gel column (2.0 × 80 cm, eluted with $CHCl_3$/MeOH, 10:1, v/v) to obtain **8** (15 mg), **9** (5.1 mg), and **10** (20 mg). Fraction 4-2 (800 mg) was subjected to chromatography over RP C-18 (3.0 × 50 cm, eluted with MeOH/H_2O, 30−70%, v/v) to give five minor fractions (fractions 4-2-1−4-2-5). Fraction 4-2-2 (50 mg) was separated by preparative thin layer chromatography (P-TLC, eluted with $CHCl_3$/MeOH, 8:1, v/v) to gain **1** (5.7 mg), **2** (20 mg), and **5** (3.0 mg). Using the same methods as for fraction 4-2-2 on P-TLC with $CHCl_3$/MeOH (8:1, v/v), compounds **3** (3.6 mg) and **6** (15 mg) were obtained from fraction 4-2-3 (80 mg). Fraction 4-3 (32 mg) was separated by reverse-phase HPLC (MeOH/H_2O: 30−50%, 25 min, flow rate = 3.0 mL/min, UV 210 nm) to get **4** (2.5 mg, 10.3 min). Fraction 4-5 (600 mg) was chromatographed on a silica gel column (2.0 × 60 cm) with $CHCl_3$/MeOH (10:1, v/v) to afford three

dx.doi.org/10.1021/jf500788t | J. Agric. Food Chem. 2014, 62, 2631−2637

Table 2. ^{13}C NMR and DEPT Data of Compounds 1−5[a]

position	1[b]	2[b]	3[c]	4[c]	5[c]
1	54.2 (t)	54.2 (t)	40.3 (t)	33.4 (t)	33.2 (t)
2	187.9 (s)	186.5 (s)	19.7 (t)	20.1 (t)	20.4 (t)
3	147.9 (s)	147.0 (s)	37.7 (t)	39.3 (t)	39.4 (t)
4	145.0 (s)	143.9 (s)	44.4 (s)	45.5 (s)	45.0 (s)
5	45.8 (d)	46.3 (d)	156.8 (s)	50.8 (d)	47.1 (d)
6	23.4 (t)	22.7 (t)	113.5 (d)	23.2 (t)	25.2 (t)
7	36.5 (t)	36.8 (t)	29.8 (t)	38.0 (t)	119.1 (d)
8	45.3 (s)	45.1 (s)	42.2 (s)	50.9 (s)	139.8 (s)
9	62.2 (d)	56.4 (d)	46.0 (d)	78.8 (s)	42.4 (s)
10	43.8 (s)	43.9 (s)	38.1 (s)	49.1 (s)	38.2 (s)
11	66.2 (d)	77.5 (d)	29.1 (t)	30.0 (t)	23.9 (t)
12	37.5 (t)	40.4 (t)	18.2 (t)	28.2 (t)	33.3 (d)
13	46.5 (d)	43.3 (d)	43.8 (d)	45.1 (d)	75.1 (s)
14	41.2 (t)	43.8 (t)	42.9 (t)	39.5 (t)	32.6 (t)
15	52.0 (t)	53.8 (t)	54.9 (t)	48.1 (t)	43.6 (t)
16	82.4 (s)	89.6 (s)	83.7 (s)	83.1 (s)	23.7 (t)
17	75.5 (t)	73.5 (t)	67.9 (t)	66.8 (t)	69.1 (t)
18	111.5 (d)	111.3 (d)	27.1 (q)	29.3 (q)	29.8 (q)
19	150.5 (d)	150.0 (d)	175.5 (s)	178.5 (s)	177.6 (s)
20	15.7 (q)	16.9 (q)	23.0 (q)	18.6 (q)	17.1 (q)
1′	104.9 (s)	104.2 (s)	92.3 (s)	93.3 (s)	96.3 (s)
2′	75.3 (d)	74.6 (d)	72.9 (d)	74.0 (d)	74.6 (d)
3′	77.8 (d)	78.4 (d)	78.8 (d)	79.1 (d)	80.0 (d)
4′	71.8 (d)	71.2 (d)	70.0 (d)	71.2 (d)	71.4 (d)
5′	77.8 (d)	77.4 (d)	75.5 (d)	77.2 (d)	79.6 (d)
6′	62.8 (t)	62.4 (t)	60.9 (t)	62.4 (t)	62.6 (t)
1″			165.8 (s)	166.9 (s)	
2″			114.1 (d)	121.9 (s)	
3″			145.1 (d)	133.7 (d)	
4″			125.0 (s)	116.4 (d)	
5″			129.8 (d)	164.3 (s)	
6″			115.9 (d)	116.4 (d)	
7″			160.7 (s)	133.7 (d)	
8″			115.9 (d)		
9″			129.8 (d)		

[a] δ in parts per million, and J in hertz. NMR solvent was MeOD. [b] Obtained at 100 MHz. [c] Obtained at 150 MHz.

minor fractions (fractions 4-5-1−4-5-3). Fraction 4-5-2 (190 mg) was purified by use of Sephadex LH-20 (1.0 × 200 cm, eluted with MeOH, 100%, 1 L) and divided into two fractions (fractions 4-5-2-1 and 4-5-2-2), and then fraction 4-5-2-2 (160 mg) was isolated by P-TLC ($CHCl_3$/MeOH, 7:1, v/v) to gain **7** (7.1 mg), **11** (12 mg), and **12** (14 mg).

Acid Hydrolysis of Compounds 1−5.[15] Compounds **1**−**5** (each 1 mg) were dissolved in 25 mL of MeOH and refluxed with 1 N HCl (1 mL) for 3 h at 80 °C. The reaction mixture was then evaporated to dryness and diluted with H_2O (10 mL). After being extracted with EtOAc (3 × 10 mL), the aqueous layer was concentrated and compared with reference D-glucose by TLC ($CHCl_3$/MeOH, 2:1, v/v). Then 900 μL of hexamethyldisilazane/trimethylchlorosilane (2:1, v/v) was added in the aqueous layer, and the mixture was stirred at 60 °C for 30 min. The supernatant was subjected to GC analysis. Derivatives of D-glucose were detected from **1**−**5**, which were identified by comparison of their retention times with that of an authentic sample of D-glucose (9.53 min).

*Mascaroside I (**1**):* white amorphous powder; $[\alpha]^{22}_D$ −85.1 (*c* 0.16, MeOH); UV (MeOH) λ_{max} (log ε) 276 (3.86) nm; IR (KBr) ν_{max} 3418, 3132, 2926, 1660, 1471, 1436, 1411, 1387, 1365, 1331, 1314, 1237, 1208, 1165, 1131, 1076, 1047, 1031 cm^{-1}; ESIMS *m*/*z* 531 [M + Na]$^+$; HREIMS *m*/*z* 508.2308 [M]$^+$ (calcd for $C_{26}H_{36}O_{10}$, 508.2315). ^1H and ^{13}C NMR data are shown in Tables 1 and 2, respectively.

*Mascaroside II (**2**):* white amorphous powder; $[\alpha]^{25}_D$ −89.5 (*c* 0.16, MeOH); UV (MeOH) λ_{max} (log ε) 276 (3.93) nm; IR (KBr) ν_{max} 3850, 3429, 2923, 2853, 1661, 1555, 1435, 1076 cm^{-1}; ESIMS *m*/*z* 513 [M + Na]$^+$; HREIMS *m*/*z* 490.2199 [M]$^+$ (calcd for $C_{26}H_{34}O_9$, 490.2203). ^1H and ^{13}C NMR spectral data are shown in Tables 1 and 2, respectively.

*Paniculoside VI (**3**):* white amorphous powder; $[\alpha]^{22}_D$ −6.0 (*c* 0.27, MeOH); UV (MeOH) λ_{max} (log ε) 315 (4.03) nm; IR (KBr) ν_{max} 3431, 2924, 2853, 2070, 1722, 1630, 1605, 1514, 1461, 1378, 1262, 1167, 1070, 1034 cm^{-1}; ESIMS *m*/*z* 641 [M - H]$^+$; HREIMS *m*/*z* 642.3052 [M]$^+$ (calcd for $C_{35}H_{46}O_{11}$, 642.3040). ^1H and ^{13}C NMR spectral data are shown in Tables 1 and 2, respectively.

*Cofaryloside I (**4**):* white amorphous powder; $[\alpha]^{27}_D$ −35.1 (*c* 0.06, MeOH); UV (MeOH) λ_{max} (log ε) 259 (3.98) nm; IR (KBr) ν_{max} 3771, 3424, 2928, 2872, 2857, 1720, 1610, 1513, 1447, 1383, 1313, 1268, 1235, 1166, 1097, 1070, 1036 cm^{-1}; ESIMS *m*/*z* 657 [M + Na]$^+$; HREIMS *m*/*z* 634.3006 [M]$^+$ (calcd for $C_{33}H_{46}O_{12}$, 634.2989). ^1H and ^{13}C NMR spectral data are shown in Tables 1 and 2, respectively.

*Villanovane I (**5**):* white amorphous powder; $[\alpha]^{22}_D$ +29.3 (*c* 0.11, MeOH); UV (MeOH) λ_{max} (log ε) 318 (3.12) nm; IR (KBr) ν_{max} 3425, 2926, 2872, 1730, 1630, 1514, 1451, 1382, 1267, 1215, 1071 cm^{-1}; ESIMS *m*/*z* 519 [M + Na]$^+$; HREIMS *m*/*z* 496.2666 M$^+$ (calcd for $C_{26}H_{40}O_9$, 496.2672). ^1H and ^{13}C NMR spectral data are shown in Tables 1 and 2, respectively.

dx.doi.org/10.1021/jf500788t | J. Agric. Food Chem. 2014, 62, 2631−2637

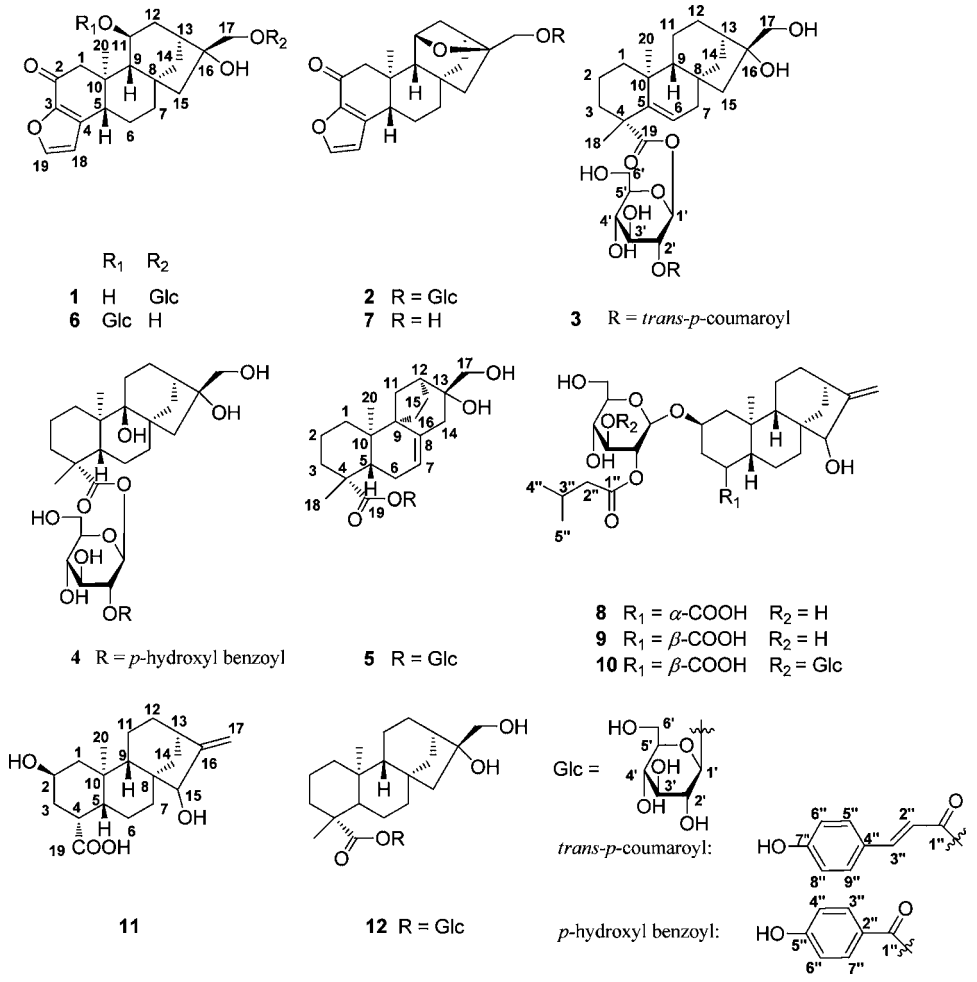

Figure 1. Structures of diterpenoid glucosides isolated from roasted coffee beans.

Cytotoxicity Assays. The cytotoxicities of compounds **1**−**5** were evaluated against HL-60, SMMC-7721, A-549, MCF-7, and SW480 cells by using the MTT [3-(4,5-dimethylthiazol-2-yl)-2,5-diphenyltetrazolium bromide] method.[16] All cells were cultured in RPMI-1640 or DMEM medium (Hyclone, Logan, UT, USA), supplemented with 10% fetal bovine serum (Hyclone) at 37 °C in a humidified atmosphere with 5% CO_2. After seeding of 1×10^5 cells/mL in a 96-well cell culture plate for 12 h before test compound addition, 100 μL of sample or standard agent was placed in each well and incubated at 37 °C for 3 days. After incubation, MTT (100 μg) was added to each well, and the incubation was continued for 4 h at 37 °C. The cells were lysed with 100 μL of 20% SDS−50% DMF after removal of 100 μL of medium. The optical density of the lysate was measured at 595 nm in a 96-well microtiter plate reader (Bio-Rad 680). The IC_{50} value of each compound was calculated by using Reed and Muench's method.[17]

RESULTS AND DISCUSSION

Structure Elucidation. The acetone extract of roasted coffee beans was extracted with ether (PE), ethyl acetate (EtOAc), and *n*-butanol. The EtOAc layer was fractionated by silica gel column chromatography in a step gradient of PE/acetone to yield four fractions, and then fraction 4 (PE/acetone, 1:1, v/v) was further purified successively on silica gel, Sephadex LH-20, and RP C-18 columns, respectively. As a result, the diterpenoid glucosides **1**−**12** were obtained in pure forms (Figure 1), of which **1**−**5** are reported for the first time in this study. Their structures were established by interpretation and full assignments of 1D and 2D NMR spectroscopic data and comparison with literature data.

Compound **1** was isolated as a white amorphous powder. The molecular formula $C_{26}H_{36}O_{10}$ was deduced from the molecular ion peak at m/z $[M]^+$ 508.2308 (calcd for $C_{26}H_{36}O_{10}$, 508.2315) in HREIMS. The IR spectrum indicated that **1** possessed hydroxyl (3418 cm^{-1}) and α,β-unsaturated ketone (1660 cm^{-1}) groups. The ^1H NMR spectrum (Table 1) of **1** displayed characteristic signals for one methyl (δ_H 0.85, s, H-20), two oxymethylenes [δ_H 3.57 (m, J = 7.2 Hz, H-17a), 4.77 (d, J = 7.6 Hz, H-17b); δ_H 3.65 (m, J = 15.6 Hz, H-6′a), 3.87 (d, J = 12.0 Hz, H-6′b)], and five oxygenated methines. The ^{13}C NMR spectrum (Table 2) showed 26 carbon resonances, attributed to a monosaccharide and an aglycone moiety. The monosaccharide was identified as glucose on the basis of comparison of chemical shifts to those found in the literature.[18] Its relative configuration was confirmed as β on the basis of the coupling constant (δ_H 4.28, m, J = 7.2 Hz, H-1′) in the ^1H NMR spectrum. The configuration of glucose was identified as D-form by acid hydrolysis. The other 20 carbon signals of the aglycone moiety were classified by ^{13}C NMR as 1 methyl, 7 methylenes (1 oxygenated), 6 methines (including 1 oxygenated, 2 olefinic), and 6 quaternary carbons (including 1 carbonyl, 2 olefinic, and 1 oxygenated). These data indicated that **1** resembled mascaroside,[19] except that a methylene (δ_C 52.0, C-15) in **1** replaced the oxymethine in mascaroside at C-15, which was further confirmed by the heteronuclear multiple-

dx.doi.org/10.1021/jf500788t | J. Agric. Food Chem. 2014, 62, 2631−2637

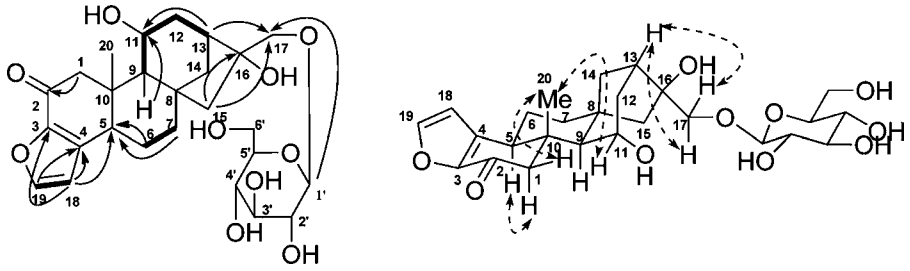

Figure 2. Key HMBC (H→C), ^{1}H–^{1}H COSY (bold), and ROESY (H←- -→H) correlations of **1**.

bond correlations (HMBC) from H_2-15 to C-9, C-13, and C-17 (Figure 2). Meanwhile, the HMBC correlations from H_2-17 to C-13, C-16, and C-1′ suggested the glucose group was coupled to C-17. The relative configuration of **1** was determined by the rotating frame Overhauser effect spectroscopy (ROESY) spectrum. On biogenetic grounds, compound **1** was confirmed as an *ent*-kauranoid with the configuration of H-20 being α-orientated. The key ROESY correlations of H-11/H-20 and H-13/H_2-17 (Figure 2) were assigned H-11 and OH-16 as α-orientated. Thus, the structure of **1** was assigned as mascaroside I.

The HREIMS data for compound **2** indicated a molecular formula of $C_{26}H_{34}O_9$. Analysis of the 1D NMR data of **2** and those of **1** (Tables 1 and 2) revealed that they were comparable. However, the carbon signals of C-11 (δ_C 77.5 for **2**, 66.2 for **1**) and C-16 (δ_C 89.6 for **2**, 82.4 for **1**) were significantly downfield shifted in **2**, and **2** being 18 mass units less than **1** suggested the presence of the ether between C-11 and C-16 in **2**. The HMBC correlations of H-11 with C-9, C-13, and C-16, of H-13 with C-16, and of H_2-15 with C-16 provided important evidence for the above inference. The glucose group was positioned at C-17 on the basis of the HMBC correlation from H_2-17 to C-13, C-16, and C-1′. Furthermore, major correlations of H-20/H-11, H-13/H_2-17 were observed in the ROESY spectrum of **2**, establishing H-11 and H_2-17 as being α-oriented. Therefore, the structure of compound **2** was identified as mascaroside II.

Compound **3**, a white amorphous powder, displayed a $[M]^+$ ion at *m*/*z* 642.3052 (calcd for $C_{35}H_{46}O_{11}$, 642.3040) in HREIMS, consistent with the molecular formula of $C_{35}H_{46}O_{11}$, indicating 13 degrees of unsaturation. IR absorption bands at 3431 and 1630 cm^{-1} were attributed to hydroxyl and double-bond groups. A *p*-coumaroyl group was confirmed by comparison of the MS and 1D NMR data of **3** with those of laevissioside A;[20] its double bond was suggested as *trans* due to the coupling constant (J = 18.0 Hz). The ^{13}C NMR spectrum (Table 2) showed the remaining 26 characteristic carbon signals for diterpenoid and β-glucose. Meanwhile, 20 carbon signals of the diterpenoid were attributed to 2 singlet methyls, 9 methylenes (1 oxygenated), 3 methines (1 olefinic), and 6 quaternary carbons (1 carboxyl, 1 oxygenated, 1 olefinic). These data revealed that **3** was similar to paniculoside IV,[21] except for the presence of two olefinic carbons (δ_C 156.8, C-5, and δ_C 113.5, C-6) in **3**. In the HMBC spectrum, the protons of C-7, C-20, and C-3 all correlated with the sp^2 quaternary carbon (δ_C 156.8, C-5), and the proton of sp^2 methine showed correlations with C-4 and C-10. Therefore, the position of the double bond was between C-5 and C-6. The β-glucose group was confirmed at C-19 by HMBC correlations of H-1′ to C-19. The HMBC correlation from H- 2′ to C-1″ (Figure 3) established that the *trans*-*p*-coumaroyl group was at C-2′. The

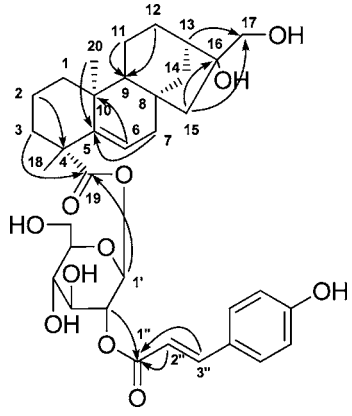

Figure 3. Key HMBC (H→C) correlations of **3**.

ROESY correlation of H-20/H-1′ assigned the relative configuration of CH_3-18 as β. Finally, the structure of **3** was confirmed as paniculoside VI.

The molecular formula of **4**, $C_{33}H_{46}O_{12}$, was determined by HREIMS (*m*/*z* 634.3006, calcd 634.2989). The IR absorption bands at 3424, 2928, and 1610 cm^{-1} suggested the presence of hydroxyl, carbonyl, and double-bond groups. The 1D NMR spectrum shows seven carbon signals (δ_C 166.9, C-1″; δ_C 164.3, C-2″; δ_C 133.7, C-3″; δ_C 133.7, C-4″; δ_C 121.9, C-5″; δ_C 116.4, C-6″; δ_C 116.4, C-7″) and two aromatic signals at δ_H 7.81 (2H, d, J = 6.6 Hz, H-2″ and H-6″), 6.71 (2H, d, J = 12.0 Hz, H-3″ and H-5″), indicating the presence of a *p*-hydroxybenzoyl group. In addition, the ^{13}C NMR spectrum exhibited another 26 carbon signals for diterpenoid and β-glucose. Comparison of the NMR data of the diterpenoid moiety of **4** with those of cofaryloside indicated they were similar.[22] In the HMBC spectrum, correlation from H-1′ to C-19 suggested the β-glucose group was linked to C-19. HMBC correlation from H-2′ (δ_H 3.55) to C-1″ confirmed the *p*-hydroxybenzoyl group at C-2′. The similar ROESY correlations with **3** indicated the relative configuration of CH_3-18 to be β. Therefore, compound **4** was assigned as cofaryloside I.

Compound **5** was obtained as a white powder, and its molecular formula was deduced as $C_{26}H_{40}O_9$ from HREIMS (*m*/*z* 496.2259, calcd 496.2672). The ^{13}C NMR spectrum (Table 2) of **5** displayed 20 carbon signals for diterpenoid, attributed to 2 methyls, 9 methylenes (1 oxygenated), 3 methines (1 olefinic), and 6 quaternary carbons (1 olefinic, 1 oxygenated, 1 carboxyl), suggesting **5** may be analogous to **4**. However, this assignment was in disagreement with HMBC correlations between H-20 and two quaternary sp^3 carbons (δ_C 38.2, C-10 and δ_C 42.4, C-9). Furthermore, comparison of chemical shifts of **5** showed resemblance to villanovane,[23] which was confirmed by the HMBC correlations from H-7, H-11, H-12, H_2-14, H_2-15, and H_2-16 to C-9, and the ^{1}H–^{1}H

dx.doi.org/10.1021/jf500788t | J. Agric. Food Chem. 2014, 62, 2631–2637

correlation spectrometry (COSY) correlations of H-11, H-15/H-12, and H-15/H-16 (Figure 4).

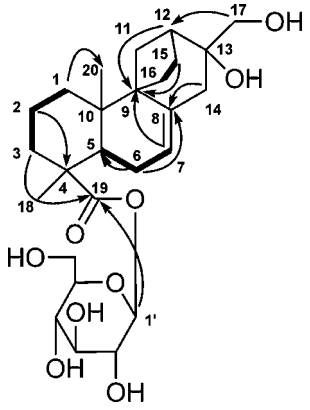

Figure 4. Key HMBC (H→C) and ^{1}H−^{1}H COSY (bold) correlations of **5**.

Comparison of 1D NMR data of **5** with those of villanovane suggested a double-bond and a glucose group were present in **5**, which were consistent with the IR absorption bands at ν_{max} 1631 and 3425 cm^{-1}. The relative configuration of glucose was confirmed as β-based on a coupling constant of 12 Hz for H-1′ (δ_H 6.40). Its position was confirmed at C-19 on the basis of HMBC correlation from H-1′ to C-19. The olefinic group involving C-7 and C-8 was supported by the HMBC correlations from H-5 and H_2-6 to C-7. Furthermore, the key correlations of H-12/H-20 and H-5/H-18 in the ROESY spectrum assigned the relative configurations of C-15, C-16, and C-18 as β. Hence, compound **5** was characterized as villanovane I.

The known compounds isolated were identified by comparison of their NMR data with literature data as mozambioside (**6**),[24] bengalensol (**7**),[25] 19-*norkaur*-16-en-18-oic acid-15-hydroxy-2-[[2-*O*-(3-methyl-1-oxobutyl)-β-D-glucopyranosyl]oxy]-(2β,4α,15α)- (**8**),[26] 19-*norkaur*-16-en-18-oic acid-15-hydroxy-2-[[2-*O*-(3-methyl-1-oxobutyl)-β-D-glucopyranosyl]oxy]-(2β,4β,15α)- (**9**),[26] 19-*norkaur*-16-en-18-oic acid-2-[[3-*O*-β-D-glucopyranosyl-2-*O*-(3-methyl-1-oxobutyl)-β-D-glucopyranosyl]oxy]-15-hydroxy-(2β,4α,15α)- (**10**),[26] 2β,16α,17-trihydroxy-*ent*-kauran-19-oic acid (**11**),[27] and paniculoside IV (**12**).[21]

The evaluation of cytotoxicities of compounds **1**−**12** showed that they were inactive against all test cells.

In conclusion, the present investigation on diterpenoid glucosides has revealed a wide structural diversity and upgrades our knowledge on the composition of roasted coffee. This is the first report about *ent*-atisans from Rubiaceae. Our work lays the chemical foundation for further bioactive research of coffee.

■ ASSOCIATED CONTENT

Supporting Information

^{1}H and ^{13}C NMR, DEPT, HSQC, HMBC, ^{1}H−^{1}H COSY, and ROESY spectra of compounds **1**−**5**. This material is available free of charge via the Internet at http://pubs.acs.org.

■ AUTHOR INFORMATION

Corresponding Author

*(M.Q.) E-mail: mhchiu@mail.kib.ac.cn. Phone: (86) 0871-65223255.

Notes

The authors declare no competing financial interest.

■ ACKNOWLEDGMENTS

This work was supported financially by Research Foundation of Coffee Engineering Research Centre of CHINA (2013P001), the National Special Program of Basic Research (SB2007FY400), the Knowledge Innovation Program of CAS (Grant No. Qian-2011), as well as Foundation of Yunnan Tobacco Industry Group (2010.2012) and State Key Laboratory of Phytochemistry and Plant Resources in West China (P2010-ZZ14).

■ REFERENCES

(1) Guo, R. Q.; Huang, J. Development status analysis of Yunnan arabica coffee industry. *Guangdong Agric. Sci.* **2009**, *3*, 209−211.
(2) Agardh, E. E.; Ostenson, C. G. Coffee consumption, type 2 diabetes and impaired glucose tolerance in Swedish men and women. *J. Intern. Med.* **2004**, *255*, 645−652.
(3) Salazar-Martinez, E.; Willett, W. C.; Hu, F. B. Coffee consumption and risk for type 2 diabetes mellitus. *Ann. Intern. Med.* **2004**, *140*, 1−8.
(4) Rosengreen, A.; Doterval, A.; Thele, D.; Johanssens, S. Coffee and incidence of diabetes in Swedish women: a perspective 18-year follow-up study. *Intern. Med.* **2004**, *255*, 89−95.
(5) Lindsay, J.; McDowell, I. Risk factors for Alzheimer's disease: a prospective analysis from the canadian study of health and aging. *Am. J. Epidemiol.* **2002**, *156*, 445−453.
(6) Larsson, S. C.; Wolk, A. Coffee consumption and risk of liver cancer: a meta analysis. *Gastroenterology* **2007**, *132*, 1740−1745.
(7) Ranheim, T.; Halvorsen, B. Coffee consumption and human health-beneficial or detrimental? Mechanisms for effects of coffee consumption on different risk factors for cardiovascular disease and type 2 diabetes mellitus. *Mol. Nutr. Food Res.* **2005**, *49*, 274−284.
(8) Kurzrock, T.; Speer, K. Diterpenes and diterpene esters in coffee. *Food Rev. Int.* **2001**, *17*, 433−450.
(9) Cardenas, C.; Quesada, A. R.; Medina, M. A. Anti-angiogenic and anti-Inflammatory properties of kahweol, a coffee diterpene. *PLoS One* **2011**, *6*, 1−9.
(10) Lee, K. J.; Choi, J. H.; Jeong, H. G. Hepatoprotective and antioxidant effects of the coffee diterpene kahweol and cafestol on carbon tetrachloride-induced liver damage in mice. *Food Chem. Toxicol.* **2007**, *45*, 2118−2125.
(11) Luke, K. T.; Velta, L. S.; Lee, W. W. Isolation and identification of kahweol palmitate and cafestol palmitate as active constituents of green coffee beans that enhance glutathione *S*-transferase activity in the mouse. *Cancer Res.* **1982**, *42*, 1193−1198.
(12) Niu, X. M.; Li, S. H.; Mei, S. X.; Na, Z.; Zhao, Q. S.; Lin, Z. W.; Sun, H. D. Cytotoxic 3,20-epoxy-*ent*-kaurane diterpenoids from *Isodon eriocalyx* var. *laxiflora*. *J. Nat. Prod.* **2002**, *65*, 1892−1896.
(13) Li, X.; Xiao, W. L.; Pu, J. X.; Ban, L.-L.; Shen, Y. H.; Weng, Z.-Y.; Li, S. H.; Sun, H. D. Cytotoxic *ent*-kaurene diterpenoids from *Isodon phyllostachys*. *Phytochemistry* **2006**, *67*, 1336−1340.
(14) Feifei, W.; Masaru, T. Roasting process of coffee beans as studied by nuclear magnetic resonance: time course of changes in composition. *J. Agric. Food Chem.* **2012**, *60*, 1005−1012.
(15) Du, X. G.; Guo, D. A. Neuroprotective xanthone glycosides from *Swertia punicea*. *J. Nat. Prod.* **2010**, *73*, 1422−1426.
(16) Monks, A.; Scudiero, D. Feasibility of a high-flux anticancer drug screen using a diverse panel of cultured human tumor cell lines. *J. Natl. Cancer Inst.* **1991**, *83*, 757−766.
(17) Reed, L. J.; Muench, H. A simple method of estimating fifty percent endpoints. *Am. J. Hyg.* **1938**, *27*, 493−497.
(18) Russell, B. W.; Gary, R. E.; Courtney, M. S. Acetylated dammarane-type bisdesmosides from *Combretum inflatum*. *J. Nat. Prod.* **2013**, *76*, 1592−1597.

(19) Richter, H.; Spiteller, G. A new furokaurane glycoside from green coffee-beans. *Chem. Ber.* **1979**, *112*, 1088−1092.
(20) Li, M. M.; Zhao, Q. S. Four new labdane-type diterpenoid glycosides from *Diplopterygium laevissimum*. *Nat. Prod. Bioprospect.* **2013**, *3*, 38−42.
(21) Xing, F. C.; Im, S. L. Diterpenoids with inhibitory activity against NFAT transcription factor from *Acanthopanax koreanum*. *Phytother. Res.* **2004**, *18*, 677−680.
(22) Richter, H.; Obermann, H.; Spiteller, G. A new kauran-18-oic acid glucopyranosyl ester from green coffee-beans. *Chem. Ber.* **1977**, *110*, 1963−1970.
(23) Bohlmann, F.; Robinson, H. Epoxycannabinolide and diterpenes with a new carbon skeleton from *Villanova titicaensis*. *Liebigs Ann. Chem.* **1984**, *2*, 250−258.
(24) Roland, P.; Armin, G. Crystal structure of mozambioside, a diterpene glycoside of *Coffea* pseudozanguebariae. *Phytochemistry* **1990**, *29*, 990−992.
(25) Choudhury, M. H.; Quamrul, H. Bengalensol, a new 16-epicafestol derivative from the leaves of *Coffea* Bengalensis. *Nat. Prod. Lett.* **1994**, *5*, 55−60.
(26) Jia, L.; Lin, F. Three new *ent*-kaurane diterpenoids from *Siegesbeckia pubescens* Helv. *Chim. Acta* **2012**, *95*, 221−226.
(27) Emika, O.; Satoshi, K. *ent*-Kaurenoic acids from *Mikania hirsutissima*. *Phytochemistry* **2004**, *65*, 885−890.

MATERIALS AND METHODS

Reagents and Standards. The standard PAH mixture in 1 mL of acetonitrile (Supelco, Bellefonte, PA, USA) consisted of 10 μg/mL of naphthalene, acenaphthene, acenaphthylene, fluorene, anthracene, phenanthrene, fluoranthene (F), pyrene, B*a*A, Ch, B*b*F, B*k*F, B*a*P, D*b*A, B*g*P, and IP. PAH standard solution was stored in amber flasks at −20 °C.

Ethanol, methanol, acetonitrile, ethyl acetate, hexane, and dichloromethane were of HPLC grade and were provided by Merck (Darmstadt, Germany). 1,1-Diphenyl-2-picrylhydrazyl (DPPH) was purchased from Sigma-Aldrich (St. Louis, MO, USA). Water was purified with a Milli-Q System (Millipore, Bedford, MA, USA). Amber glassware was carefully washed and rinsed with distilled solvent (acetone and hexane) before use.

Marinated Meat Samples and Cooking Conditions. *Preparation of Marinated Meat Samples.* Three different types of beer marinades were tested: Pilsner beer, nonalcoholic Pilsner beer, and Black beer, coded PB, P0B, and BB, respectively. PB contained 5.2% alcohol and was made from water, barley malt, unmalted cereals (maize and barley), and hops; P0B contained 0.5% alcohol and was made from water, barley malt, unmalted cereals (maize), glucose−fructose syrup, flavors, and hops; and BB contained 5.0% alcohol and was made from water, barley malt, sugar, color E150C (ammonia caramel), and hops. All beers were purchased at local supermarkets.

Loin pork steaks were obtained from a local supermarket in Porto, Portugal. Loin pork steaks presented similar dimensions (0.75 cm thick) and weight (about 100 g each). A total of 32 pork loin steaks were used for determination of PAHs: 8 for each marinade and 8 as control samples (unmarinated). Marinade conditions were selected according to previous works:[11,12] marinating time was 4 h at 5 °C, and the proportion of meat amount and marinade volume was 1:1 (g/mL). No other ingredients were added, besides beer. Before cooking, pork samples were removed from the marinade and dried slightly. Four hours of marinating time was selected on the basis of the best beer marinating time for HA inhibition.[11] Recently, Farhadian et al.[14] observed lower PAH concentration in almost all of the analyzed samples with 4 h of marinating.

Cooking Conditions. A bed of charcoal was prepared and ignited in a garden-type grill (35 cm width, 52 cm length, and 15 cm height). When all flames had subsided, pork samples were barbecued at 15 cm distance from the heat source. The grilling temperature was 200−230 °C, and internal temperature reached the minimum 75 °C measured by a digital thermocouple (0560 9260, Testo 926, Lenzkirch, Germany) with a surface probe (0603 1992, Testo 926, Lenzkirch, Germany). Samples were turned once during grilling at half of the total cooking time (10 min). Charcoal was replaced between grilling each type of marinated meat.

After cooking, the eight steaks prepared for each type of marinade were divided in two homogeneous groups of four steaks each. Each group was mixed with a knife mill (Grindomix GM 200, Retsh, Hann, Germany) to obtain a uniform, representative, and homogeneous sample for duplicate analyses. The samples were codified, frozen, and freeze-dried (Cryodos-90, Telstar, Terrassa, Spain). Grilled pork sample codes were as follows: control (unmarinated pork), PBp (pork marinated in Pilsner beer), P0Bp (pork marinated in nonalcoholic Pilsner beer), and BBp (pork marinated in black beer). Average cooking losses were around 54−66 and 50−60% for unmarinated and marinated samples, respectively.

Determination of Marinades Radical-Scavenging in DPPH Reaction. *Extraction of phenolic compounds* of beer marinades was performed according to the method of Zhao et al.[15] and Viegas et al.[12] with some modifications. Marinades were degassed with intensive stirring for 15 min at room temperature. Fifteen milliliters of each sample was extracted during 15 min with 15 mL of ethyl acetate by ultrasound-assisted solvent extraction (FungiLab SA, Barcelona, Spain) and centrifuged at 2000 rpm for 2 min at 20 °C (Eppendorf 5810 R centrifuge, Eppendorf, Hamburg, Germany). The supernatant was collected. Then, 6 g of NaCl was added and the pH was set to 1 (combined pH glass electrode connected to a pH-meter, MicropH 2001, Crison, Barcelona, Spain) using 1 M HCl. The resulting sample was extracted two times more with 15 mL of ethyl acetate. The pooled ethyl acetate extracts were evaporated to dryness under reduced pressure in a rotary evaporator (Rotavapor Büchi RE-111, coupled with a water bath Büchi 461, BÜCHI, Flawil, Switzerland) at 40 °C and redissolved in 10 mL of ethanol 70% (v/v).

Antiradical Activity by DPPH. Extracts of PB, P0B, and BB collected before and after 4 h of marinating were diluted in 96-well microplates (1:2; 1:4; 1:8; 1:16; 1:32; 1:62). A 100 μL amount of 150 μM DPPH and 100 μL of each extract were mixed in the microplates. Absorbances at 517 nm were measured for 2 h until the reaction reached plateau (Biotekmicroplate reader ELX 808, Biotek Corp., USA). For each extract, two readings with DPPH ($A_{extract}$) and one without the radical ($A_{blank\ 1}$) were carried out. DPPH solution were used as control ($A_{control}$), and ethanol 70% was used as blank ($A_{blank\ 2}$). The radical-scavenging activity was expressed as a percentage and calculated by using the following formula:

$$\%\ \text{DPPH scavenging} = 100 - \left(\frac{A_{extract} - A_{blank\ 1}}{A_{control} - A_{blank\ 2}} \times 100 \right)$$

Analysis of PAHs. *Extraction and Cleanup.* PAH extraction and cleanup procedures were performed according to the method of Viegas et al.,[3] with some modifications. Briefly, 2 g of lyophilized meat was weighed into an EPA amber glass vial (40 mL) and was subjected to ultrasound-assisted solvent extraction with 20 mL of *n*-hexane for 1 h at room temperature. The extract obtained was filtered, and the solvent was evaporated nearly to dryness with a rotatory evaporator at room temperature. The residue was redissolved in 3 mL of *n*-hexane and loaded for cleanup in a 5 g silica cartridge (Mega BE-Si, 5 g, 20 mL, from Agilent Technologies) previously washed with 20 mL of dichloromethane, dried completely by vacuum, and conditioned with 20 mL of *n*-hexane. The cartridge was dried by vacuum and eluted with 24 mL of *n*-hexane/dichloromethane (70:30, v/v). The first 5 mL was discharged to reduce the volume of PAH fraction and because no PAHs were detected in this first fraction as described by Viegas et al.,[3] the remaining elution volume was collected in a vial and evaporated to dryness under nitrogen stream at room temperature. The residue obtained was dissolved in 100 μL of acetonitrile.

Chromatographic Conditions. Separation and quantification of PAHs were performed by liquid chromatography with fluorescence detection (HPLC-FLD) according to the method of Viegas et al.[3] A HPLC unit (Jasco, Japan) equipped with a PU-1580 HPLC pump, an AS-950 autosampler with a 20 μL loop, and a FP-920 fluorescence detector was used. PAH separations were performed with a 25 cm × 4.6 mm (length × i.d.), 5 μm particle size, Supelcosil LC-PAH (Supelco, Bellefonte, PA, USA), thermostated at 32.0 ± 0.2 °C. Borwin PDA Controller software (JMBS Developments, Le Fontanil, France) was used. Three solvents were used for mobile phase: 75% methanol in water (A), methanol (B), and ethyl acetate (C) with a flow rate 1 mL/min. The linear gradient program was as follows: 0−18 min, 0−80% B in A; 18−19 min, 80−100% B in A; 19−20 min, 100−90% B in C; 20−28.5 min, 90−82% B in C; 28.5−37.5 min, 82−80% B in C; 37.5−40 min, 80−100% B in C; 40−45 min, 100−0% B in A, followed by rinsing and re-equilibration of the column to the initial conditions. The excitation and emission wavelengths used were 270/390 nm for B*a*A and Ch; 260/430 nm for B*b*F; 290/410 for B*k*F, B*a*P, D*b*A, and B*g*P; and 293/498 for IP. Peak identification in pork samples was carried out by comparing retention times of the peaks with those obtained from a reference standard mixture of PAHs. Quantification of PAHs was performed by standard addition method using nonspiked sample and two fortified levels (10−20 ng/g).[3]

Statistics. The averages of duplicate analyses of two independent experiments were calculated for each PAH. The results were statistically analyzed by analysis of variance. Comparison of mean values was made using the Duncan test. Statistical analyses were all performed with SPSS for Windows version 21 (SPSS Inc., Chicago, IL, USA).

RESULTS AND DISCUSSION

Antiradical Activities of Beer Marinades. DPPH assay was used to evaluate the antioxidant activity of the marinades under study. The DPPH radical-scavenging activities expressed as percent of inhibition of beer marinades before the addition of meat (T0) and after 4 h of meat marinating (T4) are shown in Figure 1. All beers exhibited radical-scavenging activity. The

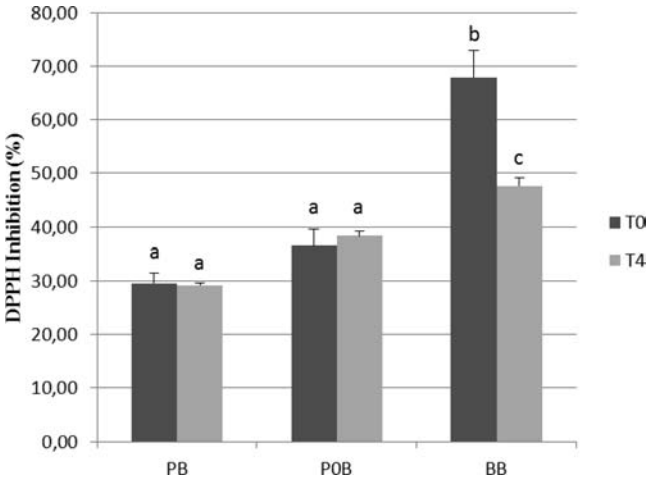

Figure 1. DPPH radical scavenging activity of beer marinades (Pilsner, nonalcoholic Pilsner, and Black beer marinades coded respectively PB, P0B, and BB) before the addition of meat to the marinade (T0) and after 4 h of meat marinating (T4). Results are expressed as percentage of inhibition (%) of DPPH. Error bars represent standard deviation obtained from triplicate experiments. Bars with different letters show significant differences ($p < 0.05$).

results expressed correspond to a 1:8 dilution of beer extracts, necessary to achieve the linearity. As can be seen, at T0, the strongest DPPH-scavenging activity was found in the BB (68.0%), followed by P0B (36.5%) and PB (29.5%). BB exhibited a significantly higher value than others; the slightly higher value of P0B was not significant when compared with PB. These results are in agreement twith those obtained by Tafulo et al.[16] and Polak et al.[17] According to these authors the differences between radical-scavenging activities of the different kinds of beers could be explained by several factors such as the type of fermentation and the presence of food coloring, sweeteners, flavors, and other additives. Ale beers have a higher antioxidant capacity than lager beers.[16] BB is an ale beer in contrast with the rest of the beers studied, which are lager beers. The presence in BB of food coloring (E150C) could be another factor that explains its higher antioxidant activity. In Tafulo et al.,[16] beers with food coloring, including E150C, showed a higher activity antioxidant than ones without it. Nonalcoholic Pilsner beer (P0B) showed a slightly higher antioxidant activity than Pilsner beer (PB). This fact could be explained by the presence in the nonalcoholic Pilsner beer of different additives such as glucose−fructose syrup and flavors. Tafulo et al.[16] also reported that beer samples with sweeteners, flavors, antioxidants, and other additives had a slightly higher antioxidant activity than the samples without it.

After 4 h of meat marinating, no significant changes were observed in radical-scavenging activity of PB and P0B. In our previous work the same behavior was observed for Pilsner beer marinade.[12] However, a significant loss of antiradical capacity was observed in BB after meat marinating. Possible interactions between beer antioxidant compounds and oxidative species of meat surface may occur.

PAH Formation in Charcoal-Grilled Pork. PAH concentrations in charcoal-grilled pork loin are presented in Table 1. All eight PAHs under study were quantified, and their sum was around 21 ng/g wet weight grilled meat. For the quantitative profile, greater contents of Ch > B*a*A > B*bF* > B*a*P were found. B*k*F, D*b*A, B*g*P, and IP were formed in very low concentrations. The four main PAHs formed in charcoal-grilled pork comprise the PAH4. Their contribution to PAH8 was around 80%. Martorell et al.[18] studied 16 PAHs (which include PAH8) in various foodstuffs and also found that lowest PAH levels corresponded to D*b*A, IP, and B*k*F.

Scarce information was found on the individual compounds of PAH4 in grilled meat; several studies describe only B*a*P composition, and few studies mention other PAHs. However, in an EFSA report[2] thousands of food items from several food groups were compared, and the highest mean value was recorded for Ch (3.20 ng/g), followed by B*a*A (1.97 ng/g) and B*b*F (1.48 ng/g); mean contents of these compounds were higher than the mean value for B*a*P (1.02 ng/g). In the present study the PAH4 profile was in agreement with the EFSA statement.

Table 1. PAH8 Formation on Charcoal-Grilled Pork Loin Unmarinated (Control) and Marinated with Pilsner Beer (PBp), Nonalcoholic Pilsner Beer (P0Bp), and Black Beer (BBp)[a]

	PAHs (ng/g wet weight grilled meat)			
PAH	control	PBp	P0Bp	BBp
B*a*A	3.93 ± 0.73 a	3.59 ± 0.90 a	3.55 ± 0.29 a	1.60 ± 0.41 b
Ch	7.45 ± 0.57 a	5.21 ± 2.24 ab	5.79 ± 1.42 ab	3.43 ± 0.49 b
B*b*F	3.23 ± 0.95 a	3.06 ± 0.90 a	2.29 ± 0.24 ab	1.42 ± 0.37 b
B*k*F	0.39 ± 0.32 a	0.61 ± 0.37 a	0.71 ± 0.24 a	0.42 ± 0.17 a
B*a*P	2.71 ± 0.82 a	2.17 ± 0.76 ab	2.03 ± 0.20 ab	1.07 ± 0.08 b
D*b*A	0.24 ± 0.34 a	0.61 ± 0.65 a	0.27 ± 0.16 a	0.44 ± 0.22 a
B*g*P	1.36 ± 0.45 ab	1.80 ± 0.90 b	0.60 ± 0.22 a	0.85 ± 0.13 ab
IP	1.26 ± 0.34 a	0.77 ± 0.57 ab	0.26 ± 0.20 b	0.51 ± 0.13 ab
∑PAH8	20.57	17.82	15.50	9.74

[a]Results are presented as the mean ± standard deviation, $n = 4$. Means with different letters in the same row are significantly different ($p < 0.05$). For all PAHs (except IP) LOD and LOQ were 0.003 and 0.01 ng/g wet weight grilled meat, respectively. LOD and LOQ for IP were 0.01 and 0.04 ng/g wet weight, respectively.

Table 2. Inhibitory Effects of Different Marinating Treatments or Additives on PAH Formation in Cooked Meat

marinating treatment	meat	cooking method	analyzed PAHs	inhibition (%)	ref
basic marinade (sugar, water, onion, turmeric, lemon grass, salt, garlic, coriander, cinnamon)	beef	charcoal-grilled	B*a*P, B*b*F, F	32	14
basic-oil (basic marinade, cooking oil)			B*a*P, B*b*F, F	0.0	
commercial marinade (spices, onion, garlic, salt, sugar, water, cooking oil)			B*a*P, B*b*F, F	9.0	
basic-lemon juice (basic marinade, lemon juice)			B*a*P, B*b*F, F	56	
basic-oil-lemon juice (basic marinade, cooking oil, lemon juice)			B*a*P, B*b*F, F	27	
basic-oil-tamarind (basic marinade, cooking oil, tamarind)			B*a*P, B*b*F, F	0.0	
commercial-tamarind (commercial marinade, tamarind)			B*a*P, B*b*F, F	27	
Pilsner beer	pork	charcoal-grilled	PAH8	13	present work
Pilsner beer without alcohol			PAH8	25	
Black beer			PAH8	53	
marinade (tomato juice, garlic paste, onion, sodium chloride, cumin, coriander, and black pepper)	chicken	microwave oven	U.S. EPA PAHs	89	20
		pan-fried	U.S. EPA PAHs	91	
		direct-flame butane gas	U.S. EPA PAHs	84	
		indirect-flame butane gas	U.S. EPA PAHs	92	
additives					
onion	pork (collars)	pan-fried	F, B*a*A, B*b*F, B*k*F, B*a*P, D*b*A, B*g*P	53	21
	pork (chop)		F, B*a*A, B*b*F, B*k*F, B*a*P, D*b*A, B*g*P	67	
	pork (minced chops)		F, B*a*A, B*b*F, B*k*F, B*a*P, D*b*A, B*g*P	18	
garlic	pork (collars)	pan-fried	F, B*a*A, B*b*F, B*k*F, B*a*P, D*b*A, B*g*P	66	
	pork (chop)		F, B*a*A, B*b*F, B*k*F, B*a*P, D*b*A, B*g*P	41	
	pork (minced chops)		F, B*a*A, B*b*F, B*k*F, B*a*P, D*b*A, B*g*P	0	
spices (cumin, coriander, black pepper, and rosemary)	chicken	microwave oven	U.S. EPA PAHs	56	20
		pan-fried	U.S. EPA PAHs	58	
		direct-flame butane gas	U.S. EPA PAHs	68	
		indirect-flame butane gas	U.S. EPA PAHs	80	
garlic	chicken	microwave oven	U.S. EPA PAHs	76	20
		pan-fried	U.S. EPA PAHs	31	
		direct-flame butane gas	U.S. EPA PAHs	39	
		indirect-flame butane gas	U.S. EPA PAHs	47	
spices and garlic	chicken	microwave oven	U.S. EPA PAHs	88	20
		pan-fried	U.S. EPA PAHs	90	
		direct-flame butane gas	U.S. EPA PAHs	82	
		indirect-flame butane gas	U.S. EPA PAHs	86	

Chung et al.[5] analyzed seven PAHs of the PAH8 in different pork samples and found a total of 10.18 ng/g in charcoal-grilled ones. B*a*P accounted for 2.90 ng/g. Alomirah et al.[19] screened the concentrations of 16 priority PAHs in 72 grilled and smoked food samples and presented mean results; among the PAH8, Ch (4.88 ng/g) and B*a*A (2.27 ng/g) showed the highest mean values, followed by B*b*F (1.58 ng/g) and B*a*P (1.10 ng/g), and the sum of PAH8 was 11.7 ng/g.

Considering the maximum levels of B*a*P (5 ng/g) and PAH4 (30 ng/g) described in European legislation[8] for meat and meat products that have undergone grilling and barbecuing as heating treatment, the values of B*a*P and PAH4 in control samples, 2.71 and 17.32 ng/g, respectively, were below the maximum levels, indicating that they were cooked to a well-done level appropriate for consumption.

Effects of Beer Marinades on PAH Formation. PAH8 concentrations in charcoal-grilled pork loin marinated during 4

dx.doi.org/10.1021/jf404966w | J. Agric. Food Chem. 2014, 62, 2638−2643

h with different beers are shown in Table 1. As observed for unmarinated meat, PAH8 (B*a*A, Ch, B*b*F, B*k*F, B*a*P, DbA, B*g*P, and IP) were also formed in marinated samples; however, their sum was lower in these samples when compared with control meat. With regard to the three types of beers used as marinades, the less effective in reducing the PAH8 content was PB (17.82 ng/g), followed by P0B (15.50 ng/g). BB had the strongest inhibitory effect on the PAH8 in grilled pork (9.74 ng/g), reducing by more than half the PAH8 content of the control samples. Although not statistically significant, a positive correlation was found between the higher radical-scavenging activity of marinades and a decrease of PAH8 formation (Pearson correlation = 0.606, p = 0.202).

A decrease in antioxidant activity was observed for BB after 4 h; interactions between BB antioxidant compounds and oxidative species of the meat surface may occur, possibly increasing meat resistance to the formation of PAHs.

The exact mechanism of PAH formation is not precisely known; however, it is generally considered that PAHs are formed by condensation of small organic molecules by either pyrolysis or pyrosynthesis.[6,7] At high temperatures these molecules are easily fragmented (pyrolysis) and the free radicals produced recombine to form stable polynuclear aromatic compounds (pyrosynthesis). Because the mechanism of formation of PAHs involves free radicals, it may be possible that antioxidant compounds from beer (especially BB) act as inhibitors in the free radical reaction pathways, through radical quenchers and free radical scavengers activity. Inhibitory effects of different marinating treatments and additives on PAH formation in grilled meat are scarce. Table 2 reports a summary of results from the literature and comparison with the present work. Farhadian et al.[14] evaluated the effect of seven marinade treatments of beef satay on the formation of B*a*P, B*b*F, and F. Inhibitory effects were observed in some marinades; the authors attributed the protective effect due to the presence of spices that are known to have antioxidant activity, emphasizing the sulfur compounds, present in garlic and onion, and their potential to prevent Maillard reactions and then PAH formation. Brady[20] found the highest reduction in samples treated with marinade (from 84 to 92%) followed by spice mixture and garlic paste (from 82 to 90%), spice mixture (from 56 to 80%), and garlic paste (from 31 to 76%) for different cooking methods. However, the charcoal grilling method was not evaluated, and according to EFSA[2] special attention is required for this cooking method because higher PAH content is found in charcoal-grilled products.

Janoszka[21] observed that the addition of onion (30/100 g of meat) and garlic (15/100 g of meat) caused, respectively, average decreases of 60 and 54% of the total content of PAHs (six of the PAH8) in pan-fried pork meat and also connected the effect to the antioxidant effect of polyphenols and sulfhydryl compounds, which can scavenge free radicals and destroy fatty acid hydroperoxides.

In control and marinated samples the PAH8 profiles were quite similar; the predominant PAHs were Ch > B*a*A > B*b*F > B*a*P. However, control samples had greater contents of these PAHs than marinated ones. BB caused a significant decrease these PAHs. B*k*F, D*b*A, B*g*P, and IP were formed in very low concentrations, and no relevant differences between control and marinated were achieved. EFSA[2] concluded that although PAH8 is a suitable indicator of PAHs in food, PAH4 (sum of B*a*P, Ch, B*a*A, and B*b*F) may provide enough information. In fact, the measurement of PAH4 provided a suitable overview of PAH formation and the beer effect on their formation (Figure 2).

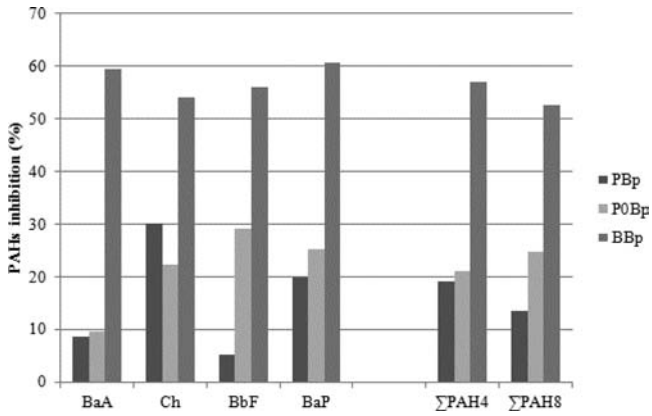

Figure 2. Percentage of inhibition of PAH formation in charcoal-grilled pork loin marinated by different beers (Pilsner, nonalcoholic Pilsner, and Black beer marinades coded respectively PBp, P0Bp, and BBp) versus unmarinated charcoal-grilled loin pork (mean value of quadruplicate analyses). B*a*A, benzo(*a*)anthracene; Ch, chrysene; B*b*F, benzo(*b*)fluoranthene; B*a*P, benzo(*a*)pyrene; ∑PAH4, sum of PAH4; ∑PAH8, sum of PAH8.

With regard to the inhibition of each individual compound, BB showed the highest percentage of inhibition for all with very similar values: 59% of B*a*A, 54% of Ch, 56% of B*b*F, and 61% of B*a*P. P0B and PB presented very similar PAH4 inhibitions, around 20%, but with regard to individual compounds, the inhibitory profile was different. For P0B it was 10% of B*a*A, 22% of Ch, 29% of B*b*F, and 25% of B*a*P. The inhibitory effect of PB was 9% for B*a*A, 30% of Ch, 5% of B*b*F, and 20% of B*a*P.

According to an EFSA report,[2] throughout Europe an exposure of 279 ng/day of PAHs from meat and meat products was estimated on the basis of the occurrence of PAH8 and average consumption of these foods (132 g). Considering an intake of 132 g of grilled pork loin (unmarinated), the uptake of 271 ng of B*a*P and 2057 ng of PAH8 will exceed the overall average dietary exposure of B*a*P (235 ng) and PAH8 (1729 ng) estimated by EFSA. If grilled pork loin marinated in Black beer is consumed, the uptake of 141 ng of B*a*P and 1286 ng in 132 g will not exceed the overall average dietary exposure. Thus, the intake of beer-marinated meat can be a suitable mitigation strategy.

AUTHOR INFORMATION

Corresponding Author

*(I.M.P.L.V.O.F.) E-mail: isabel.ferreira@ff.up.pt.

Author Contributions

‖O.V. and I.Y.-P. contributed equally to this study.

Funding

This work was supported by Projects PP-IJUP2011-332 from Universidade do Porto and PEst-C/EQB/LA0006/2013. O.V. thanks QREN for her PostDoc Grant (NORTE-07-0124-FEDER-000069), and I.Y.-P. thanks the Spanish Ministry of Education, Culture and Sport for her FPU grant.

Notes

The authors declare no competing financial interest.

REFERENCES

(1) Phillips, D. H. Polycyclic aromatic hydrocarbons in the diet. *Mutat. Res.−Genetic Toxicol. Environ. Mutagen.* **1999**, *443* (1−2), 139−147.

(2) EFSA. Scientific opinion of the panel on contaminants in the food chain on a request from the European Commission on polycyclic aromatic hydrocarbons in food. *EFSA J.* **2008**, *724*, 1−114.

(3) Viegas, O.; Novo, P.; Pinho, O.; Ferreira, I. M. P. L. V. O. A comparison of the extraction procedures and quantification methods for the chromatographic determination of polycyclic aromatic hydrocarbons in charcoal grilled meat and fish. *Talanta* **2012**, *88*, 677−683.

(4) Viegas, O.; Novo, P.; Pinto, E.; Pinho, O.; Ferreira, I. M. P. L. V. O. Effect of charcoal types and grilling conditions on formation of heterocyclic aromatic amines (HAs) and polycyclic aromatic hydrocarbons (PAHs) in grilled muscle foods. *Food Chem. Toxicol.* **2012**, *50* (6), 2128−2134.

(5) Chung, S. Y.; Yettella, R. R.; Kim, J. S.; Kwon, K.; Kim, M. C.; Min, D. B. Effects of grilling and roasting on the levels of polycyclic aromatic hydrocarbons in beef and pork. *Food Chem.* **2011**, *129* (4), 1420−1426.

(6) Chen, B. H.; Chen, Y. C. Formation of polycyclic aromatic hydrocarbons in the smoke from heated model lipids and food lipids. *J. Agric. Food Chem.* **2001**, *49* (11), 5238−5243.

(7) Sharma, R. K.; Chan, K. G.; Hajaligol, M. R. Product compositions from pyrolysis of some aliphatic α-amino acids. *J. Anal. Appl. Pyrolysis* **2006**, *75* (2), 69−81.

(8) European Commission.. Commission regulation 835/2011 of 19 August 2011 amending Regulation (EC) EC) no. 1881/2006 as regards maximum levels for polycyclic aromatic hydrocarbons in foodstuffs. *Off. J. Eur. Union* **2011**, *L215*, 4−8.

(9) Sinha, R.; Kulldorff, M.; Gunter, M. J.; Strickland, P.; Rothman, N. Dietary benzo[a]pyrene intake and risk of colorectal adenoma. *Cancer Epidemiol. Biomarkers Prev.* **2005**, *14*, 2030−2034.

(10) European Commission. Opinion of the Scientific Committee on Food on the risks to human health of polycyclic aromatic hydrocarbons in food, 2002; http://ec.europa.eu/food/fs/sc/scf/out153_en.pdf.

(11) Melo, A.; Viegas, O.; Petisca, C.; Pinho, O.; Ferreira, I. M. P. L. V. O. Effect of beer/red wine marinades on the formation of heterocyclic aromatic amines in pan-fried beef. *J. Agric. Food Chem.* **2008**, *56* (22), 10625−10632.

(12) Viegas, O.; Amaro, L. F.; Pinho, O.; Ferreira, I. M. P. L. V. O. Inhibitory effect of antioxidant-rich marinades on the formation of heterocyclic aromatic amines in pan-fried beef. *J. Agric. Food Chem.* **2012**, *60* (24), 6235−6240.

(13) Quelhas, I.; Petisca, C.; Viegas, O.; Melo, A.; Pinho, O.; Ferreira, I. M. P. L. V. O. Effect of green tea marinades on the formation of heterocyclic aromatic amines and sensory quality of pan-fried beef. *Food Chem.* **2010**, *122* (1), 98−104.

(14) Farhadian, A.; Jinap, S.; Faridah, A.; Zaidul, I. S. M. Effects of marinating on the formation of polycyclic aromatic hydrocarbons (benzo[a]pyrene, benzo[b]fluoranthene and fluoranthene) in grilled beef meat. *Food Control* **2012**, *28* (2), 420−425.

(15) Zhao, H.; Chen, W.; Lu, J.; Zhao, M. Phenolic profiles and antioxidant activities of commercial beers. *Food Chem.* **2010**, *119* (3), 1150−1158.

(16) Tafulo, P. A. R.; Queirós, R. B.; Delerue-Matos, C. M.; Sales, M. G. F. Control and comparison of the antioxidant capacity of beers. *Food Res. Int.* **2010**, *43* (6), 1702−1709.

(17) Polak, J.; Bartoszek, M.; Stanimirova, I. A. Study of the antioxidant properties of beers using electron paramagnetic resonance. *Food Chem.* **2013**, *141* (3), 3042−3049.

(18) Martorell, I.; Perelló, G.; Martí-Cid, R.; Castell, V.; Llobet, J. M.; Domingo, J. L. Polycyclic aromatic hydrocarbons (PAH) in foods and estimated PAH intake by the population of Catalonia, Spain: temporal trend. *Environ Int.* **2010**, *36* (5), 424−432.

(19) Alomirah, H.; Al-Zenki, S.; Al-Hooti, S.; Zaghloul, S.; Sawaya, W.; Ahmed, N.; Kannan, K. Concentrations and dietary exposure to polycyclic aromatic hydrocarbons (PAHs) from grilled and smoked foods. *Food Control* **2011**, *22* (12), 2028−2035.

(20) El Badry, N. Effect of household cooking methods and some food additives on polycyclic aromatic hydrocarbons (PAHs) formation in chicken meat. *World Appl. Sci. J.* **2010**, *9*, 963−974.

(21) Janoszka, B. HPLC-fluorescence analysis of polycyclic aromatic hydrocarbons (PAHs) in pork meat and its gravy fried without additives and in the presence of onion and garlic. *Food Chem.* **2011**, *126* (3), 1344−1353.

energy input level will be more favorable for producing finer emulsions. Furthermore, the application of a high energy level of emulsification may impart some novel characteristics (e.g., enhanced interdroplet interactions and, subsequently, formation of a uniform and gel-like emulsion) to the emulsions stabilized by these nanoparticles.

Another noteworthy issue is that, for any particle dispersion, interparticle interactions and particle−particle associations (or aggregation) are highly determined by the particle concentration. The concentration of particles may affect their adsorption at the oil/water interface during emulsification, as well as formation of a multilayer-structured interfacial film, since at high particle concentrations, most of the particles with good surface hydrophobicity (e.g., modified silica nanoparticles) are usually present in the aggregated form.[19] Once these aggregated particles are adsorbed at the interface, they could provide supplementary stabilization to the formed emulsions.[19] More importantly, the association or aggregation of particles in the continuous phase (which is more favorable at higher particle concentrations) may lead to formation of a gel-like network in the emulsions, as in the chitin nanocrystal case.[5] The gel-like network formation can thus impart extraordinary stability against creaming to the emulsions. Using steady viscosity and dynamic oscillatory measurements, gel-like network formation has also been confirmed for the emulsions stabilized by preheated SPI or whey proteins at high c values, produced by microfluidization as the emulsification process (e.g., 6% in the continuous phase).[19−21] If the oil fraction is high enough, the gel-like behavior can also be observed for the emulsions stabilized by SPI nanoparticles, produced even by a high-shear mixer with a low-energy input.[21]

In this work we aim to investigate the influence of the emulsification process on the interfacial and emulsifying properties of SPI nanoparticles and the properties of the resultant Pickering emulsions. The SPI nanoparticles were formed by the same process as in our previous work.[12] For comparison, three emulsification processes (I−III) with different energy input levels were applied to formulate the emulsions: (I) only high-shear homogenization; (II) combined applications of high-shear homogenization and ultrasonic treatment; (III) combined applications of high-shear homogenization and microfluidization. It is reasonably hypothesized that increasing the energy input level of emulsification may greatly improve the adsorption of the nanoparticles at the interface and, subsequently, can impart some unique characteristics to the resultant Pickering emulsions, e.g., extraordinary stability against coalescence and creaming and a gel-like emulsion structure.

MATERIALS AND METHODS

Materials. Freeze-dried SPI was the same as that applied in our previous work,[12] the protein content of which was about 91% (wet basis). Soy oil was purchased from a local supermarket in Guangzhou (China). Nile Blue A, Nile Red, and dithiothreitol (DTT) were obtained from Sigma-Aldrich (St. Louis, MO). Bovine serum albumin (BSA) was obtained from Fitzgerald Industries International Inc. (Concord, MA). All other chemicals used were of analytical grade.

SPI Nanoparticle Preparation. The SPI nanoparticles were formed according to the same process described in our previous work.[12] In brief, an SPI solution (6%, w/v) in water, containing 0.02% (w/v) sodium azide, was heated in a bath at 95 °C for 15 min. After being cooled in an ice bath to room temperature, the preheated SPI dispersion was added to the salt powder little by little to a final concentration of 300 mM. Last, the SPI nanoparticle dispersion (6%, w/v), diluted with the same buffer to an appropriate concentration (in the range of 0.01−6.0%, w/v) if needed, was applied to the emulsion preparation.

SPI Nanoparticle Characterization. The particle size (z-average diameter) of nanoparticles in the preheated SPI dispersions was determined using the dynamic light scattering (DLS) technique, using a Zetasizer Nano-ZS instrument (Malvern Instruments Ltd., Worcestershire, U.K.) equipped with a 4 mW He−Ne laser (633 nm wavelength) at 25 °C. The SPI nanoparticle dispersion (6%, w/v) was diluted with the same background buffer (containing 300 mM NaCl) to different individual c values (0.01−1.5%, w/v), and the diluted dispersions were kept at ambient temperature for 30 min, before being subjected to the determination. All the samples were centrifuged at 10000g for 20 min to remove any insolubles in the dispersions prior to the determination. The z-average diameter was obtained with a single-exponential fitting, with each datum reported as the average over three readings.

To unravel the interactive forces involved in the formation and maintenance of the nanoparticle structure, the z-average diameter of the SPI nanoparticle dispersion at c = 0.05% (w/v) in the presence of 6.0 M urea, 0.5% SDS, and 30 mM DTT, alone or in combinations, was also determined according to the same process above.

Dynamic Surface Pressure (π) Measurement. The adsorption kinetics of SPI nanoparticles at the oil/water (pH 7.0, 300 mM NaCl) interface, at varying c values of 0.01−1.5% (w/v), were determined using an optical contact angle meter (OGA-20) with an oscillating drop accessory, ODG-20 (Dataphysics Instruments GmbH, Germany), at 25 °C. The interfacial tension (γ) of the oil/water interface, formed with an oil drop submerged into a cuvette filled with the nanoparticle dispersions, was determined by the drop shape analysis.[22] The surface pressure (π) was calculated as $\gamma_s - \gamma_p$, where γ_s and γ_p are the surface tensions of the aqueous background buffer and the corresponding nanoparticle dispersion (at any test time), respectively. All the measurements with a period of up to 3 h were performed in duplicate. For each sample two consecutive measurements were performed (with the average used for statistics analysis), and each sample was replicated at least two times.

Emulsion Preparation. The SPI nanoparticle dispersions at varying c values of 0.5−6% (w/v), obtained as mentioned above, were applied to form the emulsions, with types I, II, and III corresponding to the three different emulsification processes. All the emulsions were formed at a fixed oil fraction (ϕ) of 0.2. The type I emulsions were prepared as follows: In brief, 16 mL of any SPI nanoparticle dispersion was added to a glass vial, and 4 mL of soybean oil was slowly added to the dispersion, with mixing via an Ultra Turrax homogenizer (model IKA-ULTRA-TURRAX T25 basic, IKA Works, Inc., Wilmington, NC) with a dispersing head operating at 10000 rpm. After all the oil was added, the sample was mixed for an additional 2 min. The type I emulsions were further processed using ultrasonic equipment with a probe at 250 W for 3 min to produce the type II emulsions or homogenized through a microfluidizer (M110EH model, Microfluidics International Corp., Newton, MA) for one pass at a pressure level of 40 MPa to produce the type III emulsions. These resultant emulsions (fresh) were directly subjected to analysis or stored at room temperature for various periods of time for emulsion stability evaluation, e.g., 7 or 40 days for coalescence stability analysis.

Droplet Size Distribution Profiles and Volume-Average Droplet Size ($d_{4,3}$) of Emulsions. Droplet size distribution profiles of various freshly prepared or stored (7 or 40 days) emulsions were obtained with a Malvern MasterSizer 2000 (Malvern Instruments Ltd.). Deionized water or 1.0% (w/v) SDS solution containing 300 mM NaCl was used as the dispersant. The relative refractive index of the emulsion was taken as 1.095, that is, the ratio of the refractive index of soy oil (1.456) to that of the continuous phase (1.33). Droplet size measurements are reported as the volume-average droplet size, $d_{4,3}$ ($=\sum n_i d_i^4 / \sum n_i d_i^3$), where n_i is the number of droplets with diameter d_i. All determinations were conducted on individual samples at least in duplicate.

Flocculation Index (FI, %). The FI (%) of the fresh emulsions was evaluated according to the method described by Castellani and

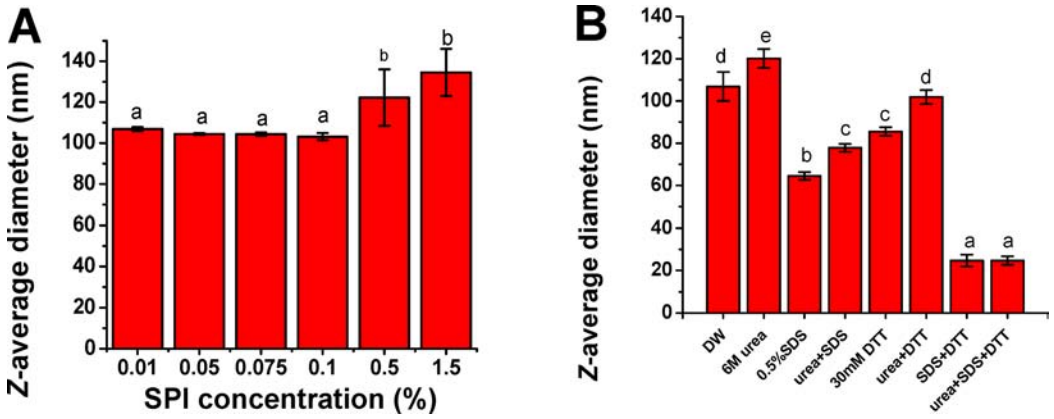

Figure 1. (A) Protein concentration dependence of the *z*-average diameter (D_z) for heat-induced SPI nanoparticles. The nanoparticles were formed by heating the SPI dispersion (c = 6%, w/v) at 95 °C for 15 min and, subsequently, electrostatic screening with addition of 300 mM NaCl. The preheated SPI dispersion was diluted with the same solvent (with 300 mM NaCl) to a specific c value in the range of 0.01−1.5% (w/v). (B) Effects of various protein-perturbing solvents on the D_z of nanoparticles in a preheated SPI dispersion at c = 0.05%. Different characters on the tops of the columns represent the significant difference at the $p < 0.05$ level (n = 3).

others.[23] The emulsions were diluted in deionized water with and without 1% (w/v) SDS, and $d_{4,3}$ of the droplets was determined as described above. The FI was calculated as follows:

$$\text{FI}\ (\%) = [d_{4,3}(\text{in water})/d_{4,3}(\text{in 1\% SDS}) - 1.0] \times 100$$

Microstructure of Fresh Emulsions. The microstructure of the fresh emulsions (types I–III), formed at varying c values of 0.5–6.0% (w/v), was evaluated by confocal laser scanning microscopy (CLSM) using a Leica TCS SP5 confocal laser scanning head mounted on a Leica DMRE-7 (SDK) upright microscope (Leica Microsystems Inc., Heidelberg, Germany). Each fresh emulsion sample (1 mL) was mixed with about 40 μL of fluorescence dye mixtures of Nile Blue (0.1%, w/v) and Nile Red (0.1%, w/v). The mixtures were then placed on concave confocal microscope slides (Sail, Sailing Medical-Lab Industries Co. Ltd., Suzhou, China), covered with glycerol-coated coverslips, and examined with a 100× magnification lens and an argon/krypton laser with an excitation line of 488 nm and a He–Ne laser with excitation at 633 nm, respectively.

Creaming Stability. The creaming stability of various emulsions was assessed visually upon quiescent storage for up to 30 days. Each emulsion (10 mL) in a glass test tube (1.5 cm internal diameter × 12 cm height) was perpendicularly stored at ambient temperature. After different periods of storage, the height of the serum (H_s) and total height of the emulsion (H_t) were recorded. The creaming index (%) was calculated as $(H_s/H_t) \times 100$. Each datum is reported as the mean ± standard deviation of three replicates performed on separated samples.

Rheological Characterization. *Steady Shear Viscosities.* Steady shear viscosities (η) of various fresh emulsions were characterized using a HAAKE RS600 rheometer (HAAKE Co., Germany) with parallel plates (d = 27.83 mm) at 25 °C. The gap between two plates was set to 1.0 mm. After 10 min of equilibration, η of the emulsions was recorded as the shear rate was increased from 1 to 100 s^{-1}.

Dynamic Oscillatory Measurements. The dynamic viscoelastic properties of the gel-like type III emulsions were characterized by the same RS600 rheometer using a small-amplitude oscillatory strain or frequency sweep mode. For the strain sweep experiments, the strain (γ) was varied from 0.002 to 1.0 at a constant frequency of 1.0 Hz, while, for the frequency sweep experiments, the frequency was varied from 0.1 to 100 rad/s at a constant strain of 0.5%. The elastic modulus (G'), loss modulus (G''), and loss tangent (tan δ) were recorded. All the experiments were carried out at 25 °C unless stated otherwise.

Amount of Adsorbed or Entrapped Proteins. The amount of adsorbed or entrapped proteins in the fresh emulsions (types I–III) was evaluated by a centrifugation method. In brief, each fresh emulsion (1.0 mL) was centrifuged at 10000*g* for 30 min at room temperature. After the centrifugation, two phases were observed: a cream layer (or concentrated oil droplets) at the top of the tube and an aqueous phase of the emulsion at the bottom. The cream layer was carefully removed using a syringe, and the subnatant was filtered through a 0.22 μm filter (Millipore Corp.). The protein concentration of the filtrate (C_f) was determined with the Lowry method using BSA as the standard. The percentage of adsorbed proteins (AP) was calculated as $[(C_o - C_f) \times 100]/C_o$, where C_o is the initial protein concentration in SPI aggregate dispersions. The amount of adsorbed proteins (g/100 mL) was calculated on the basis of the total adsorbed protein content per 100 mL of emulsion.

Statistics. An analysis of variance (ANOVA) of the data was performed, and a least significant difference (LSD) with a confidence interval of 95% was applied to compare the means of duplicate or triplicate measurements on separate samples (n = 2 or 3).

RESULTS AND DISCUSSION

SPI Nanoparticle Characteristics. Figure 1 A shows the *z*-average diameter (D_z) of SPI nanoparticles as affected by the c (in the range 0.01–1.5%, w/v) at which the DLS measurements were performed. D_z (about 103 nm) basically remained constant at c values in the range of 0.01–0.1% (w/v), but it significantly increased to 122 nm as c was increased to 0.5% (w/v) (Figure 1 A). A further increase in c to 1.5% (w/v) led to a slight but insignificant increase in D_z. D_z at c = 0.5% (w/v; 122 nm) is basically similar to that (84–112 nm) observed for the glycinin and β-conglycinin mixtures heated at 100 °C for 30 min at the same c value but without 300 mM NaCl.[24] The increases in D_z might be associated with the increased interparticle interactions and subsequent formation of larger particles.[12]

To unravel the pattern of interactive forces involved in formation and maintenance of the nanoparticle structure, we determined the D_z of nanoparticles at c = 0.05% (w/v) in the presence of various protein perturbants, including 6 M urea, 0.5% SDS, and 30 mM DTT, or their combinations, as displayed in Figure 1 B. The results interestingly showed that the presence of 0.5% SDS or 30 mM DTT led to a significant reduction in D_z, with a higher extent of reduction observed in the presence of 0.5% SDS; the presence of both 0.5% SDS and 30 mM DTT led to a considerable decrease in D_z (77% vs 39% in the presence of 0.5% SDS; Figure 1B). On the other hand, the presence of 6 M urea did not decrease D_z, regardless of the presence or absence of 0.5% SDS and/or 30 mM DTT, and in some cases, D_z on the contrary significantly increased (Figure 1

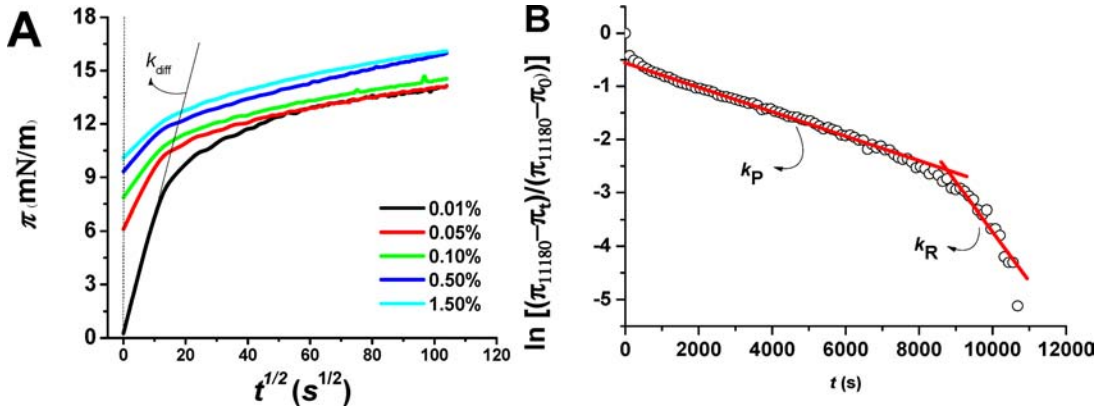

Figure 2. (A) Time evolution of the surface pressure (π) for the adsorption of SPI nanoparticles at the oil/water interface (SPI concentration in solution, 0.01−1.5%, w/v; temperature, 25 °C). (B) Typical profile of the molecular penetration and configurational rearrangement steps at the interface for SPI nanoparticles at c = 0.5%. k_P and k_R represent first-order rate constants of penetration and rearrangement, respectively.

Table 1. Characteristic Parameters, Including the Apparent Diffusion Rate ($k_{diff}°$), Constants of Penetration and Structural Rearrangement at the Interface (k_P and k_R), and Surface Pressure at the End of Adsorption (11800 s; π_{11800}), for the Adsorption of SPI Nanoparticles at the Oil/Water Interface at Varying Protein Concentrations of 0.01−1.5% (w/v)

protein concn (%)	$k_{diff}°$ [a] (mN m^{-1} $s^{-0.5}$) (LR[b])	$k_P \times 10^4$ (s^{-1}) (LR)	$k_R \times 10^4$ (s^{-1}) (LR)	π_{11800} (mN m^{-1})
0.01	0.5822 (0.9459)	−2.5609 (0.969)	−12.2 (0.808)	14.13
0.05	0.2986 (0.9274)	−2.6183 (0.979)	−11.4 (0.870)	14.14
0.1	0.2117 (0.9550)	−2.5456 (0.982)	−11.0 (0.861)	14.54
0.5	0.1779 (0.9495)	−2.4088 (0.982)	−11.1 (0.937)	15.99
1.5	0.1552 (0.9755)	−2.6482 (0.989)	−11.7 (0.949)	16.10

[a] π vs $t^{1/2}$ slope during the initial adsorption. [b] LR = linear regression coefficient.

B). Usually, SDS, urea, and DTT mainly disrupt hydrophobic interactions, hydrogen bonding, and disulfide bonding, respectively.[25,26] Thus, the observations suggest that hydrophobic interactions and disulfide bondings are the major intramolecular interactive forces maintaining the internal structure of the nanoparticles, while the hydrogen bonds play a crucial role in their external structure. The interactive force pattern seems to be a bit different from that observed for SPI nanoparticles induced by the calcium ion, where the driving forces for the nanoparticle formation and stabilization were largely attributed to hydrogen bonding and hydrophobic interactions, while disulfide bonding was minor.[27]

Interfacial Adsorption Behavior: Adsorption Kinetics and Structural Rearrangements at the Interface. The interfacial adsorption behavior of the SPI nanoparticles in relation to c was also investigated, with the aim to elucidate the role of the particle concentration in the formation dynamics of the films at the oil/water interface. The surface pressure (π) at the interface for SPI nanoparticles at any test c value (0.01−1.5%, w/v) progressively increased with time (Figure 2A), reflecting protein or particle adsorption at the interface.[22] Due to the consideration that various kinds of emulsifiers (including solid particles, globular proteins, and surfactants) exhibit high similarities in emulsification and emulsion stability,[28] the adsorption kinetics of SPI nanoparticles at the interface can also be described by three main steps: (i) diffusion of particles from the bulk onto the interface, (ii) penetration and structural deformation at the interface, and (iii) rearrangement of adsorbed nanoparticles at the interface and multilayer formation, as has been widely applied to proteins.[29] When the adsorption process is controlled by diffusion, a plot of π against $t^{1/2}$ will be linear and the slope of this plot the diffusion rate constant (k_{diff}).[29] Figure 2 A shows that only at c = 0.01% (w/v) was the adsorption of the nanoparticles at the interface diffusion-controlled, while, at c values of 0.05% (w/v) or higher, the adsorption was more complex. A similar adsorption behavior has been previously observed for native and heat-treated (at 90 or 120 °C for 20 min) SPIs.[30] At c values above 0.01% (w/v), the π value at the beginning of adsorption (0 s; π_0) was far above zero, suggesting that the initial adsorption at these c values was too fast to be detected. However, it can still be observed that π_0 progressively increased from about 0 to 10.2 mN/m as c increased from 0.01 to 1.5% (w/v; Figure 2 A). This observation reflects that increasing the particle concentration progressively accelerated the most initial diffusion and/or adsorption of the nanoparticles from the bulk onto the interface.

The increasing rate of π, or slope for the plot of π against $t^{1/2}$ during initial adsorption (e.g., less than 100 s), gradually decreased with increasing c (from 0.01% to 1.5%, w/v; Table 1), which might reflect the presence of an energy barrier at the interface.[31] On the other hand, π at the end of the adsorption period (11800 s; π_{11800}) was nearly unchanged by variation in c from 0.01% to 0.1%, irrespective of the differences in π changes during initial adsorption; π_{11800} considerably increased from about 14.5 to 16.0 mN/m when c was increased from 0.1% to 0.5% (w/v), and it did not change upon a further increase in c (to 1.5%, w/v) (Table 1). Interestingly, the changing pattern of π_{11800} upon an increase in c is basically the same as that observed for the particle size (Figure 1A), implying that the potential for these nanoparticles to be adsorbed at the interface and participate in interfacial film formation was largely determined by their particle size.

Following the initial adsorption, penetration and subsequent rearrangement of previously adsorbed nanoparticles at the interface occur. These processes can be monitored using a first-

dx.doi.org/10.1021/jf405348k | J. Agric. Food Chem. 2014, 62, 2644−2654

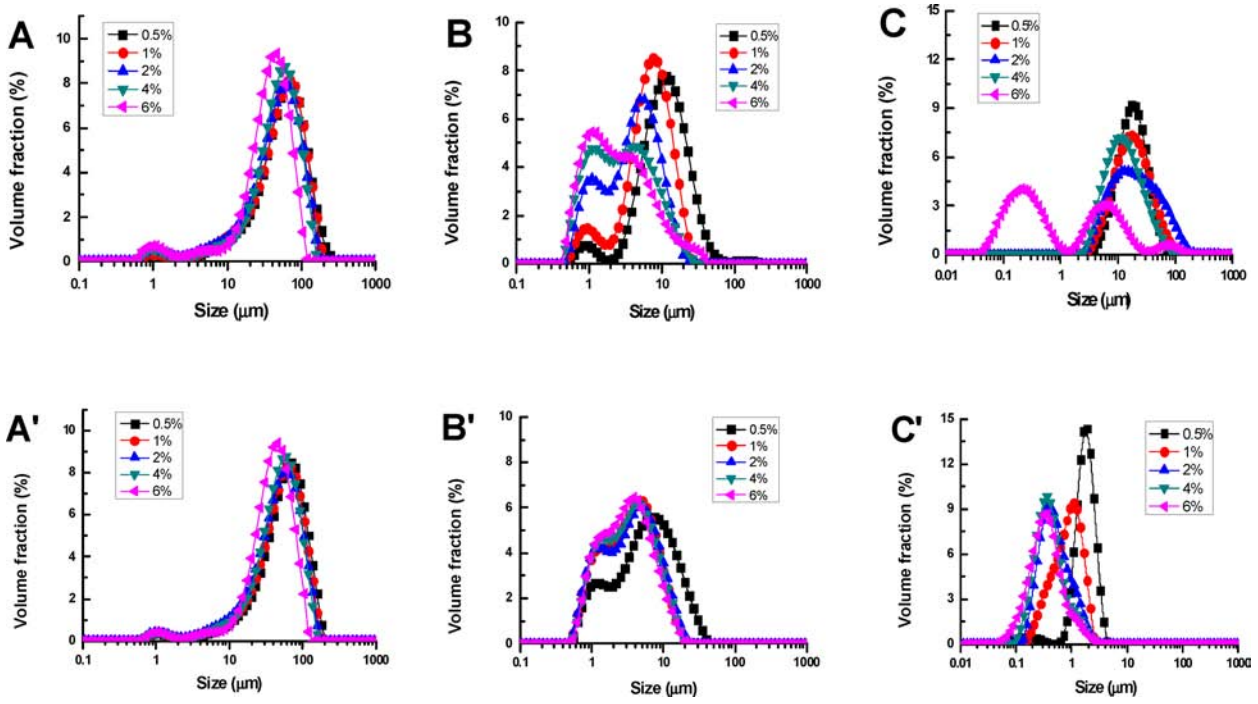

Figure 3. Typical droplet size distribution profiles of various fresh emulsions stabilized by the SPI nanoparticle aggregates at a comparable initial *c* of 0.5−6.0% (w/v), as determined with water (A−C) or 1% SDS (A′−C′) as the dispersing solvent: (A, A′) emulsification with an Ika T25 (emulsification I); (B, B′) emulsification with an Ika T25 in combination with ultrasonic equipment (emulsification II); (C, C′) emulsification with an Ika T25 in combination with a microfluidizer (emulsification III).

Table 2. Mean *z*-Average Diameter ($d_{4,3}$, in Water or 1% SDS) Values and Flocculation Index (FI, %) of Droplets in the Fresh Emulsions Stabilized by the SPI Nanoparticle Aggregates at a Comparable Initial *c* Value of 0.5−6.0% (w/v), Produced by Three Emulsification Processes (I−III)[a]

	emulsification process I[b]			emulsification process II			emulsification process III		
	$d_{4,3}$ (μm)			$d_{4,3}$ (μm)			$d_{4,3}$ (μm)		
protein concn (%)	water	SDS	FI (%)	water	SDS	FI (%)	water	SDS	FI (%)
0.5	57.3 ± 3.5 a	53.6 ± 6.4 a	6.9 ± 0.6 a	15.8 ± 2.3 a	8.6 ± 1.9 a	83.7 ± 2.5 a	23.2 ± 2.1 b	1.8 ± 0.1 a	1189 ± 81 d
1.0	53.2 ± 2.4 a	52.2 ± 1.4 a	2.0 (± 0.1 b	6.8 ± 0.8 b	3.9 ± 0.2 b	74.4 ± 2.8 b	23.1 ± 1.8 b	0.89 ± 0.01 b	2496 ± 224 b
2.0	49.4 ± 1.1 b	52.3 ± 1.6 a		4.4 ± 0.5 c	3.8 ± 0.3 b	22.2 ± 0.6 c	27.2 ± 1.2 a	0.57 ± 0.02 c	4672 ± 137 a
4.0	49.7 ± 1.3 b	50.3 ± 1.6 b		3.7 ± 0.3 c	3.8 ± 0.2 b		19.7 ± 1.3 c	0.44 ± 0.02 d	4377 ± 258 a
6.0	36.3 ± 1.7 c	38.9 ± 1.8 c		3.6 ± 0.4 c	3.9 ± 0.3 b		6.1 ± 0.5 d	0.42 ± 0.01 d	1352 ± 102 c

[a]The SPI nanoparticles were formed by heating a 6% (w/v) SPI dispersion at 95 °C for 15 min (and then immediately cooling it in an ice bath to room temperature), followed by addition of 300 mM NaCl. The heated SPI dispersion (containing the nanoparticles) was diluted with pH 7.0 water with the same ionic strength to the required initial *c* value (in the range of 0.5−4.0%, w/v). Emulsifications I−III are the same as in the caption of Figure 3. Each datum is the mean ± standard deviation of triplicate measurements on separate samples. Different online letters (a−d) represent the significant difference at the $p < 0.05$ level due to the difference in *c* (within the same column). [b]The data are the same as in our previous work.[12]

order phenomenological equation: $\ln[(\pi_{11800} - \pi_t)/(\pi_{11800} - \pi_0)] = -k_i t$, where π_{11800}, π_t, and π_0 are the π values at the final time (11800 s) of each step, at any time (t), and at the initial time (t_0), respectively, and k_i is the first-order rate constant.[32] Figure 2 B shows a typical application of the above equation to the adsorption of the nanoparticles at the interface at $c = 0.5\%$ (w/v). In general, the first slope is taken as a first-order rate constant of penetration (k_P), while the next slope refers to a first-order rate constant of molecular rearrangement (k_R) for the adsorbed nanoparticles. The results showed that k_P and k_R for the adsorbed nanoparticles were slightly affected by increasing *c* from 0.01% to 1.5% (w/v) ((−2.41 to −2.65) × 10^{-4} s^{-1} and (−11 to −12) × 10^{-4} s^{-1} for k_P and k_R, respectively; Table 1). At any *c* value, k_R for the adsorbed nanoparticles was considerably higher than k_P, indicating the greater importance of the structural rearrangement of adsorbed nanoparticles at the interface to film formation (than their penetration). The observations suggest that, after initial adsorption, penetration at the interface and subsequent structural rearrangement of adsorbed nanoparticles seem to be slightly dependent on the applied *c* in the range of 0.01−1.5% (w/v).

Emulsifying Properties and Emulsion Characteristics. *Emulsifying Ability or Emulsification Efficiency.* The emulsifying properties of these nanoparticles, including emulsifying ability, flocculated state of a droplet in fresh emulsions, and emulsion stability against coalescence and creaming, were evaluated at varying *c* values of 0.5−6.0% (w/v) and at a fixed oil fraction (ϕ) of 0.2. Three emulsification processes (I−III; see section 2.3) with different levels of energy input were

applied to form the emulsions. Figure 3 shows the typical droplet size distribution profiles of these fresh emulsions, diluted in water or 1% SDS, and the corresponding volume-average diameter ($d_{4,3}$) data are summarized in Table 2. One noteworthy point is that the data for the type I emulsions produced with only a high-shear homogenization have been reported in our previous work,[12] but are still presented herein for comparison between the different emulsification processes. In general, the emulsifying ability of a protein can be reflected in terms of the droplet size of the freshly formed emulsion in the presence of 1% SDS, with smaller sizes indicative of higher emulsifying ability, since SDS can keep individual oil droplets separate in the emulsions.

As expected, the droplet size distribution profiles and the $d_{4,3}$ data (in 1% SDS) were highly dependent on the applied emulsification process and c (Figure 3 and Table 2), indicating that the ability of these nanoparticles to help dispersion of the oil phase into an aqueous phase (at a specific ϕ) might be closely related to the interfacial area of droplets created in the emulsification and the concentration of proteins in the continuous phase. As previously indicated, the type I emulsions exhibited a prominent size distribution peak at around 60−70 μm, with $d_{4,3}$ (in water or 1% SDS) slightly decreasing with an increase in c (from 0.5% to 6.0%) (Figure 3 A,A′ and Table 2). For this type of emulsion, $d_{4,3}$ (in 1% SDS; 52−53 μm) did not significantly change upon an increase of c to 2.0% (w/v), and it progressively decreased as c further increased above 2.0% (w/v; Table 2). This observation suggests that, at c values >2.0% (w/v), the total interfacial area nonlinearly increased with c, due to enough nanoparticles being available to aid formation and stabilization of the newly created interface. The progressive increase in total interfacial area with c (above 2.0%, w/v) is very consistent with the fact that at higher c values the initial adsorption of nanoparticles at the interface was much faster (Figure 2 A), and as a consequence, more interfacial area newly created during the emulsification could be coated and stabilized. When the type I emulsions were further processed by ultrasonic equipment (II) or microfluidization (III), it was observed that, at any specific c, the size distribution profiles in the presence of 1% SDS remarkably shifted toward lower sizes, with a much higher extent of the changes observed for the type III emulsions than the type II counterparts (Figure 3 A′−C′). This can also be reflected in the changes in $d_{4,3}$ data (in 1% SDS; Table 2), confirming that the emulsification efficiency considerably increased with the energy level input order of the emulsification processes: I < II < III.

For the type II emulsions, the droplet size distribution profiles (in 1% SDS) were basically bimodal (Figure 3 B′), reflecting that the additional ultrasonic treatment increased the polydispersity of droplets. In this case, increasing c from 0.5% to 1.0% (w/v) resulted in a shift of the larger size peak toward lower sizes and an increased volume of the smaller peak, and concomitantly, $d_{4,3}$ (in 1% SDS) considerably decreased from 8.6 to 3.9 μm, while a further increase in c to 6.0% (w/v) did not significantly change the size distribution profiles and the $d_{4,3}$ data (Figure 3 B′ and Table 2). In contrast, in the case of type III emulsions, the monomodal size distribution peak (in 1% SDS) progressively shifted toward lower sizes, and $d_{4,3}$ (in 1% SDS) accordingly decreased from 1.76 to about 0.4 μm, as c increased from 0.5% to 4.0% (w/v), though the magnitude of the reduction in $d_{4,3}$ was relatively marginal (Figure 3 C′ and Table 2). The observations suggest that, in both the cases, the amount of nanoparticles at c = 1% (w/v) seemed to be enough to fully cover the newly created interfacial area during the emulsification. The progressive but slight decrease in $d_{4,3}$ upon an increase of c from 1.0% to 4.0% (w/v), in the type III emulsions, reflects that increasing the c of the nanoparticles was favorable for the coalescence stability of newly formed oil droplets during microfluidization. Considering that the initial adsorption of the nanoparticles at the interface was highly related to their concentration, and the adsorption of these nanoparticles was very fast during the initial adsorption, especially at high c values (Figure 2), it can thus be reasonably hypothesized that the droplet size in 1% SDS of the emulsions stabilized by these nanoparticles is mainly determined by the interfacial area created during the emulsification, and increasing c may facilitate the stabilization of newly created oil droplets through an enhanced rate of adsorption during the initial adsorption. In the emulsions stabilized by bare silica, it has been observed that the interfacial area was linearly proportional to the silica content.[18]

Decreases in droplet size with an increase in particle concentration have been similarly observed in emulsions stabilized by modified silica nanoparticles,[18,33] clay particles,[34] and chitin nanocrystal particles.[5] This observation is expected because more particles or nanoparticles are available to stabilize smaller oil droplets. At low c values (e.g., 0.5%, w/v) bridging flocculation and/or coalescence may take place, while, when the SPI nanoparticles are in excess of that needed to fully cover the oil droplet surface, more particles may be adsorbed to form interfacial multilayers or remain dispersed in the aqueous phase.[5,33]

Flocculated State of Droplets in Fresh Emulsions. In the protein-stabilized emulsion system, protein-coated oil droplets may be present in the flocculated form, subsequently affecting the coalescence and even creaming stability of the emulsions. At low c values, bridging flocculation may occur, while, at high c values, the flocculation may be induced by interdroplet attraction interactions (e.g., hydrophobic interactions) between adsorbed proteins on individual droplets. The flocculated state of oil droplets in various fresh emulsions (types I−III) stabilized by SPI nanoparticles was evaluated in terms of the flocculation index (FI, %) by comparison of $d_{4,3}$ between water and 1% SDS (as the dispersant), as included in Table 2. For the type I emulsions, the droplet size distribution profiles without 1% SDS were basically the same as those with 1% SDS (Figure 3 A,A′), indicating a low extent of droplet flocculation in the fresh emulsions. However, it can be still observed that FI progressively decreased from 7.0 to nearly 0 as c increased from 0.5% to 2.0% (w/v; Table 2), suggesting complete inhibition of bridging flocculation at c values above 1.0% (w/v). The decrease in FI with c can be similarly observed in the type II emulsions, where FI progressively decreased from about 84 to near 0 as c increased from 0.5% to 4.0% (w/v; Table 2). This can also be seen from the bimodal droplet size distribution profiles (in water) of this type of emulsion (Figure 3 B), wherein increasing c led to a progressive shift of the larger size distribution peak (toward lower sizes) and, concomitantly, a progressive increase in the volume fraction of the smaller size peak. In contrast, FI at any comparable c value for the type III emulsions was considerably higher than that for the type II counterparts (Table 2), indicating a much higher extent of flocculation. For this type of emulsion, FI on the contrary progressively increased from 1189% to 4672%, as c increased from 0.5% to 2.0% (w/v); when c was above 2.0% (w/v), a contrary trend was observed (Table 2). In this case, the

increasing extent of flocculation upon an increase in c to 2.0% (w/v) might be largely attributed to the enhanced attraction interactions between the adsorbed proteins, while the progressive decrease in FI at c values above 2.0% (w/v) could also be explained to be a result of inhibited flocculation, as in the type I or II emulsions.

The flocculated state of oil droplets in these fresh emulsions can be further corroborated by their CLSM observations, as illustrated in Figure 4. For the type I emulsions, only a portion of the oil droplets at c = 0.5% (w/v) were associated together, while, in the case of the type II emulsions, the microstructural morphology of oil droplets gradually changed from a clustered to a dissociated state as c increased from 0.5% to 4% (w/v; Figure 4, the top two rows). In the latter case, most of the individual oil droplets seemed to be present in the dissociated form, which is well in accordance with the droplet size data (Figure 3 A and Table 2). As compared with the type II emulsions, the extent of droplet flocculation and/or aggregation for the type III emulsions was much higher (Figure 4, middle and bottom rows), indicating a much higher interdroplet interaction of droplets. When c was high enough, e.g., 4% or above, a homogeneous network of the emulsions could be observed, which seems to be in agreement with the decrease in the extent of droplet flocculation (Table 2). On the other hand, the CLSM observations of the contour size of individual oil droplets are basically consistent with the droplet size data (in 1% SDS; Figure 3 C′ and Table 2).

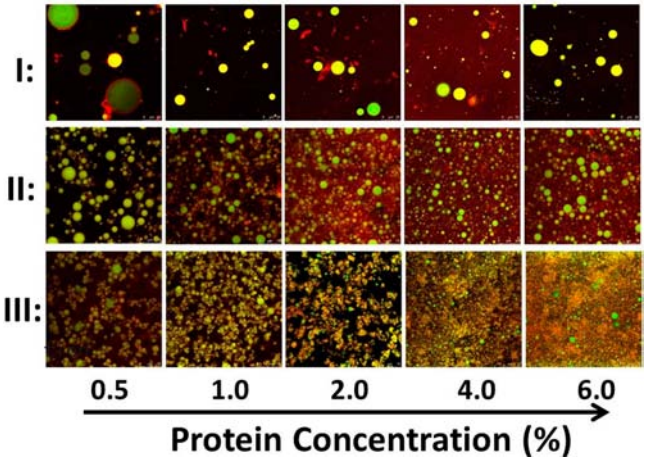

Figure 4. Typical CLSM images of emulsions I–III stabilized by the SPI nanoparticle aggregates at a comparable initial c of 0.5–6.0% (w/v). Emulsions I–III correspond to those produced by the three emulsification processes, as described in the caption of Figure 3.

Coalescence Stability. Extraordinary coalescence stability is one of the most striking features for Pickering emulsions.[33] Table 3 shows the influence of storage after specific periods (7 and 40 days) on $d_{4,3}$ (in 1% SDS) of the various fresh emulsions. In general, we can observe that the coalescence stability of the emulsions was higher at higher c values, or when a higher energy input level of emulsification was applied (Table 3). For the type I emulsions, for example, a minimal c of approximately 1% was needed to keep them stable against coalescence upon storage for 7 days, while a minimal c of 4% (w/v) was needed when the storage was extended to 40 days (Table 3). The type II emulsions, at c values >0.5% (w/v), were basically stable against coalescence upon storage for up to 40 days, though significant but marginal increases in $d_{4,3}$ (in 1% SDS) were observed at c = 1.0% or 2.0% (w/v) after more than 7 days of storage (Table 3). In this case, the emulsion at c = 0.5% (w/v) was unstable against coalescence after 40 days of storage (Table 3). In contrast, all the type III emulsions exhibited extraordinary stability against coalescence upon storage for up to 40 days, even at c = 0.5% (w/v; Table 3).

For particle-stabilized emulsions, the extraordinary coalescence stability can be largely attributed to the effective and irreversible adsorption of particles at the interface, because several thousand kT (k is the Boltzmann constant and T the temperature) of energy might be needed for one particle to desorb from the interface.[35] Besides, the steric hindrance of the particles at the interface,[5,36] as well as a network formation of flocculated particles at the interface or in the continuous phase at high solid concentrations,[5,37] can also contribute to the stability of droplets against coalescence. In the present study, the particle size analyses confirmed that increasing c above 0.1% (w/v) progressively increased the flocculation or aggregation of SPI nanoparticles (Figure 1A), which suggests that the increase in coalescence stability at higher c values might be largely due to the formation of a network involving associated nanoparticles in the system. On the other hand, it should be worth noting that the SPI nanoparticles share some common features of SPI; e.g., once the nanoparticles adsorb at the interface, unfolding or deformation of their structures and subsequent structural rearrangement may occur. This situation may become more distinct at lower c values, e.g., 0.5% (w/v) in the present work. Thus, the differences in coalescence stability at low c values between the different emulsification processes might be to a certain extent attributed to the differences in viscoelasticity and/or intermolecular interactions between adsorbed proteins of interfacial protein films. This can be indirectly corroborated

Table 3. Changes of $d_{4,3}$ (in 1% SDS; μm) of SPI-Nanoparticle-Stabilized Emulsions I–III Formed at Varying c Values of 0.5–6.0% (w/v) upon Storage for up to 40 days[a]

protein concn (%)	emulsion I			emulsion II			emulsion III		
	0 days	7 days	40 days	0 days	7 days	40 days	0 days	7 days	40 days
0.5	53.6 ± 6.4 a	64.1 ± 1.1 b	63.5 ± 0.8 b	8.6 ± 1.9 a	10.6 ± 4.3 ab	16.0 ± 3.2 b	1.8 ± 0.1 a	2.0 ± 0.2 a	2.0 ± 0.2 a
1.0	52.2 ± 1.4 a	54.4 ± 2.6 a	61.8 ± 4.4 b	3.9 ± 0.2 a	4.3 ± 0.1 b	4.3 ± 0.1 b	0.89 ± 0.01 a	1.0 ± 0.03 ab	1.2 ± 0.2 b
2.0	52.3 ± 1.6 a	49.2 ± 3.3 a	60.8 ± 2.4 b	3.8 ± 0.3 a	4.3(± 0.2 b	4.4 ± 0.5 b	0.57 ± 0.02 a	0.59 ± 0.01 a	0.64 ± 0.09 b
4.0	50.3 ± 1.6 a	51.6 ± 0.4 a	51.0 ± 2.1 a	3.8 ± 0.2 a	3.8 ± 0.3 a	3.8 ± 0.2 a	0.44 ± 0.02 a	0.45 ± 0.01 a	0.54 ± 0.07 a
6.0	38.9 ± 1.8 a	38.6 ± 2.3 a	39.4 ± 3.3 a	3.9 ± 0.3 a	3.9 ± 0.4 a	4.0 ± 0.4 a	0.42 ± 0.01 a	0.40 ± 0.01 a	0.44 ± 0.02 a

[a]Emulsification processes I–III correspond to those described in the caption of Figure 3. Each datum is the mean ± standard deviation of at least two replicates on separate samples. Different online letters (a–c) represent the significant difference at the $p < 0.05$ level between different storage periods (0–40 days) for a specific emulsion at a specific c value.

by the fact that the microfluidization treatment could improve the surface properties of heat-treated SPI through disruption of initially formed aggregates into smaller ones;[17] the heat-treated SPI with a higher surface activity exhibited a faster increase in surface pressure and dilatational modulus.[30]

Creaming Stability. The creaming behavior of these emulsions upon storage for up to 30 days was evaluated by the visual observation. As reported previously,[12] all the type I emulsions quickly developed into two layers, a creamed layer (top) and a clear serum layer (bottom), within 1 day, but prolonged storage just slightly increased the creaming index (height of the serum layer relative to the total emulsion height) (Figure 5), indicating instability against creaming. In this case, it

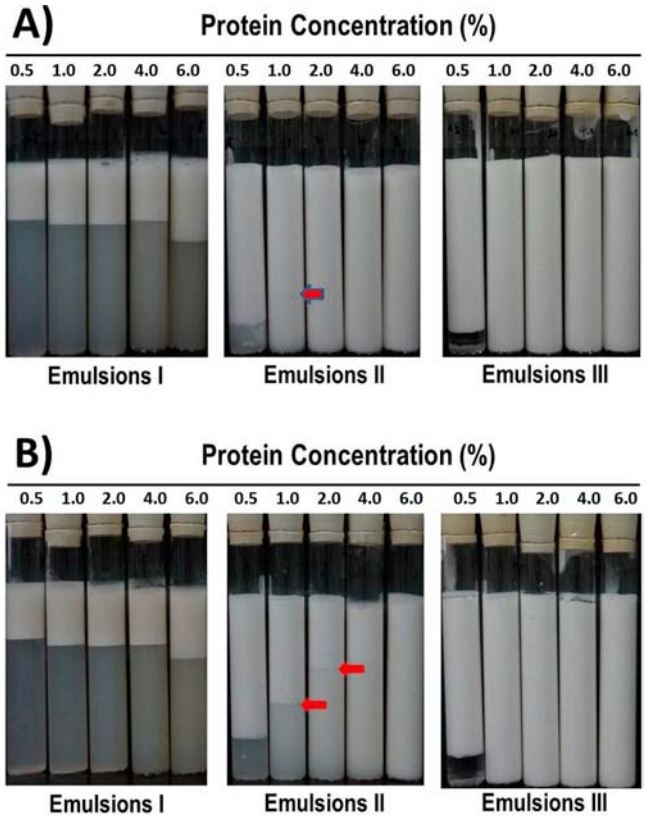

Figure 5. Visual observations of emulsions I–III stabilized by the SPI nanoparticles at varying c values of 0.5–6.0% (w/v) after storage for 1 day (A) and 30 days (B). The arrows within the figure show the position of a distinct creamed layer bottom.

can still be observed that increasing c from 0.5% to 6.0% (w/v) was favorable for the creaming stability; for example, the creaming index at 30 days decreased from about 72% to 60% as c increased from 0.5% to 6.0% (w/v) (Figure 5). The improvement of creaming stability by increasing c can be similarly observed in the type II and III emulsions (Figure 5). For the type II emulsions, no distinct creaming occurred during storage for 7 days at c values of 2.0% (w/v) or above, and when storage was extended to 30 days, a minimal c value of 4.0% (w/v) was needed to completely inhibit the creaming. In the microfluidization case, it is surprisingly observed that no creaming occurred at c values of 1.0% (w/v) or above upon storage for up to 30 days, and even at c = 0.5% (w/v) the creaming index was relatively low (approximately 15%; Figure 5), indicating extraordinary stability against creaming. The improvement of creaming stability by increasing the particle concentration has been observed for the emulsions stabilized by microcrystalline cellulose and modified starch,[3] chitin nanocrystal particles,[5] and zein colloidal particles.[7]

The c dependence of creaming behavior is very consistent with the droplet size data in water (Table 2), reflecting that, within each type of emulsion, the creaming behavior of droplets might still satisfy the Stokes rule. Compared with the type II emulsions, the type III emulsions at any test c value showed much larger $d_{4,3}$ in water but exhibited much higher creaming stability (Table 2 and Figure 5), implying that the creaming behavior in the latter case was predominated by other crucial factors rather than the droplet size in the system. In our previous work, the improved creaming stability for the type I emulsions at higher c or ϕ values has been attributed to the formation of a gel-like network involving server droplet flocculation.[12] This explanation is distinctly applicable to the extraordinary creaming stability of the type III emulsions relative to the type II counterparts, since in the former case the droplet flocculation was much higher (Table 2 and Figure 5). The importance of the gel-like network formation to the creaming stability has also been confirmed in the emulsions stabilized by preheated whey protein or SPI[19,21] and chitin nanocrystal particles.[5]

Rheological Properties of Gel-like Emulsions. To ascertain the formation of a gel-like network in the emulsions, we evaluated the flow behavior and dynamic viscoelastic properties of various freshly prepared emulsions. As expected, all the test emulsions (fresh) exhibited a shear-thinning behavior in the shear rate range of 0.2–100 s^{-1} (Figure 6), mainly reflecting deflocculation of associated droplets in the emulsions.[21,38−40] For the type I emulsions, η at a specific shear rate above 1.0 s^{-1} gradually increased upon an increase in c from 0.5% to 6.0% (w/v) (Figure 6 A), indicating enhanced association or flocculation at higher c values. In this case, all the formed emulsions exhibited a good flow behavior with very low η values, e.g., <0.2 Pa·s at a shear rate of 1 s^{-1}.

When the type I emulsions were further processed by ultrasonic treatment or microfluidization, we observed that the η values were significantly increased, with much greater increases observed for the microfluidized emulsions (type III) (Figure 6). For the type II emulsions, the flow behavior seemed to be independent of c within the c range of 0.5–4.0% (w/v); η was significantly increased only when c was increased to 6.0% (w/v; Figure 6 B). Except the situation at c = 6.0% (w/v), the type II emulsions also exhibited good flow behavior with low η values, e.g., ∼0.5 Pa·s at a shear rate of 1 s^{-1}. By comparison, the flow behavior of the type III emulsions was much poorer than that of the other two types of emulsions, especially at c values of 1.0% (w/v) or above (Figure 6 C). In this case, we can observe that, as c increased from 0.5% to 4.0% (w/v), η at any specific shear rate progressively increased to a maximum, but a further increase in c to 6.0% (w/v) on the contrary led to a considerable decrease in η (relative to that at c = 4.0%, w/v). A similar flow behavior of the type III emulsions has been observed in our previous work,[12] indicating formation of a gel-like network.

The gel-like network formation in the type III emulsions was further evaluated using dynamic viscoelastic measurements. To determine the linear viscoelastic range of measurement, we first performed a strain (γ) sweep experiment on the emulsion at the lowest c value (0.5%) at a constant frequency of 1.0 Hz. From Figure 7 A, it can be seen that the emulsion was mainly elastic in nature at a γ of less than 0.1, and there was

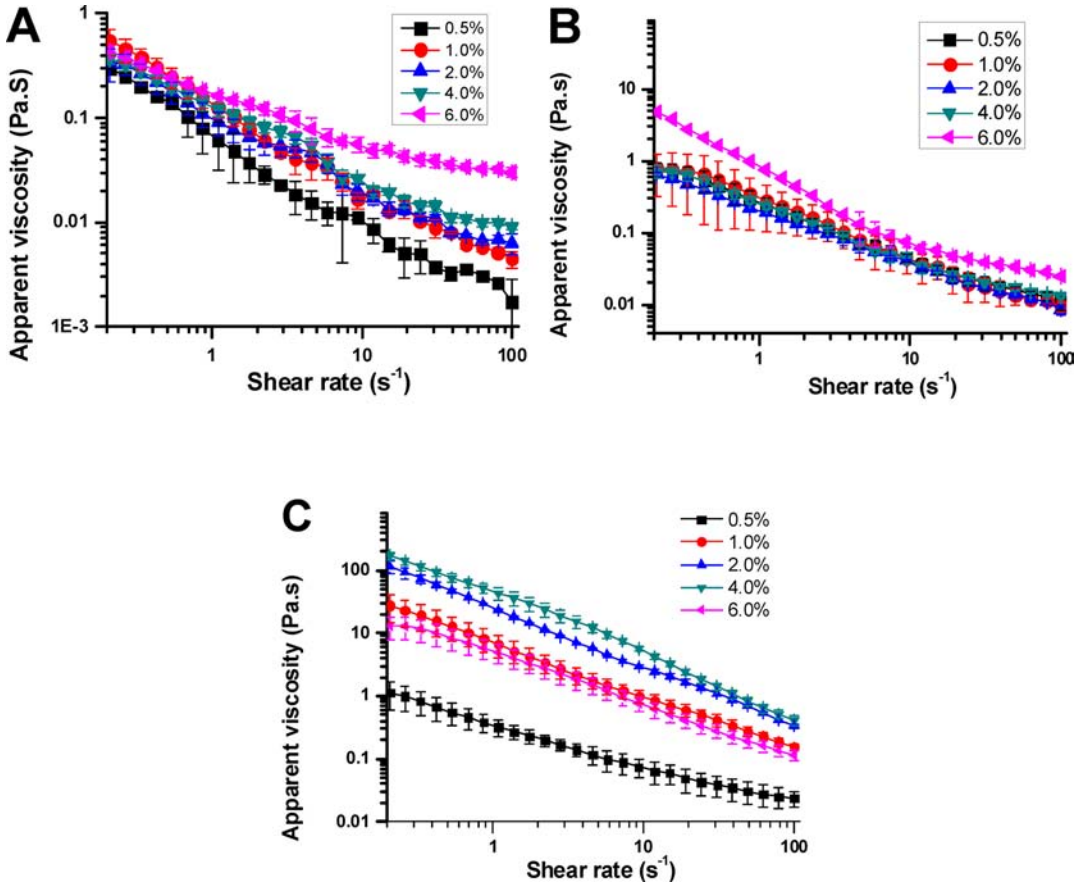

Figure 6. Typical flow behaviors of the fresh emulsions stabilized by the SPI nanoparticles at varying c values of 0.5−6.0% (w/v) formed by emulsification processes I (A), II (B), and III (C). Each datum is the mean ± standard deviation of at least duplicate measurements on separate emulsions. Emulsions I−III refer to those described in the caption of Figure 3.

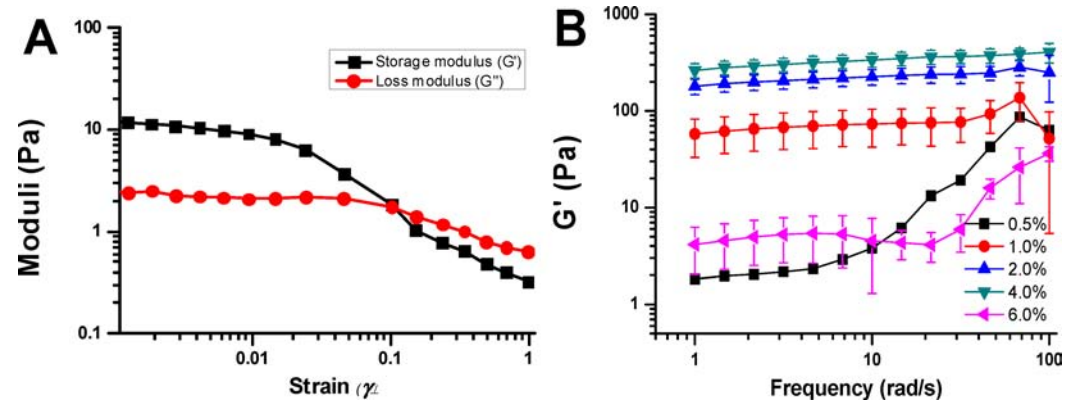

Figure 7. (A) A typical strain sweep of the emulsion stabilized by SPI nanoparticles at a c value of 0.5% (w/v), formed by emulsification III (microfluidization). (B) Frequency dependence profiles of storage moduli (G') for the fresh emulsions stabilized by SPI nanoparticles at varying c values of 0.5−6.0% (w/v), formed by emulsification III. The experiments were performed at a constant frequency of 1 rad/s or a constant strain of 0.5%. Each datum is the mean ± standard deviation of at least duplicate measurements.

approximately a linear viscoelastic range with γ below 0.01, during which the moduli were basically independent of the applied γ. Then, at a constant γ value (0.005) within the linear viscoelastic range, we performed the frequency sweep experiments of the emulsions at varying c values (0.5−6.0%, w/v), and only the storage modulus (G') data are presented in Figure 7 B (the loss modulus, G'', data not provided, due to the consideration of the simplicity within the figure). In all the cases, G' was considerably higher than G' in the low-frequency range, e.g., less than 10 rad/s (data not provided), indicating the formation of predominantly elastic gel-like emulsions. For all the test emulsions, G' progressively increased upon an increase in frequency in the test range of 1.0−100 rad/s. The frequency dependence of G' became less at higher c values (in the c range of 0.5−4.0%); for example, G' at c = 4.0% (w/v) was almost independent of the applied frequency in the test range of 1.0−100 rad/s (Figure 7 B). Similar phenomena for the frequency dependence of the moduli have been observed

for gel-like protein-stabilized emulsions or emulsion gels.[19,21,40] The G' dependence on the frequency can reflect the nature of cross-links in the gel-like network of emulsions or emulsion gels, with less dependence observed for the network consisting of more chemical cross-links.[41] Thus, the observations suggested that, upon an increase in c from 0.5% to 4.0% (w/v), the cross-links in the gel-like network of the emulsions gradually changed from noncovalent "physical" to covalent "chemical" in nature. Like the steady viscosity, the situation for the emulsion at c = 6.0% (w/v) seemed to be an exception, where the frequency dependence of G' became more distinct compared with that at c = 4.0% (w/v; Figure 7 B), indicating a loss of the gel stiffness. The seemingly abnormal loss of the gel stiffness might be largely attributed to the decreased droplet flocculation (Table 2), indirectly confirming the above argument that the gel-like network formation was mainly due to the droplet flocculation.

Amount of Adsorbed Proteins. In the protein-stabilized emulsions, the creaming or rheological behavior is not only related to interdroplet attractive and repulsion interactions, but also affected by interactions between individual proteins in the continuous phase or between the unadsorbed proteins and those adsorbed at the interface. To help unravel the role of these interactions in the rheological or creaming behavior of the emulsions, we evaluated the adsorbed (at the interface) or entrapped (within the gel-like network) protein concentration (g/100 mL of emulsion) of the three types of emulsions (I–III) by a centrifugation method, and the results are presented in Figure 8. In general, for any type of emulsion the concentration of adsorbed or entrapped proteins progressively increased with increasing c from 0.5% to 6.0% (w/v; Figure 8). This is basically consistent with the fact that, at higher c values, more proteins are adsorbed at the interface of the droplets and thus participate in the formation of interfacial protein films.

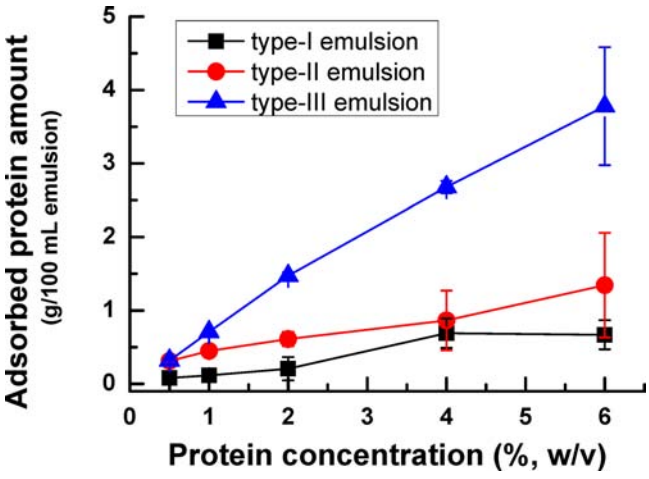

Figure 8. Amount of adsorbed proteins (g/100 mL of emulsion) for emulsions I–III stabilized by the SPI nanoparticles as a function of c (0.5–6.0%, w/v). Each datum is the mean ± standard deviation of triplicate measurements (on separate samples).

However, it can be clearly seen that, for the type I or II emulsions, the concentration of adsorbed or entrapped proteins increased at a much lower rate than that for the type III counterparts upon an increase of c (Figure 8). By calculation, in the case of the type III emulsions, more than 80% of the total proteins were adsorbed at the interface of the droplets or entrapped within the gel-like network, throughout the whole test c range, while, in the type I emulsions, the value was approximately 20%. The situation for the type II emulsions seemed to be a bit different, and in this case, the amount of adsorbed or entrapped proteins progressively decreased from about 80% to 30% with c increasing from 0.5% to 6.0% (w/v; data not shown). At higher c values, e.g., 4% or 6% (w/v), the amount of adsorbed or entrapped proteins for the type II emulsions was slightly but insignificantly higher than that of the type I emulsions (Figure 8). Interestingly, these observations are well in accordance with the rheological and creaming behavior and microstructure of these emulsions at varying c values (Figures 5–7), implying that the rheological and creaming behavior and microstructure of the emulsions stabilized by SPI nanoparticles were mainly related to the amount of adsorbed or entrapped proteins in the system.

In summary, the emulsifying properties of SPI nanoparticles (formed by combined treatments of heat pretreatment and electrostatic screening) and the properties of the resultant Pickering-like emulsions were highly dependent on the emulsification process and c in the continuous phase. In general, increasing c resulted in a progressive reduction in droplet size (in water or 1% SDS) for any type of emulsion. At any test c value, the emulsification efficiency and extent of droplet flocculation increased with an increase in the energy input level. On the other hand, we found that increasing the emulsification efficiency and/or c was favorable for formation of emulsions with higher viscosity and stiffness and greater stability against coalescence and creaming. The rheological and creaming behavior and microstructure of these emulsions were largely determined by the amount of proteins adsorbed at the interface or entrapped within the gel-like network. The results confirmed that the SPI nanoparticles exhibited excellent interfacial and emulsifying properties, as well as a Pickering-like stabilization. With these nanoparticles as the emulsifiers, the application of a high-pressure emulsification technique can produce a kind of Pickering-like emulsion with smaller droplet sizes but a gel-like network structure which exhibits excellent potential to be applied in novel functional food formulations.

AUTHOR INFORMATION

Corresponding Author

*Fax: 086-20-87114263. E-mail: chtang@scut.edu.cn.

Funding

This work is supported by the National Natural Science Foundation of China (Grant 31171632) and Program for New Century Excellent Talents in University (Grant NCET-10-0398).

Notes

The authors declare no competing financial interest.

REFERENCES

(1) Dickinson, D. Use of nanoparticles and microparticles in the formation and stabilization of food emulsions. *Trends Food Sci. Technol.* **2012**, *24*, 4–12.

(2) Dickinson, D. Stabilising emulsion-based colloidal structures with mixed food ingredients. *J. Sci. Food Agric.* **2013**, *93*, 710–721.

(3) Karger, M.; Fayazmanesh, K.; Alavi, M.; Spyropoulos, F.; Norton, I. T. Investigation into the potential ability of Pickering emulsions (food-grade particles) to enhance the oxidative stability of oil-in-water emulsions. *J. Colloid Interface Sci.* **2012**, *366*, 209–215.

(4) Simovic, S.; Prestidge, C. A. Nanoparticle layers controlling drug release from emulsions. *Eur. J. Pharm. Biopharm.* **2007**, *67*, 39–47.

(5) Tzoumaki, M. V.; Moschakis, T.; Kiosseoglou, V.; Biliaderis, C. G. Oil-in-water emulsions stabilized by chitin nanocrystal particles. *Food Hydrocolloids* **2011**, *25*, 1521−1529.
(6) Tzoumaki, M. V.; Moschakis, T.; Scholten, E.; Biliaderis, C. G. *In vitro* lipid digestion of chitin nanocrystal stabilized o/w emulsions. *Food Funct.* **2013**, *4*, 121−129.
(7) de Folter, J. W.; van Ruijven, M. W. M.; Velikov, K. P. Oil-in-water Pickering emulsions stabilized by colloidal particles from water-insoluble protein zein. *Soft Matter* **2012**, *8*, 6807−6815.
(8) Rayner, M.; Timgren, A.; Sjöö, M.; Dejmek, P. Quinoa starch granules: a candidate for stabilising food-grade Pickering emulsions. *J. Sci. Food Agric.* **2012**, *92*, 1841−1847.
(9) Tan, Y.; Xu, K.; Liu, C.; Li, Y.; Lu, C.; Wang, P. Fabrication of starch-based nanospheres to stabilize pickering emulsions. *Carbohydr. Polym.* **2012**, *88*, 1358−1363.
(10) Luo, Z.; Murray, B. S.; Yusoff, A.; Morgan, M. R. A.; Povey, M. J. W.; Day, A. J. Particle-stabilizing effects of flavonoids at the oil-water interface. *J. Agric. Food Chem.* **2011**, *59*, 2636−2645.
(11) Gupta, R.; Rousseau, D. Surface-active solid lipid nanoparticles as Pickering stabilizers for oil-in-water emulsions. *Food Funct.* **2012**, *3*, 302−311.
(12) Liu, F.; Tang, C. H. Soy protein nanoparticle aggregates as Pickering stabilizers for oil-in-water emulsions. *J. Agric. Food Chem.* **2013**, *61*, 8888−8898.
(13) McClements, D. J. Emulsion design to improve the delivery of functional lipophilic components. *Annu. Rev. Food Sci. Technol.* **2010**, *1*, 241−269.
(14) Köhler, K.; Santana, A. S.; Braisch, B.; Preis, R.; Schuchmann, H. P. High pressure emulsification with nano-particles as stabilizing agents. *Chem. Eng. Sci.* **2010**, *65*, 2957−2964.
(15) Arzeni, C.; Martínez, K.; Zema, P.; Arias, A.; Pérez, O. E.; Pilosof, A. M. R. Comparative study of high intensity ultrasonic effects on food proteins functionality. *J. Food Eng.* **2012**, *108*, 463−472.
(16) Keerati-U-Rai, M.; Corredig, M. Effect of dynamic high pressure homogenization on the aggregation state of soy protein. *J. Agric. Food Chem.* **2009**, *57*, 3556−3562.
(17) Shen, L.; Tang, C. H. Microfluidization as a potential technique to modify surface properties of soy protein isolate. *Food Res. Int.* **2012**, *48*, 108−118.
(18) Frelichowska, J.; Bolzinger, M.-A.; Chevalier, Y. Effects of solid particle content on properties of o/w Pickering emulsions. *J. Colloid Interface Sci.* **2010**, *351*, 348−356.
(19) Liu, F.; Tang, C. H. Cold, gel-like whey protein emulsions by microfluidisation emulsification: rheological properties and microstructures. *Food Chem.* **2011**, *127*, 1641−1647.
(20) Luo, L. J.; Liu, F.; Tang, C. H. The role of glycinin in the formation of gel-like soy protein-stabilized emulsions. *Food Hydrocolloids* **2013**, *32*, 97−105.
(21) Tang, C. H.; Liu, F. Cold, gel-like soy protein emulsions by microfluidization: emulsion characteristics, rheological and microstructural properties, and gelling mechanism. *Food Hydrocolloids* **2013**, *30*, 61−72.
(22) Güzey, D.; Gülseren, I.; Bruce, B.; Weiss, J. Interfacial properties and structural conformation of thermosonicated bovine serum albumin. *Food Hydrocolloids* **2006**, *20*, 669−677.
(23) Castellani, O.; Belhomme, C.; David-Briand, E.; Guérin-Dubiard, C.; Anton, M. Oil-in-water emulsion properties and interfacial characteristics of hen egg yolk phosvitin. *Food Hydrocolloids* **2006**, *20*, 35−43.
(24) Guo, J.; Yang, X. Q.; He, X. T.; Wu, N. N.; Wang, J. M.; Gu, W.; Zhang, Y. Y. Limited aggregation behavior of β-conglycinin and its terminating effect on glycinin aggregation during heating at pH 7.0. *J. Agric. Food Chem.* **2012**, *60*, 3782−3791.
(25) Gezimati, J.; Creamer, L. K.; Singh, H. Heat-induced interactions and gelation of mixtures of β-lactoglobulin and α-lactalbumin. *J. Agric. Food Chem.* **1997**, *45*, 1130−1136.
(26) Schmitt, C.; Moitzi, C.; Bovay, C.; Rouvet, M.; Bovetto, L.; Donato, L.; Leser, M. E.; Schurtenberger, P.; Stradner, A. Internal structure and colloidal behaviour of covalent whey protein microgels obtained by heat treatment. *Soft Matter* **2010**, *6*, 4876−4884.
(27) Zhang, J.; Liang, L.; Tian, Z.; Chen, L.; Subirade, M. Preparation and *in vitro* evaluation of calcium-induced soy protein isolate nanoparticles and their formation mechanism study. *Food Chem.* **2012**, *133*, 390−399.
(28) Tcholakova, S.; Denkov, N. D.; Lips, A. Comparison of solid particles, globular proteins and surfactants as emulsifiers. *Phys. Chem. Chem. Phys.* **2008**, *10*, 1608−1627.
(29) Ruíz-Henestrosa, V. P.; Sánchez, C. C.; Rodríguez Patino, J. M. Effect of sucrose on functional properties of soy globulins: adsorption and foam characteristics. *J. Agric. Food Chem.* **2008**, *56*, 2512−2521.
(30) Wang, J. M.; Xia, N.; Yang, X. Q.; Yin, S. W.; Qi, J. R.; He, X. T.; Yuan, D. B.; Wang, L. J. Adsorption and dilatational rheology of heat-treated soy protein at the oil-water interface: relationship to structural properties. *J. Agric. Food Chem.* **2012**, *60*, 3302−3310.
(31) Murray, B. S. Interfacial rheology of food emulsifiers and proteins. *Curr. Opin. Colloid Interface Sci.* **2002**, *7*, 426−431.
(32) Perez, A. A.; Carrara, C. R.; Sánchez, C. C.; Santiago, L. G.; Patino, J. M. R. Interfacial dynamic properties of whey protein concentrate/polysaccharide mixtures at neutral pH. *Food Hydrocolloids* **2009**, *23*, 1253−1262.
(33) Binks, B. P.; Whitby, C. P. Silica particle-stabilized emulsions of silicone oil and water: aspects of emulsification. *Langmuir* **2004**, *20*, 1130−1137.
(34) Whitby, C. P.; Fornasiero, D.; Ralston, J. Effect of oil soluble surfactant in emulsions stabilised by clay particles. *J. Colloid Interface Sci.* **2008**, *323*, 410−419.
(35) Dickinson, E. Food emulsions and foams: stabilization by particles. *Curr. Opin. Colloid Interface Sci.* **2010**, *15*, 40−49.
(36) Binks, B. P.; Clint, J. H.; Whitby, C. P. Rheological behavior of water-in-oil emulsions stabilized by hydrophobic bentonite particles. *Langmuir* **2005**, *21*, 5307−5316.
(37) Tambe, D. E.; Sharma, M. M. The effect of colloidal particles on fluid-fluid interfacial properties and emulsion stability. *Adv. Colloid Interface Sci.* **1994**, *52*, 1−63.
(38) Boutin, C.; Giroux, H. J.; Paquin, P.; Britten, M. Characterization and acid-induced gelation of butter oil emulsions produced from heated whey protein dispersions. *Int. Dairy J.* **2007**, *17*, 696−703.
(39) Demetriades, K.; McClements, D. J. Influences of pH and heating on physicochemical properties of whey protein-stabilized emulsions containing nonionic surfactant. *J. Agric. Food Chem.* **1998**, *46*, 3936−3942.
(40) Manoi, K.; Rizvi, S. S. H. Emulsification mechanisms and characterizations of cold, gel-like emulsions produced from texturized whey protein concentrate. *Food Hydrocolloids* **2009**, *23*, 1837−1847.
(41) Dickinson, E.; Yamamoto, Y. Rheology of milk protein gels and protein-stabilized emulsion gels cross-linked with transglutaminase. *J. Agric. Food Chem.* **1996**, *44*, 1371−1377.

chitosan, due to a high degree of deacetylation, allows it to react efficiently with negatively charged groups of proteins.[25] The addition of chitosan resulted in significant inhibition of microbial growth in Greek-style fresh pork sausages[6] and could also improve thermal gelling properties of grass carp gels and delay lipid oxidation.[26] However, the high molecular weights and high viscosity may restrict its uses;[27] the oligomers of chitosan have received considerable attention because they may have a greater biological activity than chitosan and are also water-soluble.[28]

Myosin, as one component of the myofibrillar protein matrix, is a primary gelling protein, which contributes to desirable texture and stabilization of fat and water in processed meat products. The gelation of a single myosin has been studied in detail.[29−31] Many papers have discussed the interaction between myofibrillar protein and polysaccharide,[13,17,19] but the myofibrillar protein system is complex (containing a variety of proteins such as myosin, actin, actomyosin), and it is not clear that the certain protein of the system interacts with polysaccharide. To our knowledge, no investigation has so far been reported regarding the interactions of different ionic types of polysaccharide (KCG, LBG, and water-soluble chitosan (WSC)) with myosin and those interaction-induced effects.

The objective of this study was to investigate the effects of three ionic types of polysaccharide (anionic polysaccharide KCG, neutral polysaccharide LBG, and cationic polysaccharide WSC) on the WHC and hardness of poultry myosin gels. And the changes in the properties of the gels were explained using different instrumental techniques.

MATERIALS AND METHODS

Materials. KCG and LBG were provided by Danisco (China) Co., Ltd. The viscosities of a 1.5% KCG water solution (w/w) and a 1% LBG water solution (w/w) were above 10 and 2400 mPa·S, respectively. WSC was provided by HeFei XinDe Biotechnology Co., Ltd., and the viscosity of 1% water solution (w/w) was 55 mPa·S. The chicken breast meat was purchased from a local supermarket of the Carrefour Group, and the preparations were commenced within 30 min after purchase.

Extraction of Myosin. Myosin was extracted from chicken breast muscle using a modified procedure originally reported by Wang et al.[32] and Hayakawa et al.[33] First, 150 g of minced chicken breast muscle was mixed with 400 mL of a cold solution (0.1 M KCl, 20 mM potassium phosphate, 2 mM $MgCl_2$, 1 mM EGTA, pH 7.0) containing 1 mM dithiothreitol and subsequently ground with a blender (DS-1, Shanghai Yueci Electronic Technology Co., Ltd., China). The mixture was treated with 1% Triton X-100 and homogenized for 3 min at 10000 rpm using a homogenizer (FA25 model, Fluko, China); the material was subsequently centrifuged at 8000*g* for 12 min at 4 °C in a refrigerated centrifuge (CT14RD, Techcomp Co., Ltd., Shanghai, China). The sediment was extracted with 3 volumes of a modified Guba−Straub solution (0.3 M KC1, 0.1 M KH_2PO_4, 50 mM K_2HPO_4, 1 mM EGTA, 4 mM sodium pyrophosphate, 20 mM $MgCl_2$, pH 6.5) and stirred for 15 min at 4 °C with an agitator. The extraction was centrifuged at 5000*g* for 12 min at 4 °C. The supernatant was diluted with 14 volumes of cold 1 mM EDTA−2Na solution and stored for 90 min at 4 °C. After the floating material was removed via siphon, the precipitated protein was collected by centrifugation at 10000*g* for 6 min at 4 °C and suspended using 1 volume of 0.6 M KCl buffer (0.6 M KCl, 150 mM sodium phosphate, pH 6.5). Magnesium chloride and sodium pyrophosphate were added into the protein, reaching final concentrations of 5 mM. The mixture was stirred vigorously for 30 min without foaming at 4 °C and centrifuged at 10000*g* for 20 min at 4 °C. The supernatant was rediluted with 9 volumes of cold distilled water and precipitated for approximately 12 h. The floating material and precipitated protein were re-treated as above. The solution was dialyzed against the 0.6 M KCl buffer (pH 6.5) described above. The resulting supernatant was regarded as the extraction solution of myosin.

The protein composition of the extracted myosin was validated by SDS-PAGE with a gel imaging system (Universal Hood II, Bio-Rad Co., Hercules, CA, USA). The protein concentration in this myosin solution was measured using the biuret method, and the final concentration was adjusted to 20 mg/mL myosin using the 0.6 M KCl buffer (pH 6.5) before test.

Preparation of Myosin−Polysaccharide Sols. Each polysaccharide (KCG, LBG, and WSC) was added to 80 g of myosin solution (myosin 20 mg/mL) at different concentrations (0, 0.25, 0.5, 0.75, and 1%, w/w). Deviations of weight of all ingredients were not in excess of ±0.5%. The mixture of myosin−polysaccharide was stirred for 30 min and homogenized for 1 min at 10000 rpm using a homogenizer (FA25 model, Fluko, China) in a 100 mL beaker and kept overnight (about 12 h) at 4 °C prior to treatment.

Preparation of Myosin−Polysaccharide Gels. Each myosin−polysaccharide sol prepared as described above was added to a beaker of 27 mm in diameter and 35 mm in height. The beaker was heated for 30 min in an 80 °C water bath (an additional 25 min was needed to warm the system from 20 to 80 °C) to form a gel and then immediately cooled in a water bath (about 4−10 °C) and kept overnight (10−12 h) at 4 °C before the WHC, gel hardness, low-field nuclear magnetic resonance (LF-NMR), Fourier transform infrared (FT-IR) spectroscopy, and scanning electron microscopy (SEM) measurements.

Gel Analysis. *WHC.* WHC was determined by a centrifugal method.[34] Approximately 5 g of the gel was centrifuged at 1000*g* for 10 min at 4 °C. WHC was the percentage of the gel's weight retained after centrifugation relative to its initial weight. The experiments were conducted in triplicate.

Gel Hardness. The hardness of the gels was analyzed using a TA-XT Plus Texture Analyzer (Stable Micro System Co., UK) at ambient temperatures (approximately 20 °C). The gel was subjected to a compression test using a cylindrical probe (P/0.5 in., aluminum) at a trigger type button with a 1.5 mm/s pretest speed, a 1.0 mm/s test speed, a 1.0 mm/s post-test speed, a 4.0 mm distance, and a 3 g trigger force. The maximum force of the sustained compression was the gel hardness. The experiments were conducted in six replicates.

LF-NMR Spin−Spin Relaxation Time (T_2) Measurements. The gel sample (2−4g) was placed in a ⌀ 25 mm glass tube. LF-NMR ^1H T_2 measurements were performed using the method described by Han et al.[35] with slight modifications. The data were collected using a Niumag Benchtop Pulsed NMR Analyzer MiniMR-60 (Niumag Electric Corp., Shanghai, China) operating at 23.318 MHz (proton resonances) and a τ value (time between the 90° and 180° pulse) of 200 μs. The data from 12000 echoes were acquired as 32 scan repetitions with 6.5 s between each scan. T_2 was measured in triplicate. The NMR T_2 data were analyzed using Multi-Exp Inv Analysis Software (Niumag Electric Corp.).

FT-IR Spectroscopy. The gel samples were dried for 32 h in an LGJ-12 lyophilizer (Beijing Songyuan Huaxing Technology Development Co., Ltd., China). The spectra of the gels were obtained as previously described[24] and recorded at ambient temperatures (20 °C) using 16 scans. Origin 7.5 software was used to analyze these spectra.

SEM. The gel samples were dried for 15−16 h in an LGJ-12 lyophilizer (Beijing Songyuan Huaxing Technology Development Co., Ltd., China). The SEM observations were performed with a field emission scanning electron microscope (SU8020, Hitachi, Ltd., Japan), according to a reported method.[24] Two fields from each treatment were examined, and one of the two is presented.

Myosin−Polysaccharide Sol Analysis. *Dynamic Rheological Measurements.* The dynamic oscillatory measurements were carried out with a rheometer (Discovery HR-3, TA Instruments Co., USA) in oscillatory mode, as described by Verbeken et al.[36] with a slight modification. A parallel steel plate geometry (60 mm) with a 550 μm gap was used. The samples were heated from 20 to 80 °C at 2 °C/min and cooled from 80 to 20 °C at 4 °C/min. A continuous 0.1 Hz

oscillation and a 2% strain were applied to monitor the storage modulus (G') and tan δ. All experiments were conducted in triplicate.

Statistical Analysis. The analyses of variances, means, and standard errors were determined using Excel 2003 (Microsoft Office Excel 2003 for Windows). A significance level ($P < 0.05$) was used to determine differences between the treatments.

RESULTS AND DISCUSSION

WHC. As shown in Figure 1, all three polysaccharides could improve the WHC of myosin gel, and the improvement by

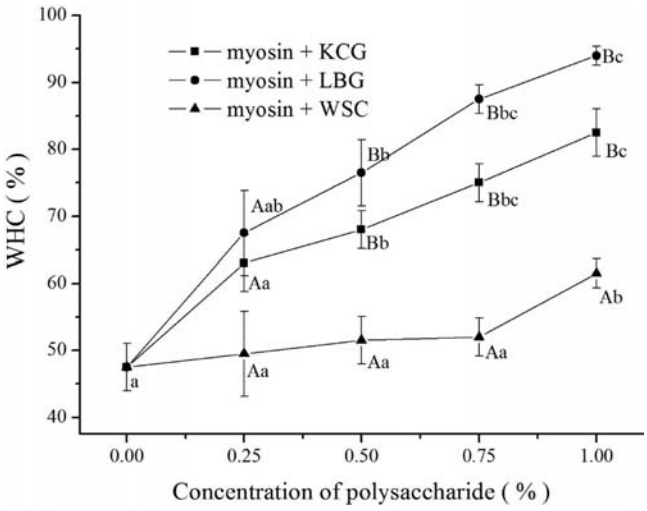

Figure 1. Effects of KCG, LBG, and WSC on the WHC of myosin gels. Different lower case letters (a–c) in the same curve indicate significant difference ($P < 0.05$). Different capital letters (A, B) among the three polysaccharides at the same concentration indicate significant difference ($P < 0.05$).

LBG was the greatest. The increase of KCG or LBG concentrations in the range of 0–1% caused a clear improvement for the WHC of myosin gel, whereas the concentration of WSC in the range of 0–0.75% had no distinctive impact ($P > 0.05$). The difference between the effect of KCG and that of LBG on the WHC was insignificant ($P > 0.05$) at equal concentrations from 0.5 to 1%; however, the addition of KCG and LBG could respectively cause significant increases ($P < 0.05$) of WHC value compared to the WSC at equal concentration. The increase of WHC indicated that more favorable physical entrapment of water occurred in the protein–gum matrices.[13] The results suggested that myosin–KCG or myosin–LBG matrices had a greater ability to entrap water than myosin–WSC matrices.

The effects of KCG, LBG, and WSC on WHC properties shown in our study were consistent with the results of other studies.[7,8,21,36,37] It is well-known that water-binding capacity involves electrostatic, hydrophobic, and hydrogen bonds, etc. LBG has the ability to form hydrogen bonds with water.[7,8] It was found that KCG was present in the interstitial spaces of the protein network, where it bound water and might form gel fragments upon cooling,[36] and thus more water was preserved in the gel network. The WHC improvement of WSC samples was due to the interaction between chitosan and protein.[37] The result suggested that the ability to effectively immobilize water increased in the order myosin–LBG, myosin–KCG, and myosin–WSC.

Gel Hardness. As shown in Figure 2, the hardness of myosin gels increased with the elevated KCG and LBG

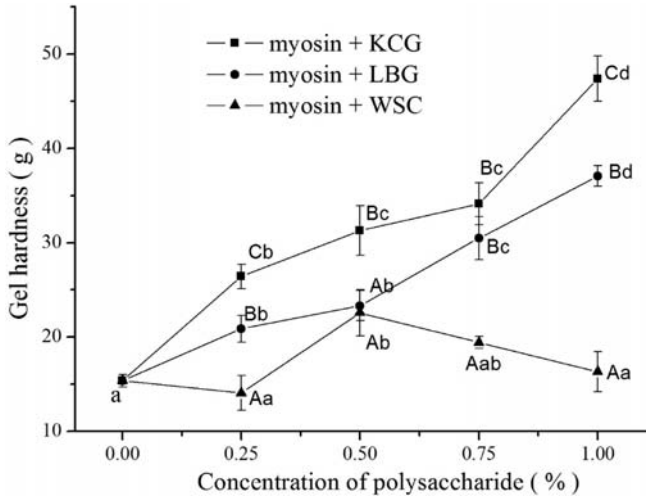

Figure 2. Effects of KCG, LBG, and WSC on the hardness of myosin gels. Different lower case letters (a–d) in the same curve indicate significant difference ($P < 0.05$). Different capital letters (A–C) among the three polysaccharides at the same concentration indicate significant difference ($P < 0.05$).

concentrations, respectively. For the myosin–WSC gel, the change of the gel hardness was insignificant ($P > 0.05$) within the range of 0.25–1.0% addition, except the addition of 0.5% WSC (Figure 2). The increasing effect of KCG in gel hardness was the greatest among the three polysaccharides.

Synergistic effects have been previously observed between carrageenan and proteins, which resulted in much stronger gels compared to protein alone. DeFreitas et al.[21] interpreted the positive influence of carrageenan on the strength of meat protein/carrageenan gels as resulting from the interaction between them. However, Verbeken et al.[36] inferred that KCG did not seem to interact with meat protein in the network formation. Hunt et al.[38] deemed that the increase in gel strength might be caused by electrostatic interactions between sulfate groups of carrageenan molecules, resulting in increased aggregation of the molecular chains of carrageenan. LBG is a nongelling polysaccharide, and Xiong et al.[8] reported that a high hardness of low-fat beef sausages containing LBG was obtained at pH 6.2. In the presence of chitosan, protein–polysaccharide conjugation may be formed between the reactive amino group of glucosamine and the glutaminyl residue of myofibrillar proteins.[26,37] The penetration force of SSMP gels increased proportionally with increasing amount of chitosan incorporated in gels.[37] The breaking force of kamaboko gels increased proportionally with the amount increase of chitosan below 1% addition and then decreased significantly when a higher amount (>1%) of chitosan was added. It was postulated that a higher concentration of chitosan could disrupt the polymerization and aggregation of myofibrils, resulting in a reduced breaking force.[26]

Some researchers reported that KCG, LBG, and WSC would be entrapped as filler ingredients to influence the formation of the continuous gel matrix, modifying the physicochemical properties of the aqueous phase and/or influencing the texture of the final product.[26,36,39] The interactions between polysaccharides and proteins in food systems are largely ascribed to electrostatic association or repulsion. Because myosin would have a negative net charge in myosin/polysaccharide systems at pH 6.5 (isoelectric pH 5.0 of myosin), it was speculated that electrostatic repulsion between the myosin and KCG with the

same charges could be enhanced and thus lead to the changes of the WHC and hardness of myosin−KCG gel. On the other hand, the electrostatic attraction between the protein and WSC with positively charged groups could also be strengthened, and the gel hardness of myosin−WSC should theoretically be increased. However, the present result (Figure 2) revealed that the increase of the myosin−WSC gel hardness was insignificant ($P > 0.05$). Many researchers ascribed the gel hardness to the polymerization of myofibrils inter- or intramolecularly, and the polymerization was relative to the deacetylation degree of chitosan.[37] This insignificant increase might be attributed to the deacetylation degree of WSC, but this mechanism is worth further investigation.

The WHC of myosin gel with LBG was greatest among the three myosin−polysaccharide systems (Figure1), whereas the gel hardness of myosin with LBG was smaller than that with KCG (Figure2). The results were similar to the result of the KCG−/LBG−blue whiting muscle system described by Pérez-Mateos et al.[40] The WHC of myosin gel with KCG was less than that with LBG, because KCG is quite difficult to hydrate within the myosystem.[40] This discrepancy could also be due to the different types of interaction (electrostatic, ionic, etc) between protein and polysaccharide and/or the differences in ability to solubilize or disperse through the protein matrix.

LF-NMR. The distributions of T_2 relaxation times on the gels with myosin−KCG, myosin−LBG, and myosin−WSC are shown in Figure 3. Three relaxation populations of myosin

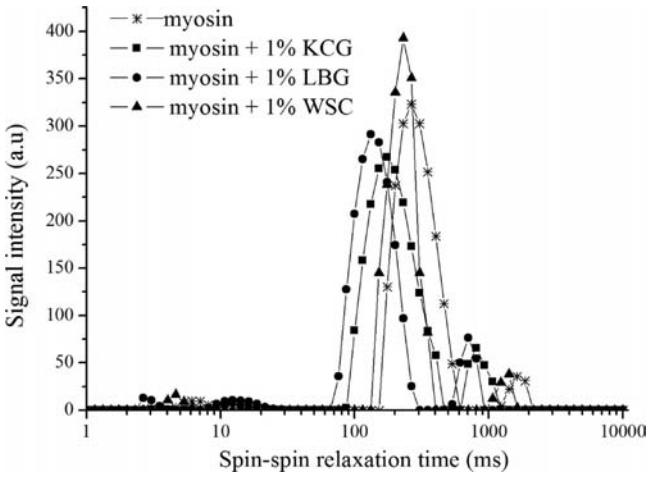

Figure 3. Effects of KCG, LBG, and WSC on the distribution of the T_2 relaxation times of myosin gels.

were centered at approximately 3.05−14.17 ms (T_{21}), 151.99−464.15 ms (T_{22}), and 1232.85−1873.82 ms (T_{23}), revealing bound, immobilized, and free water, respectively, according to the report of Bertram et al.[41] In addition, a broadening of the populations centered at 151.99−464.15 ms (T_{22}) was significant.

The positions of T_{22} and T_{23} clearly shifted toward lower relaxation times with polysaccharide added at 1% concentration (Figure 3). A statistically significant effect was found on the T_{22} and T_{23} ($P < 0.05$) with the addition of gum to myosin (Table 1); the T_{22} and T_{23} decreased in the order myosin−LBG, myosin−KCG, and myosin−WSC, respectively, which is in accordance with the result of WHC. The decrease in nuclear relaxation times indicates an overall decrease of water mobility, and the results are similar to the effect of flaxseed gum added into myofibrillar protein.[42] Hills et al.[43] showed that protein aggregation reduced the water proton relaxation time. This implied that the polysaccharide could stimulate the aggregation of myosin, which was also consistent with the subsequent increase of the storage modulus (G') induced by the addition of the three polysaccharides.

Dynamic Rheological Measurements. The thermodynamic viscoelastic behavior of myosin (Figure 4A) showed that

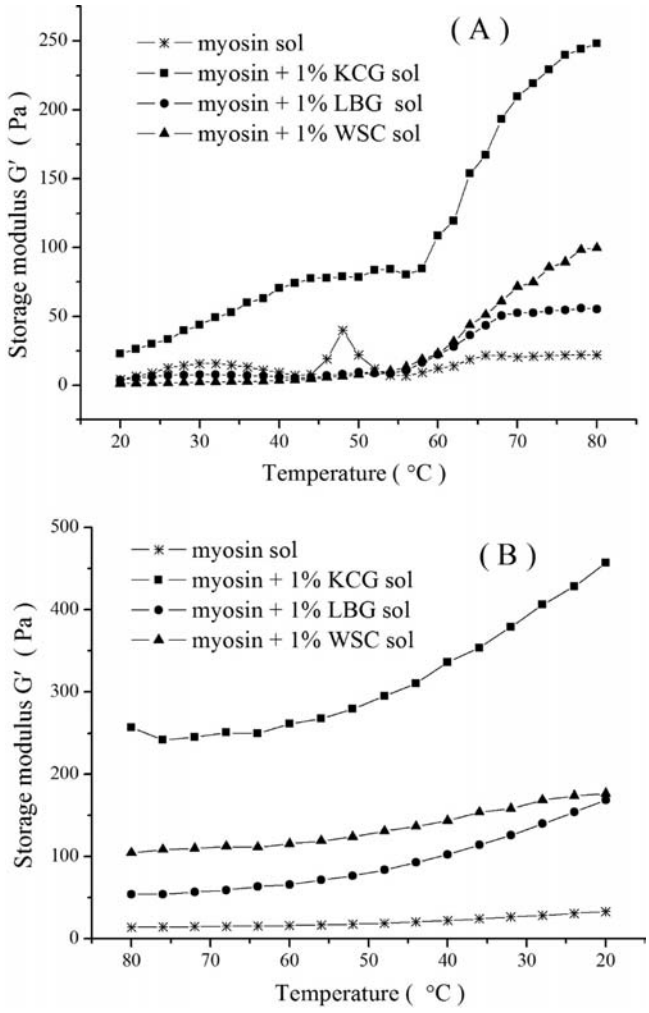

Figure 4. Effects of KCG, LBG, and WSC on the storage modulus (G') of myosin sols during heating (A) and cooling (B).

Table 1. Effects of Three Ionic Types of Polysaccharide on the Spin−Spin Relaxation Times (T_{22} and T_{23}) of Myosin Gels[a]

sample	myosin gel	myosin + 1% KCG gel	myosin + 1% LBG gel	myosin + 1% WSC gel
T_{22}	265.60 ± 17.37d	174.75 ± 13.14b	132.19 ± 0.93a	231.01 ± 0c
T_{23}	1629.75 ± 53.05d	811.13 ± 46.14b	705.48 ± 0a	1417.47 ± 60.9c

[a]Data are expressed as the mean ± SD, $n = 3$. Different letters (a−d) in the same row indicate statistically significant differences at $P < 0.05$.

the G' of the myosin suspension, reflecting the elastic portion of the gel, began to increase from 44 °C and reached a maximum value at 48 °C before declining sharply to a minimum value at 54 °C, after which an ascending curve was exhibited. This rheological transition could be ascribed to the initial association of myosin head as a result of denaturation of the S1 subfragment (42−48 °C) and the disruption of the temporary protein network due to subsequent unfolding of the myosin tail (50−55 °C).[44] Moreover, a similar G' curve was reported during heating of chicken myosin in 0.6 M NaCl at pH 7.0.[45]

The G' of myosin−polysaccharide increased with the increase of temperature, showing differences between different systems (Figure 4A). However, the G' did not decrease during heating at 48 °C. This phenomenon was similar to the effect of β-lactoglobulin added to myosin,[45] and the authors suggested that the relative importance of the various chemical bonds forming the mixed protein gel network might be different from those bonds forming the myosin gel network. The finding in our experiments suggested that the effects of the three polysaccharides were the same as the effect of β-lactoglobulin. The G' values of myosin−KCG mixtures were significantly higher than those of myosin−LBG or −WSC at the same temperature, which meant that the myosin−KCG interaction could lead to a higher elasticity of the sol/gel. These results corresponded with the gel hardness of myosin−KCG, which tended to be higher compared to the gels containing LBG or WSC. The mixtures of myosin with LBG and WSC showed similar G' evolution with heating up to 60 °C, but the myosin−WSC above 60 °C showed higher values of G'.

The G' increase of myosin−polysaccharide suggested the presence of fine gel structure containing polysaccharide sample, because G' is relative to the degree of three-dimensional network formation. Previous observations on protein−KCG systems showed synergistic effects between the two biopolymers on gelation properties at pH above the isoelectric point of proteins.[36,38,46] The main cause of these synergistic effects seems to be thermodynamic incompatibility between the different biopolymers in solution. At low pH values, sulfated polysaccharides and proteins seem to be completely compatible. When the pH increases above the isoelectric point of the protein, the net charge of the protein becomes negative. As a result, electrostatic repulsive forces between protein molecules and sulfated polysaccharides increase, promoting excluded volume effects. This may lead to a mutual concentration of both biopolymers in separate microphases and favor the gelation of the hydrocolloid.[39]

The tan δ of myosin gradually increased until 44 °C and then decreased in subsequent heating. However, the tan δ is <1 throughout heating (Figure 5), indicating that the solution is elastic more than viscous. The tan δ of myosin−KCG is similar to that of myosin−WSC, whereas the myosin−LBG mixtures had higher tan δ at the early stage of heating due to the ability of LBG to give very viscous solution.[47]

Cooling from 80 to 20 °C showed that G' values continued to increase as the temperature decreased (Figure 4B), which indicated an increase in gel hardness as the gels were cooled. Hydrogen bonds have been shown to become stronger as the temperature decreases.[48] The increase of G' is more pronounced ($P < 0.05$) in the presence of KCG and LBG, as indicated by the higher slope of the gelation curve, whereas WSC had no significant effect ($P > 0.05$) on the final elasticity of myosin gels during cooling. This observation suggested the anionic polysaccharide KCG and the neutral polysaccharide LBG could strengthen the cross-linked extent of myosin gel network when the thermal gelling of the myosin was irreversible, whereas the cationic polysaccharide WSC could not.

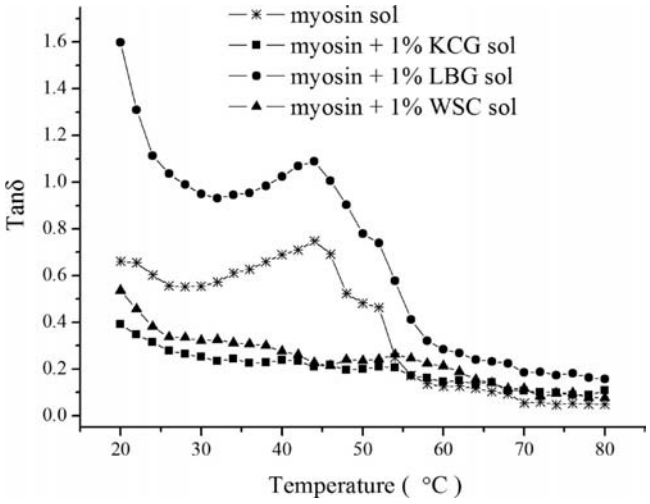

Figure 5. Effects of KCG, LBG, and WSC on the tan δ of myosin sols during heating.

In addition, the G' value is relative to the aggregation of protein[49,50] and the gel strength. Although the changes in G' of myosin−LBG were similar to those of myosin−WSC (Figure 4), the change of gel hardness is not entirely consistent with that of G'. The hardness could be also affected by other factors, such as interactions between protein and polysaccharide, [12] hydrogen bonding, and the microstructure of gels. The different extents of these influences on both hardness and G' might be why the gel hardness of myosin−LBG was much higher than that with WSC (Figure 2).

FT-IR. As shown in Table 2, myosin gel revealed transmittance bands at 3439 cm^{-1} (amide A, N−H or O−H stretching, PK1),[51] 1655 cm^{-1} (amide I, C═O and C═N stretching, PK3), and 1106 cm^{-1} (C−O and C−C stretching, PK4).[52] Among these bands, the amide A band between 3000 and 3500 cm^{-1} is known as the "water region" to assess and estimate the interaction of protein molecules with water,[51] and the amide I band between 1600 and 1700 cm^{-1} is commonly used for secondary structure analysis of proteins.[53]

Table 2. FT-IR Spectra Data for Three Kinds of Myosin−Polysaccaride Gels

		FT-IR spectra numbers (cm^{-1})			
	treatment	PK1	PK2	PK3	PK4
A	myosin gel	3439		1655	1106
B	myosin + 1% KCG gel	3358	3006	1655	1131
C	myosin + 1% LBG gel	3366	3006	1655	1106
D	myosin + 1% WSC gel	3439		1655	1106

The spectra of myosin and myosin−polysaccharide gels indicated similar patterns, which suggested that there was no major change in the functional groups of the myosin with the addition of polysaccharide. The addition of KCG and LBG caused the shift of NH-stretching left peak (PK1) to lower number and the appearance of the NH-stretching right peak (PK2). The shift of PK1 to lower number implied the

dx.doi.org/10.1021/jf405381z | J. Agric. Food Chem. 2014, 62, 2655−2662

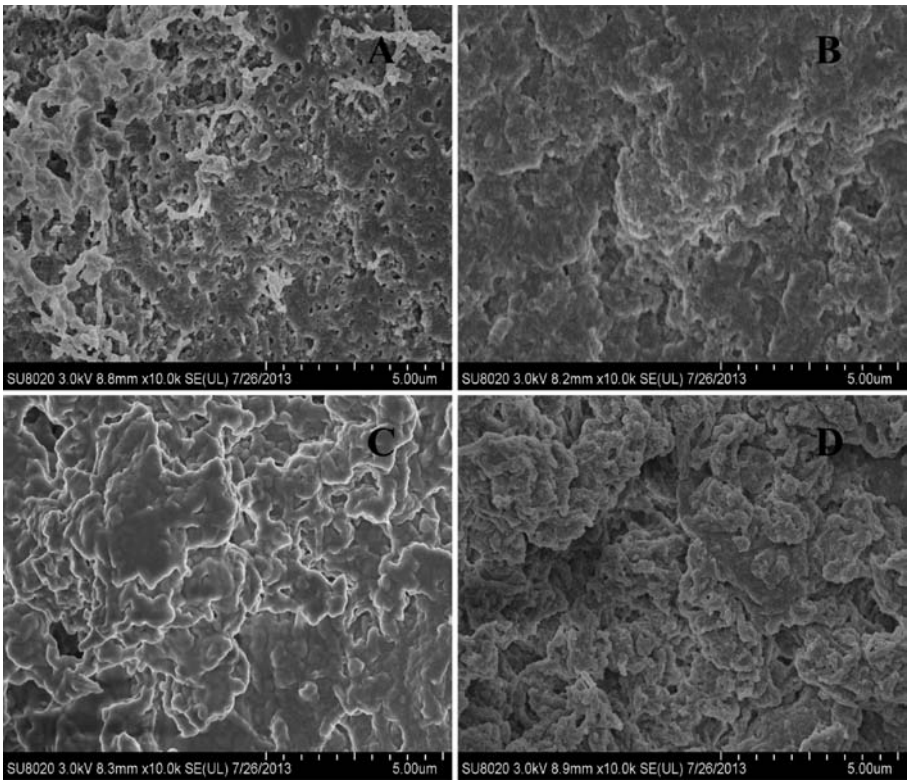

Figure 6. SEM images of (A) myosin gel, (B) myosin + 1% KCG gel, (C) myosin + 1% LBG gel, and (D) myosin + 1% WSC gel.

enhancement of hydrogen bonding within myosin molecules. A similar shift of this peak caused by interrupting intramolecular hydrogen bonding was also observed by Ma et al.[24] and García-García et al.[7] The enhancement of hydrogen bonding in gels might cause the increase of WHC (Figure 1) and gel hardness (Figure 2), but the effect of WSC on the spectral patterns of myosin gels was not obvious because the spectra did not change (Table 2).

Microstructure. The three-dimensional network structure of gels is an important determiner of sensory texture, rheological properties, and WHC. As shown in Figure 6, distinctive differences among gels were observed, which corresponded to the differences in gel hardness and WHC. The control myosin gels (Figure 6A) appeared slightly porous and consisted of protein aggregates. Cross-linking with KCG−myosin (Figure 6B) or LBG−myosin (Figure 6C) reduced the empty spaces and changed the aggregate gel structure into a fine-stranded gel network. Baeza et al.[39] also suggested that electrostatic cross-links between proteins and KCG might cause a reinforcement of the network structure. The structural difference between the control (myosin gel) and myosin−KCG/myosin−LBG gel may explain why the latter was harder (Figure 2) and more elastic (Figure 4A). On the other hand, Sun et al.[42] proposed that the finer gel network with smaller pore size held the majority of water in myofibrillar structures, and it could be concluded that the increases of the WHC in myosin−KCG and myosin−LBG might be related to a compact and dense myosin gel matrix. Although the added WSC could also cause a compact and dense myosin gel structure (Figure 6D), this addition could induce a more concavo-convex microstructure with larger cavities, a severer phase separation, and a bigger aggregation of myosin, which resulted in the weak gel hardness (Figure 2).

In addition, the amount of meat proteins interacting with polysaccharide (κ-carrageenan) to form complexes/gels increased with the concentration of meat proteins,[54] and the interactions between protein and hydrocolloid were the reason for the increased gel strength; higher protein concentration then affected the interaction by increasing gel strength.[12] These implied that the present results of low myosin concentration (20 mg/mL) could be applicable to the gelation of myosin with higher concentration in meat.

In conclusion, the additions of three polysaccharides could decrease the mobility (reducing the water relaxation time T_{22} and T_{23}) of inner water in myosin gel. The anionic polysaccharide KCG and the neutral polysaccharide LBG could strengthen the cross-linked extent of myosin gel network, thus inducing the increase of G' and forming a compact gel network with fine strands when the thermal gelling of the myosin irreversibly occurred. Moreover, KCG could enhance hydrogen bonding and electrostatic force, and LBG could enhance hydrogen bonding. These efficiencies resulted in the improvement of the WHC and hardness of myosin−KCG and myosin−LBG gels at 0.5−1.0% levels ($P < 0.05$). However, the weak molecular interaction between cationic polysaccharide WSC and myosin had an insignificant effect on the WHC and hardness of myosin−WSC gels ($P > 0.05$). Therefore, it is interesting to search for the anionic polysaccharide and neutral polysaccharide that can substitute for fat in the development of low-fat meat products.

AUTHOR INFORMATION

Corresponding Author

*(C. Chen) Phone: +86-551-62919387. Fax: +86-551-62901539. E-mail: chen_conggui@hotmail.com.

Funding

This work was financially supported by the National Natural Science Foundation of China (No. 31271893) and the Special Foundation of Anhui Testing Area (12z0102062).

Notes

The authors declare no competing financial interest.

■ ACKNOWLEDGMENTS

We thank Shi Ke-fu and Wu Shuang-shuang for their help during this experiment.

■ REFERENCES

(1) Luruena-Martínez, M.; Vivar-Quintana, A.; Revilla, I. Effect of locust bean/xanthan gum addition and replacement of pork fat with olive oil on the quality characteristics of low-fat frankfurters. *Meat Sci.* **2004**, *68*, 383−389.

(2) Ayadi, M.; Kechaou, A.; Makni, I.; Attia, H. Influence of carrageenan addition on turkey meat sausages properties. *J. Food Eng.* **2009**, *93*, 278−283.

(3) Cierach, M.; Modzelewska-Kapituła, M.; Szaciło, K. The influence of carrageenan on the properties of low-fat frankfurters. *Meat Sci.* **2009**, *82*, 295−299.

(4) Ma, F.; Chen, C.; Zheng, L.; Zhou, C.; Cai, K.; Han, Z. Effect of high pressure processing on the gel properties of salt-soluble meat protein containing $CaCl_2$ and κ-carrageenan. *Meat Sci.* **2013**, *95*, 22−26.

(5) Mao, L.; Wu, T. Gelling properties and lipid oxidation of kamaboko gels from grass carp (*Ctenopharyngodon idellus*) influenced by chitosan. *J. Food Eng.* **2007**, *82*, 128−134.

(6) Soultos, N.; Tzikas, Z.; Abrahim, A.; Georgantelis, D.; Ambrosiadis, I. Chitosan effects on quality properties of Greek style fresh pork sausages. *Meat Sci.* **2008**, *80*, 1150−1156.

(7) García-García, E.; Totosaus, A. Low-fat sodium-reduced sausages: effect of the interaction between locust bean gum, potato starch and κ-carrageenan by a mixture design approach. *Meat Sci.* **2008**, *78*, 406−413.

(8) Xiong, Y.; Noel, D.; Moody, W. Textural and sensory properties of low-fat beef sausages with added water and polysaccharides as affected by pH and salt. *J. Food Sci.* **1999**, *64*, 550−554.

(9) Schmitt, C.; Turgeon, S. L. Protein/polysaccharide complexes and coacervates in food systems. *Adv. Colloid Interface Sci.* **2011**, *167*, 63−70.

(10) Dickinson, E. Mixed biopolymers at interfaces: competitive adsorption and multilayer structures. *Food Hydrocolloids* **2011**, *25*, 1966−1983.

(11) Schmitt, C.; Sanchez, C.; Desobry-Banon, S.; Hardy, J. Structure and technofunctional properties of protein-polysaccharide complexes: a review. *Crit. Rev. Food Sci.* **1998**, *38*, 689−753.

(12) Chen, H.-H.; Xu, S.-Y.; Wang, Z. Interaction between flaxseed gum and meat protein. *J. Food Eng.* **2007**, *80*, 1051−1059.

(13) Xiong, Y. L.; Blanchard, S. P. Viscoelastic properties of myofibrillar protein-polysaccharide composite gels. *J. Food Sci.* **1993**, *58*, 164−167.

(14) Yang, Y.; Zhou, G.; Xu, X.; Wang, Y. Rheological properties of myosin-gelatin mixtures. *J. Food Sci.* **2007**, *72*, C270−C275.

(15) Chin, K. B.; Go, M. Y.; Xiong, Y. L. Konjac flour improved textural and water retention properties of transglutaminase-mediated, heat-induced porcine myofibrillar protein gel: effect of salt level and transglutaminase incubation. *Meat Sci.* **2009**, *81*, 565−572.

(16) de Jong, S.; van de Velde, F. Charge density of polysaccharide controls microstructure and large deformation properties of mixed gels. *Food Hydrocolloids* **2007**, *21*, 1172−1187.

(17) Montero, P.; Hurtado, J.; Pérez-Mateos, M. Microstructural behaviour and gelling characteristics of myosystem protein gels interacting with hydrocolloids. *Food Hydrocolloids* **2000**, *14*, 455−461.

(18) Filipi, I.; Lee, C. Preactivated ι-carrageenan and its rheological effects in composite surimi gel. *LWT−Food Sci. Technol.* **1998**, *31*, 129−137.

(19) Ramırez, J.; Barrera, M.; Morales, O.; Vázquez, M. Effect of xanthan and locust bean gums on the gelling properties of myofibrillar protein. *Food Hydrocolloids* **2002**, *16*, 11−16.

(20) Zhu, J.-H.; Yang, X.-Q.; Ahmad, I.; Li, L.; Wang, X.-Y.; Liu, C. Rheological properties of κ-carrageenan and soybean glycinin mixed gels. *Food Res. Int.* **2008**, *41*, 219−228.

(21) DeFreitas, Z.; Sebranek, J.; Olson, D.; Carr, J. Carrageenan effects on salt-soluble meat proteins in model systems. *J. Food Sci.* **1997**, *62*, 539−543.

(22) Amako, D. E.; Xiong, Y. L. Effects of carrageenan on thermal stability of proteins from chicken thigh and breast muscles. *Food Res. Int.* **2001**, *34*, 247−253.

(23) Pérez-Mateos, M.; Hurtado, J.; Montero, P.; Fernández-Martín, F. Interactions of κ-carrageenan plus other hydrocolloids in fish myosystem gels. *J. Food Sci.* **2001**, *66*, 838−843.

(24) Ma, F.; Chen, C.; Sun, G.; Wang, W.; Fang, H.; Han, Z. Effects of high pressure and $CaCl_2$ on properties of salt-soluble meat protein gels containing locust bean gum. *Innovative Food Sci. Emerging Technol.* **2012**, *14*, 31−37.

(25) Kataoka, J.; Ishizaki, S.; Tanaka, M. Effects of chitosan on gelling properties of low quality surimi. *J. Muscle Foods* **1998**, *9*, 209−220.

(26) Benjakul, S.; Visessanguan, W.; Tanaka, M.; Ishizaki, S.; Suthidham, R.; Sungpech, O. Effect of chitin and chitosan on gelling properties of surimi from barred garfish (*Hemiramphus far*). *J. Sci. Food Agric.* **2001**, *81*, 102−108.

(27) Seo, W.-G.; Pae, H.-O.; Kim, N.-Y.; Oh, G.-S.; Park, I.-S.; Kim, Y.-H.; Kim, Y.-M.; Lee, Y.-h.; Jun, C.-D.; Chung, H.-T. Synergistic cooperation between water-soluble chitosan oligomers and interferon-γ for induction of nitric oxide synthesis and tumoricidal activity in murine peritoneal macrophages. *Cancer Lett.* **2000**, *159*, 189−195.

(28) Tsigos, I.; Martinou, A.; Kafetzopoulos, D.; Bouriotis, V. Chitin deacetylases: new, versatile tools in biotechnology. *Trends Biotechnol.* **2000**, *18*, 305−312.

(29) Liu, R.; Zhao, S.-m.; Liu, Y.-m.; Yang, H.; Xiong, S.-b.; Xie, B.-j.; Qin, L.-h. Effect of pH on the gel properties and secondary structure of fish myosin. *Food Chem.* **2010**, *121*, 196−202.

(30) Cao, Y.; Xia, T.; Zhou, G.; Xu, X. The mechanism of high pressure-induced gels of rabbit myosin. *Innovative Food Sci. Emerging Technol.* **2012**, *16*, 41−46.

(31) Raghavan, S.; Kristinsson, H. G. Conformational and rheological changes in catfish myosin during alkali-induced unfolding and refolding. *Food Chem.* **2008**, *107*, 385−398.

(32) Wang, S. F.; Smith, D. M. Dynamic rheological properties and secondary structure of chicken breast myosin as influenced by isothermal heating. *J. Agric. Food Chem.* **1994**, *42*, 1434−1439.

(33) Hayakawa, T.; Yoshida, Y.; Yasui, M.; Ito, T.; Iwasaki, T.; Wakamatsu, J.; Hattori, A.; Nishimura, T. Heat-induced gelation of myosin in a low ionic strength solution containing L-histidine. *Meat Sci.* **2012**, *90*, 77−80.

(34) Kocher, P.; Foegeding, E. Microcentrifuge-based method for measuring water-holding of protein gels. *J. Food Sci.* **1993**, *58*, 1040−1046.

(35) Han, M.; Zhang, Y.; Fei, Y.; Xu, X.; Zhou, G. Effect of microbial transglutaminase on NMR relaxometry and microstructure of pork myofibrillar protein gel. *Eur. Food Res. Technol.* **2009**, *228*, 665−670.

(36) Verbeken, D.; Neirinck, N.; Van Der Meeren, P.; Dewettinck, K. Influence of κ-carrageenan on the thermal gelation of salt-soluble meat proteins. *Meat Sci.* **2005**, *70*, 161−166.

(37) Li, X.; Xia, W. Effects of chitosan on the gel properties of salt-soluble meat proteins from silver carp. *Carbohydr. Polym.* **2010**, *82*, 958−964.

(38) Hunt, A.; Park, J. W. Alaska pollock fish protein gels as affected by refined carrageenan and various salts. *J. Food Qual.* **2013**, *36*, 51−58.

(39) Baeza, R.; Carp, D.; Pérez, O.; Pilosof, A. κ-Carrageenan-protein interactions: effect of proteins on polysaccharide gelling and textural properties. *LWT−Food Sci. Technol.* **2002**, *35*, 741−747.
(40) Pérez-Mateos, M.; Montero, P. Contribution of hydrocolloids to gelling properties of blue whiting muscle. *Eur. Food Res. Technol.* **2000**, *210*, 383−390.
(41) Bertram, H. C.; Andersen, H. J.; Karlsson, A. H. Comparative study of low-field NMR relaxation measurements and two traditional methods in the determination of water holding capacity of pork. *Meat Sci.* **2001**, *57*, 125−132.
(42) Sun, J.; Li, X.; Xu, X.; Zhou, G. Influence of various levels of flaxseed gum addition on the water-holding capacities of heat-induced porcine myofibrillar protein. *J. Food Sci.* **2011**, *76*, C472−C478.
(43) Hills, B.; Takacs, S.; Belton, P. The effects of proteins on the proton NMR transverse relaxation times of water: I. Native bovine serum albumin. *Mol. Phys.* **1989**, *67*, 903−918.
(44) Wu, M.; Xiong, Y. L.; Chen, J.; Tang, X.; Zhou, G. Rheological and microstructural properties of porcine myofibrillar protein-lipid emulsion composite gels. *J. Food Sci.* **2009**, *74*, E207−E217.
(45) Vittayanont, M.; Steffe, J. F.; Flegler, S. L.; Smith, D. M. Gelation of chicken pectoralis major myosin and heat-denatured β-lactoglobulin. *J. Agric. Food Chem.* **2003**, *51*, 760−765.
(46) Nunes, M.; Raymundo, A.; Sousa, I. Rheological behaviour and microstructure of pea protein/κ-carrageenan/starch gels with different setting conditions. *Food Hydrocolloids* **2006**, *20*, 106−113.
(47) Perrechil, F.; Braga, A.; Cunha, R. Interactions between sodium caseinate and LBG in acidified systems: rheology and phase behavior. *Food Hydrocolloids* **2009**, *23*, 2085−2093.
(48) Foegeding, E. A.; Gonzalez, C.; Hamann, D. D.; Case, S. Polyacrylamide gels as elastic models for food gels. *Food Hydrocolloids* **1994**, *8*, 125−134.
(49) Yongsawatdigul, J.; Park, J. Thermal aggregation and dynamic rheological properties of Pacific whiting and cod myosins as affected by heating rate. *J. Food Sci.* **1999**, *64*, 679−683.
(50) Visessanguan, W.; Ogawa, M.; Nakai, S.; An, H. Physicochemical changes and mechanism of heat-induced gelation of arrowtooth flounder myosin. *J. Agric. Food Chem.* **2000**, *48*, 1016−1023.
(51) Perisic, N.; Afseth, N. K.; Ofstad, R.; Kohler, A. Monitoring protein structural changes and hydration in bovine meat tissue due to salt substitutes by Fourier transform infrared (FTIR) microspectroscopy. *J. Agric. Food Chem.* **2011**, *59*, 10052−10061.
(52) Naumann, D. FT-infrared and FT-Raman spectroscopy in biomedical research. *Appl. Spectrosc. Rev.* **2001**, *36*, 239−298.
(53) Carbonaro, M.; Nucara, A. Secondary structure of food proteins by fourier transform spectroscopy in the mid-infrared region. *Amino Acids* **2010**, *38*, 679−690.
(54) Farouk, M. M.; Frost, D. A.; Krsinic, G.; Wu, G. Phase behaviour, rheology and microstructure of mixture of meat proteins and kappa and iota carrageenans. *Food Hydrocolloids* **2011**, *25*, 1627−1636.

copigmentation cofactors.[15,16] However, to date there are scarce studies about the addition of these natural sources during red winemaking, probably because of the difficulty of performing this process due to the different harvesting dates for white and red grapes. Some of these studies have revealed that the effects on the final quality of the wine are different depending on the winemaking stage and duration of the application and the dose applied as well as the particular phenolic potential of the grapes in the mixture.[7,17−19] Thus, further investigations are needed to better understand the contribution of these incorporated compounds to wine color and color stability.

Generally, white grapes are harvested several weeks before red grapes. Nevertheless, in some Mediterranean regions (such as Andalucía, southwestern Spain, warm climate) red and white grape varieties with similar ripening periods are usually harvested at the same time. In this case, skins and seeds from white grape pomace are available just at the moment they are needed to be added to red winemaking. This winemaking technique may be therefore interesting as an alternative to traditional maceration to improve the quality of red wines from a warm climate as well as to exploit the white winemaking residues.

Therefore, the main objective of this work is to study the impact of adding supplementary amounts of skins and seeds from white grape pomace (var. Pedro Ximenez) during the fermentative maceration on young Syrah wines from a warm climate, especially in terms of their phenolic composition and color stability.

MATERIALS AND METHODS

Vinification Protocols and Samples. *Vitis vinifera* var. Syrah (red grape) and Pedro Ximenez (white grape) grown in the Montilla-Moriles Designation of Origin (Cordoba, southeastern Spain), with the typical climatological conditions of warm climate regions, were used in this study. These cultivars were selected because they have similar periods of ripeness (end of August) and represent the main and more extensively cultivated red and white grape varieties in the region.

Pedro Ximenez grape pomace (PXGP), the main organic vinification byproduct from Pedro Ximenez grapes, was used in the vinification experiments to ferment with Syrah grapes.

About 40 kg of industrially pressed PXGP was provided by La Unión Winery Coop. (Cordoba, Spain). It was collected from the 2012 vintage after Pedro Ximenez grapes were processed for winemaking at optimum technological maturity (density = 13.6 °Baumé). As usual, in traditional white vinifications the grapes are destemmed, so it is assumed that the pomace generated after vinification contains only some stems, which were manually separated. Therefore, the raw material used in the vinification experiments was composed by a mixture of skins and seeds.

Syrah grapes were harvested in 2012 vintage at optimum technological maturity (density = 13.1 °Baumé; total acidity = 5.21 g/L; and pH, 3.61) and good sanitary conditions. About 360 kg of grapes was manually harvested, placed in 15 kg plastic boxes, and transported to an experimental wine production center belonging to the Instituto Andaluz de Investigación y Formación Agraria, Pesquera, Alimentaria y de la Producción Ecológica (IFAPA, Cordoba, Spain).

Nine vinifications were carried out on a pilot scale using 50 L stainless steel tanks. For each vinification, 40 kg of Syrah grapes was processed. Grapes were destemmed and crushed, and the must with solid parts was homogenized and distributed into tanks for maceration. Three types of Syrah wines were elaborated, in three replicates for each one (n = 3), with the following mixtures of Syrah grapes and PXGP: (a) one monovarietal wine elaborate with 100% Syrah grapes (SY); as control; (b) two wines containing the same amount of Syrah grapes and additional 10 and 20% of PXGP (w/w as grapes). Thus, to elaborate PXGP 10% wines, 4 kg of PXGP was added to 40 kg of Syrah grapes in each replicate. In the case of PXGP 20% wines, 8 kg of PXGP was added to 40 kg of Syrah grapes for each replicate. An adequate homogenization among PXGP and Syrah grapes was assured with a gradual addition at crushing.

An identical red winemaking procedure was used for all assays. Enological treatments were adjusted at the same levels for all of the assays: 60 mg/L total sulfur dioxide and 7 g/L of total titratable acidity by adding tartaric acid. Fermentative alcoholic maceration was induced by inoculating *Saccharomyces cerevisiae* selected yeast (TTA, 30 g/hL, 25 °C, Agrovin, Spain) and occurred at controlled temperature (20−25 °C). Fermentation caps were punched down once a day during the on-skin maceration period, which lasted 14 days. After this, the mash was drawn off to remove the skins and other solid parts, and the free-run musts were left to finish the fermentation under the same conditions. To guarantee the development of malolactic fermentation, selected *Oenococcus oeni* lactic acid bacteria (VINIFERM Oe 104, UFC/mL > 10^6; Agrovin, Spain) were inoculated at the rate of 10 mL/hL at the end of alcoholic fermentation. When fermentative processes were finished, the wines were racked in 15 L stainless steel tanks and held for 2 weeks at 4 °C. They were bottled 30 days later and stored at 10−15 °C until analysis.

Must and wine samples (100 mL) were taken at the initial point or grape crushing (I), at the middle of the fermentative alcoholic maceration (FAM), just after the skin removal (SR), at the end of malolactic fermentation (MLF), and 1, 2, 3, 4, and 5 months after fermentative processes were finished (bottled wines).

Enological Parameters. The conventional enological parameters of wines (Table 1) were evaluated according to the official methods established by the European Union.[20]

Table 1. Conventional Analytical Data (Means ± SD, n = 3) of Final Red Wines

	maceration treatment[a]		
analytical data	SY	PXGP 10%	PXGP 20%
reducing sugars (g/L)	1.12 ± 0.13	1.90 ± 0.06	1.65 ± 0.11
malic acid (g/L)	<0.01	<0.01	<0.01
alcohol degree (% v/v)	12.90 ± 0.18	13.20 ± 0.12	13.10 ± 0.12
volatile acidity (g/L as acetic acid)	0.55 ± 0.09	0.57 ± 0.03	0.57 ± 0.03
total acidity (g/L as tartaric acid)	5.85 ± 0.18	5.57 ± 0.04	5.59 ± 0.04
pH	3.33 ± 0.07	3.37 ± 0.03	3.29 ± 0.03
free sulfur dioxide (mg/L)	<10	<10	<10
total sulfur dioxide (mg/L)	44.33 ± 1.25	45.31 ± 6.6	50.56 ± 7.4

[a]SY, 100% Syrah grapes; PXGP 10% and PXGP 20%, fermentation of Syrah grapes with PXGP at 10 and 20% (w/w), respectively.

Copigmented and Polymerized Anthocyanin Determination. The contribution of copigmented anthocyanins to the total wine color at pH 3.6 (% copigmented anthocyanins) and the degree of anthocyanin polymerization (% polymeric pigments) were determined following the method proposed by Boulton.[21] The wine sample pH values were first adjusted to 3.6 using 1 M NaOH or HCl.

Total Phenolic Content. Total phenolic content was determined using a modification of the Folin−Ciocalteu method.[22] Absorbance was measured at 765 nm, and the results were expressed as milligrams of gallic acid per liter (mg GAE/L).

Phenolic Compound Analysis by HPLC-DAD. An Agilent 1200 chromatographic system equipped with a quaternary pump, an UV−vis diode-array detector, an automatic injector, and ChemStation software (Palo Alto, CA, USA) was used for the HPLC separation, identification, and quantification of phenolic compounds. Prior to direct injection, the samples were filtered through a 0.45 μm nylon filter (E0034, Análisis Vínicos, Spain). All analyses were made in triplicate.

Table 2. Mean Values and Standard Deviations of the Anthocyanin Compounds (Milligrams per Liter) and Percentages of Copigmentation and Polymerization of Wines (n = 3), at Skin Removal (SR) and after 5 Months of Stabilization

		maceration treatment[a]		
	stage	SY	PXGP 10%	PXGP 20%
delphinidin-3-glucoside	SR	72.27 a ± 5.82	52.03 b ± 6.51	42.99 b ± 0.44
	5 months	0.23 a ± 0.02	4.86 b ± 0.86	nd
cyanidin-3-glucoside	SR	nd	nd	nd
	5 months	nd	nd	nd
petunidin-3-glucoside	SR	63.14 a ± 2.12	67.96 a ± 2.30	50.31 b ± 1.54
	5 months	4.01 a ± 1.87	10.51 b ± 1.10	1.88 a ± 0.79
peonidin-3-glucoside	SR	178.43 a ± 4.35	131.34 b ± 11.67	112.41 b ± 4.43
	5 months	39.18 a ± 2.43	37.06 a ± 0.88	13.99 b ± 1.02
malvidin-3-glucoside	SR	547.87 a ± 25.18	414.49 b ± 15.48	373.91 b ± 13.49
	5 months	214.61 a ± 11.63	201.52 a ± 4.73	155.23 b ± 2.49
petunidin-3-acetyl-glucoside	SR	43.17 a ± 1.90	29.34 b ± 4.39	33.60 b ± 0.99
	5 months	1.31 a ± 0.23	2.24 b ± 0.99	nd ±
peonidin-3-acetyl-glucoside	SR	46.72 a ± 6.16	28.57 b ± 0.57	21.39 b ± 1.47
	5 months	8.59 a ± 1.44	3.25 b ± 0.66	nd ±
malvidin-3-acetyl-glucoside	SR	310.46 a ± 12.40	244.20 b ± 6.03	225.32 b ± 6.43
	5 months	148.92 a ± 4.23	136.70 b ± 1.57	115.92 c ± 3.78
petunidin-3-*p*-coumaroyl-glucoside	SR	23.52 a ± 10.96	16.36 a ± 1.94	17.10 a ± 2.01
	5 months	5.27 ± 2.36	nd	nd
peonidin-3-*p*-coumaroyl -glucoside	SR	16.72 a ± 2.31	9.88 b ± 1.51	7.41 b ± 0.61
	5 months	nd	nd	nd
malvidin-3-*p*-coumaroyl -glucoside	SR	225.46 a ± 30.82	202.99 a ± 14.03	203.66 a ± 12.36
	5 months	26.51 a ± 3.03	35.18 b ± 1.51	11.43 b ± 2.78
sum of glucoside derivatives	SR	861.71 a ± 34.64	665.82 b ± 33.77	597.63 c ± 19.91
	5 months	258.04 a ± 16.22	253.97 a ± 8.37	171.11 b ± 2.20
sum of acetate derivatives	SR	400.36 a ± 19.46	302.12 b ± 3.92	280.32 b ± 6.90
	5 months	158.82 a ± 6.72	142.20 b ± 0.25	115.92 c ± 0.41
sum of *p*-coumaric derivatives	SR	265.40 a ± 43.99	229.23 a ± 15.80	228.17 a ± 14.98
	5 months	31.79 a ± 2.33	35.19 a ± 1.51	11.43 b ± 2.87
% copigmented anthocyanins (%CA)	SR	21.82 a ± 1.02	26.69 a ± 0.56	34.46 b ± 1.47
	5 months	13.56 a ± 0.23	16.06 b ± 0.25	29.51 c ± 1.02
% polymeric pigments (%PP)	SR	35.33 a ± 2.51	41.30 b ± 1.21	45.04 b ± 0.50
	5 months	66.71 a ± 0.67	70.67 a ± 1.03	54.06 b ± 0.44

[a]SY, 100% Syrah grapes; PXGP 10% and PSGP 20%, fermentation of Syrah grapes with PXGP at 10 and 20% (w/w), respectively. Different letters in the same row indicate significant differences ($p < 0.05$). nd, not detected.

The anthocyanin identification was carried out following the method described in Heredia et al.[23] Anthocyanins were separated using a Zorbax C18 column (250 × 4.6 mm, 5 μm particle size) maintained at 38 °C. Acetonitrile/formic acid/water (3:10:87) as solvent A and acetonitrile/formic acid/water (50:10:40) as solvent B were used. The elution profile was as follows: 0−10 min, 94% A−6% B; 10−15 min, 70% A−30% B; 15−25 min, 60% A−40% B; 25−35 min, 55% A−45% B; 35−40 min, 50% A−50% B; 40−42 min, 40% A−60% B; 42−43 min, 94% A−6% B. The flow rate was 0.8 mL/min, and the injection volume was 50 μL. UV−vis spectra were recorded from 200 to 800 nm with 2.0 nm bandwidth. The quantification was made at 525 nm by comparing the areas and retention times with those of the malvidin-3-glucoside standard, and anthocyanin concentration was expressed as milligrams per liter. Sums of glucosides, acetates, and *p*-coumaric derivatives were estimated by summing the content of each member identified by HPLC, respectively, and the sum of anthocyanins was obtained by summing the content of all anthocyanin compounds identified.

The identification of the noncolored phenolic compounds (low molecular weight) was carried out following the method described in Gordillo et al.[14] Individual phenolic compounds were separated using a Zorbax C18 column (250 × 4.6 mm, 5 μm particle size) maintained at 40 °C. Acetonitrile/formic acid/water (3:10:87) as solvent A and acetonitrile/formic acid/water (50:10:40) as solvent B were used. The flow rate was 0.63 mL/min, and the injection volume was 50 μL. UV−vis spectra were recorded from 200 to 800 nm with a bandwidth of 2.0 nm. The quantification was made at 280, 320, and 360 nm by comparing the areas and the retention times with the gallic acid, caffeic acid, (+)-catechin, and quercetin standards, respectively. Phenolic compound concentration was expressed as milligrams per liter. Sums of phenolic acids, monomeric flavanols, and flavonols were also estimated by summing the content of each member identified by HPLC, respectively.

Colorimetric Analysis. Color measurements were made with a Hewlett-Packard UV−vis HP8453 spectrophotometer (Palo Alto, CA, USA), using 0.2 cm path length glass cells and distilled water as reference. The whole visible spectrum (380−770 nm) was recorded (λ = 2 nm), considering the Illuminant D65 and 10° Observer as references. Wine samples were centrifuged (4190*g*, 5 min), and the supernatants were filtered through Millipore-AP20 filters (Bedford, MA, USA) prior to the spectrophotometric analysis.

The CIELAB parameters (L^*, a^*, b^*, C^*_{ab}, h_{ab}) were determined by using the original software CromaLab,[24] following the recommendations of the Commission Internationale de L'Eclairage.[25] The L^* value is the vertical axis and defines the lightness, the property according to which each color can be considered as equivalent to a member of the

dx.doi.org/10.1021/jf405574x | J. Agric. Food Chem. 2014, 62, 2663−2671

Table 3. Mean Values and Standard Deviations of Noncolored Monomeric Phenols and Total Phenolics of Wines (n = 3), at Skin Removal (SR) and after 5 Months of Stabilization

		maceration treatment[a]		
	stage	SY	PXGP 10%	PXGP 20%
phenolic acids (mg/L)				
gallic acid	SR	174.28 a ± 8.77	227.14 b ± 9.36	244.00 b ± 12.62
	5 months	149.85 a ± 7.68	195.43 b ± 4.18	214.34 b ± 20.31
GRP[b]	SR	23.47 a ± 3.69	22.43 a ± 2.53	22.27 a ± 1.88
	5 months	17.49 a ± 1.58	17.28 a ± 1.26	16.60 a ± 1.80
trans-caftaric acid	SR	21.57 a ± 1.72	16.37 b ± 0.52	16.62 b ± 1.96
	5 months	20.37 a ± 1.58	15.38 b ± 0.73	14.41 b ± 1.92
trans-coutaric acid	SR	11.62 a ± 1.23	9028 b ± 0.28	9.07 b ± 0.78
	5 months	11.41 a ± 1.45	8.84 b ± 0.39	8.75 b ± 0.77
syringic acid	SR	1.77 a ± 0.16	4.63 b ± 1.22	7.85 c ± 0.50
	5 months	2.13 a ± 1.10	5.05 a ± 4.04	5.48 a ± 0.19
flavan-3-ols (mg/L)				
(+)-catechin	SR	16.14 a ± 1.74	21.37 b ± 0.40	23.69 b ± 1.23
	5 months	15.32 a ± 0.71	18.29 b ± 0.37	20.91 c ± 1.25
(−)-epicatechin	SR	13.81 a ± 1.24	12.96 a ± 0.29	12.80 a ± 1.70
	5 months	12.90 a ± 0.79	12.92 a ± 0.39	12.57 a ± 1.16
flavonols (mg/L)				
myricetin-3-glucuronide	SR	0.81 a ± 0.11	0.67 ab ±0.02	0.57 b ± 0.18
	5 months	0.71 a ± 0.12	0.61 a ± 0.10	0.09 a ± 0.03
myricetin-3-glucoside	SR	14.95 a ± 0.11	12.15 b ± 0.12	10.36 b ± 0.95
	5 months	10.03 a ± 0.72	8.34 a ± 0.94	8.46 a ± 0.28
quercetin-3-glucuronide	SR	10.75 a ± 1.01	14.56 b ± 0.27	16.65 a ± 0.52
	5 months	7.79 a ± 0.29	11.32 b ± 0.39	11.95 b ± 0.06
quercetin-3-glucoside	SR	12.82 a ± 0.96	14.65 a ± 0.19	14.08 a ± 0.52
	5 months	7.13 a ± 0.68	9.33 b ± 0.27	9.54 b ± 0.15
laricitrin-3-glucoside	SR	8.47 a ± 1.02	7.18 b ± 0.08	3.70 c ± 0.19
	5 months	3.72 a ± 0.70	3.15 ab ±0.23	2.57 b ± 0.10
kaempferol-3-glucoside	SR	2.08 a ± 0.28	0.58 b ± 0.01	1.29 c ± 0.14
	5 months	nd	0.12 b ± 0.03	0.63 c ± 0.01
isorhamnetin-3-glucoside	SR	4.69 a ± 0.44	1.66 b ± 0.10	1.29 b ± 0.06
	5 months	1.39 a ± 0.10	1.17 b ± 0.05	0.90 c ± 0.03
syringetin-3-glucoside	SR	nd	3.47 b ± 0.08	2.65 c ± 0.26
	5 months	3.46 a ± 0.25	2.70 b ± 0.22	1.99 c ± 0.07
total phenolics (Folin−Ciocalteu) (mg GAE/L)	SR	2269.8 a ± 49.01	2416.6 a ± 105.79	2779.2 b ± 135.35
	5 months	2036.6 a ± 75.34	2278.2 b ± 93.10	2346.0 b ± 62.91

[a]SY, 100% Syrah grapes; PXGP 10% and PXGP 20%, fermentation of Syrah grapes with PXGP at 10 and 20% (w/w), respectively. Different letters in the same row indicate significant differences ($p < 0.05$). nd, not detected. [b]GRP, grape reaction product (2-*S*-glutathionyl-caftaric acid).

gray scale, between black and white, taking values within the range of 0−100, respectively. The a^* and b^* values represent the chromaticity scalar coordinates, which in turn represent opponent red−green and blue−yellow scales.

From L^*, a^*, and b^*, other parameters are defined, such as hue (h_{ab}) and chroma (C^*_{ab}). Hue angle (h_{ab}) is the attribute according to which colors have been traditionally defined as red, green, etc. On the other hand, the chroma (C^*_{ab}) is the attribute that allows each hue to be determined by its degree of difference in comparison to a gray color with the same lightness. Moreover, these colorimetric parameters can be distinguished as quantitative or qualitative color attributes as they indicate a quantitative contribution to color (L^* and C^*_{ab}) or qualitative one (h_{ab}).[26]

Also, the color differences (ΔE^*_{ab}) were calculated between the samples to state the implications of the maceration treatments on the color of the final wines, as well as to assess the color stability. It was calculated as the Euclidean distance between two points in the three-dimensional space defined by L^*, a^*, and b^*: $\Delta E^*_{ab} = [(\Delta L^*)^2 + (\Delta a^*)^2 + (\Delta b^*)^2]^{1/2}$.

Statistical Analysis. All statistical analyses were performed using Statistica v.8.0 software.[27] Univariate analysis of variance (ANOVA) was applied using the general linear model program to establish whether mean values of the physicochemical data obtained in each studied point differed significantly among the three types of wines (SY, PXGP 10% and PXGP 20%). The means values of each set of samples (n = 3) were compared by the Tukey test at a significance level of $p < 0.05$.

RESULTS AND DISCUSSION

Enological Parameters. No statistically significant difference was found among control wines and wines fermented with additional amounts of PXGP for any enological parameter analyzed. These results indicate that the general wine composition was not affected by the maceration treatment applied (Table 1).

The low values found in wines for the reducing sugars and malic acid concentration (<2.0 g/L and <0.01 mg/L, respectively) denoted the correct development of fermentative

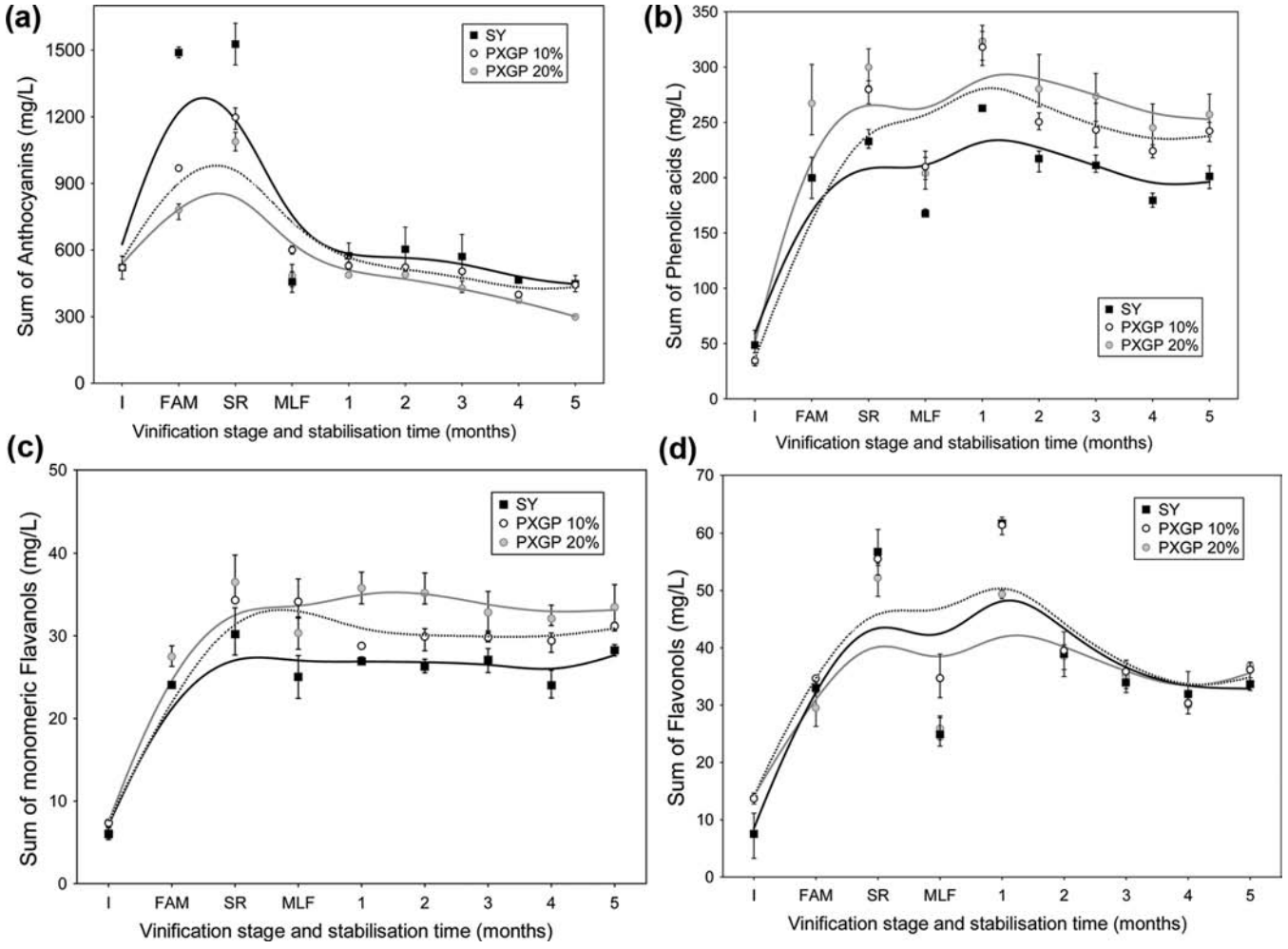

Figure 1. Evolution of the main phenolic families (mg/L ± SD, $n = 3$) in control wines (SY) and wines fermented with PXGP (10 and 20%) during the vinification process: (a) sum of anthocyanins; (b) sum of phenolic acids; (c) sum of monomeric flavanols; (d) sum of flavonols.

processes. The alcohol degree reached when fermentative processes were finished (between 12.9 and 13.2% v/v) was in accordance with the sugar concentration of Syrah grapes at ripeness. The good preservation state of wines was confirmed by the low values of the volatile acidity (around 0.5 g/L). As expected, all finished wines showed very similar values of total acidity (between 5.6 and 5.8 g/L as tartaric acid), pH (around 3.3 units), and free and total sulfur dioxide contents (<10 and between 44.3 and 50.6 mg/L, respectively) because these enological parameters were adjusted at the same levels for all assays.

Phenolic Composition and Changes during Vinification. Twenty-five monomeric phenolic compounds were identified and quantified in wines by HPLC. The comparative chromatographic analysis of samples revealed that control and fermented wines with PXGP did not differ in their phenolic profile in qualitative terms. It included several anthocyanin pigments and colorless phenols belonging to diverse phenolic families: 11 anthocyanins (including nonacylated, acetylated, and *p*-coumaroylated derivatives), 5 phenolic acids (gallic, GRP, *trans*-caftaric, *trans*-coutaric, and syringic), 2 monomeric flavanols ((+)-catechin and (−)-epicatechin), and 8 flavonols (myricetin-3-glucuronide, myricetin-3-glucoside, quercetin-3-glucuronide, quercetin-3-glucoside, laricitrin-3-glucoside, kaempferol-3-glucoside, isorhamnetin-3-glucoside, and syringetin-3-glucoside).

Table 2 summarizes the concentrations for the mentioned anthocyanins (mg/L) together with the percentage of copigmentation and polymerization of wines (mean ± SD, $n = 3$), showing the statistical differences among treatments at the end of the fermentative maceration (skin removal) and after 5 months of stabilization. In the same way, Table 3 summarizes the information relative to the colorless monomeric phenols (mg/L) and the total phenolic content (as mg GAE/L).

Results showed that the addition of PXGP at the beginning of fermentation causes a significant impact on the concentration of the most individual compounds identified and on the physicochemical transformations in which they are involved (copigmentation and polymerization). However, the effect was not the same for the different phenolic families and depended on the proportions of PXGP added. An accurate evaluation of the changes on the total levels of anthocyanins, phenolic acids, monomeric flavanols, and flavonols during the whole process of vinification allowed the stages at which the applied treatments had a greater influence on the chemical quality of wines to be established (Figure 1).

During the period of fermentative maceration, all wines elaborated with supplementary amounts of PXGP had lower levels of anthocyanins than wines elaborated by traditional maceration, although they were richer in phenolic acids and monomeric flavanols. The effect on the flavonols was quite different because additions of 10% PXGP had no significant

dx.doi.org/10.1021/jf405574x | J. Agric. Food Chem. 2014, 62, 2663−2671

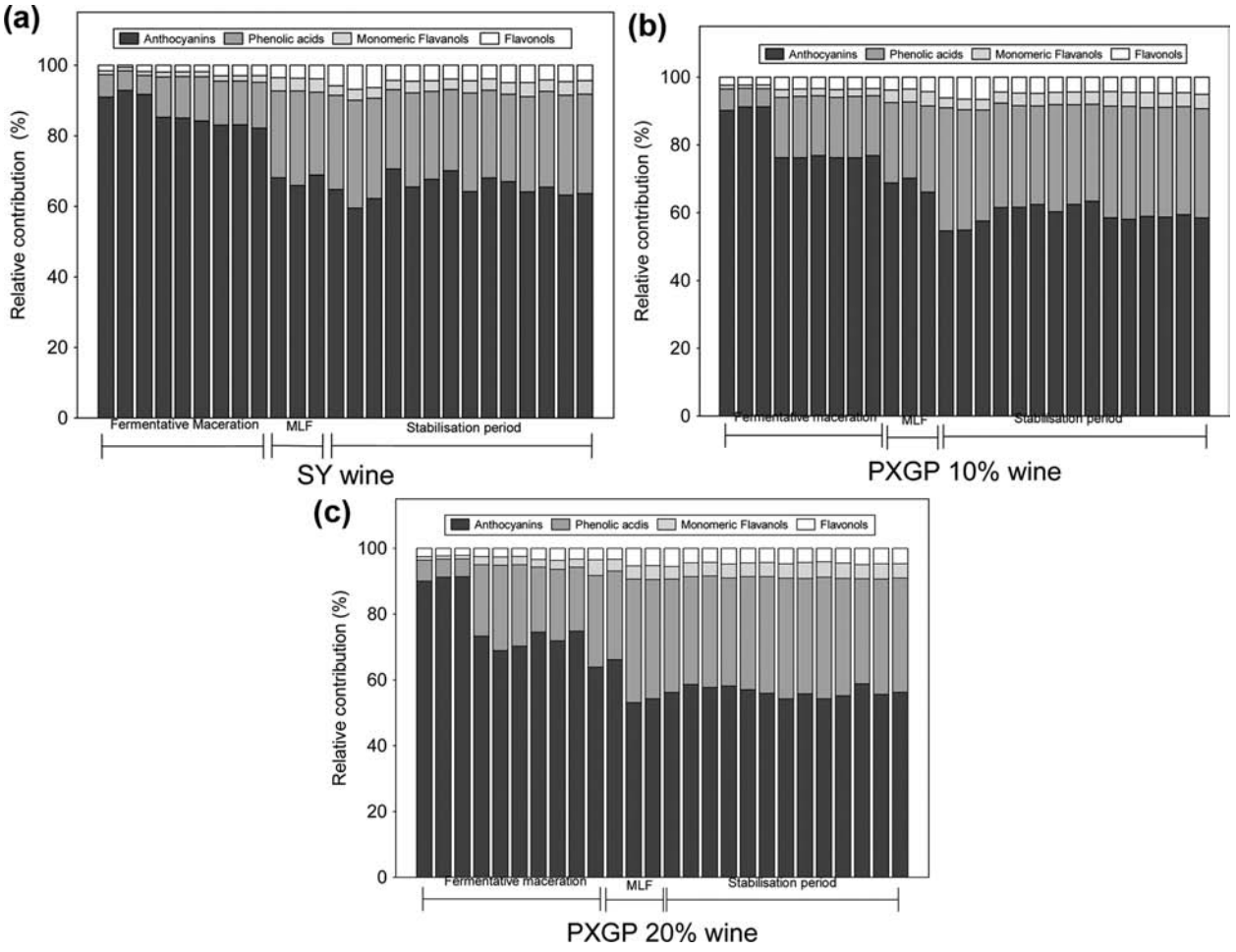

Figure 2. Relative proportion of the different phenolic families during the vinification process, according to the maceration treatment applied: (a) Syrah wines, traditional red wine vinification; (b) PXGP 10% wines, fermentative addition of PXGP at 10% (w/w); (c) PXGP 20% wines, fermentative addition of PXGP at 20%.

effect on the global content, but at higher proportions (20%) it was slightly reduced. Analogous chemical behavior was found by other authors in similar vinification experiments because two competitive effects are expected to occur simultaneously: (1) incorporation of the phenolics contained in the solid parts of grapes enhances the pool of copigmenting cofactors in the wine matrix; and (2) anthocyanin adsorption to the extra amounts of skin and seeds causes loss of color.[9,15,17]

In our winemaking conditions, significantly higher contents of gallic and syringic acids, (+)-catequin, quercetin-3-glucuronide, quercetin-3-glucoside, and syringentin-3-glucoside were found in PXGP wines at the end of the skin contact period, the effect being stronger when 20% was added (Table 3). Thus, adding PXGP at the rates studied favored the enrichment of Syrah wines in specific colorless phenolics, especially those cofactors having limited solubility.[28] Most of these compounds have been described as good copigments,[6] which support the higher grade of copigmentation reached by PXGP wines at skin removal (%CA = 34 and 27 versus 22% in PXGP 20%, PXGP 10%, and control wines).

On the other hand, the lower anthocyanin or flavonol content (only in the case of PXGP 20% wines) suggested the partial adsorption of pigments and even other phenolic compounds by extra amounts of skins and seeds, which could be especially drastic if too high proportions are added to the fermentation mash,[7] as occurred with PXGP at 20%.

Nevertheless, although the initial pigment content clearly differed for the treatments, the differences among them tended to diminish as the stabilization period proceeded (Figure 1a). A gradual decrease of total monomeric anthocyanins after skin removal was observed in the three wines, being more intense for control and PXGP 20% wines. As a consequence, the final values of total anthocyanins were almost the same order of magnitude for control and PXGP 10% wines (448.7 and 431.3 mg/L, respectively), whereas PXGP 20% wines showed the significantly lowest content (298.7 mg/L). Moreover, 10% PXGP addition seemed to protect to a larger extent the presence of bluish forms of anthocyanins (delphinidin-3-glucoside and petunidin-3-glucoside) and some acylated derivatives having chemical characteristics that great affect copigmentation (petunidin-3-acteyl-glucoside and malvidin-3-*p*-coumaroyl-glucoside), because significantly higher contents were found in the final wines.

With regard to the three groups of colorless phenols, wines elaborated with the addition of PXGP maintained the highest levels of phenolic acids (257.8 and 241.9 versus 201.3 mg/L, in 20%, 10%, and control wines, respectively), monomeric flavanols (33.5 and 31.2 versus 28.2 mg/L, respectively), and flavonols (36.2 and 36.1 versus 33.6 mg/L, respectively), and also the final total phenolic content (2346.0 and 2278.2 versus 2036.6 mg/L, respectively).

dx.doi.org/10.1021/jf405574x | J. Agric. Food Chem. 2014, 62, 2663−2671

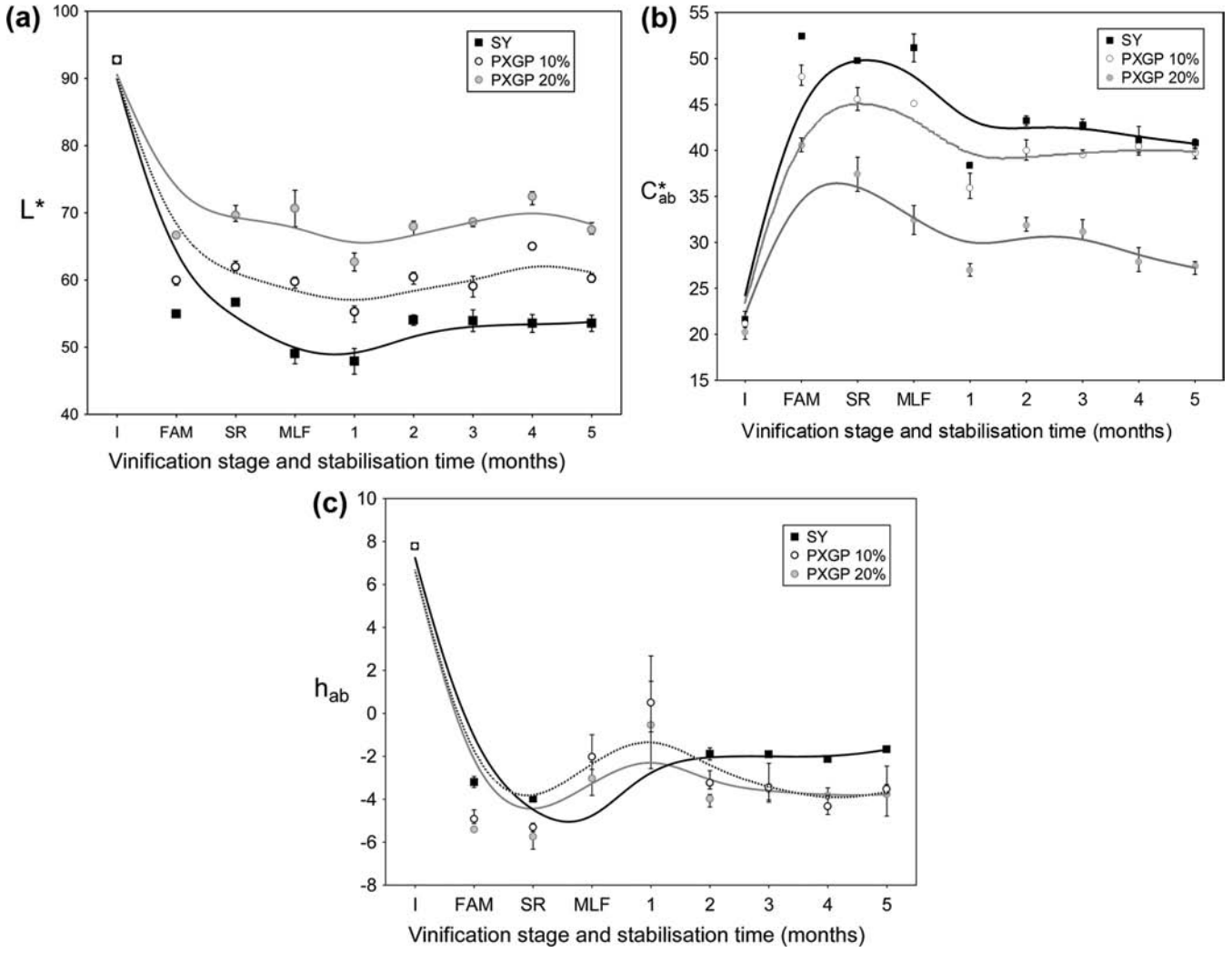

Figure 3. Changes in the color parameters (means ± SD, $n = 3$) for control wines (SY) and wines fermented with PXGP (10 and 20%) during the vinification process: (a) L^*, lightness; (b) C^*_{ab}, chroma; (c) h_{ab}, hue angle.

Table 4. Mean Values and Standard Deviations of Lightness (L^*), Chroma (C^*_{ab}), and Hue (h_{ab}) of Wines ($n = 3$), at Skin Removal (SR) and after 5 Months of Stabilization

		maceration treatment[a]		
	stage	SY	PXGP 10%	PXGP 20%
L^*	SR	56.29 a ± 0.18	61.92 b ± 0.89	69.63 c ± 1.29
	5 months	53.81 a ± 1.44	60.24 b ± 0.67	67.70 c ± 0.72
C^*_{ab}	SR	49.46 a ± 0.12	46.30 b 1.26	35.23 c ± 1.86
	5 months	41.22 a ± 0.91	40.49 a ± 1.06	27.40 b ± 0.78
h_{ab}	SR	−3.98 a ± 0.11	−4.56 b ± 0.9	−5.73 b ± 0.52
	5 months	−1.66 a ± 0.13	−3.17 a ± 0.63	−3.76 b ± 1.19

[a]SY, 100% Syrah grapes; PXGP 10% and PXGP 20%, fermentation of Syrah grapes with PXGP at 10 and 20% (w/w), respectively. Different letters in the same row indicate significant differences ($p < 0.05$).

Furthermore, the contribution of each group of pigments to the total color (copigmented and polymeric pigments) evolved differently depending on the maceration applied, which seemed to be related to the relative proportions of the different phenolic families in each wine (Figure 2). Adding 10% PXGP led to wines with the highest degree of polymerization (%PP = 70.6), meaning a higher proportion of more stable pigments than control wines (%PP = 66.7). Probably, the lower content of pigments in PXGP 10% wines at skin removal could be balanced by the relative highest proportion of copigments extracted in comparison with control wines, resulting in a better pigment/copigment ratio and higher chemical stability. On the contrary, the PXGP 20% wines reached the lowest proportion of polymeric pigments (%PP = 54.1%). This fact shows the difficulty of those wines to convert the earlier copigmentation complexes into more stable pigments despite having important amounts of copigments. Most likely, the significantly lower content of anthocyanins and flavonols from the first steps of vinification was insufficient to achieve higher chemical stability during stabilization.[2,29]

dx.doi.org/10.1021/jf405574x | J. Agric. Food Chem. 2014, 62, 2663−2671

Color Characteristics and Changes during Vinification. The evolution of CIELAB color parameters (L^*, C^*_{ab}, and h_{ab} CIELAB parameters) during the winemaking processes is shown in Figure 3, where the mean value and standard deviation for these variables are included for each set of samples.

As determined from the whole set of data, red wine color evolved in a similar way both in control and in PXGP wines. A net increase of chroma (C^*_{ab}) and decreases of lightness (L^*) and hue (h_{ab}) due to the pigment extraction characterized the fermentative maceration, whereas all of the parameters became gradually stable after the skin contact period because of the stabilization processes.

As can be seen, the maceration treatments applied induced significant differences in the color characteristics of wines and their stability depending on the doses of PXGP added. As expected, the higher color extraction corresponded to control wines, which showed the lowest values of lightness (L^*) and highest values of chroma (C^*_{ab}) at skin removal, indicating darker and more saturated color than PXGP wines (Table 4). These results were consistent with the higher content of anthocyanins in control wines during the fermentative maceration period, which reflects the better balance between the extraction and adsorption of pigments with respect to wines elaborated with higher amounts of pomace than are naturally found in a traditional red wine vinification.

However, it is interesting to note how the particular changes during the stabilization in the phenolic fractions influenced the final color of wines (Table 4), in both quantitative (C^*_{ab} and L^*) and qualitative (h_{ab}) terms.[26] At the end of the stabilization period, the addition of PXGP at 10% led to wines with comparable content in pigments relative to wines elaborated by traditional maceration, but with higher proportions of bluish anthocyanins, copigments, and polymeric pigments, which resulted in lighter wines but with comparable quantity of color (L^* = 60.24 ± 0.67 versus 53.81 ± 1.44 u; C^*_{ab} = 40.49 ± 1.06 versus 41.22 ± 0.91 u) and more notably bluish hues (negative values of hue; h_{ab} = −3.17° ± 0.63 versus −1.66° ± 0.13, in PXGP 10% and control wines, respectively).

The effect on these analytical parameters was the opposite when 20% of pomace from PXGP was added, which can be attributable to the lower phenolic potential during the whole process of vinification. In this case, it was related to significantly lighter wines with less saturated color (L^* = 67.70 ± 0.72 u; C^*_{ab} = 27.40 ± 0.78 u). In terms of total color, the highest color difference values (ΔE^*_{ab}) were found between control wine and 20% PXGP wine (14.38 u) and the least one between control wine and 10% PXGP wines (3.93 u), although in all cases they were visually perceptible (ΔE^*_{ab} > 3.0 CIELAB units).[30]

The assessment of the color differences (ΔE^*_{ab}) occurring from the skin removal to the end of the stabilization period (5 months) allowed evaluation of the color stability of each wine. The lowest values of color difference were obtained for PXGP 10% wines compared to control and PXGP 20% wines (ΔE^*_{ab} = 6.36 versus 9.53 and 8.81 u, respectively), indicating lower color variation and, thus, higher color stability. As can be observed in Figure 3b,c, the chroma decreased and the hue increased toward 0° (redness color) in all wines. This observation means that the color variation that took place during stabilization was due to a decrease of the quantity of color and bluish hue of wines (lower values of C^*_{ab} and higher values of hue). Specifically, these chromatic modifications were less intense in PXGP 10% wines (ΔC^*_{ab} = −5.7 versus −7.7 and −8.6 u; Δh_{ab} = +1.39° versus +1.97° and +2.37° in 10%, 20%, and control wines, respectively). Chemically, this may be explained by the lower loss of monomeric anthocyanins and the higher content in more stable pigments in PXGP 10% wines as a result of the phenolic compounds extracted from PXGP, which favored a better pigmet/copigment ratio and a more effective stabilization of wine color. Thus, it was confirmed that the addition of limited amounts (10%) of skins and seeds of PXGP during fermentation led to wines with more stable color that kept their vivid bluish tonalities for a longer time, and these characteristics are highly appreciated in young red wines. In the case of the higher proportions tested (20%), the adsorption of pigments during fermentation seems to have a stronger effect on the color than the copigmentation (color stabilization) due to the cofactors extracted from PXGP, as reported in the literature.[15]

On the basis of the results, it has been proved that the addition of a limited amount of skins and seeds from white grape pomace during the fermentative step of the winemaking process represents an interesting enological practice to improve the phenolic potential and color characteristic of young Syrah wines from a warm climate. The effectiveness of the fermentative addition was demonstrated by the increase of the concentration of several colorless phenolic compounds (copigments) and intermolecular copigmentation reactions in wines. Potential benefits observed in Syrah wines include greater chemical complexity and higher development of polymerization, as well as better color characteristics and color stability. However, the global effect clearly depends on the proportions of white skins and seeds applied. When too high a proportion of pressed grape pomace (20% w/w) is added to the fermentation mash, it may damage wine quality due to a higher adsorption of phenolic compounds during maceration (pigments and copigments), resulting in a net loss in color in final wines. Thus, not all proportions are acceptable to obtain phenolic and color enhancement effects.

AUTHOR INFORMATION

Corresponding Author

*(F.J.H.) Phone: +34 954556495. Fax: +34 954556110. E-mail: heredia@us.es.

Funding

This research was financially supported by the Consejería de Economía, Innovación, Ciencia y Empleo, Junta de Andalucía (Project P10-AGR06331, AGR02893 posdoctoral grant) and the Ministerio de Ciencia e Innovación (Project AGL2011-30254-C02-02), Spain.

Notes

The authors declare no competing financial interest.

ACKNOWLEDGMENTS

We thank Coop. Agric. La Unión winery (Cordoba, Spain) for supplying samples and Dr. Modesto Carballo (Biology Service, CITIUS, Universidad de Sevilla) for technical assistance.

REFERENCES

(1) Jackson, D. I.; Lombard, P. B. Environmental and management practices affecting grape composition and wine quality − a review. *Am. J. Enol. Vitic.* **1993**, *44*, 409−430.

(2) Sacchi, K. L.; Bisson, L. F.; Adams, D. O. A review of the effect of winemaking techniques on phenolic extraction in red wines. *Am. J. Enol. Vitic.* **2005**, *56*, 197−206.

(3) De Freitas, V.; Mateus, N. Chapter 3. Updating wine pigments. *Recent Advances in Polyphenol Research*; Wiley-Blackwell: Oxford, UK, 2010.
(4) He, F.; Liang, N. N.; Mu, L.; Pan, Q. H.; Wang, J.; Reeves, M. J.; Duan, C. Q. Anthocyanins and their variation in red wines I. Monomeric anthocyanins and their color expression. *Molecules* **2012**, *17*, 1571−1601.
(5) Escribano-Bailón, M. T.; Santos-Buelga, C. Anthocyanin copigmentation − evaluation, mechanisms and implications for the colour of red wines. *Curr. Org. Chem.* **2012**, *16*, 715−723.
(6) Gómez-Miguez, M.; González-Manzano, S.; Escribano-Bailón, M. T.; Heredia, F. J.; Santos-Buelga, C. Influence of different phenolic copigments on the color of malvidin 3-glucoside. *J. Agric. Food Chem.* **2006**, *54*, 5422−5429.
(7) Boulton, R. The copigmentation of anthocyanins and its role in the color of red wine: a critical review. *Am. J. Enol. Vitic.* **2001**, *52*, 67−87.
(8) Mira de Orduña, R. Climate change associated effects on grape and wine quality and production. *Food Res. Int.* **2010**, *43*, 1844−1855.
(9) Revilla, E.; Ryan, J. M.; Kovac, V.; Nemanic, J. The effect of the addition of supplementary seeds and skins during fermentation on the chemical and sensory characteristics of red wines. In *Food Flavors: Formation, Analysis and Packaging Influences*; Contis, E. T., et al., Eds.; Elsevier Science: Amsterdam, The Netherlands, 1998.
(10) Schwarz, M.; Picazo-Bacete, J. J.; Winterhalter, P.; Hermosín-Gutiérrez, I. Effect of copigments and grape cultivar on the color of red wines fermented after the addition of copigments. *J. Agric. Food Chem.* **2005**, *53*, 8372−8381.
(11) Canals, R.; Llaudy, M. C.; Canals, J. M.; Zamora, F. Influence of the elimination and addition of seeds on the colour, phenolic composition and astringency of red wine. *Eur. Food Res. Technol.* **2008**, *226*, 1183−1190.
(12) Neves, A. C.; Spranger, M. I.; Zhao, Y.; Leandro, M. C.; Sun, B. Effect of addition of commercial grape seed tannins on phenolic composition, chromatic characteristics, and antioxidant activity of red wine. *J. Agric. Food Chem.* **2010**, *58*, 11775−11782.
(13) Harbertson, J. F.; Parpinello, G. P.; Heymann, H.; Downey, M. O. Impact of exogenous tannin additions on wine chemistry and wine sensory character. *Food Chem.* **2012**, *131*, 999−1008.
(14) Gordillo, B.; Cejudo-Bastasnte, M. J.; Rodríguez-Pulido, F. J.; González-Miret, M. L.; Heredia, F. J. Application of the differential colorimetry and polyphenolic profile to the evaluation of the chromatic quality of Tempranillo red wines elaborated in warm climate. Influence of the presence of oak wood chips during fermentation. *Food Chem.* **2013**, *141*, 2184−2190.
(15) Kovac, V.; Alonso, E.; Revilla, E. The effect of adding supplementary quantities of seeds during fermentation on the phenolic composition of wines. *Am. J. Enol. Vitic.* **2005**, *46*, 363−367.
(16) Rodríguez Montealegre, R.; Romero Peces, R.; Chacón Vozmediano, J. L.; Martínez Gascueña, J.; García Romero, E. Phenolic compounds in skins and seeds of ten grape *Vitis vinifera* varieties grown in a warm climate. *J. Food Compos. Anal.* **2006**, *19*, 687−693.
(17) Diago-Santamaría, M. P.; Boulton, R. B. Effect of cofermentation of red grapes with different amounts of white skins on the color of young red wines. In *54th Annual meeting of the American Society for Enology and Viticulture*, Reno, NV; American Society for Enology and Viticulture: Davis, CA, USA, 2003
(18) Alvarez, I.; Aleixandre, J. L.; García, M. J.; Lizama, V.; Aleixandre-Tudó, J. L. Effect of the prefermentative addition of copigments on the polyphenolic composition of Tempranillo wines after malolactic fermentation. *Eur. Food Res. Technol.* **2009**, *228*, 501−510.
(19) Pedroza, M. A.; Carmona, M.; Alonso, G. L.; Salinas, M. R.; Zalacain, A. Pre-bottling use of dehydrated waste grape skins to improve colour, phenolic and aroma composition of red wines. *Food Chem.* **2013**, *136*, 224−236.
(20) UE, Official Methods to Wine Analyses, Reglamento 440/2003.
(21) Boulton, R. B. A method for the assessment of copigmentation in red wines. In *47th Annual Meeting of the American Society for Enology and Viticulture*, Reno, NV; American Society for Enology and Viticulture: Davis, CA, USA, 1996.
(22) Singleton, V. L.; Rossi, J. A. Colorimetry of total phenolics with phosphomolybdic−phosphotungstic acid reagents. *Am. J. Enol. Vitic.* **1965**, *16*, 144−158.
(23) Heredia, F. J.; Escudero-Gilete, M. L.; Hernanz, D.; Gordillo, B.; Meléndez-Martínez, A. J.; Vicario, I. M.; González-Miret, M. L. Influence of the refrigeration technique on the colour and phenolic composition of syrah red wines obtained by prefermentative cold maceration. *Food Chem.* **2010**, *118*, 377−383.
(24) Heredia, F. J.; Álvarez, C.; González-Miret, M. L.; Ramírez, A. CromaLab, Análisis de color. Registro General de la Propiedad Intelectual, 2004.
(25) CIE. *Technical Report Colorimetry*; Commission Internationale de l'Eclairage Central Bureau: Vienna, Austria, 2004.
(26) Gordillo, B.; Rodríguez-Pulido, F. J.; Escudero-Gilete, M. L.; González Miret, M. L.; Heredia, F. J. Comprehensive colorimetric study of anthocyanic copigmentation in model solutions. Effects of pH and molar ratio. *J. Agric. Food Chem.* **2012**, *60*, 2896−2905.
(27) StatSoft Inc. *STATISTICA (Data Analysis Software System)*, v 8; StatSoft Inc.: Tulsa, OK, USA, 2007.
(28) González-Neves, G.; Gil, G.; Barreiro, L.; Favre, G. Pigment profile of red wines cv. Tannat made with alternative winemaking techniques. *J. Food Compos. Anal.* **2010**, *23*, 447−454.
(29) Parker, M.; Smith, P. A.; Birse, M.; Francis, I. L.; Kwiatkowski, M. J.; Lattey, K. A.; Liebich, B.; Herderich, M. J. The effect of pre- and post-ferment additions of grape derived tannin on Shiraz wine sensory properties and phenolic composition. *Aust. J. Grape Wine Res.* **2007**, *13*, 30−37.
(30) Martínez, J. A.; Melgosa, M.; Pérez, M. M.; Hita, E.; Negueruela, A. I. Note. Visual and instrumental color evaluation in red wines. *Food Sci. Technol. Int.* **2001**, *7*, 439−444.

and water phases, have intermediate wettability, and remain intact over the lifetime of the emulsion system.[16] Recently, de Folter et al.[15] have prepared O/W Pickering emulsions with droplet sizes in a range of 10−200 μm by zein colloidal particles through an antisolvent precipitation procedure. The zein-stabilized emulsions were highly unstable to creaming, but possessed long-term stability against coalescence at pH above and below the isoelectric point of zein. Our recent study has shown that incorporation of zein colloidal particles at the surface of rthe oil droplet can act against coalescence during the formation of emulsion-based films by Pickering stabilization.[17]

In practice, there have been multiple challenges for the preparation of Pickering emulsions, including the aggregation of particles in bulk phase, low diffusive mobility that resulted low interfacial adsorption, and limited surface coverage.[16] In our previous study,[18] we have found that soy lipophilic protein (LP), one of the soy storage proteins and a natural complex of hydrophobic membrane protein and biosurfactant phospholipids, self-assembles to form nanoparticles by ultrasonical treatment. These nanoparticles have an improved diffusive mobility to the interface and then form a complex interface of aggregated protein particles and phospholipids, providing the oil droplets with the synergic improvement in coalescence and flocculation stability of emulsion.

Zein, the predominant food grade protein in corn, is a particularly abundant material extracted from corn gluten meal (CGM) and has great potential for commecialization in various industrial applications.[19] Zein with a high proportion (>50%) of hydrophobic amino acids, for example, leucine, proline, and alanine, is insoluble either in water or in oil, but it can be dissolved in a water−ethanol mixture[19] and low molecular weight charged surfactant, such as sodium dodecyl sulfate (SDS) solution.[20,21] Here we describe a method to prepare soluble complexes of hydrophobic corn protein zein colloidal particles and sodium stearate (SS), an anionic surfactant, to overcome problems exhibited by zein particles only and to produce food protein based in a Pickering emulsion with high stability. Moreover, a protein-based Pickering emulsion as a starting template for preparing oil gels without *trans* and saturated fats is also the goal of this study.

MATERIALS AND METHODS

Materials. Zein and SS (>99%) were purchased from Sigma Chemical Co. (St. Louis, MO, USA) without further purification. Low acyl gellan gum available from Kelco (Atlanta, GA, USA) was provided by Berger & Baker Food Industry Co. Ltd. (Guangzhou, China). Polydimethylsiloxane (PDMS, Sylgard184) was purchased from Dow Corning Co. (Midland, MI, USA). All other chemicals used were of analytical grades, and all solutions and dispersions were prepared using Milli-Q water.

Dispersion of Zein Colloidal Particles. Zein (0.5 wt %) was dissolved in water containing SS at concentrations of 2.5, 5, and 10 mM, respectively, under ultrasonic shear (Sonic Ruptor 400 Ultrasonic Homogenizer, OMNI, USA) with the power of 30%. The temperature of the aqueous phase was maintained below 25 °C by using an ice bath under ultrasonic shear.

Particle Size and ζ-Potential Measurements. The measurements of size distribution, ζ-potential, and polydispersity index (PDI) of zein particles were performed using a Nano ZS Zetasizer instrument (Malvern Instruments, Worcestershire, UK). Samples were diluted to 1 mg/mL with water before loading to the cuvette. All measurements were carried out at 25 °C in triplicate. A refractive index of 1.450 was used for zein dispersion and 1.331 for the continuous phase. The apparent hydrodynamic radius (R_h) of protein samples was analyzed by means of the "cumulants" method[22] and Stokes−Einstein equation (eq 1) using Dispersion Technology Software (DTS) (V4.20).

$$D = K_B T/6\pi\eta r \quad (1)$$

D is the diffusion coefficient, K_B is the Boltzmann constant, T is the absolute temperature, η is the medium viscosity, and r is the radius of the particle.

Morphology of Zein Particles Adsorbed at the Oil−Water Interface. The morphology of the zein particle monolayer trapped at the oil−water interface was observed by gel trapping technology (GTT) described by Paunov[23] with modifications. An aliquot of 5 mL of 1.0 wt % gellan gum dispersion in a 10 mL beaker was heated to 50 °C to dissolve and hydrate. Then 0.5 mL zein dispersions modified with different SS concentrations were added into the gellan gum solution, and 2 mL of soybean oil was added to form an oil−water interface. The system was kept at 50 °C for 30 min and stirred mildly with a magnetic stirrer to ensure the sufficient adsorption of zein particles at the oil−water interface. To solidify gellan gum, 2 mM $MgCl_2$ was injected into the aqueous phase with a syringe and the temperature was cooled for 1 h at ambient temperature (25 °C). The top oil phase was removed and then was replaced with 2 mL of PDMS silicone elastomer and cured for 24 h at ambient temperature. The particle monolayer on the PDMS surface could be peeled off from the aqueous gel and imaged with a field emission scanning electron microscope (SEM, LEO 1530 VP, Oberkochem, Germany).

Surface Protein Loading Measurement. The content of protein adsorbed at the oil−water interface was determined according to the method described by Akhtar et al.[24] with modifications. Freshly prepared emulsions (described as below) were centrifuged at $1 \times 10^5 g$ for 30 min at 20 °C using a Himac CS150NX Micro Ultracentrifuge (Hitachi Koki Co. Ltd., Tokyo, Japan) with an S140AT rotor. Five hundred microliters of the supernatant was collected for analysis of the protein in continuous phase. After that, the cream layers and the rest of the supernatant were carefully removed. The precipitate was carefully washed twice with water to remove any residual cream or protein in continuous phase, and after that, the precipitate was heat-dried at 50 °C for 6 h. The composition of protein adsorbed at the oil−water interface was determined using SDS-PAGE. Dispersed protein in aqueous phase was determined by using the micro-Kjeldahl method (N × 5.71) and recorded as M_D (mg), precipitated protein was determined by weighing and recorded as M_P (mg), and the weight of protein added into the emulsions was recorded as M_I (mg), so the weight of adsorbed protein was M_A (mg) = $M_I - M_D - M_P$. The surface loading of protein can be calculated with eq 2

$$\text{surface protein loading (mg/m}^2) = (M_A \times d_{3,2})/(6 \times V \times \Phi_{oil}) \times 10^{-2} \quad (2)$$

where $d_{3,2}$ (μm) is the average droplet size of the emulsions, V (mL) is the volume of emulsions, and Φ_{oil} is the volume fraction of the oil in emulsions.

Contact Angle Measurement. Contact angles of Milli-Q water on solid zein film were measured at 25 °C with the method of sessile drop by a contact angle analyzer (OCA 20 AMP, Dataphysics Instruments, Germany). A droplet of water (constant 4 μL) was deposited on the film surface with a precision syringe. The drop image was recorded immediately just after dropping from the syringe by a video camera, and the profile of the droplet was numerically solved and fitted to the Laplace−Young equation. Ten parallel measurements were performed for each film. Solid zein film was prepared by the method of participation as follows: ultrasonic treated zein dispersion (0.5 wt %) was centrifuged at 10000g for 20 min, and the supernatant was dripped on the cleaved mica and heat-dried at 40 °C for 8 h. To prepare an oil film, soybean oil was spread on the cleaved mica, and then the mica was inclined to allow the redundant oil to flow away.

Preparation and Characterization of Emulsions and Oil Gels. The O/W emulsions were prepared by homogenizing the mixture of 10 wt % soybean oil and 0.5 wt % zein particle dispersion at 10000 rpm for 2 min by using a T25 Ultraturrax homogenizer (IKA, Staufen, Germany). Oil gels were obtained by one-step freeze-drying of the

precursor emulsions (10 mL) over 24 h on a DELTA1-24/LSC freeze-dryer (Martin Christ Gefriertrocknungsanlagen GmbH, Germany) using room temperature in the drying chamber, −60 °C for the cooling unit, and a vacuum of 0.34 mbar. Emulsion droplet size distributions were measured by Mastersizer 2000 (Malvern Instruments Co. Ltd.) at 25 °C. The particle sizes measured are reported as the volume-weighted mean diameter $d_{4,3} = \Sigma n_i d_i^4 / \Sigma n_i d_i^3$, where n_i is the number of droplets with diameter d_i. Refractive indices of 1.46 and 1.33 were used for soybean oil and water, respectively. The microstructure of the emulsion was imaged by a TCS SP5 confocal laser scanning microscope (CLSM, Leica Microsystems Inc., Heidelberg, Germany), using an argon krypton laser having an excitation line of 488 nm and a helium neon laser (He/Ne) with excitation at 633 nm. Aliquots (1 mL) of emulsions were stained with 40 μL of staining solution containing 0.1 wt % Nile Red (for protein) and 0.01 wt % Nile Blue (for oil). Emulsion stability was assessed with the heating−salting test we used previously.[18] Emulsions were heated at 90 °C for 30 min in the presence of 200 mM NaCl and then analyzed for drop size distribution and mean droplet diameters ($d_{4,3}$) described above. The changes in emulsion microstructure were observed by a BX51 light microscopy (Olympus Optical Co. Ltd., Tokyo, Japan).

Statistical Analysis. Unless specified otherwise, three independent trials were carried out, each with a new batch of sample preparation. The results are presented as means ± standard deviations. Analysis of variance (ANOVA) was performed on the data using the SPSS 13.0 statistical analysis system.

RESULTS AND ANALYSIS

Complexes of Zein Particles and SS. The solubilization of zein in SDS solution occurs in two distinct stages. SDS at 4 mM, which is close to its critical micelle concentration (CMC, ≈8 mM), is incorporated into the zein structure, forming zein−SDS complexes, followed by the formation of a complete unfolding chain of zein polypeptides until the concentration of SDS reaches 200 mM.[20,21] In this study we chose SS to stabilize zein protein due to its relatively low CMC value (≈0.4 mM), which should be attributed to its strong binding capacity on the hydrophobic protein.[25]

As expected, the water-insoluble zein agglomerates could be solubilized with SS dispersion above the CMC under ultrasonic shear (Figure 1). The SS dispersions used in this study were around 10 times the CMC (2.5, 5, and 10 mM, respectively), which is predominantly self-assembled micelles with very low monomer concentration (Figure 1B, appeared turbid). Dynamic light scattering (Figure 2) revealed that the hydrodynamic size, polydispersity index (PDI), and ζ-potential of the obtained zein colloidal particles decreased sharply with increasing SS concentration up to 5 mM and then remained constant until 20 mM. Although the zein dispersion without SS had a pH value of 3.7, the addition of SS raised it to a basic range (pH 7.7−8.6) and resulted in a negative charge of the colloids. Moreover, the hydrophobic adsorption of SS also brought about negative charge. Surface charge up to −60 mV at 5 mM SS (Figure 2B) prevented the aggregation tendency of zein in aqueous phase and, therefore, enhanced the solubilization of zein. This critical SS concentration (about 5 mM) suggested the existence of a critical complexation concentration (CCC). When the SS concentration was below the CCC, the natural conformation of zein might not be disturbed. As the SS concentration rose beyond the CCC, the C_{16} alkyl chain of SS might be incorporated into the hydrophobic zein structure, forming the zein−SS complexes with partially unfolded hydrophobic microdomains, which is similar to the structure of zein−SDS (C_{12}) complexes.[20] The hydrodynamic size of the obtained zein−SS particle was 360 ± 21 nm with a PDI of 0.27 ± 0.02, slightly larger than that of zein colloidal particles prepared through antisolvent procedures (with diameters of 200 ± 20 nm and PDI of 0.18, respectively),[17,26] probably due to the structural difference between the two kinds of zein particles. The colloidal behavior of zein−SS particles is likely caused by an increase in anisotropy accompanying partial unfolding of zein proteins, which could be attributed to their large hydrodynamic size and polydispersity.

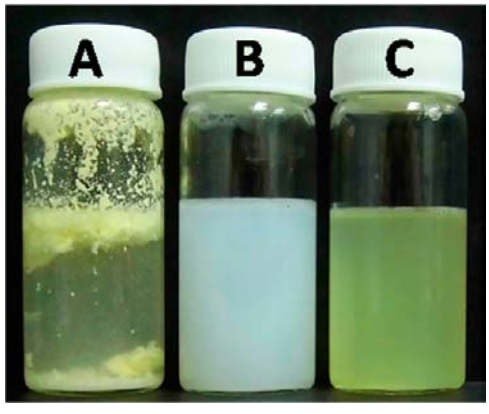

Figure 1. Dispersions of 0.5 wt % zein (A), 10 mM SS (B), and the complex of 0.5 wt % zein and SS (10 mM) (C) in water after ultrasonication.

Interface Adsorption of Zein Particles. The surface hydrophobicity and wettability of silica colloidal particle can be modified through adsorption of low molecular weight charged surfactants.[6,7] Unlike the solid silica particle, the binding of charged surfactant to protein developed from specific electrostatic interactions to nonspecific hydrophobic binding with increasing surfactant concentration, inevitably resulting in the protein unfolding. Using GTT combined with SEM, we inspected the morphology of the adsorbed zein particles monolayer at the oil−water interface (Figure 3), which revealed an enhanced adsorption and accumulation of zein colloidal particles at the interface with increasing SS concentration. In contrast to the zein dispersion in the absence of surfactant SS, an enhanced accumulation of zein particles adsorbed at the oil−water interface was observed for zein modified with 2.5 mM SS that was below the CCC (Figure 3B). The zein particles on the surface of PDMS obtained by GTT for the oil−water interface exhibited intact and isolated microspheres with uniform diameter of 200 nm (determined from the SEM images), very similar to the zein colloidal particles prepared through antisolvent procedures.[17,26] In the case of the zein modified with 10 mM SS (above the CCC), deformable particles and a densely packed layer with significant high surface overlapping at the oil−water interface were observed (Figure 3C), which might be attributed to the partially unfolded zein particles due to the nonspecific hydrophobic interaction with SS that has a concentration above the CCC. It could be concluded that the hydrophobic microdomain of partially unfolded zein molecule triggered the aggregation and the close packing of zein particles with significant high surface coverage at the oil−water interface.

The hydrophobic modification of zein particles by surfactant affects their interfacial wetting properties. We further investigated the wetting properties of zein particles by measuring the water wetting angle on macroscopic solid zein

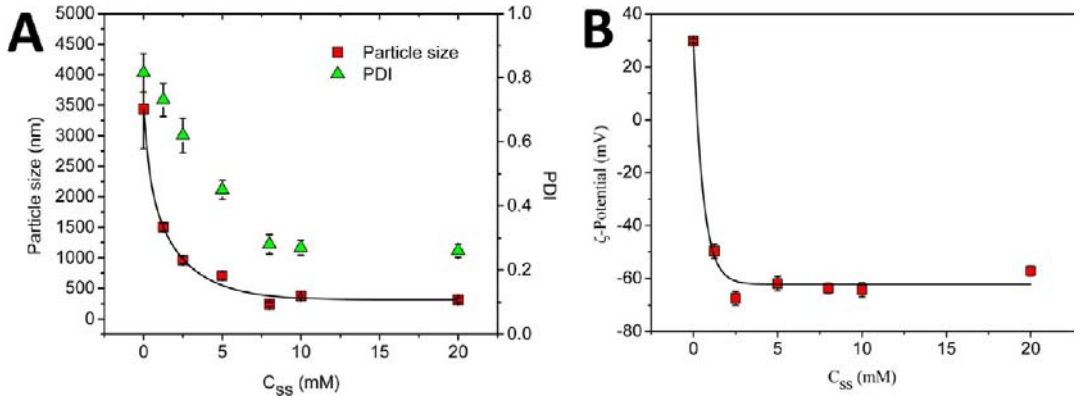

Figure 2. Changes of the particle size (A) and ζ-potential (B) of zein as a function of SS concentration.

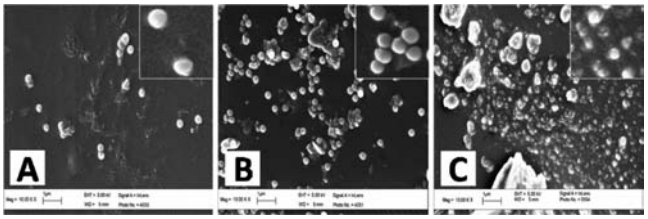

Figure 3. Morphology of the zein adsorbed on oil–water interface obtained by the method of gel trapping technology (GTT) combined with SEM: (A) pure zein; (B) zein with 2.5 mM SS; (C) zein with 10 mM SS. Scale bar = 1 μm.

films (Figure S1, Support Information), which indicated that the wetting angle of water droplets attached to the oil film was about 82°, much higher than that of zein films (60°), suggesting that the bare zein colloidal particles were more hydrophilic and not available to serve as suitable material for interfacial adsorption. de Folter et al.[15] have determined directly the oil-in water three-phase contact angle (θ_{ow}) of bare zein at low pH (pH 4.0) and confirmed the wetting properties of zein strongly favor interfacial particle adsorption with θ_{ow} close to 90°. In this work we estimated roughly the three-phase contact angle of the zein particles that was modified by surfactant SS at the oil–water interface according to GTT described by Paunov.[23] In this method the captured interfacial particle monolayer embedded within the PDMS elastomer surface could be imaged by SEM, and the position of the particles with respect to the PDMS surface has been determined from the SEM images, which gave information on the particle contact angle at the oil–water interface. In the case of bare zein and the zein particles coated by 2.5 mM SS (below CCC) (Figure 3A,B), the spherical zein particles with the average diameter of 200 nm were immersed in the PDMS (representing oil phase) above their equatorial line, protruded into water phase, and actually showed a three-phase contact angle of <90°. For the zein particles modified with 10 mM SS (above the CCC) (Figure 3C), deformed zein particles were immersed in the PDMS below their equatorial line, protruded into oil phase, and exhibited a three-phase contact angle of >90°; therefore, it could facilitate efficient packing of particles and then form a steric barrier at the interface.

We also measured the surface protein loading of the oil droplets as a function of SS concentration (Figure 4A), suggesting a nearly linear enhancement of surface zein loading with increasing SS concentration from 2.5 to 5.0 mM and then reached 9.04 ± 0.43 mg/m^2 at 10 mM. The composition and content of the adsorbed protein at the oil droplet surface was also analyzed by SDS-PAGE (Figure 4B), which revealed a gradually denser band of α-zein (22 and 24 kDa) by increasing SS concentration, further confirming enhancement of interfacial protein loading with increase of surfactant concentration. Thus, it is reasonable to speculate that the formation of zein particles–SS complexes not only improved the diffusive mobility of water-insoluble zein particles but also endowed the particles with equilibrium interfacial wetting properties,

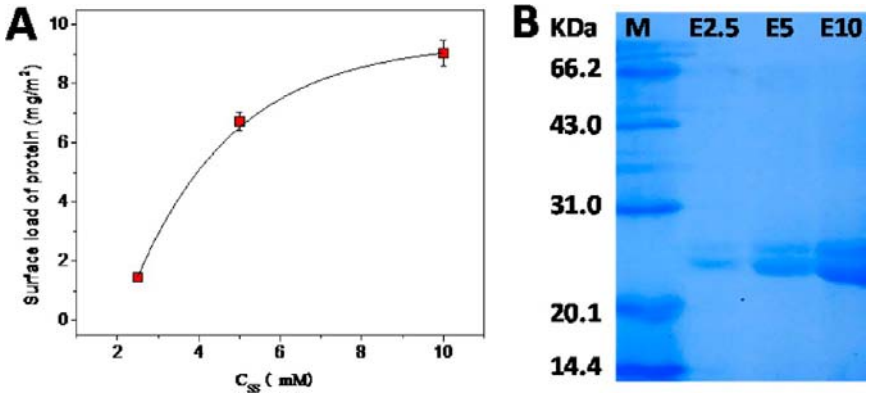

Figure 4. Surface loading (A) and interfacial composition (B) of emulsions stabilized by 0.5 wt % zein and various concentrations of SS. Lanes: M, marker; E2.5, emulsions stabilized with 0.5 wt % zein and 2.5 mM SS; E5, emulsions stabilized with 0.5 wt % zein and 5 mM SS; E10, emulsions stabilized with 0.5 wt % zein and 10 mM SS.

dx.doi.org/10.1021/jf500005y | J. Agric. Food Chem. 2014, 62, 2672–2678

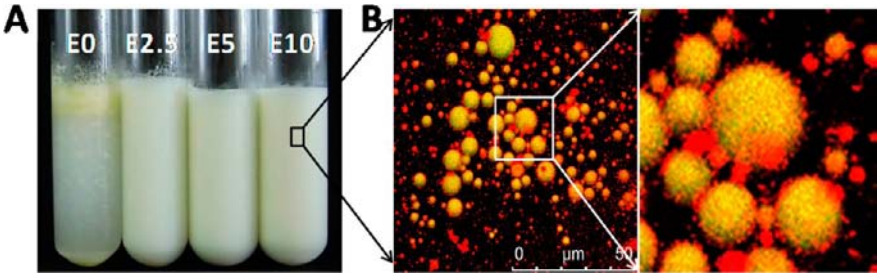

Figure 5. Emulsions appearance (A) and its CLSM (B) stabilized by 0.5 wt % zein and zein-SS: (A, left to right) 0.5 wt % zein (E0), 0.5 wt % zein and 2.5 mM SS (E2.5), 0.5 wt % zein and 5 mM SS (E5), 0.5 wt % zein and 10 mM SS (E10); (B) emulsions stained with 0.1 wt % Nile Blue and 0.01 wt % Nile Red, scale bar = 50 μm.

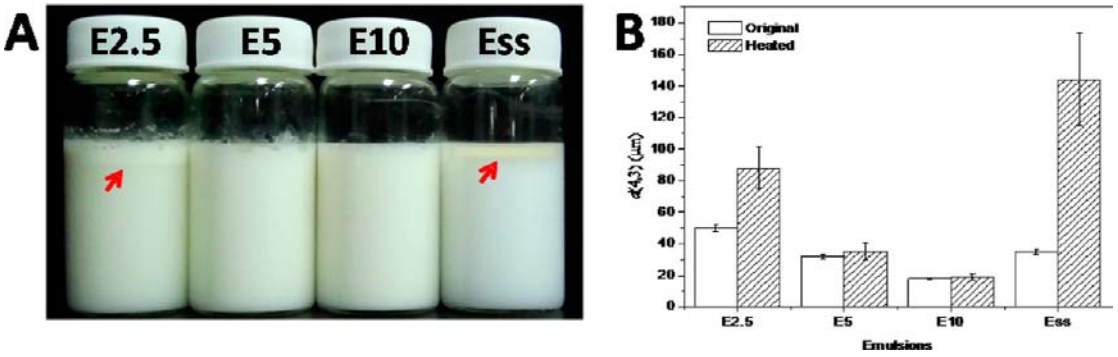

Figure 6. Appearance (A) and average droplet size (B) of emulsions after heating−salting treatment (90 °C/30 min, 200 mM NaCl): E2.5, emulsions stabilized with 0.5 wt % zein and 2.5 mM SS; E5, emulsions stabilized with 0.5 wt % zein and 5 mM SS; E10, emulsions stabilized with 0.5 wt % zein and 10 mM SS; Ess, emulsions stabilized with 10 mM SS.

evidently enhanced the surface particle coverage and steric barrier of densely packed layer at the interface, and produced Pickering emulsions with excellent stability against coalescence.

Formation of Zein-Based Pickering Emulsion. de Folter et al.[15] prepared micrometer-sized Pickering emulsions stabilized by zein colloidal particles and studied the effect of particle concentration, pH, and ionic strength on emulsion stability, indicating that under conditions where the particle volume fraction was low (<0.2 wt %) or at low pH, the resulting emulsions were not stable against coalescence. Unfortunately they did not characterize in detail the microstructure of the oil droplets to confirm the formation of Pickering emulsions. In this study we prepared O/W emulsions (Φ = 0.1) stabilized by a mixture of 0.5 wt % zein colloidal particles and surfactant SS at 0, 2.5, 5.0, and 10 mM (Figure 5A). To confirm the formation of Pickering emulsions, we characterized the microstructure of the oil droplets of the obtained emulsions by CLSM (Figure 5B), highlighting the presence of zein particles (labeled in red) adsorbed and covering almost all of the surface of the oil droplet (labeled in green). To our best knowledge, this is the first evident demonstration of the formation of protein zein particle-stabilized Pickering emulsion. In addition, CLSM also showed polydispersed zein aggregates dispersed in the continuous phase, which were further confirmed by droplet size distributions analysis. Unlike Pickering emulsion stabilized solely by particles that possessed long-term stability against coalescence but exhibited severe creaming and macroscopic phase separation,[11−13,15] the emulsion we prepared by zein particle−SS complexes exhibited no creaming and macroscopic phase separation. Binks and co-workers[6] found that synergistic stabilization of O/W Pickering emulsions occurred when positively charged silica nanoparticles were mixed with the anionic surfactant (SDS) in water, and this kind of Pickering emulsion was stable to both creaming and coalescence.

Emulsion Stability and Formation of Oil Gel. Conventionally, a particle-stabilized emulsion typically contains rather coarse droplets (~10 μm diameter or larger). The mean droplet diameter ($d_{4,3}$) of the modified zein particle stabilized emulsions we prepared was about 20−50 μm, depending on the concentration of SS (Figure S2, Supporting Information). A gradual decrease of $d_{4,3}$ and polydispersity of zein particle-stabilized emulsion upon increasing SS concentration was observed (Figure S2; Figure 6B), until a monodisperse Pickering emulsion with narrow size distribution was formed at 10 mM SS. Emulsion microstructure evaluated with an optical microscope revealed dispersed oil droplets covered with adsorbed Pickering-type particles in sample E5, which contained 5 mM SS. Interestingly, the freshly prepared emulsion prepared with 10 mM SS was characterized by unusual microstructure and high oil droplet sizes in the range of 30−40 μm, much like the fat crystals stabilized Pickering emulsion through interfacial crystallization.[14] In the same way, we have monitored the physical stability of emulsion stabilized by zein particles−SS complexes. The heating−salting stability test of emulsions, which were assayed by heating at 90 °C for 30 min in the presence of 200 mM NaCl, was assessed by creaming, mean droplet diameter ($d_{4,3}$), and microstructure with optical microscope observations, given in Figures 6 and 7. After heating−salting treatment, the emulsion stabilized by zein particles with 2.5 mM SS (E2.5, below the CCC) was slightly creamed with an increase of $d_{4,3}$ from 50.1 to 88.3 μm. For emulsions stabilized by zein particles with 5 mM SS (E5, CCC) and 10 mM SS (E10, above the CCC), there was slight flocculation but no coalescence or change of droplet size ($d_{4,3}$) (Figures 6 and 7). In contrast, the emulsion stabilized only by

dx.doi.org/10.1021/jf500005y | J. Agric. Food Chem. 2014, 62, 2672−2678

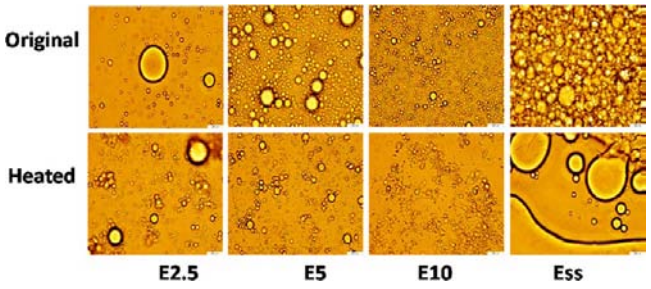

Figure 7. Optical microscope images of emulsions before and after heating–salting treatment (90 °C/30 min, 200 mM NaCl): E2.5, emulsions stabilized with 0.5 wt % zein and 2.5 mM SS; E5, emulsions stabilized with 0.5 wt % zein and 5 mM SS; E10, emulsions stabilized with 0.5 wt % zein and 10 mM SS; Ess, emulsions stabilized with 10 mM SS. Scale bar = 200 μm.

10 mM surfactant SS (Ess) was severely creamed with oil droplet collapse. Thus, it can be concluded that a synergistic improvement in coalescence stability of Pickering emulsion could be derived from a complex of zein particles and charged surfactant SS.

Pickering stabilization is known to require the presence of complete monolayer coverage of closely packed particles against coalescence.[4] The instability of E2.5 emulsion might derive from its low interface protein loading of the droplets (Figure 4) and the limited surface coverage at the oil–water interface (Figure 3B). Correspondingly, the stability of E5 and E10 emulsions against heating–salting induced creaming and coalescence, mainly due to the high interface protein loading and densely packed monolayer created by accumulated and aggregated protein particles at the interface (Figure 3C). To further evaluate the stability of the emulsions, they were freeze-dried to prepare oil gels. Generally, a weak interface of the emulsion droplet stabilized by surfactant and biopolymer could not prevent the severe coalescence between droplets during dehydration processing of freeze-drying, leading to the collapse of the emulsion and oil leakage. Now we found the zein particle stabilized O/W emulsions provided suitable templates for freeze-drying processes to produce oil gels. The appearances of the materials resulting from freeze-drying of the emulsions for surfactant-modified zein particle (E2.5, E5, and E10) and surfactant SS (Ess) stabilized system are shown in Figure 8. For E2.5 and E5 emulsions with SS concentrations between 2.5 and 5 mM, sol-like solids were formed, which had slight oil leakage, confirming the low interfacial loading and insufficient surface particles coverage. For E10 emulsions (containing 10 mM SS), however, a homogeneous and translucent gel without oil leakage was formed, meaning that the oil content entrapped in this matrix was >92% wt %. By contrast, the emulsion stabilized by 10 mM SS yielded a turbid flowing liquid, indicating that freeze-drying failed to produce an encapsulated oil gel only by surfactant SS. The strategy of structuring liquid oils into solid-like oil gels by simply freeze-drying the Pickering emulsion precursor would be meaningful, because until today the most widely used methods used to create fat-structured foods, such as chocolate, ice cream, spreads, and shortening, are given by an underlying colloidal network of polycrystalline fat crystals, which are composed of high-melting saturated or *trans* fatty acids.[27] As we know, excessive consumption of *trans* and saturated fats has been shown to have deleterious health effects including negative effects on lipoprotein profiles and increases in the incidence of heart disease and metabolic syndrome.[28]

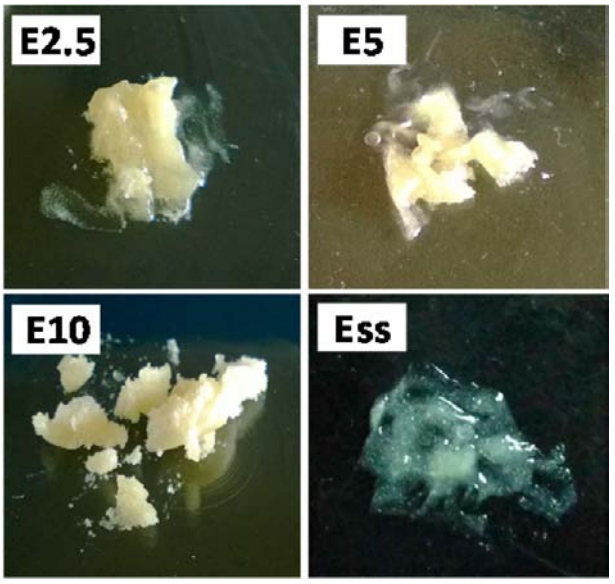

Figure 8. Visual aspect of the freeze-dried emulsions stabilized by zein–SS and sole SS: E2.5, emulsions stabilized with 0.5 wt % zein and 2.5 mM SS; E5, emulsions stabilized with 0.5 wt % zein and 5 mM SS; E10, emulsions stabilized with 0.5 wt % zein and 10 mM SS; Ess, emulsions stabilized with 10 mM SS.

General Discussion. The main challenges to the production of edible Pickering emulsions are the low interfacial adsorption and limited surface coverage due to the aggregation and low diffusive mobility of the food grade colloidal particles.[29] In this study we employed a novel strategy by taking advantage of the properties of the complexes between zein particles and small molecular weight surfactant SS to overcome simultaneously the multiple challenges exhibited by solely colloidal particles, fabricated protein-based Pickering emulsion, and oil gels with superior stability against both coalescence and creaming. For better understanding of the stabilization mechanism of zein particle–SS complexes, we provide a schematic illustrations in Figure 9.

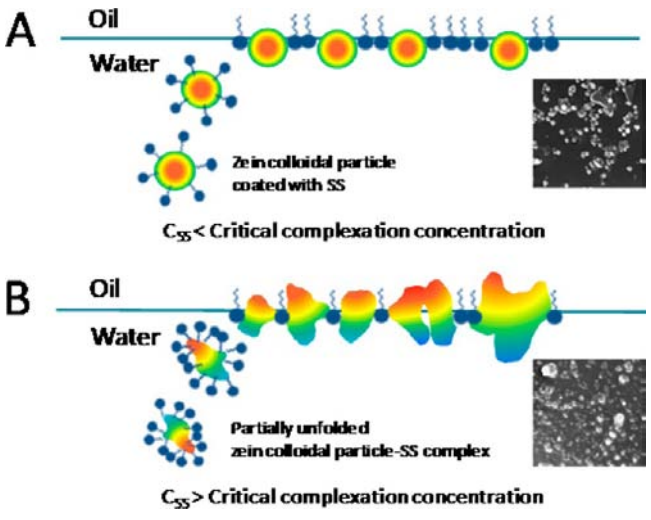

Figure 9. Schematic diagrams showing enhanced adsorption and targeted accumulation of zein particles at the interface with the synergism of SS.

dx.doi.org/10.1021/jf500005y | J. Agric. Food Chem. 2014, 62, 2672–2678

The modification of zein particles through adsorption of ionic surfactant SS affected their interfacial wetting properties. At SS concentration below the CCC (about 2.5 mM) (Figure 9A), the intact and inherently hydrophilic zein colloidal particles migrated to the oil−water interface, resulting in an unsaturated particle monolayer at the interface owing to the inefficient accumulation of particles (low surface protein loading) and weak adsorption on the interface ($\theta_{ow} < 90°$), and thus failed to provide a packed steric barrier of oil droplets against emulsion coalescence and creaming. However, at SS concentration above the CCC (about 10 mM) (Figure 9B), zein particles−SS complexes formed mainly due to nonspecific hydrophobic interaction, resulting in the partial unfolding of zein particles and the exposure of hydrophobic microdomains, not only improved the diffusive mobility of water-insoluble zein particles but also endowed the particles with equilibrium interfacial wetting properties and thus evidently enhanced the surface particle coverage and facilitated efficient packing of zein colloidal particles at the oil−water interface, producing Pickering emulsions with superior stability against both coalescence and creaming.

■ ASSOCIATED CONTENT

Supporting Information

Figures S1 and S2. This material is available free of charge via the Internet at http://pubs.acs.org.

■ AUTHOR INFORMATION

Corresponding Author

*(X.-Q.Y.) Phone: (086) 20-87114262. Fax: (086) 20-87114263. E-mail: fexqyang@scut.edu.cn, fexqyang@163.com.

Funding

This research was supported by the Chinese National Natural Science Foundation (No. 31371744 and 31301432) and the Ph. D. Programs Foundation of Ministry of Education of China (No. 20100172110021).

Notes

The authors declare no competing financial interest.

■ REFERENCES

(1) Dickinson, E. Use of nanoparticles and microparticles in the formation and stabilization of food emulsions. *Trends Food Sci. Technol.* **2012**, *24*, 4−12.

(2) Jin, H.; Zhou, W. Z.; Cao, J.; Stoyanov, S. D.; Blijdenstein, T. B. J.; de Groot, P. W. N.; Arnaudov, L. N.; Pelan, E. G. Super stable foams stabilized by colloidal ethyl cellulose particles. *Soft Matter* **2012**, *8*, 2194−2205.

(3) Adelmann, H.; Binks, B. P.; Mezzenga, R. Oil powders and gels from particle-stabilized emulsions. *Langmuir* **2012**, *28*, 1694−1697.

(4) Aveyard, R.; Binks, B. P.; Clint, J. H. Emulsions stabilized solely by colloidal particles. *Adv. Colloid Interface Sci.* **2003**, *102*, 503−546.

(5) Binks, B. P. Particles as surfactants similarities and differences. *Curr. Opin. Colloid Interface Sci.* **2002**, *7*, 21−41.

(6) Binks, B. P.; Rodrigues, J. A.; Frith, W. J. Synergistic interaction in emulsions stabilized by a mixture of silica nanoparticles and cationic surfactant. *Langmuir* **2007**, *23*, 3626−3636.

(7) Binks, B. P.; Rodrigues, J. A. Enhanced stabilization of emulsions due to surfactant induced nanoparticle flocculation. *Langmuir* **2007**, *23*, 7436−7439.

(8) Eskandar, N. G.; Simovic, S.; Prestidge, C. A. Synergistic effect of silica nanoparticles and charged surfactants in the formation and stability of submicron oil-in-water emulsions. *Phys. Chem. Chem. Phys.* **2007**, *9*, 6426−6434.

(9) Reger, M.; Sekine, T.; Okamoto, T.; Watanabe, K.; Hoffmanna, H. Pickering emulsions stabilized by novel clay-hydrophobin synergism. *Soft Matter* **2011**, *7*, 11021−11030.

(10) Sadeghpour, A.; Pirolt, F.; Glatter, O. Submicrometer-sized Pickering emulsions stabilized by silica nanoparticles with adsorbed oleic acid. *Langmuir* **2013**, *29*, 6004−6012.

(11) Yusoff, A.; Murray, B. S. Modified starch granules as particle stabilizers of oil-in-water emulsions. *Food Hydrocolloids* **2011**, *25*, 42−55.

(12) Tzoumaki, M. V.; Moschakis, T.; Kiosseoglou, V.; Biliaderis, C. G. Oil-in-water emulsions stabilized by chitin nanocrystal particles. *Food Hydrocolloids* **2011**, *25*, 1521−1529.

(13) Luo, Z.; Murray, B. S.; Ross, A. L.; Povey, M. J. W.; Morgan, M. R. A.; Day, A. J. Effects of pH on the ability of flavonoids to act as Pickering emulsion stabilizers. *Colloids Surf. B: Biointerfaces* **2012**, *92*, 84−90.

(14) Rousseau, D. Trends in structuring edible emulsions with Pickering fat crystals. *Curr. Opin. Colloid Interface Sci.* **2013**, *18*, 283−291.

(15) de Folter, J. W. J.; Van Ruijvena, M. W. M.; Velikov, K. P. Oil-in-water Pickering emulsions stabilized by colloidal particles from the water-insoluble protein zein. *Soft Matter* **2012**, *8*, 6807−6815.

(16) Dickinson, E. Food emulsions and foams: stabilization by particles. *Curr. Opin. Colloid Interface Sci.* **2010**, *15*, 40−49.

(17) Wang, L. J.; Yin, Y. C.; Yin, S. W.; Yang, X. Q.; Shi, W. J.; Tang, C. H.; Wang, J. M. Development of novel zein-sodium caseinate nanoparticle (ZP)-stabilized emulsion films for improved water barrier properties via emulsion/solvent evaporation. *J. Agric. Food Chem.* **2013**, *61*, 11089−11097.

(18) Gao, Z. M.; Wang, J. M.; Wu, N. N.; Wan, Z. L.; Guo, J.; Yang, X. Q.; Yin, S. W. Formation of complex interface and stability of oil-in-water (O/W) emulsion prepared by soy lipophilic protein nanoparticles. *J. Agric. Food Chem.* **2013**, *61*, 7838−7847.

(19) Shukl, R.; Cheryan, M. Zein: the industrial protein from corn. *Ind. Crops Prod* **2001**, *13*, 171−192.

(20) Deo, N.; Jockusch, S.; Turro, N. J.; Somasundaran, P. Surfactant interactions with zein protein. *Langmuir* **2003**, *19*, 5083−5088.

(21) Ruso, J. M.; Deo, N.; Somasundaran, P. Complexation between dodecyl sulfate surfactant and zein protein in solution. *Langmuir* **2004**, *20*, 8988−8991.

(22) Koppel, D. E. J. Analysis of macromolecular polydispersity in intensity correlation spectroscopy: the method of cumulants. *J. Chem. Phys.* **1972**, *57*, 4814.

(23) Paunov, V. N. Novel method for determining the three-phase contact angle of colloid particles adsorbed at air-water and oil-water interfaces. *Langmuir* **2003**, *19*, 7970−7976.

(24) Akhtar, M.; Dickinson, E.; Mazoyer, J.; Langendorff, V. Emulsion stabilizing properties of depolymerised pectin. *Food Hydrocolloids* **2002**, *16*, 249−256.

(25) Sparnaay, M. J. The electrical double layer. *The International Encyclopedia of Physical Chemistry and Chemical Physics, Topic 14: Properties of Interfaces*; Pergamon Press: Oxford, UK, 1972.

(26) Li, K. K.; Yin, S. W.; Yang, X. Q.; Tang, C. H.; Wei, Z. H. Fabrication and characterization of novel antimicrobial films derived from thymol-loaded zein-sodium caseinate (SC) nanoparticles. *J. Agric. Food Chem.* **2012**, *60*, 11592−11600.

(27) Rogers, M. A.; Wright, A. J.; Marangoni, A. G. Oil organogels: the fat of the future? *Soft Matter* **2009**, *5*, 1594−1596.

(28) Aro, A.; Jaughiainen, M.; Partanen, R.; Salminen, I.; Mutanen, M. Stearic acid, *trans* fatty acids, and dairy fat: effects on serum and lipoprotein lipids, apolipoproteins, lipoprotein (a), and lipid transfer proteins in healthy subjects. *Am. J. Clin. Nutr.* **1997**, *65*, 1419−1426.

(29) Dickinson, E. Stabilising emulsion-based colloidal structures with mixed food ingredients. *J. Sci. Food Agric.* **2013**, *93*, 710−721.

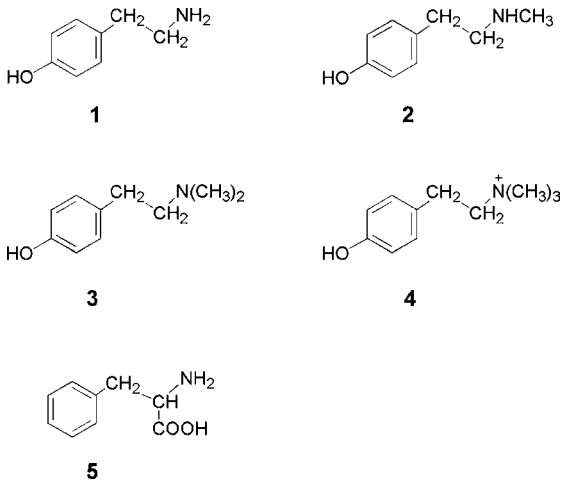

Figure 1. Chemical structures of analyzed compounds: tyramine (**1**), *N*-methyltyramine (**2**), *N,N*-dimethyltyramine (hordenine) (**3**), 2-(4-hydroxyphenyl)ethyl-trimethylazanium (candicine or *N,N,N*-trimethyltyramine) (**4**), and phenylalanine (**5**).

methyl iodide were added. The mixture was stirred at room temperature and the formation of the reaction products *N*-methyltyramine, *N,N*-dimethyltyramine, and *N,N,N*-trimethyltyramine was monitored by liquid chromatography−electrospray ionization tandem mass spectrometry (LC-ESI-MS/MS). The addition of methyl iodide (10 mL) and $KHCO_3$ (1 g) was repeated twice more. Finally, after centrifugation of the mixture, the supernatant was collected and evaporated to dryness at 40 °C in a rotary evaporator. The residue containing *N,N,N*-trimethyltyramine was dissolved in 10 mL of Milli Q-grade water and purified by flash chromatography on SepPac C18 cartridge (Phenomenex, Anzola Emilia, Italy). The sample-loaded column was washed with 100 mL of Milli Q water, and *N,N,N*-trimethyltyramine was eluted from the column by applying 50 mL of a solution of H_2O/acetonitrile (80:20). The eluted product was evaporated to dryness under a stream of air and dried overnight in vacuum over P_2O_5. The yield was 88%.

Preparation of Citrus Leaf Extracts. Citrus leaf samples were obtained from the Research Centre for Citrus Crops and the Mediterranean (CRA-ACM), Arboretum of Reggio Calabria (Italy). Four lots of 100 g were taken from different branches from each citrus plant species. Leaves, in the late development stage, were harvested in January and February. The leaves were washed with distilled water and dried with filter paper. Then 50 g of product, finely chopped, was homogenized in a blender with 100 mL of 0.2% formic acid in Milli Q-grade water and the mixture was stirred for 1 h. In these conditions the extraction yield was higher than 96% for all the analyzed compounds. Finally, the homogenate was centrifuged at 18000*g* for 30 min and the supernatant was stored in 20 mL vials at −20 °C. Citrus varieties included in this study were mandarin, sweet orange, bitter orange, chinotto (*Citrus myrtifolia*), pomelo, citron, grapefruit, bergamot, and clementine.

Preparation of Standards. Standard stock solutions of tyramine, *N*-methyltyramine, *N,N*-dimethyltyramine, and *N,N,N*-trimethyltyramine were prepared at concentration of 2 mg/L and stored at 4 °C. Prior to injection, stock solutions were appropriately diluted with water containing 0.1% formic acid before being used as working solutions. Quantitation was achieved by comparison with calibration curves obtained with the standard solutions. Additional calibration levels (2, 1, 0.5, 0.1, and 0.05 mg/L) were prepared by serial dilution with water containing 0.1% formic acid. The calibration curve was built by use of these standard solutions. The response of the MS/MS detection followed a linear calibration curve between 0.05 and 2 mg/L with a correlation coefficient of 0.99. Detection limits, determined as the compound concentration that gave a peak height 3 times that of background noise, were 0.021 mg/L for tyramine, 0.016 mg/L for *N*-methyltyramine, 0.020 mg/L for *N,N*-dimethyltyramine, and 0.009 mg/L for *N,N,N*-trimethyltyramine.

Flow Injection Analysis and HPLC-ESI-MS/MS Measurements. HPLC-ESI-MS analyses were performed with an HPLC Agilent 1100 series coupled online with an Agilent LC-MSD SL quadrupole ion trap. MS acquisition was performed by using electrospray inonization (ESI) in positive-ion mode. Nitrogen was used at a flow rate of 7 L/min and a pressure of 30 psi as both a drying and a nebulizing gas. The nebulizer temperature was set at 350 °C. The ion charge control (ICC) was applied with a target set at 30 000 and maximum accumulation time at 20 ms. Measurements were performed from the peak area of the extracted ion chromatogram (EIC). Quantitation was achieved by comparison with calibration curves obtained with standard solutions. Optimization of instrumental parameters for analyses of tyramine and its methylated derivatives was performed by continuous infusion [flow injection analysis (FIA)-ESI-MS/MS measurements] of 5 μM standard solution in 0.1% formic acid. Mass cutoff and amplitude were optimized to obtain the most efficient MS/MS transitions from the positively charged precursor ion $[M + H^+]$ to the fragment ions. Multiple reaction monitoring (MRM) was used for quantitation of analytes. The transitions utilized for MS/MS quantitation were 138.1 → 121 for tyramine, 152.1 → 121 for *N*-methyltyramine, 166.1 → 121 for *N,N*-dimethyltyramine, 180.1 → 121 for *N,N,N*-trimethyltyramine, and 166.1 → 120 for phenylalanine. LC-ESI-MS/MS analyses were performed with a 150 mm × 3.0 mm i.d., 5 μm Discovery-C8 analytical column (Supelco). The mobile phase was composed of 0.1% formic acid in water and pumped at 0.1 mL/min under isocratic conditions at room temperature. Volumes of 10−20 μL of standard solutions or samples were injected.

Statistical Analysis. Data are expressed as mean ± std of $n = 4$ determinations, each in duplicate. Differences were assessed by *t*-test, and a p value less than 0.05 was considered to be significant.

RESULTS AND DISCUSSION

Identification of *N,N,N*-Trimethyltyramine in *Citrus* Genus Plants. Recently, we reported the occurrence of secondary metabolites derived from tryptamine in *Citrus* genus plants.[28] Specifically, we described the presence of *N*-methyltryptamine and *N,N*-dimethyltryptamine in all parts of the fruit (peel and edible part) with higher levels in leaves and seeds. Interestingly, we also revealed the occurrence of *N,N,N*-trimethyltryptamine, a metabolite never described before in plants.[28] Subsequently, in several *Citrus* genus plants, we quantitated 5-hydroxytryptamine (serotonin) and its N-methylated forms such as 5-hydroxy-*N*-methyltryptamine, 5-hydroxy-*N,N*-dimethyltryptamine (bufotenine), and 5-hydroxy-*N,N,N*-trimethyltryptamine. In particular, we reported the occurrence of 5-hydroxy-*N,N,N*-trimethyltryptamine, also named bufotenidine or cinobufotenine.[29] It is worth noting that the occurrence of tyramine, *N*-methyltyramine, and *N,N*-dimethyltyramine in *Citrus* genus plants has been known for a long time, whereas the occurrence of *N,N,N*-trimethyltyramine has never been reported so far. Therefore, we sought to verify the occurrence of *N,N,N*-trimethyltyramine in the most common and economically important plants of the *Citrus* genus. Moreover, we also aimed to quantitatively compare, among them, the distribution of tyramine and its N-methylated derivatives. The analysis, performed on a lemon leaf extract and conducted with the same HPLC-ESI-MS/MS methodology previously described,[30,31] showed complete chromatographic separation of all examined metabolites in less than 30 min (Figure 2A). In particular, tyramine eluted at a retention time (T_R) of 12.7 min, followed by *N*-methyltyramine at T_R 15.5 min and *N,N*-dimethyltyramine (hordenine) at T_R 19.5 min. Interestingly, an unknown peak emerged at T_R 23.8 min. Moreover, this peak occurred at m/z 180 and showed a very

dx.doi.org/10.1021/jf5001698 | J. Agric. Food Chem. 2014, 62, 2679−2684

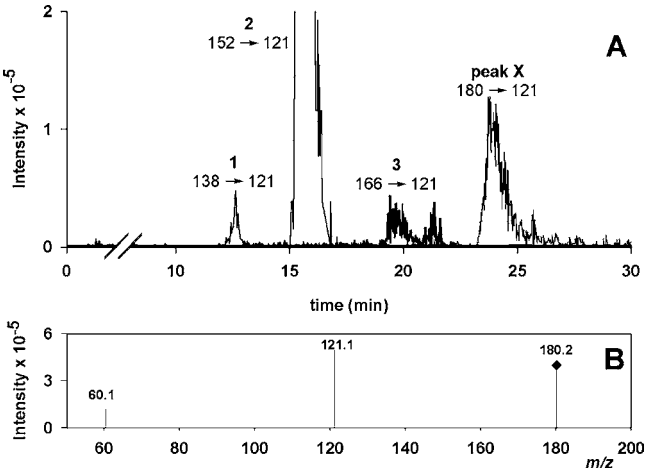

Figure 2. (A) LC-ESI-MS/MS chromatogram of lemon leaf extract. (B) MS^2 fragmentation pattern of the unknown peak (peak X) at retention time of 24 min.

simple MS/MS fragmentation pattern (Figure 2B) with only two fragments at *m/z* 60 and 121, which strongly suggested the possibility that the it might be *N,N,N*-trimethyltyramine.

Synthesis and ESI-MS^n Characterization of *N,N,N*-Trimethyltyramine. With the aim to confirm the presence of *N,N,N*-trimethyltyramine in *Citrus* genus plants, we synthesized the substance according to the method of Chen and Benoiton,[26,27] as it was not commercially available. Under the reaction conditions adopted, the methylation process of tyramine, which was used as starting substrate for the synthesis, was essentially complete in about 6 h at room temperature. Formation of *N,N,N*-trimethyltyramine and the less methylated derivatives (*N*-methyltyramine and *N,N*-dimethyltyramine) was monitored by withdrawing 50 μL of reaction mixture at preset times of 2, 6, 12, and 24 h. Each aliquot was then diluted to a final volume of 1 mL with 0.1% formic acid. Then 20 μL portions of the diluted samples were analyzed by LC-ESI-MS/MS. After 2 h, the reaction mixture contained tyramine and noticeable amounts of *N*-methyltyramine and *N,N*-dimethyltyramine compared to *N,N,N*-trimethyltyramine (Figure 3A). High levels of the desired compound were found in the reaction mixture in 6 h (Figure 3B). Conversely, other N-methylated tyramine derivatives occurred at lower levels. The synthesis was complete in 12 h of reaction, as demonstrated by the presence in the reaction mixture of only *N,N,N*-trimethyltyramine and the disappearance of other components (Figure 3C).

In order to find the optimal instrumental conditions for detection and quantitation, the synthesized *N,N,N*-trimethyltyramine was purified and subjected to mass spectrometric analysis. In particular, amplitude and cutoff, the main parameters for an ion-trap mass spectrometer to achieve the most effective collision-induced dissociation (CID) of the parent ion toward its ion fragments, were optimized. This study was performed in positive-ion mode by direct infusion of 5 μM *N,N,N*-trimethyltyramine solution in 0.1% formic acid. *N,N,N*-Trimethyltyramine showed the highest retention time relative to the less methylated tyramine derivatives and eluted at about 24 min (Figure 4A). It is interesting to note that the MS^2 fragmentation pattern of the synthesized *N,N,N*-trimethyltyramine is essentially constituted by only two ions (Figure 4B). The one at *m/z* 60 corresponds to trimethylammonium ion,

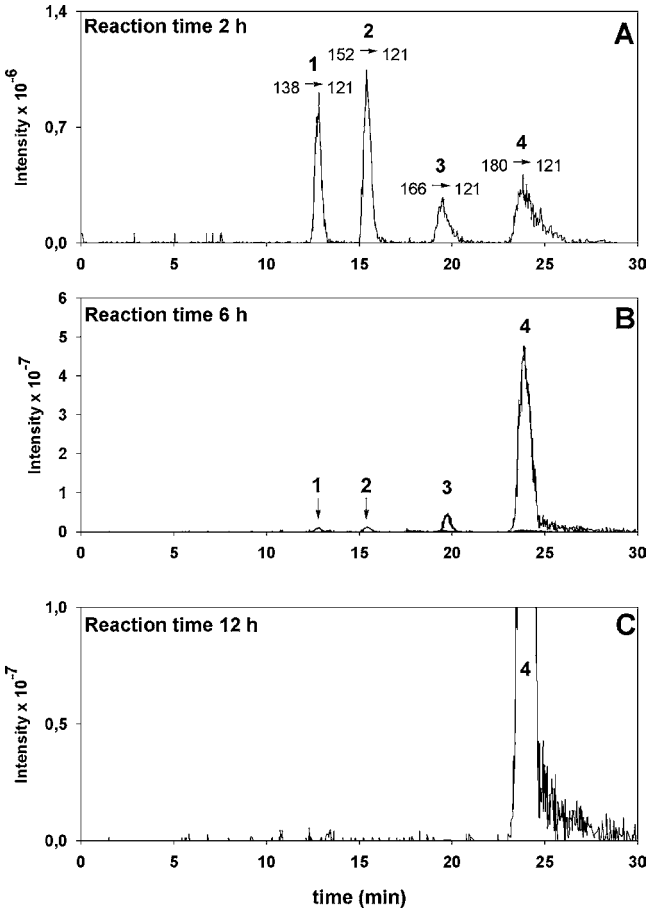

Figure 3. Time course of tyramine methylation performed according to the method of Chen and Benoiton:[26,27] products of tyramine methylation after (A) 2 h, (B) 6 h, and (C) 12 h of reaction. The MS^2 transitions used to monitor tyramine (**1**), *N*-methyltyramine (**2**), *N,N*-dimethyltyramine (**3**), and *N,N,N*-trimethyltyramine (**4**) are also reported.

which is peculiar for most betaines,[30,32] and the other, at *m/z* 121, is formed as a consequence of neutral loss of the trimethylamine moiety[33] from the parent ion. An intense fragment at *m/z* 121 is present also in the MS^2 spectra of tyramine, *N*-methyltyramine, and *N,N*-dimethyltyramine. This fragment was observed for the first time by Cram and Thompson[33] in the solvolysis of 2-arylethyl derivatives and is supposed to have the very stable bicyclo structure shown in the inset of Figure 4B. The fragment is produced from tyramine by neutral loss of ammonia, whereas *N*-methyltyramine and *N,N*-dimethyltyramine produce it by neutral loss of methylamine and dimethylamine, respectively. The MS^3 fragmentation pattern was obtained by isolating the MS^2 fragment at *m/z* 121 of the synthesized *N,N,N*-trimethyltyramine (Figure 4C). The MS^3 fragment at *m/z* 93 likely originated from C_2H_4 neutral loss from the *m/z* 121 parent ion.[33] The identity of the fragment at *m/z* 121 in the MS^2 fragmentation pattern of the synthesized *N,N,N*-trimethyltyramine was further supported by the observation that its MS^3 fragmentation pattern was the same as those of the MS^2 fragments, isolated at *m/z* 121, generated by tyramine, *N*-methyltyramine, and *N,N*-dimethyltyramine.

It is important, from an analytical point of view, to highlight that the stability of the *N*-methylated derivatives of tyramine toward in-source CID is strongly dependent on the degree of

dx.doi.org/10.1021/jf5001698 | J. Agric. Food Chem. 2014, 62, 2679−2684

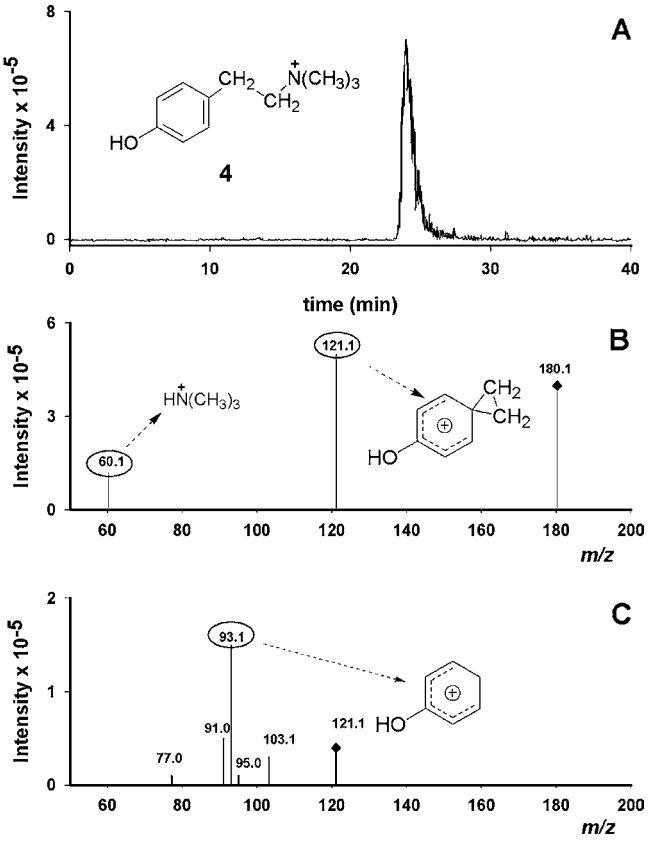

Figure 4. Mass spectrometric characterization of *N,N,N*-trimethyltyramine (**4**) standard solution. (A) Extracted-ion chromatogram at m/z 180.1 from LC-ESI-MS analysis of the synthesized *N,N,N*-trimethyltyramine (**4**) standard solution. (B) MS^2 fragmentation pattern of the peak in panel A. Arrows indicate the structure of the generated MS^2 fragments. (C) MS^3 fragmentation pattern of the peak in panel A, obtained by isolating the MS^2 fragment at m/z 121.1. Arrows indicate the structure of the MS^3 fragment at m/z 93.1, likely generated by C_2H_4 neutral loss.

methylation. In fact, we observed that about 85% of tyramine, 70% of *N*-methyltyramine, and 10% of *N,N*-dimethyltyramine was fragmented by in-source CID. Instead, no in-source fragmentation of *N,N,N*-trimethyltyramine was observed. Therefore, especially for tyramine and *N*-methyltyramine, if needed, more analytical sensitivity can be achieved by selecting the fragment at m/z 121 produced in the ion source than that at the m/z corresponding to the protonated parent molecules.

Distribution of N-Methylated Tyramine Derivatives in *Citrus* Genus Plant Leaves. Analysis of the content of tyramine and its N-methylated derivative in citrus leaf extracts was conducted by HPLC-ESI-MS/MS. From a quantitative point of view, *N,N,N*-trimethyltyramine was most abundant in the leaves of clementine (0.88 ± 0.64 mg/kg), followed by bitter orange and lemon. In contrast, substantially lower levels were found in orange, bergamot, citron, pomelo, and mandarin leaves (Table 1).

In order to unambiguously confirm the presence of *N,N,N*-trimethyltyramine in these matrices, chromatographic and mass spectrometric behaviors of the putative *N,N,N*-trimethyltyramine peak in leaf extracts were compared with those of the synthesized standard. In each case, both peaks showed the same chromatographic retention time. Moreover, under the same instrumental settings of the ion trap, the peaks showed the same fragmentation patterns and the same intensity ratios of main fragments in both MS^2 and MS^3 measurements. On the whole, these results leave no doubt that the compound eluting at about 24 min in the extracts of citrus leaves is *N,N,N*-trimethyltyramine.

Among the other analyzed metabolites, tyramine is well-represented in leaves of citrus plants. Particularly, 49.75 ± 12.16 and 21.63 ± 7.80 mg/kg tyramine were found in leaves of chinotto and clementine, respectively (Table 1), while values of 0.55 ± 0.38 and 0.41 ± 0.33 mg/kg were found in pomelo and bergamot leaves. *N*-Methyltyramine is the tyramine derivative most abundant in citrus leaves. Particularly, leaves of chinotto and clementine contained mean levels above 20 mg/kg of this metabolite, whereas leaves of bergamot, pomelo, citron, mandarin, lemon, bitter orange, and sweet orange contained amounts from a minimum of 0.45 ± 0.31 mg/kg up to a maximum of 6.91 ± 2.04 mg/kg (Table 1).

N,N-Dimethyltyramine was contained in discrete amounts only in the leaves of clementine (0.30 ± 0.19 mg/kg). In all other citrus matrices *N,N*-dimethyltyramine was at levels equal or below 0.07 ± 0.04 mg/kg (Table 1). It is important to point out that phenylalanine, an amino acid well represented in the citrus matrices,[34,35] has the same mass as *N,N*-dimethyltyramine. Fortunately, complete chromatographic separation of all examined tyramine derivatives and phenylalanine was obtained under the chromatographic conditions employed (Figure 5). In particular, phenylalanine, which in all samples examined was always present in much higher amounts than *N,N*-dimethyltyramine, was well resolved from it (Figure 6A). Therefore, phenylalanine did not interfere in the quantitation of *N,N*-dimethyltyramine in the samples examined. It is important to achieve good chromatographic resolution between these two compounds, especially when phenylalanine is much more abundant then *N,N*-dimethyltyramine, despite the fact that phenylalanine and *N,N*-dimethyltyramine seem resolvable by mass spectrometric measurements. In fact, the analytical MS^2 transition employed for *N,N*-dimethyltyramine determination was at m/z 166 → 121, while for phenylalanine it was at m/z 166 → 120. However, besides the intense peak corresponding

Table 1. Distribution of N-Methylated Tyramine Derivatives in Citrus Leaves

	content[a] (mg/kg)								
compd	citron	mandarin	pomelo	bitter orange	sweet orange	chinotto	clementine	lemon	bergamot
tyramine	1.42 ± 0.45	2.47 ± 0.47	0.55 ± 0.38	0.70 ± 0.56	5.74 ± 1.39	49.75 ± 12.16	21.63 ± 7.80	1.92 ± 1.01	0.41 ± 0.33
N- methyltyramine	0.63 ± 0.43	0.66 ± 0.52	0.58 ± 0.41	2.22 ± 0.82	6.91 ± 2.04	22.63 ± 8.62	23.25 ± 6.88	1.88 ± 0.97	0.45 ± 0.31
N,N-dimethyltyramine	0.07 ± 0.04	0.06 ± 0.04	0.03 ± 0.02	0.04 ± 0.02	0.03 ± 0.02	0.05 ± 0.03	0.30 ± 0.19	0.05 ± 0.04	0.03 ± 0.02
N,N,N-trimethyltyramine	0.01 ± 0.01	0.01 ± 0.01	0.01 ± 0.01	0.64 ± 0.50	0.01 ± 0.01	0.07 ± 0.05	0.88 ± 0.64	0.31 ± 0.19	0.01 ± 0.01

[a]Content is expressed as mean ± std of n = 4 determinations, each in duplicate.

dx.doi.org/10.1021/jf5001698 | J. Agric. Food Chem. 2014, 62, 2679−2684

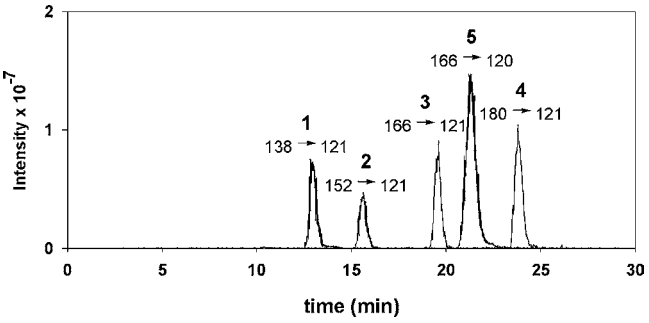

Figure 5. Chromatographic separation of standard solutions of phenylalanine and methylated tyramine derivatives by HPLC-ESI-MS/MS. For each compound, the extracted ion chromatogram (EIC) at the indicated MS^2 transition is reported. (**1**) tyramine (T_R 12.7 min); (**2**) *N*-methyltyramine (T_R 15.5 min); (**3**) *N,N*-dimethyltyramine (T_R 19.5 min); (**5**) phenylalanine (T_R 21.3 min); (**4**) *N,N,N*-trimethyltyramine (T_R 23.8 min).

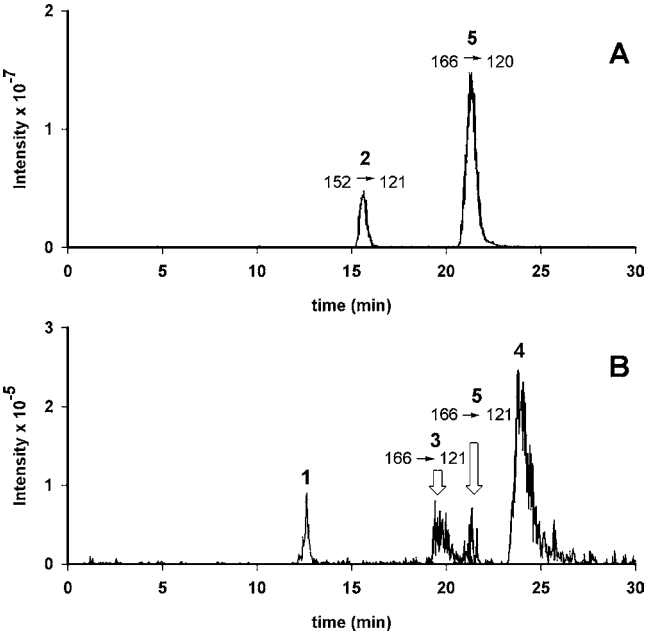

Figure 6. Representative HPLC-ESI-MS/MS chromatogram of lemon leaf extract. (A) Peaks of components present at higher levels: *N*-methyltyramine (**2**) and phenylalanine (**5**) (intensity × 10^{-7}). (B) Peaks of components present at lower levels: tyramine (**1**), *N,N*-dimethyltyramine (**3**), and *N,N,N*-trimethyltyramine (**4**) (intensity × 10^{-5}). The M + 1 peak originating from phenylalanine ^{13}C content, obtained by monitoring the MS^2 transition at 166−121, is also shown in panel B.

to the transition at *m/z* 166 → 120, phenylalanine, being much more abundant than *N,N*-dimethyltyramine in all the samples examined, also showed a peak at *m/z* 166 → 121, arising from a not-negligible ^{13}C contribution, with intensity similar to the peak at *m/z* 166 → 121 of *N,N*-dimethyltyramine. Therefore, without chromatographic resolution, the two compounds would strongly interfere (Figure 6B).

The data reported in Table 1 show that distribution of the biogenic amine tyramine and its other two methylation products, *N*-methyltyramine and *N,N*-dimethyltyramine, is somewhat uneven among the various *Citrus* species. The novelty of this work has been the identification and quantitation of *N,N,N*-trimethyltyramine in *Citrus* plant leaves. The results show that also *N,N,N*-trimethyltyramine is present at very different levels in the various plant species examined. Clementine, lemon, and bitter orange leaves contained the most significant amounts. The highest level was found in clementine leaves (0.88 mg/kg) and the lowest in citron, mandarin, pomelo, and bergamot leaves (0.01 mg/kg) ($p < 0.05$) (Table 1). From a physiological point of view, the simultaneous presence of tyramine and all other N-methylated derivatives in the leaf, a part of the plant highly specialized in biosynthesis, secretion, and accumulation of toxic substances, suggests that these substances are aimed at plant defense. It is well-known that plants under pathogenic attacks respond with the activation of defense mechanisms regulated by several phytohormones. These rapid defensive responses occur through metabolic pathways involving tryptophan, tyrosine, and phenylalanine, leading to the production and accumulation of specific metabolites aiming to prevent or alleviate the action of the pathogens.[36,37] Among the products of these enzymatic activities, an important role is played by tyramine and tryptamine, produced by the actions of tyrosine decarboxylase and tryptophan decarboxylase. These biogenic amines are precursors of many specialized defensive secondary metabolites.[38,39] In this context, the formation of *N,N,N*-trimethyltyramine may be the result of a series of reactions starting from tyrosine decarboxylation and continuing with successive methylation catalyzed by the same or a different N-methyltransferase.[29] This process is likely aimed to increase the plant's defense through formation of a final product with powerful physiological activity. Such a possibility is supported by pharmacological studies reporting that *N,N,N*-trimethyltyramine is a neuromuscular blocker of depolarizing type that possesses muscarine-like and sympathomimetic effects.[22−25] It was demonstrated that in some animals *N,N,N*-trimethyltyramine induces cardiovascular and respiratory disturbances. Furthermore, it has been shown that *N,N,N*-trimethyltyramine is a stimulant of autonomic ganglia and can liberate catecholamines from the adrenal medulla. Finally, the hypothesized defensive role of *N,N,N*-trimethyltyramine could occur in synergy with other biogenic amine derivatives also well-represented in citrus leaves, such as those arising from tryptophan.[29]

AUTHOR INFORMATION

Corresponding Author

*Phone +39-08-15665865; fax+39-08-15665863; e-mail luigi.servillo@unina2.it.

Notes

The authors declare no competing financial interest.

ACKNOWLEDGMENTS

We are grateful to Dr. Giuseppe Cicciarello, peripheral operational section of Reggio Calabria Research Centre for Citrus Crops and the Mediterranean (CRA-ACM), Acireale (Italy), for providing citrus plant materials.

REFERENCES

(1) Kutchan, T. M. A role for intra-and intercellular translocation in natural product biosynthesis. *Curr. Opin. Plant Biol.* **2005**, *8*, 292−300.

(2) Murata, J.; Roepke, J.; Gordon, H.; De Luca, V. The leaf epidermome of *Catharanthus roseus* reveals its biochemical specialization. *Plant Cell* **2008**, *20*, 524−542.

(3) Ballhorn, D. J.; Kautz, S.; Heil, M.; Hegeman, A. D. Analyzing plant defences in nature. *Plant Signal Behav.* **2009**, *8*, 743−745.

(4) Facchini, P. J. Alkaloid biosynthesis in plants: Biochemistry, cell biology, molecular regulation, and metabolic engineering applications. *Annu. Rev. Plant Physiol. Plant Mol. Biol.* **2001**, *52*, 29−66.
(5) O'Connor, S. E.; Maresh, J. Chemistry and biology of monoterpene indole alkaloid biosynthesis. *Nat. Prod. Rep.* **2006**, *23*, 532−547.
(6) St.Pierre, B.; Vazquez-Flota, F. A.; De Luca, V. Multicellular compartmentation of *Catharanthus roseus* alkaloid biosynthesis predicts intercellular translocation of a pathway intermediate. *Plant Cell* **1999**, *11*, 887−900.
(7) Irmler, S.; Schroder, G.; St. Pierre, B.; Crouch, N. P.; Hotze, M.; Schmidt, J.; Strack, D.; Matern, U.; Schroder, J. Indole alkaloid biosynthesis in *Catharanthus roseus*: new enzyme activities and identification of cytochrome P450 CYP72A1 as secologanin synthase. *Plant J.* **2000**, *24*, 797−804.
(8) Burlat, V.; Oudin, A.; Courtois, M.; Rideau, M.; St. Pierre, B. Coexpression of three MEP pathway genes and geraniol 10-hydroxylase in internal phloem parenchyma of *Catharanthus roseus* implicates multicellular translocation of intermediates during the biosynthesis of monoterpene indole alkaloids and isoprenoid-derived primary metabolites. *Plant J.* **2004**, *38*, 131−141.
(9) Gugler, K.; Funk, C.; Brodelius, P. Elicitor-induced tyrosine decarboxylase in berberine-synthesizing suspension cultures of *Thalictrum rugosum*. *Eur. J. Biochem.* **1988**, *170*, 661−666.
(10) Kawalleck, P.; Keller, H.; Hahlbrock, K.; Scheel, D.; Somssich, I. E. A pathogen-responsive gene of parsley encodes tyrosine decarboxylase. *J. Biol. Chem.* **1993**, *268*, 2189−2194.
(11) Facchini, P. J.; De Luca, V. Expression in *Escherichia coli* and partial characterization of two tyrosine/dopa decarboxylases from opium poppy. *Phytochemistry* **1995**, *38*, 1119−1126.
(12) Gallon, J. R.; Butt, V. S. L-Tyrosine decarboxylase from barley roots. *Biochem. J.* **1971**, *123*, 5P−6P.
(13) Facchini, P. J.; Huber-Allanach, K. L.; Tari, L. W. Plant aromatic-amino acid decarboxylases: evolution, biochemistry, regulation, and metabolic engineering applications. *Phytochemistry* **2000**, *54*, 121−138.
(14) Facchini, P. J.; De Luca, V. Differential and tissue-specific expression of a gene family for tyrosine/dopa decarboxylase in opium poppy. *J. Biol. Chem.* **1994**, *269*, 26684−26690.
(15) Bartley, G. E.; Breksa, A. P., III; Ishida, B. K. PCR amplification and cloning of tyrosine decarboxylase involved in synephrine biosynthesis in *Citrus*. *New Biotechnol.* **2010**, *27*, 308−316.
(16) Pellati, F.; Benvenuti, S. Fast high-performance liquid chromatography analysis of phenethylamine alkaloids in citrus natural products on a pentafluorophenylpropyl stationary phases. *J. Chromatogr. A.* **2007**, *1165*, 58−66.
(17) Nelson, B. C.; Putzbach, K.; Sharpless, K. E.; Sander, L. C. Mass spectrometric determination of the predominant adrenergic protoalkaloids in bitter orange (*Citrus aurantium*). *J. Agric. Food Chem.* **2007**, *55*, 9769−9775.
(18) Haaz, S.; Fontaine, K. R.; Cutter, G.; Limdi, N.; Perumean-Chaney, S.; Allison, D. B. *Citrus aurantium* and synephrine alkaloids in the treatment of overweight and obesity: an update. *Obes. Rev* **2006**, *7*, 79−88.
(19) Stewart, I.; Newhall, W. F; Edwards, G. J. The isolation and identification of L-synephrine in the leaves and fruit of citrus. *J. Biol. Chem.* **1964**, *239*, 85−92.
(20) Wheaton, T. A.; Stewart, I. Quantitative analysis of phenolic amines using ion exchange chromatography. *Anal. Biochem.* **1965**, *12*, 585−592.
(21) Wheaton, T. A.; Stewart, I. Biosynthesis of synephrine in citrus. *Phytochemistry* **1969**, *8*, 85−92.
(22) Urakawa, N.; Hayama, T.; Deguchi, T.; Ohkubo, Y. Some chemical and pharmacological properties of an amine (maltoxin) isolated from malt rootlet. *Jpn. J. Pharmacol.* **1959**, *9*, 41−45.
(23) Urakawa, N.; Hirabe, Y.; Ohkubo, Y. Identification of maltoxin, an active principle from malt rootlet, as candicine. *Jpn. J. Pharmacol.* **1961**, *11*, 4−10.
(24) Urakawa, N.; Deguchi, T.; Ohkubo, Y. Decamethonium-like action of maltoxin, an active principle from malt rootlet, on the frog muscle. *Jpn. J. Pharmacol.* **1960**, *10*, 1−6.
(25) Deguchi, T.; Urakawa, N.; Hayama, T.; Ohkubo, Y. Ganglion stimulating action of candicine. *Jpn. J. Pharmacol.* **1963**, *13*, 143−159.
(26) Chen, F. M. F.; Benoiton, N. L. A new method of quaternizing amines and its use in amino acid and peptide chemistry. *Can. J. Chem.* **1976**, *54*, 3310−3311.
(27) Chen, F. M. F.; Benoiton, N. L. A synthesis of N^6,N^6,N^6-trimethyl-L-lysine dioxalate in gram amounts. *Biochem. Cell Biol.* **1986**, *64*, 182−183.
(28) Servillo, L.; Giovane, A.; Balestrieri, M. L.; Cautela, D.; Castaldo, D. N-Methylated tryptamine derivatives in *Citrus* genus plants: identification of *N*,*N*,*N*-trimethyltryptamine in bergamot. *J. Agric. Food Chem.* **2012**, *60*, 9512−9518.
(29) Servillo, L.; Giovane, A.; Balestrieri, M. L.; Casale, R.; Cautela, D.; Castaldo, D. *Citrus* genus plants contain N-methylated tryptamine derivatives and their 5-hydroxylated forms. *J. Agric. Food Chem.* **2013**, *61*, 5156−5162.
(30) Servillo, L.; Giovane, A.; Balestrieri, M. L.; Bata-Csere, A.; Cautela, D.; Castaldo, D. Betaines in fruits of *Citrus* genus plants. *J. Agric. Food Chem.* **2011**, *59*, 9410−9416.
(31) Servillo, L.; Giovane, A.; Balestrieri, M. L.; Ferrari, G.; Cautela, D.; Castaldo, D. Occurence of pipecolic acid and pipecolic acid betaine (homostachydrine) in *Citrus* genus plants. *J. Agric. Food Chem.* **2012**, *60*, 315−321.
(32) Servillo, L.; Giovane, A.; Balestrieri, M. L.; Cautela, D.; Castaldo, D. Proline derivatives in fruits of bergamot (*Citrus bergamia* Risso et Poit): Presence of *N*-methylproline and 4-hydroxyprolinebetaine. *J. Agric. Food Chem.* **2011**, *59*, 274−281.
(33) Cram, D. J.; Thompson, J. A. Phenonium verus open ions in solvolyses of 3-phenyl-2-butyl tosylate and its p-nitro derivative. *J. Am. Chem. Soc.* **1967**, *89*, 6766−6768.
(34) Cautela, D.; Laratta, B.; Santelli, F.; Trifirò, A.; Servillo, L.; Castaldo, D. Estimating bergamot juice adulteration of lemon juice by high-performance liquid chromatography (HPLC) analysis of flavanone glycosides. *J. Agric. Food Chem.* **2008**, *56*, 5407−5414.
(35) Cautela, D.; Castaldo, D.; Servillo, L.; Giovane, A. Enzymes in citrus juice processing. In *Enzymes in Fruit and Vegetable Processing: Chemistry and Engineering Applications*; Bayindirdli, A., Ed.; CRC Press, Taylor & Francis Group: Boca Raton, FL, 2010; pp 197−214.
(36) Pieterse, C. M. J; Leon-Reyes, A.; Van der Ent, S.; Van Wees, S. C. M. Networking by small-molecule hormones in plant immunity. *Nat. Chem. Biol.* **2009**, *5*, 308−316.
(37) Chehab, E. W.; Kaspi, R.; Savchenko, T.; Rowe, H.; Negre-Zakharov, F.; Liebenstein, D.; Dehesh, K. Distinct roles of jasmonates and aldehydes in plant-defense responses. *PLoS One* **2008**, *3*, e1904.
(38) Kang, S.; Kang, K.; Lee, K.; Back, K. Characterization of tryptamine 5-hydroxylase and serotonin synthesis in rice plants. *Plant Cell Rep.* **2007**, *26*, 2009−2015.
(39) Facchini, P. J.; Hagel, J.; Zulak, K. G. Hydroxycinnamic acid amide metabolism: physiology and biochemistry. *Can. J. Bot.* **2002**, *80*, 577−589.

Due to the complexity of food samples, analysis of PAH metabolites remains a challenging task. A preconcentration step, which empowers detection of low concentrations and interferent removal, is required and often performed through solid-phase extraction (SPE). Among the analytical methods described in the scientific literature, reverse-phase sorbents, such as C18 cartridges, are the most applied in the analysis of biological, food, and environmental matrices.[12,17,21] Moreover, methods for the simultaneous analysis of different PAH monohydroxy derivatives are quite limited and concern mainly matrices such as foodstuffs,[17,22−25] and none about cephalopod samples. Quantitation usually relies on liquid chromatography with fluorescence detection (LC-FD) or on liquid chromatography with tandem mass detection (LC-MS-MS).[17]

This study provides the first report on the optimal conditions for the simultaneous determination of three monohydroxy derivatives of PAHs, namely, 1-hydroxynaphthalene, 2-hydroxyfluorene, and 1-hydroxypyrene, using SPE-LC-FD, for the analysis of different cephalopod matrices (edible tissues and hemolymph). The developed method was applied to samples of the major cephalopod species consumed worldwide.[26] The developed methodology allows an improved assessment of consumers' PAH exposure, as well as the possibility to explore more deeply the PAH metabolic capacity of marine species and, in particular, of cephalopods.

MATERIALS AND METHODS

Safety Considerations. The toxicity or carcinogenicity of each chemical and reagent used in this method was not precisely defined. However, each one must be treated as a potential health hazard, and exposure to these chemicals should be minimized. Some method analytes have been tentatively classified as known or suspected human or mammalian carcinogens. Pure standard materials and stock standard solutions of these compounds should be handled with suitable protection to skin, eyes, etc.

Standards and Chemicals. The standards of 1-hydroxypyrene, 2-hydroxyfluorene, and 1-hydroxynaphthalene were purchased from Sigma-Aldrich (St. Louis, MO, USA), all with ≥98% purity. Individual stock solutions were prepared at 2 mg/mL in acetonitrile/water (50:50). These solutions were stored at −20 °C, in the dark, for a maximum of 6 months. Individual intermediate standard solutions were prepared at 250, 50, and 5 μg/mL in acetonitrile/water (50:50). Working standard solutions were prepared weekly, kept in amber flasks at −20 °C, and used for calibration, accuracy, and repeatability assays of the validation study.

Given the different fluorescence sensitivity of each compound, mixed standard working solutions were prepared at different concentrations for each compound. For linearity assays, the following concentration levels were used: 750, 850, 1000, 1500, and 2000 ng/mL for 1-hydroxynaphthalene; 30, 40, 50, 60, and 75 ng/mL for 2-hydroxyfluorene; and 150, 175, 200, 250, and 300 ng/mL for 1-hydroxypyrene.

HPLC grade acetonitrile and methanol were obtained from Carlo Erba (Milan, Italy), and ethyl acetate was from Panreac (Barcelona, Spain). Double-distilled water used throughout the experiments was prepared daily from a Milli-Q system (Millipore, Bedford, MA, USA).

Sodium acetate and ascorbic acid were purchased from Merck (Darmstadt, Germany) and Sigma-Aldrich, respectively. Glacial acetic acid was obtained from Panreac, and β-glucuronidase/arylsulfatase from *Helix pomatia* (100,000 Fishman units/mL at pH 4.5 and 38 °C and 800,000 Roy units/mL at pH 6.2 and 38 °C, respectively) was purchased from Roche Diagnostics (Mannheim, Germany).

A solution of sodium acetate buffer at 0.1 M was prepared by dissolving 1.36 g of sodium acetate in 250 mL of distilled water and adjusting the pH to 5.0 with acetic acid. An ascorbic acid solution at 1 mg/mL was prepared in methanol.

Materials and Equipment. Oasis HLB (Merck) solid-phase extraction (SPE) cartridges were used. The LC apparatus consisted of two Gilson pump models 305 and 321 coupled to a Gilson autoinjector, model 234 (Gilson Medical Electronics, Villiers-le-Bel, France). A model 0305 Ultrafluor scanning fluorescence detector (LabAlliance, USA) operated at variable-wavelength program was also used. The results were recorded on UniPoint software (Gilson Medical Electronics). A 250 × 4.6 mm i.d., 5 μm, PAH C18 chromatography column (Waters, Milford, MA, USA) maintained at 30 °C was used. All chromatographic solvents were filtered through a 0.20 μm nylon membrane filter (Whatman, Dassel, Germany) and degassed for 15 min in an ultrasonic bath. All standard solutions and sample extracts were filtered through Durapore PTFE syringe filters, 0.45 μm, from Millipore (Milford, MA, USA).

Sample Collection and Characterization. Fresh squid samples were randomly acquired from November 24 to 30, 2011, at supermarkets in the city of Oporto, Portugal. All samples were *Loligo gahi*, from Argentina Southwest Atlantic Ocean (FAO: 41). After arrival at the laboratory, samples were minced and homogenized. Moreover, hemolymph samples were obtained from *Octopus vulgaris* specimen harvested live from the Northwest Atlantic Portuguese coast. Sample collection, biometric characterization (Table 1), and preparation were performed in accordance with EC regulation no. 333/2007.[27] Moisture of squids was evaluated using 10 g of homogenized sample according to Portuguese Standard NP 2282-1991 and the official AOAC method.[28]

Table 1. Squid and Octopus Sample Characterization

sample	weight (g)	total length (cm)	mantle width (cm)	arm length (cm)	moisture ± SD (%; n = 3)
			Squid		
L10A	58.70	18.50	14.5	12.5	86.8 ± 1.0
L10B	54.54	17.75	6.00	14.5	85.3 ± 1.5
L10C	64.74	24.00	10.0	14.3	ND[a]
L18A	98.55	22.00	12.3	12.5	ND
L18B	89.51	21.75	11.0	12.0	ND
L18C	85.55	21.00	11.0	11.5	ND
L19A	105.24	25.75	12.3	12.5	84.9 ± 0.5
L19B	79.70	23.75	11.0	12.3	ND
L19C	84.62	24.25	11.0	12.3	ND
L24A	83.84	24.00	10.5	12.3	85.1 ± 0.2
L24B	90.42	20.00	6.00	12.8	ND
L24C	79.37	23.25	9.75	12.8	ND
			Octopus		
H48	1025.0	48.5	10.5	39.0	80.7 ± 0.5
H51	578.8	48.5	7.0	39.0	82.8 ± 0.4
H52	927.9	46.5	9.5	37.0	81.0 ± 1.0
H53	654.0	42.0	8.0	33.0	80.8 ± 1.3
H54	868.8	46.5	6.5	38.0	83.9 ± 0.5
H55	965.3	49.5	6.5	39.5	81.9 ± 0.7

[a]ND, not determined.

Samples were kept frozen, in polycarbonate containers, at −20 °C, until analysis.

Sample Extraction, Hydrolysis, and Solid-Phase Extraction. After defrosting, samples were minced and homogenized, and 1 g was added of 1 mL of ascorbic acid (1 mg/mL) and 6 mL of acetonitrile. Once vortex stirred, the sample was ultrasonicated for 5 min and extracted by centrifugation at 4 °C and 10000*g* for 10 min. The supernatant was collected and concentrated to dryness at 37 °C under a gentle N_2 stream.

For the enzymatic hydrolysis, the extract was redissolved in 4 mL of sodium acetate buffer. Then, 20 μL of β-glucuronidase/arylsulfatase was added and the oxygen atmosphere replaced by nitrogen. After incubation at 37 °C for 45 min, the enzymatic reaction was stopped by

cooling to room temperature, and the extract was centrifuged at 10000*g*, for 10 min, at 4 °C. This supernatant was then loaded into 200 mg Oasis HLB cartridges, previously conditioned with 5 mL of water and 5 mL of methanol. The cartridges were then washed with 5 mL of water and eluted with 10 mL of methanol/ethyl acetate (50:50). Finally, the eluate was evaporated to dryness under a gentle stream of nitrogen, at 37 °C, and the dried extracts were analyzed.

Chromatographic Conditions. Quantitation of the three PAH metabolites was carried out with LC-FD analysis. The dried eluate was dissolved in 1 mL of acetonitrile/methanol (50:50) and microfiltered. A 20 μL injection volume was used with a flow rate at 1 mL/min and a gradient elution of (A) (water) and B (acetonitrile) as follows: 0−5 min, 50% acetonitrile; 5−20 min, a linear gradient from 50 to 100% acetonitrile; 20−25 min, 100% acetonitrile; 25−30 min, a linear gradient from 100 to 50% methanol; and 30−32 min, 50% acetonitrile. A variable excitation/emission wavelength program was optimized to detect the different compounds as follows: 0−6.5 min, 266/348 nm; 6.51−9 min, 266/366 nm, acetonitrile; 9.01−30 min, 346/390 nm.

Validation Assays. To verify that the analytical method complies with criteria for the performance characteristics as established by Commission Decision 2002/657/EC, the following described validation procedures were carried out.

Linearity was evaluated through a calibration curve assembled by plotting each PAH metabolite peak area versus the concentration of standard solutions, at five concentration levels. The concentration levels ranged between 750 and 2000 ng/mL for 1-hydroxynaphthalene, between 30 and 75 ng/mL for 2-hydroxyfluorene, and between 150 and 300 ng/mL for 1-hydroxypyrene. Linearity was also evaluated in matrix-matched samples at 750, 850, 1000, 1500, and 2000 ng/g; 30, 40, 50, 60, and 75 ng/g; and 150, 175, 200, 250, and 300 ng/g 1-hydroxynaphthalene,2-hydroxyfluorene, and 1-hydroxypyrene, respectively.

Detection and quantification limits (LODs and LOQs) were evaluated on the basis of the noise obtained with the analysis of unfortified blank samples (n = 6). LOD and LOQ were defined as the concentration of the analyte that produced a signal-to-noise ratio of 3 and 10, respectively, and were then tested experimentally by spiking blank samples at such levels.

Recovery assays were performed on spiked samples to determine the accuracy and precision of the method, in triplicate, under the same analytical conditions. The accuracy was evaluated through spiking blank matrix at three levels of known concentrations: 750, 1000, and 2000 ng/g 1-hydroxynaphthalene; 30, 50, and 75 ng/g o2-hydroxyfluorene; and 150, 200, and 300 ng/g 1-hydroxypyrene. Precision was evaluated though the RSD (%) of the fortified samples, in within- and between-day assays.

RESULTS AND DISCUSSION

Chromatographic Method Optimization. A gradient reversed-phase LC-FD method was developed for the simultaneous determination of 1-hydroxynaphthalene, 2-hydroxyfluorene, and 1-hydroxypyrene. Different chromatographic conditions such as stationary phase, mobile phase composition, with isocratic or gradient program, flow rate, injection volume, temperature, and wavelength program were optimized for the separation of the selected PAH derivatives. According to the scientific literature, C18 LC columns are the most employed.[19,29,30] A C18 PAH column was chosen given their specificity for the LC analysis of these molecules and, as expected, separation and sensitivity were appropriate.

During the optimization of the chromatographic method, the organic solvents most commonly used for PAH metabolite determination were evaluated. A combination of acetonitrile with water[29,31] or methanol with water[19,32] is reported by most authors, and both of these combinations were tried. In a preliminary study, an isocratic elution system, consisting of methanol or acetonitrile and water (95:5), was attempted. Given that the chromatographic separation achieved was inadequate, a gradient elution system of acetonitrile and water was established. For the simultaneous determination of the three compounds, a variable-wavelength program was optimized on the basis of previous studies.[17,25]

Because PAH metabolites are subject to thermal degradation and photodegradation, antioxidant addition should prevent or at least reduce these processes. Some authors recommended their use in the preparation of the mobile phase and standard solutions to avoid degradation and increase the stability of the analytes. The addition of ascorbic acid at 1 mg/mL to the mobile phase was tried; nonetheless, because no improvement in the standards' stability was observed, this procedure was abandoned in further studies.[9,33] The addition of *tert*-butylhydroquinone (TBHQ), a hydroquinone derivative substituted with a *tert*-butyl group, in the preparation of standard solutions has also been reported to avoid standards' degradation.[17] However, this compound shows fluorescence at the same wavelength as 2-hydroxyfluorene, causing an overload of the photomultiplier tube (PMT) of the detector. Because the aim of this study was to quantitate simultaneously 1-hydroxynaphthalene, 2-hydroxyfluorene, and 1-hydroxypyrene, TBHQ usage was also excluded. To ensure standard stability, degradation studies on working standard solutions were performed during five consecutive days, and it has been concluded that the standard solutions were stable until the third day without antioxidant addition. Representative LC-FD chromatograms of a mixed standard solution and a spiked squid sample are shown in Figure 1.

Extraction Procedure Optimization. Optimization of the extraction, enzymatic deconjugation, and purification/concentration steps was performed with a blank sample (without PAH metabolites).

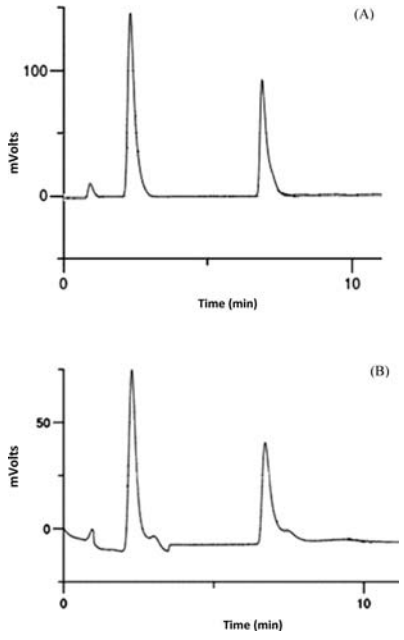

Figure 1. (A) LC-FD chromatogram of a standard solution mixture of (1) 1-hydroxynaphthalene, (2) 2-hydroxyfluorene, and (3) 1-hydroxypyrene at 1000, 50, and 200 ng/g, respectively. (B) LC-FD chromatogram of a spiked sample with (1) 1-hydroxynaphthalene, (2) 2-hydroxyfluorene, and (3) 1-hydroxypyrene at 1000, 50, and 200 ng/g, respectively.

Table 2. Validation Data Obtained for 1-Hydroxynaphthalene, 2-Hydroxyfluorene, and 1-Hydroxypyrene

			recovery (%)			RSD within-day (%)			RSD between-day (%)		
compound	LOD (ng/g)	LOQ (ng/g)	F1[a]	F2[b]	F3[c]	F1[a]	F2[b]	F3[c]	F1[a]	F2[b]	F3[c]
1-hydroxynaphthalene	225.0	750.0	98.7	110.1	107.4	9.5	4.6	15.3	6.8	0.5	12.2
2-hydroxyfluorene	9.0	30.0	70.3	77.6	79.0	6.0	7.2	6.1	1.6	0.1	7.5
1-hydroxypyrene	45.0	150.0	79.9	62.2	67.4	8.6	4.8	3.7	1.9	1.4	0.8

[a]Fortification level 1 = 750/30/150 ng/g of 1-hydroxynaphthalene/2-hydroxyfluorene/1-hydroxypyrene. [b]Fortification level 2 = 1000/50/200 ng/g of 1-hydroxynaphthalene/2-hydroxyfluorene/1-hydroxypyrene. [c]Fortification level 3 = 2000/75/300 ng/g of 1-hydroxynaphthalene/2-hydroxyfluorene/1-hydroxypyrene.

Most of the analytical methods for determining PAH metabolites were developed for human urine samples,[19] blood, and other biological fluids such as fish bile.[34] Although some analytical methods have been optimized for the determination of hydroxylated PAHs in milk and in infant foods,[17] to our knowledge no extraction procedures have been previously reported for their determination in cephalopods.

To optimize the extraction efficiency, different parameters were tested. First, as these compounds are light sensitive and easily degradable, the importance of the addition of an antioxidant to the sample was evaluated. In the present study, the action of two antioxidants, ascorbic acid and TBQH, was assessed. When ascorbic acid was used at a concentration of 1 mg/mL, better recovery rates were achieved when 1 mL of the solution was added to 1 g of sample.

With regard to the extraction solvent, and given that PAH metabolites present high solubility in acetonitrile, this solvent was chosen. Because enzymatic hydrolysis in the following step is active in aqueous media, the extraction organic solvent must be evaporated to dryness. However, the temperature applied during the evaporation step may limit the recoveries of hydroxylated metabolites. Different temperatures were tested (35, 37, 40, and 42 °C) and, in agreement with other studies,[17] the highest temperatures degrade these compounds and, therefore, 37 °C was selected. In addition, to decrease the time of the evaporation step, two volumes of extraction solvent were tested, 6 and 10 mL. Nonetheless, the best recovery results were attained with 6 mL because a reduction in the evaporation time was accomplished. It is worth noting the importance of avoiding light and maintaining a low temperature to minimize metabolite degradation. Good separation between the sample and supernatant was achieved when 10000*g* was applied for 10 min at 4 °C.

Hydrolysis Optimization. Because hydroxy metabolites are biotransformed to phase II metabolites by conjugation with glutathione, glucuronide, or sulfate, an enzymatic reaction with β-glucuronidase is crucial to liberate them and obtain free metabolites. As the enzymatic hydrolysis is a chemical reaction catalyzed by an enzyme that uses water to break molecules, the use of an aqueous buffer solution is essential. It will also keep the pH constant at the optimum value for enzyme activity. Therefore, several experimental conditions, such as pH (4.5, 5.0, and 5.5), buffer concentration (0.05, 0.1, and 0.5 M), enzyme volume, incubation time (40, 45, 50, and 60 min), and temperature (37, 40, and 42 °C) were optimized. In agreement with other authors,[17,35] it was found that 4 mL of a 0.1 M sodium acetate buffer, at pH 5, at 37 °C for 45 min, gave the best results.

On the basis of scientific evidence,[17,19,36] the addition of 20 μL of β-glucuronidase/arylsulfatase from *Helix pomatia* to 4 mL of solution is enough for the reaction to occur extensively, which was tested in this study and revealed to be clearly appropriate. Because the analyzed compounds degrade in the presence of oxygen, it is important to highlight the need to displace the oxygen present in the test tube by a nitrogen atmosphere shortly after the addition of the enzyme.

SPE Optimization. SPE is one of the most employed tools for the cleanup of PAHs[21] and their metabolites.[17,19,37] First, we attempted to choose the best sorbent to obtain higher recoveries. C18 cartridges, reversed phase silica-based sorbents, have several disadvantages such as low breakthrough volumes, instability at some pH values, and the presence of silanol groups, which can result in low recoveries for some polar compounds or lack of precision from column to column, resulting in irreproducible recoveries. PAH hydroxylated metabolites have quite polar characteristic, and it was difficult to extract them with traditional reversed-phase sorbents. Aware that the SPE method, and particularly the C18 cartridges, might impose some variability in PAH hydroxylated metabolite recoveries, hydrophilic polymeric sorbents have been chosen, and best results were obtained with the reversed phase polymeric-based cartridges Oasis HLB, which allow a hydrophilic−lipophilic balance. According to our knowledge, the use of Oasis HLB has never been reported for the analysis of PAH hydroxylated metabolites.

The initial Oasis SPE procedure was based on the C18 SPE procedures previously attempted.[17,19] However, because 1-hydroxynaphthalene and 1-hydroxypyrene metabolites were inefficiently retained, with recoveries of 34 and 32%, respectively, parameters, such as washing and elution steps, were optimized using a mixed standard working solution at 1000, 50, and 150 ng/mL 1-hydroxynaphthalene, 2-hydroxyfluorene, and 1-hydroxypyrene, respectively.

The obtained results suggested that for the washing step water is the more suitable solvent, as it has enough solvent power to remove weakly absorbed interferents without removing the strongly absorbed analytes. Washing solutions containing methanol led to substantial losses and greatly decreased 1-hydroxynaphthalene, 2-hydroxyfluorene, and 1-hydroxypyrene recoveries, from 87, 68, and 75%, respectively, to 66, 40, and 22%, respectively.

With regard to the elution step, to ensure high recoveries of all PAH metabolites, mixtures of solvents are usually recommended.[21] Different solvents and volumes were evaluated, and it was found that the presence of methanol was important; nonetheless, neither methanol nor dichloromethane, alone, eluted efficiently 1-hydroxynaphthalene (recoveries of 15 and 40%, respectively) and 1-hydroxypyrene (recoveries of 32 and 8%, respectively). In agreement with other authors,[17] 10 mL of methanol/ethyl acetate was the best approach to obtain greater recovery.

Method Validation. The developed analytical method complied with criteria for the performance characteristics as established by Commission Decision 2002/657/EC.[38]

The linearity of the method was evaluated in solvent and in matrix-matched solutions. In the working standard solutions, at five concentration levels, correlation coefficients (r^2) were 0.9987 for 1-hydroxynaphthalene and 0.9959 for 2-hydroxyfluorene and 1-hydroxypyrene. In matrix-matched solutions adequate r^2 values of 0.9949, 0.9901, and 0.9903 for 1-hydroxynaphthalene, 2-hydroxyfluorene, and 1-hydroxypyrene, respectively, were obtained.

Because no standard reference material is available for PAH metabolites in cephalopods, for accuracy and repeatability assays, recoveries were determined through a spiking matrix at three different levels, on three different days, and each extract was analyzed three times. Accuracy varied between 62.2 and 110.1%, with within-day and between-day repeatabilities ranging between 3.7 and 15.3% and between 0.1 and 12.2%, respectively (Table2).

Application to Real Samples. The optimized and validated analytical methodology was applied to the analysis of 12 squid samples of *Loligo gahi* species and to 6 hemolymph samples obtained from *Octopus vulgaris* harvested live from the Northwest Atlantic Portuguese coast. *L. gahi* is widely distributed along the Pacific coast of South America. It is the second most important loliginid squid in commercial fisheries worldwide.[39] A small part of the total catch is consumed in Europe, predominantly in Spain.[2] With regard to the selected octopus, it corresponds to the major species consumed worldwide[40] and was recently proposed as a sentinel species for the presence of contaminants in coastal waters.[13]

Of the 18 samples analyzed, 39% (7) were contaminated with 1-hydroxynaphthalene, which was the only PAH metabolite detected, ranging between 786 and 1145 ng/g (Table 3). Naphthalene, a low molecular weight PAH, which is classified as a possible carcinogen to humans (group 2B) by the International Agency for Research on Cancer (IARC), is one the most abundant compounds detected in marine organisms and it is mainly due to petrogenic pollution.[41] None of the squid samples contained detectable amounts of 2-hydroxyfluorene or 1-hydroxypyrene. Also, none of the hemolymph samples exhibited detectable amounts of metabolites, which confirms the lack of (or low) detoxification capacity of the octopus species regarding PAHs.

Table 3. PAH Metabolite Concentrations from the Analyzed Samples

sample	1-hydroxynaphthalene (ng/g)
L18A	830
L18B	786
L10B	788
L10C	<LOQ
L24A	1013
L24B	1145
L24C	<LOQ

Although some publications regarding the contamination of PAHs metabolites in fish[10,11,22−25] have been reported, the comparison with other studies is difficult, because, to our knowledge, there are no reports of the determination of PAH metabolites in mollusks, namely, in cephalopod samples. Nonetheless, the results of the present study are corroborated by a previous work[2] that evaluated the concentrations of 18 PAHs in five commercial squid species in Portugal, with different geographical origins. The results showed that low molecular weight compounds with two and three rings were the most predominant PAHs in all of the species. The detected concentrations in *L. gahi* (from the Atlantic Ocean) may mean additional carcinogenic risks for high cephalopod consumers. Moreover, in a survey that revealed the measurable presence of four low molecular weight PAHs (naphthalene, acenaphthene, fluorine, and phenanthrene) in three commonly consumed and commercially valuable fish species (sardine, chub, and horse mackerel) from the Atlantic Ocean, naphthalene was the most abundant PAH in sardine and horse mackerel, accounting for ca. 55% of the total PAHs.[41]

In contrast to our results, in a study[22] that included the analysis of PAH metabolites in the bile of flounder (*Platichthys flesus*), the major PAH metabolite detected was 1-hydroxypyrene. 1-Hydroxyphenanthrene and 3-hydroxybenzo[*a*]pyrene were also detected in 70 and 24 samples, respectively, of the 87 samples analyzed. However, the concentrations of 1-hydroxyphenanthrene and 3-hydroxybenzo[*a*]pyrene were below or near the LOQ (0.002 mg/mL bile). The bile of flounder samples from the Gulf of Gdansk presented 1-hydroxypyrene concentrations ranging from 0.019 to 0.066 mg/mL.[22]

Rey-Salgueiro et al.[37] also investigated the levels of 3-hydroxybenzo[*a*]pyrene in the bile and plasma of Nile tilapia after waterborne exposure to benzo[*a*]pyrene (10 and 100 mg/L). Metabolites were detected in bile and plasma, and conjugates of 3-hydroxybenzo[*a*]pyrene (glucuronide and/or sulfate conjugates) were the majority forms in both biological fluids, glucuronide 3-hydroxybenzo[*a*]pyrene being the main metabolite in bile. The same research group, in a previous study[17] concerning food safety of commercial milk formulas and infant cereals, reported that no hydroxy PAH metabolites (1-hydroxypyrene and 3-hydroxybenzo[*a*]pyrene) or their conjugates were detected in the analyzed foodstuffs.

AUTHOR INFORMATION

Corresponding Author

*(A.P.) Phone: +351 239 488 400. Fax: +351 239 827 126. E-mail: apena@ci.uc.pt.

Funding

We thank Fundação para a Ciência e a Tecnologia (FCT), through PTDC/AGR-AAM/102316/2008 (COMPETE and cofinanced by FEDER), for the financial support and the post-Ph.D. fellowship granted to L.J.G.S. (SFRH/BPD/62877/2009). This work received financial support from the European Union (FEDER funds through COMPETE) and National Funds (FCT, Fundação para a Ciência e Tecnologia) through Project Pest-C/EQB/LA0006/2013. The work also received financial support from the European Union (FEDER funds) within the framework of QREN through Project NORTE-07-0124-FEDER-000069. We are greatly indebted to all financing sources.

Notes

The authors declare no competing financial interest.

ABBREVIATIONS USED

PAH, polycyclic aromatic hydrocarbons; TBHQ, *tert*-butylhydroquinone

REFERENCES

(1) Lordan, S.; Ross, R. P.; Stanton, C. Marine bioactives as functional food ingredients: potential to reduce the incidence of chronic diseases. *Mar. Drugs* **2011**, *9*, 1056−100.

(2) Gomes, F.; Oliveira, M.; Ramalhosa, M. J.; Delerue-Matos, C.; Morais, S. Polycyclic aromatic hydrocarbons in commercial squids from different geographical origins: levels and risks for human consumption. *Food Chem. Toxicol.* **2013**, *59*, 46−54.
(3) *Some Non-Heterocyclic Polycyclic Aromatic Hydrocarbons and Some Related Exposures*; IARC Monographs on the Evaluation of Carcinogenic Risks to Humans 92; IARC: Lyon, France, 2010; 773 pp.
(4) WHO. *State of the Science of Endocrine Disrupting Chemicals 2012*; Geneve, Switzerland, 2013.
(5) European Commission. . Commission regulation (EU) no. 835/2011 of 19 August 2011 amending regulation (EC) no. 1881/2006 as regards maximum levels for polycyclic aromatic hydrocarbons in foodstuffs. *Off. J. Eur. Union* **2011**, *L215*, 4−8.
(6) Ramalhosa, M. J.; Paíga, P.; Morais, S.; Delerue-Matos, C.; Oliveira, M. B. P. P. Analysis of polycyclic aromatic hydrocarbons in fish: evaluation of a quick, easy, cheap, effective, rugged, and safe extraction method. *J. Sep. Sci.* **2009**, *32*, 3529−3538.
(7) Domingo, J. L.; Bocio, A.; Falcó, G.; Llobet, J. M. Benefits and risks of fish consumption Part I. A quantitative analysis of the intake of omega-3 fatty acids and chemical contaminants. *Toxicology* **2007**, *230*, 219−226.
(8) Bláha, L.; Kapplová, P.; Vondrácek, J.; Upham, B.; Machala, M. Inhibition of gap-junctional intercellular communication by environmentally occurring polycyclic aromatic hydrocarbons. *Toxicol. Sci.* **2002**, *65*, 43−51.
(9) Vuontisjärvi, H.; Keinänen, M.; Vuorinen, P. J.; Peltonen, K. A comparison of hplc with fluorescence detection and fixed wavelength fluorescence methods for the determination of polycyclic aromatic hydrocarbon metabolites in fish bile. *Polycycl. Aromat. Compd.* **2004**, *24*, 333−342.
(10) Forsberg, N. D.; Wilson, G. R.; Anderson, K. Determination of parent and substituted polycyclic aromatic hydrocarbons in high-fat salmon using a modified QuEChERS extraction, dispersive SPE and GC-MS. *J. Agric. Food Chem.* **2011**, *59*, 8108−8116.
(11) Ni, H.-G.; Guo, J.-Y. Parent and halogenated polycyclic aromatic hydrocarbons in seafood from South China and implications for human exposure. *J. Agric. Food Chem.* **2013**, *61*, 2013−2018.
(12) Beyer, J.; Jonsson, G.; Porte, C.; Krahn, M. M.; Ariese, F. Analytical methods for determining metabolites of polycyclic aromatic hydrocarbon (PAH) pollutants in fish bile: a review. *Environ. Toxicol. Pharmacol.* **2010**, *30*, 224−244.
(13) Semedo, M.; Reis-Henriques, M. A.; Rey-Salgueiro, L.; Oliveira, M.; Delerue-Matos, C.; Morais, S.; Ferreira, M. Metal accumulation and oxidative stress biomarkers in octopus (*Octopus vulgaris*) from Northwest Atlantic. *Sci. Total Environ.* **2012**, *433*, 230−237.
(14) Martí-Cid, R.; Llobet, J. M.; Castell, V.; Domingo, J. L. Evolution of the dietary exposure to polycyclic aromatic hydrocarbons in Catalonia, Spain. *Food Chem. Toxicol.* **2008**, *46*, 3163−3171.
(15) Martorell, I.; Perelló, G.; Martí-Cid, R.; Castell, V.; Llobet, J. M.; Domingo, J. L. Polycyclic aromatic hydrocarbons (PAH) in foods and estimated PAH intake by the population of Catalonia, Spain: temporal trend. *Environ. Int.* **2010**, *36*, 424−432.
(16) Hayakawa, K.; Onoda, Y.; Tachikawa, C.; Hosoi, S.; Yoshita, M.; Chung, S. W.; Kizu, R.; Toriba, A.; Kameda, T.; Tang, N. Estrogenic/antiestrogenic activities of polycyclic aromatic hydrocarbons and their monohydroxylated derivatives by yeast two-hybrid assay. *J. Health Sci.* **2007**, *53*, 562−570.
(17) Rey-Salgueiro, L.; Martínez-Carballo, E.; García-Falcón, M. S.; González-Barreiro, C.; Simal-Gándara, J. Occurrence of polycyclic aromatic hydrocarbons and their hydroxylated metabolites in infant foods. *Food Chem.* **2009**, *115*, 814−819.
(18) Jongeneelen, F. J. Benchmark guideline for urinary 1-hydroxypyrene as biomarker of occupational exposure to polycyclic aromatic hydrocarbons. *Ann. Occup. Hyg.* **2001**, *45*, 3−13.
(19) Wang, Y.; Zhang, W.; Dong, Y.; Fan, R.; Sheng, G.; Fu, J. Quantification of several monohydroxylated metabolites of polycyclic aromatic hydrocarbons in urine by high-performance liquid chromatography with fluorescence detection. *Anal. Bioanal. Chem.* **2005**, *383*, 804−809.
(20) Varanasi, U. *Metabolism of Polycyclic Aromatic Hydrocarbons in the Aquatic Environment*; CRC Press: Boca Raton, FL, USA, 1989.
(21) Marcé, R. M.; Borrull, F. Solid-phase extraction of polycyclic aromatic compounds. *J. Chromatogr., A* **2000**, *885*, 273−290.
(22) Ruczyńska, W. M.; Szlinder-Richert, J.; Malesa-Ciećwierz, M.; Warzocha, J. Assessment of PAH pollution in the southern Baltic Sea through the analysis of sediment, mussels and fish bile. *J. Environ. Monit.* **2011**, *13*, 2535−2542.
(23) Ruddock, P. J.; Bird, D. J.; McEvoy, J.; Peters, L. D. Bile metabolites of polycyclic aromatic hydrocarbons (PAHs) in European eels *Anguilla anguilla* from United Kingdom estuaries. *Sci. Total Environ.* **2003**, *301*, 105−117.
(24) Vuorinen, P. J.; Keinänen, M.; Vuontisjärvi, H.; Barsiene, J.; Broeg, K.; Förlin, L.; Gercken, J.; Kopecka, J.; Köhler, A.; Parkkonen, J.; Pempkowiak, J.; Schiedek, D. Use of biliary PAH metabolites as a biomarker of pollution in fish from the Baltic Sea. *Mar. Pollut. Bull.* **2006**, *53*, 479−487.
(25) Johnson-Restrepo, B.; Olivero-Verbel, J.; Lu, S.; Guette-Fernández, J.; Baldiris-Avila, R.; O'Byrne-Hoyos, I.; Aldous, K. M.; Addink, R.; Kannan, K. Polycyclic aromatic hydrocarbons and their hydroxylated metabolites in fish bile and sediments from coastal waters of Colombia. *Environ. Pollut.* **2008**, *151*, 452−459.
(26) FAO. *Agriculture Review of the State of World Marine Fishery Resources*; FAO Fisheries and Aquaculture Technical Paper 569; Rome, Italy, 2011.
(27) European Commission. . Commission regulation (EC) no. 333/2007 of 28 March 2007 laying down the methods of sampling and analysis for the official control of the levels of lead, cadmium, mercury, inorganic tin, 3-MCPD and benzo(a)pyrene in foodstuffs. *Off. J. Eur. Union* **2007**, *L88*, 29−38.
(28) AOAC. *Official Methods of Analysis of AOAC International*, 18th ed.; AOAC International: Arlington, VA, USA, 2007.
(29) Sarrazin, L.; Diana, C.; Wafo, E.; Pichard-Lagadec, V.; Schembri, T.; Monod, J. Determination of polycyclic aromatic hydrocarbons (PAHs) in marine, brackish, and river sediments by HPLC, following ultrasonic extraction. *J. Liq. Chromatogr. Relat. Technol.* **2006**, *29*, 69−85.
(30) Lintelmann, J.; Fischer, K.; Karg, E.; Schröppel, A. Determination of selected polycyclic aromatic hydrocarbons and oxygenated polycyclic aromatic hydrocarbons in aerosol samples by high-performance liquid chromatography and liquid chromatography-tandem mass spectrometry. *Anal. Bioanal. Chem.* **2005**, *381*, 508−519.
(31) Benlahcen, K. T.; Chaoui, A.; Budzinski, H.; Bellocq, J.; Garrigues, P. Distribution and sources of polycyclic aromatic hydrocarbons in some Mediterranean coastal sediments. *Mar. Pollut. Bull.* **1997**, *34*, 298−305.
(32) Sarrazin, L.; Diana, C.; Schembri, T.; Rebouillon, P. HPLC determination of polycyclic aromatic hydrocarbons (PAHs) in the littoral urban sewage area of Cortiou (Marseille, France). *Int. J. Environ. Stud.* **2004**, *61*, 413−425.
(33) Martínez-Salinas, R. I.; Elena Leal, M.; Batres-Esquivel, L. E.; Domínguez-Cortinas, G.; Calderón, J.; Díaz-Barriga, F.; Pérez-Maldonado, I. N. Exposure of children to polycyclic aromatic hydrocarbons in Mexico: assessment of multiple sources. *Int. Arch. Occup. Environ. Health* **2010**, *83*, 617−623.
(34) Sundt, R. C.; Beyer, J.; Vingen, S.; Sydnes, M. O. High matrix interference affecting detection of PAH metabolites in bile of Atlantic hagfish (*Myxine glutinosa*) used for biomonitoring of deep-water oil production. *Mar. Environ. Res.* **2011**, *71*, 369−374.
(35) Bouchard, M.; Krishnan, K.; Viau, C. Kinetics of tissue distribution and elimination of pyrene and 1-hydroxypyrene following intravenous administration of [^{14}C]pyrene in rats. *Toxicol. Sci.* **1998**, *46*, 11−20.
(36) Richardson, D. M.; Gubbins, M. J.; Davies, I. M.; Moffat, C. F.; Pollard, P. M. Effects of feeding status on biliary PAH metabolite and biliverdin concentrations in plaice (*Pleuronectes platessa*). *Environ. Toxicol. Pharmacol.* **2004**, *17*, 79−85.
(37) Rey-Salgueiro, L.; Costa, J.; Ferreira, M.; Reis-Henriques, A. Evaluation of 3-hydroxy-benzo[*a*]pyrene levels in Nile tilapia

(*Oreochromis niloticus*) after waterborne exposure to benzo[*a*]pyrene. *Toxicol. Environ. Chem.* **2011**, 37−41.
(38) EC. Commission decision of 12 August 2002 implementing council directive 96/23/EC concerning the performance of analytical methods and the interpretation of results. *Off. J. Eur. Communities* **2002**, *L221*, 8−36.
(39) FAO. *Cephalopods of the World. An Annotated and Illustrated Catalogue of Cephalopod Species Known to Date. Vol. 2. Myopsid and Oegopsid Squids*; Jereb, P., Roper, C. F. E, Eds.; FAO Species Catalogue for Fishery Purposes 4; Rome, Italy, 2010; pp 34−81.
(40) FAO. *Review of the State of World Marine Fishery Resources*; FAO Fisheries and Aquaculture Technical Paper; Rome, Italy, 2011; p 569.
(41) Ramalhosa, M. J.; Paíga, P.; Morais, S.; Ramos, S.; Delerue-Matos, C.; Oliveira, M. B. P. P. Polycyclic aromatic hydrocarbon levels in three pelagic fish species from Atlantic Ocean: inter-specific and inter-season comparisons and assessment of potential public health risks. *Food Chem. Toxicol.* **2012**, *50*, 162−167.

With respect to glyceollin, a recent study conducted in rats reported absorption of glyceollins across the gastro-intestinal tract following oral administration of a single 90 mg/kg dose of a mixture of glyceollin isomers I–III.[30] In that study, the average maximum plasma concentration of the three isomers combined was only 160 ng/mL; thus, it seemed plausible that glyceollin may behave similarly to other phytochemicals in being extensively metabolized. Initial characterization of plasma samples taken from the same rats that received the 90 mg/kg dose revealed sulfated metabolites.[17] The purpose of the current work is to extend this initial metabolite profiling through broader characterization of glyceollin metabolites in these same plasma samples and to expand our analyses to urine and feces samples obtained from separate groups of rats that received either a single 90 mg/kg oral dose (urine) or two weeks of daily 90 mg/kg oral doses (feces) of the same glyceollin I–III isomeric mixture used in the initial study.[29]

MATERIALS AND METHODS

Chemicals. High purity grade trifluoroacetic acid (TFA, >99%) and formic acid (>96%) were obtained from Sigma-Aldrich Chemical Co. (St. Louis, MO) as was HPLC-methanol solvent. OmniSolv LC-MS acetonitrile was purchased from EMD Millipore (Billerica, MA). A Millipore water purifying system (18.2 MΩ·cm) was used to obtain deionized water.

Extraction of Glyceollin Isomers. Using a procedure developed at the Southern Regional Research Center (SRRC, ARS, USDA, New Orleans, LA), a mixture of glyceollins I, II, and III was obtained.[6] Briefly, after slicing, soybean seeds were inoculated with *Aspergillus sojae*. The *A. sojae* (SRRC 1125) culture was grown at 25 °C in the dark on potato dextrose agar. *Conidia* were harvested from 5-day-old cultures of *A. sojae*. *Conidia* were suspended in 15 mL sterile, distilled H_2O ($1.0–3.0 \times 10^7$ conidia mL^{-1}) and mixed with sliced soybean seeds (1 kg). Three days after exposure to *Conidia*, the glyceollins were extracted from the inoculated seeds with 1 L of methanol. Notably, the process to induce glyceollins in soybean is not a traditional fermentation (soybean seeds are not heated). Typically, there are no glyceollins present in soybean unless the plant or seed was subjected to stress. Under conditions of stress, the soybean seed triggers the production of critical enzymes (phenylalanine ammonia-lyase, PAL) necessary for producing glyceollins. The glyceollins were isolated using preparative scale HPLC employing two Waters (Milford, MA) 25 × 100 mm, 10 μm particle size μBondapak C_{18} radial compression column segments; the column segments were connected in series using an extension tube. HPLC was performed on a Waters 600E liquid chromatograph equipped with a Waters UV–vis 996 detector scanning from 210 to 400 nm. The injection volume was 20 mL; the flow rate was 8.0 mL/min using the following solvent gradient: A = acetonitrile (Sigma-Aldrich), B = water (Millipore system, Billerica, MA) 5% A for 10 min, then 5% A to 90% A in 60 min followed by holding at 90% A for 20 min. The fraction containing the glyceollins was concentrated (≥98% purity) under vacuum and freeze-dried. Confirmation of individual glyceollins was based on HPLC retention times and UV–vis absorbance spectra comparison with those of authentic standards isolated at SRRC. UV–vis spectrophotometry at 285 nm was used to estimate the percentage of the three isomers used in all experiments: glyceollin I (68%), glyceollin II (21%), and glyceollin III (11%).

Glyceollin Dosing of Rats and Plasma Sample Collection. The procedures used for administration of glyceollins to rats and subsequent sample collection have been previously described.[30] Briefly, the mixture of glyceollin isomers I–III defined in the preceding section was dissolved in poloxamer and administered (90 mg/kg) via oral gavage (3 mL) to male ZDSD (Zucker Diabetic Sprague–Dawley) rats (PreClinOmics, Indianapolis, IN) that were subjected to a 12:12 h light/dark cycle. These rats are an obese prediabetic rat model of Type II diabetes.[30] This dose was selected because it was identical to that used in an oral-glucose-tolerance test to evaluate the antidiabetic potential of glyceollins.[29] Rats (approximately 500 g wt) were euthanized at various time points by decapitation; trunk blood was subsequently collected into EDTA-coated tubes supplemented with aprotinin. Plasma samples obtained 3 h after dosage were separated and stored at −80 °C. Upon thawing, 125 μL of plasma was transferred into microcentrifuge tubes to which an equivalent volume of acetonitrile was added. The mixture was vortexed, then centrifuged at 10 000 rpm for 20 min. The supernatant was subjected to mass spectrometric analysis.

Urine Sample Treatment. A urine sample obtained from a 24 h collection period that commenced following a single 90 mg/kg oral dose to a rat was acidified with 1% TFA, vortexed, and centrifuged at 10 000 rpm for 10 min. The supernatant was diluted with 1:1 0.2% formic acid in 10% acetonitrile[31] and stored at −80 °C until the subsequent LC-MS analyses.

Fecal Sample Collection. Rat fecal samples were collected prior to and after the dosage of the mixture of glyceollin isomers I–III (90 mg/kg) once daily for 2 weeks. This study was conducted to assess possible effects of glyceollin administration on the gastrointestinal microbiome, thus necessitating multiple dose administration. Both the pre- and postdosed fecal pellets were weighed, and a 1:2 (pellet weight/vol) ratio of deionized water was added to each group. A smooth paste was created in a glass mortar and pestle. The paste was then transferred to a polypropylene tube and diluted with CH_3CN 1:2 (paste wt/vol). The tubes were centrifuged for 5 min at 1000 rpm. Supernatant was collected and transferred to fresh tubes; then, approximately 0.1 g of ammonium acetate was added progressively with gentle vortexing. Tubes were subsequently centrifuged for 5 min at 1000 rpm. The supernatant (acetonitrile layer) was collected and stored at −70 °C until analysis.

Liver Microsomes Treatment with NADPH or UDPGA Cofactors. Samples were prepared in triplicate for both the control and the experimental group. For the NADPH incubations (phase I oxidation), 168 μL of 100 mM NaH_2PO_4 buffer (pH 7.4), 10 μL of 20 mg/mL rat liver microsomes, 10 μL of 20 mM $MgCl_2$, and 1 mM glyceollins I–III isomeric mixture were added to 1.5 mL Eppendorf tubes, vortexed, and incubated for 3 min at 37 °C. Subsequently, 10 μL of either 10 mM NADPH or buffer (control) was added, and the samples were incubated for 30 min at 37 °C. The incubation was stopped by adding 200 μL of cold acetonitrile, followed by vortexing, and centrifugation for 5 min at 4000 rpm. Supernatant was transferred to fresh tubes and stored at −70 °C until analysis. For the UDPGA conjugation procedure, 134 μL of 100 mM KH_2PO_4 buffer (pH 7.1), 20 μL of 20 mg/mL rat liver microsomes, and 4 μL of 5 mg/mL alamethicin were added to 1.5 mL Eppendorf tubes, vortexed, and incubated on ice for 15 min. Twenty microliters of $MgCl_2$ and 2 μL of 1 mM glyceollins I–III isomeric mixture were then added, vortexed, and incubated for 3 min. Twenty microliters of KH_2PO_4 buffer and 20 μL of 10 mM UDPGA were added to control and experimental groups, respectively. The tubes were incubated for 60 min at 37 °C. Two hundred microliters of cold acetonitrile was added to each tube to terminate the incubation. Tubes were then vortexed followed by centrifugation for 5 min at 4000 rpm. Supernatant was transferred to fresh tubes and stored at −70 °C until analysis.

Liquid Chromatography–Mass Spectrometry. LC-ESI-MS and LC-ESI-MS/MS analyses were conducted on an Agilent 1200 series LC system (Agilent, Santa Clara, CA) coupled to a 3200 QTrap triple quadrupole mass spectrometer (Applied Biosystems/MDS SCIEX, Foster City, CA). Separation was performed on an Agilent Eclipse XDB C18 column (4.6 × 150 mm ID, 5 μm). Ten microliters was injected onto the column held at 25 °C. The binary mobile phase consisted of mobile phase A (water with 0.1% formic acid) and mobile phase B (acetonitrile with 0.1% formic acid). The gradient was 0–44 min 5% B to 45% B; the flow rate was 0.500 mL/min. The UV absorbance detector was set at 285 nm.

For negative ion LC-ESI-MS and LC-ESI-MS/MS analyses, electrospray parameters were set at the following: curtain gas (CUR) of 20 psi, ionspray voltage (IS) of −4500 V, GAS1 of 60 psi, GAS2 of 60 psi, source temperature of 600 °C, CAD gas pressure of 6 psi, entrance potential (EP) of −10 V, and collision cell exit

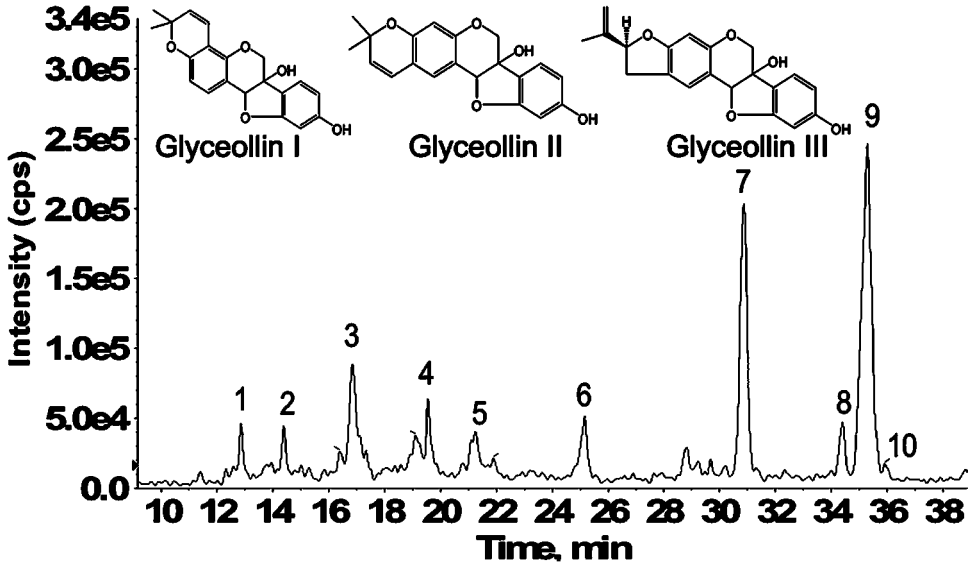

Figure 1. LC-ESI-MS/MS precursor ion scans showing total ion current of all precursors of m/z 148 from feces of rats dosed orally once daily for 2 weeks with 90 mg/kg of the glyceollin isomeric mixture. Isomeric structures of glyceollins I, II, and III are shown above the scans (inset).

potential (CXP) of −3 V. Declustering potential (DP) and collision energy (CE) were optimized to be −55 V and −34 eV, respectively. For positive ion experiments, CUR, IS, EP, CXP, DP, and CE were maintained at 10 psi, 5000 V, 10 V, 5 V, 40 V, and 30 eV, respectively. All other parameters were the same as for negative ion mode. Full scan and precursor ion scans were performed sequentially (scan rate = 1 s/200 Da). In a subsequent LC injection, product ion scans for precursors of interest were added to the sequential acquisitions.

RESULTS AND DISCUSSION

Precursor Ion Scans of *m/z* 148. In our previous work, we proposed a precursor ion scan method to screen for isomeric glyceollins and their metabolites based on a diagnostic radical product ion.[17,29] Higher-energy triple quadrupole (e.g., 34 eV E_{Lab}) CID product ion spectra of glyceollins yield an exceptionally stable radical at m/z 148, which serves as a "signature" common to the three glyceollin isomers.[17] Employing this precursor ion scanning approach, plasma, urine, and feces samples obtained from rats dosed with isomeric glyceollins I, II, and III (structures shown in Figure 1) were screened for the glyceollins and their metabolites by LC-ESI-MS and LC-ESI-MS/MS. The precursor ion scanning of m/z 148 for rat feces samples resulted in the appearance of substantially more metabolites compared to rat plasma and urine samples. Figure 1 shows a representative LC chromatogram of a rat feces sample. All three unmetabolized isomers of glyceollins (m/z 337) were detected. Peaks labeled 9, 8, and 10 on the LC chromatogram correspond to glyceollin I, II, and III, respectively.

Little is known about the metabolism of glyceollins, but our findings from rat feces indicate that extensive oxidation of glyceollins occurred. Peaks 5, 1, and 6 (Figure 1) represent m/z 148 precursors at m/z 353, 371, and 387, respectively. Relative to deprotonated glyceollins (m/z 337), these three metabolites are proposed as products of epoxidation or hydroxylation of glyceollins (m/z 353), diol addition at a double bond (m/z 371), and a combination of these two processes (m/387). Two of the three above-mentioned peaks observed in rat feces (m/z 371, 387) were also detected in rat urine, as was m/z 451 (the latter likely represents glyceollins that are both hydrolyzed and sulfated). Notably, m/z 451 had also been detected in rat plasma, along with m/z 353 and 355 (the latter representing a hydrolysis product).[17] LC-ESI-MS/MS precursor ion scanning of m/z 148 from rat feces showed additional peaks eluting at 14.4 (peak 2), 16.8 (peak 3), 19.3 (peak 4), 30.9 (peak 7), and 35.3 (peak 9) min. These chromatographic peaks correspond, respectively, to glyceollin metabolite precursors at m/z 531, 474, 433, 417, and the deprotonated glyceollin isomers at m/z 337. These five precursors of m/z 148 were also found in rat plasma, whereas m/z 531, 474, and 417 were observed in rat urine (data not shown). Sulfation and sulfation plus an oxygen of glyceollins account for the peaks observed at m/z 417 (peak 7) and 433 (peak 4), respectively, as discussed previously.[17] The two remaining precursor peaks of interest at m/z 474 and 531 were considered as phase II metabolites of glyceollins and were further investigated by tandem mass spectrometry, as discussed in the following section.

Evidence of GSH-Derived Metabolites Obtained by LC-ESI-MS and LC-ESI-MS/MS. A chromatographic peak corresponding to the m/z 531 precursor from feces samples eluted at 14.4 min (Figure 1, peak 2); an identical peak was observed in rat plasma and urine. The NI mode LC-ESI-MS/MS CID product ion mass spectrum of this m/z 531 precursor (Figure 2a) summed across the entire chromatographic peak showed a fragment at m/z 353, which corresponds to a loss of 178 Da. Appearing in Figure 2b is the NI mode LC-ESI-MS/MS CID product ion mass spectrum of m/z 474 corresponding to the chromatographic peak eluting at 17.0 min (Figure 1, peak 3). Similar to the result shown in Figure 2a, the m/z 474 also yields a fragment at m/z 353, indicating this time, a loss of 121 Da. The combined information extracted from Figure 2a,b allows the deduction that glutathione conjugation has occurred in glyceollins and that subsequent metabolic byproducts are present in the three matrices: rat plasma, urine, and feces.[32] GSH is a tripeptide (Glu-Cys-Gly) that, when conjugated to molecules via the thiol function in cysteine, is subsequently metabolized via γ-glutamyltranspeptidase to form cysteinylglycine conjugates. We propose that the loss of 178 Da (Figure 2a) involves loss of intact cysteinylglycine from the m/z 531 precursor that corresponds to a cysteinylglycine conjugate of an oxygenated form of glyceollins. Strongly supporting this

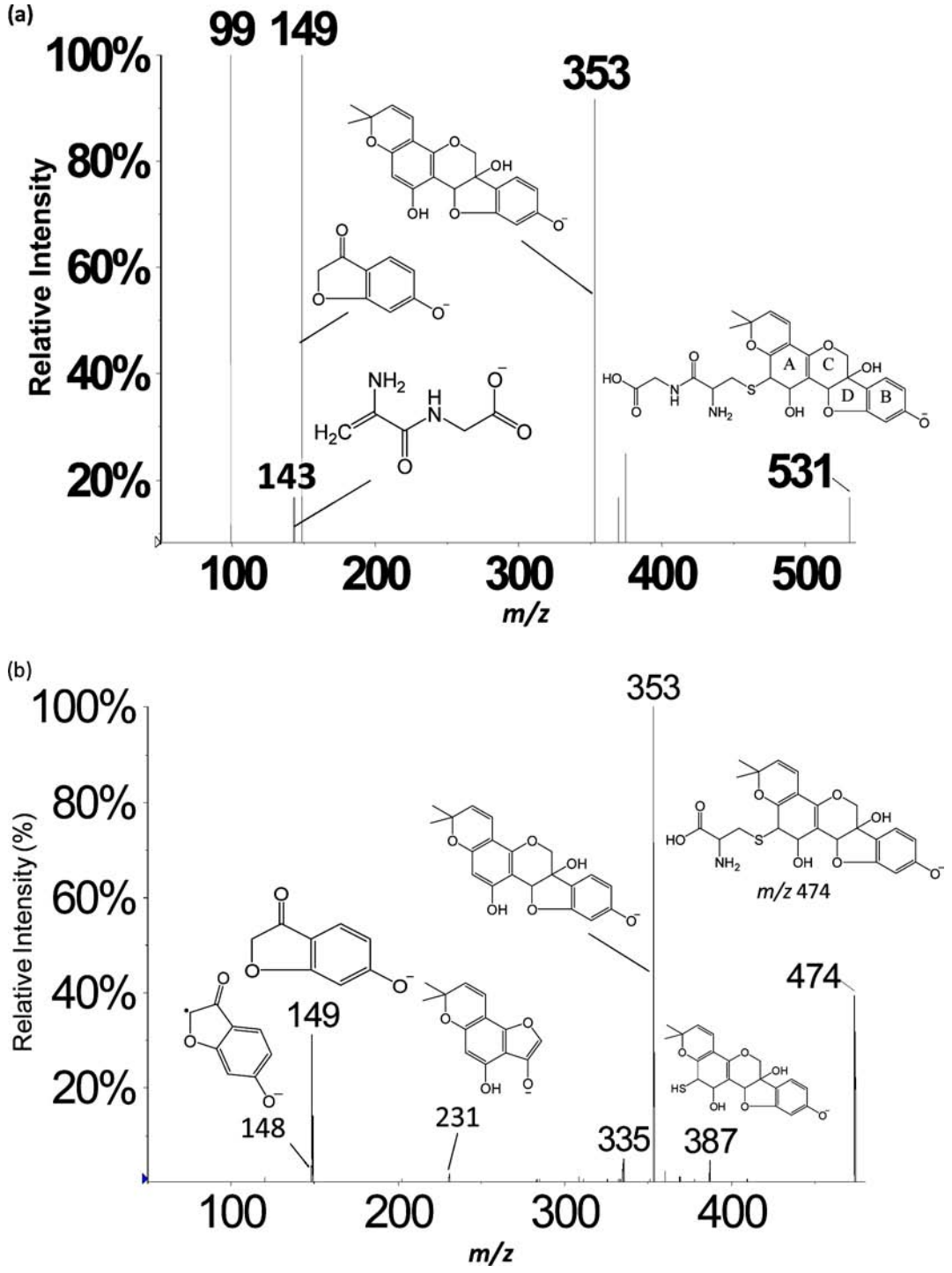

Figure 2. LC-ESI-MS/MS negative ion mode product ion mass spectra of (a) m/z 531 precursor and (b) m/z 474 precursor. One site of hydroxylation and one site of peptide addition are proposed; other isomeric structures may exist (see Scheme 1).

proposition is the appearance of a cysteinylglycine fragment ion at m/z 143 (Figure 2a). To complement this information, the 121 Da loss from the m/z 474 precursor (Figure 2b) is proposed to correspond to intact cysteine. The m/z 474 precursor is thus proposed to represent the cysteinyl conjugate of oxygenated glyceollins, which represents the second step in the metabolism of GSH conjugates via peptidase-mediated hydrolysis of the cysteinylglycine conjugate. Further evidence to support this assignment is given by the appearance of m/z 387 that corresponds to decomposition of the cysteine amino acid (Figure 2b).

The occurrence of GSH conjugation via glutathione S-transferases (GSTs) is often associated with electrophilic compounds or their metabolites.[33] With respect to phytochemicals, this pathway is the principal metabolic route in the metabolism of sulforophane,[34] which is derived from cruciferous vegetables and contains an isothiocyanate-based electrophile. Importantly, sulforophane possesses potent anticarcinogenic and cytoprotective properties[35,36] that are

dx.doi.org/10.1021/jf403498f | J. Agric. Food Chem. 2014, 62, 2692−2700

postulated to derive from its ability to induce expression of phase II enzymes, including GSTs.

Evidence obtained from the in vivo studies reported herein indicates that phase I-derived glyceollin metabolites detected in rat plasma, urine, and feces have undergone glutathione conjugation. Although NI mode LC-ESI-MS/MS CID product ion mass spectra of m/z 660 and 644 precursors (corresponding to potential oxygenated and nonoxygenated GSH-glyceollins, respectively) were acquired from rat plasma, urine, and feces samples, no intact glutathione conjugates of glyceollins were detected. This can be attributed to the fast kinetics of enzymatic glutamate cleavage[37] from the GSH–glyceollin complex that produces the cysteinylglyceine conjugate (m/z 531, Figure 2a). As mentioned above, the cysteinylglyceine conjugate can be subsequently metabolized to the cysteine conjugate. The product ion spectrum of the m/z 474 precursor (Figure 2b) corroborates the presence of cysteinyl conjugates of glyceollins. These proposed metabolites are observed in oxygenated forms (i.e., in addition to the cysteinyl sulfur linkage, an oxygen atom has been added). Complementing this finding, a +16 metabolite was also observed via precursor ion scanning following coincubation of 10 μM of the glyceollin isomeric mixture with NADPH in rat liver microsomes (data not shown). We propose that the addition of oxygen precedes the addition of GSH; initial formation of an epoxide would be consistent with this proposition. Enzymatic formation of epoxides followed by glutathione conjugation has been previously documented.[38,39] Epoxide formation at a double bond represents a reactive intermediate that is highly susceptible to GSH complex formation.

The CID product ion mass spectra of m/z 531 (Figure 2a) and 474 (Figure 2b) precursors each yield a fragment at m/z 353 corresponding to the loss of cysteinylglycine or cysteine, respectively, with abstraction of a neighboring hydrogen and double bond (or epoxide) formation on the glyceollins in each case. In addition, Figure 2a,b each shows the presence of m/z 149 (i.e., the B fragment ion formed from decomposition of the glyceollin backbone).[17] In our previous study, the CID product ion spectrum of the sulfated metabolite of glyceollins with an additional oxygen (m/z 433) showed B fragments (m/z 148 and 149) which were the same as those found for unmetabolized deprotonated glyceollins; however, A fragments (m/z 191 and 243) were shifted higher by 16 m/z units. These combined observations allowed the localization of oxygen attachment on glyceollins.[17] For the GSH enzymatic products, the appearance of the m/z 149 fragment suggests that the oxygen and cysteinylglyceine dipeptide or cysteine are not located on the B fragments. More importantly, the A fragment expected at m/z 215[17,40] has been shifted to m/z 231 (Figure 2b), thus indicating that oxygen addition had occurred on the A fragment. On the basis of our evidence for initial epoxidation followed by GSH attachment, combined with the CID data presented above, we conclude that there are four possible attachment sites for the initial oxygenated glutathione conjugates of glyceollins (Scheme 1); the oxygenated cysteinylglyceine and oxygenated cysteinyl–glyceollin conjugates would maintain these same sites of conjugation.

Assignments of oxygenated cysteinylglyceine- (m/z 531 in NI mode) and oxygenated cysteinyl–glyceollin conjugates (m/z 474 in NI mode) were further confirmed by acquiring data in the positive ion (PI) mode. Figure 3a,b show the PI mode LC-ESI-MS/MS CID product ion mass spectra of m/z 533

Scheme 1. Glutathione Conjugation to the Two Most Favorable Epoxide Forms of Glyceollin I

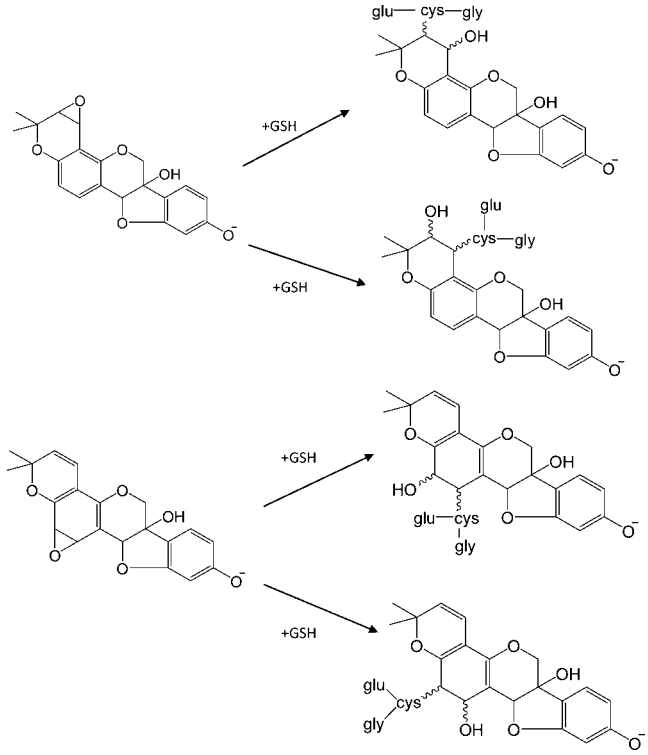

(protonated cysteinylglyceine glyceollins with an additional oxygen) and m/z 476 (protonated cysteinyl glyceollins with an additional oxygen). The appearance of m/z 355 corresponds to the loss of 178 Da from m/z 533 (Figure 3a) and 121 Da from m/z 476 (Figure 3b), indicating a loss of intact cysteinylglyceine or cysteine, respectively, that mirror the losses observed in the NI mode. Proposed fragment ion structures and decomposition mechanisms of oxygenated cysteinyl glyceollin are shown in Scheme 2. Because the CID product ion spectrum of oxygenated cysteinylglyceine glyceollins (m/z 533, Figure 3a) is similar to the CID product ion spectrum of oxygenated cysteinyl glyceollin (m/z 476, Figure 3b), the decomposition mechanisms for the two metabolites appear to be entirely analogous.

Cysteine conjugates can be further metabolized and acetylated, resulting in mercapturic acid conjugates.[41] However, these anticipated conjugates were not detected in precursor ion scans of m/z 148. Consequently, screening for mercapturic acid conjugates of glyceollins was directly performed by product ion scanning. The NI mode LC-ESI-MS/MS CID product ion mass spectrum of m/z 516 (corresponding to the previously detected oxygenated cysteinyl glyceollin, m/z 474, that had potentially undergone acetylation) was performed on rat plasma, urine, and feces samples. Only feces eluted a chromatographic peak corresponding to m/z 516 that appeared at 22.9 min. The NI mode LC-ESI-MS/MS CID product ion mass spectrum of the m/z 516 precursor showed a fragment at m/z 353 corresponding to the loss of mercapturic acid (163 Da), indicating that the precursor was indeed an oxygenated mercapturic acid conjugate of glyceollin. Other fragments similar to those in the CID product ion spectrum of deprotonated glyceollins were detected at m/z 148, 149, and 161; however, for reasons discussed below, in the case of glucuronide conjugation, the signal for m/z 148 was very low.

dx.doi.org/10.1021/jf403498f | J. Agric. Food Chem. 2014, 62, 2692–2700

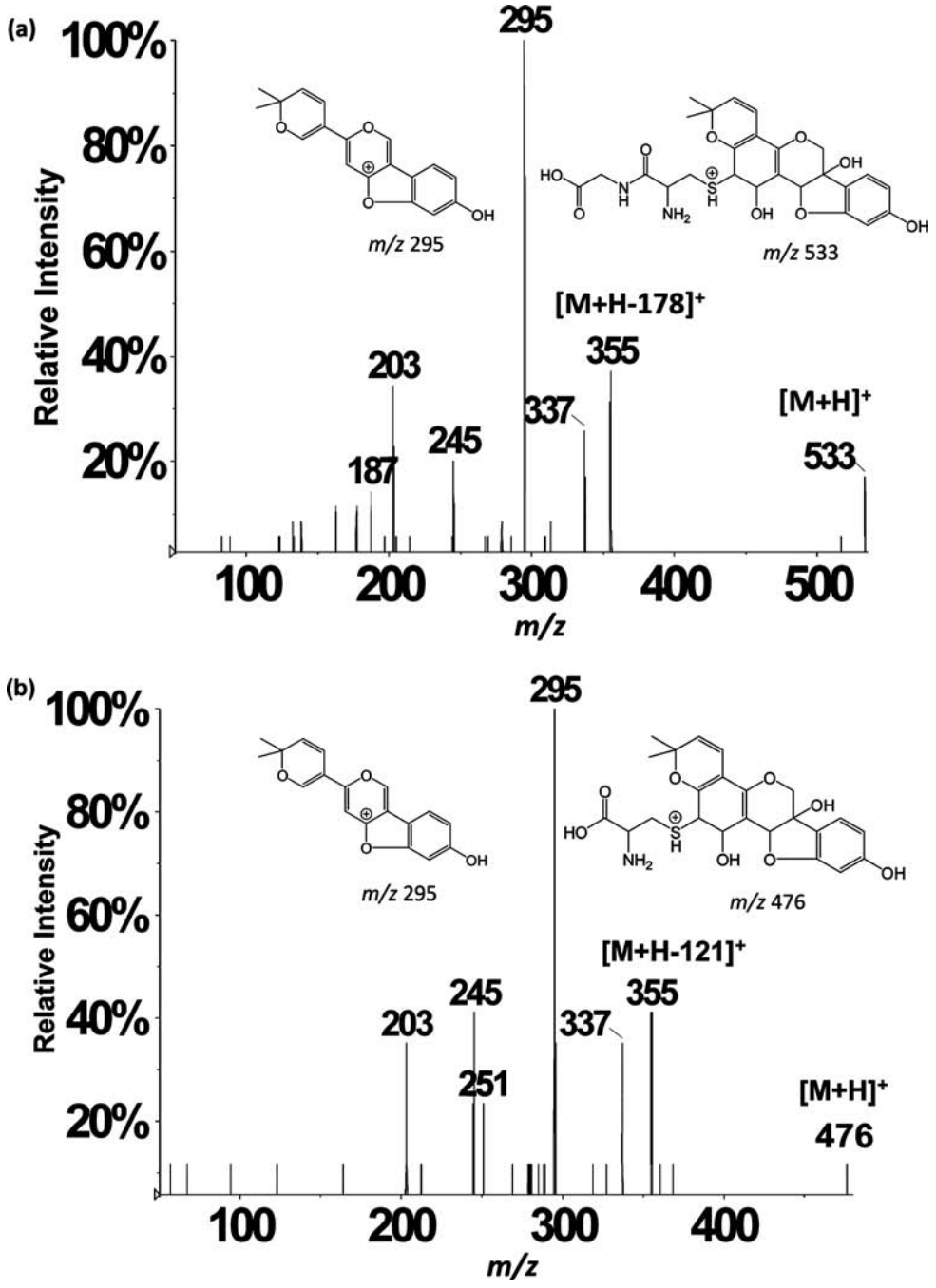

Figure 3. LC-ESI-MS/MS positive ion mode product ion mass spectra of (a) m/z 533 precursor and (b) m/z 476 precursor. Other isomeric forms of the assigned structures may also exist (see Scheme 1).

Absence of the mercapturic acid metabolite in plasma and urine may be due to insufficient formation of this metabolite upon a single dose (in contrast to multiple dosing of the rats that provided the source of the feces samples).

Glucuronidation of Glyceollins. Because glucuronide conjugates have been reported for isoflavones,[42−44] the decision was made to screen for glucuronide conjugates of glyceollins by performing product ion scans. In general, an addition of 176 Da in biological medium is well-documented to be characteristic of addition of glucuronic acid.[45,46] Thus, the LC-ESI-MS/MS CID product ion scan of m/z 513 was carried out on rat plasma, urine, and feces samples. A corresponding chromatographic peak appeared at 27.6 min from rat plasma and urine samples only. Absence of the glucuronide conjugate in feces is attributed to high levels of β-glucuronidase in the colon from bacteria.[26] The averaged product ion mass spectrum (Figure 4a) shows a peak at m/z 337 corresponding to deprotonated glyceollins produced after loss of glucuronic acid.[33] In addition, the highest abundance fragment appears at m/z 175. Even though a low abundance product ion at m/z 175 had been observed during CID of deprotonated glyceollins (m/z 337),[17,29] the high abundance of m/z 175 in Figure 4a is better rationalized as release of the glucuronate anion. No fragment ions in Figure 4 are shifted by 176 mass units relative to the product ions in the CID spectrum of m/z 337 (deprotonated glyceollins), indicating that the glucuronide moiety is the most labile

Scheme 2. Proposed Structures and Collision-Induced Dissociation Mechanisms of Oxygenated Cysteinyl Glyceollin I[a]

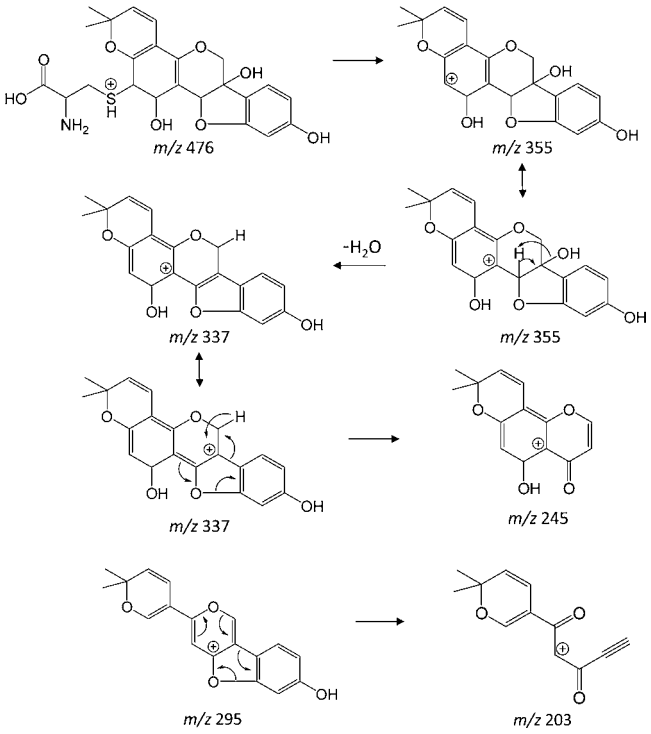

[a]One isomeric form of m/z 476 is shown, but others are possible (see Scheme 1).

substituent of the m/z 513 precursor. Accordingly, the other CID product ions are assigned as consecutive decompositions of m/z 337, including m/z 319 (water loss) and m/z 149 production. Interestingly, the m/z 148 ion was absent in these scans. This latter product ion is not always observed upon *consecutive* decompositions as it requires relatively high energy CID conditions.[17] That is, owing to the energy consumed in decomposing m/z 513 to m/z 337, less energy remains for m/z 337 to undergo consecutive decomposition, which results in more favorable kinetics for m/z 149 production relative to m/z 148. This also rationalizes the absence of m/z 513 in the scan for precursors of m/z 148.

Glucuronide conjugates of glyceollins for LC-ESI-MS/MS method development are not commercially available. Nonetheless, in vitro glucuronidation is often performed with the aid of uridine diphosphoglucuronosyl-transferase enzymes (UGTs).[27] The UGT enzymes are present in abundance in rat liver microsomes. Using this approach, glyceollins were exposed to rat liver microsomes to generate glucuronide conjugates of glyceollins. LC-ESI-MS/MS analyses were then carried out. The retention time and the similar fragmentation pattern in the product ion spectrum of m/z 513 (Figure 4b) from these in vitro incubations confirmed our assignment of the glucuronidated metabolite of glyceollins from rat plasma and urine samples.

To summarize our findings, LC-ESI-MS/MS analyses were carried out on a triple quadrupole to identify glyceollins and their metabolites from plasma, urine, and feces samples obtained from a 90 mg/kg single oral dose to rats (plasma and urine) or from 90 mg/kg/day for 14 days of dosing (feces). The precursor ion scan of m/z 148 allowed screening for the

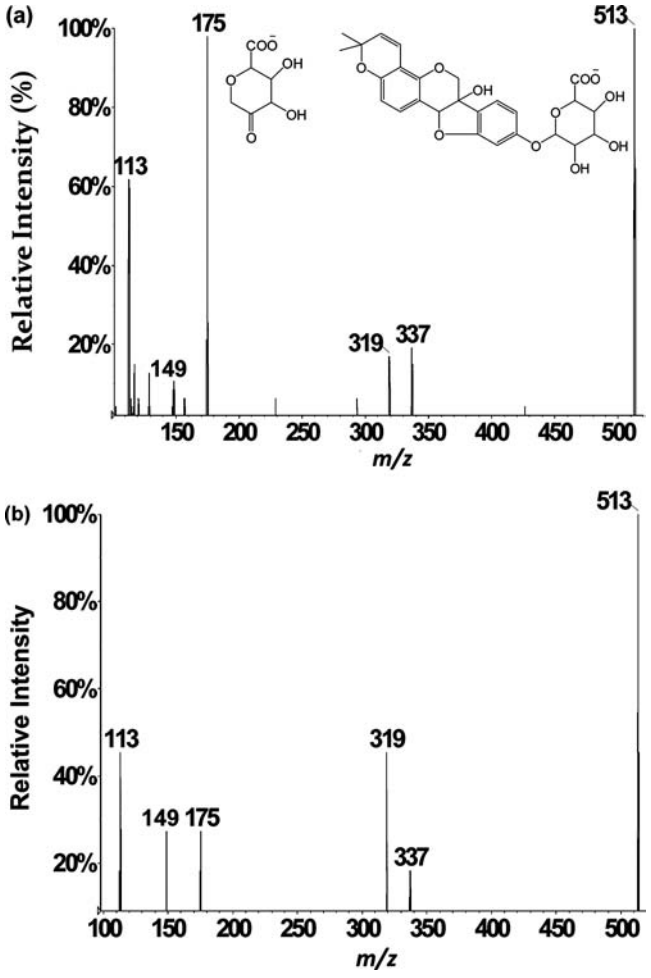

Figure 4. LC-ESI-MS/MS negative ion mode product ion spectrum of m/z 513 precursor corresponding to glucuronic acid conjugates of glyceollins acquired from (a) rat urine and (b) rat liver microsomes.

majority of the glyceollin-related compounds. Table 1 compiles a list of all metabolites found in plasma, feces, and urine of male ZDSD rats. Peaks of interest found at m/z 474 and 531 in all

Table 1. List of All Metabolites of Glyceollins Found in Plasma, Urine, and Feces[a]

	m/z value	plasma	urine	feces
phase I conjugation				
epoxidation or hydroxylation	353	√	n.d.	√
hydrolysis of a double bond	355	√	n.d.	n.d.
diol addition at a double bond	371	n.d.	√	√
diol addition at a double bond plus epoxidation or hydroxylation	387	n.d.	√	√
phase II conjugation				
sulfate conjugates	417	√	√	√
sulfate conjugates + oxygen	433	√	n.d.	√
sulfate conjugates with hydrolysis of a double bond	451	√	√	n.d.
glucuronide conjugate	513	√	√	n.d.
cysteinylglyceine + oxygen	531	√	√	√
cysteine + oxygen	474	√	√	√
mecapturic acid + oxygen	516	n.d.	n.d.	√

[a]The m/z values correspond to negative ion mode mass spectrometry. "n.d." indicates not detected.

Scheme 3. Summary of Glyceollin Metabolism in Male ZDSD Rats[a]

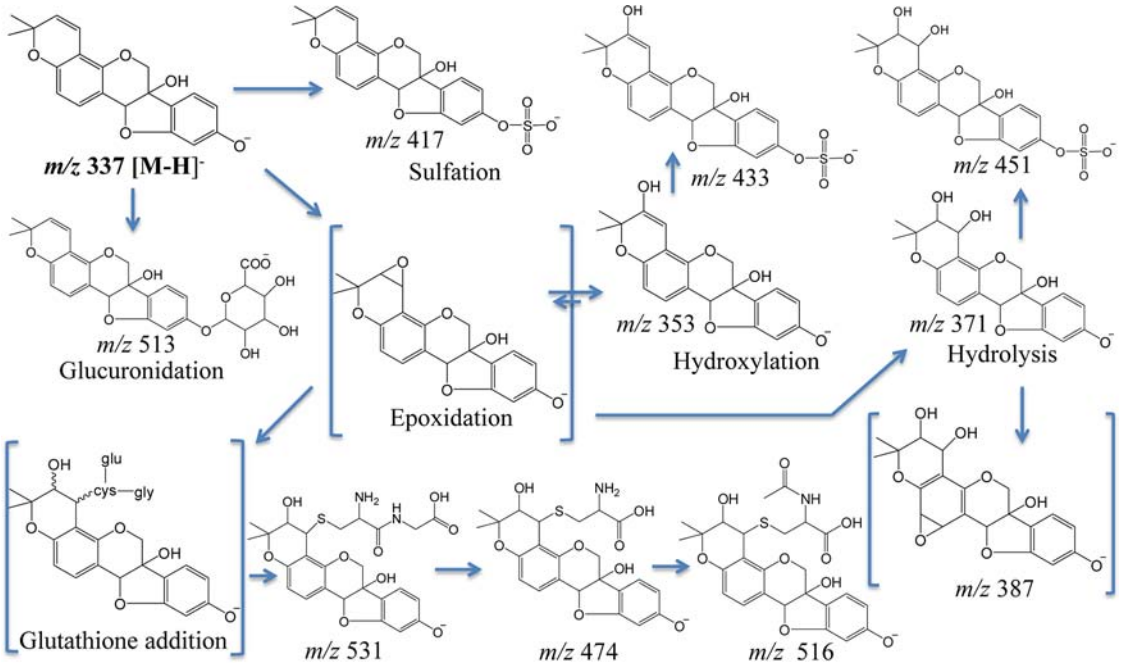

[a]Brackets surround structures most susceptible to further reaction. Structures proposed in this diagram are not intended to exclude the presence of certain other isomeric forms (see Scheme 1).

three samples were further investigated by product ion scanning. Tandem mass spectra of m/z 474 and 531 acquired in negative ion mode provided evidence for the glutathione conjugation pathway, and these two metabolites were identified as cysteinyl and cysteinylglyceine conjugates, respectively, of glyceollins with an addition of an oxygen. These assignments were substantiated by examining these conjugates in the positive ion mode. On the basis of this thorough analysis of samples derived primarily from in vivo administration of glyceollins, we proposed that the formation of the GSH-derived metabolites is preceded by epoxide formation (phase I metabolism). Four possible isomeric structures of the conjugates are proposed on the basis of tandem mass spectrometry fragmentation patterns (Scheme 1). Oxygenated forms of mercapturic acid conjugates of glyceollins (m/z 516) were found in rat feces but not in rat plasma or urine. Notably, metabolism of another phytochemical (i.e., sulforaphane) via GSH-conjugation is thought to be associated with the potent anticancer activity of this agent via induction of phase II enzymes to remove reactive oxygen species.[34] The possibility that glyceollin's promising antiproliferative effects are similarly derived from an ability to induce phase II enzymes merits exploration. With respect to the glucuronidation pathway, glucuronide conjugates of glyceollins were detected in rat plasma and urine but not in feces. Unlike the GSH conjugation pathway, glucuronidation was independent of phase I oxidation, as confirmed by in vitro glucuronidation of glyceollins by rat liver microsomes. A summary of all metabolic pathways is presented in Scheme 3.

To our knowledge, this is the first study to establish glutathione and glucuronide conjugation pathways of glyceollin metabolism. The scan for precursors of m/z 148 is thus a powerful method allowing the characterization of glyceollin metabolites, which may otherwise be difficult to pinpoint, such as the newly reported oxygenated GSH byproduct conjugates found here. These GSH byproduct conjugates yielded mostly neutral losses of the peptide portion during tandem mass spectrometry. Thus, these conjugates may have been overlooked if they were screened using conventional product ion scans that rely on the appearance of charged peptide fragments. Because the appearance of m/z 148 in precursor ion scans requires optimized CID energies, which may vary according to the particular metabolite, a caveat to this method is that all metabolites may not be detected using a single experimental condition (as was the case of mercapturic acid and glucuronide conjugates in this study). Moreover, if precursor CID does not release a conjugate that has adducted to the B fragment, then the m/z 148 ion may not be observed.

AUTHOR INFORMATION

Corresponding Author

*E-mail: richard.cole@upmc.fr. Fax: + 33 (0)1 44 27 38 43. Tel.: + 33 (0)1 44 27 32 63.

Funding

Financial support for this research was provided by the the National Science Foundation through CHE-1058764 (RBC). Additional financial support was provided by the MetaboHUB-ANR-11-INBS-0010 project (France), a Louisiana Cancer Research Consortium Seed Grant (OSP-7011-003) and through NIH RCMI 8G12MD007595-04 from the National Institute on Minority Health (RES). Lastly, access to a TGE FT-ICR FR3624 facility (France) and support for conducting the research is gratefully acknowledged.

Notes

The authors declare no competing financial interest.

ACKNOWLEDGMENTS

We thank Dr. Mark L. Heiman of NuMe Health for his expertise and input in designing the rat study. Dr. Denis McCann, Eli Lilly and Company, is also thanked for his advice

concerning metabolite extraction procedures. We thank Xavier pharmacy students, Mr. Chukwuemezie Chimezie and Ms. Adina Ewing, for their support in conducting liver microsome incubations and preparing the fecal extracts.

REFERENCES

(1) Hoyert, D.; Xu, J. *National Vital Statistics Reports* **2012**, *61*, 1−52.
(2) Xu, X.; Duncan, A. M.; Merz, B. E.; Kurzer, M. S. *Cancer Epidemiol., Biomarkers Prev.* **1998**, *7*, 1101−1108.
(3) Miyanaga, N.; Akaza, H.; Hinotsu, S.; Fujioka, T.; Naito, S.; Namiki, M.; Takahashi, S.; Hirao, Y.; Horie, S.; Tsukamoto, T.; Mori, M.; Tsuji, H. *Cancer Sci.* **2012**, *103*, 125−130.
(4) Barnes, S.; Prasain, J.; D'Alessandro, T.; Arabshahi, A.; Botting, N.; Lila, M. A.; Jackson, G.; Janle, E. M.; Weaver, C. M. *Food Funct.* **2011**, *2*, 235−244.
(5) Qi, W.; Weber, C. R.; Wasland, K.; Savkovic, S. D. *BMC Cancer* **2011**, *11*, 219.
(6) Boue, S. M.; Carter, C. H.; Ehrlich, K. C.; Cleveland, T. E. *J. Agric. Food Chem.* **2000**, *48*, 2167−2172.
(7) Burow, M. E.; Boue, S. M.; Collins-Burow, B. M.; Melnik, L. I.; Duong, B. N.; Carter-Wientjes, C. H.; Li, S.; W., T. E.; Cleveland, T. E.; McLachlan, J. A. *J. Clin. Endocrinol. Metab* **2001**, *86*, 1750−1758.
(8) Setchell, K. D. R., Adlercreutz, H. In *The Role of Gut Microflora in Toxicity and Cancer*; Rowland, I. A., Ed.; New York: Academic Press, 1988; pp 315−345.
(9) Miksicek, R. J. *Proc Soc Exp Biol Med.* **1995**, *208*, 44−50.
(10) Cassidy, A.; Bingham, S.; Setchell, K. *Br. J. Nutr.* **1995**, *74*, 587−601.
(11) Rhodes, L. V.; Tilghman, S. L.; Boue, S. M.; Wang, S.; Khalili, H.; Muir, S. E.; Bratton, M. R.; Zhang, Q.; Wang, G.; Burow, M. E.; Collins-Burrow, B. M. *Oncol. Lett.* **2012**, *3*, 163−171.
(12) Salvo, V. A.; Boue, S. M.; Fonseca, J. P.; Elliott, S.; Corbitt, C.; Collins-Burow, B. M.; Curiel, T. J.; Srivastav, S. K.; Shih, B. Y.; Carter-Wientjes, C.; Wood, C. E.; Erhardt, P. W.; Beckman, B. S.; McLachlan, J. A.; Cleveland, T. E.; Burow, M. E. *Clin. Cancer Res.* **2006**, *12*, 7159−7164.
(13) Zimmermann, C.; Tilghman, S. L; Boue, S. M; Salvo, V. A; Elliott, S.; Williams, K. Y.; Skripnikova, E. V.; Ashe, H.; Payton-Stewart, F.; Vanhoy-Rhodes, L.; Fonseca, J. P.; Corbitt, C.; Collins-Burow, B. M.; Howell, M. H.; Lacey, M.; Shih, B. Y.; Carter-Wientjes, C.; Cleveland, T. E.; McLachlan, J. A.; Wiese, T. E.; Beckman, B. S.; Burow, M. E. *J. Pharmacol. Exp. Ther.* **2010**, *332*, 35−45.
(14) Tilghman, S. L.; Boue, S. M.; Burow, M. E. *Mol. Cell. Pharmacol.* **2010**, *2*, 155−160.
(15) Wood, C. E.; Clarkson, T. B.; Appt, S. E.; Franke, A. A.; Boue, S. M.; Burow, M. E.; McCoy, T.; Cline, J. M. *Nutr. Cancer* **2006**, *56*, 74−81.
(16) Kim, H. J.; Lim, J.; Kim, W.; Kim, J. *Proc. Nutr. Soc.* **2012**, *71*, 166−174.
(17) Quadri, S. S.; Stratford, R. E.; Boué, S. M.; Cole, R. B. *Anal. Chem.* **2013**, *85*, 1727−1733.
(18) Gibson, G.; Skett, P. *Introduction to Drug Metabolism*; Blackie Academic and Professional, Champan & Hall: London, 1994.
(19) Maarit, H.; Antti, H.; Kristiina, W.; Herman, A. *J. Steroid Biochem. Mol. Biol.* **2003**, *87*, 285−299.
(20) Hu, M.; Krausz, K.; Chen, J.; Ge, X.; Li, J.; Gelboin, H. L.; Gonzalez, F. J. *Drug Metab. Dispos.* **2003**, *31*, 924−931.
(21) Chen, J.; Lin, H.; Hu, M. *Cancer Chemother. Pharmacol.* **2005**, *55*, 159−169.
(22) Hernandez-Montes, E.; Pollard, S. E.; Vauzour, D.; Jofre-Montseny, L.; Rota, C.; Rimbach, G.; Weinberg, P. D.; Spencer, J. P. E. *Biochem. Biophys. Res. Commun.* **2006**, *346*, 851−859.
(23) Graf, B. A.; Ameho, C.; Dolnikowski, G. G.; Milbury, P. E.; Chen, C.; Blumberg, J. B. *J. Nutr.* **2006**, *136*, 39−44.
(24) Manach, C.; Donovan, J. L. *Free Radical Res.* **2004**, *38*, 771−785.
(25) Kroon, P. A.; Clifford, M. N.; Crozier, A.; Day, A. J.; Donovan, J. L.; Manach, C.; Williamson, G. *Am. J. Clin. Nutr.* **2004**, *80*, 15−21.
(26) Liu, Y.; Hu, M. *Drug Metab. Dispos.* **2002**, *30*, 370−377.
(27) Bolling, B. W.; Court, M. H.; Blumberg, J. B.; Chen, C.-Y.O. *J. Nutr. Biochem.* **2010**, *21*, 498−503.
(28) Patel, K. R.; Adreadi, C.; Britton, R. G.; Horner-Glister, E.; Karmokar, A.; Sale, S.; Brown, V. A.; Brenner, D. E.; Singh, R.; Steward, W. P.; Gescher, A. J.; Brown, K. *Sci. Transl. Med.* **2013**, *5*, 1−12.
(29) Quadri, S. S.; Stratford R. E.; Boué; S. M.; Cole, R. B. *Proceedings of the 60th ASMS Conference on Mass Spectrometry and Allied Topics*, Vancouver, BC, May 22, 2012.
(30) Boué, S. M.; Isakova, I. A.; Burow, M. E.; Cao, H.; Bhatnagar, D.; Sarver, J. G.; Shinde, K. V.; Erhardt, P. W.; Heiman, M. L. *J. Agric. Food Chem.* **2012**, *60*, 6376−6382.
(31) Kemperman, R. F. J.; Horvatovich, P. L.; Hoekman, B.; Reijmers, T. H.; Muskiet, F. A. J.; Bischoff, R. *J. Proteome Res.* **2007**, *6*, 194−206.
(32) Quadri, S. S.; Stratford R. E.; S. M.; Cole, R. B. *Proceedings of the 61th ASMS Conference on Mass Spectrometry and Allied Topics*, Minneapolis, April 10, 2013.
(33) Dourado, D. F. A. R.; Fernandes, P. A.; Mannervik, B.; Ramos, M. J. *Chemistry* **2008**, *14*, 9591−9598.
(34) Watson, G. W.; Beaver, L. M.; Williams, D. E.; Dashwood, R. H.; Ho, E. *AAPS Journal* **2013**, DOI: 10.1208/s12248-013-9504-4.
(35) Fahey, J. W.; Talalay, P. *Food Chem. Toxicol.* **1999**, *37*, 973−979.
(36) Guerrero-Beltran, C. E.; Calderon-Oliver, M.; Pedraza-Chaverri, J.; Chirino, Y. I. *Exp. Toxicol. Pathol.* **2012**, *64*, 503−508.
(37) Binkley, F.; Nakamura, K. *J. Biol. Chem.* **1948**, *173*, 411.
(38) Boyland, E.; Williams, K. *Biochem. J.* **1965**, *94*, 190−197.
(39) Fjellstedt, T A; Allen, R H; Duncan, B K; Jakoby, W B. *J. Biol. Chem.* **1973**, *248*, 3702−3707.
(40) Simons, R.; Vincken, J.; Bohin, M. C.; Kuijpers, T. F. M.; Verbruggen, M. A.; Gruppen, H. *Rapid Commun. Mass Spectrom.* **2011**, *25*, 55−65.
(41) Ketterer, B.; Coles, B.; Meyer, D. J. *Environ. Health Perspect.* **1983**, *49*, 59−69.
(42) Shelnutt, S. R.; Cimino, C. O.; Wiggins, P. A.; Ronis, M. J.; Badger, T. M. *Am. J. Clin. Nutr.* **2002**, *76*, 588−594.
(43) Zhang, Y.; Song, T. T.; Cunnick, J. E.; Murphy, P. A.; Hendrich, S. *J. Nutr.* **1999**, *129*, 399−405.
(44) Zhang, Y.; Hendrich, S.; Murphy, P. A. *J. Nutr.* **2003**, *133*, 399−404.
(45) Yang, P.; Ebbert, J. O.; Sun, Z.; Weinshilboum, R. M. *J. Clin. Oncol.* **2006**, *24*, 1761−1769.
(46) Gu, J. K.; Zhong, D. F.; Chen, X. Y. *Fresenius' J. Anal. Chem.* **1999**, *365*, 553−558.

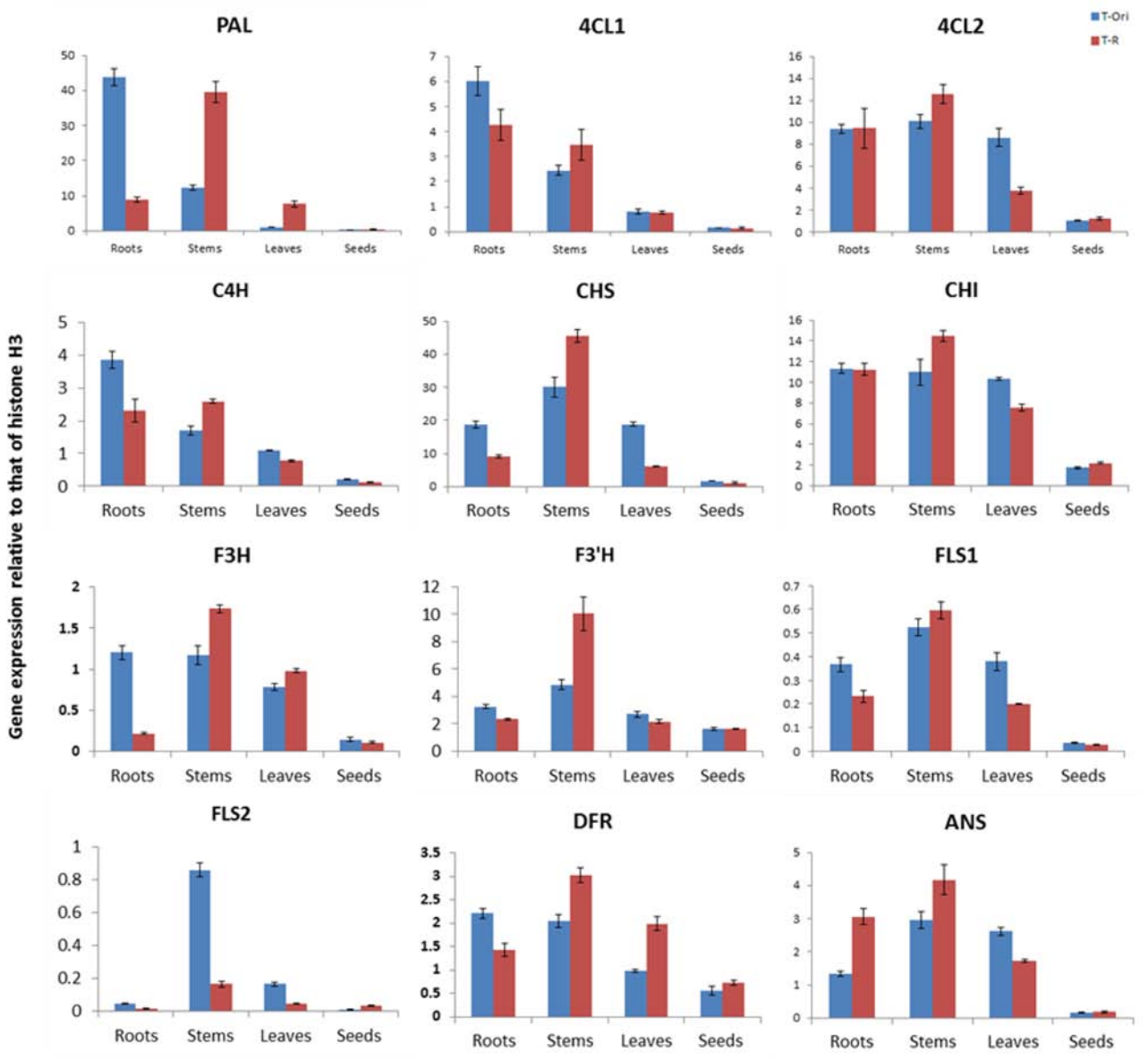

Figure 1. Expression levels of flavonoid biosynthesis genes in two different cultivars of *Fagopyrum esculentum*. T-Ori indicates Tanno-original common buckwheat; T-R indicates Tanno-rutin cultivar. The expression level of each gene is relative to that of the constitutively expressed histone H3 gene. Each value is the mean of three replicates ± SD.

MATERIALS AND METHODS

Plant Materials and Culture Conditions. Two common buckwheat cultivars, 'Tanno-Hiushinai original line' (Tanno-original) and 'Tanno-Hiushinai high rutin line' (Tanno-rutin) were bred by the Hokkaido Agricultural Research Center (Hokkaido, Japan). Seeds of the two buckwheat cultivars were germinated and cultured in a greenhouse (25 °C, 50% humidity) at Chungnam National University (Daejeon, Korea). The various plant organs were harvested when seeds were mature. Samples were rapidly frozen in liquid nitrogen after collection and stored at −80 °C until analysis.

Total RNA Extraction and Quantification of Gene Expression. Total RNA was isolated from samples of *F. esculentum* using an RNeasy Plant Mini Kit (Qiagen, Valencia, CA). For quantitative real-time polymerase chain reaction (qRT-PCR), 1 μg of total RNA was reverse transcribed using the Superscript II First-Strand Synthesis Kit (Invitrogen, Carlsbad, CA) and an oligo$(dT)_{20}$ primer.

Transcription levels were analyzed by qRT-PCR. The gene-specific primer sets were designed for qRT-PCR as described previously.[20] Gene expression was normalized to that of the histone H3 gene as a housekeeping gene.[21] QRT-PCR reactions were performed in triplicate on a MiniOpticon system (Bio-Rad Laboratories, Hercules, CA) with the Quantitect SYBR Green PCR Kit (Qiagen, Valencia, CA). The PCR protocol was as follows: denaturation for 5 min at 95 °C followed by 40 cycles of denaturation for 15 s at 95 °C, annealing for 15 s at 56 °C, and elongation for 20 s at 72 °C. PCR results were calculated as the mean of three replicated treatments.

Extraction of Flavonoids in Buckwheat. Plant materials were freeze-dried and then ground to a powder before extraction using methods described previously with some modification.[22] Powdered samples (0.10 g) were extracted with 5 mL of 80% methanol (MeOH) containing 10% acetic acid (0.1% v/v); this was followed by vortexing for 5 min at room temperature, and then the samples were extracted for 1 h at 37 °C, with 1 min of vortex every 20 min. After centrifugation at 1000 × g for 5 min, the supernatant was filtered and used for analysis.

Quantitative Analysis of Phytochemicals by HPLC. External standards were purchased from Extrasynthese (Genay, France). HPLC-grade methanol (MeOH) was purchased from Wako Pure Chemical Industries (Osaka, Japan). Acetic acid was provided from

dx.doi.org/10.1021/jf4049534 | J. Agric. Food Chem. 2014, 62, 2701−2708

Jun Sei Chemical Co., Ltd. (Kyoto, Japan). For HPLC analysis, extracts were filtered through a 0.45-μm poly filter and diluted 2-fold with MeOH prior to HPLC analysis. Samples were determined using a Futecs model NS-4000 HPLC apparatus (Daejeon, Korea) with a UV−vis detector and autosampler. The analysis was monitored at 280 nm and performed using a C18 column (250 mm × 4.6 mm, 5 μm; RStech, Daejeon, Korea). The mobile phase consisted of a mixture of (A) MeOH/water/acetic acid (5:92.5:2.5, v/v/v) and (B) MeOH/water/acetic acid (95:2.5:2.5, v/v/v); the procedure was described previously.[23] The initial mobile phase composition was 0% solvent B, followed by a linear gradient from 0% to 80% of solvent B in 48 min, then holding at 0% solvent B for an additional 10 min, and the column was maintained at 30 °C. The flow rate was set at 1.0 mL/min, and the injection volume was 20 μL. Quantification of the different compounds was based on peak areas and calculated as equivalents of representative standard compounds. All contents were expressed as microgram per milligram dry weight.

GC-TOFMS Analysis of Polar Metabolites. Polar metabolite extraction was performed as described previously.[24] A total of 20 mg of ground sample was extracted with 1 mL of a mixed solvent of methanol/water/chloroform (2.5:1:1, v/v/v). Ribitol solution (120 μL, 0.2 mg/mL) was added as an internal standard (IS). Extraction was performed at 37 °C with a mixing frequency of 1200 rpm for 30 min, using a thermomixer compact (Eppendorf AG, Germany). The solutions were then centrifuged at 16000 × g for 3 min. The polar phase (0.8 mL) was transferred into a new tube, and 0.4 mL of water was added before centrifugation to separate the nonpolar phase. The mixed contents of the tube were centrifuged at 16000 × g for 3 min. The methanol/water phase containing hydrophilic metabolites was dried in a centrifugal concentrator (CVE-2000, Eyela, Japan) for 2 h, followed by drying in a freeze-dryer for 16 h. Methoxime (MO) derivatization was performed by addition of 160 μL of methoxyamine hydrochloride (20 mg/mL) in pyridine and shaking at 30 °C for 90 min. Trimethylsilyl (TMS) etherification was performed by addition of 160 μL of MSTFA at 37 °C for 30 min. GC-TOFMS was performed using an Agilent 7890A gas chromatograph (Agilent, Atlanta, GA, USA) coupled to a Pegasus HT TOF mass spectrometer (LECO, St. Joseph, MI). Derivatized sample (1 μL) was separated on a fused-silica capillary column (30 m × 0.25 mm id) coated with 0.25 mm of CP-SIL 8 CB low bleed (Varian Inc., Palo Alto, CA, USA). The split ratio was set at 1:25. The injector temperature was 230 °C, and the flow rate of helium through the column was 1.0 mL/min. The temperature program was as follows: initial temperature of 80 °C for 2 min, followed by an increase to 320 °C at 15 °C/min, and a 10 min hold at 320 °C. The transfer line and ion-source temperatures were 250 and 200 °C, respectively. The scanned mass range was 85−600 m/z, and the detector voltage was set at 1700 V. The quantification of each analyte was based on the peak area ratio relative to that of the IS.

Statistical Analysis. Each result shown in the figure or table was the mean of three replicated treatments. Data were expressed as the mean of three independent replicates. The significant differences between treatments were statistically evaluated by the statistical analysis software (SAS), version 8.2. The GC-TOFMS data were subjected to principal component analysis (PCA) (SIMCA-P, version 13.0, Umetrics, Umeå, Sweden) to evaluate similarity/dissimilarity among groups of multivariate data. The PCA output consisted of score plots to visualize the contrast between samples and loading plots to explain the cluster separation. Unit variance scaling was used without transformation of the data.

RESULTS AND DISCUSSION

Expression of Flavonoid Biosynthetic Genes in Buckwheat. The flavonoid biosynthetic pathway is well described in plants. In this study, expression of ten flavonoid biosynthetic pathway genes (*FePAL*, *FeC4H*, *Fe4CL*, *FeCHS*, *FeCHI*, *FeF3H*, *FeF3′H*, *FeFLS*, *FeDFR*, and *FeANS*) was detected in the two cultivars of common buckwheat by qRT-PCR (Figure 1). Most genes, *FePAL*, *Fe4CL1*, *Fe4CL2*, *FeC4H*, *FeCHS*, *FeCHI*, *FeF3H*, *FeF3′H*, *FeDFR*, and *FeANS*, showed higher transcription levels in stems of the high-rutin cultivar compared with the original cultivar. In particular, the PAL gene, which plays a primary role in the flavonoid biosynthetic pathway, showed 3- and 4-fold higher expression in stems and leaves of the high-rutin cultivar. Compared with the original cultivar, *FeC4H*, *FeF3H*, and *FeDFR* also maintained higher transcript level in leaves of the high-rutin cultivar. However, the transcription levels of *FePAL*, *Fe4CL1*, *FeC4H*, *FeCHS*, *FeF3H*, *FeF3′H*, *FeFLS1*, and *FeDFR* were higher in roots of the original cultivar.

Transcription of isoforms or multicopies of CHS, CHI, 4CL, F3H, and FLS has shown the different expression levels on the regulation of the flavonoid biosynthetic pathway in many plants.[25−29] 4CL is involved in lignification and flavonoid biosynthesis; 4CL ligates coenzyme A (CoA) with hydroxycinnamic acids, such as 4-coumaric acid and caffeic acid to form the corresponding CoA thioesters.[30,31] In the present study, two 4CL isoform genes showed different transcriptional levels in buckwheat organs, and both genes exhibited higher expression in the roots and stems of buckwheat than in the leaves and seeds. This result is consistent with the physiological and morphological structures of the buckwheat plant. *Fe4CL2* showed higher activity than *Fe4CL1* in the two buckwheat cultivars (Figure 2); in particular, the highest level of *Fe4CL2* was observed in the stems of the high-rutin cultivar. Overall, our results indicated that the two 4CL isoforms may have the different functions in lignification and flavonoid biosynthesis in buckwheat. FLS is an important enzyme in the synthesis of quercetin, which is the precursor of rutin.[32] Two FLS isoform genes have been reported in tartary buckwheat, which showed differential expression and regulation levels in different buckwheat cultivars and under stress conditions.[32] In the present study, the two FLS isoform genes exhibited differential transcriptional levels in the original and high-rutin common buckwheat cultivars. Our results indicated that expression of *FeFLS2* was obviously higher in seeds of the high-rutin cultivar than seeds of the original cultivar (Figure 2). The expression level of *FeFLS1* in seeds was not significantly different between the cultivars. However, expression of *FeFLS2* in roots, stems, and leaves was 2−4 times higher in the original than in the high-rutin cultivar.

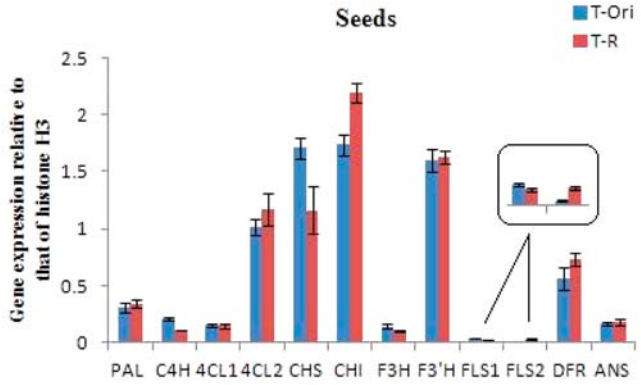

Figure 2. Expression levels of flavonoid biosynthesis genes in seeds of two different cultivars of *Fagopyrum esculentum*. T-Ori indicates Tanno-original common buckwheat; T-R indicates Tanno-rutin cultivar. The expression level of each gene is relative to that of the constitutively expressed histone H3 gene. Each value is the mean of three replicates ± SD.

dx.doi.org/10.1021/jf4049534 | J. Agric. Food Chem. 2014, 62, 2701−2708

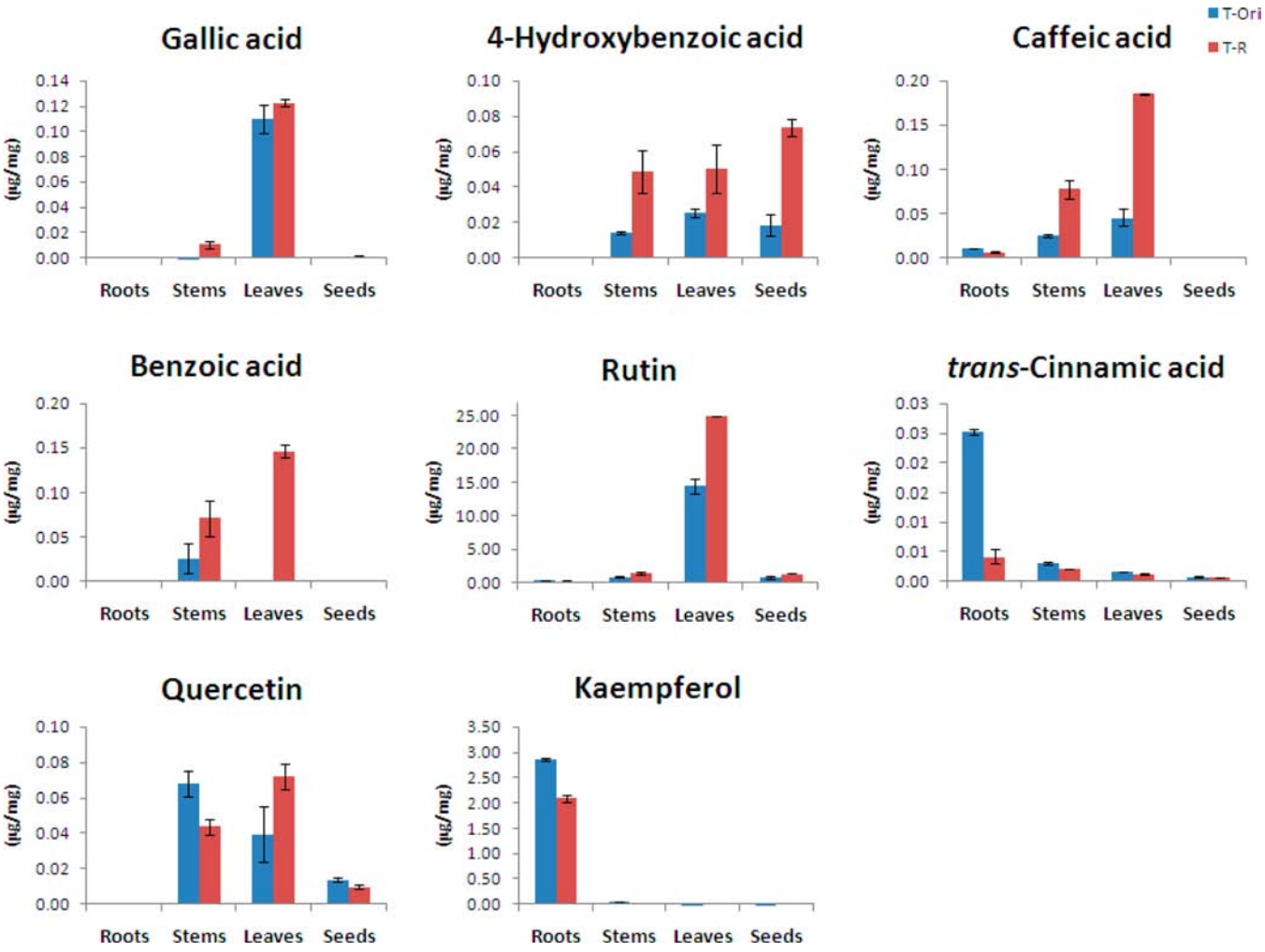

Figure 3. The accumulation of phytochemicals in two *Fagopyrum esculentum* cultivars. The plotted data and error bars indicate the means and variance of duplicate individual experiments. Each value is the mean of three replicates ± SD.

Phytochemical Content in Buckwheat. The compounds gallic acid, 4-hydroxybenzoic acid, caffeic acid, benzoic acid, rutin, *trans*-cinnamic acid, quercetin, and kaempferol were detected by HPLC analysis (Figure 3). Gallic acid, 4-hydroxybenzoic acid, caffeic acid, benzoic acid, and rutin were highly detected in leaves and stems of the high-rutin cultivar. *trans*-Cinnamic acid was 6-fold higher in roots of the original cultivar, and kaempferol was higher in roots than in other organs, particularly in the original cultivar. The primary active component, rutin, showed the highest levels of accumulation in leaves, followed by stems and seeds, and roots contained the lowest levels of this compound. Rutin content in leaves, stems, and seeds of the high-rutin cultivar were 24.86, 1.46, and 1.36 μg/mg, respectively, which was 1.73-, 1.62-, and 1.77-fold higher than that in the original buckwheat cultivar.

Buckwheat is a beneficial and healthy source of dietary rutin, and it has excellent rutin levels compared with those in other crops.[33−36] Rutin content in buckwheat depends on the variety and environmental factors.[37−40] Rutin content has shown significant variations in different growth stages of different *Fagopyrum* species.[37] The results of our study also proved that the quality of buckwheat, especially rutin content could be improved by breeding method. Our results indicated that the higher rutin content in high-rutin cultivar seeds may be directly related to *FtFLS2*, which showed higher expression levels in high-rutin cultivar seeds (Figure 2). However, even the expression pattern of PAL is correlated with its direct product, cinnamic acid, in the roots of buckwheat; this trend was not observed in the stems and leaves of the two buckwheat cultivars. The relationship between rutin content and gene expression of PAL and CHS did not show any obvious positive or negative correlation, this result was not consistent with the finding of a previous study.[37] Our results showed that the levels of flavonoid biosynthetic genes did not clearly correlate with rutin and other flavonoids in buckwheat. Similar results have been reported by previous studies,[32,41−43] which leads us to speculate that these results may be attributable to the dynamic transport of metabolites during physiological and morphological processes in plants. Otherwise, the rutin-degrading enzyme would be another factor that influences the rutin levels in different organs of buckwheat.[44,45] In addition, secondary metabolism in plants is complicated; it could be co-regulated by a complex set of regulatory networks, that is, by not only structural genes but also other classes of genes, including regulators, modifiers, transporters, and elicitors.[38,39,46−48] cDNA amplified fragment length polymorphism (AFLP) has shown that several factors involved in the regulation, metabolism, signaling, and transport of secondary metabolites contribute to the higher rutin content and overall nutritional superiority of rice-tartary over common buckwheat,[48] Study of

dx.doi.org/10.1021/jf4049534 | J. Agric. Food Chem. 2014, 62, 2701−2708

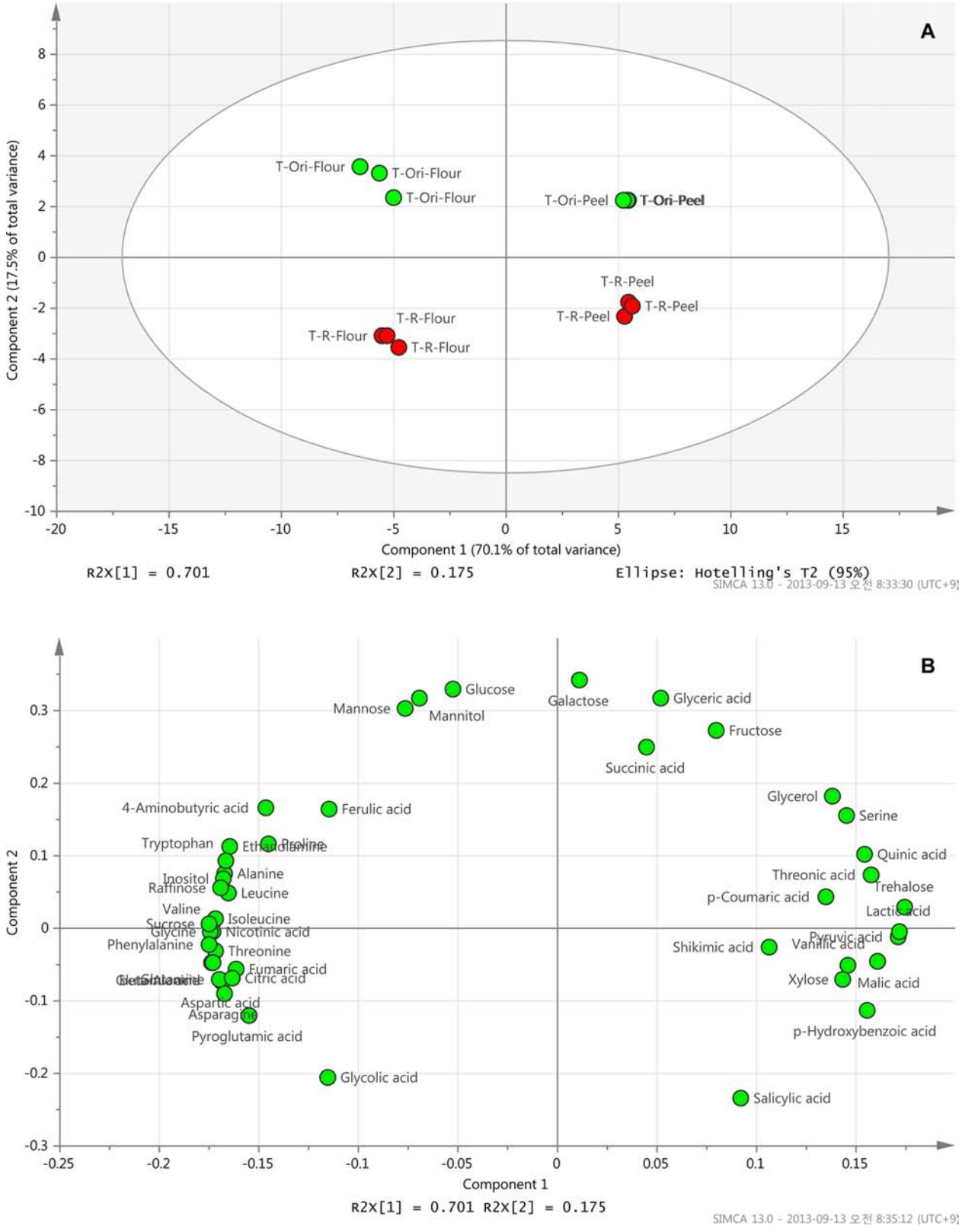

Figure 4. Scores (A) and loading plots (B) of principal components 1 and 2 of the PCA results from polar metabolite data for Tanno-rutin and Tanno-original buckwheat cultivars. T-Ori indicates Tanno-original common buckwheat; T-R indicates Tanno-rutin cultivar.

the differences in rutin or other nutritional content between Tanno-original and Tanno-rutin cultivars may be required.

Metabolic Profiling of Buckwheat. The production of secondary metabolites is strongly associated with primary metabolism pathways. Thus, we conducted comprehensive metabolic phenotyping of the primary metabolism in the peels and flower organs of buckwheat. GC-TOFMS has been one of the most popular metabolomic techniques because it can

dx.doi.org/10.1021/jf4049534 | J. Agric. Food Chem. 2014, 62, 2701−2708

determine the levels of primary metabolites such as amino acids, organic acids, and sugars by using chemical derivatization of these hydrophilic metabolites. In this study, low-molecular-weight molecules from peels and flower organs were identified using GC-TOFMS. The advantages of GC-TOFMS are the relatively high reproducibility and possible adaption for high-throughput analysis because of its rapid spectrum accumulation times. Furthermore, use of mathematical algorithms for deconvolution of closely overlapping peaks is possible because of the high mass-spectrum similarities among peaks. Forty-six metabolites, including 17 amino acids, 17 organic acids, 8 sugars, 3 sugar alcohols, and 1 amine, were detected in the peels and seed flour of two cultivars of *F. esculentum* by using GC-TOFMS (Supplementary Figure S1 and Table S1, Supporting Information). Quantification was performed using selected ions (Supplementary Table S1, Supporting Information).

According to the PCA analysis (Figure 4), the two highest-ranking principal components (PCs) accounted for 87.3% of the total variance within the data set. The first PC (PC1), accounting for 70.1% of total variance, resolved the measured metabolite profiles of buckwheat peels and flour. The second PC (PC2, 17.5% of total variance) differentiated the high-rutin from the original cultivar. There was a clear absence of significant variance within tissues of the same cultivar. PCA enables identification of compounds that exhibit the greatest variance within a population and allows closely related compounds to be identified. In PC2, the variation was mainly attributable to galactose and glucose, for which the eigenvectors were 0.34217 and 0.32803, respectively. The building blocks for secondary metabolites are derived from primary metabolism. Rutin (also called quercetin-3-*O*-rutinoside and sophorin) is the glycoside between the flavonol quercetin and the disaccharide rutinose. Thus, the levels of endogenous glucose may be lower in the high-rutin cultivar than in the low-rutin cultivar because of glycosylation reactions.[49,50] Our results suggest that these metabolites were present in lower quantities in the Tanno-rutin buckwheat than in Tanno-original. Our results showed that buckwheat peels contained amino acids and carbohydrates similar to those in flour. Tanno-original buckwheat contained a particularly high level of carbohydrates (fructose, glucose, mannose, mannitol, and sucrose) in both peels and flour (Supplementary Table S2, Supporting Information).

In this study, metabolites and flavonoid biosynthetic pathway-related genes were compared between Tanno-original and Tanno-rutin, two cultivars of common buckwheat. We found that the Tanno-rutin cultivar generally had higher rutin content in the aerial plant, indicating it could be a good alternative to culture for agricultural usage. Previously, it has been reported that hulls and flour of common buckwheat contained phenolics, flavonols, and procyanidins, and that flavonoids were more abundant in hulls than in flour.[51] The bran is considered a byproduct of buckwheat and has been proven to be a good source of flavonoids with antioxidant and antibacterial activities.[51,52] In this study, we reported the metabolites in peels and flours of the two buckwheat cultivars, which provided nutritional information about the seeds of these cultivars. The hydrophilic metabolite profile is closely related to an organism's phenotype and reveals important nutritional characteristics.[53,54] The differences between these two buckwheat cultivar seeds were identified by PCA results from the metabolite data. Even Tartary buckwheat has a high content of rutin,[3,4] but common buckwheat is cultivated more widely worldwide. This is the first report to present the theoretical basis for the high rutin content in a common buckwheat cultivar by employing the metabolomic method of analysis.

■ ASSOCIATED CONTENT

Ⓢ Supporting Information

Metabolites identified in peels and seed flour of the two cultivars and results of PCA. This material is available free of charge via the Internet at http://pubs.acs.org.

■ AUTHOR INFORMATION

Corresponding Author

*S. U. Park. Phone: +82-42-821-5730. Fax: +82-42-822-2631. E-mail: supark@cnu.ac.kr.

Author Contributions

§Xiaohua Li and Jae Kwang Kim contributed equally to this work.

Funding

This work (K11101) was supported by the Korea Institute of Oriental Medicine (KIOM) grant funded by the Korea government and also partially carried with the support of "Next-Generation BioGreen 21 Program (SSAC, Project No. 009520)" Rural Development Administration, Republic of Korea.

Notes

The authors declare no competing financial interest.

■ ACKNOWLEDGMENTS

We thank Dr.Tastsuro Suzuki (Hokkaido Agricultural Research Center, National Agriculture and Food Research Organization, Japan) for providing two common buckwheat cultivars, 'Tanno-Hiushinai original line' and 'Tanno-Hiushinai high rutin line', used in this work.

■ ABBREVIATIONS USED

HPLC, high-performance liquid chromatography; PAL, phenylalanine ammonium lyase; C4H, cinnamic acid 4-hydroxylase; CHI, chalcone isomerase; CHS, chalcone synthase; 4CL, 4-coumarate-CoA ligase; DFR, dihydroflavonol reductase; F3H, flavanone-3-hydroxylase; F3′H, flavonoid-3′-hydroxylase; FLS, flavonol synthase; ANS, anthocyanin synthase

■ REFERENCES

(1) Zhebrak, E. A.; Shirshov, V. A.; Kolchin, N. M. Fractional and amino acid composition of the proteins of diploid and tetraploid buckwheat. *Dokl. Akad. Nauk SSSR* **1967**, *174*, 975−977.

(2) Rokka, S.; Ketoja, E.; Jarvenpaa, E.; Tahvonen, R. The glycaemic and C-peptide responses of foods rich in dietary fibre from oat, buckwheat and lingonberry. *Int. J. Food Sci. Nutr.* **2013**, *64*, 528−534.

(3) Jiang, P.; Burczynski, F.; Campbell, C.; Pierce, G.; Austria, J. A.; Briggs, C. J. Rutin and flavonoid contents in three buckwheat species *Fagopyrum esculentum*, *F. Tataricum*, and *F. Homotropicum* and their protective effects against lipid peroxidation. *Food Res. Int.* **2007**, *40*, 356−364.

(4) Zielinska, D.; Turemko, M.; Kwiatkowski, J.; Zielinski, H. Evaluation of flavonoid contents and antioxidant capacity of the aerial parts of common and tartary buckwheat plants. *Molecules (Basel, Switzerland)* **2012**, *17*, 9668−9682.

(5) Peng, L. X.; Wang, J. B.; Hu, L. X.; Zhao, J. L.; Xiang, D. B.; Zou, L.; Zhao, G. Rapid and simple method for the determination of emodin in tartary buckwheat (*Fagopyrum tataricum*) by high-performance liquid chromatography coupled to a diode array detector. *J. Agric. Food Chem.* **2013**, *61*, 854−857.

(6) Sytar, O.; Brestic, M.; Rai, M. Possible ways of fagopyrin biosynthesis and production in buckwheat plants. *Fitoterapia* **2013**, *84*, 72−79.
(7) Ren, Q.; Wu, C.; Ren, Y.; Zhang, J. Characterization and identification of the chemical constituents from tartary buckwheat (*Fagopyrum tataricum* Gaertn) by high performance liquid chromatography/photodiode array detector/linear ion trap fticr hybrid mass spectrometry. *Food Chem.* **2013**, *136*, 1377−1389.
(8) Wang, M.; Liu, J. R.; Gao, J. M.; Parry, J. W.; Wei, Y. M. Antioxidant activity of tartary buckwheat bran extract and its effect on the lipid profile of hyperlipidemic rats. *J. Agric. Food Chem.* **2009**, *57*, 5106−5112.
(9) Wroblewska, M.; Brzuzan, L.; Jaroslawska, J.; Zdunczyk, Z. Effect of buckwheat sprouts and groats on the antioxidant potential of blood and caecal parameters in rats. *Int. J. Vitam. Nutr. Res.* **2011**, *81*, 286−294.
(10) Sedej, I.; Sakac, M.; Mandic, A.; Misan, A.; Tumbas, V.; Canadanovic-Brunet, J. Buckwheat (*Fagopyrum esculentum* Moench) grain and fractions: Antioxidant compounds and activities. *J. Food Sci.* **2012**, *77*, C954−C959.
(11) Guo, X.; Zhu, K.; Zhang, H.; Yao, H. Anti-tumor activity of a novel protein obtained from tartary buckwheat. *Int. J. Mol. Sci.* **2010**, *11*, 5201−5211.
(12) Durendic-Brenesel, M.; Popovic, T.; Pilija, V.; Arsic, A.; Milic, M.; Kojic, D.; Jojic, N.; Milic, N. Hypolipidemic and antioxidant effects of buckwheat leaf and flower mixture in hyperlipidemic rats. *Bosnian J. Basic Med. Sci.* **2013**, *13*, 100−108.
(13) Stringer, D. M.; Taylor, C. G.; Appah, P.; Blewett, H.; Zahradka, P. Consumption of buckwheat modulates the post-prandial response of selected gastrointestinal satiety hormones in individuals with type 2 diabetes mellitus. *Metabolism* **2013**, *62*, 1021−1031.
(14) Lee, C. C.; Shen, S. R.; Lai, Y. J.; Wu, S. C. Rutin and quercetin, bioactive compounds from tartary buckwheat, prevent liver inflammatory injury. *Food Funct.* **2013**, *4*, 794−802.
(15) Oomah, B. D.; Campbell, C.; Mazza, G. Effects of cultivar and environment on phenolic acids in buckwheat. *Euphytica* **1996**, *90*, 73−77.
(16) Ölschläger, C.; Regos, I.; Zeller, F. J.; Treutter, D. Identification of galloylated propelargonidins and procyanidins in buckwheat grain and quantification of rutin and flavanols from homostylous hybrids originating from *F. Esculentum*×*F. Homotropicum*. *Phytochemistry* **2008**, *69*, 1389−1397.
(17) Sun, Z.; Hou, S.; Yang, W.; Han, Y. Exogenous application of salicylic acid enhanced the rutin accumulation and influenced the expression patterns of rutin biosynthesis related genes in *Fagopyrum tartaricum* Gaertn leaves. *Plant Growth Regul.* **2012**, *68*, 9−15.
(18) Sun, C. X.; Hou, S. Y.; Yang, W. D. Effect of exogenous L-phentermine and UV-C on the accumulation of rutin compounds and the expression of rutin biosynthesis genes in *Fagopyrum tartaricum*. *China Agric. Sci.* **2011**, *44*, 4772−4780.
(19) Alekseeva, I. V. Evaluation of buckwheat breeding materials obtained after crossing with dwarf forms. *Fagopyrum* **1994**, *14*, 26−28.
(20) Li, X.; Park, N. I.; Xu, H.; Woo, S. H.; Park, C. H.; Park, S. U. Differential expression of flavonoid biosynthesis genes and accumulation of phenolic compounds in common buckwheat (*Fagopyrum esculentum*). *J. Agric. Food Chem.* **2010**, *58*, 12176−12181.
(21) Timotijevic, G. S.; Milisavljevic, M. D.; Radovic, S. R.; Konstantinovic, M. M.; Maksimovic, V. R. Ubiquitous aspartic proteinase as an actor in the stress response in buckwheat. *J. Plant Physiol.* **2010**, *167*, 61−68.
(22) Kim, S. J.; Zaidul, I. S. M.; Suzuki, T.; Mukasa, Y.; Hashimoto, N.; Takigawa, S.; Noda, T.; Matsuura-Endo, C.; Yamauchi, H. Comparison of phenolic compositions between common and tartary buckwheat (*Fagopyrum*) sprouts. *Food Chem.* **2008**, *110*, 814−820.
(23) Li, X.; Thwe, A. A.; Park, N. I.; Suzuki, T.; Kim, S. J.; Park, S. U. Accumulation of phenylpropanoids and correlated gene expression during the development of tartary buckwheat sprouts. *J. Agric. Food Chem.* **2012**, *60*, 5629−5635.
(24) Thwe, A. A.; Kim, J. K.; Li, X.; Bok Kim, Y.; Romij Uddin, M.; Kim, S. J.; Suzuki, T.; Park, N. I.; Park, S. U. Metabolomic analysis and phenylpropanoid biosynthesis in hairy root culture of tartary buckwheat cultivars. *PLoS One* **2013**, *8*, No. e65349.
(25) Ageorges, A.; Fernandez, L.; Vialet, S.; Merdinoglu, D.; Terrier, N.; Romieu, C. Four specific isogenes of the anthocyanin metabolic pathway are systematically co-expressed with the red colour of grape berries. *Plant Sci.* **2006**, *170*, 372−383.
(26) Jeong, S. T.; Goto-Yamamoto, N.; Hashizume, K.; Esaka, M. Expression of multi-copy flavonoid pathway genes coincides with anthocyanin, flavonol and flavan-3-ol accumulation of grapevine. *Vitis* **2008**, *47*, 135−140.
(27) Martens, S.; Preuß, A.; Matern, U. Multifunctional flavonoid dioxygenases: Flavonol and anthocyanin biosynthesis in *Arabidopsis thaliana* L. *Phytochemistry* **2010**, *71*, 1040−1049.
(28) Kumar, A.; Ellis, B. E. 4-Coumarate:CoA ligase gene family in *Rubus idaeus*: cDNA structures, evolution, and expression. *Plant Mol. Biol.* **2003**, *51*, 327−340.
(29) Lindermayr, C.; Möllers, B.; Fliegmann, J.; Uhlmann, A.; Lottspeich, F.; Meimberg, H.; Ebel, J. Divergent members of a soybean (*Glycine max* L.) 4-coumarate:coenzyme A ligase gene family. *Eur. J. Biochem.* **2002**, *269*, 1304−1315.
(30) Chen, H. C.; Song, J.; Williams, C. M.; Shuford, C. M.; Liu, J.; Wang, J. P.; Li, Q.; Shi, R.; Gokce, E.; Ducoste, J.; Muddiman, D. C.; Sederoff, R. R.; Chiang, V. L. Monolignol pathway 4-coumaric acid:coenzyme A ligases in *Populus trichocarpa*: Novel specificity, metabolic regulation, and simulation of coenzyme A ligation fluxes. *Plant Physiol.* **2013**, *161*, 1501−1516.
(31) Hu, W. J.; Kawaoka, A.; Tsai, C. J.; Lung, J.; Osakabe, K.; Ebinuma, H.; Chiang, V. L. Compartmentalized expression of two structurally and functionally distinct 4-coumarate:CoA ligase genes in aspen (*Populus tremuloides*). *Proc. Natl. Acad. Sci. U. S. A.* **1998**, *95*, 5407−5412.
(32) Li, X.; Kim, Y. B.; Kim, Y.; Zhao, S.; Kim, H. H.; Chung, E.; Lee, J. H.; Park, S. U. Differential stress-response expression of two flavonol synthase genes and accumulation of flavonols in tartary buckwheat. *J. Plant Physiol.* **2013**, *170*, 1630−1636.
(33) Fabjan, N.; Rode, J.; Kosir, I. J.; Wang, Z.; Zhang, Z.; Kreft, I. Tartary buckwheat (*Fagopyrum tataricum* Gaertn.) as a source of dietary rutin and quercitrin. *J. Agric. Food Chem.* **2003**, *51*, 6452−6455.
(34) Krkosková, B.; Mrázová, Z. Prophylactic components of buckwheat. *Food Res. Int.* **2005**, *38*, 561−568.
(35) Kalinova, J.; Triska, J.; Vrchotova, N. Distribution of vitamin e, squalene, epicatechin, and rutin in common buckwheat plants (*Fagopyrum esculentum* Moench). *J. Agric. Food Chem.* **2006**, *54*, 5330−5335.
(36) Gabrovska, D.; Fiedlerova, V.; Holasova, M.; Maskova, E.; Smrcinov, H.; Rysova, J.; Winterova, R.; Michalova, A.; Hutar, M. The nutritional evaluation of underutilized cereals and buckwheat. *Food Nutr. Bull.* **2002**, *23*, 246−249.
(37) Gupta, N.; Sharma, S. K.; Rana, J. C.; Chauhan, R. S. Expression of flavonoid biosynthesis genes vis-à-vis rutin content variation in different growth stages of *Fagopyrum* species. *J. Plant Physiol* **2011**, *168*, 2117−2123.
(38) Kalinova, J.; Vrchotova, N. Level of catechin, myricetin, quercetin and isoquercitrin in buckwheat (*Fagopyrum esculentum* Moench), changes of their levels during vegetation and their effect on the growth of selected weeds. *J. Agric. Food Chem.* **2009**, *57*, 2719−2725.
(39) Kim, H. J.; Park, K. J.; Lim, J. H. Metabolomic analysis of phenolic compounds in buckwheat (*Fagopyrum esculentum* Moench) sprouts treated with methyl jasmonate. *J. Agric. Food Chem.* **2011**, *59*, 5707−5713.
(40) Ohsawa, R.; Tsutsumi, T. Inter-varietal variations of rutin content in common buckwheat flour (*Fagopyrum esculentum* Moench.). *Euphytica* **1995**, *86*, 183−189.
(41) Buer, C. S.; Muday, G. K.; Djordjevic, M. A. Flavonoids are differentially taken up and transported long distances in *Arabidopsis*. *Plant Physiol* **2007**, *145*, 478−490.

(42) Dhaubhadel, S.; McGarvey, B. D.; Williams, R.; Gijzen, M. Isoflavonoid biosynthesis and accumulation in developing soybean seeds. *Plant Mol. Biol.* **2003**, *53*, 733−743.
(43) Li, C.; Bai, Y.; Li, S.; Chen, H.; Han, X.; Zhao, H.; Shao, J.; Park, S. U.; Wu, Q. Cloning, characterization, and activity analysis of a flavonol synthase gene *FtFLS1* and its association with flavonoid content in tartary buckwheat. *J. Agric. Food Chem.* **2012**, *60*, 5161−5168.
(44) Suzuki, T.; Kim, S. J.; Takigawa, S.; Mukasa, Y.; Hashimoto, N.; Saito, K.; Noda, T.; Matsuura-Endo, C.; Zaidul, I. S. M.; Yamauchi, H. Changes in rutin concentration and flavonol-3-glucosidase activity during seedling growth in tartary buckwheat (*Fagopyrum tataricum* Gaertn.). *Can. J. Plant Sci.* **2007**, *87*, 83−87.
(45) Suzuki, T.; Honda, Y.; Funatsuki, W.; Nakatsuka, K. Purification and characterization of flavonol 3-glucosidase, and its activity during ripening in tartary buckwheat seeds. *Plant Sci.* **2002**, *163*, 417−423.
(46) Park, N. I.; Li, X.; Thwe, A. A.; Lee, S. Y.; Kim, S. G.; Wu, Q.; Park, S. U. Enhancement of rutin in *Fagopyrum esculentum* hairy root cultures by the arabidopsis transcription factor AtMYB12. *Biotechnol. Lett.* **2012**, *34*, 577−583.
(47) Kreft, S.; Strukelj, B.; Gaberscik, A.; Kreft, I. Rutin in buckwheat herbs grown at different UV-B radiation levels: Comparison of two uv spectrophotometric and an hplc method. *J. Exp. Bot.* **2002**, *53*, 1801−1804.
(48) Gupta, N.; Naik, P. K.; Chauhan, R. S. Differential transcript profiling through cDNA-AFLP showed complexity of rutin biosynthesis and accumulation in seeds of a nutraceutical food crop (*Fagopyrum* spp.). *BMC Genomics* **2012**, *13*, No. 231.
(49) Barber, G. A. Enzymic glycosylation of quercetin to rutin. *Biochemistry* **1962**, *1*, 463−468.
(50) Materska, M. Quercetin and its derivatives: Chemical structure and bioactivity - a review. *Pol. J. Food Nutr. Sci.* **2008**, *58*, 407−413.
(51) Quettier-Deleu, C.; Gressier, B.; Vasseur, J.; Dine, T.; Brunet, C.; Luyckx, M.; Cazin, M.; Cazin, J. C.; Bailleul, F.; Trotin, F. Phenolic compounds and antioxidant activities of buckwheat (*Fagopyrum esculentum* Moench) hulls and flour. *J. Ethnopharmacol.* **2000**, *72*, 35−42.
(52) Wang, L.; Yang, X.; Qin, P.; Shan, F.; Ren, G. Flavonoid composition, antibacterial and antioxidant properties of tartary buckwheat bran extract. *Ind. Crops Prod.* **2013**, *49*, 312−317.
(53) Hoekenga, O. A. Using metabolomics to estimate unintended effects in transgenic crop plants: Problems, promises, and opportunities. *J. Biomol. Technol.* **2008**, *19*, 159−166.
(54) Kok, E. J.; Keijer, J.; Kleter, G. A.; Kuiper, H. A. Comparative safety assessment of plant-derived foods. *Regul. Toxicol. Pharmacol.* **2008**, *50*, 98−113.

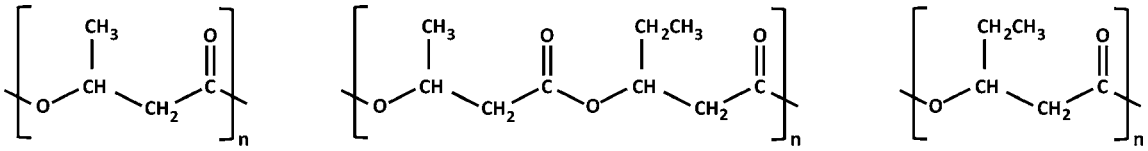

Figure 1. Chemical structures of three different types of PHA, synthesized and accumulated in certain prokaryotes.

Depending on cell needs, the cell is capable of transforming polar lipids into neutral lipids and vice versa due to the different pools present in strategic cellular locations. For instance, polar lipids are pooled and may be mobilized from the different cell membranes. Key membranes involved in the accumulation of lipids include the plasma membrane in both eukaryotes and prokaryotes, and in the case of eukaryotes the endoplasmic reticulum (ER), peroxisome, mitochondrial, plastidial (and their variants, such as apicoplastidial), or even thylakoid membranes, depending on the organism. Key intermediates, such as acetyl coenzyme A (Ac-CoA), malonyl coenzyme A (mal-CoA), acyl coenzyme A (acyl-CoA), and glycerol-3-phosphate (G3P) are also pooled in strategic cellular locations such as the cytosol, plastidial stroma, and mitochondrial intermembrane space. The distribution of the different biosynthetic enzymes plays a key role in achieving the correct lipid traffic toward accumulation. The accumulation of intracellular neutral lipid is a highly reductive process, requiring more NADPH and ATP than the storage of glucose and glucose derivatives.[8]

■ ACCUMULATION OF LIPIDS IN SINGLE-CELL MICROORGANISMS: AN OVERVIEW

Accumulation of lipids is a biological process that fulfills several roles in microorganisms. Storage of lipids contributes to cell growth, cell division, stress response, and as energy storage for survival.[9] In some cases, lipid accumulation plays a role in pathogenity.[7,10−13] Some SCM have the capacity to accumulate lipids >20% of their weight when exposed to an environmental stress, such as the lack of a key nutrient.[14−16] These are referred to as oleaginous SCM (OSCM).[17]

When growing on limiting concentrations of a key nutrient (typically nitrogen) and with sufficient or excess carbon sources, OSCM will stop their replication processes and utilize the available carbon to synthesize and store it in the way of reduced lipids. In the case of TAG and SE, the accumulation process has four main stages. In the first stage, OSCM shift their metabolic machinery to generate a pool of Ac-CoA, as well as NADPH, which is the reducing power driving fatty acid (FA) synthesis forward[18,19] The strategies vary among different classes of OSCM, and details will be discussed in the following sections. In the second stage, Ac-CoA is carboxylated to produce mal-CoA, transferred to acyl carrier protein (ACP), and further transformed into an acyl ACP by sequential turns within the fatty acid synthase (FAS). There are two types of FAS: Type I is an integrated enzyme complex (common in eukaryotic cytoplasm), and type II is a dissociated version in which all subunits are independent (common in prokaryotes and in organelles of prokaryotic origin in primary and secondary endosymbionts, such as plastids and mitochondria). Type I can be subdivided in type IA, present in fungi ($\alpha_6\beta_6$ complex in the cytoplasm), and type IB, present in animals (as cytoplasmic α_2 dimers). For reviews describing type I FAS and type II FAS, the reader is referred to the works of Schweizer and Lu et al., respectively.[20,21] In the third step, depending on the cell's needs and the type of SCM, the acyl chain might end in a specific type of lipid pool, such as membrane lipid (coupling the acyl chain to G3P, Ac-CoA, or other glycerol-based backbone to form PL or other types of polar lipid) or can eventually be incorporated into a neutral lipid droplet core (via the construction of TAG or SE molecules). The nature, location, and dynamics of this stage vary among species and are explained more in detail in the following sections. In this stage, further elongation and desaturation of the acyl chains may also occur, and these phenomena vary throughout the different domains of life. Finally, the fourth stage involves the formation of intracellular lipid droplets (LD). Variations occur depending on the organism and the environmental conditions.

In the case of prokaryotes, accumulation of TAG or SE is less common. In some members of the Gram-positive actinomycete group,[6,22] such as *Mycobacterium*, *Rhodococcus*, *Nocardia*, *Dietzia*, and *Streptomyces*, TAG are readily accumulated. Interestingly, bacterial TAG biosynthesis occurs frequently in the environment because actinomycetes are the most abundant microorganisms in soil.[22] Accumulation of TAG in Gram-negative bacteria has been reported only in species from the genus *Acinetobacter*, but only as a minor component of the neutral accumulated lipid. Wax esters are the main compound stored in these species.[6] For the rest of the Gram-negative bacteria, the main purpose of fatty acid synthesis is to become membrane lipid precursors.[6,18,23−25] However, several studies have successfully transformed model bacteria such as *Escherichia coli* by inserting the required genes to become oleaginous, with remarkable success.[26−28] In addition, TAG have been reported as major components of the neutral lipid of the cyanobacterium *Nostoc commune*, although no indications were obtained for the storage of lipid inclusions in the cells.[6,29] In the case of archaea, TAG accumulation of archaea is yet to be reported.[11]

It is more common in prokaryotes to accumulate PHA, comprising specialized lipids such as poly(3-hydroxybutyrate) (P3HB), polyhydroxyvalerate (PHV), or copolymers such as poly(3-hydroxybutyrate-*co*-3-hydroxyvalerate) (PHBV). Figure 1 shows the structures of such lipids. PHA possess thermoplastic and elastomeric properties and are recyclable materials that can be easily degraded into carbon dioxide and water.[30] The uses and applications of these polyesters have been thoroughly reviewed elsewhere.[30] The most promising are as film formation, paper coating,[31] foils and diaphragms,[32] and multiple-use packages, because the melted polymers have low viscosity, permitting the injection molding of objects with thin walls. The end product is very hard and can be used at temperatures from −30 to 120 °C.[30]

Polyhydroxyalkanoate accumulation in prokaryotes can also be divided into four stages. The first stage involves the generation of a suitable cytoplasmic Ac-CoA pool. The second one involves the synthesis of the hydroxyalkanoate (HA) monomer or monomers, which can change depending on the

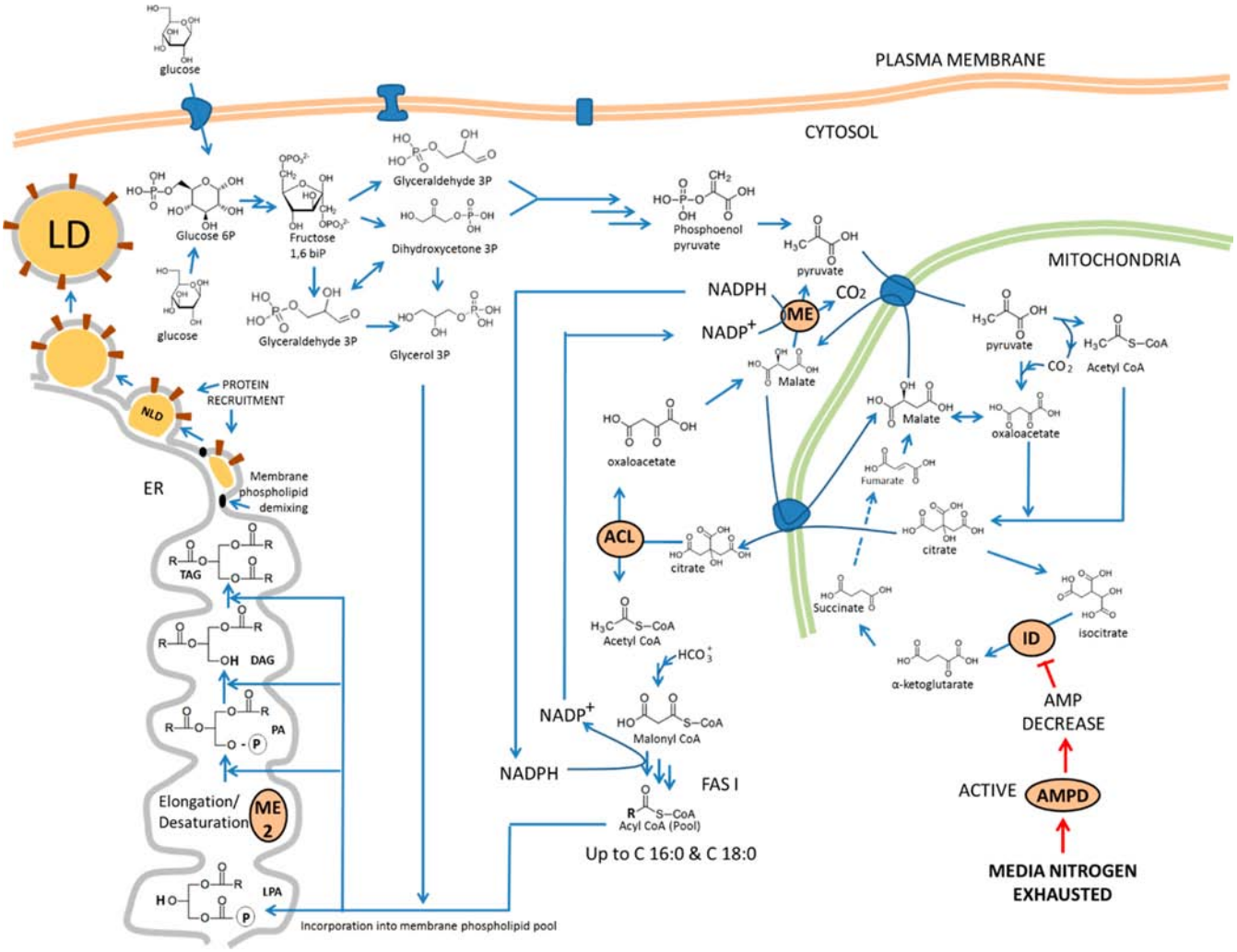

Figure 2. Schematic representation of metabolic steps involved in lipid accumulation in yeasts. The diagram also includes the connection between fatty acid synthesis, triacylglycerol synthesis, and lipid droplet formation. Abbreviations: ME, malic enzyme (cytosolic); ME 2, malic enzyme (ER membrane, responsible for fatty acid desaturation); ACL, ATP:citrate lyase; ID, isocitrate dehydrogenase; NLD, nascent lipid droplet; LD, lipid droplet; ER, endoplasmic reticulum; LPA, lysophosphatidic acid; PA, phosphatidic acid, FAS I, fatty acid synthase I; DAG, diacylglycerol; TAG, triacylglycerol; AMPD, AMP deaminase.

species and substrates. The third stage consists of polymerizing or copolymerizing the monomers into PHA chains, and the fourth one involves the formation of the intracellular PHA LD.

In both prokaryotes and eukaryotes, accumulation of neutral lipids results in the formation of intracellular fat bodies typically called lipid droplets (LD). LD are also called lipid bodies, fat bodies, or adiposomes, and in the case of plants they have also been termed oleosomes, spherosomes,[22,33] or plastoglobules, the latter if their location is inside the plastid.[11] For the present discussion, the term lipid droplet will be used. In most of the eukaryotes LD are intracellular sphere-like particles composed of a core of neutral lipids, such as TAG or SE or both, coated by a monolayer of polar lipids, mainly PL, and decorated with a series of proteins.[11,33−35] The polar heads face the cytoplasm, and the nonpolar tails face the inside, where the neutral lipids reside. The inserted proteins within the polar lipid monolayer play functional, structural, and regulatory roles in the life cycle of LD.[35−37] In the case of polyhydroxyalkanoate-accumulating prokaryotes, they form LD, which are also called lipid granules or carbonosomes.[38,39] In some higher organisms (e.g., humans), lipid droplet interaction with other cellular organelles, and their dynamics is closely related to progression of metabolic diseases, such as obesity, fatty liver, type 2 diabetes mellitus, and atherosclerosis.[36]

Therefore, it has become apparent that LD are not just a static storage compartment in the cell, but rather a dynamic organelle that interacts with other organelles within the cell and actively participates in the intricate cellular processing symphony,[40,41] to the point that some authors consider LD as specialized organelles in cells.[42]

As described in later sections, strategies for lipid accumulation in SCM vary among the different types of SCM, and it is important to understand these differences to improve and/or create productive strategies that can become economically as well as technologically feasible for the generation of biofuels as well as nutritional lipid metabolites such as long-chain polyunsaturated fatty acids (LC-PUFA).

THE CASE OF YEAST

Yeasts are single-cell eukaryotic fungi that display heterotrophic behavior. Thus, they are capable of metabolizing carbon from simple sugars or from other simple compounds such as

dx.doi.org/10.1021/jf4042134 | J. Agric. Food Chem. 2014, 62, 2709−2727

glycerol. When oleaginous yeasts encounter an environmental stress, such as a limiting nutrient (e.g., nitrogen), they shift their metabolic machinery to stop synthesizing proteins and nucleic acids and, thus, begin to allocate the available carbon in the form of reduced lipids. Other examples of limiting nutrients can be phosphorus or magnesium.[6] In practice to date, nitrogen has been extensively used because it seems to yield higher lipid accumulation when compared to other nutrients.[43] The carbon to nitrogen ratio is a useful tool to construct nitrogen-rich or nitrogen-depleted media. For example, it has been shown that for yeasts, poor lipid accumulation occurs in media in which the carbon to nitrogen (C:N) ratio is <20, whereas ideal lipid production occurs in a C:N ratio range of 30−80. The optimal C:N ratio for lipid accumulation varies greatly with the microbial species, strain, and carbon sources present in the growth medium.[44] In yeasts, oleaginicity depends on the ability to produce Ac-CoA, the necessary precursor of fatty acids, in an effective manner.[45,46]

The conversion of 1 mol of Ac-CoA to fatty acids requires the formation of 2 mol of NADPH, which constitutes the reducing power necessary to drive the reaction forward.[45−47] The metabolic steps for lipid accumulation in yeast can be divided into four main stages, as mentioned before (see Figure 2).[18,42,45−48]

Stage 1. Production of Acetyl CoA and NADPH. This stage begins with depletion of nitrogen in the medium. The cell responds by activating AMP deaminase and inducing an acute decrease of cellular AMP content. In mitochondria of oleaginous species, the decrease in cellular AMP levels causes isocitrate dehydrogenase (IDH) activity to decrease or even stop.[19] As a consequence, the production of α-ketoglurarate drops and the tricarboxylic cycle (TCA) is dramatically reduced or even stopped. Therefore, isocitrate will begin to build up inside the mitochondria. To reverse this situation, aconitase transforms isocitrate back to citrate (CIT), leading to an accumulation of CIT in mitochondria. CIT is transported by an antiport protein, known as citrate/malate translocase (CMT), from the mitochondria to the cytoplasm. In the cytoplasm, CIT is cleaved to form oxaloacetate and Ac-CoA, by ATP:citrate lyase (ACL). ACL is an enzyme that is exclusively present in oleaginous species.[18,42,49,50] Cytosolic oxaloacetate is reduced by malate dehydrogenase (MD) to form malate. Cytosolic malate is converted to pyruvate by malic enzyme (ME), encoded by *ME1*. This reaction generates NADPH[51,52] and is coupled to a series of parallel reactions as well. The first is the carboxylation of pyruvate to form oxaloacetate by pyruvate carboxylase inside mitochondria. Mitochondrial oxaloacetate is further reduced to form malate by MD. This malate is then transported outside the mitochondria and decarboxylated by ME. This reaction takes $NADP^+$ and converts it to NADPH. This NADPH is the reducing power required to convert Ac-CoA into fatty acids. Thus, pyruvate carboxylase, MD, and ME are known as the transhydrogenation machinery.[19,42] The resulting pyruvate completes the cycle and goes inside the mitochondria (Figure 2). ME is present in all fungi, but its role in supplying NADPH for de novo lipogenesis is preponderant in oleaginous species.[18] It has been found that, upon nitrogen limitation, ME changes from isoform D to isoform E, which supplies NADPH for de novo lipogenesis.[18]

Stage 2. Biosynthesis of Fatty Acyl Chains. Ac-CoA is converted by acetyl-CoA carboxylase (Acc) to mal-CoA, which is then used to synthesize fatty acids. In yeast, cytosolic Acc is encoded by *ACC1* and mitochondrial Acc is encoded by *HFA1*. The mitochondrial version closely resembles in both its molecular mass and amino acid sequence the cytoplasmic one.[20] Acc uses biotin as a cofactor to transfer CO_2 to Ac-CoA in a two-step process. It is a trifunctional enzyme, harboring a biotin carboxyl carrier protein domain, a biotin−carboxylase domain (where CO_2 binds to biotin), and a carboxyl-transferase domain (where CO_2 is transferred to Ac-CoA to yield mal-CoA).[53] The fatty acyl chain is built in a type I cytosolic fatty acid synthase (FAS I). It is an $\alpha_6\beta_6$ complex encoded by two genes, *FAS1* (β subunit) and *FAS2* (α subunit).[53] It is suggested to contain 6 equivalent sites of FA synthesis with a total of 42 catalytic domains, organized in a ring-like structure.[54] However, variations to this architecture exist and probably may affect the performance in de novo lipogenesis.[42] Loading of substrates to FAS varies among life domains. For example, Ac-CoA is always the basis of FA biosynthesis and is the substrate of β-ketoacyl ACP synthase (KSa) in bacteria.[20,21] Yeasts load Ac-CoA first to KSb through ACP before condensation.[20] The sequence of reactions in yeast FAS II is condensation of Ac-CoA with mal-CoA (via KS), reduction (via ketoacyl reductase, KR), dehydration (via a dehydratase, DH) and further reduction (via enoyl reductase EAR) in a repetitive manner until palmitoyl-ACP is formed. Release of the acyl moiety is a key step that differs from species and is currently a subject of intense research. Yeasts employ malonyl-palmitoyl transacylase (MPT) to transfer the acyl chain from acyl ACP to acyl-CoA.[18,53] In algae, the acyl chain can be released in three ways, depending on the cell's needs. First, it can be hydrolyzed from ACP as a free fatty acid by means of a thioesterase (TE). Second, it can be transferred either to G3P or monoacylglycerol-3-phosphate (MAG3P) through an acyltransferase (AT) in the chloroplast.[8,55,56] Lastly, if the acyl chain is destined to leave the plastid, it can also be released in the acyl-CoA form by acyl-coenzyme A synthetases (ACS).[8,57] It has been found that ACS play a key role in regulating in each compartment the internal acyl-CoA pools by esterification of FA to CoA. The localization of the pools is maintained due to Acyl-CoA's not being able to cross the intracellular membranes. The final fatty acid composition of different types of microalgae is in great part dependent on the activity of these enzymes. For example, microalgal chain length specific TE have been reported, which can release acyl moieties of specific length (e.g., C 12:0 or even C 8:0). This type of fatty acid is more suitable for the production of gasoline and jet fuel.[56]

In contrast, Gram-positive bacteria first form acyl-phosphate from acyl-CoA (via PlsX), which is then transferred onto G3P by PlsY. Gram-negative species use PlsB acyltransferase only to load an acyl group directly onto G3P from acyl ACP.[18,51,58]

Stage 3. Allocation of Acyl Moieties to either Polar or Neutral Lipid Pools. In yeast, acyl-CoAs released from cytosolic FAS I system are channeled to the ER membrane. There, a series of esterifications to a G3P backbone occur, also known as the Kennedy pathway. The first step consists of esterifying the acyl moiety from acyl-CoA to G3P or dihydroxyacetone 3-phosphate via glycerol-3-phosphate acyl transferase (G3PAT), on the sn-1 position. G3PAT is encoded in yeast by *GAT1* and *AYR1*, when the acceptor is G3P or dihydroxyacetone 3-phosphate, respectively.[18] Gat1 does not exhibit a particular preference for acyl-CoA, whereas AYR1 prefers palmitoyl-CoA, thus defining FA composition. A second acyl moiety can be attached on the sn-2 position to generate phosphatidate (PA), catalyzed by acyl-CoA:lysophosphatidic acyltransferase (LPAAT). PA plays a key role in the regulation

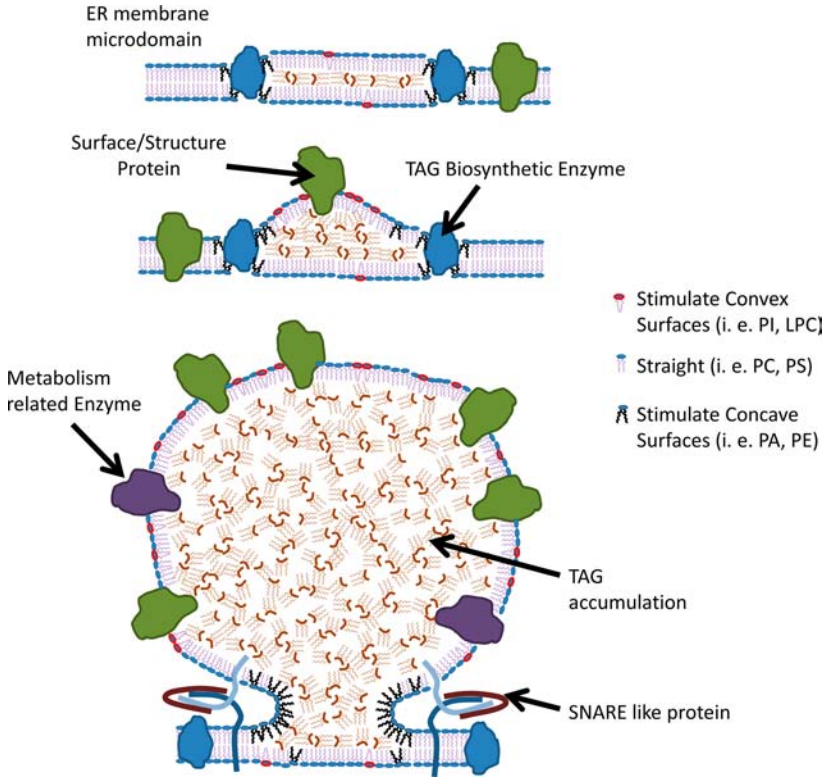

Figure 3. Model of lipid droplet formation in the ER membrane. Adapted from ref 11.

of *ACC1*, *FAS1*, and *FAS2* genes, as it is involved in an autoregulatory loop directed by the concentrations of inositol and choline in the cytosol and PA in the ER membrane.[18,20,53,59−62] Expression of upstream activating sequence (UAS_{INO})-operated genes changes in parallel to PA, inositol, and choline concentrations. In the case when PA is going to be transformed into TAG, it has to be transformed into diacylglycerol (DAG) first. This can happen in two ways. First, the phosphate group can be directly hydrolyzed by a phosphatidate phosphatase (PAP) to create DAG. PAP is encoded by *PAH1* and requires a magnesium ion to perform hydrolysis.[60,62] It is regulated by lipids, nucleotides, and phosphorylation. The second one involves synthesizing cytidine diphosphate DAG (CDP-DAG) from PA, catalyzed by CDP-DAG kinase, encoded by *CDS1*.[18,42] CDP-DAG is the precursor of the different PL in the ER membrane. It thus stays as either phosphatidylcholine (PC), phosphatidylethanolamine (PE), or another type of PL. Eventually, DAG is generated by cleavage of the PL via phospholipase C. Both alternatives are in metabolic interlock with each other. This creates a positive feedback system that channels PA into the TAG pathway if CDP-DAG concentration is higher than DAG concentration or directs PA to the membrane pool in the opposite situation.[18,60−62] Lastly, DAG is transformed into TAG by esterifying an acyl moiety from Acyl CoA catalyzed by an Acyl CoA:DAG acyltransferase (ADAT), encoded by either *DGA1* or *LRO1*,[42] depending on whether DAG is generated directly from PA via PAP or it comes from the ER membrane PL pool, respectively.

Further elongation and desaturation of fatty acids also occur in the ER membrane. Desaturation requires fatty acids to be attached to the ER membrane PL. Here another ME, different from the cytosolic malic enzyme, catalyzes the conversion of malate to pyruvate and the consequent reduction of NADP to NADPH. NADPH then couples to a series of electron transfer reactions involving cytochrome *b*5 reductase and further activating the desaturase, which adds a double bond on the fatty acid chain at the expense of converting 1 mol of oxygen into a mole of water.[3],

Ergosterol is the major sterol present in yeast. For a review in the biosynthesis of ergosterol backbone, the reader is referred to the work of Kristan.[63] Yeast SE are synthesized via transesterification of ergosterol with acyl-CoA.[5] In yeast, two acyl-CoA cholesterol acyltransferase (ACAT) related enzymes, ARE1P and ARE2P (encoded by *ARE1* and *ARE2*), catalyze the reaction. Microscopic localization of green fluorescent protein hybrids and enzyme measurements showed that both ARE1P and ARE2P are localized to the ER.[64] ARE1P esterifies ergosterol and its precursors with nearly equal efficiency with a slight preference for lanosterol, whereas ARE2P uses ergosterol as a preferred substrate.[64] An acyl-CoA-independent pathway for the formation of SEs has not been identified in yeast.

Stage 4. Lipid Droplet Biogenesis. Lipid droplet biogenesis is an area of intensive current research, and there is emerging scientific evidence showing that in yeast it takes place between the two membrane leaflets of the ER.[34,65,66] By mechanisms still not clearly understood there are spots in the ER membrane where there is a concentration of ADATs DGA1 and LRO1. The first one is responsible for TAG synthesis in the outer leaflet of the endoplasmic reticulum, whereas the second is responsible for TAG synthesis in the inner leaflet of the ER.[18,42] The synthesized TAG begin to accumulate, generating a lens-like protrusion and promoting the recruitment of structural proteins. In yeast, PAT proteins (from the initials of perilipin, adipocyte differentiation-related protein, and TIP47)[67] accumulate in the outer leaflet (see Figure 3), whereas in plants this role is played by oleosins. When there is

enough accumulation of TAG between the leaflets, the outer buds off and the lipid droplet is formed (Figure 3).[34,68−70]

There seems to be a functional relationship between the lipid droplet membrane and the ER membrane, because several studies have shown that certain functional proteins can migrate between the lipid droplet and ER membranes by mechanisms that do not require energy expenditure.[71] In yeast, most ER proteins are also detected on the lipid droplet membrane. For example, experiments using yeast mutants unable to synthesize TAG revealed that LD were not formed. However, the proteins that were present in the wild forms in LD were also present in the ER of the yeast mutants, suggesting a relationship between ER proteins and lipid droplet proteins.[68] In some cases, lipid droplet-localized proteins can relocate back to the ER, indicating that some continuity between the two organelles is maintained, even if only transiently, in a way that allows the two-way partitioning of proteins between the two compartments.[33]

In describing the functions of proteins embedded in the droplet monolayers, two mechanisms have been proposed. The first is a hydrophobic helix that interacts with the monolayer. Examples of this strategy are the multifunctional caveolin protein, which has been localized to both the plasma membrane and LD, and DGA1, the major enzyme catalyzing triacylglycerol synthesis.[33] Both have similar topology. Their long internal hydrophobic stretch may enable them to be embedded in either bilayers or monolayers. The second mechanism is best represented by the previously mentioned PAT protein family. They display a four-helix bundle with great similarity to the N-terminal domain of apolipoprotein E.[33,72] Upon binding to lipids, the apoE four-helix bundle opens to expose amphipathic helices that can bind the monolayer surfaces of lipoproteins. In an analogous manner, PAT proteins may bind to lipid droplets by embedding hydrophobic helices into the droplet surface. PAT proteins also share a common structural element: N-terminal 11-mer repeats that have an amphipathic helical structure.[73] Different PAT proteins attach to different-sized LD. It is still unclear why or how they do it.

In the specific case of perilipins (members of the PAT family), there are five groups, and their abundance has been correlated with the abundance of TAG in the lipid droplet as well.[35] Perilipins play crucial roles in regulating triacylglycerol hydrolysis by protein−protein interactions, suggesting physiological and regulatory functions.[35] It is important to mention that perilipin-like proteins are not found in plants. As was already mentioned, functionally similar oleosins and caleosins are present in plants instead.[11]

There is increasing evidence that phospholipid demixing occurs during the birth of LD.[68] The accumulation of lipids that promote concavity decreases the energy burden required for budding. It has been shown that lipid droplet PL contain more lysophospholipids and less sphingomyelin and PA compared to the total membrane.[33,68] In silico studies proposed a packing parameter *S* to quantify the degree of convexity/concavity in PL.[68] Lysophosphatidylcholine and phosphatidylinositol (PI) promote a convex shape where their lipid footprint areas are much smaller than their headgroup areas. Their *S* values are <1. Conversely, PE and PA induce a concave shape. These PL have *S* values >1.[68] Lipids with *S* values <1 adopt a convex surface, favoring lipid droplet formation. This is diagrammed in Figure 4.

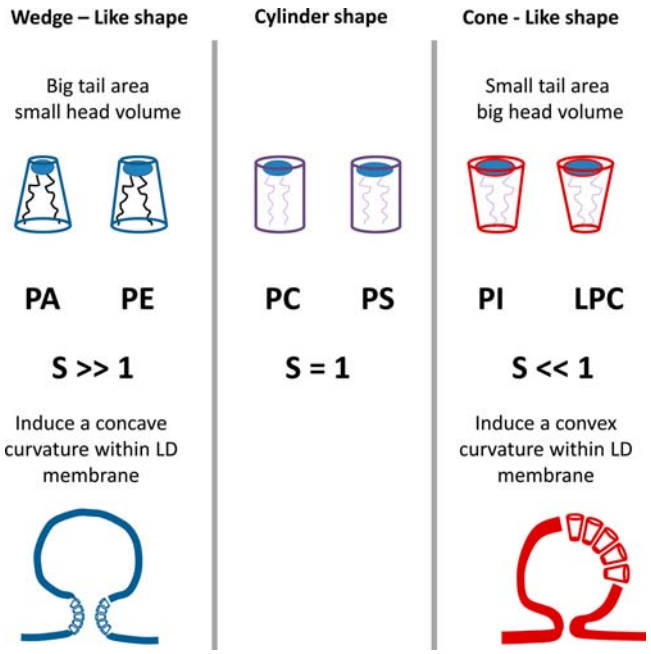

Figure 4. Configurations adopted by different phospholipids, which can affect the curvature during lipid droplet formation.[68]

THE CASE OF MICROALGAE

Eukaryotic microalgae are classified into nine divisions: Glaucophyta, Rhodophyta (red algae), Heterokontophyta, Haptophyta, Cryptophyta, Dinophyta (dinoflagellates), Euglenophyta, Chlorarachniophyta, and Chlorophyta (green algae)[55,74,75] All of these divisions include single-cell strains, which can be either motile, nonmotile, or both. In terms of their nutritional strategies, microalgae can be divided into obligate heterotrophs, obligate photoautotrophs, facultative mixotrophs, and obligate mixotrophs. Most algal divisions contain colorless heterotrophic species that can obtain organic carbon from the external environment either by taking up dissolved substances (osmotrophy) or by engulfing bacteria and other cells as particulate prey (phagotrophy).[75] In most cases, lipid accumulation strategies in microalgae and some single-cell protists (both primary and secondary endosymbionts) follow the four-stage lipid accumulation strategy described for yeast. However, several differences are present in each stage. In addition, further studies are demonstrating that lipid biosynthesis pathways in microalgae are not a simple mirror image of what happens in higher plants, which have been more thoroughly studied.[76,77] It seems likely that regulation of triacylglycerol synthesis and breakdown in microalgae tends to obey a stress response phenomenon, whereas in plants it follows a developmental phenomenon. For a review comparing lipid metabolism between microalgae and plants, see Liu.[4]

Stage 1. Production of Acetyl-CoA and NADPH. Microalgae differ from yeast in the location of the acetyl-CoA pools within the cell. Microalgae display plastidial and cytosolic acetyl-CoA pools, which are key for lipid accumulation. In contrast, yeast's main acetyl-CoA pool used for lipid accumulation is located in the cytosol. There is an additional acetyl-CoA pool present in mitochondria as well as a mitochondrial lipid biosynthesis pathway employing a type II FAS (different from plastidial FAS II) both in algae and in yeasts.[18,76,78−82] They play important roles in different cell processes, such as RNA processing, mitochondrial lipoic acid

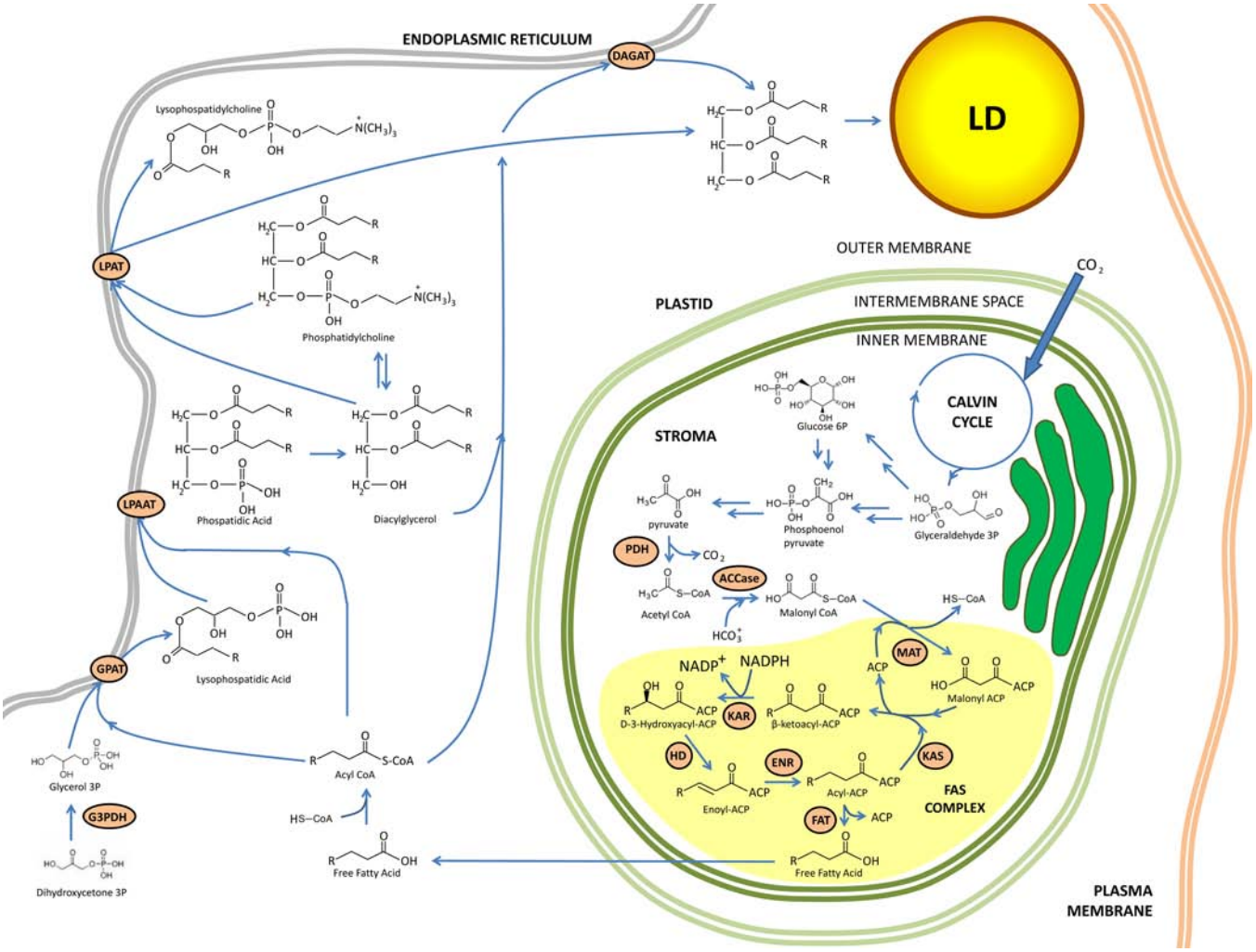

Figure 5. Simplified overview of lipid biosynthesis and lipid droplet formation in photosynthetic algae. Adapted from ref 56. Abbreviations: ER, endoplasmic reticulum; ACCase, acetyl-CoA carboxylase; ACP, acyl carrier protein; DAGAT, diacylglycerol acyltransferase; DHAP, dihydroxyacetone phosphate; ENR, enoyl-ACP reductase; FAT, fatty acyl-ACP thioesterase; G3PDH, glycerol-3-phosphate dehydrogenase; GPAT, glycerol-3-phosphate acyltransferase; HD, 3-hydroxyacyl-ACP dehydratase; KAR, 3-ketoacyl-ACP reductase; KAS, 3-ketoacyl-ACP synthase; LPAAT, lysophosphatidic acid acyltransferase; LPAT, lysophosphatidylcholine acyltransferase; MAT, malonyl-CoA:ACP transacylase; PDH, pyruvate dehydrogenase complex.

synthesis, and protein lipoylation. However, mitochondrial lipid synthesis is not the main avenue for lipid accumulation and will not be covered in the present work. For a review of mitochondrial lipid biosynthesis and its relevance in cell function, the reader is referred to the work of Hiltunen and co-workers.[78−80]

Plastids present in algae play a key role in de novo lipid biosynthesis (for a review of plastid evolution and diversification, see the work of Keeling[83]). In photoautotrophic microalgae, photosynthesis provides an endogenous source of plastidial acetyl-CoA, although more than one pathway may contribute to maintaining the acetyl-CoA pool.[55] For instance, in photoautotrophic microalgae plastidial pyruvate can be sourced via transformation of photosynthesis-derived glyceraldehyde-3-phosphate to phosphoenolpyruvate (PEP). PEP is irreversibly converted to pyruvate (see Figure 5) by pyruvate kinase (PK).[55,84] Finally, the plastidial pyruvate dehydrogenase complex (PDH) catalyzes the oxidative decarboxylation of pyruvate to produce plastidial Ac-CoA, CO_2, and NADH. PDH contains three components: E1 (pyruvate dehydrogenase, composed of E1α and E1β subunits), E2 (dihydrolipoyl acyltransferase), and E3 (dihydrolipoamide dehydrogenase). It is possible that photosynthesis-derived pyruvate is the major contributor to plastidial Ac-CoA for de novo fatty acid synthesis. However, in mixotrophic grown cultures of heterokonts such as *Nannochloropsis* sp., incorporation of acetate directly into lipids occurs.[8,85−88] The acetyl-CoA synthetase (ACSIN) converts acetate to plastidial Ac-CoA. Additionally, a study showed that under nitrogen deprivation *Chlamydomonas* is capable of changing its metabolism from converting acetate to glucose to a more direct incorporation of acetate into fatty acids by down-regulating glyoxylate cycle activity and gluconeogenesis.[4,89]

In microalgae, the cytosolic Ac-CoA pool is mainly fueled by the release of mitochondrial CIT to the cytosol and further cleaved into oxaloacetate and Ac-CoA by ACL. Cytosolic Ac-CoA is the building block used for LC-PUFA elongation in the ER. Concomitant production of NADPH by ME generates the reductive power necessary to drive plastidial de novo fatty acid synthesis forward. Availability of NADPH can increase the reaction velocity of Acc 2 (see stage 2) and ACL.[8] Fatty acid synthesis is an energy-demanding process due to the activity of

dx.doi.org/10.1021/jf4042134 | J. Agric. Food Chem. 2014, 62, 2709−2727

elongases and desaturases. For instance, the formation of a C18 FA requires 54 NADPH from oxygenic photosynthesis.[8] Other functions of malic enzyme in algae may include delivery of CO_2 from the TCA for the plastidial ribulose-1,5-bisphosphate carboxylase (Rubisco). Studies also suggest the existence of a plastidial ME (absent in yeast), which can provide electrons for plastidial FA synthesis.[8,90−92] For a review about plastidial ME see the work of Maier et al.[93]

Some microalgae are capable of accumulating intracellular starch, such as the thoroughly studied microalgal model *Chlamydomonas*. Starch synthesis is an example of how carbon partitioning might play a key role in lipid accumulation. One study showed that in wild-type *Chlamydomonas*, TAG accumulated only after the maximum amount of starch was reached, whereas starchless *Chlamydomonas* mutants initiated TAG accumulation earlier and reached a higher level than wild-type strain.[4,94] Therefore, it is possible to engineer high TAG algal strains by eliminating competing carbon utilization pathways such as starch synthesis to maximize lipid biosynthesis.

Stage 2. Biosynthesis of Fatty Acyl Chains. In algae, de novo fatty acid biosynthesis occurs primarily in the plastid. The committed step in plastidial fatty acid synthesis is the conversion of plastidial Ac-CoA to mal-CoA by Acc1. The three domains of the homomeric Acc1 are located on a multifunctional polypeptide encoded by a nuclear gene.[8,95] It works via biotin carboxylation and subsequent carboxyl transfer to Ac-CoA.[55,96] Some microalgae contain only Acc1, such as *I. galbana*. Others, such as *T. pseudonana* and *P. tricornutum*, contain two homomeric Accases, Acc1 (described above) and a cytosolic Acc (Acc2), which uses cytosolic Ac-CoA to generate mal-CoA. The latter plays a role in LC-PUFA elongation in the ER membrane.[8,97]

FAs are synthesized in microalgae's plastid via a dissociated type II FAS, containing discrete, monofunctional enzymes encoded by distinct genes.[98] In plastidial FAS II mal-CoA is loaded to ACP via malonyl-CoA:ACP transacylase encoded by *FABD*. Malonyl-ACP is used in the cyclic condensation reactions to extend the acyl group to palmitoyl ACP or stearoyl ACP. The acyl ACP can be released from FAS II in several ways: It can be hydrolyzed by a fatty acyl-ACP thioesterase located in the chloroplast envelope, forming a free fatty acid, or it can be transesterified from ACP to CoA via (ACS), or it can even be coupled to either G3P or MAG3P through an AT in the chloroplast.[8,55]

There are some heterotrophic microalgal species that contain a cytosolic type I FAS, synthesized from one or two polypeptides,[8,98] different from plastidial type II FAS. For example, *Aurantiochytrium*[99] contains a type I FAS, which synthesizes saturated C14:0 and C16:0. The synthesized free FAs and the absence of genes homologous to a type II TE may indicate integration of TE activity into the synthase.[100]

Several attempts have been made to overexpress specific enzymes in the lipid biosynthetic pathways. In the cases of Acc and KS (KS III), overexpression failed to increase lipid accumulation.[101]

Stage 3. Allocation of Acyl Moieties to either Polar or Neutral Lipid Pools. The released acyl moieties as free fatty acids destined to stay within the plastid may be further desaturated (typically to hexadecatrienoic acid HDT, C16:3*n*-4) and coupled to a monogalactosyldiacylglycerol (MGDG) backbone. MGDG, along with other types of galactosylglycerides (GG), is a major component of photosynthetic membranes in microalgae and in some cases may be even more abundant than PL.[8,74] In plants, the FA combination of GG can be traced back to their biosynthetic pathways; the so-called eukaryotic molecular species (C18/C18) of GG are synthesized outside the chloroplast in the eukaryotic pathway, and the prokaryotic molecular species (C18/C16) are synthesized in the plastid via the prokaryotic pathway.[8,102] Microalgae differ from plants in that most C20 FAs are synthesized outside the chloroplast and are present in both the eukaryotic-like (C20/C20, C18/C18) and prokaryotic-like (C18/C16, C20/C16) molecular species.[8,74,103,104] Therefore, microalgae's GG are referred to as "C20/C20" or "C20/MLC" (where MLC means medium to long chain) rather than eukaryotic- and prokaryotic-like GG.

When acyl ACP's are esterified to either G3P or MAG3P, they can join the plastidial PL pool. In plants two ATs catalyze these reactions. The first is a soluble enzyme that prefers oleoyl-ACP as substrate. The second one resides on the inner chloroplast envelope membrane and preferentially selects palmitoyl-ACP.[77] In some algal species, such as *C. reinhardtii* and *P. lutheri*, PC is absent in both plastidial and extraplastidial phospholipid pools. Instead, they contain the non-phosphorus betaine lipid diacylglyceryl-*N*,*N*,*N*-trimethylhomoserine (DGTS), which has similar physicochemical properties, as a major membrane component.[105−109] This is a significant difference against higher plants. It has been suggested that DGTS may have a role in lipid droplet formation similar to that of PC in higher plants.[105] However, they contain other types of phospholipids, such as PA, PE, and PI.[8,74]

Acyl ACPs synthesized in plastidial type II FAS can be transesterified with CoA via ACS. These enzymes regulate the acyl pools in different cellular compartments. Thus, stearoyl ACP can leave the FAS II complex via transesterification by a series of ACS responsible for maintaining both intraplastidial and cytosolic acyl-CoA pools.[8,110] In both cases, acyl-CoA is destined to leave the plastid and enter the ER membrane for further oxygen-dependent elongation and desaturation, to become long-chain polyunsaturated fatty acids (LC-PUFA), such as eicosapentaenoic acid (EPA) and docosahexaenoic acid (DHA). Two types of desaturases can be distinguished in microalgae. The first are front-end desaturases containing an N-terminal cytochrome *b*5 domain and insert the new double bond between the FA carboxyl group and a possible existing double bond. One example is the high substrate specific plastidial-located Δ12 desaturase, identified in *P. tricornutum*, which desaturates palmitoleic acid C16:1*n*-7 to hexadecadienoic acid 16:2*n*-4.[8] The second group comprises the less common *ω*6/*ω*3 desaturases capable of inserting a new double bond between the FA methyl end and a pre-existing double bond.[8,111]

Stearoyl CoA can be desaturated by an ER membrane-bound Δ9 desaturase to oleyl-CoA and then linked to a glycerol backbone for further processing. Some microalgae contain a plastidial Δ9 desaturase, capable of direct desaturation of stearoyl ACP to be then transesterified to CoA and sent to the ER for elongation and desaturation. In most microalgae, *n*-3 LC-PUFA are more abundant than *n*-6 LC-PUFA,[112] whereas in filamentous fungi, such as *mortierella* and *mucor*, *n*-6 LC-PUFA are more common.[3,19] In microalgae the most common pathways for EPA and DHA synthesis are the *n*-3 and *n*-6 pathways, but variations of the theme occur. In the *n*-3 pathway, oleic acid already linked to a glycerol backbone in the ER membrane is desaturated to linoleic acid (LA), via a Δ12

desaturase (encoded by FAD2). A third double bond inserted by an *n*-3 Δ15 desaturase gives α-linolenic acid (LNA), which is further desaturated to produce stearidonic acid (SA) by a Δ6 desaturase. SA is then elongated to C20:4 *n*-3 (eicosatetraenoic acid, EA) and finally desaturated by a Δ5 desaturase to produce EPA. In most DHA-producing microalgae, EPA undergoes an additional elongation and a Δ4 desaturation to create DHA.[112] This is a different, less complicated strategy for DHA synthesis from EPA, compared to the Sprecher pathway, present in mammals, which involves an additional elongation and a β-oxidation. In contrast to the *n*-3 pathway, some microalgae synthesize EPA via the *n*-6 pathway, following Δ6 desaturation of LA to γ-linolenic acid (GLA), elongation to dihomo-γ-linolenic acid (DGLA), creation of a fourth double bond by Δ5 desaturase to produce arachidonic acid (ARA), and a final desaturation to create EPA via a *n*-3 Δ17 desaturase.[112] Some microalgae express Δ9 elongase and Δ8 desaturase, allowing them to synthesize EPA in a different way compared to the *n*-3 and *n*-6 pathways.[112] In a variation of the *n*-3 pathway, LNA is elongated by a Δ9 elongase to eicosatrienoic acid (ETA) and desaturated by the Δ8 desaturase, creating EA. On the other hand, a variation of the *n*-6 pathway using this pair of enzymes involves Δ9 elongation of LA to eicosadienoic acid (EDA) and Δ8 desaturation to DGLA.[74] Thus, microalgae can switch from *n*-6 fatty acids to *n*-3 fatty acids via the *n*-3 Δ15 desaturase and the *n*-3 Δ17 desaturase. In some species of the Thraustochytrids, it is also possible to switch from *n*-6 docosapentaenoic acid (DPA) to DHA, via an *n*-3 Δ4 desaturase.

In addition to these pathways, there is a different *n*-3 LC PUFA biosynthetic pathway present in one of the three genera of heterotrophic Thraustochytrids, namely *Auranthiochytrium*, based on an anaerobic polyketide synthase pathway (PKS).[8,113] A large multifunctional enzyme complex carries out the multitude of individual reactions, utilizing mal-CoA and producing free *n*-3 LC-PUFAs. The major free FAs DPA (22:5*n*-6) and DHA (22:6*n*-3) are then activated to acyl-CoA and incorporated into TAGs.[8,100] Because PKS does not require aerobic desaturation, the pathway is energetically favorable compared to the membrane-bound desaturases and elongases.[114]

TAG synthesis in microalgae follows the Kennedy pathway in the ER in a similar fashion as yeast (see Figure 5). However, an acyl-CoA-independent mechanism for triacylglycerol synthesis in some plants and yeast has been reported.[55,115] This pathway uses PL as acyl donors and DAG as the acceptor, and the reaction is catalyzed by the enzyme phospholipid:DAG acyltransferase.

There are two diacylglycerol acyltransferase families identified in *Chlamydomonas*, involved in the final step of triacylglycerol synthesis: type one (DGAT), encoded by DGAT1, and type two (DGTT), encoded by five DGTT genes, which do not share sequence similarity. Two independent studies showed the expression levels of DGAT1 and DGTT1 increased considerably following nitrogen deprivation.[4,89,116] However, it remains unclear which of these DGATs are primarily responsible for the accumulation of TAGs under this condition or whether individual isoforms have specific roles.

Triacylglycerol synthesis can also occur within the plastid, through a series of acyl-ACP esterifications to plastidial G3P, catalyzed by plastidial ATs similar to the Kennedy pathway in the ER.[117] The involvement of GG (the major polar lipid family in plastidial membranes in several microalgae) in this process remains to be elucidated.

During light−dark cycles, many microalgae initiate triacylglycerol storage during the day and deplete those stores at night to support cellular ATP demands and/or cell division.[56] This cycling has to be taken into account when scaling up processes for production of lipids from algae. This variable may be key to the overall success of an open pond process or a closed photoreactor process.

Stage 4. Lipid Droplet Biogenesis. In contrast to yeast, LD can emerge from plastidial membranes. They can grow facing the cytosol or toward the inside of the plastid, facing the stroma, which is the major aqueous fluid surrounding the thylakoids inside the chloroplast.[4,117] The mechanisms underlying the orientation of lipid droplet growth in plastid membranes are not well understood. When LD grow toward the inside of the plastid (facing the stroma), they can also be called plastoglobules (PTG). PTG can be considered to be functionally equivalent to cytosolic LD, but differ in three major respects. First, they are confined to the stroma. Second, they can assume several different forms including rods, fibers, and globules; and third, they are bound by a specific family of proteins, variously termed plastoglobulins, plastid lipid-associated proteins, and fibrillins.[11] Oleosins (the major lipid droplet proteins present in plants) are not present in green algae, but a major lipid droplet protein was identified by applying proteomics in *Chlamydomonas* and shown to modulate lipid droplet size.[1] Orthologues of the major lipid droplet protein are present in other green algae. A wide variety of parameters affect the abundance of LD in *Chlamydomonas*, and there is ample evidence that turnover of LD plays crucial roles in cellular lipid or carbon homeostasis.[118]

THE CASE OF BACTERIA

In bacteria, the most frequent types of neutral and polymeric lipids synthesized and accumulated are PHA, TAG, wax esters (WE), and, to a lesser extent, SE. This review focuses on the first two. Most bacteria are capable of synthesizing either PHA or TAG. However, a special situation occurs in bacteria such as *Rhodococcus ruber*, and other related bacteria, capable of accumulating both types of lipids from unrelated carbon sources such as glucose.[7,11]

The mechanisms of wax ester accumulation have been reviewed elsewhere.[119,120] In a nutshell, an acyl-CoA is transformed to an aldehyde via an NADPH-dependent acyl-CoA reductase (encoded by *Acr1*), which is then reduced to an alcohol via an also NADPH-dependent fatty aldehyde reductase. The alcohol is then transesterified to an acyl-CoA via an enzyme displaying both wax ester synthase (WS) and acyl-CoA:diacylglycerol acyltransferase (DGAT) activities (abbreviated WS/DGAT).[7]

The only report of the presence of an sterol ester-synthesizing enzyme in prokaryotes was provided by Thornton et al.[121]

Accumulation of TAG in Bacteria. To date, triacylglycerol biosynthesis has been detected only in aerobic heterotrophic bacteria and in cyanobacteria.[6] In most bacteria, accumulation of TAG and other neutral lipids, such as WE, is stimulated by a carbon source present in excess, together with limited nitrogen in the medium.

Biosynthesis of Fatty Acyl Chains. Structurally, fluorescence staining experiments showed that lipid biosynthesis starts at peripheral lipid domains close to the cytoplasm

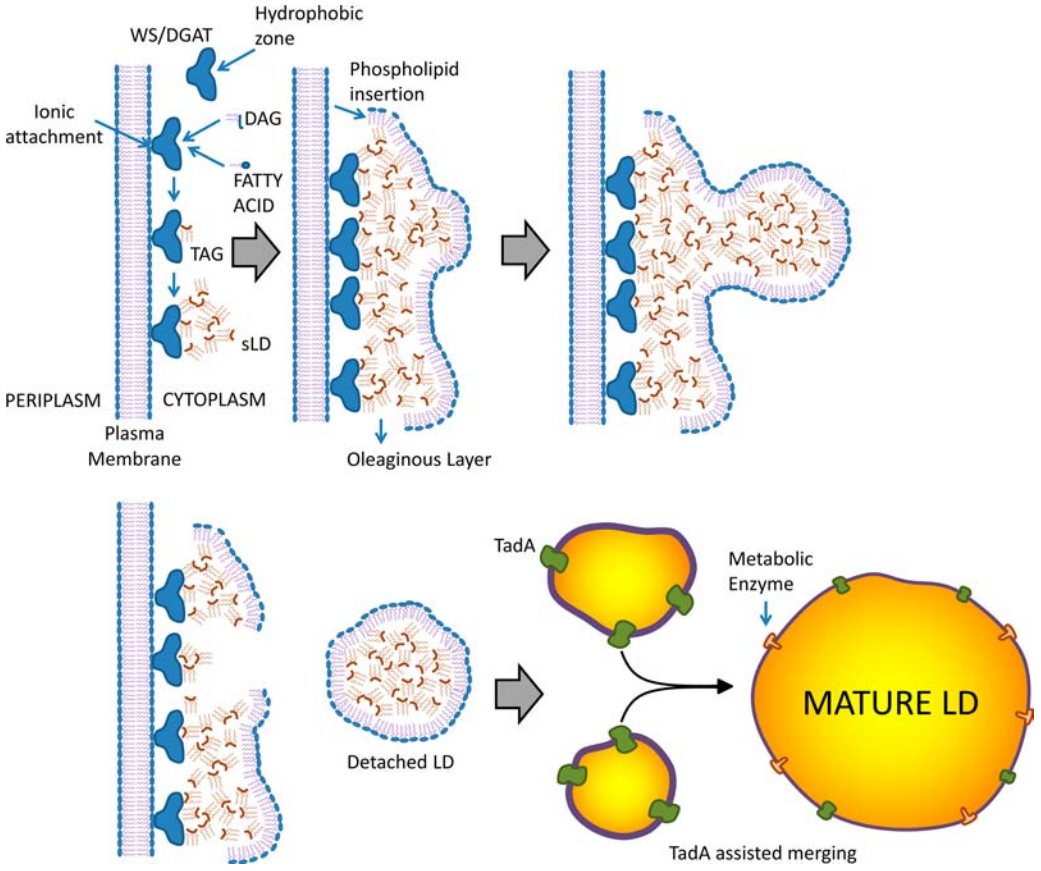

Figure 6. Suggested mechanisms of neutral LD formation in bacteria. Adapted from ref 22.

membrane.[22,122] Biochemically, fatty acid biosynthesis begins in bacteria with Acc, a heterotetrameric enzyme encoded by four genes, *accA*, *accB*, *accC*, and *accD*.[21] Fatty acids in bacteria are synthesized via a dissociated type II FAS. Each monofunctional protein is encoded by a specific gene.

Ac-CoA is converted to mal-CoA and transferred to ACP by malonyl-CoA:ACP transacylase (FabD in bacteria) to form malonyl-ACP. A first condensation of malonyl-ACP with acetyl-CoA by β-ketoacyl-ACP synthase III (FabH) to form β-ketobutyryl-ACP and CO_2 initiates a cycle that can elongate the fatty acyl-ACP by two carbon units for each cycle until a saturated fatty acid of 16 or 18 carbons is made. KSI (FabB) and KSII (FabF) are responsible for the subsequent elongation cycles of the growing acyl-ACP chain.

To balance chain initiation with growth and utilization in bacterial FASII, KSIII, enoyl-ACP reductase (FabI in bacteria), and β-ketoacyl-ACP reductase (Fab G in bacteria) are under negative feedback control by long-chain acyl-ACPs.[18] Long-chain acyl-ACPs directly control reductase activities; consequently, FASII is biased to catalyze forward if these products are withdrawn from the system by any conversion, including phospholipid or triacylglycerol synthesis.

In some bacteria, FAS II yields unsaturated fatty acids, which play a key role in bacterial membrane fluidity and function.[21,123] Unlike ER desaturases present in microalgae or yeast, which introduce double bonds into the completed fatty acid chains at the expense of oxygen, the bacterial FAS II system can also desaturate fatty acids anaerobically, because it does not require molecular oxygen.[21] FabA introduces the double bond at the 10-carbon intermediate, forming *cis*-2-decenoyl-ACP. It additionally isomerizes it into *trans*-3-decenoyl-ACP, which is further elongated by FabB.[18,21] Two genes, *fabA* and *fabB*, are the key players in this pathway and occur together in bacteria that produce unsaturated fatty acids.

Some *Rhodococcus* and *Nocardia* bacteria are capable of incorporating branched or phenylic groups into their intracellular TAG if the corresponding substrate is fed to the medium. For example, *Nocardia globerula* strain 432 accumulated TAG containing the branched fatty acid 4,8,12-trimethyltridecanoic acid after cells were fed pristane (a branched alkane),[6] and TAG with a subfraction containing phenyldecanoic acid residues were detected in cells of *R. opacus* PD630 after phenyldecane was fed as sole carbon source.[6,124]

Allocation of Acyl Moieties to either Polar or Neutral Lipid Pools. The enzymes involved in the esterification of the glycerol moiety probably act via sequential acylation of the sn-1, -2, and -3 positions of G3P, with the removal of the phosphate group occurring before the final acylation step.[6] The first esterification is catalyzed by a G3PAT using either acyl-CoA or acyl ACP to form lysophosphatidic acid. A second acylation to lysophosphatidic acid gives PA, which is the first branchpoint for the synthesis of TAG and PL, because it can be converted to CDP-DAG, the precursor of the different PL species in bacterial membranes. DAG itself is also at a metabolic branchpoint that divides phospholipid and triacylglycerol formations, because it acts as a precursor for TAG, PC, and PE biosynthesis. In addition, DAG can also be derived from PL by the action of phospholipase C[7,125] The distribution of acyl groups on the hydroxyl groups of the glycerol backbone is nonrandom, as has been demonstrated for *R. opacus* PD630.[6,126] The shorter and saturated fatty acids were esterified to the hydroxyl group at position 2, whereas

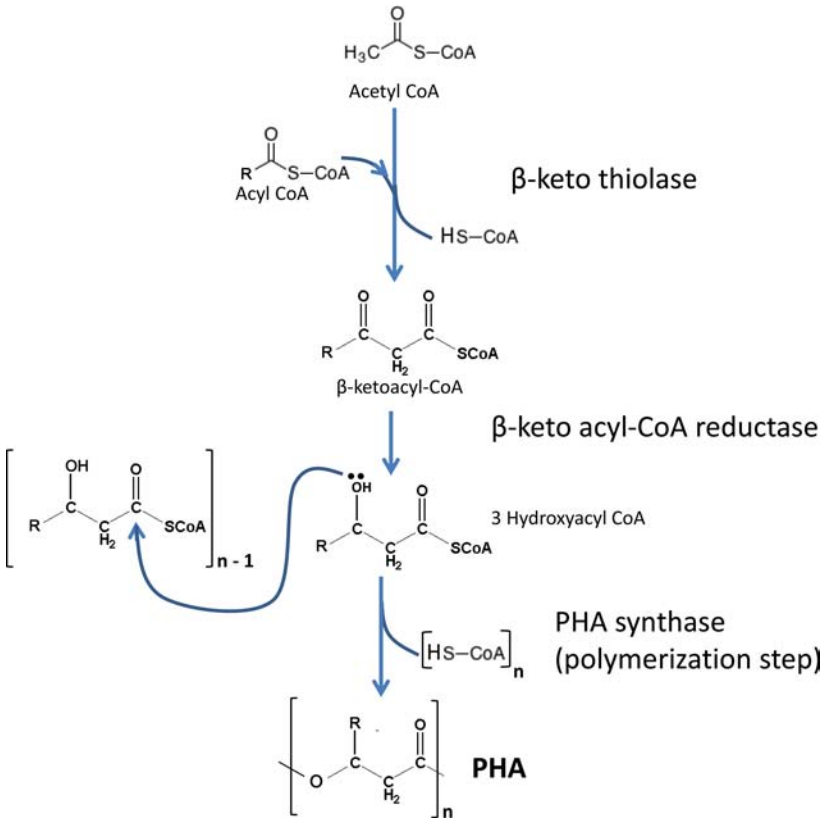

Figure 7. Biosynthesis of PHA.

unsaturated fatty acids were preferentially found at position 3. This distribution in bacterial TAG is different from the TAG of mammals and plants, where the longer unsaturated fatty acids are found at position sn-2.[127]

The final step in wax ester and triacylglycerol biosyntheses in bacteria is catalyzed by WS/DGAT.[7,127] WS/DGAT is encoded by *atfA* and is not related to any known AT involved in the formation of TAG and WE in eukaryotes. It has also been shown that WS/DGAT is localized at the bacterial cytoplasmic membrane, presumably attached to the inner leaflet of the membrane, probably via ionic interactions.[22] For a detailed review about WS/DGAT, the reader is referred to the work of Waltermann et al.[7] Alternative pathways for triacylglycerol synthesis that do not involve DAG in bacteria have also been reported and may involve an enzyme similar to that reported by Dalquist in yeast,[115] which catalyzes the formation of TAG from the transesterification of an acyl donor (e.g., acyl-CoA) to PL.[6] This follows observations that following a double knockout of WS/DGAT genes in *A. borkumensis*, cells were still capable of substantial triacylglycerol accumulation in LD.[11,128]

Triacylglycerol/Wax Ester Lipid Droplet Biogenesis. Triacylglycerol/wax ester lipid droplet biogenesis presumably begins by allocation of newly formed TAG in a hydrophobic zone within WS/DGAT. As time goes by, more WS/DGAT attaches to the membrane, and cumulative synthesis advances, presumably leading to the formation of very small triacylglycerol agglomerates, depicted by Wältermann et al. as small lipid droplets (sLD).[22] sLD apparently recruit PL from the membrane by a mechanism that is still not well understood, forming a layer toward the cytoplasmic side (see Figure 6). The agglomeration of phospholipid-coated sLD appears in microscopy as an oleaginous layer just parallel to the membrane.[22] Then, accumulation of sLD in a given point gives birth to LD, which are coated by PL and detach from the oleaginous layer. These droplets will acquire more TAG and grow. It has been suggested that acquisition of additional TAG is by merging with other LD freshly synthesized from the oleaginous layer via coalescence[22] and/or through a protein identified as TadA.[11] An interesting study by Ding and co-workers[36] examined the proteome of *Rhodococcus* sp. RHA 1 (a Gram-positive bacteria capable of accumulating TAG)[36] grown both in nitrogen-abundant (not favoring lipid accumulation) and nitrogen-depleted conditions (favoring lipid accumulation). Using a combination of techniques, including LC-MS, SDS-PAGE, and immunoblot assays, they reported 228 lipid droplet-associated proteins, which clustered primarily into metabolism-related enzymes, transcriptional regulators, ribosome proteins, and cell division-related proteins. Interestingly, they identified two major proteins, ro02104 and PspA, which constituted about 15% of the total lipid droplet protein. According to their findings, the structure predicted for ro02104 resembles that of apolipoproteins, the structural proteins of plasma lipoproteins in mammals.

Accumulation of PHA in Bacteria. In bacteria PHA comprise a complex class of storage polyesters, with almost 150 different hydroxyalkanoic acids known as constituents.[6] A wide variety of Gram-positive as well as Gram-negative bacteria synthesize PHA. Examples include *Pseudomonas*, *Bacillus*, *Ralstonia*, *Aeromonas*, and *Rhodobacter*, among others. PHA are divided into two groups on the basis of the number of constituent carbon atoms in their monomer units: short chain length PHAs (SCL PHA) and medium chain length PHAs (MCL PHA). Monomers of SCL PHA are 3−5 carbon atoms

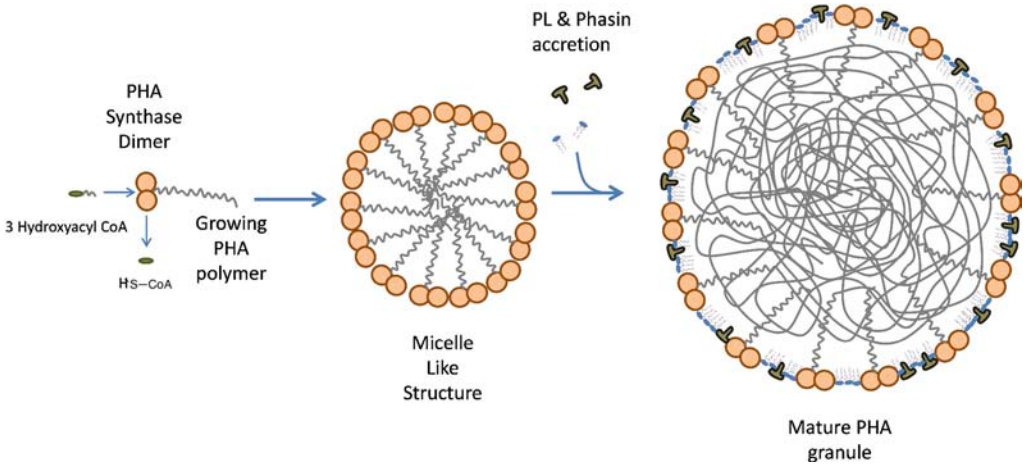

Figure 8. Proposed mechanism of PHA containing lipid droplet formation in bacteria (micelle model). Adapted from ref [22].

long, compared to 6−14 carbon atoms in MCL PHA. In addition, SCL PHA are stiff and brittle with a high degree of crystallinity, whereas MCL PHA are flexible and have low crystallinity, tensile strength, and melting point.[30]

Production of Acetyl-CoA and Synthesis of Hydroxyalkanoate Monomers. Accumulation of PHA starts with the creation of hydroxyalkanoate monomers from three different biosynthetic pathways. The first one involves incorporation of two acetyl-CoAs to form acetoacetyl-CoA, by the enzyme β-ketothiolase.[11,30,129,130] Then acetoacetyl-CoA reductase converts acetoacetyl-CoA into 3-hydroxybutyryl-CoA. This pathway creates hydroxybutyrate (HB) monomers exclusively and is used by bacteria such as *Cupriavidus necator* and *Azotobacter beijerinckii* (see Figure 7).[30,129,130] On a second pathway involving de novo fatty acid biosynthesis, monomers of different lengths can be formed by transesterifying 3-hydroxyacyl-ACP, an intermediate of FAS II to 3-hydroxyacyl-CoA, presumably by the enzyme acyl-ACP-CoA transacylase, encoded by *phaG*. This enzyme is the key link between de novo fatty acid synthesis and polyhydroxyalkanoate biosynthesis.[30,131] This pathway is of biotechnological interest because it helps generate monomers for polyhydroxyalkanoate synthesis from structurally unrelated and simple, inexpensive carbon sources such as glucose or related simple sugars. On a third embodiment, monomers of different lengths can also be sourced from fatty acid β-oxidation pathway either by conversion of 2-enoyl-CoA by an *R*-specific enoyl-CoA hydratase, encoded by *PhaJ*, or by reduction of 3-ketoacyl-CoA, presumably by FabG or PhaB.[30] In this case, the monomer composition is related to the carbon source used.

Polymerization and Copolymerization into Polyhydroxyalkanoate Chains. The resulting *R*-3-hydroxyacyl-CoA monomers are polymerized by polyhydroxyalkanoate synthase. The ability of microorganisms to synthesize a particular form of polyhydroxyalkanoate is mainly due to the substrate specificity of polyhydroxyalkanoate synthases. These enzymes are divided into four classes, depending on their structure and specificity. Class I enyzmes utilize CoA thioesters of 3-hydroxyalkanoates (3-HAs), 4-HAs, and 5-HAs comprising three to five carbon atoms.[132] Species such as *Pseudomonas putida* and *R. eutropha* possess this class of enzymes. Members of class II display major specificity for monomers ranging from 6 to 14 carbon atoms. Enzymes from both classes consist of a single subunit of an average size of 60−70 kDa and are encoded by *PhaC*. In contrast, class III and class IV synthases are encoded by two genes, PhaC/PhaE, and PhaC/PhR respectively, and consist of two subunits. Class III members are capable of polymerizing preferably monomers ranging from three to five carbons, yet can utilize monomers from six to eight carbons as well.[132] Species such as *Allochromatium vinosum* contain class III synthases, whereas class IV has been reported only in *Bacillus* sp.[38] All polyhydroxyalkanoate synthases share a conserved cysteine as a catalytic site to which the growing polyhydroxyalkanoate chain is covalently attached. The active-site cysteine, histidine, and aspartate constitute a catalytic triad similar to esterases.[38] Literature is available for an in-depth analysis of polyhydroxyalkanoate synthases.[133−139]

Polyhydroxyalkanoate Lipid Droplet Biogenesis. Two models currently exist that may explain the formation of in vivo polyhydroxyalkanoate LD (which are also called granules or carbonosomes[38,39]): the micellar and the budding models. The first one is based on the assumption that the polyhydroxyalkanoate synthase is present in the cell as a soluble enzyme, distributed throughout the cytoplasm. Once polymerization of substrate molecules (CoA-thioesters of suitable hydroxyalkanoic acids) starts, the nascent polyester chain converts the initially soluble enzyme into an amphipathic molecule and the increasingly hydrophobic polyhydroxyalkanoate chains aggregate into a micelle-like structure. Polyhydroxyalkanoate synthase remains attached to the surface of the granule and therefore becomes insoluble (see Figure 8). In this model, PL and proteins of the surrounding layer would gradually become incorporated as the self-assembled polyhydroxyalkanoate inclusion increases in size.[38,39] This model requires the polyhydroxyalkanoate granule to be localized in the cytoplasm at all stages of formation. In contrast, the budding model assumes that polyhydroxyalkanoate synthase is associated with the inner face of the cytoplasmic membrane, either inherently or as soon as a polyhydroxyalkanoate chain emerges from the enzyme. In this case, biosynthesis of the polyester would be directed into the intermembrane space where the extending chains would accumulate until eventually the granules detach from the membrane and polyhydroxyalkanoate-specific surface proteins can be attached to the growing granules.[38,39] Although the micelle model is supported by the fact that polyhydroxyalkanoate granules can be produced in vivo in the absence of membranes, most of the recently emerging evidence is in favor of the budding model.[39] The major structural proteins present

in polyhydroxyalkanoate granules are phasins (Phas). Phas may constitute approximately 5% (w/w) of total cellular proteins,[140,141] and they play a main structural role in preventing polyhydroxyalkanoate granules from aggregating and in preventing the nonspecific attachment of other proteins to polyhydroxyalkanoate granules.[140−142] In addition, phasins are presumably involved in the regulation of polyhydroxyalkanoate synthesis, polyhydroxyalkanoate degradation, polyhydroxyalkanoate granule size control,[140,141,143,144] the formation of networks on the polyhydroxyalkanoate granule surface,[145] and the distribution of polyhydroxyalkanoate granules during cell division. Another important group of proteins present in the external granule layer is the depolymerases, which are responsible of catalyzing polyhydroxyalkanoate breakdown. This is a relevant step in the role of polyhydroxyalkanoate accumulation as a survival mechanism in the absence of suitable energy/carbon sources, as was demonstrated many years ago in *R. eutropha*.[146] Two groups have been identified: intracellular (PhaZs) and extracellular depolymerases. PhaZs have been investigated much less than extracellular depolymerases, and the mechanism by which intracellular native polyhydroxyalkanoate granules can be reutilized is still not well understood.[39] Interestingly, the gene coding for PhaZs is located between two copies of *phaC1* and *phaC2* (both polyhydroxyalkanoate synthase genes) in all investigated bacteria that accumulate MCL PHA.[38] In contrast, secreted depolymerases are used by most bacteria to assimilate PHA present in the environment from, for example, other nonliving cells.[147]

Polyhydroxyalkanoate granule synthesis and phasin production are tightly regulated by the effectiveness of the transcriptional regulator PhaR. Genes encoding proteins homologous to PhaR are widely distributed among SCL PHA producing bacteria, indicating an important role in the regulation of SCL PHA biosynthesis.[39,148,149]

THE CASE OF ARCHAEA

The discovery of the Archaea domain in 1977 revealed a novel class of microorganisms encountered in exceptional ecological niches such as high (thermophiles and hyperthermophiles) or low (psychrophiles) temperatures, acidic media (acidophiles an thermoacidophiles), anaerobic atmosphere (methanogens), and high salinity (halophiles).[150,151] The unique chemical structure of their core membrane lipids is in part responsible for their adaptation to such hostile environments. Archaeal membrane lipids, in contrast to those of bacteria and eukaryotes, are made up of saturated chains containing methyl branches, attached to glycerol by ether linkages with a stereochemistry in the 2-position of the glycerol opposite that of conventional mesophilic lipids. (For a review on archaeal ether lipid structures, the reader is referred to the work of Jacquemet et al.[150]) Moreover, Archaea do not synthesize fatty acyl esters, which are the most common constituents of LD; instead, their lipids are based on isoprenoid chains.[11] Therefore, no accumulation of TAG has been reported yet in Archaea. Despite these differences, however, evidence of polyhydroxyalkanoate accumulation was first reported in Haloarchaea back in 1972.[152,153] The strains were called at that time "*Halobacterium* sp. from the Dead Sea", but later identified as *Haloarcula marismortui*.[154] Since then, strains of several other haloarchaeal genera, including *Haloferax*, *Halobiforma*, and *Haloquadratum*, have been found to accumulate PHA.[140,154] As in bacteria, Archaea produce PHA under conditions of nutrient limitation but where carbon is available in excess.[155−161] The mechanisms of polyhydroxyalkanoate accumulation within Archaea are beginning to be understood, and work is underway to elucidate the type of proteins involved in archaeal polyhydroxyalkanoate accumulation. Genes involved in polyhydroxyalkanoate biosynthesis in Haloarchaea were not recognized until recently, when the polyhydroxyalkanoate synthase genes were identified and characterized for *Haloarcula marismortui* and *Haloferax mediterranei*.[156,157,159−163] These archaeal polyhydroxyalkanoate synthases are all composed of two subunits, PhaE and PhaC, and they are homologous to class III bacterial polyhydroxyalkanoate synthases but have a longer C-terminal extension in the PhaC subunit.[162] The close similarity of archaeal and bacterial type III polyhydroxyalkanoate synthase genes and the lack of other polyhydroxyalkanoate gene types in archaea suggest that archaeal PHA originated from the horizontal transfer of an ancestral type III gene from a bacterium.[11] Some authors suggest this transfer to have occurred already before Permian times.[152]

Genome-wide analysis of *H. marismortui* ATCC 43049[162,163] revealed eight paralogues of a short-chain dehydrogenase/reductase, responsible for reduction of acetoacetyl-CoA to (*R*)-3-hydroxybutyryl-CoA (3-HB CoA), a monomer used by polyhydroxyalkanoate synthase to produce polyhydroxybutyrate (PHB). Another study[162] demonstrated that a similar paralogue in *H. hispanica*, namely *fabG1*, encodes a PHA-specific acetoacetyl-CoA reductase responsible for providing 3-HB-CoA for polyhydroxyalkanoate biosynthesis in *Haloarcula* species. The authors concluded that the polyhydroxyalkanoate biosynthesis pathway from Ac-CoA, catalyzed by β-ketoacyl thiolase, acetoacetyl-CoA reductase, and polyhydroxyalkanoate synthase, as distributed in bacteria, likely also exists in the domain of Archaea. Nonetheless, they pointed out that for PHB-accumulating haloarchaeal *Natrialba* strain 56,[157,158] no enzyme activity of acetoacetyl-CoA reductase or β-ketoacyl thiolase was detected in the crude extract, indicating that a different metabolic route toward production of PHB might be employed.

Polyhydroxyalkanoate synthase, putative enoyl-CoA hydratase, and two structural phasin-like proteins have been identified in haloarchaeal polyhydroxyalkanoate granule surfaces.[140] The phasin-like proteins in Haloarchaea share some structural features with bacterial Phas, such as the presence of hydrophobic domains and a high α-helix content.[140,164] After a genome-wide investigation into the 12 Haloarchaea that harbored the PhaP gene, most of these Archaea were found to possess a similar *pha* cluster, with five genes, namely, *maoC-gap12-phaP-phaE-phaC*, having the same organization as that in *H. mediterranei*.[140] The extensive existence of this *pha* gene cluster was suggested as an indication of an evolutionarily conserved *pha* gene cluster unique to Haloarchaea.[140]

A promising approach is to develop archaeal species as industrial scale polyhydroxyalkanoate producers. In particular, several halophilic Archaea have the advantages of utilizing much cheaper carbon sources (including waste materials), as well as having less strict sterilization requirements, plus easier and more efficient methods for polyhydroxyalkanoate extraction.[132]

FUTURE PERSPECTIVES

Microorganisms provide an exciting platform for the development of lipid technologies. In the course of evolution, they have developed elegant pathways to synthesize a wide array of lipids, providing a versatile and cost-effective approach for sourcing

lipids to virtually all sectors of industry. The understanding of the biochemical and cellular mechanisms of lipid production, accumulation, and secretion will provide valuable insights on innovations to overcome the hurdles in microbial lipid utilization.

Ongoing studies using different "omics" approaches will provide a holistic view of flows and interactions between the different metabolic pathways involved in lipid accumulation. Tools such as next-generation sequencing, transcriptome analysis, proteomics, and mass spectrometry are already clearing out the missing links in single-cell lipid biosynthesis. This information will permeate in the creation and scaleup of more efficient processes.

It is thus important to project the potential applications and envision the frontiers to which this valuable toolset can lead the diverse fields of lipid technology. For example, in the field of biotherapeutics, microbial-based approaches have the flexibility to construct platforms to manufacture personalized lipid therapies starting as simply as LC PUFA combinations, appropriate to the metabolic phenotype of each individual[165] and eventually becoming as complex and selective as personalized cancer interventions. This approach of personal medicine will carry improved benefits in the treatment of a range of conditions: in immunological diseases from infections to autoimmunities; in metabolic conditions from diabetes to cardiometabolic diseases; and in microbiota dysbiosis from IBS to IBD. Microbial technologies can also provide an alternative pathway for sourcing promising lipids and fatty acids that are unavailable in the market at present. For example, oil-producing microbes can be considered as appropriate vehicles in which foreign (plant) genes could be cloned for the production of commercially attractive fatty acids such as nervonic acid (C24:1 Δ15) obtained from Honesty (*Lunaria*),[3] which is used in small amounts in the treatment of particular neuropathies. Another example is sterculic acid {ω-(2*n*-octylcycloprop-1-enyl)-octanoic acid},[166] which has been considered as a treatment for certain cancers of the bowel. One more promising example is represented by the non-methylene-interrupted fatty acids (e.g., C20:3 Δ5, Δ11, Δ14), which can be obtained from *Juniperus chinensis* seed oil and is known to reduce the amount of arachidonic acid in certain phospholipid pools and, thus, act to alter eicosanoid signaling.[167]

In the field of energy and biofuels, understanding the mechanisms by which each group of microorganisms generates highly combustible lipids will foster the production of cost-effective fuels through sustainable processing and with improved performance. It is yet to be tested whether the biochemical mechanisms for amphipathic lipid secretion present in some microorganisms would work for the secretion of neutral lipids. This concept, if brought to practice, will significantly reduce the processing costs and render high-quality combustible lipids for the production of biofuels.

In the case of the food industry, a microbial-based approach will allow food companies to expand their core businesses by creating new product portfolios out of their current byproducts. Two promising examples are the production of cocoa butter analogues[3] and the production of high-value oils out of spent agricultural materials.

In the field of biomaterials, microbial lipids are already being used for producing biosurfactants and bioplastics, replacing synthetic analogues due to their improved biodegradability and reduced cost. Companies are now emerging worldwide taking advantage of the microbial lipid toolset. Products such as Metabolix PHA and Biomer are examples on how microbial-derived plastics are gaining momentum in the market.

Microbial biosurfactants are beginning to generate improved results against their synthetic homologues. Their specific modes of action, low toxicity, relative ease of preparation, and widespread applicability are increasing their use in applications such as emulsifiers, wetting and foaming agents, functional food ingredients, detergents in petroleum, petrochemicals, environmental management, agrochemicals, cosmetics and pharmaceuticals, commercial laundry detergents, mining and metallurgical industries (for an overview of microbial surfactant applications, see Mukherjee[168]). The scope of applications goes to such an extent that the petroleum extractive industry is already researching the use of microbial lipid-based biosurfactants for increasing oil recovery yields from subterranean depots.[168,169] The great era of chemistry culminating in the restructuring of the human condition in the 20th century has been defined by the principles of reductionism and simplicity. In contrast, the 21st century heralds the era of complexity for which the inherent biological diversity and information content of microorganisms will be key to adding value to all industrial chains.

A search performed on July 6, 2013, with the terms "microbial lipids" in the U.S. Patent Office "quick search" option retrieved 11905 results. Figure 9 shows a steady increase in U.S. patent publication since 2008, showing the increasing interest in the generation of intellectual property around this area of research.

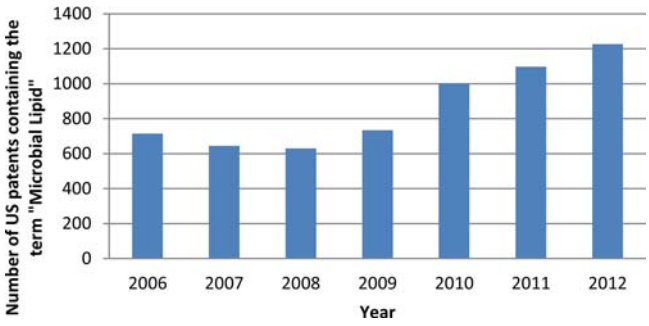

Figure 9. Number of U.S. patents containing the term "microbial lipids" per year.

Notice the increasing trend starting in 2008. The estimated patents by the end of 2013 according to the current trend will be around 1420, almost doubling the number registered in 2009.

The next step in microbial lipid technology is the integration of processes and applications to generate comprehensive, sustainable solutions. The immediate challenge is to combine desired metabolic pathways present in different species or strains to generate superior microbial species. Benefits will include improved yields, targeted lipidomic profiles, and structural features to synthesize in a sustainable and cost-effective way the lipid structures necessary to satisfy the breadth of needs of 21st century industry. For example, an appropriate integration of microbial-based lipid technologies will allow delivery of smart biofuels and even personalized edible oils derived from microorganisms and reporter-equipped biodegradable containers also derived from microorganisms. Currently the most used packaging material for commercial edible oils is polyethylene terephthalate, which is virtually a

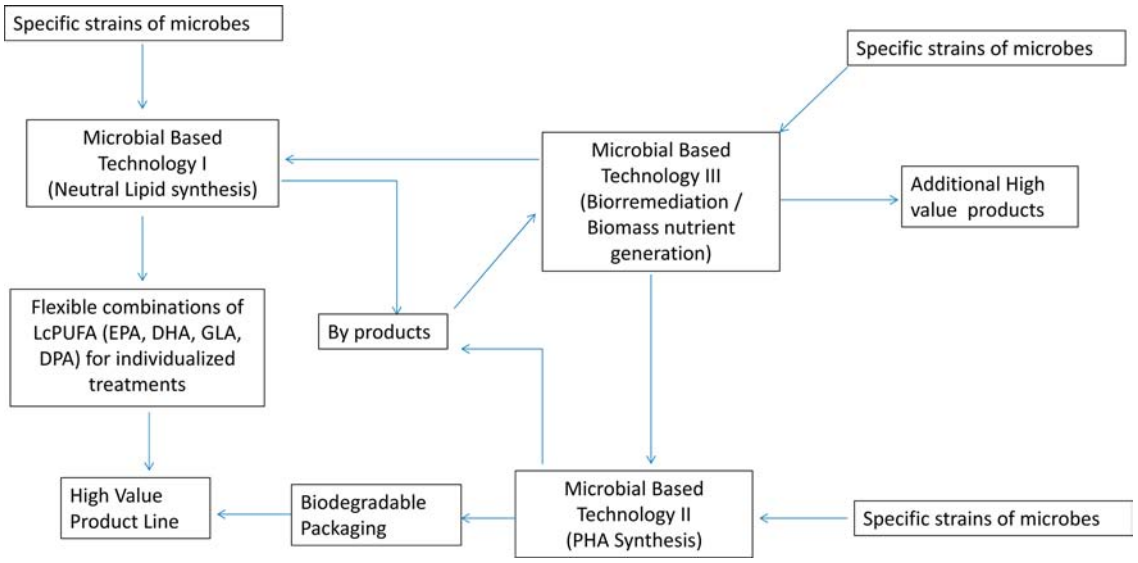

Figure 10. Conceptual flowchart for an integral, sustainable microbial-based edible oil process.

nondegradable plastic. With the appropriate use of microbial PHA, it could be possible to see in the same facility the production of high-value microbial oils (rich in a combination of LC PUFA), along with the production of polyhydroxyalkanoate-based bottles for its commercialization. Furthermore, additional microbial biotechnology platforms will be integrated to transform the byproducts either into biomass nutrients to make the process sustainable or even into another portfolio of high-value products, as a way to increase the business profitability (Figure 10). This would be a proposed example of a sustainable microbial-based industry.

Microbial lipid technologies are a valuable toolset available for the future generation of scientists, which will help them push the boundaries of production solutions ultimately toward a more sustainable society.

AUTHOR INFORMATION

Corresponding Author

*(J.B.G.) E-mail: jbgerman@ucdavis.edu.

Funding

We gratefully acknowledge funding from the National Mexican Council of Science and Technology (CONACYT) Fellowship 291795, Institute of Health U24 DK097154, National Institutes of Health awards R01HD059127, R01HD065122, R01HD061923, R21AT006180, and R01AT007079.

Notes

The authors declare no competing financial interest.

REFERENCES

(1) Merchant, S.; Kropat, J.; Liu, B.; Shaw, J. TAG, you're it! *Chlamydomonas* as a reference organism for understanding algal triacylglycerol accumulation. *Curr. Opin. Biotechnol.* **2012**, *23*, 352−363.

(2) Singh, A.; Singh, P.; Murphy, J. Mechanism and challenges in commercialization of algal biofuels. *Bioresour. Technol.* **2011**, *102*, 26−34.

(3) Ratledge, C. Microbial lipids: commercial realities or academic curiosities. In *Industrial Applications of Single Cell Oils*, 1st ed.; Kyle, D., Ratledge, C., Eds.; AOCS Press: Champaign, IL, USA, 1992; pp 1−15.

(4) Liu, B.; Benning, C. Lipid metabolism in microalgae distinguishes itself. *Curr. Opin. Biotechnol.* **2013**, *24*, 300−309.

(5) Athenstaedt, K.; Daum, G. The life cycle of neutral lipids: synthesis, storage and degradation. *Cell. Mol. Life Sci.* **2006**, *63*, 1355−1369.

(6) Alvarez, H. M.; Steinbüchel, A. Triacylglycerols in prokaryotic microorganisms. *Appl. Microbiol. Biotechnol.* **2002**, *60*, 367−376.

(7) Wältermann, M.; Stöveken, T.; Steinbüchel, A. Key enzymes for biosynthesis of neutral lipid storage compounds in prokaryotes: properties, function and occurrence of wax ester synthases/acyl-CoA:diacylglycerol acyltransferases. *Biochimie* **2007**, *89*, 230−242.

(8) Mülroth, A.; Li, K.; Rokke, G.; Winge, P.; Olsen, Y.; Hohmann-Marriott, M. F.; Vadstein, O.; Bones, A. M. Pathways of lipid metabolism in marine algae, co-expression network, bottlenecks and candidate genes for enhanced production of EPA and DHA in species of Chromista. *Mar. Drugs* **2013**, *11*, 4662−4697.

(9) Chapman, K. D.; Dyer, J. M.; Mullen, R. T. Biogenesis and functions of lipid droplets in plants. Thematic Review Series: Lipid droplet synthesis and metabolism: from yeast to man. *J. Lipid Res.* **2012**, *53*, 215−226.

(10) Mazumdar, J.; Wilson, E. H.; Masek, K.; Hunter, C. A.; Striepen, B. Apicoplast fatty acid synthesis is essential for organelle biogenesis and parasite survival in *Toxoplasma gondii*. *Proc. Natl. Acad. Sci. U.S.A.* **2006**, *103* (35), 13192−13197.

(11) Murphy, D. The dynamic roles of intracellular lipid droplets: from archaea to mammals. *Protoplasma* **2012**, *249*, 541−585.

(12) Daniel, J.; Deb, C.; Dubey, V. S.; Sirakova, T. D.; Abomoelak, B.; Morbidoni, H. R.; Kolattukudy, P. E. Induction of a novel class of diacylglycerol acyltransferases and triacylglycerol accumulation in *Mycobacterium tuberculosis* as it goes into a dormancy-like state in culture. *J. Bacteriol.* **2004**, *186*, 5017−5030.

(13) Garton, N. J.; Christensen, H.; Minnikin, D. E.; Adegbola, R. A.; Barer, M. R. Intracellular lipophilic inclusions of *Mycobacteria* in vitro and in sputum. *Microbiology* **2002**, *148*, 2951−2958.

(14) Heredia-Arroyo, T.; Wei, W.; Hu, B. Oil accumulation via heterotrophic/mixotrophic *Chlorella protothecoides*. *Appl. Biochem. Biotechnol.* **2010**, *162*, 1978−1995.

(15) Skrupski, B.; Wilson, K. E.; Goff, K. L.; Zou, J. Effect of pH on neutral lipid and biomass accumulation in microalgal strains native to the Canadian prairies and the Athabasca oil sands. *J. Appl. Phycol.* **2013**, *25*, 937−949.

(16) Ratha, S. K.; Prasanna, R.; Prasad, R. B.N.; Sarika, C.; Dhar, D. W.; Saxena, A. K. Modulating lipid accumulation and composition in microalgae by biphasic nitrogen supplementation. *Aquaculture* **2013**, *392 − 395*, 69−76.

(17) Ratledge, C. Resources conservation by novel biological processes. Part 1: Grow fats from wastes. *Chem. Soc. Rev.* **1979**, *8*, 283−296.
(18) Kosa, M.; Ragauskas, A. Lipids from heterotrophic microbes: advances in metabolism research. *Trends Biotechnol.* **2011**, *29* (2), 53−61.
(19) Wynn, J.; Hamid, A.; Li, Y.; Ratledge, C. Biochemical events leading to the diversion of carbon into storage lipids in the oleaginous fungi *Mucor circinelloides* and *Mortierella alpine*. *Microbiology* **2001**, *147*, 2857−2864.
(20) Schweizer, E.; Hofmann, J. Microbial type I fatty acid synthases (FAS): major players in a network of cellular FAS systems. *Microbiol. Mol. Biol. Rev.* **2004**, *68* (3), 501−517.
(21) Lu, Y.-J.; Zhang, Y.-M.; Rock, C. O. Product diversity and regulation of type II fatty acid synthases. *Biochem. Cell Biol.* **2004**, *82*, 145−155.
(22) Wältermann, M.; Hinz, A.; Robenek, H.; Troyer, D.; Reichelt, R.; Malkus, U.; Galla, H.; Kalscheuer, R.; Stöveken, T.; Landenberg, P.; Steinbüchel, A. Mechanism of lipid-body formation in prokaryotes: how bacteria fatten up. *Mol. Microbiol.* **2005**, *55* (3), 750−763.
(23) White, S. W.; Zheng, J.; Zhang, Y. M.; Rock, C. O. The structural biology of type II fatty acid biosynthesis. *Annu. Rev. Biochem.* **2005**, *74*, 791−831.
(24) Schujman, G. E.; Mendoza, D. Regulation of type II fatty acid synthase in Gram-positive bacteria. *Curr. Opin. Microbiol.* **2008**, *11*, 148−152.
(25) Zhang, Y. M.; Rock, C. O. Transcriptional regulation in bacterial membrane lipid synthesis. *J. Lipid Res.* **2009**, *50*, S115−S119.
(26) Steen, E. J.; Kang, Y.; Bokinsky, G.; Hu, Z.; Schirmer, A.; McClure, A.; Del Cardayre, S. B.; Keasling, J. D. Microbial production of fatty-acid-derived fuels and chemicals from plant biomass. *Nature* **2010**, *463* (7280), 559−562.
(27) Clomburg, J. M.; Gonzalez, R. Biofuel production in *E. coli*: the role of metabolic engineering and synthetic biology. *Appl. Microbiol. Biotechnol.* **2010**, *86* (2), 419−434.
(28) Handke, P.; Lynch, S. A.; Gill, R. T. Application and engineering of fatty acid biosynthesis in *Escherichia coli* for advanced fuel. *Metab. Eng.* **2011**, *13* (1), 28−37.
(29) Taranto, P. A.; Keenan, T. W.; Potts, M. Rehydration induces rapid onset of lipid biosynthesis in desiccated *Nostoc commune* (cyanobacteria). *Biochim. Biophys. Acta* **1993**, *1168*, 228−237.
(30) Philip, S.; Keshavarz, T.; Roy, I. Polyhydroxyalkanoates: biodegradable polymers with a range of applications. *J. Chem. Technol. Biotechnol.* **2007**, *82*, 233−247.
(31) Lauzier, C.; Monasterios, C.; Saracovan, I.; Marchessault, R.; Ramsay, B. Film formation and paper coating with poly(β-hydroxyalkanoate), a biodegradable latex. *Tappi J.* **1993**, *76* (5), 71−77.
(32) Babel, W.; Riis, V.; Hainich, E. Mikrobielle thermoplaste: biosynthese, eigenschaften und anwendung. *Plaste Kautschuk* **1990**, *37*, 109−115.
(33) Walther, T.; Farese, R. The life of lipid droplets. *Biochim. Biophys. Acta* **2009**, *1791*, 459−466.
(34) Spanova, M.; et al. Influence of squalene on lipid particle/droplet and membrane organization in the yeast *Saccharomyces cerevisiae*. *Biochim. Biophys. Acta* **2012**, *1821*, 647−653.
(35) Vieler, A.; Brubaker, S.; Vick, B.; Benning, C. A lipid droplet protein of *Nannochloropsis* with functions partially analogous to plant oleosins. *Plant Physiol.* **2012**, *158*, 1562−1569.
(36) Ding, Y.; Yang, L.; Zhang, S.; Wang, Y.; Du, Y.; Pu, J.; Peng, G.; Chen, Y.; Zhang, H.; Yu, J.; Hang, H.; Wu, P.; Yang, F.; Yang, H.; Steinbüchel, A.; Liu, P. Identification of the major functional proteins of prokaryotic lipid droplets. *J. Lipid Res.* **2011**, *53*, 399−411.
(37) Bartz, R.; Zehmer, J.; Zhu, M.; Chen, Y.; Serrero, G.; Zhao, Y.; Liu, P. Dynamic activity of lipid droplets: protein phosphorylation and GTP-mediated protein translocation. *J. Proteome Res.* **2007**, *6*, 3256−3265.
(38) Jendrossek, D. Polyhydroxyalkanoate granules are complex subcellular organelles (carbonosomes). *J. Bacteriol.* **2009**, *191* (10), 3195−3202.
(39) Grage, K.; Jahns, A. C.; Parlane, N.; Palanisamy, R.; Rasiah, I. A.; Atwood, J. A.; Rehm, B. H. A. Bacterial polyhydroxyalkanoate granules: biogenesis, structure, and potential use as nano-/micro-beads in biotechnological and biomedical applications. *Biomacromolecules* **2009**, *10*, 660−669.
(40) Goodman, J. The gregarious lipid droplet. *J. Biol. Chem.* **2008**, *283*, 28005−28009.
(41) Murphy, S.; Martin, S.; Parton, R. Lipid droplet-organelle interactions; sharing the fats. *Biochim. Biophys. Acta* **2009**, *1791*, 441−447.
(42) Zhu, Z.; Zhang, S.; Liu, H.; Shen, H.; Lin, X.; Yang, F.; Zhou, Y.; Jin, G.; Ye, M.; Zou, H.; Zhao, Z. A multi-omic map of the lipid-producing yeast *Rhodosporidium toruloides*. *Nat. Commun.* **2012**, *3*, 1112−1123.
(43) Moreton, R. Physiology of lipid accumulation. In *Single Cell Oil*, 1st ed.; Moreton, R., Ed.; Longman Scientific: New York, USA, 1988; pp 1−32.
(44) Beopoulos, A.; Cescut, J.; Haddouche, R.; Uribelarrea, J.-L.; Molina-Jouve, C.; Nicaud, J.-M. *Yarrowia lipolytica* as a model for bio-oil production. *Prog. Lipid Res.* **2009**, *48*, 375−387.
(45) Ratledge, C. Regulation of lipid accumulation in oleaginous micro-organisms. *Biochem. Soc. Trans.* **2002**, *30* (6), 1047−1050.
(46) Ratledge, C. Fatty acid biosynthesis in microorganisms being used for single cell oil production. *Biochimie* **2004**, *86*, 807−815.
(47) Ratledge, C. Biochemistry, stoichiometry, substrates and economics. In *Single Cell Oil*, 1st ed.; Moreton, R., Ed.; Longman Scientific: New York, USA, 1988; pp 33−64.
(48) Vorapreeda, T.; Thammarongtham, C.; CHeevadhanarak, S.; Laoteng, K. Alternative routes of acetyl-CoA synthesis identified by comparative genomic analysis: involvement in the lipid production of oleaginous yeast and fungi. *Microbiology* **2012**, *158*, 217−228.
(49) Morin, N.; Cescut, J.; Beopoulos, A.; Lelandais, G.; Le Berre, V.; Uribelarrea, J.; Molina-Jouve, C.; Nicaud, J. Transcriptomic analyses during the transition from biomass production to lipid accumulation in the oleaginous yeast *Yarrowia lipolytica*. *PLoS One* **2011**, *6* (11), 1−13.
(50) Beopoulos, A.; Mrozova, Z.; Thevenieau, F.; Le Dall, M.; Hapala, I.; Papanikolaou, S.; Chardot, T.; Nicaud, J. Control of lipid accumulation in the yeast *Yarrowia lipolytica*. *Appl. Environ. Microbiol.* **2008**, *74* (24), 7779−7789.
(51) Zhang, Y.; Adams, I.; Ratledge, C. Malic enzyme: the controlling activity for lipid production? Overexpression of malic enzyme in *Mucor circinelloides* leads to a 2.5-fold increase in lipid accumulation. *Microbiology* **2007**, *153*, 2013−2025.
(52) Rodriguez-Frómeta, R.; Gutierrez, A.; Torres-Martinez, S.; Garre, V. Malic enzyme activity is not the only bottleneck for lipid accumulation in the oleaginous fungus *Mucor circinelloides*. *Appl. Microbiol. Biotechnol.* **2013**, *97*, 3063−3072.
(53) Tehlivets, O.; Scheuringer, K.; Kohlwein, S. D. Fatty acid synthesis and elongation in yeast. *Biochim. Biophys. Acta* **2007**, *1771*, 255−270.
(54) Kolodziej, S. J.; Penczek, P. A.; Schroeter, J. P.; Stoops, J. K. Structure-function relationships of the *Saccharomyces cerevisiae* fatty acid synthase, three-dimensional structure. *J. Biol. Chem.* **1996**, *271*, 28422−28429.
(55) Hu, Q.; Sommerfeld, M.; Jarvis, E.; Ghirardi, M.; Posewitz, M.; Seibert, M.; Darzins, A. Microalgal triacylglycerols as feedstocks for biofuel production: perspectives and advances. *Plant J.* **2008**, *54*, 621−639.
(56) Radakovits, R.; Jinkerson, R.; Darzins, A.; Posewitz, M. Genetic engineering of algae for enhanced biofuel production. *Eukaryotic Cell* **2010**, *9* (4), 486−501.
(57) Groot, P. H.; Scholte, H. R.; Hulsmann, W. C. Fatty acid activation: specificity, localization and function. *Adv. Lipid Res.* **1976**, *14*, 75−126.

(58) Schujman, G. E.; Mendoza, D. Transcriptional control of membrane lipid synthesis in bacteria. *Curr. Opin. Microbiol.* **2005**, *8*, 149−153.
(59) Chen, M.; Hancock, L. C.; Lopes, J. M. Transcriptional regulation of yeast phospholipid biosynthetic genes. *Biochim. Biophys. Acta* **2007**, *1771*, 310−321.
(60) Rajakumari, S.; Grillitsch, K.; Daum, G. Synthesis and turnover of non-polar lipids in yeast. *Prog. Lipid Res.* **2008**, *47*, 157−171.
(61) Carman, G. M.; Han, G.-S. Regulation of phospholipid synthesis in yeast. *J. Lipid Res.* **2009**, *50*, S69−S73.
(62) Carman, G. M.; Han, G.-S. Phosphatidic acid phosphatase, a key enzyme in the regulation of lipid synthesis. *J. Biol. Chem.* **2009**, *284*, 2593−2597.
(63) Kristan, K.; Lanisnik Rizner, T. Steroid-transforming enzymes in fungi. *J. Steroid Biochem. Mol. Biol.* **2012**, *129*, 79−91.
(64) Zweytick, D.; Leitner, E.; Kohlwein, S. D.; Yu, C.; Rothblatt, J.; Daum, G. Contribution of Are1p and Are2p to steryl ester synthesis in the yeast *Saccharomyces cerevisiae*. *Eur. J. Biochem.* **2000**, *267*, 1075−1082.
(65) Long, A.; Manneschmidt, A.; VerBrugge, B.; Dortch, M.; Minkin, S.; Prater, K.; Biggerstaff, J.; Dunlap, J.; Dalhaimer, P. Lipid droplet *de novo* formation and fission are linked to the cell cycle in fission yeast. *Traffic* **2012**, *13*, 705−714.
(66) Choudhary, V.; Jacquier, N.; Schneiter, R. The topology of the triacylglycerol synthesizing enzyme Lro1 indicates that neutral lipids can be produced within the luminal compartment of the endoplasmic reticulum. *Commun. Integr. Biol.* **2011**, *4* (6), 781−784.
(67) Londos, C.; Sztalryd, C.; Tansey, J. T.; Kimmel, A. R. Role of PAT proteins in lipid metabolism. *Biochimie* **2005**, *87*, 45−49.
(68) Zanghellini, J.; Wodlei, F.; Grünberg, H. Phospholipid demixing and the birth of a lipid droplet. *J. Theor. Biol.* **2010**, *264*, 952−961.
(69) Wolinski, H.; Kolb, D.; Hermann, S.; Koning, R.; Kohlwein, S. A role for seipin in lipid droplet dynamics and inheritance in yeast. *J. Cell Sci.* **2011**, *124*, 3894−3904. Adeyo, O.; Horn, P.; Lee, S.; Binns, D.; Chandrahas, A.; Chapman, K.; Goodman, J. The yeast lipin orthologue Pah 1p is important for biogenesis of lipid droplets. *J. Cell Biol.* **2011**, *192* (6), 1043−1055.
(70) Adeyo, O.; Horn, P.; Lee, S.; Binns, D.; Chandrahas, A.; Chapman, K.; Goodman, J. The yeast lipin orthologue Pah1p is important for biogenesis of lipid droplets. *J. Cell Biol.* **2011**, *192* (6), 1043−1055.
(71) Bozaquel-Morais, B.; Madeira, J.; Maya-Monteiro, C.; Masuda, C.; Montero-Lomeli, M. A new fluorescence-based method identifies protein phosphatases regulating lipid droplet metabolism. *PLoS One* **2010**, *5* (10), 1−14.
(72) Wilson, C.; Wardell, M.; Weisgraber, K.; Mahley, R.; Agard, D. Three-dimensional structure of the LDL receptor-binding domain of human apolipoprotein E. *Science* **1991**, *252*, 1817−1822.
(73) Hickenbottom, S.; Kimmel, A.; Londos, C.; Hurley, J. Structure of a lipid droplet protein: the PAT family member TIP47. *Structure* **2004**, *12*, 1199−1207.
(74) Guschina, I. A.; Harwood, J. L. Lipids and lipid metabolism in eukaryotic algae. *Prog. Lipid Res.* **2006**, *45*, 160−186.
(75) Barsanti, L.; Gualtieri, P. *Algae Anatomy, Biochemistry Biotechnology*, 1st ed.; Taylor & Francis: Boca Raton, FL, USA, 2006; pp 1−33.
(76) Li-Beisson, Y.; Shorrosh, B.; Beisson, F.; Andersson, M. X.; Arondel, V.; Bates, P. D.; Baud, S.; Bird, D.; DeBono, A.; Durret, T. P.; Franke, R. B.; Graham, I. A.; Katayama, K.; Kelly, A. A.; Larson, T.; Markham, J. E.; Miquel, M.; Molina, I.; Nishida, I.; Rowland, O.; Samuels, L.; Schmid, K. M.; Wada, H.; Welti, R.; Xu, C.; Zallot, R.; Ohlrogge, J. Acyl-lipid metabolism. In *The Arabidopsis Book*; e-ISSN 1543-8120, DOI: 10.1199/tab.0161.
(77) Ohlrogge, J.; Browse, J. Lipid biosynthesis. *Plant Cell* **1995**, *7*, 957−970.
(78) Hiltunen, J. K.; Schonauer, M. S.; Autio, K. J.; Mittelmeier, T. M.; Kastaniotis, A. J.; Dieckmann, C. L. Mitochondrial fatty acid synthesis type II: more than just fatty acids. *J. Biol. Chem.* **2009**, *284*, 9011−9015.
(79) Hiltunen, J. K.; Autio, K. J.; Schonauer, M. S.; Samuli Kursu, V. A.; Dieckmann, C. L.; Kastaniotis, A. J. Mitochondrial fatty acid synthesis and respiration. *Biochim. Biophys. Acta* **2010**, *1797*, 1195−1202.
(80) Hiltunen, J. K.; Chen, Z.; Haapalainen, A. M.; Wierenga, R. K.; Kastaniotis, A. J. Mitochondrial fatty acid synthesis − an adopted set of enzymes making a pathway of major importance for the cellular metabolism. *Prog. Lipid Res.* **2010**, *49*, 27−45.
(81) Wada, H.; Shintani, D.; Ohlrogge, J. Why do mitochondria synthesize fatty acids? Evidence for involvement in lipoic acid production. *Proc. Natl. Acad. Sci. U.S.A.* **1997**, *94*, 1591−1596.
(82) Gueguen, V.; Macherel, D.; Jaquinod, M.; Douce, R.; Bourguignon, J. Fatty acid and lipoic acid biosynthesis in higher plant mitochondria. *J. Biol. Chem.* **2000**, *275*, 5016−5025.
(83) Keeling, P. J. The endosymbiotic origin, diversification and fate of plastids. *Philos. Trans. R. Soc. B* **2010**, *365*, 729−748.
(84) Andre, C.; Froehlich, J. E.; Moll, M. R.; Benning, C. A heteromeric plastidic pyruvate kinase complex involved in seed oil biosynthesis in *Arabidopsis*. *Plant Cell* **2007**, *19*, 2006−2022.
(85) Mus, F.; Toussaint, J. P.; Cooksey, K. E.; Fields, M. W.; Gerlach, R.; Peyton, B. M.; Carlson, R. P. Physiological and molecular analysis of carbon source supplementation and pH stress-induced lipid accumulation in the marine diatom *Phaeodactylum tricornutum*. *Appl. Microbiol. Biotechnol.* **2013**, *97*, 3625−3642.
(86) Kitano, M.; Matsukawa, R.; Karube, I. Enhanced eicosapentaenoic acid production by *Navicula saprophila*. *J. Appl. Phycol.* **1998**, *10*, 101−105.
(87) Schneider, J. C.; Roessler, P. Radiolabeling studies of lipids and fatty-acids in *Nannochloropsis* (Eustigmatophyceae), an oleaginous marine alga. *J. Phycol.* **1994**, *30*, 594−598.
(88) Hofmann, M.; Eichenberger, W. Radiolabeling studies on the lipid metabolism in the marine brown alga *Dictyopteris membranacea*. *Plant Cell Physiol.* **1998**, *39*, 508−515.
(89) Miller, R.; Wu, G.; Deshpande, R. R.; Vieler, A.; Gartner, K.; Li, X.; Moellering, E. R.; Zauner, S.; Cornish, A. J.; Liu, B. Changes in transcription abundance in *Chlamydomonas reinhardtii* following nitrogen deprivation predict diversion of metabolism. *Plant Physiol.* **2010**, *154*, 1737−1752.
(90) Yang, Z.-K.; Niu, Y.-F.; Ma, Y. H.; Xue, J.; Zhang, M. H.; Yang, W. D.; Liu, J. S.; Lu, S. H.; Guan, Y.; Li, H. Y. Molecular and cellular mechanisms of neutral lipid accumulation in diatom following nitrogen deprivation. *Biotechnol. Biofuels* **2013**, *6*, 67.
(91) Bellou, S.; Aggelis, G. Biochemical activites in *Chlorella* sp. and *Nannochloropsis salina* during lipid and sugar synthesis in a lab-scale open pond simulating reactor. *J. Biotechnol.* **2012**, *164*, 318−329.
(92) Kroth, P. G.; Chiovitti, A.; Gruber, A.; Martin-Jezequel, V.; Mock, T.; Parker, M. S.; Stanley, M. S.; Kaplan, A.; Caron, L.; Weber, T. A model for carbohydrate metabolism in the diatom *Phaeodactylum tricornutum* deduced from comparative whole genome analysis. *PLoS One* **2008**, *3*, e1426.
(93) Maier, A.; Zell, M. B.; Maurino, V. G. Malate decarboxylases: evolution and roles of NAD(P)-ME isoforms in species performing C_4 and C_3 photosynthesis. *J. Exp. Bot.* **2011**, *62* (9), 3061−3069.
(94) Fan, J.; Yan, C.; Andre, C.; Shanklin, J.; Schwender, J.; Xu, C. Oil accumulation is controlled by carbon precursor supply for fatty acid synthesis in *Chlamydomonas reinhardtii*. *Plant Cell Physiol.* **2012**, *53*, 1380−1390.
(95) Huerlimann, R.; Heimann, K. Comprehensive guide to acetyl-carboxylases in algae. *Crit. Rev. Biotechnol.* **2013**, *33*, 49−65.
(96) Roessler, P. G. Purification and characterization of acetyl CoA carboxylase from the diatom *Cyclotella cryptica*. *Plant Physiol.* **1990**, *92*, 73−78.
(97) Nikolau, B. J.; Ohlrogge, J. B.; Wurtele, E. S. Plant biotin-containing carboxylases. *Arch. Biochem. Biophys.* **2003**, *414*, 211−222.
(98) Ryall, K.; Harper, J. T.; Keeling, P. J. Plastid-derived type II fatty acid biosynthetic enzymes in chromists. *Gene* **2003**, *313*, 139−148.
(99) Nagano, N.; Sakaguchi, K.; Taoka, Y.; Okita, Y.; Honda, D.; Ito, M.; Hayashi, M. Detection of genes involved in fatty acid elongation

and desaturation in *Thraustochytrid* marine eukaryotes. *J. Oleo Sci.* **2011**, *60* (9), 475−481.
(100) Metz, J. G.; Kuner, J.; Rosenzweig, B.; Lippmeier, J. C.; Roessler, P.; Zirkle, R. Biochemical characterization of polyunsaturated fatty acid synthesis in *Schizochytrium*: release of the products as free fatty acids. *Plant Physiol. Biochem.* **2009**, *47*, 472−478.
(101) Dehesh, K.; Tai, H.; Edwards, P.; Byrne, J.; Jaworski, J. G. Overexpression of 3-ketoacyl-acyl-carrier protein synthase IIIs in plants reduces the rate of lipid synthesis. *Plant Physiol.* **2001**, *125*, 1103−1114.
(102) Roughan, P. G.; Slack, C. R. Cellular organization of glycerolipid metabolism. *Plant Physiol.* **1982**, *33*, 97−132.
(103) Khozin-Goldberg, I.; Didi-Cohen, S.; Shayakhmetova, I.; Cohen, Z. Biosynthesis of eicosapentaenoic acid (EPA) in the freshwater eustigmatophyte *Monodus subterraneus* (Eustigmatophyceae). *J. Phycol.* **2002**, *38*, 745−756.
(104) Khozin, I.; Adlerstein, D.; Bigongo, C.; Heimer, Y. M.; Cohen, Z. Elucidation of the biosynthesis of eicosapentaenoic acid in the microalga *Porphyridium cruentum*. II. Studies with radiolabeled precursors. *Plant Physiol.* **1997**, *114*, 223−230.
(105) Khozin-Goldberg, I.; Cohen, Z. Unraveling algal lipid metabolism: recent advances in gene modification. *Biochimie* **2011**, *93*, 91−100.
(106) Thompson, G. A. Lipids and membrane function in green algae. *Biochim. Biophys. Acta* **1996**, *1302*, 17−45.
(107) Riekhof, W. R.; Sears, B. B.; Benning, C. Annotation of genes involved in glycerolipid biosynthesis in *Chlamydomonas reinhardtii*: discovery of the betaine lipid synthase BTA1(Cr). *Eukaryotic Cell* **2005**, *4*, 242−252.
(108) Moellering, E. R.; Miller, R.; Benning, C. Molecular genetics of lipid metabolism in the model green alga *Chlamydomonas reinhardtii*. In *Lipids in Photosynthesis: Essential and Regulatory Functions*; Wada, H., Murata, N., Eds.; Springer Science: Dordrecht, The Netherlands, 2009; pp 139−155.
(109) Moellering, E. R.; Benning, C. Glycerolipid biosynthesis. In *The Chlamydomonas Sourcebook: Organellar and Metabolic Processes*, 2nd ed.; Stern, D., Harris, E. H., Eds.; Elsevier: New York, 2008; Vol. 2, pp 41−68.
(110) Fulda, M.; Shockey, J.; Werber, M.; Wolter, F. P.; Heinz, E. Two long-chain acyl-CoA synthetases from *Arabidopsis thaliana* involved in peroxisomal fatty acid β-oxidation. *Plant J.* **2002**, *32*, 93−103.
(111) Sperling, P.; Heinz, E. Desaturases fused to their electron donor. *Eur. J. Lipid Sci. Technol.* **2001**, *103*, 158−180.
(112) Alves Martins, D.; Custodio, L.; Barreira, L.; Pereira, H.; Ben-Hamadou, R.; Varela, J.; Abu-Salah, K. M. Alternative sources of *n*-3 long-chain polyunsaturated fatty acids in marine microalgae. *Mar. Drugs* **2013**, *11*, 2259−2281.
(113) Metz, J. G.; Roessler, P.; Facciotti, D.; Levering, C.; Dittrich, F.; Lassner, M.; Valentine, R.; Lardizabal, K.; Domergue, F.; Yamada, A. Production of polyunsaturated fatty acids by polyketide synthases in both prokaryotes and eukaryotes. *Science* **2001**, *293*, 290−293.
(114) Harwood, J. L.; Guschina, I. A. The versatility of algae and their lipid metabolism. *Biochimie* **2009**, *91*, 679−684.
(115) Dahlqvist, A.; Stähl, U.; Lenman, M.; Banas, A.; Lee, M.; Sandager, L.; Ronne, H.; Stymne, S. Phospholipid:diacylglycerol acyltransferase: an enzyme that catalyzes the acyl-CoA-independent formation of triacylglycerol in yeast and plants. *Proc. Natl. Acad. Sci. U.S.A.* **2000**, *97*, 6487−6492.
(116) Boyle, N. R.; Page, M. D.; Liu, B.; Blaby, I. K.; Casero, D.; Kropat, J.; Cokus, S.; Hong-Hermesdorf, A.; Shaw, J.; Karpowicz, S. J. Three acyltransferases and a nitrogen responsive regulator are implicated in nitrogen starvation-induced triacylglycerol accumulation in *Chlamydomonas*. *J. Biol. Chem.* **2012**, *287*, 15811−15825.
(117) Yu, W.-L.; Ansari, W.; Schoepp, N. G.; Hannon, M. J.; Mayfield, S. P.; Burkart, M. D. Modifications of the metabolic pathways of lipid and triacylglycerol production in microalgae. *Microb. Cell Factories* **2011**, *10*, 91.
(118) Vieler, A.; Wu, G.; Tsai, C.; Bullard, B.; Cornish, A.; Harvey, C.; Reca, I.; Thornburg, C.; Achawanantakun, R.; Buehl, C.; Campbell, M.; Cavalier, D.; Childs, K.; Clark, T.; Deshpande, R.; Erickson, E.; Ferguson, A.; Hanee, W.; Kong, Q.; Li, X.; Liu, B.; Lundback, S.; Peng, C.; Roston, R.; Sanjaya, S.; Simpson, J.; TerBush, A.; Warakanont, J.; Zäuner, S.; Farre, E.; Hegg, E.; Jiang, N.; Kuo, M.; Lu, Y.; Niyogi, K.; Ohlrogge, J.; Osteryoung, K.; Shrachar-Hill, Y.; Sears, B.; Sun, Y.; Takahashi, H.; Yandell, M.; Shiu, S.; Benning, C. Genome, functional gene annotation, and nuclear transformation of the heterokont oleaginous alga *Nannochloropsis oceanica* CCMP1779. *PLoS Genetics* **2012**, *8* (11), 1−25.
(119) Ishige, T.; Tani, A.; Sakai, Y.; Kato, N. Wax ester production by bacteria. *Curr. Opin. Microbiol.* **2003**, *6*, 244−250.
(120) Manila-Perez, E.; Lange, A. B.; Hetzler, S.; Steinbüchel, A. Occurrence, production and export of lipophilic compounds by hydrocarbonoclastic marine bacteria and their potential use to produce bulk chemicals from hydrocarbons. *Appl. Microbiol. Biotechnol.* **2010**, *86*, 1693−1706.
(121) Thornton, J.; Howard, S. P.; Buckley, J. T. Molecular cloning of a phospholipid-cholesterol acyltransferase from *Aeromonas hydrophila*: sequence homologies with lecithin-cholesterol acyltransferase and other lipases. *Biochim. Biophys. Acta* **1988**, *959*, 153−159.
(122) Christensen, H.; Garton, N. J.; Horobin, R. W.; Minnikin, D. E.; Barer, M. R. Lipid domains of mycobacteria studied with fluorescent molecular probes. *Mol. Microbiol.* **1999**, *31*, 1561−1572.
(123) Cronan, J. E.; Vagelos, P. R. Metabolism and function of the membrane phospholipids of *Escherichia coli*. *Biochim. Biophys. Acta* **1972**, *265* (25), 60.
(124) Alvarez, H. M.; Luftmann, H.; Silva, R. A.; Cesari, A. C.; Viale, A.; Wältermann, M.; Steinbüchel, A. Identification of phenyldecanoic acid as a constituent of triacylglycerols and wax esters produced by *Rhodococcus opacus* PD630. *Microbiology* **2002**, *148*, 1407−1412.
(125) Pelech, S. L.; Vance, D. E. Signal transduction via phosphatidylcholine cycles. *Trends Biochem. Sci.* **1989**, *14*, 28−30.
(126) Wältermann, M.; Steinbüchel, A. In vitro effects of sterculic acid on lipid biosynthesis in *Rhodococcus opacus* strain PD630 and isolation of mutants defective in fatty acid desaturation. *FEMS Microbiol. Lett.* **2000**, *190*, 45−50.
(127) Lehner, R.; Kuksis, A. Biosynthesis of triacylglycerols. *Prog. Lipid Res.* **1996**, *35*, 169−201.
(128) Kalscheuer, R.; Stöveken, T.; Malkus, U.; Reichelt, R.; Golyshin, P.; Sabirova, J.; Ferrer, M.; Timmis, K.; Steinbüchel, A. Analysis of storage lipid accumulation in *Alcanivorax borkumensis*: evidence for alternative triacylglycerol biosynthesis routes in bacteria. *J. Bacteriol.* **2007**, *189* (3), 918−928.
(129) Senior, P. J.; Dawes, E. A. Poly-β-hydroxybutyrate biosynthesis and the regulation of glucose metabolism in *Azotobacter beijerinckii*. *Biochem. J.* **1971**, *125*, 55−66.
(130) Senior, P. J.; Dawes, E. A. The regulation of poly-β-hydroxybutyrate metabolism in *Azotobacter beijerinckii*. *Biochem. J.* **1973**, *134*, 225−238.
(131) Rehm, B. A.; Kruger, N.; Steinbüchel, A. A new metabolic link between fatty acid de novo synthesis and polyhydroxyalkanoic acid synthesis. The phaG gene from *Pseudomonas putida* KT2440 encodes a 3-hydroxy-acyl carrier protein-coenzyme A transferase. *J. Biol. Chem.* **1998**, *273*, 24044−24051.
(132) Quillaguaman, J.; Guzmán, H.; Van-Thuoc, D.; Hatti-Kaul, R. Synthesis and production of polyhydroxyalkanoates by halophiles: current potential and future prospects. *Appl. Microbiol. Biotechnol.* **2010**, *85*, 1687−1696.
(133) Rehm, B. Genetic and biochemistry of polyhydroxyalkanoate-granule self-assembly: the key role of polyester synthases. *Biotechnol. Lett.* **2006**, *28*, 207−213.
(134) Rehm, B. H. Biogenesis of microbial polyhydroxyalkanoate granules: a platform technology for the production of tailor-made bioparticles. *Curr. Issues Mol. Biol.* **2007**, *9*, 41−62.
(135) Rehm, B. H. Polyester synthases: natural catalysts for plastics. *Biochem. J.* **2003**, *376*, 15−33.

(136) Steinbüchel, A.; Hein, S. Biochemical and molecular basis of microbial synthesis of polyhydroxyalkanoates in microorganisms. *Adv. Biochem. Eng./Biotechnol.* **2001**, *71*, 81.
(137) Stubbe, J.; Tian, J. Polyhydroxyalkanoate (PHA) homeostasis: the role of PHA synthase. *Nat. Prod. Rep.* **2003**, *20*, 445−457.
(138) Stubbe, J.; Tian, J.; He, A.; Sinskey, A. J.; Lawrence, A. G.; Liu, P. Non-template-dependent polymerization processes: polyhydroxyalkanoate synthases as a paradigm. *Annu. Rev. Biochem.* **2005**, *74*, 433−480.
(139) Valappil, S. P.; Boccaccini, A. R.; Bucke, C.; Roy, I. Polyhydroxyalkanoates in Gram-positive bacteria: insights from the genera *Bacillus* and *Streptomyces*. *Antonie van Leeuwenhoek* **2007**, *91*, 1−17.
(140) Cai, S.; Cai, L.; Liu, H.; Liu, X.; Han, J.; Zhou, J.; Xiang, H. Identification of the Haloarchaeal phasin (PhaP) that functions in polyhydroxyalkanoate accumulation and granule formation in *Haloferax mediterranei*. *Appl. Environ. Microbiol.* **2012**, *78* (6), 1946−1952.
(141) Steinbüchel, A. Considerations on the structure and biochemistry of bacterial polyhydyroxyalkanoic acid inclusions. *Can. J. Microbiol.* **1995**, *41* (Suppl. 1), 94−105.
(142) Wieczorek, R.; Pries, A.; Steinbüchel, A.; Mayer, F. Analysis of a 24-kilodalton protein associated with the polyhydroxyalkanoic acid granules in *Alcaligenes eutrophus*. *J. Bacteriol.* **1995**, *177*, 2425−2435.
(143) Handrick, R. Unraveling the function of the *Rhodospirillum rubrum* activator of polyhydroxybutyrate (PHB) degradation: the activator is a PHB-granule-bound protein (phasin). *J. Bacteriol.* **2004**, *186*, 2466−2475.
(144) York, G. M.; Stubbe, J.; Sinskey, A. J. New insight into the role of the PhaP phasin of *Ralstonia eutropha* in promoting synthesis of polyhydroxybutyrate. *J. Bacteriol.* **2001**, *183*, 2394−2397.
(145) Dennis, D.; Sein, V.; Martinez, E.; Augustine, B. PhaP is involved in the formation of a network on the surface of polyhydroxyalkanoate inclusions in *Cupriavidus necator* H16. *J. Bacteriol.* **2008**, *190*, 555−563.
(146) Hippe, H.; Schlegel, H. G. Hydrolyse von PHBS durch intracelluläre Depolymerase von *Hydrogenomanas* H16. *Arch. Mikrobiol.* **1967**, *56*, 278−299.
(147) Jendrossek, D.; Handrick, R. Microbial degradation of polyhydroxyalkanoates. *Annu. Rev. Microbiol.* **2002**, *56*, 403−432.
(148) Liebergesell, M.; Steinbüchel, A. New knowledge about the PHA-locus and P(3HB) granule-associated proteins in *Chromatium vinosum*. *Biotechnol. Lett.* **1996**, *18* (6), 719−724.
(149) Pieper-Fürst, U.; Madkour, M. H.; Mayer, F.; Steinbüchel, A. Identification of the region of a 14-kilodalton protein of *Rhodococcus ruber* that is responsible for the binding of this phasin to polyhydroxyalkanoic acid granules. *J. Bacteriol.* **1995**, *177*, 2513−2523.
(150) Jacquemet, A.; Barbeau, J.; Lemiegre, L.; Benvegnu, T. Archaeal tetraether bipolar lipids: structures, functions and applications. *Biochimie* **2009**, *91*, 711−717.
(151) Woesze, C. R.; Fox, G. E. Phylogenetic structure of the prokaryotic domain: the primary kingdoms. *Proc. Natl. Acad. Sci. U.S.A.* **1977**, *74*, 5088−5090.
(152) Legat, A.; Gruber, C.; Zangger, K.; Wanner, G.; Stan-Lotter, H. Identification of polyhydroxyalkanoates in *Halococcus* and other halaorchaeal species. *Appl. Microb. Cell Physiol.* **2010**, *87*, 119−1127.
(153) Kirk, R. G.; Ginzburg, M. Ultrastructure of two species of *halobacterium*. *J. Ultrastruct. Res.* **1972**, *41*, 80−94.
(154) Oren, A.; Ginzburg, M.; Ginzburg, B. Z.; Hochstein, L. I.; Volcani, B. E. *Haloarcula marismortui* (Volcani) sp. nov., nom. rev., an extremely halophilic bacterium from the Dead Sea. *Int. J. Syst. Evol. Microbiol.* **1990**, *40*, 209−210.
(155) Brandl, H.; Gross, R. A.; Lenz, R. W.; Fuller, R. C. Physiology and biotechnology of *Pseudomonas oleovorans* as a source of poly(*β*-hydroxyalkanoates) for potential applications as biodegradable polyesters. *Appl. Environ. Microbiol.* **1988**, *54* (8), 1977−1982.
(156) Han, J.; Lu, Q.; Zhou, J.; Xiang, H. Molecular characterization of the phaECHm genes, required for biosynthesis of poly(3-hydroxybutyrate) in the extremely halophilic archaeon *Haloarcula marismortui*. *Appl. Environ. Microbiol.* **2007**, *73*, 6058−6065.
(157) Hezayen, F. F.; Rehm, B. H.; Eberhardt, R.; Steinbüchel, A. Polymer production by two newly isolated extremely halophilic archaea: application of a novel corrosion-resistant bioreactor. *Appl. Microbiol. Biotechnol.* **2000**, *54*, 319−325.
(158) Hezayen, F. F.; Steinbüchel, A.; Rehm, B. H. Biochemical and enzymological properties of the polyhydroxybutyrate synthase from the extremely halophilic archaeon strain 56. *Arch. Biochem. Biophys.* **2002**, *403*, 284−291.
(159) Hezayen, F. F.; Tindall, B. J.; Steinbüchel, A.; Rehm, B. H. Characterization of a novel halophilic archaeon, *Halobiforma haloterrestris* gen. nov., sp. nov., and transfer of *Natronobacterium nitratireducens* to *Halobiforma nitratireducens* comb. nov. *Int. J. Syst. Evol. Microbiol.* **2002**, *52*, 2271−2280.
(160) Lu, Q.; Han, J.; Zhou, J.; Xiang, H. Genetic and biochemical characterization of the poly(3-hydroxybutyrate-*co*-3-hydroxyvalerate) synthase in *Haloferax mediterranei*. *J. Bacteriol.* **2008**, *190*, 4173−4180.
(161) Campisano, A.; Overhage, J.; Rehm, B. H. The polyhydroxyalkanoate biosynthesis genes are differentially regulated in planktonic- and biofilm-grown *Pseudomonas aeruginosa*. *J. Biotechnol.* **2008**, *133*, 442−452.
(162) Han, J.; Lu, Q.; Zhou, L.; Liu, H.; Xiang, H. Identificaction of the polyhydroxyalkanoate (PHA)-specific acetoacetyl coenzyme A reductase among multiple FabG paralogs in *Haloarcula hispanica* and reconstruction of the PHA biosynthetic pathway in *Haloferax volcanii*. *Appl. Environ. Microbiol.* **2009**, *75* (19), 6168.
(163) Baliga, N. S.; Bonneau, R.; Facciotti, M. T.; Pan, M.; Glusman, G.; Deutsch, E. W.; Shannon, P.; Chiu, Y.; Weng, R. S.; Gan, R. R.; Hung, P.; Date, S. V.; Marcotte, E.; Hood, L.; Mg, W. V. Genome sequence of *Haloarcula marismortui*: a halophilic archaeon from the Dead Sea. *Genome Res.* **2004**, *14*, 2221−2234.
(164) Neumann, L. Binding of the major phasin, PhaP1, from *Ralstonia eutropha* H16 to poly(3-hydroxybutyrate) granules. *J. Bacteriol.* **2008**, *190*, 2911−2919.
(165) Watkins, S.; Hammock, B.; Newman, J.; German, B. Individual metabolism should guide agriculture toward foods for improved health and nutrition. *Am. J. Clin. Nutr.* **2001**, *74*, 283−286.
(166) Verma, J.; Bhola, N.; Aggarwal, J. Structure of sterculic acid. *Nature* **1955**, *175*, 84−85.
(167) Berger, A. *Diet-Induced Acyl Modifications of Mouse Phospholipid Classes*. Doctoral thesis, University of California, 1992.
(168) Mukherjee, A.; Das, K. Microbial surfactants and their potential applications: an overview. In *Biosurfactants*, 1st ed; Sen, R., Ed.; Landes Bioscience and Springer Science: New York, USA, 2010; Vol. 672, pp 54−64.
(169) Youssef, N.; Simpson, D.; Duncan, K.; McInerney, M.; Folmsbee, M.; Fincher, T.; Knapp, R. In situ biosurfactant production by *Bacillus* strains injected into a limestone petroleum reservoir. *Appl. Environ. Microbiol.* **2007**, *73* (4), 1239−1247.

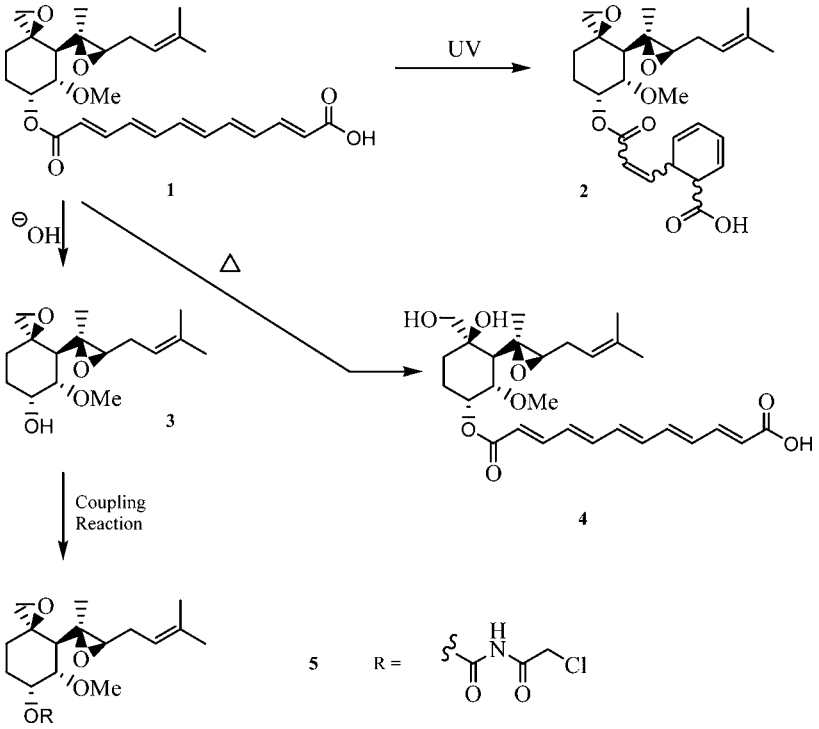

Figure 1. Fumagillin (**1**), UV-decomposed fumagillin (**2**), fumagillol (**3**), thermally decomposed fumagillin (**4**), and TNP-470 (**5**).

(Hymenoptera: Apidae), demonstrating its high virulence and ability to infect multiple bee species.[32] Recent literature reports verify the ubiquitous geographical presence of this invasive pathogen, its presence now being confirmed not only in Europe, Asia, and North America[33] but also in more remote geographical locations such as Australia,[34] South America,[32] and North Africa.[35] Evidence suggests that *N. apis* is gradually being replaced by *N. ceranae* in *A. mellifera*,[18] although *N. apis* remains more prevalent in colder climates.[16,36] Controversy regarding the greater relative virulence of *N. apis* compared with *N. ceranae* remains unresolved, with different results being obtained by different research groups.[18,36−38] Co-infection of *N. apis* and *N. ceranae* commonly occurs in *A. mellifera*[16,20] and has also been reported in *A. cerana*.[39]

N. ceranae infects the bee digestive tract midgut epithelial cells (ventriculus) of adult workers and queens.[17,40] Similar to *N. apis*, the mature spores burst forth by rupturing the epithelial cells and spill into the midgut lumen, followed by defecation with the fecal matter. Infection spreads via a fecal−oral route when adult worker bees contract the infection by cleaning up fecal material originating from infected bees or through trophallaxis of contaminated food.[41,42] Infection with *N. ceranae* has been shown to increase precocious foraging in worker bees, resulting in reduced life expectancy by 9 days on average in cage trials as compared with control groups.[43] Although outward signs of *Nosema* spp. infection cannot typically be seen, the inhibition of pollen digestion caused by the parasites leads to poor nourishment, smaller populations, reduced honey production, and higher winter colony mortality.[44] For more detailed information on the biology of *N. ceranae* as honey bee pathogen, the reader is directed to recently published reviews.[16,17,45]

FUMAGILLIN DISCOVERY AND USAGE IN APICULTURE, HUMAN MEDICINE, AND IN OTHER AGRICULTURE

Fumagillin is a naturally occurring antibiotic compound that was first isolated in 1949 from an *Aspergillus* species, designated H-3[46] and later identified as *Aspergillus fumigatus*.[47] The drug was also discovered to be a potent amebicide.[48] The structure of fumagillin was eventually elucidated[49] through an extensive series of chemical manipulations, including the hydrolysis of fumagillin to yield the alcohol fumagillol (Figure 1).

The importance of fumagillin as a treatment against the microsporidian fungal disease *N. apis* plaguing the European honey bee (*A. mellifera* L.) was soon recognized.[50,51] Fumagillin is also currently the only effective drug treatment available against *N. ceranae*.[52−54] The commercial formulation of fumagillin consists of the dicyclohexylamine (DCH) salt of fumagillin (Figure 2). The significance of the usage of fumagillin in the "salt" form is described under Toxicity of Fumagillin. On the basis of experimentation using cage bioassays, it was nevertheless purported that fumagillin provides only short-term suppression of *N. ceranae*, compared with *N. apis*, and that hyperproliferation of spores of the former results at specific and much degraded concentrations of the drug.[55]

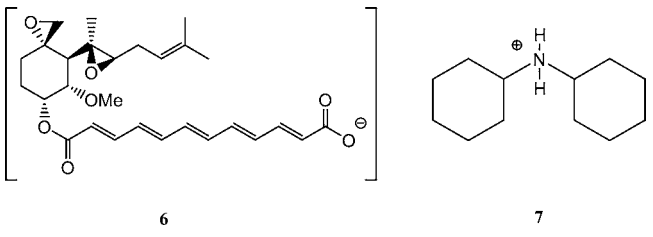

Figure 2. Fumagillin, CAS Registry No. 23110-15-8 (**6**), as the DCH CAS Registry No. 101-83-7 (**7**) salt.

dx.doi.org/10.1021/jf4055374 | J. Agric. Food Chem. 2014, 62, 2728−2737

Fumagillin was also tested for the treatment of microsporidian infections in fish.[56−59]

In human medicine, fumagillin is used as an inhibitor of microsporidian infections in patients with compromised immune systems due to acquired immunodeficiency syndrome (AIDS) or to relieve symptoms of intestinal microsporidiosis that occur after organ transplant procedures.[60−62] More interestingly, though, fumagillin and its analogues are used to treat various cancers by inhibiting the formation of new blood vessels around growing tumors (angiogenesis), thereby limiting their blood supply.[63]

The treatment of cancer tumors by inhibition of angiogenesis was first proposed in 1985.[64,65] The discovery that fumagillin inhibits angiogenesis led to a renewed interest in fumagillin as a therapeutic drug.[63] The mechanism for this activity was not clear, until the discovery of fumagillin binding to the methionine aminopeptidase type 2 (MetAP-2) protein.[66,67] The exact binding of fumagillin to the MetAP-2 enzyme was determined by crystallizing the enzyme with fumagillin covalently bound to the enzyme active site.[68] A crystallographic study then revealed that fumagillin covalently binds to a histidine moiety (His^{231}) of the enzyme, resulting in an irreversible opening of the spiro-epoxide on the cyclohexane core skeleton of fumagillin.[66,68,69]

This result prompted numerous research efforts aimed at modulating the mode of action[70,71] by preparing analogues of fumagillin via modification of the alkene side chain. First, fumagillin was hydrolyzed with a suitable base, thereby removing the side chain to yield fumagillol (Figure 1). Subsequently, a new chemical moiety could be coupled to fumagillol,[70,72,73] resulting in analogues including TNP-470 (Figure 1), which has shown promise as a potential new treatment for malaria.[69,74] Another analogue of fumagillin, named fumarranol, with the spiro-epoxide opened, exhibited an 80−100-fold lower activity than TNP-470 against malaria.[74] The low activity of fumarranol indicates the importance of the intact epoxide for biological activity of the fumagillin family of analogues. A 1000-fold decrease of MetAP-2 inhibition by fumagillin upon the opening of this cyclohexane ring spiro-epoxide was observed.[67,75,76]

Fumagillin binds only to the MetAP-2 enzyme via the epoxide group located on the cyclohexane core ring structure and not to the MetAP-1 enzyme.[66] The other remaining epoxide on the molecule is not crucial for the binding to take place and is therefore dispensable.[76]

MetAP-2 enzymes are found ubiquitously in all organisms.[69] Fumagillin acts against microsporidian as well as mammalian MetAP-2 enzyme, and the low selectivity of fumagillin between human and microsporidian MetAP-2 is the cause of its toxicity to humans as it also inhibits the human MetAP-2 enzyme necessary in protein maturation and post-translation processes.[55,77] A similar observation was recently reported whereby it was shown that fumagillin is active against honey bee MetAP-2 at low concentrations, whereas it has no therapeutic activity at those concentrations against *N. ceranae* MetAP-2.[55] The fact that fumagillin acts against both the disease and bee MetAP-2 may explain the significant bee mortality associated with fumagillin usage.[78] An earlier study supports this increased mortality associated with fumagillin usage.[79] In this study it was observed that fumagillin does not influence the mortality of healthy bees during cage trials, but when *N. apis*-infected caged bees are treated with fumagillin, at concentrations of 25.2−50 mg/L in sugar syrup, increased bee mortality was observed. Even though fumagillin degrades over time,[80,81] the repeated seasonal treatment with fumagillin that is required to control reestablishment of *N. ceranae* infections, which is not necessary for *N. apis* control, ensures that multiple generations of honey bees are exposed to low levels of fumagillin.[54,55] It is postulated that this constant low level of fumagillin in the hive creates conditions conducive to hyperproliferation of *Nosema* spp.[55] The MetAP-2 binding site amino acid sequences between human, honey bees, and *N. apis*, *N. ceranae*, and *Nosema bombi* (nosema infection of bumble bees, *Bombus* spp.) were found to be identical between honey bee and human MetAP-2, whereas the *Nosema* spp. amino acid sequences were identical and exhibited only two differences in the binding site amino acid sequences compared to human and honey bee MetAP-2 sequences.[55] The authors also speculate that the MetAP-2 enzymes may not be the only factor influencing response to fumagillin.

Semisynthetic analogues of fumagillin exhibit different properties from fumagillin regarding their potency, selectivity, and toxicity, and it has been shown that the potency of fumagillin against MetAP-2 depends not only on the covalent interaction with the spiro-epoxide but also on more complex noncovalent interactions necessary for molecular recognition of the target drug by the enzyme.[82]

TOXICITY OF FUMAGILLIN

It is important to note that the key purpose in creating new analogues of fumagillin has been the need to limit the human toxicity associated with fumagillin while retaining or enhancing the beneficial properties of the parent compound, fumagillin.[63,83−86]

Several contradictory findings have been reported in the literature regarding the toxicity of fumagillin. It is important to know that the commercial formulation of fumagillin consists of the dicyclohexylamine (DCH, DCHA) salt of fumagillin in a 1:1 stoichiometric ratio with fumagillin. When the possible adverse effects of a compound are evaluated, any additive or contaminant should also be taken into account, regardless of its concentration, as the contribution to properties such as toxicity or mutagenicity from the additive may be more significant than what is expected.[87] The authors actually used the potential carcinogenicity of DCH contamination in a cyclamate study as an example of such an effect.

It is also interesting to note that most studies on the toxicity of fumagillin itself were conducted using the fumagillin DCH salt as reagent, thereby introducing not only one but two potentially toxic compounds.[85,88−94] Experiments using the fumagillin analogue TNP-470 (AGM-1470) (Figure 1) appear to use only the pure TNP-470 in toxicity testing with no DCH included.[83,85,95−97] In other studies it is unclear whether fumagillin was used as the DCH salt, free acid, or an alternative formulation,[78,98,99] although one study was found that refers to the use of purified fumagillin with no DCH present.[63] It is important to realize this fact when the reported data on the toxicity of fumagillin, or the more frequently employed fumagillin DCH salt, are evaluated.

The toxicity of DCH in isolation has been investigated[100] and was found to induce chromosomal damage in human leucocyte cultures at low concentrations of 10^{-3}−10^{-5} M, over periods ranging from 5 to 25 h. Stoltz et al.[100] also reported that *N*-hydroxycyclohexylamine, a metabolite of DCH, exhibited equivalent toxicity. A study using a *Salmonella typhimurium* strain (TA1535/pSK1002) to verify the genotox-

icity of DCH yielded negative results.[101] Nevertheless, the same study yielded positive results using an in vivo alkaline filter elution test (AFE) with freshwater clams as test subject to detect DNA damage. *Salmonella* mutagenicity tests also proved negative for DCH in an additional study.[102] Similar negative results were reported where DCH exhibited a positive carcinogenic response in only one of six tests.[103] DCH was also reported to be a powerful inhibitor of spermidine synthesis catalyzed by extracts from *Escherichia coli* and *P. aeruginosa* in vitro.[104] A national screening program in Sweden determined that DCH is toxic to rats by several modes of action, but no mutagenic properties were reported.[105] According to the MSDS (Sigma-Aldrich product 185841 v5.0 07/24/2012), DCH exhibits serious immediate toxic effects with an LD_{50} of 373 mg/kg orally (rat). Similar data were reported with an LD_{50} of 200−373 mg/kg.[106] According to the MSDS, the compound is extremely toxic to aquatic life and should not be released into the water system. It is also tumorigenic, causing gastrointestinal and liver tumors (orally) as well as being subcutaneously carcinogenic in mice, causing tumors at the site of application.[107]

Fumagillin toxicity was extensively examined by Stanimirović et al.[88−94] In these papers it is sometimes unclear whether fumagillin DCH or DCH alone was used in their experiments as their use of the terms fumagillin and dicyclohexylamine appear to be equivalent in earlier publications.[88,89] The authors also ascribed the DCH toxicity data[96] as being that of fumagillin,[88,89,93] whereas Stoltz et al.[100] clearly examined only DCH, with no mention of fumagillin ever being made. These inconsistencies, however, should not detract from the value of their research, which is briefly summarized below.

Fumagillin was observed to exhibit significant negative chromosomal aberration effects at 50−75 mg/kg body weight in mice. Concentrations of 25, 50, and 75 mg/kg body weight were administered by gavage.[88] All experimental dosages listed above induced significant antiproliferative and genotoxic potential in mice.[89] Fumagillin exhibited clastogenic activity in human lymphocytes at concentrations equivalent to the therapeutic dose in beekeeping.[92] Genotoxicity to mouse bone marrow cells at concentrations of 10−20 mg/kg body weight administered in vivo to mice by gastric probe (5, 10, and 20 mg/kg concentrations tested), as compared to a control group, was also observed.[93] These results were confirmed with fumagillin-induced chromosomal aberrations at 10−20 mg/kg in mouse bone marrow cells.[94] In summary, the Stanimirović group concluded that fumagillin DCH is a mutagenic formulation, both in vitro and in vivo.

Fumagillin was evaluated in the United Kingdom by the Committee on Mutagenicity in 1999, with the aim of establishing a maximum residue limit (MRL) in honey after a submission by the patent holder, CEVA Animal Health.[108] No MRL recommendation could be made by the Committee on Veterinary Medicinal Products because the available toxicity data at that time were considered to be insufficient to draw any conclusions on the risk. In 2011, it was concluded that fumagillin should be considered as an in vitro mutagen, but not an in vivo mutagen.[109] Fumagillin is still not licensed for general use in beekeeping in Europe except in exceptional circumstances, when a temporary authorization to use it under veterinary supervision will be allowed.[54] Fumagillin is registered for use in the United States and Canada to treat nosema disease. Temporary authorization has been issued in exceptional conditions to use fumagillin in the United Kingdom, Spain, Belgium, Greece, Hungary, and Romania under veterinary supervision.[54]

Although fumagillin is an extremely beneficial compound in human medicine and in apiculture, some undesirable side effects cannot be ignored.[61−63,83,85,86,95] Extended usage of fumagillin over prolonged periods of time, as required by chemotherapy, caused severe body weight loss of >15% from the starting weight in human test subjects.[95] In 1952, it was reported that fumagillin was essentially nontoxic to humans at oral doses of up to 50 mg daily for durations of 2 weeks to treat intestinal amebiasis,[84] although no weight loss was observed in test subjects. A more recent study administered fumagillin orally up to 60 mg daily for 2 weeks to treat microsporidiosis in patients with HIV infection.[61] The authors acknowledged significant bone marrow toxicity of fumagillin with 4 patients of a group of 11 developing severe toxic side effects at the highest dosage administered (60 mg). These effects ceased within days of the treatment being terminated.

Common side effects in human trials in which fumagillin is administered orally are gastrointestinal-related cramping, diarrhea, and significant loss of body weight.[95] This undesirable weight loss side effect prompted recent, perhaps ethically questionable, trial use of fumagillin as a chemical mitigation for obesity.[110,111]

In beekeeping, potential toxic and undesirable consequences of fumagillin treatment have also been examined, with a limited number of effects being documented. For example, unique changes in the ultrastructure of the hypopharyngeal glands have been observed in worker bees after infection with *N. apis* and subsequent treatment with fumagillin.[98] Such alterations may influence protein secretions from these glands, although the role of fumagillin treatment on gland structure and function remain speculative from this descriptive study. Fumagillin was also noted to have a significant influence on mortality during a cage trial experiment in which honey bees (150−200 bees per cage) were fed a sugar syrup solution for 7 days using a total dose of 140 mg of fumagillin per cage, compared with unmedicated controls.[78] In contrast, a later study indicated few to no deleterious effects of fumagillin (50 mg/L fumagillin in sugar syrup) for caged *N. apis*-infected bees, also over a 7 day period.[112] This concentration is also double that currently recommended for the only commercial formulation of the drug registered in North America for apiculture (Fumagilin-B, Medivet Pharmaceuticals Ltd., DIN 02231180). Label directions for this product prescribe 9.5 g of fumagillin DCH base to prepare 380 L of syrup (25 mg/L), which is sufficient to treat 100−110 colonies (86−95 mg/colony) in the spring or 50 overwintering (190.5 mg/colony) colonies in the fall.

The majority of other reported cage experiments that evaluated bee mortality associated with fumagillin usage have found few effects. No statistically observable increase in mortality was observed when sugar syrup was fed at concentrations of 12.6, 25.2, and 50.4 mg/L ad libitum over 17 days to bees not infected by *N. apis*.[79] Field trials on overwintering bee colonies infected with *N. apis* in Ontario, Canada, showed that fumagillin treatments in the fall (25 mg/L, 440 mg/colony) significantly increased colony survival and did not harm bees at the colony level.[79] In a Polish study, fumagillin (56.8 mg/L, 71 mg/colony) increased the unit honey productivity (+19%), brood production (+20%), surplus honey production (+58%), and lifespan of worker honey bees (+20%), with no observable negative effects for *N. apis*-infected colonies in the spring.[113] A study from Alberta, Canada,

recommended fall treatments with fumagillin at increased amounts of fumagillin (22.2 mg/L, 300−400 mg/colony) to effectively treat *N. apis* infection with no noted harmful side effects.[114] Improvements in colony survival were similarly noted for fall sugar syrup treatments containing fumagillin at a lower dosages (26.4 mg/L, 200 mg/colony), also under Canadian wintering conditions.[115] Sugar syrup applications of the drug require a longer period for bees to consume and, hence, have a longer duration of treatment, compared with dusting or pollen patty applications, which are more suitable as spring treatments.[115]

Although previous studies have concluded that fumagillin has suppressed infections and reduced mortality of *Nosema* spp. infected bees in cages[79,112] and colonies,[79,113−115] a recent paper suggests that fumagillin has negative effects on bee health and leads to the hyperproliferation of *N. ceranae* spores.[55] It is, however, difficult to directly compare this with older studies because of differences in methods used to evaluate the effects of fumagillin on the parasites and bees. Previous research has evaluated bee mortality specifically at high therapeutic concentrations of fumagillin using spore counts as an indicator of the efficacy of treatment, while harmful effects on bees have been measured as differential survival of bees or colonies compared with infected, untreated controls. In Huang et al.,[55] deleterious effects on bees were confirmed by alterations in structural and metabolic midgut proteins, notably at concentrations that did not suppress microsporidia reproduction. Although the study did use spore production as a measure of fumagillin efficacy, concentrations at which hypoproliferation of spores were seen were at very low, subtherapeutic levels of fumagillin that were not examined in other studies. Such levels were estimated to represent the degraded concentrations of fumagillin 2−5.5 months after cessation of treatment to a colony.[55] Previous work examining the effects of degraded fumagillin-medicated syrup, after 44 months of storage, showed clear suppression of *N. apis* infections in caged bees with no significant deleterious effects on bee mortality.[116]

The difference between test methods employing controlled environments, as in cage trials, and field trials, where colonies are exposed to other environmental influences, also makes direct comparison among studies difficult. Field trial studies are more prone to the effects of environmental contamination by pesticides, for example, making bees more susceptible to *N. ceranae* infection.[117] Furthermore, synergistic effects exhibited by some pesticides on fumagillin[118] have been observed. The effect of other stress factors[53] and co-infection by pathogens, such as the deformed wing virus, further complicates the interpretation of results.[119] A recent publication that details a comprehensive standard approach to nosema research is of interest, as it will simplify the comparison of results obtained by different research groups.[120]

CHEMICAL ANALYSIS AND STABILITY OF FUMAGILLIN IN THE FIELD AND UNDER LABORATORY CONDITIONS

Mammalian toxicity and mutagenicity of fumagillin are well reported, and therefore it is important that the amount of fumagillin residues in honey intended for human consumption be established. The proposed structures of the main thermal and UV degradation products of fumagillin are shown in Figure 1. UV degradation products involve isomerization and cyclization of the alkene side chain, whereas the epoxide on the main cyclohexane skeleton of the active moiety remains intact.[80,81] Thermal degradation results in the opening of the epoxide situated on the cyclohexane ring. A combination of thermal and UV degradation is also likely to occur. It is important to note that the UV decomposition products of fumagillin retain their biological activity,[81] whereas the thermally degraded fumagillin does not.[54] The hydrolyzed product (fumagillol) also retains some biological activity, albeit only about 10% of that of fumagillin.[121]

Several analytical methods for the detection of fumagillin have been reported. In 1988 a reversed-phase HPLC-UV method was reported to analyze fumagillin in acetonitrile solutions using a UV detection wavelength of 351 nm, which corresponds to the maximum UV absorption of the alkene side chain of the molecule, and a detection concentration range of 0.000−0.035 mg/mL.[122] Interestingly, it was found that 254 nm UV light does not cause fumagillin to degrade, but that 336 and 351 nm UV light (fumagillin λ_{max} 351 nm) and fluorescent room lights do cause degradation. Samples in that study were prepared in acetonitrile, and it is not clear if pure fumagillin, or a salt form of fumagillin, was used. An ELISA method with a limit of detection (LOD) of 20 ng/g and an HPLC UV method (350 nm detection wavelength) with an LOD of 100 ng/g for quantitation of fumagillin and its degradation products in honey were developed.[123] Honey samples were prepared by dissolving first 5.0 g of honey in equal amounts of water (25 mL) and then dilution with acetonitrile (25 mL). Assil and Sporns[123] also describe the isolation of pure fumagillin with the elimination of the DCH and other formulation compounds from the commercial formulation. The authors also identify the UV-cyclized product neofumagillin as a further potential contaminant of honey.

Fumagillin was quantitated in rainbow trout muscle tissue, where it was tested to control myxosporidiae, by using ion-pairing liquid chromatography with UV (351 nm detection wavelength) detection.[124] Fish muscle tissue (1 g) was macerated in the presence of 8 mL of an acetonitrile/water mixture (2:6 v/v) with sample cleanup and concentration done using Bond Elut Octyl C_8 cartridge columns to give a method that has a linear range of 20−1000 ng/g.

The photostability of fumagillin was investigated, and an HPLC method reported using a UV method for detection at 350 nm.[81] The investigators found fumagillin to be extremely unstable when exposed to sunlight or fluorescent laboratory lighting in 50% ethanol solutions, with half-lives of fumagillin determined as being in the range of seconds to minutes. Nevertheless, the activity of UV-irradiated fumagillin in syrup solutions did not reduce its efficacy against nosema disease significantly, with *N. apis* being identified as the microsporidian used in the efficacy experiments.

Fumagillin and its UV and thermal decomposition products were quantitated by LC−diode array−electrospray ionization mass spectrometry.[80] The method that the researchers developed to purify and concentrate fumagillin from the honey matrix using a polymeric solid phase extraction (SPE) technique forms the basis for most of the subsequent published analytical methods.[54] Method detection limits ranging from 1−24 ng/g (for light colored honeys) to 4−45 ng/g for darker colored honeys are reported. The researchers also note that honey samples to be analyzed for fumagillin can be stored at room temperature for 1 month in the dark without influencing the fumagillin results significantly.

A multiclass LC-MS/MS method to determine a variety of antibiotics in honey, including fumagillin, was developed.[125] It

was noted that fluorescent lights and sunlight accelerate fumagillin decomposition and that sodium laboratory lights were preferred for fumagillin analysis. The method LOD for fumagillin was reported as 60 ng/g and was used to determine several other classes of compounds including tetracyclines, fluoroquinolones, macrolides, lincosamides, aminoglycosides, sulfonamides, and phenicols. Sample cleanup was done using the same SPE cartridges described earlier,[80] but sample elution consisted of a very laborious process with multiple elutions of the samples off the SPE cartridges, followed by concentration and reconstitution steps, making this very time-consuming.

A rapid LC-MS/MS method quantitating fumagillin using a QuEChERS (quick, easy, cheap, effective, rugged, and safe) sample preparation technique in conjunction with an Oasis mixed-mode weak anion-exchange SPE cartridge for concentrating fumagillin was reported, with a reported LOQ of 0.1 ng/g.[126] The additional QuEChERS step adds 30 min to the extraction, because it is still followed by an SPE.

The stability of fumagillin under various laboratory and field conditions pertaining to its thermal and UV degradation was reported.[54] It was shown that higher temperatures (40 °C) caused rapid thermal degradation of fumagillin in sugar syrup application solutions, with resulting loss of its activity. Fumagillin was undetectable in sugar syrup solutions after 20 days at this temperature. A stability study of fumagillin under various temperature conditions in the presence and absence of light was also conducted, confirming the sensitivity of fumagillin to light that is amplified by higher temperatures.[54]

The most recent published method of fumagillin analysis in honey by LC-MS/MS[127] is an optimized version of a previously published method.[80] This study provides useful information for laboratory analysis, demonstrating that fumagillin solutions stored in acetonitrile at 4 °C are stable for 6 months.[127] The authors report an LOD of 0.368−0.522 μg/kg and an LOQ of 1.564−1.112 μg/kg in honey, depending on the brand of analytical instrumentation used. They also observed that performing the SPE cleanup and sample concentration step under gravity elution yielded better sample recoveries.

None of the analytical methods for fumagillin published to date recognize the importance of the presence of DCH as a contaminant in honey or other hive products (such as wax), although the presence of DCH in solvent samples originating from the formulation is recognized in a recent paper.[127]

FUTURE OUTLOOK

It could be hypothesized that the mode of action of fumagillin against the two *Nosema* spp. in question is similar to that observed in humans against the MetAP-2 enzyme. It is important to note that fumagillin will also be acting in a similar fashion on the MetAP-2 enzyme of the host honey bee.[55] The intact epoxide on the cyclohexane ring of fumagillin is crucial for its observed activity, but the rest of the molecule is also important for enzymatic recognition. This observation is supported by the studies in the beekeeping literature.[54,81] A potential strategy for the rational design of simpler and more cost-effective compounds that mimic the chemical behavior of fumagillin[128] using the cyclohexane spiro-epoxide as a scaffold for new potential chemical treatments against nosema disease should be considered. The development of new compounds to treat nosema disease in apiculture is of utmost importance, owing to the fact that fumagillin has been extensively employed in human medicine and apiculture almost since its discovery in the early 1950s. Although there is no proof in apiculture to indicate that *Nosema* spp. have developed resistance to fumagillin, it has been reported that *Nosema* spp. infecting diamondback moth, *Pluetella xylostella*,[129] have developed resistance to fumagillin (Fumidil-B), although the identity of the *Nosema* spp. was not established.[129] Given this finding, it can be speculated that *Nosema* spp. resistance to fumagillin in apiculture may develop in the future, owing to the prolonged and intensive utilization of fumagillin dating back to the 1950s.

Numerous different fumagillin toxicity evaluations employing direct in vitro testing against isolated cancer cell lines and in vivo testing in test organisms such as mice and rabbit using the DCH salt form of fumagillin have been reported, as discussed under Toxicity of Fumagillin. In early human trials no observable side effects are noted in some studies, whereas significant weight loss and toxic effects were observed in others. A recent paper[55] proposes that fumagillin may influence the MetAP-2 enzymes in the host and in the pathogen differently due to the slight differences in the amino acid sequence of the binding site portion of the enzymes in *Nosema* spp. as compared to that in honey bees. It remains unclear whether the reduced toxicity of fumagillin and its analogues is due to inherent properties of these analogues themselves or the fact that the toxicity contribution arising from the DCH is not accounted for in studies to date.

It is also important in the evaluation of toxicity studies to take into account the interspecies differences when extrapolating animal and other data to humans.[130] In vitro testing is also not equivalent to in vivo human testing when using human and other cell cultures or bacteria such as *Salmonella* spp. When all of the currently available information is evaluated, it is evident that fumagillin is indeed cytotoxic and mutagenic in vitro and that it has undisputed negative effects in humans such as short-term toxicity, weight loss, and diarrhea. The establishment of an MRL for the presence of fumagillin in honey and other hive products is needed. Caution should be exercised during fumagillin sugar syrup solution preparation, because it could lead to elevated levels of fumagillin and DCH exposure through dermal contact and through breathing in airborne fumagillin dust.

However, a significant concern is not only fumagillin toxicity but also that of DCH, which may be present in equimolar amounts to fumagillin in bee products. As discussed under Toxicity of Fumagillin, it is evident that DCH is at least 5 times as toxic, comparing only the LD_{50} values and disregarding any additional negative effects. All published analytical methods to date evaluate only the presence of fumagillin and, in a few instances, one or two of the major metabolites or degradation products in honey. It is known that fumagillin degrades within days to weeks in honey[54] and that there is a low likelihood of fumagillin being detected in significant quantities in honey if it is applied well before the extraction process.

The contribution of DCH present in the commercial fumagillin formulation to the overall toxicity and resulting food safety implications in products destined for human consumption is definitely not negligible.[87] None of the analytical methods for analyzing fumagillin and metabolites in honey published to date even mention the presence of DCH as an analyte of concern. This is a significant oversight because the potential presence of DCH in hive products is clearly of significance for human health and food safety concerns.

The industrial use of DCH as a corrosion inhibitor and in the rubber industry (vehicle tires) could result in a background level of this compound being present in hive products,

especially in hives located close to main roads and areas of higher vehicle use.[105] This potential background level of DCH contamination needs to be further investigated to determine whether it is a real cause of concern. More importantly, the stability and presence of DCH in bee products such as honey and wax also need to be investigated. There is a clear need for the inclusion of the analysis of DCH relating to the usage of fumagillin in hive products.

Despite all of the potential shortcomings and detrimental aspects relating to fumagillin's usage in beekeeping, and their resulting implications for bee and human health, it is important to note that this is still the only effective chemical treatment currently available to treat nosema disease. The potential contamination by DCH of hive products destined for human consumption could be eliminated by exploring alternative formulation methods of fumagillin or through the development of alternative chemical treatments utilizing the current knowledge regarding the proposed mode of action of fumagillin against *Nosema* spp.

AUTHOR INFORMATION

Corresponding Author

*(J.P.v.d.H.) Phone: 1 (780) 415-8714. Fax: 1 (780) 415-4527. E-mail: johan.vandenheever@gov.ab.ca.

Notes

The authors declare no competing financial interest.

REFERENCES

(1) Ellis, J. D.; Munn, P. A. The worldwide health status of honeybees. *Bee World* **2005**, *86*, 88.

(2) Genersch, E. Honey bee pathology: current threats to honey bees and beekeeping. *Appl. Microbiol. Biotechnol.* **2010**, *87*, 87−97.

(3) Didier, E. S.; Weiss, L. M. Overview of microsporidia and microsporidiosis. *Protistology* **2008**, *5*, 243−255.

(4) Franzen, C. Microsporidia: a review of 150 years of research. *Open Parasitol. J.* **2008**, *2*, 1−34.

(5) Weiss, L. M.; Edlind, T. D.; Vossbrinck, C. R.; Hashimoto, T. Microsporidian molecular phylogeny: the fungal connection. *J. Eukaryot. Microbiol.* **1999**, *46*, 17S−18S.

(6) Sina, M.; Alastair, G.; Farmer, M.; Andersen, R.; Anderson, O.; Barta, J.; Bowser, S.; Brugerolle, G.; Fensome, R.; Fredericq, S.; James, T.; Karpov, S.; Kugrens, P.; Krug, J.; Lane, C.; Lewis, L.; Lodge, J.; Lynn, D.; Mann, D.; Maccourt, R.; Mendoza, L.; Moestrup, O.; Mozley, S.; Nerad, T.; Shearer, C.; Smirnov, A.; Spiegel, F.; Taylor, M. The new higher level classification of eukaryotes with emphasis on the taxonomy of protists. *J. Eukaryot. Microbiol.* **2005**, *52*, 399−451.

(7) Fries, I. *Nosema apis* − a parasite in the honey bee colony. *Bee World* **1993**, *74*, 5−19.

(8) Zander, E. Tierische Parasite als Krankenheitserreger bei der Biene. *Munchener Bienenzeitung* **1909**, *31*, 196.

(9) Fries, I.; Fend, F.; Da Silva, A.; Slemenda, S. B.; Pieniazek, N. J. *Nosema ceranae* n. sp. (Microspora, Nosematidae), morphological and molecular characterization of a microsporidian parasite of the Asian honey bee *Apis cerana* (Hymenoptera: Apidae). *Eur. J. Protistol.* **1996**, *32*, 356−365.

(10) Fries, I. Protozoa. In *Honey Bee Pests, Predators, and Diseases*, 3rd ed.; Morse, R. A., Ed.; A. I. Root: Medina, OH, USA, 1997; pp 57−76.

(11) Huang, W.-F.; Jiang, J.-H.; Chen, Y.-W.; Wang, C.-H. A *Nosema ceranae* isolate from the honeybee *Apis mellifera*. *Apidologie* **2007**, *38*, 30−37.

(12) Huang, W.-F.; Bocquet, M.; Lee, K.-C.; Sung, I.-H.; Jiang, J.-H.; Chen, Y.-W.; Wang, C.-H. The comparison of rDNA spacer regions of *Nosema ceranae* isolates from different hosts and locations. *J. Invertebr. Pathol.* **2008**, *97*, 9−13.

(13) Weinstein Teixeira, E.; Guimarães dos Santos, L.; Sattler, A.; Message, D.; Teles Marques Florencio Alves, M. L.; Fonseca Martins, M.; Lopes Grassi-Sella, M. *Nosema ceranae* has been present in Brazil for more than three decades infecting Africanized honey bees. *J. Invertebr. Pathol.* **2013**, *114*, 250−254.

(14) Higes, M.; Martín, R.; Meana, A. *Nosema ceranae*, a new microsporidian parasite in honeybees in Europe. *J. Invertebr. Pathol.* **2006**, *92*, 93−95.

(15) Klee, J.; Besana, A. M.; Genersch, E.; Gisder, S.; Nanetti, A.; Quyet Tam, D.; Xuan Chinh, T.; Puerta, F.; Ruz, J. M.; Kryger, P.; Message, D.; Hatjina, F.; Korpela, S.; Fries, I.; Paxton, R. J. Widespread dispersal of the microsporidian *Nosema ceranae*, an emergent pathogen of the Western honey bee, *Apis mellifera*. *J. Invertebr. Pathol.* **2007**, *96*, 1−10.

(16) Fries, I. *Nosema ceranae* in European honey bees (*Apis mellifera*). *J. Invertebr. Pathol.* **2010**, *103*, S73−S79.

(17) Higes, M.; Martín-Hernendez, R.; Meana, A. *Nosema ceranae* in Europe: an emergent type C nosemosis. *Apidologie* **2010**, *41*, 375−392.

(18) Martín-Hernández, R.; Botías, C.; Garrido-Bailón, E.; Martínez-Salvador, A.; Prieto, L.; Meana, A.; Higes, M. Microsporidia infecting *Apis mellifera*: coexistence or competition. Is *Nosema ceranae* replacing *Nosema apis*? *Environ. Microbiol.* **2012**, *14*, 2127−2138.

(19) Medici, S. K.; Sarlo, E. G.; Porrini, M. P.; Braunstein, M.; Eguaras, M. J. Genetic variation and widespread dispersal of *Nosema ceranae* in *Apis mellifera* apiaries from Argentina. *Parasitol. Res.* **2012**, *110*, 859−864.

(20) Paxton, R. J.; Klee, J.; Korpela, S.; Fries, I. *Nosema ceranae* has infected *Apis mellifera* in Europe since at least 1998 and may be more virulent than *Nosema apis*. *Apidologie* **2007**, *38*, 558.

(21) Chen, Y.; Evans, J. D.; Smith, B. I.; Pettis, J. S. *Nosema ceranae* is a long-present and wide-spread microsporidian infection of the European honey bee (*Apis mellifera*) in the United States. *J. Invertebr. Pathol.* **2008**, *97*, 186−188.

(22) Currie, R. W.; Pernal, S. F.; Guzmán-Novoa, E. Honey bee colony losses in Canada. *J. Apic. Res.* **2010**, *49*, 104−106.

(23) Cox-Foster, D. L.; Conlan, S.; Holmes, E. C.; Palacios, G.; Evans, J. D.; Moran, N. A.; Quan, P.-L.; Briese, T.; Hornig, M.; Geiser, D. M.; Martinson, V.; vanEngelsdorp, D.; Kalkstein, A. L.; Drysdale, A.; Hui, J.; Zhai, J.; Cui, L.; Hutchinson, S. K.; Simons, J. F.; Egholm, M.; Pettis, J. S.; Lipkin, W. I. A metagenomic survey of microbes in honey bee colony collapse disorder. *Science* **2007**, *318*, 283−287.

(24) Martín-Hernández, R.; Meana, A.; Prieto, L.; Salvador, A. M.; Garrido-Bailón, E.; Higes, M. Outcome of colonization of *Apis mellifera* by *Nosema ceranae*. *Appl. Environ. Microbiol.* **2007**, *73*, 6331.

(25) Higes, M.; Martín-Hernández, R.; Botías, C.; Garrido-Bailón, R.; Gonzales-Porto, A. V.; Barrios, L.; Nozal, M. J.; Bernal, J. L.; Jimenez, J. J.; Palencia, P. G.; Meana, A. How natural infection by *Nosema ceranae* causes honeybee colony collapse. *Environ. Microbiol.* **2008**, *10*, 2659−2669.

(26) Higes, M.; Martín-Hernández, R.; Garrido-Bailón, E.; Gonzalez-Porto, A. V.; Garcia-Palencia, P.; Meana, A.; del Nozal, M. J.; Mayo, R.; Bernal, J. L. Honeybee colony collapse due to *Nosema ceranae* in professional apiaries. *Environ. Microbiol. Rep.* **2009**, *1*, 110−113.

(27) vanEngelsdorp, D.; Evans, J. D.; Saegerman, C.; Mullin, C.; Haubruge, E.; Nguyen, B. K.; Frazier, M.; Frazier, J.; Cox-Foster, D.; Chen, Y.; Underwood, R.; Tarpy, D. R.; Pettis, J. S. Colony collapse disorder: a descriptive study. *PLoS One* **2009**, *4*, e6481 DOI: 10.1371/journal.pone.0006481.

(28) Botías, C.; Martín-Hernández, R.; Garrido-Bailón, E.; González-Porto, A.; Martínez-Salvador, A.; De La Rúa, P.; Meana, A.; Higes, M. The growing prevalence of *Nosema ceranae* in honey bees in Spain, an emerging problem for the last decade. *Res. Vet. Sci.* **2012**, *93*, 150−155.

(29) Martínez, J.; Leal, G.; Conget, P. *Nosema ceranae* an emergent pathogen of *Apis mellifera* in Chile. *Parasitol. Res.* **2012**, *111*, 601−607.

(30) Chaimanee, V.; Warrit, N.; Chantawannakul, P. Infections of *Nosema ceranae* in four different honeybee species. *J. Invertebr. Pathol.* **2010**, *105*, 207−210.

(31) Botías, C.; Anderson, D. L.; Meana, A.; Garrido-Bailón, E.; Martín-Hernández, R.; Higes, M. Further evidence of an Oriental

origin for *Nosema ceranae* (Microsporidia: Nosematidae). *J. Invertebr. Pathol.* **2012**, *110*, 108−113.
(32) Plischuck, S.; Martín-Hernández, R.; Prieto, L.; Lucia, M.; Botías, C.; Meana, A.; Abrahamovich, A. H.; Lange, C.; Higes, M. South American native bumblebees (Hymenoptera: Apidae) infected by *Nosema ceranae* (Microsporidia), an emerging pathogen of honeybees (*Apis mellifera*). *Environ. Microbiol. Rep.* **2009**, *1*, 131−135.
(33) Williams, G. R.; Shafer, A. B. A.; Rogers, R. E. L.; Shutler, D.; Stewart, D. T. First detection of *Nosema ceranae*, a microsporidian parasite of European honey bees (*Apis mellifera*), in Canada and central USA. *J. Invertebr. Pathol.* **2008**, *97*, 189−192.
(34) Giersch, T.; Berg, T.; Galea, F.; Hornitzky, M. *Nosema ceranae* infects honey bees (*Apis mellifera*) and contaminates honey in Australia. *Apidologie* **2009**, *40*, 117−123.
(35) Higes, M.; Martín-Hernández, R.; Garrido-Bailón, E.; Botías, C.; Meana, A. First detection of *Nosema ceranae* (Microsporidia) in African honey bees (*Apis mellifera intermissa*). *J. Apic. Res.* **2009**, *48*, 217−219.
(36) Forsgren, E.; Fries, I. Temporal study of *Nosema* spp. in a cold climate. *Environ. Microbiol. Rep.* **2013**, *5*, 78−82.
(37) Forsgren, E.; Fries, I. Comparative virulence of *Nosema ceranae* and *Nosema apis* in individual European honey bees. *Vet. Parasitol.* **2010**, *170*, 212−217.
(38) Stevanović, J.; Stanimirović, Z.; Genersch, E.; Kovacevic, S. R.; Ljubenkovic, J.; Radakovic, M.; Aleksić, N. Dominance of *Nosema ceranae* in honey bees in the Balkan countries in the absence of symptoms of colony collapse disorder. *Apidologie* **2010**, *42*, 49−58.
(39) Chen, Y.; Evans, J. D.; Zhou, L.; Boncristiani, H.; Kimura, K.; Xiao, T.; Litkowski, A. M.; Pettis, J. S. Asymmetrical coexistence of *Nosema ceranae* and *Nosema apis* in honey bees. *J. Invertebr. Pathol.* **2009**, *101*, 204−209.
(40) Traver, B. E.; Fell, R. D. Low natural levels of *Nosema ceranae* in *Apis mellifera* queens. *J. Invertebr. Pathol.* **2012**, *110*, 408−410.
(41) Higes, M.; Martín-Hernández, R.; Garcia-Palencia, P.; Martin, P.; Meana, A. Horizontal transmission of *Nosema ceranae* (Microsporidia) from worker honeybees to queens (*Apis mellifera*). *Environ. Microbiol. Rep.* **2009**, *1*, 495−498.
(42) Smith, M. L. The honey bee parasite *Nosema ceranae*: transmissible via food exchange? *PLoS One* **2012**, *7*, e43319 (accessed Feb 25, 2014).
(43) Goblirsch, M.; Huang, Z. Y.; Spivak, M. Physiological and behavioral changes in honey bees (*Apis mellifera*) induced by *Nosema ceranae* infection. *PLoS One* **2013**, *8*, e58165 (accessed Feb 25, 2014) DOI: 10.1371/journal.pone.0058165.
(44) Bailey, L.; Ball, B. V. *Honey Bee Pathology*, 2nd ed.; Academic Press: London, UK, 1991.
(45) Higes, M.; Meana, A.; Bartolomé, C.; Botías, C.; Martín-Hernández, R. *Nosema ceranae* (Microsporidia), a controversial 21st century honey bee pathogen. *Environ. Microbiol. Rep.* **2013**, *5*, 17−29.
(46) Hanson, F. R.; Eble, T. E. An antiphage agent isolated from *Aspergillus* sp. *J. Bacteriol.* **1949**, *58*, 527−529.
(47) Eble, T. E.; Hanson, F. R. Fumagillin, an antibiotic from *Aspergillus fumigatus* H-3. *Antibiot. Chemother.* **1951**, *1*, 54−58.
(48) McCowan, M. C.; Callender, M. E.; Lawlis, J. F. Fumagillin (H-3), a new antibiotic with amebicidal properties. *Science* **1951**, *113*, 202−203.
(49) Tarbell, D. S.; Carman, R. M.; Chapman, D. D.; Cremer, S. E.; Cross, A. D.; Huffman, K. R.; Kunstmann, M.; McCorkindale, N. J.; McNally, J. G., Jr.; Rosowsky, A.; Varino, F. H. L.; West, R. L. The chemistry of fumagillin. *J. Am. Chem. Soc.* **1961**, *83*, 3096−3113.
(50) Katznelson, H.; Jamieson, C. A. Control of *Nosema* disease of honeybees with fumagillin. *Science* **1952**, *115*, 70−71.
(51) Bailey, L. Effect of fumagillin upon *Nosema apis* (Zander). *Nature* **1953**, *171*, 212−213.
(52) Williams, G. R.; Sampson, M. A.; Shutler, D.; Rogers, R. E. L. Does fumagillin control the recently detected invasive parasite *Nosema ceranae* in Western honey bees (*Apis mellifera*)? *J. Invertebr. Pathol.* **2008**, *99*, 342−344.
(53) Williams, G. R.; Shutler, D.; Little, C. M.; Burgher-MacLellan, K. L.; Rogers, R. E. L. The microsporidian *Nosema ceranae*, the antibiotic Fumagilin-B®, and Western honey bee (*Apis mellifera*) colony strength. *Apidologie* **2011**, *42*, 15−22.
(54) Higes, M.; Nozal, M. J.; Alvaro, A.; Barrios, L.; Meana, A.; Martín-Hernández, R.; Bernal, J. L.; Bernal, J. The stability and effectiveness of fumagillin in controlling *Nosema ceranae* (Microsporidia) infection in honey bees (*Apis mellifera*) under laboratory and field conditions. *Apidologie* **2011**, *42*, 364−377.
(55) Huang, W.-F.; Solter, L. F.; Yau, P. M.; Imai, B. S. *Nosema ceranae* escapes fumagillin control in honey bees. *PLoS Pathol.* **2013**, *9*, e1003185 (accessed Feb 25, 2014) DOI: 10.1371/journal.ppat.1003185.
(56) Kent, M. L.; Dawe, S. C. Efficacy of fumagillin DCH against experimentally induced *Loma salmonae* (Microsporea) infections in Chinook salmon *Oncorhynus tshawytscha*. *Dis. Aquat. Org.* **1994**, *20*, 231−233.
(57) Molnar, K. Recent achievements in the chemotherapy of myxosporean infections of fish. *Acta Vet. Hung.* **1994**, *41*, 51−58.
(58) El-Matbouli, M.; Hoffmann, R. W. Prevention of experimentally induced whirling disease in rainbow trout *Oncorhynus mykiss* by fumagillin. *Dis. Aquat. Org.* **1991**, *10*, 109−113.
(59) Rigos, G. R.; Kotzamanis, I.; Gialamas, I.; Nengas, I.; Alaxis, M. Toxicity and digestability of fumagillin DCH in gilthead sea bream, *Sparus aurata* L. *J. Fish Dis.* **2000**, *23*, 161−164.
(60) Lanternier, F.; Boutboul, D.; Menotti, J.; Chandesris, M. O.; Sarfati, C.; Mamzer Bruneel, M. F.; Calmus, Y.; Mechai, F.; Viard, J. P.; Lecuit, M.; Bougnoux, M. E.; Lortholary, O. Microsporidiosis in solid organ transplant recipients: two *Enterocytozoon bieneusi* cases and review. *Transpl. Infect. Dis.* **2009**, *11*, 83−88.
(61) Molina, J. M.; Goguel, J.; Sarfati, C.; Michiels, J.-F.; Desportes-Livage, I.; Balkan, S.; Chastang, C.; Cotte, L.; Maslo, C.; Struxiano, A.; Derouin, F.; Decazes, J.-M. Trial of oral fumagillin for the treatment of intestinal microsporidiosis in patients with HIV infection. *AIDS* **2000**, *14*, 1341−1348.
(62) Molina, J.-M.; Tourneur, M.; Sarfati, C.; Chevret, S.; de Gouvello, A.; Gobert, J.-G.; Balkan, S.; Derouin, F. Fumagillin treatment of intestinal microsporidiosis. *N. Engl. J. Med.* **2002**, *346*, 1963−1969.
(63) Ingber, D.; Fujita, T.; Kishimoto, S.; Sudo, K.; Kanamaru, T.; Brem, H.; Folkman, J. Synthetic analogues of fumagillin that inhibit angiogenesis and suppress tumor growth. *Nature* **1990**, *348*, 555−557.
(64) Folkman, J. Tumor angiogenesis. *J. Adv. Cancer Res.* **1985**, *43*, 175−204.
(65) Folkman, J.; Shing, Y. Minireview: angiogenesis. *J. Biol. Chem.* **1992**, *267*, 10931−10934.
(66) Sin, N.; Meng, L.; Wang, M. Q. W.; Wen, J. J.; Bornmann, W. G.; Crews, C. M. The anti-angiogenic agent fumagillin covalently binds and inhibits the methionine aminopeptidase, MetAP-2. *Proc. Natl. Acad. Sci. U.S.A.* **1997**, *94*, 6099−6103.
(67) Griffith, E. C.; Su, Z.; Turk, B. E.; Chen, S.; Chang, Y.-H.; Wu, Z.; Biemann, K.; Liu, J. O. Methionine aminopeptidase (type 2) is the common target for angiogenesis inhibitors AGM-1470 and ovalicin. *Chem. Biol.* **1997**, *4*, 461−471.
(68) Liu, S.; Widom, J.; Kemp, C. W.; Crews, C. M.; Clardy, J. Structure of human methionine aminopeptidase-2 complexed with fumagillin. *Science* **1998**, *282*, 1324−1327.
(69) Zhang, P.; Nicholson, D. E.; Bujnicki, J. M.; Su, X.; Brendle, J. J.; Ferdig, M.; Kyle, D. E.; Milhous, W. K.; Chiang, P. K. Angiogenesis inhibitors specific for methionine aminopeptidase 2 as drugs for malaria and leishmaniasis. *J. Biomed. Sci.* **2002**, *9*, 34−40.
(70) Han, C. K.; Ahn, S. K.; Choi, N. S.; Hong, R. K.; Moon, S. K.; Chun, H. S.; Lee, S. J.; Kim, J. W.; Hong, C. I.; Kim, D.; Yoon, J. H.; No, K. T. Design and synthesis of highly potent fumagillin analogues from homology modeling for a human MetAP-2. *Bioorg. Med. Chem. Lett.* **2000**, *10*, 39−43.
(71) Weiss, L. M.; Zhou, G. C.; Zhang, H. Characterization of recombinant microsporidian methionine aminopeptidase type 2. *J. Eukaryot. Microbiol.* **2003**, *50* (Suppl.), 597−599.

(72) Baldwin, J. E.; Bulger, P. G.; Marquez, R. Fast and efficient synthesis of novel fumagillin analogues. *Tetrahedron* **2002**, *58*, 5441−5452.
(73) Lee, H. W.; Cho, C. S.; Kang, S. K.; Yoo, Y. S.; Shin, J. S.; Ahn, S. K. Design, synthesis and antiangiogenic effects of a series of potent novel fumagillin analogues. *Chem. Pharm. Bull.* **2007**, *55*, 1024−1029.
(74) Chen, X.; Xie, S.; Bhat, S.; Kumar, N.; Shapiro, T. A.; Liu, J. O. Fumagillin and fumarranol interact with *P. falciparum* methionine aminopeptidase 2 and inhibit malaria parasite growth *in vitro* and *in vivo*. *Chem. Biol.* **2009**, *16*, 193−202.
(75) Lu, J.; Chong, C. R.; Hu, X.; Liu, J. O. Fumarranol, a rearranged fumagillin analogue that inhibits angiogenesis *in vivo*. *J. Med. Chem.* **2006**, *49*, 5645−5648.
(76) Griffith, E. C.; Su, Z.; Niwayama, S.; Ramsay, C. A.; Chang, Y.-H.; Liu, J. O. Molecular recognition of angiogenesis inhibitors fumagillin and ovalicin by methionine aminopeptidase 2. *Proc. Natl. Acad. Sci. U.S.A.* **1998**, *95*, 15183−15188.
(77) Drahl, C.; Cravatt, B. F.; Sorensen, E. J. Protein-reactive natural products. *Angew. Chem., Int. Ed.* **2005**, *44*, 5788−5809.
(78) Rada, V.; Máchová, M.; Juk, J.; Marounek, M.; Dušková, D. Microflora in the honeybee digestive tract: counts, characteristics and sensitivity to veterinary drugs. *Apidologie* **1997**, *28*, 357−365.
(79) Furgala, B.; Boch, R. The effect of Fumidil B, Nosemack and Humatin on *Nosema apis*. *J. Apic. Res.* **1970**, *9*, 79−85.
(80) Nozal, M. J.; Bernal, J. L.; Martín, M. T.; Bernal, J.; Alvaro, A.; Martín, R.; Higes, M. Trace analysis of fumagillin in honey by liquid chromatography-diode array-electrospray ionisation mass spectrometry. *J. Chromatogr., A* **2008**, *1190*, 224−231.
(81) Kochansky, J.; Nasr, M. Laboratory studies on the photostability of fumagillin, the active ingredient of Fumidil B. *Apidologie* **2004**, *35*, 301−310.
(82) Arico-Muendel, C. C.; Benjamin, D. R.; Caiazzo, T. M.; Centrella, P. A.; Contonio, B. D.; Cook, C. M.; Doyle, E. G.; Hannig, G.; Labenski, M. T.; Searle, L. L.; Lind, K.; Morgan, B. A.; Olson, B.; Paradise, C. L.; Self, C.; Skinner, S. R.; Sluboski, B.; Svedsen, J. L.; Thompson, C. D.; Westlin, W.; White, K. F. Carbamate analogues of fumagillin as potent, targeted inhibitors of methionine aminopeptidase-2. *J. Med. Chem.* **2009**, *52*, 8047−8056.
(83) Didier, E. S. Effects of albendazole, fumagillin, and TNP-470 on microsporidial replication *in vitro*. *Antimicrob. Agents Chemother.* **1997**, *41*, 1541−1546.
(84) Killough, J. T.; Magill, G. B.; Smith, R. C. The treatment of amebiasis with fumagillin. *Science* **1952**, *115*, 71−72.
(85) Didier, P. J.; Phillips, J. N.; Kuebler, D. J.; Nasr, M.; Brindley, P. J.; Stoval, M. E.; Bowers, L. C.; Didier, E. S. Antimicrosporidial activities of fumagillin, TNP-470, ovalicin, and ovalicin derivatives *in vitro* and *in vivo*. *Antimicrob. Agents Chemother.* **2006**, *50*, 2146−2155.
(86) Conteas, C. N.; Berlin, O. G. W.; Ash, L. R.; Pruthi, J. S. Therapy for human gastrointestinal microsporidiosis. *Am. J. Trop. Med. Hyg.* **2000**, *63*, 121−127.
(87) Kirkby, W. W.; Salmond, G. W. A.; Davies, K. W. The assessment for safety of food additives. *J. Royal Stat. Soc. D (The Statistician)* **1972**, *21*, 47−61.
(88) Stanimirović, Z.; Stevanović, J.; Kulić, M.; Stojic, V. Frequency of chromosomal aberrations in the evaluation of genotoxic potential of dicyclohexylamine (fumagillin) *in vivo*. *Acta Vet. (Belgrade)* **2006**, *56*, 353−366.
(89) Stevanović, J.; Stanimirović, Z.; Ivana, P. I.; Lazarević, M. Monitoring of mitotic index and frequency of micronuclei in evaluation of genotoxic potential of fumagillin (dicyclohexylamine) *in vivo*. *Acta Vet. (Belgrade)* **2006**, *56*, 437−448.
(90) Stanimirović, Z.; Stevanović, J.; Bajic, V.; Radovic, I. Evaluation of genotoxic effects of fumagillin by cytogenic tests *in vivo*. *Mutat. Res.* **2007**, *628*, 1−10.
(91) Stanimirović, Z.; Ivana, P. I.; Kulišić, Z.; Milanka, D. Evaluation of genotoxic effects of fumagillin by sister chromatide exchange and chromosomal aberration tests in human cell cultures. *Acta Vet. (Belgrade)* **2007**, *57*, 257−273.
(92) Stevanović, J.; Stanimirović, Z.; Radakovic, M.; Stojic, V. *In vitro* evaluation of the clastogenicity of fumagillin. *Environ. Mol. Mut.* **2008**, *49*, 594−601.
(93) Kulić, M.; Aleksić, N.; Stanimirović, Z.; Ristić, S.; Medenica, S. Examination of genotoxic effects of fumagillin *in vivo*. *Genetika* **2009**, *41*, 329−338.
(94) Stanimirović, Z.; Aleksić, N.; Kulić, M.; Maletić, M. Fumagillin-induced chromosome aberrations in mouse bone-marrow cells. *Arch. Biol. Sci., Belgrade* **2010**, *62*, 47−55.
(95) Yanase, T.; Tamura, M.; Fujita, K.; Kodama, S.; Tanaka, K. Inhibitory effect of angiogenesis inhibitor TNP-470 on tumor growth and metastasis of human cell lines *in vitro* and *in vivo*. *Cancer Res.* **1993**, *53*, 2566−2570.
(96) Yamaoka, M.; Yamamoto, T.; Masaki, T.; Ikeyama, S.; Sudo, K.; Fujita, T. Inhibition of tumor growth and metastasis of rodent tumors by the angiogenesis inhibitor *O*-(chloroacetyl-carbamoyl)fumagillol (TNP-470; AGM-1470). *Cancer Res.* **1993**, *53*, 4262−4267.
(97) Yamaoka, M.; Yamamoto, T.; Masaki, T.; Ikeyama, S.; Sudo, K.; Fujita, T. Angiogenesis inhibitor TNP-470 (AGM-1470) potentially inhibits the tumor growth of hormone-independent human breast and prostate carcinoma cell lines. *Cancer Res.* **1993**, *53*, 5233−5236.
(98) Liu, T. P. Ultrastructural changes in the secretion granules of the hypopharangeal glands of the honeybee infected by *Nosema apis* and after treatment with fumagillin. *Tissue Cell* **1990**, *22*, 523−531.
(99) Kusaka, M.; Sudo, K.; Fujita, T.; Marui, S.; Itoh, F.; Ingber, D.; Folkman, J. Potent anti-angiogenic action of AGM-1470: comparison to the fumagillin parent. *Biochem. Biophys. Res. Commun.* **1991**, *174*, 1070−1076.
(100) Stoltz, D. R.; Khera, K. S.; Bendall, R.; Gunner, S. W. Cytogenetic studies with cyclamate and related compounds. *Science* **1970**, *167*, 1501−1502.
(101) Heil, J.; Reifferscheid, G.; Waldman, P.; Leyhausen, G.; Geurtsen, W. Genotoxicity of dental materials. *Mutat. Res.* **1996**, *368*, 181−194.
(102) Mortelmans, K.; Haworth, S.; Lawlor, T.; Speck, W.; Tainer, B.; Zeiger, E. Salmonella mutagenicity tests: II. Results from the testing of 270 chemicals. *Environ. Mutat.* **1986**, *8* (Suppl. 7), 1−119.
(103) Purchase, I. F. H.; Longstaff, E.; Ashby, J.; Styles, J. A.; Anderson, D.; Lefevre, P. A.; Westwood, F. R. An evaluation of 6 short-term tests for detecting organic chemical carcinogens. *Br. J. Cancer* **1978**, *37*, 873−903.
(104) Pegg, A. E.; Bitonti, A. J.; McCann, P. P.; Coward, J. K. Inhibition of bacterial aminopropyltransferases by *S*-adenosyl-1,8-diamino-3-thiooctane and by dicyclohexylamine. *FEBS Lett.* **1983**, *155*, 192−196.
(105) Woldegiorgis, A.; Wiklund, P.; Remberger, M.; Kaj, L.; Viktor, T.; Lilja, K.; Brorstrom-Lunden, E.; Dye, I. C. Results from the Swedish National Screening Programme 2007, Sub Report 1: Amines IVL Report B1817 (www.ivl.se), 2007; pp 1−36.
(106) Greim, H.; Bury, D.; Klimisch, H.-J.; Oeben-Negele, M.; Ziegler-Skylakakis, K. Toxicity of aliphatic amines: structure-activity relationship. *Chemosphere* **1998**, *36*, 271−295.
(107) Pliss, G. B. On the carcinogenic activity of dicyclohexylamine and dicyclohexylamine nitrite. *Vopr. Onk.* **1958**, *4*, 659−667. (Original reference in Russian; abstract accessed at http://toxnet.nlm.nih.gov on Oct 29, 2013.)
(108) COM (2009) Committees on Toxicity, Mutagenicity, Carcinogenicity of Chemicals in Food, Consumer Products and the Environment [online]. Joint Annual Report 2009 http://cot.food.gov.uk/pdfs/comsection2009.pdf (accessed Nov 30, 2012), http://www.iacom.org.uk/meetings/documents/COMfinalminsFeb2009.pdf (accessed Nov 30, 2012).
(109) COM (2011) Committees on Toxicity, Mutagenicity, Carcinogenicity of Chemicals in Food, Consumer Products and the Environment [online] http://www.iacom.org.uk/statements/documents/fumagillinfinalstatement2011_002.pdf (accessed Nov 30, 2012).

(110) Lijnen, H. R.; Frederix, L.; Van Hoef, B. Fumagillin reduces adipose tissue formation in murine models of nutritionally induced obesity. *Obesity* **2010**, *18*, 2241−2246.
(111) Scroyen, I.; Christiaens, V.; Lijnen, H. R. Effect of fumagillin on adipocyte differentiation and adipogenesis. *Biochim. Biophys. Acta* **2010**, *1800*, 425−429.
(112) Webster, T. C. Fumagillin affects *Nosema apis* and honey bees (*Hymenoptera: Apidae*). *J. Econ. Entomol.* **1994**, *87*, 601−604.
(113) Woyke, J. Increase in life-span, unit honey productivity and honey surplus with fumagillin treatment of honeybees. *J. Apic. Res.* **1984**, *23*, 209−212.
(114) Szabo, T. I.; Heikel, D. T. Effect of fumagillin treatment on *Nosema* infection, survival and populations of overwintering honeybee colonies. *J. Apic. Res.* **1987**, *26*, 186−190.
(115) Furgala, B.; Gochnauer, T. A. Chemotherapy of nosema disease. Effect of treatment method with Fumidil-B. *Am. Bee J.* **1969**, *109*, 380−381; 392.
(116) Furgala, B.; Gochnauer, T. A. Chemotherapy of nosema disease. Further studies on the residual activity of fumagillin in stored sugar syrup and "bee manipulated" sugar syrup. *Am. Bee J.* **1969**, *109*, 218−219.
(117) Pettis, J. S.; Lichtenberg, E. M.; Andree, M.; Stitzinger, J.; Rose, R.; vanEngelsdorp, D. Crop pollination exposes honey bees to pesticides which alters their susceptibility to the gut pathogen *Nosema ceranae*. *PLoS One* **2013**, *8*, e70182 (accessed Feb 25, 2014)..
(118) Johnson, R. M.; Dahlgren, L.; Siegfried, B. D.; Ellis, M. D. Acaricide, fungicide and drug interactions in honey bees (*Apis mellifera*). *PLoS One* **2013**, *8*, e54092 (accessed Feb 25, 2014)..
(119) Martin, S. J.; Hardy, J.; Villalobos, E.; Martín-Hernández, R.; Nikaido, S.; Higes, M. Do the honeybee pathogens *Nosema ceranae* and deformed wing virus act synergistically? *Environ. Microbiol. Rep.* **2013**, *5*, 506−510.
(120) Fries, I.; Chauzat, M.-P.; Chen, Y.-P.; Doublet, V.; Genersch, E.; Gisder, S.; Higes, M.; McMahon, D. P.; Martín-Hernández, R.; Natsopoulou, M.; Paxton, R. J.; Tanner, G.; Webster, T. C.; Williams, G. R. Standard methods for nosema research. In The COLOSS *BEEBOOK*: Vol. II: Standard Methods for *Apis mellifera* Pest and Pathogen Research; Dietemann, V., Ellis, J. D., Neumann, P., Eds.; *J. Apic. Res.* **2013**, *51*, http://dx.doi.org/10.3896/IBRA.1.52.1.14.
(121) Gochnauer, T. A.; Furgala, B. The nosema inhibitory activity of alcohol I, a component of fumagillin. *J. Insect Pathol.* **1962**, *4*, 489−491.
(122) Brackett, J. M.; Arguello, M. D.; Schaar, J. C. Determination of fumagillin by high performance liquid chromatography. *J. Agric. Food Chem.* **1988**, *36*, 762−764.
(123) Assil, H. I.; Sporns, P. ELISA and HPLC methods for analysis of fumagillin and its decomposition products in honey. *J. Agric. Food Chem.* **1991**, *39*, 2206−2213.
(124) Guyonnet, J.; Richard, M.; Hellings, Ph. Determination of fumagillin in muscle tissue of rainbow trout using automated ion-pairing liquid chromatography. *J. Chromatogr., B* **1995**, *666*, 354−359.
(125) Lopez, M. I.; Pettis, J. S.; Barton Smith, I.; Chu, P.-S. Multiclass determination and confirmation of antibiotic residues in honey using LC-MS/MS. *J. Agric. Food Chem.* **2008**, *56*, 1553−1559.
(126) Kanda, M.; Sasamoto, T.; Takeba, K.; Hayashi, H.; Kusano, T.; Matsushima, Y.; Nakajima, T.; Kanai, S.; Takano, I. Rapid determination of fumagillin residues in honey by liquid chromatography-tandem mass spectrometry using the QuEChERS method. *J. AOAC Int.* **2011**, *94*, 878−885.
(127) Dmitrovic, J.; Durden, D. A. Analysis of fumagillin in honey by LC-MS/MS. *J. AOAC Int.* **2013**, *96*, 687−695.
(128) Balthaser, B. R.; Maloney, M. C.; Beeler, A. B.; Porco, J. A., Jr.; Snyder, J. K. Remodelling of the natural product fumagillol employing a reaction discovery approach. *Nat. Chem.* **2011**, *3*, 969−973.
(129) Idris, A. B.; Paul, A. Y.; Noraman, M. N.; Zainal Abidin, B. A.-H. Evidence of antibiotic resistant development on *Nosema* spp, infecting diamondback moth larvae. *Resistant Pest Manage. Newsl.* **2000**, *11*, 21−23.
(130) Bajić, V.; Stanimirović, Z.; Stevanović, J. Genotoxicity potential of 8-Cl-cyclic adenosine monophosphate assessed with cytogenic tests *in vivo*. *Arch. Med. Res.* **2004**, *35*, 209−214.

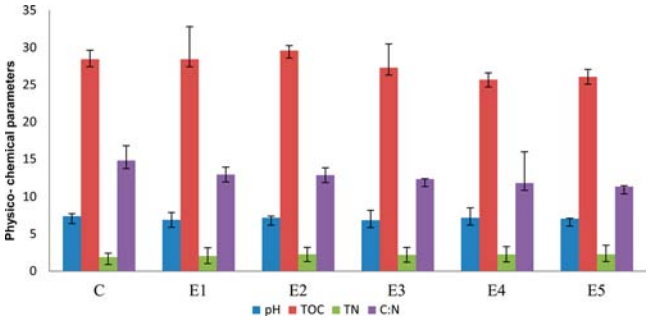

Figure 1. Physicochemical parameters of vermicompost (C, E1−E5).

(E1−E5) were increased significantly compared to control (C); data are presented in Table 1. The higher value of P was recorded at E3, which may be partially due to the earthworm's gut phosphatase and more P discharged by the added phosphobacteria in the substrate. The maximum K level was observed in E5 followed by E2, E3, E4, and E1. A higher value of Ca was observed in E1 and a similar increment of Mg level in E5. The increased level of nutrients in vermicompost was similar to that in the literature.[11,12] The transition metal concentration was decreased in vermicompost samples relative to compost (C) except Zn concentration in E3, which was slightly increased. The decrease in the metal concentration is due to the accumulation of metals (Mn, Zn, and Cu) on the earthworm body.[13] The results of the PCA are given in (Figure 2. Four principal components accounting for 99% of the total variation are retained on the basis of the eigenvalue greater-than-one rule. The first two principal components explain 80.82 and 13.90% of the variance, respectively. The third and fourth principal components are considerably less important, explaining only 3.24 and 1.82% of the variance, respectively. Accordingly, we consider only the first two components, which account for a large proportion of the variation in the data (94% of the variance). It is possible to observe that control and vermicompost treatments are separated into two different groups on the basis of their characteristics. PC1 separates the composts studied in two different groups: group 1A (C, E3) was characterized by high TOC, C:N ratio, and phosphorus; group 1B (E1, E4) was characterized by the lowest value of pH. PC2 included E2 and E5, and it is possible to separate composts that have higher TN contents (2.29%) and reduced level of C:N ratio, 11.39%, respectively. CA was used to detect similar groups to characterize the control and vermicompost samples (Figure 3); it is found that two different groups were ordinated separately from all of the treatments, which confirm PCA.

SEM was used to study the morphological results of the final control and vermicompost samples as shown in Figure 4. In the control sample the cellulose and protein groups were tightly bound with the lignin as an assortment (Figure 4C). Comparison of the micrographs of vermicompost samples E1−E5 suggests that the surface area of compost samples is higher than that of the control. Within the vermicompost samples, the highest proportion of the surface was recorded in

Table 1. AAS Data for Control and Vermicompost Samples

	concentration determined (%)					concentration determined (ppm)			
sample	P	K	Ca	Mg	Na	Fe	Mn	Zn	Cu
C	0.89	1.16	0.77	0.59	0.18	1947	211	128	60
E1	0.96	1.19	1.02	0.61	0.1	1907	187	52	41
E2	0.96	1.74	0.88	0.68	0.17	1901	183	119	3.1
E3	1	1.6	0.8	0.67	0.18	1887	209	136	53
E4	0.94	1.27	0.82	0.62	0.07	1874	192	90.33	44.3
E5	0.93	1.82	0.93	0.73	0.13	1817	167	98	16
t test[a]	0.004*	0.044**	0.039**	0.029**	0.153	0.012**	0.026**	0.159	0.038**

[a](*) $p < 0.05$ and (**) $p < 0.01$ level of significance in *t* test.

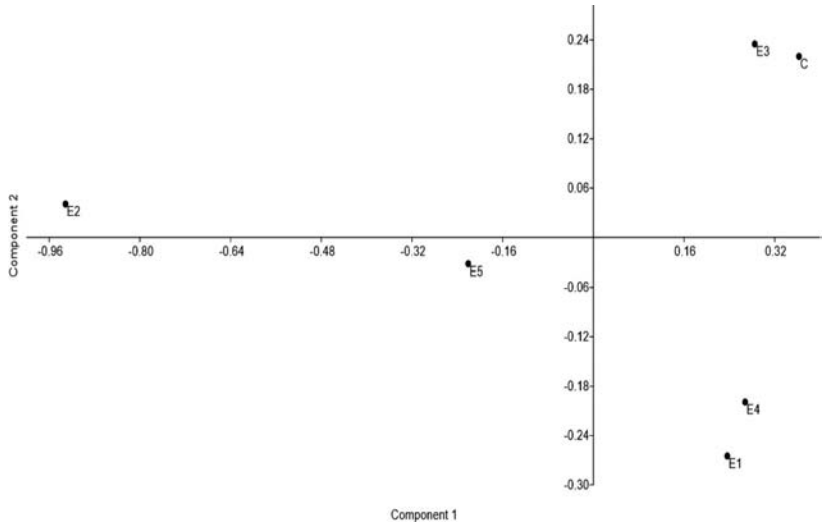

Figure 2. Principal component analysis for control and vermicomposting treatments.

dx.doi.org/10.1021/jf4054403 | J. Agric. Food Chem. 2014, 62, 2738−2741

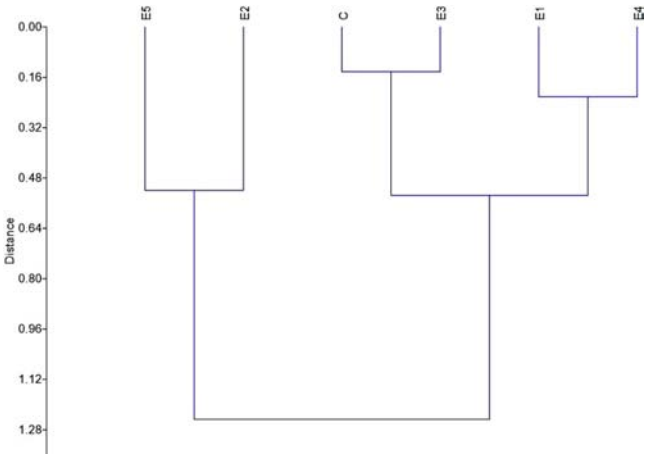

Figure 3. Cluster analysis for control and vermicomposting treatments.

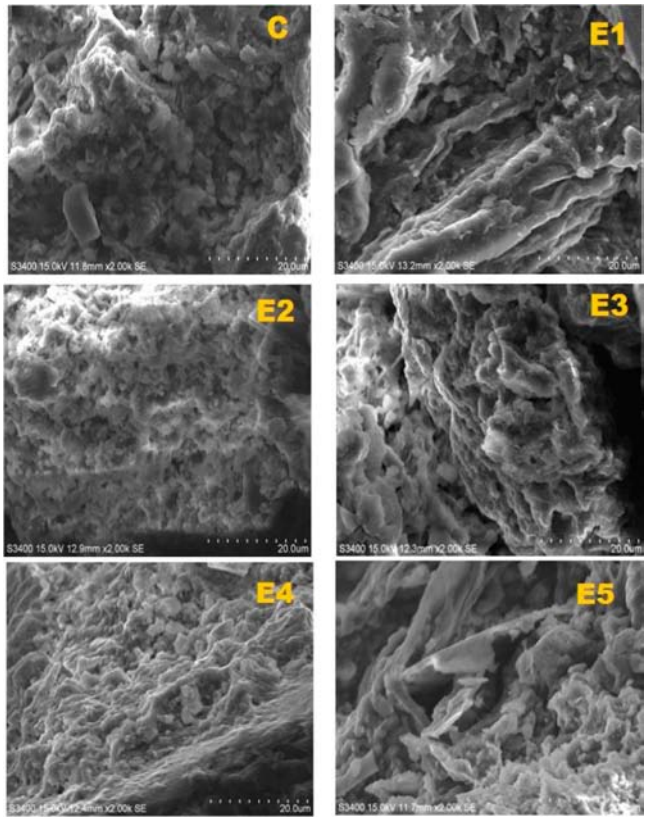

Figure 4. Micrographs by SEM of flower waste vermicompost after 80 days in the following forms: (C) control compost; (E1) vermicompost; (E2) vermicompost + *Azospirillum*; (E3) vermicompost + Phosphobacterium; (E4) vermicompost + blue-green algae; (E5) vermicompost + *Rhizobium*.

E2 followed by E4 and E5. It is observed that the particle size of the vermicompost was smaller than that of control compost. The surface area of vermicompost samples showed single particles packed together to form aggregates. Such aggregation is responsible for the uncertainty about a real surface area of vermicompost because the internal area was not fully accessible. Moreover, different morphological features occurring within vermicompost might be due to their different chemical structures.[5] In addition, in the final vermicompost product (Figure 4, E1−E5), the protein and lignin matrix is disaggregated by earthworms and microbes. The presence of earthworms and microbes shows more numerous surface irregularities that confirm the final compost has attained compost maturity.[7] These images indicate a surface region with an irregular morphology as well as a high number of pores and can corroborate the high CEC value. Similar results were reported for their vermicompost samples.[7,9]

In the past the focus of the application of the chromatography method was on the soil and compost assessment. In contrast to the assessment of soils and composts, there are hardly any methodical works on the evaluation of chromatography pictures of foods.[6,14] The chromatogram of the initial substrate shows three clear zones: (a) an absence of color in the outer zone, which reflects the lack of colloidal substances; (b) a faint brown color indicates the availability of less organic matter; (c) the inner small violet zone indicates the quantity of available minerals, which is clearly observed in E1.[6,8,14] These zones were entirely different from the final substrate in the present study. The final day of samples showed the inner zone with violet radiation confirmed the concentration of the mineralization was increased at the end of the composting process (Figure 5). E2 shows a high level of mineralization process

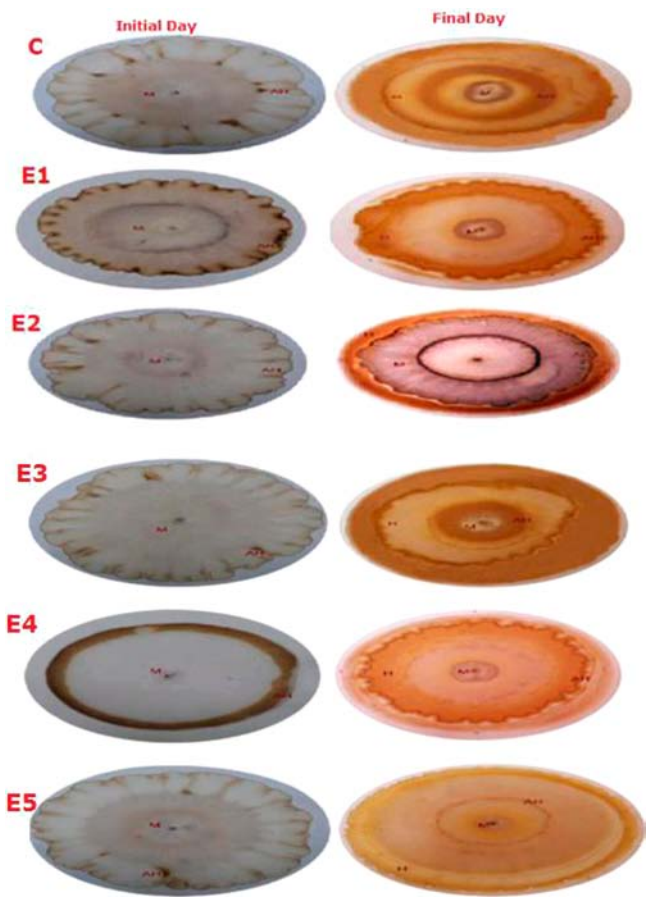

Figure 5. Biodynamic paper chromatography of flower waste vermicompost after 80 days in the following forms: (C) control compost; (E1) vermicompost; (E2) vermicompost + *Azospirillum*; (E3) vermicompost + Phosphobacterium; (E4) vermicompost + blue-green algae; (E5) vermicompost + *Rhizobium*.

followed by E5, whereas in the remaining samples the mineralization process was not clearly visible. All of the final samples showed an evenly distributed brown color in the outer zone that indicates the presence of humus substances in the final

dx.doi.org/10.1021/jf4054403 | J. Agric. Food Chem. 2014, 62, 2738−2741

samples. The existence of humus in all samples around neutral pH values is a sign of maturity of the vermicompost samples. Similar chromatography results of vermicompost samples are reported in the literature.[8,14] The R_f values of different color bands/patterns of all samples are given in Table S1 (see the Supporting Information). In this study, a circular chromatographic method has been used for the purpose of determining differences in the formation of humus in the compost and biofertilizer-enriched vermicompost samples that cannot be determined by chemical analysis.[7]

Vermicomposting led to the drop of pH, decrease in TOC and C:N ratio, and increase in nitrogen content compared to the control sample. The reduction of the C/N ratio was reported from an initial value of 15% in C and to the end of the composting (11.5%) in E5, which indicates organic carbon decomposition in the final vermicompost. However, by the employment of statistical analysis, PCA and CA, it was possible to classify and characterize the vermicompost samples. BPC and SEM techniques proved useful tools to monitor the maturity of vermicompost during the composting process. Critical investigation of our study results indicates that the epigeic earthworm *E. fetida* was capable of decomposing flower waste into nutrient-enriched products and can play a significant role in solid waste management.

D. Senthil Kumar*[,†]
P. Satheesh Kumar[§]
N. M. Rajendran[#]
V. Uthaya Kumar[⊥]
G. Anbuganapathi[†]

[†]Department of Zoology, Kandaswami Kandar's College, Paramathi-Velur, 638 182 Tamil Nadu, India
[§]Department of Biological and Environmental Sciences, University of Messina, Messina 98166, Italy
[#]Department of Chemistry, Pondicherry University, Puducherry 605 014, India
[⊥]Department of Zoology, Bharathiyar University, Coimbatore, Tamil Nadu, India

■ ASSOCIATED CONTENT

Supporting Information

Table S1. This material is available free of charge via the Internet at http://pubs.acs.org.

■ AUTHOR INFORMATION

Corresponding Author

*(D.S.K.) E-mail: drskumar1968@gmail.com.

Notes

The authors declare no competing financial interest.

■ REFERENCES

(1) Hand, P.; Hayes, W. A.; Frankland, J. C.; Satchell, J. E. The vermicomposting of cow slurry. *Pedobiologia* **1988**, *31*, 199−209.
(2) Sarkar, R. K.; Karmakar, S.; Chakraborty, A. Response of summer green gram (*Phaseolus radiatus*) to nitrogen, phosphorus application and bacterial inoculation. *Indian J. Agron.* **1997**, *38* (4), 578−581.
(3) Ramanathan, B.; Alagesan, P. Evaluation of millicompost versus vermicompost. *Curr. Sci.* **2012**, *103* (2), 140−143.
(4) Raju, A. A.; Rose, C.; Muralidhara Rao, N. Enzymatic hydrolysis of tannery fleshings using chicken intestine proteases. *Anim. Feed Sci. Technol.* **1997**, *66* (1), 139−147.
(5) Kumar, D. S.; Kumar, P. S.; Rajendran, N. M.; Anbuganapathi, G. Compost maturity assessment using physicochemical, solid-state spectroscopy, and plant bioassay analysis. *J. Agric. Food Chem.* **2013**, *61*, 11326−11331.
(6) Pfeiffer, E. *Chromatography Applied to Quality Testing*; Biodynamic Literature: Wyoning, RI, USA, 1984; 44 pp.
(7) Ravindran, B.; Dinesh, S. L.; John Kennedy, L.; Sekaran, G. Vermicomposting of solid waste generated from leather industries using epigeic earthworm *Eisenia fetida*. *Appl. Biochem. Biotechnol.* **2008**, *151*, 480−488.
(8) Perumal, K.; Vatsala, T. M. *Utilization of Local Alternative Materials in Cow Horn Manure (BD 500) Preparations: A Case Study on Biodynamic Vegetable Cultivation*; Murugappa Chettiar Research Centre: Tharamani, Chennai, India. 2002; 26 pp.
(9) Pereira, M. G.; Arruda, M. A. Z. Vermicompost as a natural absorbent material. Characterization and potentialities for cadmium absorption. *J. Braz. Chem. Soc.* **2003**, *14* (1), 39−47.
(10) Satheeshkumar, P.; Khan, A. B. Identification of mangrove water quality by multivariate statistical analysis methods in Pondicherry coast, India. *Environ. Monit. Assess.* **2012**, *184* (6), 3761−3774.
(11) Suthar, S.; Singh, S. Vermicomposting of domestic waste by using two epigeic earthworms (*Perionyx excavatus* and *Perionyx sansibaricus*). *Int. J. Environ. Sci. Technol.* **2008**, *5* (1), 99−106.
(12) Kaushik, P.; Garg, V. K. Dynamics of biological and chemical parameters during vermicomposting of solid textile mill sludge mixed with dung and agricultural residues. *Bioresour. Technol.* **2004**, *94*, 203−209.
(13) Kumar, D. S. Study on biofertilizer enriched flower waste vermicompost by using *Eisenia fetida* and its application on agriculture and aquaculture. Ph.D. thesis, Periyar University, Salem, Tamil Nadu, India, 2013; 152 pp.
(14) Ismail, S. A. Status of composting in India − an Indian earthworm's eye view. In *Proceedings Indo-US Workshop on Vermitechnology in Human Welfare*; Edwards, C. A., Jeyaraj, and Jeyaraj, I., Eds.; Coimbatore, India, 2007; pp 110−124.

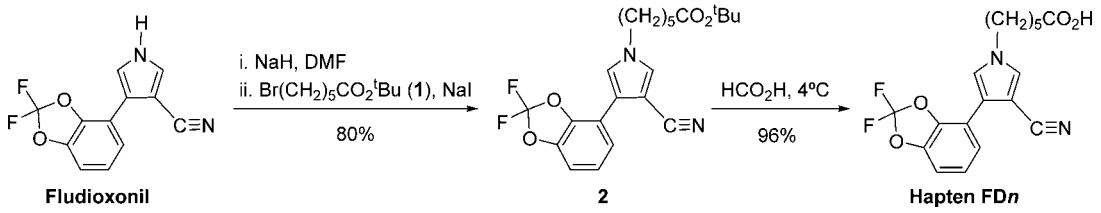

Figure 1. Synthesis of hapten FD*n*.

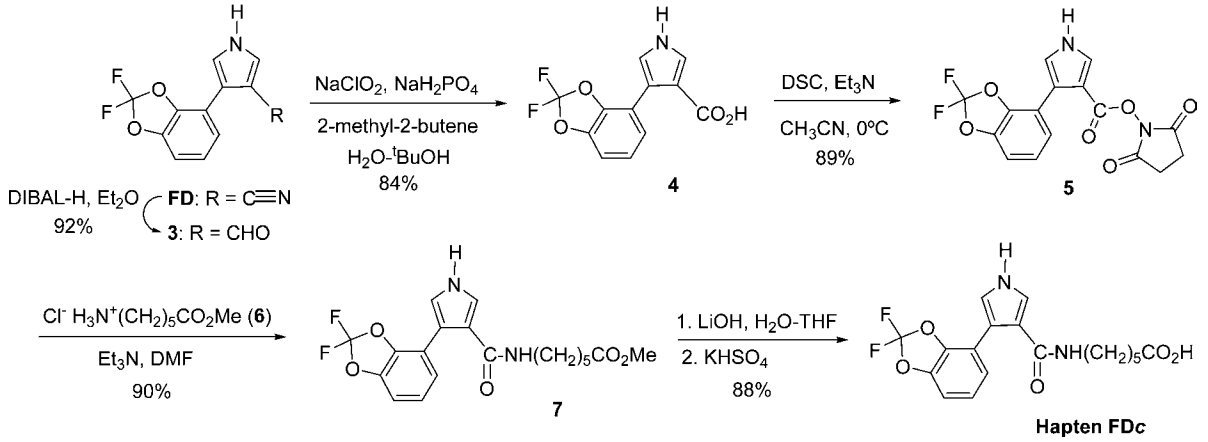

Figure 2. Synthesis of hapten FD*c*. FD, Fludioxonil.

Table 1. Assay Sensitivity in the Direct cELISA Format

	tracer conjugate							
	HRP–FD*c*				HRP–FD*n*			
Ab	[Ab][a]	[C][b]	A_{max}	IC_{50}[c]	[Ab]	[C]	A_{max}	IC_{50}
FD*c*#1	30	3	1.0	1366.4	3	100	0.8	92.0
FD*c*#2	3	10	1.8	1542.6	3	100	nd[d]	
FD*n*#1	3	100	ns		10	3	0.8	22.9
FD*n*#2	3	100	ns		30	10	1.2	129.5

[a]Antibody dilution (×10[3]). [b]Conjugate concentration in ng/mL. [c]Values in nM. [d]Signal was below 0.5.

Table 2. Assay Sensitivity in the Indirect cELISA Format

	coating conjugate							
	OVA–FD*c*				OVA–FD*n*			
Ab	[Ab][a]	[C][b]	A_{max}	IC_{50}[c]	[Ab]	[C]	A_{max}	IC_{50}
FD*c*#1	300	100	1.1	1405.7	10	1000	0.9	88.1
FD*c*#2	100	100	0.8	1329.4	10	1000	0.8	
FD*n*#1	3	1000	ns[d]		30	100	1.5	75.1
FD*n*#2	3	1000	ns		100	100	1.0	372.8

[a]Antibody dilution (×10[3]). [b]Conjugate concentration in ng/mL. [c]Values in nM. [d]Signal was below 0.5.

N,*N*′-disuccinimidyl carbonate. Activated purified haptens were coupled to bovine serum albumin (BSA), ovalbumin (OVA), and horseradish peroxidase (HRP). The amount of employed activated hapten was adjusted according to the desired final hapten density. Thus, high MRs for BSA conjugates (15 and 17 for FD*c* and FD*n*, respectively) and low MRs for OVA conjugates (2 for both haptens) were obtained as intended. On the other hand, calculated hapten densities of HRP conjugates were 6 and 4 for FD*c* and FD*n*, respectively. Unrealistically high MR values for HRP conjugates (this enzyme contains 3–4 available lysine residues) are probably due to modified molar extinction coefficients of the protein and/or the hapten after conjugation. However, adequate enzymatic activity and hapten coupling was demonstrated by competitive assay.

Antibody Affinity and Selectivity. Competitive assays were performed with FD*c*-type antibodies (obtained with BSA–FD*c* as immunizing conjugate) and FD*n*-type antibodies (from BSA–FD*n* immunized animals), using homologous conjugates (same hapten as the immunizing conjugate) and following the direct and indirect cELISA procedures. Antibody affinity was assessed by checkerboard competitive assays, running a standard curve of Fludioxonil in each microplate column (from 10 pM to 10 μM plus a blank) and assaying diverse antibody and antigen concentrations simultaneously as described in the Supporting Information. The lowest IC_{50} values with homologous

dx.doi.org/10.1021/jf5001716 | J. Agric. Food Chem. 2014, 62, 2742–2744

conjugates were obtained with antibodies from FD*n*-immunized rabbits in both cELISA formats (Tables 1 and 2). Thus, hapten FD*n* behaved better as immunogen than hapten FD*c*, so it was a better mimic of Fludioxonil. Hapten FD*n* keeps unmodified all moieties of the target molecule, and only an N−H bond is substituted by an N−C bond. Comparatively, in hapten FD*c*, the cyano group modification *probably* alters more significantly the electronic properties of the pyrrole moiety (Figures 1 and 2). Moreover, the linker in hapten FD*n* is located further to the bulky aryl moiety than in hapten FD*c*, which probably favors the aromatic portion of this hapten adopting similar conformations to those adopted by the common framework of parent Fludioxonil (see Figure S1 of Supporting Information).

With regard to selectivity, binding of the four antibodies to additional new-generation fungicides that are commonly formulated together with Fludioxonil was assessed, such as cyprodinil, pyrimethanil, mepanipyrim, azoxystrobin, boscalid, and fenhexamid. As expected, no inhibition was observed by any of the studied compounds at a concentration of 10^4 nM with any of the described antibodies.

Competitive Immunoassays. Checkerboard assays were performed with both FD*c*- and FD*n*-type antibodies using also the heterologous conjugates. Concerning the direct cELISAs, antibody FD*c*#1 bound the heterologous tracer HRP−FD*n*, and a moderate IC_{50} value to Fludioxonil was found in this case, improving the IC_{50} value that was obtained with the homologous combination. However, FD*n*-type antibodies recognized only the homologous tracer. Parallel results were observed with the indirect format (Table 2). For a particular antibody/antigen combination, the IC_{50} values stayed in the same order of magnitude in both cELISA formats. Overall, the most sensitive assay was achieved with antibody FD*n*#1 using the homologous combination. The inhibition curve of such an assay is depicted in Figure S2 in the Supporting Information, showing an IC_{50} value for Fludioxonil of 22.9 nM (equivalent to 5.7 μg/L) and an A_{max} of 0.8 absorbance unit.

Antonio Abad-Fuentes[†]
Consuelo Agulló[§]
Francesc A. Esteve-Turrillas[†]
Antonio Abad-Somovilla[§]
Josep V. Mercader*[,†]

[†]Department of Biotechnology, Institute of Agrochemistry and Food Technology, Consejo Superior de Investigaciones Científicas (IATA-CSIC), Agustí Escardino 7, 46980 Paterna, València, Spain

[§]Department of Organic Chemistry, Universitat de València, Doctor Moliner 50, 46100 Burjassot, València, Spain

■ ASSOCIATED CONTENT

Supporting Information

Synthesis details and characterization data of intermediates, haptens, and active esters; equipment, immunoreagent production, ELISA procedures, Fludioxonil most-stable conformations, and inhibition curve. This material is available free of charge via the Internet at http://pubs.acs.org.

■ AUTHOR INFORMATION

Corresponding Author

*(J.V.M.) Phone: +34-963900022. Fax: +34-963636301. E-mail: jvmercader@iata.csic.es.

Funding

This work was supported by the Spanish Ministerio de Ciencia e Innovación (MICINN) (AGL2009-12940-C02-01/02/ALI) and cofinanced by FEDER funds. F.A.E.-T. and J.V.M. were hired by CSIC with postdoctoral contracts, the former under the JAE-doc program and the latter under the Ramón y Cajal program, both cofinanced by MICINN and by the European Social Fund (ESF).

Notes

The authors declare no competing financial interest.

■ ACKNOWLEDGMENTS

We thank Ana Izquierdo-Gil, Laura López-Sánchez, and Laura Vila-Dasí for excellent technical assistance.

■ ABBREVIATIONS USED

BSA, bovine serum albumin; cELISA, competitive enzyme-linked immunosorbent assay; DSC, *N,N′*-disuccinimidyl carbonate; HRP, horseradish peroxidase; MR, molar ratios; OVA, ovalbumin

■ REFERENCES

(1) Schirra, M.; D'Aquino, S.; Cabras, P.; Angioni, A. Control of postharvest diseases of fruit by heat and fungicides: efficacy, residue levels, and residue persistence. A review. *J. Agric. Food Chem.* **2011**, *59*, 8531−8542.

(2) Rosslenbroich, H. J.; Stuebler, D. *Botrytis cinerea* − history of chemical control and novel fungicides for its management. *Crop Prot.* **2000**, *19*, 557−561.

(3) Kanetis, L.; Förster, H.; Jones, C. A.; Borkovich, K. A.; Adaskaveg, J. E. Characterization of genetic and biochemical mechanisms of fludioxonil and pyrimethanil resistance in field isolates of *Penicillium digitatum*. *Phytopathology* **2008**, *98*, 205−214.

(4) Benigni, M.; Bompeix, G. Chemical and biological control of *Sclerotinia sclerotiorum* in witloof chicory culture. *Pest Manage. Sci.* **2010**, *66*, 1332−1336.

(5) Cus, F.; Bach, B.; Barnavon, L.; Pongrac, V. Z. Analytical determination of Dolenjska region wines quality. *Food Control* **2013**, *33*, 274−280.

(6) Passarella, I.; Elia, I.; Guarino, B.; Bourlot, G.; Nègre, M. Evaluation of the field dissipation of fungicides and insecticides used on fruit bearing trees in northern Italy. *J. Environ. Sci. Health B* **2009**, *44*, 137−143.

(7) Peterson, E. C.; Gunnell, M.; Che, Y.; Goforth, R. L.; Carroll, F. I.; Henry, R.; Liu, H.; Owens, S. M. Using hapten design to discover therapeutic monoclonal antibodies for treating methamphetamine abuse. *J. Pharmacol. Exp. Ther.* **2007**, *322*, 30−39.

(8) Mercader, J. V.; Agulló, C.; Abad-Somovilla, A.; Abad-Fuentes, A. Synthesis of site-heterologous haptens for high affinity anti-pyraclostrobin antibody generation. *Org. Biomol. Chem.* **2011**, *9*, 1443−1453.

(9) Mercader, J. V.; Suárez-Pantaleón, C.; Agulló, C.; Abad-Somovilla, A.; Abad-Fuentes, A. Hapten synthesis and monoclonal antibody-based immunoassay development for the detection of the fungicide kresoxim-methyl. *J. Agric. Food Chem.* **2008**, *56*, 1541−1552.

(10) Esteve-Turrillas, F. A.; Parra, J.; Abad-Fuentes, A.; Agulló, C.; Abad-Somovilla, A.; Mercader, J. V. Hapten synthesis, monoclonal antibody generation, and development of competitive immunoassays for the analysis of picoxystrobin in beer. *Anal. Chim. Acta* **2010**, *682*, 93−103.

(11) Mercader, J. V.; Esteve-Turrillas, F. A.; Agulló, C.; Abad-Somovilla, A.; Abad-Fuentes, A. Antibody generation and immunoassay development in diverse formats for pyrimethanil specific and sensitive analysis. *Analyst* **2012**, *137*, 5672−5679.

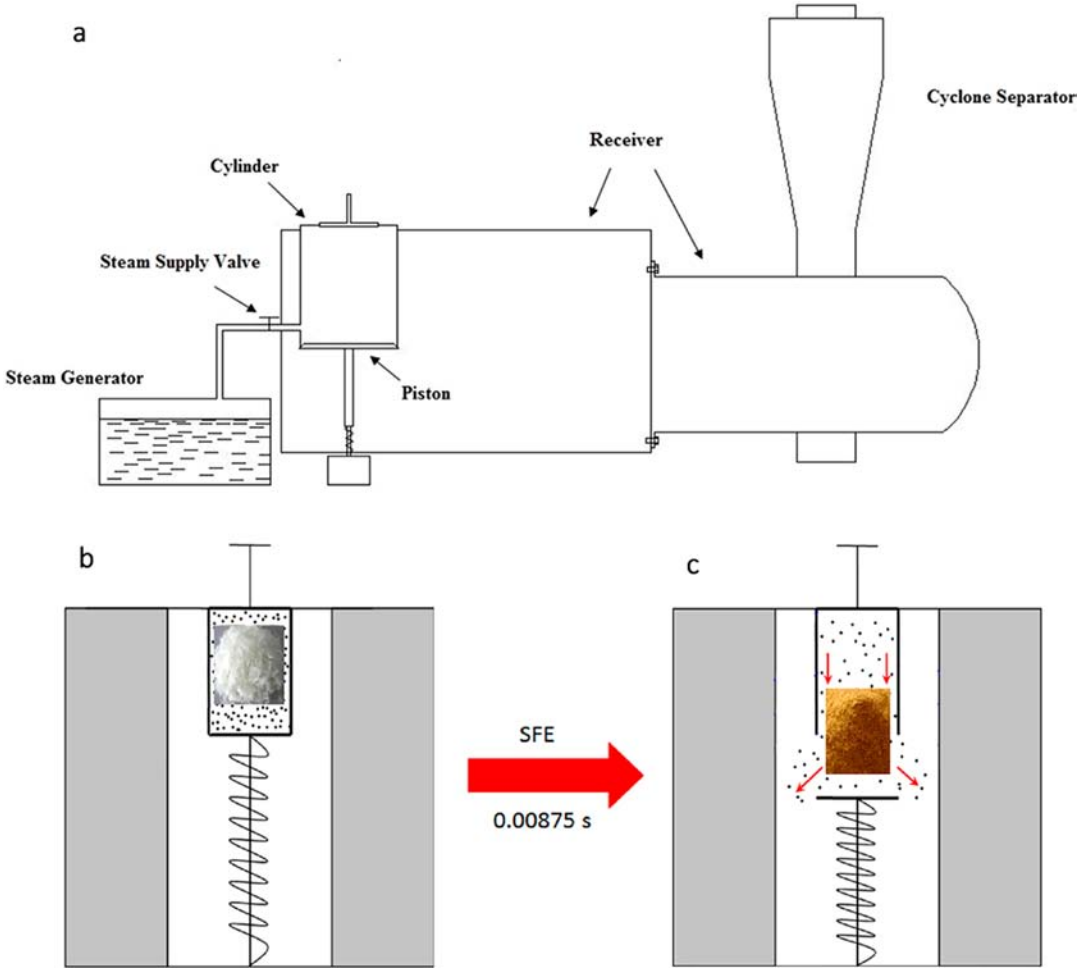

Figure 1. Structural diagram of the QBS-200B SFE test bed: (a) SFE system, (b) status of the piston in the steam boiling phase, and (c) status of the piston in the explosion phase.

pressure decreased dramatically in a very short time (within 0.00875 s). The exploded materials, together with a little water, were recovered in the receiver and frozen at −20 °C until the analyses.

Morphological Characterization. The morphology of feather fibers was observed using scanning electron microscopy (SEM, FEI Quanta 200, Eindhoven, Netherlands). The specimens were mounted on conductive adhesive tape, sputter-coated with gold palladium, and observed using a voltage of 5.0 kV.

Protein Solubility and Pepsin Digestibility. A total of 1 g of ground samples was suspended in 25 mL solutions. The suspensions were shaken in a water bath for 4 h according to the method described by Li and Lee.[16] The mixture was centrifuged at 10000*g* for 20 min at 4 °C. The soluble protein content of the supernatant was then determined using a modified Lowry procedure.[17] The total nitrogen in the original samples was measured by the Kjeldahl method. All analyses were conducted in duplicate.

Pepsin digestibility of each sample was determined by the procedure of the AOAC International using 0.2% pepsin (activity of 1:10 000) in 0.075 M HCl.[18] In this assay, 1.000 g (±0.010 g) of sample was incubated in 150 mL of pepsin solution at 45 °C for 16 h. Protein digestibility was expressed as the difference between the nitrogen content of the sample and the residual nitrogen content after pepsin digestion, divided by the nitrogen content of the sample.

Disulfide−Sulfhydryl Quantification. Disulfide (SS) and sulfhydryl (SH) contents of unexploded and exploded samples were determined according to the method of the solid-phase assay by Chan et al.,[19] with some modifications. For free sulfhydryl content determination, approximately 15 mg of the ground sample with a particle size smaller than 40 mesh was suspended in 0.8 mL of reaction buffer consisting of 8 M urea, 3 mM ethylenediaminetetraacetic acid (EDTA), 1% sodium dodecyl sulfate (SDS), and 0.2 M tris-(hydroxymethyl)aminomethane) (Tris)−HCl (pH 8.0) (buffer A). The reaction mixture was vortexed for various intervals at room temperature. After 2.5 h, 0.2 mL of 50 mM 5,5′-dithiobis(2-nitrobenzoic acid) (DTNB) in 0.2 M Tris−HCl (pH 8.0) (buffer B) was added to each sample, vortexed for 1 h, and then centrifuged at 13600*g* for 10 min at room temperature. Concurrently, a sample was incubated without DTNB as a blank. The supernatant was collected and diluted at a ratio of 1:10. The absorbance of the supernatant was read at 412 nm. An extinction coefficient of 13 600 M^{-1} cm^{-1} was used to calculate the number of thiol-containing groups.

For determination of the total sulfhydryl (SH + reduced SS) content, the assay procedure was as described for the SH assay, except for the use of different reaction buffers. The buffer consisted of 8 M urea, 3 mM EDTA, 1% SDS, and 0.2 M Tris−HCl (pH 9.5), 0.1 M Na_2SO_3, and 50 mM 2-nitro-5-thio-sulfobenzoic acid ($NTSB^{2-}$), synthesized from DTNB according to the procedure by Thannhauser et al.[20] The disulfide group content was calculated as the difference between the thiol group content before and after reduction of disulfide bonds with sulfite. From each replicate of each treatment, three measurements were taken.

Fourier Transform Infrared (FTIR) Spectroscopy. FTIR spectra of the steam-exploded samples, dried at 105 °C for 2 h, were obtained from 4000 to 400 cm^{-1} by a Nexus Thermo Nicolet spectrometer. The KBr pellet sampling method was used to prepare the thin film for testing. All sample spectra were recorded at 128 scans and 4 cm^{-1} resolution, and spectra of two replicate measurements for each sample were averaged. The infrared (IR) spectra were acquired and analyzed

dx.doi.org/10.1021/jf405498k | J. Agric. Food Chem. 2014, 62, 2745−2751

using Thermo Scientific OMNIC software package (version 8.2). Spectra were baseline-corrected, smoothed with a nine-point Savitsky–Golay function, and normalized using the amide I absorption intensity peak. Amide I was shown after band narrowing by Fourier self-deconvolution (FSD) to resolve overlapping IR bands using a half bandwidth of 30.0 cm^{-1} and enhancement factor k = 3.0. Second-derivative spectra were obtained to support the initial identification of band positions by deconvolution. The band positions obtained from the above steps were then used as the initial guess for curve-fitting of the original spectra with Gaussian bands. For the final fits, the positions, heights, and widths of all bands were varied simultaneously. The curve-fitting procedure was calculated on Peakfit version 4.12 software (SeaSolve Software, Inc.).

Statistical Analysis. Data are expressed as the mean ± standard deviation (SD). The difference between groups were tested by analysis of variation (ANOVA) and Duncan's multiple range tests (SPSS version 19.0 for Windows, SPSS, Inc., Chicago, IL). Means were compared and considered significant when $p < 0.05$.

RESULTS AND DISCUSSION

Morphological Changes of Feathers Treated by SFE. The effect of SFE on the morphology of feathers was illustrated in Figure 2. SEM of untreated and treated feathers showed

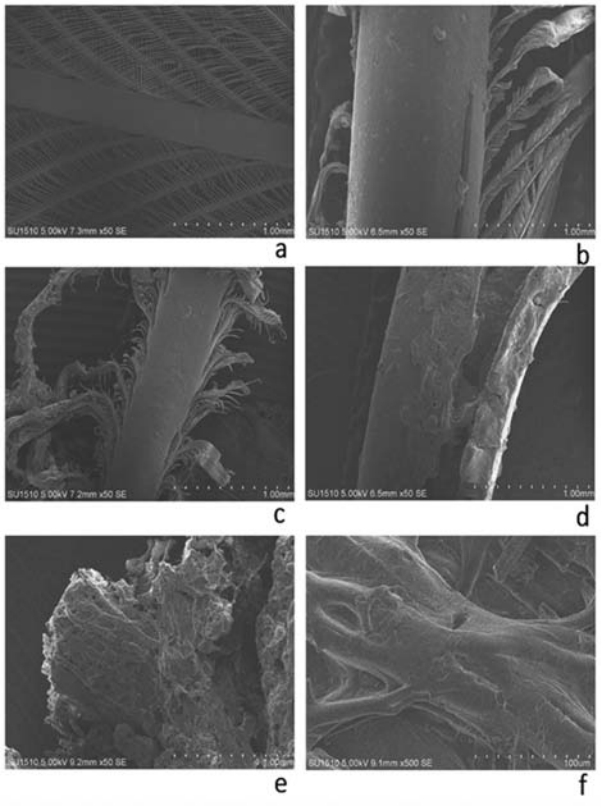

Figure 2. Scanning electron micrographs of untreated and treated feathers by SFE treatment: (a) feather fiber without treatment (50×), (b) steam exploded at 0.5 MPa (50×), (c) steam exploded at 1.0 MPa (50×), (d) steam exploded at 1.4 MPa (50×), (e) steam exploded at 1.8 MPa (50×), and (f) steam exploded at 1.8 MPa (500×).

obvious morphological changes induced by SFE treatment. As shown in Figure 2a, feathers showed a smooth surface and had a hierarchical structure beginning with the level of the central barbs, which grow directly from the quill. These central barbs are tiny "quills" that also grow barbs.[12] At lower steam pressures, feathers showed the regular and compact structure, with shrinkage folds appearing occasionally (panels b and c of Figure 2). As the pressure increased, the central axis of the feather disappeared and the original structure could not be identified. The samples gave cross-interconnected pores, which were sponge-like and had more cracks and cavities (panels d–f of Figure 2).

In SFE treatment, saturated steam with a powerful seepage force penetrates into the fibrous tissues of the materials. The material is maintained at the desired pressure for a short time and undergoes hydrolysis and other chemical processes. At the end of this period, the pressure rapidly decreases to atmosphere and most of the steam in the material will quickly expand. Accordingly, the resulting mechanical effect plays a role in forming the cavities in the surface of feather when the steam rushes out. Yu et al.[14] also demonstrated the mechanical effect of steam explosion through the characterization of the morphological changes of maize stalks in different steam pretreatment methods. We prolonged the time of the feather at 1.8 MPa to 8 min and then carried out SFE, but no additional effect was found on the treatment efficiency, indicating that the mechanical effect played an important role on the exploded feathers.

Protein Solubility and Pepsin Digestibility of Feathers Treated by SFE. Four solvents [0.05 M sodium phosphate buffer (pH 8.0), 0.05 M sodium phosphate buffer (pH 8.0) + 6 M urea, 0.2% potassium hydroxide, and 0.2% pepsin] were used to monitor dissolubility changes of the exploded samples. As shown in Figure 3, the dissolubility of feather meal in all of the

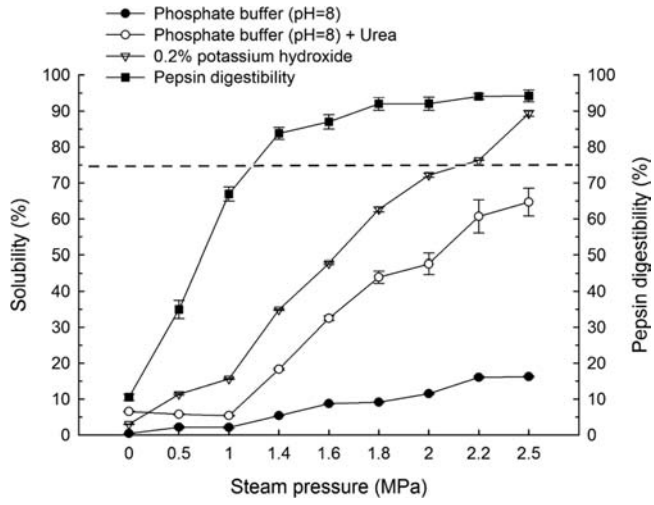

Figure 3. Solubility and pepsin digestibility of feather meal treated by SFE treatment. The dotted line is the minimum digestible protein level recommended as feather meal by the Association of American Feed Control Officials. The data are expressed as the mean ± SD (n = 3).

solvents tested in this study dramatically increased with the increase of steam pressure. The protein solubility in 0.2% potassium hydroxide solution is always the common procedure to evaluate the intensity of treatment.[21] After SFE treatment, the solubility of feather meal could reach 89.3% at 2.5 MPa from only 3.0% in the original sample. The increase may be ascribed to the increasing repulsive forces between surface groups of the exploded sample that mainly exists as the anion form. From the point of view of eco-friendly conversion and utilization of extracted keratins, it is not necessary to use 0.2% potassium hydroxide to extract feather keratins. Figure 3 also

showed that there was 16.2% of the exploded sample soluble in a 0.05 M sodium phosphate (pH 8.0) system and 64.6% of the protein soluble in a 6 M urea system at 2.5 MPa. However, the original feathers are almost insoluble in the above mild solvents. The present work also provides a mild way to extract feather keratin for exploitation of innovative biopolymers.

Feathers are rich in crude protein (90%), while without pretreatment, only 10.5% of feathers could be hydrolyzed by pepsin, because of their intact and compact structures.[4] As shown in Figure 3, pepsin digestibility sharply increased to 91.9% at 1.8 MPa, which was nearly 9 times higher than that of untreated feathers, while it changed not significantly at higher conditions ($p > 0.05$). This result reflects the very high effectiveness of SFE treatment for the improvement of the bioutilization of feather meal. Moreover, only cysteine decreased significantly from 5.07 g/100 g of crude protein for the control to 1.66 g/100 g of crude protein for the exploded sample at 1.8 MPa, while the changes of other amino acids in feather meal were not obvious during SFE treatment (data not shown). Several researchers have employed chemical treatments or screened microorganisms to increase the enzymatic accessibility of feathers.[7,22,23] Obviously, it is not environmentally friendly or requires a long production cycle and tedious preparation. SFE is a physicochemical process, which includes three phases: the steam penetration phase (3−5 s), the boiling phase (1−3 min), and the explosion phase (within 0.00875 s). The total time in high temperatures is very short, and the temperature of materials could decrease to 50 °C or lower immediately after SFE treatment, indicating that SFE treatment is a high-efficiency and environmentally friendly process for production of feather meal.

When steam pressure rose higher than 2.2 MPa, the colors of the samples were dark yellow, indicating degradation and a chemical modification of feather keratin, as demonstrated by Senoz et al.[24] The author suggested that undesired materials formed via cross-linking reactions to provide a high-temperature-resistant nature to the keratin, even when disulfide bonds were broken. In the present work, SFE allowed use of a low steam pressure (1.8 MPa) and short time (1 min) to effectively increase pepsin digestibility of feather meal.

Disulfide Bonds and Free Sulfhydryl of Feathers Treated by SFE. Figure 4 illustrated the quantitative change of the disulfide bond and free SH in feather keratins treated by SFE treatment. Obviously, SFE treatment could significantly decrease the content of the disulfide bond, which is the major factor resistant to proteolytic cleavage. With the increasing severity of the treatment, the disulfide bonds decreased from 330 to 93 nmol mg^{-1}. Because 1 mol of disulfide reacts quantitatively to yield 2 mol of cysteine residues, the free sulfhydryl increase should be accounted for the decreased disulfide cross-linking. However, as shown in Figure 4, the free sulfhydryl significantly ($p < 0.05$) decreased from 10 nmol mg^{-1} for the control to 2 nmol mg^{-1} for the exploded sample (1.0 MPa) and then increased to 31 nmol mg^{-1} at higher steam pressures. Although the sample showed the greatest increase in free sulfhydryl with the greatest decrease in disulfides, the changes were not proportional.

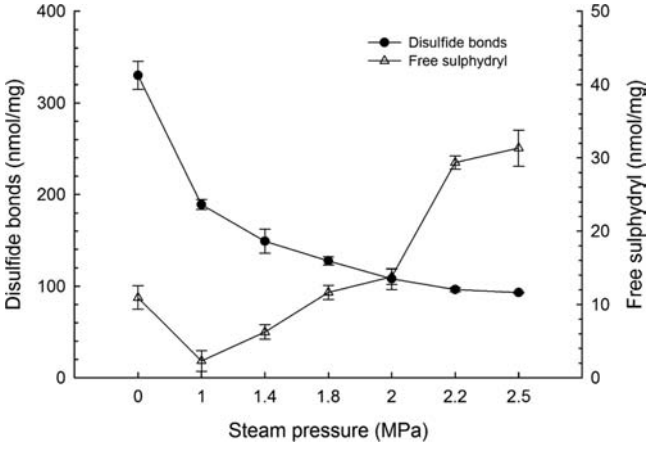

Figure 4. Changes of disulfide bonds and free thiol groups of feather keratins in SFE treatment. The data are expressed as the mean ± SD ($n = 3$).

The decrease in free sulfhydryl content of exploded samples at low pressures and then increases with increasing steam pressures, concomitant with decreases in disulfide bonds, are in general agreement with the findings among extruded samples. These authors showed large reductions in disulfide bond content and slightly increased sulfhydryl content among the extrusion of wheat meal and lentil meal.[25,26] The results indicated that feather keratins containing a high level of cysteine/cystine residues were easily denatured by SFE treatment. It is also likely that some of the free sulfhydryl groups were oxidized to sulfoxyl compounds or formed sulfur-containing volatiles, such as hydrogen sulfide, volatile organic compounds, or flavor compounds, during the process.[27,28] Furthermore, because of the involvement of mechanical force in the explosion phase, cysteine might be more prone to oxidation and then the keratin molecules was susceptible to the extrinsic factors, such as the temperature and humidity.

FTIR Spectroscopy of Feathers Treated by SFE. The secondary molecular structure of feather keratin can be changed under the influence of physicochemical forces, such as mechanical forces or chemical processes.[29] FTIR investigation can be used as an effective tool to assess the structural changes in proteins. Particularly, the amide I band in the range between 1600 and 1700 cm^{-1} and amide II band in the region of 1510 and 1580 cm^{-1} provide useful information. Amide I, the most intense absorption band in proteins, is useful for the analysis of the protein secondary structure and arises mainly from C═O stretching, with a minor contribution from C−N stretching, while the amide II band originates from the N−H bending and C−H stretching vibrations.[30] In Figure 5, the IR spectra of feather keratin are reported. As previously reported[1] and evident from the amide I peak at 1627 cm^{-1}, the feather mainly consists of β-sheet structure. A peak shift of the amide I band was observed as a function of the steam pressure from approximately 1627 cm^{-1} to a strong, broad maximum at approximately 1633 cm^{-1}, which was indicative of decreased amounts of ordered β-sheet structures and the promotion of disordered structures.[1,31]

The amide II band, much less conformationally sensitive than amide I, is related to N−H bending and C−H stretching vibrations. However, it is much more sensitive to the environment of the N−H group. Therefore, the amide II band can be used to deduce changes to the environment of the N−H groups and respond to differences in hydrogen-bonding environments.[32] In general, stronger hydrogen-bonded N−H groups absorb at higher frequencies.[1] In amide II of the steam-exploded samples, it is worth noting a significant decrease in the intensity of the absorption band at 1540 cm^{-1} with respect

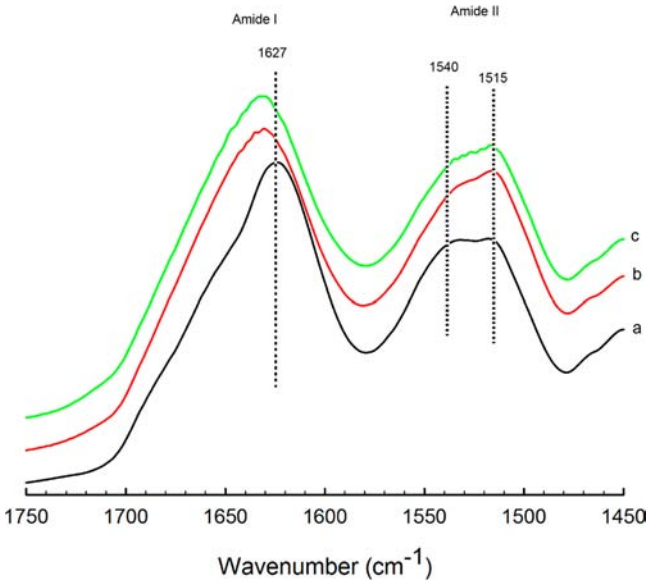

Figure 5. FTIR spectra of (a) feather and samples of the SFE process at (b) 1.0 MPa for 1 min and (c) 2.2 MPa for 1 min. For easier comparison, intensities have been normalized in all spectra. Spectra are offset, and curves are shifted vertically for clarity.

to the component at 1515 cm^{-1}. This means that less hydrogen-bonded peptide groups were contained in the samples resulting from SFE with respect to the original feather, which is in line with the solubility, as shown in Figure 3. Under high temperature and humidity, most of the hydrogen bonds in the feather were broken, as demonstrated by Xu et al.,[33] increasing accessibility of the protein bodies to enzymatic attack.

Effect of Protein Structure Modification on Pepsin Digestibility. A high cystine content (7%) is the most important property that differentiates keratins from other structural proteins, such as collagen and elastin.[34] Feather proteins in their native form are resistant to most proteases when fed to an animal. Thus, destruction of cystines to a certain extent is desirable in production of feather meal. As shown in Figure 6, when steam pressure was below 1.4 MPa, disulfide bonds of feather keratin decreased dramatically and the β-sheet contents changed slightly, with pepsin digestibility increasing

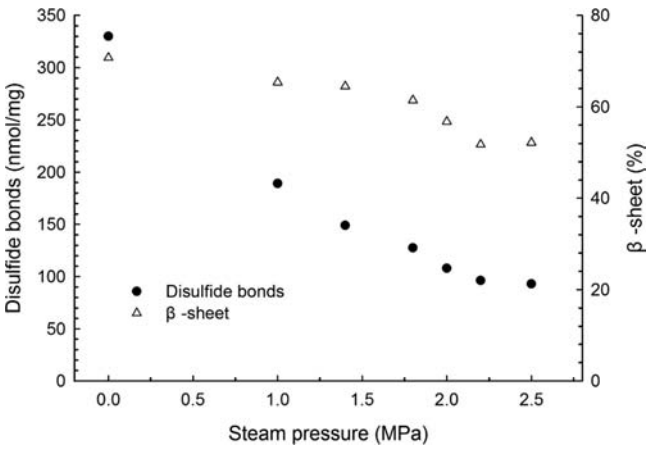

Figure 6. Changes of the relative spectral weights of the β-sheet of feather keratins in SFE treatment.

significantly (83.7%). When the pressure rose higher than 1.4 MPa, β-sheet and disulfide bond contents decreased gradually. Hence, there was a synergistic effect between hydrogen and disulfide bonds on the stability of feather keratin.

Disulfide bonds have the lowest covalent bond energy in proteins, making them the most susceptible for cleavage by thermal effect and mechanical force.[35,36] In the present work, a high negative linear correlation coefficient (R^2 = 0.98) was found between disulfide bond contents of feather keratin and pepsin digestibility, over the full investigated steam pressure range (Figure 7a). Reduction of disulfide bonds caused

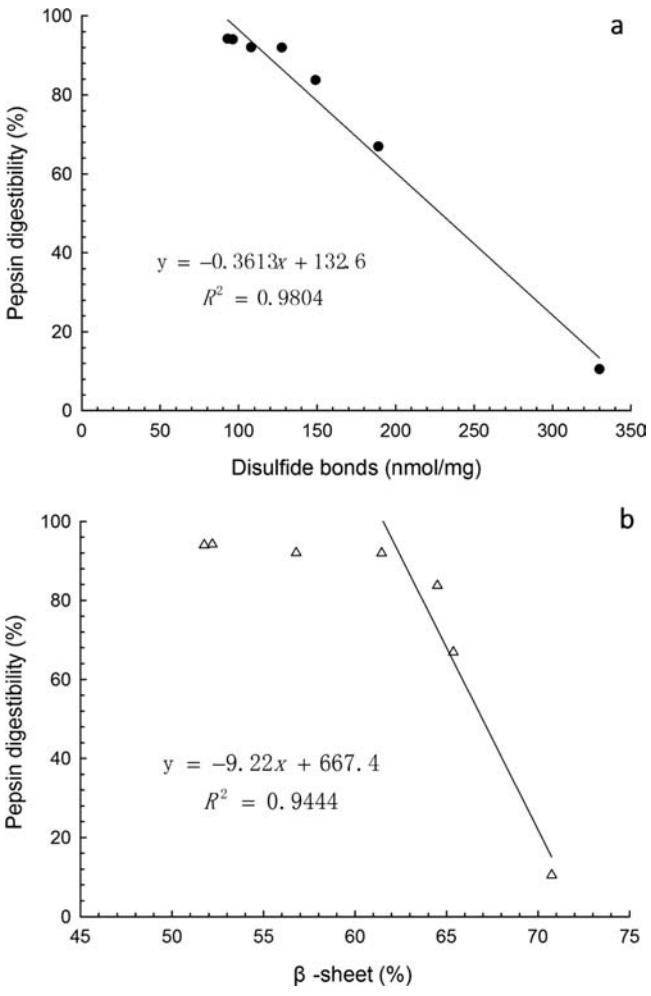

Figure 7. Correlation between pepsin digestibility and (a) disulfide bond content and (b) relative spectral weights of the β-sheet of steam-exploded samples.

disruption of the feather keratin structure and, as a consequence, an enhanced accessibility of sites susceptible to proteolysis. A similar study also found that the degree of hydrolysis by trypsin and pancreatin was strongly correlated to the degree of disulfide reduction of soy flour.[37] In contrast, Figure 7b showed that, at a lower steam pressure, a linear relationship was observed between the relative spectral weights of the β-sheet structures and pepsin digestibility (R^2 = 0.94). As steam pressure increased, the digestibility became independent of the β-sheet contents. The results partly agreed with the findings of Yu et al.,[38] who suggested that the difference in the percentage of protein secondary structure might be responsible for different feed protein digestive behaviors. Obveriously, the

dx.doi.org/10.1021/jf405498k | J. Agric. Food Chem. 2014, 62, 2745−2751

application of heat energy or mechanical energy during SFE breaked hydrogen bonds, which stabilized the β-sheet conformation, and consequently, more protein could disolve in the 6 M urea system (Figure 3). We also observed that a random coil structure was detected among the exploded samples (not shown), suggesting a good amino acid availability from the unordered secondary structure.

SFE equipment with a 5 m^3 chamber has been developed; hence, SFE treatment could be performed on a large scale.[14] Because of the structural features of the catapult explosion mode of SFE, the effective gas deflation passage of the mode has the same area as the cylinder cross-section, which ensures that the deflation time will not be prolonged. Therefore, the treatment efficiency in scale-up applications of SFE can remain consistent with the small equipment. This environmentally friendly technology, requiring little or no chemical input, is a promising route for commercial production of feather meal.

AUTHOR INFORMATION

Corresponding Author

*Telephone/Fax: +86-510-85919150. E-mail: yrj@jiangnan.edu.cn.

Funding

The authors gratefully acknowledge the support by the National Natural Science Foundation of China (31271977).

Notes

The authors declare no competing financial interest.

ABBREVIATIONS USED

SFE, steam flash explosion; SS, disulfide; SH, sulfhydryl; DTNB, 5,5′-dithiobis(2-nitrobenzoic acid); NTSB, 2-nitro-5-thio-sulfobenzoic acid; FTIR, Fourier transform infrared; FSD, Fourier self-deconvolution

REFERENCES

(1) Ullah, A.; Vasanthan, T.; Bressler, D.; Elias, A. L.; Wu, J. Bioplastics from feather quill. *Biomacromolecules* **2011**, *12*, 3826−3832.

(2) Poole, A. J.; Church, J. S.; Huson, M. G. Environmentally sustainable fibers from regenerated protein. *Biomacromolecules* **2009**, *10*, 1−8.

(3) Jin, E.; Reddy, N.; Zhu, Z.; Yang, Y. Graft polymerization of native chicken feathers for thermoplastic applications. *J. Agric. Food Chem.* **2011**, *59*, 1729−1738.

(4) Onifade, A. A.; Al-Sane, N. A.; Al-Musallam, A. A.; Al-Zarban, S. A review: Potentials for biotechnological applications of keratin-degrading microorganisms and their enzymes for nutritional improvement of feathers and other keratins as livestock feed resources. *Bioresour. Technol.* **1998**, *66*, 1−11.

(5) Fraser, R. D.; Parry, D. A. The structural basis of the filament-matrix texture in the avian/reptilian group of hard β-keratins. *J. Struct. Biol.* **2011**, *173*, 391−405.

(6) Daroit, D. J.; Correa, A. P. F.; Brandelli, A. Production of keratinolytic proteases through bioconversion of feather meal by the Amazonian bacterium *Bacillus* sp. P45. *Int. Biodeterior. Biodegrad.* **2011**, *65*, 45−51.

(7) Coward-Kelly, G.; Chang, V. S.; Agbogbo, F. K.; Holtzapple, M. T. Lime treatment of keratinous materials for the generation of highly digestible animal feed: 1. Chicken feathers. *Bioresour. Technol.* **2006**, *97*, 1337−1343.

(8) Martins, V. G.; Costa, J. A. V.; Silveira, S. T.; Brandelli, A.; Prentice, C. Protein and amino acid solubilization using *Bacillus cereus*, *Bacillus velesensis*, and *Chryseobacterium* sp. from chemical extraction protein residue. *Food Bioprocess Technol.* **2011**, *4*, 116−123.

(9) Gong, L.; Huang, L.; Zhang, Y. Effect of steam explosion treatment on barley bran phenolic compounds and antioxidant capacity. *J. Agric. Food Chem.* **2012**, *60*, 7177−7184.

(10) Martin-Sampedro, R.; Capanema, E. A.; Hoeger, I.; Villar, J. C.; Rojas, O. J. Lignin changes after steam explosion and laccase-mediator treatment of eucalyptus wood chips. *J. Agric. Food Chem.* **2011**, *59*, 8761−8769.

(11) Zhang, Y. P.; Yang, R. J.; Zhao, W.; Hua, X.; Zhang, W. B. Application of high density steam flash-explosion in protein extraction of soybean meal. *J. Food Eng.* **2013**, *116*, 430−435.

(12) Zhao, W.; Yang, R. J.; Zhang, Y. Q.; Wu, L. Sustainable and practical utilization of feather keratin by an innovative physicochemical pretreatment: High density steam flash-explosion. *Green Chem.* **2012**, *14*, 3352−3360.

(13) Wang, K.; Jiang, J. X.; Xu, F.; Sun, R. C. Influence of steaming pressure on steam explosion pretreatment of Lespedeza stalks (*Lespedeza cyrtobotrya*). II. Characteristics of degraded lignin. *J. Appl. Polym. Sci.* **2010**, *116*, 1617−1625.

(14) Yu, Z.; Zhang, B.; Yu, F.; Xu, G.; Song, A. A real explosion: The requirement of steam explosion pretreatment. *Bioresour. Technol.* **2012**, *121*, 335−341.

(15) Zhang, Y. Z.; Chen, H. Z. Multiscale modeling of biomass pretreatment for optimization of steam explosion conditions. *Chem. Eng. Sci.* **2012**, *75*, 177−182.

(16) Li, M.; Lee, T. C. Effect of extrusion temperature on solubility and molecular weight distribution of wheat flour proteins. *J. Agric. Food Chem.* **1996**, *44*, 763−768.

(17) Peterson, G. L. A simplification of the protein assay method of Lowry et al. which is more generally applicable. *Anal. Biochem.* **1977**, *83*, 346−356.

(18) AOAC International. *Official Methods of Analysis*, 17th ed.; AOAC International: Gaithersburg, MD, 2000.

(19) Chan, K.; Wasserman, B. P. Direct colorimetric assay of free thiol groups and disulfide bonds in suspensions of solubilized and particulate cereal proteins. *Cereal Chem.* **1993**, *70*, 22−26.

(20) Thannhauser, T. W.; Konishi, Y.; Scheraga, H. A. Analysis for disulfide bonds in peptides and proteins. *Methods Enzymol.* **1987**, *143*, 115−119.

(21) Parsons, C.; Hashimoto, K.; Wedekind, K.; Baker, D. Soybean protein solubility in potassium hydroxide: An in vitro test of in vivo protein quality. *J. Anim. Sci.* **1991**, *69*, 2918.

(22) Mokrejs, P.; Svoboda, P.; Hrncirik, J.; Janacova, D.; Vasek, V. Processing poultry feathers into keratin hydrolysate through alkaline-enzymatic hydrolysis. *Waste Manage. Res.* **2011**, *29*, 260−267.

(23) Rahayu, S.; Syah, D.; Thenawidjaja Suhartono, M. Degradation of keratin by keratinase and disulfide reductase from *Bacillus* sp. MTS of Indonesian origin. *Biocatal. Agric. Biotechnol.* **2012**, *1*, 152−158.

(24) Senoz, E.; Wool, R. P.; McChalicher, C. W. J.; Hong, C. K. Physical and chemical changes in feather keratin during pyrolysis. *Polym. Degrad. Stab.* **2012**, *97*, 297−307.

(25) Li, M.; Lee, T. C. Effect of extrusion temperature on the solubility and molecular weight of lentil bean flour proteins containing low cysteine residues. *J. Agric. Food Chem.* **2000**, *48*, 880−884.

(26) Anderson, A.; Ng, P. Changes in disulfide and sulfhydryl contents and electrophoretic patterns of extruded wheat flour proteins. *Cereal Chem.* **2000**, *77*, 354−359.

(27) Rebello, C.; Schaich, K. Extrusion chemistry of wheat flour proteins: II. Sulfhydryl−disulfide content and protein structural changes. *Cereal Chem.* **1999**, *76*, 756−763.

(28) Zhang, Y.; Chien, M.; Ho, C. T. Comparison of the volatile compounds obtained from thermal degradation of cysteine and glutathione in water. *J. Agric. Food Chem.* **1988**, *36*, 992−996.

(29) Bragulla, H. H.; Homberger, D. G. Structure and functions of keratin proteins in simple, stratified, keratinized and cornified epithelia. *J. Anat.* **2009**, *214*, 516−559.

(30) Jackson, M.; Mantsch, H. H. The use and misuse of FTIR spectroscopy in the determination of protein structure. *Crit. Rev. Biochem. Mol. Biol.* **1995**, *30*, 95−120.

(31) Khurana, R.; Fink, A. L. Do parallel β-helix proteins have a unique Fourier transform infrared spectrum? *Biophys. J.* **2000**, *78*, 994−1000.
(32) Almutawah, A.; Barker, S. A.; Belton, P. S. Hydration of gluten: A dielectric, calorimetric, and Fourier transform infrared study. *Biomacromolecules* **2007**, *8*, 1601−1606.
(33) Xu, W. L.; Ke, G. Z.; Wu, J. H.; Wang, X. G. Modification of wool fiber using steam explosion. *Eur. Polym. J.* **2006**, *42*, 2168−2173.
(34) Kornillowicz-Kowalska, T.; Bohacz, J. Biodegradation of keratin waste: Theory and practical aspects. *Waste Manage.* **2011**, *31*, 1689−1701.
(35) Aslaksen, M. A.; Romarheim, O. H.; Storebakken, T.; Skrede, A. Evaluation of content and digestibility of disulfide bonds and free thiols in unextruded and extruded diets containing fish meal and soybean protein sources. *Anim. Feed Sci. Technol.* **2006**, *128*, 320−330.
(36) Zhu, X.; Jin, Z.; Liu, D. Study on the mechanism of feather keratin extrusion. *J. Chin. Cereals Oils Assoc.* **1998**, *13*, 16−19.
(37) Faris, R. J.; Wang, H.; Wang, T. Improving digestibility of soy flour by reducing disulfide bonds with thioredoxin. *J. Agric. Food Chem.* **2008**, *56*, 7146−7150.
(38) Yu, P. Q.; McKinnon, J. J.; Christensen, C. R.; Christensen, D. A. Using synchrotron-based FTIR microspectroscopy to reveal chemical features of feather protein secondary structure: Comparison with other feed protein sources. *J. Agric. Food Chem.* **2004**, *52*, 7353−7361.

Table 1. Effects of CeO_2 and ZnO Nanoparticles on Sugar Content of Cucumber Fruit[a]

	reducing sugar	nonreducing sugar	total sugar	starch
control	3.72 ± 0.27ab	23.3 ± 3.00b	27.0 ± 2.73b	70.9 ± 11.3b
CeO_2 400 mg/kg	3.11 ± 0.34b	8.31 ± 0.96c	11.4 ± 1.09c	90.7 ± 5.9 ab
CeO_2 800 mg/kg	5.35 ± 0.56a	37.2 ± 4.05a	42.5 ± 4.39a	90.6 ± 4.5ab
ZnO 400 mg/kg	4.98 ± 0.64ab	33.9 ± 2.41ab	38.9 ± 3.04ab	110.8 ± 2.6a
ZnO 800 mg/kg	4.50 ± 0.42ab	30.4 ± 0.74ab	34.9 ± 0.96ab	81.0 ± 2.9b

[a]Data are average of four replicates ± standard deviation.

showed the first evidence that fullerol greatly increased bitter melon water content and fruit yield and improved fruit quality by increasing the phytomedicine content.[12] Servin et al. reported an increase in phosphorus and potassium concentration in cucumber fruit of plants exposed to 750 mg/kg of TiO_2 NPs.[13] In addition, Rico et al. reported that CeO_2 at 500 mg/kg soil modified the quality of rice grains.[14]

Cucumber is one of the very low calorie vegetables. In addition it contains many nutrient elements, including Ca, Fe, Mg, P, K, Na, Mn, S, and Zn. According to USDA National Nutrient Database, 100 g of fresh cucumber provides as much as 147 mg of K, which is an important intracellular electrolyte.[15] In addition, cucumber contains phenolic compounds (*p*-coumaric, caffeic, and ferulic acids and *p*-coumaric acid methyl ester), and those compounds act as protective scavengers against oxygen-derived free radicals and reactive oxygen species (ROS) that play a role in cardiovascular disease prevention and anticancer activity.[16−18] The aim of this study was to study the effect of ZnO and CeO_2 NPs on the nutritional quality of cucumber fruit. Carbohydrates, proteins, antioxidants, and mineral nutrient were analyzed by using several biochemical and spectroscopic techniques.

MATERIALS AND METHODS

Characterization of NPs. The CeO_2 and ZnO NPs (Meliorum Technologies, NY, U.S.) used in this study were obtained from the University of California Center for Environmental Implications of Nanotechnology. According to the supplier, the primary size for those two NPs is 10 nm. The characterization of both NPs, including hydrodynamic size, ζ-potential, and pH, were previously reported by Keller et al.[5] Stock solutions were prepared by adding 1000 mg of nanoparticles to 1.0 L of deionized water. The dispersed nanoparticles were sonicated for 30 min in a water bath and immediately applied to the substrate.

Experimental Design and Growth Conditions. CeO_2 NPs and ZnO NPs were used, separately, at 400 and 800 mg/kg. Pots containing substrate without the addition of NPs were included as a control. Each treatment had four replicate (pots), and each pot contained two plants. More details regarding the experimental design, soil, and greenhouse conditions were introduced in previous a study.[11]

Mineral Content. Dried cucumber fruits were ground to pass a 40-mesh screen (0.425 mm) with a stainless Wiley mill (Thomas Scientific, Swedesboro, NJ). Subsequently, the samples were digested with a mixture of H_2O_2 and plasma pure HNO_3 (v/v: 4:1) using microwave oven (CEM Corp, Mathews, NC, U.S.).[14] The standard reference materials NIST 1547 and 1570a were also digested and analyzed as samples. The recoveries for all elements were between 90 and 99%. The macro- and micronutrient elements were analyzed using inductively coupled plasma optical emission spectrometry (Perkin-Elmer Optima 4300 DV).

Determination of Total Soluble and Reducing Sugars. The total soluble sugars were extracted by the method of Verma and Dubey.[19] One hundred grams of dried cucumber tissue was ground in 10 mL of 80% ethanol and then boiled (80 °C) in a water bath for 30 min. After cooling to room temperature, the extracts were centrifuged at 22000*g* (Thermo Scientific, Soruall T1, U.S.) for 20 min. The extraction was repeated three times, and all the supernatants were combined. Total soluble sugar content was measured following the method of Dubois et al.[20] while reducing sugar content was determined according to the procedure of Nelson-Somogyi.[21] The nonreducing sugar content was reported as the difference between total and reducing sugars.

Determination of Starch in Fruit. The starch extraction was performed following the method of Verma and Dubey.[19] The residue from sugar extraction was dried at 80 °C for 24 h. To the dried residue was added 2 mL of DI water, and the mixture was boiled in a water bath for 15 min. The suspension was cooled to room temperature, and 2 mL of concentrated H_2SO_4 was added. The suspension was stirred for 15 min, and the final volume was adjusted to 10 mL using water. The supernatant was centrifuged at 3000*g* for 20 min, and the extraction was repeated using 50% H_2SO_4. The supernatants were combined and diluted with water to the 50 mL mark. The starch content was quantified following the method of Dubois et al.[20]

Protein Fractionation. Protein extraction and fractionation was conducted according to Chen and Bushak.[22] Dried cucumber fruit (500 mg) was extracted sequentially with 8 mL each of water, 0.5 mol/L NaCl, 70% ethanol, and 0.05 M acetic acid. The extracted protein in each step was labeled as albumin, globulin, prolamin, and glutelin fractions, respectively. The protein content was quantified by the Bradford method.[23]

Total Phenolics and Total Flavonoids. Total phenolic content was determined by the spectrophotometric method followed by Dewanto et al.[24] At room temperature, Folin−Ciocalteu phenol reagent (0.2 mL) was added to each sample (0.1 mL). After 1 min, 3 mL of 5% Na_2CO_3 solution was added to the mixture and the mixture was allowed to stand for 1 h in a dark place. The absorbance was measured at 760 nm using a Perkin-Elmer Lambda 14 UV/Vis Spectrometer (single-beam mode, Perkin-Elmer, Uberlinger, Germany). Total phenolic contents of the sample were expressed on a fresh weight basis as mg of gallic acid equivalent (GAE) g^{-1}.

Total flavonoid content of cucumber fruit was measured using the method of Jia et al.[25] Briefly, to 500 μL of each sample was added 75 μL of 5% $NaNO_2$. After 5 min, to the mixture were sequentially added 150 μL 10% $AlCl_3$, 500 μL 1 M NaOH, and 275 μL of DI water. The absorbance was measured at 510 nm using a spectrophotometer. The total flavonoid content was expressed as catechin equivalents.

Fourier Transform Infrared (FTIR) Spectra Acquisition. The dried cucumber fruits were ground, and the powder was analyzed using FTIR spectroscopy (Perkin-Elmer, Spectrum 100, Universal ATR Sampling Accessory) in a range of 650−3950 cm^{-1}. The second derivative spectrum was collected using Spectrum software (Version 6.0.2.0025, Perkin-Elmer, Shelton, CT). A total of 3 replicates per treatment were used for the analysis.

μ-XRF Analysis. Fruits were carefully washed with DI water to eliminate any surface contaminants. Then, they were transversally cut and frozen in liquid nitrogen for 30 min. The samples were fixed with Tissue Tek (Sakura Finetek USA, Torrance, CA) and sectioned with a cryomicrotome (Triangle Biomedical Sciences, Durham, NC) at −20 °C to a thickness of 30 μm. Subsequently, the samples were mounted onto Kapton tape and freeze-dried for 1 h in a Labconco freeze-dryer (FreeZone 4.5, Kansas City, MO) with operating conditions of −53 °C and 0.140 mBar pressure.

X-ray fluorescence imaging was obtained at beamline 10-2 at the Stanford Synchrotron Radiation Lightsource (Menlo Park, CA). Standard operating conditions were 3 GeV beam energy and 80−

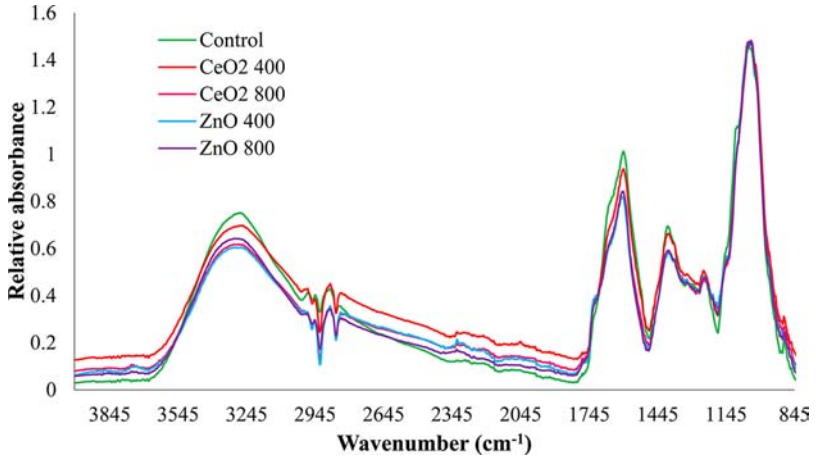

Figure 1. FTIR spectra of cucumber fruit treated with 0, 400, and 800 mg/kg ZnO NPs and 400 and 800 mg/kg CeO_2 NPs. Spectra are means of three replicates.

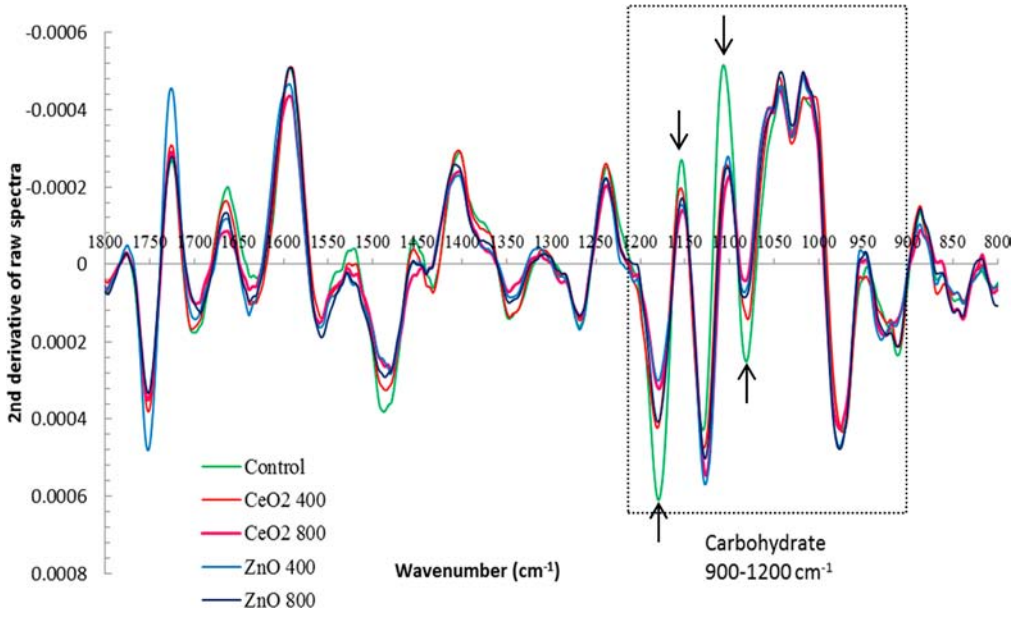

Figure 2. Second derivative of FTIR band in the region of 800−1800 cm^{-1}.

100 mA beam current. Incident X-ray energy was set to 10 keV, and a Si (111) monochromator was used. SMAK[27] software was used for data analyses.

Data Analysis. The treatments from two NPs at two concentrations and four replicate/treatments were allocated in a completely random design. All data including sugars, starch, protein, mineral nutrients, and antioxidant were analyzed by using PROC GLM in SAS software (Version 9.1.3, SAS Institute, Cary, NC).

RESULTS AND DISCUSSION

Effects of NPs on Fruit Carbohydrates (Sugar and Starch) Content. Sugars, starches, and fiber are main components of carbohydrates in cucumber fruit. Among them, "soluble sugars and starch are important parameters to evaluate the quality of fruits."[26,27] As shown in Table 1, reducing sugars (glucose and fructose) were not modified by CeO_2 NPs. This implies that the sweet taste of cucumber fruit was not affected. However, the nonreducing sugar (sucrose) was impacted by CeO_2 NPs. At 400 mg/kg treatment, the content of nonreducing sugars was significantly decreased compared to control, while at 800 mg/kg, the nonreducing sugars content was significantly increased, compared to control. Typically, sugars are a source of carbon and energy.[28] On the other hand, sugars such as glucose, fructose, and sucrose also act as signaling molecules in plant responses under biotic and abiotic stresses.[29,30] Among them, sucrose contributes to stress-related responses.[31] It has been reported that some of the defense-related genes were upregulated in rice leaves when sucrose was fed to the roots.[32] In this study, the upregulation of sucrose by CeO_2 NPs was a possible indicator of stress.

In contrast, ZnO NPs at both concentrations did not impact the reducing and nonreducing sugar contents (Table 1). Leaves are plant's main photosynthetic organs. Sugar and starch are synthesized in the chloroplasts of leaves and are translocated from leaves to fruits. Previous studies reported that reduced photosynthetic rate led to a decrease in the concentration of soluble sugars, and often starch accumulation in leaves.[33] In our study, the photosynthetic rate in leaves was not decreased by ZnO NPs.[11] This explained well that ZnO NPs did not change the carbohydrate composition in fruit.

dx.doi.org/10.1021/jf405476u | J. Agric. Food Chem. 2014, 62, 2752−2759

Table 2. Effect of CeO_2 and ZnO NPs on Protein Fractionation and Antioxidant Content of Cucumber Fruit[a]

	albumin	globulin	prolamin	glutelin	phenolic	flavonoid
control	2.32 ± 0.83 a	0.75 ± 0.11 b	2.50 ± 0.15 a	0.20 ± 0.03 b	0.689 ± 0.027 a	0.537 ± 0.056 a
CeO_2 400 mg/kg	6.82 ± 0.91 a	1.32 ± 0.17 a	2.61 ± 0.54 a	0.07 ± 0.02 c	0.662 ± 0.041 ab	0.596 ± 0.076 a
CeO_2 800 mg/kg	5.31 ± 1.61 a	0.44 ± 0.07 b	2.84 ± 0.11 a	0.25 ± 0.00 b	0.517 ± 0.043 b	0.403 ± 0.047 a
ZnO 400 mg/kg	5.68 ± 0.74 a	1.28 ± 0.08 a	3.57 ± 0.15 a	0.18 ± 0.04 bc	0.557 ± 0.026 ab	0.505 ± 0.003 a
ZnO 800 mg/kg	4.93 ± 0.47 a	0.86 ± 0.04 ab	3.68 ± 0.21 a	0.39 ± 0.01 a	0.582 ± 0.016 ab	0.426 ± 0.003 a

[a]Data are average of four replicates ± standard deviation.

Table 3. Effect of CeO_2 and ZnO Nanoparticle on Mineral Content of Cucumber Fruit (mg/kg)[a]

	K	Ca	Mg	S	P	Na	Fe	Cu	Mn	Mo	Zn
control	60224 a	7249 a	3349 c	3443 a	1136 a	589 a	12.7 a	62.6 a	25.2 b	22.9 a	36.1 c
CeO_2 400 mg/kg	64018 a	8907 a	3934 ab	3538 a	1174 a	580 a	14.6 a	60.5 a	28.1 ab	5.48 c	38.3 c
CeO_2 800 mg/kg	58837 a	8436 a	3452 c	3260 a	1134 a	522 a	9.34 a	57.3 ab	24.4 b	9.93 bc	37.7 c
ZnO 400 mg/kg	60225 a	6900 a	3956 a	3344 a	1087 a	527 a	14.6 a	47.2 c	32.0 a	13.8 b	61.3 b
ZnO 800 mg/kg	56533 a	6988 a	3583 bc	3481 a	1059 a	544 a	6.41 a	50.7 bc	27.1 b	10.7 bc	89.1 a

[a]Data are average of four replicates ± standard deviation.

Starch is another important carbohydrate in fruits. From Table 1, it seems that all NP treatments increased the starch content compared to control, but only at 400 mg/kg ZnO NPs, the difference was significantly increased. Previous reports showed that copper stress induced the overaccumulation of starch and sucrose in cucumber plants.[34] Another report indicates that salinity stress stimulated the starch accumulation in chloroplasts and resulted in increased accumulation of starch and total sugars in *Thellungiella halophile* leaves.[35] This could indicate that starch and sucrose increased in cucumber fruit as a result of stress caused by the NPs.

FTIR Analysis. As a rapid and noninvasive tool, Fourier transform infrared spectroscopy is used to identify changes in functional groups in plant tissues. FTIR spectra of cucumber fruit from plants treated with CeO_2 and ZnO NPs are shown in Figure 1. As seen in this figure, the band area of the carbohydrate region (900−1200 cm^{-1}) was reduced by all NP treatments, compared with the control. Furthermore, the difference between NP treatments and control can be seen in the lignin area (1635 cm^{-1}). The data also showed band differences in control and NP treated plants in the lipid region located between 2840 and 2960 cm^{-1}. In this region, control and 400 mg/kg CeO_2 NP treatments were similar; however, the 800 mg/kg CeO_2 NP treatment and both ZnO NP concentrations reduced this band area. In addition, it was observed that the band areas at 1350−1420 cm^{-1} and 1520−1650 cm^{-1} decreased in all NP treatments. The spectrum at 400 mg/kg CeO_2 NPs was similar to that of the control, while those of the other three treatments were apparently lower than that of the control.

For a better understanding of the fingerprint of carbohydrates, second derivatives of spectra were collected at the 800−1800 cm^{-1} region. The plots of the second derivative spectra are shown in Figure 2. Carbohydrates (glucose, fructose, and sucrose) showed intense characteristic bands in the fingerprint region (900−1400 cm^{-1}).[36,37] It is clear from the spectra that the bands at 1181, 1153, 1106, and 1083 cm^{-1} were lower in the NP treatments, compared to control. According to Duarte et al.,[37] spots 1153 and 1083 cm^{-1} are related to sucrose while 1108 cm^{-1} corresponds to fructose and glucose. Although it is difficult to quantify based on those bands, the spectra revealed that NPs changed the carbohydrate pattern in cucumber fruit.

Effects of NPs on Fruit Protein Fractions and Antioxidant Content. Although cucumber is a low protein vegetable, protein is an important factor contributing to the sweet taste of cucumber fruit.[38] The effect of ZnO and CeO_2 NPs on the four soluble protein fractions is presented in Table 2. Generally, albumin and prolamin fractions are the predominant proteins in cucumber fruit, which represents 84%−92% of the fruit protein. Globulin and glutelin fractions are present to a lesser extent. Results showed that neither CeO_2 nor ZnO NPs significantly affected albumin and prolamin fractions. However, compared to control, globulin content was significantly increased by CeO_2 NPs at 400 mg/kg treatment. Glutelin content was also significantly decreased by CeO_2 NPs at 400 mg/kg. Those results indicated that CeO_2 NPs at 400 mg/kg changed the protein content in fruit. CeO_2 NPs at 800 mg/kg did not affect any of the protein fractions. More studies are needed in order to explain the different response at 400 and 800 mg/kg treatments. ZnO NPs at 400 mg/kg treatment increased globulin content while those at 800 mg/kg treatment increased glutelin content. Du et al. reported that salt stress increased the soluble protein content of cucumber seedlings.[39] Several proteins such as heat shock protein, catalase, and glutathione *S*-transferase are related to stress response.[40] Those proteins were upregulated under abiotic or biotic stress. It is possible that protein increased as a response to NP induced stress.

Phenolic compounds including flavonoids and phenolic acids are the most frequently examined group of antioxidants, and they are highly correlated with the total antioxidant activity.[41,42] This is an important trait in cucumber because phenolic compounds haven been associated with a reduction in breast and prostate cancer risks.[43] As shown in Table 2, none of the CeO_2 and ZnO concentrations impacted flavonoid content. However, CeO_2 NPs at 800 mg/kg significantly decreased the phenolic content. As a result of this treatment there was an increase in total sugar content but a decrease in phenolic content. This indicates that, at this concentration, CeO_2 NP impacted the nutritional quality of the fruit.

Effects of NPs on the Fruit Mineral Composition. The uptake of nutrients by plant roots is affected by abiotic and biotic stressors including soil composition, cation exchange capacity, pH of the soil solution, microorganisms, and metal immobilization in root cell walls, among others.[44,45] Cucumber

dx.doi.org/10.1021/jf405476u | J. Agric. Food Chem. 2014, 62, 2752−2759

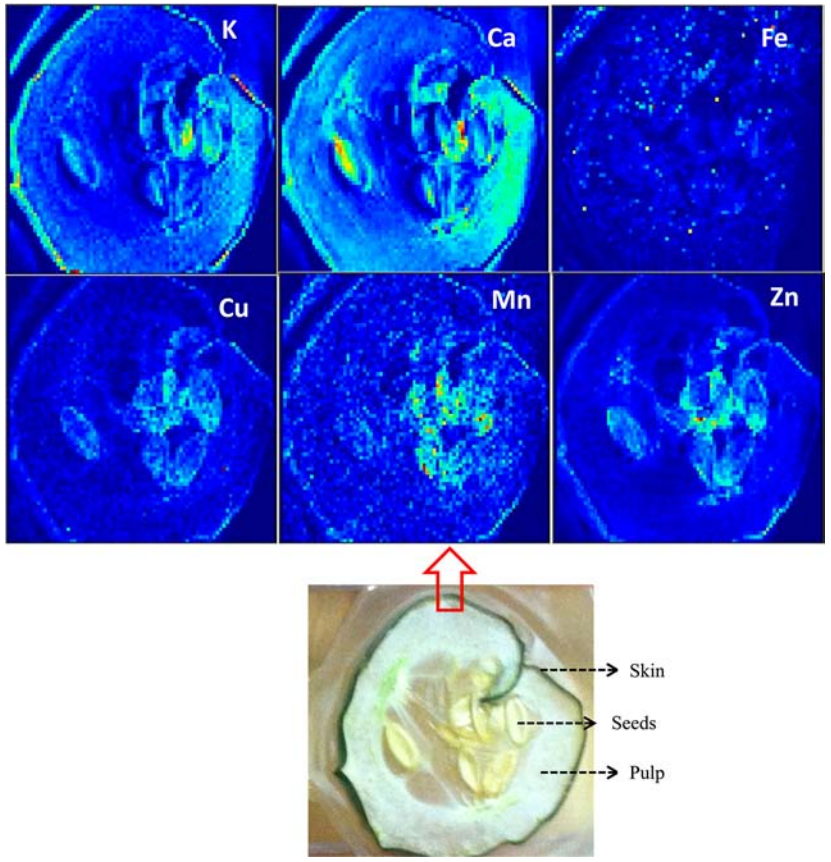

Figure 3. μ-XRF temperature map from a cross cut cucumber fruit showing normalized K, Ca, Fe, Cu, Mn, and Zn intensities. The image corresponds to control fruit. Red represents higher intensity, and dark blue represents the absence of the element.

is a source of vitamins, potassium, magnesium, and phosphorus required for human nutrition.[46] The influence of both the CeO_2 and ZnO NPs on the cucumber fruit mineral content is shown in Table 3. As seen in this table, from all macronutrients analyzed, only Mg showed significant differences in the NP treated plants. At 400 mg/kg, both the CeO_2 and ZnO NPs increased Mg in cucumber fruit by 17% and 18%, respectively ($p \leq 0.05$). Magnesium is an essential element for human health. It is obtained from foods and concentrates in bones and muscle.[47] Magnesium participates in multiple functions including energy production, protein synthesis, cell membranes and chromosomes, ion transport across cell membrane, and cell migration and interacts with protein, fiber, vitamin D, calcium, and zinc.[48] Magnesium is essential in plants as it is the core of the chlorophyll molecule. Mg^{2+} enters the root cortex cells through the apoplast.[49] However, it is not clear how Mg^{2+} enters the symplast and then the xylem apoplast.[50] To this end, we cannot explain why the CeO_2 NPs increased Mg translocation to cucumber fruit. However, other NPs like CuO NPs have been found to increase the production of indole-3-acetic acid in bacteria,[51] and this growth hormone induces the expression of two aquaporins in tomato (*Lycopersicon esculentum* Mill.). Magnesium has been found to be transported through the *rca* channel in wheat root.[52] Thus, it is possible that the CeO_2 NPs promote the expression of aquaporins or other channels, like the MRS2, which is Mg^{2+} transporter to the shoot, enhancing Mg^{2+} uptake.[53]

CeO_2 and ZnO NPs changed the fruit profile of micronutrients Cu, Mo, Mn, and Zn. As expected, Zn was increased at both ZnO NP concentrations. Previous reports have shown that ZnO NPs at 200 mg/kg soil and above increased the concentration of Zn in roots and shoots of corn plants.[54] At all concentrations, both the CeO_2 and ZnO NPs significantly reduced molybdenum concentration in cucumber fruit (Table 3). Reductions were in the range of 57 to 76% for CeO_2 NPs and about 40 to 53% for the ZnO NP treatments. Previous studies have shown that Mo is taken up by plants as MoO_4^{2-}.[55] Reports indicate that Mo uptake is reduced by sulfate and increased by phosphate.[56] In addition, previous work with alfalfa showed that Mo is complexed with malate.[55] As shown in Table 3, P and S were at the same levels in control and NP treated plants; thus, we cannot conclude about the role of P or S in Mo uptake. Perhaps the NPs altered the production of organic acids like citrate or malate, and then, they reduced Mo uptake. Studies about the effects of CeO_2 and ZnO NPs on organic acid production are currently being performed in order to explain the uptake of some micronutrients. The reduction in Mo in CeO_2 and ZnO NPs treated cucumber might not represent a concern to human health as it has been documented that most people in the U.S. consume more than sufficient amounts of this trace mineral in their diets.[48]

Manganese was increased by ZnO NPs at 400 mg/kg. A previous study showed that 34% of Zn/ZnO NPs was bound to Mn−Fe oxides.[57] At this time we cannot explain why this could increase Mn uptake. Additionally, we do not know the effect ZnO NPs produce in Nramp transporters, which are associated with Mn uptake by plants.[58] The increase of Mn in ZnO NPs treatment might not represent a health concern especially in diets that include the consumption of foods high in phytic acid (beans, seeds, nuts, whole grains, and soy products), oxalic acid

Table 4. Comparison of Effects of CeO_2 NPs and ZnO NPs on Cucumber Fruit Quality[a]

	soluble sugar	starch	protein fractionation	phenolic	flavonoid	mineral
CeO_2 NPs 400 mg/kg	−		globulin +; glutelin −			Mg +, Mo −
CeO_2 NPs 800 mg/kg	+			−		Mo −
ZnO NPs 400 mg/kg		+	globulin +			Mg, Mn +; Cu, Mo −
ZnO NPs 800 mg/kg			glutelin +			Cu, Mo −

[a]+ means positive impact; − means negative impact; blank means no impact.

(spinach, cabbage, and sweet potatoes), and tannins (tea), compounds that might slightly inhibit manganese absorption. Intake of minerals including iron, calcium, and phosphorus have been found to limit retention of manganese.[48]

Copper was also reduced by ZnO NPs. Previous studies have shown that ZnO NPs dissociate releasing Zn ions into the medium,[59] and according to Alloway, Zn decreases the uptake of Cu because both metals are taken up by the same transporter.[60] Some experts propose that Cu deficiency rather than excess Cu increases the risk of cardiovascular diseases.[48] More studies are needed in order to understand the effects of CeO_2 and ZnO NPs at the root surface interface and their effect on nutrient uptake by plants.

Micro-XRF Analysis of Mineral Localization in Cucumber Fruit. ICP-OES data only reflect total mineral concentration in cucumber fruit. In order to detect whether NPs altered the mineral distribution pattern, the μ-XRF technique was applied. Because of the limited beam time, only two macronutrients Ca and K and four micronutrients including Fe, Cu, Mn, and Zn were analyzed. The mineral distribution between CeO_2 treated and control plants was very similar. This indicates that CeO_2 NPs did not change the nutrient element distribution in cucumber plant. The micro-XRF intensity map of the cucumber fruit cross-section is shown in Figure 3. In general, K and Ca were localized in skin, pulp, and seeds, while iron was almost evenly distributed in the whole cross section. Figure 3 also shows that Cu, Zn, and Mn were more concentrated in seeds and at lower concentration in the skin.

As revealed by ICP-OES results, Cu concentration was reduced by ZnO NPs. Furthermore, μ-XRF results indicate that Cu is mainly present in cucumber seeds (Figure 3). Therefore, the next generation could also be impacted. Cu is an essential element for plant growth because they participate in many important physiological processes such as photosynthesis and respiration.[61] It has been reported that soaking seeds in Cu sulfate solution may enhance plant growth and development and, even, improve the nutritional quality of fruit.[62] Thus, a reduction in Cu in cucumber seeds suggests that ZnO NPs may have a negative impact on the growth of next plant generation. More studies are needed in order to solve this knowledge gap.

Conclusions. In summary, at the concentration tested, the ZnO NPs did not show negative impact on carbohydrate, protein, and antioxidant contents compared to control. To some extent, ZnO NPs increased starch and protein content, which might result in an increased caloric value of a food that is typically characterized by its low caloric content. However, it is not clear if the increased starch and protein contents are indicators of stress induced by ZnO NPs. Both ZnO NP treatments significantly decreased the concentration of the micronutrients Cu and Mo. Since both Cu and Mo are important minerals in plant tissues and participate in many processes, the quality of fruit in the next generation of cucumber plants may be impacted.

CeO_2 NPs not only decreased Mo concentration, they also altered the nonreducing sugars and phenolic content and they also changed the fractionation of proteins (Table 4). This suggests that CeO_2 NPs impacted the fruit flavor and reduced the antioxidant capacity. Furthermore, as previously reported,[11] the fruits were grouped by size as large, medium, and small and the total weight of each group was recorded. The fresh weight of large cucumbers was reduced by 31.4% by CeO_2 NPs at 800 mg/kg (Table S1 in the Supporting Information). More studies have to be performed in order to determine the effects of NPs on other parameters such as lignin and pectin that can influence fruit weight. The above-mentioned results suggest that, at the concentration tested, both CeO_2 and ZnO NPs impacted the nutritional quality of cucumber.

■ ASSOCIATED CONTENT

Supporting Information

Table providing average weight of large, medium, and small cucumber fruits harvested from plants grown in CeO_2 NP amended soil. This material is available free of charge via the Internet at http://pubs.acs.org.

■ AUTHOR INFORMATION

Corresponding Author

*E-mail: jgardea@utep.edu. Phone: 915-747-5359. Fax: (915) 747-5748.

Funding

This material is based upon work supported by the National Science Foundation and the Environmental Protection Agency under Cooperative Agreement Number DBI-0830117. The authors also acknowledge USDA Grant No. 2011-38422-30835 and NSF Grant No. CHE-0840525. J.L.G.-T. acknowledges the Dudley family for the Endowed Research Professorship and the Academy of Applied Science/US Army Research Office, Research and Engineering Apprenticeship program (REAP) at UTEP, Grant No. W11NF-10-2-0076, Subgrant 13-7.

Notes

The authors declare no competing financial interest.

■ ACKNOWLEDGMENTS

Any opinions, findings, and conclusions or recommendations expressed in this material are those of the authors and do not necessarily reflect the views of the National Science Foundation or the Environmental Protection Agency. This work has not been subjected to EPA review and no official endorsement should be inferred.

■ REFERENCES

(1) Rico, C. M.; Majumdar, S.; Duarte-Gardea, M.; Peralta-Videa, J. R.; Gardea-Torresdey, J. L. Interaction of nanoparticles with edible plants and their possible implications in the food chain. *J. Agric. Food Chem.* **2011**, *59*, 3485−3498.

(2) Priester, J. H.; Ge, Y.; Mielke, R. E.; Horst, A. M.; Cole Moritz, S.; Espinosa, K.; Gelb, J.; Walker, S. L.; Nisbet, R. M.; Schimel, J. P.;

Palmer, R. G.; Hernandez-Viezcas, J. A.; Zhao, L.; Gardea-Torresdey, J. L.; Holden, P. A. Soybean susceptibility to manufactured nanomaterials with evidence for food quality and soil fertility interruption. *Proc. Natl. Acad. Sci. U.S.A.* **2012**, *109*, 2451−2456.

(3) Hong, J.; Peralta-Videa, J. R.; Gardea-Torresdey, J. L. Nanomaterials in agricultural production: benefits and possible threats? In *Sustainable Nanotechnology and the Environment: Advances and Achievements*; Sharma, V., Shamin, A. N., Eds.; ACS Symposium Series; American Chemical Society: Washington, DC, 2013; Vol. *1124*, pp 73−90.

(4) Diatloff, E.; Smith, F. W.; Asher, C. J. Effects of lanthanum and cerium on the growth and mineral nutrition of corn and mungbean. *Ann. Bot.* **2008**, *101*, 971−982.

(5) Keller, A. A.; Wang, H.; Zhou, D.; Lenihan, H. S.; Cherr, G.; Cardinale, B. J.; Miller, R.; Ji, Z. Stability and aggregation of metal oxide nanoparticles in natural aqueous matrices. *Environ. Sci. Technol.* **2010**, *344*, 1962−1967.

(6) Schwabe, F.; Schulin, R.; Limbach, L. K.; Stark, W.; Burge, D. Influence of two types of organic matter on interaction of CeO_2 nanoparticles with plants in hydroponic culture. *Chemosphere* **2013**, *91*, 512−520.

(7) Zhang, P.; Ma, Y.; Zhang, Z.; He, X.; Zhang, J.; Guo, Z.; Tai, R.; Zhao, Y.; Chai, Z. Biotransformation of ceria nanoparticles in cucumber plants. *ACS Nano* **2012**, *6*, 9943−9950.

(8) Wang, Q.; Ma, X.; Zhang, W.; Pei, H.; Chen, Y. The impact of cerium oxide nanoparticles on tomato (*Solanum lycopersicum* L.) and its implications for food safety. *Metallomics* **2012**, *4*, 1105−1112.

(9) Wang, Q.; Ebbs, S. D.; Chen, Y.; Ma, X. Trans-generational impact of cerium oxide nanoparticles on tomato plants. *Metallomics* **2013**, *5*, 753−759.

(10) Hernandez-Viezcas, J. A.; Castillo- Michel, H.; Andrews, J. C.; Cotte, M.; Rico, C. M.; Peralta-Videa, J. R.; Priester, J. H.; Holden, P. A.; Gardea-Torresdey, J. L. *In situ* synchrotron fluorescence mapping and coordination of CeO_2 and ZnO nanoparticles in soil cultivated soybean (*Glycine max*). *ACS Nano* **2013**, *26*, 1415−1423.

(11) Zhao, L.; Sun, Y.; Hernandez-Viezcas, J. A.; Servin, A.; Hong, J.; Niu, G.; Peralta-Videa, J. R.; Duarte-Gardea, M.; Gardea-Torresdey, J. L. Influence of CeO_2 and ZnO nanoparticles on cucumber physiological markers and bioaccumulation of Ce and Zn: A life cycle study. *J. Agric. Food Chem.* **2014**, *61*, 11945−11951.

(12) Kole, C.; Kole, P.; Randunu, K. M.; Choudhary, P.; Podila, R.; Ke, P. C.; Rao, A. M.; Marcus, R. K. Nanobiotechnology can boost crop production and quality: first evidence from increased plant biomass, fruit yield and phytomedicine content in bitter melon (*Momordica charantia*). *BMC Biotechnol.* **2013**, *13*, 37 DOI: 10.1186/1472-6750-13-37.

(13) Servin, A. D.; Morales, M. I.; Castillo-Michel, H.; Hernadez-Viezcas, J. A.; Munoz, B.; Zhao, L.; Nunez, J. E.; Peralta-Videa, J. R.; Gardea-Torresdey, J. L. Synchrotron verification of TiO_2 accumulation in cucumber fruit: A possible pathway of TiO_2 nanoparticle transfer from soil into the food chain. *Environ. Sci. Technol.* **2013**, *47*, 11592−11598.

(14) Rico, C.; Morales, M.; Barrios, A.; McCreary, R.; Hong, J.; Lee, W.; Nunez, J.; Peralta-Videa, J.; Gardea-Torresdey, J. L. Effect of cerium oxide nanoparticles on the quality of rice (*Oryza sativa* L.) grains. *J. Agric. Food Chem.* **2013**, *61*, 11278−11285.

(15) *USDA National Nutrient Data Base* (http://www.fns.usda.gov).

(16) Daayf, F.; Ongena, M.; Boulanger, R.; Hadrami, I. E.; Belanger, R. R. Induction of Phenolic compounds in two cultivars of cucumber by treatment of healthy and powdery mildew-infected plants with extracts of *Reynoutria sachalinensis*. *J. Chem. Ecol.* **2000**, *26*, 1579−1593.

(17) Yao, L. H.; Jiang, Y. M.; Shi, J.; Tomas-Barberan, F. A.; Dalta, N.; Singanusong, R.; Chen, S. S. Flavonoids in food and their health effect. *Plant Foods Hum. Nutr.* **2004**, *59*, 113−122.

(18) Del Rio, D.; Rodriguez-Mateos, A.; Spencer, J.; Tognolini, M.; Borges, G.; Crozier, A. Dietary (poly) phenolics in human health: Structures, bioavailability, and evidence of protective effects against chronic diseases. *Antioxid. Redox Signaling* **2013**, *18*, 1118−1892.

(19) Verma, S.; Dubey, R. S. Effect of cadmium on soluble sugars and enzymes of their metabolism in rice. *Biol. Plant.* **2001**, *44*, 117−123.

(20) Dubois, M.; Gilles, K. A.; Hamilton, J. K.; Rebers, P. A.; Smith, F. Colorimetric method for determination of sugars and related substances. *Anal. Chem.* **1956**, *26*, 350−356.

(21) Somogyi, M. Notes on sugar determination. *J. Biol. Chem.* **1952**, *195*, 19−23.

(22) Chen, C. H.; Bushuk, W. Nature of proteins in triticale and its parental species 1. Solubility characteristic and amino acid composition of endosperm proteins. *Can. J. Plant Sci.* **1970**, *50*, 9−14.

(23) Bradford, M. M. A rapid and sensitive method for the quantitation of microgram quantities of protein utilizing the principle of protein-dye binding. *Anal. Biochem.* **1976**, *72*, 248−254.

(24) Dewanto, V.; Wu, X.; Adonm, K. K.; Liu, R. H. Thermal processing enhances the nutritional value of tomatoes by increasing total antioxidant activity. *J. Agric. Food. Chem.* **2002**, *50*, 3010−3014.

(25) Jia, Z.; Tang, M.; Wu, J. The determination of flavoid contents in mulberry and they scavenging effects on superoxide radicals. *Food Chem.* **1999**, *64*, 555−559.

(26) Ruiz, J. M.; Romero, L. Commercial yield and quality of fruits of cucumber plants cultivated under greenhouse conditions: response to increases in nitrogen fertilization. *J. Agric. Food Chem.* **1998**, *46*, 4171−4173.

(27) Ho, L. C. The mechanism of assimilate partitioning and carbohydrate compartmentation in fruit in relation to the quality and yield of tomato. *J. Exp. Bot.* **1996**, *47*, 1239−1243.

(28) Koch, K. Sucrose metabolism: regulatory mechanisms and pivotal roles in sugar sensing and plant development. *Curr. Opin. Plant Biol.* **2004**, *7*, 235−246.

(29) Levitz, S. M. Interactions of Toll-like receptors with fungi. *Microbes Infect.* **2004**, *6*, 1351−1355.

(30) Zaragoza, O.; Rodrigues, M. L.; De Jesus, M.; Frases, S.; Dadachova, E.; Casadevall, A. The capsule of the fungal pathogen *Cryptococcus neoformans*. *Adv. Appl. Microbiol.* **2009**, *68*, 133−216.

(31) Moghaddam, M. R. B.; Ende, W. V. D. Sugars and plant innate immunity. *J. Exp. Bot.* **2012**, DOI: 10.1093/jxb/ers129.

(32) Gómez-Ariza, J.; Campo, S.; Rufat, M.; Estopa, M.; Messeguer, J.; San Segundo, B.; Coca, M. Sucrose-mediated priming of plant defence responses and broad-spectrum disease resistance by over-expression of the maize pathogenesis-related PRms protein in rice plants. *Mol. Plant−Microbe Interact.* **2007**, *20*, 832−842.

(33) Goodman, R. N.; Kiraly, Z.; Wood, K. R. *The Biochemistry and Physiology of Plant Disease*; University of Missouri Press: Columbia, 1986.

(34) Alaoui-Sosse, B.; Genet, P.; Vinit-Dunand, F.; Toussaint, M.; Epron, D.; Badot, P. Effect of copper on growth in cucumber plants (*Cucumis sativus*) and its relationships with carbohydrate accumulation and changes in ion contents. *Plant Sci.* **2004**, *166*, 1213−1218.

(35) Wang, X.; Chang, L.; Wang, B.; Wang, D.; Li, P.; Wang, L.; Yi, X.; Huang, Q.; Peng, M.; Guo, A. Comparative proteomics of *Thellungiella halophila* leaves from plants subjected to salinity reveals the importance of chloroplastic starch and soluble sugars in halophyte salt tolerance. *Mol. Cell. Proteomics* **2013**, *12*, 2174−2195.

(36) Leopold, L. F.; Leopold, N.; Diehl, H.; Socaciu, C. Quantification of carbohydrates in fruit juices using FTIR spectroscopy and multivariate analysis. *Spectroscopy* **2011**, *26*, 93−104.

(37) Duarte, I. F.; Barros, A.; Delgadillo, I.; Almeida, C.; Gil, A. A. M. Application of FTIR spectroscopy for the quantification of sugars in Mango juice as a function of ripening. *J. Agric. Food. Chem.* **2002**, *50*, 3104−3111.

(38) Gajc-Wolska, J.; Szwacka, M.; Malepszy, S. The evaluation of cucumber fruit quality (*Cucumis sativus* L.) transgenic line with thaumatin gene. *Folia Hort.* **2005**, *17*, 23−28.

(39) Du, C.; Fan, H.; Guo, S.; Tezuka, T. Applying spermidine for differential responses of antioxidant enzymes in cucumber subjected to short-term salinity. *J. Am. Soc. Hortic. Sci.* **2010**, *135*, 18−24.

(40) Chan, Z. Proteomic responses of fruits to environmental stresses. *Front. Plant Sci.* **2013**, DOI: 10.3389/fpls.2012.00311.

(41) Chinnici, F.; Bendini, A.; Gaiani, A.; Riponi, C. S. Radical scavenging activities of peels and pulps from cv. Golden Delicious apples as related to their phenolics composition. *J. Agric. Food. Chem.* **2004**, *52*, 4684−4689.
(42) Tsao, R.; Yang, R.; Xie, S.; Sockovie, E.; Khanizadeh, S. Which polyphenolic compounds contribute to the total antioxidant activities of apple? *J. Agric. Food. Chem.* **2005**, *53*, 4989−4995.
(43) Ingram, D.; Sanders, K.; Kolybaba, M.; Lopez, D. Case-control study of phytoestrogens and breast cancer. *Lancet* **1997**, *9083*, 990−994.
(44) Fernandes, J. C.; Henriques, F. S. Biochemical, physiological, and structural effects of excess copper in plants. *Bot. Rev.* **1991**, *57*, 246−273.
(45) Brady, N. C.; Weil, R. R. *The Nature and Properties of Soils*, 12th ed.; Prentice-Hall: Upper Saddle River, NJ, 1998.
(46) Ekholm, P.; Reinivuo, H.; Mattila, P.; Pakkala, H.; Koponen, J.; Happonen, A.; Hellstrom, J.; Ovaskainen, M. L. Changes in the mineral and trace element contents of cereals, fruits and vegetables in Finland. *J. Food Compos. Anal.* **2007**, *20*, 487−495.
(47) Carson, B. L.; Ellis, H. V., III; McCann, J. L. *Toxicology and Biological Monitoring of Metals in Humans*; Lewis Publishers: Chelsea, MI, 1986; pp 140−144.
(48) Linus Pauling Institute. Micronutrient Information. Magnesium. Available from: http://lpi.oregonstate.edu/infocenter/minerals/magnesium/.
(49) Kuhn, A. J.; Schroder, W. H.; Bauch, J. The kinetics of calcium and magnesium entry into mycorrhizal spruce roots. *Planta* **2000**, *210*, 488−496.
(50) Shaul, O. Magnesium transport and function in plants: the tip of the iceberg. *BioMetals* **2002**, *15*, 309−323.
(51) Dimkpa, C. O.; Zeng, J.; McLean, J. E.; Britt, D. W.; Zhan, J.; Anderson, A. J. Production of indole-3-acetic acid via the indole-3-acetamide pathway, in the plant-beneficial bacterium *Pseudomonas chlororaphis* O6 is inhibited by ZnO nanoparticles but enhanced by CuO nanoparticles. *Appl. Environ. Microbiol.* **2012**, *78*, 1404−1410.
(52) Pineros, M.; Tester, M. Calcium channels in higher plant cells: Selectivity, regulation and pharmacology. *J. Exp. Bot.* **1997**, *48*, 551−557.
(53) Karley, A. J.; White, P. J. Moving cationic minerals to edible tissues: potassium, magnesium, calcium. *Plant Biol.* **2009**, *12*, 291−298.
(54) Zhao, L.; Peralta-Videa, J. R.; Ren, M.; Varela-Ramirez, A.; Li, C.; Hernandez-Viezcas, J. A.; Aguilera, R. J.; Gardea-Torresdey, J. L. Transport of Zn in a sandy loam soil treated with ZnO NPs and uptake by corn plants: Electron microprobe and confocal microscopy studies. *Chem. Eng. J.* **2012**, *184*, 1−8.
(55) Steinke, D. R.; Majak, W.; Sorensen, T. S.; Parvez, M. Chelation of molybdenum in *Medicago sativa* (alfalfa) grown on reclaimed mine tailings. *J. Agric. Food Chem.* **2008**, *56*, 5437−5442.
(56) Tejada-Jimenez, M.; Chamizo-Ampudia, A.; Galvan, A.; Fernandez, E.; Llamas, A. Molybdenum metabolism in plants. *Metallomics* **2013**, *5*, 1191−1203.
(57) Zhao, L.; Peralta-Videa, J. R.; Hernandez-Viezcas, J. A.; Hong, J.; Gardea-Torresdey, J. L. Transport and retention behavior of ZnO nanoparticles in two natural soils: Effect of surface coating and soil composition. *J. Nano Res.* **2012**, *17*, 229−242.
(58) Pitman, J. K. Managing the manganese: molecular mechanisms of manganese transport and homeostasis. *New Phytol.* **2005**, *167*, 733−742.
(59) Bandyopadhyay, S.; Peralta-Videa, J. R.; Plascencia-Villa, G.; Jose-Yacaman, M.; Gardea-Torresdey, J. L. Comparative toxicity assessment of CeO_2 and ZnO nanoparticles towards *Sinorhizobium meliloti*, a symbiotic alfalfa associated bacterium: Use of advanced microscopic and spectroscopic techniques. *J. Hazard. Mater.* **2012**, *241*−*242*, 379−386.
(60) Alloway, B. J. *Zinc in Soils and Crop Nutrition*, 2nd ed.; IZA and IFA: Brussels, Belgium, and Paris, France, 2008.
(61) Van Assche, F.; Clijsters, H. Effects of metals on enzyme activity in plant. *Plant , Cell Environ.* **1990**, *13*, 195−206.
(62) Allowag, B. J. Study on trace element copper in Japan. *Proc. Soil Sci.* **1984**, Vol. *4*.

MATERIALS AND METHODS

Vineyards. In 2012, two cv. Grenache Noir vineyards, site 1 (s1) and site 2 (s2), located in Southern France and frequently subject to drought were studied. The vines in these vineyards are grafted onto the 110 Richter rootstock, trained on a vertical trellis, and pruned as a bilateral cordon. At site 1, plant spacing was 2.25 (between rows) × 0.7 (between plants in a row), giving a plant density of 6350 plants/ha. The rows were aligned in a north/south orientation. At site 2, plant spacing was 2.10 (between rows) × 1.0 (between plants in row), giving a density of 4760 plants/ha. The rows were aligned in an east/west orientation.

Vine Irrigation Treatments. Water was applied with a drip irrigation system, once per week, to generate the various treatments. For irrigated treatments, irrigation was initiated following the first detection of a water deficit. The amount of water supplied depended on the desired intensity of the water deficit. Four different irrigation treatments were applied: irrigation before veraison only (bV), irrigation after veraison only (aV), irrigation before and after veraison (TOT), and no irrigation (DRY). Each irrigation treatment was organized into two rows at s2 and two blocks at s1.

Monitoring of Berry Ripening. Berry ripening was monitored during the last month of maturation. We sampled berries in clusters (200 berries) to ensure that the berries sampled were representative of all cluster positions within the canopy and all positions within the cluster.[17] Fresh berries were analyzed on the day of sampling: pH, sugars (Brix), and titratable acidity. The harvest date for each treatment was determined from these analysis results.

Vine Water Status Measurement. Vine water status was evaluated for each treatment by measuring predawn leaf water potential by the pressure chamber technique.[18] This parameter has been reported to reflect the nature of the soil, climatic conditions, and irrigation. Indeed, it provides information about the water status of the soil layers explored by the roots, because there is an equilibrium between vine water status and soil water status just before dawn.[19] This parameter was monitored from June to September, with at least four replicates for each date. We also determined the carbon isotope composition of grape sugars ($\delta^{13}C$) at maturity.

Sampling, Measurement of Mean Berry Volume, and Preparation of Grape Juices for Aroma and Nitrogen Composition Analysis. Sampling was performed weekly, during the last few weeks of the ripening period, for each treatment. We picked 20 clusters evenly distributed over the two faces of the row, from 20 vines (10 vines from each of the two rows at site 2, and each of the two blocks at site 1). In the laboratory, the clusters were cut into small fragments (each containing between 5 and 10 berries), mixed, and 1 kg of fragments was isolated and stored at −20 °C for grape juice preparation.

Mean berry volume was determined by immersing 100 fresh berries in a graduated cylinder containing water and measuring the displacement of the water. These volumes were used to obtain per-berry measurements, to prevent possible dilution effects due to the irrigation of the vine in some treatments.

Grape juice was prepared from 1 kg of frozen cluster fragments, which were destemmed and defrosted overnight at 4 °C. The berries were then crushed in a blender for 20 s, and the juice obtained was filtered and stored at −20 °C until analysis.

Harvest and Winemaking. At maturity, 100 kg of clusters was picked manually. The vine yield of each treatment was estimated by weighing and counting the clusters present on each of 20 plants.

At site 1, the grapes are used to produce red wines. Clusters were mechanically destemmed and placed in a 1 hL stainless steel tank. SO_2 (3 g/hL) was added to the must, which was then inoculated with yeasts (20 g/hL) (Zymaflore X5, Laffort, France). Alcoholic fermentation and maceration were carried out over a period of 7 days, at temperatures of 24−30 °C. The mixture was pressed, and a malolactic fermentation was performed, with the addition of 1 g/hL of Vitilactic F (Martin Vialatte, France), at 18 °C, before the addition of 4 g/hL SO_2. Tartaric stabilization was then carried out over 15 days at 0 °C, followed by filtration (5 μm pores), before bottling.

At site 2, the grapes are used to produce rosé wines. Clusters were mechanically destemmed and placed in a 1 hL stainless steel tank. SO_2 (3 g/hL) was added to the must, which was allowed to macerate for 24 h at 18 °C before the addition of 2 g/hL SO_2 and pressing. Enzyme (2 g/hL; Lafazym, Laffort, France) was then added, and the mixture was allowed to settle for 18 h at 12 °C. The mixture was clarified and inoculated with 20 g/hL yeast (Zymaflore X5, Laffort, France). Alcoholic fermentation was carried out at 16−23 °C, with monitoring. At the end of the alcoholic fermentation, SO_2 was added to the wine at a concentration of 4 g/hL, before tartaric stabilization for 15 days at 0 °C, filtration (1 and 0.65 μm pores), and bottling.

Analyses. *Analysis of Amino Acids and Ammonium in Grape Juice.* The amino acid content of grape juice was determined with a specific amino acid analyzer (Biochrom 30), according to the protocol used by Crépin et al.[20]

Ammonium was quantified spectrophotometrically in grape juices with an enzyme kit (Enzytec kit, R-biopharm, Germany), according to the manufacturer's instructions.

Dimethyl Sulphide Potential (DMSP) Analysis. Must and wine DMSP were analyzed with a modified version of the protocol described by Ségurel et al.[21] Briefly, the sample (8 mL of must or wine) was mixed with sodium hydroxide (300 mg, to obtain a 1 N solution), sodium chloride (1 g), and DMSPA-d_6 (4.5 μg in aqueous solution as an internal standard). DMSPA-d_6 was synthesized in our laboratory as described by Smith et al.[22] This compound was used as an internal standard, leading to a modification of the protocol suggested by Ségurel et al.,[21] who introduced the standard (DMS-d_6) after heating the sample. We heated the sample at 100 °C for 1 h, resulting in the hydrolysis of DMS precursors and DMSPA-d_6 to generate DMS and DMS-d_6, respectively. Calibration was performed on a model must and wine, according to the same sample preparation protocol, with serial dilutions of SMM. For the model must, SMM concentrations varied between 0 and 2775 μg/L (between 0 and 485 μg/L for wine), and DMSPA-d_6 concentration was 570 μg/L (303 μg/L for wine). Six calibration points were used for each matrix. The resulting curves were linear ($[DMS]/[DMS\text{-}d_6] = 0.8449 \times A_{m/z62}/A_{m/z68} + 0.009$; $R^2 = 0.997$ and $[DMS]/[DMS\text{-}d_6] = 0.9930 \times A_{m/z62}/A_{m/z68} - 0.017$; $R^2 = 0.999$ for wine and grape juice, respectively).

Statistical Analyses. Principal component analysis and Tukey tests were performed with Xlstat software (Addinsoft, France).

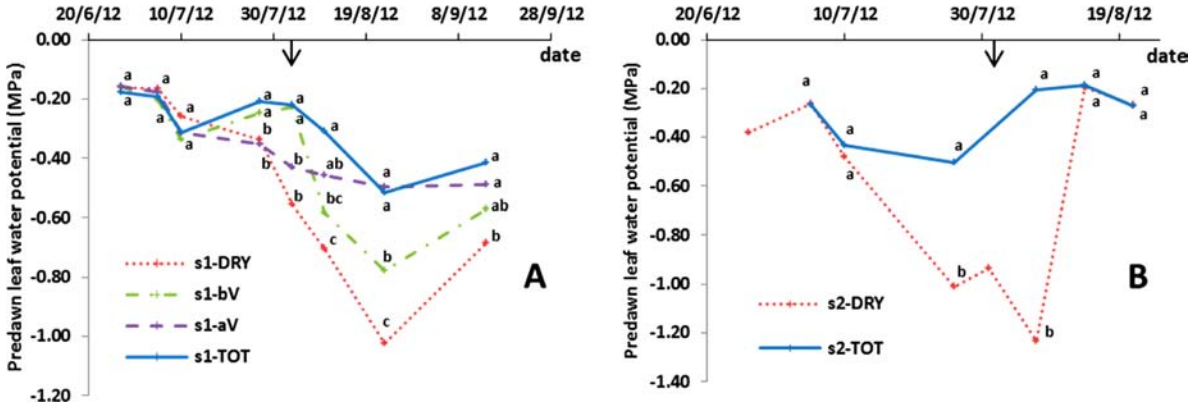

Figure 1. Predawn leaf water potential monitoring for the various irrigation treatments during maturation (site 1 (A) and site 2 (B)). Each point is the mean of at least four replicates. Statistically significant differences in the Tukey test ($p < 0.05$) are indicated by different letters. The arrows on the *x*-axis indicate the dates of veraison.

RESULTS/DISCUSSION

Vine Water Status. The different irrigation treatments presented differed in terms of water status (Figure 1). At site 1 (Figure 1A), the predawn leaf water potential measurements were lowest between August 20th and 30th; there were significant differences between treatments (except for TOT and aV, consistent with the irrigation treatments applied). At site 2 (Figure 1B), predawn leaf water potential was lowest from the end of July to the start of August, with significant differences between treatments. Veraison occurred at about August 3rd at site 1 and August 1st at site 2, and water deficit had no impact on veraison date, as reported by Tregoat.[23]

The carbon isotope composition of grape sugar ($\delta^{13}C$) was used as an integrative indicator of vine water deficit during the ripening period. At site 1, s1-DRY was the treatment associated with the highest degree of stress (−23.16 ‰), followed by s1-bV (−24.15 ‰), s1-aV (−24.42 ‰), and then s1-TOT (−25.34 ‰). At site 2, s2-DRY was the treatment resulting in the greatest water deficit (−22.87 ‰), followed by s2-TOT (−25.22 ‰).

Berry Ripening under Different Water Deficit Conditions. At both sites, sugars accumulated and titratable acidity decreased earlier for the TOT treatment than for the DRY, aV, and bV treatments, consistent with the observations reported by Ojeda.[24] The harvest dates for each treatment were therefore determined on the basis of the results for the monitoring of berry ripening. At maturity, sugar concentrations reached 240 and 247 g/L, and the titratable acidity was 2.8 and 2.5 g (H_2SO_4)/L for s1-DRY and s1-TOT, respectively; sugar concentrations were 190 and 233 g/L, and titratable acidity was 2.75 and 2.5 g (H_2SO_4)/L for s2-DRY and s2-TOT, respectively. Water deficit has been reported to inhibit sugar accumulation in grape berries, by decreasing phloem sugar unloading,[25] potentially accounting for the low sugar concentration of s2-DRY grapes at maturity.

Changes in the Yeast Assimilable Amino Acid Content of Berries during Maturation. Yeast assimilable nitrogen (YAN) consists of ammonium and free primary amino acids;[26,27] secondary amino acids, such as proline and hydroxyproline, are not metabolized by yeast under the conditions usually prevailing during winemaking.[28] Bell and Henschke [16] summarized a large number of published results, showing that amino acid composition varies considerably, according to many factors, including grape cultivar, rootstock, site, seasonal conditions, level of maturity, viticultural practices, soil management techniques, and the health status of the grapes.

We monitored the amino acid content of berries during the last few weeks of maturation (Figure 2). For each irrigation

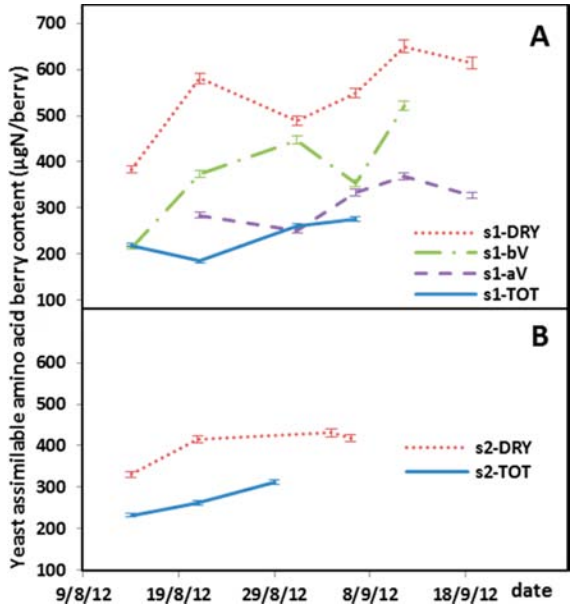

Figure 2. Changes in the yeast assimilable amino acid content of berries during ripening in different water deficit conditions (site 1 (A) and site 2 (B)). The standard deviations indicated are the mean analytical standard deviations.

treatment, the yeast assimilable amino acid content of the berry increased during ripening, this increase being most pronounced for the treatments involving a water deficit (DRY and bV). At maturity, the yeast assimilable amino acid content of berries from vines subjected to the s1-DRY treatment was more than twice that of berries from vines subjected to the s1-TOT treatment (614 and 276 μg N/berry, respectively), and s1-bV and s1-aV displayed intermediate behavior (521 and 327 μg N/berry, respectively) (Figure 2A); the yeast assimilable amino acid content for s2-DRY was 35% greater than that for s2-TOT (418 and 313 μg N/berry, respectively) (Figure 2B). At both sites, greater water deficiencies were associated with the accumulation of larger amounts of yeast assimilable amino

dx.doi.org/10.1021/jf404758g | J. Agric. Food Chem. 2014, 62, 2760−2766

acids in the berry during ripening. The differences were more marked when expressed as concentrations: at site 1, the yeast assimilable amino acid concentrations recorded were 391, 286, 211, and 153 mg N/L for s1-DRY, s1-bV, s1-aV, and s1-TOT, respectively; at site 2, we obtained values of 440 and 209 mg N/L for s2-DRY and s2-TOT, respectively. These observations are consistent with those reported by Morgan, who observed higher levels of solute accumulation in the organs of plants subjected to water deficit than in well-watered plants.[29] Some sugars and amino acids may be recycled to the grape, to sustain ripening.[30] Glutamine and glutamic acid are the only amino acids that decrease in concentration during ripening, this decrease being smaller at higher water deficits (DRY and bV) (data not shown). As reported by Stines,[31] glutamine can act as a precursor for the biosynthesis of other amino acids, potentially accounting for the decrease in glutamine and glutamic acid levels during ripening.

Changes in the Proline/Arginine Ratio during Ripening. Arginine and proline are generally the most abundant amino acids in grapes, together with alanine, gamma aminobutyric acid, and glutamine.[31] The proline/arginine ratio is considered to be a good indicator of the nitrogen nutritional status of the musts from different grape varieties.[16] Indeed, proline cannot be assimilated by yeast, whereas arginine is the most important amino acid for yeast in the must. A lower proline/arginine ratio would therefore be expected to result in a more fermentable must for the same total amino acid concentration. Grenache Noir has been reported to accumulate large amounts of arginine at early stages of maturation (19.7°B) and large amounts of proline when more mature (24°B).[26] In our experiments, the proline/arginine ratio increased during maturation (Figure 3), consistent with the observations of

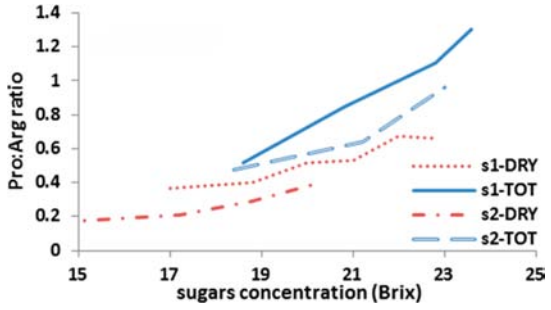

Figure 3. Changes in proline/arginine ratio during maturation as a function of berry sugar concentration, for the DRY and TOT treatments at sites 1 and 2.

Kliewer.[26] The change in this ratio during ripening differed between the DRY and TOT treatments: at the same range of maturity (between 18.8 and 22.8°B), the proline/arginine ratio was lower for the DRY treatment at the two sites, indicating that the amino acid nitrogen fraction was more assimilable by yeast in water-deficient berries. Moreover, the proline/arginine ratio increased more rapidly in the s1-TOT treatment than in the s1-DRY treatment, for the same range of maturity. Water deficiency at the end of the maturation period favored the accumulation of arginine in berries: the arginine content of s1-DRY berries was 2.5 times higher than that of s1-TOT berries at ripeness (363 and 144 μg N/berry for s1-DRY and s1-TOT, respectively; 230 and 173 μg N/berry for s2-DRY and s2-TOT, respectively).

Changes in Berry Ammonium Content during Maturation. Ammonium is the second component of YAN. In our experiments, ammonium levels decreased during ripening, for all irrigation treatments, consistent with previous observations.[16,32] At site 1 (Figure 4A), berry ammonium levels

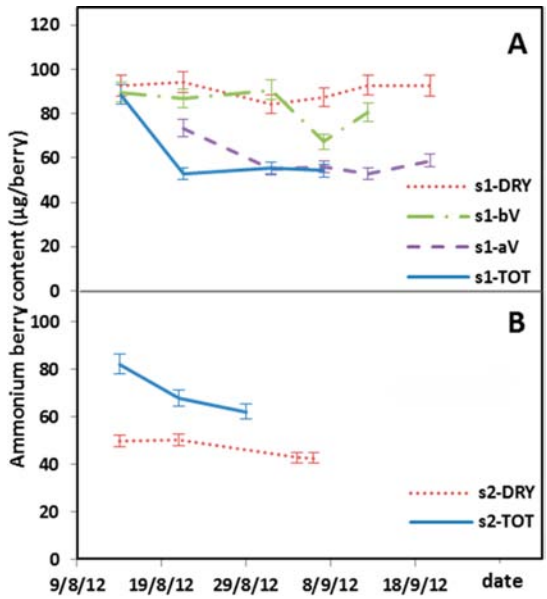

Figure 4. Changes in the ammonium content of the berries during ripening, for the various water deficit conditions (site 1 (A) and site 2 (B)). The standard deviations indicated are the mean analytical standard deviations.

decreased slowly or remained stable in water-deficient treatments (s1-DRY and s1-bV) and were higher than those for the non water-deficient treatments at maturity (s1-aV and s1-TOT). Ammonium, like other solutes, accumulated in larger amounts in water-deficient organs.[29] The higher berry ammonium contents observed in water-deficient treatments may reflect higher levels of transpiration, resulting in a greater uptake of soil water, which contains nutrients such as ammonium.[30] The opposite situation was observed at site 2 (Figure 4B), where s2-TOT berries had higher ammonium contents than s2-DRY berries. Predawn leaf water potential was lower at site 2 than at site 1 (Figure 1B), consistent with a high level of water stress. It is possible that the considerable water deficiency generated by the s2-DRY treatment limited water uptake by the roots more strongly, resulting in lower levels of ammonium accumulation in the berries.

Berries from the water-deficient vines at the two sites had higher ammonium concentrations than berries from irrigated vines: 59, 44, 38, and 30 mg N/L for the s1-DRY, s1-bV, s1-aV, and s1-TOT treatments, respectively, and 47 and 41 mg N/L for s2-DRY and s2-TOT, respectively.

Proportion of the YAN in the Form of Ammonium. The ammonium/YAN ratio decreased during maturation, for all irrigation treatments at both sites. This is not surprising, given the decrease in ammonium levels and the increase in assimilable amino acid levels occurring during ripening. At maturity, the ammonium/YAN ratio varied between 13 and 16% at site 1 and between 9 and 17% at site 2. The lowest ratios were those for s1-DRY and s2-DRY, raising questions about a possible increase in amino acid synthesis or accumulation in the berries of vines subjected to water deficit.

dx.doi.org/10.1021/jf404758g | J. Agric. Food Chem. 2014, 62, 2760−2766

Changes in the DMSP Content of Berries during Maturation. The DMSP content of berries increased during ripening, for all irrigation treatments (Figure 5). In s1-DRY, a large increase in the DMSP content of berries was observed during the last two weeks of maturation, consistent with previous observations showing a large increase in the DMSP content of berries at the end of maturation and over mature[12] (Figure 5A). At maturity, the DMSP content of berries was higher for DRY treatments than for TOT treatments. At site 1, berry DMSP level was 272, 191, 174, 86 ng/berry (173, 105, 112, and 45 μg/L) for s1-DRY, s1-bV, s1-aV, and s1-TOT, respectively; at site 2, berry DMSP level was 238 and 208 ng/berry (250, 139 μg/L) for s2-DRY and s2-TOT, respectively. The smaller difference in berry DMSP content between the two treatments observed at site 2 (Figure 5B) may be due to large differences in maturity.

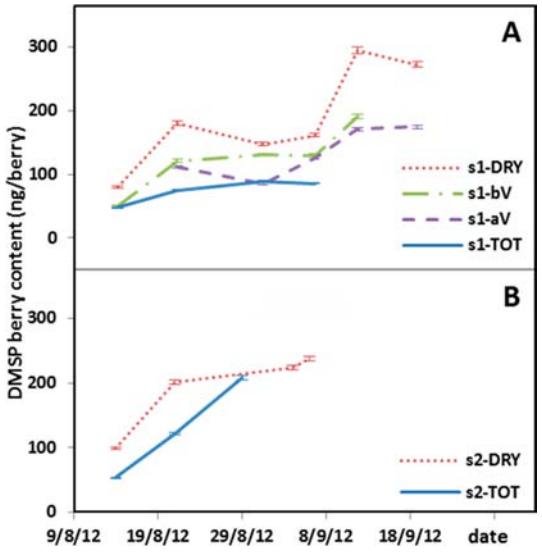

Figure 5. Changes in the DMSP level of berries during ripening under different water deficit conditions (site 1 (A) and site 2 (B)). The standard deviations indicated are the mean analytical standard deviations.

Global Analysis of Grape Juice. At the end of the experiments, 31 samples were available, corresponding to the grape samples for the different irrigation treatments at the two sites collected during the maturation period. We investigated the general impact of vine water stress, by carrying out principal component analysis (PCA) with all the available analytical data: berry ammonium, yeast assimilable amino acid, and DMSP contents (Figure 6). The first axis of this PCA was strongly linked to the variables "yeast assimilable amino acids (YAAA)" and "DMSP" and accounted for 62% of total variability. The second axis was strongly linked to the variable "Ammonium (NH_4^+)" and accounted for 34% of total variability. Amino acid and DMSP contents were found to be correlated (R^2 = 0.85), whereas no correlation could be established between ammonium content and the other two variables. The composition of the DMSP may account for this observation, as the DMSP reflects mostly SMM content in grapes,[13] SMM being an amino acid derivative. Thus, vine water deficit may favor high berry YAN content and concentration and a high berry DMSP.

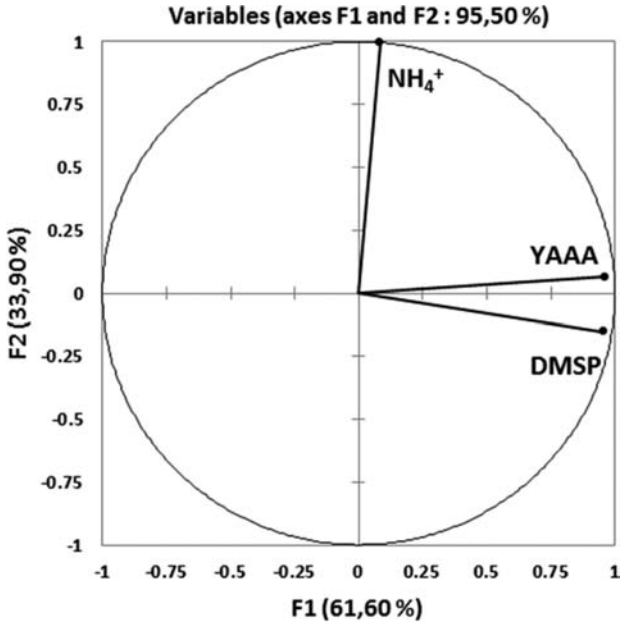

Figure 6. Correlation circle for principal component analysis, based on 31 observations and the ammonium (NH_4^+), the yeast assimilable amino acid (YAAA), and the DMSP levels of berries during maturation, for all irrigation treatments at sites 1 and 2.

Relationship between DMSP and YAN Concentration in Grape Juice at Maturity and Wine DMSP Concentration. The DMSP concentration of must at maturity was greater for water-deficient treatments (DRY) than for the other treatments, at both sites (Figure 7, dark histograms). In the red wines produced from site 1 grapes, DMSP (Figure 7, pale histograms) followed the same pattern as the DMSP of the corresponding grapes. Thus, a higher grape DMSP concentration was associated with a higher DMSP concentration of the wine. For the rosé wines produced from site 2 grapes, wine DMSP concentration was low and similar for the two treatments, despite large differences in must DMSP concentration between the two treatments. This probably reflects the characteristics of the rosé winemaking process, in which there is little extraction from berry skins, the chief source of the DMSP.[14]

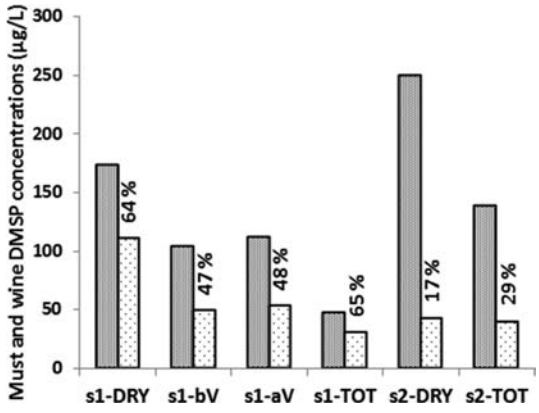

Figure 7. DMSP concentrations in the musts (dark histograms) and wines (pale histograms) and corresponding DMSP preservation rate during fermentation (percentage annotated), for all irrigation treatments at sites 1 and 2.

The wine DMSP/must DMSP ratio provided information about the preservation of DMSP during fermentation. This

dx.doi.org/10.1021/jf404758g | J. Agric. Food Chem. 2014, 62, 2760−2766

ratio was very high for s1-DRY (64%), probably due to the high YAN concentration of the must (450 mg N/L). Indeed, levels of SMM (the main component of DMSP in grapes [13]) have been reported to be better preserved during fermentation with higher concentrations of YAN in model must.[14] The two intermediate treatments, s1-bV and s1-aV, had lower YAN concentrations (330 and 250 mg N/L, respectively) and a lower DMSP preservation rate (47 and 48%, respectively). However, the preservation rate for s1-TOT was high (65%), despite the YAN concentration being lower for this treatment than for the other treatments (183 mg N/L). At site 2 (rosé wines), the wine DMSP/must DMSP ratio was lower than those obtained for the red wines from site 1, for the reasons explained above. This ratio was higher for s2-TOT than for s2-DRY, even though YAN concentration was higher for s2-DRY (s2-DRY: 485 mg N/L; s2-TOT: 250 mg N/L). Therefore, not only YAN concentration impacted DMSP preservation. At both sites, the fermentability of the different musts was satisfactory in terms of their YAN concentrations at maturity.

Thus, generally speaking, water deficit affected both YAN and DMSP levels in grapes, potentially resulting in a better preservation of DMSP during alcoholic fermentation, although DMSP content was variable and depended on the wine considered. One possible consequence of this finding is that "stressed" wines may have a longer aroma shelf life, due to the role of DMS, at the ranges of concentration reported here, in enhancing the fruity notes of Grenache Noir wines.[7] However, further studies are required to confirm these preliminary results.

AUTHOR INFORMATION

Corresponding Author

*E-mail: royerdup@supagro.inra.fr. Tel.: (33) (0)4 99 61 23 11.

Funding

We thank Fondation Jean Poupelain for the financial support.

Notes

The authors declare no competing financial interest.

ABBREVIATIONS USED

DMS/DMS-d_6,dimethyl sulfur/dimethyl sulfur deuterated; SMM,(*S*)-methylmethionine; DMSO,dimethylsulfoxide; DMSP,dimethyl sulfur potential; YAN,yeast assimilable nitrogen; bV,before veraison; aV,after veraison; TOT,total; SO_2,sulfur dioxide; NH_4^+,ammonium; DMSPA-d_6,dimethyl sulfoniopropionate deuterated; YAAA,yeast assimilable amino acids; HS-SPME,head space − solid phase micro extraction; GC−EIMS,gas chromatography−electronic impact mass spectrometry; PDMS,polydimethylsiloxane; PCA,principal component analysis

REFERENCES

(1) Hidalgo Fernández, L. *Tratado de viticultura general*. Mundi-Prensa Libros: Madrid, 2002; p 288.

(2) Planton, S. At the continental scale: the models viewpoint. *C. R. Geosci.* **2003**, *335*, 535−543.

(3) IPCC, *Climate change 2007: The physical science basis*; Geneva, 2007.

(4) Jones, G.; Duchene, E.; Tomasi, D.; Yuste, J.; Braslavska, O.; Schultz, H.; Martinez, C.; Boso, S.; Langellier, F.; Perruchot, C. In *Changes in European winegrape phenology and relationships with climate*, XIV International GESCO Viticulture Congress, Geisenheim, Germany, 23−27 August, 2005, Groupe d'Etude des Systemes de Conduite de la vigne (GESCO), 2005; pp 54−61.

(5) Cheynier, V.; Schneider, R.; Salmon, J.-M.; Fulcrand, H. Chemistry of Wine. In *Comprehensive Natural Products II*; Lew, M., Hung-Wen, L., Eds.; Elsevier: Oxford, 2010; pp 1119−1172.

(6) Mora, S. J.; Knowles, S. J.; Eschenbruch, R.; Torrey, W. J. Dimethyl sulphide in some Australian red wines. *Vitis* **1987**, *26*, 79−84.

(7) Segurel, M. Contribution des précurseurs glycosidiques et du sulfure de diméthyle des baies de Vitis Vinifera L.cv. Grenache noir et Syrah à l'arôme des vins da la vallée du Rhône. Ecole Nationale Supérieure Agronomique de Montpellier, 2005.

(8) Spedding, D. J.; Raut, P. The influence of dimethyl sulphide and carbon disulphide in the bouquet of wines. *Vitis* **1982**, *21*, 240−246.

(9) Anocibar Beloqui, A.Les composés soufrés volatils des vins rouges. PhD Dissertation. Université Victor Segalen Bordeaux II, Bordeaux, France, 1998; p 169

(10) Escudero, A.; Campo, E.; Farina, L.; Cacho, J.; Ferreira, V. Analytical characterization of the aroma of five premium red wines. Insights into the role of odor families and the concept of fruitiness of wines. *J. Agric. Food Chem.* **2007**, *55*, 4501−4510.

(11) San-Juan, F.; Ferreira, V.; Cacho, J.; Escudero, A. Quality and aromatic sensory descriptors (mainly fresh and dry fruit character) of spanish red wines can be predicted from their aroma-active chemical composition. *J. Agric. Food Chem.* **2011**, *59*, 7916−7924.

(12) Dagan, L. Potentiel aromatique des raisins de Vitis Vinifera L. cv. Petit Manseng et Gros Manseng. Contribution à l'arôme des vins de pays Côtes de Gascogne. Ecole Nationale Supérieure Agronomique de Montpellier, 2006.

(13) Loscos, N.; Segurel, M.; Dagan, L.; Sommerer, N.; Marlin, T.; Baumes, R. Identification of (*S*)-methylmethionine in Petit Manseng grapes as dimethyl sulphide precursor in wine. *Anal. Chim. Acta* **2008**, *621*, 24−29.

(14) Dagan, L.; Schneider, R. Le sulfure de diméthyle: Quels moyens pour gérer ses teneurs dans les vins en bouteilles? *Actes de colloque "Arôme du vin" - Toulouse* **2012**, 7−10.

(15) Marais, J. Effect of storage time and temperature on the formation of dimethyl sulphide and on white wine quality. *Vitis* **1979**, *18*, 254−260.

(16) Bell, S. J.; Henschke, P. A. Implications of nitrogen nutrition for grapes, fermentation and wine. *Aust. J. Grape Wine Res.* **2005**, *11*, 242−295.

(17) Carbonneau, A. Observations sur vigne. Codification des données agronomiques. *Vitis* **1981**, *5*, 9−13.

(18) Scholander, P. F.; Bradstreet, E. D.; Hemmingsen, E.; Hammel, H. Sap pressure in vascular plants negative hydrostatic pressure can be measured in plants. *Science* **1965**, *148*, 339−346.

(19) Katerji, N.; Hallaire, M. Les grandeurs de référence utilisables dans l'étude de l'alimentation en eau des cultures. *Agronomie* **1984**, *4*, 999−1008.

(20) Crepin, L.; Nidelet, T.; Sanchez, I.; Dequin, S.; Camarasa, C. Sequential use of nitrogen compounds by *Saccharomyces cerevisiae* during wine fermentation: a model based on kinetic and regulation characteristics of nitrogen permeases. *Appl. Environ. Microbiol.* **2012**, *78*, 8102−8111.

(21) Segurel, M. A.; Razungles, A. J.; Riou, C.; Salles, M.; Baumes, R. L. Contribution of dimethyl sulfide to the aroma of syrah and grenache noir wines and estimation of its potential in grapes of these varieties. *J. Agric. Food Chem.* **2004**, *52*, 7084−7093.

(22) Smith, G. C.; Clark, T.; Knutsen, L.; Barrett, E. Methodology for analyzing dimethyl sulfide and dimethyl sulfoniopropionate in seawater using deuterated internal standards. *Anal. Chem.* **1999**, *71*, 5563−5568.

(23) Tregoat, O.; Van Leeuwen, C.; Choné, X.; Gaudillere, J. Etude du régime hydrique et de la nutrition azotée de la vigne par des indicateurs physiologiques. Influence sur le comportement de la vigne et la maturation du raisin (*Vitis vinifera* L. cv Merlot, 2000, Bordeaux). *J. Int. Sci. Vigne Vin.* **2002**, *36*, 133−142.

(24) Ojeda, H.; Andary, C.; Kraeva, E.; Carbonneau, A.; Deloire, A. Influence of pre-and postveraison water deficit on synthesis and

concentration of skin phenolic compounds during berry growth of *Vitis vinifera* cv. Shiraz. *Am. J. Enol. Vitic.* **2002**, *53*, 261−267.
(25) Wang, Z. P.; Deloire, A.; Carbonneau, A.; Federspiel, B.; Lopez, F. An in vivo experimental system to study sugar phloem unloading in ripening grape berries during water deficiency stress. *Ann. Bot.* **2003**, *92*, 523−528.
(26) Kliewer, W. Free amino acids and other nitrogenous fractions in wine grapes. *J. Food Sci.* **1970**, *35*, 17−21.
(27) Ough, C. Acids and amino acids in grapes and wines. In *Wine Analysis*; Springer: Berlin Heidelberg, 1988; pp 92−146.
(28) Ingledew, W.; Magnus, C.; Sosulski, F. Influence of oxygen on proline utilization during the wine fermentation. *Am. J. Enol. Vitic.* **1987**, *38*, 246−248.
(29) Morgan, J. M. Osmoregulation and water stress in higher plants. *Ann. Rev. Plant Physiol.* **1984**, *35*, 299−319.
(30) Keller, M. Deficit irrigation and vine mineral nutrition. *Am. J. Enol. Vitic.* **2005**, *56*, 267−283.
(31) Stines, A.; Grubb, J.; Gockowiak, H.; Henschke, P. A.; Høj, P. B.; van Heeswijck, R. Proline and arginine accumulation in developing berries of Vitis vinifera L. in Australian vineyards: Influence of vine cultivar, berry maturity and tissue type. *Aust. J. Grape Wine Res.* **2000**, *6*, 150−158.
(32) Lafon-Lafourcade, S.; Guimberteau, G. Evolution des amino-acides au cours de la maturation des raisins. *Vitis* **1962**, *3*, 130−135.

bromophenol, 2,4-, 2,6-, and 3,5-dibromophenol (99% each), and 2,4,6-tribromophenol were from Sigma-Aldrich (Taufkirchen, Germany), and 3-bromophenol was from Alfa Aesar (Karlsruhe, Germany).

Whisky Samples. A total of 20 whiskies of different origins were analyzed for the content of bromophenols especially in Islay whiskies, which are described in more detail in the following. Three of the nine Islay whisky distilleries on this island, i.e., Laphroaig, Lagavulin, and Ardbeg (not available), reportedly have a significant marine flavor which includes notes of iodine and seaweed. This characteristic note has not been described for two further Islay whiskies analyzed by us, i.e., Bowmore and Bruichladdich. Origins and qualities of non-Islay whiskies will be listed below.

Laphroaig, 10 years. Laphroaig is the southernmost distillery on Islay. The storehouses are directly located at the sea, and during high tide, they are bathed by the ocean.[18] Compared to other distilleries, there is a later cut from spirit collection to feints at Laphroaig, and for this reason it contains more peaty phenolic compounds.[4] It is exclusively aged in American oak barrels. It is known for the strongest marine flavor of all Islay malts.[4] The flavor is described, among others, as peaty, medicinal with nuances of iodine, machine room, and smoky, well-rounded by the sweet flavor of oak.[4,19] The taste includes iodine, smoky, strong distinctive salty taste, and sharp finish.[19] The salty water, the salty marine air, the peaty water, and the peat itself are key factors for the generation of the unique flavor and taste. The malt is known to contain 40 ppm of phenolic compounds.[18] It has been claimed that the nearness to the sea is the reason for the salty character of the spirit and that the exchange of salty air and barrel contribute to the unique flavor.[19]

Lagavulin, 16 years. The Lagavulin distillery is only two kilometers north of Laphroaig.[4] The distillery is also directly located at the sea.[4] The flavor notes include peat, iodine, and flowery while the taste has been reported as smoky, very peaty, salty, full-bodied, and recalling dried seaweed.[4,19]

Bowmore, 12 years. Distillery also located directly at the sea. The flavor includes musk, as well as earthy and nutty notes. Taste attributes are dry, charcoal, moderately peaty, smoky, slightly bitter, and very complex.[19]

Bruichladdich, 10 years. Flavor: nutty, sweet, light, slightly peaty. Taste: mild, smokey, slightly sweet, intense, strong finish.[19]

Non-Islay Whisky. The following samples from Scotland were analyzed: Jura Superstition, Glen Scotia, Johnnie Walker RedLabel, Old Pulteney (12 years), Speyside Single Malt (18 years), The Glenlivet (12 years), Glenfiddich (12 years), Ballantines Gold (12 years), Chivas Regal (12 years), Ballentines Finest, and Glen Garioch (8 years). Samples of other origins were Jameson (Ireland), Jim Beam (USA), Jack Daniels Nr. Seven (USA), the flavored whisky Southern Comfort (USA), and Hohenheimer Whisky (Germany).

Sample Cleanup. The derivatization with acetic acid anhydride/$NaHCO_3$ was performed in a downscaled way according to the procedures reported for benzotriazoles.[20,21] $NaHCO_3$ (40 mg) was weighed into a 2 mL sample vial, and 1 mL of whisky, 10 μL of the internal standard, 3,5-dibromophenol (10 ng/μL in ethanol), and 40 μL of acetic anhydride were added. After the reaction (visible by the development of CO_2), 200 μL of *n*-hexane was pipetted into the vial. After shaking and phase separation, the upper organic phase was separated and used for analysis.

Gas Chromatography with Electron Capture Negative Ion Mass Spectrometry (GC/ECNI-MS). GC/ECNI-MS measurements were carried out with a 7890/5975C system (Agilent, Waldbronn, Germany). Helium (purity 99.9990%) was used as the carrier gas in constant flow mode (1.2 mL/min). A 15 m long ZB-1 column (internal diameter 0.25 mm, film thickness 0.1 μm, Phenomenex, Aschaffenburg, Germany) was used in combination with the following GC oven program: After 1 min at 50 °C, the temperature was raised at 10 °C/min to 250 °C (0 min hold time). Sample solutions (2 μL) were injected splitless into a PTV injector programmed as follows: 80 °C (hold time 0.01 min), then at 500 °C/min to 300 °C. The ion source temperature was set at 150 °C. Methane (purity 99.9995%) was used as moderation gas at an ion gauge pressure of 1.6×10^{-4} Torr. Mass spectra were recorded in the full scan range from m/z 50 to m/z 500. Quantification was carried out in the selected ion monitoring mode using m/z 79 and m/z 81 (Br^- ion isotopes suitable for all organobromine compounds[22]), m/z 250 and m/z 252 (M^- of free dibromophenols and fragment ion of the *O*-acetylated dibromophenols ($[M - C_3H_2O + H]^-$), and m/z 330 and m/z 332 (M^- of free tribromophenols and fragment ion of *O*-acetylated tribromophenols ($[M - C_3H_2O + H]^-$); and m/z 372 and m/z 374 (M^- of *O*-acetylated tribromophenols) were monitored for confirmation throughout the run.

For *O*-acetylated dibromophenols the abundance of M^- was about 7% of m/z 79 while it was ~18% for 2,4,6-tribromophenol. Accordingly, the LOQ would have been higher by ~factor 14 or ~5.5. However, the presence of the verification ions (M^-) along with the retention time was used for verification of the compounds in samples with response to m/z 79 and 81. Vice versa, the absence of di- and tribromophenols in our samples was based on the lack of response to m/z 79 and 81 in the corresponding GC/MS-ECNI-MS chromatograms.

RESULTS AND DISCUSSION

GC/ECNI-MS Method for the Analysis of *O*-Acetylated Bromophenols in Whiskies. Phenolic compounds and especially bromophenols are difficult to analyze in free form by gas chromatography.[7] Especially when present at low amounts (<1 ng injected), GC peaks of bromophenols were characterized by severe peak broadening within a few runs.[23] Only very clean GC/MS systems and frequent instrumental maintenance allowed for the determination of free bromophenols in the low pg range.[23] Moreover, the direct analysis of bromophenols from whisky proved to be difficult. For this reason we chose to convert the bromophenols into *O*-acetylated derivatives according to other studies on halophenols.[5,7,24−26] The protocol followed our recent method for the derivatization of benzotriazoles in dishwasher tabs.[21] This procedure turned out to be easy to perform and resulted in sharp and abundant peaks due to the high sensitivity of GC/ECNI-MS-SIM for polyhalogenated compounds including *O*-acetylated di- and tribromophenols.

The GC/ECNI-MS mass spectra of the *O*-acetylated bromophenols were dominated by the bromide ion isotopes (m/z 79 and 81). For *O*-acetylated 2,4,6-tribromophenol, M^- (m/z 370) was also detected at ~20% of the base peak along with $[M - CH_3CO + H]^-$ at m/z 328 (Figure 2a). The latter fragmentation was also detected in the mass spectrum of *O*-acetylated 2,4-dibromophenol (m/z 250) but at lower abundance (Figure 2b). Other *O*-acetylated dibromophenols showed the same mass spectra except that m/z 250 had even lower abundance than in the 2,4-dibromophenol derivative. While quantification was based on m/z 79 and m/z 81, the mentioned high mass ions were also recorded for verification (see Materials and Methods).

Once these parameters were set up, the method was developed by using 3,5-dibromophenol as internal standard. 3,5-Dibromophenol is not naturally occurring and has only been detected at traces as a transformation product of the anthropogenic polybrominated diphenyl ether congener BDE 196.[23] Initial measurements confirmed that the IS was not present in the whisky samples. Linearity, tested with solutions of bromophenols in ethanol/water (40:60, v/v), was established in the range 20−1,000 pg injected on the column for di- and tribromophenols corresponding to 100−5,000 pg/mL bromophenols in whisky ($R^2 > 0.999$). The signal-to-noise (S/N) approach was used to establish the limit of detection (S/N = 3) and the limit of quantification (S/N = 10). The limit of

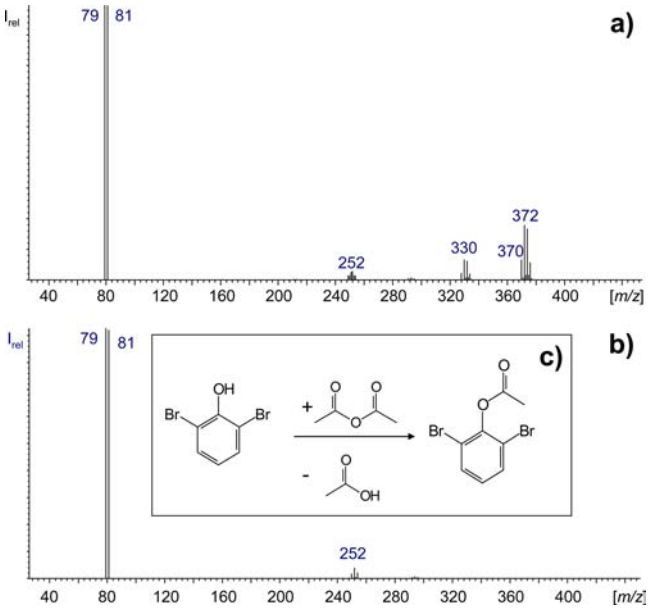

Figure 2. GC/ECNI-MS spectra of *O*-acetylated (a) 2,4,6-tribromophenol and (b) 2,6-dibromophenol along with (c) an inset of the reaction scheme of the *O*-acetylation of 2,6-bromophenol with acetic acid anhydride.

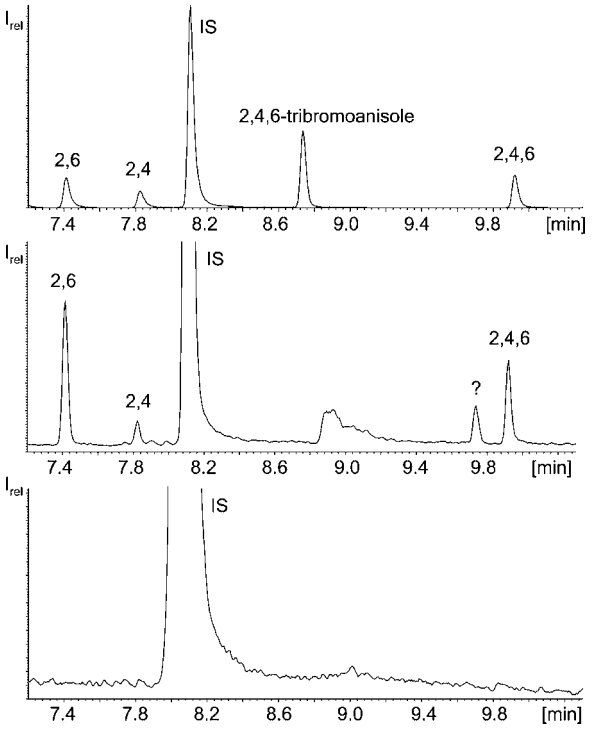

Figure 3. GC/ECNI-MS-SIM chromatograms (m/z 79) of (a) a 50 pg standard solution of *O*-acetylated 2,6-dibromophenol ("2,6"), 2,4-dibromophenol ("2,4"), 3,5-dibromophenol ("IS"), 2,4,6-tribromophenol ("2,4,6"), and 2,4,6-tribromoanisole and a sample of (b) Lagavulin containing *O*-acetylated bromophenols and (c) Jameson (without *O*-acetylated bromophenols). The peak labeled with a question mark ("?") in panel b denotes a yet unknown brominated compound.

quantification of dibromophenols and tribromophenols was estimated at ~2 pg (~10 pg/mL in whisky, i.e., ~40% ethanol in water). However, monobromophenols did not provide the required sensitivity for GC/ECNI-MS determination (limit of detection >100 pg/μL[23]). Samples were analyzed at least in duplicate, and the standard deviation was generally <10%.

Initial experiments on the acetylation procedure demonstrated that this method produced between 95 and 98% of *O*-acetylated bromophenols. This efficiency was in the same range as reported in other studies.[7] More, no enrichment step was used which could reduce the recovery and with the use of the internal standard the results obtained with our method can be considered quantitative. However, the response of the internal standard 3,5-dibromophenol was about 1 order of magnitude lower than the ones of the target analytes. The relative standard deviations of the analyte response factors in the calibration solutions were between 11 and 15%, which represents the accuracy of the method.

The GC/ECNI-MS chromatograms could be well-analyzed and compared with the standard (Figure 3a). In Lagavulin, 2,4- and 2,6-dibromophenols as well as 2,4,6-tribromophenol could be identified (Figure 3b). The most abundant peak originated from 2,6-dibromophenol. Except for the three bromophenols, one further minor peak was detected which eluted slightly before 2,4,6-tribromophenol from the GC column. Due to the low amounts available, the compound gave only response to m/z 79 and m/z 81, so that its identity could not be determined. By contrast, a sample of Jameson (Ireland) did not show the presence of any bromophenols, even after selective zoom into the *y*-axis (Figure 3c). This whisky sample did not indicate the presence of any brominated compound.

Application of the Method of Bromophenol Determination to Whisky Samples. By means of standard compounds we were able to identify the bromophenols in the Islay whiskies (Figure 3). The highest amounts were generally determined for 2,6-dibromophenols. In addition to 2,6-dibromophenol, 2,4-dibromophenol was detected in only three and 2,4,6-tribromophenol in only two samples (Table 1), i.e., those with the highest concentrations of 2,6-dibromophenol (Laphroaig > Lagavulin > Bowmore). The concentration of 2,4-dibromophenol was about 1 order of magnitude lower than that of 2,6-dibromophenol (Table 1). Lagavulin showed the highest level of 2,4,6-tribromophenol (Table 1). The two Islay whiskies with characteristic iodine flavor (Lagavulin and Laphroaig) contained >300 ng/L 2,6-dibromophenol. This concentration is about 3 orders of magnitude higher than the taste threshold of this compound in water.[5] The highest level was detected in Laphroaig, i.e., the sample with the most intense taste and the most distinct marine flavor.[4] Typically, whisky is served in portions of 20 mL, which corresponds with 8 ng of bromophenols per serving (and 1 ng per sample aliquot analyzed).

The sample with the third highest bromophenol content was Bowmore, i.e., another Islay whisky, which reportedly is not characterized by a distinct iodine flavor.[4] Surprisingly, some other whiskies also contained low amounts of bromophenols whose origins remained unclear. However, the measured bromophenol concentrations were generally more than 1 order of magnitude lower than in the two Islay whiskies with distinct iodine flavor (Table 1). These amounts corresponded with <1 ng per serving. Although even these 2,6-dibromophenol levels exceeded the taste threshold concentration for 2,6-dibromophenol in water,[5] the abundance of 2,6-dibromophenol was deemed too low for contributing a "marine" note to the whiskies, which is in accordance with flavor descriptions.[4]

Relevance of the Findings and Potential Origins of the Bromophenols. Assumedly, the ethanolic solutions and

dx.doi.org/10.1021/jf405006e | J. Agric. Food Chem. 2014, 62, 2767−2771

Table 1. Concentration of Simple Di- and Tribromophenols in Whisky [ng/L]

whisky	origin	2,6-dibromophenol	2,4-dibromophenol	2,4,6-tribromophenol
Lagavulin	Islay/Scotland	324	44	112
Laphroaig	Islay/Scotland	398	31	24
Bowmore	Islay/Scotland	88	9	nd
Bruichladdich	Islay/Scotland	12	nd	nd
Jura Superstition	Scotland	40	nd	nd
Glen Scotia	Scotland	22	nd	nd
Johnnie Walker Red Label	Scotland	22	nd	nd
Old Pulteney	Scotland	21	nd	nd
Speyside Single Malt	Scotland	17	nd	nd
The Glenlivet	Scotland	17	nd	nd
Glenfiddich	Scotland	11	nd	nd
Ballantines Gold	Scotland	10	nd	nd
Chivas Regal	Scotland	nd	nd	nd
Ballentines Finest	Scotland	nd	nd	nd
Glen Garioch	Scotland	nd	nd	nd
Jameson	Ireland	nd	nd	nd
Hohenheimer Whisky	Germany	nd	nd	nd
Jim Beam	USA	nd	nd	nd
Jack Daniels no. 7	USA	nd	nd	nd
Southern Comfort	USA	nd	nd	nd

the presence of many other flavor compounds in whisky increase the flavor threshold of 2,6-dibromophenol. For instance, the flavor threshold of 2,6-dibromophenol in prawn meat was 2 orders of magnitude higher than in water (i.e., 60 ng/kg vs 0.5 g/L).[27] Accordingly, the flavor threshold value of 2,6-dibromophenol in prawn meat was at the borderline of whiskies with a distinct iodine flavor and those without.[27] Unfortunately, we were lacking a trained panel with expertise in flavor evaluation. Hence, we could not verify the explicit or additive contribution of 2,6-dibromophenol to the iodine-flavored Islay whiskies. Nevertheless, the low amounts of the possible character impact compound 2,6-dibromophenol required to generate iodine-flavored Islay whiskies suggest that such a marine flavor could be easily imitated (or adjudged) by the addition of only nanogram amounts to the spirits. For this reason a more thorough investigation of the impact of bromophenols on the flavor of whisky should be carried out in the future. Likewise the route by which the bromophenols enter the whisky should be investigated in more detail. The direct uptake of bromophenols from marine air on the one hand and the bromination of existing phenol (40 ppm of phenolic compounds in Laphroaig[18]) on the other hand appear to be the most likely sources.

As we could show in this study, bromophenols could be determined for the first time in Scotch Islay whiskies. Due to the excellent sensitivity of GC/ECNI-MS-SIM, the di- and tribromophenols could be determined without utilization of an enrichment step. Yet, further research will be required to determine the role of monobromophenols which could not be detected with this approach. Such results could be obtained in the future by using purge-and-trap techniques for sample enrichment, which will increase sensitivity and enable the use of GC/EI-MS for analysis.[7] Future sensory evaluation should aim at elucidating the contribution of the bromophenols to the specific flavor of Scotch Islay whiskies. In the positive case, this flavor impression could be imitated by the addition of small amounts to the whiskies. Likewise their natural formation and their point of entrance during the whisky production should be a matter of future research.

AUTHOR INFORMATION

Corresponding Author

*Fax: +49 711 459 24377. E-mail: walter.vetter@uni-hohenheim.de.

Notes

The authors declare no competing financial interest.

REFERENCES

(1) http://www.scotch-whisky.org.uk/news-publications/news/scotch-whisky-exports-grow-in-value-and-volume/#.UnfHO1PwN8E, last accessed Nov 6, 2013.

(2) Wishart, D. The flavour of whisky. *Significance* **2009**, 20−26.

(3) Harrison, B. M.; Priest, F. G. Composition of peats used in the preparation of malt for Scotch whisky production - influence of geographical source and extraction depth. *J. Agric. Food Chem.* **2009**, *57*, 2385−2391.

(4) Jackson, M. *Whisky*; Dorong Kindersley: London, Munich, 2005.

(5) Whitfield, F. B.; Last, J. H.; Shaw, K. J.; Tindale, C. R. 2,6-Dibromophenol: the cause of an iodoform-like off-flavour in some Australian crustacea. *J. Sci. Food Agric.* **1988**, *46*, 29−42.

(6) Boyle, J. L.; Lindsay, R. C.; Stuiber, D. A. Contributions of bromophenols to marine-associated flavors of fish and seafood. *J. Aquat. Food Prod. Technol.* **1993**, *1* (Issue 3−4), 43−63.

(7) Blythe, J. W.; Heitz, A.; Joll, C. A.; Kagi, R. I. Determination of trace concentrations of bromophenols in water using purge-and-trap after in situ acetylation. *J. Chromatogr. A* **2006**, *1102*, 73−83.

(8) Whitfield, F. B.; Helidoniotis, F.; Shaw, K. J.; Svoronos, D. Distribution of bromophenols in species of marine algae from Eastern Australia. *J. Agric. Food Chem.* **1999**, *47*, 2367−2373.

(9) Boyle, J. L.; Lindsay, R. C.; Stuiber, D. A. Occurrence and properties of flavor-related bromophenols found in the marine environment - A Review. *J. Aquat. Food Prod. Technol.* **1993**, *2* (Issue 2), 75−112.

(10) Vetter, W. Marine halogenated natural products of environmental and food relevance. *Rev. Environ. Contam. Toxicol.* **2006**, *188*, 1−57.

(11) Gribble, G. W. *Naturally Occurring Organohalogen Compounds—A Comprehensive Update*; Springer: Wien, 2010.

(12) Gribble, G. W. The natural production of organobromine compounds. *Environ. Sci. Pollut. Res.* **2000**, *7*, 37−49.

(13) Flodin, C.; Whitfield, F. B. Biosynthesis of bromophenols in marine algae. *Water Sci. Technol.* **1999**, *40*, 53−58.

(14) Reineke, N.; Biselli, S.; Franke, S.; Francke, W.; Heinzel, N.; Hühnerfuss, H.; Iznaguen, H.; Kammann, U.; Theobald, N.; Vobach, M.; Wosniok, W. Brominated indoles and phenols in marine sediment and water extracts from the North and Baltic Seas-concentrations and effects. *Arch. Environ. Contam. Toxicol.* **2006**, *51*, 186−196.
(15) Vetter, W.; Schlabach, M.; Kallenborn, R. Evidence for the presence of natural halogenated hydrocarbons in Southern Norwegian and polar air. *Fresenius Environ. Bull.* **2002**, *11*, 170−175.
(16) Melcher, J.; Schlabach, M.; Strand Andersen, M.; Vetter, W. Contrasting the seasonal variability of halogenated natural products and anthropogenic hexachlorocyclohexanes in the Southern Norwegian atmosphere. *Arch. Environ. Contam. Toxicol.* **2008**, *55*, 547−557.
(17) Vetter, W.; Haase-Aschoff, P.; Rosenfelder, N.; Komarova, T.; Mueller, J. F. Determination of halogenated natural products in passive samplers deployed along the Great Barrier Reef, Queensland/Australia. *Environ. Sci. Technol.* **2009**, *43*, 6131−6137.
(18) http://de.wikipedia.org/wiki/Laphroaig, last accessed Nov 6, 2013.
(19) Lerner, D. *Schottischer Whisky*; Könemann, Cologne, 1998.
(20) Pervova, M. G.; Kirichenko, V. E.; Saloutin, V. I. Determination of 1,2,3-benzotriazole in aqueous solutions and air by reaction-gas-liquid chromatography. *J. Anal. Chem.* **2010**, *65*, 276−279.
(21) Vetter, W.; Lorenz, J. Determination of benzotriazoles in dishwasher tabs from Germany and estimation the discharge into German waters. *Environ. Sci. Pollut. Res.* **2013**, *20*, 4435−4440.
(22) Vetter, W. A GC/ECNI-MS method for the identification of lipophilic anthropogenic and natural brominated compounds in marine samples. *Anal. Chem.* **2001**, *73*, 4951−4957.
(23) Bendig, P.; Vetter, W. UV induced formation of bromophenols from polybrominated diphenyl ethers. *Environ. Sci. Technol.* **2013**, *47*, 3665−3670.
(24) Abrahamsson, K.; Xie, T. M. Direct determination of trace amounts of chlorophenols in fresh water, waste water and sea water. *J. Chromatogr.* **1983**, *279*, 199−208.
(25) Chau, A. S.; Coburn, J. A. Determination of pentachlorophenol in natural and waste waters. *J.—Assoc. Off. Anal. Chem.* **1974**, *57*, 389−393.
(26) Bao, M. L.; Pantani, F.; Barbieri, K.; Burrini, D.; Griffini, O. Direct acetylation followed by solid-phase disk extraction and GC-ITDMS for the determination of trace phenols in water. *Chromatographia* **1996**, *42*, 227−233.
(27) Chung, H. Y.; Ma, W. C. J.; Kim, J.-S. Seasonal distribution of bromophenols in selected Hong Kong seafood. *J. Agric. Food Chem.* **2003**, *51*, 2619−2624.

There are also some research studies concerning hydrolyzing flavonol glycosides into their corresponding flavonols and determining them in an indirect way.[32] Gallic acid (GA) and chlorogenic acid (CGA), the main phenolic acids and depsides of tea, although quite low in contents relative to other phenolic acids and depsides such as isochlorogenic acid, *p*-coumaric acid, *p*-coumaric quinovic acid, and caffeic acid, were detected by Yin et al.[13] The pretreatment and evolution system of ISO14502-2 ("determination of content of catechins in green tea − using the method of HPLC) is a promising method for routine analysis of catechins in tea. In addition, the determination of caffeine content of tea by HPLC was reported by Lin et al.,[17] Blahova and Lehotay,[21] and Prayong et al.[24]

Previous studies reported that caffeine and polyphenols such as (−)-gallocatechin, (−)-epigallocatechin, (−)-epigallocatechin gallate, (−)-epicatechin, gallocatechin gallate, and (−)-epicatechin gallate in oolong tea, which was obtained from three main production sites in China, that is, Fujian, Taiwan, and Guangdong, were simultaneously determined using HPLC.[20] In addition, five catechins in green tea,[25] catechins and caffeine in green tea leaves,[22] or caffeine and catechins in tea extracts[23] were simultaneously determined using HPLC. However, little information is available on the simultaneous determination of caffeine and polyphenols in Wuyi Rock tea. In this paper, the method of high-performance liquid chromatography coupled with photodiode array detector (HPLC-PDAD) at three different wavelengths [detection wavelength at 278 nm (Det.278 nm), reference wavelength at 360 nm (ref.360 nm); detection wavelength at 330 nm (Det.330 nm), reference wavelength at 380 nm (ref.300 nm); and detection wavelength at 370 nm (Det.370 nm), reference wavelength at 290 nm (ref.290 nm)] for the simultaneous determination of caffeine (CAF), catechins (EGC, C, EGCG, EC, GCG, ECG), and polyphenols (GA, CGA, myricetin, myricetin glycoside, quercetin, quercetin glycoside) in 'Wuyi Rougui' and 'Wuyi Shuixian', the two major cultivars of Wuyi Rock tea, was developed. The objective of this study was to evaluate the tea quality of 'Wuyi Rougui' and 'Wuyi Shuixian' and provide the method for clarifying the cause of "cultivated varieties flavor" of Wuyi Rock tea.

MATERIALS AND METHODS

Samples. Wuyi Rock teas (*C. sinensis* L.), including 10 'Wuyi Rougui' samples and 10 'Wuyi Shuixian' samples, were obtained from Wuyishan Jiejieqing Tea Co., Ltd., in Fujian province, China; Wuyishan Xiangjiang Tea Co., Ltd., in Fujian province, China; Wuyishan Qinpin Tea Co., Ltd., in Fujian province, China; Wuyishan Yanshang Tea Co., Ltd., in Fujian province, China; Wuyishan Huahui Tea Co., Ltd., in Fujian province, China; Wuyishan Mangtingfeng Tea Co., Ltd., in Fujian province, China; Wuyishan Kaimingxuan Tea Co., Ltd., in Fujian province, China; and Wuyishan Qingpao Tea Co., Ltd., in Fujian province, China.

Table 1. Factors and Levels of Orthogonal Experiment

	factors		
level	concn of HCl solution (mol/L)	hydrolysis temp (°C)	hydrolysis time (h)
1	1	70	0.5
2	2	80	1.0
3	3	90	1.5

Chemicals. EGC, C, EGCG, E, GCG, and ECG were purchased from Shanghai Ronghe Pharmacy Co., Ltd. (China). Myricetin, quercetin, CGA, and GA were obtained from Chengdu Must Biotechnology Co., Ltd. (China). Caffeine was purchased from Sigma Chemical Co. Ltd. (USA). HCl, acetic acid, vitamin C, and ethylenediaminetetraacetic acid (EDTA) were manufactured by Sinopharm Chemical Reagent Co., Ltd. (China). The above reagents were of analytical grade. Acetonitrile and methanol, of HPLC grade, were the products of Merck Co. Ltd. (Germany). The water used was redistilled and ion free.

Table 2. Linear Range, Linear Equation, Correlation Coefficient (r), and Limit of Quantification (LOQ) of Standard Compounds

compd	linear range (mg/L)	linear eq[a]	r	LOQ[b] (mg/L)
GA	0−100	$Y = 39.80X + 27.03$	0.999	0.012
EGC	0−200	$Y = 1.82X - 3.69$	0.999	0.317
C	0−200	$Y = 1.45X + 0.86$	0.999	0.345
CGA	0−100	$Y = 24.13X - 6.45$	0.999	0.021
CAF	0−150	$Y = 42.86X - 235.03$	0.962	0.015
EGCG	0−200	$Y = 11.33X - 29.49$	0.996	0.043
EC	0−200	$Y = 7.23X - 1.48$	0.999	0.064
GCG	0−200	$Y = 13.05X - 14.51$	0.999	0.038
ECG	0−200	$Y = 16.27X + 21.84$	0.999	0.030
myricetin	0−100	$Y = 4.47X - 5.81$	0.999	0.431
quercetin	0−100	$Y = 11.94X + 17.01$	0.995	0.121

[a] Y stands for the area of the peak. X stands for the amount of corresponding compound, mg/L. [b] Signal to noise ratio (S/N) is 10.

Selection of Detection Wavelength. Stock solutions (1000 μg/mL) of each standard were prepared individually by dissolving the required weight of each compound in corresponding solutions. Further diluted solutions (20 μg/mL) of each standard were also prepared individually and then injected into HPLC separately to get their retention time and spectrogram from 200 to 400 nm. After the comparison of each spectrum, the detection wavelength and its reference wavelength were selected.

Elution Program. The analyses of polyphenols and caffeine in tea were carried out by the following HPLC method. An Agilent 1200 series liquid chromatography system (Agilent Corp., USA), comprising a vacuum degasser (part G1322A), a quaternary pump (part G1311A), an autosampler (part G1313A), a column oven compartment (part G1316A), and a photodiode array detector (PDAD) (part G1314A), was used. The column was C18 reverse-phase Zorbax Ecllpse XDB-18 (5 μm, 4.6 mm × 250 mm, P/N 990967-902).

The elution program was according to method ISO 14502-2 with some modifications. Two mobile phases were employed in gradient HPLC elution. Mobile phase A was prepared with 90 mL of acetonitrile, 20 mL of acetic acid, and 2.0 mL of EDTA water solution (10 mg/mL) and subsequently made up to a volume of 1000 mL with water. Mobile phase B was mixed with 800 mL of acetonitrile, 20 mL of acetic acid, and 2.0 mL of EDTA water solution (10 mg/mL) and subsequently made up to a volume of 1000 mL with water. Both mobile phases (A and B) should be filtered through a 0.45 μm filter before use. Column oven temperature was set at 35 °C. The flow rate of the mobile phase was 1.0 mL/min. The injection volume was 20 μL. All of the above paremeters were concordant with the ISO 14502-2 method. To get a better separation, there were some changes in gradient elution program as follows: 100% (v/v) mobile phase A for 10 min, then (over another 10 min) a linear gradient to 80% (v/v) mobile phase A and 20% (v/v) mobile phase B, then (over 5 min) a linear gradient again to 50% (v/v) mobile phase A and 50% (v/v) mobile phase B, held at this composition for 8 min. Finally, it was reset to 100% (v/v) mobile phase A and allowed to equilibrate before the next injection.

Standard Preparation. GA (10 mg), EGC (20 mg), C (20 mg), CGA (10 mg), CAF (15 mg), EGCG (20 mg), E (20 mg), GCG (20 mg), ECG (20 mg), myricetin (10 mg), and quercetin (10 mg) were weighed and mixed together. Then the mixture was dissolved in a 20

Table 3. Spiked Recoveries and Relative Standard Deviations (RSDs) of Standard Compounds (n = 3)

compd	spiked (g/kg)	recovery (%)	RSD (%)
GA	5	98.73	3.86
	25	97.51	2.19
	50	98.90	1.93
EGC	5	97.40	3.48
	25	98.92	2.27
	50	98.20	2.37
C	5	98.67	3.57
	25	99.57	2.72
	50	98.13	1.26
CGA	5	98.20	3.73
	25	97.75	2.09
	50	97.60	2.34
CAF	5	98.93	1.11
	25	98.41	0.71
	50	98.20	1.27
EGCG	5	99.60	2.41
	25	99.43	1.79
	50	100.30	1.44
EC	5	99.33	2.33
	25	98.30	1.50
	50	98.37	0.65
GCG	5	100.10	3.21
	25	99.44	2.56
	50	99.07	1.71
ECG	5	99.80	2.63
	25	99.43	1.89
	50	98.70	1.41
myricetin	5	81.13	4.52
	25	82.41	3.79
	50	83.11	3.62
quercetin	5	88.73	4.17
	25	89.89	3.14
	50	92.10	3.00

mL one-mark volumetric flask with methanol to form the stock mixture solution.

Five milliliters of the stock solution was dispensed to 25, 50, and 100 mL one-mark volumetric flasks, respectively. All of these flasks were diluted with mobile phase to form working standard solutions A, B, and C and then injected into the HPLC. The peak area responses were obtained. Each peak was identified by comparing their retention time and UV spectra with those of the respective standard. A standard graph for each component was prepared by plotting concentration versus peak area.

Extraction Preparation of Sample of Wuyi Rock Tea. The method of extraction from Wuyi Rock tea was used according to the method of ISO 14502-2 with some modifications. Tea leaves (0.2 g) were mixed with 5 mL of 70% (v/v) aqueous methanol at 70 °C by a vortex mixer. After bathing at 70 °C for 10 min, the tube was removed, allowed to cool, and then centrifuged for 10 min at 3500g and 4 °C, and the supernatant was collected. The precipitation was extracted according to the above extraction procedure. The collected supernatants from the above extraction were mixed, then diluted to 10 mL with 70% (v/v) aqueous methanol, and filtered through a 0.22 μm filter. The filtrate was collected for the following analysis.

Method of Hydrolyzing Flavonol Glucosides to Flavonols in Wuyi Rock Tea. As flavonol glucosides present as *O*-glycosides with sugars bound at the C3 position and they can be hydrolyzed into their corresponding flavonols,[32] the quantity of flavonols in the hydrolyzed solution was used to assess the flavonol glucosides in tea sample according to the method of Wang and Helliwell.[32]

There were two steps for preparing the sample of hydrolyzed solution from flavonol glucosides in Wuyi Rock tea. The first step was 5 mL of filtrate of tea sample extraction, which was prepared by using the procedure of Extraction Preparation of Sample of Wuyi Rock Tea above, transferred into a tube, and then mixed with 5 mL of HCl solution at different concentrations on the basis of the following test design. The second step was the mixture bathed with different combinations of temperature and time span according to the following test design and then cooled rapidly to 20 °C, after which 70% (v/v) aqueous methanol was added to 25 mL.

The hydrolysis conditions for flavonoid glycosides including concentration of HCl solution, hydrolysis temperature, and hydrolysis time are shown in the following Single-Factor Test and Orthogonal Experiment. All hydrolyzed solutions should be filtered through 0.22 μm filters before injection into the HPLC.

Single-Factor Test. Effects of different concentrations of HCl solution, hydrolysis temperatures, and hydrolysis times on the content of flavonols and the yield of hydrolysate from flavonol glucosides were conducted, respectively. Specific designs were as follows: the experiment at different concentrations of HCl solution (0, 1.5, 3.0, 4.5, 6.0, 7.5, and 9.0 mol/L) on the flavonol content from the hydrolysis of flavonol glucosides was conducted by hydrolyzing at 80 °C for 1 h, respectively, whereas the experiment of different hydrolysis temperatures (60, 70, 80, 90, and 100 °C) was conducted using 1.5 mol/L HCl solution and hydrolyzing for 1 h, respectively. In addition, the experiment of different hydrolysis times (0, 0.5, 1, 1.5, 2, and 2.5 h) was also conducted using 1.5 mol/L HCl solution and hydrolyzing at 80 °C, respectively.

Orthogonal Experiment. On the basis of the result of the above single-factor test, selection of three factors and three levels of orthogonal experiment is shown in Table 1. The test plan of an orthogonal experiment [$L_9(3)^4$] design for optimizing parameters of hydrolyzing flavonol glucosides to corresponding flavonols in Wuyi Rock tea is shown in Table 4.

Reliability and Quantification of Caffeine and Some Selected Polyphenols in Samples of Wuyi Rock Tea. The UV spectrum of each standard compound after subtraction of the corresponding UV base spectrum was normalized automatically using a computer, and the plots were superimposed.

Peaks were considered to be chromatographically pure when there was exact coincidence to their corresponding UV spectra. Chromatographic peaks in the samples were indentified by comparing their retention times and UV spectra with those of the reference standards. The linear relationship, limit of quantification (LOQ), recovery, and relative standard deviation (RSD) are shown in Tables 2 and 3 to evaluate the quality of this method.

EGC, C, EGCG, EC, GCG, ECG, GA, CGA, myricetin, quercetin, and caffeine were detected and calculated from the sample extraction directly without hydrolysis. The myricetin glycoside and quercetin glycoside were detected in an indirect way by quantitating myricetin and quercetin in sample extraction after hydrolysis.

Statistical Analyses. All statistical analyses, including the design of orthogonal test and independent-sample t test, were carried out with PASW (IBM SPSS Statistics) statistical software (version 19.0).

RESULTS AND DISCUSSION

Chromatographic Performance of Working Standard Solution. HPLC of caffeine and some selected tea polyphenols in their working standard solution at various concentrations was

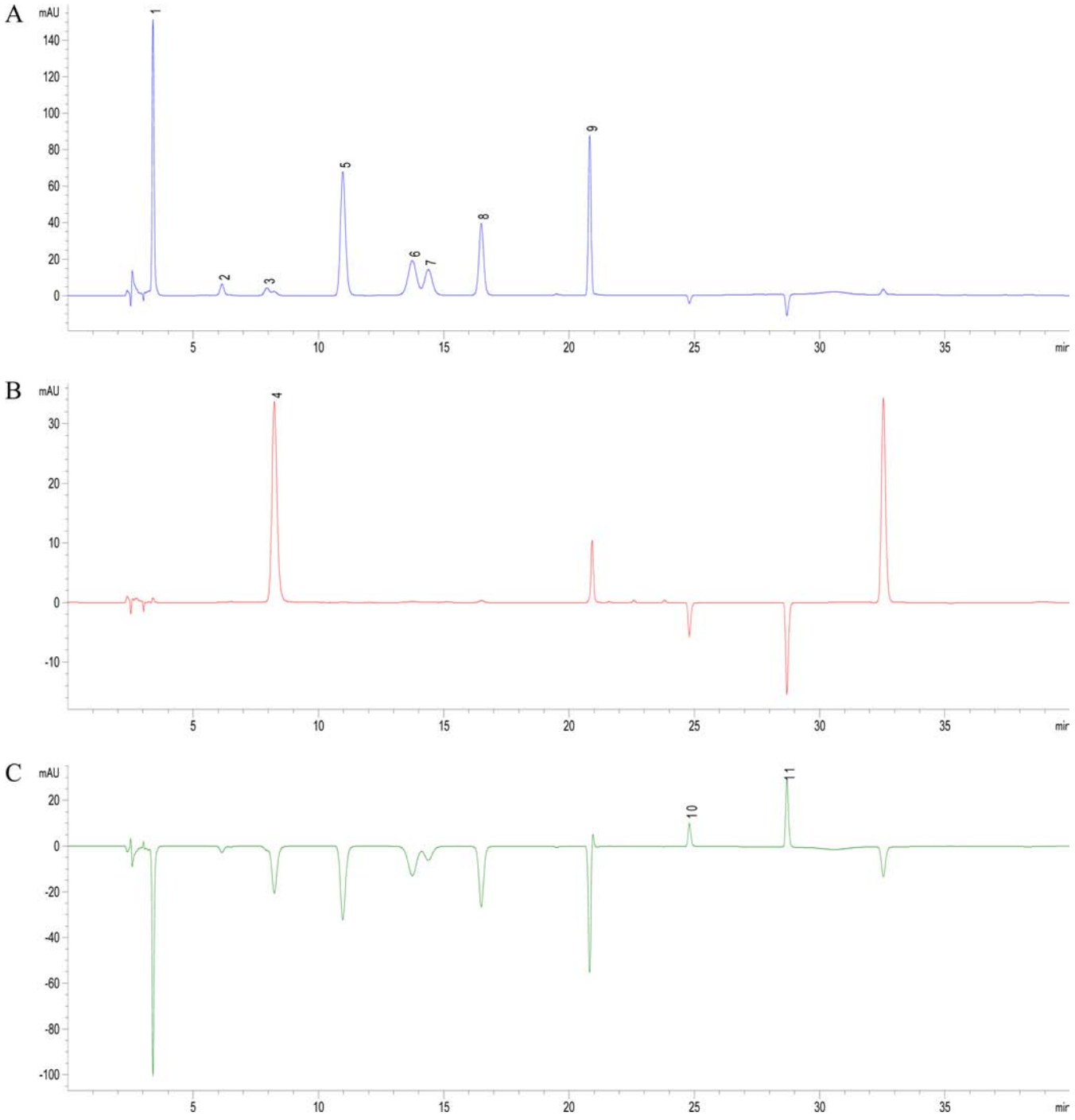

Figure 1. HPLC chromatogram of the working standard solution C mixture containing 25 μg/mL GA (1), 50 μg/mL EGC (2), 50 μg/mL C (3), 25 μg/mL CGA (4), 37.5 μg/mL CAF (5), 50 μg/mL EGCG (6), 50 μg/mL EC (7), 50 μg/mL GCG (8), 50 μg/mL ECG (9), 25 μg/mL myricetin (10), and 25 μg/mL quercetin (11) at different wavelengths under the experimental conditions. (A) GA (1), EGC (2), C (3), CAF (5), EGCG (6), EC (7), GCG (8), and ECG (9) were detected at acquisition wavelength of 278 nm and at reference wavelength of 360 nm. (B) CGA (4) was detected at acquisition wavelength of 330 nm and at reference wavelength of 380 nm. (C) Myricetin (10) and quercetin (11) were detected at acquisition wavelength of 370 nm and at reference wavelength of 290 nm.

recorded. There were negative peaks in a single wavelength. Therefore, it was important to select the proper wavelength for detection. Figure 1 shows the detection wavelength, reference wavelength, and retention time for each compound of standard solution C. These were slightly overlapping near C (3) and CGA (4), EGCG (6), and EC (7), whereas separation of other compounds performed well at corresponding wavelengths. Considering the sensitivity for quantitative determination, GA, C, CAF, EGCG, EC, GCG, and ECG were detected at 278 nm with the reference wavelength at 360 nm. CGA was detected at 330 nm with the reference wavelength at 380 nm. Myricetin and quercetin were detected at 370 nm with the reference wavelength at 290 nm.

Reliability of the Method. The linear range, linear equation of the working curve, coefficient of correlation (r), and LOQ for each standard are shown in Table 2. The results

dx.doi.org/10.1021/jf4056314 | J. Agric. Food Chem. 2014, 62, 2772−2781

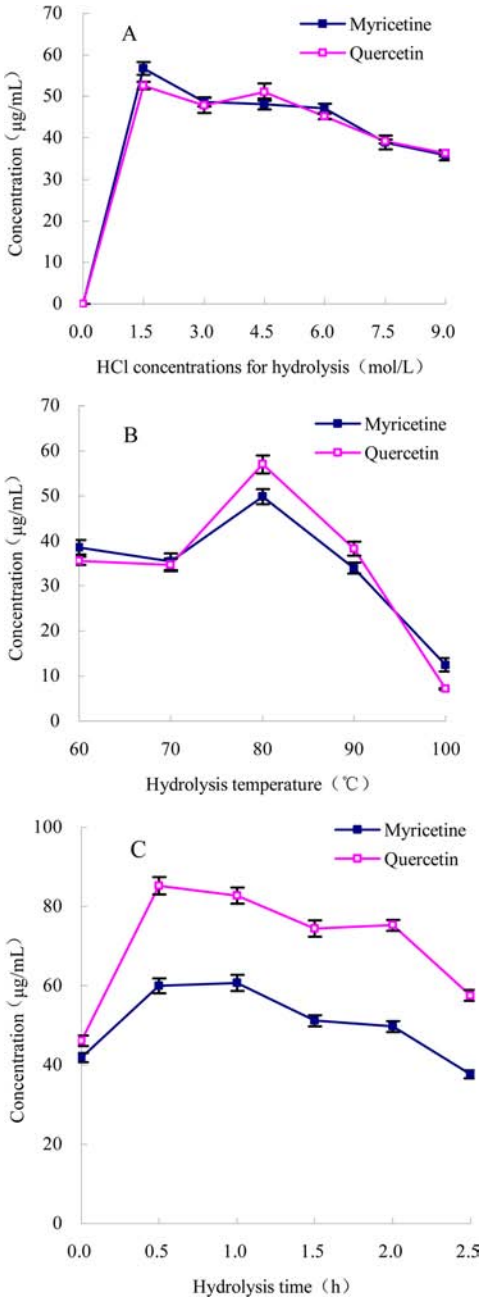

Figure 2. Effect of three factors on the hydrolysis of the flavonols: (A) HCl concentrations for hydrolysis; (B) hydrolysis temperature; (C) hydrolysis time.

indicated that there were low limits of quantification (LOQs) for GA, CGA, CAF, EGCG, EC, GCG, ECG, and quercetin with the range of these being 0.01−0.15 mg/L. Relatively speaking, higher LOQs for EGC, C, and myricetin in the range of 0.30−0.45 mg/L were observed. The correlation coefficient (r) was >0.96 in the analysis of each compound.

As shown in Table 3, recoveries were determined in triplicate in Wuyi Rock tea by spiking pure standards to the extraction solution prior to the sample analysis. The mean recoveries and RSDs of the method for determination of GA, EGC, C, CGA, EGCG, EC, and GCG were 97.5−100.3% and within the range ±3.9% (n = 3), respectively.

The method of indirect determination for the quantification of myricetin and quercetin, which are flavonols, the hydrolysates from flavonol glucosides, could be influenced by hydrolysis. The mean recoveries and RSDs of the method for determination of myricetin and quercetin in Wuyi Rock tea were 82.1−92.1% and within the range of ±4.5% (n = 3), respectively. By multiplying their corresponding recoveries as the correction coefficient with quantificaiton, more reliable results could be obtained.

The above results confirmed that the development of the method in this study was an accurate and precise method for the determination of caffeine and selected polyphenols in Wuyi Rock tea.

Factors Affecting Hydrolysis of Flavonol Glucosides to Flavonols in Wuyi Rock Tea. *Results of Single-Factor Test. 1. Concentrations of HCl Solution.* Figure 2A shows that both myricetin content and quercetin content increased sharply with the concentration of HCl solution from 0 to 1.5 mol/L HCl and reached peak values at 1.5 mol/L HCl, whereas the contents of myricetin and quercetin both decreased gradually with increasing concentration of HCl solution from 1.5 to 9.0 mol/L. These results indicated that the concentration of 1.5 mol/L HCl solution was an appropriate concentration of HCl for hydrolyzing flavonol glucosides to flavonols in Wuyi Rock tea at 80 °C for 1 h.

2. Hydrolysis Temperature. As shown in Figure 2B, contents of myricetin and quercetin in Wuyi Rock tea exhibited a slight change when the hydrolyzing temperature was raised from 60 to 70 °C, whereas both myricetin content and quercetin content increased rapidly with increasing hydrolysis temperature from 70 to 80 °C, reaching peak values at 80 °C and then decreasing sharply with increasing hydrolysis temperature from 80 to 100 °C. These results suggested that 80 °C was a proper hydrolysis temperature for hydrolyzing flavonol glucosides to flavonols in Wuyi Rock tea at a concentration of 1.5 mol/L HCl solution for 1 h.

3. Hydrolysis Time. Quercetin content in Wuyi Rock tea exhibited a sharp increase from 0 to 0.5 h of hydrolysis, a slight decrease from 0.5 to 1 h, a gradual decrease from 1 to 2 h, and a rapid decrease from 2 to 2.5 h (Figure 2C). These results showed that 0.5−1 h of hydrolysis might be a proper hydrolysis time for hydrolyzing flavonol glucosides to quercetin in Wuyi Rock tea at 80 °C and a concentration of 1.5 mol/L HCl solution.

As shown in Figure 2C, myricetin content in Wuyi Rock tea exhibited a rapid increase from 0 to 0.5 h of hydrolysis, but almost no change of myricetin content from 0.5 to 1 h, and then showed a gradual decrease from 1 to 2.5 h. From the above results it could be concluded that 0.5−1 h of hydrolysis might be a suitable hydrolysis time for hydrolyzing flavonol glucosides to myricetin in Wuyi Rock tea at 80 °C and a concentration of 1.5 mol/L HCl solution.

Results of Design of Orthogonal Experiment. The hydrolysis conditions, including concentration of HCl solution, hydrolysis temperature, and hydrolysis time, for flavonoid glycosides to myricetin and quercetin, which were based on an orthogonal experiment $L_9(3)^4$ design, were determined. As shown in Table 4, the order of important factors of the hydrolysis conditions for hydrolyzing flavonoid glycosides to myricetin in Wuyi Rock tea was hydrolysis temperature (factor B), concentration of HCl (factor A), and hydrolysis time (factor C). In addition, Table 4 also shows that hydrolysis at a concentration of 2 mol/L HCl solution and at 70 °C for 1.5 h was the most beneficial hydrolysis condition for hydrolyzing flavonoid glycosides to myricetin in Wuyi Rock tea.

Table 4. Test Plans and Results of Range Analysis Based on an Orthogonal Experiment $L_9(3)^4$ Design for Hydrolyzing Flavonol Glucosides to Corresponding Flavonols in Wuyi Rock Tea

	factors				results	
expt	factor A: concn of HCl solution (mol/L)	factor B: hydrolysis temperature (°C)	factor C: hydrolysis time (h)	error analysis	myricetin (μg/mL)	quercetin (μg/mL)
1	1	70	0.5	1	36.7	28.3
2	1	80	1.0	2	29.0	38.0
3	1	90	1.5	3	48.8	46.4
4	2	70	1.0	3	64.3	70.8
5	2	80	1.5	1	41.6	73.8
6	2	90	0.5	2	49.5	78.6
7	3	70	1.5	2	56.5	66.5
8	3	80	0.5	3	42.5	67.3
9	3	90	1.0	1	47.7	87.0
myricetin (μg/mL)						
k_1	41.2	56.7	46.3			
k_2	55.9	40.7	50.7			
k_3	52.7	52.5	52.9			
R	14.7	15.9	6.6			
superior level	A_2	B_1	C_3			
important order of factor	B > A > C					
quercetin (μg/mL)						
k_1	28.7	42.1	44.3			
k_2	56.8	45.5	49.8			
k_3	56.1	53.9	47.5			
R	28.1	11.8	5.5			
superior level	A_2	B_3	C_2			
important order of factor	A > B > C					

Table 5. ANOVA of Myricetin and Quercetin Output after Hydrolysis

	factor	variance	df	F value	F critical value	signif ($P < 0.05$)
myricetin	concn of HCl	360.3	2	0.575	19.0	
	hydrolysis temp	409.2	2	0.653	19.0	
	hydrolysis time	68.1	2	0.109	19.0	
	error	626.4	2			
quercetin	concn of HCl	1546.3	2	402.0	19.0	*
	hydrolysis temp	221.4	2	57.5	19.0	*
	hydrolysis time	46.2	2	12.0	19.0	
	error	3.8	2			

Table 4 shows that the order of important factors of the hydrolysis conditions for hydrolyzing flavonoid glycosides to quercetin in Wuyi Rock tea was concentration of HCl (factor A), hydrolysis temperature (factor B), and hydrolysis time (factor C). In addition, Table 4 also shows that hydrolyzing at a concentration of 2 mol/L HCl solution and at 90 °C for 1 h might be the best hydrolysis condition for hydrolyzing flavonoid glycosides to quercetin in Wuyi Rock tea.

Further analysis of variance (ANOVA) indicated that there were no significant ($P > 0.05$) differences among different concentrations of HCl solution for hydrolyzing flavonoid glycosides to myricetin in Wuyi Rock tea; the same results were also found among different hydrolysis temperatures or among different hydrolysis times (Table 5). However, there were significant ($P < 0.05$) differences among different concentrations of HCl solution or among different hydrolysis temperatures for hydrolyzing flavonoid glycosides to quercetin in Wuyi Rock tea, whereas there were no significant ($P > 0.05$) differences among different hydrolysis times (Table 5).

From the above results it could be concluded that the best hydrolysis conditions (hydrolyzing at a concentration of 2 mol/L HCl solution and at 90 °C for 1 h) for hydrolyzing flavonoid glycosides to quercetin in Wuyi Rock tea could be considered as the best hydrolysis conditions for hydrolyzing flavonoid glycosides to their corresponding flavonols including quercetin and myricetin in Wuyi Rock tea.

Typical Chromatographic Performance of Wuyi Rock Tea Sample. As shown in Figure 3A,B, a typical chromatogram of tea polyphenols and caffeine in nonhydrolyzed extraction of Wuyi Rock tea sample was observed at different

dx.doi.org/10.1021/jf4056314 | J. Agric. Food Chem. 2014, 62, 2772−2781

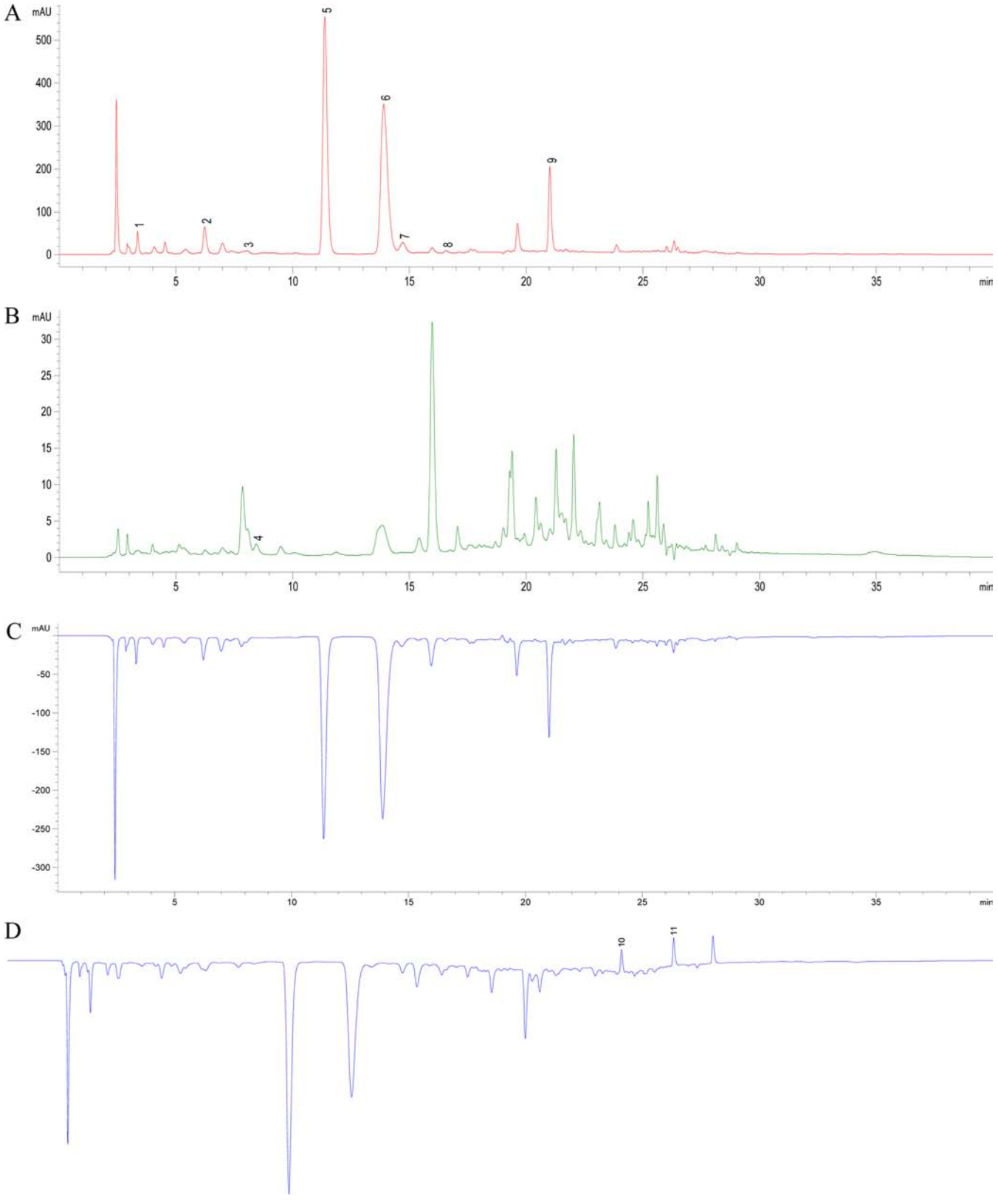

Figure 3. Typical chromatogram of tea sample extraction at different wavelengths under the experimental conditions. The sample contains GA (1), EGC (2), C (3), CGA (4), CAF (5), EGCG (6), EC (7), GCG (8), ECG (9), myricetin (10), and quercetin (11). (A) Tea sample extraction without hydrolysis was detected at acquisition wavelength of 278 nm and at reference wavelength of 360 nm. (B) Tea sample extraction without hydrolysis was detected at acquisition wavelength of 330 nm and at reference wavelength of 380 nm. (C) Tea sample extraction without hydrolysis was detected at acquisition wavelength of 370 nm and at reference wavelength of 290 nm. (D) Tea sample extraction after hydrolysis was detected at acquisition wavelength of 370 nm and at reference wavelength of 290 nm.

dx.doi.org/10.1021/jf4056314 | J. Agric. Food Chem. 2014, 62, 2772−2781

Table 6. Contents of Tea Polypheols and Caffeine in 'Wuyi Rougui' and 'Wuyi Shuixian' Samples

	'Wuyi Rougui' (g/kg)			'Wuyi Shuixian' (g/kg)			asymp signif (2-tailed)[a]	
compd	range	av	SD	range	av	SD	Mann− Whitney *U*	Kolmogorov−Smirnov *Z*
GA	1.17−2.02	1.50	0.24	0.91−1.91	1.40	0.37	0.353	0.400
EGC	41.20−61.61	48.34	6.66	21.08−30.56	26.12	3.03	0.000*	0.000*
C	0−11.69	5.98	4.54	0−12.72	4.58	4.46	0.613	0.759
CGA	0.54−0.85	0.65	0.10	0−1.68	0.28	0.60	0.023*	0.003*
CAF	22.82−27.26	24.58	1.48	19.34−30.22	23.16	3.18	0.165	0.164
EGCG	59.32−81.04	69.46	6.65	57.83−88.49	72.14	9.68	0.631	0.988
EC	3.58−6.55	5.58	0.97	3.73−6.98	5.41	1.00	0.529	0.400
GCG	0.58−1.13	0.80	0.14	0−1.75	0.83	0.68	0.971	0.400
ECG	8.80−10.78	9.47	0.72	6.44−9.82	8.09	0.98	0.004*	0.003*
myricetin glycosides	2.82−4.91	3.88	0.61	1.00−2.61	1.76	0.40	0.000*	0.000*
myricetin	none detected			none detected				
quercetin glycosides	1.19−1.99	1.64	0.25	1.46−2.73	1.86	0.41	0.529	0.759
quercetin	none detected			none detected				

[a]*, $P < 0.05$.

acquisition wavelengths and at different reference wavelengths. Contents of GA, EGC, C, CAF, EGCG, EC, and ECG were detected at an acquisition wavelength of 278 nm and at a reference wavelength of 360 nm (Figure 3A), whereas CGA content was detected at an acquisition wavelength of 330 nm and at a reference wavelength of 380 nm (Figure 3B).

No target substances (myricetin and quercetin) in nonhydrolyzed extraction of Wuyi Rock tea sample were detected at an acquisition wavelength of 370 nm and a reference wavelength at 290 nm (Figure 3C). In contrast, contents of myricetin and quercetin in hydrolyzed extraction of Wuyi Rock tea sample were detected at an acquisition wavelength of 370 nm and a reference wavelength of 290 nm (Figure 3D). These results indicated that myricetin and quercetin could be detected in hydrolyzed extraction of Wuyi Rock tea sample, which implied myricetin and quercetin might be hydrolyzed from their corresponding glycosides. Thus, the contents of myricetin glycosides and quercetin glycosides could be determined by detecting the content of corresponding myricetin and quercetin.

From the above results it could be concluded that caffeine and some selected polyphenols such as GA, EGC, C, EGCG, EC, ECG, and CGA in nonhydrolyzed extraction of Wuyi Rock tea sample could be simultaneously detected, whereas other polyphenols such as myricetin and quercetin also could be simultaneously detected in hydrolyzed extraction of Wuyi Rock tea sample.

Quantification of Caffeine and Selected Polyphenols in Wuyi Rock Tea Samples. In this effort, the developed HPLC method for simultaneous determination of caffeine and some selected polyphenols was successfully applied in the determination of 20 samples of Wuyi Rock tea, including 10 samples of 'Wuyi Rougui' and 10 samples of 'Wuyi Shuixian'. The results showed that, except for myricetin and quercentin, the other nine kinds of polyphenols (GA, EGC, C, EGCG, EC, ECG, CGA, myricetin glycosides, and quercetin glycosides) and caffeine were all detected in the above 20 samples of Wuyi Rock tea (Table 6).

Until now, the distribution of caffeine and selected polyphenols in two cultivar sets of Wuyi Rock tea was still unclear. The Mann−Whitney *U* test and Kolmogorov−Smirnov test, methods of nonparametric statistics, were used for evaluating the differences of caffeine and selected polyphenols in 'Wuyi Rougui' and 'Wuyi Shuixian', two cultivar sets of Wuyi Rock tea. The results indicated that both the Mann−Whitney *U* test and Kolmogorov−Smirnov test showed significant ($P < 0.05$) differences of ECG, CGA, ECG, and myricetin glycosides in 'Wuyi Rougui' and 'Wuyi Shuixian', which might be credited with causing the different tastes between these two cultivar sets of Wuyi Rock tea. However, there were no significant ($P > 0.05$) differences of GA, C, CAF, EGCG, EC, GCG, and quercetin glycosides in 'Wuyi Rougui' and 'Wuyi Shuixian' (Table 6).

It also could be found from this effort that contents of C, GCG, and CGA in 'Wuyi Rougui' and 'Wuyi Shuixian' were at low levels (Table 6). In addition, some peaks of other unknown substances overlapped slightly with the peak of CGA (Figure 3B). The above observation might result in the accuracy of the quantification of C, GCG, and CGA in Wuyi Rock tea.

In conclusion, due to the very many kinds of flavonoid glycosides in tea and the lack of commercial standards of flavonoid glycosides, it is critical to develop a rapid and cheap method for determining the flavonoid glycosides of tea. The contents of myricetin glycosides and quercetin glycosides in Wuyi Rock tea could be determined by detecting the content of corresponding myricetin and quercetin. Developing the optimized hydrolysis conditions for hydrolyzing flavonoid glycosides to their corresponding flavonols including quercetin and myricetin in Wuyi Rock tea was regarded as a key technology for determining the content of corresponding myricetin and quercetin. In our work, hydrolysis at a concentration of 2 mol/L HCl solution and at 90 °C for 1 h was found to be optimal for hydrolyzing flavonoid glycosides to myricetin and quercetin in Wuyi Rock tea. Caffeine and seven kinds of polyphenols (GA, EGC, C, EGCG, EC, ECG, and CGA) in 20 samples of Wuyi Rock Tea were simultaneously determined using a simple and fast reverse-phase high-performance liquid chromatography procedure coupled with a photodiode array detector (RP-HPLC-PDAD), which was developed in this effort. This work also showed that there were significant ($P < 0.05$) differences of ECG, CGA, ECG, and myricetin glycosides in 'Wuyi Rougui' and 'Wuyi Shuixian', which were credited with causing the different tastes between these two cultivar sets of Wuyi Rock Tea. Therefore, it was suggested that the application of RP-HPLC-DAD, the method developed in this study, might be a promising method for simultaneously determing caffeine and some selected polyphenols in Wuyi Rock tea, evaluating the tea quality of 'Wuyi

Rougui' and 'Wuyi Shuixian', and clarifying the cause of "cultivated varieties flavor" of Wuyi Rock tea. In addition, a simple and fast method for determining the flavonoid glycosides in Wuyi Rock tea, except myricetin glycosides and quercetin glycosides, should be further developed.

AUTHOR INFORMATION

Corresponding Author

*(H.-T.L.) E-mail: hetonglin@126.com.

Funding

This work was supported by the National Natural Science Foundation of China (Grant 31270735), the Key Science and Technology Program of Fujian Province of China (Grant 2013N5009), the Science and Technology Program of General Administration of Quality Supervision, Inspection and Quarantine of China (Grant 2013QK318), and the Program for New Century Excellent Talents in Fujian Province University of China (Grant NCETFJ-200720).

Notes

The authors declare no competing financial interest.

ABBREVIATIONS USED

RP-HPLC-PDAD, reverse-phase high-performance liquid chromatography procedure coupled with photodiode array detector; GA, gallic acid; EGC, epigallocatechin; C, catechin; CGA, chlorogenic acid; EGCG, epigallocatechin gallate; EC, epicatechin; GCG, gallocatechin gallate; ECG, epicatechin gallate; CAF, caffeine; UV, ultraviolet; PDAD, photodiode array detector; HPLC, high-performance liquid chromatography; ISO, International Organization for Standardization; Det.278 nm, detection wavelength at 278 nm; ref.360 nm, reference wavelength at 360 nm; Det.330 nm, detection wavelength at 330 nm; ref.380 nm, reference wavelength at 380 nm; Det.370 nm, detect wavelength at 370 nm; ref.290 nm, reference wavelength at 290 nm; EDTA, ethylenediaminetetraacetic acid; LOQ, limit of quantification; RSD, relative standard deviation; ANOVA, analysis of variance; asymp signif (2-tailed), asymptotic significance (two-tailed)

REFERENCES

(1) Higdon, J. V.; Frei, B. Tea catechins and polyphenols: health effects, metabolism, and antioxidant functions. *Crit. Rev. Food Sci. Nutr.* **2003**, *43*, 89−143.

(2) Sakakibara, H.; Honda, Y.; Nakagawa, S.; Ashida, H.; Kanazawa, K. Simultaneous determination of all polyphenols in vegetables, fruits, and teas. *J. Agric. Food Chem.* **2003**, *51*, 571−581.

(3) Du, G. J.; Zhang, Z.; Wen, X. D.; Yu, C.; Calway, T.; Yuan, C. S.; Wang, C. Z. Epigallocatechin gallate (EGCG) is the most effective cancer chemopreventive polyphenol in green tea. *Nutrients* **2012**, *4*, 1679−1691.

(4) Kuroda, Y.; Hara, Y. Antimutagenic and anticarcinogenic activity of tea polyphenols. *Mutat. Res.−Rev. Mutat. Res.* **1999**, *436*, 69−97.

(5) Bustos, I.; Garcia-Cayuela, T.; Hernandez-Ledesma, B.; Pelaez, C.; Requena, T.; Carmen Martinez-Cuesta, M. Effect of flavan-3-ols on the adhesion of potential probiotic lactobacilli to intestinal cells. *J. Agric. Food Chem.* **2012**, *60*, 9082−9088.

(6) Chang, Y. C.; Chen, P. N.; Chu, S. C.; Lin, C. Y.; Kuo, W. H.; Hsieh, Y. S. Black tea polyphenols reverse epithelial-to-mesenchymal transition and suppress cancer invasion and proteases in human oral cancer cells. *J. Agric. Food Chem.* **2012**, *60*, 8395−8403.

(7) Gorjanovic, S.; Komes, D.; Pastor, F. T.; Belscak-Cvitanovic, A.; Pezo, L.; Hecimovic, I.; Suznjevic, D. Antioxidant capacity of teas and herbal infusions: polarographic assessment. *J. Agric. Food Chem.* **2012**, *60*, 9573−9580.

(8) Jimenez, R.; Duarte, J.; Perez-Vizcaino, F. Epicatechin: endothelial function and blood pressure. *J. Agric. Food Chem.* **2012**, *60*, 8823−8830.

(9) Soares, S.; Kohl, S.; Thalmann, S.; Mateus, N.; Meyerhof, W.; De Freitas, V. Different phenolic compounds activate distinct human bitter taste receptors. *J. Agric. Food Chem.* **2013**, *61*, 1525−1533.

(10) Tanaka, M.; Zhao, J.; Suyama, A.; Matsui, T. Epigallocatechin gallate promotes the vasorelaxation power of the antiatherosclerotic dipeptide Trp-His in contracted rat aorta. *J. Agric. Food Chem.* **2012**, *60*, 9048−9054.

(11) Zhou, L.; Elias, R. J. Investigating the hydrogen peroxide quenching capacity of proteins in polyphenol-rich foods. *J. Agric. Food Chem.* **2011**, *59*, 8915−8922.

(12) Zhu, L. F.; Xu, M.; Zhu, H. T.; Wang, D.; Yang, S. X.; Yang, C. R.; Zhang, Y. J. New flavan-3-ol dimer from green tea produced from camellia taliensis in the Ai-Lao Mountains of southwest China. *J. Agric. Food Chem.* **2012**, *60*, 12170−12176.

(13) Yin, J.; Andersen, M. L.; Skibsted, L. H. Reduction of ferrylmyoglobin by theanine and green tea catechins. Importance of specific acid catalysis. *J. Agric. Food Chem.* **2013**, *61*, 3159−3166.

(14) Anesini, C.; Ferraro, G. E.; Filip, R. Total polyphenol content and antioxidant capacity of commercially available tea (*Camellia sinensis*) in Argentina. *J. Agric. Food Chem.* **2008**, *56*, 9225−9229.

(15) Bandaruk, Y.; Mukai, R.; Kawamura, T.; Nemoto, H.; Terao, J. Evaluation of the inhibitory effects of quercetin-related flavonoids and tea catechins on the monoamine oxidase − a reaction in mouse brain mitochondria. *J. Agric. Food Chem.* **2012**, *60*, 10270−10277.

(16) Roberts, E. A. H.; Wood, D. J. Separation of tea polyphenols on paper chromatograms. *Biochem. J.* **1953**, *53*, 332−336.

(17) Lin, Y. S.; Wu, S. S.; Lin, J. K. Determination of tea polyphenols and caffeine in tea flowers (*Camellia sinensis*) and their hydroxyl radical scavenging and nitric oxide suppressing effects. *J. Agric. Food Chem.* **2003**, *51*, 975−980.

(18) Hadad, G. M.; Salam, R. A. A.; Soliman, R. M.; Mesbah, M. K. Rapid and simultaneous determination of antioxidant markers and caffeine in commercial teas and dietary supplements by HPLC-DAD. *Talanta* **2012**, *101*, 38−44.

(19) Srividhya, B.; Raj, V.; Subramanian, R. Determination of catechins and antioxidant properties of commercial green and black teas. *Asian J. Chem.* **2011**, *23*, 4603−4605.

(20) Wang, Y.; Li, Q.; Wang, Q.; Li, Y.; Ling, J.; Liu, L.; Chen, X.; Bi, K. Simultaneous determination of seven bioactive components in oolong tea *Camellia sinensis*: quality control by chemical composition and HPLC fingerprints. *J. Agric. Food Chem.* **2012**, *60*, 256−260.

(21) Blahova, E.; Lehotay, J. Sample preparation and HPLC determination of catechins in green tea. *Chem. Anal.−Warsaw* **2006**, *51*, 795−807.

(22) Choung, M. G.; Lee, M. S. Optimal extraction conditions for simultaneous determination of catechins and caffeine in green tea leaves. *Food Sci. Biotechnol.* **2011**, *20*, 327−333.

(23) He, Q.; Lv, Y.; Zhou, L.; Shi, B. Simultaneous determination of caffeine and catechins in tea extracts by HPLC. *J. Liq. Chromatogr. Relat. Technol.* **2010**, *33*, 491−498.

(24) Prayong, P.; Weerapreeyakul, N.; Sripanidkulchai, B. Validation of isocratic eluting and stepwise flow rate gradient for HPLC determination of catechins, gallic acid and caffeine in tea. *Sci. Asia* **2007**, *33*, 113−117.

(25) Sun, X. L.; Liu, S. H.; Wang, L.; Li, W. G.; Zhao, C. J.; Zu, Y. G. Simultaneous determination of five catechins in green tea using high performance liquid chromatography. *Bull. Bot. Res.* **2011**, *31*, 377−380.

(26) Hollman, P. C. H.; Arts, I. C. W. Flavonols, flavones and flavanols − nature, occurrence and dietary burden. *J. Sci. Food Agric.* **2000**, *80*, 1081−1093.

(27) Jiang, L.; Shen, X.; Shoji, T.; Kanda, T.; Zhou, J.; Zhao, L. Characterization and activity of anthocyanins in zijuan tea (*Camellia sinensis* var. kitamura). *J. Agric. Food Chem.* **2013**, *61*, 3306−3310.

(28) Price, K. R.; Rhodes, M. J. C.; Barnes, K. A. Flavonol glycoside content and composition of tea infusions made from commercially

available teas and tea products. *J. Agric. Food Chem.* **1998**, *46*, 2517−2522.
(29) Fieschi, M.; Codignola, A.; Luppi Mosca, A. M. Mutagenic flavonol aglycones in infusions and in fresh and pickled vegetables. *J. Food Sci.* **1989**, *54*, 1492−1495.
(30) Ligor, M.; Kornysova, O.; Maruska, A.; Buszewski, B. Determination of flavonoids in tea and rooibos extracts by TLC and HPLC. *J. Planar Chromatogr.−Modern TLC* **2008**, *21*, 355−360.
(31) Apak, R.; Cekic, S. D.; Cetinkaya, A.; Filik, H.; Hayvali, M.; Kilic, E. Selective determination of catechin among phenolic antioxidants with the use of a novel optical fiber reflectance sensor based on indophenol dye formation on nano-sized TiO_2. *J. Agric. Food Chem.* **2012**, *60*, 2769−2777.
(32) Wang, H.; Helliwell, K. Determination of flavonols in green and black tea leaves and green tea infusions by high-performance liquid chromatography. *Food Res. Int.* **2001**, *34*, 223−227.

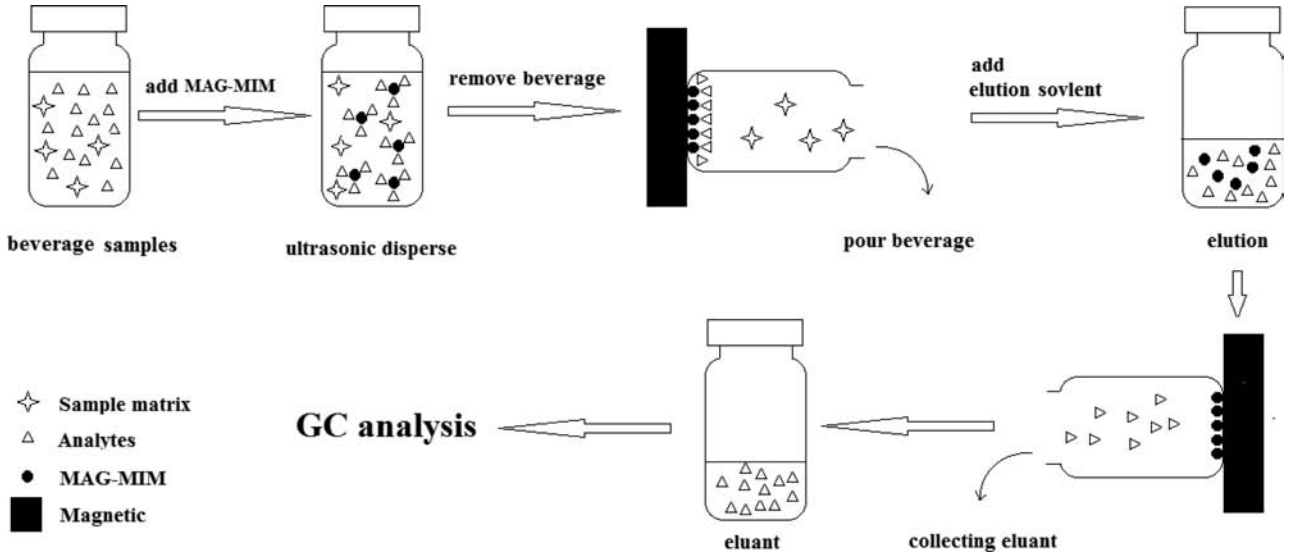

Figure 1. The MAG-MIM-dSPE procedure.

after removal of template molecules from polymers, leaving behind cavities for subsequent rebinding, which can selectively rebind target molecules from a mixture of closely related compounds. Compared with biological macromolecules such as antibodies, receptors, and enzymes, MIPs are much more stable and can be used under more demanding conditions.[36] However, most MIPs suffer from problems of poor recognition in water and template leakage at the present stage.

Furthermore, magnetic particles can be collected and separated from the liquid phase under an external magnetic field, which avoids tedious filtration or centrifugation procedures and allow particles to be easily retrieved at low cost.[37−39] If some magnetic components are encapsulated into MIPs, the resulting composite magnetic MIPs would not only have susceptible magnetic characteristics but also have high selectivity for the target molecule. Composite magnetic MIPs have been prepared, as reported in the literature, and they all exhibited higher recognition selectivity and certain magnetic responses to external magnetic fields.[40−43]

The aim of this work was to develop a new MAG-MIM-dSPE-GC method using composite magnetic dummy molecularly imprinted microspheres (MAG-MIM) as the adsorbents for dSPE in the selective extraction and determination of five phthalates from plastic bottled beverages. The new MAG-MIM adsorbents, which were synthesized by coprecipitation coupled with aqueous suspension polymerization using diisononyl phthalate as the dummy template, improve the poor selectivity of MIPs in a water environment and eliminate the effect of template leakage of MIPs upon quantitative analysis. The MAG-MIM-dSPE-GC method combines the quick separation of magnetic particles, special selectivity of MIM, and high extraction efficiency of dSPE and potentially could be applied to selective screening of phthalates in beverages.

EXPERIMENTAL PROCEDURES

Chemicals and Reagents. Butyl benzyl phthalate (BBP), diethyl phthalate (DEP), dibutyl phthalate (DBP), diisooctyl phthalate (DIOP), diisononyl phthalate (DINP), and dioctyl phthalate (DNOP) were obtained from Crystal Pure Industrial Co., Ltd. (Shanghai, China). Methanol (HPLC grade) was from Xingke Biochem. Co., Ltd. Chloroform, dichloromethane, poly(vinylpyrrolidone) (PVP), and ammonia were purchased from Huaxin Chemical Reagent Co., Ltd. (Baoding, China). Acetone, ethyl acetate, methanol, ethanol, and acetic acid were obtained from Huadong Chemical Reagent Co. (Tianjin, China). Iron(II) chloride tetrahydrate ($FeCl_2{\cdot}4H_2O$), iron(III) chloride hexahydrate ($FeCl_3{\cdot}6H_2O$), oleic acid, 2,2-azobis(isobutyronitrile) (AIBN), methacrylic acid (MAA), and acetonitrile were obtained from Kermel Chemical Reagents Center (Tianjin, China). Ethylene glycol dimethacrylate (EGDMA) was obtained from Sigma-Aldrich (St. Louis, MO). A Nd−Fe−B magnet (80 × 60 × 17 mm) was purchased from a local market in Baoding, China. All the reagents used in this work were of analytical grade (purity ≥99%). Double deionized water was filtered through a 0.45 μm filter membrane before use.

Instrumentation and Conditions. Chromatographic analysis was performed on a Shimadzu GC-2014 system equipped with a split/splitless injector and an FID detector (Shimadzu, Japan). High-purity nitrogen (99.999%) was used as carrier gas. A GH-300 high-purity hydrogen generator and a GA-2000A air pump (Beijing ZXHL Co., Ltd., China) were used to supply hydrogen gas and auxiliary gas (supply oxygen) at the rate of 40 and 400 mL/min, respectively. The capillary column was KB-1 (100% dimethyl polysiloxane as stationary phase, 30 m × 0.25 mm × 0.25 μm, Kromat, Delran, NJ), and its flow rate was set at 1.7 mL/min with a split ratio of 10. An N-2000 workstation (Zheda Zhineng, Hangzhou, China) was used as the data acquisition system. The temperature-programmed mode was as follows: the initial oven temperature was 150 °C for 2.0 min and then increased to 285 °C at the rate of 25 °C/min and held for 10 min. The temperatures of the injection port and FID detector were set at 290 °C and 300 °C, respectively. A Fourier transform infrared (FT-IR) spectrometer (Shimadzu, Japan) was employed to examine infrared spectra of obtained particles. Magnetic properties were measured with a LakeShore 7307 (Lakeshore Cryotronic) vibration magnetometer (VSM) at 300 K. The obtained particles were also characterized by thermogravimetric analysis (TGA, SDTA851E). The morphology of MAG-MIM was characterized by field-emission scanning electron microscopy (FE-SEM), S-4200 (Hitachi, Ontario, Canada). The morphology of Fe_3O_4 magnetite was characterized by transmission electron microscopy (TEM; JEM-100SX, JEOL, Tokyo, Japan).

Preparation of Fe_3O_4 Magnetite with a Hydrophobic Shell. The Fe_3O_4 magnetites with a hydrophobic shell were prepared by the coprecipitation method as follows: $FeCl_2{\cdot}4H_2O$ (0.02 mol) and $FeCl_3{\cdot}6H_2O$ (0.03 mol) were dissolved into 100 mL of deaerated deionized water, 2.0 mL of oleic acid was added dropwise into the solution, and then the mixture was placed in an ultrasonic environment for 20 min under vigorous stirring. Fifteen milliliters of aqueous ammonia was added drop by drop when the temperature of the water bath was elevated to 60 °C. After 30 min, when the temperature was elevated to

dx.doi.org/10.1021/jf4051705 | J. Agric. Food Chem. 2014, 62, 2782−2789

80 °C, another 2.0 mL of oleic acid was added. After 2.0 h, magnetic precipitates were isolated from the solvent by a permanent magnet and washed several times with highly purified deaerated water and ethanol to remove unreacted ferric chloride and oleic acid.

Preparation of MAG-MIM. The MAG-MIM were prepared as follows: Fe_3O_4 magnetite (4.0 mmol), diisononyl phthalate (DINP) (2.0 mmol), and MAA (8.0 mmol) were added into 20 mL of chloroform. After EGDMA (50 mmol) and AIBN (1.2 mmol) were added, the solution was sonicated for 5.0 min to fully dissolve them. Finally, the solution was added dropwise to PVP solution (27 mmol of PVP dissolved into 120 mL of water) by stirring at 600 rpm and heated at 60 °C for 24 h. After polymerization, the obtained MAG-MIM particles were separated, washed with methanol−acetic acid (9:1, v/v) and methanol, respectively, under ultrasound to remove template and unreacted reagents, and then dried under vacuum at 45 °C for 24 h. To verify the effectiveness of the cleaning process, the washing solvent (10 mL) was evaporated, and the sample mixture was redissolved in acetone (0.5 mL) before injection into the gas chromatograph. The magnetic nonimprinted microspheres (MAG-NIM) were prepared and processed similarly as above, except that template was not added.

MAG-MIM-dSPE Procedure. Plastic bottled beverages were obtained from local supermarkets in Baoding, and the MAG-MIM-dSPE procedure was performed as shown in Figure 1. MAG-MIM (100 mg) were added into a 10 mL beverage sample and entirely dispersed by ultrasound at room temperature. After 10 min, phase separation was performed by magnetic separation with a applied magnetic field (Nd−Fe−B magnet) in the bottom of bottle, and then the MAG-MIM were eluted with 7.0 mL ethyl acetate−acetic acid (85:15, v/v) to desorb analytes from the adsorbents. Finally, the eluent was evaporated under a gentle nitrogen stream, and the sample was reconstituted with 0.5 mL of acetone for further GC analysis.

RESULTS AND DISCUSSION

Preparation of MAG-MIM. The preparation of MAG-MIM particles involved the synthesis of hydrophobic superparamagnetic Fe_3O_4 particles, MIM functionalization of the magnetic particles, and removal of the template to generate the recognition sites. Hydrophobic superparamagnetic Fe_3O_4 particles were prepared by a modified coprecipitation method, and the TEM image of the hydrophobic Fe_3O_4 particles showed that their sizes were on nanoscale (Figure 2A). The surface of magnetite was hydrophobic with a coating of oleic acid, which avoided electrostatic agglomeration and ensured the uniform dispersion of magnetic nanoparticles in the polymerization solution and homogeneous embedding. Ultrasound treatment was employed for modification of Fe_3O_4, making the procedure simple, rapid, and easily controlled. This strategy was successful in the fabrication of magnetically susceptible polymer-supported imprinted microspheres. To improve binding capacity, selectivity, and compatibility of MAG-MIM in water, aqueous suspension polymerization was adopted. Moreover, diisononyl phthalate (DINP) was chosen as the template mimic, which eliminated the effect of template leaking during quantitative analysis and demonstrated special recognition ability for the five phthalates.

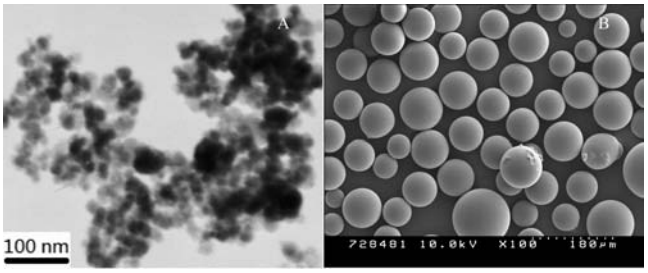

Figure 2. (A) Transmission electron microscopy (TEM) of Fe_3O_4 microspheres and (B) scanning electron microscopy (SEM) of MAG-MIM.

In the oil-in-water suspension polymerization, MAA was a common monomer, and EGDMA as a cross-linker maintained the stability of imprinting sites while making the polymer easier to be handled and processed. Generally, the molar ratios between template and monomer play an important role in the affinity and imprinting effect of MIM toward its template molecule. Therefore, the molar ratios between template and monomer of 1:2, 1:3, 1:4, and 1:6 were investigated, while a molar ratio of 4:25 between monomer and cross-linker was selected to ensure the formation of the defined recognition sites. When porogens had poor hydrogen bonding capacity, the interaction between template and functional monomer was mainly influenced by the dielectric constant of the solvent. The aprotic porogen with a small dielectric constant favored the formation of a higher concentration of template−monomer complexes, which resulted in MIM with high affinity and selectivity.[44] Therefore, taking hydrogen bonding capacity and dielectric constants of porogens into consideration, chloroform and toluene were investigated as porogens for the entire synthetic process. Figure 2B shows that the morphology of MAG-MIM was regular spherical when using chloroform as porogen and a molar ratio of 1:4:25 for template, monomer, and cross-linker. With further consideration to the mechanical strength and special affinity to phthalates, 20 mL of chloroform was chosen as porogenic solvent. Although water was considered to weaken, and even to eliminate, the noncovalent interaction (hydrogen bond, van der Waals force, etc.) between functional monomer and template, the MAG-MIM prepared by aqueous suspension polymerization using PVP as dispersing agent exhibited good recognition performance.

The GC-FID trace of washing solvent after five washes (Figure 8A) proved that methanol can dissolve and wash out DINP,[45,46] allowing MAG-MIM to be cleaned. The preparation method for MAG-MIM applied in this work was aqueous suspension polymerization, and the solvent was water in which methanol can effectively disperse and wash out the DINP template. Moreover, some added acetic acid can destroy the hydrogen bond for imprinting and help methanol wash out the template. Actually, on the basis of the dummy template strategy adopted in this work, residual DINP template on MIM was not washed out and leaked during the extraction procedure but would still not affect the quantitative determination because the leaked template can be fully separated from the analytes during GC separation.

Characterization of MAG-MIM. The products of Fe_3O_4 and MAG-MIM were investigated by FT-IR spectroscopy (Figure 3A). A sharp and strong Fe−O stretching peak (≈584 cm^{-1}) was observed in the trace of Fe_3O_4, while this characteristic peak was not in the trace of MAG-MIM, indicating that Fe_3O_4 magnetite of MAG-MIM was coated with polymers. The band at 1732 cm^{-1} was assigned to the absorption of COOH, and the band at 1233 cm^{-1} was ascribed to stretching vibrations of C−O−C in MAG-MIM. The characteristic bands at 2900 cm^{-1} and 1800 cm^{-1} of diisononyl phthalate still markedly existed in the spectra of MAG-MIM without extraction of the template, but they greatly weakened after extraction. In addition, the GC-FID trace of washing solvent after five washes (Figure 8A) show that MAG-MIM had

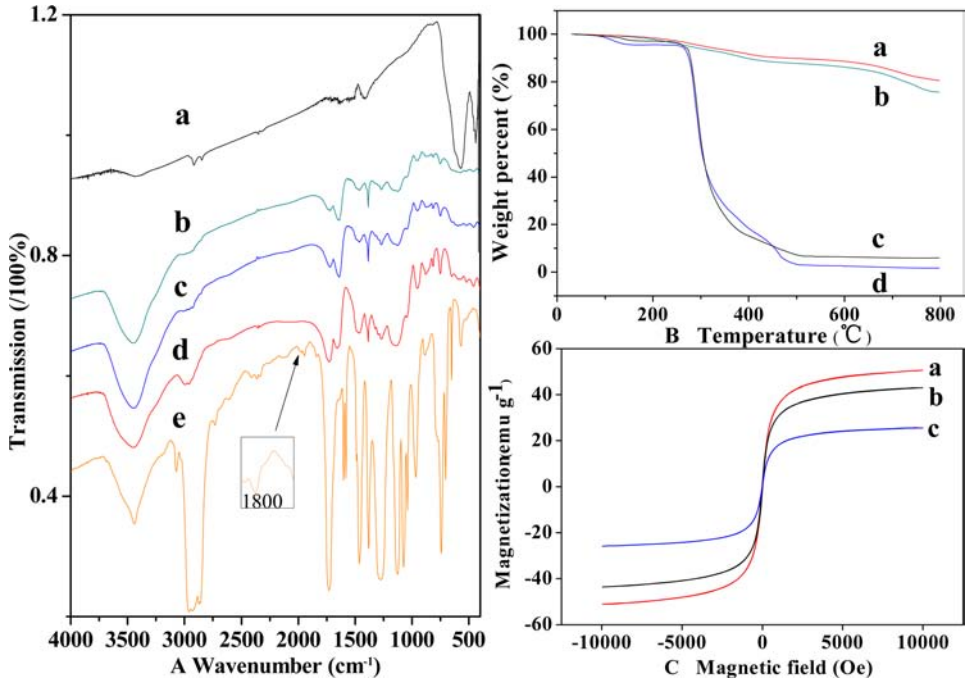

Figure 3. (A) FT-IR spectra of Fe_3O_4 particles (a), MAG-NIM (b), MAG-MIM after extraction of the template (c), MAG-MIM without extraction of the template (d), and diisononyl phthalate (e). (B) TGA of Fe_3O_4 (a), hydrophobic Fe_3O_4 (b), MAG-MIM (c), and MAG-NIM (d). (C) VSM of Fe_3O_4 (a), hydrophobic Fe_3O_4 (b), and MAG-MIM (c).

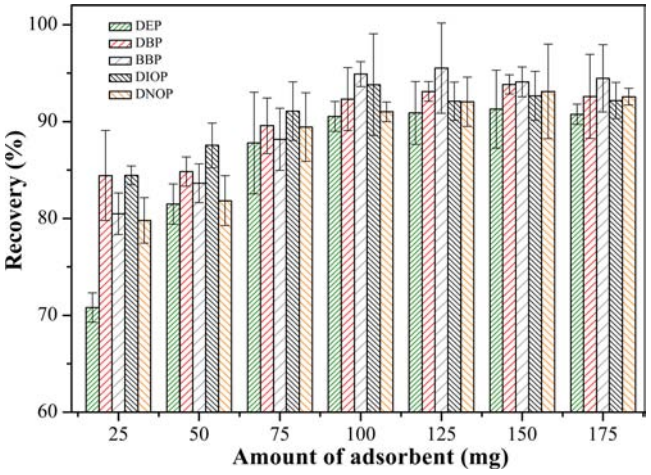

Figure 4. Effect of MAG-MIM amounts in dSPE.

been cleaned. All these observations indicated that MAG-MIM were prepared well.

Figure 3B shows the TGA curve of MAG-MIM and MAG-NIM compared with Fe_3O_4 magnetite and hydrophobic Fe_3O_4 magnetite. There was no dramatic weight loss below temperature of 240 °C, which means that all materials were stable under 240 °C. Significant weight loss occurred from 270 °C to 450 °C owing to the thermal degradation of MIM polymer (c) and NIM polymer (d). The outside layer of beads was a polymer mixture resulting from a different degree of polymerization. This caused the inflection (e.g., at about 10%) and different degradation rates in the TGA trace of MIM (c) and NIM (d). The remaining weight was attributed to the existence of Fe_3O_4 particles, and the quantity of loss of hydrophobic Fe_3O_4 magnetite (b) was more than Fe_3O_4 magnetite (a) without chemical modification, respectively.

The magnetic properties of the obtained materials were analyzed by VSM at room temperature, and the results are illustrated in Figure 3C. It is obvious that there was no hysteresis; both remanence and coercivity were zero, suggesting that the materials were superparamagnetic. The saturation magnetization (M_s) values of Fe_3O_4 magnetite, hydrophobic Fe_3O_4 magnetite, and MAG-MIM were about 51, 44, and 26 emu/g, respectively. The decrease of the M_s value was due to the coating of a hydrophobic layer and an organic polymer shell layer. Although the M_s value of MAG-MIM was reduced to 26 emu/g, they were susceptible to magnetic fields and could be easily separated from a suspension.

Optimization of MAG-MIM-dSPE Procedures. Various factors influencing the MAG-MIM-dSPE extraction effect were investigated, and the results are shown in Figures 4–6. Regarding the MAG-MIM particles that were dispersed in 10 mL of sample solution to rebind the five phthalates during the extraction procedure, the amount of adsorbent used should provide sufficient binding sites for the analytes and achieve good recoveries. Therefore, the minimum amount of MAG-MIM to achieve efficient recoveries was investigated, and Figure 4 shows that the recoveries for the five phthalates were more than 90.5% when 100 mg of MAG-MIM was added to samples, while the recoveries kept constant with a further increase to 175 mg. Therefore, 100 mg of MAG-MIM was selected as the optimal amount of dSPE adsorbent.

When 100 mg of MAG-MIM was dispersed in a sample solution, the analytes should contact the surface of sorbents and attain adsorption−desorption equilibrium in the appropriate time. As shown in Figure 5A, the influence of adsorption time was studied, and extraction equilibria were obtained in a short time. DBP and BBP achieved the largest extraction recoveries in 3 min, while DEP, DIOP, and DNOP needed 10 min to ensure full extraction because the structures of DBP and BBP matched the binding sites of MAG-MIM better than DEP, DIOP, and

dx.doi.org/10.1021/jf4051705 | J. Agric. Food Chem. 2014, 62, 2782−2789

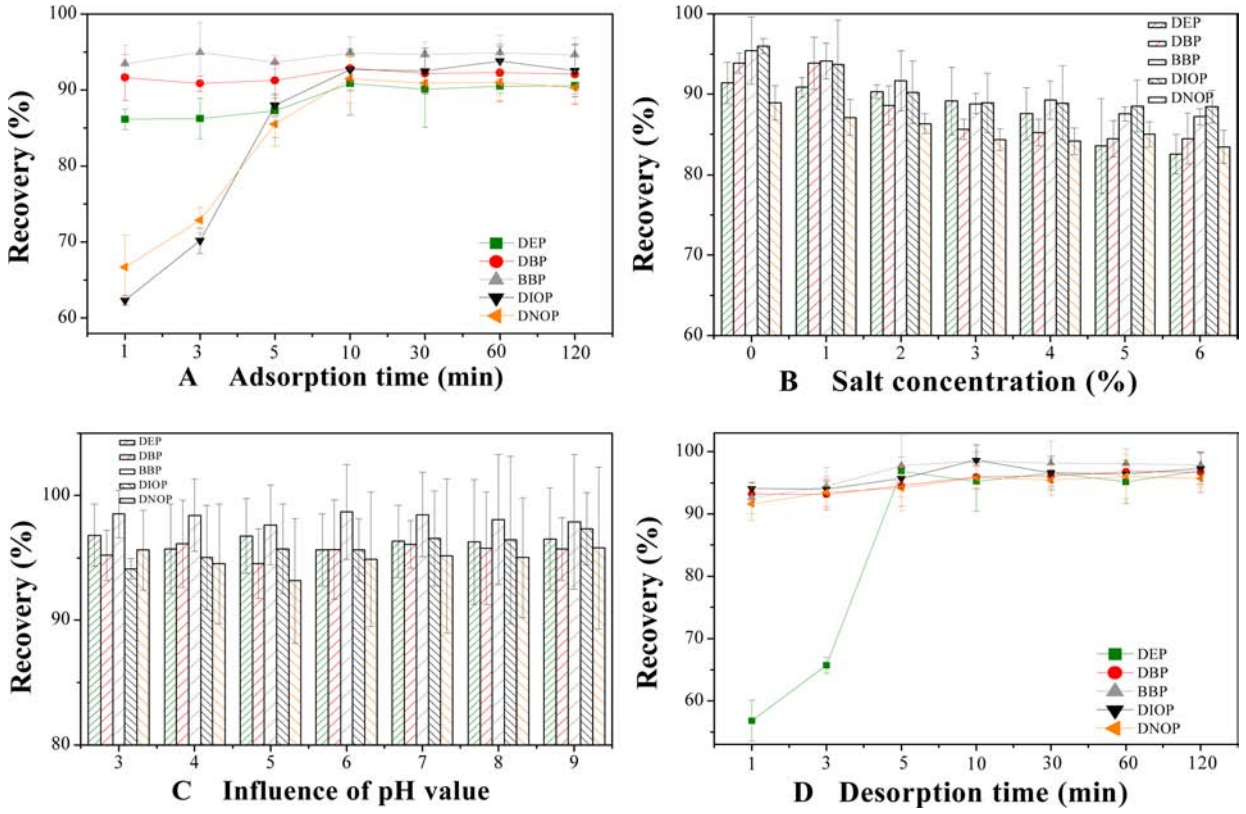

Figure 5. Effect of adsorption time (A), salt concentration (B), pH value (C), and desorption time (D) in MAG-MIM-dSPE.

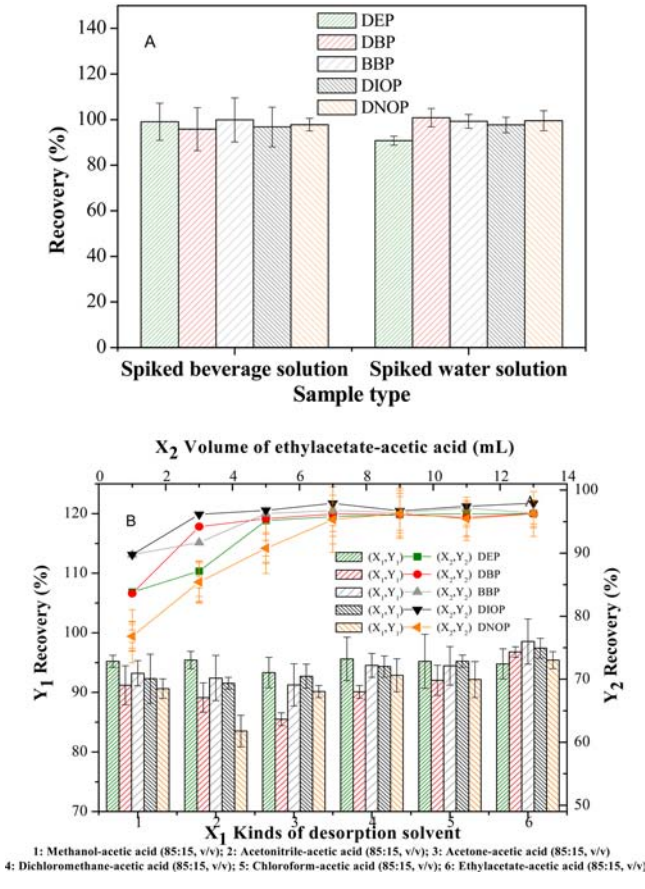

Figure 6. Effect of organic matter in (A) beverages and (B) desorption solvent in MAG-MIM-dSPE.

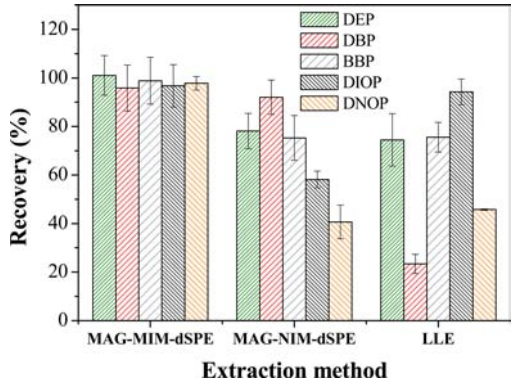

Figure 7. Comparison of MAG-MIM-dSPE, MAG-NIM-dSPE, and simple ethyl acetate extraction.

DNOP. Therefore, the time of adsorption was determined for 10 min.

Generally, an increase in ionic strength decreased the concentration of analytes in sample solution and enhanced the extraction efficiency of MAG-MIM. To evaluate the possibility of a salting out effect, extraction efficiency was studied with an increase in sodium chloride concentration over a range of 0−6% (w/v). As shown in Figure 5B, there was almost constant extraction recovery with an increase of salt concentration from 0% to 1% and then a slight decrease in recovery with a further increase to 6% in salt concentration, which indicated that the ionic strength of the samples hardly interfere with extraction efficiency. Similarly, when the influence of pH was investigated, as shown in Figure 5C, there was no obvious variation in extraction efficiency in a pH range from 3.0 to 9.0 probably because the phthalate structures

dx.doi.org/10.1021/jf4051705 | J. Agric. Food Chem. 2014, 62, 2782−2789

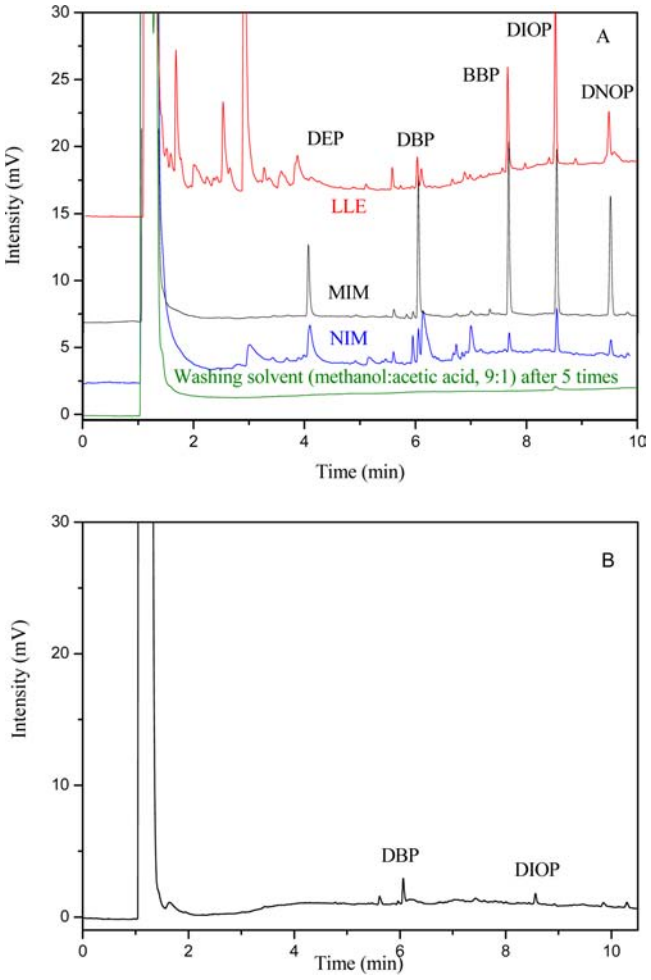

Figure 8. Chromatograms of (A) spiked beverage sample and (B) real sample.

were stable and the MAG-MIM-dSPE extraction procedure was not easily affected by an acid or alkaline environment. Considering that the beverage samples were neutral or slightly acidic, pH was not adjusted for further experiments. The effect of organic matter in the sample matrix was also investigated. The beverage samples used in this work were vitamin drinks, and most of the compounds in the sample matrixes were water-soluble vitamins (such as vitamins B6, B12, and C and niacinamide). These vitamins were hardly absorbed by MAG-MIM in the aqueous matrix, so there was very little effect on the recovery of PAEs (Figure 6A).

After phase separation by an applied magnetic field in the bottom of bottle, the MAG-MIM adsorbent was eluted to desorb the analytes. The phthalates were extracted well by most organic solvents. The solvent molecules were adsorbed easily on the surface of the adsorbent polymer to replace the analyte molecules. A small amount of acetic acid was added to contribute to the destruction of the hydrogen bonds between analytes and binding sites on the adsorbents. Therefore, different kinds and volumes of organic solvents coupled with 15% acetic acid were investigated. Figure 6B shows that 7.0 mL of ethyl acetate−acetic acid (85:15, v/v) was used as the desorption solvent to strip the adsorbed analytes from MAG-MIM.

The time of desorption also investigated as shown in Figure 5D. The new adsorption−desorption equilibria were obtained in a short time. The polarity of DEP can be inferred from its structure, so the extraction equilibrium in strong hydrophobic solvent would take a longer time than that of other analytes. Considering time efficiency, 5 min was selected as the optimum desorption time.

Moreover, the MAG-MIM-dSPE method was compared with MAG-NIM-dSPE in parallel using simple ethyl acetate extraction according to their optimization steps. Recoveries with MAG-MIM-dSPE for phthalates were more than those with MAG-NIM-dSPE or liquid−liquid extraction (LLE), as shown in Figure 7, obtained for spiked beverages (0.040 μg/mL). The chromatograms of MAG-MIM-dSPE, MAG-NIM-dSPE, and LLE are shown in Figure 8A, and the effect of nonselective uptake (interferences) from LLE was worse than that of MAG-NIM-dSPE. The lack of selectivity aggravated the serious inaccuracies in determination. There were many impurity peaks that interfered with the determination of the phthalates as shown in the chromatograms of MAG-NIM-dSPE and LLE. MAG-MIM-dSPE-GC background from the beverage matrix was more or less identical to that of MAG-NIM-dSPE-GC. For example, a peak (≈6 min) was observed in the chromatogram of LLE and MAG-NIM-dSPE-GC, while it did not appear in the chromatogram of MAG-MIM-dSPE-GC. The reason for this may be the effective utilization of functional groups on polyacrylate during the templating process of MAG-MIM, resulting in relatively reduced nonselective binding for the beverage constituents. All aforementioned details indicate that the templating of MIM was successful. In summary, the utility of MAG-MIM-dSPE is reliable for selective screening of phthalates in beverages.

Validation of the MAG-MIM-dSPE-GC Method. To validate the analytical methodology of the MAG-MIM-dSPE-GC method, several parameters such as linearity, recovery,

Table 2. Recoveries in the MAG-MIM-dSPE-GC Method for Spiked Beverage (n = 3)

	0.0040 μg/mL		0.040 μg/mL		0.40 μg/mL	
spiked level of analytes	recovery (%)	RSD (%)	recovery (%)	RSD (%)	recovery (%)	RSD (%)
DEP	100.5	6.7	96.1	4.6	95.8	3.3
DBP	101.3	4.6	95.0	3.6	97.9	2.5
BBP	89.5	5.2	93.4	2.7	100.2	2.1
DIOP	92.9	5.9	96.4	3.5	99.2	3.6
DNOP	97.9	4.9	94.4	3.8	98.2	2.4

Table 1. Features of the MAG-MIM-dSPE-GC Method

compounds	regression equation	r^2	LOD (μg/L)	LOQ (μg/L)	RSD
DEP	$Y = 4.57 \times 10^3X + 215.3$	0.9995	1.2	4.0	4.3
DBP	$Y = 4.76 \times 10^3X + 1.10 \times 10^3$	0.9997	0.60	2.0	3.1
BBP	$Y = 7.01 \times 10^3X + 389.4$	0.9991	0.53	1.8	6.9
DIOP	$Y = 6.95 \times 10^3X + 3.56 \times 10^3$	0.9991	0.56	1.9	5.3
DNOP	$Y = 6.40 \times 10^3X + 883.3$	0.9998	0.74	2.5	4.9

dx.doi.org/10.1021/jf4051705 | J. Agric. Food Chem. 2014, 62, 2782−2789

Table 3. Comparison of Different Analytical Methods for Screening of Phthalates

sample matrix	treatment method	detection method	recovery (%)	LOD	estimated time (min)	RSD (%)	ref no.
soybean milk	SPE	GC-MS	75.8−107.5	13−22 μg/L	>100	1.8−10.08	10
water	SPME	GC-ECD	109−116	1−4 ng/L	>70	4−10	16
vegetable oil	HS-SPME	GC-ECD/MSD	−[a]	0.06−0.3 mg/kg	60−70	14−23	17
water	DLLME	GC-MS	68.1−88.9	2−8 ng/L	<45	4.6−6.8	19
water	LPME	GC-FID	84−102	0.43−4.3 μg/L	<30	5.2−6.4	21
beverage, water, and perfume	MSPE[b]	GC-MS	64.6−125.6	4.9−38 ng/L	<30	2−16.5	47
urine	MSPE[b]	GC-MS	92.6−98.8	0.025−0.05 ng/mL	200	5.28−11.45	48
beverage	dSPE	GC-FID	89.5−101.3	0.53−1.2 μg/L	40	2.1−6.7	present

[a]Not given in the literature. [b]Magnetic solid-phase extraction, the same as dSPE.

reproducibility, limit of detection (LOD), and limit of quantification (LOQ) were evaluated. All parallel experiments were repeated three times, and the results are tabulated in Table 1. The linearity of the MAG-MIM-dSPE-GC method was tested using the areas of chromatographic peaks measured at nine increasing spiked levels in a range of 0.0040−0.40 μg/mL. Good linearities were obtained throughout the concentration range for all analytes with the correlation coefficient (r^2) ≥ 0.9991. Analyses of reproducibility of intraday and interday were carried out for spiked beverage samples (0.08 μg/mL), and RSD values of intraday and interday were less than 6.9% and 7.2%, respectively. The LOD values calculated on the basis of S/N = 3 were in a range of 0.53−1.2 μg/L for all analytes. On the basis of S/N = 10, the LOQ values of analytes were from 1.8 to 4.0 μg/L. Spiked recoveries were determined to validate the method on the basis of the obtained linearity (taking the form of $Y = aX + b$). Recoveries were calculated as:

$$R = \frac{P - b}{a \times C_s} \times 100\%$$

In the equation, R stands for the recovery value, P is the peak area, C_s is the actual concentration, and a and b are two coefficients of the obtained linear equation. The average recoveries for the five phthalates in spiked samples were in a range of 89.5−101.3% (Table 2), which demonstrated that the proposed MAG-MIM-dSPE-GC technique was reliable. The parameters of the present MAG-MIM-dSPE-GC method (such as recovery, LOD, RSD, and estimated time) were justified briefly in comparison with other procedures reported in the literature, indicating that the method is reliable and practical (Table 3).

Real Sample Analysis. To demonstrate the suitability and application of the MAG-MIM-dSPE-GC method for actual samples, five brands of vitamin beverage products collected from local markets in Baoding were pretreated and analyzed under optimal MAG-MIM-dSPE-GC conditions. Figure 8B shows that trace levels of DBP and DIOP at concentrations of 5.7 μg/L and 4.0 μg/L were observed in one of the beverage products, and water-soluble vitamins (such as vitamins B6, B12, and C and niacinamide) (which are the main components in beverage matrixes) did not interfere with the screening of the phthalates.

AUTHOR INFORMATION

Corresponding Author

*Tel: +86-312-5079788. Fax: +86-312-5971107. E-mail: yanhy@hbu.edu.cn.

Funding

The project was sponsored by National Natural Science Foundation of China (31301464, 21175031) and the Natural Science Foundation of Hebei Province (B2012201052).

Notes

The authors declare no competing financial interest.

REFERENCES

(1) Swan, S. H. Environmental phthalate exposure in relation to reproductive outcomes and other health endpoints in humans. *Environ. Res.* **2008**, *108*, 177−184.
(2) Heudorf, U.; Mersch-Sundermann, V.; Angerer, J. Phthalates: toxicology and exposure. *Int. J. Hyg. Environ. Health* **2007**, *210*, 623−634.
(3) Fromme, H.; Küchler, T.; Otto, T.; Pilz, K.; Müller, J.; Wenzel, A. Occurrence of phthalates and bisphenol A and F in the environment. *Water Res.* **2002**, *36*, 1429−1438.
(4) Sathyanarayana, S.; Karr, C. J.; Lozano, P.; Brown, E.; Calafat, A. M.; Liu, F.; Swan, S. H. Baby care products: Possible sources of infant phthalate exposure. *Pediatrics* **2008**, *121*, 260−268.
(5) Benson, R. Hazard to the developing male reproductive system from cumulative exposure to phthalate esters-dibutyl phthalate, diisobutyl phthalate, butylbenzyl phthalate, diethylhexyl phthalate, dipentyl phthalate, and diisononyl phthalate. *Regul. Toxicol. Pharmacol.* **2009**, *53*, 90−101.
(6) Hauser, R.; Duty, S.; Godfrey-Bailey, L.; Calafat, A. M. Medications as a source of human exposure to phthalates. *Environ. Health Persp.* **2004**, *112*, 751−753.
(7) Schettler, T. Human exposure to phthalates via consumer products. *Int. J. Androl.* **2006**, *29*, 134−139.
(8) Kole, P. L.; Venkatesh, G.; Kotecha, J.; Sheshala, R. Recent advances in sample preparation techniques for effective bioanalytical methods. *Biomed. Chromatogr.* **2011**, *25*, 199−217.
(9) Chen, Y.; Guo, Z.; Wang, X.; Qiu, C. Sample preparation. *J. Chromatogr. A* **2008**, *1184*, 191−219.
(10) He, J.; Lv, R.; Zhu, J.; Lu, K. Selective solid-phase extraction of dibutyl phthalate from soybean milk using molecular imprinted polymers. *Anal. Chim. Acta* **2010**, *661*, 215−221.
(11) Del Carlo, M.; Pepe, A.; Sacchetti, G.; Compagnone, D.; Mastrocola, D.; Cichelli, A. Determination of phthalate esters in wine using solid-phase extraction and gas chromatography-mass spectrometry. *Food Chem.* **2008**, *111*, 771−777.
(12) Fatoki, O. S.; Noma, A. Solid phase extraction method for selective determination of phthalate esters in the aquatic environment. *Water Air Soil Pollut.* **2002**, *140*, 85−98.
(13) Luks-Betlej, K.; Popp, P.; Janoszka, B.; Paschke, H. Solid-phase microextraction of phthalates from water. *J. Chromatogr. A* **2001**, *938*, 93−101.
(14) Penalver, A.; Pocurull, E.; Borrull, F.; Marce, R. M. Determination of phthalate esters in water samples by solid-phase microextraction and gas chromatography with mass spectrometric detection. *J. Chromatogr. A* **2000**, *872*, 191−201.

(15) Cao, X. L. Determination of phthalates and adipate in bottled water by headspace solid-phase microextraction and gas chromatography/mass spectrometry. *J. Chromatogr. A* **2008**, *1178*, 231−238.
(16) Prokůpková, G.; Holadová, K.; Poustka, J.; Hajšlová, J. Development of a solid-phase microextraction method for the determination of phthalic acid esters in water. *Anal. Chim. Acta* **2002**, *457*, 211−223.
(17) Holadová, K.; Prokůpková, G.; Hajšlová, J.; Poustka, J. Headspace solid-phase microextraction of phthalic acid esters from vegetable oil employing solvent based matrix modification. *Anal. Chim. Acta* **2007**, *582*, 24−33.
(18) Liang, P.; Xu, J.; Li, Q. Application of dispersive liquid-liquid microextraction and high-performance liquid chromatography for the determination of three phthalate esters in water samples. *Anal. Chim. Acta* **2008**, *609*, 53−58.
(19) Farahani, H.; Norouzi, P.; Dinarvand, R.; Ganjali, M. R. Development of dispersive liquid-liquid microextraction combined with gas chromatography-mass spectrometry as a simple, rapid and highly sensitive method for the determination of phthalate esters in water samples. *J. Chromatogr. A* **2007**, *1172*, 105−112.
(20) Psillakis, E.; Kalogerakis, N. Hollow-fibre liquid-phase microextraction of phthalate esters from water. *J. Chromatogr. A* **2003**, *999*, 145−153.
(21) Xu, J.; Liang, P.; Zhang, T. Dynamic liquid-phase microextraction of three phthalate esters from water samples and determination by gas chromatography. *Anal. Chim. Acta* **2007**, *597*, 1−5.
(22) Yan, H.; Wang, H.; Qiao, J.; Yang, G. Molecularly imprinted matrix solid-phase dispersion combined with dispersive liquid-liquid microextraction for the determination of four Sudan dyes in egg yolk. *J. Chromatogr. A* **2011**, *1218*, 2182−2188.
(23) Anastassiades, M.; Lehotay, S. J.; Stajnbaher, D.; Schenck, F. J. Fast and easy multiresidue method employing acetonitrile extraction/partitioning and dispersive solid-phase extraction for the determination of pesticide residues in produce. *J. AOAC Int.* **2003**, *86*, 412−431.
(24) Fontana, A. R.; Camargo, A.; Martinez, L. D.; Altamirano, J. C. Dispersive solid-phase extraction as a simplified clean-up technique for biological sample extracts. Determination of polybrominated diphenyl ethers by gas chromatography-tandem mass spectrometry. *J. Chromatogr. A* **2011**, *1218*, 2490−2496.
(25) Román, I. P.; Chisvert, A.; Canals, A. Dispersive solid-phase extraction based on oleic acid-coated magnetic nanoparticles followed by gas chromatography−mass spectrometry for UV-filter determination in water samples. *J. Chromatogr. A* **2011**, *1218*, 2467−2475.
(26) Peng, Y.; Xie, Y.; Luo, J.; Nie, L.; Chen, Y.; Chen, L.; Du, S.; Zhang, Z. Molecularly imprinted polymer layer-coated silica nanoparticles toward dispersive solid-phase extraction of trace sulfonylurea herbicides from soil and crop samples. *Anal. Chim. Acta* **2010**, *674*, 190−200.
(27) Wulff, G.; Sarhan, A.; Zabrocki, K. Enzyme-analogue built polymers and their use for the resolution of racemates. *Tetrahedron Lett.* **1973**, *14*, 4329−4332.
(28) Vlatakis, G.; Andersson, L. I.; Müller, R.; Mosbach, K. Drug assay using antibody mimics made by molecular imprinting. *Nature* **1993**, *361*, 645−647.
(29) Scorrano, S.; Longo, L.; Vasapollo, G. Molecularly imprinted polymers for solid-phase extraction of 1-methyladenosine from human urine. *Anal. Chim. Acta* **2010**, *659*, 167−171.
(30) Lv, Y. K.; Wang, L. M.; Yang, L.; Zhao, C. X.; Sun, H. W. Synthesis and application of molecularly imprinted poly(methacrylic acid)-silica hybrid composite material for selective solid-phase extraction and high-performance liquid chromatography determination of oxytetracycline residues in milk. *J. Chromatogr. A* **2012**, *1227*, 48−53.
(31) He, J.; Lv, R.; Zhu, J.; Lu, K. Selective solid-phase extraction of dibutyl phthalate from soybean milk using molecular imprinted polymers. *Anal. Chim. Acta* **2010**, *661*, 215−221.
(32) Tamayo, F. G.; Martin-Esteban, A. Selective high performance liquid chromatography imprinted-stationary phases for the screening of phenylurea herbicides in vegetable samples. *J. Chromatogr. A* **2005**, *1098*, 116−122.
(33) Li, J.; Jiang, F.; Wei, X. Molecularly imprinted sensor based on an enzyme amplifier for ultratrace oxytetracycline determination. *Anal. Chem.* **2010**, *82*, 6074−6078.
(34) Liang, R.; Zhang, R.; Qin, W. Potentiometric sensor based on molecularly imprinted polymer for determination of melamine in milk. *Sens. Actuators, B* **2009**, *141*, 544−550.
(35) Pasetto, P.; Maddock, S. C.; Resmini, M. Synthesis and characterisation of molecularly imprinted catalytic microgels for carbonate hydrolysis. *Anal. Chim. Acta* **2005**, *542*, 66−75.
(36) Jung, B. M.; Kim, M. S.; Kim, W. J.; Chang, J. Y. Molecularly imprinted mesoporous silica particles showing a rapid kinetic binding. *Chem. Commun.* **2010**, *46*, 3699−3701.
(37) Zhang, Y.; Liu, R.; Hu, Y.; Li, G. Microwave heating in preparation of magnetic molecularly imprinted polymer beads for trace triazines analysis in complicated samples. *Anal. Chem.* **2009**, *81*, 967−976.
(38) Chen, L.; Liu, J.; Zeng, Q.; Wang, H.; Yu, A.; Zhang, H.; Ding, L. Preparation of magnetic molecularly imprinted polymer for the separation of tetracycline antibiotics from egg and tissue samples. *J. Chromatogr. A* **2009**, *1216*, 3710−3719.
(39) Meng, J.; Bu, J.; Deng, C.; Zhang, X. Preparation of polypyrrole-coated magnetic particles for micro solid-phase extraction of phthalates in water by gas chromatography-mass spectrometry analysis. *J. Chromatogr. A* **2011**, *1218*, 1585−1591.
(40) Kan, X.; Zhao, Q.; Shao, D.; Geng, Z.; Wang, Z.; Zhu, J. J. Preparation and recognition properties of bovine hemoglobin magnetic molecularly imprinted polymers. *J. Phys. Chem. B* **2010**, *114*, 3999−4004.
(41) Mehdinia, A.; Roohi, F.; Jabbari, A. Rapid magnetic solid phase extraction with in situ derivatization of methylmercury in seawater by Fe_3O_4/polyaniline nanoparticle. *J. Chromatogr. A* **2011**, *1218*, 4269−4274.
(42) Zhang, Z.; Tan, W.; Hu, Y.; Li, G. Simultaneous determination of trace sterols in complicated biological samples by gas chromatography-mass spectrometry coupled with extraction using β-sitosterol magnetic molecularly imprinted polymer beads. *J. Chromatogr. A* **2011**, *1218*, 4275−4283.
(43) Tan, C. J.; Chua, H. G.; Ker, K. H.; Tong, Y. W. Preparation of bovine serum albumin surface-imprinted submicrometer particles with magnetic susceptibility through core-shell miniemulsion polymerization. *Anal. Chem.* **2008**, *80*, 683−692.
(44) Wu, L.; Zhu, K.; Zhao, M.; Li, Y. Theoretical and experimental study of nicotinamide molecularly imprinted polymers with different porogens. *Anal. Chim. Acta* **2005**, *549*, 39−44.
(45) Sun, H.; Yang, Y.; Li, H.; Zhang, J.; Sun, N. Development of multiresidue analysis for twenty phthalate esters in edible vegetable oils by microwave-assisted extraction−gel permeation chromatography−solid phase extraction−gas chromatography−tandem mass spectrometry. *J. Agric. Food Chem.* **2012**, *60*, 5532−5539.
(46) Reid, A. M.; Brougham, C. A.; Fogarty, A. M.; Roche, J. J. Accelerated solvent-based extraction and enrichment of selected plasticisers and 4-nonylphenol, and extraction of tin from organotin sources in sediments, sludges and leachate soils. *Anal. Chim. Acta* **2009**, *634*, 197−204.
(47) Luo, Y. B.; Yu, Q. W.; Yuan, B. F.; Feng, Y. Q. Fast microextraction of phthalate acid esters from beverage, environmental water and perfume samples by magnetic multi-walled carbon nanotubes. *Talanta* **2012**, *90*, 123−131.
(48) Rastkari, N.; Ahmadkhaniha, R. Magnetic solid-phase extraction based on magnetic multi-walled carbon nanotubes for the determination of phthalate monoesters in urine samples. *J. Chromatogr. A* **2013**, *1286*, 22−28.

Table 1. Neonicotinoid Insecticides and Metabolites Analyzed in This Study

Compound	Chemical structure	Water solubility (g/L) [a]	log K_{ow} [a]
CPMF [b]	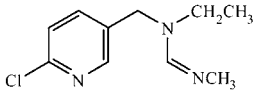	— [c]	—
Dinotefuran	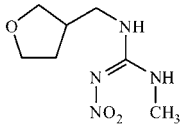	54.3	−0.644
CPMA [b]	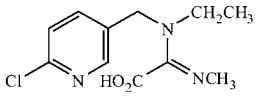	—	—
Nitenpyram	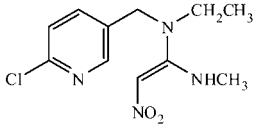	≥59	−0.66
Thiamethoxam	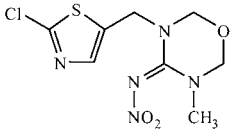	4.1	−0.13
Clothianidin	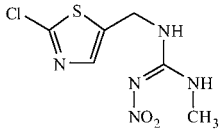	0.340	0.7
Imidacloprid	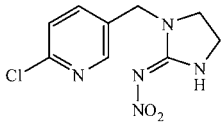	0.61	0.57
Thiacloprid amide [d]	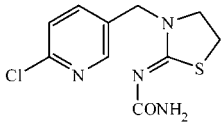	—	—
Acetamiprid	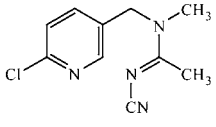	4.25	0.80
Thiacloprid	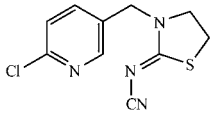	0.185	0.73

[a] All values were obtained from ref 2. [b] Major metabolite of nitenpyram. [c] Not reported. [d] Major metabolite of thiacloprid.

and *N*-(6-chloro-3-pyridylmethyl)-*N*-ethyl-*N*′-methylformamidine (CPMF)], and a major metabolite of thiacloprid (thiacloprid amide), all of >95% purity, were purchased from Wako Pure Chemical Industries (Osaka, Japan), Dr. Ehrenstorfer (Augsburg, Germany), and Fluka-Sigma-Aldrich (Steinheim, Germany), respectively. Pesticide analysis grade and HPLC grade organic solvents, HPLC grade formic acid, and other analytical grade reagents were obtained from Kanto Chemical Co. (Tokyo, Japan) or Wako Pure Chemical Industries. Pure water for sample preparation and LC-MS/MS analysis was prepared in the laboratory by means of a water purification system (Milli-Q, Millipore Corp., Bedford, MA, USA). ENVI-Carb II/PSA SPE cartridges (500 mg of graphitized carbon black and 500 mg of ethylenediamine-*N*-propyl silica gel) and ENVI-Carb/LC-NH_2 SPE cartridges (500 mg of graphitized carbon black and 500 mg of aminopropyl silica gel) were purchased from Supelco (Bellefonte, PA, USA).

Stock and Working Solutions. Stock solutions of CPMA in water and the other target compounds in methanol were prepared, and the solutions were stored in the dark at 4 and −20 °C, respectively. Multicomponent working solutions (1, 10, and 100 mg/L) were prepared by diluting each stock solution with 20:80 (v/v) methanol/water at every recovery test and LC-MS/MS analyses, and the working solutions were used as calibration standards and for spiking agricultural samples.

Agricultural Samples. Green peppers and tomatoes were used as model agricultural crops. Green peppers and tomatoes were chopped and homogenized by a home food processor (KC-D627, TWINBIRD Corp., Niigata, Japan). For the preparation of spiked samples for recovery tests, green peppers and tomatoes were grown on arable land of the Japan Plant Protection Association (Miyazaki, Japan) without the use of neonicotinoid insecticides. The absence of the target compounds in the vegetables was confirmed by LC-MS/MS prior to each experiment. For the recovery tests, a homogenized sample (5 g) was spiked with 50 μL of the 1, 10, or 100 mg/L multicomponent working solution (0.01, 0.10, or 1.00 mg/kg, respectively). The spiked samples were exposed to the target compounds for 30 min prior to extraction.

In addition to the spike−recovery tests, we also conducted tests on green peppers and tomatoes sprayed with commercial formulations of the target compounds. The plants were grown in a plastic greenhouse on arable land of the National Institute for Agro-Environmental Sciences and, at the harvesting stage, were sprayed with a mixture of four neonicotinoid insecticide formulations: Mospilan (water-soluble powder), containing 20.0% acetamiprid (Nippon Soda Co., Tokyo, Japan); Admire (water-soluble granules), containing 20% imidacloprid (Bayer Crop Science, Tokyo, Japan); Bariard (water-soluble granules), containing 30% thiacloprid (Bayer Crop Science); and Actara (water-soluble powder), containing 10% thiamethoxam (Syngenta Japan K.K., Tokyo, Japan), all diluted with water according to the manufacturers' instructions. The samples were harvested at 1, 3, and 7 days after spraying. After harvesting, the samples were chopped and homogenized by a home food processor.

Sample Preparation. *Proposed Water-Based Extraction Method.* A 5 g aliquot of homogenized sample was weighed into a 100 mL centrifuge tube, and 25 mL of water was added to the tube. The sample was shaken vigorously for 30 min on a shaker (SA-400, Yamato Scientific Co., Tokyo, Japan) and then centrifuged at approximately 1400*g* for 20 min. The sample mixture was suction-filtered through a glass fiber filter (60 mm in diameter, GF-B, Kiriyama Glass Co., Tokyo, Japan), and the solid residue on the filter was washed with 15 mL of water. The volume of the extract was brought to exactly 50 mL with water, and then 2 mL aliquots (equivalent to 0.2 g of sample) were added to 10 mL of acetonitrile. The solution obtained by adding 2 mL aliquots to 10 mL of acetonitrile was cleaned up according to the procedure established by Kobayashi,[16] as follows. The solution was loaded onto an ENVI-Carb II/PSA SPE cartridge preconditioned with 5 mL of acetone and 5 mL of *n*-hexane. The target compounds were eluted with 5 mL of acetonitrile/toluene (3:1, v/v). The eluate was concentrated and evaporated to dryness with a gentle stream of nitrogen. The residue was reconstituted with 1 mL of 20:80 (v/v) methanol/water, and the resulting solution was filtered with a polytetrafluoroethylene membrane syringe-driven filter unit (0.45 μm, GL Sciences Inc., Tokyo, Japan).

Japanese Official Method (Reference Method). To verify the applicability of the proposed water extraction method, we used the

dx.doi.org/10.1021/jf405311y | J. Agric. Food Chem. 2014, 62, 2790−2796

Table 2. Detection Parameters, Calibration Data, and Limits of Detection of Target Compounds

compound	retention time (min)	transition mass (m/z)[a]	transition mass (m/z)[b]	cone voltage (V)	collision energy (eV)	calibration curve	linearity (μg/L)	correlation coefficient (r)	limit of detection (μg/L)
CPMF	2.01	212 → 126	212 → 157	20	33	$y = 1015.23x - 36.43$	0.10−5	0.9997	0.05
dinotefuran	2.66	203 → 129	203 → 157	12	26	$y = 319.99x + 6.97$	0.10−5	0.9997	0.05
CPMA	2.90	256 → 126	256 → 176	20	25	$y = 271.39x - 0.90$	0.10−5	0.9997	0.05
nitenpyram	3.31	271 → 225	271 → 130	10	31	$y = 104.36x + 6.11$	0.5−5	0.9996	0.10
thiamethoxam	5.69	292 → 211	292 → 181	17	26	$y = 224.32x + 6.14$	0.05−5	1.0000	0.02
clothianidin	7.86	250 → 169	250 → 132	13	24	$y = 226.19x + 37.17$	0.5−5	0.9995	0.10
imidacloprid	8.07	256 → 175	256 → 209	22	25	$y = 188.91x + 1.54$	0.05−5	0.9998	0.03
thiacloprid amide	8.13	271 → 126	271 → 228	25	25	$y = 530.47x - 5.39$	0.05−5	0.9998	0.01
acetamiprid	8.62	223 → 126	223 → 90	20	32	$y = 1837.52x + 21.67$	0.05−5	1.0000	0.01
thiacloprid	9.74	253 → 126	253 → 56	25	36	$y = 2146.54x + 0.60$	0.05−5	1.0000	0.01

[a]MS-MS transition used for quantification. [b]MS-MS transition used for conformation.

Japanese official method[26] as a reference method as follows. Acetonitrile (50 mL) was added to 20 g of homogenized sample, and the slurry was extracted for 3 min with a high-speed homogenizer (Polytron PT2100, Kinematica AG, Lucerne, Switzerland). The sample mixture was suction-filtered, and the solid residue on the filter was extracted again with 20 mL of acetonitrile. The volume of the combined extracts was brought to exactly 100 mL with acetonitrile, and 20 mL aliquots of the extract (equivalent to 4 g of sample) were mixed with 10 g of sodium chloride and 20 mL of 0.5 M phosphate buffer (pH 7). The resulting mixture was shaken vigorously for 10 min and then allowed to stand for about 10 min. After the aqueous phase was discarded, the acetonitrile phase was dried with anhydrous sodium sulfate and filtered, and the filtrate was concentrated and evaporated to dryness with a gentle stream of nitrogen. The residue was reconstituted in 2 mL of acetonitrile/toluene (3:1, v/v), and the resulting solution was loaded onto an ENVI-Carb/LC-NH_2 SPE cartridge preconditioned with 10 mL of acetonitrile/toluene (3:1, v/v). After the target compounds were eluted with 20 mL of acetonitrile/toluene (3:1, v/v), the eluate was concentrated. The residue was reconstituted in 10 mL of acetone. The resulting solution was concentrated, and 5 mL of acetone was added to the residue. The acetone was evaporated under a gentle stream of nitrogen. After the residue was reconstituted with 1 mL of methanol, the solution was diluted five times with methanol/water (20:80, v/v) and filtered through a polytetrafluoroethylene membrane syringe-driven filter unit.

Evaluation of Matrix Effects. To evaluate matrix effects, we used the proposed water extraction method and the reference method described above to prepare cleaned up extracts of nonspiked samples. The cleaned up extracts were dissolved in 1 mL of methanol/water (20:80, v/v), and then 0.04 μg of each target compound was added to the extracts. Matrix effects were evaluated according to a method described in an earlier paper,[27] and the magnitude of the effects was calculated by means of the following equation:

$$\text{matrix effect (\%)} = \left[\frac{\text{peak area of standards in cleaned up extract}}{\text{peak area of standards in pure solvent}} - 1\right] \times 100$$

LC-MS/MS Analysis. LC-MS/MS analysis was carried out with an HPLC system (Alliance 2695 series, Waters, Milford, MA, USA) equipped with a pump, a degasser, an autosampler, and a column oven. The target compounds were separated on an Atlantis T3 analytical column (50 mm × 2.1 mm i.d., 3.5 μm particle size) fitted with an Atlantis T3 guard column Atlantis T3 (10 mm × 2.1 mm i.d., 3.5 μm particle size), both from Waters. The column oven temperature was kept at 30 °C. The injection volume was 10 μL, and the flow rate was 0.2 mL min^{-1}. Mobile phases A and B were methanol and 5 mM ammonium acetate containing 0.1% formic acid, respectively. A gradient mobile was used, with the A:B ratio varied as follows: 0 min, 20:80; 5 min, 20:80; 10 min, 95:5; 13 min, 95:5; 13.5 min, 20:80; 25 min, 20:80.

The MS/MS system (Quattro Micro API, Micromass, Manchester, UK) was a triple-quadrupole tandem mass spectrometer equipped with an electrospray ionization (ESI) interface. For all compounds, the MS instrument was operated in the ESI positive-ion mode at a desolvation temperature of 350 °C and a source temperature of 120 °C and at an ESI voltage of 3.9 kV. Nitrogen was used as the desolvation gas at a flow rate of 600 L/h. For collision-induced dissociation, argon gas was used as the collision gas at a pressure of 4.5×10^{-3} mbar in the collision cell. Mass spectrometric detection was performed in multiple reaction monitoring mode. The multiple reaction monitoring transitions were selected and tuned by direct syringe pump infusion of a 5.0 mg/L standard solution of each compound prepared in methanol/water 20:80 (v/v) into the spectrometer at a flow rate of 10 μL/min. The dwell time for each transition was 300−600 ms. Optimized MS/MS transitions as well as specific cone voltages and collision energies are summarized in Table 2.

Under the chromatographic conditions described, calibration graphs were constructed by plotting peak areas versus concentrations. Excellent linearity and regression coefficient (r) were achieved for all of the target compounds in this study (Table 2). The limit of detection for each compound was determined as the lowest concentration of each compound that gave a signal-to-noise ratio of at least 3.

RESULTS AND DISCUSSION

Optimization of LC-MS/MS Conditions. To achieve good separation of the target compounds with high sensitivity, we analyzed all samples using a slightly modified version of the LC gradient program reported by Kobayashi.[16] This gradient program resulted in good sensitivity and peak shape for all of the target compounds. We optimized the MS parameters and multiple reaction monitoring transitions for the maximum abundance of fragmented ions under ESI positive-ion mode conditions by infusing standard solutions of the target compounds into the mass spectrometer (Table 2). Full-scan spectra were measured for selection of the most abundant m/z values. For each target compound, the addicted ion $[M + H]^+$ was determined as a precursor ion. The optimal collision energy for each target compound was selected, which yielded the most abundant product ion by dissociation of each precursor ion in the collision cell.

Matrix Effects. Matrix effects have been widely studied and are recognized as a source of error in quantitative LC-ESI-MS/MS analysis of food samples.[28] Matrix effects result from competition between matrix ions and analyte ions in the sprayed solution for access to the droplet.[29] Depending on the environment in which ionization and ion evaporation take place, this competition can either suppress or enhance the efficiency of analyte ion formation.[30]

We evaluated matrix effects on the results of analysis of the target compounds in green peppers and tomatoes by means of the proposed water-based extraction method and the reference method (Figure 1). For all of the target compounds, the

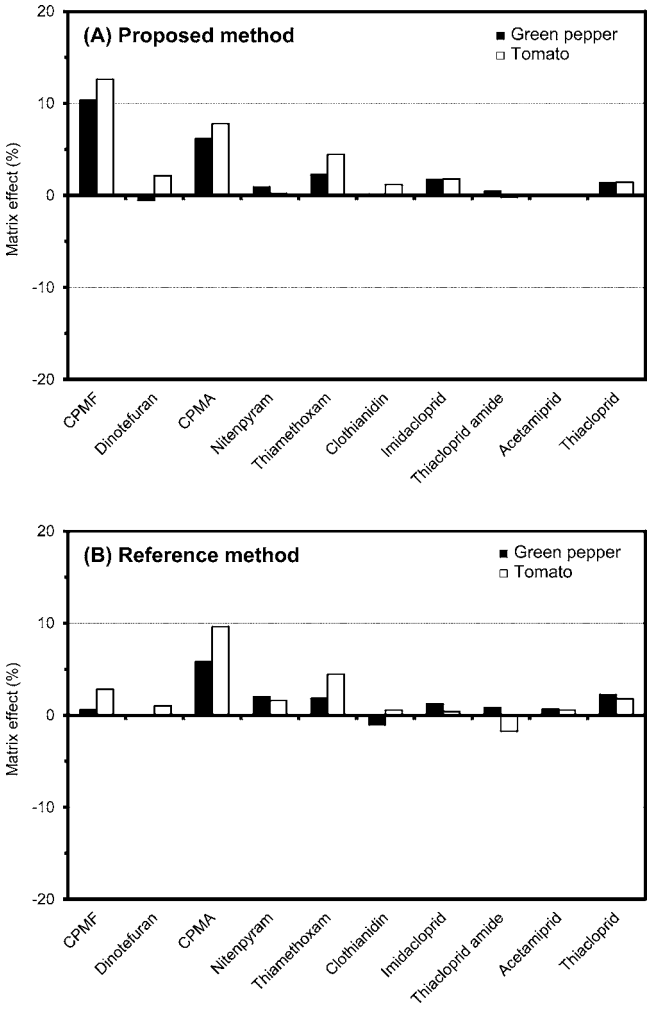

Figure 1. Matrix effects in the proposed water-based extraction method and the reference method.

magnitude of the matrix effect was between −1.7 and +12.6%; this result indicates that for all the combinations of target compounds and matrices in this study, there was no substantial signal suppression or enhancement (matrix effect within ±20%) that interfered with accurate determination by LC-MS/MS analysis according to the criteria explained by Mol et al.[31] On the basis of our results, we performed calibration of the target compounds with external standards diluted with 20:80 (v/v) methanol/water. Some studies[21,32,33] on the QuEChERS method reported that matrix-matched calibration was performed because there was substantial signal suppression and enhancement for the combinations of some pesticides and matrices. On the other hand, matrix effects in the proposed method were not significant; therefore, the target compounds in this study could be analyzed with good precision by calibration with external standards. From the viewpoint of calibration of the target compounds without matrix-matched standards, the proposed method might have an advantage over the QuEChERS method.

Precision and Accuracy of the Proposed Water-Based Extraction Method. We conducted recovery tests on samples spiked with the target compounds at three concentrations (0.01, 0.10, and 1.00 mg/kg; Table 3). The recoveries and relative standard deviations were in the range of 71.2−112.8 and ≤7.5%, respectively, except for the recoveries of imidacloprid (122.3 ± 2.5%) and nitenpyram (121.7 ± 4.9%) in tomato samples spiked at 0.01 mg/kg. For most of the target compounds, the recoveries and relative standard deviations were within the criteria specified in Japanese and European guidelines for validation of pesticide residue analysis methods (70−120 and <20%, respectively).[34,35] These results are indicative of the good precision and accuracy of the proposed water-based extraction method. Although the water solubility and octanol−water partition coefficients of CPMA, CPMF, and thiacloprid amide have not been reported, these metabolites are thought to be at least as hydrophilic as the respective parent compounds. Xiao et al.[20] reported that neonicotinoid insecticides in bovine tissues can be recovered almost completely by means of extraction with pressurized pure water. Our results confirmed that the hydrophilic neonicotinoid insecticides and their metabolites targeted in this study could be extracted into water and recovered, suggesting that the proposed environmentally friendly water-based extraction method is potentially useful for the analysis of hydrophilic pesticides such as neonicotinoid insecticides and related metabolites.

Table 3. Recoveries of Target Compounds from Artificially Spiked Agricultural Samples Using the Proposed Water-Based Extraction Method (n = 4)

		green pepper		tomato	
compound	spiked concentration (mg/kg)	recovery (%)	RSD[a] (%)	recovery (%)	RSD[a] (%)
CPMF	0.01	88.6	6.4	99.8	6.7
	0.10	71.2	5.0	75.9	6.4
	1.00	106.1	0.7	85.0	3.5
dinotefuran	0.01	112.8	4.3	96.9	4.7
	0.10	81.8	4.0	77.1	6.2
	1.00	100.7	0.4	93.1	1.9
CPMA	0.01	88.8	2.3	93.0	4.5
	0.10	82.3	7.5	80.2	6.9
	1.00	100.1	0.8	97.6	1.9
nitenpyram	0.01	94.3	3.1	121.7	4.1
	0.10	83.5	4.7	96.6	4.3
	1.00	95.0	0.8	104.5	1.6
thiamethoxam	0.01	90.0	4.0	104.6	4.4
	0.10	84.0	5.4	85.7	6.8
	1.00	102.8	0.4	100.2	2.1
clothianidin	0.01	110.7	1.9	104.0	4.5
	0.10	85.0	2.9	87.0	7.4
	1.00	105.2	0.5	108.0	2.2
imidacloprid	0.01	106.2	2.4	122.3	2.0
	0.10	97.2	6.0	96.2	6.5
	1.00	103.9	0.3	100.5	1.8
thiacloprid amide	0.01	87.2	3.2	105.1	2.5
	0.10	81.9	5.6	86.5	6.3
	1.00	96.4	2.1	98.7	1.1
acetamiprid	0.01	86.8	2.9	100.6	1.5
	0.10	81.7	5.1	82.8	6.6
	1.00	101.4	0.2	102.2	1.4
thiacloprid	0.01	82.7	2.6	100.1	1.5
	0.10	79.0	6.1	81.9	5.5
	1.00	98.0	1.1	101.3	1.0

[a]Relative standard deviation.

Applicability of the Proposed Method to Samples Sprayed with Commercial Insecticide Formulations. We evaluated the relationship between the analytical results obtained by means of the proposed water-based extraction method and the reference method with green pepper and tomato samples that had been sprayed with four commercial neonicotinoid insecticide

dx.doi.org/10.1021/jf405311y | J. Agric. Food Chem. 2014, 62, 2790−2796

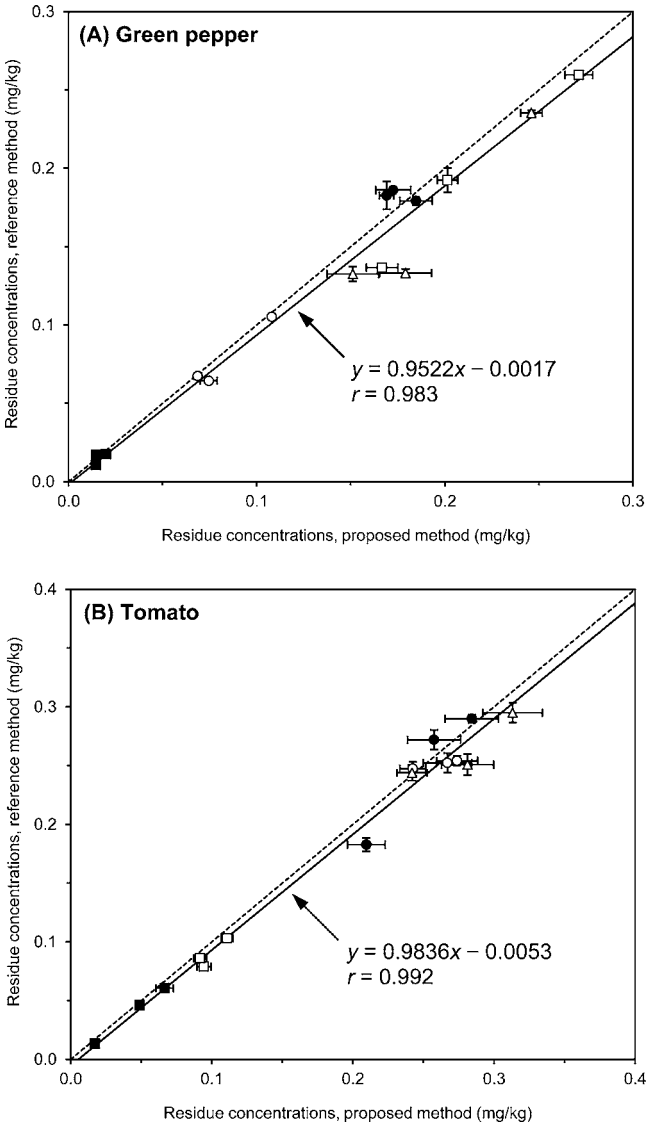

Figure 2. Relationship between residue concentrations in green pepper and tomato samples determined by the proposed water-based extraction method and by the reference method: (○) acetamiprid; (□) clothianidin (a metabolite of thiamethoxam); (△) imidacloprid; (●) thiacloprid; (■) thiamethoxam. Each point is the average of four replicate determinations. The dotted line corresponds to a perfect correlation ($y = x$).

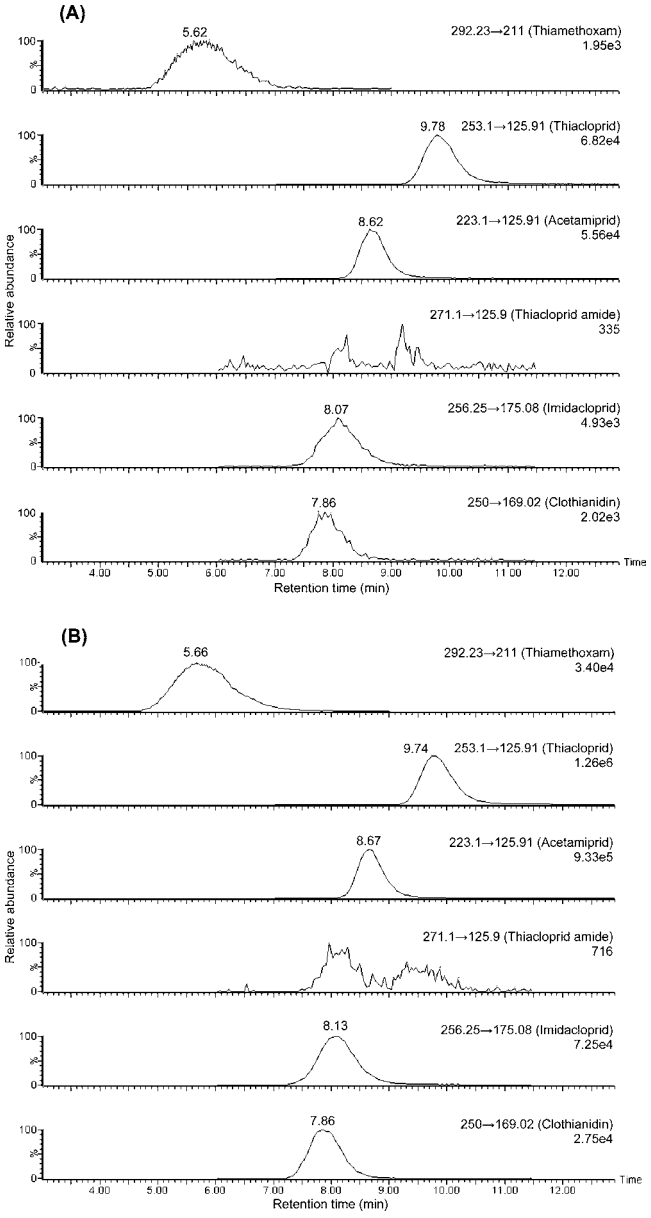

Figure 3. Chromatograms of target compounds obtained from tomato samples harvested 7 days after being sprayed with mixtures of the insecticide formulations by the proposed water-based extraction method (A) and by the reference method (B).

formulations (Figure 2). Acetamiprid, imidacloprid, thiacloprid, thiamethoxam, and clothianidin (a metabolite of thiamethoxam) were detected at >0.01 mg/kg in the samples. The residual concentrations of the target compounds in the green pepper samples determined by means of the proposed method and the reference method were 0.015−0.27 and 0.017−0.26 mg/kg, and those in the tomato samples were 0.017−0.31 and 0.013−0.30 mg/kg, respectively. The residual concentration of thiacloprid amide in the samples was <0.01 mg/kg. Figure 3 shows chromatograms of target compounds obtained from green pepper and tomato samples harvested 7 days after being sprayed with mixtures of the insecticide formulations. The slopes of the simple linear regression equations describing the relationship between the pesticide concentrations detected by means of the proposed method and the reference method were approximately 1; specifically, the slope for the green pepper samples was 0.95 ($r = 0.98$) and that for the tomato samples was 0.98 ($r = 0.99$), indicating that the concentrations detected by means of the two methods were equivalent. Our results suggest that the proposed method can be also applicable for spraying crops and market samples with hydrophilic pesticides.

The proposed environmentally friendly water-based extraction method for agricultural samples here demonstrates that (1) the consumed volume of organic solvent (25 mL per sample) is much less than the volume consumed by the official Japanese multiresidue method (150 mL per sample) and (2) it has simple procedures without liquid−liquid partitioning and can simultaneously and suitably recover hydrophilic pesticides as well as polar metabolites such as CPMA and CPMF that cannot be simultaneously recovered by the official Japanese multiresidue method. To secure food safety, this proposed method could be utilized for regular monitoring of neonicotinoid insecticides and their metabolites in high water content crops, such as green

dx.doi.org/10.1021/jf405311y | J. Agric. Food Chem. 2014, 62, 2790−2796

peppers and tomatoes, and for monitoring before shipment of these crops.

■ ASSOCIATED CONTENT

Supporting Information

Residue concentrations in green pepper and tomato samples sprayed with formulations 1, 3, and 7 days after insecticide application determined by the proposed method and by the reference method ($n = 4$). This material is available free of charge via the Internet at http://pubs.acs.org.

■ AUTHOR INFORMATION

Corresponding Author

*(E.W.) Phone: +81 29 838 8306. Fax: +81 29 838 8199. E-mail: eikiw@affrc.go.jp.

Notes

The authors declare no competing financial interest.

■ ACKNOWLEDGMENTS

We thank Takahiro Ara and Hiroshi Yamagushi (National Institute for Agro-Environmental Sciences) for their support in the growth of crop samples sprayed with commercial formulations of pesticides. We also thank Yutaka Takagi (Japan Plant Protection Association) for providing blank samples for recovery tests.

■ REFERENCES

(1) In *Nicotinoid Insecticides and Nicotinic Acetylcholine Receptor*; Yamamoto, I., Casida, J. E., Eds.; Springer: Tokyo, Japan, 1999.

(2) In *The Pesticide Manual*, 15th ed.; Tomlin, C. D. S., Ed.; British Crop Protection Council: Hampshire, UK, 2009.

(3) Navalón, A.; González-Casado, A.; El-Khattabi, R.; Vilchez, J. L.; Fernández-Alba, A. R. Determination of imidacloprid in vegetable samples by gas chromatography-mass spectrometry. *Analyst* **1997**, *122*, 579−581.

(4) MacDonald, L. M.; Meyer, T. R. Determination of imidacloprid and triadimefon in white pine by gas chromatography/mass spectrometry. *J. Agric. Food Chem.* **1998**, *46*, 3133−3138.

(5) Mateu-Sánchez, M.; Moreno, M.; Arrebola, F. J.; Martínez Vidal, J. L. Analysis of acetamiprid in vegetables using gas chromatography-tandem mass spectrometry. *Anal. Sci.* **2003**, *19*, 701−704.

(6) Obana, H.; Okihashi, M.; Akutsu, K.; Kitagawa, Y.; Hori, S. Determination of acetamiprid, imidacloprid, and nitenpyram residues in vegetables and fruits by high-performance liquid chromatography with diode-array detection. *J. Agric. Food Chem.* **2002**, *50*, 4464−4467.

(7) Watanabe, E.; Baba, K.; Eun, H. Simultaneous determination of neonicotinoid insecticides in agricultural samples by solid-phase extraction cleanup and liquid chromatography equipped with diode-array detection. *J. Agric. Food Chem.* **2007**, *55*, 3798−3804.

(8) Wu, Q.; Li, Z.; Wang, C.; Wu, C.; Wang, W.; Wang, Z. Dispersive solid-phase extraction clean-up combined with dispersive liquid-liquid microextraction for the determination of neonicotinoid insecticides in vegetables samples by high-performance liquid chromatography. *Food Anal. Methods* **2011**, *4*, 559−566.

(9) Wang, P.; Yang, X.; Wang, J.; Cui, J.; Dong, A. J.; Zhao, H. T.; Zhang, L. W.; Wang, Z. Y.; Xu, R. B.; Li, W. J.; Zhang, Y. C.; Zhang, H.; Jing, J. Multi-residue method for determination of seven neonicotinoid insecticides in grains using dispersive solid-phase extraction and dispersive liquid-liquid micro-extraction by high performance liquid chromatography. *Food Chem.* **2012**, *134*, 1691−1698.

(10) Campillo, N.; Viñas, P.; Férez-Melgarejo, G.; Hernández-Córdoba, M. Liquid chromatography with diode array detection and tandem mass spectrometry for the determination of neonicotinoid insecticides in honey samples using dispersive liquid-liquid micro-extraction. *J. Agric. Food Chem.* **2013**, *61*, 4799−4805.

(11) Hou, R.-Y.; Jiao, W.-T.; Qian, X.-S.; Wang, X.-H.; Xiao, Y.; Wan, X.-C. Effective extraction method for determination of neonicotinoid residues in tea. *J. Agric. Food Chem.* **2013**, *61*, 12565−12571.

(12) Tapparo, A.; Giorio, C.; Soldà, L.; Bogialli, S.; Marton, D.; Marzaro, M.; Girolami, V. UHPLC-DAD method for the determination of neonicotinoid insecticides in single bees and its relevance in honeybee colony loss investigations. *Anal. Bioanal. Chem.* **2013**, *405*, 1007−1014.

(13) Obana, H.; Okihashi, M.; Akutsu, K.; Kitagawa, Y.; Hori, S. Determination of neonicotinoid pesticide residues in vegetables and fruits with solid phase extraction and liquid chromatography mass spectrometry. *J. Agric. Food Chem.* **2003**, *51*, 2501−2505.

(14) Di Muccio, A.; Fidente, P.; Barbini, D. A.; Dommarco, R.; Seccia, S.; Morrica, P. Application of solid-phase extraction and liquid chromatography−mass spectrometry to the determination of neonicotinoid pesticide residues in fruit and vegetables. *J. Chromatogr., A* **2006**, *1108*, 1−6.

(15) Yáñez, K. P.; Bernal, J. L.; Nozal, M. J.; Martín, M. T.; Bernal, J. Determination of seven neonicotinoid insecticides in beeswax by liquid chromatography coupled to electrospray-mass spectrometry using a fused-core column. *J. Chromatogr., A* **2013**, *1285*, 110−117.

(16) Kobayashi, H. Development of residue analysis for pesticides by LC/MS and LC/MS/MS methods. *Bunseki Kagaku* **2009**, *58*, 985−997 (in Japanese).

(17) Liu, S.; Zheng, Z.; Wei, F.; Ren, Y.; Gui, W.; Wu, H.; Zhu, G. Simultaneous determination of seven neonicotinoid pesticide residues in food by ultraperformance liquid chromatography tandem mass spectrometry. *J. Agric. Food Chem.* **2010**, *58*, 3271−3278.

(18) Kamel, A. Refined methodology for the determination of neonicotinoid pesticides and their metabolites in honey bees and bee products by liquid chromatography−tandem mass spectrometry (LC-MS/MS). *J. Agric. Food Chem.* **2010**, *58*, 5926−5931.

(19) Xie, W.; Han, C.; Qian, Y.; Ding, H.; Chen, X.; Xi, J. Determination of neonicotinoid pesticides residues in agricultural samples by solid-phase extraction combined liquid chromatography−tandem mass spectrometry. *J. Chromatogr., A* **2011**, *1218*, 4426−4433.

(20) Xiao, Z.; Li, X.; Wang, X.; Shen, J.; Ding, S. Determination of neonicotinoid insecticides residues in bovine tissues by pressurized solvent extraction and liquid chromatography−tandem mass spectrometry. *J. Chromatogr., B* **2011**, *879*, 117−122.

(21) Zhang, F.; Li, Y.; Yu, C.; Pan, C. Determination of six neonicotinoid insecticides residues in spinach, cucumber, apple and pomelo by QuEChERS method and LC−MS/MS. *Bull. Environ. Contam. Toxicol.* **2012**, *88*, 885−890.

(22) Xiao, Z.; Yang, Y.; Li, Y.; Fan, X.; Ding, S. Determination of neonicotinoid insecticides residues in eels using subcritical water extraction and ultra-performance liquid chromatography-tandem mass spectrometry. *Anal. Chim. Acta* **2013**, *777*, 32−40.

(23) Jovanov, P.; Guzsvány, V.; Franko, M.; Lazić, S.; Sakač, M.; Šarić, B.; Banjac, V. Multi-residue method for determination of selected neonicotinoid insecticides in honey using optimized dispersive liquid-liquid microextraction combined with liquid chromatography-tandem mass spectrometry. *Talanta* **2013**, *111*, 125−133.

(24) Yoshida, T.; Murakawa, H.; Toda, K. Determination of nitenpyram and its metabolites in agricultural products by using hydrophilic interaction liquid chromatography-tandem mass spectrometry. *J. Pestic. Sci.* **2013**, *38*, 27−32.

(25) Watanabe, E.; Kobara, Y.; Baba, K.; Eun, H. Reduction of hazardous organic solvent in sample preparation for hydrophilic pesticide residues in agricultural products with conventional liquid chromatography. *J. Agric. Food Chem.* **2013**, *61*, 4792−4798.

(26) Japanese Ministry of Health, Labour and Welfare. Analytical methods for residual compositional substances of agricultural chemicals, feed additives, and veterinary drugs in food; http://www.mhlw.go.jp/english/topics/foodsafety/positivelist060228/dl/060526-1a.pdf (accessed Nov 19, 2013).

(27) Stahnke, H.; Kittlaus, S.; Kempe, G.; Alder, L. Reduction of matrix effects in liquidchromatography−electrospray ionization−mass spectrometry by dilution of the sample extracts: how much dilution is needed? *Anal. Chem.* **2012**, *84*, 1474−1482.

(28) Niessen, W. M. A.; Manini, P.; Andreoli, R. Matrix effects in quantitative pesticide analysis using liquid chromatography−mass spectrometry. *Mass Spectrom. Rev.* **2006**, *25*, 881−899.
(29) Choi, B. K.; Hercules, D. M.; Gusev, A. I. Effect of liquid chromatography separation of complex matrices on liquid chromatography−tandem mass spectrometry signal suppression. *J. Chromatogr., A* **2001**, *907*, 337−342.
(30) Soler, C.; Mañes, J.; Picó, Y. Routine application using single quadrupole liquid chromatography−mass spectrometry to pesticides analysis in citrus fruits. *J. Chromatogr., A* **2005**, *1088*, 224−233.
(31) Mol, H. G. J.; Plaza-Bolaños, P.; Zomer, P.; deRijk, T. C.; Stolker, A. A. M.; Mulder, P. P. J. Toward a generic extraction method for simultaneous determination of pesticides, mycotoxins, plant toxins, and veterinary drugs in feed and food matrixes. *Anal. Chem.* **2008**, *80*, 9450−9459.
(32) Kmellár, B.; Fodor, P.; Pereja, L.; Ferrer, C.; Martínez-Uroz, M. A.; Valverde, A.; Fernandez-Alba, A. R. Validation and uncertainty study of a comprehensive list of 160 pesticide residues in multi-class vegetables by liquid chromatography−tandem mass spectrometry. *J. Chromatogr., A* **2008**, *1215*, 37−50.
(33) Lee, S. W.; Choi, J.-H.; Cho, S.-K.; Yu, H.-A.; El-Aty, A. M. A.; Shim, J.-H. Development of a new QuEChERS method based on dry ice for the determination of 168 pesticides in paprika using tandem mass spectrometry. *J. Chromatogr., A* **2011**, *1218*, 4366−4377.
(34) Japanese Ministry of Health, Labour and Welfare. Revision of guideline on validation of analytical methods for residual compositional substances of agricultural chemicals, feed additives, and veterinary drugs in food; http://www.mhlw.go.jp/topics/bukyoku/iyaku/syoku-anzen/zanryu3/dl/101224-1.pdf (in Japanese) (accessed Nov 19, 2013).
(35) European Commission. Method validation and quality control procedures for pesticide residues analysis in food and feed, Document no. SANCO/10684/2009; http://ec.europa.eu/food/plant/protection/resources/qualcontrol_en.pdf#search=%27No.%20SANCO/10684/2009%27 (accessed Nov 19, 2013).

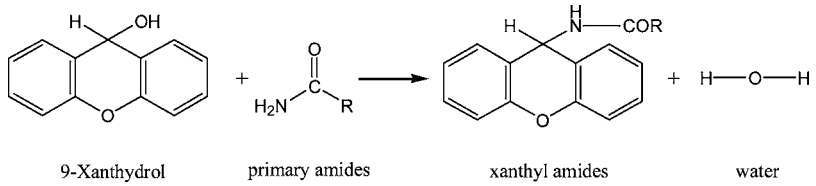

Figure 1. Formation of xanthyl amides from 9-xanthydrol and primary amides.

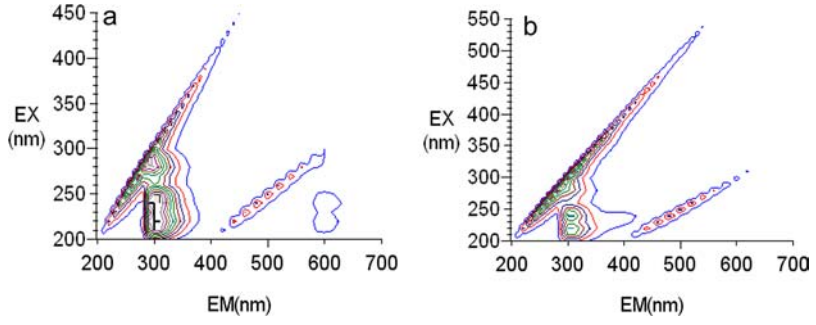

Figure 2. Three-dimensional fluorescence spectra of (a) XEC and (b) Xurea.

Chinese yellow-rice wine. However, the method needed different excitation and emission wavelengths at different times. After that, Wang et al.[30] developed an HPLC−FLD procedure (λ_{ex} of 234 nm and λ_{em} of 600 nm) to simultaneously detect EC and urea in Chinese yellow-rice wine. The method featured high recovery and good repeatability. However, their report did not provide any spectral information about the analytes. Moreover, the understanding of the derivatization conditions is insufficient, and the detection limit for urea is too high to monitor its variation in the brewing process of some alcoholic beverages. Therefore, in this work, we further studied the HPLC−FLD method and applied it to more alcoholic beverages. First, we systematically investigated the excitation wavelength and emission wavelength of the derivatized analytes. Then, the derivatization and separation conditions of analytes were optimized. Next, the parameters of the developed method were evaluated. Finally, we applied the developed method to the analysis of real samples from the Chinese market.

MATERIALS AND METHODS

Reagents and Solvents. Milli-Q-RG (Millipore, Milford, MA) high-purity water was used for dissolution of chemicals and dilution. Acetic acid, ethanol, hydrochloric acid, 1-propanol, and sodium acetate, purchased from Merck (Darmstadt, Germany), were of analytical grade. Acetonitrile of HPLC grade was purchased from Merck. EC (99%) and urea (99%) were purchased from Sigma Chemical Co. (St. Louis, MO). 9-Xanthydrol (99%) was purchased from Fluka Chemicals Co. (Buchs, Switzerland).

Samples. Red wines, grape brandies, and Chinese rice wines were purchased from the Chinese market. All of the information regarding the samples was obtained from the sample labels. The alcoholic strength of red wines, grape brandies, and Chinese rice wines ranged from 11.5 to 12% (v/v), 38 to 40% (v/v), and 15 to 16% (v/v), respectively. The red wines were made from *Cabernet Sauvignon* grapes grown in the Huaizhuo basin district (Hebei Province, P. R. China); we studied 2008, 2010, and 2011 vintages. The grape brandies were produced by three different manufacturers (namely, Greet Wall, The Dynasty, and Zhang Yu Wine Co. Ltd.) and aged for 3−15 years. The Chinese rice wines were produced by four different manufacturers (namely, Jiashan Youhua, Tapai, Gu Yue Long Shan, and Fuchunjiang Wine Co. Ltd.). All of the companies are from Zhejiang Province, P. R. China. All of the Chinese rice wines were semidry rice wines.

Sample Derivatization. The derivatization reaction was conducted in chromatographic vials as follows: 0.4 mL of the 9-xanthydrol solution (0.02 mol of 9-xanthydrol per liter in 1-propanol) was added to 0.6 mL of a sample or standard, and then 0.1 mL of hydrochloric acid (1.5 mol/L) was slowly added.

To ensure the reaction reached completion, the solution was homogenized and held for 30 min in the dark before being injected into chromatographic system for analysis. Three repeated injections of standard solutions, at six concentrations, were used to generate calibration curves.

HPLC−FLD. The experiments were conducted on an Agilent 1200 series analytical HPLC system equipped with a quaternary solvent delivery system and a G1321A fluorescence detector. The separations were performed on an Agilent Zorbax Eclipse XDB-C18 column (250 mm × 4.6 mm, 5 μm). The flow rate was 1.0 mL/min, the oven temperature 30 °C, and the injection volume 20 μL. The excitation and emission wavelengths were 240 and 308 nm, respectively. Phase A was sodium acetate (pH 7.2, adjusted with acetic acid). Phase B was acetonitrile. Elution was conducted using a gradient program as indicated in Table S1 of the Supporting Information. Quantitation was performed in accordance with an external standard method.

Validation. Method validation was performed following the recommendation of the International Conference on Harmonization.[31] The method was validated for linearity, stability, limits of detection (LOD), limits of quantification (LOQ), precision, and accuracy.

RESULTS AND DISCUSSION

Fluorescence Characteristics. To optimize fluorescence detection, 1 mg/L EC and urea in anhydrous alcohol were derivatized to obtain the three-dimensional spectra of xanthyl EC (XEC) and xanthyl urea (Xurea) (Figure 2). It is evident that XEC and the Xurea have similar fluorescence characteristics, which is consistent with the work of Francis et al.[27] This similarity is caused by their similar molecular structures. The diagonal bands in panels a and b of Figure 2 could be the result of Rayleigh and Raman scattering by solvent molecules. This possibility is supported by the fact that these diagonal signals were present in the contour plot of the blank working solutions. Both XEC and Xurea exhibit maximal fluorescence at 308 nm after excitation at 213 or 240 nm.

For the detection of fluorescence from Xurea, Herbert et al.[26] used excitation and emission wavelengths of 233 and 600 nm, respectively. Francis et al.[27] later verified that the peak at 592

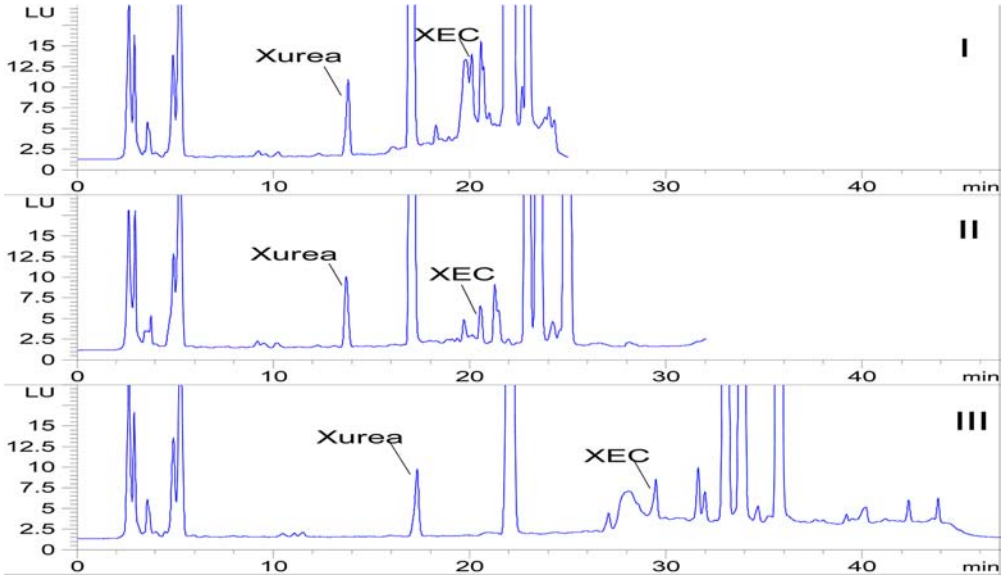

Figure 3. Determination of urea and EC in a 20% alcohol/water mixture using three gradient programs.

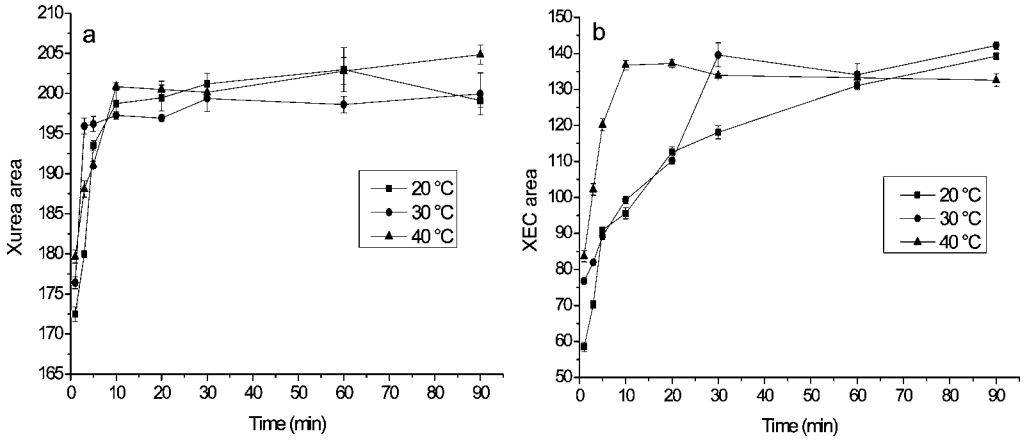

Figure 4. Formation of Xurea (a) and XEC (b) as a function of reaction time and temperature.

nm (corresponding to 600 nm) was actually an artifact of the instrumentation. They observed similar maxima at 211 and 240 nm in the excitation spectrum and 298 nm in the emission spectrum. Our results are consistent with the report of Francis et al.;[27] the slight discrepancies in the emission maxima were due (in part) to the different slit widths used in each instrument.

For the detection of the fluorescence of XEC, Herbert et al.[17] used excitation and emission wavelengths of 233 and 600 nm, respectively. Mihucz et al.[28] later detected XEC at λ_{ex} and λ_{em} wavelengths of 238 and 300 nm, respectively, because they observed that the peak at 300 nm was more intense than that at 600 nm. Our results are consistent with the report of Mihucz et al.

Although wavelengths of 213 or 240 nm could excite the same intense peak at 308 nm, we chose an excitation wavelength of 240 nm and an emission wavelengths of 308 nm for the characterization of XEC and Xurea. This is because high-energy photons will be absorbed by mainly the solvent and can damage the fluorescence spectrophotometer. The use of the same excitation and emission wavelengths allowed the use of HPLC–FLD for the simultaneous determination of XEC and Xurea.

Chromatographic Separation. To achieve successful resolution of XEC and Xurea, three gradient elution programs were tested (Table S1 of the Supporting Information). Figure 3 shows a chromatogram of the derivatized urea and EC in a 20% alcohol/water mixture. An amino group ($-NH_2$) results in Xurea being more polar than XEC, which has an ethoxy group ($-OCH_2CH_3$). This characteristic allowed easy separation of XEC and Xurea. In all cases, we observed insufficient separation of XEC. This may be due to the presence of the 9-xanthydrol derivatives in the reagent, which have polarities that are similar to that of XEC and exhibit strong fluorescence at λ_{ex} and λ_{em} wavelengths of 240 and 308 nm, respectively. Alternatively, the MS detector can provide excellent selectivity for XEC and demonstrate no other interference signal.[34]The best analytical frequency, chromatographic resolution (not satisfactory but acceptable for XEC), and peak shape were obtained adopting gradient program II. Under this condition, XEC and Xurea are detected at 20.6 and 13.8 min, respectively.

Optimization of the Derivatization Condition. The derivatization kinetics was determined by using standard solutions [1 mg/L for both EC and urea in a 40% (v/v) alcoholic solution] reacting at different temperatures. Because a higher temperature can accelerate the reaction of urea to form

dx.doi.org/10.1021/jf405400y | J. Agric. Food Chem. 2014, 62, 2797–2802

EC, the derivatization was conducted at a relatively low temperature (20, 30, or 40 °C). To evalute the stability of the derivatized analytes, a wide reaction time range (5−90 min) was chosen.

It can be observed in Figure 4a that the three curves are almost superimposed, demonstrating that temperature has very little effect on the formation of Xurea. In contrast, the temperature had a strong effect on the formation of XEC (Figure 4b). This is because oxygen is more electronegative than nitrogen. This causes the EC to be less susceptible (than the urea) to nucleophilic attack by the hydroxyl group in 9-xanthydrol. The temperature in this experimental range can provide sufficient activation energy, which ensures the complete formation of Xurea in 10 min. With regard to EC reacting with 9-xanthydrol to form XEC, however, the rate of XEC formation increases with an increasing temperature because of the greater kinetic energy of the reacting molecules. To ensure the complete formation of XEC, the derivative should be held at 40 °C for 10 min, 30 °C for 30 min, or 20 °C for at least 60 min. For simultaneous determination of EC and urea, considering both efficiency and operability, we determined that the derivative reaction should be performed at 30 °C for 30 min. These conditions ensured the completion of the derivative reaction. In addition, the derivatized products were stable in 60 min, with a difference between the maximal signal and the minimal signal of 5% for XEC and 1% for Xurea.

In general, the samples vary in alcoholic strength. To standardize the derivatization and to improve the reproducibility of the method, it is necessary to make the alcoholic strength of the samples uniform. Moreover, in an alcohol/water mixture, the alcoholic strength can have an effect on solubility, stability, and reaction rates. Choosing the appropriate alcoholic strength allows for thermodynamic and kinetic control over a derivative reaction. Thus, the effect of the alcoholic strength on the derivatization response was evaluated. As shown in Figure 5, the alcoholic strength clearly influences the peak area of XEC

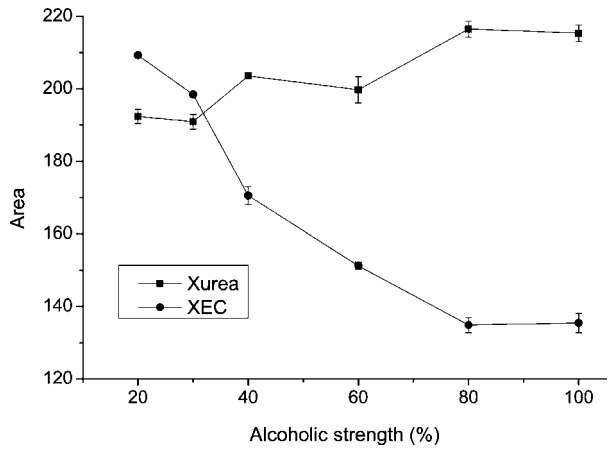

Figure 5. Effect of alcoholic strength on the response of Xurea and XEC (the derivative reaction was conducted at 30 °C for 30 min).

or Xurea. A higher alcoholic strength favors the derivatization of urea but adversely affects the derivatization of EC. The latter result is in agreement with the findings of Roberto et al.,[32] who reported that the extent of EC derivatization decreases with an increasing alcoholic strength. The different responses of urea and EC derivatization can partly be explained by the Hughes−Ingold rules.[33] An alcoholic strength of 20% (v/v) is considered to be more suitable for simultaneous determination of EC and urea in alcoholic beverages. This is true for the three following reasons.

(1) With an increasing alcoholic strength, the response of XEC decreases sharply while that of Xurea increases mildly. Choosing a 20% (v/v) alcohol/water mixture as the solvent can significantly improve the detection sensitivity for EC but slightly decrease that of urea.

(2) Alcoholic beverages generally contain EC and urea at levels of micrograms per liter and milligrams per liter, respectively. Moreover, the response of the fluorescence detector to Xurea is more significant than the response to XEC. Therefore, we must give priority to EC detection sensitivity.

(3) Alcoholic beverages generally contain 10−40% alcohol. Choosing a 20% (v/v) alcohol/water mixture as the solvent results in no dilution or trace dilution of the sample, which can significantly improve the detection limits of EC and urea.

Method Validation. *Linearity, LOD, and LOQ.* Considering the levels of EC and urea normally found in alcoholic beverages, and the maximal or recommended limits set in some countries, the linearity of EC detection was studied in the range from 10 to 500 μg/L, while the linearity of the urea detection was tested in the range from 0.01 to 100 mg/L. The regression equations used for EC and urea determination were $Y = 30.5X + 6.4$ and $Y = 53.3X + 4.3$, respectively. In the equations, Y is the peak area and X is the EC or urea concentration. The correlation coefficients (R^2) of both analytes were >0.999, which indicates excellent linearity over the tested concentration ranges. The LOD (signal-to-noise ratio of 3) and LOQ (signal-to-noise ratio of 10) for both analytes were as follows: 4.8 and 16 μg/L for EC and 0.003 and 0.01 mg/L for urea, respectively.

Precision and Accuracy. To determine the precision and accuracy of the method, intraday and interday repeatability and recovery experiments were performed. To simplify processing, red wine, Chinese rice wine, and grape brandy were chosen for the precision and accuracy experiment because they present more complex compositions and demonstrate greater applicability of the method. Three samples were spiked with EC and urea, at low and high fortification levels, and were analyzed accordingly. The results are listed in Table 1 and show great repeatability for both analytes because the intraday RSD values were <3.7% and the interday values were <4.8%. The data showed satisfactory accuracy of the proposed method as recoveries of all analytes were in the range from 90.7 to 104.8%.

Application of the Method. The new method was applied to alcoholic beverages for the assessment of EC and urea levels. Nine types of red wines, 12 types of Chinese rice wines, and 5 types of grape brandies were analyzed, at least in duplicate, and the results are summarized in Table 2. The levels of EC in red wines, Chinese rice wines, and grape brandies ranged from "detected but not quantified" to 22.4 μg/L, detected but not quantified to 225.0 μg/L, and 44.2 to 78.3 μg/L, respectively. Correspondingly, the levels of urea in these beverages ranged from 1.2 to 2.8 mg/L, 5.1 to 17.7 mg/L, and 0.3 to 0.7 mg/L, respectively. The high level of EC (average value of 76.3 μg/L) in Chinese rice wine may be caused by their special production process, which includes wine boiling, jar filling, and storage. The high standard deviations of the EC and urea concentrations in the Chinese rice wines are the result of the various raw materials and the production processes that are used in their manufacture. A proportion of 8.3% of the Chinese rice wines contained >200 μg/L EC. This is above the Canadian

Table 1. Mean Recoveries and Intraday and Interday Precisions (n = 6) of EC and Urea Measurements from Red Wine, Chinese Rice Wine, and Grape Brandy at Two Fortification Levels

			intraday		interday	
sample	analyte	added concentration (EC, μg/L; urea, mg/L)	RSD (%)	recovery (%)	RSD (%)	recovery (%)
red wine	EC	10	2.1	99.5	3.2	101.0
		500	3.1	100.2	2.8	97.3
	urea	0.01	1.3	101.1	3.1	94.2
		100	1.9	101.7	4.6	104.8
Chinese rice wine	EC	10	2.9	93.8	2.8	103.6
		500	3.1	101.2	4.2	100.0
	urea	0.01	1.2	90.7	2.1	95.8
		100	1.7	101.4	3.7	101.9
grape brandy	EC	10	1.9	98.3	1.0	104.6
		500	1.2	97.8	2.9	103.1
	urea	0.01	2.9	101.2	3.8	103.2
		100	3.7	99.7	4.8	98.3

Table 2. EC and Urea Contents of Alcoholic Beverages

	EC (μg/L)		urea (mg/L)	
samples	range of average values ± the standard deviation		range of average values ± the standard deviation	
red wines	nd[a] to 22.4	13.7 ± 7.6	1.2−2.8	2.1 ± 0.6
Chinese rice wines	nd[a] to 225.0	76.3 ± 75.9	5.1−17.7	8.8 ± 4.5
grape brandies	44.2−78.3	61.3 ± 24.1	0.3−0.7	0.5 ± 0.3

[a]Detected but not quantified.

limits for EC in Japanese sake (200 μg/L). Red wines and grape brandies have the normal EC levels that are within the limits of the Canadian legislation.

The developed method demonstrated good linearity, recoveries, and repeatability for the simultaneous analysis of EC and urea in alcoholic beverages. The advantages of the method presented here are the simplicity of sample preparation and the simultaneous determination of the two analytes within a short period of time. This method is very useful for the study of the kinetics of EC formation from urea in alcoholic beverages during storage. The method will also be helpful for the further investigation of the mechanism of the formation of EC by urea alcoholysis in the brewing process of alcoholic beverages. In addition, this method is compatible with the legal requirements for the maximal limits of EC content in beverages and therefore can be used to screen alcoholic beverages that have EC contents that are higher than the legal limit.

■ ASSOCIATED CONTENT

Supporting Information

Mobile phase gradients (Table S1). This material is available free of charge via the Internet at http://pubs.acs.org.

■ AUTHOR INFORMATION

Corresponding Authors

*E-mail: liuhaokd@tom.com (Hao Liu). Telephone: +86-022-60601599.

*E-mail: zj96sk@163.com (Jian Zhang). Telephone: +86-022-60601599.

Funding

This work was supported by the National Natural Science Foundation of China (31101275 and 31201354), the National Science and Technology Support Program (2012BAK17B11), the National High-tech R&D Program (863 Program) of China (2012AA021302), and the Science and Technology Support Project of Tianjin (12ZCZDNC01600).

Notes

The authors declare no competing financial interest.

■ REFERENCES

(1) *Alcoholic beverage consumption and ethyl carbamate*; IARC monographs on the evaluation of carcinogenic risks to humans; International Agency for Research on Cancer (IARC): Lyon, France, 2010; Vol. *96*.

(2) Vahl, M. A survey of ethyl carbamate in beverages, bread and acidified milks sold in Denmark. *Food Addit. Contam.* **1993**, *10*, 585−592.

(3) Weber, J. V.; Sharypov, V. I. Ethyl carbamate in foods and beverages: A review. *Environ. Chem. Lett.* **2009**, *7*, 233−247.

(4) Hasnip, S.; Crews, C.; Potter, N.; Christy, J.; Chan, D.; Bondu, T.; Matthews, W.; Walters, B.; Patel, K. Survey of ethyl carbamate in fermented foods sold in the United Kingdom in 2004. *J. Agric. Food Chem.* **2007**, *55*, 2755−2759.

(5) Canas, B. J.; Harvery, D. C.; Robinson, L. R.; Sulivan, M. P.; Joe, F. L. J.; Diachenko, G. W. Ethyl carbamate levels in selected foods and beverages. *J.—Assoc. Off. Anal. Chem.* **1989**, *72*, 873−876.

(6) Conacher, H. B. S.; Page, B. D. Ethyl carbamate in alcoholic beverages, a Canadian case history. In *Proceedings of the Euro food toxicity, interdisciplinary conference on natural toxicants in food*; European Society of Toxicology: Zurich, 1986; pp 237−242.

(7) U.S. Food and Drug Administration (FDA). Center for Food Safety and Nutrition. Information on Ethyl Carbamate (Urethane) in Foods and Beverages, 2000 (http://www.cfsan.fda.gov/~frf/ecin-tro.html).

(8) Lachenmeier, D. W.; Lima, M.; Nóbrega, I.; Pereira, J.; Kerr-Corrêa, F.; Kanteres, F.; Rehm, J. Cancer risk assessment of ethyl carbamate in alcoholic beverages from Brazil with special consideration to the spirits cachaca and tiquira. *BMC Cancer* **2010**, *10*, 266.

(9) Ough, C. S.; Stevens, D.; Almy, J. Preliminary comments on effects of grape vineyard nitrogen fertilization on the subsequent ethyl carbamate formation in wines. *Am. J. Enol. Vitic.* **1989**, *40*, 219−220.

(10) Valero, E.; Mauricio, J. C.; Milan, M. C.; Ortega, J. M. Changes in the urea content of wine under different fermentation and aging conditions by two *Saccharomyces cerevisae* races. *Biotechnol. Lett.* **1999**, *21*, 555−559.

(11) Ough, C. S.; Crowell, E. A.; Mooney, L. A. Formation of ethyl carbamate precursors during grape juice (chardonnay) fermentation. I. Addition of amino acids, urea, and ammonia: Effects of fortification on intracellular and extracellular precursors. *Am. J. Enol. Vitic.* **1988**, *39*, 243−249.

(12) Ough, C. S.; Crowell, E. A.; Gutlove, B. R. Carbamyl compound reactions with ethanol. *Am. J. Enol. Vitic.* **1988**, *39*, 239−242.

(13) Aresta, M.; Boscolo, M.; Franco, D. W. Copper(II) catalysis in cyanate conversion into ethyl carbamate in spirits, and relevant reactions. *J. Agric. Food Chem.* **2001**, *49*, 2819−2824.

(14) Stevens, D. F.; Ough, C. S. Ethyl carbamate formation: Reaction of urea and citrulline with ethanol in wine under low to normal temperature conditions. *Am. J. Enol. Vitic.* **1993**, *44*, 309−312.

(15) Uthurry, C. A.; Varela, F.; Colomo, B.; Suárez Lepe, J. A.; Lombardero, J.; García del Hierro, J. R. Ethyl carbamate concentrations of typical Spanish red wines. *Food Chem.* **2004**, *88*, 329−336.

(16) Butzke, C. E.; Bisson, L. F. *Ethyl carbamate preventative action manual*; Center for Food Safety and Applied Nutrition, U.S. Food and Drug Administration: Silver Spring, MD, 1997.

(17) Herbert, P.; Santos, L.; Bastos, M.; Barros, P.; Alves, A. New HPLC method to determine ethyl carbamate in alcoholic beverages using fluorescence detection. *J. Food Sci.* **2002**, *67*, 1616−1625.
(18) Lachenmeier, D. W.; Nerlich, U.; Kuballa, T. Automated determination of ethyl carbamate in stone-fruit spirits using headspace solid-phase microextraction and gas chromatography-tandem mass spectrometry. *J. Chromatogr., A* **2006**, *1108*, 116−120.
(19) Zhang, Y.; Zhang, J. Optimization of headspace solid-phase microextraction for analysis of ethyl carbamate in alcoholic beverages using a face-centered cube central composite design. *Anal. Chim. Acta* **2008**, *627*, 212−218.
(20) Jagerdeo, E.; Dugar, S.; Foster, G. D.; Schenck, H. Analysis of ethyl carbamate in wines using solid-phase extraction and multidimensional gas chromatography/mass spectrometry. *J. Agric. Food Chem.* **2002**, *50*, 5797−5802.
(21) González-Rodríguez, J.; Pérez-Juan, P.; Luque de Castro, M. D. Method for monitoring urea and ammonia in wine and must by flow injection-pervaporation. *Anal. Chim. Acta* **2002**, *471*, 105−111.
(22) Nagel, C. W.; Weller, K. M. Colorimetric determination of urea in wine. *Am. J. Enol. Vitic.* **1989**, *40*, 143−144.
(23) Francis, P. S. The determination of urea in wine: A review. *Aust. J. Grape Wine Res.* **2006**, *12*, 97−106.
(24) Francis, P. S.; Lewis, S. W.; Lim, K. F. Analytical methodology for the determination of urea: Current practice and future trends. *TrAC, Trends Anal. Chem.* **2002**, *21*, 389−400.
(25) Phillips, R. F.; Burnett, M. P. The use of xanthydrol as a reagent for the characterisation of primary amides. *J. Am. Chem. Soc.* **1943**, *65*, 1355−1357.
(26) Veiga, M. J.; Herbert, P.; Simões, T.; Oliveira, A.; Alves, A. Poster P-III-16: Determination of urea in port wine by HPLC with fluorescence detection after derivatization with 9-xanthydrol. Presented at the 4th International Conference on Instrumental Methods of Analysis: Modern Trends and Applications, October 2−6, 2005, Iraklion, Crete, Greece.
(27) Clark, S.; Francis, P. S.; Conlan, X. A.; Barnett, N. W. Determination of urea using high-performance liquid chromatography with fluorescence detection after automated derivatisation with xanthydrol. *J. Chromatogr., A* **2007**, *1161*, 207−213.
(28) Ajtony, Z.; Szoboszlai, N.; Bencs, L.; Viszket, E.; Mihucz, V. G. Determination of ethyl carbamate in wine by high performance liquid chromatography. *Food Chem.* **2013**, *141*, 1301−1305.
(29) Xiong, Z. H.; Zhong, Q. D.; Xing, J. T. A rapid detection method for production quality control of Chinese yellow rice wine. CN 102353728, February 15, 2012.
(30) Wang, R. Y.; Wu, H. M.; Zhou, X. P.; Chen, L. Simultaneous detection of ethyl carbamate and urea in Chinese yellow rice wine by HPLC-FLD. *J. Liq. Chromatogr. Relat. Technol.* **2014**, *37*, 39−47.
(31) International Conference on Harmonization (ICH). Validation of analytical procedures: Text and methodology Q2 (R1) (http://www.ich.org).
(32) Roberto, R. M.; Belén, S. V. Determination of ethyl carbamate in cider spirits by HPLC-FLD. *Food Control* **2009**, *20*, 139−143.
(33) Hughes, E. D.; Ingold, C. K. Mechanism of substitution at a saturated carbon atom. Part IV. A discussion of constitutional and solvent effects on the mechanism, kinetics, velocity, and orientation of substitution. *J. Chem. Soc.* **1935**, 244−255.
(34) Edit, D.; Attila, G.; Éva, S. B.; Mihály, D. Determination of ethyl carbamate in pálinka spirits by liquid chromatography-electrospray tandem mass spectrometry after derivatization. *Food. Res. Int.* **2010**, *43*, 2452−2455.

Table 1. Size of the PCR Products Using Universal Primers and Species-Specific Primers

species	PCR amplicon with universal primers (bp)	access number	species-specific primers	PCR amplicon with species-specific primers (bp)
E. encrasicolus	431	JX070003	Fw: CCCAAAAAGGTAAGGAGAAAG	597
	643−665	JX070004-JX070011	Rev: TGCAACATTGCAACAAAACTT	
E. mordax	472	JX070012-JX070023	Fw: TGAAAAGACATTCTCACGTTGTG	380
			Rev: ACGGTCCTCCTCTCACAGTC	
E. ringens	422−454	JX070024-JX070033	Fw: TGAAAAAGGGAATGGGGTTT	250
			Rev: CGGTCCTTTTAGGGTTAGGG	
E. japonicus	443	KF479206	Fw: CCCAAAAAGGTAAGGAGAAAG	598
	641−664	KF479207-KF479213	Rev: TGCAACATTGCAACAAAACTT	

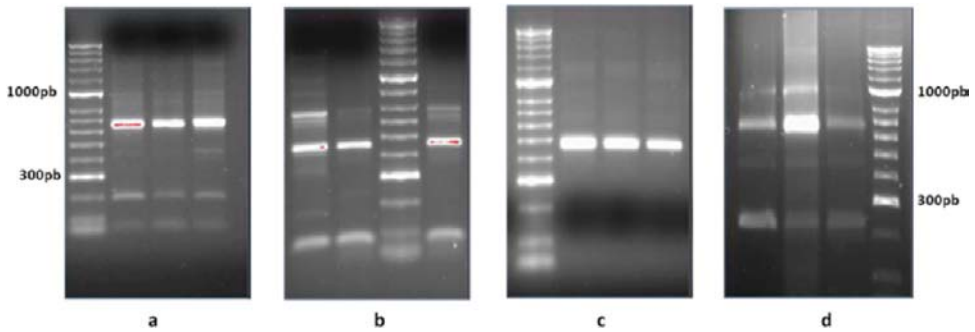

Figure 1. Amplification products of 5S rDNA using universal primers in three independent individuals of (a) *E. encrasocilus*, (b) *E. mordax*, (c) *E. ringens*, and (d) *E. japonicus*. In addition to the main amplification product, some secondary bands appeared due to different types of 5 S rDNA.

processed, and this presents additional difficulty for morphological identification. The results of this study should ensure the traceability of products to prevent fraud, improve food safety, and assist in implementing initiatives such as appellations of origin.

MATERIALS AND METHODS

Chemicals. The DNA extraction kit was purchased from Bio101 (Vista, CA, USA) and the DNA purification kit from Macherey-Nagel (Bethlehem, PA, USA). The PCR reagents and restriction enzyme were obtained from Fermentas (Massachusetts, USA) and Euro-Clone (Milano, Italy). Clonation DNA was purchased from Promega (Madison, WI, USA). The chemicals were purchased from Sigma-Aldrich (St. Louis, MO, USA) and Bio-Rad (Hercules, CA, USA).

Animal Sampling and DNA Isolation. For the analysis of the 5S rDNA multigene family in the four species of the Engraulidae family, the following were used: fresh samples of *Engraulis encrasicolus* from the Gulf of Cadiz, samples of *Engraulis mordax* from Baja California in Mexico, *Engraulis ringens* from Valparaiso in Chile, and *Engraulis japonicus* from the Sea of Japan. All samples were collected and preserved in absolute ethanol. Total genomic DNA was extracted from 150 mg of muscle sections with FastDNA kit for 40 s, at a speed of 5 m/s, in a FP120 Fastprep instrument (Bio101, Inc., Vista, CA).

PCR Amplification, Cloning, and Sequencing. The 5S rDNA gene was amplified with the two universal primers 5S1F (5′-TACGCCCGATCTCGTCCGATC-3 ′) and 5S2R (5′-CAGGCTGG-TATGGCCGTAAGC-3′).[15] PCR was performed in a final volume of 50 μL containing 4 μL of genomic DNA, 3 mM $MgCl_2$, 200 μM dNTP (Fermentas), 0.2 μM of each primer, 2 units of Taq polymerase (Euro-Clone, Italy), and the appropriate buffer for the enzyme. The reaction was carried out using an initial cycle of 5 min at 94 °C and 35 cycles of 45 s at 94 °C, 45 s at 59 °C, and 1 min at 72 °C and a final extension of 10 min at 72 °C. Products were visualized by agarose gel 2% with ethidium bromide (0.5 μg/mL) after electrophoresis. The PCR products obtained were purified using the NucleoSpin extraction kit (Macherey-Nagel, Inc., Bethlehem, PA) and cloned using the pGEM cloning kit from T Easy Vector Systems (Promega, Madison, WI). The sequencing was carried out using a sequencing kit (BigDye Terminator v 3.1 Cycle Sequencing Kit, Applied Biosystems). Sequencing peaks were analyzed with Chromas 2.0, and the sequences obtained were aligned using the ClustalW and BioEdit programs

Design of Species-Specific Primers of 5S rDNA. Alignment of the 5S rDNA sequences of the four species studied reveals a significant difference in the NTS between *E. encrasicolus* on the one hand and *E. japonicus*, *E. mordax*, and *E. ringens* on the other and a similarity of 83% between *E. encrasicolus* and *E. Japonicus*. Therefore, to differentiate between these species, species-specific primers were designed (Table 1) and located in the NTS using the Primer 3 program.

The multiplex PCR for the simultaneous identification of the different species of anchovy was performed in a final volume of 50 μL containing 2 μL of DNA (80−100 ng), 0.2 μM of each primer, 3 mM $MgCl_2$, 200 mM dNTP, 2 units of the Taq polymerase enzyme, and appropriate buffer for the enzyme. The reaction was carried out under the same conditions as those described above. PCR products were purified and directly sequenced to verify that the amplified products are the same as previously designed. These primers not only indicate the presence or absence of amplification but also allow the product size to be differentiated, which also facilitates the reading of the results.

Sequences of *E. encrasicolus* and *E. japonicus* showed a high degree of similarity, which hinders identification using specific primers. We used the same pair of primers for the two species and were able to distinguish between them using the RFLP restriction enzyme *BspLU11I*. The digestion reaction was carried out in a final volume of 20 μL with 2 μL of PCR product, 1 μL of enzyme, and 2 μL of the appropriate buffer.

RESULTS

In eukaryotes, rDNA (rDNA) is generally arranged in two different gene clusters (multigene families), each composed of

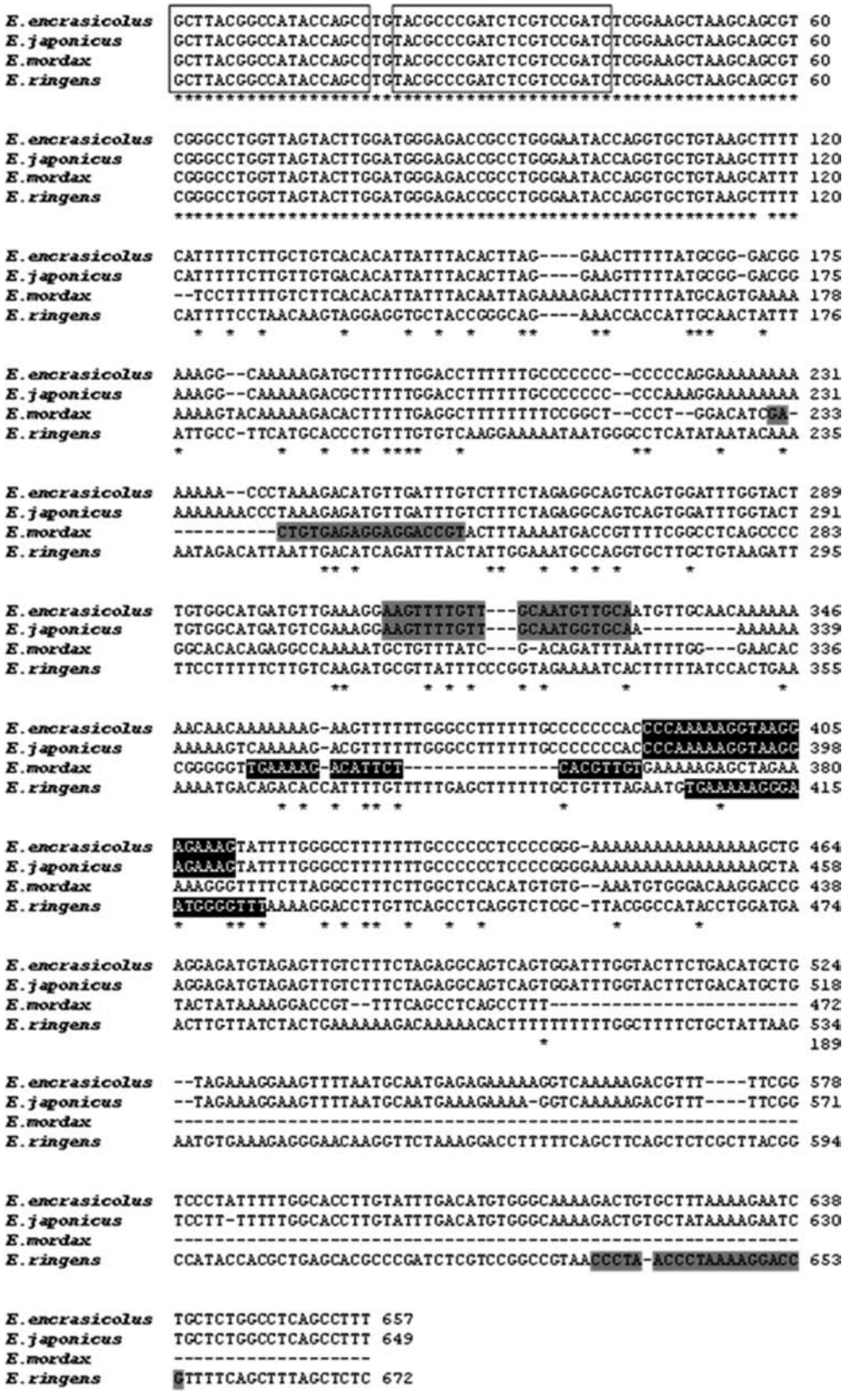

Figure 2. Alignment of the 5S consensus sequences of the four species of *Engraulis*. Consensus sequence were obtained from three individuals of each species (*E. encrasicolus* nine clones, *E. japonicus* eight clones, *E. ringens* 10 clones, and *E. mordax* 12 clones). Sequences of each clone are deposited in GenBank with an access number shown in Table 1. Universal primers (described in Table 1) are framed, and species-specific primers (Table 1) are shaded (Fw sequences shaded in black and Rev sequences shaded in gray).

hundreds to thousands of gene copies, one the major cluster (45S rDNA) and the other the minor cluster (5S rDNA). The 5S rRNA gene consists of one highly conserved sequence of 120 base pairs (bp), which is separated from the next unit by a

dx.doi.org/10.1021/jf405680g | J. Agric. Food Chem. 2014, 62, 2803−2808

nontranscribed spacer (NTS). Although the 5S rRNA gene is highly conserved, the NTSs are variable both in length and in sequence. The fast rate of base substitution, together with gene conversion, should make NTS sequences candidates as markers for species identification.

The aim of this study is to differentiate between four very similar species of the Engraulidae family: *E. encrasocilus*, *E. mordax*, *E. ringens*, and *E. japonicus*, which are of considerable commercial interest in Europe, Asia, and Latin America; reliable differentiation should help to prevent fraud and labeling errors.

Repeat units of 5S rDNA were amplified using universal primers.[15] Several products were obtained among them, which varied depending on the length of the NTS. The coding region of 120 bp showed a high degree of conservation among the four species.

We found many products of 5S rDNA which differed, for example, between *E. encrasocilus*, *E. ringens*, and *E. japonicus* by the length of their NTS, mainly due to the presence of several repeated sequences of poly A, poly C, and poly G or due to fouling by pseudogenes (Figure 1, Table 1).

However, because of the presence of many products and dimer bands, 5S rDNA amplification is not sufficient to differentiate reliably between these species. The high degree of polymorphism observed between the NTS sequences of these four species of *Engraulis*, after aligning their 5S rDNA sequences, means that this characteristic could be useful for differentiating between the species, therefore species-specific primers were designed for the zones of variability (Figure 2, Table 1).

Multiplex PCR was performed with the four pairs of primers designed to discriminate rapidly the four species of *Engraulis*. The results obtained show that these primers indicate not only presence or absence of amplification but also the difference in size of the amplification product, which facilitates reading (Figure 3, Table 1).

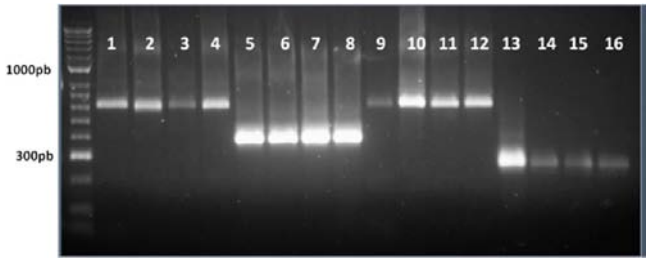

Figure 3. Electrophoretic patterns of multiplex PCR with species-specific primers as described in Table 1 in four independent individuals of each of the four species of *Engraulis*: (1–4) *E. encrasicolus*, (5–8) *E. mordax*, (9–12) *E. japonicus*, and (13–16) *E. ringens*..

In the case of *E. encrasicolus* and *E. japonicus*, it was difficult to design specific primers for each of the species because their sequences are very similar and there were areas where polymorphism is present in the form of sequences of poly A and poly T; consequently, the only solution was to use a restriction enzyme. By analyzing the sequences of all the specific primer clones of the two species, it was found that the enzyme *BspLU11I* allows differentiation to be made between these two species because two different banding patterns were obtained. *E. encrasicolus* has two different alleles for the enzyme *BspLU11I*, whereas *E. japonicus* has one allele with a unique restriction site (Figure 4).

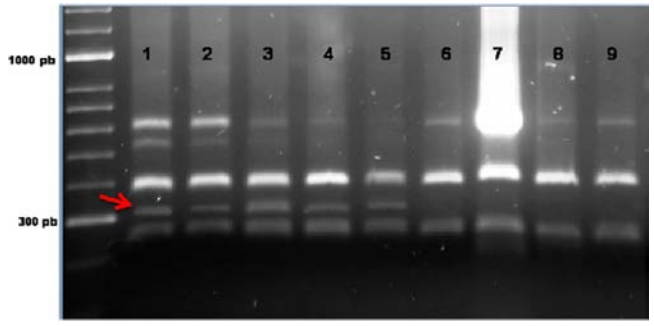

Figure 4. Electrophoretic patterns of digestion with restriction enzyme *BspLU11I* of the PCR products with species-specific primers for *E. encrasicolus* (from 1 to 5) and *E. japonicus* (from 6 to 9). The arrow indicates the differential band. Each lane is from an independent individual.

DISCUSSION

In this paper, we study the identification of four species of anchovy: one European (*E. encrasicolus*), which is in great demand for the European market and for which there has been a significant decrease in the fishing grounds, another Japanese (*E. japonicus*) which is marketed in much of Asia, and two species from the Americas (*E. mordax* and *E. ringens*) that are being imported into Europe in order to increase supply to match the high demand.

Consumers in all markets of the world increasingly expect the seafood industry to devise and implement measures for the safety and traceability of food products to ensure that these products are of sufficient quality, authentic, and properly labeled with all the necessary information. The industry is therefore increasingly seeking fast and reliable techniques for controlling seafood safety and preventing fraud, especially with respect to species of fish that are morphologically similar but very different in commercial value, such as anchovies.

The European anchovy *E. encrasicolus* has been the target of identification studies using PCR-RFLP of cytochrome *b*, versus *Sardinella aurita*,[8] in semipreserved products and in paste.[10] A phylogenetic study has also been made of the Engraulidae family in which the genetic distances between various species is highlighted.[9]

In this study, the repeating units of 5S rDNA have been used as a molecular marker to differentiate rapidly the four species of the Engraulidae family by multiplex PCR . These repeating units showed a 5S rRNA with 120 bp, which is highly conserved among many taxa, separated by NTS noncoding segments of rDNA which evolve much faster than the coding region, and appear to be specific for each species. The 5S rDNA has been widely used as a molecular marker to differentiate closely related species due to the peculiarity of its structure and organization. Thus, in several studies it has been used as a marker to discriminate fish species[16−19] and in one study linked to other genes such U snRNA.[20]

The variations found between the NTS of the different species studied are due to insertions/deletions, repeats, and pseudogenes that have been the main source of variation in the size of 5S rDNA units. These have been characterized in several other organisms and appear to be very useful as markers in the

characterization of species.[21−23] Precise species-specific primers have also been designed for the four species of *Engraulis* which showed considerable differences in the size of the gene (Table 1).

In the four species, amplification with the universal primers gave more than one product; this is probably because the particular organization of this gene appears to be very common in fish. This means that the genes are in different genomic locations and must be independently assessed.[17,24,25]

As in most tandemly repeated multigene families under concerted evolution, our results also revealed homogeneity of the 5S rDNA, but in both *E. encrasicolus* and *E. japonicus*, the elements homogenized by repetition are two widely divergent units, one short NTS I (about 450 bp) and a long NTS II (about 640 bp). Also in *E. encrasicolus* and *E. japonicus*, the duplication observed in NTS II, with base substitutions and insertions/deletions represents most of the difference in length between the two types of NTS. A similar situation has also been described in other genera including *Coregonus*, *Brycon*, and *Leporinus*.[26−28]

However, unlike in other fish species that also have several size classes of 5S rDNA, the comparison between the two classes of NTS revealed that the sequence identity is extremely low in the spacer region.[29]

Unexpectedly, the NTS sequences of the two species *E. encrasicolus* and *E. japonicus* maintain a very high degree of conservation (91% for NTS I and 89% for NTS II) as a result of some particular homogenization mechanism such as gene conversion or unequal crossing;[30] similar results have been found in NTS sequences between two species of shark.[12] The closeness of the genetic distance observed between these two species has also been described by analysis of cytochrome *b* nucleotide divergence, showing values of 0.04, whereas in our study we have obtained a value of 0.045.[31]

The presence of several types of product of 5S rDNA is not sufficient to identify conclusively each species; it can even lead to confusing results. Therefore it was decided to design species-specific primers to give reliable results.

Ultimately, these results should be of great interest for product traceability in the marketing of these species, given the overexploitation of anchovy fisheries in Europe and the continued periods of closure imposed. Imports of other anchovy species have been increasing significantly as suppliers try to alleviate this shortage. These imported products may be frozen or processed, which presents additional difficulties for morphological identification. In conclusion, these results allow anchovy products to be reliably traced, with the object of preventing fraud, improving food safety, and implementing initiatives such as appellations of origin.

AUTHOR INFORMATION

Corresponding Author

*Phone: +34956016181. Fax: +34956016448. E-mail: laureana.rebordinos@uca.es.

Present Address

[†]H.C.: Laboratoire Pluridisciplinaire, Université Abdelmalek Essâadi, Faculté Polydisciplinaire, B.P. 745, Poste Principale 92004, Larache, Morocco.

Funding

This work was supported by grants from the Junta de Andalucía (Spain) to the PAI BIO-219 group.

Notes

The authors declare no competing financial interest.

REFERENCES

(1) *The State of World Fisheries and Aquaculture*; FAO Fisheries and Aquaculture Department: Rome, 2012.

(2) Rasmussen, R. S.; Morrissey, M. T. DNA-based methods for the identification of commercial fish and seafood species. *Comp. Rev. Food Sci. Food Saf.* **2008**, *7*, 280−295.

(3) Garcia-Vazquez, E.; Perez, J.; Martinez, J. L.; Pardiñas, A. F.; Lopez, B.; Karaiskou, N.; Casa, M. F.; Machado-Schiaffino, G.; Triantafyllidis, A. High level of mislabeling in Spanish and Greek hake markets suggests the fraudulent introduction of African species. *J. Agric. Food Chem.* **2001**, *59*, 475−480.

(4) Chuang, P. S.; Chen, M. I.; Shiao, J. C. Identification of tuna species by a real-time polymerase chain reaction technique. *Food Chem.* **2012**, *133*, 1055−1061.

(5) Pascoal, A.; Ortea, I.; Gallardo, J. M.; Cañas, B.; Barros-Velázquez, J.; Calo-Mata, P. Species identification of the Northern shrimp (*Pandalus borealis*) by polymerase chain reaction−restriction fragment length polymorphism and proteomic analysis. *Anal. Biochem.* **2012**, *421*, 56−67.

(6) Li, X.; Li, J.; Zhang, S.; He, Y.; Pan, L. Novel Real-Time PCR Method Based on Growth Hormone Gene for Identification of *Salmonidae* Ingredient in Food. *J. Agric. Food Chem.* **2013**, *61*, 5170−5177.

(7) Prado, M.; Boix, A.; Von Holst, C. Development of a real-time PCR method for the simultaneous detection of mackerel and horse mackerel. *Food Control* **2013**, *34*, 19−23.

(8) Sebastio, P.; Zanelli, P.; Neri, T. M. Identification of Anchovy (*Engraulis encrasicholus* L.) and Gilt Sardine (*Sardinella aurita*) by Polymerase Chain Reaction, Sequence of Their Mitochondrial Cytochrome b Gene, and Restriction Analysis of Polymerase Chain Reaction Products in Semipreserves. *J. Agric. Food Chem.* **2001**, *49*, 1194−1199.

(9) Santaclara, F. J.; Cabado, A. G.; Vieites, J. M. Development of a method for genetic identification of four species of anchovies, *E. encrasicolus*, *E. anchoita*, *E. ringens* and *E. japonicus*. *Eur. Food Res. Technol.* **2006**, *223*, 609−614.

(10) Rea, S.; Storani, G.; Mascaro, N.; Stocchi, R.; Loschi, A. R. Species identification in anchovy pastes from the market by PCR-RFLP technique. *Food Control* **2009**, *20*, 515−520.

(11) Cross, I.; Rebordinos, L. Species identification of *Crassostrea* and *Ostrea* oysters by polymerase chain reaction amplification of 5S rRNA gene. *AOAC Int.* **2006**, *89*, 144−148.

(12) Pinhal, D.; Gadig, O. B. F.; Martins, C. Genetic identification of the sharks *Rhizoprionodon porosus* and *R. lalandii* by PCR-RFLP and nucleotide sequence analyses of 5S rDNA. *Conserv. Genet. Resour.* **2009**, *1*, 35−38, DOI: 10.1007/s12686-009-9008-9.

(13) Tognoli, C.; Saroglia, M.; Terova, G.; Gornati, R.; Bernardini, G. Identification of fish species by 5S rRNA gene amplification. *Food Chem.* **2011**, *129*, 1860−1864.

(14) Fernandez-Tajes, J.; Méndez, J. Identification of the razor clam species *Ensis arcuatus*, *E. siliqua*, *E. directus*, *E. macha*, and *Solen marginatus* using PCR-RFLP analysis of the 5S rDNA region. *J. Agric. Food Chem.* **2007**, *55*, 7278−7282.

(15) Pendás, A.; Morán, P.; Freije, J.; García-Vázquez, E. Chromosomal mapping and nucleotide sequence of two tandem repeats of Atlantic salmon 5S rDNA. *Cytogenet. Cell Genet.* **1994**, *67*, 31−36.

(16) Campo, D.; Machado-Schiaffino, G.; Perez, J.; Garcia-Vazquez, E. Phylogeny of the genus *Merluccius* based on mitochondrial and nuclear genes. *Gene* **2007**, *406*, 171−179.

(17) Morescalchi, M. A.; Liguori, I.; Rocco, L.; Archimandritis, A.; Stingo, V. Karyotypic characterization and genomic organization of the 5S rDNA in *Polypterus senegalus* (Osteichthyes, Polypteridae). *Genetica* **2008**, *132*, 179−186.

(18) Merlo, M. A.; Cross, I.; Chairi, H.; Manchado, M.; Rebordinos, L. Analysis of three multigene families as useful tools in character-

ization of two closely related species, *Dicentrarchus labrax*, *Dicentrarchus punctatus* and their hybrids. *Genes Genet. Syst.* **2010**, *85*, 341−349.
(19) Rojo-Bartolomé, I.; Diaz de Cerio, O.; Cancio, I. 5S rRNA in gonads, a powerful marker for the identification of sex in fish. *Comp. Biochem. Physiol., Part A* **2012**, *163*, S55−S60.
(20) Manchado, M.; Rebordinos, L.; Infante, C. U1 and U2 small nuclear RNA genetic linkage: a novel molecular tool for identification of six sole species (Soleidae, Pleuronectiformes). *J. Agric. Food Chem.* **2006**, *54*, 3765−3767.
(21) Martins, C.; Wasko, A. P.; Oliveira, C.; Porto-Foresti, F.; Parise-Maltempi, P. P.; Wright, J. M.; Forestia, F. Dynamics of 5S rDNA in the tilapia (*Oreochromis niloticus*) genome, repeat units, inverted sequences, pseudogenes and chromosome loci. *Cytogenet. Genome Res.* **2002**, *98*, 78−85.
(22) Martins, C.; Wasko, A. P. Organization and evolution of 5S ribosomal DNA in the fish genome. In *Focus on Genome Research*, Williams, C. R., Eds.;Nova Biomedical Books: Hauppauge, NY, 2004; pp 335−363
(23) Pichiri, G.; Nieddu, M.; Manconi, S.; Casu, C.; Coni, P.; Salvadori, S.; Mezzanotte, R. Isolation and characterization of two different 5S rDNA in *Anguilla anguilla* and in *Anguilla rostrata*, possible markers of evolutionary divergence. *Mol. Ecol. Notes* **2006**, *6*, 638−641.
(24) Martins, C.; Galetti, P. M. Two 5S rDNA arrays in Neotropical fish species, is it a general rule for fishes? *Genetica* **2001**, *111*, 439−446.
(25) Qin, Q.; He, W.; Liu, S.; Wang, J.; Xiao, J.; Liu, Y. Analysis of 5S rDNA organization and variation in polyploid hybrids from crosses of different fish subfamilies. *J. Exp. Zool.* **2010**, *314*, 403−411.
(26) Sajdak, S. L.; Reed, K. M.; Phillips, R. B. Intraindividual and interspecies variation in the 5S rDNA of Coregonid fish. *J. Mol. Evol.* **1998**, *46*, 680−688.
(27) Wasko, A. P.; Martins, C.; Wright, J. M.; Galetti, P. M. Molecular organization of 5S rDNA in fishes of the genus *Brycon*. *Genome* **2001**, *44*, 893−902.
(28) Ferreira, I. A.; Oliveira, C.; Venere, P. C.; Galetti, P. M.; Martins, C. 5S rDNA variation and its phylogenetic inference in the genus *Leporinus* (Characiformes, Anostomidae). *Genetica* **2007**, *129*, 253−257.
(29) Martins, C.; Wasko, A. P.; Oliveira, C.; Wright, J. M. Nucleotide sequence of 5S rDNA and localization of the ribosomal RNA genes to metaphase chromosomes of the Tilapiine cichlid fish, *Oreochromis niloticus*. *Hereditas* **2000**, *133*, 39−46.
(30) Dover, G. A. Linkage disequilibrium and molecular drive in the rDNA gene family. *Genetics* **1989**, *122*, 249−252.
(31) Jérome, M.; Lemaire, C.; Bautista, J. M.; Fleurence, J. L.; Etienne, M. Molecular phylogeny and species identification of sardines. *J. Agric. Food Chem.* **2003**, *51*, 43−50.

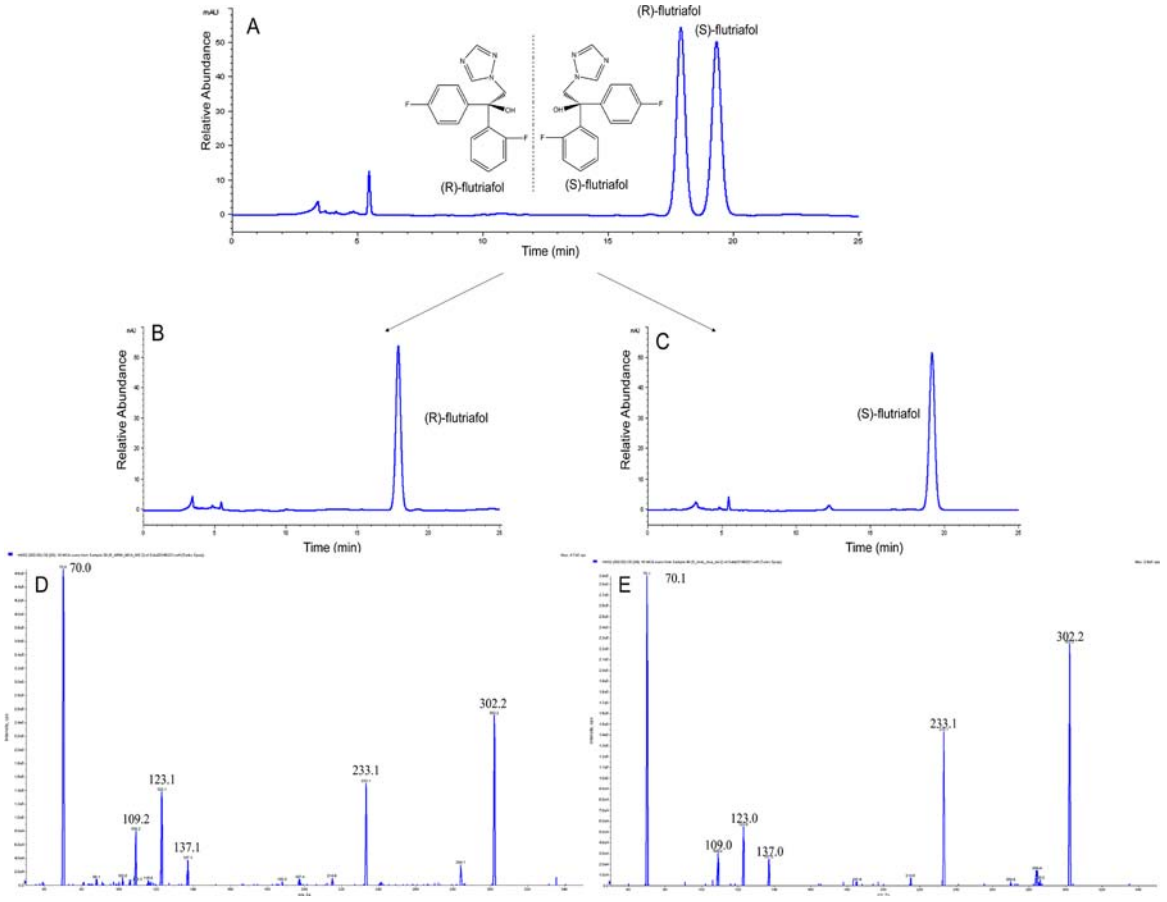

Figure 1. Chromatograms and mass spectra of flutriafol enantiomers: (A) HPLC chromatogram of racemic flutriafol; (B) chromatogram of (*R*)-flutriafol. (C) chromatogram of (*S*)-flutriafol; (D) mass spectra of (*R*)-flutriafol; (E) mass spectra of (*S*)-flutriafol.

column to remove pigments and fatty acids from extracts. To the best of our knowledge, the current report is the first time to present the enantioselective analysis of flutriafol in environment and food samples (cucumber, tomato, grape, pear, wheat, soil, and water). The time-dependent density functional (TDDFT) methodology was applied to predict the electronic circular dichroism (ECD) spectra of flutriafol. The absolute configuration of flutriafol enantiomers was measured through the combination of experimental and predicted ECD spectra. This analytical method developed was validated by its application to the real samples.

MATERIALS AND METHODS

Chemical and Materials. The standard of *rac*-flutriafol (>97.3% purity) was obtained from the China Shanghai Pesticide Research Institute (Shanghai, China). HPLC-grade acetonitrile was purchased from Fisher Scientific (Shanghai, China). Purified water was obtained by using MUL-9000 water purification systems (Nanjing Zongxin Water Equipment Co. Ltd., China). The mobile phase was filtered through a 0.22 μm filter membrane (Tengda, Tianjin, China). Sodium chloride, anhydrous sodium sulfate, acetonitrile, acetone, and hexane of analytical grade were purchased from commercial sources.

A stock solution of racemic flutriafol standard (200 mg/L) was prepared in acetonitrile−water (60/40, v/v). Standard working solutions of *rac*-flutriafol at 0.2, 0.5, 1, 2, 5, 10, and 20 mg/L were prepared in acetonitrile/water (60/40, v/v) from the stock solution by serial dilution. Accordingly, the matrix-matched standard solutions were obtained at 0.2, 0.5, 1, 2, 5, 10, and 20 mg/L concentrations of *rac*-flutriafol by adding appropriate amounts of standards to the control matrix extract. Enantiomers of flutriafol (purity ≥97.0%) were obtained from Daicel (Shanghai, China). Stock standard (500 mg/L) of each enantiomer was prepared in methanol. All solutions were protected against light and stored at −20 °C.

The Cleanert Florisil and Cleanert C18 (500 mg, 6 mL) were purchased from Agela Technologies (Tianjin, China). The samples were comminuted and blended by FeiGe DL-5200B centrifuge (Shanghai, China), Joyoung Soymilk Maker (Hangzhou, China), and Jinyi SK-1 Ultra-Turrax homogenizer (Jiangsu, China).

Apparatus and Chromatographic Conditions. The chromatographic separation of the enantiomers of flutriafol was performed on an Agilent 1200 HPLC system (Agilent, USA) with chiral Lux Cellulose-2 (cellulose tris(3-chloro-4-methyl phenyl carbamate), 250 mm × 4.6 mm id)) (Phenomenex, China) using a mixture of acetonitrile and water (40:60, v/v) as the mobile phase at a flow rate of 0.8 mL/min with the injection volume of 20 μL. The column was kept at 30 °C, with a UV detection at 210 nm. Capacity factor (k), separation factor (α), and resolution factor (Rs) were calculated from the formulas

$$k = (t - t_0)/t_0$$

$$\alpha = k_2/k_1$$

$$\mathrm{Rs} = 2(t_2 - t_1)/(W_1 + W_2)$$

where t is the retention time, t_0 is the void time at given conditions, and k is the retention factor. Parameter k_1 is the capacity factor of the first eluted enantiomer: $(t_1 - t_0)/t_0$. k_2 is the capacity factor of the second eluted enantiomer: $(t_2 - t_0)/t_0$. W_1 and W_2 are the corresponding baseline peak widths for first and second eluted enantiomers. Triplicate determination was made for the measurement of the mean values.

dx.doi.org/10.1021/jf405689n | J. Agric. Food Chem. 2014, 62, 2809−2815

Circular Dichroism Spectroscopy and ECD Calculations. The absolute configuration determination of the flutriafol enantiomers was carried out using a Jasco J815 circular dichroism spectropolarimeter (Tokyo, Japan) at room temperature in methanol. The spectrum was collected over a wavelength range of 200−400 nm at scan speed of 100 nm/min. A quartz cell with a path length of 0.5 cm was used for the scan, and the average of three scans was reported. The geometry of the flutriafol enantiomers was optimized and predicted by Gaussian 09 software using density functional theory (DFT) at a level of B3LYP/6-31+G* in methanol with a conductor-like polarizable continuum model (CPCM) solvent model.[17,18]

Extraction and Cleanup for Water. Water (100 mL) samples spiked at three concentration levels were prepared by the addition of appropriate amounts of standard solutions of racemic flutriafol to tap water. The C18 SPE was preconditioned using 6 mL of methanol followed by 6 mL of purified water. 100 mL of the water sample was slowly uploaded to a SPE cartridge at a flow rate of 2 mL/min, and the effluent was discarded. 10 mL of methanol was used to elute target analytes and collected. The eluate was evaporated to dryness using a rotary evaporator (30 °C). The residue was redissolved in 1 mL of acetonitrile−water (40:60, v/v) and filtered through a 0.22 μm filter membrane for HPLC analysis.

Extraction and Cleanup for Vegetables and Fruits. A 20 g minced sample was added into a 100 mL Teflon centrifuge tube and spiked with different concentrations of flutriafol standard solutions. The tubes containing the spiked samples were vortexed for 30 s and allowed to stand overnight at room temperature to distribute the pesticide evenly. 40 mL of acetonitrile was added to the tube and then homogenized at high speed for 3 min, followed by sonication for 10 min. Subsequently, 6 g of anhydrous magnesium sulfate ($MgSO_4$) and 1.5 g sodium chloride (NaCl) were added. The tube was vortexed vigorously for 2 min and then centrifuged for 5 min at 4,000 rpm. The supernatant acetonitrile (20 mL) was evaporated to dryness and redissolved in 5 mL of a mixture of hexane−acetone (98:2, v/v) followed by cleanup with Florisil-SPE conditioned with 4 mL of hexane. The SPE cartridge was rinsed with 6 mL of hexane−acetone (95:5, v/v) and eluted with 5 mL of hexane−acetone (85:15, v/v) three times sequentially. All eluates were collected and evaporated to dryness under vacuum at 40 °C. The sample was dissolved in 1 mL of acetonitrile−water (40:60, v/v) and filtered through a 0.22 μm filter for HPLC analysis.

Extraction and Cleanup for Wheat and Soil. A 15 g sample of soil or wheat was weighed into a 100 mL Teflon centrifuge tube and spiked with different concentrations of flutriafol standard solutions. The samples were allowed to stand overnight at room temperature. Then, 5 mL of water and 30 mL of acetonitrile were added to the tube and then homogenized at high speed for 3 min, followed by sonication for 10 min. The mixture was homogenized, and 4 g of anhydrous $MgSO_4$ and 1 g of NaCl were added. The tube was vortexed vigorously for 2 min and centrifuged for 5 min at 4,000 rpm. The acetonitrile (15 mL) was concentrated to dryness under vacuum at 40 °C. The residue was transferred with 5 mL of hexane−acetone (98:2, v/v) to a Florisil-SPE column conditioned with 4 mL of hexane. The SPE cartridge was rinsed with 6 mL of hexane−acetone (95:5, v/v) and eluted with 5 mL of hexane−acetone (85:15, v/v) three times sequentially. All eluate was evaporated to dryness with a vacuum rotary evaporator at 40 °C and dissolved in 1 mL of acetonitrile−water (40:60, v/v) for HPLC analysis.

Method Validation. The specificity, linearity, limit of detection (LOD) and limit of quantification (LOQ), matrix effect, accuracy, precision, and stability were applied to evaluate the performance of the method.

A total of 35 blank samples, five samples of each matrix, were applied to verify the absence of interfering substances. The linearity of calibration curves was evaluated based on the peak areas of the standard solutions and the different matrices at seven concentrations ranging from 0.1 to 10 mg/L in triplicate. The linearity was determined by linear regression analysis of both standard solution and matrix-matched calibration curves.

The matrix-dependent LOD and LOQ were determined using the blank and calibration standards of the vegetables, fruits, wheat, soil, and water matrices. The LOD and LOQ for enantiomers of flutriafol were considered as concentrations in a sample matrix resulting in peak areas with signal-to-noise (S/N) ratio of 3 and 10, respectively.

The recoveries were carried out to investigate the accuracy and precision of the method. Soil and water samples from trial plots were located in the Nanjing region in Jiangsu. Other samples were purchased from regional retailers. Five replicates of spiked sample at three different levels from 0.004 to 1 mg/kg were prepared on three consecutive days. The flutriafol was extracted and purified according to the above procedure. The average recoveries and intraday and interday relative standard deviations (RSD) were used to evaluate accuracy and precision.

It has been reported that some kinds of chiral pesticides, such as pyrethroids, could undergo epimerization under certain conditions.[19] Two optically pure flutriafol enantiomers were determined under the same conditions to evaluate the stability of the flutriafol enantiomers during analysis and storage in solvent and matrices. Stability of the stock solutions and the spiked sample matrix-matched standard was tested monthly, and all the samples used in the stability test were stored at −20 °C. The results of the stability tests were compared with those concluded from the freshly prepared samples using Student's t test ($P < 0.05$).

RESULTS AND DISCUSSION

Chromatographic Condition Optimization. A number of the chiral stationary phases (CSPs) were used for chiral separations by HPLC in various chemical fields. The polysaccharide-based CSPs, especially cellulose- and amylase-based polysaccharide columns with higher recognition abilities, are the most used.[20,21] Zhang et al. reported that the two enantiomers of flutriafol could be baseline separated on polysaccharide-based CSPs by reversed-phase HPLC−MS/MS.[22] Ying et al. reported that the flutriafol enantiomers were separated using Chrialcel OD and Chrialcel OJ column by normal phase HPLC.[23] Despite chiral separation, the retention time was not less than 25 min in all reports. In this study, the two enantiomers of flutriafol were completely separated with the Lux Cellulose-2 column under reversed-phase conditions using acetonitrile−water (40:60, v/v) as the mobile phase at a flow rate of 0.8 mL/min with the good resolution factor (Rs) of 1.82. The consumption of solvents was reduced within 20 min.

The methanol and acetonitrile may induce different effects for the separation of the flutriafol on the same column. The flutriafol enantiomers were separated with all Rs higher than 1.54 using a mixture of acetonitrile and water as mobile phase at the rate of 65:35 to 30:70 (v/v). When the percentage of acetonitrile in the eluent increased, a decrease in the retention factors was observed and a worse resolution was obtained. Therefore, a solvent system mixture of acetonitrile−water (40:60, v/v) was used as mobile phase at a flow rate of 0.8 mL/min based on retention time and satisfactory separation (Figure 1). The effect of column temperature on the chiral separation also was evaluated. The result showed a slightly better separation and better peak shape at 30 °C.

The Absolute Configuration and Elution Order Determination of Flutriafol Enantiomers. The each enantiomer was stereochemically determined by circular dichroism (CD) spectroscopy. The two CD curves were almost mirror imaged, and the curves of the predicted ECD and experimental ECD were very similar (Figure 2). The absolute configuration of enantiomers was measured through the combination of experimental and predicted ECD spectra. The configurations of the flutriafol enantiomers that eluted from the

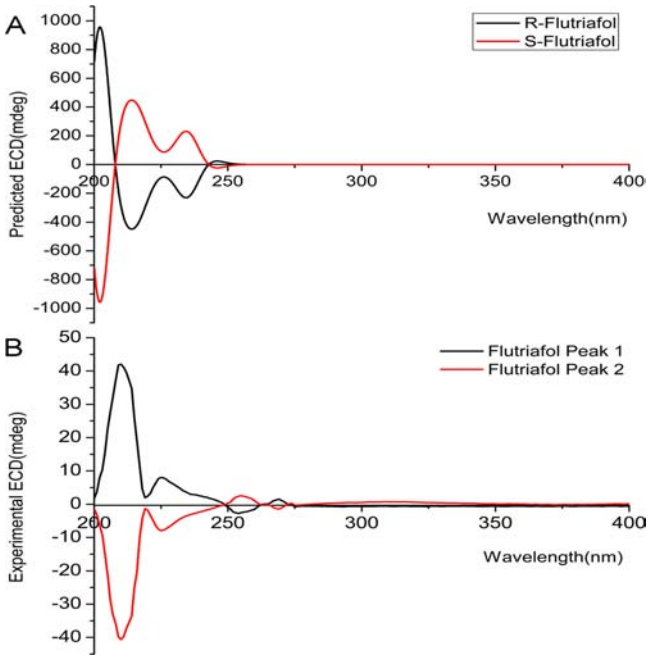

Figure 2. The predicted and experimentally measured ECD spectra of flutriafol enantiomers: (A) predicted ECD spectra; (B) experimentally measured ECD spectra.

HPLC were determined based on the predicted ECD spectra by the TDDFT methodology. Accordingly, peak 1 and peak 2 of the chromatograms shown in Figure 1 were assigned to (*R*)-flutriafol and (*S*)-flutriafol, respectively. Chang et al. had confirmed that (*S*)-flutriafol was (+)-flutriafol and the (*R*)-flutriafol corresponded to (−)-flutriafol.[24] As can be seen from Figure 1, (−)-flutriafol was first eluted under the above conditions, and the mass spectra of the two enantiomers of flutriafol are also provided.

Sample Preparation. The QuEChERS method is a major development for sample preparation in pesticide residue analysis.[25] The magnesium sulfate reduces the water phase and promotes the partitioning of the pesticides into the organic phase.[26] The dispersive cleanup procedure of QuEChERS is faster and easier. However, some food colorings and lipidic soluble materials could not been removed by primary secondary amine (PSA), C18, and graphitized carbon black (GCB). It is not as effective as using SPE columns, and the QuEChERS method has a high requirement in the device.[27−29] Flutriafol was extracted based on the modified QuEChERS method assisted with ultrasound extraction. The flutriafol was concentrated by 10 or 7.5 times, and a further cleanup step was improved using SPE columns.

The Cleanert Florisil, Cleanert NH_2, and Cleanert C18 were used for the cleanup procedure. The pigments and interferences were not efficiently removed and diminished by NH_2-SPE, whereas the C18-SPE was satisfactorily utilized for water sample and the Florisil-SPE could remove the visible pigments of vegetables, soil, and fruits. The chromatograms showed very clean baseline and separation. Methanol was selected as the eluting solvent in Cleanert C18 because of lower toxicity and higher efficiency for the analytes than acetonitrile.[9]

Specificity, Linearity, and Matrix Effect. No interference was detected at the retention time of flutriafol in blank samples of different matrices, and this showed the specificity of the method. Linear regression results of standard solution and matrix-matched calibration curves within the range of 0.1−10 μg/mL for each enantiomer of flutriafol are summarized in Table 1. Table 1 indicates the slopes, *P* values, and correlation

Table 1. Comparison of Matrix-Matched Calibration and Solvent Calibration

calibration (matrix)	calibration range (mg/kg)	regression equation	R^2	*P* value
		(*R*)-Flutriafol		
solvent	0.1−10	$y = 80.27x + 1.11$	0.9999	
soil	0.1−10	$y = 78.271x - 2.5071$	0.9993	0.0579
water	0.1−10	$y = 75.782x - 3.7409$	0.9996	0.823
cucumber	0.1−10	$y = 76.622x - 0.4451$	0.9997	0.0832
tomato	0.1−10	$y = 81.998x + 0.4045$	0.9995	0.0889
pear	0.1−10	$y = 81.02x - 2.0206$	0.9991	0.676
wheat	0.1−10	$y = 81.268x - 0.9632$	0.9989	0.187
grape	0.1−10	$y = 81.845x + 1.1147$	0.9992	0.249
		(*S*)-Flutriafol		
solvent	0.1−10	$y = 80.642x - 1.3033$	0.9999	
soil	0.1−10	$y = 78.604x - 2.6554$	0.9994	0.0525
water	0.1−10	$y = 75.105x - 3.6976$	0.9998	0.0946
cucumber	0.1−10	$y = 76.604x - 0.7979$	0.9995	0.114
tomato	0.1−10	$y = 81.472x + 1.4445$	0.9997	0.117
pear	0.1−10	$y = 81.042x - 3.4951$	0.9989	0.623
wheat	0.1−10	$y = 81.292x - 0.6155$	0.9990	0.176
grape	0.1−10	$y = 81.515x + 2.3394$	0.9993	0.0721

coefficients of determination (R^2) of both matrix-matched and standard solution calibration curves. Excellent linearities were observed for the enantiomers ($R^2 \geq 0.9989$), which were adequate for enantiomeric-specific quantitative trace analysis. The response of standard solution and matrix-matched calibration curves were compared to matrix-matched calibration curves using two-tailed paired *t* test with a probability of 95%. Table 1 showed that no significant matrix-induced enhancement or suppression effects were observed for the two enantiomers. The *P* values implied that the data between pure solvent and sample matrices were not significantly different ($P > 0.05$) and the matrix effect could be negligible.

LODs and LOQs. The LODs for both enantiomers were estimated to be 0.001 mg/kg in water, 0.012 mg/kg in grape, cucumber, pear, and tomato, and 0.015 mg/kg in wheat and soil. The LOQs were estimated at 0.003−0.05 mg/kg for the two enantiomers based on five replicate extractions and analyses of seven spiked samples at low concentration levels. The low detection limits indicated that chiral HPLC was capable of the quantitation of flutriafol enantiomers in the food and environmental matrices.

Accuracy and Precision. The analytical precision and accuracy, expressed with the RSD and the recoveries, was evaluated by spiking the blank samples at three different

dx.doi.org/10.1021/jf405689n | J. Agric. Food Chem. 2014, 62, 2809−2815

Table 2. Accuracy and Precision of the Proposed Method in the Seven Matrices (n = 5)

		intraday (n = 5)						
		day 1		day 2		day 3		
matrix	spiked level (mg/kg)	av recoveries (%)	RSD (%)	av recoveries (%)	RSD (%)	av recoveries (%)	RSD (%)	interday (n = 15) RSD (%)
				(*R*)-Flutriafol				
soil	0.02	88.5	6.6	87.3	4.3	91.5	3.8	5.9
	0.1	90.2	4.2	89.2	3.9	92.3	4.3	5.2
	0.5	91.1	5.6	94.1	2.5	90.5	4.1	3.8
water	0.004	98.2	3.2	93.4	2.7	99.4	5.6	5.1
	0.02	98.5	3.9	93.8	4.3	101.2	4.9	5.4
	0.1	95.1	2.2	91.8	3.1	98.2	3.6	3.9
cucumber	0.02	92.5	4.6	90.5	5.1	95.3	5.3	4.2
	0.1	91.1	4.1	87.7	3.7	90.5	4.9	4.5
	0.5	85.3	5.2	84.2	3.6	87.8	4.2	3.7
tomato	0.02	90.8	4.2	88.9	3.8	96.1	5.3	4.9
	0.1	92.1	2.5	91.1	2.9	88.3	3.3	3.0
	0.5	85.6	2.9	83.8	3.4	87.8	3.5	3.3
pear	0.02	92.2	5.1	87.5	3.2	95.2	6.5	7.3
	0.1	85.4	2.4	83.5	3.5	89.3	5.1	5.4
	0.5	85.8	3.8	83.5	6.9	88.9	4.9	4.4
wheat	0.05	92.6	4.3	89.9	5.3	94.1	7.1	6.5
	0.25	90.4	3.1	88.6	4.8	93.1	4.7	4.6
	1	89.8	2.9	92.3	3.4	87.1	3.8	3.5
grape	0.02	91.9	3.4	87.9	3.2	94.3	4.3	4.1
	0.1	85.1	3.5	83.8	2.8	88.9	2.9	3.8
	0.5	90.7	4.8	88.9	3.3	92.1	4.4	4.7
				(*S*)-Flutriafol				
soil	0.02	92.7	5.2	89.3	3.6	93.4	7.5	6.7
	0.1	94.9	4.8	91.8	3.3	96.7	5.8	5.2
	0.5	90.5	6.7	93.5	3.1	89.5	7.2	5.7
water	0.004	97.1	6.2	92.1	5.3	102.1	7.3	7.5
	0.02	97.1	5.2	94.3	5.8	99.5	3.6	5.3
	0.1	94.1	2.6	90.9	2.3	97.1	4.6	3.9
cucumber	0.02	96.1	3.8	94.3	4.8	101.7	6.7	5.2
	0.1	94.2	3.9	92.7	3.3	96.8	3.8	3.4
	0.5	84.6	5.9	83.1	5.8	88.3	5.5	5.7
tomato	0.02	101.4	5.8	95.4	4.5	103.4	4.1	4.9
	0.1	94.5	2.2	92.4	3.2	90.8	3.8	2.9
	0.5	86.7	3.6	84.2	2.8	87.2	5.9	4.0
pear	0.02	91.1	4.3	88.3	5.9	96.2	7.2	7.9
	0.1	87.1	6.3	84.2	4.6	87.8	6.8	5.2
	0.5	84.2	7.2	82.9	6.2	89.1	7.8	7.6
wheat	0.05	95.8	5.1	90.7	4.7	95.2	5.8	5.6
	0.25	93.2	2.8	87.9	3.5	94.1	6.2	4.3
	1	90.8	8.3	90.8	7.5	88.8	3.9	7.1
grape	0.02	95.2	7.5	92.1	6.5	97.1	5.8	5.2
	0.1	87.7	2.5	84.8	3.8	87.4	4.7	4.3
	0.5	87.1	5.8	85.9	5.4	89.2	6.2	5.1

concentrations with five replications on three consecutive days (Table 2). As shown in Table 2, the method presented satisfactory mean recoveries and precision for both enantiomers. The average recoveries ranged from 83.5% to 101.2% with intraday RSD 2.2−7.3% for (*R*)-flutriafol and ranged from 82.9% to 103.4% with intraday RSD 2.2−7.9% for (*S*)-flutriafol. The chromatograms of the flutriafol in the blank samples and the spiked pear at 0.5 mg/kg are shown in Figure 3. Further statistical analysis using one-way analysis of variance at 95% confidence limit showed no significant difference of interday and intraday assays. The results demonstrated that this method could achieve a satisfactory precision and accuracy for the enantiomeric analysis of flutriafol in food and environmental matrices. In addition, an evaluation of the stability of the two enantiomers was conducted, and no significant difference (P > 0.05) was observed under the solvent and matrix storage treatment as described in Materials and Methods.

Application to Authentic Samples. The effectiveness of this method in measuring trace levels of *rac*-flutriafol was monitored by analyzing seven different samples obtained from field and local market (Nanjing, China). Each kind of sample was analyzed in quintuplicate. The results showed three positive pear samples with flutriafol residues in the range of 0.009−0.019 mg/kg. The enantiomers of flutriafol were not found in other real samples. The typical chromatograms of pear

dx.doi.org/10.1021/jf405689n | J. Agric. Food Chem. 2014, 62, 2809−2815

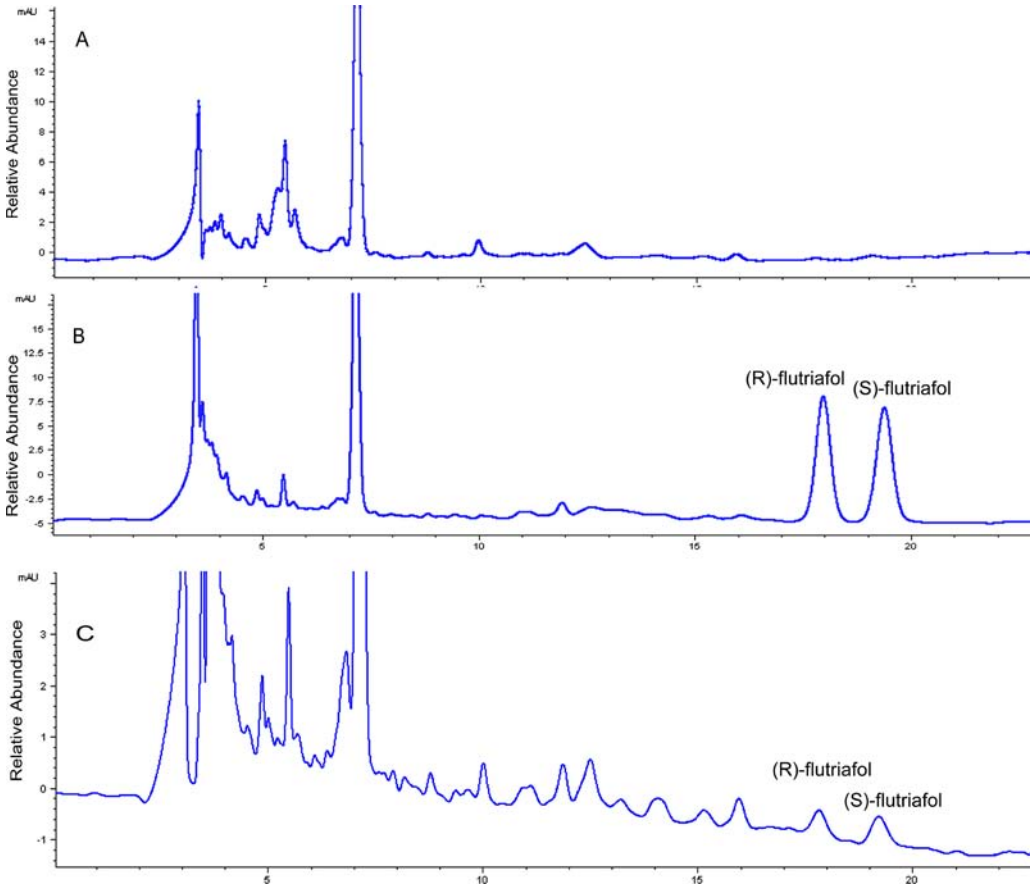

Figure 3. The typical chromatograms of pear sample: (A) blank pear sample; (B) pear sample spiked with 0.5 mg/kg; (C) authentic pear sample.

are presented in Figure 3 with 0.0151 and 0.0158 mg/kg for (*R*)-flutriafol and (*S*)-flutriafol, respectively.

In the present study, a simple and reliable enantioselective method using chiral HPLC for the simultaneous quantitative determination of flutriafol enantiomers in food and environment matrices (cucumber, tomato, grape, pear, wheat, soil, and water) has been successfully established and validated. Target compounds were extracted and purified based on the modified QuEChERS method. In addition, the absolute configurations and elution order of flutriafol enantiomers were determined by a combination of experimental and predicted ECD spectra. Adequate analytical performance characteristics were obtained in terms of linearity range and precision for both enantiomers of flutriafol in seven matrices. Satisfactory results were obtained in the real samples. The purpose of the current work was not only to establish a novel valid chiral HPLC method to separate the two enantiomers of the flutriafol but also to develop a method of quantitative determination of the two enantiomers of flutriafol in the food and environmental samples. The developed chiral HPLC method may be used to facilitate further studies in tracing the different toxicities, bioactivities, metabolism, and environmental behavior of each enantiomer, which could help minimize the hazards posed by flutriafol to humans, animals, and ecological health.

AUTHOR INFORMATION

Corresponding Author

*Tel: +86 25 84395479. Fax: +86 25 84395479. E-mail: wangmha@njau.edu.cn.

Funding

This work was supported by the Special Fund for Agro-scientific Research in the Public Interest (201203022) and the National "863" High-Tech Research Program of China (2011AA100806).

Notes

The authors declare no competing financial interest.

ACKNOWLEDGMENTS

We are grateful to Hu Zhang (Zhejiang Academy of Agricultural Sciences) for calculating the absolute configuration of flutriafol enantiomers by Gaussian 09 software.

REFERENCES

(1) Koeller, K. M.; Wong, C. Enzymes for chemical synthesis. *Nature* **2001**, *409* (6817), 232−240.

(2) Yoon, T. P.; Jacobsen, E. N. Privileged chiral catalysts. *Science* **2003**, *299* (5613), 1691−1693.

(3) Wang, M.; Zhang, Q.; Cong, L.; Yin, W.; Wang, M. Enantioselective degradation of metalaxyl in cucumber, cabbage, spinach and pakchoi. *Chemosphere* **2014**, *95*, 241−246.

(4) Perez-Fernandez, V.; Garcia, M. A.; Marina, M. L. Chiral separation of agricultural fungicides. *J. Chromatogr. A* **2011**, *1218* (38), 6561−6582.

(5) Liu, W.; Gan, J.; Schlenk, D.; Jury, W. A. Enantioselectivity in environmental safety of current chiral insecticides. *Proc. Natl. Acad. Sci. U.S.A.* **2005**, *102* (3), 701−706.

(6) Perez-Fernandez, V.; Garcia, M. A.; Marina, M. L. Chiral separation of metalaxyl and benalaxyl fungicides by electrokinetic chromatography and determination of enantiomeric impurities. *J. Chromatogr. A* **2011**, *1218* (30), 4877−4885.

(7) Armstrong, D. W.; Reid, G. L., III; Hilton, M. L.; Chang, C. Relevance of enantiomeric separations in environmental science. *Environ. Pollut.* **1993**, *79* (1), 51−58.
(8) Lewis, D. L.; Garrison, A. W.; Wommack, K. E.; Whittemore, A.; Steudler, P.; Melillo, J. Influence of environmental changes on degradation of chiral pollutants in soils. *Nature* **1999**, *401* (6756), 898−901.
(9) Li, Y.; Dong, F.; Liu, X.; Xu, J.; Li, J.; Kong, Z.; Chen, X.; Zheng, Y. Enantioselective determination of triazole fungicide tebuconazole in vegetables, fruits, soil and water by chiral liquid chromatography/tandem mass spectrometry. *J. Sep. Sci.* **2012**, *35* (2), 206−215.
(10) Griffiths, K. M.; Bacic, A.; Howlett, B. J. Sterol composition of mycelia of the plant pathogenic ascomycete *Leptosphaeria maculans*. *Phytochemistry* **2003**, *62* (2), 147−153.
(11) Yang, L.; Li, Z.; Li, Y. Bioactivity investigation of triazole fungicide enantiomers. *Chin. J. Pestic. Sci.* **2002**, *4*, 67−70.
(12) Belluck, D. A.; Benjamin, S. L.; Dawson, T. Groundwater contamination by atrazine and its metabolites. Risk Assessment, Policy, and Legal Implication. In *Pesticide Transformation Products*; ACS Symposium Series; American Chemical Society: Washington, DC, 1991; pp 254−273.
(13) Yu, P.; Jia, C.; Song, W.; Liu, F. Dissipation and Residues of Flutriafol in Wheat and Soil Under Field Conditions. *Bull. Environ. Contam. Toxicol.* **2012**, *89* (5), 1040−1045.
(14) Gilbert-Lopez, B.; Garcia-Reyes, J. F.; Molina-Diaz, A. Determination of fungicide residues in baby food by liquid chromatography-ion trap tandem mass spectrometry. *Food Chem.* **2012**, *135* (2), 780−786.
(15) Wang, P.; Jiang, S.; Liu, D.; Wang, P.; Zhou, Z. Direct enantiomeric resolutions of chiral triazole pesticides by high-performance liquid chromatography. *J. Biochem. Biophys. Methods* **2005**, *62* (3), 219−230.
(16) Shen, Z.; Zhang, P.; Xu, X.; Wang, X.; Zhou, Z.; Liu, D. Gender-Related Differences in Stereoselective Degradation of Flutriafol in Rabbits. *J. Agric. Food Chem.* **2011**, *59* (18), 10071−10077.
(17) Ding, S.; Jia, L.; Durandin, A.; Crean, C.; Kolbanovskiy, A.; Shafirovich, V.; Broyde, S.; Geacintov, N. E. Absolute configurations of spiroiminodihydantoin and allantoin stereoisomers: Comparison of computed and measured electronic circular dichroism spectra. *Chem. Res. Toxicol.* **2009**, *22* (6), 1189−1193.
(18) Zhang, H.; Wang, X.; Zhuang, S.; Jin, N.; Wang, X.; Qian, M.; Xu, H.; Qi, P.; Wang, Q.; Wang, M. Enantioselective Analysis and Degradation Studies of Isocarbophos in Soils by Chiral Liquid Chromatography-Tandem Mass Spectrometry. *J. Agric. Food Chem.* **2012**, *60* (41), 10188−10195.
(19) Liu, W.; Gan, J. J.; Lee, S.; Werner, I. Isomer selectivity in aquatic toxicity and biodegradation of cypermethrin. *J. Agric. Food Chem.* **2004**, *52* (20), 6233−6238.
(20) Ward, T. J.; Ward, K. D. Chiral separations: fundamental review 2010. *Anal. Chem.* **2010**, *82* (12), 4712−4722.
(21) Ward, T. J.; Baker, B. A. Chiral separations. *Anal. Chem.* **2008**, *80* (12), 4363−4372.
(22) Zhang, H.; Qian, M.; Wang, X.; Wang, X.; Xu, H.; Wang, Q.; Wang, M. HPLC−MS/MS enantioseparation of triazole fungicides using polysaccharide-based stationary phases. *J. Sep. Sci.* **2012**, *35* (7), 773−777.
(23) Zhou, Y.; Ling, L.; Kunde, L.; Xinping, Z.; Weiping, L. Enantiomer separation of triazole fungicides by high-performance liquid chromatography. *Chirality* **2009**, *21* (4), 421−427.
(24) Chang, M.; Kim, T. H.; Kim, H. Stereoselective synthesis of (+)-flutriafol. *Tetrahedron: Asymmetry* **2008**, *19* (12), 1504−1508.
(25) Koesukwiwat, U.; Lehotay, S. J.; Miao, S.; Leepipatpiboon, N. High throughput analysis of 150 pesticides in fruits and vegetables using QuEChERS and low-pressure gas chromatography-time-of-flight mass spectrometry. *J. Chromatogr. A* **2010**, *1217* (43), 6692−6703.
(26) Li, J.; Dong, F.; Xu, J.; Liu, X.; Li, Y.; Shan, W.; Zheng, Y. Enantioselective determination of triazole fungicide simeconazole in vegetables, fruits, and cereals using modified QuEChERS (quick, easy, cheap, effective, rugged and safe) coupled to gas chromatography/tandem mass spectrometry. *Anal. Chim. Acta* **2011**, *702* (1), 127−135.
(27) Schenck, F. J.; Lehotay, S. J. Does further clean-up reduce the matrix enhancement effect in gas chromatographic analysis of pesticide residues in food. *J. Chromatogr. A* **2000**, *868* (1), 51−61.
(28) Schenck, F. J.; Lehotay, S. J.; Vega, V. Comparison of solid-phase extraction sorbents for cleanup in pesticide residue analysis of fresh fruits and vegetables. *J. Sep. Sci.* **2002**, *25* (14), 883−890.
(29) Okihashi, M.; Kitagawa, Y.; Akutsu, K.; Obana, H.; Tanaka, Y. Rapid method for the determination of 180 pesticide residues in foods by gas chromatography/mass spectrometry and flame photometric detection. *J. Pestic. Sci.* **2005**, *30* (4), 368−377.

characterization of monoclonal antibody-based direct and indirect cELISAs, samples of strawberries, cucumbers, and tomatoes were fortified with kresoxim-methyl and extracted using the QuEChERS (Quick, Easy, Cheap, Effective, Rugged, and Safe) methodology[14] in order to evaluate immunoassay performance. Validation of the newly developed rapid methods was carried out by comparison with GC−MS through Deming regression analysis and Bland−Altman plots using samples from sprayed crops.

MATERIALS AND METHODS

Reagents and Instruments. The employed monoclonal antibody (KM*o*#117) and the homologous assay conjugates using horseradish peroxidase (HRP−KM*o*) and ovalbumin (OVA−KM*o*) were generated in our lab, and their preparation was as described elsewhere.[13] The affinity to kresoxim-methyl of monoclonal antibody (mAb) KM*o*#117 clearly improves that of a former antibody that we produced some years ago, at the beginning of this project.[12] Rabbit anti-mouse immunoglobulin polyclonal antibody conjugated to peroxidase (RAM−HRP) was from Dako (Glostrup, Denmark). *o*-Phenylenediamine was purchased from Sigma/Aldrich (Madrid, Spain). 96-well Costar flat-bottom high-binding polystyrene ELISA plates were purchased from Corning (Corning, NY, USA). ELISA absorbances were read with a PowerWave HT from BioTek Instruments (Winooski, VT, USA). Microwells were washed with an ELx405 microplate washer also from BioTek Instruments.

Pestanal-grade kresoxim-methyl (methyl (*E*)-methoxyimino[α-(*o*-tolyloxy)-*o*-tolyl]acetate, CAS registry number 143390-89-0, M_w 313.35) was purchased from Fluka/Riedel-de-Haën (Seelze, Germany). Other pesticide standards were also from Fluka/Riedel-de-Haën or from BASF (Limburgerhof, Germany), Bayer CropScience (Frankfurt, Germany), Dr. Ehrenstorfer (Augsburg, Germany), or Syngenta (Basel, Switzerland). Triphenylphosphate (TPP) was from Sigma/Aldrich (Madrid, Spain), and primary−secondary amine (PSA) for dispersive solid phase extraction cleanup was from Scharlab (Barcelona, Spain). Chromatographic determinations were carried out with a 6890N GC apparatus furnished with a 7683 series autosampler, a HP-5MS (30 m × 0.25 mm × 0.25 μm) capillary column, and a quadrupole 5973N mass detector, all from Agilent Technologies (Santa Clara, CA, USA).

Immunoassays. *General Procedures.* Eight-point standard curves, including a blank, were prepared in borosilicate glass tubes by 10-fold serial dilution in PBS starting from a 100 μg/L solution also in PBS. Pesticide concentrated stock solutions (100 mg/L) in anhydrous *N*,*N*-dimethylformamide—kept at −20 °C in amber glass vials—were used to prepare the first standard point. Experimental values were fitted using the SigmaPlot software (Systat Software Inc., Chicago, IL, USA) to a four-parameter logistic equation:

$$y = (A_{max} - A_{min})/[1 + (x/C)^B] + A_{min}$$

were A_{max} is the absorbance that was reached in the absence of analyte, A_{min} is the background signal, C is the analyte concentration at the inflection point of the sigmoidal curve, and B is the slope at the inflection point. Curves were normalized, and average values were calculated from independent experiments.

The concentration of kresoxim-methyl inducing a 50% inhibition (IC_{50}) of the reaction between antibody and hapten conjugate was taken as the key criterion for assay characterization. The limit of detection (LOD) was calculated as the analyte concentration causing a 10% inhibition (IC_{10}) of the immunochemical reaction. Cross-reactivity (CR) was estimated as a percentage value from the quotient between the IC_{50} value for kresoxim-methyl and the IC_{50} for the studied compound, both in molar concentration units.

Antigen-Coated Indirect Competitive ELISA. Microplates were coated by overnight incubation with 100 μL per well of OVA−KM*o* conjugate solution in 50 mM carbonate buffer, pH 9.6. All incubation steps were performed at room temperature with sealed plates, and after each step, microwells were washed four times with washing solution (150 mM NaCl with 0.05% (v/v) Tween 20). The competitive step was carried out during 1 h with 50 μL per well of analyte solution in PBS plus 50 μL per well of a dilution of antibody KM*o*#117 in PBST (PBS containing 0.05% (v/v) Tween 20). Retained mAb was amplified by incubation during 1 h with 100 μL per well of RAM−HRP diluted 1/2000 in PBST. Finally, a signal was generated with 100 μL per well of 0.012% (v/v) H_2O_2 in 62 mM phosphate and 25 mM citrate, pH 5.4 containing 2 g/L of *o*-phenylenediamine. Ten minutes later, enzymatic activity was stopped with 100 μL per well of 2.5 M H_2SO_4. Absorbance was immediately read at 492 nm using 650 nm as reference wavelength.

Antibody-Coated Direct Competitive ELISA. Polystyrene plates were coated by overnight incubation with 100 μL per well of a solution of antibody KM*o*#117 in 50 mM carbonate buffer, pH 9.6. All incubation steps were carried out at room temperature, and after each incubation step, microwells were washed as described above. The competitive step was performed during 1 h with sequential addition of 50 μL per well of analyte solution in PBS and 50 μL per well of a solution of tracer HRP−KM*o* in PBST. Signal was generated and plates were read as before.

Solvent, Detergent, and Buffer Studies. The influence of acetonitrile was evaluated using kresoxim-methyl standard curves in PBS with different solvent contents, whereas antibody or tracer solutions were prepared in PBST. Variation of A_{max} and IC_{50} values due to Tween 20 concentration was also assessed. Moreover, a central composite design was followed for buffer studies, consisting of a two-level full factorial design (α = 1.414) with two factors (pH and ionic strength) and three replicates that included 12 cube, 12 axial, and 15 center points; that is, 39 randomized assays under 9 different buffer conditions (Table S1 in the Supporting Information). The corresponding 9 buffers were set up from a 40 mM citrate, 40 mM phosphate, and 40 mM Tris solution, as described elsewhere.[15] Ionic strength and pH values of each buffer were adjusted using 2 M NaCl and 5 M HCl, respectively. All buffers contained 0.05% (v/v) Tween 20. Kresoxim-methyl was prepared in Milli-Q water, and antibody or tracer solutions were diluted in the studied buffers. A_{max} and IC_{50} values of the 39 resulting curves were fitted as functions of pH and ionic strength using the Minitab software (Minitab Inc., State College, PA, USA).

Sample Treatment and Analysis. Tomatoes, cucumbers, and strawberries were obtained from local supermarkets and extracted using the QuEChERS method.[14] Briefly, 20 g of homogenate was mixed under vigorous stirring with 2 g of sodium acetate and 8 g of anhydrous magnesium sulfate in 20 mL of acetonitrile containing 1% (v/v) acetic acid. The organic phase was separated by centrifugation at 2200*g* during 5 min, and a 10 mL aliquot was cleaned up by vortexing with PSA (500 mg) in the presence of 1.5 g of anhydrous magnesium sulfate. After a second centrifugation step, extracts were filtrated with a Teflon filter (0.2 μm) and stored at −20 °C. Extracts were fortified with kresoxim-methyl, diluted 50-fold in PB (100 mM phosphate, pH 7.4), and analyzed by the developed cELISAs using antibody or tracer solutions prepared in PBT (PB containing 0.05% (v/v) Tween 20). A kresoxim-methyl standard curve in PB was run in each plate.

In order to better simulate real-world situations, greenhouse strawberry crops were sprayed with a nebulizer using a commercial kresoxim-methyl formulation from BASF (Stroby), which was prepared as recommended by the manufacturer (100 mg/L kresoxim-methyl in water containing 20% (v/v) alkyl polyglycol ether). Samples were collected at different days to obtain positive samples covering a wide range of kresoxim-methyl concentrations, homogenized, and stored frozen at −20 °C. Residues were extracted by the described QuEChERS procedure and analyzed by the optimized cELISAs and GC−MS. Immunochemical determinations were performed as described for spiked samples. For chromatographic analysis, one microliter of clean extract containing 500 μg/L of TPP as internal standard was injected in splitless mode at 280 °C, employing helium as carrier with a steady flow of 1 mL/min. The temperature of the oven (110 °C) was held during 1 min; then, it was increased at a rate of 15 °C/min until 280 °C and kept constant at the final temperature during 15 min. Electron impact ionization at 70 eV was

used with the ion source at 225 °C. The employed quantification ions were m/z 116 and 131 for kresoxim-methyl and m/z 325 and 326 for TPP. Retention times were 11.0 and 14.0 min for kresoxim-methyl and TPP, respectively. For method validation, Deming regression and Bland–Altman analysis were applied using the SigmaPlot software (version 12.0).

RESULTS AND DISCUSSION

Assay Selectivity. Two mAb-based immunoassays for kresoxim-methyl were studied. Both assays employed mAb KM*o*#117 and the homologous conjugate but different cELISA formats (for hapten structure, see Figure S1 in the Supporting Information). Immunoassay selectivity with structurally related compounds was assessed toward the main strobilurin fungicides (trifloxystrobin, azoxystrobin, picoxystrobin, dimoxystrobin, metominostrobin, orysastrobin, pyraclostrobin, and fluoxastrobin; see Figure S2 in the Supporting Information). In both cELISA formats, antibody KM*o*#117 was highly selective to kresoxim-methyl (CR values with other strobilurins were below 1%). On the other hand, recognition toward chemicals potentially present in real samples was verified using active principles that are commonly formulated together with kresoxim-methyl, such as boscalid, fenpropimorph, epoxiconazole, propiconazole, tebuconazole, and pyrimethanil, and none of them was noticeably recognized by mAb KM*o*#117.

Tolerance to Solvents and Detergents. QuEChERS methodology for pesticide extraction from food matrices consists of a liquid phase extraction of homogenates with acetonitrile. Hence, tolerance of the described cELISAs to that solvent was appraised. The A_{max} and IC_{50} values of inhibition curves that had been run in the presence of different amounts of acetonitrile (from 0.5% to 10%, v/v) were compared to those obtained in the absence of solvent (see Figure 1). Only a slight influence over the assay signal was observed, and up to 2% acetonitrile was fairly well tolerated by the studied immunoassays.

Immunochemical competitive reactions are usually performed in the presence of different additives. Tween 20 is a common detergent for unspecific binding minimization; however, it has been often shown to exert a negative effect over the analytical parameters of immunoassays for small organic analytes.[16] The relative variation of A_{max} and IC_{50} values in the presence of different concentrations of Tween 20 (from 0% to 0.1%, v/v), taking 0.025% as a reference detergent concentration, is depicted in Figure 1. A similar behavior was observed with the two studied cELISAs, i.e., Tween 20 increased the A_{max} of both assays, but it also increased the IC_{50} value.

Influence of pH and Ionic Strength. The analytical influence of physicochemical conditions such as pH and ionic strength was evaluated. Competitive assays were performed following a biparametric study with composite design in which the center point conditions (pH = 7.5 and I = 175 mM at 25 °C) were similar to those of PBS. A series of buffers were prepared with a mixture of citrate, phosphate, and Tris in order to cover a wide effective pH range. The ionic strength of each buffer was fixed with NaCl, and Tween 20 was added. Figure 2 shows the overlaid contour plots for the responses (A_{max} and IC_{50} values) to pH and ionic strength changes of the two studied immunoassays, taking the results at center point conditions as the reference values. A constricted area for acceptable pH and ionic strength variations (the area stretching changes on A_{max} and IC_{50} values below ±20%; area in white color) was found for the indirect cELISA. With this assay, at pH 7.5, ionic strength values below 150 mM increased both A_{max} and IC_{50} values above tolerable levels (>120%), whereas values over 200 mM decreased excessively the A_{max} (<80%). On the contrary, the direct cELISA was very robust—A_{max} and IC_{50} changes stayed below ±20%—to alterations of either pH or ionic strength conditions (white area in lower graph of Figure 2).

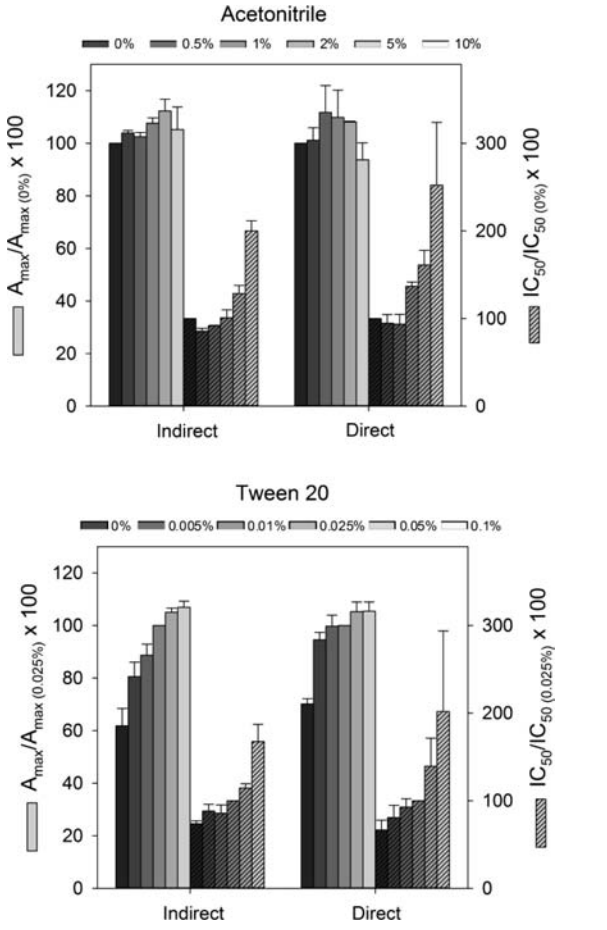

Figure 1. Influence of acetonitrile (upper graph) and Tween 20 (lower graph) contents over A_{max} and IC_{50} values of the studied immunoassays.

Immunoassay Validation. The assays were validated by investigating the LOD, LOQ, trueness, and repeatability. Final assay conditions of the developed cELISAs and the optimized standard inhibition curves can be found in Table 1. Optimum antibody concentrations were 100 and 300 μg/L for the indirect and direct format, respectively, whereas optimum assay conjugate concentrations were 100 μg/L for the former and 30 μg/L for the latter. Signals in the absence of analyte (A_{max}) were high (around 2.0), background signals (A_{min}) were low, and slopes were moderate (between −1.0 and −1.2). Under those conditions, the IC_{50} values for kresoxim-methyl were below 1 μg/L for both cELISAs, and the LODs were around 0.10 μg/L. Attempts to reduce these values by decreasing immunoreagent concentrations just resulted in lower A_{max} without a concomitant effect on assay sensitivity.

To evaluate the trueness and precision, the described immunoassays were applied to the analysis of kresoxim-methyl in diverse fortified foodstuffs. Nowadays, this pesticide is employed against a variety of plant diseases in cucumber,

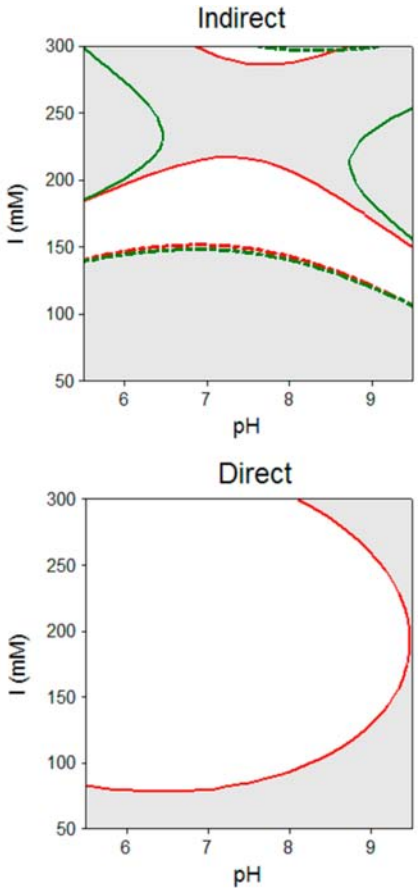

Figure 2. Overlaid contour plots for the A_{max} and IC_{50} dependence upon pH and ionic strength conditions of the studied immunoassays. White areas set the limits of acceptable pH and *I* conditions; those with A_{max} (red) and IC_{50} (green) variations between 80% (solid line) and 120% (dashed line), taking as a reference (100%) the average of the A_{max} and IC_{50} values of the center point conditions of the composite design.

tomato, and strawberry crops. Extracts of those food samples were prepared following a QuEChERS procedure that was essentially based on the AOAC Official Method 2007.01 for pesticide extraction from food matrices.[17] Homogenized foodstuffs were treated with acetonitrile in the presence of buffered saline and $MgSO_4$, and then a cleanup step using PSA was performed. Extracts from kresoxim-methyl-free samples (as judged by GC−MS) were fortified at four concentration levels and analyzed with the optimized immunoassays after a simple dilution in buffer. In general, quantitative recoveries (between 70% and 120%) and good precision values (relative standard deviation below 20%) were retrieved with each cELISA (Table 2), in accordance with the EU validation guidelines for pesticide residue analysis in food.[18] For both immunoassays, the limit of quantification (LOQ) for the studied foodstuffs was set at 0.01 mg/kg, which is lower than the European MRLs for kresoxim-methyl in these food products (0.05, 0.5, and 1.0 mg/kg for cucumbers, tomatoes, and strawberries, respectively).

As further validation of the developed cELISAs, strawberry samples from crops that we had sprayed with a commercial formulation of kresoxim-methyl were employed as model and relevant commodity in order to evaluate the performance of our novel analytical methods under real-like conditions. Fruits were extracted following a QuEChERS procedure and then analyzed

Table 1. Conditions and Parameters of the Optimized Immunoassays[a]

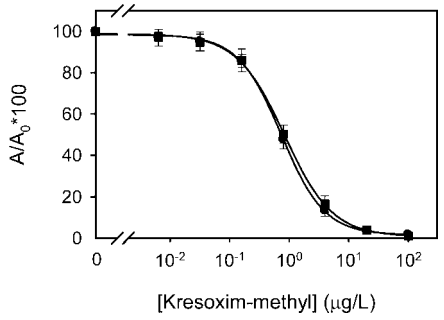

	immunoassay	
	indirect cELISA	direct cELISA
mAb	KM*o*#117	KM*o*#117
	100 μg/L	300 μg/L
conjugate	OVA−KM*o*	HRP−KM*o*
	100 μg/L	30 μg/L
A_{max}	2.390 ± 0.254	2.037 ± 0.208
A_{min}	0.039 ± 0.015	0.021 ± 0.009
slope	−1.198 ± 0.059	−1.082 ± 0.056
IC_{50} (μg/L)	0.738 ± 0.032	0.838 ± 0.044
LOD (μg/L)	0.103	0.097
buffer	PB + 0.025% Tween 20	PB + 0.025% Tween 20
time (h)	2.5	1.5

[a]Values are the mean of 16 independent experiments.

by the optimized immunoassays and by GC−MS (Table S2 in the Supporting Information). Trueness of the developed cELISAs was also assessed by statistical method comparison using the Deming regression, which accounts for errors in observations on both methods. Orthogonal regression analysis showed that the results provided by both cELISAs were statistically comparable to those retrieved by the reference method; i.e., the 95% confidence intervals for the intercept and for the slope included 0 and 1, respectively (Table 3). The corresponding regression lines can be seen in Figure S3 in the Supporting Information. Moreover, good correlation between the studied immunochemical technique and the reference chromatography approach was evidenced by the Bland−Altman plot (Figure 3), as the average values of both methods were randomly distributed around the average difference, and they were mostly inside the limits of agreement (average difference ±1.96 s), meaning that only random deviations occurred.

In summary, two mAb-based immunoassays to kresoxim-methyl—one indirect and one direct cELISA—have been characterized, optimized, and validated using food samples. These assays showed no CR with the most common strobilurin pesticides or a series of fungicides potentially present in relevant foodstuffs. A relative tolerance to acetonitrile contents was observed, and lower influence of pH and ionic strength changes over assay analytical parameters was found with the direct assay. Both immunoassays showed IC_{50} values below 1 μg/L under optimized conditions. The LOQs were fixed at 10 μg/kg from the analysis of fortified tomato, cucumber, and strawberry samples which had been extracted by the QuEChERS method. Overall, good recoveries and precision values were found. Method trueness was also demonstrated by comparison with a reference chromatographic method through statistical analysis using Deming regression and Bland−Altman plot.

dx.doi.org/10.1021/jf500287t | J. Agric. Food Chem. 2014, 62, 2816−2821

Table 2. Recoveries and Precision Values Obtained by Analyzing Replicate Spiked Samples (n = 4)

		indirect			direct		
sample	spiked [KM][a] (μg/kg)	found [KM] (μg/kg)	RSD (%)	recovery (%)	found [KM] (μg/kg)	RSD (%)	recovery (%)
tomato	10	9.1 ± 0.8	8.8	91.3 ± 7.7	11.6 ± 1.4	12.1	75.5 ± 21.9
	30	29.1 ± 3.8	13.1	97.0 ± 12.8	32.8 ± 4.8	14.6	95.8 ± 15.2
	100	103.2 ± 7.5	7.3	103.2 ± 7.5	110.8 ± 3.9	3.5	110.8 ± 3.9
	300	313.2 ± 28.8	9.2	104.4 ± 9.6	361.2 ± 9.3	2.6	120.5 ± 3.1
cucumber	10	8.1 ± 0.9	11.1	81.3 ± 9.1	7.5 ± 1.1	14.7	75.4 ± 10.7
	30	30.4 ± 5.5	18.1	101.2 ± 18.2	29.5 ± 3.3	11.2	98.3 ± 10.9
	100	104.4 ± 6.4	6.1	104.4 ± 6.4	116.3 ± 4.0	3.4	116.3 ± 4.0
	300	306.0 ± 12.3	4.0	102.0 ± 4.1	336.0 ± 26.4	7.9	112.0 ± 8.8
strawberry	10	9.7 ± 1.9	19.6	97.2 ± 18.7	11.5 ± 1.6	13.9	115.1 ± 15.8
	30	29.0 ± 5.3	18.3	96.7 ± 17.6	34.4 ± 5.6	16.3	114.7 ± 18.7
	100	100.0 ± 19.2	19.2	100.0 ± 19.2	120.3 ± 8.3	6.9	120.3 ± 8.3
	300	308.4 ± 60.9	19.7	102.8 ± 20.3	360.6 ± 12.0	3.3	120.7 ± 4.0

[a]KM: kresoxim-methyl.

Table 3. Correlation between the Developed Immunoassays and GC−MS by Deming Regression of In-Field Treated Samples

cELISA	intercept	95% confidence interval for intercept	slope	95% confidence interval for slope	r^a	N^b
indirect	0.015 ± 0.027	[−0.045; 0.074]	1.03 ± 0.04	[0.94; 1.12]	0.9838	14
direct	0.055 ± 0.026	[−0.003; 0.112]	0.99 ± 0.03	[0.91; 1.06]	0.9882	14

[a]Correlation coefficient. [b]Number of samples.

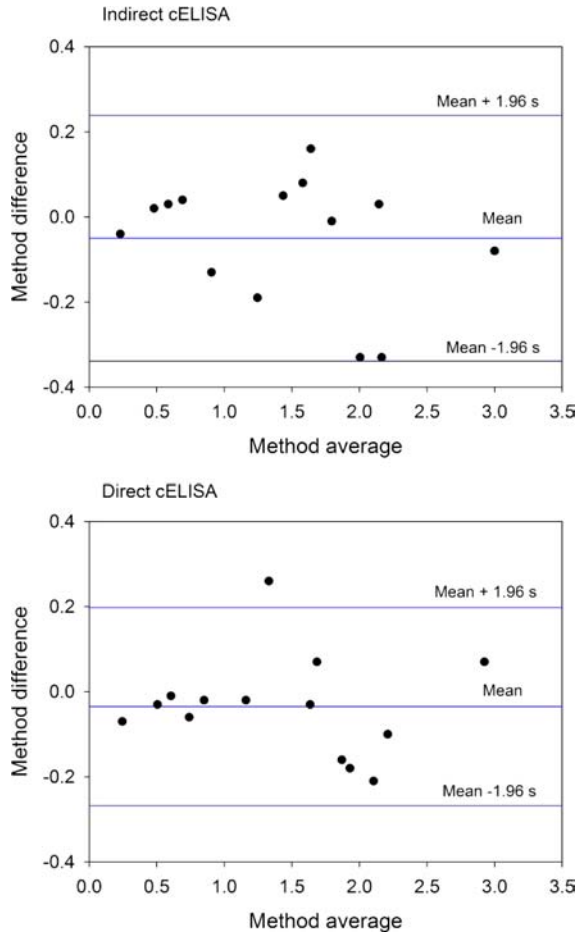

Figure 3. Bland−Altman dispersion for comparison of results obtained by the developed cELISAs and by a reference chromatographic method. Samples were analyzed three times by the immunochemical methods and twice by GC−MS.

■ ASSOCIATED CONTENT

Ⓢ Supporting Information

Studied buffer conditions, chemical structure of hapten KMo, chemical structures of strobilurins, raw data from the analysis of in-field treated samples, and Deming regression lines. This material is available free of charge via the Internet at http://pubs.acs.org.

■ AUTHOR INFORMATION

Corresponding Authors

*E-mail: antonio.abad@uv.es (A.A.-S.). Tel: +34-963544509. Fax: +34-963544328.

*E-mail: aabad@iata.csic.es (A.A.-F.). Tel: +34-963900022. Fax: +34-963636301.

Author Contributions

‡These authors contributed equally to this work

Funding

This work was supported by the Spanish *Ministerio de Ciencia e Innovación* (MICINN) (AGL2006-12750-C02-01/02/ALI and AGL2009-12940-C02-01/02/ALI) and cofinanced by FEDER funds. R.L.-M. was hired by MICINN under a predoctoral FPI grant. F.A.E.-T. and J.V.M. were hired by CSIC with postdoctoral contracts, the former under the JAE-doc program and the latter under the *Ramón y Cajal* program, both cofinanced by MICINN and by the European Social Fund (ESF).

Notes

The authors declare no competing financial interest.

■ ACKNOWLEDGMENTS

We thank Ana Izquierdo-Gil and Laura López-Sánchez for excellent technical assistance. Limited amounts of the described immunoreagents are available upon request.

REFERENCES

(1) Bartlett, D. W.; Clough, J. M.; Godwin, J. R.; Hall, A. A.; Hamer, M.; Parr-Dobrzanski, B. The strobilurin fungicides. *Pest Manage. Sci.* **2002**, *58*, 649−662, DOI: 10.1002/Ps.520.

(2) Balba, H. Review of strobilurin fungicide chemicals. *J. Environ. Sci. Health, Part B* **2007**, *42*, 441−451, DOI: 10.1080/03601230701316465.

(3) Ypema, H. L.; Gold, R. E. Modification of a naturally occurring compound to produce a new fungicide. *Plant Dis.* **1999**, *83*, 4−19, DOI: 10.1094/pdis.1999.83.1.4.

(4) Environmental Protection Agency (1998). Kresoxim-methyl pesticide fact sheet. http://oaspub.epa.gov/apex/pesticides/f?p=CHEMICALSEARCH:31:17590345896928::NO:1,3,31,7,12,25:P3_XCHEMICAL_ID:1460. Accessed 17.12.13.

(5) Australian Pesticides and Veterinary Medicines Authority (2000). Evaluation of the new active Kresoxim-methyl in the product Stroby WG fungicide. https://portal.apvma.gov.au/pubcris. Accessed 17.12.13.

(6) European Food Safety Authority. Conclusion on the peer review of the pesticide risk assessment of the active substance kresoxim-methyl. *EFSA J.* **2010**, DOI: 10.2903/j.efsa.2010.1891.

(7) Das Capital Management and Advisors (2011). Rallis India. http://www.dascap.com/house_view_pdf/Rallis.pdf. Accessed 17.12.13.

(8) Cabras, P.; Angioni, A.; Garau, V. L.; Pirisi, F. M.; Brandolini, V. Gas chromatographic determination of azoxystrobin, fluazinam, kresoxim-methyl, mepanipyrim, and tetraconazole in grapes, must, and wine. *J. AOAC Int.* **1998**, *81*, 1185−1189.

(9) Christensen, H. B.; Granby, K. Method validation for strobilurin fungicides in cereals and fruit. *Food Addit. Contam.* **2001**, *18*, 866−874, DOI: 10.1080/02652030121435.

(10) Sannino, A.; Bolzoni, L.; Bandini, M. Application of liquid chromatography with electrospray tandem mass spectrometry to the determination of a new generation of pesticides in processed fruits and vegetables. *J. Chromatogr. A* **2004**, *1036*, 161−169, DOI: 10.1016/j.chroma.2004.02.078.

(11) Koesukwiwat, U.; Lehotay, S. J.; Miao, S.; Leepipatpiboon, N. High throughput analysis of 150 pesticides in fruits and vegetables using QuEChERS and low-pressure gas chromatography-time-of-flight mass spectrometry. *J. Chromatogr. A* **2010**, *1217*, 6692−6703, DOI: 10.1016/j.chroma.2010.05.012.

(12) Mercader, J. V.; Suárez-Pantaleón, C.; Agulló, C.; Abad-Somovilla, A.; Abad-Fuentes, A. Hapten synthesis and monoclonal antibody-based immunoassay development for the detection of the fungicide kresoxim-methyl. *J. Agric. Food Chem.* **2008**, *56*, 1545−1552, DOI: 10.1021/Jf073039x.

(13) López-Moreno, R.; Mercader, J. V.; Agulló, C.; Abad-Somovilla, A.; Abad-Fuentes, A. Structure-immunogenicity relationship of kresoxim-methyl regioisomeric haptens. *Org. Biomol. Chem.* **2013**, *11*, 7361−7371, DOI: 10.1039/c3ob41570h.

(14) Anastassiades, M.; Lehotay, S. J.; Stajnbaher, D.; Schenck, F. J. Fast and easy multiresidue method employing acetonitrile extraction/partitioning and "dispersive solid-phase extraction" for the determination of pesticide residues in produce. *J. AOAC Int.* **2003**, *86*, 412−431.

(15) Abad-Fuentes, A.; Esteve-Turrillas, F. A.; Agulló, C.; Abad-Somovilla, A.; Mercader, J. V. Development of competitive enzyme-linked immunosorbent assays for boscalid determination in fruit juices. *Food Chem.* **2012**, *135*, 276−284, DOI: 10.1016/j.foodchem.2012.04.090.

(16) Mercader, J. V.; Suárez-Pantaleón, C.; Agulló, C.; Abad-Somovilla, A.; Abad-Fuentes, A. Hapten synthesis and monoclonal antibody-based immunoassay development for detection of the fungicide trifloxystrobin. *J. Agric. Food Chem.* **2008**, *56*, 2581−2588, DOI: 10.1021/Jf800157s.

(17) Lehotay, S. J. Determination of pesticide residues in foods by acetonitrile extraction and partitioning with magnesium sulfate: Collaborative study. *J. AOAC Int.* **2007**, *90*, 485−520.

(18) European Commission DG SANCO (2007). Method validation and quality control procedures for pesticide residues analysis in food and feed. http://www.eurl-pesticides.eu/docs/public/tmplt_article.asp?CntID=615&LabID=100&Lang=EN. Accessed 17.12.13.

casein-stabilized emulsions has been studied,[10] and improved stability against creaming has been reported.[11] However, studies on the oxidative stability of transglutaminase-cross-linked caseinate-stabilized emulsions are inconsistent. Whereas improved oxidate stability of flaxseed oil emulsions was recently reported when caseinate molecules were cross-linked prior to emulsification step,[12] no improvement or decreased oxidative stability was reported for cross-linked caseinate-stabilized fish oil emulsions.[13] In this work, analytical ultracentrifugation was used to gain insight into the state of aggregation in which sodium caseinate existed at the interface. Analytical ultracentrifugation is a versatile tool that can be used in the investigation of polymer size, polymer shape, molecular self-association, and molecular interactions.[14,15] In particular for proteins, analytical centrifugation is one of the classical methods used for the determination of oligomeric states and macromolecular interactions.[9] Due to the relatively large size of these macromolecules, the sedimentation profiles observed under gravitational fields lend this technique a high resolution.[10] The objective of this work was to investigate the oxidative stability of transglutaminase cross-linked caseinate-stabilized fish oil emulsions as a function of homogenization pressure.

MATERIALS AND METHODS

Chemicals. Sodium caseinate powder was provided by Tatua Co-operative Dairy Co. Ltd. (Tatuanui, New Zealand) and used in all experiments except for proton nuclear magnetic resonance (NMR) spectroscopy, in which sodium caseinate (Alanate 180) from New Zealand Milk Products (North America) Inc. (Santa Rosa, CA, USA) was used. Activa transglutaminase-T1 enzyme product, with maltodextrin and transglutaminase declared as main ingredients and with a commercially reported enzyme activity of 100 U/g, was provided by Ajinomoto North America, Inc. (Eddyville, IA, USA). The following were purchased from Sigma-Aldrich Co. (St. Louis, MO, USA): 2,2′-azinobis(3-ethylbenzothiazoline-6-sulfonic acid) (ABTS) stock solution at 1.8 mM, 2-propanol, 30% hydrogen peroxide, ammonium thiocyanate, barium chloride dehydrate, disodium phosphate, ferric chloride hexahydrate, ferrous sulfate heptahydrate, isooctane, menhaden fish oil, potassium persulfate, sodium chloride, and triple-distilled peppermint oil. The following were purchased from Mallinckrodt Chemicals Inc. (St. Louis, MO, USA): butanol, hexane, and methanol. Ethyl acetate, glacial acetic acid, and sodium acetate trihydrate were purchased from J. T. Baker (Phillipsburg, NJ, USA). Iron powder was purchased from Acros Organics and hexane from EMD Chemicals (Philadelphia, PA, USA). Distilled water was used to prepare all aqueous solutions. Dilute solutions of hydrochloric acid and sodium hydroxide ($\leq$5 N) were used for pH adjustments.

Proton Nuclear Magnetic Resonance Spectroscopy. Proton NMR spectroscopy was carried out using a Varian 300 MHz NMR spectrometer (Varian, Inc., Palo Alto, CA, USA). Two percent (w/v) sodium caseinate solutions were either not treated by homogenization (0 kpsi, 0 MPa) or homogenized at 40 kpsi (276 MPa) under five passes using a Nano DeBEE 45 high-pressure homogenizer (BEE International, South Easton, MA, USA). Both solutions were freeze-dried and subsequently lyophilized from deuterium oxide of 99.9% isotopic purity (Sigma) twice. The samples were then dissolved to 2% (w/v) in deuterium oxide and analyzed. A homogenization pressure of 40 kpsi was selected for NMR studies because this is the highest pressure reached by the homogenizer. It is hypothesized that if protein interactions were promoted in protein solutions by the homogenization pressure, they should become evident after processing at highest homogenization pressures. However, in emulsion-making, a lower pressure (20 kpsi, 137.9 MPa) was selected because at higher homogenization pressures larger particle sizes were observed due to droplet coalescence promoted by the higher temperatures reached at 40 kpsi as compared to 20 kpsi.

Caseinate-Stabilized Emulsion Preparation. *Emulsification via High-Pressure Homogenization.* A 1% (w/v) sodium caseinate solution with 0.05 M sodium chloride and 0.05 M disodium phosphate was prepared at room temperature, during which the mixing time for ensuring complete solvation of the protein was at least 3 h. The pH was eventually adjusted to 7.0. A 4% (v/v) fish oil-in-water coarse emulsion was made using a VirtiShear homogenizer (SP Scientific, Gardiner, NY, USA) at 30000 rpm for 10 s, immediately followed by HPH using a Nano DeBEE 45 high-pressure homogenizer (BEE International) under three or eight passes at either 5 kpsi (34.5 MPa) or 20 kpsi (137.9 MPa). Samples from coarse emulsions were used as controls (~0 kpsi). For temperature control during HPH, a counter-current heat exchanger that was connected to a 2 °C water bath was positioned downstream of the emulsifying cell. Each emulsion sample batch consisted of 100 mL and was prepared in triplicate.

Enzymatic Cross-Linking of Interfacial Protein in Emulsions. The transglutaminase enzyme product was added to emulsion samples prepared at 20 kpsi at different concentrations (0, 5, 10, and 25 mg/mL of emulsion). Fifty milliliters of each emulsion batch added with transglutaminase was incubated for 1 h at 37 °C to avoid acceleration of oil oxidation. The emulsions were then immersed in boiling water for 4 min for enzyme inactivation and quickly cooled in water to room temperature.

Recovery of Interfacial Protein for Analytical Ultracentrifugation Analysis. To analyze the mass distribution of protein at the oil/water interface, emulsions homogenized at 0, 5, and 20 kpsi were made using a volatile oil that could be removed from the emulsion. Thus, peppermint oil was used in place of fish oil. The emulsion samples were ultracentrifuged at 46000*g* for at least 3 h at 2 °C using an Optima XL-I ultracentrifuge (Beckman Coulter, Brea, CA, USA). Immediately after ultracentrifugation, the supernatant was removed with a syringe needle, and then distilled water was added to disperse the residual cream in the centrifugation tube. The dispersed cream was frozen in liquid nitrogen and freeze-dried at −55 °C and 0 mbar using a FreezeMobile freeze-dryer (The VirTis Co., Gardner, NY, USA), during which frozen peppermint oil and water sublimed. After freeze-drying, the residual protein was redissolved in deionized water to a concentration of 2 mg/mL and subjected to overnight dialysis against a buffer of 0.05 M sodium chloride and 0.05 M disodium phosphate, at pH 7, using a Spectra/Por 4 standard regenerated cellulose dialysis membrane of 12−14 kDa molecular weight cutoff (Spectrum Laboratories, Inc., Rancho Dominguez, CA, USA).

Characterization of Oils. The suitability of using peppermint oil to replace fish oil, in the sample preparation of interfacial caseinate for analysis by analytical centrifugation, lies in its similarity in its influence on protein interfacial behavior. Although oil viscosity influences emulsion drop size, it is not the critical factor at issue. Because protein interfacial behavior is influenced by hydrophobicity of oil, it was relevant to gain an understanding about the partition coefficient of peppermint oil and its interfacial tension with water compared with those of fish oil, to validate its appropriateness.

Determination of Logarithm of Partition Coefficient. The solubility of oil in hexane could be determined by UV absorbance measurement.[16] Both fish oil and peppermint oil were assayed. Oil (25 μL) was added to a mixture comprising 20 mL of hexane and 20 mL of deionized water and vortexed for 5 min. The mixture was left to stand for phase separation until both phases became clear. UV absorbance was read at 250 nm on a Beckman Coulter DU 700 series UV−vis spectrophotometer (Beckman Coulter, Brea, CA, USA) for the hexane phase in duplicates, against a standard curve of oil in hexane within a 0−0.125% (v/v) concentration range. The logarithm of the ratio of oil concentrations in hexane and deionized water, log $P_{\text{hexane/water}}$, was calculated.

Measurement of Interfacial Tension with Water. The interfacial tension of fish oil/water and peppermint oil/water interfaces was measured in triplicate by a platinum ring (diameter = 6.1 cm, ratio of radii of ring to wire = 55.6) attached to a CSC DuNouy tensiometer 70545 (CSC Scientific Co., Inc., Fairfax, VA, USA). Each measurement was taken 30 min after layering of oil above the water at room temperature, in a glass dish having inner diameter = 4.7 cm and height

= 2.9 cm). The reading was adjusted by a correction factor read from the manual of the tensiometer.

Ferric Thiocyanate Peroxide Value Assay. To monitor oil oxidation, primary oxidation products were measured by the ferric thiocyanate peroxide value assay. Emulsions from each treatment, cross-linked at various transglutaminase concentrations homogenized at 0, 5, or 20 kpsi, were analyzed. The procedure for the assay was modified from that of Ogawa et al.,[17] and the exact details were reported in our earlier work.[18] Triplicate samples were removed over a period of 12 days for the determination of oxidative stability.

Emulsion Drop Size Measurement. Triplicate emulsion samples were diluted 100-fold with deionized water, and each triplicate was measured twice for particle size (*Z*-average) at 25 °C by dynamic light scattering (DLS), using a Zetasizer Nano ZS90 with optical arrangement at 90° (Malvern Instruments Ltd., Worcestershire, UK). During size measurement, the refractive indices of water and oil were set at 1.33 and 1.46, respectively, whereas the dispersant viscosity was that of water at 25 °C (i.e., 0.89 cP).

According to Thomas,[19] and as previously reported in our earlier work,[18] the average value of *Z*-average (Z_{av}) was converted to the average Sauter mean diameter (d_{32}) as

$$\text{av } d_{32} = Z_{av} \times (1 + Q)^2 \tag{1}$$

where Q was the average experimentally determined polydispersity obtained during particle size measurement.

Intrinsic Rate of Oxygen Depletion Calculation. It must be emphasized that the average emulsion drop size has a strong implication on the total interfacial area per volume subjected to contact with dissolved oxygen in the emulsion. Hence, the intrinsic rate of oxidation, which takes into account the interfacial area, is a more accurate indicator of the rate of oxidation in the average emulsion drop than the change of peroxide value of the emulsion over time. The intrinsic rate of oxidation has an especially strong bearing on the oxidative stability of emulsions with very fine drops, which are often desirable due to the slowing of creaming/sedimentation according to Stokes' law.

The calculation steps were reported in our earlier work.[18] The total rate of oxygen depletion during oxidation of oil was proportional to $(\partial(\text{Abs}_t - \text{Abs}_0))/(\partial t)$ and in turn $(6/d_{32}) \times$ intrinsic rate of oxygen depletion per unit of interfacial area of the emulsion drops, where Abs_0 was the average absorbance reading at 510 nm of an emulsion sample from peroxide value assay corrected by that of the blank at time = 0; Abs_t was the absorbance at 510 nm from peroxide value assay at time = t; and $(6/d_{32t})$ represented the ratio of the total surface area of the emulsion drops to total volume of the drops at time = t.

Hence, the relative intrinsic rate of oxygen depletion per unit of interfacial area of the emulsion drops was calculated as

$$\frac{\partial(\text{Abs}_t - \text{Abs}_0)}{\partial t} \times \frac{d_{32t}}{6} \tag{2}$$

Analytical Ultracentrifugation. Sedimentation velocity experiments were performed in an Optima XL-A ultracentrifuge (Beckman CoulterS). The samples analyzed included protein dissolved directly as it was in buffer, as well as freeze-dried protein recovered from emulsions after the sublimation of peppermint oil and redissolved in buffer. The final protein concentration ranged from 0.5 to 2.0 mg/mL as determined by the Lowry protein assay. Solvent densities and viscosities, along with the partial specific volume, were calculated with SEDNTERP (v. 1.09). The estimation of the partial specific volume ($\bar{v}$) was done according to the method of Cohn and Edsall:[20] $\bar{v} = (\sum \bar{v}_i n_i M_i)/(\sum n_i M_i)$, where n_i is the number of moles of ith component and M is its molecular weight. Solvent densities are extrapolated from the polynomial fit to

$$\Delta\rho_c = a + bC^{1/2} + cC + dC^2 + eC^3 + fC^4 - \rho_{water} \tag{3}$$

where $\Delta\rho_c$ is the density increment at a certain concentration, a–f are coefficients, C is the concentration of the solute, and ρ_{water} is the density of water.[21] Boundary positions were determined using the absorbance (280 nm) and interference (675 nm) optics, with scans taken every 4 min over 8 h at 45000 rpm. The $c(s)$ distributions were calculated using SEDFIT (v. 12.0b).[22] To assess the formation of higher order species, the weighted average sedimentation coefficients of the species was obtained by integration of the entire $c(s)$ distribution. The hydrodynamic movement of a particle can be described by the Svedberg equation: $M = (RTs)/(D(1 - \bar{v}\rho_{solv}))$, where M is molar mass, R is the gas constant, T is the temperature, D is the solute diffusion coefficient, $\bar{v}$ is the partial specific volume of the particle, and ρ_{solv} is the density of the solvent.[23] The sedimentation and diffusion of a particle in a section-shaped cell under a centrifugation field is described by the Lamm equation:

$$\frac{\partial\chi}{\partial t} = \frac{1}{r}\frac{\partial}{\partial r}\left[rD\frac{\partial\chi}{\partial r} - s\omega^2 r^2\chi\right] \tag{4}$$

SEDFIT employs a numerical solution to the Lamm equation that generates a $c(s)$ distribution describing the sedimenting solutes in the solution under a centrifugal field.[24]

Enzymatic Cross-Linking Turbidity Assay. It is expected that an increase in transglutaminase concentration will lead to an increase in cross-linking of caseinate. The turbidity assay was done as a quick qualitative verification of the relative extent of enzymatic cross-linking. Although the Zetasizer instrument may be used to measure particle size distribution in the sodium caseinate solutions to infer turbidity, the credibility of the results from the Zetasizer may be affected by the inherently high polydispersity at 1% (w/v). Hence, turbidity was analyzed by measuring the sample absorbance at 340 nm on a Beckman Coulter DU 700 series UV–vis spectrophotometer at room temperature. The transglutaminase enzyme product was added to 1% (w/v) sodium caseinate solutions (with 0.05 M sodium chloride and 0.05 M disodium phosphate, at pH 7) at 0, 5, 10, and 25 mg/mL and incubated in a 37 °C water bath for 1 h before being boiled for 4 min for enzyme inactivation. Sodium caseinate solutions with 5, 10, and 25 mg/mL of the enzyme product added and boiled immediately without an incubation step were prepared as positive controls. Triplicate measurements of the absorbance of the sodium caseinate solutions were taken. The mean increase in turbidity due to enzymatic cross-linking was reported by the subtraction of the mean absorbance of a positive control from the mean absorbance of the corresponding sample. Statistical analysis for mean comparison was done using the Tukey–Kramer test.

ABTS Decolorization Assay. For the ABTS assay, sample solutions of 1% (w/v) sodium caseinate (with 0.05 M sodium chloride and 0.05 M disodium phosphate, at pH 7) were subjected to enzymatic cross-linking at 5, 10, and 25 mg/mL of the transglutaminase enzyme product (37 °C for 1 h) followed by enzyme inactivation (100 °C for 4 min). Positive controls were added with the corresponding amounts of the transglutaminase enzyme product but subjected only to boiling for 4 min. The negative controls consisted of the native protein solution.

The assay is based on the quenching of the ABTS cationic radical, observed as the loss of blue-green color at 734 nm. The assay could be indicative of the scavenging capability of radicals such as reactive oxygen species or radical species formed from oil oxidation at the oil/water interface. In particular, the assay was chosen because it can be set up such that the sample pH is not altered, and neither does it involve the use of organic solvents. As such, the assay is free of complications from pH- and solvent-induced changes in solubility, structure, and/or state of aggregation of the protein. Although antioxidative mechanisms may be diverse, in the work of Moure et al.[25] involving protein analysis, the assay yielded results that generally agreed with the overall trend in antioxidant properties measured by different methods. The procedure for the assay was modified from that reported by Moure et al.[25] Two parts volume of 1.8 mM ABTS stock solution and five parts volume of 2.45 mM potassium persulfate in 0.02 M disodium phosphate solution were mixed together, adjusted to pH 7, and incubated for 1 h at room temperature in the dark to generate the blue-green ABTS radical cation. Duplicate measurements of radical scavenging capacity were done by mixing 20 μL of the sample or control with 2 mL of the radical solution and, after 15 min, reading the

absorbance at 734 nm on a Jasco V-650 spectrophotometer (Jasco Spectroscopic Co., Easton, MD, USA). The relative antioxidant capacity of the samples was inferred by comparing the mean absorbance values using the Tukey–Kramer method.

RESULTS

Figure 1 shows that the homogenizing pressure in HPH had no effect on the molecular structure of sodium caseinate in

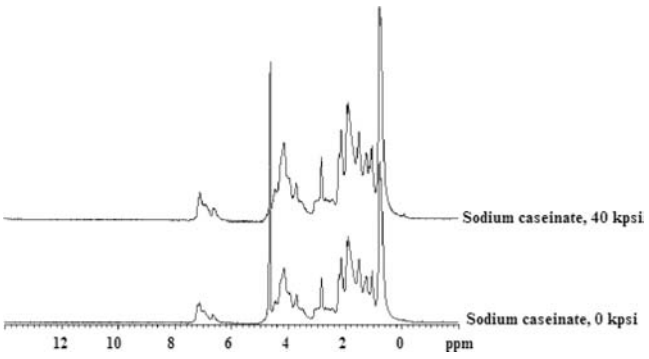

Figure 1. One-dimensional NMR spectra of 2% (w/v) sodium caseinate solutions that were not treated by homogenization (0 kpsi) and homogenized at 40 kpsi under five passes.

solution. Thus, it could be established that during emulsification by HPH, the homogenizing pressure would not exert any influence on the chemical antioxidant property of sodium caseinate in the continuous phase. Despite this, emulsions made by HPH (5 and 20 kpsi) showed slower initial rates of formation of primary oxidation products compared to a coarse emulsion (0 kpsi), as shown by the slope of the oxidation curves in Figure 2. The mean peroxide value (PV) of the coarse

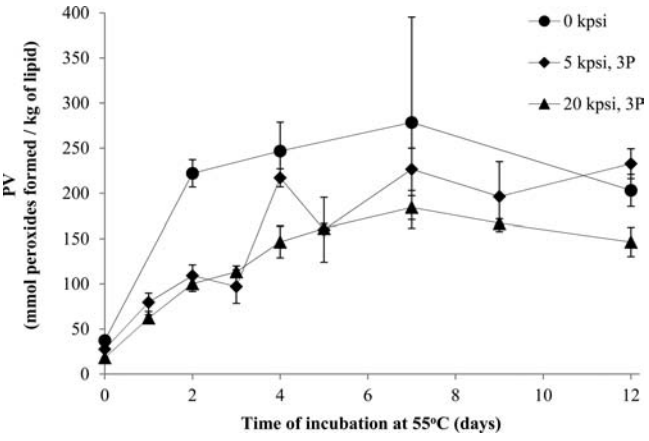

Figure 2. Plots showing the effect of high-pressure homogenization on the peroxide value with increasing incubation time (number of passes = 3) of emulsion samples. A decrease in PV at longer times is due to the conversion of primary to secondary oxidation products. Error bars indicate the standard deviation from the mean of triplicate readings.

emulsion declined considerably at longer incubation time (from days 7 to 12), reflecting further aggravated oil oxidation with the conversion of primary to secondary oxidation products. Between homogenizing pressures, the intrinsic rate of oxidation in emulsions at 20 kpsi was slower than for the emulsions made at 5 kpsi, as shown in Figure 3.1 by a steeper slope of the oxidation curve at 5 kpsi and early incubation times. By day 4 of incubation, emulsions formed at 20 kpsi were at a significantly

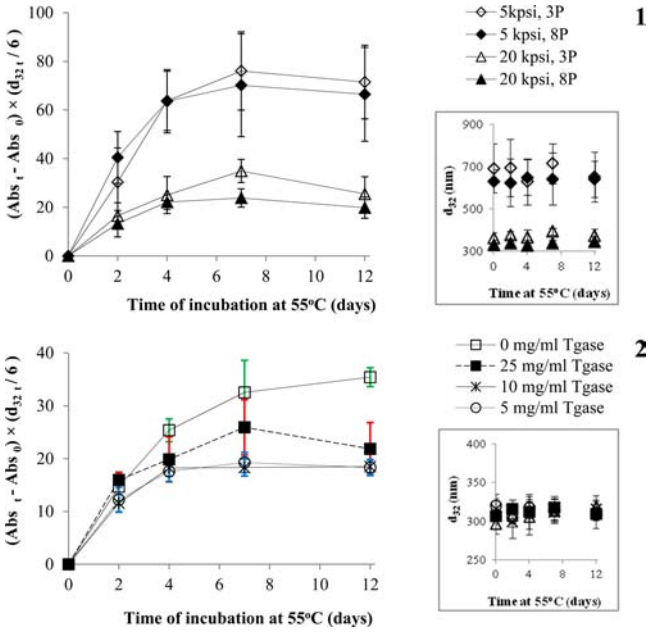

Figure 3. Plots of the relative intrinsic rate of oxygen depletion in fish oil per unit interfacial area, as influenced by (1) homogenization pressure and number of passes (P) and (2) use of different concentrations of the transglutaminase (Tgase) enzyme product at homogenization conditions of 20 kpsi and 3P. Error bars indicate the standard deviation from the mean of oxygen depletion. (Insets) Plots of the variation of the saunter mean diameter d_{32} of emulsions with time, with error bars indicating the standard deviation from the mean of six measurements from triplicates.

lower intrinsic state of oxidation than those formed at 5 kpsi. The difference in the intrinsic rate of oxidation between 5 and 20 kpsi homogenizing pressures is much more pronounced (Figure 3.1) than that in the PV values (Figure 2). This can be explained by the difference in the interfacial area available for oxidation. Compared to emulsions prepared at 5 kpsi, those made at 20 kpsi had significantly ($p < 0.05$) smaller mean d_{32} and thus larger total interfacial area per volume available for reaction with dissolved oxygen.

The addition of transglutaminase to emulsions did not lead to any significant difference in drop size, as shown in the inset of Figure 3.2. No sedimentable aggregates were formed. Even though the total interfacial area per volume was similar, there was improved emulsion oxidative stability at 5 and 10 mg/mL dosage of the enzyme product compared to no dosage. However, when the enzyme product concentration increased further (25 mg/mL), the beneficial effect of the use of transglutaminase apparently decreased. The general trend in the results suggested that there was an optimal enzyme level for emulsion oxidative stability.

Peppermint oil seemed to be a reasonable replacement of fish oil, as suggested by the results displayed in Table 1. From Table 1, the mean logarithm of partition coefficient of the peppermint oil was within 24% difference from that of the fish oil. The mean oil/water interfacial tension of the peppermint oil was within 32% difference from that of the fish oil. Figure 4 shows how homogenizing pressure affected the state of aggregation in solvated and interfacial caseinate. As seen in Figure 4.1, there was a slight increase in the mass of caseinate aggregates in the continuous phase of emulsions with increasing pressure. However, for interfacial caseinate, higher homogenizing pressure led to increased formation of larger species, as

dx.doi.org/10.1021/jf403285z | J. Agric. Food Chem. 2014, 62, 2822–2829

Table 1. Physical Properties of Fish Oil and Peppermint Oil[a]

oil	log $P_{hexane/water}$	oil/water interfacial tension (mN/m)
fish	1.37 ± 0.02 (SD)	12.0 ± 0.2 (SD)
peppermint	1.05 ± 0.04 (SD)	15.8 ± 0.3 (SD)

[a]SD stands for the standard deviation based on duplicate measurements for the logarithm of the partition coefficient, log $P_{hexane/water}$, and triplicate measurements for oil/water interfacial tension.

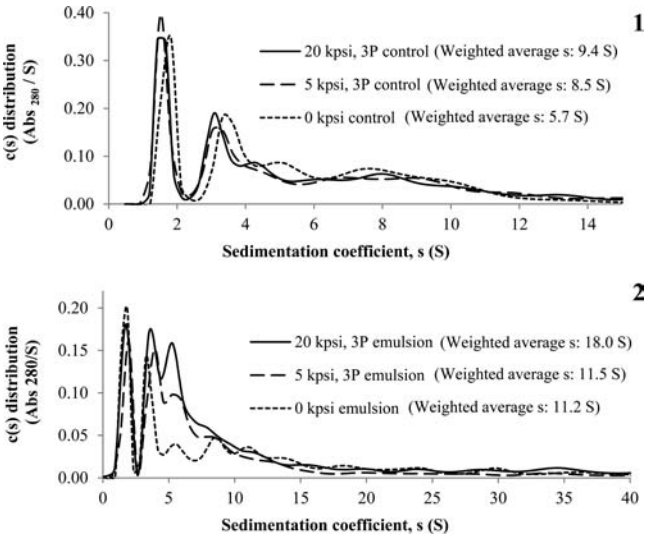

Figure 4. Sedimentation coefficient distribution plots for (1) sodium caseinate solutions homogenized under three passes (P) at 0, 5, and 20 kpsi, which served as controls, and (2) interfacial protein isolated from sodium caseinate emulsions made under three passes at 0, 5, and 20 kpsi. The weighted average sedimentation coefficient, *s*, of each sample is indicated.

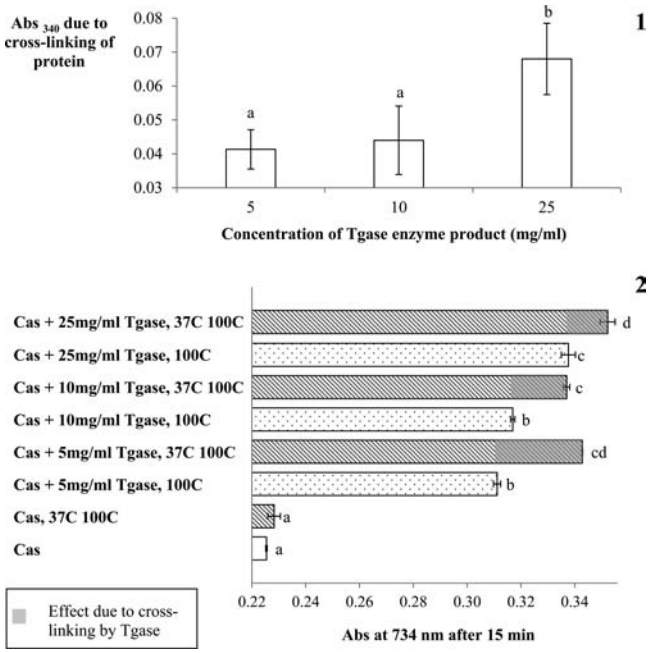

Figure 5. Results of spectrophotometric assays of 1% (w/v) sodium caseinate (Cas) solutions: (1) Turbidity measured at 340 nm as a function of concentration of the transglutaminase (Tgase) enzyme product during enzymatic cross-linking. Error bars indicate the standard deviation from the mean values derived from three measurements. (2) Absorbance measurements at 734 nm in the 2,2′-azinobis(3-ethylbenzothiazoline-6-sulfonic acid) (ABTS) assay. Prior to the ABTS assay, the samples (which contained Tgase) were subjected to treatment at 37 °C for 1 h followed by 100 °C for 4 min, whereas the positive controls (which also contained Tgase) were subjected to treatment at 100 °C for 4 min. Means with different letters are significantly different from one another at $p < 0.01$, according to the Tukey–Kramer test. Error bars indicate the standard deviation from the mean absorbance values derived from two measurements.

indicated in Figure 4.2 and by an upward shift in the weighted average sedimentation coefficient (from 11.2 S for 0 kpsi to 18 S for 20 kpsi).

Figure 5.1 depicts the results of the turbidity assay, with increase in transglutaminase concentration causing an increase in the cross-linking of caseinate. Figure 5.2 shows the results of the ABTS decolorization assay. The native sodium caseinate solution had the lowest mean absorbance reading at 734 nm, inferring higher antioxidant capacity than any other treated sample. Heat treatment at 37 °C and boiling of the native caseinate solution did not change the absorbance and antioxidant capacity significantly. Boiled protein samples containing the enzyme product had much higher absorbance at 734 nm overall due to the presence of maltodextrin in the commercial product. Generally, the higher the dosage of the enzyme product, the higher was the absorbance. However, at every enzyme product concentration, an additional 60 min of incubation at 37 °C (followed by boiling) led to even higher absorbance, indicating the reduction of chemical antioxidant capacity due to enzymatic cross-linking of caseinate.

DISCUSSION

The poor oxidative stability exhibited by coarse emulsions (0 kpsi) was expected because these emulsions are prone to creaming, due to the large particle size, which causes the oil droplets to become directly exposed to oxygen in the headspace. On the other hand, in emulsions made by homogenization, the increase in interfacial area due to smaller particle size would be expected to increase its susceptibility to react with oxygen present in the continuous phase, when oxygen concentration is not limiting. This was supported by Lethuat et al.,[26] who measured the rate of formation of conjugated diene in sunflower oil emulsions stabilized by bovine serum albumin. However, Let et al.[27] reported that milk-stabilized fish oil emulsions with smaller drops (and therefore larger interfacial area) were less oxidized than emulsions with larger drops. Similarly, higher lipid oxidative stability of caseinate-stabilized emulsion with smaller droplets was also reported by Ries et al.[28] In the present study, oxidative stability increased with decreasing emulsion droplet size. Figure 2 shows that the increase in PV versus time for the 20 kpsi emulsion was not significantly ($p < 0.05$) faster than that for the 5 kpsi emulsion. However, when particle size is taken into account, as shown in Figure 3.1, the lower the homogenizing pressure, the lower was the intrinsic emulsion oxidative stability. From the d_{32} results in the different test scenarios, the varying total interfacial areas per volume of emulsion could be evaluated. It was estimated that regardless of the total interfacial area in each test scenario, there was excessive caseinate at 1% (w/v) to permit maximum protein load at the plateau region of the interfacial adsorption isotherm, which was deduced to be around 3 mg/m^2 oil according to Tornberg's work.[29] As such, the protein load per unit interfacial area in each test scenario

could be reasonably assumed the same. Thus, it was not probable that the more oxidatively stable emulsions had significantly higher protein loads. It was unlikely that they had significantly thicker interfacial layers either, because the thickness of adsorbed caseinate (and casein) was found to be insensitive to adsorption conditions but constant at ∼10−15 nm.[30−32] The next section discusses the disparity in the observed emulsion oxidative stability from a molecular viewpoint (of how cross-linking might alter the chemical antioxidant property) and a physical standpoint (of how cross-linked interfacial caseinate might serve as a physical barrier against oil oxidation).

Analytical Ultracentrifugation Findings Show Higher State of Interfacial Protein Aggregation at Higher Homogenizing Pressure. Sodium caseinate in water at pH 7 is translucent in appearance at as low a concentration of 0.5% (w/v) and thus not completely soluble. Owing to this physical character, attempts to analyze the conformation of interfacial caseinate were met with obstacles. FTIR for studying protein secondary structure was not considered in this case, because the protein in question essentially lacks any defined secondary structure. Khun and Cunha[33] used sodium dodecyl sulfate−polyacrylamide gel electrophoresis (SDS-PAGE) under non-reducing and reducing conditions to demonstrate the formation of disulfide linkages in interfacial whey protein with increase in homogenizing pressure. This method is, however, not applicable for the study of interfacial sodium caseinate because, first, sodium caseinate does not possess substantial sulfur amino acid residues and, second, the method dissociates any electrostatic and hydrophobic interactions that could have contributed to interfacial caseinate polymerization. In a preliminary experiment, native PAGE assay on a 15% criterion precast Tris-HCl gel (from Bio-Rad) was found not useful for the analysis of sodium caseinate either, as it was impossible to separate sodium caseinate into bands due to the size of molecular aggregates being >200 kDa. In another previous instance, sodium caseinate at pH 7 was found not soluble enough to be analyzed by multiangle laser light scattering-size exclusion chromatography (MALLS-SEC).

To our knowledge, the present study was the first time analytical ultracentrifugation was demonstrated to be a viable method for experimentally examining the state of protein aggregation at an oil−water interface. The analytical ultracentrifugation results of interfacial caseinate elucidated an upward shift in the order of oligomer species and molecular weight, when the homogenizing pressure increased. These results were in agreement with the trend in the high-performance liquid chromatography (HPLC) results published by Lee et al.,[34] which showed dimensionally larger aggregates in interfacial whey protein from emulsions subjected to higher homogenizing pressure. The increased aggregation in interfacial caseinate was an indication of cross-linking in its random coil structure. Slight increases in sedimentation coefficient patterns were observed in homogenized protein solutions, with values gradually increasing with increase in homogenization pressure (Figure 4.1). However, protein recovered for the interface dramatically increased the values for sedimentation coefficient with increasing pressure, presumably due to protein aggregation promoted by interactions between pressure and temperature. Similar observations have been reported for casein micelles subjected to static high-pressure treatments, where aggregation of casein micelles was reported for skim milk exposed to 200 MPa and mild temperature (40 °C), whereas deaggregation was observed at similar pressure levels but lower temperatures.[35]

Cross-Linking of Caseinate Was Associated with Decreased Chemical Antioxidant Property. The samples in the present study were all controlled for the starting level of dissolved oxygen by using the same source of water. To understand how cross-linking of caseinate would influence its inherent antioxidant property, the ABTS decolorization assay at 734 nm was performed on sodium caseinate solution samples dosed with different concentrations of the transglutaminase product, which also contained maltodextrin. When activated, transglutaminase catalyzes the formation of a covalent bond between the free ε-amine group of a protein-bound lysine and the γ-carboxyamide group of a protein-bound glutamine.[36] It was acknowledged that during enzyme inactivation by boiling, the process might cause the removal of dissolved oxygen and/or trigger the Maillard reaction between caseinate and maltodextrin; hence, the impact of boiling was also tested in the ABTS assay.

In all of the samples, absorbance due to turbidity was checked and verified to be negligible at 734 nm and hence would not significantly interfere with true absorbance due to the blue-green ABTS radical. In light of this, Figure 5.2 clearly shows that transglutaminase-induced cross-linking caused a reduction in antioxidant capacity, across the three enzyme product concentrations tested (5, 10, and 25 mg/mL dosage of the enzyme product or 50, 100, and 250 U/g sodium caseinate). Despite this, the emulsion oxidative stability in all three cases was better than without the use of transglutaminase (Figure 3.2). Because the improvement in emulsion oxidative stability could not be explained from a chemical standpoint, the cross-linked interfacial caseinate layer must have played a dominant role in terms of physical barrier property against oxidation. Considering that Kellerby et al.[37] did not observe improvement in the oxidative stability of sodium caseinate-based menhaden oil-in-water emulsions at a transglutaminase activity of 10 U/g protein, the present finding suggests a minimum enzyme activity needed to boost the physical barrier property of interfacial caseinate.

The results in Figure 3.2 also suggested a maximum in emulsion oxidative stability at an optimum transglutaminase activity, similar to the findings of Bao et al.[38] for spray-dried microalgal oil encapsulated by cross-linked sodium caseinate (with transglutaminase) as a function of the cross-linking time. Protein cross-linking could possibly reduce the solvent accessibility of some amino acids with antioxidant activity, such as tryptophan, tyrosine, histidine, methionine, and cysteine; however, the decline in emulsion oxidative stability from 10 to 25 mg/mL dosage of the enzyme product did not seem to be a case of cross-linking induced reduction in solvent accessibility of antioxidant amino acids prevailing over the interfacial physical barrier property. This was because as the dosage of the enzyme product increased, the reduction in antioxidant property owing to cross-linking decreased (see shaded regions in Figure 5.2). There was no significant difference ($p > 0.05$) in the average emulsion drop size between the 10 and 25 mg/mL dosed emulsions (inset in Figure 3.2), thus ruling out the possibility of different interfacial areas for oxygen transfer affecting the oxidation rates. The early stages of milk protein−carbohydrate Maillard reaction had been reported by Calligaris et al.[39] to generate oxidative species. Puscasu and Birlouez-Aragon[40] reported on how intermediary and/or advanced Maillard reaction products formed from milk protein

(α-lactalbumin) and lactose exhibited pro-oxidant property. Albeit scarce, and although the antioxidative property of Maillard reaction products is more widely recognized in general, reports on the pro-oxidant property of milk protein−carbohydrate Maillard reaction products do exist. In Figure 5.2, the increase in absorbance of the boiled-only protein−carbohydrate samples (without the 37 °C incubation) with increasing enzyme product dosage might be attributed to (i) a correspondingly higher formation of pro-oxidant Maillard reaction products and/or (ii) increasing protein−maltodextrin conjugation, leading to lessening solvent accessibility of amino acids with antioxidant activity. Hence, a plausible reason for the decline in emulsion oxidative stability in the 25 mg/mL dosed emulsion was that either or both the aforementioned points started to offset the effect of interfacial barrier resistance to oxygen transfer as a result of greater cross-linking in the interfacial caseinate.

Cross-Linking of Interfacial Caseinate Might Promote Tighter Packing and Hence Enhance Emulsion Oxidative Stability. The influential role of cross-linked interfacial caseinate in improving emulsion oxidative stability, as implied by the results of the ABTS assay on transglutaminase-treated systems, could similarly be inferred when interfacial cross-linking was induced by HPH.

Such a view is substantiated by the works of Lefèvre and Subirade[41] and Lee et al.[34,42] on whey protein adsorbed at the oil/water interface. These authors reported the formation of intermolecular β-sheet, which led to protein aggregation in the interfacial membranes. Lee et al.[34] also detected an increase in intermolecular β-sheet in the interfacial protein of whey protein-stabilized emulsions subjected to higher homogenizing pressure, further demonstrating how HPH could promote condensed interfacial packing that could boost the physical interfacial barrier property against oxidation.

The ability to analyze the density of the HPH-induced interfacial caseinate in situ was met with paramount technical challenge, because the dynamics of conformational behavior accompanying interfacial adsorption during HPH needed to be captured. Neutron scattering and dual polarizing interferometry are both advanced techniques suitable for analyzing the thickness of the interfacial film or the variation of density along the film thickness, but only under static experimental conditions when the film is preformed or immobilized. Molecular dynamics simulations may hold the key to better understanding of the conformational dynamics. The following proposes what might have happened at a higher homogenizing pressure of 20 kpsi as opposed to 5 kpsi, such that it promoted higher emulsion oxidative stability:

For simplicity, sodium caseinate at pH 7 could be molecularly viewed as a polyelectrolyte chain. At 20 kpsi, there was a higher convection rate and thus greater kinetic energy accompanying the turbulence in HPH, which could better overcome the adsorption energy barriers[43] arising from increasing repulsive electrostatic and/or steric interaction forces of protein molecules already adsorbed,[44] whereas free interfacial area continued to diminish. According to the simulation study by Aguilera-Granja and Kikuchi,[45] the polyelectrolyte chains approaching the adsorbent surface experienced such strong electrostatic repulsion that in avoidance they preferentially adsorbed almost as a monolayer with a dominantly high train fraction rather than the loops and tails combined because such a conformation considerably lowered the free energy in the system by exposing hydrophobic functional groups to the oil phase. As such, a tighter packing in the foremost subinterfacial layer to the oil, comprising a higher density of train segments, could be envisioned for HPH at 20 versus 5 kpsi. At sufficiently high surface coverage, the closer local proximity among the train segments could have promoted intermolecular cross-linking and thus led to the analytical ultracentrifugation finding of more interfacial protein oligomers of higher species during HPH at 20 kpsi. The postulated denser subinterfacial layer of train segments probably provided additional resistance to oxygen diffusion from the continuous phase to the oil, thus increasing the physical interfacial barrier property against oxidation. Furthermore, densification of a β-casein cross-linked adsorbed onto polystyrene beads was recently reported by Partanen et al.[46]

AUTHOR INFORMATION

Corresponding Author

*(M.F.S.M.G.) E-mail: msanmart@purdue.edu. Phone: +1 (765) 496-1140. Fax: +1 (765) 494-7953.

Present Addresses

§(P.Y.P.) Sensient Flavors LLC, 5600 W. Raymond St., Indianapolis, IN 46241, USA.

⊗(J.W.B.) 3024 Newquay Lane, Richmond, VA 23236, USA.

Notes

The authors declare no competing financial interest.

ACKNOWLEDGMENTS

The authors would like to thank Ajinomoto North America, Inc., for providing the transglutaminase enzyme used in this study.

REFERENCES

(1) Dickinson, E.; Rolfe, S. E.; Dalgleish, D. G. Competitive adsorption of α_{s1}-casein and β-casein in oil-in-water emulsions. *Food Hydrocolloids* **1988**, *265*, 395−405.

(2) Dickinson, E. Properties of emulsions stabilized with milk proteins: overview of some recent developments. *J. Dairy Sci.* **1997**, *80*, 2607−2619.

(3) Allen, J. C.; Wrieden, W. L. Influence of milk-proteins on lipid oxidation in aqueous emulsion: I. Casein, whey protein and α-lactalbumin. *J. Dairy Res.* **1982**, *49*, 239−248.

(4) Hu, M.; McClements, D. J.; Decker, E. A. Lipid oxidation in corn oil-in-water emulsions stabilized by casein, whey protein isolate, and soy protein isolate. *J. Agric. Food Chem.* **2003**, *51*, 1696−1700.

(5) Faraji, H.; McClements, D. J.; Decker, E. A. Role of continuous phase protein on the oxidative stability of fish oil-in-water emulsions. *J. Agric. Food Chem.* **2004**, *52*, 4558−4564.

(6) Horn, A. F.; Nielsen, N. S.; Jensen, L. S.; Horsewell, A.; Jacobsen, C. The choice of homogenisation equipment affects lipid oxidation in emulsions. *Food Chem.* **2012**, *134*, 803−810.

(7) Ho, B. *Water Vapour Permeabilities and Structural Characteristics of Casein Films and Casein-Lipid Emulsion Films*. M.S. thesis, University of California, Davis, CA, 1992.

(8) Yang, L.; Paulson, A. T. Effects of lipids on mechanical and moisture barrier properties of edible gellan film. *Food Res. Int.* **2000**, *33*, 571−578.

(9) Kuraishi, C.; Yamazaki, K.; Susa, Y. Transglutaminase: its utilization in the food industry. *Food Rev. Int.* **2001**, *17*, 221−246.

(10) Dickinson, E.; Yamamoto, Y. Rheology of milk protein gels and protein-stabilized emulsion gels cross-linked with transglutaminase. *J. Agric. Food Chem.* **1996**, *44*, 1371−1377.

(11) Faergemand, M.; Murray, B. S.; Dickinson, E. Cross-linking of milk proteins with transglutaminase at the oil-water interface. *J. Agric. Food Chem.* **1998**, *45*, 2514−2519.

(12) Ma, H.; Forssell, P.; Kylli, P.; Lampi, A. M.; Buchert, J.; Boer, H.; Partanen, R. Transglutaminase catalyzed cross-linking of sodium caseinate improves oxidateive stability of flaxseed oil emulsion. *J. Agric. Food Chem.* **2012**, *60*, 6223−6229.
(13) Kellerby, S. S.; Gu, Y. S.; McClements, D. J.; Decker, E. Lipid oxidation in a menhaden oil-in-water emulsion stabilized by sodium caseinate cross-linked with transglutaminase. *J. Agric. Food Chem.* **2006**, *54*, 10222−10227.
(14) Schuck, P. On the analysis of protein self-association by sedimentation velocity analytical ultracentrifugation. *Anal. Biochem.* **2003**, *320*, 104−124.
(15) Schuck, P.; Perugini, M. A.; Gonzales, N. R.; Howlett, G. J.; Schubert, D. Size-distribution analysis of proteins by analytical ultracentrifugation: strategies and application to model systems. *Biophys. J.* **2002**, *82*, 1096−1111.
(16) Kulkarni, A. R.; Soppimath, K. S.; Aminabhavi, T. M. Effect of cosolvent and non-ionic surfactant on partition coefficient of *Azadirachta indica* A. Juss. (neem) seed oil in water-hexane at (298.15, 303.15, 308.15, and 313.15) K. *J. Chem. Eng. Data* **2000**, *45*, 75−77.
(17) Ogawa, S.; Decker, E. A.; McClements, D. J. Influence of environmental conditions on the stability of oil in water emulsions containing droplets stabilized by lecithin-chitosan membranes. *J. Agric. Food Chem.* **2003**, *51*, 5522−5527.
(18) Phoon, P. Y.; Narsimhan, G.; San Martin-Gonzalez, M. F. Effect of thermal behaviour of β-lactoglobulin on the oxidative stability of menhaden oil-in-water emulsions. *J. Agric. Food Chem.* **2013**, *61*, 1954−1967.
(19) Thomas, J. C. The determination of log normal particle size distributions by dynamic light scattering. *J. Colloid Interface Sci.* **1986**, *117*, 187−192.
(20) Cohn, E. J.; Edsall, J. T. *Proteins, Amino Acids and Peptides as Ions and Dipolar Ions*; Reinhold: New York, 1943; Chapter 4, p 157.
(21) Laue, T. M.; Shah, B. D.; Ridgeway, T. M.; Pelletier, S. L. *Analytical Ultracentrifugation in Biochemistry and Polymer Science*; Royal Society of Chemistry: London, UK, 1992; pp 90−125.
(22) Schuck, P. Size distribution analysis of macromolecules by sedimentation velocity ultracentrifugation and Lamm equation modeling. *Biophys. J.* **2000**, *78*, 1606−1619.
(23) Schuck, P.; MacPhee, C. E.; Howlett, G. J. Determination of sedimentation coefficients for small peptides. *Biophys. J.* **1998**, *74*, 466−474.
(24) Brown, P. H.; Schuck, P. A new adaptive grid-size algorithm for the simulation of sedimentation velocity profiles in analytical ultracentrifugation. *Comput. Phys. Commun.* **2007**, *178*, 105−120.
(25) Moure, A.; Domínguez, H.; Parajó, J. C. Antioxidant properties of ultrafiltration-recovered soy protein fractions from industrial effluents and their hydrolysates. *Process Biochem.* **2006**, *41*, 447−456.
(26) Lethuaut, L.; Métro, F.; Genot, C. Effect of droplet size on lipid oxidation rates of oil-in-water emulsions stabilized by protein. *J. Am. Oil Chem. Soc.* **2002**, *79*, 425−430.
(27) Let, M. B.; Jacobsen, C.; Sørensen, A. D. M.; Meyer, A. S. Homogenization conditions affect the oxidative stability of fish oil enriched milk emulsions: lipid oxidation. *J. Agric. Food Chem.* **2007**, *55*, 1773−1780.
(28) Ries, D.; Ye, A.; Haisman, D.; Singh, H. Antioxidant properties of caseins and whey proteins in model oil-in-water emulsions. *Int. Dairy J.* **2010**, *20*, 72−78.
(29) Tornberg, E. Functional characterisation of protein stabilised emulsions: emulsifying behaviour of proteins in a valve homogenizer. *J. Sci. Food Agric.* **1978**, *29*, 867−879.
(30) Caldwell, K. D.; Li, J.; Li, J.-T.; Dalgleish, D. G. Adsorption behaviour of milk proteins on polystyrene latex: a study based on sedimentation field-flow fractionation and dynamic light scattering. *J. Chromatogr., A* **1992**, *604*, 63−71.
(31) Leaver, J. D.; Brooksbank, D. V.; Horne, D. S. Influence of glycosylation and surface charge on the binding of κ-casein to latex particles. *J. Colloid Interface Sci.* **1994**, *162*, 463−469.
(32) Helstad, K. M. *Nanorheological Studies of Caseins*. Ph.D. thesis, Lund University, Lund, Sweden, 2007.
(33) Kuhn, K. R.; Cunha, R. L. Flaxseed oil−whey protein isolate emulsions: effect of high pressure homogenization. *J. Food Eng.* **2012**, *111*, 449−457.
(34) Lee, S.-H.; Lefèvre, T.; Subirade, M.; Paquin, P. Effects of ultra-high pressure homogenization on the properties and structure of interfacial protein layer in whey protein-stabilized emulsion. *Food Chem.* **2009**, *113*, 191−195.
(35) Anema, S. G.; Lowe, E. K.; Stockman, R. Particle size changes and casein solubilization in high-pressure treated skim milk. *Food Hydrocolloids* **2005**, *19*, 257−267.
(36) Folk, J. E.; Finlayson, J. S. The ε-(γ-glutamyl) lysine crosslink and the catalytic role of transglutaminases. *Adv. Protein Chem.* **1977**, *31*, 1−133.
(37) Kellerby, S. S.; Gu, Y. S.; McClements, D. J.; Decker, E. A. Lipid oxidation in a menhaden oil-in-water emulsion stabilized by sodium caseinate cross-linked with transglutaminase. *J. Agric. Food Chem.* **2006**, *54*, 10222−10227.
(38) Bao, S.-S.; Hu, X.-C.; Zhang, K.; Xu, X.-K.; Zhang, H.-M.; Huang, H. Characterization of spray-dried microalgal oil encapsulated in cross-linked sodium caseinate matrix induced by microbial transglutaminase. *J. Food Sci.* **2011**, *76*, E112−E118.
(39) Calligaris, S.; Manzocco, L.; Anese, M.; Nicoli, M. C. Effect of heat-treatment on the antioxidant and pro-oxidant activity of milk. *Int. Dairy J.* **2004**, *14*, 421−427.
(40) Puscasu, C.; Birlouez-Aragon, I. Intermediary and/or advanced Maillard products exhibit prooxidant activity on Trp: in vitro study on α-lactalbumin. *Food Chem.* **2002**, *78*, 399−406.
(41) Lefèvre, T.; Subirade, M. Formation of intermolecular β-sheet structures: a phenomenon relevant to protein film structure at oil-water interfaces of emulsions. *J. Colloid Interface Sci.* **2003**, *263*, 59−67.
(42) Lee, S.-H.; Lefèvre, T.; Subirade, M.; Paquin, P. Changes and roles of secondary structures of whey protein for the formation of protein membrane at soy oil/water interface under high-pressure homogenization. *J. Agric. Food Chem.* **2007**, *55*, 10924−10931.
(43) McClements, D. J. *Food Emulsions: Principles, Practices, and Techniques*, 2nd ed.; CRC Press: Boca Raton, FL, USA, 2004; p 190.
(44) Mohan, S.; Narsimhan, G. Coalescence of protein-stabilized emulsions in a high-pressure homogenizer. *J. Colloid Interface Sci.* **1997**, *192*, 1−15.
(45) Aguilera-Granja, F.; Kikuchi, R. Polymer statistics IV. Simulation of adsorption of polymers and polyelectrolytes on surfaces. *Physica A* **1992**, *189*, 108−126.
(46) Partanen, R.; Forssell, P.; Mackie, A.; Blomberg, E. Interfacial cross-linking of β-casein changes the structure of the adsorbed layer. *Food Hydrocolloids* **2013**, *32*, 271−277.

polymerase (PARP), and GAPDH were purchased from Cell Signaling Technology, Inc. (Danvers, MA, USA). The antibody against cyclin E was obtained from Santa Cruz Biotechnology (Dallas, TX, USA). Other chemicals and reagents were of high quality and obtained from commercial sources.

Heat-Processing of Ginsenoside Re. Ginsenoside Re was steamed at 120 °C for 3 h using an autoclave as reported previously.[12,13] The reaction was conducted in aqueous solution to contain approximately 5 mM ginsenoside Re. After drying at 50 °C for 3 days, untreated and heat-processed ginsenoside Re at 120 °C were prepared.

Analysis of Ginsenosides. Untreated and heat-processed ginsenoside Re were weighed (10 mg) and completely dissolved in 1 mL of 50% methanol and then filtered through a 0.45 μm syringe filter for high-performance liquid chromatography (HPLC) analysis. The analytical reversed-phase HPLC system consisted of a solvent degasser (Agilent, G1322A), binary pump (Agilent, G1312C), an autosampler (Agilent, G1329B), and model ZAM 3000 evaporative light scattering detector (ELSD) (Young Lin, South Korea). ELSD conditions were optimized in order to achieve maximum sensitivity: temperature of the nebulizer was set for 50 °C, and N_2 was used as the nebulizing gas at a pressure of 2.0 bar. A Phenomenex Luna C18 column (150 × 4.6 mm, 5 μm) was used, and the mobile phase consisted of a binary gradient of solvent A (acetonitrile:water:5% acetic acid in water = 15:80:5) and solvent B (acetonitrile:water = 80:20) at a flow rate of 1.0 mL/min. The gradient flow program was as follows: initial; 0% B, 6 min; 30% B, 18 min; 50% B, 30 min; 100% B. Ginsenosides were identified by the comparison of retention times with those of standard samples. The standard solutions containing 1−50 μg of each ginsenoside were injected into the HPLC, and all calibration curves showed good linearity (R^2 > 0.995). The analysis was repeated two times for the verification of repeatability.

Antiproliferative Effect on Gastric Cancer Cells. The human gastric cancer AGS cell line was purchased from the American Type Culture Collection (ATCC, Manassas, VA, USA). The cells were grown in RPMI1640 medium (Cellgro, Manassas, VA, USA) supplemented with 10% fetal bovine serum (Gibco BRL, Carlsbad, MD, USA), 100 units/mL penicillin, and 100 μg/mL streptomycin and incubated at 37 °C in a humidified atmosphere with 5% CO_2. AGS cells were treated with different concentrations of compounds for 24 h, and cell proliferation was measured using the Cell Counting Kit-8 (CCK-8, Dojindo Laboratories, Japan) according to the manufacturer's recommendations. CCK-8 allows sensitive assays by utilizing the highly water-soluble tetrazolium salt, WST-8, which is reduced by dehydrogenase activities in cells to give a yellow-color formazan dye, which is soluble in the tissue culture media. The amount of the formazan dye, generated by the activities of dehydrogenases in cells, is directly proportional to the number of living cells. Briefly, cells seeded in 96-well plates were treated with various concentrations of compounds. After incubation for the indicated times, 10 μL of CCK-8 reagent was added to each well. Cell proliferation was assessed by scanning with a microplate reader at 450 nm.

Hoechst Staining. Cells in 6-well plates were treated with the indicated compounds and incubated for 24 h at 37 °C. After the cells were washed twice with cold PBS, the cells were then incubated with 1 μg/mL Hoechst 33342 (Sigma-Aldrich, St. Louis, MO, USA) for 15 min in the dark at 37 °C before image acquisition. Stained cells were subsequently examined using an inverted fluorescence microscope.

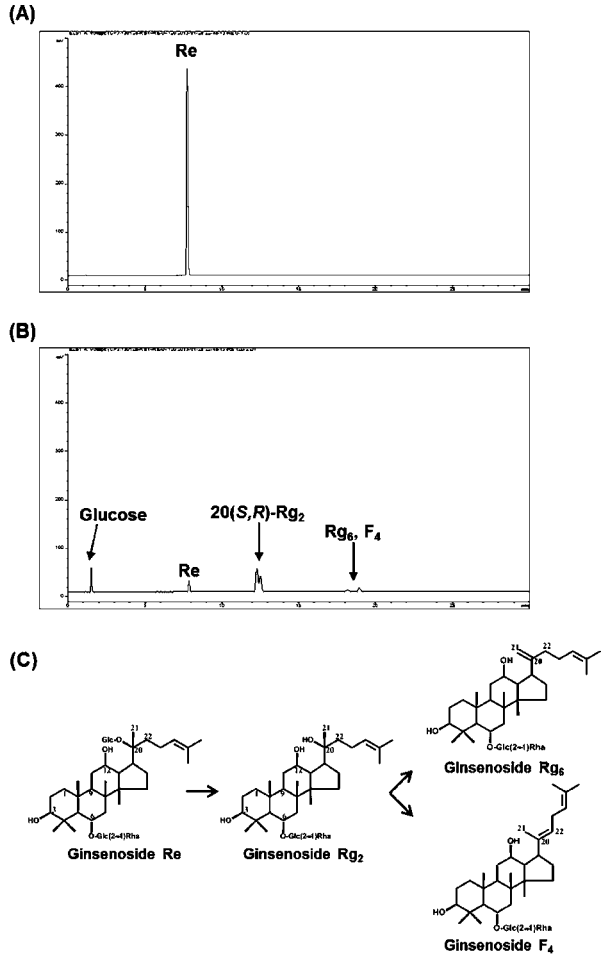

Figure 1. Comparison in the HPLC chromatograms of ginsenoside Re before and after heat-processing at 120 °C. (A) HPLC chromatogram of ginsenoside Re before heat-processing. (B) HPLC chromatogram of ginsenoside Re after heat-processing. (C) Proposed reaction scheme for the heat-treatment of ginsenoside Re. -Glc: D-glucopyranosyl. -Rha: L-rhamnopyranosyl.

Flow Cytometric Assay. To detect changes in cell cycle distribution, the treated cells were collected, washed with cold PBS, and fixed in 70% ethanol at 4 °C for 30 min. The cells were then washed twice with PBS and resuspended in 500 μL of a propidium iodide (PI) staining solution containing 40 μg/mL PI and 20 μg/mL RNase A in PBS. Then, the cells were incubated at room temperature for 30 min in the dark and analyzed with a FACSCalibur flow cytometer (Becton-Dickinson, San Jose, CA, USA) and the ModFit LT V2.0 computer program. Apoptotic cell death was assessed by annexin-V/PI double staining using an Annexin-V-FLUOS Staining Kit (Roche, Penzberg, Germany) according to the manufacturer's recommendations. At least 20,000 events were evaluated in each experiment.

Caspase Activity Assay. Caspase-3, -8, and -9 activities were determined by using caspase-3, -8, and -9 fluorometric assay kits according to the protocol of the manufacturer (BioVison, Milpitas, CA, USA). In brief, a total of 1.6 × 10^6 cells were seeded in 100 mm dishes and incubated for 24 h at 37 °C. Heat-processed ginsenoside Re at 40 and 80 μg/mL and ginsenoside Rg6/F4 mixture at 50 μg/mL were directly added to the dishes and incubated for an additional 24 h. In order to examine the possible effects of ginsenoside on caspase-dependent apoptosis, AGS cells were also pretreated with 50 μM Z-VAD-fmk

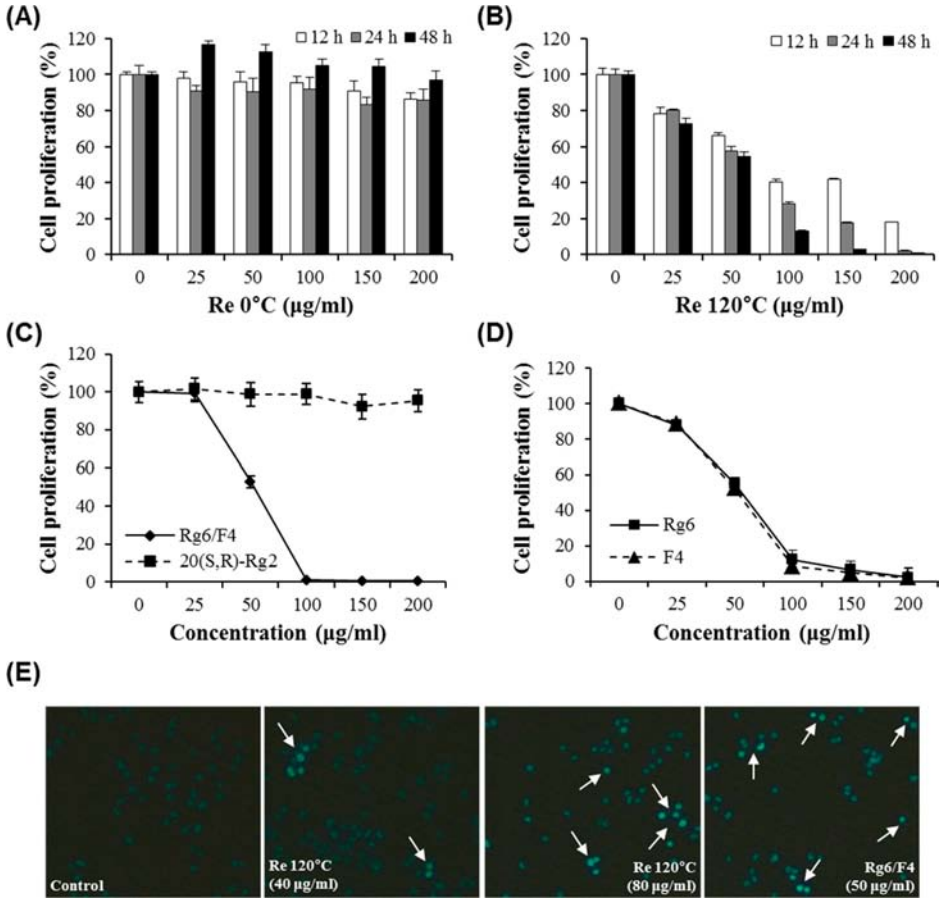

Figure 2. Changes in effects of ginsenoside Re upon heat-processing on AGS cell proliferation. AGS cells were treated with the indicated concentrations of ginsenoside Re (A) and heat-processed ginsenoside Re (B) for 12, 24, and 48 h, and cell proliferation was examined by CCK-8 assay. (C) AGS cells were treated with the indicated concentrations of ginsenosides 20(*S*,*R*)-Rg2 and Rg6/F4 mixtures for 24 h, and cell proliferation was examined by CCK-8 assay. (D) AGS cells were treated with the indicated concentrations of ginsenosides Rg6 and F4 for 24 h, and cell proliferation was examined by CCK-8 assay. (E) AGS cells were treated with the indicated concentrations of heat-processed ginsenoside Re for 24 h, and subjected to Hoechst staining assay. Apoptotic cells (bright blue fluorescent) are indicated with a white arrow. Each value represents the mean ± SEM of three independent experiments.

(pan-caspase inhibitor) for 2 h prior to ginsenoside treatment. The cells (1.0×10^6 cells) were lysed in the supplied 50 μL of lysis buffer and incubated for 10 min in an ice bath. Then, 50 μL of 10 mM dithiothreitol 2× reaction buffer and 5 μL of the 1 mM substrates for caspase-3, -8, and -9 were added to each of the lysed samples and incubated for an additional 1.5 h at 37 °C. Subsequently, caspase activities were measured by comparing relative fluorescent intensities using a Tecan Infinite M1000 plate reader (Männedorf, Switzerland) equipped with a 400 nm excitation filter and 505 nm emission filter.

Western Blotting Analysis. AGS cells (8×10^5 cells) were grown in 60 mm dishes and treated with heat-processed ginsenoside Re at 40 and 80 μg/mL and ginsenoside Rg6/F4 mixture at 50 μg/mL for 24 h. Whole-cell extracts were then prepared according to the manufacturer's instructions using RIPA buffer (Cell Signaling, MA, USA) supplemented with 1× protease inhibitor cocktail and 1 mM phenylmethylsulfonyl fluoride (PMSF). Proteins (whole-cell extracts, 30 μg/lane) were separated by electrophoresis in a precast 4−15% Mini-PROTEAN TGX gel (Bio-Rad, Hercules, CA, USA) blotted onto PVDF transfer membranes and analyzed with epitope-specific primary and secondary antibodies. Bound antibodies were visualized using ECL Advance Western Blotting Detection Reagents (GE Healthcare, U.K.) and a LAS 4000 imaging system (Fujifilm, Japan).

Statistical Analysis. Statistical significance was determined through one-way analysis of variance (ANOVA) followed by a multiple comparison test with a Bonferroni adjustment. *P* values of less than 0.05 were considered statistically significant.

RESULTS AND DISCUSSION

Anticancer effects of several ginsenosides have been identified. In particular, diol type ginsenosides were shown to trigger apoptotic cell death.[21] Ginsenoside Rg3 induces senescence-like growth arrest in human glioma cancer through Akt, which is associated with increased ROS levels and p53/p21-dependent signaling pathways.[22] Ginsenoside Rg3 and Rh2 have also been known to induce apoptosis by the activation of caspase-3 and Bax protein, inhibition of Bcl-2 protein, and production of intracellular ROS in human hepatocellular carcinoma cells.[16] Ginsenoside Rg5 blocks the cell cycle of human hepatoma SK-HEP-1 cells via downregulation of cyclin E-dependent kinase activity.[14] In addition, ginsenoside F2 has been reported to induce apoptosis in breast cancer stem cells by activating the intrinsic apoptotic pathway and mitochondrial dysfunction.[23] However, apart from our previously published investigation, there is no report of positive evidence to show antiproliferative efficacy of ginsenosides Rg6 and/or F4.[24]

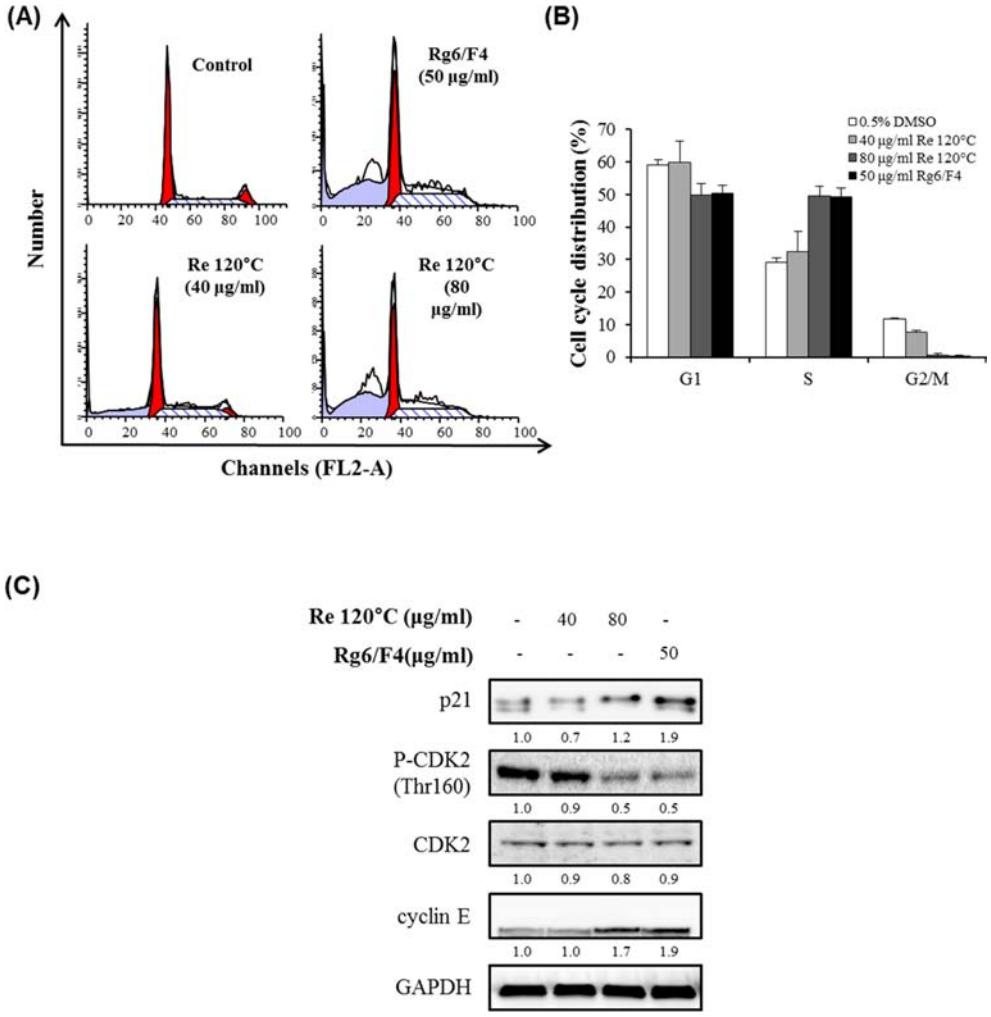

Figure 3. Effects of heat-processed ginsenoside Re and ginsenoside Rg6/F4 mixtures on AGS cell cycle. (A, B) AGS cells were treated with the indicated concentrations of heat-processed ginsenoside Re and ginsenoside Rg6/F4 mixtures for 24 h, and FACS analysis/PI staining was then performed to assess cell cycle distribution. Each value represents the mean ± SEM of three independent experiments. (C) The protein levels of p21, p-CDK2, CDK2, and cyclin E were detected by Western blot analysis using their respective antibodies. GAPDH was used as an internal control. A representative immunoblot of three independent experiments is shown. Density ratios over GAPDH were measured by densitometer.

Figure 1 shows HPLC chromatograms comparing ginsenoside Re before and after heat-processing at 120 °C. Native ginsenoside Re (1000.0 μg/mL) was detected at about 7.8 min (Figure 1A). Following heat treatment, the peak of ginsenoside Re (52.1 μg/mL) decreased, and the peaks of ginsenoside 20(*S*)-Rg2 (168.9 μg/mL), 20(*R*)-Rg2 (125.4 μg/mL), Rg6 (20.7 μg/mL), and F4 (35.4 μg/mL) appeared (Figure 1B). Therefore, we can deduce that ginsenoside Re was transformed into ginsenosides 20(*S*,*R*)-Rg2, Rg6, and F4 by heat-processing (Figure 1C).

Figures 2A and 2B show a comparison of antiproliferative effects of ginsenoside Re and heat-processed ginsenoside Re at 120 °C in AGS cells. Heat-processed ginsenoside Re was found to significantly suppress cell proliferation in a dose- and time-dependent manner, whereas ginsenoside Re had no effect up to 48 h. Because of evident cytotoxicity at 24 h by heat-processed ginsenoside Re (IC_{50}: 79 μg/mL), we pursued the following experiments at this time point. Figure 2C shows the comparison of antiproliferative effects of ginsenosides 20(*S*,*R*)-Rg2 and ginsenoside Rg6/F4 mixtures. The ginsenoside Rg6/F4 mixture strongly suppressed cell proliferation in a dose-dependent manner (IC_{50}: 49 μg/mL), but ginsenosides 20(*S*,*R*)-Rg2 had no effect (IC_{50} > 200 μg/mL). Ginsenosides Rg6 and F4 exhibited almost the same cytotoxic effect against AGS cells (IC_{50}: 49 μg/mL) (Figure 2D) and less cytotoxic activity against normal porcine kidney proximal tubular epithelial LLC-PK1 cells (IC_{50}: 96 μg/mL). As shown in Figure 2E, changes in apoptosis (nuclear pyknosis and chromatin condensation) were observed under a fluorescence microscope. The number of apoptotic cells, displayed with bright blue fluorescence, was also increased after treatments with heat-processed ginsenoside Re and ginsenoside Rg6/F4 mixtures (Figure 2E).

The effects of heat-processed ginsenoside Re and ginsenoside Rg6/F4 mixture on the cell cycle distribution at 24 h are shown in Figures 3A and 3B. The population of cells in S phase was increased by treatment with heat-processed Re at 40 and 80 μg/mL in a dose-dependent manner (32.5 ± 6.29 and 49.6 ± 2.99% versus 29.1 ± 1.30%). Ginsenoside Rg6/F4 mixture at 50 μg/mL also promoted similar accumulation of cells in S phase to heat-processed ginsenoside Re (49.4 ± 2.57% versus 29.1 ± 1.30%). During S phase, active CDK2−cyclin E complexes predominate and require phosphorylation of CDK2 at Thr160.[25] Inhibition of CDK2−cyclin E complexes can also be attributed to association with p27 and p21.[26] As shown in Figure 3C,

dx.doi.org/10.1021/jf5000776 | J. Agric. Food Chem. 2014, 62, 2830−2836

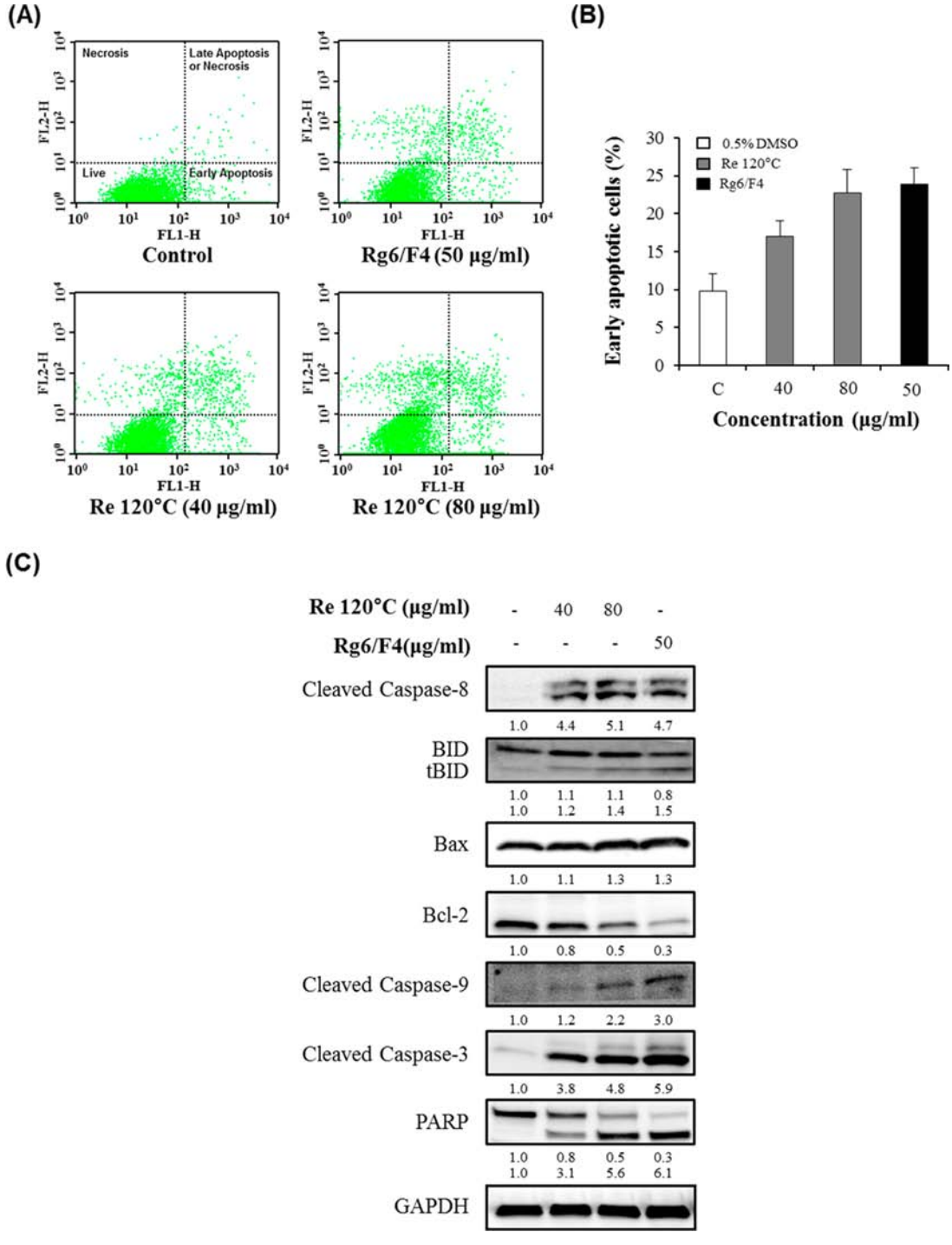

Figure 4. Effects of heat-processed ginsenoside Re and ginsenoside Rg6/F4 mixtures on apoptosis in AGS cells. (A, B) AGS cells were treated with the indicated concentrations of heat-processed ginsenoside Re and ginsenoside Rg6/F4 mixtures for 24 h, and FACS analysis/AV-PI double-staining was then performed to assess apoptotic cell death. Each value represents the mean ± SEM of three independent experiments. (C) The protein levels of cleaved caspase-8, BID, Bax, Bcl-2, cleaved caspase-9, cleaved caspase-3, and PARP were detected by Western blot analysis using their respective antibodies. GAPDH was used as an internal control. A representative immunoblot of three independent experiments is shown. Density ratios over GAPDH were measured by densitometer.

heat-processed ginsenoside Re and ginsenoside Rg6/F4 mixture elevated p21 and cyclin E protein levels and inhibited phosphorylation of CDK2 at Thr160. Consequently, both of them induced p21-mediated S phase arrest.

Exposure to heat-processed ginsenoside Re and ginsenoside Rg6/F4 mixture resulted in significant apoptosis (Figures 4A and 4B). Heat-processed ginsenoside Re at 40 and 80 μg/mL caused 17.0 ± 2.08% and 22.8 ± 3.01% early apoptotic cell populations, respectively, compared with control value showing 9.7 ± 2.29. Ginsenoside Rg6/F4 mixture at 50 μg/mL also promoted similar induction of apoptosis to heat-processed ginsenoside Re (23.8 ± 2.25% versus 9.7 ± 2.29%). Since apoptosis is one of the mechanisms by which cells undergo death, we also confirmed the molecular mechanisms of

dx.doi.org/10.1021/jf5000776 | J. Agric. Food Chem. 2014, 62, 2830−2836

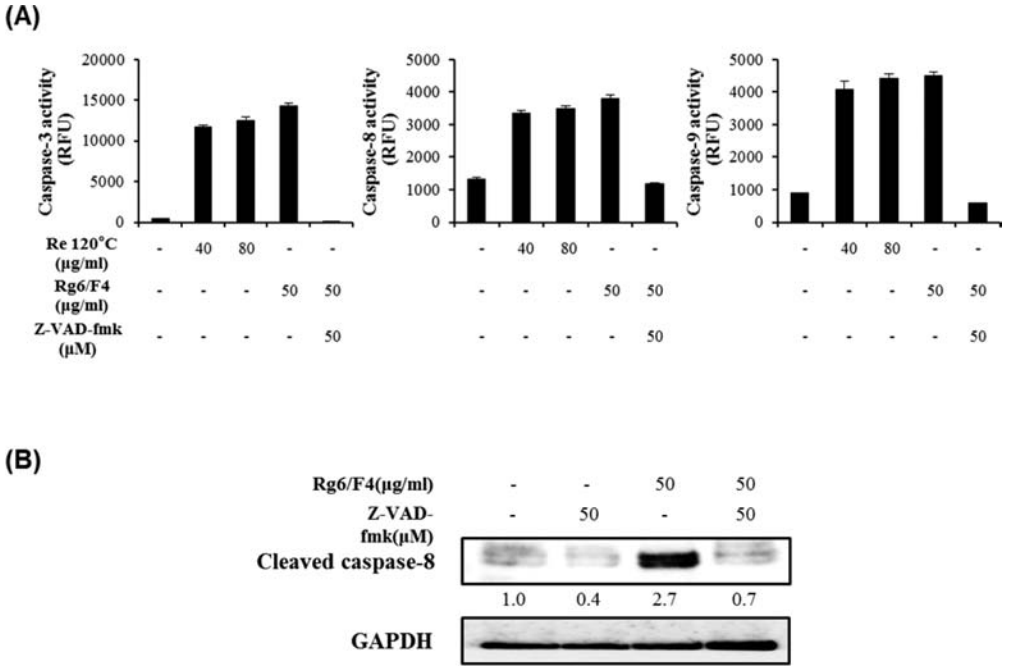

Figure 5. Involvement of caspases in the heat-processed ginsenoside Re and ginsenoside Rg6/F4 mixture-induced apoptosis in AGS cells. (A) AGS cells were pretreated with or without 50 μM Z-VAD-fmk for 2 h, followed by exposure to the indicated concentrations of heat-processed products of ginsenoside Re for 24 h, and the activity levels of caspase-3, -8, and -9 were then estimated. Each value represents the mean ± SEM of three independent experiments. (B) AGS cells were pretreated with or without 50 μM Z-VAD-fmk for 2 h, followed by exposure to 50 μg/mL ginsenoside Rg6/F4 mixtures for 24 h, and the protein level of cleaved caspase-8 was detected by Western blot analysis using its respective antibody. GAPDH was used as an internal control. A representative immunoblot of three independent experiments is shown. Density ratios over GAPDH were measured by densitometer.

apoptotic effects by Western blotting. Western blotting results on the protein levels related to caspases and apoptosis are shown in Figure 4C. Treatment of heat-processed ginsenoside Re and ginsenoside Rg6/F4 mixture increased the level of cleaved caspase-8. While the level of full-length BID (22 kDa) gradually decreased, the level of the active form of tBID (15 kDa) increased after treatment with heat-processed ginsenoside Re and ginsenoside Rg6/F4 mixture. The level of proapoptotic protein Bax was slightly increased by treatment with ginsenoside Rg6/F4 mixture, but the level of antiapoptotic protein Bcl-2 markedly decreased by the same condition. Protein levels of cleaved caspase-9 and -3 increased after treatment with heat-processed ginsenoside Re and ginsenoside Rg6/F4 mixtures. The level of full-length PARP (116 kDa) decreased, whereas the level of cleaved PARP (89 kDa) increased by treatment with heat-processed ginsenoside Re and ginsenoside Rg6/F4 mixtures.

Histograms in Figure 5A show the effect of the pan-caspase inhibitor Z-VAD-fmk on cell proliferation to further confirm the role played by caspases in ginsenoside Rg6/F4 mixture-induced apoptosis. The activities of caspase-3, caspase-8, and caspase-9 were significantly increased by treatment with the products of heat-processed ginsenoside Re and ginsenoside Rg6/F4 mixture. However, Z-VAD-fmk completely inhibited ginsenoside Rg6/F4 mixture-induced caspase activity to near basal levels. As shown in Figure 5B, pretreatment with Z-VAD-fmk completely suppressed the cleavage of caspase-8 by ginsenoside Rg6/F4.

In the present study, we investigated the anticancer effects of heat-processed ginsenoside Re on AGS human gastric cancer cells. Ginsenoside Re was transformed into less-polar ginsenosides, namely, Rg2, Rg6, and F4 by heat-processing. Among them, we discovered that ginsenosides Rg6 and F4 have

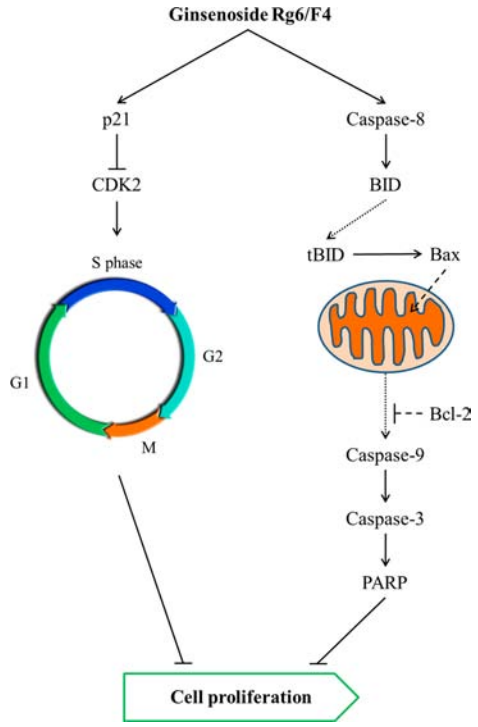

Figure 6. Schematic description of the anticancer mechanism of ginsenoside Rg6 and F4 in AGS cells.

anticancer activity through p21-mediated S phase arrest and caspase-dependent apoptosis (Figure 6). The present study provides a new insight on the mechanism of beneficial effects of heat-processed ginseng on gastric cancer.

dx.doi.org/10.1021/jf5000776 | J. Agric. Food Chem. 2014, 62, 2830−2836

AUTHOR INFORMATION

Corresponding Author

*K.S.K.: phone, 82-31-750-5402; fax, 82-31-750-5416; e-mail, kkang@gachon.ac.kr. D.-W.E.: phone, 82-33-651-3428; fax, 82-33-610-3430; e-mail, edwjyh@gnah.co.kr.

Author Contributions

‡H.-J.J. and I.-H.H. contributed equally to the work described in this study.

Funding

This research was carried out with the support of the Korea Institute of Science and Technology institutional program (2Z04210). This research was also funded by Gangneung Asan Hospital Biomedical Research Center Promotion Fund.

Notes

The authors declare no competing financial interest.

REFERENCES

(1) Ferlay, J.; Shin, H. R.; Bray, F.; Forman, D.; Mathers, C.; Parkin, D. M. Estimates of worldwide burden of cancer in 2008: GLOBOCAN 2008. *Int. J. Cancer* **2010**, *127*, 2893−2917.

(2) Hou, I. C.; Amarnani, S.; Chong, M. T.; Bishayee, A. Green tea and the risk of gastric cancer: Epidemiological evidence. *World J. Gastroenterol.* **2013**, *19*, 3713−3722.

(3) Jain, V. K.; Cunningham, D.; Rao, S. Chemotherapy for operable gastric cancer: current perspectives. *Indian J. Surg. Oncol.* **2011**, *2*, 334−342.

(4) Wargovich, M. J.; Morris, J.; Brown, V.; Ellis, J.; Logothetis, B.; Weber, R. Nutraceutical use in late-stage cancer. *Cancer Metastasis Rev.* **2010**, *29*, 503−510.

(5) Aggarwal, B. B.; Bhardwaj, A.; Aggarwal, R. S.; Seeram, N. P.; Shishodia, S.; Takada, Y. Role of resveratrol in prevention and therapy of cancer: preclinical and clinical studies. *Anticancer Res.* **2004**, *24*, 2783−2840.

(6) Horie, N.; Hirabayashi, N.; Takahashi, Y.; Miyauchi, Y.; Taguchi, H.; Takeishi, K. Synergistic effect of green tea catechins on cell growth and apoptosis induction in gastric carcinoma cells. *Biol. Pharm. Bull.* **2005**, *28*, 574−579.

(7) Riles, W. L.; Erickson, J.; Nayyar, S.; Atten, M. J.; Attar, B. M.; Holian, O. Resveratrol engages selective apoptotic signals in gastric adenocarcinoma cells. *World J. Gastroenterol.* **2006**, *12*, 5628−5634.

(8) Kamangar, F.; Gao, Y. T.; Shu, X. O.; Kahkeshani, K.; Ji, B. T.; Yang, G.; Li, H. L.; Rothman, N.; Chow, W. H.; Zheng, W. Ginseng intake and gastric cancer risk in the Shanghai Women's Health Study cohort. *Cancer Epidemiol. Biomarkers Prev.* **2007**, *16*, 629−630.

(9) Yun, T. K.; Choi, S. Y. A case-control study of ginseng intake and cancer. *Int. J. Epidemiol.* **1990**, *19*, 871−876.

(10) Yun, T. K.; Choi, S. Y. Preventive effect of ginseng intake against various human cancers: a case-control study on 1987 pairs. *Cancer Epidemiol. Biomarkers Prev.* **1995**, *4*, 401−408.

(11) Yun, T. K.; Choi, S. Y. Non-organ specific cancer prevention of ginseng: a prospective study in Korea. *Int. J. Epidemiol.* **1998**, *27*, 359−364.

(12) Lee, W.; Park, S. H.; Lee, S.; Chung, B. C.; Song, M. O.; Song, K. I.; Ham, J.; Kim, S. N.; Kang, K. S. Increase in antioxidant effect of ginsenoside Re-alanine mixture by Maillard reaction. *Food Chem.* **2012**, *135*, 2430−2435.

(13) Yamabe, N.; Kim, Y. J.; Lee, S.; Cho, E. J.; Park, S. H.; Ham, J.; Kim, H. Y.; Kang, K. S. Increase in antioxidant and anticancer effects of ginsenoside Re-lysine mixture by Maillard reaction. *Food Chem.* **2013**, *138*, 876−883.

(14) Lee, K. Y.; Lee, Y. H.; Kim, S. I.; Park, J. H.; Lee, S. K. Ginsenoside-Rg5 suppresses cyclin E-dependent protein kinase activity via up-regulating p21Cip/WAF1 and down-regulating cyclin E in SK-HEP-1 cells. *Anticancer Res.* **1997**, *17*, 1067−1072.

(15) Lee, J. G.; Baek, S. H.; Lee, Y. Y.; Park, S. Y.; PARK, J. H. Anti-complementary Ginsenosides Isolated from Processed Ginseng. *Biol. Pharm. Bull.* **2011**, *34*, 898−900.

(16) Park, H. M.; Kim, S. J.; Kim, J. S.; Kang, H. S. Reactive oxygen species mediated ginsenoside Rg3- and Rh2-induced apoptosis in hepatoma cells through mitochondrial signaling pathways. *Food Chem. Toxicol.* **2012**, *50*, 2736−2741.

(17) Kim, S. J.; Kim, J. D.; Ko, S. K. Changes in ginsenoside composition of ginseng berry extracts after a microwave and vinegar process. *J. Ginseng Res.* **2013**, *37*, 269−272.

(18) Shih, P. H.; Yeh, C. T.; Yen, G. C. Effects of anthocyanidin on the inhibition of proliferation and induction of apoptosis in human gastic adenocarcinoma cells. *Food Chem. Toxicol.* **2005**, *43*, 1557−1566.

(19) Barranco, S. C.; Townsend, C. M., Jr.; Casartelli, C.; Macik, B. G.; Burger, N. L.; Boerwinkle, W. R.; Gourley, W. K. Establishment and characterization of an in vitro model system for human adenocarcinoma of the stomach. *Cancer Res.* **1983**, *43*, 1703−1709.

(20) Liu, J. D.; Lin, S. Y.; Ho, Y. S.; Pan, S.; Hung, L. F.; Tsai, S. H.; Lin, J. K.; Liang, Y. C. Involvement of c-jun N-terminal kinase activation in 15-deoxy-delta12, 14-prostaglandin J2 and prostaglandin A1-induced apoptosis in AGS gastric epithelial cells. *Mol. Carcinog.* **2003**, *37*, 16−24.

(21) Wang, W.; Zhao, Y.; Rayburn, E. R.; Hill, D. L.; Wang, H.; Zhang, R. In vitro anti-cancer activity and structure-activity relationships of natural products isolated from fruits of *Panax ginseng*. *Cancer Chemother. Pharmacol.* **2007**, *59*, 589−601.

(22) Sin, S.; Kim, S. Y.; Kim, S. S. Chronic treatment with ginsenoside Rg3 induces Akt-dependent senescence in human glioma cells. *Int. J. Oncol.* **2012**, *41*, 1669−1674.

(23) Mai, T. T.; Moon, J.; Song, Y.; Viet, P. Q.; Phuc, P. V.; Lee, J. M.; Yi, T. H.; Cho, M.; Cho, S. K. Ginsenoside F2 induces apoptosis accompanied by protective autophagy in breast cancer stem cells. *Cancer Lett.* **2012**, *321*, 144−153.

(24) Wang, C. Z.; Aung, H. H.; Ni, M.; Wu, J. A.; Tong, R.; Wicks, S.; He, T.C.k; Yuan, C. S. Red American ginseng: ginsenoside constituents and antiproliferative activities of heat-processed *Panax quinquefolius* roots. *Planta Med.* **2007**, *73*, 669−674.

(25) Gu, Y.; Rosenblatt, J.; Morgan, D. O. Cell cycle regulation of CDK2 activity by phosphorylation of Thr160 and Tyr15. *EMBO J.* **1992**, *11*, 3995−4005.

(26) Poon, R. Y.; Jiang, W.; Toyoshima, H.; Hunter, T. Cyclin-dependent kinases are inactivated by a combination of p21 and Thr-14/Tyr-15 phosphorylation after UV-induced DNA damage. *J. Biol. Chem.* **1996**, *271*, 13283−13291.

Although the antioxidant properties of MR mixtures are well-known and the above-mentioned mechanism for antioxidant properties of reductones is discussed, the antioxidant properties of single compounds are rarely determined. The motivation of the present work was to expend the knowledge about the antioxidant properties of single MR products. 1-DG **3** and GLUC **4** seemed to be a promising starting point, because they are both important intermediates of the MR and possess a structure that should have antioxidant abilities.

Thus, three different methods were used to measure the antioxidant capacity of the two MR intermediates: the spectrophotometric assays TEAC and FCR as well as EPR spectroscopy. In addition, both substances were compared to different MR products and the two reducing carbohydrates D-glucose and D-fructose.

Furthermore, MR model experiments (pH 5 and 8; 80, 100, and 130 °C; with and without L-alanine addition) with D-glucose and D-fructose, as well as with synthesized 1-DG **3** and GLUC **4**, were conducted and investigated in terms of antioxidant abilities, 1,2-dicarbonyl content, and browning.

MATERIALS AND METHODS

Chemicals. 2,2′-Azinobis(3-ethylbenzothiazoline-6-sulfonic acid) diammonium salt (ABTS), benzoyl hydrazine, ethyl vinyl ether, Folin−Ciocalteu's phenol reagent, D-*arabino*-hexo-2-ulose (GLUC **4**), glyoxal (GO; 40 wt % in water), 6-hydroxy-2,5,7,8-tetramethylchroman-2-carboxylic acid (trolox), (−)-2,3-*O*-isopropylidene-D-erythronolactone, potassium nitrosodisulfonate (Fremy's salt), potassium persulfate, and 3-hydroxy-2-methyl-4*H*-pyran-4-one (maltol **2**) were purchased from Sigma-Aldrich (Steinheim, Germany); Dowex 50W X8 and *o*-phenylenediamine (OPD) were purchased from Fluka (Steinheim, Germany); acetic acid, benzaldehyde, ethanol, D-fructose, D-glucose, potassium hydrogen phosphate anhydrate, potassium dihydrogen phosphate anhydrate, phenyl hydrazine, sodium dihydrogen phosphate dihydrate, and *p*-toluidine were purchased from Merck (Darmstadt, Germany); L-alanine was purchased from Roth (Karlsruhe, Germany); methanol was purchased from VWR (Darmstadt, Germany); gallic acid monohydrate was purchased from Serva (Heidelberg, Germany); diacetyl (DA), *tert*-butyllithium, methylglyoxal (MGO; 40 wt % in water), and tetrahydrofuran were purchased from Acros (Geel, Belgium). The quinoxaline standard mix for HPLC was prepared in our working group.[16]

Synthesis of 1-Deoxy-D-*erythro*-hexo-2,3-diulose (1-DG 3). 1-DG **3** was synthesized using the method of Glomb and Pfahler.[17] The purity of the product was >98%.

Synthesis of D-*arabino*-Hexo-2-ulose (GLUC 4). The synthesis of GLUC **4** followed the description of Hellwig et al.[18] as well as Usui et al.[19] with minor modifications. In both syntheses purities of >98% were obtained. The commercially purchased GLUC **4** was used as a reference substance.

High-Performance Liquid Chromatography (HPLC). For HPLC analysis the following system was used: degasser, Knauer Degasys DG-1300; pump, Shimadzu LC-9A; column oven, Shimadzu CTO-10AS VP; guard column, Macherey-Nagel CC 8/4 Nucleosil 120-5 C18; column, Macherey-Nagel EC 250/4.6 Nucleosil 120-5 C18; detector, Shimadzu SPD-M10A; communication module, Shimadzu CBM-10A; software, Shimadzu CLASS-LC10 v1.64A; injection volume, 40 μL; eluent, water/methanol gradient; flow rate, 1 mL/min; oven temperature, 35 °C.

HPLC Analysis of 1,2-Dicarbonyl Compounds. For the determination of 1,2-dicarbonyl compounds, the samples were derivatized with *o*-phenylenediamine (OPD) after the defined reaction time (postderivatization). The resulting quinoxalines were separated via HPLC on an RP-18 column (see above). The mobile phase consisted of water (solvent A) and methanol (solvent B). The gradient started with 20% of solvent B. After 4 min, it was changed to 33% B within 7 min. In the next 8 min B was increased to 65% (held for 7 min). Then the gradient was changed to 100% B in 2 min. Afterward, B was decreased to 0% in 4 min (held for 5 min). In the following 3 min B was increased to 30% (held for 1 min). For equilibration B was decreased to 20% in 4 min (held for 7 min). The identification and quantification (at 318 nm) was carried out with a standard mix of eight 1,2-dicarbonyls (GLUC, 1-DG, 3-deoxyglucosone, 3-deoxypentosone, 1,4-dideoxyglucosone, GO, MGO, and DA) in different dilutions.[16]

Electron Paramagnetic Resonance (EPR) Spectroscopy. EPR measurements were performed with a Magnettech MiniScope MS 100 spectrometer. Potassium nitrosodisulfonate (Fremy's salt) was used as a stabilized radical. The following settings were used: magnetic flux density, 339.700 mT; sweep, 6.983 mT; sweep time, 30 s; modulation, 0.1500 mT; microwave attenuation, 10 dB; gain, 6; measurement interval, 1 measurement in 40 s; measurement time, 30 min.

Recording of EPR Radical Scavenging Kinetics. The solution of Fremy's salt was prepared in phosphate buffer (pH 7.4). One hundred microliters of Fremy's salt solution (1 mmol/L) and 100 μL of sample (diluted with water) were mixed for 10 s. The mixture was filled in a 50 μL capillary and sealed on one side with modeling clay. Solution and modeling clay were separated by an air buffer. The measurement was performed in comparison to a blank sample that consisted of 100 μL of Fremy's salt solution (1 mmol/L) and 100 μL of phosphate buffer (pH 7.4). For the calculation of the antioxidant activity/capacity, the measurement point at 30 min was used (antioxidant activity/capacity after 30 min: AC_{30}/AA_{30}). The antioxidant potential was calculated between 5 and 10 min (AP_{5-10}) as well as between 20 and 30 min (AP_{20-30}).[20]

UV−Vis Spectroscopy. For the browning measurements as well as for the TEAC and Folin−Ciocalteu assays, a Bio-Tek Instruments UVIKON XL photospectrometer was used. Semimicro disposable cuvettes were purchased from VWR.

Browning Measurements. All samples were diluted 1:20 with water, centrifuged (10 min; 20 °C; 14000 rpm), and measured at 420 nm in comparison to water.

TEAC Assay. The reagents and all standards were prepared in PBS buffer (pH 7.2−7.4). Ten trolox standards (0.025−0.45 mmol/L) were used for the calibration. The samples were diluted with water to fit the calibration curve. For the measurement, 500 μL of ABTS solution (0.5 mmol/L), 100 μL of sample, and 200 μL of potassium persulfate solution (10 mmol/L) were mixed in a cuvette. After exactly 6 min, the mixture was measured at 734 nm in comparison to an empty cuvette.

Folin−Ciocalteu Assay. The calibration was performed with five gallic acid standards (10−80 μg/mL). The samples were diluted with water to fit the calibration curve. Two hundred microliters of sample, 1000 μL of Folin−Ciocalteu phenol reagent (diluted 1:10 with water), and 800 μL of sodium carbonate solution (7.5 wt %) were mixed. The mixture was incubated for 15 min at 35 °C and measured at 736 nm compared to a blank sample (water instead of sample). To convert the results from gallic acid equivalents (GAE) to trolox equivalents (TE), different samples of trolox were measured with respect to gallic acid.

Carbohydrate Reaction Mixtures. Model reactions under typical Maillard conditions were conducted. For that purpose aqueous solutions of D-glucose or D-fructose (0.2 mol/L) with or without L-alanine (0.2 mol/L) were prepared. The pH value was adjusted to 5.0 ± 0.1 or 8.0 ± 0.1 with 0.1 N HCl or 0.1 N NaOH. The solutions were sealed in ampules and were thermally treated in a heating block at 80 ± 1, 100 ± 1, or 130 ± 1 °C for a defined reaction time (0−300 min). A part of the sample was trapped with OPD solution (0.5 mmol/L) for the determination of the 1,2-dicarbonyl compounds. The remaining amount of sample was kept underivatized for further analysis (browning measurement, EPR spectroscopy, and FCR assay).

1,2-Dicarbonyl Reaction Mixtures. For 1,2-dicarbonyl reaction mixtures, aqueous solutions of 1-DG **3** and GLUC **4** (0.02 mol/L) with or without L-alanine (0.2 mol/L) were used. The reactions were conducted under the same conditions as the carbohydrate reaction mixtures.

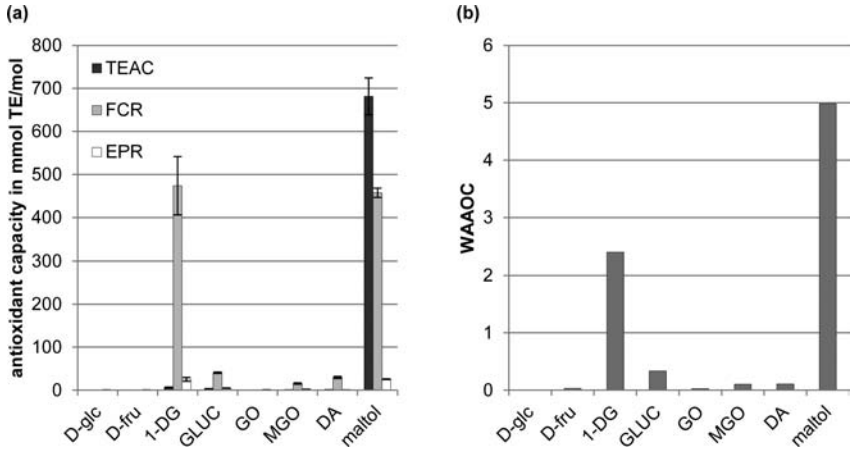

Figure 2. Results of the antioxidant capacity (a) and the WAAOC (b) of the two reductones and six reference substances measured with three different methods. Abbreviations: TEAC, trolox equivalent antioxidant capacity; FCR, Folin−Ciocalteu reagent; EPR, electon paramagnetic resonance; WAAOC, weighted-average antioxidant capacity; D-glc, D-glucose; D-fru, D-fructose; 1-DG, 1-deoxy-D-*erythro*-hexo-2,3-diulose (**3**); GLUC, D-*arabino*-hexo-2-ulose (**4**); GO, glyoxal; MGO, methylglyoxal; DA, diacetyl; maltol, 3-hydroxy-2-methyl-4*H*-pyran-4-one (**2**).

RESULTS AND DISCUSSION

Antioxidant Capacity and WAAOC. The antioxidant capacity of six different MR products, including 1-DG **3** and GLUC **4**, as well as the antioxidant capacity of the reducing carbohydrates D-glucose and D-fructose was measured with three methods (Figure 2a). The results were expressed with respect to trolox as millimoles of trolox equivalents (TE) per mole of sample to allow comparison of the results with other studies.[15] The values of all samples were below 1000 mmol TE/mol in every assay, showing that none of the used substances had an antioxidant capacity that was comparatively as high as the capacity of trolox. Because of the different mechanisms of the various tests, the results for single substances differed strongly. This is a well-known issue, which requires the use of different methods in the first place.[15,21] To generate a single value out of different antioxidant capacities from different assays, the calculation of the weighted-average antioxidant capacity (WAAOC) as described by Tabart et al.[15] was used.

The results of the WAAOC (Figure 2b) showed that the two C6-1,2-dicarbonyls (1-DG **3** and GLUC **4**) had a higher antioxidant capacity than their precursors (D-glucose and D-fructose) as well as their short-chain cleavage products (e.g., glyoxal, methylglyoxal, and diacetyl). The reductone ether maltol **2** showed a higher capacity than the two C6-1,2-dicarbonyls. The reactivities of 1-DG **3** and GLUC **4** differed considerably even though both possess an isomer with reductone structure. The WAAOC of 1-DG **3** was >7 times higher than the WAAOC of GLUC **4**.

EPR Radical Scavenging Kinetics. To allow statements about the velocity and progression of radical scavenging reactions, EPR experiments were conducted. The analysis of EPR kinetics generates two different measures: the antioxidant capacity (AC) and the antioxidant potential (AP), which both are illustrated in Figure 3.[20] According to the definition, the AC is the amount of reduced radical at a specific point in time. The AC is expressed with respect to the used amount of antioxidant (units of AC: moles of reduced radical per mole of defined antioxidant). Many samples contain an unknown type and/or amount of antioxidant or a mixture of different antioxidants; in such cases the antioxidant activity (AA) is mostly used. This measure is expressed with respect to the volume of sample

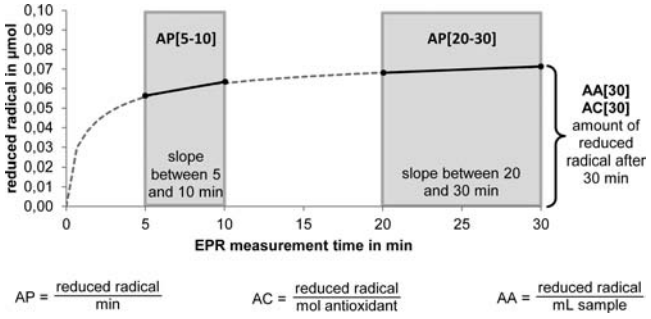

Figure 3. Graphical illustration of the antioxidant activity after 30 min (AA_{30}), the antioxidant capacity after 30 min (AC_{30}), the antoxidant potential between 5 and 10 min (AP_{5-10}), and the antioxidant potential between 20 and 30 min (AP_{20-30}).[20]

solution (units of AA: moles of reduced radical per liter of sample). The AP describes the velocity of the radical scavenging reaction and is expressed in moles of reduced radical per minute. Mathematically this is the slope of kinetics at a specific point in time. In practical terms the slope of a partial regression line can be used to calculate the AP.

All EPR kinetics for this work were recorded in a time frame of 30 min. Fast antioxidants, such as trolox, showed a high AP in the first minutes, followed by a fast decrease of the AP to 0 mol reduced radical/min within several minutes and consequently reached their maximal (final) AC in a short time frame. However, most samples did not deplete their potential to 0 mol reduced radical/min within 30 min, and accordingly their final AC could not be measured. Therefore, the AP and AC of selected points in time are suitable to compare different samples. In this work the AC, the AA after 30 min (AC_{30}/AA_{30}), and the potentials between 5 and 10 min (AP_{5-10}) as well as between 20 and 30 min (AP_{20-30}) were used. With the help of these two potentials, the depletion of the AP of different samples over time could be compared.

From eight tested substances just the two C6-1,2-dicarbonyls and maltol **2** (10 mmol/L solutions) showed a radical reduction of >5% in 30 min (Figure 4a). The used amount of radical in each measurement was 0.1 μmol, and accordingly a radical reduction of 0.05 μmol equals 5%. 1-DG **3** and maltol **2** exhibited similar radical reduction abilities after 30 min: 73 and

dx.doi.org/10.1021/jf404322r | J. Agric. Food Chem. 2014, 62, 2837−2844

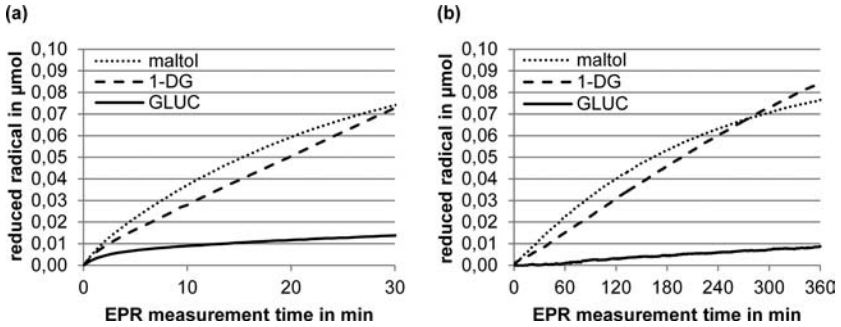

Figure 4. EPR kinetics of GLUC **4**, 1-DG **3**, and maltol **2** as 10 mmol/L solutions (a) and 1 mmol/L solutions (b).

74%, respectively, equaling AC_{30} values of 73 and 74 mmol reduced radical/mol. Within the standard deviation their AC_{30} was identical, but their potentials differed. Whereas the potential of 1-DG **3** was almost constant over 30 min, the AP_{20-30} of maltol **2** decreased about 50% in comparison to the AP_{5-10}. GLUC **4** also showed a constant potential over 30 min but an AC_{30} of only 14 mmol reduced radical/mol.

Measurements over a period of 6 h with 1 mmol/L solutions (Figure 4b) showed identical behaviors of the AP of the three different substances. Additionally, 1-DG **3** showed a higher AC after 360 min as maltol **2**, because of its constant AP. It became apparent that the final AC of 1-DG **3** would be higher than the one of maltol **2**. But even in 6 h the final ACs could not be measured. Therefore, single-point EPR measurements of a 0.25 mmol/L 1-DG solution were performed over a time period of 139 h (Figure 5). The potential decreased slightly in

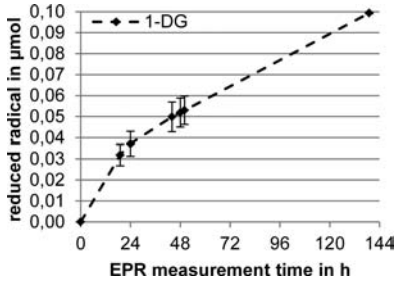

Figure 5. EPR single-point measurements of 1-DG **3** as 0.25 mmol/L solution compared to a blank sample (water and 1 mmol/L Fremy's salt). The radical concentration is depleted after 139 h.

the first 24 h and stayed constant for the next days. After 139 h, the radical concentration was nearly depleted, but the potential of 1-DG **3** was not 0 mol reduced radical/min. Even with a measurement this long, the final AC of 1-DG **3** could not be determined.

The slow reactivity over a long time frame seemed to be characteristic for 1-DG **3** and GLUC **4**. This behavior was the reason for the comparably low AC of the reductones in photometrical assays such as TEAC and FCR, which are designed for fast-reacting antioxidants.

The different radical scavenging behaviors of 1-DG **3**, GLUC **4**, and maltol **2** could be explained by the isomeric composition of each substance. Maltol **2** (Figure 6) reacted relatively rapidly compared to 1-DG **3** and GLUC **4** because only one isomeric form exists in aqueous solution, which is the antioxidative form of this compound. 1-DG **3** and GLUC **4** form different amounts of isomers in aqueous solution, and only the particular reductone isomer is considered to react antioxidatively.

Kaufmann et al.[22] identified up to 15 isomers of 1-DG **3** in aqueous solution. All of them are cyclic hemiacetals that do not possess a reductone structure and thus should not be antioxidative. Solely the enediol tautomer **3b** of the open chain form **3a** (Figure 6) is actually a reductone. But the open chain form **3a** acts only as an intermediate during the rearrangement of different cyclic isomers. The relative quantity of any open chain isomers could not be determined with high-resolution NMR[22] and therefore can be considered as a low percentage (the lowest percentage of a determinable isomer was <3% in this case). A simplified diagram of the equilibria of isomeric forms **3a**−**e** is given in Figure 6. Besides the equilibrium between the open chain isomer **3a** and a specific cyclic isomer such as **3c**, there are equilibria to the particular hydrated forms **3d**/**e**. Thus, the effective reductone concentration of a 1-DG **3** solution equals the undeterminable low relative quantity of the antioxidative enediol tautomer **3b**. The removal of this reductone form from the equilibrium leads, according to Le Chatelier's principle, to the re-formation of this particular form over time. This could explain the low but constant AP of 1-DG **3**.

The even lower potential of GLUC **4** could also be explained by the isomeric composition. Freimund et al.[23] and Kaufmann et al.[24] identified four cyclic isomers of GLUC **4** in aqueous solution, and all of them were hydrates. Thus, a chain opening during a rearrangement of the main isomers leads always to a hydrated open chain isomer **4e**. The quantity of unhydrated open chain isomer **4a** can be estimated lower than in the case of 1-DG **3**. Accordingly, the effective reductone concentration, represented by the relative quantity of the open chain enediol tautomer **4b**, is lower, too.

Antioxidant Properties of the Carbohydrate Reaction Mixtures. The aim of the analysis of the carbohydrate reaction mixtures was to establish a possible correlation between the 1,2-dicarbonyl content, which was determined with HPLC-DAD analysis, and the antioxidant activity, measured with the FCR assay and EPR spectroscopy. However, the results did not show such a correlation. Instead, there was a general correlation between the browning and the antioxidant activity. Both measures increased with the heating time, depending on the used carbohydrate, the amino catalysis, the pH value, and the temperature. The trends of browning and AA (determined with FCR) for the reaction mixture of D-fructose and L-alanine at 130 °C and pH 5/8 are shown in Figure 7. Reaction mixtures with higher temperatures, with pH 8 (instead of 5), with D-fructose (instead of D-glucose), and with L-alanine addition produced a higher antioxidant activity and stronger browning. The absence of a correlation between single 1,2-dicarbonyls and the antioxidant activity could originate in the minor

dx.doi.org/10.1021/jf404322r | J. Agric. Food Chem. 2014, 62, 2837−2844

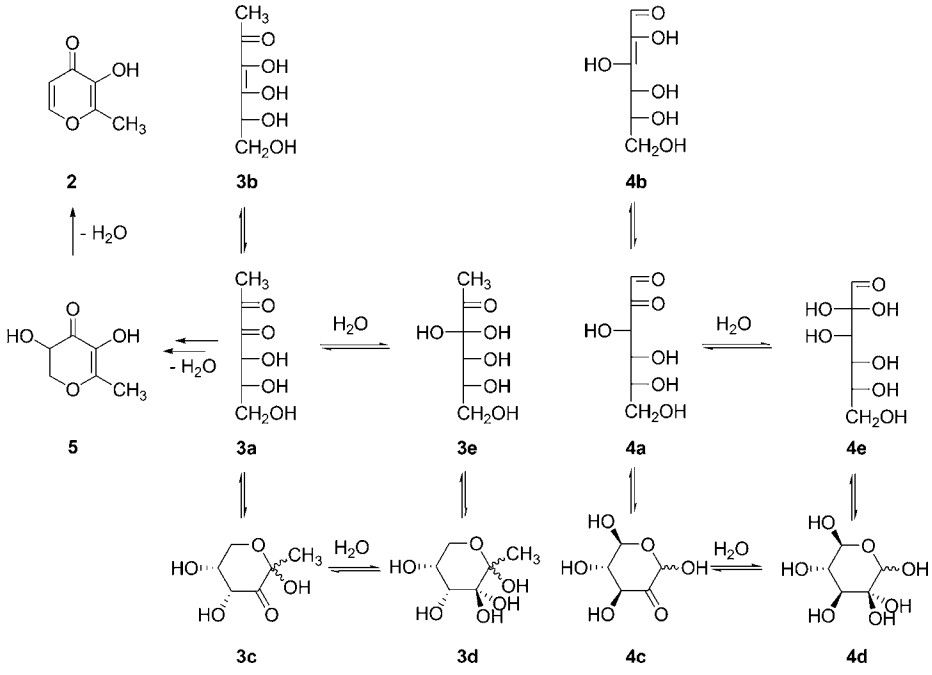

Figure 6. Structures and simplified isomeric equilibria of 3-hydroxy-2-methyl-4*H*-pyran-4-one (maltol **2**), 1-deoxy-D-*erythro*-hexo-2,3-diulose (1-DG **3**), D-*arabino*-hexo-2-ulose (GLUC **4**), and 2,3-dihydro-3,5-dihydroxy-6-methyl-4*H*-pyran-4-one (hydroxydihydromaltol **5**).[22−24,26] **2**, **3b**, **4b**, and **5** show (stabilized) enediol structures of reductones.

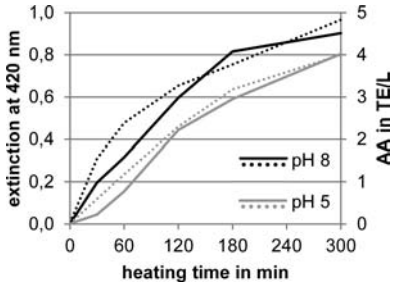

Figure 7. Browning (line) and antioxidant acitivity (AA) determined with FCR (dotted line) of the reaction mixtures of D-fructose and L-alanine at 130 °C and pH 8 (black)/pH 5 (gray) as a function of heating time.

concentrations of these particular substances and in the high amount of different antioxidative substances that were formed simultaneously in the MR. The highest 1,2-dicarbonyl content was detected in the reaction mixture of D-fructose and L-alanine at pH 5 and 130 °C. The summarized concentration of all identified 1,2-dicarbonyls had increased to 1.5 mmol/L within 180 min. In all reaction mixtures of D-fructose (with and without L-alanine addition) at 130 °C (pH 5 and 8), combined concentrations of around 1 mmol/L could be determined. At these concentrations the summarized relative quantity of 1-DG **3** and GLUC **4** was between 17 and 25% (around 0.17−0.25 mmol/L), but the used carbohydrate concentration was 0.2 mol/L, so only around 0.1% of the carbohydrate was degraded to the two 1,2-dicarbonyls. Because of the broad variety of other MR products, the antioxidant activity of this small amount of slowly reacting 1,2-dicarbonyls could easily be overlaid by antioxidative MR products, especially when the formed products were fast-reacting antioxidants.

Antioxidant Properties of the 1,2-Dicarbonyl Reaction Mixtures. To limit the product range of the MR to the direct degradation products of 1-DG **3** respectively, GLUC **4** appropriate reaction mixtures of these single 1,2-dicarbonyls were examined. The decomposition of the 1,2-dicarbonyls was measured with the help of HPLC-DAD analysis.

The results showed that 1-DG **3** decomposed more quickly than GLUC **4** under identical conditions. Furthermore, the degradation of both 1,2-dicarbonyls was faster with the addition

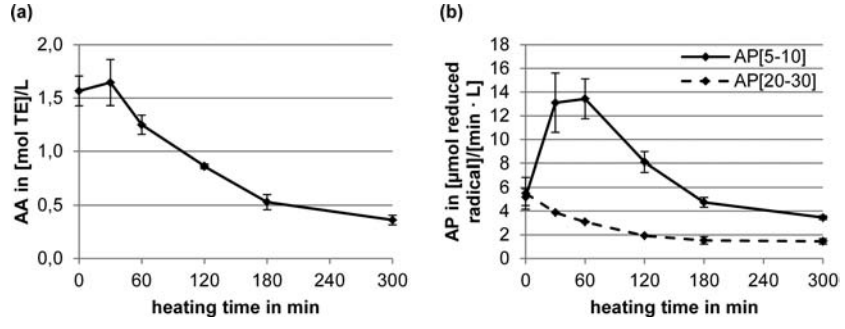

Figure 8. Antioxidant activity (AA) determined with FCR assay (a) and antioxidant potentials (AP) determined with EPR analysis (b) of the 1-DG **3** reaction mixture without L-alanine addition at 130 °C and pH 5.

dx.doi.org/10.1021/jf404322r | J. Agric. Food Chem. 2014, 62, 2837−2844

of L-alanine, and the temperature had a stronger influence than the pH value.

Reaction mixtures of 1-DG **3** (without L-alanine addition) at high temperatures (130 °C) showed a decrease of the AA, which could be determined with the FCR assay (Figure 8a). Nevertheless, a correlation to the remaining 1-DG **3** concentration could not be established. The reaction mixtures of 1-DG and L-alanine did not show such a relationship, possibly because of the much faster degradation of 1-DG **3** and the consequently more rapid formation of fractional antioxidative degradation products.

More detailed information was revealed by the EPR data: the formed antioxidative compounds are mainly fast-reacting antioxidants, and in most cases the low AP of 1-DG **3** was overlaid by the summarized potential of these fast-reacting compounds within the EPR measurement time of 30 min. But, finally, it was possible to establish a correlation between the antioxidant properties and the 1,2-dicarbonyl content in the form of the remaining 1-DG **3** concentration at least for the reaction mixtures without L-alanine.

Figure 8 shows the antioxidant properties and Figure 9 the kinetics of the reaction mixture of 1-DG **3** (without L-alanine addition) at 130 °C and pH 5. Before the heat treatment (0 min), the kinetics of the sample equals the typical nearly linear kinetics of 1-DG (compare to Figure 4). Under heat treatment the AP_{5-10} increased strongly after a short time (30–60 min) and fell after 60 min (Figures 8b and 9). The same trend could be observed for the AA_{30} (Figure 9), but the AP_{20-30} (Figure 8b) was reduced while the AP_{5-10} and the AA_{30} grew. The increase of the AP_{5-10} and the simultaneous decrease of the AP_{20-30} indicated the formation of fast-reacting antioxidants. Their comparably low AC was depleted in a small time frame and was added to the remaining AC of 1-DG **3** in the first minutes of the reaction (Figure 9). The AP_{20-30} equaled the AP of the remaining 1-DG **3** concentration that was increasing over the course of the heating time. In fact, there was a correlation between the relative 1-DG **3** concentration and the relative decrease of the AP_{20-30} for all of the reaction mixtures of 1-DG **3** without L-alanine addition independent from the chosen reaction conditions. Figure 10 shows the correlations for three reaction mixtures at pH 5.

Even though the AP of 1-DG **3** was comparably low, the proof that the antioxidant properties of 1-DG **3** were higher than the antioxidant properties of the corresponding degradation products was possible, at least for a part of the reaction mixtures.

The GLUC **4** reaction mixtures did not show a correlation at all because of the lower AP of GLUC **4** in comparison to 1-DG **3**. The AP of the remaining GLUC **4** concentration in the samples could possibly be determined within an EPR measurement over a longer time frame.

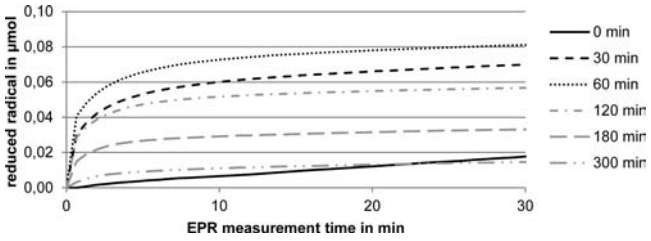

Figure 9. EPR kinetics of the 1-DG reaction mixture without L-alanine addition at 130 °C and pH 5 determined with EPR analysis.

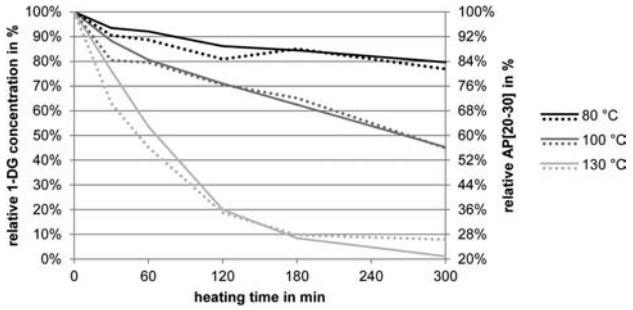

Figure 10. Correlation between the relative 1-DG **3** concentration (line) and the relative antioxidant potential between 20 and 30 min (AP_{20-30}; dotted line) and of the 1-DG **3** reaction mixtures without L-alanine addition at pH 5.

Degradation of 1-DG 3. To measure the 1-DG concentration and to determine the 1,2-dicarbonyl degradation products, 1-DG **3** reaction mixtures were analyzed with HPLC-DAD. The 1,2-dicarbonyl cleavage and elimination products were glyoxal (GO), methylglyoxal (MGO), diacetyl (DA), and 1,4-dideoxyglucosone (1,4-DDG). However, 1,4-DDG and GO could not be detected in all reaction mixtures. 1,4-DDG appeared only in reaction mixtures of 1-DG **3** and L-alanine at pH 5 and, as an exception, in the reaction mixture without amino acid addition at 100 °C and pH 8. The retro-aldol cleavage product GO was detected in all reaction mixtures with L-alanine at pH 8. At pH 5 it was exclusively formed at 130 °C with L-alanine. In Figure 11 the reaction mixture at pH 5 and 130 °C without L-alanine addition is shown. The concentrations of the 1,2-dicarbonyl degradation products suggested that other compounds were formed during the decomposition of 1-DG **3**. These compounds could be secondary products of the 1,2-dicarbonyls or could be formed through independent pathways.[25] However, the short-chain 1,2-dicarbonyls were not antioxidative. Thus, the observed changes of the antioxidant properties of the 1-DG **3** reaction mixtures could not be explained by the formation of short-chain 1,2-dicarbonyl compounds. Possibly degradation products with reductone ether structure were important for the summarized antioxidant properties of the samples. An example for such a substance formed from 1-DG **3** is hydroxydihydromaltol **5**,[13,25] which has strong structural similarities to maltol **2**, and according to Baltes et al.,[26] a small amount of maltol **2** is formed as a degradation product of hydroxydihydromaltol **5** (Figure 6).

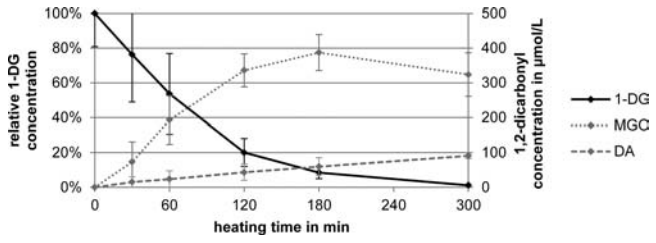

Figure 11. 1-DG **3** degradation (black line, relative 1-DG **3** concentration) and 1,2-dicarbonyl content (gray lines) of the 1-DG **3** reaction mixture without L-alanine addition at 130 °C and pH 5 determined with HPLC-DAD analysis. Abbreviations: MGO, methylglyoxal; DA, diacetyl.

Degradation of GLUC 4. In the corresponding GLUC **4** reaction mixtures the short-chain cleavage products GO, MGO, and 3-deoxypentosone (3-DP) were identified (Figure 12).

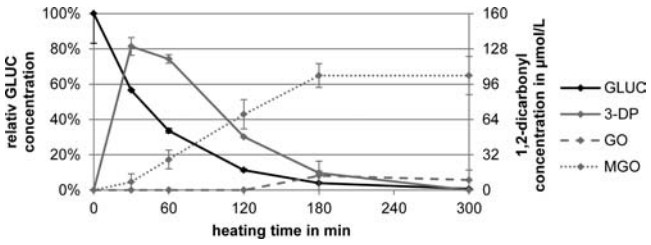

Figure 12. GLUC **4** degradation (black line, relative GLUC **4** concentration) and 1,2-dicarbonyl content (gray lines) of the D-GLUC reaction mixture without L-alanine addition at 130 °C and pH 5 determined with HPLC-DAD analysis. Abbreviations: 3-DP, 3-deoxypentuolose; GO, glyoxal; MGO, methylglyoxal.

These degradation products could be detected under all conditions. Similar to the 1-DG **3** reaction mixtures, the changes of the antioxidant properties were more likely caused by degradation products other than short-chain 1,2-dicarbonyl compounds.

In conclusion, the thermal degradation of 1-DG **3** and GLUC **4** leads to fast-reacting antioxidants, which increase the AP_{5-10} rapidly after short heating times. However, the formed antioxidants are obviously MR products other than the short-chain 1,2-dicarbonyls, because of their lack of antioxidative properties. The reductone ether maltol **2** shows high ACs/APs, and it could be assumed that substances with a related structure play an important part as fast-reacting antioxidants. The antioxidative properties of 1-DG **3** and GLUC **4** are remarkable because of their radical scavenging ability, which is slow compared to other antioxidants but lasts for a longer time (up to 139 h; Figure 5). This behavior causes low results in classical antioxidant assays such as FCR and TEAC, and only EPR measurements could reveal the antioxidant properties of the two reductones and showed their uncommon radical scavenging abilities. The AP of both C6-1,2-dicarbonyls can be measured as soon as the AP of fast antioxidants is depleted. In the case of the 1-DG **3** reaction mixtures without L-alanine addition, the AP_{5-10} could be assigned to the fast-reacting compounds and at the same time the AP_{20-30} could be correlated to the 1-DG **3** concentration.

AUTHOR INFORMATION

Corresponding Author

*(P.T.H.) Phone: +49-30-31472806. Fax: +49-30-31472585. E-mail: paul.haase@tu-berlin.de.

Author Contributions

‖C.K. and P.T.H. contributed equally to this work.

Notes

The authors declare no competing financial interest.

ABBREVIATIONS USED

AA_{30}, antioxidant activity after 30 min; AC_{30}, antioxidant capacity after 30 min; AP_{5-10}, antioxidant potential between 5 and 10 min; AP_{20-30}, antioxidant potential between 20 and 30 min; ARP, Amadori rearrangement product; DAD, diode array detector; 1-DG, 1-deoxyglucosone (1-deoxy-D-*erythro*-hexo-2,3-diulose) (**3**); EPR, electron paramagnetic resonance; D-fru, D-fructose; FCR, Folin−Ciocalteu reagent; D-glc, D-glucose; GLUC, D-glucosone (D-*arabino*-hexo-2-ulose) (**4**); HPLC, high-performance liquid chromatography; MR, Maillard reaction; NMR, nuclear magnetic resonance; RP, reversed phase; TEAC, trolox equivalent antioxidant capacity; WAAOC, weighted-average antioxidant capacity

REFERENCES

(1) Hodge, J. E. Chemistry of browning reactions in model systems. *J. Agric. Food Chem.* **1953**, *1*, 928−943.

(2) Maillard, L.-C. Action des acides aminés sur les sucres; formation des mélanoïdines par voie méthodique. *C. R. Acad. Sci.* **1912**, *154*, 66−68.

(3) Ledl, F.; Schleicher, E. Die Maillard-Reaktion in Lebensmitteln und im menschlichen Körper − neue Ergebnisse zu Chemie, Biochemie und Medizin. *Angew. Chem.* **1990**, *102*, 597−626.

(4) Gobert, J.; Glomb, M. A. Degradation of glucose: reinvestigation of reactive α-dicarbonyl compounds. *J. Agric. Food Chem.* **2009**, *57*, 8591−8597.

(5) Kawakshi, S.; Tsunehiro, J.; Uchida, K. Autoxidative degradation of Amadori compounds in the presence of copper ion. *Carbohydr. Res.* **1991**, *211*, 167−171.

(6) Hyghues-Despointes, A.; Yaylayan, V. A. Retro-aldol and redox reactions of Amadori compounds: mechanistic studies with variously labeled D-[^{13}C]glucose. *J. Agric. Food Chem.* **1996**, *44*, 672−681.

(7) Yilmaz, Y.; Toledo, R. Antioxidant activity of water-soluble Maillard reaction products. *Food Chem.* **2004**, *93*, 273−278.

(8) Morales, F. J.; Babbel, M.-J. Antiradical efficiency of Maillard reaction mixtures in a hydrophilic media. *J. Agric. Food Chem.* **2002**, *50*, 2788−2792.

(9) Ninomiya, M.; Matsuzaki, T.; Shigematsu, H. Formation of reducing substances in the Maillard reaction between D-glucose and γ-aminobutyric acid. *Biosci., Biotechnol., Biochem.* **1992**, *56* (5), 806−807.

(10) Dittrich, R.; El-Massry, F.; Kunz, K.; Rinaldi, F.; Peich, C. C.; Beckmann, M. W.; Pischetsrieder, M. Maillard reaction products inhibit oxidation of human low-density lipoproteins in vitro. *J. Agric. Food Chem.* **2003**, *51*, 3900−3904.

(11) Pischetsrieder, M.; Rinaldi, F.; Gross, U.; Severin, T. Assessment of the antioxidative and prooxidative activities of two aminoreductones formed during the Maillard reaction: effects on the oxidation of β-carotene, N^{α}-acetylhistidine, and *cis*-alkenes. *J. Agric. Food Chem.* **1998**, *46*, 2945−2950.

(12) Ledl, F.; Fritsch, G. Formation of pyrrolinone reductones by heating hexoses with amino acids. *Z. Lebensm.-Unters. -Forsch.* **1984**, *178* (1), 41−44.

(13) Belitz, H.-D.; Grosch, W.; Schieberle, P. *Lehrbuch der Lebensmittelchemie*, 6th ed.; Springer: Berlin, Germany, 2008.

(14) Voigt, M.; Smuda, M.; Pfahler, C.; Glomb, M. A. Oxygen-dependent fragmentation reactions during the degradation of 1-deoxy-D-*erythro*-hexo-2,3-diulose. *J. Agric. Food Chem.* **2010**, *58*, 5685−5691.

(15) Tabart, J.; Kevers, C.; Pincemail, J.; Defraigne, J.-O.; Dommes, J. Comparative antioxidant capacities of phenolic compounds by various tests. *Food Chem.* **2009**, *113*, 1226−1233.

(16) Pfeifer, Y. V.; Kroh, L. W. Investigation of reactive α-dicarbonyl compounds generated from the Maillard reactions of l-methionine with reducing sugars via their stable quinoxaline derivates. *J. Agric. Food Chem.* **2010**, *58*, 8293−8299.

(17) Glomb, M. A.; Pfahler, Ch. Synthesis of 1-deoxy-D-*erythro*-hexo-2,3-diulose, a major hexose Maillard intermediate. *Carbohydr. Res.* **2000**, *329*, 515−523.

(18) Hellwig, M.; Degen, J.; Henle, Th. 3-Deoxygalactosone, a "new" 1,2-dicarbonyl compound in milk products. *J. Agric. Food Chem.* **2010**, *58*, 10752−10760.

(19) Usui, T.; Yoshino, M.; Watanabe, H.; Hayase, F. Determination of glyceraldehyde formed in glucose degradation and glycation. *Biosci., Biotechnol., Biochem.* **2007**, *71* (9), 2162−2168.

(20) Rohn, S.; Kroh, L. W. Electron spin resonance − a spectroscopic method for determining the antioxidant activity. *Mol. Nutr. Food Res.* **2005**, *49*, 898−907.

(21) Frankel, E. N.; Meyer, A. S. The problem of using one-dimensional methods to evaluate multifunctional food and biological antioxidants. *J. Sci. Food Agric.* **2000**, *80*, 1925−1941.
(22) Kaufmann, M.; Haase, P. T.; Mügge, C.; Kroh, L. W. Milieu dependence of isomeric composition of 1-deoxy-D-*erythro*-hexo-2,3-diulose in aqueous solution determined by high-resolution NMR spectroscopy. *Carbohydr. Res.* **2012**, *364*, 15−21.
(23) Freimund, S.; Baldes, L.; Huwig, A.; Giffhorn, F. Enzymatic synthesis of D-glucosone 6-phosphate (D-*arabino*-hexos-2-ulose 6-(dihydrogen phosphate)) and NMR analysis of isomeric forms. *Carbohydr. Res.* **2002**, *337*, 1585−1587.
(24) Kaufmann, M.; Haase, P. T.; Mügge, C.; Kroh, L. W. Milieu dependence of isomeric composition of D-*arabino*-hexo-2-ulose in aqueous solution determined by high-resolution NMR spectroscopy. *J. Agric. Food Chem.* **2013**, *61* (43), 10220−10224.
(25) Voigt, M.; Glomb, M. A. Reactivity of 1-desoxy-D-*erythro*-hexo-2,3-diulose: a key intermediate in the Maillard chemistry of hexoses. *J. Agric. Food Chem.* **2009**, *57*, 4765−4770.
(26) Kim, M.-O.; Baltes, W. On the role of 2,3-dihydro-3,5-dihydroxy-6-methyl-4(*H*)-pyran-4-one in the Maillard Rreaction. *J. Agric. Food Chem.* **1996**, *44*, 282−289.

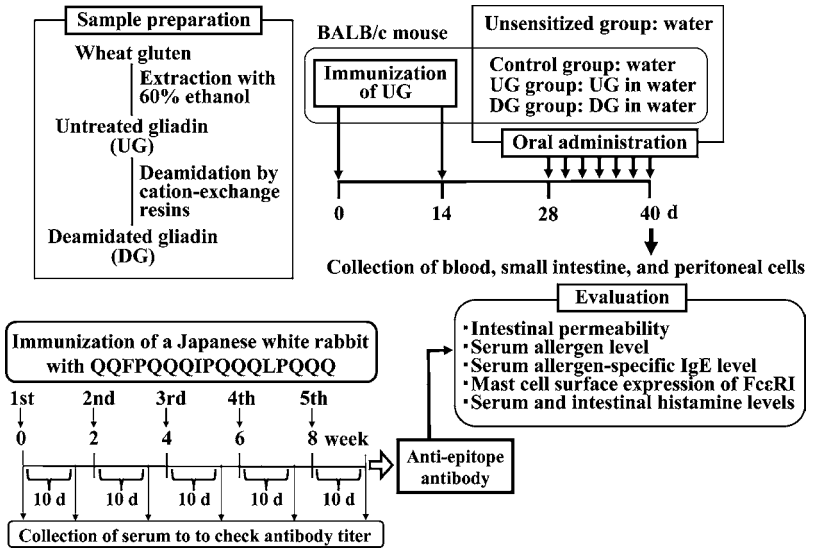

Figure 1. Preparation of deamidated gliadin and evaluation of its in vivo allergenicity by using anti-epitope antibody prepared by immunization with a peptide containing three epitopes.

IgE, and an increase in the level of IgE potently enhances the expression of FcεRI, the high-affinity IgE receptor, on the surface of mast cells.[33−38] Although the deamidated gliadin obtained by cation-exchange treatment has low reactivity with the sera of wheat-allergy patients, retention of its low allergenicity after digestion needs to be confirmed. Therefore, prior to an oral challenge to wheat-allergy patients, we evaluated the allergenicity of deamidated gliadin by measuring the intestinal permeability, serum allergen level, serum allergen-specific IgE level, mast-cell-surface expression of FcεRI, and serum and intestinal histamine levels of gliadin-sensitized mice.

MATERIALS AND METHODS

Deamidation of Wheat Gliadin. Wheat gliadin was extracted from gluten (Nakarai Tesque, Kyoto, Japan) with 60% ethanol. After being concentrated under vacuum, the extract was lyophilized. A cation-exchange resin of the carboxylate type (WK-11, Mitsubishi Chemical Corp., Tokyo, Japan) was washed with 1 N NaOH and then packed into a glass column (5750 × 50 mm, Nippon Flex Co., Aichi, Japan), after which the column was equilibrated with 60% (v/v) ethanol. Then 30 mL of 10 mg/mL undeamidated gliadin (UG) in 60% (v/v) ethanol was loaded onto the column, and the column was eluted with 60% (v/v) ethanol at 5 mL/min. Fractions were collected over 220 min. Deamidated gliadin (DG) obtained as the eluate was concentrated under vacuum and lyophilized.

Degree of Deamidation. The degree of deamidation was obtained from the ratio of amount of acid amide removed by treatment with cation-exchange resin to total acid amide in UG, as described previously.[24,27] Briefly, the acid amides in UG and DG were both completely deamidated by heating in a HCl solution, and the amount of ammonia produced was measured by Conway's micro-diffusion method[39] and the indophenol method.[40] Then the amount of acid amide deamidated was calculated by subtracting the amount of ammonia produced by DG from that produced by UG.

Preparation of Rabbit Anti-Gliadin-Epitope Antibody. As QQFPQQQ, QQIPQQQ, and QQLPQQQ are the major epitope sequences of gliadin, a peptide (QQFPQQQIPQQQLPQQQ) that comprised these three major epitope sequences was synthesized and conjugated to keyhole limpet hemocyanin (KLH). We used the hydrophobic tag-assisted liquid-phase method[41,42] in combination with linker strategy[43,44] to prepare the desired sequence, followed by addition of a cysteine residue to its N-terminus. After deprotection of all protective groups, including the tag, the peptide was conjugated to KLH through the maleimide−thiol reaction.

As shown in Figure 1, Japanese white female rabbits (Nippon Bio-Supply Center, Tokyo, Japan) were subcutaneously immunized with 2 mg of the three-epitope peptide in phosphate-buffered saline (PBS) emulsified with the same volume of Freund's complete adjuvant (Difco Laboratories, Detroit, MI) for the first and second immunization, and Freund's incomplete adjuvant (Difco Laboratories, Detroit, MI) was used for subsequent immunization. Blood was collected from the central artery in the ear 10 days after each immunization to check the antibody titer. Sera containing the anti-gliadin-epitope antibody were collected 10 days after the fifth immunization. This experiment was performed in accordance with the Guidelines for Animal Experiments of the College of Bioresource Sciences of Nihon University (approval no. 09-12).

Binding Capacity of Rabbit Anti-Gliadin-Epitope Antibody. For the identification of IgG-binding sequence in the 17-mer three-epitope peptide, 11 7-mer overlapping peptides with an offset of one amino acid were synthesized. The hydrophobic tag-assisted liquid-phase method was also used to produce these peptides.

Reactivity of the 7-mer overlapping peptides, 17-mer three-epitope peptide, UG, and DG with the anti-gliadin-epitope antibody was measured by use of an inhibition enzyme-linked immunosorbent assay (ELISA) conducted as follows: Either 0.3 mg of peptide (7-mer or 17-mer) in 30 μL of dimethyl sulfoxide or 3 μg of gliadin (UG or DG) in 30 μL of 60% ethanol (v/v) was mixed with 270 μL of rabbit anti-gliadin-epitope antibody or pooled serum from patients RAST-positive to wheat in 0.2% bovine serum albumin (BSA)/phosphate-buffered saline containing 5% Tween20 (PBST), and the samples were incubated for 1 h at 37 °C. Sera were donated from wheat-allergy outpatients (8 females and 12 males, mean age 24.2 years, range 0−53 years, mean total IgE 21 076 IU/mL, range 1030−84 616 IU/mL) who were under treatment at Yokohama City University Hospital after a full explanation of contents of the study. Flat-bottomed microtiter plates were coated with 100 μL of 10 μg/mL gliadin in 60% ethanol at 4 °C overnight and blocked with a 2% BSA/PBST solution for 2 h at 37 °C. The mixture of peptide/gliadin and antibody was added to the wells, and the platers were further incubated for 1 h at 37 °C. Then horseradish peroxidase (HRP)-conjugated goat anti-rabbit IgG was reacted for 1 h at 37 °C with the rabbit anti-gliadin-epitope antibody bound to the gliadin that had been coated onto the wells. The wells were washed five times with PBST at every step. As a substrate for HRP, 100 μL of 0.04% *o*-phenylenediamine containing H_2O_2 was added. The reaction was allowed to proceed for 20 min at room temperature and then stopped by adding 100 μL of 2 N H_2SO_4. The optical density of the formazan at 490 nm was measured with a

dx.doi.org/10.1021/jf4034078 | J. Agric. Food Chem. 2014, 62, 2845−2852

microtiter plate reader. The inhibition percent was determined according to the following formula:

$$\text{inhibition (\%)} = \frac{\text{OD}_{490\,\text{nm}}\ \text{without peptide} - \text{OD}_{490\,\text{nm}}\ \text{with peptide}}{\text{OD}_{490\,\text{nm}}\ \text{without peptide}} \times 100$$

Animals. Male BALB/c mice, 5 weeks old, were purchased from Japan SLC Inc. (Shizuoka, Japan). All mouse experiments were performed in accordance with the Guidelines for Animal Experiments of the College of Bioresource Sciences of Nihon University (approval no. AP11B088). Water was made available continuously through automatic ports, and a commercial mouse diet was provided ad libitum.

Sensitization and Intragastric Challenge. As illustrated in Figure 1, mice were sensitized twice, 2 weeks apart, with 50 μg of UG in the presence of 1 mg of aluminum hydroxide (Imject Alum; Thermo Scientific, Kanagawa, Japan) as an adjuvant by intraperitoneal injection. Two weeks after the second sensitization, the mice were orally administered 10 mg of UG or DG in 500 μL of water via an intragastric feeding needle (5202; Fuchigami Instrument Co., Kyoto, Japan) every other day for a total of seven times. Before each intragastric challenge, the animals were deprived of their diet for 4 h. Then 40 min after the final administration, the mice were anesthetized by barbital, and thereafter peritoneal cells, blood samples, and each part of the small intestines were collected. For collection of peritoneal cells, 3 mL of a Tyrode buffer ([10 mM *N*-(2-hydroxyethyl)-piperazine-*N*′-ethanesulfonic acid (HEPES), pH 7.4, containing 130 mM NaCl, 5.6 mM glucose, 1.4 mM $CaCl_2$, 1 mM $MgCl_2$, 5 mM KCl, and 0.1% (w/v) BSA] was injected into the peritoneal cavity, after which the abdomen was gently massaged for about 60 s. The peritoneal cavity was then carefully opened, and the peritoneal cell-containing fluid was aspirated by use of a Pasteur pipet. Blood samples were withdrawn from the postcaval vein, and the sera were separated by centrifugation at 1300*g* and 20 °C for 15 min after clotting. The duodenum, jejunum, and ileum were excised and rinsed with PBS.

Intestinal Permeability. Intestinal permeability was evaluated by the amount of HRP (molecular mass 40 kDa; Wako Pure Chemical Industries, Osaka, Japan) that passed through the wall of the jejunum according to the method of Isobe et al.[45] Briefly, 0.1 mL of 0.1 mg/mL HRP in PBS was injected into the lumen of a closed loop of a 5-cm length of jejunum, and the loop was then placed in 5 mL of PBS and incubated at 37 °C for 30 min. Then 50 μL of the outside solution was collected into the well of a microtiter plate, and the concentration of HRP that had permeated from the lumen through the intestinal wall was measured by adding 100 μL of 0.04% *o*-phenylenediamine with H_2O_2 to the outside solution.

Level of Epitope Absorbed into the Blood. The level of epitope absorbed from the intestinal lumen into the blood was evaluated by performing a competitive inhibition ELISA with the anti-gliadin-epitope antibody as described above. A serum sample in 0.3% BSA/PBST was mixed with the same amount of rabbit anti-gliadin-epitope antibody in 0.3% BSA/PBST, and the mixture was incubated for 1 h at 37 °C for the antigen−antibody reaction to be completed before its addition to gliadin-coated plates.

Level of Gliadin-Specific IgE in Blood. For determination of the level of gliadin-specific IgE in the serum, 100 μL of 5 μg/mL rat anti-mouse IgE antibody (eBioscience, Inc., San Diego, CA) in a 0.05 M sodium carbonate buffer at pH 9.6 was added to a microtiter plate, and the plate was allowed to stand at 4 °C overnight. Nonspecific binding was blocked by with the addition of 200 μL of 2% BSA/PBST and incubation at 37 °C for 1 h. Then 100 μL of test serum diluted 10× with 0.3% BSA/PBST was added to each well, and incubation was continued for 2 h at 37 °C. Biotinylated gliadin, prepared by use of a biotin labeling kit (Dojindo Laboratories, Kumamoto, Japan), was diluted 500× with 0.3% BSA/PBST, and a 100-μL aliquot of it was added to each well, followed by incubation for 2 h at 37 °C. A 100-μL aliquot of HRP-conjugated streptavidin (Funakoshi Co., Tokyo, Japan) diluted 3000× with 0.3% BSA/PBST was added to each well, and incubation was continued for another 1 h at 37 °C. The wells were washed five times with PBST at every step. As a substrate for HRP, 100 μL of 0.04% *o*-phenylenediamine containing H_2O_2 was added to the wells. The reaction was allowed to proceed for 20 min at room temperature and then stopped by adding 100 μL of 2 N H_2SO_4. The optical density was measured at 490 nm with a microtiter plate reader.

Detection of Peritoneal Mast Cells. Mast cells were separated from macrophages and small lymphocytes in the peritoneal cell population by sedimentation at 150*g* for 10 min at room temperature, and the pellet was resuspended in Tyrode buffer. Mast cells, detected by their expression of the high-affinity IgE receptor (FcεRI) and c-kit, were stained with anti-FcεRI (fluorescein isothiocyanate-conjugated) antibody (diluted 1000×) and anti-c-kit (phycoerythrin-conjugated) antibody (diluted 2000×) at 4 °C for 30 min. These antibodies were purchased from eBioscience (San Diego, CA). Flow cytometry was performed with a LSRII flow cytometer (BD Biosciences, San Jose, CA), and data were analyzed with FlowJo 6.4.2 software (Tree Star Inc., Ashland, OR).

Total Histamine in Gut and Free Histamine in Plasma. Total histamine level in the gut, including that in mast cells and basophils, was measured to estimate the inflammatory status of the small intestines. The first 5 cm of the duodenum and ileum, distal from the ligament of Treitz, was collected and flushed with 5 mL of cold 0.9% NaCl solution. After being weighed, the tissue was homogenized with 1 mL of 0.9% NaCl. Then 200 μL of 1.2 N perchloric acid was added to the homogenate, which was subsequently centrifuged for 10 min at 13000*g*. The supernatant was then collected. This procedure was repeated, and the supernatants were pooled and stored at −20 °C until further analysis.

For measurement of the level of free histamine in the plasma, 500 μL of a mouse plasma sample was mixed with the same amount of 1 N perchloric acid, and then centrifuged for 10 min at 13000*g*. The supernatant was collected and stored at −20 °C until further analysis.

The histamine level was measured by fluorometric analysis as described by Komatsu.[46] After 1 mL of each sample had been mixed with 0.135 mL of 1 N NaOH containing 0.75 mg of NaCl, 1.75 mL of a 3:2 (v/v) mixture of *n*-butanol and chloroform was added, and the mixture was stirred for 5 min. After centrifugation at 500*g* for 5 min, 1.5 mL of the organic solvent layer was recovered and mixed with 1.5 mL of *n*-heptane and 0.6 mL of 0.1 N HCl, and the mixture was stirred for 5 min. After further centrifugation at 500*g* for 5 min, 1.5 mL of the HCl layer recovered was mixed with 0.12 mL of 1 N NaOH and 0.1 mL of 0.2% *o*-phthalaldehyde (Wako Pure Chemical Industries, Osaka, Japan). The reaction was allowed to proceed for 40 min at 4 °C and terminated by adding 0.05 mL of 0.5 N H_2SO_4. The fluorescence intensity (excitation at 360 nm and emission at 440 nm) was measured by use of a microtiter plate reader.

Statistical Analysis. All data were expressed as the mean ± standard error of the mean (SEM), and the significance of differences (P values) between groups was evaluated by using Tukey−Kramer test.

RESULTS

Degree of Deamidation. Wheat gliadin was effectively deamidated with the cation-exchange resin of the carboxylate type. The acid amide deamidated amounted to 421.3 μmol/g of protein. As the amount of acid amide in UG was about 1784.8 μmol/g of protein, the degree of deamidation was 23.6%.

Reactivity of Rabbit Anti-Gliadin-Epitope Antibody with Synthetic Peptides. The inhibition rate of synthetic peptides with rabbit anti-QQFPQQQIPQQQLPQQQ IgG is shown in Table 1. The reactivity of QQIPQQQ, one of the major epitope peptides of gliadin, was the highest among the 11 7-mer overlapping peptides synthesized, its inhibition rate being approximately 42%. The reactivity of QFPQQQI and QQLPQQQ was also high, with inhibition rates of 32% and 15%, respectively. The inhibition rate of QQFPQQQ was about 7%. Therefore, rabbit anti-QQFPQQQIPQQQLPQQQ IgG was able to detect the major epitope peptides of wheat gliadin

Table 1. ELISA Inhibition Rate of Synthetic Peptides with Rabbit Anti-QQFPQQQIPQQQLPQQQ IgG

synthetic peptide	inhibition rate[a] (%)	synthetic peptide	inhibition rate[a] (%)
QQFPQQQ	6.94 ± 3.18	QIPQQQL	5.68 ± 3.14
QFPQQQI	32.30 ± 1.52	IPQQQLP	1.19 ± 0.94
FPQQQIP	5.54 ± 0.91	PQQQLPQ	4.95 ± 4.52
POOOIPQ	10.97 ± 0.71	QQQLPQQ	12.95 ± 1.60
QQQIPQQ	3.96 ± 1.32	QQLPQQQ	15.31 ± 2.05
QQIPQQQ	42.35 ± 1.59	full-length	76.07 ± 1.48

[a]Each value is the mean ± SE of seven experiments.

and will be referred to as anti-gliadin-epitope antibody hereafter.

Reactivity of Rabbit Anti-Gliadin-Epitope Antibody and Patients' Serum with UG and DG. The reactivity of anti-gliadin-epitope antibody was compared with that of the patients' serum. Figure 2 shows the reactivity of anti-gliadin-epitope antibody and wheat-allergy patients' serum with UG or DG. The rabbit anti-gliadin-epitope antibody showed reactivity similar to that of the wheat-allergy patients' serum, and the inhibition rate by DG was lower than that by UG.

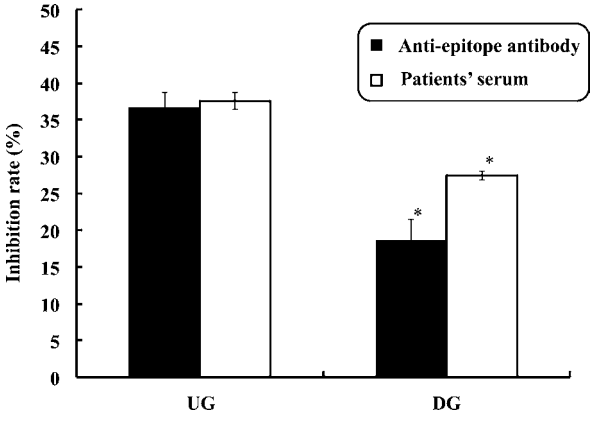

Figure 2. Reactivity of anti-gliadin-epitope antibody and wheat-allergy patients' serum with UG and DG. Asterisk-marked values of DG are significantly different from the corresponding UG value at $P < 0.05$. Each value is the mean of four experiments, with SE shown as a vertical bar.

Intestinal Permeability. Allergic inflammation may enhance intestinal permeability, permitting large molecules such as proteins to be absorbed from the small intestines. Figure 3 presents the permeability of the jejunum from mice orally administered water, UG, or DG after sensitization with UG. The oral administration of UG after sensitization with it greatly enhanced intestinal permeability of HRP. On the other hand, intestinal permeability for the UG-sensitized DG-administered group was almost the same as that of the unsensitized group or UG-sensitized water-administered group.

Level of Epitope Absorbed into the Blood. The low digestibility and high intestinal permeability of proteins may promote the absorption of antigens and epitope peptides into the blood. As shown in Figure 4, the level of epitope in the blood absorbed from the small intestine was much higher for mice orally administered UG after sensitization with it than for those orally administered DG or water. However, orally administered DG and/or its hydrolysates seem to have been absorbed from the small intestines to some extent after 30 min of incubation.

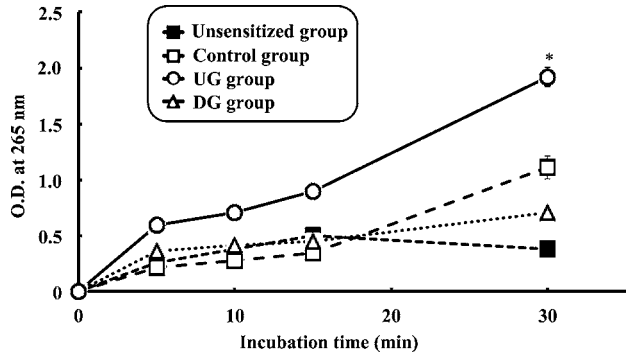

Figure 3. Permeability of small intestines from mice orally administered water, UG, or DG after sensitization with UG. Asterisk-marked values are significantly different from the corresponding values for unsensitized mice at $P < 0.05$. Each value is the mean of seven experiments, with SE shown as a vertical bar.

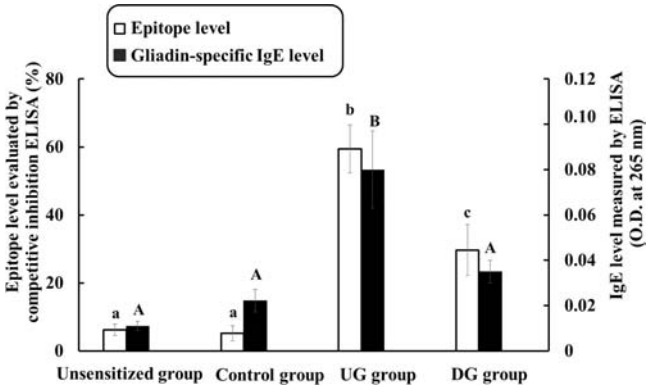

Figure 4. (Open bars) Epitope level and (solid bars) gliadin-specific IgE level in serum. Values with different letters are significantly different at $P < 0.01$. Each value is the mean of seven experiments, with SE shown as a vertical bar.

Gliadin-Specific IgE Level in the Blood. Figure 4 shows the level of IgE specific for gliadin in the blood of mice orally administered UG, DG, or water after UG sensitization. Oral administration of UG after sensitization with it significantly enhanced the level of gliadin-specific IgE in the blood, whereas that of DG scarcely changed it.

Peritoneal Mast Cells. Mast cells, defined as FcεRI+ and c-kit+ cells, play a key role in allergic reactions, and these cells degranulate to release chemical mediators such as histamine when IgE binds to FcεRI on their surface. Figure 5 presents flow cytometric dot plots of FcεRI- and c-kit-expressing cells. The percentage of FcεRI+ and c-kit+ cells in the UG-sensitized orally administered UG group was much higher than in any of the other groups, being approximately 20% of total cells. On the other hand, the percentage of FcεRI+ and c-kit+ cells from UG-sensitized orally administered DG mice was only about 3%. The results are also shown graphically in Figure 5.

Total Histamine in Gut and Free Histamine in Plasma. Figure 6 shows the level of total histamine in the small intestines. This level in the UG-sensitized, orally administered UG group was almost double that in the other groups, whereas the level for the UG-sensitized, orally administered DG group was almost the same as for the unsensitized and control groups.

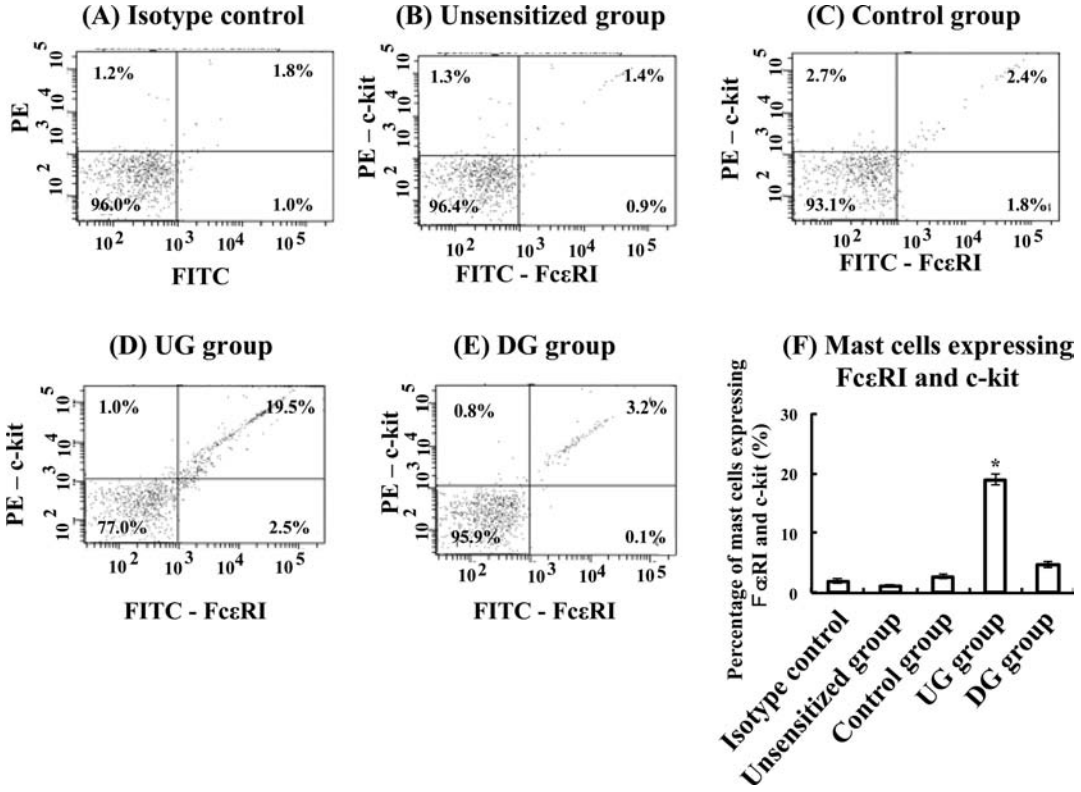

Figure 5. (A–E) Flow cytometric dot plots of FcεRI and c-kit expression on mast cells. (F) Percentage of mast cells expressing FcεRI and c-kit. Asterisk-marked values are significantly different from those of unsensitized mice at $P < 0.05$. Each value is the mean of seven experiments, with SE shown as a vertical bar.

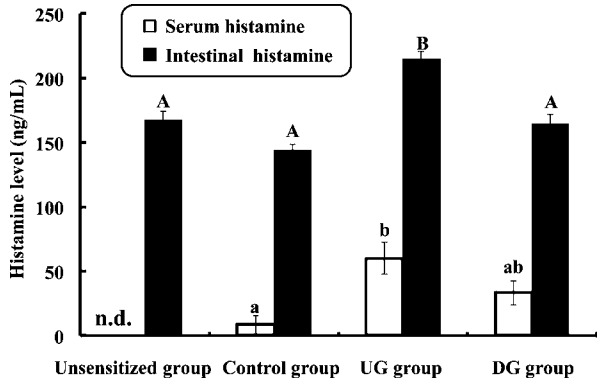

Figure 6. (Open bars) Free histamine level in the serum and (solid bars) total histamine level in the small intestine. Values with different letters are significantly different at $P < 0.01$. Each value is the mean of seven experiments, with SE shown as a vertical bar.

Similarly, oral administration of UG after sensitization with it enhanced the free histamine level in the serum, as shown in Figure 6. The free histamine level in the serum of mice orally administered DG was lower than that of the mice orally administered UG, though there was no significant difference between the two groups.

DISCUSSION

Certain tandem sequence motifs that have glutamine residues in wheat gliadin have been reported to constitute the primary structure of IgE-binding epitopes.[9,14,15] Therefore, deamidation would be an effective means to reduce wheat allergenicity, although it may not be applicable to patients with celiac disease or to those who are sensitive to deamidated proteins.[47−49] Hydrochloric acid treatment has generally been used for deamidation of wheat protein.[50,51,47] However, hydrochloric acid simultaneously causes hydrolysis of peptide bonds, which produces bitter-tasting peptides and reduces the processing properties of wheat such as extensibility and elasticity. The cation-exchange resin treatment used in this study does not cause peptide-bond hydrolysis and rather improves the processing properties.[24,29] Therefore, deamidation by cation-exchange resins will provide proteins with health benefits and enhanced sensory properties.

Deamidation is thus expected to reduce the allergenicity of wheat gliadin. However, gliadin in gluten deamidated to the degree of 36−51% by hydrochloric acid still reacted with the sera of patients suffering from wheat allergy to some extent.[49] Maruyama et al.[50] reported that gluten treated with hydrochloric acid showed reduced reactivity with the sera of patients allergic to wheat and that gluten with more than 50% deamidation showed markedly decreased IgE-binding capacity. Similarly, gliadin with 52% deamidation generated by treatment with hydrochloric acid showed low reactivity with IgE antibody.[51] Yong et al.[23] reported that wheat gluten deamidated by protein glutaminase had low allergenicity when the deamidation degree reached 72%. These findings indicate that more than 50% deamidation is required to reduce the reactivity of gliadin deamidated by acid or enzyme, probably because of the exposure of inner epitope structure to the surface during acidic hydrolysis and enzymatic reaction. On the other hand, 28% deamidated wheat gliadin achieved with cation-exchange resin treatment scarcely reacted with IgE in the sera of patients allergic to wheat.[29] The low reactivity of this deamidated gliadin

dx.doi.org/10.1021/jf4034078 | J. Agric. Food Chem. 2014, 62, 2845−2852

with IgE could be due to the effective deamidation of glutamine residues on the surface of protein by cation-exchange resin.

As shown in our previous study, deamidation increased the solubility of gliadin in water and sodium chloride solutions[25] and enhanced its digestibility by pancreatin.[29] Thus, a further reduction in its allergenicity may occur during digestion. This study was therefore conducted to examine the in vivo allergenicity of DG by using wheat-allergy model mice. Although the degree of deamidation of DG used in this study was only 23.6%, oral administration of DG to mice did not induce allergic reactions. Therefore, the epitope sequences in the inner part of the gliadin structure were assumed to be effectively hydrolyzed during digestion.

When an allergic protein is orally administered to mice after immunization, the protein cross-links IgE molecules, thereby inducing an allergic reaction. Allergic inflammation in the small intestines may enhance intestinal permeability and increase the number of mucosal mast cells and eosinophils in the small intestines.[32,52] Therefore, we examined the permeability of HRP through the jejunum of DG-administered mice. The administration of UG significantly enhanced the intestinal permeability, whereas that of DG scarcely altered it (Figure 3). The considerable rise in serum allergen level after UG administration may be attributed to the increase in intestinal permeability because of probable absorption of large molecules of UG from the small intestines. As the serum allergen level of DG-administered mice was lower than that of UG-administered mice (Figure 4), the epitope structure in DG would have been more extensively hydrolyzed by digestive enzymes in the gut than that in UG. However, the serum allergen level of DG-administered mice was still higher than that of water-administered mice. This result indicates absorption of DG to some extent. The serum IgE level, surface expression of FcεRI, and intestinal histamine level of DG-administered mice were almost the same as those of water-administered mice, indicating that administration of DG did not cause an allergic reaction.

The mechanism of antibody production after immunization with a peptide or protein is not yet completely understood. In this study, a 17-mer peptide (QQFPQQQIPQQQLPQQQ) having three major epitope sequences of gliadin (QQFPQQQ, QQIPQQQ, and QQLPQQQ) was synthesized, and rabbits were immunized with it. The obtained antibody notably recognized QQIPQQQ, one of the major epitopes. Its reactivity with QQLPQQQ was also high. Therefore, these two epitope sequences can be considered to promote antibody production. On the other hand, it recognized QFPQQQI much more than QQFPQQQ, which is another major epitope sequence. The reason for this might be due to differences in the mechanism of antibody recognition between rabbits and human or to the order of connected epitope peptide sequences. However, reactivity of the antibody from rabbits immunized with UG and DG was almost the same as that of patients' serum, indicating that the antibody from rabbit serum can be used for detecting epitope sequences in vivo.

In conclusion, the deamidated gliadin was confirmed to have low allergenicity even in vivo, suppressing the enhancement in intestinal permeability, serum allergen level, serum allergen-specific IgE level, mast-cell-surface expression of FcεRI, and serum and intestinal histamine levels. As deamidated gliadin exhibits a high foaming property,[25] deamidation by cation-exchange treatment with no peptide-bond hydrolysis is a promising technique for production of bread and cakes with low allergenicity and better expansibility.

AUTHOR INFORMATION

Corresponding Author

*Phone +81-0-466-84-3946; fax +81-0-466-84-3946; e-mail kumagai@brs.nihon-u.ac.jp.

Notes

The authors declare no competing financial interest.

ABBREVIATIONS

AEDS, atopic eczema/dermatitis syndrome; DG, deamidated gliadin; FcεRI, high-affinity IgE receptor; HMW glutenin, high-molecular-weight glutenin; HRP, horseradish peroxidase; KLH, keyhole limpet hemocyanin; UG, undeamidated gliadin; WDEIA, wheat-dependent exercise-induced anaphylaxis

REFERENCES

(1) Moneret-Vautrin, D. A.; Morisset, M. Adult food allergy. *Curr. Allergy Asthma Rep.* **2005**, *5*, 80−85.

(2) Hischenhuber, C.; Crevel, R.; Jarry, B.; Mäki, M.; Moneret-Vautrin, D. A.; Romano, A.; Troncone, R.; Ward, R. Safe amounts of gluten for patients with wheat allergy or coeliac disease. *Aliment. Pharmacol. Ther.* **2006**, *23*, 559−575.

(3) Scibilia, S.; Pastorello, E. A.; Zisa, G.; Ottolenghi, A.; Bindslev-Jensen, C.; Pravettoni, V.; Scovena, E.; Robino, A.; Ortolani, C. Wheat allergy: A double-blind, placebo-controlled study in adults. *J. Allergy Clin. Immunol.* **2006**, *117*, 433−439.

(4) Jävinen, K. M.; Turpeinent, M.; Suomalainen, H. Concurrent cereal allergy in children with cow's milk allergy manifested with atopic dermatitis. *Clin. Exp. Allergy* **2003**, *33*, 1060−1066.

(5) Roehr, C. C.; Edenharter, G.; Reimann, S.; Ehlers, I.; Worm, M.; Zuberbier, T.; Niggemann, B. Food allergy and non-allergic food hypersensitivity in child and adolescents. *Clin. Exp. Allergy* **2004**, *34*, 1534−1541.

(6) Venter, C.; Pereira, B.; Grundy, J.; Clayton, C. B.; Arshad, S. H.; Dean, T. Prevalence of sensitization reported and objectively assessed food hypersensitivity amongst six-year-old children. *Pediatr. Allergy Immunol.* **2006**, *17* (5), 356−363.

(7) Palosuo, K.; Varjonen, E.; Nurkkala, J.; Kalkkinen, N.; Harvima, R.; Reunala, T.; Alenius, H. Transglutaminase-mediated cross-linking of a peptic fraction of ω-5 gliadin enhances IgE reactivity in wheat-dependent, exercise-induced anaphylaxis. *J. Allergy Clin. Immunol.* **2003**, *111*, 1386−1392.

(8) Lehto, M.; Palosuo, K.; Varjonen, E.; Majuri, M. L.; Andersson, U.; Reunala, T.; Alenius, H. Humoral and cellular responses to gliadin in wheat-dependent, exercise-induced anaphylaxis. *Clin. Exp. Allergy* **2003**, *33*, 90−95.

(9) Matsuo, H.; Morita, E.; Tatham, S. A.; Morimoto, K.; Horikawa, T.; Osuna, H.; Ikezawa, Z.; Kaneko, S.; Kohno, K.; Dekio, S. Identification of the IgE binding epitope in ω-5 gliadin, major allergen in wheat-dependent exercise-induced anaphylaxis. *J. Biol. Chem.* **2004**, *279* (13), 12135−12140.

(10) Matsuo, H.; Kohno, K.; Niihara, H.; Morita, E. Specific IgE determination to epitope peptides of ω-5 gliadin and high molecular weight glutenin subunit is a useful tool for diagnosis of wheat-dependent exercise-induced anaphylaxis. *J. Immunol.* **2005**, *175*, 8116−8122.

(11) Varjonen, E.; Vainio, E.; Kalimo, K. Antigliadin IgE-indicator of wheat allergy in atopic dermatitis. *Allergy* **2000**, *55*, 386−391.

(12) Takizawa, T.; Arakawa, H.; Tokuyama, K.; Morikawa, A. Identification of allergen fractions of wheat flour responsible for anaphylactic reactions to wheat products in infants and young children. *Int. Arch. Allergy Immunol.* **2001**, *125*, 51−56.

(13) Battais, F.; Pineau, F.; Popineau, Y.; Aparicio, C.; Kanny, G.; Guerin, L.; Moneret-Vautrin, D. A.; Denery-Papini, S. Food allergy to wheat: Identification of immunogloglin E and immunoglobulin G-binding proteins with sequential extracts and purified proteins from wheat flour. *Clin. Exp. Allergy* **2003**, *33*, 962−970.

(14) Watanabe, M.; Tanabe, S.; Suzuki, T.; Ikezawa, Z.; Arai, S. Primary structure of an allergenic peptide occurring in the chymotryptic hydrolysate of gluten. *Biosci. Biotechnol. Biochem.* **1995**, *59* (8), 1596−1597.
(15) Tanabe, S.; Arai, S.; Yanagihara, Y.; Mita, H.; Takahashi, K.; Watanabe, M. A major wheat allergen has a Gln-Gln-Gln-Pro-Pro motif identified as an IgE-binding epitope. *Biochem. Biophys. Res. Commun.* **1996**, *219*, 290−293.
(16) Matsudomi, N.; Sasaki, T.; Kato, A.; Kobayashi, K. Conformational changes and functional properties of acid-modified soy protein. *Agric. Biol. Chem.* **1985**, *49*, 1251−1256.
(17) Goulet, G.; Amiot, J.; Simard, C.; Delisle, J.; Brisson, G. J. Effect of mild autoclaving and deamidisation on the nutritive value of protein fractions. *J. Sci. Food Chem.* **1985**, *36*, 305−310.
(18) Lakkis, J.; Villota, R. Comparative performance of chemically and enzymically modified whey protein. *Food Chem.* **1992**, *43*, 93−105.
(19) Wagner, J. R.; Guéguen, J. Effects of dissociation, deamidation, and reducing treatment on structural and surface active properties of soy glycinine. *J. Agric. Food Chem.* **1995**, *42*, 1993−2000.
(20) Chan, W. M.; Ma, C. Y. Acid modification of proteins from soymilk residue (okara). *Food Res. Int.* **1999**, *32*, 119−127.
(21) Kato, A.; Tanaka, A.; Matsudomi, N.; Kobayashi, K. Deamidation of food proteins by protease in alkaline pH. *J. Agric. Food Chem.* **1987**, *35*, 224−227.
(22) Kumagai, H.; Shizawa, Y.; Sakurai, H.; Kumagai, H. Influence of phytate removal and structural modification on the calcium-binding properties of soybean globulins. *Biosci. Biotechnol. Biochem.* **1998**, *62*, 341−346.
(23) Yong, Y. H.; Yamaguchi, S.; Gu, Y. S.; Mori, T.; Matsumura, Y. Effects of enzymatic deamidation by protein-glutaminase on structure and functional properties of α-zein. *J. Agric. Food Chem.* **2004**, *52*, 7094−7100.
(24) Kumagai, H.; Norimatsu, Y.; Hashizume, N.; Sakurai, H.; Kumagai, H. Deamidation of wheat-flour gluten with ion-exchange resin. *Nippon Shokuhin Kagaku Kogaku Kaishi* **2001**, *48*, 884−890 (in Japanese).
(25) Norimatsu, Y.; Kumagai, H.; Nagai, R.; Sakurai, H.; Kumagai, H. Deamidation of wheat-flour gluten with ion-exchange resin and its functional properties. *Nippon Shokuhin Kagaku Kogaku Kaishi* **2002**, *49*, 639−645 (in Japanese).
(26) Kumagai, H.; Ishida, S.; Koizumi, A.; Sakurai, H.; Kumagai, H. Preparation of phytate-removed deamidated soybean globulins by ion exchangers and characterization of their calcium-binding ability. *J. Agric. Food Chem.* **2002**, *50*, 172−176.
(27) Kumagai, H.; Koizumi, A.; Suda, A.; Sato, N.; Sakurai, H.; Kumagai, H. Enhanced calcium absorption in the small intestine by a phytate-removed deamidated soybean globulin preparation. *Biosci. Biotechnol. Biochem.* **2004**, *68*, 1598−1600.
(28) Kumagai, H.; Koizumi, A.; Sato, N.; Ishizawa, Y.; Suda, A.; Sakurai, H.; Kumagai, H. Effect of phytate removal and deamidation of soybean proteins on calcium absorption in *in situ* rats. *BioFactors* **2004**, *22*, 21−24.
(29) Kumagai, H.; Suda, A.; Sakurai, H.; Kumagai, H.; Arai, S.; Inomata, N.; Ikezawa, Z. Improvement of digestibility, reduction in allergenicity, and induction of oral tolerance of wheat gliadin by deamidation. *Biosci. Biotechnol. Biochem.* **2007**, *71* (4), 977−985.
(30) Kumagai, H.; Sato, N.; Ikeda, M.; Sakurai, H.; Kumagai, H. Increase in solubility and function to promote calcium absorption of soybean β-conglycinin by deamidation. *J. Clin. Biochem. Nutr.* **2008**, *43*, 240−242.
(31) Spreeuwel, J. P. V.; Lindeman, J.; Maanen, J. V.; Meyer, C. Increased numbers of IgE containing cells in gastric and duodenal biopsies. An expression of food allergy secondary to chronic inflammation? *J. Clin. Pathol.* **1984**, *37*, 601−606.
(32) Yamamoto, T.; Fujiwara, K.; Yoshida, M.; Kageyama-Yahara, N.; Kuramoto, H.; Shibahara, N.; Kadowaki, M. Therapeutic effect of Kakkonto in a mouse model of food allergy with gastrointestinal symptoms. *Int. Arch. Allergy Immunol.* **2009**, *148*, 175−185.
(33) Hsu, C.; MacGlashan, D., Jr. IgE antibody up-regulates high affinity IgE binding on murine bone marrow-derived mast cells. *Immunol. Lett.* **1996**, *52*, 129−134.
(34) Shaikh, N.; Rivera, J.; Hewlett, B. R.; Stead, R. H.; Zhu, F.; Marshall, J. Mast cell FcεRI expression in the rat intestinal mucosa and tongue is enhanced during *Nippostrogylus brasiliensis* infection and can be up-regulated by *in vivo* administration of IgE. *J. Immunol.* **1997**, *158*, 3805−3812.
(35) Yano, K.; Yamaguchi, M.; de Mora, F.; Lantz, C. S.; Butterfield, J. H.; Costa, J. J.; Gail, S. J. Production of macrophage inflammatory protein-1α by human mast cells: Increased anti-IgE-dependent secretion after IgE-dependent enhancement of mast cell IgE-binding ability. *Lab. Invest.* **1997**, *77*, 185−193.
(36) Yamaguchi, M.; Lantz, C. S.; Oettgen, H. C.; Katona, I. M.; Fleming, T.; Miyajima, I.; Kinet, J.-P.; Galli, S. J. IgE enhances mouse mast cell FcεRI expression *in vitro* and *in vivo*: Evidence for a novel amplification mechanism in IgE-dependent reactions. *J. Exp. Med.* **1997**, *185*, 663−672.
(37) Boesiger, J.; Tsai, M.; Maurer, M.; Yamaguchi, M.; Brown, L. F.; Claffey, K. P.; Dvorak, H. F.; Galli, S. J. Mast cells can secrete vascular permeability factor/vascular endothelial cell growth factor and exhibit enhanced release after immunoglobulin E-dependent upregulation of Fcε receptor I expression. *J. Exp. Med.* **1998**, *188* (6), 1135−1145.
(38) Yamaguchi, M.; Sayama, K.; Yano, K.; Lantz, C. S.; Noben-Trauth, N.; Ra, C.; Costa, J. J.; Galli, S. J. IgE enhances Fcε receptor I expression and IgE-dependent release of histamine and lipid mediators from human umbilical cord blood-derived mast cell: Synergistic effect of IL-4 and IgE on human mast cell Fcε receptor I expression and mediator release. *J. Immunol.* **1999**, *162*, 5455−5465.
(39) Conway, E. J.; Byrne, A. An absorption apparatus for the micro-determination of certain volatile substances. I. The micro-determination of ammonia. *Biochem. J.* **1993**, *27*, 419−429.
(40) Akamatsu, S. Some micromethods for enzyme studies. *J. Biochem.* **1952**, *39*, 203−210.
(41) Okada, Y.; Suzuki, H.; Nakae, T.; Fujita, S.; Abe, H.; Nagano, K.; Yamada, T.; Ebata, N.; Kim, S.; Chiba, K. Tag-assisted liquid-phase peptide synthesis using hydrophobic benzyl alcohols as supports. *J. Org. Chem.* **2013**, *78*, 320−327.
(42) Tana, G.; Kitada, S.; Fujita, S.; Okada, Y.; Kim, S.; Chiba, K. A practical solution-phase synthesis of an antagonistic peptide of TNF-α based on hydrophobic tag strategy. *Chem. Commun.* **2010**, *46*, 8219−8221.
(43) Fujita, Y.; Fujita, S.; Okada, Y.; Chiba, K. Soluble tag-assisted peptide head-to-tail cyclization: Total synthesis of Mahafacyclin B. *Org. Lett.* **2013**, *15*, 1155−1157.
(44) Kitada, S.; Fujita, S.; Okada, Y.; Kim, S.; Chiba, K. Total synthesis of α-conotoxin MII using a soluble-tag-assisted method. *Tetrahedron* **2013**, *69*, 2555−2559.
(45) Isobe, N.; Suzuki, M.; Ods, M.; Tanabe, S. Enzyme modified cheese exerts inhibitory effect on allergen permeation in rats suffering from indomethacin-induced intestinal inflammation. *Biosci. Biotechnol. Biochem* **2008**, *72* (7), 1740−1745.
(46) Komatsu, M. Studies on histamine in bronchial asthma. *Allergy* **1978**, *27* (2), 67−74 (in Japanese).
(47) van de Wal, Y.; Kooy, Y.; van Veelen; Peña, S.; Mearin, L.; Papadopoulos, G.; Koning, F. Cutting edge: Selective deamidation by tissue transglutaminase strongly enhances gliadin-specific T cell reactivity. *J. Immunol.* **1998**, *161*, 1585−1588.
(48) Denery-Papini, S.; Bodinier, M.; Larré, C.; Brossard, C.; Pineau, F.; Triballeau, M.; Pierri, M.; Battais, F.; Mothes, T.; Paty, E.; Moneret-Vautrin, D.-A. Allergy to deamidated gluten in patients tolerant to wheat: Specific epitopes linked to deamidation. *Allergy* **2012**, *67*, 1023−1032.
(49) Leduc, V.; Moneret-Vautrin, D.-A.; Guerin, L.; Morisset, M.; Kanny, G. Anaphylaxis to wheat isolate: Immunochemical study of case proved by means of double-blind, placebo-controlled food challenge. *J. Allergy Clin. Immunol.* **2003**, *111* (4), 897−899.
(50) Maruyama, N.; Sugiura, F.; Kishimoto, T.; Ichise, K.; Takeuchi, Y.; Sawada, T.; Tsuda, A.; Utsumi, S. Decreased IgE-binding with

wheat gluten by deamidation. *Biosci. Biotechnol. Biochem.* **1999**, *63* (3), 567−569.
(51) Gourbeyre, P.; Denery-Papini, S.; Larre, C.; Gaudin, J. C.; Brossard, C.; Bodinier, M. Wheat gliadins modified by deamidation are more efficient than native gliadins in inducing a Th2 response in Balb/c mice experimentally sensitized to wheat allergens. *Mol. Nutr. Food Res.* **2012**, *56*, 336−344.
(52) Brandt, E. B.; Strait, R. T.; Hershko, D.; Wang, Q.; Muntel, E. E.; Scribner, T. A.; Zimmermann, N.; Finkelman, F. D.; Rothenberg, M. E. Mast cells are required for experimental oral allergen-induced diarrhea. *J. Clin. Invest.* **2003**, *112*, 1666−1677.

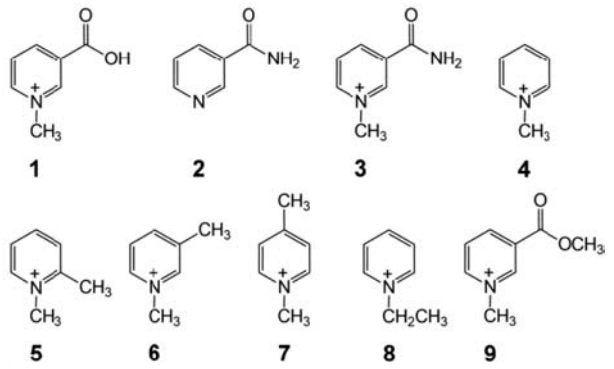

Figure 1. Chemical structures of trigonelline, nicotinamide, 1-methylnicotinamide, methyl derivatives of pyridine, and trigonelline methyl ester.

Therefore, the aim of the present study was to identify pyridinium compounds formed upon coffee roasting and to investigate their influence on experimentally induced arterial thrombosis in rats.

MATERIALS AND METHODS

Animal Studies. Animals were purchased from and housed in the Centre of Experimental Medicine of Medical University in Bialystok according to Good Laboratory Practice rules. Male Wistar rats (180–200 g) were used in all experiments. Animals were housed in a room with a 12 h light/dark cycle, grouped in cages as appropriate, and allowed to have access to tap water and a standard rat chow. All of the procedures involving animals and their care were approved by a local bioethics committee and conducted in accordance with the institutional guidelines that are in compliance with national and international laws and Guidelines for the Use of Animals in Biomedical Research.[24]

Chemicals and Materials. Trigonelline hydrochloride was obtained from Fluka (Steinheim, Germany). Methanol and formic acid (LC-LC-MS grade) were from Sigma-Aldrich (Schnelldorf, Germany). All other reagents were from Sigma-Aldrich, unless noted otherwise, and were of the highest purity available. 1-Methylpyridinium chloride (1-methylpyridine, **4**), 1,2-dimethylpyridinium chloride (1,2-dimethylpyridine, **5**), 1,3-dimethylpyridinium chloride (1,3-dimethylpyridine, **6**), 1,4-dimethylpyridinium chloride (1,4-dimethylpyridine, **7**), 1-ethylpyridinium chloride (1-ethylpyridine, **8**), and trigonelline methyl ester (**9**) (see Figure 1), as standards for chemical analysis and drugs for pharmacological experiments, were synthesized using the methods in the literature. The 6-Keto-$PGF_{1\alpha}$ ELISA kit was purchased from Cayman Chemical Company (Ann Arbor, MI, USA) and rat plasminogen activator inhibitor −1 (PAI-1) ag/activity Zymutest Kits from HYPHEN BioMed (Neuville sur Oise, France), whereas the rat tissue plasminogen activator (t-PA) activity kit was obtained from Innovative Research Inc. (Novi, MI, USA). Reagents to prothrombin time (PT), activated partial thromboplastin time (aPTT), and fibrinogen (Fg) level measurements were purchased from Bio-Ksel (Grudziadz, Poland). Moreover, collagen (Chrono-log Corporation, Havertown, PA, USA), pentobarbital (Biovet, Pulawy, Poland), and trisodium citrate (Avantor Performance Materials, Gliwice, Poland) were used in the study. Solid-phase extraction columns Bakerbond CBA, 500 mg and 3 mL (J.T. Baker, Phillipsburg, NJ, USA), were obtained from Witko (Lodz, Poland). The column used was 100 mm × 2.1 mm, i.d., 1.7 μm Acquity UPLC BEH C18 with a 5 mm × 2.1 mm, i.d. guard column of the same material (Waters, Milford, MA, USA).

Coffee Samples. Coffee (*C. arabica*) samples (150 g) were roasted using coffee roaster KN-8828D (Hottop, Cranston, RI, USA) at 220 °C. The roasting process was manually controlled by following audible cues of the beginning of a "first crack" (14.5 min), the beginning of a "second crack" (19 min), and the end of a "second crack" (23 min). Objective color measurements were obtained by a CM-3600d (Konica Minolta, Tokyo, Japan) spectrophotometer in the CIE Lab scale (L^*, a^*, and b^*).[25] The spectrophotometer had a 4-mm diameter viewing area and was equilibrated and calibrated with a standard tile before experiments. The samples were illuminated with standard D_{65} light, and the colorimetric normal observer angle was 10°. Coffee samples were made into pellets (13 × 1 mm) by a hydraulic press at a pressure of 6 tons. Color attributes were measured at six different points of each pellet on white and black backing. Each value reported is the mean of 12 measurements ± SEM. Three different roasting degrees were obtained: light (roasting time 14.5 min, $L^* = 51.62 \pm 0.23$, $a^* = 12.44 \pm 0.08$, and $b^* = 27.09 \pm 0.15$), medium-dark (roasting time 19 min, $L^* = 32.01 \pm 0.29$, $a^* = 9.00 \pm 0.09$, and $b^* = 11.12 \pm 0.16$), and dark roasted coffee (roasting time 23 min, $L^* = 25.98 \pm 0.44$, $a^* = 3.67 \pm 0.08$, and $b^* = 4.24 \pm 0.10$). The coffee samples were ground using a MKM 6003 coffee grinder (Bosch, Stuttgart, Germany).

Extract Preparation. Roasted and ground coffee were prepared using different extraction methods. Ground coffee (1.875 g) was suspended in a final volume of 50 mL of (A) medium temperature water at 60 °C or (B) hot water at 90 °C. Extracts were then cooled down to room temperature, filtered using a paper filter, and centrifuged for 15 min at 5500 rpm and a temperature of 15 °C. The supernatant was brought up to pH 8 with 0.5 M NaOH prior to further purification with the use of solid-phase extraction.

Trigonelline Pyrolysate Preparation. Crystalline trigonelline was ground in a porcelain mortar and placed as a thin layer (2–3 mm) on a Petri dish; the sample was then placed in a laboratory oven LE/4/11/R6 (Nabertherm, Bremen, Germany) and heated in a dry nitrogen atmosphere at 100 °C for 1 h. In the next step, the temperature was raised to 200 °C, and the sample was heated for additional 25 min. Trigonelline pyrolysate was cooled down to room temperature and extracted two times by chloroform. Extracted samples were dried at reduced pressure (0.1 mbar, RT). Samples of 2 mg and 0.2 mg of pyrolysate per 1 mL of Millipore-grade water were used for further analysis.

Solid-Phase Extraction (SPE) of Pyridinium Compounds from Coffee Extracts. Because of the cationic nature of pyridinium compounds, ion exchange chromatography with the use of propylcarboxylic acid Bakerbond CBA columns (J.T. Baker, Phillipsburg, NJ, USA) was chosen as a method of extraction. A portion of supernatant (5 mL) obtained after coffee extract preparation was loaded into a CBA column (500 mg), preconditioned with a methanol and water (each 5 mL). After penetration of column packing by a coffee solution, the column was washed with water followed by methanol (5 mL). The analyte was eluted with 0.2 M formic acid in water (5 mL). This acid fraction was transferred into a glass vial prior to UPLC/MS analyses.

Ultraperformance Liquid Chromatography–Electrospray Ionization Mass Spectrometry of Pyridinium Compounds in Trigonelline Pyrolysate and Coffee Extracts. All analyses of pyridinium compounds in coffee extracts and trigonelline pyrolysate were performed with an Aquity ultraperformance liquid chromatography system UPLC (Waters, Milford, MA, USA) coupled online to a photodiode array (PDA) spectrometer for UV/vis measurements and an LCT Premier XE oa-TOF mass spectrometer (Waters MicroMass, Manchester, UK). Separations were accomplished on 100 mm × 2.1 mm, i.d., 1.7 μm Acquity UPLC BEH C18 column with a 5 mm × 2.1 mm, i.d. guard column of the same material (Waters, Milford, MA, USA) maintained at 40 °C. Samples were eluted using 90% of 2 mM nonafluoropentanoic acid aqueous solution and 10% of methanol solution at a flow rate of 0.3 mL/min. The injection volumes and temperature for both sample and standard solutions were 0.2–2 μL and 4 °C, respectively. The mass spectrometer was operated in "W mode" with lock mass correction. Lock mass solution (leucine-enkephalin, reference mass: $[M]^+$ 556.2771 and $[M+H]^+$ 557.2801) was prepared fresh at a concentration of 0.5 ng/μL in water/acetonitrile (50:50; v/v) and stored at 4 °C until further use. Standards were prepared in Millipore-grade water. Ion chromatograms of pyridine derivative standards obtained at different m/z from mass spectrometer are presented in Figure 2. External calibration curves were established in the concentration range from 0.05 to 5 μM for

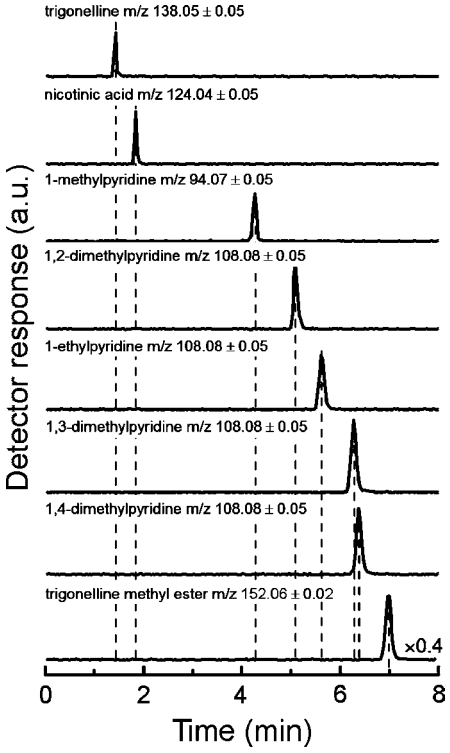

Figure 2. Ion-chromatograms of 500 nM standards of pyridine derivatives obtained at different m/z. Retention times: trigonelline, (**1**, t_R = 1.44 min); nicotinic acid, (**2**, t_R = 1.85 min); 1-methylpyridine, (**4**, t_R = 4.27 min); 1-ethylpyridine, (**8**, t_R = 5.10 min); 1,2-dimethylpyridine, (**5**, t_R = 5.62 min); 1,3-dimethylpyridine, (**6**, t_R = 6.27 min); 1,4-dimethylpyridine, (**7**, t_R = 6.38 min), and trigonelline methyl ester, (**9**, t_R = 7.00 min).

mass spectrometry and 5−1000 μM for UV/vis measurements. Analytes not falling within the given range were adequately diluted with water and reinjected. The amount of the compounds in the samples was calculated from the respective linear regression equation, r^2 > 0.999. Data acquisition and analyses were performed using MassLynx 4.1 data system software (Waters, Milford, MA, USA) and OriginPro 9.0c (OriginLab, Northampton, MA, USA).

Drugs Administration. 1-Methylpyridine (100 mg/kg/d), 1,3-dimethylpyridine (30, 100, 300 mg/kg/d), 1,4-dimethylpyridine (30, 100, 300 mg/kg/d), or vehicle was administered per os once a day for 10 days preoperatively. The animals received the examined drugs dissolved in drinking water or drinking water (vehicle) daily for 10 days via an intragastric probe.

Induction of Arterial Thrombosis. Male Wistar rats were anesthetized by intraperitoneal injection of pentobarbital (40 mg/kg) and placed in a supine position on a heated operation table. Arterial thrombosis was induced by electrical stimulation of the common carotid artery, according to methods previously described.[23,26−28] Briefly, the anode, a stainless steel L-shaped wire, was inserted under the artery and connected to a circuit with a constant current generator. The cathode was a subcutaneous metal needle attached to the hindlimb. The stimulation (1 mA) took 10 min. Forty-five minutes after stimulation, the segment of the common carotid artery with the formed thrombus was clipped at both sides, dissected, opened lengthwise, and the thrombus completely removed, air-dried in 37 °C, and weighed 24 h after the end of the experiment. After the removal of the formed thrombus, blood samples were taken from the heart. Platelet aggregation was assessed in whole blood directly after the experiment. The rest of the blood samples were drawn into 3.13% trisodium citrate in a volume ratio of 10:1, then centrifuged at 3500g in 4 °C for 20 min, and plasma was deep-frozen (−70 °C) in aliquots of 1 mL until further assays could be performed.

Measurement of Platelet Aggregation. Platelet aggregation was assessed in whole blood directly after the experiment by measuring electrical impedance in a Chronolog aggregometer (Chrono-log Corporation, Havertown, PA, USA) according to the method described by Cardinal et al.[29] Blood samples were drawn into 3.13% trisodium citrate in a volume ratio of 10:1. Collagen (5 μg/mL) was added after 15 min of incubation at 37 °C with 0.9% NaCl in a volume ratio of 1:2. Then changes in impedance were registered for 6 min. The results were expressed as percentages using four parameters: maximal extension, slope of platelet aggregation, lag phase, and area under the curve. In addition, in an in vitro study blood samples were mixed with 1,3-dimethylpyridine, 1,4-dimethylpyridine, or vehicle solution before incubation.

Plasma Level of 6-Keto-$PGF_{1\alpha}$, a Stable Metabolite of Prostacycline (PGI_2), Fibrynolysis, and Coagulation Parameters, and Blood Cell Count. Plasma level of 6-keto-$PGF_{1\alpha}$ was measured by ELISA technique in a microtiter plate at 25 °C using a microplate reader (Dynex Technologies, Chantilly, VA, USA) to monitor the changes in absorbance at 405 nm according to the manufacturer's directions. Concentrations of active rat PAI-1 and active rat t-PA were analyzed using ELISA techniques at 25 °C using a microplate reader according to the kit manufacturer's instructions. Both rat PAI-1 and rat t-PA kits were used in a bioimmunoassay for measuring rat PAI-1 and rat t-PA activities in rat plasma collected on trisodium citrate anticoagulant. The stop solutions changed the color from blue to yellow, and the intensity of the color was measured at 450 nm. PT and aPTT were automatically determined with a Coag-Chrom 3003 coagulometer (Bioksel, Grudziadz, Poland) adding routine laboratory reagents to the collected rat plasma. Fg was evaluated according to Clauss method.[30] Blood cell count was assessed by an animal blood counter (ABC Vet, Horiba ABX, Monpellier, France).

Fibrin Generation. Fibrin generation was estimated according to our modification[32,33] of the method of He et al.[31] Briefly, blood samples were drawn from the left ventricle of thrombotic rats, and platelet-rich plasma (PRP) was gained by centrifugation of citrated blood (1:10, 3.13%) at 300g at 4 °C for 20 min. A fibrin generation curve was created by adding thrombin (1 IU/mL) and $CaCl_2$ (36 mM) to the Tris buffer (66 mM Tris and 130 mM NaCl, pH 7.4) and

Table 1. Quantitative Analysis of Alkylpyridinium Derivatives Present in the Roasted Coffee Extracts[a]

roasting time (min)	extraction method	concentration of 1-ethylpyridine (μM)	1-methylpyridine (μM)	1,2-dimethylpyridine (μM)	1,3-dimethylpyridine (μM)	1,4-dimethylpyridine (μM)
14.5	water 60 °C	ND	4.8 ± 0.8	ND	ND	ND
	water 90 °C	ND	4.0 ± 0.3	ND	ND	ND
19.0	water 60 °C	0.07 ± 0.02	206 ± 3	NQ	0.03 ± 0.01	ND
	water 90 °C	0.23 ± 0.03	218 ± 3	NQ	0.14 ± 0.02	NQ
23.0	water 60 °C	0.50 ± 0.03	302 ± 2	0.05 ± 0.03	0.94 ± 0.06	NQ
	water 90 °C	0.69 ± 0.02	320 ± 10	0.11 ± 0.03	1.8 ± 0.2	NQ

[a]All values represent the mean ± SEM for at least n = 3. The calibration curve was r^2 > 0.999 within the given concentration range. ND, concentration below detection level; NQ, concentration below quantitation level.

dx.doi.org/10.1021/jf5008538 | J. Agric. Food Chem. 2014, 62, 2853−2860

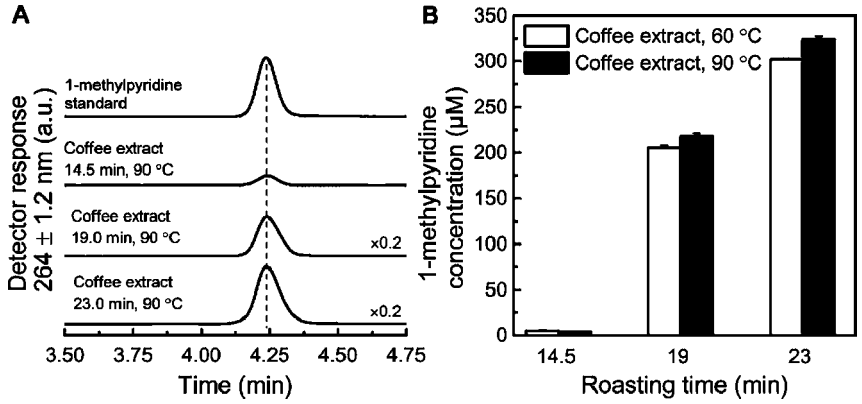

Figure 3. Influence of coffee roasting time and extraction procedure on the concentration of the main trigonelline thermal degradation product, 1-methylpyridine, in the coffee extracts samples. (A) Chromatograms obtained at 264 ± 1.2 nm with the use of a photodiode array detector (PDA) for 50 μM 1-methylpyridine standard and coffee samples of different roasting degrees. (B) Concentration of 1-methylpyridine in the coffee extract.

mixing with the platelet-rich plasma samples directly in the microplate wells. Optical density was measured via a microplate reader (Dynex Technologies, Chantilly, VA, USA) at 405 nm in 1 min intervals for 6 min and expressed as area under the curve (AUC).

Statistical Analysis. The data are shown as the mean ± SEM and analyzed using the nonparametric Mann−Whitney test. P values less than 0.05 were considered significant, less than 0.01 highly significant, and less than 0.001 extremely significant.

RESULTS AND DISCUSSION

The discrepancies between the results of the studies on coffee consumption in relation to the risk of cardiovascular disease and at the same time clear evidence for the beneficial role of coffee drinking from both epidemiologic[34] and experimental studies[11,13] encouraged us to search for new compounds in roasted coffee that could possibly improve endothelial function.

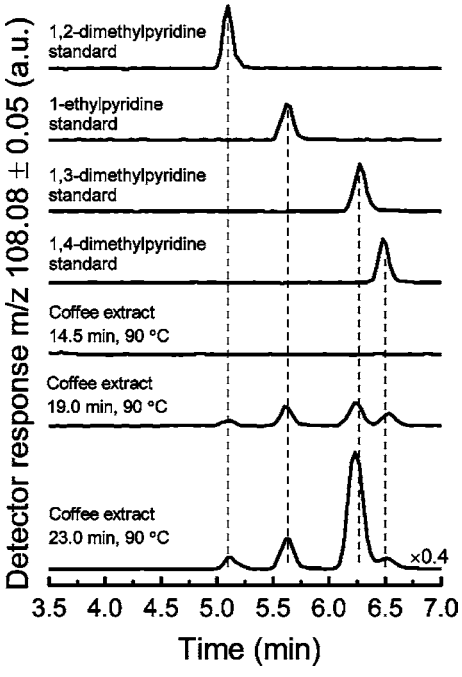

Figure 4. Influence of coffee roasting time on the profile of trigonelline thermal degradation products. Ion chromatograms obtained at m/z 108 ± 0.05 for 500 nM standards of 1-ethylpyridine, 1,2-, 1,3-, and 1,4-dimethylpyridine, and coffee extract samples (roasting time and extraction temperature are as indicated).

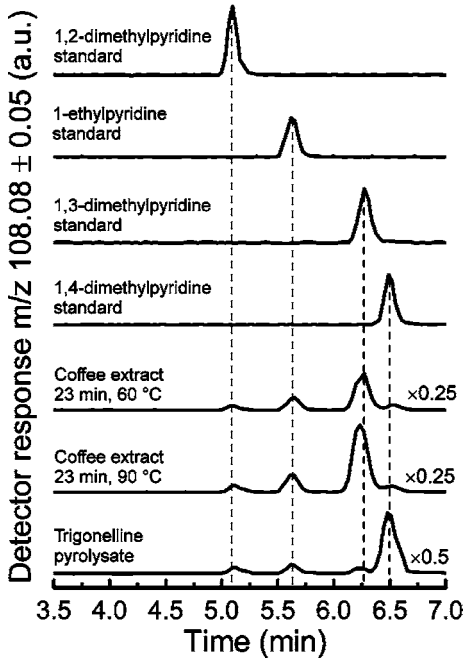

Figure 5. Difference between the profile of trigonelline thermal degradation products in coffee extracts and trigonelline pyrolysate. Ion chromatograms obtained at m/z 108 ± 0.05 for 500 nM standards of 1-ethylpyridine, 1,2-, 1,3-, and 1,4-dimethylpyridine, a dark roasted coffee sample, and trigonelline pyrolysate.

Table 2. Results of the Quantitative Analysis of Thermal Degradation Products of Trigonelline[a]

compd	quantity (mg)
trigonelline	0.91 ± 0.02
nicotinic acid	0.012 ± 0.001
1-methylpyridine	0.015 ± 0.001
1,2-dimethylpyridine	$(2.6 \pm 0.4) \times 10^{-6}$
1,3-dimethylpyridine	$(1.8 \pm 0.2) \times 10^{-6}$
1,4-dimethylpyridine	$(4.4 \pm 0.5) \times 10^{-5}$
1-ethylpyridine	$(6.8 \pm 0.8) \times 10^{-6}$
trigonelline methyl ester	$(6.3 \pm 1) \times 10^{-5}$
	0.94 ± 0.02

[a]The Major Products Identified in 1 mg of Trigonelline Pyrolysate.

dx.doi.org/10.1021/jf5008538 | J. Agric. Food Chem. 2014, 62, 2853−2860

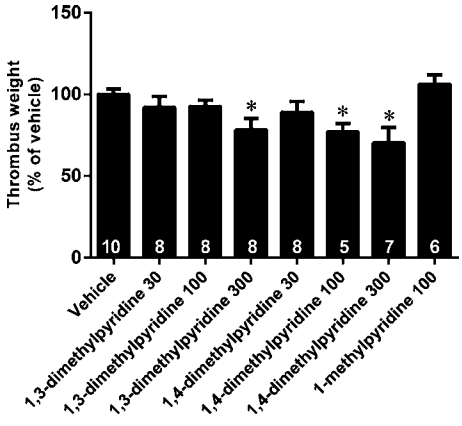

Figure 6. Columns represent the dry thrombus weight in Wistar rats treated (per os for 10 days) with vehicle, 1,3-dimethylpyridine (30, 100, and 300 mg/kg/d), 1,4-dimethylpyridine (30, 100, and 300 mg/kg/d), and 1-methylpyridine (100 mg/kg/d). Digits inside columns indicate *n* number. * $p < 0.05$ vs vehicle, Mann–Whitney test. Results are shown as the mean ± SEM.

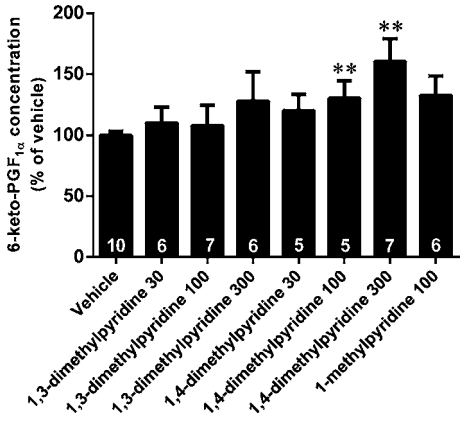

Figure 7. Columns represent the 6-keto-$PGF_{1\alpha}$ concentration in Wistar rats treated (per os for 10 days) with vehicle, 1,3-dimethylpyridine (30, 100, and 300 mg/kg/d), 1,4-dimethylpyridine (30, 100, and 300 mg/kg/d), and 1-methylpyridine (100 mg/kg/d). Digits inside columns indicate *n* number. ** $p < 0.01$ vs vehicle, Mann–Whitney test. Results are shown as the mean ± SEM.

As various factors could be responsible for the conflicting results of the studies on coffee drinking such as daily consumption and the type of coffee[35] or the role of coffee preparation,[36,37] we have focused our attention only on a selected group of compounds, pyridine derivatives (see Figure 1), present in the roasted coffee extracts and formed upon trigonelline pyrolysis.

As was shown previously by Stadler et al.,[19] during the roasting process nonvolatile alkylpyridinium salts are formed. Under a specific physiochemical condition, trigonelline, one of the most abundant compounds in green coffee, undergoes thermal degradation with subsequent formation of 1-methylpyridine and nicotinic acid, as major products, and dialkylpyridinium salts as minor products. There is a lack of information on the adverse effects of alkylpyridinium, especially dialkylpyridinium compounds. Some studies indicate that 1-methyl substituted analogues are less toxic than pyridine itself [38] but may activate cytochrome P450 CYP1A enzyme.[39] However, Szafarz et al.[40] did not observe any changes in basic biological parameters after intravenous administration of 1,4-dimethylpyridine at a dose of 100 mg/kg.

We have monitored the formation of 1-methylpyridine in coffee extracts using a photodiode array detector (PDA) coupled with a liquid chromatograph, by an increase in absorbance at 264 ± 1.2 nm. The concentration of 1-methylpyridine found in coffee extracts, expressed in μmol/L, is presented in Table 1 and Figure 3. Our findings are consistent with the previous results presented by Stadler et al.[19] Decomposition of trigonelline and subsequent formation of 1-methylpyridine increases with roasting time and higher temperature of extraction.

The formation of 1-methylpyridine, as expected, is also accompanied by the formation of dialkylpyridinium compounds as shown in Figure 4. Using a new chromatographic method with the mobile phase modifier, ion-pairing reagent, we were able to differentiate four different isomers with ions of identical m/z 108.08 ± 0.05 (Figure 4). As the formation of three dimethylpyridinium salts is known in the literature, the new entity was characterized and assigned to 1-ethylpyridine, mainly by comparison with its authentic standard. The formation of compounds specified by m/z equals 108.08 was also correlated with the formation of 1-methylpyridine and the degree of coffee roasting. The concentration of dialkylpyridinium compounds

Table 3. Platelet Aggregation, Platelet Count, and Fibrinolysis Parameters Measured in Rats Treated (per os for 10 days) with Vehicle, 1,3-Dimethylpyridine (30, 100, and 300 mg/kg/d), 1,4-Dimethylpyridine (30, 100, and 300 mg/kg/d), and 1-Methylpyridine (100 mg/kg/d)[a]

		1,3-dimethylpyridine			1,4-dimethylpyridine			1-methylpyridine
	vehicle	30	100	300	30	100	300	100
n	10	8	8	8	7	5	7	6
MaxA	100 ± 4.9	85.0 ± 6.1	85.3 ± 4.7	77.2 ± 5.1**	108.7 ± 3.7	111.0 ± 7.9	106.3 ± 3.9	109.4 ± 7.7
Slp	100 ± 4.1	93.7 ± 7.9	88.0 ± 4.0	80.9 ± 5.6*	105.3 ± 2.8	111.7 ± 6.0	109.3 ± 4.4	112.9 ± 5.1
Lag	100 ± 4.2	130.6 ± 6.1**	130.8 ± 6.8**	143.1 ± 8.4***	92.1 ± 3.2	98.4 ± 3.2	92.1 ± 6.0	99.0 ± 8.6
AUC	100 ± 7.1	78.8 ± 8.4	75.1 ± 7.2	68.2 ± 7.5**	106.5 ± 7.6	109.0 ± 5.9	105.2 ± 14.3	105.2 ± 14.3
PLT (10^3/mm^3)	555.3 ± 13.7	556.1 ± 16.8	546.6 ± 16.5	537.2 ± 18.7	533.6 ± 20.6	580.4 ± 16.2	562.4 ± 16.3	560.8 ± 21.3
PAI-1 activity	100 ± 5.6	89.1 ± 33.1	119.1 ± 14.9	101.1 ± 22.8	101.4 ± 15.6	107.5 ± 11.7	104.5 ± 9.7	88.1 ± 14.7
t-PA activity	100 ± 9.7	98.7 ± 10.7	103.7 ± 19.4	105.7 ± 8.2	131.6 ± 6.4*	108.5 ± 20.5	91.1 ± 7.2	133.9 ± 29.9

[a] *n*, number of animals; MaxA, maximal extension; Slp, slope of platelet aggregation; Lag, lag phase; and AUC, area under the curve. PAI-1 activity and t-PA activity expressed as % of vehicle; PLT, platelet count; * $p < 0.05$, ** $p < 0.01$, *** $p < 0.001$ vs vehicle, Mann–Whitney test. Results are shown as the mean ± SEM.

dx.doi.org/10.1021/jf5008538 | J. Agric. Food Chem. 2014, 62, 2853–2860

was 2 to 3 orders of magnitude lower than that of 1-methylpyridine. The main dialkylpyridinium compound, which is formed during coffee roasting is 1,3-dimethylpyridine. The concentrations of alkylpyridiniums salts present in the coffee extracts are listed in Table 1. We were not able to quantitate the amount of 1,4-dimethylpyridine due to the high concentration of 1,3-dimethylpyridine present in the extract.

As trigonelline, in contrast to caffeine, undergoes significant thermal degradation upon coffee roasting, including decarboxylation and demethylation (both processes take place in the temperature range typical for coffee roasting), it may be expected that similar products could be formed upon coffee roasting and trigonelline pyrolysis. Indeed, the analysis of trigonelline pyrolysate indicated the formation of similar products. The main dialkylpyridinium product formed from pyrolysis of trigonelline was not, however, as expected 1,3-dimethylpyridine but 1,4-dimethylpyridine, which is shown in Figure 5. The formation of 1-ethylpyridine and trigonelline methyl ester was also observed. The data of quantitative analysis of products formed during pyrolysis of trigonelline are presented in Table 2.

For some reason, the formation of 1,3-dimethylpyridine is favored during coffee roasting compared to pyrolysis of trigonelline itself, probably due to a great variety of other compounds being present in coffee beans. We assume that the formation of 1,3-dimethylpyridine rather than 1,4-dimethylpyridine in roasted coffee might be due to the direct reduction of trigonelline. In the case of thermal decomposition of pure trigonelline, bimolecular reactions might be preferred.

The influence of 1-methylpyridine, and 1,3- and 1,4-dimethylpyridine on the hemostasis and thrombotic processes is not known. To investigate that, we chose the model of experimental arterial thrombosis induced by electrical stimulation of carotid artery of rat. This experimental model enables simultaneous measurement of platelet aggregation and many other coagulation and fibrinolysis parameters. Although thrombus formation was initiated by electrical stimulation producing arterial injury that is unrelated to clinical thrombosis, platelet-rich thrombus morphology suggests that the growth of intravascular thrombotic material in response to electric injury is physiologically relevant.[27] Importantly, in this model platelets make a major contribution to the development of thrombosis as the inhibition of platelet activation by ASA and carbon monoxide or stimulation of endothelial release of PGI_2 by angiotensin-converting enzyme inhibitors or 1-methylnicotinamide afforded pronounced antithrombotic effects.[18,23,25,33,41] The collagen-induced platelet aggregation, and the markers of coagulation and fibrinolysis were also examined ex vivo. We administered these compounds at a dose of 100 mg/kg/d per os for 10 days to rats before the development of arterial thrombosis.

1-Methylpyridine had no effect on thrombus formation. Since we observed rather a trend to enhance the antithrombotic effect of the 100 mg/kg/d dose of 1-methylpyridine (106.3 ± 5.6% of control, for doses of 100 mg/kg/d; ns, Figure 6), other doses of this compound have not been elucidated. Moreover, we did not further evaluate this compound as a potential antithrombotic agent. By contrast, 1,3- and 1,4-dimethylpyridine inhibited arterial thrombus formation. 1,4-Dimethylpyridine at doses of 100 and 300 mg/kg/d decreased thrombus weight to 77.0 ± 5.2% ($p < 0.05$) and 71.3 ± 10.3% ($p < 0.05$), respectively. 1,3-Dimethylpyridine was effective at a dose of 300 mg/kg/d decreasing thrombus weight to 78.4 ± 6.9%. Not only did 1,3- and 1,4-dimethylpyridine appear to inhibit the progress of electrically induced carotid artery thrombosis but also was a more significant effect observed when we administered these pyridines in higher doses. These results indicate a new class of compounds with mild antithrombotic properties which can be found in coffee extracts.

We have further examined possible mechanisms of pharmacological activity of pyridine derivatives formed from trigonelline thermal decomposition. Since we have previously proven an important role of prostacyclin in the effect of many substances influencing endothelial function including structurally related pyridine derivatives such as 1-methylnicotinamide, we tried to elicit the contribution of prostacyclin to the antithrombotic effect of dimethylpyridinium compounds. Prostacyclin is produced in endothelial cells from prostaglandin H_2 by the action of the enzyme prostacyclin synthase and is a potent vasodilator and inhibitor of platelet aggregation.[42] We have found a dose-dependent increase in plasma level of 6-keto-$PGF_{1\alpha}$ (a stable metabolite of prostacyclin) in rats receiving 1,4-dimethylpyridine. 1,4-Dimethylpyridine increased the plasma level of 6-keto-$PGF_{1\alpha}$ to 130.3 ± 14.2% ($p < 0.01$) and 160.2 ± 18.9% ($p < 0.01$), at doses of 100 and 300 mg/kg/d, respectively. 1-Methylpyridine and 1,3-dimethylpyridine showed only a trend to increase the plasma level of 6-keto-$PGF_{1\alpha}$ (Figure 7). Prostacyclin (PGI_2) is thought to be one of the most important prostanoids in regulating the homeostasis of the cardiovascular system.[43,44] It is clear that pharmacological stimulation of PGI_2 in vivo might be beneficial in vascular diseases. So far, prostacyclin or its stable analogues have been widely used in the treatment of pulmonary hypertension[45] and have been proven effective in cases of peripheral arterial disease[46] or liver injury.[47]

We simultaneously measured collagen induced platelet aggregation after thrombus formation in rat arteries. We found that 1,3-dimethylpyridine exerted an antiaggregatory effect, decreasing collagen induced platelet aggregation (Table 3) in thrombotic animals. Both 1,3-dimethylpyridine and 1,4-dimethylpyridine (10^{-5}, 10^{-4}, and 10^{-3} M) did not significantly change platelet aggregation in in vitro experiments (data not shown). Since platelet activation is crucial in arterial thrombosis development, the antiplatelet activity of 1,3-dimethylpyridine could be responsible for its antithrombotic effect. The lack of influence of 1,4-dimethylpyridine on platelets, while stimulating prostacyclin release, was rather surprising and suggests a different mechanism of action. Thus, we performed in vitro experiments in which we incubated whole blood with various concentrations of examined compounds, but they both failed to directly influence platelet aggregation. It seems that the site of 1,3-dimethylpyridine action is not direct or that it acts through active metabolites.

Furthermore, we measured typical coagulation parameters, like prothrombin time (PT), activated partial thromboplastin time (aPTT), and fibrinogen (Fg) level using routine laboratory methods. 1-Methylpyridine and 1,3- and 1,4-dimethylpyridine failed to influence the activity of rat plasminogen activator inhibitor-1 (PAI-1) (Table 3), PT, aPTT, Fg, and blood cell count (data not shown). 1,3-Dimethylpyridine decreased fibrin formation in platelet-reach plasma, but not in platelet-poor plasma (data not shown), while 1-methylpyridine and 1,4-dimethylpyridine produced no effect (data not shown). 1,4-Dimethylpyridine increased slightly tissue plasminogen activator (t-PA) activity only at lowest

dose. 1-Methylpyridine and 1,3- and 1,4-dimethylpyridine at higher doses failed to influence t-PA activity (Table 3).

Inhibition of fibrin generation in platelet-reach but not in platelet-poor plasma by 1,3-dimethylpyridine suggests platelet involvement in the antithrombotic effect of this compound. This effect is in line with the inhibitory effect of 1,3-dimethylpyridine on platelet aggregation in whole blood. According to the fibrinolytic parameters analysis, we may also assume that the fibrinolytic system is not involved in the anithrombotic effect of dimethylpiridinium salts.

In conclusion, we demonstrated here that pyridinium compounds present in roasted coffee possess the antithrombotic prostacyclin releasing (1,4-dimethylpyridine) and platelet inhibiting (1,3-dimethylpyridine) properties. Although they have a cationic chemical nature and their permeability through cell membranes might be difficult, they can reach relatively high dose-dependent concentration in blood.[22] This property would be important for all orally administered formulations. We may hypothesize that 1,3-dimethylpyridine could be a promising agent preventing atherothrombosis development, where the platelets play a crucial role, whereas 1,4-dimethylpyridine could be beneficial in states with impaired prostacyclin endothelial production. Our findings on the novel in vivo biological activity of dimethylpiridinium compounds may have potentially important therapeutic implications and warrant further studies, although low concentration of dialkylpyridinium salts in the roasted coffee probably limits their contribution to the overall antithrombotic functions of coffee beverages.

■ ASSOCIATED CONTENT

Supporting Information

Description of the synthesis of pyridinium derivatives (1-methylpyridine, 1,2-, 1,3-, and 1,4-dimethylpyridine, 1-ethylpyridine, and trigonelline methyl ester). This material is available free of charge via the Internet at http://pubs.acs.org.

■ AUTHOR INFORMATION

Corresponding Author

*Tel: +48 857485601. Fax: +48 857485601. E-mail: kalaskab@gmail.com.

Funding

This work was supported by the European Union from the resources of the European Regional Development Fund under the Innovative Economy Programme (grant coordinated by JCET-UJ, No. POIG.01.01.02-00-069/09).

Notes

The authors declare no competing financial interest.

■ REFERENCES

(1) Nurminen, M. L.; Niittynen, L.; Korpela, R.; Vapaatalo, H. Coffee, caffeine and blood pressure: a critical review. *Eur. J. Clin. Nutr.* **1999**, *53*, 831−839.

(2) Noordzij, M.; Uiterwaal, C. S.; Arends, L. R.; Kok, F. J.; Grobbee, D. E.; Geleijnse, J. M. Blood pressure response to chronic intake of coffee and caffeine: a meta-analysis of randomized controlled trials. *J. Hypertens.* **2005**, *23*, 921−928.

(3) Farag, N. H.; Vincent, A. S.; McKe, B. S.; Whitsett, T. L.; Lovallo, W. R. Hemodynamic mechanisms underlying the incomplete tolerance to caffeine's pressor effects. *Am. J. Cardiol.* **2005**, *95*, 1389−1392.

(4) Smits, P.; Thien, T.; van 't Laar, A. Circulatory effects of coffee in relation to the pharmacokinetics of caffeine. *Am. J. Cardiol.* **1985**, *56*, 958−963.

(5) Karatzis, E.; Papaioannou, T. G.; Aznaouridis, K.; Karatzi, K.; Stamatelopoulos, K.; Zampelas, A.; Papamichael, C.; Lekakis, J.; Mavrikakis, M. Acute effects of caffeine on blood pressure and wave reflections in healthy subjects: should we consider monitoring central blood pressure? *Int. J. Cardiol.* **2005**, *98*, 425−430.

(6) Robertson, D.; Frölich, J. C.; Carr, R. K.; Watson, J. T.; Hollifield, J. W.; Shand, D. G.; Oates, J. A. Effects of caffeine on plasma renin activity, catecholamines and blood pressure. *N. Engl. J. Med.* **1978**, *298*, 181−186.

(7) Papamichael, C. M.; Aznaouridis, K. A.; Karatzis, E. N.; Karatzi, K. N.; Stamatelopoulos, K. S.; Vamvakou, G.; Lekakis, J. P.; Mavrikakis, M. E. Effect of coffee on endothelial function in healthy subjects. The role of caffeine. *Clin. Sci.* **2005**, *109*, 55−60.

(8) Wu, J. N.; Ho, S. C.; Zhou, C.; Ling, W. H.; Chen, W. Q.; Wang, C. L.; Chen, Y. M. Coffee consumption and risk of coronary heart diseases: a meta-analysis of 21 prospective cohort studies. *Int. J. Cardiol.* **2009**, *137*, 216−225.

(9) Greenberg, J. A.; Chow, G.; Ziegelstein, R. C. Caffeinated coffee consumption, cardiovascular disease, and heart valve disease in the elderly (from the Framingham Study). *Am. J. Cardiol.* **2008**, *102*, 1502−1508.

(10) Bidel, S.; Hu, G.; Sundvall, J.; Kaprio, J.; Tuomilehto, J. Effects of coffee consumption on glucose tolerance, serum glucose and insulin levels-a cross-sectional analysis. *Horm. Metab. Res.* **2006**, *38*, 38−43.

(11) Buscemi, S.; Verga, S.; Batsis, J. A.; Tranchina, M. R.; Belmonte, S.; Mattina, A.; Re, A.; Rizzo, R.; Cerasola, G. Dose-dependent effects of decaffeinated coffee on endothelial function in healthy subjects. *Eur. J. Clin. Nutr.* **2009**, *63*, 1200−1205.

(12) Natella, F.; Nardini, M.; Belelli, F.; Pignatelli, P.; Di Santo, S.; Ghiselli, A.; Violi, F.; Scaccini, C. Effect of coffee drinking on platelets: inhibition of aggregation and phenols incorporation. *Br. J. Nutr.* **2008**, *100*, 1276−1282.

(13) Toda, E.; Ishida, H.; Aoki, T.; Urano, T.; Takahari, Y.; Tamura, N.; Goto, S. Possible mechanism of preventive effects of coffee intake on the formation of arterial occlusive thrombosis. *Tokai J. Exp. Clin. Med.* **2010**, *35*, 133−136.

(14) Spiller, M. A. The Chemical Components of Coffee. In *Caffeine*; Spiller, G. A., Ed.; CRC Press Inc.: Boca Raton, FL, 1998; pp 97−161.

(15) Bonita, J. S.; Mandarano, M.; Shuta, D.; Vinson, J. Coffee andcardiovascular disease: in vitro, cellular, animal, and human studies. *Pharmacol. Res.* **2007**, *55*, 187−198.

(16) Yukawa, G. S.; Mune, M.; Otani, H.; Tone, Y.; Liang, X. M.; Iwahashi, H.; Sakamoto, W. Effects of coffee consumption on oxidative susceptibility of low-density lipoproteins and serum lipid levels in humans. *Biochemistry* **2004**, *69*, 70−74.

(17) Bydlowski, S. P.; Yunker, R. L.; Rymaszewski, Z.; Subbiah, M. T. Coffee extracts inhibit platelet aggregation in vivo and in vitro. *Int. J. Vitam. Nutr. Res.* **1987**, *57*, 217−223.

(18) Chlopicki, S.; Swies, J.; Mogielnicki, A.; Buczko, W.; Bartus, M.; Lomnicka, M.; Adamus, J.; Gebicki, J. 1-Methylnicotinamide (MNA), a primary metabolite of nicotinamide, exerts anti-thrombotic activity mediated by a cyclooxygenase-2/prostacyclin pathway. *Br. J. Pharmacol.* **2007**, *152*, 230−239.

(19) Stadler, R. H.; Varga, N.; Hau, J.; Vera, F. A.; Welti, D. H. Alkylpyridiniums. 1. Formation in model systems via thermal degradation of trigonelline. *J. Agric. Food Chem.* **2002**, *50*, 1192−1199.

(20) Somoza, V.; Lindenmeier, M.; Wenzel, E.; Frank, O.; Erbersdobler, H. F.; Hofmann, T. Activity-guided identification of a chemopreventive compound in coffee beverage using in vitro and in vivo techniques. *J. Agric. Food Chem.* **2003**, *51*, 6861−6869.

(21) Gebicki, J.; Marcinek, A.; Chlopicki, S.; Adamus, J. PCT International Application. WO 2008104920 A1, 2008.

(22) Lang, R.; Wahl, A.; Skurk, T.; Yagar, E. F.; Schmiech, L.; Eggers, R.; Hauner, H.; Hofmann, T. Development of a hydrophilic liquid interaction chromatography-high-performance liquid chromatography-tandem mass spectrometry based stable isotope dilution analysis and pharmacokinetic studies on bioactive pyridines in human plasma and urine after coffee consumption. *Anal. Chem.* **2010**, *82*, 1486−1497.

(23) Mogielnicki, A.; Kramkowski, K.; Pietrzak, L.; Buczko, W. N-methylnicotinamide inhibits arterial thrombosis in hypertensive rats. *J. Physiol. Pharmacol.* **2007**, *58*, 515−527.
(24) Giles, A. R. Guidelines for the use of animals in biomedical research. *Thromb. Haemost.* **1987**, *58*, 1078−1084.
(25) CIE Colorimetry Committee. Technical notes: working program on colour differences. *J. Opt. Soc. Am.* **1974**, *64*, 896−897.
(26) Schumacher, W. A.; Heran, C. L.; Youssef, S.; Megill, J. R.; Michel, I.; Durham, S. K. Comparison of a thromboxane receptor antagonist and aspirin in experimental arterial thrombosis. *Haemostasis* **1993**, *23*, 219−228.
(27) Guarini, S. A highly reproducible model of arterial thrombosis in rats. *J. Pharmacol. Toxicol. Methods* **1996**, *35*, 101−105.
(28) Kaminska, M.; Mogielnicki, A.; Stankiewicz, A.; Kramkowski, K.; Domaniewski, T.; Buczko, W.; Chabielska, E. Angiotensin II via AT_1 receptor accelerates arterial thrombosis in renovascular hypertensive rats. *J. Physiol. Pharmacol.* **2005**, *56*, 571−585.
(29) Cardinal, D. C.; Flower, R. J. The electronic aggregometer: a novel device for assessing platelet behavior in blood. *J. Pharmacol. Methods* **1980**, *3*, 135−158.
(30) Clauss, A. Gerinnungsphysiologische schnellmethode zur bestimmung des fibrinogens. *Acta Haematol.* **1957**, *17*, 237−246.
(31) He, S.; Antovic, A.; Blomback, M. A simple and rapid laboratory method for determination of haemostasis potential in plasma. II. Modifications for use in routine laboratories and research work. *Thromb. Res.* **2001**, *103*, 355−361.
(32) Buczko, W.; Mogielnicki, A.; Kramkowski, K.; Chabielska, E. Aspirin and the fibrinolytic response. *Thromb. Res.* **2003**, *110*, 331−334.
(33) Kramkowski, K.; Leszczynska, A.; Mogielnicki, A.; Chlopicki, S.; Fedorowicz, A.; Grochal, E.; Mann, B.; Brzoska, T.; Urano, T.; Motterlini, R.; Buczko, W. Antithrombotic properties of water-soluble carbon monoxide-releasing molecules. *Arterioscler., Thromb., Vasc. Biol.* **2012**, *32*, 2149−2157.
(34) Lopez-Garcia, E.; van Dam, R. M.; Willett, W. C.; Rimm, E. B.; Manson, J. E.; Stampfer, M. J.; Rexrode, K. M.; Hu, F. B. Coffee consumption and coronary heart disease in men and women: a prospective cohort study. *Circulation* **2006**, *113*, 2045−2053.
(35) Montagnana, M.; Favaloro, E. J.; Lippi, G. Coffee intake and cardiovascular disease: virtue does not take center stage. *Semin. Thromb. Hemost.* **2012**, *38*, 164−177.
(36) Silletta, M. G.; Marfisi, R.; Levantesi, G.; Boccanelli, A.; Chieffo, C.; Franzosi, M.; Geraci, E.; Maggioni, A. P.; Nicolosi, G.; Schweiger, C.; Tavazzi, L.; Tognoni, G.; Marchioli, R. Coffee consumption and risk of cardiovascular events after acute myocardial infarction: results from the GISSI (Gruppo Italiano per lo Studio della Sopravvivenza nell'Infarto miocardico)-Prevenzione trial. *Circulation* **2007**, *116*, 2944−2951.
(37) Di Castelnuovo, A.; di Giuseppe, R.; Iacoviello, L.; de Gaetano, G. Consumption of cocoa, tea and coffee and risk of cardiovascular disease. *Eur. J. Intern. Med.* **2012**, *23*, 15−25.
(38) D'Souza, J.; Caldwell, J.; Smith, R. L. Species variations in the N-methylation and quaternization of [^{14}C]pyridine in vivo. *Xenobiotica* **1980**, *10*, 151−157.
(39) Iba, M. M.; Fung, J.; Giannone, J. V.; Okey, A. B. Comparative induction of CYP1A1 expression by pyridine and its metabolites. *Arch. Biochem. Biophys.* **2000**, *378*, 299−310.
(40) Szafarz, M.; Szymura-Oleksiak, J.; Zakrzewska, A.; Walczak, M.; Kus, K.; Gonciarz, A. Liquid chromatography-mass spectrometry method for the analysis of 1,4-dimethylpyridinium in rat plasma-application to pharmacokinetic studies. *Biomed. Chromatogr.* **2013**, *27*, 73−79.
(41) Wojewódzka-Zelezniakowicz, M.; Chabielska, E.; Mogielnicki, A.; Kramkowski, K.; Karp, A.; Opadczuk, A.; Domaniewski, T.; Malinowska-Zaprzałka, M.; Buczko, W. Antithrombotic effect of tissue and plasma type angiotensin converting enzyme inhibitors in experimental thrombosis in rats. *J. Physiol. Pharmacol.* **2006**, *57*, 231−245.
(42) Morita, I. Distinct functions of COX-1 and COX-2. *Prostaglandins Other Lipid Mediators* **2002**, *68/69*, 165−175.
(43) Cheng, Y.; Austin, S. C.; Rocca, B.; Koller, B. H.; Coffman, T. M.; Grosser, T.; Lawson, J. A.; FitzGerald, G. A. Role of prostacyclin in the cardiovascular response to thromboxane A2. *Science* **2002**, *296*, 539−541.
(44) Kawabe, J.; Ushikubi, F.; Hasebe, N. Prostacyclin in vascular diseases. - Recent insights and future perspectives. *Circ. J.* **2010**, *74*, 836−843.
(45) Wise, H.; Jones, R. L. Focus on prostacyclin and its novel mimetics. *Trends. Pharmacol. Sci.* **1996**, *17*, 17−21.
(46) Szczeklik, A.; Gryglewski, R. J.; Nizankowski, R.; Skawiński, S.; Głuszko, P.; Korbut, R. Prostacyclin therapy in peripheral arterial disease. *Thromb. Res.* **1980**, *19*, 191−199.
(47) Ohta, S.; Nakamuta, M.; Fukushima, M.; Kohjima, M.; Kotoh, K.; Enjoji, M.; Nawata, H. Beraprost sodium, a prostacyclin (PGI) analogue, ameliorates concanavalin A-induced liver injury in mice. *Liver Int.* **2005**, *25*, 1061−1068.

XXX-3′; this is an adaptor sequence that attaches to the 5′ end of the mRNA template; X stands for undisclosed nucleotides protected by the manufacturer). The RACE ready cDNA was synthesized by a SMARTScribe reverse transcriptase. Then, 3′-RACE PCR was performed using the 3′-RACE Ready cDNA as a template, a Universal Primer A Mix (long, 5′-*CTAATACGACTCACTATAGGGC*AAGCAGTGGTATCAACGCAGAGT-3′; short, 5′-*CTAATACGACTCACTATAGGGC*-3′), and a gene-specific degenerate primer p320 (5′-GGTTACGGTCAATGTATGTGAT-3′) obtained from the PCP N-terminal amino acid sequence. 5′-RACE PCR was performed using the 5′-RACE Ready cDNA as a template, a Universal Primer A Mix, and a gene-specific primer p5-320-2 (5′-ATTGTATGTGAGTTGCATCATGTC-3′) designed on the basis of the sequence of 3′-RACE products. Finally, the complete cDNA sequence of PCP was revealed by combining the product sequences of 3′-RACE PCR and the 5′-RACE PCR. The accession number of the PCP cDNA sequence is JN571084.1.

Primary Cell Acquisition and Cell Cultures. Primary lymphocytes were acquired from murine spleens as previously described.[14] In brief, the total splenocytes were obtained from spleens excised from euthanized mice, and the splenic T cells were either positively or negatively purified using a MACS system with microbeads of anti-CD90, -CD4, -CD8, or anti-B220 antibodies (Miltenyi Biotec, Bergisch Gladbach, Germany), respectively. The purity of the purified T cells used in this study was >95%. The cells were seeded in 96-well flat-bottom plates (Corning, Lowell, MA, USA) at 4×10^6 cells/mL and were stimulated with or without PCP at indicated concentrations, ConA (5 μg/mL) or LPS (1 μg/mL), for 72 h. In some experiments, the purified T cells were seeded in rat anti-mouse CD3/CD28 antibody-coated 96-well plates. All cells were grown in a CO_2 incubator under humidified atmosphere of 5% CO_2 at 37 °C.

Mice and Animal Experiments. Female 6−8-week-old BALB/c were purchased from the National Laboratory Animal Center (Taipei, Taiwan) and used for splenic cell acquisition and in vivo studies.

To assess the in vivo effect of PCP, mice were ip injected with 50 μg/100 μL OVA adsorbed on aluminum hydroxide adjuvant or with adjuvant i alone as a nonimmunized vehicle. The mice were randomly grouped into four (n = 6 each). The first two groups were orally administered by gavage 0.5 mL of PCP solution (2 mg/mL in PBS) at 50 mg/kg body weight (1 mg/mouse) once daily and immunized with OVA or with saline vehicle, respectively. The two other groups were given an equal volume of PBS and immunized with OVA or with saline vehicle, respectively. OVA-immunized mice were immunized on days 0 and 14. Blood samples (100 μL per mouse) were collected from tail veins at various time points (days 0, 10, and 24) after immunization.

To evaluate the potential of PCP to attenuate Th2-dominat allergic response, an OVA-induced atopic dermatitis (AD) murine model, which was developed by Spergel and his collegues,[15] was performed. In brief, female BALB/c mice aged 6−8 weeks were randomly divided into three groups, each consisting of four mice (n = 4). The back skin of all the mice was shaved and tape stripped six times with 3M tape to simulate the skin injury inflicted by scratching in patients with AD. The first group of mice was orally administered daily 200 μL of PBS and sensitized daily in the sensitizing periods with 20 μL of saline vehicle placed on a 1 cm^2 patch of sterile gauze, which is secured to the skin with a transparent bio-occlusive dressing to repel licking by the mice. The other group of mice was administered daily 200 μL of PBS and sensitized with 20 μL of skin-patched OVA (100 mg/mL) in the manner described above. The last group of mice was administered daily 200 μL of PCP (5 mg/mL) and sensitized with skin-patched OVA (100 mg/mL) in the manner described above. There were two sensitizing periods in the AD model; the first period began from day 3 to day 8, and the second period began from day 22 to day 27. Oral administration began on day 0 and terminated on day 32, the end point of the AD model. Blood samples (100 μL per mouse) were collected on day 8 via tail veins of the mice. The lymphocytes of the mice were obtained from the axillary nodes, the brachial nodes, and the inguinal nodes and cultured in the presence or absence of OVA (100 mg/mL) for 48 h. The cell-free culture supernatant was collected for cytokine quantification via ELISA.

Cell Proliferation Analysis by BrdU Incorporation Assay. Cell proliferation was measured using a cell proliferation ELISA BrdU (colorimetric) kit (Roche, Basel, Switzerland) according to the user's manual. Data acquisition was carried out by measuring A_{450} on a Bio-Rad microplate reader (Bio-Rad Laboratories).

Cytokines and Igs Quantification by ELISA. The level of cytokines IFN-γ, IL-2, IL4, IL-5, and TNF-α presented in the cell-free culture supernatants were measured by sandwich ELISA using OptEIA murine IFN-γ, IL-2, IL-4, IL-5, and TNF-α ELISA kits (eBioscience, San Diego, CA, USA), respectively, following the manufacturer's protocols. The levels of the total Igs and the OVA-specific Igs presented in mouse serum were measured by sandwich ELISA using a Mouse MonoAb ID Kit (Invitrogen) and indirect ELISA, respectively, according to the user's manual. Data acquisition was carried out by measuring A_{450} on a Bio-Rad microplate reader. The results were expressed as ELISA units (EU), which were calculated by comparison with mouse IgG standards.

Cytokine Gene Expression Analysis by Quantitative Real-Time PCR. Complementary DNA samples were obtained from T cells treated with or without PCP (100 μg/mL). Gene expression was assessed by quantitative real-time PCR according to the manufacturer's protocol. The results were normalized to endogenous genes (β-actin or GAPDH). The expression level of each target gene was calculated by cycle threshold (Ct) analysis. The sense and antisense primer pairs are β-actin, 5′-GTGGGCCGCTCTAGGCACC-3′ and 5′-CTCTTTGATGTCACGCACGA-3′; G3PDH, 5′-ATGAATACGGCTACAGCA-3′ and 5′-TGGAAATTGTGAGGGAGAT-3′; T-bet, 5′-GGAGAACTTTGAGTCCAT-3′ and 5′-GTAGAAACGGCTGGGAA-3′; GATA3, 5′-CTGCGGACTCTACCATA-3′ and 5′-TTAGCGTTCCTCCTCCA-3′; ROR γ T, 5′-TGAGATTGCCCTCTACAC-3′ and 5′-GCAGAGATGATGATGGAAA-3′; and Foxp3, 5′-TGAGTTTCGCAAGAAGAG-3′ and 5′-GGTTTCCATAGGTACACG-3′.

Detection of Cell Surface Marker and Intracellular IFN-γ by Flow Cytometry. Mouse splenocytes and MACS-purified cells were treated with the indicated samples for 72 h and then collected and suspended in FACS buffer and stained with FITC- or PE-conjugated antibodies specific for CD3, CD4, CD8 (BD Biosciences), CD44, and CD69 (eBioscience) at 4 °C for 0.5 h. Flow cytometry data were acquired on a FACScan (Becton Dickinson and Co., Franklin Lakes, NJ, USA) and analyzed by CellQuest software.

To estimate intracellular production of IFN-γ and granzyme B in T cells by PCP, $CD4^+$ and $CD8^+$ cells isolated from splenocytes by the MACS purification system were incubated with the indicated stimulants or medium alone in the presence of anti-CD3/CD28 antibodies for 72 h. After incubation, brefeldin A (10 μg/mL; eBioscience) was added to block cytokine release. After an additional 6 h, cells were washed, fixed in Fixation Solution (eBioscience), and incubated in the dark at room temperature for 30 min. Then, the cells were permeabilized using the Permeabilization Buffer (eBioscience), stained with PE-conjugated mAbs specific for mouse IFN-γ and granzyme B (eBioscience), and analyzed by flow cytometry.

Immunoprecipitation of STAT4 and STAT6. Isolated $CD90^+$ cells were stimulated with 100 μg per mL of PCP for 4, 8, 16, and 24 h, respectively, in the presence or absence of anti-CD3/CD28 antibodies. Then, the cells were homogenized in RIPA buffer. The homogenate was centrifuged, and the supernatant was collected for total protein detection. The supernatant was immunoprecipitated using the mouse monoclonal antibodies against STAT4 or STAT6 (Santa Cruz Biotechnology, Dallas, TX, USA) overnight with gentle mixing at 4 °C. After incubation with STAT4 or STAT6 antibodies, the lysate was incubated with Protein G plus/Protein A agarose for 3 h with gentle mixing at 4 °C. The solution was then centrifuged, and the pellet was suspended in 20 μL of SDS sample buffer and subjected to SDS-PAGE and Western blot analysis. Blots were incubated with mouse anti-phosphotyrosine antibodies (Merck KGaA) and subsequently detected using a HRP-conjugated anti-mouse IgG (KPL, Gaithersburg, MD, USA). Membranes were washed extensively with Tris-buffered saline with Tween 20. Proteins were detected using the Western Lightning Chemiluminescence Reagent Plus (PerkinElmer, Waltham, MA, USA) and subjected to X-ray autoradiography. In addition, antibodies were

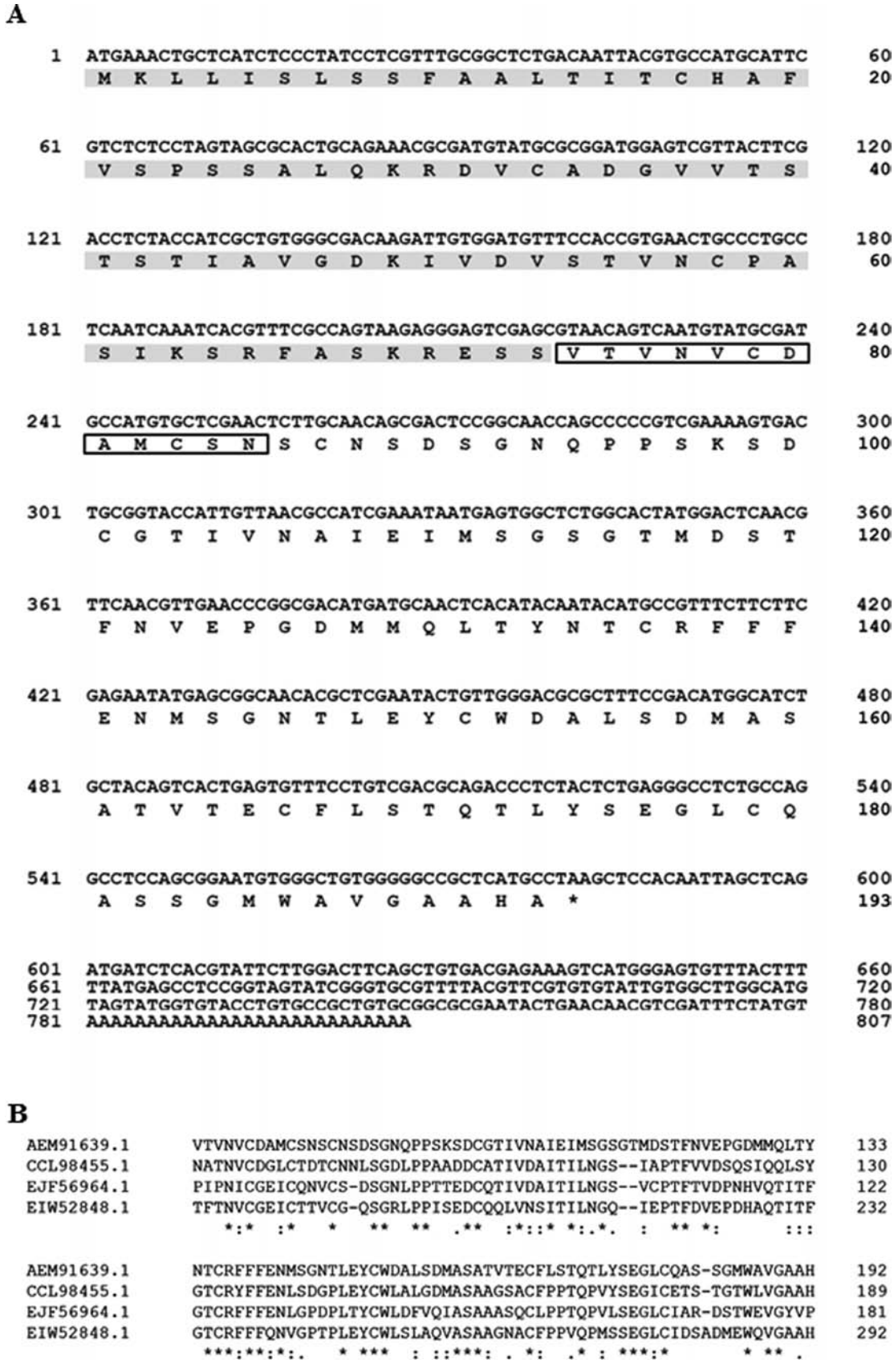

Figure 1. Complete cDNA sequence of PCP gene cloned via RACE PCR. (A) The full-length cDNA sequence of PCP was generated by combining the 3′- and 5′-RACE products. The N-terminal amino acid sequence is boxed, the signal peptide sequence is indicated by a gray background, and the stop codon is indicated by an asterisk. (B) Multiple alignment of PCP amino acid sequence with sequences of proteins from Polyporaceae fungi was performed by ClustalW omega program on the Web site of EMBL-EBI (http://www.ebi.ac.uk/Tools/msa/clustalo/). Identical, highly similar, and similar residues are marked with asterisks, colons, and dots, respectively.

Table 1. Homology Analysis of PCP Amino Acid Sequence with Proteins from Polyporaceae Fungi

species	name	accession no.	length	identity (%)	similarity (%)	gap (%)
P. cocos	PCP	AEM91639.1	193			
F. radiculosa	predicted protein	CCL98455.1	190	49	65	1
T. versicolor	TRAVEDRAFT_31886	EIW52848.1	293	46	60	3
D. squalens	DICSQDRAFT_157655	EJF56964.1	182	43	59	9

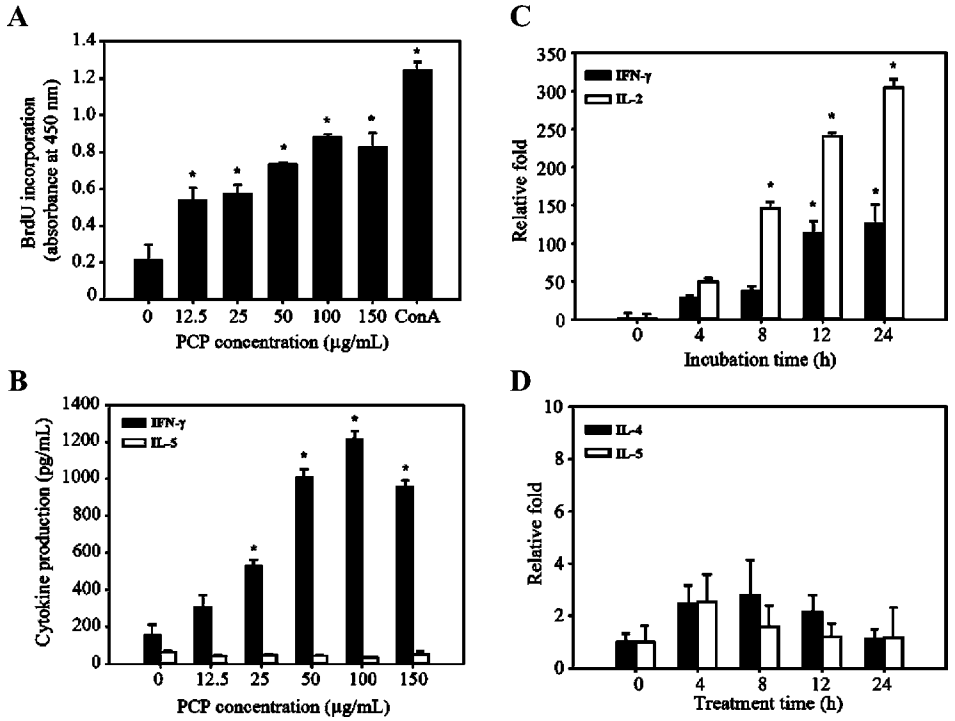

Figure 2. PCP activates murine splenocytes. (A) Mouse splenocytes were incubated with PCP at the indicated concentrations or ConA (5 μg/mL) as a positive control for 54 h. Cell proliferation was determined by measuring BrdU incorporation into DNA for an additional 18 h. (B) Mouse splenocytes were incubated with PCP at the indicated concentrations for 72 h. Culture supernatants were collected to determine their IFN-γ and IL-5 levels by sandwich ELISA methods. Statistical difference was compared to the level in untreated control cells (∗, $P < 0.05$). (C, D) Mouse splenocytes were treated with PCP at each time point. RNAs from treated cells were isolated and subjected to RT-PCR using specific primer sets for mouse Th1-associated cytokines (C; IFN-γ and IL-2), Th2-associated cytokines (D; IL-4 and IL-5), and β-actin. The values were normalized by dividing by the amount of β-actin gene expression in real-time PCR analysis. Each bar of the histogram represents a minimum of three experiments, and data are presented as the mean ± SD (∗, $P < 0.05$ compared to the culture medium control (0 h).

removed by 2% SDS, 62.5 mM Tris, pH 6.8, 100 mM β-mercaptoethanol buffer. The membrane was reprobed with rabbit anti-mouse STAT4 or STAT6 antibodies (Santa Cruz Technology) and detected with HRP-conjugated anti-rabbit IgG (KPL) as a loading control.

Statistical Analysis. All in vitro data are presented as means ± SD of three independent experiments ($n = 3$). All animal experiment data are presented as means ± SE of at least two independent experiments performed in quadruplicate or hexaplicate. Statistical comparison was made by one-way ANOVA followed by a Duncan multiple-comparisons test. Differences were considered as statistically significant when the P values were <0.05.

RESULTS

Cloning the PCP Gene. The N-terminal sequence of PCP was VTVNVXDAMXSN. This sequence was used to design degenerate primers to clone the PCP gene. 3′-RACE was performed using a gene-specific primer p320 (5′-GGTTAC-GGTCAATGTATGTGAT-3′). A 700 bp product, PR320-700, was obtained. This product contained the sequence of the N-terminal sequence of PCP (Figure S1 of the Supporting Information). Another primer, p5-320-2 (5′-ATTGTATG-TGAGTTGCATCATGTC-3′), was made to perform 5′-RACE PCR. A 550 bp product, PR5-320-2-550, was generated. The 83rd to 94th amino acid residues of the translated PR5-320-2-550 sequence were the same as the N-terminal amino acid sequence of PCP (Figure S2 of the Supporting Information). We merged PR320-700 and PR5-320-2-550 to acquire the complete cDNA sequence of PCP (Figure 1A).

It was an 807 bp nucleotide sequence. It had a 579 bp ORF and encoded 193 amino acids. It also had a putative signal peptide at the first 19 amino acid residues as shown in Figure S3 of the Supporting Information. The accession number of this sequence is JN571084.

We also performed sequence homology analysis on PCP using the NCBI protein Blast tool (Figure 1B and Table 1). The sequence of PCP shared 49% identical sequence with a *Fibroporia radiculosa* predicted protein (CCL98455.1), 46% identical sequence with a *Trametes versicolor* hypothetical protein TRAVEDRAFT_31886 (EIW52848.1), and 43% identical sequence with a *Dichomitus squalens* hypothetical protein DICSQDRAFT_157655 (EJF56964.1). Notably, these proteins were all derived from fungi of the Polyporaceae family, suggesting that PCP might be related to a universally expressed fungal protein.

PCP Activates Murine T Cells in the Presence of Co-stimulatory Signals. To determine the induction of PCP on mouse splenocytes, we first estimated the regulation of cell proliferation and cytokine secretion under PCP stimulation measured by using BrdU incorporation and sandwich ELISA methods. As shown in Figure 2A, PCP was able to induce an enhancement of cell proliferation in a dose-dependent manner. Upon stimulation with 100 μg/mL PCP, the maximum BrdU incorporation rate in splenocytes was observed. In particular, PCP induced a 4−5-fold-increased BrdU incorporation as compared to medium alone. Meanwhile, the similarity in cytokine production results showed that PCP markedly activated mouse splenocytes to increase their secretion of IFN-γ in vitro, whereas there was no significant change on IL-5 production (Figure 2B). In the presence of PCP (100 μg/mL), the amount of IFN-γ secreted was up to 1225 pg/mL; however, the incubation of PCP failed to enhance IL-5 production in mouse splenocytes. Because IFN-γ is a cytokine strongly associated with a Th1 response and impedes the development of Th2 responses, we suggested that PCP might up-regulate Th1-mediated immunity. To test this possibility, we further examined the effect of PCP on Th1- and Th2-associated cytokine gene expression. Stimulation of mouse splenocytes with PCP (100 μg/mL) resulted in a time-dependent increase in IFN-γ and IL-2 mRNA expression as measured by quantitative real-time PCR (Figure 2C). In contrast, the mRNA expression of IL-4 and IL-5 in mouse splenocytes was insignificantly increased upon PCP treatment between 4 and 8 h in comparison with those in control untreated cells (Figure 2D). These results suggested that PCP directly enhanced mouse splenocyte activation and promoted Th1-associated cytokine production.

In addition, we tested if $CD4^+$ and $CD8^+$ T cell populations in the spleen were changed through induction of PCP at different concentrations characterized by flow cytometry. CD69 is the earliest activation marker newly synthesized and expressed during T lymphocyte activation.[16] Accordingly, we also investigated the expression of CD69 on $CD4^+$ and $CD8^+$ T cells upon PCP stimulation. Slight increases in $CD4^+$ and $CD8^+$ T cell populations were observed in splenocytes upon PCP stimulation (Figure 3A). However, remarkable increases of CD69-positive cells were seen in both $CD4^+$ and $CD8^+$ T cells after PCP stimulation (Figure 3A).

To further clarify the PCP-induced lymphocyte population, we utilized the MACS system with specific magnetic beads to obtain purified lymphocytes. Because CD28 co-stimulation is also important in T cell activation,[17] $CD90^+$ cells, which are composed mainly of CD4 and CD8 T cell subsets, were isolated from BALB/c mice by positive selection and stimulated in vitro using plate-bound anti-CD3 and anti-CD28 antibodies. Different concentrations of PCP were introduced to the culture system, and cell proliferation was analyzed by BrdU incorporation analysis. PCP treatment increased the proliferation rate of sorted $CD90^+$ cells upon CD3/CD28-mediated activation in a dose-dependent manner (Figure 3B). The maximum response of $CD90^+$ cells was achieved at a concentration of 100 μg/mL of PCP, whereas PCP resulted in a slight increase in cell proliferation of non-$CD90^+$ cells (mainly B cells). $CD4^+$ and $CD8^+$ T cells were isolated from total splenocytes, and the cell proliferation upon PCP stimulation in a combination of anti-CD3/CD28 antibodies was analyzed. The results provided strong evidence for $CD4^+$ and $CD8^+$ T cell proliferation (Figure 3C). These results

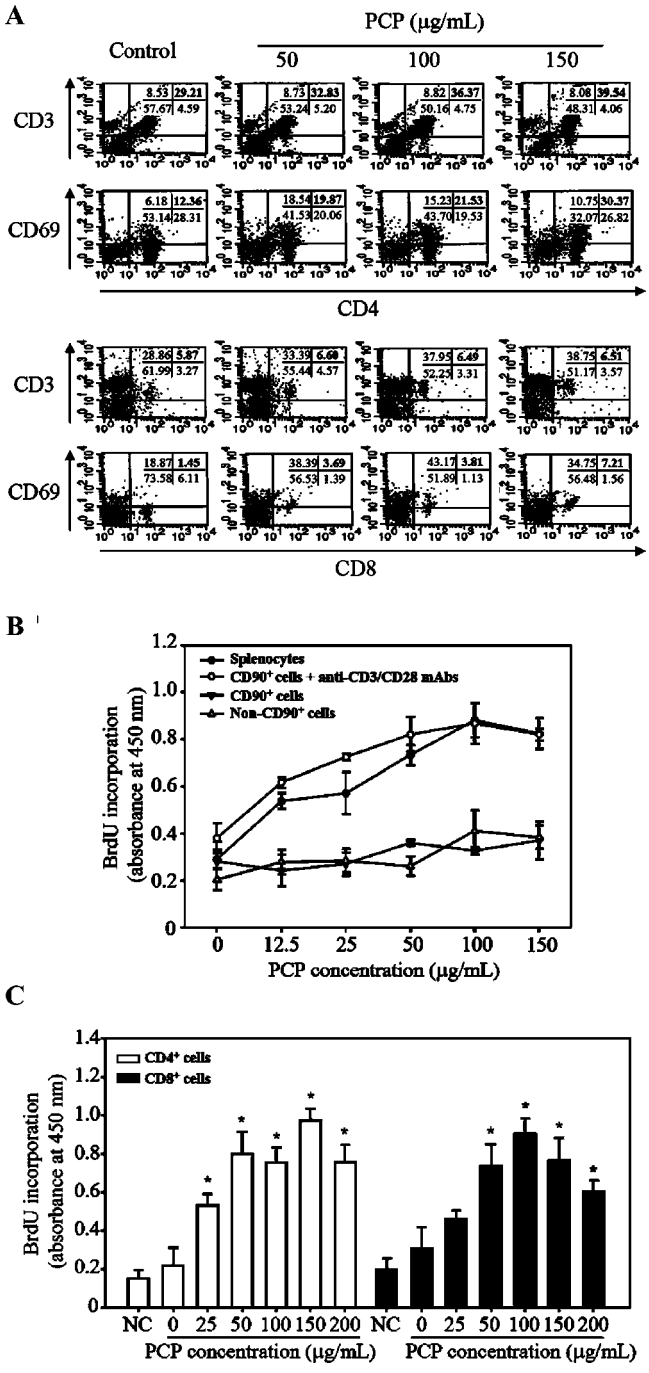

Figure 3. PCP activates murine $CD90^+$ T lymphocytes. (A) Splenocytes were stimulated with PCP (50, 100, and 150 μg/mL), ConA (5 μg/mL), and LPS (1 μg/mL) in combination with anti-CD3/CD28 antibodies for 72 h, and cells were then stained with PE-conjugated anti-CD3 and CD69 antibodies and FITC-conjugated anti-CD4 and CD8 antibodies, respectively. The flow cytometry data are representative of three independent sets of analyses. (B) $CD90^+$ cells were sorted from BALB/c mouse splenocytes using anti-CD90 coated magnetic microbeads. Anti-CD3/CD28 stimulated $CD90^+$ cells, unstimulated $CD90^+$ cells, non-$CD90^+$ cells, and splenocytes were cultured in medium containing various concentrations of PCP for 54 h. (C) Purified $CD4^+$ and $CD8^+$ T cells were activated with anti-CD3/CD28 antibodies in the presence of various concentrations of PCP for 54 h. Cell proliferation was quantified by measuring BrdU incorporation into DNA for an additional 18 h. NC, negative control (medium alone). (*, $P < 0.05$ compared to the anti-CD3/CD28 alone control.)

dx.doi.org/10.1021/jf405507e | J. Agric. Food Chem. 2014, 62, 2861−2871

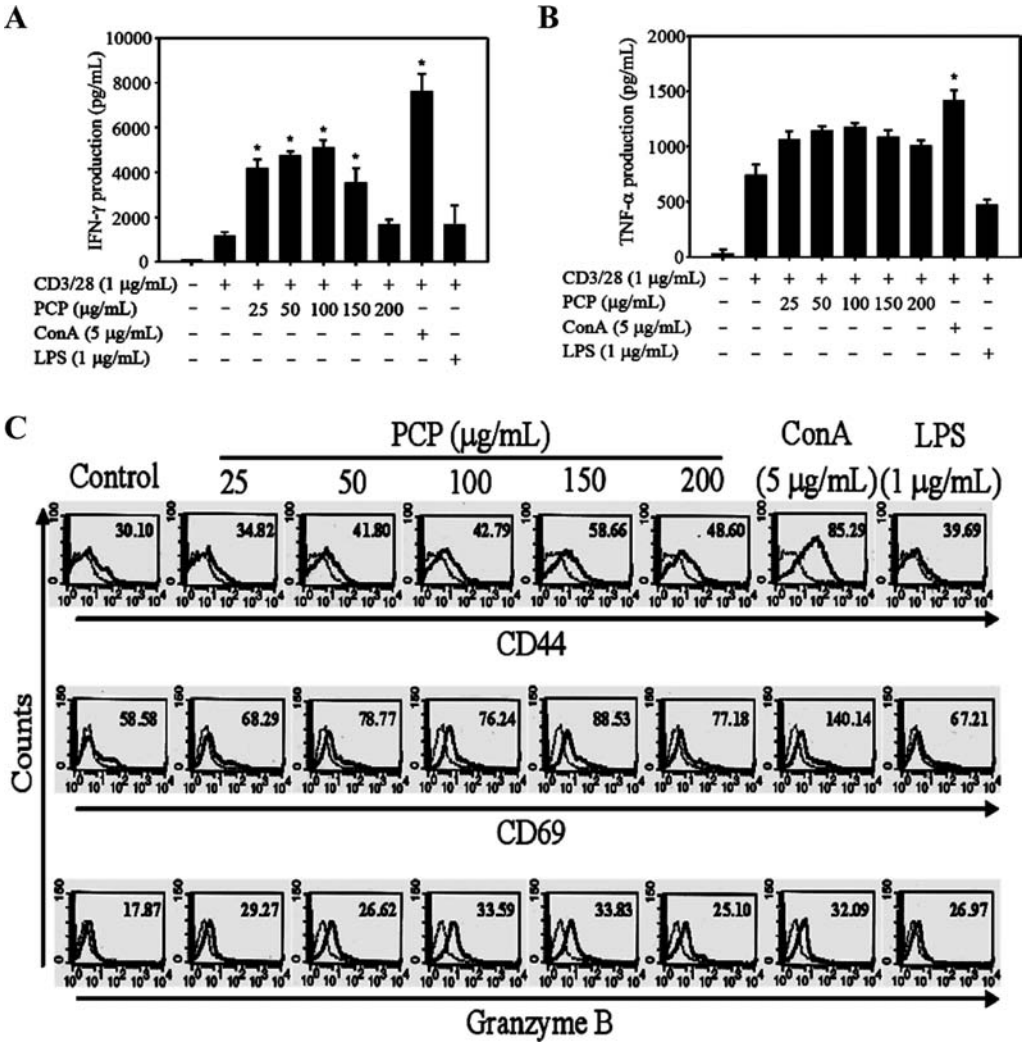

Figure 4. PCP activates murine CD8$^+$ T lymphocytes. (A) Purified CD8$^+$ T cells were activated with anti-CD3/CD28 antibodies in the presence of various concentrations of PCP for 72 h. Culture supernatants were collected to determine the production of IFN-γ and TNF-α measured by sandwich ELISA methods. (B) Purified CD8$^+$ T cells were stimulated with PCP (25−200 μg/mL), ConA (5 μg/mL), and LPS (1 μg/mL) in combination with anti-CD3/CD28 antibodies for 72 h, and cells were then stained with PE-conjugated anti-CD44 and CD69 antibodies and intracellularly stained with PE-conjugated anti-mouse granzyme B antibodies, respectively. The flow cytometry data are representative of three independent sets of analyses. The shaded area shows the unstained control. The solid line indicates the cell surface expression of CD44 and CD69, and intracellular granzyme B level in CD8$^+$ T cells, respectively. The histograms were quantified and represented as mean fluorescence intensity (MFI).

indicated that PCP could enhance the activation of both CD4$^+$ and CD8$^+$ T cells in the presence of a CD3/CD28 co-stimulation signal, demonstrating the up-regulation of cell proliferation and the early activation molecule CD69 expression believed to be involved in transmission of co-stimulatory signals in T cells.

PCP Enhances the Effector Functions of Purified CD8$^+$ and CD4$^+$ T Cells. To clarify whether PCP induced CD8$^+$ T cell activation, we also evaluated distinct cytokine production, the expression of activation markers CD44 and CD69, and the levels of granzyme B on sorted CD8$^+$ T cells. It is well-known that granzyme B is a serine proteinase released by effector CD8$^+$ T cells to kill abnormal cells. CD8$^+$ T cells can also produce cytokines such as TNF-α and IFN-γ. As shown in Figure 4A, PCP exhibited potential activating effects on CD8$^+$ T cells inducing significant increases in the production of IFN-γ and TNF-α secretion; whereas there was no detectable difference in IL-2 levels between the PCP-treated cells and the anti-CD3/CD28 alone control (data not shown). Moreover, we also observed PCP-induced up-regulation of CD44 and CD69 expression on CD8$^+$ T cells in combination with anti-CD3/CD28 antibodies (Figure 4B). A significant increase in intracellular granzyme B levels was also observed in PCP-treated cells when compared to anti-CD3/CD28 control cells. In this study, we demonstrated that PCP was able to activate CD8$^+$ T cells and enhance their effector functions.

To demonstrate that PCP prompted T helper cell development, CD4$^+$ T cells were activated with anti-CD3/CD28 antibodies and cultured in PCP-containing medium at different concentrations to evaluate T helper cell associated cytokine production and transcription factor gene expression. The mRNA levels of respective transcription factors were determined by using a quantitative real-time PCR after various incubation times. PCP treatment (100 μg/mL) increased the mRNA level of T-bet by almost 4.6-fold, whereas it showed only slight fluctuations in relative gene expression levels of

GATA-3, RORγt, and Foxp3 (Figure 5A). To determine whether PCP stimulated phosphorylation of STAT4 (Th1

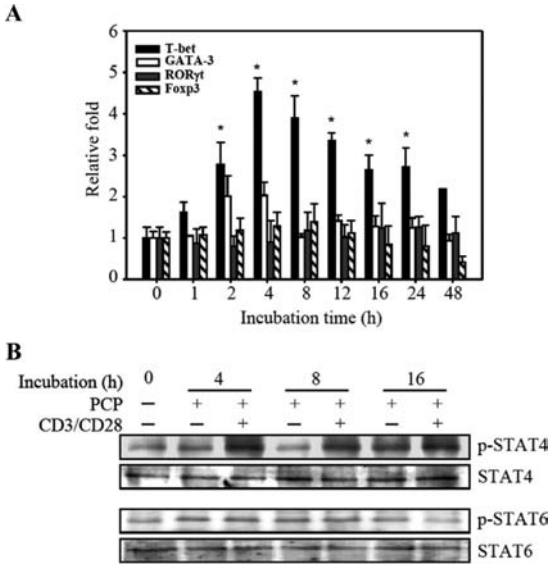

Figure 5. PCP induces the expression of T-bet and the phosphorylation of STAT4 in $CD4^+$ T lymphocytes. (A) Purified $CD4^+$ T cells were treated with PCP in combination with anti-CD3/CD28 antibodies at each time point. RNAs from treated cells were isolated and subjected to RT-PCR using specific primer sets for mouse Th1-associated transcription factor T-bet, Th2-associated transcription factor GATA-3, Th17-associated transcription factor RORγt, Treg-associated transcription factor Foxp3, and β-actin. The values were normalized by dividing by the amount of β-actin gene expression. (∗, $P < 0.05$ compared to the anti-CD3/CD28 alone control (0 h).) (B) Cell lysates from control or PCP-treated $CD4^+$ T cells at the indicated times were immunoprecipitated with anti-STAT4 and STAT6 antibodies and then resolved by SDS-PAGE. Blots were probed with anti-phosphotyrosine (upper panel) or anti-STAT4 and STAT6 (lower panel) antibodies in each group.

transcription factor) or STAT6 (Th2 transcription factor), the cell lysates from control and PCP-stimulated $CD4^+$ T cells with or without combination of anti-CD3/CD28 antibodies were precipitated with antibodies against STAT4 or STAT6. The immunoprecipitates were then detected using either anti-phosphotyrosine or anti-STAT4 or anti-STAT6 antibodies. In the present study, PCP was demonstrated to stimulate STAT4 tyrosine phosphorylation in a time-dependent manner, whereas treatment with PCP (100 μg/mL) had no effect on STAT6 tyrosine phosphorylation compared to anti-CD3/CD28 control cells at indicated time (Figure 5B). In addition, the secretion of Th1-associated cytokines including IFN-γ and IL-2 was dramatically increased under PCP stimulation in the presence of anti-CD3/CD28 antibodies; however, Th2-associated cytokines containing IL-4 and IL-5 were not altered in their secretion levels (Figure 6A). The maximum IFN-γ and IL-2 production was observed at concentrations ranging from 50 to 150 μg/mL of PCP. As shown in Figure 6B, the flow cytometry results also indicated that $CD4^+$ T cells expressed high levels of activation markers CD44 and CD69 after incubation with PCP in the presence of anti-CD3/CD28 antibodies and also increased intracellular production of IFN-γ, but not IL-4 (data not shown). These results implied that PCP specifically primed naive $CD4^+$ T cell differentiation into the Th1 subset.

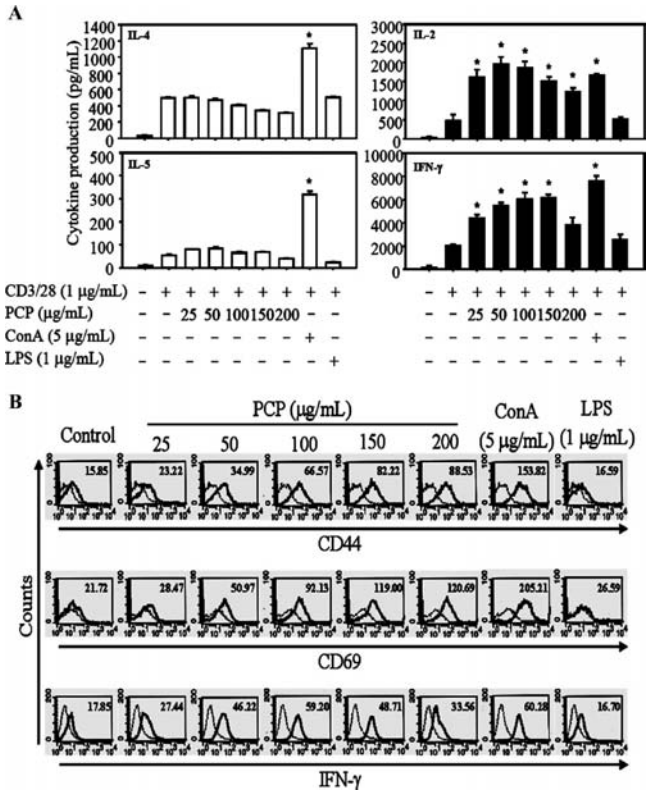

Figure 6. PCP activates murine $CD4^+$ T lymphocytes. (A) Purified $CD4^+$ T cells were incubated with PCP at the indicated concentrations (25, 50, 100, 150, and 200 μg/mL) in combination with anti-CD3/CD28 antibodies for 72 h. Culture supernatants were collected to determine the production of Th1-associated cytokines including IFN-γ and IL-2, and Th2-associated cytokines including IL-4 and IL-5 measured by sandwich ELISA methods. Statistical difference was compared to the level in anti-CD3/CD28 alone control cells (∗, $P < 0.05$.) (B) Purified $CD4^+$ T cells were stimulated with PCP (25−200 μg/mL), ConA (5 μg/mL), and LPS (1 μg/mL) in combination with anti-CD3/CD28 antibodies for 72 h, and cells were then stained with PE-conjugated anti-CD44 and CD69 antibodies and intracellularly stained with PE-conjugated anti-mouse IFN-γ antibodies, respectively. The flow cytometry data are representative of three independent sets of analyses. The shaded area shows the unstained control. The solid line indicates the cell surface expression of CD44 and CD69 and intracellular IFN-γ level in $CD4^+$ T cells, respectively. The histograms were quantified and represented as mean fluorescence intensity (MFI).

Oral Administration of PCP Enhances Th1-Related Immunoglobulin and Cytokine Production by Murine Splenocytes. Sensitization of BALB/c mice with ip injection of OVA protein absorbed to aluminum hydroxide two times as described previously[18] led to the development of an antigen-specific Th2-type response to OVA. The above results suggested that PCP could up-regulate Th1-mediated responses in vitro. Therefore, it was examined whether PCP was involved in the modulation of the Th1 pathway by using the animal model containing the OVA-sensitized murine model to confirm the influence of PCP on $CD4^+$ T cells. In our preliminary study, we fed BALB/c mice varying dosages of PCP (0.5, 1, or 2 mg per mouse) or PBS every day and collected sera on day 7 for the measurement of IFN-γ. We found that the optimal dose was 1 mg per mouse of PCP for maximal induction of IFN-γ in vivo (data not shown); therefore, this dosage was employed for further experiments.

dx.doi.org/10.1021/jf405507e | J. Agric. Food Chem. 2014, 62, 2861−2871

Immunized and nonimmunized mice were orally administered PCP (1 mg per mouse once daily) or an equal volume of PBS as a control for 24 days. As shown in Figure 7A, the production of total IgG1 in sera of PCP-treated mice was suppressed as compared with that of PBS-treated mice, especially in both OVA-immunized and nonimmunized mice on day 24. On the other hand, PCP-treated mice showed a significant increase of total IgG2a levels after administration for 10 days. In OVA-immunized mice, the serum level of OVA-specific IgG1 was significantly decreased when mice were administered PCP, whereas the level of OVA-specific IgG2a was highly increased in a statistically significant manner on day 24. There were a slight decrease on IgE levels and no significant change in IgA and IgG2b after administration of PCP in all situations (data not shown).

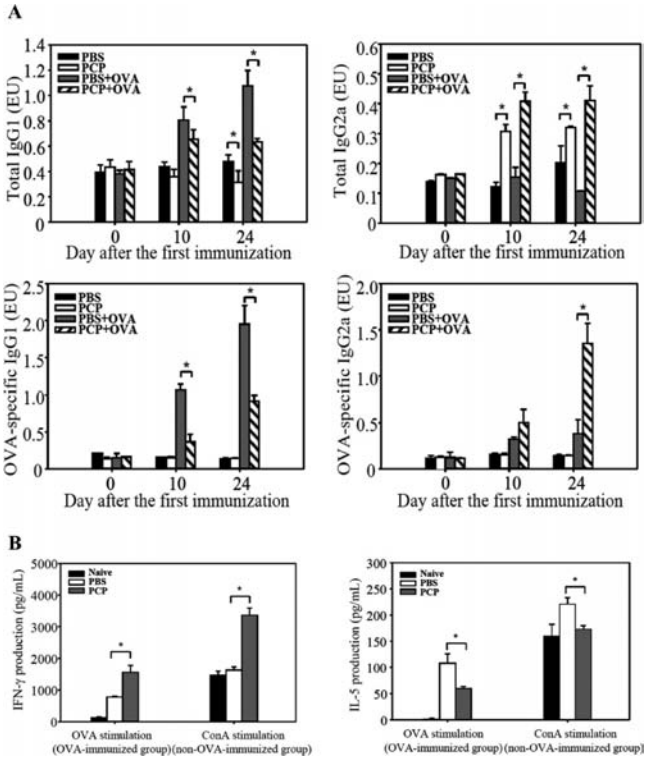

Figure 7. Orally administered PCP activates Th1-associated immunoglobulin and cytokine production in mice. (A) BALB/c mice were injected intraperitoneally with or without OVA under PCP or PBS treatment and their serum total and anti-OVA IgG1 and IgG2a responses determined. Mice administered orally PCP (1 mg per mouse once daily) or PBS were immunized with or without 50 μg of OVA on days 0 and 14, and serum samples were collected on days 0, 10, and 24 after the first immunization. Data represent the mean ± SE, and each group had six mice (∗, $P < 0.05$ among the different groups.) (B) Splenocytes from treated BALB/c mice were prepared on day 24 and incubated with 10 μg/mL OVA or 1 μg/mL ConA for 72 h, respectively. The culture supernatants were collected and used to determine their IFN-γ and IL-5 production. Naive mice had neither additional administration nor immunization with OVA and were used as a negative control. Data represent the mean ± SE ($n = 5$; ∗, $P < 0.05$ among the different groups).

It has been reported that cytokines play an important role in antibody response. Accordingly, we investigated the regulatory effect of PCP on Th1 and Th2 responses in PCP- and PBS-treated mice. On day 24, mice from each group were sacrificed to obtain splenocytes and then incubated in the presence of OVA (OVA-immunized group) and ConA (nonimmunized group) for 3 days, and then culture supernatants were collected to measure the levels of IFN-γ and IL-5. Following in vitro stimulation with ConA, oral administration of PCP increased the IFN-γ level and decreased the IL-5 level compared with oral administration of PBS (Figure 7B, top panel). Moreover, there was no difference in cytokine production by splenocytes stimulated with ConA between PBS-treated and naive mice. In addition, the level of IFN-γ was enhanced by OVA stimulation, and oral administration of PCP further increased the IFN-γ production by splenocytes from OVA-immunized mice. Unlike the induction of IFN-γ, the level of IL-5 significantly decreased in OVA-immunized mice after oral administration of PCP compared with oral administration of PBS (Figure 7B, bottom panel). These results indicated that PCP changed the balance of Th1/Th2 cell immune responses from Th2 dominant to Th1 dominant in OVA-immunized mice.

Oral Administration of PCP Allays IL-4 and IgE Production in a Murine AD Model. To evaluate the potential of PCP to attenuate Th2-dominat allergic response, an OVA-induced AD murine model was performed. The mice were sensitized by OVA and orally administered PCP or saline. At the end of the animal experiment, the lymph nodes were collected for cytokine production quantification and the serum was collected for immunoglobulin measurement. OVA sensitization caused a reduction in IFN-γ production by the lymphocytes; however, PCP administration restored IFN-γ production to normal range found for the control mice that were sensitized by saline (Figure 8A). In addition, OVA

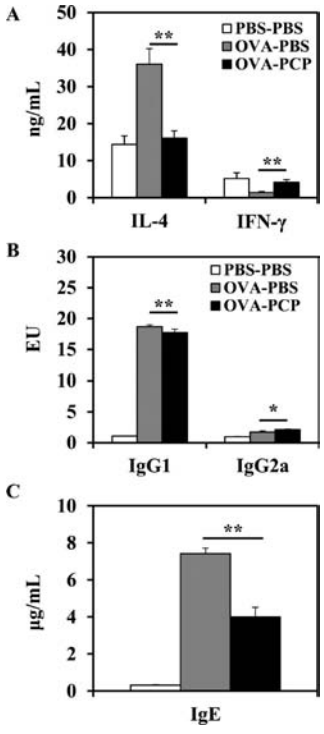

Figure 8. Orally administered PCP alleviates Th2-associated cytokines and immunoglobulin production in mice. (A) IFN-γ and IL-4 production by lymph node cells was detected after 48 h of incubation. ($n = 5$; ∗, $P < 0.05$, and ∗∗, $P < 0.001$, among the different groups.) OVA-specific (B) IgG1 and IgG2a and (C) IgE present in mice serum were detected by ELISA. Data represent the mean ± SE ($n = 5$; ∗, $P < 0.05$ among the different groups).

dx.doi.org/10.1021/jf405507e | J. Agric. Food Chem. 2014, 62, 2861−2871

sensitization also caused a significant increase in lymphocyte IL-4 production, whereas PCP administration restored IFN-γ production to normal range found for the control mice (Figure 8B). The IgE level in serum surged in the mice sensitized with OVA; however, PCP administration significantly reduced this effect by 46% (Figure 8C). In addition, PCP also increased the IgG2a level and reduced the IgG1 level in OVA-sensitized mice (Figure 8D,E). Altogether, oral administration of PCP was capable of alleviating the production of Th2 cytokine and Th2 immunoglobulins.

DISCUSSION

In our previous study we characterized the biochemical features and the TLR4/MyD88-mediated macrophage activating effect of PCP.[6] In this study we determined the complete cDNA sequence of the PCP gene. Taking advantage of the sequence information, we were able to compare the biochemical features that we previously acquired with the sequence-derived biochemical data obtained from bioinformatics tools. The predicted molecular weight (MW) of PCP from the N-terminus to the first stop codon is 12.8 kDa (Figure S4 of the Supporting Information). We previously showed that PCP is a heterodimeric protein consisting of 14.3 and 21.3 subunits. Interestingly, these subunits had identical N-terminal amino acid sequences and the same amino acid composition.[6] This suggested that the difference in MW of the subunits might result from different post-translational modification, such as N- and O-linked glycosylation that was also demonstrated in our previous paper. On the basis of the sequence we obtained in this study, it could be inferred that PCP is composed of two identical 12.8 kDa protein subunits; however, these subunits are asymmetrically modified. It was plausible that the 14.3 and 21.3 kDa subunits were conjugated to a 1.5 kDa glycan and a 8.5 kDa glycan, respectively. Neverthless, further studies are required to clarify these assumptions. The predicted p*I* value of PCP was 3.8 (Figure S4 of the Supporting Information), meaning that PCP carried a negative charge when suspended in the Tris buffer, pH 8.2. This negative charge made it possible for anion-exchange chromatographic purification for PCP. In addition, using YinOYang 1.2 prediction and the NetNGly 1.0 prediction software, we showed that PCP could have O-glycosylation at the 39th and 97th residues and N-glycosylation at the 142nd residue. This finding corresponded well with our previous prediction.[6]

Homology analysis of the PCP amino acid sequence revealed an interesting finding. PCP shared a similar sequence with other fungal proteins from the Polyporaceae family, including *F. radiculosa*, *T. versicolor*, and *D. squalens*. Although *F. radiculoss* and *D. squalens* are mainly studied for their lignin digestion activities, *T. versicolor* is a known for its immunomodulatory and tumor-resisting capabilities.[19] We have recently discovered the critical contribution of *T. versicolor* protein in regard to the immunomodulatory effects of the fungus. The current finding suggested that PCP might be related to a ubiquitously expressed protein conserved in the Polyporaceae family. It would be of great scientific value to investigate the existence and function of such protein in other Polyporaceae fungi.

T lymphocytes play a critical role in the development of adaptive immune response.[20] Recent studies have implicated efficient antigen presentation and T cell priming as being central for the practical implementation of clinical applications. Our results collectively showed a pronounced elevation of MHC class II and CD86 expression on mouse peritoneal macrophages in response to PCP, suggesting PCP had the capability of strengthening APCs that are necessary for T cell activation and proliferation. Accordingly, we further characterized the effects of PCP on $CD4^+$ and $CD8^+$ T cell responses. According to our data, PCP increased cell proliferation and activation marker expression of splenic $CD4^+$ and $CD8^+$ T and induced a predominant IFN-γ response in vitro. Naive T cells are activated antigens presented on APCs.[21] Among PCP-induced $CD8^+$ T cell activation, the increased proliferation of $CD8^+$ T cells was accompanied by differentiation into granzyme B-producing cells. Effector $CD8^+$ CTLs play a pivotal role in the successful clearance of viruses, intracellular microorganisms, and tumors.[22] Therefore, PCP might have a beneficial effect on these circumstances as well. Furthermore, the combined role of PCP as antigen and immunomodulator has led to the suggestion that it might provide an important link between innate and adaptive immune responses.

$CD4^+$ T cells have regulatory functions as helper cells that can initiate and potentiate immune reactions.[23] In this study, we have also shown that PCP is a potent regulator of IFN-γ production and Th1 differentiation in $CD4^+$ T cells. PCP induced IFN-γ and IL-2 production dose-dependently in vitro. To further examine this issue, we systematically evaluated the quantitative and kinetic parameters of PCP-induced activation of T helper lineage-specific transcription factors in $CD4^+$ T cells. T-bet is a transcription factor that stimulates Th1 response while inhibiting Th2 response.[24] We showed that PCP enhanced STAT4 phosphorylation, promoted downstream immune signaling, and increased T-bet expression. In addition, the expression of Th2 signaling proteins (STAT6 and GATA-3) induced by PCP was similar to that of control cells, indicating that PCP had no effect on this pathway. These findings support the point that PCP up-regulates Th1 cell-mediated immune responses.

On the basis of the in vitro data, PCP was demonstrated to be able to regulate Th1 and Th2 balance via Th1 cytokine induction. This effect might result from the activation of T-bet, which induces Th1 transition and IFN-γ synthesis.[25] T-bet can also mediate B-cell IgG2a class-switch recombination and IFN-γ secretion.[26] Accordingly, we showed that PCP down-regulates GATA-3, IL-4, and IL-5 while up-regulating T-bet and IFN-γ.

To clarify the Th1/Th2 modulating abilities of PCP, we examined the effects of oral administration of PCP on antibodies and cytokine production. As a result, we showed that oral PCP increased Th1 response including induction of OVA-specific IgG2a and IFN-γ. On the other hand, oral PCP suppressed OVA-specific IgG1 and IL-5 production. These findings suggested suppression of humoral immune response and antibody class switch recombination.[27] Taken together, PCP might be a regulator of Th1/Th2 balance that favored Th1 response.

We showed in this study that PCP might be a potent antiallergic agent that activates Th1 $CD4^+$ T cells and suppresses Th2 cells, which are the major effectors in allergic responses such as asthma and allergic rhinitis.[28]

Atopic dermatitis is characterized by an itchy, inflammatory skin condition with a predilection for skin flexures. It is also characterized by high serum IgE and a Th2-dominat immune response such as the production of IL-4 and IL-5.[29,30] In this study, we showed that PCP could induce a Th1 response in vitro and in vivo, indicating the potential of PCP to be utilized to regulate T cell response. In addition, we demonstrated the effect of PCP to alleviate Th2 cytokine and IgE production in

an AD murine model. These data exhibited the potential of PCP to be utilized to regulate allergic response.

In conclusion, we cloned the gene of PCP, verified its biochemical characteristics, and demonstrated that PCP is a T cell-activating agent that induces Th1 response in vitro and in vivo. Moreover, PCP could alleviate the Th2-dominant cytokine and IgE production in a murine atopic dermatitis model. These findings showed some unique properties of a newly cloned protein from *P. cocos*, enabling further studies and application.

■ ASSOCIATED CONTENT

Supporting Information

The nucleotide sequence and translation result of primer 320 product (Figure S1), the nucleotide sequence and translation result of primer 5−320−2 product (Figure S2), signal peptide prediction of PCP (Figure S3), and the theoretical pI/M_w for amino acid sequence deduced from cDNA sequence terminated translation at the first stop codon. This material is available free of charge via the Internet at http://pubs.acs.org.

Accession Codes

The complete cDNA sequence of PCP is published in GenBank under accession no. JN571084.1.

■ AUTHOR INFORMATION

Corresponding Author

*(F.S.) Phone: 886-2-33664846. Fax: 886-2-23673103. E-mail: fsheu@ntu.edu.tw.

Author Contributions

‖Y.-T.L. Y.-C.K., and H.-H.C. contributed equally to this work.

Funding

This work was supported by a grant from the National Science Council of Taiwan (NSC-99-2628-B-002-003-MY3).

Notes

The authors declare no competing financial interest.

■ ABBREVIATIONS USED

APC, antigen-presenting cells; ConA, concanavalin A; FPLC, fast protein liquid chromatography; Ig, immunoglobulin; IL-1β, interleukin-1 beta; IFN, interferon; LAL, Limulus amoebocyte lysate; LPS, lipopolysaccharide; MHC, major histocompatibility complex; MyD88, myeloid differentiation factor 88; NF-κB, nuclear factor-kappa B; OVA, ovalbumin; qPCR, quantitative real-time polymerase chain reaction; STAT, signal transducer and activator of transcription protein; TLR, Toll-like receptor; TNF-α, tumor necrosis factor-alpha

■ REFERENCES

(1) Lee, K. Y.; You, H. J.; Jeong, H. G.; Kang, J. S.; Kim, H. M.; Rhee, S. D.; Jeon, Y. J. Polysaccharide isolated from *Poria cocos* sclerotium induces NF-κB/Rel activation and iNOS expression through the activation of p38 kinase in murine macrophages. *Int. Immunopharmacol.* **2004**, *4*, 1029−1038.

(2) Gapter, L.; Wang, Z.; Glinski, J.; Ng, K. Y. Induction of apoptosis in prostate cancer cells by pachymic acid from *Poria cocos*. *Biochem. Biophys. Res. Commun.* **2005**, *332*, 1153−1161.

(3) Zhang, G. W.; Liu, H. Y.; Xia, Q. M.; Li, J. Q.; Lu, H.; Zhang, Q. H.; Yao, Z. F. Anti-rejection effect of ethanol extract of *Poria cocos* wolf in rats after cardiac allograft implantation. *Chin. Med. J. (Engl.)* **2004**, *117*, 932−935.

(4) Chen, W.; An, W.; Chu, J. Effect of water extract of *Poria* on cytosolic free calcium concentration in brain nerve cells of neonatal rats. *Zhongguo Zhong Xi Yi Jie He Za Zhi* **1998**, *18*, 293−295.

(5) Schinella, G. R.; Tournier, H. A.; Prieto, J. M.; Mordujovich de Buschiazzo, P.; Rios, J. L. Antioxidant activity of anti-inflammatory plant extracts. *Life Sci.* **2002**, *70*, 1023−1033.

(6) Chang, H. H.; Yeh, C. H.; Sheu, F. A novel immunomodulatory protein from *Poria cocos* induces Toll-like receptor 4-dependent activation within mouse peritoneal macrophages. *J. Agric. Food Chem.* **2009**, *57*, 6129−6139.

(7) Nascimbeni, M.; Shin, E. C.; Chiriboga, L.; Kleiner, D. E.; Rehermann, B. Peripheral $CD4^+CD8^+$ T cells are differentiated effector memory cells with antiviral functions. *Blood* **2004**, *104*, 478−486.

(8) Rammensee, H. G. Chemistry of peptides associated with MHC class I and class II molecules. *Curr. Opin. Immunol.* **1995**, *7*, 85−96.

(9) Mosmann, T. R.; Coffman, R. L. TH1 and TH2 cells: different patterns of lymphokine secretion lead to different functional properties. *Annu. Rev. Immunol.* **1989**, *7*, 145−173.

(10) Infante-Duarte, C.; Horton, H. F.; Byrne, M. C.; Kamradt, T. Microbial lipopeptides induce the production of IL-17 in Th cells. *J. Immunol.* **2000**, *165*, 6107−6115.

(11) Dickensheets, H. L.; Venkataraman, C.; Schindler, U.; Donnelly, R. P. Interferons inhibit activation of STAT6 by interleukin 4 in human monocytes by inducing SOCS-1 gene expression. *Proc. Natl. Acad. Sci. U.S.A.* **1999**, *96*, 10800−10805.

(12) Yin, Z.; Braun, J.; Neure, L.; Wu, P.; Liu, L.; Eggens, U.; Sieper, J. Crucial role of interleukin-10/interleukin-12 balance in the regulation of the type 2 T helper cytokine response in reactive arthritis. *Arthritis Rheum.* **1997**, *40*, 1788−1797.

(13) Kuan, Y. C.; Wu, T. J.; Kuo, C. Y.; Hsu, J. C.; Chang, W. Y.; Sheu, F. Molecular cloning of a new immunomodulatory protein from *Anoectochilus formosanus* which induces B cell IgM secretion through a T-independent mechanism. *PLoS One* **2011**, *6*, e21004.

(14) Kuan, Y. C.; Wu, Y. J.; Hung, C. L.; Sheu, F. *Trametes versicolor* protein YZP activates regulatory B lymphocytes − gene identification through de novo assembly and function analysis in a murine acute colitis model. *PLoS One* **2013**, *8*, e72422.

(15) Spergel, J.; Mizoguchi, E.; Brewer, J.; Martin, T.; Bhan, A.; Geha, R. Epicutaneous sensitization with protein antigen induces localized allergic dermatitis and hyperresponsiveness to metacholine after single exposure to aerosolized antigen in mice. *J. Clin. Invest.* **1998**, *101*, 1614−1622.

(16) Pitsios, C.; Dimitrakopoulou, A.; Tsalimalma, K.; Kordossis, T.; Choremi-Papadopoulou, H. Expression of CD69 on T-cell subsets in HIV-1 disease. *Scand. J. Clin. Lab. Invest.* **2008**, *68*, 233−241.

(17) Hombach, A.; Wieczarkowiecz, A.; Marquardt, T.; Heuser, C.; Usai, L.; Pohl, C.; Seliger, B.; Abken, H. Tumor-specific T cell activation by recombinant immunoreceptors: CD3 zeta signaling and CD28 costimulation are simultaneously required for efficient IL-2 secretion and can be integrated into one combined CD28/CD3 zeta signaling receptor molecule. *J. Immunol.* **2001**, *167*, 6123−6131.

(18) Ohkawara, Y.; Lei, X. F.; Stampfli, M. R.; Marshall, J. S.; Xing, Z.; Jordana, M. Cytokine and eosinophil responses in the lung, peripheral blood, and bone marrow compartments in a murine model of allergen-induced airways inflammation. *Am. J. Respir. Cell Mol. Biol.* **1997**, *16*, 510−520.

(19) Chu, K. W.; Ho, S. S.; Chow, H. L. *Coriolus versicolor*: a medicinal mushroom with promising immunotherapeutic values. *J. Clin. Pharmacol.* **2002**, *42*, 976−984.

(20) Prigent, P.; El Mir, S.; Dreano, M.; Triebel, F. Lymphocyte activation gene-3 induces tumor regression and antitumor immune responses. *Eur. J. Immunol.* **1999**, *29*, 3867−3876.

(21) Mahajan, S. D.; Aalinkeel, R.; Schwartz, S. A.; Chawda, R. P.; Nair, M. P. Effector cell mediated cytotoxicity measured by intracellular Granzyme B release in HIV infected subjects. *Biol. Proc. Online* **2003**, *5*, 182−188.

(22) Kaech, S. M.; Wherry, E. J.; Ahmed, R. Effector and memory T-cell differentiation: implications for vaccine development. *Nat. Rev. Immunol.* **2002**, *2*, 251−262.

(23) Gergely, P. Drug-induced lymphopenia: focus on $CD4^+$ and $CD8^+$ cells. *Drug Saf.* **1999**, *21*, 91−100.

(24) Peng, S. L. The T-box transcription factor T-bet in immunity and autoimmunity. *Cell. Mol. Immunol.* **2006**, *3*, 87−95.
(25) Szabo, S. J.; Kim, S. T.; Costa, G. L.; Zhang, X.; Fathman, C. G.; Glimcher, L. H. A novel transcription factor, T-bet, directs Th1 lineage commitment. *Cell* **2000**, *100*, 655−669.
(26) Gerth, A. J.; Lin, L.; Peng, S. L. T-bet regulates T-independent IgG2a class switching. *Int. Immunol.* **2003**, *15*, 937−944.
(27) Mizoguchi, C.; Uehara, S.; Akira, S.; Takatsu, K. IL-5 induces IgG1 isotype switch recombination in mouse CD38-activated sIgD-positive B lymphocytes. *J. Immunol.* **1999**, *162*, 2812−2819.
(28) Umetsu, D. T.; DeKruyff, R. H. Th1 and Th2 $CD4^+$ cells in human allergic diseases. *J. Allergy Clin. Immunol.* **1997**, *100*, 1−6.
(29) Tanaka, M.; Aiba, S.; Matsumura, N.; Aoyama, H.; Tabata, N.; Sekita, Y.; Tagami, H. IgE-mediated hypersensitivity and contact sensitivity to multiple environmental allergens in atopic dermatitis. *Arch. Dermatol.* **1994**, *130*, 1393−1401.
(30) Kim, G. D.; Kim, T. H.; Jang, A. H.; Ahn, H. J.; Park, Y. S.; Park, C. S. α-Lipoic acid suppresses the development of DNFB-induced atopic dermatitis-like symptoms in NC/Nga mice. *Exp. Dermatol.* **2011**, *20*, 97−101.

phase.[20] Excessive macrophage activation is involved in many diseases, such as atherosclerosis. It has recently been suggested that activated macrophages within injured/inflamed arteries are the potential targets of dietary quercetin metabolites.[21] The presence of 50 μM quercetin glucuronide regulates the coronary venular barrier function through improving blood-borne inflammatory mediators and pharmacological tools in a novel microvascular wall model.[22] Taken together, inflamed macrophages may be selected as a good target for evaluating the antiinflammatory potential of quercetin and its metabolites. Changes in pro-/antiinflammatory cytokine secretion levels by target cells may be a good marker for inflammation status.

Cumulative data imply that quercetin (Q) can be absorbed and metabolized into quercetin-3-glucuronide (Q3G) in vivo. However, little is known about the differences in antiinflammatory effects between Q and Q3G administration. To clarify this puzzle, this study investigated the prophylactic or therapeutic effects of Q and Q3G administration on lipopolysaccharide (LPS)-induced inflammation in peritoneal macrophages from female BALB/c mice using ex vivo models. Changes in pro-/antiinflammatory cytokine secretion profiles by macrophages were determined using enzyme-linked immuno-sorbent assay (ELISA) to unravel the possible immunomodulatory or antiinflammatory mechanisms of Q or Q3G.

MATERIALS AND METHODS

Chemicals. Quercetin (Q) is a typical flavonoid existing in many plants. Quercetin-3-glucuronide (Q3G) is a major quercetin metabolite found in the serum in humans. In this study, both quercetin dihydrate ($C_{15}H_{10}O_7 \cdot 2H_2O$; 338.27 g/mol) (Sigma-Aldrich Co., Steinheim, Switzerland) and quercetin-3-glucuronide ($C_{21}H_{18}O_{13}$; 478.37 g/mol) (Carbosynth Limited, Berkshire, UK) were purchased at the highest available purity (>98%, HPLC). The chemical structures of Q and Q3G are shown in Figure 1. Quercetin was dissolved in

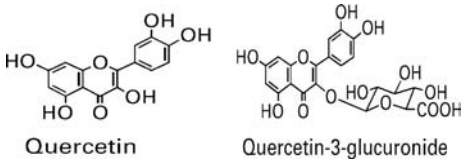

Figure 1. The chemical structures of quercetin and quercetin-3-glucuronide.

dimethyl sulfoxide (DMSO, Wako, Osaka, Japan) to prepare a stock solution at a concentration of 20 mM and sterilized using a filter (Millipore, Carrigtwohill, Cork, Ireland) with 0.2 μm pore size. Quercetin-3-glucuronide (Q3G) was dissolved in phosphate-buffered saline (PBS, 137 mM NaCl, 2.7 mM KCl, 8.1 mM Na_2HPO_4, 1.5 mM KH_2PO_4, pH 7.4, 0.2 μm filtered) to prepare a stock solution at a concentration of 2 mM and sterilized using a filter (Millipore, Carrigtwohill, Cork, Ireland) with 0.2 μm pore size. The stock solution was stored at −80 °C for future use.

Experimental Mice. Female BALB/cByJNarl mice (7 weeks old) were obtained from the National Laboratory Animal Center, National Applied Research Laboratories, National Science Council in Taipei, Taiwan, ROC, and maintained in the Department of Food Science and Biotechnology at National Chung Hsing University, Taiwan, ROC. The mice were housed and kept on a chow diet (laboratory standard diet, Diet MF 18, Oriental Yeast Co., Ltd., Osaka, Japan). The animal room was kept on a 12-h-light and 12-h-dark cycle. Constant temperature (25 ± 2 °C) and relative humidity (50−75%) were maintained. After acclimation for 1 week, the mice were sacrificed to obtain peritoneal macrophages. BALB/c strain mice weighting 20−25 g were used throughout the experiment. The animal use protocol for these experiments was reviewed and approved by the Institutional Animal Care and Use Committee (IACUC), National Chung Hsing University, Taiwan, ROC.

Source of Mouse Primary Peritoneal Macrophages. The primary peritoneal macrophages from mice were collected according to the method described previously.[23,24] Briefly, the adult female BALB/c mice were anesthetized with diethyl ether, bled using a retro-orbital venous plexus puncture to collect blood, and immediately euthanized by CO_2 inhalation. Peritoneal macrophages were prepared by lavaging the peritoneal cavity with 2 aliquots of 5 mL of sterile Hank's balanced salts solution (HBSS) ((50 mL of 10× HBSS (Hyclone Laboratories Inc., South Logan, UT), 2.5 mL of antibiotic−antimycotic solution (100× PSA) containing 10 000 units of penicillin, 10 mg of streptomycin, and 25 μg of amphotericin B per mL in 0.85% saline (Atlanta Biologicals Inc., Norcross, GA); 20 mL of 3% bovine serum albumin (BSA, Sigma-Aldrich Co., St. Louis, MO) in PBS; 2.5 mL of 7.5% $NaHCO_3$ (Wako, Osaka, Japan), 425 mL sterile water)) for a total of 10 mL through the peritoneum. The peritoneal lavage fluid was centrifuged at 400g for 10 min at 4 °C. The cell pellets were collected and resuspended in tissue culture medium (TCM, a serum replacement; Celox Laboratories Inc., Lake Zurich, IL); suspended in a medium consisting of 10 mL of TCM, 500 mL of Roswell Park Memorial Institute (RPMI) 1640 medium (Atlanta Biologicals Inc., Norcross, GA), and 2.5 mL of antibiotic−antimycotic solution (100× PSA). The peritoneal adherent cells (>90% of macrophages) from each animal were adjusted to 2×10^6 cells/mL in TCM medium with a hemocytometer using the trypan blue dye exclusion method.

Mouse Peritoneal Macrophage Cultures with Q and Q3G and Cell Viability Determination. To evaluate the possible cytotoxic effect of the test samples, the cell viability of mouse primary peritoneal macrophages treated with Q or Q3G was determined using 3-(4,5-dimethylthiazol-2-diphenyl)-2,5-tetrazolium bromide (MTT) assay. Briefly, peritoneal macrophages (2×10^6 cells/mL in TCM medium, 50 μL/well) in the absence or presence of Q (0.8, 8, 40, 100, and 200 μM in TCM medium; 50 μL/well), or Q3G (0.8, 1.6, 8, 40, 100, and 200 μM in TCM medium; 50 μL/well), respectively, were cocultured in 96-well plates at 37 °C in a humidified incubator with 5% CO_2 and 95% air for 48 h. An endotoxin and B-cell mitogen, lipopolysaccharide (LPS, Sigma-Aldrich Co., L-2654, St. Louis, MO) at a final concentration of 2.5 μg/mL in culture was selected as a positive control in every individual experiment. Aliquots of 10 μL of 5 mg/mL MTT (Sigma, St. Louis, MO) in PBS were added to each well in the 96-well plate. The plates were incubated for another 4 h. The culture medium was then discarded. The plates were carefully washed with PBS buffer twice. Aliquots of 100 μL of DMSO were added to each well and oscillated for 30 min to extract formed insoluble formazan. The absorbance was measured at 550 nm on a plate reader (ELISA reader, ASYS Hitech, GmbH, Austria). The cell viability was calculated using the absorbance (A) at 550 nm; cell viability (% of control) = $[(A_{\text{sample}} - A_{\text{sample blank}})/(A_{\text{control}} - A_{\text{blank}})] \times 100$. The remaining cell viability showed that Q or Q3G treatments lower than 50 μM did not have cytotoxicity on peritoneal macrophages.

Antiinflammation Assessments of Q and Q3G Administrations Ex Vivo. To verify the antiinflammatory potential of Q and Q3G, Q and Q3G were prepared and administered to mouse primary macrophages in the absence or presence of LPS under two different ex vivo experimental models, including prophylactic and therapeutic models. Dexamethasone (Dex), a potent glucocorticoid drug having antiinflammatory and immunosuppressant functions, was chosen as a positive control in this study.

A Prophylactic Ex Vivo Model. To avoid excessive high concentrations administered in vivo, noncytotoxic concentrations of Q or Q3G at 25 and 10 μM based on the in vitro study were selected to conduct antiinflammation assessments ex vivo. Accordingly, concentrations of 25 and 10 μM Q or Q3G responded to 1×10^6 cells/mL in vitro. On the basis of our preliminary results, we presumed that there are a total of 6×10^6 peritoneal macrophages in a 20 g normal mouse, reflecting its corresponding doses of Q or Q3G were 0.15 and 0.06 μmol/mouse for treating a total of 6×10^6 peritoneal macrophages/mouse in vivo. In our preliminary results, intraperitoneal

administrations with Q or Q3G, even at 0.30 μmol/mouse, over 24 h did not significantly affect the body weight and cause toxic signs in the experimental mice. Each animal received an appropriate concentration of Q or Q3G dissolved in a volume of 100 μL of sterilized PBS using aliquots from a single lot of Q or Q3G (both at 0.06 and 0.15 μmol/mouse), respectively, to evaluate the prophylactic (preventive) Q or Q3G effects on LPS-induced inflammation ex vivo. The negative control animals received the same volume of PBS, and the positive control animals received the same volume of Dex (0.03 μmol/mouse). At 12 h after Q, Q3G, PBS, or Dex injection, all of the experimental animals were sacrificed. The peritoneal macrophages were collected as described previously. The isolated macrophages were cultured in the absence or presence of LPS (Sigma-Aldrich Co., L-2654, St. Louis, MO) at a final concentration of 25 μg/mL in 6-well plates. The plate was incubated at 37 °C in a humidified incubator with 5% CO_2 and 95% air for 48 h. The plates were centrifuged at 400*g* for 10 min. The cell culture supernatants were collected and stored at −80 °C for cytokine assays.

A Therapeutic Ex Vivo Model. We found that administration with an intraperitoneal (i.p.) injection of LPS at a concentration of 10 mg/kg body weight (BW) might induce acute systemic inflammation.[25,26] To obtain inflamed macrophages in vivo, a series of preliminary experiments were conducted to determine the effective LPS dosage for inducing moderate systemic inflammation and inflamed macrophages. We found that mice administered with an intraperitoneal injection of LPS at a concentration of 8 mg/kg BW over 12 h could induce moderate systemic inflammation and inflamed macrophages in mice. Therefore, LPS i.p. was administered at a concentration of 8 mg/kg BW for 12 h to induce inflammation in vivo. We further presumed a total of 6×10^6 peritoneal macrophages in a 20 g normal mouse, reflecting a corresponding concentration about 25 μg/mL LPS to stimulate 1×10^6 peritoneal macrophages/mL in vitro. Dex was found to have antiinflammatory effects to inhibit LPS-induced inflammation in J774 macrophages at 0.1−10 μM in vitro.[27] We adopted 1 μM Dex as a positive control to treat inflamed peritoneal macrophages in vitro. To evaluate the therapeutic (curative) effects of Q or Q3G on LPS-induced inflammation ex vivo, each animal was first challenged with *Escherichia coli* LPS (O127:B8, Sigma-Aldrich Co., L-3129, St. Louis, MO) to induce moderate systemic inflammation to obtain inflamed macrophages in vivo. Mice were given an intraperitoneal injection of LPS from *E. coli* O127:B8 at a dose of 8 mg/kg body weight (BW). Each animal received this dose of LPS in a volume of 100 μL of LPS dissolved in sterilized PBS using aliquots from a single lot of LPS. The negative control animals received the same volume of PBS. At 12 h after LPS or PBS injection, all experimental animals were sacrificed. The inflamed or normal peritoneal macrophages were collected. The isolated inflamed or normal macrophages (1×10^6 cells/mL) were cultured in the absence or presence of Q or Q3G at the indicated final concentrations of 0.4, 0.8, 4, 20, and 50 μM in 6-well plates. Dex (1 μM) was chosen as a positive control. The plate was incubated at 37 °C in a humidified incubator with 5% CO_2 and 95% air for 48 h. The plates were centrifuged at 400*g* for 10 min. The supernatants in cell cultures were collected and stored at −80 °C for cytokine assays.

Proinflammatory and Antiinflammatory Cytokine Level Measurement in Macrophage Cultures Using ELISA. The macrophage culture supernatants in each individual treatment were collected to measure proinflammatory cytokines (TNF-*α*, IL-1*β*, and IL-6) and antiinflammatory cytokine (IL-10) levels using sandwich ELISA kits. The TNF-*α*, IL-1*β*, IL-6, and IL-10 concentrations were assayed according to the cytokine ELISA protocol from the manufacturer's instructions (mouse DuoSet ELISA Development system, R&D Systems, Minneapolis, MN). The sensitivity of these cytokine assays was <15.6 pg/mL.

Statistical Analysis. Values are expressed as means ± SD and analyzed statistically using one-way ANOVA followed using Duncan's New Multiple Range test or followed by unpaired Student's *t*-test. Differences among treatments were considered statistically significant if $P < 0.05$. Statistical tests were performed using SPSS version 12.0.

RESULTS AND DISCUSSION

The differences in antiinflammatory effects between Q and Q3G remain unclear. Normal and inflamed macrophages were collected from mouse peritoneal cavities and cultured with Q and Q3G in prophylactic or therapeutic ex vivo experimental models, respectively, to clarify these therapeutic effects.

Q and Q3G Treatment In Vitro Effects on Mouse Peritoneal Macrophage Cell Viabilities. To avoid excessive cytotoxicity at high concentrations or doses, Q (at the indicated final concentrations of 0.4, 4.0, 20, 50, and 100 μM) or Q3G (at the indicated final concentrations of 0.4, 0.8, 4.0, 20, 50, and 100 μM) treatments were first selected to assess their effects on primary peritoneal macrophage cell viabilities. The remaining cell viability was determined using the MTT assay showing that either Q or Q3G treatments at concentrations lower than 50 μM did not produce cytotoxic effects on the macrophages (Figure 2). Therefore, appropriate concentrations of Q or Q3G

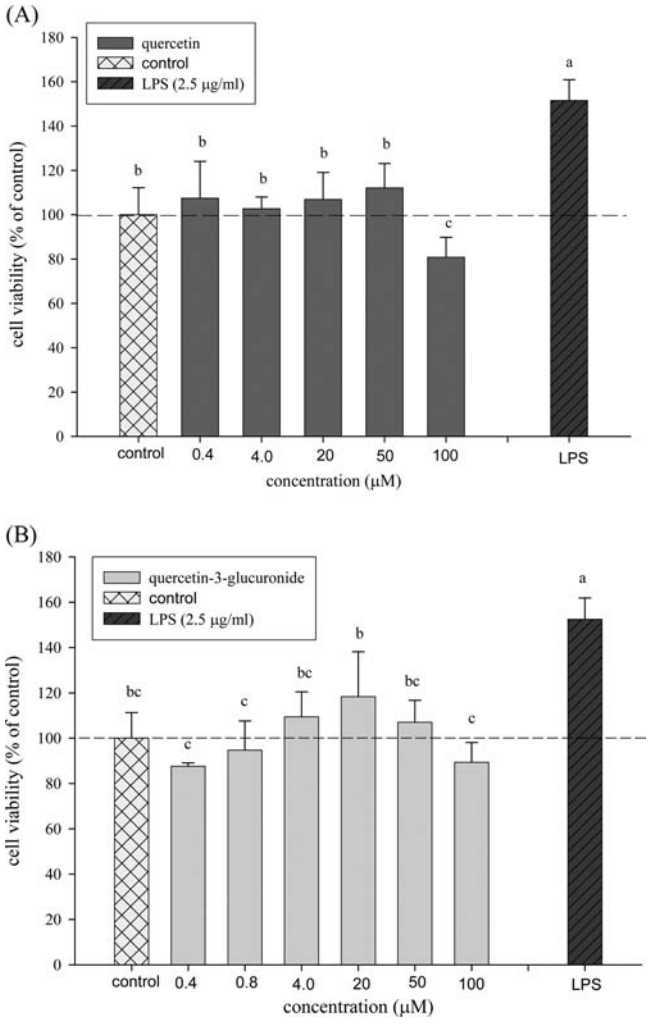

Figure 2. Effects of quercetin (A) and quercetin-3-glucuronide (B) administration in vitro on cell viabilities of primary peritoneal macrophages from female BALB/c mice. Values are means ± SD (n = 3 biological determinations), analyzed using one-way ANOVA, followed by Duncan's new multiple range test. Bars not sharing a common small letter are significantly different ($P < 0.05$) from each other. Lipopolysaccharide (LPS, 2.5 μg/mL) was selected as a positive control. Cell viability (% of control) = $[(A_{sample} - A_{sample\ blank})/(A_{control} - A_{blank})] \times 100$.

Table 1. Effects of Quercetin in a Prophylactic Ex Vivo Model on Cytokine Secretions by LPS-Stimulated Peritoneal Macrophages from Female BALB/c Mice[a,b,c,d]

			quercetin (μmol/mouse)			
	cytokines[e]	treatment[f]	0	0.06	0.15	Dex[g] (0.03 μmol/mouse)
proinflammatory cytokines	TNF-α (pg/mL)	medium	246 ± 62	199 ± 63	190 ± 80	243 ± 47
		LPS	545 ± 109*	609 ± 290	609 ± 192	551 ± 173
	IL-1β (pg/mL)	medium	36.6 ± 8.2	35.6 ± 14.8	30.9 ± 6.8	34.6 ± 21.6
		LPS	90.1 ± 32.1*	74.4 ± 9.4	77.0 ± 9.9	98.0 ± 49.4
	IL-6 (pg/mL)	medium	2613 ± 757	2150 ± 1017	1717 ± 558	2648 ± 759
		LPS	4645 ± 1623*	4050 ± 1780	3375 ± 768	4635 ± 1925
antiinflammatory cytokine	IL-10 (pg/mL)	medium	208 ± 108 A	105 ± 95.7 AB	32.4 ± 26.0 B	224 ± 148 A
		LPS	711 ± 206 A,*	423 ± 216 AB	287 ± 36.3 B	755 ± 388 A
ratios of pro-/antiinflammatory cytokine	TNF-α/IL-10	medium	1.66 ± 1.52 B	3.50 ± 3.21 AB	7.21 ± 3.34 A	1.59 ± 1.07 B
		LPS	0.81 ± 0.28 C	1.56 ± 0.63 AB	2.08 ± 0.46 A	0.89 ± 0.41[x BC]
	IL-1β/IL-10	medium	0.22 ± 0.12 B	0.56 ± 0.42 B	1.24 ± 0.52 A	0.18 ± 0.08 B
		LPS	0.13 ± 0.05 C	0.22 ± 0.12 AB	0.27 ± 0.04 A	0.15 ± 0.07 AB
	IL-6/IL-10	medium	15.0 ± 6.6 B	32.6 ± 22.8 B	65.9 ± 25.5 A	15.3 ± 7.4 B
		LPS	6.62 ± 2.20 B	10.1 ± 2.1 A	11.8 ± 2.1 A	6.79 ± 1.75 B

[a]Values are means ± SD (n = 4 biological determinations), analyzed using one-way ANOVA, followed by Duncan's new multiple range test. [b]Values within same row not sharing a common capital letter are significantly different (P < 0.05) from each other. [c]Asterisk (*) within same cytokine item means significantly different (P < 0.05) from TCM medium alone in the absence of quercetin treatment. [d]The original cell density was 1×10^6 cells/mL. [e]The sensitivity of the ELISA kits used in this study was <15.6 pg/mL. [f]Lipopolysaccharide (LPS, 25 μg/mL) was selected to induce inflammation in vitro. [g]Dexamethasone (Dex) was administrated i.p. to serve as a positive control.

Table 2. Effects of Quercetin-3-glucuronide in a Prophylactic Ex Vivo Model on Cytokine Secretions by LPS-Stimulated Peritoneal Macrophages from Female BALB/c Mice[a,b,c,d]

			quercetin-3-glucuronide (μmol/mouse)			
	cytokines[e]	treatment[f]	0	0.06	0.15	Dex[g] (0.03 μmol/mouse)
proinflammatory cytokines	TNF-α (pg/mL)	medium	246 ± 62 B	373 ± 62 A	310 ± 87 AB	243 ± 47 B
		LPS	545 ± 109*	707 ± 160	708 ± 51	551 ± 173
	IL-1β (pg/mL)	medium	36.6 ± 8.2	50.3 ± 6.7	47.8 ± 18.7	34.6 ± 21.6
		LPS	90.1 ± 32.1*	113 ± 15	112 ± 40	98.0 ± 49.4
	IL-6 (pg/mL)	medium	2613 ± 757	3617 ± 1001	3293 ± 1142	2648 ± 759
		LPS	4645 ± 1623*	5515 ± 1647	5177 ± 1289	4635 ± 1925
antiinflammatory cytokine	IL-10 (pg/mL)	medium	208 ± 108	205 ± 58	248 ± 81	224 ± 148
		LPS	711 ± 206*	487 ± 46	714 ± 151	755 ± 388
ratios of pro-/antiinflammatory cytokine	TNF-α/IL-10	medium	1.66 ± 1.52	1.98 ± 0.85	1.40 ± 0.71	1.59 ± 1.07
		LPS	0.81 ± 0.28 B	1.47 ± 0.41 A	1.02 ± 0.21 AB	0.89 ± 0.41 B
	IL-1β/IL-10	medium	0.22 ± 0.12	0.27 ± 0.10	0.19 ± 0.03	0.18 ± 0.08
		LPS	0.13 ± 0.05 B	0.23 ± 0.04 A	0.16 ± 0.07 AB	0.15 ± 0.07 AB
	IL-6/IL-10	medium	15.0 ± 6.6	19.7 ± 10.4	13.7 ± 3.2	15.3 ± 7.4
		LPS	6.62 ± 2.20 B	11.5 ± 4.0 A	7.56 ± 2.80 AB	6.79 ± 1.75 B

[a]Values are means ± SD (n = 4 biological determinations), analyzed using one-way ANOVA, followed by Duncan's new multiple range test. [b]Values within same row not sharing a common capital letter are significantly different (P < 0.05) from each other. [c]Asterisk (*) within same cytokine item means significantly different (P < 0.05) from TCM medium alone in the absence of quercetin treatment. [d]The original cell density was 1×10^6 cells/mL. [e]The sensitivity of the ELISA kits used in this study was <15.6 pg/mL. [f]Lipopolysaccharide (LPS, 25 μg/mL) was selected to induce inflammation in vitro. [g]Dexamethasone (Dex) was administrated i.p. to serve as a positive control.

at the indicated concentrations of 0.4, 0.8, 4.0, 20, and 50 μM were adopted to treat inflamed macrophages (1×10^6 cells/mL) in vitro. However, to avoid excessive high doses in vivo, medium noncytotoxic concentrations of Q or Q3G at 25 and 10 μM based on this in vitro study were selected to conduct the in vivo antiinflammation assessments. We presumed that there are a total of 6×10^6 peritoneal macrophages in a 20 g normal mouse according to our previous studies, reflecting the corresponding Q or Q3G doses were 0.15 and 0.06 μmol/mouse, respectively.

Q and Q3G Administration Effects on Cytokine Secretions Using LPS-Stimulated Macrophages in a Prophylactic Ex Vivo Model. To unravel the Q and Q3G administration effects on pro-/antiinflammatory cytokine secretions using LPS-stimulated macrophages in a prophylactic ex vivo model, Q or Q3G (both at 0.06 and 0.15 μmol/mouse) were administered i.p. to female BALB/c mice, respectively. The negative control animals received the same volume of PBS, and the positive control animals received the same volume of Dex (0.03 μmol/mouse). At 12 h after Q, Q3G, PBS, or Dex injection, all experimental animals were sacrificed to collect peritoneal macrophages. The peritoneal macrophages were cultured for 48 h in the absence or presence of LPS. Table 1 shows the intraperitoneal injection effects with Q in a prophylactic ex vivo model on cytokine secretions by LPS-stimulated peritoneal macrophages from female BALB/c mice.

Table 3. Effects of Quercetin in a Therapeutic Ex Vivo Model on Cytokine Secretions by Normal or Inflamed Peritoneal Macrophages from Female BALB/c Mice Intraperitoneally Injected with Phosphate-Buffered Saline or 8 mg/kg BW Lipopolysaccharide for 12 h[a,b,c]

			quercetin (μM)						
	cytokines[d]	groups	0	0.4	0.8	4	20	50	Dex[e]
pro- inflammatory cytokines	TNF-α (pg/mL)	normal	248 ± 144	303 ± 171	285 ± 171	308 ± 211	263 ± 174	315 ± 270	153 ± 119
		inflamed	41.2 ± 9.4 A	41.5 ± 5.3 A	43.1 ± 15.9 A	36.8 ± 6.6 A	16.2 ± 9.8 B	9.8 ± 7.6 B	8.9 ± 7.3 B
	IL-1β (pg/mL)	normal	23.2 ± 4.9 A	25.4 ± 7.6 A	23.1 ± 8.4 A	23.1 ± 9.2 A	19.7 ± 9.4 A	27.0 ± 6.0 A	4.8 ± 3.3 B
		inflamed	50.2 ± 13.6	53.1 ± 28.6	42.5 ± 12.6	40.7 ± 10.8	36.9 ± 11.3	31.7 ± 10.3	36.7 ± 16.2
	IL-6 (pg/mL)	normal	3100 ± 1867	2858 ± 1417	2118 ± 1145	2248 ± 1172	2025 ± 1082	1891 ± 1233	2083 ± 1608
		inflamed	1275 ± 529 A	1110 ± 460 A	895 ± 452AB	815 ± 374 ABC	404 ± 284 BC	335 ± 358 C	304 ± 253 C
antiinflammatory cytokine	IL-10 (pg/mL)	normal	171 ± 91.3	160 ± 79.8	169 ± 105	176 ± 111	360 ± 294	165 ± 126	303 ± 227
		inflamed	1929 ± 535 A	1590 ± 404A B	1672 ± 640 AB	1613 ± 570 AB	1797 ± 579 A	940 ± 600 BC	777 ± 206 C
ratios of pro-/anti inflammatory cytokine	TNF-α/IL-10	normal	1.45 ± 0.37 AB	1.88 ± 0.39 AB	1.80 ± 0.58 AB	1.76 ± 0.58 AB	1.00 ± 0.93B C	1.93 ± 1.22 A	0.49 ± 0.09 C
		inflamed	0.02 ± 0.01 A	0.03 ± 0.01 A	0.03 ± 0.01 A	0.02 ± 0.00 A	0.01 ± 0.00 B	0.01 ± 0.00 B	0.01 ± 0.01 B
	IL-1β/IL-10	normal	0.17 ± 0.08 AB	0.18 ± 0.05 A	0.17 ± 0.06 AB	0.16 ± 0.06 AB	0.08 ± 0.06 BC	0.23 ± 0.12 A	0.03 ± 0.03 C
		inflamed	0.03 ± 0.00 BC	0.03 ± 0.01 ABC	0.03 ± 0.01 BC	0.03 ± 0.01 BC	0.02 ± 0.01 C	0.04 ± 0.02 AB	0.05 ± 0.02 A
	IL-6/IL-10	normal	17.8 ± 4.4 A	18.7 ± 4.5 A	13.8 ± 4.4 A	14.4 ± 4.8 A	8.0 ± 6.7 B	12.7 ± 5.1 AB	7.3 ± 1.7 B
		inflamed	0.65 ± 0.24 A	0.69 ± 0.23 A	0.56 ± 0.30 AB	0.53 ± 0.26 AB	0.20 ± 0.08 C	0.29 ± 0.19 BC	0.36 ± 0.24 BC

[a]Values are means ± SD (n = 5−6 biological determinations), analyzed using one-way ANOVA, followed by Duncan's new multiple range test. [b]Values within same row not sharing a common letter are significantly different ($P < 0.05$) from each other. [c]The original cell density was 1×10^6 cells/mL. [d]The sensitivity of the ELISA kits used in this study was <15.6 pg/mL. [e]Dexamethasone (Dex, 1 μM) was selected as a positive control.

dx.doi.org/10.1021/jf405630h | J. Agric. Food Chem. 2014, 62, 2872−2880

Table 4. Effects of Quercetin-3-glucuronide in a Therapeutic Ex Vivo Model on Cytokine Secretions by Normal or Inflamed Peritoneal Cells from Female BALB/c Mice Intraperitoneally Injected with Phosphate-Buffered Saline or 8 mg/kg BW Lipopolysaccharide for 12 h[a,b,c]

			quercetin-3-glucuronide (μM)						
	cytokines[d]	groups	0	0.4	0.8	4	20	50	Dex[e]
pro- inflammatory cytokines	TNF-α (pg/mL)	normal	248 ± 144	340 ± 165	281 ± 161	312 ± 187	311 ± 218	322 ± 241	153 ± 119
		inflamed	46.2 ± 14.8 A	49.9 ± 20.3 A	49.5 ± 21.7 A	45.7 ± 13.9 A	49.0 ± 10.6 A	48.2 ± 14.4 A	13.4 ± 9.2 B
	IL-1β (pg/mL)	normal	23.2 ± 4.9 AB	28.6 ± 7.6 A	24.3 ± 10.0 AB	24.4 ± 11.8 AB	15.2 ± 4.1 B	19.3 ± 10.3 AB	4.8 ± 3.3 B
		inflamed	49.4 ± 15.8	42.1 ± 13.0	44.9 ± 8.7	38.2 ± 11.3	38.0 ± 12.1	37.8 ± 15.7	33.9 ± 17.2
	IL-6 (pg/mL)	normal	3100 ± 1867	3007 ± 1586	2611 ± 1445	2453 ± 1452	2359 ± 1356	2143 ± 1206	2083 ± 1608
		inflamed	1300 ± 447 A	1220 ± 581 A	1222 ± 463 A	1009 ± 360 A	1078 ± 444 A	1191 ± 517 A	352 ± 199 B
antiinflammatory cytokine	IL-10 (pg/mL)	normal	171 ± 91 AB	177 ± 101 AB	164 ± 92 AB	177 ± 107 AB	149 ± 93 AB	120 ± 36 B	303 ± 227 A
		inflamed	2121 ± 417 A	1568 ± 221 B	1595 ± 320 B	1454 ± 235 B	1776 ± 283 B	1500 ± 294 B	836 ± 210 B
ratios of pro-/anti inflammatory cytokine	TNF-α/IL-10	normal	1.45 ± 0.37 B	2.08 ± 0.59 AB	1.75 ± 0.31 AB	1.76 ± 0.22 AB	2.06 ± 0.69 AB	2.54 ± 1.76 A	0.49 ± 0.09 C
		inflamed	0.02 ± 0.01	0.03 ± 0.02	0.03 ± 0.01	0.03 ± 0.01	0.03 ± 0.01	0.03 ± 0.01	0.02 ± 0.02
	IL-1β/IL-10	normal	0.15 ± 0.07 AB	0.17 ± 0.08 A	0.15 ± 0.05 AB	0.13 ± 0.07 AB	0.12 ± 0.06 AB	0.14 ± 0.06 AB	0.04 ± 0.06 C
		inflamed	0.03 ± 0.02	0.03 ± 0.01	0.03 ± 0.01	0.03 ± 0.01	0.02 ± 0.01	0.02 ± 0.01	0.04 ± 0.02
	IL-6/IL-10	normal	17.8 ± 4.4 A	18.5 ± 5.8 A	17.3 ± 5.8 A	14.9 ± 5.0 A	17.4 ± 4.8 A	18.8 ± 11.5 A	7.3 ± 1.7 B
		inflamed	0.62 ± 0.24 AB	0.77 ± 0.36 AB	0.79 ± 0.30 AB	0.71 ± 0.24 AB	0.63 ± 0.31 AB	0.81 ± 0.33 A	0.42 ± 0.20 B

[a]Values are means ± SD (n = 6 biological determinations), analyzed using one-way ANOVA, followed by Duncan's new multiple range test. [b]Values within same row not sharing a common capital letter are significantly different ($P < 0.05$) from each other. [c]The original cell density was 1×10^6 cells/mL. [d]The sensitivity of the ELISA kits used in this study was <15.6 pg/mL. [e]Dexamethasone (Dex, 1 μM) was selected as a positive control.

dx.doi.org/10.1021/jf405630h | J. Agric. Food Chem. 2014, 62, 2872−2880

The results showed that LPS stimulation in vitro significantly ($P < 0.05$) increased TNF-α, IL-1β, IL-6, and IL-10 secretions by peritoneal macrophages compared with those stimulated by TCM medium alone. Quercetin administration in vivo significantly ($P < 0.05$) decreased IL-10 (an antiinflammatory cytokine) secretions, but increased TNF-α/IL-10, IL-1β/IL-10, and IL-6/IL-10 (pro-/antiinflammatory cytokines) secretion ratios by the macrophages in dose-dependent manners in the absence or presence of LPS in vitro. Our results indicated that quercetin administration in a prophylactic ex vivo model might activate macrophages but enhance inflammation in the macrophages in the absence or presence of LPS. It was found that Dex treatment i.p. could effectively inhibit LPS-induced systemic inflammation in mice.[28] However, we found that Dex treatment in this prophylactic ex vivo model did not significantly ($P > 0.05$) affect TNF-α, IL-1β, IL-6, and IL-10 secretions by peritoneal macrophages in the absence or presence of LPS. Our results further suggested that Dex treatment for antiinflammation might not have a prophylactic effect.

Table 2 shows the intraperitoneal injection effects with Q3G in a prophylactic ex vivo model on cytokine secretions by LPS-stimulated peritoneal macrophages from female BALB/c mice. The results showed that Q3G administration in vivo did not significantly ($P > 0.05$) affect TNF-α, IL-1β, IL-6, and IL-10 secretions by peritoneal macrophages in the absence or presence of LPS. However, Q3G administration in vivo at 0.06 μmol/mouse significantly ($P < 0.05$) increased TNF-α/IL-10, IL-1β/IL-10, and IL-6/IL-10 (pro-/antiinflammatory cytokines) secretion ratios by the macrophages in the presence of LPS in vitro. Our results indicated that Q3G administration in a prophylactic ex vivo model slightly enhanced inflammation in macrophages in the presence of LPS.

In comparison with Q, Q3G, and Dex administration effects on LPS-stimulated inflammation using mouse peritoneal macrophages in the prophylactic ex vivo model, we found that Dex did not have a prophylactic effect on LPS-induced inflammation (Tables 1 and 2). Dex, a glucocorticoid, is widely used to treat many inflammatory and autoimmune diseases, including rheumatoid arthritis, bronchospasm, and idiopathic thrombocytopenic purpura. Importantly, our results indicated that Dex administration did not exert a prophylactic effect on LPS-induced inflammation. However, Dex treatment may still have therapeutic (curative) effects on inflammatory diseases.[29] In contrast to Dex administration effects, our results indicated that Q and Q3G administration, particularly Q, in a prophylactic ex vivo model might activate macrophages but enhance inflammation (Tables 1 and 2). Quercetin is found to have diverse physiological effects, such as antioxidant and antiinflammatory effects in different tissues.[30,31] Our results further suggest that Q treatment in a prophylactic manner might have an immuno-stimulatory effect on macrophages. Quercetin-3-glucuronide that is a major quercetin metabolite was also found to have antioxidant functions in vitro and to regulate coronary venular barrier function through improving blood-borne inflammatory mediators and pharmacological tools in a novel microvascular wall model.[22] Q3G was found in this study to have less effective immunostimulatory functions on macrophages than quercetin in a prophylactic ex vivo model. We hypothesized that a glycoside in Q3G might enhance its water solubility in blood but might disturb its uptake by macrophages in vivo.[32] Most recently, we proved that quercetin uptake improved metabolism in mouse primary immune cells, including macrophages and splenocytes (data not shown); however, the immunostimulatory mechanisms of Q and Q3G on macrophages in a prophylactic ex vivo model remain to be further studied.

Q and Q3G Administration Effects on Cytokine Secretions Using LPS-Induced Inflamed Macrophages in a Therapeutic Ex Vivo Model. We assumed that Q and Q3G administration might have therapeutic or curative potential against normal or inflamed macrophages through regulating pro- and antiinflammatory cytokine secretion profiles. Normal or inflamed peritoneal macrophages were obtained from female BALB/c mice intraperitoneally injected with PBS or 8 mg/kg BW LPS for 12 h, respectively. To unravel the Q and Q3G administration effects on in vitro on pro-/antiinflammatory cytokine secretions, Q or Q3G at the indicated noncytotoxic concentrations (0, 0.4, 0.8, 4, 20, and 50 μM) were added to normal or inflamed peritoneal macrophage cultures for 48 h. Table 3 shows the quercetin administration effects in a therapeutic ex vivo model on cytokine secretions using normal or inflamed peritoneal macrophages from female BALB/c mice intraperitoneally injected with PBS or LPS for 12 h. The results showed that quercetin treatments at >20 μM in vitro significantly ($P < 0.05$) decreased TNF-α, IL-6 (proinflammatory cytokines) or IL-10 (antiinflammatory cytokine) secretions as well as TNF-α/IL-10 and IL-6/IL-10 (pro-/antiinflammatory cytokines) secretion ratios by normal or inflamed macrophages. Our results indicated that Q exerted antiinflammatory effects on normal or inflamed macrophages through decreasing pro-/antiinflammatory cytokine secretion ratios.

In addition, Q might have a therapeutic effect on spontaneous or LPS-induced inflammation in vivo. Dex (1 μM) was also selected as a positive control in this therapeutic ex vivo model. Importantly, Dex treatment in vitro significantly ($P < 0.05$) decreased TNF-α, IL-1β, IL-6 (proinflammatory cytokines) and IL-10 (antiinflammatory cytokine) secretions as well as TNF-α/IL-10 and IL-6/IL-10 (pro-/antiinflammatory cytokines) secretion ratios by normal or inflamed macrophages. Our results indicated that Dex exerted strong antiinflammatory or immunosuppressive effects on normal or inflamed macrophages, evidencing that Dex has a therapeutic effect on spontaneous or LPS-induced inflammation in vivo (Table 3). Our results have proven that Dex administration exerted a therapeutic but not prophylactic effect on inflammation (Tables 1 and 3). Dex was found to have antiinflammatory and immunosuppressive functions to inhibit LPS-induced inflammation in J774 macrophages at 0.1−10 μM in vitro.[27] The results from this study are identical to previous published reports.[29]

Table 4 shows Q3G administration effects in a therapeutic ex vivo model on cytokine secretions by normal or inflamed peritoneal macrophages from female BALB/c mice intraperitoneally injected with PBS or LPS for 12 h. The results showed that Q3G treatment in vitro significantly ($P < 0.05$) decreased IL-1β (proinflammatory cytokine) and IL-10 (antiinflammatory cytokine) secretions by normal or inflamed macrophages. However, Q3G treatment at 50 μM significantly ($P < 0.05$) increased the TNF-α/IL-10 (pro-/antiinflammatory cytokines) secretion ratio by normal macrophages, suggesting that Q3G had less therapeutic effects on inflammation. In contrast, the presence of high concentrations of Q3G might enhance spontaneous inflammation. Conjugated quercetin glucuronides were suggested to be bioactive metabolites and

precursors of aglycone in vivo. The cardiovascular and central nervous system seemed to be the major targets of the conjugated quercetin glucuronides circulating in the human bloodstream.[33] However, it was found that Q3G treatment could not mediate TNF-α, IL-1β, and IL-6 mRNA expression levels in LPS-stimualted RAW264.7 cells, suggesting that Q3G had less antiinflammatory potential than Q.[34] Importantly, our results evidenced that Q3G had less therapeutic effects on LPS-induced inflammation than Q using an ex vivo model.

IL-10 is produced in late stage inflammation by immune effector cells to inhibit the synthesis of other cytokines; therefore, IL-10 has been recognized as an antiinflammatory cytokine.[20] In contrast to antiinflammatory cytokines, proinflammatory cytokines, such as IL-1β, IL-6, and TNF-α, present their maximum secretion at 12−48 h, when inflammation starts.[35,36] Undoubtedly, cytokine secretion profiles can reflect the status of inflammatory cells. This study established both prophylactic and therapeutic ex vivo models to verify the antiinflammatory potential of Q and Q3G using mouse primary macrophages in the absence or presence of LPS. Our results indicated that these prophylactic and therapeutic ex vivo models were suitable for evaluating the antiinflammatory potential of Q and Q3G and suggesting appropriate concentrations or doses of Q and Q3G administered in vitro and in vivo.

Quercetin is a flavonoid and phenolic compound that has been an interesting resource from functional food products and other foods targeted for reducing age-related macular degeneration risk.[37] We found that quercetin exists in different fruit juices and might have the ability to regulate Th1/Th2 and pro-/antiinflammatory cytokine secretion profiles in splenocytes.[38] It was suggested that particularly efficient compounds found among polyphenol-rich extracts should be carefully considered for medicinal and other applications.[39] We have evidenced that quercetin might be ingested in vitro, although a small quantity metabolized by immune cells, indicating that certain flavonoid compounds may exert their effects via directly entering cells (data not shown). We further proved that quercetin, but not its metabolite Q3G, exerted antiinflammatory effects in a therapeutic manner; however, there is a limitation to this ex vivo study. We assumed that the absorption rate of Q, Q3G, and Dex by macrophages might be low in this acute experimental model. Q, Q3G, and Dex were administered i.p. for only 12 h in the present study; therefore, it is too soon to conclude that those drugs had no prophylactic effects against inflammation. Studies targeting oral administration of Q for alleviating chronic inflammation and confirming a therapeutic effect in an in vivo model should be performed in the future. Importantly, we found an antiinflammatory signal pathway effect of Q at the molecular level. Q exerted antiinflammatory effects through modulating Toll-like receptor (TLR)2 and Janus kinase 2/signal transducers and activators of transcription 3 (JAK2/STAT3) pathways and inhibiting STAT3 tyrosine 705 phosphorylation within inflamed cells (data not shown).

This study isolated primary peritoneal macrophages in the absence or presence of LPS from female BALB/c mice to evaluate Q and Q3G antiinflammatory potential using both prophylactic and therapeutic ex vivo models. The results showed that either Q or Q3G treatments lower than 50 μM did not produce in vitro cytotoxic effects on the macrophages. Noncytotoxic concentrations or doses of Q and Q3G were adopted to evaluate their antiinflammatory potential. The results showed that Q or Q3G administration in a prophylactic ex vivo model might activate macrophages but enhance inflammation status in the absence or presence of LPS. However, Q3G was found to have fewer immunostimulatory functions on macrophages. Quercetin and Dex exerted antiinflammatory effects on normal or inflamed macrophages, suggesting that Q and Dex, but not Q3G, might have a therapeutic effect on spontaneous or LPS-induced inflammation ex vivo. Overall, Q and Q3G administrations in a prophylactic manner might act as an immunostimulatory agent, but Q exhibited better ability than its metabolite Q3G. In addition, both Q and Dex might have a therapeutic, but not prophylactic, effect on spontaneous or LPS-induced inflammation ex vivo.

AUTHOR INFORMATION

Corresponding Author

*Phone/Fax: + 886-4-22851857. E-mail: jinlin@nchu.edu.tw.

Funding

This study was kindly supported by Research Grant NSC99-2628-B-005-004-MY3 from the National Science Council, Taipei, Taiwan, ROC.

Notes

The authors declare no competing financial interest.

ABBREVIATIONS USED

Dex, dexamethsaone; DMSO, dimethyl sulfoxide; ELISA, enzyme-linked immunosorbent assay; IL, interleukin; LPS, lipoolysaccharide; MTT, 3-(4,5-dimethylthiazol-2-diphenyl)-2,5-tetrazolium bromide; Q, quercetin; Q3G, quercetin-3-glucuronide; TNF, tumor necrosis factor

REFERENCES

(1) Chirumbolo, S. Quercetin in cancer prevention and therapy. *Integr. Cancer Ther.* **2013**, *12*, 97−102.

(2) Kleemann, R.; Verschuren, L.; Morrison, M.; Zadelaar, S.; van Erk, M. J.; Wielinga, P. K.; Kooistra, T. Anti-inflammatory, anti-proliferative and anti-atherosclerotic effects of quercetin in human in vitro and in vivo models. *Atherosclerosis* **2011**, *218*, 44−52.

(3) Liang, W.; Luo, Z.; Ge, S.; Li, M.; Du, J.; Yang, M.; Yan, M.; Ye, Z.; Luo, Z. Oral administration of quercetin inhibits bone loss in rat model of diabetic osteopenia. *Eur. J. Pharmacol.* **2011**, *670*, 317−324.

(4) Nabavi, S. M.; Nabavi, S. F.; Habtemariam, S.; Moghaddam, A. H.; Latifi, A. M. Ameliorative effects of quercetin on sodium fluoride-induced oxidative stress in rat's kidney. *Ren. Fail.* **2012**, *34*, 901−906.

(5) Boesch-Saadatmandi, C.; Wagner, A. E.; Wolffram, S.; Rimbach, G. Effect of quercetin on inflammatory gene expression in mice liver in vivo − role of redox factor 1, miRNA-122 and miRNA-125b. *Pharmacol. Res.* **2012**, *65*, 523−530.

(6) Drummond, E. M.; Harbourne, N.; Marete, E.; Martyn, D.; Jacquier, J.; O'Riordan, D.; Gibney, E. R. Inhibition of proinflammatory biomarkers in THP1 macrophages by polyphenols derived from chamomile, meadowsweet and willow bark. *Phytother. Res.* **2013**, *27*, 588−594.

(7) Kao, T. K.; Ou, Y. C.; Raung, S. L.; Lai, C. Y.; Liao, S. L.; Chen, C. J. Inhibition of nitric oxide production by quercetin in endotoxin/cytokine-stimulated microglia. *Life Sci.* **2010**, *86*, 315−321.

(8) Suematsu, N.; Hosoda, M.; Fujimori, K. Protective effects of quercetin against hydrogen peroxide-induced apoptosis in human neuronal SH-SY5Y cells. *Neurosci. Lett.* **2011**, *504*, 223−227.

(9) Manach, C.; Texier, O.; Regerat, F.; Agullo, G.; Demigne, C.; Remesy, C. Dietary quercetin is recovered in rat plasma as conjuated derivatives of isorhamnetin and quercetin. *J. Nutr. Biochem.* **1996**, *7*, 375−380.

(10) Moon, J. H.; Tsushida, T.; Nakahara, K.; Terao, J. Identification of quercetin 3-*O*-β-D-glucuronide as an antioxidant metabolite in rat

plasma after oral administration of quercetin. *Free Radic. Biol. Med.* **2001**, *30*, 1274−1285.
(11) Cornish, K. M.; Williamson, G.; Sanderson, J. Quercetin metabolism in the lens: role in inhibition of hydrogen peroxide induced cataract. *Free Radic. Biol. Med.* **2002**, *33*, 63−70.
(12) Chong, N. J.; Aziz, Z. A systemic review on the chemical constituents of *Centella asiatica*. *Res. J. Pharm. Biol. Chem. Sci.* **2011**, *2*, 445−459.
(13) Roy, D. C.; Barman, S. K.; Shaik, M. Current updates on *Centella asiatica*: Phytochemistry, pharmacology and traditional uses. *Med. Plant Res.* **2013**, *3*, 20−36.
(14) Wei, Y.; Xie, Q.; Dong, W.; Ito, Y. Separation of epigallocatechin and flavonoids from *Hypericum perforatum* L. by high-speed counter-current chromatography and followed by preparative liquid chromatography. *J. Chromatogr. A* **2009**, *1216*, 4313−4318.
(15) Cheng, H. L.; Zhang, L. J.; Liang, Y. H.; Hsu, Y. W.; Lee, I. J.; Liaw, C. C.; Hwang, S. Y.; Kuo, Y. H. Anti-inflammatory and antioxidant flavonoids and phenols from *Cardiospermum halicacabum*. *J. Tradit. Complement. Med.* **2013**, *3*, 33−40.
(16) Fan, D.; Zhou, X.; Zhao, C.; Chen, H.; Zhao, Y.; Gong, X. Anti-inflammatory, anti-viral and quantitative study of quercetin-3-*O*-*β*-D-glucuronide in *Polygonum perfoliatum* L. *Fitoterapia* **2011**, *82*, 805−810.
(17) Pacifico, S.; D'Abrosea, B.; Scognamiglio, M.; Gallicchio, M.; Galasso, S.; Monaco, P.; Fiorentino, A. Antioxidant polyphenolic constituents of *Vitis* × *Labruscana* cv. 'Isabella' leaves. *Open Nat. Prod. J.* **2013**, *6*, 5−11.
(18) Shirai, M.; Moon, J. H.; Tsushida, T.; Terao, J. Inhibitory effect of a quercetin metabolite, quercetin 3-*O*-*β*-D-glucuronide, on lipid peroxidation in liposomal membranes. *J. Agric. Food Chem.* **2001**, *49*, 5602−5608.
(19) Hopkins, S. J. The pathophysiological role of cytokines. *Leg. Med.* **2003**, *5*, S45−57.
(20) Lin, J. Y.; Li, C. Y. Proteinaceous constituents of red cabbage juice increase IL-10, but decrease TNF-*α* secretions using LPS-stimulated mouse splenocytes. *J. Food Drug Anal.* **2010**, *18*, 15−23.
(21) Kawai, Y.; Nishikawa, T.; Shiba, Y.; Saito, S.; Murota, K.; Shibata, N.; Kobayashi, M.; Kanayama, M.; Uchida, K.; Terao, J. Macrophage as a target of quercetin glucuronides in human atherosclerotic arteries—Implication in the anti-atherosclerotic mechanism of dietary flavonoids. *J. Biol. Chem.* **2008**, *283*, 9424−9434.
(22) Juchem, G.; Weiss, D. R.; Knott, M.; Senftl, A.; Forch, S.; Fischlein, T.; Kreuzer, E.; Reichart, B.; Laufer, S.; Nees, S. Regulation of coronary venular barrier function by blood borne inflammatory mediators and pharmacological tools: insights from novel microvascular wall models. *Am. J. Physiol.: Heart Circ. Physiol.* **2012**, *302*, H567−H581.
(23) Lin, J. Y.; Tang, C. Y. Strawberry, loquat, mulberry, and bitter melon juices exhibit prophylactic effects on LPS-induced inflammation using murine peritoneal macrophages. *Food Chem.* **2008**, *107*, 1587−1596.
(24) Liu, C. J.; Lin, J. Y. Anti-inflammatory and anti-apoptotic effects of strawberry and mulberry fruit polysaccharides on lipopolysaccharide-stimulated macrophages through modulating pro-/anti-inflammatory cytokines secretion and Bcl-2/Bak protein ratio. *Food Chem. Toxicol.* **2012**, *50*, 3032−3039.
(25) Lin, J. Y.; Lai, Y. S.; Liu, C. J.; Wu, A. R. Effects of lotus plumule supplementation before and following systemic administration of lipopolysaccharide on the splenocyte responses of BALB/c mice. *Food Chem. Toxicol.* **2007**, *45*, 486−493.
(26) Lin, J. Y.; Wu, A. R.; Liu, C. J.; Lai, Y. S. Suppressive effects of lotus plumule (*Nelumbo nucifera* Geartn.) supplementation on LPS-induced systemic inflammation in a BALB/c mouse model. *J. Food Drug Anal.* **2006**, *14*, 273−278.
(27) Korhonen, R.; Lahti, A.; Hamalainen, M.; Kankaanranta, H.; Moilanen, E. Dexamethasone inhibits inducible nitric oxide synthase expression and nitric oxide production by destabilizing mRNA in lipopolysaccharide-treated macrophages. *Mol. Pharmacol.* **2002**, *62*, 698−704.
(28) Yang, Y. H.; Aeberli, D.; Dacumos, A.; Xue, J. R.; Morand, E. F. Annexin-1 regulates macrophage IL-6 and TNF via glucocorticoid-induced leucine zipper. *J. Immunol.* **2009**, *183*, 1435−1445.
(29) Provan, D.; Stasi, R.; Newland, A. C.; Blanchette, V. S.; Bolton-Maggs, P.; Bussel, J. B.; Chong, B. H.; Cines, D. B.; Gernsheimer, T. B.; Godeau, B.; Grainger, J.; Greer, I.; Hunt, B. J.; Imbach, P. A.; Lyons, G.; McMillan, R.; Rodeghiero, F.; Sanz, M. A.; Tarantino, M.; Watson, S.; Young, J.; Kuter, D. J. International consensus report on the investigation and management of primary immune thrombocytopenia. *Blood* **2010**, *115*, 168−186.
(30) Ishisaka, A.; Ichikawa, S.; Sakakibara, H.; Piskula, M. K.; Nakamura, T.; Kato, Y.; Ito, M.; Miyamoto, K. I.; Tsuji, A.; Kawai, Y.; Terao, J. Accumulation of orally administered quercetin in brain tissue and its antioxidative effects in rats. *Free Radic. Biol. Med.* **2011**, *51*, 1329−1336.
(31) Yoon, J. S.; Chae, M. K.; Lee, S. Y.; Lee, E. J. Anti-inflammatory effect of quercetin in a whole orbital tissue culture of Graves' orbitopathy. *Br. J. Ophthalmol.* **2012**, *96*, 1117−1121.
(32) Wiczkowski, W.; Romaszko, J.; Bucinski, A.; Szawara-Nowak, D.; Honke, J.; Zielinski, H.; Piskula, M. K. Quercetin from shallots (*Allium cepa* L. var. aggregatum) is more bioavailable than its glucosides. *J. Nutr.* **2008**, *138*, 885−888.
(33) Terao, J.; Murota, K.; Kawai, Y. Conjugated quercetin glucuronides as bioactive metabolites and precursors of aglycone in vivo. *Food Funct.* **2011**, *2*, 11−17.
(34) Boesch-Saadatmandi, C.; Loboda, A.; Wagner, A. E.; Stachurska, A.; Jozkowicz, A.; Dulak, J.; Doring, F.; Wolffram, S.; Rimbach, G. Effect of quercetin and its metabolites isorhamnetin and quercetin-3-glucuronide on inflammatory gene expression: role of miR-155. *J. Nutr. Biochem.* **2011**, *22*, 293−299.
(35) Loram, L. C.; Themistocleous, A. C.; Fick, L. G.; Kamerman, P. R. The time course of inflammatory cytokine secretion in a rat model of postoperative pain does not coincide with the onset of mechanical hyperalgesia. *Can. J. Physiol. Pharmacol.* **2007**, *85*, 613−620.
(36) Takacs, T.; Farkas, G., Jr.; Czako, L.; Jarmay, K.; Mandi, Y.; Lonovics, J. Time-course changes in serum cytokine levels in two experimental acute pancreatitis models in rats. *Res. Exp. Med. (Berlin)* **1996**, *196*, 153−161.
(37) Gliszczyńska-Świglo, A.; Woude, H.; Haan, L.; Tyrakowska, B.; Aarts, M. M. J. G.; Rietjens, I. M. C. M. The role of quinone reductase (NQO1) and quinone chemistry in quercetin cytotoxicity. *Toxicol. Vitro* **2003**, *17*, 423−431.
(38) Liu, C. J.; Lin, J. Y. Anti-inflammatory effects of phenolic extracts from strawberry and mulberry fruits on cytokine secretion profiles using mouse primary splenocytes and peritoneal macrophages. *Int. Immunopharmacol.* **2013**, *16*, 165−170.
(39) Metodiewa, D.; Jaiswal, A.; Ceans, N.; Dickancatte, E.; Segura-Aguilar, J. Quercetin may act as a cytotoxic prooxidant after its metabolic activation to semiquinone and quinoidal product. *Free Radic. Biol. Med.* **1998**, *26*, 107−116.

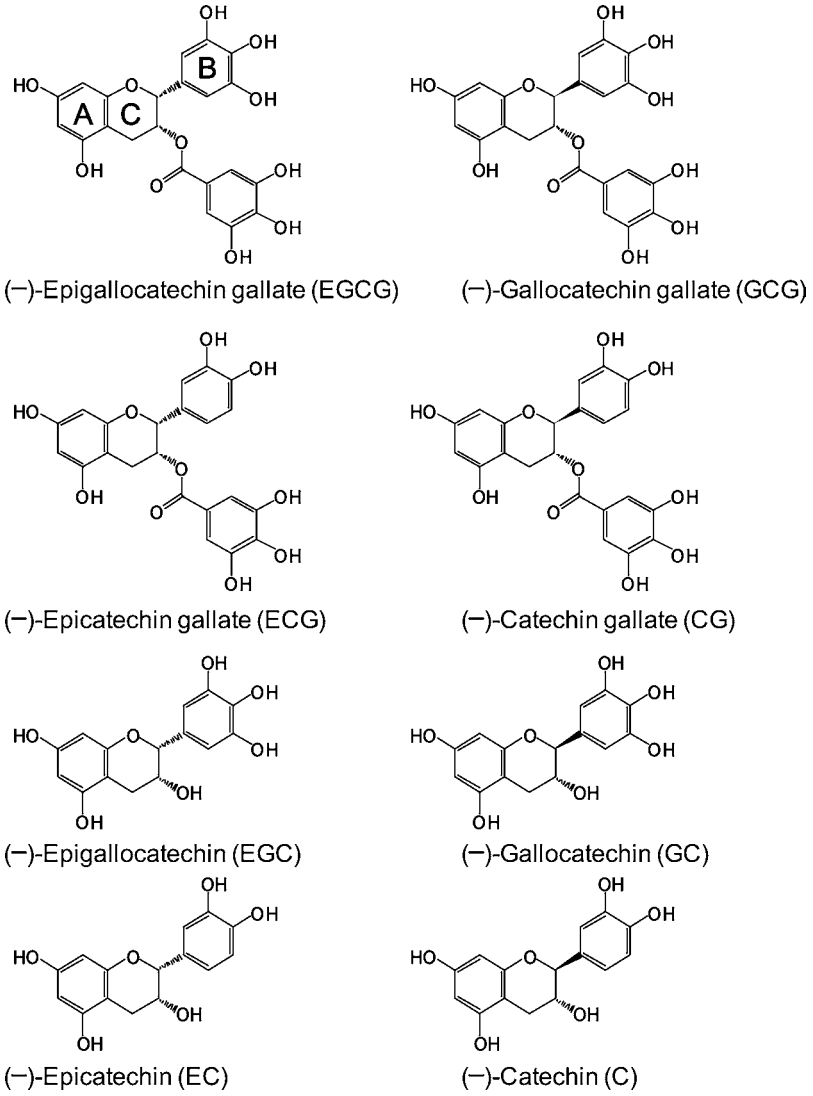

Figure 1. Chemical structures of various green tea catechins and heat-epimerized tea catechins: (left) green tea catechins; (right) heat-epimerized tea catechins.

is also a hydrophobic molecule. However, we provided direct experimental evidence that the EGCG molecule interacts with a lipid bilayer containing dimyristoylphosphatidylcholine by solid-state ^{31}P and ^{2}H nuclear magnetic resonance (NMR).[28] We also showed that ECG and EGCG interact with the surface of lipid membranes through the trimethylammonium group in phosphatidylcholine (PC) by using solution NMR techniques.[29] Therefore, it is possible that the interaction between green tea catechins with a galloyl moiety and phosphatidylcholine leads to the precipitation of micellar cholesterol and, as a result, the micellar solubility of cholesterol is decreased. In this study, the mechanisms underlying the EGCG-mediated decrease in the micellar solubility of cholesterol were examined.

MATERIALS AND METHODS

The purified catechins, EGCG, GCG, ECG, CG, EGC, GC, EC, and C, were purchased from Wako Pure Chemicals (Osaka, Japan). The purity of all catechins was confirmed to be >98% by NMR analysis. PC from egg yolk, phosphatidic acid (PA) from egg yolk, phosphatidylethanolamine (PE) from egg yolk, phosphatidylinositol (PI) from soybean, phosphatidylserine (PS) from soybean, 1-palmitoyl-2-oleoylphosphatidylcholine (POPC), and 1,2-dioleoylphosphatidic acid (DOPA) were purchased from Sigma-Aldrich Co. LLC (St. Louis, MO, USA). Sodium 2,2-silapentane-5-sulfonate (DSS), 2-(9-anthroyloxy)stearic acid (2-AS), and 12-(9-anthroyloxy)stearic acid (12-AS) were purchased from Wako. Deuterium oxide (D_2O; deuterium purity, 99.8%) was purchased from Kanto Chemicals Co. (Tokyo, Japan).

Effects of EGCG, EGC, and GCG on the Micellar Solubility of Cholesterol and PC *in Vitro*. The effects of purified catechins on the micellar solubility of cholesterol and PC were examined as described in our previous study.[17] A bile salt micellar solution containing 6.6 mmol/L sodium taurocholate, 0.6 mmol/L PC, 0.5 mmol/L cholesterol, 132 mmol/L NaCl, and 15 mmol/L sodium phosphate (pH 6.8) was prepared by sonication and stored at 37 °C for at least 24 h. Various amounts of EGCG, EGC, or GCG in deionized water (100 μL) stored at 37 °C were added to the 3 mL micellar solutions. The mixture was incubated for 1 h at 37 °C. The supernatant was passed through a 0.2 μm syringe filter (25 mm; GDD/X; Whatman Inc., Piscataway, NJ, USA), and the cholesterol and fatty acid contents originating from the phospholipids were analyzed by gas chromatography using an SPB-1 column (Supelco, Bellefonte, PA, USA) and a DB-WAX column (Agilent Technologies, Santa Clara, CA, USA), respectively.

Effect of EGCG on the Micellar Solubility of Cholesterol and Different Types of Phospholipids *in Vitro*. Five types of bile salt micellar solutions containing 0.6 mmol/L PC, PA, PE, PI, or PS were prepared as previously described. The effects of EGCG on the micellar

solubility of both cholesterol and the phospholipids were examined as previously described.

Effect of EGCG on the Vesicular Solubility of Different Phospholipids *in Vitro*. For the purpose of conveniently examining the interaction between EGCG and phospholipids, five vesicular solutions containing 0.6 mmol/L PC, PA, PE, PI, or PS in ultrapure water were prepared by sonication and stored at 37 °C. Various amounts of EGCG in ultrapure water (in a volume of 200 μL) were added to the 6 mL vesicular solutions. The mixture was incubated for 1 h at 37 °C and then centrifuged at 25000*g* for 1 h. In a preliminary study, we confirmed that centrifugation did not precipitate the phospholipids from vesicular solution. The supernatant was passed through a 0.2 μm syringe filter (25 mm; GDD/X; Whatman), and the phospholipids in the filtrate were chemically analyzed as previously described.[30]

Effects of EGCG, GCG, and EGC on the Vesicular Solubility of PC *in Vitro*. A vesicular solution containing 0.6 mmol/L PC in ultrapure water was prepared by sonication and stored at 37 °C. The effects of EGCG, GCG, and EGC on the vesicular solubility of PC were examined as previously described.

Determination of the Apparent Equilibrium Dissociation Constant (K_D) for the Binding of Eight Green Tea Catechins to POPC Using an SPR-Based Biosensor Assay. Experiments were performed using L1 sensor chips (GE Healthcare U.K. Ltd., Buckinghamshire, England) on a Biacore X100 Plus package analytical system (GE Healthcare) at the Biomedical Research Core of the Tohoku University Graduate School of Medicine. The running buffer used for all experiments was a 0.01 mmol/L phosphate buffer containing 2.7 mmol/L KCl and 137 mmol/L NaCl (pH 6.8). The washing solution was 40 mmol/L *N*-octyl-β-D-glucopyranoside. All solutions were freshly prepared, degassed, and filtered through a 0.2 μm filter. A 50 μmol amount of POPC (the ligand; phase transition temperature, −2 °C) or DOPA (the control ligand; phase transition temperature, −8 °C) in $CHCl_3$ was placed in a round-bottomed glass flask, and the solvent was removed under nitrogen. POPC was then resuspended in 0.5 mL of the running buffer, and DOPA was resuspended in 0.5 mL of the running buffer containing 500 mmol/L NaCl to suppress the electrostatic repulsion between DOPA and the alkyl surface of the L1 sensor chip for effective immobilization because DOPA is negatively charged. The resulting phospholipid suspension was mixed vigorously and then recapitulated by five freeze−thaw cycles. To obtain homogeneous liposomal solutions, the liposomal solutions were then passed through 50 nm pore polycarbonate filters 20 times using a mini-extruder (Avanti Polar Lipids Inc., Alabaster, AL, USA). The liposomal solutions were diluted 20-fold with the running buffer with or without 500 mmol/L NaCl. The final concentration of POPC or DOPA in the liposomal solution was 0.5 mmol/L.

The liposome was immobilized on the L1 sensor chip surface using the method of Subasinghe et al.[31] with some modifications. The alkyl surface of the L1 sensor chip was cleaned by a 50 μL injection of 40 mmol/L *N*-octyl-β-D- glucopyranoside at a flow rate of 10 μL/min. The POPC or DOPA liposomal solution was then immediately applied to the L1 sensor chip surface at a flow rate of 5 μL/min. The immobilization levels of POPC and DOPA were equalized as accurately as possible using an "aim for immobilized level" command. To remove any multilamellar structures from the synthetic phospholipid bilayer surface, 2 μL of 10 mmol/L sodium hydroxide was injected at a flow rate of 5 μL/min. Generally, the injection of bovine serum albumin solution is recommended for sealing the remainder of the alkyl surface of the L1 sensor chip, which is not bound to the phospholipid bilayer. However, in preliminary studies, we observed that EGCG (one of the analytes) nonspecifically and tightly bound to bovine serum albumin and the surface of the L1 sensor chip. Therefore, 5 μL of a 1 mmol/L EGCG solution prepared in the running buffer was repeatedly injected until the baseline elevation stopped to suppress nonspecific binding to the gap. Then, the running buffer was injected until a stable baseline was achieved. The aim of this injection was to dissociate the EGCG from the phospholipid bilayer. The operating temperature was 25 °C.

An SPR-based biosensor assay was performed using the single-cycle kinetics method.[32] This method involves the sequential injection of various concentrations of an analyte without any regeneration steps. Eight green tea catechin solutions were prepared at 5−80 μmol/L (green tea catechins with a galloyl moiety) and 50−800 μmol/L (green tea catechins without a galloyl moiety) in running buffer. To associate the green tea catechins with POPC or DOPA, the green tea catechin solutions were injected over the lipid surface at a flow rate of 5 μL/min for 1,080 s. To dissociate the POPC− or DOPA−green tea catechin complexes, the green tea catechin solutions were replaced with the running buffer at a flow rate of 5 μL/min for 180 s. The sensorgrams obtained from the injection of the running buffer were subtracted from the sensorgrams obtained from the injection of green tea catechin solutions. Then, the sensorgram obtained from the reference flow cell, in which DOPA was immobilized, was subtracted from the sensorgram obtained from the measurement flow cell, in which POPC was immobilized, to yield apparent binding responses. The sensorgrams did not have appropriate curvature for curve fitting to determine association and dissociation rates. Furthermore, an unexpected finding was that EGCG weakly bound to DOPA in a dose-dependent manner. Therefore, the apparent K_D for the eight green tea catechins to POPC were calculated from the equilibrium resonance signals as a function of analyte concentration according to the manufacturer's instructions (Biacore X100 evaluation software).[33]

^{1}H NMR Measurement of EGCG in the Absence and Presence of Bile Salt Micelles. A bile salt micellar solution (in D_2O) containing 6.6 mmol/L sodium taurocholate, 0.6 mmol/L PC, 0.5 mmol/L cholesterol, 132 mmol/L NaCl, and 15 mmol/L NaD_2PO_4 (pD 6.8) was prepared by sonication and stored at room temperature overnight. EGCG was then added to 1 mL of the micellar solution. The amount of EGCG added was adjusted to 0.5 mmol/L of micelles. Then, 20 μL of a 1 mg/mL DSS solution was added to the micellar solution as an internal standard, and the mixture was incubated for 1 h at room temperature. ^{1}H NMR spectra were recorded on an AVANCE III 400 (Bruker BioSpin, Billerica, MA, USA) operating at a resonance frequency of 399.7 MHz with 20 Hz spinning at 300 K. Typically, an excitation pulse length of 14.0 μs and a pulse delay time of 1.0 μs were used. Signal assignments were performed as described in our previous study.[29]

NOESY Experiments on Bile Salt Micelle/EGCG Samples. Preparation of a bile salt micellar solution (in D_2O) and addition of EGCG and DSS solution were performed as described above. NOESY spectra were acquired on an AVANCE III 400 (Bruker BioSpin) operating at a resonance frequency of 399.7 MHz with 0 Hz spinning at 300 K. The typical acquisition parameters used were as follows: a pulse delay of 2.0 s, 0.03 and 0.3 s acquisition times in the f_1 and f_2 axes, respectively, a mixing time of 800 ms, 64 scans, and 1,024 data points acquired in both the f_1 and f_2 axes. The sine-bell-squared function was adopted as a window function.

Measuring the Fluorescence of 2-AS or 12-AS in Bile Salt Micelles in the Presence of EGCG. A bile salt micellar solution containing 6.6 mmol/L sodium taurocholate, 0.6 mmol/L PC from egg yolk, 0.5 mmol/L cholesterol, 132 mmol/L NaCl, and 15 mmol/L NaH_2PO_4 (pH 6.8) containing 1 mmol/L 2-AS or 12-AS was prepared by sonication and stored at room temperature overnight. The micellar solutions (100 μL) were incubated with 100 μL of phosphate-buffered saline (PBS) containing EGCG for 20 min at 20 °C. The amount of EGCG added was adjusted to 0, 0.1, 0.3, 0.5, 0.7, 1.0, and 2.0 mmol/L of micelles. The fluorescence of 2-AS (excitation, 362 nm; emission, 446 nm) or 12-AS (excitation, 381 nm; emission, 446 nm) in the bile salt micellar solution was measured.[27] The fluorescence intensity was calculated as the percentage of the fluorescence intensity of 2-AS or 12-AS in the absence of EGCG.

Binding Analyses of EGCG to Cholesterol by an SPR-Based Biosensor Assay. Binding analyses were performed using L1 sensor chips on the Biacore X100 Plus package analytical system. Preparations of 0.5 mmol/L POPC or DOPA liposomes with or without 0.05 mmol/L or 0.15 mmol/L cholesterol and immobilizations to the phospholipid bilayer with or without cholesterol on the surface of the L1 sensor chip were performed as described above with some

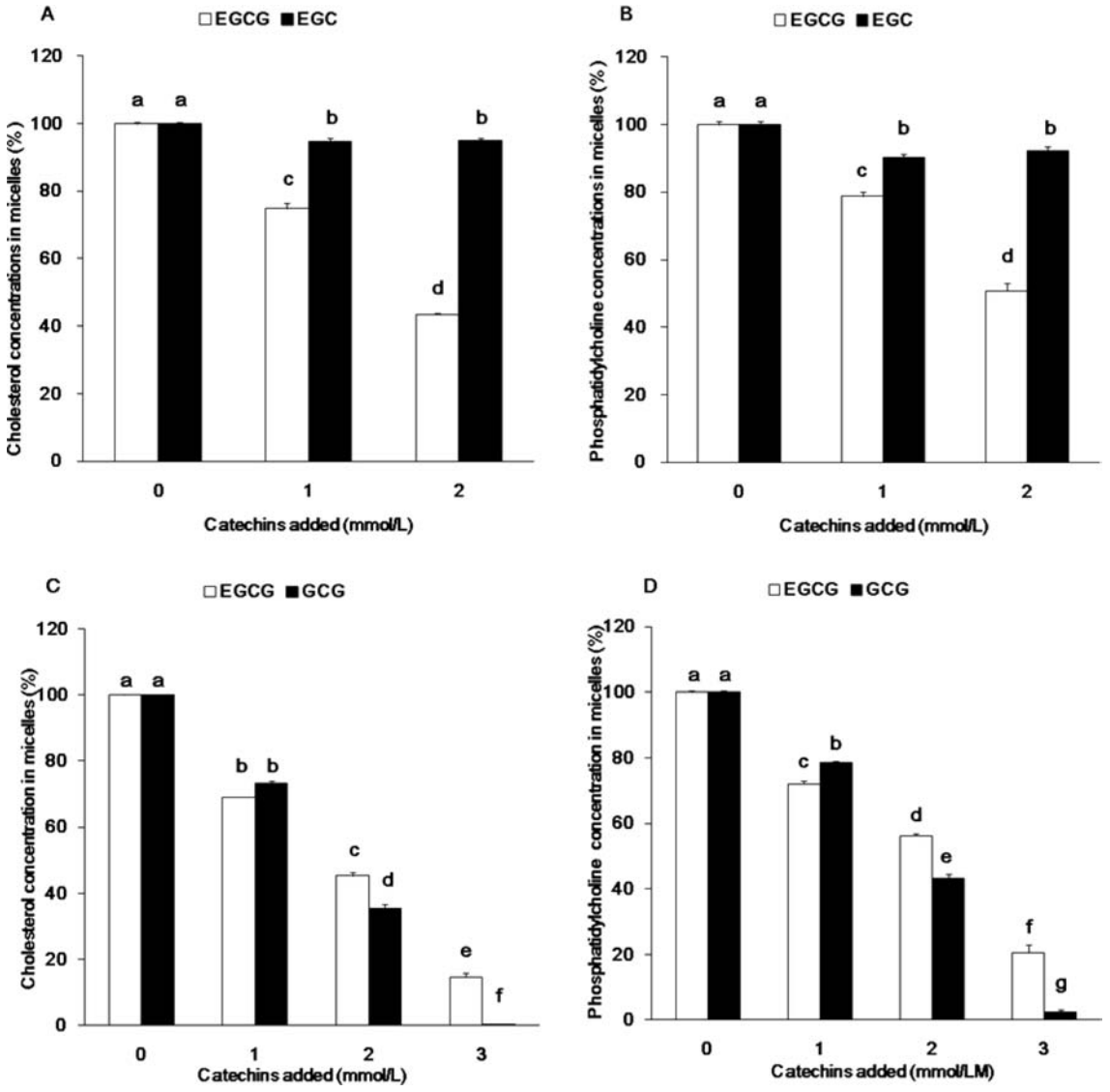

Figure 2. Effect of green tea catechins on micellar solubility of cholesterol and phosphatidylcholine *in vitro*. Comparison of effect of epigallocatechin gallate (EGCG) and epigallocatechin (EGC) on the micellar solubility of cholesterol (A) and phosphatidylcholine (B) *in vitro*. Comparison of the effect of EGCG and gallocatechin gallate (GCG) on micellar solubility of cholesterol (C) and phosphatidylcholine (D) *in vitro*. Various amounts of EGCG, EGC, or GCG in deionized water (100 μL) stored at 37 °C were added to 3 mL micellar solutions. The micellar cholesterol and phosphatidylcholine concentration at 0 mmol/L tea catechins was adjusted to 100%. Data are means ± SE of triplicate experiments. Means not sharing a common letter differ significantly ($P < 0.05$). Two-way ANOVA: (A–D) effect of catechins type, $P < 0.0001$; effect of catechin concentration, $P < 0.0001$; interaction between catechins type and catechin concentration, $P < 0.0001$.

modification. The 10 mmol/L sodium hydroxide injection was avoided because this decreased immobilization levels, particularly in the measurement flow cell, in which cholesterol was immobilized. EGCG solutions were prepared at concentrations from 0.05 to 1.6 mmol/L using the running buffer. The solutions were injected over the lipid surface at a flow rate of 5 μL/min for 60 s. The solutions were then replaced by the running buffer at a flow rate of 5 μL/min for 60 s. The operating temperature was routinely 25 °C.

Statistical Analysis. Data are expressed as the means ± standard error (SE). Statistical analysis of the data was performed by two-way ANOVA followed by a Bonferroni/Dunn test to evaluate the significance of differences between pairs of means. Differences were considered significant at $P < 0.05$.

RESULTS

Effects of EGCG, EGC, and GCG on the Micellar Solubility of Cholesterol and PC *in Vitro*. In the absence of green tea catechins, the amounts of cholesterol incorporated into the bile micelles in Figure 2A,C were 94.2% and 91.0%, respectively. These values were adjusted to 100% in Figure 2. EGCG and GCG effectively decreased the micellar solubilities of cholesterol and PC in a dose-dependent manner (Figure 2C,D). EGC slightly decreased the micellar solubilities of cholesterol and PC (Figure 2A,B). The concentrations of micellar cholesterol and PC following the addition of GCG were significantly lower than those following the addition of EGCG at concentrations of 2 and 3 mmol/L of micelles (Figure 2C,D).

Effects of EGCG on the Micellar Solubility of Cholesterol and Different Phospholipids *in Vitro*. In the absence of EGCG, the percentages of cholesterol incorporated into the bile micelles containing PC, PA, PE, PI, and PS were 85.5%, 91.0%, 95.4%, 84.0%, and 94.8%, respectively. These values were adjusted to 100% in Figure 3A. When the bile salt

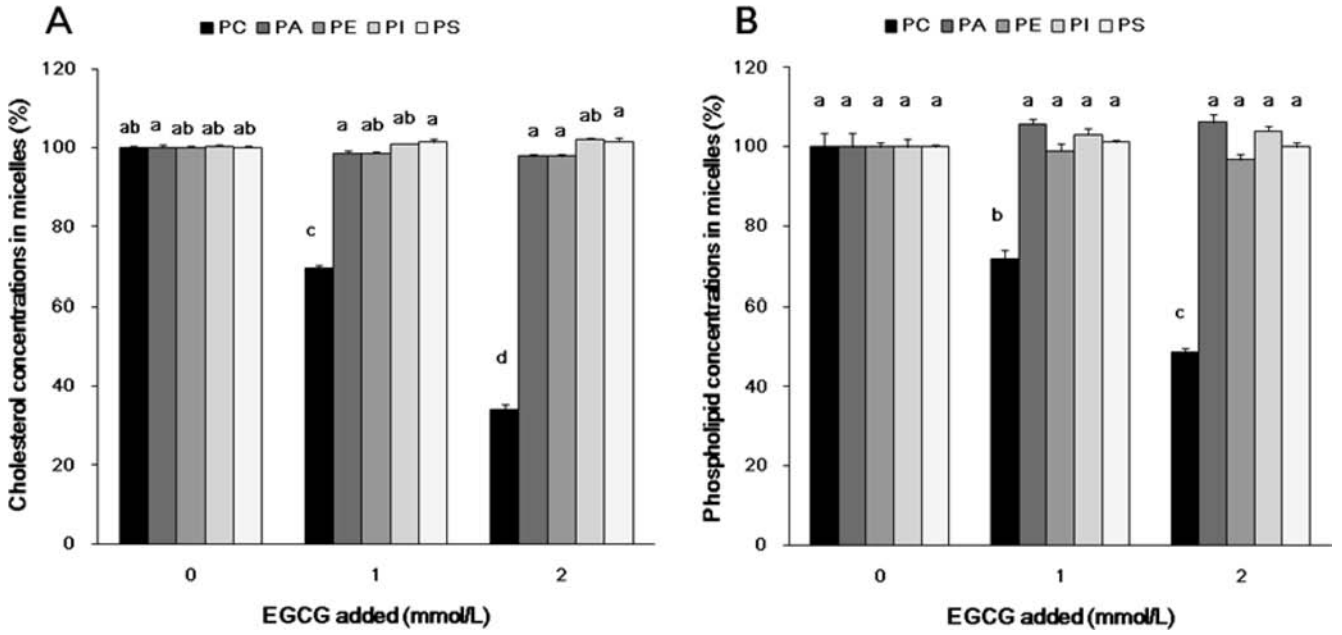

Figure 3. Effect of epigallocatechin gallate on the micellar solubility of cholesterol (A) and different phospholipids (B) *in vitro*. Various amounts of epigallocatechin gallate (EGCG) in deionized water (100 μL) stored at 37 °C were added to 3 mL micellar solution containing 0.6 mmol/L phosphatidylcholine (PC), phosphatidic acid (PA), phosphatidylethanolamine (PE), phosphatidylinositol (PI), or phosphatidylserine (PS). The micellar cholesterol and phospholipid concentrations at 0 mmol/L of EGCG were adjusted to 100%. EGCG was added at 1 and 2 mmol/L. Data are means ± SE of triplicate experiments. Means not sharing a common letter differ significantly ($P < 0.05$). Two-way ANOVA: (A, B) effect of phospholipid type, $P < 0.0001$; effect of EGCG concentration, $P < 0.0001$; interaction between phospholipid type and EGCG concentration, $P < 0.0001$.

micelles contained a phospholipid other than PC, neither cholesterol nor the phospholipid was eliminated following the addition of EGCG. (Figures 3A,B).

Effect of EGCG on the Vesicular Solubility of Different Phospholipids *in Vitro*. EGCG effectively decreased the vesicular solubility of PC and slightly decreased the vesicular solubility of PS (Figure 4). EGCG did not decrease the vesicular solubilities of PA, PE, or PI.

Effects of EGCG, GCG, and EGC on the Vesicular Solubility of PC *in Vitro*. EGCG and GCG similarly and effectively decreased the vesicular solubility of PC in a dose-dependent manner (Figure 5). EGC slightly decreased the vesicular solubility of PC (Figure 5). The concentrations of vesicular PC following the addition of EGCG or GCG were significantly lower than those following the addition of EGC at concentrations of 0.5, 1, and 2 mmol/L of vesicles (Figure 5).

Determination of the Apparent K_D for the Binding of Eight Green Tea Catechins to POPC by an SPR-Based Biosensor Assay. We immobilized DOPA in the reference flow cell as the control ligand because green tea catechins were not expected to interact with DOPA based on the result shown in Figure 4. However, the green tea catechins weakly bound to DOPA, and the resonances in the reference flow cell with immobilized DOPA were slightly elevated. Therefore, we calculated the apparent K_D values for the eight green tea catechins to POPC. The immobilization levels of POPC in the measurement flow cell and DOPA in the reference flow cell were 5,705.6 and 5,090.3 resonance units (RU), respectively. Figure 6 shows the sensorgrams of sequentially injected EGCG and EGC obtained using a single-cycle kinetics method. The sensorgrams were obtained by subtracting of the sensorgram obtained for the reference flow cell from the sensorgram obtained for the measurment flow cell. The binding of EGCG

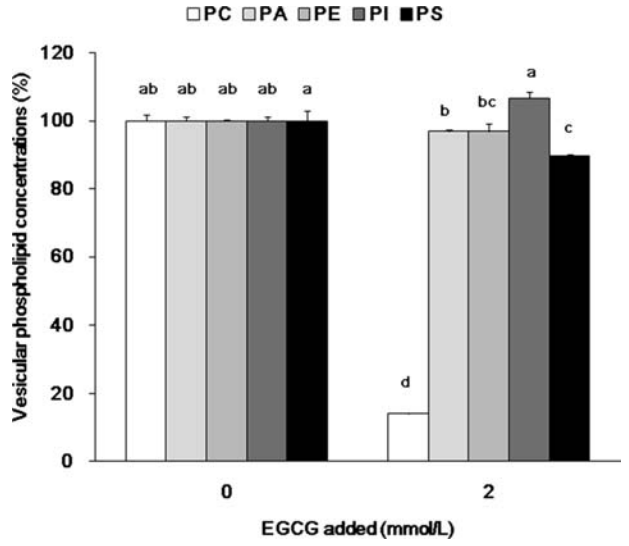

Figure 4. Effect of epigallocatechin gallate on the vesicular solubility of different phospholipids *in vitro*. Various amounts of epigallocatechin gallate (EGCG) in ultrapure water (200 μL) were added to the vesicular solutions (6 mL). The mixture was incubated for 1 h at 37 °C and then centrifuged at 25000*g* for 1 h. In a preliminary study, we confirmed that centrifugation did not precipitate the phospholipids from the vesicular solution. The vesicular phospholipid concentration at 0 mmol/L EGCG was adjusted to 100%. EGCG was added at 2 mmol/L. Data are means ± SE of triplicate experiments. Means not sharing a common letter differ significantly ($P < 0.05$). Two-way ANOVA: effect of phospholipid type, $P < 0.0001$; effect of EGCG concentration, $P < 0.0001$; interaction between phospholipid type and EGCG concentration, $P < 0.0001$.

dx.doi.org/10.1021/jf405591g | J. Agric. Food Chem. 2014, 62, 2881−2890

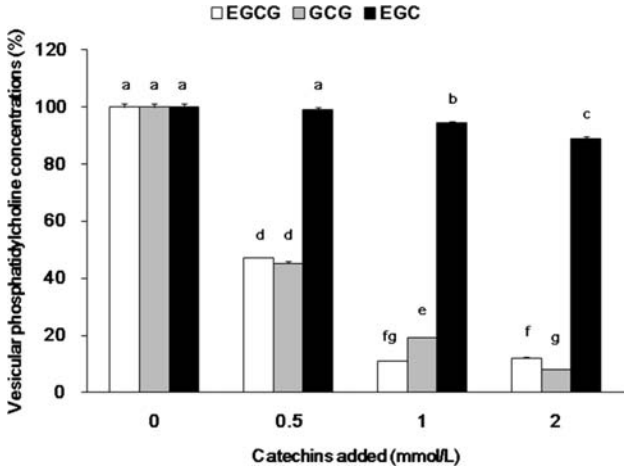

Figure 5. Effect of epigallocatechin gallate, gallocatechin gallate, and epigallocatechin on the vesicular solubility of phosphatidylcholine *in vitro*. Various amounts of epigallocatechin gallate (EGCG), gallocatechin gallate (GCG), and epigallocatechin (EGC) in ultrapure water (200 μL) were added to the PC vesicles (6 mL). The mixture was incubated for 1 h at 37 °C, and then centrifuged at 25000*g* for 1 h. The vesicular phosphatidylcholine concentration at 0 mmol/L of tea catechins was adjusted to 100%. Tea catechins were added at 0.5, 1, and 2 mmol/L. Data are means ± SE of triplicate experiments. Means not sharing a common letter differ significantly ($P < 0.05$). Two-way ANOVA: effect of phospholipid type, $P < 0.0001$; effect of EGCG concentration, $P < 0.0001$; interaction between phospholipid type and EGCG concentration, $P < 0.0001$.

and EGC to POPC was initially fast but then slowed, and concentration-dependent binding was observed (Figure 6A,B). Table 1 shows the apparent K_D for eight green tea catechins to POPC. The apparent K_D values of the green tea catechins with a galloy moiety to POPC were lower than those of the green tea catechins without a galloyl moiety. These results show that green tea catechins with a galloyl moiety have higher affinity for POPC than those without a galloyl moiety.

Table 1. Apparent Equilibrium Dissociation Constants for the Binding of Eight Green Tea Catechins to POPC Obtained from Surface Plasmon Resonance-Based Biosensor Assays[a]

	apparent K_D (mol/L)
EGCG	1.535×10^{-5}
GCG	2.485×10^{-5}
ECG	2.888×10^{-5}
CG	3.662×10^{-5}
EGC	6.685×10^{-4}
GC	9.488×10^{-4}
EC	1.036×10^{-3}
C	4.316×10^{-4}

[a]Eight green tea catechin solutions were prepared at 5−80 μmol/L (green tea catechins with a galloyl moiety) and 50−800 μmol/L (green tea catechins without a galloyl moiety) in the running buffer. To measure the association of green tea catechin with POPC or DOPA, the solutions were injected over the lipid surface at a flow rate of 5 μL/min for 1,080 s. To measure the dissociation of the POPC− or DOPA−green tea catechin complex, the green tea catechin solutions were then replaced with the running buffer at a flow rate of 5 μL/min for 180 s. The sensorgrams obtained from the injection of the running buffer were subtracted from the sensorgrams obtained from the injection of the green tea catechin solutions. Then, the sensorgram obtained from the reference flow cell, in which DOPA was immobilized, was subtracted from the sensorgram obtained from the measurement flow cell, in which POPC was immobilized, to yield the apparent binding responses. Because the sensorgrams did not have the appropriate curvature for curve fitting to determine the association and dissociation rates and because EGCG weakly bound to DOPA, the apparent equilibrium dissociation constants (K_D) for eight green tea catechins to POPC were calculated from the equilibrium resonance signals as a function of analyte concentration according to the manufacturer's instructions (Biacore X100 evaluation software).[33]

^{1}H NMR Measurement of EGCG in the Absence and Presence of Bile Salt Micelles. Interaction of EGCG with the bile salt micelles resulted in a considerable shift of the A-

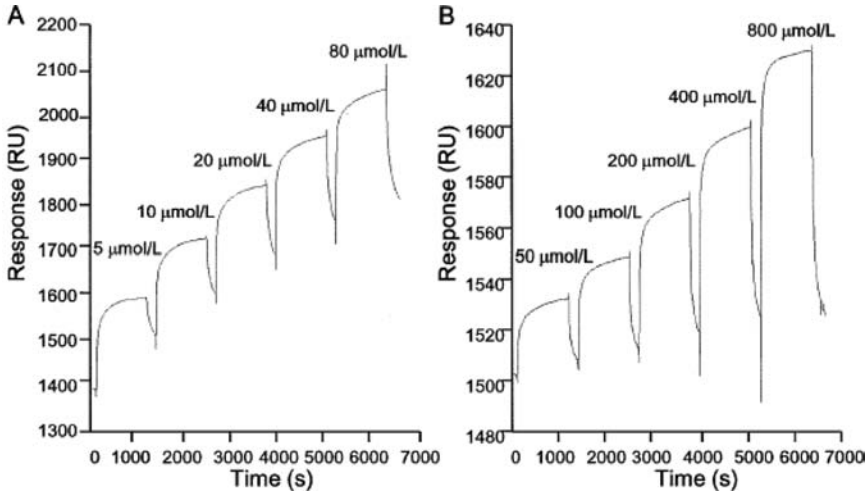

Figure 6. Sensorgrams showing the binding of various concentrations of (−)-epigallocatechin gallate (A) and (−)-epigallocatechin (B) obtained from single-cycle kinetics assays. EGCG in running buffer at 5, 10, 20, 40, and 80 μmol/L (A) and EGC in running buffer at 50, 100, 200, 400, and 800 μmol/L (B) were sequentially injected over the lipid surface at a flow rate of 5 μL/min for 1,080 s. To dissociate the POPC− or DOPA−green tea catechin complex, the green tea catechin solutions were then replaced with the running buffer at a flow rate of 5 μL/min for 180 s. The sensorgrams obtained from the injection of the running buffer were subtracted from the sensorgrams obtained from the injection of the green tea catechin solutions. Then, the sensorgram obtained from the reference flow cell, in which DOPA was immobilized, was subtracted from the sensorgram obtained from the measurement flow cell, in which POPC was immobilized, to yield the apparent binding responses.

ring (6- and 8-H), the B-ring (2′- and 6′-H), C-ring (2- and 3-H), and the galloyl moiety (2″- and 6″-H) signals in EGCG (Figure 7). These changes of chemical shift following the

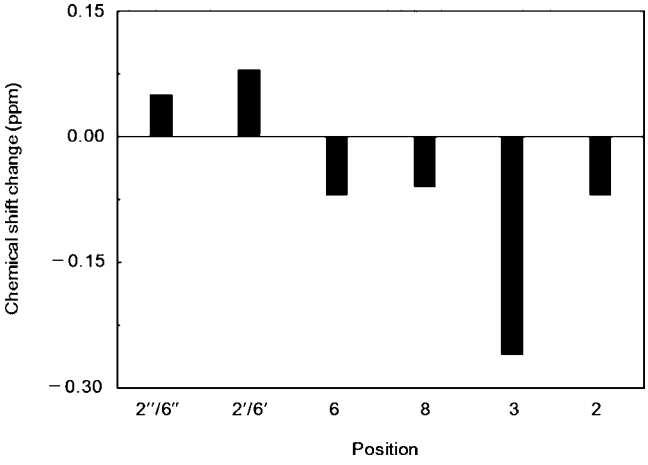

Figure 7. Change values of the chemical shift of (−)-epigallocatechin gallate following its addition to the bile salt micelles. The changes of (−)-epigallocatechin gallate (EGCG) signals in the presence of the bile salt micelles are compared to those in the absence of the bile salt micelles.

addition of EGCG to the bile salt micelles were similar to those to isotropic bicelles, which are composed of PC and frequently used as a lipid bilayer model, in our previous study.[29] These observations suggest that EGCG interacts with PC in the bile salt micells as well as in lipid bilayers. 4α- and 4β-H signals were not observed because they overlapped large signals derived from several molecules that existed in the bile salt micelles.

NOESY Experiment on Bile Salt Micelles/EGCG Samples. NOESY experiments are suitable for estimating both intermolecular and intramolecular proton distances up to 5 Å.[34] NOESY spectra were first measured with various mixing times. By increasing the mixing time, an NOE was observed. We found that a mixing time of 800 ms was optimal for observing the cross-peak in the bile salt micelle/EGCG sample. Figure 8A shows the NOESY spectra of EGCG interacting with bile salt micelles containing cholesterol and PC prepared with D_2O at 300 K. Intermolecular NOE was observed between the γ-H of the PC molecule and the 2″- and 6″-H on the galloyl moiety in EGCG (Figure 8B). An intermolecular NOE between cholesterol and EGCG was not observed. Several intramolecular cross-peaks in the EGCG molecule were observed between the protons on the B-ring and the protons on the galloyl moiety (data not shown).

Measuring the Fluorescence of 2-AS or 12-AS in Bile Salt Micelles in the Presence of EGCG. The localization of EGCG in bile salt micelles containing cholesterol and PC was investigated by fluorescence quenching of 2-AS and 12-AS with EGCG. Fluorescence was measured using a Flex Station II system (Molecular Devices, Sunnyvale, CA, USA). The anthroyl group of 2-AS should be located on the surface of the bile salt micelles, whereas that of 12-AS should be located in the hydrophobic core of the bile salt micelles. EGCG effectively quenched the fluorescence of 2-AS in a dose-dependent manner (Figure 9). EGCG (at 0.1, 0.3, 0.5, 0.7, 1, and 2 mmol/L) more strongly quenched the fluorescence of 2-AS than that of 12-AS (Figure 9).

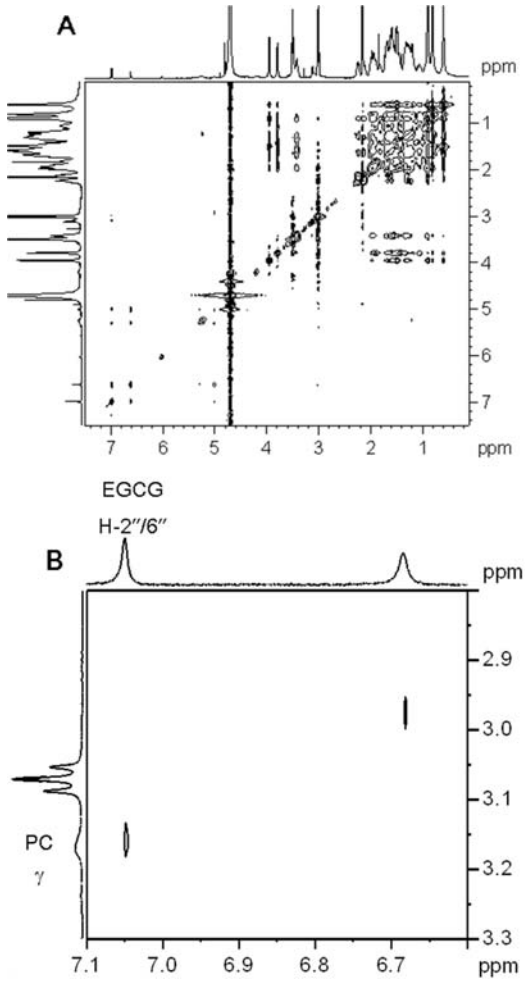

Figure 8. NOESY spectra of epigallocatechin gallate and bile salt micelles containing cholesterol and phosphatidylcholine, with a 800 ms mixing time at 300 K. (A) Overall view of the NOESY spectra. (B) Enlarged view of the NOESY spectra.

Binding Analyses of EGCG to Cholesterol by an SPR-Based Biosensor Assay. Four immobilization experiments were performed (reference flow cell/measurement flow cell: 0.5 mmol/L POPC/0.5 mmol/L POPC and 0.05 mmol/L cholesterol, 0.5 mmol/L POPC/0.5 mmol/L POPC and 0.15 mmol/L cholesterol, 0.5 mmol/L DOPA/0.5 mmol/L DOPA and 0.05 mmol/L cholesterol, and 0.5 mmol/L DOPA/0.5 mmol/L DOPA and 0.15 mmol/L cholesterol). The immobilization levels of phospholipid on the measurement flow cell and the reference flow cell were equalized as accurately as possible. The EGCG binding to cholesterol was not observed in any immobilization experiments (data not shown).

■ DISCUSSION

We previously showed that the addition of green tea catechins with a galloyl moiety to a bile salt micellar solution precipitated cholesterol and decreased the micellar solubility of cholesterol in a dose-dependent manner.[16] In contrast, green tea catechins without a galloyl moiety did not precipitated cholesterol. When purified EGCG was added to the bile salt micellar solution, the amount of EGCG precipitated from the micellar solution was highly positively correlated with the amount of cholesterol precipitated (correlation coefficient = 0.99). These results strongly suggested that EGCG eliminated the cholesterol from

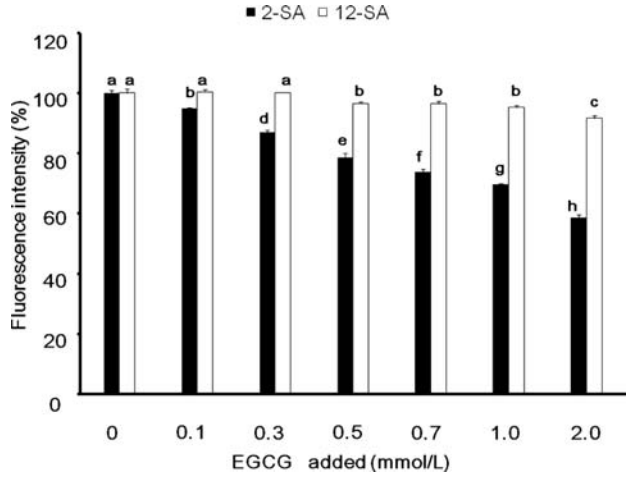

Figure 9. Effects of epigallocatechin gallate on the fluorescence intensity of 2-(9-anthroyloxy) stearic acid or 12-(9-anthroyloxy)stearic acid in bile salt micelles. A bile salt micellar solution containing 1 mmol/L 2-AS or 12-AS was prepared by sonication and stored at room temperature overnight. The micellar solutions (100 μL) were incubated with 100 μL of PBS containing epigallocatechin gallate (EGCG) for 20 min at 20 °C. The amounts of EGCG added were adjusted to 0, 0.1, 0.3, 0.5, 0.7, 1.0, and 2.0 mmol/L micelles. The fluorescence of 2-AS or 12-AS in the bile salt micellar solution were measured. The fluorescence intensity was calculated as the percentage of the fluorescence intensity of 2-AS or 12-AS in the absence of EGCG. Data are means ± SE of triplicate experiments. Means not sharing a common letter differ significantly ($P < 0.05$). Two-way ANOVA: effect of AS type, $P < 0.0001$; effect of EGCG concentration, $P < 0.0001$; interaction between AS type and EGCG concentration, $P < 0.0001$.

the bile salt micelles and co-precipitated with cholesterol. Therefore, we hypothesized that the micellar cholesterol-lowering activities of green tea catechins with a galloyl moiety could be a major cause for the inhibition of cholesterol absorption in rats.[16,17]

In the present study, we showed for the first time that green tea catechins with a galloyl moiety, but not those without a galloyl moiety, eliminated not only cholesterol but also PC from bile salt micelles (Figure 2). When bile salt micelles contained a phospholipid other than PC, neither cholesterol nor the phospholipid was eliminated by the addition of EGCG (Figure 3A,B). The same phenomenon was also observed in vesicles containing various phospholipids. EGCG effectively eliminated only the PC in the vesicles (Figure 4). We also showed that EGCG and GCG, but not EGC, effectively decreased the vesicular solubility of PC in a dose-dependent manner (Figure 5). Furthermore, we showed that green tea catechins with a galloyl moiety had higher affinity for POPC than those without a galloyl moiety in an SPR-based biosensor assay (Figure 6A,B and Table 1). The different affinity to PC between green tea catechins with a galloyl moiety and those without a galloyl moiety may be a reason why the concentrations of vesicular PC following the addition of EGCG or GCG were significantly lower than those following the addition of EGC (Figure 5). These observations suggest that green tea catechins with a galloyl moiety interact with PC and the binding of EGCG to PC decreases PC solubility. In our preliminary study, when a bile salt micellar solution containing 0.5 mmol/L cholesterol was prepared by sonication in the absence of phospholipids, the amount of cholesterol incorporated into the bile salt micelles was extremely low, and no more than 2.47% was incorporated, whereas the rest of the cholesterol was precipitated. These results suggest that because PC is eliminated from the bile salt micelles through its interaction with green tea catechins with a galloyl moiety, the micellar solubility of cholesterol is reduced; therefore, the cholesterol precipitated.

The result from Figure 7 suggested that EGCG interacted with PC in the bile salt micelles. To clearly investigate how EGCG interacts with the PC in a bile salt micellar solution and whether the interaction between EGCG and PC indirectly leads to the precipitation of cholesterol from the bile salt micelles or the formation of a complex containing EGCG, PC, and cholesterol, we performed a NOESY experiment and estimated the location of EGCG in the bile salt micelles containing cholesterol and PC. Intermolecular NOE was observed between the γ-H of PC and 2″- and 6″-H on the galloyl moiety of EGCG when EGCG was added to the bile salt micelles containing cholesterol and PC (Figure 8B). The cation−π interaction between the trimethylammonium group of PC and the galloyl moiety of EGCG was inferred from this observation. Furthermore, several intramolecular cross-peaks in the EGCG molecule were observed between the protons on the B-ring and the protons on the galloyl moiety (data not shown). Therefore, there is a strong possibility that the cation−π interaction between the trimethylammonium group of PC and the galloyl moiety of EGCG may lead not only to a considerable shift of the galloyl moiety (2″- and 6″-H) signals in EGCG but also to a considerable shift of the A-ring (6- and 8-H), the B-ring (2′- and 6′-H), and the C-ring (2- and 3-H) signals in EGCG (Figure 7). In contrast, the intermolecular NOE between cholesterol and EGCG was not observed. These observations support our expectation that EGCG specifically interacts with only PC, but not cholesterol in the bile salt micelles, and agree with the results of our previous study in which we showed that EGCG specifically interacts with isotropic bicelles, which are composed of PC and frequently used as lipid bilayer models.[29]

When the localization of EGCG in the bile salt micelles containing cholesterol and PC was investigated, EGCG effectively quenched the fluorescence of 2-AS in a dose-dependent manner (Figure 9). Because the trimethylammonium group of PC is a hydrophilic group, it should be located on the surface of the bile salt micelles. Therefore, this observation suggests that EGCG is located on the surface of the bile salt micelles via its interaction with micellar PC. The concentration of EGCG added to the micelles in this experiment was less than the amount that precipitated following the addition of EGCG to the bile salt micelles. It is thought that PC could be eliminated from the bile salt micelles by increasing the EGCG concentration added to the micelles.

The results from our previous study suggested that cholesterol directly precipitated with EGCG.[16] To investigate whether EGCG interacts with cholesterol, we performed binding analyses using an SPR-based biosensor assay. Binding of EGCG to cholesterol was not observed (data not shown). This observation strongly suggests that EGCG does not directly interact with cholesterol in a bile salt micelle. The results from the present study suggest that EGCG formed a complex with PC, and then this complex interacts with cholesterol. Hénin et al. showed that cholesterol and dimyristoylphosphatidylcholine formed a complex with a 1:1 stoichiometry in a fully hydrated cholesterol−dimyristoylphosphatidylcholine bilayer through

molecular dynamics simulations.[35] Furthermore, in preliminary studies, we observed that cholesterol and PC formed a complex with a 1:1 stoichiometry in $CDCl_3$ (data not shown). These observations suggest that cholesterol and PC form a complex in bile salt micelles and that the interaction between EGCG and PC leads to the formation of a complex containing EGCG, PC, and cholesterol. However, we could not provide direct evidence that the interaction between EGCG and PC leads to the formation of a complex containing EGCG, PC, and cholesterol in the present study. We could not assign all spectra in the bile salt micelles in the NOESY study, because too many protons derived from several molecules existed in the bile salt micelles. Furthermore, NOESY experiments are suitable for estimating specific interactions, but not nonspecific interactions. If cholesterol nonspecifically interacts with the EGCG/PC complex, it would be difficult to observe the intermolecular NOE between the protons in the cholesterol molecule and the EGCG/PC complex. Further research is required to confirm these results.

We previously suggested the possibility that the B-ring and the plane of the ring in the galloyl moiety in EGCG or ECG were stacked via the $\pi-\pi$ interaction in lipid bilayers and that the cation$-\pi$ interaction between the trimethylammonium group of PC and the galloyl moiety in EGCG or ECG was enhanced by the $\pi-\pi$ interaction between the B-ring and the plane of the ring in their galloyl moiety of EGCG or ECG.[36] Several intramolecular cross-peaks were observed between the protons on the B-ring and the protons on the galloyl moiety in the EGCG molecule in the NOESY experiment in this study (data not shown). The intramolecular NOE between the protons on the B-ring and the protons on the galloyl moiety was also observed in our previous NOESY experiment using bicelle/EGCG and ECG samples.[29] Therefore, there is a strong possibility that the intramolecular interactions in the EGCG molecule enhanced the cation$-\pi$ interaction between the trimethylammonium group of PC and the galloyl moiety of EGCG in bile salt micelles as well as in lipid bilayers.

Both exogenous and endogenous phospholipids exist in the intestinal lumen. The dietary intake of phospholipids is typically estimated to be 2−8 g/day in humans, and the biliary pathway delivers 10−20 g/day to the intestinal lumen.[37] The predominant phospholipid in the intestinal lumen is PC. Therefore, the intestinal lumen can be a suitable environment for the inhibitory effect of EGCG on cholesterol absorption because the interaction between green tea catechins with a galloyl moiety and PC is important in eliminating cholesterol from bile salt micelles.

In conclusion, our study showed that EGCG decreased the micellar solubility of cholesterol via specific interaction with PC, but not through a direct interaction with cholesterol. At any rate, the limited solubility of cholesterol by green tea catechins with a galloyl moiety can be a major cause of the inhibition of cholesterol absorption.[16,17] In this study, we could not sufficiently describe the mechanism underlying the EGCG-mediated elimination of cholesterol from bile salt micelles. Therefore, detailed studies are necessary to understand how green tea catechins with a galloyl moiety cause the precipitation of cholesterol from bile salt micelles.[16,17]

AUTHOR INFORMATION

Corresponding Author

*Tel.: 001-81-548-54-1247. Fax: 001-81-548-54-0763. E-mail: m-kobayasi@itoen.co.jp.

Notes

The authors declare no competing financial interest.

ABBREVIATIONS USED

EGCG, epigallocatechin gallate; ECG, epicatechin gallate; EGC, epigallocatechin; EC, epicatechin; GCG, gallocatechin gallate; CG, catechin gallate; GC, gallocatechin; C, catechin; PC, phosphatidylcholine; PA, phosphatidic acid; PE, phosphatidylethanolamine; PI, phosphatidylinositol; PS, phosphatidylserine; POPC, 1-palmitoyl-2-oleoylphosphatidylcholine; DOPA, 1,2-dioleoylphosphatidic acid; SPR, surface plasmon resonance; NOE, nuclear Overhauser effect; NOESY, NOE-correlated spectroscopy; DSS, sodium 2,2-silapentane-5-sulfonate; 2-AS, 2-(9-anthroyloxy)stearic acid; 12-AS, 12-(9-anthroyloxy)stearic acid

REFERENCES

(1) Subramanian, N.; Venkatesh, P.; Ganguli, S.; Sinkar, V. P. Role of polyphenol oxidase and peroxidase in the generation of black tea theaflavins. *J. Agric. Food Chem.* **1999**, *47*, 2571−2578.

(2) Chen, Z.-Y.; Xhu, Q. Y.; Tsang, D.; Huang, Y. Degradation of green tea catechins in tea drinks. *J. Agric. Food Chem.* **2001**, *49*, 477−482.

(3) Seto, R.; Nakamura, H.; Nanjo, F.; Hara, Y. Preparation of epimers of tea catechins by heat treatment. *Biosci. Biotechnol. Biochem.* **1997**, *61*, 1434−1439.

(4) Miura, Y.; Chiba, T.; Tomita, I.; Koizumi, H.; Miura, S.; Umegaki, K.; Hara, Y.; Ikeda, M.; Tomita, T. Tea catechins prevent the development of atherosclerosis in apoprotein E-deficient mice. *J. Nutr.* **2001**, *131*, 27−32.

(5) Murase, T.; Nagasawa, A.; Suzuki, J.; Hase, T.; Tokimitsu, I. Beneficial effects of tea catechins on diet-induced obesity: stimulation of lipid catabolism in the liver. *Int. J. Obes.* **2000**, *26*, 1459−1464.

(6) Ikeda, I.; Hamamoto, R.; Uzu, K.; Imaizumi, K.; Nagao, K.; Yanagita, T.; Suzuki, Y.; Kobayashi, M.; Kakuda, T. Dietary gallate esters of tea catechins reduce deposition of visceral fat, hepatic triacylglycerol, and activities of hepatic enzymes related to fatty acid synthesis in rats. *Biosci. Biotechnol. Biochem.* **2005**, *69*, 1049−1053.

(7) Kajimoto, O.; Kajimoto, Y.; Yabune, M.; Nakamura, T.; Kotani, K.; Suzuki, Y.; Nozawa, A.; Nagata, K.; Unno, T.; Sagesaka-Mitane, Y.; Kakuda, T.; Yoshikawa, T. Tea catechins with a galloyl moiety reduce body weight and fat. *J. Health Sci.* **2005**, *51*, 161−171.

(8) Tian, W. X. Inhibition of fatty acid synthase by polyphenols. *Curr. Med. Chem.* **2006**, *13*, 967−977.

(9) Okuda, T.; Kimura, Y.; Yoshida, T.; Hatano, T.; Okuda, H.; Arichi, S. Studies on the activities of tannins and related compounds from medicinal plants and drugs. I. Inhibitory effects on lipid peroxidation in mitochondria and microsomes of liver. *Chem. Pharm. Bull.* **1983**, *31*, 1625−1631.

(10) Yoshino, K.; Tomita, I.; Sano, M.; Oguni, I.; Hara, Y.; Nakano, M. Effects of long term dietary supplement of tea polyphenols on lipid peroxide levels in rats. *Age* **1994**, *17*, 79−85.

(11) Kada, T.; Kaneko, K.; Matsuzaki, S.; Matsuzaki, T.; Hara, Y. Detection and chemical identification of natural bioantimutagens. A case of the green tea factor. *Mutat. Res.* **1985**, *150*, 127−132.

(12) Fujiki, H.; Suganuma, M.; Okabe, S.; Sueoka, N.; Komori, A.; Sueoka, E.; Kozu, T.; Tada, Y.; Suga, K.; Imai, K.; Nakachi, K. Cancer inhibition by green tea. *Mutat. Res.* **1998**, *402*, 307−310.

(13) Ikeda, I.; Tsuda, K.; Suzuki, Y.; Kobayashi, M.; Unno, T.; Tomoyori, H.; Goto, H.; Kawata, Y.; Imaizumi, K.; Nozawa, A.; Kakuda, T. Tea catechins with a galloyl moiety suppress postprandial hypertriacylglycerolemia by delaying lymphatic transport of dietary fat in rats. *J. Nutr.* **2005**, *135*, 155−159.

(14) Chan, P. T.; Fong, W. P.; Cheung, Y. L.; Huang, Y.; Ho, W. K. K.; Chen, Z. Y. Jasmine green tea epicatechins are hypolipidemic in hamsters (*Mesocricetus auratus*) fed a high fat diet. *J. Nutr.* **1999**, *129*, 1094−1101.

(15) Koo, S. I.; Noh, S. K. Green tea as inhibitor of the intestinal absorption of lipids: potential mechanism for its lipid-lowering effect. *J. Nutr. Biochem.* **2007**, *8*, 179−183.
(16) Ikeda, I.; Imasato, Y.; Sasaki, E.; Nakayama, M.; Nagao, H.; Takeo, T.; Yayabe, F.; Sugano, M. Tea catechins decrease micellar solubility and intestinal absorption of cholesterol in rats. *Biochim. Biophys. Acta* **1992**, *1127*, 141−146.
(17) Ikeda, I.; Kobayashi, M.; Hamada, T.; Tsuda, T.; Goto, H.; Imaizumi, K.; Nozawa, A.; Sugimoto, A.; Kakuda, T. Heat-epimerized tea catechins rich in gallocatechin gallate and catechin gallate are more effective to inhibit cholesterol absorption than tea catechins rich in epigallocatechin gallate and epicatechin gallate. *J. Agric. Food Chem.* **2003**, *51*, 7303−7307.
(18) Muramatsu, K.; Fukuyo, M.; Hara, Y. Effect of green tea catechins on plasma cholesterol level in cholesterol-fed rats. *J. Nutr. Sci. Vitaminol.* **1986**, *32*, 613−622.
(19) Yang, T. T. C.; Koo, M. W. L. Chinese green tea lowers cholesterol level through an increase in fecal lipid excretion. *Life Sci.* **2000**, *66*, 411−423.
(20) Kobayashi, M.; Unno, T.; Suzuki, Y.; Nozawa, A.; Sagesaka, Y.; Kakuda, T.; Ikeda, I. Heat-epimerized tea catechins have the same cholesterol-lowering activity as green tea catechins in cholesterol-fed rats. *Biosci. Biotechnol. Biochem.* **2005**, *69*, 2455−2458.
(21) Kajimoto, O.; Kajimoto, Y.; Yabune, M.; Nozawa, A.; Nagata, K.; Kakuda, T. Tea catechins reduce serum cholesterol levels in mild and borderline hypercholesterolemia patients. *J. Clin. Biochem.* **2003**, *33*, 101−111.
(22) Kajimoto, O.; Kajimoto, Y.; Takeda, M.; Nozawa, A.; Suzuki, Y.; Kakuda, T. A beverage containing tea catechins with a galloyl moiety reduce serum cholesterol level in hypercholesterolemis women. *Health Sci.* **2006**, *22*, 60−71 (in Japanese with English summary)..
(23) Zheng, X. X.; Xu, Y. L.; Li, S. H.; Hui, R.; Huang, X. H. Green tea intake lowers serum total and LDL cholesterol in adults: A meta-analysis of 14 randomized controlled trials. *Am. J. Clin. Nutr.* **2011**, *94*, 601−610.
(24) Kim, A.; Chiu, A.; Barone, M. K.; Avino, D.; Wang, F.; Coleman, C. I.; Phung, O. J. Green tea catechins decrease total and low-density lipoprotein cholesterol: A systematic review and meta-analysis. *J. Am. Diet. Assoc.* **2011**, *111*, 1720−1729.
(25) Raederstorff, D. G.; Schlachter, M. F.; Elste, V.; Weber, P. Effect of EGCG on lipid absorption and plasma lipid levels in rats. *J. Nutr. Biochem.* **2003**, *14*, 326−332.
(26) Vermeer, M. A.; Mulder, T. P.; Molhuizen, H. O. Theaflavins from black tea, especially theaflavin-3-gallate, reduce the incorporation of cholesterol into mixed micelles. *J. Agric. Food Chem.* **2008**, *56*, 12031−12036.
(27) Kajiya, K.; Kumazawa, S.; Nakayama, T. Steric effects of interaction of tea catechins with lipid bilayers. *Biosci. Biotechnol. Biochem.* **2001**, *65*, 2638−2643.
(28) Kumazawa, S.; Kajiya, K.; Naito, A.; Saito, H.; Tuzi, S.; Tanio, M.; Suzuki, M.; Nanjo, F.; Suzuki, E.; Nakayama, T. Direct evidence of interaction of a green tea polyohenol, epigallocatechin gallate, with lipid bilayers by solid-state nuclear magnetic resonance. *Biosci. Biotechnol. Biochem.* **2004**, *68*, 1743−1747.
(29) Uekusa, Y.; Kamihira, M.; Nakayama, T. Dynamic behavior of tea catechins interacting lipid membranes as determined by NMR spectroscopy. *J. Agric. Food Chem.* **2007**, *55*, 9986−9992.
(30) Ikeda, I.; Wakamatsu, K.; Inayoshi, A.; Imaizumi, K.; Sugano, M.; Yazawa, K. α-Linolenic, eicosapentaenoic and docosahexaenoic acids affect lipid metabolism differently in rats. *J. Nutr.* **1994**, *124*, 1898−1906.
(31) Subasinghe, S.; Unabia, S.; Barrow, C. J.; Mok, S. S.; Aguilar, M. I.; Small, D. H. Cholesterol is necessary both for the toxic effect of Aβ peptides on vascular smooth muscle cells and Aβ binding to vascular smooth muscle cell membranes. *J. Neurochem.* **2003**, *84*, 471−479.
(32) Karlsson, R.; Katsamba, P. S.; Nordin, H.; Pol, E.; Myszka, D. Analyzing a kinetic titration series using affinity biosensors. *Anal. Biochem.* **2006**, *34*, 136−147.
(33) O'Shannessy, D. J.; Winzor, D. J. Interpretation of deviations from pseudo-first-order kinetic behavior in the characterization of ligand binding by biosensor technology. *Anal. Biochem.* **1996**, *236*, 275−283.
(34) Lee, S.; Kim, Y. Solution structure of neuromedin B by ^{1}H nuclear magnetic resonance spectroscopy. *FEBS Lett.* **1999**, *460*, 263−269.
(35) Hénin, J.; Chipot, C. Hydrogen-bonding patterns of cholesterol in lipid membranes. *Chem. Phys. Lett.* **2006**, *425*, 329−335.
(36) Uekusa, Y.; Kamihira-Ishijima, M.; Sugimoto, O.; Ishii, T.; Kumazawa, S.; Nakamura, K.; Tanji, K.; Naito, A.; Nakayama, T. Interaction of epicatechin gallate with phospholipid membranes as revealed by solid-state NMR spectroscopy. *Biochim. Biophys. Acta* **2011**, *1808*, 1654−1660.
(37) Cohn, J. S.; Kamili, A.; Wat, E.; Chung, R. W.; Tandy, S. Dietary phospholipids and intestinal cholesterol absorption. *Nutrients* **2010**, *2*, 116−127.

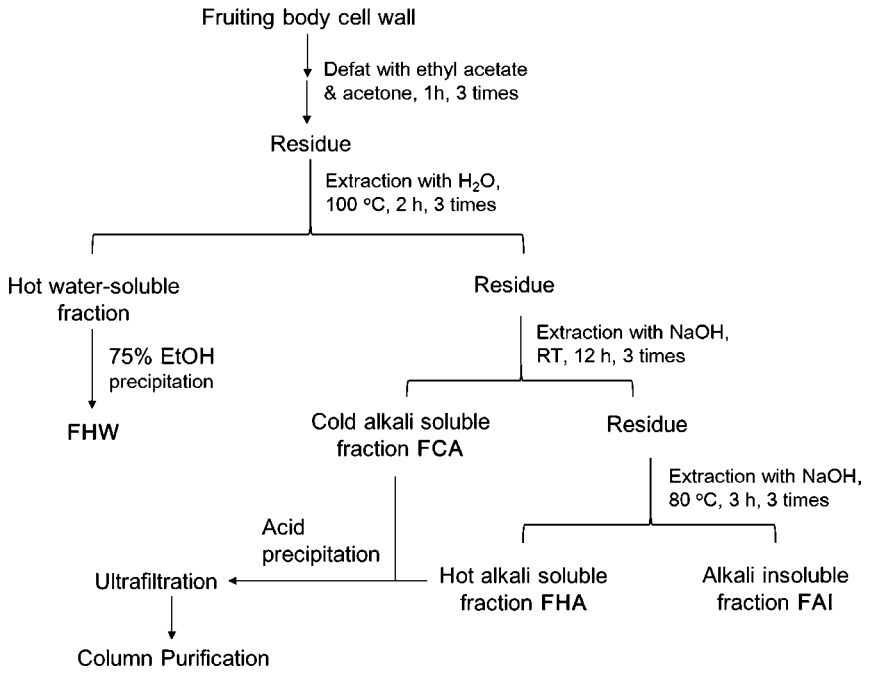

Figure 1. Fractionation scheme of mushroom cell wall of PTR fruiting body.

dietary fiber. This paper focuses on the fractionation of the major soluble MCW polysaccharides from PTR fruiting body and their structural elucidation by use of chemical, spectroscopic, and microscopic techniques.

MATERIALS AND METHODS

Cultivation of Fruiting Body and Preparation of Mushroom Cell Wall. Fruiting body was obtained from the incubation of PTR sclerotium embedded in soil kept in a greenhouse under humid and warm conditions (30−35 °C) for 2 months. The harvested fruiting body was freeze-dried and stored at −20 °C before use. Freeze-dried sample of fruiting body was pulverized into powders to pass through a screen with an aperture of 0.5 mm by using a cyclotech mill (Tecator, Höganäs, Sweden). The milled powders were suspended in distilled water and ultrasonicated at 300 W with a 30% duty cycle for 10 min (Sonics & Materials Vibracell, model VC 600) for cell breakage. The degree of cell breakage was monitored by a phase contrast microscope (PCM, Eclipse 80i, Nikon). Cleaved mushroom cells were washed sequentially with wash solution A [1 mM phenylmethanesulfonyl fluoride (PMSF)], wash solution B [5% (w/v) NaCl, 1 mM PMSF], wash solution C [2% (w/v) NaCl, 1 mM PMSF], wash solution D [1% (w/v) NaCl, 1 mM PMSF], and then wash solution A again to remove intracellular contaminants.[16] Each step was repeated three times until no carbohydrate and protein could be determined from the washed buffer using the phenol−sulfuric acid method and bicinchoninic acid (BCA) protein assay,[17,18] respectively. The isolated MCW was lyophilized prior to its fractionation.

Fractionation and Purification of MCW from PTR Fruiting Body. MCW of PTR fruiting body was fractionated according to the scheme shown in Figure 1. After the successive extraction using hot water, cold alkali, and hot alkali solution (1 M NaOH), three soluble MCW fractions including the hot water-soluble fraction (FHW), the cold alkali-soluble fraction (FCA), and the hot alkali-soluble fraction (FHA) were obtained from the supernatants after centrifugation (4000*g* for 10 min at 4 °C), leaving behind an alkali-insoluble residue (FAI). The FHW fraction was concentrated and subjected to ethanol fractional precipitation up to 75% ethanol. The supernatants of the two alkali-soluble fractions FCA and FHA were precipitated using 75% ethanol to precipitate the polysaccharides and then washed five times using 75% ethanol until the washings were neutral. FAI was washed with Milli-Q water five times to remove any residual chemicals.

FCA and FHA were subjected to further fractionation by membrane ultrafiltration (Millipore, stirred ultrafiltration 8040) with molecular weight (MW) cutoff of 10000 Da to give two fractions (FCA-I and -II; FHA-I and -II) with MW >10000 and <10000 Da, respectively. As larger MW fractions, FCA-I and FHA-I were further purified by gel filtration on a Sephacryl S-1000 Superfine column combined with a Sephacryl S-400 high-resolution column (90 × 2.6 cm i.d., Amersham Pharmacia Biotech, UK) eluted with 0.2 M NaCl at 1.5 mL/min. Being smaller MW fractions, FCA-II and FHA-II were further purified to a single fraction by a Sephacryl S-200 high-resolution column (70 × 2.6 cm i.d., Amersham Pharmacia Biotech, UK) eluted with 0.2 M NaCl at 1.5 mL/min. All of these purified fractions were desalted by gel filtration on a Sephadex G10 column (70 × 2.6 cm i.d.; Amersham Pharmacia Biotech, UK) eluted with distilled water and then freeze-dried prior to further analyses.

Chemical Composition Analysis. The carbohydrate content of the MCW was estimated by using the phenol−sulfuric acid method,[17] whereas the uronic acid was determined colorimetrically according to the *m*-hydroxydiphenyl−sulfuric acid method.[19] Protein content was analyzed using the bicinchoninic acid (BCA) protein assay as described previously.[18]

The monosaccharide composition of the purified polysaccharides from the MCW of PTR fruiting body was determined by the alditol acetate derivatives of the sugars after acid hydrolysis, reduction, and acetylation as described previously[20] using a gas chromatograph (GC) (6890N, Agilent Technology, USA) fitted with an Alltech DB-225 capillary column (15 m × 0.25 mm i.d., 0.25 μm film) and coupled with a mass spectrometer (MS) (5973N, Agilent Technology, USA)]. The oven temperature program were as follows: initial temperature, 170 °C; temperature raised at 2 °C/min to 220 °C, and final hold for 15 min. Helium was used as carrier gas at a flow rate of 1.0 mL/min. The injector temperature and interface temperature were set at 250 and 280 °C, respectively. The MS conditions were as follows: ion source temperature at 250 °C, ionization energy at 70 eV, detector voltage at 1.5 kV, and mass range from 50 to 400.[20] Individual sugars were corrected for losses during hydrolysis and derivatization as well as their different responses to the MS detector.[20]

Linkage Analysis by Methylation. The purified polysaccharides from fruiting body cell wall material (FCWM) were permethylated to partially methylated alditol acetates (PMAA) using methyl iodide and solid NaOH in dry DMSO as described in a modified protocol reported previously.[21] The PMAA samples were then analyzed by GC-

MS with an Alltech DB-225 capillary column (15 m × 0.25 mm i.d., 0.25 μm film) as mentioned above. The oven temperature was increased from 130 to 220 °C by 4 °C/min. The MS detector conditions were the same as mentioned above. Each PMAA was identified by matching its mass spectrum with the literature database.[22]

Molecular Mass and Size. The molecular parameters (including molecular mass and size) of purified polysaccharide were determined using a size exclusion chromatograph (SEC) (Agilent 1200 series LC system) coupled with a multiangle laser light scattering (MALLS) photometer (DAWN EOS, Wyatt Technology Co., USA) and refractive index detector (RI, G1362A, Agilent Technologies Inc., USA). The purified soluble MCW polysaccharide fractions were dissolved in 0.15 M NaCl to a concentration of 1.0 mg/mL and filtered through a 0.22 μm nylon syringe filter before determination. A serial column that combined TSK G-5000 (30 cm × 7.5 mm i.d., Supelco, USA) with TSK G-3000 columns was then employed to separate the samples at 30 °C. The predegassed 0.15 M NaCl aqueous solution was applied as the elution buffer at a flow rate of 0.5 mL/min. A specific refractive index increment (dn/dc) value of the polysaccharides in 0.15 M NaCl aqueous solution was determined with a differential refractometer (OPTILAB DSP) (λ = 690 nm) to be 0.140 mL/g. Astra software (Wyatt Technology Co.) was utilized for data recording and further analysis.

Infrared Spectrum Analysis. The infrared spectra of the purified MCW polysaccharides, hot water-soluble fractions, and alkali-insoluble fractions from MCW of PTR fruiting body were recorded with a Fourier transform infrared spectrometer (FT-IR, Nicolet 670) in the range of 4000−400 cm^{-1} using a KBr disk method.

Microscopic Analysis. The protocols used were according to the previous analysis of MCW polysaccharides from PTR sclerotium[16] and hyper-branched glucans.[14] To observe the microstructure of a single molecule, sodium dodecyl sulfate (SDS) (used as a small molecular surfactant to disperse the entangled molecules) was added to a 1 mg/mL FHA-I aqueous solution at a ratio of 1:1 (w/w) and heated together at 80 °C for 2 h. The solution was diluted stepwise to a final concentration of 5 μg/mL and was heated to 80 °C for 2 h with constant stirring.

The holey carbon film (200 mesh, Beijing Zhongjingkeyi Technology, China), supported by a copper grid, was used to prepare the sample for the TEM viewing. After filtration through a 0.22 μm nylon syringe filter, a droplet of the sample (5 μg/mL) was deposited on the specimen, which was finally dried in air at ambient temperature and humidity. The molecular morphology of the prepared samples was performed on a TEM (H-7650, Hitachi, Japan) at an accelerating voltage of 80 kV.

To observe the AFM image, 5 μL of filtered sample solution (5 μg/mL) was pipetted briefly onto the freshly cleaved surface of a mica disc (Ted Pella, Inc., USA). The surface was air-dried for 20 min in a covered Petri dish and then washed with a large amount of distilled water before fixing with ethanol. After the surface was dried under the same condition as the TEM sample, it was examined using an AFM (Nanoscope III, Velco Instruments Inc., USA) in the tapping mode, which was equipped with a Si probe (Tap 150-G-10, Ted Pella, Inc., USA) with a quoted spring constant of 1.5−15 N/m at a cantilever driving frequency of 300 kHz and a scanning frequency of 1−2 Hz. Nanoscope software was used to obtain and process AFM images.

RESULTS AND DISCUSSION

Cell Wall Content and Composition. The cell wall content of PTR fruiting body was determined to be 46.6 ± 0.9% dry weight (DW), which was significantly less than that from sclerotium (78.4 ± 0.7% DW) according to our previous analysis of sclerotial cell wall.[14] In general, PTR fruiting body MCW contained 74.6% carbohydrate, 4.27% uronic acids, and 3.27% protein (Table 1). In contrast, the chemical composition of the mycelial cell wall was found to contain 79.0% carbohydrates, 5.1% uronic acids, and 3.8% proteins, whereas that of sclerotial cell wall contained 71.6% carbohydrates, 1.6% uronic acids, and 7.0% proteins (unpublished data).

Table 1. Composition of Fractions from Fruiting Body Cell Wall[a]

sample	% DW	total carbohydrate (%)	uronic acid (%)	protein (%)
FHW	3.37 ± 0.13	42.7 ± 0.4	0.22 ± 0.04	49.4 ± 0.61
FCA	20.5 ± 0.16	90.1 ± 0.4	0.76 ± 0.07	8.18 ± 0.38
FHA	52.4 ± 0.77	98.5 ± 0.8		
FAI	17.6 ± 0.54	72.9 ± 0.4	5.96 ± 0.23	
MCW		74.6 ± 0.8	4.27 ± 0.18	3.27 ± 0.03

[a]Data are the mean ± SD (n = 3).

Four crude fractions (FHW, FCA, FHA, and FAI) were obtained from the MCW of PTR fruiting body, and their chemical compositions are shown in Table 1. Hot-water-soluble fraction (FHW) accounted for only 3.4% DW of the MCW of PTR fruiting body, whereas the two alkali-soluble fractions constituted 72.9% of the MCW (20.5 and 52.4% for FCA and FHA, respectively). The relative percentage of these two alkali-soluble fractions (FCA and FHA) was similar to that of mycelial cell wall (22.0 and 47.0% for mycelial cold-alkali and hot-alkali fractions, respectively) but was different from sclerotial cell wall with the main component being the cold alkali-soluble fraction (41.2 and 35.3% for sclerotial cold-alkali and hot-alkali fractions, respectively).[14] FAI constituted 17.6% of MCW, which was similar to that from mycelial and sclerotial alkali-insoluble cell residues (19.0 and 16.9%, respectively) (unpublished data). FHW had a very high level of protein (49.4% by weight), indicating the existence of proteins or glycoproteins in the outer layer of the MCW of PTR fruiting body. A relatively lower level of proteins (8.18%) found in the FCA fraction suggested the existence of proteins in the middle layer of the MCW of PTR fruiting body. Levels of uronic acids were very low among the MCW fractions except for FAI. The alkali-soluble fractions (FCA and FHA) of the PTR fruiting body were predominantly composed of carbohydrates, whereas the FAI fraction contained 72.9% carbohydrates, which was higher compared with that in mycelial and sclerotial alkali-insoluble residues (45.7 and 57.4%, respectively) (unpublished data).

On the basis of the fractionation, the arrangement of the cell wall components in PTR fruiting body from outer layer to inner layer was suggested to be in the following order: proteins or glycoproteins, polysaccharides, complex of polysaccharide and chitin.

Purification of Polysaccharides from PTR Fruiting Body MCW. Other than FHW, which had little amount, FCA and FHA were purified by using membrane filtration and column chromatography. After purification by use of membrane filtration, fractions with larger molecular weight (MW > 10000) were obtained and then further purified using column chromatography to give a single fraction (FCA-I and FHA-I). Fractions with smaller MW (<10000) (FCA-II and FHA-II) obtained from membrane separation were then subjected to column chromatography purification, but very little amount of samples could be recovered (<7% of total fraction). Therefore, the analysis of purified MCW polysaccharides was mainly focused on two high MW soluble fractions (FCA-I and FHA-I).

Monosaccharide Composition of Polysaccharides from PTR Fruiting Body MCW. The monosaccharide composition of FHW was mainly glucose with small amounts

Table 2. Chemical Composition of Cell Wall Polysaccharide Fractions from PTR Fruiting Body[a]

	monosaccharides (%)						
sample	xylose	mannose	galactose	glucose	glucosamine[b]	total carbohydrate (%)	uronic acid (%)
FHW	3.19	19.64	3.45	73.72		42.2	0.22
FCA-I		22.22	11.24	66.54		92.1	0.77
FHA-I				100.00		97.4	
FAI				72.23	27.77	72.9	5.96

[a]Data are the means of triplicates. [b]Glucosamine is derived from chitin

of mannose, galactose, and xylose as shown in Table 2. Compared with FHW, the cold alkali-soluble polysaccharide (FCA-I) contained more mannose and galactose, but without xylose. After purification, protein was not detected in FCA-I, although 8.17% protein was found in FCA. FHA-I as the main fraction of PTR fruiting body MCW was composed of almost purely glucose (Table 2). Different from the other soluble MCW fractions, FAI contained 72.2% glucose [similar to the total carbohydrate content of 72.9% (Table 1)], whereas 27.3% of this fraction was composed of glucosamine (the structural subunit of chitin). FAI was thus composed of an insoluble glucan−chitin complex that is commonly found in fungi.

Glycosidic Linkages of FHA-I. Due to the poor solubility of FCA-I and FAI in DMSO, linkage analysis was performed only on FHA-I. PMAAs in the GC-MS chromatogram of FHA-I were identified by their retention time in the total ion chromatogram (TIC) and by comparison with mass spectrum patterns from the literature database.[22] The glycosidic linkages and their corresponding percentages are listed in Table 3. The molar ratio of monosaccharide residues was calculated according to the peak areas and response factors for individual sugars in the TIC as mentioned above.

Table 3. Peak Area and Molar Ratio of Glycosidic Linkages in FHA-I by Methylation Analysis[a]

		FHA-I	
linkage pattern	retention time (min)	peak area (%)	molar ratio
T-Glc*p*[b]	13.999	26.61	5.64
1,3-Glc*p*	16.991	5.13	1.00
1,6-Glc*p*	17.972	10.93	2.13
1,4-Glc*p*	18.170	32.05	6.25
1,3,6-Glc*p*	21.097	8.19	1.48
1,4,6-Glc*p*	21.319	17.09	3.08
TU/BP[c]		1.05	
DB[d]			0.52

[a]Data are the means of triplicates. [b]Glc*p*, glucopyranose. [c]TU/BP, terminal units/branching points. [d]DB = (NT + NB)/(NT + NB + NL), the degree of branching, where NT, NB, and NL are the numbers of the terminal residues, branch residues, and linear residues, respectively.

Consistent with the results of polysaccharides from PTR sclerotium MCW,[14] FHA-I consisted of a nonreducing terminal glucose, 1,3-D-Glc*p*, 1,4-D-Glc*p*, 1,6-D-Glc*p*, 1,3,6-D-Glc*p*, and 1,4,6-D-Glc*p*. The molar ratios of these six sugar residues were similar to those polysaccharides from PTR sclerotial MCW.[14] However, the percentages of 1,4-D-Glc*p* and 1,3,6-D-Glc*p* in FHA-I had obviously increased, whereas residues of T-D-Glc*p* and 1,4,6-D-Glc*p* had decreased. The major glycosidic linkage in FHA-I was 1,4-D-Glc*p* residues (32.1%), followed by T-D-Glc*p* (26.6%) (Table 3). The major branched sugar residues in FHA-I were 1,4,6-D-Glc*p*, which accounted for 17.1% of the total sugar residues, whereas 8.19% of 1,3,6-D-Glc*p* existed in this fraction. The ratio between terminal units (T-D-Glc*p*) and branching points (1,4,6-D-Glc*p* and 1,3,6-D-Glc*p*) was 1.05 (TU/BP ratio) (Table 3). Consistent with the structure of polysaccharides from PTR sclerotial MCW,[14] the data from the above methylation analysis suggested that FHA-I was also mainly composed of →1)-D-Glc*p*-(4→ residues as the backbone with some →1)-D-Glc*p*-(6→ residues in the side chains, whereas some →1)-D-Glc*p*-(3→ residues might exist in the backbone or side chains. The major branching points of FHA-I were at *O*-4 and/or *O*-6 positions of the Glc*p* chain. The degree of branching (DB) of FHA-I was calculated by the equation [DB = $(N_T + N_B)/(N_T + N_B + N_L)$] to be 52%. With such a high DB value, FHA-I would be likely to be a hyper-branched glucan consistent with polysaccharides purified from PTR sclerotial MCW.[14]

Molecular Mass and Size of FHA-I. The SEC chromatogram of FHA-I indicated that there was only a very small shoulder peak (<9% total peak area) present in front of the major peak (Figure 2) that might be caused by the aggregation of the polysaccharide. The values of M_w, M_n, root-mean-square (RMS) radius/radius of gyration ($\langle S^2 \rangle^{1/2}$) of the samples were obtained by computing a classical Zimm plot from light-scattering data (data not shown).[23] The d_f value can be determined from the relationship between M_w and RMS radius and v according to eqs 1 and 2, known as the inverse power law functions.[24]

$$\text{RMS radius} = kM_w^{\ v} \quad (1)$$

$$d_f = 1/v \quad (2)$$

From the slope of the angular dependence (Figure 3), the M_w of the FHA-I was estimated to be 4.224×10^6 g/mol, whereas its RMS radius was calculated to be 30.4 nm (Table 4). FHA-I, which was purified from FHA, accounted for 52.4% DW of the PTR fruiting body MCW, indicating that this fraction is the major structural skeleton in the cell wall. The value of M_w/M_n is known as the polydispersity index, which reflects MW homogeneity and a value of 1 for monodispered molecules.[25] The value of M_w/M_n (1.089) for FHA-I (Table 4) indicated the relatively high purity of FHA-I.

According to previous studies, the exponent v in eq 2 reflects the molecular shape of a polymer with values of 0.33, 0.50−0.60, and 1.0 representing a sphere, random coil, and rigid rod, respectively.[26,27] The small RMS radius of FHA-I (30.4 nm) (Table 4) suggested that this macromolecule might exist as a compact conformation in aqueous solution.[28,29] The v value of FHA-I was found to be 0.33, and its corresponding d_f value was 3.06 (Table 4), indicating that the conformation of the FHA-I was spherical.[26,27,30] As described in previous studies,[31−33] this was consistent with the highly branched structure suggested by the above linkage analysis (Table 3).

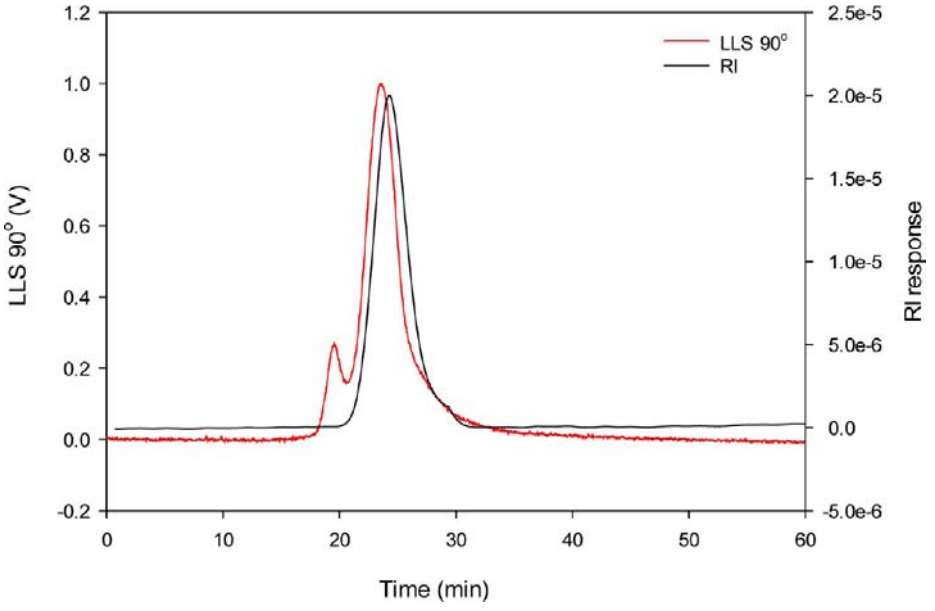

Figure 2. SEC-MALLS chromatograms of FHA-I.

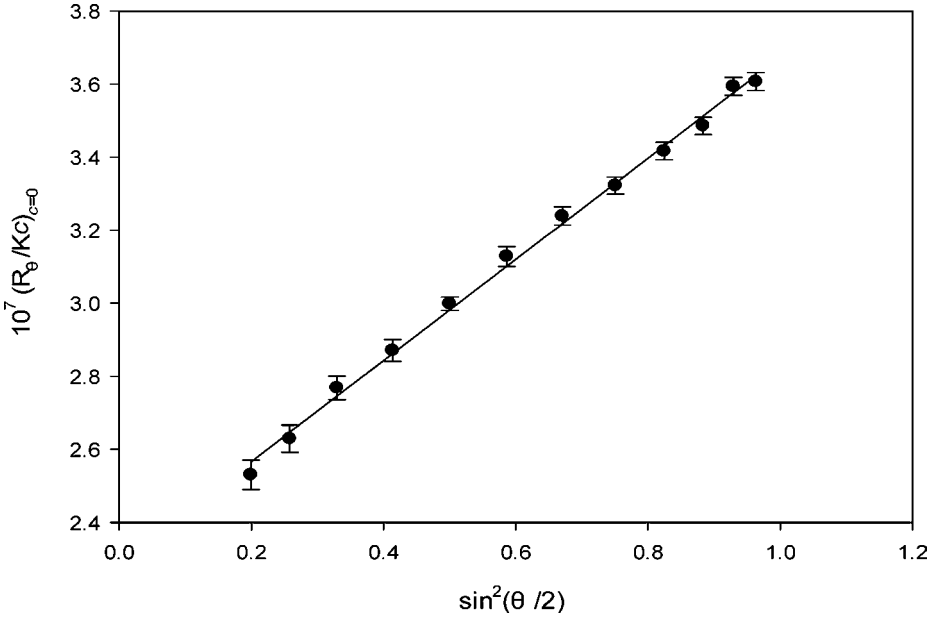

Figure 3. Angular dependence of $(R_\theta/Kc)_{c=0}$ for FHA-I, where K is the optical constant, c is the concentration, R_θ is the Rayleigh ratio, and θ is the scattering angle.

Table 4. Results of SEC-MALLS for FHA-I[a]

sample	$M_w \times 10^{-6}$ (g/mol)	RMS radius (nm)	M_w/M_n	d_f	ν
FHA-I	4.224 ± 0.77	30.4 ± 4.9	1.089	3.06	0.33 ± 0.08

[a]Data are the mean ± SD. M_w, weight-average molecular mass; M_n, number-average molecular mass; d_f, fractal dimension; ν, exponent in eq 1.

IR Spectrum of Polysaccharides from PTR Fruiting Body of MCW. All of the IR spectra of the four fractions from MCW (Figure 4) exhibited an absorption peak at ~900 cm^{-1}, which was similar to the characteristic absorption peak for the β configuration of glucan (890 cm^{-1}).[34] The absorption peak at 834 cm^{-1} of FCA-I indicated the existence of an α configuration of glucan. The unique absorption of double peaks at 1661 and 1629 cm^{-1} combined with the peak at 1565 cm^{-1} in the spectrum of FAI indicated that a secondary amide group (−CO−NH−C) existed in this fraction due to the presence of a large amount of chitin and was consistent with the monosaccharide composition data (Table 2) for a glucan−chitin complex.

Molecular Morphology of FHA-I. To further observe the microstructure of the spherical FHA-I, SDS was added to break the hydrogen bonds inside the sphere. Both branched conformations and crossed chains were observed under this condition (Figure 5). Figure 5A shows part of a particular FHA-I molecule with an extended conformation. Similar to the hyper-branched PTR sclerotium MCW cold alkali-soluble fraction (SCA-I),[15] a high degree of branching was observed from the TEM image of FHA-I (Figure 5A) with a large

dx.doi.org/10.1021/jf500112j | J. Agric. Food Chem. 2014, 62, 2891−2899

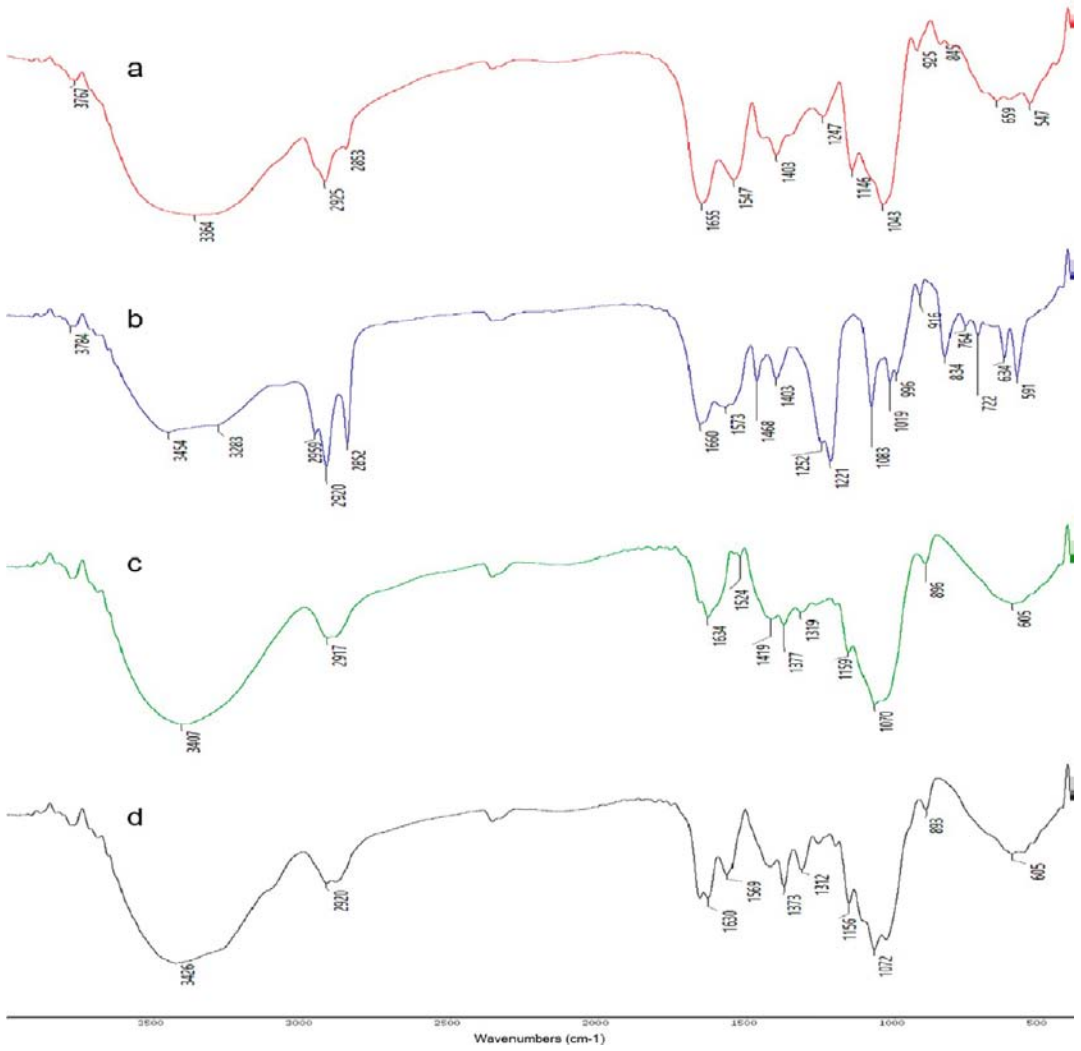

Figure 4. IR spectrum of polysaccharide fractions derived from mushroom cell wall of PTR fruiting body: (a) FHW; (b) FCA-I; (c) FHA-I; (d) FAI.

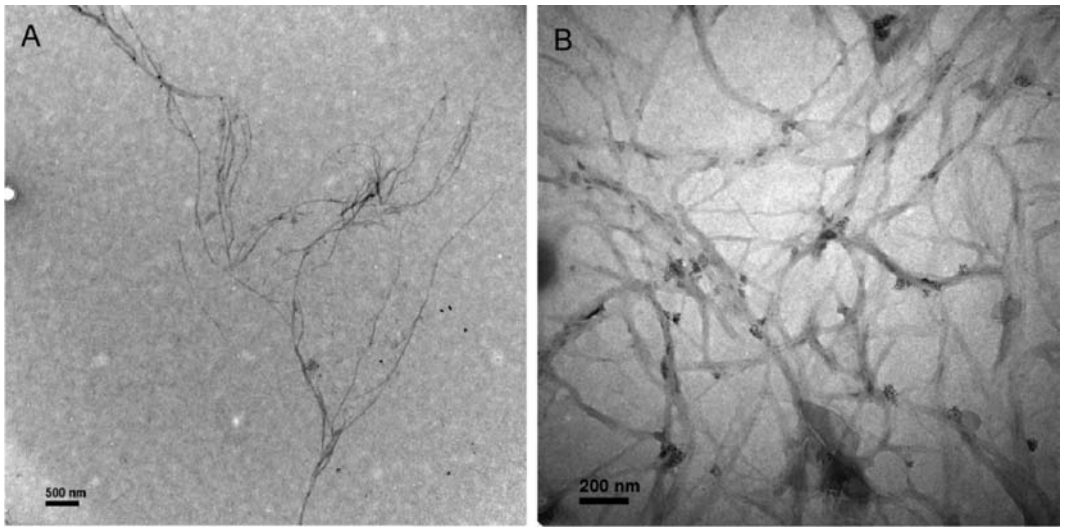

Figure 5. TEM images of FHA-I in SDS solution: (A) unfolded conformation; (B) entangled chains.

number of the polymer chains entangled together in the fully extended state shown in Figure 5B.

Branched conformation of FHA-I molecule in SDS could also be found in AFM (Figure 6A), which was similar to the result in TEM (Figure 5). Furthermore, the thickness of the molecules (indicated by the red pointers in the cross-section line in Figure 6B) varied from 4.8 to 40.4 nm, indicating that multiple chains of FHA-I molecules rather than a single-chain

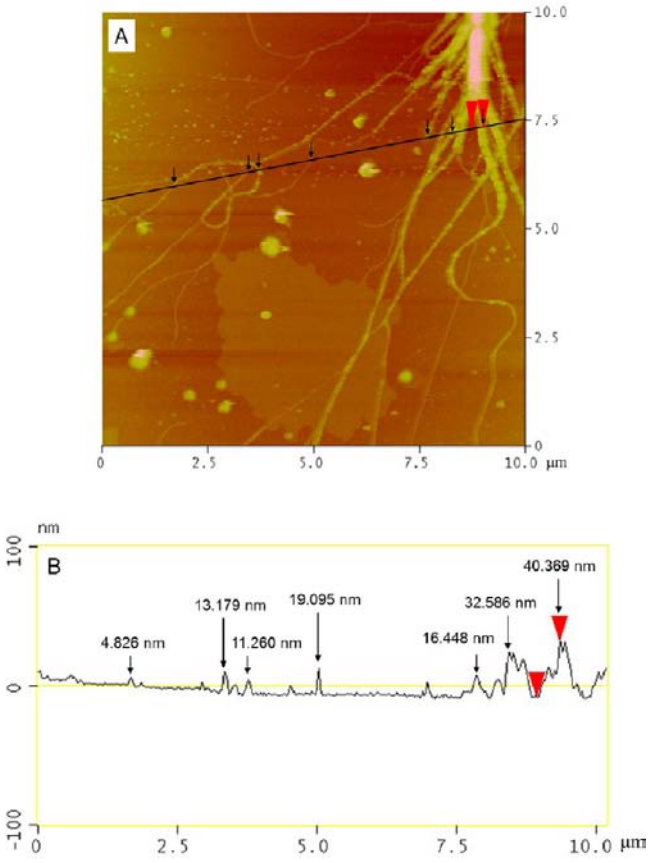

Figure 6. Tapping mode AFM images (A) and cross-sectional profile (B) of FHA-I dispersed in 80 °C SDS solution.

one existed in the SDS medium. With such thickness, it was possible that up to eight chains of macromolecules might be stacked up or bundled together to give such a dimension.

Mushroom Cell Wall Structure of PTR Fruiting Body. A sandwich model was proposed to represent the amount and chemical nature of the cell wall components sequentially extracted from the MCW of PTR fruiting body (Figure 7). Apart from proteins, a small amount of glycan−protein complexes could be found in the first fraction of MCW (Table 1), all of which could be linked with other cell wall components via noncovalent bonding because these proteins and glycan−protein complexes could be extracted using boiling water.[16] The second fraction of MCW is mainly composed of cold alkali-soluble heteropolysaccharides with glucose, mannose, and galactose (Table 2) with small amounts of proteins (Table 1), suggesting that the glycans are associated with proteins via noncovalent linkage because these proteins could be removed in the purification procedure. The third fraction of MCW could be considered as the main structural skeleton due to its abundance, and it is composed of hyper-branched glucans (Table 3 and Figure 6). The MCW polysaccharides in this fraction could be removed using alkali solution at 80 °C. The innermost fraction of MCW could be composed of glucan−chitin complexes, which contain >70% glucan and <30% chitin (Table 2). This protective barrier could not be removed by hot alkali solution. The normalized relative percentage of the above four fractions in MCW was found to be 3.6:21.9:55.7:18.8 from outer layer to inner layer on the basis of the results in Table 1.

The cell wall structure of other mushroom fruiting bodies has not been studied in detail, but some cell wall polysaccharides have been derived and characterized.[35,36] A cold alkali-soluble polysaccharide has been purified from the fruiting body of *Laetiporus sulphureus* (Bull.: Fr.) Murr and was named latiglucan I, which was characterized to be a linear β-1,3-glucan (molecular weight = 1.8×10^5 Da) constituting 42.7% by weight of the fruiting body.[36] The structure of some polysaccharides obtained from the fruiting body of *Pleurotus* species other than PTR has also been investigated. For instance, the main MCW polysaccharides of the fruiting body of *P. ostreatus* and *P. eryngii* were branched β-1,3-/1,6-glucan and linear α-1,3-glucan, respectively.[6] Furthermore, the fruiting body of *P. florida* contained two different types of glucans: a water-soluble one consisting of a main chain of α-1,3-linked D-glucan partially substituted at *O*-3 and *O*-6 by β-D-glucose[37] and a water-insoluble β-1,3-/1,6-D-glucan.[38] The structure and degree of branching (DB) of MCW polysaccharide from PTR fruiting body therefore are unique as compared with those found previously in other *Pleurotus* species.

Despite the fact that mushroom cell wall is composed of a water-soluble fraction, an alkali-soluble fraction, and an alkali-insoluble fraction that are similar to the cell wall in lower fungi,

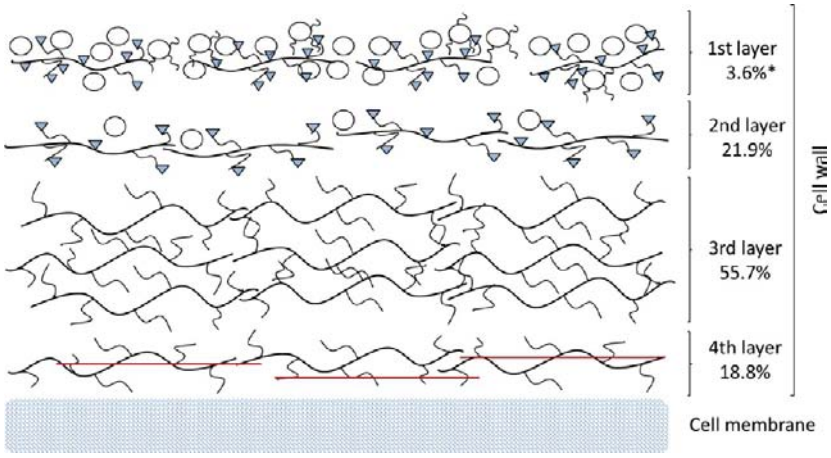

Figure 7. Proposed cell wall structure of PTR fruiting body. (*) The normalized relative percentage of individual cell wall fractions is not shown in an absolute scale. Symbol key: (open circles) protein; (open circles with "legs") glycoprotein; (lines with "legs") glucan; (red line) chitin; (blue triangles) other sugar residues (including mannose, galactose, and xylose).

dx.doi.org/10.1021/jf500112j | J. Agric. Food Chem. 2014, 62, 2891−2899

the structure of mushroom cell wall of PTR fruiting body is more complicated than and very different from the cell wall of lower fungi in terms of the chemical fine structure of the cell wall polysaccharides.[39−41] Such differences could mainly be found in the alkali-soluble fractions. This fraction has been characterized to be β-glucans in the cell wall of yeast and filamentous fungi, which is mainly composed of a long β-1,3 main chain or short β-1,6-linked side chains.[42−45] However, many more β-1,4 residues was found in the alkali-soluble fractions of MCW in PTR fruiting body. β-1,4-Glucose is commonly recognized as the sugar residue of structural polysaccharides of plant cell wall, such as cellulose.[46−48] More mannose, galactose, and xylose were found in the alkali-soluble cell wall polysaccharides from the fruiting body in PTR. Moreover, differing from the linear structure of β-glucans found in the cell wall of lower fungi, the alkali-soluble fractions from MCW of PTR fruiting body are mainly hyper-branched polymer with a relatively higher DB (52%) than that of lower fungal cell wall polysaccharides mainly composed of linear β-1,3-/1,4-glucan with 4% of β-1,6 branch points.[42] The innermost fraction of MCW is composed of glucan−chitin complexes, which account for only <20% by weight. The relative thickness of this fraction in MCW of PTR fruiting body is therefore thinner than that of lower fungi, which accounts for about 40% of their cell wall.[42]

In summary, the fruiting body of PTR has 47% MCW by dry weight, of which the main components (total 78% of MCW) are the alkali-soluble fractions (FCA and FHA), and this was in contrast with the cell wall of filamentous fungi and yeast. The major fraction of FCWM in PTR is hyper-branched β-1,4-glucans with 52% DB on the *O*-6 position as compared to the linear β-1,3-glucans with very few branches on the *O*-6 position found in the cell wall of lower fungi. These results provide some new insights in the study of the structural organization of fungal cell wall, especially for higher fungi. Mushroom fruiting body of PTR thus represents a potential source of novel dietary fiber with unique structural features that might have potential applications in the food industry. Furthermore, research on the biological functions and physiological activities of the fractionated cell wall components of FCWM from PTR is currently underway.

AUTHOR INFORMATION

Corresponding Author

*(P.C.K.C.) Phone: 852 39436144. Fax: 26037246. E-mail: petercheung@cuhk.edu.hk.

Funding

This project was financially supported by the Research Committee of CUHK Directed Grant for Research (No. 2030435).

Notes

The authors declare no competing financial interest.

ACKNOWLEDGMENTS

The technical support provided by technicians from the School of Life Sciences and the Department of Physics of CUHK for AFM, SEM, and HPSEC-LLS was gratefully acknowledged.

ABBREVIATIONS USED

AFM, atomic force microscopy; BCA, bicinchoninic acid; DB, degree of branching; DW, dry weight; FAI, alkali-insoluble residue; FCA, cold alkali-soluble fraction; FCWM, fruiting body cell wall material; FHA, hot alkali-soluble fraction; FHW, hot water-soluble fraction; GC, gas chromatograph; MALLS, multiangle laser light scattering; MCW, mushroom cell wall; MS, mass spectrometry; MW, molecular weight; NMR, nuclear magnetic resonance; PCM, phase contrast microscope; PMAA, partially methylated alditol acetates; PMSF, phenylmethanesulfonyl fluoride; PTR, *Pleurotus tuber-regium*; RI, refractive index; RMS, root-mean-square; SDS, sodium dodecyl sulfate; SEC, size exclusion chromatograph; TEM, transmission electron microscopy; TIC, total ion chromatogram; TU/BP, terminal units/branching points

REFERENCES

(1) Cheung, P. C. K. Mini-review on edible mushrooms as source of dietary fiber: preparation and health benefits. *Food Sci. Hum. Wellness* **2013**, *2*, 162−166.

(2) Wong, S. M.; Wong, K. K.; Chiu, L. C. M.; Cheung, P. C. K. Non-starch polysaccharides from different developmental stages of *Pleurotus tuber-regium* inhibited the growth of human acute promyelocytic leukemia HL-60 cells by cell-cycle arrest and/or apoptotic induction. *Carbohydr. Polym.* **2007**, *68*, 206−217.

(3) Lau, B. F.; Abdullah, N.; Aminudin, N. Chemical composition of the tiger's milk mushroom, *Lignosus rhinocerotis* (Cooke) Ryvarden, from different developmental stages. *J. Agric. Food Chem.* **2013**, *61*, 4890−4897.

(4) Wong, K.; Cheung, P. C. K. Sclerotium of culinary-medicinal King Tuber oyster mushroom, *Pleurotus tuberregium* (Fr.) Singer (Agaricomycetideae): its cultivation, biochemical composition, and biopharmacological effects (review). *Int. J. Med. Mushrooms* **2008**, *10*, 303−313.

(5) Michalenko, G. O.; Hohl, H. R.; Rast, D. Chemistry and architecture of the mycelial wall of *Agaricus bisporus*. *J. Gen. Microbiol.* **1976**, *92*, 251−262.

(6) Synytsya, A.; Míčková, K.; Synytsya, A.; Jablonský, I.; Spěváček, J.; Erban, V.; Kováříková, E.; Čopíková, J. Glucans from fruit bodies of cultivated mushrooms *Pleurotus ostreatus* and *Pleurotus eryngii*: structure and potential prebiotic activity. *Carbohydr. Polym.* **2009**, *76*, 548−556.

(7) Di Mario, F.; Rapana, P.; Tomati, U.; Galli, E. Chitin and chitosan from Basidiomycetes. *Int. J. Biol. Macromol.* **2008**, *43*, 8−12.

(8) Wong, K. H.; Lai, C. K. M.; Cheung, P. C. K. Immunomodulatory activities of mushroom sclerotial polysaccharides. *Food Hydrocolloids* **2011**, *25*, 150−158.

(9) Zhang, M.; Cui, S. W.; Cheung, P. C. K.; Wang, Q. Antitumor polysaccharides from mushrooms: a review on their isolation process, structural characteristics and antitumor activity. *Trends Food Sci. Technol.* **2007**, *18*, 4−19.

(10) Wong, K. H.; Cheung, P. C. K. Dietary fibers from mushroom sclerotia: 1. Preparation and physicochemical and functional properties. *J. Agric. Food Chem.* **2005**, *53*, 9395−9400.

(11) Wong, K. H.; Wong, K. Y.; Kwan, H. S.; Cheung, P. C. K. Dietary fibers from mushroom sclerotia: 3. In vitro fermentability using human fecal microflora. *J. Agric. Food Chem.* **2005**, *53*, 9407−9412.

(12) Oso, B. A. *Pleurotus tuber-regium* from Nigeria. *Mycologia* **1977**, 271−279.

(13) Lam, K.; Chi-Keung Cheung, P. Non-digestible long chain β-glucans as novel prebiotics. *Bioact. Carbohydr. Diet. Fibre* **2013**, *2*, 45−64.

(14) Chen, L.; Xu, W.; Lin, S.; Cheung, P. C. K. Cell wall structure of mushroom sclerotium (*Pleurotus tuber regium*): Part 1. Fractionation and characterization of soluble cell wall polysaccharides. *Food Hydrocolloids* **2014**, *36*, 189−195.

(15) Chen, L.; Zhang, B.; Chen, J.; Cheung, P. C. K. Cell wall structure of mushroom sclerotium (*Pleurotus tuber-regium*): Part 2. Fine structure of a novel alkali-soluble hyper-branched cell wall polysaccharide. *Food Hydrocolloids* **2014**, *38*, 48−55.

(16) Chen, L.; Zhang, B. B.; Cheung, P. C. Comparative proteomic analysis of mushroom cell wall proteins among the different developmental stages of *Pleurotus tuber-regium*. *J. Agric. Food Chem.* **2012**, *60*, 6173−6182.
(17) DuBois, M.; Gilles, K. A.; Hamilton, J. K.; Rebers, P. A.; Smith, F. Colorimetric method for determination of sugars and related substances. *Anal. Chem.* **1956**, *28*, 350−356.
(18) Hill, H. D.; Straka, J. G. Protein determination using bicinchoninic acid in the presence of sulfhydryl reagents. *Anal. Chem.* **1988**, *170*, 203−208.
(19) Blumenkrantz, N.; Asboe-Hansen, G. New method for quantitative determination of uronic acids. *Anal. Biochem.* **1973**, *54*, 484−489.
(20) Zhang, B. B.; Cheung, P. C. K. Use of stimulatory agents to enhance the production of bioactive exopolysaccharide from *Pleurotus tuber-regium* by submerged fermentation. *J. Agric. Food Chem.* **2011**, *59*, 1210−1216.
(21) Oxley, D.; Currie, G.; Bacic, A. Linkage analysis using the NaOH methylation method. In *Purifying Proteins for Proteomics: A Laboratory Manual*; Simpson, R. J., Ed.; Cold Spring Harbor Laboratory Press: Cold Spring Harbor, NY, USA, 2004; pp 629−632.
(22) CCRC. http://www.ccrc.uga.edu/specdb/ms/pmaa/pframe.html (accessed July 28, 2012).
(23) Tao, Y. Z.; Zhang, L. N. Determination of molecular size and shape of hyperbranched polysaccharide in solution. *Biopolymers* **2006**, *83*, 414−423.
(24) Hanselmann, R.; Burchard, W.; Ehrat, M.; Widmer, H. M. Structural properties of fractionated starch polymers and their dependence on the dissolution process. *Macromolecules* **1996**, *29*, 3277−3282.
(25) Huang, Z. P.; Huang, Y. N.; Li, X. B.; Zhang, L. N. Molecular mass and chain conformations of *Rhizoma Panacis Japonici* polysaccharides. *Carbohydr. Polym.* **2009**, *78*, 596−601.
(26) Sato, T.; Norisuye, T.; Fujita, H. Double-stranded helix of xanthan: dimensional and hydrodynamic properties in 0.1 M aqueous sodium chloride. *Macromolecules* **1984**, *17*, 2696−2700.
(27) Kato, T.; Okamoto, T.; Tokuya, T.; Takahashi, A. Solution properties and chain flexibility of pullulan in aqueous solution. *Biopolymers* **1982**, *21*, 1623−1633.
(28) Huang, Z. P.; Zhang, L. N.; Duan, X. B.; Liao, Z. Q.; Ding, H.; Cheung, P. C. K. Novel highly branched water-soluble heteropolysaccharides as immunopotentiators to inhibit S-180 tumor cell growth in BALB/c mice. *Carbohydr. Polym.* **2012**, *87*, 427−434.
(29) Zhang, Y. F.; Wang, J. G.; Zhang, L. N. Creation of highly stable selenium nanoparticles capped with hyperbranched polysaccharide in water. *Langmuir* **2010**, *26*, 17617−17623.
(30) Picton, L.; Bataille, I.; Muller, G. Analysis of a complex polysaccharide (gum arabic) by multi-angle laser light scattering coupled on-line to size exclusion chromatography and flow field flow fractionation. *Carbohydr. Polym.* **2000**, *42*, 23−31.
(31) Zhou, Y. F.; Yang, B.; Ren, X. Y.; Liu, Z. Z.; Deng, Z.; Chen, L. M.; Deng, Y. B.; Zhang, L. M.; Yang, L. Q. Hyperbranched cationic amylopectin derivatives for gene delivery. *Biomaterials* **2012**, *33*, 4731−4740.
(32) Huang, L.; Yao, Y. Particulate structure of phytoglycogen nanoparticles probed using amyloglucosidase. *Carbohydr. Polym.* **2011**, *83*, 1665−1671.
(33) Meléndez, R.; Meléndez-Hevia, E.; Canela, E. I. The fractal structure of glycogen: a clever solution to optimize cell metabolism. *Biophys. J.* **1999**, *77*, 1327−1332.
(34) Kiho, T.; Sakushima, M.; Wang, S. R.; Nagai, K.; Ukai, S. Polysaccharides in fungi. XXVI. Two branched (1−3)-β-D-glucans from hot water extract of *Yu ěr*. *Chem. Pharm. Bull. (Tokyo)* **1991**, *39*, 798−800.
(35) Villares, A.; Mateo-Vivaracho, L.; Guillamón, E. Structural features and healthy properties of polysaccharides occurring in mushrooms. *Agriculture* **2012**, *2*, 452−471.
(36) Olennikov, D. N.; Agafonova, S. V.; Borovskii, G. B.; Penzina, T. A.; Rokhin, A. V. Alkali-soluble polysaccharides of *Laetiporus Sulphureus* (Bull.: Fr.) Murr fruit bodies. *Appl. Biochem. Microbiol.* **2009**, *45*, 626−630.
(37) Santos-Neves, J. C.; Pereira, M. I.; Carbonero, E. R.; Gracher, A. H. P.; Alquini, G.; Gorin, P. A. J.; Sassaki, G. L.; Iacomini, M. A novel branched $\alpha\beta$-glucan isolated from the basidiocarps of the edible mushroom *Pleurotus florida*. *Carbohydr. Polym.* **2008**, *73*, 309−314.
(38) Rout, D.; Mondal, S.; Chakraborty, I.; Islam, S. S. The structure and conformation of a water-insoluble (1→3)-,(1→6)-β-D-glucan from the fruiting bodies of *Pleurotus florida*. *Carbohydr. Res.* **2008**, *343*, 982−987.
(39) Latgé, J. P. The cell wall: a carbohydrate armour for the fungal cell. *Mol. Microbiol.* **2007**, *66*, 279−290.
(40) Klis, F. M.; Boorsma, A.; De Groot, P. W. Cell wall construction in *Saccharomyces cerevisiae*. *Yeast* **2006**, *23*, 185−202.
(41) Klis, F. M.; Mol, P.; Hellingwerf, K.; Brul, S. Dynamics of cell wall structure in *Saccharomyces cerevisiae*. *FEMS Microbiol. Rev.* **2002**, *26*, 239−256.
(42) Fontaine, T.; Simenel, C.; Dubreucq, G.; Adam, O.; Delepierre, M.; Lemoine, J.; Vorgias, C. E.; Diaquin, M.; Latgé, J. P. Molecular organization of the alkali-insoluble fraction of *Aspergillus fumigatus* cell wall. *J. Biol. Chem.* **2000**, *275*, 27594−27607.
(43) Kapteyn, J. C.; Hoyer, L. L.; Hecht, J. E.; Muller, W. H.; Andel, A.; Verkleij, A. J.; Makarow, M.; Van Den Ende, H.; Klis, F. M. The cell wall architecture of *Candida albicans* wild-type cells and cell wall-defective mutants. *Mol. Microbiol.* **2000**, *35*, 601−611.
(44) Shahinian, S.; Bussey, H. β-1,6-Glucan synthesis in *Saccharomyces cerevisiae*. *Mol. Microbiol.* **2000**, *35*, 477−489.
(45) Shematek, E. M.; Braatz, J. A.; Cabib, E. Biosynthesis of the yeast cell wall. I. Preparation and properties of β-(1−3) glucan synthetase. *J. Biol. Chem.* **1980**, *255*, 888−894.
(46) Keegstra, K. Plant cell walls. *Plant Physiol.* **2010**, *154*, 483−486.
(47) Somerville, C. Cellulose synthesis in higher plants. *Annu. Rev. Cell Dev. Biol.* **2006**, *22*, 53−78.
(48) Astbury, W. T.; Davies, M. M. Structure of cellulose. *Nature* **1944**, *154*, 84.

and baking. Additionally, changes in free amino acids were also determined during fermentation, especially to evaluate tryptophan consumption by yeasts.

MATERIALS AND METHODS

Chemicals and Consumables. Acetonitrile (HPLC grade), ethanol (HPLC grade), and melatonin (*N*-acetyl-5-methoxytryptamine) (>98%) were obtained from Sigma-Aldrich (Steinheim, Germany). Formic acid (98%) and high-purity (>98%) alanine (Ala), arginine (Arg), asparagine (Asn), aspartic acid (Asp), glutamic acid (Glu), glutamine (Gln), glycine (Gly), histidine (His), isoleucine (Ile), leucine (Leu), lysine (Lys), methionine (Met), phenylalanine (Phe), proline (Pro), serine (Ser), tryptophan (Trp), tyrosine (Tyr), valine (Val), and γ-aminobutyric acid (GABA) were purchased from Merck Co. (Darmstadt, Germany). Ultrapure water was used throughout the experiments (Milli Q-System, Millipore, Milford, MA, USA). Syringe filters (nylon, 0.45 μm) were purchased from Waters (Milford, MA). ZORBAX Rapid Resolution SB-C18 column (50 mm × 4.6 mm i.d., 3.5 μm) and SeQuant ZIC-HILIC column (150 mm × 4.6 mm i.d., 3.5 μm) were supplied by Agilent Technologies (Waldbronn, Germany) and Merck Co. (Darmstadt, Germany), respectively.

Preparation of Dough and Breads. All-purpose wheat flour (Söke Un, Turkey), sugar (Bal Küpü, Turkey), salt (Billur Tuz, Turkey), and instant baker's yeast (*Saccharomyces cerevisiae*) (Yuva, Turkey) for preparing breads were purchased from a local market. Breads were prepared using the AACC (American Association of Cereal Chemists) Method 10-10.03 (1983) with some modification.[16] 100 g of wheat flour, 38 mL of water, and 20 mL of yeast suspension composed of 5.3 g of instant yeast and 11 mL of sugar−salt solution containing 6 g of sugar and 1.5 g of salt were mixed with a mixer until dough development. After the dough was divided into equal pieces, the pieces were fermented at 30 °C for 0 (control), 30, 60, 90, 120, and 180 min. During fermentation, punching was carried out every 30 min. Before baking, a small piece of fermented dough was set apart and stored at −20 °C for melatonin and amino acid analysis. Following fermentation, the dough was baked in a temperature-controlled oven (Memmert Une 400, Germany) at 215 °C for 17 min.

Analysis of Melatonin and Melatonin Isomer. *Extraction.* Crumb and crust samples were ground with a grinder prior to analysis. Two grams of sample (dough, ground crumb, and ground crust) was extracted with ethanol in three stages (5−2.5−2.5 mL) by vortexing (3 min). After centrifugation (7500*g* for 5 min) in each stage, supernatants were collected in a test tube and evaporated to dryness under a gentle stream of nitrogen. The final residue was redissolved in 1 mL of ethanol−water (50:50, v/v). After centrifugation (13000*g*) supernatant was passed through a 0.45 μm syringe filter into an autosampler vial prior to LC−MS/MS analysis.

LC−ESI-MS/MS analysis. The analysis of melatonin and its isomer was carried out according to the method described previously.[14] Melatonin was determined by using an Agilent 1200 series HPLC system coupled to an Agilent 6460 triple quadrupole mass spectrometer (Waldbronn, Germany). The chromatographic separations were performed on a ZORBAX Rapid Resolution SB-C18 column (50 mm × 4.6 mm i.d., 3.5 μm) using a mixture of 0.1% formic acid in water and 0.1% formic acid in acetonitrile (65:35, v/v) at a flow rate of 0.5 mL/min at 40 °C. The injection volume was 5 μL. The electrospray source had the following settings: drying gas (N_2) flow of 10 L/min at 325 °C, nebulizer pressure of 30 psi, sheath gas (N_2) flow of 10 L/min at 375 °C, nozzle voltage of 1000 V, and positive capillary voltage of 4000 V. MS data were acquired in the positive mode, and melatonin was identified by multiple reaction monitoring (MRM). Fragmentor voltage of precursor ion was 80 V. The ion transitions for melatonin were determined as 233.2 → 174.2 (collision energy of 10 V) and 233.2 → 216.2 (collision energy of 4 V). A dwell time was set at 250 ms for each.

The 233.2 → 174.2 MRM transition was selected to quantitate melatonin. Concentration of melatonin was calculated by means of external calibration curves covering the range between 0.05 and 20 μg/L. Working solutions of melatonin were prepared in ethanol−water (50:50, v/v). Determination of the melatonin isomer was semi-quantitative, and its content was calculated from total ion chromatogram (sum of the area of the MRM transitions (233.2 → 174.2 and 233.2 → 216.2) of melatonin). The linearity was evaluated by plotting the peak area against the concentrations of melatonin standards. Limit of detection (LOD) and limit of quantitation (LOQ) were determined at a signal-to-noise ratio of 3 and 10, respectively.

Analysis of Free Amino Acids. *Extraction.* One gram of sample (dough, ground crumb, and ground crust) was extracted with water in three stages (10, 5, and 5 mL) by vortexing (3 min). After centrifugation (7500*g* for 5 min) in each stage, supernatants were collected in a test tube. Combined extract was diluted subsequent to centrifugation with a mixture of acetonitrile−water (50:50, v/v), and a part of the diluted extract was filtered through a 0.45 μm syringe filter into an autosampler vial prior to LC−MS/MS analysis.

LC−ESI-MS/MS Analysis. The analysis of free amino acids was carried out according to the method described previously.[17] An Agilent 1200 series HPLC system coupled to an Agilent 6460 triple quadrupole mass spectrometer (Waldbronn, Germany) was used. The chromatographic separations were performed on a SeQuant ZIC-HILIC column (150 mm × 4.6 mm i.d., 3.5 μm) using a gradient mixture of 0.1% formic acid in water (A) and 0.1% formic acid in acetonitrile (B) at flow rate of 0.75 mL/min at 40 °C. The eluent composition starting with 25% of A was linearly increased to 60% in 5 min and was held for 5 min. Then, it was linearly decreased to its initial conditions (25% of A) in 5 min. Electrospray ionization was operated in positive mode. The electrospray source had the following settings: drying gas (N_2) flow of 10 L/min at 325 °C, nebulizer pressure of 30 psi, sheath gas (N_2) flow of 10 L/min at 375 °C, nozzle voltage of 1000 V, and capillary voltage positive of 4000 V. Amino acids were identified by their specific MRM transitions, and the dwell time was 0.1 s for all. Concentration of amino acids was calculated by means of external calibration curves built for individual amino acids in a range between 0.1 and 5.0 mg/L.

Statistical Analysis. The results were reported as mean ± standard deviations. Significant differences ($p < 0.05$) were evaluated by Duncan test after the analysis of variance (ANOVA), by using SPSS 17.0 statistical package.

RESULTS AND DISCUSSION

Evaluation of Analytical Method. The chromatographic separation and ion transitions of melatonin and its isomer are given in Figure 2. Retention time, specific MRMs (233.2 → 174.2 and 233.2 → 216.2), and fragment ion ratios acquired from the standard compound were used to confirm the presence of melatonin in the samples. Figure 2A illustrates the chromatogram of 1 ng/mL melatonin standard for the MRM transitions of 233.2 → 174.2 (upper panel) and 233.2 → 216.2 (bottom panel). Since relative abundance of the fragment ion of 174.2 was higher than that of 216.2 for melatonin, the fragment ion of 174.2 was used for the quantitation of melatonin. The ratio of 174.2/216.2 for melatonin was found to be 14.2 ± 2.0.

The fragment ion 174.2 originates from the cleavage of amide substituent ($-NH_2COCH_3$) from main ion and 216.2 by OH removal. Although the melatonin isomer has the same fragment ions, their ratios were found to be quite different. The abundance of fragment ion 216.2 was much higher than that of 174.2 in the fragmentation pattern of the isomer. Diamantini et al.[18] indicated that 174.2 is the base peak for all isomers except where the substituent is bound to nitrogen of the pyrole ring. Therefore, the possible molecular structure of the melatonin isomer, **2**, was proposed as shown in Figure 1. However, the position of the methoxy group on the indole ring could not be determined by tandem mass spectrometry. The purification of the isomer is needed for the identification of exact molecular structure by using either NMR spectroscopy or X-ray

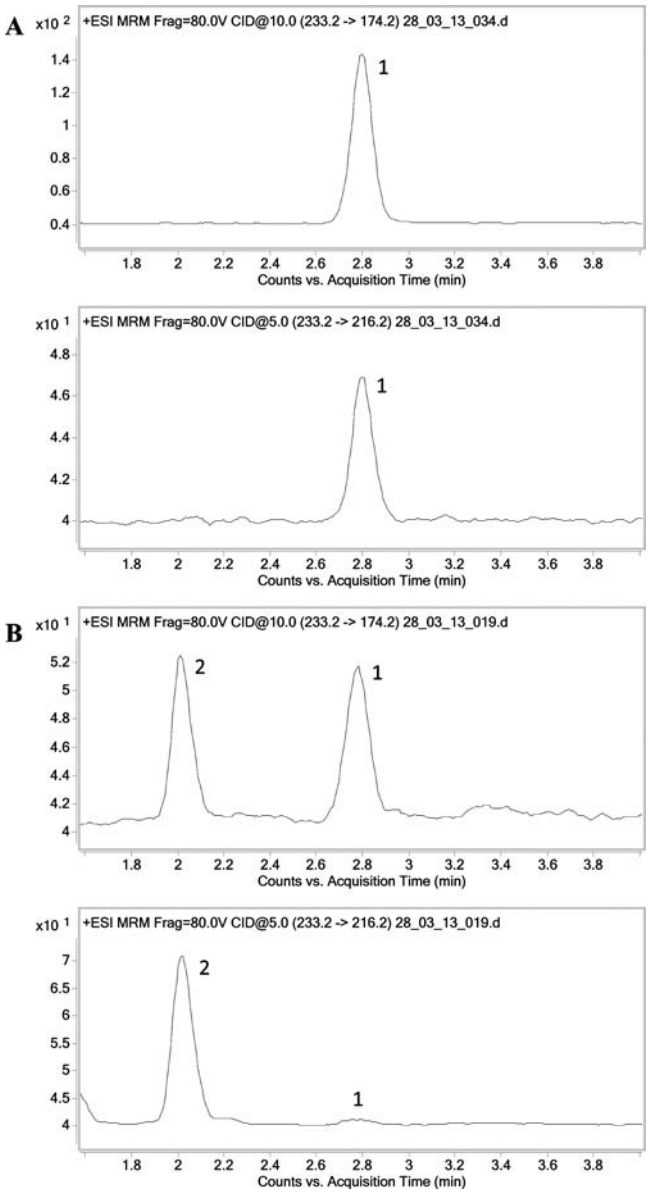

Figure 2. LC–MS/MS chromatograms for (A) 1.0 ng/mL melatonin standard, (B) bread crumb (nonfermented). Upper panel illustrates the MRM of 233.2 → 174.2, and lower panel illustrates the MRM of 233.2 → 216.2 (1, melatonin; 2, melatonin isomer).

diffraction spectroscopy. Other investigators have also observed similar fragmentation patterns.[12,19] Vitalini et al.[11] used MS/MS and Orbitrap MS with a collision cell, but they did not mention the 233.2 → 216.2 transition for the detection of melatonin and its isomer.

Figure 2B illustrates the chromatogram of bread crumb prepared from nonfermented dough for the MRM transitions of 233.2 → 174.2 (upper panel) and 233.2 → 216.2 (bottom panel). As shown in Figure 2B, bread crumb contained melatonin isomer having relatively shorter retention time (2.1 min) than melatonin (2.8 min). Differently from melatonin, relative abundance of the fragment ion of 216.2 was higher than that of 174.2 and the ratio of 216.2/174.2 for melatonin isomer was found to be 2.9 ± 0.2. Since there was no standard compound found for the melatonin isomer, it was specifically distinguished from melatonin by retention time and fragment ion ratio. For quantitation of melatonin isomer, calibration curve of melatonin was used. Although the abundant ion of 216.2 is suitable for the quantitation of the isomer, its abundance in fragmentation of melatonin itself was very low, i.e., the transition ratio of 233.2/216.2 is quite different as mentioned. Thus, sum of the ions of 174.2 and 216.2 was used for calibration and quantitation of the isomer in the samples as reported previously.[14]

An external calibration was built for 0.05–20 ng/mL with melatonin standard, and a good linearity was obtained for the fragment ion 174.2 and for the sum of both fragments. Linearity equations of $y = 595.1x + 68.3$ and $y = 629.5x + 54.1$ and good correlation coefficients (R^2 = 0.9998 and 0.9997, respectively) were obtained in both quantitations. LOD values of melatonin were 0.03, 0.05, and 0.03 ng/g and LOQ values of melatonin were 0.10, 0.18, and 0.09 ng/g for dough, bread crumb, and bread crust samples respectively.

Formation of Melatonin. Figure 3A illustrates the effect of fermentation time on melatonin in bread dough. According to

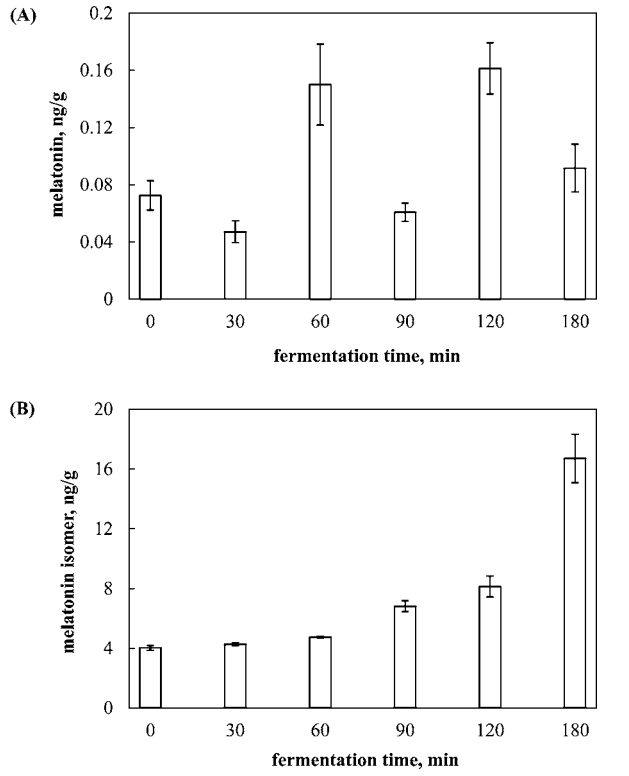

Figure 3. Change of the concentrations of (A) melatonin and (B) melatonin isomer in bread dough during fermentation (on dry matter basis).

results, nonfermented dough was found to contain 0.07 ng/g melatonin. At the end of the 30, 60, 90, 120, and 180 min of fermentation, 0.05 (<LOQ), 0.15, 0.06 (<LOQ), 0.16, and 0.09 (<LOQ) ng/g melatonin was detected, respectively. There was no trend in melatonin concentration as a result of dough fermentation. Melatonin concentrations ranged between 0.19 and 0.63 ng/g and between 0.14 and 0.82 ng/g for crumb and crust parts, respectively. Favorable conditions attained during certain stages of baking could be the reason for the occurrence of melatonin at higher concentrations in crumb than dough. The results suggested that *Saccharomyces cerevisiae* was ineffective in changing melatonin concentration during bread dough fermentation. However, some authors have previously

reported that melatonin concentration was increased by anaerobic activity of yeasts. Rodriguez-Naranjo et al.[9] reported that, although melatonin is absent in grape and musts, it is synthesized during the wine fermentation process. According to the results reported by Garcia-Moreno et al.,[10] a second fermentation step caused melatonin formation in beer. Rodriguez-Naranjo et al.[13] also reported that the synthesis of melatonin largely depends on the growth phase of the yeast. It should be mentioned that bread dough fermentation is mainly an aerobic process unlike the fermentation of beer and wine.

Formation of Melatonin Isomer. The melatonin isomer content of nonfermented dough was estimated to be 4.02 ng/g (Figure 3B). The initial concentration might come from both the yeast culture and the flour since flour has also a natural microbial load. The concentration of isomer in dough increased up to 16.71 ng/g during fermentation. At the beginning its concentration was slightly increased; however, this change was not significant in 30 and 60 min fermented dough samples ($p > 0.05$). Similar trends were also observed for almost all amino acids. This might be because of the limited activity of yeasts in the early stages of dough fermentation. Instant baker's yeast requires some time to revive and adapt to a new environment to show maximum activity. After 60 min of fermentation an apparent increase was observed in melatonin isomer concentration. Gomez et al.[12] also reported that concentration of isomer increased during a laboratory scale wine making process and in an aqueous medium containing yeast and nutrients.

Effect of Baking on Melatonin Isomer. Compared to their corresponding dough, both the crumb and crust parts of breads baked at 215 °C for 17 min contained significantly lower amounts of melatonin isomer (Figure 4). This indicated that

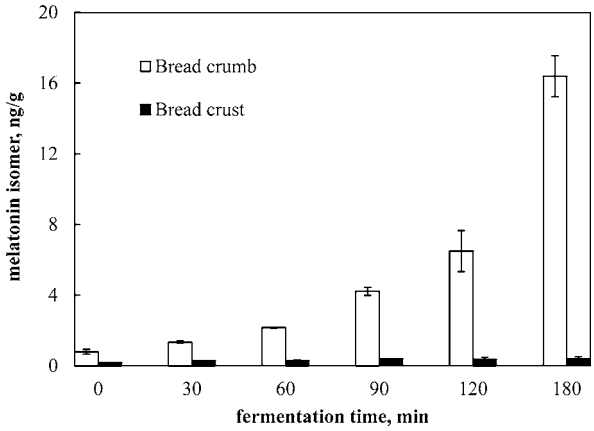

Figure 4. Effect of baking on the resulting concentration of melatonin isomer in crust and crumb for different fermentation times of bread dough (on dry matter basis).

melatonin isomer is not stable at elevated temperatures attained during baking of bread. In the crust part, approximately 95% of melatonin isomer was degraded during baking. On the other hand, a different degradation trend was observed in the crumb samples. As the fermentation time increased, the degree of degradation was found to be decreasing. This must be due to the accumulation of CO_2 and ethanol leading to a spongelike texture in oven spring, which limits the heat transfer into the loaf during baking. The degradation was 80, 69, 54, and 38% in the crumb samples fermented for 0, 30, 60, and 90 min. Also, no significant degradation was observed in the samples of 120 and 180 min fermented dough after baking ($p > 0.05$).

Consumption of Free Amino Acids. Free amino acids are important growth factors for fermentative microorganisms.[20] They utilize tryptophan as the source of nitrogen and yield metabolites such as indolacetic acid, tryptophol, or biogenic amines.[21] Changes in the concentrations of 18 proteinogenic free amino acids and γ-aminobutyric acid (GABA) are given in Table 1. At the beginning the rate of utilization was limited and a significant decrease was observed usually after 60 min of fermentation. At the end of the 180 min, fermentation resulted in a considerable reduction (approximately 50%) in the total free amino acid content of dough. It was shown that the consumption of total amino acids followed first order kinetics ($r^2 = 0.94$, $k = 0.0037$ 1/min, see Supporting Information). In the dough after 180 min of fermentation the highest rates of reduction were observed in Asn and Glu (82% and 76%, respectively). Meanwhile no statistically significant ($p > 0.05$) reduction was observed in Gly, Lys, and Pro. It was previously reported that the more preferred nitrogen sources for yeasts are Gln and Asn whereas Pro is qualified as a poor nitrogen source.[22,23] In contrast to the other amino acids, GABA concentration increased during fermentation. The increased amount of GABA is found mainly in fermented foods, and it is formed from Glu by the enzyme glutamate decarboxylase.[24] The initial concentration in dough might be due to the activities of natural microflora and the endogenous enzymes of flour.

The decrease in the concentration of tryptophan followed first order kinetics ($r^2 = 0.97$, $k = 0.0043$ 1/min, see Supporting Information). Trp concentration decreased by a ratio of 58% during 180 min of fermentation. Although Trp is the precursor of melatonin, it is unknown whether melatonin isomer is synthesized via tryptophan or not. Sprenger et al.[25] found that melatonin appears more quickly when there is a precursor (Trp, serotonin, or *N*-acetylserotonin) in the growth medium. Rodriguez-Naranjo et al.[13] reported that melatonin did not form at all when it was absent from synthetic grape must medium. Contrastingly, in a previous study, there were no significant differences in the melatonin content between red wine samples in which Trp was added and not added.[9] Gomez et al.[12] also reported that the production of melatonin and its isomer during the process of wine fermentation is independent of external Trp. Reduction of Trp content during dough fermentation could be attributed to the fact that Trp might be utilized by yeast to synthesize melatonin and melatonin isomer with its enzyme system.

Effect of Baking on Free Amino Acids. Figure 5 illustrates the effect of baking on total free amino acids and tryptophan contents of bread fermented for 120 min. In the baking process (215 °C for 17 min), loss of amino acids was most likely to occur in the crust part as a result of the Maillard reaction. With regard to dough, 71% of total amino acids and 46% of Trp were lost in the crumb part during baking. The loss increased to 89% for total amino acids and 89% for Trp in the crust part (Figure 5). It was previously reported that Trp degradation in cookie model systems was temperature and time dependent.[26] Considering a possible effect of Trp rich food intake on melatonin and its isomer synthesis, the reducing effect of baking should be taken into consideration.

The results revealed for the first time the formation of melatonin isomer in bread dough during yeast fermentation. Its quantities formed in dough were significantly higher than those of melatonin itself. The formation rate of melatonin isomer and the degradation rate of Trp were compatible with each other.

Table 1. Concentration of Free Amino Acids (μg/g) in Dough during Fermentation[a]

	fermentation time, min					
	0	30	60	90	120	180
Ala	395.0 ± 32.9 a	369.5 ± 0.5 a	354.8 ± 12.7 ab	303.7 ± 19.0 bc	277.0 ± 25.8 c	161.8 ± 18.3 d
Arg	250.9 ± 14.6 a	244.5 ± 13.8 ab	231.5 ± 7.14 ab	221.2 ± 9.7 bc	201.5 ± 12.0 c	138.2 ± 1.8 d
Asn	169.1 ± 12.1 a	149.4 ± 0.1 a	119 ± 4.6 b	73.0 ± 2.7 c	42.9 ± 13.9 d	30.6 ± 10.4 d
Asp	232.9 ± 2.6 a	226.3 ± 0.0 a	220.7 ± 1.3 ab	195.6 ± 12.9 bc	184.3 ± 21.4 c	76.2 ± 10.8 d
Glu	1142.8 ± 3.9 a	791.7 ± 41.4 b	693.9 ± 0.1 c	545.5 ± 11.0 d	493.8 ± 26.5 e	272.5 ± 9.8 f
Gln	272.4 ± 26.0 a	260.7 ± 19.4 ab	232.4 ± 16.2 abc	192.4 ± 25.7 bcd	170.0 ± 40.3 cd	157.3 ± 29.9 d
Gly	76.8 ± 6.2 a	83.8 ± 0.5 a	79.3 ± 9.3 a	86.6 ± 14.1 a	93.5 ± 12.6 a	87.6 ± 11.3 a
His	26.0 ± 2.7 a	24.2 ± 1.9 a	19.5 ± 0.8 ab	15.4 ± 4.3 b	15.3 ± 5.4 b	14.0 ± 3.0 b
Ile	129.4 ± 28.3 a	124.6 ± 18.4 ab	103.2 ± 13.3 ab	82.7 ± 25.1 ab	79.3 ± 29.0 ab	62.8 ± 25.3 ab
Leu	180.8 ± 4.7 a	171.9 ± 9.2 a	139.1 ± 4.9 b	109.5 ± 4.2 c	102.1 ± 5.2 cd	92.0 ± 4.7 d
Lys	133.7 ± 25.5 a	140.4 ± 21.2 a	129.9 ± 26.3 a	109.6 ± 34.6 a	120.7 ± 35.8 a	136.9 ± 28.0 a
Met	75.6 ± 15.9 a	67.3 ± 13.9 ab	45.0 ± 7.3 ab	40.9 ± 13.4 ab	41.7 ± 16.7 ab	37.1 ± 14.5 b
Phe	198.5 ± 38.8 a	190.3 ± 36.2 ab	168.2 ± 25.2 ab	141.6 ± 29.5 ab	130.0 ± 46.6 ab	97.7 ± 37.8 b
Pro	126.5 ± 5.9 a	126.3 ± 1.4 a	131.1 ± 1.8 a	130.3 ± 0.3 a	135.9 ± 7.8 a	133.5 ± 2.8 a
Ser	118.8 ± 9.7 a	112.9 ± 7.5 ab	104.5 ± 6.6 ab	83.9 ± 12.9 abc	75.0 ± 27.0 bc	65.3 ± 15.7 c
Trp	597.3 ± 27.2 a	526.1 ± 23.4 b	480.0 ± 17.8 b	426.8 ± 26.9 c	372.6 ± 7.7 d	251.9 ± 1.8 e
Tyr	24.9 ± 4.3 a	23.6 ± 2.3 a	23.1 ± 2.3 a	22.3 ± 2.9 ab	21.7 ± 4.5 ab	14.2 ± 3.7 b
Val	157.9 ± 25.9 a	145.9 ± 19.5 a	137.3 ± 14.1 a	122.1 ± 14.3 ab	104.5 ± 31.0 ab	73.1 ± 23.9 b
GABA	163.5 ± 25.2 a	239.1 ± 13.3 b	269.9 ± 11.3 bc	292.9 ± 17.0 c	307.6 ± 18.7 c	298.1 ± 11.4 c
total	4472.0 ± 293.8 a	4018.6 ± 93.7 ab	3682.8 ± 112.2 bc	3196.3 ± 196.3 cd	2969.7 ± 377.7 d	2200.8 ± 261.4 e

[a]Values followed by different spaced letters are significantly different within each row ($p < 0.05$). Concentrations were given on dry matter basis.

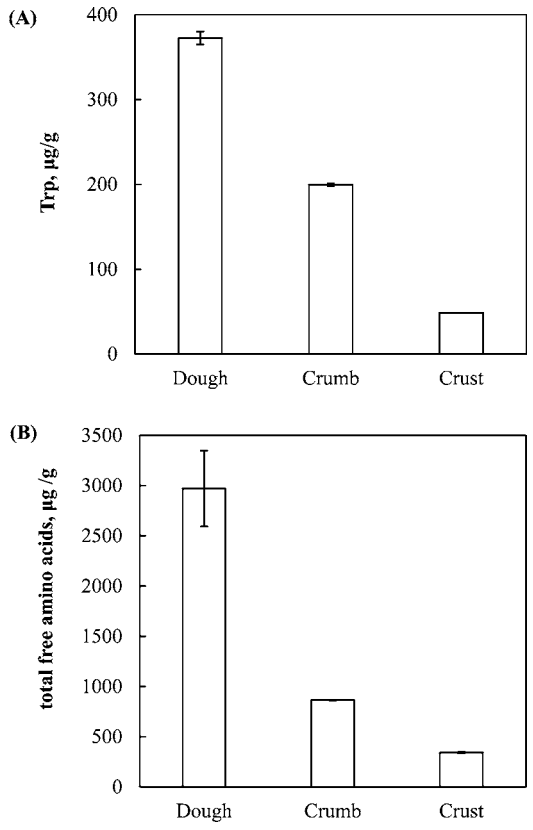

Figure 5. Baking effect on (A) tryptophan and (B) total free amino acid content of breads fermented for 120 min (on dry matter basis).

This indicated a potential role of Trp in the formation mechanism during yeast fermentation. At extreme conditions applied during baking, concentration of melatonin isomer significantly decreased in bread. Comparing to crumb, this effect was more pronounced in the crust part expectedly, in which higher temperatures were attained during the process. It is a fact that the degradation products of melatonin and its isomer are unknown, but this needs further clarification. Primarily, the precise structure of the melatonin isomer needs to be revealed. Since bread as a yeast leavened staple food appears as the major source of melatonin isomer, its biological consequences should be investigated in depth.

■ ASSOCIATED CONTENT

Supporting Information

Figure depicting degradation kinetics of total amino acids and tryptophan in bread dough during fermentation. This material is available free of charge via the Internet at http://pubs.acs.org.

■ AUTHOR INFORMATION

Corresponding Author

*Tel: +90-312-2977108. Fax: +90-312-2992123. E-mail: vgokmen@hacettepe.edu.tr.

Notes

The authors declare no competing financial interest.

■ REFERENCES

(1) Reiter, R. J. Pineal Melatonin - Cell biology of its synthesis and of its physiological interactions. *Endocr. Rev.* **1991**, *12*, 151−180.

(2) Reiter, R. J. The melatonin rhythm - both a clock and a calendar. *Experientia* **1993**, *49*, 654−664.

(3) Reiter, R. J.; Paredes, S. D.; Manchester, L. C.; Tan, D. X. Reducing oxidative/nitrosative stress: a newly-discovered genre for melatonin. *Crit. Rev. Biochem. Mol.* **2009**, *44*, 175−200.

(4) Tan, D. X.; Manchester, L. C.; Terron, M. P.; Flores, L. J.; Reiter, R. J. One molecule, many derivatives: A never-ending interaction of melatonin with reactive oxygen and nitrogen species. *J. Pineal Res.* **2007**, *42*, 28−42.

(5) Tan, D. X.; Hardeland, R.; Manchester, L. C.; Rosales-Corral, S.; Coto-Montes, A.; Boga, J. A.; Reiter, R. J. Emergence of naturally occurring melatonin isomers and their proposed nomenclature. *J. Pineal Res.* **2012**, *53*, 113−121.

(6) Hardeland, R.; Poeggeler, B. Non-vertebrate melatonin. *J. Pineal Res.* **2003**, *34*, 233−241.
(7) Park, S.; Lee, K.; Kim, Y. S.; Back, K. Tryptamine 5-hydroxylase-deficient Sekiguchi rice induces synthesis of 5-hydroxytryptophan and *N*-acetyltryptamine but decreases melatonin biosynthesis during senescence process of detached leaves. *J. Pineal Res.* **2012**, *52*, 211−216.
(8) Tan, D. X.; Hardeland, R.; Manchester, L. C.; Korkmaz, A.; Ma, S. R.; Rosales-Corral, S.; Reiter, R. J. Functional roles of melatonin in plants, and perspectives in nutritional and agricultural science. *J. Exp. Bot.* **2012**, *63*, 577−597.
(9) Rodriguez-Naranjo, M. I.; Gil-Izquierdo, A.; Troncoso, A. M.; Cantos-Villar, E.; Garcia-Parrilla, M. C. Melatonin is synthesised by yeast during alcoholic fermentation in wines. *Food Chem.* **2011**, *126*, 1608−1613.
(10) Garcia-Moreno, H.; Calvo, J. R.; Maldonado, M. D. High levels of melatonin generated during the brewing process. *J. Pineal Res.* **2013**, *55*, 26−30.
(11) Vitalini, S.; Gardana, C.; Simonetti, P.; Fico, G.; Iriti, M. Melatonin, melatonin isomers and stilbenes in Italian traditional grape products and their antiradical capacity. *J. Pineal Res.* **2013**, *54*, 322−333.
(12) Gomez, F. J. V.; Raba, J.; Cerutti, S.; Silva, M. F. Monitoring melatonin and its isomer in Vitis vinifera cv. Malbec by UHPLC-MS/MS from grape to bottle. *J. Pineal Res.* **2012**, *52*, 349−355.
(13) Rodriguez-Naranjo, M. I.; Torija, M. J.; Mas, A.; Cantos-Villar, E.; Garcia-Parrilla, M. D. Production of melatonin by Saccharomyces strains under growth and fermentation conditions. *J. Pineal Res.* **2012**, *53*, 219−224.
(14) Kocadağlı, T.; Yılmaz, C.; Gökmen, V. Determination of melatonin and its isomer in foods by liquid chromatography tandem mass spectrometry. *Food Chem.* **2014**, *153*, 151−156.
(15) Spadoni, G.; Diamantini, G.; Bedini, A.; Tarzia, G.; Vacondio, F.; Silva, C.; Rivara, M.; Mor, M.; Plazzi, P. V.; Zusso, M.; Franceschini, D.; Giusti, P. Synthesis, antioxidant activity and structure-activity relationships for a new series of 2-(*N*-acylaminoethyl)indoles with melatonin-like cytoprotective activity. *J. Pineal Res.* **2006**, *40*, 259−269.
(16) *AACC International Approved Methods of the American Association of Cereal Chemists*, 8th ed.; Method 10-10B, approved January 1983, revised 1985; The Association: St. Paul, MN, USA.
(17) Kocadağlı, T.; Özdemir, K. S.; Gökmen, V. Effects of infusion conditions and decaffeination on free amino acid profiles of green and black tea. *Food Res. Int.* **2013**, *53*, 720−725.
(18) Diamantini, G.; Tarzia, G.; Spadoni, G.; D'Alpaos, M.; Traldi, P. Metastable ion studies in the characterization of melatonin isomers. *Rapid Commun. Mass Spectrom.* **1998**, *12*, 1538−1542.
(19) Rodriguez-Naranjo, M. I.; Gil-Izquierdo, A.; Troncoso, A. M.; Cantos, E.; Garcia-Parrilla, M. C. Melatonin: A new bioactive compound in wine. *J. Food Compos. Anal.* **2011**, *24*, 603−608.
(20) Martinez-Anaya, M. A., Associations and Interactions of Microorganisms in Dough Fermentations: Effects on Dough and Bread Characteristics. In *Handbook of Dough Fermentations*; Kulp, K., Lorenz, K., Eds.; CRC Press: Boca Raton, FL, 2003; pp 63−95.
(21) Rosazza, J. P.; Juhl, R.; Davis, P. Tryptophol formation by Zygosaccharomyces priorianus. *Appl. Microbiol.* **1973**, *26*, 98−105.
(22) Cooper, T. G. Nitrogen metabolism in Saccharomyces cerevisiae. In *The Molecular Biology of the Yeast Saccharomyces*; Strathern, J. N., Jones, E. W., Broach, J. R., Eds.; Cold Spring Harbor Laboratory: Cold Spring Harbor, NY, 1982; pp 39−99.
(23) Magasanik, B. Regulation of nitrogen utilization. In *The Molecular and Cellular Biology of the Yeast Saccharomyces: Gene Expression*; Jones, E. W., Pringle, J. R., Broach, J. R., Eds.; Cold Spring Harbor Laboratory Press: Cold Spring Harbor, NY, 1992; pp 283−317.
(24) Dhakal, R.; Bajpai, V. K.; Baek, K. H. Production of GABA (gamma-aminobutyric acid) by microorganisms: a review. *Braz. J. Microbiol.* **2012**, *43*, 1230−1241.
(25) Sprenger, J.; Hardeland, R.; Fuhrberg, B.; Han, S. Z. Melatonin and other 5-methoxylated indoles in yeast: Presence in high concentrations and dependence on tryptophan availability. *Cytologia* **1999**, *64*, 209−213.
(26) Morales, F. J.; Acar, O. C.; Serpen, A.; Arribas-Lorenzo, G.; Gökmen, V. Degradation of free tryptophan in a cookie model system and its application in commercial samples. *J. Agric. Food Chem.* **2007**, *55*, 6793−6797.

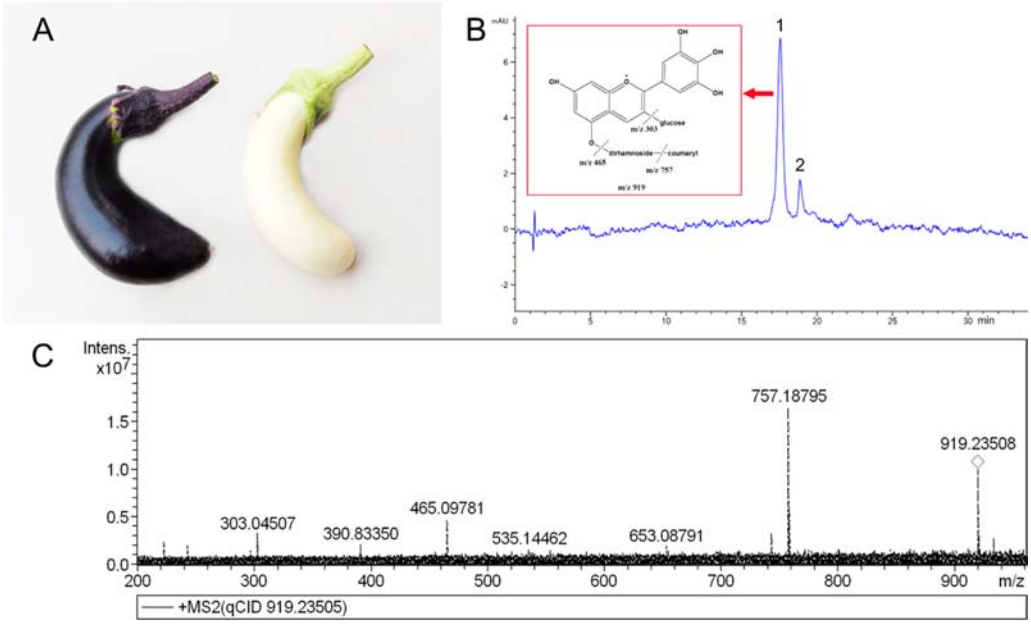

Figure 1. Anthocyanin component analysis in the fruit of eggplant. (A) Photographs of the two eggplant cultivars (Zi Chang on the left and Bai Xue on the right) used in this study. (B) HPLC profiles of anthocyanins in Zi Chang skin. Peak numbers refer to the anthocyanins listed in Table 1. Structures and major cleavage of delphinidin-3-glucoside-5-(coumaryl)dirhamnoside in reference to peak 1 is framed in the red box. (C) LC-MS/MS ion graphs of the major anthocyanin delphinidin-3-glucoside-5-(coumaryl)dirhamnoside (*m/z* 919.2, 757.2, 465.1, 303.0 ($[M + H]^+$)) from the Zi Chang cultivar.

On the basis of the extensive studies reported, it is obvious that the increased expression of some structural genes is directly associated with enhanced levels of anthocyanin accumulation.[14,15] Moreover, transcriptional activation of anthocyanin biosynthesis-related transcription factors always accounts for tissue specific upregulation of structural genes in nature conditions.[16,17] Numbers of regulatory genes including R2R3MYB transcription factors, basic helix−loop−helix (bHLH) transcription factors, MADS transcriptional factors, and WD40 proteins have been cloned from many plants, such as *Arabidopsis*, potato, petunia, and other species.[18] In addition, the two major families of anthocyanin biosynthesis-related regulatory proteins, R2R3MYB and bHLH transcription factors, are found to form regulatory complexes with WD40 proteins in regulating the expression of structural genes.[19,20] Therefore, expression analysis of anthocyanin structural genes and associated transcriptional factors should be helpful for the explanation of tissue specific pigment accumulation in eggplant fruit skin.

In this article, the purple cultivar Zi Chang and the control cultivars Bai Xue that has no pigment accumulation in the fruit were used for this study (Figure1A). Anthocyanin production in eggplant was analyzed by high-performance liquid chromatography−electrospray ionization tandem mass spectrometry (HPLC-ESI-MS/MS). To investigate the molecular mechanism of anthocyanin biosynthesis, the dynamic transcriptional levels of anthocyanin structural genes and regulatory transcriptional factors were analyzed by quantitative real-time reverse transcription polymerase chain reaction (qRT-PCR) in the fruit skin and the flesh in these two cultivars. Then, the tissue specific expression gene *SmMYB1* was transformed into wild eggplant under the drive of the 35s promoter. In the regenerating shoots with abundant anthocyanin accumulation, we examined the expression level of *SmMYB1* and some vital structural genes of the anthocyanin biosynthetic pathway. This work expanded our knowledge about anthocyanin accumulation and the underlying molecular mechanism in eggplant. It will be helpful for the breeding of high anthocyanin content eggplant cultivars in both traditional breeding and genetic engineering.

MATERIALS AND METHODS

Plant Materials. Eggplant (*S. melongena* L.) seeds of the white cultivar (Bai Xue) and the purple cultivar (Zi Chang) were obtained from Chongqing Academy of Agriculture Sciences. The seeds were sown directly into soil and grown in a greenhouse with a 16 h photoperiod at 28 °C. The fruits of eggplant were harvested at 12−15 days after anthesis. Both the skin and the flesh of Bai Xue are white. Zi Chang has purple pigment accumulated in the skin but not in the flesh (Figure 1A). The fruit skins of the two cultivars were manually peeled in the thickness of about 2 mm. The fruit flesh was cut into tiny cubes. All the samples were frozen in liquid nitrogen and stored at −80 °C for RNA extraction and other analyses.

RNA Extraction and qRT-PCR Analysis. The skin and flesh samples of the two cultivars were grounded into powder in liquid nitrogen. Total RNA was isolated from various tissues for three biological repeats using RNAiso reagent according to the manufacturer's instruction (Takara, Dalian, PRC). RNA samples (1 μg) were reverse transcripted into complementary DNA (cDNA) with an oligo(dT)20 primer and M-MLV reverse transcriptase (Promega, Madison, WI) following the manufacturer's protocol. The synthesized cDNAs were diluted five times in H_2O for qRT-PCR analysis.

qRT-PCR was carried out using the CFX96 Real-Time System (C1000 thermal cycler). All reactions were performed using the GoTaq qPCR Master Mix according to the manufacturer's instructions. Reactions were performed in triplicate using 5 μL of Master Mix, 0.25 μM each primer, 1 μL of diluted cDNA, and DNase-free water to a final volume of 10 μL. The PCR amplification was as follows: 1 cycle of 3 min at 95 °C, 40 cycles of denaturation for 15 s at 95 °C, annealing for 30 s at 60 °C, and elongation for 15 s at 72 °C. Amplification was followed by a melting curve analysis with continual fluorescence data acquisition during the 60−95 °C melt. Melt curve analysis of qPCR samples revealed that there was only one product for

dx.doi.org/10.1021/jf404574c | J. Agric. Food Chem. 2014, 62, 2906−2912

each gene primer reaction. The primers used for qPCR analysis were designed by Primer Premier 5 and are listed in Supplementary Table 1 (Supporting Information). The PCR products were sequenced to confirm the specific amplifications. The gene expression was normalized to *SmGAPDH* as a reference gene. Values reported here were calculated from three biological repeats for each sample.

Gene Cloning and Sequence Analysis. The full-length coding sequence of anthocyanin biosynthesis-related transcription factors were cloned from eggplant by RT-PCR with degenerate primers and finally named *SmMYB1*, *SmMYB2*, *SmAN11*, *SmbHLH1*, and *SmMADS1*, respectively, referring to the corresponding genes from tomato and potato. Sequence similarities were calculated with DNAMAN version 5.2.2. The phylogenetic and molecular evolutionary analysis was used with MEGA (Molecular Evolutionary Genetics Analysis) version 3.1.

Chemicals. Anthocyanin (delphinidin 3-rutinoside chloride) for external standards was purchased from Phytolab (Germany). HPLC-grade formic acid and methanol (MeOH) were bought from Sigma. All the other solvents were provided from Aldrich (St. Louis, MO).

Anthocyanin Extraction and HPLC-ESI-MS/MS Analysis. Anthocyanin extraction of eggplant was carried out as the same way as for radish.[21] The extract was filtered through a 0.2 μm PTFE syringe filter. The samples were then analyzed by an Agilent Technologies 1200 Series HPLC (Agilent Technologies, Palo Alto, CA), equipped with an Agilent 1200 HPLC variable wavelength detector. The results were analyzed by Agilent 1200 HPLC ChemStation software. The chromatographic separation was performed on a Zorbax Stablebond Analytical SB-C18 column (4.6 mm × 250 mm, 5 μm, Agilent Technologies, Rising Sun, MD). The injection sling was 10 μL. Elution was performed using mobile phase A (aqueous 5% formic acid solution) and mobile phase B (methanol). The detection was at 520 nm, and the column oven temperature was set at 40 °C. The flow rate was 1 mL/min. The gradient program is described as follows: 0−5 min, 10−20% B; 5−10 min, 20−30% B; 10−15 min, 30−40% B; 15−25 min, 40% B; 25−30 min, 40−60% B; 31−32 min, 90% B; 32−35 min, 10% B. Quantification of the different anthocyanins was based on peak areas and calculated as equivalents of the standard compounds. All contents were expressed as milligrams per grams of dry weight. Low-resolution electrospray mass spectrometry was performed with a solariX ion trap mass spectrometer (Bruker Daltoniks, Billerica, MA). The experimental conditions were as follows: ESI interface, nebulizer, 50 psi; dry gas, 15.0 psi; dry temperature, 320 °C; MS/MS, scan from m/z 200 to 2000; ion trap, scan from m/z 200 to 2000; source accumulation, 50 ms; ion accumulation time, 300 ms; flight time to acq. cell, 1 ms; smart parameter setting (SPS), compound stability, 50%; trap drive level, 60%.

Total Anthocyanin Analysis. Spectrophotometric differential pH method was used for the measurement of total anthocyanins. The protocols are described as follows. Frozen samples (100 mg) were crushed into powder in liquid nitrogen and then extracted separately with 2 mL of pH 1.0 buffer and 2 mL of pH 4.5 buffer. In addition, pH 1.0 buffer contains 50 mM KCl and 150 mM HCl, while pH 4.5 buffer contains 400 mM sodium acetate and 240 mM HCl. The mixtures were centrifuged at 14 000*g* for 10 min at 4 °C. The supernatants were gathered for measurement of absorbance at 510 nm. The amount of total anthocyanin was calculated according to the equation which follows:

$$\text{amount } (\text{mg g}^{-1}\text{ FW}) = (\text{A1} - \text{A2}) \times 484.8/24.825 \times \text{dilution factor}$$

A1 represents the absorbance of supernatants gathered from pH 1.0 buffer solution at 510 nm while A2 represents the other. The value 484.8 represents the molecular mass of cyaniding-3-glucoside chloride, while 24 825 reflects its molar absorptivity at 510 nm. The total anthocyanins of sample were analyzed in triplicate.

Vector Construction and Transformation of Eggplant. The complement DNA was synthesized with total RNA with M-MLV (Promega, Madison, WI) as the recommendation of manufacturer. The full-length coding sequence of *SmMYB1* was cloned into pBI121 for the replacement of GUS. Primers used for amplification of *SmMYB1* are SmMYB1-con-F, GCGATCTAGAAATAAAATGAATAATCCTCC, and SmMYB1-con-R, GACTGAGCTCCGAAAACAGACAATATTACTA. The binary vector pBI121-SmMYB1 containing the *SmMYB1* cDNA driven by the 35S promoter was transferred into *Agrobacterium tumefaciens* strain LBA4404 by the freeze−thaw method. Eggplant (*S. melongena*) 'Bai Xue' was used for the generation of transgenic callus by Agrobacterium-mediated transformation, using the protocol previously reported.[22]

RESULTS AND DISCUSSION

Identification and Quantitative Analyses of Anthocyanins. By analyzing the extracts from the fruit of Zi Chang and Bai Xue cultivar with LC-MS/MS, two kinds of anthocyanins were separated and identified (Table 1 and Figure1B,C). Then, the MS/MS (m/z) fragmentation pattern was applied to verify the identity of anthocyanins in purple fruit skin with the information provided by earlier reports.[12] These results show that delphinidin may be the unique aglycone present in all eggplant fruits.[10−12] However, the major component of anthocyanin in Zi Chang cultivar is delphinidin-3-glucoside-5-(coumaryl)dirhamnoside, which is apparently different from the anthocyanins identified in other cultivars. These results show that the purple eggplant cultivars reported up to now share the same pattern of anthocyanidin biosynthesis but with different modification patterns. The total anthocyanins content from Zi Chang skin was found to be 1.24 mg/g of dry weight. (Table 2). The content of major identity delphinidin-3-glucoside-5-(coumaryl)dirhamnoside is 1.10 mg/g, while the minor identity is only 0.14 mg/g. So, eggplant should be classified in the food category containing simple anthocyanins in contrast with cabbage and radish.[12,14,21] Consequently, it is the major anthocyanin delphinidin-3-glucoside-5-(coumaryl)-dirhamnoside that contributes to the purple color in fruit skin principally.

Table 1. Anthocyanins Identified in the Eggplant Zi Chang Skin

no.[a]	RT[b] (min)	$[M + M]^+$ (m/z)	MS/MS (m/z)	anthocyanin
1	17.56	919	757/465/303	delphinidin-3-glucoside-5-(coumaryl)dirhamnoside
2	18.86	757		delphinidin-3-glucoside-5-dirhamnoside

[a]No. corresponds to the elution order by HPLC analysis in Figure 1B. [b]RT is the retention time.

Table 2. Anthocyanin Content (mg/g dry wt) in the Two Eggplant Cultivars (Zi Chang, Bai Xue) (n = 3)

no.[a]	anthocyanin	ZC-S[b]	ZC-F	BX-S	BX-F
1	delphinidin-3-glucoside-5-(coumaryl) dirhamnoside	1.10	nd[c]	nd	nd
2	delphinidin-3-glucoside-5-dirhamnoside	0.14	nd	nd	nd

[a]No. corresponds to the elution order by HPLC analysis in Figure 1B. [b]ZC-S, Zi Chang skin; ZC-F, Zi Chang flesh; BX-S, Bai Xue skin; and BX-F, Bai Xue flesh. [c]nd is not detected.

Isolation and Sequence Analysis of Anthocyanin Biosynthesis Regulatory Genes from *S. melongena* L. Given that the gene sequences encoding anthocyanin biosynthesis enzymes can be found partially in the database of the

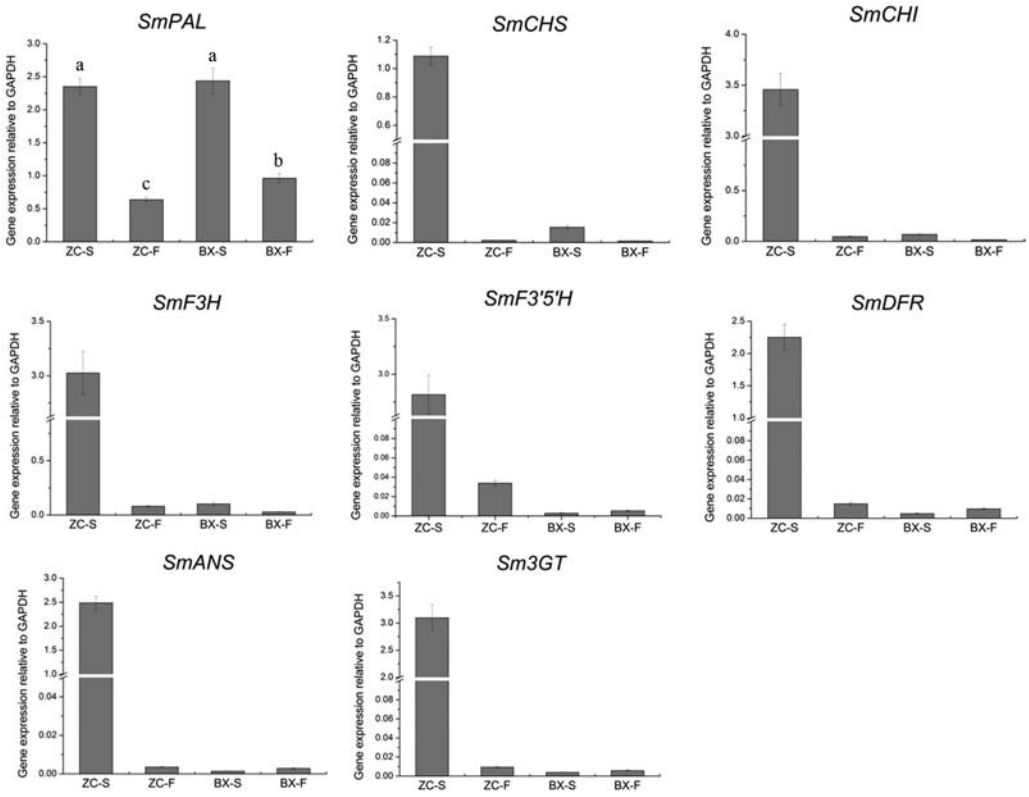

Figure 2. Expression analysis of anthocyanin biosynthesis genes in the skin and the flesh of two eggplant cultivars. ZC-S, Zi Chang skin; ZC-F, Zi Chang flesh; BX-S, Bai Xue skin; and BX-F, Bai Xue flesh. Error bars represent the standard error of the mean (n = 3). Statistical significance of the differences between samples was calculated with ANOVA by paired-group comparisons. Different letters indicate significance at $P < 0.05$.

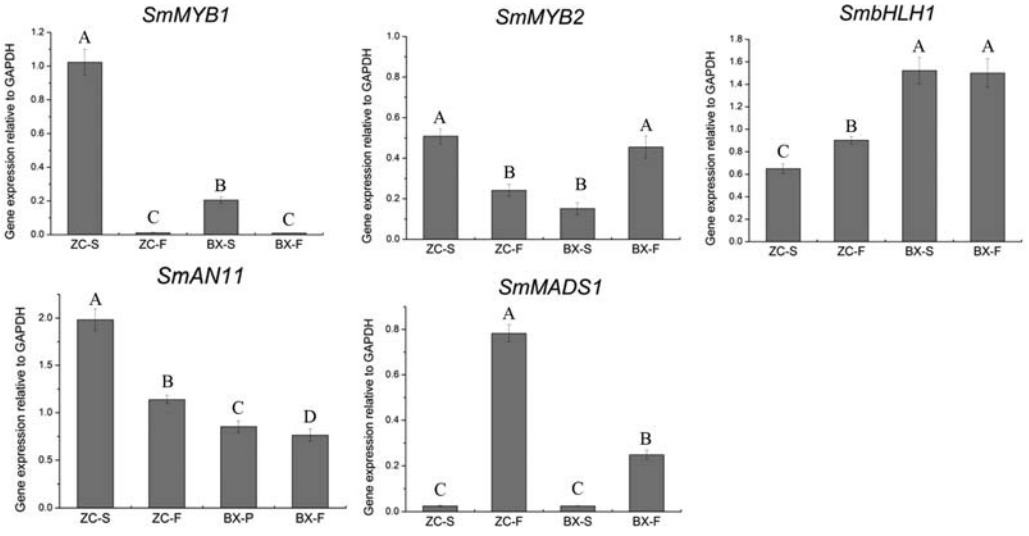

Figure 3. Expression analysis of anthocyanin biosynthesis-associated transcriptional factors in the skin and the flesh of two eggplant cultivars. ZC-S, Zi Chang skin; ZC-F, Zi Chang flesh; BX-S, Bai Xue skin; and BX-F, Bai Xue flesh. Error bars represent the standard error of the mean (n = 3). Statistical significance of the differences between samples was calculated with ANOVA by paired-group comparisons. Different letters indicate significance at $P < 0.05$.

Institute for Genomic Research, our research focused on the cloning of regulatory gene sequences with primers designed according to conserved sequences from other species. Then, the full-length coding sequences of a bHLH transcriptional factor (*SmbHLH1*), a MADS transcriptional factor (*SmMADS1*), two R2R3MYB transcriptional factors (*SmMYB1* and *SmMYB2*), and a WD40 protein (*SmAN11*) are obtained. The gene identities were further verified by sequence alignment with orthologous sequences from other plants. The results of sequence alignment show that the orthologous genes from different eggplant cultivars share the same predicted protein sequence in spite of some inconsistencies in the nucleotide sequence. Then, it is reasonable to speculate that the accumulation of anthocyanins in purple eggplant may be the result of the alternation in expression level of some transcription factors.

dx.doi.org/10.1021/jf404574c | J. Agric. Food Chem. 2014, 62, 2906−2912

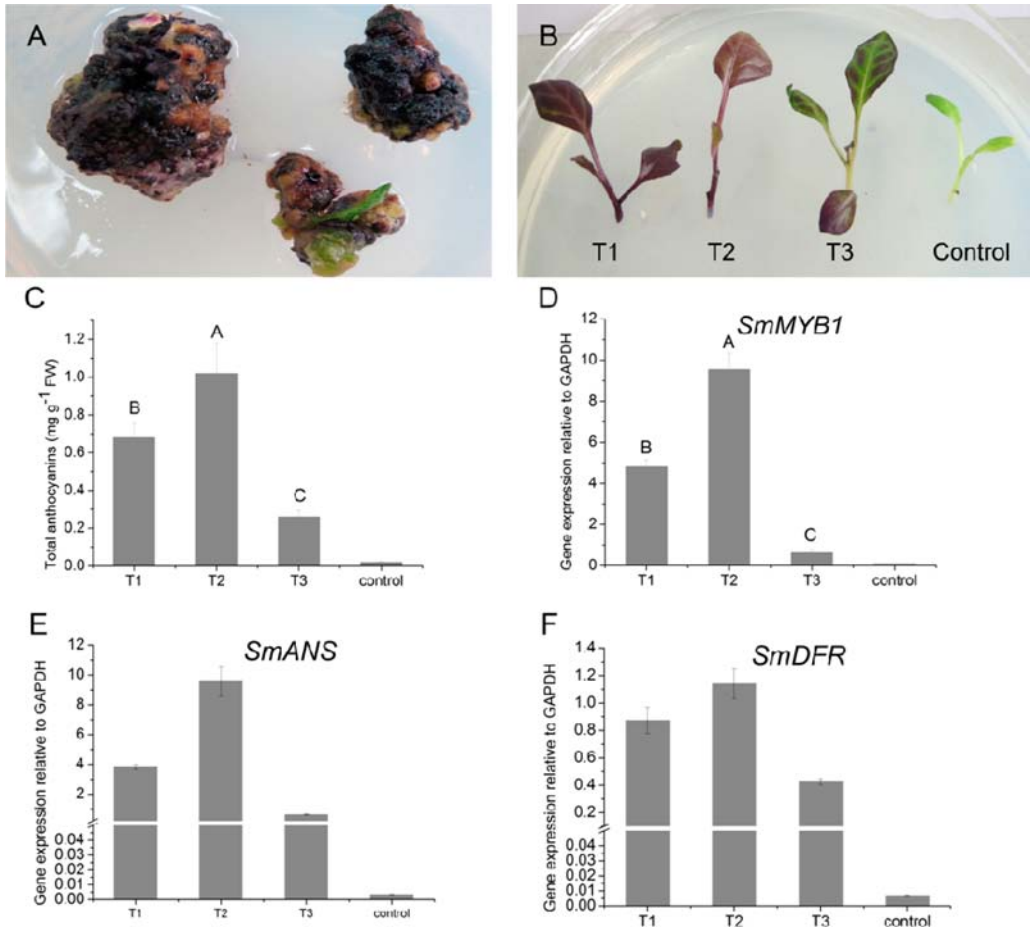

Figure 4. Overexpression of SmMYB1 in eggplant elevates the expression levels of structure genes and anthocyanin production. (A) Pigmented callus transformed with 35S-SmMYB1. (B) Three independent regenerating shoot lines transformed with 35S-SmMYB1 with one regenerating shoot transformed with empty vector. (C) Anthocyanin content in different lines of shoot. (D) transcriptional analysis of SmMYB1 in different regeneration shoots. (E, F) transcriptional analysis of anthocyanin biosynthesis genes SmANS (E) and SmDFR (F) in different regeneration shoots.

Expression Analysis of Anthocyanin Biosynthetic Genes in the Skin and Flesh of Different Eggplant Cultivars. For the purpose of investigating the molecular mechanisms underlying anthocyanin biosynthesis in eggplant, the transcriptional level of anthocyanin synthetic genes including *SmPAL*, *SmCHS*, *SmCHI*, *SmF3H*, *SmF3′5′H*, *SmDFR*, *SmANS*, and *Sm3GT* were examined in the skin and the flesh from two eggplant cultivars (Figure 2). The expression levels of all these genes except *SmPAL* are dramatically upregulated in the Zi Chang fruit skin compared with the other three tissues. Especially, the expression levels of *SmF3′5′H*, *SmDFR*, *SmANS*, and *Sm3GT* are upregulated to at least 1000 fold in the purple fruit skin. From the results reported previously,[23,24] the phenomenon that small amounts of transcripts of all the structural genes were always detected in the green cultivars with no visible anthocyanin pigmentation was apparently observed. Here, we speculate that sufficient transcripts of some structural genes are essential for a large amount of anthocyanin production in the fruit skin of the Zi Chang cultivar.

Expression Analysis of Anthocyanin Biosynthesis-Associated Regulatory Genes in the Skin and the Flesh of Different Eggplant Cultivars. According to recent research, anthocyanin structural genes are regulated by a complex composed of MYB, bHLH, and WD40 proteins from three different families of transcriptional factors.[18] MYB and bHLH transcription factors play essential roles in activating anthocyanin biosynthetic genes among various plant species, while WD40 proteins play a critical role in the process of complex formation. In addition, the transcriptional factor of MADS family is also found to be involved in anthocyanin accumulation in sweet potato.[25] Therefore, expression analysis of anthocyanin biosynthesis-associated regulatory genes provides critical information to reveal the molecular mechanisms of pigment accumulation in eggplant fruit skin. The expression level analyses of *SmMYB1*, *SmMYB2*, *SmbHLH1*, *SmAN11*, and *SmMADS1* are shown in Figure 3. The R2R3MYB gene *SlANT1* was identified from tomato as a transcriptional regulator of anthocyanin biosynthesis, modification, and transport.[26] Hence, two MYB genes were cloned and designated as *SmMYB1* and *SmMYB2* because of high similarity with *SlANT1*. Sequence analysis of SmMYB1 reveals that the predicted protein contains a R2R3 DNA binding domain that is involved in the interaction with bHLH cofactor (Supplementary Figure 1, Supporting Information). *SmMYB1* was the only transcription factor that was significantly upregulated in the fruit skin of the Zi Chang cultivar. The enhanced expression of the MYB gene in certain tissue was in accordance with the anthocyanin distribution pattern of the two cultivars. These results indicate that SmMYB1 may play a major role in the anthocyanin biosynthesis regulation. It is worth mentioning that SmMYB2 is unlikely necessary for the anthocyanin

biosynthesis in purple eggplant for the reason that the transcripts of *SmMYB2* are little to detect by qPCR. The expression analyses of *SmbHLH1* and *SmAN11* in the different cultivars show that these two genes are not accounted for the transcriptional activation of anthocyanin structural genes in purple eggplant. Furthermore, *SlTDR4*, which is the orthologous gene of *SmMADS1*, was proved to be an important switch that regulates the process of fruit ripening in an ethylene-independent manner including the accumulation of pigments.[27] However, the transcripts of *SmMADS1* in fruit skin in contrast with flesh indicate that the pathway of anthocyanin biosynthesis is probably independent of *SmMADS1*.

Overexpression of SmMYB1 in Transgenic Eggplant. Phylogenetic analysis shows that SmMYB1 lays in the same cluster with the anthocyanin synthesis activator SlANT1 and CaMYB1 (Supplementary Figure 1, Supporting Information). To further study the function of the *SmMYB1* gene, the full-length coding sequence of *SmMYB1* driven by the 35S promoter was overexpressed in the callus of eggplant. Compared with the kanamycin resistant callus transformed by the empty vector, there were large amounts of anthocyanin accumulation on the surface of kanamycin resistant callus transformed by the vector containing the *SmMYB1* gene (Figure 4A). Overexpression of the *SmMYB1* gene resulted in the high level of anthocyanin accumulation in purple regeneration shoots (Figure 4B,C). Furthermore, the expression of *SmMYB1* and two key anthocyanin biosynthesis genes in regenerating shoots was confirmed by qRT-PCR (Figure 4D−F). The enhanced expression of SmMYB1 was in accordance with a coordinated increase in transcript levels of SmANS and SmDFR. In addition, the enhanced expression of SmMYB1 was also in accordance with the total anthocyanin content in regenerative shoots. These results demonstrate that overexpression of SmMYB1 is able to activate anthocyanin biosynthesis by the way of significantly raising the expression level of anthocyanin structural genes.

In this study, delphinidin-3-glucoside-5-(coumaryl)-dirhamnoside was identified as the major anthocyanin in Chinese purple eggplant cultivar Zi Chang. In contrast to the control, SmF3′5′H that mainly catalyzes the hydroxylation at the 3′- and 5′-position of the B ring is dramatically upregulated at the transcript level.[28] Therefore, delphinidin should be the unique aglycone in the purple eggplant skin despite a lack of MS/MS (m/z) data of peak 2. Furthermore, the substantially upregulation of most of anthocyanin structural genes provides a reasonable explanation for large amounts of pigmentation accumulation in Zi Chang fruit skin. By expression analysis of flavonoid biosynthetic regulatory genes, *SmMYB1* is found to be significantly upregulated in the tissue where considerable pigments accumulate. Similarity and phylogenetic analysis of SmMYB1 with other MYBs from various species suggests that SmMYB1 might participate in the activating of anthocyanin biosynthesis in eggplant.[29,30] Moreover, the pigments displayed in the kanamycin resistant callus and regenerating shoots confirmed the hypothesis proposed above. Besides, the total anthocyanins content of other tissues in Zi Chang cultivar was measured by the spectrophotometric differential pH method (Supplementary Figure 3, Supporting Information). The distribution pattern of anthocyanin content agrees well with the expression level of *SmMYB1* in the tissues above (Supplementary Figure 4, Supporting Information). Therefore, all of these results prove that SmMYB1 plays an important role in activating anthocyanin biosynthesis in Zi Chang fruit skin by transcriptional activation of anthocyanin structural genes.

Owing to the great benefits anthocyanins bring to human health, foods rich in anthocyanins are attracting more and more attention from the public gradually. Since eggplant is an important food crop world widely cultivated, the consumption of high anthocyanin-containing fruit in the diet will raise the intake of health-promoting phytonutrients undoubtedly. Unfortunately, the existing cultivars of eggplant only have purple pigments accumulated in the skin but not in the flesh. Although we can elevate the anthocyanin content of eggplant fruit by overexpression of exogenous genes like tomato, the potential risks still exist.[6] Hence, an intragenic approach that improves the agricultural traits of the crop by modifying the genome of the plant provides us a new method to elevate the anthocyanin content of eggplant fruit.[31] However, the isolation of anthocyanin biosynthesis activator gene *SmMYB1* made an important progress toward the breeding of high anthocyanin-containing eggplant with little potential risk.[32] In summary, this work not only promotes our understanding of the molecular mechanisms underlying anthocyanin biosynthesis in eggplant but also provides a candidate gene for the development of eggplant cultivar that is rich of anthocyanins.

■ ASSOCIATED CONTENT

Ⓢ Supporting Information

Table of primers used for RT-PCR; figures describing protein sequence alignment of SmMYB with MYBs from other plants, showing phylogenetic analysis of SmMYB1 and other MYBs, showing anthocyanin content in different tissues from Zi Chang cultivar, and depicting the expression level of SmMYB1 in different tissues of Zi Chang cultivar. This material is available free of charge via the Internet at http://pubs.acs.org.

■ AUTHOR INFORMATION

Corresponding Authors

*(S.T.) E-mail: tiansbing@aliyun.com.

*(G.C.) Phone: 0086 23 65112674; fax: 0086 23 65112674; e-mail: chenguoping@cqu.edu.cn.

Funding

This work was supported by National Natural Science Foundation of China (nos. 31100089 and 31171968) and Technology System of National *Bulk* Vegetable Industry--Eggplant Breeding Position (CARS-25-A-06).

Notes

The authors declare no competing financial interest.

■ ABBREVIATIONS USED

PAL, phenylalanine ammonia lyase; CHS, chalcone synthase; CHI, chalcone isomerase; F3H, flavone 3-hydroxylase; F3′5′H, flavonoid 3′,5′-hydroxylase; DFR, dihydroflavonol reductase; ANS, anthocyanidin synthase; HPLC, high-performance liquid chromatography; ESI-MS/MS, elctrospray ionization tandem mass spectrometry; qRT-PCR, quantitative real-time reverse transcription PCR

■ REFERENCES

(1) Harborne, J. B.; Williams, C. A. Advances in flavonoid research since 1992. *Phytochemistry* **2000**, *55*, 481−504.

(2) Toufektsian, M. C.; de Lorgeril, M.; Nagy, N.; Salen, P.; Donati, M. B.; Giordano, L.; Mock, H. P.; Peterek, S.; Matros, A.; Petroni, K.; Pilu, R.; Rotilio, D.; Tonelli, C.; de Leiris, J.; Boucher, F.; Martin, C.

Chronic dietary intake of plant-derived anthocyanins protects the rat heart against ischemia-reperfusion injury. *J. Nutr.* **2008**, *138*, 747−752.
(3) Paredes-Lopez, O.; Cervantes-Ceja, M. L.; Vigna-Perez, M.; Hernandez-Perez, T. Berries: Improving human health and healthy aging, and promoting quality life—A review. *Plant Foods Hum. Nutr.* **2010**, *65*, 299−308.
(4) de Pascual-Teresa, S.; Moreno, D. A.; Garcia-Viguera, C. Flavanols and anthocyanins in cardiovascular health: A review of current evidence. *Int. J. Mol. Sci.* **2010**, *11*, 1679−703.
(5) Guarnieri, S.; Riso, P.; Porrini, M. Orange juice vs vitamin C: Effect on hydrogen peroxide-induced DNA damage in mononuclear blood cells. *Br. J. Nutr.* **2007**, *97*, 639−643.
(6) Butelli, E.; Titta, L.; Giorgio, M.; Mock, H. P.; Matros, A.; Peterek, S.; Schijlen, E. G.; Hall, R. D.; Bovy, A. G.; Luo, J.; Martin, C. Enrichment of tomato fruit with health-promoting anthocyanins by expression of select transcription factors. *Nat. Biotechnol.* **2008**, *26*, 1301−1308.
(7) Meiers, S.; Kemeny, M.; Weyand, U.; Gastpar, R.; von Angerer, E.; Marko, D. The anthocyanidins cyanidin and delphinidin are potent inhibitors of the epidermal growth-factor receptor. *J. Agric. Food Chem.* **2001**, *49*, 958−962.
(8) Williams, R. J.; Spencer, J. P.; Rice-Evans, C. Flavonoids: Antioxidants or signalling molecules? *Free Radical Biol. Med.* **2004**, *36*, 838−849.
(9) Cao, G.; Sofic, E.; Prior, R. L. Antioxidant capacity of tea and common vegetables. *J. Agric. Food Chem.* **1996**, *44*, 3426−3431.
(10) Noda, Y.; Kneyuki, T.; Igarashi, K.; Mori, A.; Packer, L. Antioxidant activity of nasunin, an anthocyanin in eggplant peels. *Toxicology* **2000**, *148*, 119−123.
(11) Matsubara, K.; Kaneyuki, T.; Miyake, T.; Mori, M. Antiangiogenic activity of nasunin, an antioxidant anthocyanin, in eggplant peels. *J. Agric. Food Chem.* **2005**, *53*, 6272−6275.
(12) Wu, X.; Prior, R. L. Identification and characterization of anthocyanins by high-performance liquid chromatography-electrospray ionization-tandem mass spectrometry in common foods in the United States: Vegetables, nuts, and grains. *J. Agric. Food Chem.* **2005**, *53*, 3101−3113.
(13) Winkel-Shirley, B. Flavonoid biosynthesis. A colorful model for genetics, biochemistry, cell biology, and biotechnology. *Plant Physiol.* **2001**, *126*, 485−493.
(14) Yuan, Y.; Chiu, L. W.; Li, L. Transcriptional regulation of anthocyanin biosynthesis in red cabbage. *Planta* **2009**, *230*, 1141−1153.
(15) Crifò, T.; Petrone, G.; Lo Cicero, L.; Lo Piero, A. R. Short cold storage enhances the anthocyanin contents and level of transcripts related to their biosynthesis in blood oranges. *J. Agric. Food Chem.* **2011**, *60*, 476−481.
(16) Butelli, E.; Licciardello, C.; Zhang, Y.; Liu, J.; Mackay, S.; Bailey, P.; Reforgiato-Recupero, G.; Martin, C. Retrotransposons control fruit-specific, cold-dependent accumulation of anthocyanins in blood oranges. *Plant Cell* **2012**, *24*, 1242−1255.
(17) Chiu, L. W.; Zhou, X.; Burke, S.; Wu, X.; Prior, R. L.; Li, L. The purple cauliflower arises from activation of a MYB transcription factor. *Plant Physiol.* **2010**, *154*, 1470−1480.
(18) Gonzalez, A.; Zhao, M.; Leavitt, J. M.; Lloyd, A. M. Regulation of the anthocyanin biosynthetic pathway by the TTG1/bHLH/Myb transcriptional complex in Arabidopsis seedlings. *Plant J. Cell Mol. Biol.* **2008**, *53*, 814−827.
(19) Albert, N. W.; Lewis, D. H.; Zhang, H.; Schwinn, K. E.; Jameson, P. E.; Davies, K. M. Members of an R2R3-MYB transcription factor family in Petunia are developmentally and environmentally regulated to control complex floral and vegetative pigmentation patterning. *Plant J. Cell Mol. Biol.* **2011**, *65*, 771−784.
(20) Spelt, C.; Quattrocchio, F.; Mol, J. N.; Koes, R. Anthocyanin1 of petunia encodes a basic helix-loop-helix protein that directly activates transcription of structural anthocyanin genes. *Plant Cell* **2000**, *12*, 1619−1632.
(21) Park, N. I.; Xu, H.; Li, X.; Jang, I. H.; Park, S.; Ahn, G. H.; Lim, Y. P.; Kim, S. J.; Park, S. U. Anthocyanin accumulation and expression of anthocyanin biosynthetic genes in radish (*Raphanus sativus*). *J. Agric. Food Chem.* **2011**, *59*, 6034−6039.
(22) Filippone, E.; Lurquin, P. F. Stable transformation of eggplant (Solanum melongena L.) by cocultivation of tissues withAgrobacterium tumefaciens carrying a binary plasmid vector. *Plant Cell Rep.* **1989**, *8*, 370−373.
(23) Feyissa, D. N.; Lovdal, T.; Olsen, K. M.; Slimestad, R.; Lillo, C. The endogenous GL3, but not EGL3, gene is necessary for anthocyanin accumulation as induced by nitrogen depletion in Arabidopsis rosette stage leaves. *Planta* **2009**, *230*, 747−754.
(24) Palapol, Y.; Ketsa, S.; Lin-Wang, K.; Ferguson, I. B.; Allan, A. C. A MYB transcription factor regulates anthocyanin biosynthesis in mangosteen (*Garcinia mangostana* L.) fruit during ripening. *Planta* **2009**, *229*, 1323−1334.
(25) Lalusin, A.; Nishita, K.; Kim, S.-H.; Ohta, M.; Fujimura, T. A new MADS-box gene (*IbMADS10*) from sweet potato (*Ipomoea batatas* (L.) Lam) is involved in the accumulation of anthocyanin. *Mol. Genet. Genomics* **2006**, *275*, 44−54.
(26) Mathews, H.; Clendennen, S. K.; Caldwell, C. G.; Liu, X. L.; Connors, K.; Matheis, N.; Schuster, D. K.; Menasco, D. J.; Wagoner, W.; Lightner, J.; Wagner, D. R. Activation tagging in tomato identifies a transcriptional regulator of anthocyanin biosynthesis, modification, and transport. *Plant Cell* **2003**, *15*, 1689−1703.
(27) Bemer, M.; Karlova, R.; Ballester, A. R.; Tikunov, Y. M.; Bovy, A. G.; Wolters-Arts, M.; Rossetto Pde, B.; Angenent, G. C.; de Maagd, R. A. The tomato FRUITFULL homologs TDR4/FUL1 and MBP7/FUL2 regulate ethylene-independent aspects of fruit ripening. *Plant Cell* **2012**, *24*, 4437−4451.
(28) Seitz, C.; Eder, C.; Deiml, B.; Kellner, S.; Martens, S.; Forkmann, G. Cloning, functional identification and sequence analysis of flavonoid 3′-hydroxylase and flavonoid 3′,5′-hydroxylase cDNAs reveals independent evolution of flavonoid 3′,5′-hydroxylase in the Asteraceae family. *Plant Mol. Biol.* **2006**, *61*, 365−381.
(29) Feng, S.; Wang, Y.; Yang, S.; Xu, Y.; Chen, X. Anthocyanin biosynthesis in pears is regulated by a R2R3-MYB transcription factor PyMYB10. *Planta* **2010**, *232*, 245−255.
(30) Lin-Wang, K.; Bolitho, K.; Grafton, K.; Kortstee, A.; Karunairetnam, S.; McGhie, T. K.; Espley, R. V.; Hellens, R. P.; Allan, A. C. An R2R3MYB transcription factor associated with regulation of the anthocyanin biosynthetic pathway in Rosaceae. *BMC Plant Biol.* **2010**, *10*, 50.
(31) Rommens, C. M. All-native DNA transformation: A new approach to plant genetic engineering. *Trends Plant Sci.* **2004**, *9*, 457−64.
(32) Rommens, C. M. Intragenic crop improvement: Combining the benefits of traditional breeding and genetic engineering. *J. Agric. Food Chem.* **2007**, *55*, 4281−4288.

Table 1. Strains, Plasmids, and Primers Used in This Study

strain, plasmid, or primer	description	source or reference
	Strains	
B. subtilis		
168	*trpC2*	25
total-tat_2	*trpC2*; *tatAc*::Em; *tatAy-tatCy*::Sp; *tatAd-tatCd*::Km; Em^r; Sp^r; Km^r	21
tatAyCy	*trpC2*; *tatAy-tatCy*::Sp; Sp^r	21
tatAdCd	*trpC2*; *tatAd-tatCd*::Km; Km^r	21
	Plasmids	
pUC18	pUC origin, P_{lac}, Ap^r	TaKaRa
pWH1520	*E. coli*–*B. subtilis* shuttle vector, *pBC16 ori*, *pBR ori*, P_{xylA}, *xylR*, Tc^r, Ap^r	26
pWYM20	pWH1520 derivative, secretion expression vector coding for YwbN-MPH	this study
pWTM20	pWH1520 derivative, secretion expression vector coding for TorA-MPH	23
pWM20	pWH1520 derivative, cytoplasmic expression vector coding for MPH	23
	Primers	
P1	GAATTCCATGAGCGATGAACAGAAA	this study
P2	CTGCAGCTGAGGCAACAAGCGGAGCGA	this study
P3	CTGCAGCACCGCAGGTGCGC	this study
P4	AAGCTTTCACTTGGGGTTGACGAC	this study
P5	GGTACCTCTAGAGGGTATTAATAATGAGCGATGAACAGAAA	this study
P6	GCATGCTCAGTGGTGGTGGTGGTGCTTGGGGTTGACGAC	this study

TatA complex is then recruited to form a pore through which substrates are translocated.[19] *E. coli* usually does not secrete Tat substrates into the growth medium because of the presence of the outer membrane.

The *Bacillus subtilis* Tat machinery lacks TatB and consists of three TatA (namely, TatAd, TatAy, and TatAc) and two TatC (TatCd and TatCy).[20] The TatA and TatC proteins form two active Tat translocation complexes, TatAdCd and TatAyCy, which display different substrate specificities.[21] Recently, a working model has been proposed for *B. subtilis*, in which the TatA protein has a dual function, because it can complement for the absence of both TatA and TatB in *E. coli*.[22] Moreover, Tat pathway specificity in *B. subtilis* is determined by twin-arginine signal peptide interactions with TatCd or TatCy.[21] In *B. subtilis*, Tat substrates can be secreted directly into culture media because of the absence of an outer membrane.

In a previous study, the twin-arginine signal peptide of TorA from *E. coli* directed secretion of MPH via the *B. subtilis* Tat pathway into the culture medium.[23] In this study, the MPH secretion directed by the *B. subtilis* YwbN signal peptide was achieved, leading to 1.8-fold improvement in extracellular MPH activity compared to the activity achieved with the TorA signal peptide. Furthermore, we demonstrated that the MPH secretion was specifically mediated by the TatAyCy system.

MATERIALS AND METHODS

Strains, Plasmids, Primers, and Culture Conditions. The strains, plasmids, and primers used in this study are listed in Table 1. *E. coli* DH5α was used for construction of recombinant plasmids. *B. subtilis* 168 was used for expressing recombinant MPH. All strains were grown at 37 °C in Luria–Bertani (LB) medium.[24] If necessary, media were supplemented with ampicillin (Ap; 100 μg/mL), tetracycline (Tc; 15 μg/mL), erythromycin (Em; 5 μg/mL), spectinomycin (Sp; 100 μg/mL), or kanamycin (Km; 10 μg/mL). When the *B. subtilis* culture reached an OD_{600} of 0.6, 0.5% xylose was added to induce protein expression for 24 h at 37 °C.

Construction of Recombinant *B. subtilis* 168. The nucleotide sequence encoding the twin-arginine signal peptide of *B. subtilis* YwbN was amplified from *B. subtilis* 168 chromosomal DNA[25] using primers P1 and P2, digested with *Eco*RI/*Pst*I and ligated into *Eco*RI/*Pst*I digested pUC18 to generate pUY18. The *mpd* gene was amplified from *Stenotrophomonas* sp. YC-1 chromosomal DNA[9] using primers P3 and P4, digested with *Pst*I/*Hin*dIII, and ligated into *Pst*I/*Hin*dIII-digested pUY18 to generate pUYM18. The *ywbN–mpd* fusion gene was amplified from pUYM18 using primers P5 and P6, digested with *Kpn*I/*Sph*I, and subcloned into *Kpn*I/*Sph*I-digested pWH1520,[26] an *E. coli–B. subtilis* shuttle vector, to create pWYM20. All plasmid constructions were verified by DNA sequence analysis. Transformation of plasmid into *B. subtilis* 168 was carried out according to the method by Sadaie and Kada.[27]

Western Blot Analysis. Cells were resuspended in lysis buffer with 5 mg/mL lysozyme, incubated at 37 °C for 30 min, and disrupted by sonication. Extracellular proteins were precipitated by adding 10% trichloroacetic acid for 12 h at 4 °C. Samples of total cell protein and extracellular protein were analyzed on 12% sodium dodecyl sulfate–polyacrylamide gel electrophoresis (SDS–PAGE)[24] and electrophoretically transferred onto a nitrocellulose membrane with a tank transfer system. After blocking non-specific binding sites with 3% bovine serum albumin (BSA) in TBST solution (20 mM Tris–HCl at pH 7.5, 150 mM NaCl, and 0.05% Tween-20), the membrane was incubated with rabbit anti-MPH serum at a 1:1000 dilution at 30 °C for 2 h and washed with TBST. Subsequently, the membrane was allowed to react with alkaline phosphatase-conjugated goat anti-rabbit IgG antibody (Promega) at a 1:2000 dilution at 30 °C for 1 h. The membrane was then stained with NBT/BCIP (Novagen) for visualizing antigen–antibody conjugates. The rabbit polyclonal antiserum was raised against the purified His_6-tagged MPH as described by Yang et al.[23]

MPH Assays. MPH activity was measured with MP as the substrate by monitoring an increase in absorbance at 405 nm (ε_{405} = 17 700 M^{-1} cm^{-1} for *p*-nitrophenol) at 30 °C.[28] For each assay, 100 μL of concentrated supernatant and 5 μL of 10 mg/mL MP (methanol stock solution) were added to 895 μL of 100 mM phosphate buffer (pH 7.4). One unit of activity was defined as the formation of 1 μmol of *p*-nitrophenol per minute.

Purification of His_6-Tagged MPH. For purification of the recombinant MPH from the culture supernatant of *B. subtilis* 168 carrying pWYM20, 5 mL of preculture was inoculated into 1 L of LB medium and grown to an OD_{600} of 0.6 at 37 °C. Subsequently, 0.5% xylose was added to induce protein expression at 37 °C for 24 h. The culture supernatant was concentrated 10-fold by ultrafiltration and dialyzed overnight against 20 mM *N*-2-hydroxyethylpiperazine-*N*′-2-ethanesulfonic acid (HEPES) buffer (pH 7.5). Recombinant His_6-tagged MPH was purified using nickel–nitrilotriacetic acid (Ni–NTA) affinity chromatography, following the procedure described by Fu et al.[28] In brief, the concentrated fraction was loaded onto a Ni–NTA column (Novagen). His_6-tagged MPH tightly bound to the Ni–NTA

matrix and fusion proteins were eluted with elution buffer (20 mM Tris-HCl, 0.5 mM NaCl, and 300 mM imidazole at pH 7.9). The purity of purified MPH was examined by 12% SDS–PAGE. Protein concentrations were determined by the Bradford method.[24] The N-terminal sequence of purified MPH was determined by high-performance liquid chromatography–electrospray ionization mass spectrometry (HPLC–EIMS).

Pesticide Degradation Experiments. *B. subtilis* 168 cells harboring pWYM20 or pWTM20 were grown to an OD_{600} of 0.6 and then induced with 0.5% xylose for 24 h at 37 °C. Cells and supernatant were separated by centrifugation. Subsequently, 0.4 mM MP was added to the supernatant. Samples were incubated for 2 h at 30 °C and 150 rpm on a shaker. Then, residual pesticides were extracted twice with ethyl acetate, and the amounts of pesticides were determined by gas chromatography (GC). The detection conditions for GC were the same as those described by Yang et al.[23] Degradation of pesticide residues on cabbage was also performed as described by Yang et al.[23] using the supernatant of *B. subtilis* 168 cultures expressing YwbN–MPH.

RESULTS AND DISCUSSION

Tat-Dependent Secretion of MPH Directed by the YwbN Signal Peptide. Protein substrates of the Tat pathway are folded prior to translocation and are targeted to the Tat machinery by cleavable N-terminal signal peptides containing an almost invariant pair of arginine residues.[11,12] In a previous work, MPH was secreted by the *B. subtilis* Tat pathway into the growth medium when fused to the twin-arginine signal peptide of TorA from *E. coli*.[23] In this study, to enhance secretion of MPH to extracellular milieu, we used the twin-arginine signal peptide of YwbN from *B. subtilis*. A secretory expression vector pWYM20 coding for YwbN–MPH fusion protein was constructed and transformed into *B. subtilis* 168. A typical cleavage site (ASA-A) for signal peptidase I[29] was designed for producing mature MPH with an authentic N-terminal sequence of AAPQVR by cleaving the YwbN signal peptide.

To evaluate the efficiency of *B. subtilis* as the host strain for the Tat-dependent secretion of MPH, the distribution of MPH in cell lysate and culture supernatant was determined by western blotting with MPH antiserum. After 24 h of induction, the *B. subtilis* culture was fractionated into cells and culture supernatant and then these fractions were probed with anti-MPH serum. As shown in Figure 1, two specific bands corresponding to the unprocessed YwbN–MPH precursor (37 kDa) and the mature-sized MPH (32 kDa) were detected in the cell lysate of *B. subtilis* 168. As expected, mature-sized MPH was found predominantly in the culture supernatant of *B. subtilis* 168.

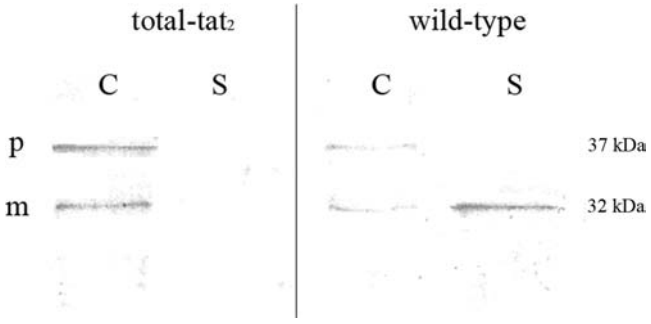

Figure 1. Secretion of MPH by the Tat pathway in *B. subtilis*. The culture of *B. subtilis* 168/pWYM20 or 168 total-tat_2/pWYM20 was fractionated into cells (C) and supernatant (S). The samples were used for SDS–PAGE and western blot using anti-MPH serum. p, YwbN–MPH precursor; m, mature-sized MPH. The protein sample loaded onto each lane in SDS–PAGE was 10 μg.

To determine whether the translocation of MPH was mediated specifically by the Tat pathway of *B. subtilis*, the secretory expression vector pWYM20 was also transformed into 168 total-tat_2 mutant strain, in which all *tat* genes encoding Tat translocases have been inactivated by insertional mutagenesis.[21] In contrast to wild-type strain, no secreted MPH was found in the culture supernatant of total-tat_2 mutant (Figure 1). Interestingly, mature-sized MPH was also found in the cellular fraction of the 168 total-tat_2 mutant, possibly resulting from proteolysis of YwbN–MPH. The degradation of TorA or YwbN chimeric proteins has previously been reported,[11,23] suggesting that the Tat signal peptides may be easily accessible to proteases. As shown in Figure 2, extracellular MPH activity

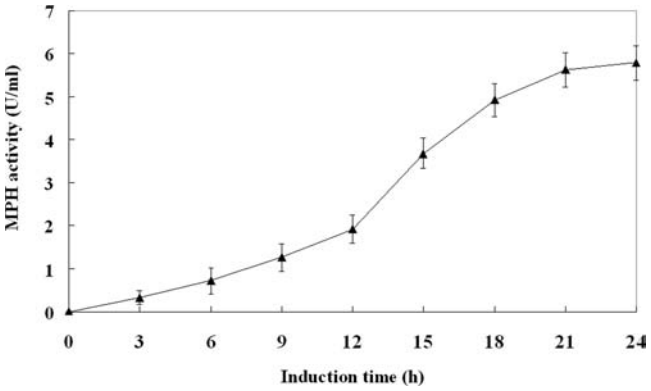

Figure 2. Extracellular MPH activity in *B. subtilis* 168 cultures capable of secreting MPH with the *B. subtilis* YwbN signal peptide. Cells were cultured in LB medium containing 15 μg/mL tetracycline at 37 °C and 250 rpm and then induced at OD_{600} = 0.6 by adding 0.5% xylose. The data are the mean ± standard deviation of three replicates.

of *B. subtilis* 168 cultures expressing YwbN–MPH increased gradually after induction and accumulated to a maximum level (5.78 units/mL) at 24 h. In contrast, no MPH activity was detected in the culture supernatant of 168 total-tat_2 mutant strain expressing YwbN–MPH fusion protein. These results clearly showed that MPH could be secreted by *B. subtilis* 168 in a strictly Tat-dependent manner.

Secretion of MPH with the YwbN Signal Peptide Is TatAyCy-Dependent. The *B. subtilis* Tat machinery comprises two active Tat translocation complexes with distinct substrate specificities: PhoD is secreted by the TatAdCd complex, whereas YwbN is secreted by the TatAyCy complex.[21] To examine whether the MPH secretion directed by the YwbN signal peptide would also be TatAyCy-dependent, we expressed the YwbN–MPH fusion protein in a *tatAyCy* or *tatAdCd* mutant strain. Secretion of MPH by these *tat* mutant strains was verified by western blot with MPH antiserum. MPH was detected in the culture medium of the *tatAdCd* mutant producing YwbN–MPH, which indicated that the *tatAdCd* mutant was still capable of secreting MPH, relying on using the other TatAyCy system. In contrast, MPH was not secreted into the culture medium of the *tatAyCy* mutant expressing YwbN–MPH (data not shown).

To further demonstrate whether the MPH secretion was specifically mediated by the TatAyCy system, extracellular MPH activity was also detected with these *tat* mutant strains. As a result, no MPH activity was detected in the culture

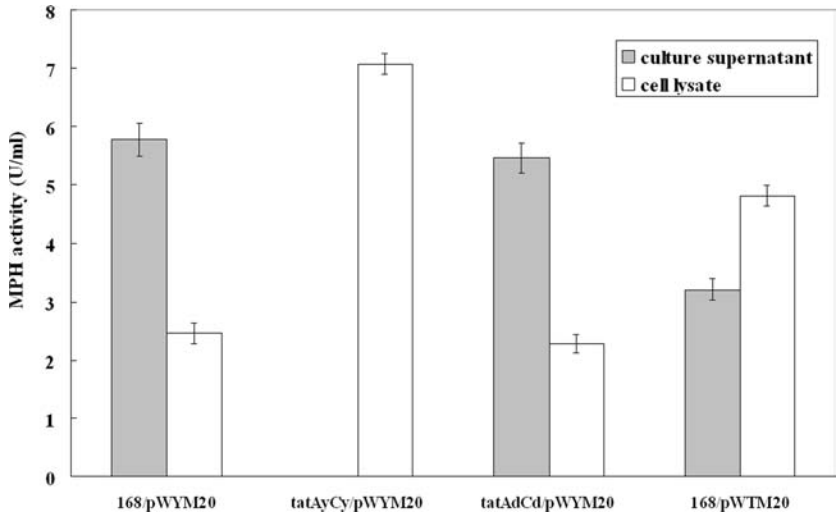

Figure 3. Specific MPH activities of the culture supernatant and total cell lysate derived from *B. subtilis* 168 and its *tat* mutant strains. 168/pWYM20, *B. subtilis* 168 expressing YwbN−MPH; *tatAyCy*/pWYM20, *tat* mutant strain of *B. subtilis* 168 lacking functional TatAyCy translocase; *tatAdCd*/pWYM20, *tat* mutant strain of *B. subtilis* 168 lacking functional TatAdCd translocase; and 168/pWTM20, *B. subtilis* 168 expressing TorA−MPH. Cells carrying pWYM20 or pWTM20 were incubated at 37 °C for 24 h after induction with 0.5% xylose. The data are the mean ± standard deviation of three replicates.

Table 2. Purification of Recombinant His_6-Tagged MPH from 1 L of Culture Supernatant by Metal Affinity Chromatography

purification step	total protein (mg)	total activity (units)	specific activity (units/mg of protein)	yield (%)	fold
culture supernatant	426	5260	12	100	1
Ni−NTA column	13	4576	352	87	29

supernatant of the *tatAyCy* mutant expressing YwbN−MPH. In contrast, MPH activity (5.46 units/mL) was found in the culture supernatant of the *tatAdCd* mutant expressing YwbN−MPH (Figure 3). These results indicated that the YwbN signal peptide directed MPH secretion in a strictly TatAyCy-dependent manner.

Efficiency of Tat-Dependent Secretion of MPH in *B. subtilis* 168. The majority of total MPH activity (70%) was found in the supernatant of *B. subtilis* 168 cultures expressing YwbN−MPH. The cell lysate contained lower activity (30% of total), and the data are consistent with the MPH immunoblots. Extracellular MPH activity of *B. subtilis* cultures expressing YwbN−MPH was 1.8-fold higher than that of *B. subtilis* cultures expressing TorA−MPH (Figure 3). Enhanced secretion of MPH activity was achieved with the YwbN signal peptide, indicating that the selection of Tat signal peptides is crucial to improve Tat-dependent protein secretion efficiency.

To determine the amount of MPH that was secreted by *B. subtilis* 168, the recombinant MPH was purified from 1 L of culture supernatant by metal affinity chromatography using a Ni−NTA column following the procedures described in the Materials and Methods. His_6-tagged MPH tightly bound to the Ni−NTA matrix, and fusion proteins were eluted with elution buffer containing 300 mM imidazole, thereby allowing for their one-step purification to electrophoretic homogeneity. The purified His_6-tagged MPH gave a single band appearing at the position of 32 kDa in SDS−PAGE (data not shown), which is in good agreement with the molecular mass estimated from the deduced amino acid sequence of the fusion protein. From 1 L of culture supernatant, we routinely obtained 13 mg of purified MPH with a purification of 29-fold, 87% final yield, and a specific activity of 352 units/mg. The data on the purification are summarized in Table 2. The N-terminal sequence of the purified MPH was determined by HPLC−EIMS as AAPQVR, demonstrating that the YwbN signal peptide had been processed correctly.

Degradation of Methyl Parathion by Recombinant *B. subtilis*. In this study, *B. subtilis* 168 cultures capable of secreting MPH (pWYM20) degraded MP 12-fold faster than *B. subtilis* 168 cultures expressing cytoplasmic MPH (pWM20). In contrast, no MP degradation was observed with *B. subtilis* 168 transformed with the empty vector pWH1520. Extracellular secretion of MPH is advantageous over intracellular production, because it allows MPH to freely bind extracellular substrates. This will greatly improve the application efficiency of the engineered strain to degrade organophosphorus pesticides in farm products and contaminated soil and water.

In this study, the supernatant can be separated from the cells by one-step centrifugation and used as the crude enzyme for the removal of pesticide residues on vegetables. The removal efficiencies for MP and chlorpyrifos on cabbage were 99 and 96%, respectively. Moreover, the supernatant containing secreted MPH was shown to effectively degrade MP (Figure 4). In contrast, the supernatant from *B. subtilis* cultures expressing YwbN−MPH (pWYM20) degraded MP 2-fold faster than the supernatant from *B. subtilis* cultures expressing TorA−MPH (pWTM20), which indicated that the efficiency of MPH secretion had been improved by use of the YwbN signal peptide.

To test whether extracellular secretion of MPH inhibits cell growth, the growth kinetics of cells carrying pWYM20 or pWH1520 were compared. No growth inhibition was observed for cells expressing YwbN−MPH. The two cultures showed the same growth profile and reached the same final cell density after 48 h of incubation. To monitor the stability of MPH activity of the concentrated supernatant, the activity was

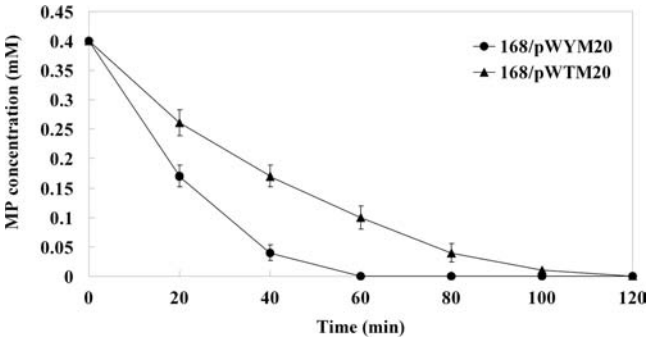

Figure 4. Degradation of MP by the culture supernatant of *B. subtilis* 168 cells capable of secreting MPH with the *B. subtilis* YwbN signal peptide (pWYM20) or *E. coli* TorA signal peptide (pWTM20). Methyl parathion was added at an initial concentration of 0.4 mM. The data are the mean ± standard deviation of three replicates.

determined each day over a 2-week period. MPH activity of the concentrated supernatant remained at essentially the original level over the duration of 2 weeks (Figure 5). The stability of

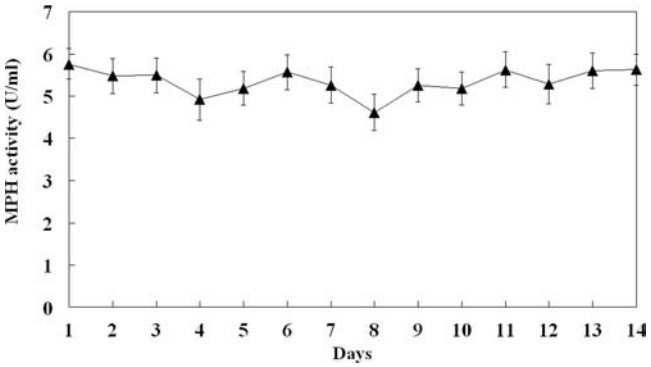

Figure 5. Stability of MPH activity of the culture supernatant of *B. subtilis* 168 cells capable of secreting MPH with the *B. subtilis* YwbN signal peptide (pWYM20) over the duration of 2 weeks. MPH activity was measured with MP as the substrate. The data are the mean ± standard deviation of three replicates.

the MPH activity observed here is in line with the results of previous studies in which MPH was secreted by *B. subtilis* 168 with the TorA signal peptide of *E. coli*.[23]

The suitability and popularity of *B. subtilis* as one of the main hosts for recombinant protein production are due to several reasons: generally recognized as safe as a result of its lack of pathogenicity and the absence of endotoxins, the absence of an outer membrane, easy for genetic manipulation and handling, and capable of large-scale fermentation.[25] These merits make recombinant *B. subtilis* a promising candidate for extracellular production of MPH for practical industrial applications, for example, enzyme-based products.

In previous studies, the YwbN signal peptide directed secretion of the *B. subtilis* subtilisin via the TatAyCy route. In contrast, the YwbN signal peptide directed secretion of the *Bacillus licheniformis* α-amylase and the *E. coli* SufI in a Tat-independent manner.[29] The *E. coli* phytase AppA was shown to export TatAdCd dependently when fused to the twin-arginine signal peptide of PhoD.[30] Tat-dependent secretion of the green fluorescent protein was reported, albeit in an inactive form.[31] Thus far, there are no reports of TatAyCy-dependent export of an active heterologous protein in *B. subtilis*. In this study, active MPH was exported to the extracellular environment via the *B. subtilis* TatAyCy system when fused to the twin-arginine signal peptide of YwbN. Here, we demonstrated for the first time TatAyCy-dependent secretion of an active heterologous protein in *B. subtilis*. In future studies, we will further explore the capability of the *B. subtilis* TatAyCy system for secretion of other heterologous proteins.

AUTHOR INFORMATION

Corresponding Authors

*Telephone/Fax: 86-21-34206723. E-mail: pingxu@sjtu.edu.cn.
*Telephone: 86-22-23507800. Fax: 86-22-66229562. E-mail: zhouqx523@yahoo.com.
*Telephone/Fax: 86-22-23503866. E-mail: yang_chao2008@hotmail.com.

Author Contributions

†Ruihua Liu and Zhenqiang Zuo contributed equally to this work.

Funding

The authors gratefully acknowledge the financial support from the National High Technology Research and Development Program of China ("863" Program, 2013AA06A210), the National Natural Science Foundation of China (31300032), the Open Project Funding of the State Key Laboratory of Microbial Metabolism, Shanghai Jiao Tong University (MMLKF13-06), the Project of Tianjin, China (13JCQNJC09700), and the Open Project Funding of the Key Laboratory of Original Agro-environment Quality of Ministry of Agriculture and Tianjin Key Laboratory of Agro-environment and Safe-product (2013-KF-06).

Notes

The authors declare no competing financial interest.

REFERENCES

(1) Singh, B. K.; Walker, A. Microbial degradation of organophosphorus compounds. *FEMS Microbiol. Rev.* **2006**, *30*, 428−471.
(2) Singh, B. K. Organophosphorus-degrading bacteria: Ecology and industrial applications. *Nat. Rev. Microbiol.* **2009**, *7*, 156−164.
(3) Bai, Y.; Zhou, L.; Wang, J. Organophosphorus pesticide residues in market foods in Shaanxi area, China. *Food Chem.* **2006**, *98*, 240−242.
(4) Salas, J.; Noa, M.; Perez, N.; Gutierrez, R.; Zazueta, H.; Osuna, I. Organophosphorus pesticide residues in Mexican commercial pasteurized milk. *J. Agric. Food Chem.* **2003**, *51*, 4468−4471.
(5) Uchimiya, M.; Wartelle, L.; Boddu, V. Sorption of triazine and organophosphorus pesticides on soil and biochar. *J. Agric. Food Chem.* **2012**, *60*, 2989−2997.
(6) Mulbry, W. W.; Karns, J. S. Parathion hydrolase specified by the *Flavobacterium opd* gene: Relationship between the gene and protein. *J. Bacteriol.* **1989**, *171*, 6740−6746.
(7) Serdar, C. M.; Gibson, D. T. Enzymatic hydrolysis of organophosphates: Cloning and expression of a parathion hydrolase gene from *Pseudomonas diminuta*. *Biotechnology* **1985**, *3*, 567−571.
(8) Cui, Z.; Li, S.; Fu, G. Isolation of methyl parathion-degrading strain M6 and cloning of the methyl parathion hydrolase gene. *Appl. Environ. Microbiol.* **2001**, *67*, 4922−4925.
(9) Yang, C.; Liu, N.; Guo, X.; Qiao, C. Cloning of *mpd* gene from a chlorpyrifos-degrading bacterium and use of this strain in bioremediation of contaminated soil. *FEMS Microbiol. Lett.* **2006**, *265*, 118−125.
(10) Richins, R. D.; Kaneva, I.; Mulchandani, A.; Chen, W. Biodegradation of organophosphorus pesticides by surface-expressed organophosphorus hydrolase. *Nat. Biotechnol.* **1997**, *15*, 984−987.
(11) Thomas, J. D.; Daniel, R. A.; Errington, J.; Robinson, C. Export of active green fluorescent protein to the periplasm by the twin-

arginine translocase (Tat) pathway in *Escherichia coli*. *Mol. Microbiol.* **2001**, *39*, 47−53.
(12) DeLisa, M. P.; Tullman, D.; Georgiou, G. Folding quality control in the export of proteins by the bacterial twin-arginine translocation pathway. *Proc. Natl. Acad. Sci. U. S. A.* **2003**, *100*, 6115−6120.
(13) Palmer, T.; Berks, B. C. The twin-arginine translocation (Tat) protein export pathway. *Nat. Rev. Microbiol.* **2012**, *10*, 483−496.
(14) Berks, B. C. A common export pathway for proteins binding complex redox cofactors? *Mol. Microbiol.* **1996**, *22*, 393−404.
(15) Bogsch, E. G.; Sargent, F.; Stanley, N. R.; Berks, B. C.; Robinson, C.; Palmer, T. An essential component of a novel bacterial protein export system with homologues in plastids and mitochondria. *J. Biol. Chem.* **1998**, *273*, 18003−18006.
(16) Sargent, F.; Bogsch, E. G.; Stanley, N. R.; Wexler, M.; Robinson, C.; Berks, B. C.; Palmer, T. Overlapping functions of components of a bacterial Sec-independent protein export pathway. *EMBO J.* **1998**, *17*, 3640−3650.
(17) Sargent, F.; Stanley, N. R.; Berks, B. C.; Palmer, T. Sec-independent protein translocation in *Escherichia coli*: A distinct and pivotal role for the TatB protein. *J. Biol. Chem.* **1999**, *274*, 36073−36082.
(18) Alami, M.; Lüke, I.; Deitermann, S.; Eisner, G.; Koch, H. G.; Brunner, J.; Müller, M. Differential interactions between a twin-arginine signal peptide and its translocase in *Escherichia coli*. *Mol. Cell* **2003**, *12*, 937−946.
(19) Gohlke, U.; Pullan, L.; McDevitt, C. A.; Porcelli, I.; de Leeuw, E.; Palmer, T.; Saibil, H. R.; Berks, B. C. The TatA component of the twin-arginine protein transport system forms channel complexes of variable diameter. *Proc. Natl. Acad. Sci. U. S. A.* **2005**, *102*, 10482−10486.
(20) Jongbloed, J. D. H.; Martin, U.; Antelmann, H.; Hecker, M.; Tjalsma, H.; Venema, G.; et al. TatC is a specificity determinant for protein secretion via the twin-arginine translocation pathway. *J. Biol. Chem.* **2000**, *275*, 41350−41357.
(21) Jongbloed, J. D.; Grieger, U.; Antelmann, H.; Hecker, M.; Nijland, R.; Bron, S.; van Dijl, J. M. Two minimal Tat translocases in *Bacillus*. *Mol. Microbiol.* **2004**, *54*, 1319−1325.
(22) Barnett, J. P.; Eijlander, R. T.; Kuipers, O. P.; Robinson, C. A minimal Tat system from a Gram-positive organism: A bifunctional TatA subunit participates in discrete TatAC and TatA complexes. *J. Biol. Chem.* **2008**, *283*, 2534−2542.
(23) Yang, C.; Song, C.; Freudl, R.; Mulchandani, A.; Qiao, C. Twin-arginine translocation of methyl parathion hydrolase in *Bacillus subtilis*. *Environ. Sci. Technol.* **2010**, *44*, 7607−7612.
(24) Sambrook, J.; Russel, D. W. *Molecular Cloning: A Laboratory Manual*, 3rd ed.; Cold Spring Harbor Laboratory Press: Cold Spring Harbor, NY, 2001.
(25) Kunst, F.; Ogasawara, N.; Moszer, I.; et al. The complete genome sequence of the Gram-positive bacterium *Bacillus subtilis*. *Nature* **1997**, *390*, 249−256.
(26) Rygus, T.; Hillen, W. Inducible high-level expression of heterologous genes in *Bacillus megaterium* using the regulatory elements of the xylose-utilization operon. *Appl. Microbiol. Biotechnol.* **1991**, *35*, 594−599.
(27) Sadaie, Y.; Kada, T. Formation of competent *Bacillus subtilis* cells. *J. Bacteriol.* **1983**, *153*, 813−821.
(28) Fu, G.; Cui, Z.; Huang, T.; Li, S. Expression, purification, and characterization of a novel methyl parathion hydrolase. *Protein Expression Purif.* **2004**, *36*, 170−176.
(29) Kolkman, M. A. B.; van der Ploeg, R.; Bertels, M.; van Dijk, M.; van der Laan, J.; van Dijl, J. M.; Ferrari, E. The twin-arginine signal peptide of *Bacillus subtilis* YwbN can direct either Tat- or Sec-dependent secretion of different cargo proteins: Secretion of active subtilisin via the *B. subtilis* Tat pathway. *Appl. Environ. Microbiol.* **2008**, *74*, 7507−7513.
(30) Gerlach, R.; Pop, O.; Muller, J. P. Tat dependent export of *E. coli* phytase AppA by using the PhoD-specific transport system of *Bacillus subtilis*. *J. Basic Microbiol.* **2004**, *44*, 351−359.
(31) Meissner, D.; Vollstedt, A.; van Dijl, J. M.; Freudl, R. Comparative analysis of twin-arginine (Tat)-dependent protein secretion of a heterologous model protein (GFP) in three different Gram-positive bacteria. *Appl. Microbiol. Biotechnol.* **2007**, *76*, 633−642.

investigate the effects of silica nanoparticles prepared using the sol−gel process (nanosilica sol) on the activity and thermostability of the β-CGTase from *B. circulans* STB01 and the mechanisms by which this unique additive might activate and/or stabilize the enzyme. Silica nanoparticles had small size, high surface energy, and unsaturated chemical bonds on the surface,[17] so they showed not only flexibility like organic materials but also thermal stability, chemical stability, and high strength like inorganic materials.[18] Nanosilica sols have been available for some time,[19,20] but the ability of unmodified silica nanoparticles to stabilize proteins has not, to our knowledge, been investigated. The data presented here provide an effective approach for improving the thermostability of CGTases, or related enzymes, and give a deeper understanding of the mechanism by which PEG molecules and silica nanoparticles enhance the thermostability of proteins.

MATERIALS AND METHODS

Materials. The *cgt* gene encoding wild-type β-CGTase was from *B. circulans* STB01, and the β-CGTase was produced with *Bacillus subtilis* WB600 harboring plasmid *cgt*/pST.

Nanosilica sol (Bindzil 2034DI, particle diameter approximately 20 nm, pH 4.2, 33 wt % solid content) was purchased from Eka Chemicals Co. (Sweden).

Production and Purification of β-CGTase. A single colony of *B. subtilis* WB600 harboring plasmid *cgt*/pST was inoculated into 50 mL of LB medium containing kanamycin (5 μg/mL) and gibberellin (5 μg/mL) and grown at 37 °C overnight. The overnight culture (2 mL) was then diluted into 50 mL of terrific broth with kanamycin (5 μg/mL) and gibberellin (10 μg/mL) and incubated on a rotary shaker (200 rpm) at 37 °C for 48 h. The CGTase present in the supernatant was purified as previously described.[16] The purified enzymes were aliquoted and stored at −80 °C.

Protein Concentration Determination. The protein concentration was quantified using the Bio-Rad protein assay reagent kit, which employs the Bradford method.[21] Bovine serum albumin was used as the standard.

β-CGTase Assay. Enzyme assays was performed by incubating 0.1 mL of appropriately diluted purified enzyme with 0.9 mL of 1% (w/v) maltodextrin (DE = 5, Roquette Freres) in 10 mM phosphate buffer (pH 6.5) at 50 °C for 10 min.

The β-cyclization activity was determined by using the phenolphthalein method.[22] Corresponding samples containing inactivated enzyme were used as controls. One unit of each activity was defined as the amount of enzyme required to produce 1 μmol of β-cyclodextrin per minute under the assay conditions.

Thermostability Determination. The thermostability of the β-CGTase was determined by incubating the purified enzyme, at a concentration of approximately 3.2×10^{-8} M, in 10 mM phosphate buffer (pH 6.5) at 60 °C. Samples were taken at several time intervals, and the residual β-cyclization activity was determined.

Kinetic Parameters. To determine the kinetic parameters (K_m, V_{max}, and K_{cat}/K_m), the purified enzymes were assayed at substrate (maltodextrin, DE = 5) concentrations ranging from 0.1 to 10 mg/mL under standard assay conditions. The enzymes were prepared at a concentration of 1.1×10^{-8} M in 10 mM phosphate buffer (pH 6.5). Kinetic parameters (K_m and V_{max}) were determined by the Michaelis−Menten and Hanes−Woof plots. The specificity constants, K_{cat}/K_m, were calculated to determine the substrate specificity of each enzyme.

Surface Hydrophobicity Analysis. Surface hydrophobicity (S_o) of the enzymes were measured using 1-anilino-8-naphthalenesulfonate (ANS) as the fluorescence probe.[23,24] Protein dispersions were diluted (0.02, 0.04, 0.06, 0.08, and 0.1 mg/mL) in 10 mM phosphate buffer solution (pH 6.5), and then aliquots (10 μL) of ANS (8.0 mM in the same buffer) were added to 2 mL of each sample. Fluorescence intensity (FI) was measured using an F-7000 fluorescence spectrometer (Hitachi, Ltd., Tokyo, Japan) with an excitation wavelength of 390 nm and an emission wavelength of 470 nm. S_o was calculated by linear regression analysis using the initial slope of the FI versus protein concentration plot. Measurements were performed in triplicate.

Atomic Force Microscopy (AFM) Analysis. The β-CGTase samples (50 μL; 3.2×10^{-8} M) in the presence or absence of additives were deposited onto freshly cleaved mica coverslips (Goodfellow, Cambridge, UK). After 10 min, the samples were washed with water and air-dried. Imaging was performed at room temperature using a scanning probe microscope (Dimension ICON, Bruker, Germany), in tapping mode with a drive frequency of ∼300 kHz and a root-mean-square amplitude of 0.7 V. RTESPA probes (Digital Instruments, Santa Barbara CA, USA) were used in the analysis.

Intrinsic Fluorescence Analysis. Intrinsic fluorescence spectra of β-CGTase samples (0.1 mg/mL), in the presence or absence of additives, were measured in 10 mM phosphate buffer (pH 6.5) at room temperature with a fluorescence spectrophotometer (F-7000; Hitachi, Japan). The emission spectra from 300 to 400 nm were recorded at an excitation wavelength of 295 nm and a scanning speed of 1200 nm/min. The excitation and emission slit widths were 2.5 nm. All spectra were performed in triplicate and corrected for the corresponding protein-free sample.

Far-UV Circular Dichroism (CD) Analysis. The CD spectra (190−250 nm) were determined on a MOS-450 CD spectropolarimeter (Biologic, Claix, Charente, France) with a 1 mm path length cell at room temperature. The final spectra were the average of four scans with a bandwidth of 0.1 nm, a step resolution of 0.1 nm, and a scan rate of 1 nm/s. The CD spectra of β-CGTase (0.1 mg/mL) with or without additives were recorded in 10 mM phosphate buffer (pH 6.5); blank spectra of protein-free buffer solutions were subtracted to correct for background effects. The CD data were expressed in terms of mean residue ellipticity, $[\theta]$, in degree·cm^2·dmol^{-1}. Analysis of the protein secondary structure was performed using Dichroweb.[25]

Statistical Analysis. Experimental results are reported as the average of triplicate measurements. Statistical analyses were carried out using the statistical package from SPSS Inc., Chicago, IL, USA. Significant differences ($p < 0.05$) between means were identified by one-way analysis of variance (ANOVA) and the Student−Newman−Keuls (SNK) procedure.

RESULTS

PEG 1000 and Nanosilica Sol Activate the Cyclization Activity of β-CGTase. The effects of the addition of PEG 1000 and/or nanosilica sol on the β-cyclodextrin formation activity of the β-CGTase *B. circulans* STB01 at 50 °C are presented in Table 1. The addition of 0.05% (w/v) nanosilica sol resulted in a modest enhancement of the formation of β-cyclodextrin. Addition of 10% (w/v) PEG 1000 produced a similar enhancement. Titration of nanosilica sol in reaction mixtures also containing 10% PEG 1000 increased the enhancement of β-cyclodextrin formation, with 0.02, 0.05, or 0.10% nanosilica sol producing statistically significant increases.

Table 1. Activation of β-CGTase by PEG 1000 and Nanosilica Sol

additive	relative activity[a] (%)
10% (w/v) PEG 1000	109.8 ± 1.2ab
0.05% (w/v) nanosilica sol	106.7 ± 1.6a
10% (w/v) PEG 1000−0.01% (w/v) nanosilica sol	112.4 ± 2.2bc
10% (w/v) PEG 1000−0.02% (w/v) nanosilica sol	115.0 ± 2.8cd
10% (w/v) PEG 1000−0.05% (w/v) nanosilica sol	117.2 ± 1.4d
10% (w/v) PEG 1000−0.1% (w/v) nanosilica sol	115.0 ± 0.9cd

[a]Values are the means ± SD ($n = 3$), given as percent of activity relative to the activity of the control that had no added additives. Means with different letters within the same row are significantly different ($p < 0.05$).

dx.doi.org/10.1021/jf500322b | J. Agric. Food Chem. 2014, 62, 2919−2924

Table 2. Kinetic Parameters of β-CGTases with PEG 1000 and/or Nanosilica Sol Added[a]

additive[b]	K_m (mg/mL)	V_{max} [μmol/(min·mL)]	K_{cat} ($\times 10^2$ s^{-1})	K_{cat}/K_m [$\times 10^2$ mL/(mg·s)]
none	3.42 ± 0.62c	0.54 ± 0.08b	8.18 ± 1.21b	2.39 ± 0.08a
PEG	1.43 ± 0.18a	0.35 ± 0.05a	5.30 ± 0.76a	3.71 ± 0.06c
NSS	2.11 ± 0.15b	0.43 ± 0.04a	6.52 ± 0.60a	3.09 ± 0.07b
PEG + NSS	1.29 ± 0.11a	0.32 ± 0.03a	4.85 ± 0.45a	3.76 ± 0.03c

[a]Values are the means ± SD (n = 3). Means with different letters within the same column are significantly different ($p < 0.05$). [b]PEG, 10% (w/v) PEG 1000; NSS, 0.05% (w/v) nanosilica sol.

The greatest increase in β-cyclodextrin formation, 17.2%, was achieved by a combination of 10% PEG 1000 with 0.05% nanosilica sol. To investigate the underlying mechanism of this enhancement, the kinetics of the cyclization reaction were investigated. The results are presented in Table 2. Addition of either PEG 1000 or nanosilica sol, alone, significantly increases the K_{cat}/K_m value, with PEG 1000 increasing the K_{cat}/K_m value significantly more than does nanosilica sol. The primary contributor to this increase in efficiency is a decrease in apparent K_m, because both additives decrease K_{cat} somewhat. The simultaneous addition of 10% PEG 1000 and 0.05% nanosilica sol produced the greatest increase in the mean value of K_{cat}/K_m, although this increase was not significantly different from that observed with 10% PEG 1000 alone. This increase in efficiency was due to a decrease in the apparent K_m, because the apparent K_{cat} actually decreased by approximately 40%.

Mixtures of PEG 1000 with Nanosilica Sol Increase β-CGTase Thermostability. The effects of the addition of 10% PEG 1000 and/or nanosilica sol on the thermostability of β-CGTase at 60 °C are shown in Figure 1. Addition of 10% PEG 1000 alone significantly enhanced the thermostability of the β-CGTase, increasing the half-life approximately 6-fold at 60 °C. Addition of 0.05% nanosilica sol alone, in contrast, had essentially no effect on the thermostability of β-CGTase. However, simultaneous addition of both 10% PEG 1000 and 0.01−0.05% nanosilica sol enhanced the thermostability of β-CGTase to a greater extent than the addition of either substance alone. The enhancement increased gradually with increasing concentration of nanosilica sol. However, addition of 0.1% nanosilica sol decreased the thermostability rapidly to the level a little lower than that with 10% PEG 1000 added individually. At the point of greatest stabilization (10% PEG 100 with 0.05% nanosilica sol) the β-cyclodextrin-forming activity remaining after incubation at 60 °C for 60 min was 61.3% of that possessed by a mixture of β-CGTase with the same additives that had not undergone heating.

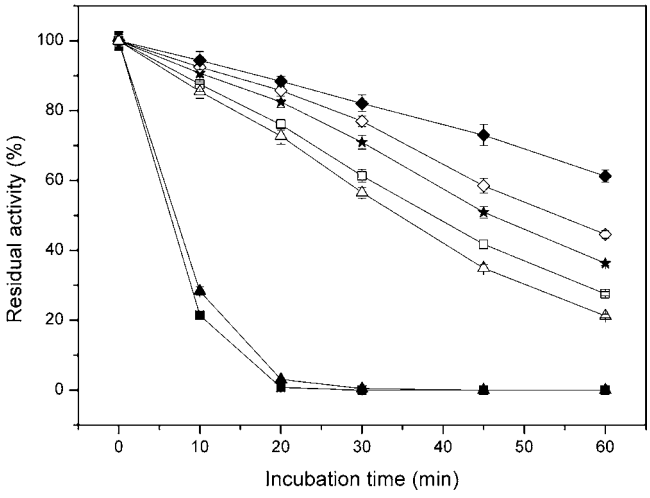

Figure 1. Effects of PEG 1000 and nanosilica sol on the thermostability of wild-type β-CGTase. β-CGTase without additives was incubated at 60 °C for up to 60 min with (■) no additives, (□) 10% (w/v) PEG 1000, (▲) 0.05% (w/v) nanosilica sol, (★) 10% (w/v) PEG 1000−0.01% (w/v) nanosilica sol, (◇) 10% (w/v) PEG 1000−0.02% (w/v) nanosilica sol, (◆) 10% (w/v) PEG 1000−0.05% (w/v) nanosilica sol, or (△) 10% (w/v) PEG 1000−0.1% (w/v) nanosilica sol. The activity before incubation was set as 100%. Each value represents the mean of three independent measurements, and the deviation from the mean is <5%.

Surface Hydrophobicity Analysis. A fluorescence method, using ANS as the probe, was used to determine the surface hydrophobicity (S_o) of β-CGTase samples after incubation at 60 °C for 20 min. The results are presented in Table 3. Incubation of β-CGTase at 60 °C for 20 min increased its S_o significantly by nearly 8.8-fold. The addition of 10% PEG 1000, either alone or together with nanosilica sol, further enhanced the S_o of the enzyme. Interestingly, the addition of 0.05% nanosilica sol alone reduced the S_o of the enzyme by nearly 40%.

Table 3. Surface Hydrophobicity (S_o) and Estimated Secondary Structural Content of β-CGTase before and after Incubation at 60 °C for 20 min

sample	S_o value[a]	α-helix (%)	β-sheet (%)	turn (%)	random coil (%)
control[b]	2.5 ± 0.1a	27.0	21.7	20.0	31.3
no additive[b,c]	24.4 ± 0.8c	20.0	7.8	9.8	62.4
PEG[b,c]	30.9 ± 0.9d	32.2	19.5	20.3	28.0
NSS[b,c]	15.4 ± 0.7b	20.8	24.4	21.2	33.6
PEG + NSS[b,c]	32.1 ± 0.7d	36.9	17.3	18.9	27.2

[a]Values are the means ± SD (n = 3). Means with different letters within the same column are significantly different ($p < 0.05$). [b]Control, β-CGTase before heating; No additive, β-CGTase without additives; PEG, β-CGTase with 10% (w/v) PEG 1000; NSS, β-CGTase with 0.05% (w/v) nanosilica sol; PEG + NSS, β-CGTase with 10% (w/v) PEG 1000 and 0.05% (w/v) nanosilica sol. [c]Samples after heating at 60 °C for 20 min.

Aggregation State of β-CGTase Proteins under Heat Treatment Revealed by Atomic Force Microscopy. AFM was used to determine the surface morphology and aggregation state of the enzyme under heat treatment. The results are presented in Figure 2. Before heat treatment, the β-CGTase was seen as small dots or assemblies (Figure 2a,A). After being incubated at 60 °C for 20 min, the β-CGTase was seen in dramatically larger circular assemblies (Figure 2b,B). Addition of 10% PEG 1000 alone appeared to form a gel around the aggregated β-CGTase protein (Figure 2c,C), whereas addition of nanosilica sol formed a crust-like matrix that makes the protein more difficult to see (Figure 2d,D). Adding both 10% PEG and 0.05% nanosilica sol formed a surface that was much

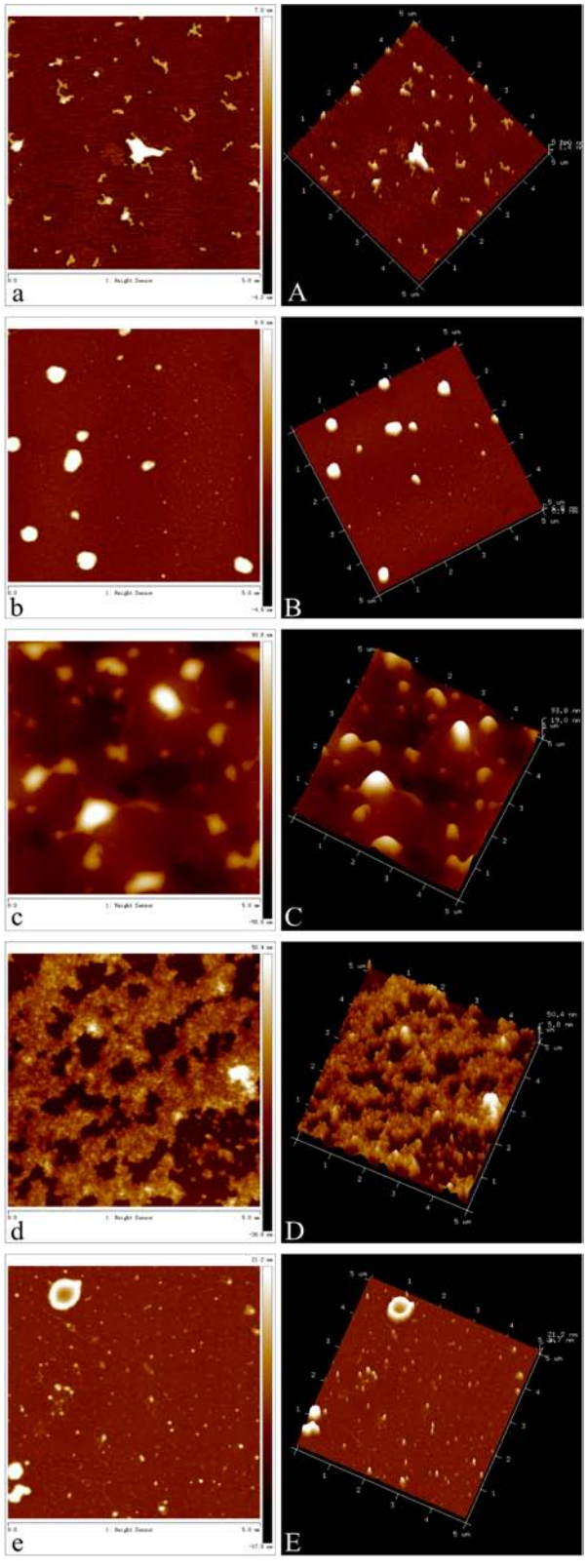

Figure 2. AFM images obtained using tapping mode: (a) β-CGTase without additives prior to heat treatment; (b) β-CGTase without additives incubated at 60 °C for 20 min; (c) as in (b), but with addition of 10% (w/v) PEG 1000; (d) as in (b), but with addition of 0.05% (w/v) nanosilica sol; (e) as in (b), but with addition of both 10% (w/v) PEG 1000 and 0.05% (w/v) nanosilica sol. All scan sizes: μm × μm. (A), (B), (C), (D), and (E) are 3D images corresponding to (a), (b), (c), (d), and (e), respectively.

more uniform than that produced by either PEG 1000 or nanosilica sol alone (Figure 2e,E), featuring fewer large aggregates than seen without the addition of additives (Figure 2b,B).

Intrinsic Protein Fluorescence Spectra. The β-CGTase from *B. circulans* contains 13 tryptophan residues per chain, 3 of which (W75, W101, and W258) are within approximately 15 Å of the active site tyrosine.[26] Variations in the β-CGTase microenvironment caused by the addition of PEG 1000 and/or nanosilica sol were investigated using the intrinsic fluorescence of the β-CGTase protein. The results are presented in Figure 3a. The fluorescence spectrum of β-CGTase without additives,

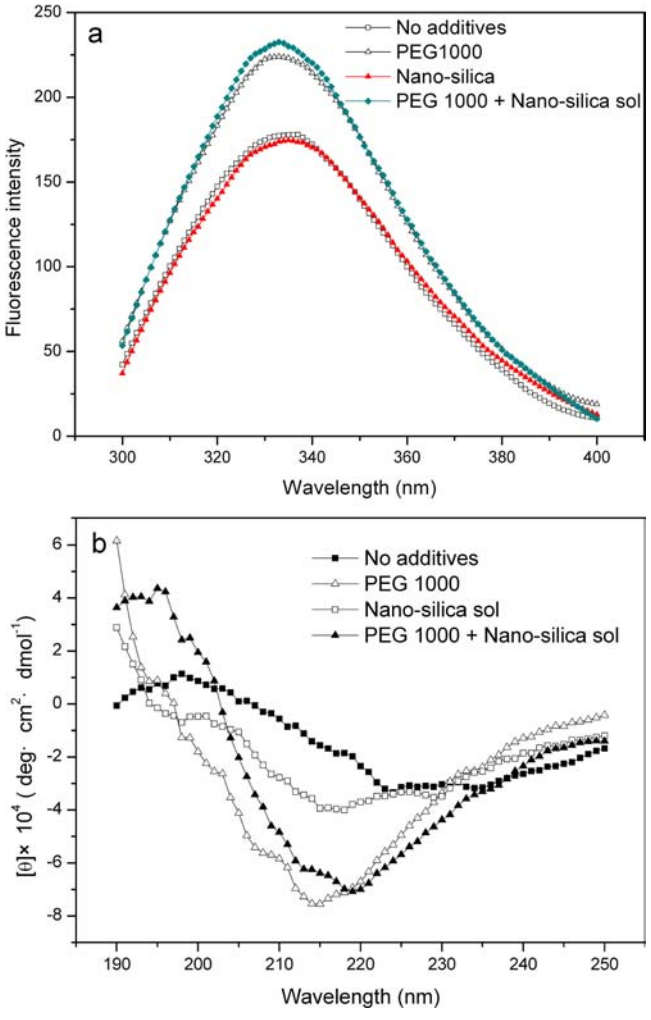

Figure 3. Intrinsic fluorescence spectra (a) and far-UV CD spectra (b) of β-CGTase samples incubated at 60 °C for 20 min in the absence of additives or in the presence of 10% (w/v) PEG 1000, 0.05% (w/v) nanosilica sol, or a combination of 10% (w/v) PEG 1000 and 0.05% (w/v) nanosilica sol.

excited at 295 nm, had a maximum fluorescence emission at 335 nm (data not shown). The fluorescence maximum exhibited a slight red shift, to 337 nm, and the fluorescence intensity decreased substantially after incubation for 20 min at 60 °C. The addition of 10% PEG 1000 to the incubation mixture increased the maximum fluorescence intensity by approximately 26%. In contrast, the addition of 0.05% nanosilica sol decreased the maximum fluorescence intensity slightly and caused a slight blue shift in the fluorescence

dx.doi.org/10.1021/jf500322b | J. Agric. Food Chem. 2014, 62, 2919−2924

maximum, to 335 nm. Addition of both 10% PEG 1000 and 0.05% nanosilica sol enhanced the maximum fluorescence intensity to a greater extent than 10% PEG 1000 alone and caused a more significant blue shift in the fluorescence maximum, to 333 nm.

Circular Dichroism Spectra. CD measurements in the far UV (190−250 nm) were performed to investigate the secondary structure of β-CGTase after incubation at 60 °C for 20 min. The results are presented in Figure 3b. These data, and the web tool Dichroweb, were used to determine the detailed secondary structural specifications of β-CGTase; the results are summarized in Table 3. Before heating, the β-CGTase without additives has relatively balanced content (20−32%) of α-helix, β-sheet, turn, and random coil, whereas additions of 10% PEG 1000 and/or 0.05% nanosilica sol show almost no effect on the secondary structure (data not shown). After heating in the absence of additives, the α-helix, β-sheet, and turn contents decreased by 7.0, 13.9, and 10.2%, respectively, whereas the random coil content increased significantly, by 31.3%. Random coil is the main secondary structural element seen in the heated β-CGTase. Addition of 10% PEG 1000 during the incubation dramatically decreases the amount of random coil and increases the content of α-helix, β-sheet, and turn by 12.2, 11.7, and 10.5%, respectively. Addition of 0.05% nanosilica sol during the incubation also dramatically decreases the content of random coil and increases the content of β-sheet (by 16.6%) and turn (by 11.4%). However, the addition of nanosilica sol has almost no effect upon the content of α-helix, increasing it by a mere 0.8%. Combining 10% PEG 1000 with 0.05% nanosilica sol gives the greatest decrease in random coil content (35.2%) and the greatest increase in the α-helix content (16.9%). The increases in β-sheet and turn content are still substantial, but they are lower than those caused by either 10% PEG 1000 or 0.05% nanosilica sol alone.

DISCUSSION

The aims of this study were to investigate the effect of silica nanoparticles and the combination of silica nanoparticles with PEG 1000 on the activity and thermostability of the β-CGTase from *B. circulans* STB01, as well as to analyze the mechanisms through which the activation or stabilization was achieved. We found that the addition of silica nanoparticles, by themselves, induced a modest increase in the production of β-cyclodextrin by β-CGTase at 60 °C, but a negligible increase in thermostability. However, when these same silica nanoparticles were combined with 10% PEG 1000, they offered a statistically significant increase in both activity and thermostability at 60 °C.

Activation and stabilization of enzymes by the addition of various forms of PEG are not unprecedented. Addition of 10% (w/v) PEG 3000 to the reaction mixture was shown to increase the activity of the β-CGTase from *Bacillus agaradhaerens* LS-3C[27] and the cyclomaltodextrin glycosyltransferase from *Bacillus macerans*.[28] PEGs of various types have been also been found to stabilize a number of enzymes, including α-amylase,[29,30] chymotrypsin,[31] and penicillin G acetylase.[32] On the other hand, the only data available about the activation of enzymes with silica nanoparticles appear to involve the covalent immobilization of enzymes to the silica surface, such as the investigations of Wang et al. with papain.[33] This paper is the first to show that nanosilica sol alone is of little use as an additive but that it augments the activating and stabilizing effects of PEG 1000.

Several different techniques were employed to ascertain the mechanism or mechanisms by which the activation and stabilization were achieved. Evaluation of the kinetic parameters revealed that addition of 10% PEG or the combination of 10% PEG and nanosilica sol decreased the substrate K_m by 58.2 and 62.3%, respectively, while decreasing K_{cat}. This suggests that PEG, or the combination of PEG with nanosilica sol, has an effect upon the interaction of the enzyme with the substrate, rather than increasing the fraction of active enzyme molecules or increasing the rate at which the enzyme molecules perform the required chemistry. The AFM images, which showed that the PEG 1000−nanosilica sol−enzyme mixture combined to form a gel network that was much more uniform than that produced in the absence of either PEG or the nanosilica sol, are consistent with this interpretation. According to the study of Wang et al.,[34] nanosilica particles may interact with the random coils of PEG to form stable PEG−SiO_2 complexes through hydrogen bonding, which may prevent the enzyme from aggregating. In fact, these data suggest that the effect may, at least in part, be a reflection of an interaction of the PEG and nanosilica sol with the substrate. However, when the concentration of nanosilica was increased to 0.1%, combinations of nanosilica sol with 10% PEG 1000 decreased the thermostability rapidly, compared with the addition of 0.05% nanosilica sol−10% PEG 1000. Perhaps excess nanosilica sol might cause more silica nanoparticles to be liberated, which might promote the formation of a crust-like matrix, like that seen in the AFM image containing only nanosilica sol and protein, which can damage the gel formed by the combination of nanosilica sol and PEG with the β-CGTase protein.

The surface hydrophobicity data, intrinsic fluorescence data, and CD spectra are all consistent with the PEG 100−nanosilica sol network having an effect upon the stability of the enzyme. Denaturation of enzymes in aqueous solution occurs through disruption of hydrophobic interactions and hydration of the polypeptide.[35] The surface hydrophobicity data demonstrate that the combination of PEG 1000 with nanosilica sol may expel the water molecules around the enzyme, which may help prevent the heat-induced exposure of hydrophobic amino acids to the solvent. Similarly, the dramatic decrease in fluorescence intensity and red shift of the fluorescence maximum that accompanied heating of β-CGTase to 60 °C, which indicate a shift of its tryptophan residues to a more hydrophilic environment, were prevented by the addition of PEG 1000 or PEG 1000−nanosilica sol. Finally, the CD data generally support the notion that the addition of PEG 1000−nanosilica sol to the mixture preserved secondary structure in the protein.

AUTHOR INFORMATION

Corresponding Authors

*(Z.G.) Phone/fax: 86-510-85329237. E-mail: zhengbiaogu@jiangnan.edu.cn

*(Z.L.) E-mail: zfli@jiangnan.edu.cn.

Funding

Financial support for this work was obtained from the National Natural Science Foundation of China (No. 31101228), the Natural Science Foundation of Jiangsu Province (BK2011152), the Twelfth Five-Year National Key Technology Research and Development Program of the Ministry of Science and Technology of China (No. 2012BAD34B07), the Fok Ying-Tong Education Foundation, China (No. 131069), and the

Priority Academic Program Development of Jiangsu Higher Education Institutions.

Notes

The authors declare no competing financial interest.

REFERENCES

(1) Li, Z. F.; Li, B.; Liu, Z. G.; Wang, M.; Gu, Z. B.; Du, G. C.; Wu, J.; Chen, J. Calcium leads to further increase in glycine-enhanced extracellular secretion of recombinant alpha-cyclodextrin glycosyltransferase in *Escherichia coli*. *J. Agric. Food Chem.* **2009**, *57*, 6231−6237.

(2) Ferrarotti, S. A.; Bolivar, J. M.; Mateo, C.; Wilson, L.; Guisan, J. M.; Fernandez-Lafuente, R. Immobilization and stabilization of a cyclodextrin glycosyltransferase by covalent attachment on highly activated glyoxyl-agarose supports. *Biotechnol. Prog.* **2006**, *22*, 1140−1145.

(3) Li, Z. F.; Wang, M.; Wang, F.; Gu, Z. B.; Du, G. C.; Wu, J.; Chen, J. γ-Cyclodextrin: a review on enzymatic production and applications. *Appl. Microbiol. Biotechnol.* **2007**, *77*, 245−255.

(4) Howard, L. R.; Brownmiller, C.; Prior, R. L.; Mauromoustakos, A. Improved stability of chokeberry juice anthocyanins by β-cyclodextrin addition and refrigeration. *J. Agric. Food Chem.* **2013**, *61*, 693−699.

(5) Becker, P.; Abu-Reesh, I.; Markossian, S.; Antranikian, G.; Markl, H. Determination of the kinetic parameters during continuous cultivation of the lipase-producing thermophile *Bacillus* sp. IHI-91 on olive oil. *Appl. Microbiol. Biotechnol.* **1997**, *48*, 184−190.

(6) Mozhaev, V. V. Mechanism-based strategies for protein thermostabilization. *Trends Biotechnol.* **1993**, *11*, 88−95.

(7) Tonkova, A. Bacterial cyclodextrin glucanotransferase. *Enzyme Microb. Technol.* **1998**, *22*, 678−686.

(8) Leemhuis, H.; Kelly, R. M.; Dijkhuizen, L. Engineering of cyclodextrin glucanotransferases and the impact for biotechnological applications. *Appl. Microbiol. Biotechnol.* **2010**, *85*, 823−835.

(9) Penninga, D.; Strokopytov, B.; Rozeboom, H. J.; Lawson, C. L.; Dijkstra, B. W.; Bergsma, J.; Dijkhuizen, L. Site-directed mutations in tyrosine 195 of cyclodextrin glycosyltransferase from *Bacillus circulans* strain 251 affect activity and product specificity. *Biochemistry* **1995**, *34*, 3368−3376.

(10) Ben Mabrouk, S.; Aghajari, N.; Ben Ali, M.; Ben Messaoud, E.; Juy, M.; Haser, R.; Bejar, S. Enhancement of the thermostability of the maltogenic amylase MAUS149 by Gly312Ala and Lys436Arg substitutions. *Bioresour. Technol.* **2011**, *102*, 1740−1746.

(11) Gribenko, A. V.; Patel, M. M.; Liu, J.; McCallum, S. A.; Wang, C. Y.; Makhatadze, G. I. Rational stabilization of enzymes by computational redesign of surface charge-charge interactions. *Proc. Natl. Acad. Sci. U.S.A.* **2009**, *106*, 2601−2606.

(12) Kusano, M.; Yasukawa, K.; Inouye, K. Effects of the mutational combinations on the activity and stability of thermolysin. *J. Biotechnol.* **2010**, *147*, 7−16.

(13) Chou, H. H.; Chang, S. W.; Lee, G. C.; Chen, Y. S.; Yeh, T. N.; Akoh, C. C.; Shaw, J. F. Site-directed mutagenesis improves the thermostability of a recombinant *Picrophilus torridus* trehalose synthase and efficiency for the production of trehalose from sweet potato starch. *Food Chem.* **2010**, *119*, 1017−1022.

(14) Sheth, S. R.; Leckband, D. Measurements of attractive forces between proteins and end-grafted poly(ethylene glycol) chains. *Proc. Natl. Acad. Sci. U.S.A.* **1997**, *94*, 8399−8404.

(15) Azevedo, A. M.; Cabral, J. M. S.; Prazeres, D. M. F.; Gibson, T. D.; Fonseca, L. P. Thermal and operational stabilities of *Hansenula polymorpha* alcohol oxidase. *J. Mol. Catal. B−Enzym.* **2004**, *27*, 37−45.

(16) Li, C.; Ban, X.; Gu, Z.; Li, Z. Calcium ion contribution to thermostability of cyclodextrin glycosyltransferase is closely related to calcium-binding site CaIII. *J. Agric. Food Chem.* **2013**, *61*, 8836−8841.

(17) Zhang, M. Q.; Rong, M. Z.; Zhang, H. B.; Friedrich, K. Mechanical properties of low nano-silica filled high density polyethylene composites. *Polym. Eng. Sci.* **2003**, *43*, 490−500.

(18) Chronakis, I. S. Novel nanocomposites and nanoceramics based on polymer nanofibers using electrospinning process − a review. *J. Mater. Process. Technol.* **2005**, *167*, 283−293.

(19) Ab Rahman, I.; Padavettan, V. Synthesis of silica nanoparticles by sol-gel: size-dependent properties, surface modification, and applications in silica-polymer nanocomposites − a review. *J. Nanomater.* **2012**, 1−15.

(20) Trewyn, B. G.; Slowing, I. I.; Giri, S.; Chen, H. T.; Lin, V. S. Y. Synthesis and functionalization of a mesoporous silica nanoparticle based on the sol-gel process and applications in controlled release. *Acc. Chem. Res.* **2007**, *40*, 846−853.

(21) Bradford, M. M. A rapid and sensitive method for the quantitation of microgram quantities of protein utilizing the principle of protein-dye binding. *Anal. Biochem.* **1976**, *72*, 248−254.

(22) Makela, M.; Korpela, T.; Laakso, S. Colorimetric determination of β-cyclodextrin: two assay modifications based on molecular complexation of phenolphthalein. *J. Biochem. Biophys. Methods* **1987**, *14*, 85−92.

(23) Hou, D. H.; Chang, S. K. C. Structural characteristics of purified glycinin from soybeans stored under various conditions. *J. Agric. Food Chem.* **2004**, *52*, 3792−3800.

(24) Liu, Y.; Zhao, G. L.; Zhao, M. M.; Ren, J. Y.; Yang, B. Improvement of functional properties of peanut protein isolate by conjugation with dextran through Maillard reaction. *Food Chem.* **2012**, *131*, 901−906.

(25) Whitmore, L.; Wallace, B. A. Protein secondary structure analyses from circular dichroism spectroscopy: methods and reference databases. *Biopolymers* **2008**, *89*, 392−400.

(26) Uitdehaag, J. C. M.; van Alebeek, G.; van der Veen, B. A.; Dijkhuizen, L.; Dijkstra, B. W. Structures of maltohexaose and maltoheptaose bound at the donor sites of cyclodextrin glycosyltransferase give insight into the mechanisms of transglycosylation activity and cyclodextrin size specificity. *Biochemistry* **2000**, *39*, 7772−7780.

(27) Martins, R. F.; Hatti-Kaul, R. *Bacillus agaradhaerens* LS-3C cyclodextrin glycosyltransferase: activity and stability features. *Enzyme Microb. Technol.* **2003**, *33*, 819−827.

(28) Delbourg, M. F.; Drouet, P.; Demoraes, F.; Thomas, D.; Barbotin, J. N. Effect of PEG and other additives on cyclodextrin production by *Bacillus-macerans* cyclomaltodextrin-glycosyl-transferase. *Biotechnol. Lett.* **1993**, *15*, 157−162.

(29) Mukerjea, R.; Slocum, G.; Mukerjea, R.; Robyt, J. F. Significant differences in the activities of alpha-amylases in the absence and presence of polyethylene glycol assayed on eight starches solubilized by two methods. *Carbohydr. Res.* **2006**, *341*, 2049−2054.

(30) Yoon, S. H.; Robyt, J. F. Activation and stabilization of 10 starch-degrading enzymes by Triton X-100, polyethylene glycols, and polyvinyl alcohols. *Enzyme Microb. Technol.* **2005**, *37*, 556−562.

(31) Otamiri, M.; Adlercreutz, P.; Mattiasson, B. A differential scanning calorimetric study of chymotrypsin in the presence of added polymers. *Biotechnol. Bioeng.* **1994**, *44*, 73−78.

(32) Kazan, D.; Erarslan, A. Stabilization of *Escherichia coli* penicillin G acylase by polyethylene glycols against thermal inactivation. *Appl. Biochem. Biotechnol.* **1997**, *62*, 1−13.

(33) Wang, Q.; Zhou, L. Y.; Jiang, Y. J.; Gao, J. Improved stability of the carbon nanotubes-enzyme bioconjugates by biomimetic silicification. *Enzyme Microb. Technol.* **2011**, *49*, 11−16.

(34) Wang, D. P.; Yang, M. Q.; Dong, Z. X.; Bo, S. Q.; Ji, X. L. Interaction between poly(ethylene oxide) and silica nanoparticles in dilute solutions. *Chin. J. Polym. Sci.* **2013**, *31*, 1290−1298.

(35) Costa, S. A.; Tzanov, T.; Carneiro, A. F.; Paar, A.; Gubitz, G. M.; Cavaco-Paulo, A. Studies of stabilization of native catalase using additives. *Enzyme Microb. Technol.* **2002**, *30*, 387−391.

study of tissues (histological observations) and cells (cytological observations) confirms the biochemical assays: on the one hand, during grape berry development there are textural changes in the cell walls that lead to softening of the cell walls;[29] and on the other hand, green-berry tissues are rich in phenolic compounds. During berry development, phenolic compound content decreases until veraison (grape color change) and then stabilizes until maturity.[30−32] Tannins in the internal cell fractions are polymerized to a lesser degree than those in the cell wall.[32,33] All of these histological and cytological phenomena are essential to the extraction of both juice from the pulp and phenolic and aromatic compounds from the skin. The degree of extraction of these compounds has a significant influence on the duration of maceration and the quality of the resulting wine. Thus, the red wines of Bordeaux ought to be quite tannic to be well structured and to have good aging potential.[34] Throughout maceration, tannins are extracted from either skins or seeds, but during conventional winemaking it is very difficult both to extract seed tannins and to know how much tannin is extracted from seeds. Therefore, the availability of a technique which enhances the extraction of tannins is advantageous in that such a technique may produce a better tannin balance. Moreover, in the case of harvests that are not fully ripe, maceration ought to be of longer duration to improve the extraction rate. However, this may concomittantly release unwanted flavors (vegetable aromas, for example). Thus, the use of a technique that reduces maceration time may avoid such complications. According to recent studies, the development of an extraction process such as PEF technology in the wine industry seems to be one of the less time-consuming and more energy-efficient[18,20] alternatives. Indeed, this method has proved highly efficient in terms of both molecule extraction and yield.[15−20]

In previous works, we studied the effects of PEF treatment on must and wine composition.[19,20] The present work is complementary to our previous study and shows the effects of PEF treatment on the histocytological structure and the cell wall composition of berry, providing a better understanding of how polyphenol extraction can be modified by PEF. The objective was to study the effects on grape berries of two pulsed field treatments of medium strength. Light and transmission electron microscopy were both used to observe structural changes to the skin cell walls of treated grape berries. These observations completed the results obtained in biochemical analyses of skin cell walls of the grape berries examined.

MATERIALS AND METHODS

Plant Material. One hundred and twenty kilograms of grapes berries of *Vitis vinifera* L. cv. Cabernet Sauvignon were manually harvested at maturity (sugars = 225 g/L; extractability of anthocyanins = 50%; total polyphenols richness = 48) in a Bordeaux vineyard in September 2009. These berries were then destemmed by hand.

PEF Treatments. Three batches of 20 kg of lightly crushed and pressed berries were prepared, two of which were subjected to two different PEF treatments. The third batch corresponded to the control group. The PEF parameters described below were chosen in to compare the effects of a treatment of short duration (1 ms) and high strength (4 kV/cm) with the effects of a treatment of long duration (200 ms) and low strength (0.7 kV/cm). Cabernet Sauvignon grape berries were placed between two parallel stainless steel electrodes, and PEF was subsequently applied. [PEF1: E = 4 kV/cm; t_{PEF} = 1 ms, W = 3.99 Wh/kg (n = 1; t_i = 10 μs; Δt = 10 ms; Δt_t = 10 s; N = 100). PEF2: E = 0.7 kV/cm; t_{PEF} = 200 ms; W = 31 Wh/kg (n = 100; t_i = 100 μs; Δt = 10 ms; Δt_t = 10 s; N = 20).] N series of pulses were used for the treatment. Each series consisted of n pulses, pulse duration (t_i), time interval between pulses (Δt), and there was a pause (Δt_t) after each train of pulses. The effective time of the PEF treatment was regulated by the variation of the number of series N and is calculated as $t_{PEF} = nNt_i$. A sample of grape berries (0.7−4.2 kg) was placed in the PEF treatment cell between two stainless plane electrodes (230 mm × 265 mm). The distance between electrodes was 70 mm for PEF1 and 12 mm for PEF2. The value of the electric field E was evaluated as $E = U/d$, where U is the applied voltage. The initial conductivity of the samples was approximately 2.5 mS/cm. The specific energy consumption was calculated using the following formula: $W = UIt_{PEF}/m$, where m is the mass of grapes. These protocols allowed fine regulation of the treatment without any noticeable temperature elevation ($\Delta T \leq 6$ °C for PEF1 and $\Delta T \leq 14$ °C for PEF2) during the PEF treatment.

Three batches of 50 "control" berries were collected on the same day as the treated berries and stored in the same way to await the different biochemical analyses.

Microscopy Skin Characterization and Cytological Preparation for Light and Transmission Electron Microscopy (Method Described by Colin et al.[35]). A first sampling of 10 berries from each batch, treated and untreated, was carried out immediately after the various PEF treatments (day 0) to observe the immediate effects of the treatment on their cellular structure. A second sampling was carried out after the end of alcoholic fermentation (day 14) to note the indirect effect of the treatment on extraction from cells.

For each PEF treatment, 10 berries were randomly selected and immediately prepared for microscopy as described by McManus[36] for fixation and by Thiéry[37] for staining. Control (untreated) and treated berries were dissected into four sections each, always in the same manner and fixed (4 °C for 90 min in 2.5% glutaraldehyde in a phosphate buffer, pH 7.2), then washed in the same buffer, and postfixed (4 °C for 90 min in osmium tetroxide). The berry pieces were dehydrated progressively in successive baths of ethyl alcohol from 40% (v/v) to absolute (100% v/v) and were then embedded in epoxy resin (Epon).

Light Microscopy (MO). Semithin sections (2 μm thick) were stained via the periodic acid Schiff (PAS) method for the detection of polysaccharides.[37] Two hundred cross sections were observed by light microscopy for each treatment mode. Ten cross sections per treatment mode were photographed using an Olympus camera. The PAS-stained sections were used to determine the general histocytological morphology and to evaluate the polysaccharide content of the cell walls according to the different shades of pink obtained (negative PAS = light pink, positive PAS = dark and intense pink).

Transmission Electron Microscopy (TEM). Thin sections were cut using an ultramicrotome UCT (LEICA, Vienna, Austria) and picked up on 150-mesh copper grids. The sections were counterstained with uranyl acetate and lead citrate.[38] One hundred cross sections were examined for each treatment using a transmission electron microscope at 120 kV (Tecnai 12, FEI) and photographed with an ORIUS 832-11 MPixel (Gatan) camera.

Biochemical Analysis of Total Flavan-3-ols and Pectic Fractions of Skin Cell Walls. Frozen berries were peeled with a razor blade to retain only their skins. The skins were then very finely ground in a mortar under liquid nitrogen until a powder form was obtained.

Extractions of Cell Wall Fraction.[32,39] The cell wall isolation procedure followed the method described by Harris et al.[40] with slight modifications to allow us to perform the assay of tannins and polysaccharides on the same extraction sample.

One and a half grams of "skin powder" was suspended in 10 mL of 0.2 M Tris-HCl buffer, pH 7.5, containing 2.5% (w/v) EDTA (homogenization buffer) and homogenized at 4 °C to prevent the activation of the pectolytic enzymes[41] and the polyphenol oxidases.[42] This sample was then centrifuged at 15000 rpm for 20 min at 4 °C. The resulting pellet was resuspended in 10 mL of homogenization buffer and recentrifuged at 15000 rpm for 30 min at 4 °C. The pellet was further resuspended twice in 10 mL of 2.5 M saccharose and recentrifuged at 15000 rpm for 30 min at 4 °C. The pellet was

resuspended six more times in 10 mL of homogenization buffer and centrifuged anew after each resuspension, each time with different settings: 16000 rpm, 30 min, 4 °C; 14000 rpm, 30 min, 4 °C; 10000 rpm, 20 min, 4 °C; 9000 rpm, 15 min, 4 °C; 8000 rpm, 10 min, 4 °C; 5000 rpm, 10 min, 4 °C. The pellet was resuspended in 10 mL of Triton X-100 0.1% and recentrifuged at 3000 rpm for 10 min at 4 °C. The pellet was resuspended twice in 10 mL of homogenization buffer and recentrifuged at 3000 rpm for 10 min at 4 °C and at 2000 rpm for 5 min at 4 °C. The sample was subsequently filtered through a 3 μm PTFE filter and dried in an oven at 35 °C. This fraction was designated the "cell wall fraction of the skin".

Extraction of Polysaccharidic Fractions of the Cell Wall Fraction of the Skin (Adapted from Saulnier and Thibault [43]). For all samples, extraction and analysis were performed in triplicate. One-tenth of a gram of the cell wall fraction of the skin was suspended in a mixture of 20 μL of ethanol 95% and 20 mL of distilled water, stirred for 24 h at room temperature, and centrifuged at 1200 rpm for 30 min. The resulting supernatant corresponded to the PSE fraction (polysaccharides soluble in water). The pellet was resuspended in 20 mL of ammonium oxalate 2% (w/p), stirred for 2 h at room temperature, and centrifuged at 1200 rpm for 30 min. The resulting supernatant corresponded to the PSOX fraction (polysaccharides soluble in ammonium oxalate). The pellet was again suspended in 20 mL of 0.05 N HCl, stirred for 2 h at 85 °C, and centrifuged at 1200 rpm for 30 min. The resulting supernatant corresponded to the PSH fraction (polysaccharides soluble in acid). The pellet was once more suspended in 20 mL of 0.05 N NaOH, stirred for 2 h at 4 °C, and centrifuged at 1200 rpm for 30 min. The resulting supernatant corresponded to the PSOH fraction (polysaccharides soluble in sodium hydroxide). The pellet corresponded to the residual matter and was designated RP (residual pellet).

Extraction of Tannins.[44] For all samples, extraction was performed in triplicate. Either 0.1 g of the cell wall fraction of the skin and the residual pellet or 10 mL of pectic fraction was suspended in 10 mL of methanol containing 0.1% HCl. This solution was stirred for 3 h at 20 °C. The extract was filtered through 20 μm PTFE filters. For pectic fractions, this extract was designated the "phenolic extract of the skin pectic fraction". In the same manner as for the cell wall fraction of the skin and the residual pellet, the powder remaining on the filter was suspended in 10 mL of methanol containing 0.1% HCl (v/v) and stirred anew for 3 h at 20 °C. The resulting extract was filtered through 20 μm PTFE filters. This extract was designated the "phenolic extract of skin cell wall" from the cell wall fraction or the "phenolic extract of the residual pellet" from the residual pellet.

Analysis of Tannins by Reverse Phase HPLC following Phloroglucinolysis.[33,34,45] The mean degree of polymerization (mDP) and the subunit composition of procyanidins in the different fractions were analyzed. Six hundred microliters of phenolic extract, desiccated under nitrogen flow, plus 200 μL of reagent (0.2 Nmethanol-HCl + ascorbic acid + phloroglucinol) were mixed and incubated at 50 °C for 20 min. The reaction was stopped with 200 μL of sodium acetate. This extract was filtered and placed in a 2 mL HPLC sealed vial. Ten microliters was injected into the HPLC for analysis (column, 250 × 4.6 μm, 5 μm, ODS (Beckman, Roissy Charles de Gaulle, France): precolumn, 10 × 4.6 mm, 5 μm, BDS C18 (Thermo Hypersil); flow rate, 1 mL/min; solvent A, water/acetic acid (19:1 v/v); solvent B, MeOH/acetic acid (19:1 v/v); gradient, 5% B from 0 to 30 min, 20% B from 30 to 55 min, 40% B from 55 to 60 min, 90% B from 60 to75 min, 5% B from 75 to 80 min; injection volume, 10 μL; detection wavelength, 280 nm.

Spectrophotometric Analysis of Polysaccharides.[46] One hundred and fifty microliters of extract diluted at 1/10 plus 750 μL of 95% H_2SO_4 were stirred for 3 min at 0 °C and then for 6 min at 100 °C and then cooled for 10 min at 0 °C. After the addition of 15 μL of 3-hydroxydiphenyl (MHDP), the extracts were left in the dark for 20 min at room temperature before dosing at a wavelength of 520 nm.

Statistical Data Treatment. Two-way analysis of variance (ANOVA) could not be performed (non-normality of the residues and/or nonhomogeneity of the variance). We thus performed nonparametric tests. The statistical significance of differences was determined by the Freidman test ($\alpha = 0.05$) for paired samples and by the Kruskal and Wallis test ($\alpha = 0.05$) for unpaired samples. Experimental data detected as being significantly different are marked in the tables with different letters.

RESULTS

Immediate and Long-Term Effects of Different Pulsed Electric Field Treatments on Skin Histocytological Structure. Skin histocytological structures of grape berries were observed in both light microscopy (200 cross sections) and transmission electron microscopy (100 cross sections) for the two PEF treatment modes. Observations were carried out soon after treatment (day 0) to observe the immediate effects of PEF treatment and at the end of the alcoholic fermentation (day 14) to note the modifications to the cell structure of the grape berry skin.

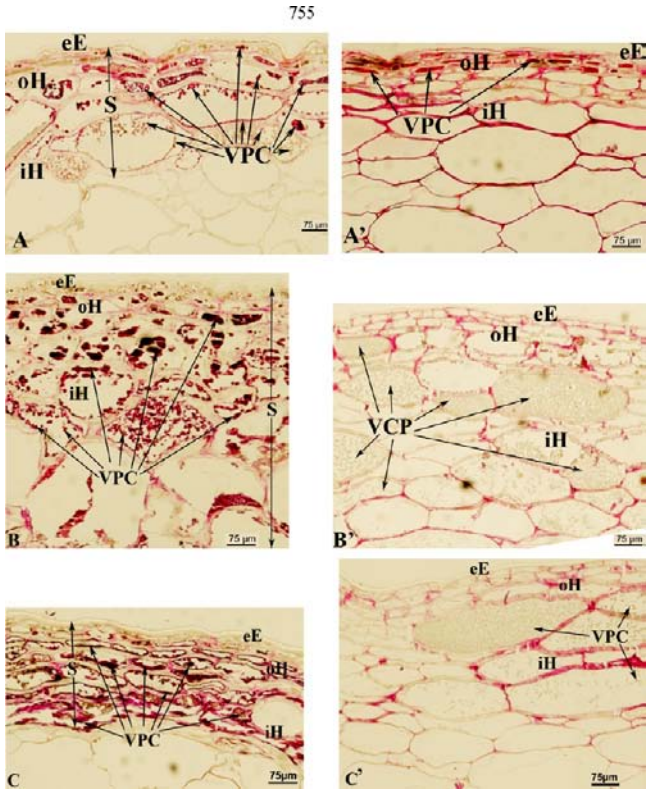

Figure 1. Evolution of the skin cross sections immediately after PEF treatments (day 0) (A, untreated (0 kV/cm); B, PEF1-treated (4 kV/cm; 1 ms; 4 Wh/kg); C, PEF2-treated (0.7 kV/cm; 200 ms; 31 Wh/kg)) and 14 days after PEF treatments (day 14) (A′, untreated (0 kV/cm); B′, PEF1-treated (4 kV/cm; 1 ms; 4 Wh/kg); C′, PEF2-treated (0.7 kV/cm; 200 ms; 31 Wh/kg)), under optical microscopy. eE, external epidermis; oH, outer hypodermis; iH, inner hypodermis; S, skin; VPC, vacuolar phenolic compounds.

Control Berries (Figures 1, 2, and 4). At day 0, all berry skins observed were characterized by one layer of epidermal cells and by five to six layers of hypodermal cells (Figure 1A), which were found to be rich in organelles (o) such as mitochondria (m) (Figure 2A). Vacuolar polyphenols (VPC) appeared as dense amorphous precipitates from the epidermis and the outer hypodermis (Figures 1A and 2A) and as gray granules originating from the inner hypodermis (Figures 1A and 2B). Despite slight staining with PAS (Figure 1A), it was

dx.doi.org/10.1021/jf404804d | J. Agric. Food Chem. 2014, 62, 2925−2934

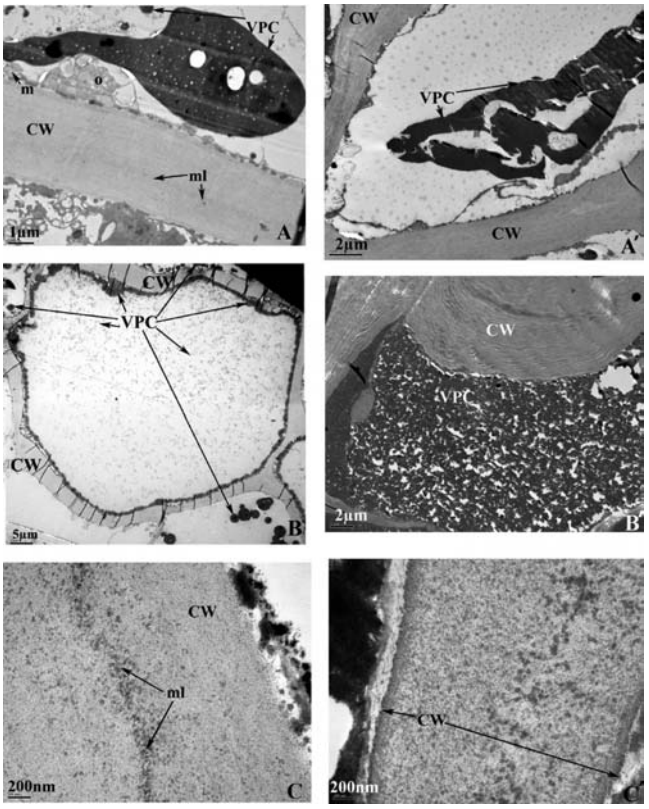

Figure 2. Skin cross sections of (A, B, C) untreated-berries (0 kV/cm) and of (A′, B′, C′) PEF1-treated berries (4 kV/cm; 1 ms, 4 Wh/kg) observed at day 0, under transmission electron microscopy: (A, A′) outer hypodermis; (B, B′) inner hypodermis; (C, C′) outer hypodermis. CW, cell wall; o, organelles; ml, middle lamella; m, mitochondria; VPC, vacuolar phenolic compounds.

possible to observe that the cell walls (CW) showed no signs of deterioration (Figure 2A–C).

At 14 days, almost all of the vacuolar polyphenols had been evacuated (Figure 1A′). Very few vacuolar polyphenols were still present in the epidermis and outer hypodermis, where they appeared as very dense, dark red or brown, amorphous precipitates. Curiously, contrary to day 0, cell walls were found to show homogeneous dark pink PAS staining (Figure 1A′), and the contrast under TEM was seen to be homogeneous and electron-dense (Figure 4A,B). Most organelles, such as plastids (p), were senescent (Figure 4B).

PEF 1 (4 kV/cm, 1 ms, 4 Wh/kg) (Figures 1, 2, and 4). At day 0, the skin of all treated berries was more distended (Figure 1B) than that of the control batch (Figure 1A). Vacuolar polyphenols of the epidermis (Figure 2A′) and hypodermis (Figure 2B′) were less dispersed and more condensed in the vacuole. Small spherical structures, which were localized only at the middle lamella level in the control batch (Figure 2C′), were observed over a large portion of the hypodermis cell wall thickness (Figure 2C′).

At day 14 (Figure 1B′), the hypodermis of all treated berry skins contained no vacuolar phenolic compounds with a dense dark red or brown aspect, as was the case in the control batch. However, it was richer in vacuolar phenolic compounds in the form of small gray granules dispersed throughout the vacuolar space. It can therefore be concluded that these phenolic compounds were probably chemically different from those present in the control berries at the same time. Furthermore, the cell walls of the outer hypodermis showed perforations (Figure 4A′, arrowed). At the inner hypodermis, fiber cell wall polysaccharides were more distended than in the control batch (Figure 4, panel B vs panel B′).

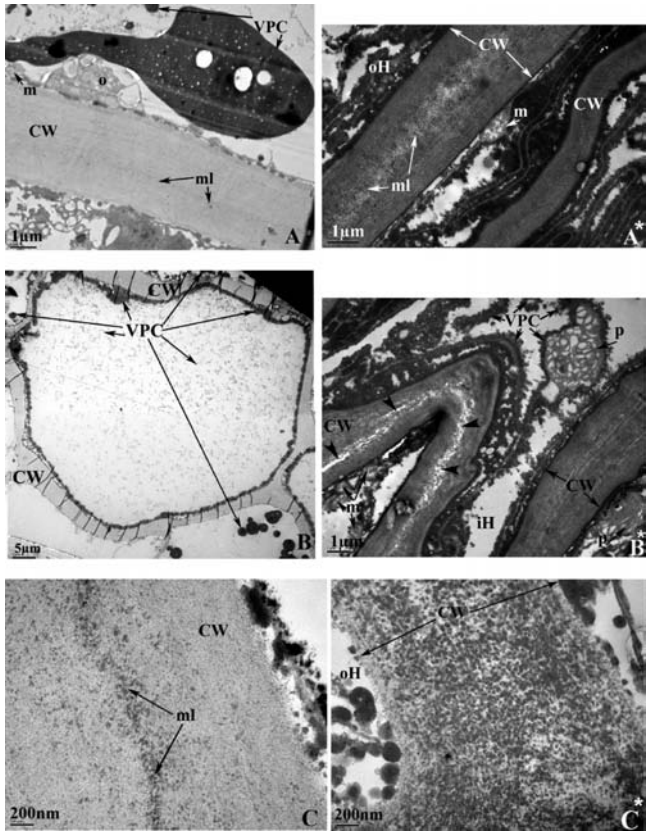

Figure 3. Skin cross sections of (A, B, C) untreated berries (0 kV/cm) and of (A*, B*, C*) PEF2-treated berries (0.7 kV/cm; 200 ms, 31 Wh/kg) observed at day 0, under transmission electron microscopy: (A, A*) outer hypodermis; (B, B*) inner hypodermis; (C, C*) outer hypodermis. CW, cell wall; iH, inner hypodermis; m, mitochondria; ml, middle lamella; o, organelles; oH, outer hypodermis; p, plastid; VPC, vacuolar phenolic compounds.

PEF 2 (0.7 kV/cm, 200 ms, 31 Wh/kg) (Figures 1, 3, and 4). At day 0, in contrast to PEF1, the skin of all treated berries was seen to be much more degraded than in the control batch, especially in the deepest layers of the inner hypodermis of the skin (Figure 1C). The vacuolar polyphenols of the outer cell layers of the skin appeared denser and more contrasted, as was the case for PEF1. The outer hypodermis cells (Figure 3A*), and even more so those of the inner hypodermis (Figure 3B*), were disorganized, showing destructuring of the middle lamella of cell walls (arrowed) and organelles, such as mitochondria (m) or plastids (p), that had been disrupted. At highest magnification, the aspect of the cell wall appeared unstructured, with the presence of small spherical structures throughout the whole thickness (Figure 3C*).

At day 14 the skin of the treated berries was, in 80% of cases, less rich in vacuolar polyphenols than that of the untreated berries. However, some areas could be observed in which phenolic compounds of a dense gray appearance persisted in the cells (Figure 1C′). In all cases, cell wall structure and the organization of the polysaccharide fibers had a very different

dx.doi.org/10.1021/jf404804d | J. Agric. Food Chem. 2014, 62, 2925–2934

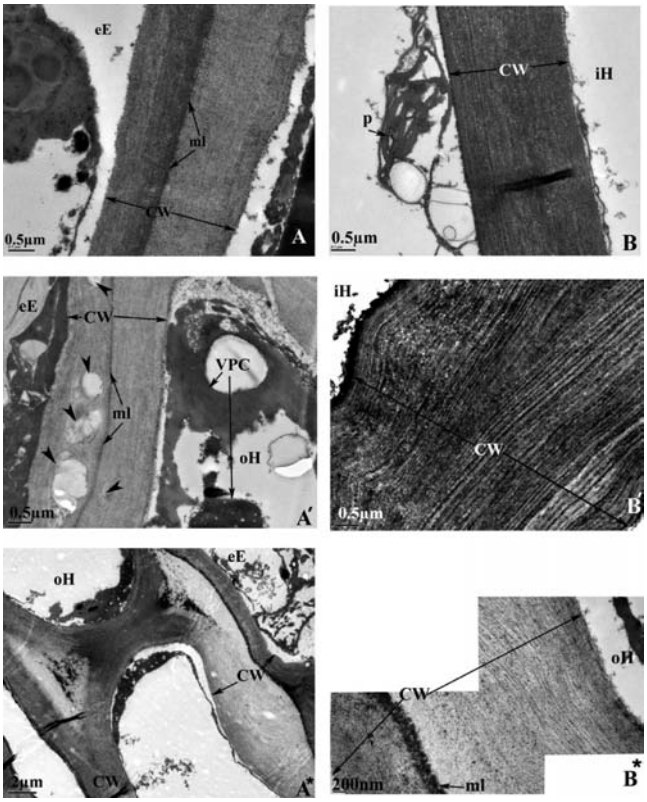

Figure 4. Skin cross sections of (A, B) untreated berries (0 kV/cm), (A′, B′) PEF1-treated berries (4 kV/cm; 1 ms, 4 Wh/kg), and (A*, B*) PEF2-treated berries (0.7 kV/cm; 200 ms, 31 Wh/kg) observed at day 14, under transmission electron microscopy: (A, A′, A*, B*) outer hypodermis; (B, B′) inner hypodermis. CW, cell wall; eE, external epidermis; iH, inner hypodermis; ml, middle lamella; oH, outer hypodermis; p, plastid; VPC, vacuolar phenolic compounds.

appearance from the control batch. In treated skins, cell angles were observed to be rather distended with high-contrast deposits and perforations that evoke meatus (Figure 4A*). Tangential walls of contiguous layers of cells were asymmetrical on either side of the middle lamella (Figure 4B*). Moreover, the middle lamella was observed under TEM as being more highly contrasted and electron dense (Figure 4B*), which could be one of the consequences of changes in the wall that contained more sites where the counterstaining metal salts of the different sections could be lodged. In conclusion, the immediate impact of PEF1 was characterized by a distension of the skin and a condensation of most of the vacuolar polyphenols. The impact on the cell walls was more limited, but remained significant, at 14 days after perforations were first observed. The immediate impact of PEF2 was much more pronounced: the skin became very dense, the polyphenols were more highly concentrated, and, more especially, the cell walls were greatly modified. They were observed at 14 days as being very eroded and degraded.

Immediate Effects of Pulsed Electric Field Treatments on Skin Cell Wall Condensed Tannins. PSE and PSOX fractions correspond to the easily extractable peripheral pectic fractions, whereas PSH and PSOH fractions correspond to the internal pectic fractions that are only extractable with greater difficulty.[42] The residual pellet (RP) corresponds to the "heart" of the cell wall.

Control Berries (Table 1). The pectic fractions richest in condensed tannins were PSH and PSOH, which were internal and strongly bonded with the cell wall fibers. The larger condensed tannins with the highest mDP were found in the PSH fraction.

PEF 1 (4 kV/cm, 1 ms, 4 Wh/kg) (Table 1). In the different peripheral cell wall fractions (PSE; PSOX), the treatment did not have a marked effect. However, levels of condensed tannins in the PSE fraction (TPSE) tended to be higher (C, 0.17, vs PEF1, 0.24) and mDP tended to decrease (C, 3.42, vs PEF1, 2.91), reflecting a probable decondensation of tannins and their accumulation in this fraction. In the PSOX fraction, tannin levels (TPSOX) tended to be lower (C, 0.29, vs PEF1, 0.2) and mDP tended to increase (C, 2.43, vs PEF1, 3.26), reflecting a probable loss of tannins further to their condensation in this fraction.[32] In the different internal cell wall fractions (PSOH,

Table 1. Effects of PEF1 and PEF2 on the Total Tannins and mDP of the PSE, PSOX, PSH, PSOH, and RP Polysaccharide Fractions in Berry Skins[a]

tannins of polysaccharide fractions		C	PEF1 (4 kV/cm, 1 ms, 4 Wh/kg)	PEF2 (0.7 kV/cm, 200 ms, 31 Wh/kg)
TPSE	total tannins (mg/g of skin)	0.17 ± 0.11 a*	0.24 ± 0.17 ab*	0.42 ± 0.04 b*
	mDP	3.42 ± 0.88 a*	2.91 ± 0.49 a*	3.17 ± 2.78 a*
TPSOX	total tannins (mg/g of skin)	0.29 ± 0.08 a*	0.20 ± 0.03 a*	0.14 ± 0.05 b*
	mDP	2.43 ± 0.50 a*	3.26 ± 0.72 a*	2.79 ± 1.13 a*
TPSH	total tannins (mg/g of skin)	2.81 ± 0.83 a*	1.13 ± 1.36 a*	2.17 ± 1.59 a*
	mDP	15.83 ± 5.07 a*	58.03 ± 68.8 a*4	13.84 ± 1.22 a*
TPSOH	total tannins (mg/g of skin)	2.57 ± 1.85 a*	5.19 ± 5.49 a*	9.29 ± 8.03 b*
	mDP	3.59 ± 3.75 a*	1.63 ± 0.25 a*	1.64 ± 0.13 a*
TRP	total tannins (mg/g of skin)	0.75 ± 0.15 a*	0.66 ± 0.64 a*	1.67 ± 0.87 a*
	mDP	5.79 ± 2.11 a*	2.64 ± 0.32 a*	4.79 ± 1.99 a*

[a]Values are means ± standard deviations. (*) Significant difference in Kruskal and Wallis test (α = 0.1). PEF1, treatment 1 of pulsed electric field; PEF2, treatment 2 of pulsed electric field; C, control berries; TPSE, tannins of PSE; TSPOX, tannins of PSOX; TPSH, tannins of PSH; TPSOH, tannins of PSOH; TRP, tannins of RP; PSE, extracted polysaccharide fraction in water; PSOX, extracted polysaccharide fraction in oxalate; PSH, extracted polysaccharide fraction in acid; PSOH, extracted polysaccharide fraction in sodium hydroxide; RP, pellet of residual polysaccharide fractions.

dx.doi.org/10.1021/jf404804d | J. Agric. Food Chem. 2014, 62, 2925−2934

PSH, RP), the same phenomenon was observed because levels of condensed PSH tannins (TPSH) tended to be lower (C, 2.81, vs 1.13), and mDP levels tended to increase (C, 15.83, vs PEF1, 58.03), as was the case for the PSE fraction. The tannin level of the PSOH fraction (TPSOH) tended to be higher (C, 2.57, vs PEF1, 5.19), and mDP tended to decrease (C, 3.59, vs PEF1, 1.63), as was the case for the PSOX fraction. Moreover, in the residual pellet (TRP), mDP tended to decrease (C, 5.79, vs PEF1, 2.64), whereas levels of condensed tannins showed no variation (C, 0.75, vs PEF1, 0.66). This could reflect a breakdown of the tannins present in this fraction and a leakage of decondensed tannins into adjacent fractions.

PEF2 (0.7 kV/cm, 200 ms, 31 Wh/kg) (Table 1). The two peripheral cell walls (PSE; PSOX) were affected by the treatment as compared to the control batch. The level of condensed PSE tannins (TPSE) increased significantly (C, 0.17, vs PEF2, 0.42) and mDP also tended to increase (C, 3.42, vs PEF2, 4.26). In the PSOX fraction the level of condensed tannins (TPSOX) decreased significantly (C, 0.29, vs PEF2, 0.14) and mDP also tended to increase (C, 2.43, vs PEF2, 2.79). It is conceivable that either the TPSOX were depleted after their condensation in this fraction or a part of TPSOX was decondensed under the action of PEF2, which spontaneously migrated from this fraction to accumulate in PSE, in which bonds are of the same nature, and spontaneously condensed in this fraction where the amount of condensed tannins increased. This migration would thus explain the large increase in the level of TPSE, whereas mDP also showed an increase. The PSE fraction was enriched in condensed tannins from TPSE and TPSOX (therefore, the average value of mDP was higher in these fractions), contributing to the significant decrease in the level of TPSOX. Among the internal fractions (PSOH; PSH; RP) only PSOH was significantly affected; mDP tended to decrease (C, 3.59, vs PEF2, 1.64), reflecting a rupture due to treatment, and the level of condensed tannins (TPSOH) increased (C, 2.57, vs PEF2, 9.29), reflecting an accumulation of these tannins. Moreover, the mDP of condensed PSH tannins (TPSH) tended to be lower than in the control batch (C, 15.83, vs PEF2, 13.84), reflecting a rupture, whereas the level of TPSH tended to decrease (C, 2.81, vs PEF2, 2.17). This decrease in the level of TPSH can be explained by a leakage of TPSH to the PSOH fraction, contributing to the increased levels of TPSOH. In the RP, mDP tended to decrease as compared with the control batch (C, 5.79, vs PEF2, 4.79) and the level of condensed tannins (TRP) increased (C, 0.75, vs PEF2, 1.67), reflecting an accumulation of these decondensed tannins.

Finally, whereas PEF1 did not significantly affect the tannic skeleton of skin cell walls, the consequences of PEF2 were much more significant: the tannic skeleton of skin cell walls was highly disorganized, especially the external fractions.

Immediate Effects of Different Pulsed Electric Field Treatments on Skin Cell Wall Polysaccharidic Fractions. The peripheral pectic fractions PSE and PSOX are easily extractable because they are connected by weak bonds. The internal pectic fractions PSH and PSOH are not easily extractable because they are connected by strong bonds. Each of the fractions contains mainly galacturonic acid, arabinose, and galactose, which correspond to pectic compounds.[43] It is thus possible to refer indifferently to the polysaccharide fraction or the pectic fraction.

Control Berries (Table 2). In descending order, the most abundant polysaccharide fraction corresponded to the PSE fraction, which is the most easily extractable, followed by PSOH, PSOX, and PSH.

Table 2. Effects of PEF1 and PEF2 on the Contents of External Polysaccharide Fractions (PSE, PSOX) and Internal Polysaccharide Fractions (PSH, PSOH) in Berry Skins[a]

polysaccharide content (mg/g of skin)	C	PEF1 (4 kV/cm, 1 ms, 4 Wh/kg)	PEF2 (0.7 kV/cm, 200 ms, 31 Wh/kg)
PSE fractions	8.80 ± 2.25 a*	9.71 ± 3.12 a*	3.88 ± 2.66 b*
PSOX fractions	1.32 ± 0.36 a*	1.57 ± 0.47 a*	2.54 ± 0.73 b*
PSH fractions	0.70 ± 0.07 a*	0.56 ± 0.07 b*	0.55 ± 0.16 c*
PSOH fractions	2.59 ± 0.50 a*	1.76 ± 0.74 a*	1.55 ± 0.63 b*

[a]Values are means ± standard deviations. (*) Significant difference in Kruskal and Wallis test ($\alpha = 0.1$). PEF1, treatment 1 of pulsed electric field; PEF2, treatment 2 of pulsed electric field; C, control berries; PSE, extracted polysaccharide fraction in water; PSOX, extracted polysaccharide fraction in oxalate; PSH, extracted polysaccharide fraction in acid; PSOH, extracted polysaccharide fraction in sodium hydroxide.

PEF 1 (4 kV/cm, 1 ms, 4 Wh/kg) (Table 2). This treatment mode did not cause changes in the distribution of pectic fractions in the cell walls. Furthermore, external fractions of cell wall were not significantly affected (Table 2) because the levels of PSE and PSOX remained stable, but these fractions tended to increase, which seems to imply a slightly increased density of weak bonds (noncovalent) in the cell wall. However, PEF1 significantly modified the internal fractions, showing decreased levels of PSH, which is the cause of disruption of strong bonds (covalent) and a rearrangement of molecular bonds at this level.

PEF2 (0.7 kV/cm, 200 ms, 31 Wh/kg) (Table 2). This treatment mode significantly affected all polysaccharidic fractions of the cell walls, principally in the peripheral fractions. At the periphery of the cell wall, the PSOX level was increased significantly and may have been enriched by some of the PSE, the level of which decreased (Table 2). However, the density of weak bonds (noncovalent) decreased in PSE and increased in PSOX; therefore, the molecular affinity of these fractions was totally modified. Toward the inside of the cell wall, as was the case for PEF1 but more pronounced, levels of PSH and PSOH were decreased significantly (Table 2), which is the cause of a decrease of strong bonds (covalent) and of an upheaval and rearrangement of molecular bonds at this level.

As seen above in the case of the tannic skeleton, PEF1 had only a slight impact on the pectic skeleton of skin cell walls. Conversely, the consequences of PEF2 were more far-reaching seeing as this treatment mode caused the disorganization of cell wall polysaccharides and molecular bonds, which induced a modification of polyphenol extraction phenomenon.[47−49]

DISCUSSION

The main action of PEF is the induction of a phenomenon of electroporation in the form of hydrophilic pores on small portions of cell membranes of the cells facing the electrodes. Cells exposed to the transmembrane energy of an external electric field undergo a reorganization of membrane phospholipids.[4,5] In this way, the shape and size of the affected cells directly influences the phenomenon of electroporation. Grape berries being composed of heterogeneous tissues, with cell shape and membrane potential variables,[21−27] the spread and consequences of PEF are not homogeneous in the skin.

Moreover, the presence of the cell walls is an important factor in the spread of PEF. Few studies have examined the influence of PEF on the walls. Furthermore, Janositz and Knorr[3] have demonstrated, with tobacco cells and protoplasts, the protective effect of cell walls vis-a-vis PEF treatment, having observed that protoplast cell size increased slightly after reversible permeabilization by PEF treatment with few pulses. In the present study, PEF treatment has been shown for the first time to have an effect on several cellular compartments such as cell walls in addition to the membranes: the skin of the treated berries was, overall, only slightly affected by the PEF1 treatment (4 kV/cm, 1 ms, 4 Wh/kg), but very largely degraded following the PEF 2 treatment (0.7 kV/cm, 200 ms, 31 Wh/kg).

The most striking histological effect observed immediately after the PEF1 treatment concerned the thickness of the skin that was much greater than in the control batch, the most strongly affected cells being the large cells of the inner hypodermis.[19,20] From a cytological point of view, skin-cell membranes of treated berries were found to be little affected by PEF1, which is logical in view of the PEF1 parameters (pulses of short duration (1 ms) and high strength (4 kV/cm)) that had induced electroporation on a lesser scale[4] and which remained reversible. Conversely, cell walls of treated berries were more highly affected by PEF1 than membranes and, especially, the aspect of cell walls of the inner hypodermis immediately after the treatment (Figure 2). At the end of 14 days, cell walls were more distended in the inner hypodermis, showing certain areas with perforations in the outer hypodermis (Figure 3), which confirmed our findings that the consequences of PEF are not homogeneous.[21−27] In this way, cytological observations revealed modifications of the polysaccharide skeleton interior, as did biochemical analysis of the pectic fractions (galacturonic acid, arabinose, and galactose).[43]

Pectic cell wall organization was only slightly but measurably affected further to the treatment: external fractions (PSE, PSOX) tended to increase, which probably increased the number of weak bonds,[43] and the quantity of internal fractions (PSH, PSOH) was decreased, which also decreased the number of strong bonds.[43] It can be hypothesized that the disappearance of PSH and PSOH had disturbed the microfibrillar interactions of cell walls,[29] thus freeing new space at the heart of the cell walls into which water may penetrate, thus inducing a stretching thereof. The distension of the walls that was observed immediately after the treatment would then allow the expansion of these cells, which would explain the thickening of the treated skin. The largest cells being the most strongly affected,[3,7,13] this expansion was most noticeable at the inner hypodermis, which is made up of very large cells.[23,25] Moreover, this upheaval of pectic skeleton has probably induced a change of affinity for the various parietal molecules such as polyphenols.[47−50,53] With regard to the polyphenolic organization of the treated skin, biochemical analysis of the cell walls of total tannins in the different pectic fractions did not reveal any significant effect. However, a trend was observed: levels of TPSOX (inside the external pectic fraction) and TPSH (inside the internal pectic fraction) decreased, and their mDP increased. Following PEF1 treatment, PSOX and PSH fractions were depleted of total tannins because of the condensation of these tannins (mDP increased). It was possible to confirm this observation with TEM observations, in which structures resembling small balls were observed in the middle lamella walls (Figure 2). These structures may correspond to the condensation of TPSH in the space freed by the disappearance of the PSH pectic fraction. Renard et al.[50] demonstrated that affinity and binding between cell wall procyanidins and polysaccharides in apples increased with the degree of polymerization of these phenolic compounds. Thus, in the present case, this polymerization may help strengthen cell walls[32] and slow extraction phenomena.[51,52] This would explain why, at day 14, the hypodermis of treated berries was still rich in vacuolar phenolic compounds (Figure 1). However, TPSOX, TPSH, and TRP were highly condensed by the PEF1 treatment, inducing, on the one hand, a strong bond with pectic compounds, particularly in the PSOX fraction where the number of noncovalent bonds probably increased, thus limiting their depolymerization.[53] On the other hand, the formation of new spaces in the heart of the cell walls resulted in a diminished extractability of these tannins, which are more strongly encapsulated within microfibrillar pores and therefore strongly adsorbed by cell wall components.[47] Thus, PEF1 slowed the phenomena of diffusion and extraction of most tannins from the skin of treated berries. It was also noted that the cytological aspect of vacuolar phenolic compounds was modified after the PEF1 treatment: they appeared more condensed in the cell vacuoles. This seems to demonstrate that the PEF1 treatment had had an effect mainly on vacuolar phenolic compounds.[20] Therefore, it can be seen that phenolic compounds and skin cell wall pectic fraction skeletons were little affected by the PEF1 treatment, and it can be confirmed that the polyphenols affected by high-intensity short duration PEF treatment are the vacuolar tannins rather than the cell wall tannins.[20] In this way, PEF1 can be considered as a treatment that has little immediate destructive effect on cells, this effect remaining reversible, which explains the increase in skin size, without cell destruction. However, in the longer term, the skins of treated berries release their condensed tannins less easily, as they are strongly bonded to the affected pectic cell wall fractions. Their liberation takes place with a "delayed action effect", which implies a lower rate of tannin extraction from the skins during maceration[20]

With regard to the PEF2 treatment, the skin structure of the treated berries was very largely degraded following the treatment. It was observed that the histological (Figure 1) and cytological (Figure 3) impacts on the cells were very significant. PEF2 was of lesser intensity, but was of longer duration than PEF1, which explains the more destructive effects of the PEF2 treatment.[4,5,7] As berries are composed of heterogeneous tissues,[23,25] with cells of differing shapes and sizes, PEF propagation cannot be uniform,[3,7,13] which partly explains this result. Moreover, the increase in treatment energy (W = 31 Wh/kg) applied caused a higher degree of cell lysis[19] than was the case for PEF1 (W = 4 Wh/kg). In parallel, TEM observations revealed skin cells with severely affected membranes and organelles, with distension of the cell walls and rupture of the middle lamella (Figure 2). These effects can be compared with the structural changes induced by PEF treatment on bacteria[10,54] or yeast,[6,11] in which a much greater critical electric field strength is required to obtain this result. This is mainly related to their diameter, which is much smaller, and to their cell wall thickness, which is greater than that of grape skin cells.[3,7,13] The cytological structure of the cell walls was very largely modified by the PEF2 treatment, which explains the modified aspect of the cell walls observed with TEM (Figure 2). This finding was confirmed by biochemical studies in which analysis of the polysaccharide fractions revealed that the entire pectic skeleton had been disrupted. The whole polysaccharide mesh was greatly weakened, only

one internal fraction being strengthened. Except for PSOX, which increased, the quantities of all fractions were significantly decreased, which probably caused a loss of PSE, which is the most easily extractable fraction,[42] and a reduction in the number of binding sites between polysaccharides and phenolic compounds.[47,53]

In the same way, biochemical analysis of total cell wall tannins demonstrated that the treatment profoundly modified the organization of the tannic skeleton. In the external fractions of the cell walls, TPSE were ruptured (mDP was decreased) contributing to the increase of their numbers in this fraction and probably inducing a decrease in their affinity for the polysaccharides of this fraction.[53] At the same time, TPSOX became even more condensed (mDP was increased), which increased their affinity for the PSOX polysaccharide fraction, for which the numbers of weak bonds were increased. In the internal fractions of the cell walls, TPSOH were ruptured (mDP decreased) and remained in this fraction, whereas TPSH were also ruptured (mDP decreased) but migrated to the PSOH fraction in view of TPSH values, which decreased (Figure 2). Despite this enrichment in tannins, cell walls may have been weakened by a loss of the protective effect of the phenolic compounds against pectin depolymerization.[32,53] The PEF2 treatment induced, on the one hand, an overall decrease in the number of weak bonds due to the loss of peripheral pectic fractions and loss of the strong bonds due to the loss of the internal pectic fraction and, on the other hand, a liberation of the majority of the cell wall tannins, which implies an overall decrease in the affinity of polyphenols for the cell wall fraction. In this way, the biochemical and physical structures of the cell walls were weakened by treatment, favoring the early release of cellular polyphenols, which explains why, at day 14, the skin vacuolar tannins of treated berries were depleted. The destructuring of the cell walls by the treatment facilitated the extraction and diffusion of phenolic compounds. This hypothesis seems to confirm the results of Delsart et al.[19,20] concerning musts. These phenomena may have been facilitated at all layers of the skin by modification of the skeleton of tannins and the pectic fibers[55,56] combined with ion leakage in cells and cell walls brought about by PEF treatment.[7] Thus, low-intensity, long-duration PEF treatment profoundly modified the organization of the skin cell walls, which explains how the application of a PEF treatment enhanced phenolic compound extraction.[15,18] This treatment mainly affected the cells wall tannins[20] and severely affected cell wall protection. This suggests a more rapid release of cellular tannins due to the parietal system being disrupted and thus becoming more permeable to intracellular compounds. The extraction of polyphenols during maceration is facilitated by PEF2 treatment of the grapes.

In conclusion, the comparison of the impact of two types of PEF treatment on the structure of grape berry skin allowed the very different consequences of the two treatment modes to be brought to light. In the case of PEF treatment of high intensity, short duration, and low energy, the effects on the structure of phenolic compounds and pectic cell walls of the skin were measurable but relatively limited. This study demonstrated a strengthening of the phenolic skeleton of skin cell walls, which has a protective effect, slowing polyphenol extraction phenomena. In the case of PEF treatment of higher strength, longer duration, and high energy, the consequences for the parietal structures of the skin were very significant, the pectic and phenolic skeletons being largely disorganized, which facilitated polyphenol extraction. Thus, the choice of treatment modality is of prime importance because this choice can modify the kinetics of polyphenol extraction and, thus, wine quality. Moreover, it appears that there is a correlation between the mDP of tannins, astringency, and structure of wine, which has an influence on wine quality (low mDP tannins seem less astringent than strong mDP tannins).[34] The availability of a technique that allows the extraction of more and better skin tannins during maceration or a technique that reduces maceration time, especially in the case of unripe harvests, and which, in addition, lead to a reduction of mDP (which is relatively high when the harvest is unripe), may be interesting from a qualitative point of view.[34,38] This study is a first approach to the study of the impact of PEF on cell walls, and further research is required to better understand exactly which cell wall compounds are affected by PEF treatments and to better comprehend the mechanisms involved in improving the extractability of tannins by PEF treatment.

AUTHOR INFORMATION

Corresponding Author

*(L.G.) Phone: +33 5 57 57 58 54. Fax: +33 5 57 57 58 13. E-mail: laurence.geny@u-bordeaux2.fr.

Funding

This work was supported by the Conseil Interprofessionnel des Vins de Bordeaux−33000 Bordeaux and by ADEME.

Notes

The authors declare no competing financial interest.

ACKNOWLEDGMENTS

We thank Alan Metcalfe for corrections made to the text and Dr. Warren Albertin for expertise in statistical analysis.

ABBREVIATIONS USED

eE, external epidermis; oH, outer hypodermis; iH, inner hypodermis; S, skin; VPC, vacuolar phenolic compounds; CW, cell wall; o, organelles; ml, middle lamella; p, plastid; m, mitochondria; mDP, mean degree of polymerization; PSE, extracting polysaccharide fraction in water; PSOX, extracting polysaccharide fraction in oxalate; PSH, extracting polysaccharide fraction in acid; PSOH, extracting polysaccharide fraction in sodium hydroxide; RP, residual-pellet polysaccharide fractions; TPSE, tannins of PSE; TSPOX, tannins of PSOX; TPSH, tannins of PSH; TPSOH, tannins of PSOH; TRP, tannins of RP; PEF1, treatment 1 of pulsed electric field; PEF2, treatment 2 of pulsed electric field; C, control berries; TEM, transmission electron microscopy; MO, optical microscopy

REFERENCES

(1) Chang, D. C. Cell poration and cell fusion using an oscillating electric field. *Biophys. J.* **1989**, *56*, 641−652.

(2) Fincan, M.; Dejmek, P. In situ visualization of the effect of a pulsed electric field on plant tissue. *J. Food Eng.* **2002**, *55* (3), 223−230.

(3) Janositz, A.; Knorr, D. Microscopic visualization of pulsed electric field induced changes on plant cellular level. *Innovative Food Sci. Emerging Technol.* **2010**, *11* (4), 592−597.

(4) Kandušer, M.; Šentjurc, M.; Miklavčič, D. The temperature effect during pulse application on cell membrane fluidity and permeabilization. *Bioelectrochemistry* **2008**, *74* (1), 52−57.

(5) Kandušer, M.; Miklavčič, D. Electroporation in biological cell and tissue: an overview. In *Electrotechnologies for Extraction from Food*

Plants and Biomaterials; Vorobiev, Lebovka, Eds.; Springer Science +Business Media: Dordrecht, The Netherlands, 2008; pp 1−37.
(6) Harrison, S. L.; Barbosa-Cánovas, G. V.; Swanson, B. G. Saccharomyces cerevisiae structural changes induced by pulsed electric field treatment. *Lebensm. Wiss. Technol.* **1997**, *30*, 236−240.
(7) Ersus, S.; Barrett, D. M. Determination of membrane integrity in onion tissues treated by pulsed electric fields: use of microscopic images and ion leakage measurements. *Innovative Food Sci. Emerging Technol.* **2010**, *11* (4), 598−603.
(8) Beveridge, J. R.; Macgregor, S. J.; Marsili, L.; Anderson, J. G.; Rowan, N. J.; Farish, O. Comparison of the effectiveness of biphase and monophase rectangular pulses for the inactivation of micro-organisms using pulsed electric fields. *IEEE Trans. Plasma Sci.* **2002**, *30*, 1525−1531.
(9) El Zakhem, H.; Lanoisellé, J. L.; Lebovka, N. I.; Nonus, M.; Vorobiev, E. Influence of temperature and surfactant on *Escherichia coli* inactivation in aqueous suspensions treated by moderate pulsed electric fields. *Int. J. Food Microbiol.* **2007**, *120* (3), 259−265.
(10) Chen, Y.; Yu, L. J.; Rupasinghe, H. V. Effect of thermal and non-thermal pasteurisation on the microbial inactivation and phenolic degradation in fruit juice: a mini-review. *J. Sci. Food Agric.* **2013**, *93* (5), 981−986.
(11) Huang, K.; Yu, L.; Liu, D.; Gai, L.; Wang, J. Modeling of yeast inactivation of PEF-treated chinese rice wine: effects of electric field intensity, treatment time and initial temperature. *Food Res. Int.* **2013**, *54* (1), 456−467.
(12) Angersbach, A.; Heinz, V.; Knorr, D. Effects of pulsed electric fields on cell membranes in real food systems. *Innovative Food Sci. Emerging Technol.* **2000**, *1*, 135−149.
(13) Zimmermann, U. Electrical breakdown, electropermeabilization and electrofusion. *Rev. Physiol., Biochem. Pharmacol.* **1986**, *105*, 175−256.
(14) Grimi, N.; Lebovka, N. I.; Vorobiev, E.; Vaxelaire, J. Effect of a pulsed electric field treatment on expression behavior and juice quality on Chardonnay grape. *Food Biophys.* **2009**, *4*, 191−198.
(15) Donsì, F.; Ferrari, G.; Fruilo, M.; Pataro, G. Pulsed electric fields − assisted vinification. *Proc. Food Sci.* **2011**, *1*, 780−785.
(16) López, N.; Puértolas, E.; Condón, S.; Álvarez, I.; Raso, J. Application of pulsed electric fields for improving the maceration process during vinification of red wine: influence of grape variety. *Eur. Food Res. Technol.* **2008**, *227* (4), 1099−1107.
(17) López, N.; Puértolas, E.; Condón, S.; Álvarez, I.; Raso, J. Effects of pulsed electric fields on the extraction of phenolic compounds during the fermentation of must of Tempranillo grapes. *Innovative Food Sci. Emerging Technol.* **2008**, *9* (4), 477−482.
(18) Puértolas, E.; López, N.; Saldaña, G.; Álvarez, I.; Raso, J. Evaluation of phenolic extraction during fermentation of red grapes treated by a continuous pulsed electric fields process at pilot-plant scale. *J. Food Eng.* **2010**, *98* (1), 120−125.
(19) Delsart, C.; Cholet, C.; Ghidossi, R.; Grimi, N.; Gontier, E.; Gény, L.; Vorobiev, E.; Mietton-Peuchot, M. Effects of pulsed electric fields on Cabernet Sauvignon grape berries and on the characteristics of wines. *Food Bioprocess Technol.* **2013**, 1−13, DOI: 10.1007/s11947-012-1039-7.
(20) Delsart, C.; Ghidossi, R.; Poupot, C.; Cholet, C.; Grimi, N.; Vorobiev, E.; Milisic, V.; Mietton-Peuchot, M. Enhanced extraction of phenolic compounds from Merlot grapes by pulsed electric field treatment. *Am. J. Enol. Vitic.* **2012**, *63* (2), 205−211.
(21) Pratt, C. Reproductive anatomy in cultivated grapes − a review. *Am. J. Enol. Vitic.* **1971**, *22* (2), 92−109.
(22) Considine, J. A.; Knox, R. B. Development and histochemistry of the cells, cell walls and cuticle of the dermal system of the grape, *Vitis vinifera* L. *Protoplasma* **1979**, *99*, 347−365.
(23) Hardie, W. J.; O'Brien, T. P.; Jaudzens, V. G. Morphology, anatomy and development of the pericarpe after anthesis in grape, *Vitis vinifera* L. *Aust. J. Grape Wine Res.* **1996**, *2* (2), 97−142.
(24) Ollat, N.; Diakou-Verdin, P.; Carde, J. P.; Barrieu, F.; Gaudillere, J. P.; Moing, A. Grape berry development: a review. *J. Int. Sci. Vigne Vin* **2002**, *36* (3), 109−131.
(25) Fougère-Rifot, M.; Park, H. S.; Bouard, J. Ontogenèse du péricarpe de la baie de *Vitis vinifera* L. var. Merlot de la fécondation à la maturité. *J. Int. Sci. Vigne Vin* **1997**, *31* (3), 109−118.
(26) Fougère-Rifot, M.; Cholet, C.; Bouard, J. Evolution des parois des cellules de l'hypoderme de la baie de raisin lors de leur transformation en cellules de pulpe. *J. Int. Sci. Vigne Vin* **1996**, *30* (2), 47−51.
(27) Huang, X. H.; Huang, H. B.; Wang, H. C. Cell wall of loosening skin in post-veraison grape berries lose structural polysaccharides and calcium while accumulate structural proteins. *Sci. Hortic.* **2005**, *104*, 249−263.
(28) Park, H. S.; Fougère-Rifot, M.; Bouard, J. Les tanins vacuolaires de la baie de *Vitis vinifera* L. var. Merlot à maturité. In *Œnologie 95, 5ème Symposium International d'Œnologie*; Tec&Doc: Paris, France, 1995; pp 115−118.
(29) Goulao, L. F.; Oliveira, C. M. Cell wall modifications during fruit ripening: when a fruit is not the fruit. *Trends Food Sci. Technol.* **2008**, *19*, 4−25.
(30) Pirie, A.; Mullin, M. G. Concentration of phenolics in the skin of grape berries during fruit development and ripening. *Am. J. Enol. Vitic.* **1980**, *28* (4), 204−209.
(31) Cholet, C.; Darné, G. Evolution of the contents in soluble phenolic compounds, in proanthocyanic tannins and in anthocyanins of shot grape berries of *Vitis vinifera* L. during their development. *J. Int. Sci. Vigne Vin* **2004**, *38* (3), 171−180.
(32) Gagné, S.; Saucier, C.; Gény, L. Composition and cellular localization of tannins in Cabernet Sauvignon skins during growth. *J. Agric. Food Chem.* **2006**, *54* (25), 9465−9471.
(33) Lacampagne, S. Localization and characterization of grape skin tannins: impact of cell wall physicochemical organization on tannin component, fruit quality and typicality of the Bordeaux grape. Ph.D. Thesis, Doctorat de l'Université Bordeaux2, 2010; 202 pp (http://www.theses.fr/2010BOR21762/document).
(34) Chira, K.; Pacella, N.; Jourdes, M.; Teissedre, P. L. Chemical and sensory evaluation of Bordeaux wines (Cabernet-Sauvignon and Merlot) and correlation with wine age. *Food Chem.* **2010**, *126* (4), 1971−1977.
(35) Colin, L.; Cholet, C.; Gény, L. Relationships between endogenous polyamines, cellular structure and arrested growth of grape berries. *Aust. J. Grape Wine Res.* **2002**, *8* (2), 101−108.
(36) McManus, J. F. A. Histological and histochemical uses of periodic acid. *Stain Technol.* **1948**, *23* (3), 99−108.
(37) Thiéry, J. P. Mise en évidence des polysaccharides sur coupes fines en microscopie électronique. *J. Microscopie* **1967**, *6* (7), 987−1018.
(38) Reynolds, E. The use of lead citrate at high pH as an electron opaque stain in electron microscopy. *J. Cell. Biol.* **1963**, *17*, 208−212.
(39) Gény, L.; Saucier, C.; Bracco, S.; Daviaud, F.; Glories, Y. Composition and cellular localization of tannins in grape seeds during maturation. *J. Agric. Food Chem.* **2003**, *51* (27), 8051−8054.
(40) Harris, P. J. Cell walls. In *Isolation of Membranes and Organelles from Plant Cells*; Hall, J. L., More, A. L., Eds.; Academic Press: New York, 1983; pp 25−83.
(41) Deytieux-Belleau, C.; Vallet, A.; Donèche, B.; Geny, L. Pectin methylesterase and polygalacturonase in the developing grape skin. *Plant Physiol. Biochem.* **2008**, *46* (7), 638−646.
(42) Rapeanu, G.; Van Loey, A.; Smout, C.; Hendrickx, M. Thermal and high-pressure inactivation kinetics of polyphenol oxidase in Victoria grape must. *J. Agric. Food Chem.* **2005**, *53* (8), 2988−2994.
(43) Saulnier, L.; Thibault, J. F. Extraction and characterization of pectic substances from pulp of grape berries. *Carbohydr. Polym.* **1987**, *7*, 329−343.
(44) Revilla, E.; Ryan, J. M.; Martin-Ortega, G. Comparison of several procedures used for the extraction of anthocyanins from red grapes. *J. Agric. Food Chem.* **1998**, *46* (11), 4592−4597.
(45) Kennedy, J. A.; Hayasaka, Y.; Vidal, S.; Waters, E. J.; Jones, G. P. Composition of grape skin proanthocyanidins at different stages of berry development. *J. Agric. Food Chem.* **2001**, *49* (11), 5348−5355.

(46) Robertson, G. L. The fractional extraction and quantitative determination of pectic substance in grapes and musts. *Am. J. Enol. Vitic.* **1979**, *30*, 182−186.
(47) Bindon, K. A.; Madani, S. H.; Pendleton, P.; Smith, P.; Kennedy, J. A. Factors affecting skin tannin extractability in ripening grapes. *J. Agric. Food Chem.* **2014**, *62* (5), 1130−1141.
(48) Hernández-Hierro, J. M.; Quijada-Morín, N.; Martínez-Lapuente, L.; Guadalupe, Z.; Ayestarán, B.; Rivas-Gonzalo, J. C.; Escribano-Bailón, M. T. Relationship between skin cell wall composition and anthocyanin extractability of *Vitis vinifera* L. cv. Tempranillo at different grape ripeness degree. *Food Chem.* **2014**, *146*, 41−47.
(49) Ortega-Regules, A.; Romero-Cascales, I.; Ros-García, J. M.; López-Roca, J. M.; Gómez-Plaza, E. A first approach towards the relationship between grape skin cell-wall composition and anthocyanin extractability. *Anal. Chim. Acta* **2006**, *563* (1−2 special issue), 26−32.
(50) Renard, C. M. G. C.; Baron, A.; Guyot, S.; Drilleau, J. F. Interactions between apple cell walls and native apple polyphenols: quantification and some consequences. *Int. J. Biol. Macromol.* **2001**, *29* (2), 115−125.
(51) Saunder, J. A.; Lin, C. H.; Hou, B. H.; Cheng, J.; Tsengawa, N.; Lin, J. J.; Smith, C. R.; Macintoch, M. S.; Wert, S. V. Rapid optimization of electroporation conditions for plant cells protoplasts, and pollen. *Mol. Biotechnol.* **1995**, *3*, 181−190.
(52) Wu, F. S.; Feng, T. Y. Delivery of plasmid DNA into intact plant cells by electroporation of plamolysed cells. *Plant Cell Rep.* **1999**, *18*, 381−386.
(53) Le Bourvellec, C.; Guyot, S.; Renard, C. M. G. C. Non-covalent interaction between procyanidins and apple cell wall material: Part I. Effect of some environmental parameters. *Biochim. Biophys. Acta−Gen. Subj.* **2004**, *1672* (3), 192−202.
(54) Calderón-Miranda, M. L.; Barbosa-Cánovas, G. V.; Swanson, B. G. Inactivation of *Listeria innocua* in liquid whole egg by pulsed electric fields and nisin. *Int. J. Food Microbiol.* **1999**, *51* (1), 7−17.
(55) Barnavon, L.; Doco, T.; Terrier, N.; Ageorges, A.; Romieu, C.; Pellerin, P. Involvement of pectin methyl-esterase during the ripening of grape berries: cDNA isolation, transcript expression and changes in the degree of methyl-esterification of cell wall pectins. *Phytochemistry* **2001**, *58*, 693−701.
(56) Cabanne, C.; Donèche, B. Changes in polygalacturonase activity and calcium content during ripening of grape berries. *Am. J. Enol. Vitic.* **2001**, *5* (4), 331−335.

Some of these compounds were detected for the first time in the genus *Brassica* and species *B. napus*.

MATERIALS AND METHODS

Chemicals. NaOH and HCl were purchased from Sangon Biological Engineering Technology and Service Co., Ltd. (Shanghai, China). Methanol, formic acid, acetone, and acetonitrile were of HPLC grade (Sigma, St. Louis, MO). Water was purified using a Milli-Q system (Millipore, Bedford, MA). Procyanidin B2, (−)-epicatechin, and quercetin-3-*O*-β-D-glucoside were purchased from Sigma. Isorhamnetin-3-*O*-glucoside was purchased from ChromaDex (Irvine, CA). Sephadex LH-20 was purchased from GE Healthcare BioSciences AB (Uppsala, Sweden).

Plant Materials and Sample Collection. According to previous research, some flavonoids and hydroxycinnamic acid derivatives normally combine with other seed coat components, which makes them difficult to identify. The flavonoid and hydroxycinnamic acid derivative contents of rapeseed accumulate in the early periods of seed development and reach their peak about 5 weeks after flowering (WAF).[23] In the present study, *B. napus* L. var. *napus* (cv.Yang 6) grown in a greenhouse at approximately 25 °C with a 16 h light/8 h dark cycle was used as the plant material. Two weeks after seedling development, rapeseed lines were planted into 15 cm diameter pots filled with the same soil (20% vermiculite and 80% orchid soil). The plants were vernalized for 2 months at 4 °C. Each flower on the primary raceme was tagged on the day of pollination. Developing seeds were harvested at 5 WAF for phenolic analysis. Five pods from individual plants of one rapeseed line were collected, pooled, and immediately frozen in liquid nitrogen for further analysis.

Preparation of Crude Methanol Extract. The powder (40 g) of dissected rapeseeds was extracted with 200 mL of 80% methanol in an ultrasonicator bath at 4 °C for 1 h. The supernatant was collected after centrifugation (10 000 rpm, 10 min, 4 °C) and stored at −80 °C. The pellet was again extracted overnight with 100 mL of the same extraction buffer at 4 °C under agitation (200 rpm). The supernatant from the second extraction was collected and pooled with the supernatant collected from the previous day. The extracts were subsequently concentrated using a vacuum rotary evaporator at 35 °C, and the slurry was washed with ddH_2O to a final volume of 4 mL. Finally, the obtained crude extract was diluted with 5 volumes of methanol, filtered through a 0.45 μm Teflon membrane (Interchim, Montluc-on, France), and analyzed by HPLC-PDA−ESI(−)-MS^n (IonTrap) and HPLC-DAD−ESI(−)-HRMS (Q-TOF).

Preparation of Sephadex LH-20 Column Chromatography Fractions. Column chromatography of the crude extract described above was carried out according to the method described by Yang et al.[26] with several modifications. The crude extract (2 mL) was loaded onto a 22 mm i.d. × 470 mm length glass column packed with 25 g of Sephadex LH-20 medium resin (dry particle size 18−118 μm); the resin was swelled in ddH_2O overnight and equilibrated with ddH_2O before use. Finally, the column was eluted with the solvents listed in Table 1. The elution speed was controlled to 1 mL min^{-1}, and 150 mL of each collection was produced. The column was regenerated by washing with 10 column volumes of ddH_2O. Each fraction was again concentrated using a vacuum rotary evaporator at 35 °C, and the slurry was washed with ddH_2O to a final volume of 3 mL, which was transferred into a 10 mL glass tube and evaporated using nitrogen flow. Finally, the slurry was washed with 1 mL to 2 mL 80% methanol, filtered with Teflon membrane, and analyzed with HPLC−PDA−ESI(−)/MSn (LCQ) and HPLC−DAD−ESI(−)/HRMS (Q-TOF).

Table 1. Eluotropic Series for Sephadex LH-20 Column Chromatography

fraction	H_2O concn (%)	MeOH concn (%)	acetone concn (%)
F1	100	0	0
F2	70	30	0
F3	50	50	0
F4	50	40	10
F5	50	30	20
F6	50	20	30
F7	50	10	40
F8	40	0	60

Alkaline Hydrolysis of Crude Extracts. Alkaline hydrolysis of the crude extracts was carried out according to the method described by Lin et al.[8] with minor modifications. The crude extract (0.4 mL) was evaporated by nitrogen flow, and the residue was mixed with 0.3 mL of 2 N NaOH under a N_2 atmosphere for 18 h. Then, 0.1 mL of HCl (37%) was added to the reaction mixture to adjust the pH to 1.0, and 1.6 mL of methanol was added. After filtering through a Teflon membrane, the extract was analyzed by HPLC-PDA−ESI(−)-MS^n (IonTrap) and HPLC-DAD−ESI(−)-HRMS (Q-TOF).

HPLC-PDA−ESI(−)-MS^n (IonTrap) Analysis. The crude extract, alkaline-hydrolyzed extract, and eight fractions of the crude extract were analyzed using an LCQ Deca XP MAX (ThermoFinnigan, San Jose, CA) instrument to determine the UV absorption characteristics and MS^n fragmentation patterns of the flavonoids and other compounds. The instrument was operated using Xcalibur version 1.4 software. An LCQ Deca XP MAX system with an ion-trap mass spectrometer including an LC pump, a Finnigan Surveyor autosampler, and a Thermo Finnigan Surveyor PDA detector was used. Separation was performed on an RP-C18 column (150 mm × 4.6 mm, 5 μm, Agilent Technologies, Waldbronn, Germany) at 30 °C. The flow rate was set to 0.8 mL min^{-1}, and the injection volume was set to 10 μL. The mobile phase consisted of a combination of solvent A (0.1% formic acid in water, v/v) and solvent B (0.1% formic acid in acetonitrile, v/v). The linear gradient was as follows: 4%−20% B (v/v) for 40 min, 35% B for 60 min, 100% B for 61 min, hold at 100% B for 76 min, 4% B for 77 min, and hold at 4% B to 86 min. UV−vis spectra were recorded from 200 to 600 nm. The mass analyzer was a ThermoFinnigan LCQ IonTrap instrument coupled with an ESI source. The instrument was set to negative ion mode with an m/z range of 90−2000. The following conditions were adopted: capillary temperature of 300 °C, sheath gas of 70 arbitrary units, capillary voltage of 20 V, and tube lens of 70 V. Under 50% normalized collision energy, the most intense ion was selected to obtain the MS^2, MS^3, and MS^4 data. The collision gas used was nitrogen.

HPLC-DAD−ESI(−)-HRMS (Q-TOF) Analysis. The extracts were subjected to HPLC-DAD−ESI(−)-HRMS (Q-TOF) analysis to determine their exact molecular mass, identify the elemental composition of the compounds, and verify the result of MS^n (IonTrap) analysis. An Ultimate 3000 series instrument (Dionex Sunnyvale, CA) coupled with an Ultimate 3000 pump including an autosampler, a column compartment, and a DAD detector was used for liquid chromatography. Separation was performed using the same gradient described above; here, an Ultimate XB-C18 column (3.5 μm, 2.1 mm × 150 mm, Welch) and a Phenomenex precolumn (2 mm × 4 mm, Torrance, CA) were used at 30 °C. The flow rate was set to 0.2 mL min^{-1}, and the injection volume was 10 μL. The DAD was set to 520, 330, and 280 nm to record peaks, and UV−vis spectra were recorded from 190 to 800 nm. A Bruker Daltonik (Bremen, Germany) maXis Q-TOFHRMS instrument with an ESI source was used for mass analysis. The instrument was operated by the microTOF control (Bruker Daltonik) software package. Negative ion mode and an m/z range of 100−2000 were selected during operation. The nebulizer gas (N_2) pressure was 1.5 bar, the drying gas flow was 6 L min^{-1}, the drying gas temperature was 180 °C, and the capillary voltage was 2500 V.

RESULTS AND DISCUSSION

Confirmation of Flavonol Glycosides. The structures of the compounds identified in seeds of *B. napus* L. var. *napus* are shown in Figure 1. The HPLC−UV (330 nm) profiles of flavonoids and hydroxycinnamic acid derivatives obtained from the crude extracts and chromatography fractions are presented in Figure 2. Fifteen flavonol glycosides were successfully

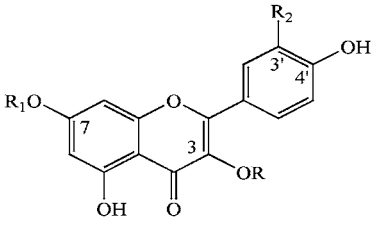

Flavonols and their glycosides:
Kaempferol: $R=R_1=R_2=H$ (MW=286 Da)
Quercetin: $R=R_1=H$, $R_2=OH$ (MW=302 Da)
Isorhamnetin: $R=R_1=H$, $R_2=OMe$ (MW=316 Da)
Glycosides: R or R and R_1=glycosyls

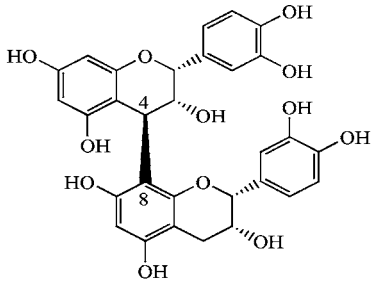

Procyanidin B2 ([DP 2], MW=578 Da)

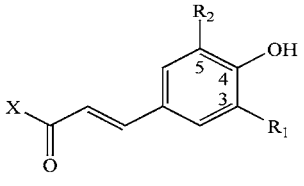

Hydroxycinnamoyls (the mass data):
p-Coumaroyl: $R_1=R_2=H$ (+146 Da)
Caffeoyl: $R_1=OH$, $R_2=H$ (+162 Da)
Feruloyl: $R_1=OMe$, $R_2=H$ (+176 Da)
Hydroxyferuloyl: $R_1=OMe$, $R_2=OH$ (+192 Da)
Sinapoyl: $R_1=R_2=OMe$ (+206 Da)

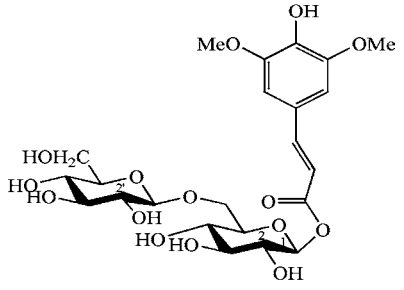

1-Sinapoylgentiobiose (MW=548 Da)

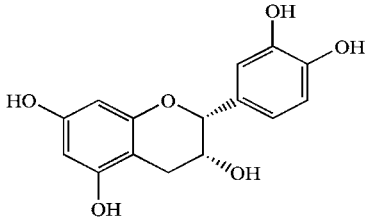

(-)-Epicatechin (MW=290 Da)

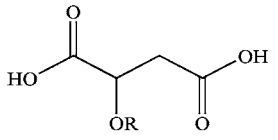

Malic acid (R=H, MW=134 Da)

Figure 1. Structures of compounds identified in seeds of *B. napus* L. var. *napus*.

identified according to their retention times, UV−vis wavelength maxima (λ_{max}), MS^2, MS^3, and MS^4 ion characteristics, alkaline hydrolysis patterns, and HRMS profiles. The corresponding chemical information of the identified phenolic compounds is listed in Table 2.

On the basis of previous conclusions,[8,14,16] the identified flavonol glycosides were analyzed according to their UV wavelength maxima (λ_{max}) and MS^n fragments. For example, the UV spectra of the 3-*O*-glycosides and 3-*O*-,7-*O*-diglycosides in both quercetin and isorhamnetin showed λ_{max} at approximately 255−270 nm (band II) and 345−355 nm (band I), respectively. The 7-*O*-glycosides in quercetin and isorhamnetin showed λ_{max} at 255−270 nm (band II) and 370 nm (band I), respectively. By contrast, the λ_{max} values of 3-*O*-glycosides, 3-*O*-,7-*O*-diglycosides, and 7-*O*-glycosides on kaempferol were detected at around 255−270 nm (band II), 345−350 nm (band II), and 365 nm (band I), respectively.

During the formation of flavonol derivatives in Cruciferae, glycosylation initially occurs at 3-OH and then at 7-OH. During MS^n analysis with negative ionization, the major MS^2 product ions resulting from the loss of 7-*O*-glycosides were first detected, followed by the main MS^3 product ions formed by the loss of 3-*O*-glycosides.[16,27] According to the size of the MS^n fragments, losses of glucosyl (162 Da) and sophorosyl (2-*β*-D-glucopyranosyl-D-glucopyranosyl)/sophorotriosyl (2-*β*-D-glucopyranosyl-20-*β*-D-glucopyranosyl-D-glucopyranosyl) (120 Da/180 Da) were also detected. Several compounds could be confirmed on the basis of the chemical formulas obtained from HRMS analysis and alkaline hydrolysis characteristics. For instance, kaempferol-3-*O*-sophoroside-7-*O*-glucoside (peak 5), which has been previously reported,[21] exhibited UV spectra with λ_{max} at 255 and 350 nm. The major MS^2 fragment at m/z 609 obtained from the loss of a glucosyl (162 Da) was first detected, followed by two major MS^3 fragments, including an ion fragment at m/z 429 from the partial loss of a sophorosyl (180 Da) and a parent ion at m/z 285 from the complete loss of a sophorosyl. The presence of peak 5 after alkaline hydrolysis indicates the presence of glucosyl rather than caffeoyl in this compound, which is in agreement with the HRMS analysis.

In summary, 15 glucosylated flavonols were successfully identified (Table 2), including 6 isomers of kaempferol diglucoside and 2 isomers of quercetin triglucoside. We found that the number of glycosides varied among the different flavonol derivatives. The 15 glucosylated flavonols consisted of 9 glycosylated kaempferol compounds, 3 glycosylated quercetin compounds, and 3 glycosylated isorhamnetin compounds. Five

dx.doi.org/10.1021/jf404826u | J. Agric. Food Chem. 2014, 62, 2935−2945

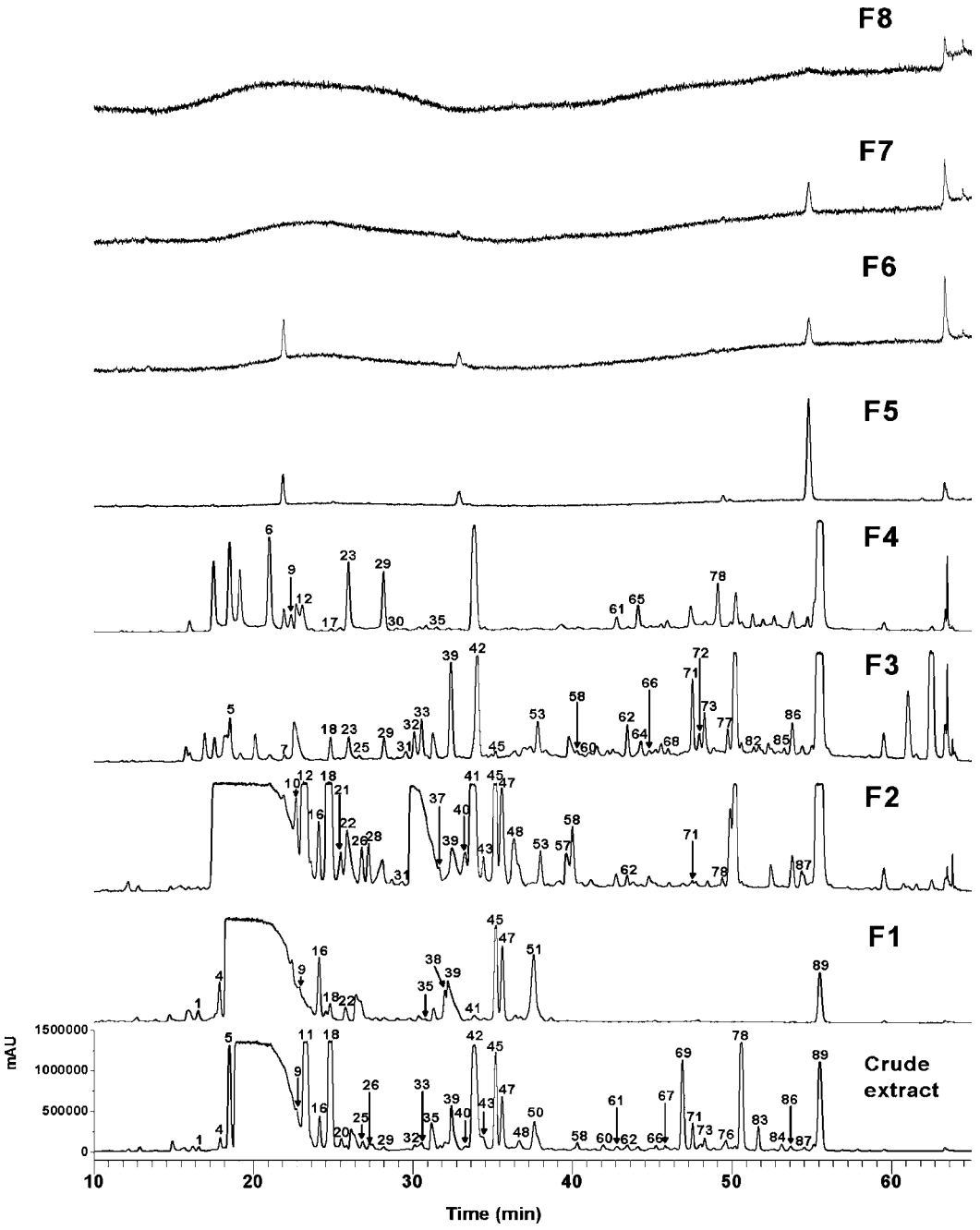

Figure 2. LC chromatograms (330 nm) for the crude extracts and column chromatography fractions (F1−F8) of phenolic compounds in rapeseed. Peaks: (1) qn-3-*O*-sophoroside-7-*O*-glucoside; (4) km-*O*-diglucoside; (5) km-3-*O*-sophoroside-7-*O*-glucoside; (6) sinapoylhexose; (7) km-3-*O*-caffeoylsophoroside-7-*O*-glucoside; (9) procyanidin B2; (10) qn-3-*O*-sinapoylsophoroside-7-*O*-glucoside; (11) *cis*-sinapic acid; (12) sinapoylhexose; (16) km-3-*O*-sinapoylsophorotrioside-7-*O*-glucoside; (17) (−)-epicatechin; (18) km-3-*O*-sinapoylsophoroside-7-*O*-glucoside; (20) putative hydroxycinnamic acid derivative; (21) km-3-*O*-glucoside-7-*O*-glucoside; (22) km-3-*O*-feruloylsophoroside-7-*O*-glucoside; (23) sinapoylhexose; (25) km-3-*O*-*p*-coumaroylsophoroside-7-*O*-glucoside; (26) is-3-*O*-glucoside-7-*O*-glucoside; (28) sinapoylgentiobiose; (29) sinapoylhexose; (30) [DP 3]; (31) km-3-*O*-sophoroside; (32) qn-3-*O*-sophoroside; (33) km-3-*O*-diglucoside; (35) [DP 4]; (37) km-3-*O*-caffeoyldiglucoside-7-*O*-glucoside; (38) km-3-*O*-sinapoylsophotrioside-7-*O*-glucoside; (39) is-3-*O*-diglucoside; (40) km-3-*O*-disinapoylgalloyldiglucoside; (41) km-*O*-dihydroxyferuloylsinapoyldiglucoside; (42) km-7-*O*-sophoroside; (43) qn-3-*O*-sinapoylsophoroside-7-*O*-glucoside; (45) km-3-*O*-sinapoyldiglucoside-7-*O*-glucoside; (47) is-3-*O*-sinapoyldiglucoside-7-*O*-glucoside; (48) is-*O*-glucoside-sulfate; (50) [DP 2]; (51) sinapoylmalic acid; (53) km-3-*O*-sinapoylsophoroside; (57) km-3-*O*-sinapoyldiglucoside-7-*O*-glucoside; (58) km-3-*O*-sinapoylsophoroside-7-*O*-glucoside; (60) is-3-*O*-sinapoylglucoside-sulfate-7-*O*-glucoside; (61) km-3-*O*-glucoside; (62) km-3-*O*-sophoroside-7-*O*-sinapoylglucoside; (64) km-3-*O*-disinapoylhydroxyferuloyldiglucoside; (65) is-3-*O*-glucoside; (66) km-3-*O*-sinapoylsophoroside-7-*O*-sinapoylglucoside; (67) km-3-*O*-disinapoylhydroxyferuloyldiglucoside; (68) km-3-*O*-sinapoyltriglucoside-7-*O*-sinapoylglucoside; (69) disinapoylgentiobiose; (71) km-3-*O*-sinapoyldiglucoside-7-*O*-sinapoylglucoside; (72) is-3-*O*-sinapoylglucoside-7-*O*-glucoside; (73) km-3-*O*-sinapoylglucoside-7-*O*-glucoside; (76) putative hydroxycinnamic acid derivative; (77) km-3-*O*-trisinapoylhydroxyferuloylsophoroside; (78) 1,2-disinapoylglucoside; (82) km-3-*O*-disinapoylhydroxyferuloylglucoside-7-sinapoylglucoside; (83) 1,2,2′-trisinapoylgentiobiose; (84) putative hydroxycinnamic acid derivative; (85) km-3-*O*-sinapoylsophoroside; (86) km-3-*O*-sinapoylsophoroside-7-*O*-sinapoylglucoside; (87) putative hydroxycinnamic acid derivative; (89) putative hydroxycinnamic acid derivative.

dx.doi.org/10.1021/jf404826u | *J. Agric. Food Chem.* 2014, 62, 2935−2945

Table 2. HPLC-PDA–ESI(−)-MS^n/HRMS Data and Putative Identification of Flavonoids and Hydroxycinnamic Acid Derivatives in Seeds of *B. napus* L. var. *napus*

peak	t_R (min)	measd m/z $[M - H]^-$	calcd formula $[M - H]^-$	error (ppm)	major and important MS^2 ions (m/z) (%)	major and important MS^3 ions (m/z) (%)	major and important MS^4 ions (m/z) (%)	UV λ_{max} (nm)	tentative identification[a]
1	16.57	787.1945	$C_{33}H_{39}O_{22}$	−0.9	625 (100)	445 (23), 301 (85), 300 (100)	nt[b]	255, 355	qn-3-*O*-sophoroside-7-*O*-glucoside
2	17.40	787.1938	$C_{33}H_{39}O_{22}$	0.0	625 (100)	463 (100), 300 (42)	nd[c]	nd	qn-3-*O*-diglucoside-7-*O*-glucoside[d]
3	17.63	933.2529	$C_{39}H_{49}O_{26}$	−1.1	771 (100)	429 (51), 284 (100)	nt	265, 345	km-3-*O*-triglucoside-7-*O*-glucoside[d]
4	17.89	609.1469	$C_{27}H_{29}O_{16}$	−1.3	447 (100), 285 (30)	nd	nd	nd	km-*O*-diglucoside
5	18.50	771.1997	$C_{33}H_{39}O_{21}$	−1.0	609 (100)	429 (33), 285 (48), 284 (100)	nt	255, 350	km-3-*O*-sophoroside-7-*O*-glucoside
6	21.00	385.1137	$C_{17}H_{21}O_{10}$	0.9	247 (100), 223 (11), 205 (6)	nt	nd	240, 330	sinapoylhexose[d]
7	21.96	933.2307	$C_{42}H_{45}O_{24}$	0.0	771 (100)	609 (100), 447 (11), 429 (29), 285 (5)	nd	268, 330	km-3-*O*-caffeoylsophoroside-7-*O*-glucoside[d]
8	22.21	431.1923	$C_{20}H_{31}O_{10}$	−0.1	359 (69), 281 (83), 223 (100)	nt	nd	nd	putative hydroxycinnamic acid derivative
9	22.50	577.1361	$C_{30}H_{25}O_{12}$	−1.7	425 (100), 407 (44), 289 (18)	nt	nd	202, 280	procyanidin B2 ([DP 2])
10	22.82	993.2525	$C_{44}H_{49}O_{26}$	0.5	831 (78), 625 (100)	nd	nd	255, 330	qn-3-*O*-sinapoylsophoroside-7-*O*-glucoside
11	23.26	223.0616	$C_{11}H_{11}O_5$	−1.6	193 (100), 164 (74)	nt	nd	nd	*cis*-sinapic acid
12	23.40	385.1141	$C_{17}H_{21}O_{10}$	−0.3	247 (69), 223 (100)	208 (32), 179 (21), 164 (100)	nd	nd	sinapoylhexose
13	23.92	547.1670	$C_{23}H_{31}O_{15}$	0.9	411 (36), 223 (100)	208 (100), 179 (40)	nd	nd	sinapoylgentiobiose[d]
14	23.93	977.2584	$C_{44}H_{49}O_{25}$	−1.6	815 (100), 785 (24), 771 (57)	609 (100)	nd	nd	km-3-*O*-sinapoyldiglucoside-7-*O*-glucoside[d]
15	24.08	719.1148	$C_{28}H_{31}O_{20}S$	−1.9	639 (100), 477 (50), 315 (23)	nd	nd	nd	is-*O*-diglucoside-sulfate[e]
16	24.17	1139.3100	$C_{50}H_{59}O_{30}$	−0.3	977 (100), 771 (21), 609 (12), 285 (15)	nd	nd	270, 335	km-3-*O*-sinapoylsophorotrioside-7-*O*-glucoside[d]
17	24.46	289.0714	$C_{15}H_{13}O_6$	1.2	245 (100), 205 (38), 179 (22)	203 (100), 187 (39)	nt	220, 280	(−)-epicatechin
18	24.84	977.2581	$C_{44}H_{49}O_{25}$	−1.3	815 (100), 609 (10)	609 (100), 591 (33), 285 (7)	429 (100), 284 (71), 285 (23)	270, 335	km-3-*O*-sinapoylsophoroside-7-*O*-glucoside
19	24.91	1045.2459	$C_{47}H_{49}O_{27}$	0.7	977 (49), 815 (100), 609 (39), 447 (20), 285 (9)	nd	nd	nd	putative kaempferol derivative
20	25.28	729.2621	$C_{33}H_{45}O_{18}$	−1.3	533 (17), 341 (100), 179 (29)	nd	nd	nd	putative hydroxycinnamic acid derivative
21	25.50	609.1479	$C_{27}H_{29}O_{16}$	−2.9	489 (35), 447 (100), 285 (22)	284 (100), 243 (51)	nd	nd	km-3-*O*-glucoside-7-*O*-glucoside[d]
22	25.80	947.2457	$C_{43}H_{47}O_{24}$	0.6	785 (100), 609 (19)	609 (100), 623 (79) 591 (62)	429 (100), 284 (27)	270, 330	km-3-*O*-feruloylsophoroside-7-*O*-glucoside[d]
23	25.99	385.1144	$C_{17}H_{21}O_{10}$	−0.1	325 (71), 295 (100), 265 (63),223 (21)	223 (100)	nt	240, 325	sinapoylhexose[d]
24	26.64	547.1662	$C_{23}H_{31}O_{15}$	1.2	223 (100), 205 (27)	208 (100), 164 (77)	nt	nd	sinapoylgentiobiose[d]
25	26.71	917.2351	$C_{42}H_{45}O_{23}$	0.7	755 (100)	609 (100), 591 (7)	nd	nd	km-3-*O*-*p*-coumaroylsophoroside-7-*O*-glucoside[d]
26	26.81	639.1561	$C_{28}H_{31}O_{17}$	0.8	477 (100), 315 (21)	315 (40),314 (100)	nd	nd	is-3-*O*-glucoside-7-*O*-glucoside[d]
27	27.02	465.0715	$C_{13}H_{21}O_{18}$	4.0	421 (44), 379 (100), 283 (11), 223 (26)	nd	nd	nd	putative hydroxycinnamic acid derivative
28	27.26	547.1666	$C_{23}H_{31}O_{15}$	0.5	385 (34), 223 (100)	208 (100), 179 (42)	nd	240, 325	sinapoylgentiobiose[d]
29	28.21	385.1135	$C_{17}H_{21}O_{10}$	1.3	325 (69), 295 (100), 265 (81), 223 (24)	223 (100)	nt	240, 325	sinapoylhexose[d]
30	28.50	865.1994	$C_{45}H_{37}O_{18}$	−1.0	577 (62), 451 (71), 407 (100), 289 (78)	nt	nd	240, 280	[DP 3]
31	29.31	609.1460	$C_{27}H_{29}O_{16}$	0.2	447 (100), 429 (31)	285 (100)	nd	nd	km-3-*O*-sophoroside[d]
32	30.02	625.1410	$C_{27}H_{29}O_{17}$	0.0	463 (100), 445 (44), 300 (81)	300 (100)	nd	265, 345	qn-3-*O*-sophoroside[d]
33	30.60	609.1452	$C_{27}H_{29}O_{16}$	1.4	44 (53), 285 (100)	257 (100), 241 (41)	nd	265, 335	km-3-*O*-diglucoside[d]
34	30.85	753.2260	$C_{34}H_{41}O_{19}$	−1.5	529 (100), 487 (42)	427 (22), 223 (100)	nt	nd	disinapoylgentiobiose[d]
35	30.90	1153.2634	$C_{60}H_{49}O_{24}$	−1.3	865 (43), 575 (100), 413 (35), 289 (42)	nd	nd	nd	[DP 4]

dx.doi.org/10.1021/jf404826u | J. Agric. Food Chem. 2014, 62, 2935−2945

Table 2. continued

peak	t_R (min)	measd m/z $[M - H]^-$	calcd formula $[M - H]^-$	error (ppm)	major and important MS^2 ions (m/z) (%)	major and important MS^3 ions (m/z) (%)	major and important MS^4 ions (m/z) (%)	UV λ_{max} (nm)	tentative identification[a]
36	31.34	719.1154	$C_{28}H_{31}O_{20}S$	−2.6	639 (100), 403 (27), 315 (12)	315 (100), 211 (69)	nd	nd	is-*O*-diglucoside-sulfate[e]
37	31.73	933.2311	$C_{42}H_{45}O_{24}$	−0.5	771 (100), 609 (10)	609 (100)	447 (100), 285 (46)	nd	km-3-*O*-caffeoyldiglucoside-7-*O*-glucoside[e]
38	32.02	1139.3083	$C_{50}H_{59}O_{30}$	1.2	977 (100), 815 (53)	nd	nd	270, 320	km-3-*O*-sinapoylsophotrioside-7-*O*-glucoside[d]
39	32.40	639.1570	$C_{28}H_{31}O_{17}$	−0.5	477 (45), 315 (100), 313 (46)	300 (100)	nt	256, 350	is-3-*O*-diglucoside[d]
40	33.28	1173.2715	$C_{56}H_{53}O_{28}$	1.2	815 (100)	609 (100)	nd	275, 330	km-3-*O*-disinapoylgalloyldiglucoside[e]
41	33.74	1199.2885	$C_{58}H_{55}O_{28}$	0.5	993 (11), 771 (27), 609 (49), 427 (100), 285 (12)	nd	nd	nd	km-*O*-dihydroxyferuloylsinapoyldiglucoside[e]
42	34.10	609.1469	$C_{27}H_{29}O_{16}$	−1.3	447 (9), 429 (100), 285 (91)	369 (44), 339 (100). 327 (65), 309 (72)	nd	nd	km-7-*O*-sophoroside[d]
43	34.44	993.2521	$C_{44}H_{49}O_{26}$	−0.3	831 (100)	669 (67), 625 (100), 463 (32), 301 (29)	nd	265, 330	qn-3-*O*-sinapoylsophoroside-7-*O*-glucoside[d]
44	34.61	681.1662	$C_{30}H_{33}O_{18}$	1.5	476 (100), 315 (29)	315 (100)	nt	nd	is-3-*O*-glucoside-7-*O*-acetylglucoside[e]
45	35.20	977.2586	$C_{44}H_{49}O_{25}$	−1.8	815 (100), 653 (28), 609 (4)	653 (100), 447 (14), 285 (4)	nd	265, 330	km-3-*O*-sinapoyldiglucoside-7-*O*-glucoside[e]
46	35.23	609.1467	$C_{27}H_{29}O_{16}$	−1.0	490 (7), 429 (21), 355 (10), 284 (100)	nt	nd	nd	km-*O*-sophoroside[d]
47	35.70	1007.2683	$C_{45}H_{51}O_{26}$	−0.9	845 (100)	683 (100), 639 (21), 477 (43), 315 (14)	nd	265, 330	is-3-*O*-sinapoyldiglucoside-7-*O*-glucoside
48	36.65	557.0624	$C_{22}H_{21}O_{15}S$	1.4	477 (100), 395 (7), 315 (18)	315 (100)	nd	265, 320	is-*O*-glucoside-sulfate
49	37.28	977.2578	$C_{44}H_{49}O_{25}$	−0.9	815 (100)	653 (100)	353 (68), 285 (100)	nd	km-3-*O*-sinapoyldiglucoside-7-*O*-glucoside[e]
50	37.42	577.1359	$C_{30}H_{25}O_{12}$	−1.3	451 (35), 425 (100), 407 (41), 289 (19)	407 (100)	nt	nd	[DP 2]
51	37.58	339.0720	$C_{15}H_{15}O_9$	0.3	223 (100)	208 (100), 179 (41), 164 (55)	nd	240,330	sinapoylmalic acid
52	37.60	223.0616	$C_{11}H_{11}O_5$	−1.6	208 (100), 179 (32), 164 (51)	nt	nd	nd	*trans*-sinapic acid
53	37.86	815.2046	$C_{38}H_{39}O_{20}$	−0.7	623 (66), 609 (100), 591 (34)	429 (100), 284 (20)	nd	nd	km-3-*O*-sinapoylsophoroside[d]
54	37.92	679.1519	$C_{30}H_{31}O_{18}$	−0.4	631 (82), 479 (89), 223 (100)	nt	nd	nd	putative hydroxycinnamic acid derivative
55	38.15	917.2144	$C_{45}H_{41}O_{21}$	0.2	639 (19), 577 (67), 407 (100), 223 (79)	nt	nd	nd	putative hydroxycinnamic acid derivative
56	38.31	865.2005	$C_{45}H_{37}O_{18}$	−2.3	695 (37), 587 (76), 407 (84), 289 (100)	nt	nd	nd	[DP 3]
57	39.23	977.2586	$C_{44}H_{49}O_{25}$	−1.8	815 (100), 653 (30)	653 (100), 447 (59), 285 (7)	nd	nd	km-3-*O*-sinapoyldiglucoside-7-*O*-glucoside[e]
58	40.26	977.2585	$C_{44}H_{49}O_{25}$	−1.7	609 (100), 815 (36)	429 (100), 285 (65)	nd	265, 330	km-3-*O*-sinapoylsophoroside-7-*O*-glucoside[d]
59	40.40	947.2469	$C_{43}H_{47}O_{24}$	−0.7	785 (100)	609 (47), 591 (100)	nd	nd	km-3-*O*-feruloyldiglucoside-7-*O*-glucoside[e]
60	41.05	925.1709	$C_{39}H_{41}O_{24}S$	0.5	763 (100)	601 (100), 557 (57), 315 (29)	nd	275, 330	is-3-*O*-sinapoylglucoside-sulfate-7-*O*-glucoside[e]
61	42.74	447.0934	$C_{21}H_{19}O_{11}$	−0.3	357 (23), 285 (100). 284 (80)	nt	nd	265, 345	km-3-*O*-glucoside
62	43.40	977.2574	$C_{44}H_{49}O_{25}$	−0.6	609 (100)	429 (71), 285 (100)	nd	265, 340	km-3-*O*-sophoroside-7-*O*-sinapoylglucoside
63	43.84	947.2471	$C_{43}H_{47}O_{24}$	−0.8	644 (35), 609 (100), 285 (38)	nd	nd	nd	km-3-*O*-diglucoside-7-*O*-feruloylglucoside[e]
64	44.28	1213.3035	$C_{59}H_{57}O_{28}$	0.6	815 (21), 609 (100), 285 (29)	nd	nd	270, 330	km-3-*O*-disinapoylhydroxyferuloyldiglucoside[e]
65	44.25	477.1047	$C_{22}H_{21}O_{12}$	−1.8	315 (43), 314 (100)	285 (100), 243 (55)	nd	265, 355	is-3-*O*-glucoside
66	45.27	1183.3156	$C_{55}H_{59}O_{29}$	−0.7	977 (15), 815 (100), 609 (21), 285 (7)	609 (100), 429 (42), 285 (23)	nd	270, 330	km-3-*O*-sinapoylsophoroside-7-*O*-sinapoylglucoside[e]
67	45.90	1213.3039	$C_{59}H_{57}O_{28}$	0.2	1080 (11), 609 (100), 285 (21)	nd	nd	nd	km-3-*O*-disinapoylhydroxyferuloyldiglucoside[e]

dx.doi.org/10.1021/jf404826u | J. Agric. Food Chem. 2014, 62, 2935−2945

Table 2. continued

peak	t_R (min)	measd m/z $[M - H]^-$	calcd formula $[M - H]^-$	error (ppm)	major and important MS^2 ions (m/z) (%)	major and important MS^3 ions (m/z) (%)	major and important MS^4 ions (m/z) (%)	UV λ_{max} (nm)	tentative identification[a]
68	46.00	1345.3681	$C_{61}H_{69}O_{34}$	−0.4	977 (100), 815 (23)	785 (17), 771 (100), 753 (21)	nd	275, 330	km-3-*O*-sinapoyltriglucoside-7-*O*-sinapoylglucoside[e]
69	46.71	753.2253	$C_{34}H_{41}O_{19}$	−0.7	529 (100)	289 (64), 223 (76), 205 (100),	nt	nd	disinapoylgentiobiose[d]
70	46.82	845.2157	$C_{39}H_{41}O_{21}$	−1.3	683 (100), 477 (13), 459 (10)	477 (38), 353 (100), 315 (30)	nd	nd	is-3-*O*-sinapoylglucoside-7-*O*-glucoside[e]
71	47.6	1183.3162	$C_{55}H_{59}O_{29}$	−1.2	815 (100), 623 (37)	609 (100)	nd	270, 330	km-3-*O*-sinapoyldiglucoside-7-*O*-sinapoylglucoside[e]
72	48.01	845.2161	$C_{39}H_{41}O_{21}$	−1.8	683 (100), 477 (21), 357 (7)	353 (100), 329 (57), 315 (63)	nt	270, 330	is-3-*O*-sinapoylglucoside-7-*O*-glucoside[e]
73	48.29	815.2042	$C_{38}H_{39}O_{20}$	−0.2	653 (100), 447 (11), 284 (4)	353 (100), 285 (29)	nd	265, 330	km-3-*O*-sinapoylglucoside-7-*O*-glucoside[e]
74	49.45	753.2259	$C_{34}H_{41}O_{19}$	−1.6	529 (100)	289 (61), 223 (21), 205 (100)	nt	nd	disinapoylgentiobiose[d]
75	49.54	949.2999	$C_{44}H_{53}O_{23}$	−1.6	753 (39), 725 (100)	419 (100), 223 (11)	nd	nd	putative hydroxycinnamic acid derivative
76	49.64	757.2353	$C_{37}H_{41}O_{17}$	−0.5	561 (100), 337 (49), 223 (19)	337 (100), 223 (22), 216 (40)	nd	235, 330	putative hydroxycinnamic acid derivative
77	49.75	1419.3633	$C_{70}H_{68}O_{32}$	−0.8	1213 (2), 1195 (2), 815 (100), 609 (16)	609 (100), 591 (16), 284 (14)	429 (100), 284 (43)	270, 330	km-3-*O*-trisinapoylhydroxyferuloylsophoroside[e]
78	50.60	591.1725	$C_{28}H_{31}O_{14}$	−0.9	367 (100), 223 (91)	352 (40), 223 (37), 205 (100), 179 (4)	nd	245, 320	1,2-disinapoylglucoside
79	50.63	1205.3333	$C_{40}H_{69}O_{41}$	−1.1	1130 (7), 941 (8), 835 (6), 613 (100), 427 (11), 223 (12)	nd	nd	nd	putative hydroxycinnamic acid derivative
80	50.66	1237.2697	$C_{60}H_{53}O_{29}$	−1.5	1013 (23), 911 (34), 705 (100), 613 (67), 223 (19),	nd	nd	nd	putative hydroxycinnamic acid derivative
81	50.94	1419.3629	$C_{70}H_{68}O_{32}$	−0.6	1051 (45), 889 (29), 815 (100), 653 (24), 591 (19)	609 (38), 591 (89), 285 (100),	nd	nd	km-3-*O*-trisinapoylhydroxyferuloyldiglucoside[e]
82	51.50	1419.3643	$C_{70}H_{68}O_{32}$	−1.5	1213 (25), 1051 (100), 815 (39), 609 (16), 591 (23)	751 (100), 591 (79)	nd	nd	km-3-*O*-disinapoylhydroxyferuloylglucoside-7-sinapoylglucoside[e]
83	51.67	959.2833	$C_{45}H_{51}O_{23}$	−0.7	735 (100), 529 (8), 511 (11)	528 (87), 511 (100), 385 (21), 223 (27)	nd	230, 330	1,2,2′-trisinapoylgentiobiose
84	53.11	787.2461	$C_{38}H_{43}O_{18}$	−0.8	739 (15), 591 (100), 367 (56), 223 (31)	223 (100)	nt	235, 290, 325	putative hydroxycinnamic acid derivative
85	53.32	815.2053	$C_{38}H_{39}O_{20}$	−1.6	623 (77), 609 (100), 591 (41)	429 (70), 308 (29), 285 (100)	nd	265, 330	km-3-*O*-sinapoylsophoroside[d]
86	53.78	1183.3155	$C_{55}H_{59}O_{29}$	−0.6	815 (80), 609 (100)	429 (33), 285 (100)	nd	nd	km-3-*O*-sinapoylsophoroside-7-*O*-sinapoylglucoside[e]
87	54.49	841.2780	$C_{38}H_{49}O_{21}$	−1.0	635 (100), 617 (23), 371 (39)	575 (40), 473 (82), 455 (100), 429 (62)	nd	nd	putative hydroxycinnamic acid derivative
88	55.15	591.1728	$C_{28}H_{31}O_{14}$	−1.5	531 (33), 367 (100), 205 (31)	223 (45), 205 (100), 190 (41)	nd	235, 330	1,6-disinapoylglucoside
89	55.62	757.2359	$C_{37}H_{41}O_{17}$	−0.5	595 (100), 223 (47)	401 (100)	nd	nd	putative hydroxycinnamic acid derivative
90	56.92	959.2828	$C_{45}H_{51}O_{23}$	−0.1	735 (100)	331 (71), 247 (100)	nd	235, 330	trisinapoylgentiobiose[d]
91	57.87	739.2108	$C_{33}H_{39}O_{19}$	−1.5	515 (100), 353 (41), 223 (10)	379 (87), 353 (100), 191(33)	nd	235, 330	sinapoylhydroxyferuloylgentioside[d]

[a]Abbreviations: km, kaempferol; qn, quercetin; is, isorhamnetin; DP, degree of polymerization of the epicatechin unit. [b]nt = no test was made. [c]nd = not detected. [d]Chemicals identified for the first time in *B. napus*. [e]Chemicals identified for the first in the genus *Brassica*.

dx.doi.org/10.1021/jf404826u | J. Agric. Food Chem. 2014, 62, 2935−2945

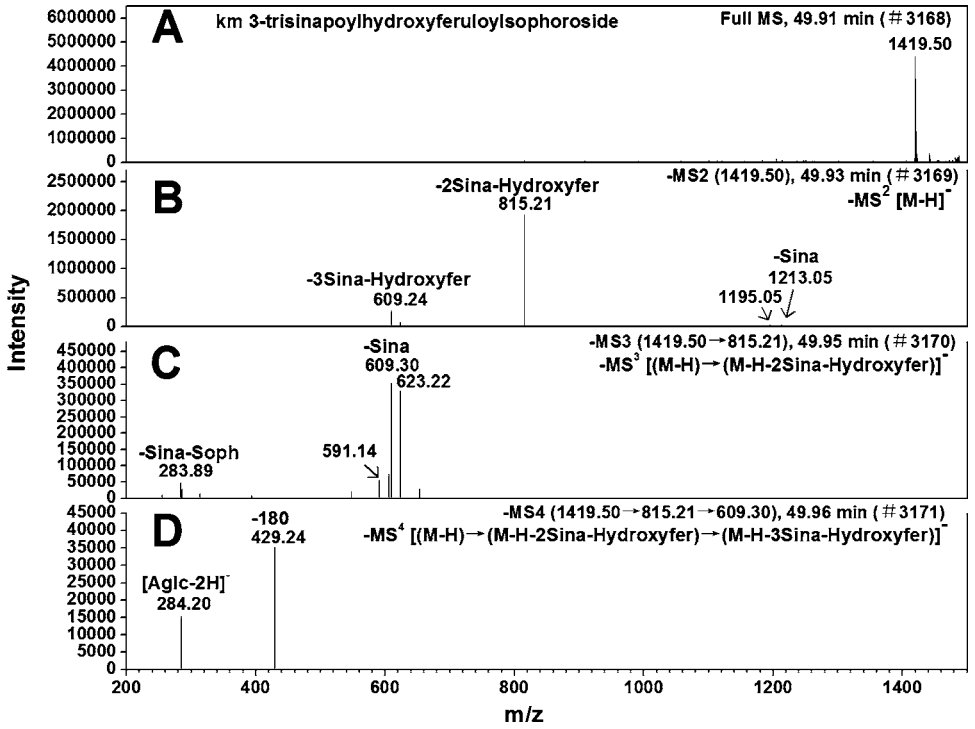

Figure 3. MS^n analysis of kaempferol-3-*O*-trisinapoylhydroxyferuloylsophoroside (peak 77), (km = kaempferol). (A) $[M - H]^-$, (B) MS^2 $[M - H]^-$, (C) MS^3 $[(M - H) \rightarrow (M - H - 2Sina - hydroxyfer)]^-$, (D) MS^4 $[(M - H) \rightarrow (M - H - 2Sina - hydroxyfer) \rightarrow (M - H - 3Sina - Hydroxyfer)]^-$.

of these compounds have previously been reported in *B. napus* and genus *Brassica*; these compounds include quercetin-3-*O*-sophoroside-7-*O*-glucoside,[11,21,28] kaempferol-*O*-diglucoside, [24] kaempferol-3-*O*-sophoroside-7-*O*-glucoside,[11,21,28] kaempferol-3-*O*-glucoside,[11,16,20,29] and isorhamnetin-3-*O*-glucoside.[11,22] Ten of the flavonols, including quercetin-3-*O*-diglucoside-7-*O*-glucoside,[13,16,17,27] kaempferol-3-*O*-triglucoside-7-*O*-glucoside,[12,13,16,17,27] kaempferol-3-*O*-glucoside-7-*O*-glucoside,[8,11,16] isorhamnetin-3-*O*-glucoside-7-*O*-glucoside,[8,11,28] kaempferol-3-*O*-sophoroside,[8,10,11,28] quercetin-3-*O*-sophoroside,[8,10] kaempferol-3-*O*-diglucoside,[13,14,16,29] isorhamnetin-3-*O*-diglucoside,[16] kaempferol-7-*O*-sophoroside,[8] and kaempferol-*O*-sophoroside,[8] have previously been reported in the genus *Brassica.* For example, km-3-*O*-sophoroside (peak 31) presented MS^2 fragments at m/z 447 and 429 from the loss of a glucosyl (162 Da) and the partial loss of a sophorosyl (180 Da). Qn-3-*O*-sophoroside (peak 32) presented MS^2 fragments at m/z 463 and 445 from the loss of a glucosyl (162 Da) and the partial loss of a sophorosyl (180 Da). The parent ions of peaks 31 and 32 were respectively observed at m/z 285 and 300 from the complete loss of a glucosyl. Thus, peaks 31 and 32 may be concluded to contain sophorose. Consistent with the alkaline hydrolysis characteristics and HRMS data, we found that peaks 31 and 32 feature λ_{max} at 265 and 345 nm, respectively, which indicate that peaks 31 and 32 are kaempferol-3-*O*-sophoroside and quercetin-3-*O*-sophoroside, respectively.

Confirmation of Acylated Flavonol Glycosides. In *Brassica*, acyl groups on flavonol glycosides were mainly observed in *p*-coumaroyl, caffeoyl, feruloyl, hydroxyferuloyl, and sinapoyl. Acylation greatly affects the UV absorption of flavonol glycosides. For example, the λ_{max} of flavonol glycosides (band I) normally shifts to 310−312 nm when they are combined with *p*-coumaroyl. However, the λ_{max} of band I may also shift to 320−340 nm when the flavonol glycosides are combined with caffeoyl, feruloyl, hydroxyferuloyl, and sinapoyl.[14,16,25,28]

Acylated flavonol glycosides, such as flavonol-3-*O*-acylglycoside-7-*O*-acylglycoside, produce a major MS^2 ion peak from the loss of 7-acyl and glucosyl as well as a parent peak of flavonol from the loss of 3-acyl and glucosyl. *p*-coumaroyl, galloyl, caffeoyl, feruloyl, hydroxyferuloyl, and sinapoyl could be identified from losses of 146, 152, 162, 176, 192, and 206 Da, respectively. As such, deduction of unknown compounds according to the glycosyl products of flavonols after alkaline hydrolysis of acylated flavonol glycosides, accompanied by their UV absorption characteristics, MS^n fragments, and HRMS analysis results, is possible. For instance, Olsson et al.[21] characterized kaempferol-3-*O*-sinapoylsophoroside-7-*O*-glucoside (peak 18) with λ_{max} at 265 and 330 nm, which are considered typical UV absorption peaks of acylated flavonol glycosides. This compound presents a major MS^2 fragment at m/z 815 from the loss of 162 Da and three MS^3 fragments at m/z 609, 591, and 285 from the loss of 206 Da (sinapoyl), 224 Da (sinapic acid), and all acyl and glycosyl groups, respectively. The MS^3 fragment at m/z 609 can be further fragmented into an ion peak at m/z 429, which indicates the presence of sophorosyl.

In this study, we identified 35 acylated flavonol glycosides, including 29 kaempferol derivatives, 3 quercetin derivatives, and 4 isorhamnetin derivatives (Table 2). These flavonols were also clarified in terms of different numbers of glucosyls. Of these 35 compounds, 31 were found for the first time in rapeseed and 21 were discovered for the first time in the genus *Brassica*.

Seven derivatives of kaempferol sinapoyltriglucosides were distributed as peaks 14, 18, 45, 49, 57, 58, and 62. Peaks 14, 45, 49, and 57 were identified as isomers of kaempferol-3-*O*-sinapoyldiglucoside-7-*O*-glucoside, and peaks 18 and 58 were

identified as isomers of kaempferol-3-*O*-sinapoylsophoroside-7-*O*-glucoside on the basis of ion peaks (loss of 180 Da) in the MS^3 spectra. Peak 62 was detected with an ion peak at m/z 609 from losses of (206 Da) and glucosyl (162 Da). We thus hypothesize that sinapoyl is ligated to 7-glucosyl. Peaks 18, 58, and 62 have been previously reported in rapeseed.[21,30] Peak 14 was reported for the first time in *B. napus*, and peaks 45, 49, and 57 were discovered for the first time in the genus *Brassica*.

Ion fragments of peaks 3, 7, and 37 obtained from low-resolution MS in negative mode were found at m/z 933. However, the λ_{max} (band 1) of peak 7 observed at 330 nm was obviously smaller than that of peak 3; this result indicates that peak 7 is an acylated flavonol glycoside. Whereas peak 3 was observed even after alkaline hydrolysis, peak 7 disappeared. HRMS analysis demonstrated that peak 7 ($C_{42}H_{45}O_{24}$) possesses three more carbon atoms than peak 3 ($C_{39}H_{49}O_{26}$). An MS^3 ion fragment from the loss 180 Da was observed after further analysis of peak 7, which indicates that the peak is kaempferol-3-*O*-caffeoylsophoroside-7-*O*-glucoside. We also confirmed that peak 37 is kaempferol-3-*O*-caffeoyldiglucoside-7-*O*-glucoside.

Peaks 66, 71, and 86 showed the same molecular mass, and peaks 66 and 71 were further ascertained as acylated flavonol glycosides according to their UV absorption characteristics. The major MS^2 fragment of peaks 66 and 71 was found at m/z 815 (from the loss of 368 Da), while the major MS^3 fragment of peak 86 was observed at m/z 609 (from the loss of 206 Da). The parent ions of these compounds were about 285 Da, arising from the complete loss of acyl and glucosyl. The m/z 609 ions of peaks 66 and 86 could be fragmented into other ions at m/z 429 from the loss of 180 Da. Thus, we can identify peaks 66, 71, and 86 as kaempferol-3-*O*-sinapoylsophoroside-7-*O*-sinapoylglucoside, kaempferol-3-*O*-sinapoyldiglucoside-7-*O*-sinapoylglucoside, and kaempferol-3-*O*-sinapoylsophoroside-7-*O*-sinapoylglucoside, respectively.

Figure 3 depicts the MS^n spectra of peak 77, which was identified as kaempferol-3-*O*-trisinapoylhydroxyferuloylsophoroside. The spectra of peak 77 show λ_{max} at 270 and 330 nm, which implies that peak 77 is an acylated flavonol glycoside. Further MS^n analysis proved the presence of sinapoyl and hydroxyferuloyl in this compound. Two isomers of kaempferol-3-*O*-trisinapoylhydroxyferuloylsophoroside at peaks 81 and 82 were successfully identified. Peaks 64 and 67 were similarly identified as isomers of kaempferol-3-*O*-disinapoylhydroxyferuloyldiglucoside. Peaks 40 and 44 were identified as kaempferol-3-*O*-disinapoylgalloyldiglucoside and 3-*O*-glucoside-7-*O*-acetylglucoside, respectively. Multiple acylated flavonol glycosides have never been reported in rapeseed, and 21 of these compounds were discovered for the first time in the genus *Brassica* (Table 2). Several compounds found in our work have been previously reported in the genus *Brassica*; these compounds include quercetin-3-*O*-sinapoylsophoroside-7-*O*-glucoside,[21] kaempferol-3-*O*-sinapoylsophoroside-7-*O*-glucoside,[21,31] isorhamnetin-3-*O*-sinapoyldiglucoside-7-*O*-glucoside,[22] kaempferol-3-*O*-sophoroside-7-*O*-sinapoylglucoside,[30] kaempferol-3-*O*-caffeoylsophoroside-7-*O*-glucoside,[8,11] kaempferol-3-*O*-sinapoyldiglucoside-7-*O*-glucoside,[11,16,17,29] kaempferol-3-*O*-sinapoylsophorotrioside-7-*O*-glucoside,[8] kaempferol-3-*O*-feruloylsophoroside-7-*O*-glucoside,[8,28] kaempferol-3-*O*-*p*-coumaroylsophoroside-7-*O*-glucoside,[8,28] kaempferol-3-*O*-sinapoylsophotrioside-7-*O*-glucoside,[8,10,12] quercetin-3-*O*-sinapoylsophoroside-7-*O*-glucoside,[11] kaempferol-3-*O*-sinapoylsophoroside,[8,11] kaempferol-3-*O*-sinapoylsophoroside-7-*O*-glucoside,[12] and kaempferol-3-*O*-sinapoylsophoroside.[8]

Confirmation of Sulfated Flavonol Glycosides. In the present study, we identified four sulfated isorhamnetin compounds. Peak 48 was previously reported by Auger et al.,[22] whereas peaks 15, 36, and 60 have never been reported in the genus *Brassica*. Peak 36 was identified as an isorhamnetin-*O*-diglucoside-sulfate, which presents an MS^2 fragment at m/z 639 from the loss of a SO_3^{2-} (80 Da) and an MS^3 parent fragment at m/z 315. Peaks 15 and 60 were confirmed as isorhamnetin-*O*-diglucoside-sulfate and isorhamnetin-3-*O*-sinapoylglucoside-sulfate-7-*O*-glucoside, respectively. Among the four isorhamnetins found, three were reported for the first time in the genus *Brassica*; only isorhamnetin-*O*-glucoside-sulfate has been previously reported.[22]

Confirmation of Flavanol and its Oligomers. Flavanols show λ_{max} at 202 and 280 nm. The molecular mass of flavanol polymers can be determined as follows: $290 + 288(n - 1)$, where n stands for the number of polymers. A previous report found that fragments of 290 or 288 Da are always lost during the fragmentation of these polymers.[32]

Using (−)-epicatechin and procyanidin B2 as standards, we identified six (−)-epicatechins and their oligomers [DP 2], [DP 3], and [DP 4] [DP = degree of polymerization of the (−)-epicatechin unit] on the basis of their UV absorption characteristics, MS^n fragments, and HRMS analysis results. Identification of these compounds was performed in accordance with previous research.[22,23] We observed that flavanols and their oligomers are generally found in F4 fractions obtained by column chromatography and that isomers of flavanol oligomers in F4 are obviously more abundant than those in crude extracts. These results indicate the possibility of polymer degradation during the experiment and that flavanol polymers are abundant in seeds of *B. napus*.

Confirmation of Hydroxycinnamic Acid Derivatives. Hydroxycinnamic acid derivatives in *Brassica* principally include *p*-coumalic acid, caffeic acid, ferulic acid, hydroxyferulic acid, and sinapic acid, which could be combined with glucose, gentiobiose, quinic acid, malic acid, and malonic acid to form hydroxycinnamic acid derivatives.[19,23,33] The λ_{max} of these derivatives ranged from 230 to 250 nm and from 320 to 330 nm.[14]

Hydroxycinnamoyl or hydroxycinnamic acid may be lost during MS^n analysis, and the presence of gentiobiose can be deduced from the loss of 306 Da. Peak 78 was defined as 1,2-disinapoylglucoside, which has been previously reported.[30] 1,2-Disinapoylglucoside shows an MS^2 ion fragment at m/z 367 from the loss of 224 Da and MS^3 fragments at m/z 352, 223, and 179 from losses of 15 Da (a methyl on sinapoyl), 144 Da (a glucosyl without H_2O), and 188 Da (a sinapoyl without H_2O), respectively.

Eighteen phenypropanoid derivatives were determined according to their retention times, UV absorption characteristics, MS^2 and MS^3 fragments, and HRMS molecular ions $[M - H]^-$. Most of these compounds were derivatives of sinapic acid in conjunction with monosaccharides or disaccharides. While all of the hydroxycinnamic acid derivatives obtained have been previously reported in the genus *Brassica*, 11 of them were discovered for the first time in *B. napus* (Table 2). Four isomers of sinapoylhexose (peaks 6, 12, 23, and 29) were further identified; of these, peaks 12, 23, and 29 were reported for the first time in *B. napus*. Three isomers of sinapoylgentiobiose (peaks 24, 28, and 34) and three isomers of disinapoylgentio-

biose (peaks 34, 69, and 74) were reported for the first time in *B. napus*. A trisinapoylgentiobiose (peak 90) and a sinapoylferuloylgentiobiose (peak 91) were also discovered in this study.

Among the hydroxycinnamic acid derivatives observed, seven have been previously reported in both *B. napus* and genus *Brassica*; these compounds include *cis*-sinapic acid,[33] sinapoylhexose,[19,24] sinapoylmalic acid,[30] *trans*-sinapic acid,[33] 1,2-disinapoylglucoside,[30] 1,2,2′-trisinapoylgentiobiose,[14,16,30] and 1,6-disinapoylglucoside.[8,12,30] Another 11 of these acid derivatives, including sinapoylhexose,[12] sinapoylgentiobiose,[8] sinapoylhexose,[8] sinapoylgentiobiose,[8,12] sinapoylgentiobiose,[8,12] sinapoylhexose,[17] disinapoylgentiobiose,[8,12,14] disinapoylgentiobiose,[8,12] disinapoylgentiobiose,[12] trisinapoylgentiobiose,[12] and sinapoylhydroxyferuloylgentioside,[8] have also been previously reported in the genus *Brassica*

Unknown Flavonoids and Hydroxycinnamic Acid Derivatives. Although multiple phenolic compounds were successfully identified in this research, many chemical compounds remain unknown. These compounds may include specific hydroxycinnamic acid derivatives and flavonoids and always present in conjunction with several unknown chemical groups. For instance, peak 19 was ascertained as a kaempferol combined with three hexoses, a sinapine, and an unknown 68 Da group. Twelve unknown hydroxycinnamic acid derivatives (peaks 8, 20, 27, 54, 55, 75, 79, 80, 84, 87, and 89) produced MS^n fragments of sinapoyl, feruloyl, and gentiobiose. Peaks 20, 75, 76, and 84 exhibited an unknown compound (196 Da) during MS^n analysis. Further confirmation of these unknown compounds must be carried out by purification of single components and subsequent application of infrared spectroscopy and/or nuclear magnetic resonance spectroscopy.

The UV absorption characteristics and MS^n fragments of the target compounds were principally investigated to identify new components by HPLC analysis. HPLC analysis of the crude extracts of flavonoids and hydroxycinnamic acid derivatives in rapeseed is limited by the fact that many of the compounds are simultaneously washed away during the determination, thereby leading to UV spectrum overlaps and identification difficulties.[23] As well, minute amounts of certain compounds may be neglected because of their weak signals in the UV spectra. Sephadex LH-20 column chromatography was performed to separate the crude methanol extract of rapeseed into different fractions that could be further analyzed by HPLC-PDA−ESI(−)-MS^n (LCQ) and HPLC-DAD−ESI(−)-HRMS (Q-TOF), thereby allowing comprehensive and detailed characterization of the crude extract. Although some of the compounds may be dehydrated during subsequent concentration, no adverse effects on their identification were noted. Alkaline hydrolysis transformed acylated flavonol glycosides into glycosylated chemicals of the parent ion, thereby promoting the identification of acylated compounds. Compounds released after alkaline hydrolysis also directly demonstrate the type of phenypropanoid available.[14,16,34]

The development of HPLC-PDA−ESI(−)-MS^n/HRMS greatly facilitates the identification of unknown compounds according to their molecular mass; this analytical technique further allows calculation and deduction of the element composition of relevant chemical compounds. Several flavonol derivatives were identified in this research, 70% of which were confirmed as kaempferol derivatives, 20% of which were isorhamnetin derivatives, and 10% of which were quercetin derivatives. In a previous study, the kaempferol content was found to be higher than those of quercetin and isorhamnetin.[23] Epicatechin, a compound related to the flavonoid biosynthetic pathway, varies obviously in content in differently colored rapeseed.[23] A comprehensive dissection of flavonoid biosynthesis patterns indicates that kaempferol formation is related to epicatechin accumulation.[35,36] In the present study, we found that sinapic acid, the main derivative of phenypropanoids in rapeseed, greatly increases after alkaline hydrolysis. This result suggests that sinapic acid is the main antinutritional factor of rapeseed.

In conclusion, we detected 91 flavonoids and hydroxycinnamic acid derivatives in *B. napus* L. var. *napus* seeds through HPLC-PDA−ESI(−)-MS^n/HRMS (IonTrap and Q-TOF) analysis. Seventy-eight of these compounds were identified tentatively; 55 of the compounds were reported for the first time in *B. napus*, and 24 were reported for the first time in the genus *Brassica*. Comprehensive interpretation of flavonoids and hydroxycinnamic acid derivatives in rapeseed is fundamental to studies on the antinutrition properties of rapeseed. The results of this study improve the scientific knowledge of the phenolic composition of rapeseed and provide a reliable guide for selecting rapeseed for breeding with better seed quality. We also successfully prove that HPLC-PDA−ESI(−)-MS^n/HRMS is a highly efficient and elaborate technique for plant phenolic analysis and chemical identification.

AUTHOR INFORMATION

Corresponding Author

*Phone: +86 514 87997303. E-mail: wangyp@yzu.edu.cn.

Author Contributions

[§]Y.S. and J.J. contributed equally to this work.

Funding

This study was supported by NSFC projects (Grants 31330057 and 31171581), the Priority Academic Program Development of Jiangsu Higher Education Institutions, and an SRFDP project (Grant 20123250110009).

Notes

The authors declare no competing financial interest.

ABBREVIATIONS USED

HPLC, high-performance liquid chromatography; HRMS, high-resolution mass spectrometry; PDA, photodiodide array; ESI, electrospray ion source

REFERENCES

(1) Schwender, J.; Hay, J. O. Predictive modeling of biomass component tradeoffs in *Brassica napus* developing oilseeds based on *in silico* manipulation of storage metabolism. *Plant Physiol.* **2012**, *160*, 1218−1236.

(2) Cartea, M. E.; Francisco, M.; Soengas, P.; Velasco, P. Phenolic compounds in *Brassica* vegetables. *Molecules* **2011**, *16*, 251−280.

(3) Agudo, A.; Cabrera, L.; Amiano, P.; Ardanaz, E.; Barricarte, A.; Berenguer, T.; Chirlaque, M. D.; Dorronsoro, M.; Jakszyn, P.; Larranaga, N.; Martınez, C.; Navarro, C.; Quiros, J. R.; Sanchez, M. J.; Tormo, M. J.; Gonzalez, C. A. Fruit and vegetable intakes, dietary antioxidant nutrients, and total mortality in spanish adults: findings from the spanish cohort of the european prospective investigation into cancer and nutrition (EPIC-Spain). *Am. J. Clin. Nutr.* **2007**, *85*, 1634−1642.

(4) Higdon, J. V.; Delage, B.; Williams, D. E.; Dashwood, R. H. Cruciferous vegetables and human cancer risk: epidemiologic evidence and mechanistic basis. *Pharm. Res.* **2007**, *55*, 224−236.

(5) Lam, T. K.; Gallicchio, L.; Lindsley, K.; Shiels, M.; Hammond, E.; Tao, X. G.; Chen, L.; Robinson, K. A.; Caulfield, L. E.; Herman, J. G.; Guallar, E.; Alberg, A. J. Cruciferous vegetable consumption and lung

cancer risk: a systematic review. *Cancer Epidemiol., Biomarkers Prev.* **2009**, *18*, 184−195.
(6) He, F.; Pan, Q. H.; Shi, Y.; Duan, C. Q. Biosynthesis and genetic regulation of proanthocyanidins in plants. *Molecules* **2008**, *13*, 674−703.
(7) Lipsa, F. D.; Snowdon, R.; Friedt, W. Quantitative genetic analysis of condensed tannins in oilseed rape meal. *Euphytica* **2012**, *184*, 195−205.
(8) Lin, L. Z.; Sun, J. H.; Pei, C.; Harnly, J. UHPLC-PDA-ESI/HRMS/MS^n analysis of anthocyanins, flavonol glycosides, and hydroxycinnamic acid derivatives in red mustard greens (*Brassica juncea* Coss). *J. Agric. Food Chem.* **2011**, *59*, 12059−12072.
(9) Badani, A. G.; Snowdon, R. J.; Wittkop, B.; Lipsa, F. D.; Baetzel, R.; Horn, R.; Haro, A. D.; Font, R.; Friedt, W. Colocalization of a partially dominant gene for yellow seed colour with a major QTL influencing acid detergent fibre (ADF) content in different crosses of oilseed rape (*Brassica napus*). *Genome* **2006**, *49*, 1499−1509.
(10) Romani, A.; Vignolini, P.; Isolani, L.; Ieri, F.; Heimler, D. HPLC-DAD/MS characterization of flavonoids and hydroxycinnamic derivatives in turnip tops (*Brassica rapa* L. subsp. *sylvestris* L.). *J. Agric. Food Chem.* **2006**, *54*, 1342−1346.
(11) Ferreres, F.; Valentao, P.; Pereira, J. A.; Bento, A.; Noites, A.; Seabra, R. M.; Andrade, P. B. HPLC-DAD-MS/MS-ESI screening of phenolic compounds in *Pieris brassicae* L. reared on *Brassica rapa* var. *rapa* L. *J. Agric. Food Chem.* **2008**, *56*, 844−853.
(12) Ferreres, F.; Fernandes, F.; Sousa, C.; Valentao, P.; Pereira, J. A.; Andrade, P. B. Metabolic and bioactivity insights into *Brassica oleracea* var. *acephala*. *J. Agric. Food Chem.* **2009**, *57*, 8884−8892.
(13) Ferreres, F.; Fernandes, F.; Oliveira, J. M. A.; Valentao, P.; Pereira, J. A.; Andrade, P. B. Metabolic profiling and biological capacity of *Pieris brassicae* fed with kale (*Brassica oleracea* L. var. *acephala*). *Food Chem. Toxicol.* **2009**, *47*, 1209−1220.
(14) Olsen, H.; Aaby, K.; Borge, G. I. A. Characterization and quantification of flavonoids and hydroxycinnamic acids in curly kale (*Brassica oleracea* L. convar. *acephala* var. *sabellica*) by HPLC-DAD-ESI-MS^n. *J. Agric. Food Chem.* **2009**, *57*, 2816−2825.
(15) Olsen, H.; Aaby, K.; Borge, G. I. A. Characterization, quantification, and yearly variation of the naturally occurring polyphenols in a common red variety of curly kale (*Brassica oleracea* L. convar. *acephala* var. *sabellica* cv. 'Redbor'). *J. Agric. Food Chem.* **2010**, *58*, 11346−11354.
(16) Lin, L. Z.; Harnly, J. M. Identification of the phenolic components of collard gerrns, kale, and chinese broccoli. *J. Agric. Food Chem.* **2009**, *57*, 7401−7408.
(17) Lin, L. Z.; Harnly, J. M. Phenolic component profiles of mustard green, Yuchoy, and 15 other *Brassica* vegetables. *J. Agric. Food Chem.* **2010**, *58*, 6850−6857.
(18) Cuyckens, F.; Ma, Y. L.; Pocsfalvi, G.; Claeys, M. Tandem mass spectral strategies for the structural characterization of flavonoid glucosides. *Analusis* **2000**, *28*, 888−895.
(19) Frolov, A.; Henning, A.; Bottcher, C.; Tissier, A.; Strack, D. An UPLC-MS/MS method for the simultaneous identification and quantitation of cell wall phenolics in *Brassica napus* seeds. *J. Agric. Food Chem.* **2013**, *61*, 1219−1227.
(20) Qu, C. M.; Fu, F. Y.; Lu, K.; Zhang, K.; Wang, R.; Xu, X. F.; Wang, M.; Lu, J. X.; Wan, H. F.; Tang, Z. L.; Li, J. N. Differential accumulation of phenolic compounds and expression of related genes in black- and yellow-seeded *Brassica napus*. *J. Exp. Bot.* **2013**, *64*, 2885−2898.
(21) Olsson, L. C.; Veit, M.; Weissenbock, G.; Bornman, J. F. Differential flavonoid response to enhanced UV-B radiation in *Brassica napus*. *Phytochemistry* **1998**, *49*, 1021−1028.
(22) Auger, B.; Marnet, N.; Gautier, V.; Maia-Grondard, A.; Leprince, F.; Renard, M.; Guyot, S.; Nesi, N.; Routaboul, J. M. A detailed survey of seed coat flavonoids in developing seeds of *Brassica napus* L. *J. Agric. Food Chem.* **2010**, *58*, 6246−6256.
(23) Jiang, J.; Shao, Y.; Li, A.; Lu, C.; Zhang, Y.; Wang, Y. P. Flavonoid profiling and gene expression in developing seeds of yellow- and black-seeded *Brassica napus*. *J. Integr. Plant Biol.* **2013**, *55*, 537−551.
(24) Farag, M. A.; Eldin, M. G. S.; Kassem, H.; Fetouh, M. A. E. Metabolome classification of *Brassica napus* L. organs via UPLC−QTOF−PDA−MS and their anti-oxidant potential. *Phytochem. Anal.* **2012**, *24*, 277−287.
(25) Lin, L. Z.; Sun, J. H.; Chen, P.; Harnly, J. A. LC-PDA-ESI/MS^n identification of new anthocyanins in purple bordeaux radish (*Raphanus sativus* L. variety). *J. Agric. Food Chem.* **2011**, *59*, 6616−6627.
(26) Yang, B.; Kortesniemi, M.; Liu, P. Z.; Karonen, M.; Salminen, J. P. Analysis of hydrolysable tannins and other phenolic compounds in emblic leafflower (*Phyllanthus emblica* L.) fruits by high performance liquid chromatography-electrospray ionization mass spectrometry. *J. Agric. Food Chem.* **2012**, *60*, 8672−8683.
(27) Llorach, R.; Gil-Izquierdo, A.; Ferreres, F.; Tomas-Barberan, F. A. HPLC-DAD-MS/MS ESI characterization of unusual highly glucosylated acylated flavonoids from cauliflower (*Brassica oleracea* L. var. *botrytis*) agroindustrial byproducts. *J. Agric. Food Chem.* **2003**, *51*, 3895−3899.
(28) Rochfort, S. J.; Imsic, M.; Jones, R.; Trenerry, V. C.; Tomkins, B. Characterization of flavonol conjugates in immature leaves of pak choi [*Brassica rapa* L. ssp. *chinensis* L. (Hanelt.)] by HPLC-DAD and LC-MS/MS. *J. Agric. Food Chem.* **2006**, *54*, 4855−4860.
(29) Gonzales, G. B.; Rae, K.; Coelus, S.; Struijs, K.; Smagghe, G.; Camp, J. V. Ultra(high)-pressure liquid chromatography-electrospray ionization-time-of-flight-ion mobility-high definition mass spectrometry for the rapid identification and structural characterization of flavonoid glycosides from cauliflower waste. *J. Chromatogr., A* **2014**, *1323*, 39−48.
(30) Baumert, A.; Milkowski, C.; Schmidt, J.; Nimtz, M.; Wray, V. Formation of a complex pattern of sinapate esters in *Brassica napus* seeds, catalyzed by enzymes of a serine carboxypeptidase-like acyltransferase family? *Phytochemistry* **2005**, *66*, 1334−1345.
(31) Lee, R. W. H.; Malchev, I. T.; Rajcan, I.; Kott, L. S. Identification of putative quantitative trait loci associated with a flavonoid related to resistance to cabbage seedpod weevil (*Ceutorhynchus obstrictus*) in canola derived from an intergeneric cross, *Sinapis alba* × *Brassica napus*. *Theor. Appl. Genet.* **2014**, *127*, 419−428.
(32) Lin, L. Z.; Harnly, J. M. A screening method for the identification of glycosylated flavonoids and other phenolic compounds using a standard analytical approach for all plant materials. *J. Agric. Food Chem.* **2007**, *55*, 1084−1096.
(33) Liu, Q.; Wu, L.; Pu, H. M.; Li, C. Y.; Hu, Q. H. Profile and distribution of soluble and insoluble phenolics in chinese rapeseed (*Brassica napus* L.). *Food Chem.* **2012**, *135*, 616−622.
(34) Vallejo, F.; Tomas-Barberan, F. A.; Ferreres, F. Characterisation of flavonols in broccoli (*Brassica oleracea* L. var. *italica*) by liquid chromatography−UV diode-array detection−electrospray ionization mass spectrometry. *J. Chromatogr., A* **2004**, *1054*, 181−193.
(35) Winkel-Shirley, B. Flavonoid biosynthesis. A colorful model for genetics, biochemistry, cell biology, and biotechnology. *Plant Physiol.* **2001**, *126*, 485−493.
(36) Lepiniec, L.; Debeaujon, I.; Routaboul, J. M.; Baudry, A.; Pourcel, L.; Nesi, N.; Caboche, M. Genetics and biochemistry of seed flavonoids. *Annu. Rev. Plant Biol.* **2006**, *57*, 405−30.

This study was a part of the Novinpak project. The first objective of the latter was to develop a monolayer PET bottle containing recycled PET (RPET) and suitable for wine. In addition, this bottle had to be light and suitable for incorporation in present industrial recycling and recovery processes. The second objective concerned gas management during bottling (dissolved oxygen (DO_2), headspace or gaseous oxygen ($HspO_2$), and dissolved carbon dioxide (DCO_2)) that ensured satisfactory conservation of rosé wine. Indeed, the oxygen content of headspace and wine during bottling can be the equivalent of several months of O_2 ingress through packaging.[25,26] The management of both dissolved and headspace gases during bottling and the choice of packaging are the key factors in the control of the quality and shelf life of wine. Bottling is the last step before selling wine, and O_2 trapped during bottling is consumed by wine and has consequences on wine aging.[6,25,27−29] The final objective of the project was to be able to ensure the good conservation of the organoleptic quality of wine by gas management during bottling and oxygen ingress management during storage. Several research teams and companies worked on this project in order to attain these objectives. Wine color and aroma evolution were studied, and sensory evaluation was performed. Life cycle analyses of glass and PET bottles were compared. Inertness, food contact suitability, and the barrier properties of PET were also studied. These studies are not reported in the present paper. Our study examines the limits of a standard monolayer PET bottle for wine packaging, with regard to the three main gases present in headspace and in wine (O_2, CO_2, N_2) and their exchanges with air in order to propose monolayer packaging for the wine targeted and its required shelf life. The impact on wine aging during 372 days of storage and SO_2 content are also examined. To the best of our knowledge, this is the first complete gas balance study for PET and glass bottles in time.

MATERIALS AND METHODS

A Cinsault rosé wine was bottled at Pech Rouge Experimental Unit (INRA, UEPR, Gruissan) in 75 cL colorless glass and PET bottles. Gas management in the bottling line used achieved homogeneous bottling with negligible losses of CO_2 and a low DO_2 content.[26,27] Two PET bottles were studied: a 38 g standard PET bottle (PET38) and a 38 g 100% recycled PET bottle (PET38R). Different methods were used to measure fSO_2, TSO_2, and headspace and dissolved gases (O_2, CO_2, N_2) for one year as described in Table 1. Analyses were scheduled throughout bottle storage to characterize the changes in the wines. A PreSens probe was used for frequent measurement of $HspO_2$ and DO_2 in the same three bottles for 372 days (noninvasive analyses). However, it was not possible to measure $HspCO_2$, $HspN_2$, or DCO_2 using this method. We therefore used other methods such as polarography and gas chromatography (invasive analyses) to measure all these parameters (gas balance) in three different bottles on several dates.

Experimental Bottling. The line was first purged with N_2 from preparation tank to head filler machine (to $HspO_2$ < 1% (v/v)). The preparation tank was filled by gravity with rosé wine. The wine was sparged with N_2 gas until DO_2 reached 0.3 mg/L. DCO_2 was then regulated with CO_2 gas using a porous injector bolted to the bottom of the preparation tank until DCO_2 reached 1 g/L. DCO_2 was monitored by sampling in the preparation tank using a Carbodoseur (Dujardin-Salleron laboratories, Noizay, France). Wine was forced into the circuit by N_2 to the filler tank through the filtration skid using overpressure of 150 kPa applied to the preparation tank. Bottles were blanketed before filling. Filled bottles were placed in the capping machine, where a screwcap was crimped. To achieve good bottling homogeneity, we discarded the first three and the last three bottles as DO_2 at the beginning and the end of bottling is higher than during the rest of the process.[27,30] Certain bottling parameters, kind of bottles, headspace and wine volume, and gas management are summarized in Table 2. Bottles were stored upright for 12 months in a thermostatically controlled room (20 ± 0.7 °C) with a relative humidity (RH) of 68 ± 9% (monitored but not controlled). Half of the bottles were stored in light (400 Lux) 24 h a day and 7 days a week and the other half stored in the dark (packed in cardboard boxes).

Table 1. Summary of Analyses Performed during Storage*

analyses	method	no. of bottles/ procedure	dates of analyses (days after bottling)
DO_2 (mg/L) converted in (mg/bt)	polarography	3	0 ($12 < n < 18$), 35, 91, 162, 278, 372
	luminescence	3	1, 7, 15, 21 and approx each month from 0 to 372
$HspO_2$ (% (v/v)) converted in (mg/bt)	micro gas chromatography	3	0 ($12 < n < 18$), 35, 91, 162, 278, 372
	luminescence	3	1, 7, 15, 21 and approx each month from 0 to 372
DCO_2 (mg/L)	volumetry	3	0 ($12 < n < 18$), 35, 91, 162, 278, 372
P_{aphro} (hPa)	pressure potentiometer	3	0 ($12 < n < 18$), 35, 91, 162, 278, 372
alcohol (%), TA (g/L H_2SO_4), pH	FTIR	3	0, 35, 91, 162, 278, 372
RS (mg/L)	FTIR	3	0
VA (g/L H_2SO_4)	enzymatic	3	0, 35, 91, 162, 278, 372
fSO_2 (mg/L), TSO_2 (mg/L)	colorimetric	3	0, 35, 91, 162, 278, 372

*At least 3 bottles per procedure were analyzed for each analysis. At t = 0, "n" represents the number of bottles analyzed per procedure. To monitor bottling homogeneity throughout the process, dissolved and headspace gases were measured in a larger number of bottles ($12 < n < 18$).

Determination of Headspace and Wine Volume with Unfilled Level. O_2 trapped in headspace directly determines consumption by wine after bottling.[28] To be able to compare procedures, the same screwcap was used whatever the packaging and the headspace volume/wine volume ratios ($Hsp_{vol}/wine_{vol}$) were as close as possible in each procedure. The unfilled level, directly related to headspace and wine volumes, was set before bottling. Different unfilled levels and volumes of reverse osmosis water (22 °C) were tested by Sidel Blowing Service (Le Havre, France) on several bottles of each procedure. It appeared that correlation between Hsp_{vol} measured and the unfilled level was good ($R^2 \approx 0.98$, data not shown). Experiments conducted at UEPR indicated the accuracy and reproducibility of this method for wine (data not shown). To achieve the closest $Hsp_{vol}/wine_{vol}$ in all procedures, the headspace level at 20 °C was set at 46 mm for PET bottles and 60 mm for glass bottles. As a result, the wine volume was not exactly the same for each packaging type (Table 2).

Noninvasive Analyses. On line O_2 monitoring was performed using a PreSens luminescent probe (PreSens Precision Sensing GmbH, Regensburg, Germany) and PSt3 O_2-sensitive optical spots (PreSens Precision Sensing GmbH; oxygen range, 0−22 mg/L; limit of detection, 15 μg/L; accuracy, ±1% at 100% air-saturation and ±0.15% at 1% air-saturation) integrated at four checkpoints on the bottling line and at the top and bottom of the preparation and filler tank. In bottles, DO_2 and $HspO_2$ were also measured using this method.[22] Data acquisition was performed using PST3v541 software (PreSens Precision Sensing GmbH). Analytical monitoring was performed on 19 dates of analyses after bottling (Table 1). The system measured oxygen partial pressure (PO_2) in hPa. It could also express the values in mg/L or in % (v/v) according to the phase studied, temperature, and pressure. Headspace was measured in % (v/

Table 2. Bottling Parameters at $t = 0$*

	unfilled level (mm)	vol (mL) Hsp	vol (mL) wine	($Hsp_{vol}/wine_{vol}$) (%)	DO_2 (mg/bt)	$HspO_2$ (mg/bt)	TO_2 (mg/bt)	DCO_2 (mg/bt)	$HspCO_2$ (mg/bt)
instrument					Orbisphere	PreSens		Carbodoseur	μGC
no. of samples					$12 < n < 18$	$n = 6$		$12 < n < 18$	$12 < n < 18$
PET38	46	20.5	742.4	2.76	1.37 ± 0.20	4.05 ± 0.48	5.42	623 ± 20	4.08 ± 1.94
PET38R	46	20.5	742.4	2.76	1.66 ± 0.10	4.28 ± 0.32	5.94	601 ± 37	4.03 ± 2.06
GLASS	60	19.4	751.4	2.58	1.19 ± 0.29	4.46 ± 0.32	5.65	617 ± 24	3.51 ± 0.95

*Averages and standard deviations of bottling parameters: "n" represents the number of samples per analysis. TO_2 is the sum of DO_2 measured by Orbisphere probe and $HspO_2$ measured by PreSens spots.

v) and converted into milligrams per bottle (mg/bt) according to Hsp_{vol}, using eq 1:

$$HspO_2 = \frac{HspO_2'}{100} \times Hsp_{vol} \times \frac{M_{O_2}}{V_M \times \frac{T + 273.15}{273.15}} \quad (1)$$

$HspO_2$ is headspace oxygen (mg/bt), $HspO_2'$ is headspace oxygen (% (v/v)), Hsp_{vol} is headspace volume (mL), T is wine temperature (°C), M_{O_2} is the molar mass of oxygen (32 g/mol), and V_M is the molar volume (22.414 L/mol). DO_2 values were measured in mg/L and converted into mg/bt as the volume of wine in the bottle was known.

Invasive Analyses. DO_2 was measured using an Orbisphere 31110A polarographic probe equipped with a 25 μm 2956A membrane (Hach Ultra Analytics, Trappes, France). The membrane range of O_2 measurement was 0.25 Pa to 50 kPa (limit of detection, 1 μg/L; accuracy, 0.02 μg/L). The probe was connected to an Orbisphere Moca 3600 single channel microprocessor analyzer for oxygen measurements. Results were expressed in mg/L and converted into mg/bt according to the volume of wine. At $t = 0$, the Orbisphere probe was used to measure DO_2 in bottles because the response time of PreSens spots in liquid is greater than in gas. As a result, measurement of DO_2 should take place at least 40 min after bottling with the PreSens probe, whereas it can be measured immediately after bottling with the Orbisphere probe (Table 2).

$HspO_2$, headspace CO_2 ($HspCO_2$), headspace N_2 ($HspN_2$), and aphrometric pressure (P_{aphro}) were measured by gas chromatography (μGC, micro GC CP4900, Varian, Les Ullis, France) (accuracy = 0.25%). A specific sampling system was set up, consisting of a peek tube with a needle, a Genie 170 membrane to prevent any liquid contamination, a four-way valve to purge the needle or to load the sample into the injectors, and an electronic manometer to measure the internal pressure of the sample (P_{aphro}). After the piercing of the screwcap, the internal pressure was monitored and then the sample was pumped for 30 s through the circuit to ensure satisfactory clearance. A 400 μL sample was then injected in the columns. The results were expressed in % (v/v) and converted into mg/bt using eq 2:

$$Hsp_{gas} = \frac{Hsp_{gas}' P_{tot} Hsp_{vol} \times 10^{-6}}{\left(\frac{R}{M_{gas}} \times 10^3\right)(273.15 + T)} \quad (2)$$

Hsp_{gas} is gas headspace (mg/bt), Hsp_{gas}' is gas headspace (% (v/v)), Hsp_{vol} is headspace volume (mg/L), M_{gas} is the molar mass of gas (O_2, 32 g/mol; CO_2, 44 g/mol; or N_2, 28 g/mol), R is the universal gas constant (8.314 J/mol/K), T is headspace temperature (°C), and P_{tot} is total pressure (hPa), the sum of atmospheric and aphrometric pressure of the day 3

$$P_{tot} = P_{atm} + P_{aphro} \quad (3)$$

DCO_2 was measured by sampling in the preparation tank or bottles. Determination was performed using a Carbodoseur (repeatability 90 mg/L).[31] Results were expressed in mg/L and converted into mg/bt.

The methods used to determine alcohol content (% vol), total and volatile acidity (TA and VA: g/L H_2SO_4), pH, and free and total SO_2 (fSO_2 and TSO_2: mg/L) are reported in Table 1.

Calculation of Gas Flow Directions inside the Bottle and between Bottle and Air. In glass bottles, exchanges with air can only take place through the screwcap. As monolayer PET is gas-permeable, exchanges can also take place through the bottle wall as well. In general, as soon as a difference in the concentration of a chemical species appears in an environment, matter flows appear to reach balance. In our case, diffusion was the main driver for gas exchange between bottle and air and between headspace and wine. To determine gas exchange direction between bottle and air, we used the comparison of partial pressure of each gas in the headspace (P_{HspO_2}, P_{HspCO_2}, P_{HspN_2}) and the partial pressure of each dissolved gas (P_{DO_2}, P_{DCO_2}, P_{DN_2}) with the partial pressure of each gas in air at RH 68% (as monitored in our experiment). The partial pressure of each gas was expressed in hPa using results of the headspace composition in a bottle given by μGC in % (v/v). We consider that the air in the headspace was water vapor saturated. Oxygen partial pressure in headspace is given by eq 4:

$$P_{HspO_2} = \frac{HspO_2'}{100} \times (P_{tot} - P_{w(T)}) \quad (4)$$

P_{HspO_2} is the partial pressure of O_2 in headspace (hPa), $HspO_2'$ is headspace O_2 measured by μGC (% (v/v)), P_{tot} is total pressure (hPa) (eq 3), and $P_{w(T)}$ is the saturated water vapor pressure (hPa).

The saturated water vapor pressure at a known temperature can be expressed using Campbell's eq 5 in this form (T expressed in °C):

$$P_{w(T)} = \exp\left(52.57 - \frac{6690.9}{T + 273.15} - 4.681 \times \ln(T + 273.15)\right) \quad (5)$$

Equation 6 was deduced from eqs 4 and 5 and used to calculate oxygen partial pressure in the headspace using $HspO_2'$:

$$P_{HspO_2} = \frac{HspO_2'}{100} \times \left(P_{tot} - \exp\left(52.57 - \frac{6690.9}{T + 273.15} - 4.681 \times \ln(T + 273.15)\right)\right) \quad (6)$$

Similarly we calculated P_{HspN_2} (partial pressure of N_2 in headspace) and P_{HspCO_2} (partial pressure of CO_2 in headspace) using $HspN_2'$ (headspace N_2 in (% (v/v))) and $HspCO_2'$ (headspace CO_2 in (% (v/v))).

We calculated the partial pressure of O_2 in air at RH 68% (P_{O_2atm}) using eq 7 (pressure in hPa):

$$P_{O_2atm} = (P_{atm} - 0.68P_{w(T)}) \times 0.2095 \quad (7)$$

Likewise, we calculated the partial pressure of N_2 and CO_2 in air at RH 68% (P_{N_2atm}, P_{CO_2atm}) using eqs 8 and 9:

$$P_{N_2atm} = (P_{atm} - 0.68P_{w(T)}) \times 0.7808 \quad (8)$$

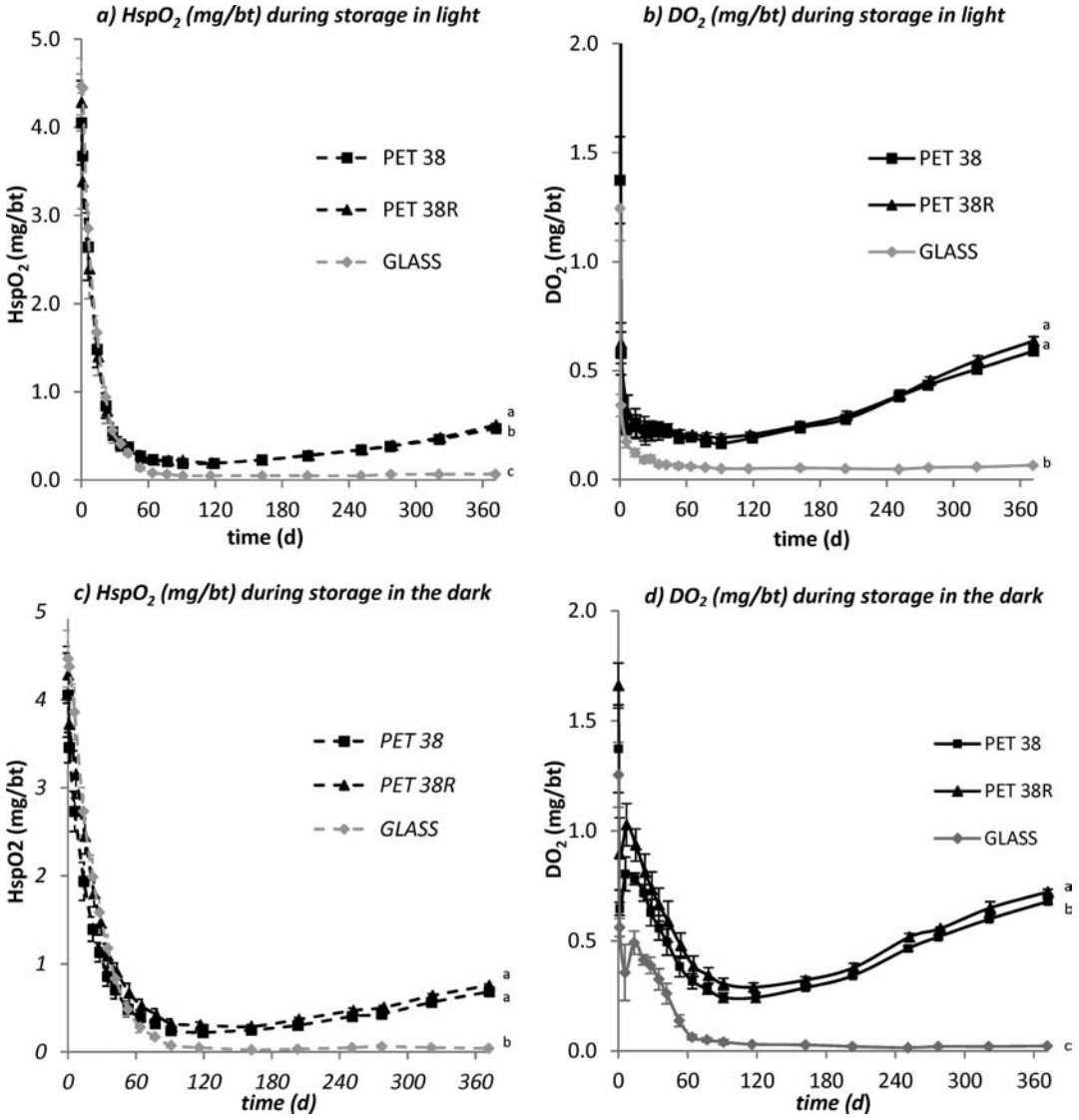

Figure 1. $HspO_2$ and DO_2 for PET and glass bottles during storage time in light (a, b) and in the dark (c, d). Averages and standard deviations are calculated from 3 bottles per procedure. Data were analyzed by analysis of variance (ANOVA) at 372 days, followed by Newman−Keuls multiple comparison tests ($\alpha = 0.05$). Similar letters denote no significant differences between the tested groups. $HspO_2$ and DO_2 values were obtained by PreSens, except for DO_2 at t = O where values were obtained by using an Orbisphere probe. Dotted lines with squares, triangles, and diamonds indicate $HspO_2$ of PET38, PET38R, and glass bottles respectively. Continuous lines with squares, triangles, and diamonds indicate DO_2 of PET38, PET38R, and glass bottles respectively.

$$P_{CO_2atm} = (P_{atm} - 0.68P_{w(T)}) \times 0.0003 \quad (9)$$

We compared $P_{Hsp_{gas}}$ with P_{gasatm} to identify gas flow directions between bottle and air 10 (pressures in hPa):

$$Hsp_{gas}{}^{\%} = \frac{P_{Hsp_{gas}}}{P_{gasatm}} \times 100 \quad (10)$$

$Hsp_{gas}{}^{\%}$ is expressed as the gas saturation percentage in air at RH 68%. As long as $Hsp_{gas}{}^{\%}$ is below 100% (respectively above 100%), gas from the air tends to diffuse through the bottle wall into the headspace to reach equilibrium (respectively headspace gas tends to diffuse from bottle to air).

Furthermore, we were interested in exchanges in the bottle between headspace and wine. O_2, N_2, and CO_2 are present in the headspace and are also dissolved in the wine. These exchanges are governed by both Fick's law and Henry's law: the solubility of a gas in a liquid is directly proportional to the partial pressure of the gas above the liquid. To calculate the pressure of dissolved gases (P_{Dgas}), we used formulas that took into account O_2 and N_2 dissolution in water, for lack of bibliographical references on wine. For dissolved gases, we were able to measure DCO_2 and DO_2 as described above, but we could not measure DN_2. It was estimated using eq 11 based on Dalton's law (3% is an estimate for water, ethanol, and the vapor pressure of noble gases):

$$P_{DN_2} = 0.97 \times P_{tot} - P_{DO_2} - P_{DCO_2} \quad (11)$$

DO_2 was given using Orbisphere probe in mg/L and was used to calculate partial pressure of O_2 dissolved in wine (hPa). The solubility of oxygen in water was used here and can be described by the Bunsen absorption coefficient $\alpha(T)$ (eq 12):[32]

$$P_{DO_2} = \frac{DO_2 \times 1013.25}{\alpha(T) \times 1000 \times \frac{32}{22.41 \times \frac{T+273.15}{273.15}}} \quad (12)$$

P_{DO_2} is the partial pressure of dissolved O_2 (hPa), DO_2 is oxygen concentration (mg/L), T is temperature (°C), and $\alpha(T)$ is the Bunsen absorption coefficient ($mL(O_2)/mL$), that determines the partition between gas and liquid phases (eq 13) (T expressed in °C):

dx.doi.org/10.1021/jf405392u | J. Agric. Food Chem. 2014, 62, 2946−2955

$$\alpha(T) \times 10^3 = 48.998 - 1.335T + 2.755 \times 10^{-2} \times T^2 - 3.220 \times 10^{-4} \times T^3 + 1.598 \times 10^{-6} \times T^4 \quad (13)$$

As this solubility was given for dissolved oxygen in water, we used it for wine as well.

DCO_2 was given by Carbodoseur methodology in mg/L, and the partial pressure of dissolved CO_2 (P_{DCO_2}) was then calculated. The formula according to the OIV Reference Method at 20 °C (OIV, 2008) was used for calculations and applications in wine. Equation 14 takes into account the temperature correction factor as proposed by Liger-Belair.[33]

$$P_{DCO_2} = \left(\frac{DCO_2}{\exp\left(2984 \times \frac{1}{293.15} - \frac{1}{T + 273.15}\right)} \times \frac{1}{0.01951(0.86 - 0.01E)(1 - 0.00144 \times RS)} \right) \times \frac{1}{100} \quad (14)$$

P_{DCO_2} is the partial pressure of dissolved CO_2 (hPa), DCO_2 is CO_2 concentration (mg/L), T is wine temperature (°C), E is the alcohol content (12.6% vol alcohol), and RS is the residual sugar in wine (0.23 g/L).

As explained for eq 10, if we compare P_{Dgas} (partial pressure of dissolved gases) with P_{gasatm} (partial pressure of gas in air at RH 68%), we can understand the direction of gas flows between wine and air (eq 15) (pressures are expressed in hPa).

$$Dgas^{\%} = \frac{P_{Dgas}}{P_{gasatm}} \times 100 \quad (15)$$

$Dgas^{\%}$ is expressed as the percentage of gas saturation in air at RH 68% (% (sat)). Equations 10 and 15 are also used to deduce the direction of gas exchanges between headspace and wine. As long as $Dgas^{\%}$ is below $Hsp_{gas}{}^{\%}$ (respectively above), gas tends to dissolve from the headspace into the wine (respectively to diffuse from wine to headspace).[25,28]

Wine. The wine was a Cinsault rosé "Vin de Pays d'Oc" (12.6% vol alcohol; RS, 0.23 g/L; TA, 3.40 g/L H_2SO_4; VA, 0.17 g/L H_2SO_4; pH, 3.28; free and total SO_2, 36 and 130 mg/L, respectively).

Bottling Raw Materials. PET bottles were 75 cL colorless Bordeaux bottles supplied by Sidel. The OTRs of PET38 and PET38R bottles were respectively 0.0637 ± 0.0008 and 0.0527 ± 0.0009 mg/bt/day. Glass bottles were 75 cL colorless Bordeaux bottles (BSN Glasspack SA, Villeurbanne, France). PET and glass bottles were capped with Novatwist 30H60 screwcaps (Novembal, Edison, NJ, USA) with Saranex seals (OTR: 0.0016 mg/cap/day). These caps were made of PE (polyethylene) and PP (polypropylene) and were 100% recyclable. The OTR values mentioned above were measured using a Mocon Ox-Tran 2/20 (Mocon, Minneapolis, MN. Tests were carried out by Sidel on an entire bottle at 23 °C (RH 60%), and the test gas was ambient air. Tests were performed on five bottles per procedure. Bottles of pure N_2 and pure CO_2 (food quality, purity ≥99.9%, Air Liquide, France) were used to manage gases during bottling as described above.

Bottling Line. The bottling line used consisted of three components: (1) a filtration skid with one preparation tank (105 L), 2 cartridge housings for 1 μm prefiltration, and 0.65 μm filtration membrane cartridges; (2) a single head filler MTB 1/1 (Perrier, Le Cheylard, France) with a 46 L tank; (3) a single head capping machine (TM3, Zalkin, Rueil-Malmaison, France).

Data Analysis. Statistical analyses were performed with analysis of variance (ANOVA) and Newman−Keuls multiple comparisons test (α = 0.05) using XLSTAT version 2007.1 program (Addinsoft, Paris, France).

RESULTS AND DISCUSSION

Bottling. Results showed inter- and intraprocedure homogeneity (Table 2). $HspO_2$ formed the major part of total oxygen content (TO_2) ($HspO_2 \approx 75\%$ TO_2) because of the low wine level (wine volume of 742.4 mL instead of 750 mL). Furthermore, average DO_2 was 1.38 mg/bt whereas average $HspO_2$ was higher (4.27 mg/bt). Another study conducted at UEPR showed that $HspO_2$ could reach 0.38 mg/bt to 3.58 mg/bt according to Hsp_{vol}, the kind of stopper, and the use of inert gas, whereas average DO_2 was 3.91 mg/bt.[28] TO_2 was between 5.40 mg/bt and 5.95 mg/bt. However these results could have been lower if the headspace had been flushed with N_2 before capping and PET bottles had a wine volume of 750 mL. Average DCO_2 was 615 mg/bt (≈800 mg/L), and $HspCO_2$ formed less than 1% of the total carbon dioxide content (TCO_2) at bottling.

Evolution of Headspace and Dissolved Oxygen. Figures 1a and 1b represent $HspO_2$ and DO_2 evolution for PET and glass bottles during storage in light. O_2 decreased in both graphs whatever the packaging because of consumption by wine.[28] This decrease was not linear and was faster during the first month.[6,25] After 3 months, it increased for PET but remained stable for glass, and at 12 months, $HspO_2$ and DO_2 were 0.59/0.59, 0.63/0.64, and 0.07/0.07 mg/bt respectively for PET38, PET38R, and glass. The Newman−Keuls multiple comparison test showed that differences between procedures were significant (α = 0.05) for $HspO_2$ and DO_2 between PET and glass (for DO_2 there was no difference between PET and RPET).

Figures 1c and 1d represent $HspO_2$ and DO_2 during storage in the dark. We found the same behavior as previously. However, O_2 consumption was slower: on day 7, $HspO_2$ and DO_2 values were higher than in light, and this was still the case after 372 days. The estimated average rate of TO_2 consumption in 7 days in light was 0.49 ± 0.02 mg/bt/d (PET and glass), whereas it was 0.25 ± 0.03 mg/bt/d in the dark (Table 3). Data were analyzed by Newman−Keuls multiple comparison tests, and there was a statistical difference (α = 0.05) between O_2 consumption rate in light and O_2 consumption rate in the dark. Furthermore, a transient increase in DO_2 was observed between 7 and 20 days. This means that, during this time, the rate of oxygen dissolution in wine was higher than consumption. This phenomenon was observed by Dimkou et al. (2011) for wine samples in glass bottles closed with a screwcap.[6] The increase was not observed for wine stored in

Table 3. Estimated Average Rates of TO_2 Consumption between 0 and 7 Days for PET and Glass Bottles Stored in Light and in the Dark*

	TO_2 consumption rate (mg/bt/d)	
	light	darkness
PET38	0.49 ± 0.02 a	0.25 ± 0.03 b
PET38R	0.44 ± 0.01 a	0.28 ± 0.02 b
glass	0.44 ± 0.02 a	0.25 ± 0.05 b

*TO_2 consumption rate is an average of oxygen consumption for the first 7 days calculated with the following formula: TO_2 consumption rate = $(TO_{2_{t=0}} - TO_{2_{t=7}})/7$. Averages and standard deviations were based on 3 bottles per procedure. Data were analyzed by ANOVA followed by Newman−Keuls multiple comparison tests (α=0.05). Similar letters denote no significant differences between the tested groups.

dx.doi.org/10.1021/jf405392u | J. Agric. Food Chem. 2014, 62, 2946−2955

Table 4. fSO_2 during Storage Time for PET and Glass Bottles*

	fSO_2 (mg/L)				
	0[b]	35[b]	162[b]	278[b]	372[b]
PET38	37 ± 1 a	24 ± 2 a	11 ± 0 b	3 ± 1 b	3 ± 1 b
PET38R	36 ± 1 a	24 ± 2 a	11 ± 1 b	3 ± 0 b	3 ± 2 b
glass	38 ± 1 a	26 ± 1 a	28 ± 1 a	19 ± 4 a	19 ± 1 a

*Averages and standard deviations are based on 6 bottles per procedure (3 bottles in light + 3 bottles in the dark), except for glass bottles at 162 days (n = 4). Data were analyzed at each date by ANOVA followed by Newman−Keuls multiple comparison tests (α = 0.05). Similar letters denote no significant differences between the tested groups. [b]Time (d).

light, probably because of faster O_2 consumption than dissolution from headspace to wine. DO_2 was subsequently close to minimum on the 14th day in light but did not reach minimum in darkness before the 60th day, meaning that after the consumption of initial DO_2, O_2 consumption was limited by the diffusion from headspace into wine for bottles stored in light. At 12 months, $HspO_2$ and DO_2 were 0.68/0.68, 0.76/0.72, and 0.04/0.02 mg/bt respectively for PET38, PET38R, and glass. PET38 and PET38R exhibited similar but statistically different behavior.

Evolution of SO_2. Table 4 represents losses of fSO_2 during storage. As there were no significant differences between storage in light and in the dark (data not shown), values represent averages at each month. Similar profiles were obtained for TSO_2 (data not shown). At bottling, fSO_2 was higher than 30 mg/L, and after one month, around 30% of initial fSO_2 had been lost, whatever the packaging. In the early stages of storage, fSO_2 decrease was consistent with other studies[6,7] and was associated with the oxygen present at bottling, especially with $HspO_2$, which represented, in our case, 75% of TO_2 at t = 0. These results showed the importance of managing O_2 and SO_2 at bottling: the results would have been better if the headspace had been flushed by N_2 just before capping.[6] In wine, the reaction between oxygen and SO_2 is extremely slow.[9] Sulfites react with the products of wine oxidation and in particular with the hydrogen peroxide that is produced when polyphenols are oxidized.[10,11] Finally, after 162 days, fSO_2 in PET reached around 10 mg/L. It is widely accepted that below this limit wine is not protected anymore. Godden et al. (2001) showed that, below this concentration, the sensory perception of a Semillon wine was affected by oxidized aroma, in contrast with wines that retained higher concentrations of SO_2, and had higher scores for citrus and fruity aromas.[8] After one year, wine in glass bottles had still 19 ± 1 mg/L of fSO_2. Data were analyzed by Newman−Keuls multiple comparison tests at 372 days and the difference between PET and glass was significant (α = 0.05). These results corroborated those found in an experiment conducted on a Sauvignon Blanc wine using 75 cL glass bottles containing 6.26 mg/bt of TO_2 just after closure and stored at 17.1 °C, where fSO_2 losses were 44% after one month.[25] Another study showed that, for a white wine packed in 3 L PET containers and stored 12 months at 20 °C, fSO_2 fell from 30 to 12 mg/L in the first month, then, to less than 4 mg/L after 12 months (similar results were found for rosé and red wines), whereas fSO_2 in glass fell from 30 to 14 mg/L in the first month and then to 10 mg/L after 12 months.[4] The same behavior was observed for 18.7 cL PET bottles with 2% oxygen scavenger and stored at 20−25 °C: in a white wine, the initial fSO_2 was 36 mg/L and then decreased to 9 mg/L at 12 months, in contrast with 18 mg/L in glass bottles.[5] After 12 months of storage of different wines, those stored in PET generally contain less SO_2 than those stored in glass.

Evolution of Headspace and Dissolved Carbon Dioxide. The results shown in Table 5 were obtained using a Carbodoseur for DCO_2 and μGC for $HspCO_2$. As there were no differences between storage in light or away from light (data not shown), values are averages for each month. At 162 days, TCO_2 losses were 21% for PET38 and PET38R. Finally, after 372 days, TCO_2 decreased by more than 40% for PET, whereas it remained almost stable for glass bottles. This decrease could have consequences on the perception of the wine.[24] Lonvaud-Funel (1976) showed that, for a red wine with different low DCO_2 contents (below 600 mg/L), differences can be detected by an untrained jury.[23] Furthermore the diffusion of O_2 in wine is facilitated when the CO_2 concentration decreases.[34] In our experiment, $HspCO_2$ represented less than 4% of TCO_2 at any time during storage. It appeared that DCO_2 was very close to TCO_2 and could be compared directly with it. DCO_2 losses were observed in different wines stored in 75 cL PET bottles with no special barrier to prevent CO_2 permeation,[15,19] and also in 25 cL PET bottles where the DCO_2 content decreased in wine whose initial DCO_2 was more than 100 mg/L.[2]

Table 5. TCO_2 during Storage Time for PET and Glass Bottles*

	TCO_2 (mg/bt)			CO_2 losses (%)	
	0**	162**	372**	0−162**	0−372**
PET38	627 ± 19 a	498 ± 10 b	370 ± 0 b	21	41
PET38R	605 ± 37 a	478 ± 23 c	357 ± 30 b	21	41
glass	621 ± 25 a	590 ± 15 a	633 ± 33 a	5	−2

*The results were obtained using a Carbodoseur for DCO_2 and the μGC for $HspCO_2$ (TCO_2 = $HspCO_2$ + DCO_2). Averages and standard deviations are based on 6 bottles per procedure (3 bottles in light + 3 bottles in the dark). Data were analyzed at each date by ANOVA followed by Newman−Keuls multiple comparison tests (α = 0.05). Similar letters denote no significant differences between the tested groups. **Time (d).

Evolution of Other Parameters. There were no significant differences in alcohol content, residual sugars, TA, VA, and pH after 372 days of storage (data not shown).

Direction of Gas Flows inside the Bottle and between Bottle and Air. As results for PET38R were close to those for PET38, and as there were no fundamental differences between storage in light or in the dark, the results for glass and PET38 bottles stored in light are presented here. Figure 2a covers glass bottles and represents $HspO_2^{\%}$ and $DO_2^{\%}$.

These values were calculated using eqs 4 to 15 cited previously. As $HspO_2^{\%}$ and $DO_2^{\%}$ were below 100% saturation, O_2 tended to permeate into the bottle from air to reach

dx.doi.org/10.1021/jf405392u | J. Agric. Food Chem. 2014, 62, 2946−2955

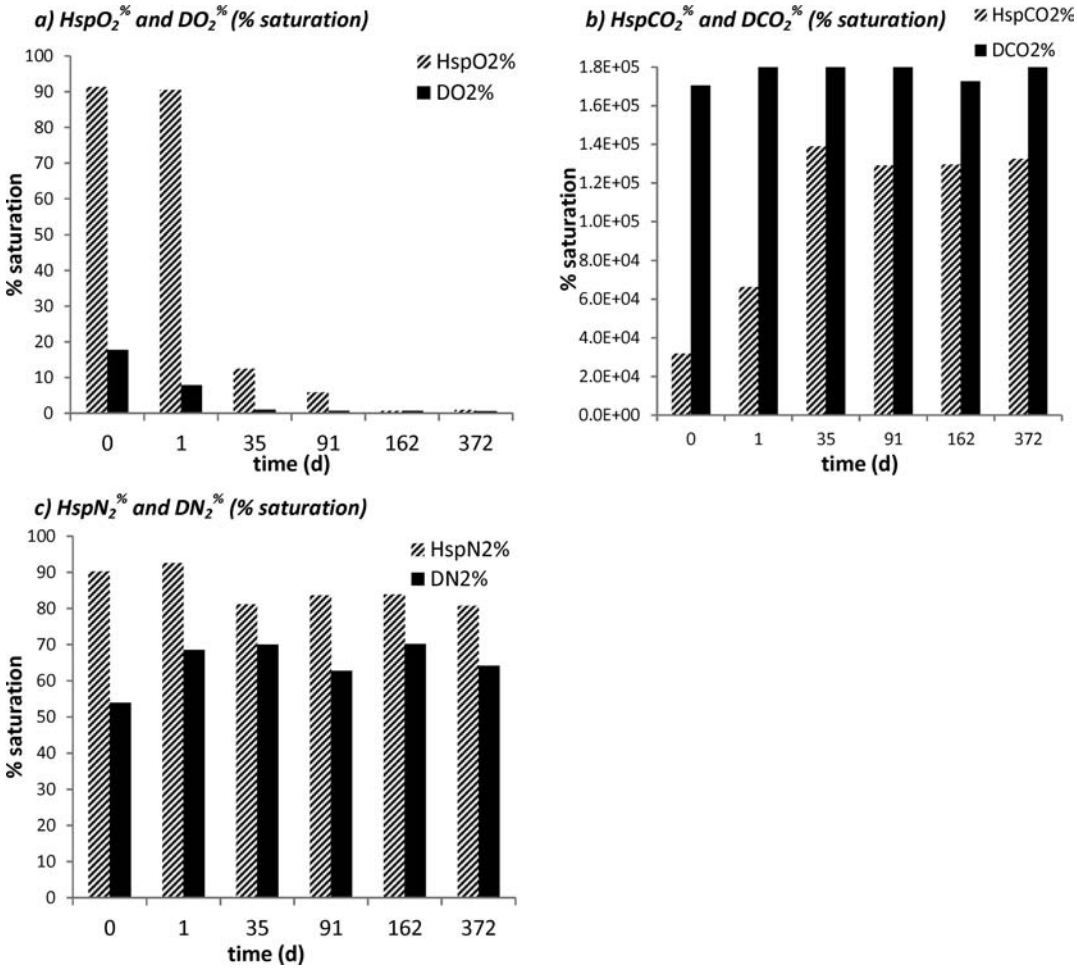

Figure 2. Comparison of $Hsp_{gas}^{\%}$ and $Dgas^{\%}$ with saturation of each gas in air at RH 68% for glass bottles stored in light. Hsp_{gas} were measured using the μGC, DO_2 was measured using the Orbisphere, DCO_2 was measured using the Carbodoseur, and DN_2 was calculated as described previously (eq 11). For panels a, b, and c respectively, solid squares indicate $DO_2^{\%}$, $DCO_2^{\%}$, and $DN_2^{\%}$ and striped squares indicate $HspO_2^{\%}$, $HspCO_2^{\%}$, and $HspN_2^{\%}$.

equilibrium. Furthermore, whatever the date of analyses, $DO_2^{\%}$ was lower than $HspO_2^{\%}$, so O_2 tended to dissolve in wine.[28] During the first month, $HspO_2^{\%}$ and $DO_2^{\%}$ decreases were due to wine oxygen consumption (as seen in Figure 1). After three months, DO_2 content was very low and remained stable at around 0.1 mg/bt (0.12 mg/L), corresponding to $P_{DO_2} \approx 1$ hPa ($P_{HspO_2} \approx 2$ hPa). These results were consistent with those found of Vidal and Moutounet (2006) in which DO_2 reached value of 0.06 mg/L in a rosé wine after 150 days of storage at 20 °C.[28] Figure 2b concerns CO_2. As $HspCO_2^{\%}$ and $DCO_2^{\%}$ were far above 100% saturation, CO_2 tended to diffuse from the bottle. In contrast with O_2, $HspCO_2^{\%}$ was lower than $DCO_2^{\%}$ and so CO_2 tended to diffuse from the wine to the headspace. After one month, $HspCO_2^{\%}$ and $DCO_2^{\%}$ remained stable for P_{HspCO_2} (≈460 hPa) and P_{DCO_2} (≈560 hPa), showing that diffusion through screwcaps is negligible in glass bottles. Finally, N_2 displayed the same behavior as O_2 (Figure 2c). N_2 was below 100% saturation, and so it tended to permeate into the bottle, and as $DN_2^{\%}$ was below $HspN_2^{\%}$, N_2 dissolved in wine in the first month and then equilibrium was nearly attained for P_{HspN_2} (≈640 hPa) and P_{DN_2} (≈520 hPa).

Figure 3 is for PET38. In the first month, O_2 consumption by wine was the dominant factor in oxygen kinetics, but after 3 months both $HspO_2^{\%}$ and $DO_2^{\%}$ increased (Figure 3a). This meant that wine O_2 consumption became slower than O_2 ingress. Between 91 and 372 days, P_{HspO_2}, (respectively P_{DO_2}) increased from 11 hpa (respectively 7 hPa) to 28 hpa (respectively 25 hPa). For CO_2 (Figure 3b), during first month, a phase of equilibrium between $HspCO_2^{\%}$ and $DCO_2^{\%}$ was observed like for glass bottles before P_{HspCO_2} and P_{DCO_2} decreased by respectively 148 hPa (0.24 mg/L) and 171 hPa (235 mg/L) between 91 and 372 days. Finally for N_2, differences with glass bottles could be seen after 1 month (Figure 3c): $HspN_2^{\%}$ and $DN_2^{\%}$ increased. Between 91 and 372 days, P_{HspN_2} (respectively P_{DN_2}) increased slightly from 607 hPa (respectively 480 hPa) to 616 hPa (respectively 561 hPa).

These results could be compared with those of P_{aphro} (Table 6). Standard deviations showed that there was substantial variability within each procedure. It was observed for PET bottles that P_{aphro} decreased from 41 ± 33 hPa to −68 ± 21 hPa during one year of storage. For glass bottles, P_{aphro} decreased but remained positive. As standard deviations were substantial, it was difficult to make a conclusion although a decrease of P_{aphro} for PET bottles could be expected: eq 11 cited previously can be used for partial pressure in bottle headspace:

$$0.97(P_{aphro} + P_{atm}) = P_{HSO_2} + P_{HSCO_2} + P_{HSN_2} \quad (16)$$

dx.doi.org/10.1021/jf405392u | J. Agric. Food Chem. 2014, 62, 2946−2955

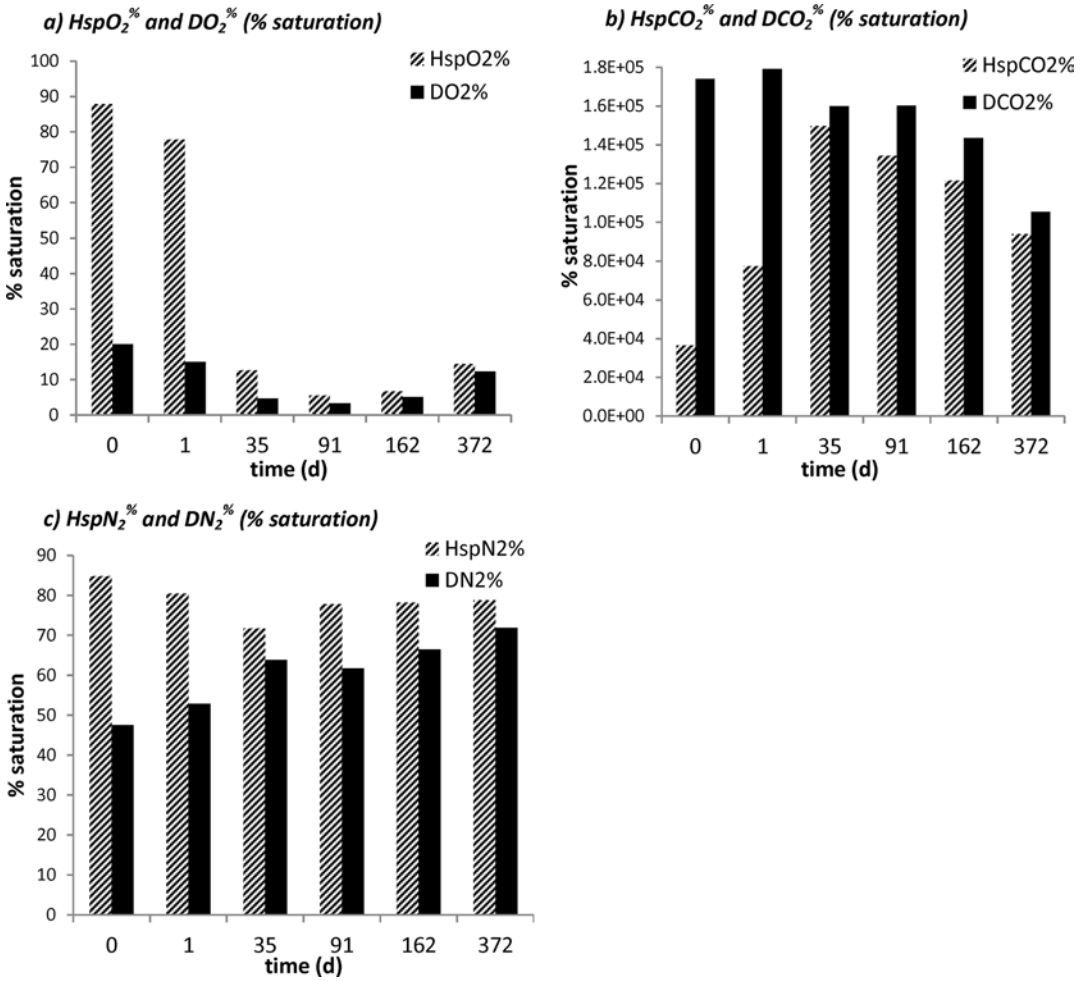

Figure 3. Comparison of $Hsp_{gas}^{\%}$ and $Dgas^{\%}$ with saturation of each gas in air at RH 68% for PET38 bottles stored in light. Hsp_{gas} were measured using the μGC, DO_2 was measured using the Orbisphere, DCO_2 was measured using the Carbodoseur, and DN_2 was calculated as described previously (eq 11). For panels a, b, and c respectively, solid squares indicate $DO_2^{\%}$, $DCO_2^{\%}$, and $DN_2^{\%}$ and striped squares indicate $HspO_2^{\%}$, $HspCO_2^{\%}$, and $HspN_2^{\%}$.

Table 6. P_{aphro} during Storage Time for PET and Glass Bottles*

	P_{aphro} (hPa)				
	1**	91**	162**	278**	372**
PET38	30 ± 38	−3 ± 19	−5 ± 17	−48 ± 32	−76 ± 19
PET38R	55 ± 22	17 ± 9	13 ± 10	−44 ± 15	−59 ± 20
PET average	41 ± 33	7 ± 18	4 ± 16	−46 ± 24	−68 ± 21
glass	167 ± 19	94 ± 19	111 ± 6	79 ± 28	84 ± 29

*P_{aphro} is measured by μGC. Averages and standard deviations are based on 6 bottles per packaging (3 bottles in light + 3 bottles in the dark), except for PET38R bottles at 1 day (n = 5). **Time (d).

P_{atm} varied slightly during one year (<1%). For PET38 bottles, between 91 and 372 days, P_{HspO_2} (respectively P_{HspN_2}) increased by 16 hPa (respectively 8 hPa) whereas P_{HspCO_2} decreased by 148 hPa. This balance between CO_2 losses and O_2 ingress can explain the observed decrease of P_{aphro} during storage.

O_2 Balance during One Year of Storage. To estimate O_2 ingress from bottling to one year of storage, we used TO_2 values at bottling and OTR of PET bottles and screwcaps given by Sidel (Table 7). After one year of storage, we could estimate O_2 ingress for each procedure, which was 4 to 5 times higher for PET bottles than for glass bottles. These values were between 25 and 30 mg/bt/year for PET bottles whereas they were estimated at 6 mg/bt/year for glass bottles. The oxygen content of wine saturated from air at atmospheric pressure is about 6 or 8 mg/L, depending on wine composition and temperature.[35] In our experiment, the rosé wine was saturated with O_2 approximately 4 times. Furthermore, these results showed the importance of O_2 management at bottling in PET bottles because TO_2 at bottling represented around 3 months of O_2 ingress through packaging.

Effect of Light and Packaging on the Evolution of Bottled Wine. After 372 days of storage, it appeared that light had an influence on O_2 consumption, which was faster in light, especially during the first week, where $HspO_2$ and DO_2

dx.doi.org/10.1021/jf405392u | J. Agric. Food Chem. 2014, 62, 2946−2955

Table 7. Evaluation of O_2 Ingress with TO_2 at Bottling and OTR of Bottles and Screwcaps*

	O_2 ingress through packaging** (mg/bt/year)	TO_2 trapped at bottling (mg/bt)	estimated TO_2 ingress (mg/bt/year)
PET38	23.8 ± 0.3	5.42 ± 0.68	29.3 ± 1.0
PET38R	19.8 ± 0.3	5.94 ± 0.42	25.7 ± 0.8
glass	0.6	5.70 ± 0.47	6.3

*Estimated TO_2 ingress is equal to O_2 ingress through packaging (OTR × 365 days) plus TO_2 trapped at bottling. **Tests carried out by Sidel at 23 °C RH = 60% under air. These OTR take into account bottle and screwcap. The OTR of glass bottle represents only the OTR of the screwcap.

decreased strongly. DO_2 then reached a minimum on day 14 in light against day 60 in darkness, meaning that O_2 consumption in light was soon limited by diffusion from the headspace into the wine. In contrast, light had no influence on parameters such as fSO_2, $HspCO_2$, and DCO_2. To the best of our knowledge, this is the first time that oxygen consumption kinetics in wine are reported to be accelerated by light although the impact on wine sensory quality was not investigated in the present study.

The impact of PET could be seen in different parameters. Wine stored in a monolayer PET bottle with no oxygen scavenger aged faster than in a glass bottle. After 162 days of storage, fSO_2 in a PET bottle reached the critical value of 10 mg/L, which meant that wine was not protected anymore, whereas wine in a glass bottle was still protected after a year. At the same time, after 3 months, $HspO_2$ and DO_2 in PET bottles increased, meaning that wine O_2 consumption became slower than O_2 ingress. Furthermore, O_2 at bottling played a key role in wine conservation because in our case it represented 3 months of O_2 ingress through PET packaging. TCO_2 losses were more than 40% after one year for PET bottles whereas it remained stable for glass bottles. These losses were linked to PET permeability and to a low bottle weight. CO_2 losses and O_2 ingress during storage seemed to be similar overall for PET38 and PET38R.

This experimental bottling enabled us to draw up the first complete gas balance for a bottle of wine including the three main gases present in headspace and in wine (O_2, CO_2, N_2) and their exchanges with air. The goal of the work reported here was to assess the limits of a monolayer PET bottle. According to this study, it appeared that a 38 g monolayer PET bottle was not sufficient to conserve wine for one year, given the losses of fSO_2 and CO_2 and the increase of O_2 content during storage. The next step in the study was to find a solution to increase the wine conservation period to 12 months using better gas management during bottling and by adding oxygen scavengers in PET packaging.

AUTHOR INFORMATION

Corresponding Author

*Phone: (33) 468 49 74 00. E-mail: vidaljc@supagro.inra.fr.

Funding

This work was performed within the NOVINPAK project (www.novinpak.org) and carried out with the financial support of OSEO (French state agency for innovation, Hérault, France), the ERDF (European Regional Development Funds, European Community) and the Languedoc-Roussillon Region.

Notes

The authors declare no competing financial interest.

ACKNOWLEDGMENTS

The authors thank companies and research centers associated with this project, namely, UCCOAR-Val d'Orbieu (Carcassonne, France), SIDEL Blowing Service (Le Havre, France), Pure Environnement (Perpignan, France), CNRS-PBS (Rouen, France), IRSTEA (Montpellier, France), UMR-SPO (INRA, Montpellier, France), UMR-IATE (INRA, Montpellier, France), and more specifically, the coordinators of the project, namely, Perrine Languet of UCCOAR-Val d'Orbieu and Marie-Hélène Lemaistre of SIDEL Blowing Service. The authors also thank Emilie Devic and Fabien Dell'Ova (UEPR, Gruissan, France) for analytical and technical aid.

ABBREVIATIONS USED

α(T), Bunsen absorption coefficient (mL(O_2)/mL); bt, bottle; d, day; Dgas, dissolved gas (O_2, CO_2, N_2) (mg/bt); $Dgas^{\%}$, dissolved gas (O_2, CO_2, N_2) (% of saturation of gas in air at RH 68%); *E*, alcohol content (% vol alcohol); fSO_2, free sulfites (mg/L); FTIR, Fourier transform infrared spectroscopy; Hsp_{gas}, headspace gas (O_2, CO_2, N_2) (mg/bt); Hsp_{gas}', headspace gas (O_2, CO_2, N_2) (% (v/v)); $Hsp_{gas}{}^{\%}$, headspace gas (O_2, CO_2, N_2) (% of saturation of gas in air at RH 68%); Hsp_{vol}, headspace volume (mL); LCA, life cycle analysis; M_{gas}, molar mass of gas (O_2, CO_2, N_2) (g/mol); OTR, oxygen transmission rate (mg/bt/d); P_{aphro}, aphrometric pressure (hPa); P_{atm}, atmospheric pressure (hPa); P_{Dgas}, partial pressure of dissolved gas (O_2, CO_2, N_2) (hPa); P_{gasatm}, partial pressure of gas (O_2, CO_2, N_2) in air at RH 68% (hPa); $P_{Hsp_{gas}}$, partial pressure of gas (O_2, CO_2, N_2) in headspace (hPa); P_{tot}, total pressure (hPa); $P_{w(T)}$, saturated water vapor pressure (hPa); PE, polyethylene; PET, polyethylene terephthalate; PP, polypropylene; RH, relative humidity (%); RPET, recycled PET; RS, residual sugar (g/L); *T*, temperature (°C); TA, total acidity (g/L H_2SO_4); TCO_2, total carbon dioxide (mg/bt); TO_2, total oxygen (mg/bt); TSO_2, total sulfites (mg/L); UEPR, experiment unit at Pech Rouge; VA, Volatile acidity (g/L H_2SO_4); V_M, molar volume (L/mol); $wine_{vol}$, wine volume (mL); μGC, micro gas chromatography

REFERENCES

(1) Gérand, Y.; Languet, P.; Lemaistre M. H.; Desoutter, L.; Roux P. PET/Recycled PET mix vs. Glass in the Packaging Industry: Southern France wine sector with a focus on the end-of-life effects. [avniR] 2nd LCA Conference, 6−7 November 2012, 289−294.

(2) Boidron, J. N.; Bar, M. Influence du matériau sur l'évolution du vin conditionné en contenant de faible volume. *Connaiss. Vigne Vin* **1988**, *22* (1), 73−83.

(3) Welle, F.; Ewender, J. Are PET-bottles suitable also for wine, liqueur and spirits? *Dtsch. Lebensm.-Rundsch.* **2002**, *98*, 79−81.

(4) Ough, C. S. Use of PET Bottles for Wine. *Am. J. Enol. Vitic.* **1987**, *38*, 100−104.

(5) Matthews, I.; Vale, C. Study of suitability of 187mL PET bottles for packaging wine in Australia. *Aust. N. Z. Wine Ind. J.* **2009**, *24* (Issue 1), p31.

(6) Dimkou, E.; Ugliano, M.; Diéval, J. B.; Vidal, S.; Aagaard, O.; Rauhut, D.; Jung, R. Impact of Headspace Oxygen and Closure on Sulfur Dioxide, Color, and Hydrogen Sulfide Levels in a Riesling Wine. *Am. J. Enol. Vitic.* **2011**, *62* (3), 261−269.

(7) Brajkovitch, M.; Tibbits, N.; Peron, G.; Lund, C. M.; Dykes, S.; Kilmartin, P. A.; Nicolau, L. Effect of Screwcap and Cork Closures on SO_2 levels and Aromas in a Sauvignon Blanc Wine. *J. Agric. Food Chem.* **2005**, *53*, 1006−10011.

(8) Godden, P.; Francis, L.; Field, J.; Gishen, M.; Coulter, A.; Valente, P.; Høj, P.; Robinson, E. Wine bottle closures: physical

characteristics and effect on composition and sensory properties of a Semillon wine 1. Performance up to 20 months post-bottling. *Aust. J. Grape Wine Res.* **2001**, *7*, 64−105.
(9) Waterhouse, A. L.; Laurie, V. F. Oxidation of Wine Phenolics: A Critical Evaluation and Hypotheses. *Am. J. Enol. Vitic.* **2006**, *57*, 306−313.
(10) Danilewicz, J. C.; Seccombe, J. T.; Whelan, J. Mechanism of Interaction of Polyphenols, Oxygen, and Sulfur Dioxide in Model Wine and Wine. *Am. J. Enol. Vitic.* **2008**, *59* (2), 128−136.
(11) Danilewicz, J. C.; Wallbridge, P. J. Further studies on the Mechanism of Interaction of Polyphenols, Oxygen, and Sulfite in Wine. *Am. J. Enol. Vitic.* **2010**, *61* (2), 166−175.
(12) Wirth, J.; Caillé, S.; Souquet, J. M.; Samson, A.; Dieval, J. B.; Vidal, S.; Fulcrand, H.; Cheynier, V. Impact of post-bottling oxygen exposure on the sensory characteristics and phenolic composition of Grenache rosé wines. *Food Chem.* **2012**, *132*, 1862−1871.
(13) Buiatti, S.; Celotti, E.; Ferrarini, R.; Zironi, R. Wine Packaging for Market in Containers Other than Glass. *J. Agric. Food Chem.* **1997**, *45*, 2081−2084.
(14) Pati, S.; Mentana, A.; La Notte, E.; Del Nobile, M. A. Biodegradable poly-lactic acid package for the storage of carbonic maceration wine. *Food Sci. Technol.* **2010**, *43*, 1573−1579.
(15) Ghidossi, R.; Poupot, C.; Thibon, C.; Pons, A.; Darriet, P.; Riquier, L.; De Revel, G.; Mietton Peuchot, M. The influence of packaging on wine conservation. *Food Control* **2012**, *23*, 302−311.
(16) Galassi, S. Packaging of wines in containers other than glass. *Ind. Bevande* **1985**, *14* (75), 30−35.
(17) Mentana, A.; Pati, S.; La Notte, E.; Del Nobile, M. A. Chemicals changes in Apulia table wines as affected by plastic packages. *Food Sci. Technol.* **2009**, *42*, 1360−1366.
(18) Giovanelli, G.; Brenna, O. V. Oxydative stability of red wine stored in packages with different oxygen permeability. *Eur. Food Res. Technol.* **2006**, *226*, 169−179.
(19) Jung, R.; Schüssler, C.; Hamdorf, B.; Lay, J.; Seckler, F.; Seckler, J. Oxygen transfer into wines through alternative packaging materials. *Mitt. Klosterneuburg* **2011**, *61*, 82−90.
(20) Oliveira, V.; Lopes, P.; Cabral, M.; Pereira, H. Kinetics of Oxygen Ingress into Wine Bottles Closed with Natural Cork Stopeers of Diferent Qualities. *Am. J. Enol. Vitic.* **2013**, *64* (3), 395−399.
(21) Lopes, P.; Saucier, C.; Glories, Y. Nondestructive Colorimetric Method To Determine the Oxygen Diffusion Rate through Closures Used in Winemaking. *J. Agric. Food Chem.* **2005**, *53*, 6967−6973.
(22) Dieval, J. B.; Vidal, S.; Aagaard, O. Measurement of the Oxygen Transmission Rate of co-extruded wine bottle closures using a luminescence-based Technique. *Packag. Technol. Sci.* **2011**, *24*, 375−385.
(23) Lonvaud-Funel, A. Recherches sur le gaz carbonique des vins. Thèse doctorat 3^{e} cycle, Université de Bordeaux II, 1976.
(24) Blankenhorn, D. Die Bedeutung von CO_2 für die Weinbereitung. *Rebe und Wein* **2002**, *55* (11), 14−15.
(25) Vidal, J. C.; Moutounet, M. Impact of operating conditions during bottling and of technical cork permeability on the oxygen content and evolution of bottled Sauvignon Blanc wine. *Internet J. Vitic. Enol.* **2011**, *4*/3, 1−15, www.infowine.com.
(26) Vidal, J. C.; Devic, E.; Dell'Ova F. Bottling of small volumes of experimental wines with precise management of dissolved gases. *35th World Congress of Vine and Wine, Izmir*, 20 juin 2012.
(27) Vidal, J. C.; Boulet, J. C.; Moutounet, M. Les apports d'oxygène au cours des traitements des vins. Bilan des observations sur site, 3^{éme} partie. *Rev. Fr. Oenol.* **2004**, *205*, 25−33.
(28) Vidal, J. C.; Moutounet, M. Monitoring of oxygen in the gas and liquid phases of bottles of wine at bottling and during storage. *J. Int. Sci. Vigne Vin* **2006**, *40* (1), 35−45.
(29) Castellari, M.; Simonato, B.; Tornielli, G. B.; Spinelli, P.; Ferrarini, R. Effects of different enological treatments on dissolved oxygen in wines. *Ital. J. Food Sci.* **2004**, *16* (3), 387−396.
(30) Karbowiak, T.; Gougeon, R. D.; Alinc, J. B.; Brachais, L.; Debeaufort, F.; Voilley, A.; Chassagne, D. Wine Oxydation and the Role of Cork. *Crit. Rev. Food Sci.* **2009**, *50* (1), 20−52.
(31) Vidal, J. C.; Gianduzzo, A.; Chauvet, V.; Sirena, I. Validation of a laser spectroscopic method for the determination of dissolved carbon dioxide in bottles of still wine. *Bulletin de l'OIV* **2011**, *85* (974−975−976), 173−188.
(32) Huber, C. Appendix. In *Instruction manual-Fibox 3-trace v3*; PreSens Precision Sensing GmbH: Regensburg, Germany, 2006; pp 62−66.
(33) Liger-Belair, G. The Physics and Chemistry behind the bubbling properties of Champagne and Sparkling Wines: A State of the Art Review. *J. Agric. Food Chem.* **2005**, *53*, 2788−2802.
(34) Devatine, A.; Chiciuc, I.; Mietton-Peuchot, M. The protective role of dissolved carbon dioxide against wine oxidation: a simple and rational approach. *J. Int. Sci. Vigne Vin* **2011**, *45* (3), 189−197.
(35) Singleton, V. L. Oxygen with phenols and related reaction in musts, wines and model systems: observation and practical implications. *Am. J. Enol. Vitic.* **1987**, *38*, 69−77.

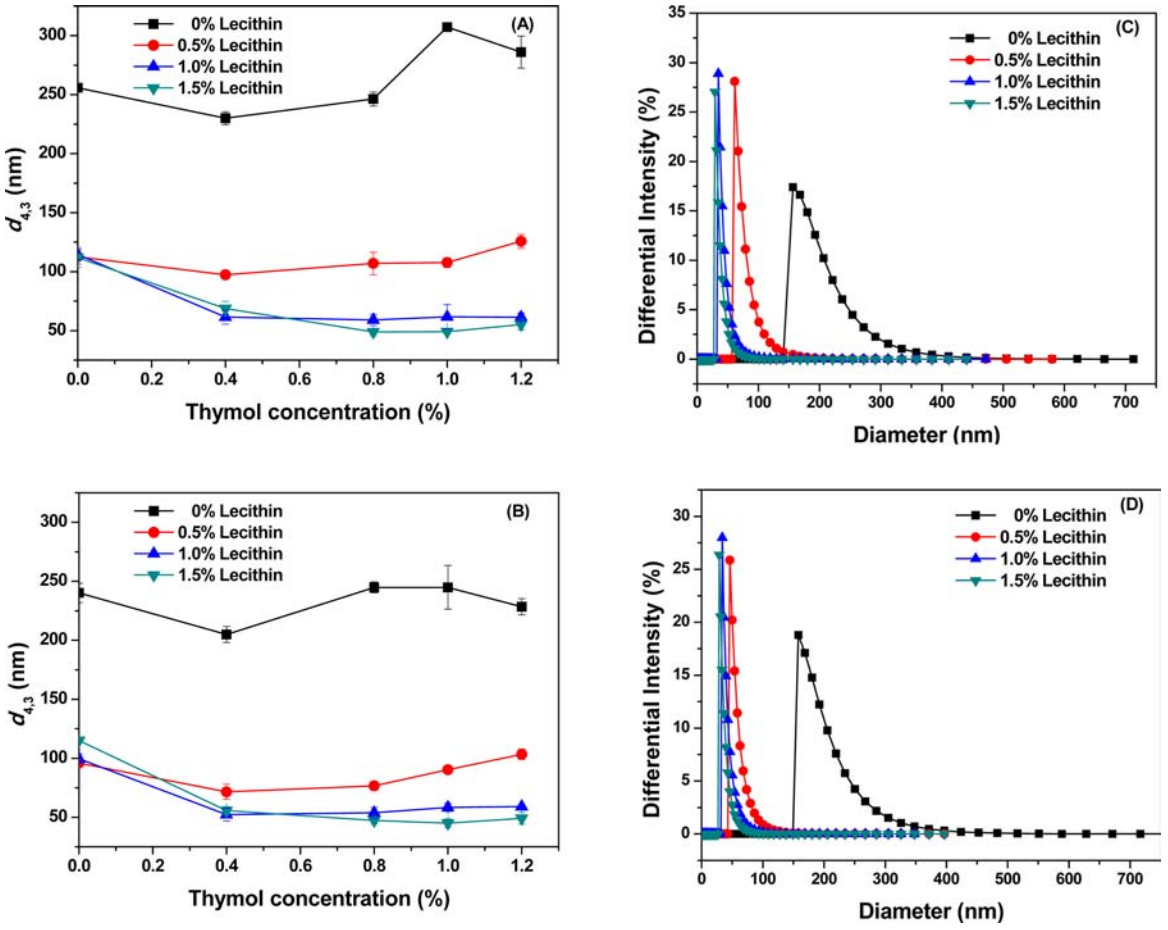

Figure 1. Volume fraction−length mean particle diameter ($d_{4,3}$) of thymol dispersions prepared with 0.2% (w/v) type A (A) and type B (B) gelatin and different amounts of lecithin. Size distributions are shown in C and D for samples containing 0.8% thymol emulsified by gelatins A and B, respectively. Error bars are standard deviations from duplicates.

MATERIALS AND METHODS

Materials. Thymol (99% purity) and type A gelatin were purchased from Acros Organics (Morris Plains, NJ, USA). Type B gelatin, soy lecithin (phosphatidylcholines), and other chemicals, such as PG and methanol, were obtained from Fisher Scientific (Pittsburgh, PA, USA).

Preparation of Nanodispersions. The 0−0.06 g of gelatin was dissolved in 9 mL of deionized water. Different amounts of lecithin (0, 0.05, 0.1, and 0.15 g) were added into the gelatin solution, followed by vortexing for 1 h at room temperature (21 °C), and the pH was 6.8. The working thymol solution was prepared separately by dissolving various amounts (0, 0.04, 0.08, 0.10, and 0.12 g) in 1 mL of PG. The gelatin/lecithin sample and thymol solution were mixed and emulsified at 15,000 rpm for 2 min using a model Cyclone I.Q.^{2} microprocessor homogenizer (The VirTis Co., Inc., Gardiner, NY, USA).

Particle Size Measurement. Particle size distributions of dispersions were measured using a Delas nano-ζ potential and sub-micrometer particle size analyzer (Beckman Coulter, Inc., Brea, CA, USA). The volume−length mean particle diameter ($d_{4,3}$) was calculated from the number of particles (n_i) with the corresponding diameter (d_i) based on the following equation:

$$d_{4,3} = \frac{\sum_{i=1} n_i d_i^4}{\sum_{i=1} n_i d_i^3} \quad (1)$$

Turbidity. The absorbance of dispersions was measured at 600 nm (Abs_{600}) as the indicator of turbidity using a UV−vis spectrophotometer (model Biomate 5, Thermo Electron Corp., Woburn, MA, USA).

Transmission Electron Microscopy. The morphology of thymol dispersions prepared with gelatin alone, lecithin alone, and gelatin−lecithin blend was characterized using a Zeiss Libra 200 transmission electron microscope (Carl Zeiss SMT Inc., Oberkochen, Germany). A 5 μL aliquot of the emulsion was placed onto a copper grid and stained with a drop of 2% (w/w) uranyl acetate solution. After 2 min, the grid was tapped with filter paper, followed by air-drying at room temperature (21 °C) before imaging.

Quantification of Protein in the Serum of Dispersions. The nanodispersions were prepared with the aqueous phase with 0.2% (w/v) gelatin B and 1.0% (w/v) lecithin at pH 7.0. After homogenizing 0.8% (w/v) thymol as discussed previously, nanodispersions were adjusted to pH 2.0−6.0 using 1.0 M HCl or pH 8.0 using 1.0 M NaOH. The gelatin B−lecithin blend without thymol was also prepared using the same procedures. All samples were centrifuged at 16,110g for 30 min at 25 °C using an Optima MAX ultracentrifuge (Beckman Coulter) to obtain the supernatant for protein assay. Because thymol interferes with protein assay, 200 μL of the supernatant was mixed with 6 mL of an acetone−hexane (1:1, v/v) mixture to extract thymol and precipitate protein. [27] After vigorous mixing and centrifugation at 6,700g for 5 min using an Eppendorf MiniSpin plus centrifuge (Hamburg, Germany), the supernatant (organic phase) was discarded, and the bottom protein precipitate was re-dissolved in 300 μL of 100 mM NaOH and was quantified using the bicinchoninic acid (BCA) method (Thermo Fisher Scientific Inc., Morris Plains, NJ, USA). Gelatin was used as a reference protein in the BCA assay.

ζ Potential. The ζ potentials of thymol dispersions were measured using a DelasTM nano-ζ potential and sub-micrometer particle size analyzer (Beckman Coulter). Samples were diluted 100 times using

dx.doi.org/10.1021/jf405828s | J. Agric. Food Chem. 2014, 62, 2956−2962

deionized water and adjusted to pH 3.0−7.0 before analysis. Three dispersion replicates were tested for three times each.

Storage Stability. Storage stability of thymol dispersions at room temperature (21 °C) was assessed over a period of 1 month. The dispersions were monitored weekly for changes in particle size.

Statistical Analysis. Analysis of variance (ANOVA) test was conducted using the SPSS 16.0 statistical analysis system (SPSS Inc., Chicago, IL, USA). The least significant difference (LSD) test was used to determine the significant difference of mean values at a P level of 0.05.

RESULTS AND DISCUSSION

Effects of Gelatin Type and Lecithin Concentration on Particle Dimension at Neutral pH. The $d_{4,3}$ and particle size distribution of dispersions prepared with two types of gelatin and different amounts of lecithin are shown in Figure 1. The $d_{4,3}$ of dispersions prepared with gelatin alone was around 250 nm. Blending lecithin with gelatin significantly decreased the $d_{4,3}$ when compared to gelatin alone without thymol ($P < 0.05$), indicating the formation of gelatin−lecithin complexes. When thymol was present, the $d_{4,3}$ of the dispersions prepared with gelatin−lecithin blends further decreased, which may have resulted from the increased particle packing due to the strengthened intraparticle attraction by hydrophobic thymol. Generally speaking, $d_{4,3}$ decreased with an increase in lecithin concentration until about 1% (w/v), above which there was no significant further decrease in $d_{4,3}$ ($P > 0.05$). The increase of lecithin content also corresponded to the narrowed particle size distributions of dispersions containing 0.8% thymol (Figure 1C,D). A greater amount of lecithin enables the stabilization of a larger interfacial area, leading to smaller particles, until the radius of droplet curvature reaching a critical value beyond which no further decrease in the particle size is enabled.[28] Furthermore, a greater $d_{4,3}$ was observed at a higher thymol concentration between 0.4 and 1.2% (w/v) when 0.5% (w/v) lecithin and 0.2% (w/v) gelatin were used. In contrast, there was no significant change in $d_{4,3}$ when 0.4−1.2% (w/v) thymol was dispersed by 0.2% (w/v) gelatin and 1 or 1.5% (w/v) lecithin ($P > 0.05$). Therefore, the combination of 1% (w/v) lecithin and 0.2% (w/v) gelatin was sufficient to disperse 1.2% (w/v) thymol.

When two gelatin types were compared, it was observed that dispersions prepared with gelatin A had significantly bigger $d_{4,3}$ than those with gelatin B when 0 and 0.5% (w/v) lecithin was used ($P < 0.05$, Figure 1A,B), which indicates that complexes formed with gelatin B are more effective in dispersing thymol. As discussed previously, gelatin A has pI ∼ 8−9 and has net positive charges at neutral pH. [17] In contrast, gelatin B has pI ∼ 4−5 and is net negatively charged at neutral pH. [17] The electrostatic attraction between gelatin A and highly negatively charged lecithin may enable the formation of more compact complexes than those of gelatin B, which may reduce the ability to disperse thymol. When more lecithin (1 and 1.5% (w/v)) was used with 0.2% (w/v) gelatin, the $d_{4,3}$ of the dispersions prepared with gelatin B was slightly smaller than those with gelatin A, which indicates that the effect of gelatin type was not significant when a sufficient amount of lecithin was used. Furthermore, it was observed that dispersions prepared with gelatin A precipitated after storage for 2 to 3 days at room temperature (21 °C), while those prepared with gelatin B were stable after several months. This likely is due to the net surface charge being smaller for samples with gelatin A, due to opposite charges between gelatin A and lecithin but the same types of net charges for the case of gelatin B and lecithin. Based on this set of experiments, gelatin B and 1% (w/v) lecithin were chosen for further studies.

Effects of Gelatin B Concentration on Dispersion Properties at Neutral pH. Appearance, Abs_{600}, and $d_{4,3}$ of thymol dispersions prepared with 1% (w/v) lecithin, 0.8% (w/v) thymol, and 0−0.6% (w/v) gelatin B are presented in Figure 2. The dispersion prepared with lecithin only was very turbid

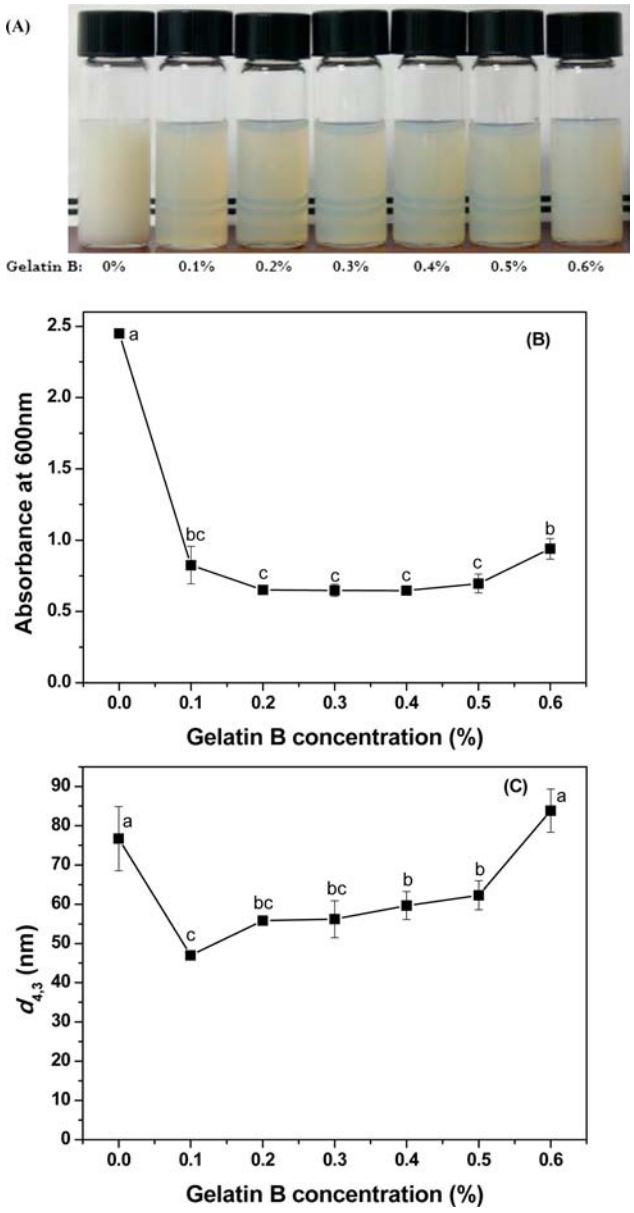

Figure 2. Appearance (A), absorbance at 600 nm (B), and volume−length mean particle diameter ($d_{4,3}$) of thymol dispersions prepared with 0−0.6% (w/v) gelatin B, 1% (w/v) lecithin, and 0.8% (w/v) thymol. Error bars are standard deviations from duplicates. Different letters next to symbols indicate significant differences in the mean ($P < 0.05$).

(Figure 2A), which became translucent after blending with gelatin B. The dispersions prepared with intermediate gelatin B concentrations (0.2−0.5% (w/v)) showed the lowest turbidity. The sample with 0.6% (w/v) gelatin B was more turbid, possibly because of the limited solubility of gelatin B. The Abs_{600} data (Figure 2B) generally agreed with the visual

dx.doi.org/10.1021/jf405828s | J. Agric. Food Chem. 2014, 62, 2956−2962

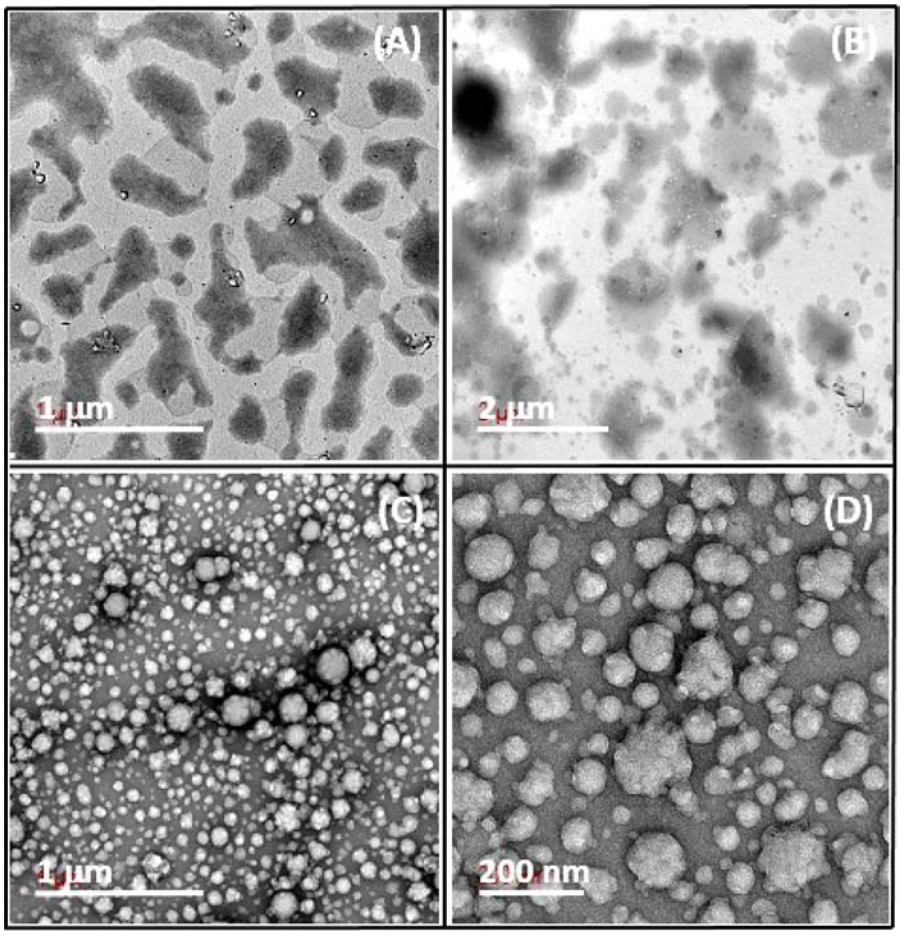

Figure 3. TEM images of dispersions prepared with 0.8% (w/v) thymol and 1.0% (w/v) lecithin only (A), 0.2% (w/v) gelatin B only (B), and their blend (C and D, in two magnifications).

appearance (Figure 2A). No obvious differences in Abs_{600} of treatments with 0.2−0.5% (w/v) gelatin B indicate the 0.8% (w/v) thymol was well dispersed at these conditions. Conversely, a sharp decrease in $d_{4,3}$ was observed when gelatin B concentration increased from 0 to 0.1% (w/v), followed by gradual increases in particle dimension as gelatin B concentration further increased. The $d_{4,3}$ was not significantly different for the treatments with 0.2−0.5% (w/v) gelatin B ($P > 0.05$), while that with 0.6% (w/v) gelatin B was significantly bigger than other treatments with gelatin B ($P < 0.05$, Figure 2C). In a study encapsulating drug Amphotericin B, the lipophilic drug was mixed with lecithin in an organic solvent mixture of dimethyl sulfoxide and methanol, followed by mixing with an aqueous gelatin solution to form sub-micrometer particles. [29] Confocal laser scanning microscopy and fluorescent resonance energy transfer analyses showed that lecithin was present in the particle interior and gelatin was present on the particle surface. This study suggests that the more hydrophobic lecithin is preferably in contact with the lipophilic drug, while the hydrophilic gelatin binds with lecithin on the particle surface. In our study, if thymol particles are preferentially emulsified by lecithin, the particles with adsorbed gelatin B would be bigger than those with lecithin only. The expectation from this sequential adsorption of lecithin and gelatin on thymol particles is opposite to the data in Figure 2C. Therefore, it is more likely that gelatin B forms complexes with lecithin, which adsorb on thymol particles simultaneously during emulsification. Since 0.2% (w/v) of gelatin B was sufficient to form a translucent dispersion, this concentration was selected for further studies.

Morphology of Thymol Particles. The morphology of thymol particles (Figure 3) was studied for dispersions prepared with 0.8% (w/v) thymol dispersed by 0.2% (w/v) gelatin B alone, 1.0% (w/v) lecithin alone, and their combination. The dispersion prepared with the blend (Figure 3C,D) had mostly spherical particles with a mean diameter of 60 nm that agrees with the $d_{4,3}$ of 49 nm (Figure 1B) and the translucent appearance (Figure 2A). In contrast, bigger and irregular particles were observed for dispersions prepared with lecithin only (Figure 3A) and gelatin B only (Figure 3B), which agrees with the turbid appearance of both dispersions (Figure 2B for the sample dispersed with lecithin only; the other sample is not shown). The heterogeneity of particle structures (Figure 3) overall agrees with the particle size distributions in Figure 1D. Lecithin used in this study (phosphatidylcholines) is soluble in hexane and its poor water solubility can contribute to turbidity (Figure 2) and irregular structures (Figure 3A). In contrast, 0.2% (w/v) gelatin B is dissolved in water as a transparent solution, but the turbid dispersion and irregular big particles after emulsifying thymol indicate the weak emulsifying property of gelatin. In addition, the particle dimension observed by transmission electron microscopy (TEM) was bigger than the $d_{4,3}$ values of dispersions made with gelatin B alone (250 nm, Figure 1B) or lecithin alone (76 nm, Figure 2C). The

dx.doi.org/10.1021/jf405828s | J. Agric. Food Chem. 2014, 62, 2956−2962

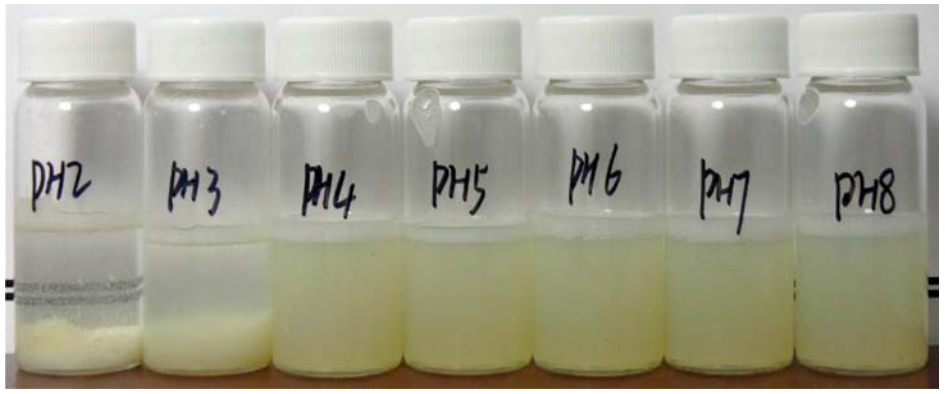

Figure 4. Appearance of aqueous mixtures with 1.0% (w/v) lecithin and 0.2% (w/v) gelatin B adjusted to different pH.

difference can be contributed by sample preparation with (in light scattering) and without (in TEM) dilution. Dilution can separate weakly flocculated particles/structures, lowering the measured particle dimension.

Effects of pH on Dispersion Stability. The stability of dispersions prepared with 0.8% (w/v) thymol, 0.2% (w/v) gelatin B, and 1% (w/v) lecithin was investigated at pH 2.0−8.0. The first set of samples was prepared for aqueous mixtures of gelatin B and lecithin without thymol to study the complex formation of the two molecules. Figure 4 shows that samples at pH 4.0−8.0 were turbid and those at pH 2 and 3 precipitated quickly. The turbidity is due to the poor water solubility of lecithin, as discussed previously. The precipitation at pH 3.0 contrasts with stable samples with gelatin or lecithin alone (not shown). After centrifugation of the mixture at pH 3.0, the serum contained 0.0169% (w/v) protein (gelatin), less than 10% of the total gelatin concentration (0.2% (w/v)), which indicates the co-precipitation of lecithin and gelatin B.

In the second set of treatments, thymol dispersions prepared at pH 7.0 were adjusted to pH 2.0−6.0. Like the mixture (Figure 4), dispersions at pH 2.0 and 3.0 also showed significant precipitation. The dispersion at pH 4.0 showed some precipitated structures, while dispersions at pH 5.0−7.0 were stable. The acidification increased the $d_{4,3}$ (Table 1), with that at pH 5.0 being significantly bigger ($P < 0.05$). In comparison, the $d_{4,3}$ of gelatin−lecithin mixture (without thymol) was not significantly different at pH 5.0−7.0 ($P > 0.05$) but was significantly bigger than comparable samples with thymol at pH 6.0 and 7.0 ($P < 0.05$). This suggests that the adsorption of gelatin B−lecithin complexes on thymol particles resulted in much ordered structures. The inclusion of thymol in nanoparticles increases the overall hydrophobicity that can cause some particle aggregation when repulsive electrostatic interactions are weakened below pH 5.0, as discussed further in subsequent text for ζ-potential data.

Table 1. Volume Fraction−Length Mean Diameter ($d_{4,3}$, nm) of Dispersions with 0.8% (w/v) Thymol Dispersed by 0.2% (w/v) Gelatin B and 1.0% (w/v) Lecithin at pH 7.0 and after Acidification to pH 5.0 and 6.0, with Comparison to the Blend (without Thymol) Prepared at Identical Conditions[a]

	$d_{4,3}$		
	pH 5	pH 6	pH 7
with thymol	159.3 ± 11.9a	58.9 ± 2.0cde	45.3 ± 2.1e
without thymol	135.2 ± 3.0ab	132.7 ± 4.9ab	109.1 ± 7.7ab

[a]Numbers are mean ± standard deviation from triplicates. Different letters represent significant differences in the mean.

To further study the surface composition of thymol particles, the protein content in the serum of dispersions with and without thymol after centrifugation was measured as the content of free gelatin (Table 2). At pH 5.0, close to the pI of gelatin B, [17] the protein content in the thymol dispersion serum was lower than that at pH 6.0 and 7.0 ($P < 0.05$), which was in agreement with the significantly bigger particles at pH 5.0 (Table 1). Conversely, similar to $d_{4,3}$ (Table 1), there was no significant difference in the serum protein content in the blend dispersions (without thymol) at pH 5.0−7.0 ($P > 0.05$). Because gelatin only solutions had the gradually decreased protein contents after acidification to 5.0 and centrifugation (Table 2), similar serum protein contents in the blend dispersions suggest the complex formation between gelatin B and lecithin that resulted in the stability at pH 5.0−7.0. The thymol dispersion at pH 5.0 did not show visible precipitation, and the lowered serum protein content after centrifugation is likely due to the sedimentation of aggregated particles (Table 1).

ζ Potential of Thymol Dispersions. To study the role of electrostatic interactions on dispersion formation and stability, ζ potentials of thymol dispersions prepared with gelatin B alone, lecithin alone, and their blend were measured (Figure 5). The ζ potentials of dispersions prepared with lecithin only were highly negative at pH 3.0−7.0, with a reduced magnitude at a lower pH. This is due to the presence of ionized phosphate group of lecithin that is protonated to a greater extent at a lower pH, as previously reported. [30] In comparison, dispersions prepared with gelatin B only showed the characteristics expected from gelatin B, with ζ potential being zero at about pH 4.8 that corresponds to the pI of gelatin B. At pH 6.0 and 7.0, the negative ζ potential of dispersions prepared with gelatin B only had much smaller magnitudes than those prepared with lecithin.

For dispersions prepared with gelatin B−lecithin blend, ζ potentials at pH 5.0, 6.0, and 7.0 were close to those prepared with lecithin alone. Besides, thymol dispersion prepared with the blend exhibited similar ζ potential at pH 5.0, 6.0, and 7.0, which contradicts with the different $d_{4,3}$ and serum protein content of thymol nanodispersions at pH 5.0, 6.0, and 7.0 (Tables 1 and 2). The ζ -potential data suggest additional colloidal forces causing particle aggregation at pH 5.0. It may be caused by the increased particle hydrophobicity due to gelatin B at the acidity close to its pI (Figure 5). The strong electrostatic

Table 2. Percentages of Total Protein in the Serum of Dispersions with 0.8% (w/v) Thymol Dispersed by 0.2% (w/v) Gelatin B and 1.0% (w/v) Lecithin at pH 7.0 and after Acidification to pH 5.0 and 6.0, with Comparison to the Blend or Gelatin B Only (without Thymol) Prepared at Identical Conditions[a]

	protein % in the serum		
	pH 5	pH 6	pH 7
thymol dispersion	49.51 ± 12.28f	73.23 ± 1.39bcde	83.73 ± 0.57ab
gelatin B–lecithin blend	67.06 ± 1.52cdef	71.75 ± 2.55bcde	56.93 ± 4.37ef
gelatin B only	75.32 ± 0.82bcd	87.18 ± 1.23ab	93.25 ± 1.73a

[a]Numbers are mean ± standard deviation from triplicates. Different letters represent significant differences in the mean.

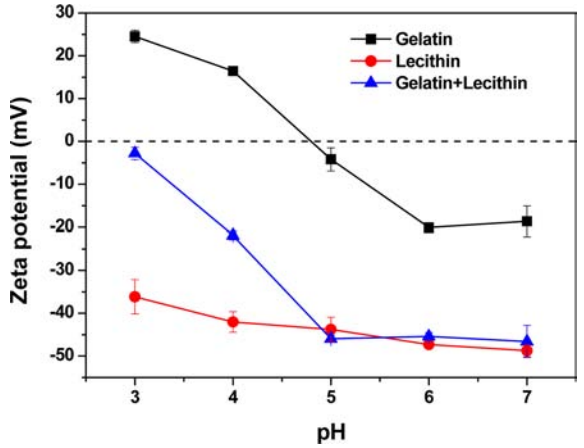

Figure 5. ζ potential of dispersions with 0.8% (w/v) thymol dispersed by 0.2% (w/v) gelatin B alone, 1.0% (w/v) lecithin alone, or their blend at pH 3.0–7.0. Error bars are standard deviations from triplicates.

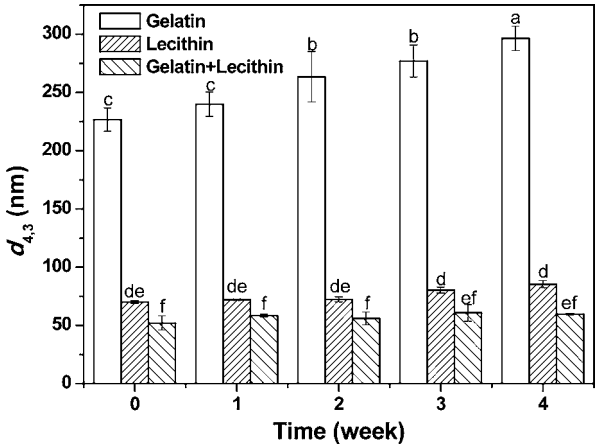

Figure 6. Changes of $d_{4,3}$ of dispersions with 0.8% (w/v) thymol dispersed by 1.0% (w/v) lecithin alone, 0.2% (w/v) gelatin B alone, or their blend at pH 7.0 during storage at room temperature (21 °C) for 4 weeks. Error bars are standard deviations from triplicates. Different letters above bars indicate significant differences in the mean of the same sample ($P < 0.05$).

repulsion at pH 5.0 was able to limit the particle aggregation (Table 1) so that the overall dispersion showed the absence of macroscopic precipitation.

At pH 4.0, ζ potential of the thymol nanodispersion prepared by the gelatin B–lecithin blend reduced to about one-half of the dispersion prepared with lecithin only (Figure 5), indicating that gelatin B also had a significant influence on the droplet surface charge. At pH 4.0, gelatin B is positively charged and neutralizes negative charges of lecithin. The reduced ζ potential at pH 4.0 may have caused some precipitation of thymol particles, as discussed previously. At pH 3.0, as gelatin B had more positive charges, the ζ potential of the dispersion prepared with the blend decreased further in magnitude to be close to zero, which caused severe precipitation. Therefore, electrostatic interactions are the major colloidal force responsible for the stability of thymol dispersions prepared with gelatin B–lecithin blend. The stable dispersions at pH 5.0 and above are significant for their applications, as many foodborne pathogens can grow in low-acid foods (>pH 4.6).

Storage Stability of Dispersions at Neutral pH. The storage stability of dispersions containing 0.8% (w/v) thymol at neutral pH was evaluated by measuring $d_{4,3}$ weekly for 1 month at room temperature (21 °C). Figure 6 shows that the dispersion prepared with lecithin–gelatin B blend had a constant $d_{4,3}$ of around 55 nm during storage. In contrast, $d_{4,3}$ of dispersions prepared with gelatin B alone increased significantly after 4 weeks ($P < 0.05$), from 220 to 280 nm. For dispersions prepared with lecithin alone, $d_{4,3}$ also increased from 68 to 85 nm. Because thymol has a solubility of about 0.048% (w/v) in water, [7] Ostwald ripening has been observed to cause the increase of particle size in thyme oil nanodispersions emulsified by Tween 80, which can be eliminated by blending with lipids with low water solubility.[31,32] The use of low water solubility lipids however reduced the loading and antimicrobial efficacy of essential oils. Therefore, stable thymol nanodispersions prepared by the gelatin B–lecithin blend are promising for use as antimicrobial delivery systems. Furthermore, in our recent studies, the minimum inhibitory concentration of thymol increased or remained unchanged after encapsulation in whey protein–maltodextrin conjugates[33,34] and sodium caseinate,[35] respectively. Whey proteins have more ordered secondary structures and are more hydrophobic than caseins.[36] Since gelatin is less hydrophobic than whey proteins and caseins and does not have secondary structures,[36] impacts of gelatin on antimicrobial activity of thymol may be insignificant. Characterizations of antimicrobial activities of these dispersions and their impact on sensory properties of food products are underway.

In conclusion, gelatin B and lecithin, both GRAS emulsifers, can be used as a blend to prepare translucent thymol nanodispersions with a mean diameter of about 50 nm at pH 5.0 and above. The synergistic surface activity of the blend is likely due to complex formation of the blend. The electrostatic repulsion, contributed mostly by lecithin, prevented particles from aggregation. The blend complexes on thymol particle surface prevented Ostwald ripening and maintained particle dimension during storage at neutral pH. Therefore, the stable nanodispersions prepared from GRAS ingredients have great potential to incorporate lipophilic food antimicrobials such as thymol in low-acid foods to enhance the microbiological safety.

dx.doi.org/10.1021/jf405828s | J. Agric. Food Chem. 2014, 62, 2956–2962

AUTHOR INFORMATION

Corresponding Author

*Phone: (865) 974-6196. Fax: (865) 974-7332. E-mail: qzhong@utk.edu.

Funding

This work was supported by the University of Tennessee and the USDA National Institute of Food and Agriculture.

Notes

The authors declare no competing financial interest.

REFERENCES

(1) Holley, R. A.; Patel, D. Improvement in shelf-life and safety of perishable foods by plant essential oils and smoke antimicrobials. *Food Microbiol.* **2005**, *22*, 273−292.

(2) Weiss, J.; Gaysinsky, S.; Davidson, M.; McClements, J. Nanostructured encapsulation systems: Food antimicrobials. *Global Issues in Food Science and Technology*; Academic Press: London, England, 2009; pp 425−480.

(3) Smith-Palmer, A.; Stewart, J.; Fyfe, L. Antimicrobial properties of plant essential oils and essences against five important food-borne pathogens. *Lett. Appl. Microbiol.* **1998**, *26*, 118−122.

(4) Hammer, K. A.; Carson, C.; Riley, T. Antimicrobial activity of essential oils and other plant extracts. *J. Appl. Microbiol.* **1999**, *86*, 985−990.

(5) Elgayyar, M.; Draughon, F.; Golden, D.; Mount, J. Antimicrobial activity of essential oils from plants against selected pathogenic and saprophytic microorganisms. *J. Food Prot.* **2001**, *64*, 1019−1024.

(6) Dorman, H.; Deans, S. Antimicrobial agents from plants: Antibacterial activity of plant volatile oils. *J. Appl. Microbiol.* **2000**, *88*, 308−316.

(7) Chen, H.; Davidson, P. M.; Zhong, Q. Impacts of sample preparation methods on solubility and anti-listerial characteristics of essential oil components in milk. *Appl. Environ. Microbiol.* **2014**, *80*, 907−916.

(8) Shah, B.; Davidson, P. M.; Zhong, Q. Nanocapsular Dispersion of Thymol for Enhanced Dispersibility and Increased Antimicrobial Effectiveness against Escherichia coli O157:H7 and Listeria monocytogenes in Model Food Systems. *Appl. Environ. Microbiol.* **2012**, *78*, 8448−8453.

(9) Delgado, B.; Palop, A.; Fernández, P. S.; Periago, P. M. Combined effect of thymol and cymene to control the growth of Bacillus cereus vegetative cells. *Eur. Food Res. Technol.* **2004**, *218*, 188−193.

(10) Juneja, V. K.; Thippareddi, H.; Friedman, M. Control of Clostridium perfringens in cooked ground beef by carvacrol, cinnamaldehyde, thymol, or oregano oil during chilling. *J. Food Prot.* **2006**, *69*, 1546−1551.

(11) Del Nobile, M. A.; Conte, A.; Cannarsi, M.; Sinigaglia, M. Strategies for prolonging the shelf life of minced beef patties. *J. Food Saf.* **2009**, *29*, 14−25.

(12) Donsì, F.; Annunziata, M.; Vincensi, M.; Ferrari, G. Design of nanoemulsion-based delivery systems of natural antimicrobials: Effect of the emulsifier. *J. Biotechnol.* **2012**, *159*, 342−350.

(13) Terjung, N.; Löffler, M.; Gibis, M.; Hinrichs, J.; Weiss, J. Influence of droplet size on the efficacy of oil-in-water emulsions loaded with phenolic antimicrobials. *Food Funct.* **2012**, *3*, 290−301.

(14) McClements, D. J. *Food emulsions: Principles, practice, and techniques*; CRC Press: Boca Raton. FL., 1999.

(15) Weiss, J.; Gaysinsky, S.; Davidson, M.; McClements, J. Nanostructured encapsulation systems: Food antimicrobials. In *Global Issues in Food Science and Technology*; Barbosa-Cánovas, I. G., Mortimer, A., Lineback, D., Spiess, W., Buckle, K., Colonna, P., Eds.; Academic Press: New York, 2009.

(16) Gioffrè, M.; Torricelli, P.; Panzavolta, S.; Rubini, K.; Bigi, A. Role of pH on stability and mechanical properties of gelatin films. *J. Bioact. Compat Polym.* **2012**, *27*, 67−77.

(17) Gómez-Guillén, M.; Giménez, B.; López-Caballero, M.; Montero, M. Functional and bioactive properties of collagen and gelatin from alternative sources: A review. *Food Hydrocolloids* **2011**, *25*, 1813−1827.

(18) van Nieuwenhuyzen, W.; Tomás, M. C. Update on vegetable lecithin and phospholipid technologies. *Eur. J. Lipid Sci. Technol.* **2008**, *110*, 472−486.

(19) Shchipunov, Y. A.; Schmiedel, P. Phase behavior of lecithin at the oil/water interface. *Langmuir* **1996**, *12*, 6443−6445.

(20) Arnold, G.; Schuldt, S.; Schneider, Y.; Friedrichs, J.; Babick, F.; Werner, C.; Rohm, H. The impact of lecithin on rheology, sedimentation and particle interactions in oil-based dispersions. *Colloids Surf., A* **2012**, *418*, 147−156.

(21) ARSDR. Environmental Health and Medicine Education. *Ethylene Glycol and Propylene Glycol Toxicity*, http://www.atsdr.cdc.gov/csem/csem.asp?csem=12&po=14 (accessed Nov. 19, 2013).

(22) Center for the Evaluation of Risks to Human Reproduction; NTP-CERHR Expert Panel report on the reproductive and developmental toxicity of propylene glycol. *Reprod. Toxicol.* **2004**, *18*, 533−579.

(23) El Maghraby, G. M. Transdermal delivery of hydrocortisone from eucalyptus oil microemulsion: Effects of cosurfactants. *Int. J. Pharm.* **2008**, *355*, 285−292.

(24) Kale, N. J.; Allen, L. V. Studies on microemulsions using Brij 96 as surfactant and glycerin, ethylene glycol and propylene glycol as cosurfactants. *Int. J. Pharm.* **1989**, *57*, 87−93.

(25) Stilbs, P.; Rapacki, K.; Lindman, B. Effect of alcohol cosurfactant length on microemulsion structure. *J. Colloid Interface Sci.* **1983**, *95*, 583−585.

(26) Rao, J.; McClements, D. J. Formation of flavor oil microemulsions, nanoemulsions and emulsions: Influence of composition and preparation method. *J. Agric. Food Chem.* **2011**, *59*, 5026−5035.

(27) Martín-Hernández, C.; Bénet, S.; Marvin-Guy, L. F. Characterization and quantification of proteins in lecithins. *J. Agric. Food Chem.* **2005**, *53*, 8607−8613.

(28) Yang, T.-S.; Liu, T.-T.; Hu, T.-F. Effects of Lecithin and Pectin on Riboflavin-Photosensitized Oxidation of Orange Oil in a Multilayered Oil-in-Water Emulsion. *J. Agric. Food Chem.* **2011**, *59*, 9344−9350.

(29) Jain, S.; Valvi, P. U.; Swarnakar, N. K.; Thanki, K. Gelatin Coated Hybrid Lipid Nanoparticles for Oral Delivery of Amphotericin B. *Mol. Pharm.* **2012**, *9*, 2542−2553.

(30) Chuah, A. M.; Kuroiwa, T.; Kobayashi, I.; Nakajima, M. Effect of chitosan on the stability and properties of modified lecithin stabilized oil-in-water monodisperse emulsion prepared by microchannel emulsification. *Food Hydrocolloids* **2009**, *23*, 600−610.

(31) Chang, Y.; McLandsborough, L.; McClements, D. J. Physical properties and antimicrobial efficacy of thyme oil nanoemulsions: influence of ripening inhibitors. *J. Agric. Food Chem.* **2012**, *60*, 12056−12063.

(32) Ziani, K.; Chang, Y.; McLandsborough, L.; McClements, D. J. Influence of surfactant charge on antimicrobial efficacy of surfactant-stabilized thyme oil nanoemulsions. *J. Agric. Food Chem.* **2011**, *59*, 6247−6255.

(33) Shah, B.; Davidson, P. M.; Zhong, Q. Antimicrobial activity of nanodispersed thymol in tryptic soy broth. *J. Food Prot.* **2013**, *76*, 440−447.

(34) Xue, J.; Davidson, P. M.; Zhong, Q. Thymol Nanoemulsified by Whey Protein-Maltodextrin Conjugates: The Enhanced Emulsifying Capacity and Antilisterial Properties in Milk by Propylene Glycol. *J. Agric. Food Chem.* **2013**, *61*, 12720−12726.

(35) Pan, K.; Chen, H.; Davidson, P. M.; Zhong, Q. Thymol nanoencapsulated by sodium caseinate: Physical and anti-listerial properties. *J. Agric. Food Chem.* **2014**, *62*, 1649−1657.

(36) Voutsinas, L. P.; Cheung, E.; Nakai, S. Relationships of hydrophobicity to emulsifying properties of heat denatured proteins. *J. Food Sci.* **1983**, *48*, 26−32.

helical cavity. The objectives of this study were to determine the effects of these treatments on the formation of soluble and insoluble complexes and their complexation yields and physicochemical properties.

MATERIALS AND METHODS

Materials. Potato starch was obtained from Penford Food Ingredients (Centennial, CO, USA) and used without further treatment. Isoamylase (specific activity = 59000 units/mg protein) was purchased from Hayashibara Biochemical Laboratories Inc. (Okayama, Japan). β-Amylase from *Bacillus cereus* (specific activity = 2484 units/mg protein) was purchased from Megazyme International Ireland Ltd. (Wicklow, Ireland). Stearic acid was from Sigma-Aldrich (St. Louis, MO, USA). All other chemicals were of ACS grade.

Acetylation of Starch. Acetylation was carried out following the method described by Wang and Wang.[20] Starch (160 g, dry basis (db)) was weighed into a 2 L reaction vessel, and water was added to make up a final weight of 457.2 g. The mixture was stirred and hydrated for 30 min, and then the pH was adjusted to 8−8.5 with 1 M NaOH. Acetic anhydride (6.4 g, 4% based on starch db) was used for a low acetylation, or 9.6 g (8% based on starch db) was used for a high acetylation. Acetic anhydride was added very slowly to the starch mixture while the starch slurry pH was maintained between 8 and 8.5 and stirred. After the addition of acetic anhydride, the slurry was left to stand for 60 min with stirring. The resulting mixture was adjusted with 1 M HCl to a pH of 5.5, washed with a 3-fold volume of deionized water, filtered, and dried in an oven at 40 °C for 24 h. The acetyl content of starches was determined according to the method of McComb and McCready[21] and expressed as DS.[22]

Enzymatic Modification of Starch. *Debranching.* Starch (15 g wet basis) was added to 400 mL of water (3.75% w/v) and placed in a boiling water bath for 1 h with constant stirring to achieve complete gelatinization. The solution was equilibrated in a water bath at 45 °C and adjusted to pH 3.5 with 0.5 M HCl; 0.5% (v/w starch db) isoamylase was added, and then the mixture was incubated at 45 °C with constant stirring for 48 h. The starch was recovered with a 4-fold volume of pure ethanol, centrifuged, dried at 40 °C for 48 h, and milled using a UDY cyclone mill (UDY Corp., Ft. Collins, CO, USA) fitted with a 0.5-mm screen.

β-Amylase Treatment. A portion of the debranched starch was further subjected to β-amylase hydrolysis to reduce the DP. After incubation with isoamylase for 48 h, the starch slurry was adjusted to pH 6.5 with 0.5 M NaOH, and incubated with 0.5% (v/w starch db) β-amylase at 40 °C for 4 h. The enzyme reaction was terminated by boiling for 15 min. Starch was recovered by precipitating with 4-fold volume of pure ethanol, dried at 40 °C for 48 h and milled using the UDY cyclone mill fitted with a 0.5-mm screen.

Characterization of Starch Structure. The molecular size distribution of debranched unacetylated and acetylated starch with or without β-amylase treatment prior to complexation was characterized using a high-performance size exclusion chromatography (HPSEC) system (Waters Corp., Milford, MA, USA). Starch (10 mg) was dissolved in 5 mL of 90% dimethyl sulfoxide (DMSO), boiled for 1 h, and filtered through a 5.0 μm filter prior to injection into the HPSEC system. The HPSEC system consisted of a guard column (OHpak SB-G, 6.0 × 500 (mm) i.d. × length), two Shodex columns (OHpak KB-804 and KB-802, both 8.0 × 300 (mm) i.d. × length), a 200 μL injector valve (model 7725i, Rheodyne, Cotati, CA, USA), an inline degasser, a model 515 HPLC pump, and a model 2414 refractive index detector. The mobile phase of 0.1 M ammonium acetate with 0.02% sodium azide was eluted at a flow rate of 0.4 mL/min. The temperature of the columns was maintained at 55 °C and that of the detector at 40 °C. Dextran standards with molecular weights of 5,200, 11,600, 23,800, 48,600, 273,000, and 410,000 g/mol from Waters Corp. (Milford, MA, USA) and 1,050,000 g/mol from Sigma-Aldrich (St. Louis, MO, USA) were used to establish the calibration curve. An Ultrahydrogel 250 column (Waters Corp., Milford, MA, USA) was used for analyzing the molecular size distribution of starches recovered after complexation with stearic acid.

Amylopectin chain-length distribution was characterized by high-performance anion exchange chromatography equipped with pulsed amperometric detection (HPAEC-PAD) according to the method of Wong and Jane.[23] The HPAEC-PAD system (Dionex ICS-3000, Sunnyvale, CA, USA) consisted of the components of an AS40 autosampler, a single pump, detector/chromatography module (DC), a 4 × 50 mm CarboPac PA1 guard column, and a 4 × 250 mm CarboPac PA1 analytical column. Starch (20 mg) was boiled in 3.2 mL of distilled water for 1 h, cooled, and then filtered through a 0.45 μm filter (NYL w/GMF, Whatman, Clifton, NJ, USA) prior to injection into the HPAEC-PAD system. The mobile phase consisted of two eluents, A (150 mM NaOH) and B (150 mM NaOH containing 500 mM sodium nitrate) and was eluted at a flow rate of 1 mL/min. The gradient program was as follows: 94% of eluent A at 0 min, 92% at 11 min, 87% at 31 min, 80% at 81 min, 75% at 105 min, and 94% at 106 min. Column temperature was at 25 °C, and injection volume was 25 μL. Sugar standards, including glucose (DP1), maltose (DP2), maltotriose (DP3), maltotetraose (DP4), maltopentoase (DP5), maltohexaose (DP6), and maltoheptaose (DP7), were used as calibration standards to identify the chromatographic peaks. Each successive peak after DP 7 was considered to represent one glucose unit longer than the previous peak. The chains were divided into DP ranges and classified as follows: A chains (DP 6−12), B1 chains (DP 13−24), B2 chains (DP 25−36), and B3+ chains (DP 37+).[24] The average chain length was calculated as the cumulative sum of the product of DP and percentage relative areas for all the identified peaks.

Complexation of Starch and Stearic Acid. The starch solution (3.75% w/v) after debranching and with or without the β-amylase treatment as previously described was adjusted to pH 7.0 prior to the addition of 1 g of stearic acid. The mixture was heated at 80 °C for 30 min with continuous stirring, and then the temperature was lowered and maintained at 45 °C overnight with continuous stirring. Then the starch−stearic acid mixture was centrifuged at 7000*g* for 10 min, from which the precipitate, that is, "insoluble complex", was obtained, and the "soluble complex" was recovered from the supernatant by precipitation with a 4-fold volume of pure ethanol. Uncomplexed stearic acid was removed from both the insoluble and soluble complexes by rinsing with 95% ethanol using a labquake shaker rotisserie (Barnstead/Thermolyne, Dubuque, IA, USA) at room temperature for 2 h. Complexes were recovered by centrifugation at 7000*g* for 10 min, dried at 40 °C for 48 h, milled using a mortar and pestle, sieved through a 250 mm sieve, and stored for further analysis.

Hydrolysis of Complexes and Stearic Acid Analysis. To the complex (100 mg), both soluble and insoluble, was added 10 mL of 1 M HCl, and the mixture was heated in a boiling water bath for 1 h. The complex mixture was cooled, and 5 mL of hexane was added to extract the released stearic acid by rotation on the rotary shaker for 1 h. The hexane layer was recovered, and the previous step was repeated with another 5 mL of hexane for 1 h. Boron trifluoride−methanol (BF_3) was added to the recovered hexane phase to prepare fatty acid methyl esters (FAMEs), and an internal standard of methyl heptadecanoate (~1 mg) was subsequently added. The fatty acid methyl esters extracted in the hexane layer were injected into a gas chromatography (GC) system (GC-2010, Shimadzu, Kyoto, Japan) equipped with a BP 21 capillary column (30 m × 0.25 mm i.d.; SGE Inc., Austin, TX, USA) with a flame ionization detector (FID), and responses were collected by a Shimadzu GCsolution Workstation 2.3 (Kyoto, Japan). The carrier gas was helium at a flow rate of 30 mL/min, and the temperature of the column oven was equilibrated at 130 °C for 2 min, ramped at 10 °C/min to 250 °C, and maintained at 250 °C for 3 min. The injector and detector temperatures were set at 250 and 270 °C, respectively. Stearic acid was methylated, and the concentrations of stearic acid were determined from a standard curve prepared by using stearic acid solution (0.1, 0.2, 0.4, 0.6, 0.8, and 1.0 mg/mL) containing the internal standard of methyl heptadecanoate (0.5 mg/mL).

Physicochemical Properties. The thermal stability of all complexes was measured using a differential scanning calorimeter (DSC, Pyris-Diamond, PerkinElmer, Shelton, CT, USA). Starch samples (approximately 8 mg) were weighed into aluminum pans,

16 μL of distilled water was added with the aid of a microsyringe, and the pans were hermetically sealed. The pans were equilibrated for at least 1 h at room temperature before scanning. The samples were scanned from 25 to 180 °C at a rate of 10 °C/min. The onset temperature (T_o), peak temperature (T_p), conclusion temperature (T_c), and enthalpy (ΔH) of the endotherms were calculated using the Pyris data analysis software.

The powder X-ray diffraction pattern of complexes was determined using a diffractometer (PW1830 MPD, Philips, Almelo, The Netherlands). The generator voltage was set at 45 kV and the current at 40 mA. The sample was scanned over the 2θ angular range from 5° to 35° with a step size of 0.02° and time of 1 s per step.

Statistical Analysis. All measurements were conducted in replication, and the data were analyzed using JMP software (SAS Institute Inc., Cary, NC, USA); the means were compared using Tukey's honestly significant differences (HSD) test.

RESULTS AND DISCUSSION

Degree of Substitution. The DS values of the prepared low acetylated and high acetylated starches were 0.041 and 0.078, respectively. After both acetylated starches were debranched and treated with or without β-amylase and complexed with stearic acid, the insoluble and soluble fractions were recovered and analyzed for their structures and properties. It was found that the soluble fractions had significantly higher DS of acetylation, 82−173% higher, than their insoluble counterparts for the same treatment (Table 1). The differences in DS between the soluble and insoluble fractions of acetylated starch complexes were apparently responsible for the type of complexes formed because starch solubility increases with an increase in acetyl groups. A further increase in DS was observed when acetylation was combined with β-amylase treatment for both soluble and insoluble fractions. Because starch was acetylated in its native state, most acetyl groups were present in the amorphous lamella close to the branching points. Therefore, most acetyl groups were retained after β-amylase hydrolysis, resulting in an increase in DS of acetylation for samples treated with β-amylase.

Wulff et al.[19] reported that for the formation of soluble complexes of fenchone, a minimum DS of 0.16 was required for acetylated amylose, and only insoluble complexes were formed when acetylated amylose with a DS < 0.16 was used. In the present study, soluble complexes were produced from acetylated potato starch with DS ≥ 0.063. The difference in the DS observed in the two studies might be because starch was used in the present study, whereas amylose was used in the study by Wulff et al.[19] Although a different guest molecule was used in the present study, these results imply that amylopectin chains participated in complexation, and the required DS of acetylation for soluble complex formation was proportional to the DP of amylose and amylopectin chains. Nevertheless, the present results are in agreement with Wulff et al.[19] that there is a minimum DS of acetylation for the formation of soluble complex.

Table 1. Degree of Substitution (DS) of Acetylated Starches and Stearic Acid Complexes[a]

starch	β-amylase treatment	type of complex	DS
low acetylated starch	N/A[b]	N/A	0.041 ± 0.001f
low acetylated starch complex	no	soluble	0.063 ± 0.002d
		insoluble	0.029 ± 0.000g
	yes	soluble	0.093 ± 0.002b
		insoluble	0.034 ± 0.000f
high acetylated starch	N/A	N/A	0.078 ± 0.001c
high acetylated starch complex	no	soluble	0.089 ± 0.002b
		insoluble	0.049 ± 0.001e
	yes	soluble	0.133 ± 0.002a
		insoluble	0.052 ± 0.002e

[a]At least replicate samples were prepared for each complex. Data of two measurements with standard deviation. Means in a column not sharing the same letter are significantly different based on Tukey's honestly significant difference test ($p < 0.05$). [b]N/A, not applicable.

Complex Recovery and Complexation Yield. The recovery of complex was calculated by comparing the weight of recovered fractions to the weight of initial materials. The highest recovery for the insoluble complex was 0.72 g/g from the unacetylated starches with the β-amylase treatment. The recovery of unacetylated insoluble complex is in agreement with previous studies,[5,25] in which only insoluble fractions were reported. The total recovery, including both soluble and insoluble complexes, was highest for the unacetylated starch and decreased with increasing acetylation, which was probably because the increased solubility of starches from acetylation resulted in a significant reduction complex recovery (Table 2).

Table 2. Complex Recovery and Percentage Stearic Acid Content Recovered from All Complexes[a]

starch	type of complex	β-amylase treatment	recovery (g/g)	stearic acid in complex (mg/g)
unacetylated	soluble	no	0.24 ± 0.00d	15.7 ± 1.5f
	insoluble	no	0.58 ± 0.00a	42.7 ± 5.6d
	soluble	yes	0.11 ± 0.01e	33.8 ± 5.4de
	insoluble	yes	0.72 ± 0.04a	63.1 ± 1.2c
low acetylated	soluble	no	0.26 ± 0.00cd	23.4 ± 1.3ef
	insoluble	no	0.32 ± 0.01cd	101.0 ± 5.9b
	soluble	yes	0.28 ± 0.01cd	34.6 ± 2.9de
	insoluble	yes	0.47 ± 0.01b	123.1 ± 4.2a
high acetylated	soluble	no	0.26 ± 0.02cd	36.8 ± 7.4d
	insoluble	no	0.28 ± 0.02cd	40.3 ± 3.8d
	soluble	yes	0.38 ± 0.02bc	61.2 ± 12.2c
	insoluble	yes	0.36 ± 0.02c	16.6 ± 1.9f

[a]Data of at least two measurements with standard deviation. Means in a column not sharing the same letter are significantly different based on Tukey's honestly significant difference test ($p < 0.05$).

These results support previous findings that the presence of acetyl groups increased the solubility of starch and prevented the precipitation of starch−stearic acid complexes after complexation, thereby resulting in a lower recovery for insoluble complexes but a higher recovery for soluble complexes.

The additional β-amylase treatment increased recovery for the insoluble fractions of acetylated and unacetylated starches and for the soluble fractions of high acetylated starch. When acetylated starches received the β-amylase treatment, there was presumably an increase in favorable chain lengths of starch chains for the formation of both insoluble and soluble complexes, thus resulting in an increase in complexation.

However, for β-amylase-treated unacetylated starches the recovery of the insoluble complex increased, which was probably due to the absence of acetyl groups. The absence of acetyl groups may have led to an increase in starch reassociation and a reduction in solubility of unacetylated starches, which ultimately prevented complexes from staying in solution. The recovery of soluble fractions from acetylated-only starch was similar to that from the unacetylated starch at 0.26 g/g, implying that acetylation alone might not be sufficient to increase the recovery of soluble complexes. The recovery of soluble fractions of acetylated starches increased when the β-amylase treatment was incorporated, and this increase became more noticeable with the high acetylated starch. The increase in recovery of the soluble fraction of high acetylated was ascribed to the increase in the acetyl groups that promoted the preference of stearic acid to interact with the hydrophobic cavity of starch helix. This may be ascribed to the alignment of acetyl groups toward the cavity, thereby increasing overall hydrophobicity of the cavity and encouraging more stearic acid interaction, and this increased complexation.[26]

Stearic acid was recovered from all starch complexes, and the amount of stearic acid recovered was higher in the insoluble fractions than in the soluble fractions except for the high acetylated and β-amylase treated starch (Table 2). The highest amounts of stearic acid were recovered from the insoluble fractions of low acetylated starches fractions without (101.0 mg/g) and with (123.1 mg/g) the β-amylase treatment. Lui et al.[27] reported that acetylated pea starch with DS of 0.1 had a reduced iodine affinity of ∼4.4% compared to native pea starch with a value of ∼6.4%. They concluded that acetyl groups interfered with complex formation and reduced complexation yield. Similarly, Wulff et al.[19] reported that the complexing ability of amylose with fenchone decreased when amylose was modified with hydroxypropyl, hydroxyethyl, acetyl, and carboxymethyl groups. In contrast, the present results show that although acetylation of starch decreased the recovery of the insoluble fractions, the amount of complexed stearic acid was increased by 95−135% at a low acetylation level with or without the β-amylase treatment, but then decreased at a high acetylation level.

For the soluble complexes, both acetylation and β-amylase treatment enhanced the complexation of stearic acid. The high acetylated, β-amylase-treated starch had the highest amount of complexed stearic acid (61.2 mg/g), which was about 81% higher than the amount of stearic acid recovered from the soluble fraction of unacetylated starch (33.8 mg/g). The present results demonstrate that there is an optimum DS of acetylation to increase the amount of complexed stearic acid with starch in both soluble and insoluble complexes. This supports our hypothesis that apart from acetylation, an optimum starch chain length may also be critical for increasing the complexation yield of stearic acid and formation of soluble complexes.

Molecular Size Distribution. The molecular size distributions of debranched unacetylated and acetylated starches prior to complexation with stearic acid are displayed in Figure 1. For the unacetylated starches, the chromatogram shifted to lower DP with the β-amylase treatment, and the proportion of amylose fraction between 26 and 31 min was clearly reduced. The hydrolysis by β-amylase reduced the molecular size of amyloses to the range of amylopectin long chains and also lowered the molecular size of amylopectin chains. For the acetylated starches, the proportion of the amylose fraction

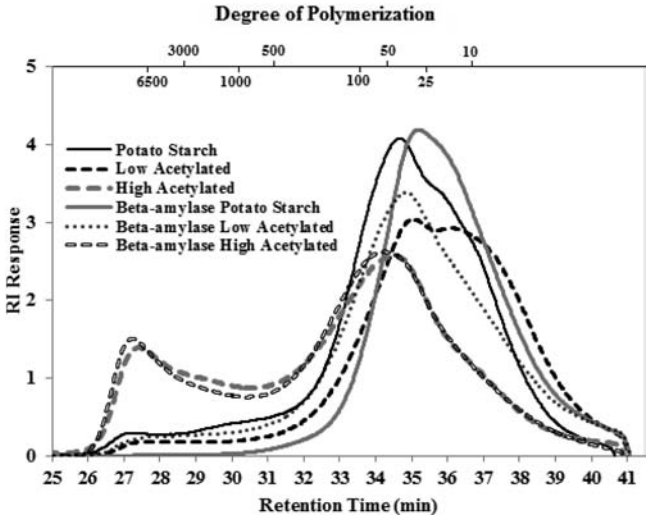

Figure 1. Normalized HPSEC profiles of debranched only or debranched and β-amylase-treated unacetylated and low and high acetylated potato starch.

increased with acetylation, and a further increase was noted with the additional β-amylase treatment. This increase was attributed to an increase in the hydrodynamic volume of the starch due to the presence of acetyl groups rather than an increase in the proportion of amylose. This supports previous DS results (Table 1) that during β-amylase hydrolysis of acetylated starch most acetyl groups were retained and responsible for the increased hydrodynamic volume of the acetylated starches.

The molecular size distributions of recovered soluble and insoluble fractions of all starches are presented in Figure 2. All starches displayed a peak at ∼14.5 min, signifying the presence of amylose fractions. The peak at 14.5 min (∼DP 3400) was more pronounced in the insoluble fractions than in the soluble fractions, became larger with acetylation, and then further increased when combined with the β-amylase treatment. These results support previous findings (Figure 1) that the increase in amylose fraction was due to the presence of acetyl groups not hydrolyzed by β-amylase. The acetylated fractions not treated with β-amylase also displayed two additional peaks at ∼19.5 min of DP 67 and ∼21 min of DP 23, which represent the long and short chains of amylopectin, respectively. However, the acetylated and β-amylase-treated starch fractions only had an additional peak around 19 min (DP 96).

It has been reported that approximately DP 18−24 glucose units are required for complexation of one fatty acid or monoacyl glycerol of 14−18 carbons,[10] DP 30−40 for two palmitic acid (C16:0),[28] DP 34 for two stearic acid,[29] and DP 40 for two docosanoic acid (C22:0).[13] Therefore, it can be deduced that the minimum chains required for complexation of one or two stearic acid would be DP 18−40, and were available in both soluble and insoluble fractions in the present study.

The chain-length distributions of recovered starch chains from the soluble and insoluble fractions without and with β-amylase treatment are presented in Figures 3 and 4, respectively. The soluble fraction displayed a more unimodal-like distribution after the β-amylase treatment (Figure 4A,C,E) with peak DP 30 and 33 for low and high acetylated starches, respectively. The insoluble fractions of all starches with or without β-amylase treatment displayed a bimodal distribution with peak DP 13−14 and 43−45. These results indicate that

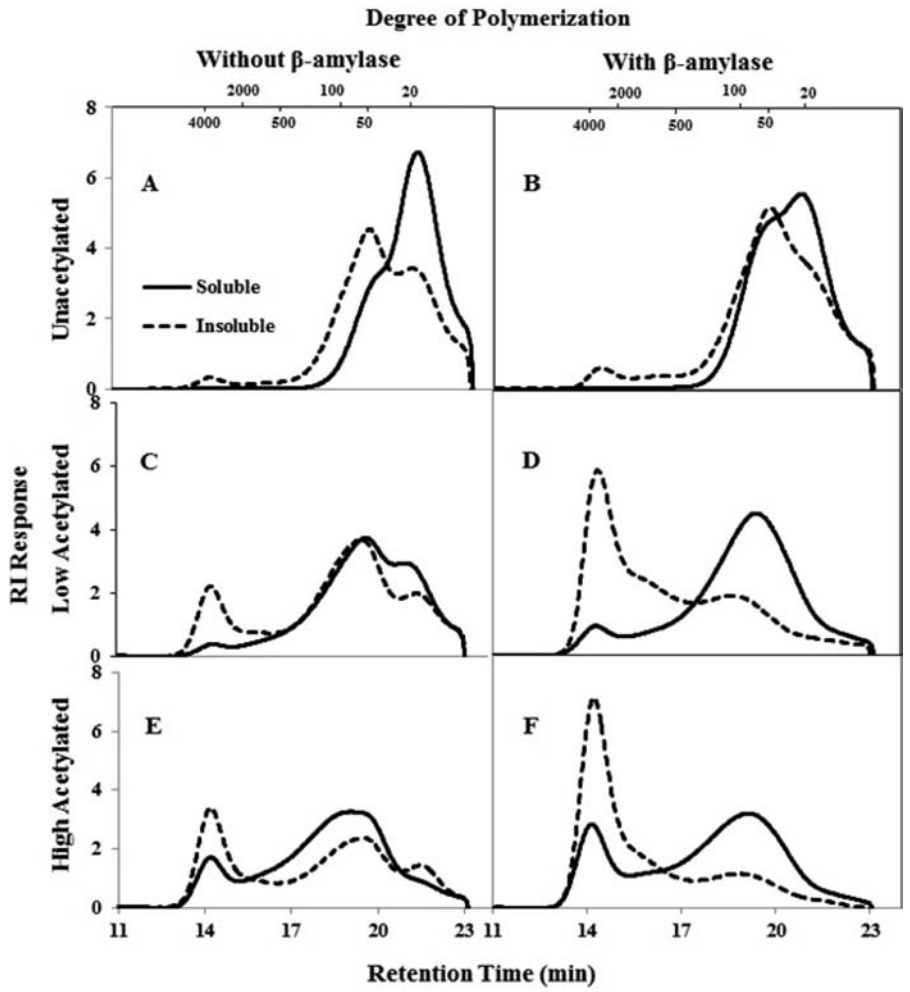

Figure 2. Normalized HPSEC profiles of recovered unacetylated and acetylated potato starches from the soluble and insoluble fractions after complexation.

upon complexation, different fractions of the starch chains form different types of complexes, that is, soluble or insoluble complex. When the amounts of complexed stearic acid (Table 2) were compared with the chain length distributions (Figures 3 and 4), it was found that the DP range 20−43 from amylopectin chains might be more favorable for soluble complex formation, and the proportion of this DP range was increased after the β-amylase treatment. The first fraction of chains consisting of ~DP 6−17 present in all unacetylated and acetylated starches was decreased after β-amylase treatment. These results are in agreement with the molecular size distribution results in Figure 2 and indicate that DP 6−17 represent chains that are too short to participate in stearic acid complexation. The present results also agree with Eliasson,[30] who found that amylopectin chains could participate in complex formation because the favorable DP for complex formation was observed in all fractions.

Characterization of Starch-Fatty Acid Complexes. *Melting Properties by Differential Scanning Calorimetry.* The melting thermogram of starch−stearic acid complex was observed in all soluble and insoluble fractions except for the soluble fractions from the low and high acetylated starch without the β-amylase treatment (Table 3). This is in contrast to the stearic acid recovery results, which showed that stearic acid was recovered from all soluble and insoluble starch fractions, which will be discussed later in this section. All unacetylated starch−stearic acid complexes displayed peak melting temperatures (T_p) of 92.4−116.1 °C, similar to those reported in previous studies,[25,31] which indicate the presence of both type I and type II starch−stearic acid complex. The type I complex has a lower T_p of around 90 °C and is formed at lower temperatures of about 60 °C; thus, it is less ordered and exhibits low heat stability.[10,32] The type II complex has a T_p of around 110 °C[31] and is formed with continuous heat treatment and rearrangement of the type I complex at higher temperatures of about 90 °C.[15] Although both type I and II starch−stearic acid complexes were present in the unacetylated starch complexes, the type II complex was more dominant as shown by its higher enthalpy value.

The low acetylated starch complexes exhibited a lower T_p than the unacetylated starch complexes for the same type of complex, and the T_p was further decreased with a higher DS of acetylation. This implies that for unacetylated starch, the nucleation rate for complexation was low, leading to sufficient propagation[10] and rearrangement of the complexes and, hence, more ordered, heat-resistant complexes were formed. In contrast, the presence of acetyl groups may hinder the rearrangement of included helices and prevented the formation of the type II complex. The T_p values of all insoluble complexes were higher than their soluble counterparts for all acetylated

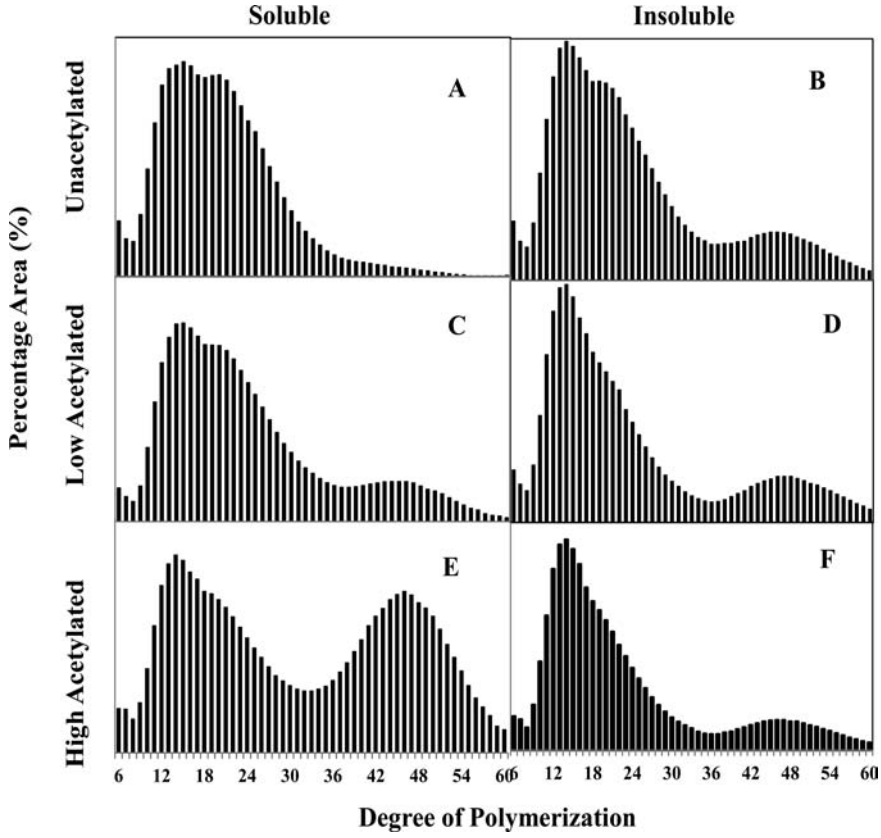

Figure 3. Normalized chain-length distributions of recovered amylopectin chains from unacetylated and acetylated potato starches without β-amylase treatment after complexation.

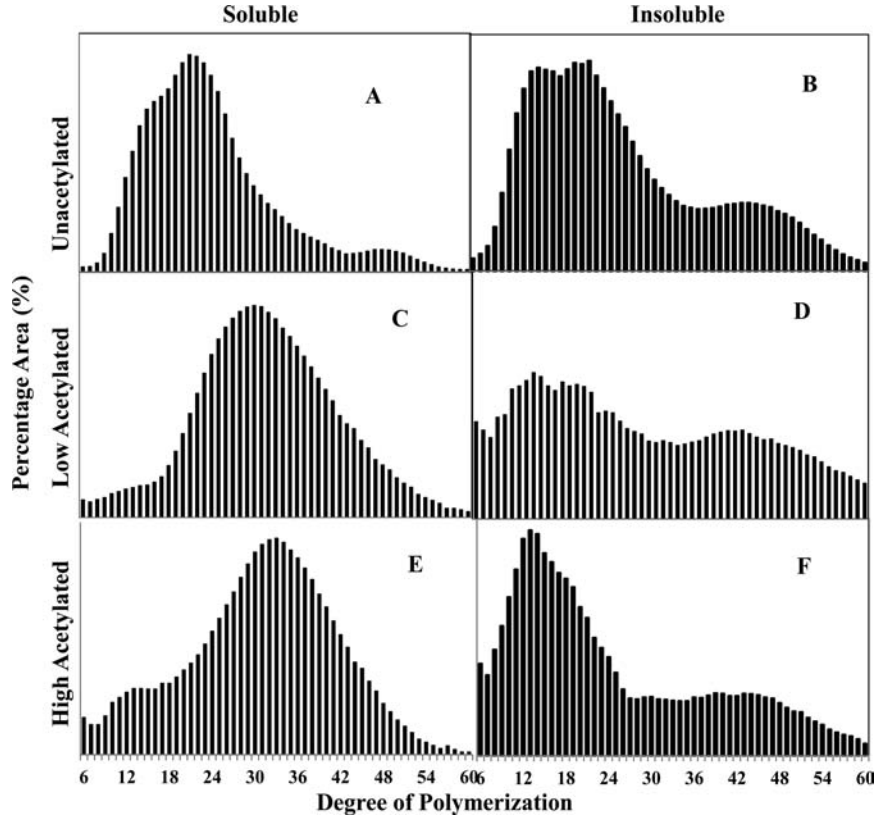

Figure 4. Normalized chain-length distributions of recovered amylopectin chains from unacetylated and acetylated potato starches with β-amylase treatment after complexation.

Table 3. Melting Temperatures and Enthalpies of Soluble and Insoluble Unacetylated and Acetylated Potato Starch−Stearic Acid Complexes[a]

			first peak				second peak			
starch	type of complex	β-amylase treatment	T_o (°C)	T_p (°C)	T_c (°C)	ΔH (J/g)	T_o (°C)	T_p (°C)	T_c (°C)	ΔH (J/g)
unacetylated	soluble	no	86.5c	92.4f	97.1c	0.67e	99.8	116.1	127.1	3.53
			(0.2)	(0.2)	(0.0)	(0.01)	(0.0)	(1.4)	(0.3)	(0.12)
	insoluble	no	101.0a	114.4a	123.7a	6.11c				
			(1.9)	(1.2)	(0.0)	(0.62)				
	soluble	yes	92.2b	110.2b	124.7a	3.61d				
			(0.1)	(0.9)	(0.1)	(0.09)				
	insoluble	yes	94.1b	107.9b	122.0a	9.68b				
			(0.8)	(1.1)	(0.3)	(0.15)				
low acetylated	soluble	no	ND[b]	ND	ND	ND				
	insoluble	no	79.2d	101.1cd	114.6b	13.92a				
			(0.0)	(0.5)	(0.8)	(0.68)				
	soluble	yes	68.5e	86.5g	95.5c	7.26c	98.3	104.9	112.0	1.19
			(0.1)	(0.6)	(2.0)	(0.23)	(3.5)	(3.4)	(5.6)	(0.45)
	insoluble	yes	77.7d	102.2c	113.9b	15.29a				
			(0.9)	(1.2)	(0.4)	(1.62)				
high acetylated	soluble	no	ND	ND	ND	ND				
	insoluble	no	77.5d	95.9ef	110.5b	10.03b				
			(0.0)	(0.6)	(2.2)	(0.17)				
	soluble	yes	68.0e	82.8g	98.0c	6.54c				
			(0.9)	(0.8)	(0.9)	(0.13)				
	insoluble	yes	79.3d	97.6de	111.5b	13.30a				
			(0.9)	(1.8)	(0.3)	(0.08)				

[a]Mean (standard deviation) of at least two measurements. Means in a column not sharing the same letter are significantly different based on Tukey's honestly significant difference test ($p < 0.05$). [b]ND, not detected.

starches; the high acetylated starch fractions did not always exhibit lower melting temperatures than their low acetylated counterparts. Previous studies[13,28] have proposed that T_p of amylose−fatty acid complexes increased with an increase in amylose size. Therefore, the present results suggest that longer starch chains are responsible for the formation of insoluble complexes and shorter starch chains for the soluble complexes, supporting the previous HPSEC results (Figure 2).

More energy was required to disrupt the insoluble complex because it is composed of more highly organized or longer helices compared with the soluble complexes. Whittam et al.[33] reported that although the same energy was required to disrupt the helical complex structures of both crystalline and amorphous complexes of amylose and alcohols (chain length of four to eight carbon atoms), the crystalline complexes required an additional energy to break the crystal lattice that is absent in amorphous complexes. Hence, this might explain why higher enthalpy values were observed for the insoluble complexes. Eliasson et al.[34] found that the enthalpy of an acetylated high-amylose maize starch−cetyltrimethylammonium bromide (CTAB) complex was lower than that of the native high-amylose maize starch−CTAB complex. They concluded that acetylation of starch decreased its tendency to crystallize or form the starch−CTAB complex. However, in the present study, the enthalpy was higher in acetylated starches than the unacetylated starches for the same treatment. Later, Karkalas et al.[15] concluded that enthalpy values of amylose−lipid complexes should not be regarded as good indicators for measuring complex formation because precise results could not always be obtained because some samples could have polymorphs in the intermediate polymorphic state or contain free amylose that could give false low-enthalpy readings.[12]

According to Lui et al.,[27] a different type of supramolecular structure of complexes could exist in acetylated starch complexes due to the presence of acetyl groups. The presence of acetyl groups may promote the formation of a complex that is not crystalline in nature, which was supported by the absence of the endotherm for the soluble complexes of acetylated starches without the β-amylase treatment. However, when acetylation was combined with the β-amylase treatment, the endotherm of the soluble complex appeared, indicating that the presence of the nonacetylated portion of the amylose and amylopectin chains may interfere with the arrangement of the included stearic acid when the other portion was more acetylated as evidenced by the increased DS after β-amylase treatment (Table 1). Therefore, when the less acetylated portion was hydrolyzed by β-amylase, stearic acid was capable of better arranging itself within the starch helical structure, thus resulting in increased crystalline structure.

X-ray Diffraction Pattern. Except the unacetylated and without β-amylase treatment (Figure 5A) all insoluble starch complexes showed the V-type diffraction patterns with characteristic peaks at diffraction angle 2θ = 7.4°, 12.9°, and 20° (Figure 5). Debranched unacetylated starch complexes (Figure 5A,B) had additional peaks at 2θ = 17.0°, 22°, and 24° for soluble complexes and at 2θ = 17.0° and 24° for insoluble complexes, which indicate the presence of retrogradation. These peaks were absent in all acetylated starch complexes because the acetyl groups hindered starch retrogradation except for the soluble low acetylated starch (Figure 5C). This may be due to the reassociation of longer chains with low DS of

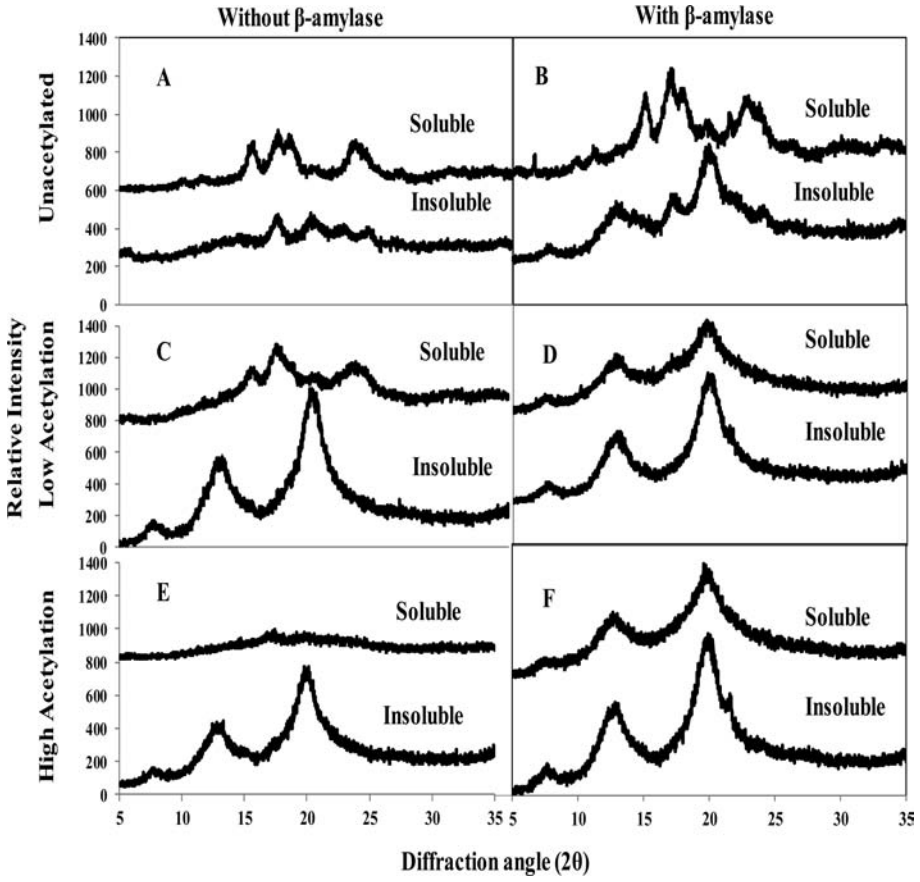

Figure 5. X-ray diffraction patterns of the soluble and insoluble fractions of debranched unacetylated and acetylated potato starches and their stearic acid complexes: (A) potato starch; (B) *β*-amylase-treated potato starch; (C) low acetylated potato starch; (D) low acetylated *β*-amylase-treated potato starch; (E) high acetylated potato starch; (F) high acetylated *β*-amylase-treated potato starch.

acetylation and not involved in stearic−acid complexation. For the unacetylated insoluble starches complexes, the additional *β*-amylase treatment increased the intensity of the V-type pattern and the peak at $2\theta = 20.0°$ increased noticeably. These results agree with previous DSC enthalpy data (Table 3) that for insoluble complexes, the additional *β*-amylase treatment resulted in starch with chain lengths that favored interaction with stearic acid instead of reassociation. The characteristic peak for the starch−stearic acid complex $2\theta = 20.0°$ was also observed in the soluble fractions of unacetylated starch complexes, indicating that native starches also formed soluble complexes, although only in small quantities. The present results again agree with previous results on the amount of complexed stearic acid (Table 2).

When low acetylation only was applied to starch, the X-ray diffraction peaks of the starch−stearic acid complex became predominant in the insoluble fraction, but the intensity of the peaks decreased at the high acetylation (Figure 5C,E). At high acetylation, the acetyl groups may interfere with proper arrangement of stearic acid in the complexes, thus resulting in complexes of low crystallites. These results support previous DSC results that for insoluble fractions, the low acetylated starch complex had higher enthalpy than the high acetylated one (Table 3). These results agree with Lui et al.,[27] who suggested that acetyl groups caused a reduction in the crystallinity of complexes and that acetylation resulted in complexes that existed mainly in the amorphous state rather than in the crystalline form. The same trend was also noted for corresponding soluble complex fractions, in which peak intensity decreased for the high acetylated-only starch complex. The characteristic peaks of starch−stearic acid complex were barely noticeable in both acetylated-only soluble starch complexes, which supports the DSC results (Table 3) and indicates that no crystalline structure was present in these soluble complexes. Nevertheless, the presence of an amorphous structure does not suggest the absence of a starch−stearic acid complex because it may still consist of unpacked helical amylose chains[28] as evidenced by the presence of complexed stearic acid (Table 2).

The V-type X-ray pattern was not evident for the soluble fractions until the *β*-amylase treatment was combined with acetylation (Figure 5D,F). This again supports previous DSC and DS findings that an optimum chain length of starch chains together with high acetyl content encouraged the formation of crystalline soluble complex. In addition, when a combination of acetylation and *β*-amylase treatment was employed, the peak intensities increased with increasing acetylation in both the soluble and insoluble complexes (Figure 5D,F). However, in the debranched-only acetylated potato starch complexes (Figure 5C,D), the reverse was noted as the peak intensities of complexes decreased with increasing acetylation, which further emphasized the importance of starch chain length in complex formation.

Some insoluble complexes showed a small peak at $2\theta = 21.5°$ (Figure 5D,F), which has been ascribed to pure stearic acid that is only physically trapped between starch helices[35] but not

dx.doi.org/10.1021/jf5004682 | J. Agric. Food Chem. 2014, 62, 2963−2972

included in the starch helix cavity. Overall, the highest crystallinity for insoluble fractions was observed for low acetylated, debranched-only starch (Figure 5C), and for the soluble fractions, the highest crystallinity was observed for high acetylated, debranched, and β-amylase-treated starch (Figure 5F), which agree with the amount of complexed stearic acid quantified (Table 2).

In conclusion, the present results show that low acetylation encouraged the formation of complexed stearic acid with debranched potato starch for insoluble complexes, whereas high acetylation increased the amount of complexed stearic acid for soluble complexes. The acetylation reduced retrogradation, increased the hydrophobicity of the cavity, and ultimately encouraged more starch−stearic acid interaction. A combination of acetylation, debranching, and β-amylase treatment was required to produce soluble, crystalline starch−stearic acid complex; soluble, amorphous starch−stearic acid complexes were formed in acetylated and debranched-only starches. Acetylation reduced melting temperature and increased the enthalpy values of all starch−stearic acid complexes compared with unacetylated ones. There was an optimum range of chain length to encourage the formation of starch−stearic acid complexes. Information on the generation and properties of soluble starch−stearic acid complex from this study may provide insight into the creation of soluble complexes between starch and other insoluble bioactive compounds and may pave the way for applications whereby soluble complexes are desired to improve bioavailability.

AUTHOR INFORMATION

Corresponding Author

*(Y.-J.W.) Phone: (479) 575-3871. Fax: (479) 575-6936. E-mail: yjwang@uark.edu.

Notes

The authors declare no competing financial interest.

ACKNOWLEDGMENTS

We appreciate Jia-Rong Jinn and Vanessa Tjarks for their technical support and Drs. Steven Ricke and Sun-Ok Lee for access to the GC.

REFERENCES

(1) Colin, J. J.; de Claubry, H. G. Sur les combinaisons de l'iodie avec les substances végétales et animales. *Ann. Chim.* **1814**, *90*, 87−100.

(2) Schoch, T. J. Fractionation of starch by selective precipitation with butanol. *J. Am. Chem. Soc.* **1942**, *64*, 2957−2961.

(3) Godet, M. C.; Trans, V.; Delage, M. M.; Buleon, A. Molecular modelling of the specific interactions involved in the amylose complexation by fatty acids. *Int. J. Biol. Marcromol.* **1993**, *15*, 11−16.

(4) Mikus, F. F.; Hixon, R. M.; Rundle, R. Complexes of fatty acids with amylose. *J. Am. Chem. Soc.* **1946**, *68*, 1115−1123.

(5) Lalush, I.; Bar, H.; Zakaria, I.; Eichler, S.; Shimoni, E. Utilization of amylose-lipid complexes as molecular nanocapsules for conjugated linoleic acid. *Biomacromolecules* **2005**, *6*, 121−130.

(6) Wulff, G.; Avgenaki, G.; Guzmann, M. S. P. Molecular encapsulation of flavors as helical inclusion complexes of amylose. *Cereal Sci.* **2005**, *41*, 239−249.

(7) Tapanapunnitikul, O.; Chaiseri, S.; Peterson, D. G.; Thompson, D. B. Water solubility of flavor compounds influences formation of flavor inclusion complexes from dispersed high-amylose maize starch. *J. Agric. Food Chem.* **2008**, *56*, 220−226.

(8) Cohen, R.; Orlova, Y.; Kovalev, M.; Ungar, Y.; Shimoni, E. Structural and functional properties of amylose complexes with genistein. *J. Agric. Food Chem.* **2008**, *56*, 4212−4218.

(9) Schoch, T. J.; Williams, C. Adsorption of fatty acid by the linear component of corn starch. *J. Am. Chem. Soc.* **1944**, *66*, 1232−1233.

(10) Putseys, J. A.; Lamberts, L.; Delcour, J. A. Amylose-inclusion complexes: formation, identity and physiochemical properties. *J. Cereal Sci.* **2010**, *51*, 238−247.

(11) Eliasson, A. C.; Krog, N. Physical properties of amylose-monoglyceride complexes. *J. Cereal Sci.* **1985**, *3*, 239−248.

(12) Raphaelides, S.; Karkalas, J. Thermal-dissociation of amylose fatty-acid complexes. *Carbohydr. Res.* **1988**, *172*, 65−82.

(13) Gelders, G. G.; Vanderstukken, T. C.; Goesaert, H.; Delcour, J. A. Amylose-lipid complexation: a new fractionation method. *Carbohydr. Polym.* **2004**, *56*, 447−458.

(14) Evans, I. D. An investigation of starch/surfactant interactions using viscosmetry and differential scanning calorimetry. *Starch/Staerke* **1986**, *38*, 227−235.

(15) Karkalas, J.; Ma, S.; Morrison, W. R.; Pethrick, R. A. Some factors determining the thermal-properties of amylose inclusion complexes with fatty-acids. *Carbohydr. Res.* **1995**, *268*, 233−247.

(16) Kubik, S.; Wulff, G. Characterization and chemical modification of amylose complexes. *Starch/Staerke* **1993**, *45*, 220−225.

(17) Rutenberg, M. W.; Solarek, D. Starch derivatives: production and uses. In *Starch: Chemistry and Technology*, 2nd ed.; Whistler, R. L., BeMiller, J. N., Paschalls, J. F., Eds.; Academic Press: Orlando, FL, USA, 1984; pp 311−388.

(18) Wulff, G.; Kubik, S. Helical amylose complexes with organic complexands. 1. Microcalorimetric and circular dichroitic investigations. *Makromol. Chem.* **1992**, *193*, 1071−1080.

(19) Wulff, G.; Steinert, A.; Holler, O. Modification of amylose and investigation of its inclusion behavior. *Carbohydr. Polym.* **1998**, *307*, 19−31.

(20) Wang, Y.-J.; Wang, L. Characterization of acetylated waxy maize starches prepared under catalysis by different alkali and alkaline-earth hydroxides. *Starch/Staerke* **2002**, *54*, 25−30.

(21) McComb, E. A.; McCready, R. M. Determination of acetyl in pectin and in acetylated carbohydrate polymers, hydroxamic acid reaction. *Anal. Chem.* **1957**, *29*, 819−820.

(22) Wurzburg, O. B. Crosslinked starches. In *Modified Starches: Properties and Uses*; Wurzburg, O. B., Ed.; CRC Press: Boca Raton, FL, USA, 1986; pp 41−53.

(23) Wong, K. S.; Jane, J. Effects of pushing agents on the separation and detection of debranched amylopectin by high performance anion-exchange chromatography with pulsed amperometric detection. *J. Liq. Chromatogr. Relat. Technol.* **1995**, *18*, 63−80.

(24) Hanashiro, I.; Abe, J. I.; Hizukuri, S. A periodic distribution of chain length of the amylopectin as revealed by high performance anion-exchange chromatography. *Carbohydr. Res.* **1996**, *147*, 342−347.

(25) Szejtli, J.; Banky-Elod, E. Inclusion complexes of unsaturated fatty acids with amylose and cyclodextrin. *Starch/Staerke* **1975**, *27*, 368−376.

(26) Fanta, G. F.; Shrogen, R. L.; Salch, J. H. Steam jet cooking of high-amylose starch-fatty acid mixtures. An investigation of complex formation. *Carbohydr. Polym.* **1999**, *38*, 1−6.

(27) Lui, H.; Arntfield, S. D.; Holley, R. A.; Aime, D. B. Amylose-lipid complex formation in acetylated pea starch-lipid systems. *Cereal Chem.* **1997**, *74*, 159−162.

(28) Godet, M. C.; Bizot, H.; Buleon, A. Crystallization of amylose-fatty acid complexes prepared with different amylose chain lengths. *Carbohydr. Polym.* **1995**, *27*, 47−52.

(29) Gelders, G. G.; Goesaert, H.; Delcour, J. A. Potato phosphorylase catalyzed synthesis of amylose-lipid complexes. *Biomacromolecules* **2005**, *6*, 2622−2629.

(30) Eliasson, A. C. Interaction between starch and lipids studied by DSC. *Thermochim. Acta* **1994**, *246*, 343−356.

(31) Biliaderis, C. G.; Page, C. M.; Maurice, T. J. On the multiple melting transitions of starch-monoglyceride systems. *Food Chem.* **1986**, *22*, 279−295.

(32) Gelders, G. G.; Duyck, J. P.; Goesaert, H.; Delcour, J. A. Enzyme and acid resistance of the amylose-lipid complexes differing in the

amylose chain length, lipid and complexation temperature. *Carbohydr. Polym.* **2005**, *60*, 379−389.
(33) Whittam, M. A.; Orford, P. D.; Ring, S. G.; Clark, S. A.; Parker, M. L.; Cairns, P.; Miles, M. J. Aqueous dissolution of crystalline and amorphous amylose-alcohol complexes. *Int. J. Biol. Macromol.* **1989**, *11*, 339−344.
(34) Eliasson, A. C.; Finstad, H.; Ljunger, L. A study of starch-lipid interactions for some native and modified maize starches. *Starch/Staerke* **1988**, *3*, 95−100.
(35) Lesmes, U.; Cohen, S. H.; Shener, Y.; Shimoni, E. Effects of long fatty acid unsaturation on the structure and controlled release properties of amylose complexes. *Food Hydrocolloids* **2009**, *23*, 667−675.

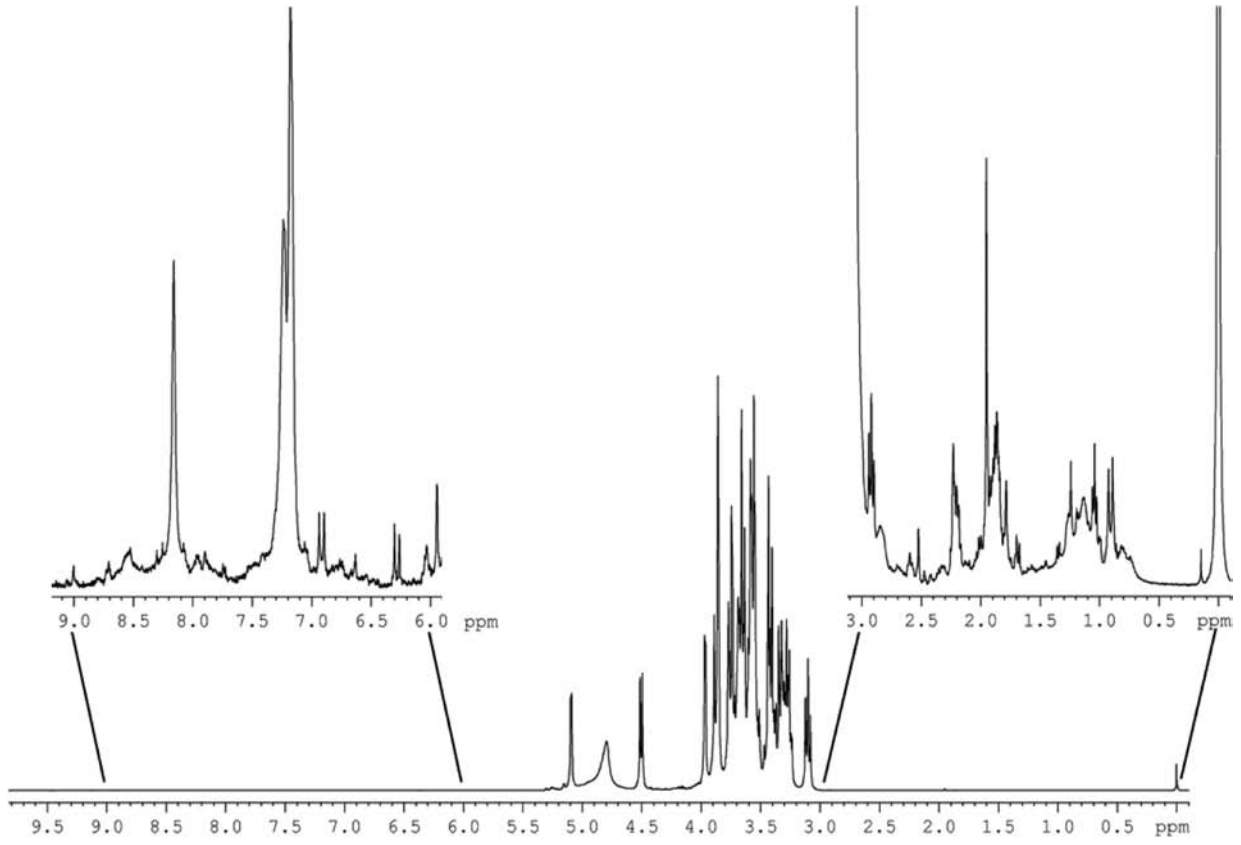

Figure 1. Spectrum of honey sample. Because the most prominent components in honey are carbohydrates, which overwhelm other compounds, the spectrum was broken into three regions: aliphatic region (0.5−3 ppm), carbohydrate region (3−6 pmm), and aromatic region (6−9 ppm).

to current environmental and living conditions. In this method not only is the presence of given individual molecules important, but their proportions are crucial. Therefore, acquiring data-rich chemical fingerprints for specific types of honeys is a next step in building chemical biomarkers profile of certain types of honeys and to identify their botanical and geographical origins. The utility of such an approach has been recently positively validated for identification of the botanical origin of some of American honeys.[12]

The aim of this study was to determine if chemical fingerprints generated using ^{1}H NMR spectroscopy and analyzed using chemometric tools might be useful to define the botanic origin of five brands of Polish unifloral honeys, namely, heather (derived from *Calluna vulgaris* L.), buckwheat (from *Fagopyrum esculentum* L.), lime (from *Tilia* L.), acacia (*Acacia* Mill.), and rape (*Brassica napus* L. var. *napus*) ones. For reference, Polish multifloral honeys were also studied.

MATERIALS AND METHODS

Honey Samples. Thirty-five honey samples of six different botanic origins (multifloral, heather, lime, rape, buckwheat, acacia) were analyzed. The origin of each honey sample was declared either by beekeepers or by the seller in the case of commercial honeys. Honey samples were stored at room temperature without daylight. Details considering geographical origin and production year of honey samples are presented in Table S1 in the Supporting Information.

Sample Preparation. Honey samples were dissolved at a concentration of 0.529 g/mL in 10% D_2O (Armar Chemicals, 100% atom % D, Switzerland). Dissolving was performed with the use of an ultrasonic bath (Cole-Parmer model 08891-26) at 298 K. After filtration, the pH was adjusted to 3.00 (± 0.01) using 2 M HCl (POCH, Poland) using a Beckman Coulter pHi 510 pH-meter. Honey solution and external standard (trimethlsilyl)tetradeuteropropionic acid sodium salt (TSP), closed in a coaxial insert tube (Wilmad Labglass), was placed in a NMR tube (5 mm o.d., 7′ Wilmad selected to 500 MHz). TSP concentration was matched in such a manner that the signal was $^{1}/_{10}$ of the maximum signal from sample (4.6 mg/mL). Each sample was analyzed in triplicate with random order.

Melissopalinological Analysis. Pollen analysis was performed in The Research Institute of Horticulture, Apicultural Division in Pulawy (Poland), an Accredited Laboratory (PCA AB 715) for performing pollen analysis, according to Polish Quality Standard number PN-88/A-77626.

Sample Solid Phase Extraction for 2D NMR Experiments. Ten grams of honey was mixed with 50 mL of acidic water (pH 2 by addition of HCl), and the mixture was subjected to an ultrasonic bath for 1 h. Undissolved particles were removed by filtration. Fluid was passed through the column (2 cm × 20 cm) with Amberlite XAD-2 (Supelco Analytical). Hydrophobic compounds remained on the Amberlite XAD-2 with a capacity of 95%;[14] other compounds such as sugars and amino acids were eluted with 100 mL of acidic water (pH 2) and 100 mL of distilled water. The hydrophobic fraction was obtained by elution with 150 mL of methanol. The methanol was evaporated on a rotary evaporator (40 °C). The acquired extract was dissolved in 600 μL of MeOD and transferred into a NMR tube.

NMR Analysis. All NMR measurements were performed with a Bruker 400 MHz Ultrashield NMR spectrometer (Bruker, GmBH, Germany) operating at a proton frequency of 400.13 MHz. Standard one-dimensional spectra with water suppression were recorded at 293 K with a relaxation delay of 3.5 s. During acquisition, 256 following scans were collected and stored in 32K data points with a spectral width of 20.55 ppm. Both phase and baseline corrections were done manually. The whole spectral set was aligned to β-glucose anomeric proton signal (doublet at 4.505 ppm). Additionally, two-dimensional HSQC experiments were acquired for spectra assignments. HSQC spectra were recorded in AntyEcho mode with a 20.55 ppm ^{1}H

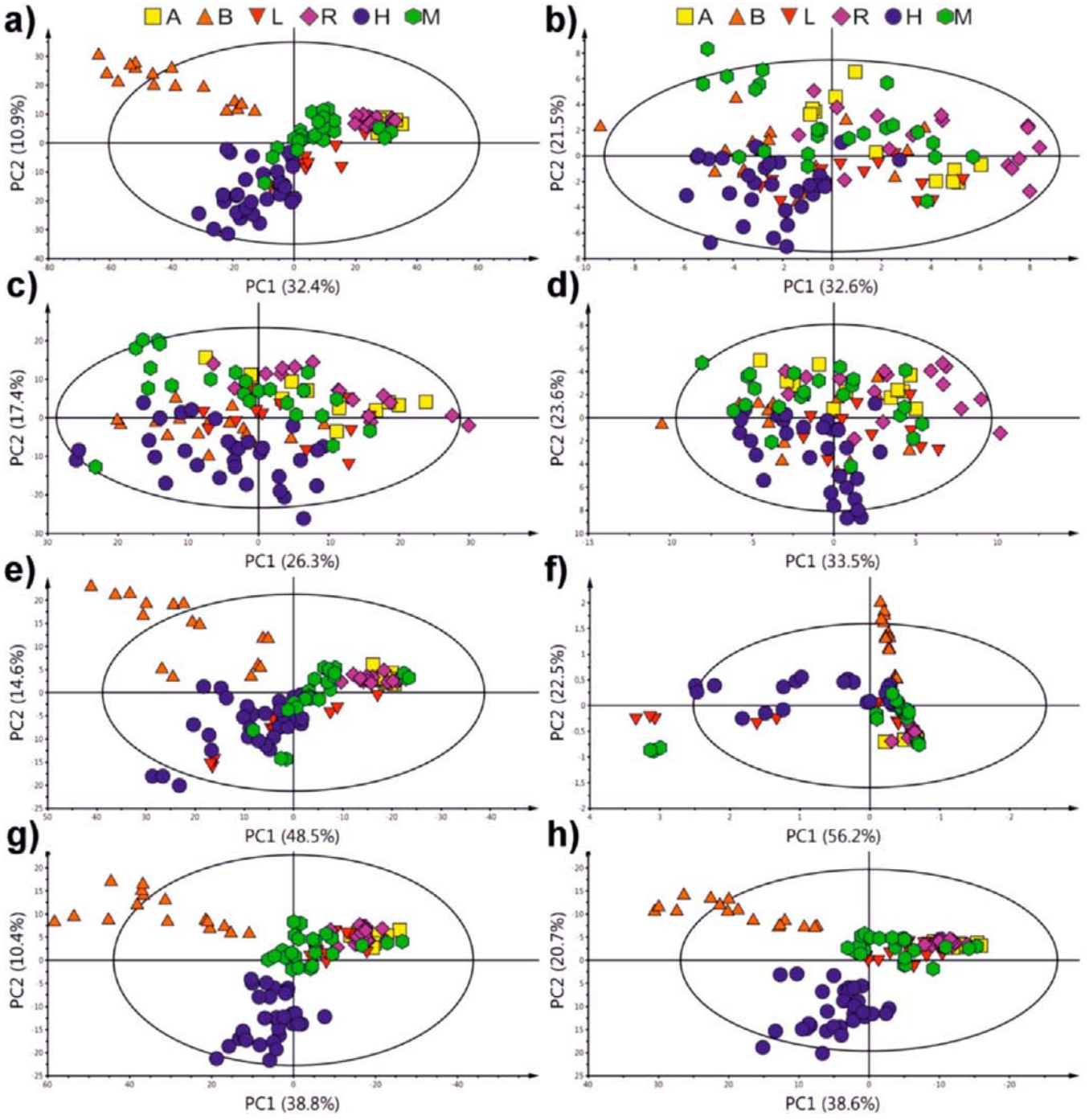

Figure 2. Influence of different spectrum regions and scaling methods on PCA results: (a) full chemical fingerprint, UV; (b) full chemical fingerprint, PAR; (c) carbohydrate region fingerprint, UV; (d) carbohydrate region fingerprint, PAR; (e) aliphatic region fingerprint, UV; (f) aliphatic region fingerprint, PAR; (g) aromatic region fingerprint, UV; (h) aromatic region fingerprint, PAR. Yellow box, acacia; orange triangle, buckwheat; red inverted triangle, lime; violet diamond, rape; blue circle, heather; green hexagon, multifloral; UV, unit variance scaling; PAR, Pareto scaling.

window and a 238 ppm ^{13}C window, 2 s realxation time, 1K data points, 64 scans, and 256 experiments.

Data Analysis. Prior to multivariate data analysis ^{1}H NMR spectra were preprocessed. In the spectral region covering the range of 0.5−10.0 ppm data reduction was conducted by segmenting the spectra into 0.005 ppm equal width integrals, which gave 1840 new variables, after exclusion of the residual water signal region laying in the range of 4.7−5.5 ppm. The obtained data set (X matrix) was exported to Microsoft Office Excel 2003 (Microsoft Corp., Redmond, WA, USA), in which normalization to the TSP integral was performed. The data matrix was transferred into SIMCA-P+ software (v 13.0, Umetrics, Umeå, Sweden), where principal component analysis (PCA) and orthogonal partial least-squares discriminant analysis (OPLS-DA) analyses were conducted. Data were scaled using Pareto and unit variance (UV) scaling. The supervised OPLS-DA models were validated by means of cross-validation analysis of variance (CV-ANOVA) at a level of statistical significance $\alpha = 0.05$ to provide evidence that the observed separation was not due to random effects. A heatmap was generated using PermutMartix software, in which column normalization (Z score) was used.[15]

dx.doi.org/10.1021/jf4056715 | J. Agric. Food Chem. 2014, 62, 2973−2981

Table 1. Parameters Obtained for OPLS-DA Models Discriminating Particular Types of Honey from All Other Studied Honey Samples

		vs REST							
		full spectrum (0.5−10 ppm)		aliphatic region (0.5−3 ppm)		carbohydrate region (3−6 ppm)		aromatic region (6−10 ppm)	
origin	code	Q2 (cum)	p value	Q2 (cum)	p value	Q2 (cum)	p value	Q2 (cum)	p value
rape	R	0.538	1.07×10^{-16}	0.462	2.40×10^{-13}	0.470	2.77×10^{-12}	0.658	3.57×10^{-20}
buckwheat	B	0.835	$<10 \times 10^{-40}$	0.864	3.52×10^{-36}	0.734	1.57×10^{-25}	0.841	$<10 \times 10^{-40}$
lime	L	0.653	2.03×10^{-21}	0.641	3.85×10^{-19}	0.600	6.76×10^{-17}	0.701	1.26×10^{-24}
heather	H	0.892	$<10 \times 10^{-40}$	0.892	$<10 \times 10^{-40}$	0.829	5.32×10^{-35}	0.906	$<10 \times 10^{-40}$
multifloral	M	0.674	4.95×10^{-15}	0.340	6.75×10^{-6}	0.314	5.37×10^{-6}	0.524	3.68×10^{-10}

RESULTS AND DISCUSSION

NMR Fingerprint of Honey. The aim of this study was to find a fast and unequivocal method to determine the botanic origin of Polish nectar honeys, collected mainly in southern Poland. During the study the differences and similarities between chemical fingerprints of each type of Polish nectar honey were identified.

Due to the variability of signal intensities in various parts of the spectra and for the purpose of discussion, spectra were divided into three sections: aliphatic region (0.5−3 ppm), carbohydrate region (3−6 ppm), and aromatic region (6−10 ppm) (Figure 1). Variable chemical composition of nectar honeys is reflected in the quantity and intensity of signals in NMR spectra. Therefore, to specify differences and similarities, multivariate data analysis has been used.

Preliminary Chemometric Analysis and Influence of Scaling Methods. Significant differences in the intensity of the three regions of the spectrum may be an issue in multivariate data analysis. There are two major scaling methods applied in NMR-based metabolomics: unit variance (UV) and Pareto scaling. Pareto scaling partially reduces the relative importance of large signals; however, it keeps somehow the structure of the original data. Pareto scaling may be sensitive to large fold changes. On the other hand, when using UV scaling, all resonances become equally important, but noise regions or signal artifacts may have a stronger influence on the results.[16] Therefore, it was essential to determine which scaling method gives the most reliable and unbiased results. For that reason, it was decided to analyze (by means of principal component analysis (PCA)) all three regions independently and compare the obtained results with the whole chemical fingerprint analysis.

When PCA was performed for the whole ^{1}H NMR fingerprint, it revealed a huge influence of the scaling method (Figure 2a,b). Contrary to UV scaling, where the majority of groups were well separated (Figure 2a), in Pareto scaling a strong overlap was observed (Figure 2b). Subsequent analysis of each region showed that it is due to the carbohydrate resonances, which overwhelm the model when using Pareto scaling. The PCA score plot based on the whole chemical fingerprint was very similar to the PCA results based solely on the carbohydrate region (Figure 2, panel b vs panel d). Interestingly enough, the carbohydrate region exhibited the lowest discrimination potential, regardless of the scaling method used (Figure 2c,d). Previously it was shown that the carbohydrate region may be sufficient for honey discrimination;[17] however, in our study it was more efficient to utilize aliphatic and aromatic regions. Both aliphatic and aromatic regions could be used for discrimination of the honeys, regardless of the used scaling method, whereas still slightly better separation was achieved with the application of UV scaling. Results for the aliphatic region showed that in Pareto scaling samples present compact groups (Figure 2f), whereas in UV scaling they were spread more (Figure 2e); however, intragroup separation was similar in both cases. Only in the case of the aromatic region did both scaling methods give almost identical results (Figure 2g,h). Therefore, UV scaling was decided to be more suitable for the comprehensive analysis of honey chemical fingerprints.

Although PCA is an unsupervised method, it gave sufficient results for most of the analyzed types of honey (Figure 2a). The best discrimination was achieved between buckwheat, heather, and (surprisingly) multifloral honeys, whereas honeys derived from rape and acacia overlapped strongly. The group resulting from multifloral honeys was always located in the center of the PCA score plot. It is in agreement with the origin of multifloral honey, which is composed from nectars of many flowers and therefore might be seen as a composite of several unifloral honey types. Consequently, many chemical markers of variable botanic origin are present in this type of honey.

Revealing Incorrect Honey Classification. To distinguish rape from acacia, a supervised chemometric modeling OPLS-DA was performed. There was no model that passed the validation procedure and crossed the level of statistical significance (α = 0.05). Hence, analysis of three spectrum fragments (aliphatic, 0.5−3 ppm; aromatic, 6−10 ppm; and whole region from 0 to 10 ppm) showed that it was not possible to distinguish between rape and acacia honeys because of unclear reasons. It suggested, however, that despite the producer's claims these two branches might be in fact rape honey, because acacia and rape flower at the same time. Trying to explain this phenomenon and confirm sources of honey species, rape and acacia honey samples were sent to The Research Institute of Horticulture, Apicultural Division in Pulawy (Poland), for pollen analysis. Melissopalinological examination revealed incorrect declaration of origin of the whole acacia group of honeys because it was indicated that their main plant source was rape (*Brassica napus*) instead of acacia (*Acacia* Mill.). All of them contained >60% of rape pollen, which in two cases amounted to >90%. Other pollens (amount of which exceeded 5%) were derived from aesculus, raspberry, corn flower, prunus, willow, and maple. These data clearly show that honeys described by producers as acacia-derived ones did not contain acacia pollen at all. Because acacia and rape flower at the same time, it seems that honey bees are preferring rape as a major collecting source. Results of melissopalinological analysis are presented in Table S2 in the Supporting Information. Therefore, all further analyses were performed using a new group of rape honeys (made by merging the "acacia" and rape groups).

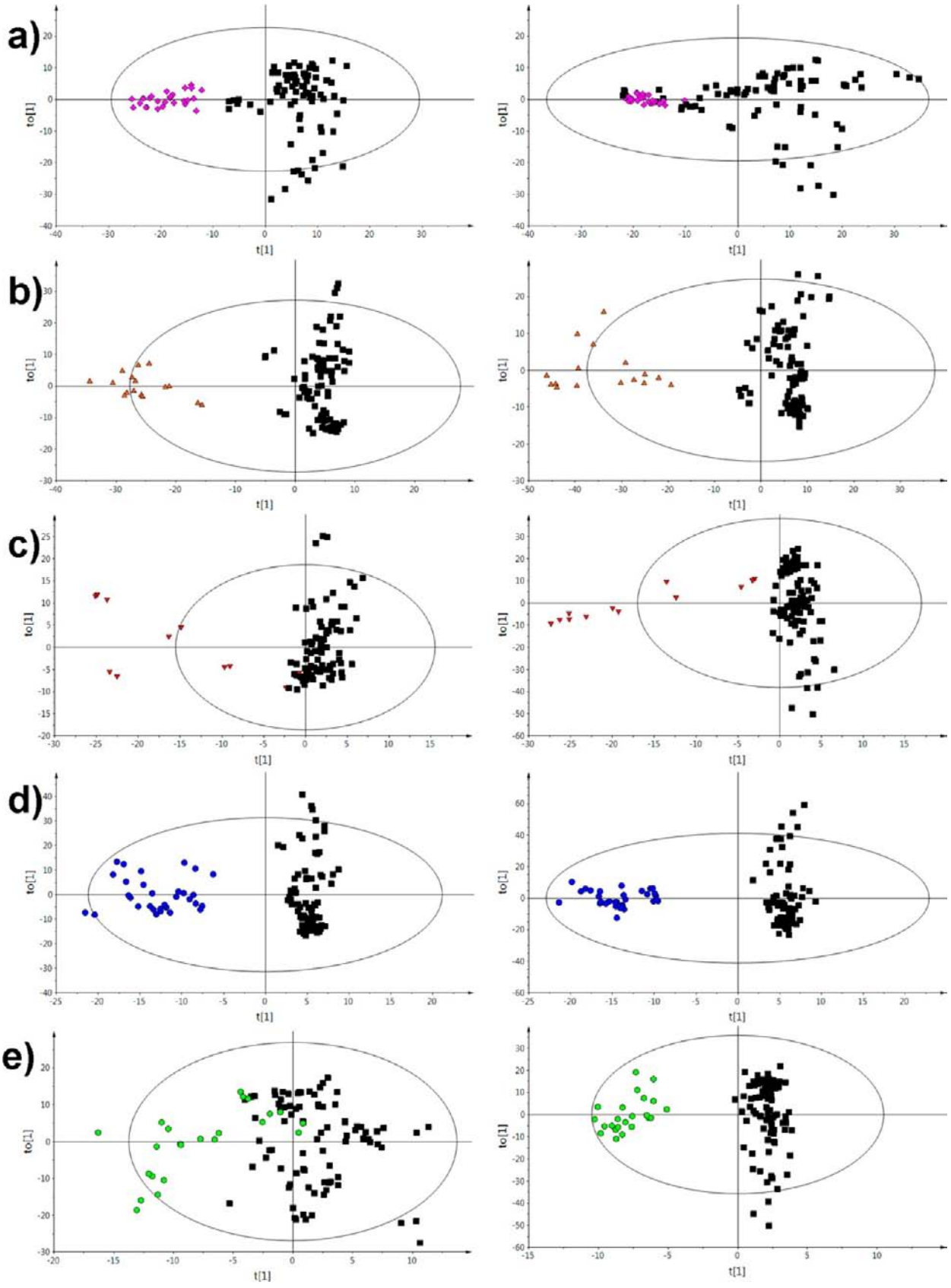

Figure 3. OPLS-DA score plot of aromatic (left) and aliphatic (right) regions corresponding with discrimination between: (a) R versus rest; (b) B versus rest; (c) L versus rest; (d) H versus rest; (e) M versus rest.

Discriminant Analysis of Honeys. Prior to identification of chemical markers specific to a particular honey type, a subsequent discriminant analysis was carried out. For each honey type an OPLS-DA model was built, discriminating it

dx.doi.org/10.1021/jf4056715 | J. Agric. Food Chem. 2014, 62, 2973−2981

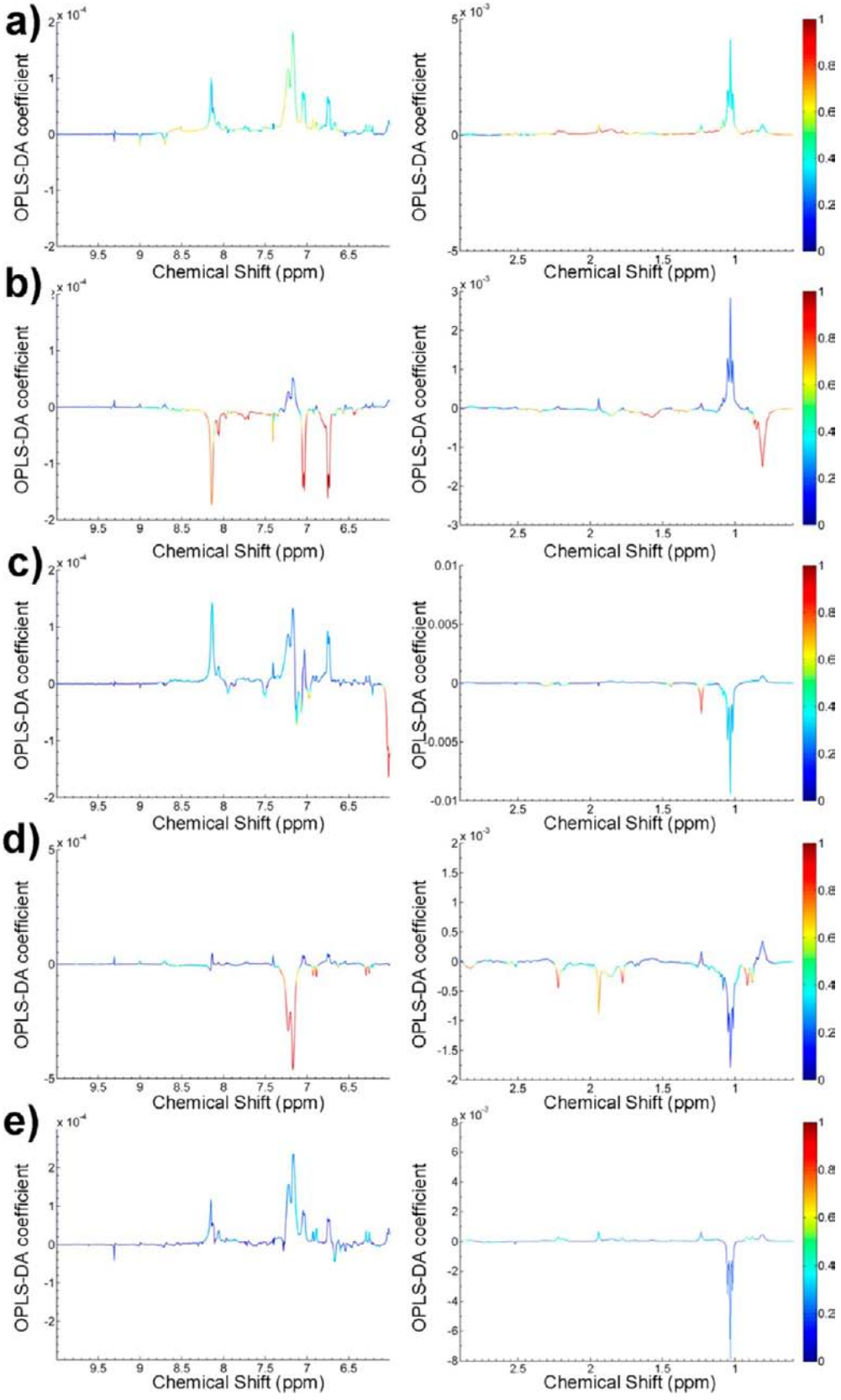

Figure 4. OPLS-DA loadings of aromatic (left) and aliphatic (right) regions corresponding with discrimination between (a) R versus rest, (b) B versus rest, (c) L versus rest, (d) H versus rest, and (e) M versus rest. The color bar corresponds to the absolute value of the correlation loading in the discrimination model.

from all the rest of the studied honey samples. Both *p* value and Q2 (cum) parameter are reported in Table 1. Selected OPLS-DA score plots for aromatic and aliphatic regions are presented in Figure 3. However, for complete interpretation, the reader is

dx.doi.org/10.1021/jf4056715 | *J. Agric. Food Chem.* 2014, 62, 2973−2981

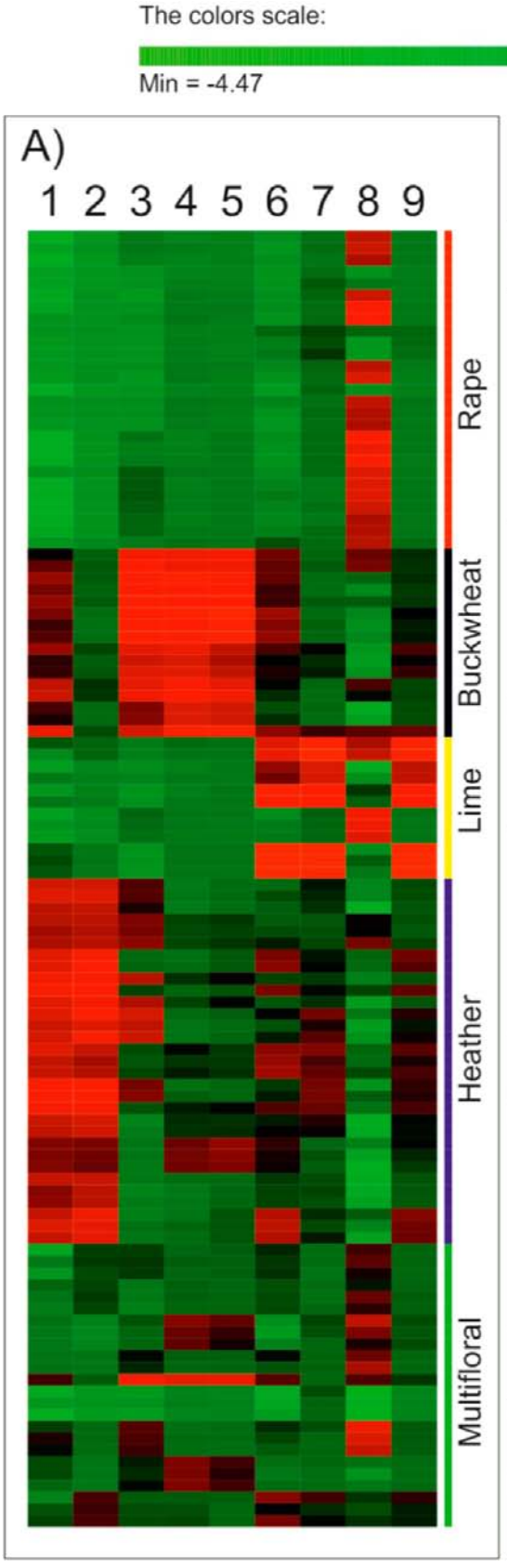

B) C)

Structure	Atom number	Chemical shift proton/carbon
1. Dehydrovomifoliol 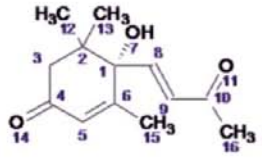	3	2.53/50.4 ppm
	5	5.94/128.8 ppm
	8	6.27/130.8 ppm
	9	6.91/145 ppm
	12	1.03/24.2 ppm
	13	1.11/22.8 ppm
	15	1.89/18.6 ppm
	16	2.32/28.3 ppm
2. Phenylacetic acid 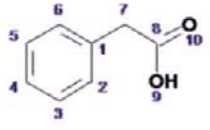	4	7.37/131 ppm
	3,5	7.29/131 ppm
	2,6	7.30/129.1 ppm
	7	3.37/50.7 ppm
3. Formic acid 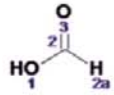	2	8.06/166.8 ppm
4. Tyrosine 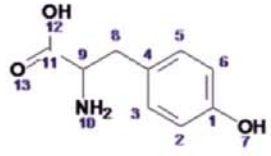	2,6	6.74/118.9 ppm
	3,5	7.04/133.8 ppm
	8	2.62/46.1 ppm
	9	overlap with carbohydrate region
5. Unknown - characteristic for Buckwheat honey	-	0.80 / 24.5 ppm
6. 4-(1-hydroxy-1-methylethyl) cyclohexa-1,3-diene-carboxylic acid 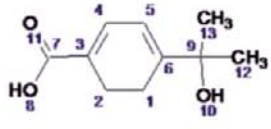	1	2.3/24 ppm
	2	2.3/24 ppm
	4	6.1/123 ppm
	5	6.9/123 ppm
	12	1.2/28 ppm
	13	1.2/28 ppm
7. Unknown - characteristic for Lime honey	-	6.02/ 118.4ppm
8. Unknown – characteristic for Rape honey	-	8.704 / 178.2 ppm
9. Unknown – characteristic for Lime honey	-	1.23/ 29.9 ppm

Figure 5. (A) Heatmap of all tested samples versus concentration of all proposed markers; (B) chemical structures of potential markers; (C) chemical shifts of markers atoms obtained in HSQC experiment.

referred to the Supporting Information, where all OPLS-DA score plots and their cross-validated counterparts are given (Figures S2−S6 in the Supporting Information). The most differing of all other honeys, in all types of comparisons, were

dx.doi.org/10.1021/jf4056715 | J. Agric. Food Chem. 2014, 62, 2973−2981

buckwheat and heather ones (Figure 3b,d). Lime presented good separation from all other samples, however, not complete; in every model, the triplicate of one sample was overlapped with other honeys (Figure 3c; Figure S4 in the Supporting Information). Finally, rape and multifloral honeys exhibited similar separation qualities (Figure 3a,e). Although OPLS-DA score plots showed good separation of multifloral honeys, it became poor in cross-validated score plots (Figure S6 in the Supporting Information). This indicates that it is hard to extract one reliable marker in such a diverse group. On the other hand, it was hard to efficiently separate rape honey; however, this group was well clustered (Figure S2 in the Supporting Information). The overlap may result from the fact that many multifloral honeys contain relatively high rape components.

For each comparison loadings plots were obtained and utilized to locate specific resonances that could be marker candidates (Figure 4).

Potential Markers of Honey. Over 600 chemical compounds have been identified in honey so far. Such a rich chemical constitution makes defining the botanic origin based on individual chemicals difficult, although possible. The presence of a single chemical compound unique for the honey may indicate its botanic origin.[18−20] However, such compounds frequently occur in low or very low concentrations, which require sophisticated analytical methods or expensive and time-consuming extraction procedures.[21−23] Instead, honey origin can be defined by determining the proportion of common, for certain groups of honeys, compounds, with flavonoids being a good example here.[24−26] In both cases, the extraction process is essential and the type of extraction procedure imposes not only the applied analytical technique but also the composition of the studied samples.

In this work, sample preparation lacking an extraction process was performed. That approach to botanical origin determination of honey has not been previously used. It allows quantitative and qualitative analyses of all chemical components present in the honey sample to be performed and thus provides comprehensive information about honey. On the basis of complete chemometric analysis, the most differentiating components between species were pointed out (Figure 4). Those components, in the form of NMR resonances, were assigned to compounds by proton−carbon correlation obtained in HSQC experiments taking also into consideration data available in the literature. To confirm correct assignment, NMR experiments of honey extracts obtained by solid phase extraction were performed. Obtained in this way spectra confirmed the original assignment of signals to analyzed compounds (Figure S7 in the Supporting Information).

Dark Monofloral Honey Markers. Heather honey, falling into the category of dark honeys, contains two dominating characteristic chemical markers. The first one was identified as dehydrovomifoliol (formed from abscisic acid), which was already reported as a marker of eucalyptus honey.[13,27] The second one is phenylacetic acid produced from phenylpyruvic acid.[28] Furthermore, high contents of lactic and acetic acids were detected in heather honey, which corresponds to the high acidity of dark-type honeys. The chemical structures of the foregoing markers are presented in Figure 5B.

The second honey tested, buckwheat honey, is also classified as a dark honey. According to recent studies, the presence of 3-methylbutanal, 3-hydroxy-4,5-dimethyl-2(5*H*)-furanone (sotolon), and β-damascenone as markers had been expected.[29] However, attendance of these markers has not been seen and, thus, new chemical markers were proposed. The first of them was tyrosine, 1 of 20 natural amino acids, present in significantly high concentrations in buckwheat honey. The second one was formic acid. The presence of both was confirmed by addition of internal standards, where an increase in the intensity of their characteristic proton NMR resonances was observed (Figure S8 in the Supporting Information). Additionally, high amounts of proline and lactic acid were detected.

Light Monofloral Honey Markers. In our studies it was not possible to identify any markers for rape honey, due to the low concentration of possible ones. However, two proton and carbon NMR resonances were found to be characteristic for this type of honey. They are seen as peaks at 8.704 and 8.328 ppm in proton spectra correlated with peaks at 178.2 and 113.1 ppm in carbon spectra. We were unsuccessful in determining their chemical origin. Additionally, an unusually low amount of proline might be considered as a characteristic feature.

Lime honey is characterized by the high level of acetic acid as well as the presence of 4-(1-hydroxy-1-methylethyl)-cyclohexane-1,3-dienecarboxylic acid. This compound was reported as characteristic for lime honey from Italy.[30] The two signals that could not be identified but were specific to these honeys occur at the following chemical shifts: 1.369/29.98 and 6.16/118.56 ppm (proton/carbon NMR).

Multifloral Honey and Common Chemicals as Markers. It is assumed that multifloral honeys are produced from the nectar of many flowering plants. Therefore, small amounts of various chemical markers in the constitution of this type of honey could be observed. Furthermore, depending on the flowering plants (or main flowering plant) different chemical markers might be detected. Analyzed samples of multifloral honeys showed a chemical composition similar to light honeys. This is mostly due to the presence of chemical compounds characteristic for lime and rape honey.

Proposed markers had been used to construct a heatmap (Figure 5a), a matrix in which the relationships between intensities of peaks characteristic for all proposed markers and groups of honey are shown. The warmth of colors in a single cell represents the amount of marker in a honey sample. This resulted in a code system that might be used to identify the botanical origin of any new honey sample by examining its NMR spectrum and relating the concentration of these markers within the heatmap. In addition, compounds commonly present in honey, such as hydroxymethylfurfural (HMF) and ethyl alcohol, detected in all tested honey samples were included in this map.

In summary, studies presented in this work indicate the possibility of using chemical fingerprinting as a tool for defining the origin of Polish monofloral honeys by analysis of proton nuclear magnetic resonance spectra of crude honey preparations. Moreover, an optimum scaling method suitable for this purpose was selected. Unit variance scaling performs better in the case of honey, where significant differences in the intensity of the spectrum regions are present. Results of chemometric analysis classified all acacia honey samples as rape. Further evaluation by pollen analysis revealed the incorrect classification of acacia honeys by the producer/beekeeper and confirmed the usefulness of the chemical fingerprinting approach. Heatmaps, which might be useful for differentiation of honeys, were constructed. They are somewhat similar to the popular barcodes used in the wholesale trade. All of this confirms that NMR-based fingerprinting combined with chemometric tools

may be considered as an alternative method of honey botanical origin determination. This method of origin determination of honey might be supplementary to or a fast replacement of pollen analysis.

■ ASSOCIATED CONTENT

Supporting Information

Figures S1−S9 and Tables S1 and 2. This material is available free of charge via the Internet at http://pubs.acs.org.

■ AUTHOR INFORMATION

Corresponding Author

*(L.Z.) Phone/fax: 0048 77 452 7115. E-mail: Lukasz.Zielinski@uni.opole.pl.

Funding

This work was supported by the Polish Ministry of Science and Higher Education. Ł.Z. and S.D. are recipients of Ph.D. scholarships under a project funded by the European Social Fund.

Notes

The authors declare no competing financial interest.

■ REFERENCES

(1) Louveaux, J.; Maurizio, A.; Vorwohl, G. Methods of melissopalinology. *Bee World* **1978**, *59*, 139−157.

(2) Molan, P. The limitations of the methods of identifying the floral source of honeys. *Bee World* **1998**, *79*, 59−68.

(3) Alissandrakis, E.; Tarantilis, P. A.; Harizanis, P. C.; Polissiou, M. Aroma investigation of unifloral Greek citrus honey using solid-phase microextraction coupled to gas chromatographic-mass spectrometric analysis. *Food Chem.* **2007**, *100*, 396−404.

(4) Stephens, J. M.; Schlothauer, R. C.; Morris, B. D.; Yang, D.; Fearnley, L.; Greenwood, D. R.; Loomes, K. M. Phenolic compounds and methylglyoxal in some New Zealand manuka and kanuka honeys. *Food Chem.* **2010**, *120*, 78−86.

(5) Ferreres, F.; Ortiz, A.; Silva, C.; Garciaviguera, C.; Tomasbarberan, F. A.; Tomaslorente, F. Flavonoids of la alcarria honey − a study of their botanical origin. *Z. Lebensm.-Unters.-Forsch.* **1992**, *194*, 139−143.

(6) Kaskoniene, V.; Venskutonis, P. R. Floral markers in honey of various botanical and geographic origins: a review. *Compr. Rev. Food Sci. Food Saf.* **2010**, *9*, 620−634.

(7) Mato, I.; Silvia-Luque, S.; Huidobro, J. F.; Simal-Lozano, J. Fumaric acid as a possible discriminant parameter of geographical origin of honey samples. *Dtsch. Lebensm.-Rundsch.* **2004**, *100*, 502−505.

(8) Andrade, P.; Ferreres, F.; Gil, M. I.; TomasBarberan, F. A. Determination of phenolic compounds in honeys with different floral origin by capillary zone electrophoresis. *Food Chem.* **1997**, *60*, 79−84.

(9) Bouseta, A.; Collin, S.; Dufour, J. P. Characteristic aroma profile of unifloral honey obtained with a dynamic headspace GC-MS system. *J. Apic. Res.* **1992**, *31*, 96−109.

(10) Tomas-Barberan, F. A.; Martos, I.; Ferreres, F.; Radovic, B. S.; Anklam, E. HPLC flavonoid profiles as markers for the botanical origin of European unifloral honeys. *J. Sci. Food Agric.* **2001**, *81*, 485−496.

(11) Jasicka-Misiak, I.; Poliwoda, A.; Deren, M.; Kafarski, P. Phenolic compounds and abscisic acid as potential markers for the floral origin of two Polish unifloral honeys. *Food Chem.* **2012**, *131*, 1149−1156.

(12) Agila, A.; Barringer, S. Application of selected ion flow tube mass spectrometry coupled with chemometrics to study the effect of location and botanical origin on volatile profile of unifloral American honeys. *J. Food Sci.* **2012**, *77*, C1103−C1108.

(13) Martos, I.; Ferreres, F.; Yao, L. H.; D'Arcy, B.; Caffin, N.; Tomas-Barberan, F. A. Flavonoids in monospecific *Eucalyptus* honeys from Australia. *J. Agric. Food Chem.* **2000**, *48*, 4744−4748.

(14) Tomas-Barberan, F. A.; Blazquez, M. A.; Garcia-Viguera, C.; Ferreres, F.; Tomas-Lorente, F. A comparative-study of different Amberlite XAD resins in flavonoid analysis. *Phytochem. Anal.* **1992**, *3*, 178−181.

(15) Caraux, G.; Pinloche, S. PermutMatrix: a graphical environment to arrange gene expression profiles in optimal linear order. *Bioinformatics* **2005**, *21*, 1280−1281.

(16) van den Berg, R. A.; Hoefsloot, H. C. J.; Westerhuis, J. A.; Smilde, A. K.; van der Werf, M. J. Centering, scaling, and transformations: improving the biological information content of metabolomics data. *BMC Genomics* **2006**, *7*, 142.

(17) Consonni, R.; Cagliani, L. R.; Cogliati, C. NMR characterization of saccharides in Italian honeys of different floral sources. *J. Agric. Food Chem.* **2012**, *60*, 4526−4534.

(18) Jerkovic, I.; Tuberoso, C. I. G.; Marijanovic, Z.; Jelic, M.; Kasum, A. Headspace, volatile and semi-volatile patterns of *Paliurus spina-christi* unifloral honey as markers of botanical origin. *Food Chem.* **2009**, *112*, 239−245.

(19) Lusic, D.; Koprivnjak, O.; Curic, D.; Sabatini, A. G.; Conte, L. S. Volatile profile of Croatian lime tree (*Tilia* sp.), fir honeydew (*Abies alba*) and sage (*Salvia officinalis*) honey. *Food Technol. Biotechnol.* **2007**, *45*, 156−165.

(20) Senyuva, H. Z.; Gilbert, J.; Silici, S.; Charlton, A.; Dal, C.; Gurel, N.; Cimen, D. Profiling Turkish honeys to determine authenticity using physical and chemical characteristics. *J. Agric. Food Chem.* **2009**, *57*, 3911−3919.

(21) Cherchi, A.; Spanedda, L.; Tuberoso, C.; Cabras, P. Solid-phase extraction and high-performance liqued-chromatographic determination of organic-acid in honey. *J. Chromatogr., A* **1994**, *669*, 59−64.

(22) Yao, L. H.; Datta, N.; Tomas-Barberan, F. A.; Ferreres, F.; Martos, I.; Singanusong, R. Flavonoids, phenolic acids and abscisic acid in Australian and New Zealand *Leptospermum* honeys. *Food Chem.* **2003**, *81*, 159−168.

(23) Yao, L. H.; Jiang, Y. M.; Singanusong, R. T.; D'Arcy, B.; Datta, N.; Caffin, N.; Raymont, K. Flavonoids in Australian *Melaleuca*, *Guioa*, *Lophostemon*, *Banksia* and *Helianthus* honeys and their potential for floral authentication. *Food Res. Int.* **2004**, *37*, 166−174.

(24) Cavazza, A.; Corradini, C.; Musci, M.; Salvadeo, P. High-performance liquid chromatographic phenolic compound fingerprint for authenticity assessment of honey. *J. Sci. Food Agric.* **2013**, *93*, 1169−1175.

(25) Keckes, S.; Gasic, U.; Velickovic, T. C.; Milojkovic-Opsenica, D.; Natic, M.; Tesic, Z. The determination of phenolic profiles of Serbian unifloral honeys using ultra-high-performance liquid chromatography/high resolution accurate mass spectrometry. *Food Chem.* **2013**, *138*, 32−40.

(26) Socha, R.; Juszczak, L.; Pietrzyk, S.; Galkowska, D.; Fortuna, T.; Witczak, T. Phenolic profile and antioxidant properties of Polish honeys. *Int. J. Food Sci. Technol.* **2011**, *46*, 528−534.

(27) Schievano, E.; Stocchero, M.; Morelato, E.; Facchin, C.; Mammi, S. An NMR-based metabolomic approach to identify the botanical origin of honey. *Metabolomics* **2012**, *8*, 679−690.

(28) Guyot, C.; Bouseta, A.; Scheirman, V.; Collin, S. Floral origin markers of chestnut and lime tree honeys. *J. Agric. Food Chem.* **1998**, *46*, 625−633.

(29) Zhou, Q. X.; Wintersteen, C. L.; Cadwallader, K. R. Identification and quantification of aroma-active components that contribute to the distinct malty flavor of buckwheat honey. *J. Agric. Food Chem.* **2002**, *50*, 2016−2021.

(30) Beretta, G.; Caneva, E.; Regazzoni, L.; Bakhtyari, N. G.; Facino, R. M. A solid-phase extraction procedure coupled to H-1 NMR, with chemometric analysis, to seek reliable markers of the botanical origin of honey. *Anal. Chim. Acta* **2008**, *620*, 176−182.

because the transesterification method used in the analysis of epoxy fatty acids does not esterify free fatty acids,[17,18] which is mainly used as an IS and because during solid phase extraction (SPE) separation of FAMEs, the FAMEs IS can be lost in the neutral fraction if it is added at the beginning. To improve the analytics of epoxy fatty acids in oils, a sensitive and accurate method used two internal standards, and this required two methylation steps.[13,18] In another study on food sample matrices, Fankhauser-Noti et al.[19] used a direct methylation method developed by Suter et al.[17] to analyze epoxy fatty acids without SPE column separation. This direct transesterification method in food matrices has a drawback that it sometimes involves use of pretreatment steps which differ per food matrix, and this limits its universal applicability to all food matrices.[17] Besides, epoxy fatty acids must be analyzed after the SPE separation step to reduce the amount of neutral fatty acids so as to be able to analyze them on a GC-FID.[8,12,18] Recently we developed a method that separates the coeluting hydroxy fatty acids and thus determined the epoxy fatty acids more accurately in oil.[8] On the basis of the fact that epoxy fatty acids are available in various fatty foods, there is a need for better methods of analysis that can be applied to a wide range of food sample types.

To analyze epoxy fatty acids from food samples, a method that can reliably extract oil from the food matrix is required. A good method for extraction of lipids from various food matrices should be able to overcome the interaction between the lipid and tissue matrix.[20] Although many methods are available for lipid extraction from various foods,[21,22] the most outstanding ones are the Folch method and Bligh and Dyer method.[20,23] These two methods have been a basis of lipid extraction, and because of their robustness, modifications have been presented by different researchers.[24,25]

In this study a universal method for the extraction of epoxy fatty acids from different fat-containing food matrices based on a modified Bligh and Dyer method was validated and implemented. This method uses a synthesized epoxy FAMEs IS at the beginning of the analysis, which reduces analytical variation within and between samples and has proved to be a robust and successful method. The method can be used to analyze epoxy fatty acids in various fat food matrices. Various food matrices have been analyzed, and results obtained are presented.

MATERIALS AND METHODS

Chemicals and Reagents. Methyl *tert*-butyl ether (MTBE) and 3-chloroperoxybenzoic acid (70−75%) were purchased from Acros Organics (Geel, Belgium). Dichloromethane (99% purity) was bought from Chem-Lab NV (Zedelgem, Belgium), and methanol was obtained from Fischer Scientific (Tournai, Belgium). Sodium methoxide solution (25% w/v) and silica gel 60 for column chromatography (particle size = 0.063−0.100 mm) were bought from Sigma-Aldrich (St. Louis, MO, USA). Methyl oleate (C18:1), methyl *cis*-10-heptadecenoate (C17:1), and a mixed FAMEs GLC 68D standard were obtained from Nu-Chek-Prep, Inc., USA. All other chemicals and reagents were of analytical grade and obtained from reliable local suppliers.

Standards. *Synthesis of Methyl cis-10,11-epoxyheptadecanoate (IS) and cis-9,10-epoxystearate.* Both epoxy FAMEs of the IS and the *cis*-9,10-epoxystearate (analyte) were synthesized on the basis of a stereospecific method described by Gunstone and Jacobsberg.[26] Briefly, the corresponding FAMEs of the IS and the analyte were reacted with 3-chloroperoxybenzoic acid in chloroform at room temperature for 4 h with periodic agitation. The formed epoxy esters were purified on dry activated silica gel column (25 g) by eluting the unreacted fatty acids with 200 mL of hexane/diethyl ether (98:2 v/v) as the mobile phase, and the epoxy FAMEs were collected with 300 mL of hexane/diethyl ether (90:10 v/v). Confirmation of the identity and purity of the synthesized compounds was done by use of gas chromatography−mass spectrometry (GC-MS).

Standard Preparations. The synthesized IS and analyte at a concentration of 20 mg mL^{-1} each were prepared in iso-octane. Stock solutions at a concentration of 10 mg mL^{-1} each were also prepared in iso-octane, and all were stored at −20 °C. From the individual stock standard solutions, working solutions were prepared by making dilutions in iso-octane to obtain a calibration range of 40, 80, 120, 160, 200 and 200, 400, 600, 800, and 1000 μg mL^{-1} for the lower and upper range, respectively. The upper range was diluted 10 times before injection on GC-FID. All necessary precautions were taken to avoid photodegradation of the light-sensitive standards, such as wrapping the standard solutions and the extracts with aluminum foil and storing them in the dark.

Samples. Validation was based on the following samples, namely, coconut oil, crisps, milk powder (infant formula), and pork samples, which were purchased from a supermarket in Belgium. Normally the samples would be brought to the laboratory on the day of analysis and analyzed immediately. A number of different food samples here referred to as market samples were screened for epoxy fatty acids, namely, mayonnaise, crisps, biscuits, peanuts, minced beef, cooked ham, butter, and a special biscuit known as speculoos, and were bought from supermarkets in Belgium and analyzed.

Sample Preparation. *Validation Samples.* A ground and homogenized sample (except oil) of 500 ± 0.50 mg was weighed into a 250 mL glass centrifuge tube and spiked with a mixture of epoxy IS and epoxy analyte at different concentrations (0−200 μg g^{-1} of sample). A fixed concentration (50 μg) of the IS was always added. Water was adjusted to reach a final water content of 14.5 g as determined by the initial water content of the sample. Thereafter, 26 mL of methanol and 11 mL of dichloromethane were added and homogenized using an Ultra-Turrax blender (Janke & Kunkel, IKA-Werk, Staufeb, Germany) for 1 min at 14000 rpm. Another 15 mL of dicholoromethane was added and then homogenized for 30 s, and finally 15 mL of water (pH ≤2) was added and homogenized for 30 s. The tubes were centrifuged at 3600*g* for 10 min, the pH of the aqueous layer was checked to be <2; if not, it was adjusted by using 5 M hydrochloric acid. The top aqueous layer was siphoned off, and the organic layer was dried on sodium sulfate over a 150 mm filter paper. The solvents were removed using a rotary evaporator and finally dried on nitrogen.

Market Samples. When the extraction procedure was applied to the screening market samples, a weight (depending on the amount of lipid in the sample) that does not exceed 200 mg of oil was taken. The IS amount always added was 10 μg, and the same extraction procedure above was followed.

Transmethylation and SPE Separation. *Transmethylation.* Base-catalyzed transmethylation procedures and the SPE separation steps followed have previously been described.[8] Briefly, 5 mL of MTBE was added to the extracted oil in a 25 mL glass centrifuge tube. Then, 2.5 mL of a 0.2 M sodium methoxide solution in methanol was added, vortexed for 1 min, and allowed to stand at room temperature for 2 min. Then 0.17 mL of 0.5 M sulfuric acid was added, and the mixture vortexed for a few seconds. Finally, 5 mL of water was added, vortexed for 30 s, and centrifuged at 3600*g* for 1 min. The organic layer was collected over a layer of sodium sulfate, and the extraction was repeated two times with 5 mL of MTBE. The organic layer was evaporated on a rotary evaporator and finally dried under a stream of nitrogen. The resultant FAME was dissolved into 2 mL of *n*-hexane/diethyl ether (98:2, v/v) and then loaded onto the silica column.

SPE Separation. The SPE cartridge column (6 mL, 6.5 cm × 1.3 cm) was filled with 1 g of activated silica and 5 mL of the elution solvent; *n*-hexane/diethyl ether (98:2, v/v) was added and thoroughly mixed in the column to prepare a slurry. Care was taken to ensure uniform packing and to avoid air bubbles by tapping the column slightly, and 1 cm of sand was added.

Column Chromatography Partitioning. An aliquot of FAMEs dissolved in 2 mL of *n*-hexane/diethyl ether (98:2, v/v) was loaded onto the prepared silica column, and the nonpolar fraction, which comprises the nonaltered FAMEs, was eluted with 15 mL of *n*-hexane/diethyl ether (98:2, v/v). The epoxy FAMEs were eluted with 15 mL of *n*-hexane/diethyl ether (90:10, v/v). This was dried using a stream of nitrogen and dissolved into 200 μL of iso-octane ready for GC-FID analysis.

Instrumentation. *GC-FID Conditions.* The epoxy FAMEs were analyzed by GC-FID using an Agilent 6890N series gas chromatograph (Agilent, USA). The samples were dissolved in iso-octane, and 0.1 μL was injected directly into the column using a cold on-column injector; separation was performed in a CP-Sil 88 for FAME (50 m × 0.25 mm i.d.) capillary column coated with a 0.2 μm film. A deactivated fused silica precolumn, 3 m × 0.25 mm i.d. (Agilent, Belgium), was fitted to protect the column. The oven temperature program was set as follows: 50 °C hold for 4 min, then ramp to 225 °C at 20 °C min^{-1}, and hold for 25 min. The flame ionization detector temperature was set at 300 °C. The detector flow rates for hydrogen, air, and helium (makeup) were 40, 400, and 20 mL min^{-1}, respectively. Helium was used as carrier gas at a flow rate of 1 mL min^{-1}. Identification of individual epoxy FAMEs was carried out by comparison of retention times with those of authentic standards (GLC 68D, Nu-Chek Prep, Inc., USA).

GC-MS Conditions. A GC-MS was used for the qualitative identification the epoxy FAMEs, especially in the screened samples. The epoxy FAMEs were injected in an Agilent 7890A GC equipped with a 5975C mass spectrometer (Agilent Technologies, Palo Alto, CA, USA). Chromatographic conditions and column were the same as those applied on GC-FID. The injection volume was 1 μL, and the programmed temperature vaporizing (PTV) injector was kept at 53 °C for 0.2 min and then ramped to 200 °C at a rate of 700 °C min^{-1}. The mass selective detector (MSD) conditions were as follows: capillary direct interface temperature, 250 °C; ionization energy, 70 eV; operating in scan mode between m/z 30 and 600; scan rate, 3.64 cycles s^{-1}.

Method Validation. The analytical method here presented was optimized using four different food matrices covering a wide category of common fat foods as indicated under Samples. Although foods were analyzed to obtain blank samples, it was not possible to obtain one without a signal of the analyte; however, the IS did not have any interfering signal. In-house validation procedures were followed as recommended by Commission Decision 2002/657/EC[27] and Ricard et al.[28] Performance criteria assessed included linearity, matrix effect, limit of detection (LOD), limit of quantification (LOQ), repeatability (intraday; RSDr), reproducibility (interday; RSDR), and stability. Because there are no certified reference materials available for epoxy fatty acids, trueness of the obtained results was assessed by the use of spiked samples.[28] The concentration levels used to spike the different food matrices were decided on after considering the epoxy levels obtained in fresh oil samples.[8] This study revealed that epoxy fatty acids occur in a wide range (0−1.4 mg g^{-1} of oil) in fresh oils.

Intraday Repeatability, Interday Reproducibility, and Stability. Precision of the method was assessed by repeatability and the intermediate precision called interday reproducibility. The repeatability was assessed by spiking the epoxy standard solutions to the different food matrices at five different concentration levels with three replicates at each level (n = 3) and analyzing on the same run of the day on GC-FID. Interday reproducibility was determined by repeating the experiment on two different days for all of the matrices. Stability was evaluated by storing the extracts at −20 °C and analyzing them after 4 months of storage.

Calibration Curves, LOD, LOQ, and Recoveries. Linearity and working ranges were evaluated by the correlation coefficient of standard calibration curve and by plotting the residuals for the curve. Because epoxy fatty acids are occurring at a wide concentration range, two calibration curves with uniformly spaced ranges were used in the beginning, 0−200 and 200−1000 μg g^{-1} of sample. The calibration curve was obtained by directly injecting to the GC the mixture of IS and analyte. The calibration and standard addition curves were constructed by plotting area ratios of analyte to IS (y) versus the concentration ratios of the analyte to that of the IS (x). During standard addition, the same concentrations as those in the calibration curve were used, and known amounts of the epoxy analyte were added to a fixed mass of each matrix separately. Regression of the calibration curve using the general linear regression model was performed to obtain the calibration curve equation (R^2, slope, and intercept). LOD and LOQ were determined from the standard addition curves using the linest function of the Microsoft Office Excel 2007 program. LOD was defined as the concentration equal to 3 (SEb/slope) and LOQ = 2 × LOD, where SEb is the standard error of the intercept.[28] Because certified reference materials are not available, it is acceptable that trueness of measurements is assessed through apparent recovery of additions of known amounts of the element to the unknown samples.[27] The same addition curves (spiked samples) used to calculate the LOD were further used to obtain the apparent recoveries of the method. Apparent recovery is defined as the quantity observed value/reference value, obtained using an analytical procedure that involves a calibration graph.[29] Quantification of the validation samples was based on external calibration curve, and for real samples it was based on the response factor of epoxystearate.

Matrix Effect Evaluation. The matrix effect was assessed by comparing the slopes of the calibration curve with that of the standard addition curves.[30] When there was no matrix effect, the same slope was obtained.

Statistical Analyses. Analytical determinations were conducted in triplicate, and when duplicate analysis was performed, evaluation of precision was done according to the method of Synek.[31] Comparison of the calibration and addition curve slopes was done by performing a one-way ANCOVA test carried out using the GraphPad Prism 6 2012 program.

RESULTS AND DISCUSSION

Method Development. During method development and validation both the Folch method and Bligh and Dyer method were applied, and the recovery results (not shown) for both methods were not different. Because the Bligh and Dyer method has an advantage of using less solvent,[23] it was chosen so as to reduce the use of expensive and hazardous solvents.[32]

An important factor during method development was that liquid−liquid extraction of oil had to optimize the solvent ratios to be used. The possible extraction agents are dichloromethane and chloroform. Because dichloromethane is less hazardous, it was preferred in the extraction. As a quality note, high-quality solvents should be used, and where such a quality is not achievable, the solvents should be distilled and the use of glassware is highly recommended.

Because the Bligh and Dyer method was initially developed using chloroform, it was required to optimize the use of dichloromethane. The ternary diagram of water + methanol + dichloromethane[21,33] was used to optimize both sample and solvent ratios required during extraction. The water content of dry samples had to be adjusted as indicated below because this had a bearing on the phase separation, which is the basis of this method. Addition of solvent mixtures in the following ratio and in the following order was optimal; water, 29 mL (considering water in the sample); dichloromethane, 22 mL; and methanol, 52 mL. The system should be monophasic; there should not be phase separation if the solvent ratio is correct and if sufficient homogenization is done. Addition of 30 mL of dichloromethane to the mixture, followed by addition of 30 mL of acidic water (pH ≤2 acidified with 6 M hydrochloric acid) and homogenizing again with an Ultra-Turrax blender for 30 s, allowed phase separation. Methanol is a poor solvent for triacylglycerols but is fully miscible with water in all proportions. It can thus serve to strip away the hydrating water and allow dichloromethane to dissolve the polar fatty

dx.doi.org/10.1021/jf405664c | J. Agric. Food Chem. 2014, 62, 2982−2988

acids. The water in the system causes the dichloromethane to separate cleanly, with the methanol component retaining the water and suppressing emulsion formation.[20]

Because epoxy standards are not available from commercial sources,[8] the IS and epoxy analyte used during this study were both synthesized by use of a solvent-based epoxidation procedure described by Gunstone and Jacobsberg.[26] Although it is possible to synthesize epoxides using hydrogen peroxide-based catalytic epoxidation, the "Tetrakis" phosphotungstate catalyst, and lipase-mediated reactions,[15,34] the internal standard used was prepared by using the method reported by Gunstone and Jacobsberg.[26] The method had a yield of >90%, which is a sign of purity. The synthesized compounds were confirmed by mass spectral data after GC-MS analysis. It is well-known that during the analysis of epoxy fatty acids, the method of sample preparation has to take into account the fact that the highly reactive epoxide ring can be opened by heat or chemicals.[35] Thus, the methylation procedure adopted for the formation of FAMEs during the study was room temperature methylation. However, this has a disadvantage that a free fatty acid cannot be used as an IS during the analysis of epoxy fatty acids. As observed by Suter et al.,[17] methylation and saponification reactions both compete in the presence of water, so care had to be taken that the reaction mixture was not kept unnecessarily long for the formed methyl esters to be saponified. Use of acidified water also helped to stop the possibility of saponification. The FAMEs were extracted twice in MTBE to increase the efficiency of the extraction procedure. During this study the use of a methylated IS was evaluated by calculating the area ratios of both the analyte and the methylated IS. It was found out that there was no change in the ratios; furthermore, during validation, the analyte and the IS were both epoxy FAMEs, which reduced variability during the analysis. However, it is important to note that care should be taken during the evaporation step not to lose the IS, so finally after the rotary evaporation step, extracts were always dried under a gentle stream of nitrogen. The use of an epoxy FAME IS has made this method more sensitive and accurate because analytical variations can be corrected by the IS added at the beginning of the extraction as recommended by Commission Decision 2002/657/EC.[27] In analytical methods where the IS may not be added at the start of the analysis, control of analytical variations is not possible.

Method Validation. *Linearity, LOD, LOQ, and Recovery.* Because the epoxy fatty acids occur over a wide range, in the beginning of method development, two calibration ranges were chosen, the low and the high ranges. Six concentration levels (0, 40, 80, 120, 160, and 200 $\mu g\ g^{-1}$) plus the blank were used during method development and validation. In both ranges the linearity was evaluated by plotting the residuals and linear regression (R^2) values. It must be emphasized that concentrations of the high-range calibration curve could not be injected directly onto the GC-FID, so they were diluted 10 times. In all the two ranges there was no sign of detector saturation, which would be a cause of loss of linearity, so a good linear range was observed in both calibration curves. When the two concentration ranges data were pooled and plotted into one calibration curve, still good linearity with a regression coefficient of 0.9994 and a slope of 1.23 was obtained. The calibration curves showed a measure of goodness-of-fit of linear regression (R^2) ranging from 0.9979 to 0.9999, whereas the standard addition curves showed coefficients (R^2) ranging from 0.9959 to 0.9973 in oil, 0.9885−0.9927 in crisps, 0.9990−0.9994 in milk powder, and 0.9915−0.9995 in pork. The curves with $R^2 \geq 0.995$ are considered linear,[36] and these results show how well the developed method can estimate epoxy fatty acids in the different matrices.

Mean percent recoveries based on spiked samples for the epoxy fatty acids in the different matrices were in the range from 94 to 115 (Table 1). The values are the mean of three replications of analysis performed on two different days.

Table 1. Intraday Precision (RSDr), Interday Precision (RSDR) Expressed as Relative Standard Deviation, and Apparent Recovery Obtained for Oil, Crisps, Pork, and Milk Powder at Five Concentration Levels of *cis*-9,10-Epoxystearate Analyte

matrix	concentration ($\mu g\ g^{-1}$)	RSDr (%)	RSDR (%)	apparent recovery (%)
oil	40	3	9	100
	80	4	4	100
	120	6	5	101
	160	8	5	101
	200	2	3	101
crisps	40	19	3	115
	80	1	5	99
	120	3	2	95
	160	4	6	97
	200	5	6	97
pork	40	10	7	96
	80	1	8	94
	120	2	3	96
	160	7	9	99
	200	5	6	96
milk powder	40	3	4	98
	80	2	5	98
	120	2	6	99
	180	3	3	101
	200	2	5	102

The LOD was determined according to the definition given by IUPAC and the regression of the calibration equation using the linest method was used. Accordingly, the LOD values ($\mu g\ g^{-1}$ of sample) determined for the different matrices validated were 2.75 in oil, 10.23 in crisps, 1.66 in milk powder, and 5.16 in pork. The lowest LOD was obtained in milk (Table 2).

Table 2. Limits of Detection (LOD) and Limits of Quantification (LOQ) Obtained for the Different Matrices

	oil	crisps	pork	milk powder
LOD ($\mu g\ g^{-1}$ of sample)	2.8	10.2	5.2	1.7
LOQ ($\mu g\ g^{-1}$ of sample)	5.5	20.5	10.3	3.3

The matrix effect on the recovery of the analytes was evaluated by comparing the slopes of the calibration curves with those of the addition curves. The comparison was done by using a statistical tool in GraphPad Prism to obtain a p value. The results of the statistical evaluation of the slopes of the calibration and addition curves are shown in Table 3. Only crisps samples appear to have a statistically significant matrix effect ($p = 0.0002$). The observed matrix effect in crisps could

Table 3. Matrix Effect Evaluation by Statistical Comparison of the Calibration Curve with the Standard Addition Curve

	calibration curve		addition curve		
matrix	slope	R^2	slope	R^2	p value[a]
oil	1.209	0.9999	1.222	0.9973	0.6019
crisps	1.180	0.9987	0.986	0.9885	0.0002*
pork	1.174	0.9998	1.185	0.9998	0.2615
milk powder	1.180	0.9987	1.200	0.9994	0.3498

[a]An asterisk indicates statistical difference within rows between the two slopes ($p < 0.05$).

be attributed to the high signal of epoxy fatty acids that is detected in the blank samples. Normally a good evaluation of matrix effect is obtained if a sample without the analyte of interest (blank) is obtained, but in all cases, it was not possible to get one. However, in other matrices for which the signal was low, it was possible to objectively evaluate whether it is the matrix interfering with the analysis or not.

Intraday Precision (Repeatability), Interday Precision (Reproducibility), and Stability. Results for intraday and interday precision measures are presented in Table 1. These results are presented as percent relative standard deviations in both cases as a measure of precision. The repeatability values presented are the highest that were obtained during the validation study. Although it was not possible to vary all factors that may affect precision as recommended in method validation studies,[27,28] the relative standard deviations obtained revealed that accurate estimation of precision was obtained. In the lower concentration ranges, higher variations of up to 19% were observed in crisps. The stability of the extracts was evaluated by reinjection of the same extracts after storage. Results after reinjection of the same extracts for all three matrices used did not show any degradation after 4 months of storage. This was true with the calibration standards, for which, when reinjected after 4 months, the slopes obtained did not differ significantly. This is a clear indication that epoxy fatty acid extracts can be stored at −20 °C for some time without any degradation.

Application of the Method on Market Samples. After validation and optimization of the analytical method, it was applied on commercially available samples collected from Belgian supermarkets. For each sample, the analytical determination was performed in duplicate. The results of the analysis are summarized in Table 4. The food samples analyzed were chosen to cover a wide range of samples of fat origin with differing physical and chemical composition. It was important to note that for samples which had a high dry matter content, their weight during analysis was reduced significantly as to avoid the solid matter covering the organic layer. Furthermore, depending on the fat content of the sample, the sample weight and the solvent ratio were increased so as to be able to recover enough fat. The results obtained indicate that the epoxy fatty acids are occurring in high amounts in most samples, although beef samples had less. The coefficient of variation for duplicate analysis ranged from 13.9 to 14.1%. It was generally observed that on a fat basis, biscuits had the highest total epoxy content. There is no clear relationship between the sample type and the total epoxy fatty acids determined. However, the levels of epoxy fatty acids are expected to depend on the amount of unsaturated fatty acids present, which are the precursors of epoxy fatty acids,[8] sensitivity to oxidation, and the level of oxidation.

The method presented and validated is accurate and reproducible and can be applied in the determination of epoxy fatty acids in a wide range of food samples of fat origin. The well-resolved and clean chromatograms obtained on real sample matrices indicate the reliability of the method for confirmatory purposes. The method developed is robust and can be applied to such a wide coverage. High recoveries for the epoxy fatty acids and the low LOD and LOQ levels indicate that the method is sensitive and can be used in risk assessment studies.

AUTHOR INFORMATION

Corresponding Author

*Ghent University, Coupure Links 653, B-9000, Belgium. Phone: +32 92 64 61 66. Fax: + 32 92 64 62 15. E-mail: Bruno.DeMeulenaer@UGent.be.

Funding

Ghent University through the Concerted Research Actions (GOA) project funded this research, K.S. was supported by the Special Research Fund (BOF) of Ghent University, and A.P.

Table 4. Epoxy Fatty Acid Levels Analyzed in Different Food Samples from Belgian Supermarkets

		epoxy fatty acid content ($\mu g\ g^{-1}$ of sample)						total epoxy	
sample	fat content[a] (%)	*trans*- 9,10-ES[b]	*cis* 9,10-ES	*trans*- 12,13-EO[c]	*trans*-9,10-EO	*cis*- 12,13-EO	*cis*- 9,10-EO	$\mu g\ g^{-1}$ of sample	$\mu g\ g^{-1}$ of fat
biscuit	12	14.90	13.92	3.89	1.03	27.40	12.67	73.81	615.08
speculoos A	19	3.58	19.16	1.06	0.76	39.13	10.80	74.49	392.05
speculoos B	19	2.91	17.55	1.11	0.97	34.63	9.41	66.58	350.42
speculoos C	18.7	3.49	12.28	1.11	1.15	22.12	6.80	46.95	251.07
speculoos D	17.4	4.04	13.96	1.25	1.94	24.58	7.99	53.76	308.97
mayonnaise A	80.3	10.92	9.50	4.15	7.00	7.27	5.25	44.09	54.91
mayonnaise B	81	17.33	7.87	4.49	6.54	6.96	5.97	49.16	60.69
mayonnaise C	81.4	10.15	5.14	3.74	4.65	4.31	4.61	32.6	40.05
peanuts A	51	9.42	129.41	4.39	4.34	4.69	18.53	170.78	334.86
peanuts B	NI[d]	4.70	47.10	2.29	3.37	2.76	14.09	74.31	ND[e]
butter	82	53.66	16.79	18.30	0.00	9.38	17.21	115.34	140.66
cooked ham	2.8	0.75	0.66	0.47	0.00	0.48	0.88	3.24	115.71
minced beef	30	1.48	1.09	1.72	0.00	0.66	0.63	5.58	18.60
walnuts	65	4.27	6.42	3.68	1.84	25.60	7.07	48.88	75.20

[a]Fat content as reported on the package label. [b]ES, epoxystearate. [c]EO, epoxyoleate. [d]NI, not indicated. [e]ND, not determined.

was supported by Federal Public Service of Health, Food Chain Safety and Environment (project RT/10 TOXAL).

Notes

The authors declare no competing financial interest.

■ ABBREVIATIONS USED

GC-FID, gas chromatography−flame ionization detector; IS, internal standard; MTBE, methyl *tert*-butyl ether; LOD, level of detection; LOQ, level of quantification; FAME, fatty acid methyl esters; GC-MS, gas chromatography−mass spectrometry; SPE, solid phase extraction; PTV, programmed temperature vaporizing; MSD, mass selective detector

■ REFERENCES

(1) Waraho, T.; McClements, D. J.; Decker, E. A. Mechanisms of lipid oxidation in food dispersions. *Trends Food Sci Technol.* **2011**, *22* (1), 3−13.

(2) Choe, E.; Min, D. B. Mechanisms and factors for edible oil oxidation. *Compr. Rev. Food Sci. Food Saf.* **2006**, *5* (4), 169−186.

(3) Tian, F.; Decker, E. A.; Goddard, J. M. Controlling lipid oxidation of food by active packaging technologies. *Food Funct.* **2013**, *4* (5), 669−680.

(4) Frankel, E. N. *Lipid Oxidation*, 2nd ed.; Oily Press: Sawston, UK, 2005.

(5) Dobarganes, M. C. Formation of epoxy-, keto- and hydroxy-fatty acids. In *Frying Oils − Chemistry*; Christie, W. W., Ed.; AOCS Lipid Library: AOCS: Champaign, IL, USA, 2009.

(6) Giuffrida, F.; Destaillats, F.; Robert, F.; Skibsted, L. H.; Dionisi, F. Formation and hydrolysis of triacylglycerol and sterols epoxides: role of unsaturated triacylglycerol peroxyl radicals. *Free Radical Biol. Med.* **2004**, *37* (1), 104−114.

(7) Schaich, K. M. Lipid oxidation: theoretical aspects. In *Bailey's Industrial Oil and Fat Products*, 6th ed.; Shahidi, F., Ed.; Wiley Interscience: Hoboken, NJ, USA, 2005; pp 269−355.

(8) Mubiru, E.; Shrestha, K.; Papastergiadis, A.; De Meulenaer, B. Improved gas chromatography-flame ionization detector analytical method for the analysis of epoxy fatty acids. *J. Chromatogr., A* **2013**, *1318*, 217−225.

(9) Greene, J. F.; Newman, J. W.; Williamson, K. C.; Hammock, B. D. Toxicity of epoxy fatty acids and related compounds to cells expressing human soluble epoxide hydrolase. *Chem. Res. Toxicol.* **2000**, *13* (4), 217−226.

(10) Hayakawa, M.; Kosaka, K.; Sugiyama, S.; Yokoo, K.; Aoyama, H.; Izawa, Y.; Ozawa, T. Proposal of leukotoxin, 9,10-epoxy-12-octadecenoate, as a burn toxin. *Biochem. Int.* **1990**, *21* (3), 573−579.

(11) Ishizaki, T.; Shigemori, K.; Nakai, T.; Miyabo, S.; Ozawa, T.; Chang, S. W.; Voelkel, N. F. Leukotoxin, 9,10-epoxy-12-octadecenoate causes edematous lung injury via activation of vascular nitric oxide synthase. *Am. J. Physiol.: Lung Cell. Mol. Physiol.* **1995**, *269* (1), L65−L70.

(12) Marmesat, S.; Velasco, J.; Dobarganes, M. C. Quantitative determination of epoxy acids, keto acids and hydroxy acids formed in fats and oils at frying temperatures. *J. Chromatogr., A* **2008**, *1211* (1−2), 129−134.

(13) Velasco, J.; Marmesat, S.; Bordeaux, O.; Márquez-Ruiz, G.; Dobarganes, C. Formation and evolution of monoepoxy fatty acids in thermoxidized olive and sunflower oils and quantitation in used frying oils from restaurants and fried-food outlets. *J. Agric. Food Chem.* **2004**, *52* (14), 4438−4443.

(14) Velasco, J.; Marmesat, S.; Berdeaux, O.; Marquez-Ruiz, G.; Dobarganes, C. Quantitation of short-chain glycerol-bound compounds in thermoxidized and used frying oils. A monitoring study during thermoxidation of olive and sunflower oils. *J. Agric. Food Chem.* **2005**, *53* (10), 4006−4011.

(15) Orellana-Coca, C.; Adlercreutz, D.; Andersson, M. M.; Mattiasson, B.; Hatti-Kaul, R. Analysis of fatty acid epoxidation by high performance liquid chromatography coupled with evaporative light scattering detection and mass spectrometry. *Chem. Phys. Lipids* **2005**, *135* (2), 189−199.

(16) Cui, P. H.; Duke, R. K.; Tattam, B. N.; Duke, C. C. Monoepoxy octadecadienoates and monoepoxy octadecatrienoates 2: mass spectral characterization. *Chem. Phys. Lipids* **2008**, *152* (2), 65−70.

(17) Suter, B.; Grob, K.; Pacciarelli, B. Determination of fat content and fatty acid composition through 1-min transesterification in the food sample; principles. *Z. Lebensm. Unters. Forsch.* **1997**, *204* (4), 252−258.

(18) Velasco, J.; Berdeaux, O.; Márquez-Ruiz, G.; Dobarganes, M. C. Sensitive and accurate quantitation of monoepoxy fatty acids in thermoxidized oils by gas−liquid chromatography. *J. Chromatogr., A* **2002**, *982* (1), 145−152.

(19) Fankhauser-Noti, A.; Fiselier, K.; Biedermann-Brem, S.; Grob, K. Assessment of epoxidized soy bean oil (ESBO) migrating into foods: comparison with ESBO-like epoxy fatty acids in our normal diet. *Food Chem. Toxicol.* **2006**, *44* (8), 1279−1286.

(20) Christie, W. W. *Lipid Analysis: Isolation, Separation, Identification and Strucutral Analysis of Lipids*, 3rd ed.; Oily Press: Sawston, UK, 2003.

(21) Bligh, E. G.; Dyer, W. J. A rapid method of total lipid extraction and purification. *Can. J. Biochem. Phys.* **1959**, *37* (8), 911−917.

(22) Folch, J.; Lees, M.; Stanley, G. H. S. A simple method for the isolation and purification of total lipids from animal tissues. *J. Biol. Chem.* **1957**, *226* (1), 497−509.

(23) Iverson, S. J.; Lang, S. L. C.; Cooper, M. H. Comparison of the Bligh and Dyer and Folch methods for total lipid determination in a broad range of marine tissue. *Lipids* **2001**, *36* (11), 1283−1287.

(24) Perez-Palacios, T.; Ruiz, J.; Ferreira, I.; Petisca, C.; Antequera, T. Effect of solvent to sample ratio on total lipid extracted and fatty acid composition in meat products within different fat content. *Meat Sci.* **2012**, *91* (3), 369−373.

(25) Dodds, E. D.; McCoy, M. R.; Rea, L. D.; Kennish, J. M. Gas chromatographic quantification of fatty acid methyl esters: flame ionization detection vs. electron impact mass spectrometry. *Lipids* **2005**, *40* (4), 419−428.

(26) Gunstone, F. D.; Jacobsberg, F. R. Fatty acids, Part 35. The preparation and properties of the complete series of methyl epoxyoctadecanoates. *Chem. Phys. Lipids* **1972**, *9* (1), 26−34.

(27) European Commission. Commission Decision 2002/657/EC of 12 August 2002 implementing Council Directive 96/23/EC concerning the performance of analytical methods and the interpretation of results. *Off. J. Eur. Communities* **2002**, *L 221*, 8−36

(28) Ricard, B.; Alicia, M.; Jordi, R.; Rius, F. X. Validation of analytical methods. *Grasas Aceites* **2002**, *53* (1), 128−143.

(29) Burns, D. T.; Danzer, K.; Townshend, A. Use of the terms "recovery" and "apparent recovery" in analytical procedures (IUPAC recommendations 2002). *Pure Appl. Chem.* **2002**, *74* (11), 2201−2205.

(30) Papastergiadis, A.; Mubiru, E.; Van Langenhove, H.; De Meulenaer, B. Development of a sensitive and accurate stable isotope dilution assay for the simultaneous determination of free 4-hydroxy-2-(*E*)-nonenal and 4-hydroxy-2-(*E*)-hexenal in various food matrices by gas chromatography−mass spectrometry. *Food Anal. Methods* **2013**, 1−8.

(31) Synek, V. Evaluation of the standard deviation from duplicate results. *Accred. Qual. Assur.* **2008**, *13* (6), 335−337.

(32) Cequier-Sánchez, E.; Rodríguez, C.; Ravelo, A. G.; Zárate, R. Dichloromethane as a solvent for lipid extraction and assessment of lipid classes and fatty acids from samples of different natures. *J. Agric. Food Chem.* **2008**, *56* (12), 4297−4303.

(33) Merzougui, A.; Hasseine, A.; Kabouche, A.; Korichi, M. LLE for the extraction of alcohol from aqueous solutions with diethyl ether and dichloromethane at 293.15 K, parameter estimation using a hybrid genetic based approach. *Fluid Phase Equilib.* **2011**, *309* (2), 161−167.

(34) Poli, E.; Clacens, J.-M.; Barrault, J.; Pouilloux, Y. Solvent-free selective epoxidation of fatty esters over a tungsten-based catalyst. *Catal. Today* **2009**, *140* (1−2), 19−22.

(35) Piazza, G. J.; Nunez, A.; Foglia, T. A. Isolation of unsaturated diols after oxidation of conjugated linoleic acid with peroxygenase. *Lipids* **2003**, *38* (3), 255−261.
(36) Van Loco, J.; Elskens, M.; Croux, C.; Beernaert, H. Linearity of calibration curves: use and misuse of the correlation coefficient. *Accred. Qual. Assur.* **2002**, *7* (7), 281−285.

Table 1. Primers and Probes Used in the NAIMA, qPCR and Microarrays

primers used for NAIMA				
target	orientation	name	sequence (5′−3′)	refs
PSTVd	antisense	T7-NAIMA-pstvd[a]	T7- TGCGGTTCCAAGGGCTAAAC	this study
	sense	SP6-NAIMA-pstvd[b]	SP6-CTGTCGCTTCGGCTACTACC	
R. solanacearum	antisense	T7-NAIMA-Rs[a]	T7- GGCCTTGCGGTCCCCCACT	this study
	sense	SP6-NAIMA-Rs[b]	SP6- TGGCGGCATGCCTTACACA	14
T7-sequence		T7-universal[c]	AATTCTAATACGACTCACTATAGGGAGA*TCCAATAGAATCACATCGCTTACAAGGCAAT*	4
SP6-sequence		SP6-universal[d]	**CATA**CGATTTAGGTGACACTATAGAA	

capture probes present on the microarray			
target	name	sequence (5′−3′)	refs
PSTVd	PSTVd-NAIMA-1	CTTCTATCTTACTTGCTTCGGGGCGAGGGT	this study
	PSTVd-NAIMA-2	TCTTACTTGCTTCGGGGCGAGGGTGTTTAG	
	PSTVd-NAIMA-3	TACTTGCTTCGGGGCGAGGGTGTTTAGC	
R. solanacearum	Rs-NAIMA-16S/1	GTGAGTAATACATCGGAACGTGCCCTGTAGTG	this study
	Rs-NAIMA-16S/2	CTTACACATGCAAGTCGAACGGCAGCGG	
	Rs-NAIMA-16S/3	GGTAGCTTGCTACCTGCCGGCGAGT	

primers used for TaqMan qPCR				
target	orientation	name	sequence (5′−3′)	refs
PSTVd	antisense	Rv_Taq_viroid	CGGTTCCAAGGGCTAAACAC	this study
	sense	Fw_Taq_viroid	CTGTCGCTTCGGCTACTACC	
	probe	Probe_Taq_viroid	FAM-AACAACTGAAGCTCCCGAGAACCGC-TAMRA	
R. solanacearum	antisense	RS-II-R	GGCACGTTCCGATGTATTACTCA	13
	sense	RS-I-F	GCATGCCTTACACATGCAAGTC	
	probe	RS-P	FAM- AGCTTGCTACCTGCCGGCGAGTG-TAMRA	

[a]All antisense primers used in NASBA contain the T7-cap sequence that is designed so that the T7 segment is bound to the 5′-end in addition to the given sequence. [b]All sense primers used in NASBA contain the SP6 sequence that is designed so that the SP6 is bound to the 5′-end in addition to the given sequence. [c]The T7-cap extension primer is composed of the T7-RNA polymerase promoter sequence (5′-end) and an abiotic cap sequence (3′-end, in italic) [d]The SP6-extension primer differs from the SP6 sequence used in sense primers in that it lacks the first four nucleotides (in bold) contained in the latter sequence.

diagnostics at the National Institute of Biology.[10,13] All of the primers were submitted to BLAST against different databases (only *R. solanacearum*, all *Ralstonia* without *R. solanacearum*, no *Ralstonia*, PSTVds, all viroids, plant) to obtain the selection of the most specific and selective primers. The primers for the multiplex template synthesis reaction were designed by addition of universal tail sequences to the target-specific sequences, as previously reported.[4] The primers designed for the NAIMA procedure are listed in Table 1. For *R. solanacearum*, the primers were highly similar (one additional nucleotide was inserted at the 3′ region of the antisense primer) to those previously described.[14] The universal primers for the second step of amplification are the same as previously reported.[4] The primers were synthesized and HPLC-purified by MWG Biotech AG (Eurofins MWG, Ebersberg, Germany). The experimental specificity of the primers and probes was assessed on samples of different species (Table 2, Table 4).

Design of Microarray Probes. The ArrayTube platform consists of a custom microprobe array integrated into a microreaction vial. The probes for the ArrayTubes (Alere Technologies, Jena, Germany) were designed in the region amplified by the NAIMA reactions. Briefly, windows of 30 nucleotides (±3 nucleotides) with a calculated T_m of 65 °C (±1 °C) were slid onto the NAIMA amplicon sequences with increments of 3 nucleotides. All of the candidate probe sequences were submitted to BLAST against different databases (as for the primer design). The candidates with best hits against the target (identity, similarity, lowest *E*-values) and the least number of hits were selected (and/or less significant scores; i.e., high *E*-values). The selected sequences were then checked for secondary structure (M-fold, at 55 °C), and those with no significant structure (ΔG positive or only slightly negative; i.e., $\Delta G > -1$ kcal/mol) were finally chosen. For *Ralstonia* species, the selection was made from the best ones, as specific as possible for *R. solanacearum* (for one probe), and for *Ralstonia* genus for the other two.

NAIMA Amplification Setup. *First Step: Multiplex Template Synthesis.* This first step consisted of a multiplexed template synthesis reaction, during which several pairs of tailed primers annealed to the specific DNA or RNA target and were extended to produce DNA templates bound to the universal regions (Figure 1). For this, 5 pmol of each of the SP6-specific and T7-specific tailed primers (i.e., two pairs of tailed primers for duplex NAIMA), 100 U SuperScriptII reverse transcriptase (Invitrogen, Carlsbad, CA), 10 mM dithiothreitol (Invitrogen, Carlsbad, CA), 1× First-Strand buffer (Invitrogen, Carlsbad, CA), 1 mM dNTP (Promega, Fitchburg, WI), and 5 μL of RNA, DNA, or RNA/DNA mixture were mixed in a final reaction volume of 10 μL. Template synthesis was carried out for 30 min at 42 °C in a Gene Amp PCR system 9700 (Applied Biosystems, Foster City, CA). The final product of this reaction (independently of whether the target is RNA or DNA) is the DNA template consisted of target region, tailed with universal sequence that is crucial for universal NASBA amplification step.

Second Step: Universal NASBA Amplification. The DNA templates from the first step were used directly in the NASBA amplification step (Figure 1) as follows: 2 μL template DNA from the first step was added to 5 μL of resuspended 2× NASBA Reaction Buffer Accusphere (Life Sciences Advance Technologies, St. Petersburg, FL) and mixed with 0.5 μL of the universal primers (T7 universal primer, SP6 universal primer; each at 50 μM). When the product was to be hybridized to the ArrayTube, an additional 1.1 μL of bio-UTP (Ambion; Foster City, CA) was added to the reaction mixture. This mixture was preincubated at 95 °C for 15 min and then incubated at

dx.doi.org/10.1021/jf5002149 | J. Agric. Food Chem. 2014, 62, 2989−2996

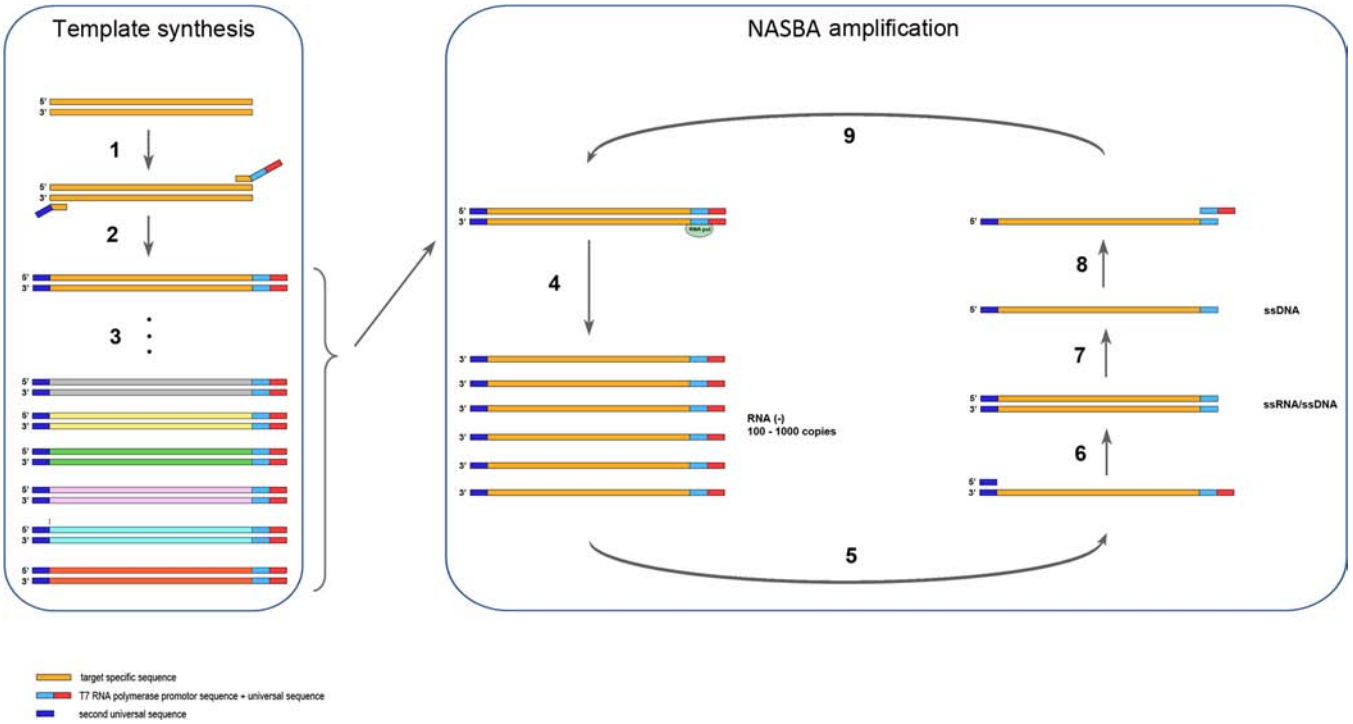

Figure 1. Schematic representation of the NAIMA amplification. The NAIMA amplification consisted of two steps: template synthesis and NASBA amplification. In the template synthesis step, the NAIMA tailed primers with sequence complementary to the target and the 5′-end sequences necessary for the multiplex amplification bind to the target (1) and are extended by the reverse transcriptase (2), producing the DNA templates for all of the targets present with identical 5′-ends (3). These templates were used in the amplification step, where T7 RNA polymerase transcribed them into several copies of antisense RNA molecules (4), and they were further reverse transcribed into single-stranded sense DNA (ssDNA) (5,6) to form an RNA−DNA duplex. The RNA−DNA duplex was later degraded by RNase H activity (7), and the ssDNA was then used as a template by the reverse transcriptase, followed by T7-cap-extension primer annealing (8) to synthesize a second DNA strand (9). These dsDNAs enter new cycles of amplification. The main product of the NAIMA amplification was antisense cRNA. Only one pair of primers was needed in this amplification step for all of the targets to be amplified.

41 °C for 2.5 min in a Gene Amp PCR system 9700 (Applied Biosystems, Foster City, CA). Afterward, 2.5 μL of resuspended NASBA Enzyme Accusphere (Life Sciences Advanced Technologies, St. Petersburg, FL) was added. NASBA Enzyme Accusphere is a cocktail of following enzymes: AMV reverse transcriptase (3.2 units/reaction), RNase H (0.04 units/reaction), and T7 RNA polymerase (16 units/reaction). The reactions were incubated at 41 °C for 40 min in a Gene Amp PCR system 9700.

Determination of NAIMA Amplification Performance and Monitoring with qPCR. The main final product of NAIMA amplification is cRNA. To estimate the amplification rate of the multiplex NAIMA amplification with qPCR, reverse transcription was performed on the NAIMA amplification products to obtain double-stranded cDNA, as previously described.[4] The primers and probes used for the qPCR detection of PSTVd and *R. solanacearum* are listed in Table 1. The qPCR reaction setup followed recommendations described by Cankar et al.,[15] and the reactions were performed as in Morisset et al.[4] using reverse-transcribed NAIMA amplification products and control samples (*R. solanacearum* DNA or reverse-transcribed PSTVd samples) (see workflow in Supporting Information Figure S1). Two dilutions of each sample were used in the qPCR, and each dilution was assayed in duplicate. The results were analyzed using the SDS 2.3 software (Applied Biosystems, Foster City, CA), after an automatic adjustment of the baseline and manual adjustment of the fluorescence threshold. The signals were considered positive if the Cq value was <40. The copy numbers of PSTVd for the sensitivity estimates were determined as described previously.[10,12] The exported data were further analyzed in a basic Excel spreadsheet. Briefly, the Cq values of the NAIMA amplification products were compared to the Cq values of the control samples. The control sample in our experiments was DNA used for NAIMA that had been diluted in the same proportion as the amplified DNA in the NAIMA reactions and reverse transcription. The differences in the Cq values between the NAIMA amplification products and the control indicated the amplification rate of the NAIMA amplification reaction. The relative efficiencies were calculated based on the assumption that the efficiency between qPCR cycles was 100% (the amount of target doubles for every cycle). The copy number estimation for PSTVd was done on the dilution series that was used in sensitivity experiments, as previously described.[12]

Array Tube Hybridization and Signal Detection. The ArrayTubes were conditioned with 500 μL of water and incubated at 55 °C in a shaking heated block for 2 min at 500 rpm. The water was then removed, and 500 μL of Nexterion hybridization buffer (Schott; Mainz, Germany) was added to the ArrayTube and incubated at 55 °C in a shaking heated block for 2 min at 500 rpm.

For the ArrayTube hybridization, 5 μL of each NAIMA amplification product was mixed with 25 μL of water and 70 μL of Nexterion hybridization buffer. This hybridization mixture was preheated to 95 °C for 4 min and cooled to 55 °C. The Nexterion hybridization buffer was removed from the ArrayTube, and 100 μL of hybridization mixture was added directly to the ArrayTube, followed by incubation at 55 °C in a shaking heated block at 500 rpm. The optimization of the hybridization time was performed on limited amounts of samples in the later stages of the experiments; however, the hybridization time of 15 min was shown to be as efficient as 60 min. Nevertheless, all of the reported tests were performed with 60 min of hybridization.

Arrays were washed by addition of 250 μL of washing buffer I that contained 2× saline-sodium citrate buffer and 0.01% Triton X-100, and the tubes were then inverted five times. The washing buffer I was removed, and 250 μL of washing buffer III containing 0.2× saline−sodium citrate buffer was added to the array, which was then inverted five times. To block the arrays, the washing buffer III was removed and 100 μL of blocking solution containing PBS, 2% milk powder, and

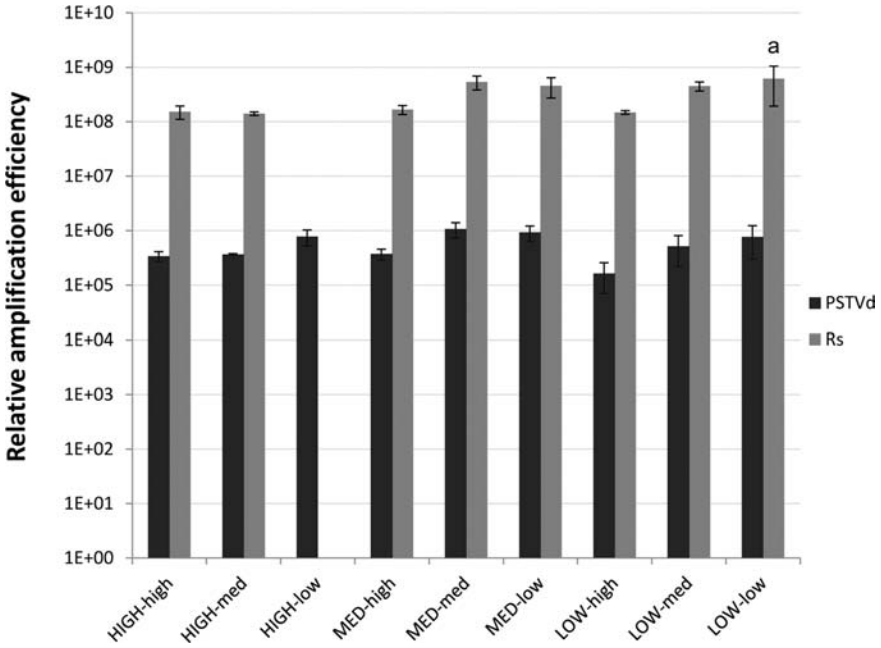

Figure 2. Efficiency of the duplex NAIMA amplification with asynchronous target concentrations. The amplification efficiency is expressed as the relative increase in copy number of the target, starting the reaction with value 1. Each bar represents the mean ± standard error of four replicates. PSTVd: HIGH, 2.5×10^4–2.5×10^6 copies; MED, 2.5×10^3–2.5×10^4 copies; LOW, 250–2500 copies. *R. solanacearum*: high, 10^8 cells/mL; med, 10^6 cells/mL; low, 10^4 cells/mL. (a) In 2 out of 4 replicates, there was no amplification.

0.005% Triton X-100 was added to the array, which was then incubated at 30 °C for 5 min without shaking. For conjugation, the blocking solution was removed and 100 μL of conjugation solution (1:100 dilution of antibiotin HRP-linked antibody (NEB, Ipswich, MA) in blocking solution) was added to the array, which was then incubated at 20 °C for 5 min without shaking. After the conjugation, the arrays were washed twice with 250 μL of PBS containing 0.1% Tween 20. For detection, the washing buffer was removed and 100 μL of SeramunGrün chip (Seramun Diagnostica, Heidesee, Germany) was added to the array. The array was scanned after 20 min incubation at room temperature, using an ATR 03 Reader (Alere Technologies, Jena, Germany). The image analysis was carried out using the IconoClust software (Alere Technologies, Jena, Germany) and the 10441_CSL_12_1.0_package analysis template. The signals were calculated within the software by the use of the proportion of the background and the mean spot intensity (241/256 × (1 − "Mean"/"Background")). The signal for each probe was considered positive if the mean of the replicates on the array diminished by a standard deviation was greater than the signal with one standard deviation of the other nonspecific probes on the array, with the confidence of the signal >0.95.

RESULTS AND DISCUSSION

In the course of the method development (Supporting Information Figure S2), the NAIMA amplification (template synthesis together with NASBA amplification, Figure 1) efficiency was always measured using qPCR as an independent assessment technique, where relative differences in the amounts of target before and after the NAIMA amplification were compared (Supporting Information Figure S1). The qPCR assay used for checking the *R. solanacearum* is routinely used in *R. solanacearum* diagnostics.[13] The sensitivity and specificity of the amplification were evaluated at different experimental stages and at two different procedure steps: after NAIMA amplification and after product hybridization on the microarray.

Primer design is of key importance, especially in multiplex reactions, due to the complexity of primer–pair combinations and issues with possible nonspecific background amplification.[16] Three different primer–pair combinations were initially designed for each pathogen target (data not shown), from which the best combination (Table 1) was chosen based on their amplification efficiencies. Likewise, different amplification protocols were initially tested for singleplex assays to obtain optimal amplification efficiency and sensitivity. Briefly, the changes included a combination of the following parameters: elimination of the denaturation step, supplying the reaction with additional reverse transcriptase enzyme, and performing both steps of the reaction in one tube. Amplification of *R. solanacearum* was not affected by changes in the protocols, whereas PSTVd amplification was shown to be more sensitive to these protocol modifications. Namely, no amplification was observed for PSTVd when the reverse transcriptase was absent from the reaction. Moreover, the absence of denaturation before NAIMA amplification decreased its efficiency. Thus, the selected protocol is the one that provides the optimal amplification efficiencies of both of these targets. The efficiencies of this duplex assay were assessed with the protocol that was optimal for both singleplex assays. For the custom-made ArrayTubes, three different probes were designed for each target (Table 1). For *R. solanacearum*, one targeted an *R. solanacearum*-specific region of the 16S rRNA gene (Rs-NAIMA-16S/3) and the two others targeted less specific sequences of the same gene, which shares a common pattern with bacteria closely related to *R. solanacearum*.

The sensitivity of the PSTVd RNA amplification in the singleplex NAIMA reactions was estimated to be from 250 to 2500 copies, four times higher than the conventional RT-PCR[12,17] and approximately 25 times lower than the reverse transcriptase (RT)-qPCR,[10] and for *R. solanacearum*, the sensitivity was 10^4 cells/mL, which is slightly lower than for the qPCR assay, where it was set between 10^2 and 10^4 cells/mL.[13] The same sensitivity for both targets was achieved when the multiplex reactions (containing both sets of primers) were

dx.doi.org/10.1021/jf5002149 | J. Agric. Food Chem. 2014, 62, 2989–2996

performed in the presence of each single target. This is the expected situation when testing actual samples, in which only one of the pathogens is usually present. Nevertheless, we also tested the sensitivities of the multiplex reactions in the presence of both targets in four parallel situations using asynchronous target concentrations, where the pathogens titers were not equal. In these cases, the multiplex amplification efficiency for *R. solanacearum* dropped significantly when the target concentration was close to or at the limit of detection of the respective NAIMA system, irrespective of the concentration of the PSTVd target in the sample (Figure 2). These results suggest that when the *R. solanacearum* target is at the limit of detection, the amplification is affected by the presence of the PSTVd target. Of note, the sensitivity of the *R. solanacearum* qPCR assay was lower than most of the other qPCR assays that are commonly used in our laboratory for routine plant health detection (data not shown). This lower qPCR sensitivity can therefore be correlated with the observed drop in the NAIMA amplification efficiency for the *R. solanacearum* system in the multiplex mode. Anyway, in the cases where the amplification was successful for *R. solanacearum* at this limit situation, it was as efficient as in the other reactions (Figure 2). However, we have shown that in the rare case where both of these targets are in the same plant sample, the NAIMA duplex would allow the detection of at least one of them and thus would trigger further analysis for quarantine-pest confirmation, with an alternative approach.

The specificities of both systems were tested on several PSTVd isolates and other related viroids (Supporting Information Table S1) as well as on several *R. solanacearum* strains and other nontarget and potentially cross-reactive strains (as listed in European Union Council Directive 2000/29/EC)[9] (Supporting Information Table S2). Moreover, we tested NAIMA on denatured bacterial suspensions without any DNA isolation and purification. The specificity of the singleplex and multiplex NAIMA assays was also compared to that of the singleplex qPCR.[13,17] The NAIMA assays showed suitable specificity for their respective targets, which matches the performance of the qPCR (Table 2).

For practical reasons, and as the microarrays were already shown to be suitable for detection of multiplex amplification products,[18−21] we have coupled the multiplex NAIMA amplification to product detection on microarrays. To do so, custom-made ArrayTubes were chosen, as this technology allows simple and relatively fast hybridization procedures. Moreover, the ArrayTubes can be scanned using a small and inexpensive benchtop machine, the ATR03 ArrayTube reader (Alere Technologies). To enable visualization of the hybridized products on the arrays, biotin was incorporated into the NAIMA amplification product. To do so, several ratios of different concentrations of biotinylated UTPs (bio-UTPs) versus nonbiotinylated UTPs were evaluated during the NAIMA reactions, with the focus on the amplification efficiency. None of the tested bio-UTP concentrations negatively affected the NAIMA amplification (data not shown), and therefore the highest tested concentration (1 mM, 20% of the total UTPs in the reaction) was used to maximize the final signal. All of the NAIMA products were checked with qPCR in parallel to the hybridization for confirmation of the array readings.

The sensitivity of the ArrayTubes detection platform was compared to that of the previously measured NAIMA amplification. For the PSTVd amplicon, similar sensitivity was

Table 2. Specificity of the NAIMA Amplification Step as Compared to qPCR[e]

Organism	Detection method	
	NAIMA	qPCR[a]
R. solanacearum[b] (Phylotypes 1, 2 and 3)	+	+
Blood disease bacterium[c] (*R. solanacearum* phylotype 4)	+	+
Ralstonia syzygii[c] (*R. solanacearum* phylotype 4)	+	+
Ralstonia mannitolilytica	+	+
Burkholderia andropogonis	-	-
Burkholderia caryophilli	-	-
Burkholderia cepacia	-	-
Burkholderia cepacia	-	-
Burkholderia glumae	-	-
Burkholderia plantarii	-	-
R.-solanacearum-negative samples[b]	-	-
Enterobacter sp.	-	-
Ochrobacterium anthropi	-	-
Paenibacillus polymyxa	-	-
Pseudomonas marginalis pv. Marginalis	-	-
Ralstonia pickettii	-	-
Potato spindle tuber viroid[b]	+	+
Tomato planta macho viroid	+	+
Tomato chlorotic dwarf viroid[b]	+	+
Chrysanthemum stunt viroid	-	-
Citrus exocortis viroid	-	-
Columnea latent viroid[b]	-	-
Eggplant latent viroid	-	-
Hop stunt viroid[b]	-	-
Peach latent mosaic viroid	-	-
Tomato apical stunt viroid[b]	-	+[d]

[a]qPCR results presented are for control samples that were not subjected to NAIMA amplification (see workflow in Supporting Information Figure S1). [b]Different isolates of the same species were tested and all showed the same result. [c]*R. syzigii* and blood-disease bacterium are part of the *R. solanacearum* species complex phylotype 4. [d]One out of two samples was positive. [e]+, target was successfully amplified and detected; −, target was not amplified and not detected.NAIMA targets are indicated with a clear background, nontarget organisms are indicated with the gray background. *R. solanacearum*-negative samples, samples of *Clavibacter michiganensis* DNA, used as the *R. solanacearum*-negative sample.

observed (250−2500 RNA copies), which is comparable to RT-PCR,[12,17] and about 25 times lower than for RT-qPCR[10] (Table 3). For the *R. solanacearum* amplicon, the sensitivity of the ArrayTubes detection (10^6 cells/mL) is about two log units lower than the NAIMA amplification sensitivity, which shows a loss of signal (Table 3) that probably occurs due to the lower numbers of incorporated biotinylated UTPs that is caused by the packed structure of the DNA chromosome. However, on the basis of the experience in our laboratory that shows that asymptomatic *R. solanacearum* infections of potato tubers show bacterial concentrations of 10^6 CFUs/mL (unpublished data), the displayed sensitivity is sufficient even for the testing of these samples.

The importance of the probe design is illustrated by the different probes used, which were mainly targeting specific regions of both of the amplicons. The probes present on the

Table 3. Sensitivity of the NAIMA Detection on the ArrayTubes in a Dilution Series[e]

Target concentration	qPCR[a]	Array readings for individual probe: PSTVd-NAIMA-1	PSTVd-NAIMA-2	PSTVd-NAIMA-3	Rs-NAIMA-16S/1	Rs-NAIMA-16S/2	Rs-NAIMA-16S/3[b]
PSTVd 1	+	+	+	+	+[c,d]	+[c]	-
PSTVd 2	+	+	+	+	-	-	-
PSTVd 3	+	+[c,d]	+[c,d]	+[c,d]	-	-	-
PSTVd 4	-	-	-	-	-	-	-
R. solanacearum 1	+	-	-	-	+	+	+[c]
R. solanacearum 2	+	-	-	-	+	+	-
R. solanacearum 3	+	-	-	-	-	-	-
R. solanacearum 4	-	-	-	-	-	-	-

[a]qPCR results are for the NAIMA amplified samples (see workflow in Supporting Information Figure S1). [b]*R. solanacearum* species-specific probe. [c]Weak signal just above the limit of the background-noise signal. [d]In one of the two replicates, the signal was negative. [e]+, positive signal for the target; −, negative signal for the target; PSTVd 1−4, decimal dilutions of PSTVd RNA from 2.5×10^3 to 2.5×10^4, to 2.5−25 copies per reaction; *R. solanacearum* 1−4, decimal dilutions of *R. solanacearum* DNA from 10^6 cells/mL to 10^3 cells/mL; the decreasing intensity of the gray background indicates the decreasing target concentration in the samples.

Table 4. Specificity of the NAIMA Detection on the ArrayTubes[d]

Target	qPCR[a]	Array readings for individual probe: PSTVd-NAIMA-1	PSTVd-NAIMA-2	PSTVd-NAIMA-3	Rs-NAIMA-16S/1	Rs-NAIMA-16S/2	Rs-NAIMA-16S/3[b]
NTC	-	-	-	-	-	-	-
PSTVd sample	+	+	+	+	-	-	-
TPMVd sample	+	-	-	-	+	+	-
TCDVd sample	+	-	-	-	+	+	-
CEVd sample	+	+[c]	+	+	-	-	-
PSTVd neg. pool	-	-	-	-		+	-
Ralstonia neg. pool	-	-	-	-	+	+	-
R.solanacearum isolate	+	-	-	-	+	+	+
R. mannitolilytica isolate	+	-	-	-	+	+	-
Bdb isolate	+	-	-	-	+	+	+
R. syzygii isolate	+	-	-	-	+	+	+
R. solanacearum and PSTVd isolates	+	+	+	+	+	+	+

[a]qPCR results are for NAIMA-amplified samples (see workflow in Supporting Information Figure S1). [b]*R. solanacearum* species-specific probe. [c]Weak signal just above the limit of the background-noise signal. [d]Target organisms are indicated with clear background, nontarget organisms are indicated with gray background. +, target was detected; −, target was not detected; NTC, replicates of negative control reactions with water instead of DNA or RNA; TPMVd, tomato planta macho viroid; TCDVd, tomato chlorotic dwarf viroid; CEVd, citrus exocortis viroid; PSTVd neg. pool, pool of different viroid RNA samples previously determined to be negative for PSTVd (tomato apical stunt viroid, chrysanthemum stunt viroid, citrus exocortis viroid, columnea latent viroid, hop stunt viroid, eggplant latent viroid); *Ralstonia* neg. pool, pool of *Ralstonia* and other species DNA samples previously determined to be negative for *R. solanacearum* (*Ralstonia pickettii*, *Burkholderia caryophilli*, *Burkholderia cepacia*, *Paenibacillus polymyxa*, *Pseudomonas marginalis* pv *Marginalis*, *Enterobacter* sp.); Bdb, blood-disease bacterium; duplex, two replicates of the duplex reaction with a target concentration of 10^8 cells/mL of *R. solanacearum* and 10^5 to 10^6 copies of PSVTd.

arrays spanned different regions than the probes used in the (RT-)qPCR assays. Often, the detection of the NAIMA products on the ArrayTubes appeared more specific than the (RT-)qPCR assays. For example, one of the probes (Rs-NAIMA-16S/3) that was designed to be specific for *R. solanacearum* was shown to provide more specific detection toward *R. solanacearum* than qPCR, as it did not detect the related *Ralstonia mannitolilytica* (Table 4). In comparison, the other two ArrayTubes probes designed to cover the wider range of the *Ralstonia* genus led to positive signals when hybridized with the NAIMA products from the reaction performed on other *Ralstonia* species or in *R. solanacearum*-negative samples. Intriguingly, some of the NAIMA reactions performed on a PSTVd RNA sample also gave positive signals when hybridized on these two ArrayTubes *Ralstonia*-specific probes. Further bioinformatic analysis of the bacterial

sequences revealed that these signals were most probably due to the presence of the ubiquitous *Ralstonia pickettii*[22] in the samples, as they came from a natural environment. For the PSTVd target, all of the ArrayTubes probes provided detection that was at least as specific as that for the RT-qPCR assay. NAIMA appeared to be even slightly more specific, as it did not detect the nontarget TPMVd and TCDVd. However, it could be argued that this difference in specificity between qPCR and NAIMA is linked to the higher sensitivity of the former rather than the better performance of the latter. Nevertheless, the general finding is that the NAIMA primers allow the amplification of a wider, less specific range of targets than the qPCR assays (because of the high specificity of the TaqMan probe), with the overall specificity of the NAIMA assay determined by the ArrayTubes probe. In addition to the above-discussed specificity, the selectivity of the multiplex assay was satisfying, as when one of the targets or both the *R. solanacearum* and PSTVd targets were present in the samples and were amplified, a signal was detected for all of the relevant ArrayTubes probes (Figure 3, Table 4).

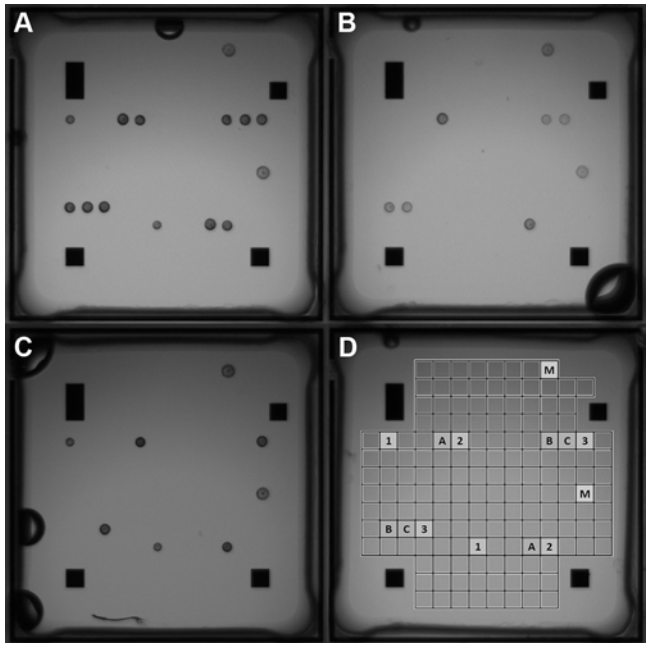

Figure 3. Samples of the scanned arrays after the hybridization of the NAIMA-amplified products. Duplex amplification was performed in the presence of both targets (A), with only the PSTVd target (B), and with only *R. solanacearum* (C). The legend for the probes is shown in (D): 1, Rs-NAIMA-16S/3; 2, Rs-NAIMA-16S/1; 3, Rs-NAIMA-16S/2; A, PSTVd-NAIMA-1; B, PSTVd-NAIMA-2; C, PSTVd-NAIMA-3.

In conclusion, the herein-proposed NAIMA method allows simultaneous, multiplex amplification and detection of RNA and DNA targets in the same reaction with satisfying performance for plant pathogen screening in terms of sensitivity and specificity. To our knowledge, this is the first report of an assay that allows both RNA and DNA target detection in a single experimental setup without PCR cycling. The time needed for the complete analysis is comparable to that of real-time PCR, although there was no particular focus on the shortening of the NAIMA procedure. As proof of concept, we tested a duplex reaction; however, the method itself has higher multiplexing capabilities, as has already been demonstrated.[4,6] As the method is isothermal, it can also be applied for on-site diagnostics after further optimization, especially as it is robust enough to detect the bacterial DNA directly from denatured bacterial suspension. Moreover, the limited size of the microarray reader and the ArrayTubes hybridization phase should allow the use of the NAIMA procedure out of the laboratory. The method as described here is a general approach for sensitive and specific multiplex RNA and DNA target identification, and it can be applied to domains of research and molecular testing where multiplex amplification and detection of DNA, RNA or both of these target types are required.

■ ASSOCIATED CONTENT

Ⓢ Supporting Information

List of PSTVd isolates used in the NAIMA amplification. List of bacterial strains tested in this study. Schematic representation of the NAIMA workflow. Schematic representation of developmental procedure. This material is available free of charge via the Internet at http://pubs.acs.org.

■ AUTHOR INFORMATION

Corresponding Author

*Phone: +386-5-9232819. Fax: +386-1-2573847. E-mail: david.dobnik@nib.si.

Present Address

‡D.M. CropDesign NV, Technologiepark 21C, 9052 Gent (Zwijnaarde), Belgium.

Author Contributions

§D.D. and D.M contributed equally to this study.

Funding

This work was financially supported by the Slovenian Research Agency (contract no. L4-3642) and the EU Framework 7 Programme (FP7-KBBE-2009-3) project 245047 (Q-DETECT: Developing Quarantine Pest Detection Methods for Use by National Plant Protection Organizations (NPPO) and Inspection Services).

Notes

The authors declare no competing financial interest.

■ ACKNOWLEDGMENTS

We thank Neil Boonham, Tom Nixon, Samantha Bennett, and Adrian Fox from the Food and Environment Research Agency (FERA) in York, UK, Jacobus T. J. Verhoeven from the National Plant Protection Organization of The Netherlands for providing us with a valuable collection of viroid-infected material, and Philippe Prior from INRA/CIRAD, France, for providing the *R. solanacearum* strains. We thank Jenny Tomlinson and Neil Boonham from FERA for providing tailored ArrayTubes and the hybridization protocol. We thank Tanja Dreo, Manca Pirc and Nataša Mehle for preparing the bacterial samples and viroid isolates used in this study. We also thank Kristina Gruden for helpful suggestions related to the experimental work.

■ ABBREVIATIONS USED

CFU, colony forming units; NAIMA, nucleic acid sequence based amplification [NASBA]-implemented microarray analysis; NASBA, nucleic acid sequence based amplification; PBS, phosphate buffered saline; PSTVd, potato spindle tuber viroid; qPCR, quantitative real-time PCR; RT-qPCR, reverse tran-

scription quantitative real-time PCR; TCDVd, tomato chlorotic dwarf viroid; TPMVd, tomato planta macho viroid

REFERENCES

(1) Defoort, J. P.; Martin, M.; Casano, B.; Prato, S.; Camilla, C.; Fert, V. Simultaneous detection of multiplex-amplified human immunodeficiency virus type 1 RNA, hepatitis C virus RNA, and hepatitis B virus DNA using a flow cytometer microsphere-based hybridization assay. *J. Clin. Microbiol.* **2000**, *38*, 1066−1071.

(2) Mercier, B.; Burlot, L.; Ferec, C. Simultaneous screening for HBV DNA and HCV RNA genomes in blood donations using a novel TaqMan PCR assay. *J. Virol. Methods* **1999**, *77*, 1−9.

(3) Xu, X. G.; Chen, G. D.; Huang, Y.; Ding, L.; Li, Z. C.; Chang, C. D.; Wang, C. Y.; Tong, D. W.; Liu, H. J. Development of multiplex PCR for simultaneous detection of six swine DNA and RNA viruses. *J. Virol. Methods* **2012**, *183*, 69−74.

(4) Morisset, D.; Dobnik, D.; Hamels, S.; Zel, J.; Gruden, K. NAIMA: target amplification strategy allowing quantitative on-chip detection of GMOs. *Nucleic Acids Res.* **2008**, *36*, e118.

(5) Compton, J. Nucleic acid sequence-based amplification. *Nature* **1991**, *350*, 91−92.

(6) Dobnik, D.; Morisset, D.; Gruden, K. NAIMA as a solution for future GMO diagnostics challenges. *Anal. Bioanal. Chem.* **2010**, *396*, 2229−2233.

(7) Hayward, A. C. Biology and Epidemiology of Bacterial Wilt Caused by *Pseudomonas solanacearum*. *Annu. Rev. Phytopathol.* **1991**, *29*, 65−87.

(8) Owens, R. A. Potato spindle tuber viroid: the simplicity paradox resolved? *Mol. Plant Pathol.* **2007**, *8*, 549−560.

(9) Council Directive 2000/29/EC of 8 May 2000 on Protective Measures against the Introduction into the Community of Organisms Harmful to Plants or Plant Products and against Their Spread within the Community. *Official J. Eur. Communities*; **2000**, *169*, 1−159.

(10) Boonham, N.; Perez, L. G.; Mendez, M. S.; Peralta, E. L.; Blockley, A.; Walsh, K.; Barker, I.; Mumford, R. A. Development of a real-time RT-PCR assay for the detection of potato spindle tuber viroid. *J. Virol. Methods* **2004**, *116*, 139−146.

(11) Markham, N. R.; Zuker, M. DINAMelt web server for nucleic acid melting prediction. *Nucleic Acids Res.* **2005**, *33*, W577−W581.

(12) Lenarčič, R.; Morisset, D.; Mehle, N.; Ravnikar, M. Fast real-time detection of potato spindle tuber viroid by RT-LAMP. *Plant Pathol.* **2012**, *62*, 1147−1156.

(13) Weller, S. A.; Elphinstone, J. G.; Smith, N. C.; Boonham, N.; Stead, D. E. Detection of *Ralstonia solanacearum* Strains with a Quantitative, Multiplex, Real-Time, Fluorogenic PCR (TaqMan) Assay. *Appl. Environ. Microbiol.* **2000**, *66*, 2853−2858.

(14) Bentsink, L.; Leone, G.; Van Beckhoven, J.; Van Schijndel, H.; Van Gemen, B.; Van Der Wolf, J. Amplification of RNA by NASBA allows direct detection of viable cells of *Ralstonia solanacearum* in potato. *J. Appl. Microbiol.* **2002**, *93*, 647−655.

(15) Cankar, K.; Štebih, D.; Dreo, T.; Žel, J.; Gruden, K. Critical points of DNA quantification by real-time PCR—effects of DNA extraction method and sample matrix on quantification of genetically modified organisms. *BMC Biotechnol.* **2006**, *6*, 37.

(16) Markoulatos, P.; Siafakas, N.; Moncany, M. Multiplex polymerase chain reaction: a practical approach. *J. Clin. Lab. Anal.* **2002**, *16*, 47−51.

(17) Verhoeven, J. T. J.; Jansen, C. C. C.; Willemen, T. M.; Kox, L. F. F.; Owens, R. A.; Roenhorst, J. W. Natural infections of tomato by *Citrus exocortis* viroid, *Columnea* latent viroid, potato spindle tuber viroid and tomato chlorotic dwarf viroid. *Eur. J. Plant Pathol.* **2004**, *110*, 823−831.

(18) Xu, J.; Zhu, S.; Miao, H.; Huang, W.; Qiu, M.; Huang, Y.; Fu, X.; Li, Y. Event-Specific Detection of Seven Genetically Modified Soybean and Maizes Using Multiplex-PCR Coupled with Oligonucleotide Microarray. *J. Agric. Food Chem.* **2007**, *55*, 5575−5579.

(19) Schmidt, A. M.; Sahota, R.; Pope, D. S.; Lawrence, T. S.; Belton, M. P.; Rott, M. E. Detection of Genetically Modified Canola Using Multiplex PCR Coupled with Oligonucleotide Microarray Hybridization. *J. Agric. Food Chem.* **2008**, *56*, 6791−6800.

(20) Kim, J. H.; Kim, S. Y.; Lee, H.; Kim, Y. R.; Kim, H. Y. An Event-Specific DNA Microarray To Identify Genetically Modified Organisms in Processed Foods. *J. Agric. Food Chem.* **2010**, *58*, 6018−6026.

(21) Tortajada-Genaro, L. A.; Santiago-Felipe, S.; Morais, S.; Gabaldón, J. A.; Puchades, R.; Maquieira, Á. Multiplex DNA Detection of Food Allergens on a Digital Versatile Disk. *J. Agric. Food Chem.* **2011**, *60*, 36−43.

(22) Gilligan, P. H.; Lum, G.; Vandamme, P.; Whittier, S. Burkholderia, Stenotrophomonas, Ralstonia, Brevundimonas, Comamonas, Delftia, Pandoraea, and Acidovorax. In *Manual of Clinical Microbiology*; Murray, P. R., Baron, E. J., Jorgenson, J. H., Pfaller, M. A., Yolken, R. H., Eds.; ASM Press: Washington, DC, 2003; pp 729−748.

technology or are due to natural variation resulting from genetic and environmental effects, interaction of genotypes with environments, or even stochastic differences between plants. For this purpose it is necessary to evaluate the reproducibility of these analytical methods and natural variation of the results of applying these methods to crop species, such as maize. Without this understanding it would be impossible to interpret the -omics data and declare equivalence. Therefore, the International Life Sciences Institute (ILSI) recommended establishing baseline ranges for natural variations and validating these -omics technologies before they can be used for regulatory assessment of biotech crops.[15] This paper is directed toward fulfilling this function for transcriptomic and metabolomic methods.

Microarray analysis of transcriptomes is available for both model and crop plants, including *Arabidopsis*, maize, rice, potato, tomato, soy, pepper, barley, *Brassica*, and sugar cane.[21] Microarrays provide high-throughput, simultaneous detection of differences in mRNA abundance between samples for thousands of genes. Use of microarray technology for safety assessment of GM crops faces some challenges. First, nucleic acid probe hybridization is not able to detect genes expressed at very low level or genes with alternate splicing forms. Second, it is difficult to achieve high reproducibility for microarray experiments due to variations resulting from sample handling, experiment processes, environmental impact on plants, and crop variety differences.[22−24]

Technologies for simultaneous analysis of metabolites have been developed[25,26] and offer the possibility of surveying significantly more metabolites than conventional chemical analyses in a much shorter time and with much lower cost per analyte. However, comparing data from different laboratories remains challenging. This challenge is usually due to relative rather than absolute quantification and different methodologies adopted by different groups, including equipment platforms and statistical analysis methods. High sample-to-sample and experiment-to-experiment variability, even within the same laboratory, and the wide concentration range of the same metabolite between plants add to the complexity of the analysis.[10] We applied microarray and metabolomic technologies to a randomized field study as conventionally used in regulatory studies. To evaluate the reproducibility and technical variations of the microarray and metabolomic technologies, the samples were tested individually or as pools of plants and RNA and metabolites were extracted and analyzed by microarray and GC-MS. Overall, we evaluated the reproducibility of the microarray and metabolomic technologies to explore the capability of these methodologies in our experimental settings to detect the natural variation of gene expression and metabolite levels between plants and maize varieties.

MATERIALS AND METHODS

Plant Tissue. Seven inbred and four non-GM commercial hybrid maize varieties were planted in a randomized plot at DuPont Stine Haskell Research Center, Newark, DE, USA. Twenty-five seeds were sowed per row for each variety. Leaves at the V5 growth stage and immature kernels at 25 days after pollination (DAP) were collected in the morning between 8:30 a.m. and 12 p.m. for microarray and GC-MS-based metabolomics.

Three leaf punches avoiding midribs were collected at the middle of the V5 leaf area and placed on dry ice immediately after harvest, transported to the laboratory on dry ice, and stored at −80 °C before processing for metabolomic analysis. The remaining leaf was collected and frozen in liquid nitrogen immediately after harvest, transported to the laboratory on dry ice, and stored at −80 °C before processing for microarray analysis.

For 25 DAP kernels, 10 kernels in the middle row of the ear were collected for metabolomics, and the remaining kernels were used for microarray analysis. The ears at 25 DAP were removed from the plants and placed on wet ice immediately after harvest and transported to the laboratory on wet ice. Immature kernels were removed from the cobs, frozen in the liquid nitrogen, and stored at −80 °C before processing for microarray and metabolomics analyses.

Mature kernels at R6 growth stage (about 60 DAP) were also collected for metabolomics analysis. The ears at R6 stage were removed from the plants and placed on wet ice immediately after harvest and transported to the laboratory on wet ice. Ten mature kernels in the middle row of the ear were removed from the cob, frozen in the liquid nitrogen, and stored at −80 °C before processing for metabolomics analyses.

For microarray analysis, tissues were ground into fine powders. For metabolomics analysis, tissues were lyophilized before they were ground to fine powders. Additional pooled samples were obtained by combining equivalent amounts of ground material from three individual plants.

Microarray. Total RNA was isolated from ground frozen tissue using the EZNA SQ RNA Isolation Kit (Omega Bio-Tek, Norcross, GA, USA), treated with DNase-I, and used for mRNA isolation with an Illustra mRNA Purification Kit (GE Biosciences, Pittsburgh, PA, USA). The total RNA and mRNA samples were visualized and quantified on a Bioanalyzer 2100 (Agilent Technologies, Santa Clara, CA, USA). Each mRNA sample was converted into double-stranded DNA by an in vitro transcription reaction and labeled with Cy3 fluorescent dye using the Low RNA Input Fluorescent Linear Amplification Kit (Agilent Technologies). The cRNA product was purified with an Agencourt RNAClean Kit (Beckman Coulter, Indianapolis, IN, USA). Hybridizations were performed overnight with equal amounts of labeled cRNA to a custom 4x44K Maize Oligo Microarray from Agilent Technologies according to Agilent's One-Color Microarray-Based Gene Expression Analysis protocol. After hybridization, the microarray slides were washed and immediately scanned with the a G2505C DNA microarray scanner (Agilent Technologies). The images were visually inspected for artifacts, and feature intensities were extracted, filtered, and normalized with Feature Extraction software (v 10.5.1.1) (Agilent Technologies). Quality control and downstream analysis were performed using data analysis tools in Genedata Expressionist and the statistical language R. Further data analysis and bioinformatic analyses were carried out according to methods described in Hayes et al.[27]

Metabolomics. Metabolites were extracted from approximately 3 mg (dry weight) of lyophilized tissues for each sample. In a 1.1 mL polypropylene microtube containing two $^{5}/_{32}$ in. stainless steel ball bearings, each sample was added with 500 μL of chloroform/methanol/water (2:5:2, v/v/v) solution containing a 0.015 mg ribitol internal standard. Samples were homogenized in a 2000 Geno/Grinder ball mill at setting 1650 for 1 min and then rotated at 4 °C for 30 min before being centrifuged at 1454*g* for 15 min at 4 °C. Aliquots (300 μL) were transferred to 1.8 mL high recovery glass autosampler vials, evaporated to dryness in a speed vac, and redissolved in 50 μL of 20 mg mL^{-1} methoxyamine hydrochloride in pyridine. The vials were capped, agitated with a vortex mixer, and incubated in an orbital shaker at 30 °C for 90 min to form methoxyamine derivatives. Next, 80 μL of *N*-methyl-*N*-(trimethylsilyl)trifluoroacetamide (MSTFA) was added to each sample to form trimethylsilyl (TMS) derivatives by a Gerstel autosampler 30 min prior to injection to minimize sample variations due to derivatization differences. This "just in time" derivatization eliminates variation due to differences in reaction time or temperature. Furthermore, the gas chromatograph inlet liner and septum were replaced daily, mitigating the known influence of sample residue in the inlet on trimethylsilylation completeness.[28] However, trimethylsilylation can vary with the sample matrix.[28] Thus, for molecules such as amino acids that present multiple reaction sites leading to the possibility of two or more chemical derivatives, the relative abundance

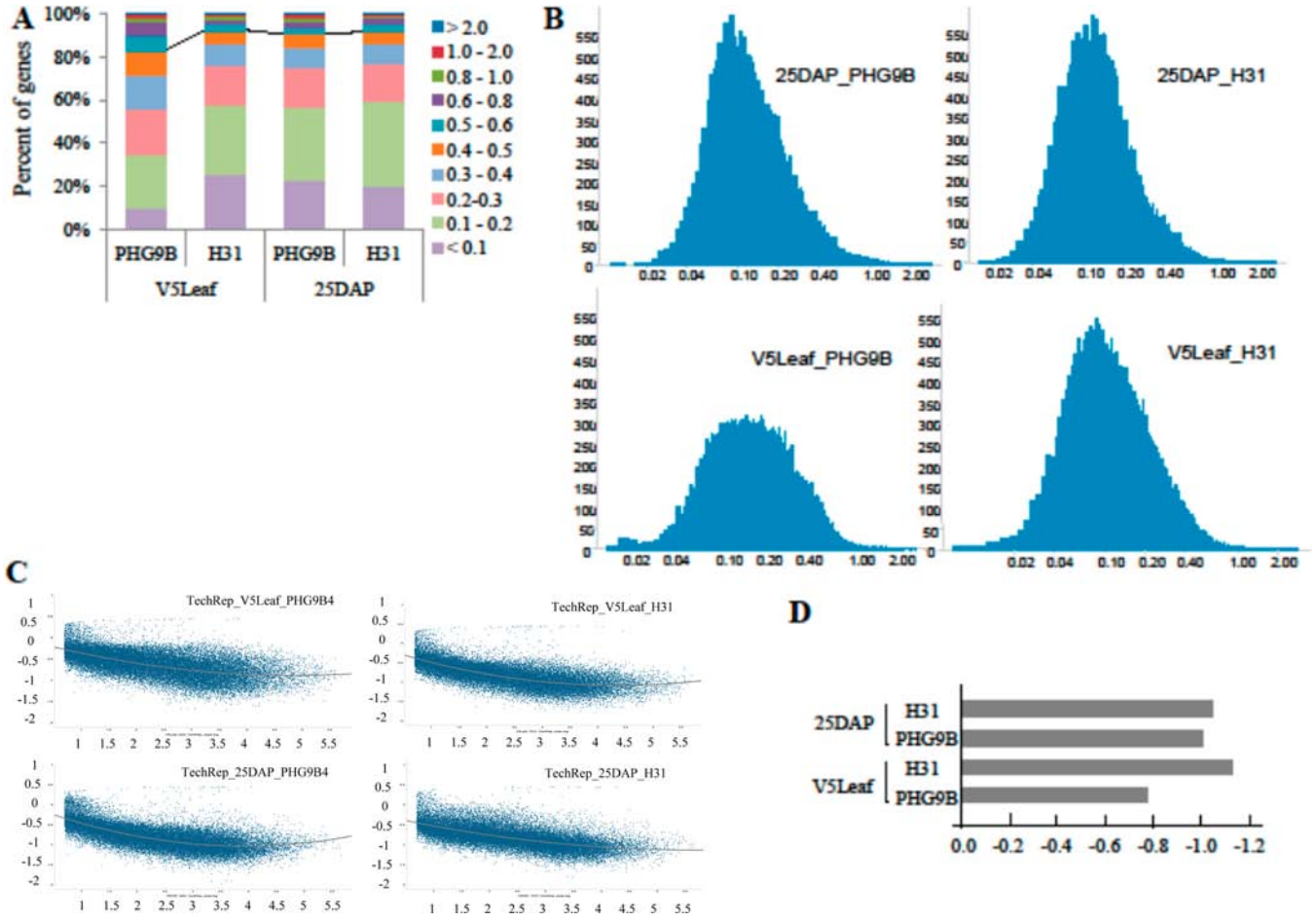

Figure 1. CVs of gene expression calculated from technical repeat microarrays: (A) percentages of genes within different CV ranges; (B) CV distributions generated by TIBCO Spotfire (*x*-axis, CV values in log scale; *y*-axis, gene counts); (C) plots of log10 (CV)s (*y*-axis) and against log10 (mean)s (*x*-axis) (curves are polynomial fittings generated by TIBCO Spotfire); (D) log10 (CV) values of inflection points calculated from curves in panel C.

of these trimethylsilylated forms can vary among the three different tissue types assayed in this study.

The derivatized samples were separated by gas chromatography on a Restek 30 m × 0.25 mm × 0.25 μm film thickness Rtx-5Sil MS column with a 10 m Integra-Guard column. One microliter injections were made with a 1:30 split ratio using a Gerstel autosampler. An Agilent 6890N gas chromatograph was programmed for an initial temperature of 80 °C for 0.5 min and increased to 350 °C at a rate of 18 °C min^{-1}, at which it was held for 2 min before being cooled rapidly to 80 °C and held there for 5 min in preparation for the next run. The injector and transfer line temperatures were 230 and 250 °C, respectively, and the source temperature was 200 °C. Helium was used as the carrier gas with a constant flow rate of 1 mL min^{-1} maintained by electronic pressure control. Data acquisition was performed on a LECO Pegasus III time-of-flight mass spectrometer with an acquisition rate of 10 spectra s^{-1} in the mass range of m/z 45−600. An electron beam of 70 eV was used to generate spectra. Detector voltage was 1750 V. An instrument autotune for mass calibration using perfluorotributylamine (PFTBA) was performed prior to each sample sequence.

Metabolomics Data Processing and Analysis. Raw Leco GC-MS .peg datafiles were converted into .netcdf (Andi) formats using Leco ChromaTof ver. 4.13 software. Data preprocessing was performed with Genedata Refiner MS ver. 5.2.1 software. For each .netcdf file, retention times were converted into retention indices using an in-house program. Preprocessing consisted of gridding chromatograms in the m/z value (80−437) and retention index dimensions, subtracting chemical noise, aligning the retention indices of each selected ion chromatogram, and detecting nominal mass peaks, using empirically optimized settings for each process. Data from each of the three tissue types were processed separately to maximize alignment and peak peaking. The resulting three matrices consisted of intensities for each m/z value−retention index combination and each sample. The aligned and denoised data matrices were passed to Genedata Analyst ver. 2.1 software, where each intensity value by sample was normalized for both the ribitol internal standard signal and sample dry weight.

Because m/z value−retention index fingerprint data are redundant, significant signatures were reduced to named known metabolites on the basis of matching both the retention index and mass spectrum to those of authentic standards. Relative quantitation of each metabolite in each sample was derived from the intensity of each metabolite's representative m/z value obtained from the Genedata Analyst output. In a few cases, peak heights obtained from ChromaTof quantification ion chromatograms were used instead when signals were below the threshold set for fingerprinting and thus not present in the Genedata Analyst output. Metabolite detection from either source was dependent on reaching a conservative limit of detection to mitigate false-positive peaks that would have an undue effect on subsequent statistical analyses. Percent CV values were calculated for each metabolite across selected samples. Data matrices were reformatted and imported into the PLS_Toolbox version 7.0.1 (Eigenvector Research, Inc.), with which principal component analysis (PCA) was performed on autoscaled (mean centered and each variable scaled to unit variance) data.

Experimental Design. For both microarray and metabolomics experiments, 11 maize varieties were used, including (1) 7 inbred lines, PHG9B (high oil), H31 (low oil), PH2WBS (high protein), PH2WBR (low protein), PH0GP (median starch), PH14T (median starch), and 658 (low starch); and (2) 4 commodity hybrid lines, 38B85, 37Y12, 34A15, and 34P88. These lines were chosen as a partial representation of the range of U.S. cultivated maize diversity and include lines differing in protein, oil, and starch contents. Three types of tissues, V5 leaf, 25 DAP immature kernel, and mature kernel, were used for metabolomic experiments. Because the mature kernels are dormant and have very limited gene expression,[29,30] only the V5 leaf and the 25 DAP immature kernels were used for microarray experiments. Due to limited tissue availability for some varieties, some microarray or metabolomic experiments were not conducted.

For microarray technical repeat controls, eight independent RNA samples were isolated from either V5 leaves or 25 DAP immature kernels of a single plant from the high-oil variety PHG9B and the low-oil line H31 and used for eight different microarray hybridizations. The signal differences among these hybridizations were considered the technical variation of the microarray methodology. Similarly, eight independent metabolite extractions were made from bulk collections of V5 leaves or 25 DAP immature kernels of PHG9B and H31 and from bulk mature kernels of PH2WBS (high-protein line) and PHG9B. They were used for independent GC-MS analyses and technical variation assessment. Multiple sample preparation and testing steps were used to evaluate the reproducibility of both technical methods. Sample variations were also evaluated by comparing data from different individual plants and different pooled plants.

qRT-PCR. Genes, primers, and probes are listed in Supplementary Table 1 in the Supporting Information. Primers and probes were designed with Primer Express 3.0.1 (Applied Biosystems, Carlsbad, CA, USA) and purchased from Integrated DNA Technologies, Inc. (Coralville, IA, USA). First-strand cDNA was synthesized from the same mRNA samples used for microarray. Fifteen pooled samples from either V5 leaf or 25 DAP kernel were chosen on the basis of sample availability. For each RT reaction, 240 ng of mRNA was used as a template in a total volume of 80 μL following the manufacturer's instruction for the SuperScript VILO cDNA synthesis kit (Invitrogen, Carlsbad, CA, USA). All qRT-PCR primers and Taqman probes were designed using the Primer Express program (Applied Biosystems) and tested for specificity by Blast search against the NCBI public sequence database. The qPCR reactions were carried out in 384-well plates in a ViiA 7 real-time-PCR machine (Applied Biosystems) using the TaqMan Gene Expression Master Mix (Applied Biosystems). The qPCR program was 50 °C for 2 min, 95 °C for 10 min, followed with 40 cycles of 95 °C for 15 s and 60 °C for 1 min. Each reaction contains 200 nM of each primer, 100 nM of probe, and 2 μL of the RT reaction solution as template in a final volume of 20 μL. Every reaction was repeated three times. The ViiA 7 software V1.2 was used to record and process the data. The Rn (normalized reporter) values of each reaction for every cycle were exported and used to calculate the single-well qPCR efficiencies using a real-time PCR Miner program.[31]

RESULTS

Microarray Reproducibility. To compare the reproducibility of expression levels of the same genes on repeated microarrays, the data were analyzed using correlation statistics. The coefficient of variation (CV) for each set of repeats was calculated and compared as an indication of reproducibility.[32] Mean CV values of gene transcripts for technical repeats were 0.25, 0.23, 0.33, and 0.23 for 25 DAP PHG9B, 25 DAP H31, V5 leaf PHG9B, and V5 leaf H31 samples, respectively, relatively low compared to the microarray literature,[33−35] indicating good technical reproducibility. Expression of most of genes on the microarrays had low CV values, with 82.4, 92.1, 90.4, and 91.6% of genes from V5 leaf PHG9B, V5 leaf H31, 25 DAP PHG9B, and 25 DAP H31 microarrays exhibiting CV values below 0.5 (Figure 1A). In addition, these CV values showed log-normal distribution centered at 0.1 (Figure 1B), indicating good reproducibility. However, the reproducibility of eight technical repeat microarrays for PHG9B V5 leaves was little higher than other technical repeat microarrays (Figure 1A). Alternatively, the CV values were log transformed and plotted against the log transformed mean values. Polynomial curve fitting showed as expected that CV values decreased as the mean intensities increased (Figure 1C). The inflection points calculated on the basis of the polynomial curves showed that technical repeat microarrays for PHG9B V5 leaves have higher background noise (Figure 1D), similar to that shown by the CV distributions (Figure 1A).

We further investigated the reproducibility of microarray results by a linear regression model correlating data between any pair of microarrays within each group. Four groups were analyzed this way for both V5 leaf and 25 DAP kernel samples, including the eight technical arrays for H31, the six individual biological repeats for H31, the eight technical arrays for PHG9B, and the nine individual biological repeats for PHG9B. The box plots represent the distributions of *R* square values of all pairwise comparisons of linear regression modeling (Figure 2). The technical replicates had consistently higher correlations

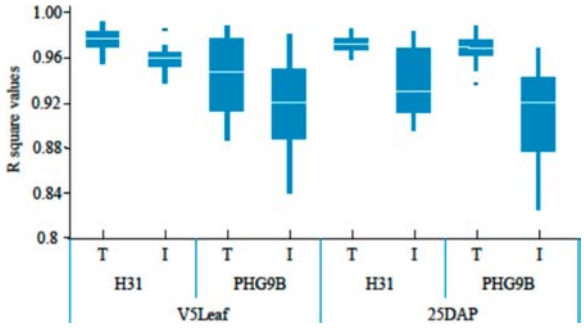

Figure 2. Technical reproducibility of microarrays. Pairwise correlation coefficients between pairs of technical replicates (T) or between pairs of biological repeats (I). Box plots were generated with TIBCO Spotfire. The white bar represents the median value. Edges of boxes represent values at 75 and 25% percentiles. Edges of bars represent the ranges of values with outside dots as outliers.

than the biological replicates (Figure 2). We conclude that gene expression variation from microarrays resulted primarily from maize variety differences rather than from plant-to-plant differences, pooled sample-to-sample differences, or technical variations, indicating that the method is sensitive enough to detect biological variation among individual or pooled plant samples.

Correlation between Gene Expression of Individual and Pooled Samples. Next, CV values for the microarrays from the six varieties analyzed both as individual samples (I) and as pooled samples (P) were calculated. For each variety, six or nine individual plants and two or three pools of samples (three plants per pool) were analyzed. The pools were created by combining equal amounts of RNA extracts from individual plants. Overall, 73.7% (34A15_I)−93.3% (38B85_P) of the genes had CV values below 0.5 from V5 leaf samples, and 73.8% (38B85_I) − 96.8% (PHG9B_P) of genes had CV values below 0.5 from 25 DAP kernel samples (Supporting Information Supplementary Table 2), representing very good experimental reproducibility. The distributions of the CV values from both 25 DAP kernel and V5 leaf samples are shown in Supplementary Figure 1 in the Supporting Information. When

dx.doi.org/10.1021/jf405652j | J. Agric. Food Chem. 2014, 62, 2997−3009

Table 1. (Rows 1 and 2) Mean Gene Expression Levels Detected in Individual Plants (I) and Pooled Plants (P) for the Same Tissue Type of a Variety Are Highly Correlated;[a] (Rows 3 and 4) Mean Gene Expression Detected Microarrays Are Not Correlated between V5 Leaf and 25 DAP[b]

row	sample	34A15	38B85	PH2WBR	PH2WBS	PHG9B	H31
1	V5 leaf	0.9932	0.9885	0.9959	0.9893	0.9937	0.9846
2	25 DAP	0.9938	0.9743	0.989	0.9836	0.9889	0.9899
3	I	0.238	0.2527	0.317	0.2757	0.283	0.2472
4	P	0.234	0.2551	0.3092	0.2595	0.2849	0.239

[a]Values are Pearson correlation coefficients (R) comparing mean gene expression intensities between all I and all P samples for each variety−tissue combination, calculated using Excel function PEARSON. [b]Values are Pearson correlation coefficients (R) comparing gene expression intensities from V5 leaf and 25 DAP for the same plant samples, calculated using Excel function PEARSON, for individual plants (I) or pooled plants (P).

the overall CV distribution patterns of individual or pooled samples were compared, microarrays for 25 DAP kernel samples showed larger CV differences, compared to V5 leaf samples. Additionally, log10 (CV) versus log10 (mean) plots were generated for all of the microarrays to reveal the relationship between CV and mean intensities (data not shown). The inflection point values were very similar to what was shown by the CV distribution patterns (Supporting Information Supplementary Figure 1).

The Pearson's correlation coefficient was calculated by comparing mean gene expressions between individual samples and pooled samples for each variety and tissue type. The R values were between 0.9743 and 0.9959 (Table 1), indicating that the signals obtained from individual plants and pooled plants were highly correlated and similar. When samples from the same variety but different tissue types were compared, the Pearson correlation R values were between 0.234 and 0.317 (Table 1), indicating significant gene expression differences between leaves and kernels, as expected. For every variety−tissue combination, the pooled samples showed a smaller mean CV value than the one from corresponding individual samples (Supporting Information Supplementary Table 3). Therefore, the plant-to-plant variation detected from the same variety was reduced by pooling three plants into a single sample, essentially transforming plant-to-plant variation into sample-to-sample variation. In addition, the distribution patterns of CV values from I and P samples were very similar (Supporting Information Supplementary Figure 2), indicating that our pooling strategy was efficient in capturing the variations existing among maize varieties while realizing a cost savings.

Gene Expression Differences between Varieties. To evaluate gene expression variation between maize varieties, mean microarray spot intensities from six or nine individual samples (I) and two or three pooled samples, with three individuals per each pool (P), were determined and used for CV calculations comparing the six varieties that had both I and P samples.

When the CV distributions of individual samples representing variety-to-variety variations (Supporting Information Supplementary Figure 2 and Table 4) were compared to the CV distributions representing plant-to-plant variation within a certain variety (Supporting Information Supplementary Figure 3 and Table 2), we found that the former were larger. For V5 leaves, 65.4% of genes showed a CV value <0.5 when different maize varieties were compared (Supporting Information Supplementary Figure 2 and Table 4), but 73.7% (34A15)−93.1% (38B85) of genes had a CV <0.5 when individual plants within a given variety were compared (Supporting Information Supplementary Figure 1 and Table 2). For 25 DAP kernels, 68% of genes showed a CV value <0.5 when different maize varieties were compared (Supporting Information Supplementary Figure 2 and Table 4), but 73.8% (38B85)−85.1% (H31) of genes had a CV <0.5 when individual plants within a given variety were compared (Supporting Information Supplementary Figure 1 and Table 2). These results indicate that higher variations exist among different maize varieties compared to those among individual plants of the same variety, likely due to the genetic differences and/or genetic and environmental interactions affecting gene expression among varieties.

In addition, the variety-to-variety variation detected in 25 DAP kernels is similar to that among V5 leaf tissues on the basis of their CV distributions (Supporting Information Supplementary Figure 2), indicating that gene expression variations among different maize varieties are similar between these two tissue types.

Confirmation of Microarray Results by qRT-PCR. To confirm the gene expression levels measured by the microarray experiments, two groups of 18 different genes were chosen for V5 leaf and 25 DAP kernel, respectively (Supporting Information Supplementary Table 1). The expression levels of these genes are ranked across all microarrays at 80 or 50% percentiles. Expression of these genes was measured by qRT-PCR reactions using the same RNA samples used for microarrays. Due to limited sample availability and possible polymorphisms among different maize varieties at primer annealing locations, we used a real-time PCR Miner program[31] that has been validated by many other groups[36−43] to monitor the single-well qRT-PCR efficiency. The *dapA* gene was used as a control for comparison between microarray and qRT-PCR data. Gene expression levels from qRT-PCR reactions were calculated on the basis of the *dapA* expression and compared to levels detected on microarrays that were also quantified on the basis of the *dapA* expression. The ratio of expression levels for each gene detected by these two techniques was log transformed for proper comparison (Figure 3).

For V5 leaf tissue samples, two genes (pco602011 and pco603626) were not amplified from any of the 15 templates by qRT-PCR and therefore not included in the analysis. Two genes, pco627753 and pco643043 (genes 2 and 11 in Figure 3A, respectively), had expression detected only in some of the samples, and four genes, pco624384, pco521467, pco652567, and pco658406 (genes 13, 14, 15, and 16 in Figure 3A, respectively), showed higher expression (ca. 2−32-fold higher), relative to microarray, in all 15 samples. For the remaining genes tested, the expression levels were close to those measured by the microarrays, although there were some variety-specific expression differences between the two techniques (Figure 3A). For 25 DAP kernel samples, one gene (pco621453) did not

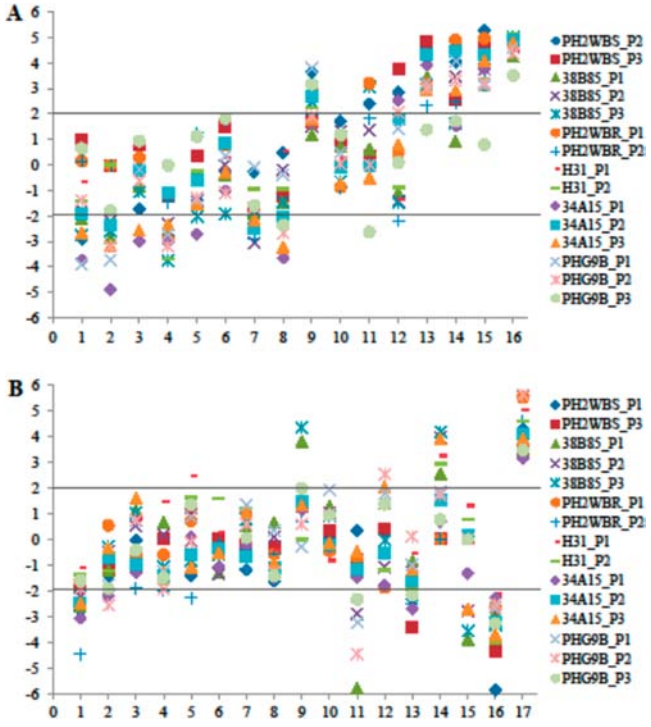

Figure 3. Gene expression analysis comparing qRT-PCR to microarray hybridization with V5 leaf (A) or 25 DAP (B) samples. Numbers are log 2 transformed ratios between expression levels detected by qRT-PCR and microarray that were defined against dapA expression levels.

show any amplification from qRT-PCR and was not included for further analysis. Two genes, pco653893 and pco598383 (genes 14 and 15 in Figure 3B, respectively), were amplified from 11 and 8 samples of 15 varieties, respectively. Two genes, pco601999 and pco632057 (genes 16 and 17 in Figure 3B, respectively), had very different expression levels from microarray across all varieties (Figure 3B). Gene 16 showed 4−60 times lower expression and gene 17 showed 8−60 times higher expression when detected by qRT-PCR compared to microarray results. The rest of the genes tested in 25 DAP kernel samples showed good consistency with microarray data (Figure 3B). A few qRT-PCR expression data points were different from the microarray data, but only for one or two maize varieties.

Metabolomic Data Analysis. The three processed data matrices contained 3891 metabolomic signatures or fingerprints (m/z value−RI combinations) for V5 leaves, 4300 for 25 DAP immature kernels, and 3891 for mature kernels. Of these, 87−103 metabolites were successfully identified in tissues examined. These numbers, reduced relative to the raw data set, take into account the elimination of the inherent redundancy in metabolomics signatures and ignore metabolites for which the identity could not be unambiguously established. The substantial reductions are due to (1) eliminating the inherent redundancy in metabolomics signatures wherein each metabolite can be represented by multiple m/z values in its electron impact mass spectrum and (2) ignoring metabolites for which the identity could not be unambiguously established.

To evaluate technical variations including the sampling, analytical, and data analysis variability, eight technical repeats were produced from V5 leaves of PHG9B and H31, 25 DAP kernels from PHG9B and H31, and mature kernels from PH2WBS and PHG9B. For each tissue−variety combination, a single bulk tissue sample was aliquoted into eight extraction tubes, producing eight metabolomic samples. Mean CV values calculated from technical repeat metabolite relative levels were

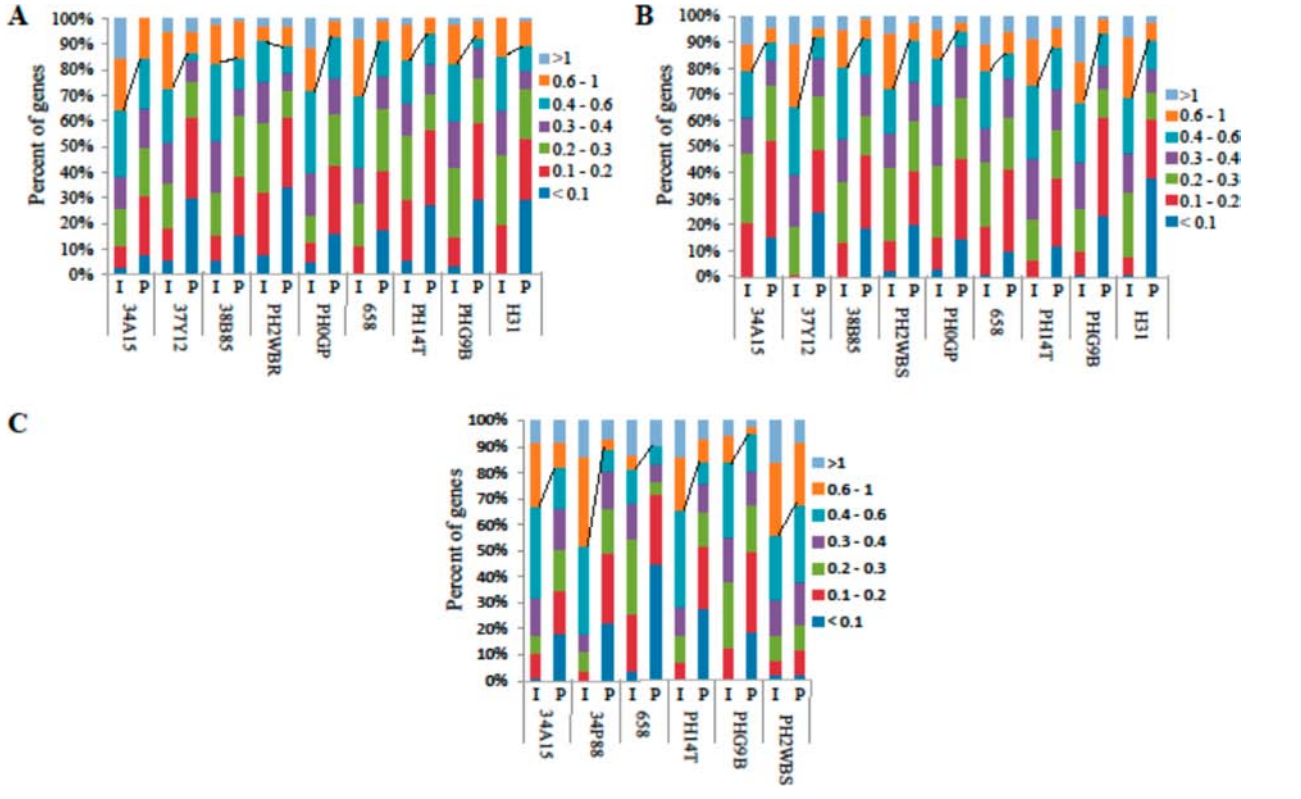

Figure 4. CV distribution of metabolite levels detected from V5 leaf (**A**), 25 DAP immature kernel (B), and mature kernels (C).

dx.doi.org/10.1021/jf405652j | J. Agric. Food Chem. 2014, 62, 2997−3009

between 0.33 and 0.54, and median values were between 0.27 and 0.46, indicating good reproducibility despite some outliers in the upper ranges (Supporting Information Supplementary Figure 3). The majority of metabolites detected showed CV values <0.6, with 76.7 and 87.4% metabolites from V5 leaves of PHG9B and H31, 76.1 and 80.2% of metabolites from 25 DAP immature kernels of PHG9B and H31, and 77.6 and 60.9% of metabolites from mature seeds of PH2WBS and PHG9B, respectively (Supporting Information Supplementary Figure 3). We also found that pooled samples had lower variances compared to the individual samples (Figure 4; Supporting Information Supplementary Table 5), similar to what was observed from the transcript data. Particularly, metabolomics for mature seed samples showed much less variation than for immature seeds (Supporting Information Supplementary Table 5), probably due to a less complex metabolome and terminal differentiation state of mature kernels.

Mean metabolite levels detected from individual and pooled samples of the same tissue–variety combination are highly correlated, with Pearson correlation *R* values all close to 1 (Table 2). For PHG9B and H31, the high correlations are observed despite the fact that the individual samples were from nine different plants, compared to the technical variation tests for which metabolites were extracted from eight aliquots of the same plant sample. These results also demonstrate consistent derivatization, GC, MS data acquisition, and data processing.

Table 2. Mean Metabolite Levels Detected from Individual Plant (I) and Pooled Plants (P) Samples for the Same Tissue Type of a Variety Are Highly Correlated[a]

variety	V5 leaf	25 DAP	mature
34A15	0.9976	0.9996	0.9732
37Y12	0.9988	0.9987	0.9921
38B85	0.9988	0.9994	
PH2WBS		0.9089	0.9952
PH2WBR	0.9985		
PH0GP	0.9970	0.9971	
658	0.9981	0.9948	0.9984
PH14T	0.9994	0.9981	0.9992
PHG9B	0.9993	0.9933	0.9940
H31	0.9980	0.9891	

[a]Pearson correlation coefficients (*R*) by Excel function PEARSON.

Tissue or Variety Separation Based on Metabolomics. When the metabolites detected from the three different tissues were compared, PCA clearly indicated tissue separation (Figure 5), reflecting tissue specificity of metabolic processes, as expected. However, PCA revealed variety specificity for only certain variety–tissue combinations. For example, for V5 leaf tissues, there was clear separation of PH2WBR, PH14T, and H31 from other varieties based on PC1 and PC3 (Figure 6A). Likewise, PH2WBS and PH2WBR in 25 DAP kernels were readily distinguished from other varieties with PC1 and PC4 (Figure 6E). For mature kernels, PH2WBS and PHG9B showed good separation from other varieties based on PC2 and PC3 (Figure 6I).

For the most part, the tissue and variety classifications observed with individual plants were also evident in pooled plant samples, although sometimes with different principal component projections (Figures 5 and 6A,J). This result suggests that pooling did not degrade the discriminating power afforded by individual samples. Interestingly, the combined percent variance included in the PCA scores plots was slightly higher for pooled samples compared to that generated for analogous individual samples, suggesting that pooling removed some uninformative signal.

Loadings associated with examples of the above variety classifications were selected graphically (Figures 6C,D; G,H; and K,L; in purple) and listed in Supplementary Table 6 in the Supporting Information. The very significant increases in the amount of amino acids in developing kernels, including glutamic acid, glutamine, histidine, leucine, lysine, pyroglutamic acid (which could be derived from glutamine during sample preparation), and tryptophan, are expected for PH2WBS, a genotype with elevated grain protein. Explanations for the genotype-specific differences (loadings) in the other tissues are less obvious. For the three examples shown, loadings from pooled plants were very similar to those from individual plants. Thus, pooling generated similar PCA scores and loadings, maintaining the ability to classify sample groups (varieties) as well as to identify the prominent metabolites underlying said classifications.

In this GC-MS metabolomic study, we also found that some metabolites were detected in only one or two tissue types. Among individual plant samples, there were 19 metabolites uniquely detected in V5 leaves, 2 only in immature kernels, and 3 only in mature kernels (Table 3). It is expected that the

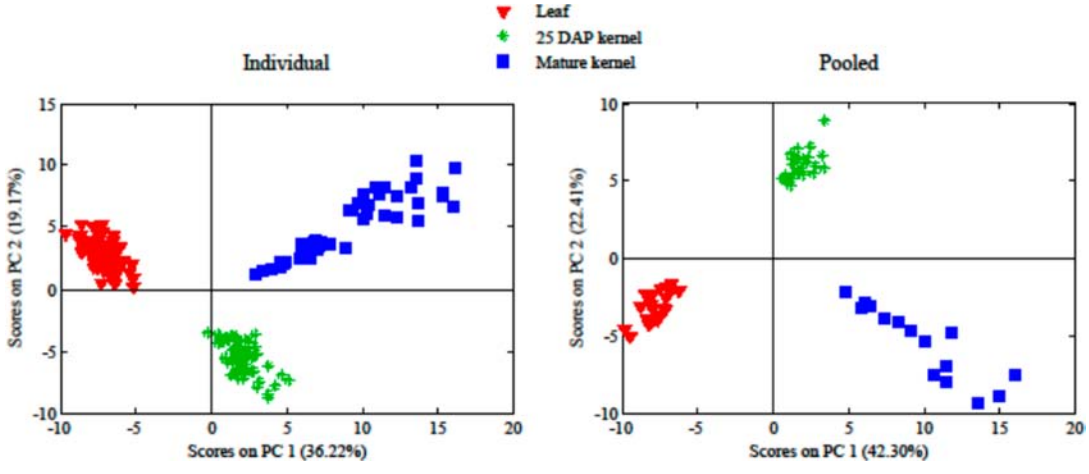

Figure 5. PCA score plots from individual or pooled plants showing tissue specificity of metabolomes.

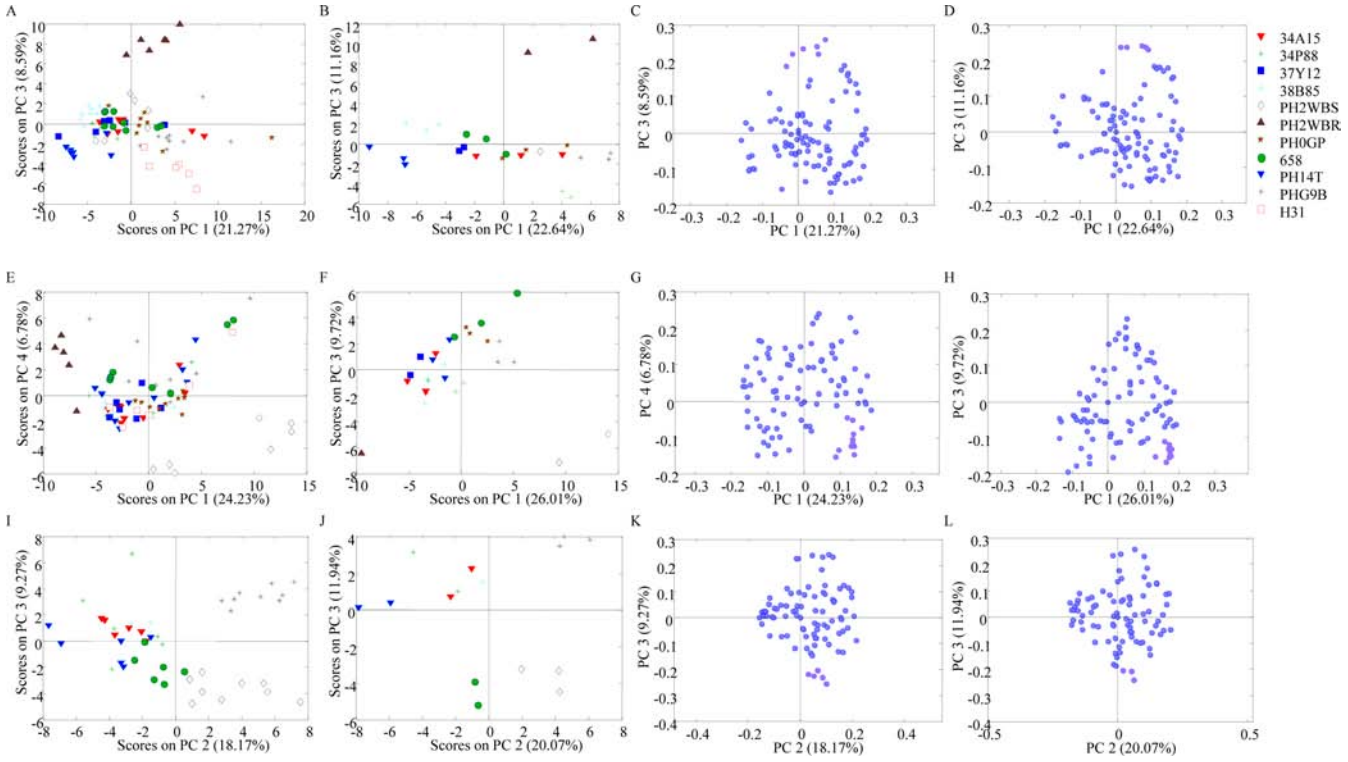

Figure 6. PCA scores and loadings plots from individual plants (A, C; E, G; I, K) or pooled plants (B, D; F, H; J, L) showing classifications of PH2WBR from the leaf metabolome (A–D), PH2WBS from the 25 DAP kernel metabolome (E–H), and PH2WBS from the mature kernel metabolome (I–L). Significant loadings are shown in purple.

Table 3. Apparent Tissue-Specific Metabolites

tissue	analyte	class
V5 leaf	tyramine	polyamine
	tryptophan	amino acid
	chlorogenic acid	phenolic acid
	citramalic acid	organic acid
	dehydroascorbic acid, secondary peak 1	vitamin
	dehydroascorbic acid, secondary peak 2	vitamin
	dehydroascorbic acid, secondary peak 3	vitamin
	heptadecanoic acid	fatty acid
	itaconic acid	organic acid
	maleic acid	organic acid
	pyruvic acid	organic acid
	salicylic acid	phenolic acid
	cis-caffeic acid	phenolic acid
	trans-caffeic acid	phenolic acid
	α-tocopherol	vitamin
	rhamnose	sugar
	trehalose	sugar
	glyceric acid-3-phosphate	phosphorylated acid
	phytol	alkane alcohol
	margaric acid	fatty acid
25 DAP	myristic acid	fatty acid
	cysteine, partial derivative	amino acid
mature kernel	adenosine-5-monophosphate	nucleic acid
	pipecolic acid	organic acid

metabolome of leaves is more divergent than that of immature or mature kernels. Some of these metabolites are present but not detected in other tissues, given our conservative limit of peak detection. Moreover, immature and mature kernels contain more polysaccharides by weight than leaves. Because approximately 3 mg dry weight samples were used for all three tissue types, it is expected that the concentration of many small molecule metabolites will be greater in leaf than in kernel samples. This could result in apparent tissue specificity, as seen in Table 3.

Range and Variations of Metabolite Abundances. We observed large ranges in relative levels for many metabolites across all varieties. The ratio between the maximum value and the minimum value detected for a metabolite in individual samples ranged from 1.8 to 1663 for V5 leaf tissues, from 3.3 to 16815 for immature kernels, and from 2.7 to 585 for mature kernels (Supporting Information Supplementary Table 7). However, when samples were pooled, the ranges narrowed to 1.4–167 for V5 leaves, 2.1–4828 for immature kernels, and 1.6–86 for mature kernels (Supporting Information Supplementary Table 7). Similarly, when the mean values within each variety for each metabolite from either individual samples or pooled samples were compared across all varieties with box plots, the pooled samples showed much narrower distribution compared to the individual samples (data not shown). This observation indicated that the biological variation among individual plants combined with variety variation was very large. However, our pooling strategy effectively decreased the biological variation between plants. The actual relative levels are specific to the current data set and should not be compared to other data sets, unless they were processed (aligned and scaled) together.

dx.doi.org/10.1021/jf405652j | J. Agric. Food Chem. 2014, 62, 2997–3009

Table 4. Metabolites with Relatively Stable or Highly Variable Levels among Different Maize Varieties and Their CV Values[a]

V5 leaf		25 DAP immature kernel		mature kernel	
0.31	**acetic acid**	**0.30**	**acetic acid**	**0.29**	**β-sitosterol**
0.30	**arabinose**	**0.39**	**arabinose**	**0.28**	**campesterol**
0.13	**β-sitosterol**	0.34	aspartic acid part. deriv	0.36	erythritol
0.23	**campesterol**	0.32	benzoic acid	**0.37**	**glycerol-3-phosphate**
0.40	cellobiose deriv 1	0.30	ethanolamine	**0.37**	**linoleic acid**
0.38	*cis*-aconitic acid	0.37	fructose deriv 1	**0.38**	**malic acid**
0.39	ferulic acid	0.39	galactose	*0.35*	*myo-inositol*
0.33	galactitol	0.24	glucose deriv 1	**0.31**	**palmitic acid**
0.24	glycerol	0.38	glyceric acid	**0.31**	**stigmasterol**
0.38	**glycerol-3-phosphate**	0.36	isoleucine part. deriv	*0.19*	*sucrose*
0.40	heptadecanoic acid	0.34	leucine part. deriv	**0.39**	**tyrosine**
0.30	**linoleic acid**	**0.36**	**malic acid**		
0.17	*myo-inositol*	0.36	mannose		
0.30	**palmitic acid**	*0.23*	*myo-inositol*		
0.17	phytol	0.25	phosphoric acid		
		0.37	serine part. deriv		
0.35	**stigmasterol**	0.30	succinic acid		
0.14	*sucrose*	*0.38*	*sucrose*		
0.36	*trans*-caffeic acid	0.31	threonine part. deriv		
0.31	xylitol	**0.35**	**tyrosine**		
0.28	xylose deriv 1				
0.32	xylose deriv 2				
1.60	2-aminobutyric acid	1.10	β-alanine part. deriv	1.24	asparagine
1.79	asparagine part. deriv	2.14	*cis*-aconitic acid	2.15	β-amyrin
1.52	aspartic acid	1.39	citric acid	2.63	cellobiose deriv 1
2.04	benzoic acid	2.26	gluconic acid	1.05	cysteine part. deriv
1.21	**dehydroascorbic acid**	**1.49**	**glutamic acid**	**1.28**	**dehydroascorbic acid**
1.54	dehydroascorbic acid second peak 1	*2.70*	*glutamine part. deriv*	1.03	GABA
1.71	ethanolamine	1.84	histidine	1.04	glucose deriv 2
1.36	**glutamic acid**	1.63	isocitric acid	1.83	glucose-6-phosphate deriv 2
2.14	*glutamine part. deriv*	1.25	linolenic acid	*1.70*	*glutamine part. deriv*
1.19	glycine	2.56	myristic acid	1.04	glyceric acid
1.22	glycine part. deriv	1.03	oleic acid	1.60	maltose
1.07	isoleucine	3.43	*p*-coumaric acid	1.25	pipecolic acid
1.11	leucine	**1.57**	**pyroglutamic acid**	1.14	pipecolic acid part. deriv
1.45	ornithine			**1.32**	**pyroglutamic acid**
1.06	serine			1.16	xylitol
1.60	trehalose			1.64	xylose deriv 2
1.21	tyrosine				

[a]CV values were calculated from metabolite levels from all individual (I) and pooled (P) samples for all varieties. Only metabolites that were detected from all I and P samples of all varieties were included for the calculation. Only metabolites with CV values of <0.30 (relatively stable) and >1.00 (highly variable) are shown. Metabolites in *italic* were found in all three tissues, and metabolites in **bold** were found in two tissues for the same category.

Multiple derivative forms for certain metabolites are characteristic of GC-MS-based metabolomics, as illustrated by asparagine in Supplementary Table 7 in the Supporting Information. Asparagine with four TMS groups (one attached to the carboxyl and three to the amines) was found in mature kernels, whereas asparagine with just three TMS moieties (one attached to the carboxyl and two to the amines) was specific to V5 leaves. This dichotomy might be explained by differential trimethylsilylation due to the different sample matrices.[28] Consequently, comparing metabolomes across tissue types or species should be undertaken with caution.

We also compared the levels of metabolites in all samples across all varieties for a given tissue type and identified metabolites that are quite stable as well as those that are highly variable among varieties. There were 21 metabolites from V5 leaves, 20 metabolites from 25 DAP immature kernels, and 11 metabolites from the mature kernels that showed a CV value of <0.4 across all varieties (Table 4), representing tissue-specific stable metabolomes. Among them, sucrose and *myo*-inositol were identified from all three tissues, and another 10 metabolites appeared in two tissue types. On the other hand, there were 17 metabolites from the V5 leaves, 13 from the 25 DAP immature kernels, and 16 from the mature kernels that showed CV values >1, indicating that these metabolites are highly variable among different maize varieties (Table 4). A partial derivative form of glutamine seemed to be highly variable in all three tissue types, and another three metabolites were highly variable for two tissue types. The high variability of the partial derivative of glutamine may be due, at least in part, to inconsistent transformation to pyroglutamic acid, which was

also highly variable in two of the tissues. The inconsistent transformation of pyroglutamic acid is a process known to be associated with trimethylsilylation.

As with gene expression levels detected from microarrays, mean metabolite abundances from individual samples or pooled samples were calculated for each variety and used to calculate CV values among varieties. For all three tissue types, metabolite variations among different varieties detected from individual or pooled samples are well-correlated. Linear regression R^2 values are 0.90, 0.92, and 0.82 for V5 leaves, 25 DAP developing kernels, and mature kernels, respectively. Furthermore, the CV distribution patterns are very similar between individual and pooled samples (Supporting Information Supplementary Figure 4). For V5 leaves, 43.7% of metabolites showed higher CV values in pooled samples compared to individual samples. In 25 DAP developing kernels and mature kernels, the numbers are 61.5 and 47.6%. This observation indicated that using pooled samples revealed variety-to-variety metabolomic variation similar to that using individual samples.

DISCUSSION

Thorough evaluation of the applicability and limitations of the -omics technologies for food safety assessment is necessary before their acceptance for this purpose. Toward this end, we evaluated high-throughput gene expression and metabolomic technologies by characterizing the transcriptomes and metabolomes of several conventional maize varieties using alternative protocols. Our observations led us to conclude that in applying these methods to regulatory issues, consideration should be given to natural variation in maize transcriptome and to the high degree of variation in metabolite concentrations between plant varieties and individuals of the same variety.

Technical Variation. To validate methods for both microarray and metabolomics, selected samples were analyzed multiple times to serve as technical repeats. The CV distribution for the technical microarrays showed small variations between different microarray runs for the same sample (Figure 1), validating the method and technical consistency. When compared to CVs detected from individual plant samples, the technical CVs are much smaller (Figure 1A; Supporting Information Supplementary Table 2), indicating that our microarray technology is consistent and sensitive enough to detect biological variations outside technical variations. The data correlation analysis among repeat arrays comparing individual samples and technical repeat samples confirmed this conclusion (Figure 2). Technical plus biological CVs detected from metabolomics, however, were much larger compared to microarrays (Supporting Information Supplemetary Figure 3). This increase is not unexpected because expression of many metabolites is dynamically affected by microenvironment. Furthermore, different metabolites have very different physical and biochemical properties as well as ranges of expression and, therefore, can be affected by the extraction and derivatization methods employed. Nevertheless, biological variability was found to be greater than analytical variability. The mean CVs observed are similar to those reported in the plant metabolomic literature.

Sample Pooling. Profiling techniques are a powerful tool for gene discovery research as long as appropriate statistical tools are used to analyze the data. Pooling of mRNA samples from different individuals of the same variety for microarray hybridizations has the following advantages: (1) controls cost, (2) generates data when the amounts of individual samples are insufficient, and (3) decreases variation between individuals. A design of multiple pools with multiple individual samples in each pool was established as a compromise.[44−47] Thus, the ability to detect the difference between biological subject-to-subject variations and the experimental technical variations is combined with the efficiency of the pooling strategy designed to reduce overall variance. The larger the individual-to-individual variability is, as compared to technical variability, the greater the reduction of variability is achieved by pooling samples.[44,45]

We designed the microarray and metabolomics experiments to include both individual samples and sample pools. Gene expression levels detected from microarray and metabolite abundances both showed very good correlation between individual and pooled samples within the same tissue type and variety (Tables 1 and 2). Using pooled samples lowered sample-to-sample variation, resulting in lower CV values (Figure 4; Supporting Information Supplementary Figure 1 and Tables 2, 3, 5, and 6). Interestingly, pooling microarray samples reduced the CV values more dramatically for 25 DAP samples compared to V5 leaf samples (Supporting Information Supplementary Figure 1C,D), presumably due to the higher transcriptome variation among 25 DAP individual samples compared to V5 leaf individual samples.

The mean CV values for each variety calculated from either individual plants or pooled samples represent variety-to-variety variations. The CV values representing variety-to-variety variations were similar when obtained from either individual plants or pooled samples for both microarrays and metabolomics (Supporting Information Supplementary Figures 2 and 4). Furthermore, the distribution patterns of variety CV values were similar for both microarrays and metabolomics. A slight increase of variation in pooled samples compared with individual samples from microarrays was detected (Supporting Information Supplementary Figure 2 and Table 3), presumably due to fewer pooled samples.

Pooling plants prior to analysis also did not adversely affect the ability to classify tissues or varieties or identify discriminating metabolites by PCA (Figures 5 and 6). In fact, pooling appeared to enhance discriminating power, presumably by eliminating some noise from the data sets. Overall, our pooling strategy of three sample pools of three is a cost-saving design that does not sacrifice analytical power.

qRT-PCR and Microarray. The use of microarray profiling for comparative assessment of biotech crops requires a gene expression sequence database for probe design, gene annotation, and expression level interpretation. For many plant species, genomes or transcriptomes have not been completely sequenced except for a few model genotypes. The maize genome has an especially high level of DNA sequence polymorphisms, approximately an order of magnitude higher than that in humans.[48−50] A high level of genotypic variation in maize introduces challenges for gene expression profiling such as microarray or PCR-based technologies, because experimental designs are based on knowledge obtained from just one or two varieties. As most of the genomic sequence and transcriptome for the varieties used in this study are not available, microarray hybridization efficiency is expected to vary between varieties. In the microarray study and in qRT-PCR, the primers and probes were designed using gene sequences of the B73 reference genome. Consequently, we observed substantial variation in single-well qRT-PCR efficiencies for the amplification of the same gene from different maize variety samples (data not

shown). This resulted in some inconsistency in expression values detected by qRT-PCR and microarrays across different varieties (Figure 3). For some genes, expression values assayed by qRT-PCR were very different from the corresponding microarray expression levels (Figure 3). This observation raises concerns about the validity of probe homology-dependent methodologies in highly diverse species. In some cases, very large variation in measured expression levels between varieties may be due to the presence or absence of variation.[51] For future studies, caution should be exercised when using microarray technology under similar circumstances. When transgenic and nontransgenic varieties are compared, pairs of lines should be used that are isogenic except for the presence of transgenes.

Metabolomics. The physiological concentration range of metabolites is very broad (Supporting Information Supplementary Table 7).[52,53] The lower technical variation for microarrays compared to metabolomics (Figure 1; Supporting Information Supplementary Figure 3) can be partially explained by quantile normalization of microarray data, which helps reduce CV. The CV ranges observed in our study are nevertheless comparable to those seen by others using different systems.[54−57]

The levels of many metabolites measured by metabolomics are extremely sensitive to not only the experimental procedures and instrument type used but also the environment from which the samples are collected. Nevertheless, large changes in the amounts of many metabolites within a plant rarely make significant overall contributions to the nutritional composition or raise safety concerns.[12,53,58−60] Genetic background strongly affects metabolite levels,[60,61] usually more than transgene insertions.[16,20,63] Per-sample cost for metabolomics is much lower compared to microarrays, allowing more sample replicates, increasing statistical power and lowering technical variation while retaining true variation in physiological metabolite levels.

GC-MS-based high-throughput metabolomics requires a uniform extraction and sample processing protocol for hundreds of metabolites differing in chemical properties and in vivo concentrations, which leads to suboptimal analytical conditions for many metabolites. Most metabolomic techniques lack sufficient analytical breadth to accurately measure hundreds of metabolites with very diverse chemical properties.[64−66] Analytical compromises must be made to achieve high-throughput and high metabolome coverage, rendering metabolomic data fundamentally different from targeted analysis of specific analytes. Even augmented with LC-MS and CE-MS, metabolomics does not cover all of the compounds presumed to be present in maize leaves or kernels. Also, metabolomics results include a large amount of unidentified metabolites that currently cannot be mapped to a biochemical pathway. Thus, a traditional metabolic pathway-centric evaluation of metabolomic data for safety assessment is not conceptually appropriate. The lack of knowledge of metabolic pathways and the limited availability of reference standards and databases also have restricted the use of metabolomic technology for tasks best served by traditional targeted analytical methods. Therefore, it might be preferable to combine nontargeted methods with multivariate tools such as PCA and hierarchical clustering to visualize sample relationships, rather than to focus on individual metabolite tolerance levels.[62]

Although our metabolomic study identified metabolites present at significantly different levels in different maize varieties, the biological significance of these differences should be interpreted with caution.[16,67] We reported relative metabolite abundances rather than absolute abundances; therefore, only metabolomic data generated using the same experimental procedures, detection methodologies, and internal controls should be compared to this data set directly. This consideration is additional to significant biological variability. As recommended by *Codex Alimentarius*,[68] "The statistical significance of any observed differences should be assessed in the context of the range of natural variations for that parameter to determine its biological significance." Our study strongly supports this recommendation.

■ ASSOCIATED CONTENT

Supporting Information

Supplementary Figures 1−4 and Tables 1−7. This material is available free of charge via the Internet at http://pubs.acs.org.

■ AUTHOR INFORMATION

Notes

The authors declare no competing financial interest.

■ ACKNOWLEDGMENTS

We express appreciation to the Wilmington Regulatory Science team for assistance in tissue generation; John Nau for carrying out the microarray experiments and data processing; Teresa Harp for carrying out the metabolomics experiments; Xiaoxiao Kong and Bonnie Hong for assistance in data analysis; Antoni Rafalski for assistance in the preparation of the manuscript; and Antoni Rafalski, Stan Luck, and Mary Locke for critical review of the manuscript.

■ ABBREVIATIONS USED

GMO, genetically modified organism; qRT-PCR, quantitative reverse transcript PCR; OECD, Organization for Economic Co-operation and Development; GM, genetically modified; ILSI, International Life Sciences Institute; mRNA, message RNA; RNA, ribonucleic acid; GC-MS, gas chromatography−mass spectrometry; DAP, days after pollination; cRNA, complementary RNA; MSTFA, *N*-methyl-*N*-(trimethylsilyl)-trifluoroacetamide; PFTBA, perfluorotributylamine; CV, coefficient of variation; PCA, principal component analysis; cDNA, complementary DNA; RT, reverse transcription; NCBI, National Center for Biotechnology Information; qPCR, quantitative PCR; LC-MS, liquid chromatography−ass spectrometry; CE-MS, capillary electrophoresis/mass spectrometry; TMS, trimethylsilyl

■ REFERENCES

(1) Fedoroff, N. V.; Battisti, D. S.; Beachy, R. N.; Cooper, P. J. M.; Fischhoff, D. A.; Hodges, C. N.; Knauf, V. C.; Lobell, D.; Mazur, B. J.; Molden, D.; Reynolds, M. P.; Ronald, P. C.; Rosegrant, M. W.; Sanchez, P. A.; Vonshak, A.; Zhu, J.-K. Radically rethinking agriculture for the 21st century. *Science* **2010**, *327*, 833−834.

(2) Godfray, H. C. J.; Beddington, J. R.; Crute, I. R.; Haddad, L.; Lawrence, D.; Muir, J. F.; Pretty, J.; Robinson, S.; Thomas, S. M.; Toulmin, C. Food security: the challenge of feeding 9 billion people. *Science* **2010**, *327*, 812−818.

(3) Park, J. R.; McFarlane, I.; Phipps, R. H.; Ceddia, G. The role of transgenic crops in sustainable development. *Plant Biotechnol. J.* **2010**, *9*, 2−21.

(4) McGloughlin, M. N. Modifying agricultural crops for improved nutrition. *New Biotechnol.* **2010**, *27*, 494−504.

(5) Domingo, J.; Bordonaba, J. G. A literature review on the safety assessment of genetically modified plants. *Environ. Int.* **2011**, *37*, 734−742.
(6) Kuiper, H. A.; Kleter, G.; Noteborn, H. P.; Kok, E. J. Assessment of food safety issues related to genetically modified foods. *Plant J.* **2001**, *27*, 503−528.
(7) Kok, E. J.; Kuiper, H. A. Comparative safety assessment for biotech crops. *Trends Biotechnol.* **2003**, *21*, 439−444.
(8) König, A.; Cockburn, A.; Crevel, R. W. R.; Debruyne, E.; Grafstroem, R.; Hammerling, U.; Kimber, I.; Knudsen, I.; Kuiper, H. A.; Peijnenburg, A. A. C. M.; Penninks, A. H.; Poulsen, M.; Schauzu, M.; Wal, J. M. Assessment of the safety of foods derived from genetically modified (GM) crops. *Food Chem. Toxicol.* **2004**, *42*, 1047−1088.
(9) Organization for Economic Cooperation and Development. *An Introduction to the Food/Feed Safety Consensus Documents of the Task Force*; Series on the Safety of Novel Foods and Feeds 14; Paris, France, 2006; pp 7−9.
(10) Chassy, B. M. Can -omics inform a food safety assessment? *Regul. Toxicol. Pharmacol.* **2010**, *58*, S62−S70.
(11) ILSI. Recent developments in the safety and nutritional assessment of nutritionally improved foods and feeds. *Compr. Rev. Food Sci. Food Saf.* **2008**, *7*, 50−113.
(12) Herman, R. A.; Chassy, B. M.; Parrott, W. Compositional assessment of transgenic crops: an idea whose time has passed? *Trends Biotechnol.* **2009**, *27*, 565−567.
(13) Davies, H. V.; Shepherd, L. V. T.; Stewart, D.; Frank, T.; Röhlig, R. M.; Engel, K.-H. Metabolome variability in crop plant species − when, where, how much and so what? *Regul. Toxicol. Pharmacol.* **2010b**, *58*, S54−S61.
(14) Harrigan, G. G.; Glenn, K. C.; Ridley, W. P. Assessing the natural variability in crop composition. *Regul. Toxicol. Pharmacol.* **2010**, *58*, S13−S20.
(15) ILSI. Nutritional and safety assessments of foods and feeds nutritionally improved through biotechnology. *Compr. Rev. Food Sci. Food Saf.* **2004**, *3*, 36−104.
(16) Harrigan, G. G.; Lundry, D.; Drury, S.; Berman, K.; Riordan, S. G.; Nemeth, M. A.; Ridley, W. P.; Glenn, K. C. Natural variation in crop composition and the impact of transgenesis. *Nat. Biotechnol.* **2010b**, *28*, 402−404.
(17) EFSA. Guidance document of the scientific panel on genetically modified organisms for the risk assessment of genetically modified plants and derived food and feed. *EFSA J.* **2006**, *99*, 1−100.
(18) Joyce, A. R.; Palsson, B. O. The model organism as a system: integrating 'omics' data sets. *Nat. Rev. Mol. Cell Biol.* **2006**, *7*, 198−210.
(19) Li, X.; Huang, K. L.; Zhu, B. Z.; Tang, M. Z.; Luo, Y. B. Potentiality of "omics" techniques for the detection of unintended effects in genetically modified crops. *J. Agric. Biotechnol.* **2005**, *13*, 1082−1088.
(20) Ricroch, A. E.; Bergé, J. B.; Kuntz, M. Evaluation of genetically engineered crops using transcriptomic, proteomic, and metabolomic profiling techniques. *Plant Physiol.* **2011**, *155*, 1752−1761.
(21) Davies, H. A role for "omics" technologies in food safety assessment. *Food Control* **2010**, *21*, 1601−1610.
(22) Baudo, M. M.; Lyons, R.; Powers, S.; Pastori, G. M.; Edwards, K. J.; Holdsworth, M. J.; Shewry, P. R. Transgenesis has less impact on the transcriptome of wheat grain than conventional breeding. *Plant Biotechnol. J.* **2006**, *4*, 369−380.
(23) Batista, R.; Saibo, N.; Lourenco, T.; Oliveira, M. M. Microarray analyses reveal that plant mutagenesis may induce more transcriptomic changes than transgene insertion. *Proc. Natl. Acad. Sci. U.S.A.* **2008**, *105*, 3640−3645.
(24) van Dijk, J. P.; Leifert, C.; Barros, E.; Kok, E. J. Gene expression profiling for food safety assessment: examples in potato and maize. *Regul. Toxicol. Pharmacol.* **2010**, *58*, S21−S25.
(25) Schauer, S.; Fernie, A. R. Plant metabolomics: towards biological function and mechanism. *Trends Plant Sci.* **2006**, *11*, 508−516.
(26) Hall, R. D. Plant metabolomics: from holistic hope, to hype, to hot topic. *New Phytol.* **2006**, *169*, 453−468.
(27) Hayes, K. R.; Beatty, M.; Meng, X.; Simmons, C. R.; Habben, J. E.; Danilevskaya, O. N. Maize global transcriptomics reveals pervasive leaf diurnal rhythms but rhythms in developing ears are largely limited to the core oscillator. *PLoS One* **2010**, *5*, e12887.
(28) Fiehn, O.; Wohlgemuth, G.; Scholz, M.; Kind, T.; Lee, D. Y.; Lu, Y.; Moon, S.; Nikolau, B. Quality control for plant metabolomics: reporting MSI-compliant studies. *Plant J.* **2008**, *53*, 691−704.
(29) McElver, J.; Tzafrir, I.; Aux, G.; Rogers, R.; Ashby, C.; Smith, K.; Thomas, C.; Schetter, A.; Zhou, Q.; Cushman, M. A.; Tossberg, J.; Nickle, T.; Levin, J. Z.; Law, M.; Meinke, D.; Patton, D. Insertional mutagenesis of genes required for seed development in *Arabidopsis thaliana*. *Genetics* **2001**, *159*, 1751−1763.
(30) Luo, M.; Liu, J.; Lee, R. D.; Guo, B. Z. Characterization of gene expression profiles in developing kernels of maize (*Zea mays*) inbred Tex6. *Plant Breed.* **2008**, *127*, 569−578.
(31) Zhao, S.; Fernald, R. D. Comprehensive algorithm for quantitative real-time polymerase chain reaction. *J. Comput. Biol.* **2005**, *12* (8), 1045−1062.
(32) Fan, J.; Tam, P.; Woude, G. V.; Ren, Y. Normalization and analysis of cDNA microarrays using within-array replications applied to neuroblastoma cell response to a cytokine. *Proc. Natl. Acad. Sci. U.S.A.* **2004**, *101*, 1135−1140.
(33) Zhou, J.; Thompson, D. K. In *Microarray Technology and Applications in Environmental Microbiology*; Sparks, D. L., Ed.; Advances in Agronomy Vol. 82; Academic Press: San Diego, CA, USA, 2004; pp 183−270.
(34) Novak, J. P.; Miller, M. C., III; Bell, D. A. Variation in fiberoptic bead-based oligonucleotide microarrays: dispersion characteristics among hybridization and biological replicate samples. *Biol. Direct* **2006**, *1*, 18.
(35) Sato, F.; Tsuchiya, S.; Terasawa, K.; Tsujimoto, G. Intra-platform repeatability and inter-platform comparability of microRNA microarray technology. *PLoS One* **2009**, *4*, e5540.
(36) Rutledge, R. G.; Stewart, D. A kinetic-based sigmoidal model for the polymerase chain reaction and its application to high-capacity absolute quantitative real-time PCR. *BMC Biotechnol.* **2008**, *8*, 47.
(37) Cruz, F.; Kalaoun, S.; Nobile, P.; Colombo, C.; Almeida, J.; Barros, L. M. G.; Romano, E.; Grossi-de-Sá, M. F.; Vaslin, M.; Alves-Ferreira, M. Evaluation of coffee reference genes for relative expression studies by quantitative real-time RT-PCR. *Mol. Breed.* **2009**, *23*, 607−616.
(38) Ruijter, J. M.; Ramakers, C.; Hoogaars, W. M. H.; Karlen, Y.; Bakker, O.; van den Hoff, M. J. B.; Moorman, A. F. M. Amplification efficiency: linking baseline and bias in the analysis of quantitative PCR data. *Nucleic Acids Res.* **2009**, *37*, e45.
(39) Capitão, C.; Paiva, J. A. P.; Santos, D. M.; Fevereiro, P. *Medicago truncatula*, water deficit modulates the transcript accumulation of components of small RNA pathways. *BMC Plant Biol.* **2011**, *11*, 79.
(40) Demidenko, N. V.; Logacheva, M. D.; Penin, A. A. Selection and validation of reference genes for quantitative real-time PCR in buckwheat (*Fagopyrum esculentum*) based on transcriptome sequence data. *PLoS One* **2011**, *6*, e19434.
(41) Graeber, K.; Linkies, A.; Wood, A. T. A.; Leubner-Metzger, G. A guideline to family-wide comparative state-of-the-art quantitative RT-PCR analysis exemplified with a Brassicaceae cross-species seed germination case study. *Plant Cell* **2011**, *23*, 2045−2063.
(42) Mafra, V.; Kubo, K. S.; Alves-Ferreira, M.; Ribeiro-Alves, M.; Stuart, R. M.; Boava, L. P.; Rodrigues, C. M.; Machado, M. A. Reference genes for accurate transcript normalization in citrus genotypes under different experimental conditions. *PLoS One* **2012**, *2*, e31263.
(43) Marum, L.; Miguel, A.; Ricardo, C. P.; Miguel, C. Reference gene selection for quantitative real-time PCR normalization in *Quercus suber*. *PLoS One* **2012**, *4*, e35113.
(44) Kendziorski, C. M.; Zhang, Y.; Lan, H.; Attie, A. D. The efficiency of pooling mRNA in microarray experiments. *Biostatistics* **2003**, *4*, 465−477.

(45) Kendziorski, C.; Irizarry, R. A.; Chen, K.-S.; Haag, J. D.; Gould, M. N. On the utility of pooling biological samples in microarray experiments. *Proc. Natl. Acad. Sci. U.S.A.* **2005**, *102*, 4252−4257.
(46) Peng, X.; Wood, C. L.; Blalock, E. M.; Chen, K. C.; Landfield, P. W.; Stromberg, A. J. Statistical implications of pooling RNA samples for microarray experiments. *BMC Bioinf.* **2003**, *4*, 26.
(47) Zhang, W.; Carriquiry, A.; Nettleton, D.; Dekkers, J. C. M. Pooling mRNA in microarray experiments and its effect on power. *Bioinformatics* **2007**, *23*, 1217−1224.
(48) Buckler, E. S.; Thornsberry, J. M. Plant molecular diversity and applications to genomics. *Curr. Opin. Plant Biol.* **2002**, *5*, 107−111.
(49) Ching, A.; Caldwell, K. S.; Jung, M.; Dolan, M.; Smith, O. S.; Tingey, S.; Morgante, M.; Rafalski, J. A. SNP frequency, haplotype structure and linkage disequilibrium in elite maize inbred lines. *BMC Genet.* **2002**, *3* (19), 3−19.
(50) Rafalski, A.; Morgante, M. Corn and humans: recombination and linkage disequilibrium in two genomes of similar size. *Trends Genet.* **2004**, *20*, 103−111.
(51) Springer, N. M.; Ying, K.; Fu, Y.; Ji, T.; Yeh, C.-T.; et al. Maize inbreds exhibit high levels of copy number variation (CNV) and presence/absence variation (PAV) in genome content. *PLoS Genet.* **2009**, *5* (11), e1000734 DOI: 10.1371/journal.pgen.1000734.
(52) Eldridge, A. C.; Kwolek, W. F. Soybean isoflavones: effect of environment and variety on composition. *J. Agric. Food Chem.* **1983**, *31*, 394−396.
(53) Gutierrez-Gonzalez, J. J.; Wu, X.; Zhang, J.; Lee, J. D.; Ellersieck, M.; Shannon, J. G.; Yu, O.; Nguyen, H. T.; Sleper, D. A. Genetic control of soybean seed isoflavone content: importance of statistical model and epistasis in complex traits. *Theor. Appl. Genet.* **2009**, *119*, 1069−1083.
(54) Morgenthal, K.; Wienkoop, S.; Scholz, M.; Selbig, J.; Weckwerth, W. Correlative GC-TOF-MS-based metabolite profiling and LC-MS-based protein profiling reveal time-related systemic regulation of metabolite-protein networks and improve pattern recognition for multiple biomarker selection. *Metabolomics* **2005**, *1*, 109−121.
(55) Sysi-Aho, M.; Katajamaa, M.; Yetukuri, L.; Orešič, M. Normalization method for metabolomics data using optimal selection of multiple internal standards. *BMC Bioinf.* **2007**, *8*, 93.
(56) Parsons, H. M.; Ekman, D. R.; Collette, T. W.; Viant, M. R. Spectral relative standard deviation: a practical benchmark in metabolomics. *Analyst* **2009**, *134*, 478−485.
(57) Toubiana, D.; Semel, Y.; Tohge, T.; Beleggia, R.; Cattivelli, L.; Rosental, L.; Nikoloski, Z.; Zamir, D.; Fernie, A. R.; Fait, A. Metabolic profiling of a mapping population exposes new insights in the regulation of seed metabolism and seed, fruit, and plant relations. *PLoS Genet.* **2012**, *8*, e1002612.
(58) Harrigan, G. G.; Stork, L. G.; Riordan, S. G.; Reynolds, T. L.; Ridley, W. P.; Masucci, J. D.; Macisaac, S.; Halls, S. C.; Orth, R.; Smith, R. G.; Wen, L.; Brown, W. E.; Welsch, M.; Riley, R.; Mcfarland, D.; Pandravada, A.; Glenn, K. C. Impact of genetics and environment on nutritional and metabolite components of maize grain. *J. Agric. Food Chem.* **2007**, *55*, 6177−6185.
(59) Skogerson, K.; Harrigan, G. G.; Reynolds, T. L.; Halls, S. C.; Ruebelt, M.; Iandolino, A.; Pandravada, A.; Glenn, K. C.; Fiehn, O. Impact of genetics and environment on the metabolite composition of maize grain. *J. Agric. Food Chem.* **2010**, *58*, 3600−3610.
(60) Zhou, J.; Harrigan, G. G.; Berman, K. H.; Webb, E. G.; Klusmeyer, T. H.; Nemeth, M. A. Stability of the compositional equivalence of grain from insect-protected corn and seed from herbicide-tolerant soybean over multiple seasons, locations and breeding germplasms. *J. Agric. Food Chem.* **2010**, *59*, 8822−8828.
(61) Reynolds, T. L.; Nemeth, M. A.; Glenn, K. C.; Ridley, W. P.; Astwood, J. D. Natural variability of metabolites in maize grain: differences due to genetic background. *J. Agric. Food Chem.* **2005**, *53*, 10061−10067.
(62) Asiago, V.; Hazebroek, J.; Harp, T.; Zhong, C. Effect of genetics and environment on the metabolome of commercial maize hybrids: a multisite study. *J. Agric. Food Chem.* **2012**, *60*, 11498−11508.
(63) Catchpole, G. S.; Beckmann, M.; Enot, D. P.; Mondhe, M.; Zywicki, B.; Taylor, J.; Hardy, N.; Smith, A.; King, R. D.; Kell, D. B.; Fiehn, O.; Draper, J. Hierarchical metabolomics demonstrates substantial compositional similarity between genetically modified and conventional potato crops. *Proc. Natl. Acad. Sci. U.S.A.* **2005**, *102*, 14458−14462.
(64) Goodacre, R.; Vaidyanathan, S.; Dunn, W. R.; Harrigan, G. G.; Kell, D. B. Metabolomics by numbers − acquiring and understanding global metabolite data. *Trends Biotechnol.* **2004**, *22*, 245−252.
(65) Rischer, H.; Oksman-Caldentey, K.-M. Unintended effects in genetically modified crops: revealed by metabolomics? *Trends Biotechnol.* **2006**, *24*, 102−104.
(66) Kusano, M.; Redestig, H.; Hirai, T.; Oikawa, A.; Matsuda, F.; Fukushima, A.; Arita, M.; Watanabe, S.; Yano, M.; Hiwasa-Tanase, K.; Ezura, H.; Saito, K. Covering chemical diversity of genetically-modified tomatoes using metabolomics for objective substantial equivalence assessment. *PLoS One* **2011**, *6*, e16989.
(67) Goodman, S. A dirty dozen: twelve *p*-value misconceptions. *Semin. Hematol.* **2008**, *45*, 135−140.
(68) Codex Alimentarius. Guideline for the conduct of food safety assessment of foods derived from recombinant-DNA plants; http://www.codexalimentarius.net/input/download/standards/10021/CXG_045e.pdf (accessed March 4, 2013).

JOURNAL OF AGRICULTURAL AND FOOD CHEMISTRY

Addition/Correction

pubs.acs.org/JAFC

Correction to Survey of Polyphenol Constituents in Grapes and Grape-Derived Products

Yanping Xu, James E. Simon, Cara Welch, JoLynne D. Wightman, Mario G. Ferruzzi, Lap Ho, Giulio M. Pasinetti, and Qingli Wu*

J. Agric. Food Chem. **2011** *59* (19), 10586–10593. 10.1021/jf202438d

There was an error in an author name in the original publication, which is corrected above.

Published: March 21, 2014

ACS Publications © 2014 American Chemical Society

Table 1. Chemical Composition of CEOs

#	Name	class	organ	*Citrus* species	Bioactivity	Structure	References
1	α-pinene	monoterpene	flower, peel, leaf	mandarin, orange, pummelo, lemon	antimicrobial		Hosni et al. (2010), Lota et al. (2002), Jabalpurwala et al. (2009), Sartorelli et al. (2007)
2	α-thujene	monoterpene	flower, peel, leaf	mandarin, orange, lime, pummelo, lemon			Jabalpurwala et al. (2009), Lota et al. (2002)
3	camphene	monoterpene	peel, leaf	lemon, lime, pummelo, mandarin, sour orange	lipid lowering		Lota et al. (2002), Bourgou et al. (2012), Vallianou et al. (2011), Sawamura et al. (1991)
4	β-pinene	monoterpene	flower, peel, leaf	mandarin, orange, pummelo, lemon	antifungal		Jabalpurwala et al. (2009), Lota et al. (2002), Hammer et al. (2003)
5	sabinene	monoterpene	flower, peel, leaf	mandarin, orange, pummelo, lemon	antifungal		Hosni et al. (2010), Lota et al. (2002), Jabalpurwala et al. (2009), Espinosa-García & Langenheim (1991)
6	α-phellandrene	monoterpene	peel, leaf	mandarin, orange	insecticidal activity	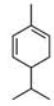	Hosni et al. (2010), Park et al. (2003)
7	δ-3-Carene	monoterpene	flower, peel, leaf	mandarin, orange, lemon	anti-inflammatory		Hosni et al. (2010), Lota et al. (2002), Jabalpurwala et al. (2009), Ocete et al. (1989)
8	α-myrcene	monoterpene	flower, peel, leaf	mandarin, orange, pummelo, lemon			Hosni et al. (2010), Lota et al. (2002)
9	β-myrcene	monoterpene	flower, leaf	mandarin, orange, pummelo, lemon	embryofoetotoxicity, antifungal	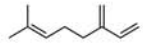	Jabalpurwala et al. (2009), Lota et al. (2002), Araujo et al. (1996), Tao et al. (2013)
10	α-terpinene	monoterpene	flower, peel, leaf	mandarin, orange, pummelo, lemon		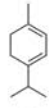	Jabalpurwala et al. (2009), Lota et al. (2002)
11	γ-terpinene	monoterpene	flower, peel, leaf	mandarin, orange, pummelo, lemon	lipid lowering, antimicrobial	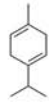	Jabalpurwala et al. (2009), Lota et al. (2002), Sartorelli et al. (2007), Takahashi et al. (2003)
12	limonene	monoterpene	flower, peel, leaf	mandarin, orange, pummelo, lemon	anti-inflammatory, antioxidant, antidiabetic, anticancer,lipid-lowering	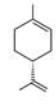	Shaw (1979), Hosni et al. (2010), Jabalpurwala et al. (2009), Lota et al. (2002), Jing et al. (2013)
13	1,8-cineole	monoterpenic oxide	leaf	lemon	antivascular, anti-inflammatory	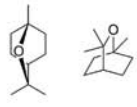	Lota et al. (2002), Santos and Rao (2000), Lahlou et al. (2002)
14	(Z)-ocimene	monoterpene	flower, peel, leaf	mandarin, orange, pummelo, lemon		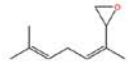	Hosni et al. (2010), Lota et al. (2002), Jabalpurwala et al. (2009)
15	(E)-ocimene	monoterpene	flower, peel, leaf	mandarin, orange, pummelo, lemon		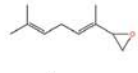	Hosni et al. (2010), Lota et al. (2002), Jabalpurwala et al. (2009)
16	trans-sabinene hydrate A		peel, leaf	pummelo, lemon			Hosni et al. (2010), Lota et al. (2002), Vekiari et al. (2002)

dx.doi.org/10.1021/jf5006148 | J. Agric. Food Chem. 2014, 62, 3011−3033

Table 1. continued

#	Name	class	organ	*Citrus* species	Bioactivity	Structure	References
17	cis-sabinene hydrate A		peel	orange, pummelo			Hosni et al. (2010)
18	p-cymene	monoterpene	flower, leaf, peel	lemon, mandarin	Antimicrobial, lipolytic effect	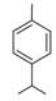	Lota et al. (2002), Vekiari et al. (2002), Sartorelli et al. (2007), Lota et al. (2001), Choi (2006)
19	α-terpinolene	monoterpene	flower, peel, leaf	mandarin, orange, lemon	radical-scavenging activity	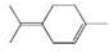	Hosni et al. (2010), Lota et al. (2002), Jabalpurwala et al. (2009), Choi et al. (2000)
20	linalool	monoterpene alcohol	flower, peel, Leaf	mandarin, orange, pummelo, lemon	antidiabetic	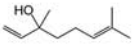	Hosni et al. (2010), Lota et al. (2002), Jabalpurwala et al. (2009), Deepa & Anuradha (2011)
21	trans-pinocarveol		peel	mandarin, orange, pummelo		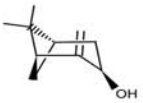	Hosni et al. (2010)
22	neo-allo-ocimene	monoterpene	flower	mandarin, orange, pummelo, lemon		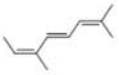	Jabalpurwala et al. (2009)
23	allo-ocimene	monoterpene	flower	mandarin, orange, pummelo, lemon			Jabalpurwala et al. (2009)
24	(Z)-epoxy-ocimene		flower	orange			Jabalpurwala et al. (2009)
25	terpinen-4-ol	monoterpenic oxide	Leaf	mandarin, orange, pummelo, lemon	antihypertension, anti-inflammatory	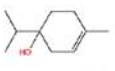	Lota et al. (2002), Lahlou et al. (2003), Hart et al. (2000)
26	β-cyclocitral	sesquiterpenoid	Peel	orange, pummelo	antimicrobial		Hosni et al. (2010), Proszenyák et al. (2007)
27	cis-linalool oxide	monoterpenic oxide	leaf	lemon		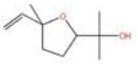	Lota et al. (2002)
28	α-p-dimethylstyrene		flower	mandarin, orange, pummelo, lemon			Jabalpurwala et al. (2009)
29	Sabinene hydrate	monoterpene	flower	orange, lemon			Jabalpurwala et al. (2009)
30	trans-para-menth-2-ene-1-ol	monoterpene alcohol	peel	mandarin, pummelo			Hosni et al. (2010)
31	carvacryl methyl oxide	monoterpene phenol derivative	peel	mandarin, orange		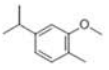	Hosni et al. (2010)
32	(Z)-limonene oxide	monoterpenic oxide	flower	lemon		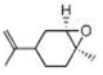	Jabalpurwala et al. (2009)
33	δ-elemene	sesquiterpene hydrocarbon	flower	lemon	anticancer	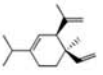	Jabalpurwala et al. (2009)
34	β-elemene	sesquiterpene hydrocarbon	leaf, peel, flower	lemon, grapefruit, orange, pummelo	anti-glioblastoma proliferation	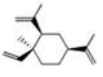	Lota et al. (2002), Zhu et al. (2011), Jabalpurwala et al. (2009)

dx.doi.org/10.1021/jf5006148 | J. Agric. Food Chem. 2014, 62, 3011−3033

Table 1. continued

#	Name	class	organ	*Citrus* species	Bioactivity	Structure	References
35	α-copaene	sesquiterpene hydrocarbon	flower, peel	mandarin, orange, pummelo, lemon	attractant for male fruit flies	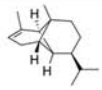	Lota et al. (2002), Nishida et al. (2000), Jabalpurwala et al. (2009)
36	β-copaene	sesquiterpene hydrocarbon	peel	mandarin, orange, pummelo		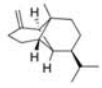	Hosni et al. (2010)
37	(E)-(E)-2,4-decadienal		peel	mandarin, orange, pummelo			Hosni et al. (2010)
38	α-bergamotene	sesquiterpene hydrocarbon	flower	lemon		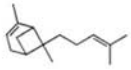	Jabalpurwala et al. (2009)
39	trans carveol	monoterpenoid alcohol	peel	mandarin, orange, pummelo		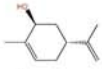	Hosni et al. (2010)
40	(E)-caryophyllene	sesquiterpene hydrocarbon	leaf, peel	lemon	antimicrobial		Lota et al. (2002), Juliani Jr et al. (2002)
41	β-caryophyllene	sesquiterpene hydrocarbon	flower	mandarin, orange, pummelo, lemon	anti-inflammatory, antibiotic, anticancer, antioxidant,	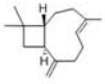	Jabalpurwala et al. (2009), Legault and Pichette (2007)
42	trans-α-bergamotene	sesquiterpene hydrocarbon	peel	lemon		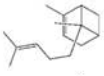	Lota et al. (2002)
43	β-ionone	isoprenoid	peel	mandarin, orange, pummelo	antimicrobial, anticancer	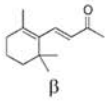	Hosni et al. (2010), Duncan et al. (2004), Radulović et al. (2006)
44	β-farnesene	sesquiterpene	flower	mandarin, orange, pummelo, lemon		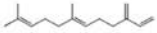	Jabalpurwala et al. (2009)
45	(E)- β-farnesene	sesquiterpene	peel	lemon	kairomone for the ladybird		Lota et al. (2002), Francis et al. (2004)
46	(E,E)-α-farnesene	sesquiterpene	peel	lemon	attractant for lepidopteran	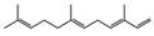	Lota et al. (2002), Pechous and Whitaker (2004)
47	farnesol	sesquiterpene	flower	mandarin, orange, pummelo	anticancer, lipid-regulation	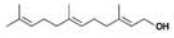	Jabalpurwala et al. (2009), Burke et al. (1997), Meigs and Simoni (1997)
48	α-humulene	sesquiterpene	peel	mandarin, orange, pummelo, lemon	anticancer		Lota et al. (2002), Hosni et al. (2010), Legault and Pichette (2007)
49	β-bisabolene	sesquiterpene	flower, peel	lemon, mandarin, orange		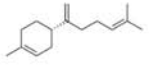	Lota et al. (2002), Jabalpurwala et al. (2009)
50	geranial	sesquiterpene aldehyde	flower, leaf	mandarin, orange, lemon	antifungal	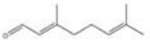	Lota et al. (2002), Jabalpurwala et al. (2009), Wuryatmo et al. (2003)
51	geraniol	terpene alcohol	flower, leaf	mandarin, orange, lemon, pummelo	antimicrobial, antioxidant, anticancer, anti-inflammatory	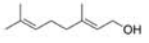	Lota et al. (2002), Jabalpurwala et al. (2009), Chen and Viljoen (2010)
52	α-citronellol	monoterpene alcohol	fower, leaf	orange, lemon		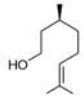	Lota et al. (2002), Jabalpurwala et al. (2009)

dx.doi.org/10.1021/jf5006148 | J. Agric. Food Chem. 2014, 62, 3011−3033

Table 1. continued

#	Name	class	organ	*Citrus* species	Bioactivity	Structure	References
53	β-citronellol	monoterpene alcohol	flower, leaf	orange, lemon, mandarin			Lota et al. (2002), Jabalpurwala et al. (2009)
54	curcumene	sesquiterpene hydrocarbon	flower	orange, lemon, pummelo	anti-inflammatory		Lota et al. (2002), Chavan et al. (2010) Jabalpurwala et al. (2009), Mujumdar et al. (2004)
55	neral	monoterpene alcohol	leaf, peel	lemon	antigungal	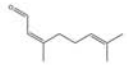	Lota et al. (2002), Wuryatmo et al. (2003)
56	nerol	monoterpene aldehyde	flower, leaf	mandarin, orange, lemon, pummelo	antimicrobial	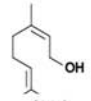	Lota et al. (2002), Jabalpurwala et al. (2009), Kotan et al. (2007)
57	calamenene	sesquiterpene	flower	lemon	anticancer		Jabalpurwala et al. (2009), Dai et al. (2012)
58	(Z)-jasmone		flower	mandarin, orange	insecticidal activity	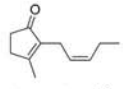	Jabalpurwala et al. (2009), Birkett et al. (2000)
59	nerolidol	sesquiterpene	flower	mandarin, orange, lemon, pummelo	insecticidal activity	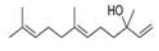	Lota et al. (2002), Arruda et al. (2005), Jabalpurwala et al. (2009)
60	thymol	monoterpene phenol	flower	mandarin, orange	antimicrobial	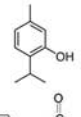	Jabalpurwala et al. (2009), Betancur-Galvis et al. (2011)
61	n-phenylformamide					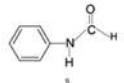	
62	aromadendrene	sesquiterpene	peel	mandarin, pummelo	antifungal		Hosni et al. (2010), Hammer et al. (2003)
63	α-terpineol	monoterpene alcohol	leaf, peel	lemon	antifungal		Lota et al. (2002), Hammer et al. (2003)
64	α-cyperone	sesquiterpene	peel	mandarin, orange, pummelo		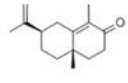	Hosni et al. (2010)
65	geranyl α-terpinene		peel	orange, pummelo		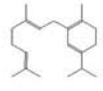	Hosni et al. (2010)
66	δ-cadinene	sesquiterpene	peel	pummelo		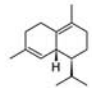	Hosni et al. (2010)
67	germacrene-B	sesquiterpene hydrocarbon	peel	pummelo		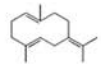	Hosni et al. (2010)
68	germacrene-D	sesquiterpene hydrocarbon	peel	mandarin, orange, pummelo, lemon	insecticidal activity	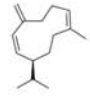	Hosni et al. (2010), Lota et al. (2002), Røstelien et al. (2000)
69	α-sinensal	sesquiterpene aldehyde	peel, leaf	mandarin, orange, lemon		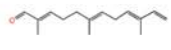	Hosni et al. (2010), Lota et al. (2002)
70	β- sinensal	sesquiterpene aldehyde	peel, leaf	orange, pummelo, lemon		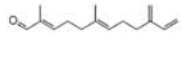	Hosni et al. (2010), Lota et al. (2002)

dx.doi.org/10.1021/jf5006148 | J. Agric. Food Chem. 2014, 62, 3011−3033

Table 1. continued

#	Name	class	organ	*Citrus* species	Bioactivity	Structure	References
71	γ-eudesmol	sesquiterpenoid	peel	pummelo		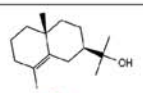	Hosni et al. (2010)
72	τ-cadinol	sesquiterpene	peel	orange, pummelo		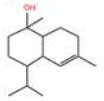	Hosni et al. (2010)
73	bicyclogermacrene	sesquiterpene hydrocarbon	peel	orange, pummelo		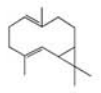	Hosni et al. (2010)
74	caryophyllene oxide	sesquiterpene oxide	leaf, peel	lemon	antifungal activity anti-inflammatory	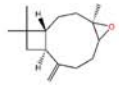	Lota et al. (2002), Yang et al. (2000), Chavan et al. (2010)
75	α-calacorene	sesquiterpene	peel	mandarin			Hosni et al. (2010)

varies significantly among the *Citrus* species and/or varieties. For example, sweet orange contains 83−97%, lemon, 54−80%, and bergamot, 25−32% limonene. [32] The nonvolatile residue, which forms about 1−15% of the oil, contains hydrocarbons, sterols, fatty acids, waxes, carotenoids, coumarins, psoralens, and flavonoids,[31] among which flavonoids are a group of components useful in differentiating between species.[17] By the end of 1970, approximately 200 different compounds had been described from orange oil, among which around 100 have been identified. In the review by Shaw,[32] the quantitative values for individual components of cold-pressed oils of different citrus species and varieties were presented, which gave us a general idea of the oil compositions of different citrus types. On the basis of previous studies,[28−30,33−36] the 75 most-reported monoterpenes and sesquiterpenes in CEOs extracted from different organs (flowers, leaves, and peels), species, and/or varieties are summarized in Table 1.

The chemical compositions of CEOs are influenced by both internal and external factors.[37,38] The genetic factors, including species, cultivars, and different parts of the fruits, are the major determinant of the composition and contents of essential oils. A comparison study of essential oils from the peels of four selected Tunisian citrus species showed that δ-cadinene, a sesquiterpene in CEOs, was found only in pummelo and α-calacorene, another sesquiterpene, was observed only in mandarin.[30] Furthermore, cultivars also influence the citrus oil profiles.[28,39] Lota et al.[28] reported that the composition and content of CEOs were different among 58 mandarin cultivars belonging to 15 different species, and the contents of the major components of these essential oils varied considerably from sample to sample. In addition, the chemical compositions of CEOs also vary significantly depending on the organs extracted. For example, terpineol-4 was one of the major compounds in the leaf oils of lemon, whereas it was not detected in peel oils.[29] Environmental factors such as soil, cultural practices, insects, ripening stage, and weather can contribute to the quantitative variations of essential oils.[38] Azizi et al.[40] compared the response of oregano (*Origanum vulgare* L.) populations to soil moisture regimens (optimal, consistent water deficiency, and water deficiency from the beginning of flowering) and nitrogen application, and they found that water deficiency after the beginning of blooming could induce an increase in essential oil content, whereas higher nitrogen levels caused a decrease. Besides soil and cultural practice factors, weather differences such as seasonal variations can also induce a difference in the composition and content of essential oils. For example, Vekiari et al.[34] measured the components of essential oil from Zambetakis (*Citrus limon* Burm.f.) at six different time intervals over a period of greater than a year. They found significant differences between the aroma profiles and quantitative variations between lemon leaves and peels and attributed those variations to the different harvest periods of citrus leaves and fruits. Their study suggested that the ripening effect influenced significantly the chemical compositions of the essential oil. Genetic and environmental factors not only influence the oil compositions and contents but also affect the bioactivity of the oils. For example, Fisher and Phillips[41] investigated the antibacterial activity of oils from lemon, sweet orange, and bergamot. They found that bergamot was the most effective among the tested oils due to its high linalool content.

CEOs and their chemical compositions possess a wide spectrum of biological activities, including antimicrobial,[34,42−49] antioxidant,[50,51] anticancer,[52−55] anti-inflammatory,[56−60] insecticidal,[61−67] embryo-fetotoxicity, [68] and metabolism disorder regulating activity.[69−76] All of the bioactivities mentioned above are summarized in Table 1. The biological activity of monocyclic monoterpene D-limonene has been evaluated by a number of studies, such as antioxidant,[77−79] anti-inflammatory, [38] anticancer,[80,81] and metabolic disorder alleviating activities.[75,82] In addition, geraniol, a terpene alcohol in CEOs, represents a new class of chemoprevention agents for cancer and other biological activities such as antimicrobial, antioxidant, anti-inflammatory, and some vascular effects.[50] Taken together, CEOs and their chemical compositions may be of great importance in many fields, from food chemistry to pharmacology and pharmaceutics.

METHODS USED IN THE ASSESSMENT OF ANTIFUNGAL ACTIVITY OF CEOS

The major methods used for the assessment of antimicrobial activity of essential oils have been summarized in several recent reviews, which include the agar diffusion test, the agar or broth dilution test, and the vapor phase test.[17,83] The particular advantages and disadvantages of these different methods are

Table 2. In Vitro Antifungal Activity of CEOs Reported in Current Literature

effective against	test CEOs	major component	test method	effects	references
Aspergillus niger	lemon (*C. limon* Burm.f.)	citral, eugenol	agar diffusion method	inhibition halo =10 mm	Souza et al. (2005)
	lemon (*C. limon* Burm.f.)		agar diffusion test	inhibition zone =7 mm	Pawar and Thaker (2006)
	sour orange (*C. aurantium* L.)		agar diffusion test	inhibition zone =6 mm	Pawar and Thaker (2006)
	orange (*C. sinensis* Osb.)	limonene (84.2%)	poisoned food assay; volatile activity assay	MIC = 600 ppm (PF[a]) MIC = 500 ppm (VA[b])	Sharma and Tripathi (2008)
	lemon (*C. limon* Burm.f.)		modified agar dilution	MIC = 0.94% (v/v)	Viuda-Martos et al. (2008)
	mandarin (*C. reticulata* Blanco)		modified agar dilution	MIC = 0.94% (v/v)	Viuda-Martos et al. (2008)
	orange (*C. sinensis* Osb.)		modified agar dilution	MIC = 0.94% (v/v)	Viuda-Martos et al. (2008)
	grapefruit (*C. paradisi* Macf.)		modified agar dilution	MIC = 0.94% (v/v)	Viuda-Martos et al. (2008)
	Citri-V[c]	limonene (603.99 mg/mL)	vapor phase test	67% reduction at 15 mg/L air	Phillips et al. (2012)
Aspergillus flavus	lemon (*C. limon* Burm.f.)		modified agar dilution	MIC = 0.94% (v/v)	Viuda-Martos et al. (2008)
	lemon (*C. limon* Burm.f.)	citral, eugenol	agar diffusion method	inhibition halo =13 mm	Souza et al. (2005)
	mandarin (*C. reticulata* Blanco)		modified agar dilution	MIC = 0.94% (v/v)	Viuda-Martos et al. (2008)
	orange (*C. sinensis* Osb.)		modified agar dilution	MIC = 0.94% (v/v)	Viuda-Martos et al. (2008)
	orange (*C. sinensis* Osb.)	limonene (31.83%), citral (31.0%)	poisoned food assay	100% inhibition at 750 ppm	Singh et al. (2010)
	orange (*C. sinensis* Osb.)	limonene	agar dilution method	MIC = 0.5% (v/v)	Bosquez-Molina et al. (2010)
	grapefruit (*C. paradisi* Macf.)		modified agar dilution	MIC = 0.94% (v/v)	Viuda-Martos et al. (2008)
	pummelo (*C. maxima* Burm.)	limonene	agar dilution method	MIC = 0.5% (v/v)	Bosquez-Molina et al. (2010)
	pummelo (*C. maxima* Burm.)	limonene (31.83%), citral (31.0%)	poisoned food assay	100% inhibition at 750 ppm	Singh et al. (2010)
	lime (*C. hystrix* DC)	limonene, citronellol, linalool	agar diffusion method; broth microdilution	MIC = 1%, 4% (v/v)	Rammance and Hongpattarakere (2011)
	acid lime (*C. aurantifolia*)	limonene, *p*-cymene	agar diffusion method; broth microdilution	MIC = 1%, 4% (v/v)	Rammance and Hongpattarakere (2011)
	orange (*C. sinensis* Osb.) vapor	limonene (96.62%)	vapor phase test	MIC = 8000 EO/air	Velázquez-Nuñez et al. (2013)
	orange (*C. sinensis* Osb.)	limonene (96.62%)	agar dilution method	MIC = 16000 mg/L	
Aspergillus fumigatu	orange (*C. sinensis* Osb.)	limonene (31.83%), citral (31.0%)	poisoned food assay	100% inhibition at 750 ppm	Singh et al. (2010)
	pummelo (*C. maxima* Burm.)	limonene (31.83%), citral (31.0%)	poisoned food assay	100% inhibition at 750 ppm	Singh et al. (2010)
Aspergillus terreus	orange (*C. sinensis* Osb.)	limonene (31.83%), citral (31.0%)	poisoned food assay	100% inhibition at 750 ppm	Singh et al. (2010)
	pummelo (*C. maxima* Burm.)	limonene (31.83%), citral (31.0%)	poisoned food assay	100% inhibition at 750 ppm	Singh et al. (2010)
Aspergillus parasiticus	lime (*C. hystrix* DC)	limonene, citronellol, linalool	agar diffusion method; broth microdilution	MIC = 1%, 4% (v/v)	Rammance and Hongpattarakere (2011)
	acid lime (*C. aurantifolia*)	limonene, *p*-cymene	agar diffusion method; broth microdilution	MIC = 1%, 4% (v/v)	Rammance and Hongpattarakere (2011)
Penicillium chrysogenum	lemon (*C. limon* Burm.f.)		modified agar dilution	MIC = 0.94% (v/v)	Viuda-Martos et al. (2008)
	mandarin (*C. reticulata* Blanco)		modified agar dilution	MIC = 0.94% (v/v)	Viuda-Martos et al. (2008)
	orange (*C. sinensis* Osb.)		modified agar dilution	MIC = 0.94% (v/v)	Viuda-Martos et al. (2008)
	orange (*C. sinensis* Osb.)	limonene (77.49%); myrcene (6.27%)	agar diffusion method; broth microdilution	inhibition zone = 18.99 mm; MIC = 9.33 μL/mL	Tao et al. (2009)
	grapefruit (*C. paradisi* Macf.)		modified agar dilution	MIC = 0.94% (v/v)	Viuda-Martos et al. (2008)
	Citri-V	limonene (603.99 mg/mL)	vapor phase test	43.8% reduction at 14 mg/L air	Phillips et al. (2012)

dx.doi.org/10.1021/jf5006148 | J. Agric. Food Chem. 2014, 62, 3011−3033

Table 2. continued

effective against	test CEOs	major component	test method	effects	references
Penicillium chrysogenum MPPLU 27	orange (*C. sinensis* Osb.)	limonene (84.2%), linalool (4.4%)	poisoned food technique; volatile activity assay	MIC = 600 ppm (PF), MIC = 500 ppm (VA)	Sharma and Tripathi (2006)
Penicillium verrucosum	lemon (*C. limon* Burm.f.)		modified agar dilution	MIC = 0.94% (v/v)	Viuda-Martos et al. (2008)
	mandarin (*C. reticulata* Blanco)		modified agar dilution	MIC = 0.94% (v/v)	Viuda-Martos et al. (2008)
	orange (*C. sinensis* Osb.)		modified agar dilution	MIC = 0.94% (v/v)	Viuda-Martos et al. (2008)
	grapefruit (*C. paradisi* Macf.)		modified agar dilution	MIC = 0.94% (v/v)	Viuda-Martos et al. (2008)
Penicillium spp.	lemon (*C. limon* Burm.f.)	citral, eugenol	agar diffusion method	not effective	Souza et al. (2005)
Penicillium digitatum	orange (*C. sinensis* Osb.)	limonene, myrcene	dry weight determination	ED_{50} = 2180.2 ppm (A1)	Caccioni et al. (1998)
	sour orange (*C. aurantium* L.)	limonene, myrcene	dry weight determination	ED_{50} = 1015.4 ppm	Caccioni et al. (1998)
	mandarin (*C. reticulata* Blanco)	limonene, α-pinene	dry weight determination	ED_{50} = 713.3 ppm	Caccioni et al. (1998)
	grapefruit (*C. paradisi* Macf.)	limonene, myrcene	dry weight determination	ED_{50} = 910.3 ppm (P1)	Caccioni et al. (1998)
	lemon (*C. limon* Burm.f.)	limonene, α-pinene	dry weight determination	ED_{50} = 1056.4 ppm (L1)	Caccioni et al. (1998)
	mandarin (*C. reticulata* Blanco)	limonene (60.74%), γ-terpinene (0.04%)	poisoned food technique	100% inhibition at 10.0 μL/mL	Tao et al. (2013)
Penicillium italicum	orange (*C. sinensis* Osb.)	limonene, myrcene	dry weight determination	ED_{50} = 5407.5 ppm (A1)	Caccioni et al. (1998)
	sour orange (*C. aurantium* L.)	limonene, myrcene	dry weight determination	ED_{50} = 1490.6 ppm	Caccioni et al. (1998)
	mandarin (*C. reticulata* Blanco)	limonene, α-pinene	dry weight determination	ED_{50} = 1977.0 ppm	Caccioni et al. (1998)
	grapefruit (*C. paradisi* Macf.)	limonene, myrcene	dry weight determination	ED_{50} = 1498.4 ppm (P1)	Caccioni et al. (1998)
	lemon (*C. limon* Burm.f.)	limonene, α-pinene	dry weight determination	ED_{50} = 2505.4 ppm (L1)	Caccioni et al. (1998)
	mandarin (*C. reticulata* Blanco)	limonene (60.74%), γ-terpinene (0.04%)	poisoned food technique	100% inhibition at 2.5 μL/mL	Tao et al. (2013)
Penicillium expansum	orange (*C. sinensis* Osb.)	limonene (90.42%), myrcene (2.81%)	agar dilution method	34.9% inhibition at 2000 ppm	Van Hung et al. (2013)
	mandarin (*C. reticulata* Blanco)	limonene (91.58%), myrcene (2.79%)	agar dilution method	39.3% inhibition at 2000 ppm	Van Hung et al. (2013)
	lime (*C. autantifolia*)	limonene (41.4%), β-pinene (18.54%)	agar dilution method	52.0% inhibition at 2000 ppm	Van Hung et al. (2013)
	pummelo (*C. grandis* Osb.)	limonene(70.46%),γ-terpinene (11.09%)	agar dilution method	53.8% inhibition at 2000 ppm	Van Hung et al. (2013)
Penicillium expansum MPPLU 24	orange (*C. sinensis* Osb.)	limonene (84.2%), linalool (4.4%)	poisoned food assay; volatile activity assay	MIC = 600 ppm (PF) MIC = 500 ppm (VA)	Sharma and Tripathi (2006)
Fusarium spp.	lemon (*C. limon* Burm.f.)	citral, eugenol	plate diffusion procedure	not effective	Souza et al. (2005)
Fusarium oxysporum	orange (*C. sinensis* Osb.)	limonene (31.83%), citral (31.0%)	poisoned food assay	100% inhibition at 750 ppm	Singh et al. (2010)
	pummelo (*C. maxima* Burm.)	limonene (31.83%), citral (31.0%)	poisoned food assay	100% inhibition at 750 ppm	Singh et al. (2010)
	mandarin (*C. reticulata* Blanco)	limonene (46.7%), geranial (19.0%)	poisoned food assay; volatile activity assay	MIC> 0.2% (v/v)	Chutia et al. (2009)
Fusarium proliferatum	orange (*C. sinensis* Osb.)	limonene (90.42%), myrcene (2.81%)	agar dilution method	59.5% inhibition at 2000 ppm	Van Hung et al. (2013)
	mandarin (*C. reticulata* Blanco)	limonene (91.58%), myrcene (2.79%)	agar dilution method	50.9% inhibition at 2000 ppm	Van Hung et al. (2013)
	lime (*C. autantifolia*)	limonene (41.4%), β-pinene (18.54%)	agar dilution method	91.5% inhibition at 2000 ppm	Van Hung et al. (2013)
	pummelo (*C. grandis* Osb.)	limonene (70.46%), γ-terpinene (11.09%)	agar dilution method	63.0% inhibition at 2000 ppm	Van Hung et al. (2013)
Alternaria alternata	mandarin (*C. reticulata* Blanco)	limonene (46.7%), geranial (19.0%)	poisoned food assay; volatile activity assay	MIC = 0.2% (v/v)	Chutia et al. (2009)

Table 2. continued

effective against	test CEOs	major component	test method	effects	references
	Citri-V		vapor phase test	34% reduction at 15 mg/L air	Phillips et al. (2012)
	orange (*C. sinensis* Osb.)	limonene (31.83%), citral (31.0%)	poisoned food assay	100% inhibition at 750 ppm	Singh et al. (2010)
	pummelo (*C. maxima* Burm.)	limonene (31.83%), citral (31.0%)	poisoned food assay	100% inhibition at 750 ppm	Singh et al. (2010)
	orange (*C. sinensis* Osb.)	limonene (84.2%), linalool (4.4%)	poisoned food assay; volatile activity assay	MIC = 600 ppm (PF) MIC = 500 ppm (VA)	Sharma and Tripathi (2006)
Rhizoctonia solani	mandarin (*C. reticulata* Blanco)	limonene (46.7%), geranial (19.0%)	poisoned food assay; volatile activity assay	MIC = 0.2% (v/v)	Chutia et al. (2009)
Curvularia lunata	mandarin (*C. reticulata* Blanco)	limonene (46.7%), geranial (19.0%)	poisoned food assay; volatile activity assay	MIC = 0.2% (v/v)	Chutia et al. (2009)
Colletotrichum gloeosporioides	lime (*C. aurantifolia*)		agar dilution method	MIC = 0.5% (v/v)	Bosquez-Molina et al. (2010)
Rhizopus spp.	lemon (*C. limon* Burm.f.)	citral, eugenol	agar diffusion method	inhibition halo =12 mm	Souza et al. (2005)
Rhizopus stolonifer	lime (*C. autantifolia*)		agar dilution method	MIC = 0.5% (v/v)	Bosquez-Molina et al. (2010)
Helminthosporium oryzae	mandarin (*C. reticulata* Blanco)	limonene (46.7%), geranial (19.0%)	poisoned food assay; volatile activity assay	MIC > 0.2% (v/v)	Chutia et al. (2009)
Phaeoramularia angolensis	pummelo (*C. maxima* Burm.)		poisoned food assay	>87% inhibition at 2500 ppm	Kuate et al. (2006)
	grapefruit (*C. paradisi* Macf.)		poisoned food assay	>64% inhibition at 2500 ppm	Kuate et al. (2006)
Botryodiplodia theobromae	orange (*C. sinensis* Osb.)	limonene (84.2%), linalool (4.4%)	poisoned food assay; volatile activity assay	MIC = 600 ppm (VA)	Sharma and Tripathi (2006)
Cladosporium fulvum	orange (*C. sinensis* Osb.)	limonene (84.2%), linalool (4.4%)	poisoned food assay; volatile activity assay	MIC = 700 ppm (PF); MIC = 500 ppm (VA)	Sharma and Tripathi (2006)
Botrytis cinerea	orange (*C. sinensis* Osb.)	limonene (84.2%), linalool (4.4%)	poisoned food assay; volatile activity assay	MIC = 500 ppm (PF); MIC = 400 ppm (VA)	Sharma and Tripathi (2006)
	lemon (*C. limon* Burm.f.)		agar dilution method	MIC = 17 or 22 μL/mL; ED 50 = 11 or 13 μL/mL	Vitoratos et al. (2013)
Cladosporium cladosporioides	orange (*C. sinensis* Osb.)	limonene (84.2%), linalool (4.4%)	poisoned food assay; volatile activity assay	MIC = 500 ppm (PF); MIC = 400 ppm (VA)	Sharma and Tripathi (2006)
Myrothecium roridum	orange (*C. sinensis* Osb.)	limonene (84.2%), linalool (4.4%)	poisoned food assay; volatile activity assay	MIC = 700 ppm (VA)	Sharma and Tripathi (2006)
Mucor hiemalis	orange (*C. sinensis* Osb.)	limonene (90.42%), myrcene (2.81%)	agar dilution method	36.5% inhibition at 2000 ppm	Van Hung et al. (2013)
	mandarin (*C. reticulata* Blanco)	limonene (91.58%), myrcene (2.79%)	agar dilution method	37.1% inhibition at 2000 ppm	Van Hung et al. (2013)
	lime (*C. aurantifolia*)	limonene (41.4%), β-pinene (18.54%)	agar dilution method	100% inhibition at 2000 ppm	Van Hung et al. (2013)
	pummelo (*C. grandis* Osb.)	limonene (70.46%), γ-terpinene (11.09%)	agar dilution method	42.1% inhibition at 2000 ppm	Van Hung et al. (2013)
Helminthosporium oryzae	orange (*C. sinensis* Osb.)	limonene (31.83%), citral (31.0%)	poisoned food assay	100% inhibition at 750 ppm	Singh et al. (2010)
	pummelo (*C. maxima* Burm.)	limonene (31.83%), citral (31.0%)	poisoned food assay	100% inhibition at 750 ppm	Singh et al. (2010)
Trichoderma viride	orange (*C. sinensis* Osb.)	limonene (31.83%), citral (31.0%)	poisoned food assay	100% inhibition at 750 ppm	Singh et al. (2010)
	pummelo (*C. maxima* Burm.)	limonene (31.83%), citral (31.0%)	poisoned food assay	100% inhibition at 750 ppm	Singh et al. (2010)
Saccharomyces cerevisiae	orange (*C. sinensis* Osb.)	limonene (77.49%), myrcene (6.27%)	agar diffusion method; broth microdilution	inhibition zone = 14.57 mm; MIC = 18.75 μL/mL	Tao et al. (2009)

[a]Citri-V, a 50:50 mix of orange/bergamot essential oils (AMPHORA, Bristol, UK). [b]PF, poisoned food technique. [c]VA, volatile activity assay.

dx.doi.org/10.1021/jf5006148 | J. Agric. Food Chem. 2014, 62, 3011−3033

extensively discussed in the book by Pauli et al.[84] and the reviews mentioned above. In this review, we summarize several of the most commonly used in vitro testing methods for the antifungal assessment of CEOs, especially the agar diffusion, the broth/agar dilution test, the broth microdilution method, and the poisoned food technique.

Agar Diffusion Test. This method was described and utilized as a standardized method for the screening of essential oils in the past decades and has been adapted in numerous ways based on the same principle.[85] The agar diffusion test is performed by placing an essential oil impregnated filter disk on the surface of agar containing the microbe to be tested, and the antifungal activity of tested essential oils is evaluated by measuring the inhibition zones. The agar diffusion method seems to be the most popular method for examining antimicrobial activity as it allows for the simultaneous testing of a large number of antimicrobials in a relatively easy and flexible manner.[86] As shown in Table 2, the agar diffusion test has been widely used in the assessment of antifungal activity of CEOs. However, it is noteworthy to point out that the size of inhibition zones is difficult to be interpreted due to the unknown diffusion coefficients, the different volatilities of single constituents, and other factors such as agar type, agar−agar content, pH, and volume of agar.[83] In particular, the results obtained from this method have shown misleadingly low antifungal activity when the components have low water solubility. [83]

Broth/Agar Dilution Test. The dilution test is another in vitro method widely used for assessing the antifungal activity of CEOs (Table 2). In the broth dilution test, a concentration series of the antifungal substance is established using a broth medium, which is seeded with fungal strains, whereas in the agar dilution test, a concentration gradient of the tested substance is placed onto an agar plate.[83] For both methods, a minimum inhibition concentration (MIC) is used to evaluate the antifungal activity of the tested substance(s), which presents the lowest concentration of tested substance(s) that prevents the growth of seeded fungal strains. The advantages and disadvantages of these two dilution test methods have been summarized in detail by Jiang.[86] Generally, in the agar dilution method, the agar with supplements is able to adequately support fungus growth, whereas in the broth dilution method, lack of or poor growth of many anaerobic microorganisms was observed because of insufficient supplements. The agar dilution test has been declared to be the "gold standard" as it overcomes some limitations of the agar diffusion method, primarily the capability to draw a quantitative conclusion by determining the MIC value of the tested substance(s).[86−88] This method can also be used to test the susceptibility of a number of substance(s) in one plate simultaneously, as well as to test fastidious organisms due to the agar being able to adequately support microorganism growth.[86] However, it is not used frequently due to its high-cost, labor-intensive, and time-consuming properties. [83]

Broth Microdilution Method. Broth microdilution is another quantitative reference method for the fungitoxicity test of CEOs, which allows for the simultaneous testing of multiple antimicrobials with ease, particularly when commercially prepared microtiter trays are used.[16,86,89] In the study by Jiang,[86] the agar diffusion, the broth/agar dilution test, and the broth microdilution method have been compared on several bacterial strains. Jiang suggested that the broth microdilution be used for MIC determination, compared to other methods, due to its time and labor savings, as well as its capability of quantitative determination. However, inconsistent and unreliable results can occur when some fastidious anaerobes are tested because of their poor growth due to excessive exposure to oxygen during the setup procedure.

Poisoned Food Technique. The poisoned food technique has been used widely in the antifungal assessment of CEOs (Table 2). In this method, the fungitoxicity was expressed in terms of percentage of mycelia growth inhibition and calculated as follows: percentage of mycelial growth inhibition = $(dc - dt)/dc \times 100$, where dc = average diameter of fungal colony in control and dt = average diameter of fungal colony in treatment.[90,91]

As shown in Table 2, there are other methods that have been used for the antifungal activity test of CEOs, such as mycelium dry weight determination test[20,91,92] and volatile activity assay.[20,93] As for the vapor phase test of CEOs, the related methodology has been discussed and summarized in the reviews by Cavanagh[94] and Laid and Phillips;[95] however, there is no standardized method available. In general, a seeded agar plate is placed upside down onto a reservoir, which comprises a certain amount of volatile oil. In this case the generated inhibition zone is considered to be a criterion for the antimicrobial activity.[83]

In general, each method has its own advantages and disadvantages. Antifungal tests of essential oils are difficult to perform because of their high volatility, which can result in distorted results. Another problem is the hydrophobicity of the essential oils, which sometimes demands the use of surfactants that might lead to noteworthy differences between outcomes.

■ IN VITRO ANTIFUNGAL EFFECTS OF CEOS

The antimicrobial property of CEOs was recognized a long time ago.[17] In the past decades, the antifungal activity of CEOs has attracted the attention of many researchers.[19,21,22,96−98] Table 2 summarizes the in vitro antifungal effects of CEOs reported in the current literature. In vitro experiments are valuable precursors to more costly food trials and enable the identification of effective essential oils and determination of the concentrations required for inhibition of a specific pathogen or a spectrum of pathogens.[99] The following part of this review will focus on the antifungal activity of CEOs against some food spoilage or phytopathogenic fungal species, especially *Aspergillus* and *Penicillium* species.

Aspergillus is a genus consisting of several hundred species, which are highly aerobic and found in almost all oxygen-rich environments. *Aspergillus* species are common contaminants of starchy foods such as bread and potatoes. The current literature has shown that CEOs have a broad anti-*Aspergillus* spectrum including *A. niger*, *A. flavus*, *A. fumigatus*, *A. terreus*, and *A. parasiticus* (Table 2). Among these species, *A. niger* and *A. flavus* are the most commonly used strains in the antifungal test of CEOs (Table 2).[2,10,16,19,21,22,89,93,100]

The first anti-*Aspergillus* research of CEOs can be traced back to 1985, when Karapinar[101] found that CEOs could inhibit the growth and aflatoxin formation of *A. parasiticus*. In 2006, Pawar and Thaker[100] compared the effects of 75 plant essential oils on the hyphal growth and spore formation of *A. niger*, among which the essential oils of sour orange (*Citrus aurantium* L.), bergamot (*Citrus bergamia* Risso and Poit), lemon (*Citrus limon* Burm.f.), and *Citrus bigaradia* Hook.f. exhibited inhibitory effects. In agreement with this, Viuda-Martos et al.[21] reported that lemon, mandarin, grapefruit, and sweet orange essential

oils could reduce or inhibit the growth of *A. niger* and *A. flavus* in a dose-dependent manner, with sweet orange essential oil being the most effective against *A. niger* and mandarin being the best inhibitor of *A. flavus*. Sharma and Tripathi[91] found that the sweet orange essential oil treatment resulted in the flattening and ultimate death of *A. niger* hyphae, and limonene was the major component (84.2%) of the oil. The study conducted by Singh et al.[19] found that pummelo (*Citrus maxima* Burm.) and sweet orange (*Citrus sinensis* Osb.) essential oils and their combination were all effective against *A. flavus*, with the essential oil of pummelo being the most effective. In the study by Rammanee and Hongpattarakere,[16] the essential oils prepared from citrus epicarps exhibited stronger antifungal activity to all *Aspergillus* strains than their ethyl acetate extracts. In particular, the essential oils from kaffir lime (*Citrus hystrix* DC) and acid lime (*Citrus aurantifolia* Swingle) were most inhibitory to mold growth as well as aflatoxin production among all of the tested citrus cultivars. On the basis of the studies mentioned above, it can be concluded that the CEOs are effective against *Aspergillus* species.

The genus *Penicillium* is another prevalent airborne fungus, which belongs to the same family as *Aspergillus*. There are over 300 different species described in the genus. *P. digitatum*, *P. italicum*, and *P. chrysogenum* are among the most reported *Penicillium* species that have been used for the fungitoxicity test of CEOs. In 1995, Caccioni and his colleagues[102] found that CEOs could exert an important bioregulatory action on the fungal spores of *P. digitatum* (Pers.) Sacc. and *P. italicum* Wehm, which are the two most dangerous postharvest pathogens of citrus fruit. Viuda-Martos et al.[21] found that lemon, mandarin, grapefruit, and sweet orange essential oils had the capacity to reduce or inhibit the growth of *P. chrysogenum* in a dose−response manner, and grapefruit was the best inhibitor among those four CEOs, followed by lemon essential oil. Tao et al.[89] reported that Bingtang sweet orange essential oil exhibited high antifungal activity against *P. chrysogenum* ATCC 10106, with an inhibition zone of 18.99 mm. In a study by Sharma and Tripathi,[93] sweet orange essential oil completely inhibited the radial growth and spore germination of *P. chrysogenum* and *P. expansum*, as well as other postharvest pathogens. Van Hung et al.[103] compared the antifungal activity of the essential oils from four citrus species and found that pummelo essential oil was the most effective against *P. expansum*. In addition, CEOs have been reported to have antifungal activity against *Penicillium* spp.[2] and *P. verrucosum* (Table 2).[21]

Besides these most studied *Aspergillus* and *Penicillium* species, CEOs have also been reported to have antifungal activity against *Fusarium*,[2,19,20,103] *Alternaria*[19,20,93] (Table 2), and other fungal strains.[97,98]

Furthermore, the vapor phase of CEOs has also been assessed for their antifungal activity, and they exhibited antifungal activity against several fungal strains, such as *A. flavus*[10] and *Alternaria alternata*.[22] The study performed by Velázquez-Nuñez et al.[10] showed that the vapor state was more effective than the liquid state of orange peel essential oil in antifungal activity, and lower concentrations were required to achieve the same antifungal effect. The advantages of vapor phase of essential oils over the direct application of the oils themselves have been summarized in the review by Cavanagh,[94] such as reduced toxicity and ease of application. The author also suggested that the vapor phase of essential oils had great potential for use in fungal control and/or treatment.

On the basis of the reports mentioned above, we may conclude that CEOs are effective in inhibiting the growth of mycelia and spores and in reducing the production of mycotoxins against different fungal species. The essential oils from the same citrus species have about the same antifungal activity, but it also varies from cultivar to cultivar. On the basis of GC-MS analysis data, different chemical compositions have been identified in different CEOs, among which limonene was found to be the major component (Table 2). Table 2 shows the concentrations of limonene varied from 31.83 to 96.62% in the essential oil samples used for the antifungal experiments. From this information, the fungitoxicity of CEOs can be attributed to their chemical composition and the concentration of active compounds. This conclusion is in agreement with the reports that the antifungal activity of CEOs relied on their chemical composition.[1,17] However, the exact active compounds that contribute to the fungitoxicity of CEOs still need to be further clarified in future studies.

Antifungal Activity of CEOs on Food. To explore the potential of CEOs as alternative additives or fungicides on food, their antimicrobial effectiveness, especially antibacterial activity, has been investigated by using several common foodborne pathogens. CEOs have been reported to be effective against a number of bacteria that cause food spoilage or poisoning, but their antibacterial activities on the strains tested were less effective in food systems than in vitro.[41,104] The antifungal assessments of CEOs on food, however, have not been performed until recently. For example, Bosquez-Molina et al.[3] reported that the Mexican lime essential oils had inhibitory effects against *Colletotrichum gloeosporioides* and *Rhizopus stolonifer* growth of storage rots in papaya fruit. Vitoratos et al.[98] found that lemon essential oils were very effective against the fungus *Botrytis cinerea* in tomatoes, strawberries, and cucumbers.

The fungitoxicity assessment on food is necessary and essential for the screening and confirmation of the antifungal activity of CEOs before they are applied in the food industry, as the efficacy of bioactive compounds might decay due to possible interactions of these compounds with the food matrix. For example, Phillips et al.[22] assessed the antifungal effects of CEOs both in vitro and on food, including tomatoes and grain, against three fungal strains (*A. niger*, *P. chrysogenum*. and *Alternaria alternata*). They found that citrus essential oil vapors completely inhibited the mycelial growth and spore germination of those three fungi in in vitro tests; however, similar results were not observed on tomatoes or grain. It is important to point out that higher concentrations of CEOs or their chemical components should be used in food products to obtain the same effect observed in in vitro experiments, as highly hydrophobic and volatile active substances are often bound by food surfaces.[1] Unfortunately, Dusan and his colleagues[105] demonstrated that higher dose of essential oils showed detrimental effects on intestinal cells. Therefore, animal and human toxicity studies of CEOs should be carried out before their commercial use.

Antifungal Components of CEOs and Their Mechanism of Action. CEOs are a complex mixture of volatile compounds. The antifungal activity of CEOs has been attributed to a single major compound or to the synergistic or antagonistic effect of different compounds.[106] Some authors suggested that the flavonoids likely play a contributing role in the antifungal activity of CEOs.[107] However, more and more authors tend to attribute the antifungal function to the presence

Table 3. Antifungal Effects of CEOs on Food Reported in Current Literature

test CEO	effective against	test food	effect	reference
lime (*C. aurantifolia*)	*Rhizopus stolonifer*	papaya fruits	reduction of up to 40% of decay	Bosquez-Molina et al. (2010)
lime (*C. aurantifolia*)	*Colletotrichum gloeosporioides*	papaya fruits	reduction of up to 50% of decay	Bosquez-Molina et al. (2010)
bergamot		grapes	log UFC value for molds reduced	Sánchez-González et al. (2011)
50:50 mix of orange/bergamot	*Aspergillus niger*	grain	reduction of 70.8% of growth	Phillips et al. (2012)
50:50 mix of orange/bergamot	*Penicillium chrysogenum*	grain	reduction of 57.8% of growth	Phillips et al. (2012)
50:50 mix of orange/bergamot	*Alternaria alternata*	tomatoes	not effective	Phillips et al. (2012)
lemon (*C. limon* Burm.f.)	*Botrytis cinerea*	strawberries	100% inhibition at 0.05 μL/mL	Vitoratos et al. (2013)
lemon (*C. limon* Burm.f.)	*Botrytis cinerea*	cucumber	39% inhibition at 0.05 μL/mL	Vitoratos et al. (2013)

of the volatile compounds of CEOs, mainly terpenoids, especially monoterpenes and sesquiterpenes.[108−113] In the following, the antifungal effective components in CEOs (Tables 3 and 4) and their suggested mechanisms of action are reviewed.

Antifungal Activity of Flavonoids in CEOs. Flavonoids are a group of polyphenolic compounds that include flavanone, flavone and polymethoxy flavone aglycones, flavanone- and flavone-*O*-glycosides, and flavone-*C*-glycosides.[114] Citrus flavonoids have been reported to have many biological activities, such as antioxidant, antimicrobial, and anti-inflammatory properties.[114−119] The antifungal activity of citrus flavonoids has been investigated by many authors in the past decades. To our knowledge, citrus flavanones including naringin, hesperidin, neohesperidin, eriodictyol, prunin, and hesperitin glucoside[116,120,121] and polymethoxylated flavones such as sinensetin, nobiletin, heptamethoxy flavone, quercetogetin, and tangeretin[107,120,122] have been reported to have antifungal activity. The research conducted by Ortuño et al.[120] found that polymethoxylated flavones were more active than the flavanones, with nobiletin being the most effective one.

The polymethoxylated flavones in CEOs have also been examined for their antifungal activity. Del Río et al.[107] reported that sinensetin, nobiletin, heptamethoxyflavone, quercetogetin, and tangeretin could confer resistance against *Phytophthora citrophthora*, *P. digitatum*, and *Geotrichum* species. Almada-Ruiz et al.[123] found that 3,5,6,7,3′,4′-hexamethoxyflavone, 3,5,6,7,8,3′,4′-heptamethoxyflavone, 5,6,7,8,4′-pentamethoxyflavone, and 5,6,7,8,3′,4′-hexamethoxyflavone were effective in inhibiting mycelial growth of *Colletotrichum gloeosporioides* (Penz) Penz & Sacc, a major plant pathogen of fruits that causes significant damage to crops in tropical, subtropical, and temperate regions. These studies suggested that the polymethoxylated flavones in CEOs could be involved in the antifungal activity; however, this postulation was not convincing as polymethoxylated flavones occurred at low levels in CEOs. Another reason that polymethoxylated flavones were not suggested as the major antifungal component is that the citrus essential oil vapors have been reported to have antifungal activity,[95] and polymethoxylated flavones were not detected in the vapor state of CEOs. The antifungal activity of the flavonoids in CEOs still needs to be clarified.

Antifungal Activity of Terpenoids in CEOs. Terpenoids are a group of secondary metabolites in higher plants and are believed to have evolved in defense against herbivores and pathogens. Terpenoids, especially sesquiterpenes and monoterpenes, have been considered to be the most possible antifungal candidates in CEOs.[92,124] Caccioni and Guizzardi[124] found citrus oxygenated monoterpenes exhibited the highest antifungal activity among examined compounds. Caccioni et al.[92] reported that there was a positive correlation between the monoterpene content of the essential oils from various citrus species and the pathogen fungus inhibition. More recently, an increasing body of research has found that the terpenoids in CEOs, including citral, geranial, eugenol, γ-terpinene, *p*-cymene, myrcene, thymol, and carvacrol, had a wide spectrum of fungitoxicity.[2,11,125−130] Among these compounds, citral and limonene have been suggested as the most significant antifungal candidates of CEOs.

Citral is an acyclic α,β-unsaturated monoterpene aldehyde with two isomers, geranial and neral. The antifungal activity of citral has been demonstrated by several authors, either in CEOs or in other plant essential oils.[131,132] In the works carried out by Caccioni and his colleagues,[92,102] citral proved to have the best antifungal activity against *P. digitatum* and *P. italicum*, among the tested components including nonanal, citral, α-pinene, myrcene, α-phellandrene, and D-limonene. Souza et al.[2] determined the antifungal activity of different phytochemicals from lemon essential oils and found that citral, eugenol, and myrcene were fungitoxic. Overall, citral showed the best fungitoxicity. Wuryatmo et al.[133] examined the inhibitory effects of vapor citral, its isomers geranial and neral, and related compounds (such as *R*-citronellal, *S*-citronellol, and citronellic acid) on *P. digitatum*, *P. italicum*, and *Geotrichum candidum*, the major fungi responsible for postharvest spoilage of citrus. They found that the inhibitory effect of citral and its isomers differed among the three fungi, and citral was the most effective one even at lower concentrations. The above studies showed that citral and its isomers likely played important roles in the antifungal activities of CEOs, with citral having the most significant role.

Recently, more and more studies have suggested that limonene played an important role in the antifungal activity of CEOs.[3,16,20,89,92,93,103] Singh et al.[19] studied both CEOs and their major component limonene for their antifungal activity and found that limonene showed a better effect against *A. flavus* compared to the whole oils, even at lower concentrations. Mahdavi et al.[134] compared the antifungal effects of limonene and orange peel extract and found that limonene (*S*)-(−) isomer had better antifungal effect than its (*R*)-(−) isomer, whereas orange peel extract did not show any antifungal activity against the tested fungi. In addition, several studies have showed that limonene also had inhibitory activity against a wide range of fungi, including *A. niger*, *P. digitatum*, *Rhizoctonia solani*, *Fusarium oxysporum*, and *Fusarium verticillioides*, compared to other monoterpenes.[135,136] On the basis of the studies mentioned above, we can conclude that limonene has a higher antifungal activity against a wide range of fungi than other terpenoids and it is most likely one of the major contributors to the fungitoxicity of the CEOs.

The fungitoxicity of CEOs may be determined by their complex chemical compositions and the concentration profiles

Table 4. Antifungal Activity of Citrus-Derived Compounds

phytochemicals in CEO	type	effective against	test method	effect	reference
terpenes					
limonene	monoterpene	*Fusarium verticillioides*	modified semisolid agar antifungal susceptibility method	MIC = 1000 mL/L	Dambolena et al. (2008)
limonene	monoterpene	*Aspergillus flavus*	agar diffusion method; broth microdilution	MIC = 2.70 mg/mL MFC[a] = 3.15mg/mL	Rammance and Hongpattarakere (2011)
limonene	monoterpene	*Aspergillus parasiticus*	agar diffusion method; broth microdilution	MIC = 3.15 mg/mL MFC = 3.60 mg/mL	Rammance and Hongpattarakere (2011)
(*R*)-(+)-limonene	monoterpene	*Aspergillus niger*	agar well diffusion, paper disc diffusion	inhibition zone = 9 mm (30 μL) for agar well diffusion method	Mahdavi et al. (2011)
		Penicillium sp.	agar well diffusion, paper disc diffusion	inhibition zone = 3 mm (30 μL) for agar well diffusion method	Mahdavi et al. (2011)
		Aspergillus sp.	agar well diffusion, paper disc diffusion	inhibition zone = 7.5 mm (30 μL) for agar well diffusion method	Mahdavi et al. (2011)
		Candida albicans	agar well diffusion, paper disc diffusion	inhibition zone = 4 mm (30 μL) for agar well diffusion method	Mahdavi et al. (2011)
(*S*)-(+)-limonene	monoterpene	*Aspergillus niger*	agar well diffusion, paper disc diffusion	inhibition zone = 5.5 mm (30 μL) for agar well diffusion method	Mahdavi et al. (2011)
		Penicillium sp.	agar well diffusion, paper disc diffusion	inhibition zone = 3.5 mm (30 μL) for paper disc diffusion method	Mahdavi et al. (2011)
		Aspergillus sp.	agar well diffusion, paper disc diffusion	inhibition zone = 15 mm (30 μL) for agar well diffusion method	Mahdavi et al. (2011)
		Candida albicans	agar well diffusion, paper disc diffusion	inhibition zone = 9.5 mm (30 μL) for agar well diffusion method	Mahdavi et al. (2011)
DL-limonene	monoterpene	*Aspergillus flavus*	poisoned food assay	100% inhibition at 750 ppm	Singh et al. (2010)
D-limonene	monoterpene	*Penicillium italicum*	poisoned food technique	42.84% inhibition at 1.519 μL/mL	Tao et al. (2013)
		Penicillium digitatum	poisoned food technique	53.2% inhibition at 24.296 μL/mL	Tao et al. (2013)
citral	monoterpene	*Penicillium digitatum*	agar diffusion test		Caccioni et al. (1995)
		Penicillium italicum	agar diffusion test		Caccioni et al. (1995)
citral	monoterpene	*Aspergillus niger*	plate diffusion procedure	MIC = 0.5% (v/v)	Souza et al. (2005)
		Aspergillus flavus	plate diffusion procedure	MIC = 0.5% (v/v)	Souza et al. (2005)
		Fusarium spp.	plate diffusion procedure	MIC = 0.5% (v/v)	Souza et al. (2005)
		Penicillium spp.	plate diffusion procedure	MIC = 2.0% (v/v)	Souza et al. (2005)
		Rhizopus spp.	plate diffusion procedure	MIC = 8.0% (v/v)	Souza et al. (2005)
citral	monoterpene	*Aspergillus fumigatus*	AFST-EUCAST[b]	MIC = 78 μg/mL	Mesa-Arango et al. (2009)
		Candida krusei	AFST-EUCAST	MIC = 270.8 μg/mL	Mesa-Arango et al. (2009)
citral vapor	monoterpene	*Penicillium digitatum*	agar diffusion test	effective at 15 μL/L	Wuryatmo et al. (2003)
		Penicillium italicum	agar diffusion test	effective at 2−6 μL/L	Wuryatmo et al. (2003)
		Geotrichum candidum	agar diffusion test	effective at 15 μL/L	Wuryatmo et al. (2003)

dx.doi.org/10.1021/jf5006148 |J. Agric. Food Chem. 2014, 62, 3011−3033

Table 4. continued

phytochemicals in CEO	type	effective against	test method	effect	reference
geranial vapor	monoterpene	*Penicillium digitatum*	agar diffusion test	effective at 15 μL/L	Wuryatmo et al. (2003)
		Penicillium italicum	agar diffusion test	effective at 15 μL/L	Wuryatmo et al. (2003)
		Geotrichum candidum	agar diffusion test	effective at 15 μL/L	Wuryatmo et al. (2003)
neral vapor	monoterpene	*Penicillium digitatum*	agar diffusion test	effective at 15 μL/L	Wuryatmo et al. (2003)
		Penicillium italicum	agar diffusion test	effective at 15 μL/L	Wuryatmo et al. (2003)
		Geotrichum candidum	agar diffusion test	effective at 15 μL/L	Wuryatmo et al. (2003)
eugenol	monoterpene	*Aspergillus flavus*	plate diffusion procedure	MIC = 2.0% (v/v)	Souza et al. (2005)
		Penicillium spp.	plate diffusion procedure	MIC = 4.0% (v/v)	Souza et al. (2005)
		Fusarium spp.	plate diffusion procedure	MIC = 4.0% (v/v)	Souza et al. (2005)
		Rhizopus spp.	plate diffusion procedure	MIC = 4.0% (v/v)	Souza et al. (2005)
thymol	monoterpene phenol	*Fusarium verticillioides*	modified semisolid agar antifungal susceptibility	MIC = 1000 mL/L	Dambolena et al. (2008)
myrcene	monoterpene	*Fusarium* spp.	plate diffusion procedure	inhibition halo =12 mm	Souza et al. (2005)
		Rhizopus spp.	plate diffusion procedure	inhibition halo =11 mm	Souza et al. (2005)
β-myrcene	monoterpene	*Penicillium italicum*	poisoned food technique	24.69% inhibition at 0.186 μL/mL	Tao et al. (2013)
	monoterpene	*Penicillium digitatum*	poisoned food technique	22.37% inhibition at 2.972 μL/mL	Tao et al. (2013)
citronellal	monoterpenoid	*Aspergillus flavus*	agar diffusion method; broth microdilution	MIC = 4.05 mg/mL; MFC = 4.05 mg/mL	Rammance and Hongpattarakere (2011)
citronellal	monoterpenoid	*Aspergillus parasiticus*	agar diffusion method; broth microdilution	MIC = 4.05 mg/ML; MFC = 4.05 mg/mL	Rammance and Hongpattarakere (2011)
β-citronellal	monoterpene	*Penicillium italicum*	poisoned food technique	11.22% inhibition at 0.015 μL/mL	Tao et al. (2013)
	monoterpene	*Penicillium digitatum*	poisoned food technique	52.90% inhibition at 0.240 μL/mL	Tao et al. (2013)
citronellal	monoterpenoid	*Aspergillus flavus*	agar diffusion method; broth microdilution	MIC = 3.60 mg/mL; MFC = 4.05 mg/mL	Rammance and Hongpattarakere (2011)
citronellal	monoterpenoid	*Aspergillus parasiticus*	agar diffusion method; broth microdilution	MIC = 3.60 mg/mL; MFC = 4.05 mg/mL	Rammance and Hongpattarakere (2011)
terpinen-4-ol	monoterpenoid alcohol	*Penicillium italicum*	poisoned food technique	24.69% inhibition at 0.186 μL/mL	Tao et al. (2013)
	monoterpenoid alcohol	*Penicillium digitatum*	poisoned food technique	22.37% inhibition at 2.972 μL/mL	Tao et al. (2013)
flavonoids					
polymethoxylated flavones	from clementine oil	*Phytophthora citrophthora*	agar diffusion test	72% inhibition	Del Río et al. (1998)

dx.doi.org/10.1021/jf5006148 | J. Agric. Food Chem. 2014, 62, 3011−3033

Table 4. continued

phytochemicals in CEO	type	effective against	test method	effect	reference
		Penicillium digitatum	agar diffusion test	100% inhibition	Del Río et al. (1998)
		Geotrichum sp.	agar diffusion test	47% inhibition	Del Río et al. (1998)
polymethoxylated flavones	from sweet orange oil	*Phytophthora citrophthora*	agar diffusion test	14% inhibition	Del Río et al. (1998)
		Penicillium digitatum	agar diffusion test	100% inhibition	Del Río et al. (1998)
		Geotrichum sp.	agar diffusion test	34% inhibition	Del Río et al. (1998)
polymethoxylated flavones	from sour orange oil	*Phytophthora citrophthora*	agar diffusion test	100% inhibition	Del Río et al. (1998)
		Penicillium digitatum	agar diffusion test	77% inhibition	Del Río et al. (1998)
		Geotrichum sp.	agar diffusion test	57% inhibition	Del Río et al. (1998)
3,5,6,7,3′,4′-hexamethoxyflavone	polymethoxylated flavones (from orange essential oil)	*Colletotrichum gloeosporioides* (Penz) Penz & Sacc	agar diffusion test	effective at 100 μL/mL	Almada-Ruiz et al. (2003)
3,5,6,7,8,3′,4′-heptamethoxyflavone	polymethoxylated flavones (from orange essential oil)	*Colletotrichum gloeosporioides* (Penz) Penz & Sacc	agar diffusion test	effective at 100 μL/mL	Almada-Ruiz et al. (2003)
5,6,7,8,4′-pentamethoxyflavone	polymethoxylated flavones (from orange essential oil)	*Colletotrichum gloeosporioides* (Penz) Penz & Sacc	agar diffusion test	100% inhibition at 100 μL/mL	Almada-Ruiz et al. (2003)
5,6,7,8,3′,4′-hexamethoxyflavone	polymethoxylated flavones (from orange essential oil)	*Colletotrichum gloeosporioides* (Penz) Penz & Sacc	agar diffusion test	100% inhibition at 100 μL/mL	Almada-Ruiz et al. (2003)
nobiletin	polymethoxylated flavone	*Penicillium digitatum*	agar diffusion test	75% inhibition after 100 h	Ortuño et al. (2006)
hesperidin	polymethoxylated flavone	*Fusarium semitectum*	agar dilution method	39% inhibition at 0.25 mM	Salas et al. (2011)
		Penicillium expansum	agar dilution method	11% inhibition at 0.25 mM	Salas et al. (2011)
		Aspergillus parasiticus	agar dilution method	33% inhibition at 0.25 mM	Salas et al. (2011)
		Aspergillus flavus	agar dilution method	33% inhibition at 0.25 mM	Salas et al. (2011)
hesperidin	flavanone	*Penicillium digitatum*	agar diffusion test	38% inhibition after 100 h	Ortuño et al. (2006)
naringin	flavanone	*Penicillium digitatum*	agar diffusion test	25% inhibition after 100 h	Ortuño et al. (2006)
naringin	flavanone	*Fusarium semitectum*	agar dilution method	29% inhibition at 0.25 mM	Salas et al. (2011)
		Penicillium expansum	agar dilution method	22% inhibition at 0.25 mM	Salas et al. (2011)
		Aspergillus parasiticus	agar dilution method	41% inhibition at 0.25 mM	Salas et al. (2011)
		Aspergillus flavus	agar dilution method	41% inhibition at 0.25 mM	Salas et al. (2011)
neohesperidin	flavanone glucoside	*Fusarium semitectum*	agar dilution method	50% inhibition at 0.25 mM	Salas et al. (2011)
		Penicillium expansum	agar dilution method	44% inhibition at 0.25 mM	Salas et al. (2011)
		Aspergillus parasiticus	agar dilution method	38% inhibition at 0.25 mM	Salas et al. (2011)

dx.doi.org/10.1021/jf5006148 | J. Agric. Food Chem. 2014, 62, 3011−3033

Table 4. continued

phytochemicals in CEO	type	effective against	test method	effect	reference
		Aspergillus flavus	agar dilution method	41% inhibition at 0.25 mM	Salas et al. (2011)
hesperetin glucoside	flavanone glucoside	*Fusarium semitectum*	agar dilution method	43% inhibition at 0.25 mM	Salas et al. (2011)
		Penicillium expansum	agar dilution method	33% inhibition at 0.25 mM	Salas et al. (2011)
		Aspergillus parasiticus	agar dilution method	38% inhibition at 0.25 mM	Salas et al. (2011)
		Aspergillus flavus	agar dilution method	41% inhibition at 0.25 mM	Salas et al. (2011)
prunin	flavanone glucoside	*Fusarium semitectum*	agar dilution method	29% inhibition at 0.25 mM	Salas et al. (2011)
		Penicillium expansum	agar dilution method	44% inhibition at 0.25 mM	Salas et al. (2011)
		Aspergillus parasiticus	agar dilution method	38% inhibition at 0.25 mM	Salas et al. (2011)
		Aspergillus flavus	agar dilution method	41% inhibition at 0.25 mM	Salas et al. (2011)

[a]MFC, minimum fungicidal concentration. [b]AFST-EUCAST, Antifungal Susceptibility Testing Subcommittee of the European Committee on Antibiotic Susceptibility Testing.

of their constituents. The terpenoids, especially citral and limonene, most likely play an important role in the antifungal activity of the CEOs. However, the total number of compounds in CEOs that have antifungal activity has not been defined yet. Furthermore, the antagonistic, synergistic, or additive antifungal activities of different components in CEOs on fungal species and/or strains have not yet been explored.

Mechanism of Action of Antifungal Compounds in CEOs. The antifungal activities of CEOs against a wide range of fungal species and their potential active compounds have been clearly demonstrated, as can be seen from the studies mentioned above. However, the antifungal mechanism of the compounds in CEOs remains poorly understood.

The difficulties for exploring the mechanism of action of the natural bioactive compounds have been summarized in detail in a previous review.[137] Generally speaking, the antifungal effects of the natural products can be influenced by a wide variety of factors, such as the different quantitative and qualitative ratios of the compounds in essential oils, their target microorganisms, and the minimum inhibitory concentrations. In addition, the methods used to test the antifungal activities, including the procedures adopted for the extraction, diffusion, and dilution of the substances, can also have an effect. In addition, the different components of an essential oil can have antagonistic, synergistic, or additive effects on microbial cells, which can influence their overall antifungal activity. To solve these problems, Caccioni et al.[92] proposed a holistic approach to explore the antifungal mechanism of CEOs, and found that the antifungal performances of CEOs could be the result of a certain quantitative balance of various components.

Many papers have suggested that the cell membrane is the possible target of bioactive volatile compounds because of the fact that essential oils are mixtures of molecules characterized by their poor solubility in water and high hydrophobicity.[1,17,83,95] Several studies have showed that terpenes and phenolic compounds can disrupt the membrane of both fungi and bacteria.[138,139] Terpenes have been suggested to have the ability to disrupt and penetrate the bacterial cell wall, which can lead to the denaturing of proteins and destruction of the cell membrane.[17] The antimicrobial activity of the active compounds in essential oils can be explained by the lipophilic character of the monoterpenes contained in the oils. Monoterpenes act by disrupting the microbial cytoplasmic membrane, resulting in the loss of membrane impermeability. If the disturbance of membrane integrity occurs, then its functions are compromised not only as a barrier but also as a matrix for enzymes and as an energy transducer.[137,139−142] In a more recent study by Tao et al.,[143] the antifungal activity of mandarin essential oils against *P. italicum* and *P. digitatum* was attributed to the monoterpenes in the oils, such as limonene, octanal, and citral. They also suggested that mandarin essential oils generated cytotoxicity by disrupting cell membrane integrity, causing the leakage of cell components.

Generally, the antimicrobial mechanism of action of the bioactive compounds of essential oils can be explained by the degradation of the cell wall, the disruption of cytoplasmic membrane, or membrane proteins (Figure 1).[17,144] This leads to cytoplasmic leakage, cell lysis, and eventually cell death. However, the exact mechanism of the antimicrobial action of the compounds in essential oils remains poorly characterized, and further studies on the antifungal mechanism of the active compounds in CEOs are especially needed.

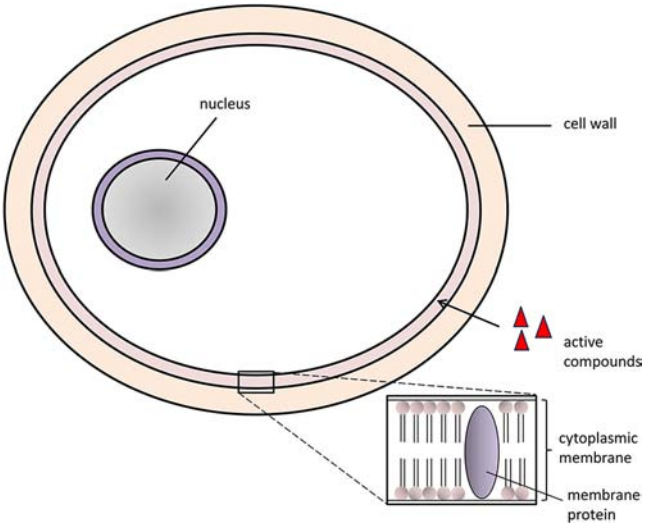

Figure 1. Possible targets or mechanisms of action of antimicrobial compounds of essential oils. The antimicrobial mechanism of the bioactive compounds of essential oils can be explained by the degradation of the cell wall or the disruption of cytoplasmic membrane or membrane proteins, which lead to cytoplasmic leakage, cell lysis, and eventually cell death.

APPLICATIONS OF CEOS IN THE FOOD INDUSTRY

Use of CEOs for Postharvest Disease Control. Alternative measures have been developed for crop protection, including biological agents, mineral salts, and plant extracts, as the use of synthetic fungicides in crops and trees can result in problems such as environmental pollution, phytotoxicity, and selection of resistant pathogen populations.[145] Of various biological approaches, the use of plant essential oils as fungicides for postharvest disease control is becoming popular throughout the world.[146,147] Several plant essential oils, such as thyme and lemongrass oils, have been demonstrated to be effective in stopping disease development caused by plant pathogens.[99,148−150] For example, Plotto et al.[149] explored the potential of several plant essential oils as natural postharvest disease control of tomato (*Lycopersicon esculentum*) and found that emulsions of oils of thyme and oregano at 5000 and 10000 ppm when used as dip treatments reduced disease development in tomatoes inoculated with *Botrytis cinerea* and *Alternaria arborescens*.

Both in vitro and on food assessments of CEOs have been performed to explore their potential as alternative fungicides to prevent or control postharvest disease.[3,22,96,97,103] Kuate and his colleagues[97] studied the effects of 22 varieties of citrus essential oils on in vitro growth and sporulation of *Phaeoramularia angolensis*, causing citrus leaf and fruit spot disease, and found that both pummelo and grapefruit oils were very effective against it. Lazar-Baker et al.[96] found lemon essential oils exhibited the strongest antifungal activity among tested oil samples in controlling brown rot caused by postharvest pathogen *Monilinia fructicola* in nectarines. In addition, in a recent study performed by Vitoratos et al.,[98] lemon essential oils were found to be very effective in controlling disease severity of infected fruits by *Botrytis cinerea* in tomatoes, strawberries, and cucumbers. Taken together, these studies suggested that CEOs have the potential to replace synthetic fungicides in the management of postharvest diseases of fruits and vegetables.

Use of CEOs in Fresh or Fresh-Cut Food Production. Food spoilage fungi can produce mycotoxins and cause food decay, which causes considerable economic losses and constitutes a health risk for consumers. Following the natural food preservation trends, research has been focused on the effect of essential oils on microbial inhibition of fresh and fresh-cut products in recent years. Plant essential oils stand out as an excellent alternative to chemical preservatives to extend the foodstuffs' shelf life, owing to their antimicrobial properties against both food pathogens and food spoilage organisms, as well as their aromas and flavors. In a previous review by Fisher and Phillips,[17] the applications of CEOs in different kinds of food including fish, meat, dairy products, fruits, and vegetables to control fungi spoilage and mycotoxin production were summarized. They concluded that CEOs could fulfill the requirements of both the food industry and the consumer for natural antimicrobials.

With fresh-cut fruit and vegetable salads becoming more and more popular among consumers, the fresh-cut industry has become one of the most successful businesses within the food-processing industry in recent years. However, fruit decay and loss of quality caused by microbial growth, including *Pseudomonas* spp., *E. herbicola*, *E. agglomerans*, lactic acid bacteria, molds, and yeasts, seriously limit the safety and shelf life of fresh-cut fruits and vegetables.[151] In addition, the sensorial appeal of fresh-cut fruits and vegetables, such as flavor and aroma, is another major indicator of shelf life and freshness from the view of consumers. The studies mentioned above showed that essential oils can serve as candidates to solve these problems owing to their antimicrobial activity and aroma nature. Ayala-Zavala and his colleagues[151] summarized the successful and unsuccessful uses of essential oils and their combinations for enhancing safety, aroma, and appearance of fresh-cut fruits and vegetables. For example, oregano and thyme essential oils exhibited excellent antimicrobial and sensorial efficacy in fresh-cut lettuce and carrots.[152] However, and according to their study, most of the present research has focused on the antibacterial effects of plant essential oils in fresh-cut fruits and vegetables, whereas the antifungal efficacy of plant essential oils, especially CEOs, have not been well investigated in the current literature.

Although plant essential oils including CEOs can be used as alternative food preservatives for improving the quality and sensorial appeal of fresh-cut fruits and vegetables, it needs to be pointed out that the antifungal compounds derived from plants may impart a strong flavor to the food they applied to, thus restricting their applicability to only those products with compatible flavor. In view of this problem, researchers have proposed different ideas, such as using the plant extract not only as a preservative but also as a flavor component or applying only some of the most active components rather than the whole extracts.[1] In a word, in this field there is still a lot of work that needs to be done.

Use of CEOs in Edible Coatings of Fruits during Storage. Recently, the use of essential oils in edible coatings has become one of the most important practices in preserving fruit quality during storage.[1,153] More and more research has shown that bioactive edible coatings enriched with essential oils exhibited excellent antimicrobial effects while maintaining fruit qualities.[154−156] The advantages and limitations of this promising technology were discussed in the review by Sánchez-González et al.[153] According to their research, the major advantage of this technology was that the edible coatings

can gradually release those antimicrobial compounds in essential oils over time, maintaining a proper concentration of antimicrobial components on the product surface during the storage period. CEOs have been applied in the edible films of oranges and papaya fruits during storage to extend their shelf life.[3,157] In addition, Sánchez-González et al.[156] applied bergamot essential oil to biodegradable coatings based on hydroxypropylmethylcellulose or chitosan for cold-stored grapes as an environmentally friendly, healthy treatment to better preserve fresh fruit quality and safety during postharvest cold storage. In their study, chitosan coatings containing bergamot oil were found to be more effective than pure hydroxypropylmethylcellulose and chitosan coatings owing to their highest antimicrobial activity and the greatest control of respiration rates.

Besides the whole essential oils mentioned above, some individual compounds in CEOs have also been applied to food to explore their antifungal potential. In a series of subsequent semicommercial and commercial trials carried out by du Plooy et al.,[158] excellent disease control was achieved with the amended essential oil coatings and terpenoid components such as D-limonene and *R*-(−)-carvone, whereas the overall fruit quality was maintained. More recently, Vu and his colleagues[159] observed that coatings with limonene reduced the decay of strawberries at most time points during the experiment, compared to chitosan alone, peppermint coatings, or uncoated strawberries. They also reported that a limonene coating did not cause any phytotoxicity during the experiment, and the appearance of strawberries was not changed compared to other groups.

The application of CEOs or their individual compounds in the edible film of coatings for foods eliminates the need for synthetic food preservatives, thereby complying with consumer preferences and organic requirements and reducing environmental pollution. However, several issues still need to be resolved such as the absorption of aromatic volatile constituents by the food product and altered sensory characteristics. In addition, the reactions of plant essential oils or their active compounds with lipids, proteins, carbohydrates, and other additives may result in an overall decrease in the activity of the antimicrobial compounds.[160] Taken together, the efficacy of amended coatings as viable alternatives or supplements to existing fruit protection strategies needs to be demonstrated in more semicommercial and commercial trials taking into consideration all factors such as costs and legal and safety issues.

In conclusion, CEOs have obvious in vitro and on food antifungal activities against a wide array of fungal species, and their fungitoxicity may be attributed to the chemical compositions, molecular structure, and concentrations of the bioactive compounds. Compared with the traditional food preservative, the application of CEOs can reduce environmental pollution, eliminate the need for synthetic fungicides, and make good use of the byproducts of the citrus-processing industry. In view of their good fungitoxic function, natural aromas and flavors, as well as their environmentally friendly property, CEOs are potentially an excellent alternative to traditional preservatives in developing highly efficient, safe, and economic fungicides for the future food industry. The fungitoxicity research of CEOs will be of great utility for the utilization of citrus byproducts and for postharvest disease control of fruits and vegetables in the agricultural industry. For a better application of the antifungal activity of CEOs, the antagonistic, synergistic, or additive effects of different components of CEOs will be likely the focus of future studies. Moreover, the antifungal mechanism of action of CEOs and their active components need further investigation. Finally, more on food studies in combination with commercial application trials would be necessary before CEOs can be applied fully as natural fungicides in the future food industry.

AUTHOR INFORMATION

Corresponding Authors

*(L.W.S.) Mail: Plant Biology Division, The Samuel Roberts Noble Foundation, 2510 Sam Noble Parkway, Ardmore, OK 73401, USA. Phone: 1 (580) 224-6710. Fax: 1 (580) 224-6692. E-mail: lwsumner@noble.org.

*(Z.Z.) Mail: College of Horticulture and Landscape Architecture, Southwest University, Chongqing 400716, China. Phone: 86-23-68250229. Fax: 86-23-68251274. E-mail: zzqswu@yahoo.com.

Author Contributions

All authors reviewed the final manuscript.

Funding

This work was supported by the Fundamental Research Funds for the Central Universities (XDJK2013A014), the China Scholarship Council (CSC), the National Natural Science Foundation of China (31171930), the Graduate Student Innovation Fund of Southwest University to L.J. (kb2011005), the Program for Chongqing Innovation Team of University (KJTD201333), and the "111" Project (B12006). L.J. and L.W.S. were supported by the Samuel Roberts Noble Foundation. L.W.S. was supported in part by National Science Foundation awards (1139489, 1024974, and 1124719).

Notes

The authors declare no competing financial interest.

ABBREVIATIONS USED

CEOs, citrus essential oils; MIC, minimum inhibition concentration

REFERENCES

(1) da Cruz Cabral, L.; Pinto, V. F.; Patriarca, A. Application of plant derived compounds to control fungal spoilage and mycotoxin production in foods. *Int. J. Food Microbiol.* **2013**, *166*, 1−14.

(2) Souza, E. L. d.; Lima, E. d. O.; Freire, K. R. d. L.; Sousa, C. P. d. Inhibitory action of some essential oils and phytochemicals on the growth of various moulds isolated from foods. *Braz. Arch. Biol. Technol.* **2005**, *48*, 245−250.

(3) Bosquez-Molina, E.; Jesús, E. R.-d.; Bautista-Baños, S.; Verde-Calvo, J. R.; Morales-López, J. Inhibitory effect of essential oils against *Colletotrichum gloeosporioides* and *Rhizopus stolonifer* in stored papaya fruit and their possible application in coatings. *Postharvest Biol. Technol.* **2010**, *57*, 132−137.

(4) Navarro García, V. M.; Gonzalez, A.; Fuentes, M.; Aviles, M.; Rios, M. Y.; Zepeda, G.; Rojas, M. G. Antifungal activities of nine traditional Mexican medicinal plants. *J. Ethnopharmacol.* **2003**, *87*, 85−88.

(5) Cheng, S. S.; Chung, M. J.; Lin, C. Y.; Wang, Y. N.; Chang, S. T. Phytochemicals from *Cunninghamia konishii* Hayata act as antifungal agents. *J. Agric. Food Chem.* **2012**, *60*, 124−128.

(6) Al-Ja'fari, A. H.; Vila, R.; Freixa, B.; Tomi, F.; Casanova, J.; Costa, J.; Cañigueral, S. Composition and antifungal activity of the essential oil from the rhizome and roots of *Ferula hermonis*. *Phytochemistry* **2011**, *72*, 1406−1413.

(7) Li, W. R.; Shi, Q. S.; Ouyang, Y. S.; Chen, Y. B.; Duan, S. S. Antifungal effects of citronella oil against *Aspergillus niger* ATCC 16404. *Appl. Microbiol. Biotechnol.* **2013**, *97*, 7483−7492.
(8) Sheikh, M.; Safiuddin, A.; Khan, Z.; Rizvi, R.; Mahmood, I. Antibacterial and antifungal potential of some medicinal plants against certain phytopathogenic micro-organisms. *Arch. Phytopathol. Plant Prot.* **2013**, *46*, 1070−1080.
(9) Soidrou, S.; Farah, A.; Satrani, B.; Ghanmi, M.; Jennan, S.; Hassane, S.; Lachkar, M.; El Abed, S.; Ibnsouda Koraichi, S.; Bousta, D. Fungicidal activity of four essential oils from *Piper capense*, *Piper borbonense* and *Vetiveria zizanoides* growing in Comoros against fungi decay wood. *J. Essent. Oil Res.* **2013**, *25*, 1−8.
(10) Velázquez-Nuñez, M. J.; Avila-Sosa, R.; Palou, E.; López-Malo, A. Antifungal activity of orange (*Citrus sinensis* var. Valencia) peel essential oil applied by direct addition or vapor contact. *Food Control* **2013**, *31*, 1−4.
(11) Vogt, V.; Cifuente, D.; Tonn, C.; Sabini, L.; Rosas, S. Antifungal activity *in vitro* and *in vivo* of extracts and lignans isolated from *Larrea divaricata* Cav. against phytopathogenic fungus. *Ind. Crop Prod.* **2013**, *42*, 583−586.
(12) Xu, L. X.; Xue, J. H.; Wu, P.; Wang, D.; Lin, L. J.; Jiang, Y. M.; Duan, X. W.; Wei, X. Y. Antifungal activity of hypothemycin against *Peronophythora litchii* in vitro and in vivo. *J. Agric. Food Chem.* **2013**, *61*, 10091−10095.
(13) Peretto, G.; Du, W. X.; Avena-Bustillos, R. J.; Berrios, J. D. J.; Sambo, P.; McHugh, T. H. Optimization of antimicrobial and physical properties of alginate coatings containing carvacrol and methyl cinnamate for strawberry application. *J. Agric. Food Chem.* **2014**, *62*, 984−990.
(14) Chambers, A. H.; Evans, S. A.; Folta, K. M. Methyl anthranilate and γ-decalactone inhibit strawberry pathogen growth and achene germination. *J. Agric. Food Chem.* **2013**, *61*, 12625−12633.
(15) Chanthaphon, S.; Chanthachum, S.; Hongpattarakere, T. Antimicrobial activities of essential oils and crude extracts from tropical *Citrus* spp. against food-related microorganisms. *Songklanakarin J. Sci. Technol.* **2008**, *30*, 125−131.
(16) Rammanee, K.; Hongpattarakere, T. Effects of tropical citrus essential oils on growth, aflatoxin production, and ultrastructure alterations of *Aspergillus flavus* and *Aspergillus parasiticus*. *Food Bioprocess. Technol.* **2011**, *4*, 1050−1059.
(17) Fisher, K.; Phillips, C. Potential antimicrobial uses of essential oils in food: is citrus the answer? *Trends Food Sci. Technol.* **2008**, *19*, 156−164.
(18) Blanco Tirado, C.; Stashenko, E. E.; Combariza, M. Y.; Martinez, J. R. Comparative study of Colombian citrus oils by high-resolution gas chromatography and gas chromatography-mass spectrometry. *J. Chromatogr., A* **1995**, *697*, 501−513.
(19) Singh, P.; Shukla, R.; Prakash, B.; Kumar, A.; Singh, S.; Mishra, P. K.; Dubey, N. K. Chemical profile, antifungal, antiaflatoxigenic and antioxidant activity of *Citrus maxima* Burm. and *Citrus sinensis* (L.) Osbeck essential oils and their cyclic monoterpene, DL-limonene. *Food Chem. Toxicol.* **2010**, *48*, 1734−1740.
(20) Chutia, M.; Deka Bhuyan, P.; Pathak, M. G.; Sarma, T. C.; Boruah, P. Antifungal activity and chemical composition of *Citrus reticulata* Blanco essential oil against phytopathogens from North East India. *LWT−Food Sci. Technol.* **2009**, *42*, 777−780.
(21) Viuda-Martos, M.; Ruiz-Navajas, Y.; Fernández-López, J.; Pérez-Álvarez, J. Antifungal activity of lemon (*Citrus lemon* L.), mandarin (*Citrus reticulata* L.), grapefruit (*Citrus paradisi* L.) and orange (*Citrus sinensis* L.) essential oils. *Food Control* **2008**, *19*, 1130−1138.
(22) Phillips, C. A.; Laird, K.; Allen, S. C. The use of Citri-V® − an antimicrobial citrus essential oil vapour for the control of *Penicillium chrysogenum*, *Aspergillus niger* and *Alternaria alternata in vitro* and on food. *Food Res. Int.* **2012**, *47*, 310−314.
(23) Kabara, J. Phenols and chelators. In *Food Preservatives*; Russell, N. J., Gould, G. W., Eds.; Blackie: London, UK, 1991; pp 200−214.
(24) Liu, C. H.; Cheng, Y. J.; Zhang, H. Y.; Deng, X. X.; Chen, F.; Xu, J. Volatile constituents of wild citrus Mangshanyegan (*Citrus nobilis* Lauriro) peel oil. *J. Agric. Food Chem.* **2012**, *60*, 2617−2628.
(25) Asikin, Y.; Taira, I.; Inafuku-Teramoto, S.; Sumi, H.; Ohta, H.; Takara, K.; Wada, K. The Composition of volatile aroma components, flavanones, and polymethoxylated flavones in Shiikuwasha (*Citrus depressa* Hayata) peels of different cultivation lines. *J. Agric. Food Chem.* **2012**, *60*, 7973−7980.
(26) Afek, U.; Sztejnberg, A.; Carmely, S. 6,7-Dimethoxycoumarin, a citrus phytoalexin conferring resistance against *Phytophthora gummosis*. *Phytochemistry* **1986**, *25*, 1855−1856.
(27) Lota, M. L.; de Rocca Serra, D.; Tomi, F.; Casanova, J. Chemical variability of peel and leaf essential oils of mandarins from *Citrus reticulata* Blanco. *Biochem. Syst. Ecol.* **2000**, *28*, 61−78.
(28) Lota, M. L.; de Rocca Serra, D.; Tomi, F.; Casanova, J. Chemical variability of peel and leaf essential oils of 15 species of mandarins. *Biochem. Syst. Ecol.* **2001**, *29*, 77−104.
(29) Lota, M. L.; de Rocca Serra, D.; Tomi, F.; Jacquemond, C.; Casanova, J. Volatile components of peel and leaf oils of lemon and lime species. *J. Agric. Food Chem.* **2002**, *50*, 796−805.
(30) Hosni, K.; Zahed, N.; Chrif, R.; Abid, I.; Medfei, W.; Kallel, M.; Brahim, N. B.; Sebei, H. Composition of peel essential oils from four selected Tunisian *Citrus* species: evidence for the genotypic influence. *Food Chem.* **2010**, *123*, 1098−1104.
(31) Tranchida, P. Q.; Bonaccorsi, I.; Dugo, P.; Mondello, L.; Dugo, G. Analysis of *Citrus* essential oils: state of the art and future perspectives. A review. *Flavour Fragrance J.* **2012**, *27*, 98−123.
(32) Shaw, P. E. Review of quantitative analyses of citrus essential oils. *J. Agric. Food Chem.* **1979**, *27*, 246−257.
(33) Jabalpurwala, F. A.; Smoot, J. M.; Rouseff, R. L. A comparison of citrus blossom volatiles. *Phytochemistry* **2009**, *70*, 1428−1434.
(34) Vekiari, S. A.; Protopapadakis, E. E.; Papadopoulou, P.; Papanicolaou, D.; Panou, C.; Vamvakias, M. Composition and seasonal variation of the essential oil from leaves and peel of a Cretan lemon variety. *J. Agric. Food Chem.* **2002**, *50*, 147−153.
(35) Bourgou, S.; Rahali, F. Z.; Ourghemmi, I.; Saïdani Tounsi, M. Changes of peel essential oil composition of four Tunisian citrus during fruit maturation. *Sci. World J.* **2012**, *2012*, 1−12.
(36) Sawamura, M.; Shichiri, K.-i.; Ootani, Y.; Zheng, S. H. Volatile constituents of several varieties of pummelos and characteristics among *Citrus* species (food & nutrition). *Agric. Biol. Chem.* **1991**, *55*, 2571−2578.
(37) Minh Tu, N. T.; Thanh, L. X.; Une, A.; Ukeda, H.; Sawamura, M. Volatile constituents of Vietnamese pummelo, orange, tangerine and lime peel oils. *Flavour Fragrance J.* **2002**, *17*, 169−174.
(38) Bakkali, F.; Averbeck, S.; Averbeck, D.; Idaomar, M. Biological effects of essential oils − a review. *Food Chem. Toxicol.* **2008**, *46*, 446−475.
(39) Merle, H.; Morón, M.; Blázquez, M. A.; Boira, H. Taxonomical contribution of essential oils in mandarins cultivars. *Biochem. Syst. Ecol.* **2004**, *32*, 491−497.
(40) Azizi, A.; Yan, F.; Honermeier, B. Herbage yield, essential oil content and composition of three oregano (*Origanum vulgare* L.) populations as affected by soil moisture regimes and nitrogen supply. *Ind. Crop Prod.* **2009**, *29*, 554−561.
(41) Fisher, K.; Phillips, C. The effect of lemon, orange and bergamot essential oils and their components on the survival of *Campylobacter jejuni*, *Escherichia coli* O157, *Listeria monocytogenes*, *Bacillus cereus* and *Staphylococcus aureus in vitro* and in food systems. *J. Appl. Microbiol.* **2006**, *101*, 1232−1240.
(42) Espinosa-García, F. J.; Langenheim, J. H. Effects of sabinene and γ-terpinene from coastal redwood leaves acting singly or in mixtures on the growth of some of their fungus endophytes. *Biochem. Syst. Ecol.* **1991**, *19*, 643−650.
(43) Hammer, K.; Carson, C.; Riley, T. Antifungal activity of the components of *Melaleuca alternifolia* (tea tree) oil. *J. Appl. Microbiol.* **2003**, *95*, 853−860.
(44) Juliani, H. R., Jr.; Biurrun, F.; Koroch, A. R.; Oliva, M.; Demo, M. S.; Trippi, V. S.; Zygadlo, J. A. Chemical constituents and antimicrobial activity of the essential oil of *Lantana xenica*. *Planta. Med.* **2002**, *68*, 762−764.

(45) Kotan, R.; Kordali, S.; Cakir, A. Screening of antibacterial activities of twenty-one oxygenated monoterpenes. *Z. Naturforsch. C* **2007**, *62*, 507.
(46) Proszenyák, Á.; Charnock, C.; Hedner, E.; Larsson, R.; Bohlin, L.; Gundersen, L. L. Synthesis, antimicrobial and antineoplastic activities for agelasine and agelasimine analogs with a β-cyclocitral derived substituent. *Arch. Pharm.* **2007**, *340*, 625−634.
(47) Radulović, N.; Stojanović, G.; Palić, R. Composition and antimicrobial activity of *Equisetum arvense* L. essential oil. *Phytother. Res.* **2006**, *20*, 85−88.
(48) Sartorelli, P.; Marquioreto, A. D.; Amaral-Baroli, A.; Lima, M. E. L.; Moreno, P. R. H. Chemical composition and antimicrobial activity of the essential oils from two species of *Eucalyptus*. *Phytother. Res.* **2007**, *21*, 231−233.
(49) Yang, D.; Michel, L.; Chaumont, J. P.; Millet-Clerc, J. Use of caryophyllene oxide as an antifungal agent in an *in vitro* experimental model of onychomycosis. *Mycopathologia* **2000**, *148*, 79−82.
(50) Chen, W.; Viljoen, A. Geraniol − a review of a commercially important fragrance material. *S. Afr. J. Bot.* **2010**, *76*, 643−651.
(51) Legault, J.; Pichette, A. Potentiating effect of β-caryophyllene on anticancer activity of α-humulene, isocaryophyllene and paclitaxel. *J. Pharm. Pharmacol.* **2007**, *59*, 1643−1647.
(52) Burke, Y. D.; Stark, M. J.; Roach, S. L.; Sen, S. E.; Crowell, P. L. Inhibition of pancreatic cancer growth by the dietary isoprenoids farnesol and geraniol. *Lipids* **1997**, *32*, 151−156.
(53) Dai, Y.; Harinantenaina, L.; Brodie, P. J.; Callmander, M. W.; Randrianasolo, S.; Rakotobe, E.; Rasamison, V. E.; Kingston, D. G. Isolation and synthesis of two antiproliferative calamenene-type sesquiterpenoids from *Sterculia capuronii* from the Madagascar rain forest. *Bioorg. Med. Chem.* **2012**, *20*, 6940−6944.
(54) Duncan, R. E.; Lau, D.; El-Sohemy, A.; Archer, M. C. Geraniol and ß-ionone inhibit proliferation, cell cycle progression, and cyclin-dependent kinase 2 activity in MCF-7 breast cancer cells independent of effects on HMG-CoA reductase activity. *Biochem. Pharmacol.* **2004**, *68*, 1739−1747.
(55) Zhu, T.; Zhao, Y.; Zhang, J.; Li, L.; Zou, L.; Yao, Y.; Xu, Y. β-Elemene inhibits proliferation of human glioblastoma cells and causes cell-cycle G0/G1 arrest via mutually compensatory activation of MKK3 and MKK6. *Int. J. Oncol.* **2011**, *38*, 419.
(56) Mujumdar, A.; Naik, D.; Misar, A.; Puntambekar, H.; Dandge, C. CNS depressant and analgesic activity of a fraction isolated from an ethanol extract of *Curcuma amada* rhizomes. *Pharm. Biol.* **2004**, *42*, 542−546.
(57) Chavan, M.; Wakte, P.; Shinde, D. Analgesic and anti-inflammatory activity of caryophyllene oxide from *Annona squamosa* L. bark. *Phytomedicine* **2010**, *17*, 149−151.
(58) Santos, F.; Rao, V. Antiinflammatory and antinociceptive effects of 1,8-cineole a terpenoid oxide present in many plant essential oils. *Phytother. Res.* **2000**, *14*, 240−244.
(59) Ocete, M.; Risco, S.; Zarzuelo, A.; Jimenez, J. Pharmacological activity of the essential oil of *Bupleurum gibraltaricum*: anti-inflammatory activity and effects on isolated rat uteri. *J. Ethnopharmacol.* **1989**, *25*, 305−313.
(60) Hart, P.; Brand, C.; Carson, C.; Riley, T.; Prager, R.; Finlay-Jones, J. Terpinen-4-ol, the main component of the essential oil of *Melaleuca alternifolia* (tea tree oil), suppresses inflammatory mediator production by activated human monocytes. *Inflamm. Res.* **2000**, *49*, 619−626.
(61) Francis, F.; Lognay, G.; Haubruge, E. Olfactory responses to aphid and host plant volatile releases: (*E*)-β-farnesene an effective kairomone for the predator *Adalia bipunctata*. *J. Chem. Ecol.* **2004**, *30*, 741−755.
(62) Park, I. K.; Lee, S. G.; Choi, D. H.; Park, J. D.; Ahn, Y. J. Insecticidal activities of constituents identified in the essential oil from leaves of *Chamaecyparis obtusa* against *Callosobruchus chinensis* (L.) and *Sitophilus oryzae* (L.). *J. Stored Prod. Res.* **2003**, *39*, 375−384.
(63) Nishida, R.; Shelly, T. E.; Whittier, T. S.; Kaneshiro, K. Y. α-Copaene, a potential rendezvous cue for the Mediterranean fruit fly, *Ceratitis capitata*? *J. Chem. Ecol.* **2000**, *26*, 87−100.
(64) Pechous, S. W.; Whitaker, B. D. Cloning and functional expression of an (*E*,*E*)-α-farnesene synthase cDNA from peel tissue of apple fruit. *Planta* **2004**, *219*, 84−94.
(65) Birkett, M. A.; Campbell, C. A.; Chamberlain, K.; Guerrieri, E.; Hick, A. J.; Martin, J. L.; Matthes, M.; Napier, J. A.; Pettersson, J.; Pickett, J. A. New roles for *cis*-jasmone as an insect semiochemical and in plant defense. *Proc. Natl. Acad. Sci. U.S.A.* **2000**, *97*, 9329−9334.
(66) Arruda, D. C.; D'Alexandri, F. L.; Katzin, A. M.; Uliana, S. R. Antileishmanial activity of the terpene nerolidol. *Antimicrob. Agents Chemother.* **2005**, *49*, 1679−1687.
(67) Røstelien, T.; Borg-Karlson, A. K.; Fäldt, J.; Jacobsson, U.; Mustaparta, H. The plant sesquiterpene germacrene D specifically activates a major type of antennal receptor neuron of the tobacco budworm moth *Heliothis virescens*. *Chem. Senses* **2000**, *25*, 141−148.
(68) Araujo, I. B.; Souza, C. A. M.; De-Carvalho, R. R.; Kuriyama, S. N.; Rodrigues, R. P.; Vollmer, R. S.; Alves, E. N.; Paumgartten, F. J. R. Study of the embryo-foetotoxicity of α-terpinene in the rat. *Food Chem. Toxicol.* **1996**, *34*, 477−482.
(69) Vallianou, I.; Peroulis, N.; Pantazis, P.; Hadzopoulou-Cladaras, M. Camphene, a plant-derived monoterpene, reduces plasma cholesterol and triglycerides in hyperlipidemic rats independently of HMG-CoA reductase activity. *PLoS One* **2011**, *6*, e20516.
(70) Takahashi, Y.; Inaba, N.; Kuwahara, S.; Kuki, W. Effects of γ-terpineneon lipid concentrations in serum using triton *WR1339*-treated rats. *Biosci., Biotechnol., Biochem.* **2003**, *67*, 2448−2450.
(71) Lahlou, S.; Figueiredo, A. F.; Magalhães, P. J. C.; Leal-Cardoso, J. H. Cardiovascular effects of 1,8-cineole, a terpenoid oxide present in many plant essential oils, in normotensive rats. *Can. J. Physiol. Pharmacol.* **2002**, *80*, 1125−1131.
(72) Deepa, B.; Anuradha, C. V. Linalool a plant derived monoterpene alcohol rescues kidney from diabetes-induced nephropathic changes via blood glucose reduction. *Diabetol. Croat.* **2011**, *40*, 121.
(73) Lahlou, S.; Interaminense, L. F. L.; Leal-Cardoso, J. H.; Duarte, G. P. Antihypertensive effects of the essential oil of *Alpinia zerumbet* and its main constituent, terpinen-4-ol, in DOCA-salt hypertensive conscious rats. *Fundam. Clin. Pharmacol.* **2003**, *17*, 323−330.
(74) Meigs, T. E.; Simoni, R. D. Farnesol as a regulator of HMG-CoA reductase degradation: characterization and role of farnesyl pyrophosphatase. *Arch. Biochem. Biophys.* **1997**, *345*, 1−9.
(75) Jing, L.; Zhang, Y.; Fan, S.; Gu, M.; Guan, Y.; Lu, X.; Huang, C.; Zhou, Z. Preventive and ameliorating effects of citrus D-limonene on dyslipidemia and hyperglycemia in mice with high-fat diet-Induced obesity. *Eur. J. Pharmacol.* **2013**, *715*, 46−55.
(76) Choi, H. S. Lipolytic effects of citrus peel oils and their components. *J. Agric. Food Chem.* **2006**, *54*, 3254−3258.
(77) Clegg, R. J.; Middleton, B.; Bell, G. D.; White, D. A. Inhibition of hepatic cholesterol synthesis and *S*-3-hydroxy-3-methylglutaryl-CoA reductase by mono and bicyclic monoterpenes administered *in vivo*. *Biochem. Pharmacol.* **1980**, *29*, 2125−2127.
(78) Clegg, R. J.; Middleton, B.; Bell, G. D.; White, D. A. The mechanism of cyclic monoterpene inhibition of hepatic 3-hydroxy-3-methylglutaryl coenzyme A reductase *in vivo* in the rat. *J. Biol. Chem.* **1982**, *257*, 2294−2299.
(79) Yang, X.; Zhao, H.; Wang, J.; Meng, Q.; Zhang, H.; Yao, L.; Zhang, Y.; Dong, A.; Ma, Y.; Wang, Z. Chemical composition and antioxidant activity of essential oil of pine cones of *Pinus armandii* from the Southwest region of China. *J. Med. Plants Res.* **2010**, *4*, 1668−1672.
(80) Miller, J.; Thompson, P.; Hakim, I.; Chow, H. H. S.; Thomson, C. D-Limonene: a bioactive food component from citrus and evidence for a potential role in breast cancer prevention and treatment. *Oncol. Rev.* **2011**, *5*, 31−42.
(81) Sun, J. D-Limonene: safety and clinical applications. *Altern. Med. Rev.* **2007**, *12*, 259−264.
(82) Victor Antony Santiago, J.; Jayachitra, J.; Shenbagam, M.; Nalini, N. Dietary D-limonene alleviates insulin resistance and oxidative stress−induced liver injury in high-fat diet and L-NAME-treated rats. *Eur. J. Nutr.* **2012**, *51*, 57−68.

(83) Lang, G.; Buchbauer, G. A review on recent research results (2008−2010) on essential oils as antimicrobials and antifungals. A review. *Flavour Fragrance J.* **2012**, *27*, 13−39.
(84) Pauli, A.; Schilcher, H. *In vitro* antimicrobial activities of essential oils monographed in the European Pharmacopoeia, 6th ed. In *Handbook of Essential Oils: Science, Technology, and Applications*; Baser, K. H. C., Buchbauer, G., Eds.; Taylor & Francis: Boca Raton, FL, USA, 2010; pp 353−547.
(85) Nweze, E.; Mukherjee, P.; Ghannoum, M. Agar-based disk diffusion assay for susceptibility testing of dermatophytes. *J. Clin. Microbiol.* **2010**, *48*, 3750−3752.
(86) Jiang, L. *Comparison of Disk Diffusion, Agar Dilution, and Broth Microdilution for Antimicrobial Susceptibility Testing of Five Chitosans*. Ph.D. dissertation, Louisiana State University, 2011.
(87) Kim, J. S.; Kim, Y. The inhibitory effect of natural bioactives on the growth of pathogenic bacteria. *Nutr. Res. Pract.* **2007**, *1*, 273−278.
(88) Varela, N. P.; Friendship, R.; Dewey, C.; Valdivieso, A. Comparison of agar dilution and E-test for antimicrobial susceptibility testing of *Campylobacter coli* isolates recovered from 80 Ontario swine farms. *Can. J. Vet. Res.* **2008**, *72*, 168.
(89) Tao, N. G.; Liu, Y. J.; Zhang, M. L. Chemical composition and antimicrobial activities of essential oil from the peel of bingtang sweet orange (*Citrus sinensis* Osbeck). *Int. J. Food Sci. Technol.* **2009**, *44*, 1281−1285.
(90) Grover, R.; Moore, J. Toxicometric studies of fungicides against brown rot organisms *Sclerotinia fructicola* and *S. laxa*. *Phytopathology* **1962**, *52*, 876−880.
(91) Sharma, N.; Tripathi, A. Effects of *Citrus sinensis* (L.) Osbeck epicarp essential oil on growth and morphogenesis of *Aspergillus niger* (L.) Van Tieghem. *Microbiol. Res.* **2008**, *163*, 337−344.
(92) Caccioni, D. R. L.; Guizzardi, M.; Biondi, D. M.; Agatino, R.; Ruberto, G. Relationship between volatile components of citrus fruit essential oils and antimicrobial action on *Penicillium digitatum* and *Penicillium italicum*. *Int. J. Food Microbiol.* **1998**, *43*, 73−79.
(93) Sharma, N.; Tripathi, A. Fungitoxicity of the essential oil of *Citrus sinensis* on post-harvest pathogens. *World J. Microbiol. Biotechnol.* **2006**, *22*, 587−593.
(94) Cavanagh, H. M. A. Antifungal activity of the volatile phase of essential oils: a brief review. *Nat. Prod. Commun.* **2007**, *2*, 1297−1302.
(95) Laird, K.; Phillips, C. Vapour phase: a potential future use for essential oils as antimicrobials? *Lett. Appl. Microbiol.* **2012**, *54*, 169−174.
(96) Lazar-Baker, E.; Hetherington, S.; Ku, V.; Newman, S. Evaluation of commercial essential oil samples on the growth of postharvest pathogen *Monilinia fructicola* (G. Winter) honey. *Lett. Appl. Microbiol.* **2011**, *52*, 227−232.
(97) Kuate, J.; Foko, J.; Ndindeng, S.; Jazet-Dongmo, P.; Fouré, E.; Damesse, F.; Bella, M.; Ducelier, D. Effect of essential oils from citrus varieties on *in vitro* growth and sporulation of *Phaeoramularia angolensis* causing citrus leaf and fruit spot disease. *Eur. J. Plant. Pathol.* **2006**, *114*, 151−161.
(98) Vitoratos, A.; Bilalis, D.; Karkanis, A.; Efthimiadou, A. Antifungal activity of plant essential oils against *Botrytis cinerea*, *Penicillium italicum* and *Penicillium digitatum*. *Not. Bot. Horti Agrobot.* **2013**, *41*, 86−92.
(99) Combrinck, S.; Regnier, T.; Kamatou, G. P. P. *In vitro* activity of eighteen essential oils and some major components against common postharvest fungal pathogens of fruit. *Ind. Crop Prod.* **2011**, *33*, 344−349.
(100) Pawar, V.; Thaker, V. *In vitro* efficacy of 75 essential oils against *Aspergillus niger*. *Mycoses* **2006**, *49*, 316−323.
(101) Karapinar, M. The effects of citrus oils and some spices on growth and aflatoxin production by *Aspergillus parasiticus* NRRL 2999. *Int. J. Food Microbiol.* **1985**, *2*, 239−245.
(102) Caccioni, D.; Deans, S.; Ruberto, G. Inhibitory effect of citrus fruit essential oil components on *Penicillium italicum* and *P. digitatum*. *Petria* **1995**, *5*, 177−181.
(103) Van Hung, P.; Chi, P. T. L.; Phi, N. T. L. Comparison of antifungal activities of Vietnamese citrus essential oils. *Nat. Prod. Res.* **2013**, *27*, 506−508.
(104) Fisher, K.; Rowe, C.; Phillips, C. The survival of three strains of *Arcobacter butzleri* in the presence of lemon, orange and bergamot essential oils and their components *in vitro* and on food. *Lett. Appl. Microbiol.* **2007**, *44*, 495−499.
(105) Dušan, F.; Marián, S.; Katarína, D.; Dobroslava, B. Essential oils—their antimicrobial activity against *Escherichia coli* and effect on intestinal cell viability. *Toxicol. in Vitro* **2006**, *20*, 1435−1445.
(106) Deba, F.; Xuan, T. D.; Yasuda, M.; Tawata, S. Chemical composition and antioxidant, antibacterial and antifungal activities of the essential oils from *Bidens pilosa* Linn. var. *Radiata*. *Food Control* **2008**, *19*, 346−352.
(107) Del Río, J. A.; Arcas, M. C.; Benavente-García, O.; Ortuño, A. Citrus polymethoxylated flavones can confer resistance against *Phytophthora citrophthora*, *Penicillium digitatum*, and *Geotrichum* species. *J. Agric. Food Chem.* **1998**, *46*, 4423−4428.
(108) Alma, M. H.; Nitz, S.; Kollmannsberger, H.; Digrak, M.; Efe, F. T.; Yilmaz, N. Chemical composition and antimicrobial activity of the essential oils from the gum of Turkish pistachio (*Pistacia vera* L.). *J. Agric. Food Chem.* **2004**, *52*, 3911−3914.
(109) Bezić, N.; Skočibušić, M.; Dunkić, V. Phytochemical composition and antimicrobial activity of *Satureja montana* L. and *Satureja cuneifolia* Ten. essential oils. *Acta Bot. Croat.* **2005**, *64*, 313−322.
(110) Rasooli, I.; Moosavi, M.; Rezaee, M.; Jaimand, K. Susceptibility of microorganisms to *Myrtus communis* L. essential oil and its chemical composition. *J. Agric. Sci. Technol.* **2002**, *4*, 127−133.
(111) Rodov, V.; Ben-Yehoshua, S.; Fang, D. Q.; Kim, J. J.; Ashkenazi, R. Preformed antifungal compounds of lemon fruit: citral and its relation to disease resistance. *J. Agric. Food Chem.* **1995**, *43*, 1057−1061.
(112) Sonboli, A.; Babakhani, B.; Mehrabian, A. Antimicrobial activity of six constituents of essential oil from *Salvia*. *Z. Naturforsch. C* **2006**, *61*, 160−164.
(113) Tepe, B.; Akpulat, H. A.; Sokmen, M.; Daferera, D.; Yumrutas, O.; Aydin, E.; Polissiou, M.; Sokmen, A. Screening of the antioxidative and antimicrobial properties of the essential oils of *Pimpinella anisetum* and *Pimpinella flabellifolia* from Turkey. *Food Chem.* **2006**, *97*, 719−724.
(114) Mencherini, T.; Campone, L.; Piccinelli, A. L.; García Mesa, M.; Sánchez, D. M.; Aquino, R. P.; Rastrelli, L. HPLC-PDA-MS and NMR characterization of a hydroalcoholic extract of *Citrus aurantium* L. var. amara peel with antiedematogenic activity. *J. Agric. Food Chem.* **2012**, *61*, 1686−1693.
(115) Tripoli, E.; Guardia, M. L.; Giammanco, S.; Majo, D. D.; Giammanco, M. Citrus flavonoids: molecular structure, biological activity and nutritional properties: a review. *Food Chem.* **2007**, *104*, 466−479.
(116) Mandalari, G.; Bennett, R.; Bisignano, G.; Trombetta, D.; Saija, A.; Faulds, C.; Gasson, M.; Narbad, A. Antimicrobial activity of flavonoids extracted from bergamot (*Citrus bergamia* Risso) peel, a byproduct of the essential oil industry. *J. Appl. Microbiol.* **2007**, *103*, 2056−2064.
(117) Xu, J. J.; Wu, X.; Li, M. M.; Li, G. Q.; Yang, Y. T.; Luo, H. J.; Huang, W. H.; Chung, H. Y.; Ye, W. C.; Wang, G. C.; Li, Y. L. Antiviral activity of polymethoxylated flavones from "Guangchenpi", the edible and medicinal pericarps of *Citrus reticulata* 'Chachi'. *J. Agric. Food Chem.* **2013**, 1−31.
(118) Chanet, A.; Milenkovic, D.; Manach, C.; Mazur, A.; Morand, C. Citrus flavanones: what is their role in cardiovascular protection? *J. Agric. Food Chem.* **2012**, *60*, 8809−8822.
(119) Hwang, S. L.; Shih, P. H.; Yen, G. C. Neuroprotective effects of citrus flavonoids. *J. Agric. Food Chem.* **2012**, *60*, 877−885.
(120) Ortuño, A.; Báidez, A.; Gómez, P.; Arcas, M. C.; Porras, I.; García-Lidón, A.; Río, J. A. D. *Citrus paradisi* and *Citrus sinensis* flavonoids: their influence in the defence mechanism against *Penicillium digitatum*. *Food Chem.* **2006**, *98*, 351−358.

(121) Salas, M. P.; Céliz, G.; Geronazzo, H.; Daz, M.; Resnik, S. L. Antifungal activity of natural and enzymatically-modified flavonoids isolated from citrus species. *Food Chem.* **2011**, *124*, 1411−1415.
(122) Liu, L.; Xu, X.; Cheng, D.; Yao, X.; Pan, S. Structure−activity relationship of citrus polymethoxylated flavones and their inhibitory effects on *Aspergillus niger*. *J. Agric. Food Chem.* **2012**, *60*, 4336−4341.
(123) Almada-Ruiz, E.; Martínez-Téllez, M. Á.; Hernández-Álamos, M. M.; Vallejo, S.; Primo-Yúfera, E.; Vargas-Arispuro, I. Fungicidal potential of methoxylated flavones from citrus for *in vitro* control of *Colletotrichum gloeosporioides,* causal agent of anthracnose disease in tropical fruits. *Pest Manage. Sci.* **2003**, *59*, 1245−1249.
(124) Caccioni, D. R. L.; Guizzardi, M. Inhibition of germination and growth of fruit and vegetable postharvest pathogenic fungi by essential oil components. *J. Essent. Oil Res.* **1994**, *6*, 173−179.
(125) Mesa-Arango, A. C.; Montiel-Ramos, J.; Zapata, B.; Durán, C.; Betancur-Galvis, L.; Stashenko, E. Citral and carvone chemotypes from the essential oils of Colombian *Lippia alba* (Mill.) NE Brown: composition, cytotoxicity and antifungal activity. *Mem. Inst. Oswaldo Cruz* **2009**, *104*, 878−884.
(126) Azaz, A. D.; Irtem, H. A.; Kurkcuoglu, M.; Baser, K. C. Composition and the *in vitro* antimicrobial activities of the essential oils of some *Thymus* species. *Z. Naturforsch. C* **2004**, *59*, 75−80.
(127) Baratta, M. T.; Dorman, H. D.; Deans, S. G.; Biondi, D. M.; Ruberto, G. Chemical composition, antimicrobial and antioxidative activity of laurel, sage, rosemary, oregano and coriander essential oils. *J. Essent. Oil Res.* **1998**, *10*, 618−627.
(128) Russo, M.; Galletti, G. C.; Bocchini, P.; Carnacini, A. Essential oil chemical composition of wild populations of Italian oregano spice (*Origanum vulgare* ssp. hirtum (Link) letswaart): a preliminary evaluation of their use in chemotaxonomy by cluster analysis. 1. Inflorescences. *J. Agric. Food Chem.* **1998**, *46*, 3741−3746.
(129) Park, M. J.; Gwak, K. S.; Yang, I.; Kim, K. W.; Jeung, E. B.; Chang, J. W.; Choi, I. G. Effect of citral, eugenol, nerolidol and α-terpineol on the ultrastructural changes of *Trichophyton mentagrophytes*. *Fitoterapia* **2009**, *80*, 290−296.
(130) Dharmawan, J.; Kasapis, S.; Sriramula, P.; Lear, M. J.; Curran, P. Evaluation of aroma-active compounds in Pontianak orange peel oil (*Citrus nobilis* Lour. Var. *microcarpa* Hassk.) by gas chromatography-olfactometry, aroma reconstitution, and omission test. *J. Agric. Food Chem.* **2008**, *57*, 239−244.
(131) Onawunmi, G. O. Evaluation of the antimicrobial activity of citral. *Lett. Appl. Microbiol.* **1989**, *9*, 105−108.
(132) Caccioni, D. R. L.; Deans, S. G. Action of citrus fruits essential oils on germination of *Penicillium digitatum* and *Penicillium italicum*. In *International Symposium on Industrial Crops and Products*; Pisa, Italy, 1993; pp 22−24.
(133) Wuryatmo, E.; Klieber, A.; Scott, E. S. Inhibition of citrus postharvest pathogens by vapor of citral and related compounds in culture. *J. Agric. Food Chem.* **2003**, *51*, 2637−2640.
(134) Mahdavi, O. S.; Moodi Mohammad, A.; Norozian, A. S. M. B.; Mosavi, S. J.; Ghazi, M. S. S. A. M.; Jabbari, S. S. M.; Kheradi, E.; Salehi, M. The effects of limonene and orange peel extracts on some spoilage fungi. *Int. J. Mol. Clin. Microbiol.* **2011**, *1*, 82−86.
(135) Dambolena, J. S.; López, A. G.; Cánepa, M. C.; Theumer, M. G.; Zygadlo, J. A.; Rubinstein, H. R. Inhibitory effect of cyclic terpenes (limonene, menthol, menthone and thymol) on *Fusarium verticillioides* MRC 826 growth and fumonisin B1 biosynthesis. *Toxicon* **2008**, *51*, 37−44.
(136) Marei, G. I. K.; Abdel Rasoul, M. A.; Abdelgaleil, S. A. M. Comparative antifungal activities and biochemical effects of monoterpenes on plant pathogenic fungi. *Pestic. Biochem. Physiol.* **2012**, *103*, 56−61.
(137) Lanciotti, R.; Gianotti, A.; Patrignani, F.; Belletti, N.; Guerzoni, M.; Gardini, F. Use of natural aroma compounds to improve shelf-life and safety of minimally processed fruits. *Trends Food Sci. Technol.* **2004**, *15*, 201−208.
(138) Cox, S. D.; Mann, C. M.; Markham, J. L.; Bell, H. C.; Gustafson, J. E.; Warmington, J. R.; Wyllie, S. G. The mode of antimicrobial action of the essential oil of *Melaleuca alternifolia* (tea tree oil). *J. Appl. Microbiol.* **2000**, *88*, 170−175.
(139) Sikkema, J.; De Bont, J.; Poolman, B. Mechanisms of membrane toxicity of hydrocarbons. *Microbiol. Rev.* **1995**, *59*, 201−222.
(140) Sikkema, J.; De Bont, J.; Poolman, B. Interactions of cyclic hydrocarbons with biological membranes. *J. Biol. Chem.* **1994**, *269*, 8022−8028.
(141) Turina, A. d. V.; Nolan, M.; Zygadlo, J.; Perillo, M. Natural terpenes: self-assembly and membrane partitioning. *Biophys. Chem.* **2006**, *122*, 101−113.
(142) Gill, A.; Holley, R. Disruption of *Escherichia coli,.Listeria monocytogenes* and *Lactobacillus sakei* cellular membranes by plant oil aromatics. *Int. J. Food Microbiol.* **2006**, *108*, 1−9.
(143) Tao, N. G.; Jia, L.; Zhou, H. E. Anti-fungal activity of *Citrus reticulata* Blanco essential oil against *Penicillium italicum* and *Penicillium digitatum*. *Food Chem.* **2013**, *153*, 265−271.
(144) Burt, S. Essential oils: their antibacterial properties and potential applications in foods − a review. *Int. J. Food Microbiol.* **2004**, *94*, 223−253.
(145) Terzi, V.; Morcia, C.; Faccioli, P.; Vale, G.; Tacconi, G.; Malnati, M. *In vitro* antifungal activity of the tea tree (*Melaleuca alternifolia*) essential oil and its major components against plant pathogens. *Lett. Appl. Microbiol.* **2007**, *44*, 613−618.
(146) Camele, I.; De Feo, V.; Altieri, L.; Mancini, E.; De Martino, L.; Luigi Rana, G. An attempt of postharvest orange fruit rot control using essential oils from Mediterranean plants. *J. Med. Food* **2010**, *13*, 1515−1523.
(147) Mari, M.; Neri, F.; Bertolini, P. Novel approaches to prevent and control postharvest diseases of fruits. *Stewart Postharvest Rev.* **2007**, *3*, 1−7.
(148) Kumar, A.; Shukla, R.; Singh, P.; Prasad, C. S.; Dubey, N. K. Assessment of *Thymus vulgaris* L. essential oil as a safe botanical preservative against post harvest fungal infestation of food commodities. *Innovative Food Sci. Emerging Technol.* **2008**, *9*, 575−580.
(149) Plotto, A.; Roberts, D.; Roberts, R. Evaluation of plant essential oils as natural postharvest disease control of tomato (*Lycopersicon esculentum*). In *XXVI International Horticultural Congress: Issues and Advances in Postharvest Horticulture 628*; Acta Horticulturae: Toronto, Canada, 2002; pp 737−745.
(150) Tripathi, P.; Dubey, N.; Shukla, A. Use of some essential oils as post-harvest botanical fungicides in the management of grey mould of grapes caused by *Botrytis cinerea*. *World J. Microbiol. Biotechnol.* **2008**, *24*, 39−46.
(151) Ayala-Zavala, J. F.; González-Aguilar, G. A.; Del-Toro-Sánchez, L. Enhancing safety and aroma appealing of fresh-cut fruits and vegetables using the antimicrobial and aromatic power of essential oils. *J. Food Sci.* **2009**, *74*, R84−R91.
(152) Gutierrez, J.; Barry-Ryan, C.; Bourke, P. The antimicrobial efficacy of plant essential oil combinations and interactions with food ingredients. *Int. J. Food Microbiol.* **2008**, *124*, 91−97.
(153) Sánchez-González, L.; Vargas, M.; González-Martínez, C.; Chiralt, A.; Cháfer, M. Use of essential oils in bioactive edible coatings: a review. *Food Eng. Rev.* **2011**, *3*, 1−16.
(154) Avila-Sosa, R.; Palou, E.; Jiménez Munguía, M. T.; Nevárez-Moorillón, G. V.; Navarro Cruz, A. R.; López-Malo, A. Antifungal activity by vapor contact of essential oils added to amaranth, chitosan, or starch edible films. *Int. J. Food Microbiol.* **2012**, *153*, 66−72.
(155) Avila-Sosa, R.; Hernández-Zamoran, E.; López-Mendoza, I.; Palou, E.; Munguía, M. T. J.; Nevárez-Moorillón, G. V.; López-Malo, A. Fungal inactivation by Mexican oregano (*Lippia berlandieri* Schauer) essential oil added to amaranth, chitosan, or starch edible films. *J. Food Sci.* **2010**, *75*, M127−M133.
(156) Sánchez-González, L.; Pastor, C.; Vargas, M.; Chiralt, A.; González-Martínez, C.; Cháfer, M. Effect of hydroxypropylmethylcellulose and chitosan coatings with and without bergamot essential oil on quality and safety of cold-stored grapes. *Postharvest Biol. Technol.* **2011**, *60*, 57−63.

(157) Cháfer, M.; Sánchez-González, L.; González-Martínez, C.; Chiralt, A. Fungal decay and shelf life of oranges coated with chitosan and bergamot, thyme, and tea tree essential oils. *J. Food Sci.* **2012**, *77*, E182−E187.
(158) du Plooy, W.; Regnier, T.; Combrinck, S. Essential oil amended coatings as alternatives to synthetic fungicides in citrus postharvest management. *Postharvest Biol. Technol.* **2009**, *53*, 117−122.
(159) Vu, K.; Hollingsworth, R.; Leroux, E.; Salmieri, S.; Lacroix, M. Development of edible bioactive coating based on modified chitosan for increasing the shelf life of strawberries. *Food Res. Int.* **2011**, *44*, 198−203.
(160) Ayala-Zavala, J.; Del-Toro-Sánchez, L.; Alvarez-Parrilla, E.; González-Aguilar, G. High relative humidity in-package of fresh-cut fruits and vegetables: advantage or disadvantage considering microbiological problems and antimicrobial delivering systems? *J. Food Sci.* **2008**, *73*, R41−R47.

levels. Hence, it is not known if UV-B radiation affects ergothioneine concentrations in mushrooms.

In addition to ergothioneine, polyphenolic compounds have been shown to contribute to mushroom antioxidant activity. Polyphenolics are naturally occurring chemicals that belong to diverse classes, including isoflavones, lignans, flavones, stilbenes, flavanones, flavonols, and anthocyanidins, among others. Several studies have found polyphenolic compounds in mushrooms. For example, Liu et al. (2012)[18] measured the flavonol quercetin in wild edible mushrooms from China, while Kim et al. (2008)[19] found naringin, resveratrol, quercetin, naringenin, kaempferol, hesperetin, formononetin, and biochanin A in edible and medicinal mushrooms from Korea. Kim et al. (2008)[19] reported that the antioxidant activity, including free radical scavenging activity of edible and medicinal mushrooms, was well correlated with concentrations of polyphenolic compound measured in mushrooms. It has been reported that UV-B irradiation increased amounts of some polyphenolic compounds, specifically flavonoids naringenin, rutin, and quercetin in tomato fruits[20] and some flavonols and flavonoids in apples,[21] but no reports have been found for mushrooms.

This study intended to fill these gaps by investigating the effects of UV-B radiation at different levels on the natural bioactive compounds: ergothioneine, phytosterols, and polyphenolic compounds in mushroom powders made of brown, white (*Agaricus bisporus*), oyster (*Pleurotus ostreatus*), and shiitake (*Lentinula edodes*) mushrooms, used as dietary supplement ingredients.

MATERIALS AND METHODS

Mushroom Powder Preparation. All mushrooms were grown, harvested, and handled in the Monterey Mushroom, Inc., facility under commercial practices. Fresh mushrooms of brown, white (*Agaricus bisporus*), oyster (*Pleurotus ostreatus*), and shiitake (*Lentinula edodes*) varieties were sliced to 0.3 cm thickness with an Urschel slicer (Valparaiso, IN) and placed in twelve clear plastic bags, with each bag containing approximately 2.26 kg of the sliced material. The bags were labeled with mushroom and assigned treatment type. There were three treatment groups: treatment group one was a control group with no UV-B treatment; in group two (low treatment), the mushrooms were exposed to 80−90 mJ/cm^2 UV-B irradiation for 25 s at 49−54 °C expected to produce 100−200 IU/g (2.5−5 μg/g) vitamin D_2; and in group three (high treatment), the mushrooms were exposed to 2800−2900 mJ/cm^2 UV-B irradiation at 60−66 °C for 10 min to produce 6000−8000 IU/g (150−200 μg/g) vitamin D_2.

For high UV-B radiation treatment, 2.26 kg each of four sliced mushroom samples (white, brown, oyster, and shiitake) were distributed onto the UV line conveyor in a monolayer (1.25 cm thickness) across the width of the conveyor, with 60 cm separating different mushroom type samples. The UV line (Monterey Mushrooms, Inc., proprietary) was set up with commercial UV specifications. The final energy output was measured in mJ/cm^2 with an EIT radiometer UV Power Puck II (Watsonville, CA 95076). After 10 min UV exposure, UV-treated mushrooms were directly placed on trays for dehydration. Low UV-B radiation treatment followed the same technique, with the UV line specifications modified to produce low UV-B levels by removing bulbs and adjusting the conveyor speed to obtain low energy readings. Total exposure time was 25 s, and the treated mushrooms were placed on trays for dehydration. For control samples with no UV treatment, sliced mushroom were directly placed on trays for dehydration.

Trays were loaded into a Harvest Saver (tray dryer) dehydrator (Commercial Dehydrator Systems, Inc.) for 16 h at 93.3 °C, and an empty tray was placed in between each tray with samples to prevent cross contamination. After the dehydration cycle, each sample was placed in a laminated prelabeled bag and sealed. A coffee grinder was used for grinding samples. After each sample, the coffee grinder was washed and dried before the next sample. Mushroom powder samples were placed in laminated bags, sealed and labeled accordingly.

The samples were shipped on dry ice overnight to the USDA laboratories. The samples were stored at −20 °C away from light exposure until the analysis. Moisture content was determined gravimetrically for each mushroom powder sample after drying the mushroom powder in an oven at 110 °C overnight. Each sample of mushroom powder was analyzed in triplicate to test for analytical variability.

Reagents and Materials. Standards of ergosterol (purity >95%), cycloartenol (purity >90%), cholesterol, methimazole, and ergothioneine (purity >99% for all) were purchased from Sigma Aldrich (St. Louis, MO, USA); standards of β-sitosterol, campesterol, stigmasterol, brassicasterol, sitostanol (stigmastanol), lupeol, and campesterol-d_3 (purity >98% for all) were from Santa Cruz Biotechnology, Inc. (Dallas, TX, USA). Stock solutions were individually prepared from neat materials at concentrations of 1 mg/mL in methanol, acetone, isopropanol, or their mixtures, depending on the compound solubility, and stored at −18 °C. A standard mixture of phytosterols at 10 μg/mL in methanol/acetone was prepared and used as a spiking solution for recovery experiments.

Standards of genistein, daidzein, glycetein, daidzin, and genistin were obtained from LC Laboratories (Woburn, MA). Standards of biochanin A, *trans*-resveratrol, quercetin dehydrate, kaempferol, coumestrol, naringin, formononetin, delphinidin, naringenin, eriodictyol, enterodiol, rutin hydrate, and cyanidin were purchased from Sigma Aldrich (St. Louis, MO, USA). (±)-Equol, matairesinol, (±)-enterolactone, apigenin, hesperetin, luteolin, and piceatannol were from the Cayman Chemical Company (Ann Harbor, MI). Genistein-d_4 was from the CDN Isotopes (Pointe-Claire, Quebec, Canada). All standards were ≥95% purity. A standard mixture of polyphenols at 10 μg/mL in methanol was prepared and used as a spiking solution for recovery experiments. Concentrations were not corrected for the purity of the standards.

All solvents were HPLC grade. Methanol was purchased from Sigma Aldrich (St. Louis, MO, USA), and acetone was from EMD Chemicals (Gibbstown, NJ, USA). Isopropanol was purchased from Honeywell Burdick and Jackson (Muskegon, MI, USA). Certified ACS grade hexane was purchased from Fisher Scientific (Fair Lawn, NJ, USA). Deionized water of 18.2 Ω-cm was prepared with an E-Pure model D4641 from Barnstead/Thermolyne (Dubuque, IA, USA). Formic acid (88% purity) was obtained from Spectrum Quality Products Inc. (New Brunswick, NJ, USA). Potassium hydroxide (KOH) pellets (purity 86.8%) and anhydrous sodium sulfate (purity 99.49%) were obtained from Mallinckrodt, Inc. (Paris, KY, USA). Pyridine (purity 99.8%) was from Sigma-Aldrich. *N*,*O*-Bis-(trimethylsilyl)trifluoroacetamide (BSTFA) and trimethylchlorosilane (TCMS) were purchased from Fisher Scientific (Pittsburgh, PA, USA).

National Institute of Standards and Technology (NIST) Standard Reference Material (SRM) 3251 *Serenoa repens* extract was purchased from NIST (Gaithersburg, MD, USA).

Phytosterol Analysis. The sample preparation method was based on that of Laakso (2005)[22] with some modifications. Briefly, mushroom powder samples (100 mg) were spiked with an internal standard (ISTD) of cholesterol (2 μg), then saponified with 2.0 mL of 3 N KOH in methanol by sonication (Branson 5510 Ultrasonicator, Branson Ultrasonics (Danbury, CT, USA)) for 10 min and heating in a water bath at 60 °C for 60 min. Phytosterols were extracted by adding 2 mL of hexane to the samples, vortexing, and then centrifuging to allow separation of the layers. The top organic layer was removed into a clean centrifuge vial, and then the extraction was repeated two more times. The combined hexane extract was then evaporated to dryness at room temperature under nitrogen. Pyridine (25 μL) was added, and the extract was derivatized with 25 μL of BSTFA + 1% TCMS by placing in a water bath at 60 °C for 30 min. After hexane (950 μL) was added, the extract was transferred to an autosampler vial and subjected to gas chromatographic (GC) analysis.

Table 1. Average Retention Times (t_R), Multiple Reaction Monitoring (MRM) Transitions, Collision Energy (CE) for Each Transition, and the Lowest Calibrated Level (LCL)

TMS ether of	t_R (min)	quantifier (m/z)	CE (V)	qualifier (m/z)	CE (V)	LCL ($\mu g\ g^{-1}$)
cholesterol	6.788	368.3 → 159.2	40	368.3 → 145.1	40	ISTD
brassicasterol	6.943	470.4 → 201.3	20	470.4 → 69	20	0.025
ergosterol	7.15	363.2 → 143	40	363.2 → 128	40	0.01
campesterol	7.223	382.3 → 145.1	40	382.3 → 105	40	0.01
stigmasterol	7.328	484.4 → 169.3	40	484.4 → 145	40	0.025
campesterol-d_3	7.422	346.3 → 121.1	10	346.3 → 95.1	10	ISTD
β-sitosterol	7.625	396.3 → 381.3	10	396.3 → 213.1	10	0.05
stigmastanol	7.69	473.3 → 161.2	20	473.3 → 75.1	20	0.01
cycloartenol	8.058	393.3 → 81.2	30	393.3 → 69.2	30	0.01
lupeol	8.14	369.3 → 109.1	10	369.3 → 94.9	10	0.05

The detection and quantification of the trimethylsilyl (TMS) ethers of sterols was performed using an Agilent (Little Falls, DE, USA) 7000B with high sensitivity electron ionization (EI) source triple-quadrupole mass spectrometer (GC–MS/MS). The GC was an Agilent 7890A gas chromatograph operated in low pressure vacuum outlet mode.[23] The GC column was a 15 m × 0.53 mm × 1 μm film thickness SLT-5 MS (Supelco, Bellefonte, PA, USA) connected to a 5 m × 0.18 mm noncoated guard column from Restek (Bellefonte, PA, USA). Ultrahigh purity He was used as a carrier gas at 2 mL min^{-1} constant flow rate as described previously.[24] At the transfer line the GC column was connected to a ∼17 cm × 0.53 mm i.d. piece of phenyl-methyl deactivated guard column (Restek).

The GC oven temperature program was as follows: 70 °C held for 1.5 min, ramped 80 °C min^{-1} to 180 °C, then ramped 40 °C min^{-1} to 250 °C, followed by 70 °C min^{-1} to 290 °C, and held 4.5 min. The total run time was 9.7 min. The transfer line was at 250 °C, and ion source was set at 320 °C. The MS/MS collision gas was nitrogen at 1.5 mL min^{-1}, and the quench gas was He at 2.25 mL min^{-1}. The EI energy was −70 eV, quadrupole temperatures were set at 150 °C, and the solvent delay was 6 min. An Agilent Multimode Inlet (MMI) was operated as a programmable temperature vaporizer (5 μL injection volume) with solvent vent mode of He flow at 55 mL min^{-1}. The MMI temperature program was 70 °C held for 0.31 min (at which point the vent was closed), then ramped to 420 °C at 320 °C min^{-1}, and held at 420 °C for the rest of the GC run.

Each phytosterol individual standard solution at 1000 ng mL^{-1} was derivatized individually with pyridine and BSTFA + TCMS as described above and injected in full scan mode to determine the most intense ions of the corresponding TMS ether. Product ion and collision energy experiments were performed to determine the optimum two product ions, collision energies, and ratios between quantifier and qualifier ions. The method detection limit was defined as a compound's lowest calibrated level. Multiple reaction monitoring (MRM) transitions, collision energy for each transition, average retention times (t_R), and the lowest calibration levels are presented in Table 1. In the finalized MRM method, a dwell time of 2.5 ms and the "wide" MS resolution were used for all transitions. The MRM transitions were monitored in one time segment from 6 to 9 min. Cholesterol was used as a main ISTD, and campesterol-d_3 was used as a backup if needed. Calibration curves were linear from 0.01 to 0.05 to 10 μg/mL for all sterols. Due to the abundance of ergosterol relative to the other sterols in mushroom powder, its calibration curve was from 1 to 50 μg/mL. Separate extraction was performed for ergosterol analysis, the mass of extracted mushroom powder was 20–30 mg, and the extracts were diluted in hexane 10 times prior to GC–MS/MS analysis.

Ergothioneine Analysis. Mushroom powder (100 mg) was placed into a 15 mL polypropylene centrifuge tube, 10 μg of ISTD methimazole was added, and the sample was extracted with 10 mL of 4:1 (v:v) methanol/water by vigorous shaking for 20 min in a shaker, following by centrifugation at 3650 rcf (×g) for 3 min. After centrifugation, 0.1 mL of the extract was transferred to an autosampler vial containing 0.9 mL of 3:7 (v:v) methanol/water, and the extract was subjected to LC–MS/MS analysis.

An HPLC column (Luna C8(2) 3 μm, 100 Å, 100 × 4.6 mm) integrated with a 4 × 3 mm i.d. Security Guard C8 column (Phenomenex Inc., Torrance, CA, USA) was used for separation. An isocratic program of 0.1% formic acid buffer (A) at 30% and MeOH (B) at 70% with a constant flow rate of 0.4 mL min^{-1} was applied with an injection volume of 20 μL, and the column oven was at 30 °C. The total run time was 5 min. The calibration curves were linear from 0.001 to 2.5 μg/mL of ergothioneine with 0.1 μg of the ISTD. The method detection limit was 1 μg/g ergothioneine.

The mass spectrometer was an API 3000 (Applied Biosystems/MDS Sciex, Ontario, Canada) with electrospray ionization (ESI) operated in the positive mode. The ion spray potential was 4500 V, and the source temperature was set at 500 °C. MRMs of m/z 230.2 → 127.1 and m/z 230.2 → 186.1 were used for ergothioneine (t_R = 2.75 min) and MRMs of m/z 114.9 → 57.1 and m/z 114.9 → 74.1 were used for methimazole (t_R = 3.05 min) with dwell times of 250 ms.

Polyphenolic Compound Analysis. Mushroom powder (100 mg) was placed into a 15 mL polypropylene centrifuge tube, 1 μg of an ISTD genistein-d_4 was added, and the sample was extracted with 5 mL of 4:1 (v:v) methanol/water by sonication for 30 min at room temperature. A 0.5 mL aliquot of the extract was filtered through a 0.2 μm PVDF filter and transferred into an autosampler vial, 0.5 mL of DI water was added to each vial, and the extract was subjected to LC–MS/MS analysis.

A Luna C8(2) 3 μm, 100 Å, 100 × 4.6 mm column with a 4 × 3 mm i.d. Security Guard C8 column (Phenomenex Inc.) was used for separation. The binary gradient of 0.2 mM ammonium formate buffer at pH 4.7 (A) and MeOH (B) at a constant flow rate of 0.4 mL min^{-1} was applied with an injection volume of 20 μL. Column oven temperature was at 40 °C. The gradient program started at 70% A held for 1 min, then ramped to 90% B over the course of 7 min, and held for 2 min. Re-equilibration time at 70% A was 4 min. The mass spectrometer with ESI was operated in the negative mode. The detailed information on the LC–MS/MS method used for polyphenols is reported elsewhere.[25] The calibration curves were linear from 0.001 to 2.5 μg/mL. The method detection limit was 0.1 μg/g.

Vitamin D Analysis. Vitamin D analysis was performed as previously described in detail by Byrdwell (2013)[26] using a "dilute-and-shoot" method and analyzed using liquid chromatography quadruple parallel mass spectrometry (MS) with UV detection at 265 nm. Comparison of MS and UV results is a separate study, which will be presented in a future work.

Each mushroom powder sample was prepared in 5 replicate analytical samples, which were each run in triplicate. A set of three calibration standards were bracketed before, between, and after the five samples. Samples that were expected to have low values (control and low treatment) used a low set of standards, consisting of 500, 1000, and 2000 IU. Samples that were expected to have higher values (high treatment) used a higher set of standards, consisting of 1000, 2000, and 5000 IU.

Statistical Analysis. Statistical data analysis was performed with the SAS System for Windows version 9.4 (SAS Institute Inc., Cary, NC, USA). Analysis of variance (ANOVA) was conducted to investigate the effects and interactions of treatment and mushroom type on ergosterol, campesterol, ergothioneine, and vitamin D. Dunnett's and Bonferroni tests were used with $p = 0.05$ significance.

RESULTS AND DISCUSSION

Sample Preparation Method Evaluation. Phytosterol recoveries were evaluated using reagent spikes (300 mg of anhydrous Na_2SO_4) and matrix spikes (100 mg of mushroom powder) fortified with 2.5 and 5 mg/g of phytosterol standard mixture. Five replicate samples were prepared for both reagent spikes and matrix spikes at each spiking level (see Table 2).

Table 2. % Recoveries of Phytosterols (and % RSDs)[a]

	reagent spike		matrix spike	
	2.5 mg/g	5 mg/g	2.5 mg/g	5 mg/g
brassicasterol	113 (6)	104 (12)	89 (3)	103 (5)
ergosterol	95 (9)	80 (7)	n/a	n/a
campesterol	107 (5)	104 (7)	107 (20)	113 (7)
stigmasterol	98 (12)	107 (4)	120 (14)	**133** (5)
β-sitosterol	112 (2)	105 (5)	120 (2)	118 (6)
stigmastanol	108 (12)	106 (13)	**121** (9)	119 (15)
cycloartenol	105 (17)	108 (17)	**125** (8)	106 (4)
lupeol	107 (11)	110 (6)	117 (8)	112 (6)

[a] $n = 5$; bold indicates recoveries outside of 70−120%; n/a, not applicable.

Unfortified mushroom powder and reagent blank samples (1 mL of DI water) were analyzed along with the spiked samples. Due to the abundance of ergosterol in mushroom powder, it was impossible to calculate its recoveries for fortified mushroom powder samples, therefore only reagent spike recoveries were evaluated in its case.

Campesterol and ergosterol were measured in mushroom powders used for the fortification experiments. Campesterol recoveries were calculated after subtracting the amounts found in the control mushroom powder from the amounts measured in the fortified mushroom powder. However, this was impossible for ergosterol, as the mushroom powders contained a very high amount of ergosterol.

The recoveries of phytosterols from reagent spike samples were within satisfactory limits of 95−113% (5−17% RSDs) for the 2.5 mg/g spiking level and 80−110% (4−17% RSDs) for the 5 mg/g level. For fortified mushroom powders, however, the recoveries ranged from 89 to 125% (2−20% RSDs) for 2.5 mg/g and 103−133% (4−15% RSDs) for the 5 mg/g spiking level. Cycloartenol and stigmasterol (125 and 133%, respectively) recoveries were outside of satisfactory limits of 70−120%. RSDs for 5 replicate measurements in the recovery experiment were at or below 20%, indicating acceptable method performance.

To estimate the accuracy of measurements (or "trueness") of the developed method, the standard reference material SRM 3251 *Serenoa repens* extract with certified values for campesterol, β-sitosterol, and stigmasterol was analyzed in 5 replicates. Due to high amounts of these sterols in the reference material, only small portions of the material (20−28 mg) were extracted. The measured values were in good agreement with certified values for campesterol and stigmasterol (see Table 3). The average accuracy measured as a percent of measured concentration vs certified concentration was 97% for campesterol and 93% for stigmasterol. For β-sitosterol concentrations measured in SRM 3251, the average accuracy was 124%. β-Sitosterol has the highest concentration in SRM 3251, and even after extraction of small amounts of the reference material, several serial dilutions 1:10 and 1:100 were required to fit its concentration in the calibration curve range. In contrast to the SRM material, β-sitosterol concentrations in mushrooms are very low[9] and were not measured in mushroom samples in our study. RSDs for five parallel measurements of selected phytosterols in SRM 3251 were 11−16%, indicating the method's acceptable repeatability.

Table 3. Determined Phytosterol Concentrations in SRM 3251 *Serenoa repens* Extract

	certified value, mg g^{-1} ± SD	measd value, mg g^{-1} ± SD, $n = 5$	% accuracy (RSD), $n = 5$
campesterol	0.533 ± 0.031	0.519 ± 0.081	97 (16)
β-sitosterol	1.666 ± 0.064	2.065 ± 0.321	124 (16)
stigmasterol	0.247 ± 0.040	0.231 ± 0.037	93 (11)

For evaluating egrothioneine recoveries, the mushroom powder was spiked with ergothioneine standard solution at the levels 0.5, 2, and 5 mg/g ergothioneine. Five replicate samples were prepared as described above for each spiking level. Unfortified mushroom powder and reagent blank samples were analyzed along with the spiked samples, and ergothioneine concentrations for the recovery calculations were adjusted for the amount measured in unfortified mushroom powder. The ergothioneine recoveries were 109 ± 20%, 105 ± 8%, and 119 ± 10% for the spiking levels of 0.5, 2, and 5 mg/g, respectively.

The recoveries of polyphenols from fortified mushroom powder samples were evaluated at spiking levels of 5 and 10 μg/g for five replicates per level. Unfortified mushroom powder and reagent blank samples were analyzed along with the spiked samples. No polyphenols were detected in the reagent blank and unfortified mushroom powder samples used in the recovery study. The recoveries of polyphenols were satisfactory (70−120%) with the exception of naringin (63%) and matairesinol (65%) at the 5 μg/g spiking level, and enterolactone (123%) at the 10 μg/g spiking level (see Table 4).

Phytosterols. Only ergosterol and campesterol were present for determination in the mushroom powder samples. Matrix spike sample recoveries were 107−113%, and precision measurement of duplicate samples was 3−20%.

Ergosterol concentrations were 2.4−4.0 mg/g dw (shiitake), 2.9−4.5 mg/g dw (oyster), 4.6−6.2 mg/g dw (brown), and 4.6−5.2 mg/g dw (white) mushroom powder samples (Figure 1). A Bonferroni test showed significantly higher ($p < 0.05$) ergosterol levels in brown and white mushroom powder than in the oyster and shiitake (See Figure 2). This is consistent with the recent findings by Villares et al. (2014)[8] reporting ergosterol concentrations in *A. bisporus* (white and brown) mushrooms (6.42 mg/g dry wt) being significantly greater ($p < 0.05$) than in *L. edodes* (shiitake) (3.64 mg/g dw) and *P. ostreatus* (oyster) (3.31 mg/g dw).

When examining the effect of UV-B treatment among different types of mushroom powder samples, shiitake and oyster mushroom powders had significantly lower concentrations of ergosterol in high UV-B treatment samples compared to control. For brown mushroom powders, samples from high UV-B treatments had significantly lower concen-

Table 4. % Average Recoveries (and % RSDs) of Polyphenolic Compounds in Spiked Mushroom Powder[a]

	spiking levels	
compound	5 μg/g	10 μg/g
naringin	**63** (12)	107 (20)
daidzein	104 (13)	89 (10)
daidzin	79 (15)	78 (20)
genistein	77 (13)	91 (13)
glycitein + biochanin A	113 (9)	118 (16)
genistin	119 (15)	70 (19)
resveratrol	78 (16)	85 (**21**)
quercetin	117 (15)	100 (15)
kaempferol	95 (13)	98 (12)
coumestrol	97 (9)	92 (18)
naringenin	115 (14)	110 (13)
hesperetin	118 (15)	95 (5)
luteolin	117 (**21**)	116 (11)
apigenin	109 (19)	93 (16)
matairesinol	**65** (19)	110 (17)
enterolactone	72 (9)	**123** (14)
equol	83 (13)	120 (4)
eriodictyol	83 (16)	78 (**23**)
enterodiol	118 (11)	96 (15)
rutin	96 (16)	111 (12)
formonetin	89 (15)	89 (19)
cyanidin	80 (10)	102 (16)
delphinidin	**127** (10)	101 (20)
piceatannol	104 (12)	77 (11)

[a] $n = 5$; bold indicates recoveries outside of 70−120% and RSDs >20%.

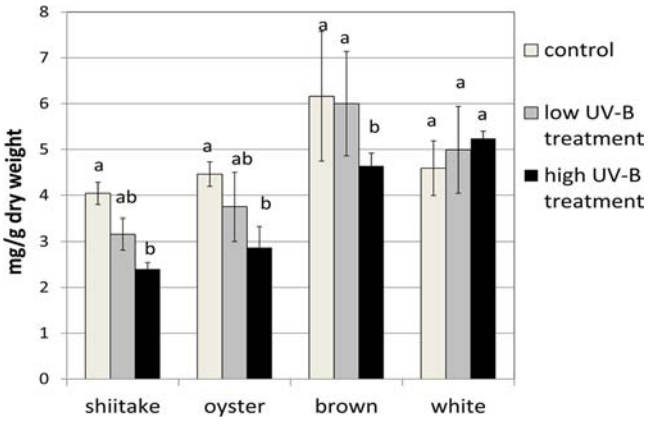

Figure 1. Ergosterol average concentrations (mg/g dry weight) in different types of mushroom powder in control and different treatment conditions; error bars represent standard deviations for $n = 3$. Any two values with no letter in common are significantly ($p < 0.05$) different according to the Bonferroni test within any specific mushroom type.

trations of ergosterol compared to low UV-B treatment and control (see Figure 1).

No statistical difference in ergosterol concentrations was observed for white mushroom powder samples exposed to different treatments. Simon et al. (2011)[27] observed the same effect when ergosterol concentrations remained stable in the same type of mushrooms (*Agaticus bisporus)* exposed to UV-B light. These observations may warrant future studies to better understand a mechanism of ergosterol conversion to vitamin D_2 in different types of mushrooms exposed to UV-B radiation.

Only a small portion of ergosterol converts to vitamin D under UV-B treatment, where ergosterol concentrations in mushrooms are in mg/g levels, and the amounts of formed vitamin D are in μg levels, therefore mushroom powder used as a dietary supplement ingredient provides high levels of ergosterol. According to Phillips et al. (2011),[9] the potential contribution of ergosterol by fresh mushrooms is 0.27−0.86 mg/g. Nuts and seeds are regarded as foods providing the highest amounts of ergosterol: 0.95−4.01 mg/g.[28] In comparison, mushroom powder made of brown mushrooms in our study provides up to 6 mg/g of ergosterol.

Besides ergosterol, campesterol was measured in mushroom powder samples in our study in concentrations of 31−41 μg/g dw (shiitake), 15−20 μg/g dw (oyster), 36−42 μg/g dw (brown), and 38−43 μg/g dw (white) mushroom powder samples (Figure 3). Campesterol concentrations were significantly lower ($p < 0.05$) in oyster mushroom powder compared to three other types (Figure 4). Shiitake mushroom powder had significantly lower concentrations of campesterol in high UV-B treated samples compared to low UV-B treated samples (Figure 3). This is an interesting finding, as we are not aware of any published studies to date reporting the effects of UV-B radiation on campesterol concentrations.

Compared to other studies, concentrations of campesterol in our study were 10 times lower compared to concentrations of campesterol found by Phillips et al. (2011)[9] in morel mushrooms (12.3−45.4 μg/g fresh weight). However, they were comparable with campesterol concentrations measured in *Tuber* fermentation mycelia (15−24 μg/g dw) by Tang et al. (2012).[29] Also, brassicasterol was measured in morel mushrooms[9] and *Tuber* fermentation mycelia,[29] but was not detected in mushroom powder in our study.

Polyphenolic Compounds. No individual polyphenolic compounds were detected in mushroom powder samples in our study (method detection limit 0.1 μg/g). In contrast, quercetin was measured in concentrations 9.64−66.74 μg/g dry weight in wild edible mushrooms from China by other researchers.[18] Another study analyzed phenolic compounds in edible and medicinal mushrooms from Korea and measured naringin (not detected (nd)−38 μg/g), resveratrol (nd−12 μg/g), quercetin (nd−52 μg/g), naringenin (nd−36 μg/g), kaempferol (nd−53 μg/g), hesperetin (nd−3 μg/g), formononetin (nd−1 μg/g), and biochanin A (nd−3 μg/g).[19] Similar to our study, rutin was not detected in mushrooms from Korea. Another study found no flavonoids or lignans in the cultivated mushrooms (white and brown *A. bisporus*, *L. edodes*, and *P. zostreatus*).[30]

Previously published studies have reported that UV-B irradiation increased concentrations of selected polyphenolic compounds, such as flavonoids and flavonols in tomatoes[20] and apples,[21] however the measured amounts were in low mg/g levels, while polyphenolic compounds reported in mushrooms are usually reported in the low μg/g range. According to Kalac (2013),[1] wild and cultivated mushrooms as well as several specific mushroom species may greatly differ in polyphenolics composition and concentrations. Polyphenolic compounds easily degrade when exposed to light, elevated temperatures, and pH changes.[31,32]As it was described by other researchers, elevated temperatures, for example, boiling mushrooms in water, resulted in decreased amounts of total polyphenols and ergothioneine.[33] A recent study indicated that up to 73% of flavonoids were lost during freeze-drying of a perennial herb *Centella asiatica*.[34] It is unclear if polyphenolic compounds were not detected in the mushroom powder samples due to

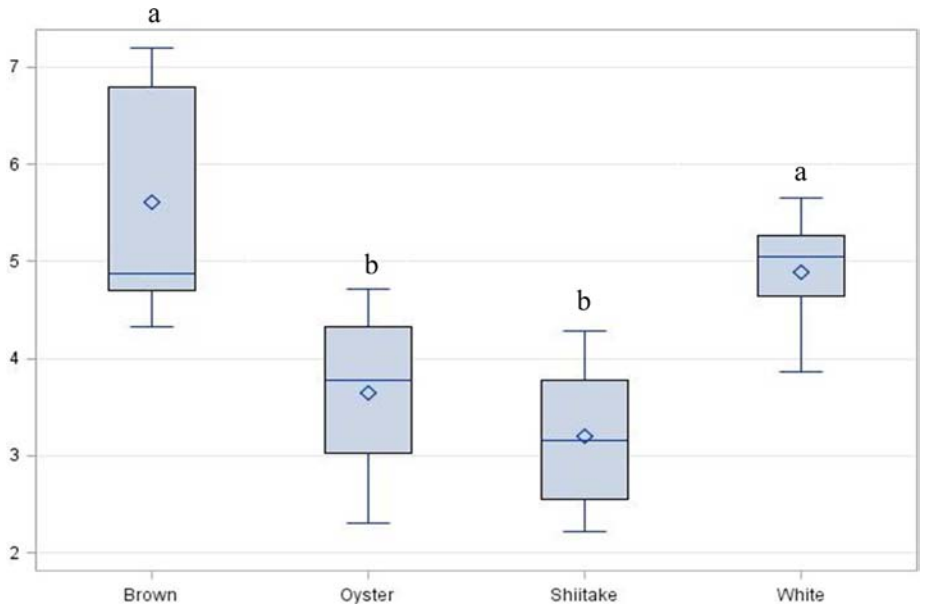

Figure 2. Distribution of ergosterol mean concentrations (mg/g dry weight) among different mushroom powder types. Any two values with no letter in common are significantly ($p < 0.05$) different according to the Bonferroni test.

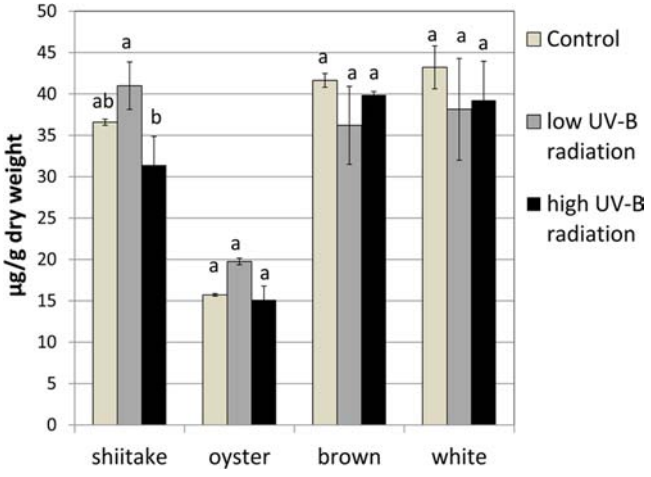

Figure 3. Campesterol average concentrations (μg/g dry weight) in different types of mushroom powder in control and different treatment conditions; error bars represent standard deviations for $n = 3$. Any two values with no letter in common are significantly ($p < 0.05$) different according to the Bonferroni test within any specific mushroom type.

compositional differences in mushroom types, or degradation during the drying process to produce mushroom powder.

Ergothioneione. Ergothioneine recoveries in matrix spike samples were 67−115%, and precision for replicate samples was 0.1−8%. Ergothioneine concentrations found in mushroom powder samples were 0.37−0.48 mg/g dw (brown), 0.81−0.92 mg/g dw (white), 7.2−7.9 mg/g dw (shiitake), and 9.7−10.4 mg/g dw (oyster) (Figure 5). Ergothioneine average concentrations were significantly greater in oyster mushroom powders compared to shiitake, and both types had significantly higher concentrations compared to brown and white (Figure 5). For comparison, Nguyen et al. (2012) found 2 mg/g dw ergothioneine in the cultivated mushroom *Flammulina velutipes*.[33] Other researchers measured 0.21 mg/g, 1.98 mg/g, and 2.59 mg/g dw of ergothioneine in white, shiitake, and oyster mushrooms, respectively.[17] While these amounts are approximately four times lower than amounts of ergothioneine measured in our work, they follow the same trend with oyster mushrooms having the highest amount of ergothioneine, followed by shiitake and white mushrooms. Ey et al. (2007)[16] measured 119 μg/g wet weight of ergothioneine in oyster mushrooms (*Pleurotus ostretus*). Assuming the moisture content of these mushroom was ≈90%, this corresponds to 12 mg/g dw of ergothioneine, which is similar to the 9.7−10.4 mg/g dw of ergothioneine measured in our study. Ergothioneine concentrations were not appreciably affected by UV-B radiation for all mushroom types, except shiitake, for which concentrations of ergothioneine decreased significantly from control to low and high UV-B treatments (Figure 5). This is an important finding, as to our knowledge this is the first study investigating ergothioneine concentration changes in UV-B exposed mushrooms.

Mushrooms can serve as an excellent source of the naturally occurring antioxidant ergothioneine. Shiitake and oyster mushroom powders in this study had the highest amounts of ergothioneine, and only 0.5−1 g of these mushroom powder supplements is needed to provide 4−5 mg of ergothioneine, compared to the need for a ≈70 g serving of fresh mushrooms to receive a similar amount of ergothioneine.

Vitamin D. Vitamin D average concentrations ($n = 5$) and standard deviations, expressed in IU/g, are given in Table 5. % precision for replicate samples ($n = 5$) ranged from 0.53 to 3.14%. No vitamin D was measured in control samples of oyster and shiitake mushroom powder. For statistical analysis, zeroes were used for these samples. In contrast, control samples of brown and white mushroom powder had 179 ± 4 (brown) and 179 ± 5 (white) IU/g of vitamin D. For low UV-B treatment, which was expected to increase vitamin D levels to 100−200 IU/g, vitamin D measured value was close to expected only for shiitake mushroom powder (217 ± 7 IU/g). Vitamin D concentrations measured in brown (1942 ± 30 IU/g) and white (2156 ± 43 IU/g) mushroom powder exposed to low UV-B radiation were statistically greater than expected. For high UV-B treatment, expected to increase vitamin D levels to 6000−8000 IU/g, the vitamin D concentration measured in

dx.doi.org/10.1021/jf403852k | J. Agric. Food Chem. 2014, 62, 3034−3042

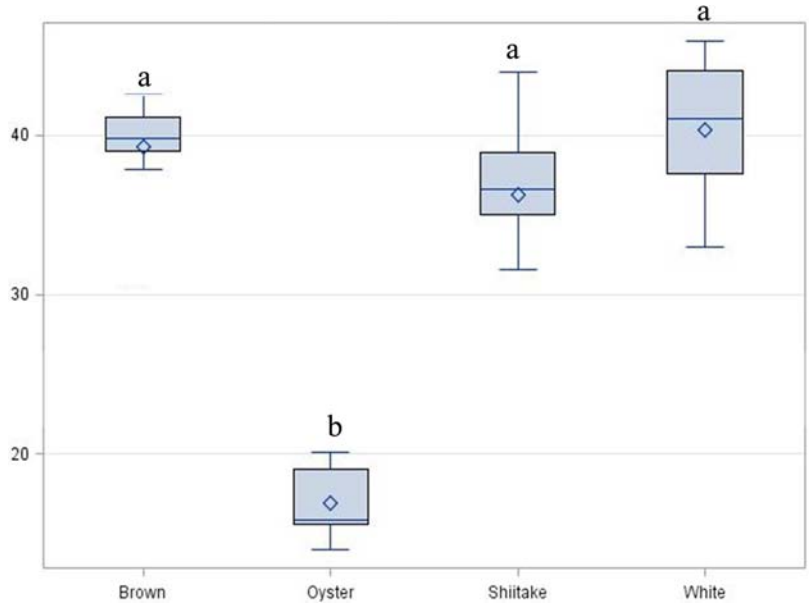

Figure 4. Distribution of campesterol mean concentrations (μg/g dry weight) among different mushroom powder types. Any two values with no letter in common are significantly ($p < 0.05$) different according to the Bonferroni test.

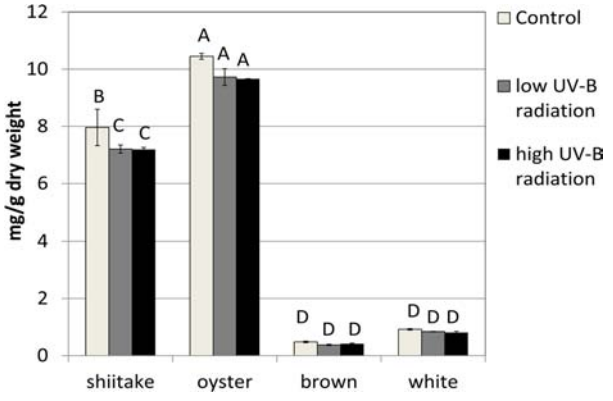

Figure 5. Ergothioneine average concentrations (mg/g dry weight) in different types of mushroom powder in controls and different treatment conditions, error bars represent standard deviations for $n = 3$. Any two values with no letter in common are significantly ($p < 0.05$) different according to the Bonferroni test.

Table 5. Vitamin D Average Concentrations and Standard Deviations ($n = 5$), IU/g in Mushroom Powder Samples[a]

	shiitake	oyster	brown	white
control	nd[b] (**I**)	nd (**I**)	179 ± 4 (**H**)	179 ± 5 (**H**)
low UV-B treatment (expected 100–200 IU/g)	217 ± 7 (**H**)	1245 ± 9 (**F**)	1942 ± 30 (**E**)	2156 ± 43 (**D**)
high UV-B treatment (expected 6000–8000 IU/g)	1036 ± 13 (**G**)	4411 ± 23 (**C**)	6292 ± 109 (**A**)	4739 ± 61 (**B**)

[a]Bold letters in parentheses represent level of statistical difference. Any of the twelve values with no letter in common are significantly different ($p < 0.05$) according to the Bonferonni test. [b]Not detected.

brown mushroom powder (6292 ± 109 IU/g) was at the expected level. Concentrations of vitamin D for oyster (4441 ± 23 IU/g), white (4739 ± 61 IU/g), and shiitake (1036 ± 13 IU/g) mushrooms were statistically lower than expected.

It is interesting to note that shiitake mushroom powder had the lowest levels of ergosterol (significantly lower than in other mushroom powder samples), and the lowest levels of vitamin D were produced in these samples.

This study investigated effects of UV-B radiation on the bioactive natural compounds in different types of mushroom powders used as dietary supplement ingredients. Mushroom antioxidant, ergothioneine, concentrations were 0.37–0.48 mg/g dw (brown), 0.81–0.92 mg/g dw (white), 7.2–7.9 mg/g dw (shiitake), and 9.7–10.4 mg/g dw (oyster) mushroom powder samples, and were mostly not affected by UV-B radiation. Polyphenolic compounds were not detected. Mushrooms' most abundant phytosterol, ergosterol, concentrations were highest for brown (2.9–4.5 mg/g dw) followed by white (4.6–5.2 mg/g dw), oyster (2.9–4.5 mg/g dw), and shiitake (2.4–4.0 mg/g dw) mushroom powder samples. Ergosterol concentrations were significantly higher in brown and white mushroom powders compared to oyster and shiitake, and significantly decreased with the increased level of UV-B treatment for all mushroom powder types, except for white. Campesterol concentrations were greatest for white (38–43 μg/g dw), followed by brown (36–42 μg/g dw), shiitake (31.4–41.0 μg/g dw), and oyster (15.1–19.8 μg/g dw), and were significantly lower in oyster mushroom powder samples compared to the other three types. Campesterol concentrations significantly decreased in shiitake mushroom powder in high UV-B treated samples compared to low UV-B treated samples. These results provide some new information on UV-B radiation effects on the important natural bioactive compounds in mushrooms, and suggest that mushroom powder dietary supplements not only provide vitamin D but also may be a good source of phytosterols and ergothioneine.

AUTHOR INFORMATION

Corresponding Author

*E-mail: yelena.sapozhnikova@ars.usda.gov.

Funding

The authors acknowledge the Monterey Mushrooms, Inc., for providing funding for this research (Trust Fund #293-1935-289).

Notes

Disclaimer. Mention of trade names or commercial products in this publication is solely for the purpose of providing specific information and does not imply recommendation or endorsement by the U.S. Department of Agriculture. USDA is an equal opportunity employer.

The authors declare no competing financial interest.

■ ACKNOWLEDGMENTS

Technical assistance of Tawana Simons and Annastassia Gallo, USDA/ARS is greatly appreciated. The authors acknowledge Dr. John Phillips, USDA/ARS, for assistance with statistical data analysis.

■ REFERENCES

(1) Kalac, P. A review of chemical composition and nutritional value of wild-growing and cultivated mushrooms. *J. Sci. Food Agric.* **2013**, *93*, 209−218.

(2) Guillamon, E.; Garcia-Lafuente, A.; Lozano, M.; D'Arrigo, M.; Rostagno, M. A.; Villares, A.; Martinez, J. A. Edible mushrooms: Role in the prevention of cardiovascular diseases. *Fitoterapia* **2010**, *81*, 715−723.

(3) Diyabalanage, T.; Mulabagal, V.; Mills, G.; DeWitt, D. L.; Nair, M. G. Health-beneficial qualities of the edible mushroom, *Agrocybe aegerita*. *Food Chem.* **2008**, *108*, 97−102.

(4) Roupas, P.; Keogh, J.; Noakes, M.; Margetts, C.; Taylor, P. The role of edible mushrooms in health: Evaluation of the evidence. *J. Funct. Foods* **2012**, *4*, 687−709.

(5) Chang, S.-T. Overview of mushroom cultivation and utilization as functional foods. In *Mushrooms as functional foods*; John Wiley & Sons, Inc.: 2009; pp 1−33.

(6) Hernando, I.; Sanjuan, N.; Perez-Munuera, I.; Mulet, A. Rehydration of freeze-dried and convective dried *Boletus edulis* mushrooms: Effect on some quality parameters. *J. Food Sci.* **2008**, *73*, E356−E362.

(7) Schneider, I.; Kressel, G.; Meyer, A.; Krings, U.; Berger, R. G.; Hahn, A. Lipid lowering effects of oyster mushroom (*Pleurotus ostreatus*) in humans. *J. Funct. Foods* **2011**, *3*, 17−24.

(8) Villares, A.; Mateo-Vivaracho, L.; Garcia-Lafuente, A.; Guillamon, E. Storage temperature and UV-irradiation influence on the ergosterol content in edible mushrooms. *Food Chem.* **2014**, *147*, 252−256.

(9) Phillips, K. M.; Ruggio, D. M.; Horst, R. L.; Minor, B.; Simon, R. R.; Feeney, M. J.; Byrdwell, W. C.; Haytowitz, D. B. Vitamin D and sterol composition of 10 types of mushrooms from retail suppliers in the United States. *J. Agric. Food Chem.* **2011**, *59*, 7841−7853.

(10) Institute of Medicine of the National Academies. *Dietary reference intakes for calcium and vitamin D*, Revised March 2011; The National Academies Press: Washington, DC, 2010. http://www.iom.edu/Reports/2010/Dietary-Reference-Intakes-for-Calcium-and-Vitamin-D.aspx.

(11) U.S. Department of Agriculture, Agricultural Research Service. USDA National nutrient database for standard reference, release 24. Nutrient data laboratory home page. http://www.ars.usda.gov/ba/bhnrc/ndl.

(12) Bedner, M.; Schantz, M. M.; Sander, L. C.; Sharpless, K. E. Development of liquid chromatographic methods for the determination of phytosterols in standard reference materials containing *Saw palmetto*. *J. Chromatogr. A* **2008**, *1192*, 74−80.

(13) Cheah, I. K.; Halliwell, B. Ergothioneine; antioxidant potential, physiological function and role in disease. *Biochim. Biophys. Acta* **2012**, *1822*, 784−793.

(14) Akanmu, D.; Cecchini, R.; Aruoma, O. I.; Halliwell, B. The antioxidant action of ergothioneine. *Arch. Biochem. Biophys.* **1991**, *288*, 10−16.

(15) Aruoma, O. I.; Spencer, J. P.; Mahmood, N. Protection against oxidative damage and cell death by the natural antioxidant ergothioneine. *Food Chem. Toxicol.* **1999**, *37*, 1043−1053.

(16) Ey, J.; Schomig, E.; Taubert, D. Dietary sources and antioxidant effects of ergothioneine. *J. Agric. Food. Chem.* **2007**, *55*, 6466−6474.

(17) Dubost, N. J.; Ou, B.; Beelman, R. B. Quantification of polyphenols and ergothioneine in cultivated mushrooms and correlation to total antioxidant capacity. *Food Chem.* **2007**, *105*, 727−735.

(18) Liu, Y. T.; Sun, J.; Luo, Z. Y.; Rao, S. Q.; Su, Y. J.; Xu, R. R.; Yang, Y. J. Chemical composition of five wild edible mushrooms collected from Southwest China and their antihyperglycemic and antioxidant activity. *Food Chem. Toxicol.* **2012**, *50*, 1238−1244.

(19) Kim, M. Y.; Seguin, P.; Ahn, J. K.; Kim, J. J.; Chun, S. C.; Kim, E. H.; Seo, S. H.; Kang, E. Y.; Kim, S. L.; Park, Y. J.; Ro, H. M.; Chung, I. M. Phenolic compound concentration and antioxidant activities of edible and medicinal mushrooms from Korea. *J. Agric. Food. Chem.* **2008**, *56*, 7265−7270.

(20) Castagna, A.; Dall'Asta, C.; Chiavaro, E.; Galaverna, G.; Ranieri, A. Effect of post-harvest UV-B irradiation on polyphenol profile and antioxidant activity in flesh and peel of tomato fruits. *Food Bioprocess Technol.* **2013**, 1−10.

(21) Hagen, S. F.; Borge, G. I. A.; Bengtsson, G. B.; Bilger, W.; Berge, A.; Haffner, K.; Solhaug, K. A. Phenolic contents and other health and sensory related properties of apple fruit (*Malus domestica borkh., cv. Aroma*): Effect of postharvest UV-B irradiation. *Postharvest Biol. Technol.* **2007**, *45*, 1−10.

(22) Laakso, P. Analysis of sterols from various food matrices. *Eur. J. Lipid Sci. Technol.* **2005**, *107*, 402−410.

(23) Koesukwiwat, U.; Lehotay, S. J.; Leepipatpiboon, N. Fast, low-pressure gas chromatography triple quadrupole tandem mass spectrometry for analysis of 150 pesticide residues in fruits and vegetables. *J. Chromatogr. A* **2011**, *1218*, 7039−7050.

(24) Sapozhnikova, Y.; Lehotay, S. J. Multi-class, multi-residue analysis of pesticides, polychlorinated biphenyls, polycyclic aromatic hydrocarbons, polybrominated diphenyl ethers and novel flame retardants in fish using fast, low-pressure gas chromatography−tandem mass spectrometry. *Anal. Chim. Acta* **2013**, *758*, 80−92.

(25) Sapozhnikova, Y. Development of liquid chromatography−tandem mass spectrometry method for analysis of polyphenolic compounds in liquid samples of grape juice, green tea and coffee. *Food Chem.* **2014**, *150*, 87−93.

(26) Byrdwell, W. C. Quadruple parallel mass spectrometry for analysis of vitamin D and triacylglycerols in a dietary supplement. *J. Chromatogr. A* **2013**, *1320*, 48−65.

(27) Simon, R. R.; Phillips, K. M.; Horst, R. L.; Munro, I. C. Vitamin D mushrooms: Comparison of the composition of button mushrooms (*Agaricus bisporus*) treated postharvest with UVB light or sunlight. *J. Agric. Food. Chem.* **2011**, *59*, 8724−8732.

(28) Phillips, K. M.; Ruggio, D. M.; Ashraf-Khorassani, M. Phytosterol composition of nuts and seeds commonly consumed in the United States. *J. Agric. Food. Chem.* **2005**, *53*, 9436−9445.

(29) Tang, Y.; Li, H. M.; Tang, Y. J. Comparison of sterol composition between *Tuber fermentation mycelia* and natural fruiting bodies. *Food Chem.* **2012**, *132*, 1207−1213.

(30) Mattila, P.; Konko, K.; Eurola, M.; Pihlava, J. M.; Astola, J.; Vahteristo, L.; Hietaniemi, V.; Kumpulainen, J.; Valtonen, M.; Piironen, V. Contents of vitamins, mineral elements, and some phenolic compounds in cultivated mushrooms. *J. Agric. Food. Chem.* **2001**, *49*, 2343−2348.

(31) Heras-Ramirez, M. E.; Quintero-Ramos, A.; Camacho-Davila, A. A.; Barnard, J.; Talamas-Abbud, R.; Torres-Munoz, J. V.; Salas-Munoz, E. Effect of blanching and drying temperature on polyphenolic compound stability and antioxidant capacity of apple pomace. *Food Bioprocess Technol.* **2012**, *5*, 2201−2210.

(32) Khanal, R. C.; Howard, L. R.; Prior, R. L. Effect of heating on the stability of grape and blueberry pomace procyanidins and total anthocyanins. *Food Res. Int.* **2010**, *43*, 1464−1469.
(33) Nguyen, T. H.; Nagasaka, R.; Ohshima, T. Effects of extraction solvents, cooking procedures and storage conditions on the contents of ergothioneine and phenolic compounds and antioxidative capacity of the cultivated mushroom *Flammulina velutipes*. *Int. J. Food Sci. Technol.* **2012**, *47*, 1193−1205.
(34) Zainol, M. M.; Abdul-Hamid, A.; Bakar, F. A.; Dek, S. P. Effect of different drying methods on the degradation of selected flavonoids in *Centella asiatica*. *Int. Food Res. J.* **2009**, *16*, 531−537.

tional markers of sunburning predisposition, with the aim of developing high-throughput methods useful in exploring the phenotypical variability of the grapes' susceptibility to sunburn damage.

MATERIALS AND METHODS

All of the *Vitis vinifera* L. accessions tested were grown in the same germplasm collection vineyard, located at the Regional Research Station of Riccagioia (Lombardy region, northern Italy) already described in a previous paper.[14] The experimental layout provided for the selection of 17 Lombard germplasm accessions named Bianca Botticina, Bianca Gabana, Pinot bianco, Chiavennasca bianca, Colombaia bianca, Croatina bianca, Erbamat, Favorita, Invernenga, Cortese, Marzemino bianco, Pollini A, Malvasia Istriana, Verdicchio, Uva bianca dura invernale, Verdea, and Vernassa. For each accession one shaded bunch was chosen. On August 29, 2012, at 12.30 p.m. solar time, the bunches were exposed to direct sunlight by leaf removal from the southwestern side facing the sun; the epicuticular waxes were mechanically removed through a slight rubbing of the berry surface with paper towels to facilitate the sunburning symptoms' appearance and to exclude the wax heterogeneity as an additional source of variability. After 5 h, at 5.30 p.m., all of the bunches were collected.

To describe grape temperatures during the experiment, the BerryTone model[21] was used to simulate the hourly temperature of the bunches. The model has been fed maximum and minimum daily air temperatures gathered by the weather station located in the vineyard.

All grape samples were kept at 10 °C and analyzed within 24 h from their harvesting. Forty berries were selected for each accession. Twenty of them were taken from the inner part of the shaded side of the cluster, with the purpose of describing the varietal reflectance spectra (control berries). Twenty berries on the exposed side of each bunch were also sampled (exposed berries). The most symptomatic berries (visual evidence of browning/discoloration), if present, were taken. When no symptoms were clearly visible, the most exposed berries were chosen. Before the spectrophotometric analysis, epicuticular waxes, still present in the control berries, were mechanically removed with a paper towel to avoid their interference with the optical properties.[10] Overall, 680 reflectance spectra were obtained using a Jaz System spectrometer (Ocean Optics), completed with a channel with a DPU module and an ILX511b detector, an OFLV-3 filter, an L2 lens, and a 50 μm slit as installed options. A reflection probe QR600-7-VIS125 consisting of a tight bundle of seven optical fibers (600 μm in diameter), in a stainless steel ferrule (six illumination fibers around one read fiber), was coupled to the spectrophotometer. The instrument was set up with a NIR−vis light source (Ocean Optics) 4095 power setting and an integration time automatically corrected by the instrument. Collected spectra ranged between 341 and 1025 nm and had a spectral resolution of about 0.3 nm. In this work, the visible spectral changes (450−750 nm) will be presented and discussed. Each spectrum was set up to be the average of nine spectra, which were directly calculated by the instrument. The spectra were converted in percentage of reflectance (%R) after a calibration with a blank, obtained by using a white Spectralon surface (Labsphere). The relationship between reflectance signal and chromophore content is nonlinear. Thus, the reflectance spectra were converted to approximate to the (quasi)linear relationship between pigment content and optical reflectance-based indices using reciprocal reflectance ($1/R$) spectra. The difference between exposed and shaded spectra was than calculated (Figure 3a). To make the browning contribution more apparent, a normalization to chlorophyll red maximum (678 nm) was also performed before the differential spectra were calculated, obtaining the "$1/R$ (chlorophyll normalized)" spectra (Figure 3b).

Chlorophyll content was estimated by using a reflectance index previously developed by Merzlyak and Solovchenko:[22]

$$\text{chlorophyll index} = R_{800}/R_{678}$$

This index was developed in apple fruits, but we decided to apply it to grapes because (i) the optical effect of chlorophylls in the red region is clearly identified in white grape spectra and (ii) no interferences from other white grape pigments are expected at these wavelengths.[14]

The index was computed on the basis of the average control spectrum of each cultivar. The objective was to evaluate the berry susceptibility to sunburn in relation to the initial chlorophyll content.

A browning intensity index was developed to evaluate the degree of sunburning symptoms in each accession. It was calculated as the difference of the inverse reflectance spectra, normalized to chlorophyll "$1/R$ (chlorophyll normalized)" at the maximum absorption wavelength (490 nm) of melanin-like pigments.

$$\text{browning intensity index} = \frac{100R_{e678}}{R_{e490}} - \frac{100R_{s678}}{R_{s490}}$$

where R_{e678} = exposed berries' reflectance at 678 nm, R_{e490} = exposed berries' reflectance at 490 nm, R_{s678} = shaded berries' reflectance at 678 nm, and R_{s490} = shaded berries' reflectance at 490 nm.

The statistical significance of the differences between reflectance data from exposed and control skins was estimated for each wavelength according to the classical computation of the mean confidence intervals per p = 0.95, with the lower limit = $M - (t_{0.95})(s_m)$ and the upper limit = $M + (t_{0.95})(s_m)$, where M = average value, t = Student's t per p = 0.95, and s_m = standard error (standard deviation/number of berries$^{1/2}$). This analysis, as well as correlations and ANOVA models, was performed by SPSS statistical software (version PASW Statistics 19, SPSS Inc., Chicago, IL, USA).

RESULTS

During the experiment, the global solar radiation ranged from 2.6 to 2.7 MJ m^{-2} h^{-1} and the air temperature from 24.3 to 29.2 °C. The hourly course of berry temperature for the day of the experiment was simulated with reference to a southwestern exposed part of the bunch in comparison to the shaded side (Figure 1). The exposed berries reached a maximum temperature of 34.2 °C at 2:00 p.m. At the same time the control berries were at 30.4 °C and the air at 29.2 °C. The difference between air and berry temperature was maximum at 1:00 and 2:00 p.m., when 6.1 °C was reached. At that time the difference between exposed and shaded berries was 4.3 °C.

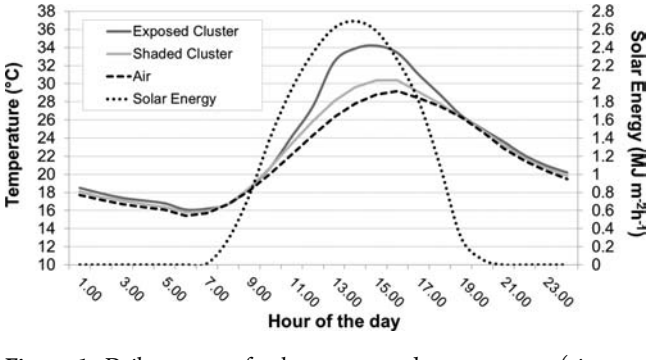

Figure 1. Daily course of solar energy and temperatures (air, sun-exposed and shaded berries). Bunches were exposed on August 29, 2012, at 12.30 p.m. solar time for 5 h.

Reflectance spectra were measured and their relative standard error was calculated for control and exposed berries to describe sunburning effects (Figure 2). Reflectance spectra minima indicate the presence of compounds absorbing in the corresponding spectral band. Figure 3 represents the variation of reciprocal reflectance ($1/R$) (Figure 3a) and $1/R$ (chlorophyll normalized) (Figure 3b) spectra in relation to sunburning. In Figure 3, when the interval of confidence overlaps zero, no significant compositional changes occurred in relation to sunlight exposure of berries. If it is above zero, new

dx.doi.org/10.1021/jf405772f | J. Agric. Food Chem. 2014, 62, 3043−3046

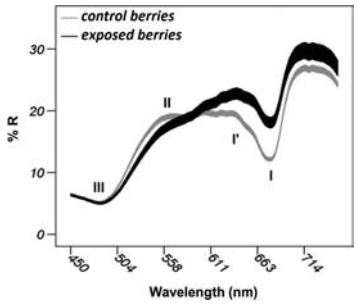

Figure 2. Control and exposed berry average spectra (±standard errors). Roman numbers indicate spectral regions of specific absorption interest.

molecules absorbing in the corresponding wavelength range have been generated (e.g., melanin-like pigments). Differences lower than zero are indicative of chromophore loss as a consequence of sunburn-induced bleaching.

It is possible to note three spectral regions (Figure 2) related to different grape skin compounds. Molecules related to region I (chlorophylls, Figure 2) evidently undergo degradation during sunburn (Figure 3a). In Figure 2, region II mainly indicates a difference between control and exposed spectra, related to the formation of brown compounds. In Figure 3 the absorption signature of melanin-like pigments clearly appears. The maximum of reciprocal reflectance ($1/R$) spectra (Figure 3a) underwent an 18 nm shift toward shorter wavelength after normalization to the chlorophyll red absorption maximum (Figure 3b). Region III (Figure 2) indicates a strong overlapping absorption by several chromophores (e.g., chlorophylls, carotenoids, melanin-like pigments).

DISCUSSION

In the red region, a broad band of combined chlorophyll *a* and *b* absorption was detected in the control and exposed berry spectra (Figure 2, region I). In Figure 2 the minimum of reflectance near 678 nm should be mostly due to chlorophyll *a* (spectral region I), whereas the little shoulder near 650 nm should be related to chlorophyll *b* absorption (spectral region I′), as suggested by Merzlyak et al.[23]

In comparison with the control spectrum, the exposed one (Figure 2) showed a decrease in reflectance in region II. This trend, emerging during browning, may be explained by the generation of melanin-like pigments,[5,24] for example, via the oxidation of polyphenols by polyphenol oxidases.[25]

In the blue and green region (Figure 2, region III), no significant difference was recorded. In this region, different molecules absorb, including chlorophylls. Chlorophylls underwent degradation (Figure 3a). Nevertheless, the expected increase in reflectance in the Soret band (see band III in Figure 2) was not detected, probably due to accumulation of other chromophores, most probably the browning pigments.[20] The normalization of reciprocal reflectance spectra to chlorophyll allows the exclusion of the overlap in region III between the absorption of chlorophylls and melanin-like pigments. Thus, the hypsochromic shift of the melanin-like pigments λ_{max} between panels a and b of Figure 3 should be related to the removal of this overlapping contribution by chlorophylls to overall.

Figure 4 shows the correlation between the varietal (shaded bunches) chlorophyll concentrations and the browning intensity index and, thus, melanin-like pigment generation. A quadratic model was able to describe the nonlinear relationship. As expected in oxidative processes, the reaction kinetics appears above a threshold. After a chlorophyll index value of about 2, the production of melanin-like compounds suddenly increased. Below the threshold, no relationships could be detected. Thus, it is possible to suggest a central role of photo-oxidation in the sunburn symptom physiology. For this reason it is possible to

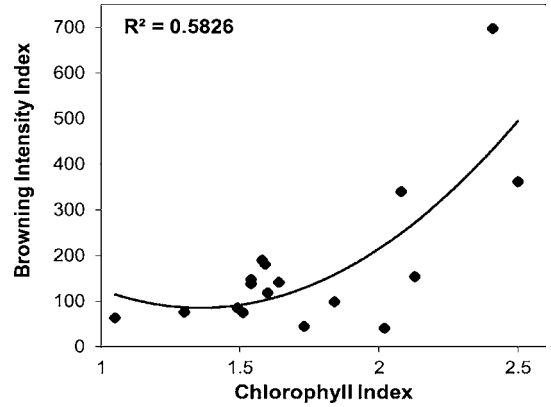

Figure 4. Nonlinear correlation between chlorophyll index and browning intensity index ($p < 0.01$).

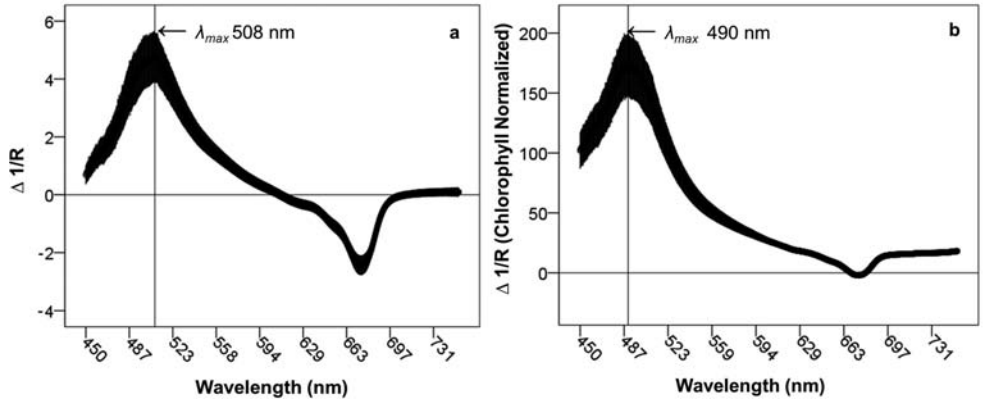

Figure 3. Differences (mean ± confidence interval 95%) in the (a) reciprocal reflectance ($1/R$) and (b) $1/R$ (chlorophyll normalized) spectra between exposed and shaded berries.

dx.doi.org/10.1021/jf405772f | J. Agric. Food Chem. 2014, 62, 3043−3046

propose the use of a chlorophyll index threshold as a marker for grapes' susceptibility to sunburning browning. Further experiments could confirm this hypothesis, studying the kinetics of browning of individual berries and relating the parameters of these kinetics to the initial chlorophyll content.

With the development of rapid, noninvasive, and low-cost methods, reflectance spectroscopy could support grapevine variety characterization with respect to sunburn susceptibility, as well as the study of the physiological processes involved in the symptoms' appearance.

AUTHOR INFORMATION

Corresponding Author

*(L.R.) E-mail: laura.rustioni@unimi.it. Phone: 0039 02503 16556. Fax: 0039 02503 16553.

Funding

The research leading to these results has received funding from the European Community's Seventh Framework Programme (FP7/2007-2013) under Grant Agreement FP7-311775, Project Innovine. Publication of the COST Action FA1003 "East-West Collaboration for Grapevine Diversity Exploration and Mobilization of Adaptive Traits for Breeding".

Notes

The authors declare no competing financial interest.

ACKNOWLEDGMENTS

We thank Dr. Marina Fogarty for revision of the English text.

REFERENCES

(1) Abbott, J. A. Quality measurement of fruit and vegetables. *Postharvest Biol. Technol.* **1999**, *15*, 207−225.

(2) Krasnow, M. N.; Matthews, M. A.; Smith, R. J.; Benz, J.; Weber, E.; Shackel, K. A. Distinctive symptoms differentiate four common types of berry shrivel disorder in grape. *Calif. Agric.* **2010**, *64*, 3.

(3) Jones, A. L.; Aldwinckle, H. S. *Compendium of Apple and Pear Diseases*; American Phytopathological Society: St. Paul, MN, USA, 1990.

(4) Schrader, L. E.; Zhang, J.; Sunday, J.. Environmental stresses that cause sunburn of apple. *Acta Hortic.* **2003**, *618*, 397−405.

(5) Vaughn, K. C.; Duke, S. O. Function of polyphenol oxidase in higher plants. *Physiol. Plant.* **1994**, *60*, 106−112.

(6) Bramlage, W. J.; Weis, S. A. Effect of temperature, light, and rain fall on superficial scald susceptibility in apples. *J. Am. Soc. Hortic. Sci.* **1997**, *32*, 808−811.

(7) Butler, W. L.; Norris, K. H. The spectrophotometry of dense light-scattering material. *Arch. Biochem. Biophys.* **1960**, *87*, 31−40.

(8) Gitelson, A. A.; Gritz, U.; Merzlyak, M. N. Relationships between leaf chlorophyll content and spectral reflectance and algorithms for non-destructive chlorophyll assessment in higher plant leaves. *J. Plant Physiol.* **2003**, *160*, 271−282.

(9) Solovchenko, A.; Merzlyak, M. Optical properties and contribution of cuticle to UV protection in plants: experiments with apple fruit. *Photochem. Photobiol. Sci.* **2003**, *2*, 861−866.

(10) Rustioni, L.; Maghradze, D.; Failla, O. Optical properties of berry epicuticular waxes in four Georgian grape cultivars (*Vitis vinifera* L.). *S. Afr. J. Enol. Vitic.* **2012**, *33* (2), 138−143.

(11) McClure, W. F. A spectrophotometric technique for studying the browning reaction in tobacco. *Trans. ASAE* **1975**, *18*, 380−383.

(12) Merzlyak, M. N.; Gitelson, A. A.; Chivkunova, O. B.; Rakitin, V. Y. Non-destructive optical detection of leaf senescence and fruit ripening. *Physiol. Plant.* **1999**, *106*, 135−141.

(13) Solovchenko, A. E.; Merzlyak, M. N.; Pogosyan, S. I. Non-destructive estimation pigment content, ripening, quality and damage in apple fruit with spectral reflectance in the visible range. *Fresh Produce* **2010**, *4* (1), 91−102.

(14) Rustioni, L.; Basilico, R.; Fiori, S.; Leoni, A.; Maghradze, D.; Failla, O. Grape colour phenotyping: development of a method based on the reflectance spectrum. *Phytochem. Anal.* **2013**, *24*, 453−459.

(15) Saure, M. C. External control of anthocyanin formation in apple. *Sci. Hortic.* **1990**, *42*, 181−218.

(16) Rustioni, L.; Di Meo, F.; Guillaume, M.; Failla, O.; Trouillas, P. Tuning color variation in grape anthocyanins at the molecular scale. *Food Chem.* **2013**, *141*, 4349−4357.

(17) Di Meo, F.; Sancho Garcia, J. C.; Dangles, O.; Trouillas, P. Highlights on anthocyanin pigmentation and copigmentation: a matter of flavonoid Π-stacking complexation to be described by DFT-D. *J. Chem. Theory Comput.* **2012**, *8*, 2034−2043.

(18) Knee, M. Anthocyanin, carotenoid, and chlorophyll changes in peel of Cox's Orange Pippin apples during ripening on and off the tree. *J. Exp. Bot.* **1972**, *23*, 184−196.

(19) Merzlyak, M. N.; Chivkunova, O. B. Light induced pigment changes and evidence for anthocyanin photoprotection in apples. *J. Photochem. Photobiol. (B)* **2000**, *55*, 155−163.

(20) Chivkunova, O. B.; Solovchenko, A. E.; Sokolova, S. G.; Merzlyak, M. N.; Reshetnikova, I. V.; Gitelson, A. A. Reflectance spectral features and detection of superficial scald-induced browning in storing apple fruit. *J. Russ. Phytopathol. Soc.* **2001**, *2*, 73−77.

(21) Cola, G.; Failla, O.; Mariani, L. BerryTone − a simulation model for the daily course of grape berry temperature. *Agric. For. Meteorol.* **2009**, *149* (8), 1215−1228.

(22) Merzlyak, M. N.; Solovchenko, A. E. Photostability of pigments in ripening apple fruit: a possible photoprotective role of carotenoids during plant senescence. *Plant Sci.* **2002**, *163* (4), 881−888.

(23) Merzlyak, M. N.; Solovchenko, A. E.; Gitelson, A. A. Reflectance spectral features and non-destructive estimation of chlorophyll, carotenoid and anthocyanin content in apple fruit. *Postharvest Biol. Technol.* **2003**, *27*, 88−103.

(24) Butt, V. S. Oxygenation and oxidation in the metabolism of aromatic compounds. *Proc. Phytochem. Soc. Eur.* **1985**, *25*, 349−365.

(25) Lurie, S.; Pesis, E.; Ben-Arie, R. Darkening of sunscald on apples in storage is a non-enzymatic and non-oxidative process. *Postharvest Biol. Technol.* **1991**, *1*, 119−125.

Table 1. Primers Selected for the Gene Expression Analyses of Strawberry Fruits Treated with Chitosan, COA, and BTH Commercial Formulations[a]

Gene	NCBI accession number	Primer sequence (forward/reverse)	Amplicon size	PCR efficiency (%)	R^2 of standard curve
Calcium-dependent protein kinase (CDPK)	AF035944.1	TCCGTTTTGAAGAACCCAAC/ CCGTCCTCAGTTTCTGCTTC	160	100.7	0.997
K^+ channel	DQ022747.1	ATGAGGGTGACTCCAAAGGA/ TGGCTGAAACCTGTTAGTGC	235	105.9	0.995
Cytosolic ascorbate peroxidase (APX)	AF159630.1	CACAAGGAACGGTCTGGATT/ CGCAGCGTATTTCTCAACAA	174	98.5	0.994
Glutathione S-transferase (GST)	AY902368.1	TTCTCATTCACAACGGCAAA/ TCCTGCTCATCTCCTTTCGT	228	103.5	0.990
Phenylalanine ammonia-lyase (PAL)	AB360394.1	GATTTGAGGCATTTGGAGGA/ CTTGCCTTAGCCTTTGCATC	217	101.6	0.990
Chalcone synthase (CHS)	AB201755	GCCGAGGAGTTGACAGAGTC/ TTTCAATGGCTTTCGCTTCT	190	103.0	0.996
Chalcone isomerase (CHI)	AB201754	TGATGATTGGCATCTCCAAA/ TGCCTTGTTTTCTGCTTCCT	233	104.4	0.994
Flavanone 3-hydroxylase (F3H)	AB201760.1	TTGTCCATAGCGACATTCCA/ AGTTGCTCCTTTGCATGCTT	176	104.7	0.998
Flavonol synthase (FLS)	DQ087252.1	CAACGAGGCCATATCCAAGT/ TGGTAGAAGGTGGCCAAATC	194	96.2	0.996
Dihydroflavonol 4-reductase (DFR)	AY691918.1	AGCAAGCAGCATGGAAGTTT/ CTTTCGGATGCTCGTAGAGG	228	97.7	0.995
Anthocyanidin synthase (ANS)	AY695817.1	AGTGCGTACCCAACTCCATC/ TGTGCTGGATATGCTCGAAG	240	101.4	0.995
Flavonoid 3-O-glucosyl transferase (UFGT)	AY695815.1	GTGGTCACTTCGGGACAACT/ AGTTTCTGATCGCCGAAGAA	219	104.7	0.987
Polygalacturonase (PG)	DQ458990.1	CGGAAGTCTCGGAAGATACG/ CCATGGGCAGTATTCTTGGT	208	97.2	0.992
Polygalacturonase-inhibiting protein (PGPI)	EU117213.1	CTGGCTCAGTCCCTGACTTC/ AGCTTGTTGTGGGAGAGGAA	217	101.1	0.999
β-1,3-Glucanase (βglu)	AY989819.1	TATGGACGAAACGGTGACAA/ AGGGTTGCACATTTTTCTGG	223	100.3	0.993
Endo-β-1,4-glucanase (endoβglu)	AJ006348.1	GCTAAACGCCAGGTGGATTA/ AAATGCATCCGAGCTATTGG	240	101.9	0.995
Class III chitinase (Chi3)	AF134347.1	ACCAAGTTCAGCTCGCAGAT/ TCCTAATGGCCTTGAAGTGG	177	102.8	0.990
Pathogenesis-related protein 1 (PR-1)	AB462752.1	ACATGGGATGCCAATCTAGC/ CCACAGGTTCACAGCAGATG	214	106.7	0.996
18S Ribosomal RNA *	AF163494.1	CGCCAAGGAACTTGAATGAA/ TTGCGTTCAAAGACTCGATG	198	102.7	0.996
Actin*	AB116565.1	CGAGGCTCAATCCAAAAGAG/ GGGGCCTCAGTTAGGAGAAC	159	97.3	0.994
Glyceraldehyde 3-phosphate dehydrogenase (GAPDH2)*	AF421145.1	TTCCGTGTACCCACTGTTGA/ TCACCAATGAAGTCGGTTGA	170	106.6	0.971
Histone H4*	AB197150.1	TCAAGCGTATCTCCGGTCTC/ AGTGTCCTTCCCTGCCTCTT	163	106.2	0.996

[a]PCR amplification efficiencies and regression coefficients for the standard curves are reported for each primer pair. *, reference genes.

3-hydroxylase (F3H), dihydroflavonol 4-reductase (DFR), flavonol synthase (FLS), anthocyanidin synthase (ANS), and flavonoid 3-*O*-glucosyltransferase (UFGT); cell-wall degradation enzymes, including *endo-β*-1,4-glucanase (endo*β*Glu), polygalacturonase (PG), polygalacturonase-inhibiting protein (PGIP); and encoding of PR proteins, including *β*-1,3-glucanase (*β*Glu), class III Chitinase (Chi3), and PR-1. In the same way, the enzyme activities related to PAL, *β*Glu, total Chitinase (Chi), and guaiacol peroxidase (GPX) were tested. The results of this study provide new information on the effect of resistance inducers on strawberry fruit.

MATERIALS AND METHODS

Fruit Material. Experiments were carried out on fruits of strawberries cv. Camarosa grown according to organic agriculture practices, from commercial orchards located in the Marche region, central-eastern Italy. The fruits were selected for the absence of defects, uniformity in size, and degree of ripening (2/3 of surface red), and they were used for the experiments on the day of their harvest.

Treatments. The physiological changes in the strawberry fruit were analyzed following treatments with commercial elicitor formulations: 1% (w/v) chitosan (Chito Plant, ChiPro GmbH, Bremen, Germany), 1% (v/v) COA (Fitocalcio, Agrisystem, Lamezia Terme, CZ, Italy), and 1% (w/v) BTH (Bion, Syngenta, Milano, MI, Italy). The commercial products were prepared by dissolving or diluting them in distilled water. Distilled water was used as the control.

Strawberry fruits (800 g) were pooled together and randomized, and then they were immersed for 30 s in 1 L of one of the three resistance inducers or water. After the treatments, the strawberries were dried in air for 30 min and then subdivided into 4 groups of 200 g each. After air drying, one group was stored at −80 °C (0.5 h post-treatment), and the other groups were arranged in small plastic boxes that were placed in bigger covered plastic boxes. These groups were stored up to a total of 6, 24, and 48 h post-treatment, at 20 °C and 95%−98% relative humidity. At each time, fruits corresponding to 20 g were randomly selected and stored in two separated tubes at −80 °C, until RNA extraction. The experiments were repeated at least twice.

Gene Expression Analysis. Gene expression analysis on the strawberry fruit after the treatments with the different resistance inducers was performed by RT-qPCR, using a SYBR-green dye system, according to Minimum Information for Publication of Quantitative Real-Time PCR Experiments (MIQE) guidelines.[17] The comparative $-\Delta\Delta C_t$ method[18] was used to evaluate the relative quantities of each of the amplified products in the samples.

RNA Extraction. High quality total RNA was obtained from the fruit according to the protocol of Landi and Romanazzi.[19] Briefly, 10 g of strawberry tissue samples including both achenes and receptacle was ground in liquid nitrogen, and 400 mg of the resulting fruit powders was randomly collected for RNA extraction. Extraction buffer was added (1 mL; 100 mM Tris-HCl, pH 8.0, 25 mM EDTA, pH 8.0, 2% [w/v] CTAB [Sigma], 2% [v/v] β-mercaptoethanol, 2.5 M NaCl, and 2% [w/v] soluble PVP-40), and the samples were incubated at 65 °C for 30 min. The supernatants were transferred to new tubes with an equal volume of chloroform/isoamyl alcohol (24:1) and centrifuged at 10,000*g* for 5 min at 4 °C. This last step was repeated two more times. The total RNA were precipitated in 0.25 vol 10 M LiCl, with the reaction left to proceed overnight at 4 °C. The samples were then centrifuged at 10,000*g* for 30 min at 4 °C, washed in 70% ethanol, dried, and resuspended in 50 μL of double-distilled diethyl pyrocarbonate water. RNA integrity was verified by agarose gels that were stained using SYBRSafe (Invitrogen, Carlsbad, CA, USA). RNA purity was assessed based on an absorbance ratio of 1.80 to 1.90 at 260/280 nm, using BioPhotometer plus (Eppendorf Inc., Westbury, NY, USA) and 1.8 to 2.0 at 230/260 nm.

Reverse Transcription. A total of 40 ng to 50 ng RNA was used for cDNA synthesis with reverse-transcription PCR, using iScript TM cDNA synthesis kits (Bio-Rad, Hercules, CA, USA), according to the manufacturer's instructions. From each RNA extraction, cDNA synthesis was performed twice, and the products were mixed before the gene expression studies.

Primers and Reference Gene Selection. Specific primer sets were designed using the Primer3 software (http://biotools.umassmededu/bioapps/primer3_www.cgi) from the specific sequence of *Fragaria* × *ananassa* deposited in NCBI GenBank (Table 1). The primer pairs were chosen and validated in silico using primer BLAST-specific analysis (http://www.ncbi.nlm.nih.gov/Blast.cgi) and then according to the melting profiles obtained from the quantitative real-time PCR conditions (qPCR), as described later.

The relative expression stabilities of the candidate reference genes of 18S-rRNA, actin, histone H4, and GAPDH2 were validated using the geNorm method, using the 3.5 version.[20]

Quantitative Real-Time PCR. qPCR reactions were performed in 96-well clear multiplate PCR plates (Bio-Rad, Hercules, CA, USA) using the iQ SYBR Green Supermix (Bio-Rad) on an iCycler iQ Real-Time PCR Detection System (Bio-Rad) under the following conditions: an initial denaturating cycle (5 min at 95 °C), followed by 40 cycles of three steps of denaturation, annealing, and polymerization (30 s at 95 °C, 20 s at 55 °C, and 30 s 72 °C). PCR amplification was carried out in a total volume of 22 μL, containing 9 μL of diluted (1:10) cDNA (duplicates), 0.25 μM of each primer, and 11 μL of iQ SYBR Green Supermix. All of the assays included no-RT and no-template controls, to determine the nonspecific amplification. To determine the specificity of the amplicons, melting curve analysis was performed over the range of 55 to 98 °C. The qPCR efficiency (E) of each primer pair was determined using standard curves generated according to the equation $E = 10^{-1/\text{slope}}$ of five triplicate cDNA pool dilutions (undiluted, 0.25, 0.0625, 0.015, and 0.003).

Enzyme Activities. Spectrophotometric assays were used to determine the βGlu EC 3.2.1.6, Chi EC 3.2.1.14, PAL EC 4.3.1.24, and GPX EC 1.11.1.7 activities of the strawberry fruits at 0.5, 6, 24, and 48 h post-treatment with chitosan, COA, and BTH. Frozen fruits (1 g fresh weight) were ground, and βGlu and Chi were extracted using 1% (w/v) polyvinylpolypyrrolidone in 50 mM sodium acetate buffer (pH 5.0) containing 1 mM dithiothreitol and 0.2% (w/v) phenylmethylsulfonyl fluoride. The PAL was obtained using 100 mM potassium phosphate buffer (pH 8.0) containing 1% (w/v) polyvinylpolypyrrolidone and 1.4 mM β-mercaptoethanol. The GPX was obtained with 100 mM potassium phosphate buffer (pH 7.3) containing 1 mM EDTA. The homogenates were centrifuged at 15000*g* for 15 min at 4 °C, and the resulting supernatants were used as the crude enzyme extracts. The protein content in the enzyme extracts was determined according to the Bradford assay[21] (Sigma-Aldrich), using bovine serum albumin as the standard. βglu activity was assayed according to Derckel et al.[22] The Chi and PAL activities were measured according to Trotel-Aziz, et al.[23] and the GPX according to Amako et al.[24] All of the enzyme activities were analyzed using a UV 1800 spectrophotometer (Shimadzu Corp., Tokyo, Japan). For all of the assays, the absorbance was measured against a blank (crude protein extract in incubation mixture). The specific activities of the enzymes are expressed as Units (U) mg^{-1} protein.

Data Analysis. The gene expression study was performed using the $-\Delta\Delta C_t$ method.[18] According to this method, the expression of target genes was given as the mean fold-changes in gene expression normalized to an endogenous reference gene and compared to the untreated controls. For each individual sample, three replications were analyzed. The gene expression calculations were performed using the Excel program Gene Expression Analysis for iCycler iQ Real Time PCR Detection System (Bio-Rad). The calculations in this spreadsheet were derived from the algorithms outlined by Vandesompele et al.[20] All of the analyses were performed twice.

For the analysis of the enzyme activities, for each individual sample three replications were analyzed. The experiments were performed twice. The data from each sampling point are shown as the mean ± SD and were statistically evaluated by ANOVA, followed by individual comparisons using Duncan's Multiple Range Test, at $p \leq 0.05$.

RESULTS

Selection of Appropriate References Genes for RT-qPCR in the Treated Strawberry Fruits. For this study, the RT-qPCR was set up for analysis of the strawberry fruits treated for 30 s with the three elicitors. The specific primer sets identified for all of the genes analyzed showed specific single-peak melting curves (data not shown), which confirmed the homogeneity and specificity of the amplicons produced in the RT-qPCR for each of the 18 target genes. No amplification was observed in any of the control assays, which confirmed that the samples were free of contamination with genomic DNA or RNA, or the cDNA template (data not shown). The amplification efficiency (E) ranged from 96.2% to 106.2%, according to the standard curve analysis in RT-qPCR of each gene-specific primer pair (Table 1).

The validation of four putative candidate reference genes, 18S-RNA, actin, glyceraldehyde 3-phosphate dehydrogenase (GAPDH2), and histone H4, according the geNorm method, showed differences within the treatments. However, these reference genes had M values <1.1, which is below the default limit of $M < 1.5$ (Figure 1). For the analysis, the two most stable genes were selected. In particular, on strawberry fruits treated with COA, among these reference genes the most stable were the 18S-RNA and GAPDH2 genes ($M = 0.49$) (Figure 1A). According to the analysis of reference genes on the strawberry fruits treated with BTH, the genes for actin and histone H4 were the most stable ($M = 0.43$) (Figure 1B). Using chitosan and the water control, the best expression stability was using the 18S-RNA and actin genes. In particular, the M value was 0.46 in samples treated with chitosan (Figure 1C), and 0.51 in the control samples (Figure 1D).

Effects of Three Resistance Inducers on the Expressions of Defense Genes. The biochemical reactions in the cell that are catalyzed by enzymes and genes that were up-regulated in strawberry fruits after the chitosan, COA, and BTH treatments are illustrated schematically in Figure 2.

The expression level of the 18 genes was compared to water control treatment, and it was defined as fold-stimulation over the control according to these analysis times, as shown in Figures 3 and 4. In general, the shortest time from the treatment of 0.5 h had no significant effects across these data (except where specified below).

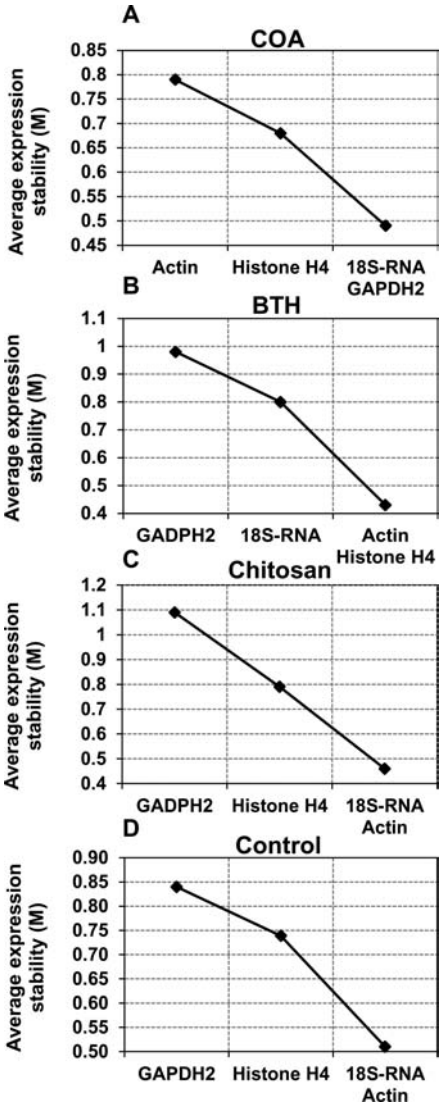

Figure 1. Stability of the reference genes in strawberry fruit. Stability value (*M*) for a set of reference genes was analyzed with the geNorm algorithm. Strawberry fruits were treated with COA (A), BTH (B), chitosan (C), and water, as the control (D). The reference genes on the *X*-axis are ranked from left to right based on their mean gene expression stability. In each panel, the genes on the right show the highest expression stability among the reference genes. See Table 1 for the names of the reference genes.

The expression levels of CDPK were increased in the strawberry fruit treated with BTH, by 2.8-fold (6 h post-treatment), 2.5-fold (24 h post-treatment), and 3.6-fold (48 h post-treatment). This gene was affected by chitosan only at 24 h post-treatment, with a 2.7-fold increase seen. There were no changes in CDPK gene expression with COA (Figure 3). For the gene encoding a K^+ channel protein, the transcript levels increased with all of the resistance inducers tested. In particular, after chitosan and COA, the K^+ channel expression increased at 6, 24, and 48 h post-treatment by 8.3-fold, 15.4-fold, and 9.7-fold, respectively, with chitosan, and 13.3-fold, 8.8-fold, and 13.4-fold, respectively, with COA. After the BTH treatment, a significant increase of the transcript was observed only after 48 h post-treatment, with an 11.4-fold increase (Figure 3).

The genes encoding for enzymes involved in the scavenging of oxygen species that were analyzed here were those of APX and GST. These showed increased gene expression with BTH at 6, 24, and 48 h post-treatment of 7.4-fold, 3.8-fold, and 1.8-fold, respectively, for APX, and of 3.2-fold, 4.9-fold, and 1.7-fold, respectively, for GST (Figure 3).

For the expression patterns of the flavonoid upstream pathway gene PAL and for the genes that are more related to biosynthesis across the different flavonoids branches, as CHS, CHI, F3H, DFR, FLS, ANS, and UFGT, different data were obtained according to the resistance inducers tested (Figure 3). The PAL gene was up-regulated at 24 and 48 h post-treatment by 4.0-fold and 4.5-fold, respectively, after chitosan treatment, and 6.1-fold and 5.0-fold, respectively, after COA treatment, with no significant changes in transcription with BTH. Conversely, CHS gene expression was enhanced only after BTH treatment, by 3.2-fold (6 h post-treatment), 2.9-fold (24 h post-treatment), and 5.6 fold (48 h post-treatment). Among the CHS downstream pathway genes, the CHI gene showed increased expression after the chitosan and BTH treatments. In particular, it increased by 7.5-fold (24 h post-treatment) and 4.9-fold (48 h post-treatment) with chitosan, and 3.5-fold (6 h post-treatment), 2.9-fold (24 h post-treatment), and 4.8-fold (48 h post-treatment) with BTH. The DFR and F3H genes were up-regulated after the BTH treatment. For DFR, the transcript levels were increased by 9.6-fold at 48 h post-treatment, while for the F3H gene, the increase was 3.2-fold at both 6 and 48 h post-treatment. For the flavonoid biosynthetic pathway, the gene showing the highest expression levels was FLS. The expression of the FLS gene increased following the treatments with each of the elicitors tested, although at different times of treatment. In particular, at 6, 24, and 48 h post-treatment, the increases were 5.2-fold, 6.7-fold, and 11.4-fold, respectively, for chitosan, and 12.8-fold, 20.4-fold, and 14.1-fold, respectively, for COA; BTH only produced a significant increase in FLS gene expression at 48 h post-treatment of 4.3-fold (Figure 3). For the ANS gene, which leads to anthocyanin and proanthocyanidin synthesis, the only significant increases in gene expression were seen for the chitosan treatment: 8.9-fold (6 h post-treatment), 7.4-fold (24 h post-treatment), and 12.6-fold (48 h post-treatment). UFGT gene expression was increased after BTH treatment, by 2.6-fold (6 h post-treatment), 3.2-fold (24 h post-treatment), and 2.0-fold (48 h post-treatment), while with COA it increased by 2.5-fold at 6 h post-treatment and 3.0-fold at 24 h post-treatment. No significant increase in UFGT transcript induction was seen after the chitosan treatment (Figure 3).

According to the cell wall degrading enzymes (Figure 4), for PG gene expression, there was a similar pattern across all of these resistance inducers, with a significant increase at 6 h post-treatment, which was lost at 24 h post-treatment but returned again at 48 h post-treatment. In particular, at 6 and 48 h post-treatment there were 3.8-fold and 5.6-fold increases, respectively, with chitosan, 7.2-fold and 7.4-fold, respectively, with COA, and 4.7-fold and 14.1-fold, respectively, with BTH; COA also showed significant up-regulation of the PG transcript at 24 h post-treatment of 2.5-fold. However, the PGIP transcripts showed an inverted pattern of expression compared to that of the PG gene, with maximum gene expression at 24 h post-treatment using all of the elicitors. Here, significant gene up-regulation was seen at 0.5, 6, 24, and 48 h post-treatment with the chitosan and COA treatments, as 2.9-fold, 3.7-fold, 3.9-fold, and 3.4-fold, and as 3.1-fold, 5.9-fold, 8.7-fold, and 3.7-fold, respectively. With BTH, PGIP gene expression was only significantly increased at 6 and 24 h post-treatment, by 4.4-fold

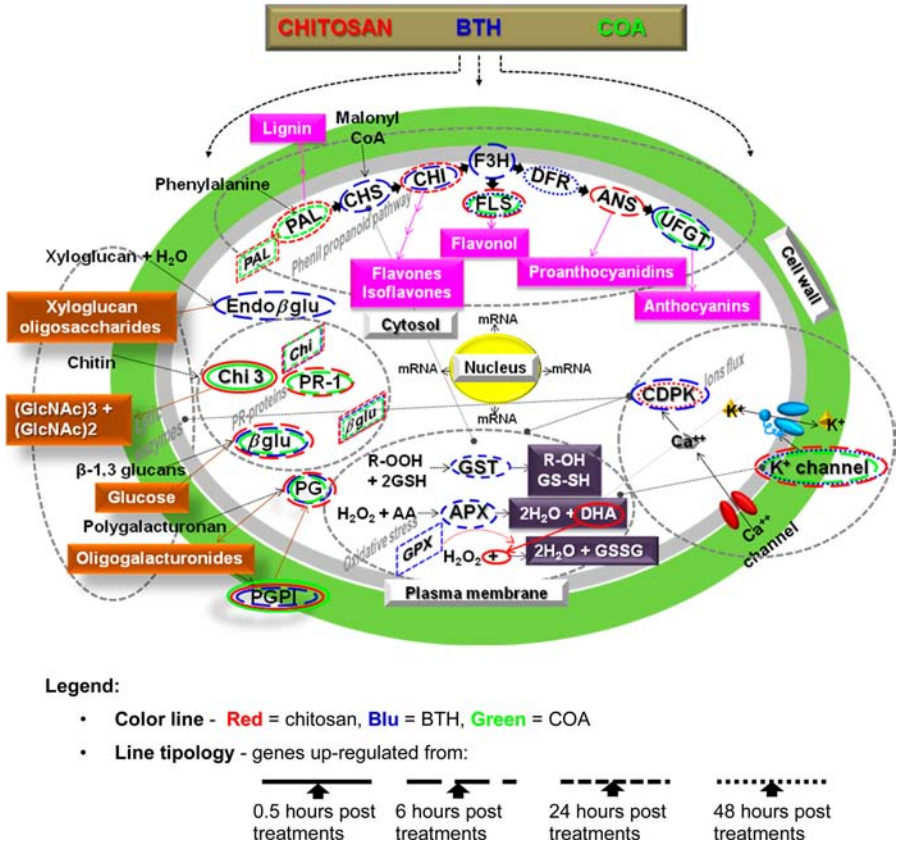

Figure 2. Gene expression and enzyme activity involved in resistance induced by chitosan, COA, and BTH (see legend). The metabolic roles of both the genes and enzymes analyzed are shown. Genes associated with ion fluxes, CDPK, the K^+ channel; genes associated with oxidative stress, GST, APX; genes associated with secondary metabolism, such as phenylpropanoid, PAL, CHS, CHI, F3H, FLS, DFR, ANS, and UFGT; genes associated with cell-wall degradation enzymes, endoβgluc, PG, and PGPI, some of which are known as PR proteins, as βglu, Chi3, and with the addition of the PR-1 protein. The up-regulation of genes by the resistance inducers and post-treatment times are shown with circular lines surrounding the abbreviated gene names, with different colors and typologies (see legend). The metabolic reactions of the analyzed enzyme activities are also shown: GPX, PAL, Chi, and βglu, surrounded by square lines (see legend).

and 3.3-fold, respectively. The βGlu gene expression was significantly increased with all of the resistance inducers tested. Starting from 6 h post-treatment, with chitosan there was a consistent increase through 24 and 48 h post-treatment, of 16.7-fold, 16.2-fold, and 21.3-fold, respectively. For BTH and COA, while remaining significantly increased, at 24 h post-treatment the effects were reduced, with increased βGlu gene expression at 6, 24, and 48 h post-treatment of 10.3-fold, 2.9-fold, and 16.6-fold, respectively, for BTH, and 14.4-fold, 4.5-fold, and 10.3-fold, respectively, for COA. The other two genes involved on plant-cell degradation, as those for endoβGlu and Chi3, showed different results again. endoβGlu gene expression was only significantly increased with BTH treatment, by 5.4-fold (6 h post-treatment), 5.8-fold (24 h post-treatment), and 12.9-fold (48 h post-treatment). Conversely, Chi3 gene expression was significantly increased only after chitosan and COA, showing increases at 0.5, 6, 24, and 48 h post-treatment of 2.7-fold, 13.6-fold, 13.6-fold, and 22.0-fold, respectively, for chitosan, and 1.4-fold, 9.4-fold, 8.6-fold, and 5.5-fold, respectively, for COA.

As for Chi3, expression of the gene coding for PR protein-1 (PR-1) was only significantly increased with chitosan and COA (Figure 4). After chitosan treatment, the PR-1 transcript levels were significantly increased at 6, 24, and 48 h post-treatment, by 7.6-fold, 13.0-fold, and 23.1-fold, respectively. The different effects with COA showed the increased PR-1 transcript level at 6, 24, and 48 h post-treatment of 17.8-fold, 9.7-fold, and 5.1-fold, respectively.

The relationships between the paired resistance inducers and these gene responses were then calculated with respect to the numbers of genes showing the same response (unvaried, up-regulated, or down-regulated) of the total set of 18 genes analyzed. The highest similitude level was seen at 0.5 h post-treatment, as at this time, a few of the genes showed some changes with the elicitors: chitosan/COA, 100%; BTH/chitosan, 88%; and BTH/COA, 88%. The similitude levels across these elicitors then differed substantially at 6, 24, and 48 h post-treatment. In particular, the paired chitosan/COA gene expression similarity was the greatest, at 88%, 72%, and 88%, respectively, with BTH/chitosan at 33%, 38%, and 28%, respectively, and BTH/COA, at 38%, 33%, and 27%, respectively (Figure 5).

Effects of Three Resistance Inducers on Enzyme Activity. For strawberry fruits, the PAL, βGlu, Chi, and GPX enzymatic activities were also assayed following the 30-s chitosan, COA, and BTH treatments, at 0.5, 6, 24, and 48 h post-treatment (Figure 6).

The control PAL activity (12.4−15.58 U mg^{-1} protein) increased after chitosan and COA treatments only. In particular, for chitosan treatment, PAL activity was significantly increased at 24 and 48 h post-treatment, by 11.8 units mg^{-1} protein (1.9-fold) and 17.9 U mg^{-1} protein (2.1-fold),

dx.doi.org/10.1021/jf404423x | J. Agric. Food Chem. 2014, 62, 3047−3056

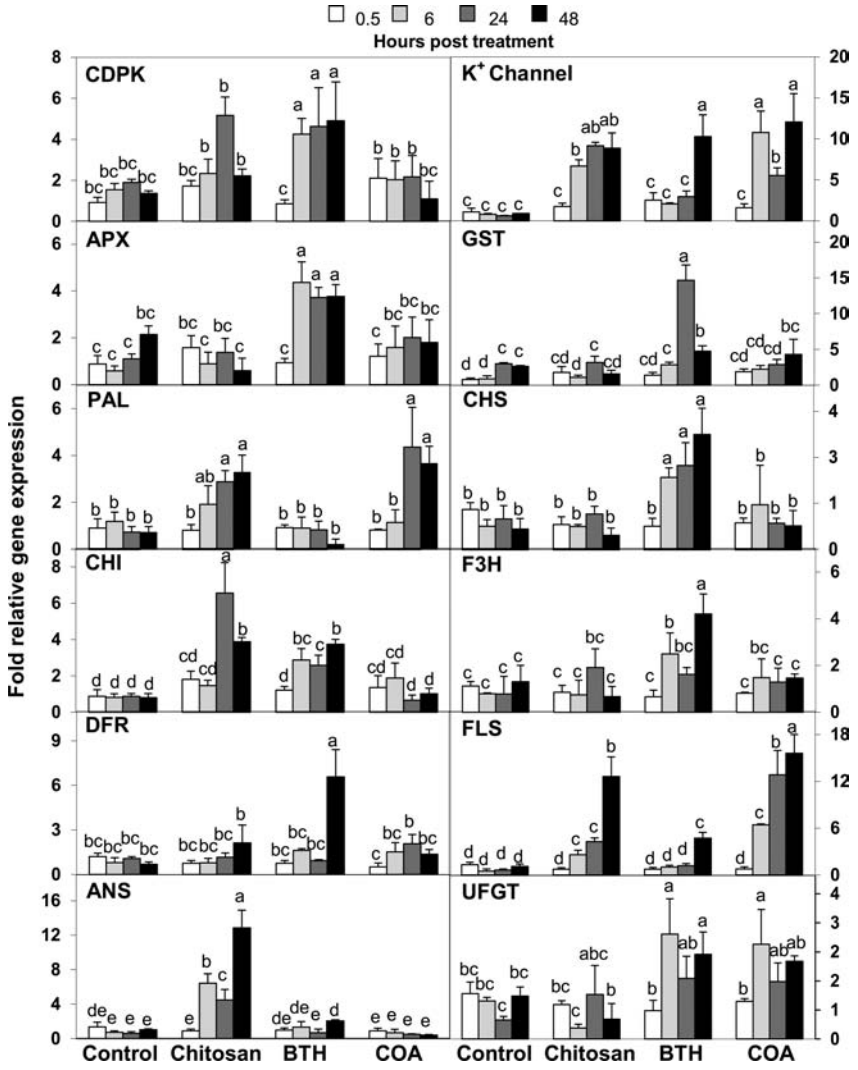

Figure 3. Relative gene expression of defense genes in strawberry fruit after treatment with resistance inducers. Strawberry fruits were treated with chitosan, BTH, and COA, and with water as the control. The relative gene expression of the defense genes (as indicated) is referred to as 0.5, 6, 24, and 48 h post-treatment. Data are the means + SD, and values with the same letter are not statistically different, according to Duncan's multiple range test, at $P \leq 0.05$. See Table 1 for the names of the genes.

respectively. Similarly, for COA treatment, the increases were 9.1 U mg^{-1} protein (1.7-fold) and 12.9 U mg^{-1} protein (1.8-fold), respectively.

The control βGlu activity (2.2−3.2 U mg^{-1} protein) increased with all of the inducers. For both chitosan and COA, this was significant at 24 and 48 h post-treatment, with 1.9 U mg^{-1} protein (1.7-fold) and 1.8 U mg^{-1} protein (1.6-fold) increases, respectively, for chitosan and 4.8 U mg^{-1} protein (2.7-fold) and 4.5 U mg^{-1} protein (2.4-fold) increases, respectively, for COA. With BTH, the βGlu activity was increased only at 48 h post-treatment by 5.6 U mg^{-1} protein (2.8-fold).

The control total Chi activity (0.9−1.4 U mg^{-1} protein) also increased with all of the elicitors tested. At 24 and 48 h post-treatment, these increases in Chi activity were of 0.8 U mg^{-1} protein (1.8-fold) and 1.8 U mg^{-1} protein (2.9-fold), after chitosan treatment, 1.4 U mg^{-1} protein (2.4-fold) and 1.6 U mg^{-1} protein (2.7-fold), with COA, and only at 48 h post-treatment of 2.7 U mg^{-1} protein (3.0-fold), with BTH.

For the control GPX activity (10.1−16.0 U mg^{-1} protein), this was significantly increased only after BTH treatment at 6 and 24 h post-treatment by 5.4 U mg^{-1} protein (1.4-fold) and 14.2 U mg^{-1} protein (2.4-fold), respectively.

DISCUSSION

The ability to quickly induce defense mechanisms is a characteristic of incompatible (resistant) plant−pathogen interactions, whereby the plant can efficiently block pathogen penetration. The application of resistance inducers promotes increases in the potential immunity of susceptible plants and allows the plants to combat possible future pathogen infections. In the present study, we investigated the gene expression of selected markers associated with defense mechanisms of strawberry fruits exposed to resistance inducers.

This study determined the relationships between the different resistance inducers of BTH, chitosan, and COA that have been shown to be effective in the control of post-harvest diseases of strawberry[4] and 18 defense-related genes that are associated with different biological processes. With this aim, we set up an analytical protocol based on RT-qPCR, and we defined the appropriate reference genes for the strawberry fruits under elicitor stress conditions. It is known that the expression

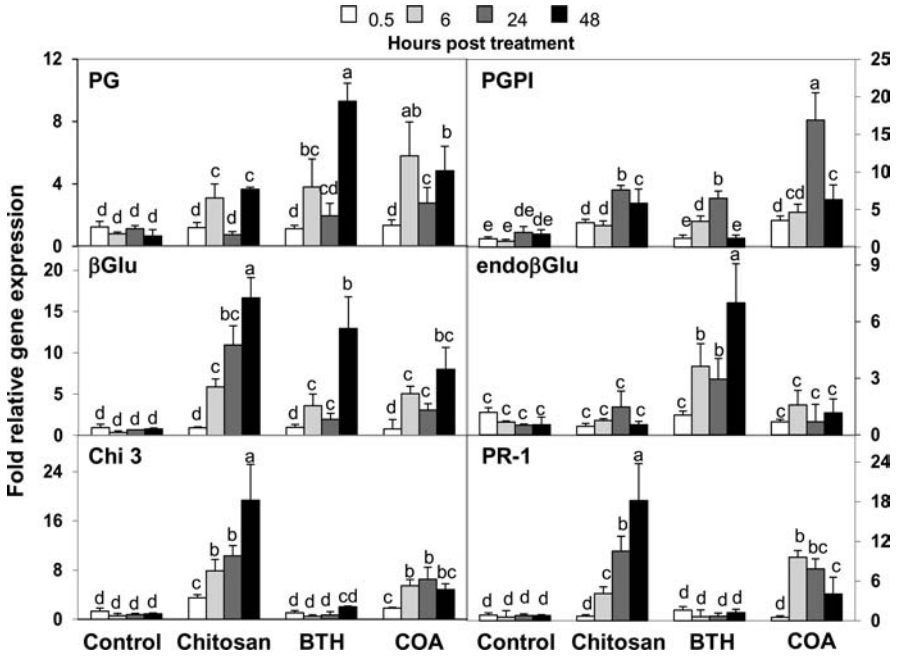

Figure 4. Relative gene expression of defense genes in strawberry fruit after treatment with resistance inducers. The strawberry fruits were treated with chitosan, BTH, and COA, and with water as the control. The relative gene expression of the defense genes (as indicated) are referred to as 0.5, 6, 24, and 48 h post-treatment. Data are the means + SD, and values with the same letter are not statistically different, according to Duncan's multiple range test, at $P \leq 0.05$. See Table 1 for the names of the genes.

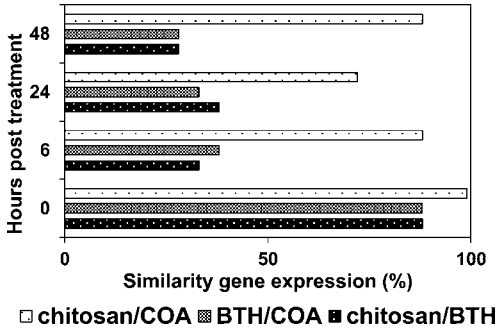

Figure 5. Relationships between the resistance inducers used and the correspondent gene responses in treated strawberry fruit. The relationships between the resistance inducers and gene responses calculated according to the numbers of genes showing the same induction response of the total genes analyzed.

stability of reference genes varies with the environment, plant growth, plant tissue, and different biotic and abiotic stress.[17] Therefore, normalization of the relative RT-qPCR data using suitable reference genes is a crucial prerequisite for obtaining reliable data. Our results showed differences between the elicitor treatments and suggested the appropriate reference gene selection for RT-qPCR analysis for new materials.

Our data show that the target genes analyzed associated with plant natural defense mechanisms are involved in different ways according to the elicitors. The earliest responses of plant cells to elicitors involve changes in membrane potential, Ca^{2+} signaling, and the production of ROS. [25] Our study shows the more constant involvement of the CDPK transcript, which is known in plants as a Ca^{2+}-binding sensor protein[26] in the strawberry fruit BTH response, with chitosan effects only seen at 24 h post-treatment in these strawberry fruits. However, although the expression of the K^+ channel was enhanced following the use of all of these elicitors, its early activation was only seen in the strawberry fruits treated with chitosan and COA; with BTH, there was only an enhancement of this gene at 48-h post-treatment. CDPKs have roles in early signal processes for multifaceted functions in the complex immune and stress signaling networks, including for oxidative burst, stomatal movements, hormonal signaling, and gene regulation.[27] In the same way, K^+ channel activation during stress is accompanied by an oxidative burst.[28] Our data suggest differences between these chitosan, COA, and BTH treatments in the activation of strawberry fruit plasma-membrane ion fluxes. This might be associated with different innate immunity signal transduction in these fruit, which might involve downstream signaling events, such as oxidative stress.[29] In this regard, the genes associated with the nonenzymatic components of the antioxidative defense system that were analyzed in this study, such as APX and GST, which can remove H_2O_2 from the cell,[30] were up-regulated in these strawberry fruits treated with BTH; likewise, the enzyme activity of GPX increased only after the BTH treatment. Our data suggest the involvement of oxidative stress in strawberry fruits treated with BTH, although we do not exclude the involvement of oxygen scavenger enzymes belonging to other biosynthetic pathways using the other elicitors, as previously hypothesized.[3,4]

Furthermore, as some of the major secondary metabolites in plants, phenolic compounds are well-known to have antioxidant properties[31] and to lead to the synthesis of phytoalexins, which are known to have antimicrobial activity.[32] In the present study, differences in the expression of the genes involved in the phenylpropanoid pathway were observed according to the elicitor used and the time from the treatment. In particular, the BTH treatment enhanced the expression of most of these genes. Some increases were apparent from 6 h post-treatment (CHS, F3H, CHI, and UFGT), while others were more delayed to 48 h post-treatment (FLS, DFR). Chitosan up-regulated

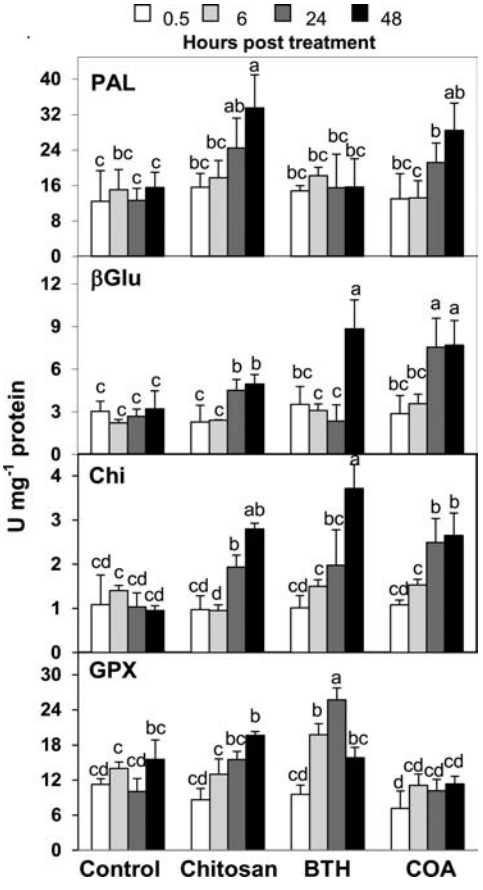

Figure 6. Enzyme activities of defense enzymes in strawberry fruits after treatment with resistance inducers. The strawberry fruits were treated with chitosan, BTH, and COA, and with water as the control. The enzyme activities (as indicated) are referred to as 0.5, 6, 24, and 48 h post-treatment. Data are the means + SD, and values with the same letter are not statistically different, according to Duncan's multiple range test, at $P \leq 0.05$.

PAL, CHI, FLS, and ANS; COA only up-regulated PAL and FLS, and usually from 6 h post-treatment. Between these genes, there was the remarkable involvement of the FLS and ANS genes, which encode the main enzymes that lead to the flux of anthocyanin and proanthocyanidin synthesis.[33] Interestingly, the PAL gene, which is pivotal for the phenylpropanoid pathway that includes, among others, the lignin branch pathway[34] was enhanced only in strawberry fruit treated with the chitosan and COA elicitors, while the downstream gene CHS, which is the key enzyme of flavonoid synthesis[35,36] was up-regulated in the strawberry fruit treated with the BTH elicitor.

Although our data suggest the prevalent involvement of flavonoid branches relative to all of the elicitors, the involvement of other pathway branches for lignin synthesis can be proposed as among the effects of the chitosan and COA treatments. The analysis of the PAL enzyme activity confirmed these PAL gene expression data.

Genes involved in cell-wall-modifying processes, such as PG, PGIP, and endoβGlu were also analyzed. Here, their expression patterns provided evidence for the synchronized expression of PG and PGIP according to all of the elicitors analyzed. In particular, the complementary gene expressions of the PG and PGPI transcripts with time could suggest a feedback mechanism, where PGPI gene expression is modulated in response to plant PG gene expression. PG is involved in pectin metabolism in the production of oligogalacturonides, which can elicit different cellular responses during plant−pathogen interactions in strawberry fruit.[37] The PGIPs that have roles in strawberry defense[38] are extracellular plant proteins that can inhibit fungal endopolygalacturonases, while endoβGlu acts on hemicellulose degradation.[39] Differences between the resistance inducers were seen for endoβGlu gene expression, which was only affected by BTH treatment. The role of this enzyme in plant defense is still unknown, although it is clear that also in this case, the elicitor typology affected the gene expression.

However, the βGlu and Chi enzymes that are involved in cell-wall degradation are those most frequently analyzed in terms of these plant−elicitor interactions.[3] βGlu, which is also a PR-2 protein,[13] showed both early gene expression and enzyme activity enhancement with all of the tested elicitors. This emphasizes the wide involvement of some structural genes in immune responses. However, related to the Chi group, our study shows Chi3 (PR-8 family) up-regulation by the chitosan and COA elicitors but not by BTH, while the total Chi enzyme activity was up-regulated with all of the elicitors tested. Our data thus indicate that there are roles for other classes of Chi following BTH treatment. The differences observed associated with Chi3 as well as in the PR-1 gene expression might be related to the elicitor-specific induction of these PR proteins in strawberry fruit and to the relationships between elicitors doses and the plant species.[13] Our study shows different levels of involvement of these genes that are associated with plant defense that depends on the resistance inducer applied. Usually, gene activation was apparent from 6 h post-treatment. Only the PGPI and Chi3 genes were up-regulated at the first time point of 0.5 h post-treatment and only when using the chitosan and COA elicitors. In this regard, starting from 6 h post-treatment, the highest similarities in the changes in gene expression were seen between the commercial formulations of chitosan and COA (>70%), compared to the similarities between BTH and both chitosan and COA (both <40%). Microarray analysis of *Arabidopsis thaliana* in response to treatment with chitin showed 43% similarity with the genes that are up-regulated by salicylic acid treatment,[40] and BTH is a light-resistant form of this SAR signaling compound. Thus, a similar level of similarity is seen in the present study in terms of the relationship between the gene expression responses of strawberry fruit treated with chitosan, which is the N-deacetylated form of chitin, and BTH, which is, as indicated, an analogue of salicylic acid. This suggests that the expression of these defense genes occurs according to the nature of the elicitor.

In investigating the possible similarities between the actions of these resistance inducers, both chitosan and COA provide a protective physical barrier to pathogen invasion, although in different ways. Chitosan forms a surface coating on the fruit, while COA uses calcium to reinforce the structural composition of the plant cell wall, through the binding of pectins with salts.[4,11] Instead, as an analogue of salicylic acid, BTH is known to primarily induce the expression of SAR without interactions with the plant cell wall.

In conclusion, in this study we set up the relevant RT-qPCR method to test for different gene expressions in strawberry fruits treated with different resistance inducers. Our data show different suitable combinations for reference genes according to the resistance inducer, also indicating the importance of the validation of the reference genes before the experiments. In this study, all of the resistance inducers analyzed had previously

been shown to reduce both gray mold and Rhizopus rot disease in postharvest strawberry fruit,[4] and here, they triggered the expression of a large number of genes that lead to the physiological events involved in plant defense. This supports the effectiveness of these compounds for the induction of resistance in strawberry fruit. However, there were differences between the elicitor resistance at both the transcriptional level of the genes analyzed and the enzyme activities of some of their products that were observed at different times from treatments. This suggests that there is a similarity between chitosan and COA in their target defense gene activation, while their gene responses differ from those due to BTH. This study thus indicates that the composition of the resistance inducers and their interaction with the host plant determine the pattern of induction of the specific defense-marker genes. Information gained with this study can be useful to choose proper resistance inducers for gray mold management.

AUTHOR INFORMATION

Corresponding Author

*Tel: +39-071-2204336. Fax: +39-071-2204856. E-mail: g.romanazzi@univpm.it.

Funding

This work was supported by EUBerry Project [EU FP7 KBBE 2010-4, Grant Agreement No. 265942].

Notes

The authors declare no competing financial interest.

ACKNOWLEDGMENTS

Thanks are expressed to Mark Davey for critical revision of the manuscript.

REFERENCES

(1) Capocasa, F.; Scalzo, J.; Mezzetti, B.; Battino, M. Combining quality and antioxidant attributes in the strawberry: The role of genotype. *Food Chem.* **2008**, *111*, 872−878.

(2) Mũnoz, Z.; Moret, A. Sensitivity of *Botrytis cinerea* to chitosan and acibenzolar-S-methyl. *Pest Manag. Sci.* **2010**, *66*, 974−979.

(3) Wang, S. Y.; Gao, H. Effect of chitosan-based edible coating on antioxidants, antioxidant enzyme system, and postharvest fruit quality of strawberries (*Fragaria* × *ananassa* Duch.). *LWT–Food Sci. Technol.* **2012**, *52*, 71−79.

(4) Romanazzi, G.; Feliziani, E.; Santini, M.; Landi, L. Effectiveness of postharvest treatment with chitosan and other resistance inducers in the control of storage decay of strawberry. *Postharvest Biol. Technol.* **2013**, *75*, 24−27.

(5) Walters, D. R.; Ratsep, J.; Havis, N. D. Controlling crop diseases using induced resistance: challenges for the future. *J. Exp. Bot.* **2013**, *64*, 1263−1280.

(6) Mikulic-Petkovsek, M.; Schmitzer, V.; Slatnar, A.; Weber, N.; Veberic, R.; Stampar, F.; Munda, A.; Koron, D. Alteration of the content of primary and secondary metabolites in strawberry fruit by *Colletotrichum nymphaeae* infection. *J. Agric. Food Chem.* **2013**, *61*, 5987−5995.

(7) El Ghaouth, A.; Arul, J.; Grenier, J.; Asselin, A. Antifungal activity of chitosan on two post harvest pathogens of strawberry fruits. *Phytopathology* **1992**, *82*, 398−402.

(8) Romanazzi, G.; Mlikota Gabler, F.; Margosan, D.; Mackey, B. E.; Smilanick, J. L. Effect of chitosan dissolved in different acids on its ability to control postharvest gray mold of table grape. *Phytopathology* **2009**, *99*, 1028−1036.

(9) Friedrich, L.; Lawton, K.; Dincher, S.; Winter, A.; Staub, T.; Uknes, S.; Métraux, J. P.; Kessmann, H.; Ryals, J. Benzothiadiazole induces systemic acquired resistance in tobacco. *Plant J.* **1996**, *10*, 61−70.

(10) Figueroa, C. R.; Opazo, M. C.; Vera, P.; Arriagada, O.; Díaz, M.; Moya-León, M. A. Effect of postharvest treatment of calcium and auxin on cell wall composition and expression of cell wall-modifying genes in the Chilean strawberry (*Fragaria chiloensis*) fruit. *Food Chem.* **2012**, *132*, 2014−2022.

(11) Hernández-Muñoz, P.; Almenar, E.; Del Valle, V.; Velez, D.; Gavara, R. Effect of chitosan coating combined with postharvest calcium treatment on strawberry (*Fragaria* × *ananassa*) quality during refrigerated storage. *Food Chem.* **2008**, *110*, 428−435.

(12) Pieterse, C. M. J.; Leon-Reyes, A.; Van Der Ent, S.; Van Wees, S. C. M. Networking by small-molecule hormones in plant immunity. *Nat. Chem. Biol.* **2009**, *5*, 308−316.

(13) van Loon, L. C.; Rep, M.; Pieterse, C. M. J. Significance of inducible defense-related proteins in infected plants. *Annu. Rev. Phytopathol.* **2006**, *44*, 135−162.

(14) Ribeiro, C.; Vicente, A. A.; Teixeira, J. A.; Miranda, C. Optimization of edible coating composition to retard strawberry fruit senescence. *Postharvest Biol. Technol.* **2007**, *44*, 63−70.

(15) Hukkanen, A. T.; Kokko, H. I.; Buchala, A. J.; McDougal, G. J.; Stewart, D.; Kärenlampi, S. O.; Karjalainen, R. O. Benzothiadiazole induces the accumulation of phenolics and improves resistance to powdery mildew in strawberry. *J. Agric. Food Chem.* **2013**, *55*, 1862−1870.

(16) Cao, S.; Hu, Z.; Zheng, Y.; Yang, Z.; Lu, B. Effect of BTH on antioxidant enzymes, radical-scavenging activity and decay in strawberry fruit. *Food Chem.* **2011**, *125*, 145−149.

(17) Bustin, S.; Benes, V.; Garson, J. A.; Hellemans, J.; Huggett, J.; Kubista, M.; Mueller, R.; Nolan, T.; Pfaffl, M. W.; Shipley, G. L.; Vandesompele, J.; Wittwer, C. T. The MIQE guidelines: minimum information for publication of quantitative real time PCR experiments. *Clin. Chem.* **2009**, *55*, 611−622.

(18) Livak, K. J.; Schmittgen, T. D. Analysis of relative gene expression data using real-time quantitative PCR and the 2-ΔΔC(T) method. *Methods* **2001**, *25*, 402−408.

(19) Landi, L.; Romanazzi, G. Seasonal variation of defense-related gene expression in leaves from Bois noir affected and recovered grapevines. *J. Agric. Food Chem.* **2011**, *59*, 6628−6637.

(20) Vandesompele, J.; De Preter, K.; Pattyn, F.; Poppe, B.; Van Roy, N.; De Paepe, A.; Speleman, F. Accurate normalization of real-time quantitative RT-PCR data by geometric averaging of multiple internal control genes. *Genome Biol.* **2002**, *3*, RESEARCH0034.

(21) Bradford, M. M. A rapid and sensitive method for quantification of microgram quantities of protein utilizing the principle of protein-dye binding. *Anal. Biochem.* **1976**, *72*, 248−254.

(22) Derckel, J. P.; Baillieul, F.; Manteau, S.; Audran, J. C.; Haye, B.; Lambert, B.; Legendre, L. Differential induction of grapevine defenses by two strains of *Botrytis cinerea*. *Phytopathology* **1999**, *89*, 197−203.

(23) Trotel-Aziz, P.; Couderchet, M.; Vernet, G.; Aziz, A. Chitosan stimulates defense reactions in grapevine leaves and inhibits development of *Botrytis cinerea*. *Eur. J. Plant Pathol.* **2006**, *114*, 405−413.

(24) Amako, K.; Chen, G. X.; Asada, K. Separate assay specific for ascorbate peroxidase and guaiacol peroxidase and for the chloroplastic and cytosolic isozymes of ascorbate peroxidase in plants. *Plant Cell Physiol.* **1994**, *35*, 497−504.

(25) (a) Amborabé, B. E.; Bonmort, J.; Fleurat-Lessard, P.; Roblin, G. Early events induced by chitosan on plant cells. *J. Exp. Bot.* **2008**, *59*, 2317−2324. (b) Boudsocq, M.; Sheen, J. CDPKs in immune and stress signaling. *Trends Plant Sci.* **2013**, *18*, 30−40.

(26) Harmon, A. C.; Gribskov, M.; Harper, J. F. CDPKs: a kinase for every Ca^{2+} signal? *Trends Plant Sci.* **2000**, *5*, 154−159.

(27) Boudsocq, M.; Sheen, J. CDPKs in immune and stress signaling. *Trends Plant Sci.* **2013**, *18*, 30−40.

(28) Demidchik, V.; Cuin, T. A.; Svistunenko, D.; Smith, S. J.; Miller, A. J.; Shabala, S.; Yurin, V. Arabidopsis root K^+-efflux conductance activated by hydroxyl radicals: single-channel properties, genetic basis and involvement in stress-induced cell death. *J. Cell Sci.* **2010**, *123*, 1468−1479.

(29) Ma, W.; Smigel, A.; Tsai, Y. C.; Braam, J.; Berkowitz, G. A. Innate immunity signaling: cytosolic Ca^{2+} elevation is linked to downstream nitric oxide generation through the action of calmodulin or a calmodulin-like protein. *Plant Physiol.* **2008**, *148*, 818−828.
(30) Sharma, P.; Jha, A. B.; Dubey, R. S.; Pessarakli, M. Reactive oxygen species, oxidative damage, and antioxidative defense mechanism in plants under stressful conditions. *J. Bot.* **2012**, DOI: http://dx.doi.org/10.1155/2012/217037.
(31) Buer, C. S.; Imin, N.; Djordjevic, M. A. Flavonoids: new roles for old molecules. *J. Integr. Plant Biol.* **2010**, *52*, 98−111.
(32) Naoumkina, M. N.; Zhao, Q.; Gallego-Giraldo, L.; Dai, X.; Zhao, P. X.; Dixon, R. A. Genome-wide analysis of phenylpropanoid defence pathways. *Mol. Plant Pathol.* **2010**, *11*, 829−846.
(33) Vannozzi, A.; Dry, I. B.; Fasoli, M.; Zenoni, S.; Lucchin, M. Genome-wide analysis of the grapevine stilbene synthase multigenic family: genomic organization and expression profiles upon biotic and abiotic stresses. *BMC Plant Biol.* **2012**, *12*, 130.
(34) Zhong, R.; Ye, Z. H. Transcriptional regulation of lignin biosynthesis. *Plant Signal. Behav.* **2009**, *4*, 1028−1034.
(35) Lunkenbein, S.; Coiner, H.; Ric de Vos, C. H.; Schaart, J. G.; Boone, M. J.; Krens, F. A.; Schwab, W.; Salentijn, E. M. J. Molecular characterization of a stable antisense chalcone synthase phenotype in strawberry (*Fragaria* x *ananassa*). *J. Agric. Food Chem.* **2006**, *54*, 2145−2153.
(36) Dao, T. T. H.; Linthorst, H. J. M.; Verpoorte, R. Chalcone synthase and its functions in plant resistance. *Phytochemistry* **2011**, *10*, 397−412.
(37) Osorio, S.; Bombarely, A.; Giavalisco, P.; Usadel, B.; Stephens, C.; Aragüez, I.; Medina-Escobar, N.; Botella, M. A.; Fernie, A. R.; Valpuesta, V. Demethylation of oligogalacturonides by FaPE1 in the fruits of the wild strawberry *Fragaria vesca* triggers metabolic and transcriptional changes associated with defence and development of the fruit. *J. Exp. Bot.* **2011**, *62*, 2855−2873.
(38) Mehli, L.; Schaart, J. G.; Kjellsen, T. D.; Tran, D. H.; Salentijn, E. M. J.; Schouten, H. J.; Iversen, T. H. A gene encoding a polygalacturonase inhibiting protein (PGIP) shows developmental regulation and pathogen-induced expression in strawberry. *New Phytol.* **2004**, *163*, 99−110.
(39) Mercado, J. A.; Trainotti, L.; Jiménez-Bermúdez, L.; Santiago-Doménech, N.; Posé, S.; Donolli, R.; Barceló, M.; Casadoro, G.; Pliego-Alfaro, F.; Quesada, M. A. Evaluation of the role of the endo-[beta]-(1,4)-glucanase gene FaEG3 in strawberry fruit softening. *Postharvest Biol. Technol.* **2010**, *55*, 8−14.
(40) Ramonell, K. M.; Zhang, B.; Ewing, R. M.; Chen, Y.; Xu, D.; Stacey, G.; Somerville, S. Microarray analysis of chitin elicitation in *Arabidopsis thaliana*. *Mol. Plant Pathol.* **2002**, *3*, 301−311.

and identify the metabolizing enzymes responsible for its hydrolysis.

MATERIALS AND METHODS

Chemicals and Reagents. Flucetosulfuron Technical (purity, 98.4%) was provided by LG Life Sciences Ltd. (Daejeon, Korea). Pooled HLMs were purchased from BD Gentest (Woburn, MA). Glucose-6-phosphate, glucose-6-phosphate dehydrogenase, and nicotinamide adenine dinucleotide ($NADP^+$) were purchased from Sigma-Aldrich (St. Louis, MO). Various esterase inhibitors, such as bisnitrophenyl phosphate (BNPP), calcium chloride, cobalt chloride, dibucaine, ethylenediaminetriacetic acid (EDTA), eserine, magnesium chloride, mercuric chloride, and quinidine, were also purchased from Sigma-Aldrich (St. Louis, MO).

Potassium phosphate monobasic/dibasic and sodium hydroxide (NaOH) were purchased from Daejung Chem (Ansan, Korea). The solvents were high-performance liquid chromatography (HPLC) grade (Burdick and Jacson, MI), and the other chemicals were of the highest quality available.

Preparation of *threo*-Flucetosulfuron. Flucetosulfuron (0.03 g) was dissolved in acetonitrile (10 mL) and injected into a Waters Delta Prep-4000 preparative chromatography system equipped with a Waters deltapak column (50 mm i.d. × 300 mm, 15 μm, 100 A). An isocratic mobile phase was used where A:B = 64:36 at a flow rate of 20.0 mL/min for 120 min (A, buffer solution with 0.02 M ammonium acetate; B, 0.1 M acetic acid). The first fraction (retention time of 80−90 min) was collected (150−170 mL) and partitioned twice with 70 mL of dichloromethane. The dichloromethane layer was washed with 100 mL of distilled water, dried over 30 g of sodium sulfate, and evaporated under reduced pressure at 30 °C to obtain 2.6−4.0 mg of *threo*-flucetosulfuron from one fractionation/purification cycle. About 0.3 g of *threo*-flucetosulfuron was obtained by repeating this process several times.

Preparation of *erythro*-Flucetosulfuron. A second HPLC fraction (retention time of 94−110 min) was collected (~250 mL) and processed as described above for *threo*-flucetosulfuron, producing 23−26 mg of *erythro*-flucetosulfuron from one cycle of the fractionation/purification process. After repeating the same processes many times, about 2.0 g of *erythro*-flucetosulfuron was obtained.

Metabolism of Flucetosulfuron in HLMs. The incubation mixtures containing 0.5 mg of pooled HLMs (H161, Gentest) were reconstituted in 50 mM phosphate buffer (pH 7.4) and preincubated for 5 min at 37 °C. The reaction was initiated by adding the *threo*- or *erythro*-flucetosulfuron isomer (100 μM) and the NADPH-generating system (0.8 mM $NADP^+$, 10.0 mM glucose-6-phosphate, 1.3 mM $MgCl_2$, and 1.0 unit/mL glucose-6-phosphate dehydrogenase) and further incubated for 30 min at 37 °C in a shaking water bath. The reaction was terminated by the addition of 250 μL of acetonitrile, and the samples were centrifuged at 15000*g* for 5 min at 4 °C. Control incubations were conducted with denatured HLMs, which had been boiled in water for 5 min at 100 °C. To confirm whether metabolite formation was NADPH-dependent, NADPH-free incubations were also performed.

Synthesis of *threo*-*N*-(4,6-Dimethoxypyrimidin-2-ylcarbomoyl)-2-(2-fluoro-1-hydroxy propyl)pyrimidine-3-sulfonamid (TM1). *threo*-Flucetosulfuron (149 mg, 1 equiv) was dissolved in 30 mL of acetonitrile in a round-bottom flask (100 mL), 7.5 mL of 0.1 M NaOH solution (30 mg, ~2.5 equiv) was added dropwise, and the reaction mixture was stirred for 1.5 h. The reaction mixture was then transferred to a separatory funnel (250 mL), and 20 mL of distilled water was added. The reaction mixture was washed twice with 25 mL of dichloromethane. The water layer was adjusted to pH 3.0 with 0.1 N HCl to obtain TM1 as a white solid, which was filtered, washed with distilled water, and dried under nitrogen purging for 10 h (90 mg, yield 70%).

Synthesis of *erythro*-*N*-(4,6-Dimethoxypyrimidin-2-ylcarbomoyl)-2-(2-fluoro-1-hydroxy propyl)pyrimidine-3-sulfonamid (EM1). *erythro*-Flucetosulfuron (487 mg, 1 equiv) was dissolved in 100 mL of acetonitrile in a round-bottom flask (250 mL), 25 mL of 0.1 M NaOH solution (100 mg, ~2.5 equiv) was added dropwise, and the reaction mixture was stirred for 1.5 h. The workup process was the same as described above for TM1. EM1 was obtained as a white solid (370 mg, yield 89%).

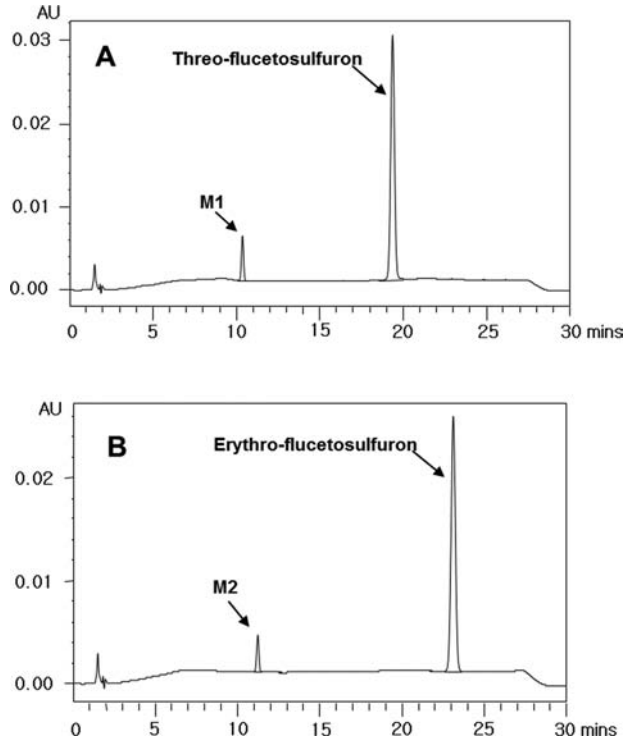

Figure 1. Formation of metabolite M1 from *threo*-flucetosulfuron (A) and M2 from *erythro*-flucetosulfuron (B) when flucetosulfurons (100 μM) were incubated with 0.125 mg human liver microsomes for 30 min at 37 °C.

Metabolite Identification. First, 2 μL of the supernatant from each metabolic reaction was analyzed using HPLC and LC-MS/MS. Again, tandem mass spectrometry (MS/MS) analysis of metabolites, TM1, EM1, and the parent flucetosulfuron isomers was conducted to compare their fragmentation patterns. Solutions of the synthesized metabolites (TM1 and EM1) were prepared in acetonitrile at 10 mg/kg level, and 20 μL of a 1:1 mixture each of TM1 and EM1 solution and the corresponding metabolic reaction supernatant was analyzed using HPLC for confirmation.

Optimization of Metabolic Conditions and Kinetic Studies. The metabolic reactions described earlier were performed with various concentrations of HLMs (0.16, 0.24, 0.32, 0.48, 0.64, 0.96, and 1.28 mg/mL) and each flucetosulfuron isomer (10, 20, 100, 200, 1000, 2000, and 10000 μM) and for 10, 20, 30, 60, 120, 180, and 240 min in a total volume of 250 μL. The incubation mixtures containing pooled HLMs were preincubated for 5 min at 37 °C. The metabolites TM1 and EM1 in the reaction mixture were determined using HPLC analysis.

Optimized conditions were used to analyze enzyme kinetics. These used an incubation time of 30 min (0.16 mg/mL HLMs) and a concentration range of each flucetosulfuron isomer (10, 20, 100, 200, 1000, 2000, and 10000 μM).

Inhibition of Metabolism by Specific Esterase Inhibitors. Incubation mixtures containing 0.16 mg/mL HLMs and one of the following esterase-selective inhibitors [BNPP (100 μM), calcium chloride (1000 μM), cobalt chloride (1000 μM), dibucaine (100 μM), EDTA (3000 μM), eserine (100 μM), magnesium chloride (1000 μM), mercuric chloride (200 μM), and quinidine (100 μM)] were preincubated for 5 min at 37 °C. The reaction was initiated by adding each flucetosulfuron isomer (100 μM) and incubating for a further 30 min at 37 °C in a shaking water bath.

The percentage inhibition was calculated using the ratio of the amount of metabolite (TM1 or EM1) formed in the presence of the

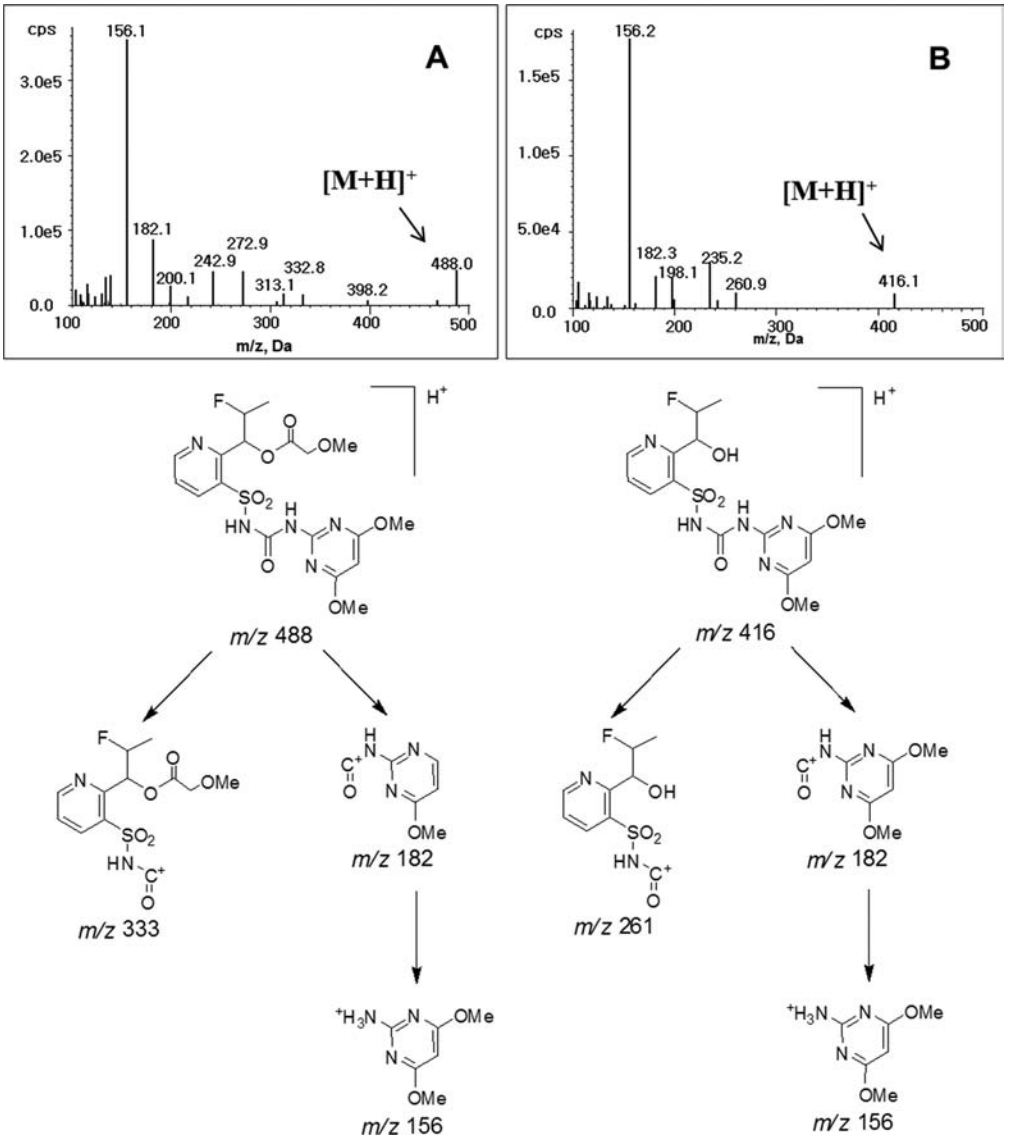

Figure 2. LC-MS/MS spectra and fragmentation of m/z 488 from flucetosulfuron ((A) $[M + H]^+$), and of m/z 416 from metabolite of *erythro* isomer ((B) $[M + H]^+$).

specific inhibitor to the amount formed under control conditions in the absence of inhibitor.

Analytical Instruments and Conditions. *HPLC.* The concentrations of flucetosulfuron isomers and metabolites (TM1 and EM1) were measured using a Waters Alliance 2690 HPLC equipped with a Capcell pak C18 UG120 column (4.6 mm i.d. × 150 mm, 3 μm; Shiseido, Tokyo, Japan) at 40 °C. The mobile phase consisted of 20 mM ammonium acetate buffer with 0.1 M acetic acid (A) and acetonitrile (B). The gradient conditions used were as follows: 20% B at 0 min, 27% B at 4 min, 30% B at 25 min, and 20% B at 28−33 min. The injection volume was 10 μL, and peaks were detected at 254 nm (UV 4890 detector; Waters, Milford, CA). Stock solutions (1 mM) were prepared by dissolving flucetosulfuron isomers, TM1, and EM1 in acetonitrile and diluting serially with acetonitrile to obtain final standard concentrations of 0.05, 0.1, 0.2, 1.0, 10, and 100 μM. The calibration curve was fitted with high linearity ($r^2 > 0.999$).

LC-MS/MS. For the identification of flucetosulfuron and its metabolites, a quadrupole MS/MS (API2000, Applied Biosystems, Foster City, CA) coupled with an Agilent 1100 series HPLC system (Agilent, Wilmington, DE) was used. The separation was performed on a Capcell pak C18 UG120 column (4.6 mm i.d. × 150 mm, 3 μm; Shiseido, Tokyo, Japan) by using a mobile phase consisting of 10 mM ammonium acetate with 0.1% formic acid (A) and acetonitrile (B) at a flow rate of 1.0 mL/min. Mass spectra were recorded by electrospray ionization in positive mode. The turbo ion spray interface was operated at 4500 V and 550 °C. The operating conditions, optimized by flow injection of analytes, were as follows: nebulizer gas flow, 50 psi; curtain gas flow, 10 psi; and collision energy, 30 eV. Quadrupole Q1 and Q3 were set on unit resolution.

Nuclear Magnetic Resonance (NMR) Analysis. ^{1}H and ^{13}C NMR spectra were recorded on a 400 MHz NMR spectrometer (Jeol JNM-LA400 with LFG, JEOL, Japan) in $CDCl_3$ (99.8%, Merck) at 297 K. TMS was used as reference ($\delta = 0$).

Data Analysis. Results are expressed as mean ± standard deviation (SD) of estimates obtained from pooled HLMs in triplicate experiments. In the microsomal incubation studies, the apparent kinetic parameters of metabolite formation (TM1 and EM1) (K_m and V_{max}) were determined by fitting a one-enzyme Michaelis−Menten equation ($V = V_{max} \times [S]/(K_m + [S])$ or a Hill equation ($V = V_{max} \times [S]^n/(K_m + [S]^n)$). The calculated parameters were the maximum rate of formation (V_{max}), the Michaelis constant (apparent K_m), intrinsic clearance (CL_{int} = V_{max}/apparent K_m), and Hill coefficient (n). Calculations were performed using Minitab 16 software (Minitab Inc., State College, PA).

dx.doi.org/10.1021/jf4048836 | J. Agric. Food Chem. 2014, 62, 3057−3063

Table 1. ^{1}H and ^{13}C NMR Data for TM1 and EM1

	^{1}H NMR Data			
	TM1		EM1	
proton	δ ($CDCl_3$)	J (Hz)	δ ($CDCl_3$)	J (Hz)
4	8.83 (dd)	1.5, 4.8	8.82 (dd)	1.5, 4.8
5	7.52 (dd)	4.7, 8.0	7.52 (dd)	4.6, 8.2
6	8.59 (dd)	1.5, 8.0	8.67 (dd)	1.5, 8.2
7	5.82 (s)		5.80 (s)	
13[a]	7.27 (s)		7.25 (s)	
15[a]	12.99 (s)		13.00 (s)	
18	5.45 (m)		5.65 (m)	
19	5.14 (m)		4.83 (m)	
20[b]	4.39 (d)	9.1	4.11 (d)	9.5
21[c]	1.47 (3H, dd)	6.3, 24.1	1.39 (3H, dd)	6.1, 24.8
25, 26	3.96 (6H, s)		3.98 (6H, s)	
	^{13}C NMR Data			
	TM1		EM1	
carbon	δ ($CDCl_3$)	J (Hz)	δ ($CDCl_3$)	J (Hz)
1	140.6		140.8	
2	157.5		157.5	
4	148.7		148.8	
5	133.5		134.5	
6	123.3		123.4	
7	85.6		85.6	
8, 12	172.0		171.0	
10	152.7		152.9	
14	155.4		155.4	
18[d]	72.2 (d)	18.1	72.0 (d)	24.8
19[d]	92.1 (d)	72.6	92.6 (d)	182.6
21[d]	17.7 (d)	22.9	16.4 (d)	21.9
25, 26	55.0		55.0	

[a]NH. [b]OH. [c]H−F coupling. [d]C−F coupling.

RESULTS AND DISCUSSION

Preparation of Flucetosulfuron Isomers. Flucetosulfuron consists of *threo*-flucetosulfuron and *erythro*-flucetosulfuron, and these isomers could be separated using HPLC, in which *threo*-flucetosulfuron eluted before *erythro*-flucetosulfuron.[17] These two flucetosulfuron isomers were isolated using preparative HPLC and purification processes. Because one cycle of the fractionation/purification process produced only a small quantity of each isomer, the same processes were repeated many times to obtain larger amounts with high purity for use in the metabolic studies. About 0.3 g of *threo*-flucetosulfuron and 2.0 g of *erythro*-flucetosulfuron were obtained with 99.8% and 99.7% purity, respectively. LC-MS/MS analysis showed $[M + H]^+$ at m/z 488, clearly confirming the identity of both isomers.

Flucetosulfuron Metabolism by HLMs and Analysis of Metabolites. *threo*-Flucetosulfuron and *erythro*-flucetosulfuron, which were isolated using preparative HPLC, were incubated with HLMs in the presence of NADPH; one metabolite, M1, was observed in the *threo*-flucetosulfuron reaction mixture, while another metabolite, M2, was observed in the *erythro*-flucetosulfuron reaction mixture. No metabolites were formed in reactions using denatured HLMs, suggesting that these were responsible for the formation of M1 and M2 from flucetosulfuron isomers (Figure 1). However, those metabolites were not oxidation products resulting from CYP450 activity in HLMs because they were also formed in NADPH-free reactions. On LC-MS/MS analysis, M1 and M2 gave the same $[M + H]^+$ at m/z 416, indicating a cleavage reaction, rather than insertion of oxygen, when compared with the parent flucetosulfuron isomers ($[M + H]^+ = m/z$ 488). MS/MS analysis of flucetosulfuron ($[M + H]^+$ at m/z 488) in the microsomal reaction mixture showed fragment ions at m/z 156, 182, and 333 (Figure 2A), while the MS/MS spectrum of MI and M2 ($[M + H]^+ = m/z$ 416) showed fragmentation ions at m/z 156, 182, and 261 (Figure 2B). This result suggested that the metabolites were hydrolysis products, which could be formed by cleavage of the flucetosulfuron ester bond.

Identification of M1 and M2. Because LC-MS/MS analysis indicated that M1 and M2 were hydrolysis products of the parent compounds, TM1 and EM1 were prepared from each flucetosulfuron isomer by chemical hydrolysis to confirm their identity. TM1 and EM1 were synthesized with good yields, and their structures were confirmed unambiguously using LC-MS/MS ($[M + H]^+ = m/z$ 416) and ^{1}H and ^{13}C NMR as *N*-(4,6-dimethoxypyrimidin-2-ylcarbomoyl)-2-(2-fluoro-1-hydroxypropyl)pyrimidine-3-sulfonamid (Table 1 and Figure 3) Finally, by comparing LC-MS/MS and MS/MS fragmentation spectra and co-chromatography, M1 and M2 were identified as TM1 and EM1, respectively. Although various studies of pesticide metabolism by HLMs showed that NADPH-dependent oxidation by CYP450s was a major metabolic pathway,[8,10,18−21] only a hydrolysis product was formed in the present study. Hydrolytic metabolism of sulfonylureas has only been reported in soil and water to date.[7−15]

Liver microsomes are a rich source of enzymes, such as CYP450s, FMOs, carboxylesterases, reductases (azo-, carbonyl, and quinone), and aldehyde dehydrogenases for phase I

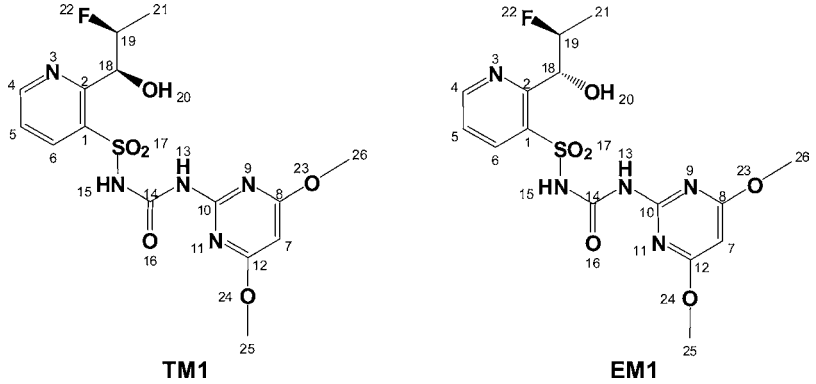

Figure 3. Chemical structure of TM1 and EM1.

dx.doi.org/10.1021/jf4048836 | J. Agric. Food Chem. 2014, 62, 3057−3063

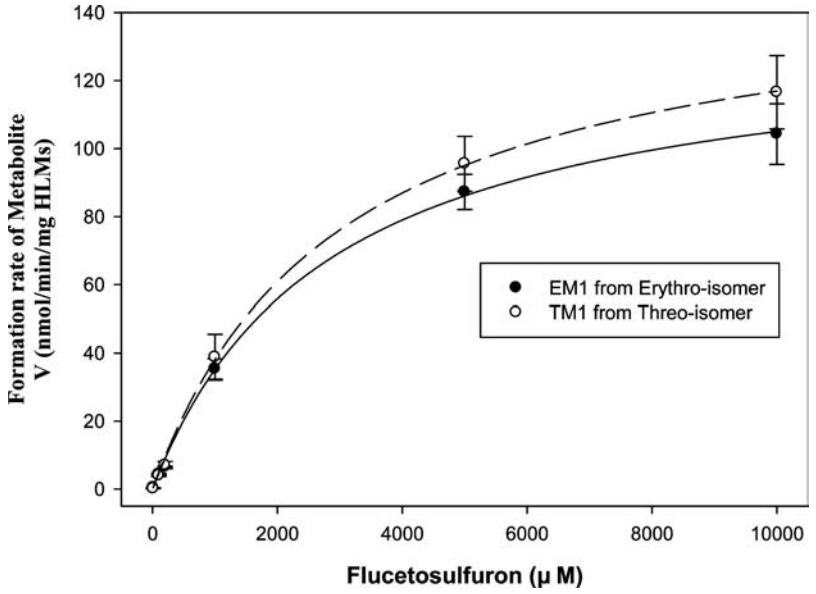

Figure 4. Formation pattern of metabolite EM1 from *erythro*-flucetosulfuron and TM1 from *threo*-flucetosulfuron when flucetosulfurons (100 μM) were incubated with 0.16 mg human liver microsomes for 30 min at 37 °C.

Table 2. Enzyme Kinetic Parameters for the Production of the Metabolite EM1 from *erythro*-Flucetosulfuron and TM1 from *threo*-Flucetosulfuron When Flucetosulfuron Isomers Were Incubated with 0.16 mg Human Liver Microsomes for 30 min at 37 °C

	threo-flucetosulfuron	*erythro*-flucetosulfuron
V_{max} (nmol/min/mg HLMs)*[a]	151.41 ± 2.75	134.38 ± 2.48
K_m (μM)*	2957.37 ± 155.74	2798.53 ± 152.81
CL_{int} [V_{max}/K_m (μL/min/mg HLMs)]	51.20 ± 9.30	48.02 ± 8.86

[a]*P value: 0.21and 0.24 for *threo*-flucetosulfuron and *erythro*-flucetosulfuron.

reactions,[22] and these results indicated the involvement of hydrolysis enzymes in HLM-mediated metabolism of flucetosulfuron.

Enzyme kinetics to establish the optimal metabolic transformation of flucetosulfuron by HLMs, protein (HLMs) concentration, substrate (each flucetosulfuron isomer) concentration, and incubation time were optimized, resulting in the use of 100 μM of each isoform of flucetosulfuron, 0.16 mg/mL of HLMs, and 30 min incubations. Under these optimized metabolic conditions, the formation pattern of TM1 and EM1 from each flucetosulfuron isomer by HLMs was best fitted to a Michaelis−Menten equation ($V = V_{max} \times [S]/(K_m + [S])$), while the Hill model and two-enzyme model did not significantly improve the regression (Figure 4). No significant difference was observed in V_{max} and K_m values for the formation of TM1 and EM1 from *threo*- and *erythro*-flucetosulfuron, respectively (Table 2). The CL_{int} values of TM1 and EM1 were 51.2 and 48.0 μL/min/mg protein for *threo*-flucetosulfuron and *erythro*-flucetosulfuron, respectively. In this study, there was no difference in the kinetics of TM1 and EM1 formation, while previous metabolic studies of endosulfan (α-, β-) showed stereoselectivity by CYP450s and permethrin (*cis*-, *trans*-) showed stereoselectivity of carboxylesterases.[8,16]

Identification of Esterases Involved in the Hydrolysis of Flucetosulfuron. Because the metabolites were formed through ester bond cleavage and the major xenobiotic metabolizing esterases include A-esterases (paraoxonases/arylesterases), cholinesterases, and carboxyesterases,[21] identification of the esterase responsible for hydrolysis was performed through an

Table 3. Effects of Esterase Inhibitors on the Production of Metabolite TM1 from *threo*-Flucetosulfuron and EM1 from *erythro*-Flucetosulfuron When Flucetosulfurons (100 μM) Were Incubated with 0.16 mg Human Liver Microsomes for 30 min at 37 °C

			specific activity (μmol/min/mg protein)[a]			
inhibitor	target esterase	concentration (μM)	TM1	inhibition (%)	EM1	inhibition (%)
control			5.31 ± 0.08		5.28 ± 0.18	
$HgCl_2$*[b]	general esterases	200	0.45 ± 0.09	91.5	0.41 ± 0.02	92.3
$CaCl_2$**[c]	A-esterases	1000	5.15 ± 0.05	2.9	4.88 ± 0.20	6.4
$CoCl_2$	A-esterases	1000	5.05 ± 0.08	4.9	5.17 ± 0.05	7.6
$MgCl_2$	A-esterases	1000	5.09 ± 0.10	4.0	4.95 ± 0.40	6.2
EDTA	A-esterases	3000	5.46 ± 0.15	−2.9	5.44 ± 0.19	−3.1
BNPP*	carboxylesterases	100	0.84 ± 0.19	84.1	0.76 ± 0.02	85.7
eserine*	cholinesterases	100	0.63 ± 0.40	88.2	0.57 ± 0.01	89.1
dibucaine*	cholinesterases	100	2.99 ± 0.15	43.6	3.18 ± 0.15	39.7
quinidine*	cholinesterases	100	2.89 ± 0.20	45.5	2.94 ± 0.20	43.3

[a]Each value represents the mean of two determinations. [b]*Significant difference at $\alpha = 0.05$. [c]**A-esterase activator.

dx.doi.org/10.1021/jf4048836 | J. Agric. Food Chem. 2014, 62, 3057−3063

inhibition study with class-specific esterase inhibitors[23] (Table 3). The concentration of each inhibitor was adopted from previous studies of their inhibitory effects on their target esterases. Addition of Hg^{2+} into the metabolic mixture significantly inhibited the production of TM1 and EM1, suggesting that arylesterases,[24] carboxylesterases,[21,25] and cholinesterases[26] were involved. However, treatment with an activator (Ca^{2+}) or inhibitor (Mg^{2+}, Co^{2+}, and EDTA) for A-esterases[27] did not produce any significant effect on metabolite formation, indicating that flucetosulfuron-metabolizing enzymes were not A-esterases.[28,29] The specific carboxylesterase inhibitor, BNPP,[21,30,31] produced almost complete suppression (>80%) of metabolite formation, and addition of eserine,[23,32] dibucaine, and quinidine, which are specific cholinesterase inhibitors, also reduced metabolite formation. These results indicated that the formation of TM1 and EM1 must be mediated by microsomal carboxylesterases and cholinesterases. Such hydrolytic reactions by carboxylesterases were reported with organophosphate pesticides,[33] pyrethroids,[14,16] and pyribenzoxim.[21] Although cholinesterase-mediated pesticide hydrolysis has not been reported, cocaine and heroin were hydrolyzed by both carboxylesterase and cholinesterase.[34,35]

In conclusion, the primary metabolic pathway for flucetosulfuron in HLMs involved hydrolysis, producing TM1 and EM1. The esterase-specific inhibition study showed that carboxylesterases and cholinesterases were responsible for the formation of these metabolites. Metabolite formation kinetics did not show any significant difference between *threo*- and *erythro*-isomers. On the basis of these findings, a metabolic pathway for both flucetosulfuron isomers was proposed (Figure 5).

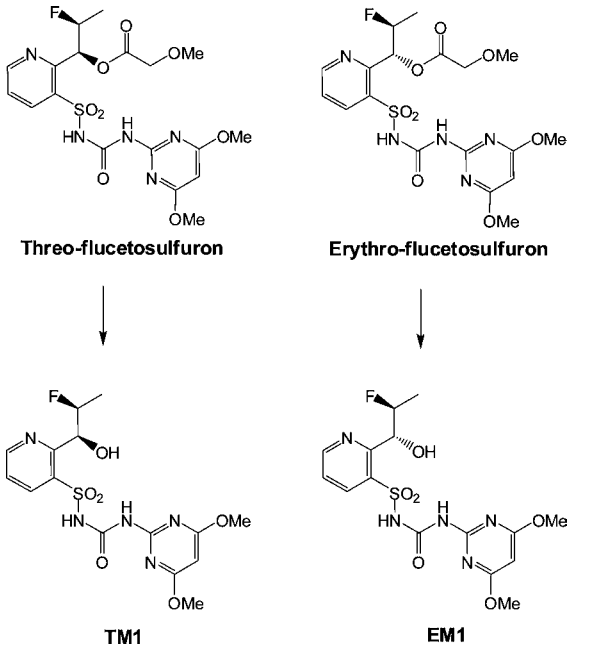

Figure 5. Metabolic pathway for flucetosulfuron in human liver microsomes.

AUTHOR INFORMATION

Corresponding Author

*Phone: +82-2-880-4644. Fax: +82-2-873-4415. E-mail: kjh2404@snu.ac.kr.

Notes

The authors declare no competing financial interest.

ACKNOWLEDGMENTS

We thank LG Life Sciences, Korea, for providing the chemicals.

REFERENCES

(1) Alister, M.; Timothy, D. Review of the activity fate and mode of action of sulfonylurea herbicide. *Pestic. Sci.* **1988**, *22*, 195−219.

(2) Brown, H. M. Mode of action, crop selectivity, and soil relations of the sulfonylurea herbicides. *Pestic. Sci.* **1990**, *29*, 263−281.

(3) JanjicV.JovanovicL.BlanusaT.MilosevicD.Sulfonylurea herbicides—mode of action. In *Plant Physiology in the New Millennium*; Yugoslav Society of Plant Physiology—Agriculture Research Institute: Belgrade, 2002.

(4) Duggleby, R. G.; McCourt, J. A.; Guddat, L. W. Structure and mechanism of inhibition of plant acetohydroxyacid synthase. *Plant Physiol. Biochem.* **2008**, *46*, 309.

(5) McCourt, J. A. Herbicide-binding sites revealed in the structure of plant acetohydroxyacid synthase. *Proc. Natl. Acad. Sci. U. S. A.* **2006**, *103*, 569−573.

(6) Kim, D.; Koo, S.; Lee, J.; Hwang, K.; Kim, T.; Kang, K.; Hwang, K.; Joe, G.; Cho, J.; Kim, D. Flucetosulfuron: a new sulfonylurea herbicide. The BCPC International Congress: Crop Science and Technology, Glasgow, November 10−12, 2003; *The BCPC International Congress: Crop Science and Technology; Proceedings of an International Congress Held at the SECC, Glasgow, Scotland, UK, 10−12 November 2003*; British Crop Protection Council, 2003; Vol. *1* and *2*, pp 87−92.

(7) Kim, K.-A.; Kim, M.-J.; Park, J.-Y.; Shon, J.-H.; Yoon, Y.-R.; Lee, S.-S.; Liu, K.-H.; Chun, J.-H.; Hyun, M.-H.; Shin, J.-G. Stereoselective metabolism of lansoprazole by human liver cytochrome P450 enzymes. *Drug Metab. Dispos.* **2003**, *31*, 1227−1234.

(8) Lee, H.-K.; Moon, J.-K.; Chang, C.-H.; Choi, H.; Park, H.-W.; Park, B.-S.; Lee, H.-S.; Hwang, E.-C.; Lee, Y.-D.; Liu, K.-H. Stereoselective metabolism of endosulfan by human liver microsomes and human cytochrome P450 isoforms. *Drug Metab. Dispos.* **2006**, *34*, 1090−1095.

(9) Liu, K.-H.; Kim, J.-H. In vitro dermal penetration study of carbofuran, carbosulfan, and furathiocarb. *Arch. Toxicol.* **2003**, *77*, 255−260.

(10) Mutch, E.; Williams, F. M. Diazinon, chlorpyrifos and parathion are metabolised by multiple cytochromes P450 in human liver. *Toxicology* **2006**, *224*, 22−32.

(11) Godin, S. J.; Crow, J. A.; Scollon, E. J.; Hughes, M. F.; DeVito, M. J.; Ross, M. K. Identification of rat and human cytochrome P450 isoforms and a rat serum esterase that metabolize the pyrethroid insecticides deltamethrin and esfenvalerate. *Drug Metab. Dispos.* **2007**, *35*, 1664−1671.

(12) Scollon, E. J.; Starr, J. M.; Godin, S. J.; DeVito, M. J.; Hughes, M. F. In vitro metabolism of pyrethroid pesticides by rat and human hepatic microsomes and cytochrome P450 isoforms. *Drug Metab. Dispos.* **2009**, *37*, 221−228.

(13) Nishi, K.; Huang, H.; Kamita, S. G.; Kim, I. H.; Morisseau, C.; Hammock, B. D. Characterization of pyrethroid hydrolysis by the human liver carboxylesterases hCE-1 and hCE-2. *Arch. Biochem. Biophys.* **2006**, *445*, 115−123.

(14) Crow, J. A.; Borazjani, A.; Potter, P. M.; Ross, M. K. Hydrolysis of pyrethroids by human and rat tissues: examination of intestinal, liver and serum carboxylesterases. *Toxicol. Appl. Pharmacol.* **2007**, *221*, 1−12.

(15) Soderlund, D. M.; Casida, J. E. Effects of pyrethroid structure on rates of hydrolysis and oxidation by mouse liver microsomal enzymes. *Pestic. Biochem. Physiol.* **1977**, *7*, 391−401.

(16) Ross, M. K.; Borazjani, A.; Edwards, C. C.; Potter, P. M. Hydrolytic metabolism of pyrethroids by human and other mammalian carboxylesterases. *Biochem. Pharmacol.* **2006**, *71*, 657−669.

(17) KOPAC. Flucetosulfuron. In *Analytical Methods of Pesticides*; Korea Pesticide Analytical Council, 2009; http//www.kopac.or.kr.

(18) Lang, D. H.; Rettie, A. E.; Böcker, R. H. Identification of enzymes involved in the metabolism of atrazine, terbuthylazine,

ametryne, and terbutryne in human liver microsomes. *Chem. Res. Toxicol.* **1997**, *10*, 1037−1044.
(19) Coleman, S.; Linderman, R.; Hodgson, E.; Rose, R. L. Comparative metabolism of chloroacetamide herbicides and selected metabolites in human and rat liver microsomes. *Environ. Health Perspect.* **2000**, *108*, 1151.
(20) Abass, K.; Reponen, P.; Turpeinen, M.; Jalonen, J.; Pelkonen, O. Characterization of diuron *N*-demethylation by mammalian hepatic microsomes and cDNA-expressed human cytochrome P450 enzymes. *Drug Metab. Dispos.* **2007**, *35*, 1634−1641.
(21) Kim, J.-H. Characterization of Pyribenzoxim Metabolizing Enzymes in Rat Liver Microsomes. *J. Toxicol. Public Health* **2006**, *22*, 1−8.
(22) Parkinson, A. *Biotransformation of Xenobiotics*; McGraw-Hill: New York, 2001.
(23) Ecobichon, D. Characterization of the esterases of canine serum. *Can. J. Biochem.* **1970**, *48*, 1359−1367.
(24) Iatsimirskaia, E.; Tulebaev, S.; Storozhuk, E.; Utkin, I.; Smith, D.; Gerber, N.; Koudriakova, T. Metabolism of rifabutin in human enterocyte and liver microsomes: kinetic parameters, identification of enzyme systems, and drug interactions with macrolides and antifungal agents. *Clin. Pharmacol. Ther.* **1997**, *61*, 554−562.
(25) Ali, B.; Kaur, S.; James, E. C.; Parmar, S. S. Identification and characterization of hepatic carboxylesterases hydrolyzing hydrocortisone esters. *Biochem. Pharmacol.* **1985**, *34*, 1881−1886.
(26) Frasco, M. F.; Colletier, J. P.; Weik, M.; Carvalho, F.; Guilhermino, L.; Stojan, J.; Fournier, D. Mechanisms of cholinesterase inhibition by inorganic mercury. *FEBS J.* **2007**, *274*, 1849−1861.
(27) Erdös, E. G.; Debay, C. R.; Westerman, M. P. Activation and inhibition of the arylesterase of human serum. *Nature* **1959**, *184*, 430.
(28) Gonzalvo, M. C.; Gil, F.; Hernández, A. F.; Villanueva, E.; Pla, A. Inhibition of paraoxonase activity in human liver microsomes by exposure to EDTA, metals and mercurials. *Chem.−Biol. Interact.* **1997**, *105*, 169−179.
(29) Gan, K. N.; Smolen, A.; Eckerson, H. W.; La Du, B. N. Purification of human serum paraoxonase/arylesterase. Evidence for one esterase catalyzing both activities. *Drug Metab. Dispos.* **1991**, *19*, 100−106.
(30) Simeon, V.; Reiner, E.; Škrinjarić-Špoljar, M.; Krauthacker, B. Cholinesterases in rabbit serum. *Gen. Pharmacol.: Vasc. Syst.* **1988**, *19*, 849−853.
(31) Reiner, E.; Pavković, E.; Radić, Z.; Simeon, V. Differentiation of esterases reacting with organophosphorus compounds. *Chem.−Biol. Interact.* **1993**, *87*, 77−83.
(32) Augustinsson, K.-B. Electrophoretic separation and classification of blood plasma esterases. *Nature* **1958**, *181*, 1786−1789.
(33) Devonshire, A. L.; Moores, G. D. A carboxylesterase with broad substrate specificity causes organophosphorus, carbamate and pyrethroid resistance in peach-potato aphids (*Myzus persicae*). *Pestic. Biochem. Physiol.* **1982**, *18*, 235−246.
(34) Stewart, D. J.; Inaba, T.; Tang, B. K.; Kalow, W. Hydrolysis of cocaine in human plasma by cholinesterase. *Life Sci.* **1977**, *20*, 1557−1563.
(35) Lockridge, O.; Mottershaw-Jackson, N.; Eckerson, H. W.; La Du, B. N. Hydrolysis of diacetylmorphine (heroin) by human serum cholinesterase. *J. Pharmacol. Exp. Ther.* **1980**, *215*, 1−8.

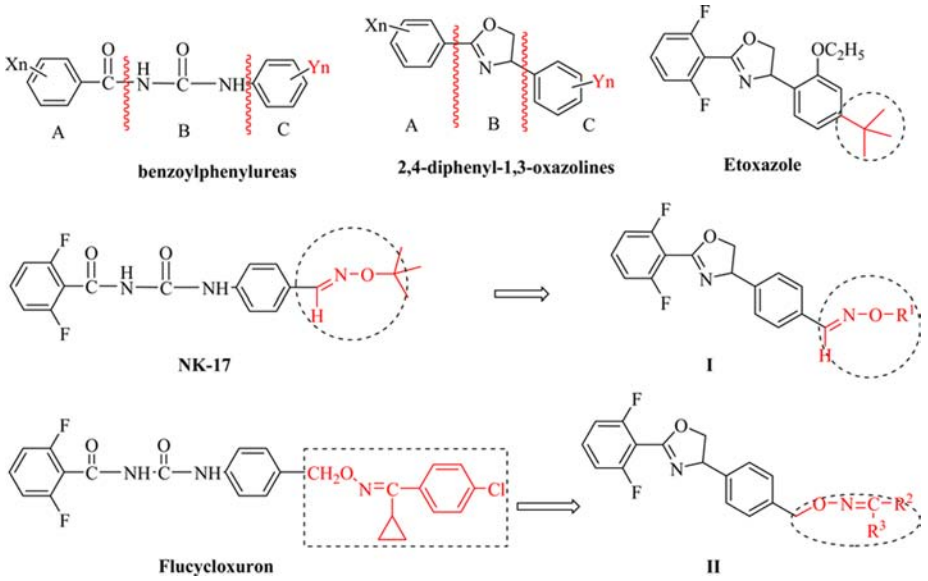

Figure 1. Design of the target compounds **I** and **II**.

Scheme 1. Synthetic Route of 6

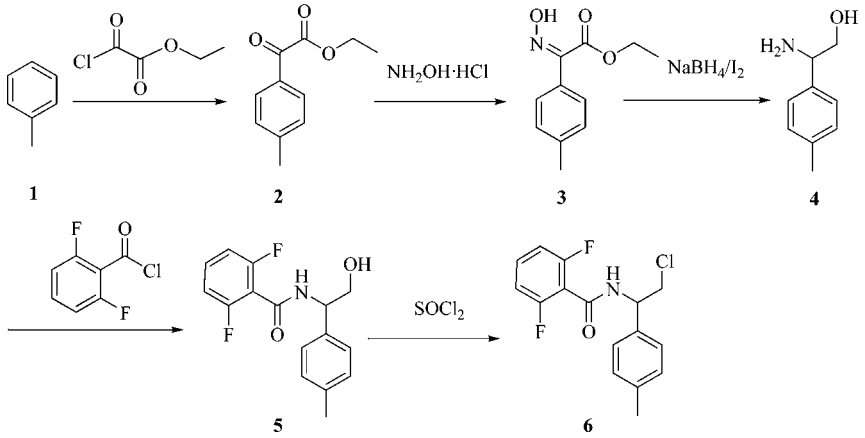

group at the 4-phenyl moiety of 2,4-diphenyl-1,3-oxazoline were designed by referring to benzoylphenylurea NK-17, which was discovered by our research group and showed excellent larvicidal activity.[3] Similarly, another series of compounds **II** were designed by referring to the commercial benzoylphenylurea flucycloxuron which was created by Solvay-Duphar B.V. as a CSI and also contained an oxime ether group.[14] The acaricidal activity of all the target compounds (**I-a**−**I-l** and **II-a**−**II-n**) against *T. cinnabarinus* was assayed in the laboratory. Furthermore, the effects of the **II-l** on *T. cinnabarinus* and *Panonychus citri* (*P. citri*) were evaluated in the field.

In 2004, diflubenzuron, a CSI belonging to benzoyphenylurea, was testified to act on the target site of sulfonylurea receptor (SUR) protein by means of the isotope labeling technology,[15] and later the mechanism of NK-17 was also proposed to bind to the same site of SUR by fluorescence polarization (FP) method in our previous report.[16] Since numerous experimental data had indicated that the action mechanism of etoxazole was similar to that of the benzoylphenylureas, we would like to know if etoxazole and the target compounds (**I-a**−**I-l** and **II-a**−**II-n**) that we synthesized in this paper can also bind to the same site of SUR. To raise awareness to the mode of action of the target compounds and help to discover some superior compounds, in this paper, we preliminarily determined the affinity activity of all the target compounds binding to the SUR in vitro by FP method, and the results were discussed.

MATERIALS AND METHODS

Instruments and Chemicals. ^{1}H NMR spectra were recorded at 300 or 400 MHz by respectively using a Bruker AV300 spectrometer or a Bruker AV400 spectrometer with $CDCl_3$ or DMSO-d_6 as solvent and tetramethylsilane as the internal standard. Chemical shift values (δ) are reported in parts per million (ppm). High-resolution mass spectrometry (HRMS) was obtained by means of FTICR-MS (Ionspec 7.0T). The melting points were obtained utilizing an X-4 binocular microscope melting point apparatus (Beijing Tech Instruments Co., Beijing, China) and are uncorrected. Yields were not optimized. The values of the FP were obtained by CARY eclipse fluorescence spectrophotometer (Agilent Technologies, Santa Clara, CA, USA). All of the reaction reagents were analytically or chemically pure, which were dried and distilled according to standard methods before use when necessary. All other biochemical reagents used in the FP determination were of the highest purity grade from Sigma-Aldrich Chemical Co., Ltd.

General Synthetic Procedure for Compound 6 (Scheme 1). *Synthesis of Ethyl 2-p-Tolyl-2-oxoacetate (2).* To a solution of ethyl chloroglyoxylate (4.5 g, 33 mmol) in anhydrous dichloromethane (50 mL) was added anhydrous $AlCl_3$ (4.40 g, 33 mmol), and the mixture

dx.doi.org/10.1021/jf500461a | J. Agric. Food Chem. 2014, 62, 3064−3072

Scheme 2. General Synthetic Route of the Target Compounds I-a−I-l

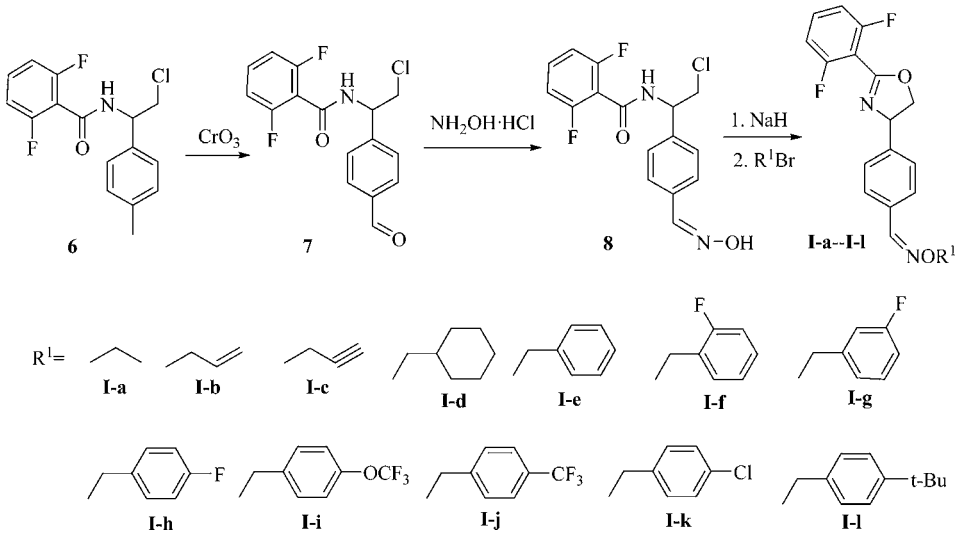

was stirred at room temperature until $AlCl_3$ was dissolved. The mixture was cooled to −10 °C, toluene (2.76 g, 30 mmol) in dichloromethane (50 mL) was added dropwise over a period of 2 h, and then the reaction mixture was stirred at room temperature for another 5 h until the reaction was complete, indicated by TLC. The mixture was poured to ice−water (80 mL), and the value of the pH was adjusted to 2. After the organic phase was separated, the aqueous phase was extracted with dichloromethane. The combined organic phase was washed with saturated brine, dried over anhydrous sodium sulfate, filtered, and concentrated in vacuo to give **2** as a yellow liquid (5.08 g, yield 88%). ^{1}H NMR (400 MHz, $CDCl_3$): δ 7.91 (d, J = 8.0 Hz, 2H), 7.31 (d, J = 8.0 Hz, 2H), 4.45 (q, J = 7.2 Hz, 2H), 2.45 (s, 3H), 1.42 (t, J = 7.2 Hz, 3H).

*Synthesis of Ethyl 2-(Hydroxyimino)-2-(p-tolyl)acetate (**3**).* To a solution of **2** (86.21 g, 450 mmol) in ethanol (400 mL) was added hydroxylamine hydrochloride (52.98 g, 760 mmol), and the mixture was refluxed for 8 h and monitored by TLC. After removal of ethanol, the solid residue obtained was redissolved in ethyl acetate. The mixture was washed twice with water, dried with anhydrous sodium sulfate, filtered, and concentrated in vacuo to give a crude product, which was purified by recrystallization using carbon tetrachloride and petroleum ether to give **3** (45.80 g). The mother liquid was purified by flash chromatography on silica gel with petroleum ether and ethyl acetate (v/v = 20:1, 10:1) to give another portion of **3** (21.5 g). Overall yield: 72%. Mp: 116−117 °C. ^{1}H NMR (300 MHz, $CDCl_3$): δ 8.65 (s, 1H), 7.42 (d, J = 8.1 Hz, 2H), 7.25 (d, J = 8.1 Hz, 2H), 4.35 (q, J = 7.2 Hz, 2H), 2.39 (s, 3H), 1.36 (t, J = 7.2 Hz, 3H).

*Synthesis of 2-Amino-2-(p-tolyl)ethanol (**4**).* To a solution of compound **3** (25.25 g, 120 mmol) in anhydrous tetrahydrofuran (200 mL) under stirring was added sodium borohydride (13.83 g, 370 mmol). Iodine (46.37 g, 180 mmol) in THF (180 mL) was added dropwise over a period of 6.5 h at 0 °C. Afterward, the reaction mixture was refluxed for 5 h. The excess reducing agent was quenched with methanol at 0 °C, and then the solvent was removed. After the residue was added to a solution of 5% sodium hydroxide in water, the mixture was refluxed for 5 h. When it was complete, indicated by TLC, the reaction mixture was cooled to room temperature and extracted by dichloromethane. Then, the organic layer was dried by sodium sulfate, filtered, and concentrated to give **4** as a yellow solid (17.45 g, yield 94%). Mp: 68−70 °C. ^{1}H NMR (400 MHz, $CDCl_3$): δ 7.22 (d, J = 8.0 Hz, 2H), 7.16 (d, J = 8.0 Hz, 2H), 4.01 (dd, J = 8.4, 4.4 Hz, 1H), 3.72 (dd, J = 10.8, 4.4 Hz, 1H), 3.53 (dd, J = 10.8, 8.4 Hz, 1H), 2.34 (s, 3H).

*Synthesis of 2,6-Difluoro-N-(2-hydroxy-1-(p-tolyl)ethyl)-benzamide (**5**).* To a mixture of **4** (5.0 g, 33 mmol) and triethylamine (5.51 g, 40 mmol) in anhydrous tetrahydrofuran (70 mL) at 0 °C was added dropwise a solution of 2,6-difluorobenzoyl chloride (6.14 g, 35 mmol) in tetrahydrofuran (60 mL) over a period of 2.5 h, and then the reaction mixture was warmed to room temperature for 5 h until the reaction was complete. The mixture was filtered, concentrated, and purified by recrystallization using ethyl acetate and petroleum ether to give **5** as a solid (4.57 g). The mother liquid was concentrated and purified by flash chromatography on silica gel with petroleum ether and ethyl acetate (v/v = 2:1) to give another portion of **5** (2.89 g). Overall yield: 77%. Mp: 125−127 °C. ^{1}H NMR (400 MHz, $CDCl_3$): δ 7.43−7.35 (m, 1H), 7.28 (d, J = 8.0 Hz, 2H), 7.20 (d, J = 8.0 Hz, 2H), 6.97 (t, J = 8.0 Hz, 2H), 6.55 (d, J = 6.8 Hz, 1H), 5.55 (dd, J = 12.8, 5.2 Hz, 1H), 4.02−3.91 (m, 2H), 2.35 (s, 3H).

*Synthesis of N-(2-Chloro-1-(p-tolyl)ethyl)-2,6-difluorobenzamide (**6**).* To a solution of **5** (41.7 g, 140 mmol) in chloroform (120 mL) was added dropwise thionyl chloride (19.59 g, 165 mmol) in chloroform (60 mL) over a period of 70 min. The reaction mixture was refluxed for 100 min until the reaction was complete. After the value of the pH of the mixture was adjusted to 8 with saturated sodium bicarbonate solution, the organic phase was separated, washed with saturated brine, dried with magnesium sulfate, filtered and concentrated to give **6** as a white solid (41.7 g, yield 94%). Mp: 62−63 °C. ^{1}H NMR (300 MHz, $CDCl_3$): δ 7.44−7.37 (m, 1H), 7.29 (d, J = 8.1 Hz, 2H), 7.21 (d, J = 8.1 Hz, 2H), 6.97 (t, J = 8.1 Hz, 2H), 6.53 (d, J = 6.0 Hz, 1H), 5.56 (dd, J = 12.9, 5.1 Hz, 1H), 4.03−3.91 (m, 2H), 2.36 (s, 3H).

General Synthetic Procedure for the Target Compounds I-a−I-l (Scheme 2). *Synthesis of N-(2-Chloro-1-(4-formylphenyl)-ethyl)-2,6-difluorobenzamide (**7**).* To a solution of **6** (10.0 g, 32 mmol) in glacial acetic acid (60 mL) was added dropwise concentrated sulfuric acid (7 mL) over a period of 1 h at the temperature range of −10 °C to −5 °C. Then powdered CrO_3 was added, after which the reaction mixture was stirred for 6 h. The reaction mixture was poured to ice−water (300 mL) and extracted by ethyl acetate (100 mL × 5). The combined organic phase was successively washed with water, saturated sodium bicarbonate, and saturated brine and dried with anhydrous magnesium sulfate. After filtration, the solvent was removed under reduced pressure to give a crude black residue. The residue was added to a mixture of methanol (30 mL) and concentrated hydrochloric acid (10 mL), and then the reaction was stirred under tepidity for 5 h. The reaction mixture was cooled to room temperature, concentrated under reduced pressure, and then extracted by ethyl acetate (50 mL × 3). The organic layer was washed with saturated sodium bicarbonate solution and saturated brine successively, dried with anhydrous magnesium sulfate, filtered and concentrated under reduced pressure. The residue was purified by flash chromatography on silica gel with petroleum ether and ethyl acetate (v/v = 3:1) to give **7** as a yellow oil (4.1 g, yield 41%). ^{1}H NMR (400 MHz, $CDCl_3$): δ 10.03 (s, 1H), 7.93 (d, J = 8.4 Hz, 2H), 7.59 (d, J = 8.4 Hz, 2H), 7.47−

dx.doi.org/10.1021/jf500461a | J. Agric. Food Chem. 2014, 62, 3064−3072

Scheme 3. General Synthetic Route of the Target Compounds II-a−II-n

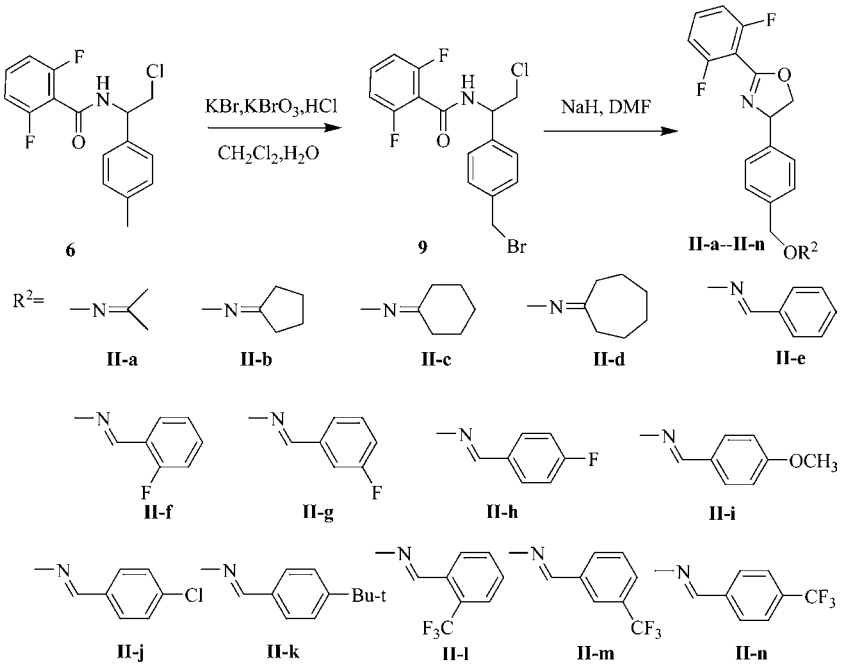

7.40 (m, 1H), 7.00 (t, J = 8.4 Hz, 2H), 6.73 (d, J = 7.6 Hz, 1H), 5.71−5.67 (m, 1H), 4.05 (dd, J = 11.6, 4.4 Hz, 1H), 3.97 (dd, J = 11.6, 4.4 Hz, 1H).

*Synthesis of N-(2-Chloro-1-(4-((hydroxyimino)methyl)phenyl)-ethyl)-2,6-difluorobenzamide (**8**).* To a mixture of **7** (2.43 g, 8 mmol), triethylamine (1.90 g, 19 mmol), and hydroxylamine hydrochloride (1.30 g, 19 mmol) in anhydrous tetrahydrofuran (50 mL) were added molecular sieves (4 Å), and then the mixture was refluxed for 4 h and monitored with TLC. After the reaction was complete, the mixture was filtered to remove molecular sieves, concentrated in vacuo, and purified by flash chromatography on silica gel with petroleum ether and ethyl acetate (v/v = 3:1) to give **8** as a white solid (1.93 g, yield 76%). ^{1}H NMR (400 MHz, DMSO-d_6): δ 11.26 (s, 1H), 9.47 (d, J = 8.4 Hz, 1H), 8.14 (s, 1H), 7.61 (d, J = 8.4 Hz, 2H), 7.61−7.57 (m, 1H), 7.49 (d, J = 8.4 Hz, 2H), 7.22−7.13 (m, 2H), 5.34−5.29 (m, 1H), 3.95 (dd, J = 11.2, 4.8 Hz, 1H), 3.80 (dd, J = 11.2, 9.6 Hz, 1H).

*Synthesis of 4-(2-(2,6-Difluorophenyl)-4,5-dihydrooxazol-4-yl)-benzaldehyde O-Ethyl Oxime (**I-a**).* To a mixture of **8** (0.82 g, 2.4 mmol) in *N*,*N*-dimethylformamide (DMF) (30 mL) stirred for 10 min at 0 °C was added sodium hydride (0.23 g, 10 mmol), and the reaction mixture was stirred for 1 h. After ethyl iodide (0.57 g, 4 mmol) was added, the reaction mixture was stirred for another 2 h. When the reaction was complete, as indicated by TLC, ethyl acetate (150 mL) was added. The mixture was washed with a large amount of water three times and saturated brine once, dried with anhydrous magnesium sulfate, filtered, and concentrated under reduced pressure. The residue was purified by flash chromatography on silica gel with petroleum ether and ethyl acetate (v/v = 12:1) to give the target compound **I-a** as an oil (0.51 g, yield 64%). ^{1}H NMR (400 MHz, $CDCl_3$): δ 8.07 (s, 1H), 7.60 (d, J = 8.4 Hz, 2H), 7.48−7.40 (m, 1H), 7.35 (d, J = 8.4 Hz, 2H), 7.00 (t, J = 8.0 Hz, 2H), 5.48 (dd, J = 10.4, 8.4 Hz, 1H), 4.83 (dd, J = 10.4, 8.4 Hz, 1H), 4.28 (t, J = 8.4 Hz, 1H), 4.23 (q, J = 7.2 Hz, 2H), 1.33 (t, J = 7.2 Hz, 3H). HRMS (ESI): calcd for $C_{18}H_{16}F_2N_2O_2Na$ $[M + Na]^+$ 353.1072, found 353.1073.

Compounds **I-b**−**I-l** were synthesized according to a method similar to that for **I-a** using the corresponding alkyl bromide instead of ethyl iodide.

*Data for 4-(2-(2,6-Difluorophenyl)-4,5-dihydrooxazol-4-yl)-benzaldehyde O-Allyl Oxime (**I-b**).* Oil; yield 58%. ^{1}H NMR (400 MHz, $CDCl_3$): δ 8.12 (s, 1H), 7.60 (d, J = 8.0 Hz, 2H), 7.48−7.41 (m, 1H), 7.35 (d, J = 8.0 Hz, 2H), 7.01 (t, J = 8.0 Hz, 2H), 6.10−6.00 (m, 1H), 5.48 (dd, J = 10.4, 8.4 Hz, 1H), 5.36 (dd, J = 17.2, 1.6 Hz, 1H), 5.26 (dd, J = 10.4, 1.2 Hz, 1H), 4.83 (dd, J = 10.4, 8.4 Hz, 1H), 4.68 (d, J = 5.6 Hz, 2H), 4.28 (t, J = 8.0 Hz, 1H). HRMS (ESI): calcd for $C_{19}H_{16}F_2N_2O_2Na$ $[M + Na]^+$ 365.1072, found 365.1075.

*Data for 4-(2-(2,6-Difluorophenyl)-4,5-dihydrooxazol-4-yl)-benzaldehyde O-Prop-2-yn-1-yl Oxime (**I-c**).* Oil; yield 47%. ^{1}H NMR (300 MHz, $CDCl_3$): δ 8.13 (s, 1H), 7.62 (d, J = 8.1 Hz, 2H), 7.49−7.39 (m, 1H), 7.36 (d, J = 8.1 Hz, 2H), 7.01 (t, J = 8.1 Hz, 2H), 5.49 (dd, J = 10.2, 8.2 Hz, 1H), 4.83 (dd, J = 10.2, 8.2 Hz, 1H), 4.78 (d, J = 2.1 Hz, 2H), 4.27 (t, J = 8.1 Hz, 1H), 2.51 (t, J = 2.4 Hz, 1H). HRMS (ESI): calcd for $C_{19}H_{14}F_2N_2O_2Na$ $[M + Na]^+$ 363.0916, found 363.0912.

*Data for 4-(2-(2,6-Difluorophenyl)-4,5-dihydrooxazol-4-yl)-benzaldehyde O-Cyclohexylmethyl Oxime (**I-d**).* Oil; yield 44%. ^{1}H NMR (400 MHz, $CDCl_3$): δ 8.07 (s, 1H), 7.59 (d, J = 8.0 Hz, 2H), 7.47−7.42 (m, 1H), 7.34 (d, J = 8.0 Hz, 2H), 7.00 (t, J = 8.0 Hz, 2H), 5.48 (dd, J = 10.0, 8.8 Hz, 1H), 4.82 (dd, J = 10.0, 8.8 Hz, 1H), 4.27 (t, J = 8.0 Hz, 1H), 3.98 (d, J = 6.4 Hz, 2H), 1.82−1.72 (m, 5H), 1.31−1.21 (m, 6H). HRMS (ESI): calcd for $C_{23}H_{24}F_2N_2O_2Na$ $[M + Na]^+$ 421.1698, found 421.1693.

*Data for 4-(2-(2,6-Difluorophenyl)-4,5-dihydrooxazol-4-yl)-benzaldehyde O-Benzyl Oxime (**I-e**).* Yellow oil; yield 50%. ^{1}H NMR (400 MHz, $CDCl_3$): δ 8.14 (s, 1H), 7.60 (d, J = 8.0 Hz, 2H), 7.47−7.31 (m, 8H), 7.01 (t, J = 8.0 Hz, 2H), 5.48 (dd, J = 12.0, 8.0 Hz, 1H), 5.21 (s, 2H), 4.83 (dd, J = 12.0, 8.0 Hz, 1H), 4.27 (t, J = 8.0 Hz, 1H). HRMS (ESI): calcd for $C_{23}H_{19}F_2N_2O_2$ $[M + H]^+$ 393.1409, found 393.1402.

*Data for 4-(2-(2,6-Difluorophenyl)-4,5-dihydrooxazol-4-yl)-benzaldehyde O-(2-Fluorobenzyl) Oxime (**I-f**).* Oil; yield 63%. ^{1}H NMR (400 MHz, $CDCl_3$): δ 8.13 (s, 1H), 7.60 (d, J = 8.0 Hz, 2H), 7.49−7.41 (m, 2H), 7.34 (d, J = 8.0 Hz, 2H), 7.32−7.28 (m, 1H), 7.16−7.12 (m, 1H), 7.10−7.05 (m, 1H), 7.01 (t, J = 8.0 Hz, 2H), 5.48 (dd, J = 10.4, 8.0 Hz, 1H), 5.28 (s, 2H), 4.83 (dd, J = 10.4, 8.0 Hz, 1H), 4.27 (t, J = 8.0 Hz, 1H). HRMS (ESI): calcd for $C_{23}H_{17}F_3N_2O_2Na$ $[M + Na]^+$ 433.1134, found 433.1129.

*Data for 4-(2-(2,6-Difluorophenyl)-4,5-dihydrooxazol-4-yl)-benzaldehyde O-(3-Fluorobenzyl) Oxime (**I-g**).* Oil; yield 53%. ^{1}H NMR (400 MHz, $CDCl_3$): δ 8.15 (s, 1H), 7.60 (d, J = 8.0 Hz, 2H), 7.48−7.40 (m, 1H), 7.35 (d, J = 8.0 Hz, 2H), 7.32−7.30 (m, 1H), 7.19−7.11 (m, 1H), 7.03−6.98 (m, 3H), 5.48 (dd, J = 10.4, 8.4 Hz, 1H), 5.19 (s, 2H), 4.83 (dd, J = 10.4, 8.4 Hz, 1H), 4.27 (t, J = 8.4 Hz,

dx.doi.org/10.1021/jf500461a | J. Agric. Food Chem. 2014, 62, 3064−3072

1H). HRMS (ESI): calcd for $C_{23}H_{17}F_3N_2O_2Na$ $[M + Na]^+$ 433.1134, found 433.1130.

*Data for 4-(2-(2,6-Difluorophenyl)-4,5-dihydrooxazol-4-yl)-benzaldehyde O-(4-Fluorobenzyl) Oxime (**I-h**).* White solid; mp 97−100 °C; yield 69%. ^{1}H NMR (400 MHz, $CDCl_3$): δ 8.12 (s, 1H), 7.59 (d, J = 8.0 Hz, 2H), 7.48−7.38 (m, 3H), 7.34 (d, J = 8.0 Hz, 2H), 7.07−6.99 (m, 4H), 5.48 (dd, J = 10.4, 8.0 Hz, 1H), 5.16 (s, 2H), 4.83 (dd, J = 10.4, 8.0 Hz, 1H), 4.27 (t, J = 8.0 Hz, 1H). ^{13}C NMR (100 MHz, $CDCl_3$): δ 163.8, 162.5, 162.5, 161.4, 160.0, 159.9, 157.8, 148.7, 143.6, 133.3, 133.3, 132.6, 132.5, 132.4, 131.6, 130.3, 130.3, 127.6, 127.0, 115.4, 115.2, 112.1, 112.1, 112.1, 111.9, 111.9, 75.7, 74.7, 70.0. HRMS (ESI): calcd for $C_{23}H_{17}F_3N_2O_2Na$ $[M + Na]^+$ 433.1134, found 433.1130.

*Data for 4-(2-(2,6-Difluorophenyl)-4,5-dihydrooxazol-4-yl)-benzaldehyde O-(4-(Trifluoromethoxy)benzyl) Oxime (**I-i**).* White solid; mp 102−103 °C; yield 65%. ^{1}H NMR (400 MHz, $CDCl_3$): δ 8.13 (s, 1H), 7.59 (d, J = 8.4 Hz, 2H), 7.47−7.42 (m, 3H), 7.35 (d, J = 8.0 Hz, 2H), 7.21 (d, J = 8.0 Hz, 2H), 7.00 (t, J = 8.0 Hz, 2H), 5.48 (dd, J = 10.4, 8.0 Hz, 1H), 5.20 (s, 2H), 4.82 (dd, J = 10.4, 8.0 Hz, 1H), 4.27 (t, J = 8.0 Hz, 1H). HRMS (ESI): calcd for $C_{24}H_{17}F_5N_2O_3Na$ $[M + Na]^+$ 499.1052, found 499.1050.

*Data for 4-(2-(2,6-difluorophenyl)-4,5-dihydrooxazol-4-yl)-benzaldehyde O-(4-(Trifluoromethyl)benzyl) Oxime (**I-j**).* White solid; mp 91−93 °C; yield 56%. ^{1}H NMR (400 MHz, $CDCl_3$): δ 8.15 (s, 1H), 7.62 (d, J = 8.0 Hz, 2H), 7.59 (d, J = 8.0 Hz, 2H), 7.52 (d, J = 8.0 Hz, 2H), 7.47−7.40 (m, 1H), 7.35 (d, J = 8.0 Hz, 2H), 7.00 (t, J = 8.0 Hz, 2H), 5.48 (dd, J = 10.4, 8.0 Hz, 1H), 5.25 (s, 2H), 4.82 (dd, J = 10.4, 8.0 Hz, 1H), 4.27 (t, J = 8.0 Hz, 1H). HRMS (ESI): calcd for $C_{24}H_{17}F_5N_2O_2Na$ $[M + Na]^+$ 483.1102; 483.1104.

*Data for 4-(2-(2,6-Difluorophenyl)-4,5-dihydrooxazol-4-yl)-benzaldehyde O-(4-Chlorobenzyl) Oxime (**I-k**).* Yellow solid; mp 77−80 °C; yield 83%. ^{1}H NMR (400 MHz, DMSO-d_6): δ 8.33 (s, 1H), 7.72−7.62 (m, 3H), 7.44 (s, 4H), 7.37 (d, J = 8.0 Hz, 2H), 7.30 (t, J = 8.0 Hz, 2H), 5.52 (t, J = 9.2 Hz, 1H), 5.17 (s, 2H), 4.86 (t, J = 9.2 Hz, 1H), 4.20 (t, J = 8.4 Hz, 1H), HRMS (ESI): calcd for $C_{23}H_{18}ClF_2N_2O_2$ $[M + H]^+$ 427.1019, found 427.1020.

*Data for 4-(2-(2,6-difluorophenyl)-4,5-dihydrooxazol-4-yl)-benzaldehyde O-(4-tert-Butylbenzyl) Oxime (**I-l**).* Yellow solid; mp 70−73 °C; yield 75%. ^{1}H NMR (300 MHz, $CDCl_3$): δ 8.13 (s, 1H), 7.60 (d, J = 8.1 Hz, 2H), 7.49−7.33 (m, 7H), 7.01 (t, J = 8.1 Hz, 2H), 5.48 (dd, J = 10.2, 8.4 Hz, 1H), 5.18 (s, 2H), 4.83 (dd, J = 10.2, 8.7 Hz, 1H), 4.27 (t, J = 8.4 Hz, 1H), 1.32 (s, 9H). HRMS (ESI): calcd for $C_{27}H_{26}F_2N_2O_2Na$ $[M + Na]^+$ 471.1855, found 471.1858.

General Synthetic Procedure for the Target Compounds II-a−II-n (Scheme 3). *Synthesis of N-(1-(4-(Bromomethyl)phenyl)-2-chloroethyl)-2,6-difluorobenzamide (**9**).*[17,18] To a solution of **6** (5.0 g, 16.1 mmol) in dichloromethane (40 mL) were successively added water (40 mL), potassium bromide (1.9 g, 16.1 mmol), and potassium bromate (1.33 g, 8.05 mmol), and then a solution of concentrated hydrochloric acid (6.1 mL) in water (14 mL) was added dropwise at 0 °C. The reaction mixture was stirred for 25 h until reaction was complete. The organic phase was separated and washed with saturated sodium carbonate. The water phase was extracted with dichloromethane. Then the combined organic phase was washed with brine, dried over anhydrous magnesium sulfate, and concentrated to give a white solid, which was purified by recrystallization using toluene and petroleum ether to give **9** as crystals (3.5 g, yield 56%). Mp: 127−128 °C. ^{1}H NMR (400 MHz, $CDCl_3$): δ 7.45−7.36 (m, 5H), 6.97 (t, J = 8.0 Hz, 2H), 6.62 (d, J = 7.6 Hz, 1H), 5.61−5.57 (m, 1H), 4.49 (s, 2H), 4.04−3.91 (m, 2H).

*Synthesis of Cyclopentanone O-(4-(2-(2,6-Difluorophenyl)-4,5-dihydrooxazol-4-yl)benzyl) Oxime (**II-b**).* To a mixture of cyclopentanone oxime (0.51 g, 5.15 mmol) in DMF (50 mL) was added sodium hydride (0.49 g, 20.59 mmol). The mixture was stirred for 40 min, and then **9** (1.00 g, 2.57 mmol) was added. The reaction mixture was stirred at 0 °C until TLC showed that the reaction was finished. The reaction mixture was extracted with ethyl acetate, and the organic layer was dried over anhydrous magnesium sulfate, filtered, and concentrated to give a reddish brown oil. The crude was purified by flash chromatography on silica gel with petroleum ether and ethyl acetate (v/v = 10:1) to give the target **II-b** as a yellow oil (0.65 g, yield 69%). ^{1}H NMR (400 MHz, $CDCl_3$): δ 7.49−7.31 (m, 1H), 7.38 (d, J = 8.0 Hz, 2H), 7.32 (d, J = 8.0 Hz, 2H), 7.00 (t, J = 8.0 Hz, 2H), 5.47 (dd, J = 10.0, 8.4 Hz, 1H), 5.07 (s, 2H), 4.81 (dd, J = 10.0, 8.4 Hz, 1H), 4.30 (t, J = 8.4 Hz, 1H), 2.44 (t, J = 6.8 Hz, 2H), 2.36 (t, J = 6.8 Hz, 2H), 1.77−1.71 (m, 4H). HRMS (ESI): calcd for $C_{21}H_{21}F_2N_2O_2$ $[M + H]^+$ 371.1566, found 371.1570.

Compounds **II-a** and **II-c−II-n** were synthesized according to a method similar to that for **II-b**.

*Data for Propan-2-one O-(4-(2-(2,6-Difluorophenyl)-4,5-dihydrooxazol-4-yl)benzyl) Oxime (**II-a**).* Yellow oil; yield 52%. ^{1}H NMR (400 MHz, $CDCl_3$): 7.41−7.46 (m, 1H), 7.37 (d, J = 7.6 Hz, 2H), 7.32 (d, J = 7.6 Hz, 2H), 7.00 (t, J = 8.0 Hz, 2H), 5.49−5.44 (m, 1H), 5.06 (s, 2H), 4.83−4.79 (m, 1H), 4.32−4.28 (m, 1H), 1.88 (s, 3H), 1.87 (s, 3H). HRMS (ESI): calcd for $C_{19}H_{19}F_2N_2O_2$ $[M + H]^+$ 367.1229, found 367.1224.

*Data for Cyclohexanone O-(4-(2-(2,6-Difluorophenyl)-4,5-dihydrooxazol-4-yl)benzyl) Oxime (**II-c**).* Yellow oil; yield 40%. ^{1}H NMR (400 MHz, $CDCl_3$): 7.46−7.41(m, 1H), 7.36 (d, J = 8.0 Hz, 2H), 7.32 (d, J = 8.0 Hz, 2H), 7.00 (t, J = 8.4 Hz, 2H), 5.52−5.42 (m, 1H), 5.05 (s, 2H), 4.85−4.78 (m, 1H), 4.32−4.28 (m, 1H), 2.50 (t, J = 6.2 Hz, 2H), 2.24−2.15 (m, 2H), 1.64−1.66 (m, 4H), 1.59−1.61(m, 2H). HRMS (ESI): calcd for $C_{22}H_{23}F_2N_2O_2$ $[M + H]^+$ 385.1722, found 385.1722.

*Data for Cycloheptanone O-(4-(2-(2,6-Difluorophenyl)-4,5-dihydrooxazol-4-yl)benzyl) Oxime (**II-d**).* Yellow oil; yield 46%. ^{1}H NMR (400 MHz, $CDCl_3$): δ 7.46−7.41 (m, 1H), 7.37 (d, J = 8.0 Hz, 2H), 7.32 (d, J = 8.0 Hz, 2H), 7.00 (t, J = 8.0 Hz, 2H), 5.47 (dd, J = 10.4, 8.0 Hz, 1H), 5.06 (s, 2H), 4.81 (dd, J = 10.4, 8.4 Hz, 1H), 4.30 (t, J = 8.4 Hz, 1H), 2.59−2.54 (m, 2H), 2.38−2.34 (m, 2H), 1.73−1.56 (m, 8H). HRMS (ESI): calcd for $C_{23}H_{25}F_2N_2O_2$ $[M + H]^+$ 399.1879, found 399.1875.

*Data for Benzaldehyde O-(4-(2-(2,6-Difluorophenyl)-4,5-dihydrooxazol-4-yl)benzyl) Oxime (**II-e**).* Yellow oil; yield 68%. ^{1}H NMR (400 MHz, $CDCl_3$): 8.13 (s, 1H), 7.64−7.54 (m, 2H), 7.45−7.41(m, 3H), 7.41−7.30 (m, 5H), 7.00 (t, J = 8.4 Hz, 2H), 5.53−5.42 (m, 1H), 5.21 (s, 2H), 4.88−4.76 (m, 1H), 4.27−4.31(m, 1H). HRMS (ESI): calcd for $C_{23}H_{19}F_2N_2O_2$ $[M + H]^+$ 393.1409, found 393.1408.

*Data for 2-Fluorobenzaldehyde O-(4-(2-(2,6-Difluorophenyl)-4,5-dihydrooxazol-4-yl)benzyl) Oxime (**II-f**).* Yellow oil; yield 61%. ^{1}H NMR (300 MHz, $CDCl_3$): δ 8.38 (s, 1H), 7.81 (t, J = 6.6 Hz, 1H), 7.45−7.32 (m, 6H), 7.15−6.96 (m, 4H), 5.48 (dd, J = 10.2, 8.1 Hz, 1H), 5.22 (s, 2H), 4.82 (dd, J = 10.2, 8.4 Hz, 1H), 4.31 (t, J = 8.1 Hz, 1H). ^{13}C NMR (100 MHz, $CDCl_3$): δ 164.1, 162.6, 162.5, 161.7, 160.0, 157.6, 147.93, 147.90, 141.6, 136.8, 134.5, 134.4, 132.5, 132.4, 132.33, 130.28, 130.2, 129.0, 126.8, 123.2, 123.2, 116.9, 116.7, 113.4, 113.2, 112.1, 112.1, 111.8, 76.3, 74.8, 70.1. HRMS (ESI): calcd for $C_{23}H_{18}F_3N_2O_2$ $[M + H]^+$ 411.1315, found 411.1307.

*Data for 3-Fluorobenzaldehyde O-(4-(2-(2,6-Difluorophenyl)-4,5-dihydrooxazol-4-yl)benzyl) Oxime (**II-g**).* Yellow oil; yield 32%. ^{1}H NMR (300 MHz, $CDCl_3$): δ 8.08 (s, 1H), 7.47−7.26 (m, 8H), 7.09−6.93 (m, 3H), 5.47 (dd, J = 10.2, 8.1 Hz, 1H), 5.20 (s, 2H), 4.80 (dd, J = 10.2, 8.4 Hz, 1H), 4.28 (t, J = 8.1 Hz, 1H). ^{13}C NMR (100 MHz, $CDCl_3$): δ 164.1, 162.6, 162.5, 161.7, 160.0, 157.6, 147.93, 147.90, 141.6, 136.8, 134.5, 134.4, 132.5, 132.4, 132.3, 130.3, 130.2, 129.0, 126.8, 123.25, 123.22, 116.9, 116.7, 113.4, 113.2, 112.1, 112.1, 111.8, 76.3, 74.8, 70.1. HRMS (ESI): calcd for $C_{23}H_{18}F_3N_2O_2$ $[M + H]^+$ 411.1315, found 411.1315.

*Data for 4-Fluorobenzaldehyde O-(4-(2-(2,6-Difluorophenyl)-4,5-dihydrooxazol-4-yl)benzyl) Oxime (**II-h**).* Yellow solid; mp 85−87 °C; yield 33%. ^{1}H NMR (400 MHz, $CDCl_3$): δ 8.10 (s, 1H), 7.60−7.52 (m, 2H), 7.47−7.39 (m, 3H), 7.35 (d, J = 8.0 Hz, 2H), 7.07−6.98 (m, 4H), 5.48 (dd, J = 10.4, 8.0 Hz, 1H), 5.19 (s, 2H), 4.82 (dd, J = 10.4, 8.4 Hz, 1H), 4.29 (t, J = 8.0 Hz, 1H). ^{13}C NMR (100 MHz, $CDCl_3$): δ 147.9, 141.6, 137.0, 132.5, 132.4, 132.3, 128.9, 126.8, 115.9, 115.7, 112.1, 111.8, 76.1, 74.8, 70.1. HRMS (ESI): calcd for $C_{23}H_{18}F_3N_2O_2$ $[M + H]^+$ 411.1315, found 411.1313.

*Data for 4-Methoxybenzaldehyde O-(4-(2-(2,6-Difluorophenyl)-4,5-dihydrooxazol-4-yl)benzyl) Oxime (**II-i**).* Yellow oil; yield 46%. ^{1}H NMR (400 MHz, $CDCl_3$): δ 8.08 (s, 1H), 7.51 (d, J = 8.8 Hz, 2H), 7.46−7.39 (m, 3H), 7.34 (d, J = 8.0 Hz, 2H), 7.00 (t, J = 8.0 Hz, 2H), 6.88 (d, J = 8.8 Hz, 2H), 5.50− 5.46 (m, 1H), 5.18 (s, 2H), 4.84−4.79

Table 1. Acaricidal Activities of the Target Compounds against *T. cinnabarinus* in the Laboratory

	acaricidal act. (%) at concn (mg L^{-1})											
	eggs of *T. cinnabarinus*						larvae of *T. cinnabarinus*					
compd	10	1	0.1	0.01	0.001	0.0001	10	1	0.1	0.01	0.001	0.0001
I-a	100	100	100	100	100	90	100	100	100	100	100	80
I-b	100	100	100	100	100	88	100	100	100	100	100	95
I-c	100	100	100	100	100	95	100	100	100	100	100	95
I-d	100	100	100	100	100	85	100	100	100	100	100	90
I-e	100	100	100	100	95	57	100	100	100	100	100	75
I-f	100	100	100	100	100	75	100	100	100	100	100	80
I-g	100	100	100	100	100	85	100	100	100	100	100	75
I-h	100	100	100	100	100	75	100	100	100	100	100	85
I-i	100	100	100	100	100	100	100	100	100	100	100	100
I-j	100	100	100	100	100	100	100	100	100	100	100	100
I-k	100	100	100	100	90	60	100	100	100	100	100	70
I-l	100	100	100	100	100	80	100	100	100	100	100	96
II-a	100	100	100	100	100	78	100	100	100	100	100	85
II-b	100	100	100	100	100	0	100	100	100	100	100	90
II-c	100	100	100	100	97	75	100	100	100	100	100	80
II-d	100	100	100	100	100	0	100	100	100	100	100	95
II-e	100	100	100	100	100	90	100	100	100	100	100	96
II-f	100	100	100	100	100	100	100	100	100	100	100	100
II-g	100	100	100	100	100	90	100	100	100	100	100	100
II-h	100	100	100	100	100	85	100	100	100	100	100	100
II-i	100	100	100	100	100	85	100	100	100	100	100	90
II-j	100	100	100	100	100	86	100	100	100	100	100	85
II-k	100	100	100	100	100	75	100	100	100	100	100	100
II-l	100	100	100	100	100	100	100	100	100	100	100	100
II-m	100	100	100	100	100	100	100	100	100	100	100	100
II-n	100	100	100	100	100	95	100	100	100	100	100	100
etoxazole	100	100	78	56	30	0	100	100	80	65	40	0

(m, 1H), 4.31−4.27 (m, 1H), 3.82 (s, 3H). HRMS (ESI): calcd for $C_{24}H_{21}F_2N_2O_3$ $[M + H]^+$ 445.1334, found 445.1335.

*Data for 4-Chlorobenzaldehyde O-(4-(2-(2,6-Difluorophenyl)-4,5-dihydrooxazol-4-yl)benzyl) Oxime (**II-j**).* Yellow solid; mp 78−80 °C; yield 58%. ^{1}H NMR (400 MHz, $CDCl_3$): 8.07 (s, 1H), 7.50 (d, J = 8.0 Hz, 2H), 7.42 (d, J = 7.6 Hz, 3H), 7.38−7.28 (m, 4H), 6.98 (t, J = 9.2 Hz, 2H), 5.49−5.44 (m, 1H), 5.19 (s, 2H), 4.83−4.78 (m, 1H), 4.30−4.26 (m, 1H). HRMS (ESI): calcd for $C_{23}H_{18}ClF_2N_2O_2$ $[M + H]^+$ 427.1019, found 427.1026.

*Data for 4-(tert-Butyl)benzaldehyde O-(4-(2-(2,6-Difluorophenyl)-4,5-dihydrooxazol-4-yl)benzyl) Oxime (**II-k**).* Yellow oil; yield 58%. ^{1}H NMR (400 MHz, $CDCl_3$): δ 8.11 (s, 1H), 7.50 (d, J = 8.0 Hz, 2H), 7.43−7.36 (m, 5H), 7.33 (d, J = 7.6 Hz, 2H), 6.97 (t, J = 8.4 Hz, 2H), 5.45 (t, J = 9.2 Hz, 1H), 5.19 (s, 2H), 4.79 (t, J = 9.2 Hz, 1H), 4.27 (t, J = 8.2 Hz, 1H), 1.31 (s, 9H). ^{13}C NMR (100 MHz, $CDCl_3$): δ 162.6, 162.5, 160.02, 159.96, 157.6, 153.2, 149.0, 141.5, 137.2, 132.5, 132.4, 132.3, 129.4, 128.9, 126.9, 126.7, 125.7, 112.1, 111.8, 107.5, 107.3, 107.1, 75.9, 74.8, 70.1, 34.8, 31.2. HRMS (ESI): calcd for $C_{27}H_{27}F_2N_2O_2$ $[M + H]^+$ 449.2035, found 449.2032.

*Data for 2-(Trifluoromethyl)benzaldehyde O-(4-(2-(2,6-Difluorophenyl)-4,5-dihydrooxazol-4-yl)benzyl) Oxime (**II-l**).* Yellow oil; yield 70%. ^{1}H NMR (400 MHz, $CDCl_3$): δ 8.51 (d, J = 2.0 Hz, 1H), 8.02 (d, J = 7.6 Hz, 1H), 7.61 (d, J = 7.6 Hz, 1H), 7.50−7.31 (m, 7H), 6.94 (t, J = 8.4 Hz, 2H), 5.46 (dd, J = 10.0, 8.0 Hz, 1H), 5.23 (s, 2H), 4.78 (dd, J = 10.0, 8.4 Hz, 1H), 4.26 (t, J = 8.4 Hz, 1H). ^{13}C NMR (100 MHz, $CDCl_3$): δ 164.1, 162.6, 162.5, 161.7, 160.0, 157.6, 147.93, 147.90, 141.6, 136.8, 134.5, 134.4, 132.5, 132.4, 132.33, 130.28, 130.2, 129.0, 126.8, 123.25, 123.22, 116.9, 116.7, 113.4, 113.2, 112.1, 112.1, 111.8, 76.3, 74.8, 70.1. HRMS (ESI): calcd for $C_{24}H_{18}F_5N_2O_2$ $[M + H]^+$ 461.1283, found 461.1287.

*Data for 3-(Trifluoromethyl)benzaldehyde O-(4-(2-(2,6-Difluorophenyl)-4,5-dihydrooxazol-4-yl)benzyl) Oxime (**II-m**).* Yellow oil; yield 54%. ^{1}H NMR (400 MHz, $CDCl_3$): δ 8.15 (s, 1H), 7.84 (s, 1H), 7.74 (d, J = 7.6 Hz, 1H), 7.61 (d, J = 7.6 Hz, 1H), 7.51−7.39 (m, 4H), 7.36 (d, J = 8.0 Hz, 2H), 7.00 (t, J = 8.0 Hz, 2H), 5.48 (dd, J = 10.0, 8.4 Hz, 1H), 5.23 (s, 2H), 4.82 (dd, J = 10.0, 8.4 Hz, 1H), 4.30 (t, J = 8.4 Hz, 1H). ^{13}C NMR (100 MHz, $CDCl_3$): δ 164.1, 162.6, 162.5, 161.7, 160.0, 157.6, 147.93, 147.90, 141.6, 136.8, 134.5, 134.4, 132.5, 132.4, 132.33, 130.28, 130.2, 129.0, 126.8, 123.25, 123.22, 116.9, 116.7, 113.4, 113.2, 112.1, 112.1, 111.8, 76.3, 74.8, 70.1. HRMS (ESI): calcd for $C_{24}H_{18}F_5N_2O_2$ $[M + H]^+$ 461.1283, found 461.1282.

*Data for 4-(Trifluoromethyl)benzaldehyde O-(4-(2-(2,6-difluorophenyl)-4,5-dihydrooxazol-4-yl)benzyl) Oxime (**II-n**).* Yellow oil; yield 53%. ^{1}H NMR (400 MHz, $CDCl_3$): 8.15 (s, 1H), 7.69 (d, J = 8.0 Hz, 2H), 7.61 (d, J = 8.0 Hz, 2H), 7.44−7.42 (m, 3H), 7.36 (d, J = 8.0 Hz, 2H), 7.00 (t, J = 8.0 Hz, 2H), 5.52−5.44 (m, 1H), 5.23 (s, 2H), 4.87−4.78 (m, 1H), 4.27−4.32 (m, 1H). HRMS (ESI): calcd for $C_{24}H_{18}F_5N_2O_2$ $[M + H]^+$ 461.1283, found 461.1285.

Biological Assay. All biological assays were performed on representative test organisms prepared in the laboratory. Each bioassay was replicated three times at 25 ± 1 °C for the statistical requirements. Percentage mortalities were evaluated according to a percentage scale of 0−100, in which 0 indicates no activity and 100 indicates total kill. When the percentage mortality of the blank control was less than 5%, the results of the treats were directly used. However, if the percentage mortality of the blank control was less than 20% and more than 5%, the results were corrected by means of $V = ((X - Y)/X) \times 100$ (V = value of corrected mortality, X = livability of the blank control, Y = livability of the treat). Etoxazole was evaluated using the entirely same procedure as contrast.[19]

Acaricidal Activity against Eggs and Larvae of Spider Mite (*Tetranychus cinnabarinus*). The acaricidal activities of all the target compounds and the contrast etoxazole against eggs and larvae of spider mite (*T. cinnabarinus*) were measured on the basis of previously reported procedure.[20,21]

dx.doi.org/10.1021/jf500461a | J. Agric. Food Chem. 2014, 62, 3064−3072

Table 2. Effect of Acaricidal Program on Spider Mite in the Field in 2013

trial sites	treatments[a]	% effect of II-l 3 days[b]	7 days	14 days	% effect of etoxazole 3 days	7 days	14 days
		P. citri					
Jingzhou, Hubei Province[c]	10	64	81	82			
	15	74	87	86			
	22	74	88	91	55	80	87
Changsha, Hunan Province[d]	10	70	84	88			
	15	77	88	91			
	22	82	91	94	81	90	93
Guilin, Guangxi Autonomous Region[e]	10	79	95[f]	97[g]			
	15	79	95[f]	98[g]			
	22	83	98[f]	99[g]	85	99[f]	97[g]
		T. cinnabarinus					
Tianjin City[h]	10	85	91	89			
	15	88	92	91			
	22	90	93	92	91	94	92

[a]Treatments: the unit of concentration is mg kg^{-1}. [b]The number of days between spraying insecticides and investigating the effects. [c]The amount sprayed is about 1000 g ha^{-1}. [d]The amount sprayed is about 2000 g ha^{-1}. [e]The amount sprayed is about 900 g ha^{-1}. [f]10 days. [g]15 days. [h]The amount sprayed is about 750 g ha^{-1}.

Affinity of the Target Compounds and Etoxazole Binding to SUR. *Preparation of SUR.* According to our previous reported method, the buffer of SUR was prepared from German cockroach (*Blattella germanica*, *B. germanica*) through the process of chopping, homogenization, centrifugation, etc.[15]

Assay of Binding to SUR. The affinity of the target compounds and etoxazole to SUR was tested using a method similar to our previously published method. After the superior concentration of *N*-phenyl-1-naphthylamine (1-NPN) that acted as fluorescence probe was determinated, ligands such as etoxazole and the target compounds in different concentrations were respectively added to a mixture solution containing SUR, buffer, and 1-NPN. After the mixture was incubated for 1 h at room temperature, the binding affinity was tested by FP.[16]

Evaluation of Acaricidal Activity in the Field. The field trials were carried out between April and June in 2013. The trial against *T. cinnabarinus* in tomato field was performed in the trial area of Institute of Plant Protection, Tianjin Academy of Agricultural Science, Tianjin City, China. Moreover, the trials against *Panonychus citri* (*P. citri*) in orange orchard were performed in the trial area of Institute of Plant Protection, Hunan Academy of Agricultural Science, Changsha City; Citrus Institute of Guangxi, Guilin City; and College of Agricuture, Yangtze University, Jingzhou City. The treated plots of tomatoes or oranges were designed in a random block array with four replicates. The untreated plots served as a blank control. The formulation of compound **II-l** and etoxazole (2.5% emulsifiable concentrates (EC)) was prepared in our research group. They were diluted to 10, 15, or 22 mg kg^{-1} before use. The amount sprayed on the field area varied from 750 to 2000 g ha^{-1} at different sites. The control effects expressed as percentages were arcsine transformed to homogenize variances before analysis, which of different spraying treatments were examined using analysis of variance (ANOVA).[22]

RESULTS AND DISCUSSION

Synthesis. *N*-(2-Chloro-1-(*p*-tolyl)ethyl)-2,6-difluorobenzamide (**6**), as a critical intermediate for all the target compounds, was synthesized from toluene (**1**) as shown in Scheme 1. Ethyl 2-oxo-2-(*p*-tolyl)acetate (**2**) was obtained by Friedel–Crafts acylation of toluene with ethyl 2-chloro-2-oxoacetate. **2** was reacted with hydroxylamine hydrochloride to afford hydroxyimino compound **3**, which was further reduced by sodium borohydride and iodine to give α-amino alcohol **4**. After **4** was reacted with 2,6-difluorobenzoyl chloride to give the corresponding benzamide **5**, the hydroxyl in **5** was converted to chloro group in **6** by thionyl chloride using chloroform as solvent.

The target compounds **I-a**–**I-l** were synthesized from **6** as shown in Scheme 2. The methyl group in **6** was oxidized with CrO_3 in the presence of concentrated sulfuric acid and glacial acetic acid to give aldehyde **7**, which was further reacted with hydroxylamine hydrochloride to afford **8** containing an oxime moiety. **8** was treated with sodium hydride and reacted with a series of alkyl or substituted-benzyl bromide to give 2,4-diphenyl-1,3-oxazolines **I-a**–**I-l** containing oxime ether moiety after nucleophilic cyclization and substitution.

The target compounds **II-a**–**II-n** were also synthesized from compound **6** as shown in Scheme 3. The key intermediate **9** was obtained through bromination of **6** according to the reported method using water as solvent, in which the reaction temperature was strictly maintained between 0 °C and 5 °C to minimize the formation of byproduct. A series of oximes were successfully reacted with **9** in the presence of sodium hydride to give the target compounds **II-a**–**II-n** via cyclization and substitution.

Acaricidal Activity against Eggs and Larvae of *T. cinnabarinus* in the Laboratory. Table 1 shows acaricidal activities of the target compounds **I-a**–**I-l** and **II-a**–**II-n** against eggs and larvae of *T. cinnabarinus*, with etoxazole, the only 2,4-diphenyl-1,3-oxazoline acaricide widely used in China, as a contrast. The result showed that all of the target compounds had much higher activities than etoxazole, as the ovicidal and larvicidal activities of the target compounds **I-a**–**I-l** and **II-a**–**II-n** against *T. cinnabarinus* were all over 90% at 0.001 mg L^{-1}, but etoxazole gave only 30% and 40% respectively at the same concentration. Therefore, the modification at the para site of the 4-phenyl moiety of 2,4-diphenyl-1,3-oxazolines was favorable to the acaricidal activity, which was in accordance with our design ideas. Especially, **I-i** and **I-j**, respectively bearing trifluoromethoxyl and trifluoromethyl group at the para position of the benzyl moiety, showed the highest ovicidal and larvicidal activities at 0.0001 mg L^{-1}. Compounds **II-l** and **II-m**, that bear a trifluoromethyl at the ortho and meta positions of the benzene ring, respectively, had obviously higher ovicidal and larvicidal activities than the others.

dx.doi.org/10.1021/jf500461a | J. Agric. Food Chem. 2014, 62, 3064–3072

Evaluation of Acaricidal Activity of II-l in the Field. Based on the comprehensive analysis of bioactivity, physical properties, synthetic procedure, and so on, compound **II-l**, which had exhibited excellent acaricidal activity in the laboratory, was chosen to evaluate the acaricidal activity in the field. 2.5% EC of **II-l** and etoxazole were separately prepared and evaluated for the control of *P. citri* in Jingzhou City (Hubei Province, South China), Changsha City (Hunan Province, South China), and Guilin City (Guangxi Zhuang Autonomous Region, South China) and *T. cinnabarinus* in Tianjin City (North China). Part of the result of the field trials is shown in Table 2. It was shown that **II-l** at the concentration of 22 mg kg^{-1} had a better control effect than etoxazole at the same concentration. The data of the field trial in Jingzhou showed that, 3 days after the spray, the control efficiency of **II-l** against *P. citri* at 22 mg L^{-1} was 75%, whereas that of etoxazole was 55% at the same condition; this phenomenon suggested that the speed of action of **II-l** was faster than that of etoxazole. Fourteen days after the spray, the control efficiency of **II-l** and etoxazole was respectively 91% and 87%. The control efficiency of **II-l** and etoxazole against *P. citri* in Changsha and Guilin was similar, if not identical, to that in Jingzhou. In Tianjin, the control efficiency of both **II-l** and etoxazole against *T. cinnabarinus* at 22 mg L^{-1} was 92% when tested 14 days after the spray. Therefore, it was suggested that **II-l** could be considered as an alternative to the excessively employed acaricide for further development on the basis of the field trials.

Affinity of the Target Compounds Binding to SUR. The binding affinity of each series of the target compounds to the isolated SUR were tested by FP method with etoxazole as a contrast.[23] Since the accurate determination of concentration and stability of the SUR have not been realized up to now, in order to make the data comparable and minimize the errors, the binding affinity was assayed within the same set of experiments and containing 5 replicates. In the paper, that is to say, the target compounds **I-a**–**I-l** and etoxazole were tested with the same vesicle prepared, and so were compounds **II-a**–**II-n**.

In the buffer solution having the most proper concentration of 1-NPN-SUR, each of the target compounds **I-a**–**I-l** and etoxazole in different concentrations was separately added, and the FP data were recorded (Figure 2). From the figure we could find all the FP data were related to the concentration of the added compounds, which meant all these compounds could replace 1-NPN and then bind with SUR by themselves. The affinity with SUR is relevant to the value of the FP: the more decreased polarization was tested, the stronger affinity was exhibited. Thus from the figure, the order of affinity of these compounds was approximately deduced as **I-i** > **I-j** > **I-d** > **I-f** > **I-b** > **I-c** > **I-l** > **I-a** > **I-e** > **I-g** > **I-h** > **I-k** > etoxazole. The result indicated that the binding affinity to SUR of the target compounds **I-a**–**I-l** in vitro was almost consistent with their acaricidal activity against *T. cinnabarinus* in vivo, since **I-i** and **I-j** showed the strongest acaricidal activity against eggs and larvae of *T. cinnabarinus* in vivo, and **I-k** exhibited the lowest activity among the target compounds **I-a**–**I-l**.

Likewise, the FP data against the concentration of **II-a**–**II-n** and etoxazole are shown in Figure 3, from which the affinity order was deduced as **II-m** > **II-l** > **II-f** > **II-g** > **II-k** > **II-n** > **II-h** > **II-j** > **II-e** > **II-i** > **II-a** > **II-c** > **II-d** > **II-b** > etoxazole. The result was also almost consistent with the acaricidal activity against *T. cinnabarinus* in vivo, supported by the fact that **II-m** and **II-l** had the highest acaricidal activity, and **II-a**–**IId** had relatively lower activity in vivo. Therefore, it was verified that

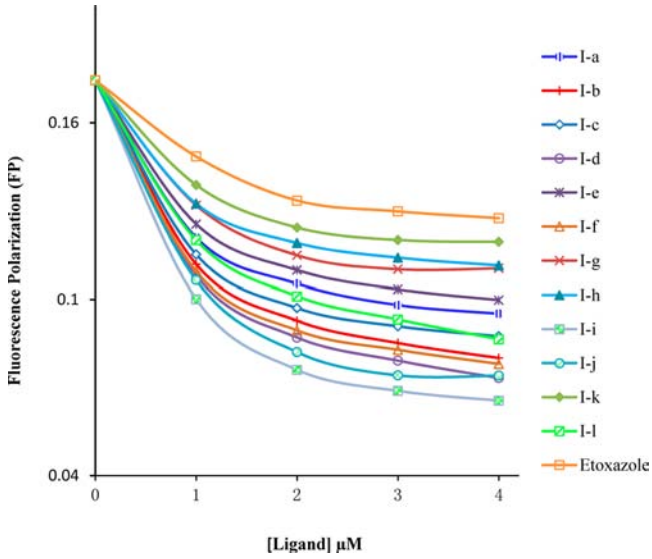

Figure 2. Binding curves of compounds **I-a**–**I-l** and etoxazole to sulfonylurea receptor.

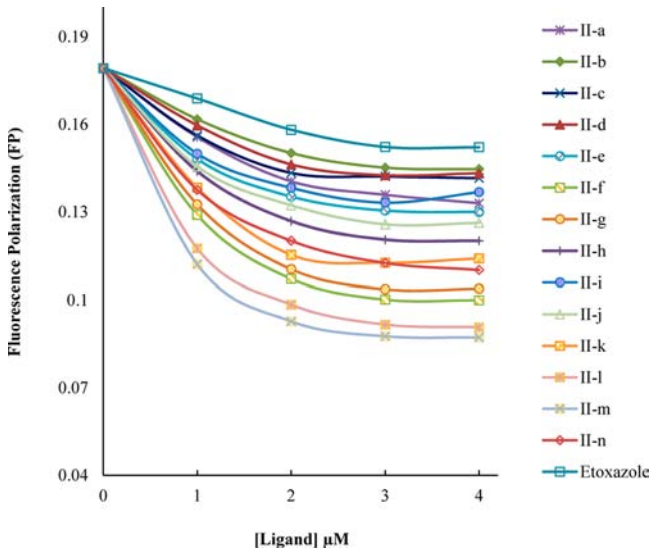

Figure 3. Binding curves of the compounds **II-a**–**II-n** and etoxazole to sulfonylurea receptor.

the target compounds and etoxazole could act on the site of SUR to suppress the chitin synthesis in mite body.

In summary, two series of novel 2,4-diphenyl-1,3-oxazoline compounds both containing an oxime ether group were designed and synthesized on the basis of etoxazole, flucycloxuron, and NK-17. The bioassay results indicated that all of the target compounds exhibited considerable acaricidal activities against *T. cinnabarinus* in the laboratory. Especially, compound **II-l**, 2-(trifluoromethyl)benzaldehyde *O*-(4-(2-(2,6-difluorophenyl)-4,5-dihydrooxazol-4-yl)benzyl) oxime, showed 100% ovicidal activities and 100% larvicidal activities at 0.0001 mg L^{-1}, much higher than etoxazole, thus it was selected to proceed to field trial. The field trial results from four sites in different parts of China clearly showed that **II-l** had nearly equivalent activity with etoxazole against *T. cinnabarinus* and *P. citri* at the same doses. Furthermore, when the fluorescence polarization method was employed to study the action mechanism, the target compounds and etoxazole were all

dx.doi.org/10.1021/jf500461a | J. Agric. Food Chem. 2014, 62, 3064–3072

speculated to act on the SUR then resulting in the suppression of chitin biosynthesis. Because of the easy preparation, good acaricidal activity, and unique mechanism, the new 2,4-diphenyl-1,3-oxazoline compound was expected to be developed as a promising candidate. Further research on acute toxicity, field residues, and their inhibitory activities against resistant mite species is ongoing and will be reported in the future.

AUTHOR INFORMATION

Corresponding Author

*E-mail: liuyuxiu@nankai.edu.cn (Yuxiu Liu); yangxl@cau.edu.cn (Xinling Yang); wangqm@nankai.edu.cn (Qingmin Wang).

Author Contributions

Yongqiang Li, Chaojie Li, Yanlong Zheng, Xingcun Wei, Qiaoqiao Ma, and Peng Wei contributed equally to this work.

Funding

This work was supported by the National Key Project for Basic Research (2010CB126100) and the National Natural Science Foundation of China (21132003, 21372131, 21102077) and the National 12th Five-year Key Technology R&D Program (2011BAE06B08-04).

Notes

The authors declare no competing financial interest.

REFERENCES

(1) Van Daalen, J. J.; Meltzer, J.; Mulder, R. Selective insecticide with a novel mode of action. *Naturwissenschaften* **1972**, *59*, 312−313.

(2) Oberlander, H.; Silhacek, D. L. Mode of action of insect growth regulators in Lepidopteran tissue culture. *Pestic. Sci.* **1998**, *54*, 300−302.

(3) Qian, X. H.; Lee, P. W.; Cao, S. China: Forward to the Green Pesticides via a Basic Research Program. *J. Agric. Food. Chem.* **2010**, *58*, 2613−2623.

(4) Suzuki, J.; Ishida, T.; Shibuya, I.; Toda, k. Development of a new acaricide, Etoxazole. *J. Pestic. Sci.* **2001**, *26*, 215−223.

(5) Suzuki, J.; Ishida, T.; Kikuchi, Y.; Ito, Y.; Morikawa, C.; Tsukidate, Y.; Tanji, I.; Ota, Y.; Toda, K. Synthesis and activity of novel acaricidal/insecticidal 2,4-diphenyl-1,3-oxazolines. *J. Pestic. Sci.* **2002**, *27*, 1−8.

(6) Nauen, R.; Smagghe, G. Mode of action of etoxazole. *Pest Manage. Sci.* **2006**, *62*, 379−382.

(7) Leeuwen, T. V.; Demaeght, P.; Osborne, E. J.; Dermauw, W.; Gohlke, S.; Nauen, R.; Grbic, M.; Tirry, L.; Merzendorfer, H.; Clark, R. M. Population bulk segregant mapping uncovers resistance mutations and the mode of action of a chitin synthesis inhibitor in arthropods. *Proc. Natl. Acad. Sci. U.S.A.* **2012**, *109* (12), 4407−4412.

(8) Nakagawa, Y.; Izumi, K.; Oikawa, N.; Kurozumi, A.; Iwamura, H.; Fujita, T. Quantitative structure-activity relationships of benzoylphenylurea larvicides: VII. Separation of effects of substituents in the multisubstituted anilide moiety on the larvicidal activity against Chilo suppressalis. *Pestic. Biochem. Physiol.* **1991**, *40* (1), 12−26.

(9) Minakuchi, C.; Suzuki, J.; Toda, K.; Akamatsu, M.; Nakagawa, Y. Estimation of the hydrophobicity of 2,4-diphenyl-1,3-oxaline analogs and QSAR analysis of their ovicidal activity against Tetranycus urticae. *Bioorg. Med. Chem. Lett.* **2006**, *16*, 4080−4084.

(10) Suzuki, J.; Tanji, I.; Ota, Y.; Toda, K.; Nakagawa, Y. QSAR of 2,4-diphenyl-1,3-oxazolines for ovicidal activity against the two-spotted spider mite Tetranychus urticae. *J. Pestic. Sci.* **2006**, *31* (4), 409−416.

(11) Roy, K.; Paul, S. Exploring 2D and 3D QSARs of 2,4-Diphenyl-1,3-oxazolines for Ovicidal Activity Against Tetranychus urticae. *QSAR Comb. Sci.* **2009**, *28*, 406.

(12) Liu, Y. X.; Wei, X. C.; Li, Y. Q.; Yang, N.; Wang, Q. M. Design, synthesis and acaricidal/insecticidal activities of etoxazole analogues. *New J. Chem.* **2013**, *37*, 1803−1810.

(13) Lee, C. W.; Chung, J. D. Characteristics and ring-opening isomerization polymerization of 2-(1,3,3-trimethyl-6-azabicyclo[3,2,1]-oct-6-yl)-4,5-dihydro-1,3-oxazoline (TAO). *Polymer (Korea)* **2012**, *36* (3), 262−267.

(14) Yang, X. L.; Wang, D. Q.; Chen, F. H.; Zhang, Z. N. The synthesis and larvicidal activity of N-aroyl-N′-(5-aryl-2-furoyl)ureas. *Pestic. Sci.* **1998**, *52*, 282−286.

(15) Abo-Elghar, G. E; Fujiyoshi, P.; Matsumura, F. Significance of the sulfonylurea receptor (SUR) as the target of diflubenzuron in chitin synthesis inhibition in Drosophila melanogaster and Blattella germanica. *Insect Biochem. Mol. Biol.* **2004**, *34*, 743−752.

(16) Li, Y. Q.; Qin, Y. G.; Yang, N.; Sun, Y. F.; Yang, X. L.; Sun, R. F.; Wang, Q. M.; Ling, Y. Studies on insecticidal activities and action mechanism of novel benzoylphenylurea candidate NK-17. *PLoS One* **2013**, *8* (6), e66251.

(17) Adimurthy, S.; Ghosh, S.; Patoliya, P. U.; Ramachandraiah, G.; Agrawal, M.; Gandhi, M. R.; Upadhyay, S. C.; Ghosh, P. K.; Ranu, B. C. An alternative method for the regio- and stereo selective bromination of alkenes, alkynes, toluene derivatives and ketones using a bromide/bromate couple. *Green Chem.* **2008**, *10*, 232−237.

(18) Kikuchi, D.; Sakaguchi, S.; Ishii, Y. An alternative method for the selective bromination of alkylbenzenes using $NaBrO_3/NaHSO_3$ reagent. *J. Org. Chem.* **1998**, *63*, 6023−6026.

(19) Abbott, W. S. A method of computing the effectiveness of an insecticide. *J. Econ. Entomol.* **1925**, *18*, 265−267.

(20) Kuhn, D. G.; Kameswaran, V. Insecticidal, acaricidal and molluscicidal 1-(substituted)thioalkylpyrroles. U.S. Patent 5,302,383, 1993.

(21) Wang, Y. J.; Ou, X. M.; Pei, H.; Lin, X. M.; Yu, K. Toxicities of novel insecticide chlorfenpyr against several insects in lab. *Agrochem. Res. Appl.* **2006**, *10*, 20−23.

(22) Siegel, S.; Castellan, N. J., Jr. *Nonparametric statistics for the behavioral sciences*; McGraw-Hill Book Co.: Singapore, 1988.

(23) Harris, A.; Cox, S.; Burns, D.; Norey, C. Miniaturization of fluorescence polarization receptor-binding assays using CyDye-labeled ligands. *J. Biomol. Screen.* **2003**, 8410−8420.

attention has been paid to new methods such as those based on multidimensional systems comprising liquid chromatography (LC) to separate peptides or proteins and MS to analyze them.[15] Chromatography and MS-based techniques have become much more widely used for analyses of proteins and peptides.[16−35]

IDMS is a primary method in the metrological field. It allows highly accurate and precise measurements of various substances and has been used widely since its development in the 1980s.[17−19] It has been used to detect and quantify drugs, hormones, pesticides and veterinary drug residues in serum, and other organic small molecules with high accuracy. With the development of the life science and biotechnology industries, IDMS methods have been further developed to quantify proteins,[21−35] nucleic acids,[36] and other biological macromolecules.[37−40] Especially, IDMS has been successfully applied into analyses with milk powders and shows several advantages. Zhang et al. developed an IDMS method to quantify12 mycotoxins in milk-based infant formula and foods. The average recoveries in fortified milk, milk-based infant formula, milk powder, and baby yogurt ranged from 89% to 126% with CVs of <20%. The validated method provides sufficient selectivity, sensitivity, accuracy, and reproducibility to screen for aflatoxin M1 at nanogram per kilogram concentrations and other mycotoxins, without using standard addition or matrix-matched calibration to compensate for matrix effects.[20] In 2008, Burkitt et al. first reported the accurate quantification of a protein in solution by an IDMS method.[21] In that study, the absolute concentration of a protein was determined using an SI-traceable peptide quantification method in which a standard peptide was quantified by amino acid analysis with IDMS, and amino acid standards of known purity were used. This allowed fully SI-traceable measurements of protein concentration. However, this method was not used to determine the protein content in mixtures or complex matrices. In another study, researchers enzymatically digested a protein into polypeptides; then, using an isotope-labeled peptide as an internal standard, they measured the specific peptide content by an IDMS method and further calculated the total protein content. This allowed them to accurately determine the protein content in mixtures and matrices.[22]

εIn recent years, LC−MS/MS and IDMS have been used to detect protein allergens in food. Weber et al. developed a LC−MS/MS method of the tryptic digest of a cleaned-up food matrix extract for the detection of milk allergens.[23] Careri et al. developed MS-based technology for the detection and quantification of contaminant or allergen traces.[24]Cryar developed IDMS method for the analysis of lysozyme in wine and the production of CRMs.[25] To date, there have been no reports on quantitation of β-LG in milk powders by HPLC−IDMS. Development of an SI-traceable quantification method for β-LG in milk powders can improve the accuracy and reliability of β-LG detection. Such a method would benefit the development of a β-LG CRM and improve the comparability of β-LG quantification results among different laboratories.

MATERIALS AND METHODS

Chemicals and Reagents. DL-Dithiothreitol (DTT), iodoacetamide (IAM), ammonium bicarbonate, D_3-leucine, perfluoroheptanoic acid, β-LG, and trypsin were purchased from Promega Co.. The specific activity of the trypsin is 18704 U/mg (BAEE as substrate). The trypsin is diluted in 50 mM acetic acid with a protein concentration of 0.5 mg/mL. RapiGest SF was obtained from Waters Co. Ltd. (Milford, MA, USA).The peptides of TPEVDDEALEK (TK-11) and isotope-labeled TPEVDDEAL*EK (L-TK-11, where L* is D_3-Leu) were synthesized by GL Biochem. Co. Ltd. (Shanghai, China). The CRMs of proline, valine, leucine, and phenylalanine were obtained from the National Institute of Metrology (NIM, Beijing, China). Milk powder samples were obtained from domestic manufacturers.

Reagent Preparation. To prepare 50 mmol/L ammonium bicarbonate (pH = 8.0), 0.179 g of ammonium bicarbonate was dissolved in 45 mL of water, and then the pH was adjusted to 8.0 with aqueous ammonia. To prepare 1 mg/mL RapiGest SF, approximately 1 mg of solid RapiGest SF was dissolved in 1 mL of 50 mmol/L ammonium bicarbonate buffer. To prepare 0.1 mol/L DTT: 0.154 g of DTT was dissolved in 0.01 mol/L NaOAc (pH = 5.2) and then filtered through a 0.22 μm filter. To prepare 0.1 mol/L IAM: 0.185 g of IAM was dissolved in 10 mL of pure water. The peptides and β-LG solutions were prepared as follows: each peptide/protein (TK-11, L-TK-11, and β- LG) was dissolved in pure water containing 0.1% formic acid to a final concentration of 1 mg/mL. The peptide solutions were distributed into 1.5 mL centrifuge tubes and stored at −80 °C until analysis.

Peptide or Protein Hydrolysis. 1 mg of TK-11 or β-LG was weighed with a balance capable of 1 μg imprecision, and it was dissolved in about 1 g of 0.1 mol/L HCl. The mass of the HCl was weighed with a balance capable of 0.01 mg imprecision. 100 μL of TK-11(1 mg/mL) or β-LG (1 mg/mL) was added to a 2 mL ampule and lyophilized. Then 500 μL of 6 mol/L HCl was added. The solution was flushed with nitrogen for 2 min before sealing. Then the ampules were put into an oven and hydrolysis was carried out at 110.0 ± 0.5 °C for 48 h for TK-11 and for 24 h for β-LG. Isotope-labeled amino acids were added to the mixture after hydrolysis, and then the mixture was flushed with nitrogen and dried. Finally, it was reconstituted with 0.1% formic acid and filtered for instrumental analysis.

Enzymatic Digestion. Approximately 2.7 mg of β-LG was dissolved in 600 μL of RapiGest SF buffer. Then, 30 μL of 0.1 mmol/L DTT was added and the mixture was incubated in a water bath at 60 °C for 30 min before addition of 60 μL of 0.1 mol/L IAM. The mixture was cooled to room temperature and then kept in the dark for 40 min. Then, 30 μL of trypsin was added and the mixture was kept at 37 °C for 48 h for digestion. An additional 5 μL of trypsin was added to the digestion mixture every 24 h. The proteolysis reaction was terminated by adding 200 μL of 0.1 mmol/L HCl. The mixture was kept at −80 °C until instrumental analysis.

Protein Identification. The digested samples were analyzed by a Synapt G1 mass spectrometer (UBA171, Waters) with a capture column (5 μm Symmetry C_{18}, 180 μm × 20 mm) and an analytical column (1.7 μm BEH130 C_{18}, 100 μm × 100 mm). The column temperature was 35 °C and the sample temperature was 8 °C during analysis. The injection volume was 2 μL, and the flow rate was 0.5 μL/min. The mobile phase A was pure water from a Milli Q system with 0.1% formic acid, and the mobile phase B was MeCN. The sample loading time was 3 min, and the trapping flow rate was 5 μL/min. The separation was performed as per the gradient shown in Table S1 in the Supporting Information.The total runtime was 60 min.

The operating parameters of the nano-ESI source were set as follows: positive ionization mode; capillary voltage, 3.0 kV; source temperature, 100 °C; desolvation nitrogen gas flow rate, 500 L/h; nano gas pressure, 2.0 bar; sampling cone voltage, 30 V. The mass to charge ratios of the target fragment ions were captured from m/z 100 to m/z 2000. The data were processed with MassLynx 4.1, and the data acquisition time was from 8 to 37 min.

Protein identification was carried out with Proteinlynx, with the following parameters: databank was Swiss-Prot; fixed modification was carbamidomethyl C; variable modifications were deamidation N, deamidation Q, and oxidation M; minimum fragment ion matches per peptide was 3; minimum fragment ion matches per protein was 7; minimum peptide matches per protein was 1.

Determination of the Mass Fraction of Pure TK-11 or β-LG in Solid Powder by Acid Hydrolysis. The mass fraction of pure peptide or pure protein in the solid powder was determined by HPLC−IDMS after acid hydrolysis. The exact mass fraction of proline,

valine, leucine, or phenylalanine in the hydrolyzed mixture was quantitatively determined by HPLC−IDMS with amino acid CRMs as standards and relative isotope-labeled amino acids as internal standards. An Agilent ZORBAX SB-Aq column (3.5 μm, 2.1 × 150 mm) was used for separation. The column temperature was 40 °C during analysis. The injection volume was 20 μL, and the flow rate was 0.2 mL/min. The mobile phase A was 0.8 mmol/L perfluoroheptanoic acid with 0.05% TFA, and the mobile phase B was MeCN. The gradient is shown in Table S2 in the Supporting Information.

A Thermo-Finnigan TSQ quantum triple quadrupole mass spectrometer (San Jose, CA, USA) equipped with an ESI ion source was used for detection. The ESI ionization was operated in positive mode, and the multiple reaction monitor (MRM) mode was used for detection of Pro (116 → 70), L-Pro (121 → 74), Val (118 → 72), L-Val (123 → 76), Leu (132 → 86), L-Leu (142 → 96), Phe (166 → 120), and L-Phe (175 → 128). The flow rate of sheath gas and auxiliary gas was 30 and 10 arbitrary units (au), respectively. The capillary temperature was set at 270 °C, and the spray voltage was set at 3000 V.

The mass fraction of each amino acid was calculated according to formula 1:[22,27,41]

$$c = \frac{Pm_s[R_s(I_1 - I_2) - (I_1R_2 - I_2R_1)}{M(R_1 - R_2)} \quad (1)$$

where c is the mass fraction of each amino acid (g/g); m_s is the absolute mass of isotope-labeled amino acid in the sample solution (g); R_s is the ratio of the peak area of an amino acid to its isotope-labeled one of the sample; I_1 is the mass ratio of an amino acid to its isotope-labeled one of the high-level standard; I_2 is the mass ratio of an amino acid to its isotope-labeled one of the low-level standard; R_1 is the peak area ratio of an amino acid to its isotope-labeled one of the high-level standard; R_2 is the peak area ratio of an amino acid and its isotope-labeled one of the low-level standard; M is the absolute mass of the sample (g); and P is the purity of the amino acid CRM.

The mass fraction of pure TK-11 or pure β-LG in the solid was calculated according to formula 2, as follows:

$$c = \frac{c_1 \cdot MW_P}{c_0 \cdot MW_{AA} \cdot N} \quad (2)$$

where c is the mass fraction of the pure peptide or protein in the solid matrix; c_1 is the mass fraction of each amino acid (g/g); MW_P is the molecular mass of the peptide or protein; MW_{AA} is the molecular mass of the amino acid; N is the number of specific amino acids in one peptide or protein molecule; and c_0 is the gravimetric prepared solid concentration (g/g).

Determination of the Mass Fraction of β-LG in Milk Powders by Proteolysis. 0.1 g of milk powder was dissolved in 0.8 mL of commercial extraction buffer (R-Biopharm, R4902). The solution was incubated in a water bath at 60 °C for 15 min and was shaken every 2 min. Then 15.2 mL of 50 mmol/L ammonium bicarbonate was added into the sample and was centrifuged at 8437*g* for 20 min. 3 mL of the supernatant was taken out and diluted three times with 50 mmol/L of ammonium bicarbonate. 2.7 g of the diluted sample solution was added into the ultrafiltration tube with the cutoff molecular mass of 3 kDa, and was centrifuged at 6500*g* for 15 min to remove the extraction buffer. Then the sample was rinsed 5 times by adding 1 mL of 50 mmol/L ammonium bicarbonate and centrifuging. Finally, 100 μL of L-TK-11 solution was added into the ultrafiltration tube and mixed well with the sample. 100 μL of the solution was taken out for proteolysis according to the protocol described in Enzymatic Digestion except the proteolysis time was 16 h.

A ZORBAX SB-Aq column (3.5 μm particle size, 2.1 × 150 mm; Agilent, Palo Alto, CA, USA) was used to separate the digested mixture. The column temperature was 40 °C during the analysis. The injection volume was 10 μL, and the flow rate was 0.2 mL/min. The mobile phase A was water containing 0.1% formic acid, and the mobile phase B was acetonitrile containing 0.1% formic acid. The gradient is shown in Table S3 in the Supporting Information.

The Thermo-Finnigan TSQ equipped with an ESI ion source was used for IDMS analysis. The ESI ionization was operated in positive mode, and selected ion mode (SIM) was used to monitor TK-11 (m/z = 623) and L-TK-11 (m/z = 625). The flow rate of sheath gas and auxiliary gas was 30 and 10 arbitrary units (au), respectively. The capillary temperature was set at 270 °C, and the spray voltage was set at 3000 V.

The mass fraction of TK-11 in the proteolysis mixture was calculated according to formula 1, where c is the mass fraction of TK-11 in the proteolysis mixture (g/g); m_s is the mass of L-TK-11 added to the sample (g); R_s is the peak area ratio of TK-11 to L-TK-11 of the sample; I_1 is the mass ratio of TK-11 to L-TK-11 of the high-level standard; I_2 is the mass ratio of TK-11 to L-TK-11 of the low-level standard; R_1 is the peak area ratio of TK-11 to L-TK-11 of the high-level standard; R_2 is the peak area ratio of TK-11 to L-TK-11 of the low-level standard; M is the mass of the proteolysis sample (g); and P is the mass fraction of pure TK-11 determined by the HPLC−IDMS method.

The mass fraction of β-LG in the solid matrix was calculated according to formula 3:

$$c = \frac{c_1 \cdot MW_P}{c_0 \cdot MW_{pep}} \quad (3)$$

where c is the mass fraction of β-LG in the solid matrix (g/g); c_1 is the mass fraction of TK-11 (g/g); MW_{pep} is the molecular mass of TK-11; MW_P is the molecular mass of β-LG; and c_0 is the gravimetric prepared milk concentration (g/g).

RESULTS AND DISCUSSION

Selection of a Specific Peptide for β-LG Quantification. As different protein molecules may produce the same peptides after proteolysis, a specific peptide is generally filtered and selected for quantification to avoid interference from other peptides. To select a peptide specific to β-LG, pure β-LG was digested with trypsin and the peptides were analyzed. The total ion chromatogram and identified TK-11 are shown in Figure S1 in the Supporting Information. The identified peptides covered 59% for the amino acid sequence of the target protein. Among all the identified peptides, TK-11 (TPEVDDEALEK) had the strongest signal intensity and the peptide sequence was only found in the Swiss-Prot entries of LACB_BOVIN (P02754) and LACB_BUBBU (P02755), which show a difference of two amino acid residues. Therefore, TK-11 was chosen for peptide-based quantification of β-LG.

Optimization of Hydrolysis Times for TK-11 and β-LG. The mass fraction of TK-11 or β-LG was determined by amino acid analysis coupled with the IDMS method. However, the hydrolysis time should be optimized to ensure the complete hydrolysis of the target peptide or protein. TK-11 and β-LG were hydrolyzed according to the above protocol. The ratio of each amino acid to its isotope-labeled one vs hydrolysis time was plotted to determine the optimum hydrolysis time (Figure S2a,b in the Supporting Information).

The ratio rapidly increased at the early stage of the hydrolysis reaction (Figure S2 in the Supporting Information). For TK-11, the ratio reached a plateau after 48 (Figure S2 in the Supporting Information), and 48 h was therefore selected as the optimum time for TK-11 hydrolysis. Similarly, 24 h was selected as the best time for β-LG hydrolysis.

Determination of the Mass Fraction of Pure TK-11 or β-LG in a Solid Matrix. We used nine vials of TK-11 or β-LG for mass fraction determination by the IDMS procedure. The average mass fraction of TK-11 was 79.1% with a relative standard deviation of 5.6%, and the average mass fraction of β-LG was 82.9% with a relative standard deviation of 3.7%.

Optimization of Proteolysis Conditions for β-LG. The proteolysis reaction reaches a chemical equilibrium. To ensure that the reaction proceeded efficiently, we optimized the following conditions: digestion time, amount of denaturing agent and reductive alkylation reagent, and time and temperature of reductive alkylation.

To optimize the digestion time, β-LG was digested according to the above protocol for various times. The ratio of TK-11 to L-TK-11 vs proteolysis time was plotted to determine the optimum time for proteolysis (Figure 1). As shown in Figure 1,

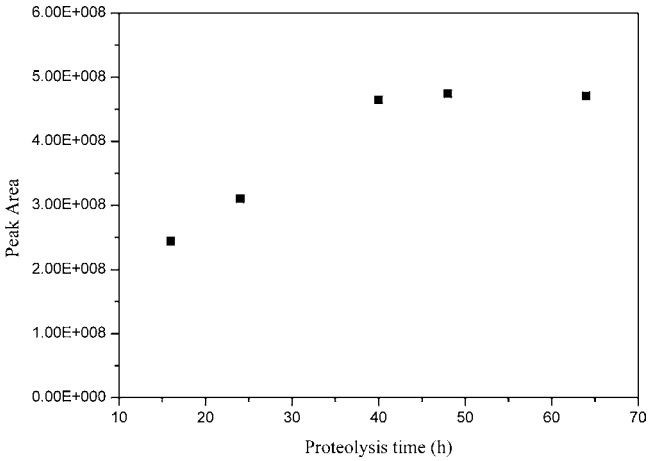

Figure 1. Optimization of proteolysis time for β-LG.

the proteolysis reaction occurred rapidly in the early stages, but reached a plateau after 48 h. Therefore, the proteolysis time of 48 h was used for proteolysis of β-LG.

Next, we optimized the amounts of denaturing agent and reductive alkylation reagent. We conducted four parallel experiments with different amounts of denaturing agent and reductive alkylation reagent (Table 1). As shown in Figure S3

Table 1. Optimization of Amounts of Denaturing Agent and Reductive Alkylation Reagent for Hydrolysis Reaction

	amount of reagent (μL)			
reagent	expt 1	expt 2	expt 3	expt 4
0.1% RapiGest SF	100	100	×[a]	×
DTT	5	×	5	×
IAM	10	×	10	×
trypsin	5	5	5	5

[a]×: Reagent omitted.

in the Supporting Information, the maximum peak area was observed in Experiment No. 3, indicating that those experimental conditions gave the best proteolysis efficiency for β-LG. Experiment No. 3 contained reducing reagents but lacked denaturants.

Then, we optimized the amount of reductive reagent by digesting β-LG according to the above protocol with various amounts of DTT. The peak area of TK-11 vs quantity of the reducing reagent was plotted to determine the optimum amount of DTT (Figure S4 in the Supporting Information).

As shown in Figure S4 in the Supporting Information, the peak area of TK-11 increased with increasing amounts of DTT. The maximum peak area was observed in the reaction containing 35 μL of DTT solutions; therefore, this amount of DTT was used for the proteolysis reactions.

Finally, we optimized the temperature by conducting the reductive alkylation reaction at different temperatures for various times (Figure S5 in the Supporting Information). As shown in Figure S5 in the Supporting Information, the optimum temperature and duration of the reductive alkylation reaction were 60 °C and 15 min, respectively.

Determination of Proteolytic Efficiency. As the proteolysis reaction reaches a chemical equilibrium, or the inhibitors may exist in the extraction buffer, the proteolysis efficiency of β-LG cannot reach 100% even in the optimized digestion conditions.

To determine the proteolytic efficiency of pure β-LG, the mass fraction of β-LG in solid was simultaneously determined by amino acid based IDMS and peptide-based IDMS. As amino acid analysis is a traditional method for protein quantitation, the proteolytic efficiency can be calculated by comparing the ratio of the mass fraction obtained by peptide-based IDMS with that obtained by amino acid based IDMS, assuming complete hydrolysis. The proteolytic efficiency was determined to be 75.7% with a relative standard deviation of 3.0% for seven repeats.

However, the inhibitors in the extraction buffer will depress the proteolytic efficiency greatly. Therefore, ultrafiltration was performed to remove the extraction buffer with 50 mmol/L ammonium bicarbonate to avoid the inhibitory effect of the extraction buffer, which was described in Determination of the Mass Fraction of β-LG in Milk Powders by Proteolysis. In order to determine the proteolytic efficiency of β-LG in milk powders when extraction buffer was applied, some amount of pure β-LG was taken out and treated as the sample according to the protocol described in the section Determination of the Mass Fraction of β-LG in Milk Powders by Proteolysis. Then the proteolytic efficiency can be calculated by comparing the ratio of the mass fraction obtained by peptide-based IDMS to the gravimetric prepared value. However, due to the different β-LG concentrations and different operations, the proteolytic efficiency varied for each run. Nine runs for 3 β-LG levels (0.01 g/g, 0.05 g/g, 0.10 g/g) were carried out for proteolytic efficiency investigation. The proteolytic efficiency was from 6.1% to 15.1% with an average of 11.0% (Table 2). Compared with the proteolytic efficiency of 38% of pure β-LG with digestion time of 16 h, the depression of the inhibitors was also significant even after buffer exchange.

Method Performance of the Peptide-Based β-LG Quantitation by HPLC–IDMS. The performance of the

Table 2. The Spiked Recoveries of Three Milk Powders with Different β-LG Levels

sample no.	level (g/g)	recovery (%) (n = 7)	CV (%) (n = 7)	proteolytic effic (%)
1	0.01	90.0–108.5	8.4	10.7
	0.05	86.2–98.3	4.1	15.1
	0.1	108.1–117.7	2.8	11.1
2	0.01	92.7–111.6	7.1	10.2
	0.05	86.0–98.6	5.1	12.8
	0.1	89.4–108.0	6.5	6.1
3	0.01	96.9–118.3	9.0	14.6
	0.05	96.2–108.7	5.2	10.0
	0.1	96.2–110.1	5.5	8.8

peptide-based HPLC−IDMS was evaluated for quantitation of both pure β-LG and β-LG in milk powder.

For the quantitation of pure β-LG in solution, a pure β-LG CRM developed by NIM was used to evaluate the accuracy and repeatability of the method. The bias, which can reflect the accuracy of the method, was calculated according to the formula 4

$$A = \frac{|c - c_0|}{c_0} \times 100\% \quad (4)$$

where c is the measured mass fraction of β-LG by TK-11 coupled with the IDMS method (g/g); c_0 is the certified value of β-LG (g/g); and A is the relative bias. The relative bias was determined to be 1.9%, and the relative standard deviation was 3.0% for seven repeats. The limits of detection (LOD) and quantification (LOQ) were calculated based on the S/N ratio of 3 and 10 by single point calibration shown in formula 5, which were 4.8×10^{-8}g/g and 1.6×10^{-7}g/g pure β-LG in solution, respectively. The relative expanded uncertainty was evaluated[42] and it was 4.2% with a coverage factor of 2, which corresponded to a 95% confidence level.

$$m_{\text{sample}} = \frac{R_{\text{h-sample}}}{R_{\text{h-STD}}} \cdot R_{\text{m-STD}} \cdot M_{\text{sample}} \quad (5)$$

where $R_{\text{m-STD}}$ is the mass ratio of TK-11 to L-TK-11 in the standard solution; $R_{\text{h-STD}}$ is the peak height ratio of TK-11 to L-TK-11 of the standard solution; M_{sample} is the mass of L-TK-11 in the sample solution (g); m_{sample} is the mass of TK-11 in the sample solution (g); and $R_{\text{h-sample}}$ is the ratio of signal-to-noise.

For quantitation of β-LG in milk powder, the pure β-LG was added into the native milk powders. And it was treated following the protocol of Determination of the Mass Fraction of β-LG in Milk Powders by Proteolysis. The recovery was calculated as the ratio of the measured concentration difference of the spiked and native milk samples to the concentration of the addition. Therefore, the recovery can be obtained although there is β-LG in native milk powder. As the proteolytic efficiency varied from sample to sample, the proteolytic efficiency for each sample was measured for correction with pure β-LG in extraction buffer as described in Determination of Proteolytic Efficiency. Then the recovery can be obtained by formulas 6 and 7.

$$c_0 = \frac{m_0}{m_s} \cdot P \quad (6)$$

$$R = \frac{c_1 - c_2}{E \cdot c_0} \times 100\% \quad (7)$$

where m_0 is the mass of the pure β-LG added into the spiked sample (g); P is the mass fraction of pure β-LG; m_s is the mass of the sample (g); c_0 is the β-LG concentration added into the sample (g/g); c_1 and c_2 are the measured concentrations of the β-LG in spiked and native samples, respectively (g/g); E is the proteolytic efficiency; and R is the recovery.

Three different brands of milk powders with 3 different spiked levels of each brand were analyzed in the recovery study. The recoveries ranged from 86.0% to 118.3% with maximum CV of 9% (Table 2). The LOD and LOQ were calculated based on the S/N ratio of 3 and 10 by single point calibration, which were 4.8×10^{-5} g/g and 1.6×10^{-4} g/g β-LG in milk powder, respectively. The relative expanded uncertainty was evaluated,[42] and it was 5.9% with a coverage factor of 2, which corresponded to 95% confidence level.

Compared with previously reported methods, the LOD of the proposed method is comparable to that by instrumental methods, such as CE-MS (10^{-6} g/g), LC−MS (10^{-6} g/g), CE (10^{-5}g/g), and HPLC (10^{-6} g/g).[9,11,16] However, the LOD of the proposed method is considerably higher than LOD values reported for ELISA methods (10^{-8} to 10^{-12} g/g).[4,7] However, the proposed HPLC−IDMS method is a potential primary method, which has advantages for a better recovery of 86.0−118.3% and a lower average standard deviation compared with other methods reported.[4,16]

Determination of the Mass Fraction of β-LG in Milk Powders by HPLC−IDMS. Ten samples from the domestic market were analyzed, covering defatted, full cream, infant formula, and partially hydrolyzed formula milk powders. All samples were analyzed according to the protocol described in Determination of the Mass Fraction of β-LG in Milk Powders by Proteolysis. Two subsamples were taken out for each sample, and 3 repeat analyses were performed for each subsample. The results are shown in Table 3, and the typical total ion and extracted ion chromatograms are shown in Figure 2. All of the ten samples were successfully analyzed by the proposed IDMS method with CVs of <5.6%. The contents of β-LG ranged from 0.02 g/g to 0.04 g/g for most samples except one brand had a higher β-LG content of 0.13 g/g.

Table 3. The Mass Fractions of β-LG in 9 Milk Powder Matrices by HPLC−IDMS

sample no.	β-LG content (g/g)	CV (%)
1	0.03	1.9
2	0.02	1.4
3	0.04	1.4
4	0.02	1.4
5	0.03	1.6
6	0.03	5.6
7	0.04	2.8
8	0.13	3.7
9	0.04	5.1

As no β-LG free milk was available, the extraction buffer was used as the blank and negative control. No TK-11 peak was detected of the negative control. To reduce the chance of the false positive, all the samples were treated identically without digestion and analyzed by HPLC−IDMS. No TK-11 peak was detected for all the samples except partially hydrolyzed formula milk powder, demonstrating that no free TK-11 or similar m/z interferences with the same retention time of TK-11 appeared in the samples except partially hydrolyzed formula milk powder. As the proposed method cannot differentiate the intact β-LG from β-LG segments, the proposed method is not suitable for partially hydrolyzed formula milk samples. Though the β-LG content can be calculated for the partially hydrolyzed formula milk sample, it did not reflect the real content; therefore, the result of the partially hydrolyzed formula milk sample was not included in Table 3. In addition, the single charged TK-11(m/z = 1245) and L-TK-11(m/z = 1248), instead of double charged TK-11(m/z = 623) and L-TK-11(m/z = 625), were also captured by HPLC−IDMS to confirm the results of the ten samples, and no clear difference was observed, which demonstrates the reliability of the proposed method.

dx.doi.org/10.1021/jf4054337 | J. Agric. Food Chem. 2014, 62, 3073−3080

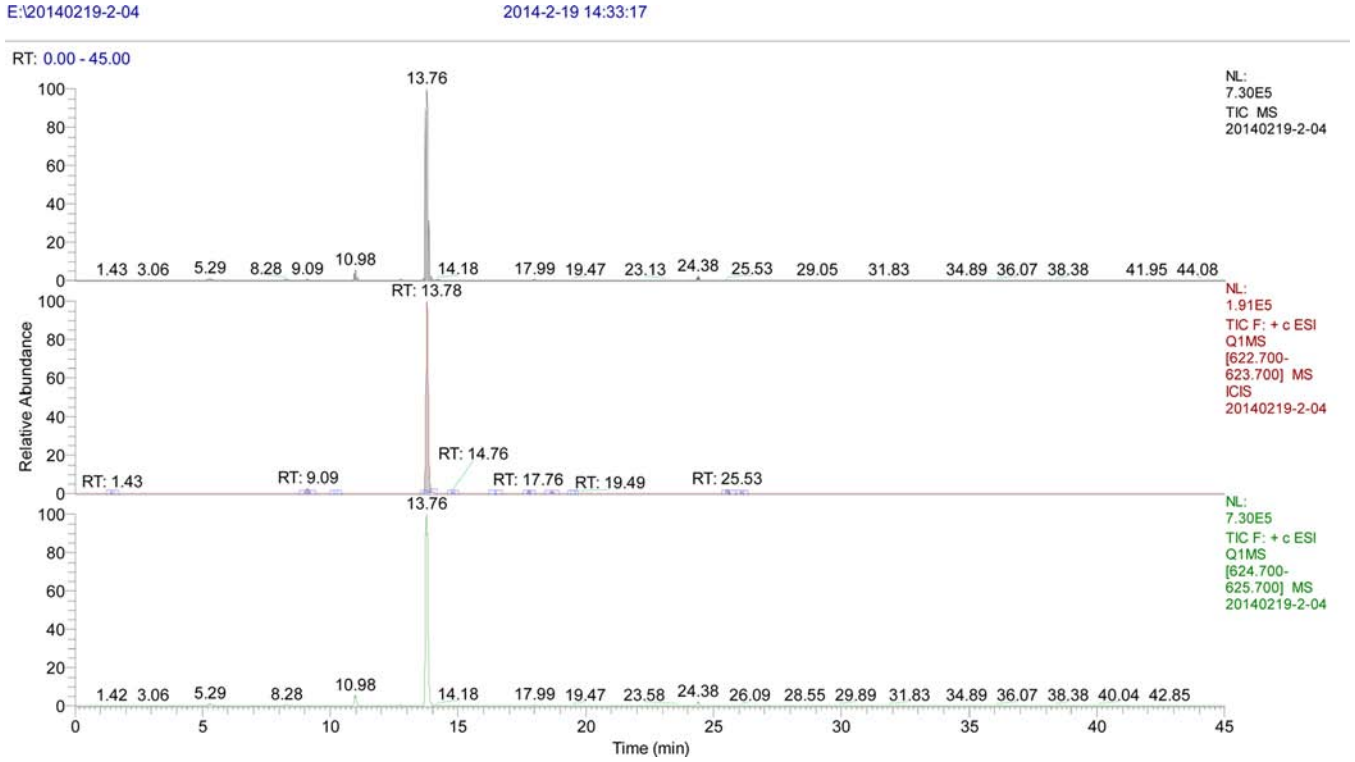

Figure 2. The typical total ion and extracted ion chromatograms of a real sample by HPLC−IDMS.

The quantification results are SI-traceable via the amino acid CRM and IDMS methods (Figure 3). This method is accurate and sufficiently sensitive to detect β-LG in milk powders. It will be useful to develop both pure β-LG CRM and CRM of β-LG in milk powders. The method is also expected to improve the comparability of β-LG quantification results among different laboratories.

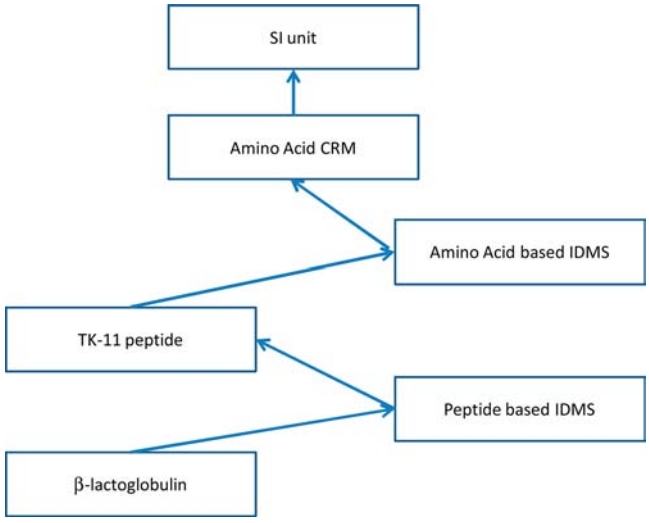

Figure 3. Traceability chain for β-LG quantification.

■ ASSOCIATED CONTENT

Ⓢ Supporting Information

Table S1, gradient of mobile phases for separation of the digested peptides from pure β-LG by UPLC-Q-TOF; Table S2, gradient of mobile phases for separation of Pro, Val, Leu, and Phe in the amino acid mixture by HPLC−IDMS; Table S3, gradient of mobile phases for separation of TK-11 from other digested peptides within 45 min by HPLC−IDMS; Figure S1a, the total ion chromatogram of protein identification by UPLC-Q-TOF; Figure S1b, the fragments of TK-11 corresponded to its sequence; Figure S2, optimization of hydrolysis time for TK-11 (a) and β-LG (b) according to the peak area ratio of each amino acid to its isotope-labeled one; Figure S3, comparison of the different amount of denaturing agent and reductive alkylation reagent addition: effect on the proteolysis efficiency; Figure S4, comparison of the different amount of DTT: effect on the peak area of TK-11; Figure S5, comparison of the different temperature and duration of reductive alkylation reaction: effect on peak area of TK-11. This material is available free of charge via the Internet at http://pubs.acs.org.

■ AUTHOR INFORMATION

Corresponding Author

*Tel: +86-10-64434898. Fax: +86-10-64434898. E-mail: yangyi@mail.buct.edu.cn.

Author Contributions

†These authors contributed equally to this work.

Funding

This project was supported by General Administration of Quality Inspection of scientific research project (2013QK048) and Key Projects in the National Science & Technology Pillar Program (2012BAK26B04).

Notes

The authors declare no competing financial interest.

■ ABBREVIATIONS USED

β-lactoglobulin, β-LG; CRM, certified reference material; IDMS, isotope dilution mass spectrometry; TK-11, peptide with the sequence TPEVDDEALEK; NIM, National Institute

of Metrology; CV, coefficient of variation; LOQ, limit of quantitation; LOD, limit of detection; DTT, dithiothreitol; IAM, iodoacetamide

REFERENCES

(1) El-Agamy, E. I. The challenge of cow milk protein allergy. *Small Ruminant Res.* **2007**, *68*, 64−72.

(2) Brownlow, S.; Morais Cabral, J. H.; Cooper, R.; Flower, D. R.; Yewdall, S. J.; Polikarpov, I.; North, A. C.; Sawyer, L. Bovine b-lactoglobulin at 1.8 Å resolution-still an enigmatic lipocalin. *Structure* **1997**, *5*, 481−495.

(3) Miantyijarv, R.; Rautiainen, J.; Virtanen, T. Lipocalins as allergens. *Bichim. Biophys. Acta* **2000**, *14*, 308−317.

(4) Pelaez-Lorenzo, C.; Diez-Masa, J. C.; Vasallo, I.; Frutos, M. D. Development of an optimized ELISA and a sample preparation method for the detection of *β*-lactoglobulin traces in baby foods. *J. Agric. Food Chem.* **2010**, *58*, 1664−1671.

(5) Bremer, M. G.; Kemmers-Voncken, A. E.; Boers, E. A.; Frankhuizen, R.; Haasnoot, W. Enzyme-linked immunosorbent assay for the detection of bovine rennet whey powder in milk powder and buttermilk powder. *Int. Dairy J.* **2008**, *18*, 294−302.

(6) Khuda, S.; Slate, A.; Pereira, M.; Al-Taher, F.; Jackson, L.; Diaz-Amigo, C.; Bigley, E. C.; Whitaker, T.; Williams, K. Effect of processing on recovery and variability associated with immunochemical analytical methods for multiple allergens in a single matrix: dark chocolate. *J. Agric. Food Chem.* **2012**, *60*, 4204−4211.

(7) Monaci, L.; Tregoat, V.; Hengel, A. J.; Anklam, E. Milk allergens, their characteristics and their detection in food: a review. *Eur. Food Res. Technol.* **2006**, *223*, 149−179.

(8) Middleton, N.; Reid, J. R.; Coolbear, T.; Jelen, P. Proliferation and intracellular glutathione in Jurkat T cells with concentrated whey protein products. *Int. Dairy J.* **2003**, *13*, 565−573.

(9) Yang, Y.; Zhao, S.; Ding, X.; Li, Y.; Wang, Z. Analysis of a-lactalbumin, beta-lactoglobulin A and B in whey protein powder, colostrum, raw milk, and infant formula by CE and LC. *Dairy Sci. Technol.* **2011**, *91*, 213−225.

(10) Vallejo-Cordoba, B. Rapid separation and quantification of major caseins and whey proteins of bovine milk by capillary electrophoresis. *J. Capillary Electrophor.* **1997**, *4*, 219−224.

(11) Figeys, D.; Oostveen, I.; Ducret, A.; Aebersold, R. Protein identification by capillary zone electrophoresis/ microelectrospray ionization-tandem mass spectrometry at the subfemtomole level. *Anal. Chem.* **1996**, *68*, 1822−1828.

(12) Cianciulli, C.; Hahne, T.; Wätzig, H. Capillary gel electrophoresis for precise protein quantitation. *Electrophoresis* **2012**, *33*, 3276−3280.

(13) Monaci, L.; Visconti, A. Mass spectrometry-based proteomics methods for analysis of food allergens. *Trends Anal. Chem.* **2009**, *28*, 581−591.

(14) Picariello, G.; Mamone, G.; Addeo, F.; Ferranti, P. The frontiers of mass spectrometry-based techniques in food allergenomics. *J. Chromatogr. A* **2011**, *1218*, 7386−7398.

(15) Careri, M.; Mangia, A. Analysis of food proteins and peptides by chromatography and mass spectrometry. *J. Chromatogr. A.* **2003**, *1000*, 609−635.

(16) Monaci, L.; van Hengel, A. J. Development of a method for the quantification of whey allergen traces in mixed-fruit juices based on liquid chromatography with mass spectrometric detection. *J. Chromatogr. A* **2008**, *1192*, 113−120.

(17) Cohen, A.; Hertz, H. S.; Mandel, J.; Paule, R. C.; Schaffer, R.; Shiegoski, L. T.; Sun, T.; Welch, M. J.; White, E. Total serum cholesterol by isotope dilution/mass spectrometry: a candidate definitive method. *Clin. Chem.* **1980**, *5*, 854−860.

(18) Patterson, D. G.; Patterson, M. B.; Culbreth, P. H.; Fast, D. M.; Holler, J. S.; Sampson, E. J.; Bayse, D. D. Determination of steroid hormones in a human-serum reference material by isotope dilution-mass spectrometry: a candidate definitive method for cortisol. *Clin. Chem.* **1984**, *30*, 619−626.

(19) Patterson, D. G.; Hampton, L.; Lapeza, C. R.; Belser, W. T.; Green, V.; Alexander, L.; Needham, L. L. High-resolution gas chromatographic/high-resolution mass spectrometric analysis of human serum on a whole-weight and lipid basis for 2, 3, 7, 8-tetrachlorodibenzo-p-dioxin. *Anal. Chem.* **1987**, *59*, 2000−2005.

(20) Zhang, K.; Wong, J. W.; Hayward, D. G. Determination of mycotoxins in milk-based products and infant formula using stable isotope dilution assay and liquid chromatography tandem mass spectrometry. *J. Agric. Food Chem.* **2013**, *61*, 6265−6273.

(21) Burkitt, W. I.; Pritchard, C.; Arsene, C.; Henrion, A.; Bunk, D.; O'Connor, G. Toward système international d'Unité-traceable protein quantification: from amino acids to proteins. *Anal. Biochem.* **2008**, *376*, 242−251.

(22) Kaiser, P.; Akerboom, T.; Ohlendorf, R.; Reinauer, H. Liquid chromatography-isotope dilution-mass spectrometry as a new basis for the reference measurement procedure for hemoglobin A_{1c} determination. *Clin. Chem.* **2010**, *56*, 750−754.

(23) Weber, D.; Raymond, P.; Ben-Rejeb, S.; Lau, B. Development of a liquid chromatography-tandem mass spectrometry method using capillary liquid chromatography and nanoelectrospray ionization-quadrupole time-of-flight hybrid mass spectrometer for the detection of milk allergens. *J. Agric. Food Chem.* **2006**, *54*, 1604−1610.

(24) Careri, M.; Costa, A.; Elviri, L.; Lagos, J. B.; Mangia, A.; Terenghi, M.; Cereti, A.; Garoffo, L. P. Use of specific peptide biomarkers for quantitative confirmation of hidden allergenic peanut proteins Ara h 2 and Ara h 3/4 for food control by liquid chromatography-tandem mass spectrometry. *Anal. Bioanal. Chem.* **2007**, *389*, 1901−1907.

(25) Cryar, A.; Pritchard, C.; Burkitt, W.; Walker, M.; O'Connor, G.; Quaglia, M. A mass spectrometry-based reference method for the analysis of lysozyme in wine and the production of certified reference materials. *J. Assoc. Public Anal. (Online)* **2012**, *40*, 77−80.

(26) Brun, V.; Masselon, C.; Garin, J.; Dupuis, A. Isotope dilution strategies for absolute quantitative proteomics. *J. Proteomics* **2009**, *72*, 740−749.

(27) Kato, M.; Kato, H.; Eyama, S.; Takatsu, A. Application of amino acid analysis using hydrophilic interaction liquid chromatography coupled with isotope dilution mass spectrometry for peptide and protein quantification. *J. Chromatogr. B* **2009**, *877*, 3059−3064.

(28) Pritchard, C.; Quaglia, M.; Mussell, C.; Burkitt, W. I.; Parkes, H.; O'Connor, G. Fully traceable absolute protein quantification of somatropin that allows independent comparison of somatropin standards. *Clin. Chem.* **2009**, *55*, 1984−1990.

(29) Abdel Rahmana, A. M.; Lopata, A. L.; Randell, E. W.; Helleur, R. J. Absolute quantification method and validation of airborne snow crab allergen tropomyosin using tandem mass spectrometry. *Anal. Chim. Acta* **2010**, *681*, 49−55.

(30) Kilpatrick, Eric. L.; Liao, W. L.; Camara, J. E.; Turko, I. V.; Bunk, D. M. Expression and characterization of ^{15}N-labeled human C-reactive protein in Escherichia coli and Pichia pastoris for use in isotope-dilution mass spectrometry. *Protein Expression Purif.* **2012**, *85*, 94−99.

(31) Konopka, A.; Boehm, M. E.; Rohmer, M.; Baeumlisberger, D.; Karas, M.; Lehmann, W. D. Improving the precision of quantitative bottom-up proteomics based on stable isotope-labeled proteins. *Anal. Bioanal. Chem.* **2012**, *404*, 1079−1087.

(32) Lai, C.; Su, R.; Zhang, M.; Xiong, Y.; Qing, H.; Deng, Y.; Zhang, Y. Quantification of Cry1Ab in genetically modified maize leaves by liquid chromatography multiple reaction monitoring tandem mass spectrometry using ^{18}O stable isotope dilution. *Analyst* **2012**, *137*, 2699−2705.

(33) McGrath, S. C.; Schieltz, D. M.; McWilliams, L. G.; Pirkle, J. L.; Barr, J. R. Detection and quantification of ricin in beverages using isotope dilution tandem mass spectrometry. *Anal. Chem.* **2011**, *83*, 2897−2905.

(34) Ordóñez, Y. N.; Deitrich, C. L.; Montes-Bayón, M.; Blanco-González, E.; Feldmann, J.; Sanz-Medel, A. Species specific isotope dilution versus internal standardization strategies for the determination

of Cu, Zn-superoxide dismutase in red blood cells. *J. Anal. At. Spectrom.* **2011**, *26*, 150−155.
(35) Dizdaroglu, M.; Reddy, P. T.; Jaruga, P. Identification and quantification of DNA repair proteins by liquid chromatography/isotope-dilution tandem mass spectrometry using their fully ^{15}N-labeled analogues as internal standards. *J. Proteome Res.* **2011**, *10*, 3802−3813.
(36) Wang, J.; Yuan, B.; Guerrero, C.; Bahde, R.; Gupta, S.; Wang, Y. Quantification of oxidative DNA lesions in tissues of long-evans cinnamon tats by capillary high-performance liquid chromatography-tandem mass spectrometry coupled with stable isotope-dilution method. *Anal. Chem.* **2011**, *83*, 2201−2209.
(37) Lee, H. S.; Lee, J. M.; Park, S. R.; Lee, J. H.; Kim, Y. G. Development and validation of primary method for the determination of glucose in human serum by isotope dilution liquid chromatography tandem mass spectrometry and comparison with field methods. *Bull. Korean Chem. Soc.* **2013**, *34*, 1698−1702.
(38) Yerramsetty, V.; Reo, M.; Cohen, J.; Hegeman, A.; Ismail, B. Development of a simple, fast, and accurate method for the direct quantification of selective estrogen receptor modulators using stable isotope dilution mass spectrometry. *J. Agric. Food Chem.* **2013**, *61*, 7028−7037.
(39) Mayr, C. M.; Schieberle, P. Development of stable isotope dilution assays for the simultaneous quantitation of biogenic amines and polyamines in foods by LC-MS/MS. *J. Agric. Food Chem.* **2012**, *60*, 3026−3032.
(40) Janssens, G.; Mangelinckx, S.; Courtheyn, D.; Prévost, S.; Poorter, D. G.; Kimpe, D. N.; Bizec, L. B. Application of gas chromatography-mass spectrometry/combustion/isotope ratio mass spectrometry (GC-MS/C/IRMS) to detect the abuse of 17β-estradiol in cattle. *J. Agric. Food Chem.* **2013**, *61*, 7242−7249.
(41) Cuadros-Rodríguez, L.; Bagur-González, M. G.; Sánchez-Viñas, M.; González-Casado, A.; Gómez-Sáez, A. M. Principles of analytical calibration/quantification for the separation sciences. *J. Chromatogr. A* **2007**, *1158*, 33−46.
(42) Wu, L.; Yang, B.; Bi, J.; Wang, J. Development of bovine serum albumin certified reference material. *Anal. Bioanal. Chem.* **2011**, *400*, 3443−3449.

Table 1. Compound Information and Composition of Stock Solutions: Retention Indices I on Stabilwax DA Column, log K_{aw}, and log K_{ow} Taken from the Experimental Data Database of EPI Suite v4.11 of the U.S. Environmental Protection Agency,[35] if Not Stated Otherwise

							stock 2 concentration	
compound	retention index I	CAS Registry No.	purity (%)	quant ion m/z	log K_{aw} (25 °C)	log K_{ow}	mmol L^{-1}	g L^{-1}
alcohols								
1-propanol	600	71-23-8	≥99.9	31	−3.52	0.25	40.1	2.41
2-propanol	445	67-63-0	≥99.9	59	−3.48	0.05	39.2	2.36
2-methylpropanol	651	78-83-1	≥99.8	43	−3.40	0.76	43.3	3.21
1-butanol	719	71-36-3	≥99.9	56	−3.44	0.88	43.7	3.24
2-butanol	580	78-9-2	≥99.8	45	−3.43	0.61	43.5	3.23
tert-butanol	429	75-6-0	≥99.8	59	−3.43	0.35	31.6	2.34
2-methylbutanol	790	137-32-6	≥99.5	56	−3.24	1.29	37.2	3.28
3-methylbutanol	794	123-51-3	≥99.8	42	−3.24	1.16	36.7	3.24
1-pentanol	832	71-41-0	≥99	42	−3.27	1.51	37.0	3.26
3-pentanol	666	584-02-1	≥99.5	59	−3.09	1.21	37.0	3.26
3-methylpentanol	896	589-35-5	99	56	−3.14[a]	1.75[a]	32.3	3.30
1-hexanol	920	111-27-3	98	56	−3.16	2.03	31.8	3.25
2-ethylhexanol	1048	104-76-7	≥99.5	57	−2.97	2.73[a]	38.4	5.00
aldehydes								
acetaldehyde	81	75-07-0	≥99.5	29	−2.56	−0.34	35.6	1.57
benzaldehyde	1131	100-52-7	≥99	77	−2.96	1.48	39.6	4.20
trans-2-nonenal	1108	18829-56-6	97	70	−2.02[a]	3.06[a]	36.2	5.08
esters								
ethyl acetate	354	141-78-6	≥99.9	70	−2.26	0.73	40.7	3.59
ethyl butanoate	600	105-54-4	99	71	−1.79	1.85[a]	37.8	4.40
ethyl 3-methylbutanoate	629	108-64-5	98	88	−1.54	2.26[a]	33.2	4.32
3-methylbutyl acetate	674	123-92-2	>99	43	−1.62	2.25	33.6	4.38
ethyl hexanoate	800	123-66-0	99	88	−1.53[a]	2.83[a]	30.3	4.37
ethyl octanoate	1000	106-32-1	≥98	88	−1.28[a]	3.81[a]	35.2	6.07
ethyl decanoate	1200	110-38-3	99	88	−1.04[a]	4.79[a]	34.4	6.90
diethyl succinate	1246	123-25-1	99	101	−4.67	1.20	35.8	6.24
2-phenethyl acetate	1463	103-45-7	99	104	−3.11[a]	2.30[a]	37.7	6.20
terpenes								
geraniol	1446	106-24-1	98	69	−3.33	3.56	34.6	5.33
limonene	765	5989-27-5	97	68	0.12	4.57	37.0	5.04
linalool	1090	78-70-6	≥97	71	−3.06	2.97	33.8	5.22

[a]Values estimated by EPI Suite v4.11 programs HenryWin v3.2 and KOWWIN v1.68.

Standard and Sample Preparation. Two stock solutions were made; the first (stock 1) was used for extraction phase evaluation and method optimization and contained 500 μL L^{-1} of each analyte, except of the aldehydes and limonene, which were added to the compound set later. The second stock solution (stock 2) was prepared to adjust for the differences in sensitivity between analytes and was composed to cover the whole linear range of all analytes for a more efficient calibration procedure. The composition of the second stock solution is given in Table 1. The highest concentrated calibration solution was prepared with 200 μL of stock 2 filled to 200 mL with water; the lower concentration levels were prepared by a serial dilution with a dilution factor of 2, resulting in a 14-point calibration spanning a concentration factor of 8192.

Forty-six beers from 6 German varieties, Altbier (A, n = 4), Helles (H, n = 6), Kölsch (K, n = 6), Pilsener Bier (P, n = 25), Schwarzbier (S, n = 1), and Weizenbier (wheat beer) (W, n = 4), were analyzed. Three varieties are produced with top-fermenting yeast; they were Kölsch, which is a light lager; Weizenbier, in which a major proportion of barley is replaced by malted wheat; and Altbier, a dark lager that gets its color from roasted malt. The other three varieties are produced with bottom-fermenting yeast and are Helles, a light lager; Schwarzbier, a dark lager; and Pilsener Bier, which is a pale lager with a hoppy aroma. Two Pilsener beers and one Weizen beer were alcohol-free beers (designated \alc). Top- or warm-fermenting yeast ferments at temperatures of 15−25 °C, whereas bottom- or cold-fermenting yeast ferments at temperatures of 6−14 °C and can also use melibiose, which top-fermenting yeast cannot.[15] The fermentation at higher temperatures is faster and results in higher concentrations of higher alcohols and esters.[16] Traditionally, top-fermenting yeast is also known as ale yeast and bottom-fermenting yeast as lager yeast, although the brewing procedure of some top-fermented beers are also subjected to cold storage for conditioning.

The beer samples have been cooled on ice to minimize the loss of volatile compounds to the gas phase before they were diluted by a factor of 10. Because precise measurement of the liquid volume of beer is difficult due to foam formation, 10 g of beer has been weighed in a 100 mL volumetric flask, which was then filled with water. The gas content of the diluted solution was then low enough to be handled by a volumetric pipet.

Ten milliliters of each standard or sample solution was transferred into a 20 mL amber headspace vial (BGB Analytik AG, Boeckten, Switzerland), with an 8 × 3 mm PTFE laminated magnetic stir bar (VWR International GmbH, Darmstadt, Germany). The vials were

dx.doi.org/10.1021/jf405832u | J. Agric. Food Chem. 2014, 62, 3081−3091

Table 2. Properties of Sorbent Materials Used (Manufacturer's Data, If Not Stated Otherwise)

sorbent	sorbent type	specific surface area (m^2 g^{-1})	temperature limit (°C)	water affinity	typical applications
Carbopack C	graphitized carbon black	10	500	relatively low	low to medium boilers (C12−C20)
Carboxen 1000	carbon molecular sieve	1200	225	moderate	permanent gases, volatiles (C2−C5)
Carbosieve S III	carbon molecular sieve	975	400	moderate	volatile organics (C2−C5)
Tenax GR	70% porous organic polymer/30% graphitized carbon	24	350	low	volatiles, flavors
Tenax TA	porous organic polymer	35	350	low	volatiles and semivolatiles (C7−C26)
HayeSep D	porous organic polymer	795	290	low	volatiles (C1−C6)
MWCNT	multiwall carbon nanotubes	211[a]	na[b]	na	na
PDMS and PDMS blue	silicone rubber	absorbent	250	low	unpolar volatiles, semivolatiles
Carbowax 20M	polyethylene glycol	absorbent	225	high	polar semivolatiles

[a]BET measurement. [b]na, not available.

closed by magnetic screw caps with rubber/PTFE septa (BGB Analytik AG).

Sorbent Materials. Nine sorbent materials were tested for their extraction efficiency for the target analytes; they were Carbopack C (CC), Carboxen 1000 (C1000), Carbosieve S III (CSIII), Tenax TA (TTA) (poly(2,6-diphenyl)-*p*-phenyloxide), Tenax GR (TGR) (Tenax TA with graphitized carbon), HayeSep D (HSD) (divinylbenzene (DVB)), multiwalled carbon nanotubes (MWCNTs) (Baytubes C 150 HP, Bayer Material Science, Leverkusen, Germany), polydimethylsiloxane (PDMS), and Carbowax 20 M (polyethylene glycol (PEG) with a molecular weight of 20000) (more information can be found in Table 2). PDMS and PDMS blue (PDMSb) particles were prepared from white silicone and IceBlue septa (Restek Corp., Bellefonte, PA, USA), which have been frozen with liquid nitrogen and were ground and sieved subsequently. Carbowax 20 M could be applied only as a fraction of 10% in a mixed-bed trap with PDMS because it melts at desorption temperature and might drip out of the trap or block it, after cooling again. A two-sorbent bed, prepared of two-thirds Tenax GR and one-third Carbosieve S III, was used on the basis of previous experiences,[18] resulting in a total of 11 different ITEX traps tested.

Sample Extraction and Injection. Sample extraction and injection were executed by a CTC Combi PAL autosampler (Axel Semrau, Sprockhövel, Germany), holding a thermostatic TrayCooler2 for 20 mL headspace vials, a heatable Single Magnet Mixer (SMM) (Chromtech, Idstein, Germany), and the ITEX II option kit (CTC Analytics AG, Zwingen, Switzerland), consisting of a heated syringe holder for a 1.3 mL gastight Hamilton syringe with side port (Hamilton, Bonaduz, Switzerland) and the ITEX trap heater. The extraction was performed by custom-made macros. Only the optimized ITEX procedure, used for sample analysis, is presented here; more details regarding method development are given under Results and Discussion.

The samples were incubated and stirred at 70 °C for 20 min in the SMM to equilibrate the sample headspace prior to extraction. During the incubation time, the ITEX trap was heated to 250 °C while being flushed with 5 mL min^{-1} of nitrogen for 10 min, for preconditioning. After the trap was cooled to 30 °C and the incubation time was over, 65 extraction strokes of 1 mL were performed with a flow of 100 μL s^{-1}. Then 1 mL of helium was aspirated and dispensed at an unconnected ATAS GL Optic 3 injection port (Axel Semrau) to remove residual carbon dioxide of the sample from the void volume of the trap. Following the transfer of the trap to the split/splitless injector (SSL), 500 μL of helium was aspirated as desorption gas and, after the trap was heated to 250 °C, injected with a desorption flow of 50 μL s^{-1}. The whole procedure for each sample (including incubation/equilibration, extraction, injection, and needle flushing) takes about 42 min and can be performed in parallel to the GC analysis, thus making the GC temperature program the total analysis time-determining step.

GC-MS Measurements. All measurements were made using a Thermo Trace GC Ultra, coupled to a Thermo DSQ II single-quadrupole mass spectrometer (S+H Analytik, Mönchengladbach, Germany). The GC was equipped with an Optic 3 programmable temperature vaporizer with a nitrogen-cooled cold trap for on-column focusing and a SSL injector, where the column was connected. Injection was performed into the SSL set to 200 °C in splitless mode; the column flow was set to 1.5 mL min^{-1} constant flow for 31 min and was then raised to 2 mL min^{-1} until the end of the temperature program, to accelerate the elution of low volatile compounds. After injection, the analytes were transferred to an uncoated 0.53 mm inner diameter (i.d.) fused silica capillary (BGB Analytik AG) and cryofocused in the cold trap at −150 °C. After a hold time of 2 min, the trap was heated at 50 °C s^{-1} to 250 °C and the analytes were transferred to the chromatographic column. Separation of compounds was performed on a Stabilwax-DA fused-silica capillary column (cross-bonded Carbowax (PEG)) with 60 m length, 0.32 mm i.d., and 1 μm film thickness (Restek GmbH, Bad Homburg, Germany). The GC oven temperature program started at 35 °C for 5 min and then rose at 5 °C min^{-1} to 110 °C, was held for 2 min, and heated further at 10 °C min^{-1} to 200 °C with a hold time of 10 min. The MS transfer line was set to 220 °C, and the ion source temperature was 200 °C. Electron ionization (EI), with an ionization energy of 70 eV, was used in scan mode (m/z 29−200), with a scan rate of 500 amu s^{-1}. Instrument automation, data acquisition, and data processing were performed using the Xcalibur 1.4 data system (S+H Analytik).

RESULTS AND DISCUSSION

Method Optimization. The ITEX procedure comprises three main steps: sample extraction, sample injection, and trap conditioning for the next analysis; several parameters can be optimized in each of these steps. The extraction parameters, next to the choice of the most suitable extraction material, are the temperatures of the trap and the sample solution and the number, volume, and flow of the extraction strokes. The parameters for injection are the desorption gas volume and flow and the desorption temperature; trap conditioning includes conditioning temperature and time.

Two of the extraction parameters will not be discussed here. The first is the choice of the extraction material, which will be covered in the next section, because it was performed after the optimization of the parameters, and the second is the trap temperature, which should normally be set to the lowest possible value, due to the exothermic nature of the sorption process. Sample temperatures were tested from 40 to 80 °C in intervals of 10 °C. The majority of analytes show increasing extraction efficiency in the whole tested range, but about a third of the analytes begin to lose sensitivity when the temperature is raised from 70 to 80 °C. Here it is an advantage of ITEX that the sorption material is located outside the heated sample vial, because a similar loss of sensitivity has been observed for the

analysis of terpenes using HS-SPME already at temperatures above 40 °C.[24] The extraction flow and the number of extraction strokes have to be optimized together, because their combination defines the efficiency and duration of the extraction procedure. An extraction flow of 10 μL s^{-1} gives the highest peak areas for all compounds, which drop to 33−94% of the area at 50 μL s^{-1} and 28−88% at 100 μL s^{-1}, with averages of 63 and 52%, respectively. On the other hand, when 10 extraction strokes is defined as 100%, the extracted amount increases to 119−1337% for 100 extraction strokes, with an average of 626%. The average peak areas for 25, 50, and 75 extraction strokes were 228, 299, and 399%, respectively. No analyte reached equilibrium within the tested 100 extraction strokes. As an increase in the number of extraction strokes by a factor of 10 results in about 6 times larger peak areas, whereas the same increase of the extraction flow only halves the peak areas, a high number of extraction strokes with a high flow gives a better extraction efficiency in the same extraction time. Consequently, 65 extraction strokes with an extraction flow of 100 μL s^{-1} was chosen, which was the maximum to be performed in parallel to the GC oven run time.

Desorption volumes of 100, 500, and 1000 μL were tested. An increase of the resulting peak areas for most compounds can be observed from 100 to 500 μL, whereas a further increase is visible only for low-volatile compounds, such as geraniol, ethyl decanoate, or diethyl succinate, when the desorption volume is raised from 500 to 1000 μL. Because the gain in sensitivity was not significant and limited to a few compounds, a desorption volume of 500 μL was chosen. The desorption flow showed a similar behavior, with a decline of peak areas from a flow of 10 to 50 μL s^{-1}, whereas only the peak areas of the low-volatile compounds further decrease at a flow of 100 μL s^{-1}. As the reproducibility got better with higher desorption flows, 50 μL s^{-1} was used. The optimization results also agree with the ones found for environmental contaminants in an earlier work.[18]

Choice of Extraction Phase Material. The comparison of the extraction materials was performed with a 5 μg L^{-1} standard solution and the optimized method parameters given before, but with adapted desorption temperatures for each trap. On the basis of previous experiences, which indicated that the best desorption efficiency is reached at high desorption temperatures,[18] the desorption temperature was set at or near the maximum temperature for each sorbent (see Table 2). The desorption temperatures were set to 300 °C for Carbopack C, Carbosieve S III, Tenax GR, Tenax TA, and the MWCNTs, to 250 °C for HayeSep D and PDMS, and to 200 °C for the trap containing Carbowax 20 M and C1000.

A summary of the total extracted amounts with each trap is given in Figure 1. The best overall extraction yield was achieved with HayeSep D, Tenax GR, Tenax TA, and Carbopack C; the PDMS -based absorbent traps were in a medium range, and the traps using molecular sieves and carbon nanotubes had the lowest yield. Information on the extracted amount per compound can be found in Table 3. HSD was most effective for the trapping of long-chain esters and terpenes, but less suitable for the more polar alcohols, for which TTA was the best sorbent. TGR had a lower efficiency for alcohols than TTA and was best suited for short-chain esters. CC as an apolar material also had the highest yields for esters and long-chain alcohols, but, complementary to HSD, very low efficiency for long-chain esters and terpenes, which may be caused by irreversible adsorption or the degradation of analytes; similar reasons might be responsible for the low extraction yields of the

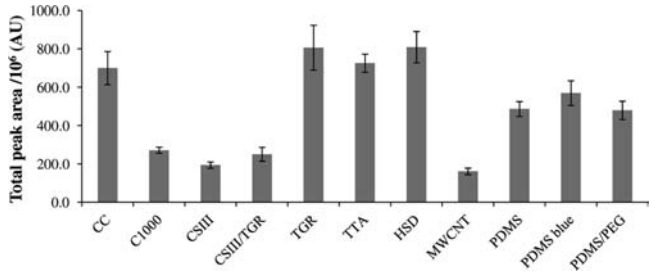

Figure 1. Summarized peak areas with average repeatability of all analytes (CC (Carbopack C), C1000 (Carboxen 1000), CSIII (Carbosieve S III), TGR (Tenax GR), TTA (Tenax TA), HSD (HayeSep D), MW CNT (multiwalled carbon nanotubes), PDMS (polydimethylsiloxane), PEG (polyethylene glycol)).

traps containing carbon molecular sieves. It has been found that the surface of carbon-based adsorbents can be activated during the conditioning, even with a stream of inert gas, and then cause analyte loss by transformation reactions, especially for alcohols and carbonyl compounds.[25] This may also apply for the MWCNTs, for which more research is currently being carried out. Because the sensitivity for esters was generally better than for alcohols and the differences in the total extracted amount were quite small, the carbon-based adsorbents were excluded and TTA was initially chosen as sorbent material.

However, when the linear range was determined during method evaluation, it proved to be quite limited for TTA (see Table 4), which led to an inferior repeatability for beer samples relative to standard solutions because of competition and displacement effects of ethanol. Moreover, the compound set was extended with aldehydes, including benzaldehyde, which can be formed as a degradation product of Tenax TA during thermal desorption.[26] When the carbon- and Tenax-based sorbents were ruled out because of their reactivity with alcohols and carbonyl compounds or interfering degradation product formation, only HSD- and the PDMS-based traps remained. However, HSD as adsorbent material would suffer from the same competition effects as TTA while the equilibrium conditions of absorbent materials do not vary until loadings of several percent are present.[27] This rendered a re-evaluation of sorbent materials for the enhanced compound set unnecessary and, consequently, the trap containing PDMS blue was used, which had the best performance of the remaining sorbents and promised to possess a wider linear range, being an absorbent material.

Method Performance Parameters. Method performance parameters were evaluated for the initially used TTA trap and the finally used PDMSb trap. The method detection limit (MDL), precision, and linear range were determined for both traps, the recovery and extracted analyte fraction only for the latter one. The results are summarized in Table 4.

The MDL of each analyte was determined by using a procedure of the U.S. Environmental Protection Agency, as the minimum concentration of an analyte that can be reported greater than zero with a confidence of 99%. It is based on the standard deviation of a seven-fold analysis with an analyte concentration resulting in a signal-to-noise ratio of about 3−5.[28] The linear range was determined as result in a constant slope between the calibration points. The precision was calculated as the average of all calibration points within the linear range, and a range factor (RF) was defined by dividing

Table 3. Comparison of Extraction Trap Efficiencies by the Average Peak Areas of a Triplicate Analysis of a 5 μg L^{-1} Standard Solution and the Average of the Relative Standard Deviations of All Compounds[a]

	peak area/1,000,000										
	CC	C1000	CSIII	CSIII/TGR	TGR	TTA	HSD	MW CNT	PDMS	PDMS blue	PDMS/PEG
alcohols											
1-propanol	5.2	7.6	7.8	2.7	7.6	6.4	2.0	0.1	3.7	3.4	2.7
2-propanol	0.3	0.6	0.8	nd	0.5	0.4	0.4	nd	0.3	0.3	0.2
2-methylpropanol	0.6	1.4	1.2	1.2	1.2	5.1	1.5	1.6	1.0	0.9	0.8
1-butanol	2.8	0.7	3.0	1.0	4.9	4.8	4.4	0.1	1.9	2.4	1.8
2-butanol	10.8	18.5	16.1	2.5	22.2	14.5	14.3	0.07	28.7	41.0	36.2
tert-butanol	14.4	31.5	11.4	4.8	27.6	5.5	24.7	0.7	22.1	12.2	11.9
2-methylbutanol	5.7	5.4	3.7	2.5	9.1	7.4	6.6	0.3	3.1	4.1	3.3
3-methylbutanol	5.6	7.0	2.3	2.1	5.8	4.6	3.9	1.2	1.9	2.5	2.0
1-pentanol	4.3	2.6	1.9	1.5	3.4	6.0	4.4	0.2	1.9	2.5	2.1
3-pentanol	4.0	3.7	6.3	1.1	7.9	30.4	4.9	0.2	6.4	6.5	7.6
3-methylpentanol	6.3	2.6	1.6	1.6	8.0	8.3	5.9	0.4	3.1	3.9	3.0
1-hexanol	9.0	3.0	1.9	2.3	10.2	12.9	7.9	1.2	4.4	5.0	3.9
2-ethylhexanol	24.0	4.0	3.1	4.4	24.1	40.5	39.2	6.7	24.9	14.4	11.8
esters											
ethyl acetate	10.4	26.1	20.9	15.9	21.9	18.7	20.2	4.5	10.1	6.5	6.5
ethyl butanoate	144.1	69.3	37.3	43.9	129.8	109.3	145.2	7.2	56.1	39.7	47.6
ethyl 3-methylbutanoate	34.8	9.7	4.6	12.5	94.0	36.7	38.3	4.1	26.8	37.7	16.6
3-methylbutyl acetate	113.4	7.5	10.4	18.0	61.3	1.4	33.9	47.2	49.6	99.3	57.2
ethyl hexanoate	111.5	16.1	7.5	23.7	134.9	118.1	92.8	11.2	40.6	71.8	52.2
ethyl octanoate	73.7	7.1	5.9	28.5	85.1	154.5	124.8	35.3	115.6	73.8	55.0
ethyl decanoate	114.5	40.8	41.8	73.5	129.5	114.3	181.7	32.8	58.5	126.8	141.4
diethyl succinate	0.07	0.7	0.3	0.3	1.4	0.7	1.7	0.05	0.8	0.5	0.7
2-phenethyl acetate	1.2	2.1	1.2	4.4	10.8	6.6	23.5	0.7	9.8	4.5	5.8
terpenes											
geraniol	0.3	2.2	2.1	0.8	3.2	2.2	6.5	0.4	2.2	3.4	3.6
linalool	3.3	1.4	1.0	1.2	1.8	16.5	20.6	5.1	13.2	6.3	5.6
sum	700.3	271.6	194.1	250.4	806.2	725.8	809.3	161.3	486.7	569.4	479.5
av RSD (%)	12.3	5.8	8.4	14.4	14.5	6.5	10.1	10.4	8.0	11.3	10.0

[a]CC, Carbopack C; C1000, Carboxen 1000; CSIII, Carbosieve S III; TGR, Tenax GR; TTA, Tenax TA; HSD, HayeSep D; MW CNT, multiwalled carbon nanotubes; PDMS, polydimethylsiloxane.

the upper limit of the linear range by the lower limit, for an easier comparison of linear ranges between sorbent materials. The MDLs achieved with the TTA trap ranged from 0.01 to 17.5 μg L^{-1} with a median of 0.2 μg L^{-1}, except for benzaldehyde, for which no quantitation was possible because of artifact formation by TTA during desorption. The average MDL for the alcohols is 1 μg L^{-1}, whereas it is 0.17 μg L^{-1} for the esters without diethyl succinate (2.1 μg L^{-1} when included), which is mainly influenced by the much higher air−water partitioning coefficient (K_{aw}, see Table 1) of most of the esters rather than by the selectivity of TTA toward the analytes. K_{aw} of diethyl succinate is 3 orders of magnitude lower than of the other esters and the lowest of all analytes. Precision with TTA was consistent in a narrow band between 6.2 and 10.0%, but the linear range was quite limited, and RF spanned from 25 to 540, with an average of 136 and a median of 88, giving <2 orders of magnitude for most analytes. The precision achieved for beer samples was worse than for standard solutions (>20% RSD), due to the low RF, the wide range of analyte concentrations in the samples, and competition effects, even when the beer has been diluted by a factor of 50. Zapata et al. experienced similar problems with mass saturation of TTA and solved it by using a stronger sorbent (Bond Elut ENV) and very small sample amounts (10 μL, diluted by a factor of 5) to achieve quantitative analyte extraction.[13] A different approach has been chosen here, where an absorbent material was used, which does not suffer from competition and saturation effects.[29]

The MDLs for the PDMSb trap were mostly higher than for TTA, ranging from 0.3 to 13 μg L^{-1}, with a median of 1.6 μg L^{-1}. They were lower for diethyl succinate, which had by far the highest MDL with TTA, 2-phenethyl acetate, and geraniol; furthermore, the quantitation of benzaldehyde was possible with PDMSb, because no artifacts were formed by the sorbent. The largest difference was observed with 3-methylbutyl acetate, for which the MDL was 410 times higher with PDMSb, but apart from this, the difference was about a factor of 10 and the sensitivity was still good enough to dilute the samples by a factor of 10 before the analysis. The same trend for the sensitivities of alcohols and esters that has been observed with TTA also applied for the extraction with PDMSb. The precision was less consistent, ranging from 1.2% for 3-pentanol to 19.9% for *trans*-2-nonenal, but overall it was better, with <5% for the majority of analytes. The linear range improved, as expected, using a sorbent based on analyte partitioning rather than adsorption. RF was between 32 and 4485, with an average of 666 and a median of 391, being about 5 times larger. The

dx.doi.org/10.1021/jf405832u | J. Agric. Food Chem. 2014, 62, 3081−3091

Table 4. Method Performance Parameters of the Evaluated ITEX Traps[a]

	Tenax TA				PDMS blue					
			linear range				linear range			
	MDL (μg L^{-1})	RSD (%)	μg L^{-1}	RF	MDL (μg L^{-1})	RSD (%)	μg L^{-1}	RF	recovery (%)	F_e (%)
alcohols										
1-propanol	2.1	6.2	3.2−80	25	7.0	1.7	37.7−2410+	64+	97.2	30.3
2-propanol	3.6	9.9	3.6−236	66	11.3	7.8	36.8−2343+	64+		8.2
2-methylpropanol	1.6	9.7	3.2−241	75	13.0	8.8	50.1−3208+	64+	105.8	12.6
1-butanol	0.3	8.4	0.4−41	103	5.0	1.8	12.7−1620	128	121.4	2.5
2-butanol	1.1	8.8	1.6−242	151	3.1	2.1	6.3−3225+	512+	120.9	5.3
tert-butanol	0.3	8.9	0.6−47	78	2.2	4.5	2.3−146	64	104.5	5.6
2-methylbutanol	0.1	7.7	0.3−10	33	1.6	2.1	1.6−3276+	2048+	109.3	5.8
3-methylbutanol	0.1	7.4	0.3−24	80	3.0	4.2	6.3−3236+	512+	110.4	9.3
1-pentanol	0.2	7.1	0.2−81	405	1.4	7.6	6.4−204	32	100.0	7.2
3-pentanol	3.1	8.6	3.3−815	247	4.3	1.2	6.4−3260+	510+	131.7	6.2
3-methylpentanol	0.3	7.0	0.3−33	110	1.5	7.1	1.6−1648	1030	111.0	6.6
1-hexanol	0.08	6.9	0.2−16.3	82	1.1	3.5	1.6−1627	1017	117.3	6.4
2-ethylhexanol	0.08	7.3	0.08−33	413	1.8	15.3	2.4−1250	521	102.4	5.8
aldehydes										
acetaldehyde	3.1	8.3	3.1−157	51	5.1	2.3	6.1−784	128	113.3	15.9
benzaldehyde					7.2	9.3	4.1−1050	256	106.0	5.6
trans-2-nonenal	0.2	7.8	0.2−25.4	127	0.5	19.9	0.6−1269	256	112.3	11.9
esters										
ethyl acetate	0.1	8.5	0.1−54	540	0.6	1.8	0.4−1794	4485	106.8	9.8
ethyl butanoate	0.02	7.3	0.04−3.5	88	0.5	2.3	0.5−1099	2198	108.4	24.9
ethyl 3-methylbutanoate	0.06	7.3	0.4−26	65	0.5	2.2	0.5−68	136	115.4	38.9
3-methylbutyl acetate	0.01	8.1	0.04−1.1	28	4.1	1.9	4.3−1095	255	121.3	34.7
ethyl hexanoate	0.08	9.3	0.2−18	90	0.4	3.2	0.5−546	1092	120.7	35.8
ethyl octanoate	0.01	8.6	0.02−1.7	85	0.5	4.4	0.7−379	541	123.3	37.3
ethyl decanoate	0.1	10.0	0.2−26	130	0.7	6.4	0.8−108	135	125.2	47.3
diethyl succinate	17.5	7.6	21−1040	50	2.1	6.3	6.1−3120	511	91.8	3.6
2-phenethyl acetate	1.0	8.9	1.0−155	155	0.3	2.9	0.8−194	243	96.1	3.8
terpenes										
geraniol	5.8	9.3	5.8−667	115	0.8	4.0	2.6−1334	513	103.7	5.7
limonene	0.07	9.5	0.08−4.2	53	0.7	11.6	1.2−1260	1050	122.6	77.9
linalool	0.06	7.5	0.2−44	220	0.9	8.4	0.9−163	272	109.5	2.3

[a]Method detection limit (MDL), precision (as relative standard deviation (RSD)), linear range (absolute and range factor (RF) from lowest to highest concentration, + indicates upper limit not reached within applied concentration range), recovery from spiked samples and extracted analyte fraction (F_e).

limit of the linear range was not reached within the applied concentration range for 1-propanol, 2-propanol, 2-methylpropanol, 2-butanol, 2-methylbutanol, 3-methylbutanol, and 3-pentanol, which could make the difference even bigger.

When the MDLs are compared to those of a solid phase dynamic extraction (SPDE) method for a similar compound set, which was previously used to analyze wine samples,[30] the ITEX method is more or less sensitive, depending on the applied sorbent material. Compared to the results with TTA, the MDLs of the SPDE method are lower for diethyl succinate and 2-phenethyl acetate, equal for ethyl hexanoate and 3-pentanol, and between 1.3 and 570 times higher for the other compounds, with a median of 3.6. With the PDMSb phase, the MDLs of the ITEX method are lower by a factor of 4 for 7 of 22 analytes, equal for 2-phenethyl acetate, and higher by an average factor of 5 for the other 14 compounds, analyzed in both methods. The lower MDL using the TTA phase should be caused by stronger sorption of the analytes and the larger sorbent volume of ITEX, compared to the 4.5 μL PEG phase that was used in SPDE. On the other hand, PEG is more polar than PDMS, making the SPDE method more sensitive for 9 of 13 of the analyzed alcohols. As no data on the linear range of the SPDE method are available, it is difficult to estimate if the smaller sorbent volume has negative effects on the extraction capacity. Liu et al. presented a method for similar analytes from beer samples, using sol−gel-derived SPME fibers. The limits of detection are comparable to those of the ITEX method with TTA sorbent and lower than ITEX with PDMSb, but the linear range of the SPME method is smaller.[31] The detection limits of the earlier mentioned ITEX method for quantitative extraction by Zapata et al. are between 3 and 117 times larger than for the method presented here; however, they were still low enough for the analysis in natural abundance in beer and wine. A comparison of linear ranges is not feasible because it has been determined only in the expected analyte range.[13]

The recovery was calculated by the analysis of pure and spiked beer samples, which were measured undiluted, diluted by a factor of 10, and diluted by a factor of 100; the spike was

Table 5. Lowest and Highest Detected Analyte Concentrations, with Relative Standard Deviation (RSD), Median and Number of Samples in which the Analytes Have Been Detected, and Average (⌀) Concentrations of All Analytes in the Different Beer Varieties (Altbier (A), Helles (H), Kölsch (K), Pilsener Bier (P), Schwarzbier (S), and Wheat Beer (W), and \alc without Alcohol) with the Average Sum of Each of the Four Analyte Classes

						$\mu g\ L^{-1}$							
	lowest ($\mu g\ L^{-1}$)	highest ($\mu g\ L^{-1}$)	RSD (%)	median ($\mu g\ L^{-1}$)	samples (n)	⌀ (A)	⌀ (H)	⌀ (K)	⌀ (P)	⌀ (P\alc)	⌀ (S)	⌀ (W)	⌀ (W\alc)
alcohols													
1-propanol	761	23400	1.7	7400	46	8530	7330	10100	9630	848	5020	10500	1660
2-propanol													
2-methylpropanol	5190	84300[a]	7.7	31000	46	22700	32900	34500	38200	7540	17100	46400	5190
1-butanol	36	676	2.2	124	16	86	113	630	323	nd	36	78	191
2-butanol	73	73	1.6		1	nd[b]	nd	nd	nd	nd	nd	73	nd
tert-butanol	25	46	3.5	28	6	31	25	nd	25	nd	nd	44	nd
2-methylbutanol	1010	21700	2.1	14000	46	9820	12100	14300	14800	1090	8610	11300	1640
3-methylbutanol	1800	57900[a]	4.2	38400[a]	46	37700	39200	40600	37900	2460	29300	46900	4030
1-pentanol	14	102	7.1	24	32	24	19	28	23	93	nd	nd	nd
3-pentanol	nd	nd	nd	nd	0	nd	nd	nd	nd	nd	nd	nd	nd
3-methylpentanol	nd	nd	nd	nd	0	nd	nd	nd	nd	nd	nd	nd	nd
1-hexanol	12	55	3.3	30	44	27	23	39	33	12	16	20	23
2-ethylhexanol	22	43	12.9	27	10	nd	38	32	23	nd	nd	nd	nd
∑ (alcohols)						78900	91600	99900	99000	12000	60100	115000	12800
aldehydes													
acetaldehyde	2640	13200[a]	2.3	5470	46	3220	7290	4960	6870	3190	4140	6830	3480
benzaldehyde	nd	nd	nd	nd	0	nd	nd	nd	nd	nd	nd	nd	nd
trans-2-nonenal	6	6	52.2	6	2	nd	6	nd	6	nd	nd	nd	nd
∑ (aldehydes)						3220	7290	4960	6880	3190	4140	6830	3480
esters													
ethyl acetate	706	32500[a]	1.8	10300	46	9680	9470	15000	10400	753	6560	21300	1010
ethyl butanoate	2	159	2.1	65	45	65	61	82	64	2	47	89	6
ethyl 3-methylbutanoate	5	6	2.8	5	5	5	nd	nd	5	nd	nd	nd	nd
3-methylbutyl acetate	47	3540	1.8	884	45	770	807	1230	854	47	599	2240	394
ethyl hexanoate	9	501	3.2	208	46	203	210	196	221	10	191	313	26
ethyl octanoate	7	850	4.4	295	46	448	316	449	297	9	253	375	20
ethyl decanoate	9	166	6.4	65	44	108	69	72	60	10	71	81	nd
diethyl succinate	41	1000	6.3	135	42	113	156	291	247	nd	91	107	nd
2-phenethyl acetate	18	1690	2.9	451	45	197	432	871	540	18	195	522	31
∑ (esters)						11600	11500	18200	12600	809	8000	25100	1488
terpenes													
geraniol	39	241	3.7	88	13	53	170	nd	88	nd	72	241	nd
limonene	7	20	45.7	11	6	nd	20	11	10	11	nd	nd	nd
linalool	9	32	5.4	14	19	10	17	19	13	28	nd	nd	10
∑ (terpenes)						63	207	30	111	39	72	241	10

[a]Upper limit of determined linear range exceeded. [b]nd, not detected or below MDL.

made using 1, 5, and 10 μL of the standard solution stock 2 in 100 mL of sample, respectively. In this way, the recovery for all analytes could be calculated from at least one analysis within the linear range; when two or all measurements were within the linear range, an average was calculated. The recoveries were between 91.8% for diethyl succinate and 131.7% for 3-pentanol, with an average of 111%. Considering the difficult handling of the undiluted samples, due to foam formation, that had to be transferred to the sample vials after spiking, it seems acceptable that most analytes show recoveries of 100 ± 15%. The recovery for 2-propanol could not be determined because the peak coeluted with ethanol, and in this period, the detector was turned off to avoid detector saturation when beer samples were analyzed.

The extracted fraction (F_e) of analyte, which is removed from the sample vial in each analysis, was calculated following the depletion method proposed by Zimmermann et al., by consecutive analyses from the same sample vial.[32] To that end three samples have been extracted five times each, and the logarithmic peak areas of the analytes were plotted over the number of extractions to obtain a linear graph, from which F_e could easily be calculated by the slope. F_e ranged from 2.3% for linalool to 77.9% for limonene. Here it was apparent that the octanol–water partitioning coefficient (K_{ow}, Table 1), which can be used to estimate the sorption of analytes to PDMS,[29,33]

dx.doi.org/10.1021/jf405832u | J. Agric. Food Chem. 2014, 62, 3081−3091

Table 6. Comparison of the Measured Analyte Concentrations of W01, a Regular Wheat Beer, and W01\alc, the Alcohol-free Beer of the Same Brand, with the Fraction of Analytes Lost in the Production of the Alcohol-free Version

	regular (μg L^{-1})	alcohol-free (μg L^{-1})	loss (%)		regular (μg L^{-1})	alcohol-free (μg L^{-1})	loss (%)
alcohols				**esters**			
1-propanol	14702	1662	89	ethyl acetate	22834	1012	96
2-methylpropanol	35716	5188	85	ethyl butanoate	97	6	94
1-butanol	59	191		3-methylbutyl acetate	2079	394	81
2-butanol	nd	11		ethyl hexanoate	501	26	95
tert-butanol	43	nd	≥49	ethyl octanoate	461	19	96
2-methylbutanol	8940	1640	82	ethyl decanoate	55	nd	≥87
3-methylbutanol	35952	4034	89	diethyl succinate	61	nd	≥66
1-hexanol	21	23		2-phenethyl acetate	506	31	94
aldehydes				**terpenes**			
acetaldehyde	4414	3477	21	linalool	nd	10	

has lower influence on the extraction efficiency than K_{aw}. Limonene has the highest F_e and the highest values for K_{aw} and K_{ow}, but ethyl hexanoate and linalool have similar log K_{ow} values of 2.83 and 2.97 with extracted fractions of 34.7 and 2.3%, respectively, so that the difference must originate in K_{aw}. Also, 1-pentanol and geraniol have similar log K_{aw} values of −3.27 and −3.33, respectively, but whereas log K_{ow} of geraniol is larger by a factor of 2, F_e of 1-pentanol is 2 times larger (7.2%) than for geraniol (3.56%). When F_e is plotted over log K_{aw} (Supporting Information Figure S1a)) and log K_{ow} (Figure S1b)), a roughly linear trend can be observed for K_{aw}, whereas no trend is visible for K_{ow}. However, this should be considered merely as a rule of thumb for ITEX users to estimate the probable extraction efficiency, because the system is not in equilibrium and the air−water and octanol−water partitioning coefficients that can be found in the literature can show quite large variations for some compounds.

Quantitative Analysis. An overview on the detected concentration ranges of all analytes and the number of samples, in which they were detected is given in Table 5; the results for all samples can be found in the Tables S1−S5 in the Supporting Information. 2-Propanol could not be detected in the actual beer samples because it coeluted with the ethanol peak, for which the detector was turned off to avoid saturation. If the peak would have been detected, quantitation could have been performed by the mass selective detector, but, as previous work showed, only with a high RSD of about 20%.[30] Three analytes were not detected in any beer sample; 3-pentanol, 3-methylpentanol, and benzaldehyde were always below the method detection limits. *trans*-2-Nonenal was detected in only two samples (H06 and P04) at a concentration of about 6 μg L^{-1}, making acetaldehyde the only one of the investigated aldehydes that was found in considerable amounts, with concentrations between 2.6 and 13.2 mg L^{-1}.

The sample concentration exceeded the determined linear range for four analytes, acetaldehyde, ethyl acetate, 2-methylpropanol, and 3-methylbutanol. Eleven samples contained acetaldehyde above the linear range of the method, but only four exceeded it by >20%. In the case of ethyl acetate, 5 of 46 samples had higher concentrations, 4 were about 20% higher, and 1 was 78% higher. Twenty-one samples contained 2-methylpropanol above the upper limit of the determined linear range, which was also the upper limit of the used calibration solutions, with the highest value being almost 3 times higher than the linear range. Thirty-three of 46 samples had concentrations of 3-methylbutanol above the highest concentrated calibration solution, similar to 2-methylpropanol. Finally, the problems with 2-methylpropanol and 3-methylbutanol have not been evident during the method development, because the concentration in the beer, which was used for test measurements, was within the linear ranges of each analyte. For future applications it needs to be checked if the problem can be solved by an increased calibration range, a stronger dilution of the samples, or a combination of both.

Eight analytes were detected in all 46 beer samples; they were 1-propanol, 2-methylpropanol, 2-methylbutanol, 3-methylbutanol, ethyl acetate, ethyl hexanoate, ethyl octanoate, and acetaldehyde. Ethyl butanoate, 3-methylbutyl acetate, and 2-phenethyl acetate were detected in 45 samples, and all three were missing in sample P25\alc, an alcohol-free Pilsener beer. Ethyl decanoate was not found in two alcohol-free beers, P25\alc and W01\alc, and diethyl succinate was absent in four samples (P05, P24\alc, P25\alc, and W01\alc), three of which were again alcohol-free variants.

Alcohol-free Beer. A regular wheat beer and the corresponding alcohol-free variant of the same brand were analyzed. The overlaid total ion chromatograms of the two beers are presented in Figure S2 (Supporting Information), where it can clearly be seen that the peaks of most compounds are much smaller in the alcohol-free version. A detailed view of the analytes found in these two samples, together with the fraction that was lost in the making of the alcohol-free beer, is given in Table 6. The average loss was 21% for acetaldehyde, 79% for the alcohols, and up to 88% for the esters. The levels dropped below the method detection limit for ethyl decanoate, diethyl succinate, and *tert*-butanol, for which, with the corresponding MDLs set as maximum possible remaining concentrations, the losses were at least 87, 66, and 49%, respectively. Exceptions were 1-butanol, 2-butanol, and linalool, for which the levels in the alcohol-free beer were higher than in the regular beer. However, the value for the regular beer of 1-butanol is below the lower limit of the linear range, which starts at 127 μg L^{-1}, due to sample dilution. Linalool is just above the MDL; in this way the differences might, as well as for 1-hexanol, originate in measurement uncertainty.

Variety Discrimination by Linear Discriminant Analysis (LDA). A LDA was performed with the free software environment R 3.0.1 (The R Foundation for Statistical Computing, www.r-project.org) using the "lda" function from the "MASS" package,[34] on semiquantitative data. To that end, the peak areas of quantified analytes present in almost all samples were combined with the peak areas of several

additional compounds, which were detected in many samples, resulting in 31 components as explanatory variables for the LDA, which are given in Table S6 in the Supporting Information. The number of useful discriminant functions is limited to the minimum of either the number of the groups minus one or the number of variables. Because the beer samples originated from eight different varieties, seven discriminant functions could be found. Their proportions of trace are shown in Figure 2. This shows that the first two linear discriminants explain about 95% of the between-group variance and should provide good separation. Most of the additional compounds were identified only by a mass spectral database; however, isoamyl propionate was the only one with a significant influence on the loadings on LD1 and LD2, which are given in Table S6, also. The main loadings on LD1 were given to isoamyl propionate in the positive direction and to 1-hexanol in the negative direction; the main loadings on LD2 were ethyl 3-methylbutanoate in the positive and diethyl succinate in the negative direction.

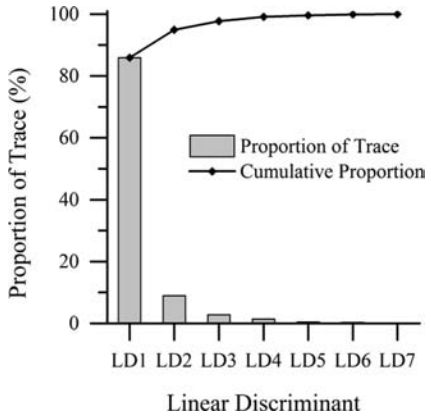

Figure 2. Proportion of trace and cumulative proportions of the seven found liniear discriminants.

Table 7 shows the prediction results using these two first discriminants. The proportion of correct predictions was almost 90%, and four of the five false predictions are between Pilsener beer and Helles, which have very similar brewing processes, their main difference being the lower hop content of Helles. Moreover, one of the falsely predicted Pilsener beers is marketed to be especially mild and another one had an increased alcohol content, which might separate them from the other beers of their variety.

A graphical representation of this situation is given in Figure S3 (Supporting Information), which shows a scatter plot based on the first two discriminant functions with boundaries for each beer variety. The distance of the two kinds of alcohol-free beers between themselves and to the rest of the beer varieties was so large that they were not included in the plot. As already discussed using Table 7 a good discrimination is achieved, and only the quite similar varieties of Pilsener beer and Helles are partially overlapping. The production conditions of these two varieties can also be quite different, as the samples originated from breweries throughout Germany, but there were also beers from Poland and Turkey and specialty beers that were brewed with higher alcohol content. On the other hand, the variations within the small groups of the top-fermenting beers Alt, Kölsch, and wheat beer were relatively small, as they are regional beers. A separation between the two general classes of top-fermenting (K, W, A) and bottom-fermenting (H, S, P) is also visible, as the top-fermenting beers are by trend more located in the lower left area of the plot, whereas the bottom-fermenting beers tend to be in the upper right-hand area.

The developed method was appropriate to perform a sensitive and robust analysis of beer samples. The performance was mostly comparable to results obtained with other microextraction techniques such as SPDE or SPME (utilizing also a special prepared coating) and in some cases also much better. The data, obtained during method evaluation, highlight that it is not always significant to have the most sensitive method, but a robust method, which also complies with factors such as precision and linear range, where it is important to choose the appropriate sorbent material for the analytical task at hand. Still, the presented ITEX method was sensitive enough to allow the dilution of the samples to minimize the influence of the matrix. A satisfying chemometric discrimination of all analyzed beer varieties was possible, and the alcohol-free beers could clearly be separated from the regular beers, also. Therefore, it would be possible to use it for quality control screening of beers to check if the well-known brand character is consistent over time to satisfy the expectations of customers.[10]

■ ASSOCIATED CONTENT

Supporting Information

Tables S1−S6 and Figures S1−S3. This material is available free of charge via the Internet at http://pubs.acs.org.

Table 7. Predicted Results of the Analyzed Samples (Altbier (A), Helles (H), Kölsch (K), Pilsener Bier (P), Schwarzbier (S), and Wheat Beer (W), and \alc without Alcohol)

	predicted variety								
variety	A	H	K	P	P\alc	S	W	W\alc	correct predictions (%)
A (n = 4)	4								100.0
H (n = 6)		5		1					83.3
K (n = 6)			5				1		83.3
P (n = 23)		3		20					87.0
P\alc (n = 2)					2				100.0
S (n = 1)						1			100.0
W (n = 3)							3		100.0
W\alc (n = 1)								1	100.0
total									89.1

dx.doi.org/10.1021/jf405832u | J. Agric. Food Chem. 2014, 62, 3081−3091

AUTHOR INFORMATION

Corresponding Author

*(M.A.J.) E-mail: maik.jochmann@uni-due.de. Phone: +49 201 183-6775. Fax: +49 201 183-6773.

Notes

The authors declare no competing financial interest.

REFERENCES

(1) Jelen, H. H.; Majcher, M.; Dziadas, M. Microextraction techniques in the analysis of food flavor compounds: a review. *Anal. Chim. Acta* **2012**, *738*, 13−26.

(2) Plutowska, B.; Chmiel, T.; Dymerski, T.; Wardencki, W. A headspace solid-phase microextraction method development and its application in the determination of volatiles in honeys by gas chromatography. *Food Chem.* **2011**, *126*, 1288−1298.

(3) Horák, T.; Čulík, J.; Kellner, V.; Čejka, P.; Hašková, D.; Jurková, M.; Dvořák, J. Determination of selected beer flavours: comparison of a stir bar sorptive extraction and a steam distillation procedure. *J. Inst. Brew.* **2011**, *117*, 617−621.

(4) Rodrigues, F.; Caldeira, M.; Camara, J. S. Development of a dynamic headspace solid-phase microextraction procedure coupled to GC-qMSD for evaluation the chemical profile in alcoholic beverages. *Anal. Chim. Acta* **2008**, *609*, 82−104.

(5) Sterckx, F. L.; Missiaen, J.; Saison, D.; Delvaux, F. R. Contribution of monophenols to beer flavour based on flavour thresholds, interactions and recombination experiments. *Food Chem.* **2011**, *126*, 1679−1685.

(6) Dong, L.; Piao, Y.; Zhang, X.; Zhao, C.; Hou, Y.; Shi, Z. Analysis of volatile compounds from a malting process using headspace solid-phase micro-extraction and GC-MS. *Food Res. Int.* **2013**, *51*, 783−789.

(7) Hrivnak, J.; Smogrovicova, D.; Nadasky, P.; Lakatosova, J. Determination of beer aroma compounds using headspace solid-phase microcolumn extraction. *Talanta* **2010**, *83*, 294−296.

(8) Lyumugabe, F.; Bajyana Songa, E.; Wathelet, J. P.; Thonart, P. Volatile compounds of the traditional sorghum beers "ikigage" brewed with *Vernonia amygdalina* "umubirizi". *Cerevisia* **2013**, *37*, 89−96.

(9) Rodriguez-Bencomo, J. J.; Munoz-Gonzalez, C.; Martin-Alvarez, P. J.; Lazaro, E.; Mancebo, R.; Castane, X.; Pozo-Bayon, M. A. Optimization of a HS-SPME-GC-MS procedure for beer volatile profiling using response surface methodology: application to follow aroma stability of beers under different storage conditions. *Food Anal. Methods* **2012**, *5*, 1386−1397.

(10) Saison, D.; De Schutter, D. P.; Vanbeneden, N.; Daenen, L.; Delvaux, F.; Delvaux, F. R. Decrease of aged beer aroma by the reducing activity of brewing yeast. *J. Agric. Food Chem.* **2010**, *58*, 3107−3115.

(11) Tsuji, H.; Mizuno, A. Volatile compounds and the changes in their concentration levels during storage in beers containing varying malt concentrations. *J. Food Sci.* **2010**, *75*, C79−C84.

(12) Vázquez-Araújo, L.; Rodríguez-Solana, R.; Cortés-Diéguez, S. M.; Domínguez, J. M. Use of hydrodistillation and headspace solid-phase microextraction to characterize the volatile composition of different hop cultivars. *J. Sci. Food Agric.* **2013**, *93*, 2568−2574.

(13) Zapata, J.; Mateo-Vivaracho, L.; Lopez, R.; Ferreira, V. Automated and quantitative headspace in-tube extraction for the accurate determination of highly volatile compounds from wines and beers. *J. Chromatogr., A* **2012**, *1230*, 1−7.

(14) Gonçalves, J.; Figueira, J.; Rodrigues, F.; Câmara, J. S. Headspace solid-phase microextraction combined with mass spectrometry as a powerful analytical tool for profiling the terpenoid metabolomic pattern of hop-essential oil derived from Saaz variety. *J. Sep. Sci.* **2012**, *35*, 2282−2296.

(15) Vidgren, V.; Multanen, J.-P.; Ruohonen, L.; Londesborough, J. The temperature dependence of maltose transport in ale and lager strains of brewer's yeast. *FEMS Yeast Res.* **2010**, *10*, 402−411.

(16) Saerens, S. M. G.; Verbelen, P. J.; Vanbeneden, N.; Thevelein, J. M.; Delvaux, F. R. Monitoring the influence of high-gravity brewing and fermentation temperature on flavour formation by analysis of gene expression levels in brewing yeast. *Appl. Microbiol. Biotechnol.* **2008**, *80*, 1039−1051.

(17) Jochmann, M. A.; Yuan, X.; Schilling, B.; Schmidt, T. C. In-tube extraction for enrichment of volatile organic hydrocarbons from aqueous samples. *J. Chromatogr., A* **2008**, *1179*, 96−105.

(18) Laaks, J.; Jochmann, M. A.; Schilling, B.; Schmidt, T. C. In-tube extraction of volatile organic compounds from aqueous samples: an economical alternative to purge and trap enrichment. *Anal. Chem.* **2010**, *82*, 7641−7648.

(19) Rasanen, I.; Viinamäki, J.; Vuori, E.; Ojanperä, I. Headspace in-tube extraction gas chromatography-mass spectrometry for the analysis of hydroxylic methyl-derivatized and volatile organic compounds in blood and urine. *J. Anal. Toxicol.* **2010**, *34*, 113−121.

(20) Akinlua, A.; Jochmann, M. A.; Laaks, J.; Ewert, A.; Schmidt, T. C. Microwave-assisted nonionic surfactant extraction of aliphatic hydrocarbons from petroleum source rock. *Anal. Chim. Acta* **2011**, *691*, 48−55.

(21) Niu, L.; Bao, J.; Zhao, L.; Zhang, Y. Odor properties and volatile compounds analysis of *Torreya grandis* aril extracts. *J. Essent. Oil Res.* **2011**, *23*, 1−6.

(22) Zapata, J.; Lopez, R.; Herrero, P.; Ferreira, V. Multiple automated headspace in-tube extraction for the accurate analysis of relevant wine aroma compounds and for the estimation of their relative liquid-gas transfer rates. *J. Chromatogr., A* **2012**, *1266*, 1−9.

(23) Socaci, S. A.; Socaciu, C.; Tofană, M.; Raţi, I. V.; Pintea, A. In-tube Extraction and GC−MS analysis of volatile components from wild and cultivated sea buckthorn (*Hippophae rhamnoides* L. ssp. Carpatica) berry varieties and juice. *Phytochem. Anal.* **2013**, *24*, 319−328.

(24) De La Calle Garcia, D.; Reichenbächer, M.; Danzer, K.; Hurlbeck, C.; Bartzsch, C.; Feller, K. H. Analysis of wine bouquet components using headspace solid-phase microextraction-capillary gas chromatography. *HRC−J. High Resol. Chromatogr.* **1998**, *21*, 373−377.

(25) Kornacki, W.; Fastyn, P.; Gierczak, T.; Gawlowski, J.; Niedzielski, J. Reactivity of carbon adsorbents used to determine volatile organic compounds in atmospheric air. *Chromatographia* **2006**, *63*, 67−71.

(26) Cao, X.-L.; Hewitt, C. N. Study of the degradation by ozone of adsorbents and of hydrocarbons adsorbed during the passive sampling of air. *Environ. Sci. Technol.* **1994**, *28*, 757−762.

(27) Pawliszyn, J. Sample preparation: quo vadis? *Anal. Chem.* **2003**, *75*, 2543−2558.

(28) U.S. Office of the Federal Register, Title 40 Code of Federal Regulations, Protection of environment, Part 136 Appendix B, revision 1.11. In [online] 7-1-09 ed.; National Archives and Records Administration: Washington, DC, 2009; p. v. http://purl.access.gpo.gov/GPO/LPS494.

(29) Poerschmann, J. Sorption of hydrophobic organic compounds on nonpolar SPME fibers and dissolved humic organic matter − part III: Application of the solubility parameter concept to interpret sorption on solid phase microextraction (SPME) fiber coatings. *J. Microcolumn Sep.* **2000**, *12*, 603−612.

(30) Laaks, J.; Letzel, T.; Schmidt, T. C.; Jochmann, M. A. Fingerprinting of red wine by headspace solid-phase dynamic extraction of volatile constituents. *Anal. Bioanal. Chem.* **2012**, *403*, 2429−2436.

(31) Liu, M.; Zeng, Z.; Xiong, B. Preparation of novel solid-phase microextraction fibers by sol-gel technology for headspace solid-phase microextraction-gas chromatographic analysis of aroma compounds in beer. *J. Chromatogr., A* **2005**, *1065*, 287−299.

(32) Zimmermann, T.; Ensinger, W. J.; Schmidt, T. C. Depletion solid-phase microextraction for the evaluation of fiber-sample partition coefficients of pesticides. *J. Chromatogr., A* **2006**, *1102*, 51−59.

(33) Dean, J. R.; Tomlinson, W. R.; Makovskaya, V.; Cumming, R.; Hetheridge, M.; Comber, M. Solid-phase microextraction as a method for estimating the octanol-water partition coefficient. *Anal. Chem.* **1996**, *68*, 130−133.

(34) Venables, W. N.; Ripley, B. D. *Modern Applied Statistics with S*, 4th ed.; Springer: New York, 2002; p *xi*, 495 pp.

(35) U.S. Environmental Protection Agency. Exposure assessment tools and models, http://www.epa.gov/opptintr/exposure/pubs/episuitedl.htm (accessed Dec 6, 2013).

This way, information about the difference in folate distribution within or between individual potatoes of the same variety, age, and size can be used to gain further insight into the divergence of reported results.

Here, we report on the development, the validation, and the application of an ultrahigh-performance liquid chromatography−tandem mass spectrometry (UHPLC-MS/MS) method, capable of providing a folate profile (encompassing six folate monoglutamates), starting from only 200 mg (FW) of potato flesh. To expand the use of our method, we opted for a single calibration curve, covering a wide dynamic range. This way, potatoes with higher folate content (obtained, for example, through biofortification via breeding[2] or genetic engineering[23−25]) can also be analyzed. The method was used to investigate the differences in folate distribution in tubers of the potato variety Désirée at different stages of maturation. Moreover, this method was used to compose, for the first time, a two-dimensional folate profile throughout potato tubers in order to visualize the biological variability both within and between potato tubers of the potato variety Désirée.

MATERIALS AND METHODS

All manipulations involving folates were done under subdued light. The air in the headspace was not displaced by use of an inert gas, but the solutions used for preparation of the stock solutions, the working solutions, and the extraction buffer were flushed with nitrogen.

Tetrahydrofolate (THF), 5-methyltetrahydrofolate (5-MTHF), 5,10-methenyltetrahydrofolate (5,10-CH+THF), 10-formyl folic acid (10-CHOFA), 5-formyl tetrahydrofolate (5-CHOTHF), and folic acid (FA) were purchased from Schirck's Laboratories (Jona, Switzerland). [$^{13}C_5$]-THF, [$^{13}C_5$]-5-MTHF, [$^{13}C_5$]-5,10-CH+THF, and [$^{13}C_5$]-FA were obtained from Merck Eprova (Schaffhausen, Switzerland) and were used as internal standards (ISs, labeling yield for all >98%) for their respective analogues. [$^{13}C_5$]-FA was also used as an IS for 5-CHOTHF and 10-CHOFA, based on its chromatographic retention characteristics.

Ultrapure water was obtained from a Synergy ultrapure water purification system (Millipore, Brussels, Belgium). Formic acid, sodium phosphate, ascorbic acid, dithiotreitol (DTT), and activated charcoal were purchased from Sigma (Diegem, Belgium). Methanol and acetonitrile of LC-MS grade were purchased from Biosolve (Valkenswaard, The Netherlands). BCR-121 wholemeal flour was obtained from the European Commission, Institute for Reference Materials and Measurement (Brussels, Belgium).

α-Amylase (type I-A, from porcine pancreas, 23.5 units/μL, EC no. 232-565-6) and protease (type XIV, from *Streptomyces griseus*, ≥3.5 units/mg, EC no. 232-909-5) were purchased from Sigma. Male rat serum was acquired from Harlan (Horst, The Netherlands). Protease was dissolved in distilled water (4 mg/mL). To remove most of the endogenous folates, protease and rat serum were mixed with a $^1/_{10}$th volume of activated charcoal and stirred for 1 h on ice, centrifuged, filtered, and divided into 500 μL aliquots. Both enzymes were stored at −80 °C. α-Amylase was used without pretreatment and stored at 4 °C.

Homogenization was either performed by manually grinding single samples in liquid nitrogen with mortar and pestle or with an IKA-18 basic Ultra-Turrax (Labo service, Kontich, Belgium). Larger volumes were mixed and subsequently divided into representative aliquots of actual samples. For ultrafiltration, 3 mL (Amicon, Millipore) 3 kDa molecular weight cutoff membrane filters were used. Ultrafiltration was done in an Eppendorf centrifuge 5804 R at 4 °C (Hamburg, Germany).

The potato variety Nicola was bought in a local supermarket (for optimization of sample preparation) or provided by a local distributor (for profiling). The potato variety Désirée, which we used for genetic engineering purposes,[25] was provided by the Laboratory of Functional Plant Biology (for determination at different stages of maturation) or bought in a local supermarket (for validation experiments).

Preparation of Stock and Working Solutions. All folate stock solutions were prepared in a 50 mM phosphate buffer, pH 7.5 or 3 (for 5,10-CH+THF, as this compound is more stable at acidic pH) containing 1% ascorbic acid and 0.5% DTT/methanol (50/50, v/v). Both standard and IS stock solutions were stored at −80 °C. Working solutions were prepared daily by appropriate dilution with the extraction buffer, which was a 50 mM phosphate buffer at pH 7.5, containing 1% ascorbic acid, 0.5% DTT, and the IS (with a concentration of 20 ng/mL for [$^{13}C_5$]-THF and 40 ng/mL for the other ISs).

Lyophilization. Dry matter content determination and freeze-drying of frozen homogeneous samples were performed by an Amsco FINN-AQUA GT4 freeze-dryer (GEA, Köln, Germany). The cycle comprised primary drying at −20 °C overnight, followed by a secondary drying step at 0 °C for three hours. The pressure for both cycles was held at 100 μbar.

Chromatography. Chromatography was performed on a Waters Acquity UHPLC system including a binary pump, controlled by analyst 1.5.2 software (AB Sciex, Toronto, Canada). The column oven temperature was maintained at 60 °C, and the autosampler was at 4 °C. An Acquity HSS T3 column (C18, 150 mm × 2.1 mm; 1.8 μm particle size, from Waters) with a VanGuard precolumn (C18, 5 mm × 2.1 mm; 1.8 μm particle size, from Waters) was used. The injection volume was 10 μL. For gradient elution, the mobile phase consisted of eluent A (0.1% formic acid in water) and eluent B (0.1% formic acid in acetonitrile) and was pumped at a flow rate of 0.6 mL/min. Initially, the same gradient was applied as described by De Brouwer et al.[26] However, we adapted this gradient to eliminate an interference coeluting with FA. The starting condition (100% A) was kept for 1 min. Subsequently, there was a nonlinear, convex increase to 95% B in 3 min, which was kept for 1 min. The mobile phase was then immediately adjusted to its initial composition and held for 3 min for re-equilibration, resulting in a total time of 8 min.

MS Instrumentation and Settings. The detection was performed by positive electrospray ionization (ESI) utilizing heated auxiliary gas (Turbospray), in the scheduled MRM mode on an Applied Biosystems API 4000 tandem mass spectrometer (Ontario, Canada). On the basis of the largest peak width at the base (5-MTHF), an MRM detection window of 30 s was chosen, together with a 0.5 s target scan time, generating at least 27 data points for 5-MTHF. The source conditions were optimized and were set as follows: source temperature, 500 °C; ion spray voltage, 3.5 kV; Q1 and Q3, unit mass resolution. The interface heater was on (100 °C); nitrogen was used for the nebulizer (gas 1), heater (gas 2), curtain, and collisionally activated dissociation (CAD) gas. Gasses 1 and 2 and the curtain gas had respective pressure settings at 70, 90, and 25 psi. The vacuum setting for CAD was set at 8, a configuration-dependent arbitrary value of the instrument. Compound parameters, together with retention times are given in Table 1.

Sample Preparation. The general sample preparation protocol included boiling, homogenization, extraction with trienzyme treatment (α-amylase, protease, and conjugase), and additional heat treatments to stop enzyme activities. The resulting solutions were ultrafiltrated at 12 851*g* for 15 min prior to UHPLC-MS/MS analysis. Before all manipulations, 1.5 mL of the extraction buffer was added to ±200 mg of fresh potato flesh, taken with a kitchen knife from the center of a single tuber. When samples were prepared in bulk (for optimization and validation purposes), a corresponding volume of extraction buffer was added to central sections of potato tubers (8−10 g, collected from 2−3 mature tubers). This quantity was afterward divided into aliquots corresponding to 200 mg of fresh potato flesh. Several variables in distinct steps of this general protocol were evaluated to obtain the best folate recovery. These included a comparison of homogenization by mixing or grinding with liquid nitrogen, boiling or not, freeze-drying or not, and varying the volumes of the three enzymes: 0, 20, 30, or 40 μL of α-amylase (0, 470, 705, or 940 units, respectively); 0 or 150 μL of the charcoal-treated protease solution (0 or 2.1 units, respectively); 100 or 150 μL of the charcoal-treated rat serum conjugase solution. Since starch is a main component of potato flesh, we opted to test three increasing volumes of α-amylase. The evaluation of boiling and

Table 1. Compound Parameters for Six Folates and Their Internal Standards[a]

	precursor ion (m/z)	product ion (m/z)	t_r (min)	DP (V)	EP (V)	CE (V)	CXP (V)
THF	446.2	299.3	3.19	70	10	30	20
		166.4		70	10	59	12
5-MTHF	460.3	313.2	3.34	70	10	30	18
		194.2		70	10	53	14
5,10-CH +THF	456.2	412.1	3.56	75	10	40	10
		282.1		75	10	65	16
10-CHOFA	470.1	295.4	3.91	65	10	35	16
		176.3		65	10	59	14
5-CHOTHF	474.2	327.2	3.96	61	10	29	8
		299.3		61	10	45	16
FA	442.1	295.3	4.09	61	10	30	18
		176.1		61	10	57	14
[$^{13}C_5$]-THF	451.1	299.3	3.19	70	10	30	20
[$^{13}C_5$]-5-MTHF	465.3	313.2	3.34	70	10	30	18
[$^{13}C_5$]-5,10-CH+THF	461.0	416.2	3.56	75	10	40	10
[$^{13}C_5$]-FA	447.2	295.3	4.09	65	10	20	16

[a] t_r, retention time; DP, declustering potential; EP, entrance potential; CE, collision energy; CXP, collision cell exit potential; V, volt. The first transition was used as quantifier, the second was used as qualifier.

lyophilization prior to storage was done in a joint experiment: skinless fresh potato was boiled or kept on ice and immediately homogenized by mixing. Subsequently, representative aliquots were weighed individually before and after lyophilization. These samples were kept at −80 °C until analysis.

VALIDATION

Selectivity. Selectivity for the folate monoglutamates was investigated by injecting aliquots of neat buffer solutions, spiked with the six monoglutamates and the four ISs (individually and together).

Sensitivity. The limit of detection (LOD) and lower limit of quantitation (LLOQ) are defined as the concentrations with a signal-to-noise ratio equal to or larger than 3 and 10, respectively. In this case, the LLOQ was arbitrarily set as the lowest point of the calibration curve because of the lack of a blank matrix. For determination of the LOD, potato matrix was diluted 1:20 in ultrapure water and boiled in the presence of light to destroy most endogenous folates. As this still yielded a measurable signal for 5-MTHF, the matrix was further diluted 1:20 and ultrafiltrated to approach a blank matrix. The matrix was prepared this way because the LOD is a qualitative descriptor of sensitivity, in contrast to the LLOQ, where possible matrix effects can affect calibration. It was then used to serially dilute the six folate standards. The average short-term noise of five independent injections of these serially diluted standards was used to correlate the peak heights with the corresponding concentrations.

Linearity and Calibration. Prior to testing the linearity of a calibration model, homoscedasticity of the calibrators was investigated. Therefore, residual plots were generated and Fisher's tests ($p < 0.01$) were performed. To obtain a linear model, the most common weighting factors ($1/\sqrt{x}$, $1/x$, $1/x^2$, $1/\sqrt{y}$, $1/y$, and $1/y^2$) and transformations (logarithmic or square rooted) were tested by comparing the sums of percent relative error (%RE, calculated as the difference between the obtained and the nominal concentration, divided by the nominal concentration and multiplied by 100), in accordance with the protocol described by Almeida et al.[27] Linearity of the most appropriate model for each folate was then tested by performing analysis of variance (ANOVA) lack of fit (LOF) tests.

Calibration curves with seven calibrators were constructed by spiking a mix of the six standards to a 1:20 dilution of potato matrix in extraction buffer. Four quality controls (QCs), including the lower and upper limits of quantitation (ULOQ), were prepared similarly but in a 1:2 diluted potato matrix, except the LLOQ QC, which was prepared in a 10-fold diluted matrix, so the endogenous folate content would not exceed the spiked concentration. The concentrations (in μg/100 g of FW) spiked to the calibrators and QCs are depicted in Table S2 (Supporting Information). After completing the sample preparation protocol, extracts of these samples were injected onto the UHPLC-MS/MS, not randomly but in increasing order of calibrator concentration. To make sure this did not contribute to heteroscedasticity, the carry-over effect was investigated by injecting a blank water sample after injection of the calibrator with the highest concentration. Lack of a significant carry-over requires that the signal obtained at the retention times of the respective folates should at all times be less than 20% or less than 5% of the LLOQ of the folate standards and ISs, respectively.

Accuracy, Precision and Measurement Uncertainty. Experiments for accuracy and precision were performed at four QC levels on three nonconsecutive days, in duplicate ($n = 3 \times 2$). Every day, fresh calibrators and QCs were prepared and analyzed as described above. Zero samples (i.e., samples with only IS spiked) were also included to subtract the endogenous folate content of the matrix. Intra- and interday precision (% relative standard deviation or %RSD), together with accuracy (%bias) were calculated as reported by Wille et al.[28] and should be less than 15%, except at the LLOQ, where they should be less than 20%. The measurement uncertainty is represented by a 95% confidence interval (CI). The interval was constructed by the combination of %bias and the %RSD (interday) of the measured value. This way, the interval becomes [measured value ± (|%bias| + 2 × %RSD)].

Matrix Effect and Recovery. To evaluate the matrix effect (ME, where percentage values <100% represent ion suppression and >100% represent ion enhancement) and recovery (REC), three separate batches of samples ($n = 3$) were prepared as suggested by Matuszewski et al.[29] Batch A contained the "neat" standards and consisted of extraction buffer, spiked at three QC levels (LOW, MED, and HIGH). Batches B and C contained 1:2 diluted potato matrix spiked after and before sample preparation, respectively. For the latter two batches, zero samples were again included. The ME and REC were then calculated as B/A*100 and C/B*100, respectively, where the zero sample signals were subtracted from B and C.

Short-Term Stability (STS) and Freeze−Thaw Stability (FTS). Aliquots of sample extracts ($n = 3$), spiked at the four QC levels, were immediately injected onto the UHPLC-MS/MS (and stayed in the autosampler at 4 °C for reanalysis after 24 h) or were frozen at −20 °C (FTS). Three freeze−thaw cycles were also performed in one day and after each cycle analysis was performed.

Analysis of Reference Material BCR-121 (Wholemeal Flour). Samples of 200 mg ($n = 5$) were treated the same way

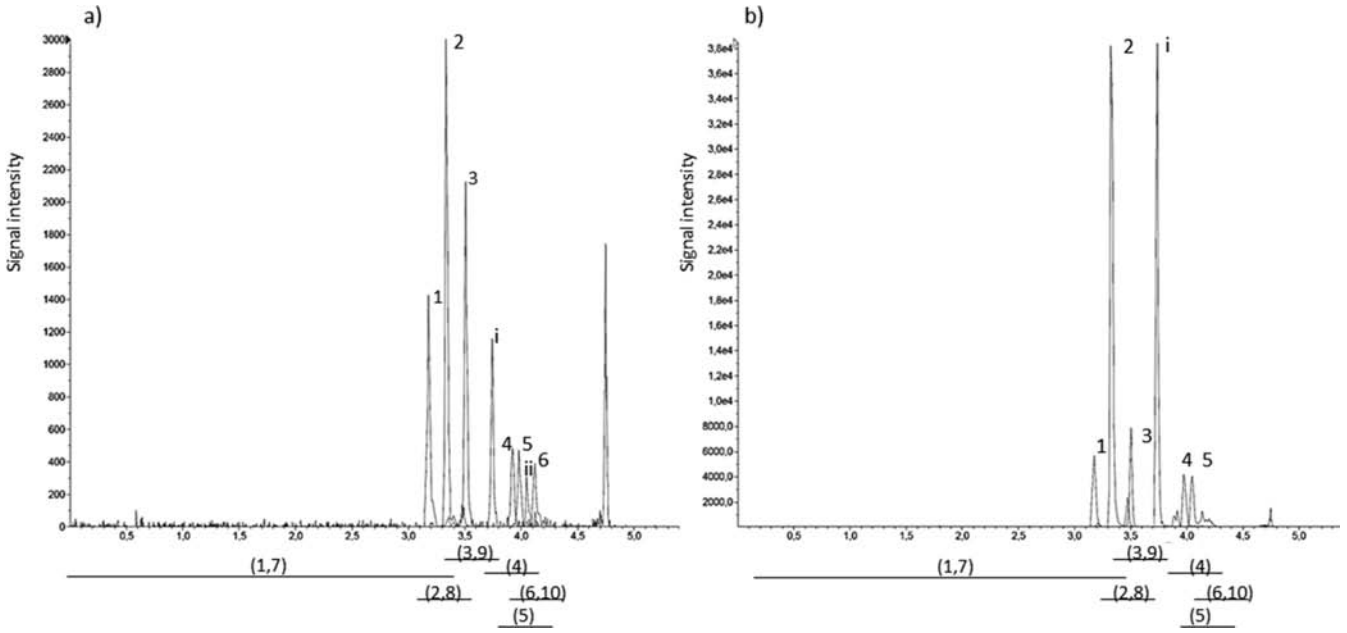

Figure 1. (a) MRM chromatogram of the lowest calibrator, i.e., spiked at the LLOQ and (b) MRM chromatogram representing the folate profile of potato variety Désirée (scan windows are depicted for each folate and its internal standard below the chromatogram). (1) THF; (2) 5-MTHF; (3) 5,10-CH+THF; (4) 10-CHOFA; (5) 5-CHOTHF; (6) FA; (7) [$^{13}C_5$]-THF; (8) [$^{13}C_5$]-5-MTHF; (9) [$^{13}C_5$]-5,10-CH+THF; (10) [$^{13}C_5$]-FA; (i) signal at first 5-CHOTHF MRM transition; (ii) signal at first FA MRM transition.

as fresh potato flesh, apart from the homogenization step, and underwent the full trienzyme treatment.

Application to the Potato Variety Désirée. The developed procedure was applied to the potato variety Désirée at three stages of maturation. Potato samples (200 mg, taken from the center of the tubers) were treated or not with conjugase to gain information about the polyglutamylation status. Immature tubers were grown at the Laboratory of Functional Plant Biology, harvested 17 weeks after plantation, and kept frozen at −20 °C until analysis. Store-bought mature tubers were kept at room temperature and analyzed that same day or after two months (when tubers were sprouting).

Folate Profiling of Potato Variety Nicola. Three potatoes with the same level of maturation and of uniform size were chosen. From each of these, a central slice was cut with a kitchen knife and divided into segments, to form a two-dimensional representation of the tuber. From the basal to the horizontal opposite apical end, 13 segments were taken, including 1 central and 2 marginal segments containing peel. From the upper surface to below, seven segments were taken, again including one central and two marginal segments. Each of these segments was further subdivided into two subsections. The first subsection was used for determination of dry matter content, the second subsection was further divided into two 200 mg sections to create genuine replicates.

RESULTS AND DISCUSSION

Eliminating Coeluting Interferences in Potato Matrix. The experiments involving sample preparation were conducted on the variety Nicola with a HPLC-MS/MS procedure as described by De Brouwer et al.[30] The initially determined total and free monoglutamate contents of this variety were respectively 21.78 ± 1.42 and 13.62 ± 0.35 μg/100 g, indicating a polyglutamylation status of 37.5%. Because of a coeluting interference, FA had to be quantified using its second MRM transition (442.1 → 176.2). To eliminate this problem, we switched the linear increase of the gradient to a convex type, which resulted in a more swift increase of mobile phase B. This modification caused a change in retention of the matrix-specific interference, now allowing a selective detection of FA with its first transition (442.1 → 295.3). Application of this gradient also improved the peak shape of 5-CHOTHF, which now eluted in a shorter time interval. Representative chromatograms, obtained with the optimized gradient, are depicted in Figure 1. Figure 1a shows a chromatogram of diluted potato extracts, spiked at the lowest calibrator level, that is, at LLOQ, while Figure 1b depicts the folate profile of potato variety Désirée. In the former, the respective scan windows of the scheduled MRM algorithm are indicated for each folate and IS at the bottom of the chromatogram. It should be noted that the fact that 10-CHOFA and 5-CHOTHF are not baseline separated does not pose a problem, since MS can distinguish these compounds. We deliberately chose not to detect or distinguish between 5,10-methylenetetrahydrofolate (5,10-CH_2THF) and 10-formyl tetrahydrofolate (10-CHOTHF), since these are highly susceptible to interconversion and oxidation at neutral (extraction protocol) and acidic (chromatographic run) pH, even with the use of antioxidants.[31,32]

Sample Preparation. Experiments involving the trienzyme treatment were performed twice. The influence of the treatment was initially investigated using a previously validated HPLC-MS/MS method.[30] α-Amylase and protease were added in increasing amounts to evaluate folate recovery, and conjugase was added in two volumes to evaluate the deconjugation efficiency (Figure S2a, Supporting Information). A one-way ANOVA and complementary t tests showed no significant impact ($p < 0.05$) on folate recovery when using α-amylase or protease, supporting the findings by Konings et al.[14] There was also no significant difference ($p < 0.05$) between the addition of 100 and 150 μL of conjugase. These results were confirmed using the newly optimized UHPLC-MS/MS

dx.doi.org/10.1021/jf500753v | J. Agric. Food Chem. 2014, 62, 3092−3100

Table 2. Sensitivity and Calibration Data

	LOD[a]	linear range[a]	slope [95% CI]	intercept [95% CI]	R^2
THF	0.0429	0.2349−234.8611	31.9469 [29.4908−34.4030]	−0.0024 [−0.0077 to 0.0028]	0.9970
5-MTHF	0.0057	0.2161−216.0722	33.5891 [29.1018−38.0763]	−0.0017 [−0.0037 to 0.0003]	0.9909
5,10-CH+THF	0.0574	0.2242−224.1688	33.8356 [30.7014−36.9699]	−0.0005 [−0.0030 to 0.0021]	0.9941
10-CHOFA	0.0474	0.2423−242.2778	38.2897 [32.7726−43.8076]	−0.0014 [−0.0021 to −0.0008]	0.9859
5-CHOTHF	0.0233	0.2252−225.1700	49.3652 [44.9580−53.7723]	−0.0001 [− 0.0009 to 0.0007]	0.9945
FA	0.0135	0.2423−242.2778	25.9820 [24.9862−26.9778]	−0.0005 [−0.0027 to 0.0017]	0.9989

[a]Values in μg/100 g.

method. Yet, although trienzyme treatment did not significantly affect folate recovery from the center of the potato matrix, we still opted to include this treatment: the resulting extracts were less gummy and easier to manipulate after consecutive heating and cooling steps. In addition, implementation of trienzyme treatment may overcome potential variability, introduced by the somewhat different composition of different sections of a tuber; for example, the dry matter content is typically lowest in the center.[33] Evaluation of the homogenization step revealed that there was no significant difference ($p < 0.05$) in folate recovery between mixing and grinding with liquid nitrogen. We therefore used mixing, which is less laborious, for further experiments and validation of the method. Since boiling prior to homogenization may aid in degrading the matrix and reducing the enzymatic and oxidative degradation of folates,[1,34−36] the impact of this manipulation on recovery was also investigated (Figure S2b, Supporting Information). In the same experiment, samples were also lyophilized or not after homogenization. The purpose of this manipulation was to find out if freeze-drying compensates for the increased variability caused by differences in moisture content, rather than preparing them for storage. Samples that were only boiled had a significantly higher folate content (13.32 ± 0.85 μg/100 g of FW, $p < 0.05$) than samples that were left untreated or that were lyophilized (with or without prior boiling). The advantage that lyophilization may offer, that is, compensating for the variable moisture content of potatoes,[2] was clearly lost, so we decided not to include a lyophilization step but to immediately freeze the samples after boiling and homogenization. Freeze-drying did provide information about the water content of the center of boiled and raw potatoes: 84.34% and 79.41%, respectively, in accordance with literature findings.[15] Therefore, freeze-drying can still be used to determine the dry matter content of frozen potato segments that do not undergo folate analysis. In conclusion, sample treatment comprised an initial boiling step followed by mixing. Subsequently, the samples were subjected to a trienzyme treatment: α-amylase (30 μL, 20 min at 37 °C) followed by an incubation with protease (150 μL, 1 h at 37 °C) and with deconjugase (100 μL rat serum, 2 h at 37 °C). The protease and conjugase incubations were each followed by a boiling step (10 min at 100 °C) to stop the respective enzyme activities. After each boiling step, samples were cooled down on ice. Samples intended for direct analysis of free monoglutamate content were spiked with water (instead of conjugase) and kept on ice (Figure S3, Supporting Information).

Validation. No signals from other folates or the IS were seen at the respective retention times of the injected standards, demonstrating the selectivity of the method. The calculated LODs of the six folates can be found in Table 2, together with the linear ranges, slopes, intercepts, and R^2 values of the final calibration curves. Visual evaluation of residual plots and performing Fisher's tests showed that the calibrator distribution was heteroscedastic. There was no carry-over: signals at the respective retention times of each folate or its IS, obtained after injection of a water sample, were all less than 5% of the LLOQ. Evaluation of several weighting factors and transformations demonstrated that applying a weighting factor of $1/x^2$ yielded the lowest sum of %RE. Subsequent performing of ANOVA LOF tests on this model showed a linear relationship for the chosen calibration ranges of all six folates. Intra- and interday precision (%RSD) and accuracy (%bias) were determined on three nonconsecutive days, in duplicate, by analyzing QCs that covered the whole calibration range (including the LLOQ and ULOQ). The data on precision and accuracy are summarized in Table 3, together with the 95% confidence limits of measurement uncertainty. Requirements for both intra- and interday precision were met for the six folates: all QCs had a % RSD lower than 15%, even at the LLOQ level. The accuracy also met acceptance criteria, except for 5-CHOTHF at its LLOQ, where accuracy was 22.69%.

The IS-corrected matrix effect exceeded the 85−115% range (Table 4, together with the recovery), though not excessive. While normalization using the IS did not compensate for matrix effects, it did compensate for the losses during sample preparation. Recoveries of more than 60% were observed for all folates at the three tested concentration levels. The (relatively) lower recovery of THF can be explained by its labile nature, while finding the actual cause for the recovery obtained for 5,10-CH+THF is more difficult: interconversion into 5-CHOTHF and the very unstable 10-CHOTHF at neutral pH, in the presence of antioxidants, has been described.[32] Subsequent oxidation of 10-CHOTHF to 10-CHOFA and other, nonfolate degradation products could result in a low recovery of 5,10-CH+THF. Alternatively, 10-CHOTHF and 5-CHOTHF might interconvert to 5,10-CH +THF at high temperature in acidic environment (as is the case during the chromatographic run). Since the recovery of 5,10-CH+THF was reproducible (%RSDs of 6.42, 13.67, and 13.58 for LOW, MED, and HIGH, respectively) and since other validation parameters yielded acceptable results, we consider quantitative determination of 5,10-CH+THF sufficiently reliable.

In general, our newly developed UHPLC-MS/MS shows improved sensitivity and precision at LLOQ, in comparison with a previously described method in rice.[26] In addition, changing to a scheduled MRM mode lowered the LODs. Although the matrix effects exceeded 15% at some instance, IS-corrected ME did not exceed the 75−125% range and given the acceptable results obtained for accuracy and precision can be regarded as "under control".

Stability. Two postextraction stability experiments were set up to find out whether or not the processed samples could be preserved over a short period of time for subsequent reanalysis. The resulting extracts could easily be kept in the autosampler

Table 3. Accuracy, Intra- and Interday Precision, and Measurement Uncertainty ($n = 3 \times 2$)

	accuracy (% bias)				intraday precision (%RSD)				interday precision (%RSD)				uncertainty [95% CI][b]			
	LLOQ	LOW	MED	HIGH	LLOQ	LOW	MED	HIGH	LLOQ	LOW	MED	HIGH	LLOQ	LOW	MED	HIGH
THF	13.93	10.16	−6.56	−1.82	1.62	3.70	6.07	1.42	2.41	3.78	6.07	8.18	[0.21−0.32]	[2.01−3.16]	[17.77−26.12]	[188.67−272.51]
5-MTHF	12.07	4.58	−0.65	1.50	3.20	2.49	6.76	4.53	4.66	9.58	8.03	5.80	[0.19−0.29]	[1.73−2.79]	[17.88−25.06]	[190.57−248.04]
5,10-CH +THF	10.49	−1.23[a]	−4.33	3.77	4.74	4.92[a]	5.46	2.48	5.41	7.08[a]	13.39	2.52	[0.20−0.30]	[1.87−2.55]	[14.77−28.12]	[212.15−253.10]
10-CHOFA	18.28	3.53	5.94	6.68	4.70	6.26	1.88	2.80	5.88	11.52	11.15	3.77	[0.20−0.37]	[1.84−3.17]	[18.42−32.92]	[221.70−295.21]
5-CHOTHF	22.69	10.70	10.94	6.87	7.34	3.38	2.87	3.94	12.00	4.10	3.40	7.33	[0.15−0.40]	[2.02−2.97]	[20.55−29.41]	[188.84−292.44]
FA	10.46	6.89	7.20	5.89	6.18	5.48	3.30	4.83	9.24	6.65	6.77	5.52	[0.19−0.35]	[2.07−3.11]	[20.59−31.36]	[213.11−300.00]

[a]Five QCs were used because one outlier confirmed with the Grubbs test ($p < 0.01$) was excluded. [b]Values in μg/100 g (calculated as [measured value ± (|%biasl + 2 × %RSD)]).

for 24 h after injection (STS, 24 h at 4 °C): the decrease was below 10% for all of the folates at the four concentration levels (Figure S4a, Supporting Information). This is sufficient to allow the samples to be reanalyzed the next morning, in case of a technical failure. The same was observed for vials with extracts that were submitted to three freeze−thaw cycles (FTS, three cycles at −20 °C) on the day of analysis. Again, the decrease did not exceed 10% (Figure S4b, Supporting Information). After performing these experiments, we concluded that reanalysis of treated samples can be performed after storage for up to 24 h at 4 °C or after freezing samples at −20 °C, followed by thawing up to three times.

Analysis of Reference Material BCR-121. Analysis of the BCR-121 wholemeal flour reference material confirmed the validity of our method: the total folate content (53.26 ± 4.93 μg/100 g of DW) as measured by UHPLC-MS/MS agreed well with the certified value (50 ± 7 μg/100 g), determined with a microbiological assay. Furthermore, the folate species concentration and distribution (1.01 ± 0.12, 5.34 ± 0.24, 5.34 ± 0.80, 10.31 ± 1.59, 29.04 ± 4.99, and 2.26 ± 0.17 μg/100 g for THF, 5-MTHF, 5,10-CH+THF, 10-CHOFA, 5-CHOTHF, and FA, respectively) were also in accordance with the literature.[18,37]

Application to Potato Tubers at Different Stages of Maturation (Variety Désirée). The folate content and distribution of individual folates (Figure 2a, b) in immature and mature Désirée tubers was comparable to those in Nicola tubers (determined with a previous method). The total folate content at these growth stages was 23.58 ± 1.51 and 24.01 ± 0.23 μg/100 g of FW, respectively, with polyglutamylation rates of only 5.4% and 5%. Hence, a comparable folate content and distribution was observed in lab-grown immature and store-bought mature potatoes. The polyglutamate content of sprouting potatoes was remarkably higher (60.49%), although their folate content had decreased (10.35 ± 0.95 μg/100 g of FW). This significantly lower folate content ($p < 0.05$) contrasts with Goyer and Navarre,[8,9] who reported a higher folate content in stored potatoes near sprouting. This discrepancy may be explained by the fact that our determination was performed on central potato flesh. Several authors[4,8,16] reported on the fact that the folate concentration is higher in potato peels, and Goyer and Navarre hypothesized that folate levels may increase when a tuber is sprouting (occurring at the peel).[8] The higher polyglutamylation level in sprouting potatoes approached the one reported by Konings et al. (90%),[14] but the distribution was different: 5-MTHF was still the predominant species, but it only accounted for 41% instead of 95% (Konings et al.)[14] of the total folate content.

Composing a Two-Dimensional Folate Profile of Mature Potato Tubers (Variety Nicola). To further investigate the biological variability, we first tried to exclude as many confounding (maturation stage, growth, harvest, and storage facilities) factors as possible: a batch of Nicola tubers at the same stage of maturation were obtained from a local distributor. From that batch, three tubers with the same dimensions were chosen for profiling of their cross sections. Comparison of genuine replicates within a tuber and corresponding segments of different potatoes were used for evaluating the variability within a certain potato variety.

Analysis of all segments resulted in a horizontal and vertical (x and y) profile, as shown in Figure 3a. In these tubers, the folate concentration was consistently higher in segments containing peel, than in central segments. The average total folate concentration of all the different segments was 17.95 ±

Table 4. Matrix Effects and Recovery (n = 3) for LOW, MED, and HIGH QCs

	matrix effects without IS (%)			matrix effects with IS (%)			recovery (%)		
	LOW	MED	HIGH	LOW	MED	HIGH	LOW	MED	HIGH
THF	80	90	92	121	110	109	63	64	74
5-MTHF	91	91	92	110	105	118	86	97	99
5,10-CH+THF	75	80	71	116	119	96	64	68	63
10-CHOFA	97	94	92	122	102	95	98	88	74
5-CHOTHF	109	98	86	124	110	89	76	94	97
FA	71	84	110	75	90	108	79	97	81

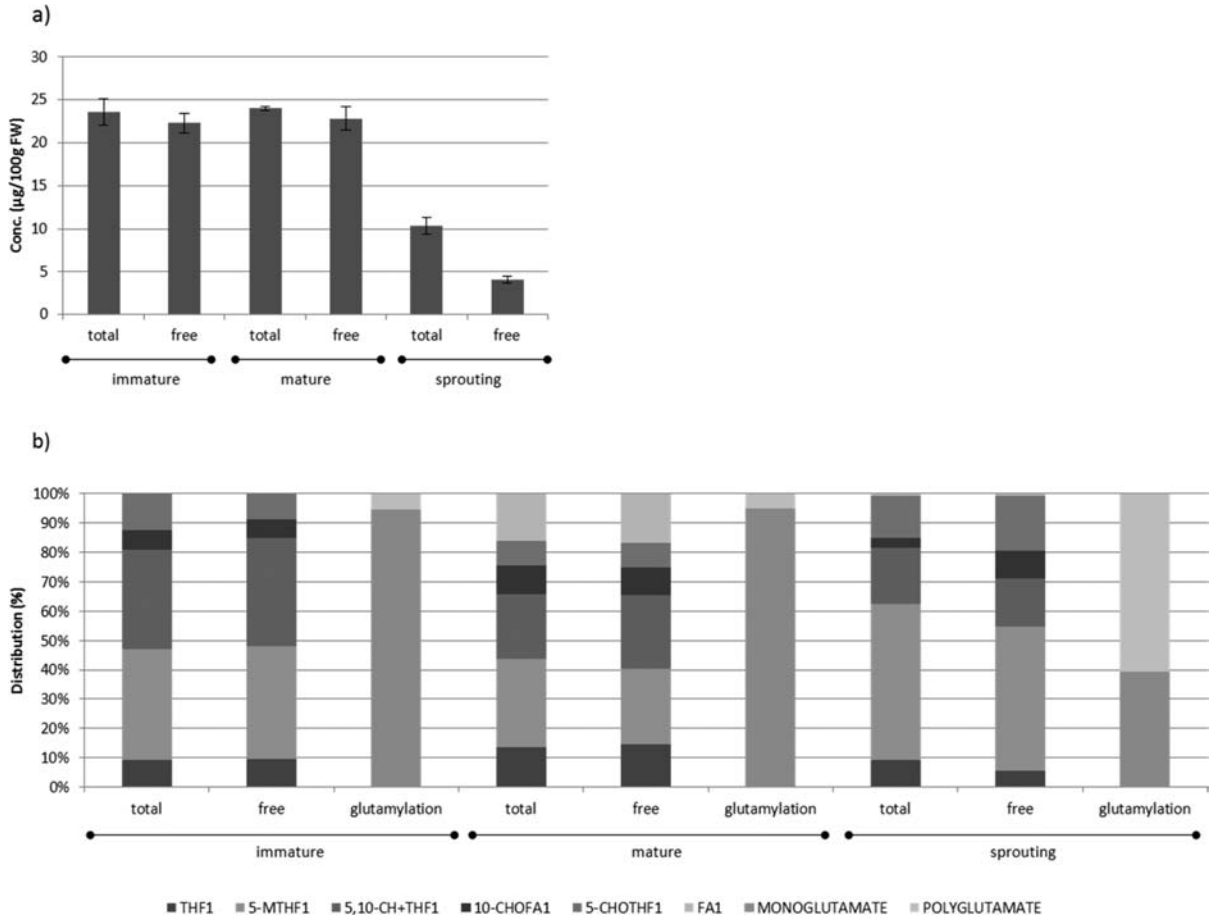

Figure 2. (a) Total and free folate monoglutamate content (error bars indicate the standard deviation) and (b) relative monoglutamate and polyglutamate distribution of immature, mature, and sprouting Désirée tubers.

3.17 μg/100 g of FW, but the average profiles of the horizontal and vertical sections (Figure 3b, c) show that this was not representative for a homogeneous distribution in the tuber: the average folate concentration in central segments was 14.08 ± 2.16 μg/100 g, increasing up to 86% toward segments containing peel (26.26 ± 11.24, 21.54 ± 5.61, 23.52 ± 3.92, and 20.31 ± 4.83 μg/100 g of FW for the peels at the basal, apical, upper, and lower ends, respectively). Interestingly, despite the increase of total folate concentration toward the peel, folate species distribution and polyglutamylation rates remained the same throughout the entire sections: 5-MTHF was still the predominant folate, representing an average 69% of the total folate. From this total folate, an average 78% was polyglutamylated. The comparable profiles of the three individual tubers also confirmed that 5-MTHF was the predominant folate in mature potato tubers variety Nicola.

The median variability (%RSD, Figure 3d) of genuine replicates within a single potato was 12%, increasing to 30% when considering corresponding segments of different potatoes. To make sure these results were not biased by the differences in dry matter content, the folate concentrations were also converted to their DW equivalents. This resulted in a moderate decrease in median variability (to 11% and 26% within and between the individual potatoes, respectively), demonstrating that folate concentrations in potato tubers may be expressed as FW as well as their DW equivalent.

The distribution of total folate, folate species, and glutamylation was similar throughout the cross sections of the three individual tubers. In addition, the "inter-tuber" variability of corresponding segments exceeded that of genuine replicates (<15%). Therefore, it is sufficient to analyze the segments from one single tuber in order to obtain a general image about a certain potato variety's folate profile and

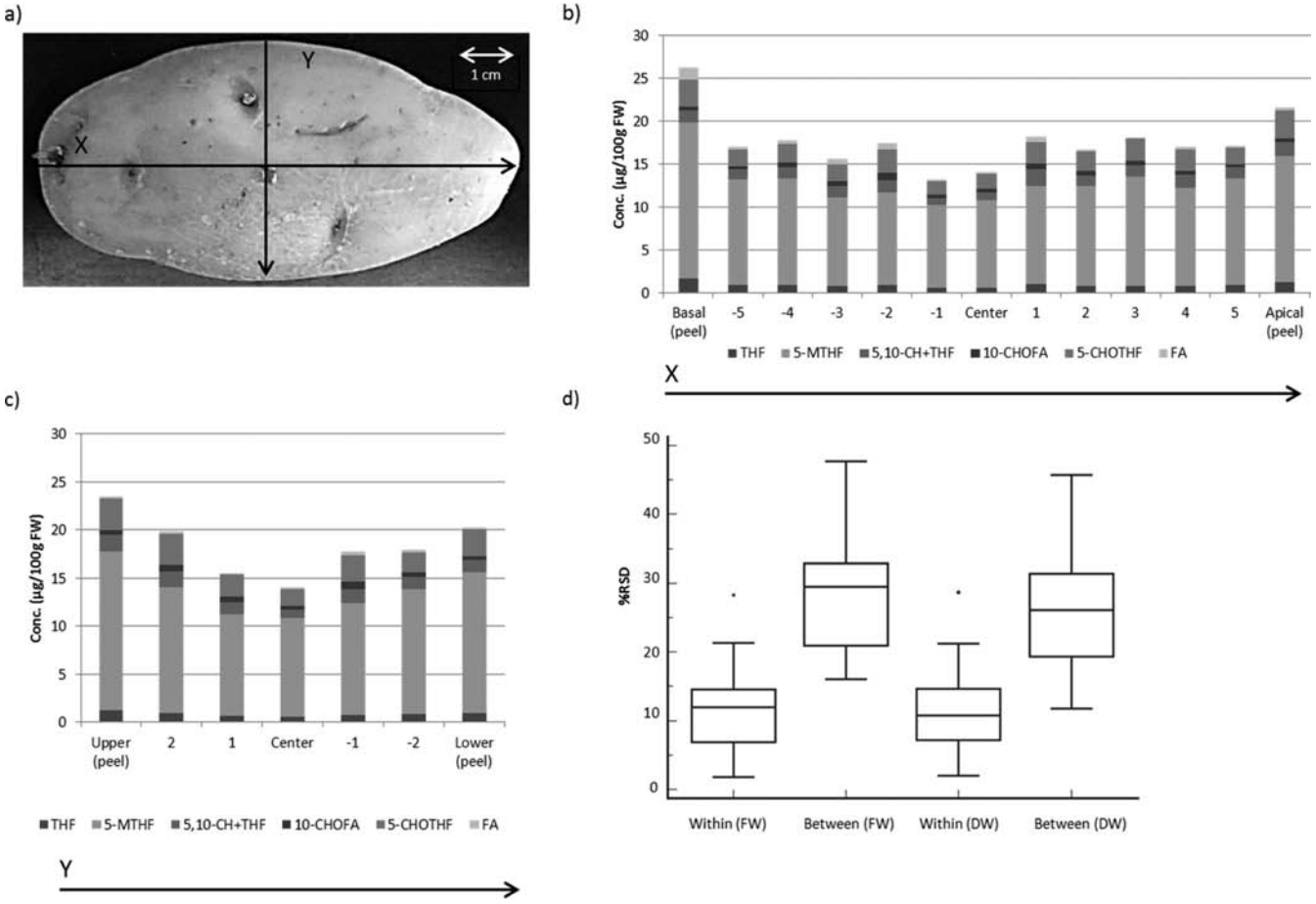

Figure 3. (a) Division of a tuber in a horizontal (x) and vertical (y) cross section. (b) Average folate profile (encompassing THF, 5-MTHF, 5,10-CH+THF, 10-CHOFA, 5-CHOTHF, and FA) of the horizontal (x) and (c) vertical (y) cross section of three potato tubers variety Nicola. (d) Boxplots demonstrating the difference in median variability within and between individual potato tubers variety Nicola, expressed as %RSD for fresh and dry weight (FW and DW, respectively).

glutamylation status at a certain stage of maturation. When knowledge about the average nutritive value (regarding absolute folate content) of a certain variety is the objective, pooling of the potato flesh will compensate for the large intravariety variability.

In conclusion, we successfully validated a UHPLC-MS/MS method for the quantitation of six folate vitamers in potato tubers. The extremely unstable folate species 5,10-CH_2THF and 10-CHOTHF prone to interconversion and oxidation were not included in the folate profile. The work is original in its application of the MS/MS technique and in the profiling of six different folate species throughout cross sections, providing a two-dimensional folate profile of a potato tuber. The use of a single, weighted calibration curve with a wide dynamic range allows determination with high sensitivity in very small amounts of potato flesh, allowing potatoes with a higher folate content (through biofortification) to be analyzed.

■ ASSOCIATED CONTENT

Ⓢ Supporting Information

Tables of literature overview of folate concentrations in raw or boiled potatoes, concentration levels spiked to seven calibrators and four quality controls; figures showing folate structure, total folate, sample processing, and stability. This material is available free of charge via the Internet at http://pubs.acs.org.

■ AUTHOR INFORMATION

Corresponding Author

*Phone: +32 9 264 81 21; fax: +32 9 264 81 83; e-mail: Christophe.Stove@UGent.be.

Funding

D.V.D.S. and W.L. gratefully acknowledge financial support from Ghent University (Bijzonder Onderzoeksfonds, BOF2009/G0A/004).

Notes

The authors declare no competing financial interest.

■ ABBREVIATIONS USED

10-CHOFA, 10-formyl folic acid; 5,10-CH+THF, 5,10-methenyltetrahydrofolate; 5-CHOTHF, 5-formyl tetrahydrofolate; 5-MTHF, 5-methyltetrahydrofolate; ANOVA, analysis of variance; BCR, community bureau of reference; CAD, collisionally activated dissociation; DTT, dithiothreitol; DW, dry weight; EC, European commission; ESI, electrospray ionization; FA, folic acid; FTS, freeze−thaw stability; FW, fresh weight; HIGH, high; HPLC, high-performance liquid chromatography; IS, internal standard; LC, liquid chromatography; LLOQ, lower limit of quantitation; LOD, limit of detection; LOF, lack of fit; LOW, low; ME, matrix effect; MED, medium; MRM, multiple reaction monitoring; MS/MS, tandem mass spectrometry; MS, mass spectrometry; PABA,

para-aminobenzoic acid; Q, quadrupole; QC, quality control; REC, recovery; RE, relative error; RSD, relative standard deviation; STS, short-term stability; THF, tetrahydrofolate; UHPLC-MS/MS, ultrahigh-performance liquid chromatography; ULOQ, upper limit of quantitation

REFERENCES

(1) Hanson, A. D.; Gregory, J. F., III. Folate biosynthesis, turnover, and transport in plants. *Annu. Rev. Plant Biol.* **2011**, *62*, 105−125.

(2) Goyer, A.; Sweek, K. Genetic diversity of thiamin and folate in primitive cultivated and wild potato (Solanum) species. *J. Agric. Food Chem.* **2011**, *59*, 13072−13080.

(3) Hurdle, A. D. F.; Barton, D.; Searles, L. H. A method for measuring folate in food and its application to a hospital diet. *Am. J. Clin. Nutr.* **1968**, *21*, 1202−1207.

(4) Augustin, J.; Swanson, B. G.; Teitzel, C.; Johnson, S. R.; Pometto, S. F.; Artz, W. E.; Huang, C. P.; Schomaker, C. Changes in the nutrient composition during commercial processing of frozen potato products. *J. Food Sci.* **1979**, *44*, 807−809.

(5) Augustin, J.; Toma, R. B.; True, R. H.; Shaw, R. L.; Teitzel, C.; Johnson, S. R.; Orr, P. Composition of raw and cooked potato peel and flesh-proximate and vitamin composition. *J. Food Sci.* **1979**, *44*, 805−806.

(6) McKillop, D. J.; Pentieva, K.; Daly, D.; Mcpartlin, J. M.; Hughes, J.; Strain, J. J.; Scott, J. M.; McNulty, H. The effect of different cooking methods on folate retention in various foods that are amongst the major contributors to folate intake in the UK diet. *Br. J. Nutr.* **2002**, *88*, 681−688.

(7) Chen, L.; Eitenmiller, R. R. Optimization of the trienzyme extraction for the microbiological assay of folate in vegetables. *J. Agric. Food Chem.* **2007**, *55*, 3884−3888.

(8) Goyer, A.; Navarre, D. A. Determination of folate concentrations in diverse potato germplasm using a trienzyme extraction and a microbiological assay. *J. Agric. Food Chem.* **2007**, *55*, 3523−3528.

(9) Goyer, A.; Navarre, D. A. Folate is higher in developmentally younger potato tubers. *J. Sci. Food Agric.* **2009**, *89*, 579−583.

(10) Bassett, M. N.; Samman, N. C. Folate content and retention in selected raw and processed foods. *Arch. Latinoam. Nutr.* **2010**, *60*, 298−305.

(11) Karatas, F.; Cansiz, A.; Cifci, H.; Serbetci, Z. Determination of folic acid level in some foodstuffs. *Chem. Nat. Compd.* **2007**, *43*, 310−312.

(12) Vahteristo, L.; Lehiokoinen, K.; Ollilainen, V.; Varo, P. Application of an HPLC assay for the determination of folate derivatives in some vegetables, fruits and berries consumed in Finland. *Food Chem.* **1997**, *59*, 589−597.

(13) Hefni, M.; Ohrvik, V.; Tabekha, M.; Witthoft, C. Folate content in foods commonly consumed in Egypt. *Food Chem.* **2010**, *121*, 540−545.

(14) Konings, E. J. M.; Roomans, H. H. S.; Dorant, E.; Goldbohm, R. A.; Saris, H. M.; Van den Brandt, P. A. Folate intake of the Dutch population according to newly established liquid chromatography data for foods. *Am. J. Clin. Nutr.* **2001**, *73*, 765−776.

(15) Stea, T. H.; Johansson, M.; Jagerstad, M.; Frolich, W. Retention of folates in cooked, stored and reheated peas, broccoli and potatoes for use in modern large-scale service systems. *Food Chem.* **2007**, *101*, 1095−1107.

(16) Phillips, K. M.; Wunderlich, K. M.; Holden, J. M.; Exler, J.; Gebhardt, S. E.; Haytowits, D. B.; Beecher, G. R.; Doherty, R. F. Stability of 5-methyltetrahydrofolate in frozen fresh fruits and vegetables. *Food Chem.* **2005**, *92*, 587−595.

(17) Holasova, M.; Fiedlerova, V.; Vavreinova, S. Determination of folates in vegetables and their retention during boiling. *Czech J. Food Sci.* **2008**, *26*, 31−37.

(18) Pawlosky, R. J.; Flanagan, V. P.; Doherty, R. F. A mass spectrometric validated high-performance liquid chromatography procedure for the determination of folates in foods. *J. Agric. Food Chem.* **2003**, *51*, 3726−3730.

(19) Phillips, K. M.; Rasor, A. S.; Ruggio, D. M.; Amanna, K. R. Folate content of different edible portions of vegetables and fruits. *Nutr. Food Sci.* **2008**, *38*, 175−181.

(20) Konings, E. J. M. A validated liquid chromatographic method for determining folates in vegetables, milk powder, liver, and flour. *J. AOAC Int.* **1999**, *82*, 119−127.

(21) Subramanian, N. K.; White, P. J.; Broadley, M. R.; Ramsay, G. The three-dimensional distribution of minerals in potato tubers. *Ann. Bot.* **2011**, *107*, 681−691.

(22) Han, J. S.; Kozukue, N.; Young, K. S.; Lee, K. R.; Friedman, M. Distribution of ascorbic acid in potato tubers and in home-processed and commercial potato foods. *J. Agric. Food Chem.* **2004**, *52*, 6516−6521.

(23) Storozhenko, S.; Ravanel, S.; Zhang, G. F.; Rebeille, F.; Lambert, W.; Van Der Straeten, D. Folate enhancement in staple crops by metabolic engineering. *Trends Food Sci. Technol.* **2005**, *16*, 271−281.

(24) Storozhenko, S.; De Brouwer, V.; Volckaert, M.; Navarette, O.; Blancquaert, D.; Zhang, G. F.; Lambert, W.; Van Der Straeten, D. Folate fortification of rice by metabolic engineering. *Nat. Biotechnol.* **2007**, *25*, 1277−1279.

(25) Blancquaert, D.; Storozhenko, S.; Van Daele, J.; Stove, C.; Visser, R. G.; Lambert, W.; Van Der Straeten, D. Enhancing pterin and *para*-aminobenzoate content is not sufficient to successfully biofortify potato tubers and *Arabidopsis thaliana* plants with folate. *J. Exp. Bot.* **2013**, *64*, 3899−3909.

(26) De Brouwer, V.; Storozhenko, S.; Stove, C. P.; Van Daele, J.; Van der Straeten, D.; Lambert, W. Ultra-performance liquid chromatography-tandem mass spectrometry (UPLC-MS/MS) for the sensitive determination of folates in rice. *J. Chromatogr. B.* **2010**, *878*, 509−513.

(27) Almeida, A. M.; Castel-Branco, M. M.; Falcao, A. C. Linear regression for calibration lines revisited: Weighting schemes for bioanalytical methods. *J. Chromatogr. B.* **2002**, *774*, 215−222.

(28) Wille, S. M. R.; Peters, F. T.; Di Fazio, V.; Samyn, N. Practical aspects concerning validation and quality control for forensic and clinical bioanalytical quantitative methods. *Accredit. Qual. Assur.* **2010**, *16*, 279−292.

(29) Matuszewski, B. K.; Constanzer, M. L.; Chavez-Eng, C. M. Strategies for the assessment of matrix effect in quantitative bioanalytical methods based on HPLC-MS/MS. *Anal. Chem.* **2003**, *75*, 3019−3030.

(30) De Brouwer, V.; Storozhenko, S.; Van de Steene, J. C.; Wille, S. M. R.; Stove, C. P.; Van der Straeten, D.; Lambert, W. Optimisation and validation of a liquid chromatography-tandem mass spectrometry method for folates in rice. *J. Chromatogr. A.* **2008**, *1215*, 125−132.

(31) De Brouwer, V.; Zhang, G. F.; Storozhenko, S.; Van der Straeten, D.; Lambert, W. pH stability of individual folates during critical sample preparation steps in prevision of the analysis of plant folates. *Phytochem. Anal.* **2007**, *18*, 496−508.

(32) Jägerstad, M.; Jastrebova, J. Occurrence, stability, and determination of formyl folates in foods. *J. Agric. Food Chem.* **2013**, *61*, 9758−9768.

(33) Glynne, M. D.; Jackson, V. G. The distribution of dry matter and nitrogen in the potato tuber. Variety, King Edward. *J. Agric. Sci.* **1919**, *9*, 237−258.

(34) Blancquaert, D.; Storozhenko, S.; Loizeau, K.; De Steur, H.; De Brouwer, V.; Viaene, J.; Ravanel, S.; Rébeillé, F.; Lambert, W.; Van Der Straeten, D. Folates and folic acid: From fundamental research toward sustainable health. *Crit. Rev. Plant Sci.* **2010**, *29*, 14−35.

(35) Scott, J.; Rébeillé, F.; Fletcher, J. Folic acid and folates: The feasibility for nutritional enhancement in plant foods. *J. Sci. Food Agric.* **2000**, *80*, 795−824.

(36) Gregory, J. F., III. Chemical and nutritional aspects of folate research: Analytical procedures, methods of folate synthesis, stability, and bioavailability of dietary folates. *Adv. Food Nutr. Res.* **1989**, *33*, 1−101.

(37) Doherty, R. F.; Beecher, G. R. A method for the analysis of natural and synthetic folate in foods. *J. Agric. Food Chem.* **2003**, *51*, 354−361.

Table 1. Key Methods Being Used for Total Phosphate or Total Phospholipid Determination

method	contributor and reference	comments
molybdenum blue	AOCS Ca 12-55[3]	standard method, tedious ashing, and calorimetric procedures
nephelometric	AOCS Ca 19-86[4]	poor accuracy, low detection limit
vanadomolybdate	Szydlowska-Czerniak and Szlyk (2003)[5]	complex sample preparation
malachite green	Szydlowska-Czerniak and Szlyk (2003)[5]	complex sample preparation
TLC	Fuchs et al. (2011)[6]	requires appropriate standards
TLC	Dynska-Kukulska (2012)[7]	requires appropriate standards
HPLC	Amalia (1997)[8]	low detection limit, low sample throughput
SPE-HPLC	Brouwers (2011)[9]	low throughput, complicated preparation
NMR	Nouri-Sorkhabi (1996)[10]	not suitable for routine analysis
NMR	Yao and Jung (2010)[11]	not suitable for routine analysis
FTIR	Nzai and Proctor (1998)[12]	workable, but limited accuracy and precision
FTIR	Nzai and Proctor (1999)[13]	workable, but limited accuracy and precision
ATR-FTIR	Kuligowski et al. (2008)[14]	workable, but limited sensitivity
FTIR/PLS	Szydlowska (2007)[15]	chemometric, limited applicability, and generality
FTIR/PLS	Meng et al. (2014)[16]	chemometric, limited applicability, and generality
FT-NIR/PLS	Rathjen et al. (1998)[17]	chemometric, limited applicability, and generality
FT-NIR/PLS	Li et al. (2009)[18]	chemometric, limited applicability, and generality

Proctor[12,13] demonstrated that the phospholipid content of soybean oil could be determined quantitatively and used FTIR as a replacement for the Bartlett and TLC methods. Although workable, these FTIR methods have relatively high coefficients of variance (CV) in terms of both accuracy and precision, ranging from 3 to 9%. Another approach, developed for phospholipid dietary supplement analysis,[14] has been to combine gel permeation chromatography (GPC) with attenuated total reflectance FTIR (ATR-FTIR) spectrometry to remove spectrally interfering triacylglycerols. Again, this is workable methodology, but complicated, and its analytical sensitivity is limited, in this case largely due to the low sensitivity of ATR. Chemometric-based FTIR methods have been developed, for both mid-FTIR[15,16] and near-FTIR[17,18] usually based on the use of partial least-squares (PLS). These methods relate the phospholipid content obtained by a standard reference method to IR spectral changes in the oil matrix. Although such methods can be viable, it can be quite difficult to devise robust and representative calibration and validate its performance; such methods tending to be heavily oil-type dependent and thus usually not applicable to a wide variety of oils and are of limited applicability. Thus, at this point in time, there is still no simple, effective, reliable, and generalized means of determining TPL in oils by FTIR spectroscopy. In this paper, a mid-FTIR method is devised that combines a single-step in-vial extraction of oil using a phospholipid-specific extraction solvent mixture that is predominantly oil-immiscible. By analyzing the solvent extract after centrifugation and using differential FTIR spectroscopy to measure a single phospholipid-specific absorption band, the TPL content can be predicted from a calibration based on a single representative PL added to the extraction solvent mixture.

MATERIALS AND METHODS

Materials. Refined soybean and canola oils were obtained locally and further degummed by silica gel column chromatography to remove any residual PL. Oil (50−100 g) was put through a 3 mm i.d. × 400 mm glass column packed with ∼200 g of 200−300 mesh activated (2 h at 105 °C) silica gel (Qingdao Haiyang Chemical Co. Ltd., China); the oil pulled through the column using a vacuum with the degummed oils was collected and used as zero-TPL reference standards. Crude rapeseed and soybean oils as well as lecithin tablets were obtained from Yihai Kerry Ltd. Co., China. Various solvents, ethanol, methanol, acetonitrile, dimethyl sulfoxide (DMSO), and dimethylformamide (DMF) were obtained from Sigma-Aldrich Co. Ltd., USA. A phosphatidylcholine (PC) phospholipid standard was purchased from Avanti Polar Lipids Inc. (Alabaster, AL, USA), which served as the sole PL standard for addition to 1:1 MeOH/CAN or degummed oils.

Phosphorus Analysis. The AOCS Ca 12-55 molybdenum blue method[3] was used to determine the phosphorus content of samples (oils or solvent extracts) by ashing them in the presence of zinc oxide followed by the visible spectrophotometric measurement of phosphorus as a blue phosphomolybdic acid complex. The phosphorus content of the sample was determined using NaH_2PO_4 as the phosphorus standard for which a standard curve was prepared, and the phosphorus content obtained was converted to TPL by multiplying the phosphate content determined by a factor of 25.

FTIR Spectroscopy and Calibration Standards. *Spectroscopy.* FT-IR spectra were collected using a Tensor 27 (Bruker Co., USA) equipped with a deuterated triglycine sulfate (DTGS) detector and purged with dry air using a Balston dryer (Balston, Lexington, MA, USA). A 25 μm CaF_2 transmission flow cell (International Crystal Laboratories, Garfield, NJ, USA) equipped with Luer-Lok fittings was employed for sample handling. The cell inlet was connected to a 10 cm, 18-gauge stainless steel aspiration needle via flexible silicone tubing to the cell Leur inlet. The cell outlet Leur fitting had a line connected to vacuum via a trap fitted with a valve to facilitate facile loading and emptying of the cell at will by aspiration. All spectra were collected using 32 scans at a resolution of 4 cm^{-1} over the spectral range of 4000−400 cm^{-1}. Each sample was analyzed in triplicate, and the spectra collected were processed and analyzed using Omnic version 7.0 (Thermo Electron Corp., USA).

Calibration Standards. PL calibrations were developed by adding the PC standard to MeOH/ACN (1:1 v/v) covering a TPL concentration range of 20−50000 ug/g. The spectra of these standards were taken and ratioed 1:1 against the spectrum of the same solvent mixture used to prepare the PC standards to produce their corresponding differential spectra. A 5-5 gap segment second-derivative of these differential spectra was also taken and multiplied by −10000 to produce positive "absorbance" values of a magnitude more readily worked with. The peak intensities (heights) of specific bands, for example, 970 cm^{-1} (asymmetric C—N stretching of $(CH)_3N^+$), 1090 cm^{-1} (C—O stretch in C—O—PO_2^-), 1172 cm^{-1} (asymmetric C—O stretch in C═O—O—C), 1243 cm^{-1} (asymmetric PO_2^- stretch), and 1740 cm^{-1} (C═O stretch), of the PL differential spectra and second-derivative differential spectra were related to the PC concentrations added. The regression equations obtained for each of these absorption bands were compared in terms of their regression statistics, and the best-performing calibration was used to calculate the PL content (μg/g) of PC-spiked canola oil as well as for crude and refined oils and lecithin tablets in subsequent validation experiments.

Sample Preparation and Analysis. Oil samples were prepared for FTIR analysis in a standardized manner using a constant oil to solvent ratio (1:2 v/v) by adding 10 mL of oil to 20 mL of 1:1 MeOH/ACN in a tarred 30 mL clinical centrifuge tube. The tube was capped, shaken

on a reciprocal shaker for 60 s, and centrifuged for 10 min at 4000 rpm to separate the oil from the PL-enriched solvent. A portion of the upper solvent layer was aspirated into the IR cell for FTIR analysis and its spectrum taken (spectrum S_1), followed by loading the solvent used to prepare the sample and collecting its spectrum (spectrum S_0). The differential spectrum of the sample was generated by subtracting S_0 from S_1; the subtraction factor used was based on the overlapping acetonitrile and methanol overtone bands, which absorb over the range of 2020−2060 cm^{-1}. Using this technique the spectral contribution of solvent is removed as well as correcting for any bias associated with solvent dilution/displacement by the sample. The absorption maximum at 1243 cm^{-1} in the differential and second-derivative spectra was measured and processed using the solvent PL-spiked calibration standard curves derived for various spectral regions to calculate the TPL content of the samples analyzed.

Method Validation. Two sets of samples were used to validate the effectiveness of the method developed: (a) ideal samples, prepared from fully degummed oil and spiked with known amounts of PC, and (b) real samples that were undefined in phospholipid composition and content. For the ideal samples, refined canola oil was used, which underwent a further laboratory degumming step and was verified to be devoid of measurable PL. This oil was serially spiked with the PC standard and extracted, and the FTIR predictions obtained using the solvent-spiked PC calibration curve were compared to the known amount of PC standard added to determine both reproducibility and accuracy. The second sample set comprised real samples for which the PL levels and composition were unknown and included four crude oils and two refined oils, as well as a commercial lecithin tablet. These were all analyzed by FTIR as well as AOCS Ca 12-55, and the relative accuracy of the FTIR method to the reference AOCS method was expressed as percent relative error for accuracy (%RA):

$$\%RA = [(TPL_{FTIR} - TPL_{AOCS})/TPL_{AOCS}] \times 100 \quad (1)$$

Reproducibility of both methods was expressed as its percent relative standard deviation (%RSD):

$$\%RSD = (SD/mean) \times 100 \quad (2)$$

RESULTS AND DISCUSSION

PL Extraction Optimization. Preliminary spectral work was carried out in relation to developing an in-vial extraction procedure of PL from a PC-spiked, degummed soybean sample using various solvents, including ethanol, methanol, acetonitrile, DMSO, and DMF using an initial solvent/oil ratio of 2:1. High and low PC-spiked soybean samples (10000 and 1000 $\mu g/g$) were extracted using each solvent and, after centrifugation, a portion of the upper solvent layer was taken for phosphate analysis by AOCS Ca 12-55 and the balance used for FTIR spectral analysis. The extract was aspirated into the IR cell, and its spectrum was taken and ratioed against the solvent used for extraction to produce a differential spectrum of the extract, the bulk of the solvent spectral contribution thus having been removed. The main spectral feature monitored in this part of the work was the ester linkage of the triglycerides, which is indicative of the relative amount of triglyceride extracted, which is known to interfere with FTIR quantitation of PL.[16] The results of the extraction procedure and the relative PL recovery obtained by coanalysis using Ca 12-55 are summarized in Table 2.

Although MeOH extracted the PL the most efficiently, spectrally it also coextracted a very substantial amount of the triglyceride. Whereas ACN does not perform as well in terms of PL extraction, spectrally it extracted almost no triglyceride. All of the other solvents performed between these two extremes in regard to PL and triglyceride extraction. As a result, MeOH was mixed with ACN in various proportions to determine if an optimal balance could be struck between maximizing the PL extraction and minimizing the extraction of triglycerides. Ratios of methanol to acetonitrile of 1:9 through 9:1 were assessed, with the recoveries presented in Table 3.

Table 2. Extraction Efficiency of Added Phospholipid Using Various Organic Solvents

solvent	phospholipid ($\mu g/mL$)	AOCS Ca 12-55 ($\mu g/mL$)	recovery (%)
DMSO	10000	5230	52
DMSO	1000	615	62
DMF	10000	7896	79
DMF	1000	724	72
MeOH	10000	9388	94
MeOH	1000	924	93
EtOH	10000	9122	91
EtOH	1000	879	88
ACN	10000	6278	63
ACN	1000	709	71

Table 3. Influence of MeOH/ACN Ratios on Phospholipid Extraction

MeOH/ACN (v/v)	PL added ($\mu g/mL$)	AOCS ($\mu g/mL$)	recovery (%)
1:9	10000	6982	70
2:8	10000	8271	83
4:6	10000	9523	95
5:5	10000	9490	95
8:2	10000	904	90
1:9	1000	803	80
2:8	1000	826	83
4:6	1000	961	96
5:5	1000	975	98
8:2	1000	954	95

It was found that for recoveries obtained from 5:5 MeOH/ACN onward, with more MeOH, the triglyceride component also increased; thus, 1:1 MeOH/ACN was considered optimal. Subsequently, the ratio of solvent/oil was assessed at 1:1 and 5:1, the former providing inadequate extraction, whereas 5:1 worked well from the standpoint of phosphate recovery but resulted in the PL extracted being too dilute for accurate quantitative analysis. As a result of these preliminary experiments, for the balance of this work, in-vial extraction was carried out using 1:1 MeOH/ACN using a 2:1 solvent to oil ratio.

FTIR Spectroscopy and Calibration Development. FTIR spectra for serially diluted PC standards prepared in 1:1 MeOH/CAN over the spectral range from 2500 to 500 cm^{-1} are presented in Figure 1 along with an inset of the variance spectrum of these spectra over the range of 4000−500 cm^{-1}. The latter represent a facsimile of an ideal PL oil extract, one in which no triglyceride is coextracted and only the phospholipid component is present in the solvent extract.

The inset variance spectrum in Figure 1 provides an overall indication of the spectral changes expected to occur when only the sample phospholipid concentration changes. Here the broad 3300 cm^{-1} band is due to the O−H stretching band of MeOH, next to which are several C−H stretching bands, which are predominantly solvent contributions that are not shown in the spectral region covered by the main spectra of Figure 1. In

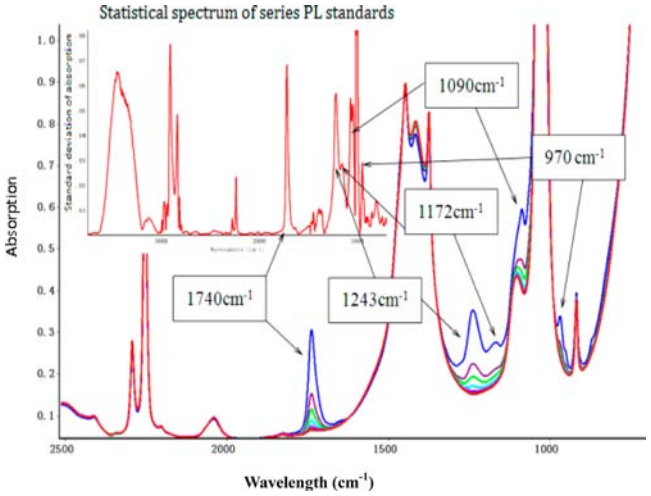

Figure 1. FTIR transmission spectra of a serial dilution of PC in 1:1 MeOH/ACN recorded in a 25 μm CaF_2 cell and their variance spectrum (inset).

the latter, the most obvious absorbance is at 1739 cm^{-1}, which is the C═O stretching mode of the ester carbonyl linkage of the lipidic component of the phospholipid. Only selected phospholipid bands are identified in Figure 1; however, all of the common phospholipid-related band assignments[22] are summarized in Table 4, reflecting the information outlined by Nzai[12] and Kuligowski,[14] although minor differences may be ascribed to the solvents the samples were measured in.

Table 4. Mid-infrared Phospholipid Band Assignments

assignment	absorption (cm^{-1})
δ CH_2 bending vibration	1451
symmetric CH_3 bending vibration	1376
asymmetric phosphate diester stretch PO_2^-	1243
symmetric phosphate diester stretch PO_2^-	1090
asymmetric ester C—O stretch in C═O—O—C	1173
symmetric ester C—O stretch in C═O—O—C	1037
asymmetric ester C–O–P stretch in C–O–PO_2^-	1068
symmetric ester C–O–P stretch	1025
asymmetric C–N stretching of $(CH_3)_3$–N^+	970

The variance spectrum of the PC serial dilution points to potential bands that may be useful for quantitation. The absorptions at 1037 and 1025 cm^{-1} bands are obviously significant; however, they are off-scale, even in such a short path length cell. Aside from these, the bands at 1740, 1243, 1172, 1090, and 973 cm^{-1} were considered as potential wavelengths for developing a PC calibration in 1:1 MeOH/ACN. Figure 2 presents the spectra of the individual solvents separately (a, b), their 1:1 mixture (c), the spectrum of an oil sample containing 5000 μg/g PC added to phospholipid-free oil and extracted into a 1:1 solvent mixture (d), and its differential spectrum (e) as well as its second-derivative spectrum (f).

The spectra of MeOH illustrate their C–O overtone band at 2040 cm^{-1}, whereas in the spectra of acetonitrile the 2070 cm^{-1} absorption could be assigned to C–N overtone band or combinations of different vibration bands related with C–N. Their combination is a good measure of the amount of solvent present. This combined spectral region (2020–2060 cm^{-1}) was used to correct for the displacement of the solvent by constituents extracted from the sample, predominantly oil

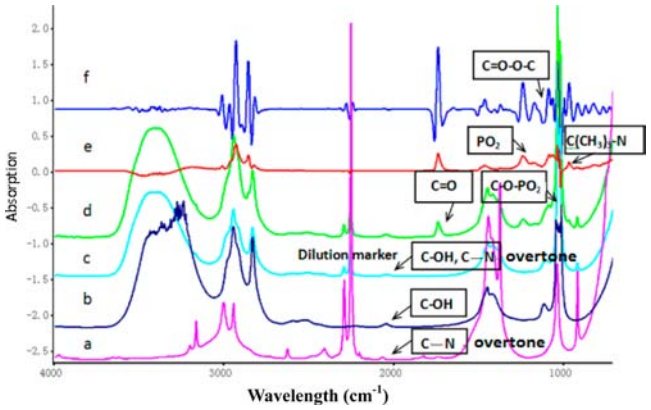

Figure 2. FT-IR spectra of (a) acetonitrile, (b) methanol, (c) mixture solution of methanol and acetonitrile with volume ratio of 1:1, (d) 5000 μg/mL PC in mixture solution, and their processed spectra (e) spectrum d − spectrum c and (f) second-derivative spectra of spectrum e.

(triglyceride). Figure 2d is a spectrum of a MeOH/ACN extract of a PC oil standard, which when ratioed against the extraction solvent spectrum is corrected for displacement by measuring the overtone band, which is thus devoid of the solvent overtone marker band (Figure 2e), indicating that spectral contribution from solvent has been removed. Figure 2f is the second-derivative spectrum of the same sample, the transform leading to sharper bands, in particular those at 1243 and 1173 cm^{-1}, which could potentially assist in quantitation. Selected phosphate bands were examined to determine whether the added PC could be tracked quantitatively, with Table 5 presenting the regression equations obtained when PC-spiked MeOH/ACN standards were analyzed in triplicate by FTIR in both their differential spectra format and their second-derivative transform.

It is clear from the regression data presented in Table 5 that the second-derivative differential spectra perform somewhat better than the simple differential spectra on the basis of their overall lower RSD. All of the phosphate-related bands used work reasonably well, with the carbonyl (γ C═O) band at 1740 cm^{-1} having the best linearity and the lowest RSD of 1.2%. However, it is well-known that the 1740 cm^{-1} phosphate ester band is problematic[12] for TPL determination because it is susceptible to interference by coextracted triglyceride absorptions that overlap. Although triglycerides have been minimized using the solvent mixture, a small and variable amount of lipid is still extracted; thus, for more reliability the PO_2^- band at 1243 cm^{-1} was chosen as the primary band for quantitative TPL analysis. The PO_2^- absorption is common to most if not all PL components found in oils and should respond to a calibration based on a single phospholipid, such as phosphatidylcholine (PC), while still responding to other PL components, such as phosphatidylethanolamines, phosphatidylinositols, and phosphatidylserines. For comparative purposes, Figure 3 presents the FTIR spectra over the spectral range of 1850–500 cm^{-1} of the 1:1 MeOH/ACN solvent and its in-vial extracts of phospholipid-free (laboratory degummed and refined) soybean oil and regular soybean oil.

In these spectra there are clear differences in the 1740 cm^{-1} band; however, as noted earlier, an undefined portion of that signal is due to coextracted triacylglycerol, which can confound quantitation. The 1243 cm^{-1} (PO_2^-) band also responds with crude soybean oil producing a higher absorbance than the

dx.doi.org/10.1021/jf404880v | J. Agric. Food Chem. 2014, 62, 3101–3107

Table 5. Calibration Regression Equations and Their Associated Statistics Obtained on the Basis of the FTIR Band Used To Measure Known Amounts of PC Spiked into MeOH/ACN Solutions

band used/measured (cm^{-1})	best fit linear regression eq	R^2	SD	%RSD
	Second-Derivative Differential Spectra			
970	PL = 3480.84 × Abs_{970} + 623.4	0.9995	336	4.0
1090	PL = 4446.50 × Abs_{1090} − 414.2	0.9995	354	4.2
1172	PL = 14404.35 × Abs_{1172} + 345.8	0.9994	393	4.7
1243	PL = 3403.60 × Abs_{1243} + 21.13	0.9999	163	1.9
1740	PL = 1453.15 × Abs_{1740} − 141.5	1.0000	103	1.2
	Differential Spectra			
970	PL = 94.97 × Abs_{970} − 2079.9	0.9958	1003	11.9
1090	PL = 51.04 × Abs_{1090} − 1776.2	0.9985	850	10.1
1172	PL = 101.34 × Abs_{1172} − 1119.6	0.9986	804	9.6
1243	PL = 56.83 × Abs_{1243} − 661.4	0.9996	404	4.8
1740	PL = 50.29 × Abs_{1740} − 182.4	0.9999	202	2.4

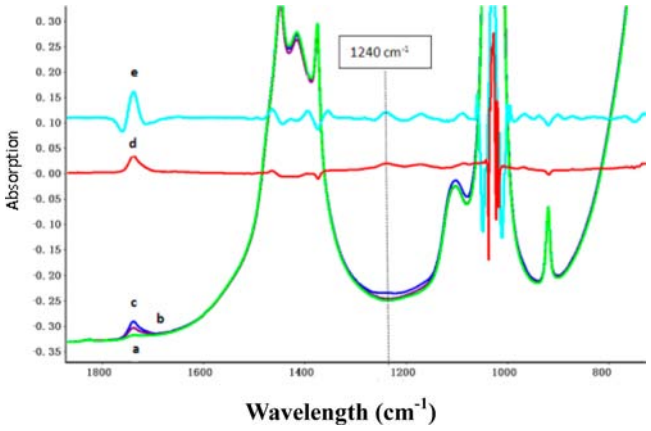

Figure 3. FT-IR spectra of (a) 1:1 methanol/acetonitrile extraction solvent, (b) 1:1 methanol/acetonitrile extract of a degummed soybean oil, (c) methanol/acetonitrile extract of soybean oil, (d) differential spectrum of soybean oil and degummed soybean oil (spectrum c − spectrum b), and (e) the second-derivative spectra of the differential spectrum of (d).

degummed sample and the solvent. Their differences are made more apparent in the differential spectrum when the degummed sample is subtracted from the regular soybean sample, with the gap segment second-derivative differential spectrum further enhancing this band as underlying absorptions associated with coextracted lipid tend to be minimized. These differential spectra have spectral attributes similar to the model PC-spiked MeOH/ACN standards once the bulk of the oil has been eliminated by the in-vial extraction and the PC component concentrated into the extraction solvent.

To evaluate the basic performance of the selected 1243 cm^{-1} band, ideal samples, canola oils spiked with known amounts of PC, were extracted in-vial and centrifuged, and their FTIR spectra were taken and processed using the 1243 cm^{-1} second-derivative calibration equations listed in Table 5 to determine how well the added PC could be determined when expressed as TPL. Table 6 presents the accuracy and precision of triplicate analyses for TPL obtained for these PC-spiked canola oils.

From the FTIR predictions obtained by analyzing the in-vial extracts of samples containing 528−30005 μg/mL of added PC, it is clear that measurements made using the 1243 cm^{-1} band of oil extracts obtained using 1:1 MeOH/ACN in a 2:1 solvent/oil ratio allow the accurate determination of the PC added to oils when extracted under these standardized conditions. The

Table 6. Accuracy and Precision of TPL[a] Determination for PC-Spiked Degummed Canola Oil Samples by FTIR Spectroscopy Using the 1243 cm^{-1} Band for Quantitation

spiked PL (μg/mL)	FTIR predicted TPL (μg/mL)	%RA	%RSD
30005	31587 ± 352	5.3	1.1
10451	10801 ± 192	3.3	1.8
6104	6073 ± 277	0.5	4.6
2035	2068 ± 8	1.6	2.8
1078	1099 ± 48	2	4.4
999	979 ± 28	2	2.9
528	514 ± 19	2.4	3.8
mean	NA	2.4	3.1

[a]Sample analyzed in triplicate.

regression relationship obtained between the FTIR predicted values versus actual spiked PL values is

$$PL_{predicted} = 1.0544 \times PL_{added} - 123.66 \quad (3)$$

$$R^2 = 0.9999 \qquad D = 134$$

Using a zero regression to remove the intercept produced the following relationship (eq 4), with only minor changes in the regression statistics, indicating that the intercept is basically not significant as it is within the SD of the original relationship.

$$PL_{predicted} = 1.0484 \times PL_{added} \quad (4)$$

$$R^2 = 0.9999 \qquad D = 162$$

Both of these relationships indicate that the in-vial extraction−FTIR phospholipid method is capable of responding linearly to PC-spiked oil within an SD of <200 μg/g. These results indicate that the basic recovery of PC added to oil is adequate as is its ability to be measured by FTIR, the key question being whether this holds for real oil samples that contain phospholipids other than simply PC.

To assess the general applicability of the in-vial solvent extraction procedure and the predictive power of the model MeOH/ACN-PC calibration, crude and refined soybean and rapeseed oils, as well as a lecithin tablet, were extracted and analyzed in triplicate by FTIR and coanalyzed as well as by AOCS Ca 12-55, with the results obtained presented in Table 7.

Because the FTIR method is a secondary method, validation of its performance requires direct comparison to an established primary method for TPL analysis such as AOCS Ca 12-55. It is

dx.doi.org/10.1021/jf404880v | J. Agric. Food Chem. 2014, 62, 3101−3107

Table 7. Comparison of the TPL[a] Obtained Using FTIR versus AOCS Ca 12-55 for Real Samples

sample	AOCS Ca 12-55	% RSD	FTIR	% RSD	% RA
crude soy 1	5786 ± 308	5.3	5602 ± 137	2.5	3.2
crude soy 2	7990 ± 365	4.6	7819 ± 235	3.0	2.1
crude rape 1	6785 ± 300	4.4	6702 ± 191	2.9	1.2
crude rape 2	8056 ± 460	5.7	8124 ± 242	3.0	0.8
refined soy	296 ± 10	3.6	302 ± 10	3.4	2.0
refined rape	203 ± 13	6.4	193 ± 7	3.9	4.7
lecithin tablet	180892 ± 7560	4.2	178869 ± 6439	3.6	1.1
mean	NA	4.9		3.2	2.2

[a]TPL content (μg/g, n = 3). Sample analyzed in triplicate.

apparent from the data presented in Table 7 that the two methods track each other well for these samples, with the AOCS method being somewhat more variable than the FTIR procedure in terms of reproducibility (RSD 4.9 vs 3.2%). This implies that the accuracy statistic obtained for FTIR is limited to some extent by the lower reproducibility of the reference method. Even so, it is clear that the FTIR procedure as developed is tracking the reference method responses well. Comparatively, Nzai et al.[12,13] used the 970−1200 cm^{-1} band area (assigned to PO_2 + P−O−C) to determine TPL of soy lecithin samples, which were compared the results obtained using Bartlett's method, a procedure similar to AOCS Ca 12-55. The CV reported for 10 duplicates having TPL contents covering 1−20% ranged from 3.6 to 9.5% for their FTIR method versus 8.9−48.7% for the reference chemical procedure. On the basis of these results, the authors implied that the FTIR method could still be used to determine the PL concentrations found in refined oil samples. The FTIR method developed here, as applied to real samples, tracked the AOCS Ca 12-55 results much better; the linear regression of the FTIR predictions versus the AOCS results presented in Table 7 produced the relationship

$$\mathrm{FTIR_{PL}} = 0.9889 \times \mathrm{AOC_{PL}} - 8.24 \quad (5)$$

$$R^2 = 0.9999 \qquad D = 95.83$$

which has a slope close to the ideal of 1.0, a negligible intercept, and an overall SD of <100 μg/g.

The key to developing this TPL methodology is the simple and efficient extraction and concentration of phospholipids using a solvent mixture which simultaneously minimizes the extraction of lipids that can spectrally interfere with quantitation. The spectrum of the extract is further simplified by accurately removing the solvent spectral contribution using the solvent overtone bands,[23] basically leaving the spectra of the phospholipids, which can be further enhanced in terms of quantitation using a second-derivative transform. With this simplified analytical system to work with, a calibration based simply on a single representative PL standard (in this case PC) to the extraction solvent becomes a possibility, focusing on phosphate bands for quantitation. Once a responsive band is found, one can assess the effect of the presence of oil on the extraction and predictions by spiking degummed oil with PC to assess both the extraction procedure and predictive capability of the solvent-spiked FTIR calibration. Validation of the extraction procedure in combination with the simplified calibration to track the TPL content of real oils is then carried out and compared by coanalysis by a reference method. The results obtained indicate that this simplified approach works adequately and that the triglycerides which usually interfere spectrally with FTIR PL quantitation have been minimized adequately. Of the phosphate bands, 1745 cm^{-1} is not in contention as it is overlapped by triglyceride ester absorptions, and 1243 cm^{-1} was found to be the most responsive in terms of quantitation of all the other bands. It appears that PC is an adequately representative calibration standard for most phospholipids and that the PO_2^- band at 1243 cm^{-1} is generally workable for TPL determination even if some residual lipid is present. The FTIR method as structured is more reproducible than AOCS Ca 12-55 and is ultimately limited in its accuracy by the reference method it is being compared to. As presented, the FTIR method developed provides a simple means for TPL determination, requiring only an in-vial extraction of the oil with solvent and centrifugation to separate the solvent from the oil, followed by FTIR analysis of the solvent. Calibration is straightforward, and the spectral manipulations required to remove the solvent contribution, obtain the second-derivative differential spectrum of the sample, and measure the absorbance at 1243 cm^{-1} can readily be programmed as a macro to directly deliver the TPL of the sample in micrograms per gram. With an FTIR configured in this manner and equipped with an autosampler, vials containing pre-extracted, centrifuged samples can be loaded into an autosampler tray and analyzed automatically in a manner similar to that of other quantitative automated FTIR methods that have been developed[24] for both oil and lubricant analysis. At a more practical level, even the manual version of this method provides a simpler, less tedious, and accurate alternative to standard chemical methods currently in use.

AUTHOR INFORMATION

Corresponding Authors

*(Y.L.) Phone: +86-10-64421335. Fax: +86-10-64416428. E-mail: liuyun@mail.buct.edu.cn.

*(F.R.v.d.V.) E-mail: frederik.vandevoort@mcgill.ca.

Funding

We gratefully acknowledge financial support from NSFC (31270858, 31070709, 31271887) and Science Technology of Department of Zhejiang Province (2013C32SA500023, 2013C32SA100035).

Notes

The authors declare no competing financial interest.

ABBREVIATIONS USED

ACN, acetonitrile; ATR, attenuated total reflectance; CV, coefficients of variance; DTGS, deuterated triglycine sulfate; DMSO, dimethyl sulfoxide; DMF, dimethylformamide; FTIR, Fourier transform infrared; GPC, gel permeation chromatography; HPLC, high-performance liquid chromatograph; MeOH, methanol; PLS, partial least-squares; PC, phosphatidylcholine; PL, phospholipid; TLC, thin layer chromatograph; TPL, total phospholipids; PLSR, partial least-squares regression; NIR, near-infrared spectra; NMR, nuclear magnetic resonance; RA, relative error; RSD, relative standard deviation

REFERENCES

(1) Liu, W. L.; Liu, J. H.; Liu, W.; Li, T.; Liu, C. M. Improved physical and in vitro digestion stability of a polyelectrolyte delivery system based on layer-by-layer self-assembly alginate-chitosan-coated nanoliposomes. *J. Agric. Food Chem.* **2013**, *61*, 4133−4144.

(2) Restuccia, D.; Spizzirri, U. G.; Puoci, F.; Cirillo, G.; Vinci, G.; Picci, N. Determination of phospholipids in food samples. *Food Rev. Int.* **2012**, *1*, 1−46.
(3) AOCS. *Official Methods and Recommended Practices of the American Oil Chemists' Society*; AOCS Press: Champaign, IL, USA, 2009; Method Ca 12−55.
(4) AOCS. *Official Methods and Recommended Practices of the American Oil Chemists' Society*; AOCS Press: Champaign, IL, USA, 2009; Method Ca 19-86.
(5) Szydłowska-Czerniak, A.; Szłyk, E. Spectrophotometric determination of total phosphorus in rape seeds and oils at various stages of technological process: calculation of phospholipids and non-hydratable phospholipids contents in rapeseed oil. *Food Chem.* **2003**, *81*, 613−619.
(6) Fuchs, B.; Suß, R.; Teuber, K.; Eibisch, M.; Schiller, J. Lipid analysis by thin-layer chromatography − a review of the current state. *J. Chromatogr., A* **2011**, *1218*, 2754−2774.
(7) Dynska-Kukulska, K.; Ciesielski, W. Methods of extraction and thin-layer chromatography determination of phospholipids in biological samples. *Rev. Anal. Chem.* **2012**, *31*, 43−56.
(8) Amalia, A. C.; Marta, I. V. B.; Guillermo, H. C. Quantitative determination of phospholipids in sunflower oil. *J. Am. Oil Chem. Soc.* **1997**, *74*, 511−514.
(9) Brouwers, J. F. Liquid chromatographic-mass spectrometric analysis of phospholipids. Chromatography, ionization and quantification. *Biochim. Biophys. Acta* **2011**, *1811*, 763−75.
(10) Nouri-Sorkhabi, M. H.; Wright, L. C.; Sullivan, D. R.; Kuchel, P. W. Quantitative ^{31}P nuclear magnetic resonance analysis of the phospholipids of erythrocyte membranes using detergent. *Lipids* **1996**, *31*, 765−770.
(11) Yao, L. X.; Jung, S. ^{31}P NMR phospholipid profiling of soybean emulsion recovered from aqueous extraction. *J. Agric. Food Chem.* **2010**, *58*, 4866−4872.
(12) Nzai, J. M.; Proctor, A. Determination of phospholipids in vegetable oil by Fourier transform infrared spectroscopy. *Food Chem.* **1998**, *75*, 1281−1289.
(13) Nzai, J. M.; Proctor, A. Soy lecithin phospholipid determination by Fourier transform infrared spectroscopy and the acid digest/arsenomolybdate method: a comparative study. *J. Am. Oil Chem. Soc.* **1999**, *76*, 61−66.
(14) Kuligowski, J.; Quintas, G.; Esteve-Turrillas, F. A. On-line gel permeation chromatography-attenuated total reflectance-Fourier transform infrared determination of reflectance-Fourier transform infrared determination of lecithin and soybean oil in dietary supplements. *J. Chromatogr., A* **2008**, *1185*, 71−77.
(15) Szydlowska-Czerniak, A. MIR spectroscopy and partial least-squares regression for determination of phospholipids in rapeseed oils at various stages of technological process. *Food Chem.* **2007**, *105*, 1179−1181.
(16) Meng, X. H.; Ye, Q.; Pan, Q. Y.; Ding, Y.; Wei, M.; Jiang, L. Z. Rapid determination of phospholipid content of vegetable oils by FT-IR spectroscopy combined with partial least-square regression. *Food Chem.* **2014**, *147*, 272−278.
(17) Rathjen, T.; Lange, R.; Steinhart, H. Analysis of lecithin by near-infrared spectroscopy. *Fett/Lipid* **1998**, *100*, 358−363.
(18) Li, H.; Goulden, M.; Cocciardi, R.; Hughes, J. Fourier transform near infrared spectroscopy as a quality control tool for the analysis of lecithin and by-products during soybean oil processing. *J. Am. Oil Chem. Soc.* **2009**, *86*, 835−841.
(19) Duevel, V.; Corn, R. M.; Liu, M. D.; Leidner, C. R. Orientation and organization in functionalized phospholipid monolayers at gold surfaces as measured by polarization modulation Fourier transform infrared spectroscopy. *J. Phys. Chem.* **1992**, *96*, 486−473.
(20) Mendelsohn, R.; Davies, M. A.; Brauner, J. W.; Schuster, H. F.; Dluhy, R. A. Quantitative determination of conformational disorder in the acyl chains of phospholipid bilayers by infrared spectroscopy. *Biochemistry* **1989**, *28*, 8934−8939.
(21) Casal, H. L. Infrared spectroscopic determination of water penetration in lipid bilayer membranes. *J. Phys. Chem.* **1989**, *93*, 4328−4330.
(22) Mohan, V. *Selective Ester Cleavage in Phospholipids*. Mississippi State University, Mississippi State, MS, USA, August 2008; pp 25−35.
(23) Meng, X. H.; Sedman, J.; van de Voort, F. R. Improving the determination of moisture in edible oils by FTIR spectroscopy using acetonitrile extraction. *Food Chem.* **2012**, *135*, 722−729.
(24) van de Voort, F. R.; Ghetler, A.; García-González, D. L.; Li, Y. D. Perspectives on quantitative Mid-FTIR spectroscopy in relation to edible oil and lubricant analysis: evolution and integration of analytical methodologies. *Food Anal. Methods* **2008**, *1*, 153−163.

competitive ELISA (dcELISA) was also described for evaluation and comparison of the IATC.

MATERIALS AND METHODS

Reagents and Apparatus. Apramycin (APR), dihydrostrepmycin, gentamicin, neomycin, and spectinomycin were purchased from Dr. Ehrenstorfer (Augsburg, Germany). Strepmycin, kanamycin, and tobramycin were obtained from China Institutes for Food and Drug Control (Beijing, PRC). Mouse anti-HRP antibody was purchased from LifeSpan Biosciences, Inc. (Seattle, WA, USA). Bovine serum albumin (BSA), ovalbumin (OVA), and 1-(3-dimethylaminopropyl)-3-ethyl carbodiimide (EDC) were obtained from Sigma Chemical Co. (St. Louis, MO, USA). CNBr-activated Sepharose 4B was purchased from GE Healthcare (Piscataway, NJ, USA). All other chemicals and solvents were of analytical grade or better and were obtained from Beijing Chemical Reagent Co. (Beijing, PRC).

Polystyrene microplate was purchased from Corning Inc. (Costar 2592, Corning, NY, USA). Empty SPE cartridges (Bond Elut reservoir, 1 mL) and polyethylene frits ($^1/_4$ in. diameter) were provided by Agilent Technologies (Santa Clara, CA, USA). The ELISA plate reader was obtained from TECAN Inc. (Durham, NC, USA).

Buffers and Solutions. The following buffers were used: (1) coating buffer was 0.05 M carbonate buffer, pH 9.6; (2) blocking buffer consisted of 0.01 M phosphate-buffered saline (PBS), pH 7.4, 0.5% BSA, and 0.05% Tween 20; (3) washing buffer was PBS with 0.05% Tween 20; (4) antibody dilution buffer was PBS, pH 7.4, containing 0.2% albumin; (5) enzyme-labeled secondary antibody dilution buffer was antibody dilution buffer containing 5% albumin; (6) substrate was 0.1% TMB and H_2O_2 in 0.05 M citrate buffer, pH 4.5; and (7) 2 M H_2SO_4 was the stopping reagent. Standard stock solutions (1 mg/mL) of analyte were prepared by dissolving an appropriate amount of standard drug in dimethylformamide (DMF). The individual stock solutions of analyte were stored at −20 °C in amber glass bottles. Working standards of APR and related antibiotics were prepared by diluting the stock solution in PBS (0.01 M, pH 7.4).

Synthesis of Complete Antigens. *APR-GA−BSA_1 (120:1).* APR (51 mg) and BSA (44.6 mg) were dissolved in 0.1 M carbonate buffer (10 mL, pH 9.5). Glutaraldehyde (0.5 mL, 0.1%) was added dropwise to the mixture, which was gently stirred for 5 h at room temperature. Then, sodium borohydride (0.05 mL, 10% solution) was dropped into the reaction system for another 1 h. The reaction mixtures were dialyzed against 0.01 M PBS for 3 days.

APR-GA−OVA_1 (80:1). APR-GA−OVA_1 was prepared according to the same method as used for APR-GA−BSA_1 by using 51 mg of APR and 45 mg of OVA.

APR-GA−OVA_2 (120:1). APR-GA−OVA_2 was prepared according to the same method as used for APR-GA−BSA_1 by using 51 mg of APR and 30 mg of OVA.

APR-EDC−BSA_2 (80:1). APR (51 mg) was dissolved in 0.1 M carbonate buffer (5 mL, pH 9.5), and the pH of the buffer was adjusted to pH 7.0 with 0.1 M PBS. EDC (40 mg) was added to the APR solution and stirred at room temperature overnight. BSA (67 mg) was dissolved in 5 mL of 0.01 M carbonate buffer (pH 8.0) and added dropwise to the active solution with continuous stirring and further stirred at room temperature for 4 h. The APR−BSA conjugates were dialyzed against 0.01 M PBS (pH 7.0) at 4 °C for 72 h.

APR-EDC−OVA_3 (120:1). APR-EDC−OVA_3 was prepared according to the same method as used for APR-EDC−BSA_2 by using 51 mg of APR and 30 mg of OVA.

Synthesis of HRP−APR Conjugate. HRP (10 mg) was dissolved in 1 mL of distilled water. One milliliter of 0.06 M sodium periodate and 1 mL of 0.16 M ethanediol solution were added into the HRP solution independently, which was stirred for 1 h at 4 °C. Then APR (28.7 mg) was added in the mixture and the reaction continued for 3 h at room temperature. Sodium borohydride (1 mL, 0.5% solution) was dropped into the reaction system for another 2 h at 4 °C. The reaction mixtures were dialyzed against 0.01 M PBS for 3 days.

Production of Antibodies. Female BALB/c mice were immunized for mAb production. The first injection consisted of immunogen emulsified with Freund's complete adjuvant at a dosage of 100 μg/mouse. Subsequent booster immunizations were administered biweekly with the same dosage of immunogen emulsified with Freund's incomplete adjuvant. After the fifth immunization, the mouse exhibiting the highest antibody titer was sacrificed, and the splenocytes were fused with SP2/0 myeloma cells. The growing hybridoma cells were screened for antibody production by a noncompetitive indirect ELISA and an indirect competitive ELISA using APR-EDC−BSA_2 as coating antigen with the amount of 100 μL/well.[23] The positive hybridomas were subcloned twice by limiting dilution, and the positive clones were used for ascites production. The antibody was purified from ascites using saturated ammonium sulfate, and the purified mAb was stored at −20 °C in 500 μL aliquots.

Preparation of Immunogels and Test Column. *Goat Anti-mouse IgG Antibody Immobilized Gels (Coupled Gels).* Briefly, freeze-dried CNBr-activated Sepharose 4B gel powder (1.0 g) was washed on a sintered glass filter (G3) using 100 mL of 1 mM HCl. Four hundred microliters of goat anti-mouse IgG (2.0 mg/mL) and 1 mL of coupling buffer (0.1 M $NaHCO_3$, 0.5 M NaCl, pH 8.3) were mixed with the gel on a shaker for 2 h at room temperature.The gel was washed with 20 mL of coupling buffer to remove the excess of antibody. After this, the unlinked active groups were blocked with 12 mL of blocking buffer (0.2 M glycine, 0.1 M $NaHCO_3$, 0.5 M NaCl, pH 8.0) for 2 h at room temperature. Afterward, three cycles of washing were conducted to wash away the excess glycine. Each cycle consisted of a wash with 0.1 M acetate buffer, pH 4.0, containing 0.5 M NaCl (10 mL) followed by a wash with coupling buffer (10 mL). The prepared gel was suspended in PBS containing 0.03% Proclin 300 and stored at 4 °C.

Glycine Immobilized Gels (Blocked Gels). Freeze-dried CNBr-activated Sepharose 4B gel powder (2.0 g) was washed on a sintered glass filter (G3) using 200 mL of 1 mM HCl. The gel was washed with 100 mL of coupling buffer to adjust the pH. Then, blocking buffer (50 mL) was added for blocking with 2 h at room temperature. Afterward, three cycles of washing were conducted to wash away the excess glycine. Each cycle consisted of a wash with 0.1 M acetate buffer, pH 4.0, containing 0.5 M NaCl (50 mL) followed by a wash with coupling buffer (50 mL). The prepared gel was suspended in PBS containing 0.03% Proclin 300 and stored at 4 °C.

Anti-APR Antibody Immobilized Gels (Anti-APR Gels). Coupled gels and blocked gels (1:4, v/v) were mixed well in a 10 mL polyethylene centrifuge tube, and then anti-APR antibodies (dilution 1/50000) were added into the mixture quickly in equal proportion volume of coupled gel. The mixture was shaken for 5 min at 400 rpm.

Anti-HRP Antibody Immobilized Gels (Anti-HRP Gels). Anti-HRP gels were prepared according to the same method as used for anti-APR gels by using mouse anti-HRP antibodies with 2000-fold dilution.

Development of IATC Assay. *Preparation of Test Column.* The test column consisted of three layers, which is a test layer, a control layer, and an air layer. Assembled steps were as follow: anti-HRP gels (200 μL) were added into the 1 mL empty cartridge with a frit at the bottom, and the excess liquid was pushed away from the outlet of the syringe. The second frit was used to cover the control layer, and the third frit was inserted to form the air layer, which is designed to prevent diffusion of the color reagents. Then, by a a similar step, an aliquot of 200 μL of anti-APR gels was added to prepare the test layer and the last frit was covered on the top of the test layer.

Assay Procedure. Drug standard solution (or sample) was added into the test column, which is passed through the cartridge with a constant speed. One milliliter of PBST (containing 0.1% Tween 20) was used for the washing step. Then 150 μL of APR−HRP conjugate prepared in PBS was added and incubated for 5 min. Another 7 mL of PBST was added to wash away the excess enzyme tracer. Then, 300 μL of the chromogenic substrate was added and squeezed out after 10 s of incubation. The color shown in the layers could be observed to detect the presence of APR.

Development of dcELISA. dcELISA was performed as follows: Polystyrene microtiter plate wells were coated with 100 μL of goat anti-mouse IgG for 2 h of incubation at 37 °C. After coating, plates were blocked for 1 h at 37 °C with 150 μL/well of blocking solution.

One hundrec microliters of anti-APR antibody was added in each well for 0.5 h at 37 °C. The solution was then discarded, and plates were washed three times with washing solution. Then, 50 μL of drug standard solution (or sample) and 50 μL/well of HRP-labeled APR prepared in PBS were added and incubated for 45 min at 37 °C. The final washing procedure was followed by a color development, which was initiated by adding 100 μL of the substrate/chromogen solution. The solution was incubated for 15 min at 37 °C before the enzymatic reaction was stopped by adding 2 M H_2SO_4 (50 μL/well). The optical density (OD) of each well was measured at 450 nm.

The B/B_0 ratio was selected to express the competitive inhibition curve, where B_0 and B are the absorbances obtained from binding at zero and certain concentrations of APR standard. A four-parameter logistic equation was used to fit the immunoassay data. Calculations were performed using OrginPro 8.0 software (OriginLab Corp., Northampton, MA, USA). The IC_{50} value, assay dynamic range, and limit of detection (LOD) served as criteria to evaluate the dcELISA. These different characteristics represent the analyte concentrations obtained at 50%, between 20 and 80%, and at 90%, respectively.

RESULTS AND DISCUSSION

Synthesis of Immunogen and mAb Production. The hapten design and the synthesis of the required immunogens are critical to the success of rapid immunoassays. Because it is a small molecule, APR lacks immunogenicity. To generate a specific antibody, APR should be conjugated with macromolecules to elicit an immune response via an active group, such as a carboxyl or an amino group. As shown in Figure S1 in the Supporting Information, there are six hydroxyl groups and four amino groups in the APR molecule, which allowed us to involve them in linkage with the protein. In this study, the glutaraldehyde method and EDC method was used to conjugate APR to carrier proteins (BSA and OVA). Theoretically, any of the four amino groups could be linked with the carrier, and both methods are nondirectional reaction.

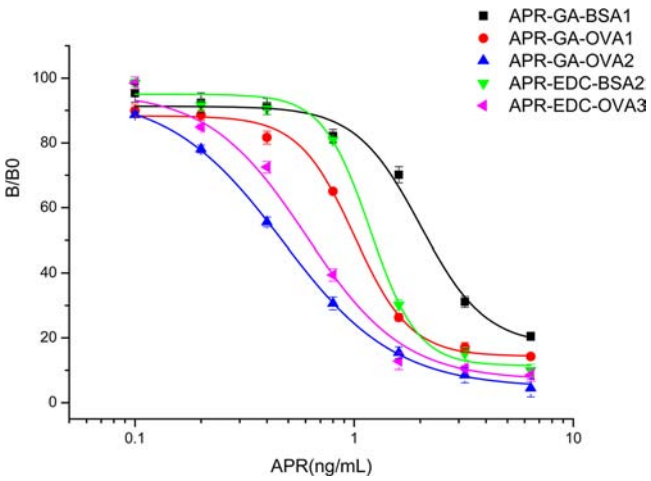

Figure 1. Standard curves of apramycin icELISA using homologous and heterologous coating antigens based on monoclonal antibody. For the concentrations of coating antigen and corresponding antibody, refer to Table S2 in the Supporting Information.

Two immunogens (APR-GA−BSA and APR-EDC−BSA) were used to immunize mice for mAb production. Mouse serum had been collected and detected after the third immunization. The results found that the titer of mouse 3, which was immunized by APR-GA−BSA, was the best with a titer of 2000, so mouse 3 was selected for the next cell fusion. During hybridoma screening, four wells of the culture supernatants were screened to contain APR-specific antibody by using indirect competitive ELISA (icELISA) after three cycles of subcloning. The results are summarized in Table S1 in the Supporting Information. Then mAb secreted by APR-2A2 was the most sensitive with an IC_{50} of 1.2 ng/mL, and its isotype was IgG_{2b}, whereas the type of light chain was κ. Therefore, APR-2A2 was chosen for further study.

Both homologous and heterologous coating antigens were utilized to further evaluate the performance of mAb. Inhibition curves of the APR using five different coating antigens are shown in Figure 1. There was a remarkable difference in the sensitivity of the antibodies, and the three heterologous coating antigens, with carrier protein OVA, expressed much higher sensitivity and affinity. The lowest IC_{50} value (0.46 ng/mL) and highest dilution of mAb (0.3 μg/mL) and antigen (0.16 μg/mL) were observed in APR-GA−OVA_2 (Supporting Information Table S2). That is, assay sensitivity may be improved using a heterologous coating antigen strategy, whereas a combination of antibody and coating antigen is proper.[23]

IATC Method. The principle of the IATC assay was similar to that of the dcELISA, and the main difference between them is the difference in type and carrier for immobilizing antibody. In IATC, there are three layers, including test, air, and control layers. For the test layer, CNBr-activated Sepharose 4B beads were utilized as the medium to immobilize capture antibody by cyanogen bromide method. APR in sample and HRP−APR conjugate compete with each other for the limited antibody on the column. After the addition of enzyme substrate and color development, the test result can be determined by the naked eye; a negative sample will produce a blue line on the column, whereas a positive sample will not produce any visible line at the respective position. While in the control layer, anti-HRP antibodies were immobilized on the gel beads and could recognize HRP enzyme to lead the color appearance after substrate existence. Compared with dcELISA, this method does not need multiple wash steps, and the washing buffer could easily drive the unbound components through the frit with 20 μm pore size, whereas the 40 μm beads bound with capture antibody and binding antigens were retained in the column.

There are four amino and six hydroxyl groups in APR, which make the drug very hydrophilic. Therefore, nonspecific sorption effect should be paid more attention for APR detection. In this study, the concentration of HRP−APR conjugate was optimized first. Six columns were divided into three groups, and one group consisted of test layers without anti-APR antibodies to control unspecific interaction (designed as control). A series of enzyme tracers (diluted with PBS at 5000, 10000, and 20000) were added to test columns in each group. The results showed that in the control group, a weak blue color appeared on the test layer in 5000-fold dilution, which means a little enzyme tracer existed with unspecific absorption on the bead, but the others did not appear. Meanwhile, the test layer showed better color intensity in 10000-fold dilutions in the test group. Thus, the concentration of 10000-fold dilution was chose for the next study (Supporting Information Figure S3).

Washing buffer is also important for eliminating nonspecific absorption. Different concentrations of Tween 20 (0.1, 0.5, and 1.0%) in washing buffer and different volumes (3, 5, 7, and 9 mL) were investigated. The results revealed that the optimal ratio of Tween 20 was 1.0% (v/v), and the amount of washing buffer was 7 mL.

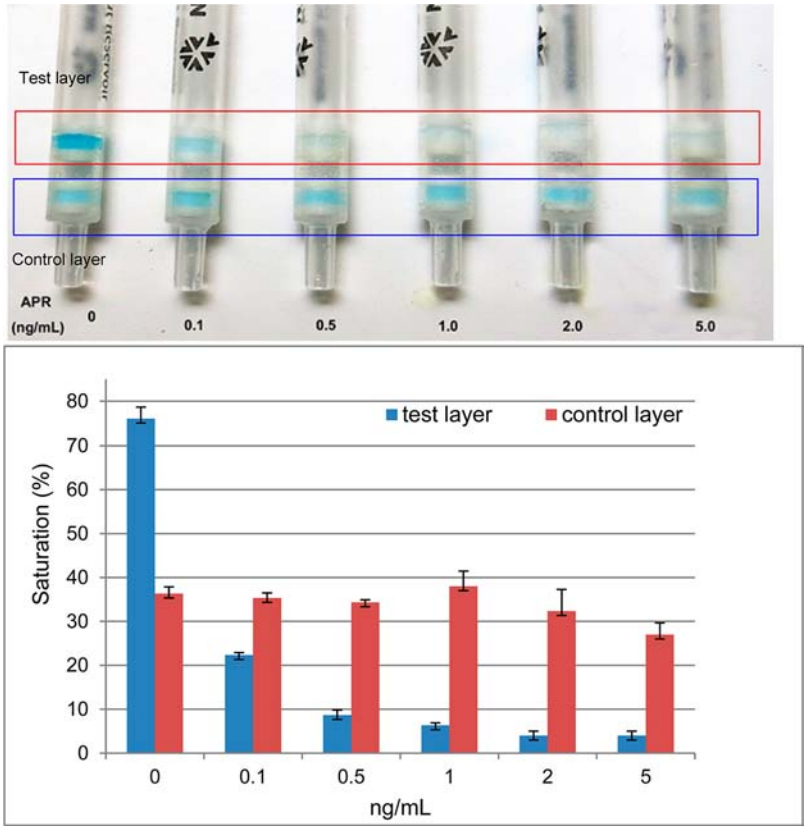

Figure 2. (a, top) Set of results for IATC assay in standard solution. From left to right, the concentrations of APR were 0, 0.1, 0.5, 1.0, 2.0, and 5.0 ng/mL, respectively. The LOD of the method could be set as 0.5 ng/mL. (b, bottom) Color intensity of the test layers and control layers.

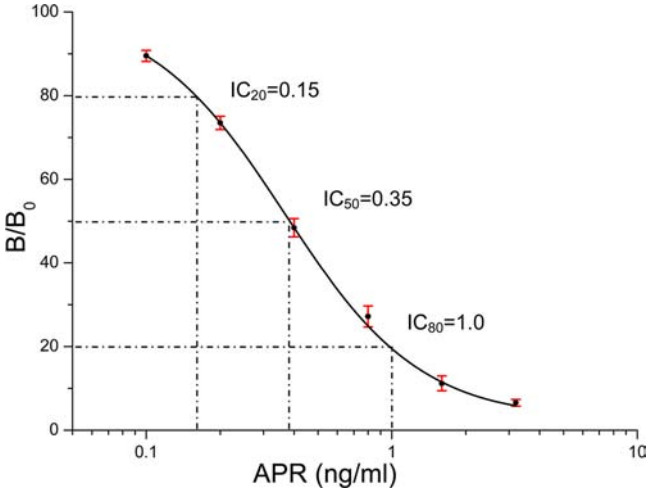

Figure 3. Standard curve of APR in buffer solution by dcELISA.

Figure 2a illustrates a set of results for IATC assay in standard solution with the concentrations of APR from 0 to 5.0 ng/mL. With the increase of drug concentration, the color fades in the test layer. When the concentration was higher than the cutoff level (defined as LOD), it could occupy enough binding sites of antibodies and lead to color disappearance. The LOD of this method was 0.5 ng/mL.

More intuitive results could be seen by quantifying the color intensity in Figure 2b. According to the method published in a previous study,[24] the IACT results were taken by a digital camera (Canon Powershot G15) and the images were saved in JPG format. The software "Adobe Photoshop 7.0.1" was used to evaluate the colors inside the test columns as saturation (parameter *S*, HSB mode). The value of parameter *S* was obtained three times, and the average value and standard deviation were calculated. Compared with observation by the naked eye, it has higher resolution to decide the cutoff value clearly. Furthermore, color quantization plays an important role for further semiquantitative analysis.

The specificity of the IATC was evaluated by determining the cross-reactivity using other common aminoglycoside drugs with high concentrations. As shown in Figure S2 (Supporting Information), 0.5 ng/mL of APR and 500 ng/mL of strepmycin (STR), gentamicin (GEN), kanamycin (KANA), and neomycin (NEO) diluted in the standard solution were respectively applied to the IATC assay. The results showed that there was no elimination of the color intensity in the test layers for the other four aminoglycoside drugs, which indicated that the assay is highly specific for the detection of APR.

dcELISA Method. To compare with the IATC, a dcELISA assay was developed and optimized on the basis of the anti-APR antibody secreted by APR-2A2. By using checkerboard titration and contrast test, many factors, such as the concentrations of the reactants (goat anti-mouse IgG antibody with 4000, anti-APR antibody with 50000, enzyme tracer with 10000), the best pH (7.4), the optimum ionic strength (0.1 M), and reaction time (see Materials and Methods), were optimized and selected in this study (detailed data not shown). Figure 3 shows the competitive inhibition standard curves for APR after fitting with Origin Pro 8.0 software. The dynamic range IC_{20}–IC_{80} was calculated as 0.15–1.0 ng/mL, and the IC_{50} and LOD of the dcELISA were 0.35 and 0.1 ng/mL, respectively, after optimization.

dx.doi.org/10.1021/jf405379r | J. Agric. Food Chem. 2014, 62, 3108–3113

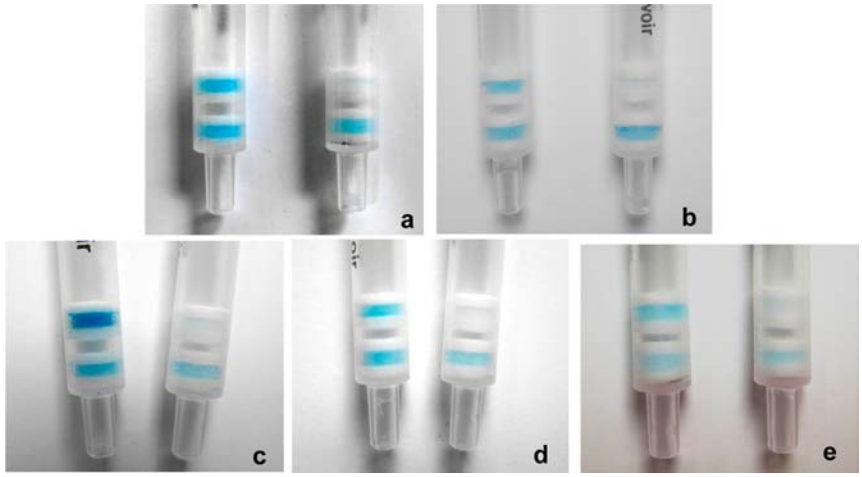

Figure 4. Results of IATC assay for different food matrices: (a) pork; (b) chicken; (c) raw milk; (d) pig liver; (e) chicken liver. Blank samples appear on the left in each panel; and spiked samples at LOD levels appear on the right.

Table 1. Recoveries of APR in Spiked Samples by dcELISA (n = 3)

sample	spiked (μg/kg)	mean recovery (%)	CV (%)
raw milk	3	103.0	5.6
	6	97.0	3.8
	12	95.6	10.1
pork	2	87.5	4.4
	4	77.0	7.5
	8	101.5	4.9
chicken	2	85.5	6.7
	4	105.5	8.6
	8	93.4	10.3
pig liver	3	80.5	5.0
	6	97.0	6.6
	12	87.2	6.8
chicken liver	20	103.5	8.9
	40	87.5	11.2
	80	93.1	5.8

The specificity of the ELISA was evaluated by determining the cross-reactivity using other common aminoglycoside drugs. Negligible cross-reactivity (<1%) was found for strepmycin, gentamicin, dihydrostrepmycin, kanamycin, tobramycin, spectinomycin, and neomycin.

Sample Analysis for dcELISA and IATC. The IATC and dcELISA assays were applied to analyze raw milk, chicken, pork, chicken liver, and pig liver. The blank samples used in the study were certified by LC-MS/MS for free APR. To eliminate interference of sample matrix, muscle and liver samples were deproteinized by trichloroacetic acid, adjusted to neutral by 1 M NaOH, and then diluted by PBS in different folds, and milk samples were diluted directly by PBS (see Table 2).

Loading volume plays a key role in improving the sensitivity of assay. For the IATC method, the loading volume of sample was not restricted, which was generally from 0 to 5 times bed volumes. Therefore, at the beginning of the study, samples were only prepared with 2−4-fold dilution. It was found that the samples containing free APR did not bind anti-APR antibody effectively, and the color appeared after addition of the enzyme tracer, especially in livers. In contrast, the color disappeared after protein precipitation was developed. This means that the protein in the sample matrix interferes the inhibition effect and affects the sensitivity of the method. Thus, for tissue samples, deproteinization steps were employed in the sample preparation. The cutoff value for raw milk was 3 ng/mL, those for pork and chicken muscles were 3 μg/kg, and those for chicken liver and pig liver were 10 μg/kg, which are summarized in Table 2 and shown in Figure 4.

For the ELISA method, in general, the loading volume of sample was 50 μL, so sample extracts needed to be diluted

Table 2. Comparison between dcELISA and IATC

	dcELISA	IATC
carrier	polystyrene well	gel bead
type	semiquantitative	qualitative
instrument	yes	no
sample treatment	depro[a] + centri[b] + dilution	depro[a] + centri[b] + dilution
dilution factor	raw milk (1:10), pork and pig liver (1:7.5), chicken (1:6), chicken liver (1:27)	1:2
method LOD (ng/mL)	0.1	0.5
sample LODs/cutoff (μg/kg)	raw milk (3), pork (2), chicken (2), pig liver (3), chicken liver (20)	raw milk (3), pork (3), chicken (3), pig liver (10), chicken liver (10)
detection time[c] (min)	90−120	15−20

[a]Deproteinization. [b]Centrifugation. [c]Include sample treatment.

dx.doi.org/10.1021/jf405379r | J. Agric. Food Chem. 2014, 62, 3108−3113

more to eliminate interference of sample matrix. When the blank samples were spiked at three concentration levels, the mean recovery ranged from 80.5 to 105.5%, with intra-assay CVs ranging from 3.8 to 11.2%; the detection limit for raw milk was 2 ng/mL, those for pork, chicken, and pig liver were 3 μg/kg, and that for chicken liver was 20 μg/kg (Tables 1 and 2).

Comparison of Two Assays. Compared with dcELISA, IATC was a new type of detection mode. Table 2 lists the difference between IATC and dcELISA. In the term of methodology itself, it is not more sensitive than dcELISA, but for the test samples, it has unique advantages. First, the loading volume is very broad, from 0 to 5 times the column bed, which could improve the sensitivity of detection effectively, whereas the volume of the ELISA microplate is only 300 μL and the loading volume is usually from 50 to 100 μL. Second, the operation is very simple and rapid and without instruments; the naked eye can be used for judgment, and repeated plate washings are avoided.

From the results of the experiments, similar sensitivities for the samples were found in two kinds of methods, which indicated that the IATC method could also act as an effective screening method for APR residues in food.

■ ASSOCIATED CONTENT

Ⓢ Supporting Information

Additional figures and tables. This material is available free of charge via the Internet at http://pubs.acs.org.

■ AUTHOR INFORMATION

Corresponding Author

*(S.D.) E-mail: dingsy@cau.edu.cn. Phone: +86-1062732802. Fax: +86-10-62731032.

Author Contributions

‖F.X. and W.J. contributed equally to this work.

Funding

This work was supported by the Special Fund for Agro-scientific Research in the Public Interest (201203069-2), the fund of modern agriculture industry system innovation in Beijing city team, and Key Projects in the National Science and Technology Pillar Program during the 12th Five-Year Plan Period (2011BAK10B01, 2012BAK17B00).

Notes

The authors declare no competing financial interest.

■ REFERENCES

(1) Canas-Rodriguez, A.; Ruiz-Poveda, S. G.; Coronel-Borges, L. A. Synthesis of apramycin analogs. *Carbohydr. Res.* **1987**, *159*, 217−227.

(2) Fernandez Suarez, A.; Ellis, R.; Bizec, B. L. Apramycin. *FAO JECFA Monographs* **2012**, *No. 12*, 35−69.

(3) Cracknell, V. C.; Andreotis, J.; Facibeni, G.; Owais, E.; Pradella, G. An evaluation of apramycin soluble power for the treatment of naturally acquired *Escherichia coli* infections in broilers. *J. Vet. Pharmacol. Ther.* **1986**, *9*, 273−279.

(4) Choi, M. J.; Lim, S. K.; Nam, H. M.; Kim, A. R.; Jung, S. C.; Kim, M. N. Apramycin and gentamicin resistances in indicator and clinical *Escherichia coli* isolates from farm animals in Korea. *Foodborne Pathog. Dis.* **2011**, *8*, 119−123.

(5) Fessler, A. T.; Kadlec, K.; Schwarz, S. Novel apramycin resistance gene apmA in bovine and porcine methicillin-resistant *Staphylococcus aureus* ST398 isolates. *Antimicrob. Agents Chemother.* **2011**, *55*, 373−375.

(6) Council Regulation (EU) No. 37/2010 on pharmacologically active substances and their classification regarding maximum residue limits in foodstuffs of animal origin. *Off. J. Eur. Union* **2010**, *L15*, 1−72.

(7) FDA. Part 556 tolerances for residues of new animal drugs in food, http://www.accessdata.fda.gov/scripts/cdrh/cfdocs/cfcfr/CFRSearch.cfm?CFRPart=556 (page last updated 06/01/2013).

(8) MHLW. Provisional Maximum Residue Limits for Agricultural Chemicals in Foods, http://www.mhlw.go.jp/english/topics/mrls/mrls.html, 2003.

(9) McGlinchey, T. A.; Rafter, P. A.; Regan, F.; McMahon, G. P. A review of analytical methods for the determination of aminoglycoside and macrolide residues in food matrices. *Anal. Chim. Acta* **2008**, *624*, 1−15.

(10) Turnipseed, S. B.; Clark, S. B.; Karbiwnyk, C. M.; Andersen, W. C.; Miller, K. E.; Madson, M. R. Analysis of aminoglycoside residues in bovine milk by liquid chromatography electrospray ion trap mass spectrometry after derivatization with phenyl isocyanate. *J. Chromatogr., B* **2009**, *877*, 1487−1493.

(11) Zhang, L. Y.; Wang, Z. Y.; Chang, B. Y.; Yang, W. J. Determination of apramycin in animal feeds by solid-phase extraction and liquid chromatography with precolumn derivatization and fluorescence detection. *J. AOAC Int.* **2007**, *90*, 885−891.

(12) Kajita, H.; Akutsu, C.; Hatakeyama, E.; Komukai, T. Simultaneous determination of aminoglycoside antibiotics in milk by liquid chromatography with tandem mass spectrometry. *Shokuhin Eiseigaku Zasshi. (J. Food Hyg. Soc. Jpn.)* **2008**, *49*, 189−195.

(13) Zhao, F.; Yue, Z.; Xiao, C.; Ye, G.; Wu, W.; Hu, X. Determination of apramycin residues in animal tissues by high pressure liquid chromatography-tandem mass spectrometry. *J. Food Saf. Qual.* **2013**, *4*, 159−164.

(14) Kumar, P.; Rubies, A.; Companyo, R.; Centrich, F. Determination of aminoglycoside residues in kidney and honey samples by hydrophilic interaction chromatography-tandem mass spectrometry. *J. Sep. Sci* **2012**, *35*, 2710−2717.

(15) Mortensen, J. E.; Nanavaty, J.; Veenhuizen, M. F.; Shryock, T. R. Reviewing apramycin's properties and use in controlling colibacillosis is in pigs. *Vet. Med.* **1996**, *91*, 473−477.

(16) Lourenco, F. R.; Barbosa, E. A.; Pinto, T. J. A. Microbiological assay for apramycin soluble powder. *Lat. Am. J. Pharm.* **2011**, *30*, 554−557.

(17) Jiang, W.; Wang, Z.; Beier, R. C.; Jiang, H.; Wu, Y.; Shen, J. Simultaneous determination of 13 fluoroquinolone and 22 sulfonamide residues in milk by a dual-colorimetric enzyme-linked immunosorbent assay. *Anal. Chem.* **2013**, *85*, 1995−1999.

(18) Burkin, M.; Galvidis, I. Immunochemical detection of apramycin as a contaminant in tissues of edible animals. *Food Control* **2013**, *34*, 408−413.

(19) Galvidis, I. A.; Burkin, M. A. Monoclonal antibody-based enzyme-linked immunosorbent assay for the aminoglycoside antibiotic kanamycin in foodstuffs. *Russ. J. Bioorg. Chem.* **2010**, *36*, 722−729.

(20) Zhang, H.; Wang, S.; Fang, G. Applications and recent developments of multi-analyte simultaneous analysis by enzyme-linked immunosorbent assays. *J. Immunol. Methods* **2011**, *368*, 1−23.

(21) Beloglazova, N. V.; Goryacheva, I. Y.; Mikhirev, D. A.; de Saeger, S.; Niessner, R.; Knopp, D. New immunochemically-based field test for monitoring benzo[*a*]pyrene in aqueous samples. *Anim. Sci.* **2008**, *24*, 1613−1617.

(22) Yuan, M.; Sheng, W.; Zhang, Y.; Wang, J.; Yang, Y.; Zhang, S.; Goryacheva, I. Y.; Wang, S. A gel-based visual immunoassay for non-instrumental detection of chloramphenicol in food samples. *Anal. Chim. Acta* **2012**, *751*, 128−134.

(23) Chen, Y. Q.; Shang, Y. H.; Wu, X. P.; Qi, Y. T.; Xiao, X. L. Enzyme-linked immunosorbent assay for the detection of neomycin in milk: effect of hapten heterology on assay sensitivity. *Food Agric. Immunol.* **2007**, *18*, 117−128.

(24) Beloglazova, N. V.; Goryacheva, I. Y.; Rusanova, T. Y.; Yurasov, N. A.; Galve, R.; Marco, M. P.; De Saeger, S. Gel-based immunotest for simultaneous detection of 2,4,6-trichlorophenol and ochratoxin A in red wine. *Anal. Chim. Acta* **2010**, *672*, 3−8.

suppression in positive ionization mode. Esterified xanthophylls tend to elute together with the bulk of triglycerides during RP-LC (e.g., on a C18 column), and this can hamper correct quantification or even identification. Triglycerides do not ionize in negative APCI mode and one could therefore suggest using negative APCI mode instead. However, some carotenoids do not ionize in negative ionization mode.[17] For proper identification and quantification of esterified carotenoids in samples with high lipid content, it is therefore essential that these lipids are removed before detection.

Saponification is most often used to hydrolyze glycerolipid interferences during carotenoid analysis. Ester bonds of other plant metabolites such as carotenoids are however also hydrolyzed during saponification, thus altering the natural carotenoid composition.[18] Preparative column chromatography has been used to separate lipids from carotenoids.[18] This procedure is, however, tedious if performed manually and expensive if performed automatically. Beyond that, this separation procedure has to be optimized for every different matrix as the composition of glycerolipids and carotenoids is matrix dependent.

Triacylglycerol hydrolases or lipases are an important group of biotechnologically relevant enzymes that find immense applications in food, dairy, detergent, and pharmaceutical industries. Lipases act under aqueous conditions on the carboxyl ester bonds present in triacylglycerols to liberate fatty acids and glycerol. The reaction is catalyzed at the lipid−water interface.[19] Lipase enzymes have, however, not only been tested for the cleavage of triacylglycerides. Several publications have been written on the use of lipase enzymes for the hydrolysis of carotenoid esters to their free form.[10,20] Conversion rates from esterified to free carotenoids ranged from 0 to 89% and are largely dependent on the type of enzyme. As free carotenoids have been reported to have a better bioavailability, the aim of these studies was to create more elegant alternatives for chemical saponification of marigold flower extracts and red paprika extracts on an industrial scale.

Breithaupt et al. were the first to report the use of lipase enzymes for the selective removal of triacylglycerides for the identification of carotenoid esters in potatoes.[21] During the first cleanup step, open bed column chromatography was used to obtain a fraction containing the carotenoid esters. This fraction was then further purified by the selective enzymatic cleavage of residual triacylglycerides with two commercial lipase enzymes. To our knowledge this is the only peer-reviewed publication written on the selective removal of triacylglycerides with the emphasis on the preservation of the natural carotenoid ester composition. As this procedure involves a fractionation step, the full natural carotenoid profile is, however, lost. Furthermore, open bed column chromatography is often laborious and tedious. Therefore, the aim of this study was to optimize this method to an efficient one-step enzymatic cleanup method without prefractionation to simplify the method and to preserve the natural carotenoid profile of the samples.

MATERIALS AND METHODS

Chemicals. LC-MS grade methanol, acetonitrile, and ethyl acetate were purchased from Biosolve (Valkenswaard, The Netherlands). Ultrapure water with a resistivity of 18.2 MΩ·cm at 25 °C was generated with a Millipore system. Dichloromethane (DCM) for gas chromatography, *n*-hexane for gas chromatography, acetone for gas chromatography, sodium hydrogen carbonate, potassium phosphate, and sodium chloride for analysis were purchased from Merck (Darmstadt, Germany). Ammonium acetate, (D-Ala^2)-leucin enkephalin, bile salts, and butylated hydroxytoluene (BHT) were purchased from Sigma-Aldrich (Bornem, Belgium). Commercially available mixtures to calibrate the mass spectrometer, namely, MSCAL5-1EA (caffeine, tetrapeptide "Met-Arg-Phe-Ala", Ultramark) for positive ion mode and MSCAL6-1EA (sodium dodecyl sulfate, taurocholic acid sodium salt, Ultramark) for negative ion mode, were purchased from Supelco (Bellefonte, PA, USA).

Capsanthin, astaxanthin dipalmitate, and astaxanthin were purchased from Carotenature (Ostermundigen, Switzerland). β-Carotene and β-sitosterol were purchased from Sigma-Aldrich (Bornem, Belgium). Paprika oleoresin 65000 CU (900 g) was obtained from Natural Spices (Mijdrecht, The Netherlands), and Asta Krill 8 (60 softgels of approximately 1 g) was obtained from Swanson vitamins (Fargo, ND, USA). The content of the Asta Krill 8 soft gels consists of *Euphausia superba* Antarctic krill oil combined with an astaxanthin-rich extract from the microalga *Haematococcus* (as stated by the supplier). The food grade enzyme formulations Lipozyme TL 100 L (100 KLU/g) and Lipozyme CALB L (5 KLU/g) were kindly provided by Novozymes (Bagsvaerd, Denmark). Sodium lauryl sulfate, glycerol dioleate, and glycerol trioleate were obtained from Chem Service (West Chester, PA, USA). Extra virgin olive oil was obtained from a local store.

Preparation of Standard Solutions. Standard stock solutions and working solutions were prepared for each analyte separately at a concentration of approximately 200 μg/mL. Stock solutions for glycerolipids were prepared in methanol. The stock solution of β-sitosterol was prepared in methanol + 0.1% BHT. Stock solutions for carotenoids were prepared in DCM + 0.1% BHT. Standard stock and working solutions were stored at −25 °C in the dark under an inert atmosphere (nitrogen). Dilutions of the stock solutions were prepared in DCM + 0.1% BHT for analysis.

Instrumental Analysis. All analyses were performed with an ultrahigh-performance liquid chromatography−photodiode array−accurate mass mass spectrometry (UHPLC-PDA-am-MS) configuration. The LC system consisted of an Accela quaternary solvent manager, a "Hot Pocket" column oven (Thermo Fisher Scientific, Bremen, Germany), and a CTC PAL autosampler (CTC Analytics, Zwingen, Switzerland). The LC system was hyphenated to an Accela PDA detector and an Orbitrap mass spectrometer (Exactive, Thermo Fisher Scientific, Bremen, Germany).

The method of analysis was previously described by Bijttebier et al.[17] Briefly, 1.25 μL was injected on a thermostatically heated (35 °C) Acquity UPLC HSS C18 SB column (2.1 mm × 100 mm, 1.8 μm; Waters, Milford, MA) and chromatographically separated by gradient elution. The mobile phase solvents consisted of 50:22.5:22.5:5 (v/v/v/v) water + 5 mM ammonium acetate/methanol/acetonitrile/ethyl acetate (A) and 50:50 (v/v) acetonitrile/ethyl acetate (B), and the gradient was set as follows (min/%A): 0.0/90, 0.1/90, 0.8/70, 20.0/9, 20.1/0, 20.4/0, 20.5/90, 23.0/90. APCI was used as MS ionization technique, and polarity switching was applied. The scanning range was set to m/z 90−1400 and a mass resolution of 50,000 fwhm was applied. The corona discharge current was set at 5 μA, the vaporizer and capillary temperatures were set at 450 °C, and a capillary voltage of ±25 V was used for both positive and negative APCI. Lock mass correction with (D-Ala)^2-leucin enkephalin was applied, and mass deviations of no more than 2 ppm were observed. The PDA detector was set to scan from 190 to 800 nm. Xcalibur software (Thermo Fisher Scientific) was used to process the data.

Sample Preparation. Red paprika fruits (*Capsicum annuum*) were bought in a local store. After removing the stems and kernels, they were cut into pieces, frozen with liquid nitrogen and immediately freeze-dried. After drying they were milled and homogenized with a Grindomix GM 200 from Retsch (Haan, Germany) at 10,000 rpm and stored in the dark under nitrogen at −25 °C. Before sample preparation, the sample was allowed to equilibrate to room temperature. To 20 g of freeze-dried paprika were added 20 g of sodium hydrogen carbonate and 330 mL of 70:30 acetone/methanol +

Table 1. Summary of the Accurate Masses Obtained for the MS Protonated and Deprotonated Molecules and Product Ions in Positive and Negative APCI Mode and the Maximum Absorbances, Used for the Identification of the Compounds Described Throughout the Paper

					positive APCI mode		negatve APCI mode	
sample matrix[a]	component	molecular formula	retention time (min)	UV_{max}	detected protonated molecules	in source fragments	detected radical ions or adducts	in source fragments
1	β-carotene[b]	$C_{40}H_{56}$	16.5	430; 455; 482	537.445	445.382	536.439	
1	capsanthin diester (C12:0, C12:0)	$C_{64}H_{100}O_5$	19.29	460	949.764	749.587; 549.409	948.757	
1	capsanthin diester (C12:0, C14:0)	$C_{66}H_{104}O_5$	19.94	463	977.795	749.587; 549.409	976.788	
1	capsanthin diester (C14:0, C14:0)	$C_{68}H_{108}O_5$	20.53	473	1005.830	777.617	1004.820	776.611; 227.202
1	capsanthin diester (C14:0, C16:0)	$C_{70}H_{112}O_5$	21.05	462	1033.860	805.648; 777.617; 549.409	1032.850	776.611; 548.400
2	astaxanthin[b]	$C_{40}H_{52}O_4$	7.85	481	597.393	579.383	596.386	504.324
2	astaxanthin monoester (C18:4)	$C_{58}H_{78}O_5$	14.25	478	855.591	579.383; 837.581	854.584	578.376
2	astaxanthin monoester (C18:3)	$C_{58}H_{80}O_5$	14.93	481	857.606	579.383; 839.597	856.600	578.376
2	astaxanthin monoester (C18:2)	$C_{58}H_{82}O_5$	15.68	481	859.622	579.383; 841.612	858.616	578.376
2	astaxanthin monoester (C18:1)	$C_{58}H_{84}O_5$	16.55	481	861.638	579.383; 835.623	860.631	578.376
2	astaxanthin diester (C18:2, C18:3)	$C_{76}H_{110}O_6$	18.75	480	1119.840	839.597; 841.612; 560.364	1118.830	840.606; 838.591
1	diglyceride (C18:3, C18:3)	$C_{39}H_{64}O_5$	11.5	nd[c]	613.482	595.471; 335.258	nd	277.217
1	diglyceride (C18:2, C18:3)	$C_{39}H_{66}O_5$	12.4	nd	615.498	597.487; 337.273; 335.258	nd	279.233; 277.217
1, 3	diglyceride (C18:2, C18:2)	$C_{39}H_{68}O_5$	13.31	nd	617.513	599.503; 337.274	nd	279.233
1, 3	diglyceride (C18:1, C18:2)	$C_{39}H_{70}O_5$	14.36	nd	619.529	601.518; 337.273; 339.289	nd	279.232; 281.248
3	diglyceride (C18:1, C18:1)	$C_{39}H_{72}O_5$	15.58	nd	621.544	603.534; 339.289	nd	339.289
2	diglyceride (C16:1, C14:0)	$C_{33}H_{62}O_5$	13.08	nd	539.467	521.456; 311.258; 285.242	nd	227.201; 253.217
1	diglyceride (C18:3, C16:0)	$C_{37}H_{66}O_5$	13.49	nd	591.498	573.487; 313.273; 335.258	nd	277.217; 255.233
3	diglyceride (C18:2, C16:0)	$C_{37}H_{68}O_5$	14.43	nd	593.513	575.503; 313.273; 337.274	nd	nm[d]
2	diglyceride (C18:1, C14:0)	$C_{35}H_{66}O_5$	14.46	nd	567.498	549.487; 339.289; 285.243	nd	281.248; 227.201
2, 3	diglyceride (C18:1, C16:0)	$C_{37}H_{70}O_5$	15.83	nd	595.529	577.518; 339.289; 313.273	nd	255.233; 281.248
1	triglyceride (C18:2, C18:2, C18:2)	$C_{57}H_{98}O_6$	19.7	nd	879.743	599.502	nd	279.233
1	triglyceride (C18:1, C18:2, C18:2)	$C_{57}H_{100}O_6$	20.36	nd	881.758	601.518; 599.503	nd	279.233; 281.248
1, 3	triglyceride (C18:1, C18:1, C18:2)	$C_{57}H_{102}O_6$	21.0	nd	883.774	603.534; 601.518	nd	279.233; 281.248
3	triglyceride (C18:1, C18:1, C18:1)	$C_{57}H_{104}O_6$	21.53	nd	885.790	603.534	nd	nm
3	triglyceride (C18:1, C18:1, C18:0)	$C_{57}H_{106}O_6$	22.16	nd	887.806	605.549; 603.534	nd	nm
1	triglyceride (C18:2, C18:2, C16:0)	$C_{55}H_{98}O_6$	20.48	nd	855.743	599.502; 575.503	nd	279.233; 255.233
1, 2, 3	triglyceride (C18:1, C18:2, C16:0)	$C_{55}H_{100}O_6$	21.3	nd	857.759	577.519; 575.503; 601.519	nd	255.233; 281.248; 279.233
3	triglyceride (C18:1, C18:1, C16:0)	$C_{55}H_{102}O_6$	21.66	nd	859.774	577.518	nd	nm
2	triglyceride (C18:1, C14:0, C16:0)	$C_{51}H_{96}O_6$	21.45	nd	805.728	577.519; 549.488; 523.472	nd	281.248; 255.233; 227.201
2	triglyceride (C14:0, C16:1, C16:0)	$C_{49}H_{92}O_6$	20.79	nd	777.696	549.488; 523.472; 521.457	nd	255.233; 227.201; 253.217
1	β-sitosterol[b]	$C_{29}H_{50}O$	15.36	nd	nd	397.383	nd	
1	β-sitosteryl glucoside	$C_{35}H_{60}O_6$	8.13	nd	nd	397.383	635.453[e]	575.432
1	β-sitosteryl linolenoyl glucoside (C18:3)	$C_{53}H_{88}O_7$	17.0	nd	nd	397.383	895.667[e]	
1	β-sitosteryl linoleoyl glucoside (C18:2)	$C_{53}H_{90}O_7$	18.09	nd	nd	397.383	897.682[e]	

dx.doi.org/10.1021/jf405477s | J. Agric. Food Chem. 2014, 62, 3114−3124

Table 1. continued

sample matrix[a]	component	molecular formula	retention time (min)	UV_{max}	positive APCI mode: detected protonated molecules	positive APCI mode: in source fragments	negatve APCI mode: detected radical ions or adducts	negatve APCI mode: in source fragments
1	β-sitosteryl oleoyl glucoside (C18:1)	$C_{53}H_{92}O_7$	19.42	nd	nd	397.383	899.698[e]	
1	β-sitosteryl palmitoyl glucoside (C16:0)	$C_{51}H_{90}O_7$	20.06	nd	nd	397.383	873.682[e]	

[a]1, paprika oleoresin; 2, Asta Krill 8 soft gels; 3, in-house paprika extract with olive oil spike. [b]Identification with standard. [c]nd, not detected. [d]nm, not measured. [e]Acetate adduct.

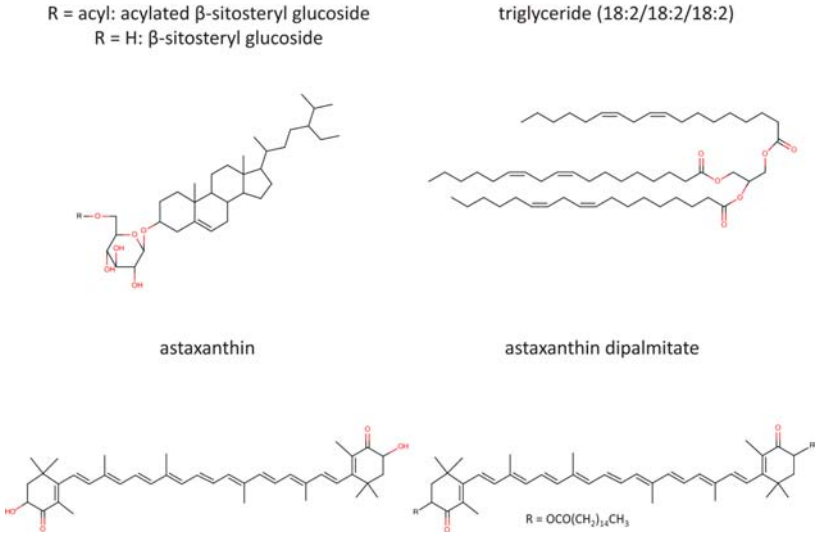

Figure 1. Representative structures of the different compound groups.

0.1% (v/v) BHT. The bottle was flushed with N_2 gas and closed. After shaking for 30 min and subsequent centrifugation for 5 min at 5000 rpm, the solvent was transferred into a round-bottom flask. This extraction procedure was repeated two more times. The three supernatants were pooled, evaporated, and dissolved in 20 mL of DCM + 0.1% BHT. The extract was stored in the dark under nitrogen at −25 °C. For the lipase treatment, an aliquot of the extract was evaporated and dissolved in the solvent of the treatment.

A commercially available paprika oleoresin was bought and stored at 4 °C. Before hydrolysis with lipase enzymes, the bottle was shaken vigorously by hand for 30 s and an aliquot was taken for enzymatic hydrolysis. The Asta Krill 8 soft gels were bought and stored at 4 °C. The oil present in the Asta Krill 8 soft gels was obtained by cutting the soft gels open. This oil was subsequently used for lipase assays.

Lipase Efficiency and Selectivity Determination. A UV wavelength of 440 nm was chosen to compare carotenoid profiles in the samples before and after lipase treatment without interferences from glycerolipids because di- and triacylglycerides do not absorb light in this region. To compare the lipid profile before and after enzymatic hydrolysis, the total ion current (TIC) signal obtained by the Orbitrap MS detector in positive APCI mode was used. Due to the high lipid content of the samples used during this study, lipids dominated the TIC chromatograms before the enzyme assay. Identification of glycerolipids was achieved with the protonated molecules and in-source product ions generated during am-MS detection. The order of the fatty acids bound to glycerol (i.e. *sn*-1, *sn*-2, or *sn*-3 position of the glycerol backbone) could not be deduced from the spectra during the experiments, and the lipids were therefore noted as "TG(C18:2, C18:2, C16:0)" instead of "TG(C18:2/C18:2/C16:0)". The decline of the level of individual lipids by lipase treatment was monitored with the extracted ion chromatograms (EIC) of selected ions. Loss in ionization efficiency during the elution of high lipid concentrations can lead to an underestimation of the percentage of lipids hydrolyzed.[22] Lipid hydrolysis rates are therefore most probably higher in practice than described in this paper.

The spectral and chromatographic data used for compound identification are listed in Table 1. Mass accuracies of <2 ppm were obtained during analysis. The identities of the compounds are tentative but reliable as the mass/charge (m/z) values and molecular formulas of the (de-)protonated molecules and product ions in am-MS are in agreement with the proposed structures. Furthermore, the fragmentation pathways of the identified carotenoids and lipids correspond to the fragmentation patterns of analytical standards of structural homologues analyzed with the same method. Confirmation of the proposed carotenoid backbones was obtained by the PDA spectra. Representative structures for the different compound groups are given in Figure 1.

RESULTS AND DISCUSSION

Lipase Treatment. *Application of the Lipase Enzymes As Described by Breithaupt et al. .*[21] The lipase procedure described by Breithaupt et al. was used as a starting point for method optimization.[21] The fractionation by column chromatography described in this procedure was not applied to preserve the natural carotenoid profile of the samples.[21] The procedure by Breithaupt et al. described the use of the enzyme formulations Novozym 868 L (6 kilo lipase units (KLU)/g) and Lipolase (100 KLU/g) (Novozymes, Bagsvaerd, Denmark) which are no longer commercially available.[21] Therefore, new enzyme formulations Lipozyme TL 100 L and Lipozyme CALB L were selected. Lipozyme TL 100 L (100 KLU/g) is the new food grade formulation of Lipolase and contains the identical enzyme. The enzyme formulation Novozym 868 L contained an enzyme from *Candida antarctica* (A), and a replacement was not readily found. Novozym 435 was tested by Zorn et al. for its

dx.doi.org/10.1021/jf405477s | J. Agric. Food Chem. 2014, 62, 3114−3124

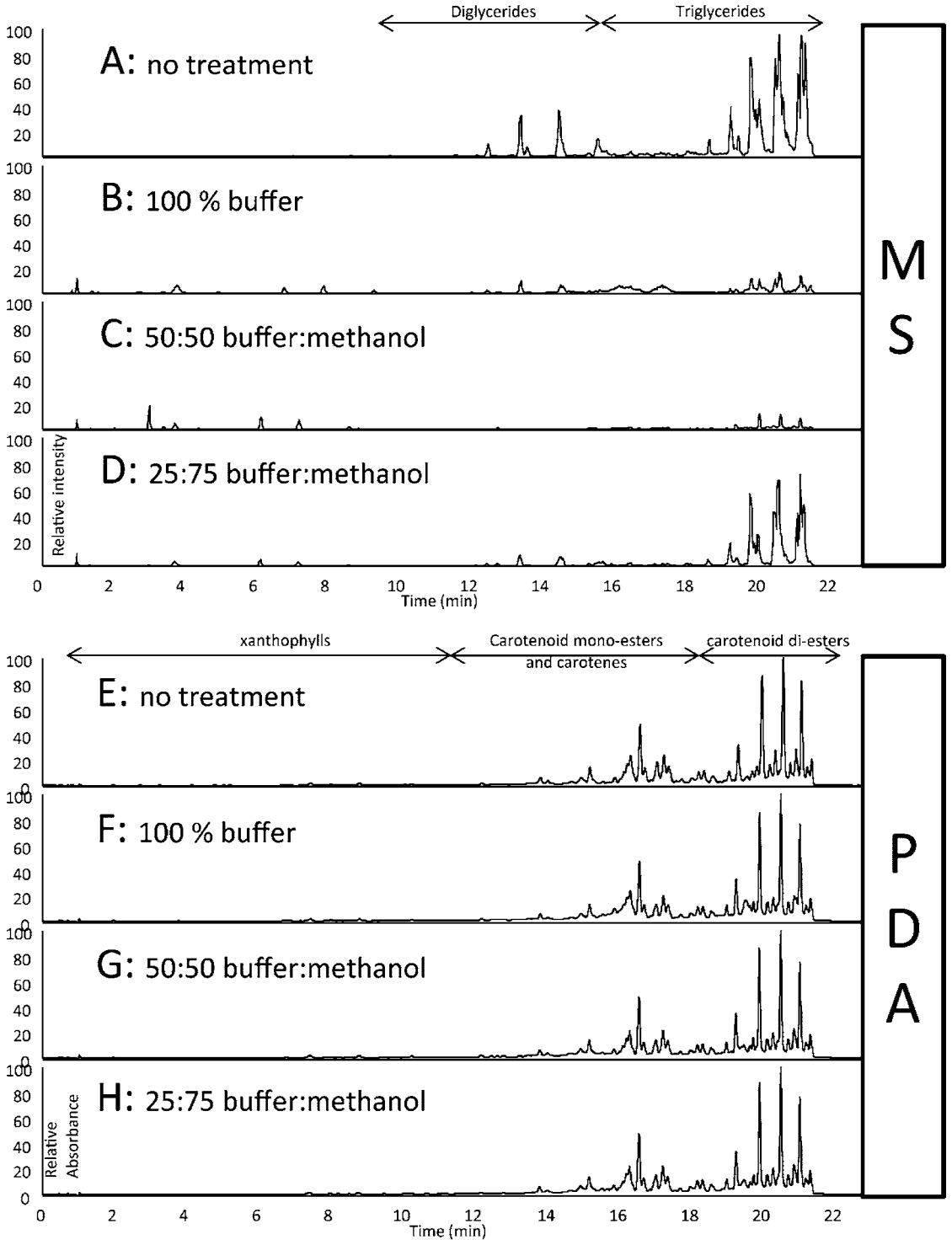

Figure 2. Chromatograms (fixed scale) of paprika oleoresin before and after lipase treatment with different solvent compositions (100 μL of oleoresin in 20 mL of solvent, 2 h at 40 °C, 25 μL of sodium *n*-octyl sulfate, 30 mg of bile salts, and 250 μL of sodium chloride solution (5 mM), 1 mL of 5 KLU of Lipozyme CALB L and 1 mL of 100 KLU of Lipozyme TL 100 L): full scan MS signal (A) before lipase treatment, (B) after lipase treatment with 100% aqueous phosphate buffer (0.1 M, pH 7.4, 10 mL), (C) after lipase treatment with 50:50 (v/v) aqueous phosphate buffer/methanol, and (D) after lipase treatment with 25:75 (v/v) aqueous phosphate buffer/methanol; UV signal at 440 nm (E) before lipase treatment, (F) after lipase treatment with 100% aqueous phosphate buffer, (G) after lipase treatment with 50:50 (v/v) aqueous phosphate buffer/methanol, and (H) after lipase treatment with 25:75 (v/v) aqueous phosphate buffer/methanol. The arrows indicate the elution order of the compound groups.

ability to hydrolyze carotenoids esterified with fatty acids and showed no significant activity toward these compounds.[10] Lipozyme CALB L (5 KLU/g) was therefore chosen because it contains the same lipase enzyme from *Candida antarctica* (B) as Novozym 435.

The altered Breithaupt et al. procedure was tested on an in-house produced paprika extract.[21] An aliquot of the paprika DCM extract (1 mL) was transferred into an Erlenmeyer flask covered in aluminum foil and subsequently dried under a gentle stream of N_2 gas. A potassium phosphate buffer solution (0.1

Table 2. Percentage of Di- (DG) and Triglycerides (TG) Hydrolyzed upon Lipase Treatment (A) under Different Solvent Compositions with an Incubation Time of 2 h for the Paprika Oleoresin, (B) under Different Solvent Compositions with an Incubation Time of 2 h for the in-House Prepared Paprika Extract Spiked with Olive Oil, and (C) with Different Incubation Times for the Paprika Oleoresin in 50:50 Phosphate Buffer/Methanol[a]

(A) solvent composition paprika oleoresin				(B) solvent composition paprika extract + olive oil			(C) incubation time paprika oleoresin		
	100% phosphate buffer	50:50 phosphate buffer/ MeOH	25:75 phosphate buffer/ MeOH		100% phosphate buffer	50:50 phosphate buffer/ MeOH	1 h	2 h	3 h
no. of replicates:	1	2	2	no. of replicates:	1	1	2	2	2
TG (C18:2, C18:2, C18:2)	90	97	39	TG (C18:1, C18:1, C18:2)	9	77	96	97	99
TG (C18:1, C18:2, C18:2)	87	98	44	TG (C18:1, C18:1, C18:1)	50	55	96	97	99
TG (C18:2, C18:2, C16:0)	90	98	40	TG (C18:1, C18:2, C16:0)	21	86	97	97	99
TG (C18:1, C18:1, C18:2)	92	98	51	TG (C18:1, C18:1, C16:0)	37	70	97	98	99
TG (C18:1, C18:2, C16:0)	86	97	32	TG (C18:1, C18:1, C18:0)	44	88	95	97	99
DG (C18:3, C18:3)	94	98	96	DG (C18:1, C18:1)	−60	−33	97	97	99
DG (C18:2, C18:3)	78	96	83	DG (C18:1, C16:0)	−120	−32	93	94	98
DG (C18:2, C18:2)	68	92	64	DG (C18:1, C18:2)	−138	−71	84	88	96
DG (C18:3, C16:0)	88	98	82	DG (C18:2, C16:0)	4	51	95	97	99
DG (C18:1, C18:2)	79	96	75	DG (C18:2, C18:2)	19	47	89	93	98

[a]Tested solvent compositions for (A) and (B): 100:0 (v/v), 50:50 (v/v), and 25:75 (v/v) aqueous phosphate buffer (0.1 M, pH 7.4, 10 mL)/MeOH. Tested incubation times for (C): 1, 2, and 3 h. Method conditions: 100 μL of oleoresin or extract spiked with 300 μL of olive oil, 20 mL of solvent, incubation at 40 °C, 25 μL of sodium *n*-octyl sulfate, 30 mg of bile salts, and 250 μL of 5 mM NaCl. Enzyme formulations: 1 mL of 5 KLU of Lipozyme CALB L and 1 mL of 100 KLU of Lipozyme TL 100 L for (A), 1 mL of 100 KLU of Lipozyme TL 100 L for (B).

M, pH 7.4, 10 mL), 30 mg of bile salts, and 250 μL of sodium chloride solution (5 mM) were added. As the paprika extract is an apolar extract, it does not dissolve in the aqueous buffer solution. Therefore, the solution was continuously stirred magnetically during preincubation and incubation to increase the surface area at the lipid−water interface. After a preincubation time of 30 min at 40 °C, the enzymes were added. In the procedure of Breithaupt et al., the enzyme formulations Novozym 868 L and Lipolase were diluted and subsequently added to the Erlenmeyer flask at levels of 0.024 and 0.4 KLU, respectively.[21] The same level of lipase units was added to the incubation mixture for the two selected lipase enzymes (0.024 KLU of Lipozyme CALB L and 0.4 KLU of Lipozyme TL 100 L). After addition of the diluted enzyme formulations, the mixture was incubated for 2 h at 40 °C. After incubation, the carotenoids were extracted immediately using a mixture of 1:1:1 methanol/ethyl acetate/hexane (v/v/v) using a separation funnel. The upper apolar layer, containing the carotenoids and remaining glycerolipids, was collected. This extraction procedure was repeated three times, and the extracts were combined. After extraction, the polar phase containing glycerol and fatty acids was discarded. The combined extracts (upper layers) were washed twice with 100 mL of water to remove all alkali and acids. The organic layer was dried over anhydrous sodium sulfate and subsequently evaporated to dryness at 35 °C under a gentle stream of N_2. The dried extract was dissolved in 1 mL of DCM + 0.1% BHT. Analysis with LC-PDA-am-MS showed that there was no clear signal drop of glycerolipids before and after hydrolysis. This low hydrolysis rate could be due to several factors. No lipid concentrations or conversion factors were mentioned in the study of Breithaupt et al., therefore making comparison impossible.[21] The enzyme/lipid concentration ratios could be too low to hydrolyze a significant level of glycerolipids. Furthermore, the used enzyme formulations were not identical to those applied by Breithaupt et al.[21] On the other hand, as mentioned before, the apolar paprika extract did not dissolve in the aqueous buffer solution. Therefore, only a low contact surface area was available for the enzymes to catalyze the hydrolysis of glycerolipids. Several method parameters were therefore adjusted to optimize the enzymatic hydrolysis of glycerolipids.

Optimization of the Lipase Treatment. Zorn et al. reported the use of purified soy lecithin to improve emulsification during enzymatic hydrolysis of carotenoid esters in paprika oleoresins.[10] It was therefore decided to add 25 μL of sodium *n*-octyl sulfate as emulsifying agent before preincubation to all of the experiments described below. This detergent was chosen as it was more readily available than lecithin and thought to be less prone to being a source of natural plant metabolites. To improve the rate of hydrolysis of the glycerolipids, 1 mL of each of the enzyme formulations, corresponding to approximately 5 KLU of Lipozyme CALB L and 100 KLU of Lipozyme TL 100 L, was added to the incubation mixtures. According to the manufacturer, the enzyme formulations that were used during the current study have sales values of approximately 40 and 80 euro/kg. The cost of the enzymes was thus approximately 0.12 euro per analysis, which is a relatively small cost in sample preparation.

Solvent Composition. A commercial paprika oleoresin was chosen for the optimization of the lipase treatment as it contains high concentrations of both carotenoids and lipids. Because of the high viscosity of the oleoresin, an aliquot of only 100 μL was used per test, and 20 mL of solvent was added. This solution contained much higher concentrations of lipids compared to the in-house prepared paprika extract used under Application of the Lipase Enzymes As Described by Breithaupt et al. As solvent, different ratios of phosphate buffer and methanol were tested. The addition of methanol could

dx.doi.org/10.1021/jf405477s | J. Agric. Food Chem. 2014, 62, 3114−3124

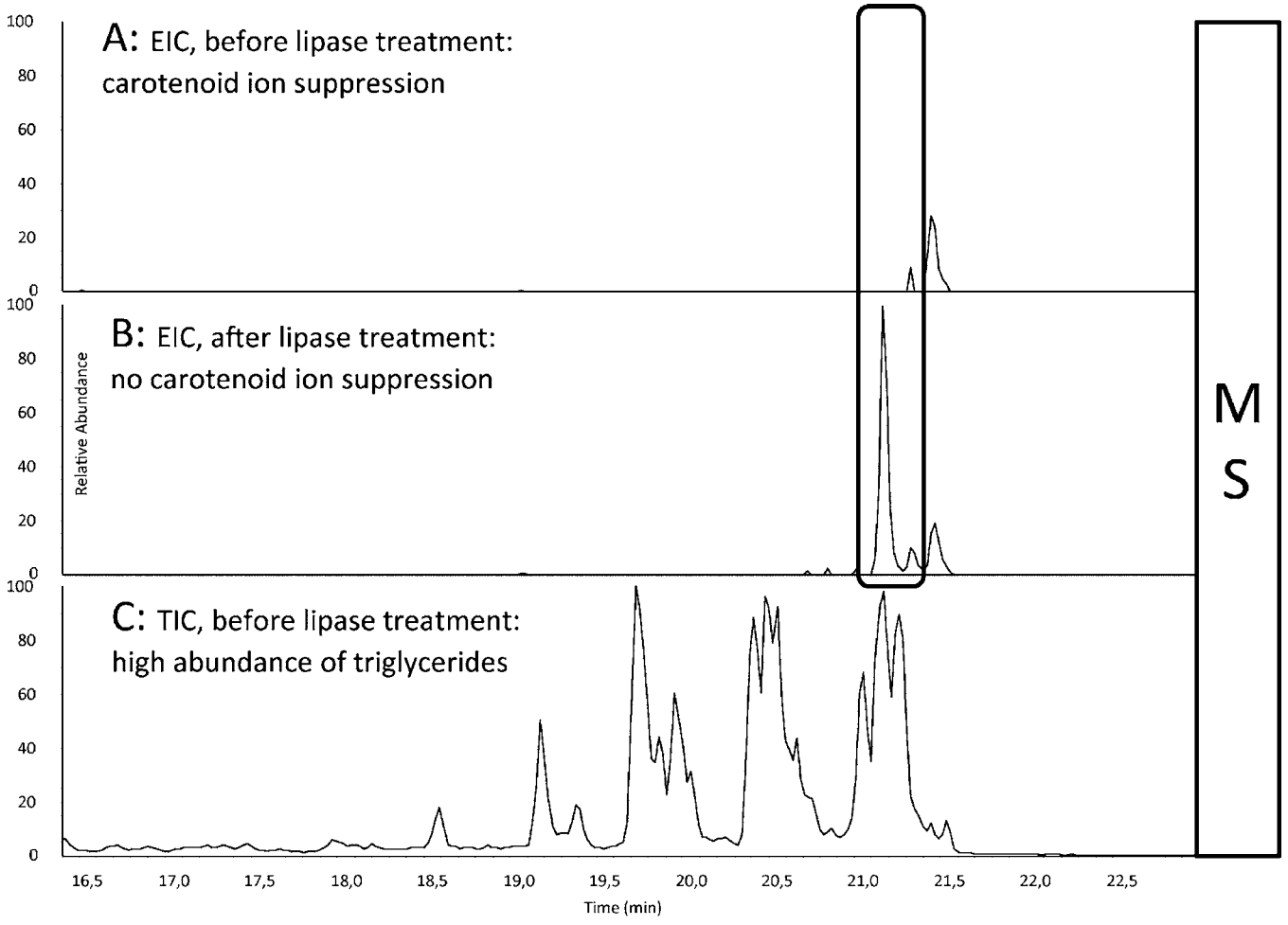

Figure 3. Extracted ion chromatograms (EIC) of the isomers of a capsanthin diester (C14:0, C16:0) in the paprika oleoresin before (A) and after (B) lipase treatment (50:50 (v/v) phosphate buffer/methanol) and the total ion chromatogram (TIC) chromatogram of the paprika oleoresin before lipase treatment (C).

improve the solubility of the oleoresin. Although organic solvents are also known to denature enzymes and thus inhibit their mode of action, lipases are known to have high stability in organic solvents.[19] Three different solvent combinations were tested: 20 mL of phosphate buffer, 20 mL of 50:50 (v/v) phosphate buffer/methanol, and 20 mL of 25:75 (v/v) phosphate buffer/methanol. The samples were all prepared in duplicate and compared to the untreated paprika oleoresin. Unfortunately, one of the samples prepared with 100% phosphate buffer was biased by a human error, and only one sample of that experiment could therefore be used for comparison. To study the removal of glycerolipids by enzymatic hydrolysis, five triglycerides (TGs) and five diglycerides (DGs) that were highly abundant in the TIC MS signal before hydrolysis were selected. The results of these tests are shown in Figure 2 and Table 2A.

On average, approximately 89, 98, and 41% of the selected TGs were hydrolyzed by the lipases with 100% phosphate buffer, 50:50 (v/v) phosphate buffer/methanol and 25:75 (v/v) phosphate buffer/methanol, respectively (calculated against the untreated sample). On average, approximately 81, 96, and 80% of the selected DGs were hydrolyzed by the lipases with 100% phosphate buffer, 50:50 (v/v) phosphate buffer/methanol and 25:75 (v/v) phosphate buffer/methanol, respectively (calculated against the untreated sample). These results show that using 75% methanol as solvent inhibits the enzyme activity compared to the other solvent compositions. This could be due to enzyme denaturation or immiscibility of the phosphate buffer and/or bile salts in 75% methanol. During both the enzymatic assay with aqueous phosphate buffer and 50:50 (v/v) phosphate buffer/methanol as solvents, high percentages of DGs and TGs were hydrolyzed. The results in Table 2A indicate that the addition of methanol as solvent improves the hydrolysis rate, probably due to a better miscibility, and thus increased contact between the lipids and the enzymes. In the MS full scan chromatograms B and C in Figure 2, the levels of DGs and TGs have clearly diminished compared to the levels in chromatogram A. In chromatogram C the natural carotenoid profile of carotenoid diesters becomes visible, indicating higher intensities for carotenoids than lipids. Figure 3 shows the extracted ion chromatograms of the isomers of a capsanthin diester (C14:0, C16:0) in the paprika oleoresin before (A) and after (B) hydrolysis with 50:50 (v/v) phosphate buffer/methanol as solvents. The signal of the most intense isomer of the capsanthin diester (C14:0, C16:0) at 21.1 min is completely suppressed in the sample without enzymatic hydrolysis by coelution with a very high concentration of TGs. The less intense isomer at 21.5 min does not suffer from suppression effects, as it elutes in a region that is less populated by TGs.

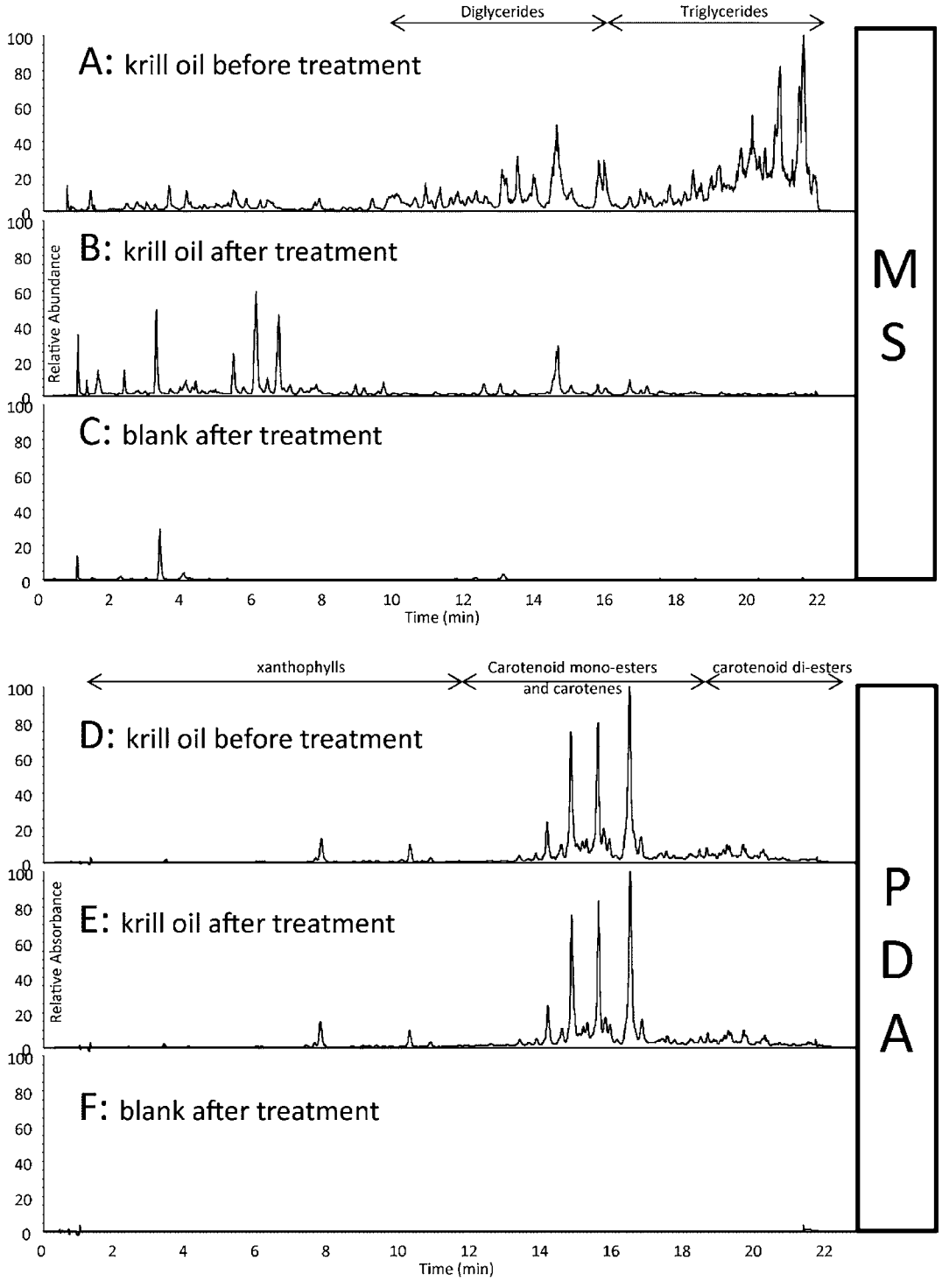

Figure 4. Total ion current MS chromatograms (fixed scale) of Asta Krill 8 oil before (A) and after lipase treatment in 50:50 phosphate buffer/methanol under optimized conditions (B) and for lipase treatment without a sample (blank) (C); chromatograms of the UV signal at 440 nm (fixed scale) for Asta Krill 8 oil before (D) and after lipase treatment under optimized conditions (E) and for lipase treatment without a sample (blank) (F). The arrows indicate the elution order of the compound groups.

Next to the rate of hydrolysis of the DGs and TGs, the PDA chromatograms were studied to compare the composition of carotenoids in the extract before and after the enzymatic assay (E, F, G and H in Figure 2). The elution profiles of the carotenoids in all chromatograms overlap completely before and after lipase treatment, indicating that the natural carotenoid profile is preserved during enzymatic hydrolysis. In both chromatograms of the untreated and treated sample, the carotenoid profile predominantly consists of esterified carotenoids: only very few, low abundant free carotenoid peaks are present.

To confirm that DGs and TGs are better hydrolyzed when 50:50 (v/v) phosphate buffer/methanol is used, both solvents (100% phosphate buffer and 50:50 (v/v) phosphate buffer/methanol) were compared in another enzymatic assay, using only 1 mL of Lipozyme TL 100 L. Previous tests had shown

dx.doi.org/10.1021/jf405477s | J. Agric. Food Chem. 2014, 62, 3114−3124

that Lipozyme TL 100 L is the most active of the two enzymes in lipid hydrolysis (data not shown). As sample matrix, an in-house produced paprika extract (1 mL of DCM extract, evaporated to dryness) was spiked with 300 μL of extra virgin olive oil to obtain a sample with a very high lipid content. The concentration of TGs was much higher in comparison to when only 100 μL of paprika oleoresin was used as test sample. This was observed from the flat and broad TG peaks that were obtained during analysis with MS because of saturated column stationary phase material and saturated detector signals (chromatograms not shown). Results showed that after 2 h of enzymatic incubation, TGs were up to almost 9 times more efficiently hydrolyzed in the 50:50 (v/v) phosphate buffer/methanol solution compared to in the 100% phosphate buffer solution (77 and 8.8% conversion for TG (C18:1, C18:1, C18:2), respectively) (Table 2B). The greater difference in lipid conversion during this test compared to the previous one can be explained by the very high amount of lipids (addition of 300 μL of olive oil). For some DGs, higher concentrations were found in the sample extract after lipase treatment (Table 2B), owing to the very high level of TGs and consequently the high conversion of TGs into DGs. This higher abundance of lipids because of olive oil spiking emphasizes the higher reaction rate when 50:50 (v/v) aqueous phosphate buffer/methanol is used as solvent. On the basis of the results of the above-mentioned experiments, 50:50 (v/v) buffer/methanol in the presence of sodium *n*-octyl sulfate was chosen as incubation solvent for future hydrolysis experiments.

Incubation Time. Three different incubation times were tested with 50:50 (v/v) phosphate buffer/methanol as incubation solvent. The commercial paprika oleoresin was used as sample matrix. The samples were all prepared in duplicate as described above. The results of these tests are shown in Table 2C. On average, approximately 96, 97, and 99% of the selected TGs and 92, 94, and 98% of the selected DGs were hydrolyzed by the lipases with an incubation time of 1, 2, and 3 h, respectively (calculated against the untreated sample). The small decline in DG and TG concentration after 1 h of incubation indicates that the enzymatic hydrolysis reaction rate decreases significantly within 1 h. This observation could be the result of first- or more likely second-order reaction kinetics. Although incubation times of <1 h are possible, 2 h was chosen for later experiments within the scope of the present work as the method was considered as sufficiently optimized for analytical purposes. The optimized enzymatic hydrolysis consists of the following steps:

- weigh 100 μL of oleoresin and add internal standard;
- add 20 mL of 50:50 (v/v) phosphate buffer (0.1 M, pH 7.4)/methanol;
- add 25 μL of sodium *n*-octyl sulfate, 30 mg of bile salts, and 250 μL of NaCl solution (5 mM);
- preheat for 30 min at 40 °C while stirring;
- add 1 mL of 5 KLU of Lipozyme CALB L and 1 mL of 100 KLU of Lipozyme TL 100 L;
- incubate for 2 h at 40 °C while stirring;
- add 20 mL of 1:1 ethyl acetate/hexane, shake vigorously and transfer the apolar fraction;
- wash the polar fraction twice with 30 mL of 1:1:1 (v/v/v) methanol/ethyl acetate/hexane;
- back-extract combined apolar fraction twice with 100 mL of water;
- dry extract with Na_2SO_4 and evaporate;
- dissolve in 1 mL of DCM + 0.1% BHT.

Repeatability. Enzymatic hydrolysis of the paprika oleoresin was carried out in 5-fold to test the repeatability of the optimized method. The average hydrolysis rates of the selected individual TGs ranged between 97.5 and 98.4%. The relative standard deviations (RSDs) ranged between 1.1 and 1.7%, indicating that lipid hydrolysis is repeatable. The average hydrolysis rates of the selected individual DGs ranged between 91 and 98% (calculated against the untreated sample). The RSDs ranged between 1.0 and 5.4%. The larger variations during DG hydrolysis can be explained by the conversion of TGs into specific DGs. For example, DG (C18:2, C18:2) can be formed from TG (C18:2, C18:2, C18:2) or TG (C18:1, C18:2, C18:2) or TG (C18:2, C18:2, C16:0). Depending on which fatty acid side chain is hydrolyzed first, the monitored amount of DG (C18:2, C18:2) will differ. DGs that are less likely to be formed because of a lower concentration in the TG profile, for example, DG (C18:3, C18:3) or DG (C18:3, C16:0), will show a smaller variability.

To investigate the recovery of the carotenoids after enzymatic hydrolysis, five highly abundant carotenoids were selected. Their chromatographic peaks were integrated in the PDA chromatogram at 440 nm and compared to the respective areas in the analysis of the untreated sample. The average recoveries of the four capsanthin diesters and β-carotene ranged between 96 and 105%, which shows that esterified carotenoids were not hydrolyzed during the enzymatic assay (calculated against the untreated sample).

To test the applicability of the method to other matrices, the optimized lipase procedure was applied in 4-fold on oil that was obtained from commercial krill oil soft gels. The samples were treated with the optimized conditions (2 h, 50:50 (v/v) phosphate buffer/methanol). The oil contains high amounts of both TGs and DGs that dominate the TIC signal in the MS chromatogram (chromatogram A, Figure 4). Chromatogram B in Figure 4 shows the TIC MS chromatogram after lipase treatment: the majority of the lipids were removed by the enzymatic hydrolysis. To study the removal of glycerolipids by the lipase assay in more detail, three TGs and three DGs that were highly abundant in the TIC MS signal before the enzymatic assay were selected. On average, approximately 99.9 and 99.6% of the selected TGs and DGs were hydrolyzed by the enzymes, respectively (calculated against the untreated sample). A higher percentage of lipids was hydrolyzed compared with the paprika oleoresin, most probably because of high levels of phospholipids present in the sample (368 mg of phospholipids/g of lipids according to the manufacturer). Phospholipids are known as great emulsifiers, which augments the contact area between glycerolipids and enzymes.[10]

The carotenoid profile of PDA chromatograms D and E in Figure 4 completely match, indicating that esterified carotenoids were not hydrolyzed during the enzymatic assay. To investigate the recovery of the carotenoids after enzymatic hydrolysis in more detail, five astaxanthin esters with a high PDA signal and free astaxanthin were selected (free astaxanthin and its esters were the main carotenoids present in the sample). Their chromatographic peaks were integrated in the PDA chromatogram at 440 nm, and the ratios of esterified astaxanthin versus free astaxanthin were calculated for each ester. These ratios were subsequently compared to the respective ratios in the untreated sample. Decrease in the ratio during the hydrolysis by lipase enzymes would indicate

hydrolysis of esterified carotenoids. The recoveries (average of four samples) of the five individual astaxanthin ratios ranged between 98 and 101%. This shows that esterified astaxanthin compounds were not hydrolyzed into free astaxanthin during the lipase assay.

The lipase treatment was performed on paprika oleoresin in duplicate over three different days using the optimized incubation conditions (50:50 (v/v) phosphate buffer/methanol, 2 h incubation) to investigate the consistency in hydrolysis rates for between- and within-day experiments. The average hydrolysis rates for the individual TGs ranged between 97.0 and 98.0% with RSDs ranging between 1.2 and 1.9%. The average hydrolysis rates for the individual DGs ranged between 89.6 and 97.5% with RSDs ranging between 1.5 and 6.9%. These average hydrolysis rates are in line with the hydrolysis rates obtained during the repeatability experiments. The RSDs are slightly higher than the RSDs obtained during the repeatability experiments. These data indicate the consistency in hydrolysis rates for between- and within-day experiments.

Applicability of the Lipase Treatment to Other Natural Compounds. Comparison of chromatograms A and B in Figure 4 shows that after sample treatment with lipase enzymes new peaks appear in the first half of the MS TIC chromatogram. To study if these signals were caused by conversion of sample compounds or by sample preparation, a method blank was prepared. Chromatogram F in Figure 4 shows the PDA chromatogram of the method blank: no peaks are visible at a wavelength of 440 nm. Chromatogram C in Figure 4 shows the MS TIC chromatogram of the method blank: only a few of the additional peaks that appear after hydrolysis by lipases can be related to sample preparation. This means that compounds originating from the sample extract, other than carotenoids, were converted into new compounds, probably by the cleavage of ester bonds. These peaks could not be related to products of DG and TG hydrolysis (FAs and MGs): accurate mass confirmed that these compounds were removed by liquid−liquid extraction after the lipase assay. These new peaks, however, could be products of phospholipid hydrolysis, as Asta Krill 8 oil contains high levels of phospholipids.

Other interesting groups of secondary metabolites such as phytosterols can also occur esterified with fatty acids. Phytosterols occur in four common forms: as the free alcohol, as fatty acid esters, as steryl glycosides, and as acylated steryl glycosides (Figure 1).[23,24] The different derivatives of β-sitosterol were identified by a common product ion at m/z 397.383 in positive APCI mode, corresponding to the breakage of the C−O-bond at the β-sitosterol moiety (Table 1). The β-sitosteryl glucoside and β-sitosterol peaks in paprika oleoresin before (B) and after (A) enzymatic hydrolysis did not change significantly. On the other hand, the acylated steryl glycosides (C18:3, C18:2, C18:1, and C16:0, respectively) almost completely disappeared by the lipase treatment. The acylated steryl glycosides were not hydrolyzed during lipase treatment to form β-sitosteryl glucoside as no elevated peak area was observed for this compound. However, a low abundant peak appeared in the chromatogram after the enzymatic assay, which corresponded to $C_{39}H_{66}O_9$ (m/z 677.464 in negative APCI mode), presumably due to conversion of acylated β-sitosteryl glucosides into β-sitosteryl glucoside ethyl ester by transesterification. Care should thus be taken when the lipase hydrolysis is used for the analysis of compounds other than carotenoids.

To conclude, carotenoid esters were not hydrolyzed by the cleanup protocol, thereby preserving the natural carotenoid composition of the sample. Even for samples with very high lipid loadings, the greater part of the lipids was selectively removed by this cleanup procedure, thereby enabling the exclusion of the fractionation step and significantly simplifying the procedure. The method was optimized on an analytical scale to enable the identification and quantification of carotenoids in lipid-rich matrices by LC-MS analysis. Next to vegetable and algal oils, the method could prove its use in the analysis of carotenoids in lipid-rich biological samples (e.g., to study the bioavailability of carotenoids and their metabolization in the human body).

AUTHOR INFORMATION

Corresponding Author

*(S.B.) Phone: + 32 14 33 50 54. Fax + 32 14 31 94 72. E-mail: sebastiaan.bijttebier@vito.be.

Notes

The authors declare no competing financial interest.

REFERENCES

(1) Armstrong, G. A.; Hearst, J. E. Genetics and molecular biology of carotenoid pigment biosynthesis. *J. Fed. Am. Soc. Exp. Biol.* **1996**, *10*, 228−37.

(2) Tanaka, T.; Shnimizu, M.; Moriwaki, H. Cancer chemoprevention by carotenoids. *Molecules* **2012**, *17*, 3202−3242.

(3) Riccioni, G. Carotenoids and cardiovascular disease. *Curr. Atheroscler. Rep.* **2009**, *11*, 434−439.

(4) Wojcik, M.; Burzynska-Pedziwiatr, I.; Wozniak, L. A. Review of natural and synthetic antioxidants important for health and longevity. *Curr. Med. Chem.* **2010**, *17*, 3262−3288.

(5) Ozawa, Y.; Sasaki, M.; Takahashi, N.; Kamoshita, M.; Miyake, S.; Tsubota, K. Neuroprotective effects of lutein in the retina. *Curr. Pharm. Des.* **2012**, *18*, 51−56.

(6) Agarwal, M.; Parameswari, R.; Vasanthi, H. R.; Das, D. K. Dynamic action of carotenoids in cardioprotection and maintenance of cardiac health. *Molecules* **2012**, *17*, 4755−4769.

(7) Chatterjee, M.; Roy, K.; Janarthan, M.; Das, S.; Chatterjee, M. Biological activity of carotenoids: its implications in cancer risk and prevention. *Curr. Pharm. Biotechnol.* **2012**, *13*, 180−190.

(8) Ilic, D.; Misso, M. Lycopene for the prevention and treatment of benign prostatic hyperplasia and prostate cancer: a systematic review. *Maturitas* **2012**, *72*, 269−276.

(9) Su, Q.; Rowley, K. G.; Balazs, N. D. H. Carotenoids: separation methods applicable to biological samples. *J. Chromatogr., B* **2002**, *781*, 393−418.

(10) Zorn, H.; Breithaupt, D. E.; Takenberg, M.; Schwack, W.; Berger, R. G. Enzymatic hydrolysis of carotenoid esters of marigold flowers (*Tagetes erecta* L.) and red paprika (*Capsicum annuum* L.) by commercial lipases and *Pleurotus sapidus* extracellular lipase. *Enzyme Microb. Technol.* **2003**, *32*, 623−628.

(11) Thompson, G. R.; Grundy, S. M. History and development of plantsterol and stanol esters for cholesterol-lowering purposes. *Am. J. Cardiol.* **2005**, *96* (IA), 3D−9D.

(12) Miao, F.; Lu, D.; Li, Y.; Zeng, M. Characterization of astaxanthin esters in *Haematococcus pluvialis* by liquid chromatography−atmospheric pressure chemical ionization mass spectrometry. *Anal. Biochem.* **2006**, *352*, 176−181.

(13) BASF. Technical information animal nutrition: Lucantin® Pink data sheet, http://www.basf.com/group/corporate/en/brand/LUCANTIN (accessed Nov 20, 2013).

(14) Li, J.; Zhu, D.; Niu, J.; Shen, S.; Wang, G. An economic assessment of astaxanthin production by large scale cultivation of *Haematococcus pluvialis*. *Biotechnol. Adv.* **2011**, *29*, 568−574.

(15) Rodríguez-Bernaldo de Quirós, A.; Costa, H. S. Analysis of carotenoids in vegetable and plasma samples: a review. *J. Food Compos. Anal.* **2006**, *19*, 97−111.
(16) van Breemen, R. B. Mass spectrometry of carotenoids. *Curr. Protoc. Food Anal. Chem.* **2001**, F2.4.1−F2.4.13.
(17) Bijttebier, S. K. A.; D'Hondt, E.; Hermans, N.; Apers, S.; Voorspoels, S. Unravelling ionization and fragmentation pathways of carotenoids using orbitrap technology: a first step towards identification of unknowns. *J. Mass Spectrom.* **2013**, *48*, 740−754.
(18) Britton, G.; Liaaen-Jensen, S.; Pfander, H.; Mercadante, A. Z.; Egeland, E. S. In *Carotenoids: Spectroscopy − Vol. 1B*, 1st ed.; Birkhäuser Verlag: Basel, Germany, 1995.
(19) Gupta, R.; Gupta, N.; Rathi, P. Bacterial lipases: an overview of production, purification and biochemical properties. *Appl. Microbiol. Biotechnol.* **2004**, *64*, 763−781.
(20) Breithaupt, D. E.; Bamedi, A.; Wirt, U. Carotenol fatty acid esters: easy substrates for digestive enzymes? *Comp. Biochem. Physiol. Part B* **2002**, *132*, 721R−728R.
(21) Breithaupt, D. E.; Bamedi, A. Carotenoids and carotenoid esters in potatoes (*Solanum tuberosum* L): new insights into an ancient vegetable. *J. Agric. Food Chem.* **2002**, *50*, 7175−7181.
(22) Brouwers, J. F. Liquid chromatographic−mass spectrometric analysis of phospholipids. Chromatography, ionization and quantification. *Biochim. Biophys. Acta* **2011**, *1811*, 763−775.
(23) Moreau, R. A.; Whitaker, B. D.; Hicks, K. B. Phytosterols, phytostanols, and their conjugates in foods: structural diversity, quantitative analysis, and health-promoting uses. *Prog. Lipid Res.* **2002**, *41*, 457−500.
(24) Yamauchi, R.; Aizawa, K.; Inakuma, T.; Kato, K. Analysis of molecular species of glycolipids in fruit pastes of red bell pepper (*Capsicum annuum* L.) by high-performance liquid chromatography-mass spectrometry. *J. Agric. Food Chem.* **2001**, *49*, 622−627.

type of solvent used in the extraction with the yield and efficiency achieved in the flavonoid extraction. Most of the papers are aimed at finding the solvents with the best extraction power,[16,19] but very few authors have considered the effect that solvents can have on the analysis of the compounds.[20]

Therefore, the aim of this work was to propose a quality control method of the floral bioresidues from *C. sativus* L. by the analysis of phenolic compounds after extraction with different solvents.

MATERIALS AND METHODS

Chemicals. All reagents and solvents employed were of HPLC purity or analytical grade. Standards of kaempferol 3-*O*-glucoside (purity > 99%), kaempferol aglycone (purity > 99%), and delphinidin 3,5-di-*O*-glucoside were purchased from Extrasynthese (Genay, France). Kaempferol 3-*O*-sophoroside was isolated as described Sánchez et al.[21] Ultrahigh-purity water was produced using a Milli-Q System from Millipore (Bedford, MA, USA). Acetonitrile (ACN), ethanol, acetone, *tert*-butyl methyl ether (TBME), *n*-butanol, dichloromethane, methanol, hydrochloridric acid (HCl), trifluoroacetic acid (TFA), anisaldehyde, sulfuric acid, glacial acetic acid, and formic acid were supplied from Scharlau (Barcelona, Spain).

Plant Material. The floral bioresidues from the production of saffron spice were obtained from the company Agrícola Técnica de Manipulación y Comercialización S.L. (Minaya, Spain) after separation of the stigma from the flower of saffron during the 2010−2011 harvest. Stigma separation was performed using traditional procedures for the Protected Designation of Origin "Azafrán de La Mancha" according to DOCM.[22] Floral bioresidues were formed by all parts of the flowers except the stigmas.

Fresh floral bioresidues from *C. sativus* L. were freeze-dried in a LyoAlfa 6-50 freeze-dryer (Telstar, Terrassa, Spain) for 48 h to constant weight.[14] The conditions used for freeze-drying the samples were as follows: mass load, 100 g; initial temperature, −50 ± 2 °C; and pressure, 10^{-3} mbar. They were crushed, sieved through a 500 μm mesh size, and then stored at −20 °C until their further analysis.

Isolation of Anthocyanins. *Sample Preparation for High-Speed Counter-Current Chromatography (HSCCC).* Floral bioresidues (835 g) were extracted with 25 L of water/HCl (100:1, v/v) at 40 ± 5 °C by stirring for 1 h and then decanted and filtered through a fabric filter. The supernatant was filtered through a Buchner funnel (sintered disk of porosity grade 2) and concentrated with a rotary evaporator under vacuum and freeze-dried. This crude extract was redissolved in water, centrifuged at 3000 rpm for 5 min, and filtered with a paper filter prior to the application onto an Amberlite XAD-7 column (Fluka, 100 × 7 cm), conditioned with 2 L of methanol and then with 2 L of water. The column was rinsed with 3 L of water, and anthocyanins were eluted with 2 L of a mixture of water/ACN/TFA (49.5:50:0.5, v/v/v). The eluate was concentrated, dissolved in water, and freeze-dried. An amount of 3.9 g of purified XAD-7 extract was obtained from 74.1 g of crude extract.

High-Speed Counter-Current Chromatography. The XAD-7 extract was fractioned with a CCC-1000 high-speed countercurrent chromatograph manufactured by Pharma-Tech Research Corp. (Baltimore, MD, USA) equipped with three preparative coils and connected in series (tubing diameter of 2.6 mm and total volume of 850 mL).

TBME/*n*-butanol/water/ACN (1:3:5:1, v/v/v/v) acidified with 0.5% TFA was used as solvent system. The elution mode was head to tail with the lighter (organic) phase acting as the stationary phase and the aqueous phase acting as the mobile phase. The flow rate was set at 3 mL min^{-1} and delivered by a BT 3020 HPLC pump (Jasco, Gross-Umstadt, Germany). The separation was run at a speed of 1000 rpm. One gram of XAD-7 extract was dissolved in 25 mL of a mixture of the upper (organic) and lower (aqueous) phases (50:50, v/v) and injected into the system by a loop injection. Volumes of 12 mL were collected with a fraction collector. Elution was monitored with a K-2501 UV−vis absorbance detector (Knauer, Berlin, Germany) at 280 nm to detect anthocyanins and also flavonols.

Thin-Layer Chromatography (TLC). The screening of the composition of the volumes collected by HSCCC was performed by TLC using water/methanol/dichloromethane (3:27:75, v/v/v) in silica gel 60 F254 aluminum plates and water/ACN/TFA (90:9.5:0.5, v/v/v) in C18 plates. Anthocyanins were visualized under a UV lamp at 254 and 366 nm, and then TLC plates were sprayed with anisaldehyde/sulfuric acid/glacial acetic acid spray reagent and heated at 100 °C. Tubes with a similar anthocyanin composition were reunited. After the evaporation of organic solvents, the fractions were frozen and freeze-dried. The HSCCC fractions with their corresponding retention times (t_R) are shown in Table 1.

Table 1. Isolated Amounts and Retention Times (t_R) of the Fractions Obtained by HSCCC

fraction	t_R (min)	isolated amount (mg)
F1	204−212	301.93
F2	212−220	77.54
F3	220−232	46.24
F4	232−252	35.20
F5	252−308	39.43
F6	308−324	<2.00
F7	324−336	<2.00
F8	336−364	<2.00
F9	364−380	1.89
F10	coil residue	18.38
F11	cleaning in methanol	36.42

Preparative HPLC-UV. Fractions 3 and 4 obtained from HSCCC were purified by preparative HPLC from Knauer (Berlin, Germany). Preparative HPLC consisted of an HPLC pump WellChrom K-1001, solvent organizer K-1500 and degasser, and a UV detector K-2600. The separation was carried out on a 250 × 10 mm, 5 μm, RP-18 Luna (18/2) column from Phenomenex (Aschaffenburg, Germany). The eluents were water/ACN/formic acid, 92:3:5, v/v/v, as solvent A and water/ACN/formic acid, 45:50:5, v/v/v, as solvent B, operating in the following gradient: 0 min, 2% B; 20 min, 14% B; 25 min, 14% B; 40 min, 18% B; 45 min, 18% B; 50 min, 90% B; 55 min, 2% B, followed by a 5 min equilibration period. The flow rate was 4 mL min^{-1}, and the detector was set at 280 and 520 nm. Two fractions were collected and freeze-dried due to their highest absorbance at 520 nm, which were the two isolated anthocyanins (t_R = 32.0−36.0 min for the first isolated anthocyanin and t_R = 44.0−47.3 min for the second isolated anthocyanin) from floral bioresidues.

Extraction of Floral Bioresidues. Floral bioresidues (0.5 g) were extracted with 25 mL of water/ACN/TFA (47:50:3, v/v/v) according to the method of Nørbæk et al.[13] Other solvents, such as water/HCl (100:1, v/v), water/ACN/HCl (50:50:1, v/v/v), water/ethanol/HCl (50:50:1, v/v/v), and water/acetone/HCl (50:50:1, v/v/v), were also used to extract floral bioresidues at the same ratio (0.5 g in 25 mL). Extracts were shaken for 1 h at 500 rpm followed by centrifugation at 3500 rpm for 5 min to remove the material plant. The supernatants of these extracts were separated, and their pH values were measured.

Addition of Acetonitrile to the Supernatant of Water/HCl (100:1, v/v) Extracts. Acetonitrile was added to the supernatant of the extract prepared with water/HCl (100:1, v/v) in a 50% ratio.

TFA (in a 3% ratio) or HCl (in a 1% ratio) was added to the supernatant of the extract prepared with water/HCl (100:1, v/v).

Acetonitrile in various ratios (from 10 to 50%, v/v) with TFA in a 50:3 ratio (ACN/TFA, v/v) or acetonitrile from 10 to 50% (v/v) with HCl in a 50:1 ratio (ACN/HCl, v/v) was added to the supernatant of the extracts prepared with water/HCl (100:1, v/v). These solutions were shaken for 1 h at 500 rpm, and their pH values were measured.

Addition of Acetonitrile to a Solution of Delphinidin 3,5-Di-*O*-glucoside. A commercial standard (5 mg) of delphinidin 3,5-di-*O*-glucoside was dissolved in 25 mL of water/HCl (100:1, v/v) by shaking for 1 h at 500 rpm.

Table 2. Regression Curve, Linearity, Limit of Detection (LOD), and Limit of Quantification (LOQ) by HPLC-DAD

	detection wavelength (nm)	t_R (min)	regression eq	R^2	concentration range (mg L^{-1})	LOD (mg L^{-1})	LOQ (mg L^{-1})
kaempferol 3-*O*-sophoroside	266	23.57 ± 0.01	$A = 38714C + 459.51$	0.9992	0.01−700.00	0.06	27.91
kaempferol 3-*O*-glucoside	266	27.35 ± 0.01	$A = 2 \times 10^6C + 156.68$	0.9992	0.01−12.00	0.01	0.22
kaempferol	266	37.04 ± 0.01	$A = 99973C + 48.749$	0.9997	0.04−90.00	0.11	1.51
delphinidin 3,5-*O*-diglucoside	520	16.55 ± 0.01	$A = 36784C - 256.13$	0.9993	15.00−300.00	7.04	7.23
petunidin 3,5-*O*-diglucoside	520	18.67 ± 0.01	$A = 31447C + 3.728$	0.9997	1.00−85.00	0.84	3.06

Table 3. HPLC-DAD-ESI-MS^n of the Main Flavonols and Anthocyanins of the Extracts of Floral Bioresidues Prepared with Water/HCl (100:1, v/v), ACN/Water/TFA (50:47:3, v/v/v), ACN/Water/HCl (50:50:1, v/v/v), Ethanol/Water/HCl (50:50:1, v/v/v), and Acetone/Water/HCl (50:50:1, v/v/v)

peak	t_R (min)	compound identity	UV−vis Abs[a] λ_{max} (nm)	$[M]^+$ (m/z)	$[M-H]^-$ (m/z)	aglycone (m/z)	MS^2 $[M]^+/[M-H]^-$ (m/z) (%[b])	MS^3 $[M]^+/[M-H]^-$ (m/z) (%)
		flavonols						
1	15.65	kaempferol 3-*O*-sophoroside-7-*O*-glucoside	266, 320sh, 348		771	286	609 (100)	429 (79), 285 (100)
2	19.28	kaempferol 3,7-di-*O*-glucoside	265, 317sh, 344		609	286	447 (100), 285	255, 284 (100), 285 (53), 327
3	19.74	kaempferol 3,7,4′-tri-*O*-glucoside	265, 292sh, 330		771	286	609 (100)	255 (32), 284 (71), 285 (100), 309 (15), 429 (76)
4	21.72	quercetin 3-*O*-sophoroside	254, 295sh, 352		625	302	300 (100), 445 (31), 463 (14), 505 (15)	271 (100), 255 (65)
5	22.55	isorhamnetin 3,4′-di-*O*-glucoside	250, 265, 344		639	316	313 (65), 315 (100), 477 (24)	300 (100)
6	23.57	kaempferol 3-*O*-sophoroside	265, 292sh, 347		609	286	284 (92), 285 (100), 429 (64), 447 (6)	255 (100)
7	25.32	kaempferol 3-*O*-rutinoside	269, 292sh, 348		593	286	255 (56), 284 (100), 429 (30), 447 (11)	255 (100)
8	27.35	kaempferol 3-*O*-glucoside	265sh, 292sh, 348		447	286	447 (100)	255 (62), 284 (100), 327 (11)
9	27.52	kaempferol 7-*O*-glucoside	265, 317sh, 365		447	286	285 (100), 327 (4)	151 (100), 257 (53)
10	37.04	kaempferol	269sh, 366		285	286	241, 151 (100)	168 (100)
		anthocyanins						
11	16.55	delphinidin 3,5-di-*O*-glucoside	275, 328sh, 520	627		302	465 (36), 303 (100)	257 (100)
12	18.67	petunidin 3,5-di-*O*-glucoside	273, 341sh, 521	641		316	479 (35), 317 (100)	302 (100)
13	19.16	delphinidin 3-*O*-glucoside	276, 343, 522	465		302	303 (100)	257 (100)
14	20.65	malvidin 3,5-di-*O*-glucoside	275, 522	655		330	493 (34), 331 (100)	315 (100)
15	21.51	petunidin 3-*O*-glucoside	277, 343, 524	479		316	317 (100)	302 (100)

[a]sh, shoulder. [b]%, relative height of ion in mass spectrum.

Acetonitrile in a 50% ratio (v/v) and TFA in a 3% ratio (v/v) were added to the solution of delphinidin 3,5-di-*O*-glucoside prepared above.

The solvents of this mixture composed of 47% of the solution of delphinidin 3,5-di-*O*-glucoside, 3% of TFA, and 50% of acetonitrile were removed by rotary evaporation under vacuum. The concentrate obtained was redissolved in water/HCl (100:1, v/v) by shaking for 1 h at 500 rpm.

HPLC-DAD-ESI-MS^n Analysis. All extracts of floral bioresidues were analyzed by HPLC with diode array detector coupled to electrospray ionization tandem mass spectrometry techniques (HPLC-ESI-DAD-MS^n). XAD-7 extracts as well as HSCCC fractions, preparative HPLC fractions, and commercial standards were redissolved in water/HCl (100:1, v/v/v) and also analyzed by HPLC-ESI-DAD-MS^n. All of the samples were filtered through PTFE filters with 0.45 μm pore size and 11 mm diameter (Millipore).

Separation was carried out on a Luna RP-18 column (150 × 2.0 mm, 3 μm, Phenomenex) at a flow rate of 0.2 mL min^{-1}, using an injection volume of 5 μL. Water/ACN/formic acid, 95:3:2 (v/v/v) (A), and water/ACN/formic acid, 48:50:2 (v/v/v) (B), were used as mobile phases with the following gradient: 0 min, 2% B; 20 min, 14% B; 25 min, 14% B; 40 min, 18% B; 45 min, 18% B; and 70 min, 90% B, followed by a 10 min equilibration period. ESI-MS^n measurements were performed on a Bruker Esquire-LC multiple ion trap mass spectrometer (Bruker Daltonics, Bremen, Germany). Mass spectral analyses were recorded under the following operating conditions for negative and positive ion modes: capillary, −3500 V; capillary exit offset, 70 V; end plate offset, −500 V; skimmer, 40 V; dry gas (N_2), 11 L min^{-1}; dry temperature, 330 °C; nebulizer, 60 psi; scan range, m/z 50−3000. Esquire NT 4.0 software (Bruker Daltonics) was used for analysis and data collection.

HPLC-DAD Analysis. To quantify, all extracts of floral bioresidues were analyzed by HPLC-DAD. XAD-7 extracts as well as HSCCC fractions, preparative HPLC fractions, and commercial standards were redissolved in water/HCl (100:1, v/v/v) and also analyzed by HPLC-DAD.

Aliquots of 30 μL of the samples were filtered through a PTFE filter (0.45 μm) and analyzed by reverse-phase HPLC technique, using an Agilent 1200 chromatograph (Palo Alto, CA, USA) operating with a 250 × 4.6 mm, 5 μm, Develosil ODS-HG-5 chromatographic column (Phenomenex, Le Pecq Cedex, France) at 40 °C. Eluents were water/TFA (99.5:0.5, v/v) (A) and ACN (B) with the following elution gradient: 0 min, 0% B; 30 min, 30% B; 40−45 min, 80% B; 50 min, 20% B, followed by a 5 min equilibration period. The flow rate was 1.0

dx.doi.org/10.1021/jf4057023 | J. Agric. Food Chem. 2014, 62, 3125−3133

mL min^{-1} and the DAD (Hewlett-Packard, Waldbronn, Germany) was set at 266 nm for flavonols and at 520 nm for anthocyanins.

Internal Validation of the HPLC-DAD Method. The linearity of the detector response for the prepared standards was assessed by means of linear regression regarding the amounts of each standard, measured in milligrams, and the area of the corresponding peak on the chromatogram. Six-point calibration curves of kaempferol 3-*O*-sophoroside and kaempferol aglycone were used (Table 2). The rest of the flavonols were quantified using a six-point calibration curve of kaempferol 3-*O*-glucoside. Most anthocyanins were quantified using a six-point calibration curve of delphinidin 3,5-di-*O*-glucoside (isolated as under Isolation of Anthocyanins). Petunidin 3,5-di-*O*-glucoside was quantified using a six-point calibration curve of petunidin 3,5-di-*O*-glucoside (isolated as under Isolation of Anthocyanins). Signal-to-noise ratios of 3:1 and 10:1 were used for estimating the limits of detection (LOD) and quantification (LOQ) of the method, respectively.

The repeatability of the injection integration was determined for standard phenolics and the samples. A standard solution containing kaempferol 3-*O*-sophoroside, kaempferol 3-*O*-glucoside, kaempferol aglycone, delphinidin 3,5-di-*O*-glucoside, and petunidin 3,5-di-*O*-glucoside was injected 10 times, and the RSD were calculated for both the retention time and integration area. Floral bioresidues were also extracted 10 times to evaluate the repeatability of the extraction process. The mean amount and RSD values of each compound were calculated.

The accuracy of the method was determined by analyzing the recovery percentage of the main constituents in the extracts. The samples were spiked with three different amounts of standard compounds before extraction. The spiked samples were extracted in triplicate and analyzed under the previously established optimal conditions. The obtained average contents of the target compounds were used as the "real values" to calculate the spike recoveries.

Statistical Analysis. One-way analysis of variance (ANOVA) was performed on each determination. Mean values were compared by Tukey's test at $p < 0.05$ using SPSS 19.0 for Windows (SPSS Inc., Chicago, IL, USA).

RESULTS AND DISCUSSION

Phenolic Identification by HPLC-DAD-ESI-MS^n. As can be observed in Table 3, 15 phenolic compounds were tentatively identified in the 5 different extracts, which included 10 flavonols and 5 anthocyanins. The flavonol fraction was mainly composed by kaempferol, isorhamnetin, and quercetin glycosides. Seven glycosides of kaempferol, namely, kaempferol 3-*O*-sophoroside-7-*O*-glucoside (compound **1**, $[M - H]^-$ at m/z 771), kaempferol 3,7-di-*O*-glucoside (compound **2**, $[M - H]^-$ at m/z 609), kaempferol 3,7,4′-tri-*O*-glucoside (compound **3**, $[M - H]^-$ at m/z 771), kaempferol 3-*O*-sophoroside (compound **6**, $[M - H]^-$ at m/z 609), kaempferol 3-*O*-rutinoside (compound **7**, $[M - H]^-$ at m/z 593), kaempferol 3-*O*-glucoside (compound **8**, $[M - H]^-$ at m/z 447), kaempferol 7-*O*-glucoside (compound **9**, $[M - H]^-$ at m/z 447), and kaempferol aglycone (compound **10**, $[M - H]^-$ at m/z 285) were identified on the basis of MS^2 and MS^3 fragmentation patterns and their maximum wavelengths in the UV–vis absorption spectrum, by comparison with previously published data.[13] Identification of compound **6** as kaempferol 3-*O*-sophoroside was also confirmed after comparison of their $[M - H]^-$ ions, MS^2 product ions, and retention times with those of their corresponding standard isolated from floral bioresidues (see Chemicals). Compounds **8** and **10** were also identified as kaempferol 3-*O*-glucoside and kaempferol aglycone, respectively, by comparison of their $[M - H]^-$ ions, MS^2 product ions, and retention times with those of their corresponding commercial standards (see Chemicals). Compounds **4** and **5** with $[M - H]^-$ ions at m/z 625 and 639 were identified as quercetin 3-*O*-sophoroside and isorhamnetin 3,4′-di-*O*-glucoside, respectively, by comparison of their MS^2 profiles and their maximum wavelengths in the UV–vis absorption spectrum with published data.[13]

With respect to the anthocyanins, isolation of the major anthocyanins by HSCCC was carried out, as can be seen in Figure 1. HSCCC is a liquid–liquid chromatographic technique

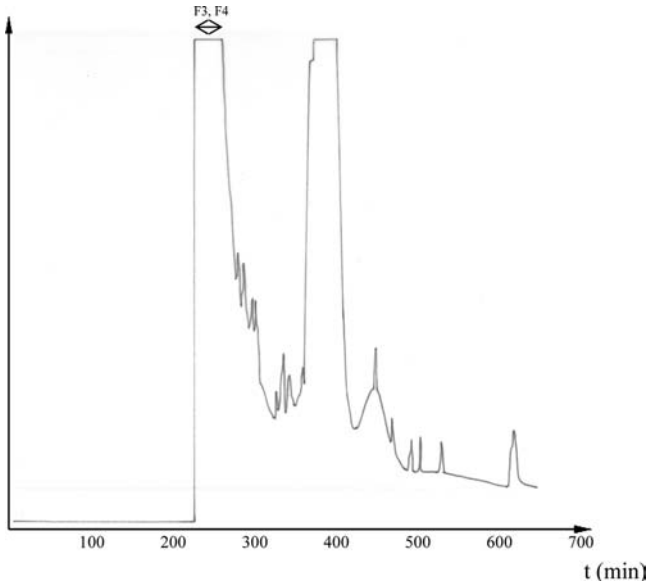

Figure 1. HSCCC chromatogram at 280 nm of the XAD-7 extract of floral bioresidues obtained from the production of saffron spice.

based on partitioning of compounds between two immiscible liquid phases.[23] The two main advantages of HSCCC compared to classical liquid chromatography are its solute loading capacity and the absence of an adsorptive matrix, which prevents irreversible adsorption of the solutes.[24] The separation was finished after 6 h. Nine major fractions were observed in the CCC separations of the XAD-7 extract of floral bioresidues. All fractions were analyzed by HPLC-DAD-ESI-MS^n. HSCCC fractions 3 and 4 were selected to be subjected to preparative HPLC separation because they showed two anthocyanins with the highest DAD signals and the lowest interferences with other phenolic compounds (Figure 1). The identification of individual anthocyanins was based on the data from HPLC-ESI-MS^n analysis, their maximum wavelengths in the UV–vis absorption spectrum, and comparison with literature data of anthocyanins.[13] The first preparative HPLC fraction (29.01 mg) contained delphinidin 3,5-di-*O*-glucoside in a purity of 90%. Upon HPLC-ESI-MS^n analysis, a molecular ion $[M - H]^+$ at m/z 627 was obtained along with fragments at m/z 465 and 303, respectively. The second preparative HPLC fraction (4.07 mg) contained petunidin 3,5-di-*O*-glucoside in a purity of 86%. Its structure was confirmed by HPLC-ESI-MS^n measurements. The molecular ion at m/z 641 yielded fragments of m/z 479 and 317, respectively.

On the basis of the MS^2 fragmentation pattern obtained, their maximum wavelengths in the UV–vis absorption spectrum, and published data,[13] five anthocyanins were identified in the extracts of floral bioresidues (Table 3): delphinidin 3,5-di-*O*-glucoside (compound **11**, $[M - H]^+$ at m/z 627), petunidin 3,5-di-*O*-glucoside (compound **12**, $[M - H]^+$

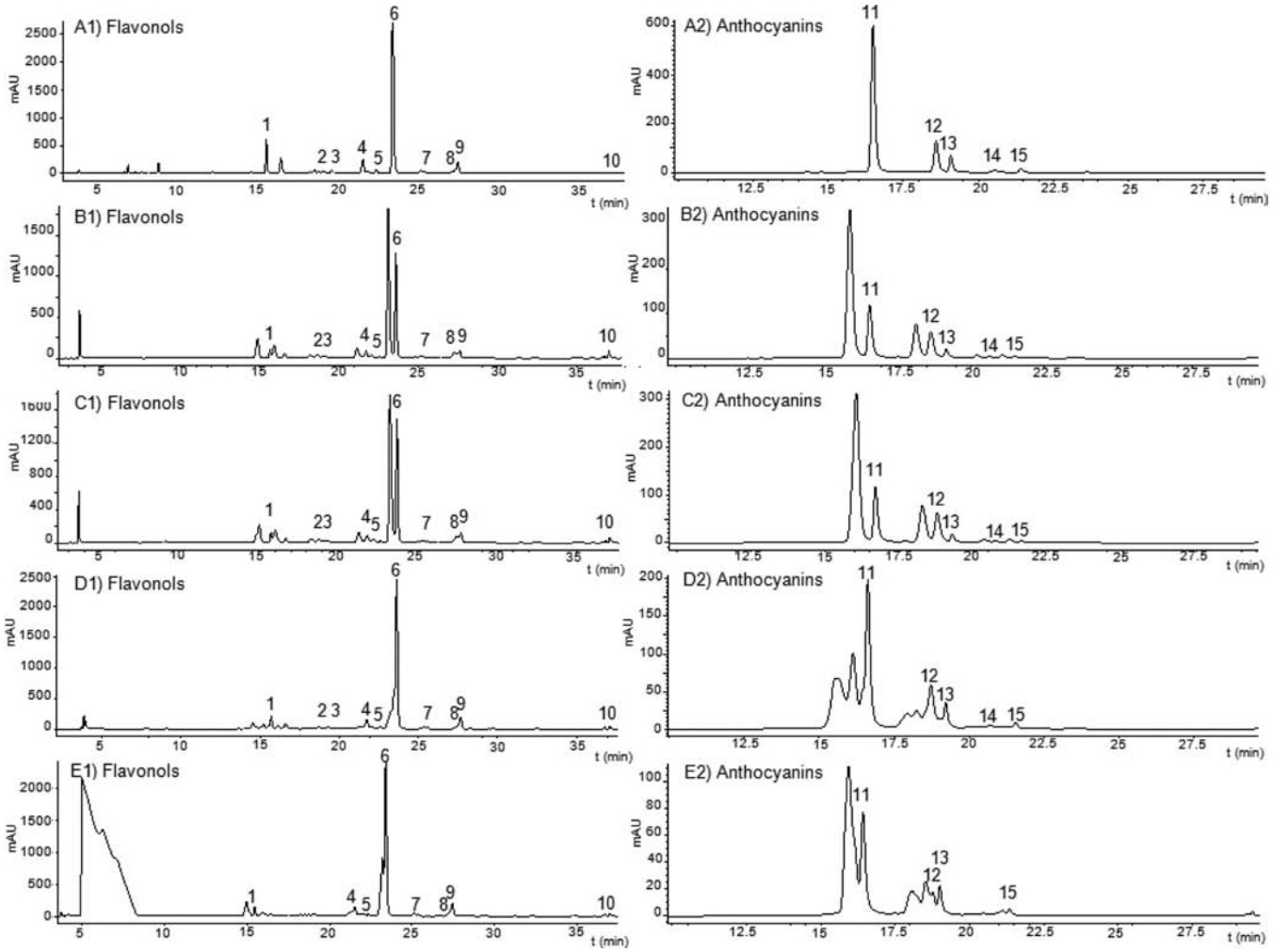

Figure 2. HPLC-DAD chromatograms of flavonols at 266 nm (1) and anthocyanins at 520 nm (2) of extracts of floral bioresidues prepared with water/HCl (100:1, v/v) (A), ACN/water/TFA (50:47:3, v/v/v) (B), ACN/water/HCl (50:50:1, v/v/v) (C), ethanol/water/HCl (50:50:1, v/v/v) (D), and acetone/water/HCl (50:50:1, v/v/v) (E). Phenolic compounds corresponding to each number can be seen in Table 3.

at m/z 641), delphinidin 3-*O*-glucoside (compound **13**, $[M - H]^+$ at m/z 465), malvidin 3,5-di-*O*-glucoside (compound **14**, $[M - H]^+$ at m/z 655), and petunidin 3-*O*-glucoside (compound **15**, $[M - H]^+$ at m/z 479). Identification of delphinidin 3,5-di-*O*-glucoside and petunidin 3,5-di-*O*-glucoside was also confirmed by comparison with the retention time and fragmentation profile of the standards isolated from floral bioresidues under Isolation of Anthocyanins. In the case of delphinidin 3,5-di-*O*-glucoside, these data were also compared with the commercial standard (see Chemicals).

Phenolic Profile by HPLC-DAD. HPLC-DAD chromatograms of flavonols (266 nm) and anthocyanins (520 nm) obtained from the five different extracts of floral bioresidues are shown in Figure 2. The extracts showed very different chromatographic profiles of flavonols and anthocyanins. The water/HCl extract showed a very good chromatographic separation of the compounds (Figure 2A1,A2). Moreover, the chromatographic peaks obtained showed high symmetry, with symmetry factors between 0.8 and 1.2. This extract showed the least number of phenolic compounds, but their peak areas were much higher than those of the rest of the extracts. Extracts prepared with water/ACN/TFA or water/ACN/HCl (water/ACN/TFA(HCl)) (Figure 2B1,B2,C1,C2) also showed a very good chromatographic separation with symmetrical peaks, but new chromatographic peaks were present that had not been detected in the water/HCl extracts (Figure 2A1,A2). Extracts prepared with water/ethanol/HCl (Figure 2D1,D2) or water/acetone/HCl (Figure 2E1,E2) showed poor peak shapes and a very low chromatographic separation efficiency in comparison with extracts prepared with water/HCl or water/ACN/TFA(HCl). Moreover, acetone interferes in the chromatogram obtained at 266 nm, the wavelength used for the flavonol identification. Therefore, the mixtures of water/ethanol/HCl or water/acetone/HCl were excluded as extractants for the determination of phenolic compounds in floral bioresidues.

Internal Validation of the HPLC-DAD Method. The HPLC-DAD method was validated by defining the linearity, LOD, LOQ, precision, specificity, and robustness. A high repeatability in the retention times was obtained with RSD values of <2% for both standards and extracts. Linearity, LOD, LOQ, accuracy, and precision were evaluated for quantitative purposes (Table 2). Linear behavior was observed in the ranges studied for all of the phenolic compounds considered, presenting good correlation coefficients (between 0.9992 and 0.9997). LOD and LOQ values ranged from 0.01 to 7.04 mg L^{-1} and from 0.22 to 27.91 mg L^{-1}, respectively, which suggested full capacity for the quantification of each phenolic compound investigated. The precision of the injection integration exhibited RSD values

dx.doi.org/10.1021/jf4057023 | J. Agric. Food Chem. 2014, 62, 3125−3133

Table 4. Quantification of Flavonols and Anthocyanins of Different Extracts of Bioresidues by HPLC-DAD[a] in Equivalents (mg L^{-1}) of Kaempferol 3-*O*-Glucoside[A], Kaempferol 3-*O*-Sophoroside[B], Kaempferol Aglycone [C], Delphinidin 3,5-Di-*O*-glucoside[D], and Petunidin 3,5-Di-*O*-glucoside[E]

	water/HCl (100:1, v/v)	water/ACN/TFA (47:50:3, v/v/v)	water/ACN/HCl (50:50:1, v/v/v)	water/ethanol/HCl (50:50:1, v/v/v)	water/acetone/HCl (50:50:1, v/v/v)
flavonols					
kaempferol 3-*O*-sophoroside-7-*O*-glucoside[A]	1.89 ± 0.05d	0.15 ± 0.01a	0.22 ± 0.01a	0.51 ± 0.03c	0.38 ± 0.01b
kaempferol 3,7-di-*O*-glucoside[A]	0.18 ± 0.01	<LOQ	<LOQ	<LOD	<LOD
kaempferol 3,7,4′-tri-*O*-glucoside[A]	0.16 ± 0.01	<LOQ	<LOQ	<LOD	<LOD
quercetin 3-*O*-sophoroside[A]	1.32 ± 0.01e	0.23 ± 0.02a	0.30 ± 0.01b	0.63 ± 0.01d	0.38 ± 0.03c
isorhamnetin 3,4′-di-*O*-glucoside[A]	0.28 ± 0.01b	0.01 ± 0.00a	0.01 ± 0.00a	0.05 ± 0.00a	0.04 ± 0.01a
kaempferol 3-*O*-sophoroside[B]	638.43 ± 11.43c	245.59 ± 23.84a	263.22 ± 1.39a	569.09 ± 16.00b	579.21 ± 36.24b
kaempferol 3-*O*-rutinoside[A]	0.21 ± 0.03c	0.01 ± 0.00a	0.01 ± 0.00a	0.15 ± 0.01b	0.21 ± 0.03c
kaempferol 3-*O*-glucoside[A]	0.05 ± 0.00a	0.55 ± 0.02d	0.46 ± 0.01c	0.06 ± 0.00a	0.10 ± 0.01b
kaempferol 7-*O*-glucoside[A]	0.17 ± 0.01b	0.09 ± 0.01a	0.16 ± 0.02b	0.18 ± 0.01b	0.24 ± 0.02c
kaempferol[C]	8.80 ± 2.97b	8.79 ± 2.75b	5.43 ± 1.46ab	3.47 ± 0.93a	3.59 ± 1.47a
anthocyanins					
delphinidin 3,5-di-*O*-glucoside[D]	183.95 ± 1.20d	47.88 ± 4.37b	45.21 ± 0.52b	79.14 ± 3.68c	30.82 ± 5.19a
petunidin 3,5-di-*O*-glucoside[E]	51.30 ± 0.34d	28.64 ± 2.54bc	28.12 ± 0.15b	31.77 ± 1.26c	10.31 ± 2.20a
delphinidin 3-*O*-glucoside[D]	27.91 ± 0.19c	14.18 ± 0.84a	13.36 ± 0.11a	17.39 ± 1.11b	13.65 ± 0.63a
malvidin 3,5-di-*O*-glucoside[D]	11.86 ± 0.08b	8.87 ± 0.28a	8.71 ± 0.06a	9.31 ± 0.98a	<LOD
petunidin 3-*O*-glucoside[D]	11.40 ± 0.10c	8.93 ± 0.32a	8.64 ± 0.10a	9.94 ± 0.74b	8.36 ± 0.15a

[a]Data expressed as mean ± SD (n = 5). Different letters within a row indicate significant differences ($p < 0.05$). <LOD, not detected. <LOQ, not quantified.

lower than 1 and 10% for both standards and extracts, respectively. Accuracy was evaluated from recovery studies. The high recovery values (close to 100%) and a high repeatability indicated a satisfactory accuracy in the proposed method. Furthermore, the accuracy was independent of the compound concentration and their chemical structure.

The HPLC-DAD method in extracts of floral bioresidues prepared with water/HCl (100:1, v/v),water/ACN/TFA (47:50:3, v/v/v), or water/ACN/HCl (50:50:1, v/v/v) can be considered selective, precise, and accurate.

Quantitative Analysis. Table 4 shows the composition in flavonols and anthocyanins of the five different extracts of floral bioresidues, although the HPLC-DAD method for the water/acetone/HCl and water/ethanol/HCl extracts was not validated. Extracts prepared with water/HCl and water/ACN/TFA(HCl) showed all identified flavonols and anthocyanins (Figure 2; Table 4). However, extracts prepared with water/ethanol/HCl and water/acetone/HCl did not show kaempferol 3,7-di-*O*-glucoside and kaempferol 3,7,4′-tri-*O*-glucoside. Malvidin 3,5-di-*O*-glucoside was not detected in water/acetone/HCl extract.

Nørbæk et al. extracted saffron tepals with water/ACN/TFA (47:50:3, v/v/v) for flavonol and anthocyanin determination.[13] In this work, an extract (Figure 2B1,B2) was prepared according to themethod of Nørbæk et al.,[13] and another extract was prepared with water/ACN/HCl (50:50:1, v/v/v) (Figure 2C1,C2) to determine if the use of different acids in different proportion could affect the phenolic composition. The use of TFA or HCl in the extractants composed by water/ACN did not significantly modify the phenolic composition or extraction, because both extracts showed the same number of phenolic compounds and very similar contents (Figure 2B1,B2,C1,C2; Table 4).

Kaempferol 3-*O*-sophoroside constituted between 96 and 99% of total flavonols identified in all extracts (Table 4). This compound has also been identified in saffron spice samples.[25] The rest of the flavonols identified were present in only trace amounts. These results showed that the quantification of this single compound could be sufficient for the rapid quality control of flavonols in this plant material by the food industry. The water/HCl extract showed the highest concentration of kaempferol 3-*O*-sophoroside, followed by water/ethanol/HCl and water/acetone/HCl extracts. The lowest concentrations were observed in water/ACN/TFA(HCl) extracts. With regard to the chromatograms of the detected flavonols at 266 nm, kaempferol 3-*O*-sophoroside (compound **6**, t_R = 23.57 min) was the main flavonol in extracts prepared with water/HCl, water/ethanol/HCl, and water/acetone/HCl (Figure 2A1,D1,E1). Extracts prepared with water/ACN/TFA(HCl) showed a compound with a t_R = 23.09 min prior to kaempferol 3-*O*-sophoroside having a peak area higher than that of kaempferol 3-*O*-sophoroside (Figure 2B1,C1). The fragmentation pattern of this compound was exactly equal to that of kaempferol 3-*O*-sophoroside (Table 3) isolated from floral bioresidues (see Chemicals).

Delphinidin 3,5-di-*O*-glucoside, followed by petunidin 3,5-di-*O*-glucoside and delphinidin 3-*O*-glucoside, was the main anthocyanin in all of the extracts studied (Table 4). Malvidin 3,5-di-*O*-glucoside and petunidin 3-*O*-glucoside were present in lower concentrations. The water/HCl extract showed much higher concentrations of the five anthocyanins identified than those of the rest of the extracts. The anthocyanin concentration was higher in water/ethanol/HCl extract than in water/ACN/TFA(HCl) extracts. The lowest concentration of the five anthocyanins identified was observed in the water/acetone/HCl extract. With regard to the chromatograms of the anthocyanins detected at 520 nm, delphinidin 3,5-di-*O*-

dx.doi.org/10.1021/jf4057023 | J. Agric. Food Chem. 2014, 62, 3125−3133

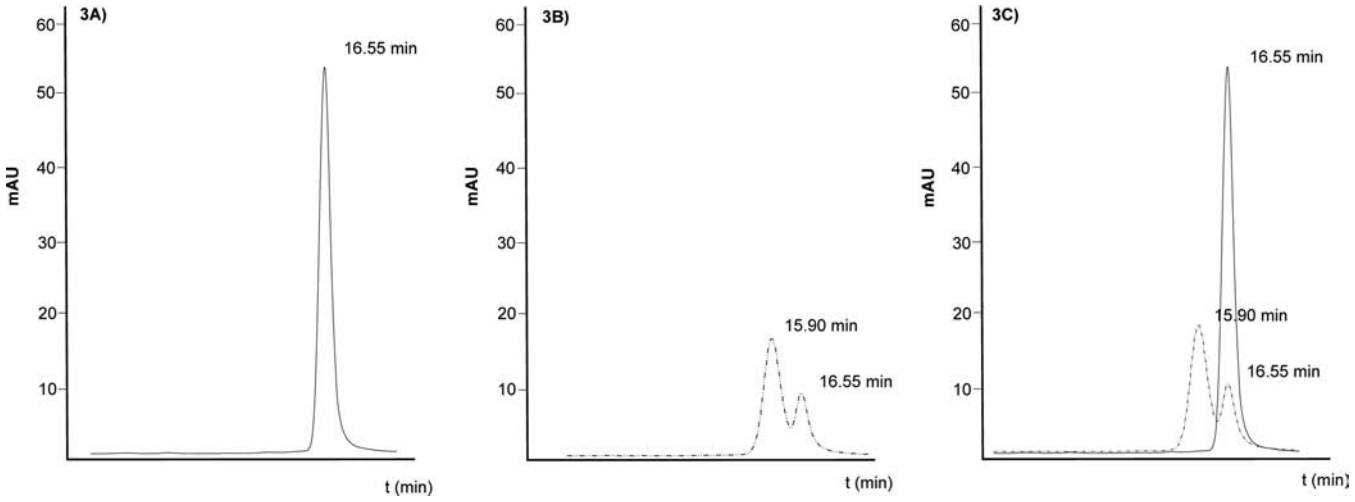

Figure 3. Commercial standard of delphinidin 3,5-di-*O*-glucoside by HPLC-DAD at 520 nm of (A) delphinidin 3,5-di-*O*-glucoside dissolved in water/HCl (100:1, v/v) and (B) solution composed of 47% of the solution analyzed in Figure 2A with the addition of 3% of TFA and 50% of acetonitrile. (C) Overlay of panels A and B.

glucoside (compound **11**, t_R = 16.55 min) was the major anthocyanin in the water/HCl extract (Figure 2A2). The rest of the extracts (Figure 2B2,C2,D2,E2) showed other anthocyanins with lower retention times (t_R = 15.62 and 15.90 min) having peak areas much higher than that of delphinidin 3,5-di-*O*-glucoside. When ESI-MS^n analysis was performed (Table 3), their fragmentation profiles were equal to that of the commercial standard of delphinidin 3,5-di-*O*-glucoside (Table 3) and to that of anthocyanins isolated from floral bioresidues (section Isolation of Anthocyanins).

Effect of Solvent on the Analysis of Phenolic Compounds. *Extracts of Floral Bioresidues.* As mentioned before, extracts prepared with water/HCl showed only one major flavonol, kaempferol 3-*O*-sophoroside (Figure 2A1), and one major anthocyanin, delphinidin 3,5-di-*O*-glucoside (Figure 2A2). However, extracts prepared with water/ACN/TFA(HCl) showed two major flavonols (Figure 2B1,C1) and two major anthocyanins (Figure 2B2,C2). In both cases, a compound with a t_R prior to kaempferol 3-*O*-sophoroside (at 266 nm) and another compound with a t_R prior to delphinidin 3,5-di-*O*-glucoside (at 520 nm) were observed. These compounds showed fragmentation patterns exactly equal to those of kaempferol 3-*O*-sophoroside and delphinidin 3,5-di-*O*-glucoside, respectively (Table 3). In the case of water/ethanol/HCl and water/acetone/HCl extracts, the same effect was observed. Due to less efficient separation of the phenolic compounds in these two extracts, this study was focused on the comparison between water/HCl with water/ACN/TFA(HCl) extracts.

First, it was hypothesized that water/ACN/TFA(HCl) extracts were capable of extracting more phenolic compounds than the water/HCl extracts. On the other hand, it could be also the case that ACN or the acids were responsible for this effect. To rule out any of these hypotheses, an extract of floral bioresidues in water/HCl (100:1, v/v) was prepared, the plant material was discarded after centrifugation, and only the supernatant of the water/HCl extracts was used. Then, ACN without acids (TFA and HCl) and/ on the other hand, TFA or HCl without ACN were added to the supernatant of the water/HCl extracts to determine whether ACN or the acids may be responsible for producing two main flavonol and two main anthocyanin peaks in the water/ACN/TFA(HCl) extracts instead of a single compound. ACN, TFA, and HCl were added in similar ratios to the initial extracts where this effect was observed, that is, ACN at 50%, TFA at 3%, and HCl at 1%. The flavonol and anthocyanin composition by HPLC-DAD was unchanged when TFA or HCl was added to the supernatant of the water/HCl extract. However, the same two flavonol and two anthocyanin peaks found in the extracts prepared with water/ACN/TFA(HCl) were observed (Figure 2B2,C2) when ACN without acids was added to the supernatant of the water/HCl extract in a 50% ratio. These results showed that water/ACN/TFA(HCl) did not extract more phenolic compounds from floral bioresidues than water/HCl. ACN caused a splitting of the chromatographic peaks of kaempferol 3-*O*-sophoroside and delphinidin 3,5-di-*O*-glucoside detected in the water/HCl extract.

Commercial Standard of Delphinidin 3,5-Di-O-glucoside. To confirm the results obtained under Extracts of Floral Bioresidues, the commercial standard of delphinidin 3,5-di-*O*-glucoside was dissolved in water/HCl (100:1, v/v) as the extract of floral bioresidues had been prepared previously. The chromatogram at 520 nm of the delphinidin 3,5-di-*O*-glucoside is shown in Figure 3A. ACN was added in a 50% ratio and, then, the same splitting of the chromatographic peak of the delphinidin 3,5-di-*O*-glucoside into two peaks was also observed for the commercial standard (Figure 3B), as had been produced in the water/ACN/TFA(HCl) extracts of floral bioresidues. The t_R of the first anthocyanin generated by the addition of ACN was 15.9 min; however, the second anthocyanin detected showed the same t_R as delphinidin 3,5-di-*O*-glucoside (Figure 3C). The percentage of peak area of the first anthocyanin with respect to the sum of areas of the first and second anthocyanins was 65 ± 2%. The first anthocyanin generated by addition of ACN had a fragmentation pattern similar to that of delphinidin 3,5-di-*O*-glucoside (Table 3).

When the solvents were removed under vacuum and the delphinidin 3,5-di-*O*-glucoside was redissolved in water/HCl (100:1, v/v), the chromatogram at 520 nm was exactly equal to the initial chromatogram of the delphinidin 3,5-di-*O*-glucoside dissolved in water/HCl (100:1, v/v) without the addition of ACN (Figure 3A). The first anthocyanin generated by the addition of ACN was not found in the chromatogram, and the

dx.doi.org/10.1021/jf4057023 | J. Agric. Food Chem. 2014, 62, 3125−3133

peak area of the delphinidin 3,5-di-*O*-glucoside increased again. Some authors stated that the chromatographic splitting of peaks can occur if the sample solvent is of higher strength than the HPLC mobile phase,[26] but really the mechanism or why this happens is still unknown.

Study of the Lowest Solvent Volume Capable of Splitting the Chromatographic Peaks of Phenolic Compounds. Different ratios (from 10 to 50) of ACN were added to the supernatant of water/HCl extracts to find the lowest ratio of ACN capable of producing the chromatographic splitting of the peak of delphinidin 3,5-di-*O*-glucoside. The pH values of the extracts prepared with water/HCl and all of the solutions containing this extract, ACN, and TFA(HCl) in different ratios ranged from 0.90 to 1.16. The effect of the chromatographic splitting of the peak of delphinidin 3,5-di-*O*-glucoside into two peaks was progressive when ACN in different ratios was added. Changes in the chromatograms at 520 nm were not observed when ACN was added in ratios from 10 to 30%. With ACN ratios from 30 to 40%, the separation between the two peaks was greater when the ratios of ACN were also higher. The chromatographic splitting resulting into two well-separated peaks was observed when ACN was added in a 40% ratio to the supernatant of the water,HCl extract. The sum of areas at 520 nm of the two peaks generated by ACN addition was approximately equal to the original peak area of the delphinidin 3,5-di-*O*-glucoside in the water/HCl extract.

The appearance of new chromatographic peaks due to the addition of solvents could produce an erroneous quantification of flavonols and anthocyanins, because the original chromatographic peak and the chromatographic peak generated by the solvent effect correspond to the same compound. Hence, both chromatographic peak areas should be added to be considered as a single compound. The best choice is the complete evaporation of the organic solvent used for extraction prior to analysis. Then the concentrated samples could be redissolved in appropriate solvents for HPLC analysis, as water acidified with HCl.

The FDA[27] proposed HCl to be GRAS (generally recognized as safe) as a direct ingredient of food, so this could be of great relevance for the food industry because floral bioresidues are rich natural sources of antioxidants according to the proposal established by Serrano-Díaz et al.[1] In conclusion, the analytical HPLC-DAD method proposed allows the quantification of phenolic compounds in floral bioresidues with good selectivity, sensitivity, and accuracy. The extract prepared with water/HCl (100:1, v/v) would be best suited for the quality of these products.

AUTHOR INFORMATION

Corresponding Author

*(G.L.A.) Phone: +34 967 599310. Fax: +34 967 599238. E-mail: Gonzalo.Alonso@uclm.es.

Funding

This study was supported by the Consejería de Educación y Ciencia of the JCCM, FSE, and FEDER (project ref POIC10-0195-9848) and the Ministerio de Educación (PNMRH del PN de I−D+i 2008−2011, ref EX2009-0395).

Notes

The authors declare no competing financial interest.

ACKNOWLEDGMENTS

We thank the Agrícola Técnica de Manipulación y Comercialización S.L. company (Minaya, Spain) for providing the samples. We also thank Marco A. García for technical assistance.

REFERENCES

(1) Serrano-Díaz, J.; Sánchez, A. M.; Maggi, L.; Martínez-Tomé, M.; García-Diz, L.; Murcia, M. A.; Alonso, G. L. Increasing the applications of *Crocus sativus* flowers as natural antioxidants. *J. Food Sci.* **2012**, *77*, 1162−1168.

(2) Ulbricht, C.; Conquer, J.; Costa, D.; Hollands, W.; Iannuzzi, C.; Isaac, R.; Jordan, J. K.; Ledesma, N.; Ostroff, C.; Grimes Serrano, J. M.; Shaffer, M. D.; Varghese, M. An evidence-based systematic review of saffron (*Crocus sativus*) by the natural standard research collaboration. *J. Dietary Suppl.* **2011**, *8*, 58−114.

(3) Licón, C.; Carmona, M.; Llorens, S.; Berruga, M. I.; Alonso, G. L. Potential healthy effects of saffron spice (*Crocus sativus* L. stigmas) consumption. In *Saffron. Functional Plant Science and Biotechnology 4*, Special Issue 2; Husaini, A. M., Ed.; Global Science Books: Japan, 2010; pp 64−73.

(4) Kyriakoudi, A.; Tsimidou, M. Z.; O'Callaghan, Y. C.; Galvin, K.; O'Brien, N. M. Changes in total and individual crocetin esters upon in vitro gastrointestinal digestion of saffron aqueous extracts. *J. Agric. Food Chem.* **2013**, *61*, 5318−5327.

(5) Geromichalos, G. D.; Lamari, F. N.; Papandreou, M. A.; Trafalis, D. T.; Margarity, M.; Papageorgiou, A.; Sinakos, Z. Saffron as a source of novel acetylcholinesterase inhibitors: molecular docking and in vitro enzymatic studies. *J. Agric. Food Chem.* **2012**, *60*, 6131−6138.

(6) Serrano-Díaz, J.; Sánchez, A. M.; Martínez-Tomé, M.; Winterhalter, P.; Alonso, G. L. A contribution to nutritional studies on *Crocus sativus* flowers and their value as food. *J. Food Compos. Anal.* **2013**, *31*, 101−108.

(7) Garvi Palazón, J. Cosechadora de azafrán. Spanish Patent ES2005088, 1987.

(8) Gracia, L.; Pérez, C.; Gracia-López, C.; Guerrero Muñoz, J. Método automatizado del corte de la flor del azafrán para liberación y separación de sus estigmas. Spanish Patent ES20080002387, 2008.

(9) Emadi, B. Separating saffron flower parts using vertical air column. *World Acad. Sci., Eng. Technol.* **2009**, *49*, 25−28.

(10) Alonso, G. L. et al. *White Book, Saffron in Europe. Problems and Strategies for Improving the Quality and Strengthen Competitiveness*; Alexandros: Athens, Greece, 2007; http://www.europeansaffron.eu/ (accessed Oct 10, 2012).

(11) Zheng, C. J.; Li, L.; Ma, W. H.; Han, T.; Qin, L. P. Chemical constituents and bioactivities of the liposoluble fraction from different medicinal parts of *Crocus sativus*. *Pharm. Biol.* **2011**, *49*, 756−763.

(12) Bergoin, M. Application du concept de raffinage végétal au safran du Quercy (*Crocus sativus*) pour la valorisation intégrée des potentiels aromatiques et colorants. Doctoral Thesis, Institut National Polytechnique de Toulouse, France, 2005.

(13) Nørbæk, R.; Brandt, K.; Nielsen, J. K.; Ørgaard, M.; Jacobsen, N. Flower pigment composition of *Crocus* species and cultivars used for a chemotaxonomic investigation. *Biochem. Syst. Ecol.* **2002**, *30*, 763−791.

(14) Serrano-Díaz, J.; Sánchez, A. M.; Alvarruiz, A.; Alonso, G. L. Preservation of floral bio-residues by hot air convection. *Food Chem.* **2013**, *141*, 1536−1543.

(15) Termentzi, A.; Kokkalou, E. LC-DAD-MS (ESI$^+$) analysis and antioxidant capacity of *Crocus sativus* petal extracts. *Planta Med.* **2008**, *74*, 573−581.

(16) Xu, B. J.; Chang, S. K. C. A comparative study on phenolic profiles and antioxidant activities of legumes as affected by extraction solvents. *J. Food Sci.* **2007**, *72*, 159−166.

(17) Barnes, J. S.; Nguyen, H. P.; Shen, S.; Schug, K. A. General method for extraction of blueberry anthocyanins and identification using high performance liquid chromatography−electrospray ioniza-

tion−ion trap−time of flight−mass spectrometry. *J. Chromatogr., A* **2009**, *1216*, 4728−4735.
(18) Sultana, B.; Anwar, F.; Ashraf, M. Effect of extraction solvent/technique on the antioxidant activity of selected medicinal plant extracts. *Molecules* **2009**, *14*, 2167−2180.
(19) Razali, N.; Mat-Junit, S.; Abdul-Muthalib, A. F.; Subramaniam, S.; Abdul-Aziz, A. Effects of various solvents on the extraction of antioxidant phenolics from the leaves, seeds, veins and skins of *Tamarindus indica* L. *Food Chem.* **2012**, *131*, 441−448.
(20) Reichardt, C. *Solvents and Solvent Effects in Organic Chemistry*, 3rd ed.; Wiley: Weinheim, Germany, 2003.
(21) Sánchez, A. M.; Jerz, G.; Serrano-Díaz, J.; Alonsa, G. L.; Winterhalter, P. In *Flavonol Composition and Isolation of Kaempferol 3-O-sophoroside from Saffron (Crocus sativus L.) Floral Bio-residues*, Proceeding 40, Frankfurt, Sept 12−14, 2011; Gesellschaft Deutscher Chemiker, Ed.; Deutscher Lebensmittelchemikertag: Halle, Germany, pp 231.
(22) DOCM. Especificaciones para los azafranes protegidos por esta Denominación de Origen, que comprende aquellos azafranes producidos en una zona geográfica delimitada de la Comunidad Autónoma de Castilla-La Mancha. Diario oficial Castilla La Mancha, 19 February 1999, no. 10, pp 1098−1112.
(23) Ito, Y. High-speed countercurrent chromatography. *CRC Crit. Rev. Anal. Chem.* **1986**, *17*, 65−143.
(24) Degenhardt, A.; Knapp, H.; Winterhalter, P. Separation and purification of anthocyanins by high-speed countercurrent chromatography and screening for antioxidant activity. *J. Agric. Food Chem.* **2000**, *48*, 338−343.
(25) Carmona, M.; Sánchez, A. M.; Ferreres, F.; Zalacain, A.; Tomás-Barberán, F. A.; Alonso, G. L. Identification of the flavonoid fraction in saffron spice by LC/DAD/MS/MS: comparative study of samples from different geographical origins. *Food Chem.* **2007**, *100*, 445−450.
(26) Zuo, Y.; Chen, H.; Deng, Y. Simultaneous determination of catechins, caffeine and gallic acids in green, polong, black and pu-erh teas using HPLC with a photodiode array detector. *Talanta* **2002**, *57*, 307−316.
(27) U.S. FDA (Food and Drug Administration). *Fed. Regist.* **1984**, *49* (82), 17966−17968.

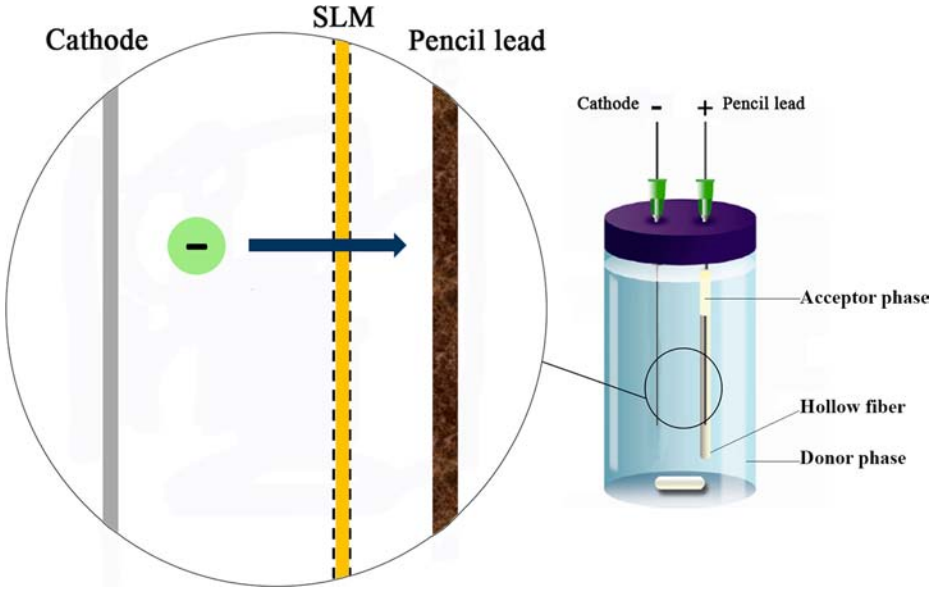

Figure 1. Equipment used for the EM-SPME method, and mechanism of transportation across liquid−liquid—liquid−solid boundaries.

electrical resistance of the system, which reduces the extraction efficiency as a result of diminishing the strength of the electrical field and lengthening the extraction time.[21] EME conjugated with dispersive liquid−liquid microextraction (EME-DLLME) is another route to transferring the analytes into an organic solvent.[22,23] However, EME-DLLME is an off-line coupling of two extraction techniques and requires sufficient time for conducting both procedures.

Rezazadeh et al. have introduced electromembrane surrounded solid phase microextraction (EM-SPME) as a simple and effective method to benefit from high extraction efficiency, sample cleanup, and fast kinetics related to EME technique as well as solid phase microextraction (SPME) compatibility with GC.[24] EM-SPME setup was the same as that of EME, unless one of the electrodes, located in the lumen of the hollow fiber, was substituted with a conductive sorbent. EM-SPME was implemented for extraction of basic drugs utilizing a platinum electrode and a piece of pencil lead as anode and cathode, respectively.[24] Thus, the basic analytes migrated in an electrical field from aqueous sample solution through a liquid membrane and into an aqueous acceptor phase, and then they were adsorbed on the solid sorbent, which acted as cathode. It was shown that EM-SPME has a great potential as a microextraction technique and could be established as a simple and inexpensive method for analysis of nonvolatile or ionizable compounds in complex matrices.[24]

The present study was focused on EM-SPME of acidic herbicides, to explore the capacity of the technique for extraction of this class of analytes by means of a sorbent as anode. Hence, the suggested method followed by GC combined with flame ionization detection (GC-FID) was exploited, for the first time, for extraction of CPA herbicides from plant tissue. In this work, an electrical field was applied to cause the CPAs, which existed in aqueous sample solution as anions, to migrate through the supported liquid membrane (SLM) into an aqueous phase inside the lumen of the hollow fiber. Using organic liquid membrane (SLM), not only the selectivity can be increased but also the sample cleanup highly improves and makes it possible to apply high voltages that increase extraction recoveries. Afterward, the target analytes were adsorbed on the solid adsorbent, which was also the anode. After derivatization to enhance the volatility of the CPAs, the carbonaceous sorbent was directly introduced into the GC-FID injection port. The goal of this work is to examine the possibility of employing EM-SPME as an effective and relatively fast extraction technique for analysis of both acidic and basic compounds in complicated matrices.

EXPERIMENTAL SECTION

EM-SPME Equipment. The equipment used for the extraction procedure is illustrated in Figure 1. A 24 mL vial with an internal diameter of 2.5 cm and a height of 5.5 cm was exploited. The platinum electrode employed in this work, with a diameter of 0.25 mm, was acquired from Pars Pelatine (Tehran, Iran). The electrodes were connected to a power supply model 8760T3 with a programmable voltage in the range of 0−600 V and a current output within the range of 0−500 mA from Paya Pajoohesh Pars (Tehran, Iran). During the extraction, the EM-SPME unit was stirred with a speed in the range of 100−1250 rpm via a heater−magnetic stirrer, model 3001 from Heidolph (Kelheim, Germany), using a 1.5 cm × 0.3 cm magnetic bar. A 40 kHz and 0.138 kW ultrasonic water bath with temperature control (Tecno-GazSpA, Parma, Italy) and a Sepand Teb Azma centrifuge (Tehran, Iran) were employed to carry out pretreatment steps for real samples.

Chemicals and Materials. 2-Methyl-4-chlorophenoxyacetic acid (MCPA) and 2,4-dichlorophenoxyacetic acid (2,4-D), were purchased from Aldrich (Milwaukee, WI, USA). 1-Octanol, 1-hexanol, 1-undecanol, 1-dodecanol, and tetrabutylammonium iodide (TBA), were supplied by Merck (Darmstadt, Germany). All of the chemicals used were of analytical reagent grade. The porous hollow fiber, utilized for supporting the liquid membrane, was a PPQ3/2 polypropylene hollow fiber from Membrana (Wuppertal, Germany), with inner diameter of 0.6 mm, wall thickness of 200 μm, and pore size of 0.2 μm. Ultrapure water was prepared by a Young Lin 370 series aquaMAX purification instrument (Kyounggi-do, Korea).

The HB pencil lead fibers with the diameter of 0.3 mm (Owner, Seoul, Korea) were purchased from a local market. The fibers were conditioned via heating under N_2 atmosphere from room temperature to 350 °C with a ramp of 3 °C min^{-1}, held for 120 min at 350 °C, and then were allowed to cool to ambient temperature.

Standard Solutions and Real Samples. A stock solution, containing 1 mg mL^{-1} of each analyte, was prepared in methanol and stored at −4 °C, protected from light. Working standard solutions were prepared by dilution of the stock solution with methanol.

dx.doi.org/10.1021/jf500017r | J. Agric. Food Chem. 2014, 62, 3134−3142

The whole wheat plant was analyzed as the real sample. For analysis of the target herbicides in the plant tissue, wheat was harvested after 1 h, 2 days, and 6 days following field spraying. The whole wheat plants were first washed and completely blended. A 20 mL aliquot of a 100 mM NaOH solution was subsequently added to 100 g of the blended sample, and the sample was immersed in the ultrasonic water bath. After 2 min of sonication (at 25 ± 3 °C), the sample was centrifuged at 2500 rpm for 10 min to separate the phases. The final liquid phase was diluted (1:9) with pure water and, following pH adjustment (pH 9.0), was transferred into the EM-SPME vial for analysis.

Gas Chromatography Conditions. Separation and detection of MCPA and 2,4-D were executed through an Agilent 7890A gas chromatograph (Palo Alto, CA, USA), equipped with a split−splitless injector, and a flame ionization detector. A 30 m HP-5 Agilent fused-silica capillary column (0.32 mm, i.d.; 0.25 μm, film thickness) was exploited for separation of the target compounds. Helium (purity, 99.999%) was utilized as carrier gas at the constant flow rate of 2.0 mL min^{-1}. The temperatures of injector and detector were set at 290 and 300 °C, respectively. The injection port was operated at the splitless mode. The oven temperature program was 100 °C for 2 min, increasing to 220 °C with a ramp of 9 °C min^{-1}, then increasing to 280 °C at 100 °C min^{-1}, and eventually holding at 280 °C for 3 min.

EM-SPME Procedure. A 24 mL aliquot of the sample solution, containing the analytes in aqueous medium, was transferred into the sample vial. To impregnate the organic liquid membrane in the pores of the hollow fiber wall, a 2.8 cm piece of the hollow fiber was cut out and dipped into 1-octanol for 5 s, and subsequently the excess of the organic solvent was gently wiped away by blowing air with a Hamilton syringe. Pure water, as the acceptor phase, was introduced into the lumen of the hollow fiber by means of a microsyringe, and the lower end of the hollow fiber was mechanically sealed afterward. The pencil lead fiber (the anode) was placed in the lumen of the hollow fiber. After that, the hollow fiber, containing the anode, together with the SLM and the acceptor solution was directed into the sample solution. The platinum cathode was led directly into the sample solution. The electrodes were subsequently connected to the power supply, and the extraction unit was placed on a stirrer with stirring rate of 700 rpm. When the extraction was accomplished, the pencil lead was retracted into the SPME syringe needle. The tractable nature of the pencil lead facilitated its insertion into the SPME syringe. The carbonaceous fiber was well fitted into the syringe by some wearing on top of it, where it was in contact with the needle. Then, the pencil lead was immersed in a concentrated TBA solution, as derivatization reagent, and withdrawn very fast and immediately inserted into the GC injection port for thermal desorption of the analytes at 290 °C for 2 min. The contact time of the fiber and TBA solution should be long enough to form a stagnant thin layer of derivatization reagent around the fiber but it must be too short to prevent dissolving of analytes in TBA solution.

Data Analysis and Statistical Methods. Response surface methodology (RSM) is effective for responses that are influenced by many factors as well as by their interactions and was originally described by Box and Wilson.[25] Optimization of the parameters affecting the extraction efficiency of the analytes by PEME was performed by a face-centered central composite design. In all cases, design generation and statistical analyses were performed by the software package Design-Expert version 8.0.5 trial for Windows (State-Ease, MN, USA).

RESULTS AND DISCUSSION

In order to figure out how the impressive parameters affected the final signals of the analytes, a number of experiments were designed. Two different influential parameters in the final chromatographic signals included EM-SPME related variables and those linked to GC analysis (i.e., derivatization process and desorption conditions). GC instrument associated parameters were optimized in terms of derivatization procedure, TBA concentration, injection port temperature, carrier gas flow rate, and desorption time. EM-SPME affected parameters consisted of SLM composition, compositions of donor and acceptor phases, extraction time, applied voltage, and stirring rate. It is obvious that stirring of the sample solution possesses a positive impact upon the kinetics and efficiency of extraction via enhancing the mass transfer of the analytes and decreasing the thickness of the double layer around the SLM. The influence of the stirring rate on extractability was investigated up to 1250 rpm. A stirring rate of 700 rpm was selected, because of creation of an intense vortex in the sample solution and bubble formation around the hollow fiber at higher rates. The SLM composition was optimized separately, and other EM-SPME variables, comprising extraction time, applied voltage, and pHs of sample solution and acceptor phase, were evaluated by means of experimental design methodology.

Derivatization Procedure and GC Analysis. Direct injection port derivatization with ion-pair reagents, known as tetraalkylammonium salt pyrolysis derivatization method, is a rapid and simple alternative to conventional derivatization techniques for aliphatic and aromatic acids.[26,27] The product of the reaction of an acidic analyte with tetraalkylammonium salt is a carboxylate ion pair, which is derivatized to its corresponding volatile alkyl ester in a high-temperature GC injection port.

$$RCOOH + N(Bu)_4{}^+X^- \leftrightarrow RCOO^-N(Bu)_4{}^+ + HX \quad (1)$$

$$RCOO^-N(Bu)_4 \leftrightarrow RCOO\,Bu + N(Bu)_3 \quad (2)$$

Two different methods were tested to form the carboxylate ion pair. In the first technique, TBA was added to the acceptor phase of EM-SPME and once the extraction was completed, the pencil lead was directly introduced into the GC injection port. The second method of carboxylate ion pair production was through the immersion of pencil lead in a TBA solution following accomplishment of EM-SPME. Comparison of the attained results demonstrated that good derivatization performance was gained by immersion of the SPME fiber in TBA solution. The main point of the injection port derivatization technique is that both analyte and derivatization reagent should simultaneously exist in the injection port during the process. When TBA was added into the acceptor solution, its adsorption on the surface of the pencil lead was difficult since both of them have positive charges. The charge of TBA is positive in the neutral acceptor phase while the positive charges of pencil lead is attributed to the connection of the fiber to the positive pole of the power supply during the extraction procedure. Therefore, the derivatization efficiency decreases due to reduction of the TBA concentration in the injection port. However, immersion of the fiber into a concentrated TBA solution occurred after completion of the extraction and disconnection of the electrical field. In this way, a thin stagnant layer of TBA solution was formed on the surface of the fiber by means of the porous nature of the pencil lead. When the fiber together with the TBA solution layer is introduced into the GC injection port, the TBA solvent (methanol) is evaporated and thus a considerable amount of TBA is available. Hence, desorption of both TBA and analytes lead to formation of derivatized analytes.

The TBA concentration was assessed thereafter, to find the best derivatization conditions. The concentration of the derivatization reagent in methanol was varied in the range of 30−400 mM. After EM-SPME of the analytes, the carbonaceous fiber was immersed in 30 μL of TBA solution and instantly inserted into the GC injection port. It was noticed that

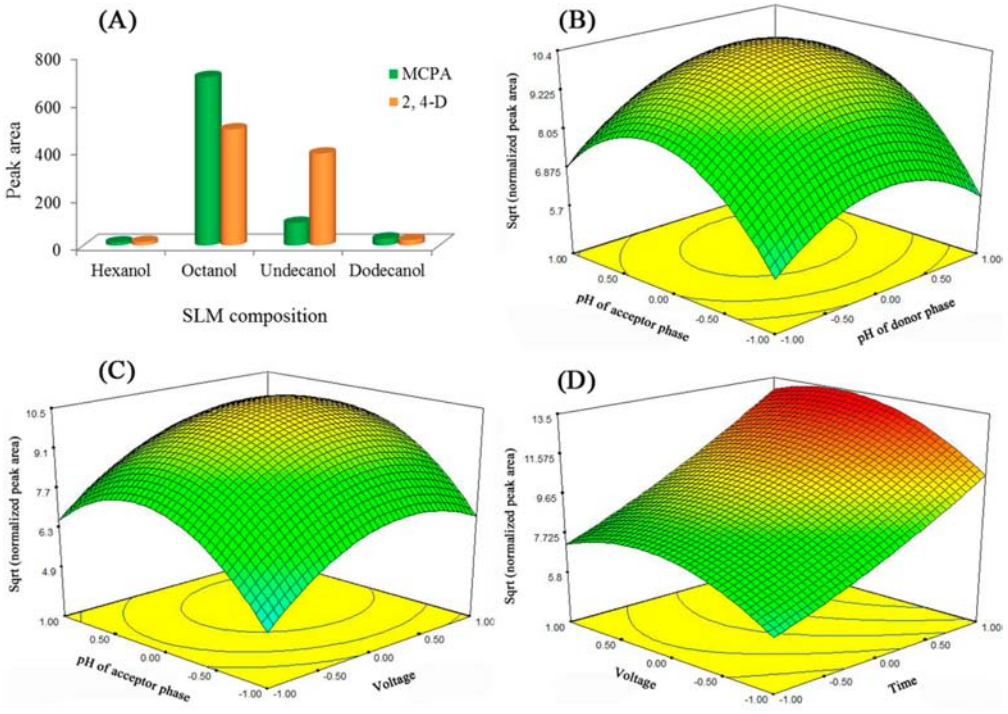

Figure 2. (A) Optimization of membrane composition, (B) response surface of the square root of the normalized peak area vs pH of donor phase and pH of acceptor phase, (C) response surface of the square root of the normalized peak area vs pH of the acceptor phase and applied voltage, and (D) response surface of the square root of the normalized peak area vs extraction time and applied voltage.

the peak areas of both CPA herbicides initially increased via enhancing the concentration of the derivatization reagent up to 200 mM and then reached a plateau with a further rise in TBA concentration. Therefore, 200 mM TBA in methanol was selected as the derivatization solution.

Another effective parameter on the efficiency of the analyte desorption as well as the injection port derivatization process is the injection port temperature that was considered in the range of 250−300 °C. The peak areas of the derivatized analytes were enhanced by raising the temperature to 290 °C. Since no changes in the derivatization yields were observed at higher temperatures, 290 °C was chosen to reach the maximum desorption and derivatization efficiencies and also prevent the entrance of the pencil lead from interfering with compounds going into the GC injection port.

The carrier gas flow rate can influence the derivatization efficiency through altering the delay time of the analytes in the injection port of the GC apparatus. The flow rate of the carrier gas was scrutinized in the range of 1−4 mL min^{-1}. The maximum peak areas for butyl esters of the herbicides were achieved at a flow rate of 2 mL min^{-1}.

Furthermore, desorption time was explored in the range of 0.5−5.0 min while the desorption temperature was 290 °C. The efficiency of thermal desorption improved as the desorption time was increased from 0.5 to 2.0 min. The chromatographic signals slightly increased after 2.0 min, but desorption of some interferences from the pencil lead fiber resulted in crowded chromatograms. Consequently, the desorption time of 2.0 min was selected.

EM-SPME Affecting Parameters. *Composition of Organic Liquid Membrane.* One of the most significant parameters, which could influence the extractability of analytes in EM-SPME technique, is the SLM composition. Extraction selectivity, range of applied voltage, extraction efficiency, and extraction time are directly affected by the composition of organic liquid membrane. Analytes should have a proper affinity for SLM so that adequate selectivity and favorable extraction efficiency could be acquired. In fact, SLM provides the major electrical resistance for the system and the range of applied voltage could be extended via raising the electrical resistance of SLM. Accordingly, system stability and extractability may improve utilizing organic solvents with high electrical resistance such as SLM. Nevertheless, the organic phase should possess satisfactory conductivity to enable ion transportation across the phases. Regarding all of these factors, 1-hexanol, 1-octanol, 1-undecanol, and 1-dodecanol were tested as the organic liquid membrane. It was proved that long-chain alcohols are the most desirable organic solvents for extraction of acidic compounds.[6,28] Among the examined alcohols, 1-hexanol has the least electrical resistance, and a system operated with 1-hexanol, such as the SLM, underwent instability problems owing to increasing the electric current (Figure 2A). Therefore, 1-hexanol offered nonrepeatable results, and the chromatographic signals substantially declined, which was probably caused by the enhancement of electrochemical reactions due to increasing the electric current of the system. On the other hand, 1-dodecanol could not provide a continuous electric field in the entire system, since it possesses a low electrical conductivity; for this reason, the extractability diminished using 1-dodecanol as the SLM. 1-Undecanol was capable of effectively extracting the 2,4-D, although it was not a suitable solvent for MCPA. Ultimately, 1-octanol was chosen as the SLM due its ability to give the best results for both of the analytes.

Optimization of Extraction Time, Applied Voltage, and pHs of the Sample Solution and Acceptor Phase Using Central Composite Design. The experiments for optimization of the rest of the EM-SPME affected parameters were modeled through face-centered central composite design

dx.doi.org/10.1021/jf500017r | J. Agric. Food Chem. 2014, 62, 3134−3142

Table 1. Experimental Factors, Levels, and Analysis of Variance (ANOVA) for the Response Surface Quadratic Model

factor	symbol	level (−1)	level (0)	level (+1)
extraction time (min)	t	5	12:30	20
applied voltage (V)	V	20	50	80
pH of donor phase	pH_d	7	10	13
pH of acceptor phase	pH_a	1	7	13

source	sum of squares	d.f.	mean square	F-value	p-value	
block	61.46	1	61.46			
model	204.54	14	14.61	26.34	<0.0001	significant
A: t	122.78	1	122.78	221.34	<0.0001	
B: V	14.64	1	14.64	26.4	0.0002	
C: pH_d	2.19	1	2.19	3.95	0.0702	
D: pH_a	12.12	1	12.12	21.85	0.0005	
AB	0.9	1	0.9	1.62	0.2267	
AC	1.13	1	1.13	2.03	0.1798	
AD	1.1	1	1.1	1.98	0.1844	
BC	0.051	1	0.051	0.093	0.7661	
BD	1.14×10^{-5}	1	1.14×10^{-5}	2.05×10^{-5}	0.9965	
CD	0.96	1	0.96	1.74	0.2123	
$\hat{A}^2$	0.28	1	0.28	0.5	0.4935	
$\hat{B}^2$	5.32	1	5.32	9.6	0.0092	
$\hat{C}^2$	5.03	1	5.03	9.07	0.0108	
$\hat{D}^2$	11.34	1	11.34	20.44	0.0007	
residual	6.66	12	0.55			
lack of fit	6.3	10	0.63	3.56	0.2392	not significant
pure error	0.35	2	0.18			
cor total	272.66	27				
R^2	0.9685					
adj R^2	0.9317					

(FCCCD) methodology. CCD is one of the most frequently used response surface designs; it is a second-order model, correlating the response functions with the independent factors. In this way, the amount of response can be predicted at any point within the factor domain, even though that point is not incorporated in the design. CCD consists of factorial points, center points, and star (axial) points. One type of CCD is FCCCD that is considered unity in α (star point). In this step, 1-octanol was exploited as the SLM for all of the experiments, and the sample solution was stirred at a speed of 700 rpm. To find the optimal conditions, four variables, including extraction time (t), applied voltage (V), and pHs of donor (pH_d) and acceptor (pH_a) phases, had to be assessed. It should be noted that to investigate the composition of donor and acceptor phases, experiments were designed by changing the concentration of HCl and NaOH solutions in the range of 0−100 mM. However for graphical presentation and to obtain a total view of the effect of the concentration of H^+ or OH^- on extractability, the results should be changed to pH. Therefore, 28 experiments were executed, in order to figure out the optimum conditions with four factors and four center points. The normalized peak area for each run was selected as the response objective for the study.[6,12,13] To normalize the peak areas, all of the experiments were first conducted and then the peak area of each analyte was divided by its smallest peak area that was attained from the entire experiments. The normalized peak areas for the analytes were subsequently added for each run and utilized in the calculation of the total normalized peak area. Analysis of variance (ANOVA) in Table 1 depicts that the model is well fitted to the significant variables by means of multiple regression analysis. Meanwhile, an acceptable coefficient of determination ($R^2 = 0.9685$) was gained, indicating that the obtained equation had good adequacy to be correlated with the experimental results. The model is described as follows:

$$\begin{aligned}\sqrt{(\text{normalized peak area})} &= 10.28 + 2.61t + 0.9V + 0.35pH_d + 0.82pH_a \\ &\quad + 0.24tV + 0.27t\,pH_d - 0.26t\,pH_a + 0.057V\,pH_d \\ &\quad + 0.00084V\,pH_a + 0.25pH_d pH_a + 0.34t^2 - 1.47V^2 \\ &\quad - 1.43pH_d{}^2 - 2.15pH_a{}^2\end{aligned}$$

Three-dimensional representation of response surfaces, seen in Figure 2B−D, displays the interaction among the independent variables and assists in establishing the optimum operating conditions for the desirable responses. Parts B−D of Figure 2 illustrate that the response for the analytes is enhanced via increasing the extraction time. Nonetheless, an average amount of applied voltage was appropriate for effective extraction; as low voltages could not provide the needed driving force, and high voltages led to system instabilities and increasing the likelihood of electrochemical reactions as a result of increasing the electric current. Results in Table 1 confirm that the pH of sample solution is not an essential factor. This could be justified by the fact that both of the analytes were ionized within the preferred range for this parameter (Table 1) and that OH^- had little competition with the analytes, owing to its low affinity for the SLM. Consequently, favorable extraction recoveries could be achieved throughout the selected range of

Table 2. Accuracy, Precision, And Relative Recovery of EM-SPME Method for Determination of MCPA and 2,4-D

		accuracy (error %)		precision (CV %)		
analyte	concn (ng mL^{-1})	intraassay (n = 3)	interassay (n = 3)	intraassay (n = 5)	interassay (n = 3)	RR%
MCPA	20	−1.8	−3.4	7.7	8.8	98.2
	100	−4.3	+0.6	7.0	10.3	95.7
	400	+0.8	+1.4	8.5	11.1	100.8
2,4-D	20	+4.8	+9.5	6.0	10.0	104.8
	100	+3.3	−5.5	5.2	9.3	103.3
	400	−5.0	+6.4	7.6	12.0	95.0

Table 3. Comparison of Figures of Merit of EM-SPME with Other Analytical Techniques for Determination of MCPA and 2,4-D

analytical method[a]	analyte	matrix	LOD (ng mL^{-1})	linearity (ng mL^{-1})	extraction time (min)	R^2	RSD%	ref
EME-CE	2,4-D	river water	10	30−500	24	>0.997	<4.8	29
SPME-GC-MS	MCPA	aqueous	0.2		50	0.999	9	30
SPME-GC-MS	2,4-D	aqueous	1.0		50	0.999	8	30
SPE-EME-CE	MCPA	river water	0.5	1.5−300	34	0.997	7.4	31
SPE-GC-MS	MCPA	aqueous	2	3−200	38	0.998	2.9	32
SPE-GC-MS	2,4-D	aqueous	3	6−200	38	0.999	6.0	32
EM-SPME-GC-FID	MCPA	plant tissue	0.5	1.0−500.0	20	0.9958	7.7	this work
EM-SPME-GC-FID	2,4-D	plant tissue	5.0	10.0−500.0	20	0.9984	6.0	this work

[a]CE = capillary electrophoresis; SPE = solid phase extraction.

pH_d. On the other hand, the extraction efficiency was small at large pH values of the acceptor phase, due to the OH^- predomination in the electrostatic migration toward the pencil lead electrode. At moderately low pH values of the acceptor phase, the extraction yield severely declined; because the analytes occurred primarily as their neutral forms (this phenomenon verified that the extraction mechanism was through the electrokinetic migration of anionic species). Desirability function was considered to find the optimal conditions. To this end, a desirability of 1.0 was assigned to the maximum, 0.0 to the minimum, and 0.5 to the middle responses. Hence, according to the analysis, the plots in Figure 2 and the desirability score of 1, the values of 50 V and 20 min were chosen as the optimum voltage and extraction time, respectively. Additionally, the pH amounts of sample solution and acceptor phase were adjusted to 9.0 and 7.0, respectively, for the remaining experiments.

Evaluation of Method Performance. The applicability of the proposed EM-SPME technique was evaluated for extraction of the acidic herbicides, according to the recommendations of the Food and Drug Administration (FDA). With this aim, linearity was investigated in pure water via the analysis of extracts acquired from the aliquots of each sample in triplicate. The extraction recovery (ER%) was defined as the percentage of the number of moles of the analyte adsorbed on the sorbent (n_f) to those originally present in the sample solution (n_i).

$$\mathrm{ER\%} = \frac{n_f}{n_i} \times 100 \tag{3}$$

The coefficient of variation (CV%) was determined by intra- and interassays and by five- and three-replicate measurements, at three concentrations of 20, 100, and 400 ng mL^{-1}, respectively. Accuracy was determined through the triplicate analysis of samples containing known amounts of the analytes at three concentrations within the expected range. The relative recovery (RR%) and accuracy (error%) were calculated by the equations below:

$$\mathrm{RR\%} = \frac{C_{found} - C_{real}}{C_{added}} \times 100 \tag{4}$$

$$\mathrm{error\%} = 100 - \mathrm{RR\%} \tag{5}$$

where C_{found}, C_{real}, and C_{added} are the concentrations (ng mL^{-1}) of analyte after addition of a given amount of standard into the real sample, the concentration of analyte in the real sample, and the concentration of a known amount of standard spiked into the real sample, respectively.

The investigation of the figures of merit confirmed that EM-SPME could also be effectively implemented for the extraction of acidic analytes using pencil lead as sorbent. The method was linear in the ranges of 1.0−2000.0 and 10.0−2000.0 ng mL^{-1} for the analyses of MCPA and 2,4-D, respectively, with coefficients of determination (R^2) larger than 0.9958. Limits of detection (LODs) were 0.5 ng mL^{-1} for MCPA and 5.0 ng mL^{-1} for 2,4-D, and ERs% were 4.8% and 0.6% for MCPA and 2,4-D, respectively. The precision of the technique was evaluated via the intra- and interassay CVs% varied in the ranges of 5.2−8.5% and 8.8−12.0%, respectively (Table 2). Moreover, the calculated error% for the analytes in the range of −5.5% to +9.5% depicted that the EM-SPME method offered acceptable accuracy for analysis of these acidic herbicides.

Comparison of the EM-SPME with other analytical techniques for determination of MCPA and 2,4-D is shown in Table 3. However, EM-SPME requires simple and low-cost equipment; it offers excellent LODs in fairly short times compared to the other reported methods. Since the organic liquid membrane amplifies the electrical resistance of the system, it is practically feasible to apply high voltages that strengthen the electric field and improve the extraction recovery. Furthermore, uncrowded chromatograms are attained, even by extraction from very dirty matrices. Thus, the use of expensive extraction and analysis methods, such as in-tube SPME and mass spectrometry detection, is avoidable. The present work was the first attempt to extract acidic herbicides by means of EM-SPME method. It was proved that EM-SPME even possesses a great potential for the extraction of acidic

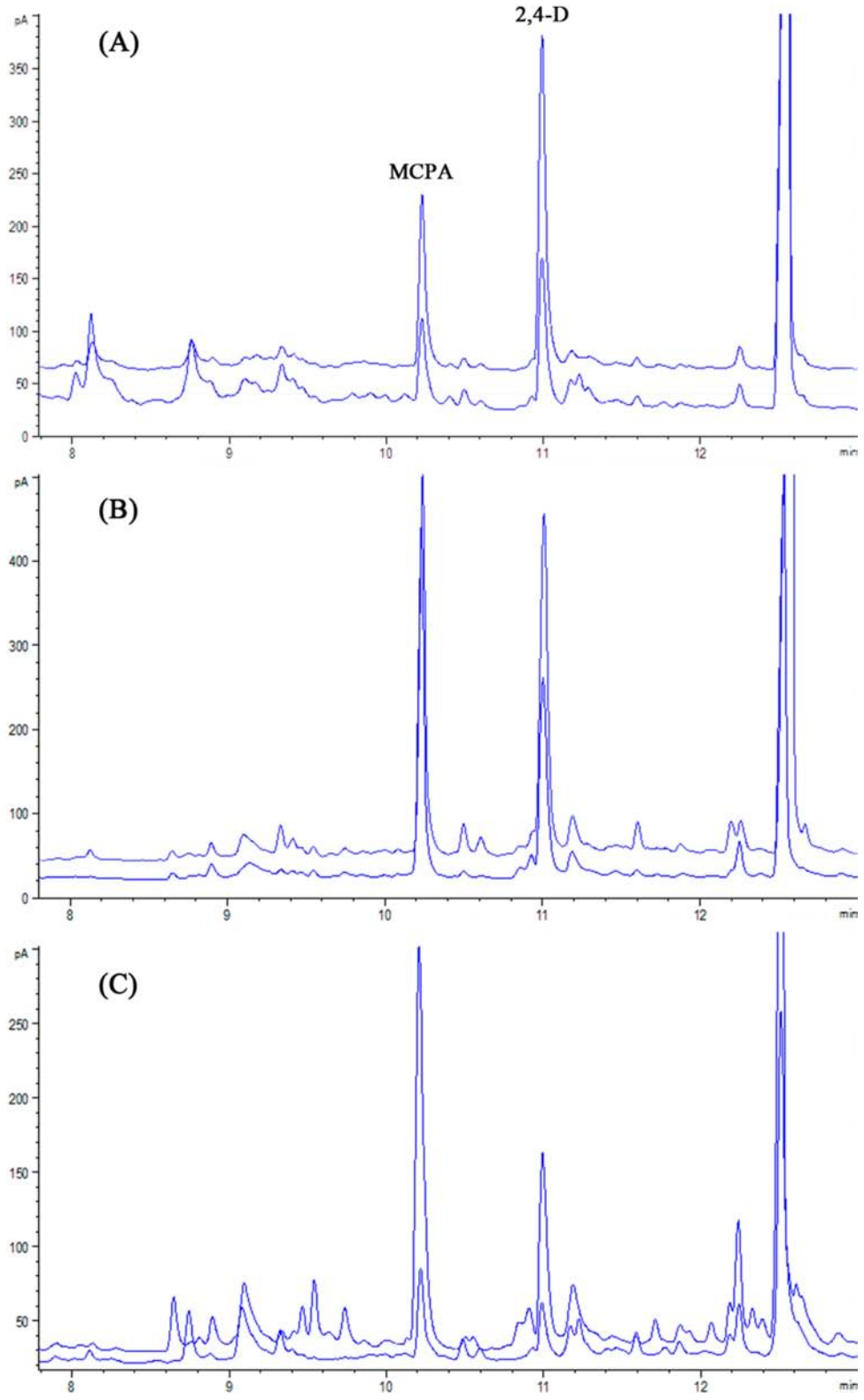

Figure 3. Chromatograms obtained by extraction of herbicides from wheat plant tissues collected after (A) 1 h, (B) 2 days, and (C) 6 days from field spraying.

compounds utilizing a sorbent as anode. Since the use of a thin hydrophobic SLM (which also acts as the principal electric resistance) significantly decreases the electric current of the system, the pencil lead could be successfully employed as both the sorbent and the anode electrode. The conducting nature, good thermal stability, low cost, and high adsorption capacity of the pencil lead made it an exceptional choice for EM-SPME–GC-FID technique. EM-SPME is a newborn extraction method, and more studies are required to figure out the best conditions for it and to develop qualified sorbents for analysis of various compounds. Indeed, the ability of this technique to efficiently

dx.doi.org/10.1021/jf500017r | J. Agric. Food Chem. 2014, 62, 3134–3142

extract the acidic and basic targets from complicated matrices is undeniable.

Analysis of Real Samples. EM-SPME was performed for analysis of the model herbicides in wheat plant tissue, to scrutinize its practical applicability. The entire wheat plant was blended and prepared, as explained in Standard Solutions and Real Samples. The pH of the final 10-fold diluted liquid extract was adjusted to 9.0 through the addition of proper amounts of hydrochloric acid solution, and quantitative analysis was conducted under optimal conditions. The chromatograms which were gained from EM-SPME of three samples, collected after 1 h, 2 days, and 6 days from field spraying, are displayed in Figure 3. The obtained results could be justified by taking into account that the reported concentration values are related to the analytes which were absorbed into the plant tissue. For preparing the real samples, whole wheat plants were first washed to remove the nonabsorbed herbicides and then were used for quantitative analysis. Whereof 1 h is not sufficient time for absorption, the obtained value for 1 h is lower than 48 h.

Since real samples (wheat plant tissue) were transformed into dirty complex solutions, some experiments were required to determine the accuracy of analysis as well as the matrix effects. Based on the FDA's definition, a matrix effect is the direct or indirect alteration or interference in response, owing to the existence of unintended analytes or other interfering substances in the sample. The error% was determined via the addition of 500 ng mL^{-1} of each analyte into the real samples, and EM-SPME was implemented afterward. Results in Table 4

Table 4. Determination of MCPA and 2,4-D in Plant Tissues Collected after 1 h, 2 days, and 6 days from Field Spraying

sample	analyte	C_{real} ($\mu g\ mL^{-1}$)	C_{added} ($\mu g\ mL^{-1}$)	C_{found} ($\mu g\ mL^{-1}$)	RR%	RSD%
1 h	MCPA	0.23	0.50	0.74	102	6.4
	2,4-D	0.76	0.50	1.23	94	9.8
48 h	MCPA	1.41	0.50	1.87	91	6.7
	2,4-D	1.19	0.50	1.67	97	8.5
6 days	MCPA	0.20	0.50	0.72	105	3.8
	2,4-D	0.16	0.50	0.61	91	8.6

demonstrate that there is no significant matrix effect in the examined real samples and that the obtained precision values are admissible. Accordingly, the calibration curves could be exploited directly in the analysis of real samples.

AUTHOR INFORMATION

Corresponding Author

*Tel.: +98 21 82883417. Fax: +98 21 88006544. E-mail: yyamini@modares.ac.ir.

Notes

The authors declare no competing financial interest.

REFERENCES

(1) Yaron, B.; Gerstl, Z.; Spencer, W. F. *Advances in Soil Science*; Springer: New York, 1985; Vol. 3.

(2) Pedersen-Bjergaard, S.; Rasmussen, K. E. Electrokinetic Migration Across Artificial Liquid Membranes: New Concept for Rapid Sample Preparation of Biological Fluids. *J. Chromatogr. A* **2006**, *1109*, 183−190.

(3) Eibak, L. E. E.; Gjelstad, A.; Rasmussen, K. E.; Pedersen-Bjergaard, S. Exhaustive Electromembrane Extraction of Some Basic Drugs From Human Plasma Followed by Liquid Chromatography−Mass Spectrometry. *J. Pharm. Biomed. Anal.* **2012**, *57*, 33−38.

(4) Eibak, L. E. E.; Hegge, A. B.; Rasmussen, K. E.; Pedersen-Bjergaard, S.; Gjelstad, A. Alginate and Chitosan Foam Combined with Electromembrane Extraction for Dried Blood Spot Analysis. *Anal. Chem.* **2012**, *84*, 8783−8789.

(5) Eibak, L. E. E.; Gjelstad, A.; Rasmussen, K. E.; Pedersen-Bjergaard, S. Kinetic Electromembrane Extraction Under Stagnant Conditions—Fast Isolation of Drugs from Untreated Human Plasma. *J. Chromatogr. A* **2010**, *1217*, 5050−5056.

(6) Seidi, S.; Yamini, Y.; Rezazadeh, M.; Esrafili, A. Low-Voltage Electrically-Enhanced Microextraction as a Novel Technique for Simultaneous Extraction of Acidic and Basic Drugs from Biological Fluids. *J. Chromatogr. A* **2012**, *1243*, 6−13.

(7) Basheer, C.; Lee, J.; Pedersen-Bjergaard, S.; Rasmussen, K. E.; Lee, H. K. Simultaneous Extraction of Acidic and Basic Drugs at Neutral Sample pH: A Novel Electro-Mediated Microextraction Approach. *J. Chromatogr. A* **2010**, *1217*, 6661−6667.

(8) Sun, H.; Wang, Y. Hollow Fiber Liquid-Phase Microextraction with in Situ Derivatization Combined with Gas Chromatography−Mass Spectrometry for the Determination of Root Exudate Phenylamine Compounds in Hot Pepper (Capsicum annuum L.). *J. Agric. Food Chem.* **2013**, *61*, 5494−5499.

(9) Chao, Y. Y.; Lee, C. H.; Chien, T. Y.; Shih, Y. H.; Lu, Y. A.; Kuo, T. H.; Huang, Y. L. Effects of Push/Pull Perfusion and Ultrasonication on the Extraction Efficiencies of Phthalate Esters in Sports Drink Samples Using On-line Hollow-Fiber Liquid-Phase Microextraction. *J. Agric. Food Chem.* **2013**, *61*, 8063−8071.

(10) Šlampová, A.; Kubáň, P.; Boček, P. Electromembrane Extraction Using Stabilized Constant D.C. Electric Current—A Simple Tool for Improvement of Extraction Performance. *J. Chromatogr. A* **2012**, *1234*, 32−37.

(11) Rezazadeh, M.; Yamini, Y.; Seidi, S.; Esrafili, A. Pulsed Electromembrane Extraction: A New Concept of Electrically Enhanced Extraction. *J. Chromatogr. A* **2012**, *1262*, 214−218.

(12) Rezazadeh, M.; Yamini, Y.; Seidi, S.; Esrafili, A. One-Way and Two-Way Pulsed Electromembrane Extraction for Trace Analysis of Amino Acids in Foods and Biological Samples. *Anal. Chim. Acta* **2012**, *773*, 52−59.

(13) Arjomandi-Behzad, L.; Yamini, Y.; Rezazadeh, M. Pulsed Electromembrane Method for Simultaneous Extraction of Drugs with Different Properties. *Anal. Biochem.* **2013**, *438*, 136−143.

(14) Hasheminasab, K. S.; Fakhari, A. R.; Shahsavani, A.; Ahmar, H. A New Method for the Enhancement of Electromembrane Extraction Efficiency Using Carbon Nanotube Reinforced Hollow Fiber for the Determination of Acidic Drugs in Spiked Plasma, Urine, Breast Milk and Wastewater Samples. *J. Chromatogr. A* **2013**, *1285*, 1−6.

(15) Hasheminasab, K. S.; Fakhari, A. R. Development and Application of Carbon Nanotubes Assisted Electromembrane Extraction (CNTs/EME) for the Determination of Buprenorphine as a Model of Basic Drugs from Urine Samples. *Anal. Chim. Acta* **2013**, *767*, 75−80.

(16) Petersen, N. J.; Jensen, H.; Hansen, S. H.; Rasmussen, K. E.; Pedersen-Bjergaard, S. Drop-to-Drop Microextraction Across a Supported Liquid Membrane by an Electrical Field Under Stagnant Conditions. *J. Chromatogr. A* **2009**, *1216*, 1496−1502.

(17) Petersen, N. J.; Jensen, H.; Hansen, S. H.; Foss, S. T.; Snakenborg, D.; Pedersen-Bjergaard, S. On-Chip Electro Membrane Extraction. *Microfluid. Nanofluid.* **2010**, *9*, 881−888.

(18) Petersen, N. J.; Foss, S. T.; Jensen, H.; Hansen, S. H.; Skonberg, C.; Snakenborg, D.; Kutter, J. P.; Pedersen-Bjergaard, S. On-Chip Electro Membrane Extraction with Online Ultraviolet and Mass Spectrometric Detection. *Anal. Chem.* **2011**, *83*, 44−51.

(19) Petersen, N. J.; Pedersen, J. S.; Poulsen, N. N.; Jensen, H.; Skonberg, C.; Hansen, S. H.; Pedersen-Bjergaard, S. On-Chip Electromembrane Extraction for Monitoring Drug Metabolism in Real Time by Electrospray Ionization Mass Spectrometry. *Analyst* **2012**, *137*, 3321−3327.

(20) Hosseiny Davarani, S. S.; Morteza-Najarian, A.; Nojavan, S.; Pourahadi, A.; Beigzadeh Abbassi, M. Two-Phase Electromembrane

Extraction Followed by Gas Chromatography-Mass Spectrometry Analysis. *J. Sep. Sci.* **2013**, *36*, 736−743.
(21) Gjelstad, A.; Jensen, H.; Rasmussen, K. E.; Pedersen-Bjergaard, S. Kinetic Aspects of Hollow Fiber Liquid-Phase Microextraction and Electromembrane Extraction. *Anal. Chim. Acta* **2012**, *742*, 10−16.
(22) Guo, L.; Lee, H. K. Electro Membrane Extraction Followed by Low-Density Solvent Based Ultrasound-Assisted Emulsification Microextraction Combined with Derivatization for Determining Chlorophenols and Analysis by Gas Chromatography−Mass Spectrometry. *J. Chromatogr. A* **2012**, *1243*, 14−22.
(23) Seidi, S.; Yamini, Y.; Rezazadeh, M. Combination of Electromembrane Extraction with Dispersive Liquid−Liquid Microextraction Followed by Gas Chromatographic Analysis as a Fast and Sensitive Technique for Determination of Tricyclic Antidepressants. *J. Chromatogr. B* **2013**, *913*−*914*, 138−146.
(24) Rezazadeh, M.; Yamini, Y.; Seidi, S.; Ebrahimpor, B. Electromembrane Surrounded Solid Phase Microextraction: A Novel Approach for Efficient Extraction from Complicated Matrices. *J. Chromatogr. A* **2013**, *1280*, 16−22.
(25) Box, G. E. P.; Wilson, K. B. On the Experimental Attainment of Optimum Conditions. *J. R. Stat. Soc.: Ser. B* **1951**, *13*, 1−45.
(26) Bailey, J. J. Determination of Aliphatic and Aromatic Acids by Pyrolysis of Their Tetramethylammonium Salts. *Anal. Chem.* **1967**, *39*, 1485−1489.
(27) Schwarze, J. W.; Gilmour, M. N. Gas-Chromatographic Determination of C1 to C7 Monocarboxylic Acids and Lactic Acid by Pyrolysis of the Tetrabutyl Ammonium Salts. *Anal. Chem.* **1969**, *41*, 1686−1687.
(28) Balchen, M.; Gjelstad, A.; Rasmussen, K. E.; Pedersen-Bjergaard, S. Electrokinetic Migration of Acidic Drugs Across a Supported Liquid Membrane. *J. Chromatogr. A* **2007**, *1152*, 220−225.
(29) Tabani, H.; Fakhari, A. R.; Zand, E. Low-Voltage Electromembrane Extraction Combined with Cyclodextrin Modified Capillary Electrophoresis for the Determination of Phenoxy Acid Herbicides in Environmental Samples. *Anal. Methods* **2013**, *5*, 1548−1555.
(30) Rodriguez, I.; Rubi, E.; Gonzalez, R.; Quintana, J. B.; Cela, R. On-Fibre Silylation Following Solid-Phase Microextraction for the Determination of Acidic Herbicides in Water Samples by Gas Chromatography. *Anal. Chim. Acta* **2005**, *537*, 259−266.
(31) Tabani, H.; Fakhari, A. R.; Shahsavani, A.; Behbahani, M.; Salarian, M.; Bagheri, A.; Nojavan, S. Combination of Graphene Oxide-Based Solid Phase Extraction and Electromembrane Extraction for the Preconcentration of Chlorophenoxy Acid Herbicides in Environmental Samples. *J Chromatogr. A* **2013**, *1300*, 227−235.
(32) Pereiro, I. R.; Irimia, R. G.; Cano, E. R.; Tottijos, R. C. Optimisation of a Gas Chromatographic−Mass Spectrometric Method for the Determination of Phenoxy Acid Herbicides in Water Samples as Silyl Derivatives. *Anal. Chim. Acta* **2004**, *524*, 249−256.

Table 1. Central Composite Experimental Design in Coded and Actual Levels of Variables and the Response Functions

	2,4-D		α-NAA		Kn			
experiment number	coded level (x_1)	actual level (X_1)	coded level (x_2)	actual level (X_2)	coded level (x_3)	actual level (X_3)	biomass (g L^{-1} DW, Y_1)	TI content (mg/g of DW, Y_2)
1	−1.000	0.500	1.000	1.500	1.000	0.150	58.90	31.23
2	0.000	1.000	0.000	1.000	0.000	0.100	61.90	37.53
3	0.000	1.000	0.000	1.000	0.000	0.100	60.80	37.98
4	0.000	1.000	0.000	1.000	0.000	0.100	62.20	37.33
5	0.000	1.000	0.000	1.000	0.000	0.100	60.40	37.21
6	−1.000	0.500	−1.000	0.500	−1.000	0.050	55.34	33.18
7	−1.000	0.500	−1.000	0.500	1.000	0.150	48.13	23.30
8	1.000	1.500	−1.000	0.500	1.000	0.150	49.83	23.70
9	1.000	1.500	1.000	1.500	1.000	0.150	63.56	39.00
10	0.000	1.000	0.000	1.000	1.682	0.184	54.16	28.20
11	0.000	1.000	0.000	1.000	0.000	0.100	61.90	38.10
12	1.682	1.841	0.000	1.000	0.000	0.100	57.24	30.00
13	−1.000	0.500	1.000	1.500	−1.000	0.050	51.70	24.90
14	0.000	1.000	−1.682	0.159	0.000	0.100	59.27	32.43
15	1.000	1.500	1.000	1.500	−1.000	0.050	56.87	31.00
16	0.000	1.000	1.682	1.841	0.000	0.100	55.17	29.50
17	0.000	1.000	0.000	1.000	0.000	0.100	60.80	38.12
18	−1.682	0.159	0.000	1.000	0.000	0.100	47.15	24.20
19	1.000	1.500	−1.000	0.500	−1.000	0.050	54.87	33.98
20	0.000	1.000	0.000	1.000	−1.682	0.016	49.67	26.23

suspension cultures of *Glycine max* to maximize isoflavone production using RSM. In the present study, RSM was employed to optimize a proper medium for biomass and isoflavone content in *G. max* cell suspension culture.

MATERIALS AND METHODS

Chemicals. All of the isoflavone standards (daidzein, genistein, and glycitein), PGRs [2,4-dichlorophenoxyacetic acid (2,4-D), 1-naphthalene acetic acid (α-NAA), and kinetin (Kn)], and fluorescein diacetate (FDA) used in the present study were purchased from Sigma-Aldrich, St. Louis, MO. High-performance liquid chromatography (HPLC)-grade solvents were obtained from Sisco Research Laboratories (SRL, Mumbai, India). Sucrose and agar were obtained from Himedia Lab (Mumbai, India). All other analytical-grade chemicals were obtained from Merck (Darmstadt, Germany).

Plant Material and Surface Sterilization. Seeds of cv. JS 335 of *G. max* were collected from AICRP, Soybean, GKVK campus, Bangalore, India. Uniform size soybean seeds were handpicked, surface-sterilized, germinated, and maintained using a standardized protocol.[24] Seeds were surface-sterilized using 70% (v/v) ethanol for 30 s, followed by 0.2% (w/v) carbendazium for 5 min and 0.1% (w/v) mercuric chloride for 1 min. The surface-sterilized seeds were rinsed 3 times in sterile distilled water and then cultured in Petri dishes containing Murashige and Skoog (MS) basal medium[25] for the germination. The medium pH was set up to 5.8 and then autoclaved at 121 °C for 20 min. The cultures were maintained at a light intensity of 57 μmol m^{-2} s^{-1} (illumination supplied by cool-white fluorescent tubes) with a 16 h photoperiod at 25 ± 2 °C.

Callus and Cell Suspension Culture and Initiation. The 3-week-old *in vitro* germinated seedlings were used as a source of explants for initiation of callus cultures. Cotyledonary nodal leaves were incised into small pieces (9−10 mm) and aseptically transferred to callus induction medium containing full-strength MS solid medium supplemented with 3% sucrose, 0.8% (w/v) agar, and different concentrations of three variables (2,4-D, α-NAA, and Kn), as mentioned in Table 1. The media pH was adjusted to 5.7 before autoclaving (121 °C and 1.2 kg/cm^2 pressure for 20 min). Cultures were routinely subcultured every 3 weeks, and further, the suspension cultures were initiated from friable callus. For this, the callus cultures were propagated in 150 mL Erlenmeyer flasks containing 40 mL of MS liquid medium supplemented with three different variables and 3% sucrose. Cultures were incubated on a rotary shaker at 100 rpm with a 16 h light/8 h dark photoperiod at 26 ± 1 °C. Cell suspension cultures were established uniformly after 8−10 passages, and then regular subcultures were performed by transferring a packed cell volume (PCV) of cells to fresh medium with 2 week intervals. All experiments had at least three replicates, and each growth regulator combination treatment was repeated 3 times.

Growth Parameters. To analyze biomass, the cell growth was measured as dry weight (dw) basis. Cells were harvested by filtration after 18 days of inoculation (three flasks per treatment) and then recovered from the filter paper (Whatmann No. 1) after washing 3 times with distilled water. The dry weight was measured after drying the fresh cell mass in an oven at 45 ± 2 °C until it reached a constant weight, and thus, fresh weight (fw) and dw of cells were estimated. Growth of cells was determined using the growth index (GI) using the following formula on a dw basis:

$$\mathrm{GI} = \frac{\text{final weight of biomass} - \text{initial weight of biomass}}{\text{initial weight of biomass}}$$

Microscopic Observations. To determine the viability of cells, 10 mL of suspension culture was incubated for 15 min with 30 μM FDA at 1 mg/mL stock in dimethyl sulfoxide (DMSO). The extracellular fluorescence in the cells was discolored by 10 volumes of fresh medium followed by resuspension by fresh culture medium. Dye loaded with live cells was monitored in fluorescence microscopy using an Olympus BX 51 (Japan) microscope equipped with camera ProResC5 and an ultraviolet (UV) light source.

Isoflavone Extraction. The soybean-powdered sample (400 mg) from each treatment was finely ground and extracted with 2 mL of concentrated HCl and 10 mL of ethanol for 2 h in a boiling water bath using a standard method,[26] which relies on acid hydrolysis of 12 endogenous isoflavone isomers to their respective aglycone forms. The resulting suspensions were cooled and centrifuged at 111800*g* for 10 min, and further, the supernatant was filtered through a syringe filter (Whatman 0.5 μm, 13 mm diameter).

Chromatographic Conditions. The HPLC analysis of isoflavones in extracts was performed using a Shimadzu chromatograph (LC 10-AS HPLC), equipped with dual pump, UV detector (SPD 10A), and a C-18 silica column (Sunfire; 5 μm, with dimensions of 250 × 4.6 mm). The isoflavone separation and its elution were employed by a binary gradient mode,[12] and the chromatographic conditions were followed as mentioned in the earlier publication.[12]

Isoflavone Standards. All three isoflavone standards were identified by their retention times and co-chromatography with standard compounds. The relative individual isoflavone concentration in the sample was calculated manually on the basis of each peak area. Individual isoflavone concentrations were expressed as micrograms per gram on a dw basis. A mixture of the standards was analyzed, and the total isoflavone (TI) concentration was the sum of aglycones (daidzein, glycitein, and genistein).[27]

Optimization of Isoflavones and Biomass Using RSM. *Central Composite Design (CCD) and RSM.* RSM is a combination of mathematical and statistical techniques useful for empirical model building and search optimum conditions of factors for desirable responses. The natural response surface in the optimum region was illustrated by performing a Box−Behnken and CCD.[19,28] CCD was employed to study the interaction of process variables, and the optimum process condition for biomass and TI content was obtained by applying RSM.[21,29] Statistical analysis was implemented using a linear regression model in the SPSS software.

The experimental design was constructed using a five-level, three-factor variable, and second-order CCD with five replications on the center points (0, 0, and 0) in coded levels of variables (−1.682, −1, 0, 1, and 1.682).[28,29] The total number of experiments was 20 with two replications to evaluate error. The three independent variables for biomass (Y_1) and TI (Y_2) content responses were concentrations of 2,4-D (X_1), α-NAA (X_2), and Kn (X_3). The experimental design in the actual (X) and coded (x) levels of variables was represented in Table 1. A second-degree polynomial with linear, quadratic, and interaction effects (in the coded level of variables) by the method of least-squares represents the response functions (y_{ijk}) of biomass and TI content in the cell suspension culture denoted in the following equation:

$$y_{ijk} = b_0 + \sum_{i=1}^{n} b_i x_i + \sum_{i=1,i\le j}^{n} \sum_{j=1,i\le j}^{n} b_{ij} x_i x_j + \varepsilon_{ijk}$$

The numbers for variables represented by n and i, j, and k are integers. The coefficients of the polynomials are denoted by b_0, b_i, and b_{ij}, and ε_{ijk} is the random error. When $i < j$, b_{ij} represents the interaction effects of the variables x_i and x_j. The response surface graphs are obtained from the regression equations in the actual level of variables, keeping the response function on the z axis, with x and y axes representing the two independent variables while keeping the other variable (third) constant at its center (corresponding to the 0 level in coded level) points. To assess the empirical model in a statistical manner, analysis of variance (ANOVA) was carried out using software SPSS version 17.0 (SPSS Inc., Chicago, IL) at the level of $p < 0.05$. The efficiency of the polynomial model equation was calculated by means of the coefficient of correlation (R), and its statistical significance was evaluated by the F test. When detailed ANOVA was performed in the coded level of variables, the effects of individual variables were identified. Stepwise deletion of individual non-significant ($p < 0.10$) terms was performed, followed by recalculation of the coefficients of the TI regression equation, to attain the final regression equation in the coded level, which was further converted to the actual level of variables.

Optimization Conditions. Canonical analysis[28] was employed to analyze the optimal conditions, in which the levels of control variables (x_1, x_2, and x_3) (within the experimental range) were determined to obtain the maximum yield of biomass and TI production individually. Stationary points in the response surface were defined by the translation and rotation of the response function (y_k),[19] the axes of which correspond toward the principal axes of the contour system. Moreover, the roots (λ_1, λ_2, and λ_3) of the auxiliary equation ($\lambda^2 - \lambda + 1 = 0$) were calculated initially to know the optimum nature. If all of the roots have negative values, the response function is maximal and vice versa. The stationary point was defined as a saddle point, if the roots have positive and negative values,[19] and when the contours are superimposed, the optimum levels of the variables are further attained.

RESULTS AND DISCUSSION

Despite the fact that phytoalexins (daidzein and genistein) were released only under stress conditions, enhancing their level in *in vitro* cultures could be achieved by the elicitation approach. In the preliminary screening experiments, various concentrations of PGRs [2,4-D, α-NAA, indole-3-acetic acid (IAA), and indole-3-butyric acid (IBA)] with a single concentration of Kn were treated in *G. max* cell suspension cultures. Interestingly, we found that the α-NAA and Kn combination improved the isoflavone content but biomass was better with 2,4-D and Kn (data not shown). However, optimization of selective media with enriched cell growth and bioactive content is laborious and time-consuming, as suggested by various researchers.[21,22] As a result, the PGRs, such as 2,4-D, α-NAA, and Kn, were selected for statistical optimization studies by employing RSM for the first time. In the present study, optimization of the medium constituents for increased production of the isoflavone content with profound biomass in *G. max* suspension cultures was achieved. In the same way, this RSM technique has been applied successfully nowadays in many biotechnological and biochemical studies, such as *in vitro* growth characteristics of *Centella asiatica*,[30] β-carotene in *D. carota*,[22] lycopene from suspension cultures of *L. esculantum*,[23] micropropagation of *Dianthus caryophyllus*,[31] and isoflavone extraction from *G. max*,[29,32] respectively.

The results on the TI content in the present investigation demonstrated daidzein as a major component (63%), followed by genistein (30%) and glycitein (7%), and TI was not detected in the spent media. The outcome of three independent variables (concentrations of 2,4-D, α-NAA, and Kn) on the response functions Y_1 and Y_2 was summarized in Table 1. The results on the ANOVA (in the coded level of variables) are shown in Table 2 for all three response functions. The roots (λ_1, λ_2, and λ_3) of the auxiliary equation of isoflavone and biomass are calculated and depicted in Table 3. The three-dimensional and contour plots represented in Figures 1 and 2 aid in envisaging the consequence

Table 2. ANOVA for the Biomass (Y_1) and TI Content (Y_2) in the Coded Level of Variables[a]

source of variation	coefficient of the polynomial for Y_1	F value	coefficient of the polynomial for Y_2	F value
constant	61.283		37.642	
x_1	2.052	7.22[b]	1.818	11.0625[c]
x_2	1.169	2.349 (NS)[d]	0.516	0.889 (NS)
x_3	0.673	0.776 (NS)	−0.184	0.113 (NS)
x_1^2	−2.897	11.744[c]	−3.293	28.717[c]
x_2^2	−1.124	0.636 (NS)	−1.927	6.415[b]
x_3^2	−2.996	12.77[c]	−3.252	27.823[c]
x_1x_2	1.075	1.160 (NS)	1.584	4.919[e]
x_1x_3	0.208	0.0431 (NS)	0.159	0.049 (NS)
x_2x_3	3.267	10.72[c]	4.311	36.453[c]
TLE		3.445[e]		4.022[b]
TQE		9.7411[c]		25.094[c]
TIE		3.9748[b]		13.807[c]
R	0.915		0.963	

[a] x_1, concentration of 2,4-D (mg/L); x_2, concentration of α-NAA (mg/L); x_3, concentration of Kn (mg/L); TLE, total linear effect; TQE, total quadratic effect; and TIE, total interaction effect. [b] Significant at $p \le 0.05$. [c] Significant at $p \le 0.01$. [d] NS = non-significant at $p \le 0.10$. [e] Significant at $p \le 0.10$.

dx.doi.org/10.1021/jf500207x | J. Agric. Food Chem. 2014, 62, 3143−3149

Table 3. Results of the Optimization Study

parameters		biomass, Y_1	TI content, Y_2
roots of the auxiliary equation	λ_1	−5.794	−3.293
	λ_2	−0.35	−0.66
	λ_3	−7.87	−9.68
optimum conditions in the coded level	x_1	2.218	0.67
	x_2	9.055	1.537
	x_3	5.126	1.00
optimum conditions in the actual level	x_1	2.109	1.335
	x_2	5.527	1.768
	x_3	0.356	0.15
optimized level of the response function		70.6	38.59

of three independent variables on response functions generated by the regression equation.

Biomass. The biomass (Y_1) content in suspension cultures for the 20 experiments is shown in Table 1. An extensive variation in the content ranged from 47.15 to 63.56 g/L on a dw basis upon the variable conditions. Plots were designed for each pair of variables, while the third variable was considered as a constant at the middle level. The consequence of 2,4-D and α-NAA on biomass with Kn as the constant value in soybean cell suspension cultures was illustrated in Figure 1a. Similarly, Figure 1b represented the influence of 2,4-D and Kn with α-NAA as a constant value on biomass in cell cultures. Besides, the effect of α-NAA and Kn with 2,4-D as a constant value on the biomass was depicted in Figure 1c.

Fitness of the second-order polynomial to predict biomass in independent variable terms was put in view by the high correlation coefficient (R = 0.915; $p \leq 0.01$) value (Table 2). Amid the variables, the total quadratic effect (significant at $p \leq 0.01$) predominates over the total interactive effect ($p \leq 0.05$) and linear effect ($p \leq 0.1$). The effect of 2,4-D on the yield of biomass has a significant effect ($p \leq 0.05$) on the individual variables, while α-NAA and Kn have no significant results (Table 2). The individual quadratic effects of "2,4-D" and "Kn" variables are significant ($p \leq 0.01$), and α-NAA has no significant results. Nevertheless, interactive effects of α-NAA and Kn concentrations have a predominant effect on the yield of biomass ($p \leq$

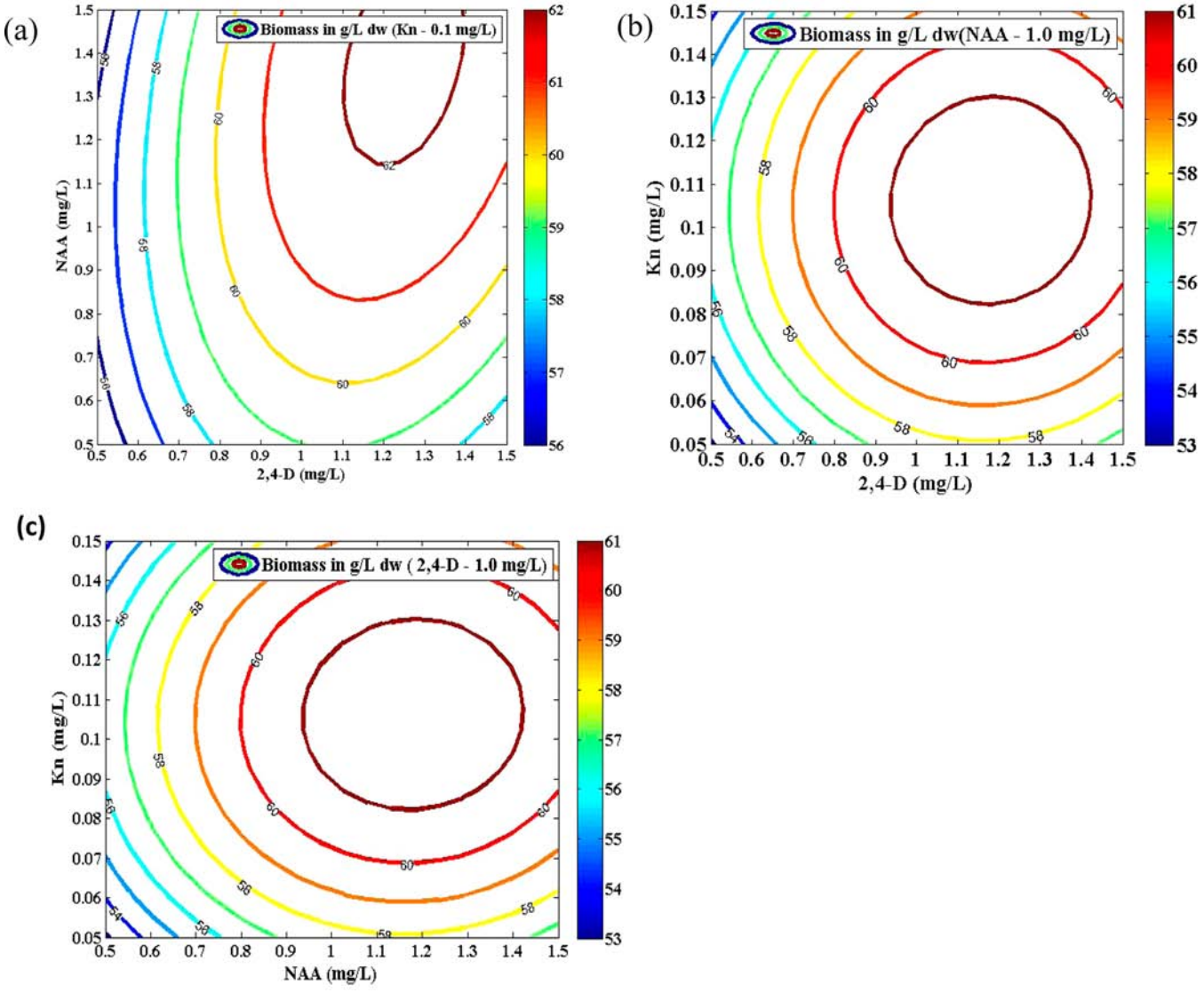

Figure 1. Contour plots for the effects of variables on biomass (Y_1) in the cell suspension cultures of *G. max*: (a) Kn as a constant value of 0.1 mg/L, (b) α-NAA as a constant value of 1.0 mg/L, and (c) 2,4-D as a constant value of 1.0 mg/L.

dx.doi.org/10.1021/jf500207x | *J. Agric. Food Chem.* 2014, 62, 3143−3149

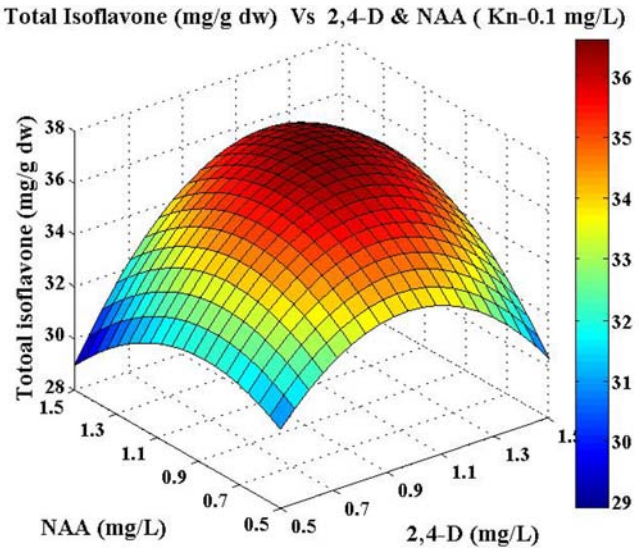

Figure 2. Response surface for the effects of variables on the total isoflavones (Y_2) in the cell suspension cultures of *G. max* with Kn as a constant value of 0.1 mg/L.

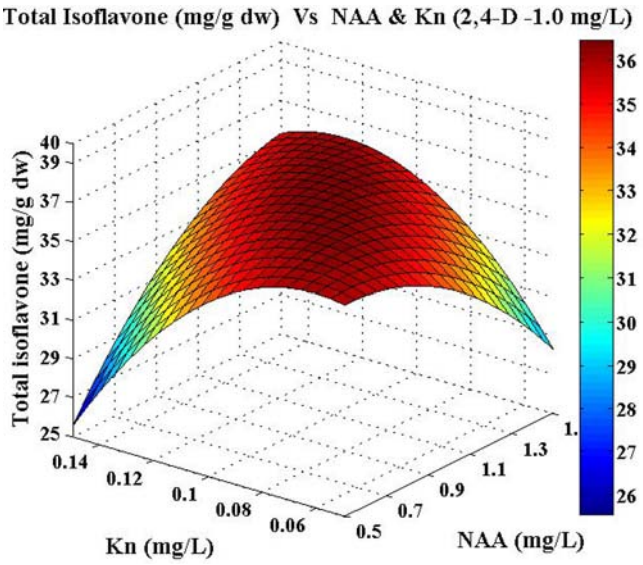

Figure 4. Response surface for the effects of variables on the TI (Y_2) in the cell suspension cultures of *G. max* with 2,4-D as a constant value of 1.0 mg/L.

0.01), while there is no significant effect of the interaction among 2,4-D−α-NAA and 2,4-D−Kn.

TI Content. The TI content (Y_2) ranged from 23.30 to 39 mg/g of dw with respect to the experimental conditions illustrated in Table 1. In Figure 2, the results of 2,4-D and α-NAA on TI with Kn as the constant value in soybean cell suspension cultures were depicted as response surface. Correspondingly, the influence of 2,4-D and Kn with α-NAA as a constant value on the TI content in cell cultures was shown in Figure 3. The effect of α-NAA and Kn with 2,4-D as a constant value on the TI was portrayed in Figure 4.

TI content in the proposed model depicted a high multiple correlation coefficient (R = 0.963;$p \leq 0.01$), pointing out the aptness of the second-order polynomial to calculate the Y_2 values of three independent variables (Table 2). With these variables,

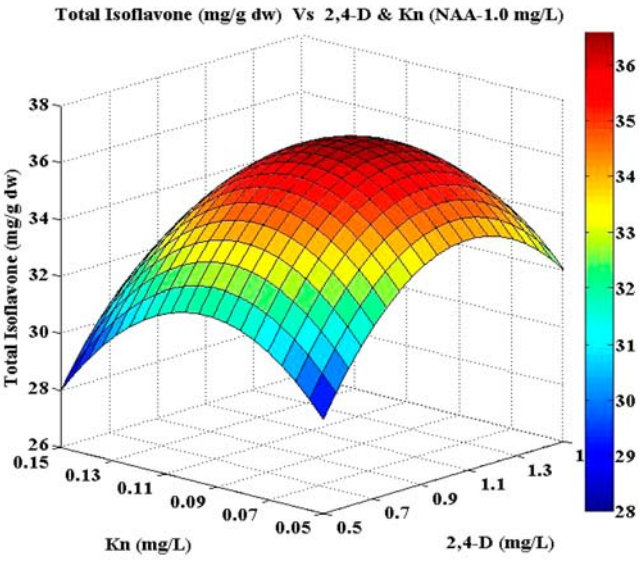

Figure 3. Response surface for the effects of variables on the TI (Y_2) in the cell suspension cultures of *G. max* with α-NAA as a constant value of 1.0 mg/L.

total quadratic and interactive effects ($p \leq 0.01$) dominate over the linear effects ($p \leq 0.05$) and the interaction among α-NAA and Kn is significant in comparison to 2,4-D and α-NAA. There are significant individual quadratic effects for 2,4-D and Kn ($p \leq 0.01$), followed by α-NAA ($p \leq 0.05$).

Optimization. The optimization process for maximizing biomass (Y_1) and TI content (Y_2) was conducted separately. The roots (λ_1, λ_2, and λ_3) of the auxiliary equation were shown in Table 3. However, the roots of the auxiliary equation for biomass and TI content indicate (negative values) maximization of the response function. For this reason, the canonical test was applied and the optimum conditions in coded and actual levels of variables were obtained (Table 3). Consequently, the maximum value for the yield of biomass is 70.62 g/L dw, and the maximum TI content is 38.59 mg/g of dw. The predicted optimized levels for all three variables are represented in Table 3 for production of biomass and TI content confirmed experimentally. By optimization, we achieved 38.59 mg/g of dw of isoflavones in JS 335, which was approximately 37 times greater than that of the field-grown greenhouse soybean plants, along with 7% of biomass as dry matter.

It is noteworthy to find a region with a "sweet spot" for multiple responses, which could be accomplished by superimposing the contours. The superimposed contour plot for optimization of Y_1 and Y_2 was given in Figure 5. The effect of x_1, x_2, and x_3 terms on Y_1 and Y_2 is positive. The optimum value of x_1 is between 1.33 and 2.10 mg/L, specifically at an average of 1.72 mg/L for x_1. The optimum value for x_2 is between 1.76 and 5.52 mg/L, which is at an average of 3.64 mg/L for x_2. The optimum value for x_3 is between 0.35 and 0.15, which is at an average of 0.25 mg/L for x_3. The contour plots against x_1 (α-NAA) and x_3 (Kn) constructed independently and later on superimposed (Figure 5) were used to identify the levels of the two variables. Moreover, the optimum conditions for the responses were found from the superimposed graph. At this point, we preferred a value of biomass to be more than 65 g/L dw and TI production to be more than 30 g/L dw (Figure 5). The optimum region was depicted obviously as the hatched zone in Figure 5. The results obtained by superimposition were validated (TI, 37.34 mg/g of

dx.doi.org/10.1021/jf500207x | J. Agric. Food Chem. 2014, 62, 3143−3149

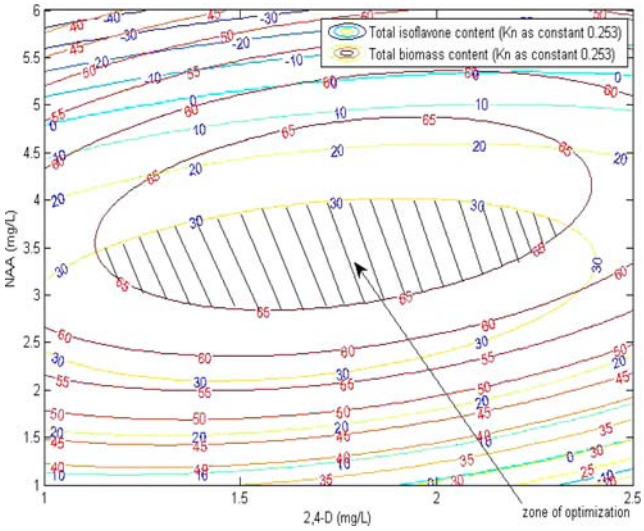

Figure 5. Superimposed contour plots with the optimized region of the responses.

dw; biomass, 67.83 g/L dw), in which callus formed in the optimized medium was found to be friable, soft, and pale greenish brown, and the same was used for the cell suspension culture initiation (Figure 6) and analysis of the responses.

Figure 6. *G. max in vitro* cultures on the MS medium with optimized concentrations of 1.72 mg/L 2,4-D, 3.64 mg/L α-NAA, and 0.25 mg/L Kn: (a) cell suspension cultures in shake flasks, (b) cell suspension cultures in round-bottom- and cylindrical-shaped flasks, and (c) FDA staining of cell suspension cultures for confirmation of viability (bar = 124 μm).

Microscopic Observation. Also, the viability of cells was confirmed by staining with FDA, followed by visualization under fluorescence microscopy. Microscopic observations of cell suspension cultures showed fluorescence yellow for viable cells (Figure 6).

In the present study, the daidzein content was more in cell suspension cultures compared to genistein and glycitein. However, in seeds of soybean, genistein levels are reported to be high.[7] Still, the results were consistent with the earlier reports of *in vitro* cultures of soybean,[3,16] which show the predominant production of daidzein than that of genistein. Similarly, the interactive effects of α-NAA and Kn concentrations positively influenced the biomass yield; however, no such effect was found for 2,4-D−α-NAA and 2,4-D−Kn. Significant individual quadratic effects were found for 2,4-D and Kn ($p \leq 0.01$). This in correspondence with earlier reports[31] in *D. caryophyllus* L., in which optimization of PGRs and $AgNO_3$ using RSM exhibited better callus growth with a high concentration of α-NAA. However, the results, in contrast with earlier reports of soybean cell cultures,[3] show that 2,4-D influences the biomass as well as isoflavone content. In *C. asiatica* cell suspension cultures, RSM applied for the optimization of sucrose, IAA, and 6-benzylaminopurine (BAP) and results revealed sucrose as a prime factor for cell growth.[30] Several studies found the significance of applying RSM.[22] RSM was used for the optimization of basal media components (sucrose, nitrogen, and phosphorus) for maximum production of β-carotene from *D. carota* cells. In addition, a 3.7-fold increase in lycopene production was observed by optimizing several lycopene extraction parameters in *L. esculentum* cell cultures.[23] To maximize the isoflavone content using RSM, acid hydrolysis conditions in soybean hypocotyls[32] and ethanol extraction and purification in soybean sprouts[29] were optimized. Biomass (7% dw) achieved in the study is considered as high for secondary metabolite production in plants. This result is in agreement with the earlier study[3] that high producing soybean cultivar strains contained a significant level of isoflavones. As a part of optimization, we obtained 37.34 mg/g of dw of isoflavones.

Because large-scale production of isoflavones for therapeutic and commercial purposes could not be achieved by natural sources, the development of cell culture technology has had a great scope in recent years.[5] Besides, various factors influenced the stimulation of isoflavone synthesis, such as manipulation of the basal nutrient medium components, physical factors, and PGRs.[33] Although there are several reports that dealt with media components, there is none on the optimization of PGRs and the same is essential before performing elicitation, precursor feeding, and biotransformation and bioreactor studies. It was hypothesized that, in most of the Fabaceae plants, 2,4-D and Kn combination was selected best for both cell growth and isoflavone content,[3,15] while its mechanism in the biosynthetic pathway is still not understood.[33] Nevertheless, a rather interesting feature in the present study was α-NAA having a more predominant role than 2,4-D.

Furthermore, as suggested by earlier reports, the isoflavone content varies with the genotype of the species.[3,16,18] Nonetheless, it could be hypothesized that variability in isoflavone composition observed within the cell suspension compared to seeds[7] might be due to the effect of PGRs on metabolic pathways (differentiation), somaclonal variation,[3] or differential gene expression. However, it was obvious that *in vitro* plant tissues represent a high level of variability in the gene expression pattern.[34] Moreover, the isoflavone pathway is one of the most complex metabolic pathways involved in plants,[11] elicited by several stress agents.[16] Overall, the optimization studies using RSM augmented the isoflavone content as well as biomass.

It is evident from the study that RSM is a reliable experimental tool, not only achieving optimized media with pronounced biomass and isoflavone content but also simplifing the time course of experiments. Results also suggested that soybean cell suspension cultures could be used as a fascinating model system for augmenting isoflavones. In future, research efforts pertaining to elicitation, scale up in bioreactors, selection of high producing cell lines, and mechanism of isoflavone biosynthesis in cell suspension cultures could be attempted to assess the possibility of an enhancement strategy with a prospective value in the nutraceutical viewpoint.

AUTHOR INFORMATION

Corresponding Author

*Telephone: +91-821-2516501. Fax: +91-821-2517233. E-mail: parvatamg@yahoo.com.

Funding

M. K. Akitha Devi is thankful to Council for Scientific and Industrial Research (CSIR), New Delhi, India, for her fellowship.

Notes

The authors declare no competing financial interest.

■ ACKNOWLEDGMENTS

The authors thank R. Manikantan, Scientist, Council for Scientific and Industrial Research–National Aerospace Laboratories (CSIR–NAL), Bangalore, India, for his support in designing the RSM experiment and analysis and Dr. K. Udayashankar, Chief Scientist, CSIR-CFTRI, Mysore, for his support in data interpretation.

■ REFERENCES

(1) Hussain, M. S.; Fareed, S.; Ansari, S.; Rahman, M. A.; Ahmad, I. Z.; Saeed, M. Current approaches toward production of secondary plant metabolites. *J. Pharm. Bioanal. Sci.* **2012**, *4*, 10–20.

(2) Verpoorte, R.; Johan, M. Engineering secondary metabolite production in plants. *Curr. Opin. Biotechnol.* **2002**, *13*, 181–187.

(3) Federici, E.; Touche, A.; Choquart, S.; Avanti, O.; Fay, L.; Offord, E.; Courtois, D. High isoflavone content and estrogenic activity of 25 year-old *Glycine max* tissue cultures. *Phytochemistry* **2003**, *64*, 717–724.

(4) Roberts, S. C. Production and engineering of terpenoids in plant cell culture. *Nat. Chem. Biol.* **2007**, *3*, 387–395.

(5) Huang, T. K.; McDonald, K. A. Bioreactor systems for *in vitro* production of foreign proteins using plant cell cultures. *Biotechnol. Adv.* **2012**, *30*, 398–409.

(6) Wilson, S. A.; Roberts, S. C. Recent advances towards development and commercialization of plant cell culture processes for the synthesis of biomolecules. *Plant Biotechnol. J.* **2012**, *10*, 249–268.

(7) Sakthivelu, G.; Akitha Devi, M. K.; Giridhar, P.; Rajasekaran, T.; Ravishankar, G. A.; Nikolova, M. T.; Angelov, G. B.; Todorova, R. M.; Kosturkova, G. P. Isoflavone composition, phenol content, and antioxidant activity of soybean seeds from India and Bulgaria. *J. Agric. Food Chem.* **2008**, *56*, 2090–2095.

(8) Akitha Devi, M. K.; Gondi, M.; Sakthivelu, G.; Giridhar, T.; Rajasekaran, T.; Ravishankar, G. A. Functional attributes of soybean seeds and products, with reference to isoflavone content and antioxidant activity. *Food Chem.* **2009**, *114*, 771–776.

(9) Qian, Y.; Guan, T.; Huang, M.; Cao, L.; Li, Y.; Cheng, H.; Jin, H.; Yu, D. Neuroprotection by the soy isoflavone, genistein, via inhibition of mitochondria-dependent apoptosis pathways and reactive oxygen induced-NF-κB activation in a cerebral ischemia mouse model. *Neurochem. Int.* **2012**, *60*, 759–767.

(10) Dixon, R. A. Natural products and plant disease resistance. *Nature* **2001**, *411*, 843–847.

(11) Yu, O.; Shi, J.; Hession, A. O.; Maxwell, C. A.; McGonigle, B.; Odell, J. T. Metabolic engineering to increase isoflavone biosynthesis in soybean seed. *Phytochemistry* **2003**, *63*, 753–763.

(12) Akitha Devi, M. K.; Giridhar, P. Variations in physiological response, lipid peroxidation, antioxidant enzymes activities, proline and isoflavones content in soybean varieties subjected to drought stress. *Proc. Natl. Acad. Sci., India, Sect. B* **2013**, DOI: 10.1007/s40011-013-0244-0.

(13) Gutierrez-Gonzalez, J. J.; Guttikonda, S. K.; Tran, L. S.; Aldrich, D. L.; Zhong, R.; Yu, O.; Nguyen, H. T.; Sleper, D. A. Differential expression of isoflavone biosynthetic genes in soybean during water deficits. *Plant Cell Physiol.* **2010**, *51*, 936–948.

(14) Cloutier, M.; Bouchard-Marchand, E.; Perrier, M.; Jolicoeur, M. A predictive nutritional model for plant cells and hairy roots. *Biotechnol. Bioeng.* **2008**, *99*, 189–200.

(15) Fedoreyev, S. A.; Pokushalova, T. V.; Veselova, M. V.; Glebko, L. I.; Kulesh, N. I.; Muzarok, T. I.; Seletskaya, L. D.; Bulgakov, V. P.; Zhuravlev, Y. N. Isoflavonoid production by callus cultures of *Maackia amurensis*. *Fitoterapia* **2000**, *71*, 365–372.

(16) Gueven, A.; Knorr, D. Isoflavonoid production by soy plant callus suspension culture. *J. Food Eng.* **2011**, *103*, 237–243.

(17) Luczkiewicz, M.; Glod, D. Callus culture of *Genista* plants—*In vitro* material producing high amounts of isoflavones of phytoestrogenic activity. *Plant. Sci.* **2003**, *165*, 1101–1108.

(18) Shinde, A. N.; Malpathak, N.; Fulzele, D. P. Enhanced production of phytoestrogenic isoflavones from hairy root cultures of *Psoralea corylifolia* L. using elicitation and precursor feeding. *Biotechnol. Bioprocess Eng.* **2009**, *14*, 288–294.

(19) Myers, R. H.; Montgomery, D. C.; Anderson-Cook, C. M. *Response Surface Methodology: Product and Process Optimization Using Designed Experiments*, 3rd ed.; John Wiley and Sons: Hoboken, NJ, 2009.

(20) Li, Y. L.; Fang, Z. X.; You, J. Application of Box–Behnken experimental design to optimize the extraction of insecticidal Cry1Ac from soil. *J. Agric. Food Chem.* **2013**, *61*, 1464–1470.

(21) Kathiresan, S.; Sarada, R.; Bhattacharya, S.; Ravishankar, G. A. Culture media optimization for growth and phycoerythrin production from *Porphyridium purpureum*. *Biotechnol. Bioeng.* **2007**, *96*, 456–463.

(22) Hanchinal, V. M.; Survase, S. A.; Sawant, S. K.; Annapure, U. S. Response surface methodology in media optimization for production of β-carotene from *Daucus carota*. *Plant Cell, Tissue Organ Cult.* **2008**, *93*, 123–132.

(23) Lu, C. H.; Engelmann, N. J.; Lila, M. A.; Erdman, J. W., Jr. Optimization of lycopene extraction from tomato cell suspension culture by response surface methodology. *J. Agric. Food Chem.* **2008**, *56*, 7710–7714.

(24) Akitha Devi, M. K.; Sakthivelu, G.; Giridhar, P.; Ravishankar, G. A. Protocol for augmented shoot organogenesis in selected variety of soybean [*Glycine max* L. (Merr.)]. *Indian J. Exp. Biol.* **2012**, *50*, 729–734.

(25) Murashige, T.; Skoog, F. A revised medium for rapid growth and bioassys with tobacco tissue cultures. *Physiol. Plant.* **1962**, *15*, 472–497.

(26) Vyn, T. J.; Yin, X.; Bruulsema, T. W.; Jackson, J. C.; Rajcan, I.; Bruder, S. M. Potassium fertilization effects on isoflavones concentrations in soybean. *J. Agric. Food Chem.* **2002**, *50*, 3501–3506.

(27) Kumar, V.; Rani, A.; Dixit, A. K.; Bhatnagar, D.; Chahan, G. S. Relative changes in tocopherols, isoflavones, total phenolic content, and antioxidative activity in soybean seeds at different reproductive stages. *J. Agric. Food Chem.* **2009**, *57*, 2705–2710.

(28) Box, G. E. P.; Hunter, W. G.; Hunter, J. S. *Statistics for Experimenters: An Introduction to Design, Data Analysis, and Model Building*, 2nd ed.; John Wiley and Sons: Hoboken, NJ, 2005.

(29) Cho, S. Y.; Lee, Y. N.; Park, H. J. Optimization of ethanol extraction and further purification of isoflavones from soybean sprout cotyledon. *Food Chem.* **2009**, *117*, 312–317.

(30) Omar, R.; Abdullah, M. A.; Hasan, M. A.; Marziah, M. Development of growth medium for *Centella asiatica* cell culture via response surface methodology. *Am. J. Appl. Sci.* **2004**, *1*, 215–219.

(31) Gutiérrez-Miceli, F. A.; Arias, L.; Juarez-Rodríguez, N.; Abud-Archila, M.; Amaro-Reyes, A.; Dendooven, L. Optimization of growth regulators and silver nitrate for micropropagation of *Dianthus caryophyllus* L. with the aid of a response surface experimental design. *In Vitro Cell. Dev. Biol.* **2010**, *46*, 57–63.

(32) Chiang, W. D.; Shih, C. J.; Chu, Y. H. Optimization of acid hydrolysis conditions for total isoflavones analysis in soybean hypocotyls by using RSM. *Food Chem.* **2001**, *72*, 499–503.

(33) Luczkiewicz, M. T. *Research into Isoflavonoid Phyto-oestrogens in Plant Cell Cultures: Bioactive Molecules and Medicinal Plants*; Springer-Verlag: Berlin, Germany, 2008; pp 55–84.

(34) Stockigt, J.; Obitz, P.; Falkenhagen, H.; Lutterbach, R.; Endre, S. Natural products and enzymes from plant cell cultures. *Plant Cell, Tissue Organ Cult.* **1995**, *43*, 97–109.

the pith cells of the stalk ranging from 10% to 25%, with glucose and fructose as the main reducing sugars.[11] As a result, they have a smaller grain yield and thicker, taller stalks when compared to grain sorghums.[11] There is a growing interest worldwide in using sweet sorghum as a replacement crop for sugar cane in the production of biofuels. Advantages of sweet sorghum over cane sugar include reduced water requirements, shorter growing periods, and reduced cultivation cost.[10] Sweet sorghum can grow in marginal lands and therefore does not have to compete with food production.[10,12] This is an attractive element to sweet sorghum, as biofuel production from sweet sorghum can add to the food supply instead of competing with it.

Biofuel production of sweet sorghum results in the generation of a large amount of biomass[13] comprised of stalks, leaves, and leaf sheaths, which is commonly treated as waste or utilized as a fodder. In addition, these products, particularly the leaves and leaf sheaths, have been used by traditional healers in Africa and India for anemia, epilepsy, stomach ache, and, interestingly, cancer.[14] Having been reported to be high in phenolic acids and other compounds,[15] it has been shown that sorghums contain high levels of small-molecule bioactive compounds in the stalk, leaf, leaf sheath, glumes, and seed[16−19] with reported bioactive properties.[20−22] Apigeninidin and luteolinidin belong to the 3-deoxyanthocyanidin subclass of flavonoids (Figure 1) and are reported to be expressed in the

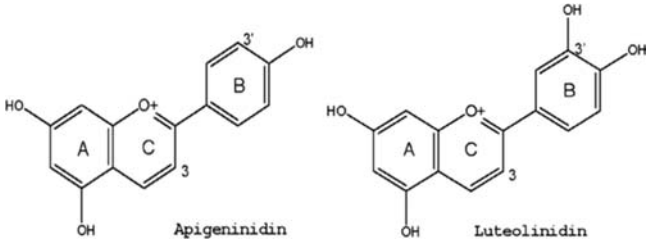

Figure 1. Structures of 3-deoxyanthocyanidins reported in this study.[30]

glume, grain, leaf, and leaf sheath[16−18] in *S. bicolor*. Furthermore, these compounds have been shown to be potent inhibitors of the HT-29 colon cancer cell line.[23]

This combination of biomass and bioactive compounds makes an attractive combination for generating large quantities of bioactive compounds for human health. In a process developed by Great Valley Energy LLC, processing of sweet sorghum strips the inner sugary cells of the pith from the outer dermal layer, resulting in two fractions, the pith and dermal layer. Currently, it is unknown if these fractions contain 3-deoxyanthocyanidins or the contribution of these compounds to its bioactivity. The pith is then further processed into biofuel, while the dermal layer can be processed to make other byproducts in a "biorefinery" approach to making biofuels. In this approach, the entire above ground sweet sorghum plant is utilized in creating products, which adds value to the process, reducing the costs of generating biofuels.[24] The aims of this study are to (1) determine the content and composition of the pith and dermal layer from the Dale and M81E varieties, (2) characterize the antiproliferative and proapoptotic activities of these extracts in human colon cancer HCT116 cells and colon cancer stem cells, (3) assess the bioactivity of apigeninidin and luteolinidin, and (4) determine if p53, a critical tumor suppressor protein, is necessary for in vitro anticancer activity.

MATERIALS AND METHODS

Chemicals and Reagents. For quantification of total phenolic and antioxidant activity, sodium bicarbonate, monobasic sodium phosphate, dibasic sodium phosphate, and sodium chloride were purchased from Fisher Scientific (Pittsburgh, PA), potassium persulfate was purchased from Mallinckrodt Chemicals (Hazelwood, MO), and 2,2′-azinobis(3-ethylbenzothiazoline-6-sulfonic acid) (ABTS) reagent, Folin−Ciocalteu reagent, Trolox, and gallic acid were purchased from Sigma (St. Louis, MO).

For cell culture and experiments, 5-fluorouracil (5-FU) was purchased from Sigma, apigeninidin and luteolinidin were purchased from Santa Cruz Biotechnology (Santa Cruz, CA) and Indofine Chemical Co. (Hillsborough, NJ), respectively, McCoy's medium and colon cancer stem cell medium were obtained from Sigma and Celprogen (San Pedro, CA), respectively, and fetal bovine serum and streptomycin/penicillin mixture were procured from Fisher Scientific.

Sweet Sorghum Materials and Extraction Preparation. Sweet sorghum materials from the Dale and M81E varieties used in this study were grown in Bakersfield, CA, and generously provided by Great Valley Energy LLC (Bakersfield, CA). Two extraction solvents were utilized for the study. Acetone (80%) was identified in the literature and empirically as a superior extraction solvent for sweet sorghum dermal and pith layers. Ethanol (80%) was used as a GRAS alternative. Fresh sweet sorghum sample (2 g) was extracted with 20 mL of extraction solvent chilled to −20 °C. This was to prevent excessive heating during the homogenization of the sample. This mixture was then homogenized for 2 min using an IKA T25 digital ultra TURRAX at 10 000 rpm. The tubes were then vortexed, and the resulting mixture was then centrifuged at 4000 rpm for 5 min. The supernatant was filtered using a 0.45 μm PTFE syringe filter (Tisch Scientific, North Bend, OH). The resulting pellet was then resuspended in 20 mL of extraction solvent by vortexing for 1 min and centrifuged, and the supernatant was collected and filtered. This was repeated for a third round of extraction, after which the filtrates were combined and the final volume was brought to 100 mL. The phenolic extracts were then stored at −20 °C until analysis for total phenolics and antioxidant activity and by LC−MS.

Phenolic-enriched extracts were prepared by extracting 2 g of sample in 20 mL of extraction solvent chilled to −20 °C. This mixture was homogenized for 2 min with an IKA T25 Digital Ultra TURRAX set to 10 000 rpm. The homogenate was then placed on a reciprocal shaker overnight in the dark at 4 °C to allow for diffusion of phenolics to create an enriched extract. The mixture was then centrifuged, and the supernatant was filtered with 0.45 μm PTFE filters (Tisch Scientific). Extracts prepared with 80% acetone were dried in a Buchi rotavapor (Flawil, Switzerland) to remove the acetone. The aqueous portion was then lyophilized, which yielded a brown powder. This was redissolved in 80% ethanol, aliquoted, and stored at −80 °C. Extracts prepared with 80% ethanol were concentrated under a nitrogen flow in a 35 °C water bath for 10 h. The extracts were then aliquoted and stored at −80 °C.

Quantification of Dry Matter, Total Phenolics, and Antioxidant Activity. Dry matter quantification was determined by freeze-drying 2 g samples in triplicate and measuring changes in mass due to water loss. The results are expressed as percent dry matter.

For quantification of total phenolics, the Folin−Ciocalteu assay was used as described in Singleton's work[25] with minor modifications. In triplicate, 35 μL of extract, standard, or solvent was added to individual wells of a 96-well plate followed by the addition of 150 μL of 1 N Folin−Ciocalteu reagent. The contents were mixed and allowed to react for 5 min under dark conditions. After 5 min, 115 μL of 7.5% sodium bicarbonate was added, and the contents were mixed and incubated in the dark at 45 °C for 30 min. The plate was then cooled for 1 h in the dark at room temperature. Finally, the absorbance was measured at 765 nm with a Biotek Synergy 2 plate reader (Winooski, VT). Gallic acid was used as a standard, and equivalency was calculated from a linear regression of standard concentrations. Data are reported as mean milligrams of gallic acid equivalents per gram of sweet sorghum sample (mg of GAE/g) ± standard error.

Antioxidant activity was measured by the ABTS assay as previously described[26,27] with minor modifications. In brief, 3 mM ABTS radical and 8 mM potassium persulfate were mixed in equal parts and reacted for at least 12 h at room temperature in the dark. Then this solution was mixed 1:30 with pH 7.4 phosphate buffer to create a working ABTS solution. In triplicate, 290 μL of the working solution was added to 10 μL of sample, standard, or solvent in a 96-well plate. This was allowed to react for 30 min at room temperature under dark conditions, after which the absorbance was measured at 734 nm using the aforementioned plate reader. The antioxidant activity is expressed as mean (n = 3) milligrams of Trolox equivalents per gram of sweet sorghum sample (mg of TE/g) ± standard error.

LC−MS Analysis. For LC−MS analysis, ethanolic extracts prepared from the pith and dermal layer of the Dale variety were concentrated 10-fold in triplicate before 1 μL of sample was injected into a Waters Acquity UPLC system fitted with a Waters Acquity UPLCT3 column (1.8 μM, 1.0 × 100 mm). The sample was injected into 100% solvent A (water, 0.1% formic acid), and this was held for 1 min. This was followed by a 12 min linear gradient to 95% solvent B (acetonitrile, 0.1% formic acid). The flow rate was held constant at 200 μL/min for the complete run. The column temperature was 50 °C, and the samples were held at 5 °C.

Eluent from the UPLC system was infused into a Waters Xevo G2 Q-Tof MS instrument fitted with an electrospray source. Data were collected in the positive ion mode, scanning from 50 to 1200 at a rate of 0.2 s per scan, alternating between MS and MS^E mode. The collision energy was set to 6 V for MS mode and 15−30 V for MS^E mode. The capillary voltage was set to 2200 V, the source temperature was 150 °C, the desolvation temperature was 350 °C, and the desolvation gas flow rate was 800 L/h of nitrogen. Waters raw data files were converted to .cdf format using Databridge software (Waters), and feature detection was performed using XCMS. Raw peaks were normalized to total ion signal in R. The UPLC−MS system was quality checked by making five injections of a standard solution containing a 2 μg/mL concentration each of caffeine, reserpine, sulfadimethoxine, and terfenadine in 50% methanol. The performance was evaluated using the final three injections, and acceptable performance is indicated by a retention time error of ±0.05 min, peak area RSD of <25%, and mass accuracy of <3 ppm error for all four compounds. Calibration was performed prior to analysis via sodium formate, with mass accuracy within 1 ppm. Compounds were identified by comparing MS spectra obtained from LC−MS analysis to the NIST, METLIN, and MassBank databases using 10 ppm as the upper limit for accuracy. In cases where spectra were not obtainable, accurate mass was used to identify the compounds.

Cell Lines and Culturing Procedures. HCT116 and HCT116 $p53^{-/-}$ cells were generously provided by Dr. Bert Vogelstein (School of Medicine, Johns Hopkins University, Baltimore, MD). Colon cancer stem cells (CCSCs) positive for CD34, CD44, and CD133 were purchased from Celprogen. All cells were maintained at a temperature of 37 °C and 5% CO_2. HCT116 cells were maintained in McCoy's medium with 5% FBS. For experiments, HCT116 cells were treated in 10% charcoal stripped serum McCoy's medium. CCSCs were maintained in colon cancer stem cell medium. For experiments, CCSCs were treated in serum-free colon cancer stem cell medium (Celprogen). Concentrated extracts were dosed in medium normalized to total phenolic content as assessed by Folin−Ciocalteu assay. We used 80% ethanol and 5-FU as negative and positive controls, respectively.

Lentiviral shRNA Mediated Knockdown of p53 in CCSCs. CCSCs were infected with lentiviral particles encoding shRNA targeting p53 (Santa Cruz Biotechnology) according to the supplier's protocol. Briefly, CCSCs were infected at a multiplicity of infection of 10 in CCSC growth medium containing 5 μg/mL Polybrene at 37 °C and 5% CO_2. After 24 h, the medium was replaced, and the cells were cultured for 2 d. Infected cells were then selected in the presence of puromycin (7.5 μg/mL) for an additional 5 d.

Proliferation and Apoptosis. Cell proliferation was assessed via 5-bromo-2′- deoxyuridine (BrdU) assay (Cell Signaling Technologies, Beverly, MA) and cell counting using an automated cell counter (Nexcelom Bioscience, Lawrence, MA). Briefly, HCT116 cells and CCSCs were grown in 96-well plates at 2×10^4 cells per well. After 24 h, the medium was aspirated, and the cells were treated with controls and sweet sorghum extracts. The treatments were added in triplicate at a volume of 150 μL per well and then allowed to incubate for 20 h at 37 °C. At this point, BrdU was added at a concentration of 10 μM per well, and the treatments were incubated at 37 °C for an additional 4 h to allow incorporation of BrdU into cellular DNA (24 h total). The medium was removed, and the BrdU assay was performed according to the manufacturer's protocol. For cell counting, cells were seeded at 1×10^5 cells per well in 12-well plates. After 24 h, control compounds and sweet sorghum extracts were added at a volume of 1 mL per well. After 24 h, the cells were removed from the plates and counted according to the manufacturer's protocol.

Apoptosis was analyzed by measuring active caspase activity with a Caspase-Glo 3/7 assay kit (Promega Corp., Madison, WI) and confirmed with the terminal deoxynucleotidyl transferase dUTP nick end labeling (TUNEL) method. For measuring caspase activity, cells were seeded and treated with control compounds and test extracts the same as in the cell counting experiments. After 24 h of incubation, 100 μL of HCT116 cells and CCSCs were transferred into a white 96-well plate, and the Caspase-Glo 3/7 assay was performed according to the company's protocol. The data were normalized to cell count and are expressed as percentages of the solvent control. For TUNEL, cells were seeded into four-well chambered glass slides at a density of 1×10^5 cells per chamber. After the treatments, the slides were prepared and analyzed for TUNEL staining according to the manufacturer's protocols (Roche Diagnostics, Indianapolis, IN). For analysis, 10 images from each well were taken, containing at least 50 cells per image. The cells were counted, and the data are expressed as the percentage of TUNEL positive cells to total cells (percent apoptosis).

Colony Formation Assay. The colony formation assay was performed as described[28] with slight modifications. Colon cancer stem cells were seeded at 1.5×10^5 cells per well in a six-well tissue culture plate (TPP, St. Louis, MO). After adhesion (24 h), the cells were treated with controls and test compounds for 24 h. The cells were then replated at a density of 100 cells per well in another six-well tissue culture plate, and colony formation was measured as described.[29]

Statistical Analysis. Data are presented as means ± standard error. Statistical significance was determined by one-way ANOVA, followed by the posthoc Fisher least significant difference test for multiple means comparisons using IBM's SPSS version 21. Means not sharing the same letter are statistically significant (P < 0.05).

RESULTS AND DISCUSSION

Sweet sorghum processing generates significant amounts of biomass containing bioactive phytochemicals and represents a promising source of human health-promoting bioactive compounds. In this study, the dermal layer and pith of two varieties of sweet sorghum were grown, processed, and

Table 1. Determination of TP, ABTS, and Dry Matter of the Pith and Dermal Layer from the Dale and M81E Sweet Sorghum Varieties[a]

	Dale		M81E	
	dermal layer	pith	dermal layer	pith
TP[b]	172 ± 6 a	127 ± 5 b	225 ± 11 c	88 ± 3 d
ABTS[c]	570 ± 54 a	248 ± 12 b	365 ± 12 c	128 ± 12 d
dry matter	39.0 ± 0.7 a	21.6 ± 0.2 b	42.2 ± 0.8 c	21.5 ± 0.3 b

[a]Values are presented as means (n = 3) ± standard error. Different online Roman letters within a row indicate significant differences (P < 0.05) among the entries. [b]Total phenolics analyzed by the Folin−Ciocalteu method, expressed as milligrams of gallic acid equivalents per 100 g of fresh mass. [c]Antioxidant activity as analyzed by ABTS assay, expressed as milligrams of Trolox equivalents per 100 g.

Table 2. Sweet Sorghum Compounds Identified by LC−MS Analysis

identity	formula[a]	t_R (min)	obsd mass	exact mass[b]	Δppm	intensity,[d] dermal layer	intensity,[d] pith	ref[e]
vanillic acid	$C_8H_8O_4$	2.79	169.050	169.0495	2	100.9 ± 3.8	68.2 ± 7.4[f]	16
p-coumaric acid	$C_9H_8O_3$	0.85	165.055	165.0546	2	534.9 ± 14.6	492.0 ± 23.8	16
ferulic acid	$C_{10}H_{10}O_4$	3.12	195.067	195.0652	9	27.6 ± 1.8	14.3 ± 1.5[f]	16
caffeic acid	$C_9H_8O_4$	3.16	181.050	181.0495	2	152.4 ± 1.3	26.5 ± 4.5[f]	16
apigeninidin	$C_{15}H_{11}O_4^+$	4.29	255.066	255.0660[c]	0	96.5 ± 20.2	7.9 ± 0.7[f]	16−18
luteolinidin	$C_{15}H_{11}O_5^+$	5.97	271.061	271.0607[c]	2	151.4 ± 30.8	7.8 ± 2.0[f]	16−18
malvidin 3-*O*-glucoside	$C_{23}H_{25}O_{12}^+$	4.76	493.134	493.1314[c]	3	168.6 ± 5.7	12.7 ± 1.4[f]	17
apigenin	$C_{15}H_{10}O_5$	4.04	271.061	271.0607	3	71.2 ± 53.8	8.6 ± 1.2	16
luteolin	$C_{15}H_{10}O_6$	5.48	287.056	287.0556	3	47.3 ± 54.2	4.6 ± 3.0	16,31
trans-resveratrol	$C_{14}H_{12}O_3$	8.48	229.087	229.0859	4	28.8 ± 3.3	37.6 ± 2.9	16
luteoferol	$C_{15}H_{14}O_6$	4.26	291.087	291.0863	2	16.3 ± 0.8	6.4 ± 0.3[f]	

[a]Formulas are based on [M]. [b]Exact masses are based on $[M + H]^+$ unless otherwise indicated. [c]Mass based on [M]. [d]Normalized peak intensities based on peak areas normalized to the total ion signal in R. [e]References which have previously identified the compound listed. [f]Significant differences ($P < 0.05$) observed among dermal and pith extracts.

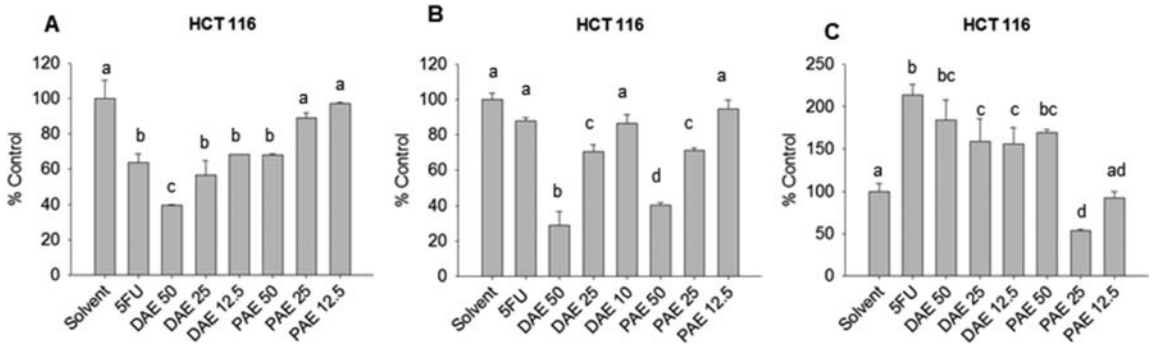

Figure 2. Antiproliferative proapoptotic activities of Dale dermal and pith phenolics measured by (A) cell count, (B) BrdU assay, and (C) Caspase 3/7 Glo assay. HCT116 cells were treated for 24 h with acetone extracts (DAE and PAE) at 10, 12.5, 25, and 50 μg of GAE/mL before estimation of proliferation and apoptosis. Values are presented as percentages of the solvent control. For cell count and Caspase 3/7 Glo, means ($n = 2$) ± standard deviation are presented. For BrdU, means ($n = 3$) ± standard error are presented. Different letters indicate significant differences ($P < 0.05$) among treatments. Solvent = solvent control, and 5-FU = 5-fluorouracil (18 μg/mL).

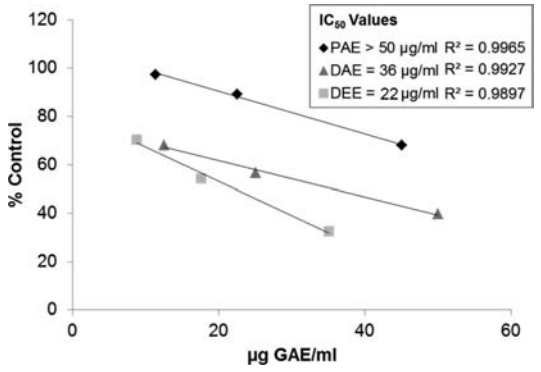

Figure 3. Dose−response curves for HCT116 cells. Cells were treated for 24 h with pith and dermal phenolic-rich extracts prepared by extraction with either acetone (AE) or ethanol (EE). The response is based on cell proliferation as estimated by cell counting. Simple linear regression was used to estimate IC_{50} values. Values are presented as percentages of the solvent control (*y* axis) at a specific dose of the respective phenolic-rich extract in micrograms of GAE per milliliter (*x* axis).

analyzed for total phenolics and antioxidant activity. The effects of sweet sorghum pith and dermal layer extracts on colon cancer stem cell proliferation, apoptosis, and stemness were also studied. For cell-based experiments, cells were dosed with sweet sorghum phenolic-rich extracts based on micrograms of gallic acid equivalents per milliliter of medium (μg of GAE/mL), which was determined by the Folin-Ciocalteu assay.

Dry Matter, Total Phenolics, Antioxidant Activity, and LC−MS Analysis. For dry matter content, we observed similar levels of dry matter in pith and dermal samples across both the Dale and M81E varieties. The dry matter content is summarized in Table 1. The dry matter of the pith from Dale and M81E was 22%. The dry matter content of the dermal layer was 39% and 42% for Dale and M81E, respectively (Table 1). These findings are in agreement with previously published data reporting dry matter content for the pith of sweet sorghum stalks of 30%,[15] reflecting the high moisture content necessary to store and concentrate sugars. To the best of our knowledge, this is the first study reporting the difference between the moisture content in pith cells and dermal cells of sweet sorghum.

We next sought to characterize the total phenolics and antioxidant activities of sweet sorghum stalk components. Acetone (80%) extracts were used to determine total phenolics and antioxidant activities of sorghum samples by Folin−Ciocalteu and ABTS, respectively (Table 1). The total phenolic content of the dermal layer was higher than that of the pith in both varieties by 35% and 155% in Dale and M81E, respectively. A similar relationship was also observed for the antioxidant activity. Among the two varieties, Dale dermal extracts yielded more Trolox equivalents, yet fewer gallic acid equivalents as assessed by ABTS and Folin−Ciocaltue assays,

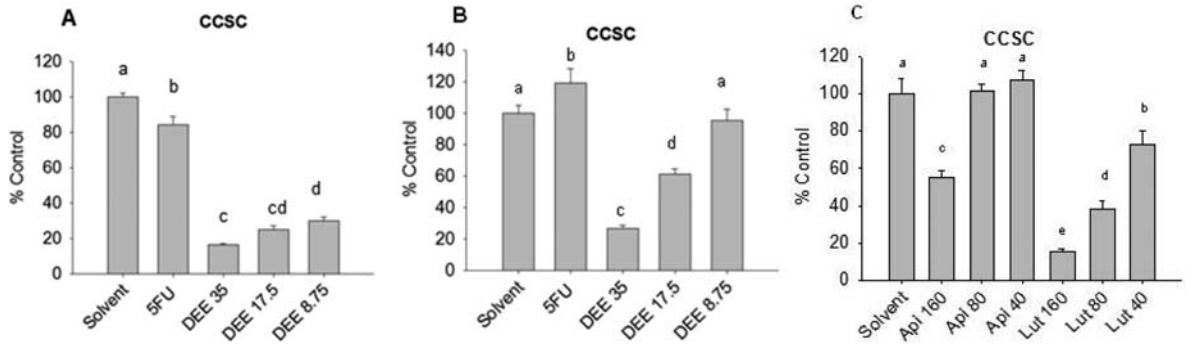

Figure 4. Antiproliferative activities of Dale dermal phenolics measured by (A) cell count and (B) BrdU assay. (C) Antiproliferative activities of apigeninidin and luteolinidin measured by BrdU. Colon cancer stem cells (CCSCs) were treated for 24 h with dermal phenolic-rich ethanol extracts of the Dale variety (DEE) at 8.75, 17.5, and 35 μg of GAE/mL before estimation of proliferation. Values are presented as percentages of the solvent control. For cell count, means (n = 2) ± standard deviation are presented. For BrdU, means (n = 3) ± standard error are presented. Different letters indicate significant differences (P < 0.05) among treatments. Solvent = solvent control, and 5-FU = 5-fluorouracil (18 μg/mL).

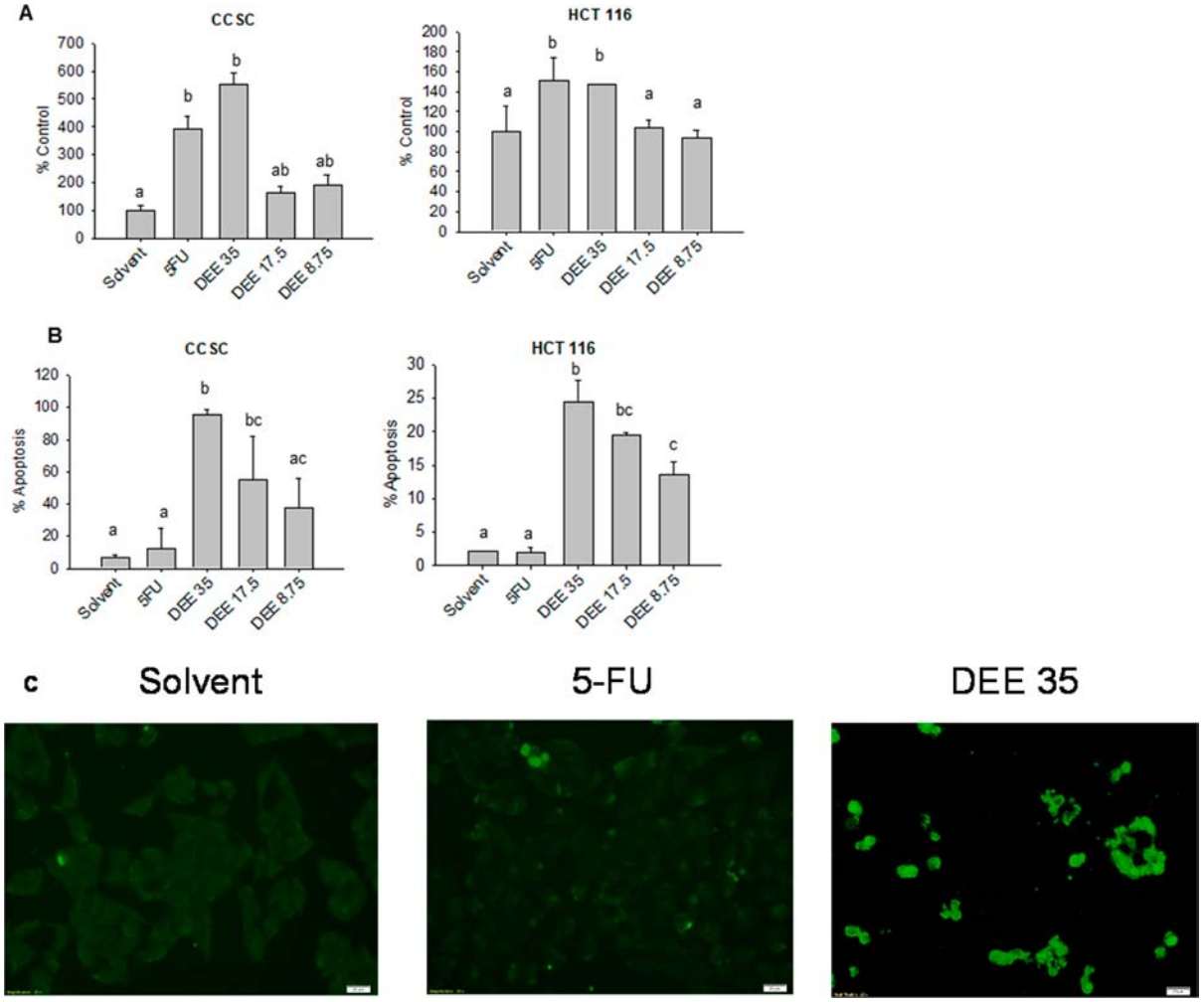

Figure 5. Proapoptotic activities of Dale dermal phenolics measured by (A) Caspase 3/7 Glo assay and (B) TUNEL assay. Colon cancer stem cells (CCSCs) and HCT116 cells were treated for 24 h with dermal phenolic-rich ethanol extracts of the Dale variety (DEE) at 8.75, 17.5, and 35 μg of GAE/mL before being tested. Values are presented as mean (n = 2) percentages of the solvent control ± standard deviation. (C) Representative images of CCSCs from TUNEL assay. Different letters indicate significant differences (P < 0.05) among treatments. Solvent = solvent control, and 5-FU = 5-fluorouracil (18 μg/mL).

respectively (P < 0.05). When the pith and dermal layer are combined, there is no difference between the gallic acid equivalents of Dale and M81E, but there are significantly more Trolox equivalents. This could be a result of a difference in the compositions of the phenolics, antioxidant, and other reducing substances contained in the two varieties. Reducing sugars such as sucrose, fructose, and glucose are concentrated in the pith of sweet sorghum and contribute to total phenolic readings.

dx.doi.org/10.1021/jf405415u | J. Agric. Food Chem. 2014, 62, 3150−3159

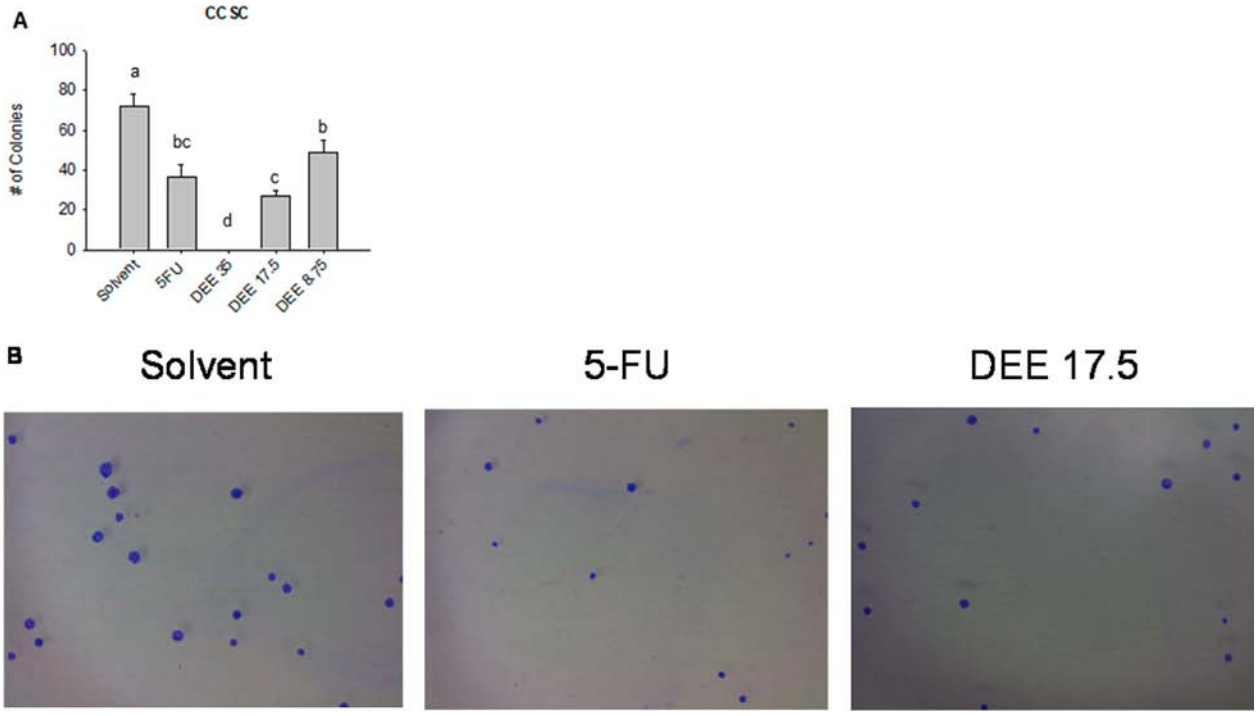

Figure 6. Effects of Dale dermal phenolics on colony formation. (A) Colon cancer stem cells (CCSCs) were treated for 24 h with dermal phenolic-rich ethanol extracts of the Dale variety (DEE) at 8.75, 17.5, and 35 μg of GAE/mL before estimation of colony formation by colony forming assay. (B) Representative images taken from the colony forming assay. Values are presented as the mean (n = 3) number of colonies formed containing at least 50 cells ± standard error. Different letters indicate significant differences ($P < 0.05$) among treatments. Solvent = solvent control, and 5-FU = 5-fluorouracil (18 μg/mL).

Reducing sugars are known to be approximately twice as concentrated in the pith as in other components of the stalk,[15] and differences in reducing sugars could explain this discrepancy.

We next sought to analyze bioactive compounds from the pith and dermal components of sweet sorghum stalk by LC–MS analysis. We were able to identify phenolic acids, flavonoids, and stilbenoids from the phenolic extracts of the sweet sorghum pith and dermal layer, which are summarized in Table 2. These compounds have been identified previously in sorghum and have also been reported to have potent in vitro and in vivo anticancer activities. For example, we were able to identify luteolinidin and apigenidin, which have been previously reported in the leaf sheaths and leaves of sorghum.[17,18] These compounds have been reported to have anticancer activities toward a number of cancer cell lines, including liver, leukemia, and colon.[22,23,30] Previous studies have identified primarily two major classes of bioactive phenolic compounds, phenolic acids and flavonoids, in sorghums and sweet sorghums. These investigations primarily focused on the grains or seed heads from grain sorghum for its relevance as a staple in human diets. Other investigations have focused on the leaf, leaf sheath, infected sorghum seedlings, and glume,[17−19,31] and these parts of the plants are pertinent to traditional medicine. These studies have identified multiple phenolic compounds with potent in vitro and in vivo activities. These include phenolic acids, anthocyanidins, and flavones. Few studies have investigated sweet sorghum with respect to its bioactive content, especially the stalk components, pith and dermal layer. On the basis of these observations, we hypothesized that extracts from the sweet sorghum stalk components pith and dermal layer containing multiple bioactives would suppress proliferation and induce apoptosis in colon cancer cells.

Anticancer Activities of Sweet Sorghum Pith and Dermal Extracts. Early in the pathogenesis of colorectal cancer, hyperproliferation of colonocytes resulting from a deregulation of cellular proliferation and a suppression of apoptosis results in the formation of aberrant crypt foci and, subsequently, adenomas. Colon stem cells, residing in the base of the crypt, are responsible for renewing the colonic epithelium during one's lifetime.[32,33] Furthermore, they are long-lived, self-renewing cells and have a high capacity for proliferation, a combination that makes them a likely candidate to acquire the mutations necessary to give rise to colon cancers.[34] Today's therapies are ineffective at targeting cancer stem cells, only targeting the bulk of the rapidly dividing tumor cells.[6] Therefore, effective treatment strategies for colon cancer should suppress proliferation and induce apoptosis in the rapidly dividing tumor mass as well as the cancer stem cells. This would rid the tumor mass of the tumor-promoting stem cells as well as remove the bulk of the tumor. We assessed the pith's and dermal layer's bioactivity by measuring (1) antiproliferative effects in colon cancer HCT116 cells and CCSCs as evaluated by cell count and BrdU assay, (2) proapoptotic effects in HCT116 cells and CCSCs as evaluated by activated caspase 3/7 activity and subsequently confirmed by TUNEL assay, and (3) self-renewal capability in CCSCs as analyzed by colony forming assay.

Differential Activities of Pith and Dermal Extracts. To investigate the differences in the anticancer effects between pith and dermal extracts, colon cancer HCT116 cells were treated with phenolic-rich extracts prepared from Dale pith 80% acetone extract (PAE) and Dale dermal 80% acetone extract

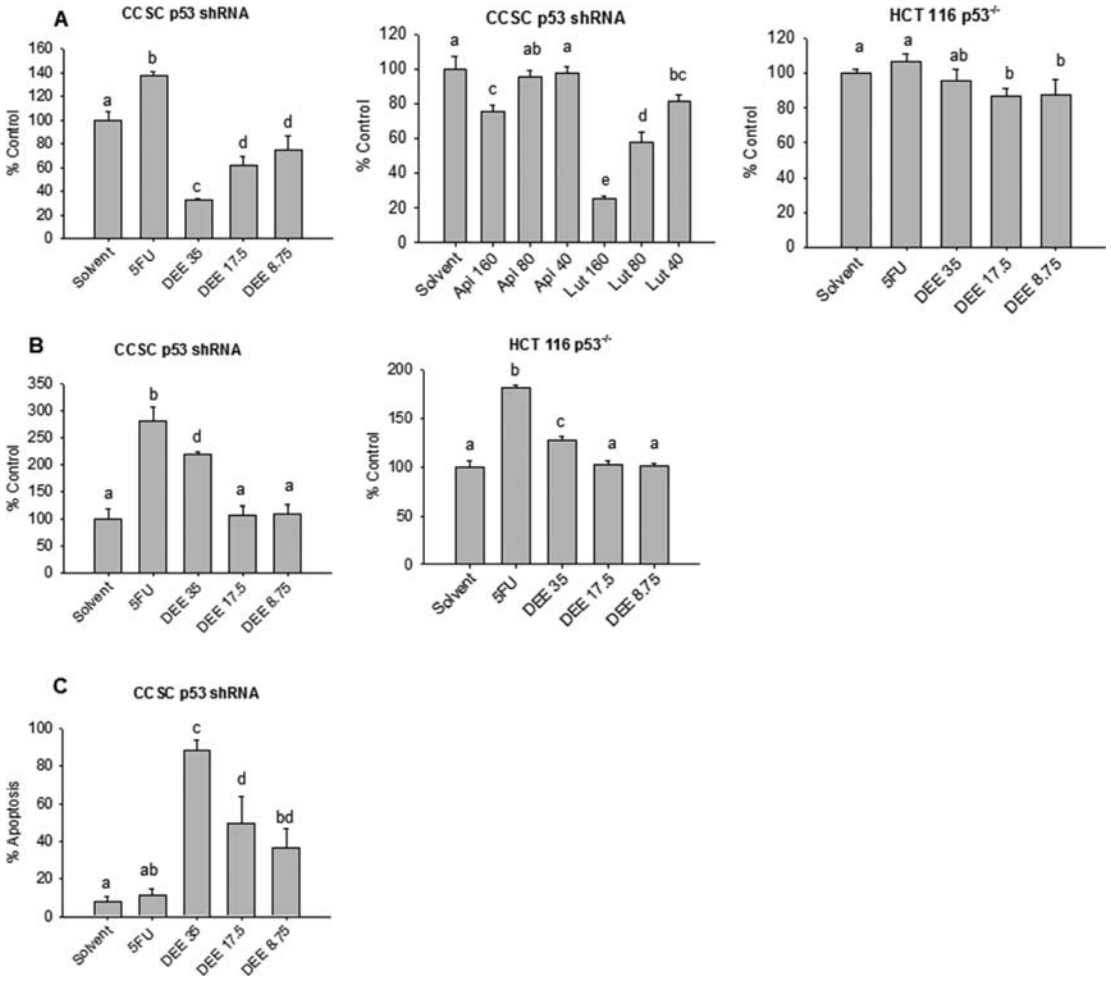

Figure 7. Antiproliferative and proapoptotic activities of Dale dermal phenolics in a p53-independent manner as measured by (A) BrdU assay, (B) Caspase 3/7 Glo assay, and (C) TUNEL assay. The antiproliferative effects of apigeninidin and luteolinidin were also measured by BrdU assay. Colon cancer stem cells (CCSCs) with p53 shRNA and HCT116 $p53^{-/-}$ cells were treated for 24 h with dermal phenolic-rich ethanol extracts of the Dale variety (DEE) at 8.75, 17.5, and 35 μg of GAE/mL before being tested. For BrdU assay, values are presented as mean (n = 3) percentages of the solvent control ± standard error. For Caspase 3/7 Glo and TUNEL assays, values are presented as mean (n = 2) percentages of the solvent control ± standard deviation. Different letters indicate significant differences ($P < 0.05$) among treatments. Solvent = solvent control, and 5-FU = 5-fluorouracil (18 μg/mL).

(DAE) for 24 h as shown in Figure 2. Extract from DAE suppressed cell proliferation more than PAE, as shown by cell count and BrdU assays. This may be due to higher levels of reducing sugars in the pith. At 25 μg of GAE/mL, DAE suppressed the cell count 43% compared to only an 11% reduction for PAE. IC_{50} values were calculated for PAE and DAE. The IC_{50} for PAE was calculated to be above 50 μg of GAE/mL, while DAE was calculated to be 36 μg of GAE/mL. DAE was also able to induce apoptosis at lower concentrations than the pith as measured by caspase activity. At concentrations of 12.5, 25, and 50 μg of GAE/mL, DAE was able to increase active caspase levels to 155%, 159%, and 184% of that of a solvent control, respectively. Only 50 μg of GAE/mL of PAE was able to increase active caspases 3 and 7 in HCT116 cancer cells (169%, $P < 0.05$). These data implicated DAE as a more effective antiproliferative and proapoptotic extract than PAE, and therefore, further experiments focused solely on extracts from the dermal layer of the Dale variety. These differences in bioactivities between the pith and dermal layer of the Dale variety stalk may be explained by the differences in their composition and content of bioactive compounds. These results are analogous to differences observed in the bioactivities of different parts of edible fruits. For example, only the ethanolic extracts from the peel of mango, but not the flesh, induced apoptosis in cervical cancer HeLa cells.[35] Interestingly, our LC−MS analysis showed marked and significant differences between extracts from the dermal layer and pith (Table 2). For example, the ethanolic pith extract contained only 8% of the apigeninidin and 5% of the luteolinidin as compared to the levels of these compounds in the ethanolic dermal extract on the basis of relative peak intensities. This may explain the increased potency observed in dermal extracts.

Solvent-Dependent Activities of Dermal Extracts. Previous quantitative and in vitro experiments demonstrated that aqueous acetone makes a good extraction solvent for dermal phenolic compounds with antioxidant and anticancer activity. However, acetone is not an environmentally safe solvent for extraction of bioactive compounds, especially for extracts intended for human consumption. Turkmen and colleagues[36] tested the ability of different organic solvents with varying percentages of water to extract phenolics from mate and black tea. They found that while 100% ethanol was

ineffective at extracting tea polyphenols, addition of 20% water increased polyphenol extraction by approximately 27-fold when compared to 100% ethanol. Furthermore, 80% ethanol yielded approximately 60% of the phenolics as compared to 80% acetone. On this basis, we hypothesized that ethanol, a GRAS organic solvent, with water could be used to extract phenolics from the sweet sorghum dermal layer with effectiveness similar to that of aqueous acetone. Similar to Turkmen's findings, 80% ethanol yielded approximately 84% of the phenolics compared to 80% acetone (data not shown). We next tested the bioactivity of the phenolic-rich dermal extract prepared from 80% ethanol (DEE) in HCT116 and compared it to that of DAE. As demonstrated by Figure 3, DEE had a superior IC_{50} value of 22 μg of GAE/mL compared to the IC_{50} of 36 μg of GAE/mL for DAE. Given the GRAS status of ethanol and the greater in vitro bioactivity against HCT116 cells, further experiments utilized DEE. We further tested DEE for proapoptotic activities by the Caspase 3/7 Glo assay and TUNEL assay. When compared to the solvent control, DEE at all concentrations significantly increased apoptosis. Furthermore, this increase in apoptosis was more than that for the positive control, 5-FU. Our findings highlight the important aspect of solvent selection when extracting and analyzing in vitro bioactivities of plant-based extracts.

DEE Effectively Eliminates Colon Cancer Stem Cells. There is growing evidence that cancers arise from a small population of adult cancer stem cells. They are also resistant to many standard of care therapies (e.g., chemotherapy and radiotherapy), and the inability to rid the body of these persistent cells is thought to be a primary cause of colon cancer recurrence.[7] There is a need for standardized bioactive compounds and extracts that can effectively eliminate these cells, as current anticancer drugs often fail.[7] We tested DEE against colon cancer stem cells and compared it to 5-FU, a common chemotherapeutic for the treatment of colon cancer. We treated colon cancer stem cells with DEE at 8.75, 17.5, and 35 μg of GAE/mL and 5-FU (18 μg/mL, 100 μM) for 24 h and measured proliferation and apoptosis (Figures 4 and 5). DEE potently suppressed proliferation to 73% of the control, as measured by BrdU, and increased the percentage of TUNEL positive cells (Figure 5B) from 7% to 95% of total cells ($P < 0.05$). Imaging of TUNEL stained cells (Figure 5C) shows increases in DNA fragmentation (increased fluorescence) and changes in cell morphology consistent with apoptosis. We further tested the antiproliferative activity of apigeninidin and luteolinidin against CCSCs with BrdU assay, and IC_{50} values were calculated as demonstrated in Figure 4C. Luteolinidin suppressed CCSC proliferation more than apigeninidin, as demonstrated by a lower IC_{50} value of 76 μg/mL as compared to >160 μg/mL.

To further assess DEE's ability to target CCSC properties other than proliferation and apoptosis, the self-renewal capability of CCSCs' self-renewal was measured by colony forming assay (Figure 6). We treated CCSCs with DEE and found a dose-dependent suppression in colony formation. Figure 6B shows representative images collected from the colony forming assay and demonstrates the decreased colony number and size associated with treatment in comparison to the control. At the highest concentration, DEE completely suppressed CCSC colony formation, and this activity was greater than that of 5-FU treatment. This demonstrates that, in addition to the antiproliferative and proapoptotic activities, DEE alters the stemlike properties by inhibiting colon cancer stem cell self-renewal.

There has been little research done on the in vitro anticancer activities of sorghum stalk, especially sweet sorghum, on cancer cells and advanced cancer stem cells. Research from Yang et al.[23] demonstrated that grain extracts from pigmented grain sorghums contained high levels of 3-deoxyanthocyanins and had strong antiproliferative activities in vitro against colon cancer HT-29 cells. Furthermore, they tested the antiproliferative effects of individual 3-deoxyanthocyanidins. They reported IC_{50} values ranging from 180 to 557 μg/mL for crude extracts and from approximately 13 to 20 μg/mL for 3-deoxyanthocyanidins. In agreement with Yang's findings, we too have demonstrated that phenolic-rich extract from the dermal layer of sweet sorghum stalks contains 3-deoxyanthocyanidins and has potent antiproliferative and proapoptotic activities. The fact that dermal phenolic-rich extract has activities in colon cancer cells and colon cancer stem cells highlights a need for further research of sweet sorghum's anticancer activity in vivo for its potential as a chemotherapeutic agent against colon cancer.

Effects of p53 on the Anticancer Activity of DEE. The p53 tumor suppressor gene is an integral regulator of cell cycle control, DNA repair, and apoptosis.[3] It is estimated that half of all tumors carry some form of mutated p53 and the synergy of phytochemicals may provide p53-dependent and -independent mechanisms to compensate.[37,38] Effective preventive and therapeutic colon cancer strategies should successfully target p53-dependent and -independent pathways. To test the p53 dependency of DEE's anticancer activity, we treated HCT116 $p53^{-/-}$ cells carrying p53 deletions in both alleles of the p53 gene with DEE for 24 h and measured changes in proliferation and caspase activity (Figure 7). We observed no significant changes between HCT116 $p53^{-/-}$ cells treated with DEE and solvent controls in cellular proliferation as measured by the BrdU assay, indicating that DEE's ability to suppress cellular proliferation is p53-dependent. However, we did observe a significant increase in active caspase activity at the highest dose of DEE. This indicates that DEE may act through p53-independent pathways of apoptosis only at concentrations at and above 35 μg of GAE/mL, and this may also be true of DEE's antiproliferative effects.

We further tested p53 dependency in CCSCs by knocking down p53 expression with lentiviral infection containing p53 shRNA (CCSC p53 shRNA). The shRNA is constitutively expressed due to the presence of a strong promoter binding to p53 mRNA, preventing its translation. In this model of p53 knockdown, DEE suppressed proliferation up to 33% of the control and elevated apoptosis of CCSC p53 shRNA cells in a dose-dependent fashion as measured by BrdU and TUNEL assays (Figure 7). We further tested the antiproliferative effects of apigeninidin and luteolinidin in CCSC p53 shRNA cells with BrdU (Figure 7). We show that both of the 3-deoxyanthocyanidins suppress proliferation in p53 knockdown cells with IC_{50} values of >160 and 103 μg/mL for apigeninidin and luteolinidin, respectively. In agreement with previous results, the antiproliferative effect of luteolinidin surpassed that of apigeninidin. Our findings may be due to the slight variation in structure, as luteolinidin contains one extra hydroxyl group on the 3′ carbon of the B-ring of the flavonoid structure, and it has been shown to have a 3-fold increase in antioxidant activity when compared to apigeninidin.[39] Our findings agree with

those of Marko et al.,[40] who reported increased activity of anthocyanidins with a higher degree of B-ring hydroxylation.

In this study, we demonstrated differential activity observed between CCSCs and the early-stage HCT116 cell lines. This differential activity is thought to be a result of the selective toxicity of complex bioactive extracts against cancer cells as compared to normal epithelial cells. Earlier staged and more differentiated cancer cell lines more resemble the normal differentiated epithelial cells than do more advanced cancer cell lines. This was demonstrated in work by Seeram et al.[41] with total cranberry extract in four colon cancer cell types (SW480, SW620, HCT116, and HT29). SW480 and SW620 represent two cell lines from the same patient, the former representing the earlier staged primary tumor and the latter derived from a metastasis. Total cranberry extract showed 35% more antiproliferative activity against the advanced metastatic SW620 cell line compared to SW480 cells. HCT116 and HT29 cells are colon cancer cell lines representing early- and late-stage disease, respectively. Total cranberry extract showed greater proliferation inhibition activity in the advanced HT29 cell line compared to HCT116 cells. These reports corroborate our findings that sweet sorghum extract was more efficacious against CCSCs as compared to HCT116 cells. While our results point to p53-independent activity, more work is needed to conclude the dermal extract's mechanisms of action.

In the present study, we have shown for the first time that the dermal layer of sweet sorghum is rich in total phenolics and antioxidants, including 3-deoxyanthocyanidins, with potent in vitro anticancer activity against colon cancer HCT116 cells and CCSCs. This activity was greater than that of the pith, and we believe this to be due to the different compositions of phenolics as illustrated in Table 2. Furthermore, we demonstrated that the ethanolic extract was more potent in suppressing the proliferation of colon cancer cells, highlighting the importance of solvent selection in developing natural-based phenolic-rich extracts. In addition to being a source of renewable biofuel, sweet sorghum may also serve as a source of health-promoting compounds for the prevention and treatment of inflammatory diseases such as colon cancer. For this to be a reality, further research is needed to determine potential toxicities and the bioactivities of sweet sorghum dermal extracts in vivo.

AUTHOR INFORMATION

Corresponding Author

*Phone: 814-865-6842. Fax: 814-863-6132. E-mail: juv4@psu.edu.

Author Contributions

A.R.M. conducted research, writing of the manuscript, and contributed to the study's design. L.R. provided intellectual contributions, study design, and assisted in research. J.V. provided intellectual contributions, study design, and review of the manuscript.

Funding

This research was funded by Great Valley Energy LLC, Bakersfield, CA.

Notes

The authors declare the following competing financial interest(s): patent pending. Brian M. Pellens and D. Edward Settle, the Managing Principals of Great Valley Energy LLC, approached the authors with the idea of studying the bioactive and antioxidant properties of sweet sorghum fractions. They have applied for a patent for sorghum extract and its therapeutic uses. In recognition of the authors' contribution, they have invited the authors to be named as co-inventors.

ACKNOWLEDGMENTS

We thank the Proteomics and Metabolomics Facility at Colorado State University for performing the LC-MS analysis of the pith and dermal samples and Sridhar Radhakrishnan and Venkata Rohit for laboratory assistance and manuscript review.

REFERENCES

(1) Cancer Facts & Figures 2012. http://www.cancer.org/acs/groups/content/@epidemiologysurveilance/documents/document/acspc-031941.pdf (accessed Apr 4, 2012).

(2) Reddy, L.; Odhav, B.; Bhoola, K. D. Natural products for cancer prevention: A global perspective. *Pharmacol. Ther.* **2003**, *99*, 1−13.

(3) Ruhul Amin, A. R. M.; Kucuk, O.; Khuri, F. R.; Shin, D. M. Perspectives for cancer prevention with natural compounds. *J. Clin. Oncol.* **2009**, *27*, 2712−2725.

(4) Worthley, D.; Whitehall, V. Colorectal carcinogenesis: Road maps to cancer. *World J. Gastroenterol.* **2007**, *13*, 3783−3908.

(5) Tsvetkov, P.; Asher, G.; Reiss, V.; Shaul, Y.; Sachs, L.; Lotem, J. Inhibition of NAD(P)H:quinone oxidoreductase 1 activity and induction of p53 degradation by the natural phenolic compound curcumin. *Proc. Natl. Acad. Sci. U.S.A.* **2005**, *102*, 5535−5540.

(6) Bitarte, N.; Bandres, E.; Boni, V.; Zarate, R.; Rodriguez, J.; Gonzalez-Huarriz, M.; Lopez, I.; Javier Sola, J.; Alonso, M. M.; Fortes, P.; Garcia-Foncillas, J. MicroRNA-451 is involved in the self-renewal, tumorigenicity, and chemoresistance of colorectal cancer stem cells. *Stem Cells* **2011**, *29*, 1661−1671.

(7) Li, Y.; Wicha, M. S.; Schwartz, S. J.; Sun, D. Implications of cancer stem cell theory for cancer chemoprevention by natural dietary compounds. *J. Nutr. Biochem.* **2011**, *22*, 799−806.

(8) Lin, L.; Liu, Y.; Li, H.; Li, P.-K.; Fuchs, J.; Shibata, H.; Iwabuchi, Y.; Lin, J. Targeting colon cancer stem cells using a new curcumin analogue, GO-Y030. *Br. J. Cancer* **2011**, *105*, 212−220.

(9) Radhakrishnan, S.; Reddivari, L.; Sclafani, R.; Das, U. N.; Vanamala, J. Resveratrol potentiates grape seed extract induced human colon cancer cell apoptosis. *Front. Biosci., Elite Ed.* **2011**, *3*, 1509−1523.

(10) Reddy, B.; Ramesh, S.; Reddy, P.; Kumar, A.; Sharma, K.; Karuppan Chetty, S.; Palaniswamy, A. *Sweet Sorghum: Food, Feed, Fodder, and Fuel Crop*; International Crops Research Institute for the Semi-Arid Tropics: Patancheru, Andhra Pradesh, India, 2007; pp 1−24.

(11) Ritter, K. B.; McIntyre, C. L.; Godwin, I. D.; Jordan, D. R.; Chapman, S. C. An assessment of the genetic relationship between sweet and grain sorghums, within *Sorghum bicolor* ssp. *bicolor* (L.) Moench, using AFLP markers. *Euphytica* **2007**, *157*, 161−176.

(12) Saballos, A. Development and utilization of sorghum as a bioenergy crop. In *Genetic Improvement of Bioenergy Crops*; Vermerris, W., Ed.; Springer: New York, 2008; pp 211−239.

(13) Zhao, Y. L.; Dolat, A.; Steinberger, Y.; Wang, X.; Osman, A.; Xie, G. H. Biomass yield and changes in chemical composition of sweet sorghum cultivars grown for biofuel. *Field Crops Res.* **2009**, *111*, 55−64.

(14) Akande, I.; Oseni, A.; Biobaku, O. Effects of aqueous extract of *Sorghum bicolor* on hepatic, histological and haematological indices in rats. *J. Cell Anim. Biol.* **2010**, *4*, 137−142.

(15) Billa, E.; Koullas, D. P.; Monties, B.; Koukios, E. G. Structure and composition of sweet sorghum stalk components. *Ind. Crops Prod.* **1997**, *6*, 297−302.

(16) Bröhan, M.; Jerkovic, V.; Collin, S. Potentiality of red sorghum for producing stilbenoid-enriched beers with high antioxidant activity. *J. Agric. Food Chem.* **2011**, *59*, 4088−4094.

(17) Polycarpe Kayodé, A. P.; Nout, M. J. R.; Linnemann, A. R.; Hounhouigan, J. D.; Berghofer, E.; Siebenhandl-Ehn, S. Uncommonly high levels of 3-deoxyanthocyanidins and antioxidant capacity in the

leaf sheaths of dye sorghum. *J. Agric. Food Chem.* **2011**, *59*, 1178−1184.
(18) Njongmeta, N. Extractability profiling and antioxidant activity of flavonoids in sorghum grain and non-grain materials. Ph.D. Thesis, Texas A&M University, 2010.
(19) Kwon, Y. S.; Kim, C. M. Antioxidant constituents from the stem of *Sorghum bicolor*. *Arch. Pharm. Res.* **2003**, *26*, 535−539.
(20) Yip, E. C. H.; Chan, A. S. L.; Pang, H.; Tam, Y. K.; Wong, Y. H. Protocatechuic acid induces cell death in HepG2 hepatocellular carcinoma cells through a c-Jun N-terminal kinase-dependent mechanism. *Cell Biol. Toxicol.* **2006**, *22*, 293−302.
(21) Ferguson, L. R.; Zhu, S.; Harris, P. J. Antioxidant and antigenotoxic effects of plant cell wall hydroxycinnamic acids in cultured HT-29 cells. *Mol. Nutr. Food Res.* **2005**, *49*, 585−593.
(22) Woo, H. J.; Oh, I. T.; Lee, J. Y.; Jun, D. Y.; Seu, M. C.; Woo, K. S.; Nam, M. H.; Kim, Y. H. Apigeninidin induces apoptosis through activation of Bak and Bax and subsequent mediation of mitochondrial damage in human promyelocytic leukemia HL-60 cells. *Process Biochem.* **2012**, *47*, 13−16.
(23) Yang, L.; Browning, J. D.; Awika, J. M. Sorghum 3-deoxyanthocyanins possess strong phase II enzyme inducer activity and cancer cell growth inhibition properties. *J. Agric. Food Chem.* **2009**, *57*, 1797−1804.
(24) Cherubini, F. The biorefinery concept: Using biomass instead of oil for producing energy and chemicals. *Energy Convers. Manage.* **2010**, *51*, 1412−1421.
(25) Singleton, V.; Orthofer, R.; Lameula-Raventós, M. Analysis of total phenols and other oxidation substrates and antioxidants by means of folin-ciocalteu reagent. *Methods Enzymol.* **1999**, *299*, 152−178.
(26) Awika, J. M.; Rooney, L. W.; Wu, X.; Prior, R. L.; Cisneros-Zevallos, L. Screening methods to measure antioxidant activity of sorghum (*Sorghum bicolor*) and sorghum products. *J. Agric. Food Chem.* **2003**, *51*, 6657−6662.
(27) Reddivari, L.; Hale, A.; Miller, J. C., Jr. Determination of phenolic content, composition and their contribution to antioxidant activity in specialty potato selections. *Am. J. Potato Res.* **2007**, *84*, 275−282.
(28) Ottinger, S.; Klöppel, A.; Rausch, V.; Liu, L.; Kallifatidis, G.; Gross, W.; Gebhard, M.-M.; Brümmer, F.; Herr, I. Targeting of pancreatic and prostate cancer stem cell characteristics by *Crambe crambe* marine sponge extract. *Int. J. Cancer* **2012**, *130*, 1671−1681.
(29) Apel, A.; Herr, I.; Schwarz, H.; Rodemann, H. P.; Mayer, A. Blocked autophagy sensitizes resistant carcinoma cells to radiation therapy. *Cancer Res.* **2008**, *68*, 1485−1494.
(30) Shih, C. H.; Siu, S. O.; Ng, R.; Wong, E.; Chiu, L. C. M.; Chu, I. K.; Lo, C. Quantitative analysis of anticancer 3-deoxyanthocyanidins in infected sorghum seedlings. *J. Agric. Food Chem.* **2007**, *55*, 254−259.
(31) Rey, J.-P.; Pousset, J.-L.; Levesque, J.; Wanty, P. Isolation and composition of a natural dye from the stem of *Sorghum bicolor* (L.) Moench subsp. *americanum caudatum*. *Cereal Chem.* **1993**, *70*, 759−760.
(32) Kelloff, G. J.; Schilsky, R. L.; Alberts, D. S.; Day, R. W.; Guyton, K. Z.; Pearce, H. L.; Peck, J. C.; Phillips, R.; Sigman, C. C. Colorectal adenomas: A prototype for the use of surrogate end points in the development of cancer prevention drugs. *Clin. Cancer Res.* **2004**, *10*, 3908−3918.
(33) Zeki, S. S.; Graham, T. A.; Wright, N. A. Stem cells and their implications for colorectal cancer. *Nat. Rev. Gastroenterol. Hepatol.* **2011**, *8*, 90−100.
(34) Li, L.; Neaves, W. B. Normal stem cells and cancer stem cells: The niche matters. *Cancer Res.* **2006**, *66*, 4553−7.
(35) Kim, H.; Kim, H.; Mosaddik, A.; Gyawali, R.; Ahn, K. S.; Cho, S. K. Induction of apoptosis by ethanolic extract of mango peel and comparative analysis of the chemical constitutes of mango peel and flesh. *Food Chem.* **2012**, *133*, 416−422.
(36) Turkmen, N.; Sari, F.; Velioglu, Y. S. Effects of extraction solvents on concentration and antioxidant activity of black and black mate tea polyphenols determined by ferrous tartrate and Folin−Ciocalteu methods. *Food Chem.* **2006**, *99*, 835−841.
(37) Liu, R. Potential synergy of phytochemicals in cancer prevention: Mechanism of action. *J. Nutr.* **2004**, *134*, 3479S−3485S.
(38) Vousden, K. H.; Lu, X. Live or let die: The cell's response to p53. *Nat. Rev. Cancer* **2002**, *2*, 594−604.
(39) Awika, J. M.; Rooney, L. W.; Waniska, R. D. Properties of 3-deoxyanthocyanins from sorghum. *J. Agric. Food Chem.* **2004**, *52*, 4388−4394.
(40) Marko, D.; Puppel, N.; Tjaden, Z.; Jakobs, S.; Pahlke, G. The substitution pattern of anthocyanidins affects different cellular signaling cascades regulating cell proliferation. *Mol. Nutr. Food Res.* **2004**, *48*, 318−325.
(41) Seeram, N. P.; Adams, L. S.; Hardy, M. L.; Heber, D. Total cranberry extract versus its phytochemical constituents: Antiproliferative and synergistic effects against human tumor cell lines. *J. Agric. Food Chem.* **2004**, *52*, 2512−2517.

glucans,[19,20,22,26,27] and for a specific MW, gelation rate can be increased by increasing concentration.[19] Low molecular weight β-glucans (≤100,000) produced gels with greater G′ values than higher MW β-glucans,[20,22,27] although large deformation measurements obtained opposite results, whereby gels from high molecular weight β-glucans formed harder gels, more resistant to mechanical stress.[19,20,27] β-Glucan source was the other significant parameter in determining gelation rate and gel elasticity. β-Glucans where β-(1→3) linked cellotriosyl units form a greater proportion of the molecular structure gel faster and produce more elastic gels. Therefore, when comparing 10% oat, barley, and lichenan β-glucan gels with similar M_w values, melting temperature and rate of gelation decreased in the order lichenan, barley, and oat.[19] Essentially, lichenan solutions gelled very quickly and, once gelled, required more heat to melt. Conversely, oat β-glucan required the most time to gel and the least amount of heat to melt. Structurally, lichenan has the highest proportion of β-(1→3) linked cellotriosyl units, followed by barley and then oats. Similarly, Tosh et al.[22] found that storage modulus G′ declined in the order lichenan, wheat, rye, barley, and oat for 6% β-glucan gels aged 7 days at 5 °C. There was a significant positive relationship between the proportion of β-(1→3) linked cellotriosyl units in the polymer and G′.

Given the health benefits of β-glucans and the relative unpalatability of highly viscous, high MW β-glucan drinks with a slimy mouth feel, the prospect of delivering the fiber in gel form is attractive. This would be a method for delivery not only of β-glucan but, potentially, for other bioactive food components, such as anthocyanins and carotenoids, as well. In light of the variability of β-glucan gel properties based on MW and fine structure, the aim of our research was to examine whether β-glucan gels could be prepared from a mix of low and high MW polymers, thus exploiting the properties of each with respect to gelation (high molecular weight β-glucans produce stronger gels, but take a long time to gel, whereas low molecular weight β-glucan gels faster and produces more elastic gels). To this end, high and low MW β-glucans were mixed in different proportions and the resultant systems subjected to small deformation oscillatory (G′, G″) and large deformation measurements. These gels were also examined using microscopy and differential scanning calorimetry (DSC) to assess gel structure and thermal properties. Model food gels containing glucose with differing high molecular weight:low molecular weight (HMW:LMW) ratios were produced and analyzed to examine viscoelastic and mechanical properties.

2. MATERIALS AND METHODS

2.1. Sample Preparation. Unhydrolyzed oat β-glucan was prepared as previously described,[28] with modifications as reported in Tosh et al.[22] A low molecular weight fraction was prepared for use in the mixed molecular weight gels by hydrolyzing the unhydrolyzed oat β-glucan with acid as described by Tosh et al.[21] For the model food gel, LMW and HMW oat β-glucan were a gift from Megazyme International (Bray, County Wicklow, Ireland).

Mixed molecular weight gels for small (small amplitude oscillatory testing) and large deformation mechanical testing were prepared by solubilizing either HMW or LMW oat β-glucan or a mixture of the two in 20 mM phosphate/1 mM NaN_3 buffer (pH7.0) with a 3, 4, and 5% total β-glucan concentration. Solubilization took place at 90 °C with constant stirring for 3 h. The mixtures had HMW:LMW ratios of 0:100, 25:75, 50:50, 75:25, and 100:0 (the 25:75 ratio was not prepared for all analyses). Gels were set in 2.5 cm diameter molds 1 mm deep for 3, 5, or 7 day rheological tests at 25 °C. For large deformation tests, the gels prepared from HMW and LMW oat β-glucans and the mixtures thereof were set in 2 cm diameter molds 6 mm deep for 7 days at 25 °C. The freshly prepared, nongelled samples were used for apparent viscosity measurements.

Model food gels with a HMW:LMW ratio of 0:100, 50:50, and 75:25 were prepared at 4% (w/w of gum and water) by vigorously mixing the gum in boiling 0.05% potassium sorbate in distilled water with an immersion blender. Food coloring and orange oil were added, and citric acid was used to maintain a pH of 4−5. The control gels were prepared as described while the sample gels were augmented by the addition of 50 g of glucose. The β-glucan solutions were set in 2.5 cm diameter 1 mm deep molds for rheology and 2 cm diameter 9 mm deep molds for large deformation tests. Gels were aged 7 days at 21−24 °C.

2.2. Characterization. The β-glucan content of samples was determined according to AOAC Method 995.16 using an enzymatic analysis kit from Megazyme (Bray, County Wicklow, Ireland).

Molecular weight (M_w) and polydsipersity (Pd) determinations for oat samples were made using a HPSEC system equipped with multiple detectors. The chromatographic system consisted of a Shimadzu (Shimadzu Scientific Instruments Inc., Kyoto, Japan) SCL-10Avp system controller, a SIL-10ADvp autosampler, and a LC-10ATvp pump. Detection was achieved using a Viscotek (Malvern Instruments Ltd., Worcestershire, U.K.) model 305 triple detector array, which housed two analytical columns maintained at 40 °C, an Ultrahydrogel linear (Waters, Milford, CT) column, and a Shodex (Showa Denko, K.K., Tokyo, Japan) OHpak Kb-806M column and three detectors: an RI, differential pressure (DP), and laser light scattering detector. The light scattering detector was equipped with both right angle and low angle detection. Samples were separated in 0.1 M $NaNO_3$ with 5 mM NaN_3 at a flow rate of 0.6 mL/min. Data integration and analysis was done using Viscotek OmniSEC software. A refractive index increment (dn/dc) of 0.146 mL/g was used for calculations, and pullulan standards were used to calculate instrument constants.

Structural determinations were made by subjecting β-glucans to hydrolysis with lichenase and evaluating the proportion of the resulting two main structural components, β-(1→3) linked cellotriosyl and β-(1→3) linked cellotetraosyl. Enzyme incubation conditions and separation and analysis of released oligosaccharides are as described by Tosh et al.,[21] with the exception that data analysis was performed with Dionex Chromeleon software, version 6.5 (Dionex Corp., Sunnyvale, CA).

2.3. Rheology. Apparent viscosity measurements were taken using a controlled strain rheometer (ARES, TA Instruments, New Castle, DE) fitted with a cone and plate geometry (cone angle of 0.04 radians, 50 mm diameter). Apparent viscosity was measured in a shear rate range of 100−0.1 s^{-1}, and viscoelastic parameters G′, G″, and tan δ were obtained in the linear viscoelastic range (2% strain) using a parallel plate (25 mm plate, 1 mm gap) configuration from 0.01 to 10 Hz. For mixed molecular weight gels, viscosity and viscoelastic measurements were taken at 25 °C, while viscoelastic measurements for the model food gel were done at 37 °C. All measurements were performed in triplicate at minimum.

2.4. Large Deformation Mechanical Testing. Compression tests were performed using a TA.HD plus texture analyzer (Stable Micro Systems, Ltd., Godalming, Surrey, U.K.) equipped with a 38 mm diameter cylinder probe. Gels were compressed using a crosshead speed of 0.3 mm/s. Gels on a Teflon sheet were placed on the stationary bottom plate of the instrument, and mineral oil was applied to the top of the gel to prevent friction during compression and to allow for biaxial expansion of the gel. Force−displacement curves were used to determine hardness at 40% compression and Young's modulus (E). Measurements are the mean of at least 10 replicates for the mixed molecular weight gels and 6 replicates for the model food gels.

2.5. Differential Scanning Calorimetry (DSC). Gels for DSC analysis were prepared as outlined in section 2.1 and ,after setting 7 days, were weighed (80−90 mg) into high volume DSC pans. Using a model 2920 DSC from TA Instruments (TA Instruments, New Castle, DE), a temperature ramp of 5−120 °C was applied to the samples and reference pan containing 10 mM sodium phosphate buffer/1 mM

NaN_3. The peak temperature, calculated as the temperature at which point the heat flow was at a minimum, was obtained using Universal Analysis software (TA Instruments, New Castle, DE).

2.6. Microscopy. Micrographs were taken for 3, 4, and 5% LMW oat gels and HMW oat viscous solutions and mixed oat gels at HMW:LMW ratios of 50:50 and 75:25. Microscopic slides were prepared by creating an enclosed space for the β-glucan solutions to gel using 3 coverslips as described by Tosh et al.[21] Microscopic observation was conducted using a Zeiss Axioskop2 light microscope (Carl Zeiss MicroImaging Inc., Thornwood, NY) equipped with a 63× phase contrast oil immersion lens. A Spot CCD camera and Advanced Spot software (Diagnostic Instruments, Inc., Burlingame, CA) was used to capture images.

2.7. Statistical Analysis. Significant differences between measurements were determined using the data analysis package in Microsoft Excel or SigmaPlot 12.0. Two tailed *t* tests were used to determine significance in peak melting temperatures (T_p), and one way analysis of variance was used for hardness and firmness values. A confidence interval of 95% was required for determining significance ($P < 0.05$).

3. RESULTS AND DISCUSSION

3.1. Mixed Molecular Weight Oat β-Glucan Gels. Characteristics of each β-glucan used are given in Table 1.

Table 1. Characteristics of Oat β-Glucan (BG) High Molecular Weight (HMW) and Low Molecular Weight (LMW) Samples

	purity % (dwb)[a]	M_w[b]	Pd[c]	MR[d]
	Mixed MW Gels			
oat BG-HMW	92.0 ± 1.3	1,190,500	1.20	2.36
oat BG-LMW	92.0 ± 1.3	31,200	1.27	2.55
	Model Food Gels			
oat BG-HMW	95.8 ± 2.0	580,000	1.5	nd[e]
oat BG-LMW	93.5 ± 0.3	145,000	1.7	nd

[a]Dry weight basis. [b]Weight average molecular weight. [c]Polydispersity (weight average/number average molecular weight). [d]Molar ratio, peak area of DP3/DP4 × 1.321. [e]Not determined.

The original oat gum, with a weight average molecular weight (M_w) of 1,190,000, was used to prepare a LMW fraction, with a M_w of 31,200. The purity of the HMW glucan used in the mixed molecular weight gels was 92.0% and did not change during the preparation of the LMW fraction, although the molar ratio (MR) increased from 2.36 to 2.55 and the polydispersity (Pd) increased from 1.20 to 1.27.

Hydrolysis with lichenase yields 3-*O*-β-cellobiosyl-D-glucose (DP3) and 3-*O*-β-cellotriosyl-D-glucose (DP4) in proportion to the number of β-(1→3) cellotriosyl and β-(1→3) cellotetrosyl units, respectively. These two oligosaccharides represent the majority of the structure of cereal and lichenan β-glucans, but it is the relative proportion of the two that differentiates the samples. The MR of β-glucan, calculated as (DP3/DP4) × 1.321, has been used to characterize the relative proportion of these two oligosaccharides and typical values for oat, barley and lichenan are 1.9−2, 3−3.8 and 30, respectively (Cui et al.,[5] 2000; Tosh et al.,[21] 2004).

Figure 1 shows the shear rate dependence of apparent viscosity for freshly prepared 3% β-glucan solutions with HMW:LMW ratios of 0:100, 50:50, 75:25, and 100:0. These are initial measurements taken before the solutions were allowed to gel. Only the 3% is shown for simplicity, however its profile is representative of the 4 and 5% as well. As expected, for all concentration levels, the apparent viscosity declines with declining HMW β-glucan proportion in the sample. All

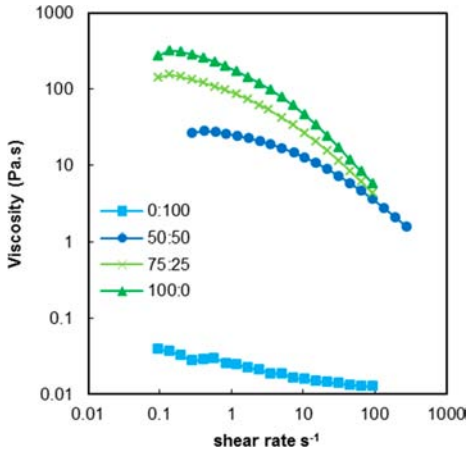

Figure 1. Shear rate dependence of viscosity for 3% β-glucan solutions with high molecular weight:low molecular weight (HMW:LMW) ratios of 0:100, 50:50, 75:25, and 100:0.

solutions were shear thinning, although the samples which included HMW β-glucan were markedly so when compared to the solution of only LMW oat β-glucan. This behavior is typical of polysaccharides because longer polymers tend to participate in more entanglements which are responsible for the shear thinning phenomenon.

Upon aging, the β-glucan solutions become more viscoelastic and, hence, more suitable for comparison by the moduli G' and G''. These were measured for the 3, 4, and 5% gels for all HMW:LMW proportions on days 3, 5, and 7 of aging. The elastic modulus G' on days 3 and 7 of aging for 3% gels at all four HMW:LMW proportions are shown in Figure 2A. The G' in the 100% and 50% LMW gels was the least frequency dependent, suggesting that the lower molecular weight β-glucan contributes to a more elastic gel structure. Low molecular weight β-glucan solutions are lower in apparent viscosity at the same concentration because they have fewer entanglements. The increased mobility of LMW β-glucans permits them to move more easily into conformations which allow the development of junction zones through hydrogen bonds. The 50% LMW gels had higher G' values than the 100% LMW gels, and the values were consistent at all frequencies, showing that they had the most stable network structure. The LMW β-glucan molecules appear to act as linker molecules between the HMW molecules so that the mixed molecular weight gels derive stiffness from both network formation and entanglements.

From a rheological perspective, a true elastic gel network has been established when G' is at least 1 order of magnitude greater than G'' and either modulus is not or is only slightly dependent on frequency.[29] The solutions prepared from 50 and 100% LMW β-glucan gelled by 3 days at all concentrations, while the 100% HMW solution did not gel, as indicated by the absence of a significant difference in magnitude between G' and G'' and the continued frequency dependence of G'. At 3% concentration, gels with 75% HMW β-glucan had G' and G'' traces that progressed from typical concentrated solution behavior (G'' predominating over G' at low frequencies while G' predominates at higher frequencies) on days 3 and 5 of aging to G' and G'' running in a parallel but frequency dependent manner by day 7. At 4%, the gels gave slightly frequency dependent but parallel G' and G'' traces by day 3 and by day 7 the moduli were frequency independent. At 5%

dx.doi.org/10.1021/jf405131d | J. Agric. Food Chem. 2014, 62, 3160−3167

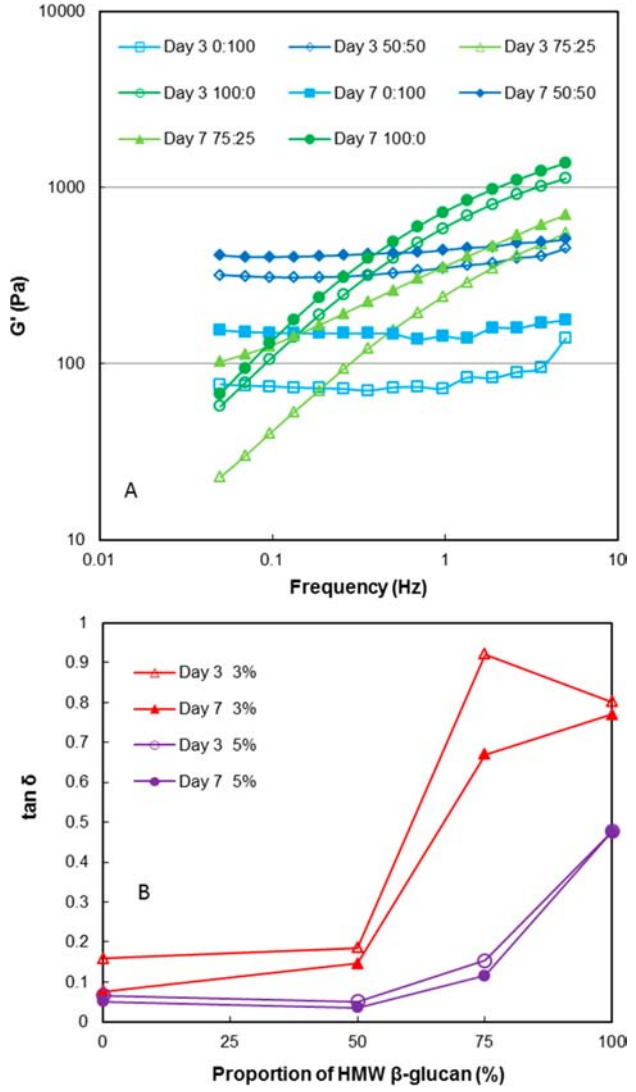

Figure 2. Frequency dependence of G' for 3% gels with high molecular weight:low molecular weight (HMW:LMW) ratios of 0:100, 50:50, 75:25, and 0:100 (A) and tan δ values at 1 Hz for 3% gels with increasing proportion of HMW β-glucan on days 3 and 7 (B).

concentration, the moduli were frequency independent by day 3.

The tan δ, which relates the energy lost to the energy stored (G''/G') in a system when subjected to a specific frequency, gives an indication of whether the system is dominated by viscous properties (tan δ >1) or solid properties (tan δ <1), and the values generally fall below 0.1 for gels, above 1 for concentrated solutions, and much higher for dilute solutions. Figure 2B shows tan δ values at 1 Hz for 3 and 5% gels on days 3 and 7. The 5% gels had lower tan δ values than the 3% gels at all HMW:LMW ratios. The tan δ values decreased from day 3 to day 7 at all points except the 100% HMW viscous solution at 5%. The effect of time was more pronounced in the 3% gels versus the 5% gels. The 4% gels had tan δ values between values for the 3 and 5% gels, however the data followed the same pattern (data not shown). More elastic gels, as indicated by lower tan δ values, were obtained when there was more LMW material in the gels. All solutions produced elastic gels or viscoelastic gels after 7 days with tan δ values below 1, however, the only samples with tan δ at or below 0.1 were the 3% gel with HMW:LMW ratio 0:100, the 4% gel with HMW:LMW 0:100 and 50:50, and the 5% gel with HMW:LMW 0:100, 50:50, and 75:25. Essentially, as the total β-glucan concentration of the gels increased, more HMW β-glucan could be incorporated while still achieving a true elastic gel. The dynamic rheological behavior of the gels can be explained by considering the mobility of the polymer molecules. The large number of entanglements encountered by the HMW β-glucan constrained their movement into suitable conformations for gelation and rearrangement into larger aggregated structures that make up the gel network. Therefore, as previously shown,[20,22,24] the low molecular weight β-glucan produced true gels because of their greater mobility. Addition of HMW β-glucan impeded the formation of intermolecular interactions and rearrangement of strands into aggregated networks.[23]

Calorimetric measurements were conducted to assess the effect of β-glucan concentration (3, 4, or 5%) and HMW:LMW ratio on the peak melting temperature (T_P) of the gels. Consistent with previous research,[20−22] the DSC endotherms were very broad, indicative of a system experiencing the effects of multiple interactions (Figure 3A). The peak temperature of the melting endotherm, which varied from 66 to 86 °C, was plotted versus the percent of HMW β-glucan in the gel for gels

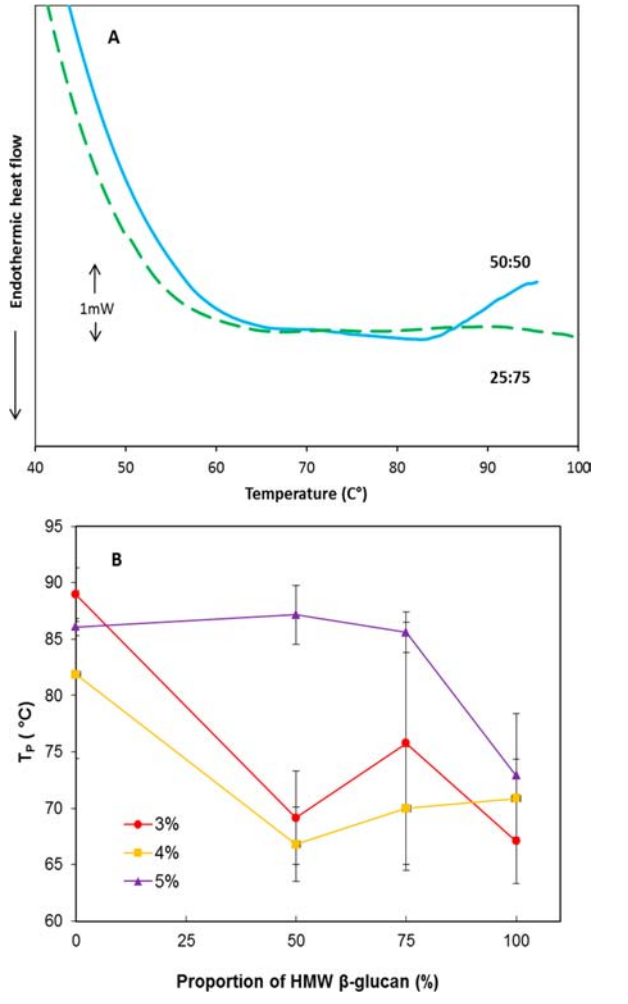

Figure 3. Typical DSC endotherms for 4% gels made using 50 and 75% high molecular weight (HMW) β-glucan (A) and peak melting temperature (T_P) of 3, 4, and 5% β-glucan gels as a function of proportion of HMW β-glucan.

dx.doi.org/10.1021/jf405131d | J. Agric. Food Chem. 2014, 62, 3160−3167

at 3, 4, and 5% (Figure 3B). The overall trend was toward higher T_P values at 0% HMW and lower T_P values at 100% HMW; however there was variability within this trend. For the 3% gels, significant differences were found between HMW:LMW ratio 0:100 and 50:50 (P = 0.00005) and 0:100 and 100:0 (P = 0.0001). For 4% gels, the T_P decreased from 100% LMW to 50%, then increased for the 75 and 100% HMW gels. A broad peak with a similar T_P was found for a 4% LMW barley β-glucan previously.[30] Significant differences were found between HMW:LMW ratios 0:100 and 100:0 (P = 0.031), 0:100 and 50:50 (P = 0.0013), and 0:100 and 75:25 (P = 0.0106). The 5% sample had a decrease in T_P from 0 to 25% HMW, then an increase until 50%, and then a decrease to 100%. At the 5% level, significant differences were observed between HMW:LMW ratios 0:100 and 100:0 (P = 0.0025).

An increase in T_P with a higher proportion of LMW β-glucan is consistent with a diffusion limited mechanism of gelation whereby β-glucan molecules in a system with a lower viscosity are able to move around and set up junction zones more quickly and easily. When the solution for gelation is composed entirely of HMW material, the entanglement that develops precludes swift movement of molecules into positions appropriate for junction zone formation and hence gelation. Rearrangement of the initial gel microstructure into aggregated structures was also constrained by HMW polymers.[23] With the exception of the 100% LMW gels, the highest T_P values were associated with the 5% gels with 0, 50, and 75% HMW. It was expected that gels of greater concentration would result in higher T_P values, given that T_P is a function of the number and stability of molecular interactions. The 3 and 4% gels generally had lower T_P values than the 5% gels, however at HMW:LMW ratio 0:100, the 3% gel had the highest T_P, although only significantly so versus the 4% gel (P = 0.035). At a HMW:LMW ratio of 0:100, the 3% concentration may have allowed more stable junction zone formation than the 4 or 5% because the molecules were more mobile. At HMW:LMW ratio 50:50, the T_P of the 5% gel was significantly higher than the 3 (P = 0.0005) or 4% (P = 0.0029) gel, at 75:25 the 5% was significantly higher than the 4% (P = 0.00096) only, and there was no significant difference in T_P among the concentrations of gels at 100:0.

The hardness (N) at 40% compression and firmness (Young's modulus) of mixed molecular weight gels varied with concentration and proportion of HMW β-glucan (Figure 4). The force required to compress the gels by 40% increased with increasing concentration and increasing proportion of HMW material, but only up to 25 or 50%. Hardness values declined between 50% and 75% HMW β-glucan across all concentrations (P > 0.05 for 3, 4, and 5% gels), and there was no significant difference between hardness values for gels with a 25:75 and 50:50 HMW:LMW ratio at the 3 and 5% concentration. However, at the 4% level, the hardness of 50:50 gels was significantly lower than that of 25:75 gels (P = 0.031). Essentially, when more than 50% of the β-glucan in the gel was HMW, the gel hardness declined. Similarly, Young's modulus increased with increasing gel concentration and the highest values were obtained for gels with either 25 or 50% HMW β-glucan. Essentially, gels with no HMW β-glucan or more than 50% HMW β-glucan deformed more with less force than did gels with an equal amount of HMW and LMW β-glucan. There was a significant difference (P < 0.05) in Young's modulus between the first two levels of HMW proportion (0 and 25%) for the 5% gels, however there was no significant

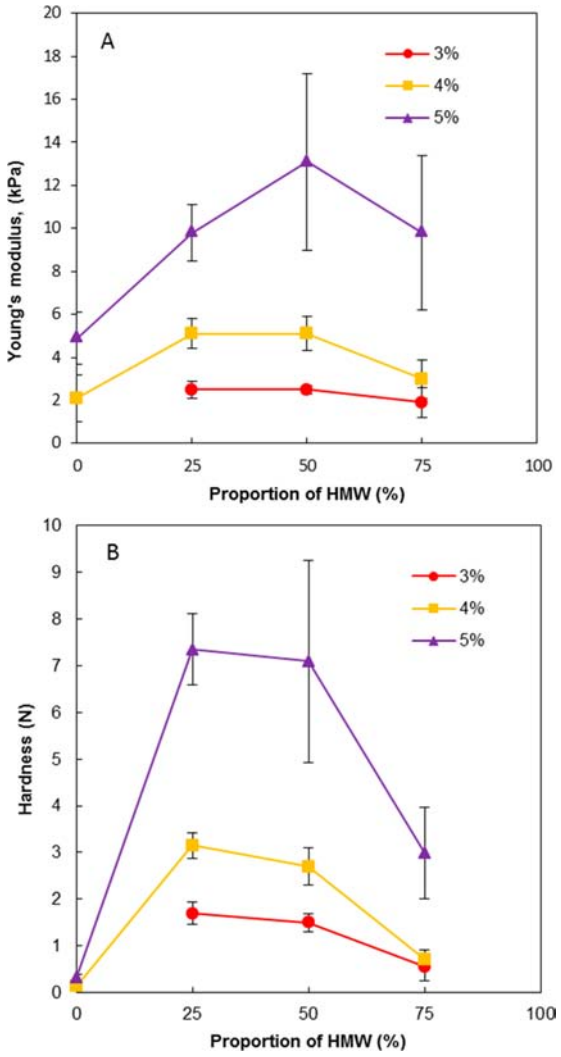

Figure 4. Firmness (A, Young's modulus) and hardness (B) for 3, 4, and 5% β-glucan gels with high molecular weight:low molecular weight (HMW:LMW) ratios of 0:100, 25:75, 50:50, and 75:25.

difference between the 50:50, 25:75, and 75:25 HMW:LMW ratios. The maximum firmness for the 4% gels occurred at 25% (5.13 kPa) and 50% (5.1 kPa) HMW β-glucan, with significantly lower values obtained at 0 and 75% HMW. As shown by small deformation measurements, the 100% LMW gels were the most elastic, indicating a structure that stored and released energy, but the gel network was weak and did not require a lot of force to compress. The addition of up to 50% HMW β-glucan increased the firmness and hardness of the gels, but this effect diminished as more HMW β-glucan was added. After 25 or 50% HMW β-glucan, the high viscosity of the mixtures hinders the movement of molecules into conformations conducive to hydrogen bonding and, therefore, junction zone formation. The LMW molecules appear to stabilize the gel structure at short distances whereas the HMW polymers contribute entanglements and longer range resistance to deformation. Hence, the gels are more viscoelastic and offer less resistance to flow. In 2003, Lazaridou et al.[20] found an increase in Young's modulus with increasing concentration for oat β-glucan gels (M_w 110,000, 6−12%), however, at constant concentration, the values initially increased with molecular weight, then decreased from M_w 65,000 to 250,000. Similarly, we found that firmness and hardness increased with the

dx.doi.org/10.1021/jf405131d | J. Agric. Food Chem. 2014, 62, 3160−3167

addition of HMW β-glucan to the gels, but after 50% addition, they decreased. By contrast, Vaikousi et al.[27] found that Young's modulus for 8% barley β-glucan gels decreased as molecular weight increased from 40,000 to 180,000, after which it stabilized.

There is substantial variation in published β-glucan gel firmness values, and the results obtained here are between the extremes of values reported thus far. Irakli et al.[26] reported Young's modulus values under 1 for 6% barley gels ranging from M_w 450,000 to 1.3 million, Lazaridou et al.[20] obtained values of 9.37−30.45 kPa for 8% β-glucan gels with molecular weights from 35,000 to 250,000, and values of 39.71 and 36.62 kPa for 8% oat beta-glucan gels where the M_w was 105,000 and 203,000, respectively, have been published.[20] Disparate results are expected given the dependency of gel properties on solubilization temperature,[31] concentration, molecular weight,[20,22,32] distribution,[19] and molecular structure .[22,32,33]

Microscopic examination of the gels reveals that the range in gel hardness and firmness results from differences in the gel network structure. The micrographs in Figure 5 show the

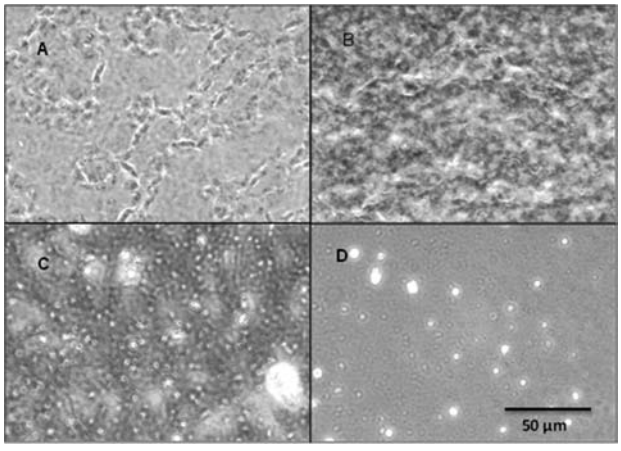

Figure 5. Micrographs obtained using phase contrast light microscopy of 4% β-glucan gels with HMW:LMW ratios of A, 0:100, B, 50:50, C, 75:25, and D, 100:0.

structure of gels with a total β-glucan concentration of 4% using phase contrast light microscopy. The aggregated β-glucan structures are clearly visible in image A, which contains only LMW β-glucan. In this sample, the β-glucan exists as hydrated fibers in a liquid solution. Low molecular weight β-glucan does not form a stable gel network that can bind sufficient water, and the network collapses easily, as indicated by the low firmness and hardness values from the large deformation tests. Gels with 50 or 75% LMW material gave the hardest, most elastic gels, as indicated respectively by the compressive force and Young's modulus data. Figure 5B shows a 50:50 gel which has a structure that is well-defined and regular in nature. In gels with a HMW:LMW ratio of 75:25 (Figure 5C) the gel structure is not as well-defined. The gelation process is diffusion limited, and the highly viscous, entangled HMW polymers retard gelation. However, the LMW polymers are able to diffuse through the solution and set up bridges between reactive sites on the longer polymers. Micrographs of gels composed entirely of HMW material (Figure 5D) do not show a regular structure, but bright spots may indicate aggregates.

During gelation, the number of hydrogen bonds between polymer molecules increases as they diffuse into conformations where runs of consecutive cellotriosyl units are aligned and form junction points. In the LMW solution, the polymers have more freedom to diffuse and the junction points form more frequently. In the solutions containing HMW β-glucan the entanglements retard the diffusion of the polymers, which hinders the formation network junction points. Each junction point that does form further impedes the mobility of the molecules, further slowing network formation. The entanglements and slow diffusion rates prevents gelling of the HMW solution. The greater mobility of the LMW polymers in solution allows them to act as linker molecules which create hydrogen bonded bridges between the slower, entangled HMW polymers. Previous investigations using atomic force microscopy have shown that HMW β-glucan tends to form larger clusters than LMW β-glucan.[24] After the initial clusters of polymers have formed, they rearrange in aggregated structures which make up the network visible in the light microscope. The dissimilarity in the aggregated network structures visible in the light microscope indicated that the differences in the initial gelation changed aggregation patterns and the final microstructure observed. Thus, mixed HMW−LMW gels exhibit high gel stiffness by maximizing both the entanglements and the number of junction points in the material.

3.2. Model Food Gel. A model food gel prepared from oat β-glucan solutions in HMW:LMW ratios of 0:100, 50:50, and 75:25 was used to assess the influence of added glucose on the gel properties. Measurements of molecular weight and purity for the β-glucans used to make model gel systems are available in Table 1. Although the terms HMW and LMW are used, it should be noted that oat β-glucans used for the model food gels were different from β-glucans used for the mixed molecular weight studies and, hence, had different molecular weights (M_w), polydispersities (Pd), and molar ratios (MR). The HMW oat β-glucan had a weight average molecular weight (M_w) of 580,000 versus 1,190,000 for the mixed molecular weight gels. Similarly, the MW of the LMW β-glucan used in the model food gel was higher (M_w 145,000 versus 31,200) than the β-glucan used for the mixed molecular weight gels. The LMW β-glucan was slightly more polydisperse than the HMW gum.

Gelled samples and controls (without added glucose) were subjected to small deformation oscillatory measurements to determine the relative contribution of viscous and elastic factors to the overall behavior of the gels. Figure 6 shows the frequency dependence of G' for samples and controls with differing HMW:LMW ratios. Overall, G' increased with increasing proportion of HMW β-glucan, however the 100% LMW gels were the least frequency dependent, regardless of the presence or absence of glucose. The 0 and 75% HMW gels without glucose had higher G' values than gels with the same ratio but no glucose. The behavior was different for the 50% HMW samples, which gave higher G' values for the sample with glucose at frequencies below 10 Hz, but lower G' values for the sample with glucose at higher frequencies. An examination of G' values shows that those without glucose were more frequency dependent at each HMW:LMW ratio.

The tan δ values at 1 Hz (Figure 7) increased with increasing proportion of HMW such that the values for 0% HMW, 50% HMW, and 75% HMW gels were 0.09, 0.3, and 0.5 respectively for gels with glucose and 0.1, 0.6, and 0.8 respectively for gels without glucose. The gels composed entirely of LMW β-glucan display more typical gel behavior, with tan δ values near 0.1, indicating behavior dominated by elastic properties. Overall, tan

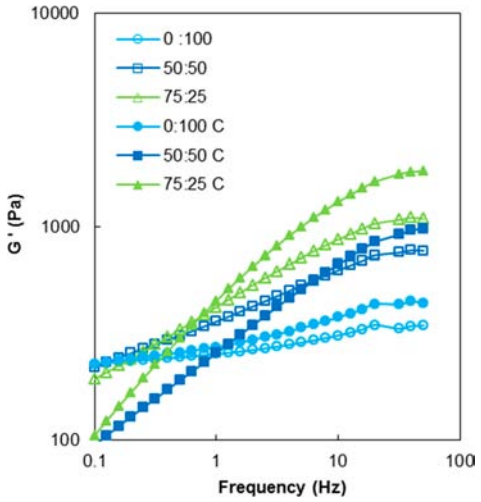

Figure 6. Frequency dependence of G' for model food gels with high molecular weight:low molecular weight (HMW:LMW) ratios of 0:100, 75:25, and 50:50.

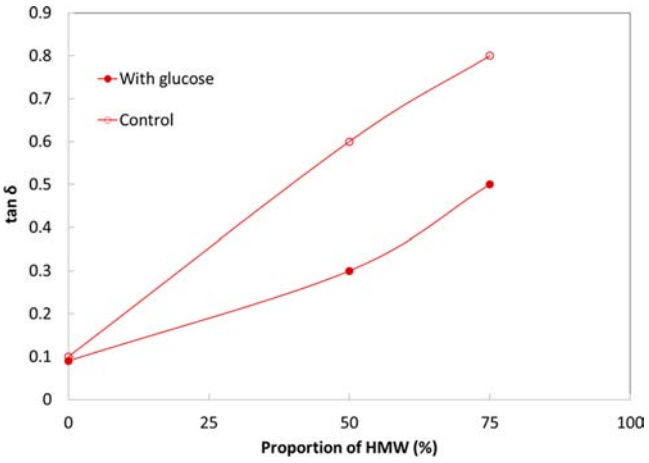

Figure 7. Tan delta at 1 Hz for model gels with high molecular weight:low molecular weight (HMW:LMW) ratios of 0:100, 50:50, and 75:25 with glucose and control gels without glucose.

δ values were slightly higher for gels without glucose, suggesting a contribution to elastic behavior by the glucose.

The hardness (N) at 40% compression and Young's modulus (E) were determined from the force displacement curves for the three model food gels and controls without glucose (Table 2). When no glucose was present, the firmness increased with increasing proportion of HMW β-glucan, and the hardness values were highest for the gel with 75% HMW. However, these trends were not observed when glucose was added to the gels, where no significant difference between hardness and firmness values was found, although the gel with 75% HMW gave the lowest hardness values. Added glucose competes for water, thereby slowing diffusion rates. Glucose may mitigate the effect of varying molecular weight by effectively increasing the concentration of β-glucan in solution and inhibiting the formation of junction zones. Additionally, these gels were less firm and required less force to compress than the similar gels prepared for the mixed molecular weight trial, perhaps reflecting the addition of a small amount of citric acid. For example, the firmness and hardness values for the 50:50 HMW:LMW gel at 4% were 5.1 and 2.7 N respectively,

Table 2. Young's Modulus and Hardness Measurements for Model Food Gels with and without Glucose

	Young's modulus[a]	hardness[a,b]
HMW:LMW[c] Ratio: Gels with Glucose		
0:100	0.86 ± 0.14 d	0.53 ± 0.10 d
50:50	0.79 ± 0.13 d	0.55 ± 0.12 d
75:25	0.88 ± 0.12 d	0.47 ± 0.10 ed
HMW:LMW Ratio Gels without Glucose (Control)		
0:100	0.51 ± 0.08 e	0.38 ± 0.04 e
50:50	0.54 ± 0.11 e	0.37 ± 0.10 e
75:25	0.82 ± 0.26 d	0.44 ± 0.12 ed

[a]Values are means ± SD. Values with different letters are significantly different ($p < 0.05$). [b]Hardness in Newtons at 40% compression (N). [c]High molecular weight:low molecular weight.

whereas for a gel prepared with the same composition but with the addition of citric acid and a small amount of flavoring, firmness and hardness values of 0.54 and 0.37 N were obtained. While the gels with citric acid gave much lower large deformation results than those without, the effects of the acid may have been mitigated by the addition of glucose as, overall, hardness and Young's modulus values were lower for the model food gels without glucose compared to gels with glucose.

3.3. Conclusions. Gel properties, as measured by small and large deformation measurements, varied with proportion of HMW or LMW β-glucan. The mix of 50% HMW and 50% LMW produced the hardest, but also the most elastic, gels. By mixing high and low molecular weight β-glucans together, the relative contribution by each type of molecule to gel structure and texture is exploited. The differences observed in gel texture based on proportion of HMW and LMW β-glucan are diminished by the incorporation of other components in the gel such as citric acid and glucose. Hence, by controll of β-glucan molecular weight and product formulations, gel properties can be controlled in order to achieve desired textural properties.

AUTHOR INFORMATION

Corresponding Author

*Tel: 00 + 1 226 217-8067. Fax: 00 + 1 226 217-8181. E-mail: Susan.Tosh@agr.gc.ca.

Present Addresses

‡Department of Agricultural and Environmental Sciences, College of Agriculture, Human and Natural Sciences, Tennessee State University, Nashville, TN. Tel: 00 + 1 615 963-5824. E-mail: ywu@Tnstate.edu.

∥Lecturer, Glycemic Index Research Unit, Temasek Polytechnic, 21 Tampines Avenue 1, Singapore 529757.

Notes

The authors declare no competing financial interest.

⊥Deceased.

REFERENCES

(1) Woodward, J. R.; Fincher, G. B.; Stone, B. A. Water soluble (1−3)(1−4)-β-glucans from barley (*Hordeum vulgare*) endosperm. II. Fine structure. *Carbohydr. Polym.* **1983**, *3*, 207−225.

(2) Wood, P. J.; Weisz, J.; Blackwell, B. A. Molecular characterization of cereal β-D-glucans. Structural analysis of oat β-D-glucan and rapid structural evaluation of β-D-glucans from different sources by HPLC of oligosaccharides released by lichenase digestion. *Cereal Chem.* **1991**, *68*, 31−39.

(3) Cui, W.; Wood, P. J.; Blackwell, B. A.; Nikiforuk, J. Physicochemical properties and structural characterization by two-dimensional NMR spectroscopy of wheat β-D-glucan-comparison with other cereal β-D-glucans. *Carbohydr. Polym.* **2000**, *41*, 249−258.
(4) Wood, P. J.; Weisz, J.; Blackwell, B. A. Structural studies of (1→3)(1→4)-β-D-glucans by $_{13}$C-nuclear magnetic resonance spectroscopy and by rapid analysis of cellulose-like regions using high performance anion exchange chromatography of oligosaccharides released by lichenase. *Cereal Chem.* **1994**, *71*, 301−307.
(5) Cui, W.; Wood, P. J. Relationships between structural features, molecular weight and rheological properties of cereal β-glucans. In *Hydrocolloids: physical chemistry and industrial applications of gels, polysaccharides and proteins*; Nishinari, K., Ed.; Elsevier Science Ltd.: Amsterdam, The Netherlands, 2000; Vol. *1*, pp 159−168.
(6) Ren, Y.; Ellis, P. R.; Ross-Murphy, S. B.; Wang, Q.; Wood, P. J. Dilute and semi-dilute solution properties of (1→3),(1→4)-β-D-glucan, the endosperm cell wall polysaccharide of oats (*Avena sativa* L.). *Carbohydr. Polym.* **2003**, *53*, 401−408.
(7) Lan-Pidhainy, X.; Brummer, Y.; Tosh, S. M.; Wolever, T. M.; Wood, P. J. Reducing β-glucan solubility in oat bran muffins by freeze-thaw treatment attenuates its hypoglycemic effect. *Cereal Chem.* **2007**, *84*, 512−517.
(8) Tosh, S. M.; Brummer, Y.; Wolever, T. M. S.; Wood, P. J. Glycemic response to oat bran muffins treated to vary molecular weight of β-glucan. *Cereal Chem.* **2008**, *85*, 211−217.
(9) Wood, P. J. Evaluation of oat bran as a soluble fibre source. Characterization of oat β-glucan and its effects on glycaemic response. *Carbohydr. Polym.* **1994**, *25*, 331−336.
(10) Braaten, J. T.; Wood, P. J.; Scott, F. W.; Wolynetz, M. S.; Lowe, M. K.; Bradley-White, P.; Collins, M. W. Oat β-glucan reduces blood cholesterol concentration in hypercholesterolemic subjects. *Eur. J. Clin. Nutr.* **1994**, *48*, 465−474.
(11) Davidson, M. H.; Dugan, L. D.; Burns, J. H.; Bova, J.; Story, K.; Drennan, K. B. The hypo-cholesterolemic effects of β-glucan in oatmeal and oat bran. *JAMA* **1991**, *265*, 1833−1839.
(12) Wolever, T. M. S.; Tosh, S. M.; Gibbs, A. L.; Brand-Miller, J.; Duncan, A. M.; Hart, V.; Lamarche, B.; Thomson, B. A.; Duss, R.; Wood, P. J. Physicochemical properties of oat β-glucan influence its ability to reduce serum LDL cholesterol in humans: a randomized clinical trial. *Am. J. Clin. Nutr.* **2010**, *92*, 723−732.
(13) Regand, A.; Chowdhury, Z.; Tosh, S. M.; Wolever, T. M. S.; Wood, P. The molecular weight, solubility and viscosity of oat β-glucan affect human glycemic response by modifying starch digestibility. *Food Chem.* **2011**, *129*, 297−304.
(14) Symons, L. J.; Brennan, C. S. The influence of (1−3) (1−4)-β-D-glucan rich fractions from barley on the physicochemical properties and in vitro reducing sugar release of white wheat breads. *J. Food Sci.* **2004**, *69*, C463−C467.
(15) Jenkins, D. J. A.; Wolever, T. M. S.; Leeds, A. R.; Gassull, M. A.; Haisman, P.; Dilawari, J.; Goff, D. V.; Metz, G. L.; Alberti, K. G. M. M. Dietary fibres, fibre analogues, and glucose tolerance: importance of viscosity. *Br. Med. J.* **1978**, *1*, 1392−1394.
(16) Battilana, P.; Ornstein, K.; Minhira, K.; Schwarz, J. M.; Acheson, K.; Schneiter, P.; Burri, J.; Jequier, E.; Tappy, L. Mechanisms of action of β-glucan in post prandial glucose metabolism in healthy men. *Eur. J. Clin. Nutr.* **2001**, *55*, 327−333.
(17) Lazaridou, A.; Biliaderis, C. G.; Izydorczyk, M. S. Cereal β-glucans. In *Functional Food Carbohydrates*; Biliaderis, C. G., Izydorczyk, M. S., Eds.; CRC Press: Boca Raton, FL, 2007; pp 1−72.
(18) Doublier, J.-L.; Wood, P. J. Rheological properties of aqueous solutions of (1→3)(1→4)-β-D-glucan from oats (*Avena sativa* L.). *Cereal Chem.* **1995**, *72*, 335−340.
(19) Böhm, N.; Kulicke, W.-M. Rheological studies of barley (1→3) (1→4)-β-D-glucan in concentrated solution: mechanistic and kinetic investigation of the gel formation. *Carbohydr. Res.* **1999**, *315*, 302−311.
(20) Lazaridou, A.; Biliaderis, C. G.; Izydorczyk, M. S. Molecular size effects on rheological properties of oat β-glucans in solution and gels. *Food Hydrocolloids* **2003**, *17*, 693−712.
(21) Tosh, S. M.; Brummer, Y.; Wood, P. J.; Wang, Q.; Weisz, J. Evaluation of structure in the formation of gels by structurally diverse (1→3)(1→4)-β-D-glucans from four cereal and one lichen species. *Carbohydr. Polym.* **2004**, *57*, 249−259.
(22) Tosh, S. M.; Wood, P. J.; Wang, Q.; Weisz, J. Structural characteristics and rheological properties of partially hydrolysed oat β-glucan: the effects of molecular weight and hydrolysis method. *Carbohydr. Polym.* **2004**, *55*, 425−436.
(23) Kontogiorgos, V.; Vaikousi, H.; Lazaridou, A.; Biliaderis, C. G. A fractal analysis approach to viscoelasticity of physically cross-linked barley β-glucan gel networks. *Colloids Surf. B* **2006**, *49*, 145−152.
(24) Agbenorhevi, J. K.; Kontogiorgos, V.; Kirby, A. R.; Morris, V. J.; Tosh, S. M. Rheological and microstructural investigation of oat β-glucan isolates varying in molecular weight. *Int. J. Biol. Macromol.* **2011**, *49*, 369−377.
(25) Moschakis, T.; Lazaridou, A.; Biliaderis, C. G. Using particle tracking to probe the local dynamics of barley β-glucan solutions. *Procedia Food Sci.* **2011**, *1*, 294−301.
(26) Irakli, M.; Biliaderis, C. G.; Izydorczyk, M. S.; Papadoyannis, I. N. Isolation, structural features and rheological properties of water-extractable β-glucans from different Greek barley cultivars. *J. Sci. Food Agric.* **2004**, *84*, 1170−1178.
(27) Vaikousi, H.; Biliaderis, C. G.; Izydorczyk, M. S. Solution flow behaviour and gelling properties of water-soluble barley (1→ 3, 1→ 4)-β-glucans varying in molecular size. *J. Cereal Sci.* **2004**, *39*, 119−137.
(28) Wood, P. J.; Weisz, J.; Fedec, P.; Burrows, V. D. Large-scale preparation and properties of oat fractions enriched in (1→3)(1→4)-β-D-glucan. *Cereal Chem.* **1989**, *66*, 97−103.
(29) Morris, E.; Nishinari, K.; Rinauda, M. Gelation of gellan-A review. *Food Hydrocolloids* **2012**, *28*, 373−411.
(30) Kontogiorgos, V.; Ritzoulis, C.; Biliaderis, C. G.; Kasapis, S. Effect of barley β-glucan concentration on the microstructural and mechanical behaviour of acid-set sodium caseinate gels. *Food Hydrocolloids* **2006**, *20*, 749−756.
(31) Tosh, S. M.; Wood, P. J.; Wang, Q. Gelation characteristics of acid-hydrolysed oat β-glucan solutions solubilized at a range of temperatures. *Food Hydrocolloids* **2003**, *17*, 523−527.
(32) Lazaridou, A.; Biliaderis, C. G. Cryogelation of cereal β-glucans: structure and molecular size effects. *Food Hydrocolloids* **2004**, *18*, 933−947.
(33) Lazaridou, A.; Biliaderis, C. G.; Micha-Screttas, M.; Steele, B. R. A comparative study on structure-function relations of mixed-linkage (1−3), (1−4) linear β-D-glucans. *Food Hydrocolloids* **2004**, *18*, 837−855.

in the molecular weight, M/G ratio, MG sequence, and the entire molecular conformation of alginates seem to be responsible for their diversity of physicochemical properties and bioactivities.[16] It has been reported that unsaturated AOS promote the growth of bifidobacteria and induce the cytotoxic cytokines in human mononuclear cells and murine macrophage RAW264.7 cells, whereas the original alginate polymers or saturated AOS have no such effects.[18,19] Further study showed that unsaturated AOS improved the growth rate of *Chlamydomonas reinhardtii* and increased the levels of the fatty acids C16:0, C18:2 cis, and C18:3 n-3 but not saturated AOS.[12] Similar structure−activity relationship profiles were also found in the inducing effects of AOS on IL-1α, IL-1β, and IL-6 secretion from RAW264.7 cells, and the most potent activities in G8 and M7 oligomers were observed.[18] Moreover, the M/G ratio also seems to influence these activities, besides the molecular sizes.[20]

In the present study, we investigated the mechanisms of the immunomodulatory effects of alginate oligosaccharides on murine macrophage RAW264.7 cells and their structure−activity relationships from the following aspects: (1) the effect of several AOS, such as guluronate oligosaccharides and mannuronate oligosaccharides prepared by enzymatic degradation, acid hydrolysis and oxidative degradation, respectively, and also the effect of G2−G9 from GOS-ED on NO production in RAW264.7 cells; in addition, we investigated (2) the potent stimulatory effect of GOS-ED on RAW264.7 macrophages activation to induce the production of NO, ROS, and TNF-α and the activation of NF-κB and MAP kinase signaling pathways.

MATERIALS AND METHODS

Reagent. Sodium alginate (1000-cps grade) was purchased from Nuotai (Shanghai, China) and used without further purification. Bacterial alginate lyase from *Pseudoalteromonas* sp. strain no. 272 was prepared as described previously.[21] Trizol reagent was purchased from Invitrogen Co. (Carlsbad, CA). 2′, 7′-Dichlorofluorescein diacetate (DCF-DA) was from Beyotime Inst Biotech (Jiangsu, China). Pyrrolidine dithiocarbamate (PDTC) and NG-nitro-L-arginine methyl ester (L-NAME) were purchased from Sigma-Aldrich (St. Louis, MO). All other chemicals were commercially available products with the highest grade.

Preparation of Alginate Oligosaccharides (AOS). Polyguluronate (PG) and polymannuronate PM (DP = 20−24) were prepared from sodium alginate as described previously.[22] The homogeneity of the prepared polyuronates was confirmed by the analysis of circular dichroic (CD) spectrum using a Jasco spectropolarimeter J-815 based on the method of Morris et al.[23] The chemical structures of PG and PM were analyzed by the infrared (IR) spectra with Bruker Vertex 70 according to the method of Linker et al.[24]

PG and PM were digested with bacterial alginate lyase[21] to produce GOS-ED and MOS-ED, which have an unsaturated terminal structure with a double bond. GOS-AH and MOS-AH, which lack the unsaturated terminal structure with a double bond, were prepared from PG and PM by the acid hydrolysis method.[12] To prepare GOS-OD and MOS-OD, which have a carboxyl group at the 1-position of the reducing end, PG and PM were incubated with 5% H_2O_2 solutions at a final concentration of 8% at 90 °C for 2 h. Before use, all alginate samples were filtered through an endotoxin-removing filter (0.22 μm) (Millipore Co., Billerica, MA). The schematic representations of chemical structures of AOS using three different preparation ways were shown in Figure 1.

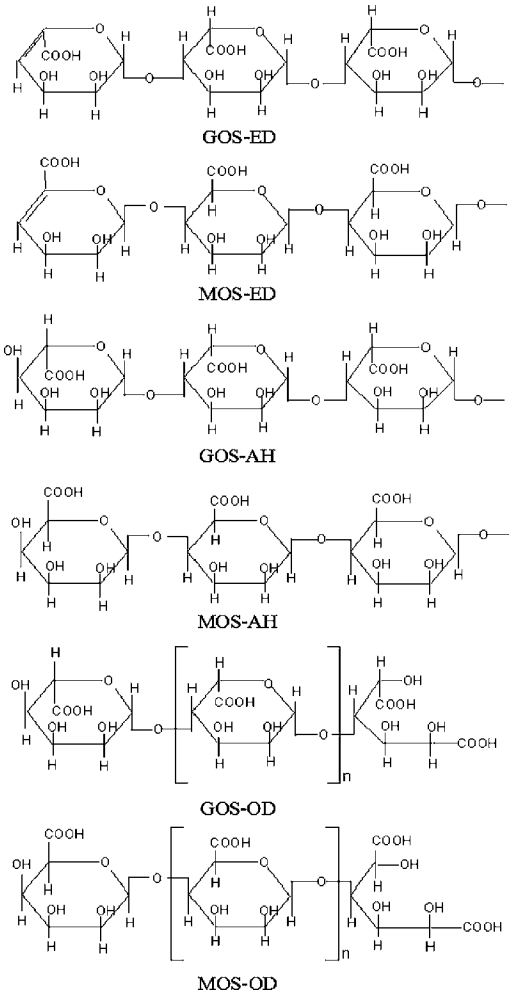

Figure 1. Schematic representation of chemical structures of guluronate and mannuronate oligosaccharides (enzymatic degradation—acid hydrolysis and oxidative degradation) used in this study.

TLC Analysis. Thin-layer chromatography (TLC) analysis was used to analyze the size and the DP of each AOS. The reaction product mixtures were loaded onto a precoated Silica Gel 60 TLC aluminum plate (2.5 cm × 7.0 cm, Merck, Germany) and developed with a solvent system consisting of *n*-butanol/formic acid/water (2:2:1 or 6:6:1, v/v/v). The developed plate was stained by dipping in a diphenylamine−aniline−phosphoric acid reagent (1 mL of 37.5% HCl, 2 mL of aniline, 10 mL of 85% H_3PO_4, 100 mL of ethyl acetate, and 2 g of diphenylamine) at RT for 3 s and then heated at 100 °C for 10 s.

Isolation and Purification of GOS-ED. The isolation and purification of each oligosaccharide derived from GOS-ED were conducted by a P-6 Bio Gel chromatography (Bio-Rad Labs, Richmond, CA) (2.6 × 100 cm) as described previously.[21] The phosphate in each fraction was removed by gel-filtration chromatography equipped with a P-2 Bio Gel (Bio-Rad Labs, Richmond, CA) (1.6 × 60 cm).

Cell Culture. Murine macrophage RAW264.7 cells, purchased from Shanghai Inst of Biochem and Cell Biol (Shanghai, China), were cultured at 37 °C in RPMI-1640 medium supplemented with 10% FBS, 100 IU/ml penicillin, and 100 μg/mL streptomycin in humidified atmosphere with 5% CO_2.

dx.doi.org/10.1021/jf405633n | J. Agric. Food Chem. 2014, 62, 3168−3176

Cytotoxicity. The cytotoxic effects of saccharide samples were assessed by measuring cell viability using a tetrazolium salt (WST-8)-based colorimetric assay in the Cell Counting Kit-8 (Dojindo, Kumamoto, Japan).[25]

NO Assay. To estimate NO level in RAW264.7 cells, nitrite, a stable reaction product of NO with molecular oxygen, was measured by Griess assay as described previously.[10] Briefly, adherent RAW264.7 cells in 96-well plates (2×10^5 cells/well) were treated with saccharide samples at the concentration of 1 mg/mL in the growth medium at 37 °C. After 24 h of treatment, 50 μL of each cultured supernatant was collected and mixed with 100 μL of Griess reagent.[10] After 10 min of incubation at RT, the optical density was measured at 540 nm using a Spectra Max microplate reader (Molecular Devices, LLC, Sunnyvale, CA). A calibration curve was made with a known concentration of $NaNO_2$ standard solution. For the time-course analysis of NO production, RAW264.7 cells were treated with tested samples at the concentration of 1 mg/mL in the growth medium at 37 °C, and nitrite levels in each cultured supernatant were measured at 3, 6, 12 and 24 h, respectively. For the concentration-dependent analysis of NO production, RAW264.7 cells were treated with varying concentrations of tested samples (0−1 mg/mL) for 24 h in the growth medium at 37 °C, and then the nitrite levels in each well were measured. LPS (1 μg/mL), which can significantly induce NO production in RAW264.7 cells, was used as positive control.

RNA Isolation, cDNA Synthesis, and RT-PCR for iNOS mRNA. Total cellular RNA was extracted from treated cells with Trizol reagent ($RNA_{fast200}$, Fastagen, China). Total RNA (1 μg) was reverse transcribed with an oligo dT primer in a 10 μL using PrimeScript first strand cDNA Synthesis Kit (TaKaRa Biotechnology Co., Ltd., Dalian, China) according to the manufacturer's instruction. PCR was performed with 1 cycle of 3 min at 95 °C, 25 cycles of 55 s at 93 °C, 45 s at 60 °C, 40 s at 72 °C and 1 cycle of 100 s at 72 °C, in a 50 μL reaction mixture containing 25 μL of Premix Taq (TaKaRa Biotechnology Co., Ltd., Dalian, China), 1 μL of forward and reverse inducible nitric oxide synthase (iNOS) primers (20 μM each) or β-actin primers (20 μM each), 5 μL of first strand cDNA, and 18 μL of nuclease-free water. The primer sequences used were 5′-CAACCAGTATTATGGCTCCT-3′ (forward) and 5′-GTGACAGCCCGGTCTTTCCA-3′ (reverse) for mouse iNOS and 5′-GGAGAAGATCTGGCACCACACC-3′ (forward) and 5′-CCTGCTTGCTGATCCACATCTGCTGG-3′ (reverse) for mouse β-actin.[10] The β-actin primer was used as an internal control. Each PCR reaction (6 μL) product was run on 1% agarose gels containing 0.1 μg/mL ethidium bromide, and the amplified products (845 bp for iNOS, 850 bp for β-actin) were observed by an G: BOX Syngene imaging system (Gene Company Ltd., Hong Kong).

Western Blot Analysis. After different treatments, cells (3×10^6 cells) were lysed in radio immunoprecipitation assay lysis buffer (Biocolors, Shanghai, China) at 4 °C for 30 min. Cell lysates (30 μg of protein for each sample) were separated by 8% SDS-polyacrylamide gel electrophoresis (SDS-PAGE), transferred onto a polyvinylidene difluoride (PVDF) membrane (Amersham Pharmacia Biotech., England, U.K.), blocked with 5% skim milk, and hybridized with antimouse iNOS antibody (dilution, 1:1,000) (Cell Signaling Technology, Inc., Beverly, MA). After incubation with a horseradish-peroxidase-conjugated secondary antibody at RT, immune-reactive proteins were detected by using a chemiluminescent ECL assay kit (Amersham Pharmacia Biosciences, England, U.K.) according to the manufacturer's instructions. Western blot bands were visualized using a LAS3000 Luminescent image analyzer (Fujifilm Life Science, Tokyo, Japan).

The analyses of IκB-α and phospho-IκB-α in cytosolic extracts and NF-κB p65 in nuclear extracts were performed. Adherent RAW264.7 cells (4×10^6 cells) were incubated with 1 mg/mL of saccharides at 37 °C for 1 h. Thereafter, the cells were washed three times with ice-cold PBS and incubated with 100 μL ice-cold cytosol extraction buffer (10 mM HEPES, pH 7.9, 1.5 mM $MgCl_2$, 10 mM KCl, 0.2% Igepal CA-630, 1 mM dithiothreitol, 20 mM β-glycerophosphate, 1 mM sodium orthoranadate, 0.5 mM phenylmethysulfonyl fluoride, 1 μg/mL leupeptin, and 1 μg/mL aprotinin) for 25 min on ice. The cytosolic extracts were collected after centrifugation at 7000*g* for 5 min at 4 °C. The nuclear pellets were resuspended in 30 μL of ice-cold nuclear extraction buffer (20 mM HEPES, pH 7.9, 1.5 mM $MgCl_2$, 0.45 M NaCl, 25% glycerol, 0.2 mM EDTA, 1 mM dithiothreitol, 0.5 mM phenylmethysulfonyl fluoride, 1 μg/mL leupeptin, and 1 μg/mL aprotinin) and incubated on ice for 25 min. The nuclear extracts were then obtained after centrifugation at 15 000*g* for 10 min at 4 °C. After protein quantitation, the nuclear and cytosolic extracts were separated by 12.5% SDS-PAGE. The Western blot analysis was conducted similar to the method described above with anti-NF-κB p65, anti-IκB-α, and antiphospho-IκB-α antibodies (Cell Signaling Technology, Inc., Beverly, MA).

For the analysis of MAP kinases, adherent RAW264.7 cells (3×10^6 cells) were treated with 1 mg/mL of each saccharide in the serum-free medium at 37 °C for 10 min. The whole-cell lysates were prepared from the treated cells. Samples containing 30 μg of proteins were subjected to SDS-PAGE in 12.5% polyacrylamide gel, and Western blot analysis using appropriate antibodies against phosphorylated and nonphosphorylated p38, JNK, and ERK MAP kinases (Cell Signaling Technology, Beverley, MA) were carried out as described above.

Intracellular ROS Measurement. The fluorescent probe DCF-DA was used to measure intracellular accumulation of ROS as described previously.[26] For this purpose, DCFH-DA solution (10 μM) was added to the suspension of each saccharide-treated cells (5×10^5 cells/ml), and the mixture was incubated at 37 °C for 20 min. Cells were then washed three times with PBS by centrifugation (1500*g*), and finally the fluorescence intensity of cell suspension was measured by the fluorescence activated cell sorting (FACS) system (Becton Deckinson, San Jose, CA) with excitation and emission wavelengths of 488 and 525 nm, respectively.

Cytokine Measurement. Adherent RAW264.7 cells in 96-well plates (2×10^5 cells/well) were treated with saccharides at the concentration of 1 mg/mL for 24 h in the growth medium at 37 °C. The levels of TNF-α in the culture medium were measured using a mouse TNF-α quantikine ELISA kit (R&D Systems, Inc., Minneapolis, MN), following the manufacturer's instructions.

Statistical Analysis. All of the experiments were repeated at least three times. The data are expressed as the means ± standard deviation (SD) and analyzed using a *t*-test or one-way ANOVA to determine any significant differences. A value of $p < 0.05$ was considered statistically significant.

RESULTS

Preparation and Structure Analysis of AOS. The CD analysis showed a high homogeneity of polyguluronate (PG) and polymannuronate (PM) (data not shown). The IR spectra

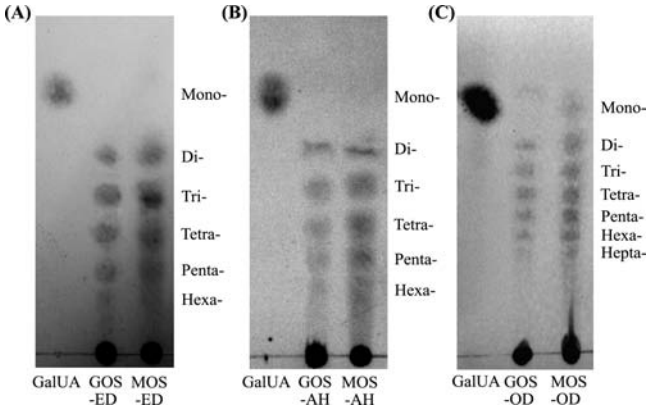

Figure 2. TLC of AOS prepared by different ways. The oligosaccharide solutions (25 mg/mL, 0.5 μL of each) were loaded onto a precoated Silica Gel 60 TLC aluminum plate and developed with a solvent system consisting of *n*-butanol/formic acid/water (2:2:1 or 6:6:1, v/v/v). The developed plate was stained by dipping in diphenylamine−aniline−phosphoric acid reagent (1 mL of 37.5% HCl, 2 mL of aniline, 10 mL of 85% H_3PO_4, 100 mL of ethyl acetate, and 2 g of diphenylamine) for 3 s and heated at 100 °C for 10 s. The average DP of GOS-ED and MOS-ED (A), GOS-AH and MOS-AH (B), and GOS-OD and MOS-OD (C) was measured using TLC analysis.

of PG and PM are very similar, but they show differences in the absorption peaks at 789 cm^{-1} and 821 cm^{-1}, indicating the unique distinction of PG and PM (data not shown).

The average DP of all kinds of AOS was measured by TLC analysis. As shown in Figure 2A−C, in all lanes, the spots corresponding to the oligosaccharides having 2−7 saccharide units were detected, whereas the spots at the origin corresponding to polysaccharides and oligosaccharides with >16 saccharide units were the most intense, indicating that AOS with average DP of 5 were obtained by three preparation ways used in this study.

GOS-ED Induces NO Production in RAW264.7 Cells. None of alginate polysaccharides (PG and PM) or AOS (-ED, -AH, and -OD) showed cytotoxic effects on RAW264.7 cells even up to a concentration of 1 mg/mL in WST-8 assay (data not shown). Hence, it is considered that any observed changes on NO production in RAW264.7 cells or related events in the following studies are not due to the cytotoxicity of alginate-derived saccharides.

Next, we investigated NO production induced by PG, PM, and AOS (GOS-ED, -AH, -OD and MOS-ED, -AH, -OD) in RAW264.7 cells. As shown in Figure 3A, only GOS-ED significantly enhanced NO production within all tested alginate polysaccharides and oligosaccharides, whereas all other saccharides showed no significant activity. Furthermore, GOS-ED-induced NO production in a time- and concentration-dependent manner, and the nitrite level reached the maximum in RAW264.7 cells treated with 1 mg/mL of GOS-ED for 24 h (Figure 3B,C).

To further analyze the structure−activity relationship of GOS-ED, the enzymatically digested PG was applied to a column Bio Gel P-6. The elution profile shown in Figure 4A

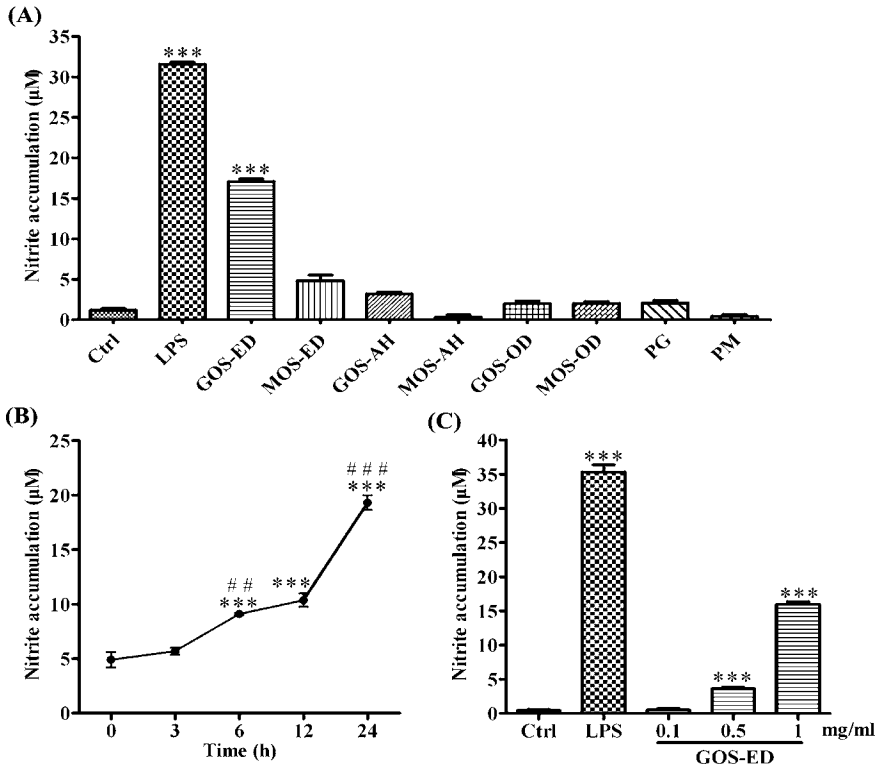

Figure 3. Effects of GOS (-ED, -AH, -OD), MOS (-ED, -AH, -OD), PG, and PM on NO production in RAW264.7 cells. Adherent RAW264.7 cells (2×10^5 cells/well) were cultured in 96-well plates. (A) RAW264.7 cells were incubated with 1 mg/mL of GOS (-ED, -AH, -OD), MOS (-ED, -AH, -OD), PG, and PM at 37 °C in the growth medium, respectively. After 24 h, the nitrite levels in the culture medium were measured by Griess assay, as described in Methods. (B) RAW264.7 cells were incubated with 1 mg/mL of GOS-ED for 3, 6, 12, and 24 h. After that, the nitrite levels in the culture medium were measured. (C) RAW264.7 cells were incubated with GOS-ED in different concentrations (0.1, 0.5, and 1 mg/mL). After 24 h, the nitrite levels in the culture medium were measured. LPS (1 μg/mL) was used as a positive control. Each value represents mean ± SD of triplicate measurements. * indicates significant differences between various time groups and 0 time group, * $p < 0.05$, ** $p < 0.01$, and *** $p < 0.001$, respectively. # indicates significant differences between time groups and previous time group, ## $p < 0.01$ and ### $p < 0.001$, respectively.

dx.doi.org/10.1021/jf405633n | J. Agric. Food Chem. 2014, 62, 3168−3176

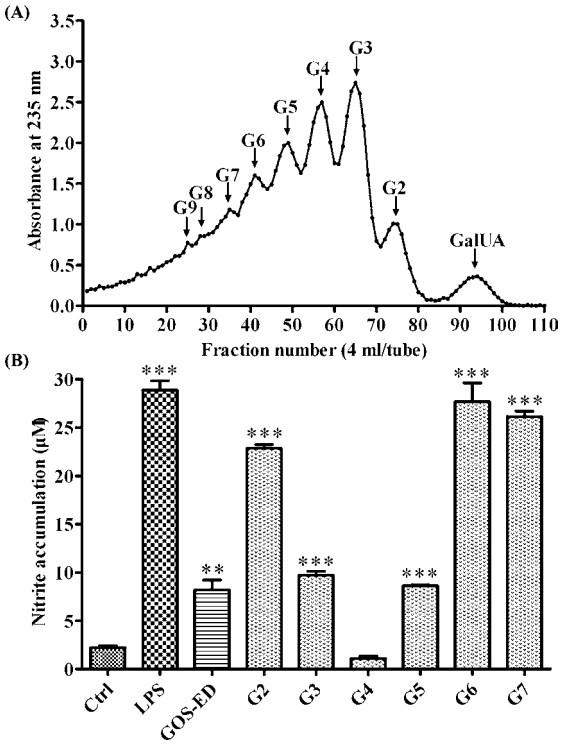

Figure 4. Effects of guluronate dimer to heptamer (G2−G7) on NO production in RAW264.7 cells. (A) GOS-ED solution (3 mL, 50 mg/mL in distilled water) was put on a column of Bio Gel P-6 equilibrated with 50 mM phosphate buffer, pH 6.5. Eluates were examined for absorbance at 235 nm. Gal UA: monomer; G2−G9: guluronate dimer-nonamer. (B) RAW264.7 cells were incubated with 0.5 mg/mL of GOS-ED and G2−G7, respectively. After 24 h, the nitrite levels in culture medium were measured. LPS (1 μg/mL) was used as a positive control. Each value represents mean ± SD of triplicate measurements.

indicated that GOS-ED was a mixture of oligomers from dimer to nonamer (G2−G9), and the fractions from G2 to G9 were obtained as relatively purified fractions. As shown in Figure 4B, purified G2, G6, and G7 fractions showed even higher activity than GOS-ED, and the highest activity was observed in G6 fraction. Meanwhile, G3 and G5 fractions showed nearly equal activity to GOS-ED, although the G4 fraction had almost no activity. The other notable founding was that G8 and G9 fractions were detected as precipitation with Griess reagent, so they were not suitable for this analysis.

GOS-ED Induces iNOS Expression in RAW264.7 Cells. As we have known, NO is produced by the activation of iNOS from L-arginine in macrophages.[27] As shown in Figure 5A−C, GOS-ED significantly induced iNOS mRNA expression in RAW264.7 cells in a time- and concentration-dependent manner. Consistent with mRNA expression, iNOS protein expression was also detected in GOS-ED-treated RAW264.7 cells (Figure 5D). In addition to GOS-ED, MOS-ED also induced iNOS mRNA and protein expression, although the expression was very low and even trace levels (Figure 5A,D). Furthermore, NO production by GOS-ED-treated RAW264.7 cells was significantly suppressed by L-NAME, a NOS inhibitor (Figure 5E).

GOS-ED Induces ROS Production in RAW264.7 Cells. As shown in Figure 6A, the intensity of the DCF fluorescence was significantly increased in GOS-ED-stimulated RAW264.7 cells compared to control cells, indicating that GOS-ED enhanced intracellular ROS production. In contrast, other saccharides including GOS (-AH, -OD), MOS (-ED, -AH, -OD), and original polymers (PG/PM) showed no statistical effect on ROS production. As shown in Figure 6B, a similar tendency was observed with the effects of G2−G9 on NO production. The purified G2, G3, and G6−G9 fractions showed higher ROS-inducing activity than GOS-ED, and the highest activity was observed in the G9 fraction. Meanwhile, the G5 fraction showed

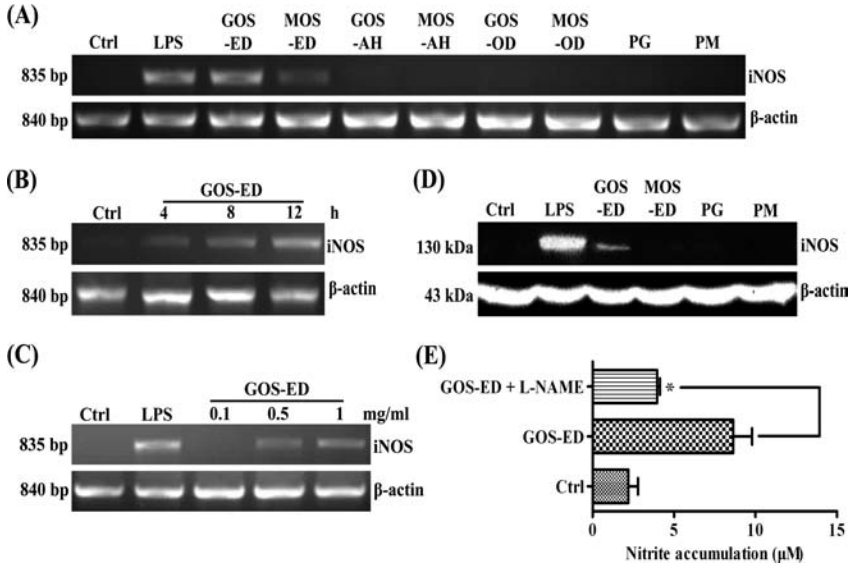

Figure 5. Effects of GOS (-ED, -AH, -OD), MOS (-ED, -AH, -OD), PG, and PM on iNOS expression in RAW264.7 cells. (A) Adherent RAW264.7 cells (2×10^6 cells/well in 6-well plates) were incubated with 1 mg/mL of GOS (-ED, -AH, -OD), MOS (-ED, -AH, -OD), PG, and PM at 37 °C in the culture medium, respectively. After 12 h of incubation, iNOS gene levels in RAW264.7 cells were analyzed by RT-PCR. (B) iNOS gene expression after 4, 8, and 12 h of stimulation with 1 mg/mL of GOS-ED was measured. (C) iNOS gene expression after 12 h stimulation with various doses (0.1, 0.5, and 1 mg/mL) of GOS-ED was measured. (D) Adherent RAW264.7 cells (2×10^6 cells/well in 6-well plates) were incubated with 1 mg/mL of GOS-ED, MOS-ED, PG, and PM at 37 °C, respectively. After 24 h of incubation, the whole-cell lysates were prepared from the treated cells and analyzed by Western blot analysis. (E) Adherent RAW264.7 cells were incubated with 1 mg/mL of GOS-ED for 24 h by the addition of the NOS inhibitor L-NAME (100 μM). The nitrite levels in the culture medium from the treated cells were measured by Griess assay. Each value represents mean ± SD of triplicate measurements. The * is representative of $p < 0.05$, when compared to control group.

dx.doi.org/10.1021/jf405633n | J. Agric. Food Chem. 2014, 62, 3168−3176

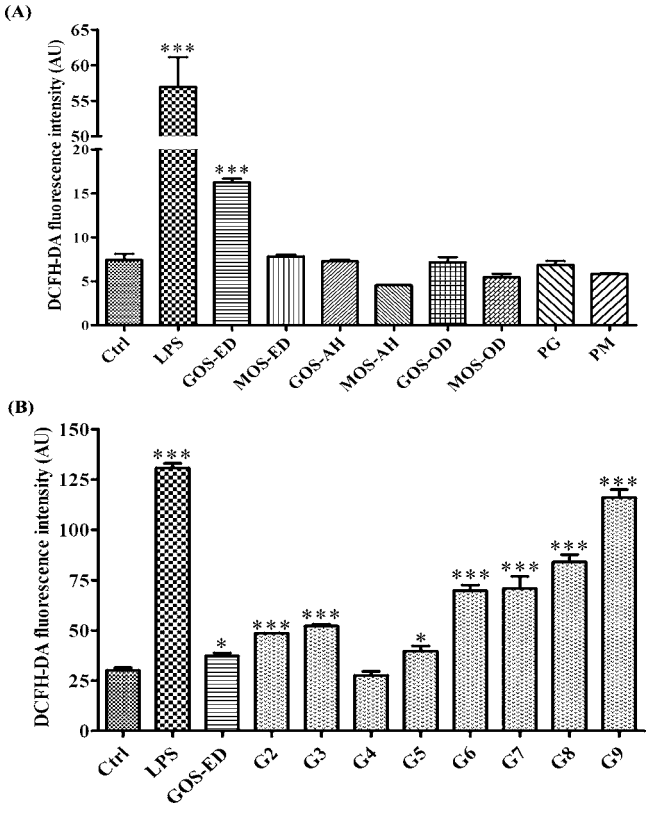

Figure 6. Effects of alginate oligosaccharides and polysaccharides on ROS production in RAW264.7 cells. (A) Adherent RAW264.7 cells (5×10^5 cells/well in 24-well plates) were incubated with 1 mg/mL of GOS (-ED, -AH, -OD), MOS (-ED, -AH, -OD), PG, and PM at 37 °C, respectively. After 24 h, intracellular ROS were measured by flow cytometry utilizing an oxidation-sensitive fluorescent probe, DCFH-DA. LPS (1 μg/mL) was used as a positive control. (B) Adherent RAW264.7 cells were incubated with 0.5 mg/mL of GOS-ED and G2−G9, respectively. After 24 h, intracellular ROS were measured. LPS (1 μg/mL) was used as a positive control. Each value represents mean ± SD of triplicate measurements. The * is representative of $p < 0.05$ and *** is representative of $p < 0.001$, when compared to the control group.

this activity nearly equal to that of the GOS-ED, whereas the G4 fraction had almost no activity.

GOS-ED Induces TNF-α Secretion in RAW264.7 Cells. As displayed in Figure 7, the levels of TNF-α secretion in the culture medium from GOS-ED- and MOS-ED-treated RAW264.7 cells were elevated in a concentration-dependent manner. A significant level of TNF-α secretion was capable to be detected at 0.1 mg/mL of GOS-ED and MOS-ED, and further increased levels were detected at 0.5 and 1 mg/mL of GOS-ED and MOS-ED. Meanwhile, the slightly stronger TNF-α-inducing activity of GOS-ED than MOS-ED was observed. On the contrary, PG or PM before depolymerization had much lower effect than oligomers on TNF-α secretion.

GOS-ED Activates the NF-κB signaling Pathway in RAW264.7 Cells. As shown in Figure 8A, the nuclear level of NF-κB p65 protein increased in GOS-ED- and MOS-ED-treated RAW264.7 cells with a greater extent than those induced by PG and PM. In addition, GOS-ED and MOS-ED, but not PG or PM, also induced both the phosphorylation and degradation of IκB-α. As the results indicated, GOS-ED and MOS-ED could induce the NF-κB activation in RAW264.7 cells. To test the potential involvement of the NF-κB activation

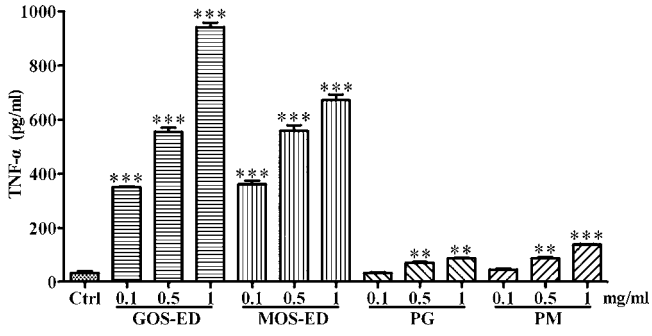

Figure 7. Effects of GOS-ED, MOS-ED, PG, and PM on TNF-α secretion in RAW264.7 cells. Adherent RAW264.7 cells (2×10^5 cells/well in 96-well plates) were incubated with various concentrations (0.1, 0.5, and 1 mg/mL) of GOS-ED, MOS-ED, PG, and PM at 37 °C, respectively. After 24 h of incubation, the TNF-α levels in the culture medium were measured by ELISA. Each value represents mean ± SD of triplicate measurements.

in GOS-ED-induced production of NO, ROS, and TNF-α, we used a NF-κB inhibitor PDTC to block the NF-κB signaling pathway. Our results demonstrated that PDTC significantly inhibited the productions of NO (Figure 8B), ROS (Figure 8C), and TNF-α (Figure 8D) in GOS-ED-treated cells, suggesting that GOS-ED-induced NO, ROS, and TNF-α production in RAW264.7 cells were partly mediated through the NF-κB signaling pathway.

GOS-ED Activates the MAP Kinase Signaling Pathway in RAW264.7 Cells. To further investigate the involvement of MAP kinase signaling pathway in immunomodulatory effects of enzymatically degraded alginate oligosaccharides and polysaccharides, RAW264.7 cells were treated with each saccharide and the levels of phosphorylated and nonphosphorylated ERK, p38, and JNK MAP kinases were analyzed by Western blot. As shown in Figure 9, a significant increase in the phosphorylation levels of ERK, p38, and JNK MAP kinases were observed in GOS-ED-treated RAW264.7 cells, whereas the phosphorylation levels of these three MAP kinases induced by MOS-ED were evidently lower than that induced by GOS-ED.

DISCUSSION

Many polysaccharides isolated from seaweeds have been recently reported to induce immune activation as molecules target to immune cells in a host immune system, such as macrophages, lymphocytes, and natural killer cells, and stimulate cytokines release and other immune responses.[28] Alginate, currently used widely in commercial enterprises, has been known to induce cytokine production *via* NF-κB signaling pathway from murine macrophage RAW264.7 cells[29] and exert antitumor activities against Sarcoma-180 solid tumor transplanted in mice without toxicity *via* the activation of the host immune system.[30] Although the properties of alginate have been widely investigated, the actual application of alginate polymers into *in vivo* system is limited due to the higher molecular weight. It is likely that the depolymerization of polymers is one possible way to overcome this drawback of alginate.[18] Our previous studies have reported that AOS-ED could stimulate RAW264.7 macrophages to produce cytokines[14] and induce multiple immunocompetent cytokines in mice *via* intraperitoneal injection,[31] suggesting that AOS-ED were potentially capable of stimulating macrophages and the host immune system activation, but the detailed mechanisms and the structure−activity relationships are unclear so

dx.doi.org/10.1021/jf405633n | J. Agric. Food Chem. 2014, 62, 3168−3176

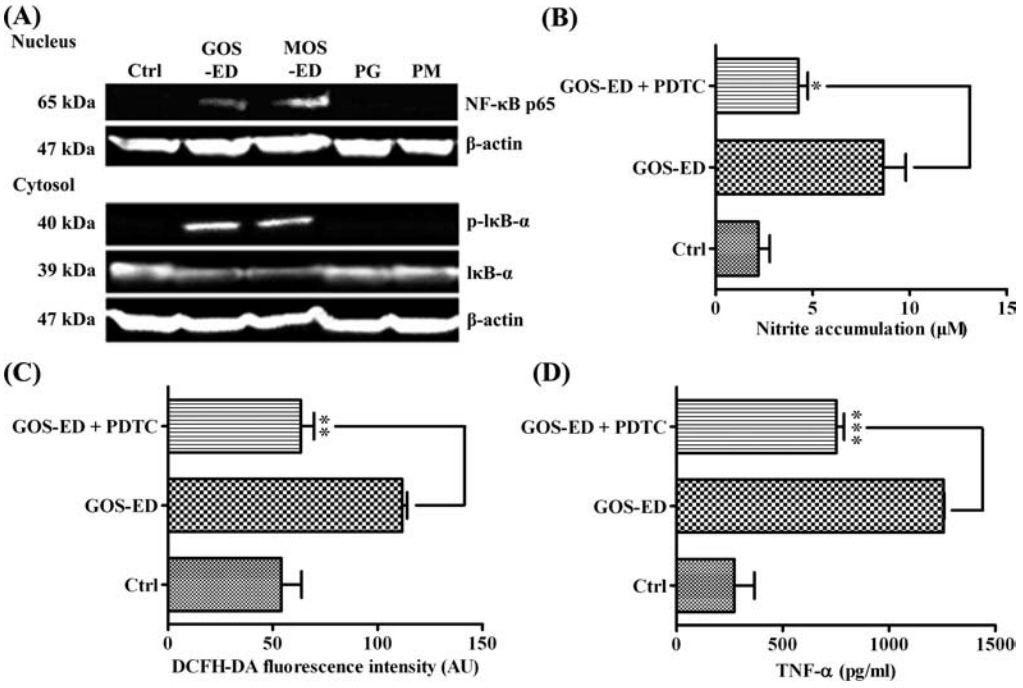

Figure 8. Effects of GOS-ED, MOS-ED, PG, and PM on the activation of NF-κB signaling pathway in RAW264.7 cells and the involvement of NF-κB in GOS-ED-induced NO, ROS, and TNF-α production. (A) RAW264.7 cells were treated with 1 mg/mL of GOS-ED, MOS-ED, PG, and PM, respectively. Afterward, Western blot analysis was conducted to detect the expression of NF-κB p65 in the nuclear extracts and the expression of IκB-α and phosphorylated IκB-α in the cytosolic extracts. (B) Adherent RAW264.7 cells were incubated with 1 mg/mL of GOS-ED for 24 h by the addition of the NF-κB signaling pathway inhibitor PDTC (50 μM). The nitrite levels in the culture medium from the treated cells were measured by Griess assay. (C) Adherent RAW264.7 cells were incubated with 1 mg/mL of GOS-ED for 24 h by the addition of the NF-κB signaling pathway inhibitor PDTC (50 μM). Intracellular ROS were measured by a FACS analysis. (D) Adherent RAW264.7 cells were incubated with 1 mg/mL of GOS-ED for 24 h by the addition of the NF-κB signaling pathway inhibitor PDTC (50 μM). The TNF-α levels in the culture medium of the treated cells were measured by ELISA. Each value represents mean ± SD of triplicate measurements. The *, **, and *** are representative of $p < 0.05$, $p < 0.01$, and $p < 0.001$, respectively, when compared to control group.

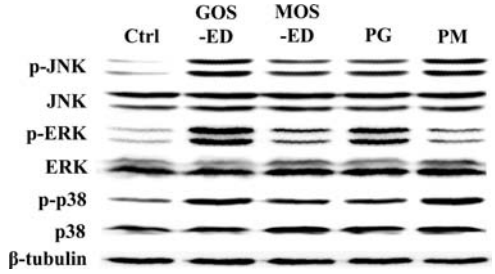

Figure 9. Effects of GOS-ED, MOS-ED, PG, and PM on the activation of MAP kinases in RAW264.7 cells. Adherent RAW264.7 cells (3×10^6 cells/3.5 cm dishes) were incubated in serum-free medium with 1 mg/mL of GOS-ED, MOS-ED, PG, and PM, respectively. The whole-cell lysates were prepared from the treated cells, and the levels of both phosphorylated and nonphosphorylated MAP kinases were analyzed by Western blot.

far. Here, we prepared GOS-ED, -AH, -OD and MOS-ED, -AH, -OD using three different depolymerized ways to compare their macrophage-activating activities and provided key insights into potential mechanisms.

Macrophages play important roles in host defense systems, and activated macrophages can kill tumor cells and pathogens either by direct contact or by releasing diffusible cytotoxic molecules, such as NO, ROS, and TNF-α.[32] As we have known, NO plays a critical role in host defense during pathogen infection and tissue damage during autoimmune responses.[33] The expression of iNOS is responsible for NO production in activated macrophages.[34] In the present study, our results revealed that GOS-ED showed significant NO-inducing activity in RAW264.7 cells in a time- and concentration-dependent manner, and this activity of GOS-ED was much higher than other oligosaccharides (GOS-AH, -OD and MOS-ED, -AH, -OD) and original polysaccharides (PG and PM). Consistent with this finding, significantly increased iNOS gene and protein expression levels were observed in GOS-ED-treated RAW264.7 cells in a time- and concentration-dependent manner, whereas MOS-ED only slightly induced iNOS gene expression. Other oligosaccharides (GOS-AH, -OD and MOS-AH, -OD) and polysaccharides (PG and PM) showed no such effects on the expression of iNOS gene and protein (Figure 5A–D). Because L-NAME, a NOS inhibitor, significantly inhibited GOS-ED-induced NO production in RAW264.7 cells (Figure 5E), GOS-ED is considered to be a potent macrophage activator capable of inducing NO production through the induction of iNOS expression. Next, the ROS and TNF-α production induced by these saccharides on RAW264.7 cells was evaluated. Our results indicated that GOS-ED significantly stimulated ROS production in RAW264.7 cells, but no significant effect was observed in other tested saccharides (Figure 6). Interestingly, contrary to the NO- and ROS-inducing activities, both kinds of AOS-ED (GOS-ED and MOS-ED), but not polysaccharides (PG and PM), significantly induced TNF-α secretion in RAW264.7 cells in a concentration-dependent manner, even though MOS-ED evidently showed lower activity than GOS-ED (Figure 7). These findings further support the notion that GOS-ED is a potent macrophage activator.

dx.doi.org/10.1021/jf405633n | J. Agric. Food Chem. 2014, 62, 3168–3176

NF-κB regulates many important biological and pathological processes in cells, and it is also a key to modulate various gene expressions involved in immune and inflammatory responses, including the production of NO, ROS, and TNF-α in macrophages.[35] In our present studies, it was found that GOS-ED showed much higher RAW264.7 macrophage-stimulating activity than other saccharides derived from alginate. Meanwhile, MOS-ED exhibited less activity on macrophage activation than GOS-ED, but the activity was higher than other saccharides, especially the induction of TNF-α production. Although alginate has been reported to stimulate RAW264.7 cells activation to release immune cytokines *via* the NF-κB signaling pathway, there has been no available information on the precise action mechanisms of AOS-ED on macrophage-stimulating activity so far. Our results showed that the NF-κB signaling pathway was potently activated in GOS-ED- and MOS-ED-treated RAW264.7 cells, whereas the activation levels in PG- or PM-treated cells were hardly distinguishable from the unstimulated control level (Figure 8A). Interestingly, the activation level of NF-κB in MOS-ED-treated RAW264.7 cells seems to be higher than that of GOS-ED-treated cells (Figure 8A). As we have known, the MAP kinase signaling pathway plays an important role in NO, ROS, and TNF-α production in activated macrophages. Our previous report showed that AOS-ED were capable of activating JNK and p38 MAP kinases involved signaling pathway leading to TNF-α secretion from RAW264.7 cells.[20] Considering the differences between GOS-ED and MOS-ED in macrophage-stimulating activities and the NF-κB-activated effects, it is speculated that the MAP kinase signaling pathway involved in GOS-ED- and MOS-ED-induced macrophage activation might be different. Our results showed that ERK, p38, and JNK MAP kinase signaling pathways were potently activated in GOS-ED-treated RAW264.7 cells, whereas the activation levels of these MAP kinases in MOS-ED-treated cells were quite low compared to the levels of unstimulated control (Figure 9), considering NO, ROS, and TNF-α production and NF-κB signaling pathway activation, suggesting that the underlying mechanisms of macrophage activation activity were different between GOS-ED and MOS-ED. To determine the possible involvement of NF-κB signaling pathway in the induction of NO, ROS, and TNF-α production by GOS-ED, NF-κB inhibitor PDTC was used to block the NF-κB activation. Our results showed that significantly inhibitory effects of PDTC on GOS-ED-inducing NO, ROS, and TNF-α production were observed (Figure 8B−D), further demonstrating that the NF-κB signaling pathway is responsible for the production of NO, ROS, and TNF-α in GOS-ED-treated RAW264.7 cells. The results obtained in this study may provide valuable basic information to the mechanisms of AOS-induced macrophage activation, especially in terms of NO, ROS, and TNF-α production in RAW264.7 cells.

It has been reported that enzymatically depolymerized alginate oligomers were capable to enhance the growth of bifidobacteria,[36] plant roots,[21] and green alga.[12,37] Our previous reports revealed that unsaturated AOS-ED were highly active inducers for cytokine production in RAW264.7 cells, whereas saturated AOS-AH showed smaller effects.[18] It seems that unsaturated terminal structure with double bonds of alginate oligomers play important roles in their biological activities, including inducing cytokines production. In fact, we presented an idea that the biological activities of AOS are strongly influenced by their molecular size, M/G composition, and the entire molecular conformation.[16] This study revealed that GOS-ED and MOS-ED showed much higher activities on the induction of NO, ROS, and TNF-α production in RAW264.7 cells than other AOS (GOS-AH, -OD, and MOS-AH, -OD) and polysaccharides (PG and PM), and these effects induced by GOS-ED were evidently greater than those of MOS-ED (Figures 3A, 6, and 7). These findings provided valuable evidence to the idea that unsaturated end structure and the composition (M/G ratio) were important structural elements for their biological activities. Previous structural studies have proposed that mannuronate and guluronate adopt different chair conformations; mannuronate block predominately forms an extended ribbon structure, whereas guluronate block forms a buckled chain.[18] Moreover, the highest NO-inducing activity among unsaturated G2−G7 fractions was found in G6 and G7 fractions (Figure 4B), which suggested that G6 and G7 oligomers were the most effective structure or molecular size in the specific activities. Interestingly, the smaller oligomer G2 also showed relatively high cytokine-inducing activities. The reason for this is uncertain now, but the finding may provide a clue to understand the recognition site or mechanism on RAW264.7 cells by alginate oligomers.

In conclusion, these results first revealed that AOS-ED but not AOS-AH, AOS-OD, or polysaccharides activated the NF-κB and MAPK signaling pathways, resulting in significant induction of NO, ROS, and TNF-α production. Our findings suggested that the structural characteristics of AOS, especially the unsaturated terminal structure, molecular size, and M/G ratio, are important in RAW264.7 macrophage activation. On the basis of these findings, it is worthwhile to develop GOS-ED as a promising agent used to regulate immune responses and vascular relaxation in functional foods and pharmacological fields.

AUTHOR INFORMATION

Corresponding Authors

*E-mail: (M.W.) min.wan@ki.se. Fax: +46-8-7360439. Tel.: +46-8-52487623.

*E-mail: (T.O.) t-oda@nagasaki-u.ac.jp. Fax: +81-95-8192799. Tel.: +81-95-8192831.

Author Contributions

*Corresponding authors contributed equally.

Funding

This work was supported financially by the project supported by the National Natural Science Foundation of China (grant no. 31000770) and Knowledge Innovation Program in Shenzhen Scientific Research and Development Funding Program (grant no. JCYJ20130329111455027).

Notes

The authors declare no competing financial interest.

ACKNOWLEDGMENTS

We are grateful to Mrs. Lijun Yao and Dr. Liyan Wang from Shenzhen University and Mr. Yi Liu from Guangdong Medical College for their technical assistance.

ABBREVIATIONS USED

AH, acid hydrolysis; AOS, alginate oligosaccharide; DP, degree of polymerization; ED, enzymatic degradation; ELISA, enzyme-linked immunosorbent assay; GOS, guluronate oligosaccharide; iNOS, inducible nitric oxide synthase; MAP kinase, mitogen-activated protein kinase; MOS, mannuronate oligosaccharide; NF-κB, nuclear factor-κB; NO, nitric oxide; OD, oxidative degradation; PG, polyguluronate; PM, polymannuronate; ROS, reactive oxygen species; TNF, tumor necrosis factor

REFERENCES

(1) Akira, S.; Uematsu, S.; Takeuchi, O. Pathogen recognition and innate immunity. *Cell* **2006**, *124*, 783−801.

(2) Klimp, A.; De Vries, E.; Scherphof, G.; Daemen, T. A potential role of macrophage activation in the treatment of cancer. *Crit. Rev. Oncol. Hematol.* **2002**, *44*, 143−161.

(3) MacMicking, J.; Xie, Q. W.; Nathan, C. Nitric oxide and macrophage function. *Annu. Rev. Immunol.* **1997**, *15*, 323−350.

(4) Kohchi, C.; Inagawa, H.; Nishizawa, T.; Soma, G. ROS and innate immunity. *Anticancer Res.* **2009**, *29*, 817−821.

(5) Ueno, H.; Yamada, H.; Tanaka, I.; Kaba, N.; Matsuura, M.; Okumura, M.; Kadosawa, T.; Fujinaga, T. Accelerating effects of chitosan for healing at early phase of experimental open wound in dogs. *Biomaterials* **1999**, *20*, 1407−1414.

(6) Peluso, G.; Petillo, O.; Ranieri, M.; Santin, M.; Ambrosic, L.; Calabró, D.; Avallone, B.; Balsamo, G. Chitosan-mediated stimulation of macrophage function. *Biomaterials* **1994**, *15*, 1215−1220.

(7) Seo, W. G.; Pae, H. O.; Kim, N. Y.; Oh, G. S.; Park, I. S.; Kim, Y. H.; Kim, Y. M.; Lee, Y. H.; Jun, C. D.; Chung, H. T. Synergistic cooperation between water-soluble chitosan oligomers and interferon-γ for induction of nitric oxide synthesis and tumoricidal activity in murine peritoneal macrophages. *Cancer Lett.* **2000**, *159*, 189−195.

(8) Wu, G. J.; Tsai, G. J. Chitooligosaccharides in combination with interferon-γ increase nitric oxide production *via* nuclear factor-κB activation in murine RAW264.7 macrophages. *Food Chem. Toxicol.* **2007**, *45*, 250−258.

(9) Nakamura, T.; Suzuki, H.; Wada, Y.; Kodama, T.; Doi, T. Fucoidan induces nitric oxide production *via* p38 mitogen-activated protein kinase and NF-κB-dependent signaling pathways through macrophage scavenger receptors. *Biochem. Biophys. Res. Commun.* **2006**, *343*, 286−294.

(10) Jiang, Z.; Okimura, T.; Yamaguchi, K.; Oda, T. The potent activity of sulfated polysaccharide, ascophyllan, isolated from *Ascophyllum nodosum* to induce nitric oxide and cytokine production from mouse macrophage RAW264.7 cells: Comparison between ascophyllan and fucoidan. *Nitric Oxide* **2011**, *25*, 407−415.

(11) Kimura, Y.; Watanabe, K.; Okuda, H. Effects of soluble sodium alginate on cholesterol excretion and glucose tolerance in rats. *J. Ethnopharmacol.* **1996**, *54*, 47−54.

(12) Yamasaki, Y.; Yokose, T.; Nishikawa, T.; Kim, D.; Jiang, Z.; Yamaguchi, K.; Oda, T. Effects of alginate oligosaccharide mixtures on the growth and fatty acid composition of the green alga *Chlamydomonas reinhardtii*. *J. Biosci. Bioeng.* **2012**, *113*, 112−116.

(13) Kawada, A.; Hiura, N.; Tajima, S.; Takahara, H. Alginate oligosaccharides stimulate VEGF-mediated growth and migration of human endothelial cells. *Arch. Dermatol. Res.* **1999**, *291*, 542−547.

(14) Yamamoto, Y.; Kurachi, M.; Yamaguchi, K.; Oda, T. Induction of multiple cytokine secretion from RAW264.7 cells by alginate oligosaccharides. *Biosci. Biotechnol. Biochem.* **2007**, *71*, 238−241.

(15) An, Q. D.; Zhang, G. L.; Wu, H. T.; Zhang, Z. C.; Zheng, G. S.; Luan, L.; Murata, Y.; Li, X. Alginate-deriving oligosaccharide production by alginase from newly isolated Flavobacterium sp. LXA and its potential application in protection against pathogens. *J. Appl. Microbiol.* **2009**, *106*, 161−170.

(16) Ueno, M.; Hiroki, T.; Takeshita, S.; Jiang, Z.; Kim, D.; Yamaguchi, K.; Oda, T. Comparative study on antioxidative and macrophage-stimulating activities of polyguluronic acid (PG) and polymannuronic acid (PM) prepared from alginate. *Carbohydr. Res.* **2012**, *352*, 88−93.

(17) Tusi, S. K.; Khalaj, L.; Ashabi, G.; Kiaei, M.; Khodagholi, F. Alginate oligosaccharide protects against endoplasmic reticulum- and mitochondrial-mediated apoptotic cell death and oxidative stress. *Biomaterials* **2011**, *32*, 5438−5458.

(18) Iwamoto, M.; Kurachi, M.; Nakashima, T.; Kim, D.; Yamaguchi, K.; Oda, T.; Iwamoto, Y.; Muramatsu, T. Structure-activity relationship of alginate oligosaccharides in the induction of cytokine production from RAW264.7 cells. *FEBS Lett.* **2005**, *579*, 4423−4429.

(19) Iwamoto, Y.; Xu, X.; Tamura, T.; Oda, T.; Muramatsu, T. Enzymatically depolymerized alginate oligomers that cause cytotoxic cytokine production in human mononuclear cells. *Biosci. Biotechnol. Biochem.* **2003**, *67*, 258−263.

(20) Kurachi, M.; Nakashima, T.; Miyajima, C.; Iwamoto, Y.; Muramatsu, T.; Yamaguchi, K.; Oda, T. Comparison of the activities of various alginates to induce TNF-α secretion in RAW264.7 cells. *J. Infect. Chemother.* **2005**, *11*, 199−203.

(21) Xu, X.; Iwamoto, Y.; Kitamura, Y.; Oda, T.; Muramatsu, T. Root growth-promoting activity of unsaturated oligomeric uronates from alginate on carrot and rice plants. *Biosci. Biotechnol. Biochem.* **2003**, *67*, 2022−2025.

(22) Haug, A.; Larsen, B.; Smidsrød, O. A study of the constitution of alginic acid by partial acid hydrolysis. *Acta Chem. Scand.* **1966**, *20*, 183−190.

(23) Morris, E. R.; Rees, D. A.; Thom, D. Characterisation of alginate composition and block-structure by circular dichroism. *Carbohydr. Res.* **1980**, *81*, 305−314.

(24) Linker, A.; Jones, R. S. A new polysaccharide resembling alginic acid isolated from *pseudomonads*. *J. Biol. Chem.* **1966**, *241*, 3845−3851.

(25) Xiong, H.; Zhang, Z. G.; Tian, X. Q.; Sun, D. F.; Liang, Q. C.; Zhang, Y. J.; Lu, R.; Chen, Y. X.; Fang, J. Y. Inhibition of JAK1, 2/STAT3 signaling induces apoptosis, cell cycle arrest, and reduces tumor cell invasion in colorectal cancer cells. *Neoplasia* **2008**, *10*, 287.

(26) Kim, A. R.; Shin, T. S.; Lee, M. S.; Park, J. Y.; Park, K. E.; Yoon, N. Y.; Kim, J. S.; Choi, J. S.; Jang, B. C.; Byun, D. S. Isolation and identification of phlorotannins from Ecklonia stolonifera with antioxidant and anti-inflammatory properties. *J. Agric. Food Chem.* **2009**, *57*, 3483−3489.

(27) Stuehr, D. J.; Gross, S. S.; Sakuma, I.; Levi, R.; Nathan, C. Activated murine macrophages secrete a metabolite of arginine with the bioactivity of endothelium-derived relaxing factor and the chemical reactivity of nitric oxide. *J. Exp. Med.* **1989**, *169*, 1011−1020.

(28) Leiro, J. M.; Castro, R.; Arranz, J. A.; Lamas, J. Immunomodulating activities of acidic sulphated polysaccharides obtained from the seaweed *Ulva rigida* C. Agardh. *Int. Immunopharmacol.* **2007**, *7*, 879−888.

(29) Yang, D.; Jones, K. S. Effect of alginate on innate immune activation of macrophages. *J. Biomed. Mater. Res., Part A* **2009**, *90*, 411−418.

(30) de Sousa, A. P. A.; Torres, M. R.; Pessoa, C.; Moraes, M. O. d.; Alves, A. P. N. N.; Costa-Lotufo, L. V. *In vivo* growth-inhibition of Sarcoma 180 tumor by alginates from brown seaweed *Sargassum vulgare*. *Carbohydr. Polym.* **2007**, *69*, 7−13.

(31) Yamamoto, Y.; Kurachi, M.; Yamaguchi, K.; Oda, T. Stimulation of multiple cytokine production in mice by alginate oligosaccharides following intraperitoneal administration. *Carbohydr. Res.* **2007**, *342*, 1133−1137.

(32) Higuchi, M.; Higashi, N.; Taki, H.; Osawa, T. Cytolytic mechanisms of activated macrophages. Tumor necrosis factor and L-arginine-dependent mechanisms act synergistically as the major cytolytic mechanisms of activated macrophages. *J. Immunol.* **1990**, *144*, 1425−1431.

(33) Bogdan, C. Nitric oxide and the immune response. *Nat. Immunol.* **2001**, *2*, 907−916.

(34) Karupiah, G.; Xie, Q. W.; Buller, R. M.; Nathan, C.; Duarte, C.; Macmicking, J. D. Inhibition of viral replication by interferon-gamma-induced nitric oxide synthase. *Science* **1993**, *261*, 1445−1448.

(35) Cieslik, K.; Zhu, Y.; Wu, K. K. Salicylate suppresses macrophage nitric-oxide synthase-2 and cyclo-oxygenase-2 expression by inhibiting CCAAT/enhancer-binding protein-β binding *via* a common signaling pathway. *J. Biol. Chem.* **2002**, *277*, 49304−49310.

(36) Akiyama, H.; Endo, T.; Nakakita, R.; Murata, K.; Yonemoto, Y.; Okayama, K. Effect of depolymerized alginates on the growth of bifidobacteria. *Biosci. Biotechnol. Biochem.* **1992**, *56*, 355.

(37) Yokose, T.; Nishikawa, T.; Yamamoto, Y.; Yamasaki, Y.; Yamaguchi, K.; Oda, T. Growth-promoting effect of alginate oligosaccharides on a unicellular marine microalga *Nannochloropsis oculata*. *Biosci. Biotechnol. Biochem.* **2009**, *73*, 450−453.

peptides interact with tight junctions or epithelial cells.[20−23] Unfortunately, the interaction between food-derived substance and epithelium is still obscure.

Gln-Ile-Gly-Leu-Phe (QIGLF) was an ACE-inhibitory peptide, with an IC_{50} value of 75 μM, identified from egg white ovalbumin. The result of simulated gastrointestinal digestion by pepsin and trypsin showed that QIGLF had a strong resistance to gastrointestinal proteases, providing a possibility for oral administration.[8] However, the bioavailability and permeability through intestinal epithelium have not been studied. Therefore, the objective of the present study was to investigate the transport of QIGLF in human intestinal Caco-2 cell monolayers. Furthermore, the effect of QIGLF on the viability of Caco-2 cells in oxidative stress induced by H_2O_2 was evaluated.

MATERIALS AND METHODS

Materials. Caco-2 cell lines were purchased from American Type Culture Collection. The ACE-inhibitory peptide QIGLF with a purity of 95% was synthesized by GL Biochem Ltd. (Shanghai, China) by the solid-phase procedure peptide using Fmoc protected amino acids synthesis methods. Dulbeco's Modified Eagle's Medium (DMEM), fetal bovine serum, penicillin-streptomycin, Hank's balanced salt solution (HBSS), and 4-(2-hydroxyethyl)-1-piperazineethanesulfonic acid (HEPES) were purchased from Gibco BRL Life Technology. Nonessential amino acid, trypsin, L-glutamine, dimethyl sulfoxide (DMSO), ethylene diamine tetraacetic acid (EDTA), cytochalasin D, wortmannin, sodium azide, glycyl-proline (Gly-Pro), 3-(4,5-dimethylthiazol-2-yl)-2,5-diphenyltetra-zolium bromide (MTT), acetonitrile, trifluoroacetic acid (TFA), and methanol were all purchased from Sigma-Adrich. 3-(4,5-Dimethylthiazol-2-yl)-5-(3-carboxymethoxyphenyl)-2-(4-sulfophenyl)-2*H*-tetrazolium (MTS) was purchased from Promega Biotechnology Co. Ltd. All other reagents were analytical grade.

Cell Culture. The Caco-2 cells were grown in Dulbecco's modified Eagle's medium containing 10% fetal bovine serum, 1% nonessential amino acid solution, 100 units/mL penicillin, 100 μg/mL streptomycin, and 4 mM L-glutamine at 37 °C in an atmosphere of 5% CO_2 and 90% relative humidity. Stock cultures were grown in 75 cm^2 tissue culture flasks and were split at 80−90% confluency using 0.25% trypsin and 0.02% EDTA solution. The cells from passage numbers of 10−20 were used and seeded on the permeable polycarbonate inserts (0.4 μm pore size, 12 mm diameter, 1.12 cm^2 grown surface, Costar, Corning, NY) in 12 transwell plates at a density of 1×10^5 cells/insert. The culture medium (0.5 mL in the apical side and 1.5 mL in the basolateral side) was replaced every 2 days for the first week and then daily until they were used for experiments 21 days after the seeding. The integrity of the cell monolayer was evaluated by measuring transepithelial electrical resistance (TEER) values with an EVOM epithelial volt/ohmmeter (Millicell-ERS, Millipore, U.S.). Only the cell monolayers with TEER values higher than 250 Ω cm^2 were used for the transport studies.

Cytotoxicity Assay. MTT was used to determine the cytotoxicity of QIGLF in Caco-2 cells as described previously.[24] Caco-2 cells were grown in 96-well culture plates and incubated with 1−10 mM QIGLF, which dissolved in DMEM, at 37 °C in 5% CO_2 for 24 h followed by addition of 0.05 mg of MTT and incubation for another 4 h. The culture medium then was replaced with 150 μL of DMSO to dissolve the MTT crystals, and the absorbance at 595 nm was measured using a multimode microplate reader (BioTek Instruments, U.S.).

Stability Assay. The stability of QIGLF in the apical surface of Caco-2 cells was studied. The Caco-2 cell monolayers were rinsed with HBSS twice and then incubated with HBSS for 30 min at 37 °C in 5% CO_2. The medium in the surface apical was replaced with 1 mM QIGLF (dissolved in HBSS, pH 7.4) and incubated at 37 °C in 5% CO_2. At the indicated time points, an aliquot of 50 μL from the apical surface was collected and analyzed by HPLC.

Transport Experiments. The transepithelial transport of ACE inhibitory peptide QIGLF was investigated as previously described by Hubatsch with minor modifications.[25] The Caco-2 cell monolayers were rinsed with HBSS twice and then incubated with HBSS for 30 min at 37 °C in 5% CO_2 before the transport experiment. We then aspirated the HBSS from both apical side and basolateral side of all wells. The peptide of 1−10 mM QIGLF in HBSS buffer (pH 7.4) was added in apical side, and fresh HBSS (pH 7.4) was added in basolateral side. All of the plates were incubated at 37 °C in 5% CO_2 for 2 h. At the appointed time points of 0, 30, 60, 90, and 120 min, an aliquot of 50 μL of sample was collected from the basolateral side. After each sampling, an equivalent volume of HBSS buffer with 25 mM HEPES was added in basolateral side to maintain a constant volume. The QIGLF concentration in each sample was determined by HPLC.

To identify which transport routes were involved in the transepithelial absorption of QIGLF, the Caco-2 cell monolayers were preincubated with transport inhibitor cytochalasin D (a tight junction disruptor, 0.5 μg/mL), wortmannin (a transcytosis inhibitor, 500 nM), sodium azide (an ATP synthesis inhibitor, 10 mM), or Gly-Pro (a peptide transport PepT 1 substrate, 10 mM) for 30 min followed by addition of 1 mM QIGLF to apical side. The cytochalasin D, wortmannin, and sodium azide were dissolved in DMSO (final concentration in HBSS 0.044%), and Gly-Pro was dissolved in HBSS. As a control, DMSO was used. All of the experiments were conducted in triplicate.

Induction of Oxidative Stress. The induction of in vitro oxidative stress was conducted as previously described by Katayama with modifications.[26,27] Caco-2 cells were seeded in 24-well culture plates (Costar, Corning, NY) at a density of 2×10^5 cells/mL and incubated at 37 °C in 5% CO_2. The oxidative stress was induced until the confluent Caco-2 cell monolayers formed by addition of H_2O_2. The Caco-2 cell monolayers were rinsed with HBSS twice, and then incubated with 1 and 5 mM QIGLF (dissolved in HBSS, pH 7.4) for 2 h followed by addition of various concentrations of H_2O_2 (250, 500, and 1000 μM) for 6 h. MTS was added in the plates (20 μL of MTS per 100 μL of culture medium was used) and incubated at 37 °C in 5% CO_2 for another 2 h followed by detection of the absorbance at 595 nm using a microplate reader (BioTek Instruments, U.S.).[28]

RP-HPLC. The peptide was quantified using a LC-2010HT HPLC system (SHIMADZU, JP) equipped with an autosampler, a quaternary pump, an online degasser, a UV detector, and a LC-2010HT workstation. The analytical column was a C18 reverse-phase column (ZORBAX SB-C18 column, 250 × 4.6 mm, particle size 5 μm, Agilent, U.S.). The mobile phases were solvent A (0.1% TFA in water) and solvent B (0.1% TFA in ACN). Samples were eluted with a gradient of solvent B from 25% to 50% in 25 min, from 50% to 100% in 10 min, and 100% for 5 min at a flow rate of 1.0 mL/min. The injection volume was 10 μL, and the absorbance detector wavelength was set at 220 nm. The peptide QIGLF concentration was calculated by a linear regression analysis of the peak area as described previously.[29]

Statistical Analysis. All data were expressed as the mean ± SD (n = 3). The difference was carried out by one-way analysis of variance (ANOVA) with the significance level at $P < 0.05$ by SPSS 19.0 software.

The apparent permeability coefficient (P_{app}, cm/s) was calculated as follows:

$$P_{app} = \frac{dQ}{dt} \times \frac{1}{A} \times \frac{1}{C_0} \quad (1)$$

where dQ/dt was the permeability rate (mmol/s); A was the area of membrane (cm^2); and C_0 was the initial concentration of QIGLF in the donor chamber (mM). After each sampling, the QIGLF concentration on the receiving side was diluted, so a correction equation was used as follows:

$$Q = C_n V + \sum_{i=0}^{n-1} C_i V_i \quad (2)$$

where Q was the accumulation of QIGLF on the receiving side (mmol); C_n and C_i were the concentrations of QIGLF in sample n and

dx.doi.org/10.1021/jf405639w | J. Agric. Food Chem. 2014, 62, 3177−3182

sample i, respectively; and V and V_i were the volumes of receiving chamber and sample i, respectively. To evaluate the kinetics in the transepithelial transport of QIGLF, K_m and V_{max} were calculated using the Michaelis−Menten equation, and the transport rate (V, μM/min cm^2) was calculated as follows:

$$V = \frac{dC}{dt} \times \frac{1}{A} \quad (3)$$

where dC/dt was the change of QIGLF concentration in basolateral side (μM/min).

RESULTS AND DISCUSSION

Validation of QIGLF. The primary structure and basic properties of QIGLF (the 204−208 residues of egg white ovalbumin, molecular weight 576.69 g/mol) were evaluated as described.[30] It was a neutral pentapeptide at pH 7.4 with a log D value of −2.287. The isoelectric point was 6.00, and the pK_a value was 3.76. Moreover, QIGLF had two intramolecular hydrogen bonds. The volume was 383.47 Å^3, and the total surface area was 603.88 Å^2 with polar surface area of 222.80 Å^2. In the present study, the retention time for QIGLF (dissolved in HBSS, pH 7.4) was 17.59 min, and the total run time was 30 min in the chromatogram of RP-HPLC analysis.

Cytotoxicity of QIGLF in Caco-2 Cells. As shown in Table 1, the result of MTT assay demonstrated that QIGLF did not have any cytotoxic effect in Caco-2 cells at the concentrations of 1−10 mM (dissolved in HBSS, pH 7.4), which were used in the transport experiments. Moreover, the transport experiments were performed within 2 h, which was much shorter than the time used for MTT assay. Therefore, the QIGLF (1−10 mM) showed no cytotoxicity in Caco-2 cell monolayers in our studies.

Table 1. Cytotoxicity of QIGLF in Caco-2 Cells As Evaluated by MTT Assay

QIGLF concentrations (mM)	absorbance at 595 nm[a,b]
0 (HBSS, control)	0.4993 ± 0.03
1	0.4932 ± 0.04
2	0.4875 ± 0.04
4	0.4814 ± 0.02
8	0.4806 ± 0.02
10	0.4796 ± 0.02

[a]No significant difference as compared to control group existed. [b]All values were the means ± SD (n = 3).

Stability of QIGLF on Caco-2 Cell Monolayers. The peptide of QIGLF at 1 mM (dissolved in HBSS, pH 7.4) was added to the apical surface Caco-2 cell monolayers and incubated 2 h. The recovery of QIGLF within 2 h was as shown in Figure 1. QIGLF was hardly degraded within 1 h, and had a good stability to Caco-2 cell monolayers with a recovery of 96.33% after 2 h incubation time. This result was associated with the strong resistance of QIGLF to gastrointestinal proteases described previously,[8] and comparable to the stability of VLPVP[31] and VYIHPF[30] to Caco-2 cell monolayers. In general, food-derived protein and peptide are degraded by proteases and peptidases in the gastrointestinal tract prior to being absorbed into the systemic blood circulation and target sites. The extensive enzyme system in gastrointestinal lumen, epithelial cells, and mucosal membrane constituted an important enzymatic barrier, and the brush border membrane enzymes might mainly cleave the peptide entered into Caco-2 cells to free amino acids or dipeptides.[32] However, QIGLF had a strong resistance to these enzymes. Iwan et al. reported that treating Caco-2 cell monolayers with diprotin A, a dipeptidyl peptidase IV inhibitor, resulted in lower degradation of β-casomorphin-5 and -7 in the donor chamber and higher transport rate.[33] Cakir-Kiefer et al. also found that the presence of bile salts appeared to modulate the peptidase activities of the Caco-2 cells leading to higher degradation of α-casozepine but lower degradation of α_{s1}-casein-(f91−97).[34]

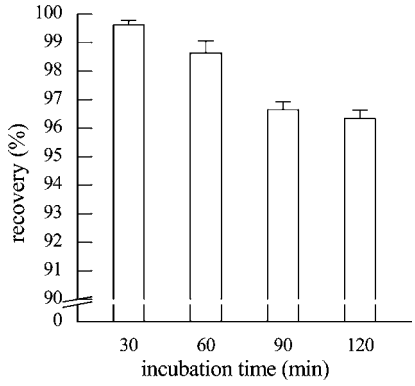

Figure 1. Stability of QIGLF (1 mM in HBSS, pH 7.4) in the AP side of Caco-2 cell monolayers within 2 h. One mM QIGLF (dissolved in HBSS, pH 7.4) was added to AP side, and samples were collected from AP side for HPLC analysis at 30, 60, 90, and 120 min. The recovery analysis revealed that the degradation of QIGLF was not significant within 2 h (P > 0.05). All values were the means ± SD (n = 3).

Transport of QIGLF across Caco-2 Cell Monolayers. The time-dependent uptake of QIGLF across Caco-2 cell monolayers was as shown in Figure 2. The accumulated amount of QIGLF in the basolateral side increased linearly up to 2 h, and the corresponding P_{app} values increased from 2.43 × 10^{-7} cm/s at 30 min to 9.11 × 10^{-7} cm/s at 120 min. Figure 3 showed the effect of QIGLF concentration in apical side on the transport. The transport kinetic parameters were also examined (K_m, 32.37 ± 12.59 mM; V_{max}, 1.23 ± 0.49 μM/min cm^2). The P_{app} value of QIGLF at 1 mM from the apical to basolateral side for 2 h was (9.11 ± 0.19) × 10^{-7} cm/s, suggesting that less than 2% QIGLF was transepithelial transported intact across Caco-2 cell monolayers. This was higher than that of KVLPVP,[35] HLPLP,[36] Gly-Ala-Hyp-Gly-Leu-Hyp-Gly-Pro,[37] VYIHPF,[30]

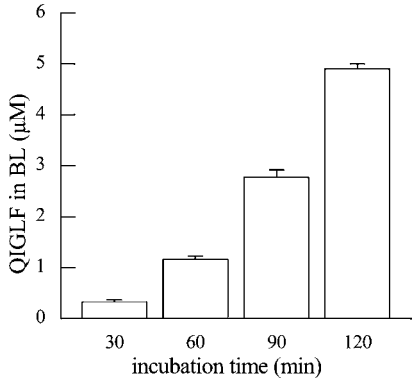

Figure 2. Effects of incubation time on the transport of QIGLF across Caco-2 cell monolayers. One mM QIGLF (dissolved in HBSS, pH 7.4) was added to AP side, and samples were collected from BL side for HPLC analysis at 30, 60, 90, and 120 min. All values were the means ± SD (n = 3).

dx.doi.org/10.1021/jf405639w | J. Agric. Food Chem. 2014, 62, 3177−3182

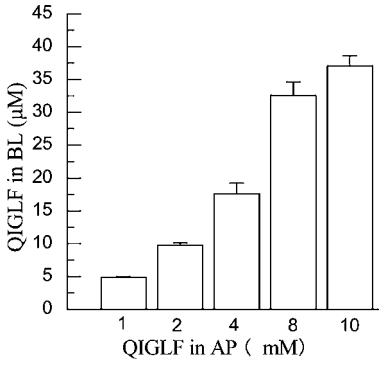

Figure 3. Effects of concentration of QIGLF on the transport across Caco-2 cell monolayers. Different concentrations of QIGLF (1, 2, 4, 8, and 10 mM; dissolved in HBSS, pH 7.4) were added to AP side, and samples were collected from BL side for HPLC analysis at 120 min. All values were the means ± SD (n = 3).

YPFPG, and SRYPSY,[38] but lower than that of VLPVP,[31] all of which had been identified with significant ACE inhibitory activities. The high absorptivity of QIGLF might be due to its hydrophobic uncharged residues such as Ile, Leu, and Phe.

Effects of Various Compounds on QIGLF Transport. To determine which transport pathways were involved in the transepithelial absorption of QIGLF, some inhibitors were added to Caco-2 cell monolayers to preincubate for 30 min before the transport experiment. As shown in Figure 4, Gly-Pro,

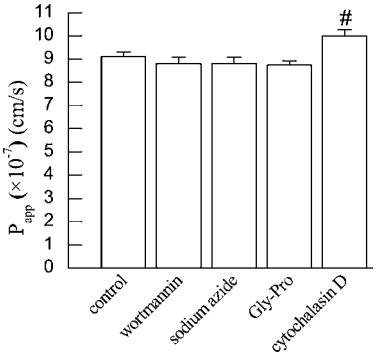

Figure 4. Effects of various compounds on the transport of QIGLF across Caco-2 cell monolayers. One mM QIGLF (dissolved in HBSS, pH 7.4) was added to AP side following the preincubation with transport inhibitors (wortmannin, sodium azide, and Gly-Pro and cytochalasin D) for 30 min, and samples were collected from BL side for HPLC analysis at 120 min. #P < 0.05 as compared to the control group. All values were the means ± SD (n = 3).

a good substrate for peptide transport PepT 1, had little effect on the transport (P > 0.05), suggesting that transport of QIGLF across the Caco-2 cell monolayers was not mediated by PepT1. The finding was unchanged when adjusted for the use of sodium azide, an ATP synthesis inhibitor, suggesting that QIGLF transport was energy-independent. It is known that PepT1 was mainly responsible for the transepithlelial transport of many di- and tripeptides, such as IRW and YPI,[29,39] bur not for the QIGLF in our present study.

Furthermore, the effect of transcytosis initiated by endocytosis at the apical cell membrane on QIGLF transepithelial transport was examined by a 30 min preincubation for Caco-2 cell monolayers with wortmannin, a transcytosis inhibitor. However, the presence of wortmannin did not significantly alter the P_{app} value of QIGLF (P > 0.05, Figure 4), suggesting that transcytosis was not the main mechanism for the transport of QIGLF.

In general, beside the transporter-mediated transport for basic molecules and the transcytosis for macromolecules, there are two other pathways for the intestinal transport of nutrients, transcellular passive diffusion for hydrophobic substances, and paracellular transport for water-soluble low-molecular substances. The transcellular passive diffusion depends on the liposolubility of substance to the lipid bilayers. However, the paracellular permeability is regulated by tight junctions, which could be evaluated by measuring the TEER. In the present study, the effect of paracellular pathway on QIGLF transport was also examined. Cytochalasin D, a tight junction disruptor, was added to Caco-2 cell monolayers and preincubated for 30 min to reduce the tight junction. The result exhibited that the TEER value decreased 10% (data not show), and the P_{app} value of QIGLF increased significantly (P < 0.05, Figure 4), suggesting that the QIGLF was transepithelial transported through Caco-2 monolayers possible mainly via paracellular pathway. This result resembled the transport route of oligopeptides VLPVL,[31] KVLPVP,[35] HLPLP,[36] Gly-Ala-Hyp-Gly-Leu-Hyp-Gly-Pro,[37] GGYR,[40] and tripeptide VPP,[41] which were all described previously. Besides cytochalasin D, bile salts[34] and sodium deoxycholate[35] were also often used to increase peptides paracellular permeability across Caco-2 cell monolayers by regulating the tight junction of Caco-2 cells and influencing the hydrolysis of peptides on the microvilli. What should be noted was that Caco-2 cell monolayers had a higher tight junction than human intestinal epithelial cells, indicating that the paracellular permeability of QIGLF across Caco-2 cell monolayers was lower than in vivo human intestine.[42]

Cytoprotective Effects of QIGLF on Caco-2 Cells Exposed to H_2O_2. To determine the effects of QIGLF on the viability of Caco-2 cells exposed to H_2O_2, Caco-2 cells were cultured with varying concentrations of QIGLF (1 and 5 mM) for 2 h followed by exposure to varying concentrations of H_2O_2 (250, 500, and 1000 μM) for another 6 h, and the cell viability was evaluated by MTS assay. As shown in Figure 5 A, the viability of Caco-2 cells decreased significantly when exposed to H_2O_2 with a dose−response effect (P < 0.05). When the concentration of H_2O_2 was up to 500 μM, 90.52% viability was maintained through the test period (P < 0.05); however, 1000 μM H_2O_2 led to only 86.90% viability remained (P < 0.01), which would bring excessive damage to Caco-2 cells. Therefore, 500 μM H_2O_2 was selected in the present study. Interestingly, treating with QIGLF could significantly improve the Caco-2 cells viability by protecting from oxidative damage induced by H_2O_2 (P < 0.05, Figure 5B). The QIGLF at high concentration of 5 mM offered a strong protection by enhancing H_2O_2-decreased cell viability up to 99.48%, with a slightly greater effect than that shown by 1 mM (95.53%), and those concentrations were all lower than the toxic concentration.

Human intestinal epithelium composes a nature barrier that selectively regulates the absorption of nutrients. However, the oxidative damage of intestinal epithelium might result in the loss of barrier function and chronic diseases.[43] It is well-known that H_2O_2 is not only an important member of the reactive oxygen species (ROS) family, but also can penetrate the cell membrane and react with intracellular metal ions to form hydroxyl radicals, both of which can cause severe damage to cultured cells. In addition, H_2O_2 and ROS are involved in the modulation of nuclear factor erythroid 2-related factor (Nrf2),

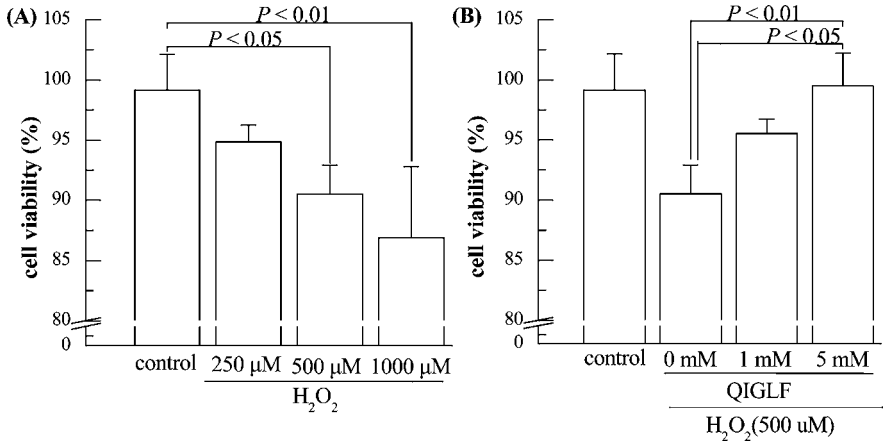

Figure 5. Cytoprotective effects of QIGLF on Caco-2 cells. (A) The cytotoxicity of H_2O_2 on viability in normal Caco-2 cells. Caco-2 cells were exposed to H_2O_2 at indicated concentrations of 250, 500, and 1000 μM for 6 h at 37 °C in 5% CO_2. (B) The cytoprotective effect of QIGLF on oxidative damage induced by H_2O_2 in Caco-2 cells. Caco-2 cells were incubated with couple concentrations of QIGLF (1 and 5 mM, dissolved in HBSS, pH 7.4) for 2 h at 37 °C in 5% CO_2 followed by the addition of 500 μM H_2O_2 for another 6 h incubation. The cell viability was evaluated by MTS assay. All values were the means ± SD (n = 3).

an emerging regulator of cellular resistance to oxidative stress.[44] In the present study, we observed that the treatment with 5 mM QIGLF could improve Caco-2 cells viability by protecting from oxidative damage induced by H_2O_2. However, QIGLF showed very low DPPH radical-scavenging activity in vitro in our previous work.[6] Thus, in synthesis, the cytoprotective effect might be involved in the Keap1/Nrf2/ARE signaling pathway, thereby upregulating the gene expression of antioxidant enzyme.

AUTHOR INFORMATION

Corresponding Author

*Tel.: +86 431 87836351. Fax: +86 431 87836391. E-mail: ljb168@sohu.com.

Funding

This work was funded by the National Natural Science Foundation of China (no. 31271907), Specialized Research Fund for the Doctoral Program of Higher Education (no. 20130061110088), and Project of National Key Technology Research and Development Program (no. 2012BAD33B03).

Notes

The authors declare no competing financial interest.

ABBREVIATIONS USED

QIGLF, Gln-Ile-Gly-Leu-Phe; ACE, angiotensin-converting enzyme; PepT1, peptide transporter 1; DMEM, Dulbeco's Modified Eagle's Medium; HBSS, Hank's balanced salt solution; HEPES, 4-(2-hydroxyethyl)-1-piperazineethanesulfonic acid; DMSO, dimethyl sulfoxide; EDTA, ethylene diamine tetraacetic acid; MTT, 3-(4,5-dimethylthiazol-2-yl)-2,5-diphenyltetra-zolium bromide; MTS, 3-(4,5-dimethylthiazol-2-yl)-5-(3-carboxymethoxyphenyl)-2-(4-sulfophenyl)-2*H*-tetrazolium; TFA, trifluoroacetic acid; TEER, transepithelial electrical resistance; Nrf2, nuclear factor erythroid 2-related factor 2

REFERENCES

(1) Yu, Z.; Yin, Y.; Zhao, W.; Yu, Y.; Liu, B.; Liu, J.; Chen, F. Novel peptides derived from egg white protein inhibiting alpha-glucosidase. *Food Chem.* **2011**, *129*, 1376−1392.

(2) Miguel, M.; Recio, I.; Gomez-Ruiz, J. A.; Ramos, M.; Lopez-Fandino, R. Angiotensin I-converting enzyme inhibitory activity of peptides derived from egg white proteins by enzymatic hydrolysis. *J. Food Prot.* **2004**, *67*, 1914−1920.

(3) Miguel, M.; Lopez-Fandino, R.; Ramos, M.; Aleixandre, A. Long-term intake of egg white hydrolysate attenuates the development of hypertension in spontaneously hypertensive rats. *Life Sci.* **2006**, *78*, 2960−2966.

(4) Majumder, K.; Wu, J. Purification and characterisation of angiotensin I converting enzyme (ACE) inhibitory peptides derived from enzymatic hydrolysate of ovotransferrin. *Food Chem.* **2011**, *126*, 1614−1619.

(5) Liu, J.; Yu, Z.; Zhao, W.; Lin, S.; Wang, E.; Zhang, Y.; Hao, H.; Wang, Z.; Chen, F. Isolation and identification of angiotensin-converting enzyme inhibitory peptides from egg white protein hydrolysates. *Food Chem.* **2010**, *122*, 1159−1163.

(6) Yu, Z.; Liu, B.; Zhao, W.; Yin, Y.; Liu, J.; Chen, F. Primary and secondary structure of novel ACE-inhibitory peptides from egg white protein. *Food Chem.* **2012**, *133*, 315−322.

(7) Yu, Z.; Yin, Y.; Zhao, W.; Wang, F.; Yu, Y.; Liu, B.; Liu, J.; Chen, F. Characterization of ACE-inhibitory peptide associated with antioxidant and anticoagulation properties. *J. Food Sci.* **2011**, *76*, C1149−C1155.

(8) Yu, Z.; Zhao, W.; Liu, J.; Lu, J.; Chen, F. QIGLF, a novel angiotensin I-converting enzyme-inhibitory peptide from egg white protein. *J. Sci. Food Agric.* **2011**, *91*, 921−926.

(9) Li, P.; Nielsen, H. M.; Mullertz, A. Oral delivery of peptides and proteins using lipid-based drug delivery systems. *Expert Opin. Drug Delivery* **2012**, *9*, 1289−1304.

(10) Hidalgo, I. J.; Raub, T. J.; Borchardt, R. T. Characterization of the human colon carcinoma cell line (Caco-2) as a model system for intestinal epithelial permeability. *Gastroenterology* **1989**, *96*, 736−749.

(11) Linnankoski, J.; Makela, J.; Palmgren, J.; Mauriala, T.; Vedin, C.; Ungell, A.-L.; Lazorova, L.; Artursson, P.; Urtti, A.; Yliperttula, M. Paracellular porosity and pore size of the human intestinal epithelium in tissue and cell culture models. *J. Pharm. Sci.* **2010**, *99*, 2166−2175.

(12) Shimizu, K.; Sato, M.; Zhang, Y.; Kouguchi, T.; Takahata, Y.; Morimatsu, F.; Shimizu, M. Molecular size of collagen peptide reverses the permeability of Caco-2 cells. *Biosci. Biotechnol. Biochem.* **2010**, *74*, 1123−1125.

(13) Artursson, P.; Palm, K.; Luthman, K. Caco-2 monolayers in experimental and theoretical predictions of drug transport. *Adv. Drug Delivery Rev.* **2001**, *46*, 27−43.

(14) Yee, S. In vitro permeability across Caco-2 cells (colonic) can predict in vivo (small intestinal) absorption in man–fact or myth. *Pharm. Res.* **1997**, *14*, 763−766.

(15) Sugano, K.; Kansy, M.; Artursson, P.; Avdeef, A.; Bendels, S.; Di, L.; Ecker, G. F.; Faller, B.; Fischer, H.; Gerebtzoff, G.; Lennernaes, H.; Senner, F. Coexistence of passive and carrier-mediated processes in drug transport. *Nat. Rev. Drug Discovery* **2010**, *9*, 597−614.
(16) Fei, Y. J.; Kanai, Y.; Nussberger, S.; Ganapathy, V.; Leibach, F. H.; Romero, M. F.; Singh, S. K.; Boron, W. F.; Hediger, M. A. Expression cloning of a mammalian proton-coupled oligopeptide transporter. *Nature* **1994**, *368*, 563−566.
(17) Vig, B. S.; Stouch, T. R.; Timoszyk, J. K.; Quan, Y.; Wall, D. A.; Smith, R. L.; Faria, T. N. Human PEPT1 pharmacophore distinguishes between dipeptide transport and binding. *J. Med. Chem.* **2006**, *49*, 3636−3644.
(18) Pappenheimer, J. R.; Dahl, C. E.; Karnovsky, M. L.; Maggio, J. E. Intestinal absorption and excretion of octapeptides composed of D amino acids. *Proc. Natl. Acad. Sci. U.S.A.* **1994**, *9*, 1942−1945.
(19) Marchiando, A. M.; Graham, W. V.; Turner, J. R. Epithelial barriers in homeostasis and disease. *Annu. Rev. Pathol.: Mech. Dis.* **2010**, *5*, 119−144.
(20) Yasumatsu, H.; Tanabe, S. The casein peptide Asn-Pro-Trp-Asp-Gln enforces the intestinal tight junction partly by increasing occludin expression in Caco-2 cells. *Br. J. Nutr.* **2010**, *104*, 951−956.
(21) Tanabe, S. Short peptide modules for enhancing intestinal barrier function. *Curr. Pharm. Des.* **2012**, *18*, 776−781.
(22) Shimizu, M. Modulation of intestinal functions by food substances. *Mol. Nutr. Food Res.* **1999**, *43*, 154−158.
(23) Shimizu, M. Interaction between food substances and the intestinal epithelium. *Biosci. Biotechnol. Biochem.* **2010**, *74*, 232−241.
(24) Van Meerloo, J.; Kaspers, G. J. L.; Cloos, J. Cell sensitivity assays: the MTT assay. *Methods Mol. Biol.* **2011**, *731*, 237−45.
(25) Hubatsch, I.; Ragnarsson, E. G. E.; Artursson, P. Determination of drug permeability and prediction of drug absorption in Caco-2 monolayers. *Nat. Protoc.* **2007**, *2*, 2111−2119.
(26) Katayama, S.; Xu, X. M.; Fan, M. Z.; Mine, Y. Antioxidative stress activity of oligophosphopeptides derived from hen egg yolk phosvitin in Caco-2 cells. *J. Agric. Food Chem.* **2006**, *54*, 773−778.
(27) Katayama, S.; Ishikawa, S.-i.; Fan, M. Z.; Mine, Y. Oligophosphopeptides derived from egg yolk phosvitin up-regulate gamma-glutamylcysteine synthetase and antioxidant enzymes against oxidative stress in Caco-2 cells. *J. Agric. Food Chem.* **2007**, *55*, 2829−2835.
(28) Cory, A. H.; Owen, T. C.; Barltrop, J. A.; Cory, J. G. Use of an aqueous soluble tetrazolium/formazan assay for cell growth assays in culture. *Cancer Commun.* **1991**, *3*, 207−12.
(29) Bejjani, S.; Wu, J. Transport of IRW, an ovotransferrin-derived antihypertensive peptide, in human intestinal epithelial Caco-2 cells. *J. Agric. Food Chem.* **2013**, *61*, 1487−1492.
(30) Chua, H. L.; Jois, S.; Sim, M. K.; Go, M. L. Transport of angiotensin peptides across the Caco-2 monolayer. *Peptides* **2004**, *25*, 1327−1338.
(31) Lei, L.; Sun, H.; Liu, D.; Liu, L.; Li, S. Transport of Val-Leu-Pro-Val-Pro in human intestinal epithelial (Caco-2) cell monolayers. *J. Agric. Food Chem.* **2008**, *56*, 3582−3586.
(32) Ohsawa, K.; Satsu, H.; Ohki, K.; Enjoh, M.; Takano, T.; Shimizu, M. Producibility and digestibility of antihypertensive β-casein tripeptides, Val-Pro-Pro and Ile-Pro-Pro, in the gastrointestinal tract: analyses using an in vitro model of mammalian gastrointestinal digestion. *J. Agric. Food Chem.* **2008**, *56*, 854−858.
(33) Iwan, M.; Jarmolowska, B.; Bielikowicz, K.; Kostyra, E.; Kostyra, H.; Kaczmarski, M. Transport of μ-opioid receptor agonists and antagonist peptides across Caco-2 monolayer. *Peptides* **2008**, *29*, 1042−1047.
(34) Cakir-Kiefer, C.; Miclo, L.; Balandras, F.; Dary, A.; Soligot, C.; Le Roux, Y. Transport across Caco-2 cell monolayer and sensitivity to hydrolysis of two anxiolytic peptides from $\alpha_{(s1)}$-Casein, α-casozepine, and $\alpha_{(s1)}$-casein-(f91−97): effect of bile salts. *J. Agric. Food Chem.* **2011**, *59*, 11956−11965.
(35) Sun, H.; Liu, D.; Li, S.; Qin, Z. Transepithelial transport characteristics of the antihypertensive peptide, Lys-Val-Leu-Pro-Val-Pro, in human intestinal Caco-2 cell monolayers. *Biosci. Biotechnol. Biochem.* **2009**, *73*, 293−298.
(36) Quiros, A.; Davalos, A.; Lasuncion, M. A.; Ramos, M.; Recio, I. Bioavailability of the antihypertensive peptide LHLPLP: transepithelial flux of HLPLP. *Int. Dairy J.* **2008**, *18*, 279−286.
(37) Shimizu, K.; Sato, M.; Zhang, Y.; Kouguchi, T.; Takahata, Y.; Morimatsu, F.; Shimizu, M. The bioavailable octapeptide Gly-Ala-Hyp-Gly-Leu-Hyp-Gly-Pro stimulates nitric oxide synthesis in vascular endothelial cells. *J. Agric. Food Chem.* **2010**, *58*, 6960−6965.
(38) Sienkiewicz-Szlapka, E.; Jarmolowska, B.; Krawczuk, S.; Kostyra, E.; Kostyra, H.; Bielikowicz, K. Transport of bovine milk-derived opioid peptides across a Caco-2 monolayer. *Int. Dairy J.* **2009**, *19*, 252−257.
(39) Miguel, M.; Davalos, A.; Manso, M. A.; de la Pena, G.; Lasuncion, M. A.; Lopez-Fandino, R. Transepithelial transport across Caco-2 cell monolayers of antihypertensive egg-derived peptides. PepT1-mediated flux of Tyr-Pro-lle. *Mol. Nutr. Food Res.* **2008**, *52*, 1507−1513.
(40) Shimizu, M.; Tsunogai, M.; Arai, S. Transepithelial transport of oligopeptides in the human intestinal cell, Caco-2. *Peptides* **1997**, *18*, 681−687.
(41) Satake, M.; Enjoh, M.; Nakamura, Y.; Takano, T.; Kawamura, Y.; Arai, S.; Shimizu, M. Transepithelial transport of the bioactive tripeptide, Val-Pro-Pro, in human intestinal Caco-2 cell monolayers. *Biosci. Biotechnol. Biochem.* **2002**, *66*, 378−384.
(42) Antunes, F.; Andrade, F.; Ferreira, D.; Nielsen, H. M.; Sarmento, B. Models to predict intestinal absorption of therapeutic peptides and proteins. *Curr. Drug Metab.* **2013**, *14*, 4−20.
(43) Ren, G.; Qiao, H. X.; Yang, J.; Zhou, C. X. Protective effects of steroids from allium chinense against H_2O_2-induced oxidative stress in rat cardiac H9C2 cells. *Phytother. Res.* **2010**, *24*, 404−409.
(44) Ma, Q. Role of Nrf2 in oxidative stress and toxicity. *Annu. Rev. Pharmacol.* **2013**, *53*, 401−42.

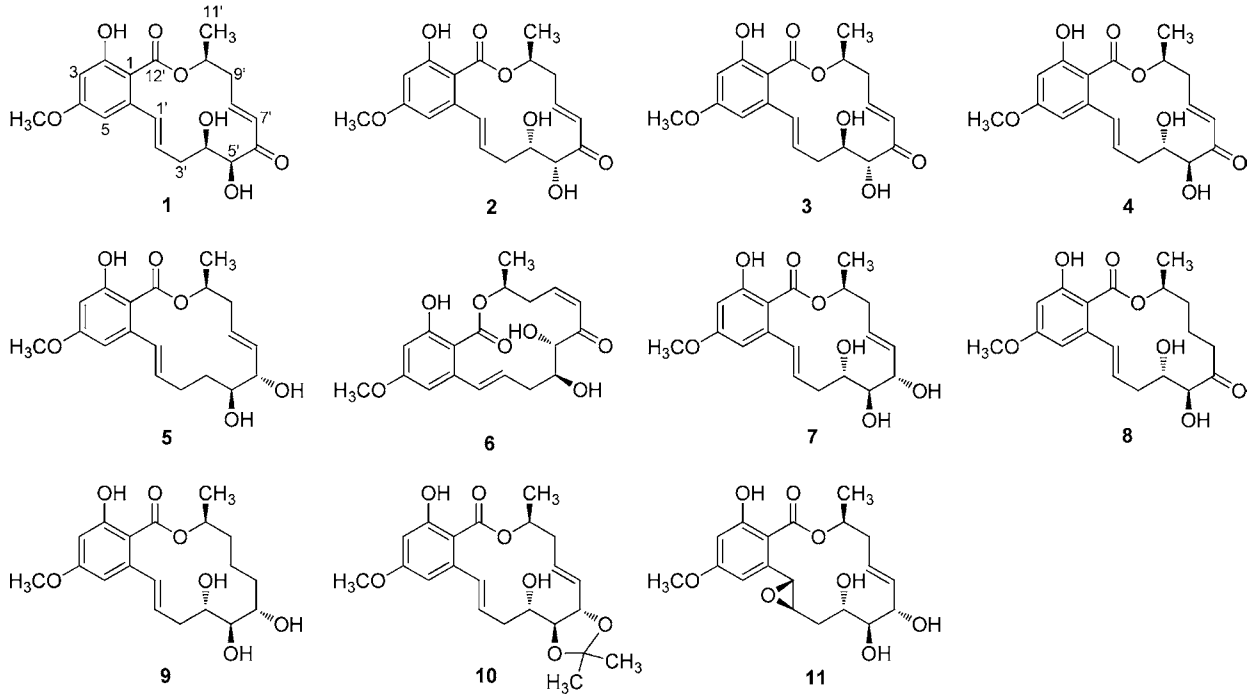

Figure 1. Structures of resorcylic acid lactones **1**−**11** isolated from *C. lunatus* (TA26-46).

Co., Ltd., Yantai, China) were used for thin layer chromatography (TLC).

Fungal Strain. The fungal strain *Cochliobolus lunatus* (TA26-46) was isolated from a piece of fresh tissue from the inner part of the sea anemone *Palythoa haddoni*, collected from the Weizhou coral reef (21° 02′ N, 109° 06′ E) in the South China Sea in April 2010. The fungus was identified as *C. lunatus* according to its morphological traits and a molecular protocol by amplification and sequencing of the DNA sequences of the ITS region of the rRNA gene. The 545 base pair ITS sequence had 100% sequence identity to that of *C. lunatus* (JN943462). The strain was deposited in the Key Laboratory of Marine Drugs, Ministry of Education of China, School of Medicine and Pharmacy, Ocean University of China, Qingdao, P.R. China, with the GenBank (NCBI) access number JF819163.

Fermentation, Extraction, and Isolation. The fungal strain *C. lunatus* (TA26-46) was fermented on solid media in 100 1-L Erlenmeyer flasks (each containing 80 g of rice, 120 mL of water, and 3.6 g of sea salt) at 28 °C for 4 weeks. The fermented solid medium was extracted three times with 300 mL of EtOAc for each Erlenmeyer flask. The combined EtOAc solution was evaporated to dryness under a vacuum to give an EtOAc extract. The EtOAc extract (80.0 g) was subjected to vacuum liquid chromatography (60.0 cm × 8.0 cm i.d.) on silica gel (100−200 mesh) using step-gradient elution with 5 L of petroleum ether/EtOAc (20:1 to 0:1, v/v) to afford five fractions (fractions 1−5). Fraction 4 was purified repeatedly by column chromatography (60.0 cm × 3.0 cm i.d.) on silica gel (200−300 mesh) eluted with 3 L of EtOAc/MeOH (v/v, 10:1) to yield **7** (2.0 g). Fraction 3 was isolated by column chromatography (60.0 cm × 3.0 cm i.d.) on silica gel (200−300 mesh) eluted with 3 L of petroleum ether/EtOAc (10:1 to 7:3, v/v), then subjected to Sephadex LH-20 column chromatography (120.0 cm × 3.0 cm i.d.) with 1 L petroleum ether/CH_2Cl_2/MeOH (2:1:1, v/v/v), and further purified by using semipreparative HPLC on an octadecylsilyl (ODS) column (150 mm × 7.8 mm i.d., 7 μm, Kromasil C18). The dried eluate was dissolved in 5 mL of MeOH and microfiltered. A 100-μL injection volume was used at a flow rate of 2 mL/min and elution of MeOH/water (11:9, v/v) to give **1** (15.0 mg), **2** (1.3 mg), **3** (2.3 mg), **4** (55.5 mg), **5** (145.5 mg), **6** (250.0 mg), **7** (5.0 mg), **8** (20.3 mg), **9** (1.5 mg), **10** (25.0 mg), and **11** (1.2 mg). The structures of the isolated compounds are depicted in Figure 1.

Cochliomycin D (1). White amorphous powder; $[\alpha]^{25}_{D}$ −125 (*c* 0.16, MeOH); UV (MeOH) λ_{max} (log ε) 198 (3.27), 232 (4.30), 271 (3.88), 312 (3.62) nm; CD (1.38 mM, MeOH) λ_{max} ($\Delta\varepsilon$) 219 (+8.07), 246 (+10.95), 273 (−14.44), 310 (−3.85), 351 (+0.31) nm; IR (KBr) ν_{max} 3747, 3648, 1700, 1650, 1540, 1510 cm^{-1}; ^1H and ^{13}C NMR data, see Tables 1 and 2; ESIMS *m*/*z* 385.1 $[M + Na]^+$, 747.2 $[2M + Na]^+$; HRESIMS *m*/*z* 385.1266 $[M + Na]^+$ (calcd for $C_{19}H_{22}O_7Na$, 385.1258).

Table 1. ^1H NMR[a] Data for 1−4 in DMSO-d_6

position	1	2	3	4
3	6.35, d (2.4)	6.31, brs	6.30, d (2.2)	6.32, d (2.3)
5	6.48, d (2.4)	6.55, brs	6.48, d (2.2)	6.45, d (2.3)
1′	6.42, d (15.9)	6.21, d (15.9)	6.24, d (15.7)	6.27, d (15.7)
2′	6.18, ddd (15.9, 7.8, 6.7)	6.33, m	6.20, ddd (15.7, 9.0, 5.2)	6.17, ddd (15.7, 10.4, 3.1)
3′	2.31, m	2.45, m	2.29, m	2.36, m
	2.20, m	2.13, m	2.12, m	2.15, m
4′	3.79, m	3.86, m	3.89, m	4.02, m
5′	4.25, t (5.9)	4.27, t (5.6)	4.30, dd (5.3, 2.6)	4.32, dd (5.1, 4.0)
7′	6.21, d (15.9)	6.13, d (16.2)	6.46, d (15.7)	6.49, d (15.7)
8′	6.82, ddd (15.9, 9.8, 5.2)	6.71, dt (16.2, 7.8)	6.80, ddd (15.7, 7.9, 5.7)	6.81, ddd (15.7, 8.7, 6.2)
9′	2.67, ddd (14.4, 5.2, 2.1)	2.59, m	2.65, m	2.58, ddd (14.4, 6.2, 2.8)
	2.40, ddd (14.4, 9.8, 7.0)	2.45, m	2.42, m	2.44, ddd (14.4, 8.7, 6.6)
10′	5.33, m	5.02, m	5.24, m	5.13, m
11′	1.32, d (6.3)	1.33, d (5.5)	1.30, d (6.3)	1.35, d (6.0)
2-OH	10.46, s	10.04, s	10.08, s	10.36, s
4′-OH	4.94, d (5.6)	4.91, d (6.1)	5.00, d (5.6)	4.99, d (5.7)
5′-OH	5.18, d (5.9)	5.02, d (5.6)	5.24, d (5.3)	5.17, d (5.1)
4-OCH_3	3.75, s	3.73, s	3.72, s	3.74, s

[a]400 MHz for **1**, 500 MHz for **2**−**4**, δ in ppm, *J* in Hz.

dx.doi.org/10.1021/jf500248z | J. Agric. Food Chem. 2014, 62, 3183−3191

Table 2. ^{13}C NMR[a] Data for 1−4 in DMSO-d_6

position	1	2	3	4
1	110.4, C	114.3, C	112.9, C	111.6, C
2	158.8, C	155.8, C	156.7, C	157.8, C
3	100.3, CH	100.5, CH	100.3, CH	100.1, CH
4	161.8, C	160.7, C	161.0, C	161.3, C
5	103.6, CH	100.9, CH	101.9, CH	102.6, CH
6	138.9, C	136.3, C	137.3, C	138.3, C
1′	129.2, CH	129.0, CH	129.2, CH	128.6, CH
2′	130.7, CH	131.3, CH	130.5, CH	130.5, CH
3′	36.5, CH_2	35.7, CH_2	36.0, CH_2	36.0, CH_2
4′	72.7, CH	71.5, CH	73.0, CH	71.9, CH
5′	75.8, CH	73.6, CH	78.8, CH	78.2, CH
6′	200.2 C	199.9, C	200.1, C	200.7, C
7′	131.0, CH	131.3, CH	129.7, CH	130.3, CH
8′	143.9, CH	143.9, CH	142.7, CH	142.4, CH
9′	37.5, CH_2	37.9, CH_2	37.5, CH_2	37.9, CH_2
10′	69.9, CH	70.5, CH	69.8, CH	70.2, CH
11′	19.7, CH_3	20.4, CH_3	19.9, CH_3	20.1, CH_3
12′	167.9, C	167.6, C	167.6, C	168.2, C
4-OCH_3	55.3, CH_3	55.3, CH_3	55.2, CH_3	55.3, CH_3

[a]100 MHz for **1**, 125 MHz for **2**−**4**, δ in ppm.

*Cochliomycin E (**2**).* White amorphous powder; $[\alpha]^{25}_D$ −73 (*c* 0.10, MeOH); UV (MeOH) λ_{max} (log ε) 198 (3.33), 223 (4.10), 271 (3.93), 312 (3.66) nm; CD (0.83 mM, MeOH) λ_{max} ($\Delta\varepsilon$) 220 (+5.53), 245 (+3.86), 278 (−1.99) nm; IR (KBr) ν_{max} 3745, 3646, 1696, 1647, 1556, 1518 cm^{-1}; ^{1}H and ^{13}C NMR data, see Tables 1 and 2; ESIMS *m*/*z* 385.1 $[M + Na]^+$; HRESIMS *m*/*z* 385.1269 $[M + Na]^+$ (calcd for $C_{19}H_{22}O_7Na$, 385.1258).

*Cochliomycin F (**3**).* White amorphous powder; $[\alpha]^{25}_D$ −23.3 (*c* 0.10, MeOH); UV (MeOH) λ_{max} (log ε) 198 (3.09), 231 (4.19), 271 (3.95), 312 (3.67) nm; CD (3.86 mM, MeOH) λ_{max} ($\Delta\varepsilon$) 228 (+2.20), 248 (+2.62), 274 (−1.77), 316 (+0.16) nm; IR (KBr) ν_{max} 3747, 3648, 1700, 1650, 1556, 1521 cm^{-1}; ^{1}H and ^{13}C NMR data, see Tables 1 and 2; ESIMS *m*/*z* 385.1 $[M + Na]^+$, 747.1 $[2M + Na]^+$; HRESIMS *m*/*z* 385.1268 $[M + Na]^+$ (calcd for $C_{19}H_{22}O_7Na$, 385.1258).

*(7′*E*)-6′-Oxozeaenol (**4**).* White amorphous powder; $[\alpha]^{25}_D$ −50 (*c* 0.20, MeOH) {literature $[\alpha]^{24}_D$ −27.0 (*c* 0.33, MeOH)};[6] CD (0.83 mM, MeOH) λ_{max} ($\Delta\varepsilon$) 235 (+12.61), 273 (−6.34), 316 (−1.07), 350 (+0.04) nm; ^{1}H and ^{13}C NMR data, see Tables 1 and 2; ESIMS *m*/*z* 385.1 $[M + Na]^+$, 747.2 $[2M + Na]^+$.

*LL-Z1640-2 (**6**).* White amorphous powder; $[\alpha]^{25}_D$ −94 (*c* 0.10, MeOH) {literature $[\alpha]^{24}_D$ −75.9 (*c* 0.41, MeOH)};[7] CD (2.21 mM, MeOH) λ_{max} ($\Delta\varepsilon$) 216 (+3.82), 247 (+7.22), 272 (−13.60), 343 (+0.71) nm.

*Specific Rotation Data for Known Compounds **5** and **7**−**11**.* *deoxy*-Aigialomycin C (**5**): $[\alpha]^{25}_D$ +43.3 (*c* 0.10, MeOH) {literature $[\alpha]^{24}_D$ +25.4 (*c* 5.4, CH_2Cl_2)}.[8] Zeaenol (**7**): $[\alpha]^{25}_D$ −79 (*c* 0.15, MeOH) {literature $[\alpha]^{24}_D$ −92 (*c* 0.54, MeOH)}.[9] LL-Z1640-1 (**8**): $[\alpha]^{25}_D$ −91.7 (*c* 0.10, MeOH) {literature $[\alpha]^{24}_D$ −80 (*c* 0.48, MeOH)}.[7] Paecilomycin F (**9**): $[\alpha]^{25}_D$ −112.5 (*c* 0.04, MeOH) {literature $[\alpha]^{24}_D$ −106.4 (*c* 0.28, MeOH)}.[10] Cochliomycin A (**10**): $[\alpha]^{25}_D$ +32.7 (*c* 0.10, MeOH) {literature $[\alpha]^{24}_D$ +10.5 (*c* 0.43, MeOH)}.[5] Aigialomycin B (**11**): $[\alpha]^{25}_D$ −26.7 (*c* 0.05, MeOH) {literature $[\alpha]^{24}_D$ −10 (*c* 0.27, $CHCl_3$)}.[2]

Preparation of the Acetonide Derivatives, 1a, 3a, and 4a. A mixture of **1** (3.0 mg), 2,2-dimethoxypropane (1.5 mL), and *p*-TsOH (0.2 mg) was stirred at room temperature for 1 h. Saturated aqueous $NaHCO_3$ (5 mL) was then added, and the reaction mixture was extracted with EtOAc (5 mL × 3). The organic solvents were removed under a vacuum, and the crude mixture was subjected to semipreparative HPLC to obtain **1a** (2.8 mg). By the same procedures, the acetonides **3a** (1.0 mg) and **4a** (2.5 mg) were prepared from **3** (1.2 mg) and **4** (3.0 mg), respectively.

*Compound **1a**.* White amorphous powder; ^{1}H NMR (500 MHz, acetone-d_6) δ 11.37 (1H, s, 2-OH), 7.21 (1H, dt, *J* = 16.7, 7.1 Hz), 7.17 (1H, dd, *J* = 15.3, 2.0 Hz), 6.51 (1H, d, *J* = 2.5 Hz, H-5), 6.44 (1H, d, *J* = 2.5 Hz, H-3), 6.15 (1H, d, *J* = 16.7 Hz), 6.07 (1H, ddd, *J* = 15.3, 10.1, 3.7 Hz), 5.40 (1H, m, H-10′), 5.04 (1H, d, *J* = 8.8 Hz, H-5′), 4.05 (1H, ddd, *J* = 8.8, 4.1, 2.9 Hz, H-4′), 3.86 (3H, s, 4-OCH_3), 2.82−2.91 (2H, m), 2.66 (1H, ddd, *J* = 15.5, 7.7, 1.2 Hz), 2.54 (1H, ddd, *J* = 16.0, 10.1, 2.7 Hz), 1.47 (3H, d, *J* = 6.3 Hz, H-11′), 1.41 (3H, s, H-14′), 1.37 (3H, s, H-15′); ^{13}C NMR (acetone-d_6, 125 MHz) δ 196.4 (C), 171.1 (C), 165.3 (C), 165.0 (C), 146.7 (C), 143.6 (CH), 135.8 (CH), 133.8 (CH), 127.0 (CH), 110.0 (C), 108.7 (CH), 105.7 (C), 101.0 (CH), 79.4 (CH), 77.6 (CH), 71.9 (CH), 56.0 (OCH_3), 38.0 (CH_2), 34.2 (CH_2), 27.3 (CH_3), 26.4 (CH_3), 20.2 (CH_3); ESIMS *m*/*z* 403.3 $[M + H]^+$, 425.3 $[M + Na]^+$, 827.5 $[2M + Na]^+$.

*Compound **3a**.* White amorphous powder; ^{1}H NMR (500 MHz, acetone-d_6) δ 11.60 (1H, s, 2-OH), 7.06 (1H, dt, *J* = 16.1, 6.2 Hz), 6.83 (1H, d, *J* = 15.6 Hz), 6.60 (1H, d, *J* = 16.1 Hz), 6.50 (1H, d, *J* = 2.2 Hz, H-5), 6.42 (1H, d, *J* = 2.2 Hz, H-3), 6.07 (1H, ddd, *J* = 15.6, 8.5, 5.9 Hz), 5.53 (1H, m, H-10′), 4.99 (1H, d, *J* = 6.7 Hz, H-5′), 4.64 (1H, ddd, *J* = 9.6, 6.7, 2.0 Hz, H-4′), 3.85 (3H, s, 4-OCH_3), 2.86 (1H, m), 2.70−2.60 (2H, m), 2.44 (1H, m), 1.56 (3H, s, H-15′), 1.47 (3H, d, *J* = 6.5 Hz, H-11′), 1.36 (3H, s, H-14′); ^{13}C NMR (acetone-d_6, 125 MHz) δ 196.6 (C), 171.3 (C), 165.2 (C), 164.8 (C), 143.2 (C), 142.3 (CH), 134.0 (CH), 130.8 (CH), 128.6 (CH), 109.8 (C), 108.5 (C), 105.9 (CH), 100.9 (CH), 81.9 (CH), 77.9 (CH), 71.7 (CH), 55.9 (OCH_3), 37.3 (CH_2), 34.4 (CH_2), 27.0 (CH_3), 25.9 (CH_3), 18.7 (CH_3); ESIMS *m*/*z* 425.0 $[M + Na]^+$.

*Compound **4a**.* White amorphous powder; ^{1}H NMR (500 MHz, acetone-d_6) δ 11.39 (1H, s, 2-OH), 7.06 (1H, dt, *J* = 15.5, 7.9 Hz), 6.96 (1H, dd, *J* = 15.5, 2.2 Hz), 6.55 (1H, d, *J* = 2.6 Hz, H-5), 6.48 (1H, d, *J* = 15.5 Hz), 6.42 (1H, d, *J* = 2.6 Hz, H-3), 6.03 (1H, ddd, *J* = 15.5, 10.0, 3.9 Hz), 5.58 (1H, m, H-10′), 4.85 (1H, d, *J* = 6.6 Hz, H-5′), 4.65 (1H, ddd, *J* = 10.9, 6.6, 2.6 Hz, H-4′), 3.85 (3H, s, 4-OCH_3), 2.69 (1H, ddd, *J* = 15.7, 6.4, 2.7 Hz), 2.65−2.60 (2H, m), 2.34 (1H, dt, *J* = 16.2, 10.5 Hz), 1.59 (3H, s, H-14′), 1.47 (3H, d, *J* = 6.5 Hz, H-11′), 1.35 (3H, s, H-15′); ^{13}C NMR (acetone-d_6, 125 MHz) δ 196.7 (C), 171.1 (C), 165.2 (C), 164.8 (C), 143.2 (C), 142.2 (CH), 133.7 (CH), 132.1 (CH), 128.8 (CH), 109.9 (C), 109.9 (C), 108.2 (CH), 101.7 (CH), 82.3 (CH), 78.5 (CH), 72.2 (CH), 55.9 (OCH_3), 37.7 (CH_2), 35.3 (CH_2), 27.0 (CH_3), 26.0 (CH_3), 19.0 (CH_3); ESIMS *m*/*z* 425.0 $[M + Na]^+$.

Preparation of Tri-*p*-bromobenzoyl Derivatives, 1b, 3b, and 4b. Cochliomycin D, **1** (2.0 mg), was treated with *p*-bromobenzoyl chloride (15 mg) and 4-*N*,*N*-dimethylaminopyridine (DMAP, 2.5 mg) in 1.5 mL of pyridine/CH_2Cl_2 (1:2) at 40 °C for 2 h. The mixture was diluted with EtOAc and washed with H_2O and 1 M $NaHCO_3$, and the organic layer was concentrated under a vacuum to obtain a colorless solid. It was then purified by Sephadex LH-20 column chromatography and semipreparative HPLC to obtain **1b** (2.9 mg). Tri-*p*-bromobenzoyl derivatives **3b** (0.5 mg) and **4b** (1.8 mg) were prepared similarly from cochliomycin F, **3** (0.3 mg), and (7′*E*)-6′-oxozeaenol, **4** (1.2 mg), respectively.

*Compound **1b**.* White amorphous powder; CD (0.87 mM, CH_2Cl_2) λ_{max} ($\Delta\varepsilon$) 262 (−11.64), 242 (+11.18) nm; ^{1}H NMR (500 MHz, $CDCl_3$) δ 8.05 (2H, d, *J* = 8.5 Hz, *p*-bromobenzoyl), 7.90 (2H, d, *J* = 8.5 Hz, *p*-bromobenzoyl), 7.75 (2H, d, *J* = 8.5 Hz, *p*-bromobenzoyl), 7.66 (2H, d, *J* = 8.5 Hz, *p*-bromobenzoyl), 7.57 (2H, d, *J* = 8.5 Hz, *p*-bromobenzoyl), 7.49 (2H, d, *J* = 8.5 Hz, *p*-bromobenzoyl), 7.11 (1H, ddd, *J* = 15.5, 8.7, 5.4 Hz), 6.93 (1H, d, *J* = 15.5 Hz), 6.88 (1H, d, *J* = 2.2 Hz, H-5), 6.73 (1H, d, *J* = 2.2 Hz, H-3), 6.34 (1H, d, *J* = 16.1 Hz), 6.12 (1H, m), 5.78 (1H, d, *J* = 3.4 Hz), 5.77 (1H, m), 5.33 (1H, m), 3.85 (3H, s, 4-OCH_3), 2.84 (1H, dt, *J* = 14.7, 7.4 Hz), 2.64 (2H, m), 2.42 (1H, m), 1.20 (3H, d, *J* = 6.3 Hz, H-11′); ESIMS *m*/*z* 933.0 $[M + Na]^+$.

*Compound **3b**.* White amorphous powder; CD (0.32 mM, CH_2Cl_2) λ_{max} ($\Delta\varepsilon$) 276 (−0.63), 249 (+5.40) nm; ^{1}H NMR (500 MHz, $CDCl_3$) δ 8.04 (2H, d, *J* = 8.5 Hz, *p*-bromobenzoyl), 7.95 (2H, d, *J* = 8.5 Hz, *p*-bromobenzoyl), 7.85 (2H, d, *J* = 8.5 Hz, *p*-bromobenzoyl), 7.66 (2H, d, *J* = 8.5 Hz, *p*-bromobenzoyl), 7.61 (2H, d, *J* = 8.5 Hz, *p*-bromobenzoyl), 7.57 (2H, d, *J* = 8.5 Hz, *p*-

dx.doi.org/10.1021/jf500248z | J. Agric. Food Chem. 2014, 62, 3183−3191

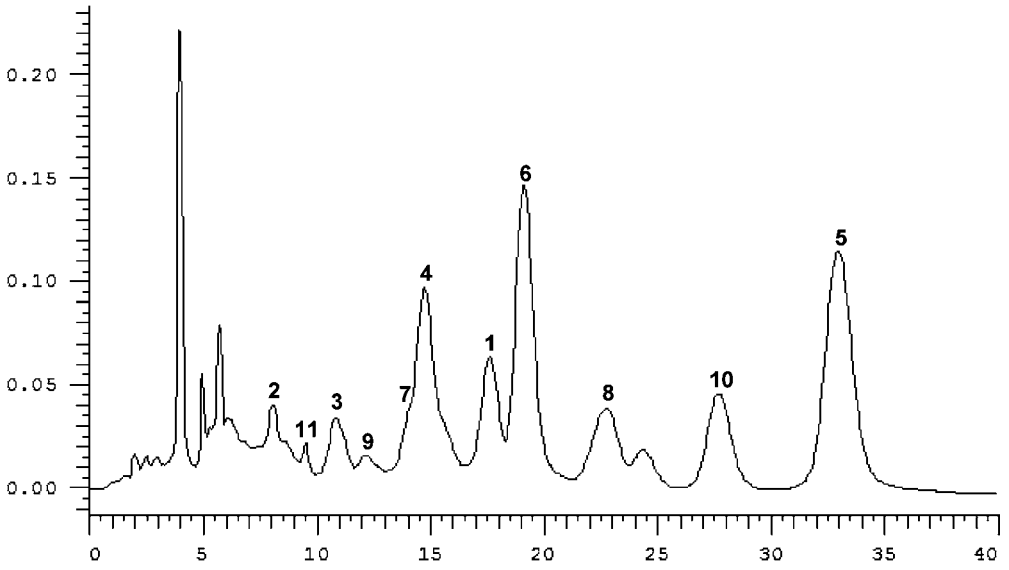

Figure 2. HPLC profile of resorcylic acid lactone constituents (fraction 3) of *C. lunatus* (TA26-46).

bromobenzoyl), 7.05 (1H, m), 6.92 (1H, d, J = 15.2 Hz), 6.88 (1H, d, J = 2.2 Hz, H-5), 6.72 (1H, d, J = 2.2 Hz, H-3), 6.52 (1H, d, J = 16.0 Hz), 6.13 (1H, m), 6.03 (1H, dd, J = 2.8, 0.5 Hz), 5.83 (1H, m), 5.32 (1H, m), 3.85 (3H, s, 4-OCH_3), 1.99−2.82 (4H, m), 1.11 (3H, d, J = 6.3 Hz, H-11′); ESIMS m/z 933.2 $[M + Na]^+$.

Compound ***4b***. White amorphous powder; CD (0.87 mM, CH_2Cl_2) λ_{max} ($\Delta\varepsilon$) 266 (+21.28), 243 (−8.26) nm; ^{1}H NMR (500 MHz, $CDCl_3$) δ 8.05 (2H, d, J = 8.5 Hz, p-bromobenzoyl), 7.77 (2H, d, J = 8.5 Hz, p-bromobenzoyl), 7.66 (2H, d, J = 8.5 Hz, p-bromobenzoyl), 7.63 (2H, d, J = 8.5 Hz, p-bromobenzoyl), 7.54 (2H, d, J = 8.5 Hz, p-bromobenzoyl), 7.41 (2H, d, J = 8.5 Hz, p-bromobenzoyl), 7.04 (1H, ddd, J = 15.5, 10.3, 5.2 Hz), 6.96 (1H, d, J = 2.3 Hz, H-5), 6.78 (1H, d, J = 2.3 Hz, H-3), 6.67 (1H, d, J = 15.5 Hz), 6.41 (1H, d, J = 15.5 Hz), 6.29 (1H, m), 6.12 (1H, d, J = 3.9 Hz), 5.95 (1H, m), 5.30 (1H, m), 3.87 (3H, s, 4-OCH_3), 2.76 (2H, m), 2.49 (1H, dd, J = 13.8 Hz, 5.1), 2.32 (1H, m), 1.02 (3H, d, J = 6.3 Hz, H-11′); ESIMS m/z 933.2 $[M + Na]^+$.

Double-Bond Isomerization of LL-Z1640-2 (6) to Yield 4. Compound **6** (3.0 mg) was dissolved in 2.0 mL of pyridine, and the solution was stirred vigorously at 50 °C for 2 h. H_2O (5 mL) was then added, and the reaction mixture was extracted with EtOAc (5 mL × 3). The organic solvents were removed under a vacuum, and the crude mixture was subjected to semipreparative HPLC to give the reaction product, the spectroscopic data of which were consistent with **4** (2.2 mg).

Biological Assays. *Antifouling Bioassay*. The antifouling activities against the larval settlement of the barnacle were determined using cyprids of *Balanus amphitrite* Darwin according to literature procedures.[11] Larval settlement assays were performed using 24-well polystyrene plates (Becton Dickinson, Franklin Lakes, NJ, USA). The tested compounds were first dissolved in a small amount of dimethyl sulfoxide (DMSO) and then diluted with filtered seawater to achieve final concentrations of 50, 20, 10, 5, 2.5, 1.25, and 0.625 μg/mL. About 15−20 competent larvae were gently transferred into each well with 1 mL of testing solution in three replicates, and wells containing larvae in filtered seawater with DMSO only served as a control. SeaNine 211 (Rohm & Haas, Philadelphia, PA, USA), a new type nontoxic antifouling agent developed by Rohm & Haas, was used as a positive control. The plates were incubated for 24−48 h at 23 °C. The effects of the test samples against biofouling were determined by examining the plates under a dissecting microscope to check for (1) settled larvae and (2) nonsettled larvae, as well as (3) any possible toxic effects of the treatments, such as death or paralysis of larvae, which were also recorded. The EC_{50} (50% inhibition of settlement of cyprids in comparison with the control) and LC_{50} (50% lethality of cyprids in comparison with the control) were calculated using the Probit software program with the means of three repeated experiments using different batches of larvae.

Antifungal Assays. Antifungal bioassays were conducted following the National Center for Clinical Laboratory Standards (NCCLS) recommendations.[12] Three phytopathogenic fungal strains, *Thielaviopsis paradoxa*, *Pestalotia calabae*, and *Glorosprium musarum*, were grown on potato dextrose agar. Targeted microbes (three to four colonies) were prepared from broth culture (28 °C for 48 h), and the final spore suspensions of fungi were 10^4 mycelial fragments/mL. Test samples (100 μM as stock solution in DMSO and serial dilutions) were transferred to a 96-well clear plate in triplicate, and the suspension of the test organisms was added to each well achieving a final volume of 200 μL. Ketoconazole was used as a positive control. After incubation, the absorbance at 492 nm was measured with a microplate reader. The minimum inhibitory concentration (MIC) was defined as the lowest test concentration that completely inhibited the growth of the test organisms.

Fungicide Screening.[13] Fungicidal activities were tested by pathogens on leaf-piece assays at a rate of 100 ppm for *Septoria tritici* on wheat and *Uromyces viciae-fabae* on bean and at rates of 200 and 60 ppm for *Phytophthora infestans* on tomato. Fungicidal activities were also evaluated in mycelial growth tests on artificial media against *Pythium dissimile*, *Alternaria solani*, *Botryotinia fuckeliana*, and *Gibberella zeae*, at rates of 20 and 2 ppm. Rates of tested compounds were adjusted to accommodate intrinsic differences in sensitivities of pathogens in the different test systems. All testing was undertaken on 96-well microtiter plates using azoxystrobin and prochloraz as positive controls. Chemicals were applied to leaf pieces prior to inoculation with spores of the pathogen or in the case of the artificial media assays. The plates were stored in controlled-environment cabinets from 4 to 14 days, depending on the assay, and disease inhibition or mycelial growth was then assessed. Each well was scored using a three-banded system, with complete inhibition of mycelial growth or disease symptoms as 99, partial inhibition as 55, and no inhibition as 0.

Fungicide Whole-Plant Assay. Fungicide whole-plant assessment was conducted against *P. infestans* and *Plasmopara viticola* on glasshouse-based whole-plant assays. All preventative, curative, and persistence tests against *P. infestans* on potato and *P. viticola* on grapevine were applied at rates of 200, 60, 20, 6, and 2 ppm as foliar sprays, whereas the preventative soil drench test against *P. infestans* on tomato was applied at rates of 20, 6, and 2 ppm/kg of soil. Mefenoxam and mandipropamid were used as positive controls. Chemical applications were made 2 days prior to inoculation for preventative foliar tests, 3 days prior to inoculation for drench tests, 6 days prior to

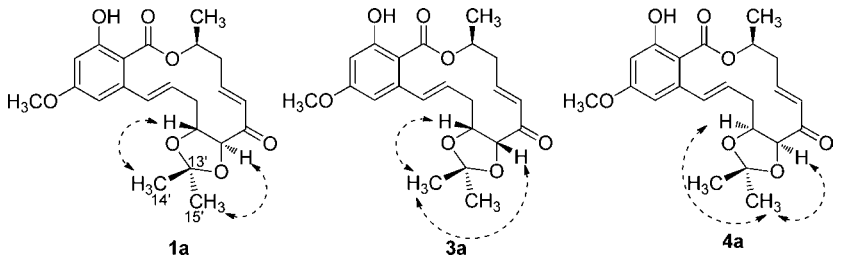

Figure 3. Structures and key NOE correlations of acetonide derivatives **1a**, **3a**, and **4a**.

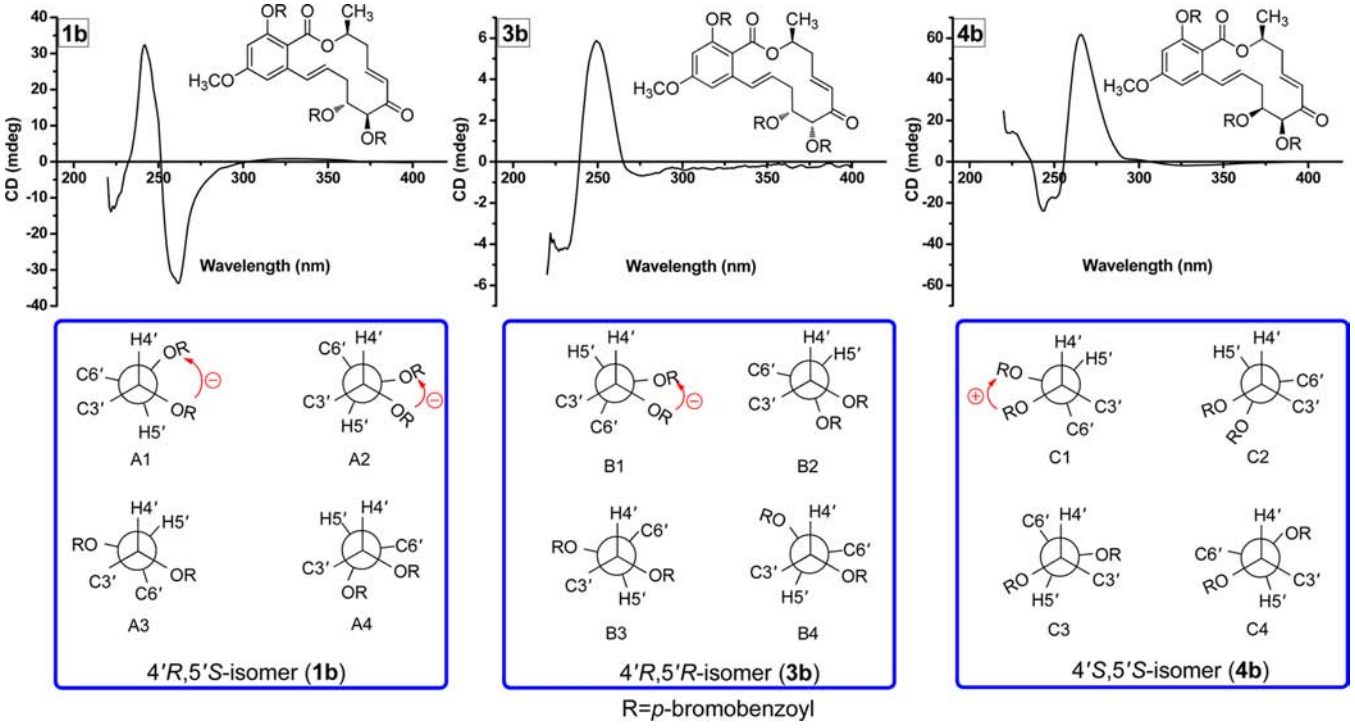

Figure 4. Structures and CD spectra of **1b**, **3b**, and **4b** and Newman projections showing possible local conformations in the 4′*R*,5′*S* (**1b**), 4′*R*,5′*R* (**3b**), and 4′*S*,5′*S* (**4b**) isomers.

inoculation for persistence tests, and 1 day after inoculation for curative tests. For the inoculation, sporangial suspensions were made up to the required rate (approximately 70000 sporangia/mL for *P. viticola* and 50000 sporangia/mL for *P. infestans*) and applied to the treated plants using a hand-held spray gun. After inoculation, the plants were kept under controlled conditions either in the glass house for trials with *P. viticola* (14 h of light/day at 100% relative humidity and 20 °C) or in a climate chamber for trials with *P. infestans* (14 h of light/day at 100% relative humidity and 18 °C). Assessments of disease development were made visually between 5 and 11 days after treatment, depending on the assay. The preventative and persistence tests against *P. infestans* also included a second evaluation of disease development 2 days after the initial assessment.

RESULTS AND DISCUSSION

An EtOAc extract from the solid fermentation of the fungus *Cochliobolus lunatus* (TA26-46) was separated by vacuum liquid chromatography on silica gel using step-gradient elution to yield five fractions (fractions 1−5). Fraction 3 showed a series of peaks in the HPLC profile (Figure 2) with similar UV absorptions at 223, 271, and 312 nm, indicative of the presence of resorcylic acid lactones.[2] Fraction 4 showed only a main peak in the HPLC profile with the same UV absorptions as the of peaks in fraction 3. Eleven resorcylic acid lactones, **1**−**11**, were isolated from fractions 3 and 4 by column chromatography and semipreparative HPLC guided by the characteristic UV absorption spectra of resorcylates.

Cochliomycin D, **1**, was isolated as a white powder, and its molecular formula was established to be $C_{19}H_{22}O_7$ (nine degrees of unsaturation) by HRESIMS. The ^{1}H NMR spectrum (Table 1) exhibited an exchangeable proton singlet at δ_H 10.46 assignable to the chelated phenolic hydrogen. The downfield ^{1}H NMR spectrum revealed two meta-coupled aromatic proton signals (δ_H 6.48, d, J = 2.4 Hz; 6.35, d, J = 2.4 Hz), and two trans double bonds (δ_H 6.42, d, J = 15.9 Hz and 6.18, ddd, J = 15.9, 7.8, 6.7 Hz; 6.21, d, J = 15.9 Hz and 6.82, ddd, J = 15.9, 9.8, 5.2 Hz). Additional resonances attributable to three oxymethines (δ_H 3.79, m; 4.25, t, J = 5.9 Hz; and 5.33, m), one oxymethyl (δ_H 3.75, s), and one methyl (δ_H 1.32, d, J = 6.3 Hz) were observed. The ^{13}C NMR spectrum (Table 2) revealed the presence of one keto carbonyl (δ_C 200.2), one ester carbonyl (δ_C 167.9), and one tetra-substituted benzene ring. These spectroscopic features suggest that **1** belongs to the family of resorcylic acid lactones and is very similar to (7′*E*)-6′-oxozeaenol, **4**.[6,9] The conspicuous differences between the ^{13}C NMR spectrum of **1** and that of **4** are the chemical shifts of C-4′ (δ_C 72.7 in **1** vs 71.9 in **4**) and C-5′ (δ_C 75.8 in **1** vs 78.2 in **4**). The planar structure of **1** was further confirmed on the basis

dx.doi.org/10.1021/jf500248z | J. Agric. Food Chem. 2014, 62, 3183−3191

of the 2D NMR [^{1}H−^{1}H correlation spectroscopy (COSY), heteronuclear multiple-quantum coherence (HMQC), and heteronuclear multiple-bond correlation (HMBC)] spectroscopic data. The connection from C-1′ to C-5′ and the local structure from C-7′ to C-11′ were addressed on the basis of the ^{1}H−^{1}H COSY correlations. A trans-olefin (C-1′/C-2′) was attached to the benzene ring at C-6 position, as indicated by the HMBCs from the olefinic proton H-1′ to C-1, C-5, and C-6 and from H-2′ to C-6. The carbonyl (δ_C 200.2) was placed at the C-6′ position, because the HMBC spectrum exhibited correlations from H-5′, H-7′, and H-8′ to this carbon. Thus, the planar structure of cochliomycin D, **1**, was established as the same as that of **4**.

Cochliomycins E and F, **2** and **3**, were also isolated as white powders, with the same molecular formula, $C_{19}H_{22}O_7$, as **1** based on HRESIMS. The ^{1}H and ^{13}C NMR spectra of **2** and **3** (Tables 1 and 2) were strikingly similar to those of **1**. Detailed analysis of the 1D and 2D NMR spectra established the same planar structures for **2** and **3** as for **1**.

Subsequently, detailed analysis of the ^{1}H and ^{13}C NMR spectra of **1**−**4** (Tables 1 and 2) revealed that these four compounds showed high similarity in NMR spectroscopic data. The significant differences among them were the carbon signals of the oxymethines at C-4′ and C-5′. These NMR features implied that **1**−**4** are diastereomers differing from each other by the absolute configurations of the 4′,5′-diol chiral centers.

The relative configurations of 4′,5′-diol in **1**, **3**, and **4** were determined by nuclear Overhauser effect (NOE) experiments of their acetonide derivatives. Compounds **1**, **3**, and **4** were treated with *p*-TsOH·H_2O in 2,2-dimethoxypropane, which gave the respective acetonide derivatives **1a**, **3a**, and **4a**. In the selective NOE experiments of **1a**, irradiation of H-4′ (δ_H 4.05) resulted in the enhancement of the signal for H_3-14′ (δ_H 1.41, s), and irradiation of H-5′ (δ_H 5.04) resulted in the enhancement of the signal for H_3-15′ (δ_H 1.37, s) (Figure 3). Therefore, H-4′ and H-5′ should be placed on opposite sides of the acetonide ring, suggesting a trans-fused acetonide in **1a**. Similarly, the selective NOE experiments indicated that both **3a** and **4a** were *cis*-acetonide derivatives (Figure 3). The acetonide formation of **2** was not conducted because of its limited quantity. It should be noted that the cis-fused acetonide derivative of **4** was reported previously,[9] but its absolute configuration has not been determined.

The absolute configurations of the 4′,5′-diol in **1**, **3**, and **4** were established by applying CD exciton chirality method.[14] To obtain derivatives suitable for CD exciton chirality analysis, additional chromophores had to be introduced into the original structures. The *p*-bromobenzoyl chromophore was selected to avoid the interference of the enone chromophore, which has an $n-\pi^*$ transition occurring around 335 nm. Acylation of **1**, **3**, and **4** with excess *p*-bromobenzoyl chloride in CH_2Cl_2 and pyridine gave their respective triacyl derivatives, **1b**, **3b**, and **4b** (Figure 4). The CD spectrum of **1b** (Figure 4) showed a negative first Cotton effect at 262 nm ($\Delta\varepsilon$ = −11.76) and a positive second Cotton effect at 242 nm ($\Delta\varepsilon$ = +11.29), suggesting negative chirality for **1b**. Furthermore, according to the Karplus formula, the $^3J_{H4'-H5'}$ value of 3.4 Hz of **1b** suggests the Newman projections of four possible conformations for the 4′*R*,5′*S* isomer, A1, A2, A3, and A4 (Figure 4). Examinations of the macrocycle conformations with a molecular model strongly suggested that conformations corresponding to the projections A3 and A4 were disfavored due to steric hindrance of the two *p*-bromobenzoyl groups. The anticlockwise manner in space of two *p*-bromobenzoyl chromophores in the projections A1 and A2 were consistent with the negative chirality of **1b**. Thus, on the basis of the exciton chirality rule, the absolute configuration of **1b** was defined as 4′*R*,5′*S*. Similarly, **3b** exhibited negative chirality in the first Cotton effect at 276 nm ($\Delta\varepsilon$ = −0.63) in its CD spectrum, consistent with the anticlockwise manner in the projection B1, suggesting the 4′*R*,5′*R* configuration, whereas **4b** showed positive chirality in the first Cotton effect at 266 nm ($\Delta\varepsilon$ = +21.28), matching the clockwise manner in the projection C1, which revealed the 4′*S*,5′*S* configuration (Figure 4). Therefore, the absolute configurations of the 4′,5′-diol in **1**, **3**, and **4** were designated as 4′*R*,5′*S*, 4′*R*,5′*R*, and 4′*S*,5′*S*, respectively.

The absolute configurations at C-10′ in **1**−**4** were determined by their CD spectra (Figure 5). The negative

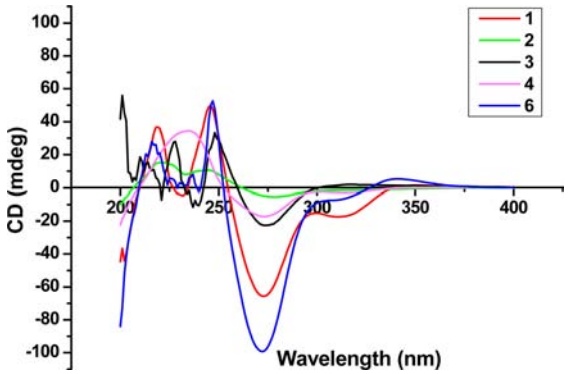

Figure 5. CD spectra of **1**−**4** and **6**.

Cotton effects around 275 nm suggested the *S* configuration at C-10′ for **1**−**4**, by comparison with that of the coisolated known compound **6** and other similar resorcylic acid lactones described in the literature.[15,16] Furthermore, **4** could be obtained by a double-bond isomerization reaction from **6**, whose absolute configuration was described as 4′*S*,5′*S*,10′*S* in the literature.[7] This isomerization experiment further confirmed the absolute configuration of **4**.

Because **1**, **3**, and **4** were determined above as having the 4′*R*,5′*S*,10′*S*, 4′*R*,5′*R*,10′*S*, and 4′*S*,5′*S*,10′*S* configurations, respectively, the absolute configuration of **2** was tentatively assigned as 4′*S*,5′*R*,10′*S*. To verify the absolute configuration of **2**, time-dependent density functional theory (TDDFT) electronic circular dichroism (ECD) calculations were applied to **2**, together with its stereoisomer **1** with the enantiomeric 4′,5′-diol. First, conformational analysis was carried out by Monte Carlo searching using molecular mechanism with the MMFF94 force field in the Spartan program.[17] The results showed four lowest-energy conformers for **1** and five for **2** whose relative energies were within 2 kcal/mol. Subsequently, the conformers were reoptimized using DFT at the B3LYP/6-31+G(d) level in a vacuum with the Gaussian 09 program.[18] The B3LYP/6-31+G(d) harmonic vibrational frequencies were further calculated to confirm their stability. The energies, oscillator strengths, and rotational strengths of the first 30 electronic excitations were calculated using the TDDFT methodology at the B3LYP/6-311++G(2d, 2p) level in a vacuum. The ECD spectra were simulated by the overlapping Gaussian function,[19] in which the first 15 velocity rotatory strengths for **1** and the first 11 for **2** were employed. To obtain the final ECD spectrum, the simulated spectra of the lowest-

dx.doi.org/10.1021/jf500248z | J. Agric. Food Chem. 2014, 62, 3183−3191

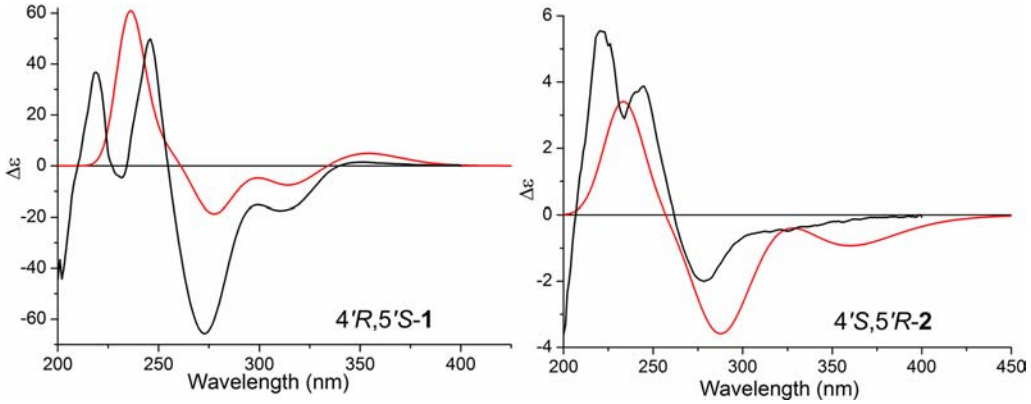

Figure 6. B3LYP/6-311++G(2d,2p)//B3LYP/6-31+G(d)-calculated ECD spectra (red) of 4′*R*,5′*S*-**1** and 4′*S*,5′*R*-**2** and experimental ECD spectra (black) of **1** (σ = 0.2) and **2** (σ = 0.4).

energy conformations were averaged according to the Boltzmann distribution theory and their relative Gibbs free energies (ΔG). In the 200−400-nm region, the experimental ECD spectrum of **1** showed a small positive first Cotton effect around 350 nm, whereas **2** showed a negative effect around this band. The calculated spectra for the two compounds matched the corresponding experimental spectra (Figure 6). Therefore, qualitative analysis of the above information confirmed the absolute configuration of **2** as 4′*S*,5′*R*,10′*S*.

The structures of the other known compounds, *deoxy*-aigialomycin C (**5**),[8] LL-Z1640-2 (**6**),[7] zeaenol (**7**),[9] LL-Z1640-1 (**8**),[7] paecilomycin F (**9**),[10] cochliomycin A (**10**),[5] and aigialomycin B (**11**),[2] were determined by comparison of their spectroscopic, MS, and specific rotation data with those in the literature. It is worth pointing out that this is the first report of **5** as a natural product. Its relative and absolute configurations were confirmed using NOE experiments of its acetonide derivative and the CD exciton chirality method with its *p*-dimethylaminobenzoyl derivative.

From the chemistry point of view, these resorcylic acid lactones might be unstable because of the existence of enone moieties and many hydroxy groups, especially phenol hydroxy groups, causing chemical conversions under acidic conditions, such as intramolecular hetero Michael addition[20] and carbon migration of hemiacetal.[3] During acquisition of their NMR spectra, all compounds were found to be quite stable, and no trace of conversions was observed in deuterated solvents (DMSO-d_6, acetone-d_6, and $CDCl_3$), even with prolonged time of more than 3 months. The stability of these lactones under various conditions is worth further investigation.

In our previous study, the resorcylic acid lactones showed potent antifouling activity against the larval settlement of the barnacle *Balanus amphitrite*.[5] In our current research, the isolated resorcylic acid lactones and the acetonide derivatives **1a** and **3a**−**6a** were also evaluated for their antifouling activities. Compounds **1**, **3**−**6**, and **6a** exhibited potent antifouling activity at nontoxic concentrations with the EC_{50} values of 17.3, 6.67, 18.1, 22.5, 1.82, and 3.85 μg/mL, respectively (Table 3), which were lower than the standard requirement of an EC_{50} value of 25 μg/mL established by the U.S. Navy program.[21] The *cis*-enone moiety in **6** (1.82 μg/mL) improved the EC_{50} value approximately 9-fold over that of **4** (18.1 μg/mL) with *trans*-enone, indicating that the *cis*-enone functionality might contribute to the antifouling activity. Moreover, the antifouling activity of **6a** (EC_{50} of 3.85 μg/mL), more than 6 times that of **4a** (EC_{50} > 25 μg/mL), also confirmed this possibility. Our previous study indicated that the acetonide functionality might have a positive effect on antifouling activity.[5] For the enone resorcylic acid lactones, however, the acetonide functionality (**1a**, **3a**, **4a**, and **6a**) was found to decrease the antifouling activity significantly (**1a**, **3a**, **4a**: EC_{50} > 25 μg/mL). Comparison of the activities of **1**−**4** indicated that the configurations of 4′,5′-diol might affect the antifouling activity, with the 4′*R*,5′*R* configuration in **3** exhibiting the highest activity. The above findings suggest that small changes in the structures, especially the enone and acetonide functionalities and hydroxy configurations, among these resorcylic acid lactones can result in obvious changes of antifouling activity. The therapeutic ratio (LC_{50}/EC_{50}) is a way of expressing the effectiveness of the compound in relation to its toxicity. A compound with LC_{50}/EC_{50} > 15 is often considered to be a nontoxic antifouling compound, and a much higher LC_{50}/EC_{50} ratio is highly recommended when selecting candidate compounds.[22] All of the active compounds, **1**, **3**−**6**, and **6a**, had high therapeutic ratios (LC_{50}/EC_{50} > 50), suggesting that they might be useful as environmentally benign antifouling agents.

Table 3. Antifouling Activity

compd	EC_{50} (μg/mL)	LC_{50}/EC_{50}
1	17.3	>50
3	6.67	>50
4	18.1	>50
5	22.5	>50
6	1.82	>50
6a	3.85	>50
SeaNine 211[a]	1.23	20.3

[a]Positive control.

Simultaneously, the antifungal activities of all isolated compounds against phytopathogenic fungi *Thielaviopsis paradoxa*, *Pestalotia calabae*, and *Glorosprium musarum* were evaluated. Noticeably, among the tested compounds, only **6** exhibited promising inhibitory activity against *P. calabae*, with an MIC value of 0.39 μM, which was approximately 25-fold more potent than that of the positive control, ketoconazole (MIC = 10 μM).

As a result of its antifungal activity, **6** was provided to Syngenta for agricultural fungicide screening. In primary- and secondary-tier fungicide assays, **6** showed moderate activity against a limited range of pathogens in laboratory-based tests. It totally inhibited the disease development of *P. infestans*

dx.doi.org/10.1021/jf500248z | J. Agric. Food Chem. 2014, 62, 3183−3191

Table 4. Fungicidal Activity of 6 on Whole-Plant Assays[a]

pathogen test method		Pi[b] drench	Pi[c] preventative		Pi[c] curative	Pi[c] persistence		Pv[d] preventative	Pv[d] curative	Pv[d] persistence
compd	rate (ppm)	eff	eff	eff le	eff	eff	eff le	eff	eff	eff
6	200	–	98	15	11	81	60	96	0	100
	60	–	98	30	11	75	40	96	0	100
	20	93	92	0	11	69	15	94	0	87
	6	86	17	0	0	63	15	91	0	93
	2	38	0	0	0	63	10	50	0	53
mefenoxam	200	–	98	98	–	–	–	100	–	–
	60	–	98	93	92	–	–	84	100	–
	20	–	98	15	89	–	–	63	100	–
	6	100	33	0	78	–	–	0	31	–
	2	100	–	–	78	–	–	–	13	–
	0.6	99	–	–	–	–	–	–	–	–
	0.2	98	–	–	–	–	–	–	–	–
mandipropamid	200	–	–	–	–	98	93	–	–	–
	60	–	–	–	–	98	88	–	–	–
	20	–	–	–	–	96	90	–	–	100
	6	–	–	–	–	91	70	–	–	100
	2	–	–	–	–	–	–	–	–	99
	0.6	–	–	–	–	–	–	–	–	93

[a]Scores are given as percentages of disease control relative to untreated plants (100 indicates complete control of disease symptoms, 0 indicates no control); –, not tested at that rate; le, late evaluation. Mefenoxam and mandipropamid as positive controls. [b]*P. infestans* (tomato). [c]*P. infestans* (potato). [d]*P. viticola* (grapevine).

(tomato) at concentrations of 200 and 60 ppm and of *U. viciae-fabae* (bean) at 100 ppm, as well as the hyphal growth of *P. dissimile* at 2 ppm.

To further characterize its fungicidal potency, **6** was assessed against *P. infestans* and *Plasmopara viticola* on glass-house-based whole-plant assays. Mefenoxam and mandipropamid were used as positive controls. The selection of the standard was based on the properties of candidate active ingredients and the nature of the assays. Mefenoxam is highly systemic; therefore, it was used as the standard in the drench and curative assays. Mandipropamid has an excellent rain-fastness and long-lasting activity because it sticks and distributes quite well in the wax layer of the cuticle, so it was used in persistence test. For the preventive test, both standards can be used, one to ensure that the method is working sufficiently. In this case, the standards serve as quality control for the respective test methods. The results indicated that **6** displayed good activity on both tests, stronger than originally observed on the primary- and secondary-tier assays (Table 4). On the preventative foliar applications against *P. infestans* (potato), **6** showed potent rate-for-rate activity, with disease control rates (DCRs) of 98%, 98%, and 92% at 200, 60, and 20 ppm, respectively, comparable to the values for the positive control mefenoxam (98%, 98%, and 98%) in the initial assessment (Table 4). Compound **6** also showed promising activity on the *P. infestans* drench test (DCR of 86% at 6 ppm). More remarkably, the DCR of **6** was 91% at 6 ppm on the preventative foliar applications against *P. viticola* (grapevine) compared to the positive control mefenoxam (6 ppm, DCR = 0), highlighting the promising activity of **6** against *P. viticola* (Table 4). In the persistence application test against *P. infestans*, **6** showed weaker activity than in the preventative application test, and it also produced no significant activity on the curative tests against either *P. infestans* or *P. viticola*.

In addition, the cytotoxicity of **6** was also determined against tumor cell lines of Hela, A549, HCT-116, HL-60, and K562. It was found that **6** showed cytotoxicity against only HCT-116 with an IC_{50} value of 3.24 μM. The antibacterial, antiviral, insecticidal, and herbicidal activities of the isolated and synthetic resorcylic acid lactones were also determined, but no significant activity was observed.

In summary, 11 resorcylic acid lactones, **1**–**11**, including three new compounds, **1**–**3**, were isolated from the sea anemone-derived fungus *C. lunatus* (TA26-46). The absolute configurations of **1**–**4** were established by the CD exciton chirality method and TDDFT ECD calculations. Compounds **1**, **3**–**6**, and **6a** exhibited potent antifouling activities against the larval settlement of the barnacle *B. amphitrite*, of which **6** showed the highest activity with low toxicity. More remarkably, **6** showed excellent agricultural fungicidal activity against *P. viticola* and *P. infestans* on the whole-plant assay, which would be helpful for the research and development of new natural potential fungicide leads.

■ ASSOCIATED CONTENT

Supporting Information

^{1}H NMR, ^{13}C NMR, ^{1}H–^{1}H COSY, and MS spectra of **1**–**3**; HMQC and HMBC spectra of **1** and **3**; ^{1}H NMR, ^{13}C NMR, 1D NOE, and MS spectra of **1a**, **3a**, and **4a**; ^{1}H NMR and MS spectra of **1b**, **3b**, and **4b**; TDDFT ECD simulation of **1** and **2**; structure and 1D NOE spectrum of compound **5a**; structure and CD spectrum of **5b** and Newman projections showing possible local conformations in the 4′*S*,5′*S* isomer (**5b**); and NMR and MS data for **5a** and **5b**. This material is available free of charge via the Internet at http://pubs.acs.org.

■ AUTHOR INFORMATION

Corresponding Author

*Tel./Fax: 86-532-82031536. E-mail: changyun@ouc.edu.cn.

Funding

This work was supported by the Program of the National Natural Science Foundation of China (Nos. 41130858, 41322037, 41376145); the Program for New Century Excellent

Talents in University, Ministry of Education of China (No. NCET-11-0472); and the Special Financial Fund of Innovative Development of Marine Economic Demonstration Project (GD2012-D01-001).

Notes

The authors declare no competing financial interest.

■ ACKNOWLEDGMENTS

We thank the Biology Team at Syngenta for the fungicide assay and Dr. Naomi Pain of Syngenta for proofreading of this manuscript. We appreciate Prof. Pei-Yuan Qian and Dr. Ying Xu, Division of Life Science, the Hong Kong University of Science and Technology, Hong Kong, China, for the antifouling bioassay.

■ REFERENCES

(1) Wicklow, D. T.; Jordan, A. M.; Gloer, J. B. Antifungal metabolites (monorden, monocillins I, II, III) from *Colletotrichum graminicola*, a systemic vascular pathogen of maize. *Mycotoxin Res.* **2009**, *113*, 1433−1442.

(2) Isaka, M.; Suyarnsestakorn, C.; Tanticharoen, M.; Kongsaeree, P.; Thebtaranonth, Y. Aigialomycins A−E, new resorcylic macrolides from the marine mangrove fungus *Aigialus parvus*. *J. Org. Chem.* **2002**, *67*, 1561−1566.

(3) Isaka, M.; Yangchum, A.; Intamas, S.; Kocharin, K.; Gareth Jones, E. B.; Kongsaeree, P.; Prabpai, S. Aigialomycins and related polyketide metabolites from the mangrove fungus *Aigialus parvus* BCC 5311. *Tetrahedron* **2009**, *65*, 4396−4403.

(4) Dong, J.-Y.; Zhu, Y.-H.; Song, H.-C.; Li, R.; He, H.-P.; Liu, H.-Y.; Huang, R.; Zhou, Y.-P.; Wang, L.; Cao, Y.; Zhang, K.-Q. Nematicidal resorcylides from the aquatic fungus *Caryospora callicarpa* YMF1.01026. *J. Chem. Ecol.* **2007**, *33*, 1115−1126.

(5) Shao, C.-L.; Wu, H.-X.; Wang, C.-Y.; Liu, Q.-A.; Xu, Y.; Wei, M.-Y.; Qian, P.-Y.; Gu, Y.-C.; Zheng, C.-J.; She, Z.-G.; Lin, Y.-C. Potent antifouling resorcylic acid lactones from the gorgonian-derived fungus *Cochliobolus lunatus*. *J. Nat. Prod.* **2011**, *74*, 629−633.

(6) Sloan, A.; Tyler, N. G.; Audrey, F. A.; David, J. K.; Susan, M.; Esperanza, J. C. B.; Qi, S.; Steven, M. S.; Mansukh, C. W.; Cedric, J. P.; Nicholas, H. O. Resorcylic acid lactones with cytotoxic and NF-κB inhibitory activities and their structure−activity relationships. *J. Nat. Prod.* **2011**, *74*, 1126−1131.

(7) Ellestad, G. A.; Lovell, F. M.; Perkinson, N. A.; Hargreaves, R. T.; McGahren, W. J. New zearalenone related macrolides and isocoumarins from an unidentified fungus. *J. Org. Chem.* **1978**, *43*, 2339−2343.

(8) Bajwa, N.; Jennings, M. P. Syntheses of *epi*-aigialomycin D and *deoxy*-aigialomycin C via a diastereoselective ring closing metathesis macrocyclization protocol. *Tetrahedron Lett.* **2008**, *49*, 390−393.

(9) Sugawara, F.; Kim, K. W.; Kobayashi, K.; Uzawa, J.; Yoshida, S.; Murofushi, N.; Takahashi, N.; Strobel, G. A. Zearalenone derivatives produced by the fungus *Drechslera portulacae*. *Phytochemistry* **1992**, *31*, 1987−1990.

(10) Xu, L.-X.; He, Z.-X.; Xue, J.-H.; Chen, X.-P.; Wei, X.-Y. β-Resorcylic acid lactones from a *Paecilomyces* fungus. *J. Nat. Prod.* **2010**, *73*, 885−889.

(11) Thiyagarajan, V.; Harder, T.; Qiu, J.-W.; Qian, P.-Y. Energy content at metamorphosis and growth rate of the early juvenile barnacle *Balanus amphitrite*. *Mar. Biol. (Berlin)* **2003**, *143*, 543−554.

(12) *Reference Method for Broth Dilution Antifungal Susceptibility Testing of Conidial Forming Filamentous Fungi*; NCCLS Document M38-A; National Committee on Clinical Laboratory Standards (NCCLS): Wayne, PA, 2002.

(13) Lin, L.; Mulholland, N.; Wu, Q.-Y.; Beattie, D.; Huang, S.-W.; Irwin, D.; Clough, J.; Gu, Y.-C.; Yang, G.-F. Synthesis and antifungal activity of novel sclerotiorin analogues. *J. Agric. Food Chem.* **2012**, *60*, 4480−4491.

(14) Isaka, M.; Chinthanom, P.; Kongthong, S.; Supothina, S.; Ittiworapong, P. Hamigeromycins C−G, 14-membered macrolides from the fungus *Hamigera avellanea* BCC 17816. *Tetrahedron* **2010**, *66*, 955−961.

(15) Snatzke, G.; Angeli, C.; Decorte, E.; Moimas, F.; Kojié-Prodié, B.; Ružić-Toroš, Z.; Sunjić, V. Preparation *via* diastereoselective hydrogenation, absolute conformation and configuration of exogeneous anabolic zeranol ((3*S*,7*R*)-3,4,5,6,7,8,9,10,11,12-decahydro-7,14,16-trihydroxy-3-methy-1*H*-2-benzoxacyclotetradecin-1-one). *Helv. Chim. Acta* **1986**, *69*, 734−748.

(16) Gelo, M.; Raza, Z.; Šunjić, V.; Guo, J.; Snatzke, G. Determination of the conformation of *E* and *Z* zearalenone and their 7α- and 7β-hydroxy congeners. *Tetrahedron: Asymmetry* **1991**, *2*, 1005−1010.

(17) *Spartan 04*; Wavefunction Inc.: Irvine, CA, 2004.

(18) Frisch, M. J.; Trucks, G. W.; Schlegel, H. B.; Scuseria, G. E.; Robb, M. A.; Cheeseman, J. R.; Scalmani, G.; Barone, V.; Mennucci, B.; Petersson, G. A.; Nakatsuji, H.; Caricato, M.; Li, X.; Hratchian, H. P.; Izmaylov, A. F.; Bloino, J.; Zheng, G.; Sonnenberg, J. L.; Hada, M.; Ehara, M.; Toyota, K.; Fukuda, R.; Hasegawa, J.; Ishida, M.; Nakajima, T.; Honda, Y.; Kitao, O.; Nakai, H.; Vreven, T.; Montgomery, J. A., Jr., Peralta, J. E.; Ogliaro, F.; Bearpark, M.; Heyd, J. J.; Brothers, E.; Kudin, K. N.; Staroverov, V. N.; Kobayashi, R.; Normand, J.; Raghavachari, K.; Rendell, A.; Burant, J. C.; Iyengar, S. S.; Tomasi, J.; Cossi, M.; Rega, N.; Millam, J. M.; Klene, M.; Knox, J. E.; Cross, J. B.; Bakken, V.; Adamo, C.; Jaramillo, J.; Gomperts, R.; Stratmann, R. E.; Yazyev, O.; Austin, A. J.; Cammi, R.; Pomelli, C.; Ochterski, J. W.; Martin, R. L.; Morokuma, K.; Zakrzewski, V. G.; Voth, G. A.; Salvador, P.; Dannenberg, J. J.; Dapprich, S.; Daniels, A. D.; Farkas, O.; Foresman, J. B.; Ortiz, J. V.; Cioslowski, J.; Fox, D. J. *Gaussian 09 Revision C.01*; Gaussian, Inc.: Wallingford, CT, 2009.

(19) Stephens, P. J.; Harada, N. ECD cotton effect approximated by the Gaussian curve and other methods. *Chirality* **2010**, *22*, 229−233.

(20) Isaka, M.; Chinthanom, P.; Veeranondha, S.; Supothina, S. Novel cyclopropyl diketones and 14-membered macrolides from the soil fungus *Hamigera avellanea* BCC 17816. *Tetrahedron* **2008**, *64*, 11028−11033.

(21) Rittschof, D. Fouling and natural products as antifoulants. In *Recent Advances in Marine Biotechnology*; Fingerman, M., Nagabhushanam, R., Thompson, M. F., Eds.; Oxford & IBH Publishing Company: New Delhi, India, 1999; pp 245−257.

(22) Qian, P.-Y.; Xu, Y.; Fusetania, N. Natural products as antifouling compounds: Recent progress and future perspectives. *Biofouling* **2010**, *26*, 223−234.

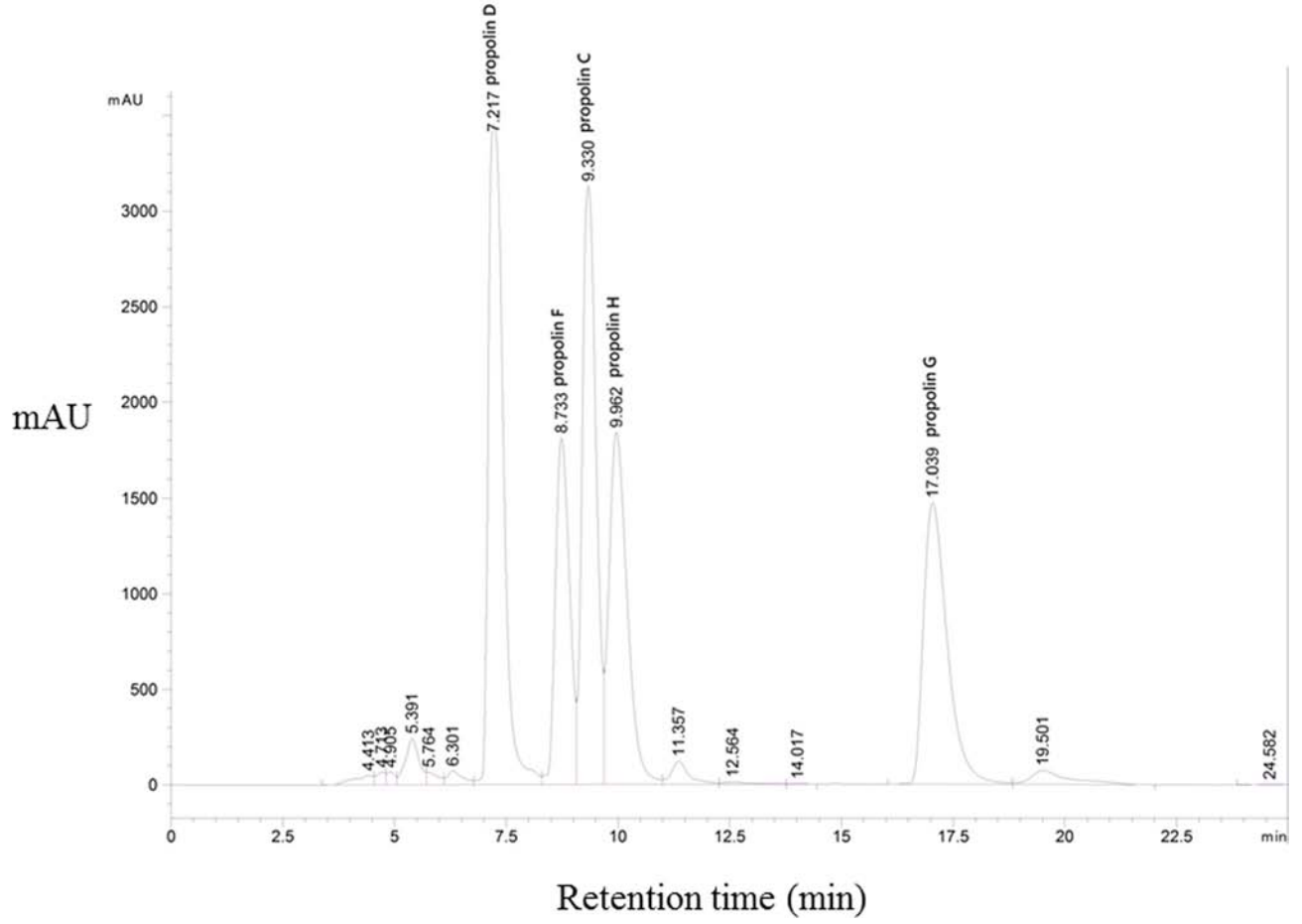

Figure 1. Separation of standard authentic compounds, using HPLC-UV. Peaks: 1, propolin D; 2, propolin F; 3, propolin C; 4, propolin H; 5, propolin G. The conditions of separation were as follows: column, Luna Phenomenex (C18, 250 mm × 4.6 mm); mobile phase, methanol/water 88.75/11.25; flow rate, 1.0 mL/min; detection, UV 280 nm; injection volume, 5 μL.

Six propolins, A–G, can be isolated from Taiwanese green propolis (TGP) and exert a broad spectrum of biological activities.[11] TGP is widely used in Taiwanese traditional medicine and reportedly exhibits anticancer,[12−18] antioxidant,[12,14,18] and antimicrobial[19] properties. Chen et al. used NMR and fast atom bombardment mass spectrometry to identify the chemical structure of propolin G and showed it to be identical to that of the compound nymphaeol C.[15] In our previous study, we found several active ingredients with TGP, including propolin G. It was revealed that propolin G can efficiently induce apoptosis in brain cancer cell lines (glioma and glioblastoma) through mitochondrial- and caspase-dependent pathways. Using the 1,2-diphenyl-2-picrylhydrazyl (DPPH) assay, we also showed that propolin G displays free radical scavenging activity and that propolin G, TGP, and Brazilian propolis (BP) extracts exert neuroprotective activity against oxidative stress in rat primary cortical neurons.[16] Because the apoptosis is an important response in physiological condition, especially in liver steatosis, we would like to investigate whether TGP and propolin G can modulate the process of liver fibrosis in hepatocytes. Propolis was collected from Chang-Hwa, a county in the middle of Taiwan. In the past, we collected propolis from northern, central, and southern Taiwan for analysis. We found that propolin G was most abundant from central Taiwan. Therefore, we utilized propolis from Chang-Hwa for this study. Therefore, we modified the previous purification method and used a prepared column and improved analysis method for mass propolin G collection (Figure 1). This study aimed to identify the underlying antifibrotic molecular mechanisms of TGP and propolin G to potentially facilitate the development of a novel treatment for liver fibrosis targeting Smad3 signaling components. According to our research, this study is the first to show that TGP and propolin G selectively down-regulate the expression of Smad2/3, but not Smads 4 and 7, mRNA, and protein in cultured rat HSCs. This process, in turn, significantly attenuates the TGF-β-induced deposition of Col Iα1 in the HSCs. Our results suggest that TGP and propolin G exert their antifibrogenic effects by directly or indirectly down-regulating Smad2/3 protein expression and phosphorylation through TGF-β signaling.

Alcoholic liver injury is a complex process involving several injury mechanisms and multiple cellular targets.[20] Ethanol oxidation and ethanol-induced injury occur in hepatocytes; thus, determining the mechanism by which ethanol primes and sensitizes hepatocytes is very important.[21] It was revealed that ethanol exposure inhibits hepatocyte regeneration in in vitro and in vivo systems.[22,23] Free radicals can bind to cellular molecules (i.e., nucleic acids, proteins, lipids, and carbohydrates),[24] induce lipid peroxidation, damage the membranes of liver cells and organelles, cause the swelling and necrosis of hepatocytes and result in the release of cytosolic enzymes such as aspartate aminotransferase (AST), alanine aminotransferase (ALT), alkaline phosphatase (ALP) into the circulating blood.[25,26] It is well-known that superoxide dismutase

(SOD), catalase (CAT), and glutathione peroxidase (GPx) act by scavenging the superoxide anion and H_2O_2 to prevent reactive oxygen species (ROS)-induced damage.[27] The present research therefore has the objective to explore the antioxidant properties and hepatoprotective effects of Taiwanese green propolis against ethanol-induced liver injury in mice. In this study, it was revealed that administration of TGP inhibited plasma or hepatic malondialdehyde (MDA) and ALT activation, whereas TGP has no influence on plasma or hepatic SOD and GPx levels in ethanol-treated mice. Further study is necessary to evaluate the effect of TGP on liver fibrosis prevention and to determine the molecular mechanisms.

MATERIALS AND METHODS

Propolis Origins. Taiwanese green propolis was collected from Taiwan. All samples were collected from May to July 2011, using propolis collectors. Propolis from the collectors at each location was gathered every month and kept at −20 °C until processed.

Extraction and Isolation of Propolin G. The TGP (50 g) was extracted with 95% ethyl alcohol (250 mL × 3), sonicated for 3 h, and left to stand for 21 h at 25 °C. The filtered ethanol extract was evaporated to dryness under reduced pressure to yield a brown gum (34.5 g), which was kept at −20 °C until used. The brown gum was dissolved in methanol and applied to an open silica column for the purification of propolin G. An *n*-hexane/EtOAc solvent system was used as the eluting solvent. Fraction 4 (*n*-hexane/EtOAc, 40:60) contained higher levels of propolin G than the other fractions. Fraction 4 was evaporated to dryness under reduced pressure to yield a yellow gum. The yellow gum was dissolved in methanol and carried out on a reversed-phase (RP) preparative high-performance liquid chromatograph (HPLC)-UV. Fractions of retention times at 17.0 min for propolin G were collected. Conditions were as follows: column, Macherey-Nagel (VP 250/10 NUCLEODUR C18 HTEC, 5 μm); solvent system, methanol/water (88:12); flow rate, 3.5 mL/min; and detection, UV 280 nm. We identified the compound as propolin G (Figure 1). The purity of the propolin G was estimated to be no less than 95% by HPLC-UV on the basis of the peak area.

Analysis Conditions. The propolin profile in the TGP extracts was analyzed with a RP HPLC-UV. The conditions were as follows: column, ZORBAX SB-C18 (4.6 × 250 mm; Agilent, Santa Clara, CA, USA); solvent system, methanol/water (88.8:11.2); flow rate, 1.0 mL/min; and detection, UV 280 nm.

Chemicals and Reagents. TGP and propolis G were stored as a stock solution in DMSO, which was used after dilution with medium for each assay. Trizol reagent and RevertAidi MMLV reverse transcriptase were obtained from Fermentas Life Science (Lithuania); Taq polymerase, dNTPs, and DNA marker were from TaKaRa Biotechnology Co. (Dalian, China). Primers for rat PAI-1, Smad3, Smad2, Smad7, Smad4, type I, type II, Col Iα1, FN, and β-actin (as internal control) were designed by our group in accordance with the gene sequence in GenBank. Cytokine recombinant human TGF-β was purchased from R&D System (Minneapolis, MN, USA). Precision protein standards and protein molecular weight markers were obtained from Bio-Rad (Hercules, CA, USA). All antibodies, including primary and secondary antibodies, were provided by Santa Cruz Biotechnology Inc. (Santa Cruz, CA, USA); Phospho-Smad3 antibody (Ser433/435) was purchased from Cell Signaling Technology Inc. (Beverly, MA, USA). All other reagents were analytically pure.

Cell Culture. HSC-T6 cells, derived from immortalized and activated rat HSCs transfected by SV40, were kindly donated by Professor Friedman from Mount Sinai Medical Center and were maintained at 37 °C in Dulbecco's modified Eagle medium (DMEM) containing 10% fetal calf serum (FCS), 100 units/mL penicillin, and 100 μg/mL streptomycin under a 5% CO_2 atm.

Cell Viability Assays. HSC-T6 cells were seeded overnight at 10000 cells/well in 96-well plates in DMEM, and the subconfluent cells in culture (75%) were washed twice with phosphate-buffered saline and serum-starved for 24 h with serum-free medium. To determine the optimal concentration of TGP or propolin G for use in these experiments, dose-dependent cytotoxicity was initially performed with different concentrations of TGP or propolin G added to culture for 48 h. Cell viability was determined by incubating each well with 10 μL of WST-1 for 4 h at 37 °C. Metabolically active cells cleave WST-1 to water-soluble formazan, which is directly quantitated with an enzyme-linked immunosorbent assay plate reader (Bio-Rad 3550). Each experiment was performed at least twice, and treatment for the cell line was done in triplicate.

Preparation of RNA and Protein Extracts. HSC-T6 cells were plated at a confluence of approximately 75% in the wells of a 6-well dish and allowed to attach overnight. Cells were treated with 10 ng/mL TGF-β for 12 h before being treated with a variety of concentrations of propolis, propolin G, or SB-431542 for 12 h to determine RNA levels and for 24 h to analyze TGF-β-regulated protein expression. Treated cells were harvested, washed, and lysed in ice-cold buffer [250 mM Tris-HCl, pH 7.4, containing a mixture of protease inhibitors (100 2 g/mL phenylmethanesulfonyl fluoride, 1 μg/mL E-64, 0.5 μg/mL leupeptin, and 1.7 μg/mL peptatin A)]. The debris was removed by centrifugation at 13000*g* for 20 min at 4 °C. Total protein amount in the extracts was measured using the Bio-Rad Bradford reagent. Total RNA was isolated from HSC-T6 cells as described by Chomczynski and Sacchi.[28]

Reverse Transcription Polymerase Chain Reaction Assay. After treatment, RNA was harvested with Trizol (Invitrogen, Carlsbad, CA, USA). For each reaction, 1 μg of total RNA was reverse-transcribed to cDNA using an RT kit (MBI) for reverse transcription polymerase chain reaction (RTPCR) (Ambion) as recommended by the manufacturer. The resulting cDNA was subsequently subjected to 40 cycles of PCR. PCR products were quantitated to confirm that they were in the linear range of amplification. PCR products were quantitated by Quantum RNA18S internal standards (Ambio). The following primers were used in this study: rat α-SMA (Genbank L26110), forward 5′-TTC GTT ACT GCT GAG CGT GAG-3′, reverse 5′-CGG GGA ATT AGG TCG ATT TC-3′ (product size 202 bp); and rat G3PDH (Genbank BC063166), forward 5′-CCC TTC ATT GAC CTC AAC TAC ATG G-3′, reverse 5′-CAT GGT GAA GAC GCC AG-3′ (product size 452 bp). The conditions for RT-PCR were as follows: cDNA synthesis and predenaturation were at 42 °C for 60 min, followed by 94 °C for 10 min. PCR amplification sequence was performed for 40 cycles at 94 °C for 45 s and at 57 °C for 45 s. After amplification, each sample was applied to 1.2% agarose/ethidium bromide gel. The resolved PCR products were photographed under UV illumination.

Western Blot. For Western blot, treated cells were harvested by the addition of ice-cold lysis buffer as described above. Centrifuged lysates (30 μg) from each sample were analyzed by SDS−polyacrylamide gel electrophoresis and transferred to a PVDF membrane by semidry transfer. The membranes were blocked for 1 h at room temperature in Tris-buffered saline containing 0.1% Tween 20 and 3% BSA. Blots were probed overnight at 4 °C with the following primary antibodies: anti-α-SMA, anti-Smad2/3, antiphospho-Smad2/3, anti-Col Iα1, and anti-β-actin antibodies. This was followed by incubation with the appropriate horseradish peroxidase-conjugated secondary antibody at a dilution of 1:1000 for 1 h. Detection was achieved by enhanced chemiluminescence (Amersham Pharmacia Biotech) followed by luminescent image analyzer (ImageQuant LAS4000). Digital data were further were quantitated by scanning densitometry using ImageQuant TL with a 1-D Analyst software package for Macintosh. The relative expression fold was all normalized with internal control (GAPDH or tubulin).

Animal Study. The animal study was approved by the Review Boards of National Ilan University with approval no. 102-8. Briefly, mice were housed in the animal center of National Ilan University according to general guidelines at 25 ± 1 °C with a 12 h dark/light cycle. For hepatic injury experiments, male 7-week-old C57BL/6J mice (approximately 21 g) were obtained from the National Laboratory Animal Center, Taipei, Taiwan. The study protocol was in accordance with the animal experimental guidelines of the Council of Agriculture, Executive Yuan. Each experimental group consisted of six mice, and

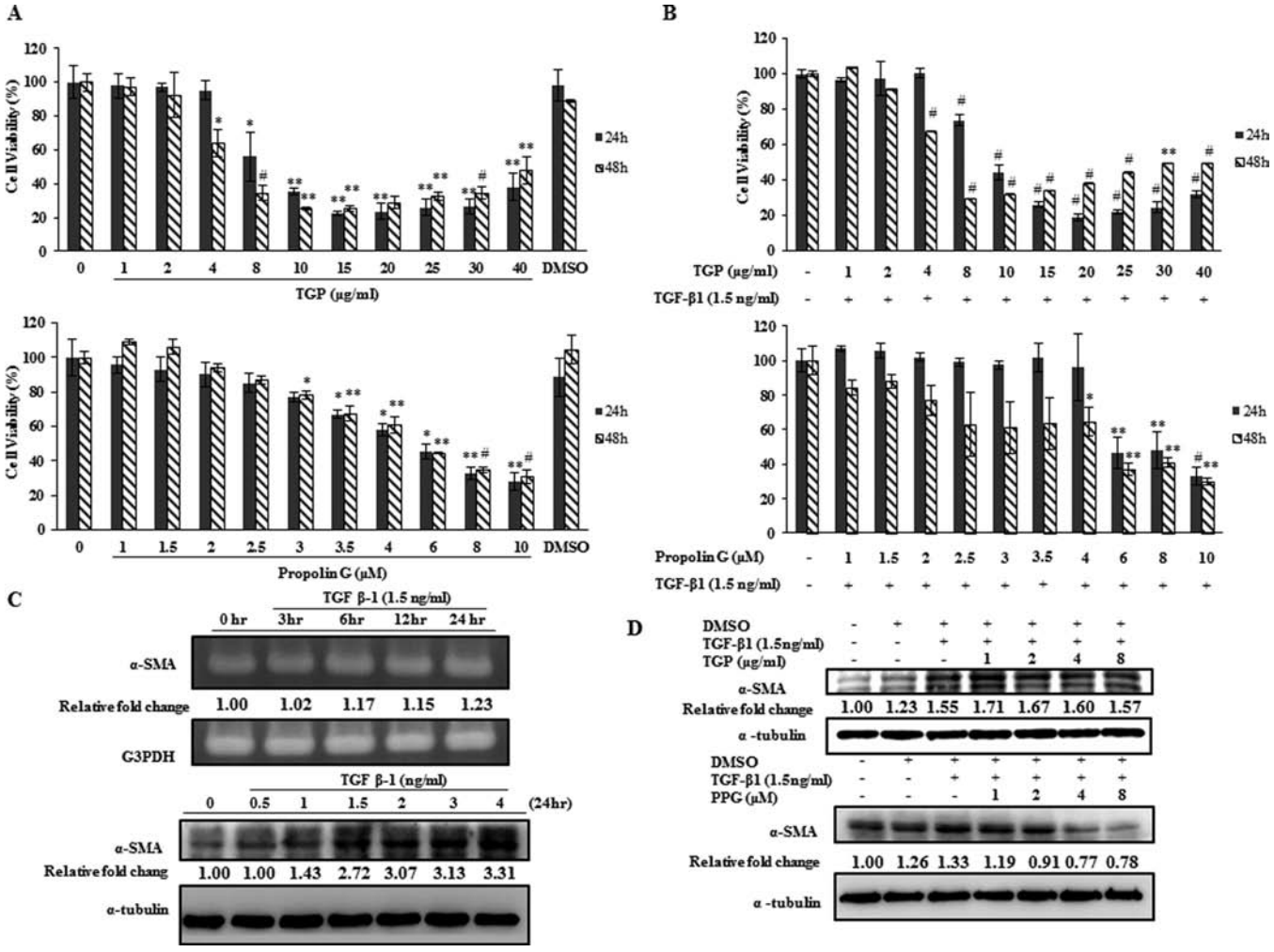

Figure 2. Inhibitory effects of TGP and propolin G on HSC-T6 cell viability. (A) HSC-T6 cells were treated with various TGP and propolin G concentrations for 24−48 h, and then cell viability was evaluated using the MTT assay. Each concentration was replicated three times. Data are expressed as mean ± standard deviation (SD). (*) $P < 0.05$, (**) $P < 0.01$, and (#) $P < 0.001$ indicate significant differences from the control group. (B) Inhibitory effects of TGP and propolin G on HSC-T6 cells in the presence of TGF-β1. Cells were treated with various TGP and propolin G concentrations in the presence of TGF-β1 (1.5 ng/mL) for 24−48 h, before the evaluation of cell viability using the MTT assay. Each concentration was replicated three times. Data are expressed as mean ± SD. (*) $P < 0.05$, (**) $P < 0.01$, and (#) $P < 0.001$ indicate significant differences from the control group. (C) Effects of TGF-β1 on α-SMA expression in HSC-T6 cells. HSC-T6 cells were treated with 1.5 ng/mL TGF-β1 for various time periods (3, 6, 12, and 24 h). α-SMA mRNA expression was then evaluated using RT-PCR. HSC-T6 cells were treated with 0−4 ng/mL TGF-β1 for 24 h. The expression of α-SMA protein was then evaluated using Western blotting (D). HSC-T6 cells were treated with 1.5 ng/mL TGF-β1 and TGP or propolin G for 24 h. The expression of α-SMA protein was then evaluated using Western blotting.

each of them was administered TGP (200 and 400 mg/kg/day) for 28 days. For injury, mice were administered alcohol (5 g/kg) followed by sacrifice after 24 h. Blood was drawn from the heart for serum analysis, and livers were quickly excised to analyze the levels of SOD, catalase, GPx, and lipid peroxide. Serum was separated by centrifugation at 3000*g* for 5 min for assays of ALT and ALS, activity, and protein levels. These samples were preserved at −80 °C until biochemical assay.

Statistical Analysis. All values are given as means ± SE. Data analysis involved one-way ANOVA with subsequent Scheffé test. * and ** indicate significant differences at the levels of $P < 0.05$ and $P < 0.01$, respectively, compared to PBS alone.

RESULTS AND DISCUSSION

Effects of TGP or Propolin G on TGF-β1-Induced α-SMA mRNA and Protein Expression in HSC-T6 Cells. To evaluate the cytotoxic effects of TGP and propolin G on HSC-T6 cells, we used the MTT assay to analyze HSC-T6 cell viability after treatment with TGP or propolin G. Our results showed that HSC-T6 cells can be treated with TGP (up to 2 ug/mL) or propolin G (up to 2 μM) for up to 48 h without any effects on cell viability (Figure 2A). The IC50 of TGP on HSC-T6 cell was 9.22 μg/mL at 24h and 7.61 μg/mL at 48 h while the IC50 of propolin G was 6.61 μM at 24h and 6.22 μM at 48h. We also evaluated the potential inhibitory effects of TGP and propolin G on TGF-β-mediated biological effects in HSC-T6 cells. To do this, we pretreated the cells with 1.5 ng/mL TGF-β before exposing them to TGP or propolin G. Around IC50 concentration, the cell viability was elevated 24h after treatment, however, with prolong treatment for 48h, the cell viability was reduced when compared with those of 24h after treatment. Thus, TGP and propolin G treatments can attenuate TGF-β-stimulated HSC cell viability in a dose-dependent manner (Figure 2B). We then analyzed the cells' responsiveness to TGF-β by evaluating α-SMA mRNA and protein expression. We observed significant up-regulation of α-SMA mRNA and protein expression following the treatment of HSC-T6 cells with 1.5 ng/mL TGF-β for 24 h (Figure 2C).

dx.doi.org/10.1021/jf500096c | J. Agric. Food Chem. 2014, 62, 3192−3201

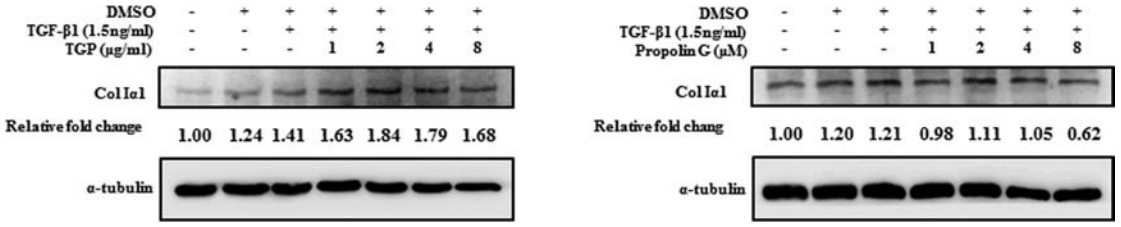

Figure 3. Effects of TGP and propolin G on Col Iα1 expression. Cells were treated with 1.5 ng/mL TGF-β1 and various TGP or propolin G concentrations for 24 h. Western blot analyses were then performed to evaluate Col Iα1 expression.

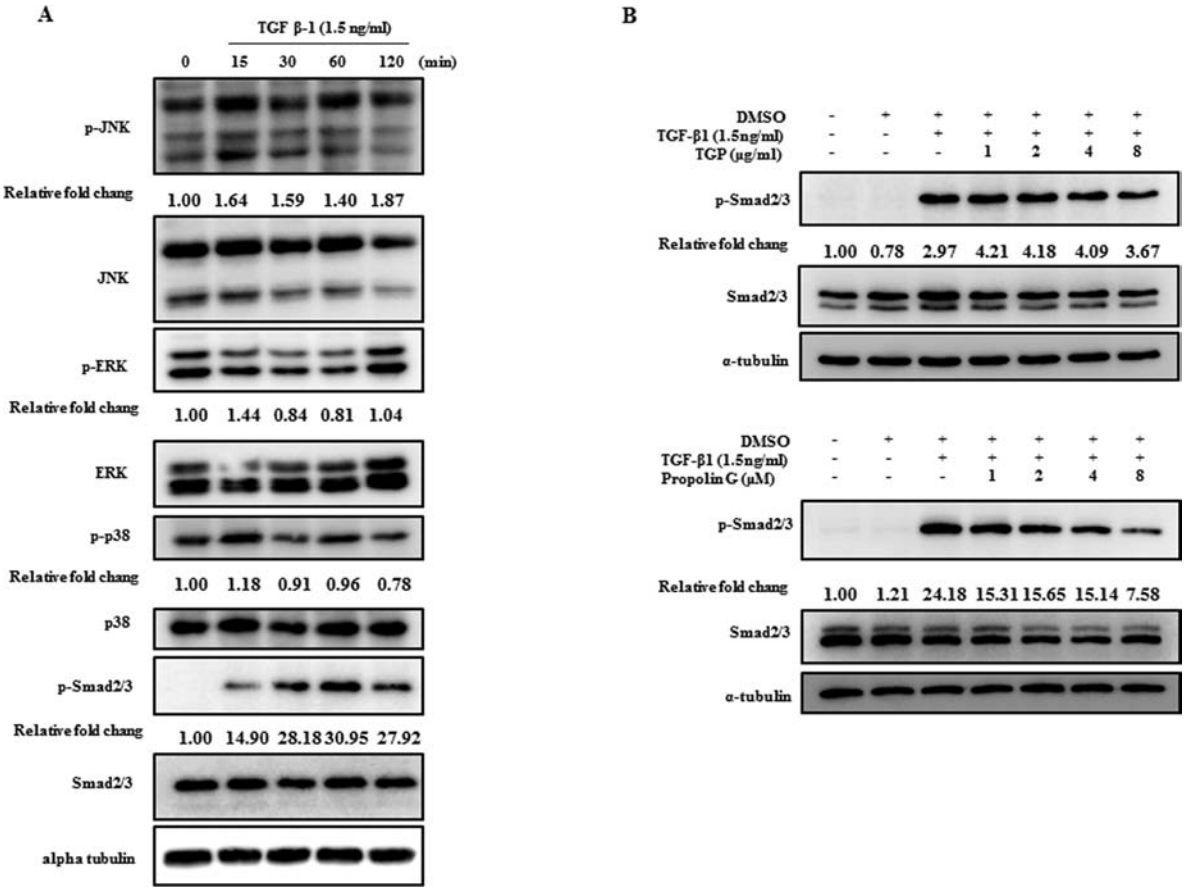

Figure 4. Effects of TGP and propolin G on Smad3 expression and phosphorylation. (A) Time-course of the effects of TGF-β1 on the phosphorylation of MAPK and Smad2/3 in HSC-T6 cells. The cells were treated with TGF-β1 (1.5 ng/mL) for various time periods (15, 30, 60, and 120 min), before Western blot analysis of JNK, extracellular signal-regulated kinase (ERK) 1/2, p38, and Smad2/3 expression. (B) TGP and propolin G down-regulated phosphor-Smad2/3 expression in HSC-T6 cells. HSC-T6 cells were pretreated with TGP or propolin G for 1 h and then treated with TGF-β1 for 1 h. Whole hepatic cell extracts were immunoblotted with the antibodies against phosphor-Smad2/3.

Furthermore, we observed the reduction of TGF-β-induced α-SMA protein expression especially after 4 μM propolin G treatment in the HSC-T6 cells (Figure 2D). However, although the inhibitory effect was more significant after 8 μM treatment, we cannot exclude the cytotoxicity effect. These results indicated that TGP and propolin G attenuated the TGF-β-dependent up-regulation of α-SMA mRNA and protein expression in HSCs. This is the first study to show that TGP and propolin G can reduce the TGF-β-induced accumulation of ECM in cultured HSC-T6 cells. One potential underlying mechanism of these effects might be the disruption of TGF-β signaling by selectively targeting Smad2/3. To evaluate this mechanism, we first investigated the cytotoxicity of TGP and propolin G to HSC-T6 cells using the MTT assay. Our results showed that TGP and propolin G have low cytotoxicity to HSCs, with an IC_{50} value of 100 μM (data not shown). The study by Well et al. described the antiproliferative activity of TGF-β in HSCs and rats, showing that the disruption of TGF-β signaling leads to increased HSC proliferation.[6] In this study, nontoxic concentrations of TGP and propolin G minimally promoted HSC-T6 cell propagation (Figure 2), indicating that these compounds might antagonize TGF-β signaling.

TGP and Propolin G Down-regulate the TGF-β-Induced Expression of Profibrotic Gene and Inhibit TGF-β-Induced Smad2/3 and Smad2/3 Phosphorylation. We used Western blotting to quantify the Col Iα1 protein level, in comparison with α-tubulin control. After pretreatment with TGF-β and treatment with TGP and propolin G in HSC-T6 cells, the expression level of Col Iα1 had no significant change after TGP or propolin G treatment except a slight reduction at

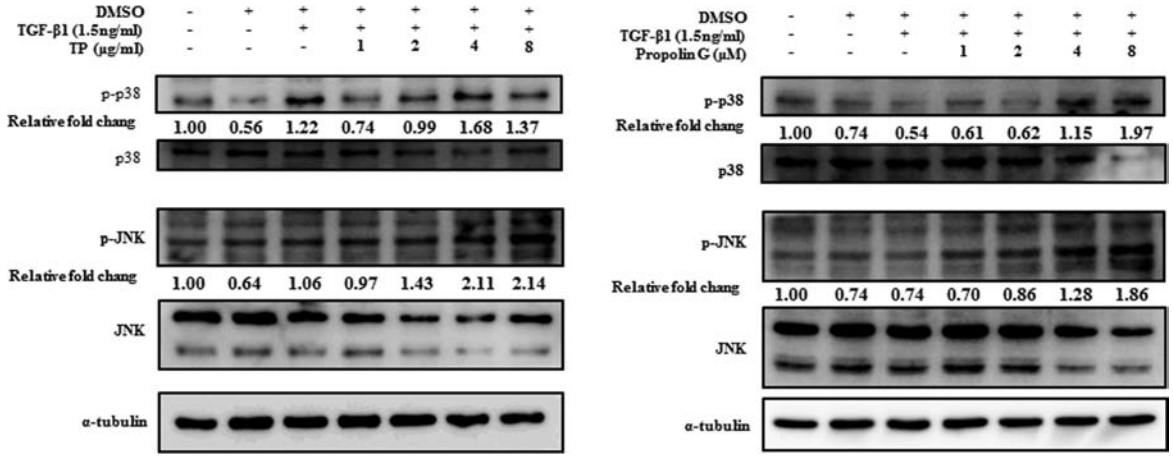

Figure 5. TGP and propolin G up-regulate phospho-JNK MAPK expression in TGF-β-stimulated HSC-T6 cells. TGP and propolin G up-regulated the expression of phospho-JNK and phospho-p38 MAPK in HSC-T6 cells. HSC-T6 cells were pretreated with TGP or propolin G for 1 h before treatment with TGF-β1 for 15 min. Whole hepatic cell extracts were immunoblotted with the antibodies against phospho-JNK and phospho-p38.

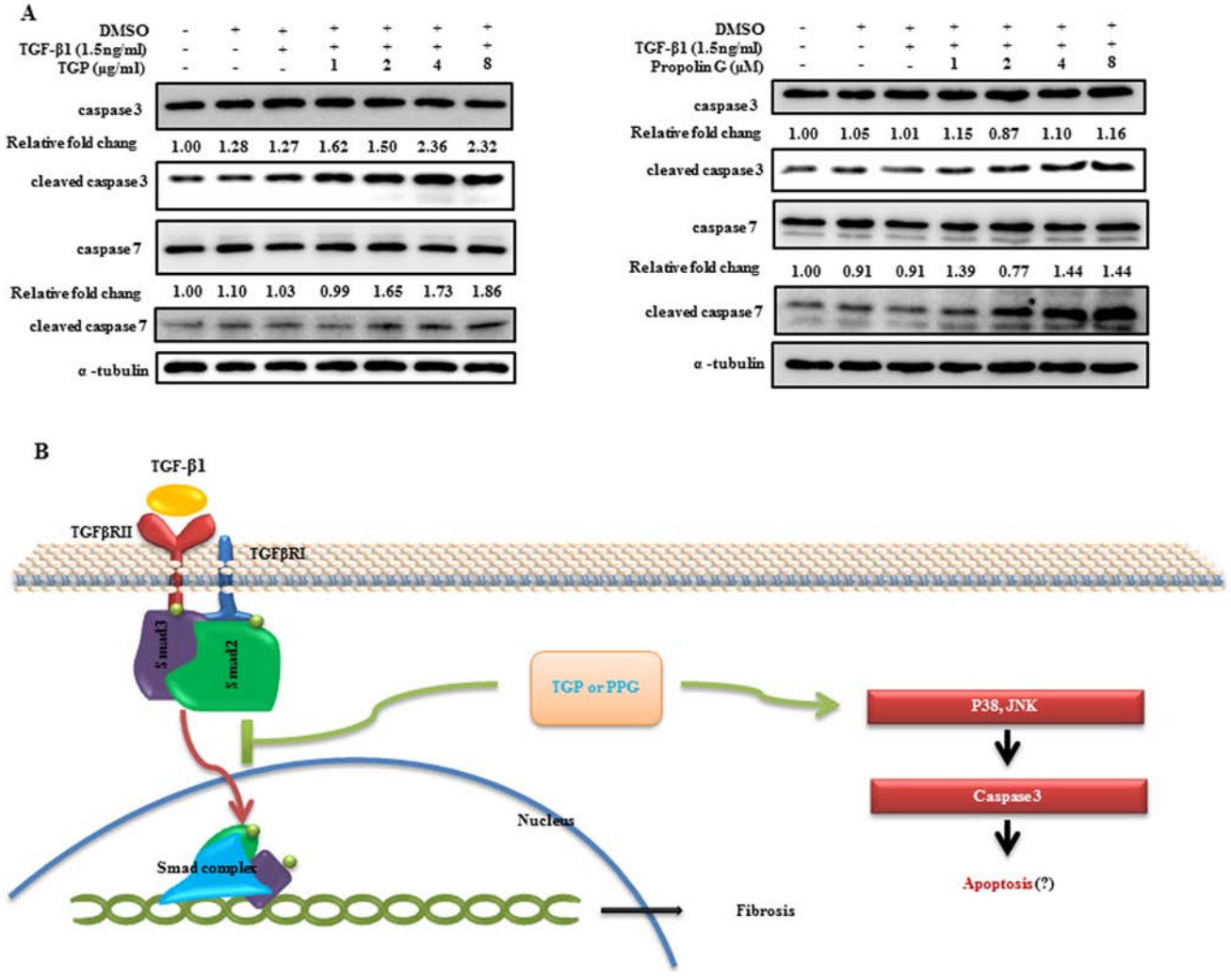

Figure 6. Effects of TGP and propolin G on the expression of apoptosis-related proteins in HSC-T6. (A) Cells were treated with 1.5 ng/mL TGF-β1 and various TGP or propolin G concentrations for 24 h. Western blotting was used to evaluate the expression of caspase-3 and caspase-7. (B) Illustration of signaling for hepatic fibrosis inhibition by TGP and propolin G.

8 μM propolin G treatment, which might be due to cytotoxicity (Figure 3). Smad3 is considered the essential mediator of TGF-β signaling, because it directly activates genes encoding transcriptional regulators and signal transducers through the Smad2/3 DNA-binding motif characteristics of the immediate early target genes of TGF-β. In this study, we used RT-PCR

dx.doi.org/10.1021/jf500096c | J. Agric. Food Chem. 2014, 62, 3192−3201

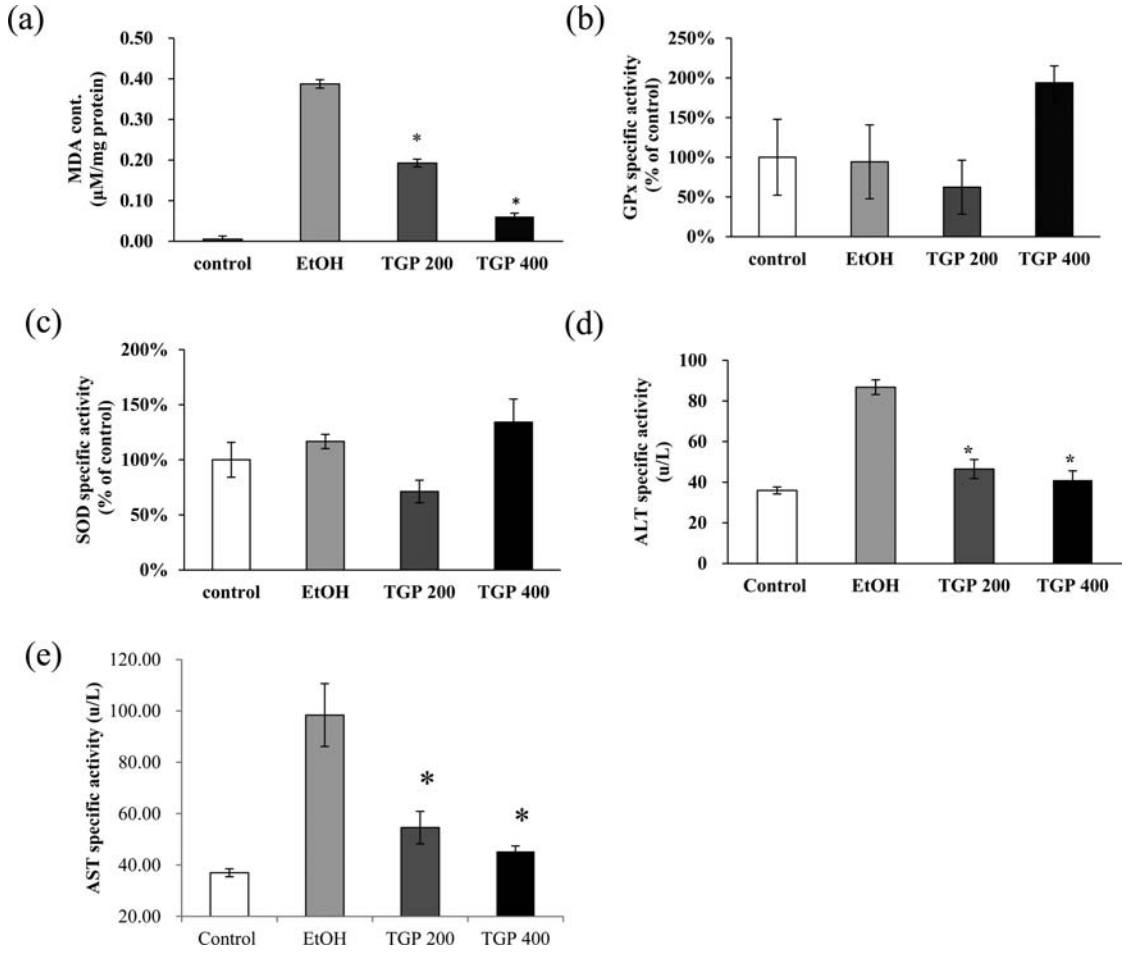

Figure 7. Effect of TGP on plasma MDA ALT levels and SOD and GPx activities in ethanol (Et)H)-treated mice. The control group received oral administration of olive oil. The EtOH group received EtOH (5 g/kg, oral). TGP (200, 400 mg/kg) + EtOH (5 g/kg) groups received TGP (200, 400 mg/kg, oral) for 4 weeks and were gavaged with EtOH (5 g/kg). TGP (200, 400 mg/kg) treatment attenuated the EtOH-induced damage of increased MDA (a) level but did not affect SOD and GPx activities. Also, TGP can reduce ALT (d) and AST (e) levels and exert liver protection function. Data are presented as mean ± standard deviation (SD) (n = 6 mice). $P < 0.05$ versus the EtOH group.

and Western blotting to evaluate the potential inhibitory effects of propolin G on TGF-β-mediated Smad2/3 and Smad2/3 phosphorylation in HSC-T6 cells. As shown in Figure 4A, TGF-β can significantly induce Smad2/3 phosphorylation in HSC-T6 cells in a time-dependent manner (from 15 to 120 min), suggesting that the phosphorylation of Smad3 by TβRII is the initial step in signal transduction. We also evaluated the potential inhibitory effects of propolin G on TGF-β-induced Smad2/3 phosphorylation in HSC-T6 cells. We observed that propolin G reduced TGF-β-induced Smad3 phosphorylation in a dose-dependent manner in the HSC-T6 cells (Figure 4B). The HSCs are considered the primary sites of hepatic fibrogenesis, and studies have shown activated HSCs to be the key sources of excess ECM proteins in liver fibrosis.[29,30] With regard to liver fibrosis, there are several pieces of evidence indicating that apoptosis played an important role in this process. For example, in CCl_4-induced acute liver fibrosis damage animal model, Fas and FasL were overexpressed in liver followed by caspase cascade activation.[30,31] In fact, in chronic hepatitis and liver damage, the progression of liver fibrosis was due to the reduced apoptosis because of other undamaged cells and growth factors contributing to tissue regeneration.[32] During liver fibrogenesis, increased extracellular TGF-β initiates TGF-β-Smad3 signaling before activated Smad3/Smad4 complexes translocate into the nucleus and immediately bind and activate target genes, including Col Iα1, TIMP-1, PAI-1, FN, and other ECM genes.[33−36] PAI-1 is a specific target gene of Smad3 and is typically used as a marker of activated TGF-β-Smad2/3 signaling.[37,38] In our study, TGP and propolin G significantly down-regulated TGF-β1-induced α-SMA mRNA and protein expression in HSCs (Figure 2), indicating that these compounds might directly or indirectly inhibit TGF-β1-Smad2/3 signaling. These results were similar to those of Tang et al. that blockage of TGF-β-Smad2/3 signaling can efficiently protect liver from fibrosis.[39] Furthermore, according to a study by Bissell et al., the down-regulation of PAI-1 protein expression could indirectly increase matrix degradation through increased plasmin activity.[40] SB-431542 is a small molecular inhibitor of the type I TGF-β receptor through a specific and competitive A TGP-binding site kinase and inhibits the phosphorylation of Smad2/3 by binding TβRI.[38] This process, in turn, inhibits the exogenous TGF-β1-induced synthesis of FN, PAI-1, and Col Iα1. In our study, TGP and propolin G down-regulated Smad2/3 mRNA and protein expression and reduced TGF-β1-induced Smad2/3 phosphorylation in HSC-T6 cells (Figure 4).

Propolin G Increases Phosphor-JNK MAPK Expression and Induces Apoptosis in TGF-β-Stimulated HSCs in

TGF-β-Stimulated HSCs. To investigate the apoptotic signaling pathways underlying the effects of propolin G on HSC-T6 cells, we evaluated the expression of two signaling proteins associated with oxidative stress: phospho-JNK MAPK and phospho-Akt. The result indicated that p-P38 and p-JNK were significantly elevated 30 min and 2 h after TGF-β treatment; this was consistent with the previous study.[41] However, we did not observe the elevation of p-ERK. We treated the HSCs with various concentrations of TGP (1−8 μg/mL) or propolin G (1−8 μM) prior to treatment with TGF-β for 15 min. Our Western blotting results showed that TGP and propolin G significantly up-regulated phospho-JNK and phospho-P38 MAPK expression in TGF-β1-stimulated cells (Figure 5). To investigate the effects of TGP and propolin G on apoptosis, we treated the HSCs with various concentrations of TGP (1−8 μg/mL) or propolin G (1−8 μM) for 24 h, before evaluating apoptosis. As shown in Figure 6A, TGP and propolin G activated caspase-7 and caspase-3 in a dose-dependent manner (Figure 6A). TGP and propolin G also activated caspase-9 and induced the cleavage of caspase-3 and PARP, in a time-dependent manner. Taken together, these results indicated that TGP and propolin G can not only attenuate TGF-β signaling via Smad2/3 inhibition but also enhance apoptosis through inducing p38 and JNK mediated caspase activity (Figure 6B). Because we cannot exclude the reduction of Smad2/3 phosphorylation by TGP or propolin G may due to cell apoptosis at this time, the results indicate TGP or propolin G can affect the process of fibrosis possibly through both TGF-β signaling inhibition and cell apoptosis below IC_{50} concentration. However, the issue of cell cytotoxicity at high dose in our findings should be carefully addressed when considering applications in the furture when compared with other low toxicity compounds.[39] On the other hand, these findings suggested that naringenin might reduce ECM components through a molecular mechanism different from SB-431542. Naringenin increases PI3K and MAPK ERK1/2 (p 38) activity in HepG2 cells in a manner similar to that of insulin. In previous studies, TGP and propolin G did not induce insulin receptor substrate phosphorylation.[42,43] Although other studies have shown that insulin- and insulin-like growth factor-I-mediated signaling pathways modulate TGF-β signaling,[44,45] the molecular details of the effects of these pathways on TGF-β signaling have yet to be fully elucidated. One mechanism by which anti-apoptotic signaling, mediated by PI3K-PKB, inhibits TGF-β signaling is the induction of interaction between PKB and Smad3, thus reducing the pool of Smad3 available for TGF-β signaling. The process is based on the down-regulating effects of insulin and insulin-like growth factors on TGF-β-regulated gene expression and can be reversed by using highly specific inhibitors of PI3K, LY294002, or wortmannin. Insulin significantly inhibits the phosphorylation of TGF-β1-induced Smad3, but not Smad2, whereas Smad2/3 protein expression remains unaffected by insulin treatment.

Ethanol Extract of Taiwanese Green Propolis against the Ethanol-Induced Hepatic Injury in Mice. We measured the activities of SOD and GPx and the MDA level in the plasma of mice. The MDA and ALT levels in EtOH-treated mice were significantly increased, as compared to that in the control group (Figure 7). Administering TGP (200 and 400 mg/kg/day) significantly inhibited the increase of MDA (Figure 7a) and GPx (Figure 7b) as well as SOD (Figure 7c). The SOD and GPx expression in the liver tissue was similar to plasma (data not shown). Furthermore, to examine whether the liver function can be rescued by TGP, we tested the ALT (Figure 7d) and AST (Figure 7e) to add support to the in vivo animal result. The data indicated that TGP can significantly reduce ALT and AST levels induced by ethanol, suggesting that TGP had a liver protection function. The production of ROS can also be evaluated indirectly by analyzing the level of MDA, a product of free radical-induced lipid peroxidation. To protect cells against oxidative damage induced by ROS, the antioxidant system in the body is activated, and endogenous antioxidant enzymes, such as SOD and GPx, scavenge ROS or prevent their formation. It has been reported that naturally fermented noni juice (NJ) contains polyphenols, polysaccharides, and some trace minerals. NJ promotes hepatoprotection against alcohol-induced injury due to regulations of lipid homeostasis, antioxidant status, alcohol metabolism (Chang et al., 2013).[46] TGP is widely used in Taiwanese traditional medicine and reportedly exhibits anticancer,[12−18] antioxidant,[12,14,18] and antimicrobial [19] properties. Interestingly, TGP has no influence on plasma or hepatic SOD and GPx levels but significantly decreased the MDA value. It is possible that TGP acts by several mechanisms, mediating a potential role in liver fibrosis retrieval in mice. Further study is necessary to evaluate the effect of TGP on liver fibrosis prevention and to determine the molecular mechanisms.

In conclusion, our results indicate that TGP and propolin G exert antifibrotic effects through the disruption of TGF-β-Smad2/3 signaling by directly or indirectly reducing Smad2/3 formation. These findings verify that Smad3 is a crucial mediator of TGF-β-modulated fibrogenic function and indicate that the inhibition of Smad2/3 protein function could potentially provide an effective strategy for the treatment of liver fibrosis. Although more detailed mechanistic studies are necessary to clarify the mechanisms of antifibrosis using TGP or propolin G, these results should encourage further studies to explore the potential antifibrosis effects of TGP or propolin G in chronic liver diseases.

AUTHOR INFORMATION

Corresponding Author

*(Y.-L.S.C.) Phone: +886-3-935-7400, ext. 7625. Fax: +886-3-9311526. E-mail: a221865880@yahoo.com.tw.

Author Contributions

Y.-L. S. Chen made contributions to concept and design and gave final approval of the manuscript to be published. C.-T. Chuang and C.-T. Chen performed experiments and collected the data for analysis. Y.-W. Chen, C.-Y. Hsieh, and K.-Y. Su provided the interpretation of data and were involved in drafting the manuscript.

Notes

The authors declare no competing financial interest.

ACKNOWLEDGMENTS

We thank Dr. Huang Yi-Tsau from the National Research Institute of Chinese Medicine, Ministry of Health and Welfare, Taipei, Taiwan, for technical support and discussion.

REFERENCES

(1) Border, W. A.; Noble, N. A. Transforming growth factor beta in tissue fibrosis. *N. Engl. J. Med.* **1994**, *331*, 1286−1292.

(2) Rojkind, M.; Giambrone, M. A.; Biempica, L. Collagen types in normal and cirrhotic liver. *Gastroenterology* **1979**, *76*, 710−719.

(3) Gressner, A. M.; Bachem, M. G. Cellular sources of noncollagenous matrix proteins: role of fat-storing cells in fibrogenesis. *Semin. Liver Dis.* **1990**, *10*, 30−46.
(4) Arthur, M. J. Fibrogenesis II. Metalloproteinases and their inhibitors in liver fibrosis. *Am. J. Physiol. Gastrointest. Liver Physiol.* **2000**, *279*, G245−G249.
(5) Friedman, S. L. Liver fibrosis − from bench to bedside. *J. Hepatol.* **2003**, *38* (Suppl. 1), S38−S53.
(6) Wells, R. G.; Fibrogenesis, V. TGF-β signaling pathways. *Am. J. Physiol. Gastrointest. Liver Physiol.* **2000**, *279*, G845−G850.
(7) Gressner, A. M.; Weiskirchen, R. Modern pathogenetic concepts of liver fibrosis suggest stellate cells and TGF-β as major players and therapeutic targets. *J. Cell. Mol. Med.* **2006**, *10*, 76−99.
(8) Liu, X.; Wang, W.; Hu, H.; Tang, N.; Zhang, C.; Liang, W.; Wang, M. Smad3 specific inhibitor, naringenin, decreases the expression of extracellular matrix induced by TGF-β1 in cultured rat hepatic stellate cells. *J. Pharm. Res.* **2006**, *23*, 82−89.
(9) Roberts, A. B.; Russo, A.; Felici, A.; Flanders, K. C. Smad3: a key player in pathogenetic mechanisms dependent on TGF-β. *Ann. N.Y. Acad. Sci.* **2003**, *995*, 1−10.
(10) Leask, A.; Abraham, D. J. TGF-β signaling and the fibrotic response. *FASEB J.* **2004**, *18*, 816−827.
(11) Lu, L. C.; Chen, Y. W.; Chou, C. C. Antibacterial activity of propolis against *Staphylococcus aureus*. *Int. J. Food Microbiol.* **2005**, *102*, 213−220.
(12) Chen, C. N.; Weng, M. S.; Wu, C. L.; Lin, J. K. Comparison of radical scavenging activity, cytotoxic effects and apoptosis induction in human melanoma cells by Taiwanese propolis from different sources. *Evidence-Based Complement. Altern. Medicine: eCAM* **2004**, *1*, 175−185.
(13) Chen, C. N.; Wu, C. L.; Lin, J. K. Apoptosis of human melanoma cells induced by the novel compounds propolin A and propolin B from Taiwenese propolis. *Cancer Lett.* **2007**, *245*, 218−231.
(14) Chen, C. N.; Wu, C. L.; Shy, H. S.; Lin, J. K. Cytotoxic prenylflavanones from Taiwanese propolis. *J. Nat. Prod.* **2003**, *66*, 503−506.
(15) Chen, C.-N.; Wu, C.-L.; Lin, J.-K. Propolin C from propolis induces apoptosis through activating caspases, Bid and cytochrome c release in human melanoma cells. *Biochem. Pharmacol.* **2004**, *67*, 53−66.
(16) Huang, W. J.; Huang, C. H.; Wu, C. L.; Lin, J. K.; Chen, Y. W.; Lin, C. L.; Chuang, S. E.; Huang, C. Y.; Chen, C. N. Propolin G, a prenylflavanone, isolated from Taiwanese propolis, induces caspase-dependent apoptosis in brain cancer cells. *J. Agric. Food Chem.* **2007**, *55*, 7366−7376.
(17) Huang, W. J.; Lin, C. W.; Lee, C. Y.; Chi, L. L.; Chao, Y. C.; Wang, H. N.; Chiou, B. L.; Chen, T. J.; Huang, C. Y.; Chen, C. N. NBM-HD-3, a novel histone deacetylase inhibitor with anticancer activity through modulation of PTEN and AKT in brain cancer cells. *J. Ethnopharmacol.* **2011**, *136*, 156−167.
(18) Popova, M.; Chen, C. N.; Chen, P. Y.; Huang, C. Y.; Bankova, V. A validated spectrophotometric method for quantification of prenylated flavanones in pacific propolis from Taiwan. *Phytochem. Anal.* **2010**, *21*, 186−191.
(19) Yang, H.-Y.; Chang, C.-M.; Chen, Y.-W.; Chou, C.-C. Inhibitory effect of propolis extract on the growth of *Listeria monocytogenes* and the mutagenicity of 4-nitroquinoline-*N*-oxide. *J. Sci. Food Agric.* **2006**, *86*, 937−943.
(20) Nanji, A. A.; Zakim, D.; Rahemtulla, A.; Daly, T.; Miao, L.; Zhao, S.; Khwaja, S.; Tahan, S. R.; Dannenberg, A. J. Dietary saturated fatty acids down-regulate cyclooxygenase-2 and tumor necrosis factor α and reverse fibrosis in alcohol-induced liver disease in the rat. *Hepatology* **1997**, *26*, 1538−1545.
(21) Tsukamoto, H.; Lu, S. C. Current concepts in the pathogenesis of alcoholic liver injury. *FASEB J.* **2001**, *15*, 1335−1349.
(22) Carter, E. A.; Wands, J. R. Ethanol inhibits hormone stimulated hepatocyte DNA synthesis. *Biochem. Biophys. Res. Commun.* **1985**, *128*, 767−774.
(23) Diehl, A. M.; Goodman, Z.; Ishak, K. G. Alcohollike liver disease in nonalcoholics. A clinical and histologic comparison with alcohol-induced liver injury. *Gastroenterology* **1988**, *95*, 1056−1062.
(24) Weber, L. W.; Boll, M.; Stampfl, A. Hepatotoxicity and mechanism of action of haloalkanes: carbon tetrachloride as a toxicological model. *Crit. Rev. Toxicol.* **2003**, *33*, 105−136.
(25) Singh, B. S. A.; Chandan, B. K.; Anand, K. K.; Suri, O. P.; Suri, K. A.; Satti, N. K. Hepatoprotective activity of verbenalin on experimental liver damage in rodents. *Fitoterapia* **1998**, *69*, 135−140.
(26) Xiong, Q.; Hase, K.; Tezuka, Y.; Tani, T.; Namba, T.; Kadota, S. Hepatoprotective activity of phenylethanoids from *Cistanche deserticola*. *Planta Med.* **1998**, *64*, 120−125.
(27) Willson, R. L. Peroxy free radicals and enzyme inactivation in radiation injury and oxygen toxicity: protection by superoxide dismutase and antioxidants? *Lancet* **1984**, *1*, 804.
(28) Chomczynski, P.; Sacchi, N. The single-step method of RNA isolation by acid guanidinium thiocyanate-phenol-chloroform extraction: twenty-something years on. *Nat Protoc.* **2006**, *1* (2), 581−585.
(29) Friedman, S. L. Molecular regulation of hepatic fibrosis, an integrated cellular response to tissue injury. *J. Biol. Chem.* **2000**, *275*, 2247−2250.
(30) Saile, B.; Knittel, T.; Matthes, N.; Schott, P.; Ramadori, G. CD95/CD95L-mediated apoptosis of the hepatic stellate cell. A mechanism terminating uncontrolled hepatic stellate cell proliferation during hepatic tissue repair. *Am. J. Pathol.* **1997**, *151*, 1265−1272.
(31) Gong, W.; Pecci, A.; Roth, S.; Lahme, B.; Beato, M.; Gressner, A. M. Transformation-dependent susceptibility of rat hepatic stellate cells to apoptosis induced by soluble Fas ligand. *Hepatology* **1998**, *28*, 492−502.
(32) Gressner, A. M.; Polzar, B.; Lahme, B.; Mannherz, H. G. Induction of rat liver parenchymal cell apoptosis by hepatic myofibroblasts via transforming growth factor beta. *Hepatology* **1996**, *23*, 571−581.
(33) Ueno, H.; Sakamoto, T.; Nakamura, T.; Qi, Z.; Astuchi, N.; Takeshita, A.; Shimizu, K.; Ohashi, H. A soluble transforming growth factor β receptor expressed in muscle prevents liver fibrogenesis and dysfunction in rats. *Hum. Gene Ther.* **2000**, *11*, 33−42.
(34) Verrecchia, F.; Chu, M. L.; Mauviel, A. Identification of novel TGF-β/Smad gene targets in dermal fibroblasts using a combined cDNA microarray/promoter transactivation approach. *J. Biol. Chem.* **2001**, *276*, 17058−17062.
(35) Goumans, M. J.; Lebrin, F.; Valdimarsdottir, G. Controlling the angiogenic switch: a balance between two distinct TGF-β receptor signaling pathways. *Trends Cardiovasc. Med.* **2003**, *13*, 301−307.
(36) Isono, M.; Chen, S.; Hong, S. W.; Iglesias-de la Cruz, M. C.; Ziyadeh, F. N. Smad pathway is activated in the diabetic mouse kidney and Smad3 mediates TGF-β-induced fibronectin in mesangial cells. *Biochem. Biophys. Res. Commun.* **2002**, *296*, 1356−1365.
(37) Shi, Y.; Massague, J. Mechanisms of TGF-β signaling from cell membrane to the nucleus. *Cell* **2003**, *113*, 685−700.
(38) Dennler, S.; Itoh, S.; Vivien, D.; ten Dijke, P.; Huet, S.; Gauthier, J. M. Direct binding of Smad3 and Smad4 to critical TGF β-inducible elements in the promoter of human plasminogen activator inhibitor-type 1 gene. *EMBO J.* **1998**, *17*, 3091−3100.
(39) Tang, L. X.; He, R. H.; Yang, G.; Tan, J. J.; Zhou, L.; Meng, X. M.; Huang, X. R.; Lan, H. Y. Asiatic acid inhibits liver fibrosis by blocking TGF-β/Smad signaling in vivo and in vitro. *PLoS One* **2012**, *7*, e31350.
(40) Bissell, D. M.; Roulot, D.; George, J. Transforming growth factor β and the liver. *Hepatology* **2001**, *34*, 859−867.
(41) Lin, Y. L.; Wu, C. F.; Huang, Y. T. Effects of rhubarb on migration of rat hepatic stellate cells. *J. Gastroenterol. Hepatol.* **2009**, *24*, 453−461.
(42) Borradaile, N. M.; de Dreu, L. E.; Huff, M. W. Inhibition of net HepG2 cell apolipoprotein B secretion by the citrus flavonoid naringenin involves activation of phosphatidylinositol 3-kinase, independent of insulin receptor substrate-1 phosphorylation. *Diabetes* **2003**, *52*, 2554−2561.

(43) Allister, E. M.; Borradaile, N. M.; Edwards, J. Y.; Huff, M. W. Inhibition of microsomal triglyceride transfer protein expression and apolipoprotein B100 secretion by the citrus flavonoid naringenin and by insulin involves activation of the mitogen-activated protein kinase pathway in hepatocytes. *Diabetes* **2005**, *54*, 1676−1683.
(44) Song, K.; Cornelius, S. C.; Reiss, M.; Danielpour, D. Insulin-like growth factor-I inhibits transcriptional responses of transforming growth factor-β by phosphatidylinositol 3-kinase/Akt-dependent suppression of the activation of Smad3 but not Smad2. *J. Biol. Chem.* **2003**, *278*, 38342−38351.
(45) Remy, I.; Montmarquette, A.; Michnick, S. W. PKB/Akt modulates TGF-β signalling through a direct interaction with Smad3. *Nat. Cell Biol.* **2004**, *6*, 358−365.
(46) Chang, Y. Y.; Lin, Y. L.; Yang, D. J.; Liu, C. W.; Hsu, C. L.; Tzang, B. S.; Chen, Y. C. Hepatoprotection of noni juice against chronic alcohol consumption: lipid homeostasis, antioxidation, alcohol clearance, and anti-inflammation. *J. Agric. Food Chem.* **2013**, *61* (46), 11016−11024.

point at which diabetic nephropathy occurs. All of the above evidence clearly indicate that MGO is a key factor in *in vivo* AGE production. Thus, scavenging reactive dicarbonyl species has been used as an effective strategy to prevent protein modification and AGE formation.[12−14] Driven by this strategy, several pharmacological reagents, such as aminoguanidine,[15,16] tenilsetam,[17,18] carnosine,[19] metformin,[20,21] and pyridoxamine,[22,23] have been developed for inhibiting the formation of AGEs and preventing the development of diabetic complications. However, all of these pharmaceutical agents have serious side effects. For example, the nucleophilic hydrazine compound aminoguanidine failed in phase III clinical trials because of the high toxicity in diabetic patients.[24] Therefore, it is critical to develop effective and safe agents to protect diabetics from complications.

Flavonoids are polyphenolic compounds that are ubiquitous in nature, many of which occur in fruits, vegetables, and beverages (tea, coffee, beer, wine, and fruit drinks). Recently, flavonoids have aroused considerable interest because of their potential beneficial effects on human health. They have been reported to reduce the risk of chronic diseases, such as cancer, cardiovascular disease, asthma, and diabetes. Certain flavonoids have shown more effective inhibition of AGE formation than aminoguanidine, a well-known AGE inhibitor.[25] For example, luteolin, rutin, (−)-epigallocatechin-3-gallate (EGCG), and quercetin demonstrated significant inhibitory effects on MGO-mediated AGE formation by 82.2, 77.7, 69.1, and 65.5%, respectively.[25] Researchers have documented the effects of added natural phenolic compounds on the generation of reactive carbonyl intermediates.[26] Previous studies in our lab have shown that EGCG from green tea, phloretin and phloridzin from apple, and genistein from soybean were able to effectively trap MGO to form mono- and di-MGO adducts.[27−29] Besides, in a study by Ma et al., phloretin or phloridzin exhibited great inhibitory effects on arginine residue modification by MGO,[30,31] which indicated that a direct capture of the reactive α-dicarbonyl species, such as MGO, would effectively inhibit the formation of AGEs and eventually benefit the prevention of diabetic complications.

In studying the mechanism that flavonoids can scavenge reactive dicarbonyl species, we revealed that the A ring of EGCG played significant role in trapping of reactive dicarbonyl species.[27−29] We also found that the A ring is the active site of phloretin or phloridzin on both MGO and glyoxal (GO) trapping. However, the structure−activity relationship (SAR) of flavonoids in scavenging reactive α-dicarbonyl species was not thoroughly investigated. In addition, the daily intake of individual flavonoids may not be high enough to significantly decrease the levels of reactive dicarbonyls in humans; however, the total intake of flavonoids from a variety of foods can reach the effective doses to trap a significant amount of exogenous and endogenous reactive dicarbonyls. Therefore, it is important to study the potential additive effects of different flavonoids. In the present study, we investigated the reaction of some naturally occurring flavonoids together with their subcomponents with MGO, in an attempt to establish the SAR of flavonoids in scavenging dicarbonyl species. The additive effects of trapping MGO at different concentrations by phloretin and quercetin were also carried out under an *in vitro* system.

MATERIALS AND METHODS

Materials. Quercetin, luteolin, epicatechin, genistein, daidzein, apigenin, phloretin, gallic acid, phloroglucinol, methylglyoxal (40% in water), 2-methylquinoxaline, and 1,2-diaminobenzene (DB) were purchased from Sigma (St. Louis, MO). Pyrogallol (Pg), pyrocatechol, resorcinol, and liquid chromatrography/mass spectrometry (LC/MS)-grade MeOH and water were purchased from Thermo Fisher Scientific (Pittsburgh, PA). High-performance liquid chromatography (HPLC)-grade solvents and other reagents were obtained from VWR Scientific (South Plainfield, NJ). HPLC-grade water was prepared using a Millipore Milli-Q purification system (Bedford, MA).

Kinetic Study of Trapping MGO by Dietary Flavonoids and Simple Phenols. MGO (0.33 mM) was mixed with 1 mM quercetin, luteolin, epicatechin, genistein, daidzein, apigenin, gallic acid, phloroglucinol, Pg, pyrocatechol, or resorcinol in pH 7.4 phosphate-buffered saline (PBS, 100 mM). The mixed solutions were incubated at 37 °C and shaken at 40 revolutions per minute (rpm) for 0, 10, 30, 60, 120, 240, 480, and 1440 min. Afterward, 200 μL of reacted mixtures were collected at each time point, 1 μL of acetic acid was added to stop the reaction, and 100 mM DB was allowed to react with the remaining MGO for 30 min. The level of methylquinoxaline was determined using the HPLC method described below.[28]

Trapping of MGO by Phloretin, Quercetin, and the Combination of Phloretin and Quercetin. MGO (300 or 60 μM) was incubated with phloretin (50 or 10 μM), quercetin (50 or 10 μM), or a combination of phloretin and quercetin (50 or 10 μM each) in pH 7.4 PBS (100 mM) at 37 °C and shaken at 40 rpm for 24 h. Then, 400 μL of each reacted mixture was collected, and 2 μL of acetic acid was added to stop the reaction. Half of this solution was used for LC/MS analysis, and the other half was used for the derivatization of the remaining MGO by adding 100 mM DB according to our previous method.[28]

Trapping of MGO by Pg. Pg (12.6 mg, 0.1 mmol) was dissolved in 10 mL of PBS (100 mM, pH 7.4) and treated with a diluted solution of MGO (0.033 or 0.1 mmol) in PBS (100 mM, pH 7.4). The mixture was incubated at 37 °C for 3 h and then quenched by adding 200 μL of acetic acid. After dilution, 100 times by MeOH, the reaction mixture was then analyzed by LC/MS.

HPLC Analysis. The level of methylquinoxaline was determined using our previous HPLC method, with slight modification.[28] Briefly, the HPLC system was equipped with a Waters 717 refrigerated autosampler, a HITACHI L-6200 Inteligent pump, and a Waters 490E programmable multi-wavelength ultraviolet−visible (UV−vis) detector. A Supelcosil C18 reversed-phase column (150 × 4.6 mm inner diameter, Supelco Co., Bellefonte, PA) was used with a flow rate of 1 mL/min. Both the column and sample temperatures were set at ambient conditions. The binary mobile phase system consisted of 5% aqueous acetonitrile with 0.2% acetic acid as A and 95% aqueous acetonitrile with 0.2% acetic acid as B. The column eluted with a binary gradient system: 100−65% A from 0 to 5 min, 65−60% A from 5 to 15 min, 60−0% A from 15 to 20 min, and then 100% A from 21 to 30 min. The injection volume was 50 μL. The wavelength of the UV detector was set at 280 nm with 100 ng/mL as the limit of detection (LOD) and 1 μg/mL as the limit of quantification (LOQ).

LC/MS Analysis. LC/MS analysis was carried out with a Thermo-Finnigan spectra system, which consisted of an Accela high-speed MS pump, an Accela refrigerated autosampler, and a LCQ Fleet ion trap mass detector (Thermo Electron, San Jose, CA) incorporated with electrospray ionization (ESI) interfaces. For the analysis of Pg or its main MGO adducts, a 150 × 3.0 mm inner diameter, 5 μm Gemini C18 column (Phenomenex, Torrance, CA) was employed with a flow rate of 0.3 mL/min in the current study. The column was eluted with 100% solvent A (100% water with 0.2% acetic acid) for 5 min, followed by linear increases in B (100% methanol with 0.2% acetic acid) to 30% from 5 to 20 min, 80% from 20 to 40 min, 100% from 40 to 50 min, and then 100% from 50 to 55 min. The column was then re-equilibrated with 100% A for 5 min. As far as phloretin, quercetin, or their major MGO adducts were concerned, a 50 × 2.0 mm inner diameter, 3 μm Gemini C18 column (Phenomenex, Torrance, CA) was used for separation at a flow rate of 0.2 mL/min. The column was

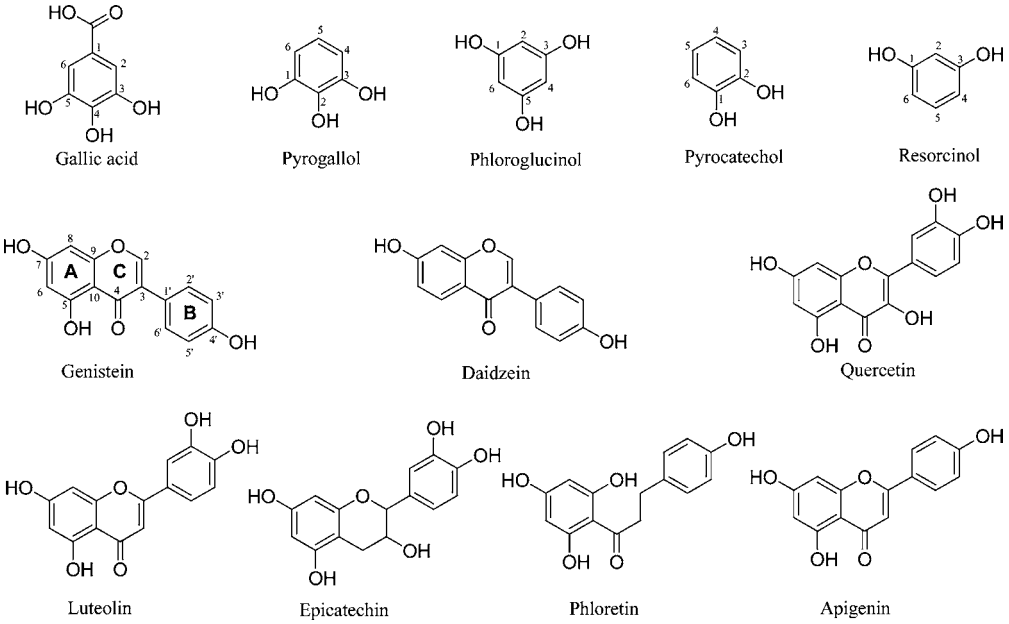

Figure 1. Chemical structures of gallic acid, pytogallol (Pg), phloroglucinol, pyrocatechol, resorcinol, genistein, daidzein, quercetin, luteolin, epicatechin, phloretin, and apigenin.

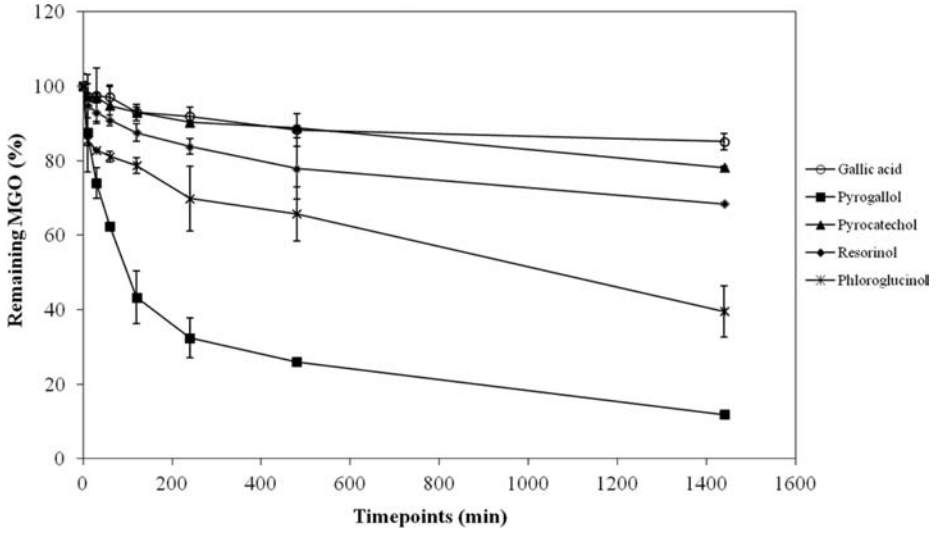

Figure 2. Trapping of MGO by gallic acid, pytogallol (Pg), phloroglucinol, pyrocatechol, and resorcinol.

eluted with 100% solvent A (100% water with 0.2% acetic acid) for 5 min, followed by linear increases in B (95% aqueous methanol with 0.2% acetic acid) to 20% from 5 to 10 min, 50% from 10 to 20 min, 100% from 20 to 28 min, and then 100% from 28 to 33 min. The column was then re-equilibrated with 100% A for 7 min. The LC eluent was introduced into the ESI interface. The negative-ion polarity mode was set for the ESI ion source with the voltage on the ESI interface maintained at approximately 5 kV. Nitrogen gas was used as the sheath gas at a flow rate of 30 arbitrary units and the auxiliary gas at 5 arbitrary units. The structural information of phloretin, quercetin, Pg, and the major MGO adducts was obtained by tandem mass spectrometry (MS/MS) through collision-induced dissociation (CID) with a relative collision energy setting of 35%. Data acquisition was performed with Xcalibur, version 2.0 (Thermo Electron, San Jose, CA).

RESULTS

Trapping of MGO by Simple Phenols. In general, flavonoids are composed of three different small units, rings A, B, and C (chalcones are ring C cleavage products). To obtain the essential SAR in trapping dicarbonyl species by dietary flavonoids, we selected some typical sub-components of flavonoids to simplify the influential factors. Five simple phenols, gallic acid, Pg, pyrocatechol, resorcinol, and phloroglucinol (Figure 1), were chosen for our current study. Among these compounds, Pg showed the highest scavenging activity by trapping almost 90% MGO within 24 h of incubation, followed by phloroglucinol, which could trap 60.5% MGO (Figure 2). Resorcinol and pyrocatechol showed relatively lower scavenging activity by trapping 31.6 and 21.8% MGO, respectively (Figure 2). In contrast, gallic acid was found to be the least active agent by trapping only 14.9% MGO within 24 h of incubation, even if it has the same *vic*-trihydroxyl groups as Pg (Figure 2).

MGO Adducts of Pg. To further investigate the MGO-trapping mechanism of Pg, the reaction of Pg and MGO was

dx.doi.org/10.1021/jf500204s | J. Agric. Food Chem. 2014, 62, 3202−3210

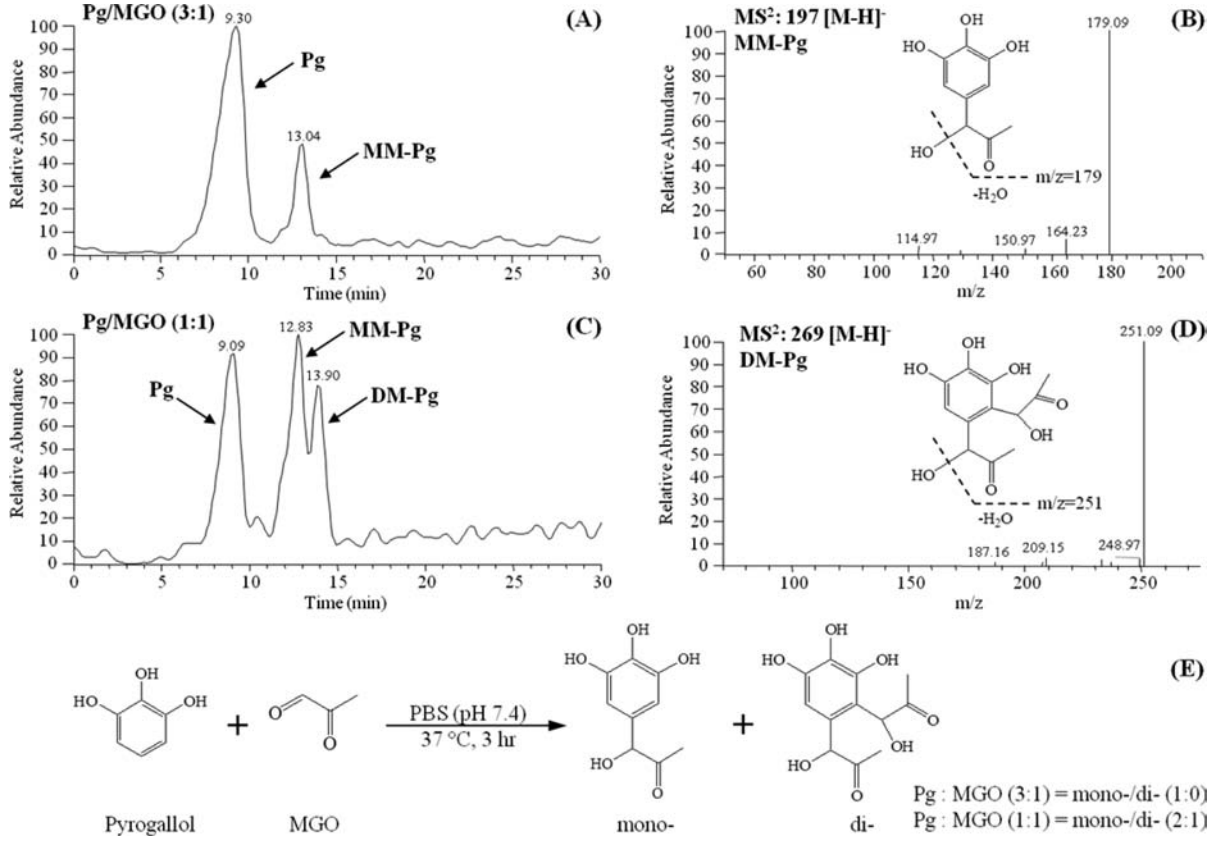

Figure 3. LC chromatogram of reaction mixtures of (A) pyrogallol (Pg) (0.1 mmol) with MGO (0.033 mmol) under a ratio of 3:1 and (C) Pg (0.1 mmol) with MGO (0.1 mmol) under a ratio of 1:1 in PBS (100 mM, pH 7.4) at 37 °C for 3 h. (B) MS/MS spectra of MM−Pg and (D) DM−Pg. (E) Chemical reaction equation of Pg and MGO (Pg = pyrogallol).

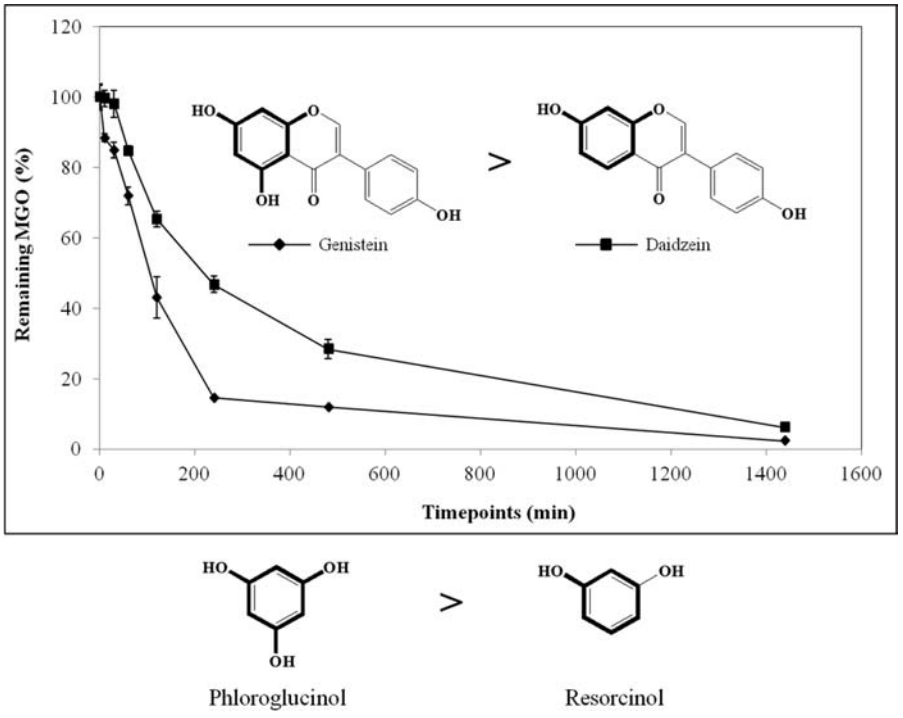

Figure 4. Trapping of MGO by genistein and daidzein.

tried at two different ratios (3:1 or 1:1 Pg/MGO). After 3 h of incubation (3:1 Pg/MGO), one major new peak [retention time (RT) of 13.04 min] appeared in the LC chromatogram (Figure 3A). This new peak had a molecular ion at m/z 197 [M − H]$^-$, which is 72 mass units (molecular weight of MGO of 72) higher than that of Pg, indicating that it is a mono-MGO

dx.doi.org/10.1021/jf500204s | J. Agric. Food Chem. 2014, 62, 3202−3210

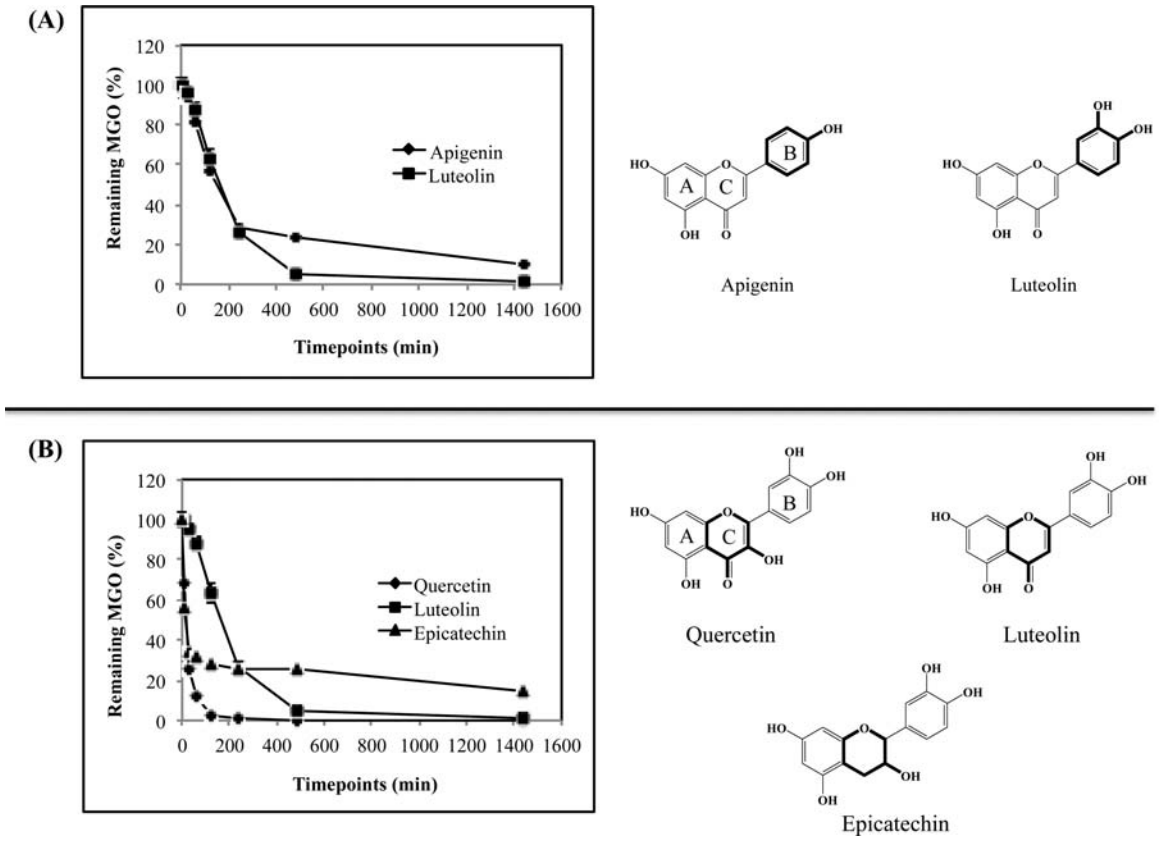

Figure 5. Trapping of MGO by (A) apigenin and luteolin and (B) quercetin, luteolin, and epicatechin.

conjugated pyrogallol (MM−Pg). Its MS^2 spectrum displayed a predominant dehydration ion at m/z 179 $[M - H_2O - H]^-$ (Figure 3B), while one more peak (RT of 13.90 min) was observed besides the peak of MM−Pg (RT of 12.83 min) with Pg and MGO at a 1:1 ratio (Figure 3C). This peak had a molecular ion at 269 $[M - H]^-$, which is 72 mass units higher than that of MM−Pg, suggesting that this product is the di-MGO conjugated pyrogallol (DM−Pg). Similarly, its MS^2 spectrum also displayed a predominant dehydration ion at m/z 251 $[M - H_2O - H]^-$ (Figure 3D). Because of the instability of these adducts, we failed to purify either MM−Pg or DM−Pg from the reaction mixture. However, the proton nuclear magnetic resonance (^{1}H NMR) spectrum (600 MHz in CD_3OD) of the crude mixture with MM−Pg as the major component showed only singlet signals for the aromatic ring protons (data not shown), suggesting that MGO was located at C-5 of Pg in MM−Pg (Figures 1 and 3B). The formation of mono- and di-MGO conjugated products of Pg was tentatively proposed in Figure 3E. The identification of position 5 as the active site of Pg further explained why gallic acid has almost no trapping effect of MGO and the B or D ring of EGCG is not the active site to trap MGO.

Effects of the A Ring on MGO-Trapping Efficacy. We used phloroglucinol and resorcinol to represent the A-ring structures of flavonoids. Our result that phloroglucinol is a better MGO scavenger than resorcinol indicates that the hydroxyl group on C-5 of the A ring will enhance the trapping efficacy of flavonoids. To test this hypothesis, we compared the MGO-trapping effects of genistein and daidzein, which have A-ring structures almost identical to phloroglucinol and resorcinol, respectively. In addition, they have the same B- and C-ring structures. Similar to our finding on phloroglucinol and resorcinol, genistein was more effective than daidzein (Figure 4). At 4 h, genistein could trap almost 90% MGO, whereas daidzein could only trap 54.5% MGO. Our results clearly support our hypothesis that the hydroxyl group on C-5 of the A ring is crucial for the trapping of MGO by flavonoids. This is also supported by our previous observation that glycosylation of the hydroxyl group at C-5 of the A ring of phloretin tended to decrease its activity.[27] In addition, glycosylation of the 5-hydroxyl group may increase the steric hindrance of position C-6 and, therefore, decrease its activity.

Effects of B and C Rings on MGO-Trapping Efficacy. By comparing the trapping of MGO by apigenin and luteolin (Figure 5A), which possess the same A and C rings but a different number of hydroxyl groups on the B ring, we found that the number of hydroxyl groups on the B ring does not play a significant role on the trapping efficacy of flavonoids, albeit that luteolin with two hydroxyl groups at C-2′ and C-3′ positions shows a slightly stronger trapping capacity than apigenin that has only one hydroxyl group on the B ring (Figure 5A). To understand how the C ring of the flavonoids affects the MGO-trapping capacity, we studied the MGO-trapping effects of quercetin, luteolin, and epicatechin, which have identical A and B rings with a different structure of the C ring. Quercetin and luteolin belong to the flavone with a double bond between C-2 and C-3 and one ketone group at C-4 (Figure 5B). Epicatechin belongs to flavan-3-ol with a hydroxy group on C-3 but with no double bond and a ketone group on the C ring. Quercetin showed the best MGO trapping efficacy, followed by luteolin and epicatechin. More than 90% MGO was trapped within 8 h by both quercetin and luteolin. Epicatechin also had strong trapping efficiency by quenching more than 85% MGO within 24 h. Both quercetin and epicatechin could

dx.doi.org/10.1021/jf500204s | J. Agric. Food Chem. 2014, 62, 3202−3210

rapidly trap MGO; almost 50% MGO was scavenged within 11.25 min.

Additive MGO-Trapping Effects by Phloretin and Quercetin. To test whether different flavonoids have additive effects in terms of trapping reactive dicarbonyl species, we investigated the MGO-trapping capability of phloretin, quercetin, or the combination of phloretin and quercetin at two different concentrations (50 and 10 μM) under a ratio of each flavonoid/MGO at 1:6 at pH 7.4 and 37 °C. Our results indicated that phloretin and quercetin trapped about 16 and 23% MGO, respectively, at a concentration of 50 μM within 24 h. About 37% MGO was trapped by the combination of phloretin and quercetin (50 μM each) (Figure 6). At a lower concentration (10 μM) with the same ratio, both phloretin and quercetin showed similar trapping capability of scavenging nearly 19 and 23% MGO within 24 h, respectively. Almost 35% MGO was trapped by the combination of phloretin and quercetin (10 μM each) (Figure 6). Our results clearly indicate that different flavonoids can additively trap MGO.

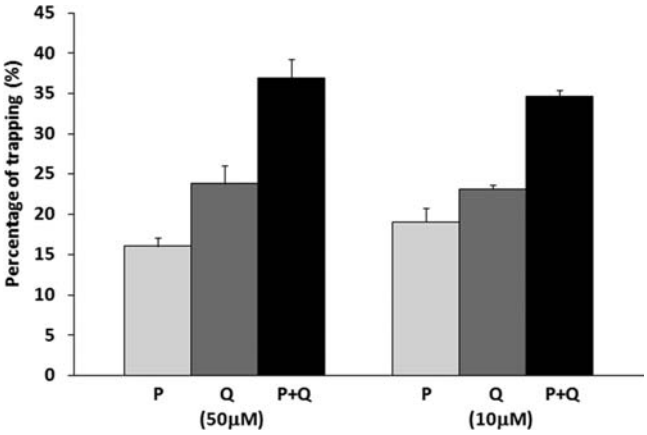

Figure 6. Tapping of MGO (300 or 60 μM) by phloretin (P), quercetin (Q), and the combination of phloretin and quercetin (P + Q, equal molar combination) at different concentrations (50 or 10 μM) in phosphate buffer (pH 7.4 and 37 °C) at 24 h. Bars on left and right sides represent the concentrations of MGO with 300 or 60 μM, respectively. Data are presented as the means ± standard deviation (SD) of three replications.

Studying the Formation of MGO Adducts of Quercetin and Phloretin by LC/MS. To understand the underlying mechanism that different flavonoids can additively trap MGO, we analyzed the formation of MGO adducts under each flavonoid along or the combination of phloretin and quercetin using LC/MS. Figure 7 shows the LC chromatograms of the reaction mixtures of quercetin with MGO (A), phloretin with MGO (B), and the combination of phloretin and quercetin (C). Both mono- and di-MGO adducts of quercetin were the major products under the ratio of quercetin/MGO at 1:6 (Figure 7A). Similar to our previous observation, mono- and di-MGO adducts of phloretin were identified as the major products for phloretin (Figure 7B). Under the combination of phloretin and quercetin, the same MGO adducts of each flavonoid were formed, which further confirmed the additive effect of phloretin and quercetin (Figure 7C).

We have confirmed the structures of the mono- and di-MGO adducts of phloretin in our previous study.[27] The structural information of the MGO adducts of quercetin was obtained using LC/MS/MS analysis under selective ion monitoring (SIM) mode (Figures 8). Three major new peaks appeared in the LC chromatogram of the reaction mixture of quercetin with MGO at a ratio of 1:6 after 24 h of incubation (Figures 7A). Two of the three peaks had the same molecular ion (m/z 373 $[M - H]^-$) and MS/MS fragments but different RTs (18.34 and 18.86 min). Both of the two compounds had the fragment ion 301 ($[M - 72 - H]^-$), showing that they both lost one MGO (m/z 72) molecule (Figure 8A), thus indicating that they are mono-MGO adducts of quercetin. Furthermore, the tandem mass spectrum of product ion 301 (MS^3, m/z 301/373) of the two compounds (Figure 8A) was almost identical to the MS^2 spectrum of authentic quercetin (MS^2, m/z 301), suggesting that the two compounds were the mono-MGO adducts of quercetin. The third peak (16.77 min) showed the molecular ion at m/z 445 $[M - H]^-$, which was 72 mass units higher than that of mono-MGO quercetin, indicating that it was the di-MGO quercetin. The tandem mass spectrum of its product ion 373 (MS^3, m/z 373/445) was almost identical to the MS^2 spectrum of mono-MGO quercetin (MS^2, m/z 373), suggesting that this peak was the di-MGO adduct of quercetin.

DISCUSSION

Flavonoids are biologically active, polyphenolic constituents of plant foods and are present in many fruits, vegetables, and beverages (tea, coffee, beer, wine, and fruit drinks), as well as dietary supplements and herbal remedies. The flavonoids are further divided into six major subclasses known as flavanols, flavanones, flavonols, flavones, isoflavones, and anthocyanidins on the basis of the connection of the B ring to the C ring, as well as the oxidation state and functional groups of the C ring.[32] All of the major classes of flavonoids are comprised of three six-membered rings: an aromatic A ring fused to a heterocyclic C ring that is attached through a single carbon−carbon bond to an aromatic B ring. Chalcone, an important precursor in the synthesis of anthocyanin pigments and other flavonoids in plants, is another type of important dietary flavonoid. In contrast to other flavonoids, the middle three carbon atoms in chalcones do not form a closed ring. Several *in vivo* and *in vitro* studies have indicated that dietary flavonoids could inhibit the formation of AGEs and prevent diabetes-related complications.[25,33,34] Previously, we found three different types of flavonoids, flavanol (EGCG), chalcone (phloretin and phloredzin), and isoflavone (genistein), could rapidly trap MGO at pH 7.4 and 37 °C and, therefore, inhibit the formation of AGEs.[27−29] We also demonstrated that the two unsubstituted carbons at the A ring of these flavonoids were the active sites for trapping reactive dicarbonyl species and forming mono- and di-MGO adducts. Most of the flavonoids have the same A-ring structure as EGCG, phloretin, phloridzin, or genistein. It is unclear whether they can also efficiently trap reactive dicarbonyl species to form mono- and di-MGO adducts. More importantly, it is largely unknown whether the number of hydroxyl groups on the A ring and the structures of B or C rings will play an important role in the trapping of reactive dicarbonyl species. To tackle these questions, we conducted the SAR studies of flavonoids as the scavengers of reactive dicarbonyl species.

We first compared the trapping efficacy of the sub-components of flavonoids, gallic acid (gallate ring of EGCG), Pg (B ring of flavonoids), pyrocatechol (B ring of flavonoids), resorcinol (A ring of flavonoids), and phloroglucinol (A ring of flavonoids). Our results showed that the MGO scavenging potency of these sub-components is in the order of Pg >

dx.doi.org/10.1021/jf500204s | J. Agric. Food Chem. 2014, 62, 3202−3210

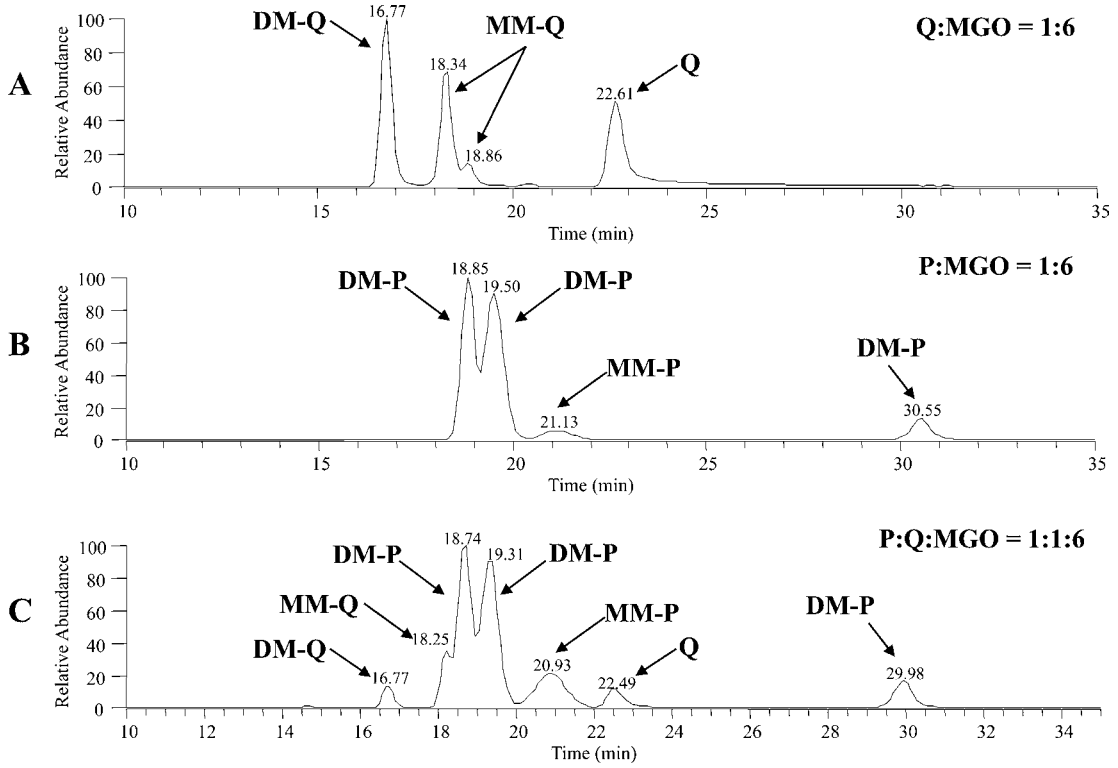

Figure 7. LC chromatogram of reaction mixtures of (A) quercetin (50 μM) with MGO (300 μM) under a ratio of 1:6 in PBS (100 mM, pH 7.4) at 37 °C for 24 h, (B) phloretin (50 μM) with MGO (300 μM) under a ratio of 1:6 in PBS (100 mM, pH 7.4) at 37 °C for 24 h, and (C) quercetin/phloretin with MGO under a ratio of 1:1:6.

phloroglucinol > resorinol > pyrocatechol > gallic acid, indicating the pivotal influence of the number and position of the hydroxyl group on the trapping activity. The trihydroxylbenzene (Pg and phloroglucinol) had a higher reactivity than the dihydroxylbenzene (pyrocatechol and resorcinol). In general, the hydroxyl group has electron-donating property. The more hydroxyl groups on the phenyl ring, the stronger the scavenging activity, because the reaction between phenol and MGO is a nucleophilic reaction. Our results also shown that the addition of a carboxyl group to position 5 of Pg almost completely diminished its trapping activity, indicating that position 5 is the active site of Pg. A further study on the trapping mechanism of Pg confirmed that MGO is conjugated at position 5 of Pg as the mono-MGO adduct of Pg, which provides the answer why gallic acid is the least active compound, albeit it has the same *vic*-trihydroxyl group as that of Pg. This also resolves the puzzle of our previous observation that the major active site of EGCG is at positions 6 and 8 of the A ring, instead of the B ring and the gallate ring, which have the *vic*-trihydroxyl group and are generally considered as the active sites for its antioxidant activities.[28] In addition, the position of the hydroxyl group also plays a significant role in contributing to the trapping capability of these small phenolic compounds. Pg with three *ortho*-hydroxyl groups demonstrated a much stronger trapping effect on MGO than phloroglucinol, which contains three *meta*-hydroxyl groups.

To extend our observation on the sub-components of flavonoids to the influence of A, B, or C ring of flavonoids on their MGO-trapping effects, we chose flavonoids containing these specific sub-components for our study. To demonstrate how the number of hydroxyl groups on the A ring of flavonoids affects the MGO-trapping efficiency, genistein and daidzein were chosen as our model compounds, because they possess identical B and C rings but with a different number of hydroxyl groups on the A ring. Genistein contains one more hydroxyl group at position C-5 than daidzein. Our finding that genistein showed stronger capability and efficacy in trapping of MGO than that of daidzein is in line with the conclusion drawn from phloroglucinol and resorcinol, which represent the A-ring structure of genistein and daidzein, respectively. In the same way, the effect of the number of hydroxyl groups on the B ring in the trapping dicarbonyl species by flavonoids was revealed by comparing the MGO-trapping capacity between apigenin and luteolin. A simple comparison among quercetin, luteolin, and epicatechin was carried out to demonstrate how the C ring of flavonoids affects the MGO-trapping ability. Even these simplified comparisons cannot provide the full picture of the essential SAR between dicarbonyl species and flavonoids; our results can still shed light on the following conclusions: (1) 1,2,3-trihydroxybenzene (Pg) has higher MGO scavenging reactivity than 1,2- and 1,3-dihydroxybenzene, and substitution at position 5 of Pg diminished the scavenging activity, indicating that position 5 is the active site of Pg; (2) the A ring is the active site of flavonoids in contributing the MGO-trapping efficacy, and the hydroxyl group at C-5 on the A ring enhances the trapping efficacy; (3) the double bond between C-2 and C-3 on the C ring could facilitate the trapping efficacy; and (4) the number of hydroxyl groups on the B ring does not significantly influence the trapping efficacy.

This is the first study to show that quercetin, luteolin, and apigenin can trap MGO at pH 7.4 and 37 °C, indicating flavonol and flavone types of flavonoids can also serve as scavengers of reactive dicarbonyl species. Further studies on the trapping mechanism of quercetin identified mono- and di-

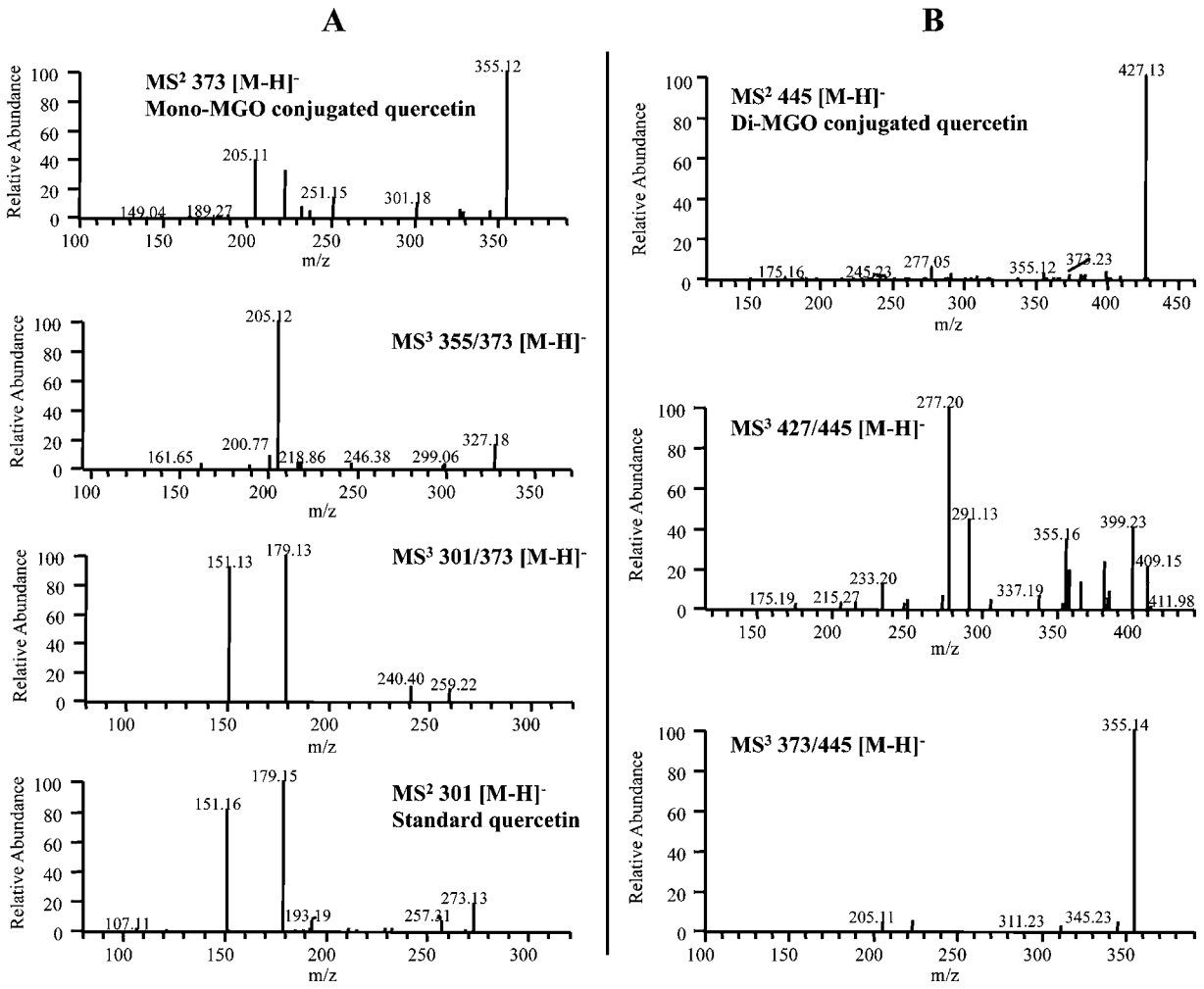

Figure 8. MS/MS spectra of (A) mono-MGO conjugated quercetin and authentic quercetin and (B) di-MGO conjugated quercetin.

MGO adducts as the major products of the reaction between quercetin and MGO. On the basis of our previous studies of EGCG, phloretin, and genistein, we suspect that the MGO conjugation should occur at positions C-6 and C-8 of the A ring. However, this needs to be further confirmed by NMR analysis of the pure mono- and di-MGO quercetin adducts. Our finding that many dietary flavonoids can trap reactive dicarbonyls through the same mechanism indicates that they may have an additive effect if not a synergistic effect. It has been reported that the total intake of flavonoids in the United States is 189.7 mg/day, which is difficult to be achieved for individual flavonoids.[35] Therefore, results on the effectiveness of the combination of individual flavonoids can be applied directly to translational studies in humans. To verify this hypothesis, phloretin and quercetin were chosen as the model compounds. Phloretin is a flavonoid found exclusively in apples and in apple-derived products. We previously reported that phloretin can effectively trap MGO.[27] Quercetin was selected because of its wide distribution in dietary plants.[36] Our results clearly indicated an additive MGO-trapping effect of these two flavonoids in two different concentrations (Figure 6). Thus, flavonoid-enriched foods and beverages as effective dietary strategies hold great promise to prevent the development of diabetic complications and, therefore, reduce the morbidity and mortality in individuals with diabetes. This topic needs to be further studied, especially under *in vivo* conditions.

AUTHOR INFORMATION

Corresponding Author

*Telephone: 704-250-5710. Fax: 704-250-5709. E-mail: ssang@ncat.edu.

Author Contributions

†Xi Shao, Huadong Chen, and Yingdong Zhu contributed equally to this work.

Funding

The authors gratefully acknowledge the financial support by United States Department of Agriculture (USDA) Grants 2009-65503-21116 and 2012-67017-30175 to Shengmin Sang.

Notes

The authors declare no competing financial interest.

ABBREVIATIONS USED

AGEs, advanced glycation end products; DM−Pg, di-MGO conjugated pyrogallol; HPLC, high-performance liquid chromatography; LC/MS, liquid chromatrography/mass spectrometry; MGO, methylglyoxal; MM−Pg, mono-MGO conjugated pyrogallol; Pg, pyrogallol; SAR, structure−activity relationship; PBS, phosphate-buffered saline

REFERENCES

(1) Kalapos, M. P. Where does plasma methylglyoxal originate from? *Diabetes Res. Clin. Pract.* **2013**, *99*, 260−271.

(2) Negre-Salvayre, A.; Salvayre, R.; Auge, N.; Pamplona, R.; Portero-Otin, M. Hyperglycemia and glycation in diabetic complications. *Antioxid. Redox Signaling* **2009**, *11*, 3071−3109.
(3) Matafome, P.; Sena, C.; Seica, R. Methylglyoxal, obesity, and diabetes. *Endocrine* **2013**, *43*, 472−484.
(4) Wang, H.; Meng, Q. H.; Gordon, J. R.; Khandwala, H.; Wu, L. Proinflammatory and proapoptotic effects of methylglyoxal on neutrophils from patients with type 2 diabetes mellitus. *Clin. Biochem.* **2007**, *40*, 1232−1239.
(5) Perkins, B. A.; Rabbani, N.; Weston, A.; Ficociello, L. H.; Adaikalakoteswari, A.; Niewczas, M.; Warram, J.; Krolewski, A. S.; Thornalley, P. Serum levels of advanced glycation endproducts and other markers of protein damage in early diabetic nephropathy in type 1 diabetes. *PloS One* **2012**, *7*, No. e35655.
(6) Singh, R.; Barden, A.; Mori, T.; Beilin, L. Advanced glycation end-products: A review. *Diabetologia* **2001**, *44*, 129−146.
(7) Crisostomo, J.; Matafome, P.; Santos-Silva, D.; Rodrigues, L.; Sena, C. M.; Pereira, P.; Seica, R. Methylglyoxal chronic administration promotes diabetes-like cardiac ischaemia disease in Wistar normal rats. *Nutr. Metab. Cardiovasc. Dis.* **2013**, *23*, 1223−1230.
(8) Lee, B. H.; Hsu, W. H.; Hsu, Y. W.; Pan, T. M. Dimerumic acid attenuates receptor for advanced glycation endproducts signal to inhibit inflammation and diabetes mediated by Nrf2 activation and promotes methylglyoxal metabolism into D-lactic acid. *Free Radicals Biol. Med.* **2013**, *60*, 7−16.
(9) Dhar, A.; Dhar, I.; Jiang, B.; Desai, K. M.; Wu, L. Chronic methylglyoxal infusion by minipump causes pancreatic β-cell dysfunction and induces type 2 diabetes in Sprague-Dawley rats. *Diabetes* **2011**, *60*, 899−908.
(10) Guo, Q.; Mori, T.; Jiang, Y.; Hu, C.; Osaki, Y.; Yoneki, Y.; Sun, Y.; Hosoya, T.; Kawamata, A.; Ogawa, S.; Nakayama, M.; Miyata, T.; Ito, S. Methylglyoxal contributes to the development of insulin resistance and salt sensitivity in Sprague-Dawley rats. *J. Hypertens.* **2009**, *27*, 1664−1671.
(11) Giacco, F.; Du, X.; D'Agati, V. D.; Milne, R.; Sui, G.; Geoffrion, M.; Brownlee, M. Knockdown of glyoxalase 1 mimics diabetic nephropathy in nondiabetic mice. *Diabetes* **2014**, *63*, 291−299.
(12) Wang, Y.; Ho, C. T. Flavour chemistry of methylglyoxal and glyoxal. *Chem. Soc. Rev.* **2012**, *41*, 4140−4149.
(13) Peng, X.; Ma, J.; Chen, F.; Wang, M. Naturally occurring inhibitors against the formation of advanced glycation end-products. *Food Funct.* **2011**, *2*, 289−301.
(14) Shapiro, H. K. Carbonyl-trapping therapeutic strategies. *Am. J. Ther.* **1998**, *5*, 323−353.
(15) Thomas, M. C.; Baynes, J. W.; Thorpe, S. R.; Cooper, M. E. The role of AGEs and AGE inhibitors in diabetic cardiovascular disease. *Curr. Drug Targets* **2005**, *6*, 453−474.
(16) Tanaka, N.; Yonekura, H.; Yamagishi, S.; Fujimori, H.; Yamamoto, Y.; Yamamoto, H. The receptor for advanced glycation end products is induced by the glycation products themselves and tumor necrosis factor-α through nuclear factor-κB, and by 17β-estradiol through Sp-1 in human vascular endothelial cells. *J. Biol. Chem.* **2000**, *275*, 25781−25790.
(17) Webster, J.; Urban, C.; Berbaum, K.; Loske, C.; Alpar, A.; Gartner, U.; de Arriba, S. G.; Arendt, T.; Munch, G. The carbonyl scavengers aminoguanidine and tenilsetam protect against the neurotoxic effects of methylglyoxal. *Neurotoxic. Res.* **2005**, *7*, 95−101.
(18) Price, D. L.; Rhett, P. M.; Thorpe, S. R.; Baynes, J. W. Chelating activity of advanced glycation end-product inhibitors. *J. Biol. Chem.* **2001**, *276*, 48967−48972.
(19) Blatnik, M.; Frizzell, N.; Thorpe, S. R.; Baynes, J. W. Inactivation of glyceraldehyde-3-phosphate dehydrogenase by fumarate in diabetes: Formation of *S*-(2-succinyl)cysteine, a novel chemical modification of protein and possible biomarker of mitochondrial stress. *Diabetes* **2008**, *57*, 41−49.
(20) Beisswenger, P.; Ruggiero-Lopez, D. Metformin inhibition of glycation processes. *Diabetes Metab.* **2003**, *29*, 6S95−6S103.
(21) Beisswenger, P. J.; Howell, S. K.; Touchette, A. D.; Lal, S.; Szwergold, B. S. Metformin reduces systemic methylglyoxal levels in type 2 diabetes. *Diabetes* **1999**, *48*, 198−202.
(22) Nagaraj, R. H.; Sarkar, P.; Mally, A.; Biemel, K. M.; Lederer, M. O.; Padayatti, P. S. Effect of pyridoxamine on chemical modification of proteins by carbonyls in diabetic rats: Characterization of a major product from the reaction of pyridoxamine and methylglyoxal. *Arch. Biochem. Biophys.* **2002**, *402*, 110−119.
(23) Voziyan, P. A.; Metz, T. O.; Baynes, J. W.; Hudson, B. G. A post-Amadori inhibitor pyridoxamine also inhibits chemical modification of proteins by scavenging carbonyl intermediates of carbohydrate and lipid degradation. *J. Biol. Chem.* **2002**, *277*, 3397−3403.
(24) Thornalley, P. J. Use of aminoguanidine (Pimagedine) to prevent the formation of advanced glycation endproducts. *Arch. Biochem. Biophys.* **2003**, *419*, 31−40.
(25) Wu, C. H.; Yen, G. C. Inhibitory effect of naturally occurring flavonoids on the formation of advanced glycation endproducts. *J. Agric. Food Chem.* **2005**, *53*, 3167−3173.
(26) Totlani, V. M.; Peterson, D. G. Reactivity of epicatechin in aqueous glycine and glucose maillard reaction models: Quenching of C_2, C_3, and C_4 sugar fragments. *J. Agric. Food Chem.* **2005**, *53*, 4130−4135.
(27) Shao, X.; Bai, N.; He, K.; Ho, C. T.; Yang, C. S.; Sang, S. Apple polyphenols, phloretin and phloridzin: New trapping agents of reactive dicarbonyl species. *Chem. Res. Toxicol.* **2008**, *21*, 2042−2050.
(28) Sang, S.; Shao, X.; Bai, N.; Lo, C. Y.; Yang, C. S.; Ho, C. T. Tea polyphenol (−)-epigallocatechin-3-gallate: A new trapping agent of reactive dicarbonyl species. *Chem. Res. Toxicol.* **2007**, *20*, 1862−1870.
(29) Lv, L.; Shao, X.; Chen, H.; Ho, C. T.; Sang, S. Genistein inhibits advanced glycation end product formation by trapping methylglyoxal. *Chem. Res. Toxicol.* **2011**, *24*, 579−586.
(30) Ahmed, M. U.; Brinkmann Frye, E.; Degenhardt, T. P.; Thorpe, S. R.; Baynes, J. W. N_ε-(Carboxyethyl)lysine, a product of the chemical modification of proteins by methylglyoxal, increases with age in human lens proteins. *Biochem. J.* **1997**, *324* (Part 2), 565−570.
(31) Odani, H.; Shinzato, T.; Usami, J.; Matsumoto, Y.; Brinkmann Frye, E.; Baynes, J. W.; Maeda, K. Imidazolium crosslinks derived from reaction of lysine with glyoxal and methylglyoxal are increased in serum proteins of uremic patients: Evidence for increased oxidative stress in uremia. *FEBS Lett.* **1998**, *427*, 381−385.
(32) Beecher, G. R. Overview of dietary flavonoids: Nomenclature, occurrence and intake. *J. Nutr.* **2003**, *133*, 3248S−3254S.
(33) Takasawa, R.; Takahashi, S.; Saeki, K.; Sunaga, S.; Yoshimori, A.; Tanuma, S. Structure−activity relationship of human GLO I inhibitory natural flavonoids and their growth inhibitory effects. *Bioorg. Med. Chem.* **2008**, *16*, 3969−3975.
(34) Maher, P.; Dargusch, R.; Ehren, J. L.; Okada, S.; Sharma, K.; Schubert, D. Fisetin lowers methylglyoxal dependent protein glycation and limits the complications of diabetes. *PloS One* **2011**, *6*, No. e21226.
(35) Chun, O. K.; Chung, S. J.; Song, W. O. Estimated dietary flavonoid intake and major food sources of U.S. adults. *J. Nutr.* **2007**, *137*, 1244−1252.
(36) Sampson, L.; Rimm, E.; Hollman, P. C.; de Vries, J. H.; Katan, M. B. Flavonol and flavone intakes in US health professionals. *J. Am. Diet. Assoc.* **2002**, *102*, 1414−1420.

limited extent, chiefly focusing on comparisons with other vegetable oils. Moreover, to our knowledge no data have been published on the factors influencing the CoQ10 content of olive oil.

The objective of this study was to investigate some factors that could influence the quantity of CoQ10 and CoQ9 in olive oils. We particularly focused on the influence of genetic factors (the cultivar) and the degree of ripeness. We also compared the composition of commercial oil blends and fresh extra virgin olive oil samples.

MATERIALS AND METHODS

Olive Oil Samples. The commercial olive oil and olive-pomace oil samples were purchased in stores in Slovenia, Spain, the United States, and Japan (seven samples of extra virgin olive oil blends, two samples of refined olive oil, two samples of olive-pomace oil) (Table 2).

Table 2. Coenzyme Q9 and Q10 Content in Olive Oils Purchased in Different Markets

description	no. of samples	content (mg/L) CoQ9	CoQ10	CoQ
olive oil (market)				
extra virgin	7	23 ± 12	56 ± 4	79 ± 12
refined	2	14 ± 9	54 ± 10	68 ± 2
olive-pomace oil	2	61 ± 19	83 ± 12	144 ± 31
Fresh olive oil (extra virgin, monocultivar)	79	21 ± 8	52 ± 17	73 ± 20

The monocultivar oil samples were provided by local producers or from local laboratories in Slovenia, Spain, Italy, Greece, France, Italy, Morocco, South Africa, Chile, and New Zealand (Tables 3 and 4). Monocultivar samples (n = 79) were stored in amber-colored glass at 4 °C in a nitrogen atmosphere until analyses. Thirteen of those samples were frozen when fresh for one season (−70 °C) and considered as fresh in the further analyses. Olive oils of the following cultivars (number of samples) were also analyzed: Picual (7 samples), Istrska belica (7), Leccino (7), Arbequina (4), Hojiblanca (4), Coratina (4), Frantoio (4), Maurino (4), Blanqueta (3), Koroneiki (3), Aglandau (2), Alfafara (2), Buga (2), Farga (2), Manzanilla (2), Olivière (2), Picholine (2), Tanche (2), Villalonga (2), and one sample per cultivar for Arbusana, Ascolano, Athinolia, Barnea, Barouni, Cacereña, Carolea, Itrana, Kalamata, Kolovi, Ladolia, Manaki, Mission, and Nocellara.

Table 4. Coenzyme Q9 and Q10 Content in Other Fresh Monocultivar Olive Oils

cultivar	no. of samples (country origin[a])	content (mg/L) CoQ9	CoQ10	CoQ
Aglandau	2 (GR)	15 ± 7	50 ± 9	65 ± 2
Alfafara	2 (ES)	11 ± 3	47 ± 23	58 ± 27
Blanqueta	3 (ES)	12 ± 2	56 ± 4	68 ± 5
Buga	2 (SI)	20 ± 4	49 ± 7	69 ± 11
Farga	2 (ES)	14 ± 4	24 ± 4	39 ± 8
Koroneiki	3 (GR)	10 ± 1	62 ± 4	71 ± 5
Manzanilla	2 (ES, SA)	17 ± 5	27 ± 3	44 ± 8
Olivière	2 (FR)	11 ± 1	52 ± 17	63 ± 15
Picholine	2 (FR)	40 ± 20	64 ± 10	104 ± 30
Tanche	2 (FR)	11 ± 2	58 ± 1	68 ± 3
Villalonga	2 (ES)	21 ± 4	81 ± 18	103 ± 14
other cultivars	14[b]	23 ± 7	49 ± 19	71 ± 23

[a]Country of origin: ES = Spain; CL = Chile; SI = Slovenia; IT = Italy; US = United States/California; SA = South Africa; GR = Greece; FR = France. [b]Other cultivars: Arbusana (CL), Ascolano (US), Athinolia (GR), Barnea (CL), Barouni (US), Cacereña (ES), Carolea (IL), Itrana (SI), Kalamata (SA), Kolovi (GR), Ladolia (GR), Manaki (GR), Mission (US), Nocellara (CL).

The monocultivar fresh samples of extra virgin olive oils for studying the CoQ10 and CoQ9 content as a function of the harvest time within a season were provided by the Experimental Centre for Olive Growing (COG) at Agricultural and Forestry Institute in Nova Gorica, Slovenia. Seventeen samples of the cultivars Istrska Belica and Leccino (9 and 8 samples, respectively) were included for the analyses. Samples were collected from an experimental groove at Beneša (Slovenia) as part of a national program to monitor the maturity of olives. Trees with a similar fruit load were selected for the monitoring program. The earliest harvest date was set for mid-October 2010, and subsequent harvest dates were approximately one week apart. COG also provided an olive maturity index (MI) for these samples that was determined[28] on a sample of 100 randomly sampled fruits.

Quantification of CoQ10 and CoQ9 Levels in the Olive Oil Samples. CoQ10 and CoQ9 levels were determined based on ESA App Note[29] (ESA, Dionex Corp.) modified as follows: Olive oil samples were diluted 1:100 shortly before the analyses

Table 3. Coenzyme Q9 and Q10 Content in Fresh Extra Virgin Olive Oils of the Cultivars Picual, Istrska Belica, Leccino, Arbequina, Hojiblanca, Coratina, Frantoio, and Maurino[a]

cultivar	no. of samples (country origin)	content (mg/L) CoQ9	CoQ10	CoQ
Arbequina	4 (2 ES, CL, US)	21 ± 10	58 ± 22	79 ± 28
Coratina	4 (ES, IT, CL, US)	30 ± 5 d,e	48 ± 5 b,c,d,g	79 ± 9 b,d
Frantoio	4 (2 CL, SA, IT)	25 ± 6	36 ± 7 a,c,f,g	61 ± 6 a,c,d,f,g
Hojiblanca	4 (ES)	24 ± 16	98 ± 22 a,b,d,e	122 ± 38 b,d,e
Istrska belica	7 (SI)	19 ± 3 a,f	30 ± 4 a,c,e,f,g	48 ± 7 a,b,c,e,f,g
Leccino	7 (4 SI, IT, ES, SA)	22 ± 7 a	41 ± 11 c,d,f,g	63 ± 18 c,d,f,g
Maurino	4 (SI)	26 ± 4 d	63 ± 11 b,d,e	89 ± 14 b,d,e
Picual	7 (6 ES, CL)	22 ± 7	63 ± 6 a,b,d,e	85 ± 13 b,d,e

[a]Country of origin: ES = Spain; CL = Chile; SI = Slovenia; IT = Italy; US = United States/California; SA = South Africa. Statistical difference (P < 0.05) in comparison with other cultivars: a, Coratina; b, Frantoio; c, Hojiblanca; d, Istrska belica; e, Leccino; f, Maurino; g, Picual.

using 2-propanol. After 30 s of vortexing at 1500 rpm at room temperature in polypropylene tubes, the solution was centrifuged for 5 min at room temperature prior to HPLC injection. Determinations of CoQ9 and CoQ10 were performed using HPLC equipment with a diode array UV−vis detector (HPLC System Gold, Beckman Coulter Ltd.) and electrochemical coulometric detector (ESA Coulochem III, Dionex Corporation). Separation was carried out at a 40 °C flow rate of 0.8 mL/min using an Ultrabase C18 column (5 μm, 4.6 × 150 mm) (Análisis Vínicos, Spain). The mobile phase was composed of solvent A (methanol/propanol/0.33 M ammonium acetate pH 4.4, 84:10:6) and solvent B (propanol/0.33 M ammonium acetate pH 4.4, 98:2). Initial conditions were 95% solvent A 5% solvent B, at min 12 the mobile phase turned to 65% solvent A 45% solvent B in 4 min. At min 33 the mobile phase composition returned to the initial conditions in 3 min. The typical sample injection volume was 50 μL. Electrochemical detection was used for the CoQ determination. The ESA Coulochem III electrochemical detector was programmed with the following settings: conditioning guard cell +400 mV, reducing cell at −500 mV followed by the analytical cell at +500 mV, full scale was 100 nA. HPLC-grade solvents were purchased from Scharlab (Spain). The CoQ9 and CoQ10 standards were purchased from Sigma-Aldrich. All other chemicals were of analytical grade and available from commercial suppliers. CoQ9 and CoQ10 concentrations were calculated using calibration curves. Stock solutions of CoQ10 and CoQ9 standards were prepared by reading their absorbance at 275 nm in ethanol. They were then used to prepare five calibration standards for each compound studied by dilution with an extraction solvent (25 pmol, 50 pmol, 75 pmol, 100 pmol, 125 pmol). Values of the slope (b), intercept (a), correlation coefficient (R), and standard deviation of the slope $V(b)$ were calculated using the 32Karat software (Beckman Coulter Ltd.).

Statistics. The results are the average of at least two replicates analyses; the standard deviation of the de novo analyses was determined to be below 10%. Average ± SD was calculated for various groups of samples (commercial samples: extra virgin olive oils, refined olive oils, and olive-pomace oils; monocultivar oil samples: a group of all monocultivar samples, a group of samples of the same cultivar). Group comparisons were performed using an unpaired t test and differences of $P < 0.05$ were considered significant. Between group comparisons for olive oils from various cultivars are presented in Table 3.

RESULTS AND DISCUSSION

CoQ10 and CoQ9 Levels in the Commercial Olive Oil Blends. We analyzed extra virgin olive oils, refined olive oils, and olive-pomace oils purchased in different markets (Table 2). Although the average levels of CoQ10 and CoQ9 in the extra virgin olive oils (56 ± 4 and 23 ± 12 mg/L, respectively) were a little higher than those in the refined olive oils (54 ± 10 and 14 ± 9 mg/L, respectively), the differences were not significant. However, higher levels of both CoQ10 and CoQ9 were observed in the olive-pomace oil (83 ± 12 and 61 ± 19 mg/L, respectively) although we note that only two samples of olive-pomace oils were investigated. Olive-pomace oil is obtained by treating olive pomace with solvents or other physical treatments[30] and this might explain the better extraction of CoQ from the fruit. Due to its undesirable organoleptic properties olive-pomace oil is considered a low-quality oil and is very rarely found in markets; it was therefore not studied further. Nevertheless, if an opportunity were to emerge for the sustainable extraction of valuable biological compounds from vegetable oils, olive pomace oil might be a valuable raw material in such processes. Such an extraction procedure was studied by Laplante et al. using mackerel and herring oils as starting material.[31]

CoQ10 and CoQ9 Levels in the Fresh Monocultivar Extra Virgin Olive Oil Samples. Commercial olive oil samples are commonly blends produced from the fruits of various cultivars. To gain an insight into preharvest factors that could affect the composition of olive oils, monocultivar samples are more appropriate. A series of 79 monocultivar olive oil samples was therefore selected; samples were provided by local producers or local laboratories from different geographical regions (Chile, Spain, Italy, Slovenia, South Africa, the United States, Greece, and France). To limit the influence of postharvest processing, only extra virgin olive oil samples were included. Although CoQ10 is relatively stable in food matrixes,[32] the included samples were either fresh or fresh-frozen.

In case of the cultivars Arbequina, Coratina, Frantoio, Hojiblanca, Istrska belica, Leccino, Maurino, and Picual, four to seven samples of olive oil per cultivar were available. Results of the determination of CoQ in those samples are presented in Table 3 together with between group statistical comparisons. For the cultivars Aglandau, Alfafara, Buga, Farga, Koroneiki, Manzanilla, Olivière, Picholine, Blanqueta, Tanche, and Villalonga, where less than four samples were available, we did not perform between group statistical comparisons (Table 4). Results for cultivars where only one sample per cultivar was available (Arbusana, Ascolano, Athinolia, Barnea, Barouni, Cacereña, Carolea, Itrana, Kalamata, Kolovi, Ladolia, Manaki, Mission, and Nocellara) are presented in aggregate form in Table 4 (other cultivars).

The average content of CoQ10 of all the monocultivar olive oil samples was 52 ± 17 mg/L and is comparable with results for the commercial extra virgin olive oil samples. However, the averages for different cultivars of which at least four samples of olive oil were available (Arbequina, Coratina, Frantoio, Hojiblanca, Istrska belica, Leccino, Maurino, and Picual) ranged from 24 ± 4 to 98 ± 20 mg/L and several statistically important differences in CoQ10 levels (Table 3) among them were observed. The highest content of CoQ10 was observed in the cultivar Hojiblanca (98 ± 22 mg/L; a statistically significant difference when compared to the Istrska belica (30 ± 4 mg/L; $P = 0.01$), Leccino (41 ± 11 mg/L; $P = 0.02$), Frantoio (36 ± 7 mg/L; $P = 0.02$), Coratina (48 ± 5 mg/L; $P = 0.03$) sets), followed by Picual (63 ± 6 mg/L; a statistically significant difference when compared to Istrska belica ($P < 0.01$), Leccino ($P < 0.01$), Frantoio ($P < 0.01$), Coratina ($P = 0.01$)), and Maurino (63 ± 11 mg/L; a statistically significant difference when compared to Istrska belica ($P = 0.01$), Leccino ($P = 0.02$), and Frantoio ($P = 0.01$)). This confirms our hypothesis that the expression of CoQ10 is also driven by genetic factors. For the Picual cultivar, our data on CoQ10 levels (63 ± 6 mg/L) are comparable with the report by Venegas et al. (77 ± 12 mg/L),[21] whereas the other cultivars were not investigated in previous studies.

The average content of CoQ9 of all the monocultivar olive oil samples was 21 ± 8 mg/L (23 ± 12 mg/L in the commercial extra virgin olive oil samples). A comparison of the CoQ9 contents between the cultivars shows less significant differences than with CoQ10. The CoQ9 levels in the studied

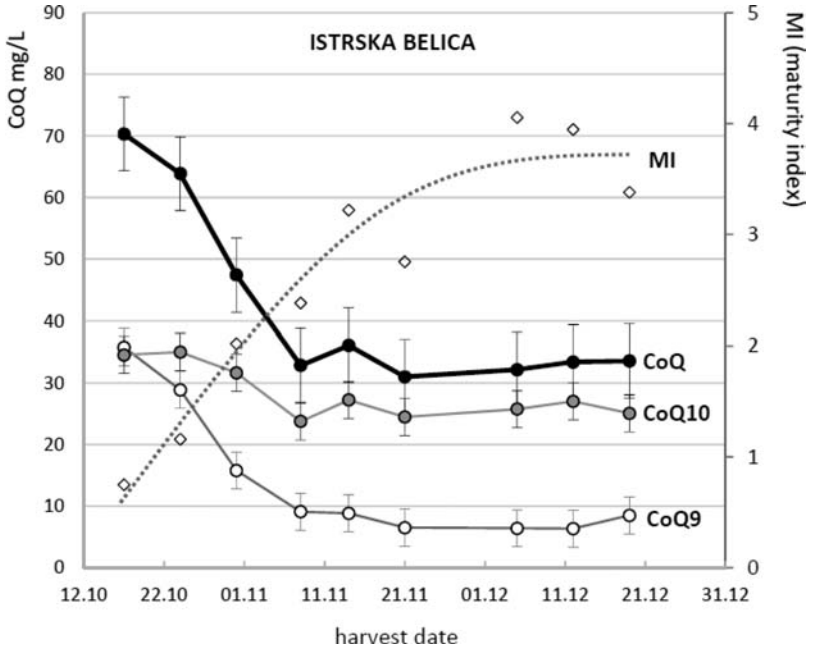

Figure 1. Coenzyme Q9 and Q10 content in olive oil as a function of harvest time for the cultivar Istrska belica (Experimental Grove, Beneša, Slovenia).

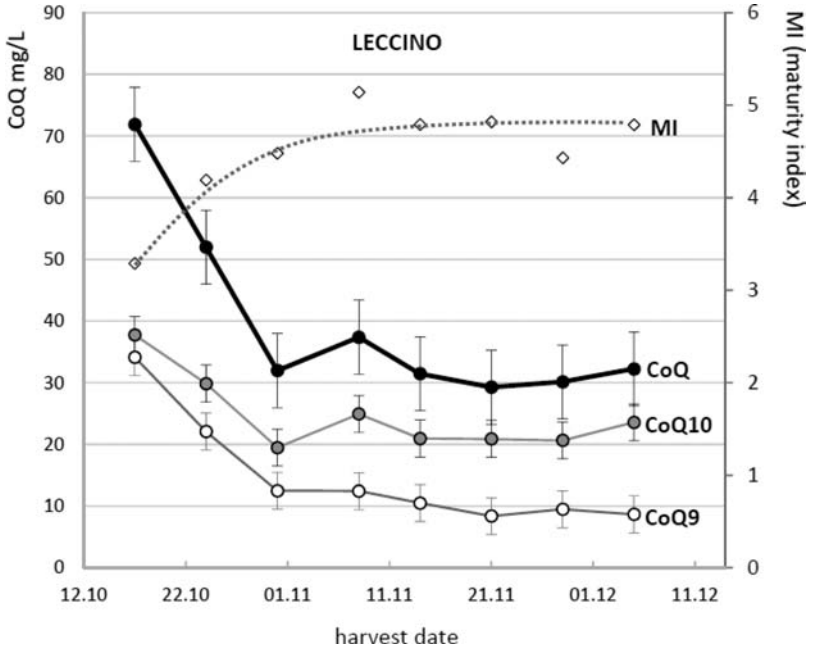

Figure 2. Coenzyme Q9 and Q10 content in olive oil as a function of harvest time for the cultivar Leccino (Experimental Grove, Beneša, Slovenia).

cultivars ranged from 10 ± 1 to 30 ± 5 mg/L. A statistical comparison of the CoQ9 content between sets of olive oils of different cultivars for which at least four samples were available showed the highest CoQ9 content in the Coratina series (30 ± 5 mg/L) with statistically significantly lower levels in Leccino (22 ± 7 mg/L; $P = 0.05$) and Istrska belica (19 ± 3 mg/L; $P = 0.01$). The observed CoQ9 levels are a little higher than reports in the literature where levels of up to 18 ± 2 mg/L were observed.[20] However, we also observed lower CoQ9 levels in some cultivars (i.e., 10 ± 1 mg/L in Koroneiki).

Foods containing over 50 mg CoQ10/kg are considered to be *very rich sources* of CoQ10.[10] We established that extra virgin olive oils generally meet this criterion and can be considered among the best natural sources of dietary CoQ10. In contrast, our results confirm that olive oils are not a very important source of CoQ9, especially when compared to other vegetable oils (i.e., corn oil with 93−373 mg CoQ9/L).[17,20]

Levels of CoQ10 and CoQ9 Content in Fresh Olive Oil with Different Harvest Times. During the maturation process, the color, oil content, and composition change dramatically in olive fruit. The magnitude of these changes depends on the cultivar and parameters such as geoclimatic and growing conditions, with processing also having an important effect.[27,33] Due to variability in cultivar response between growing seasons and the influence of varying crop loads on

dx.doi.org/10.1021/jf5002167 | J. Agric. Food Chem. 2014, 62, 3211−3216

maturation rates, the determination of the optimal harvest time of olives is difficult.

In our study we also observed relatively high average standard deviations in CoQ10 and CoQ9 contents within oil samples of the same cultivar (on average 20% and 28%, respectively). To gain further insights into the impact of preharvest conditions on the composition of olive oil, we investigated whether CoQ levels in olive oil are also affected by the degree of ripeness of olive fruit at the time of pressing.

To evaluate the possible influence of harvesting time on CoQ content in olive oil, two cultivars prevalent in Slovenia were selected. The cultivar Istrska belica (Istrian white olive) is a domestic variety grown in Slovenian Istra and the neighboring countries, while the cultivar Leccino originates in Tuscany (Italy).[34] CoQ levels were monitored in oil samples taken from an experimental groove at Beneša (Slovenia) during the approximately three-month harvesting season. We determined that the CoQ10 and CoQ9 levels in both cultivars were strongly influenced by the harvest time (Figures 1 and 2). We observed a lowering of total CoQ levels with maturation; an almost linear lowering was observed for the first 2−3 weeks of the investigation (R^2 0.98 and 0.99 for Istrska belica and Leccino, respectively) and after that the CoQ levels continued to be stable. In the case of Istrska belica, the total CoQ dropped by 53% in the first three weeks of the investigation, while in Leccino a 56% reduction was observed. The changes in the CoQ9 levels (75% and 65% for Istrska belica and Leccino, respectively) were higher than in the CoQ10 levels (29% and 47%). Although these measurements were performed on samples collected within a single season and focused only on investigation of the maturation phase, the results reveal that olive oils that are harvested early might be richer in CoQ. Further studies are needed to examine this phenomenon in greater detail and should include sampling of the same cultivars in different locations and in different growing seasons. We should note that these results cannot be simply generalized to other cultivars as it has already been established that the influence of harvest and maturity index on olive oil yield and quality can fundamentally differ between various cultivars.[33]

In conclusion, this study shows for the first time the important influence of some pre- and postharvest factors on the content of CoQ10 and CoQ9 in olive oil. By investigating the effects of the degree of ripeness on the Istrska belica and Leccino cultivars we established that the maturity of fruits significantly affects the content of CoQ in olive oil; the highest levels of both CoQ10 and CoQ9 can be found in the early maturation stages. Our investigation of CoQ10 and CoQ9 levels in numerous monocultivar samples allowed us to determine that genetic parameters (cultivars) also have an important influence on the composition of olive oils, particularly the content of CoQ10. However, we observed relatively high variations in CoQ levels also within cultivars. In addition to the maturity effects, there could be several other reasons for this, including agricultural and geo-climatic effects. Therefore, in further studies, comparisons within cultivars should be made also using samples with comparable maturity and growing conditions. While such studies would enable a comparison between only a small number of cultivars, they would provide an insight into several other possible factors influencing the composition of olive oils. Interestingly, the results of our study indicate the limited influence of postharvest processing, except when the processing technique is changed drastically, i.e. by introducing organic solvents which not only improve the extraction of oil from olive fruits but also the extraction of CoQ. However, to explore this in detail more studies are needed, covering a higher number of processed oils, preferably involving the use of the same sample of olive fruit as the starting material. These results are an important contribution to knowledge on the composition and quality of olive oils and will provide a basis for additional studies to further explore the factors influencing the contents of Coenzyme Q in olive oils.

AUTHOR INFORMATION

Corresponding Author

*Tel: +386 590 68871. Fax: + 386 1 3007981. E-mail: igor.pravst@nutris.org.

Funding

The present study was financially supported by the Nutrition Institute Research Fund (ID-M10) and by Pablo de Olavide University, Seville, Spain.

Notes

The authors declare no competing financial interest.

ACKNOWLEDGMENTS

We acknowledge the help of Viljanka Vesel (Experimental Centre for Olive Growing, Agricultural and Forestry Institute Nova Gorica, Slovenia) for providing olive oil samples from the national program monitoring olive growing. We further acknowledge the assistance of Milena Miklavčič (LABS LLC, Institute for Ecology, Olive Oil and Control, Izola, Slovenia), Vanja Dujc (Slovenia), Boris Jenko (Slovenia), Luisa Ruiz (Jefe Sección, Jefe Pnal de cata de la Comunidad Valenciana, Spain), Juan Ramón Izquierdo (Laboratorio Arbitral Agroalimentario, Madrid, Spain), Luciana Di Giacinto (C.R.A. − Centro di Ricerca per l'Olivicoltura e l'Industria Olearia, Italy), Maria Lazaraki (Chemical Laboratories of the Ministry of Economy, Competitiveness & Shipping, Greece), Christian Pinatel (Centre Technique de l'Olivier, Maison des Agriculteurs, France), Sandy Jeffery (Helluva, South Africa), Albert Viljoen (Waverley Hills Organic Farm, South Africa), Pablo Cáceres F. (Olivares de Quepu, Chile), María Luz Hurtado P. (Olave, Chile), and Steve McCulley (Appollo Olive Oil, Oregon House, CA) for support in providing the monocultivar oil samples. We also acknowledge Murray Bales for providing help with the language of this text.

REFERENCES

(1) Keys, A. B. *Seven Countries: A Multivariate Analysis of Death and Coronary Heart Disease*; Harvard University Press: Cambridge, MA, 1980.

(2) De Lorgeril, M.; Salen, P.; Martin, J. L.; Monjaud, I.; Delaye, J.; Mamelle, N. Mediterranean diet, traditional risk factors, and the rate of cardiovascular complications after myocardial infarction: Final report of the Lyon Diet Heart Study. *Circulation* **1999**, *99*, 779−785.

(3) Trichopoulou, A.; Costacou, T.; Bamia, C.; Trichopoulos, D. Adherence to a Mediterranean diet and survival in a Greek population. *New Engl. J. Med.* **2003**, *348*, 2599−2608.

(4) Scarmeas, N.; Stern, Y.; Tang, M. X.; Mayeux, R.; Luchsinger, J. A. Mediterranean diet and risk for Alzheimer's disease. *Ann. Neurol.* **2006**, *59*, 912−921.

(5) Benetou, V.; Trichopoulou, A.; Orfanos, P.; Naska, A.; Lagiou, P.; Boffetta, P.; Trichopoulos, D. Greek EPIC cohort. Conformity to traditional Mediterranean diet and cancer incidence: The Greek EPIC cohort. *Br. J. Cancer* **2008**, *99*, 191−195.

(6) Sofi, F.; Cesari, F.; Abbate, R.; Gensini, G. F.; Casini, A. Adherence to Mediterranean diet and health status: Meta-analysis. *Br. Med. J.* **2008**, 337.
(7) Granados-Principal, S.; Quiles, J. L.; Ramirez-Tortosa, C. L.; Sanchez-Rovira, P.; Ramirez-Tortosa, M. C. Hydroxytyrosol: From laboratory investigations to future clinical trials. *Nutr. Rev.* **2010**, *68*, 191−206.
(8) Omar, S. H. Oleuropein in olive and its pharmacological effects. *Sci. Pharm.* **2010**, *78*, 133−154.
(9) Martin-Pelaez, S.; Isabel Covas, M.; Fito, M.; Kusar, A.; Pravst, I. Health effects of olive oil polyphenols: Recent advances and possibilities for the use of health claims. *Mol. Nutr. Food Res.* **2013**, *57*, 760−771.
(10) Pravst, I.; Zmitek, K.; Zmitek, J. Coenzyme Q10 contents in foods and fortification strategies. *Crit. Rev. Food Sci. Nutr.* **2010**, *50*, 269−280.
(11) Crane, F. L. Biochemical functions of coenzyme Q(10). *J. Am. Coll. Nutr.* **2001**, *20*, 591−598.
(12) Littarru, G. P.; Tiano, L. Clinical aspects of coenzyme Q10: An update. *Nutrition* **2010**, *26*, 250−254.
(13) Gao, L.; Mao, Q.; Cao, J.; Wang, Y.; Zhou, X.; Fan, L. Effects of coenzyme Q10 on vascular endothelial function in humans: A meta-analysis of randomized controlled trials. *Atherosclerosis* **2012**, *221*, 311−316.
(14) Mancuso, M.; Orsucci, D.; Volpi, L.; Calsolaro, V.; Siciliano, G. Coenzyme Q10 in neuromuscular and neurodegenerative disorders. *Curr. Drug Targets* **2010**, *11*, 111−121.
(15) Kalen, A.; Appelkvist, E. L.; Dallner, G. Age-related chenges in the lipid compositions of rat and human tissues. *Lipids* **1989**, *24*, 579−584.
(16) Ely, J. T. A.; Krone, C. A.; Brief, A. Update on ubiquinone (Coenzyme Q10). *J. Orthomol. Med.* **2000**, *15*, 63−68.
(17) Rodriguez-Acuna, R.; Brenne, E.; Lacoste, F. Determination of coenzyme Q10 and Q9 in vegetable oils. *J. Agric. Food Chem.* **2008**, *56*, 6241−6245.
(18) Kamei, M.; Fujita, T.; Kanbe, T.; Sasaki, K.; Oshiba, K.; Otani, S.; Matsuiyuasa, I.; Morisawa, S. The distribution and content of ubiquinone in foods. *Int. J. Vitam. Nutr. Res.* **1986**, *56*, 57−63.
(19) Pregnolato, P.; Maranesi, M.; Mordenti, T.; Turchetto, E.; Barzanti, V.; Grossi, G. Coenzyme Q10 and Q9 content in some edible oils. *Riv. Ital. Sostanze Grasse* **1994**, *71*, 503−505.
(20) Cabrini, L.; Barzanti, V.; Cipollone, M.; Fiorentini, D.; Grossi, G.; Tolomelli, B.; Zambonin, L.; Landi, L. Antioxidants and total peroxyl radical-trapping ability of olive and seed oils. *J. Agric. Food Chem.* **2001**, *49*, 6026−6032.
(21) Venegas, C.; Cabrera-Vique, C.; Garcia-Corzo, L.; Escames, G.; Acuna-Castroviejo, D.; Carlos Lopez, L. Determination of Coenzyme Q(10), Coenzyme Q(9), and melatonin contents in virgin argan oils: Comparison with other edible vegetable oils. *J. Agric. Food Chem.* **2011**, *59*, 12102−12108.
(22) Buckland, G.; Mayén, A. L.; Agudo, A.; Travier, N.; Navarro, C.; Huerta, J. M.; Chirlaque, M. D.; Barricarte, A.; Ardanaz, E.; Moreno-Iribas, C.; Marin, P.; Quirós, J. R.; Redondo, M.-L.; Amiano, P.; Dorronsoro, M.; Arriola, L.; Molina, E.; Sanchez, M.-J.; Gonzalez, C. A. Olive oil intake and mortality within the Spanish population (EPIC-Spain). *Am. J. Clin. Nutr.* **2012**, *96*, 142−149.
(23) Gladine, C.; Meunier, N.; Blot, A.; Bruchet, L.; Pages, X.; Gaud, M.; Floter, E.; Metin, Z.; Rossignol, A.; Cano, N.; Chardigny, J. M. Preservation of micronutrients during rapeseed oil refining: A tool to optimize the health value of edible vegetable oils? Rationale and design of the Optim'Oils randomized clinical trial. *Contemp. Clin. Trials* **2011**, *32*, 233−239.
(24) Bruge, F.; Bacchetti, T.; Principi, F.; Scarpa, E.-S.; Littarru, G. P.; Tiano, L. Olive oil supplemented with Coenzyme Q10: Effect on plasma and lipoprotein oxidative status. *Biofactors* **2012**, *38*, 249−256.
(25) Zmitek, J.; Zmitek, K.; Pravst, I. Improving the bioavailability of coenzyme Q10: From theory to practice. *Agro Food Ind. Hi-Tech* **2008**, *19*, 8−10.
(26) Zmitek, J.; Smidovnik, A.; Fir, M.; Prosek, M.; Zmitek, K.; Walczak, J.; Pravst, I. Relative bioavailability of two forms of a novel water soluble Coenzyme Q10. *Ann. Nutr. Metab.* **2008**, *52*, 281−287.
(27) Charoenprasert, S.; Mitchell, A. Factors influencing phenolic compounds in table olives (*Olea europaea*). *J. Agric. Food Chem.* **2012**, *60*, 7081−7095.
(28) Matos, L. C.; Pereira, J. A.; Andrade, P. B.; Seabra, R. M.; Oliveira, M. Evaluation of a numerical method to predict the polyphenols content in monovarietal olive oils. *Food Chem.* **2007**, *102*, 976−983.
(29) ESA Analytical, Ltd. *ESA Application Note: Determination of Tocotrienols and Tocopherols*; 70-6004P IA-1; ESA Analytical, Ltd.: Aylesbury, UK, 2013; http://www.esainc.com/docs/spool/70-6004P_tocotrienols.pdf (12.12.2013).
(30) *United Nations Conference on Trade and Development: International Agreement on Olive Oil and Table Olives*; United Nations: Geneva, 2005; http://www.internationaloliveoil.org/documents/viewfile/3467-convenio03eng (12.12.2013).
(31) Laplante, S.; Souchet, N.; Bryl, P. Comparison of low-temperature processes for oil and coenzyme Q10 extraction from mackerel and herring. *Eur. J. Lipid Sci. Technol.* **2009**, 111.
(32) Pravst, I.; Prosek, M.; Wondra, A. G.; Zmitek, K.; Zmitek, J. The stability of Coenzyme Q10 in fortified foods. *Acta Chim. Slov.* **2009**, *56*, 953−958.
(33) Dag, A.; Kerem, Z.; Yogev, N.; Zipori, I.; Lavee, S.; Ben-David, E. Influence of time of harvest and maturity index on olive oil yield and quality. *Sci. Horticult.* **2011**, *127*, 358−366.
(34) Bester, E.; Butinar, B.; Bucar-Miklavcic, M.; Golob, T. Chemical changes in extra virgin olive oils from Slovenian Istra after thermal treatment. *Food Chem.* **2008**, *108*, 446−454.

MATERIALS AND METHODS

Chemicals. Benzyl-DL-arginine-*p*-nitroanilide hydrochloride (BAPNA), trypsin from porcine pancreas (1000−2000 benzyl arginine ethyl ester (BAEE) units/mg solid), and PHA-P (8754) were purchased from Sigma (St. Louis, MO, USA). All other reagents were purchased from Shanghai BOAO Biochemical Co. (China).

Sample Preparation. *C. Kkorshinskii* Kom. was collected from Liang Cheng County of Inner Mongolia (China). Leaves and tissues were air-dried, milled, and passed through a 60 mesh screen. The milled *C. korshinskii* Kom. was stored at −20 °C until further use.

Preparation of *C. korshinskii* Kom. Protein Isolates (CPI). Alkali extraction and acetone precipitation methods were used to prepare CPIs from the milled powder of *C. korshinskii* Kom.[1]

For an alkaline extraction method, the milled *C. korshinskii* Kom. was dispersed in 0.12 M NaOH with the solid to liquid ratio of 1:20 (w/v) and then incubated at 37 °C for 1 h. The slurry was centrifuged at 4000*g* for 20 min to obtain a supernatant. The pH of the supernatant was adjusted to 4.5 with 0.1 N HCl, and then the supernatant was heated in a water bath at 75 °C for 10 min. After centrifugation at 4000*g* for 20 min, the protein precipitate was freeze-dried to obtain Al-CPI.

For an acetone precipitation method, the milled *C. korshinskii* Kom. was dispersed in an extraction buffer in the ratio of 1:20 (w/v). The slurry was incubated at 4 °C for 7 h and centrifuged at 4000*g* for 20 min to obtain a supernatant. Precooled acetone was added to the supernatant, which was then incubated at −20 °C overnight. The mixture was centrifuged at 4000*g* for 20 min, and the resulting precipitate was then rinsed with precooled acetone three times. The A-CPI was obtained when the precipitate was dried under nitrogen gas.

Analysis of Nutritional Ingredients. *Approximate Composition Analysis.* The contents of moisture, crude protein, crude lipid, and ash were determined according to the standard methods described by the Association of Official Analytical Chemists (AOAC).[5] Crude fiber was determined by GB/T 5009.10-2003 (Recommended National Standard of China).[6] Samples were successively dispersed in boiling solutions of 1.25% H_2SO_4 and 1.25% NaOH. The oven-dried residual was then weighed to calculate the content of crude fiber. The carbohydrate content was determined according to the data of moisture, crude protein, crude lipid, crude fiber, and ash contents. The gross energy was calculated according to the following formula:

$$\begin{aligned}&\text{gross energy (kJ 100/g dry substance)}\\&\quad=(\text{protein}\times 16.7)+(\text{lipid}\times 37.7)\\&\qquad+(\text{carbohydrates}\times 16.7)\end{aligned}\tag{1}$$

Total Starch Analysis. Total starch was measured as described by Goni[7] with some modifications. Samples (100 mg) were dispersed in 12 mL of 2 M KOH and vigorously shaken at room temperature for 30 min. The mixture was adjusted to pH 7.0 with 0.4 M sodium acetate buffer, followed by an addition of 0.5 mL of amyloglucosidase (Aladdin, 100000 U/mL), and then incubated at 60 °C for 45 min in a shaking water bath. Glucose oxidase/peroxidase reagent (Shang Hai Rong Sheng Biotech Co., Ltd.) was utilized to measure glucose content. The conversion factor from glucose to starch was 0.9.

Soluble Sugar Analysis. Soluble sugar was extracted with 70% (v/v) ethanol, and sugar content was determined by using a phenol−sulfuric acid method.[8]

Mineral Composition. *C. korshinskii* Kom. powder was digested with the mixed acids (concentrated nitric acid, sulfuric acid, and perchloric acid in the ratio 10:0.5:2, v/v). The contents of minerals (sodium, potassium, calcium, magnesium, iron, copper, zinc, and manganese) were determined by atomic absorption spectrophotometer (Shimadzu, AA-6800) accoring to the AOAC procedure.[5] Total phosphorus was determined according to GB/T 5009.87-2003.[9] Samples (0.5 g) were digested with mixed acids to obtain a digestive solution, and then digestive solution (1 mL), $(NH_4)_6Mo_7O_{24}{\cdot}4H_2O$ reagent (2 mL), 0.5% hydroquinone solution (1 mL), 20% sodium sulfite reagent (1 mL), and water (15 mL) were added. After 0.5 h, the absorbance of the solution was observed at 660 nm with KH_2PO_4 as standard.

Amino Acid Analysis. The derivatization method described by Hainida[10] was followed by assay amino acids. The hydrolysate (1 mL) of amino acids was evaporated to dryness under vacuum and then redissolved with 1 mL of deionized water. Hydrolysate (50 uL), acetonitrile/triethylamine solution (25 μL, 43:7, v/v), and phenyl isothiocyanate (PITC)/triethylamine solution (25 μL, 1:80, v/v) were mixed and incubated for1 h at room temperature. The mixed mobile phase of acetonitrile, sodium acetate solution, and water was used. The essential amino acid (EAA) score was calculated as

$$\text{EAA score}=\frac{\text{g of EAA in 100 g crude proteins}}{\text{g of EAA in 100 g FAO/WHO (2007) reference pattern}}\tag{2}$$

Analysis of Various Antinutritional Factors (ANFs). *Trypsin Inhibitor.* Trypsin inhibitor activity (TIA) was measured according to the method of Siddhuraju.[11] Defatted ground samples (0.5 g) were incubated in 25 mL of 0.01 M NaOH at pH 9.4−9.5 for 3 h. The mixture was centrifuged at 4000*g* for 15 min, and the supernatant was collected to estimate the TIA content of material.

Lectin. The lectin content was analyzed by using the hemagglutination assay.[12] Samples (0.5 g) were incubated at room temperature in 10 mL of the phosphate buffer for 10 h with agitation using a magnetic bar. The slurry was centrifuged at 4000*g* for 20 min. The collected supernatant was then added in microtiter plates with 2% (v/v) rabbit blood erythrocyte suspension in phosphate buffer (pH 7.0). When >50% of the erythrocytes was aggregated, it was considered as agglutination. PHA-P was used as a positive control. The hemagglutination activity was defined as

$$C=(S_0\times H\times V)/(H_0\times M)\tag{3}$$

where C is the content of lectin that produced agglutination (mg/g), S_0 is the concentration of PHA-P solution (mg/mL), H is agglutinin titers (the minimum amount of samples producing hemeagglutination, 2^n), V is the volume (mL), H_0 is agglutinin titers (the minimum amount of standard producing hemeagglutination, 2^n), and M is sample quantity (g).

Phenolic Substances. The Folin−Ciocalteu method[13] was adopted to determine the total phenol and tannin levels with some slight modifications. Samples (0.2 g) were incubated with 10 mL of 70% acetone in an ultrasonic bath (frequency, 35 kHz; acoustic power, 85 W) for 20 min at room temperature. The mixture was centrifuged at 4000 rpm for 10 min. Extraction processes were performed once again. The obtained supernatants were mixed together. A certain amount of the supernatant was used to determine the content of total phenols. The tannin content was reflected by the decrease of total phenol content in the supernatant after polyvinylpyrrolidone treatment. Gallic acid was used as equivalents for total phenols and tannins.

Phytic Acid. The $FeCl_3{\cdot}6H_2O$−sulfosalicylic acid colorimetric procedure[11] was utilized to determine the content of phytic acid. Samples (0.5 g) were stirred with 10 mL of 3.5% HCl for 1 h at room temperature. The mixture was centrifuged at 4000 rpm for 10 min to obtain the supernatant. Phytic acid (98%, Guizhou Di-Da Biotech Co. Ltd.) was used as standard in the assay.

Saponins. The extraction method of total saponins was reported by Chen[14] with some slight modifications. Defatted samples (0.5 g) were incubated with 10 mL of 80% aqueous methanol in an ultrasonic bath (frequency, 35 kHz; acoustic power, 85 W) for 30 min at room temperature. The mixture was centrifuged at 3000 rpm for 10 min. Extraction processes were conducted once again. The obtained supernatants were mixed together. A certain amount of the supernatant was used to determine the content of total saponins.

Statistical Analysis. All experiments are conducted in three replicates. One-way analysis of variance (ANOVA) was carried out to compare the mean values, followed by Duncan's multiple-range tests. Significant differences in the mean values were determined at $p < 0.05$ (SPSS 19).

Table 1. Proximate Analysis of *C. korshinskii* Kom., Al-CPI, and A-CPI[a]

	C. korshinskii Kom.	Al-CPI	A-CPI
moisture (%)	6.25 ± 0.25c	8.6 ± 0.37b	10.02 ± 0.49a
ash (%)	3.63 ± 0.10c	8.95 ± 0.42a	7.28 ± 0.27b
crude protein (%)	9.09 ± 0.31c	50.06 ± 1.40a	42.59 ± 1.17b
crude fiber (%)	56.86 ± 0.97a	0.79 ± 0.03b	0.81 ± 0.02b
crude lipid (%)	1.77 ± 0.04a	0.91 ± 0.04b	ND[b]
total available carbohydrate (%)	22.40 ± 1.40c	30.70 ± 1.72b	39.30 ± 1.59a
gross energy (kJ/100 dry substance)	592.65 ± 17.70b	1382.79 ± 12.65a	1367.57 ± 8.75a

[a]Values are expressed as mean ± SD of three measurements. Values with different letters are significantly different at $p < 0.05$ within the same row. [b]ND, not detected.

RESULTS AND DISCUSSION

Analysis of Nutritional Ingredients. The proximate chemical compositions of *C. korshinskii* Kom., Al-CPI, and A-CPI are summarized in Table 1. For *C. korshinskii* Kom., crude fiber constituted about 56.9%, followed by total carbohydrate (22.4%) and crude protein (9.1%). Protein content in the plants may be varied using different growth environments and harvest times. A recent study[15] has shown that the protein level of phloem from *C. korshinskii* Kom. was about 11%. In our study, the feedstock of *C. korshinskii* Kom. was a mixture of leaves and tissues. The contents of crude protein in Al-CPI and A-CPI were 50.1 and 42.6%, respectively, which was lower than that of most protein isolate from beans, such as fava bean (81.9%), pea (88.8%), and soy (87.6%),[16] but higher than that of barley flour (35.5%).[17]

As shown in Table 2, the contents of starch in *C. korshinskii* Kom., Al-CPI, and A-CPI were not significantly different (24.1−25.4 g/100 g dry substance). In addition, the soluble sugar in A-CPI (6.5%) was about 2.5-fold that in Al-CPI (2.6%).

Table 2. Total Starch and Soluble Sugar in *C. korshinskii* Kom., Al-CPI, and A-CPI (Grams per 100 g Dry Substance)[a]

	C. korshinskii Kom. powder	Al-CPI	A-CPI
total starch	24.12 ± 0.98a	24.8 ± 0.40a	25.44 ± 0.29a
soluble sugar	5.50 ± 0.11b	2.60 ± 0.01c	6.47 ± 0.19a

[a]Values are expressed as mean ± SD of three measurements. Values with different letters are significantly different at $p < 0.05$ within the same row.

Table 3 shows that phosphorus and calcium existed in *C. korshinskii* Kom., which exceeds the demand for adults.[18] Phosphorus and calcium are the essential ingredients in human and animal skeleton series and teeth. In addition, phosphorus is a necessary component for nucleic acid, protein, and lecithin. It also participates in the metabolism process of saccharides and lipids and forms high-energy phosphate bonds to store energy. Compared with *C. korshinskii* Kom., the content of sodium in Al-CPI shows a dramatic increase, which may have resulted from the extraction solution (NaOH). However, the contents of calcium and iron in Al-CPI decreased sharply. This result may be attributed to the possibility that calcium and iron were more likely to chelate with phytic acid when Al-CPI was precipitated at pH 4.5.[19] Moreover, the contents of trace elements, such as Fe, Mn, Zn, and Cu, were higher in A-CPI than in *C. korshinskii* Kom. and Al-CPI.

Table 3. Mineral Composition of *C. korshinskii* Kom., Al-CPI, and A-CPI (Milligrams per 100 g Dry Substance)[a]

	C. korshinskii Kom. powder	Al-CPI	A-CPI
sodium	1.17 ± 0.11c	1878 ± 77a	145 ± 12b
potassium	140 ± 12a	154 ± 11a	58.82 ± 5.21b
calcium	1163 ± 44b	183 ± 17c	1712 ± 168a
phosphorus	3562 ± 88a	551 ± 17b	503 ± 16b
magnesium	24.82 ± 0.10b	15.76 ± 0.84b	284 ± 27a
iron	8.11 ± 0.23c	13.71 ± 1.01b	21.44 ± 0.40a
copper	0.22 ± 0.02c	2.64 ± 0.22b	12.91 ± 0.72a
zinc	0.40 ± 0.04c	1.49 ± 0.11b	3.32 ± 0.32a
manganese	0.61 ± 0.06b	0.49 ± 0.05b	10.48 ± 0.79a

[a]Values are expressed as mean ± SD of three measurements. Values with different letters are significantly different at $p < 0.05$ within the same row.

The compositions of essential amino acids in *C. korshinskii* Kom., Al-CPI, and A-CPI are shown in Table 4, together with those of soybean, wheat grains, rice, and FAO/WHO reference pattern. The important plant species used for humans or animals are mainly cereal grains and food legumes. Compared with animal-based proteins, many plant-based proteins do not provide essential amino acids in a balanced proportion, which restricts their potential application. The typical amino acids are lysine (Lys), threonine (Thr), and sulfur-containing acid amino acids (methionine and cysteine). The Lys content is normally deficient in cereal grains,[3] such as wheat grains, rice, and maize, but it was relatively plentiful in *C. korshinskii* Kom. (4.1 mg/100 mg crude protein), Al-CPI (3.1 mg/100 mg crude protein), and A-CPI (3.8 mg/100 mg crude protein) relative to that in cereals, but lower than that in buckwheat seeds.[29] In fish, poultry, or pig fodder, Lys was found to be the first limiting amino acid.[21] Thr is the second limiting amino acid in grain sorghum, barley, and wheat, as well as the third limiting amino acid in maize. It also becomes the first limiting amino acid when animal fodder is supplemented with lysine.[23] The content of Thr in *C. korshinskii* Kom. (4.7 mg/100 mg crude protein) or A-CPI (4.7 mg/100 mg crude protein) was even higher than that in soybean, rice, wheat grains, and FAO/WHO reference pattern for preschool children and adults.[22] However, the Thr content in Al-CPI (2.8 mg/100 mg crude protein) exceeded only rice and FAO/WHO reference pattern for adults. According to EAA scores, sulfur-containing amino acids are the first limiting amino acids for *C. korshinskii* Kom. and CPIs. Some legumes had relatively lower levels of methionine (Met) and cysteine (Cys) than animal-based proteins.[20] Met was the first limiting amino acid for soybean, the amino acid composition of which was mostly closed to animal-based protein. It has to be noted that the Met content in A-CPI (1.4 mg/100 mg crude protein) was slightly higher than that in soybean. The total amounts of aromatic amino acids (phenyl-

dx.doi.org/10.1021/jf500349s | J. Agric. Food Chem. 2014, 62, 3217−3222

Table 4. Essential Amino Acid Composition of *C. korshinskii* Kom., Al-CPI, A-CPI, Soybean, Rice, Wheat Grain, and FAO/WHO Recommended Patterns for Adults and Preschool Children

material	essential amino acid content (mg/100 mg crude protein)								
	His	Thr	Val	Met	Ile	Leu	Phe + Tyr	Lys	Try
C. korshinskii Kom.	2.2	4.7	2.5	0.9	1.7	4.2	7.5	4.1	ND[a]
Al-CPI	1.1	2.8	1.9	0.8	1.4	4.5	5.6	3.1	ND
A-CPI	1.8	4.7	3.1	1.4	2.4	6.8	8.6	4.8	ND
soybean[b]	2.5	3.8	4.6	1.2	4.6	7.7	6.1	6.1	1.24
rice[c]	1.6	2.3	4.3	1.3	2.3	4.9	5.7	2.5	0.6
wheat grains[d]	2.4	3	3.9	1.5	2.7	6.9	7.4	2.4	1.4
FAO reference pattern[e]	1.6	0.9	1.3	1.7[f]	1.3	1.9	1.9[g]	1.6	0.5
FAO reference pattern[h]	1.9	3.4	3.5	2.5[f]	2.8	6.6	6.3[g]	5.8	1.10
EAA score									
C. korshinskii Kom.	113.68	138.24	72.29	36.00	60.71	63.79	119.05	70.69	0
Al-CPI	60.00	81.18	53.43	33.20	50.00	68.03	88.73	53.62	0
A-CPI	92.63	138.82	87.71	55.60	85.71	103.64	135.71	83.10	0

[a]ND, not detectable. [b]Data from Bau et al. (1994). [c]Data from Abdel-Aal and Hucl (2002). [d]Data from Sosulski and Imafidon (1990). [e]FAO/WHO (2007) essential amino acids pattern for adults. [f]Methionine + cystine. [g]Phenylalanine + tyrosine. [h]FAO/WHO (2007) essential amino acids pattern for preschool children, individuals aged 2−5 years.

alanine and tyrosine) in *C. korshinskii* Kom. and A-CPI were 7.5 and 8.6 mg/100 mg crude protein, respectively. They are even higher than those in soybean, rice, wheat, and FAO/WHO pattern for children. Phenylalanine has been widely used as human food and animal feed additives, as well as resources to synthesize some active materials.[24] For *C. korshinskii* Kom., Al-CPI, and A-CPI, the contents of essential amino acids generally exceeded the FAO/WHO reference pattern for adults except tryptophan and sulfur-containing amino acids. The ample qualities of Lys, Thr, and aromatic amino acid make it a good alternative additive in the feed or food industry.

The compositions of nonessential amino acids in *C. korshinskii* Kom., Al-CPI, and A-CPI are shown in Figure 1. In *C. korshinskii* Kom., compared with others, proline (10.1 mg/100 mg crude protein) and glycine (3.5 mg/100 mg crude protein) ranked first and last in nonessential amino acids. Proline was adequate in the plants with high abilities of cold hardiness and drought resistance. However, in Al-CPI or A-CPI, the highest level of nonessential amino acid was aspartic acid, whereas the lowest was tyrosine.

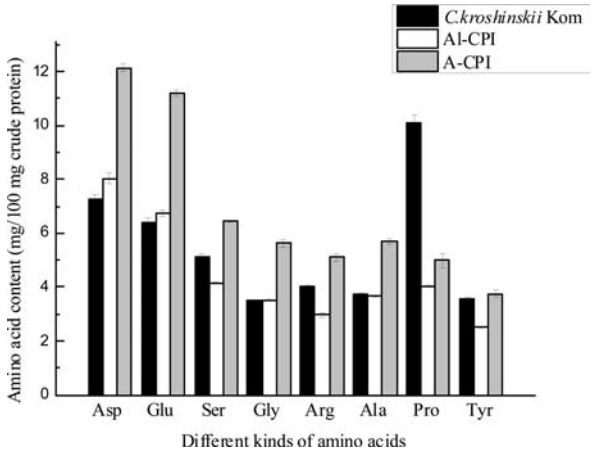

Figure 1. Nonessential amino acid composition of *C. korshinskii* Kom., Al-CPI, and A-CPI (mg/100 mg crude protein). Values are expressed as mean ± SD of triplicate measurements. All samples were significantly different ($p > 0.05$) except for aspartic acid and proline. Asp, aspartic acid; Glu, glutamic acid; Ser, serine; Gly, glycine; Arg, arginine; Ala, alanine; Pro, proline; Tyr, tyrosine.

In general, the total amount of amino acids in A-CPI was higher than that in Al-CPI. Different pH values utilized in the protein extraction processes may account for this variance. A pH of 6.8 was utilized in the extraction process of A-CPI, and most amino acids were stable at this pH.[40]

The contents of essential and nonessential amino acids in *C. korshinskii* Kom. were higher than those in Al-CPI, but lower than those in A-CPI with the exception of histidine. Different extraction methods could lead to different amino acid contents and compositions in protein isolates. Therefore, a suitable extraction method for proteins should be chosen to satisfy the demand of food and feed additives.

Analysis of Antinutritional Factors. Some ANFs exert their effects on the digestion and assimilation of some nutriments, as well as the immune system of animals. In our study, the ANF values of *C. korshinskii* Kom., Al-CPI, and A-CPI are investigated in Table 5.

Table 5. Antinutritional Factor Contents in *C. korshinskii* Kom., Al-CPI, and A-CPI (Milligrams per Gram Dry Substance)[a]

	C. korshinskii Kom.	Al-CPI	A-CPI
trypsin inhibitor[b]	2.07 ± 0.10a	ND[c]b	2.46 ± 0.10a
lectin	3.74 ± 0.0b	NDc	4.73 ± 0.0a
total phenol	10.67 ± 0.24b	19.02 ± 0.57a	NDc
tannins	7.70 ± 0.19a	5.66 ± 0.23b	NDc
phytic acid	1.70 ± 0.09a	NDc	0.96 ± 0.04b
saponin	ND	ND	ND

[a]Values are expressed as mean ± SD of three measurements. Values with different letters are significantly different at $p < 0.05$ within the same row. [b]Trypsin inhibitor, mg pure trypsin inhibited per g of dry sample. [c]ND, not detected.

The TIA contents of *C. korshinskii* Kom. and A-CPI were 2.07 and 2.46 mg pure trypsin inhibited/g dry substance, respectively. However, TIA was not detected in Al-CPI. Using the alkaline extraction, the TIA contents in protein isolates from *Vicia faba* were less than one-third of those in their raw materials.[25] The TIA value of *C. korshinskii* Kom. in this study

was lower than those of some kinds of mucuna beans (13.8−19.2 mg/g).[26,39] Combined with protease, trypsin inhibitor could lead to a decrease of protease activity and a low digestibility of proteins.

The lectin contents in *C. korshinskii* Kom. and A-CPI were 3.74 and 4.73 mg/g dry substance, respectively. However, lectin was undetectable in Al-CPI. A previous study indicated that alkaline extraction led to decreased contents of lectin in pea protein isolates (14 mg/g) compared with their raw materials (35 mg/g).[27] As a kind of glycoprotein, lectin was not digested by proteases, and it disturbed other protein digestion in humans and animals. Additionally, lectin can affect the human immune system and reduce the content of hormones secreted by the gut.[28]

The total phenols content of *C. korshinskii* Kom. (10.54 mg/g dry substance) was higher than that in *Vigna radiata* (4.5 mg/g) and lower than that in *Sesbania* (20.4−30.0 mg/g).[11] The content of total phenols in Al-CPI (19.02 mg/g) was higher than that in *C. korshinskii* Kom. Our results compared well with a previous alkaline extraction process,[29] in which the total phenols in protein isolates of buckwheat seeds (29.3 mg/g) were higher than those in their materials (6 mg/g).

The content of tannins in *C. korshinskii* Kom. was 7.61 mg/g dry substance. It was lower than that in pea (27.80−30.93 mg/g) and cowpea (22.63−26.14 mg/g).[30] Tannin content in Al-CPI was 5.66 mg/g, which was higher than that in protein isolate of mung bean (1.52 mg/g).[31] Total phenols and tannins could be united with diet proteins and digestive enzymes to form indigestible compounds, which could result in a low digestibility of food. However, in recent years, some ANFs, such as tannins and phytic acids, were also found to have some beneficial biological functions, such as oxidation resistance, antitumor promotion, and antiviral activity.

The contents of phytic acid were 1.70 and 0.96 mg/g dry substance in *C. korshinskii* Kom. and A-CPI, but it was undetectable in Al-CPI. Mwasaru[32] had reported that phytic acid contents were not detected in pigeonpea and cowpea protein isolates extracted by alkaline extraction. The phytic acid content in *C. korshinskii* Kom. was less than that in many kinds of legume beans, such as mung bean seeds (5.8 mg/g), chickpea (12.1 mg/g), cowpea (14 mg/g), and horse gram (10.2 mg/g).[33] Phytic acid could combine with minerals to form infusible precipitates, which could lead to interference with the absorption of mineral substances, especially calcium, zinc, and iron.[19]

Saponins was not detected in *C. korshinskii* Kom., A-CPI, and Al-CPI. Saponins could cause hemolysis and decrease the adsorption of nutrition in humans and animals.[34] Hydroxy steroids or bile acids can form insoluble complexes with saponins.

In an alkaline extraction process, protein extraction was followed by isoelectric precipitation. Hagerman[35] reported that phenolic substances could effectively combine with proteins during the protein isoelectric precipitation. In our study, some ANFs, such as the total phenols and tannins, in Al-CPI were higher than those in *C. korshinskii* Kom. On the other hand, the phytic acid in Al-CPI was lower than that in *C. korshinskii* Kom. Proteins and phytic acid did not combine when the pH was >11, and most of the phytic acid was removed with insoluble materials.[36] In addition, trypsin inhibitor and lectin in Al-CPI were not detected. The pH values used in the extraction process may lead to reduced bioactivity of proteins.[41]

In an acetone precipitation method, some ions derived from *C. korshinskii* Kom. may be entrapped in the extraction buffer, which might lead to an increase in the ionic strength of acetone and the precipitation efficiency of proteins.[37] This may explain the higher contents of TIA and lectin in A-CPI than those in *C. korshinskii* Kom. Additionally, phenolic substances could be solubilized in acetone during the protein precipitation,[38] which may lead to undetectable total phenols or tannins in A-CPI.

In summary, the protein contents of *C. korshinskii* Kom., Al-CPI, and A-CPI were 9.1, 50.1, and 42.6%, respectively. The contents of essential amino acids in the three materials were higher than those in FAO/WHO reference pattern for adult (2007) except sulfur-containing amino acids and tryptophan. As the limiting amino acids in cereal grains, the contents of Lys and Thr in *C. korshinskii* Kom., Al-CPI, and A-CPI exceeded those in the cereal grains, such as rice and wheat grains. The methionine in A-CPI (1.39 mg/100 mg crude protein) was even higher than that in soybean. The ANFs in *C. korshinskii* Kom. and Al-CPI were generally lower than those in other legumes except total phenols and tannins. Total phenols and tannins in Al-CPI were 19.02 and 5.66 mg/g dry substance, respectively, but they were undetectable in A-CPI. Our study provides a detailed analysis of the nutritional compositions and antinutritional factors in *C. korshinskii* Kom. and its protein isolates, indicating that they have great potential as food and feed additives.

AUTHOR INFORMATION

Corresponding Author

*(S.-R.J.) E-mail: jiashiru@tust.edu.cn. Fax: 86-22-60602298. Phone: +86-22-60601598.

Funding

We are grateful for financial support from the International Cultivation of Excellent Postdoctor (2012) by Tianjin Municipal Human Resources and Social Security Bureau, the National Natural Science Foundation of China (No. 21106105), and Changjiang Scholars and Innovative Research Team in University (No. IRT1166).

Notes

The authors declare no competing financial interest.

REFERENCES

(1) Zhong, C.; Wang, R.; Zhou, Z.; Jia, S. R.; Tan, Z. L. Functional properties of protein isolates from *Caragana korshinskii* Kom. extracted by three different methods. *J. Agric. Food Chem.* **2012**, *60*, 10337−10342.

(2) Ma, C. C.; Gao, Y. B.; Guo, H. Y.; Wang, J. L.; Wu, J. B.; Xu, J. S. Physiological adaptations of four dominant *Caragana* species in the desert region of the Inner Mongolia Plateau. *J. Arid Environ.* **2008**, *27*, 247−254.

(3) Rodríguez, C.; Frías, J.; Vidal-Valverde, V.; Hernández, A. Total chemically available (free and intrachain) lysine and furosine in pea, bean, and lentil sprouts. *J. Agric. Food Chem.* **2007**, *55*, 10275−10280.

(4) Shimelis, E. A.; Rakshit, S. K. Effect of processing on antinutrients and in vitro protein digestibility of kidney bean (*Phaseolus vulgaris* L.) varieties grown in East Africa. *Food Chem.* **2007**, *103*, 161−172.

(5) *Official Methods of Analysis*, 15th ed.; Association of Official Analytical Chemists (AOAC): Washington, DC, USA, 1990.

(6) Determination of crude fiber in vegetable foods. *Standardization Administration of the People's Republic of China (GB/T)*; The Minister of Health of the People's Republic of China; Government Printing Office: Beijing, China, 2003.

(7) Goñi, I.; Garcıa-Alonso, A.; Saura-Calixto, F. A starch hydrolysis procedure to estimate glycemic index. *Nutr. Res. (N.Y.)* **1997**, *17*, 427−437.
(8) Adebowale, Y. A.; Adeyemi, A.; Oshodi, A. A. Variability in the physicochemical, nutritional and antinutritional attributes of six *Mucuna* species. *Food Chem.* **2005**, *89*, 37−48.
(9) Determination of phosphorus in foods. *Standardization Administration of the People's Republic of China (GB/T)*; The Minister of Health of the People's Republic of China; Government Printing Office: Beijing, China, 2003.
(10) Hainida, K. I. E.; Amin, I.; Normah, H.; Mohd.-Esa, N. Nutritional and amino acid contents of differently treated roselle (*Hibiscus sabdariffa* L.) seeds. *Food Chem.* **2008**, *111*, 906−911.
(11) Siddhurajua, P.; Osoniyib, O.; Makkarc, H. P. S.; Beckera, K. Effect of soaking and ionising radiation on various antinutritional factors of seeds from different species of an unconventional legume, Sesbania, and a common legume, green gram (*Vigna radiata*). *Food Chem.* **2002**, *79*, 273−281.
(12) Dai, D. Z. Study on quantification and inactivation of lectins in feeds. Master's thesis, Zhejiang University, China, 2003.
(13) Makkar, H. P. S.; Blümmel, M.; Borowy, N. K.; Becker, K. Gravimetric determination of tannins and their correlations with chemical and protein precipitation methods. *J. Sci. Food Agric.* **1993**, *61*, 161−165.
(14) Chen, Y.; Xie, M. Y.; Gong, X. F. Microwave-assisted extraction used for the isolation of total triterpenoid saponins from *Ganoderma atrum*. *J. Food Eng.* **2007**, *81*, 162−170.
(15) Zong, S. X.; Wang, R.; Cao, C. J.; Wang, T.; Luo, Y. Q. Impact of *Chlorophorus caragana* damage on nutrient contents of *Caragana korshinskii*. *J. Plant Interact.* **2014**, *9*, 488−493.
(16) Karaca, A. C.; Low, N.; Nickerson, M. Emulsifying properties of chickpea, faba bean, lentil and pea proteins produced by isoelectric precipitation and salt extraction. *Food Res. Int.* **2011**, *44*, 2742−2750.
(17) Alu'datt, M. H.; Rababah, T.; Ereifej, K.; Alli, I.; Alrababah, M. A.; Almajwal, A.; Masadeh, N.; Alhamad, M. N. Effects of barley flour and barley protein isolate on chemical, functional, nutritional and biological properties of pita bread. *Food Hydrocolloids* **2012**, *26*, 135−143.
(18) National Academy of Sciences, National Research Council (NRC/NAS). *U.S. Recommended Dietary Allowances*; U.S. Government Printing Office: Washington, DC, USA, 1989.
(19) Liang, J. F.; Han, B. Z.; Robert, N. M. J.; Hamer, R. J. Effect of soaking and phytase treatment on phytic acid, calcium, iron and zinc in rice fractions. *Food Chem.* **2009**, *115*, 789−794.
(20) Day, L. Proteins from land plants − potential resources for human nutrition and food security. *Trends Food Sci. Technol.* **2013**, *2*, 25−42.
(21) Rawles, S. D.; Fuller, S. A.; Beck, B. H.; Gaylord, T. G.; Barrows, F. T.; McEntire, M. E. Lysine optimization of a commercial fishmeal-free diet for hybrid striped bass (*Morone chrysops* × *M. saxatilis*). *Aquaculture* **2013**, *396*−*399*, 89−101.
(22) Food and Agriculture Organization/World Health Organization (FAO/WHO). Report of a Joint WHO/FAO/UNU Expert Consultation. In *Protein and Amino Acid Requirements in Human Nutrition*; WHO Technical Report Series 935; Geneva, Switzerland, 2007.
(23) Li, D.; Xiao, C.; Qiao, S.; Zhang, J.; Johnson, E. W.; Thacker, P. A. Effects of dietary threonine on performance, plasma parameters and immune function of growing pigs. *Anim. Feed Sci. Technol.* **1999**, *78*, 179−188.
(24) Sprenger, G. A. From scratch to value: engineering *Escherichia coli* wild type cells to the production of L-phenylalanine and other fine chemicals derived from chorismate. *Appl. Microbiol. Biotechnol.* **2007**, *75*, 739−749.
(25) Gueguen, J.; Quemener, B.; Valdebourze, P. Elimination des facteurs antinutritionnels de la feverole *Vicia faba* L. et du pois *Pisum sativum* L. au cours de la preparation des isolats proteiques. *Lebensm. Wiss. Technol.* **1980**, *14*, 72−75.
(26) Siddhuraju, P.; Becker, K. Nutritional and antinutritional composition, in vitro amino acid availability, starch digestibility and predicted glycemic index of differentially processed mucuna beans (*Mucuna pruriens* var. *utilis*): an under-utilised legume. *Food Chem.* **2005**, *91*, 275−286.
(27) Le Guen, M. P.; Huisman, J.; Guéguen, J.; Beelen, G.; Verstegen, M. W. A. Effects of a concentrate of pea antinutritional factors on pea protein digestibility in piglets. *Livest. Prod. Sci.* **1995**, *44*, 157−167.
(28) Vasconcelos, I. M.; Oliveira, J. T. A. Antinutritional properties of plant lectins. *Toxicon* **2004**, *44*, 385−403.
(29) Tang, C. H.; Wang, X. Y. Physicochemical and structural characterisation of globulin and albumin from common buckwheat (*Fagopyrum esculentum* Moench) seeds. *Food Chem.* **2010**, *121*, 119−126.
(30) Khattab, R. Y.; Arntfield, S. D. Nutritional quality of legume seeds as affected by some physical treatments. Part 2. Antinutritional factors. *Food Sci. Technol.* **2009**, *42*, 1113−1118.
(31) El-Adawy, T. A. Functional properties and nutritional quality of acetylated and succinylated mung bean protein isolate. *Food Chem.* **2000**, *70*, 83−91.
(32) Mwasaru, M. A.; Muhammad, K.; Bakar, J.; Man, Y. B. C. Effects of isolation technique and conditions on the extractability, physicochemical and functional properties of pigeonpea (*Cajanus cajan*) and cowpea (*Vigna unguiculata*) protein isolates. I. Physicochemical properties. *Food Chem.* **1999**, *67*, 435−443.
(33) Sreerama, Y. N.; Sashikala, V. B.; Pratape, V. M.; Singh, V. Nutrients and antinutrients in cowpea and horse gram flours in comparison to chickpea flour: evaluation of their flour functionality. *Food Chem.* **2012**, *131*, 462−468.
(34) Cheeke, P. R. Biological effects of feed and forage saponins and their impact on animal production. *Adv. Exp. Med. Biol.* **1996**, *405*, 377−385.
(35) Hagerman, A. E.; Butler, L. G. The specificity of proanthocyanidin-protein interaction. *J. Biol. Chem.* **1981**, *256*, 4494−4497.
(36) Cheryan, M. Phytic acid interactions in food systems. *Crit. Rev. Food Sci. Nutr.* **1980**, *13*, 297−335.
(37) Crowell, A. M. J.; Wall, M. J.; Doucette, A. A. Maximizing recovery of water-soluble proteins through acetone precipitation. *Anal. Chim. Acta* **2013**, *796*, 48−54.
(38) Boudjou, S.; Oomah, B. D.; Zaidi, F.; Hosseinian, F. Phenolics content and antioxidant and anti-inflammatory activities of legume fractions. *Food Chem.* **2013**, *138*, 1543−1550.
(39) Siddhuraju, P.; Becker, K.; Makkar, H. P. S. Studies on the nutritional composition and antinutritional factors of three different germplasm seed materials of an under-utilized tropical legume, *Mucuna pruriens* var. *utilis*. *J. Agric. Food Chem.* **2000**, *48*, 6048−6060.
(40) Salcedo-Chavez, B.; Osuna-Castro, J. A.; Guevara-Lara, F. Optimization of the isoelectric precipitation method to obtain protein isolates from amaranth (*Amaranthus cruentus*) seeds. *J. Agric. Food Chem.* **2002**, *50*, 6515−6520.
(41) Gupta, P.; Dhawan, K.; Malhotra, S. P.; Singh, R. Purification and characterization of trypsin inhibitor from seeds of faba bean (*Vicia faba* L.). *Acta. Physiol. Plant.* **2000**, *22*, 433−438.

Table 1. Small Phenolic Compounds in Pretreated Stover and Their Yields (10^{-2} %)

		SECS				
	MCS	2.85[a]	3.37	3.59	3.89	3.97	4.19
syringic acid	0.00	35.98	0.00	11.12	0.00	10.20	47.98
vanillin	0.00	0.00	6.03	11.07	20.74	19.26	13.14
ferulic acid	0.00	0.00	0.00	2.41	0.00	0.00	36.04
p-hydroxybenzoic acid	7.36	36.77	72.76	25.05	45.61	27.05	37.39
syringaldehyde	0.00	7.11	4.67	6.84	4.80	0.00	20.49
vanillic acid	0.00	35.75	0.00	0.00	0.00	9.98	46.27
p-hydroxybenzaldehyde	0.00	2.28	1.72	0.00	0.00	47.24	0.00
coumaric acid	0.00	46.53	80.05	40.05	17.22	8.63	16.08
total phenolic acid	7.36	155.03	152.81	78.64	62.83	55.85	183.77
total phenolic aldehyde	0.00	9.39	12.43	17.91	25.54	66.50	33.63
total	7.36	164.42	165.24	96.55	88.36	122.36	217.40

[a]2.85 represents the sample of corn stover pretreated by steam explosion at the strength of 2.85. So do 3.37, 3.59, 3.89, 3.97, and 4.19.

(international unit) of endo-β-1,4-glucanase activity, 4.3 IU mL^{-1} of exo-β-1,4-glucanase, and 63.7 IU mL^{-1} of β-glucosidase activity. Small phenolic compound model substances, analytical grade, were purchased from Aladdin Industrial Corporation. All the other chemicals were analytical grade and purchased from Beijing Chemicals & Reagent Corp., China.

Pretreatment. The severity of steam explosion influenced the release of small phenolic compounds;[5,14] therefore, corn stover was steam exploded at various severity levels to get the exact information about the small phenolic compounds released during steam explosion. The severity of steam explosion (l g R_0) was decided by the severity factor, which was calculated as follows:[20]

$$R_0 = t \exp^{(T-100)/14.75} \quad (1)$$

where R_0 is severity factor, t is the time (min) for keeping constant pressure, and T is the temperature (°C) while keeping constant pressure.

According to eq 1, steam explosion severity (l g R_0) was designed as follows: 2.85 (1.0 MPa for 5 min), 3.37 (1.5 MPa for 3 min), 3.59 (1.5 MPa for 5 min), 3.89 (1.5 MPa for 10 min), 3.97 (1.5 MPa for 20 min), 4.19 (1.95 MPa for 5 min). The kneaded corn stover (about 200 g) was put into a batch steam explosion tank (2 L). The tank was then filled with saturated steam to the required pressure and maintained for a certain time. Finally, the pressure was discharged immediately to get the steam exploded corn stover (SECS). Corn stover was also milled with a microgrinder for plants into the size of smaller than 0.9 mm to examine the content of small phenolic compounds in raw stover.

The contents of cellulose, hemicelluloses (both of which were determined according to the literature[21]), and moisture of pretreated corn stover (Supporting Information, Figure S1) were 25.75−34.91%, 2.61−12.18%, 4.00−10.20%, respectively, and the pH was 4.0−6.0.

Washing of Pretreated Stover. The SECS and the milled corn stover (MCS) were washed separately with water by mixing in a flask with the weight ratio of solid to liquid 1:10, and then the flask was shaken at 50 °C, 150 rpm for 2 h. Finally, each mixture was separated by vacuum filtration to obtain the washing liquid of SECS, the washing liquid of MCS, the solid of steam exploded corn stover (S-SECS), and the solid of milled corn stover (S-MCS). All experiments were carried out in duplicate.

Determination of Small Phenolic Compounds in Pretreated Stover. Small phenolic compounds in washing liquid of both SECS and MCS were identified by a high-performance liquid chromatography (HPLC, Agilent 1200, Agilent Technologies, USA) with a YMC-Triart C18 column (250 × 4.6 mm L.D., YMC Co. Ltd.) and an ultraviolet detector. For each phenolic compound, the peak heights at different wavelengths were compared, and the final wavelengths to detect different small phenolic compounds were chosen as follows: 250 nm for *p*-hydroxybenzoic acid and syringaldehyde, 280 nm for syringic acid, vanillin, vanillic acid, *p*-hydroxybenzaldehyde, 320 nm for ferulic acid and coumaric acid. The elution time of each small phenolic acid were provided in Supporting Information (Table S1). The mobile phase was 60% acetic acid solution (1%) with 40% methanol at a flow rate of 0.6 mL/min. The temperature of column and detector was 30 and 35 °C, respectively. The small phenolic compound yield was calculated according to the following equation:

$$\text{PC yield (\%)} = \frac{\text{phenol weight (g)}}{\text{total material weight (g)}} \times 100\% \quad (2)$$

Cellulase Activity Analysis. Cellulase activity was tested[22,23] with 50 ± 1 mg Whatman No. 1 filter paper as substrate and 2 mL of acetic acid-sodium acetate (pH 4.8, 0.2 M) as the buffer. Cellulases were diluted 1000 times. The enzymatic hydrolysis process was carried out at 50 °C for 60 min.

The effect of small phenolic compounds, washing liquid and 5-hydroxymethylfurfural (5-HMF) on cellulase activity was examined as follows.

According to the small phenolic compounds identification results, the small phenolic compound model substances were used to examine their individual effect on cellulose activity (FPU) including vanillin, vanillic acid, coumaric acid, *p*-hydroxybenzoic acid, *p*-hydroxybenzaldehyde, syringic acid, syringaldehyde, and ferulic acid. Individual small phenolic compound was combined with enzyme and substrate immediately at the beginning of the assay. On the basis of the identified results above, the concentration of each small phenolic compound model substance was 0.05−8.00 g/L. The experiments were carried out in duplicate.

To examine the interactive effect of small phenolic compounds on cellulase activity (FPU), the small phenolic compounds mixture was prepared according to their total weight ratios of different steam exploded samples (Table 1). The small phenolic compounds mixture was added immediately while testing cellulase activity (FPU) with a total concentration 0.05−8.00 g/L. The experiments were carried out in duplicate.

When detecting the effect of washing liquid on cellulase activity (FPU), the amount of washing liquid added was calculated based on the constant ratio of cellulases to substrate in the process of enzymatic hydrolysis (0.15 mL/g). In the process of analyzing cellulase activity, 0.002 mL of cellulases was added. The equivalent volume of washing liquid should equal that from 0.002/0.15 g substrate. Buffer was added to reach 2 mL together with the washing liquid. The sample of cellulases and substrate without the washing liquid was taken as the control group.

To explore which component in the washing liquid of both SECS and MCS influences cellulase activity, the effect of 5-HMF on cellulase activity (FPU) was also carried out because 5-HMF was found in the washing liquid. The method was the same as that above. The amount of 5-HMF added was 0.2−2.0 g/L. The sample, including only cellulases and substrate without 5-HMF, was taken as the control group. The experiments were carried out in duplicate.

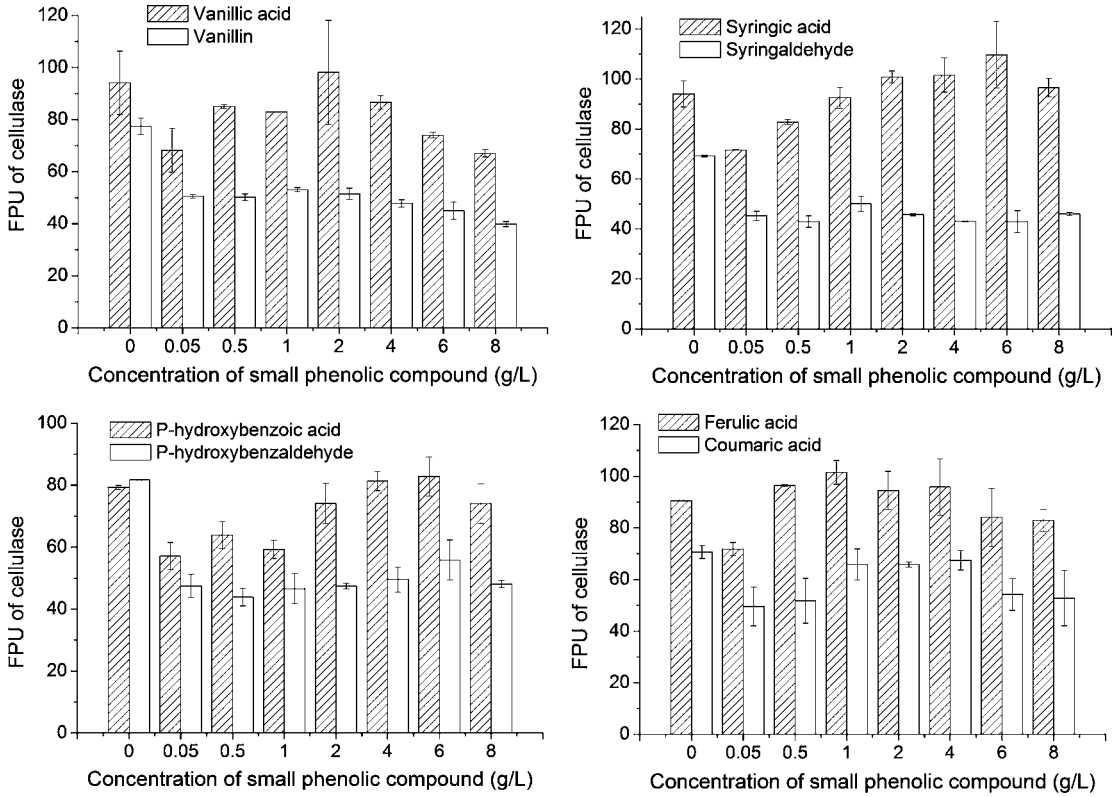

Figure 1. Effect of small phenolic compound model substance on cellulase activity. Each small phenolic compound model substance was added separately at the beginning of testing cellulase activity. Reducing sugar was tested with the DNS method.

Enzymatic Hydrolysis Process. Two assays were designed to examine the effect of small phenolic compounds on enzymatic hydrolysis.

For the first assay, the washing liquid of MCS and the washing liquid of SECS were separately put into the enzymatic hydrolysis mixture of the MCS (particle was smaller than 0.9 mm). The reaction was carried out in a 250 mL flask which was filled with 2 g (dry weight) of MCS, equivalent washing liquid (volume equal to that from 2 g of corn stover pretreated), buffer (acetic acid−sodium acetate pH 4.8, 0.2 M, the total volume of buffer and washing liquid was equal to 120 mL), and 0.6 mL of cellulases. The flask was shaken at 50 °C, 150 rpm for 48 h.

For the second assay, the enzymatic hydrolysis of pretreated corn stover before and after washing was directly compared. The reaction was carried out in a 100 mL flask which was filled with 2 g (absolute dry) of pretreated corn stover, 60 mL of buffer (acetic acid−sodium acetate pH 4.8, 0.2 M), and 0.3 mL of cellulases. The flask was covered and shaken at 50 °C, 150 rpm for 48 h.

After enzymatic hydrolysis for the required time, the flask was put into the water at 100 °C for 5 min to deactivate cellulases, and then the mixture in flask was cooled and separated by standing naturally for reducing sugar analysis.

All of the experiments were carried out in duplicate.

Reducing Sugar Analysis. While the effect of small phenolic compound model substances and small phenolic compounds mixture on cellulase activity was tested, reducing sugars were tested with the 3,5-dinitrosalicylic acid (DNS) method.[23] To exclude the color interference from the reaction between reducing phenolic aldehyde and DNS, a sample of cellulases and small phenolic compound model substances or their mixture at the same concentration without substrate was also prepared, and the optical densities of these samples (Supporting Information, Tables S2−S4) were subtracted from that of the related sample. Filter paper unit (FPU) was calculated according to the literature.[19,22]

There was 5-HMF in washing liquid, and 5-HMF might interfere with DNS by supplying active reducing groups as well as a characteristic interfering color.[24] Therefore, while the influence of washing liquid was detected, reducing sugars were all analyzed by HPLC (Agilent 1200, Agilent Technologies, USA) with an Aminex HPX-87H column (300 mm × 7.8 mm, Bio-Rad Laboratories Inc.) and a refractive index detector. The mobile phase was 0.5 mM H_2SO_4 at a flow rate of 0.6 mL/min. The temperature of column and detector was 65 and 35 °C, respectively. The content of 5-HMF in pretreated stover was also examined with this HPLC method.

While the enzymatic hydrolysis rate and yield of SECS and MCS were calculated, the content of reducing sugars in washing liquid was excluded from the sugar produced from the SECS and the MCS. The enzymatic hydrolysis yield of cellulose was calculated with the following equation,[19,22] in which the constant for cellobiose was 0.947 (324/342 = 0.947).

$$\text{enzymatic hydrolysis yield (\%)} = \frac{\text{glucose weight (g)} \times 0.9 + \text{cellobiose weight (g)} \times 0.947}{\text{cellulose weight (g)}} \times 100\% \quad (3)$$

Statistical Analysis. Experiments conducted in duplicate were analyzed at least in triplicate and expressed as mean ± standard deviation. The one-way analysis of variance test[25] was carried out using the Statistical Product and Service Solution (SPSS) 16.0 package for the effect of individual small phenolic compounds, small phenolic compounds interaction, and 5-HMF on cellulase activity. Moreover, univariate analysis of variance was also carried out with the SPSS package for the comparison of enzymatic hydrolysis of SECS before and after washing, in which two factors were analyzed: enzymatic hydrolysis time and pretreatment method (steam explosion strength, washing). Least square deviation analysis was performed to determine the significant differences of mean value ($p < 0.05$).

dx.doi.org/10.1021/jf405046m | J. Agric. Food Chem. 2014, 62, 3223−3229

RESULTS AND DISCUSSION

Analysis of Small Phenolic Compounds in Pretreated Corn Stover. To examine the effect of small phenolic compounds on cellulase activity, the compositions of water-soluble small phenolic compounds of pretreated corn stover were analyzed first. Table 1 shows that there is only *p*-hydroxybenzoic acid in washing liquid of MCS, suggesting that only *p*-hydroxybenzoic in corn stover is in the free state. However, there are other small phenolic compounds in the washing liquid of SECS including syringic acid, vanillic acid, ferulic acid, coumaric acid, syringaldehyde, *p*-hydroxybenzaldehyde, and vanillin. The amounts of different small phenolic compounds were different, and the total small phenolic compounds yield increased with the enhancement of steam explosion strength, reaching 2.17% when the strength was 4.19.

Results revealed that steam explosion caused small phenolic compounds to be released, especially for *p*-hydroxybenzoic acid and coumaric acid which were released from stover pretreated atdifferent steam explosion strengths. In corn stover, the ferulic acid mainly connects hemicelluloses and lignin with a covalent bond. Other small phenolic compounds are mainly from lignin hydrolysis.[2] For many biomass feedstocks, steam explosion pretreatment being applied to or developed for biomass conversion can transform insoluble, polymeric lignin into soluble small phenolic compounds.[26,27]

According to the small phenolic compounds identified above, eight small phenolic compound model substances were used to examine their individual effect on cellulase activity (FPU), and the influence of concentration was mainly examined.

Effect of Small Phenolic Compound Model Substances on Cellulase Activity. Results revealed that syringic acid, etc. might have a concentration-dependent stimulation effect on cellulase activity (Figure 1). At a suitable concentration (at 2−4 g/L), syringic acid, etc. might slightly stimulate cellulase activity. However, at the lower (0.05 g/L) concentration, syringic acid, etc. exhibited a significant inhibition effect on cellulase activity. At other concentrations, the slight stimulation or inhibition effect depended on different small phenolic compounds. The stimulation effect of syringic acid reached 16.65%, followed by ferulic acid, *p*-hydroxybenzoic acid, and vanillic acid (in decreasing order) at their suitable concentration. The reason for the inhibition effect of coumaric acid might be that it was insoluble in acetic acid−sodium acetate buffer at 50 °C when the concentration was higher than 2 g/L. Therefore, cellulases could hardly touch the substrate. At 0.05 g/L, the inhibitory effect of phenolic acid on cellulase activity was arranged as follows: *p*-hydroxybenzoic acid (27.96%) ≈ vanillic acid (27.55%) > syringic acid (23.84%) > ferulic acid (20.70%).

As shown in Figure 1, *p*-hydroxybenzaldehyde, etc. significantly inhibit cellulase at all concentrations. At 0.05 g/L, the inhibitory effects of different phenolic aldehydes on cellulases were arranged as *p*-hydroxybenzaldehyde (41.83%) > syringaldehyde (34.60%) > vanillin (34.71%). While at the concentration of 8 g/L, the inhibitory effects were arranged as follows: vanillin (33.51%) > *p*-hydroxybenzaldehyde (41.14%) > syringaldehyde (33.51%). These results demonstrated that the inhibitory effect of *p*-hydroxybenzaldehyde, etc. on cellulases was stronger than that of phenolic acid at the same concentration.

The above results help explain why there were contrasting reports about the effect of small phenolic compounds on cellulases.[9,28] For the enzymatic hydrolysis of steam exploded wheat straw, the concentration of small phenolic compounds in the hydrolysis mixture was 0.281−0.356 g/L.[9] Though the concrete small phenolic compounds were not identified and reported, their total concentration fell in the slight stimulation range of phenolic acid in our text.[9] Therefore, the detoxification with laccase before enzymatic hydrolysis reduced the enzymatic hydrolysis yield. The concentration of small phenolic compounds in the hydrolysis mixture of corn stover pretreated with hot water was 5 g/L, which fell in the inhibition range of small phenolic compounds, especially phenolic aldehyde in our study, so it decreased enzymatic hydrolysis yield.[28] Other reports[29] about the effect of small phenolic compounds on cellulases or enzymatic hydrolysis could also be explained by the concentration-dependent effect.

Though the inhibition or inactivation effect of small phenolic compounds on cellulases has been reported,[10,11] the mechanism of the combination between cellulases and small phenolic compoundis is not yet clear. According to the previous work, tannic acid connects with cellulases by an affinity binding.[30] For lignocellulosic substrates, the nonproductive binding and inactivation of enzymes by lignin appear to be important factors limiting catalytic efficiency.[31−33] According to the interaction mechanism between protein and small phenolic compounds in the food industry, small phenolic compounds could form a hydrophobic monolayer on the surface of protein when their concentrations were low, enhancing the hydrophobic property of protein. Cellulases are known to connect with substrates through van der Waals forces and aromatic ring polarization interaction between three exposed aromatic amino acids located in the binding site and crystal face of the pyranose ring.[34−36]

Therefore, small phenolic compounds at low concentrations might increase the hydrophobic property of the cellulase surface, which would be helpful for cellulase to connect with substrates. However, if the concentration of small phenolic compound is too low to form a hydrophobic layer on the surface of cellulase, the small phenolic compound−cellulase complex might connect substrate nonfunctionally, resulting in an inhibitory effect on cellulases. If the concentration of small phenolic compounds is too high, the hydrophobic property on the cellulase surface might increase, causing the interaction among protein molecules to result in precipitation, resulting in an inhibitory effect.[28]

The inhibitory effect of *p*-hydroxybenzaldehyde, etc. on cellulases might be similar to that of coumarin on plant growth.[37] In that there is also no active group in the molecule, making it hard to form a hydrophobic layer on the surface of cellulase. However, *p*-hydroxybenzaldehyde, etc. might connect with the aromatic ring in cellulose-binding domains through a hydrophobic interaction to hamper the binding between cellulases and substrate.

This paper mainly concerns the small phenolic compounds identified in SECS; the effects of other phenolic acid and phenolic aldehyde on cellulase activity need further research. Moreover, a more generalized conclusion about the effect of small phenolic compounds on cellulase activity and cellulose enzymatic hydrolysis could be made, which might be helpful to improve different pretreatment technologies for various plant biomass.

According to identification results of washing liquid of both SECS and MCS, there were both phenolic acid and phenolic aldehyde. The total concentration of small phenolic com-

pounds changed with different pretreatment conditions. Therefore, further research was carried out to explore how the small phenolic compounds presented in and released from pretreatment of corn stover influenced the cellulase activity and enzymatic hydrolysis of cellulose.

Effect of Small Phenolic Compounds in Pretreated Stover on Cellulase Activity. Figure 2 shows cellulase activity is stimulated by washing liquid of SECS pretreated at the strengths of 2.85−3.89, and the highest enhancement of FPU reaches 34.48%, while cellulase activity decreases only 1.72% by washing liquid of SECS pretreated at the strengths of 3.97 and 4.19.

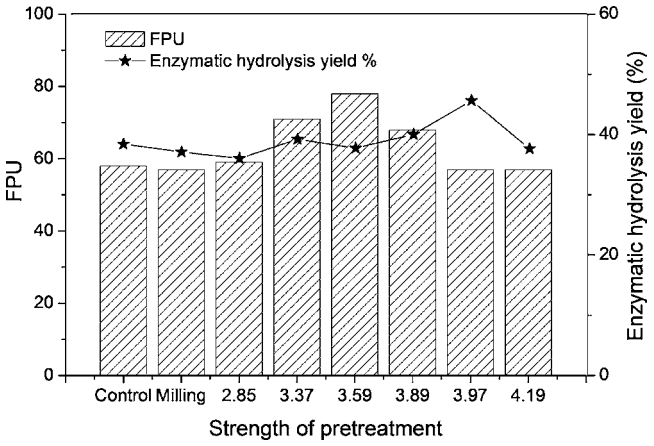

Figure 2. Effect of washing liquid on celluase activity and enzymatic hydrolysis of MCS. Reducing sugar was all analyzed with HPLC. Control represents the sample of cellulases and substrate at the same concentration without washing liquid. M indicates that the washing liquid added was from the sample of MCS. The datum 2.85 indicates that the washing liquid added was from the sample of corn stover pretreated by steam explosion at the strength of 2.85. So do 3.37, 3.59, 3.89, 3.97, and 4.19.

By composition analysis of the washing liquid of both SECS and MCS, it revealed that there were mainly sugars, 5-HMF, levulinic acid, and acetic acid.[5] While the effect of small phenolic compound on cellulase activity was tested, acetic acid−sodium acetate was taken as buffer. Therefore, the influence of small molecule acids such as levulinic acid and acetic acid could be excluded. For 5-HMF, its concentration was in the range of 0.28−0.81g/L while examining the effect of washing liquid of SECS on cellulase activity. Therefore, the effect of 5-HMF at a definite concentration on cellulase activity was also examined and shown in Figure 3. Results revealed that 5-HMF might inhibit cellulase activity at the concentration of 0.28−0.81 g/L. Therefore, it might be the small phenolic compounds in the washing liquid of SECS that stimulated cellulase activity, especially when the inhibition effect of 5-HMF was excluded.

Effect of Small Phenolic Compounds in Pretreated Stover on Enzymatic Hydrolysis. Enzymatic hydrolysis of MCS might be slightly improved by washing liquid of SECS pretreated at the strengths of 2.85−3.89, and the inhibition effect on enzymatic hydrolysis was only 2.63% for the washing liquid of SECS pretreated at the strength of 3.97 and 4.19 (Figure 2). It is different for the effect of the washing liquid on cellulase activity and enzymatic hydrolysis. This reveals that the stimulation or inhibition effect is also related to the substrate, which requires further research.

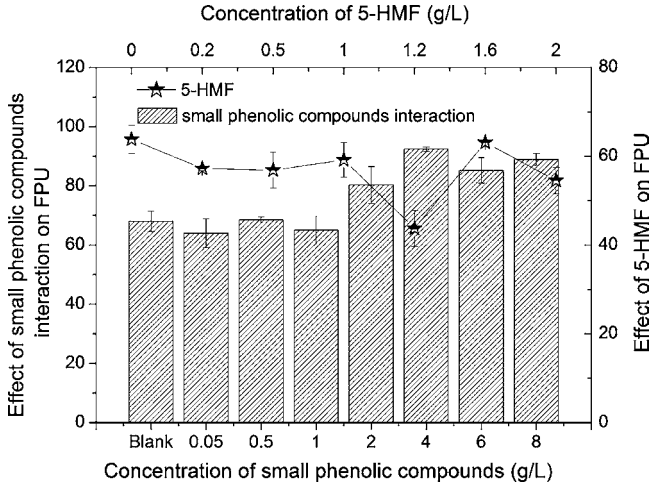

Figure 3. Left Y and bottom X is the interaction effect of individual small phenolic compound on cellulase activity. Reducing sugar was analyzed with the DNS method. Right Y and top X is the effect of 5-HMF on cellulase activity. Reducing sugar was tested with HPLC.

The average and initial enzymatic hydrolysis rates of SECS and MCS are all significantly higher than that of solid after washing steam exploded corn stover and solid after washing steam exploded corn stover, respectively (Figure 4). If the inhibition effect of 5-HMF on cellulases were excluded, the stimulation effect of phenolic acid (in pretreated stover) on enzymatic hydrolysis would be more significant. At the initial 8 h of hydrolysis, the average enzymatic hydrolysis rate of SECS increased 36.89% compared with that of the solid after washing steam exploded corn stover when the pretreatment strength was 3.97. For the last 8 h (40−48 h), the average enzymatic hydrolysis rate was 5.01 times higher than that of solid after washing steam exploded corn stover when the pretreatment strength was 3.89. These results demonstrate that water washing liquid of both SECS and MCS could stimulate enzymatic hydrolysis. Therefore, the highest enzymatic

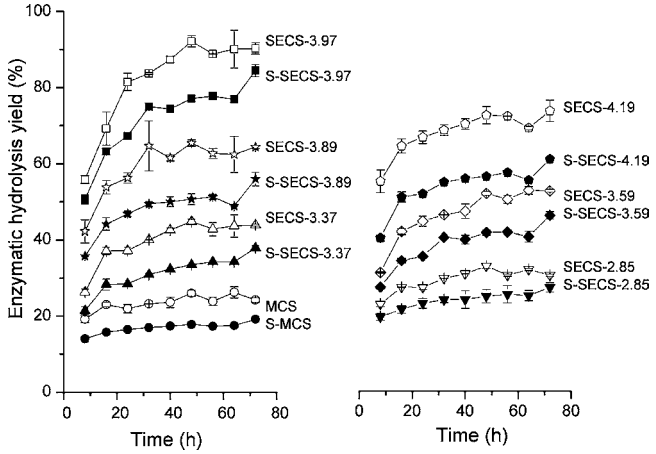

Figure 4. Effect of small phenolic compounds in pretreated stover on enzymatic hydrolysis. Reducing sugars produced at different times were analyzed with HPLC. SECS-2.85 represents the sample of corn stover pretreated by steam explosion at the strength of 2.85. So do SECS-3.37, SECS-3.59, SECS-3.89, SECS-3.97, and SECS-4.19. S-SECS-2.85 represents the solid after washing and separating corn stover pretreated by steam explosion at a strength of 2.85. So do SECS-3.37, SECS-3.59, SECS-3.89, SECS-3.97, and SECS-4.19.

dx.doi.org/10.1021/jf405046m | J. Agric. Food Chem. 2014, 62, 3223−3229

hydrolysis yield was obtained after reaction for 48 h for most SECS but 72 h for solid after washing SECS.

Results revealed that water washing liquid of both SECS and MCS could also enhance the highest enzymatic hydrolysis yield (Figure 4). Water washing liquid of MCS made the highest enzymatic hydrolysis yield increase by 37.13%, even though only *p*-hydroxybenzoic acid was identified in it. In the enzymatic hydrolysis solution of MCS, the concentration of *p*-hydroxybenzoic acid was 0.061 g/L, which would inhibit cellulases according to the analysis above. This revealed that the effect of small phenolic compounds on enzymatic hydrolysis might be related to substrates besides cellulases. As discussed above, further work is necessary to explore this finding.

The highest enhancement of enzymatic hydrolysis yield reached 20.79% when enzymatic hydrolysis was stimulated by water washing liquid of SECS pretreated at a strength of 3.97, and that pretreatment at a strength of 3.37 had the lowest stimulation effect on enzymatic hydrolysis. In the enzymatic hydrolysis solution of sample pretreated at a strength of 3.97, the concentrations of phenolic acid and phenolic aldehyde were 0.456 g/L and 0.555 g/L, respectively, while for the sample pretreated at the strength of 3.37, the concentrations of phenolic acid and phenolic aldehyde were 1.273 g/L and 0.103 g/L, respectively. When the concentration of individual small phenolic compounds was lower than 1 g/L, most of them inhibit cellulases according to Figure 1. Therefore, there might be interaction among the different small phenolic compounds. According to the content of small phenolic compounds in pretreated stover, the interaction among the different small phenolic compounds was analyzed.

Results (Figure 3) show that the mixed small phenolic compounds exhibit a slight stimulation effect on cellulase activity even at a concentration of 0.5 g/L. Moreover, compared with the effect of individual small phenolic compounds on cellulase activity, the inhibition effect of mixed small phenolic compounds at low concentration was much slighter. The highest stimulation effect reached 35.93%, which was higher than that of the individual phenolic acid (syringic acid reached the highest 16.65%). This explains why the enzymatic hydrolysis of samples pretreated at the strengths of 3.37 and 3.97 was stimulated significantly by the small phenolic compounds with a total concentration of 1.011 g/L and 1.376 g/L, respectively.

The higher enzymatic hydrolysis rate and yield of pretreated stover before washing further proved that washing liquid could stimulate enzymatic hydrolysis of cellulose. It was proven that the stimulation effect was mainly from small phenolic compounds especially phenolic acid or their interaction. Therefore, small phenolic compounds released during steam explosion should remain in the process of enzymatic hydrolysis to utilize their stimulation effect and be removed before fermentation to avoid their inhibition effect.[16] This paper also provides reference for analyzing the effect of small phenolic compounds released from other pretreatment technologies on the enzymatic hydrolysis of cellulose.

■ ASSOCIATED CONTENT

Supporting Information

Pretreated biomass composition, model phenolic compound detection on HPLC (elution time), optical densities of background/control. This material is available free of charge via the Internet at http://pubs.acs.org.

■ AUTHOR INFORMATION

Corresponding Author

*Tel: +86-10-82544982; fax: +86-10-82627071; e-mail: hzchen@home.ipe.ac.cn.

Funding

Financial support for this study was provided by the National Basic Research Program of China (973 Project No. 2011CB707401), the Beijing Key Laboratory Program of Cultivation and Development Engineering of Science and Technology Innovation Base (Z13111000280000), the National High Technology Research and Development Program of China (863 Program, SS2012AA022502).

Notes

The authors declare no competing financial interest.

■ ABBREVIATIONS USED

FPU: filter paper unit; IU: international unit; SECS: steam exploded corn stove; MCS: milled corn stover; S-SECS: solid after washing steam exploded corn stover with water; S-MCS: solid after washing milled corn stover with water; DNS: 3,5-dinitrosalicylic acid; 5-HMF: 5-hydroxymethylfurfural; HPLC: high-performance liquid chromatography; SPSS: Statistical Product and Service Solution

■ REFERENCES

(1) Chen, H. Z.; Qiu, W. H. The crucial problems and recent advance on producing fuel alcohol by fermentation of straw. *Prog. Chem.* **2007**, *19*, 1116−1121.

(2) Zhang, H. Effect of Phenolic Acids on Fermentation of Cell Walls from Crop Residues by Rumen Microorganisms. Thesis, China Agricultural University, 2005.

(3) Jung, H.; Allen, M. Characteristics of plant cell walls affecting intake and digestibility of forages by ruminants. *J. Anim. Sci.* **1995**, *73*, 2774−2790.

(4) Hartley, R. *p*-Coumaric and ferulic acid components of cell walls of ryegrass and their relationships with lignin and digestibility. *J. Sci. Food Agric.* **2006**, *23*, 1347−1354.

(5) Wang, L.; Chen, H. Z. Increased fermentability of enzymatically hydrolyzed steam-exploded corn stover for butanol production by removal of fermentation inhibitors. *Process Biochem.* **2011**, *46*, 604−607.

(6) Palmqvist, E.; Hahn-Hägerdal, B. Fermentation of lignocellulosic hydrolysates. I: inhibition and detoxification. *Bioresour. Technol.* **2000**, *74*, 17−24.

(7) Martinez, A.; Rodriguez, M. E.; Wells, M. L.; York, S. W.; Preston, J. F.; Ingram, L. O. Detoxification of dilute acid hydrolysates of lignocellulose with lime. *Biotechnol. Prog.* **2008**, *17*, 287−293.

(8) Excoffier, G.; Toussaint, B.; Vignon, M. R. Saccharification of steam-exploded poplar wood. *Biotechnol. Bioeng.* **2004**, *38*, 1308−1317.

(9) Jurado, M.; Prieto, A.; Martínez-Alcalá, Á.; Martínez, Á. T.; Martínez, M. J. Laccase detoxification of steam-exploded wheat straw for second generation bioethanol. *Bioresour. Technol.* **2009**, *100*, 6378−6384.

(10) Ximenes, E.; Kim, Y.; Mosier, N.; Dien, B.; Ladisch, M. Deactivation of cellulases by phenols. *Enzyme Microb. Technol.* **2011**, *48*, 54−60.

(11) Ximenes, E.; Kim, Y.; Mosier, N.; Dien, B.; Ladisch, M. Inhibition of cellulases by phenols. *Enzyme Microb. Technol.* **2010**, *46*, 170−176.

(12) Tejirian, A.; Xu, F. Inhibition of enzymatic cellulolysis by phenolic compounds. *Enzyme Microb. Technol.* **2011**, *48*, 239−247.

(13) Du, B.; Sharma, L. N.; Becker, C.; Chen, S. F.; Mowery, R. A.; van Walsum, G. P.; Chambliss, C. K. Effect of varying feedstock−pretreatment chemistry combinations on the formation and accumulation of potentially inhibitory degradation products in biomass hydrolysates. *Biotechnol. Bioeng.* **2010**, *107*, 430−440.

(14) Zhang, Y. Z.; Fu, X. G.; Chen, H. Z. Pretreatment based on two-step steam explosion combined with an intermediate separation of fiber cells-Optimization of fermentation of corn straw hydrolysates. *Bioresour. Technol.* **2012**, *121*, 100−104.
(15) Li, D. G.; Li, Z. X.; Qin, S. J.; Ma, H. Y. Effects of phenolic compounds on the growth and key enzymes in respiration of cerasus sachalinensis. *Acta Hortic. Sin.* **2012**, *39*, 49−56.
(16) Klinke, H. B.; Thomsen, A.; Ahring, B. K. Inhibition of ethanol-producing yeast and bacteria by degradation products produced during pre-treatment of biomass. *Appl. Microbiol. Biotechnol.* **2004**, *66*, 10−26.
(17) Chen, H.; Qiu, W. Key technologies for bioethanol production from lignocellulose. *Biotechnol. Adv.* **2010**, *28*, 556−562.
(18) Zhang, Y. Z.; Chen, H. Z. Multiscale modeling of biomass pretreatment for optimization of steam explosion conditions. *Chem. Eng. Sci.* **2012**, *75*, 177−182.
(19) Ghose, T. Measurement of cellulase activities. *Pure Appl. Chem.* **1987**, *59*, 257−268.
(20) Overend, R.; Chornet, E.; Gascoigne, J. Fractionation of lignocellulosics by steam-aqueous pretreatments [and discussion]. *Philos. Trans. R. Soc., A* **1987**, *321*, 523−536.
(21) Sluiter, A.; Hames, B.; Ruiz, R.; Scarlata, C.; Sluiter, J.; Templeton, D.; Crocker, D. *Determination of Structural Carbohydrates and Lignin in Biomass*, Laboratory Analytical Procedure; National Renewable Energy Laboratory: Golden, CO, 2008.
(22) Adney, B.; Baker, J. *Measurement of Cellulase Activities*, Laboratory Analytical Procedure; National Renewable Energy Laboratory: Golden, CO, 1996.
(23) Miller, G. L. Use of dinitrosalicylic acid reagent for determination of reducing sugar. *Anal. Chem.* **1959**, *31*, 426−428.
(24) Rivers, D. B.; Gracheck, S. J.; Woodford, L. C.; Emert, G. H. Limitations of the DNS assay for reducing sugars from saccharified lignocellulosics. *Biotechnol. Bioeng.* **2004**, *26*, 800−802.
(25) Liang, R.; Shoemaker, C. F.; Yang, X. Q.; Zhong, F.; Huang, Q. R. Stability and bioaccessibility of β-carotene in nanoemulsions stabilized by modified starches. *J. Agric. Food Chem.* **2013**, *61*, 1249−1257.
(26) Cantarella, M.; Cantarella, L.; Gallifuoco, A.; Spera, A.; Alfani, F. Effect of inhibitors released during steam-explosion treatment of poplar wood on subsequent enzymatic hydrolysis and SSF. *Biotechnol. Prog.* **2008**, *20*, 200−206.
(27) García-Aparicio, M. P.; Ballesteros, I.; González, A.; Oliva, J. M.; Ballesteros, M.; Negro, M. J. In *Effect of Inhibitors Released during Steam-Explosion Pretreatment of Barley Straw on Enzymatic Hydrolysis*; Twenty-Seventh Symposium on Biotechnology for Fuels and Chemicals, 2006; Springer: New York, 2006; pp 278−288.
(28) Kim, Y.; Ximenes, E.; Mosier, N. S.; Ladisch, M. R. Soluble inhibitors/deactivators of cellulase enzymes from lignocellulosic biomass. *Enzyme Microb. Technol.* **2011**, *48*, 408−415.
(29) Jing, X.; Zhang, X.; Bao, J. Inhibition performance of lignocellulose degradation products on industrial cellulase enzymes during cellulose hydrolysis. *Appl. Biochem. Biotechnol.* **2009**, *159*, 696−707.
(30) Olsen, S. N.; Bohlin, C.; Murphy, L.; Borch, K.; McFarland, K. C.; Sweeny, M. D.; Westh, P. Effects of non-ionic surfactants on the interactions between cellulases and tannic acid: A model system for cellulase-poly-phenol interactions. *Enzyme Microb. Technol.* **2011**, *49*, 353−359.
(31) Palonen, H.; Tjerneld, F.; Zacchi, G.; Tenkanen, M. Adsorption of *Trichoderma reesei* CBH I and EG II and their catalytic domains on steam pretreated softwood and isolated lignin. *J. Biotechnol.* **2004**, *107*, 65−72.
(32) Berlin, A.; Balakshin, M.; Gilkes, N.; Kadla, J.; Maximenko, V.; Kubo, S.; Saddler, J. Inhibition of cellulase, xylanase and β-glucosidase activities by softwood lignin preparations. *J. Biotechnol.* **2006**, *125*, 198−209.
(33) Berlin, A.; Gilkes, N.; Kurabi, A.; Bura, R.; Tu, M.; Kilburn, D.; Saddler, J. Weak lignin-binding enzymes. *Appl. Biochem. Biotechnol.* **2005**, *121*, 163−170.
(34) Kraulis, P. J.; Clore, G. M.; Nilges, M.; Jones, T. A.; Pettersson, G.; Knowles, J.; Gronenborn, A. M. Determination of the three-dimensional solution structure of the C-terminal domain of cellobiohydrolase I from *Trichoderma reesei*. A study using nuclear magnetic resonance and hybrid distance geometry-dynamical simulated annealing. *Biochemistry* **1989**, *28*, 7241−7257.
(35) Mattinen, M.-L.; Linder, M.; Teleman, A.; Annila, A. Interaction between cellohexaose and cellulose binding domains from *Trichoderma reesei* cellulases. *FEBS Lett.* **1997**, *407*, 291−296.
(36) Carrard, G.; Linder, M. Widely different off rates of two closely related cellulose-binding domains from *Trichoderma reesei*. *Eur. J. Biochem.* **2001**, *262*, 637−643.
(37) Abenavoli, M. R.; Sorgonà, A.; Sidari, M.; Badiani, M.; Fuggi, A. Coumarin inhibits the growth of carrot (*Daucus carota L.* cv. Saint Valery) cells in suspension culture. *J. Plant Physiol.* **2003**, *160*, 227−237.

To remedy the issue of environmental hazards, waste should be recycled, and new technology should be promoted. The oil and isoflavones extraction from SSR using the proposed technology was investigated. The physicochemical properties and fatty acid composition of crude oil, as well as the yield of extracted isoflavones and their components, were analyzed. Results showed that the crude oil is refined through molecular distillation and may be used as feedstuff oil. The isoflavones remaining in SSR mainly exists in the form of daidzein and genistein. This study may be referential to the comprehensive utilization of SSR.

MATERIALS AND METHODS

Materials. SSRs were donated by the PRB Biotech Co., Ltd. (Zhongshan, Guangdong, China), and the main components are shown in Table 1. Samples were stored at 4 °C inside a polythene drum until extraction. *n*-Butane (99.99%) was purchased from Shenzheng Shenyan Gas Co., Ltd. (Shenzhen, Guangdong, China). All other reagents were purchased from Sigma Chemical Co. (St. Louis, MO, USA) and of analytical grade.

Table 1. Main Components of Fresh and Defatted SSR (Dry Basic, %)

	content (%)	
main component	fresh SSR	defatted SSR
crude fat	29.2 ± 0.68	0.62 ± 0.18
crude protein	21.8 ± 0.57	29.3 ± 0.84
crude fiber	18.1 ± 0.82	24.8 ± 0.32
ash	29.5 ± 1.02	43.3 ± 0.69

Experimental Design. On the basis of previous single-factor experiments, a central composite design (CCD) was applied to evaluate the effects of extraction temperature, time, and raw material granularity (RMG) on oil yield. The coded and uncoded independent variables used in the response surface methodology (RSM) design, as well as their respective levels, are listed in Table 2.[12]

Table 2. Experimental Design and Data for the Yield of SSR Oil from the CCD[a]

				decoded value			response
run no.	coded value			X_1	X_2	X_3	Y_1
1	0	−1	1	45	45	80	21.60 ± 0.07
2	−1	0	1	40	60	80	18.38 ± 0.12
3	0	1	−1	45	75	40	28.03 ± 0.03
4	−1	0	−1	40	60	40	24.78 ± 0.17
5	1	0	1	50	60	80	20.76 ± 0.09
6	0	1	1	45	75	80	23.96 ± 0.14
7	0	0	0	45	60	60	27.80 ± 0.16
8	1	−1	0	50	45	60	22.91 ± 0.32
9	0	−1	−1	45	45	40	27.92 ± 0.06
10	0	0	0	45	60	60	27.30 ± 0.23
11	−1	−1	0	40	45	60	21.08 ± 0.19
12	1	1	0	50	75	60	23.54 ± 0.08
13	0	0	0	45	60	60	27.60 ± 0.12
14	0	0	0	45	60	60	26.90 ± 0.18
15	1	0	−1	50	60	40	23.20 ± 0.04
16	−1	1	0	40	75	60	22.50 ± 0.31
17	0	0	0	45	60	60	27.90 ± 0.03

[a] X_1 = temperature (°C), X_2 = time (min), X_3 = RMG (mesh), Y_1 = oil yield (%).

All experiments were performed randomly to minimize the effect of extraneous factors. A quadratic polynomial regression was assumed in the prediction of oil yield (Y_1) as a function of the independent variables, as shown in eq 1:

$$Y_1 = K_0 + K_1X_1 + K_2X_2 + K_3X_3 + K_{11}X_1^2 + K_{22}X_2^2 + K_{33}X_3^2 + K_{12}X_1X_2 + K_{13}X_1X_3 + K_{23}X_2X_3 \quad (1)$$

where K_0 is a constant. K_i, K_{ii}, and K_{ij} are linear, quadratic, and interactive regression coefficients, respectively. The statistical significance of the model and the goodness of fit were evaluated using analysis of variance (ANOVA). The RSM was used to investigate the effect of the process variables on the response and to determine the optimal conditions for maximum oil yield. The experimental data were statistically analyzed using Design-Expert version 8.0.0 software (StatEase Inc., Minneapolis, MN, USA).

Oil Extraction. Prior to extraction, the SSRs were dried at 60 °C to ensure that moisture content was less than 5%, and the samples were grounded into powder. Extractions were conducted by continuous *n*-butane in a 3 L extraction pot. The solvent and extracted oil were separated through low-temperature vacuum evaporation. The oil yield was calculated using the following equation:

$$\text{oil yield (\%)} = \frac{\text{the weight of extracted oil (g)}}{\text{the weight of raw materials (g)}} \times 100 \quad (2)$$

Physicochemical Analyses of Crude Oil. Assays were performed for the determination of acid value (AV), peroxide value (POV), iodine value, saponification value, and refractive index, in accordance with GB 1535-2003 (an officially recognized Chinese criterion for physicochemical property detection and quality standard of soybean oil).[13]

Fatty Acid Analysis. Fatty acid composition was determined by conversion of the oil to fatty acid methyl esters (FAMEs) and analyzed by gas chromatography−mass spectrometry (GC-MS) (Agilent Co., Santa Clara, CA, USA) equipped with a flame ionization detector (FID). FAMEs were prepared by adding 50 mg of extracted oil, which was dissolved with 4 mL of isooctane; afterward, 200 μL of sodium methoxide was mixed with the solution.[14] The mixtures were allowed to settle for 5 min, and the supernatant (0.2 μL) was injected into the gas chromatograph−mass spectrometer. The components were identified by comparing their retention time with those of the standards in the mass spectra library. In addition, their relative content was calculated from the GC peak area.

The GC-MS conditions were as follows: a polar capillary column HP-INNOWAX (30 m × 0.25 mm, 0.25 μm film thickness) was used at a column head pressure of 0.04 MPa. The oven temperature was from 120 to 220 °C at heating rate of 8 °C/min, which was held for 1 min, continuously increased to 250 °C at 4 °C/min, and held for 5 min. The detector and injector temperatures were 220 and 230 °C, respectively.[15] Helium was used as the carrier gas at approximately 40 mL/min.

Deacidification by Molecular Distillation. Crude oil deacidification was performed using a laboratory-scale molecular distillation unit (model DCH70, Meichengaoxin Separation Technology Co., Ltd., Guangzhou, Guangdong, China). The distillation unit consisted of an evaporator with an internal condenser. For feeding, a jacketed vessel equipped with a flow regulation valve and level indication was used. The vacuum was achieved using a mechanical pump and a diffusion pump. The samples were first fully melted by circulating hot water (45 °C). Then, the melted samples were placed into the circulating hot oil-heated evaporator (220 °C), with a feed flow rate from 1.5 to 2.5 mL/min under 0.05 mbar pressure.[16] Thin-film samples were achieved using a roller wiper system (475 rpm), and the condensation temperature was 25 °C. Free fatty acids were collected as the distillate, with the refined oil as the residue.

Isoflavone Extraction. The SSRs were defatted prior to isoflavone extraction. Extractions were conducted by continuous 95% (v/v) ethanol in a 3 L extraction pot under 1.0 MPa at 60 °C for 90 min. The solvent and extracted isoflavones were separated through low-

dx.doi.org/10.1021/jf405459v | J. Agric. Food Chem. 2014, 62, 3230−3235

temperature vacuum evaporation. The isoflavone yield was calculated using the following equation:

$$\text{isoflavone yield}\ (\%) = \frac{\text{the weight of extracted isoflavone (g)}}{\text{the weight of defatted SSR (g)}} \times 100 \quad (3)$$

Isoflavone High-Performance Liquid Chromatography (HPLC) Analysis. HPLC analysis was performed on a LC-10A system (Shimadzu, Kyoto, Japan) equipped with an UV detector (200−600 nm) and a Diamonsil C_{18} column (5 μm, 250 mm × 4.6 mm) at room temperature. Extracted isoflavones and standard substances were dissolved in ethanol. The injection volume was 20 μL, and the absorption was measured at 260 nm. The mobile phase was deionized water (A) and acetonitrile (B). Gradient elution was operated at a flow rate of 1.0 mL/min according to the following gradient procedure: 0.0−10.0 min, 10.0−45.0% B; 10.0−25.0 min, 45.0% B; 25.0−45.0 min, 85.0% B; 45.0−60.0 min, 10.0% B.[17] The components were identified by comparing their retention times with those of the standards, and their contents were calculated from the peak area.

Statistical Analysis. All assays were performed in triplicate, and the results were expressed as mean values ± standard deviations. ANOVA was performed, and the differences were considered statistically significant at $P < 0.05$.

RESULTS AND DISCUSSION

Model Fitting. SSR oil yield obtained for each experiment is listed in Table 2.

The response and variables were fitted to each other by multiple regressions. A good fit was obtained, and the second-order polynomial equation is shown below by eq 4:

$$Y_1 = 27.5 + 0.46{*}X_1 + 0.44{*}X_2 - 2.53{*}X_3 - 0.20{*}X_1{*}X_2 + 0.99{*}X_1{*}X_3 + 0.31{*}X_2{*}X_3 - 4.17{*}X_1^2 - 0.82{*}X_2^2 - 1.55{*}X_3^2 \quad (4)$$

Results from ANOVA showed that the polynomial model had a satisfactory P value ($P < 0.0001$), which indicated significant results at 1% (Table 3). The P value of lack-of-fit was 0.172 ($P > 0.05$), which means that each lack-of-fit was not significantly related to pure error. The large value of the multiple determination coefficient ($R^2 = 0.9886$) revealed that the model adequately represented the experimental results.

Table 3. ANOVA for Response Surface Model Fitting[a]

source	ss	df	ms	f value	P value
model	150.8	9	16.76	57.20	<0.0001[a]
X_1	1.68	1	1.68	5.75	0.0476[b]
X_2	1.55	1	1.55	5.29	NS[c]
X_3	51.16	1	51.16	174.64	<0.0001[a]
X_1X_2	0.16	1	0.16	0.53	NS[c]
X_1X_3	3.92	1	3.92	13.38	0.0081[a]
X_2X_3	0.39	1	0.39	1.33	NS[c]
X_1^2	73.32	1	73.32	249.95	<0.0001[a]
X_2^2	2.85	1	2.85	9.72	0.0169[b]
X_3^2	10.12	1	10.12	34.53	0.0006[a]
residual	2.05	7	0.29		
lack-of-fit	1.39	3	0.46	2.81	NS[c]
pure error	0.66	4	0.17		
the total correction	152.85	16			

[a]Statistically significant at $P < 0.01$. [b]Statistically significant at $P < 0.05$. [c]Not significant $P > 0.05$.

Analysis of Response Surfaces. The relationship between independent variables and responses in a three-dimensional response surface curve generated by the models is shown in Figure 1.

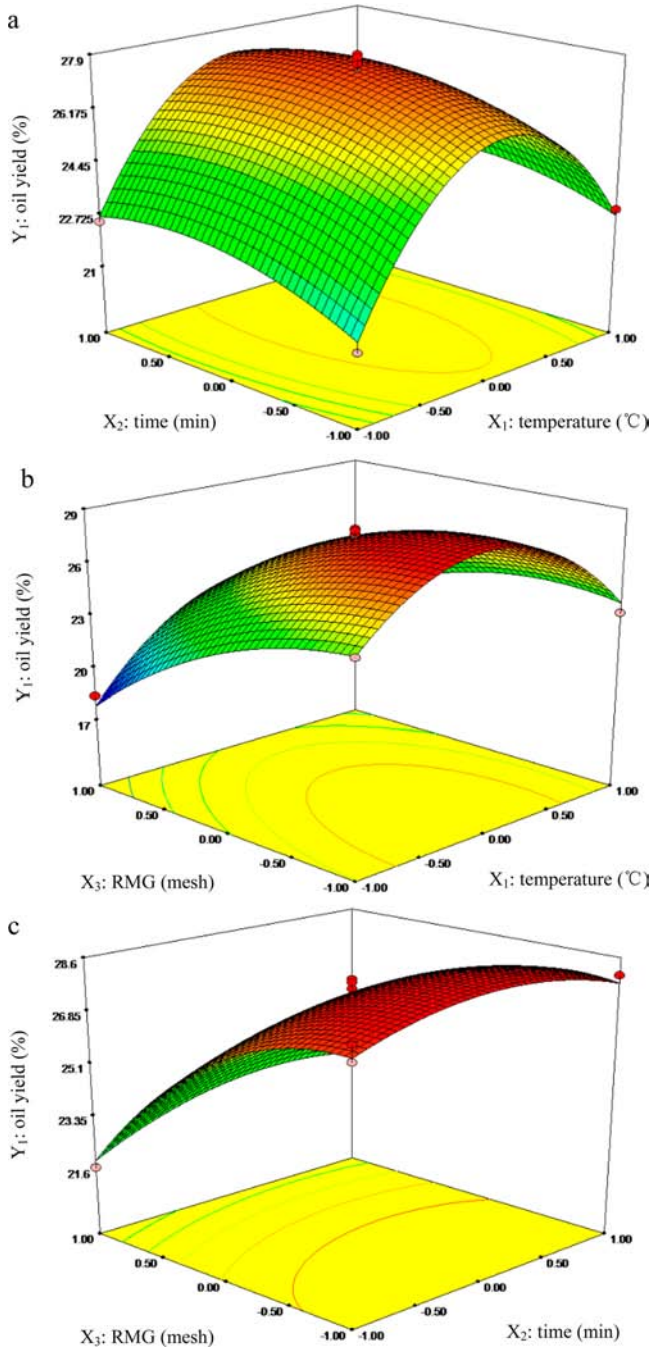

Figure 1. Three-dimensional response surface graphs for the effects on oil yield under the following parameters: (a) temperature and time; (b) RMG and temperature; and (c) time and RGM.

Time showed a positive effect on the response, which increased with a longer extraction period. This effect was more pronounced at the beginning of the extraction. When the process subsequently reached equilibrium, the freely available oil was exhausted, resulting in complete extraction with a slight increase of oil yield.[18] When the temperature increased, the response displayed an early increase and a subsequent

decreased state. Initially, high temperature reduced the viscosity of the solvent and enhanced solute vapor pressure, thereby increasing the diffusion coefficient of the oil.[19] However, when temperature was increased to a certain extent, the solvent was easily converted into gas, which decreased the mass transfer driving force and subsequently decreased the response. For RMG, the response declined dramatically when the mesh was increased from 40 to 80. Very small particles resulted in easy caking of SSR and the increase in mass transfer resistance, thereby loss of efficiency and yield decrease was caused.[20] Thus, the 40 mesh materials were enough for extraction. Results from ANOVA showed that the RMG had the maximum effect on the response, followed by the temperature. Both parameters were significant. The above analysis of response surfaces was preferential for SSR oil extraction by continuous *n*-butane.

Model Verification. With the aid of Design-Expert software, according to the solution of eq 4, the optimum conditions for maximum oil yield were 44.77 °C temperature, 61.8 min extraction time, and 43.6 mesh RMG. The predicted yield was 28.60%. The model was verified by three confirmatory tests. However, given the actual feasibility and convenience, the above condition was slightly modified as follows: 45 °C temperature, 62 min extraction time, and 45 mesh RMG. Under this condition, the actual yield was 28.43% ± 0.17%, which was relatively close to the predicted yield.

Traditional techniques, such as mechanical press extraction, can hardly extract the oil from SSR. This reason is related to the excessive degeneration of protein, which could reduce material plasticity and exploding pressure. Moreover, the phospholipids and proteins are good surfactants, which results in the decrease in interfacial tension between oil and water.[21] With petroleum ether as solvent, SSR oil can be extracted for 2 h per instance thrice.[22] After prepress, the oil yield increased by 7% through organic solvent extraction. However, the oil was further oxidized in the high-temperature process during prepress and can almost reach 18 mmol/kg. It still needs 40 min per time, twice, using subcritical fluid extraction.[23] Oil extraction from soybean using SFE is easier than that from SSR, which still requires a high pressure of 30 MPa and 4 h extraction time.[24] By using the novel extraction, the method only required 0.5 MPa and approximately 1 h extraction time. Apparently, the latter condition was more safe and efficient. Compared with these methods, continuous solvent could ensure complete oil extraction. Protection of heat-sensitive components and prevention of hazardous substances are also guaranteed in the whole low-temperature process.

The parameters were validated through comparative analysis, which showed reliable results. The developed model is advantageous for industrial production.

Physicochemical Properties. The quality and stability of the SSR oil extracted by continuous *n*-butane were determined by analyzing the physicochemical properties (Table 4).

Table 4. Physicochemical Properties of SSR Oil Extracted by Continuous Phase Transition Extraction

physicochemical index	property
refractive index (25 °C)	1.465 ± 0.08
acid value (mg KOH/g)	63.9 ± 0.10
peroxide value (mmol/kg)	9.05 ± 0.30
iodine value (g I/100 g)	138.93 ± 0.15
saponification value (mg KOH/g)	242.1 ± 0.21

Compared with the standard soybean oil in GB 1535-2003, the main drawback of the crude oil was the excess of AV (63.9 ± 0.1 mg KOH/g) and POV (9.05 ± 0.3 mmol/kg).[13] The oil is easily hydrolyzed and oxidized under acidic conditions during soy sauce fermentation.[25] The other determined indices were mostly in range. Thus, the crude oil is not appropriate for edible cooking oil but may be used for the feedstuff oil. From the main components of the defatted SSR listed in Table 1, the oil was almost extracted completely. The crude protein and fiber of defatted SSR accounted for more than half of the products. The rest of the ash was only washed away. A high amount of defatted SSR was still obtained.

Crude Oil Refining. The crude oil was refined through molecular distillation, and the results are shown in Figure 2.

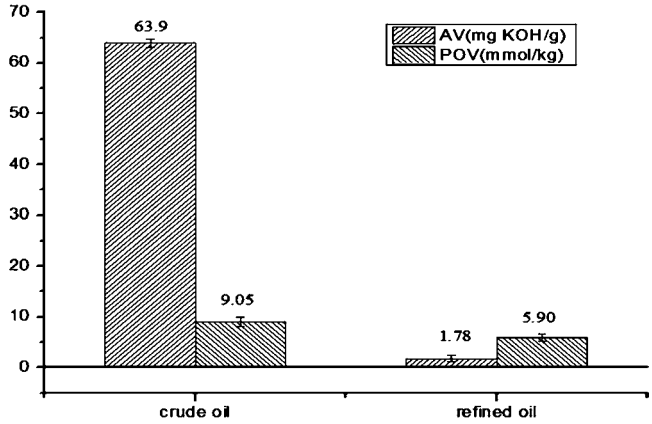

Figure 2. AV and POV of crude oil and refined oil.

Through molecular distillation, AV and POV sharply drop to 1.78 ± 0.12 mg KOH/g and 5.9 ± 0.08 mmol/kg, respectively. Compared with the conventional deacidification through alkali neutralization or esterification by adding methanol, molecular distillation avoids effluents and prevents corrosion of machines.[26] The refinement is simplified, and refined oil is easy to manufacture.

Fatty Acid Compositions and Contents. The fatty acid compositions and their relative refined oil contents were determined by GC-MS, and the results are shown in Table 5.

Table 5. Fatty Acid Compositions and Contents of Refined Oil

fatty acid composition	retention time (min)	relative content (%)
palmitic acid	11.34	13.07 ± 0.26
stearic acid	13.58	5.71 ± 0.33
oleic acid	13.84	21.44 ± 0.11
linoleic acid	14.43	50.23 ± 0.05
linolenic acid	15.22	9.54 ± 0.19

The refined oil mainly contained five fatty acids, with linoleic acid (50.23% ± 0.05%) as the principal content (>50%), followed by oleic acid (21.44% ± 0.11%). The fatty acids comprised 82% unsaturated and 18% saturated fatty acids. Compared with the first class soybean oil (GB1535-2003, China), most of the fatty acid compositions and relative content were still in range.[13]

Isoflavone Extraction and HPLC Analysis. From Figure 3, the dedicated retention times of daidzein and genistein were 15.8 and 19.6 min, respectively. No UV absorption peak was

dx.doi.org/10.1021/jf405459v | J. Agric. Food Chem. 2014, 62, 3230−3235

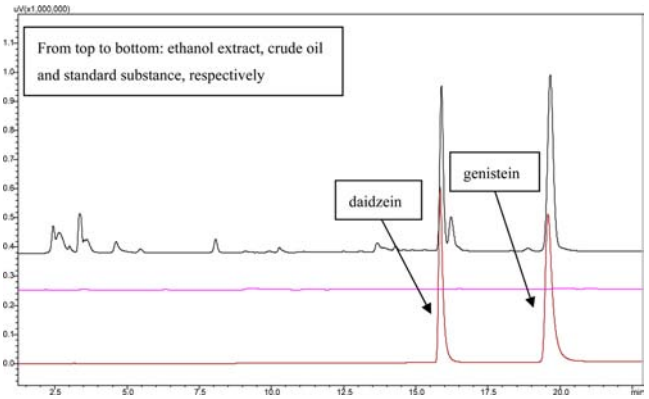

Figure 3. HPLC chromatograms of different substances.

found in the crude oil chromatogram. By contrast, two main peaks corresponding to the standard substances were observed. The results showed that isoflavones could not be extracted with oil extraction and still remained in the defatted SSR. The isoflavones mainly comprised daidzein and genistein, two kinds of aglycones.

Isoflavones reduce the risk of cardiovascular diseases and prevent certain cancers.[27] Instead of glycosidic form, aglyconic isoflavones play a major role in the biological effects. However, most isoflavones in natural food materials exist in glycosylated form and are not readily absorbed in the intestines.[28] During fermentation, glycosidic forms of isoflavones are converted to isoflavone aglycones with β-glucosidase enzymolysis. Thus, isoflavones extracted in SSR are of great value. Daidzein and genistein were calculated to be about 0.08% and 0.10%, respectively. The total isoflavones yield was 0.18% ± 0.012%. The amount of isoflavones varied according to genetics and growth location of the soybeans. The total isoflavone content ranged from 0.05% to 0.78%, with a mean of 0.1−0.2%, which indicates that, with 95% (v/v) ethanol solvent under 1.0 MPa at 60 °C temperature for 90 min, isoflavone could be extracted efficiently from defatted SSR using the proposed method.

With soybean as the main brewing material, abundant oil was remained in the SSR. The best oil extraction conditions by the novel, continuous phase transition extraction were investigated using RSM. The established optimal conditions for the maximum oil yield were *n*-butane solvent, 0.5 MPa extraction pressure, 45 °C temperature, 62 min extraction time, and 45 RGM. Under this condition, the actual yield was 28.43% ± 0.17%, relatively close to the predicted yield. Meanwhile, isoflavone was extracted from defatted SSR using the proposed method under the following parameters: solvent, 95% (v/v) ethanol; extraction pressure, 1.0 MPa; temperature, 60 °C; and extraction time, 90 min. The extracted isoflavones, with 0.18% ± 0.012% yield, mainly comprised daidzein and genistein, two kinds of aglycones. The main drawback of the crude oil was the excess of AV (63.9 ± 0.1 mg KOH/g) and POV (9.05 ± 0.3 mmol/kg). However, through molecular distillation, AV and POV could drop to 1.78 ± 0.12 mg KOH/g and 5.9 ± 0.08 mmol/kg, respectively. The refined oil may be used as feedstuff oil. The novel continuous phase transition extraction under low temperature could provide favorable conditions from the extraction of nonpolar to strongly polar substances. The proposed method is very suitable for industrial application. Results from this study may be used as reference for further development and utilization of SSR.

AUTHOR INFORMATION

Corresponding Author

*Phone: 86-020-85286234; fax: 86-020-85286234; e-mail: caoyong2181@scau.edu.cn.

Author Contributions

Lichao Zhao and Yong Zhang contributed equally to this article and should be considered cofirst authors.

Funding

The technical assistance was supported by the national forestry public welfare research (no. 201104003-03).

Notes

The authors declare no competing financial interest.

ACKNOWLEDGMENTS

We express our gratitude to PRB Biotech Co., Ltd. (Zhongshan, Guangdong, China) for donating soy sauce residues used in this study.

ABBREVIATIONS USED

SSR, soy sauce residue; RSM, response surface methodology; RMG, raw material granularity; FAMEs, fatty acid methyl esters; ANOVA, analysis of variance; GC-MS, gas chromatography−mass spectrometry; FID, flame ionization detector; HPLC, high-performance liquid chromatography; UV, ultraviolet

REFERENCES

(1) Nagai, T.; Tanoue, Y.; Kai, N.; Suzuki, N. In vitro antioxidative activity and antihypertensive activity of soy sauce cake derived from the manufacturing of Japanese style fermented soy sauce. *Int. J. Food. Sci. Nutr.* **2012**, *3*, 1118−1127.

(2) Chen, M.; Wu, H. Research development on the reutilization of soy sauce residue. *China Condiment* **2011**, *36* (8), 19−23.

(3) Pedroncelli, B.; Bonton, J. Causes of accidents by soy sauce squeezing residue and fish meal. *J. Mater. Eng. Perform.* **2009**, *2*, 1−7.

(4) Hosoda, K.; Miyaji, M.; Matsuyama, H.; Imai, Y.; Nonaka, K. Digestibility, ruminal fermentation, nitrogen balance and methane production in Holstein steers fed diets containing soy sauce cake at 10 or 20%. *Anim. Sci. J.* **2012**, *83* (3), 220−226.

(5) Seo, H.; Son, C.; Chung, C.; Jung, D.; Kim, S.; Gross, R. A.; Kaplan, D. L.; Lee, J. Production of high molecular weight pullulan by *Aureobasidium pullulans* HP-2001 with soybean pomace as a nitrogen source. *Bioresour. Technol.* **2004**, *95* (3), 293−299.

(6) Jin, H.; Lee, N.; Shin, M.; Kim, S.; Kaplan, D. L.; Lee, J. Production of gellan gum by *Sphingomonas paucimobilis* NK2000 with soybean pomace. *Biochem. Eng. J.* **2003**, *16* (3), 357−360.

(7) Umekawa, H.; Nakai, N.; Yoshida, S.; Furuichi, Y.; Matsunaga, M. Effect of Tamari soy sauce cake on blood pressure in spontaneously hypertensive rats. *J. Jpn. Soc. Food Sci.* **2006**, *53* (12), 655.

(8) Sreenath, H. K.; Moldes, A. B.; Koegel, R. G.; Straub, R. J. Lactic acid production from agriculture residues. *Biotechnol. Lett.* **2001**, *23* (3), 179−184.

(9) Latif, F.; Rajoka, M. I. Production of ethanol and xylitol from corn cobs by yeasts. *Bioresour. Technol.* **2001**, *77* (1), 57−63.

(10) Iwanaga, D.; Gray, D. A.; Fisk, I. D.; Decker, E. A.; Weiss, J.; McClements, D. J. Extraction and characterization of oil bodies from soy beans: A natural source of pre-emulsified soybean oil. *J. Agric. Food. Chem.* **2007**, *55* (21), 8711−8716.

(11) Miao, J.; Che, K.; Xi, R.; He, L.; Chen, X.; Guan, X.; Zhuang, X.; Wen, X.; Cao, Y. Characterization and benzo [a] pyrene content analysis of Camellia seed oil extracted by a novel subcritical fluid extraction. *J. Am. Oil Chem. Soc.* **2013**, *90* (10), 1503−1508.

(12) Tan, C.; Ghazali, H. M.; Kuntom, A.; Tan, C.; Ariffin, A. A. Extraction and physicochemical properties of low free fatty acid crude palm oil. *Food Chem.* **2009**, *113* (2), 645−650.

(13) Tang, X.; Long, L.; Xue, Y.; Chen, Y.; Xu, X.; Bian, Q.; Zhang, X. Soya bean oil. *Chinese National Standard*, GB 1535-2003; National Food Authority, 2003.
(14) Yang, T.; Liu, T. Optimization of production of conjugated linoleic acid from soybean oil. *J. Agric. Food. Chem.* **2004**, *52* (16), 5079−5084.
(15) He, R.; Ye, X. P.; English, B. C.; Satrio, J. A. Influence of pyrolysis condition on switchgrass bio-oil yield and physicochemical properties. *Bioresour. Technol.* **2009**, *100* (21), 5305−5311.
(16) Martinello, M.; Hecker, G.; Carmen Pramparo, M. I. A. D. Grape seed oil deacidification by molecular distillation: Analysis of operative variables influence using the response surface methodology. *J. Food Eng.* **2007**, *81* (1), 60−64.
(17) Sun, J. M.; Sun, B. L.; Han, F. X.; Yan, S. R.; Yang, H.; Akio, K. Rapid HPLC method for determination of 12 isoflavone components in soybean seeds. *Agric. Sci. China* **2011**, *10* (1), 70−77.
(18) Jokić, S.; Nagy, B.; Zeković, Z.; Vidović, S.; Bilić, M.; Velić, D.; Simándi, B. Effects of supercritical CO_2 extraction parameters on soybean oil yield. *Food. Bioprod. Process.* **2012**, *90* (4), 693−699.
(19) Kostić, M. D.; Joković, N. M.; Stamenković, O. S.; Rajković, K. M.; Milić, P. S.; Veljković, V. B. Optimization of hempseed oil extraction by n-hexane. *Ind. Crop. Prod.* **2013**, *48*, 133−143.
(20) Reverchon, E.; De Marco, I. Supercritical fluid extraction and fractionation of natural matter. *J. Supercrit. Fluids.* **2006**, *38* (2), 146−166.
(21) Campbell, K. A.; Glatz, C. E. Mechanisms of aqueous extraction of soybean oil. *J. Agric. Food. Chem.* **2009**, *57* (22), 10904−10912.
(22) Yang, Y.; Yao, S.; Wan, H.; Yu, J.; Song, H. Fat extraction from soy sauce residues and fatty acids composition analysis. *China Brewing* **2011**, *11*, 50−52.
(23) Zhong, Z. S.; Wang, Y. L.; Qi, Y. T.; Zhang, W. N. Extraction and quality analysis of soy sauce residue. *China Oils Fats* **2006**, *31* (11), 21−23.
(24) Joki, C. S.; Zekovi, C. Z.; Vidovi, C. S.; Sudar, R.; Nemet, I.; Bili, C. M.; Veli, C. D. Supercritical CO_2 extraction of soybean oil: Process optimization and triacylglycerol composition. *Int. J. Food. Sci. Technol.* **2010**, *45* (9), 1939−1946.
(25) Gong, X.; Cheng, Y. Q.; Ji, F. D.; Nirasawa, S.; Tatsumi, E.; Lu, F. Research progresses in the comprehensive utilization of soy sauce residue. *Sci. Technol. Food Ind.* [Online]. http://www.cnki.net/kcms/detail/11.1759.TS.20121122.1407.023.html.
(26) Wu, W.; Wang, C.; Zheng, J. Optimization of deacidification of low-calorie cocoa butter by molecular distillation. *LWT−Food. Sci.Technol.* **2012**, *46* (2), 563−570.
(27) Gang, L.; Yang, J.; Xin, J. F.; Yu, H. Molecular cloning and characterization of a novel β-glucosidase with high hydrolyzing ability for soybean isoflavone glycosides and glucose-tolerance from soil metagenomic library. *Bioresour. Technol.* **2012**, *123*, 15−22.
(28) Izumi, T.; Piskula, M. K.; Osawa, S.; Obata, A.; Tobe, K.; Saito, M.; Kataoka, S.; Kikuchi, M. Soy isoflavone aglycones are absorbed faster and in higher amounts than their glucosides in humans. *J. Nutr.* **2000**, *130* (7), 1695−1699.

human MFGs.[16,18,19] These studies discussed the possibility that the nonfluorescent dark domains are lipid rafts (liquid-ordered phase, L_o) enriched in SM and cholesterol[15,16] as Rd-DOPE is preferably portioned into liquid-disordered phase (L_d).[20] This proposal remains controversial as it has been demonstrated that the coexistence of phase regions [for instance, gel (L_β) + liquid crystalline (L_α) and L_d + L_o)] may not always distinguish between L_o and gel regions, thus giving misleading information about lipid surfaces when using fluorescent imaging techniques.[21] MFGM contains relatively high L_β–L_α phase transition temperature (T_m) phospholipids [for instance, 16:0-PC (DPPC) makes up ∼11.1% (w/w) and SM makes up ∼29.6% (w/w) of total polar lipids in bovine milk][2] which remain in a gel-phase state at ambient temperature, and the L_β may contribute to the dark regions on MFG surfaces by CLSM. Although the L_β phase may be transformed to the L_o phase by the inclusion of cholesterol,[21] the molar amount of cholesterol is less than the molar amounts of the high T_m phospholipids in the MFGM,[1] consequently, the existence of an L_β phase in the MFGM at ambient temperature is expected.

A supported monolayer model system was prepared from milk-derived phospholipids to examine lipid–lipid interactions and phase coexistence.[22] However, nonsupported phospholipid bilayer systems are rarely used to model the MFGM. Giant unilamellar vesicles as an artificial bilayer membrane system constructed from phospholipids with/without cholesterol have been used to mimic the morphology of native biomembranes and to investigate interactions between proteins and lipids and specific functions of lipid domains.[9,23] Techniques such as fluorescent imaging[24,25] have provided fundamental knowledge of GUV formation. In the current study, we have constructed GUVs from milk-derived phospholipids and use this as a model to examine the lipid morphology of the MFGM.

MATERIALS AND METHODS

Materials. Indium tin oxide (ITO)-coated glass slides (surface resistivity 30–60 Ω/cm^2) were purchased from Sigma-Aldrich (Saint Louis, MO). The fluorescent fatty acid-labeled phospholipid analogue 1-palmitoyl-2-{6-[(7-nitro-2-1,3-benzoxadiazol-4-yl)amino]hexanoyl}-*sn*-glycero-3-phosphocholine (16:0–12:0, NBD-PC, 1 mg/mL in chloroform) and the fluorescent headgroup-labeled phospholipid analogue 1,2-dioleoyl-*sn*-glycero-3-phosphoethanolamine-N-(lissamine rhodamine B sulfonyl) ammonium salt (18:1, Rd-DOPE, 1 mg/mL in chloroform) were chosen as fluorescent probes; 1,2-dipalmitoyl-*sn*-glycero-3-phosphocholine (16:0-PC, DPPC in powder form, L_β/L_α phase transition temperature 42 to 52 °C),[26] 1,2-dioleoyl-*sn*-glycero-3-phosphoethanolamine (18:1-PE, DOPE in powder form, L_β/L_α phase transition temperature −9.9 to −2.9 °C),[27] and sphingomyelin (SM, fractionated from bovine milk and 16:0, L_β/L_α phase transition temperature 35 to 82 °C)[28] were all provided by Avanti Polar Lipids, Inc. (Alabaster, AL). Sucrose and glucose (both anhydrous) and chloroform, acetone, methanol, and water (HPLC grade) were all sourced from Fisher Scientific (Fair Lawn, NJ). A function generator (model 72-7710) was purchased from TENMA test equipment (Springboro, OH), and a digital phosphor oscilloscope (model TDS 3012, 100 MHz, 1.25 GS/s, 10K point) was provided from Tektronix (Beaverton, OR).

Electroformation of Giant Unilamellar Vesicles (GUVs). GUVs were generated from combinations of phospholipids under an alternating current (AC) electrical field[24,29−33] with modifications. The detailed sample plan and operation are explained as follows.

Sample Plan and Preparation. GUVs were formed from unitary, binary (SM is considered as unitary), and quaternary systems including DPPC, DOPE, SM, and/or cholesterol. Two sets of sample groups were prepared for studying the effects of DPPC and SM on regulating the lipid domain formation. Set 1: DPPC, DPPC + DOPE (7/3, 1/1, 3/7, mol/mol), and DOPE; set 2: SM, SM + DOPE (7/3, 1/1, 3/7, mol/mol), and DOPE. In simulating the MFGM composition, an extra sample containing DPPC, SM, DOPE, and cholesterol (8/8/8/4, mol/mol or 28.6 mol % for polar lipids and 14.3 mol % for cholesterol) was prepared to mimic the morphology of the native MFGM. It has been reported that the weight ratio between phospholipid and cholesterol in the MFGM is 25:2, w/w (∼25:4, mol/mol, calculated based on the mean molecular weight) in which phosphatidylethanolamine (PE), phosphatidylcholine (PC), and sphingomyelin (SM) are the major phospholipid constituents (>90% w/w of total phospholipid);[1] moreover, DOPE (47.0% PE, w/w) and DPPC (32.2% PC, w/w) are the major subspecies.[34] DPPC, DOPE, and SM were chosen in this study as they are the major phospholipid species in bovine milk,[2] and they have a broad range of L_β/L_α phase transition temperatures.[26,27,35,36] Phospholipids were dissolved in chloroform to yield 10 mg/mL sample solutions which contained Rd-DOPE or NBD-PC (0.25 mol %) as a fluorescent dye during the electroformation of GUVs.

Electroformation of GUVs. Briefly, 2.5 μL lipid formula sample solutions were placed on the surface of ITO slides. After completely evaporating any residual moisture in a desiccator (room temperature, 1 h), the samples were rehydrated in 100 mM sucrose solution. GUVs were formed under AC field conditions (3 V, 10 Hz, ∼55 °C) in a custom designed chamber for 45 min.[24,32] The prepared GUVs were taken from the electroformation chamber and placed into 100 mM glucose solutions (1/4, v/v) using a wide-mouth pipet (>1 mm diameter), at which point the newly formed GUVs were ready for CLSM observation. It was reported (supported by our own observations) that aging or insufficient cleaning of ITO slides may affect the GUV electroformation process resulting in a low yield of GUVs; therefore, the ITO slides were handled by a standard cleaning procedure following a mild annealing process.[31] The fluorescent intensities at the boundary of vesicles (liquid crystalline phases) were measured to ensure that these exhibited a bilayer structure.[29] Electroformation was carried out in duplicate for each lipid combination.

CLSM Observation of GUVs. GUV preparations were pipetted onto observation slides containing a small well (∼3 mm depth) for holding GUVs without extrinsic pressure from the coverslip. An Olympus FV1000 inverted confocal laser scanning microscope (Olympus America Inc., Center Valley, PA) with oil-immersion objective lenses (40× and 60 ×) was used to observe the structural properties and morphology of GUVs. Fluorescent signal collection (for rhodamine B and NBD) and the CLSM configuration were adopted from our previous work,[16] with modification. Rd-DOPE and NBD-DLPC were excited by a diode laser (559 nm) and Ar$^+$ laser (488 nm), respectively, and the emitted spectrum was measured between 570 and 670 nm and 500–600 nm, respectively. 3D images of GUVs were constructed from a group of individual 2D images taken across a defined *z*-axis section. Differential interfacial contrast illumination was used in the transmitted light channel for determination of the positioning of GUVs. All of the image processing was carried out at 22 ± 1 °C. The operating parameters of the CLSM were not necessarily kept constant for each image as the parameters were optimized to obtain the clearest images of GUVs. This was deemed to be acceptable as relative quantification of phospholipids was not the focus of the study.

RESULTS AND DISCUSSION

1. Fluorescent Staining and Electroformation of GUVs. To test the staining ability of the headgroup dye (Rd-DOPE) and fatty acid-group dye (NBD-DLPC) for fluorescent labeling of different phospholipids and sphingolipids in the model membrane system, the two dyes were applied to two unitary GUV systems (DPPC and SM), respectively. The zwitterionic glycerophospholipid PC and the zwitterionic phosphosphingolipid SM are more enriched in the outer leaflet

monolayer in the membranes of human and animal cells; moreover, in the case of MFGM, it has also been reported that PC and SM are located on the outside layer of the MFGM.[14,37] Therefore PC and SM unitary systems were used in the preliminary experiments. The headgroup-labeled DOPE phospholipid analogue appeared to stain the surfaces of DPPC- and SM-induced GUVs systems well; the fatty acid group-labeled DLPC phospholipid analogue stained the DPPC GUV system well, whereas GUVs could not be successfully constructed from the NBD-DLPC-labeled SM system under the same GUV generation conditions. The reason for this unsuccessful construction is uncertain; it may be due to the current electroformation conditions not being capable of generating GUVs from this specific lipid combination (NBD-DLPC + SM). Consequently, headgroup-labeled Rd-DOPE, a widely used fluorescent probe in MFG studies[15,38] was used as the primary dye for probing the surface morphology of constructed GUV systems derived from milk phospholipids. No noticeable differences were apparent between headgroup-labeling and fatty acid-labeling when comparing DPPC bilayer systems (images not shown).

In previous work, Rd-DOPE was first used for labeling the surface layer of native MFGs: the dark regions, which were not stained by Rd-DOPE, were interpreted as L_o (lipid rafts) domains thought to be enriched in SM and cholesterol.[15] A possible hypothesis is that the PE-coupled headgroup fluorescent dye (Rd-DOPE) may not stain the outer monolayer components properly, which mainly consists of PC and SM. This would create unstained or heterogeneously stained regions on the surface of MFGs where dark regions occur through the absence of Rd-DOPE, and these regions may not necessarily be liquid disordered (L_o) regions. Consequently, a GUV system in which the membrane composition can be controlled is an ideal tool for testing the staining capability of fluorescent labels in different bilayer systems (such as Rd-DOPE). Electroformation of GUVs was carried out successfully where the Rd-DOPE probe was located at the periphery of the GUV, and the yield of GUVs was sufficient for further analysis.

2. GUVs Constructed From DPPC and/or DOPE. The combinations of DPPC (T_m: 42 to 52 °C) and DOPE (T_m: −9.9 to −2.9 °C) in the formulation of GUVs was based on the range of L_β/L_α phase transition temperatures. No dark regions (nonfluorescent regions) could be found in the DPPC unitary and two DPPC-DOPE binary (7/3, 1/1, mol/mol) GUVs systems (Figure 1). There were no characteristic differences in surface morphology of these samples. The 3D images (Figure 1A), that were built from 2D cross-sectional images, show that the Rd-DOPE fluorescent probe was homogenously spread on the surfaces of GUVs. Nonfluorescent regions were found on the surfaces of GUVs made from a DPPC-DOPE (3/7, mol/mol) binary system (Figure 2).

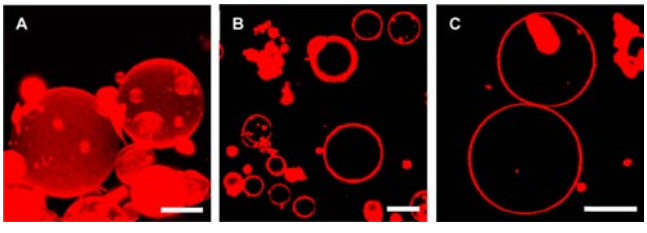

Figure 1. Comparison of GUVs formed from DPPC and/or + DOPE (unitary and binary systems). A: DPPC, 3D image; B: DPPC/DOPE, 7/3 (mol/mol), 2D image; C: DPPC/DOPE, 1/1 (mol/mol), 2D image. Scale bar: 20 μm. (Dark regions on the surface of GUVs were not commonly observed.)

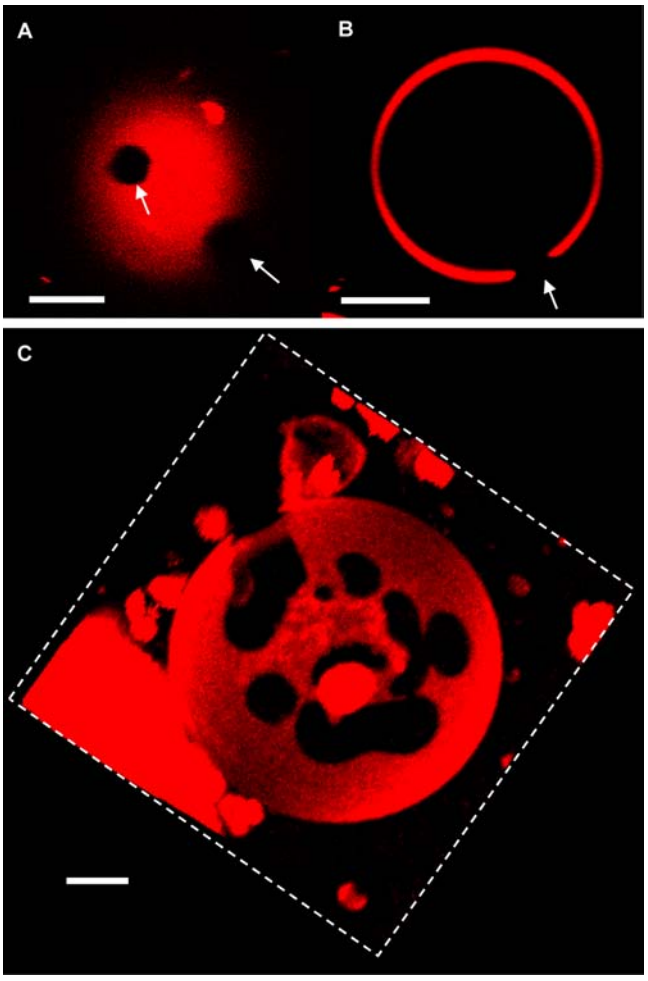

Figure 2. GUVs formed from DPPC.DOPE (3/7, mol/mol). A: 2D image taken at the top/bottom section of GUV, regular circular shape of dark regions (DRs) are shown by white arrows; B: 2D image taken in the middle section of a GUV, DR is shown by white arrow. C: 3D image showing apparent morphology of GUV in mimicking the morphology of native MFG. Scale bar: 5 μm.

Lissamine rhodamine B is a well-characterized fluorescent probe used for studying phase coexistence on GUV surfaces.[29,39] Bagatolli and Gratton[29] reported that Rd-DPPE molecules are segregated from the gel domains and locate in the liquid (crystalline) disordered domains in a DPPE-DPPC GUV system, which supports the current results where the liquid disordered domains are characterized as the location of Lissamine rhodamine B-labeled PE. Rd-DOPE, as a primary fluorescent dye, has been also used to probe the lateral segregation and morphology of the native MFGM.[4,15,16] Lopez and co-workers (2010) applied Rd-DOPE as a probe to determine the location of milk phospholipids in the MFGM and found that Rd-DOPE did not partition into the triacylglycerols interior of MFGs but was distributed heterogeneously on the surfaces of MFGs.[15] Consequently, the black interior regions of GUVs with no fluorescent emission are not considered in the current research.

In previous work,[15] the sizes of liquid-ordered or gel domains ranged from 0.6 to 2.7 μm depending on the size of the MFGs, and this is comparable with our current results as shown in Figure 2A and B from an artificial phospholipid membrane system containing only DPPC-DOPE (3/7, mol/mol). Also, the apparent morphology of the nonfluorescent emission domains, which correspond to the circular shapes on the GUV surface (Figure 2A), is in close agreement with that reported for MFGM by Lopez and co-workers.[15]

Evers et al. (2008)[40] observed heterogeneity on the MFGM using different fluorescent probes and concluded that the lack of MFGM fluorescent emission was due to the absence of an outer bilayer. Lopez et al. (2010)[15] challenged this hypothesis and suggested that the triacylglycerol inner core of the MFGs is unlikely to be directly in contact with the aqueous phase without surface coverage. Nevertheless, considering the current and widely accepted trilayer topology of the MFGM,[4,5,15,41,42] it is reasonable to expect that the primary monolayer containing glycerolphospholipids and membrane proteins located underneath the outer bilayer may still maintain the stability of MFGs.

An exposed protein inner monolayer on the surface of MFGs has been observed after centrifugal mechanical treatments;[43] therefore, the explanation of the bare surfaces on MFGs, as reported by Evers et al. (2008),[40] can be rationalized. However, this theory cannot explain the appearance of dark domains in the current GUV system containing only phospholipids, as a trilayer system is not present. Several CLSM studies[4,15,16,18,19] suggest that the dark domains on Rd-DOPE fluorescently labeled MFGM are lipid rafts[44−46] (analogous to L_o), comprising of saturated phospho/sphingo-lipids (mainly SM) and cholesterol. Dark domains, however, were generated in our artificial nonsupported model membrane system (Figures 2), containing only DPPC and DOPE (3/7, mol/mol). This phenomenon, to some extent, supports our hypothesis that the presence of nonfluorescent dark domains on the MFGM depends upon the proportion of the liquid phase: nonfluorescent regions found for DPPC/DOPE 3/7 mol/mol but not for DPPC/DOPE 7/3 nor 1/1 mol/mol. Consequently, the L_o phases (lipid rafts), which are mainly formed from SM and cholesterol,[47] and the gel phases formed by the high T_m phospholipids (DPPC ∼11.1%, w/w in total bovine milk polar lipids,[2] in this case) may both contribute to the formation of dark regions.

In previous research[4,15,16] and in our current work, CLSM characterization was carried out at ambient temperature (19−22 °C), which is lower than the T_m of DPPC required to induce gel structure formation. Bagatolli et al. (2000)[29] characterized the phase state of the lipid domain by using an excitation generalized polarization (GP) function at different temperatures. The CSLM GP images clearly show gel−liquid crystalline phase separation (DPPE/DPPC, 7/3, mol/mol) at the solid and fluid phase coexistence temperature region, 58−42 °C.[29] This is in close agreement with our results where ambient temperature is within the range of the phase coexistence temperatures (Figure 2).

The 3D image (DPPC/DOPE, 3/7, mol/mol, Figure 2C) shows more details about the gel-phase (DPPC) segregation from the liquid-phase (DOPE) in the GUV model, where irregular dendritic, flower shapes, and regular circular shapes were found. Whether the irregular shapes were formed spontaneously and individually or were formed due to the aggregation of regular circular gel-phases induced by the fluidity of liquid-phases is not known. The dark regions on GUVs (Figure 2C) are similar to the dark regions that were found on the surface of native MFGs.[15,16,18,19] It was difficult to observe gel−liquid crystalline phase separation in the GUVs systems as presented in Figure 1. This may be related to the preferred molecular arrangement of different phospholipids (DPPC and DOPE) in the nonsupported model membrane systems, as shown in Figure 3. According to the critical packing parameter

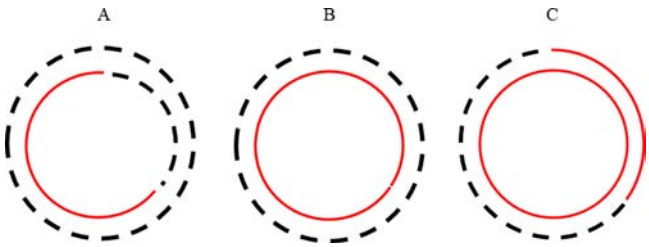

Figure 3. Highly schematic illustration of proposed molecular arrangement of GUV (bilayer) systems formed from different species of phospholipids. A: DPPC/DOPE (7/3, mol/mol); B: DPPC/DOPE (1/1, mol/mol); C: DPPC/DOPE (3/7, mol/mol). Black (dashed): DPPC; Red (solid): DOPE.

and critical packing shape of phospholipid molecules[48] it is proposed that PE is more favorably packed in the inner leaflet, with the bilayer system containing PC and/or SM, as the fatty acid tails of PE form cylindrical or inverted truncated cone shapes which favor planar bilayers or inverted micelles structures. Moreover, in this current work, the GUVs could not be constructed from the Rd-DOPE + DOPE sample under the same electroformation conditions which were used for the other samples. This negative result indirectly suggests that unlike PC and SM, PE molecules are difficult to form a flexible spherical bilayer structure, implying localization in the inner leaflet of the MFGM bilayer or GUV systems when PC and SM are present. Consequently, the outer leaflets of GUV bilayers made from DPPC and specific DPPC+DOPE mixtures (7/3 and 1/1, mol/mol) may be constructed from only DPPC (Figure 3).

It is necessary to point out that CLSM is an appropriate technique for characterizing the homogeneity of the surface of fluorescently labeled phospholipid bilayers. The characterization depends upon the instrumental configuration; by setting up a correct configuration on the CLSM, Rd-DOPE-labeled DPPC concentrated GUVs (Figure 1) may be visible. Therefore, in the current work, CLSM was applied for characterizing the "immiscible phases" on the surfaces of GUVs rather than characterizing the individual absolute ordered or disordered phases.

3. GUVs Constructed From SM and/or DOPE. In GUV systems containing only bovine milk-derived SM, the nonfluorescent regions were observed with long elongated shapes (Figure 4A and B) where the images were taken at the top and bottom section of selected GUVs. The 2D GUV image taken from the middle section (Figure 4C) is similar to the MFGM images from previous reports;[4,15,16] the tiny dark dots on the fluorescent GUV surface may contribute to the linear shaped microdomains in constructed 3D images.

Unlike DPPC, SM derived from bovine milk is a mixture of lipid molecules with different lengths of fatty acids and headgroups which gave three major peaks for the purchased sample (Avanti Polar Lipids) in HPLC-ELSD analysis. The presence of other minor SM species are also expected. This is

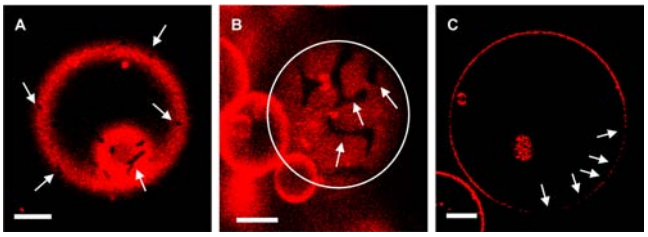

Figure 4. Dark regions (DRs, shown by white arrows) presented on GUVs formed from SM. A: 2D image, top/bottom and middle section of two GUVs, DRs were observed as elongated and dot shapes; B: 2D image, top/bottom section (in white circle), DRs were observed as irregular shapes; C: 2D image, middle section. Scale bar: 5 μm.

the same three-peak profile as our extracted bovine milk phospholipid mixture (results not shown); therefore, the proposed surface arrangement shown in Figure 3, which only represents two types of pure lipid molecules, does not apply in this case, and dark domains can occur in all SM containing samples (Figures 4, 5, and 6). These dark domains were

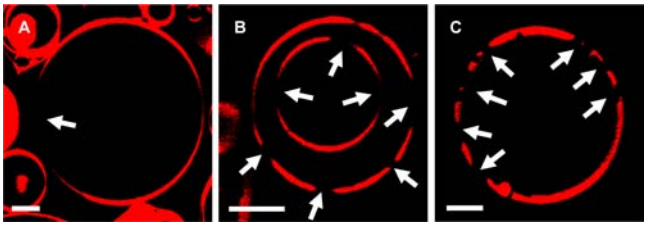

Figure 5. DRs (shown by white arrows) were found in GUVs formed from binary systems containing SM and DOPE. A: SM/DOPE, 7/3 (mol/mol); B: SM/DOPE, 1/1 (mol/mol); C: SM/DOPE, 3/7 (mol/mol). Scale bar: 5 μm.

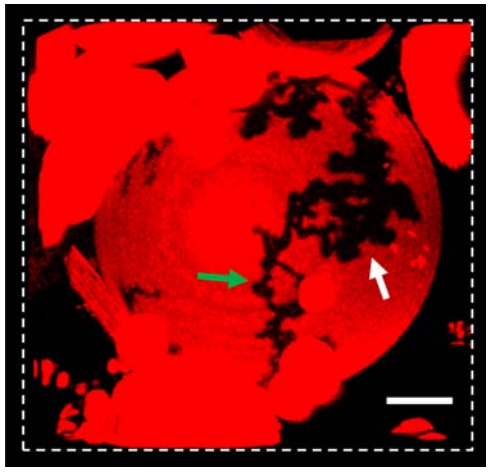

Figure 6. Apparent morphology of a GUV (SM/DOPE, 1/1, mol/mol) in a 3D image modeling part of the morphology of a native MFG. White arrow: irregular dendritic shape; green arrow: linear shape. Scale bar: 10 μm.

probably induced by heterogeneous distribution of Rd-DOPE on the surfaces of GUVs which contained different types of milk SM. The composition of milk SM in terms of fatty acid and sphingoloid population varies considerably,[2] and it was proposed that physical behavior (melting) of SM depends on both the sphingosine chain and the fatty acid distribution;[49] therefore, different physical behaviors and molecular packing of milk SM molecules in GUVs may be expected. The hosting capacity of fluorescent probes in phospholipid membranes depends on the phospholipid molecular packing,[16] consequently, the observation of phase separation, which could be induced by heterogeneous distribution of fluorescent probes in the GUV system containing different types of SM, is rationalized.

Shipley et al. (1974)[49] characterized a single lamellar bilayer structure in a SM (bovine brain) bilayer system and found phase separation for a higher degree of hydration in a SM bilayer system (>42% water, v/v) occurred at a lower phase transition temperature (25 °C). This is in close agreement with the current study where bovine milk SM is highly hydrated and characterized at ambient temperature; pulsed-field gradient NMR has shown that the lateral diffusional behavior is the same in a bilayer comprised of SM of either brain and milk origin.[50] The dark regions only account for a small proportion of GUV (SM unitary system) surfaces as discrete linear/dot shapes and larger regular shapes are not seen (Figure 4, containing only milk SM). This unique structure and morphology is probably due to the specific individual molecular profile of SMs derived from bovine milk and their packing structure in the bilayer. Filippov et al. (2006)[50] found that SM derived from brain and egg may induce larger phase coexistence areas in phospholipid bilayers than milk SM, probably due to the heterogeneous hydrocarbon chain in SM which gives a less tightly packed molecular structure. Therefore, the small dark regions could be formed by a small amount of tightly packed homogeneous hydrocarbon chains of specific SM molecules.

Bagatolli et al. (2000)[29] found similar elongated microdomains in GUV systems (DLPC/DPPC, 1/1, mol/mol) which were stained by different probes (including Rd-DPPE). Based on a previously proposed model,[51] the elongated domains were formed due to a particular topology (unlike a pure gel phase) of specific phospholipid molecules (DPPC in this case), presented as filaments of gel in a particular liquid crystalline phase. Moreover, in a good agreement with our current results shown in Figure 6 (SM/DOPE, 1/1, mol/mol), elongated and polygonal domains have also been found in other GUV systems containing only pure phospholipids, where it has been pointed out the GUV radius of curvature and fluid line defects formed by liquid crystalline domains are important for forming and shaping lipid domains.[29,52] Therefore, we can conclude that both intrinsic factors (composition, chemical and physicochemical nature of phospholipids, including hydrocarbon chain, T_m, and molecular packing shape) and extrinsic factors (size of the bilayer, environmental temperature, and physical property of liquid-domains) are important for forming lipid domains with specific morphology.

4. GUVs Mimicking the Morphology of Native MFGs. Lateral mobility of lipid domains (dark regions) with regular circular shapes was observed (Figure 7, DPPC/DOPE, 3/7, mol/mol), in good agreement with previous work where mobility of the MFGM constituents was found.[15] The composition of the mobile nonfluorescent regions is difficult to ascertain due to the complexity of the composition and structure of the MFGM; however, in artificial membrane systems with controlled composition (Figure 7), it can be concluded that the mobile microdomain was formed from a gel phase and flowed into the liquid phase. The shape and the size of nonfluorescent microdomains did not change as a function of time, as reported before in the bovine MFGM.[15] The specific shapes of nonfluorescent microdomains on the surface of

dx.doi.org/10.1021/jf500093p | J. Agric. Food Chem. 2014, 62, 3236−3243

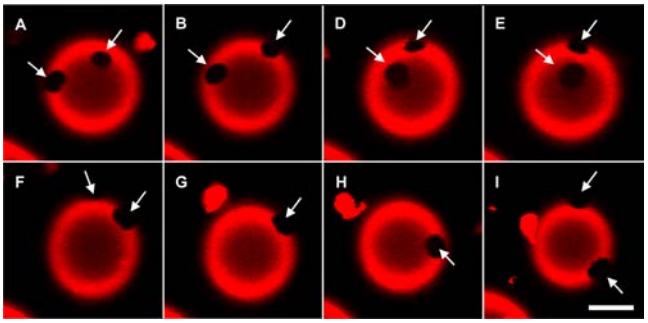

Figure 7. Monitoring mobility of DRs (pointed by arrows) on the surface of specific GUVs (DPPC/DOPE, 3/7, mol/mol). 2D images were taken at the top/bottom section of GUVs. A–I were obtained individually along a fixed time interval (20 s). Scale bar: 5 μm.

GUVs, as shown in Figures 2 and 6 (without SM, and without a combination of SM and cholesterol), shows good agreement with the previously published surface morphology of native MFG.[16] Based on the current results, we may conclude that the nonfluorescent microdomains on the surface of MFGs are not necessarily represented by the L_o phase, enriched in SM and cholesterol, but may also be formed from the gel phase containing the major MFGM phospholipid species DPPC and SM.

A lipid formulation of DOPE/DPPC/SM/cholesterol (8/8/8/4, mol/mol) was used for mimicking the composition of the native MFGM. A large integrated dark region is shown in the 3D micrograph (Figure 8). The surface morphology is in good

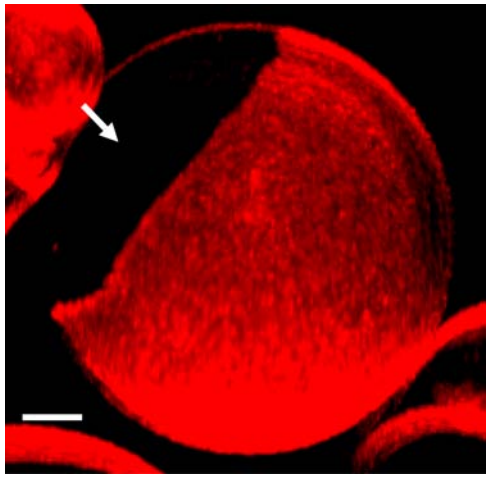

Figure 8. 3D image of a GUV formed from a lipid formula (DOPE/DPPC/SM/cholesterol, 8/8/8/4, mol/mol) mimicking the lipid composition of the native MFGM. DR is shown by the arrow. Scale bar: 5 μm.

agreement with previous GUV systems containing cholesterol where the existence of microdomains and domain patterns was regulated by the amount of cholesterol.[53] Morales-Penningston et al. (2010)[24] showed a similar pattern of microdomains on the surface of GUVs (composed from 18:0-SM/DOPC/cholesterol in the molar ratio of 0.56/0.24/0.20), where the larger and regular circular microdomains were formed by the merging of smaller separated microdomains, as induced by osmotic swelling. This osmotic swelling mechanism may explain the apparent morphology on our GUV containing cholesterol (Figure 8) as an osmotic pressure gradient is formed between the external (100 mM glucose) and internal solutions (100 mM sucrose). Cholesterol has a role in inducing domain formation[54,55] and is dependent on the amount present.[53] Scherfeld et al. (2003) reported that phase separation may be reduced by adding 10 mol % cholesterol into the phospholipid binary system (DOPC/DPPC. 0.5/0.5, mol/mol) and can increase by adding 20 mol %.[53] Cholesterol accounts for ~14 mol % in our current formulation for mimicking the lipid molar composition of MFGM, and phase separation can readily be observed with CLSM (Figure 8).

Based on CLSM experimental evidence, a model of lateral topology of MFGM lipid organization can be deduced in which PC and SM are located in the outer leaflet of the bilayer and specific phospholipids having high gel–liquid crystalline phase transition temperatures contribute to lateral segregation in the MFGM. This suggests that association of SM and cholesterol is not the only contributing factor to ordered domain formation.

AUTHOR INFORMATION

Corresponding Author

*Phone: +86 13716006816. Fax: +64 34797567. E-mail: haotian.zheng@otago.ac.nz.

Notes

The authors declare no competing financial interest.

ACKNOWLEDGMENTS

We thank the Earle Food Research Fund from the Riddet Institute, New Zealand. We also gratefully acknowledge Dr. Jakob Schweizer from Department of Biochemistry, University of Oxford, United Kingdom for the discussion in GUVs construction. We acknowledge Andrea Laubscher and other members from the Dairy Products Technology Center at the California Polytechnic State University for technical support during the course of this research.

ABBREVIATIONS USED

MFGM, milk fat globule membrane; SM, sphingomyelin; PE, phosphatidylethanolamine; PC, phosphatidylcholine; GUVs, giant unilamellar vesicles; DPPC, 1,2-dipalmitoyl-*sn*-glycero-3-phosphocholine; MFGs, milk fat globules; CLSM, confocal laser scanning microscope; Rd-DOPE, 1,2-dioleoyl-*sn*-glycero-3-phosphoethanolamine-N-(lissamine rhodamine B sulfonyl); L_o, liquid ordered; L_d, liquid disordered; ITO, indium tin oxide; DIC, differential interfacial contrast; NBD-PC, 1-palmitoyl-2-{6-[(7-nitro-2-1,3-benzoxadiazol-4-yl)amino] hexanoyl}-*sn*-glycero-3-phosphocholine; DOPE, 1,2-dioleoyl-*sn*-glycero-3-phosphoethanolamine

REFERENCES

(1) Huppertz, T.; Kelly, A. L. Physical Chemistry of Milk Fat Globules. In *Advanced Dairy Chemistry Vol. 2 Lipids*; Fox, P. F., McSweeney, P. L. H., Eds.; Springer US: New York, 2006; pp 173–212.

(2) MacGibbon, A. K. H.; Taylor, M. W. Composition and Structure of Bovine Milk Lipids. In *Advanced Dairy Chemistry Vol. 2 Lipids*; Fox, P. F., McSweeney, P. L. H., Eds.; Springer US: New York, 2006; pp 1–42.

(3) Fong, B. Y.; Norris, C. S.; MacGibbon, A. K. H. Protein and lipid composition of bovine milk-fat-globule membrane. *Int. Dairy J.* **2007**, *17*, 275–288.

(4) Lopez, C.; Briard-Bion, V.; Ménard, O.; Beaucher, E.; Rousseau, F.; Fauquant, J.; Leconte, N.; Robert, B. Fat globules selected from whole milk according to their size: Different compositions and

structure of the biomembrane, revealing sphingomyelin-rich domains. *Food Chem.* **2011**, *125*, 355−368.
(5) Mather, I. H. Milk Lipids | Milk Fat Globule Membrane. In *Encyclopedia of Dairy Sciences*, 2nd ed.; Fuquay, J. W., Ed.; Academic Press: San Diego, CA, 2011; pp 680−690.
(6) Dewettinck, K.; Rombaut, R.; Thienpont, N.; Le, T.; Messens, K.; Vancamp, J. Nutritional and technological aspects of milk fat globule membrane material. *Int. Dairy J.* **2008**, *18*, 436−457.
(7) Jimenez-Flores, R.; Brisson, G. The milk fat globule membrane as an ingredient: why, how, when? *Dairy Sci. Technol.* **2008**, *88*, 5−18.
(8) Spitsberg, V. L. Invited review: Bovine milk fat globule membrane as a potential nutraceutical. *J. Dairy Sci.* **2005**, *88*, 2289−2294.
(9) Kahya, N. Protein-protein and protein-lipid interactions in domain-assembly: Lessons from giant unilamellar vesicles. *BBA, Biochim. Biophys. Acta, Biomembr.* **2010**, *1798*, 1392−1398.
(10) Michalski, M.-C.; Januel, C. Does homogenization affect the human health properties of cow's milk? *Trends Food Sci. Technol.* **2006**, *17*, 423−437.
(11) Favé, G.; Coste, T. C.; Armand, M. Physicochemical properties of lipids: New strategies to manage fatty acid bioavailability. *Cell. Mol. Biol. (Noisy-le-grand)* **2004**, *50*, 815−831.
(12) Garcia, C.; Antona, C.; Robert, B.; Lopez, C.; Armand, M. The size and interfacial composition of milk fat globules are key factors controlling triglycerides bioavailability in simulated human gastro-duodenal digestion. *Food Hydrocolloids* **2014**, *35*, 494−504.
(13) Argov, N.; Lemay, D. G.; German, J. B. Milk fat globule structure and function: nanoscience comes to milk production. *Trends Food Sci. Technol.* **2008**, *19*, 617−623.
(14) Deeth, H. C. The role of phospholipids in the stability of milk fat globules. *Aust. J. Dairy Technol.* **1997**, *52*, 44−46.
(15) Lopez, C.; Madec, M.-N.; Jimenez-Flores, R. Lipid rafts in the bovine milk fat globule membrane revealed by the lateral segregation of phospholipids and heterogeneous distribution of glycoproteins. *Food Chem.* **2010**, *120*, 22−33.
(16) Gallier, S.; Gragson, D.; Jiménez-Flores, R.; Everett, D. Using confocal laser scanning microscopy to probe the milk fat globule membrane and associated proteins. *J. Agric. Food Chem.* **2010**, *58*, 4250−4257.
(17) Evers, J. M.; Haverkamp, R. G.; Holroyd, S. E.; Jameson, G. B.; Mackenzie, D. D. S.; McCarthy, O. J. Fluorescent probes for studying the milk fat globule (membrane). *Milchwissenschaft* **2008**, *63*, 402−405.
(18) Lopez, C.; Ménard, O. Human milk fat globules: Polar lipid composition and in situ structural investigations revealing the heterogeneous distribution of proteins and the lateral segregation of sphingomyelin in the biological membrane. *Colloids Surf., B* **2011**, *83*, 29−41.
(19) Zou, X.-Q.; Guo, Z.; Huang, J.-H.; Jin, Q.-Z.; Cheong, L.-Z.; Wang, X.-G.; Xu, X.-B. Human milk fat globules from different stages of lactation: A lipid composition analysis and microstructure characterization. *J. Agric. Food Chem.* **2012**, *60*, 7158−7167.
(20) Sengupta, P.; Jovanovic-Talisman, T.; Skoko, D.; Renz, M.; Veatch, S. L. Probing protein heterogeneity in the plasma membrane using PALM and pair correlation analysis. *Nat. Methods* **2011**, *8*, 969−975.
(21) Feigenson, G. W. Phase diagrams and lipid domains in multicomponent lipid bilayer mixtures. *BBA, Biochim. Biophys. Acta, Biomembr.* **2009**, *1788*, 47−52.
(22) Gallier, S.; Gragson, D.; Jiménez-Flores, R.; Everett, D. W. Surface characterization of bovine milk phospholipid monolayers by Langmuir isotherms and microscopic techniques. *J. Agric. Food Chem.* **2010**, *58*, 12275−12285.
(23) Menger, F. M.; Keiper, J. S. Chemistry and physics of giant vesicles as biomembrane models. *Curr. Opin. Chem. Biol.* **1998**, *2*, 726−732.
(24) Morales-Penningston, N. F.; Wu, J.; Farkas, E. R.; Goh, S. L.; Konyakhina, T. M.; Zheng, J. Y.; Webb, W. W.; Feigenson, G. W. GUV preparation and imaging: Minimizing artifacts. *BBA, Biochim. Biophys. Acta, Biomembr.* **2010**, *1798*, 1324−1332.
(25) Politano, T. J.; Froude, V. E.; Jing, B.; Zhu, Y. AC-electric field dependent electroformation of giant lipid vesicles. *Colloids Surf., B* **2010**, *79*, 75−82.
(26) Leonenko, Z. V.; Finot, E.; Ma, H.; Dahms, T. E. S.; Cramb, D. T. Investigation of temperature-induced phase transitions in DOPC and DPPC phospholipid bilayers using temperature-controlled scanning force microscopy. *Biophys. J.* **2004**, *86*, 3783−3793.
(27) Shalaev, E. Y.; Steponkus, P. L. Phase diagram of 1,2-dioleoylphosphatidylethanolamine (DOPE):water system at subzero temperatures and at low water contents. *BBA, Biochim. Biophys. Acta, Biomembr.* **1999**, *1419*, 229−247.
(28) Malmsten, M.; Bergenstahl, B.; Nyberg, L.; Odham, G. Sphingomyelin from milk - characterization of liquid-crystalline, liposome and emulsion properties. *J. Am. Oil Chem. Soc.* **1994**, *71*, 1021−1026.
(29) Bagatolli, L. A.; Gratton, E. Two photon fluorescence microscopy of coexisting lipid domains in giant unilamellar vesicles of binary phospholipid mixtures. *Biophys. J.* **2000**, *78*, 290−305.
(30) Dimitrov, D. S.; Angelova, M. I. Lipid swelling and liposome formation on solid surfaces in external electric fields. In *New Trends in Colloid Science*; Hoffmann, H., Ed.; Steinkopff: Dresden, Germany, 1987; Vol. *73*, pp 48−56.
(31) Herold, C.; Chwastek, G.; Schwille, P.; Petrov, E. P. Efficient electroformation of supergiant unilamellar vesicles containing cationic lipids on ITO-coated electrodes. *Langmuir* **2012**, *28*, 5518−5521.
(32) Veatch, S. L. Electro-formation and fluorescence microscopy of giant vesicles with coexisting liquid phases. *Methods Mol. Biol.* **2007**, *398*, 59−72.
(33) Angelova, M. I.; Dimitrov, D. S. Liposome electroformation. *Faraday Discuss. Chem. Soc.* **1986**, *81*, 303−311.
(34) Bitman, J.; Wood, D. L. Changes in milk fat phospholipids during lactation. *J. Dairy Sci.* **1990**, *73*, 1208−1216.
(35) Barenholz, Y.; Thompson, T. E. Sphingomyelins in bilayers and biological membranes. *BBA, Biochim. Biophys. Acta, Biomembr.* **1980**, *604* (C), 129−158.
(36) Contreras, F. X.; Sot, J.; Ruiz-Argüello, M. B.; Alonso, A.; Goñi, F. M. Cholesterol modulation of sphingomyelinase activity at physiological temperatures. *Chem. Phys. Lipids* **2004**, *130*, 127−134.
(37) Danthine, S.; Blecker, C.; Paquot, M.; Innocente, N.; Deroanne, C. Progress in milk fat globule membrane research: a review. *Lait* **2000**, *80*, 209−222.
(38) Zheng, H.; Jiménez-Flores, R.; Everett, D. W. Bovine milk fat globule membrane proteins are affected by centrifugal washing processes. *J. Agric. Food Chem.* **2013**, *61*, 8403−8411.
(39) Sun, Y.; Lee, C.-C.; Huang, H. W. Adhesion and merging of lipid bilayers: A method for measuring the free energy of adhesion and hemifusion. *Biophys. J.* **2011**, *100*, 987−995.
(40) Evers, J. M.; Haverkamp, R. G.; Holroyd, S. E.; Jameson, G. B.; Mackenzie, D. D. S.; McCarthy, O. J. Heterogeneity of milk fat globule membrane structure and composition as observed using fluorescence microscopy techniques. *Int. Dairy J.* **2008**, *18*, 1081−1089.
(41) Evers, J. M. The milkfat globule membrane—compositional and structural changes post secretion by the mammary secretory cell. *Int. Dairy J.* **2004**, *14*, 661−674.
(42) Michalski, M.-C.; Michel, F.; Sainmont, D.; Briard, V. Apparent [zeta]-potential as a tool to assess mechanical damages to the milk fat globule membrane. *Colloids Surf., B* **2002**, *23*, 23−30.
(43) Zheng, H.; Gordon, K. C.; Everett, D. W. Innovative application of confocal Raman microscopy to investigate the interaction between trans-2-hexenal and bovine milk fat globules. *Int. Dairy J.* **2013**, *32*, 68−70.
(44) Bacia, K.; Schwille, P.; Kurzchalia, T. Sterol structure determines the separation of phases and the curvature of the liquid-ordered phase in model membranes. *Proc. Natl. Acad. Sci. U.S.A.* **2005**, *102*, 3272−3277.
(45) Baumgart, T.; Hess, S. T.; Webb, W. W. Imaging coexisting fluid domains in biomembrane models coupling curvature and line tension. *Nature* **2003**, *425*, 821−824.

(46) Veatch, S. L.; Keller, S. L. Separation of liquid phases in giant vesicles of ternary mixtures of phospholipids and cholesterol. *Biophys. J.* **2003**, *85*, 3074−3083.
(47) Simons, K.; Ikonen, E. Functional rafts in cell membranes. *Nature* **1997**, *387*, 569−572.
(48) Israelachvili, J. N. 20 - Soft and Biological Structures. In *Intermolecular and Surface Forces*, 3rd ed.; Academic Press: San Diego, CA, 2011; pp 535−576.
(49) Shipley, G. G.; Avecilla, L. S.; Small, D. M. Phase behavior and structure of aqueous dispersions of sphingomyelin. *J. Lipid Res.* **1974**, *15*, 124−131.
(50) Filippov, A.; Orädd, G.; Lindblom, G. Sphingomyelin structure influences the lateral diffusion and raft formation in lipid bilayers. *Biophys. J.* **2006**, *90*, 2086−2092.
(51) Parasassi, T.; Ravagnan, G.; Rusch, R. M.; Gratton, E. Modulation and dynamics of phase properties in phospholipid mixtures detected by laurdan fluorescence. *Photochem. Photobiol.* **1993**, *57*, 403−410.
(52) Bagatolli, L. A.; Gratton, E. Two-photon fluorescence microscopy observation of shape changes at the phase transition in phospholipid giant unilamellar vesicles. *Biophys. J.* **1999**, *77*, 2090−2101.
(53) Scherfeld, D.; Kahya, N.; Schwille, P. Lipid dynamics and domain formation in model membranes composed of ternary mixtures of unsaturated and saturated phosphatidylcholines and cholesterol. *Biophys. J.* **2003**, *85*, 3758−3768.
(54) Bacia, K.; Scherfeld, D.; Kahya, N.; Schwille, P. Fluorescence correlation spectroscopy relates rafts in model and native membranes. *Biophys. J.* **2004**, *87*, 1034−1043.
(55) Wesolowska, O.; Michalak, K.; Maniewska, J.; Hendrich, A. B. Giant unilamellar vesicles - a perfect tool to visualize phase separation and lipid rafts in model systems. *Acta Biochim. Pol.* **2009**, *56*, 33−39.

hydrophilicity. Hepatic metabolites can then return to the intestinal lumen via the enterohepatic circulation and undergo further transformations. Then, luminal phenolic metabolites and phenolic compounds that have not been absorbed by the intestine reach the colon where they are subjected to microbial degradation.[11] Microbial metabolites are absorbed from the colon and are also subjected to the conjugation processes in the liver, resulting in their glucuronidated and sulfated derivatives. Finally, the phenolic microbial metabolites are excreted from the body via urine as hepatic conjugates.[4] The absorption, as well as the extent of hepatic conjugation and microbial deconjugation, is strongly affected by the structure of phenolic compounds.[12] Although hepatic metabolism leads to the generation of numerous combinations of methylated, glucuronidated, and/or sulfated phenolic metabolites, colonic microbial metabolism follows a general pattern leading to a relatively small number of metabolites, mainly phenolic acids and derivatives of phenylpropionic and phenylacetic acids.[5]

Direct evidence of the bioavailability of phenolic compounds can be obtained by characterizing the profile of metabolites in the plasma. This requires the use of a sensitive analytical methodology such as UHPLC with tandem MS, associated with microelution SPE (μSPE) technology, which allows the characterization of numerous metabolites in biological fluids at low concentrations, in a small volume of sample and in a short time.[13]

Among foods rich in phenolic compounds, strawberry, cranberry, and onion have previously demonstrated some beneficial effects on blood glucose regulation in rodents,[14−16] constituting a promising natural therapeutic approach in the prevention of obesity and type-2 diabetes. The purpose of the present work was thus to study the bioavailability of strawberry and cranberry phenolic compounds in a representative context of a diet-induced obesity model (rats fed a high-fat, high-sucrose diet) and compare it to a concomitant supplementation with an onion extract. Male Wistar rats were either administered a vehicle, a single intake of GlucoPhenol extract, or the same extract supplemented with an onion extract. Blood samples were collected pre- and postingestion, and plasma phenolic metabolites were characterized using an optimized UHPLC-MS/MS method, after their extraction with μSPE, and compared with the native phenolic composition of the studied extracts.

MATERIALS AND METHODS

Plant Material. Strawberry-cranberry (*Fragaria* × *ananassa*, Duch. cv. *authentique*, and *Vaccinium macrocarpon* L.) extracts blend GlucoPhenol (GP) and onion (*Allium cepa* L.) extract were provided by Nutra Canada company (total phenolic content of 18% and 45% dry weight respectively, as determined by Folin−Ciocalteu method).

Chemicals. The following phenolic standards were purchased from Sigma-Aldrich (St. Louis, MO): ellagic acid, 5-caffeoylquinic acid, protocatechuic acid, *p*-hydroxybenzoic acid, *p*-coumaric acid, vanillic acid, gallic acid, quercetin, quercetin 3-glucoside, kaempferol, myricetin, isorhamnetin, catechin, epicatechin, and rosmarinic acid. Ascorbic acid, citric acid, and hydrochloric acid were also purchased from Sigma-Aldrich (St. Louis, MO). Pelargonidin 3-glucoside was obtained from Extrasynthèse (France). Liquid chromatography grade solvents acetone, methanol, and acetonitrile were purchased from EMD Millipore Chemicals (Billerica, MA), and formic acid, glacial acetic acid, and phosphoric acid were obtained from Anachemia (Canada). Ultrapure water was obtained from a Millipore Milli-Q water purification system (Billerica, MA).

Determination of Strawberry−Cranberry and Onion Extracts Phenolic Composition. *Characterization of Anthocyanins.* The anthocyanin composition of GP extract was analyzed as previously described[17] by reverse-phase analytical HPLC using an Agilent 1100 series system (Santa Clara, CA). The separation was performed with a flow rate of 1 mL/min using a Develosil C18 reverse phase column (250 mm × 4 mm, 5 μm particle size), protected with an Ultrasep C18 guard column (Phenomenex, CA). A binary gradient of 5% formic acid in ultrapure water (solvent A) and methanol (solvent B) was as follows for the anthocyanins separation: 0−2 min, 5% B; 2−10 min, 5−20% B; 10−15 min, 20% B; 15−30 min, 20−25% B; 30−35 min, 25% B; 35−50 min, 25−33% B; 50−55 min, 33% B; 55−65 min, 33−36% B; 65−70 min, 36−45% B; 70−75 min, 45−53% B; 75−80 min, 53−55% B; 80−84 min, 55−70% B; 84−88 min, 70−5% B; 88−90 min, 5% B. Chromatographic data were acquired at 520 nm, and the quantification was performed using pelargonidin 3-glucoside as standard.

Characterization of Procyanidins. The procyanidin composition of GP extract was analyzed as previously described[18] by normal-phase analytical HPLC using an Agilent 1260/1290 infinity system (Santa Clara, CA) equipped with a fluorescence detector. The separation was performed at 35 °C with a flow rate of 0.8 mL/min using a Develosil Diol column (250 mm × 4.6 mm, 5 μm particle size), protected with a Cyano SecurityGuard column (Phenomenex, CA). The elution was performed using a solvent system comprising solvents A (acetonitrile/acetic acid 98/2 v/v) and B (methanol/ultrapure water/acetic acid 95/3/2 v/v/v) mixed using a linear gradient from 0% to 40% B for 35 min, 40% to 100% B for 5 min, 100% isocratic B over 5 min, and 100% to 0% B for 5 min. The fluorescence was monitored at excitation and emission wavelengths of 230 and 321 nm. Procyanidins with degrees of polymerization (DP) from 1 to >10 were quantified using an external calibration curve of epicatechin, taking into account their relative response factors in fluorescence.[19]

Determination of Total Ellagitannins. Total ellagitannins were estimated by reverse-phase analytical HPLC quantification of released ellagic acid following acid hydrolysis. Briefly, GP extract was dissolved in 25 mL of 50% methanol in ultrapure water containing ascorbic acid and hydrochloric acid (final concentrations of 10 mM and 1.2 M respectively). The mixture was heated to 85 °C in the dark for 2 h and then cooled in ice for 5 min. Ellagic acid separation was performed on an Agilent 1100 series HPLC system (Santa Clara, CA) using a Develosil C18 reverse phase column (250 mm × 4 mm, 5 μm particle size), protected with an Ultrasep C18 guard column (Phenomenex, CA, USA). The elution was performed at a flow rate of 1 mL/min using a solvent system comprising solvents A (methanol/ultrapure water/acetic acid 10/88/2 v/v/v) and B (methanol/ultrapure water/acetic acid 90/8/2 v/v/v) mixed using a gradient as follows: 0−15 min, 0−15% B; 15−25 min, 15−50% B; 25−34 min, 50−70% B; 34−35 min, 70−0% B. Chromatographic data were acquired at 250 nm, and the quantification was performed using ellagic acid standard.

Characterization of Phenolic Acids and Flavonoids. Phenolic acids and flavonoids were characterized using a Waters Acquity UPLC-MS/MS equipped with an H-Class quaternary pump system, a flow through needle (FTN) sample manager system, and a column manager. The MS detector was a TQD mass spectrometer equipped with a Z-spray electrospray

Table 1. Description of Phenolic Supplementation Treatments: Dose of Extract, Equivalent Phenolic Content, and Total Phenolic Intake (mg/kg of Weight Body)[a]

	dose of extract (mg/kg)		dose of phenolic compounds (mg/kg)		
group identification	GlucoPhenol	onion	GlucoPhenol	onion	total phenolic intake (mg/kg)
(1) control					0
(2) 2.7 mg/kg GP	15		2.7		2.7
(3) 5.4 mg/kg GP	30		5.4		5.4
(4) 27 mg/kg GP	150		27		27
(5) 36 mg/kg GP	200		36		36
(6) 36 mg/kg GP + O	30	68	5.4	30.6	36

[a]The experimental groups are numbered from (1) to (6).

interface. The analysis was achieved using an Agilent Plus C18 column (2.1 mm × 100 mm, 1.8 μm) (Santa Clara, CA). The separation was performed at 40 °C at a flow rate of 0.4 mL/min with a mobile phase consisting of 0.1% formic acid in ultrapure water and acetonitrile (solvent A and B, respectively) using a gradient elution as follows: 0−4.5 min, 5−20% B; 4.5−6.45 min, 20% B; 6.45−13.5 min, 20−45% B; 13.5−16.5 min, 45−100% B; 16.5−19.5 min, 100% B; 19.5−19.52 min, 100−5% B; 19.52−22.5 min, 5% B. The MS/MS analyses were carried out in negative mode using electrospray source parameters as follows: electrospray capillary voltage was 2.5 kV, source temperature was 140 °C, desolvation temperature was 350 °C, cone and desolvation gas flows were 80 l/h and 900 l/h, respectively. Data were acquired through multiple reaction monitoring (MRM) using Waters Masslynx V4.1 software. Phenolic standards were analyzed using the same parameters and used for the quantification, when available. Otherwise, the phenolic compounds were quantified using their aglycone or the most similar phenolic structure.

Animals and Plasma Preparation. Sixty male Wistar rats (Charles River, St. Constant, QC) were placed in temperature- and humidity-controlled rooms (21 ± 2 °C, 35−40%), with a daily 12h−12h light−dark cycle. Animal facilities met the guidelines of the Canadian Council on Animal Care, and the protocols were approved by the Animal Care Committee of Laval University (reference CPAUL-2011-111). Animals were acclimated to their environment for a minimum of 5 days and consumed a nonpurified rodent diet ad libitum (rodent chow no. 2918, Harlan Teklad, Madison, WI). All animals had continuous access to tap water. After the acclimation period, rats were fed a high-fat, high-sucrose (HFHS) diet containing 27% sucrose and 40% fat for 7−8 days. The day before the test, rats were fasted for 12 h. The animals were randomly allocated to 6 groups (9 to 12 per group, Table 1). A first control group (group 1) consisted of animals which only received the vehicle (0.1% citric acid in water). The animals of four groups (groups 2−5) were administered a single dose of GP extract corresponding to a phenol intake of 2.7, 5.4, 27, and 36 mg/kg, respectively. The animals of an additional experimental group (group 6) were administered a single dose of GP extract supplemented with onion extract, corresponding to a total phenol intake of 36 mg/kg (5.4 mg/kg from GP extract and 30.6 mg/kg from onion extract). Blood samples were collected from the saphenous vein with EDTA-containing syringes preingestion and at 30, 60, 120, 180, and 360 min postingestion. Plasma samples were obtained by centrifugation (3500 rpm, 10 min at 4 °C) and stored at −80 °C until analysis.

Extraction of Plasma Phenolic Compounds. Phenolic compounds extraction was realized according to a previously described methodology.[13] Waters OASIS HLB μelution plates (Milford, MA) were preconditioned using 250 μL of methanol and 250 μL of 0.2% acetic acid. Plasma samples (20 to 200 μL) were mixed with 4% phosphoric acid in ultrapure water (v/v) to disrupt phenol−protein binding prior loading into the plates. The loaded plates were washed with 200 μL of ultrapure water and 200 μL 0.2% acetic acid, and the retained phenolic compounds were then eluted with 2 × 50 μL of acetone/ultrapure water/acetic acid solution (AWA) 70/29.5/0.5 v/v/v. Rosmarinic acid (1 μg/mL final concentration) was added in AWA elution solution and used as internal standard to check the homogeneity of the SPE extraction procedure. The eluted solutions, in the collecting plates, were directly injected in UHPLC-MS/MS for phenolic acids and nonanthocyanins flavonoids analysis (negative mode). The extracts were then lyophilized and dissolved in 30 μL of 20% methanol 0.1% acetic acid for anthocyanins analysis (positive mode).

Characterization of Metabolites by UHPLC-MS. The analysis of plasma extracted phenolic metabolites was achieved with UHPLC-MS/MS using a previously developed methodology for the detection of anthocyanins and procyanidins,[13] slightly modified to also allow the detection of phenolic acids and flavonols.

The separation of phenolic acids and nonanthocyanins flavonoids was performed at 30 °C using an Agilent Plus C18 column (2.1 mm × 100 mm, 1.8 μm) (Santa Clara, CA). A flow rate of 0.4 mL/min was used with a mobile phase consisting of 0.2% acetic acid in ultrapure water and acetonitrile (solvent A and B, respectively) following this gradient elution: 0−8 min, 5−50% B; 8−9.10 min, 50−90% B; 9.10−10 min, 90% B; 10−10.10 min, 90−5% B; 10.10−13 min, 5% B. The MS/MS analyses were carried out in negative mode using electrospray source parameters as follows: electrospray capillary voltage was 3.01 kV, source temperature was 150 °C, desolvation temperature was 400 °C, and cone and desolvation gas flows were 80 l/h and 800 l/h, respectively.

The separation of anthocyanins was performed at 30 °C with a flow rate of 0.45 mL/min with a mobile phase consisting of 10% acetic acid in ultrapure water and acetonitrile (solvent A and B, respectively) using a gradient elution as follows: 0−3.50 min, 2−50% B; 3.50−4 min, 50−90% B; 4−4.50 min, 90% B; 4.50−4.55 min, 90−2% B; 4.55−6 min, 2% B. The MS/MS analyses were carried out in positive mode using electrospray source parameters as follows: electrospray capillary voltage was 1.3 kV, source temperature was 130 °C, desolvation temperature was 350 °C, and cone and desolvation gas flows were 80 l/h and 900 l/h, respectively.

Cone voltage and collision energy parameters were optimized for each compound. The identification of metabolites was performed by comparing their retention times with those of available phenolic standards and/or analyzing their fragmenta-

Table 2. Phenolic Standards, MRM Transitions, and Optimized MS Parameters Used for the Analysis of Native Phenolic Compounds and Their Metabolites by UHPLC-MS

compound	standard for quantification	ionization mode	MRM	cone voltage (V)	collision energy (eV)
phenolic acids					
p-hydroxybenzoic acid	*p*-hydroxybenzoic acid	negative	137 > 93	35	15
p-hydroxybenzoic acid glucuronide	*p*-hydroxybenzoic acid	negative	329 > 153	40	25
dimethyl ellagic acid glucuronide	ellagic acid	negative	505 > 329	40	22
protocatechuic acid	protocatechuic acid	negative	153 > 109	29	11
p-coumaric acid	*p*-coumaric acid	negative	163 > 119	35	15
anthocyanins					
pelargonidin 3-glucoside	pelargonidin 3-glucoside	positive	433 > 271	40	25
peonidin 3-galactoside	pelargonidin 3-glucoside	positive	463 > 301	40	25
flavan-3-ols					
catechin - epicatechin	epicatechin	negative	289 > 245	42	13
catechins glucuronide	epicatechin	negative	465 > 289	40	22
methyl catechins glucuronide	epicatechin	negative	479 > 303	40	22
methyl catechins sulfate	epicatechin	negative	383 > 303	45	20
flavonols					
quercetin	quercetin	negative	301 > 150	42	20
quercetin glucuronide	quercetin 3-glucoside	negative	477 > 301	40	22
quercetin diglucuronide	quercetin 3-glucoside	negative	653 > 301	40	22
quercetin sulfate	quercetin 3-glucoside	negative	381 > 301	40	20
isorhamnetin glucuronide	quercetin 3-glucoside	negative	491 > 315	40	22
isorhamnetin diglucuronide	quercetin 3-glucoside	negative	667 > 315	40	22
isorhamnetin sulfate	quercetin 3-glucoside	negative	395 > 315	40	22
isorhamnetin glucuronide sulfate	quercetin 3-glucoside	negative	571 > 315	40	22
myricetin glucuronide	quercetin 3-glucoside	negative	493 > 317	40	22
myricetin diglucuronide	quercetin 3-glucoside	negative	669 > 317	40	22

tion. Data were acquired through the multiple reaction monitoring (MRM) mode, tracking the transition of parent product ion specific for each compound. The detected metabolites were quantified using standards when available. Otherwise, a relative quantitation was achieved using the calibration curve of their aglycone or most similar phenolic structure. The phenolic standards, the MRM transitions, and the optimized MS parameters used for the characterization of phenolic metabolites in plasma are listed in Table 2.

Data Analysis. All phenolic characterizations were carried out in triplicate, and results were expressed as percentage of extract weight ± standard deviation (SD). Time 0 values being very close to 0, phenolic concentrations in rat plasma were expressed as variation of concentration from baseline (Δ mg/L for total phenolic content and Δ nM or Δ μM for individual phenolic compounds). Metabolites quantification was expressed as area under the plasma concentration (μM) time (min) curve (AUC), with AUC calculated according to the linear trapezoidal rule. Results were expressed as means ± standard error (SEM) of the mean. The main effect of phenol intake on AUC values was estimated by one-way analysis of variance (ANOVA) using the MIXED procedure in SAS 9.3 (Cary, NC). When necessary, log transformation was applied on raw data to meet the criteria for normality. A priori contrasts between selected groups were analyzed using the LSD method. The REG procedure of SAS was used to analyze if plasma metabolites concentrations (determined as AUC) followed a linear regression model with GP phenol intake and to obtain the determination coefficients (R^2). Differences were considered to be significant at $p < 0.05$.

RESULTS

Phenolic Composition of Strawberry−Cranberry and Onion Extracts. The phenolic composition of the two extracts is presented in Table 3. GP extract contained 0.8% of anthocyanins, with the main presence of pelargonidin 3-glucoside. This extract also contained about 3% of total procyanidins with a large spectrum of degree of polymerization, the monomers catechin and epicatechin representing around 0.1%. The extract presented a total ellagitannins content of 1.8%, including 0.8% of free ellagic acid. About 1.3% of phenolic acids were also identified in this extract, mainly chlorogenic acid and *p*-coumaric acid, and 1.3% of flavonols with the main presence of quercetin 3-glucoside. Conversely, onion extract did not contain any anthocyanins, procyanidins, or ellagitannins and contained almost exclusively aglycone quercetin and protocatechuic acid (about 14% and 8%, respectively). Chromatographic profiles of anthocyanidins and procyanidins of GP extract are available as Supplemental Figures S1 and S2, respectively.

Rat Plasma Phenolic Content. The evolution of the total phenolic concentration in rat plasma after ingestion of the extracts is presented in Figure 1A. The presence of phenolic compounds was detected in all treated groups, with a maximum phenolic concentration ranging from 0.5 to 8 mg/L in GP groups (groups 2−5; phenolic intake from 2.7 to 36 mg/kg) and 10 mg/L for the onion supplemented GP group (group 6; phenolic intake of 36 mg/kg). The kinetic profile of plasma total phenolic metabolites strongly differed depending on the phenolic source. GP-fed animals presented a high phenolic content 30 min after ingestion of the extract, followed by a rapid elimination of the metabolites by the organism (>85% over 360 min). GP/onion fed animals also presented a high phenolic content 30 min after ingestion of the mix, but the metabolites concentration remained high over time. Interestingly, the groups 5 and 6, which have ingested both the same dose of phenolic compounds (36 mg/kg) but from different sources, had the same phenolic concentration 30 min postingestion (about 8 mg/L; $p = 0.7829$) but a 10-fold

dx.doi.org/10.1021/jf404965z | J. Agric. Food Chem. 2014, 62, 3244−3256

Table 3. Phenolic Composition of GlucoPhenol and Onion Extracts[a]

	content (% dry weight)	
	GlucoPhenol extract	onion extract
total phenolic content	18	45
phenolic acids	**1.32 ± 0.04**	**8.49 ± 0.33**
ellagic acid	0.78 ± 0.00	0.03 ± 0.00
chlorogenic acid	0.16 ± 0.01	-
protocatechuic acid	0.04 ± 0.00	8.39 ± 0.04
p-hydroxybenzoic acid	<0.01	0.03 ± 0.00
p-coumaric acid	0.14 ± 0.00	<0.01
vanillic acid	0.03 ± 0.01	0.04 ± 0.00
caffeoyl glucoside	0.05 ± 0.00	-
feruloyl glucoside	0.06 ± 0.00	-
coumaroyl glucoside	0.05 ± 0.00	-
flavonoids	**2.26 ± 0.02**	**14.78 ± 0.27**
flavonols	**1.35 ± 0.02**	**14.78 ± 0.27**
quercetin	0.19 ± 0.02	14.50 ± 0.29
quercetin 3-glucoside	0.46 ± 0.02	0.03 ± 0.00
quercetin diglucoside	<0.01	0.03 ± 0.01
quercetin galactoside	0.02 ± 0.00	0.05 ± 0.00
quercetin rhamnoside	0.16 ± 0.00	-
quercetin xyloside	0.06 ± 0.00	<0.01
quercetin arabinoside	0.10 ± 0.01	-
kaempferol	<0.01	0.03 ± 0.00
kaempferol glucoside/galactoside	<0.01	-
myricetin	0.15 ± 0.01	<0.01
myricetin glucoside/galactoside	0.17 ± 0.00	-
isorhamnetin	0.02 ± 0.00	0.13 ± 0.01
total anthocyanins	**0.80 ± 0.01**	-
cyanidin 3-galactoside	0.10 ± 0.00	-
cyanidin 3-glucoside	0.02 ± 0.00	-
cyanidin 3-arabinoside	0.09 ± 0.00	-
pelargonidin 3-glucoside	0.35 ± 0.00	-
peonidin 3-galactoside	0.12 ± 0.00	-
peonidin 3-glucoside	0.01 ± 0.00	-
peonidin 3-arabinoside	0.07 ± 0.00	-
pelargonidin 3-(malonoyl)-glucoside	0.04 ± 0.00	-
flavan-3-ols	**0.11 ± 0.00**	-
catechin	0.05 ± 0.01	-
epicatechin	0.06 ± 0.01	-
total procyanidins	**3.24 ± 0.07**	-
monomers	0.32 ± 0.01	-
dimers	0.98 ± 0.01	-
trimers	0.46 ± 0.00	-
tetramers	0.32 ± 0.01	-
pentamers	0.17 ± 0.00	-
hexamers	0.13 ± 0.00	-
heptamers	0.06 ± 0.00	-
octamers	0.03 ± 0.00	-
nonamers	0.02 ± 0.00	-
polymers (DP > 10)	0.75 ± 0.02	-
total ellagitanins	**1.77 ± 0.07**	-

[a]Results are expressed as mean of triplicate ± SD. "-": Not detected.

difference in the phenolic concentration 360 min postingestion (about 1 mg/L for the group 5 and about 10 mg/L for the group 6; $p < 0.0001$). On the basis of mean rat body weight and blood volume (400 g and 26 mL respectively), absorption rates were estimated up to 1.4% of the total phenolic intake for GP fed rats and up to 1.8% for GP/onion fed rats.

Plasma Phenolic Metabolites: Identification, Quantification, and Kinetic Profile. The designed UHPLC-MS methods enabled the characterization of 21 phenolic compounds in rat plasma after the consumption of the extracts. These metabolites are listed in Tables 4 and 5 and their kinetic profiles are represented in Figures 1A–C.

Among anthocyanins, strictly present in GP extract, pelargonidin 3-glucoside and peonidin 3-galactoside were detected in their native form but at an extremely low level (0.01 and 0.001 nM max, respectively). A well-known metabolite

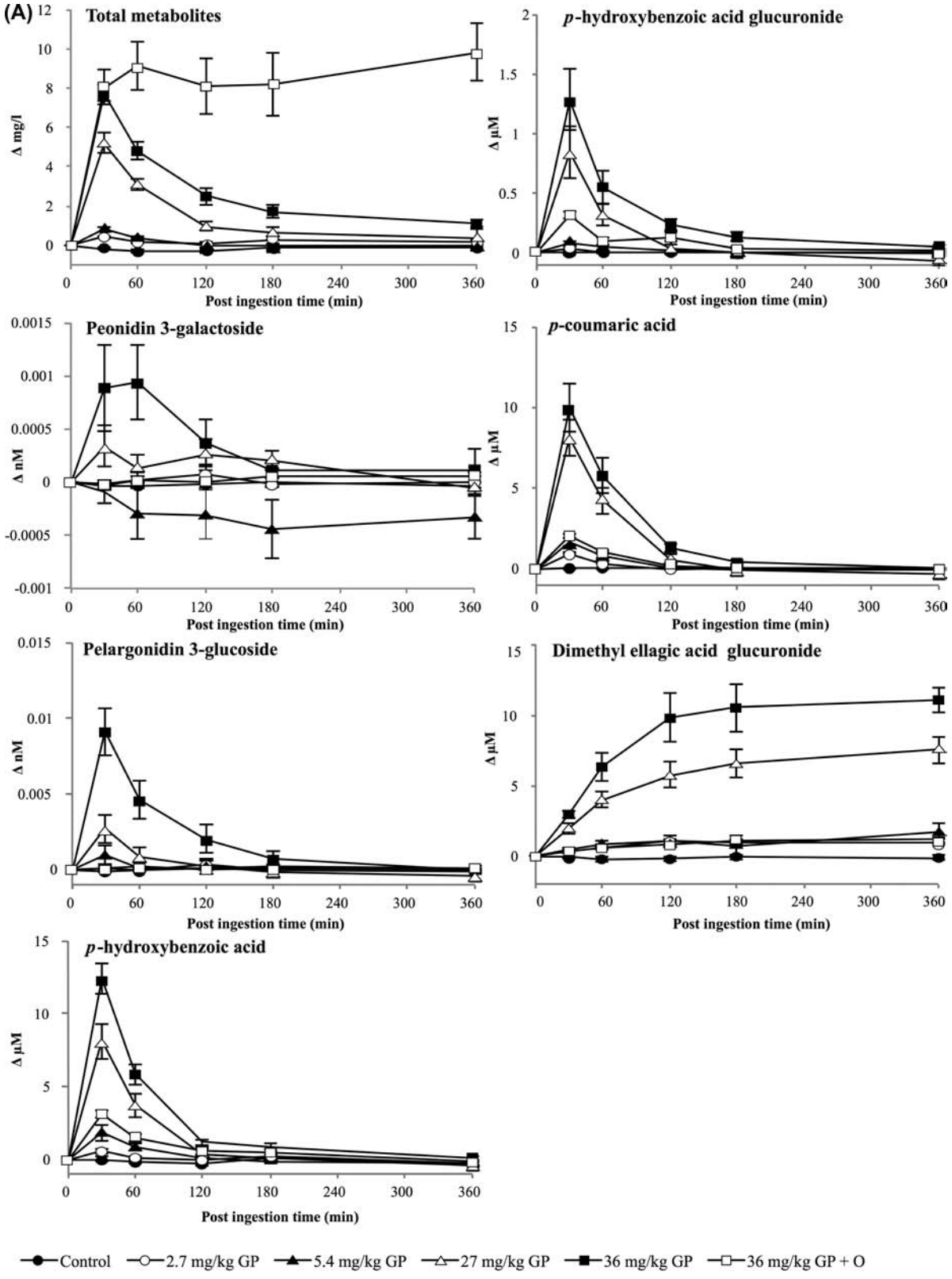

Figure 1. continued

dx.doi.org/10.1021/jf404965z | *J. Agric. Food Chem.* 2014, 62, 3244−3256

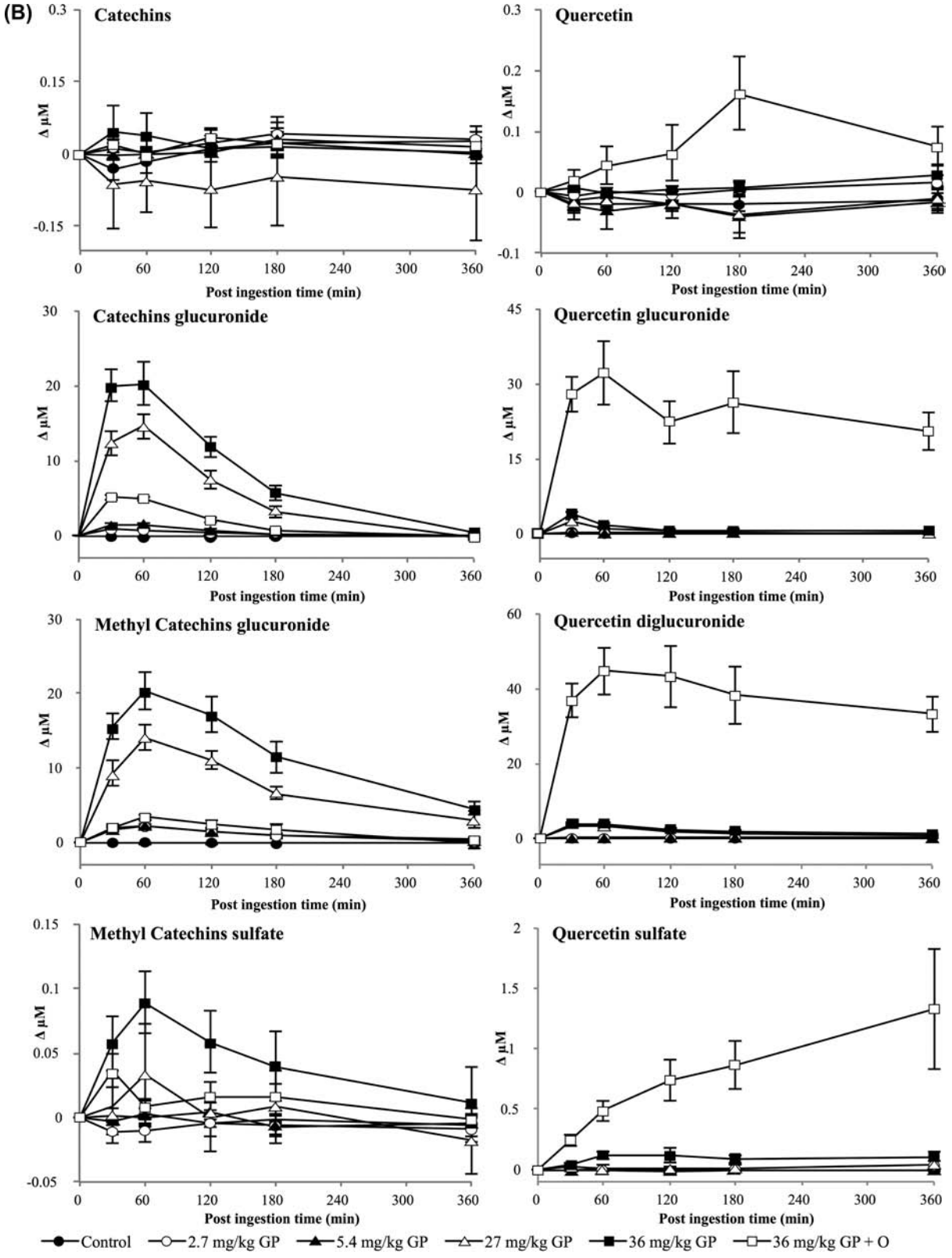

Figure 1. continued

dx.doi.org/10.1021/jf404965z | *J. Agric. Food Chem.* 2014, 62, 3244−3256

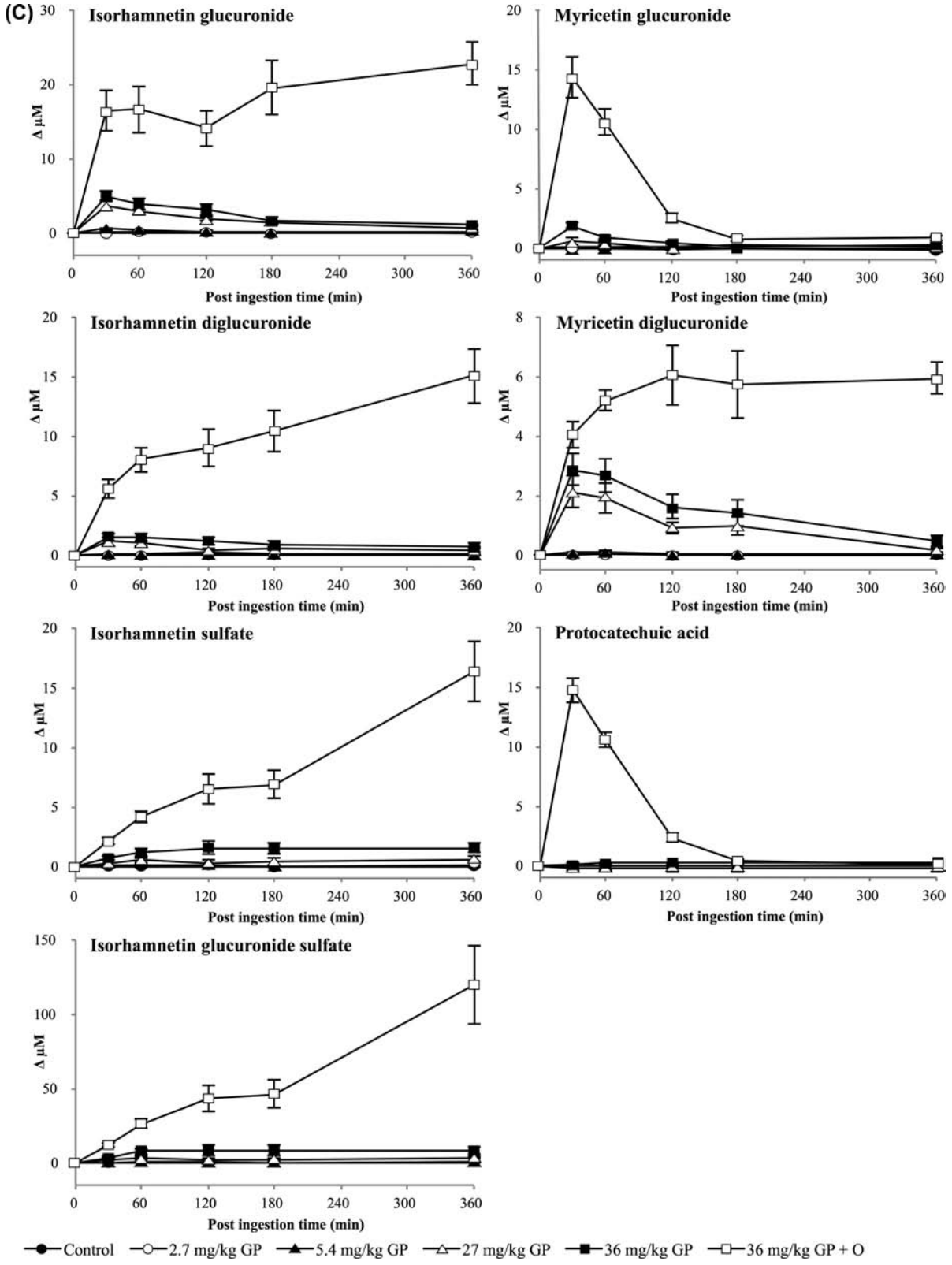

Figure 1. Evolution of the total phenolic concentration in rat plasma after ingestion of GlucoPhenol extract with or without onion extract. Results are expressed as mean of replicate (9 to 12) ± SEM. GP: GlucoPhenol; GP + O: GlucoPhenol + onion.

of pelargonidin 3-glucoside, *p*-hydroxybenzoic acid, was detected in significant amounts (12 μM max) and was also detected in its glucuronidated form, in a 10 times lower quantity. Among flavan-3-ols, also strictly present in GP extract, catechin and epicatechin were not detected in significant amounts in their native form but under conjugated forms. As the conjugated forms of catechin and epicatechin were not distinguishable by MS, these isomers were quantified together and referenced as "catechins". Catechins metabolites were detected under glucuronidated and both methylated and glucuronidated forms (until 20 μM max). A

dx.doi.org/10.1021/jf404965z | *J. Agric. Food Chem.* 2014, 62, 3244−3256

Table 4. Concentration of Total Phenolic Metabolites and Strawberry−Cranberry Phenolic Metabolites (Expressed as AUC) Found in the Plasma of Rats Fed with Different Concentrations of GlucoPhenol Extract, Co-Ingested or Not with Onion Extract[a]

	total metabolites	peonidin 3-galactoside	pelargonidin 3-glucoside	*p*-hydroxybenzoic acid	*p*-hydroxybenzoic acid glucuronide	*p*-coumaric acid
AUC						
(1) control	536 ± 82	$40.10^{-6} \pm 6.10^{-6}$	$58.10^{-6} \pm 10.10^{-6}$	192 ± 34	1.9 ± 0.3	17.2 ± 4.9
(2) 2.7 mg/kg GP	1702 ± 190*	$39.10^{-6} \pm 7.10^{-6}$	$83.10^{-6} \pm 22.10^{-6}$	253 ± 41	5.2 ± 1.4*	66.8 ± 5.0*
(3) 5.4 mg/kg GP	1907 ± 345*	$67.10^{-6} \pm 15.10^{-6}$	$91.10^{-6} \pm 22.10^{-6}$	309 ± 58	8.4 ± 1.5*	123 ± 21*
(4) 27 mg/kg GP	11623 ± 1659*	$102.10^{-6} \pm 15.10^{-6}$*	$281.10^{-6} \pm 50.10^{-6}$*	659 ± 109*	62.7 ± 13.2*	567 ± 85*
(5) 36 mg/kg GP	18830 ± 2565*	$202.10^{-6} \pm 39.10^{-6}$*	$842.10^{-6} \pm 158.10^{-6}$*	969 ± 97*	103 ± 20*	712 ± 111*
(6) 36 mg/kg GP + O	62740 ± 6942*	$202.10^{-6} \pm 39.10^{-7}$	$82.10^{-6} \pm 18.10^{-6}$	383 ± 48*	29.6 ± 4.3*	147 ± 8*
statistics						
linear regression	$p < 0.0001$	$p < 0.0001$	$p < 0.0001$	$p < 0.0001$	$p < 0.0001$	$p < 0.0001$
R^2	0.733	0.433	0.509	0.648	0.594	0.691
a priori contrasts						
(3) vs (6)	$p < 0.0001$	$p = 0.1502$	$p = 0.8045$	$p = 0.1964$	$p < 0.0001$	$p = 0.3051$
(5) vs (6)	$p < 0.0001$	$p = 0.0001$	$p < 0.0001$	$p < 0.0001$	$p = 0.0003$	$p = 0.0005$

	dimethyl ellagic acid glucuronide	catechins	catechins glucuronide	methyl catechins glucuronide	methyl catechins sulfate
AUC					
(1) control	156 ± 52	20.0 ± 3.2	20.1 ± 16.3	27.1 ± 16.6	3.8 ± 0.5
(2) 2.7 mg/kg GP	527 ± 103*	20.2 ± 5.6	117 ± 12*	404 ± 44*	3.8 ± 0.4
(3) 5.4 mg/kg GP	458 ± 147*	16.9 ± 5.8	170 ± 42*	415 ± 91*	5.2 ± 0.9
(4) 27 mg/kg GP	2039 ± 290*	22.0 ± 7.8	1970 ± 301*	2797 ± 342*	12.7 ± 3.0*
(5) 36 mg/kg GP	3325 ± 420*	22.2 ± 3.2	2949 ± 359*	4220 ± 588*	27.0 ± 3.9*
(6) 36 mg/kg GP + O	497 ± 115*	18.4 ± 5.1	644 ± 54*	904 ± 122*	7.7 ± 1.6*
statistics					
linear regression	$p < 0.0001$	$p = 0.5161$	$p < 0.0001$	$p < 0.0001$	$p < 0.0001$
R^2	0.716	0.007	0.775	0.745	0.572
a priori contrasts					
(3) vs (6)	$p = 0.8352$	$p = 0.9467$	$p = 0.0018$	$p = 0.0131$	$p = 0.2070$
(5) vs (6)	$p < 0.0001$	$p = 0.8860$	$p < 0.0001$	$p < 0.0001$	$p = 0.0004$

[a]Results are expressed as mean of replicate (9 to 12) ± SEM. GP: GlucoPhenol; GP + O: GlucoPhenol + onion. The experimental groups are numbered from (1) to (6). *$p < 0.05$ in comparison with control group.

low amount of both methylated and sulfated forms of catechins were also detected (0.1 μM max). Among phenolic acids, *p*-coumaric acid and a well-known degradation product of the ellagitannins, dimethyl ellagic acid glucuronide, were detected in significant amounts (until 10 μM). Native anthocyanidins, metabolites of flavan-3-ols and *p*-coumaric acid, presented a kinetic profile with a high concentration 30−60 min postingestion followed by a progressive decrease, whereas dimethyl ellagic acid glucuronide showed an increase of its concentration until 180 min postingestion followed by a plateau until 360 min postingestion.

Protocatechuic acid, a phenolic acid present in a very high amount in onion extract and in a low amount in GP extract, was detected in high quantities (15 μM max) and presented a kinetic profile similar to that of *p*-coumaric acid with a concentration peak at 30 min postingestion. Flavonols were the major phenolic constituents of onion extract, but they were also present in GP extract in smaller quantities. Quercetin, detected in its native aglycone form in a very low amount (0.2 μM max), was mostly detected in circulation in its conjugated forms: glucuronidated, diglucuronidated, and sulfated quercetin (30, 45, and 1.5 μM max, respectively); it was also detected as conjugates of its methylated form isorhamnetin: glucuronidated, diglucuronidated, and sulfated isorhamnetin (about 15−20 μM max). A very high concentration of both a glucuronidated and a sulfated form of isorhamnetin was also detected (about 120 μM max). Some metabolites of myricetin, present in very low quantities in GP extract, were also detected under glucuronidated and diglucuronidated forms (15 and 6 μM max, respectively). The kinetic profiles of the glucuronidated forms of quercetin were characterized by an increase of its concentration until 60 min postingestion followed by a plateau until 360 min postingestion, whereas the sulfated form of quercetin showed a continuous increase until 360 min postingestion. All the isorhamnetin metabolites also displayed a kinetic profile with a strong increase of their concentration until 360 min postingestion. Glucuronidated myricetin reached a high concentration peak 30 min postingestion followed by a rapid decline, whereas diglucuronidated myricetin reached its highest concentration 120 min postingestion and remained constant until 360 min postingestion.

Statistical Analysis: Linear Regression and A Priori Comparison between Groups. The individual metabolites, together with their AUC values and their statistical parameters, are listed in Tables 4 and 5. A linear regression analysis was performed on individual metabolite concentrations (expressed as AUC values) quantified in control and GP groups (groups 1 to 5) and GP ingested dose (phenolic intake from 0 mg/kg to 36 mg/kg). Almost all the detected phenolic metabolites fitted with the linear regression model (p max = 0.0021, R^2 ranging from 0.267 to 0.775), with the exception of native catechins and quercetin (p = 0.5161 and 0.7592, respectively). These results indicate that, in the range of tested doses, there is a relatively strong proportionality between the amount of phenolic compounds

Table 5. Concentration of Onion Phenolic Metabolites (Expressed as AUC) Found in the Plasma of Rats Fed with Different Concentrations of GlucoPhenol Extract, Co-Ingested or Not with Onion Extract[a]

	quercetin	quercetin glucuronide	quercetin diglucuronide	quercetin sulfate	isorhamnetin glucuronide	isorhamnetin diglucuronide
AUC						
(1) control	11.3 ± 3.9	15.8 ± 3.8	7.0 ± 2.2	4.2 ± 1.4	12.8 ± 3.2	3.4 ± 1.0
(2) 2.7 mg/kg GP	10.5 ± 6.2	22.0 ± 4.0	55.0 ± 6.6*	3.2 ± 1.2	59.1 ± 13.1*	22.7 ± 4.0*
(3) 5.4 mg/kg GP	7.4 ± 4.6	32.6 ± 10.0	83.5 ± 22.3*	10.2 ± 8.5	69.1 ± 14.6*	31.4 ± 10.1*
(4) 27 mg/kg GP	9.2 ± 2.3	240 ± 37*	612 ± 94*	17.2 ± 4.8*	605 ± 96*	237 ± 58*
(5) 36 mg/kg GP	8.9 ± 2.2	369 ± 63*	814 ± 111*	37.3 ± 10.7*	852 ± 125*	378 ± 86*
(6) 36 mg/kg GP + O	37.1 ± 8.8*	8629 ± 1157*	13290 ± 1529*	304 ± 77*	6481 ± 693*	3667 ± 398*
statistics						
linear regression	$p = 0.7592$	$p < 0.0001$	$p < 0.0001$	$p = 0.0021$	$p < 0.0001$	$p < 0.0001$
R^2	0.002	0.655	0.740	0.267	0.716	0.517
a priori contrasts						
(3) vs (6)	$p = 0.0005$	$p < 0.0001$	$p < 0.0001$	$p < 0.0001$	$p < 0.0001$	$p < 0.0001$
(5) vs (6)	$p = 0.0015$	$p < 0.0001$	$p < 0.0001$	$p = 0.0002$	$p < 0.0001$	$p < 0.0001$

	isorhamnetin sulfate	isorhamnetin glucuronide sulfate	myricetin glucuronide	myricetin diglucuronide	protocatechuic acid
AUC					
(1) control	4.7 ± 1.1	13.2 ± 4.9	39.2 ± 14.1	5.3 ± 1.2	15.0 ± 2.3
(2) 2.7 mg/kg GP	11.8 ± 2.6*	44.0 ± 9.1*	43.5 ± 18.4	6.1 ± 1.4	26.2 ± 4.7
(3) 5.4 mg/kg GP	12.1 ± 4.3*	62.2 ± 23.0*	51.4 ± 19.5	16.6 ± 4.5*	25.7 ± 7.0
(4) 27 mg/kg GP	215 ± 55*	997 ± 268*	129 ± 31*	381 ± 97*	49.2 ± 8.2*
(5) 36 mg/kg GP	503 ± 114*	2697 ± 734*	185 ± 26*	557 ± 127*	101 ± 18*
(6) 36 mg/kg GP + O	2942 ± 353*	20456 ± 3422*	1223 ± 124*	1949 ± 192*	1130 ± 64*
statistics					
linear regression	$p < 0.0001$	$p = 0.0002$	$p < 0.0001$	$p < 0.0001$	$p < 0.0001$
R^2	0.504	0.420	0.439	0.529	0.458
a priori contrasts					
(3) vs (6)	$p < 0.0001$	$p < 0.0001$	$p < 0.0001$	$p < 0.0001$	$p < 0.0001$
(5) vs (6)	$p = 0.0006$	$p < 0.0001$	$p < 0.0001$	$p < 0.0001$	$p < 0.0001$

[a]Results are expressed as mean of replicate (9 to 12) ± SEM. GP: GlucoPhenol; GP + O: GlucoPhenol + onion. The experimental groups are numbered from (1) to (6). *$p < 0.05$ in comparison with control group.

ingested by animals and the concentration of phenolic metabolites in plasma.

A comparison was made between the groups 5 and 6 for the total circulating phenolic concentration, expressed in AUC values (Table 4). Whereas the rats of these two groups have ingested the same phenolic dose (36 mg/kg), the total AUC value in group 6 was more than 3-fold the AUC value in group 5 ($p < 0.0001$). The groups 3 and 6 were also compared for their individual circulating metabolites concentrations, expressed in AUC values (Tables 4 and 5). These two groups have ingested the same GP dose (5.4 mg/kg), but the animals of group 6 have also received an onion supplementation, resulting in a different total phenolic intake (5.4 mg/kg and 36 mg/kg for groups 3 and 6, respectively). Protocatechuic acid and flavonol metabolites, mainly coming from onion extract, obviously presented strongly different AUC values between these two groups (from 5- to 329-fold more in group 6; $p \leq 0.0005$) as only the animals of group 6 have received the onion extract (Table 5). Among phenolic metabolites coming from GP extract (Table 4), peonidin 3-galactoside, pelargonidin 3-glucoside, *p*-hydroxybenzoic acid, *p*-coumaric acid, and methyl catechins sulfate presented as expected close AUC values in groups 3 and 6 (p value ranging from 0.1502 to 0.9467) as all the animals have received the same GP dose. However, glucuronidated metabolites showed higher AUC values in group 6 than in group 3, meaning that for the same intake of GP extract, the onion-supplemented animals have produced more glucuronide metabolites of strawberry–cranberry phenolic compounds. Indeed, *p*-hydroxybenzoic glucuronide, catechins glucuronide, and methyl catechins glucuronide AUC values were found higher in group 6 in comparison with group 3: +252% ($p < 0.0001$), +279% ($p = 0.0018$), and +118% ($p = 0.0131$), respectively. The glucuronidated dimethyl ellagic acid was an exception, because it showed similar AUC values in the two groups ($p = 0.8352$). UHPLC-MS/MS MRM profiles of *p*-hydroxybenzoic glucuronide, catechins glucuronide, and methyl catechins glucuronide are available as Supplemental Figure S3.

DISCUSSION

The present study aimed at investigating the bioavailability of strawberry and cranberry phenolic compounds after oral administration to rats, with or without onion supplementation. The human daily intake of plant phenols is estimated to be between 150 and 1000 mg.[20] In this study, the rats received a phenol intake from 2.7 to 36 mg/kg, which corresponds to a human intake from 25 to 333 mg (mean body weight of 60 kg) according to the Food and Drug Administration's (FDA) body surface area (BSA) normalization.[21] The selected doses were lower than the recommended doses in order to be relevant in a nutritional supplementation context and to be further compared with human clinical trials.

The evidence of the absorption of phenolic compounds was earlier based on the increase of the antioxidant status of the plasma after the consumption of phenolic-rich foods. This

approach has been largely criticized,[22] and direct measurements of phenolics in plasma using HPLC with DAD or MS detection have been preferred but provided limited information due to a low sensitivity. Numerous bioavailability studies were conducted using enzymatic hydrolysis but provided limited information regarding the actual metabolites present in biological fluids. To obtain an overview of the absorption and metabolism of phenolic compounds, it is essential to be able to characterize most of the circulating metabolites, generally present at low concentrations. This requires the use of an appropriate extraction method to isolate phenolic metabolites from plasma-like microelution SPE (μSPE) and a sensitive analytical methodology such as UHPLC with tandem MS for their detection and quantification. The μSPE plates are packed with a high-capacity sorbent both lipophilic and hydrophilic to give maximum retention ability for different polarity compounds from a biological matrix. In comparison with conventional SPE cartridges, μSPE plates present a better extraction recovery and a better preservation of the molecular integrity. Indeed, the eluate can directly be analyzed in the collecting plates in UHPLC-MS, and thus an evaporation step previous to the chromatographic analysis can be avoided.[13] The optimized methods developed allowed the characterization of 21 phenolic metabolites in a volume as small as 20 μL of rat plasma after their consumption of GP extract supplemented or not with onion extract.

As expected when using nutritional doses of phenolic compounds, the phenolic compound transporters and metabolic pathways were probably not saturated, which could explain the general linear increase in the concentration of plasma phenolic metabolites in response to the increase in the dose ingested of GP extract. After ingestion of the extracts, the native phenolic compounds were extensively metabolized and were thus present in the circulation almost exclusively as conjugate metabolites and microbial degradation products.

Quercetin (both aglycone and glycosides forms) was intensively conjugated in glucuronidated and diglucuronidated forms, and to a lesser extent in sulfated form. Quercetin was especially methylated at a high level into isorhamnetin, leading to the formation of isorhamnetin metabolites being present in high quantities, whereas the extracts contained only low levels of isorhamentin. Isorhamnetin glucuronide sulfate was the metabolite identified in the highest quantity in rat plasma following the extracts ingestion, showing the intensive metabolization of quercetin, with both methyl, glucuronide, and sulfate conjugations. Moreover, the presence of myricetin metabolites in onion-fed rats' plasma, even though the onion extract did not contained any myricetin, suggests a probable hydroxylation of quercetin during its metabolization. A wide variety of metabolites resulting from quercetin conjugation has been previously reported in rats and humans.[23,24] Similarly, catechins monomers have undergone extensive conjugation processes with high contents of glucuronidated forms of catechins and methylated catechins, as well as low content of sulfated forms of methylated catechins detected in strawberry−cranberry-fed animals. Such catechins conjugates were earlier reported in rat plasma.[25]

Anthocyanins constitute an exception to the classical deconjugation−reconjugation sequence involved in the metabolization of phenolic compounds as they can be absorbed in their native glycoside structure.[26] These compounds are known to be poorly available due to their microbial and spontaneous degradation and also to their high sensitivity to pH.[26−28] Pelargonidin 3-glucoside and peonidin 3-galactoside were thus detected in circulation but in extremely low concentrations. However, high amounts of a known degradation product of pelargonidin 3-glucoside, *p*-hydroxybenzoic acid,[29] and its glucuronidated conjugate were identified in rat plasma following GP extract consumption.

As expected, no polymeric phenolic compounds were detected in rat plasma. These compounds, such as procyanidins and ellagitannins, are known to be poorly absorbed.[30,31] Ellagitannins are depolymerized in stomach followed by the absorption of ellagic acid directly in the stomach or in the intestine.[31] Ellagic acid metabolization then leads to the formation of ellagic acid derivatives, like the dimethyl ellagic acid glucuronide detected here, and urolithins.[30] Procyanidins reach the colon where they are subjected to microbial degradation leading to the generation of phenolic acids, which are further absorbed and metabolized.[32] Some phenolic acids were detected here, either coming from the release from food matrix or resulting from more complex phenolic structure degradation.[4] *p*-Coumaric acid, which was present in GP extract in the same amount as chlorogenic acid, was detected in high quantities in rat plasma following their ingestion of this extract, whereas chlorogenic acid was not detected at all. Chlorogenic acid is poorly metabolized because of a lack of esterases in the intestine tissues.[10] Consequently, the only significant site for chlorogenic acid metabolism is the colonic microflora, which generates a wide variety of metabolites, including *p*-coumaric acid.[33,34] Protocatechuic acid, which constituted a major phenolic compound of onion extract, was detected in rat plasma either in its native form and/or mostly probably as a degradation product of native flavonoids such as cyanidin,[35] catechins,[36] and quercetin.[11]

Identified phenolic metabolites presented some specific kinetic profiles, reflecting the biological site of conjugation. Indeed, a low T_{max} may be indicative of conjugation taking place in the intestine before the prior passage of metabolites in the circulation, whereas a higher T_{max} may reflect a postabsorption conjugation.[28] Therefore, glucuronidated catechins conjugates, which presented a high concentration 30−60 min postingestion followed by a progressive decrease, appeared to be early conjugated in the intestine. The delay in the elimination time of methyl catechins glucuronide metabolite suggested a postabsorption methylation of glucuronidated catechins in the liver.

Similarly, glucuronidated quercetin seemed to be conjugated early in the intestine and accumulate over time, which has previously been demonstrated in humans[37] and has been attributed to the high affinity of this compound with serum albumin.[38] The increasing plasma concentration of sulfated quercetin over time probably reflects its hepatic formation. Regarding the kinetic profiles of isorhamnetin metabolites, it appears that they were likely resulting from a postabsorption methylation of already conjugated quercetin metabolites, in the liver.

Anthocyanins are highly soluble and among the few compounds that can be directly absorbed from the stomach,[39] leading to their probable rapid intestinal metabolization, as reflected by their kinetic profiles and those of their metabolites.

The kinetic profile of dimethyl ellagic acid glucuronide, a biomarker of the ellagitannins intake,[11] suggests an extensive hepatic metabolization and active enterohepatic circulation of this compound. However, the solubility of phenolic compounds should be a factor to consider as it can greatly influence the kinetics of metabolites. Indeed, because quercetin and ellagic acid

are poorly soluble, their metabolites might precipitate in blood and thus be delayed in their circulation and metabolization.

The absorption and metabolization of phenolic compounds was shown to be strongly modulated by the structure of the phenolic compounds. Indeed, although a similar phenolic metabolites absorption rate was observed 30 min postingestion in groups 5 and 6 (Figure 1A—total metabolites), which have ingested both the same phenolic amount but from different sources (GP extract or GP supplemented with onion extract), a significantly different absorption rate was observed 360 min postingestion, with the elimination of strawberry−cranberry phenolic metabolites and the accumulation of onion metabolites in rat plasma. These results support the idea that the phenolic structure prevails over the phenolic dose for absorption and metabolization. In all cases, and in accordance with previous reported data, the estimated phenolic absorption was low, as it did not exceed 2% of the ingested phenolic dose. Despite the low circulating concentrations of phenolic metabolites and their rapid elimination (for most of them), those compounds exert various regulating biological activities in vivo, which go beyond direct antioxidant activity.[40]

Phenolic compound absorption and metabolization can be modulated by phenolics themselves. Indeed, some phenolic compounds are known to specifically modify some metabolic processes that govern bioavailability, such as the modulation of gut microbiota or xenobiotics transporters activity, as well as the modulation of conjugation enzymes.[41]

Here, we observed the presence of four glucuronidated metabolites resulting from strawberry−cranberry extract phenolic compounds. Among them, three compounds, *p*-hydroxybenzoic acid glucuronide, catechins glucuronide, and methyl catechins glucuronide, which were suggested to be produced in the intestine regarding their kinetic profile, were found in 2 to almost 4 times higher concentrations in the plasma of animals that have ingested onion extract together with GP extract, for the same GP intake. On the contrary, dimethyl ellagic acid glucuronide, a highly metabolized compound whose kinetic profile indicated a hepatic conjugation, were present in the same quantities in the animals of the two groups. Glucuronidation processes of some strawberry−cranberry phenolic metabolites thus appear to be enhanced in the presence of onion phenolic compounds but specifically in the intestine. This modulation could be attributed to quercetin, which has already been demonstrated to be involved in the induction of glucuronidation enzyme UDP-glucuronosyl-transferase in intestinal cell lines in vitro and in rats in vivo.[42−44] These data therefore indicate an opportunity to increase the circulating metabolites concentration using synergistic interactions between phenolic compounds and thus to increase the bioactivity of some plant extracts by improving their oral bioavailability.

In conclusion, this study reported the use of an optimized technique combining μSPE and UHPLC-MS/MS methods for the simultaneous identification and quantification, for the first time, of about 20 phenolic metabolites in rat plasma following the ingestion of GP, a strawberry−cranberry extracts blend alone or with an onion extract. In most cases, native compounds were not detected in rat plasma and were extensively metabolized into conjugates and degradation products. Quercetin metabolites were found in greater amounts in plasma, the rats being supplemented with the onion extract or not, illustrating the differences existing between phenolic compounds in terms of absorption and metabolization. This study also highlighted a possible synergistic activity of phenolic compounds for improving bioavailability, with a possible induction of intestinal UDP-glucuronosyl-transferase by onion quercetin. This work allowed the identification and quantification of actual metabolites generated in vivo following phenolic consumption, as well as the analysis of their pharmacokinetic, data which are fundamental to unravel their mechanisms of action.

■ ASSOCIATED CONTENT

Supporting Information

HPLC chromatograms of GlucoPhenol extract anthocyanins and procyanidins (Figure S1 and Figure S2, respectively) and MRM signals of *p*-hydroxybenzoic acid glucuronide, catechins glucuronide, and methyl catechins glucuronide in rat plasma (Figure S3). This material is available free of charge via the Internet at http://pubs.acs.org.

■ AUTHOR INFORMATION

Corresponding Author

*E-mail: Yves.Desjardins@fsaa.ulaval.ca. Fax: (1) 418-656-3515. Tel.: (1) 418- 656-2131 #2359.

Notes

The authors declare no competing financial interest.

■ ACKNOWLEDGMENTS

The authors thank Dr. André Gosselin and Sébastien Léonhart from Nutra Canada and Dr. Barry Ritz from Atrium Innovations for supplying the experimental extracts and critically reviewing the manuscript. Financial support was provided by the Quebec Industrial Bioprocess Research Consortium (CRIBIQ) of the Ministry of Economic Development, Innovation, and Export Trade (MDEIE), Nutra Canada, and Atrium Innovations.

■ ABBREVIATIONS:

SPE: solid phase extraction; DP: degree of polymerization; GP: GlucoPhenol; O: onion; T_{max}: time to reach maximum concentration; AWA: acetone−water−acetic acid

■ REFERENCES

(1) Anhe, F. F.; Desjardins, Y.; Pilon, G.; Dudonne, S.; Genovese, M. I.; Lajolo, F. M.; Marette, A. Polyphenols and type 2 diabetes: A prospective review. *PharmaNutrition* **2013**, *1*, 105−114.

(2) Cherniack, E. P. Polyphenols: planting the seeds of treatment for the metabolic syndrome. *Nutrition* **2011**, *27*, 617−623.

(3) Lila, M. A. Impact of bioflavonoids from berryfruits on biomarkers of metabolic syndrome. *Funct. Foods Health Dis.* **2011**, *2*, 13−24.

(4) Aura, A. M. Microbial metabolism of dietary phenolic compounds in the colon. *Phytochem. Rev.* **2008**, *7*, 407−429.

(5) Selma, M. V.; Espin, J. C.; Tomas-Barberan, F. A. Interaction between phenolics and gut microbiota: role in human health. *J. Agric. Food Chem.* **2009**, *57*, 6485−6501.

(6) Walle, T.; Browning, A. M.; Steed, L. L.; Reed, S. G.; Walle, U. K. Flavonoid glucosides are hydrolyzed and thus activated in the oral cavity in humans. *J. Nutr.* **2005**, *135*, 48−52.

(7) Donovan, J. L.; Manach, C.; Faulks, R. M.; Kroon, P. A. Absorption and metabolism of dietary secondary metabolites. In *Plant Secondary Metabolites. Occurrence, Structure and Role in the Human Diet*; Crozier, A., Clifford, M. N., Ashihara, H., Eds; Blackwell Publishing: Oxford, 2006; pp 303−351.

(8) Gee, J. M.; DuPont, M. S.; Day, A. J.; Plumb, G. W.; Williamson, G.; Johnson, I. T. Intestinal transport of quercetin glycosides in rats involves both deglycosylation and interaction with the hexose transport pathway. *J. Nutr.* **2000**, *130*, 2765−2771.

(9) Nemeth, K.; Plumb, G. W.; Berrin, J. G.; Juge, N.; Jacob, R.; Naim, H. Y.; Williamson, G.; Swallow, D. M.; Kroon, P. A. Deglycosylation by

small intestinal epithelial cell beta-glucosidases is a critical step in the absorption and metabolism of dietary flavonoid glycosides in humans. *Eur. J. Nutr.* **2003**, *42*, 29−42.
(10) Spencer, J. P.; Chowrimootoo, G.; Choudhury, R.; Debnam, E. S.; Srai, S. K.; Rice-Evans, C. The small intestine can both absorb and glucuronidate luminal flavonoids. *FEBS Lett.* **1999**, *458*, 224−230.
(11) Rechner, A. R.; Smith, M. A.; Kuhnle, G.; Gibson, G. R.; Debnam, E. S.; Srai, S. K.; Moore, K. P.; Rice-Evans, C. A. Colonic metabolism of dietary polyphenols: influence of structure on microbial fermentation products. *Free Radical Biol. Med.* **2004**, *36*, 212−225.
(12) Scalbert, A.; Morand, C.; Manach, C.; Remesy, C. Absorption and metabolism of polyphenols in the gut and impact on health. *Biomed. Pharmacother.* **2002**, *56*, 276−282.
(13) Marti, M. P.; Pantaleon, A.; Rozek, A.; Soler, A.; Valls, J.; Macia, A.; Romero, M. P.; Motilva, M. J. Rapid analysis of procyanidins and anthocyanins in plasma by microelution SPE and ultra-HPLC. *J. Sep. Sci.* **2010**, *33*, 2841−2853.
(14) Parelman, M. A.; Storms, D. H.; Kirschke, C. P.; Huang, L.; Zunino, S. J. Dietary strawberry powder reduces blood glucose concentrations in obese and lean C57BL/6 mice, and selectively lowers plasma C-reactive protein in lean mice. *Br. J. Nutr.* **2012**, *108*, 1789−1799.
(15) Kim, M. J.; Chung, J. Y.; Kim, J. H.; Kwak, H. K. Effects of cranberry powder on biomarkers of oxidative stress and glucose control in db/db mice. *Nutr. Res. Pract.* **2013**, *7*, 430−438.
(16) Jung, J. Y.; Lim, Y.; Moon, M. S.; Kim, J. Y.; Kwon, O. Onion peel extracts ameliorate hyperglycemia and insulin resistance in high fat diet/streptozotocin-induced diabetic rats. *Nutr. Metab.* **2011**, *8*, 18.
(17) Wu, X.; Prior, R. L. Systematic identification and characterization of anthocyanins by HPLC-ESI-MS/MS in common foods in the United States: fruits and berries. *J. Agric. Food Chem.* **2005**, *53*, 2589−2599.
(18) Brownmiller, C.; Howard, L. R.; Prior, R. L. Processing and storage effects on procyanidin composition and concentration of processed blueberry products. *J. Agric. Food Chem.* **2009**, *57*, 1896−1902.
(19) Prior, R. L.; Gu, L. Occurrence and biological significance of proanthocyanidins in the American diet. *Phytochemistry* **2005**, *66*, 2264−2280.
(20) Scalbert, A.; Williamson, G. Dietary intake and bioavailability of polyphenols. *J. Nutr.* **2000**, *130*, 2073S−2085S.
(21) Guidance for Industry: Estimating the Maximum Safe Starting Dose in Initial Clinical Trials for Therapeutics in Adult Healthy Volunteers. U.S. Department of Health and Human Services, Food and Drug Administration (FDA), Center for Drug Evaluation and Research (CDER). July 2005.
(22) Lotito, S. B.; Frei, B. Consumption of flavonoid-rich foods and increased plasma antioxidant capacity in humans: cause, consequence, or epiphenomenon? *Free Radical Biol. Med.* **2006**, *41*, 1727−1746.
(23) Mullen, W.; Graf, B. A.; Caldwell, S. T.; Hartley, R. C.; Duthie, G. G.; Edwards, C. A.; Lean, M. E.; Crozier, A. Determination of flavonol metabolites in plasma and tissues of rats by HPLC-radiocounting and tandem mass spectrometry following oral ingestion of [$2^{-(14)}$C]-quercetin-4′-glucoside. *J. Agric. Food Chem.* **2002**, *50*, 6902−6909.
(24) Mullen, W.; Edwards, C. A.; Crozier, A. Absorption, excretion and metabolite profiling of methyl-, glucuronyl-, glucosyl- and sulpho-conjugates of quercetin in human plasma and urine after ingestion of onions. *Br. J. Nutr.* **2006**, *96*, 107−116.
(25) Serra, A.; Macia, A.; Romero, M. P.; Salvado, M. J.; Bustos, M.; Fernandez-Larrea, J.; Motilva, M. J. Determination of procyanidins and their metabolites in plasma samples by improved liquid chromatography-tandem mass spectrometry. *J. Chromatogr. B: Anal. Technol. Biomed. Life Sci.* **2009**, *877*, 1169−1176.
(26) Prior, R. L.; Wu, X. Anthocyanins: structural characteristics that result in unique metabolic patterns and biological activities. *Free Radical Res.* **2006**, *40*, 1014−1028.
(27) Aura, A. M.; Martin-Lopez, P.; O'Leary, K. A.; Williamson, G.; Oksman-Caldentey, K. M.; Poutanen, K.; Santos-Buelga, C. In vitro metabolism of anthocyanins by human gut microflora. *Eur. J. Nutr.* **2005**, *44*, 133−142.
(28) Crozier, A.; Jaganath, I. B.; Clifford, M. N. Dietary phenolics: chemistry, bioavailability and effects on health. *Nat. Prod. Rep.* **2009**, *26*, 1001−1043.
(29) Azzini, E.; Vitaglione, P.; Intorre, F.; Napolitano, A.; Durazzo, A.; Foddai, M. S.; Fumagalli, A.; Catasta, G.; Rossi, L.; Venneria, E.; Raguzzini, A.; Palomba, L.; Fogliano, V.; Maiani, G. Bioavailability of strawberry antioxidants in human subjects. *Br. J. Nutr.* **2010**, *104*, 1165−1173.
(30) Espin, J. C.; Gonzalez-Barrio, R.; Cerda, B.; Lopez-Bote, C.; Rey, A. I.; Tomas-Barberan, F. A. Iberian pig as a model to clarify obscure points in the bioavailability and metabolism of ellagitannins in humans. *J. Agric. Food Chem.* **2007**, *55*, 10476−10485.
(31) Clifford, M. N.; Scalbert, A. Ellagitannins - nature, occurrence and dietary burden. *J. Sci. Food Agric.* **2000**, *80*, 1118−1125.
(32) Manach, C.; Williamson, G.; Morand, C.; Scalbert, A.; Remesy, C. Bioavailability and bioefficacy of polyphenols in humans. I. Review of 97 bioavailability studies. *Am. J. Clin. Nutr.* **2005**, *81*, 230S−242S.
(33) Farah, A.; Monteiro, M.; Donangelo, C. M.; Lafay, S. Chlorogenic acids from green coffee extract are highly bioavailable in humans. *J. Nutr.* **2008**, *138*, 2309−2315.
(34) Stalmach, A.; Mullen, W.; Barron, D.; Uchida, K.; Yokota, T.; Cavin, C.; Steiling, H.; Williamson, G.; Crozier, A. Metabolite profiling of hydroxycinnamate derivatives in plasma and urine after the ingestion of coffee by humans: identification of biomarkers of coffee consumption. *Drug Metab. Dispos.* **2009**, *37*, 1749−1758.
(35) Vitaglione, P.; Donnarumma, G.; Napolitano, A.; Galvano, F.; Gallo, A.; Scalfi, L.; Fogliano, V. Protocatechuic acid is the major human metabolite of cyanidin-glucosides. *J. Nutr.* **2007**, *137*, 2043−2048.
(36) Gonthier, M. P.; Donovan, J. L.; Texier, O.; Felgines, C.; Remesy, C.; Scalbert, A. Metabolism of dietary procyanidins in rats. *Free Radical Biol. Med.* **2003**, *35*, 837−844.
(37) Hollman, P. C.; van Trijp, J. M.; Buysman, M. N.; van der Gaag, M. S.; Mengelers, M. J.; de Vries, J. H.; Katan, M. B. Relative bioavailability of the antioxidant flavonoid quercetin from various foods in man. *FEBS Lett.* **1997**, *418*, 152−156.
(38) Dangles, O.; Dufour, C.; Manach, C.; Morand, C.; Remesy, C. Binding of flavonoids to plasma proteins. *Methods Enzymol.* **2001**, *335*, 319−333.
(39) Talavera, S.; Felgines, C.; Texier, O.; Besson, C.; Lamaison, J. L.; Remesy, C. Anthocyanins are efficiently absorbed from the stomach in anesthetized rats. *J. Nutr.* **2003**, *133*, 4178−4182.
(40) Hollman, P. C.; Cassidy, A.; Comte, B.; Heinonen, M.; Richelle, M.; Richling, E.; Serafini, M.; Scalbert, A.; Sies, H.; Vidry, S. The biological relevance of direct antioxidant effects of polyphenols for cardiovascular health in humans is not established. *J. Nutr.* **2011**, *141*, 989S−1009S.
(41) Scheepens, A.; Tan, K.; Paxton, J. W. Improving the oral bioavailability of beneficial polyphenols through designed synergies. *Genes Nutr.* **2010**, *5*, 75−87.
(42) Galijatovic, A.; Walle, U. K.; Walle, T. Induction of UDP-glucuronosyltransferase by the flavonoids chrysin and quercetin in Caco-2 cells. *Pharm. Res.* **2000**, *17*, 21−26.
(43) Odenthal, J.; van Heumen, B. W.; Roelofs, H. M.; te Morsche, R. H.; Marian, B.; Nagengast, F. M.; Peters, W. H. The influence of curcumin, quercetin, and eicosapentaenoic acid on the expression of phase II detoxification enzymes in the intestinal cell lines HT-29, Caco-2, HuTu 80, and LT97. *Nutr. Cancer* **2012**, *64*, 856−863.
(44) van der Logt, E. M.; Roelofs, H. M.; Nagengast, F. M.; Peters, W. H. Induction of rat hepatic and intestinal UDP-glucuronosyltransferases by naturally occurring dietary anticarcinogens. *Carcinogenesis* **2003**, *24*, 1651−1656.

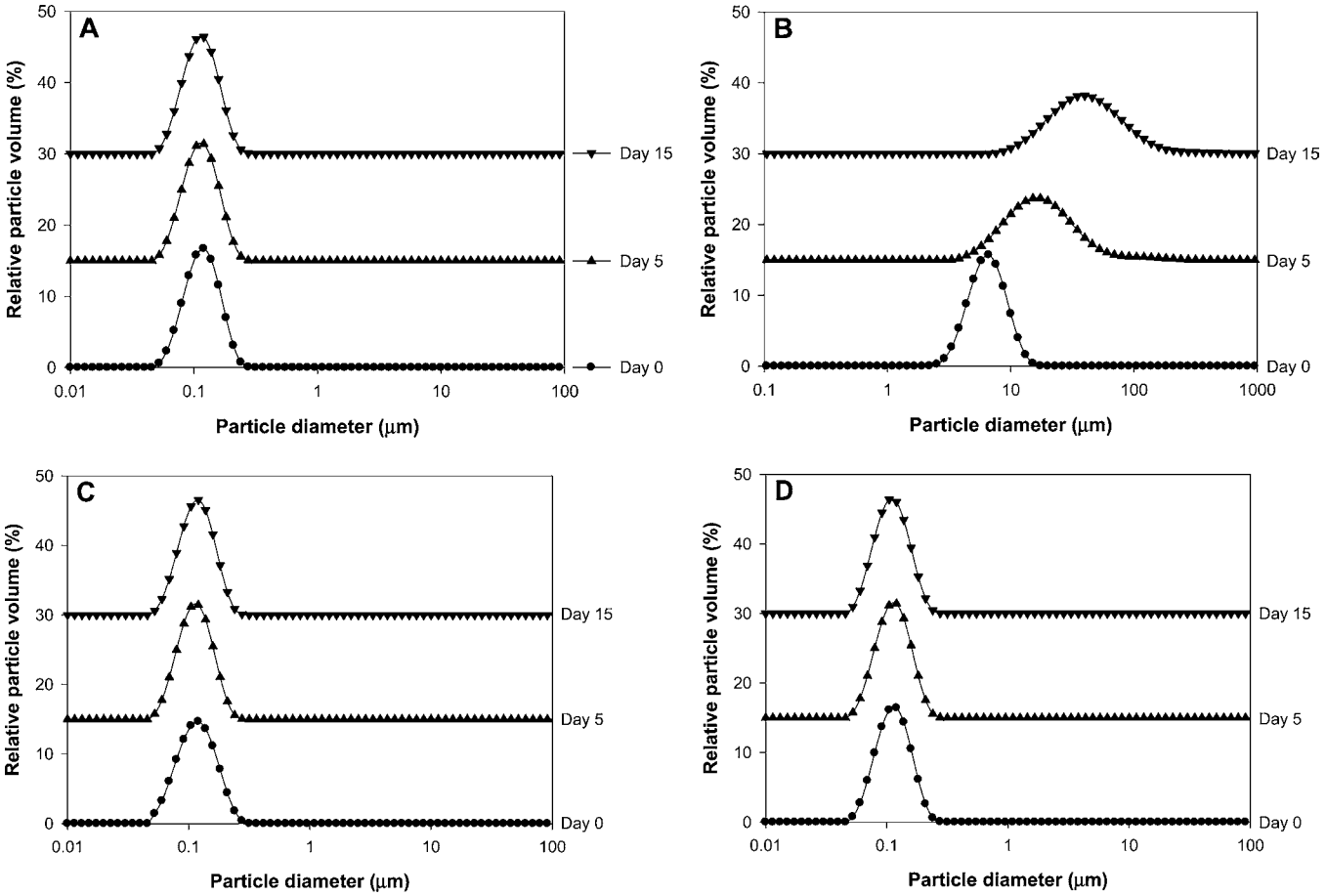

Figure 1. Evolution of the particle size distribution of SMP- or SMP/lysolecithin-stabilized orange oil-in-water emulsions (1% SMP and 5% orange oil) stored at 20 °C: (A) SMP-stabilized emulsion stored at pH 7; (B) SMP-stabilized emulsion stored at pH 3; (C) SMP/0.1% lysolecithin-stabilized emulsion at pH 3; (D) SMP/0.5% lysolecithin-stabilized emulsion at pH 3.

at 10000 rpm at room temperature. For reduction of droplet size, the premixed emulsions were homogenized by five passes through a microfluidizer (M-100L, Microfluidics, Newton, MA, USA) at 48.3 MPa. Then, the emulsion was adjusted to pH 3.0 using 1.0 and 0.1 N hydrochloric acid solutions. The final concentrations of lysolecithin in the whole emulsions varied from 0 to 0.5% (w/w), and the final concentration of SMP in the whole emulsions was 1% (w/w). To avoid the effect of light, all samples were stored in the dark before analysis.

Stability to Environmental Stresses. To determine the stability of SMP/lysolecithin-stabilized emulsions against heat treatment, emulsions were placed in glass test tubes and then incubated in a water bath for 15 min at different temperatures (30−90 °C). The emulsions were then allowed to cool to room temperature and held overnight prior to subsequent analysis. To evaluate the stability of SMP/lysolecithin-stabilized emulsions against the change in the electrostatic interaction, a series of 2.5 wt % emulsions with different NaCl concentrations was prepared by diluting the concentrated emulsions with 10 mM phosphate buffer (pH 3.0) containing different concentrations of sodium chloride. Then, the emulsions were kept at room temperature overnight prior to subsequent analysis.

Droplet Size Measurements. Mean droplet diameters of emulsions were measured using static light scattering (laser diffraction). To avoid multiple scattering effects, all emulsion samples were diluted to a droplet concentration of approximately ≈0.005% (w/w) using buffer solution at the pH of the sample and stirred continuously throughout the measurements to ensure they were homogeneous. The droplet size distribution of the emulsions was then measured using a commercial static light scattering instrument (Mastersizer 2000, Malvern Instruments, Worcestershire, UK). Droplet size data are reported as either the volume-surface mean diameter, $d_{32} = (\sum n_i d_i^3 / \sum n_i d_i^2)$, or the volume-weighted mean diameter, $d_{43} = (\sum n_i d_i^4 / \sum n_i d_i^3)$, where n_i is the number of droplets with diameter d_i. If an emulsion sample to be analyzed had phase-separated due to droplet creaming, then it was gently mixed to evenly disperse the droplets prior to collection of an aliquot for making the particle size measurements.

Electrical Charges of Oil-in-Water Emulsions. The ζ-potential of the emulsion droplets was measured using a microelectrophoresis instrument (ZetaSizer Nano, Malvern Instruments). The ζ-potential was calculated from measurement of the electrophoretic mobility of droplets in an applied oscillating electric field using laser Doppler velocimetry. Samples were prepared by diluting emulsions 1:500 with buffer solution at the pH of the sample and placing the diluted emulsions into disposable capillary cells (DTS1060, Malvern Instruments). If an emulsion sample to be analyzed had phase-separated due to creaming, then it was evenly dispersed by gentle stirring before collection of an aliquot for analysis.

Statistical Analysis. Experiments were repeated two or three times using freshly prepared samples, and the mean and standard deviations were calculated from these measurements.

RESULTS AND DISCUSSION

Influence of Lysolecithin. Previously, we examined the influence of pH on the stability of SMP-stabilized orange oil emulsions.[12] Stable orange oil emulsions with small mean droplet diameters (d_{43} < 0.15 μm) could be formed at neutral pH. However, when the emulsion was stored under acidic conditions (pH 3−5), a large increase in mean droplet diameter

dx.doi.org/10.1021/jf404983p | J. Agric. Food Chem. 2014, 62, 3257−3261

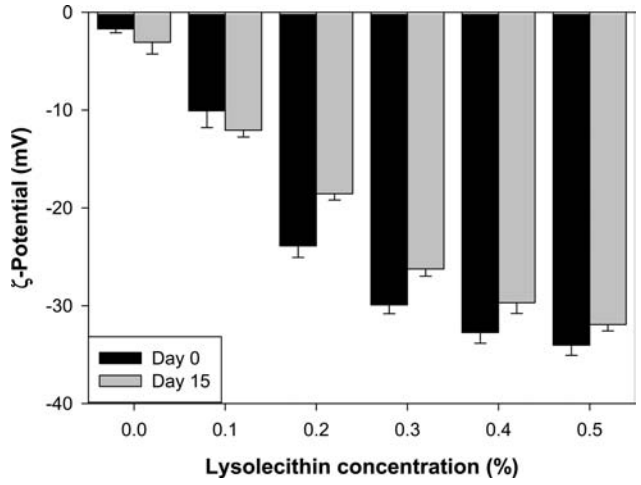

Figure 2. Influence of lysolecithin concentration on the ζ-potential of SMP-stabilized orange oil-in-water emulsions (1% SMP and 5% orange oil) at pH 3, stored at 20 °C.

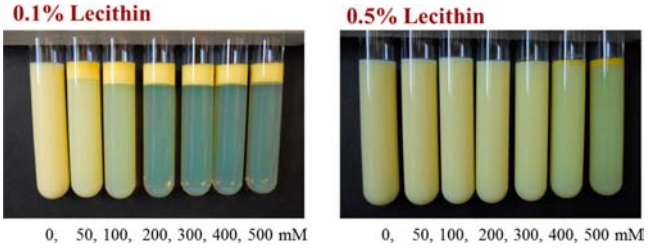

Figure 3. Photographs of SMP-stabilized orange oil-in-water emulsions (0.5% SMP, 2.5% orange oil, and 20 °C) with different NaCl concentrations.

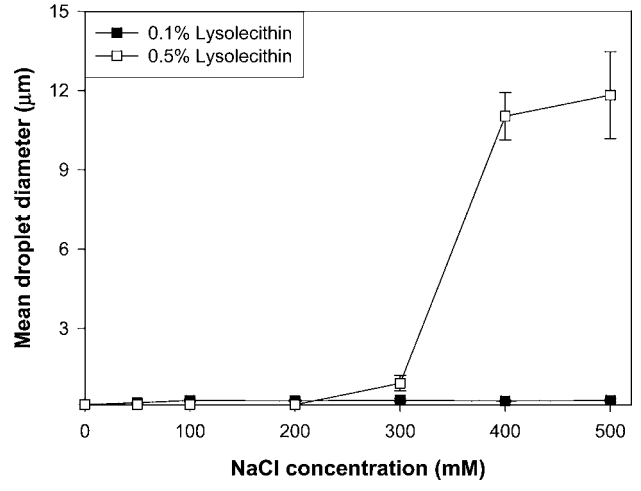

Figure 4. Influence of NaCl concentration on the mean droplet diameter of SMP-stabilized orange oil-in-water emulsions (1% SMP and 5% orange oil) at pH 3, stored at 20 °C.

was observed during storage. The reason for this phenomenon was attributed to the presence of small amounts of impurities (such as palmitic acid) in the SMP ingredient used to prepare the emulsions.[12] Because most of the palmitic acid molecules are ionized at pH values above the pK_a (≈4.9),[13] they are negatively charged. However, the predominant form of palmitic acid is neutral at pH values below the pK_a, indicating a low or almost zero net charge on the oil droplets. Therefore, the oil

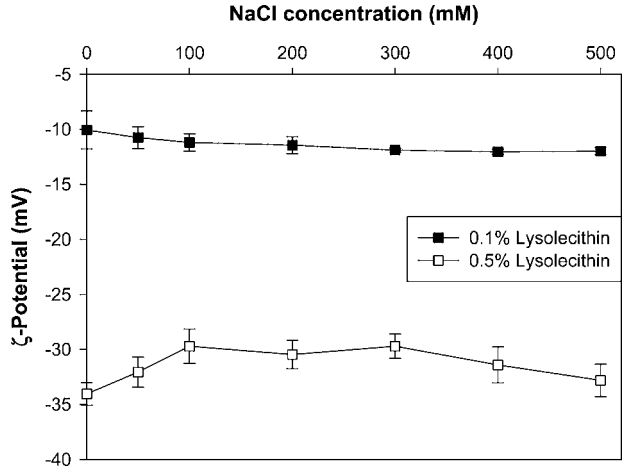

Figure 5. Influence of NaCl concentration on the electrical charge of SMP-stabilized orange oil-in-water emulsions (1% SMP and 5% orange oil) at pH 3, stored at 20 °C.

droplets have a high negative charge at high pH values, which stabilizes them from aggregation due to electrostatic repulsion. On the other hand, they have a low net charge at low pH and are therefore susceptible to aggregation due to the dominance of attractive colloidal interactions (such as van der Waals or hydrophobic attractions).

We therefore examined the impact of adding an anionic cosurfactant (lysolecithin) on the aggregation stability of orange oil-in-water emulsions under acid conditions (Figure 1). We hypothesized that this cosurfactant would improve the physical stability of the emulsions by increasing the electrostatic repulsion between the droplets. Emulsions were initially prepared under neutral pH conditions to ensure that they were stable. The initial mean droplet diameter at pH 7 was around 0.125 μm for all of the emulsions prepared (Figure 1A), independent of the lysolecithin concentration present, which suggested that the initial particle size was primarily governed by the homogenization conditions or the SMP. All of the emulsions were then adjusted to pH 3 and stored for 15 days.

In the absence of lysolecithin, the emulsions were highly unstable to droplet growth at pH 3, which was attributed to droplet coalescence during storage (Figure 1B). Conversely, in the presence of lysolecithin (0.1−0.5%), all of the emulsions were stable to droplet growth throughout 15 days of storage (Figures 1C,D). These results indicated that lysolecithin was an effective cosurfactant for improving the stability of SMP-coated droplets to growth, which can be attributed to the increased electrostatic repulsion between the droplets in the presence of this anionic surface active substance.

Figure 2 shows the ζ-potential of the SMP-stabilized orange oil emulsions with various lysolecithin concentrations. The ζ-potential of the oil droplets was close to zero (−1.7 mV) in the absence of lysolecithin, but it became increasingly negative as the amount of lecithin incorporated into the system increased. The ζ-potential reached a value of around −35 mV at 0.5% lysolecithin, which should be large enough to provide good stability through electrostatic repulsion. Theoretically, sucrose esters containing SMP are nonionic surfactants,[8] but they may have a negative charge at high pH because of the presence of ionized impurities, such as palmitic acid.[12] As described above, palmitic acid should have little charge at acid pH, which would account for the low net charge on the emulsions in the absence

dx.doi.org/10.1021/jf404983p | J. Agric. Food Chem. 2014, 62, 3257−3261

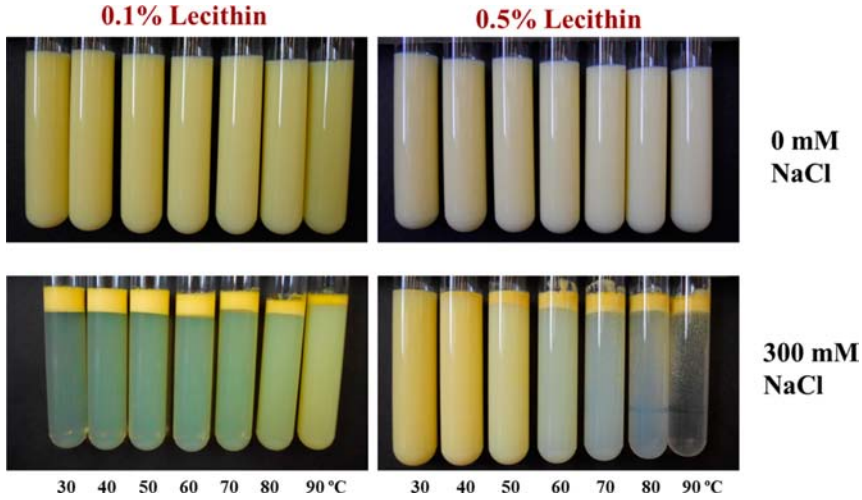

Figure 6. Photographs of 2.5 wt % orange oil-in-water emulsions stabilized by SMP and different amounts of lysolecithin after heat treatment in the presence of 0 or 300 mM NaCl.

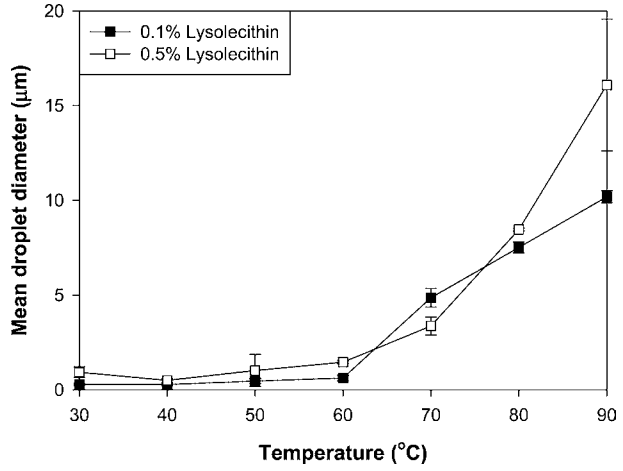

Figure 7. Influence of heat treatment on the mean droplet diameter of SMP-stabilized orange oil-in-water emulsions (0.5% SMMP, 2.5% orange oil, and 300 mM NaCl) containing lysolecithin at pH 3.

of lysolecithin. Lysolecithin has been reported to have a negative charge over a wide range of pH values.[14] Because the pK_a value of the phosphate groups on lysolecithin is typically around pH 1.5,[15] lysolecithin should still be negatively charged at pH 3.0. The presence of lysolecithin at the oil droplet surfaces would therefore account for the good stability of the orange oil emulsions to droplet growth at acidic conditions.

Influence of Ionic Strength. Commercial food and beverage products often contain different types and amounts of mineral ions, and therefore it is important to understand how ionic strength influences their stability. We therefore examined the influence of salt addition on the stability of orange oil-in-water emulsions stabilized by a combination of SMP and lysolecithin. Visual observations of orange oil emulsions containing different salt levels were made after they were stored at room temperature for 8 h. In the absence of added salts, the emulsions were visibly stable to phase separation, but in the presence of salt many of them separated into two distinct layers: a cream layer at the top and a serum layer at the bottom (Figure 3). Emulsions containing 0.1% lysolecithin were unstable to phase separation from 50 to 500 mM, whereas emulsions containing 0.5% lysolecithin were only unstable to visible phase separation at the highest salt concentrations (400 and 500 mM).

Interestingly, the particle size measurements suggested that the emulsions containing 0.1% lysolecithin remained relatively small across the entire salt range (Figure 4). We hypothesize that droplet flocculation occurred in these emulsions because they exhibited rapid creaming (indicative of an increase in particle size), but still had relatively small particle sizes when measured by static light scattering. This effect can be attributed to dissociation of flocs due to dilution and stirring within the measurement chamber of the light-scattering instrument. For the emulsions containing 0.5% lysolecithin, the mean particle diameter remained relatively small for low salt concentrations (0−300 mM NaCl), but increased steeply at higher salt levels. This result suggests that phase separation occurred due to an increase in droplet diameter (coalescence), followed by droplet creaming. Droplet aggregation can be attributed to screening of the electrostatic repulsion between negatively charged emulsion droplets at increasing ionic strength, leading to droplet flocculation and/or coalescence.[16] Emulsions containing 0.1% lysolecithin had a lower net charge than those containing 0.5% lysolecithin at all salt concentrations (Figure 5), which would account for the fact that they were less stable to salt addition. A low droplet charge leads to a lower energy barrier that has to be overcome before droplets can come into close proximity; therefore, less salt is needed to promote aggregation. However, the screening of the electrostatic repulsion between negatively charged emulsion droplets could not explain the difference in the origin of destabilization of emulsions stabilized with 0.1% (mainly flocculation) and 0.5% (mainly coalescence) lysolecithin. This effect may have been due to differences in interfacial composition: emulsions containing higher levels of lysolecithin are presumably more sensitive to electrolyte addition because of their charge characteristics. Electrolytes could change the hydrophilic−lipophilic balance and hydration conditions of the surfactants by depletion of the hydration shell around the polar head groups of surfactant molecules.[17] Because of the greater amount of lysolecithin, which is charged negatively over a broader range of pH values, the interfacial layer of emulsions containing 0.5% lysolecithin could be much more sensitive to these alterations in the physical properties of the surfactant molecules. Even if oil droplets are able to come into close

proximity due to attractive interactions, the presence of more nonpolar surfactants (SMP) within the interfacial layer of emulsions containing 0.1% lysolecithin may give better resistance against coalescence.

Influence of Temperature. Commercial food and beverage emulsions are commonly subjected to thermal processing, and so it is important to understand how heating influences their physical stability. In the absence of salt, all of the emulsions appeared to be visibly stable to phase separation after they were heated (Figure 6). In the presence of salt (300 mM NaCl), emulsions containing 0.1% lysolecithin were highly unstable to phase separation at all holding temperatures (from 30 to 90 °C). On the other hand, emulsions containing 0.5% lysolecithin were stable to phase separation at relatively low temperatures (30 and 40 °C), but unstable at higher temperatures. Previous studies have reported that SMP-stabilized emulsions were also unstable to droplet growth when they were stored at 40 °C for prolonged periods.[18] A possible reason for the destabilization of SMP-coated droplets at elevated temperatures is dehydration of the hydrophilic surfactant head groups. Dehydration leads to an alteration in the optimum curvature of the surfactant monolayer and to reduced steric repulsion between droplets.[15] The fact that the emulsions were stable to droplet aggregation in the absence of salt suggests that electrostatic repulsion was strong enough to overcome any attractive interactions in these systems. In the presence of 0.5% lecithin and 300 mM NaCl, the emulsions may have become unstable to aggregation at elevated temperatures due to the combined influence of a reduction in electrostatic repulsion and in steric repulsion.

Particle size analysis of emulsions exposed to different holding temperatures was also carried out (Figure 7). The mean droplet diameter remained relatively small (<1 μm) at low holding temperatures (30−60 and 30−50 °C for 0.1 and 0.5% lysolecithin, respectively), but increased appreciably at higher temperatures. The fact that we did not observe a large increase in mean diameter but did observe rapid phase separation at temperatures of <50−60 °C suggests that flocculation rather than coalescence occurred in this temperature range. On the other hand, the fact that we observed rapid creaming and an increase in droplet diameter at higher temperatures suggests that coalescence occurred. Droplet coalescence may have been promoted at elevated temperatures due to dehydration of the polar head groups of the surfactant molecules. At lower temperatures the surfactant molecules form a rigid monolayer that is more resistant to coalescence, but at higher temperatures they form a flexible monolayer that is more susceptible to coalescence.

AUTHOR INFORMATION

Corresponding Author

*(S.J.C.) Phone: +82 2 970 6739. Fax: +82 2 976 6460. E-mail: choisj@seoultech.ac.kr.

Funding

We thank International Fragrances and Flavors for supporting this research. This research was supported by the Basic Science Research Program through the National Research Foundation of Korea (NRF) funded by the Ministry of Science, ICT and Future Planning (2013R1A1A1008321).

Notes

The authors declare no competing financial interest.

REFERENCES

(1) Perez-Cacho, P. R.; Rouseff, R. L. Fresh squeezed orange juice odor: a review. *Crit. Rev. Food Sci. Nutr.* **2008**, *46*, 681−695.

(2) Manthey, J. A.; Bendele, P. Anti-inflammatory activity of an orange peel polymethoxylated flavone, 3′,4′,3,5,6,7,8-heptamethoxyflavone, in the rate carrageenan/paw edema and mouse lipopolysaccharide-challenge assays. *J. Agric. Food Chem.* **2008**, *56*, 9399−9403.

(3) Xiao, H.; Yang, C. S.; Li, S. M.; Jin, H. Y.; Ho, C. T.; Patel, T. Monodemethylated polymethoxyflavones from sweet orange (*Citrus sinensis*) peel inhibit growth of human lung cancer cells by apoptosis. *Mol. Nutr. Food Res.* **2009**, *53*, 398−406.

(4) Vora, J. D.; Matthews, R. F.; Crandall, P. G.; Cook, R. Preparation and chemical composition of orange oil concentrates. *J. Food Sci.* **1983**, *48*, 1197−1199.

(5) Given, P. S. Encapsulation of flavors in emulsions for beverages. *Curr. Opin. Colloid Interface Sci.* **2009**, *14*, 43−47.

(6) Velikov, K. P.; Pelan, E. Colloidal delivery systems for micronutrients and nutraceuticals. *Soft Matter* **2008**, *4*, 1964−1980.

(7) MarketsandMarkets. *Food Emulsifiers Market by Types (Mono, Diglycerides and Derivatives, Lecithin, Sorbitan Esters, Stearoyl Lactylates and Others), Applications (Bakery and Confectionery, Convenience Foods, Dairy Products, Meat Products and Others) and Geography − Global Trends and Forecast to 2018*; Pune, India, 2013.

(8) Madiedo, J. M.; Berjano, M.; Guerrero, A.; Muñoz, J.; Gallegos, C. Influence of surfactant concentration and temperature of the flow behaviour of sucrose oleate aqueous systems. *Colloid Surf. A−Physicochem. Eng. Asp.* **1994**, *82*, 59−69.

(9) Falconer, R. A.; Toth, I. Design, synthesis and biological evaluation of novel lipoamino acid-based glycolipids for oral drug delivery. *Bioorg. Med. Chem.* **2007**, *15*, 7012−7020.

(10) Healy, M. G.; Devine, C. M.; Murphy, R. Microbial production of biosurfactants. *Resour. Conserv. Recycl.* **1996**, *18*, 41−57.

(11) Nakamura, S. Using sucrose esters as food emulsifiers. *INFORM* **1997**, *8*, 866−874.

(12) Choi, S. J.; Decker, E. A.; Henson, L.; Popplewell, L. M.; Xiao, H.; McClements, D. J. Formulation and properties of model beverage emulsions stabilized by sucrose monopalmitate: influence of pH and lyso-lecithin addition. *Food Res. Int.* **2011**, *44*, 3006−3012.

(13) Moran, J. B.; Burczynski, F. J.; Cheek, R. F.; Bopp, T.; Forker, E. L. Protein binding of palmitate measured by transmembrane diffusion through polyethylene. *Anal. Biochem.* **1987**, *167*, 394−399.

(14) Ogawa, S.; Decker, E. A.; McClements, D. J. Production and characterization of O/W emulsions containing cationic droplets stabilized by lecithin-chitosan membranes. *J. Agric. Food Chem.* **2003**, *51*, 2806−2812.

(15) Israelachvili, J. *Intermolecular and Surface Forces*, 2nd ed.; Academic Press: London, UK, 1992.

(16) McClements, D. J. *Food Emulsions: Principles, Practice, and Techniques*, 2nd ed.; CRC Press: Boca Raton, FL, USA, 2005.

(17) Kawashima, Y.; Hino, T.; Takeuchi, H.; Niwa, T. Stabilization of water/oil/water multiple emulsion with hypertonic inner aqueous phase. *Chem. Pharm. Bull.* **1992**, *40*, 1240−1246.

(18) Rao, J.; McClements, D. J. Food-grade microemulsions, nanoemulsions and emulsions: fabrication from sucrose monopalmitate and lemon oil. *Food Hydrocolloids* **2011**, *25*, 1413−1423.

biochemical parameters of fatty livers to identify the potential parameters involved in cooking loss variability.

MATERIAL AND METHODS

Chemicals. Acrylamide, Bisacrylamide, Coomassie Brilliant Blue, and materials for minigels were purchased from Bio-Rad (Marnes la Coquette, France). Fastprep-24 was purchased from MP BioMedicals (Illkirch, France). All other chemicals were supplied by Sigma-Aldrich (Saint-Quentin Fallavier, France).

Animals. Fatty livers used in this experiment were issued from commercial flocks of male Mule ducks (*C. moschata* × *A. platyrhynchos*) reared until the age of 14 weeks according to standard practices. The birds were then force-fed by the distribution of a soak-corn mixture (25% grain, 35% flour, and 40% water, 3330 kcal/kg, 8.28% crude proteins and 3.38% lipids) twice daily for 12 days. The experiments described here fully comply with legislation on research involving animal subjects according to the European Communities Council Directive of Nov 24, 1986 (86/609/EC). Investigators were certificated by the French governmental authority for carrying out these experiments (accreditation no. 31-11 43 501).

Slaughter, Fatty Liver Selection, and Sampling. At the end of the force-feeding period, the slaughtering procedure was conventionally conducted in a commercial plant. Twenty minutes after bleeding, the livers were removed from the carcasses, weighed to select those with a mass ranging from 500 to 550 g (n = 100), and placed at 4 °C for 6 h. Selected livers were further sorted according to their cooking loss rate on the basis of the melting microtest method (MMTM) results. Briefly, 10 g of liver was placed in metallic spoonlike cups before being heated in an oven at 80 °C for 15 min. Immediately after, a trained operator sorted low- and high-melting samples by visually estimating the quantity of fat released during heating. On the basis of the result, the MMTM allowed two extreme groups, i.e., L+ (high melting rate or high CL) and L− (low melting rate or low CL), of 20 livers each to be distinguished.

Following this subjective classification, samples of 100 g were taken from the middle part of the big lobe of the 40 selected livers to be further controlled with a quantitative cooking yield test. Samples of 10 g were also taken from the upper part of the big lobe, to be assigned for biochemical and proteomic analysis, and immediately frozen in liquid nitrogen before storage at −80 °C until analysis.

Fatty Liver Cooking Loss Measurement. A 100 g sample of liver was placed in a perforated plastic pot to drain the exudates. The mass of each pot containing the samples was recorded to know the exact amount of raw liver placed in each perforated pot (W_{raw}). This set (liver + perforated pot) was then placed in a second pot and kept in a water bath (85 °C) for 1 h (water bath cooking). Finally, the sample was removed from the two pots, drained, gently wiped, and reweighed to determine the mass of the sample after cooking (W_{cooked}). CL (%) was then calculated according to the following formula: $CL = 100 - (W_{cooked}/W_{raw}) \times 100$.

Fatty Liver Biochemical Analysis. All biochemical analyses were performed with ground samples of liver and in duplicate to minimize technical variations.

Dry Matter. The dry matter content of the fatty livers was determined by drying a mass of ground liver (Wdm_{raw}) in an oven at 105 °C for 24 h.[8] Sand was added to previously weighed cups (Wdm_{cup}) to increase the surface of exchange. Just after being dried in the oven, the samples were placed in desiccators to be cooled to room temperature before weighing (Wdm_{dry}). The percentage of dry matter (DM) was then determined by the formula $DM\ content = ((Wdm_{dry} - Wdm_{cup})/Wdm_{raw}) \times 100$.

Lipid Content. The total lipid content of the raw samples was determined according to Folch's method.[14] After the extraction of lipids by a chloroform/methanol solution, quantification of the total lipid content of each sample was performed gravimetrically after evaporation of the chloroformic phase. The total lipid content is expressed as a percentage of dry matter for each sample.

Protein Extraction. The livers were primarily crushed into powder in liquid nitrogen. Liver lysis was then achieved using Fastprep-24 for 20 s. Briefly,[15] 1.5 mL of gelatin-degrading protease extraction buffer (50 mM Tris base, pH 7.5, 150 mM NaCl, 1 mM $CaCl_2$, 0.05% Brij 35, 10 μg/mL leupeptin, 1 mM PMSF) and 1.2 mL of casein-degrading protease extraction buffer (50 mM Tris base, pH 8.3, 20 mM EDTA, 10 mM EGTA, 0.1% β-mercaptoethanol) were added respectively to 75 and 300 mg of liver tissue to extract gelatin- and casein-degrading proteases, respectively. The samples were then centrifuged at 12000g at 4 °C for 15 min, and the fat cake (extracted lipids) was removed. This operation was repeated twice to guarantee good separation of soluble proteins from lipids and other cell components. Finally, the supernatants were collected and stored at −80 °C. The total protein concentration in the extracts (supernatants) was determined using Bradford's method with bovine serum albumin (BSA) as the protein standard. For each extraction buffer, the extractabilities (xtgelt and xtcalp for gelatin- and casein-degrading protease extraction buffers, respectively) were calculated by assuming a total protein content of 7% DM as reported in a previous study.[5]

MMP-2 Gelatin Zymography. Matrix metalloproteinase 2 (MMP-2) gelatinolytic activity was detected according to Kizaki.[15] Briefly, samples containing 40 μg of proteins were mixed (1/4, v/v) with the sample buffer (150 mM Tris base, pH 6.8, 30% glycerol, 4% SDS, 40 μM $ZnCl_2$, and 0.1% Bromophenol Blue) and loaded onto a 12% polyacrylamide gel containing 0.2% gelatin A (1 mm spacers, 5 mL per minigel). The gels were then run under denaturing but nonreducing conditions (4 °C, 125 V, 2 h). Proteolytic activity was finally achieved through washing gels for 30 min in TBS-T buffer (20 mM Tris base, 150 mM NaCl, 0.05% Tween) and 1 h in the incubation buffer (50 mM Tris−HCl, pH 7.5, 6 μM $ZnCl_2$, 5 mM $CaCl_2$, 0.05% Brij, 0.02% NaN_3) with 2.5% Triton X-100. Following that, the gels were incubated overnight (18 h) at 37 °C in the same buffer but without Triton X-100. Finally, zymograms were stained with a solution containing 0.1% Naphthol Blue Black for 2 h and then washed with a destaining solution (45% ethanol and 10% acetic acid). Digestion of the gelatin due to MMP-2 activity appeared as white bands on a dark blue background.

Cathepsin Gelatin Zymography. Cathepsin activities were detected according to Afonso.[16] Briefly, samples containing 15 μg of extracted proteins were loaded onto 0.2% gelatin gels containing SDS (12%) and run as previously described. The resulting gels were then washed twice for 30 min in a 0.1 M sodium acetate buffer solution (pH 5.2) containing 2.5% Triton X-100. Then the gels were incubated overnight with the incubation buffer (0.1 M sodium acetate + 2 mM DTT) at 37 °C. The gels were then stained in a 0.5% Coomassie Brilliant Blue R-250 solution for 2 h before being washed in a destaining solution (45% ethanol and 10% acetic acid). Digestion of the gelatin due to cathepsin activities appeared as white bands on a blue background.

Calpain Casein Zymography. Using the method of Raser,[17] calpain activities were detected on 10% polyacrylamide gels containing 0.2% casein and previously loaded with samples containing 40 μg of proteins diluted (1/4, v/v) in the calpain sample buffer (150 mM Tris base, 20% glycerol, 0.05% Bromophenol Blue, 0.75% β-mercaptoethanol). The gels were run in a calpain running buffer (192 mM glycine, 1 mM EDTA, 1 mM EGTA, 1 mM DTT, 25 mM Tris base, pH 8.3) for 2 h (4 °C, 100 V). Then the gels were washed twice in a calpain activation solution (20 mM Tris base, pH 7.4, 10 mM $CaCl_2$) for 30 min and incubated (overnight, 37 °C) in the same buffer containing 10 mM DTT. Finally, the gels were stained and destained as previously described for cathepsins. Digestion of the casein due to calpain activity appeared as white bands on a blue background.

Image Analysis. According to the procedure described by Bax,[9] the gels were scanned with an Image Scanner III using Image Master Platinum software (GE Healthcare, Uppsala, Sweden). Each liver sample was processed individually, and the value of the main bands was calculated by using an Image Master Platinum application. Each gel also included a pool of all the samples run and was used as an internal standard. Protease activity was considered as the combination of computerized measurements of both the intensity and volume of the main bands for each sample. Then the relative protease activity was estimated as protease activity/pool activity within each gel.

Statistical Analysis. For statistical analysis, the general linear model procedure of SAS software was used with a one-way ANOVA to compare L− and L+ samples. Correlations between variables were computed according to Pearson's method.[18]

In addition, a principal component analysis (PCA) was performed with all samples and the biochemical and proteomic measured variables. This statistical method calculates new variables, called principal components, which are linear combinations of the original variables to account for the variability in the data on the basis of the study of the covariances and the correlations between the original variables.[19] The results are presented in a 2D projection graph where proximate variables at the periphery of the circle are positively correlated, while those separated by 180° are negatively correlated. The closer the variables are to the periphery of the circle, the higher the coefficient of correlation between variables. Individuals are also presented in the same 2D projection. When liver samples are located in the same part of the projection with a given variable, the values of these samples for the considered variable are high. The PCA was performed with the Princomp procedure of SAS software.[18]

RESULTS AND DISCUSSION

As reported in Table 1, the mean liver masses were very similar (520 g) in both L+ and L− ducks. This value is very similar to that reported by Fernandez[20] for this typical program of force-feeding. From previous studies,[2,21] it is well-known that the greater the liver mass, the higher the cooking loss. On the contrary, in the present study, thanks to the original sorting, the mass of fatty livers cannot explain cooking loss differences as illustrated by the very low coefficient of correlation between liver mass and cooking loss ($r = 0.16$, $p > 0.05$). The percentage of cooking loss was 1.72-fold higher ($p < 0.001$) in L+ than in L− samples. This indicates that the subjective MMTM is relevant in distinguishing low- from high-melting livers. Livers from the L+ group presented higher dry matter and total lipid contents than those from the L− group ($p < 0.001$). As reported in previous studies,[3,11,21] the higher the lipid content, the higher the cooking loss ($r = 0.76$, $p < 0.001$). The buffer used for gelatin-degrading protease extraction allowed collection of similar amounts of proteins in both groups. On the contrary, the buffer used for casein-degrading protease extraction allowed collection of more proteins ($p < 0.05$) from L− than from L+ samples.

Table 1. Cooking Losses (CL) and Biochemical Characteristics of Fatty Livers from the Two Studied Groups L− (Low Cooking Loss) and L+ (High Cooking Loss)[a]

	L−	L+	p^b
CL (%)	20.9 ± 4.33	36.0 ± 9.97	***
mass (g)	519 ± 13.0	520 ± 10.2	ns
DM content (%)	63.8 ± 2.21	69.0 ± 2.23	***
lipid content (%)	53.7 ± 3.22	61.0 ± 3.04	***
xtcalp (%)	12.7 ± 3.27	9.98 ± 4.17	*
xtgelt (%)	12.1 ± 1.44	11.5 ± 2.03	ns

[a]Values are expressed as the mean ± standard deviation ($n = 20$ per group). [b]Key: ***, $p < 0.001$; **, $p < 0.01$; *, $p < 0.05$; ns, not significant ($p > 0.05$).

The MMP gelatin protease assay permitted the detection of a 72 kDa proteolytic band corresponding to MMP-2 (Figure 1b). The protocol described by Kizaki[15] allows detection of MMP-2 and MMP-9 (respectively gelatinases A and B), but in the present experiment only one isoform corresponding to MMP-2 was detected, probably because it is the most abundant MMP in the cellular extract. This gelatinolytic activity was inhibited in the presence of EDTA and DTT and in the absence of Ca^{2+} ions (data not shown). As reported in a previous study[22] on cathepsin activity in Pekin and Muscovy ducks' livers, three proteolytic bands were detected for the cathepsin proteolytic assay. The upper band being considerably smaller in Mule ducks, we chose to focus on the other two presenting molecular masses of ∼30 and ∼25 kDa, respectively (Figure 1c). Unlike MMP-2, the activities of cathepsin isoforms were not affected by the addition of DTT or EDTA, but were inhibited in the presence of PMSF (data not shown). Unfortunately, no specific antibodies directed against cathepsin isoforms from ducks are commercially available for a better identification of the detected isoforms in the present study. Moreover, an identification test of those cathepsins using mass spectrometry analysis failed to reveal reliable results. As a consequence, we chose to let the precise identification of the two detected cathepsin isoforms in the present study remain unknown and reported a total activity of cathepsins (CtsT, Figure 2) calculated as the sum of the individually detected activities. Calpain proteolytic assays revealed two bands which were active in the presence of 4 mM Ca^{2+} for the upper one and 10 mM of Ca^{2+} for the lower one (Figure 1d). These results indicate that the two bands correspond to the μ- and m-calpain isoforms, respectively. The m-calpain is also electrophoretically distinguishable from the μ-calpain because of its higher mobility in the gel.[23] To further confirm the identification of these two caseinolytic proteases, the effects of calpain inhibitors (leupeptin and E-64 both purchased from Sigma-Aldrich, Saint-Quentin Fallavier, France) were assessed before electrophoresis. As expected, the presence of these calpain inhibitors completely blocked the activity of both neutral cysteine proteases (data not shown).

Results concerning extracted protease relative activities are reported in Figure 2. In both L+ and L− samples, the zymogram profiles were similar but clearly exhibited higher values in L+ than in L− samples except for the relative activity of Ct-1. The values of protease relative activities reported in the present experiment for L− samples were close to those reported for Pekin and Muscovy force-fed ducks by Awde et al.[22] Finally, the total extracted protease activities appeared to be 1.37-fold ($p < 0.001$) higher in L+ than in L− fatty livers. Due to the fact that proteases remain active during postmortem storage, we think that these higher proteolytic activities have led to a higher degradation of cellular structure. Therefore, at the time of cooking, the overall fragility of the L+ hepatocyte structure might have been higher, and consequently, more internal fluids were released from liver cells and finally led to higher cooking loss values. This hypothesis was previously reported by Theron.[5,11]Nevertheless, it has been reported that the postmortem cooling rate largely influences the extent of cooking losses in fatty livers.[4] For example, fatty liver evisceration immediately after slaughter, associated with a rapid cooling, decreases cooking losses. On the contrary, when the livers are kept inside the carcass during postmortem cooling, the final cooking losses are increased. Besides, protease activities are known, as for other enzymes, to decrease at low temperatures.[24] As a consequence, we can hypothesize that the rate of cooling of the livers postmortem could influence the cooking losses by modulating the total activities of the proteases: the more active the proteases are (under the influence of temperature, for example) during the postmortem period, the more the structure of the hepatocytes might be altered and the more their lipid content will be exuded during cooking. In the present study, the cooling rate was the same for

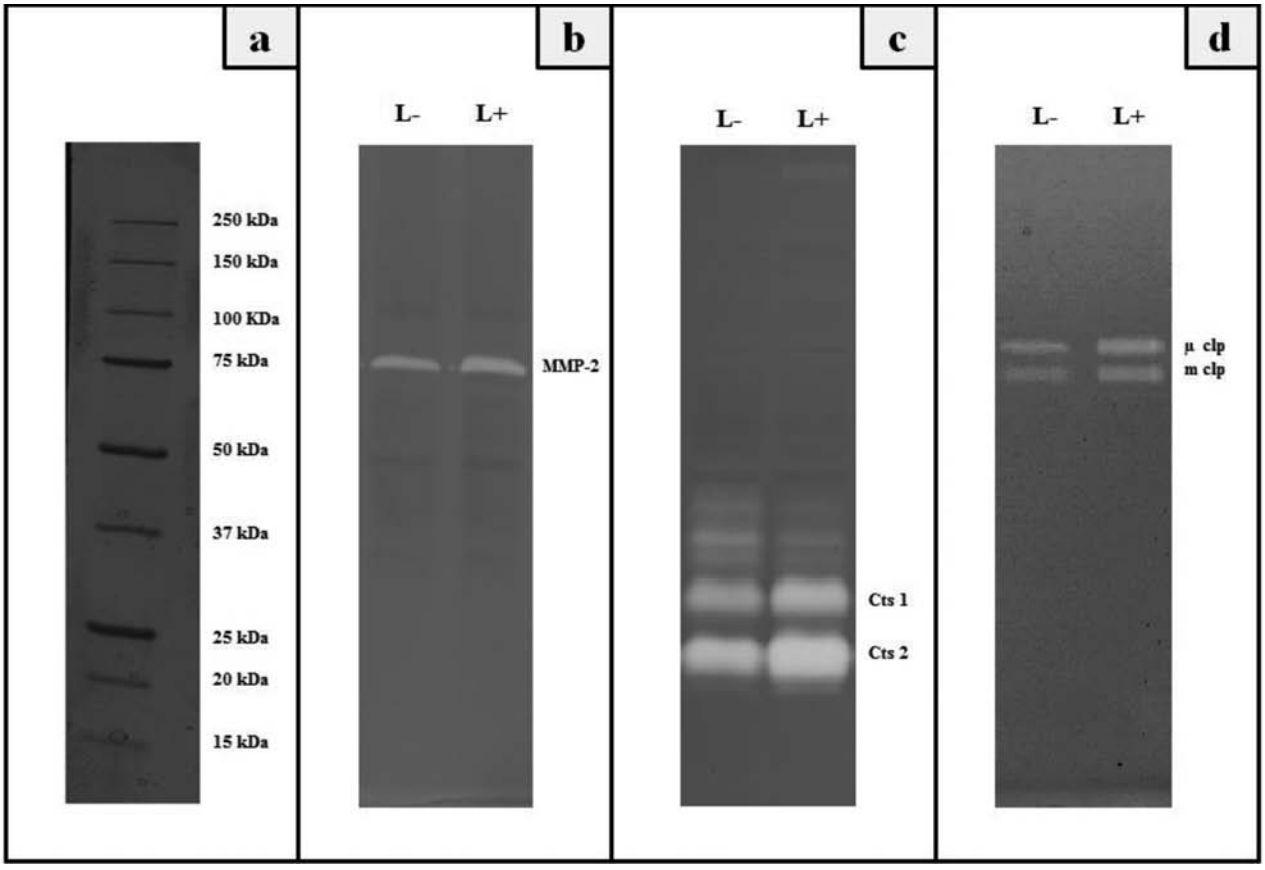

Figure 1. Molecular mass standards (a) and zymograms of the 72 kDa MMP-2 band (b), the 2 cathepsin bands (c) Cts-1 (30 kDa) and Cts-2 (25 kDa), and the μ- and m-calpain (μ-calp and m-calp) 80 kDa bands (d) analyzed by zymography in L− and L+ fatty liver samples.

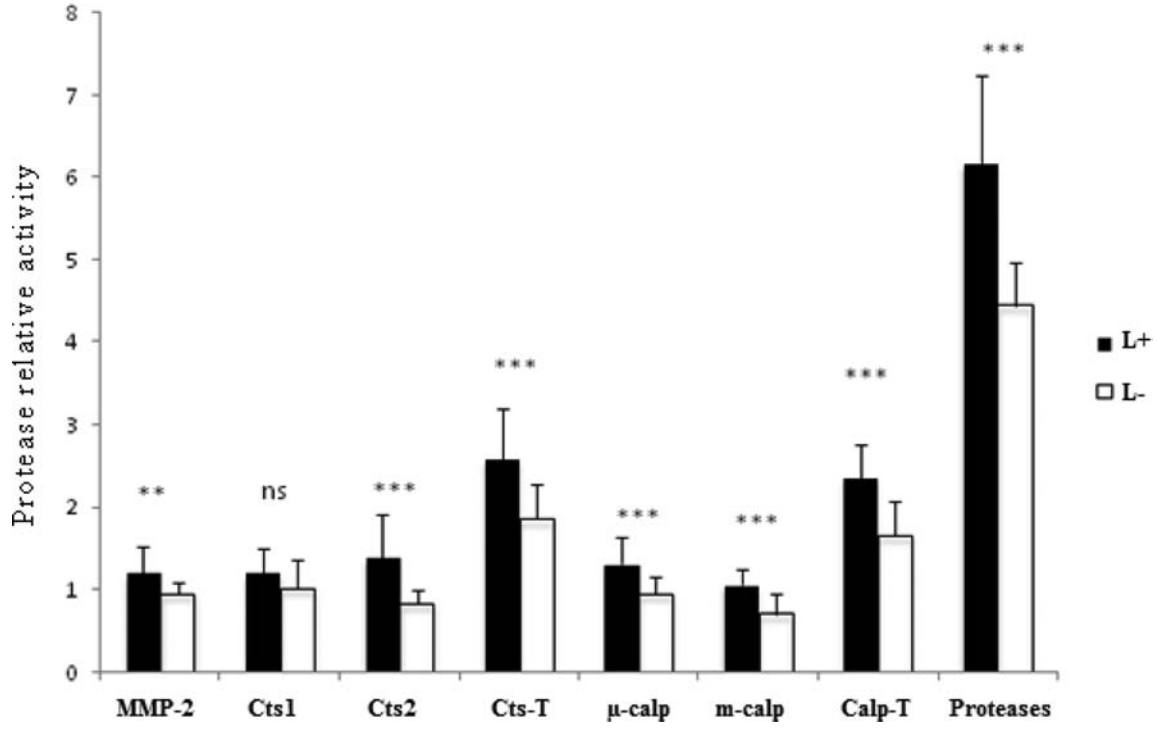

Figure 2. Protease relative activities in L+ and L− fatty liver samples. Values are the mean ± standard deviation. Key: ***, $p < 0.001$; **, $p < 0.01$; ns, not significant ($p > 0.05$). MMP-2 = matrix metalloproteinase 2, Ct-1 = cathepsin isoform 1, Ct-2 = cathepsin isoform 2, Ct-T = Ct-1 + Ct-2, μ-calp = μ-calpain, m-calp = m-calpain, Calp-T = μ-calp + m-calp, and proteases = MMP-2 + Ct-T + Calp-T.

dx.doi.org/10.1021/jf4051057 | J. Agric. Food Chem. 2014, 62, 3262−3268

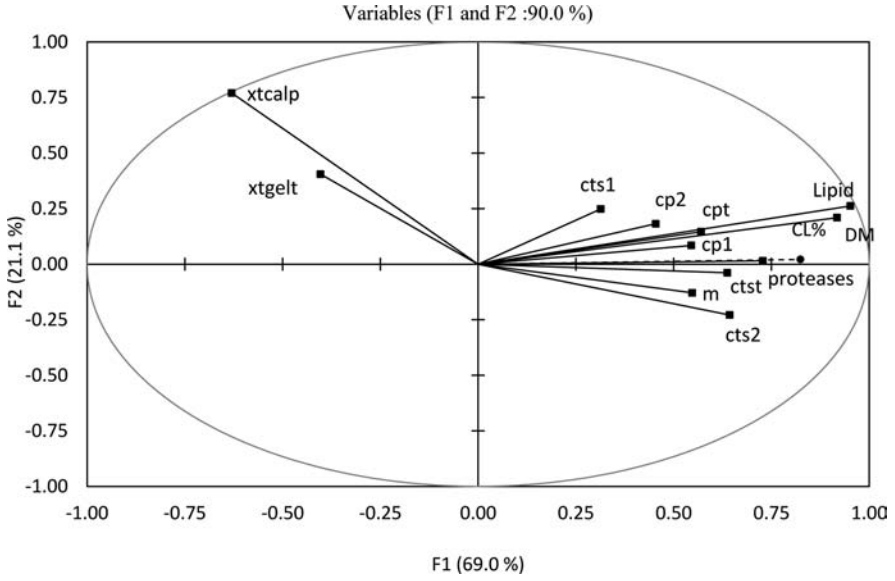

Figure 3. First two principal component score vectors showing relationships between cooking losses and liver biochemical characteristics. m = matrix metalloproteinase 2, cts1 = cathepsin isoform 1, cts2 = cathepsin isoform 2, ctst = cts1+ cts2, cp1 = μ-calpain, cp2 = m-calpain, cpt = cp1 + cp2, proteases = m + cpt + ctst, lipid = lipid content (%), DM = dry matter content (%), xtgelt = extractrability for gelatin-degrading protease buffer, and xtcalp = extractability for casein-degrading buffer. Key: ●, added variable (CL, %); ■, active variables.

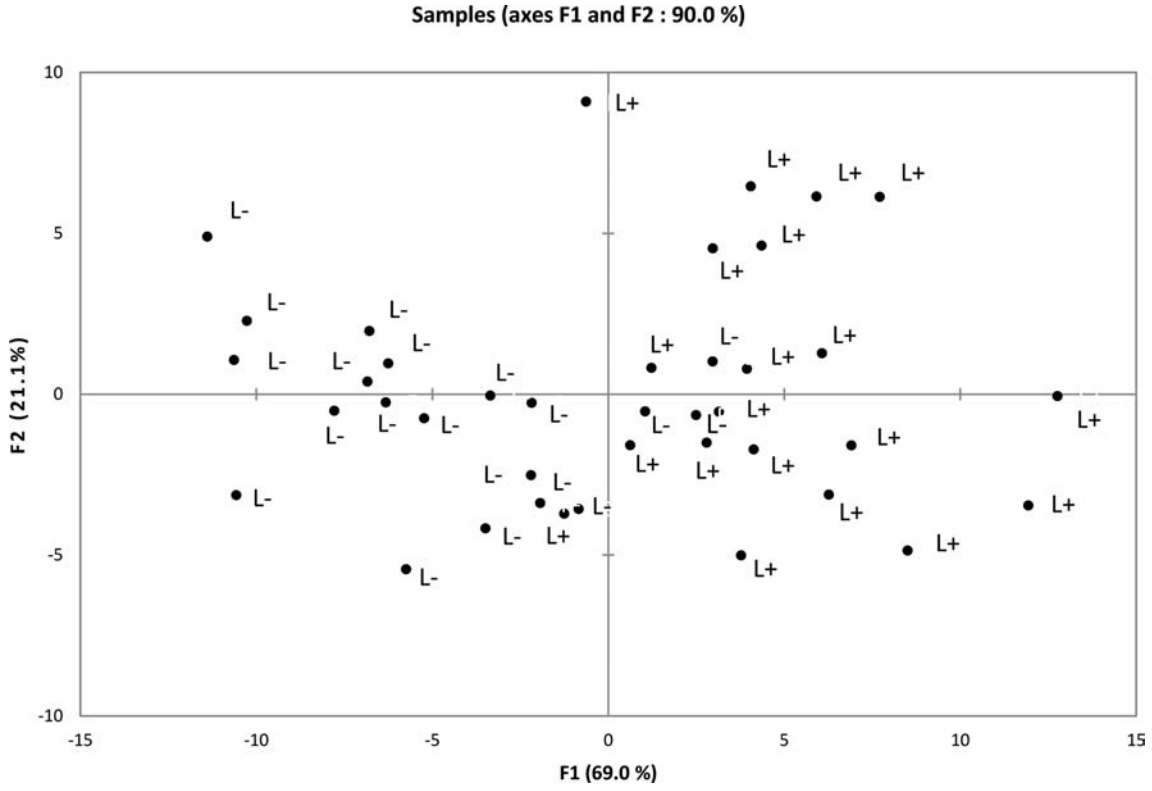

Figure 4. First two principal component score vectors showing variability according to liver groups (L+ = high cooking loss; L− = low cooking loss).

both L+ and L− livers (same process, same liver masses), but the protease activities were originally higher in L+ than in L− samples (Figure 2). Consequently, more cellular degradations occurred in L+ livers and might lead to more important cellular content releases during cooking. Nevertheless, this assumption needs to be further verified by performing SDS−PAGE with proteins extracted from fatty livers at different times postmortem. Finally, it seems that, for a given mass, the livers could differ according to the level of their metabolisms at the time of slaughtering, and this will influence the final quality of the product after cooking. When hepatic metabolisms are very active (high level of lipid accumulation, high proteolytic activities), the livers tend to be more weakened, leading to higher cooking loss values.[3,21] Differences in the levels of activity of hepatic proteases can have different origins, such as the structure of the enzyme by itself (different isoforms) or different concentrations of cellular activators (calcium content) or inhibitors (calpastatine, cystatine, or tissue inhibitors of

dx.doi.org/10.1021/jf4051057 | J. Agric. Food Chem. 2014, 62, 3262−3268

metalloproteinases). These hypotheses will have to be further investigated by comparing hepatocyte contents between L− and L+ samples.

The relationships between biochemical content, protease activities, and cooking losses are well illustrated by the principal component analysis (Figure 3) that clearly associates lipid and dry matter contents with protease activities and cooking losses along the first principal component. It also illustrates the strong correlation between DM and lipid contents (r = 0.88, p < 0.001) and their strong opposition with extractabilities (xtcalp and xtgelt) of soluble proteins. The new linear combination of original variables given by the PCA allows a good distinction of L+ and L− samples (Figure 4). Indeed, without using the CL (%) variable, 85% of the examined samples were correctly grouped according to their CL determination. By combining the results of Figures 3 and 4, it appears that L+ samples are mainly positively associated with lipid and DM contents as well as with protease activities, while the opposite is true for L− samples. On the contrary, L− samples are better associated with extractability values. Finally, we can report that the lipid and DM contents associated with the main proteolytic activities are positively associated with L+ samples, while L− samples are rather negatively associated with those variables but positively with extractability values.

In conclusion, this study demonstrates that both the lipid and DM contents as well as the main hepatic protease activities have a strong influence on cooking losses in fatty livers issued from force-fed Mule ducks. Samples issued from animals with the highest hepatic metabolisms (both lipidic and proteic) at the time of slaughter will exhibit the highest cooking loss values. It would be interesting to investigate why some ducks have a better adapted hepatic metabolism than others in their response to force-feeding and how to identify them as soon as possible to reduce final variability in cooking loss values recorded in processing plants. Associated with higher protease activities, we hypothesized that more cellular degradations occurred during the postmortem period and led to a more important weakening of cellular structures associated with higher cooking losses. New investigations are currently under way to confirm that point.

AUTHOR INFORMATION

Funding

K.P. benefited from a grant from the Royal Golden Jubilee Ph.D. program and from the French Embassy in Thailand.

Notes

The authors declare no competing financial interest.

ACKNOWLEDGMENTS

We thank La Comtesse du Barry (Gimont, France) for providing the samples used in the experiment.

REFERENCES

(1) Salichon, M.; Guy, G.; Rousselot, D.; Blum, J. Composition of the 3 Types of Foie-Gras—Goose, Mule Duck and Muscovy Duck Foie-Gras. *Ann. Zootech.* **1994**, *43*, 213−220.

(2) Blum, J. C.; Labie, C.; Raynaud, P. Influence du Poids et de la Composition Chimique du Foie Gras d'Oie sur la Fonte Mesurée Après Stérilisation à 104°C. *Sci. Aliments* **1990**, *10*, 543−554.

(3) Nir, I.; Nitsan, Z. Goose Fatty Liver Composition As Related to the Degree of Steatosis, Nutritional and Technological Treatments, and a Simplified Method for Quality Estimation. *Ann. Zootech.* **1976**, *25*, 461−470.

(4) Rousselot-Pailley, D.; Guy, G.; Sellier, N.; Blum, J. Influence des Conditions d'Abattage et de Réfrigération sur la Qualité des Foies Gras d'Oie. *INRA Prod. Anim.* **1992**, *5*, 167−172.

(5) Theron, L.; Fernandez, X.; Marty-Gasset, N.; Pichereaux, C.; Rossignol, M.; Chambon, C.; Viala, D.; Astruc, T.; Molette, C. Identification by Proteomic Analysis of Early Post-Mortem Markers Involved in the Variability in Fat Loss during Cooking of Mule Duck "Foie Gras". *J. Agric. Food Chem.* **2011**, *59*, 12617−12628.

(6) Cazeils, J. L.; Bouillier-Oudot, M.; Auvergne, A.; Candau, M.; Babile, R. Lipid Composition of Hepatocyte Plasma Membranes from Geese Overfed with Corn. *Lipids* **1999**, *34*, 937−942.

(7) Molette, C.; Théron, L.; Marty-Gasset, N.; Fernandez, X.; Rémignon, H. Current Advances in Proteomic Analysis of (Fatty) Liver. *J. Proteomics* **2012**, *75*, 4290−4295.

(8) Molee, W.; Bouillier-Oudot, M.; Auvergne, A.; Babilé, R. Changes in Lipid Composition of Hepatocyte Plasma Membrane Induced by Overfeeding in Duck. *Comp. Biochem. Physiol., B: Biochem. Mol. Biol.* **2005**, *141*, 437−444.

(9) Bax, M. L.; Chambon, C.; Marty-Gasset, N.; Remignon, H.; Fernandez, X.; Molette, C. Proteomic Profile Evolution during Steatosis Development in Ducks. *Poult. Sci.* **2012**, *91*, 112−120.

(10) Zheng, A.; Liu, G.; Zhang, Y.; Hou, S.; Chang, W.; Zhang, S.; Cai, H.; Chen, G. Proteomic Analysis of Liver Development of Lean Pekin Duck (Anas Platyrhynchos Domestica). *J. Proteomics* **2012**, *75* (17), 5396−5413.

(11) Theron, L.; Fernandez, X.; Marty-Gasset, N.; Chambon, C.; Viala, D.; Pichereaux, C.; Rossignol, M.; Astruc, T.; Molette, C. Proteomic Analysis of Duck Fatty Liver during Post-Mortem Storage Related to the Variability of Fat Loss during Cooking of "Foie Gras". *J. Agric. Food Chem.* **2013**, *61*, 920−930.

(12) Nowak, D. Enzymes in Tenderization of Meat—The System of Calpains and Other Systems—A Review. *Pol. J. Food Nutr. Sci.* **2011**, *61*, 231−237.

(13) Huff Lonergan, E.; Zhang, W.; Lonergan, S. M. Biochemistry of Postmortem Muscle—Lessons on Mechanisms of Meat Tenderization. *Meat Sci.* **2010**, *86*, 184−195.

(14) Folch, J.; Lees, M.; Sloane Stanley, G. H. A Simple Method for the Isolation and Purification of Total Lipides from Animal Tissues. *J. Biol. Chem.* **1957**, *226*, 497−509.

(15) Kizaki, K.; Ushizawa, K.; Takahashi, T.; Yamada, O.; Todoroki, J.; Sato, T.; Ito, A.; Hashizume, K. Gelatinase (MMP-2 and -9) Expression Profiles during Gestation in the Bovine Endometrium. *Reprod. Biol. Endocrinol.* **2008**, *6*, 66.

(16) Afonso, S.; Romagnano, L.; Babiarz, B. The Expression and Function of Cystatin C and Cathepsin B and Cathepsin L during Mouse Embryo Implantation and Placentation. *Development (Cambridge, U.K.)* **1997**, *124*, 3415−3425.

(17) Raser, K. J.; Posner, A.; Wang, K. K. W. Casein Zymography: A Method To Study μ-Calpain, m-Calpain, and Their Inhibitory Agents. *Arch. Biochem. Biophys.* **1995**, *319*, 211−216.

(18) The data analysis for this paper was generated using SAS/STAT software, version 8 of the SAS System for Windows, SAS Institute Inc., Cary, NC, 2011.

(19) Chriki, S.; Gardner, G.; Jurie, C.; Picard, B.; Micol, D.; Brun, J.-P.; Journaux, L.; Hocquette, J.-F. Cluster Analysis Application Identifies Muscle Characteristics of Importance for Beef Tenderness. *BMC Biochem.* **2012**, *13*, 29.

(20) Fernandez, X.; Lahirigoyen, E.; Auvergne, A.; Molette, C.; Bouillier-Oudot, M. The Effects of Stunning Methods on Product Qualities in Force-Fed Ducks and Geese. 1. Carcass Downgrading and Meat Quality. *Animal* **2010**, *4*, 128−138.

(21) Theron, L.; Cullere, M.; Bouillier-Oudot, M.; Manse, H.; Dalle Zotte, A.; Molette, C.; Fernandez, X.; Vitezica, Z. G. Modeling the Relationships between Quality and Biochemical Composition of Fatty Liver in Mule Ducks. *J. Anim. Sci.* **2012**, *90*, 3312−3317.

(22) Awde, S.; Marty-Gasset, N.; Wilkesman, J.; Rémignon, H. Proteolytic Activity Alterations Resulting from Force-Feeding in Muscovy and Pekin Ducks. *Poult. Sci.* **2013**, *92*, 2997−3002.

(23) Arthur, J. S. C.; Mykles, D. L. Calpain Zymography with Casein or Fluorescein Isothiocyanate Casein. In *Calpain Methods and Protocols*; Elce, J. S., Ed.; Methods in Molecular Biology; Humana Press: Totowa, NJ, 2000; pp 109−116.
(24) Muyan, C.; Xiumei, Z.; Tianxiang, G.; Chao, C. Effects of Temperature, pH and NaCl on Protease Activity in Digestive Tract of Young Turbot, *Scophthalmus maximus*. *Chin. J. Oceanol. Limnol.* **2006**, *24*, 300−306.

Solid-state glycation of β-Lg conserves its native-like structure[29,30,32] and its association tendency[29] and yields a heterogeneous mixture of glycoforms that differ in the degree and sites of glycation.[33] In contrast, aqueous glycation induces significant changes in the native β-Lg structure[29,34] and leads to sugar-induced protein cross-linking.[27,29,35] The effects of β-Lg glycation include improved heat stability,[10,36−38] lowered isoelectric point,[39,40] decreased surface hydrophobicity due to polar sugar groups,[10,37] and inhibition of aggregation due to the steric effect of sugar residues.[37,38]

Modification of the amine groups of amyloidogenic proteins α-synuclein[41] and insulin[42] by dicarbonyl compounds slowed their self-assembly into fibrils in vitro. On the other hand, glycation promoted the self-assembly of bovine serum albumin.[43] Glycation is likely to affect β-Lg self-assembly since almost all of the potential glycation sites are located on the regions involved in fibril formation.[18,20,23]

Liu and Zhong[44] recently prepared nanofibrils from whey protein isolate after solid-state incubation with lactose. However, the incubation produced changes in secondary structure, and Maillard reactions progressed well beyond the addition of integer numbers of sugars, due to the extreme incubation conditions (80 °C for 2 h at 70% relative humidity). Lactose-reacted β-Lg fibrils had modified functional properties, but little mechanistic information could be obtained due to the heterogeneity of the starting material.

In this study, we focused on how glycation affects the structural and chemical events involved in fibril formation and examined both the extent of glycation and the sugar type (monosaccharide or disaccharide). We glycated β-Lg under mild conditions to prevent advanced Maillard reactions and produce a well-defined starting material without marked changes to the secondary or tertiary structure of the protein. This systematic approach has produced new insights into the mechanism of amyloid-like fibril self-assembly.

MATERIALS AND METHODS

Unless otherwise mentioned, all chemicals were of analytical grade and were purchased from Sigma-Aldrich (St. Louis, MO). Unless otherwise stated, Milli-Q water was used for preparing the reagents.

Isolation of β-Lactoglobulin. β-Lg was isolated in-house from whey protein isolate 8855 (Fonterra Cooperative Ltd., Auckland, New Zealand) using the method described previously.[18] The β-Lg powder had a protein content of 97% and was a mixture of variants A and B, which did not have any glycation (Figure S1, Supporting Information).

Preparation of Glycated β-Lg. *Preliminary Experiments for Selection of Glycation Times.* A stock solution of β-Lg (pH 7) was allowed to hydrate at 4 °C overnight. The solution was then centrifuged at 44000*g* for 30 min at 20 °C, and the supernatant was filtered using a syringe filter (pore size 0.2 μm, Minisart CE, Sartorius Stedim Biotech GmbH, Goettingen, Germany). Glucose and lactose powders were mixed with the filtered β-Lg solution (molar ratio β-Lg:sugar =1:100), and the pH values of the solutions were readjusted to 7.00 ± 0.02 using 1 N NaOH. The samples were then frozen at −18 °C overnight and freeze-dried. For glycation, the freeze-dried powders were placed in a glass Petri dish and transferred to separate desiccators with a saturated potassium bromide (KBr) solution. The desiccators were sealed, and a vacuum of 125 mbar was applied to them. Then the desiccators were transferred to an oven maintained at 40.0 ± 0.5 °C. The saturated KBr solution gave a relative humidity of 80% inside the desiccators. For glucosylation, the samples were removed from the desiccators after 8, 16, or 36 h, while for lactosylation the durations were 3, 5, and 7 days. Longer heating times were not investigated since samples heated for longer than the above-mentioned times showed extensive brown discoloration indicating the presence of advanced Maillard reaction products in the samples. After completion of the glycation reaction, the samples were dissolved in Milli-Q water (pH 7) and dialyzed (molecular mass cutoff of 6−8 kDa, Spectra/Por, Spectrum Laboratories Inc., Rancho Dominguez, CA) for 48 h at 4 °C to remove the excess unreacted sugar. The dialyzed protein solution was then freeze-dried to obtain the glycated β-Lg.

Determination of the Degree of Glycation. Glycated β-Lg was dissolved in water (pH 2) and filtered using a 0.2 μm syringe filter before being subjected to RP-HPLC (C_{18}, Jupiter, Torrance, CA) at a flow rate of 1 mL/min. The compositions of the buffers were 10% (v/v) acetonitrile (MeCN) in water containing 0.1% trifluoroacetic acid (TFA) for buffer A and 90% MeCN with 0.08% TFA for buffer B. Upon loading, the sample was eluted using the following program: 2 min wash with buffer A followed by a linear gradient of buffer B from 0% to 65% in 13 min and then to 100% B in 1 min. This was followed by isocratic elution of buffer B for 5 min and then a gradient to 0% B in 1 min, after which a wash with buffer A for 2 min followed. A single large peak was eluted when the MeCN concentration was 38%, and this peak was collected and concentrated to approximately 100 μL (Savant SpeedVac SC100, Holbrook, NY) under vacuum (Varian DS 102, Varian Vacuum Technologies, Torino, Italy). The samples were stored at −86 °C until further analysis. The degree of glycation in modified β-Lg was analyzed by liquid chromatography−mass spectrometry.

RP-HPLC-purified samples (2 μL) were autoinjected into an Agilent 1200 LC system (Agilent Technologies, Santa Clara, CA) on bypass mode. The isocratic mobile phase was composed of 0.1% (v/v) formic acid/50% MeCN/water at a flow rate of 100 μL/min. The LC eluant was directed to the electrospray ionization (ESI) source at a capillary voltage of 3.4 kV of the mass spectrometer (Agilent 6520 Q-TOF, Agilent Technologies, Hanover, Germany). Sample analysis was performed in positive ion mode, and the data were stored in profile mode. MS scans (100−1700 m/z) were obtained with fragmentor and skimmer voltages at 175 and 65 V, respectively. Other source parameters were a drying gas temperature of 325 °C, gas flow rate of 6 L/min, and nebulizer gas pressure of 30 psig. The total ion chromatograms (TICs) obtained were examined and spectra deconvoluted using Agilent MassHunter Workstation Qualitative Analysis software (version B.03.01) with a BioConfirm plugin (Agilent Technologies, Santa Clara, CA). The intensity of the peaks was normalized by assigning the most intense peak in the spectrum to 100%.

Preparation of Samples for Self-Assembly Studies. The unmodified β-Lg showed only two peaks corresponding to variants A and B (Figure S1, Supporting Information). The degrees of glycation for β-Lg with glucose and lactose after different glycation times are shown in deconvoluted MS spectra in Figures S2 and S3 (Supporting Information), respectively. The degrees of glycation after 8 h of glucosylation and 3 days of lactosylation were similar, and these glycation times were selected for further investigation. From this point onward, samples made using these heating times will be referred to as low-glucose (LowGlu) and low-lactose (LowLac) β-Lg, respectively. Similarly, for the high degree of glycation, the durations selected were 36 h for glucosylation and 7 days for lactosylation. The samples made using these heating time points will be referred to as high-glucose (HighGlu) and high-lactose (HighLac) β-Lg, respectively. Fresh glycated samples were made using the selected glycation time points and analyzed by MS using the above methodology. For each of the glycation mixtures, a β-Lg sample without sugar was used as a control. The freeze-dried glycated proteins prepared as described above were stored at −18 °C until further analysis.

Self-Assembly from β-Lg. β-Lg samples intended for self-assembly were made according to a method described previously.[24] Protein concentrations in the samples were determined by spectrophotometry (Ultraspec 2000, Pharmacia Biotech, Cambridge, U.K.) using an extinction coefficient of 0.94 cm^2/mg.[45] β-Lg (with or without glycation; 1%, w/v) samples, at pH 2.00 ± 0.02 were heated in a temperature-controlled water bath (Jeio Tech, Seoul, South Korea) maintained at 80.0 ± 0.2 °C. The control sample used in the study was untreated and unglycated β-Lg. Since we were interested in investigating the effects of glycation on nucleation, heating was done

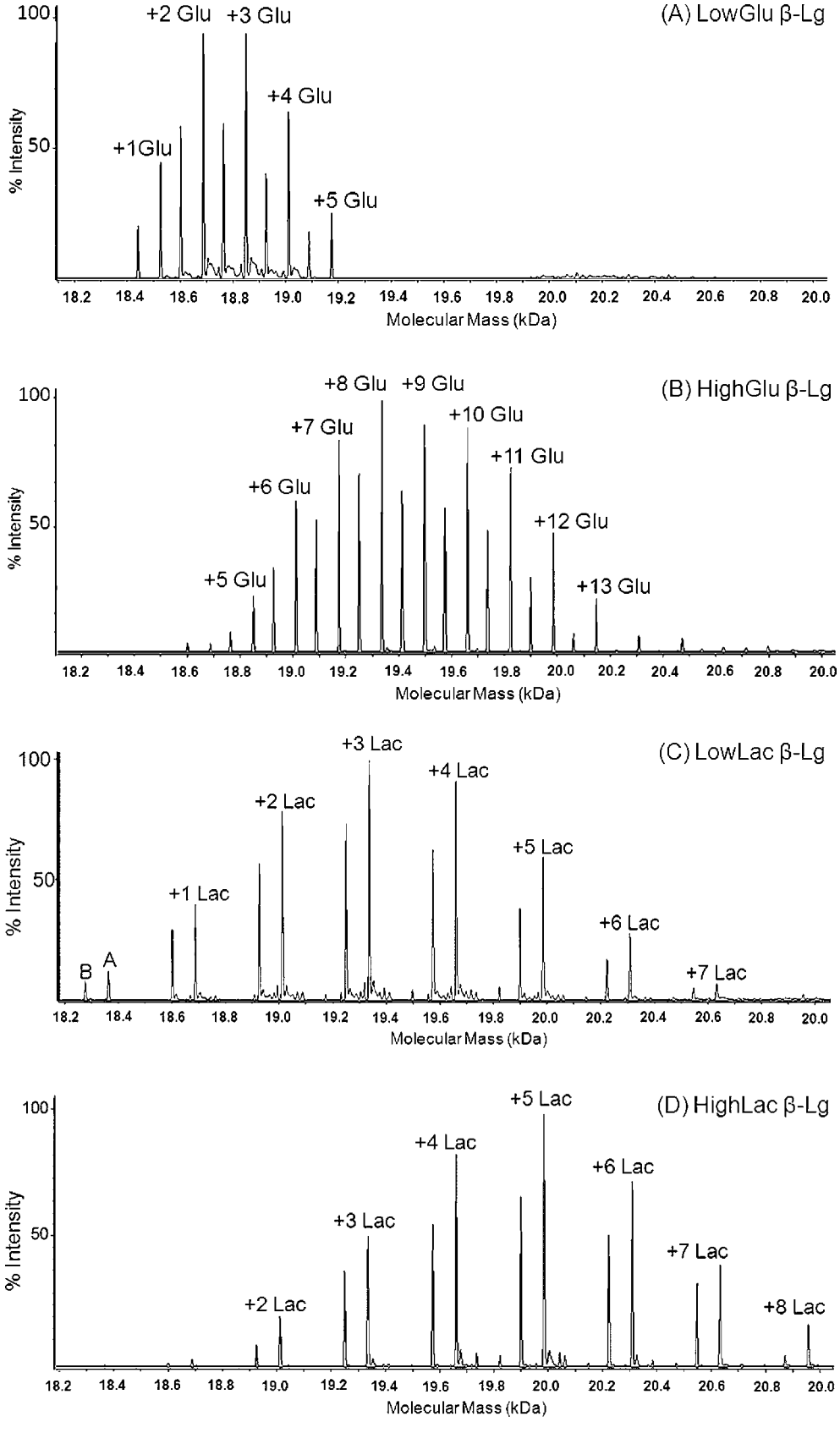

Figure 1. Deconvoluted MS spectra of glucosylated (A) LowGlu β-Lg and (B) HighGlu β-Lg and lactosylated (C) LowLac β-Lg and (D) HighLac β-Lg. Peak labels show the number of attached glucose or lactose residues.

without agitation to minimize secondary nucleation, which would otherwise obscure other phenomena. After being heated for different holding times (2−24 h), the samples were cooled rapidly using an ice bath. The cooled samples were analyzed by the thioflavin T assay and

dx.doi.org/10.1021/jf405441g | J. Agric. Food Chem. 2014, 62, 3269−3278

SDS−PAGE. The lactose used in the study was found to be stable under conditions of glycation and fibril formation (data not shown).

Thioflavin T (ThT) Fluorescence Assay. Fibril formation from β-Lg was studied by the ThT assay as previously described.[24] The fluorescence intensities in the samples were corrected against that of the unheated sample and ThT solution without any protein sample. The corrected intensities were then fitted using the mathematical model given in the following equation:

$$f_t = \alpha - \frac{\frac{\beta}{\gamma} + \alpha}{1 + \frac{\beta}{\alpha\gamma}\exp[t(\beta + \alpha\gamma)]} \quad (1)$$

where α, β, and γ are empirical constants and f_t denotes fluorescence at a given time t (h). The kinetic parameters for β-Lg self-assembly for each of the samples were calculated using the following equations:[24]

$$t_{lag} = \frac{1}{\beta + \alpha\gamma}\left(\ln\left(\frac{\alpha\gamma}{\beta}\right) - 4\frac{\alpha\gamma}{\beta + \alpha\gamma} + 2\right) \quad (2)$$

$$t_{1/2max} = \frac{\ln\left(2 + \frac{\alpha\gamma}{\beta}\right)}{\beta + \alpha\gamma} \quad (3)$$

$$\left(\frac{df}{dt}\right)_{max} = \frac{\left(\frac{\beta}{\gamma} + \alpha\right)(\beta + \alpha\gamma)}{4} \quad (4)$$

where t_{lag} represents the duration of the lag phase, $t_{1/2max}$ is the time required for attaining half of the maximum fluorescence value, and $(df/dt)_{max}$ represents the maximum rate of fluorescence increase. The value of the empirical constant α represents the fitted maximum fluorescence in the stationary phase, and is relabeled f_{max}. Equation 1 was fitted to data using SigmaPlot 12.1, and the standard deviations of t_{lag}, $t_{1/2max}$, and $(df/dt)_{max}$ were calculated using partial derivatives and the covariance matrix, as detailed in the Supporting Information.

Separation of Fibrils. Fibrils in the samples were separated using ultracentrifugation and washed using the method described previously.[18] Briefly, 9 mL volumes of heated and cooled samples were subjected to ultracentrifugation at $(2.4 \times 10^5)g$ for 1 h. The pellets obtained were dispersed in 9 mL of water and vortexed, followed by ultracentrifugation. These washing and ultracentrifugation steps were repeated twice. The washed pellet was used for analysis.

SDS−PAGE. Heated samples were analyzed by tricine SDS−PAGE methodology described elsewhere.[18] Heated samples were diluted 1:10 in reducing PAGE sample buffer (4% SDS and 100 mM dithiothreitol (DTT)). For centrifuged samples, the supernatants were diluted 1:10 while the pellets were suspended directly in the PAGE sample buffer. The PAGE gels were scanned and analyzed using Image Lab software (Bio-Rad Laboratories, Hercules, CA). The quantification of the hydrolysis of β-Lg was done as per the method described in the reference. For each of the samples, the hydrolysis rate constants (k_h) were calculated from the following equation:

$$I = I_0 e^{-k_h t} \quad (5)$$

Circular Dichroism (CD) Spectroscopy. The β-Lg solutions for CD spectroscopy were prepared in HPLC-grade water at pH 2.00 ± 0.02 according to the method described in a previous report.[18] The β-Lg concentrations for near-UV (NUV) scans (260−320 nm) and far-UV (FUV) scans (180−250 nm) were 1 and 0.01 mg/mL. Scans were recorded using a CD spectrometer (Chirascan, Applied Photophysics Ltd., Surrey, U.K.) and a cuvette of path length 10 mm either at 20 °C or continuously for 1 h at 80 °C. The time required for raising the temperature from 20 to 80 °C was excluded, and the time at which the temperature reached 80 °C was designated as 0 min. Scans were averaged sequentially to obtain data at 2 min intervals and corrected by subtracting baseline scans from each of the sample scans. Molar ellipticity was calculated using the following equation[46] with data from the β-Lg scans after baseline subtraction:

$$[\theta]^{\lambda}_{M} = \frac{100\theta_{\lambda}}{LC} \quad (6)$$

where θ_λ is the measured ellipticity (deg) at a given wavelength λ, L represents the path length of the cuvette used (cm), and C is the protein concentration (dmol/L). The data were smoothed in SigmaPlot 12.1, and the relative changes in ellipticities at 293 and 208 nm were calculated from the following equations:[18]

$$\left(\frac{\Delta[\theta]_t}{\Delta[\theta]_0}\right)_{293} = \frac{[\theta]_t - [\theta]_{60}}{[\theta]_0 - [\theta]_{60}} \quad (7)$$

$$\left(\frac{\Delta[\theta]_t}{\Delta[\theta]_{60}}\right)_{208} = \frac{[\theta]_t - [\theta]_0}{[\theta]_{60} - [\theta]_0} \quad (8)$$

θ_0 represents the ellipticity in the unheated sample, θ_t that at time t (min) during heating, and θ_{60} that at the end of the heating period after 60 min.

Transmission Electron Microscopy (TEM). Fibrils in heated solutions were separated using the methodology previously described.[24] A 200 μL volume of the heated solution was diluted 10-fold using water (pH 2) and centrifuged at 3000*g* for 15 min in a centrifuge filter (Amicon Ultra-4, Millipore) with a nominal cutoff of 100 kDa, rinsed previously with water (pH 2). The sample was washed with pH 2 water three times and recentrifuged to get fibrils in the retentate. The fibrils in the retentate were then suspended in 1 mL of the pH 2 water. For TEM, 200 μL of the suspension was mixed with 200 μL of water (pH 2) and 20 μL of BSA (0.5%, w/v) in a polypropylene tube before being stained by a negative staining protocol that is described in the reference.

RESULTS

Characterization of Glycated β-Lg. The deconvoluted MS spectra of glycated β-Lg are shown in Figure 1. All samples showed a series of peak pairs with mass increments of either 162 Da (Figure 1A,B, glucosylation) or 324 Da (Figure 1C,D, lactosylation), indicating that both variants B (18277 Da) and A (18364 Da) participated in glycation. Peaks corresponding to unglycated β-Lg appeared only in the scans of LowLac β-Lg, and at low levels in that case. Variants A and B showed a similar propensity for glycation, and the glucosylation of both variants was faster than lactosylation. The presence of multiple peaks in the spectrum suggests heterogeneity of glycoforms of β-Lg in samples with respect to the number of sugar residues attached to the β-Lg. These results are in agreement with previous studies which show similar reactivities of β-Lg A and B,[47] a heterogeneous mixture of glycoforms in samples upon glycation with respect to the number of attached sugar residues,[27,30,33,36,39] and faster rates of glucosylation than those of lactosylation of β-Lg.[10]

Unfolding Behavior of Glycated β-Lg. The effect of glycation on the β-Lg native structure and thermal unfolding was investigated using CD spectroscopy with in situ heating at 80 °C, as described previously.[18] In the NUV region, all unheated samples showed characteristic troughs at 293 and 286 nm (Figure S4A, Supporting Information) arising due to the tryptophan residue at position 19,[48] indicating that the environment around Trp19 was unaffected by glycation. In addition, the scans showed a small trough at 265 nm contributed by the phenylalanine residues in the native β-Lg structure. These troughs in the NUV region have been shown to rapidly decrease in intensity upon heating β-Lg under fibril-forming conditions.[18] Heating of glycated samples resulted in rapid loss of the characteristic troughs at 293, 286, and 265 nm. Figure 2A shows an example of scans recorded for LowGlu β-

Lg during heating, and Figure 3A shows the comparison of relative loss of ellipticities at 293 nm upon heating.

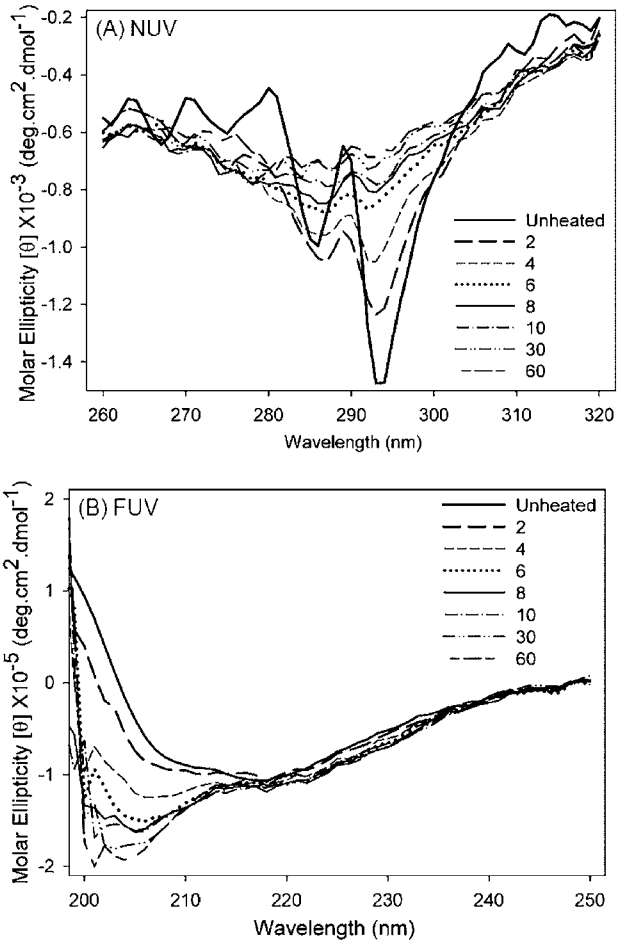

Figure 2. CD spectra of LowGlu β-Lg in the (A) NUV region (10 mg/mL β-Lg) and (B) FUV region (0.01 mg/mL β-Lg). The numbers in the legends indicate the heating time in minutes.

In the FUV region, glycated samples showed a broad trough with a minimum at 217 nm (Figure S4B, Supporting Information), indicating that in all the samples β-sheets were the dominant secondary structural conformation.[48] It has been shown that heating β-Lg at 80 °C and pH 2 resulted in a shift of the trough toward lower wavelengths,[18] representing unfolding of the secondary structure. All glycated samples showed a rapid shift in the trough during heating. Figure 2B illustrates the shift of the trough in the FUV region for LowGlu β-Lg during heating. The plot of $([\Delta\theta_t]/[\Delta\theta_{60}])_{208}$ against time comparing the change in the ellipticity at 208 nm upon heating is shown in Figure 3B.

Heat-Induced Hydrolysis. To investigate the effect of glycation on the acid hydrolysis of β-Lg, the composition of samples heated for different times was analyzed by tricine SDS−PAGE under reducing conditions. All samples showed hydrolysis of the β-Lg monomer with heating. A comparison of PAGE profiles of samples after heating for 12 h at 80 °C is shown in Figure 4. The peptide bands in glycated samples appeared less distinct than in control β-Lg. This may be attributed to the presence of a heterogeneous mixture of peptides with different degrees of glycation in the samples. In addition, the modification of amine groups on peptides may

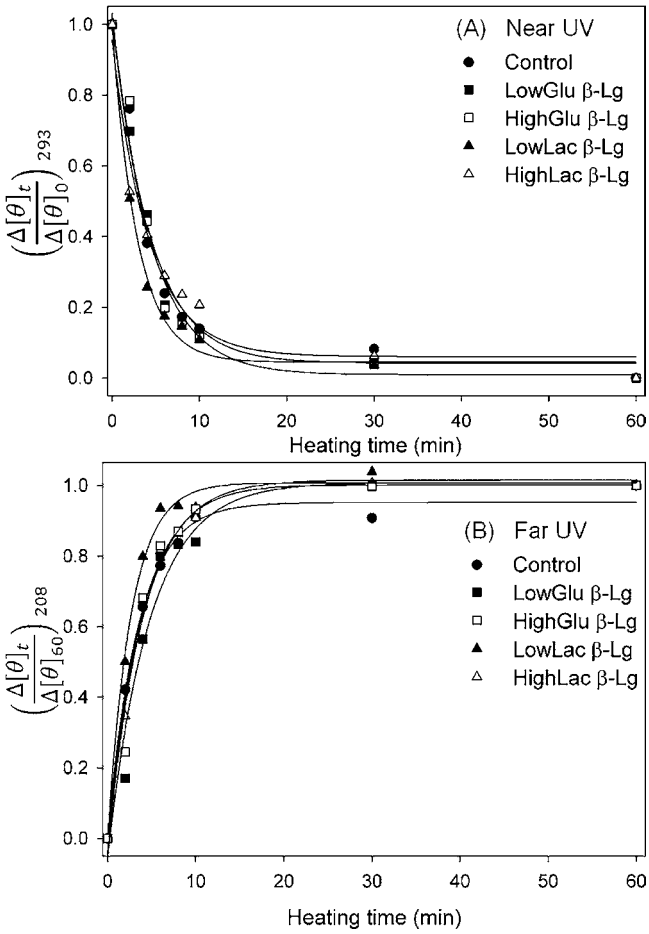

Figure 3. Relative change in ellipticity at (A) 293 nm in the NUV region and (B) 208 nm in the FUV region. Solid lines are for visual reference. For details of the *y*-axis parameters, see the Materials and Methods.

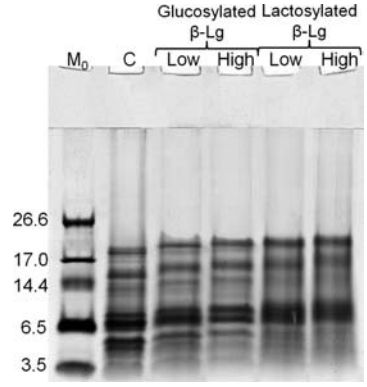

Figure 4. Tricine SDS−PAGE profiles of control and glycated samples after heating for 12 h at 80 °C. Key: M_0, molecular mass markers (kDa); C, heated control.

have altered the affinity of these peptides to bind to the staining dye.[49] Among the glycated samples, the peptide bands in lactosylated samples were the least well-defined.

The intensity of the band corresponding to the unhydrolyzed β-Lg in the SDS−PAGE gels at different times was quantified and plotted against the heating times. Hydrolysis of the monomer in all samples followed first-order exponential decay kinetics (Figure S5, Supporting Information), and the rate

dx.doi.org/10.1021/jf405441g | J. Agric. Food Chem. 2014, 62, 3269−3278

constants (k_h) were calculated using eq 5; these are listed in Table 1. Glycation reduced k_h by ~15%, and this effect was

Table 1. Rate Constants of Acid Hydrolysis of β-Lg Calculated from Eq 5

sample details	k_h ($min^{-1} \times 10^{-3}$)	adj R^2	$S_{y/x}$[c] $\times 10^{-3}$
control	2.8 (0.10)[b]	0.9921	0.50
LowGlu β-Lg[a]	2.4 (0.08)	0.9925	0.41
HighGlu-β-Lg	2.3 (0.07)	0.9752	0.40
LowLac β-Lg[a]	2.3 (0.10)	0.9609	0.55
HighLac β-Lg	2.5 (0.11)	0.9746	0.60

[a]The degrees of glycation in LowGlu and LowLac β-Lg were similar. [b]Numbers in parentheses indicate standard deviations. [c]Standard error of regression.

independent of the type of sugar or the degree of glycation. However, the glycation effect was not significant (p = 0.29) in the likelihood ratio test. The SDS–PAGE analysis of β-Lg glycation controls showed that hydrolysis rates were unaffected (p = 0.25, likelihood ratio test) by sample treatments in the absence of sugars (Figure S6 and Table S1, Supporting Information).

Self-Assembly from Glycated β-Lg. Self-assembly from glycated samples followed a three-phase sigmoidal growth pattern (Figure 5A), which is typical of β-Lg self-assembly under unstirred conditions. The ThT data were fitted well by eq 1, and results from a likelihood ratio test confirmed that the effect of glycation treatments on the parameters was statistically significant (p < 0.0001). The kinetic parameters of self-assembly calculated from eqs 2–4 are listed in Table 2. A comparison of kinetic parameters of self-assembly is shown in Figure 5B. LowGlu β-Lg and LowLac β-Lg showed only a small increase in t_{lag} (6 and 7 h, respectively, against 5.6 h for the control), whereas in HighGlu β-Lg and HighLac β-Lg the t_{lag} values were nearly twice that of the control (11.3 and 11 h, respectively).

In the growth phase, glycation greatly decreased $(df/dt)_{max}$. For glucosylated samples, this effect was more pronounced at high degrees of glycation. In contrast, lactosylation had a strong effect irrespective of the degree of glycation. The effect of glycation on the stationary phase fluorescence (f_{max}) followed a similar trend. Control β-Lg samples were freeze-dried, incubated, and dialyzed as with glycated samples but without sugars, and these controls self-assembled normally (Figure S7, Supporting Information). Thus, glucosylation and lactosylation had different effects on the different stages of self-assembly, and the effect of lactosylation was stronger than that of glucosylation.

Composition of Fibrils. Fibrils in samples heated for 24 h were separated using ultracentrifugation and analyzed using SDS–PAGE under reducing conditions. The residual ThT intensities in the supernatant samples remained low, indicating complete separation of fibrils upon ultracentrifugation (Figure S8, Supporting Information). HighGlu and HighLac β-Lg showed long t_{lag} and lower $(df/dt)_{max}$, so a heating time of 24 h was selected for studying the composition of the fibrils. Figure 6 shows the peptide bands in centrifugally-separated fibrils from glycated β-Lg. Figure 4 shows the results of analyzing noncentrifuged solutions, which contain both fibril and nonfibril material, whereas only the fibril fraction (the pellet) was analyzed in Figure 6. All pellet samples contained only peptides, indicating that the building blocks of fibrils were

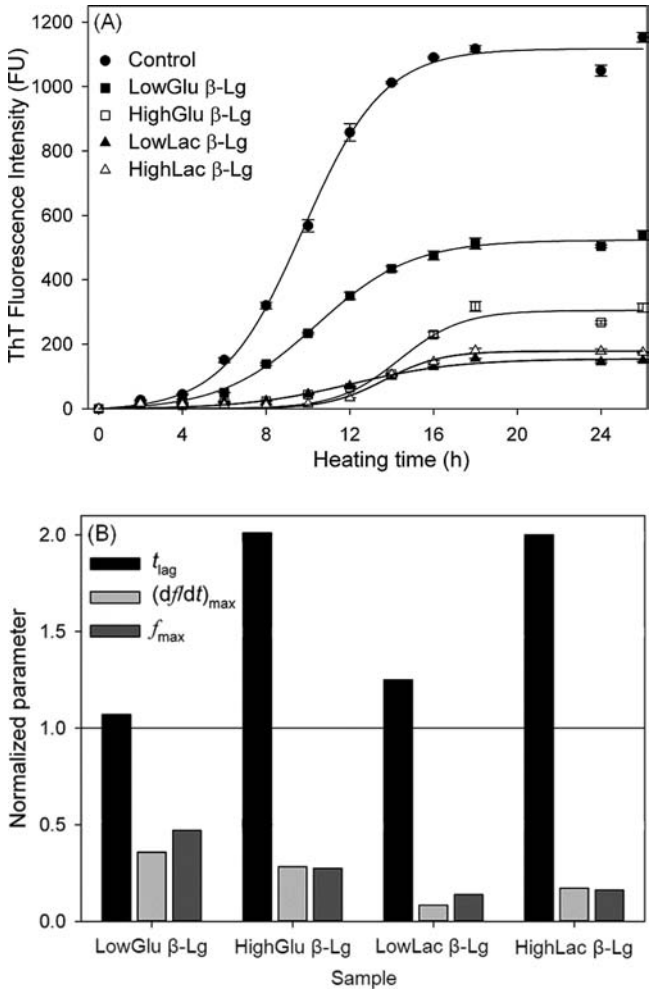

Figure 5. Self-assembly from glycated β-Lg. (A) Thioflavin T fluorescence intensity of control and glycated β-lg (1%, w/v) during heating at pH 2 and 80 °C. Each data point is an average of triplicates from two independent experiments, and error bars are standard errors. Solid lines indicate the fit to eq 1. (B) Normalized parameters of self-assembly calculated from eqs 2–4. The kinetic parameters of individual samples were normalized by those of the control sample.

predominantly peptides under the conditions used here (1% (w/v) protein, pH 2, heating at 80 °C). The unmodified control β-Lg showed seven peptide bands. The same bands appeared in all glycated samples, but they were less distinct in glycated samples and showed slightly reduced mobility, indicating that these peptides may be glycated. The lighter overall intensity in LowLac β-Lg and HighLac β-Lg lanes may result from lower fibril yields (Figure 5).

Morphology of Fibrils. The morphology of fibrils from glycated β-Lg was examined by TEM (Figure 7). The morphology of the fibrils was unaffected by glycation. The fibrils appeared long, straight, and unbranched, similar to those in unmodified β-Lg (Figure S9, Supporting Information), irrespective of glucosylation or lactosylation. Furthermore, all samples showed both long and short fibrils.

DISCUSSION

The CD studies showed that glucosylation and lactosylation had only very minor effects on the native structure of β-Lg. The structural changes in β-Lg upon heating were very fast, and CD results did not show differences between control and/or

Table 2. Kinetic Parameters Describing β-Lg Self-Assembly Calculated Using Eqs 1−4

sample details	t_{lag} (h)	$(df/dt)_{max}$ (FU·h^{-1})	$t_{1/2max}$ (h)	f_{max} (FU)
control	5.6 (0.2)[b]	158.0 (8.4)	9.1 (0.1)	1117 (16.0)
LowGlu β-Lg[a]	6.0 (0.2)	56.0 (2.9)	10.7 (0.2)	523 (6.7)
HighGlu-β-Lg	11.3 (0.7)	51.0 (10.7)	14.3 (0.4)	305 (17.0)
LowLac β-Lg[a]	7.0 (0.8)	15.5 (2.0)	12.0 (0.5)	155 (7.0)
HighLac β-Lg	11.0 (0.4)	32.7 (4.8)	13.8 (0.3)	178 (6.0)

[a]The degrees of glycation in LowGlu and LowLac β-Lg were similar. [b]Numbers in parentheses indicate standard deviations.

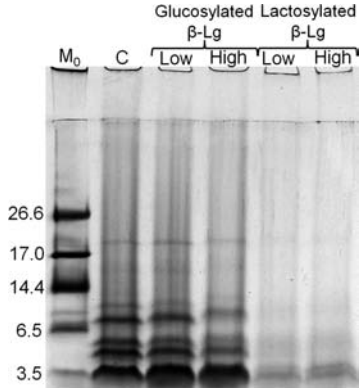

Figure 6. Tricine SDS−PAGE profiles of centrifugally precipitated fibrils made by heating glycated β-lg at 80 °C for 24 h. Key: M_0, molecular mass markers (kDa); C, nonglycated control fibrils made with the same heat treatment.

glycated samples. However, the CD method used in this study took 40−60 s to collect a spectrum, which meant that the temporal resolution was not high enough to detect subtle changes in the kinetics of unfolding. More targeted scanning of only selected wavelengths would be faster and could potentially quantify the rate of unfolding with higher precision. An innate limitation of this method is that structural changes take place during the heating of the sample to 80 °C, thus making it impossible to define an accurate $t = 0$.

Glycation produced a consistent ∼15% decrease in k_h, which we are unable to explain. However, the proportion of unhydrolyzed β-Lg monomer at any one time ("I/I_0" in Figure S5, Supporting Information) never spanned more than 10 percentage points across all treatments. Thus, glycation had a minor impact on the amount of hydrolyzed material present, and the effects of glycation on fibril formation were primarily at the self-assembly stage.

Glycation of the lysine residues on β-Lg would reduce the net charge at pH 2 by +1 per lysine, and a charge reduction alone would be expected to increase the rate of self-assembly by reducing the electrostatic repulsion between peptides. However, glycation always reduced the rate of peptide self-assembly, indicating that the charge reduction effect was counterbalanced by a more dominant assembly-inhibiting factor.

Using succinylated ovalbumin, Weijers et al.[50] have shown that the net charge on the protein influences the morphology of its aggregates. However, glycation of β-lg did not appear to modify the fibril morphology (Figure 7), even though MS spectra and SDS−PAGE patterns indicated that the fibrils must be composed of glycated peptides.

The kinetic parameters shown in Table 1 and Figure 5 reveal some important details about the effects of glycation on self-assembly. The rate of nucleation (related to t_{lag}) was largely unaffected in LowGlu and LowLac β-Lg, which had a similar number of lysine residues modified (Figure 1). The longer t_{lag} values for HighGlu β-Lg and HighLac β-Lg suggest that the amount of glycation had to reach a threshold before nucleation was adversely affected, and the size of the adduct had no effect. In contrast, fibril growth (related to $(df/dt)_{max}$) was affected by even low levels of glucosylation or lactosylation, and this effect was stronger for lactosylation than for glucosylation. In the stationary phase, increasing glucosylation progressively decreased the fibril yield (i.e., f_{max}), whereas even a small amount of lactosylation dramatically reduced the yield. Lactose is approximately twice the size of glucose, and the stronger impact of lactose on the growth kinetics and yield indicates that the effects of glycation on self-assembly are related to the size of the sugar residue.

Steric hindrance from bound sugar residues is thought to inhibit whey protein aggregation at pH 7,[37,38] and it is likely that glycation inhibited self-assembly of peptides at pH 2 by a similar mechanism. The spacing between adjacent β-strands in an amyloid fibril is on the order of 4.87 Å.[51] The hydrodynamic diameters of glucose and lactose molecules in solution are 7 and 9 Å, respectively,[52] so these adducts would certainly disrupt β-strand packing and thereby inhibit fibril assembly. In addition, the hydrophilic −OH side groups of sugar residues may interfere with hydrophobic interactions between fibril-forming peptides, which contain many hydrophobic residues.[18,20]

Glycation appears to reduce or abolish the ability of peptides to self-assemble, and glycated peptides may instead undergo further hydrolysis and/or may assemble into nonfibril aggregates,[53] reducing the potential yield of fibrils. A schematic illustrating our hypothesis is shown in Figure 8.

It may be questioned why fibril growth was sensitive to low levels of glycation, whereas nucleation was affected only by high levels of glycation. The answer lies in considering that the susceptibility of lysine residues to glycation varies from site to site. At shorter glycation times, lysines 47, 91, and 100 are preferentially glycated.[26,27,29] With an average of three bound sugar residues in LowGlu β-Lg and LowLac β-Lg (Figure1A,C), it is likely that these lysine residues were glycated. More extensive glycation in HighGlu and HighLac would also affect amine groups in the N-terminal region (Lys8 and Lys14 and the N-terminal amine). We suggest the N-terminal region containing these late-glycating lysines may be the main region involved in nucleation, whereas regions containing lysines that are preferentially glycated first are involved mainly in fibril growth.

This work has shown that even heavily glucosylated or lactosylated β-Lg retains the secondary and tertiary structures of native unglycated β-Lg. However, the steric constraints introduced by glycation substantially inhibit the self-assembly of glycated β-Lg fragments into fibrils, the effect being greater for the larger lactose moiety, even though the extent of lactosylation was smaller than that of glucosylation. We

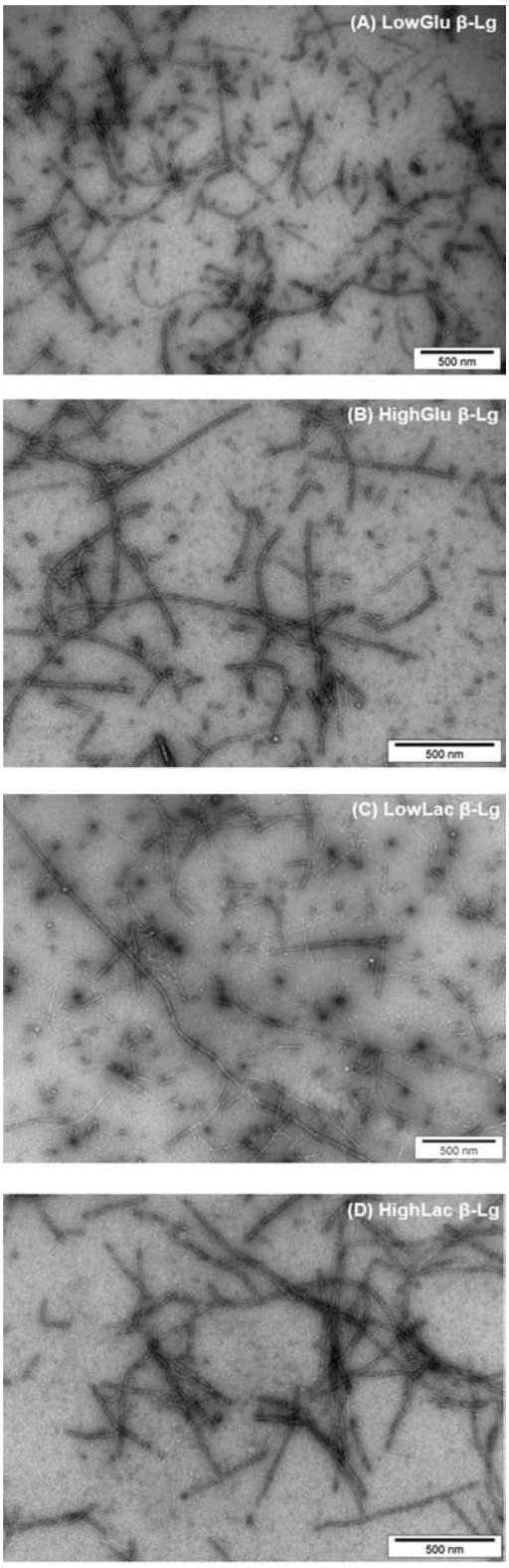

Figure 7. TEM images of fibrils from glycated β-Lg after heating for 24 h at 80 °C: (A) LowGlu β-Lg; (B) HighGlu β-Lg; (C) LowLac β-Lg; (D) HighLac β-Lg.

propose that the inhibitory effect of glycation is influenced by the location of glycated residues, which is related to the varying glycation susceptibility of different lysine residues in the natively folded protein.

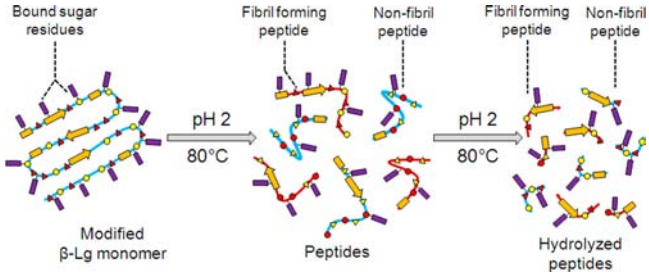

Figure 8. Proposed mechanism of inhibition of self-assembly of glycated β-Lg by the steric effect of the sugar adduct.

■ ASSOCIATED CONTENT

Supporting Information

Deconvoluted MS spectra of unglycated β-Lg (Figure S1), glucosylated and lactosylated β-Lg at different glycation times at 40 °C (Figures S2 and S3), CD spectra showing the effect of glycation on the β-Lg structure (Figure S4), residual intensities of the β-Lg band quantified from the SDS−PAGE of glycated samples (Figure S5) and β-Lg samples used as glycation controls (Figure S6), ThT intensities of β-Lg used as a glycation control (Figure S7), residual ThT intensities for supernatants for samples in Figure 6 (Figure S8), TEM image of fibrils from untreated control β-Lg after heating for 24 h (Figure S9), Tables S1 and S2 showing the kinetic parameters of acid hydrolysis and self-assembly calculated using eqs 1−5 from the data in Figures S6 and S7, and variance calculations for composite parameters. This material is available free of charge via the Internet at http://pubs.acs.org.

■ AUTHOR INFORMATION

Corresponding Author

*E-mail: s.loveday@massey.ac.nz. Phone: +64-6-3569099, ext 81375. Fax: +64-6-3505655.

Funding

This work was funded by Fonterra Cooperative Ltd. and the New Zealand Foundation for Research Science and Technology, Contract DRIX0701.

Notes

The authors declare no competing financial interest.

■ ACKNOWLEDGMENTS

We acknowledge Mr. Trevor Loo at the Institute of Fundamental Sciences (IFS) at Massey University for the MS analysis of glycated samples, and we thank Mr Doug Hopcroft at the Manawatu Microscopy and Imaging Centre Massey University for his help with the TEM imaging. We also thank Associate Professor Geoff Jones (IFS) for his guidance with statistical analysis and Dr. Gillian Norris (IFS) for useful discussions.

■ ABBREVIATIONS USED

SDS−PAGE, sodium dodecyl sulfate−polyacrylamide gel electrophoresis; HPLC, high-performance liquid chromatography; UV, ultraviolet; MS, mass spectrometry; Q-TOF, quadrupole time-of-flight; ESI, electron spray ionization

■ REFERENCES

(1) Pilkington, S. M.; Roberts, S. J.; Meade, S. J.; Gerrard, J. A. Amyloid fibrils as a nanoscaffold for enzyme immobilization. *Biotechnol. Prog.* **2010**, *26*, 93−100.

(2) Raynes, J. K.; Gerrard, J. A. Amyloid fibrils as bionanomaterials. In *Bionanotechnology: Biological Self-Assembly and Its Applications*; Rehm, B., Ed.; Horizon Scientific Press: Norfolk, U.K., 2012.
(3) Loveday, S. M.; Su, J.; Rao, M. A.; Anema, S. G.; Singh, H. Whey protein nanofibrils: the environment−morphology−functionality relationship in lyophilization, rehydration, and seeding. *J. Agric. Food Chem.* **2012**, *60*, 5229−5236.
(4) Oboroceanu, D.; Wang, L.; Magner, E.; Auty, M. A. E. Fibrillization of whey proteins improves foaming capacity and foam stability at low protein concentrations. *J. Food Eng.* **2014**, *121*, 102−111.
(5) Bolder, S. G.; Sagis, L. M. C.; Venema, P.; van der Linden, E. Effect of stirring and seeding on whey protein fibril formation. *J. Agric. Food Chem.* **2007**, *55*, 5661−5669.
(6) Hill, E. K.; Krebs, B.; Goodall, D. G.; Howlett, G. J.; Dunstan, D. E. Shear flow induces amyloid fibril formation. *Biomacromolecules* **2006**, *7*, 10−13.
(7) Loveday, S. M.; Su, J.; Rao, M. A.; Anema, S. G.; Singh, H. Effect of calcium on the morphology and functionality of whey protein nanofibrils. *Biomacromolecules* **2011**, *12*, 3780−3788.
(8) Loveday, S. M.; Wang, X. L.; Rao, M. A.; Anema, S. G.; Singh, H. Effect of pH, NaCl, $CaCl_2$ and temperature on self-assembly of β-lactoglobulin into nanofibrils: a central composite design study. *J. Agric. Food Chem.* **2011**, *59*, 8467−8474.
(9) Loveday, S. M.; Wang, X. L.; Rao, M. A.; Anema, S. G.; Singh, H. β-Lactoglobulin nanofibrils: effect of temperature on fibril formation kinetics, fibril morphology and the rheological properties of fibril dispersions. *Food Hydrocolloids* **2012**, *27*, 242−249.
(10) Medrano, A.; Abirached, C.; Panizzolo, L.; Moyna, P.; Anon, M. C. The effect of glycation on foam and structural properties of β-lactoglobulin. *Food Chem.* **2009**, *113*, 127−133.
(11) Chevalier, F.; Chobert, J. M.; Popineau, Y.; Nicolas, M. G.; Haertle, T. Improvement of functional properties of β-lactoglobulin glycated through the Maillard reaction is related to the nature of the sugar. *Int. Dairy J.* **2001**, *11*, 145−152.
(12) Nacka, F.; Chobert, J. M.; Burova, T.; Leonil, J.; Haertle, T. Induction of new physicochemical and functional properties by the glycosylation of whey proteins. *J. Protein Chem.* **1998**, *17*, 495−503.
(13) Qi, X. L.; Holt, C.; McNulty, D.; Clarke, D. T.; Brownlow, S.; Jones, G. R. Effect of temperature on the secondary structure of β-lactoglobulin at pH 6.7, as determined by CD and IR spectroscopy: a test of the molten globule hypothesis. *Biochem. J.* **1997**, *324*, 341−346.
(14) Jameson, G. B.; Adams, J. J.; Creamer, L. K. Flexibility, functionality and hydrophobicity of bovine β-lactoglobulin. *Int. Dairy J.* **2002**, *12*, 319−329.
(15) Uhrínová, S.; Smith, M. H.; Jameson, G. B.; Uhrín, D.; Sawyer, L.; Barlow, P. N. Accompanying pH-induced dissociation of the β-lactoglobulin dimer. *Biochemistry* **2000**, *39*, 3565−3574.
(16) Kella, N. K.; Kinsella, J. E. Enhanced thermodynamic stability of β-lactoglobulin at low pH. A possible mechanism. *Biochem. J.* **1988**, *255*, 113−118.
(17) Bromley, E. H. C.; Krebs, M. R. H.; Donald, A. M. Aggregation across the length-scales in β-lactoglobulin. *Faraday Discuss.* **2005**, *128*, 13−27.
(18) Dave, A. C.; Loveday, S. M.; Anema, S. G.; Loo, T. S.; Norris, G. E.; Jameson, G. B.; Singh, H. β-Lactoglobulin self-assembly: structural changes in early stages and disulfide bonding in fibrils. *J. Agric. Food Chem.* **2013**, *61*, 7817−7828.
(19) Oboroceanu, D.; Wang, L. Z.; Brodkorb, A.; Magner, E.; Auty, M. A. E. Characterization of β-lactoglobulin fibrillar assembly using atomic force microscopy, polyacrylamide gel electrophoresis, and in situ fourier transform infrared spectroscopy. *J. Agric. Food Chem.* **2010**, *58*, 3667−3673.
(20) Akkermans, C.; Venema, P.; van der Goot, A. J.; Gruppen, H.; Bakx, E. J.; Boom, R. M.; van der Linden, E. Peptides are building blocks of heat-induced fibrillar protein aggregates of β-lactoglobulin formed at pH 2. *Biomacromolecules* **2008**, *9*, 1474−1479.
(21) Kroes-Nijboer, A.; Venema, P.; Bouman, J.; van der Linden, E. Influence of protein hydrolysis on the growth kinetics of β-Ig fibrils. *Langmuir* **2011**, *27*, 5753−5761.
(22) Arnaudov, L. N.; deVries, R.; Ippel, H.; vanMierlo, C. P. M. Multiple steps during the formation of β-lactoglobulin fibrils. *Biomacromolecules* **2003**, *4*, 1614−1622.
(23) Hettiarachchi, C. A.; Melton, L. D.; Gerrard, J. A.; Loveday, S. M. Formation of β-lactoglobulin nanofibrils by microwave heating gives a peptide composition different from conventional heating. *Biomacromolecules* **2012**, *13*, 2868−2880.
(24) Loveday, S. M.; Wang, X. L.; Rao, M. A.; Anema, S. G.; Creamer, L. K.; Singh, H. Tuning the properties of β-lactoglobulin nanofibrils with pH, NaCl and $CaCl_2$. *Int. Dairy J.* **2010**, *20*, 571−579.
(25) O'Brien, J. *Heat-Induced Changes in Lactose: Isomerization, Degradation, Maillard Browning*. International Dairy Federation (IDF): Brussels, Belgium, 1995; pp 134−170.
(26) Fogliano, V.; Monti, S. M.; Visconti, A.; Randazzo, G.; Facchiano, A. M.; Colonna, G.; Ritieni, A. Identification of a β-lactoglobulin lactosylation site. *Biochim. Biophys. Acta, Protein Struct. Mol. Enzymol.* **1998**, *1388*, 295−304.
(27) Morgan, F.; Bouhallab, S.; Molle, D.; Henry, G.; Maubois, J. L.; Leonil, J. Lactolation of β-lactoglobulin monitored by electrospray ionisation mass spectrometry. *Int. Dairy J.* **1998**, *8*, 95−98.
(28) Fenaille, F.; Morgan, F.; Parisod, V.; Tabet, J. C.; Guy, P. A. Solid-state glycation of β-lactoglobulin by lactose and galactose: localization of the modified amino acids using mass spectrometric techniques. *J. Mass Spectrom.* **2004**, *39*, 16−28.
(29) Morgan, F.; Molle, D.; Henry, G.; Venien, A.; Leonil, J.; Peltre, G.; Levieux, D.; Maubois, J. L.; Bouhallab, S. Glycation of bovine β-lactoglobulin: effect on the protein structure. *Int. J. Food Sci. Technol.* **1999**, *34*, 429−435.
(30) Morgan, F.; Leonil, J.; Molle, D.; Bouhallab, S. Modification of bovine β-lactoglobulin by glycation in a powdered state or in an aqueous solution: effect on association behavior and protein conformation. *J. Agric. Food Chem.* **1999**, *47*, 83−91.
(31) French, S. J.; Harper, W. J.; Kleinholz, N. M.; Jones, R. B.; Green-Church, K. B. Maillard reaction induced lactose attachment to bovine β-lactoglobulin: electrospray ionization and matrix-assisted laser desorption/ionization examination. *J. Agric. Food Chem.* **2002**, *50*, 820−823.
(32) van Teeffelen, A. M. M.; Broersen, K.; De Jongh, H. H. J. Glucosylation of β-lactoglobulin lowers the heat capacity change of unfolding; a unique way to affect protein thermodynamics. *Protein Sci.* **2005**, *14*, 2187−2194.
(33) Morgan, F.; Leonil, J.; Molle, D.; Bouhallab, S. Nonenzymatic lactosylation of bovine β-lactoglobulin under mild heat treatment leads to structural heterogeneity of the glycoforms. *Biochem. Biophys. Res. Commun.* **1997**, *236*, 413−417.
(34) Chevalier, F.; Chobert, J. M.; Dalgalarrondo, M.; Choiset, Y.; Haertle, T. Maillard glycation of β-lactoglobulin induces conformation changes. *Nahrung-Food* **2002**, *46*, 58−63.
(35) Da Silva Pinto, M.; Bouhallab, S.; De Carvalho, A. F.; Henry, G.; Putaux, J. L.; Leonil, J. Glucose slows down the heat-induced aggregation of β-lactoglobulin at neutral pH. *J. Agric. Food Chem.* **2012**, *60*, 214−219.
(36) Broersen, K.; Voragen, A. G. J.; Hamer, R. J.; de Jongh, H. H. J. Glycoforms of β-lactoglobulin with improved thermostability and preserved structural packing. *Biotechnol. Bioeng.* **2004**, *86*, 78−87.
(37) Mulsow, B. B.; Jacob, M.; Henle, T. Studies on the impact of glycation on the denaturation of whey proteins. *Eur. Food Res. Technol.* **2009**, *228*, 643−649.
(38) Liu, G.; Zhong, Q. Thermal aggregation properties of whey protein glycated with various saccharides. *Food Hydrocolloids* **2013**, *32*, 87−96.
(39) Broersen, K.; Elshof, M.; de Groot, J.; Voragen, A. G. J.; Hamer, R. J.; de Jongh, H. H. J. Aggregation of β-lactoglobulin regulated by glucosylation. *J. Agric. Food Chem.* **2007**, *55*, 2431−2437.

(40) Chevalier, F.; Chobert, J. M.; Dalgalarrondo, M.; Haertle, T. Characterization of the Maillard reaction products of β-lactoglobulin glucosylated in mild conditions. *J. Food Biochem.* **2001**, *25*, 33−55.
(41) Lee, D.; Park, C. W.; Paik, S. R.; Choi, K. Y. The modification of α-synuclein by dicarbonyl compounds inhibits its fibril-forming process. *Biochim. Biophys. Acta, Proteins Proteomics* **2009**, *1794*, 421−430.
(42) Oliveira, L. M.; Lages, A.; Gomes, R. A.; Neves, H.; Família, C.; Coelho, A. V.; Quintas, A. Insulin glycation by methylglyoxal results in native-like aggregation and inhibition of fibril formation. *BMC Biochem.* **2011**, *12*, 41.
(43) Bouma, B.; Kroon-Batenburg, L. M. J.; Wu, Y. P.; Brunjes, B.; Posthuma, G.; Kranenburg, O.; de Groot, P. G.; Voest, E. E.; Gebbink, M. Glycation induces formation of amyloid cross-β structure in albumin. *J. Biol. Chem.* **2003**, *278*, 41810−41819.
(44) Liu, G.; Zhong, Q. Dispersible and thermal stable nanofibrils derived from glycated whey protein. *Biomacromolecules* **2013**, *14*, 2146−2153.
(45) Swaisgood, H. E., Chemistry of milk protein. In *Developments in Dairy Chemistry*, Fox, P. F., Ed.; Elsevier Applied Science: London, U.K., 1982; Vol. *1*, pp 1−59.
(46) Woody, R. W. Circular-dichroism. *Methods Enzymol.* **1995**, *246*, 34−71.
(47) Meltretter, J.; Wüst, J.; Pischetsrieder, M. Comprehensive analysis of nonenzymatic post-translational β-lactoglobulin modifications in processed milk by ultrahigh-performance liquid chromatography-tandem mass spectrometry. *J. Agric. Food Chem.* **2013**, *61*, 6971−6981.
(48) Manderson, G. A.; Creamer, L. K.; Hardman, M. J. Effect of heat treatment on the circular dichroism spectra of bovine β-lactoglobulin A, B, and C. *J. Agric. Food Chem.* **1999**, *47*, 4557−4567.
(49) Tal, M.; Silberstein, A.; Nusser, E. Why does Coomassie Brilliant Blue R interact differently with different proteins? A partial answer. *J. Biol. Chem.* **1985**, *260*, 9976−9980.
(50) Weijers, M.; Broersen, K.; Barneveld, P. A.; Stuart, M. A. C.; Hamer, R. J.; De Jongh, H. J.; Visschers, R. W. Net charge affects morphology and visual properties of ovalbumin aggregates. *Biomacromolecules* **2008**, *9*, 3165−3172.
(51) Nelson, R.; Sawaya, M. R.; Balbirnie, M.; Madsen, A. O.; Riekel, C.; Grothe, R.; Eisenberg, D. Structure of the cross-beta spine of amyloid-like fibrils. *Nature* **2005**, *435*, 773−778.
(52) Ribeiro, A. C. F.; Ortona, O.; Simões, S. M. N.; Santos, C. I. A. V.; Prazeres, P. M. R. A.; Valente, A. J. M.; Lobo, V. M. M.; Burrows, H. D. Binary mutual diffusion coefficients of aqueous solutions of sucrose, lactose, glucose, and fructose in the temperature range from (298.15 to 328.15) K. *J. Chem. Eng. Data* **2006**, *51*, 1836−1840.
(53) Dave, A. C.; Loveday, S. M.; Anema, S. G.; Jameson, G. B.; Singh, H. Modulating β-lactoglobulin nanofibril self-assembly at pH 2 using glycerol or sorbitol. *Biomacromolecules* **2014**, *15*, 95−103.

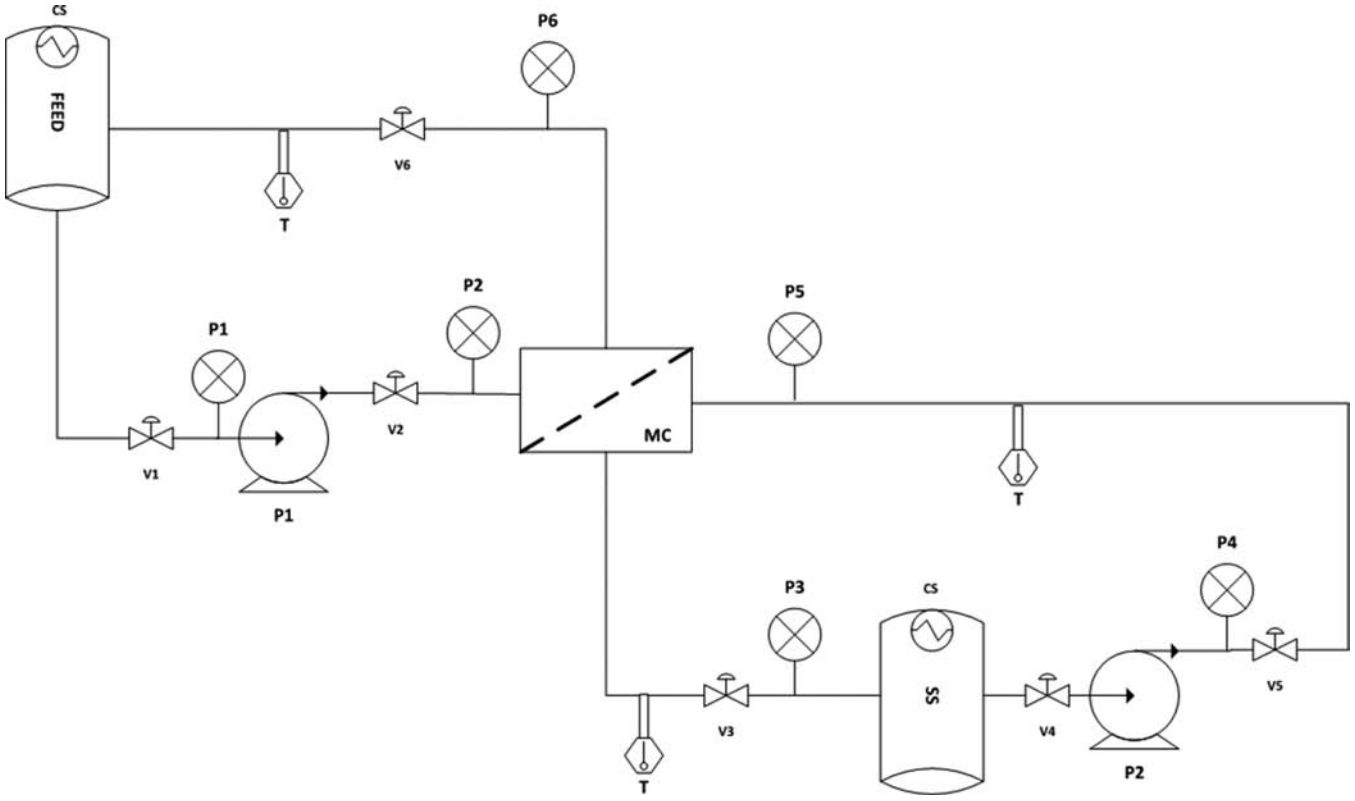

Figure 1. Model of the dealcoholization lab unit used (feed, beer tank; P1 and P2 peristaltic pumps; MC, membrane contactor; CS, cooling system; SS, stripping solution tank; V1−V6; manual valves; T, temperature controllers; P1−P6, pressure gauges.

flavor. Therefore, low-alcohol or alcohol-free beers produced by the technologies applied up to now will at best reach only approximately the high sensory quality of a "normal" beer. Nevertheless, these beers make up distinctive, high-quality products, which have earned significance in the market.[21]

The sensory quality of beer depends on the complex balance of flavor-active components. In many cases, the dealcoholization could negatively affect the organoleptic quality of beer, leading in some cases to the unacceptability of the product. The low-alcohol and alcohol-free beers are required to meet certain quality conditions regarding their stability and sensory features, which should be comparable to those of normal beers. It is likely that the sensory qualities of the beer will change over the course of the dealcoholization, where a loss of aroma, body, and flavor can be seen.[22] A reduced foaming property (especially foam head retention) is another drawback. This issue is also related to the lack of ethanol, which improves foamability and foam stability in the range of 1−3.5% v/v.[23] In any case, the addition of glycerol or other sugar alcohols can reinforce the foaming properties of beer.[24,25]

Principle of Osmotic Distillation. Osmotic distillation (OD) or evaporative pertraction (EP) is a membrane process used for removing ethanol from beverages, especially for wine partial dealcoholization. This membrane technology has been presented as a novel and promising technology to reduce the ethanol content in alcoholic beverages without unacceptably altering the organoleptic properties of the product.[26,27] OD uses hydrophobic porous membrane contactors to provide the ethanol transfer from beer to stripping solution (usually water). In this process water and beer flow countercurrently. The mechanism is similar to membrane distillation,[28] but in this case, the process is carried out at ambient temperature,[26] in which the partial pressure gradient due to the high relative volatility compared to water is the driving force for ethanol transport. Due to this mechanism the OD has also been defined "isothermal membrane distillation"[29] and in some specific cases, such as dealcoholization, the term evaporative pertraction is more precise.[30] OD is a form of dialysis, in which a liquid mixture containing a volatile component is contacted with a microporous, non-liquid-wettable membrane whose opposite surface is exposed to a second liquid phase capable of absorbing that component. The most important difference compared to more common liquid−liquid contacting processes (such as reverse osmosis) is the membrane's composition, which is porous and hydrophobic and typically made of PTFE or polypropylene.[31] The most important advantages of the membrane contactors are well-defined and constant interfacial area, high interfacial area in small volumes, small size and weight, no dispersion between phases, no need of phase separation downstream, no need to work with fluids of different densities, no flooding, loading, or foaming, wide range of operating flow-rates, flow-rates can be varied independently, and lower operating temperatures compared to distillation processes. The most important drawbacks are membrane fouling, pressure drop caused by the membrane unit, membrane lifetime, and a high stripping solution volume requirement.[32−35] The transport mechanism of ethanol by OD process can be divided into three steps: (i) evaporation of ethanol at the membrane pores on the feed side, (ii) diffusion of ethanol vapor through the membrane pores, and (iii) condensation of ethanol vapor in the stripping solution at the membrane pore exit.[36] The aim of this work was to investigate both theoretically and experimentally the effects of the different process parameters. The operating parameters which affect the

ethanol content, such as flow rate, system temperature, and types of stripping solutions, were investigated. Furthermore, the quality parameters (present gravity, pH, color, turbidity, total soluble nitrogen, CO_2) and the losses of volatile compounds of the beer were also monitored.

MATERIALS AND METHODS

Alcoholic beers of five different commercial brands were obtained. The alcoholic beers contained between 3.5% and 5% v/v. The dealcoholization tests were carried out by a small pilot plant equipped with a polypropylene hollow fiber membrane contactor (Liqui-Cel, MiniModule 1.7 × 5.5, Membrana GmbH, Wuppertal, Germany) (Figure 1). The typical membrane surface area was 0.54 m^2, with an approximate priming volume of 78 and 53 mL, for shellside and tubeside, respectively. For the first trials the membrane operating parameters were as follows: beer inlet pressure 0.3 bar gauge, beer outlet zero pressure (atmospheric), water inlet pressure 0.3 bar gauge, water outlet zero pressure, beer flow 500 mL min^{-1}, and water flow 500 mL min^{-1}. These parameters were subsequently adjusted in an experimental matrix to ascertain optimum process (below). The ethanol content of the beers and all quality parameters were determined in accordance with Analytica EBC.[37]

The aromatic profile of the beer and corresponding dealcoholized beer was analyzed by gas chromatography (Perkin-Elmer, Auto System XL, Waltham, MA). The chemical standards (acetaldehyde, *n*-propanol, 2-methyl-1-butanol, 3-methyl-1-butanol, ethyl acetate, isoamyl acetate, ethyl hexanoate, diacetyl) used for the identification and quantification of the volatile compounds of interest were purchased from Sigma-Aldrich (Milwaukee, WI). The internal standard for the determination of aldehydes and vicinal diketones, 2-chlorobenzaldehyde (Sigma-Aldrich, Milwaukee, WI), was prepared weekly in a solution of 5% ethanol with a concentration of 10 mg L^{-1}. The internal standard for determination of ethanol, higher alcohols, and esters was 1-butanol (Sigma-Aldrich, Milwaukee, WI), which was prepared weekly in water with a concentration of 60 mg L^{-1}. The gas chromatograph was equipped with an electron capture detector (ECD) for the analysis of vicinal diketones (diacetyl and 2,3-pentanedione) and with a flame ionization detector (FID) for the analysis of the other volatile compounds.The separation column was a CP-WAX 57CB wall coated open tubular (WCOT) fused silica column (polyethylene glycol stationary phase, 60 m × 0.25 mm i.d. with 0.4 μm film thickness; Chrompack, Netherlands). Ten mL of the beer samples was added to 500 μL of internal standard 2-chlorobenzaldehyde (10 mg L^{-1}) and 1 mL of the internal standard 1-butanol (60 mg L^{-1}) in a 20-mL glass vial, which was heated for 30 min at 60 °C and stirred at 250 rpm for 30 s of every minute in order to allow the volatilization and derivatization of the compounds of interest. The injection was performed by means of a 2.5-mL headspace syringe at 70 °C. The syringe was placed in the sample headspace to draw the volatile compounds and to inject them in the gas chromatograph. The injection volume was 1 mL. The front inlet temperature was 150 °C. The injection was in the splitless mode with the purge valve set at 20 mL min^{-1}. Helium was the carrier gas at a flow rate of 1.1 mL min^{-1}. The oven temperature program used was 34 °C for 2 min, followed by an increase of 45 °C min^{-1} up to 55 °C, the held for 8 min, then raised to 98 °C at 5 °C min^{-1}, and finally increased to 150 °C at 45 °C min^{-1}. The detector temperature was 200 °C.

Experimental Section. A series of experiments was performed to ascertain optimum operation of the process. The feed and stripping solutions were fed into the module by peristaltic pumps. The process temperature was controlled by a water bath fitted with temperature controllers. Six pressure gauges for inlet and outlet were installed for monitoring the pressure of the feed and stripping solutions. During processes, the beer continuously circulated from a sealed container to the dealcoholization apparatus while water flowed counter-currently on the other side of the membrane (Figure 1). Beer ethanol content was monitored throughout the process until the target level was achieved.

Experimental Conditions. The beer feed was maintained at 10, 15, or 20 °C in separate trials, in order to investigate the effect of temperature changing on separation efficiency. During these trials, the stripping water temperature was kept at 10 °C. Similarly, different amounts of stripping solution, 3, 4, 5, or 6 L were employed in separate trials, while the beer volume was 1 L for each trial. Furthermore, the effects of types of stripping solution, i.e. normal pure water and carbonated water, were investigated. Moreover, different flow rates of stripping solution were tested, namely 500 mL min^{-1} and 1 L min^{-1}. Finally, different beer brands were employed to ascertain the effect of variations in e.g. membrane fouling, different volatile concentrations, etc.

Membrane Cleaning. After dealcoholization, the membrane was cleaned by flowing filtered and deionized water in tubeside and in shellside without recycling for 15 min. Subsequently, a 0.5% (w/w) and 30 °C NaOH solution was circulated for 30 min. Finally, the system was rinsed with RO water without recycling for 10 min and then it was dried in both tube and shell side by using nitrogen gas for 20 min according to manufacturer cleaning guidelines.

RESULTS AND DISCUSSION

Different Stripping Solution Volumes. The effect of the different ratios of stripping solution (deaerated water) to beer

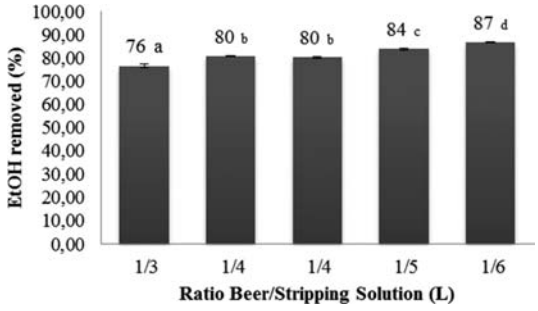

Figure 2. Percent of ethanol removed using different ratios of beer/stripping solution (% of original amount) after 4 h processing. Values with different superscript letters are statistically different ($P < 0.05$).

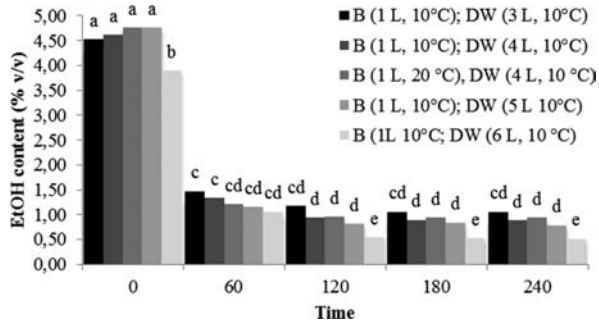

Figure 3. Decrease in ethanol during dealcoholization using different ratios of beer/stripping solution. (B: beer; DW: deaerated water). Values with different superscript letters are statistically different ($P < 0.05$).

feed in terms of ethanol flow transfer rate (mL min^{-1}) and in terms of percentage of ethanol removed (%) was measured. The different stripping solution volumes (3, 4, 5, and 6 L) noticeably influenced the percentage ethanol removed as shown in Figures 2 and 3. The matrix of experiments also included varying the feed beer temperature. The beer temperature (10 and 20 °C) did not significantly change the ethanol transfer rate and ethanol removed (Figure 3). Furthermore, Figure 3 shows that the process was essentially finished after 2 h; hence, it was

dx.doi.org/10.1021/jf405490x | J. Agric. Food Chem. 2014, 62, 3279−3286

Table 1. Representative Volatile Compounds (mg L^{-1}) and Loss Percentage (%) of Original and Dealcoholized Beer Using Different Ratios of Beer/Stripping Solution[a]

beer brand	AA	EA	EH	IAA	*n*-prop	2-MB	3-MB	DA
lager beer brand A	4.94 ab	18.35 b	0.10	1.91 d	8.55 f	9.61 e	49.53 f	0.03 a
B (1 L, 10 °C); DW (3 L, 10 °C)	2.78 a	5.34 a	0.01	0.47 bc	1.96 b	2.24 c	12.85 d	0.01 a
loss percentage (%)	43 A	70 A	87	74 A	77 B	76 AB	74 A	27 A
lager beer brand B	10.01 d	18.31 b	0.15	1.73 d	7.38 e	6.66 d	52.22 g	0.02 a
B (1 L, 10 °C); DW (4 L, 10 °C)	2.93 a	3.64 a	N.D.	0.39 ab	1.48 b	1.98 bc	10.10 c	0.02 a
loss percentage (%)	70 D	80 B		77 A	79 B	70 A	80 B	
B (1 L, 20 °C); DW (4 L, 10 °C)	4.46 ab	3.44 a	N.D.	0.29 ab	1.17 ab	1.40 abc	9.90 c	0.03 a
loss percentage (%)	55 C	81 B		83 AB	84 BC	79 B	81 B	
B (1 L, 10 °C); DW (5 L, 10 °C)	5.34 b	3.65 a	N.D.	0.25 ab	0.93 a	0.52 ab	7.75 b	0.01 a
loss percentage (%)	46 B	80 B		85 B	87 C	92 C	85 C	27 A
lager beer brand C	7.61 c	16.80 b	0.12	0.72 c	6.79 e	5.46 d	41.57 e	0.01 a
B (1 L, 10 °C); DW (6 L, 10 °C)	3.80 ab	2.67 a	N.D.	0.14 a	3.74	0.34 a	5.14 a	0.07 a
loss percentage (%)	47 A	84 B		80 AB	44 A	93 C	87 C	

[a]Acetaldehyde (AA), ethyl acetate (EA), ethyl hexanoate (EH), isoamylacetate (IAA), *n*-propanol (*n*-prop), 2-methylbutanol (2-MB), 3-methylbutanol (3-MB), diacetyl (DA). B: beer; DW: deaerated water. N.D.: not detectable. Statistical analysis was performed separately. Values in the same column with different letters are statistically different ($P < 0.05$).

Table 2. Representative Parameters of Original and Dealcoholized Beer Using Different Ratios of Beer/Stripping Solution[a]

beer brand	OG (°P)	RE (°P)	AE (°P)	EtOH (% v/v)	pH	color (EBC)	TU (EBC)	TN (mg L^{-1})	CO_2 (g L^{-1})
lager beer (brand A)	10.73 b	2.94 a	1.93 a	4.53 e	4.17 a	6.24 a	0.85 a	492 ab	5.32 cd
B (1 L, 10 °C); DW (3 L, 10 °C)	3.86 a	2.37 a	2.11 ab	1.06 d	4.15 a	6.88 b	2.54 b	518 ab	0.3 b
lager beer (brand B)	11.25 b	2.36 a	1.86 a	5.00 g	4.27 a	7.13 b	0.71 a	521 b	5.57 d
B (1 L, 10 °C); DW (4 L, 10 °C)	3.81 a	2.30 a	2.01 a	0.88 bc	4.17 a	7.49 b	1.78 ab	546 bc	0.19 ab
B (1 L, 20 °C); DW (4 L, 10 °C)	4.21 a	2.54 a	2.22 ab	0.93 c	4.24 a	7.77 b	1.07 a	535 bc	0.13 ab
B (1 L, 10 °C); DW (5 L, 10 °C)	3.89 a	2.77 a	2.55 b	0.79 b	4.27 ab	7.64 b	0.91 a	534 bc	0.44 b
lager beer (brand C)	10.94 b	3.50 a	1.90 a	4.81 f	4.42 b	7.57 b	0.65 a	549 c	5.23 d
B (1 L, 10 °C); DW (6 L, 10 °C)	3.22 a	2.40 a	2.30 ab	0.51 a	4.30 ab	7.78 b	0.92 a	569 c	0.36 ab

[a]Original gravity (OG), real extract (RE), apparent extract (AE), turbidity (TU), total nitrogen (TN). Beer (B); deaerated water (DW). Statistical analysis was performed separately. Values in the same column with different letters are statistically different ($P < 0.05$).

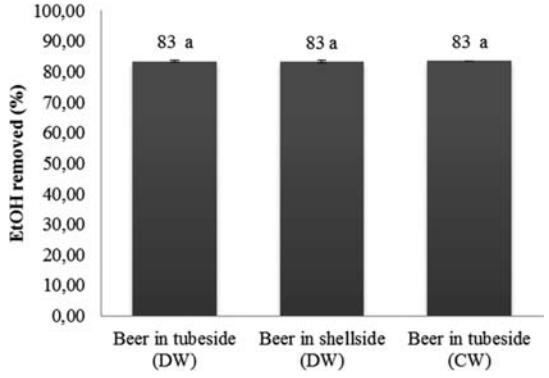

Figure 4. Percent of ethanol removed using different stripping solutions. Values with different superscript letters are statistically different ($P < 0.05$).

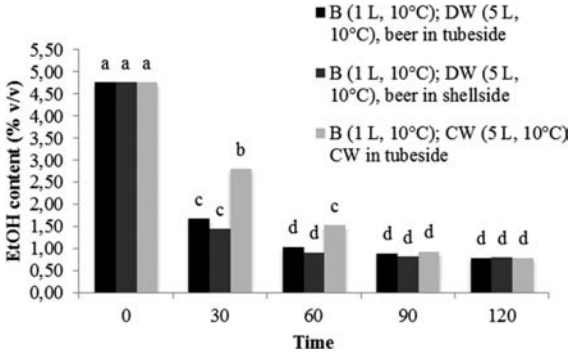

Figure 5. Decrease in ethanol during dealcoholization using different stripping solutions (B: beer; DW: deaerated water, CW: carbonated water). Values with different superscript letters are statistically different ($P < 0.05$).

not necessary to run it for 4 h. As well as the ethanol, the increase of the stripping solution quantity caused a diminution of volatile compounds concentration at the end of treatment (Table 1). The quality parameters monitored did not change significantly (Table 2), except for carbon dioxide, which was decreased considerably, and turbidity, which was increased slightly after dealcoholization.

Different Stripping Solution. The effect of different kinds of stripping solution was studied in this part of the work. Carbonated water (CW) was compared with normal deaerated water (DW) in order to reduce the loss of carbon dioxide by the end of the process. If possible, the stripping solution was pure water, which had been previously deoxygenated by boiling and/or flushing with a gas, usually nitrogen. In other words, if the stripping solution is similar to beer from a compositional point of view (especially in the case of carbon dioxide and low oxygen content), the pressure gradient between carbon dioxide in the beer and in the stripping solution would be minimal, preventing its diffusion across the membrane.[28] The amount of alcohol removed was the same with both strip solutions (Figure 4). On the contrary, the carbonation initially appeared to restrict ethanol transfer as shown in Figure 5 (mechanism

dx.doi.org/10.1021/jf405490x | J. Agric. Food Chem. 2014, 62, 3279−3286

Table 3. Representative Volatile Compounds (mg L^{-1}) and Loss Percentage (%) of Original and Dealcoholized Beer Using Different Stripping Solutions[a]

beer brand	AA	EA	EH	IAA	*n*-prop	2-MB	3-MB	DA
lager beer brand B	10.01 c	18.31 c	0.16	1.74 c	7.38 c	6.66 c	52.23 c	0.02 ab
B (1 L, 10 °C); DW (5 L, 10 °C) B in tubeside	3.86 ab	4.43 bc	0.02	0.15 a	4.28 b	0.47 a	0.22 a	0.01 a
loss percentage (%)	61 B	75 A		91 B	41 A	92 A	88 A	32 A
lager beer brand D	4.97 b	13.88 b	0.05	0.76 b	11.44 a	7.28 c	61.19 d	0.07 c
B (1 L, 10 °C); DW (5 L, 10 °C) B in shellside	2.48 a	3.06 a	N.D.	0.22 a	1.26 a	0.56 b	9.12 b	0.03 ab
loss percentage (%)	50 A	77 A		71 A	88 B	92 A	85 A	61 A
B (1 L, 10 °C); CW (5 L, 10 °C) B in shellside	2.82 a	3.79 a	N.D.	0.15 a	1.35 a	0.60 b	8.11 b	0.04 b
loss percentage (%)	43 A	72 A		80 A	88 B	91 A	86 A	46 A

[a]N.D.: not detectable. Statistical analysis was performed separately. Values in the same column with different letters are statistically different ($P < 0.05$).

Table 4. Representative Parameters of Original and Dealcoholized Beer Using Different Stripping Solutions[a]

beer brand	OG (°P)	RE (°P)	AE (°P)	EtOH (% v/v)	pH	color (EBC)	TU (EBC)	TN (mgL^{-1})	CO_2 (g L^{-1})
lager beer (brand B)	11.25 b	2.36 a	1.86 a	5.00 c	4.27 ab	7.13 a	0.71 a	521 b	5.57 d
B (1 L, 10 °C); DW (5 L, 10 °C) B in tubeside	3.89 a	2.77 a	2.55 ab	0.79 a	4.27 ab	7.64 a	0.91 ab	534 b	0.44 a
lager beer (brand D)	10.92 b	3.70 a	1.88 a	4.71 b	4.02 a	7.80 a	0.71 a	354 a	4.84 c
B (1 L, 10 °C); DW (5 L, 10 °C) B in shellside	4.80 a	3.54 a	3.19 b	0.84 a	4.17 ab	7.34 a	1.11 b	342 a	0.38 a
B (1 L, 10 °C); CW (5 L, 10 °C) B in shellside	5.00 a	3.76 a	3.45 b	0.79 a	4.39 b	7.55 a	1.21 b	346 a	1.98 b

[a]Carbonated water (CW). Statistical analysis was performed separately. Values in the same column with different letters are statistically different ($P < 0.05$).

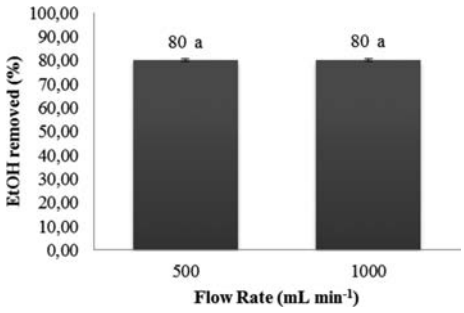

Figure 6. Percent of ethanol removed using different stripping solution flow rate (mL min^{-1}). Values with different superscript letters are statistically different ($P < 0.05$).

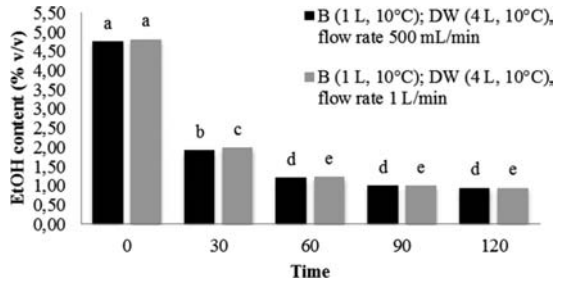

Figure 7. Decreasing ethanol during dealcoholization using different stripping solution flow rate. Values with different superscript letters are statistically different ($P < 0.05$).

unknown), but at the end of the process no difference was found. This would be explained by the equilibrium being reached between the beer and stripping solution. In other words, the ethanol concentration became the same in both beer and stripping solution. As expected, low-alcohol beer obtained using CW showed about 2 g L^{-1} of carbon dioxide, whereas the process with normal deaerated water resulted in about 0.4 g L^{-1} in each trial. The results showed that the use of carbonated water is a viable option to reduce the carbon dioxide loss, allowing a low-alcohol beer with an acceptable carbon dioxide concentration. In these experiments the final carbon dioxide level, even when carbonated water was employed as stripping solution, was low compared to a typical specification for beer, and it would have been necessary to add more before packaging in a commercial process. On the other hand, the employment of stripping solutions with higher concentrations of carbon dioxide may have resolved the problem. Concerning the most important volatile compounds, no significant difference was found when using CW or DW (i.e., similar losses) (Tables 3 and 4).

Effect of Stripping Solution Flow Rate. The effects of the stripping solution flow rate on the ethanol decrease are shown in Figure 6. In this case two different flow rates were employed: first 500 mL min^{-1} for feed and stripping solution, second 500 mL min^{-1} of feed solution and 1000 mL min^{-1} of stripping solution. A similar study was performed by Liguori et al. [38] That work showed that when increasing the stripping flow rate from 1.2 to 2.4 mL min^{-1}, a more rapid decrease in ethanol content was observed. In this case no significant effect was observed as shown in Figures 6 and 7. Figure 7 was in agreement with Diban,[30] confirming that flow rate has little influence on mass transfer resistance because the transmembrane resistance was the limiting stage in this transport mechanism. The volatile compounds and quality parameters did not change significantly when different stripping solution flow rates were employed (Tables 5 and 6).

Feed Solution and Stripping Solution Inversion. In the trials above, the stripping solution flowed in the shellside so that the beer flowed tubeside. In the following trials these operating conditions were inverted so that the beer flowed shellside and stripping solution flowed tubeside. In this dealcoholization trial 83% of ethanol was removed instead of 79% when it was used with beer tubeside (Figures 8 and 9). Thus, the beer shellside and water tubeside could be a better option. More significantly, the ethanol results after 30, 60 and

dx.doi.org/10.1021/jf405490x | J. Agric. Food Chem. 2014, 62, 3279−3286

Table 5. Representative Volatile Compounds (mg L^{-1}) and Loss Percentage (%) of Original and Dealcoholized Beer Using Different Flow Rates[a]

beer brand	AA	EA	EH	IAA	*n*-prop	2-MB	3-MB	DA
lager beer (brand B)	10.01 b	18.31 b	0.16	1.74 b	7.38 b	6.66 b	52.23 b	0.02 a
flow rate 500 mL min^{-1}	4.46 a	3.44 a	N.D.	0.30 a	1.17 a	1.41 a	9.90 a	0.03 a
loss percentage (%)	55 A	81 A		83 A	84 A	79 A	81 A	
flow rate 1000 mL min^{-1}	4.56 a	3.79 a	N.D.	0.27 a	1.01 a	0.55 a	9.20 a	0.03 a
loss percentage (%)	54 A	79 A		84 A	86 A	91 B	82 A	

[a]N.D.: not detectable. Statistical analysis was performed separately. Values on the same column with different letters are statistically different ($P < 0.05$).

Table 6. Representative Parameters of Original and Dealcoholized Beer Using Different Flow Rates[a]

beer brand	OG (°P)	RE (°P)	AE (°P)	EtOH (% v/v)	pH	color (EBC)	TU (EBC)	TN (mg L^{-1})	CO_2 (g L^{-1})
lager beer brand B	11.25 b	2.36 a	1.86 q	5.00 b	4.27 a	7.13 a	0.71 a	521 a	5.57 b
flow rate 500 mL min^{-1}	4.21 a	2.54 a	2.22 ab	0.93 a	4.24 a	7.77 a	1.07 b	535 b	0.13 a
flow rate 1000 mL min^{-1}	4.14 a	2.68 a	2.42 b	0.94 a	4.31 a	7.29 a	1.00 b	529 b	0.24 a

[a]Statistical analysis was performed separately. Values on the same column with different letters are statistically different ($P < 0.05$).

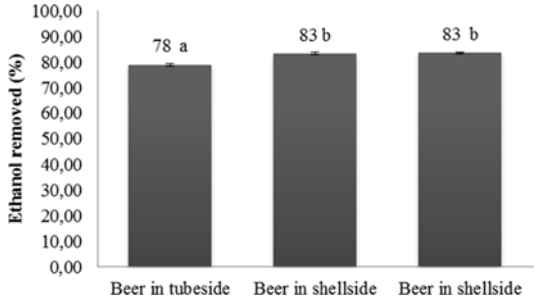

Figure 8. Percent of ethanol removed using different flowsides. Values with different superscript letters are statistically different ($P < 0.05$).

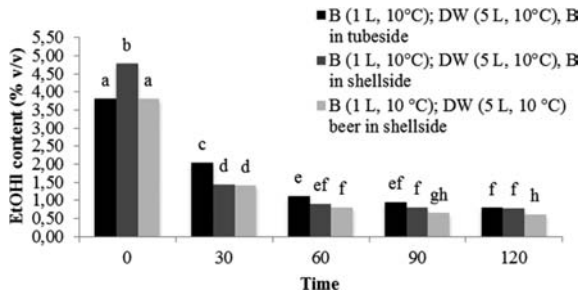

Figure 9. Decreasing ethanol during dealcoholization using different flowsides (B: beer; DW: deaerated water, CW: carbonated water). Values with different superscript letters are statistically different ($P < 0.05$).

90 min suggested that the ethanol was being removed more quickly with the beer shellside. Equilibrium may be achieved more quickly, making the process more efficient and cost-effective. With regard to the volatile compounds a larger amount of isoamyl and ethyl acetate was lost with beer in tubeside, while other compounds exhibited no significant differences (Table 7). These findings appeared to be similar to the performance of reverse osmosis when applied to dealcoholization in terms of ethanol, *n*-propanol, and esters removal (Table 8). Osmotic distillation appeared to compare favorably with vacuum distillation, which is a commonly employed dealcoholization technique and also the process with the highest ethanol and volatile compounds removal.

However, as shown in Table 8, for all dealcoholization techniques surveyed substantial losses of volatile compounds occurred, which would have had a significant effect on the flavor. However, OD compared favorably with alternative techniques such as dialysis, vacuum distillation, falling film evaporation, and reverse osmosis (Table 8).

Operating Cost Examination. A cost examination was performed in order to appraise OD as an economically viable technique. It was assumed an annual production of 100 000 hL of a low-alcohol beer with the initial ethanol content of 4.5 and a final one of 0.5% v/v. The finished plant cost (pumps, pipes, valves) emerged directly from a request for a quotation by a manufacturer, which is approximately 340 000 €, Thus, considering the plant amortization over 10 years, the annual plant cost is 34 000 €, with a cost of 0.0034 € L^{-1} of produced beer. The membrane replacement cost, assuming a membrane life of 2 years, is approximately 25 000 € per year. Membrane cost information was obtained from a private company specializing in membrane production. Finally, assuming United Kingdom industrial energy unit cost of 0.09895 € kW h^{-1}, the estimated energy cost was about 0.00021 € L^{-1} (www.energy.eu). Regarding water cost, supposing a unit water cost in United Kingdom of 1.9 € m^{-3}, the value produced is approximately 0.0114 € L^{-1}, including water required for processing and cleaning. Regarding manpower, this is always an estimate because of a wide variability across the European Member States, where the average labor cost is 23.50 € h^{-1} (Eurostat, 2013). Although membrane plants have a low requirement for supervision compared to many processes, it is important to take into account membrane maintenance, cleaning, and controlling. It could be right to consider one person per day, in this case the manpower cost would be about 50 000 € $year^{-1}$. Operating costs, investment, and membrane replacement costs could be problems that inhibit the commercialization. Improved profitability could be reached with a few process improvements such as employing sparkling and flavored water as stripping solution, thereby generating another valuable product stream.

The process settings and control was relatively simple, as well as membrane and plant cleaning. A membrane unit setup with the beer on the shellside resulted in the most efficient ethanol removal (Tables 7 and 8, Figures 8 and 9), whereas employing different temperatures and different stripping solution flow

dx.doi.org/10.1021/jf405490x | J. Agric. Food Chem. 2014, 62, 3279−3286

Table 7. Representative Volatile Compounds (mg L^{-1}) and Loss Percentage (%) of Original and Dealcoholized Beer Using Different Flowsides[a]

beer brand	AA	EA	EH	IAA	*n*-prop	2-MB	3-MB	DA
lager beer brand B	10.01 b	18.31 c	0.16	1.74 c	7.38 bc	6.66 c	52.23 c	0.02 a
beer in tubeside	4.51 a	3.99 a	N.D.	0.21 a	2.60 ab	0.51 a	7.02 a	0.02 a
loss percentage (%)	54 A	78 B		88 B	64 B	92 A	86 A	12 A
lager beer brand D	4.97 a	13.88 b	0.05	0.76 b	11.44 c	7.28 c	61.19 d	0.07 b
beer in shellside	3.49 a	3.06 a	N.D.	0.22 a	1.26 a	0.56 a	9.12 a	0.03 a
loss percentage (%)	50 A	77 B		71 A	88 C	92 A	85 A	61 B
lager beer brand E	7.61 ab	16.88 c	0.13	0.73 b	6.80 b	5.46 b	41.57 b	0.02 a
beer in shellside	3.78 a	4.39 a	N.D.	0.15 a	4.23 ab	0.46 a	6.20 a	0.02 a
loss percentage (%)	50 A	73 A		79 A	37 A	91 A	85 A	

[a]N.D.: not detectable. Statistical analysis was performed separately. Values on the same column with different letters are statistically different ($P < 0.05$).

Table 8. Aroma Compounds Loss Percentage (%) before and after Dealcoholization by Means of Falling Film Evaporation (FFE),[39] Dialysis,[40] Vacuum Distillation (VD),[41] and Reverse Osmosis (RO)[42][a]

volatile compound	dialysis	FFE	VD	RO	OD
ethanol (%)	90	89	99	91	**87**
acetaldehyde (%)	31	N.A.	60	N.A.	**54**
n-propanol (%)	94	92	100	70	**64**
iso-butanol (%)	95	95	100	66	**92**
isoamyl acetate (%)	95	25	100	89	**80**
ethyl acetate (%)	99	N.A.	100	88	**84**
total esters (%)	99	94	100	88	**85**

[a] N.A.: not analyzed.

rates did not result in improved performance. A significant decrease in the concentration of beer volatile compounds was measured after dealcoholization in all experiments, demonstrating that the volatile compounds loss is directly related to the ethanol percentage removal. This is in accordance with other studies on alcoholic beverages dealcoholization.[29,38,43−45] Furthermore, it is crucial to focus on stripping solution, which is slightly alcoholic (in this case in the range of 0.5−1% v/v) and flavored after the dealcoholization of the original beer stream. Therefore, it could be reusable in the brewing process, for instance for high gravity dilution, as brewing liquor into the mashing, sparging, or whirlpool phase, or even as a new innovative product, for example, as flavored water with a small amount of alcohol.

In this experimental work some important characteristics of the beer were not analyzed, such as the foam stability and the evaluation of flavor by trained panel, two crucial attributes and often considered weak points of low-alcohol beers. Anyway, this study was primarily proof of feasibility of the OD to produce low-alcohol beer, where the behavior of the membrane about removal of ethanol in response to the variation of process parameters was investigated. However, this data collection will be taken into account in the next step, in order to give more and more information on this method of dealcoholization.

AUTHOR INFORMATION

Corresponding Author

*Tel.: +39 075973479. E-mail: gio.defrancesco@hotmail.it.

Notes

The authors declare no competing financial interest.

ACKNOWLEDGMENTS

We gratefully acknowledge the financial support of the Italian Minister of Agriculture and the Ministry of Education, University and Research.

REFERENCES

(1) Lehnert, R.; Novak, P.; Macieira, F.; Kurec, M.; Teixeira, J. A.; Branyik, T. Optimisation of lab-scale continuous alcohol-free beer production. *Czech J. Food Sci.* **2009**, *27*, 267−275.

(2) Sohrabvandi, S.; Mortazavian, A. M.; Rezaei, K. Advanced analytical methods for the analysis of chemical and microbiological properties of beer. *J. Food Drug Anal.* **2010**, *19*, 1−21.

(3) Alcázar, Á.; Pablos, F.; Martín, M. J.; González, A. G. Multivariate characterization of beers according to their mineral content. *Talanta* **2002**, *57*, 45−52.

(4) Sohrabvandi, S. Optimization alcohol free non-alcoholic beer production produced with restricted fermentation practice, Ph.D. Thesis, University of Tehran, Iran, 2008.

(5) Bamforth, C. W. Nutritional aspects of non-alcoholic beer-A review. *Nutr. Res. (N.Y.)* **2002**, *22*, 227−237.

(6) Sohrabvandi, S.; Mousavi, S. M.; Razavi, S. H.; Mortazavian, A. M. Health-related aspects of beer: A review. *Int. J. Food Prop.* **2012**, *15*, 350−373.

(7) Sohrabvandi, S.; Mousavi, S. M.; Razavi, S. H.; Mortazavian, A. M.; Rezaei, K. Application of advanced instrumental techniques for analysis of physical and physicochemical properties of beer. *Int. J. Food Prop.* **2010**, *13*, 744−759.

(8) Bamforth, C. W. A brief history of beer. In *Proceedings of the 26th Convention of the Institute of Brewing*; Asia-Pacific, Singapore, 2002; pp 5−12.

(9) Montanari, L.; Marconi, O.; Mayer, H.; Fantozzi, P. In *Beer in health and disease prevention*. Preedy, V. R. Ed., Elsevier Inc: Burlington, MA, 2009, *114*, 61−75.

(10) Hardwick, W. A. Commercial and Economic Aspects. In *Handbook of Brewing*; Hardwick, W. A., Ed.; Marcel Dekker: New York, 1995; pp 1−35.

(11) Sohrabvandi, S.; Mousavi, S.; Razavi, S.; Mortazavian, A.; Rezaei, K. Alcohol-free beer: Methods of production, sensorial defects, and healthful effects. *Food Rev. Int.* **2010**, *26*, 335−352.

(12) Bandel, W.; Schmitz, F. J.; Ostertag, K.; Garske, F.; Breidohr, H. G. Process and apparatus for reduction of alcohol by dialysis in fermented beverages. U.S. Patent 4,664,918, 1986.

(13) Catarino, M.; Mendes, A.; Madeira, L.; Ferreira, A. Beer dealcoholization by reverse osmosis. *Desalination* **2006**, *200*, 397−399.

(14) Narziss, L.; Back, W.; Stich, S. Alcohol removal from beer by countercurrent distillation in combination with rectification. *Brauw. Int.* **1993**, *133*, 1806−1820.

(15) Wright, A.; Pyle, D. An investigation into the use of the spinning cone column for in situ ethanol removal from a yeast broth. *Process Biochem.* **1996**, *31*, 651−658.

(16) Narziss, L.; Miedaner, H.; Kern, E.; Leibhard, M. Technology and composition of non-alcoholic beers. *Brauw. Int.* **1992**, *4*, 396−410.
(17) Catarino, M. D. Production of non-alcoholic beer with reincorporation of original aroma compounds, PhD thesis, Department of Chemical Engineering University of Porto, Portugal, 2012.
(18) Perpete, P.; Collin, S. Contribution of 3-methylthiopropionaldehyde to the worty flavor of alcohol-free beers. *J. Agric. Food Chem.* **1999**, *47*, 2374−2378.
(19) Narziss, L.; Back, W. *Abriss der Bierbrauerei*; Narziss, L., Ed.; Wiley & Sons Ltd: Wenheim, Germany, 1995.
(20) Sohrabvandi, S.; Razavi, S. H.; Mousavi, S. M.; Mortazavian, A.; Rezaei, K. Application of *Saccharomyces rouxii* for the production of non-alcoholic beer. *Food Sci. Biotechnol.* **2009**, *18*, 1132−1137.
(21) Back, W. *Ausgewählte Kapitel der Brauereitechnologie*; Back, W., Ed.; Fachverlag Hans Carl: Nürnberg, Germany, 2005.
(22) Eblinger, H. M. *Handbook of Brewing*; Eblinger, H. M., Ed.; Wiley & Sons Ltd: Weinheim, Germany, 2009.
(23) Briggs, D. E.; Boulton, C. A.; Brookes, P. A.; Stevens, R. W. Chemical and physical properties of beer. In *Brewing Science and Practice*; Briggs, D. E., Boulton, C. A., Brookes, P. A., Stevens, R. W., Eds.; Woodhead Publishing Limited: Cambridge, England, 2004; pp 662−712.
(24) Dziondziak, K. Method for the production of low-alcohol or alcohol-free beer. U.S. Patent 4,814,188, 1989.
(25) Briggs, D. E.; Boulton, C. A.; Brookes, P. A.; Stevens, R. W. In *Brewing: Science and Practice*; Briggs, D. E., Boulton, C. A., Brookes, P. A., Stevens, R. W., Eds.; Woodhead Publishing Limited: Cambridge, England, 2004.
(26) Hogan, P. A.; Canning, R. P.; Peterson, P. A.; Johnson, R. A.; Michaels, A. S. A new option: Osmotic distillation. *Chem. Eng. Prog.* **1998**, *94*, 49−61.
(27) Michaels, A. S.; Canning, R. P.; Hogan, P. Methods for dealcoholization employing perstration. U.S. Patent 5,817,359, 1998.
(28) Curcio, E.; Drioli, E. Membrane distillation and related operations—A review. *Sep. Purif. Rev.* **2005**, *34*, 35−86.
(29) Fane, A. G.; Costello, M.; Hogan, P. A.; Schofield, R. W. Membrane distillation and osmotic (isothermal membrane) distillation: Factors for enhanced performance. In *Proceedings of Workshop on Membrane Distillation, Osmotic Distillation and Membrane Contactors*, Cetraro, Italy, 1998
(30) Diban, N.; Athes, V.; Bes, M.; Souchon, I. Ethanol and aroma compounds transfer study for partial dealcoholization of wine using membrane contactor. *J. Membr. Sci.* **2008**, *311*, 136−146.
(31) Gostoli, C. Thermal effects in osmotic distillation. *J. Membr. Sci.* **1999**, *163*, 75−91.
(32) Reed, B. W.; Semmens, M. J.; Cussler, E. L. Membrane contactors. In *Membrane Separation Technology Principles*; Noble, R. D., Stern, S. A., Eds.; Elsevier: Amsterdam, 1995; pp 467−498.
(33) Baker, R. W. *Membrane Technology and Applications*; John Wiley & Sons: New York, 2000; pp 405−442.
(34) Drioli, E.; Criscuoli, A. Microporous inorganic and polymeric membranes as catalytic reactors and membrane contactors. In *Membrane Science and Technology Series*; Kanellopoulos, N., Ed.; Elsevier: Amsterdam, 2000; pp 497−510.
(35) Criscuoli. A.; Curcio, E.; Drioli, E. Polymeric membrane contactors. In *Recent Research Developments in Applied Polymer Science*; Pandalai, S. G., Ed.; Transworld Research Network Publication by Research Signpost: Kerala, India, 2003; pp 1−21.
(36) Varavuth, S.; Jiraratananon, R.; Atchariyawut, S. Experimental study on dealcoholization of wine by osmotic distillation process. *Sep. Purif. Technol.* **2009**, *66*, 313−321.
(37) *Analytica-EBC*; Verlag Hans Carl: Nurnberg, Germany, 2010.
(38) Liguori, L.; Russo, P.; Albanese, D.; Di Matteo, M. Effect of process parameters on partial dealcoholization of wine by osmotic distillation. *Food Bioprocess Technol.* **2013**, *8*, 2514−2524.
(39) Zufall, C.; Wackerbauer, K. Verfahrenstechnische Parameter bei der Entalkoholisierung von Bier mittels Fallstromverdampfung und ihr Einfluss auf die Bierqualität. *Monatsschr. Brau.* **2000**, *53*, 124−137.
(40) Zufall, C.; Wackerbauer, K. Die Entalkoholisierung von Bier durch Dialyse: Verfahrenstechnische Beeinflussung der Bierqualität. *Monatsschr. Brau.* **2000**, *53*, 164−179.
(41) Zurcher, A.; Jakob, M.; Back, W. Improvements in flavor and colloidal stability of alcohol free beers. In *Proceedings of the 30th EBC Congress*, Prague, 2005.
(42) Kavanagh, T.; Clarke, B.; Gee, P.; Miles, M.; Nicholson, B. Volatile flavor compounds in low alcohol beers. *Tech. Q. Master Brew. Assoc. Am.* **1991**, *28*, 111−118.
(43) Lisanti, T. M.; Gambuti, A.; Genovese, A.; Piombino, P.; Moio, L. Partial dealcoholization of red wines by membrane contactor technique: effect on sensory characteristics and volatile composition. *Food Bioprocess Technol.* **2013**, *6*, 2289−2305.
(44) Liguori, L.; Russo, P.; Albanese, D.; Di Matteo, M. Evolution of quality parameters during red wine dealcoholization by osmotic distillation. *Food Chem.* **2013**, *140*, 68−75.
(45) Diban, N.; Arruti, A.; Barceló, A.; Puxeu, M.; Urtiaga, A.; Ortiz, I. Membrane dealcoholization of different wine varieties reducing aroma losses. Modeling and experimental validation. *Innov. Food Sci. Emerg. Technol.* **2013**, *20*, 259−268.

Table 1. Selective Synthesis of Methyl D-Glucopyranoside (2) and Methyl D-Glucofuranoside (3) Using the TCT/DMSO/MeOH System[a]

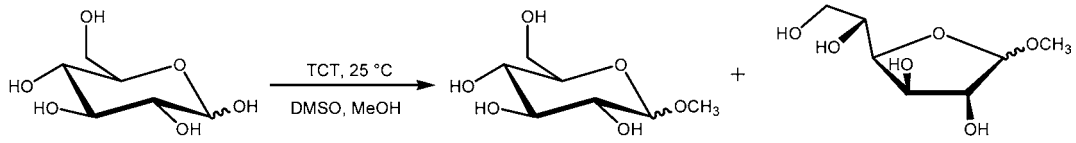

1 2 3

entry	TCT (equiv)	DMSO (equiv)	MeOH (mL)	DMSO (equiv/mL)	yield[b] (%)	product ratio[c] (2:3) (2α:2β:3α:3β)
1	1.5	34	2	17	90	100:0 52:48:0:0
2	2.0	34	2	17	92	100:0 53:47:0:0
3	1.5	25.5	3	8.5	88	100:0 51:49:0:0
4	2.0	25.5	3	8.5	97	100:0 53:47:0:0
5	1.5	17	4	4.3	96	78:22 43:35:13:9
6	2.0	17	4	4.3	97	84:16 44:40:4:12
7	1.5	8.5	5	1.7	96	57:43 31:26:13:30
8	2.0	8.5	5	1.7	97	58:42 30:28:13:29
9	1.5	1.5	15	0.1	97	0:100 0:0:62:38
10	2.0	1.5	15	0.1	98	0:100 0:0:43:57

[a] D-Glucose (300 mg), TCT (1.5 or 2.0 equiv), DMSO (1.5, 8.5, 17, 25.5, or 34 equiv), MeOH (2, 3, 4, 5, or 15 mL), 0.5 h (entries 9 and 10) or 6 h (entries 1−8), 25 °C. [b] Isolated yield. [c] Determined by ^{13}C NMR analysis.

quantitative yield, and the α and β isomers were about equally formed (Table 1, entries 1−4). Reducing the concentrations of DMSO to 4.3 or 1.7 equiv/mL resulted in an increase in the amounts of furanoside **3** to 22, 16, 43, or 42% (Table 1, entries 5−8). Further decreasing the concentration of DMSO to 0.1 equiv/mL led to the formation of furanoside in nearly quantitative yields (Table 1, entries 9 and 10). When the amount of TCT was changed from 1.5 to 2.0 equiv, the α/β ratio changed from 62:38 to 43:57. The reaction time for the pyranoside was 6 h, and that for furanoside was 0.5 h.

After the above optimization, the yields for both methyl D-glucopyranoside **2** and D-glucofuranoside **3** were nearly quantitative. The reaction yield of acetone and sugar for 1,2:5,6-di-isopropylidene-α-D-glucofuranose is >90%. For the other currently used preparation methods, the highest reported yields for D-glucofuranoside are all <80%,[7,11,20] and these products have to be separated from their isomer glucopyranoside (produced in >20% yield). The reason that **2** and **3** can be separately synthesized as the sole product with this method is probably because methanol is more polar than DMSO, and presumably when the concentration of DMSO in methanol is lower, the reaction medium is more polar and the D-glucose exists in the furanose form. In contrast, when the concentration of DMSO is higher, D-glucose exists in the pyranose form.

To validate this assumption, ^{13}C NMR analysis of the D-glucose in 3, 17, and 170 equiv of DMSO-d_6 in CD_3OD was performed. With 170 equiv of DMSO-d_6, the ^{13}C NMR spectrum revealed two hemiacetal isomers in a 13:87 ratio (Table 2, entry 2). After the addition of 0.1 equiv of TCT, only α-D-glucopyranose existed. No detectable amounts of methyl glucoside were formed within 15 min (Table 2, entry 3). With 3 equiv of DMSO-d_6, the ^{13}C NMR spectrum showed two hemiacetal isomers in a 10:90 ratio (Table 2, entry 4). Five minutes after the addition of 0.1 equiv of TCT, there were two isomers and methyl α-D-glucofuranoside in a 7:59:34 ratio (methyl α-D-glucofuranoside, β-D-glucopyranose, α-D-glucopyranose; Table 2, entry 5). This agrees with the fact that the formation rate of furanoside is higher than that of pyranoside.[1,21] With 17 equiv of DMSO-d_6, the ^{13}C NMR spectrum indicated the existence of four hemiacetal isomers in a 3:8:31:58 ratio

Table 2. ^{13}C NMR Analysis of D-Glucose Isomers at Difference Concentration of DMSO-d_6 in CD_3OD at 25 °C

entry	concn[a]	no. of major isomers	C_1 (ppm) (ratio)
1	340	2	92.15, 92.05 (38:62)
2	170	1	92.12, 92.02 (13:87)
3	170 + TCT[b]	1	92.04
4	3	1	95.51, 91.25 (10:90)
5	3 + TCT[b]	2	99.49, 91.27, 91.23 (7:59:34)[c]
6	1.5	1	94.00
7	17	2	95.56, 95.48, 91.31, 91.32 (3:8:31:58)[d]
8	17 + TCT[b]	2	95.48, 91.24 (53:47)

[a]Concn, concentration of DMSO-d_6 in CD_3OD (equiv/mL). [b]TCT = 0.1 equiv. [c]Methyl α-D-glucofuranoside:β-D-glucopyranose:α-D-glucopyranose. [d]β-D-Glucofuranose:α-D-glucofuranose:β-D-glucopyranose:α-D-glucopyranose.

(β-D-glucofuranose, α-D-glucofuranose, β-D-glucopyranose, α-D-glucopyranose; Table 2, entry 7). These are probably the four possible isomers of D-glucose. Five minutes after the addition of 0.1 equiv of TCT, there are two major isomers in a 53:47 ratio (Table 2, entry 8). This is in agreement with the fact that methyl pyranoside and furanoside were formed in roughly the same amounts (Table 1, entries 7 and 8). The isomer numbers indicated by the ^{13}C NMR analysis with 170, 17, and 3 equiv of DMSO-d_6 correlate well with the major product numbers from Table 1, entries 1, 2, and 7−10. Further increasing the concentration of DMSO-d_6 in CD_3OD to 340 equiv exhibited ^{13}C NMR signals of two isomers and decreasing that to 1.5 equiv exhibited ^{13}C NMR signals of one isomer. This again indicates that the equilibrium between pyranose and furanose is related to the solvent ratio (Table 2, entries 1 and 6). A literature survey indicates that the NMR analysis of D-glucopyranose could be performed in D_2O,[22−26] dioxane-d_8,[27] and DMSO-d_6[28] and that for D-glucofuranose in D_2O.[29,30] It is known that D-glucopyranose is dominant in aqueous solution.[31,32]

To further verify the assumption that the ratio of pyranose to furanose is controlled by the polarities of the solvents, other alcohols were used in place of methanol as the solvent. For the ethylation of glucose, 8.5, 17, and 25.5 equiv of DMSO in EtOH were used as 0.1equiv of DMSO in EtOH resulted in a poor yield. As expected, the D-glucopyranosides of the other alcohols were readily obtained as the sole product (Table 3, entries 1−12). However, the D-glucofuranosides could not be synthesized as the sole product. The proportions of the D-glucofuranosides decreased from 10 to 0% as the acceptor alcohols increased in carbon number from ethanol to *n*-pentanol with 1.7 equiv of DMSO (Table 3, entries 3, 6, 9, and 12). These results indicate that the solvent polarity is critical to the ratio of furanoside and pyranoside because all of these higher alcohols are less polar than methanol. Alkyl furanosides have been synthesized as the major products in solvents less polar than methanol, which has been attributed to metal complexions with the sugars because these glycosylation are often catalyzed by metal salts.[20]

A plausible mechanism for the synthesis of methyl D-glucofuranoside is shown in Figure 1. First, the reaction of DMSO with TCT leads to **I**, which is attacked by the C-1 hydroxyl group of D-glucofuranose to form **II**. Because DMSO is a good leaving group, the DMSO group may then be replaced by MeOH to form methyl D-glucofuranoside via an S_N2 mechanism. Another possibility is the formation of carbocation **III** from **II** and the attack of MeOH on the C-1 leading to methyl D-glucofuranoside via an S_N1 mechanism. Because only the C-1 carbon has a methoxy substituent, carbocation **III** pathway is more likely. A similar mechanism is applicable to the formation of methyl D-glucopyranose.

The reaction conditions developed here were then applied to other carbohydrates, and the results are shown in Table 4. When D-fructose was treated with TCT (2.0 equiv) in 8.5 equiv/mL of DMSO in MeOH, no products formed after 6 h (Table 4, entry 1). Reducing the amount of DMSO to 0.1 equiv/mL (Table 4, entry 2) yielded a mixture of methyl D-fructopyranoside **6a** and methyl D-fructofuranoside **6b** (**6a**:**6b** = 73:27, Table 4, entry 2) in 82% yield. Increasing the reaction time from 6 to 24 h gave a higher yield (96%) and a similar product mixture (**6a**:**6b** = 68:32, Table 4, entry 3). When the concentration of DMSO was reduced to 0.07 equiv/mL, furanoside **6b** became the major product (Table 4, entry 4). In these experiments, neither furanoside nor pyranoside could be produced as the sole product, but each could be produced as the major product by adjusting the concentration of DMSO in MeOH. The literature reports three methods for the preparation of methyl D-fructosides: an I_2/MeOH method (unspecified ratio of furanoside and pyranoside, 3 h, 61.5% yield),[12] a TsOH/MeOH method (furanoside, 12 h, 80% yield),[33] and an AcCl/MeOH method (furanoside:pyranoside = 3:1, 16 h, 92% yield).[34] Our results compare favorably with these results in terms of yields and furanoside and pyranoside selectivities.

D-Mannose could not be transformed into the furanoside even by changing the concentration of DMSO from 4.3 to 0.07 equiv/mL (Table 4, entries 5−7). This is probably because it has a C-2 axial OH and the MeOH/DMSO system cannot stabilize the D-mannofuranose. Methyl α-D-mannopyranoside was the major product in 91% yield with 0.1 equiv/mL of DMSO in MeOH and TCT (2.0 equiv) (Table 4, entry 7). This result is better than previously reported methods: HCl/MeOH (pyranoside, 2 h, 70% yield)[35] and Amberlite IRA-120/MeOH (pyranoside, 10 min, 74% yield).[36]

Treating D-arabinose with TCT (2.0 equiv) and 8.5 equiv/mL of DMSO led to only a 40% yield of pyranoside and furanoside (**8a**:**8b** = 90:10, Table 4, entry 8). When the reactions of D-arabinose with 0.1 or 0.07 equiv/mL of DMSO in MeOH were quenched after 1 h, furanoside was the major product in 73 and 97% yields, respectively (Table 4, entries 9 and 11). The pyranoside was the major product (80:20) when the reaction time was increased from 1 to 24 h (Table 4, entry 10). This method is better than the current methods in terms of yield and reaction rates. These current methods are 1% HCl/MeOH/Ag_2CO_3 (pyranoside, 24 h, no yield reported),[37] Amberlite IRA-120/MeOH (pyranoside, 12 h, 37% yield),[38] and 0.18N HCl/MeOH (furanoside, 5.5 h, 79% yield).[39]

Treating D-xylose with different concentrations of DMSO in MeOH and TCT (2.0 equiv) led to a selective synthesis of methyl D-xylofuranoside (Table 4, entries 12−15). With 8.5 equiv/mL of DMSO in MeOH, the yield was poor (Table 4, entry 12). Lowering the concentration of DMSO (0.07 equiv, Table 4, entry 13) and increasing the reaction time (24 h,

Table 3. Synthesis of Alkyl D-Glucosides Using Different TCT/DMSO/ROH Systems[a]

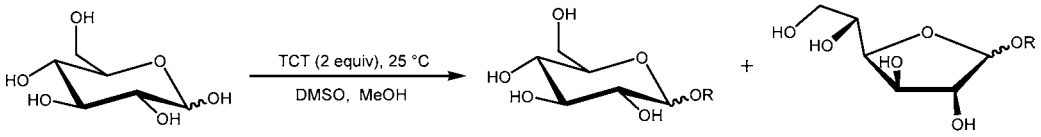

1 4 5

entry	alcohol	DMSO (equiv)	ROH (mL)	DMSO (equiv/mL)	yield[b] (%)	product ratio[c] (4:5) (4α:4β:5α:5β)
1	C_2H_5OH	25.5	3	8.5	88	100:0 44:56:0:0
2	C_2H_5OH	17	4	4.3	96	95:5 43:52:0:5
3	C_2H_5OH	8.5	5	1.7	97	90:10 43:47:0:10
4	*n*-C_3H_7OH	25.5	3	8.5	78	100:0 54:46:0:0
5	*n*-C_3H_7OH	17	4	4.3	86	90:10 32:58:2:8
6	*n*-C_3H_7OH	8.5	5	1.7	95	91:9 36:55:0:9
7	*n*-C_4H_9OH	25.5	3	8.5	77	100:0 41:59:0:0
8	*n*-C_4H_9OH	17	4	4.3	79	96:4 45:51:0:4
9	*n*-C_4H_9OH	8.5	5	1.7	94	98:2 43:55:0:2
10	*n*-$C_5H_{11}OH$	25.5	3	8.5	72	100:0 45:55:0:0
11	*n*-$C_5H_{11}OH$	17	4	4.3	74	100:0 44:56:0:0
12	*n*-$C_5H_{11}OH$	8.5	5	1.7	83	100:0 46:54:0:0

[a]D-Glucose (300 mg), TCT (2.0 equiv), DMSO (8.5, 17, or 25.5 equiv), MeOH (3, 4, or 5 mL), 6 h, 25 °C. [b]Isolated yield. [c]Determined by ^{13}C NMR analysis.

Table 4, entry 14) improved the yield to >80%. The optimized conditions were 0.1 equiv of DMSO in MeOH, 2.0 equiv of TCT in 1 h, and the furanoside was selectively synthesized in 93% total yield (pyranoside/furanoside = 7:93, Table 4, entry 15). The reaction rate of this reaction is higher than that of the known methods. The known methods are MeOH/HCl/$CaCO_3$ (furanoside, 12 h, quantitative),[40] Amberlite IRA-120/MeOH (pyranoside, 12 h, 53% yield),[38] and montmorillonite K-10 (pyranoside, 10 min, 87% yield).[41]

Methyl D-galactofuranoside could be obtained in 85% yield and methyl D-galactopyranoside in 80% yield by reacting D-galactose with TCT (2.0 equiv) and 0.1 or 8.5 equiv/mL of DMSO in MeOH (Table 4, entries 16 and 17). It is clear that the ratio of pyranoside to furanoside is controlled by the solvent polarities as in the case of methyl D-glucoside synthesis. In the above selective synthesis of methyl D-galactofuranoside, the ratio of furanoside to pyranoside was 93:7 in the crude product. The reported yields of methyl D-galactopyranoside synthesized using microwave irradiation are 100%[42] and 84%.[41] Two methods for the synthesis of methyl D-galactofuranoside as a major product catalyzed by $FeCl_3$ (furanoside:pyranoside = 75:20)[20] and in 75% yield are known.[12] Our method has better selectivity for furanoside.

In summary, a highly selective method to synthesize methyl D-glucofuranoside or pyranoside as the sole product via tuning the polarity of the solvent has been developed. The effect of the solvent polarity on the isomerization of D-glucose is supported by ^{13}C NMR analysis. Most of the reaction yields and rates for the production of methyl glycosides from D-mannose, D-fructose, D-arabinose, D-xylose, and D-galactose using the DMSO/MeOH/TCT

dx.doi.org/10.1021/jf500144b | J. Agric. Food Chem. 2014, 62, 3287−3292

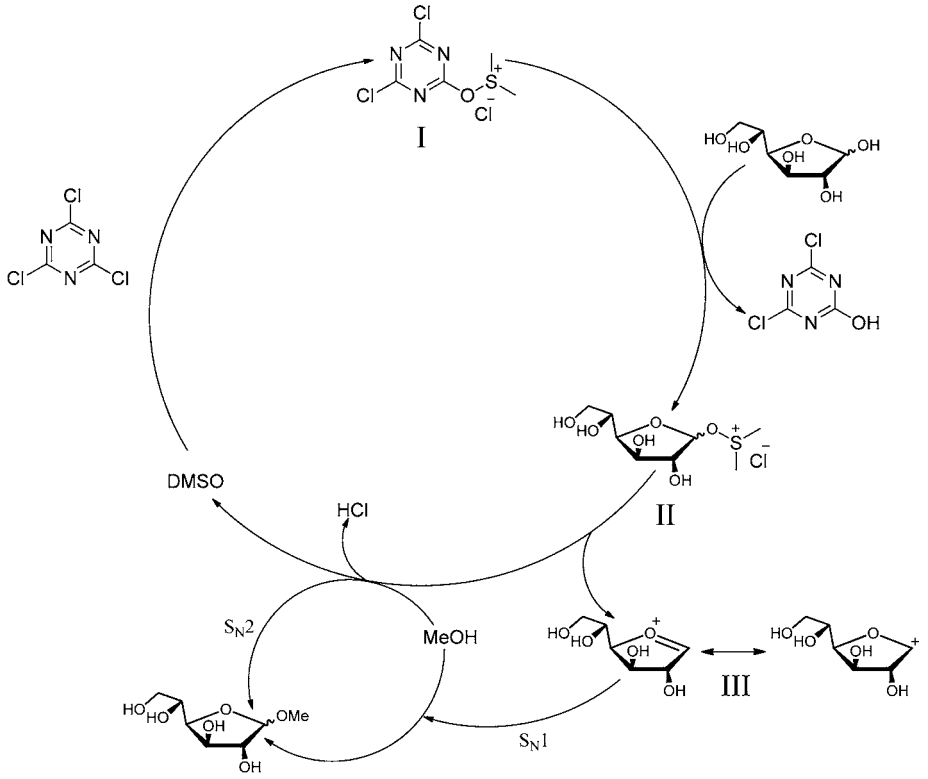

Figure 1. Plausible mechanism for the synthesis of methyl D-glucofuranoside using the TCT/DMSO/MeOH system.

Table 4. Applications of the TCT/DMSO/MeOH System to Other Monosaccharides[a]

entry	substrate	time (h)	DMSO (equiv)	MeOH (mL)	DMSO (equiv/mL)	yield[b] (product ratio[c])
1	D-fructose	6	25.5	3	8.5	0
2	D-fructose	6	1	10	0.1	82% (**6a**[d]:**6b**[e] = 73:27)
3	D-fructose	24	1	10	0.1	96% (**6a**[d]:**6b**[e] = 68:32)
4	D-fructose	3	1	15	0.07	87% (**6a**[d]:**6b**[e] = 28:72)
5	D-mannose	6	17	4	4.3	60% (**7a**)[f]
6	D-mannose	6	1	15	0.07	68% (**7a**)[f]
7	D-mannose	6	1	10	0.1	91% (**7a**)[f]
8	D-arabinose	1	25.5	3	8.5	40% (**8a**[g]:**8b**[h] = 90:10)
9	D-arabinose	1	1	10	0.1	73% (**8a**[g]:**8b**[h] = 8:92)
10	D-arabinose	24	1	10	0.1	98% (**8a**[g]:**8b**[h] = 80:20)
11	D-arabinose	1	1	15	0.07	97% (**8a**[g]:**8b**[h] = 6:94)
12	D-xylose	1	25.5	3	8.5	46% (**9a**[i]:**9b**[j] = 32:68)
13	D-xylose	1	1	15	0.07	83% (**9a**[i]:**9b**[j] = 17:83)
14	D-xylose	24	1	10	0.1	87% (**9a**[i]:**9b**[j] = 13:87)
15	D-xylose	1	1	10	0.1	93% (**9a**[i]:**9b**[j] = 7:93)
16	D-galactose	6	25.5	3	8.5	80% (**10b**)[l]
17	D-galactose	3	1	15	0.07	85% (**10a**[k]:**10b**[l] = 7:93)

[a]Sugar (300 mg), TCT (2.0 equiv), DMSO (1, 17, or 25.5 equiv), MeOH (3, 4, 10, or 15 mL), 1 h (entries 8, 9, 11−13, and 15), 3 h (entries 4 and 17), 6 h (entries 1, 2, 5−7, and 16), or 24 h (entries 3, 10, and 14), 25 °C. [b]Isolated yield. [c]Determined by ^{13}C NMR analysis. [d]**6a** = methyl D-fructopyranoside. [e]**6b** = methyl D-fructofuranoside. [f]**7a** = methyl α-D-mannopyranoside. [g]**8a** = methyl D-arabinopyranoside. [h]**8b** = methyl D-arabinofuranoside. [i]**9a** = methyl D-xylopyranoside. [j]**9b** = methyl D-xylofuranoside. [k]**10a** = methyl D-galactopyranoside. [l]**10b** = methyl D-galactofuranoside.

system are better than the currently used methods. This is a rapid, convenient, and high-yielding procedure.

■ ASSOCIATED CONTENT

Ⓢ Supporting Information

Glycosylation procedures of six sugars and ^{13}C NMR spectra of D-glucose at different concentrations of DMSO-d_6 in CD_3OD at 25 °C. This material is available free of charge via the Internet at http://pubs.acs.org.

■ AUTHOR INFORMATION

Corresponding Author

*(C.L.) Phone: +86-022-27892351. Fax: +86-022-27403475. E-mail: lichunbao@tju.edu.cn.

Author Contributions

[‖]Z.S. and L.S. contributed equally to this work.

Notes

The authors declare no competing financial interest.

REFERENCES

(1) Collins, P.; Ferrier, R. Reactions and products of reaction at the anomeric centre. In *Monosaccharides: Their Chemistry and Their Roles in Natural Products*; Wiley: New York, 1995; pp 61−97.

(2) Daniel, J. R.; Whistler, R. Sweetness−structure correlation in carbohydrates. *Cereal Chem.* **1982**, *59*, 92−95.

(3) Fischer, E. H. Alkyl derivatives of benzoin. *Ber. Dtsch. Chem. Ges.* **1893**, *26*, 2400−2412.

(4) Fischer, E. H.; Beensch, L. Synthetic glucosides. *Ber. Dtsch. Chem. Ges.* **1894**, *27*, 2478−2486.

(5) Fischer, E. H. Sugar derivatives of alcohols and ketones. *Ber. Dtsch. Chem. Ges.* **1895**, *28*, 1145−1167.

(6) Capon, B. Mechanism in carbohydrate chemistry. *Chem. Rev.* **1969**, *69*, 407−498.

(7) Kohn, P.; Samaritano, R. H.; Lerner, L. M. A new method for the synthesis of furanose derivatives of aldohexoses. *J. Am. Chem. Soc.* **1965**, *87*, 5469−5472.

(8) Green, J. W.; Pacsu, E. Glucofuranosides and thioglucofuranosides. III. New crystalline furanosides of D-galactose and L-arabinose. *J. Am. Chem. Soc.* **1938**, *60*, 2056−2057.

(9) McAuliffe, J. C.; Hindsgaul, O. Use of acyclic glycosyl donors for furanoside synthesis. *J. Org. Chem.* **1997**, *62*, 1234−1239.

(10) Dahlhoff, W.; Fenzl, W.; Koster, R. Selective syntheses of the methyl α-D-furanosides of lyxose and mannose using ethyl (dimethoxy) borane. *Liebigs Ann. Chem.* **1990**, *8*, 807−810.

(11) Verhart, C. G.; Fransen, C. T.; Zwanenburg, B.; Chittenden, G. J. Reaction of D-fructose, D-glucose and inulin with alcohols in the presence of iodine; a novel glycosidation procedure. *Recl. Trav. Chim. Pays-Bas* **1996**, *115*, 133−139.

(12) Lubineau, A.; Fischer, J. C. High-yielding one-step conversion of D-glucose and D-galactose to the corresponding methyl α- and β-glucofuranosides and galactofuranosides. *Synth. Commun.* **1991**, *21*, 815−818.

(13) Euzen, R.; Ferrieres, V.; Plusquellec, D. Synthesis of galactofuranose-containing disaccharides using thioimidoyl-type donors. *Carbohydr. Res.* **2006**, *341*, 2759−2768.

(14) Ferrieres, V.; Blanchard, S.; Fischer, D.; Plusquellec, D. A novel synthesis of D-galactofuranosyl, D-glucofuranosyl and D-mannofuranosyl L-phosphates based on remote activation of new and free hexofuranosyl donors. *Bioorg. Med. Chem. Lett.* **2002**, *12*, 3515−3518.

(15) Ferrieres, V.; Roussel, M.; Gelin, M.; Plusquellec, D. A new approach to a disaccharidic hapten containing a galactofuranosyl entity. *J. Carbohydr. Chem.* **2001**, *20*, 855−865.

(16) Ferrieres, V.; Bertho, J. N.; Plusquellec, D. A new synthesis of O-glycosides from totally O-unprotected glycosyl donors. *Tetrahedron Lett.* **1995**, *36*, 2749−2752.

(17) Roslund, M. U.; Tahtinen, P.; Niemitz, M.; Sjoholm, R. Complete assignments of the ^{1}H and ^{13}C chemical shifts and $J_{H,H}$ coupling constants in NMR spectra of D-glucopyranose and all D-glucopyranosyl-D-glucopyranosides. *Carbohydr. Res.* **2008**, *343*, 101−112.

(18) Sun, L.; Peng, G.; Niu, H.; Wang, Q.; Li, C. A highly chemoselective and rapid chlorination of benzyl alcohols under neutral conditions. *Synthesis* **2008**, *24*, 3919−3924.

(19) Sun, L.; Guo, Y.; Peng, G.; Li, C. Chemoselective etherification of benzyl alcohols using 2,4,6-trichloro-1,3,5-triazine and methanol or ethanol catalyzed by dimethyl sulfoxide. *Synthesis* **2008**, *21*, 3487−3491.

(20) Santra, S.; Jonas, E.; Bourgault, J. P.; El-Baba, T.; Andreana, P. R. Kinetic products under thermal conditions: rapid entry into α/β-D-galactofuranosides using microwave irradiation and selective lewis acids. *J. Carbohydr.Chem.* **2011**, *30*, 27−40.

(21) Bishop, C. T.; Cooper, F. P. Glycosidation of sugars. *Can. J. Chem.* **1962**, *40*, 224−232.

(22) Liu, Z.; Qian, Y.; Tang, K.; Wang, C.; Wang, D.; Wang, L.; Zhu, Y.; Wang, C. A new carbon intercalated compound of Dion-Jacobson phase HLaNb $_2$O$_7$. *J. Mater. Chem.* **2012**, *22*, 11086−11092.

(23) Bera, M.; Curtiss, A.; Musie, G. T.; Powell, D. R. New dinuclear cobalt(II) and zinc(II) complexes of a carboxylate-rich dinucleating ligand: synthesis, structure, spectroscopic characterization, and their interactions with sugars. *Inorg. Chem.* **2012**, *51*, 12093−12101.

(24) Izumikawa, M.; Takagi, M.; Shin-Ya, K. Isolation of a novel macrocyclic dilactone JBIR-101 from *Promicromonospora* sp. RL26. *J. Antibiot.* **2011**, *64*, 689−691.

(25) Lambert, J. B.; Lu, G.; Singer, S. R.; Kolb, V. M. Silicate complexes of sugars in aqueous solution. *J. Am. Chem. Soc.* **2004**, *126*, 9611−9625.

(26) Chen, A.; Johnson, J.; Charles, S.; Wu, D. Heteronuclear-detected diffusion-ordered NMR spectroscopy through coherence transfer. *J. Magn. Reson.* **1996**, *123*, 215−218.

(27) Silvestre, V.; Goupry, S.; Akoka, S.; Trierweiler, M.; Robins, R. Determination of substrate and product concentrations in lactic acid bacterial fermentations by proton NMR using the ERETIC method. *Anal. Chem.* **2001**, *73*, 1862−1868.

(28) Han, X.; Jiang, F.; Liu, X.; Ma, D.; Zhu, Q.; Ma, D. Direct conversion and NMR observation of cellulose to glucose and 5-hydroxymethylfurfural (HMF) catalyzed by the acidic ionic liquids. *J. Mol. Catal.* **2011**, *334*, 8−12.

(29) Berg, R.; Peters, J. A.; Bekkum, H. The structure and (local) stability constants of borate esters of mono- and di-saccharides as studied by ^{11}B and ^{13}C NMR spectroscopy. *Carbohydr. Res.* **1994**, *253*, 1−12.

(30) Williams, C.; Allerhand, A. Detection of β-D-glucofuranose in aqueous solutions of D-glucose. *Carbohydr. Res.* **1977**, *56*, 173−179.

(31) Angyal, S. J. The composition of reducing sugars in solution. *Adv. Carbohydr. Chem. Biochem.* **1984**, *42*, 15.

(32) Angyal, S. J. The composition of reducing sugars in solution: current aspects. *Adv. Carbohydr. Chem. Biochem.* **1991**, *49*, 19.

(33) Yu, K.; Zhao, X.; Wu, W.; Hong, Z. An efficient procedure for synthesis of fructose derivatives. *Tetrahedron Lett.* **2013**, *54*, 2788−2790.

(34) Grice, I. D.; Whelan, C.; Tredwell, G. D.; Itzstein, M. An approach towards the synthesis of sialyl nucleoside mimetics. *Tetrahedron: Asymmetry* **2005**, *16*, 1425−1434.

(35) Nandi, A.; Chattopadhyay, P. Synthesis of chiral trans-fused pyrano[3,2-*c*][2]benzoxocines from D-mannose by regioselective 8-endo-aryl radical cyclization. *Tetrahedron Lett.* **2002**, *43*, 5977−5980.

(36) Bornaghi, L. F.; Poulsen, S. A. Microwave-accelerated Fischer glycosylation. *Tetrahedron Lett.* **2005**, *46*, 3485−3488.

(37) Lucero, C. G.; Woerpel, K. A. Stereoselective C-glycosylation reactions of pyranoses: the conformational preference and reactions of the mannosyl cation. *J. Org. Chem.* **2006**, *71*, 2641−2647.

(38) McGeary, R. P.; Amini, S. R.; Tang, V. W. S.; Toth, I. Nucleophilic substitution reactions of pyranose polytosylates. *J. Org. Chem.* **2004**, *69*, 2727−2730.

(39) Mikhailopulo, I. A.; Sivets, G. G. A novel route for the synthesis of deoxy fluoro sugars and nucleosides. *Helv. Chim. Acta* **1999**, *82*, 2052−2065.

(40) Goumain, S.; Taghzouti, H.; Portella, C.; Behr, J. B.; Plantier-Royon, R. Convenient strategy for the synthesis of highly functionalizable hydroxylated unsaturated azepanes. *Tetrahedron Lett.* **2012**, *53*, 4440−4443.

(41) Bordoloi, M. Montmorillonite k-10 as a reusable catalyst for Fischer type of glycosylation under microwave irradiation. *J. Carbohydr. Chem.* **2008**, *27*, 300−308.

(42) Nuchter, M.; Ondruschka, B.; Lautenschlager, W. Microwave-assisted synthesis of alkyl glycosides. *Synth. Commun.* **2001**, *31*, 1277−1283.

less sensitive to conformational changes; thus, enzyme activity under drastic conditions may become higher than that of the free enzyme.[10,11] With these improvements, the immobilized form of *Thermomyces lanuginosus* (TL IM) was more popular in modification of fats and oils. Palm stearin (PS) is an excellent alternative for the production of plastic fats with addition of other vegetable oils because of its solid fat content (SFC) and ability to promote β' crystallization. [12]

The main objective of this paper is modification ASO and PS catalyzed by TL IM to produce desirable low-*trans* plastic fats as an alternative for plastic fats. After interesterification, the properties of produced fats [fatty acid profile, slip melting point (SMP), solid fat content (SFC), polymorphic form, and microstructure et al.] were characterized by gas chromatography (GC), differential scanning calorimetry (DSC), X-ray diffractometry (XRD), and confocal laser scanning microscopy. Also, the *sn*-2 positional fatty acid compositions were determined to check the occurrence of acyl migration side reaction.

EXPERIMENTAL PROCEDURES

Reagents and Materials. PS (SMP, 53.0 °C) was purchased from Fengyi Biotechnology Co., Ltd. (Shanghai, China). ASO were supplied by Jiujiang Regression Biotechnology Development Co., Ltd. (Jiangxi, Jiujiang, China). TL IM from *Thermomyces lanuginosus* was purchased from Novozymes A/S (Bagsvaerd, Denmark) and stored at −18 °C until use according the recommendation. The specific activity of Lipozyme TL IM, which is immobilized on silica gel, was 181 IU/g, having 0.54 g/mL bulk density, and 0.3 to 1.0 mm particle diameter. Standards of fatty acid methyl esters (FAME) (GLC-463) were purchased from Nu-Chek Prep Inc. (Elysian, MN, U.S.A.). All other chemicals used were of either HPLC or analytical reagent grade.

Interesterification. In the preliminary experiment, the interesterification conditions of PS and ASO for producing plastic fats have been screened out. Finally, PS and ASO at ratios of 70:30, 65:35, and 60:40 were successfully achieved to produce plastic fats at 60 °C for 6 h using 10% (wt) of Lipozyme TL IM as a catalyst. The react conditions of Lipozyme TL IM catalyzed interesterification were consistent to our previous reports.[13,14] In order to determine the qualities of produced plastic fats, scale-up experiments were conducted. A total of 50 g of substrate PS and ASO at ratios of 70:30, 65:35, and 60:40 were placed in 250 mL Erlenmeyer flasks with a screw cap. The melted blends were reacted with Lipozyme TL IM (10 wt % of total substrates) in a shaking water bath at 60 °C; the mixing speed was set at 220 rpm. After the reaction, TL IM was separated from the mixtures by filtering. To remove free fatty acids, the same volume of hexane and five drops of phenolphthalein solution were added to the interesterified products (IPs). The mixture was titrated with 0.5 mol/L KOH solution in 95% ethanol until a pink color appeared. IPs were washed with warm water until the pink color disappeared. The upper layer was passed through an anhydrous sodium sulfate column to remove moisture, and the solvent was completely evaporated under nitrogen with moderate heat.

Fatty Acid Composition Analysis. Samples were methylated according to the procedures described by Zhu et al.[15] with slight modification. The fats were placed in a 20 mL tube with a screw cap, saponified by 0.5 mol/L methanolic NaOH, and then methylated by boron trifluoride in methanol (14%). FAMEs were analyzed by GC using an Agilent 6890N gas chromatograph (Santa Clara, CA, U.S.A.) equipped with a flame ionization detector, an autoinjector, and a fused silica capillary column (CP-Sil 88, 100 m × 0.25 mm × 0.2 μm i.d.). The oven was heated to 45 °C and then held at this temperature for 3 min. The temperature was then increased to 175 °C at a rate of 13 °C/min and was held for 27 min. This temperature was finally increased to 215 °C at a rate of 4 °C/min and then held for 35 min. The temperature of the injector and detector were set to 250 and 260 °C, respectively. Nitrogen was used as a carrier gas at a flow rate of 52 mL/min in split mode (50:1). Fatty acid compositions were identified by comparison with the retention times of standard mixtures. Analyses were performed in triplicate.

Fatty Acid Composition at *Sn*-2 Position. *Sn*-2 positional distribution was determined by partial hydrolysis using pancreatic lipase.[15] Ten milligrams of IPs or physical blends (PBs) was dissolved in 10 mL of Tris−HCl buffer (1 mol/L, pH = 7.6), 2.5 mL of 0.05% bile salt, and 1 mL of 2.2% calcium chloride solution; 10 mg of pancreatic lipase was subsequently added to this mixture. The mixture was vortexed for at least 1 min and then placed in a water bath at 37 °C for 3 min; vortexing for 30 s followed. Four milliliters of diethyl ether was added to the mixture to extract the hydrolytic product. The upper layer was dried using a sodium sulfate column. After blowing up by nitrogen gas, applied to a thin-layer chromatography (TLC) plate (Merck KGaA, Darmstsdt, Germany) coated with silica gel G and developed with a solvent mixture comprising diethyl ether/hexane/acetic acid (50:50:1, V/V/V). The plate was air-dried for 30 min and then visualized by spraying with iodine vapor. The band corresponding to the monoacylglycerol was scrapped off, methylated, and analyzed by GC as described above. Analyses were performed in triplicate.

Analysis of TAG by RP-HPLC. The Agilent 1100 HPLC system consisted of quadruples pump with an evaporative light-scattering detector (All-tech 2000ES, U.S.A.) operating at 55 °C and a nitrogen pressure of 1.7 bar. Each sample was dissolved in hexane and 10 μL of the dissolved sample were injected and separated by the Novo-Pak C18 colomn (150 × 3.9 mm, waters, Milford, MA, U.S.A.). Elution solvent consisted of (A) acetonnitrile and B isopropanol:hexane (1:1, v/v) at the flow rate of 1.8 mL/min. [15]

Determination of SMP. The SMP of the mixture was determined according to American Oil Chemists' Society Official Method No. *Cc* 3-25 (2009)[16] using the open tube melting point method. Capillary tubes filled with a 1-cm-high column of fat were stored in a refrigerator at 10 ± 1 °C for 16 h prior to measurement in a beaker of cold water. The water was stirred and heated gradually. The temperature at which the fat in the tube began to rise because of hydrostatic pressure was recorded. This temperature was considered the SMP and determined in triplicate.

X-ray Diffraction Spectroscopy. The polymorphic forms of fat crystals in the blends were determined by Empyrean XRD (PANalytical B.V., Almelo, Netherlands) using Cu Kα radiation (voltage of 40 kV; current of 35 mA; divergence, antiscatter, and receiving slits, fixed at 0.5°, 1°, and 8 mm, respectively). The samples were melted at 70 °C, poured into a rectangular plastic mold, and tempered at 24 °C for 16 h. The short spacing was scanned at 2θ ranging from 16° to 32° at a rate of 0.01°/80 s.[15] The α polymorph was identified by a short spacing of 4.15 Å. β' forms were mainly identified by short spacings of 3.8 and

Table 1. Fatty Acid Composition (Area %) of Palm Stearin (PS), *Akebia trifoliata* Var. *australis* Seed Oil (ASO), the Physical Blends (PBs), and the Interesterified Products (IPs) of PS: ASO 70:30, 65:35, 60:40[a]

			physical blends (PS: ASO)			interesterified products (PS: ASO)		
	PS	ASO	70:30	65:35	60:40	70:30	65:35	60:40
C12:0	0.12 ± 0.01	0.07 ± 0.00	0.11 ± 0.00	0.10 ± 0.01	0.10 ± 0.00	0.11 ± 0.00	0.10 ± 0.00	0.10 ± 0.00
C14:0	1.23 ± 0.01	0.09 ± 0.01	0.89 ± 0.00	0.83 ± 0.01	0.78 ± 0.04	0.89 ± 0.00	0.83 ± 0.03	0.78 ± 0.01
C16:0	59.46 ± 0.01	21.70 ± 0.32	48.15 ± 0.11	46.24 ± 0.34	44.32 ± 0.70	48.12 ± 0.61	46.12 ± 0.29	44.47 ± 1.17
9c C16:1	ND[b]	0.19 ± 0.01	0.06 ± 0.00	0.07 ± 0.00	0.07 ± 0.00	0.06 ± 0.00	0.07 ± 0.01	0.08 ± 0.00
C18:0	5.46 ± 0.17	3.29 ± 0.15	4.80 ± 0.13	4.70 ± 0.13	4.61 ± 0.42	4.81 ± 0.05	4.71 ± 0.04	4.53 ± 0.20
9c C18:1	28.01 ± 0.16	42.40 ± 0.01	32.35 ± 0.07	33.11 ± 0.60	33.78 ± 0.18	32.33 ± 0.94	33.21 ± 0.29	33.78 ± 1.48
11c C18:1	ND	1.30 ± 0.00	0.39 ± 0.01	0.46 ± 0.04	0.52 ± 0.01	0.39 ± 0.06	0.45 ± 0.07	0.52 ± 0.00
9c12c C18:2	5.67 ± 0.02	30.54 ± 0.10	13.14 ± 0.04	14.34 ± 0.06	15.65 ± 0.49	13.18 ± 0.45	14.35 ± 0.14	15.58 ± 0.54
9t C18:1	ND	ND	ND	ND	ND	ND	ND	ND
C18:3	ND	0.43 ± 0.01	0.13 ± 0.00	0.15 ± 0.01	0.17 ± 0.01	0.13 ± 0.01	0.15 ± 0.01	0.17 ± 0.01
ΣMCFA	0.12 ± 0.01	0.07 ± 0.00	0.11 ± 0.00	0.10 ± 0.01	0.10 ± 0.00	0.11 ± 0.00	0.10 ± 0.00	0.10 ± 0.00
ΣSFA	66.28 ± 0.18	25.14 ± 0.10	53.83 ± 0.02	51.77 ± 0.49	49.70 ± 0.33	53.82 ± 1.12	51.67 ± 0.23	49.78 ± 0.95
ΣUSFA	33.68 ± 0.18	74.86 ± 0.10	46.06 ± 0.02	48.12 ± 0.48	50.19 ± 0.33	46.08 ± 1.13	48.23 ± 0.23	50.12 ± 0.95
ΣTFA	ND	ND	ND	ND	ND	ND	ND	ND
SMP(°C)	53.03 ± 0.12		49.30 ± 0.27	48.77 ± 0.06	48.03 ± 0.31	37.60 ± 0.20	34.63 ± 0.71	33.20 ± 0.66

[a]Values are the mean ± standard error. [b]ND = Not detected under this analysis condition.

Table 2. Fatty Acid Composition (Area %) at the *Sn*-2 Position of Palm Stearin (PS), *Akebia trifoliata* Var. *australis* Seed Oil (ASO), the Physical Blends (PBs), and the Interesterified Products (IPs) of PS: ASO 70:30, 65:35, 60:40[a]

			physical blends (PS: ASO)			interesterified products (PS: ASO)		
fatty acid	PS	ASO	70:30	65:35	60:40	70:30	65:35	60:40
C12:0	0.22 ± 0.01	0.04 ± 0.01	0.16 ± 0.00	0.18 ± 0.00	0.18 ± 0.00	0.21 ± 0.06	0.66 ± 0.00	0.83 ± 0.17
C14:0	1.05 ± 0.01	0.17 ± 0.01	1.13 ± 0.11	1.20 ± 0.28	0.70 ± 0.04	1.41 ± 0.15	1.21 ± 0.01	1.31 ± 0.03
C16:0	34.86 ± 0.81	8.44 ± 0.21	29.96 ± 0.00	28.19 ± 0.36	24.80 ± 0.02	49.80 ± 0.33	47.32 ± 0.46	45.93 ± 1.27
9c C16:1	1.13 ± 0.02	0.15 ± 0.02	1.00 ± 0.00	0.75 ± 0.07	0.65 ± 0.03	0.18 ± 0.01	0.20 ± 0.01	0.20 ± 0.00
C18:0	5.49 ± 0.37	2.34 ± 0.43	4.65 ± 0.21	4.94 ± 0.04	4.09 ± 0.01	9.70 ± 0.23	9.77 ± 0.07	9.91 ± 0.63
9c C18:1	45.26 ± 0.05	52.11 ± 0.06	45.84 ± 0.14	45.21 ± 0.24	48.54 ± 0.12	23.91 ± 0.69	26.69 ± 0.29	27.52 ± 1.57
9c12c C18:2	10.76 ± 0.32	35.63 ± 0.32	16.35 ± 0.31	18.62 ± 0.52	19.88 ± 0.21	12.92 ± 0.32	13.23 ± 0.12	13.70 ± 0.12
C18:3	1.23 ± 0.18	1.14 ± 0.02	0.91 ± 0.06	0.88 ± 0.01	1.16 ± 0.08	1.87 ± 0.05	0.92 ± 0.01	0.56 ± 0.01
ΣMCFA	0.22 ± 0.01	0.04 ± 0.01	0.16 ± 0.00	0.18 ± 0.00	0.18 ± 0.00	0.21 ± 0.06	0.66 ± 0.00	0.83 ± 0.17
ΣSFA	41.61 ± 0.44	10.98 ± 0.22	35.91 ± 0.11	34.53 ± 0.69	29.77 ± 0.05	61.11 ± 0.30	58.96 ± 0.38	57.98 ± 1.70
ΣUSFA	58.39 ± 0.44	89.02 ± 0.22	64.09 ± 0.11	65.47 ± 0.69	70.23 ± 0.05	38.89 ± 0.30	41.04 ± 0.38	42.02 ± 1.70
ΣTFA	ND[b]	ND	ND	ND	ND	ND	ND	ND

[a]Values are the mean ± standard error. [b]ND = Not detected under this analysis condition.

4.2 Å or three minor short spacings at 3.17, 3.97, and 4.27 Å. β forms were observed by a short spacing of 4.6 Å.[17]

Differential Scanning Calorimetry. Melting and crystallization thermograms were determined using DSC (Model No. DSC-204 F1, NETZCH Corporation, Germany) equipped with a thermal analysis data station. Nitrogen (99.99% purity) as the purge gas was used at a flow rate of 20 mL/min. An empty aluminum pan was used as a reference, and the samples were precisely weighed (7 ± 0.5 mg) for DSC analysis. The samples were heated to 80 °C and held at this temperature for 10 min. The temperature was subsequently decreased at a rate of 10 °C/min to −60 °C. After holding for 10 min at −60 °C, the temperature was returned to 80 °C at a rate of 5 °C/min and maintained for 5 min. The solid fat content (SFC, %) was determined from the melting thermograms obtained by the thermal analyzer. For calculating solid fat content SFC, each DSC thermogram was divided into 5 °C increments (0, 5, 10, 15, 20, 25, 30, 35, 40, 45, 50, and 55 °C), and the total melting energy (J/g) was converted into a percentage to determine the SFC at each temperature increment.[18]

Microstructural Analysis. The samples were melted at 70 °C in a water bath and kept at this temperature for 30 min to destroy crystal memory. About 10 mg of melted fat was placed on a preheated microscope slide and covered with a preheated coverslip with the aid of a capillary tube. The samples were cooled to 25 °C and maintained at this temperature for 20 h. The crystal morphology of the fat samples was studied under isothermal conditions (25 °C).[13] The coverslips were fixed on the stage of a Zeiss inverted microscope and observed under a Carl Zeiss 710 confocal laser scanning microscope (Carl Zeiss Inc., Oberkochen, Germany) connected to a digital video camera. All photomicrographs were obtained with a 40 × 0.75 Zeiss Plan Neofluar objective.

Induction Time of Oxidation. The induction times of produced IPs (PS:ASO 70:30) and IPs with different dosages of α-tocopherol (50, 100, and 200 ppm) were determined using a Metrohm 679 Rancimat (Brinkaman Instruments Co., Des Plains, IL, U.S.A.). For Rancimat analysis, 3.0 g of the sample was placed in a Rancimat reaction vessel kept at a constant temperature of 110 °C. A stream of air was passed through the vessel at a rate of 10 L/h. The vapors released during oxidation together with the air were passed into a flask containing 50 mL of demineralized water and an electrode for measuring conductivity.[19] Analyses were performed in triplicate.

Table 3. Triacylglycerol (TAG) Composition (Area %) of PS, ASO, the Physical Blend (PB) and Interesterified Product (IP) of PS:ASO 70:30[a]

ECN[b]	TAG	PS	ASO	PB	IP
42	LLL	ND[c]	1.17	ND	ND
44	LLO/LOL/LaPO/LaOP/OLaP	ND	10.19	3.32	0.52
44	PLL/LPL	ND	5.52	1.40	0.81
46	LOO/OLO	ND	21.56	5.49	3.90
46	PLO/OPL/POL	1.95	17.69	6.48	13.58
46	PPL/PLP	3.25	2.24	2.78	8.63
48	OOO	0.72	2.53	1.37	3.20
48	POO/OPO	10.78	15.34	13.08	27.88
48	POP/PPO	48.45	16.87	39.33	25.85
48	PPP/PLS/PSL/SPL	28.75	ND	18.27	10.11
50	POS/PSO/OPS	1.28	ND	0.76	0.99
50	SSL/SLS	2.05	4.47	3.38	1.97
50	PPS/PSP	1.67	ND	1.08	0.86
	others	1.10	2.42	1.07	1.68

[a]Abbreviations: La = lauric acid; P = palmitic acid; S = stearic acid; O = oleic acid; L = linoleic acid. [b]Equivalent carbon number (ECN) = CN-2DB, where CN is carbon number of TAG and DB is total number of double bonds in TAG. [c]ND = not detected.

Texture Profile Analysis. Textural properties (i.e., hardness, adhesiveness, and cohesiveness) of PBs and IPs were determined at 4 and 23 °C using a TA-X2 texture analyzer (Stable Micro Systems, London, U.K.). A 45° conical probe attached to a 5 kg compression load cell was inserted into the sample at 1.0 mm/s to a depth of 10 mm from the sample surface; withdrawal was performed at the same speed. Hardness and adhesiveness were respectively defined as the maximum force (g) and negative force area (g·s) of the first compression. Cohesiveness (unitless) was determined as the ratio of the positive force area during the second compression to that during the first compression. Completely melted samples were placed into 50 mL beakers and tempered at 25 °C for 24 h.[20] Specimens were prepared in triplicate for each analysis.

Statistical Analysis. Statistical analysis was performed using the SAS software package (SAS Institute, Cary, NC, U.S.A.). Duncan's multiple range test was performed to determine significant difference ($P \leq 0.05$).

RESULTS AND DISCUSSION

Total and Positional Fatty Acid Composition and SMP. The *trans* fatty acids (*TFAs*) was not detected in all samples (Table 1). ASO contained palmitic (21.70%), oleic (42.40%), and linoleic (30.54%) acids. The fatty acid profile of ASO was very similar to that of rice bran oil, in which the major fatty acids were palmitic (19.4%), oleic (45.9%), and linoleic (32.1%) acids.[21] The palmitic acid content (21.70%) in ASO was higher than that in other vegetable oils, such as soybean oil, sunflower oil, sesame seed oil, rapeseed oil, and olive oil.[17,22−25] The high palmitic and oleic acid contents of ASO imply its high oxidative stability. The *sn*-2 positional fatty acid compostion in Table 2 showed ASO contained 89.02% unsaturated fatty acids (USFAs), of which oleic acid (52.11%) and linoleic acid (35.63%) were the major fatty acids. These results demonstrated that USFAs in ASO were preferentially located at *sn*-2 position. In the case of PS, more saturated fatty acids (SFAs) were detected where palmitic acid take up to 59.49 and 34.86% of total (Table 1) and *sn*-2 positional fatty acid (Table 2). The high amount of SFAs contributed to higher SMP (53.03 °C) (Table 1).

The total fatty acid compositions PBs and IPs were altered based on the mixing ratios of PS:ASO. With increasing the weight ratio of ASO in PBs and IPs, the ΣUSFA content of PBs and IPs increased while SMP decreased. In the case of positional fatty acids, the obviously different data between PBs and IPs were detected. ΣSFA of IPs (57.98−61.11%) were significantly higher than that of PBs (29.77−35.91%). In some sense, the alteration of positional fatty acid proved the interesterification reaction occurred. Although this data also implied that the interesterification increased the saturation at the *sn*-2 position, which can be attributed to the random replacement of acyl groups in the products via a process called acyl migration. Similar phenomena have been reported previously.[24] Acyl migration is an undesirable side reaction that cannot be avoided during esterification without adopting auxiliary measures. This phenomenon can explain the changes in fatty acid composition at *sn*-2 position after interesterification.

SMP of PBs and IPs are also listed in Table 1. Both in PBs and IPs, reducing ratio of PS caused decrease of SMP. After interesterification, IPs possessed a lower SMP compared to the corresponding PBs. The differences of SMP between PBs and IPs also demonstrated the interesterification occurred. A SMP of 33.2−37.6 °C was ideal for spread fat because it is solid at room temperature and can be melted at body temperature.[6]

TAG Analysis. Table 3 showed the TAG composition of ASO, PS, PB, and IPs of PS:ASO 70:30 with different catalyzed time. The major TAG species in ASO were LLO (10.19%), LOO (21.56%), PLO (17.69), and POO (15.34), whereas POO (10.78%), POP (48.45%), and PPP (28.75%) were the dominant TAG types in PS. Therefore, the TAG species were originated from ASO and PS according to their ratio. After interesterification, however, changes of the TAG species in IP (PS:ASO 70:30) were observed compared to its PB. IP showed a reduced amount on LLO (0.52%), LOO (3.9%), PPP (10.11%), and POP (25.85%), but an increase of PLO (12.54−13.49%) and PLP (7.43−8.27%). The changes of TAG composition suggested that the fatty acid rearranged within and between TAG backbones by Lipozyme TL IM, which may alter physical properties.

SFC Value. SFC is an important determinant of the texture of bakery fats. The SFC is responsible for the various functional characteristics of bakery fat, including organoleptic properties (flavor release and thickness), physical appearance, spread-

ability, and oil exudation.[26] Figure 1 shows the SFC profiles of PS, PBs (PS:ASO 70:30; 65:35; 60:40), and IPs (PS:ASO

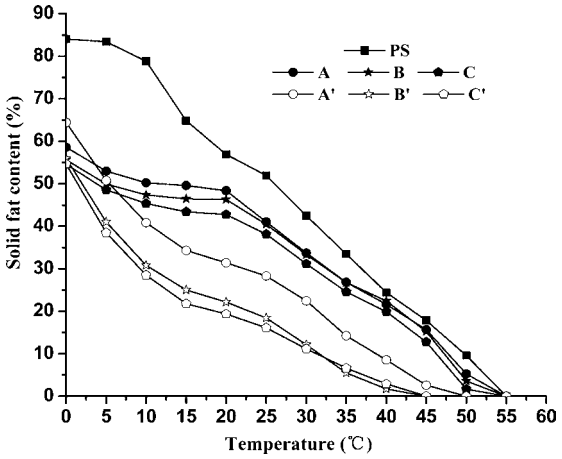

Figure 1. Solid fat content (SFC) of palm stearin (PS), the physical blends (PBs PS:ASO (wt/wt); A 70:30, B 65:35, C 60:40), and the interesterified products (IPs PS:ASO (wt/wt); A′ 70:30, B′ 65:35, C′ 60:40).

70:30; 65:35; 60:40) as a function of temperature. PS is a comparatively high melting fat that features an SFC of 24.41% even at 40 °C. Residual SFC values of 22.39%, 21.62%, and 19.88% were observed in PBs with PS:ASO ratios of 70:30, 65:35, and 60:40, respectively, at 40 °C. The sharpest decline in SFC appeared at the 25−30 °C range in PBs. In IPs, the fastest decline in SFC occurred at 0−5 °C. This shift is caused by the larger ratio of TAGs in IPs that liquefy at this temperature range. Shifts to lower temperature ranges may also explain the lower SMPs obtained in IPs compared with PBs. However, increasing the proportion of ASO decreased the prominence of the sharp drop in the 5 °C range in IPs. A similar study reported by Ming et al. shows a less pronounced drop in SFC upon decreasing the proportion of sunflower oil in enzymatic interesterified palm stearin−sunflower oil blends.[27]

SFC of IP PS:ASO 70:30 at 0−5 °C was slightly higher than that of PBs, similar to the results obtained by Kim et al. for the enzymatic interesterification of fully hydrogenated canola fat with olive oil.[28] This phenomenon may be attributed to the exchange of fatty acid residues in the two substrates to produce new TAG species after interesterification. The new species synthesized during interesterification could affect SFC profile of product at both high and low temperatures. Overall, IPs showed lower SFC contents than PBs at each temperature interval. For example, at 25 °C, IPs showed 16.11%−28.23% SFC, whereas PBs showed 38.16%−41.06% SFC. An SFC of 15%−35% at this temperature promotes the spreadability of margarine fats.[29] PBs with a higher SFC of 19.88%−21.62% at 40 °C may be used for cake manufacture.[30]

Crystallization and Melting Thermograms. The crystallization and melting properties of PS, PBs, and IPs were evaluated by DSC (Figure 2). The crystallization thermogram of PS (Figure 2A) exhibit two crystallization peaks at 2.4 and 26.4 °C, which correspond to the TAG fractions of high melting temperature and low melting temperature, respectively.[30] Figure 2A also shows the crystallization thermograms of the PS:ASO blends with different weight ratios before and after transesterification with LipozymeTL IM. Two exothermic peaks may be observed in PBs: the first occurred from 22.4 to

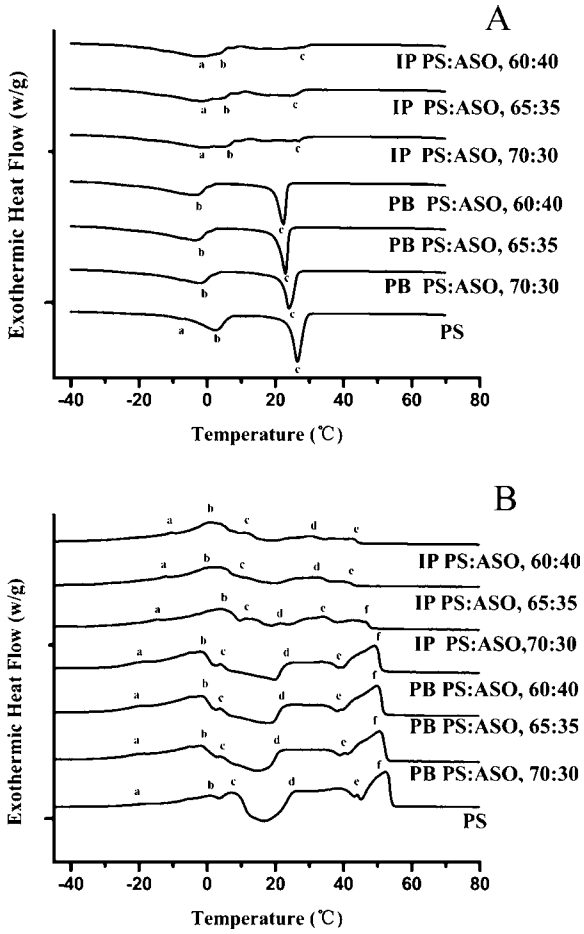

Figure 2. Differential scanning calorimetry (DSC) crystallization (A) and melting (B) thermograms of palm stearin (PS), the physical blends (PBs), and the interesterified products (IPs) of PS:ASO 70:30, 65:35, 60:40.

24 °C and the second occurred from −3.8 °C to −2.2 °C. Increasing the percentage of PS increased the representative peaks of higher-melting TAG (peak b) in terms of heights and areas and shifted them toward higher temperatures. IPs exhibited obviously broader and smaller exothermic peaks than PBs. Peak b was smaller than peak a, which indicated the formation of softer fats.

Figure 2B shows the endothermal profiles of PS and the PS:ASO blends of various ratios before and after interesterification. Five distinct melting peaks (peaks a to e) were observed in PS; peak e (at 52.4 °C) showed the largest and sharpest peak, which indicated that PS contained high-melting temperature TAGs.[23] The endothermic profiles of PBs were similar to that of PS but not to those of IPs. Five melting peaks of PBs ranging from −18.8 to 50.4 °C were observed; here, peak e, which occurred at high temperatures, showed the largest and sharpest peak. After interesterification, endothermic peaks b and c became broader and showed the largest size, whereas peaks d and e became narrower, smaller, and nearly disappeared. All of these changes indicated that most high-melting temperature TAGs are replaced by medium- and low-melting-temperature TAGs through rearrangement of fatty acids between TAGs during interesterification. The melting temperature of bakery fats normally ranges from 39 to 45 °C; IPs have this same melting point range.[22]

dx.doi.org/10.1021/jf500267e | J. Agric. Food Chem. 2014, 62, 3293−3300

Table 4. Polymorphic Forms of Palm Stearin (PS), the Physical Blends (PBs), and the Interesterified Products (IPs) of PS:ASO 70:30, 65:35, 60:40

fats	short spacing (Å)						polymorphic form
substrates							
PS	3.83 (s[a])	3.90 (s)		4.20 (m[b])		4.60 (m)	$\beta' + \beta$
physical blends (PS: ASO)							
70:30	3.82 (s)	3.90 (m)	4.14 (v[c]w[d])	4.22 (m)		4.61 (vw)	$\beta' \gg \beta + \alpha$
65:35	3.82 (s)	3.90 (m)	4.15 (vw)		4.30 (w)	4.62 (m)	$\beta' > \beta + \alpha$
60:40	3.82 (m)	3.90 (m)	4.14 (vw)	4.22 (m)	4.30 (w)	4.62 (m)	$\beta' > \beta + \alpha$
interesterified products (PS: ASO)							
70:30	3.75 (s)	3.89 (s)			4.30 (m)	4.61 (w)	$\beta' \gg \beta$
65:35	3.74 (m)	3.89 (s)			4.30 (m)	4.61 (w)	$\beta' \gg \beta$
60:40	3.73 (m)	3.89 (m)			4.29 (vw)	4.62 (vw)	$\beta' \gg \beta$

[a]s = strong. [b]m = medium. [c]v = very. [d]w = weak.

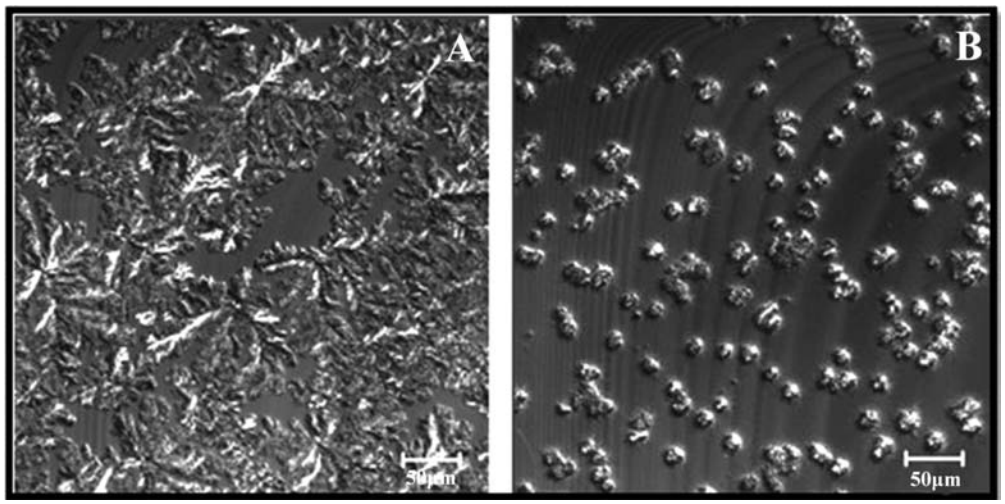

Figure 3. Crystal microstructure of the physical blend (PB, A) and the interesterified product (IP, B) of PS:ASO 70:30.

XRD Spectroscopy. Polymorphic forms of fat crystals are important criteria for determining the functional properties of bakery fats. The major polymorphs of fat crystals include the α (hexagonal), β' (orthorhombic), and β (triclinic) forms. Each polymorphic state has different properties. The α crystal form is characterized as the most unstable form and, therefore, features the lowest melting point. The β' form is a metastable and intermediate-melting polymorph. The β form is the most stable form and consequently has the highest melting point.[32] Table 4 lists the polymorphic forms of PBs and IPs analyzed by XRD.

PS was crystallized by the predominant β' (3.83, 3.90, and 4.20 Å) and β (4.60 Å) forms. PBs showed weak β crystal forms with short a spacing of 4.62 Å, strong β' forms with short spacings of 3.82, 3.90, 4.22, and 4.30 Å, and a very weak α crystal forms with a short spacing of 4.14 Å. IPs showed no α crystal forms, yielding β' forms with strong intensities (3.74, 3.89, and 4.30 Å) and β forms with weak intensity (4.61 Å) instead. We observed that the β' form increased whereas the β form decreased with increasing PS amount, which is attributed to the higher SFC and larger amount of fat crystals in samples with higher PS amounts. Similar results have previously been reported.[24] The β' form is desired for favorable molecular packing of the fatty acid chains of solid fats used to produce margarine or shortening because the small crystal size of this form stabilizes air and imparts better mouthfeel and spreadability; on the other hand, the β form comprises large crystals that give hardness as well as rough and sandy textures.[33]

Microstructural Analysis. The crystal microstructure of PBs (PS: ASO 70:30) and IPs (PS: ASO 70:30) were observed by confocal laser scanning microscopy. Figure 3 shows the distinct crystal morphologies of PBs and IPs. PBs presented very coarse, branched, and leaf-like crystals with crystal sizes of about 50−100 μm in diameter and compact packing. By contrast, IPs (PS: ASO 70:30) formed condensed, uniform, ball-like crystals with diameters of 20−30 μm. These findings agree with the XRD results, which indicated that IPs contain more β' polymorphs and less β polymorphs than PBs. Hartel reported that β' polymorphs have a spherulite-like shapes, whereas β polymorphs feature plate-shaped crystals.[34] Small, compact crystals are ideal for margarine fats and shortenings because these crystals can surround and stabilize air bubbles to impart better textural properties to a food product.

Texture Profile Analysis. Texture profile analysis was performed to evaluate the textural properties (hardness, adhesiveness, and cohesiveness) of PBs and IPs (PS:ASO 70:30) stored at room temperature (25 °C) (Figure 4). Significant changes in all textural attributes except cohesiveness were observed. PBs (3318.19 ± 86.67 g) were markedly harder than IPs (557.02 ± 12.75 g), which agrees with the SFC results, that is, the SFCs of PBs and IPs were 41.06% and 28.29%, respectively, at 25 °C. Hardness is positively related to the amount of solid fat. IPs were softer than PBs, which indicated the higher spreadablility of the former compared with the latter. PBs (PS:ASO 70:30) also showed more significant adhesive-

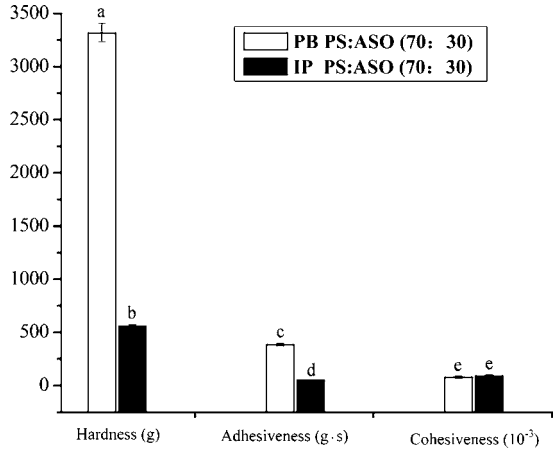

Figure 4. Hardness, adhesiveness, and cohesiveness of the physical blend (PB) and the interesterified product (IP) of PS:ASO 70:30 at 25 °C. Results are expressed as mean ± standard deviation (n = 3).

ness than IPs (PS:ASO 70:30). Adhesiveness reflects the stickiness or tackiness of plastic fats as well as the force required to remove fatty residues in the mouth, which is associated with the waxy taste of some fats. Thus, lower values of adhesiveness are preferred in edible oils.[35] IPs are potentially easier to spread and less persistent because of their lower adhesiveness. IPs possessed higher cohesiveness than PBs at 25 °C but differences between groups were not significant. Cohesiveness is related to the strength of internal bonds that make up the body of a product and describes how crumbly or brittle a food product is. IPs have stronger internal bonds and are therefore more brittle than PBs.

Induction Time of Oxidation. To develop a new lipid product, consideration of the nutritional and physical properties of the products as well as their oxidative stability is important. The oxidative stability of IPs (PS:ASO 70:30) was analyzed by measuring its induction time; longer induction times imply higher oxidative stability. Figure 5 shows that the induction time of IPs with PS:ASO 70:30 was 57 min. This induction time could be prolonged by addition of antioxidants such as α-tocopherol. In this study, the induction times of IPs fortified with 50, 100, and 200 ppm α-tocopherol significantly increased to 75, 91, and 108 min, respectively. α-Tocopherol appears to exert dose-dependent antioxidative effects from 50 to 200 ppm in ASO- and PS-based IPs.

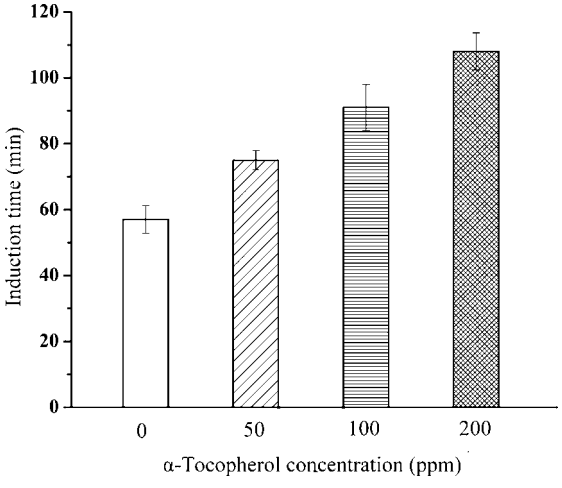

Figure 5. Induction time of the interesterified products (IPs, PS:ASO 70:30) with various antioxidant α-tocopherol concentrations.

In conclusion, the present study demonstrated the characteristics and feasibility of IPs from ASO and PS at different ratios of 70:30, 65:35, and 60:40 as plastic fats. Through analyses of fatty acid composition and physical prosperities, IPs were characterized as low TFAs, relative high content of USFAs (46.08%−50.12%), desirable physical properties (e.g., SFCs, SMPs), suitable crystal forms (β′ polymorph), and tender texture; these properties indicated IPs might be used in spreadable margarine, whereas PBs were used as shortening according to their wide SFC range. ASO can be considered as another potential resource for producing plastic fats to meet the increasing demands in the edible oil market. To make a successful application of lipase-catalyzed interesterification to produce plastic fats from ASO, we still need do further research such as how to tackle with the lipase inactivation after several recycling use.

AUTHOR INFORMATION

Corresponding Authors

*E-mail address: zhuxuemei@ncu.edu.cn. Tel: +86-791-6634810. Fax: +86-791-6634810. (X.-M. Zhu)

*E-mail address: huaxiong100@126.com (H. Xiong).

Funding

This work was supported by NSFC (31160317), Natural Science Foundation of Jiangxi Province (20122BBF60061, 20122BAB214001, 20132BA204001), SRF for ROCS, SEM [no. 20130693], Postdoctoral Science Foundation in Jiangxi Provice.

Notes

The authors declare no competing financial interest.

REFERENCES

(1) Liu, G. Y.; Ma, S. C.; Zheng, J.; Zhang, J.; Lin, R. C. Two new triterpenoid saponins from *Akebia quinata* (Thunb.) Decne. *J. Integr. Plant Biol.* **2007**, *49*, 196−201.

(2) Jiang, D.; Shi, S. P.; Cao, J. J.; Gao, Q. P.; Tu, P. F. Triterpene saponins from the fruits of *Akebia quinata*. *Biochem. Syst. Ecol.* **2008**, *36*, 138−141.

(3) Kitaoka, F.; Kakiuchi, N.; Long, C.; Itoga, M.; Yoshimatsu, H.; Mitsue, A.; Atsumi, T.; Mouri, C.; Mikage, M. Difference of ITS sequences of *Akebia* plants growing in various parts of Japan. *J. Nat. Med.* **2009**, *63*, 368−374.

(4) Du, Y. X.; Jiang, Y.; Zhu, X. M.; Xiong, H.; Shi, S. H.; Hu, J. W.; Peng, H. L.; Zhou, Q.; Sun, W. J. Physicochemical and function properties of the protein isolate and major fractions prepared from *Akebia trifoliate var. australis* seed. *Food Chem.* **2012**, *133*, 923−929.

(5) Jiang, Y.; Du, Y. X.; Zhu, X. M.; Xiong, H.; Woo, M. W.; Hu, J. W. Physicochemical and comparative properties of pectins extracted from *Akebia trifoliate var. australis* peel. *Carbohydr. Polym.* **2012**, *87*, 1663−1669.

(6) Karabulut, I.; Turan, S.; Ergin, G. Effect of chemical interesterification on solid fat content and slip melting point of fat/oil blends. *Eur. Food Res. Technol.* **2004**, *218*, 224−229.

(7) Osborn, H. T.; Akoh, C. C. Structured lipids-novel fats with medical, nutraceutical, and food applications. *Compr. Rev. Food Sci. Food Saf.* **2002**, *3*, 93−103.

(8) Noor, L. H. M. D.; Kalyana, S.; Nor, A. I. Effect of chemical interesterification on triacylglycerol and solid fat contents of palm stearin, sunflower oil and palm kernel blends. *Eur. J. Lipid Sci. Technol.* **2007**, *109*, 147−156.

(9) Yang, T.; Freukilde, M. B.; Xu, X. Applications of immobilized Termomyces lanuginose lipase in interesterification. *J. Am. Oil Chem. Soc.* **2001**, *78*, 635−640.

(10) Rodrigues, R. C.; Ortiz, C.; Berenguer-Murcia, Á.; Torres, R.; Fernández-Lafuente, R. Modifiying enzyme activity and selectivity by immobilization. *Chem. Soc. Rev.* **2013**, *42*, 6290−6307.
(11) Garcia-Galan, C.; Berenguer-Murcia, B.; Fernandez-Lafuente, R.; Rodrigues, R. C. Potential of different enzyme immobilization strategies to improve enzyme performance. *Adv. Synth. Catal.* **2011**, *353*, 2885−2904.
(12) Norizzah, A. R.; Chong, C. L.; Cheow, C. S.; Zaliha, O. Effects of chemical interesterification on physicochemical properties of palm stearin and palm kernel olein blends. *Food Chem.* **2004**, *86*, 229−235.
(13) Adhikari, P.; Shin, J. A.; Lee, J. H.; Hu, J. N.; Zhu, X. M.; Akoh, C. C.; Lee, K. T. Production of *trans*- free margarine stock by enzymatic interesterification of rice bran oil, palm stearin and coconut oil. *J. Sci. Food Agric.* **2010**, *90*, 703−711.
(14) Adhikari, P.; Hu, P.; Zhang, Y. F. Oxidative stabilities of enzymatically interesterified fats containing conjugated linoleic acid. *J. Am. Oil Chem. Soc.* **2012**, *89*, 1961−1970.
(15) Zhu, X. M.; Hu, J. N.; Xue, C. L.; Lee, J. H.; Shin, J. A.; Hong, S. T.; Sung, C. K.; Lee, K. T. Physiochemical and oxidative stability of interesterified structured lipid for soft margarine fat containing D 5-UPIFAs. *Food Chem.* **2012**, *131*, 533−540.
(16) [AOCS] American Oil Chemist's Society. *Official and recommended methods of the American Oil Chemist's Society*, 15th ed.; AOCS Press: Champaign, IL, 2009.
(17) Zeitoun, M. A. M.; Neff, W. E.; List, G. R.; Mounts, T. L. Physical properties of interesterified fat blends. *J. Am. Oil Chem. Soc.* **1993**, *70*, 467−471.
(18) Lopez, C.; Briard-Bion, V.; Camier, B.; Gassi, J. Y. Milk fat thermal properties and solid fat content in emmenta cheese: A differential scanning calorimetry study. *Br. J. Dairy. Sci.* **2006**, *89*, 2894−2910.
(19) Daniels, R. L.; Kim, H. J.; Min, D. B. Hydrogenation and interesterification effects on the oxidative stability and melting point of soybean oil. *J. Agric. Food Chem.* **2006**, *54*, 6011−6015.
(20) Kim, B. Y.; Lumor, S. E.; Akoh, C. C. *Trans*-free margarines prepared with canola oil/palm stearin/palm kernel oil-based structured lipids. *J. Agric. Food Chem.* **2008**, *56*, 8195−8205.
(21) Alim, M. A.; Lee, J. H.; Akoh, C. C.; Choi, M. S.; Jeon, M. S.; Shin, J. A.; Lee, K. T. Enzymatic transesterification of fractionated rice bran oil with conjugated linoleic acid: Optimization by response surface methodology. *Food Sci. Technol.* **2008**, *41*, 764−770.
(22) Farmani, J.; Safari, M.; Hamedi, M. Application of palm olein in the production of zero-*trans* Iranian vanaspati through enzymatic interesterification. *Eur. J. Lipid Sci. Technol.* **2006**, *108*, 636−643.
(23) Toro-Vazquez, J. F.; Briceno-Montelongo, M.; Dibildildox-Alvarado, E.; Charo-Alonso, M.; Reyes-Hernandez, J. Crystallization kinetics of palm sterain in blends with sesame seed oil. *J. Am. Oil Chem. Soc.* **2000**, *77*, 297−310.
(24) Lee, J. H.; Akoh, C. C.; Lee, K. T. Physical properties of *trans*-free bakery shortening produced by lipase-catalyzed interesterification. *J. Am. Oil Chem. Soc.* **2008**, *85*, 1−11.
(25) Kim, J.; Kim, N.; Lee, S. H.; Yoo, S. H.; Lee, S. Correlation of fatty acid composition of vegetable oils with rheological behavior and oil uptake. *Food Chem.* **2010**, *118*, 398−402.
(26) Krawczyk, G. R.; Buliga, G. S.; Bertrand, D. T.; Humphreys, W. M. Reviewing the technology of low fat spreads. *Int. News Fats, Oils Relat. Mater.* **1996**, *7*, 635−639.
(27) Ming, L. Q.; Ghazali, H. M.; Let, C. C. Use of enzymatic transesterified palm stearin-sunflower oil blends in the preparation of table margarine formulation. *Food Chem.* **1999**, *64*, 83−88.
(28) Kim, I. H.; Lee, S. M.; Lee, B. M.; Park, H. K.; Kim, J. Y.; Kwon, K. I.; Kim, J. W.; Lee, J. S.; Kim, Y. H. Interesterification of olive oil with a fully hydrogenated fat in a batch reactor using step changes in temperature. *J. Agric. Food Chem.* **2008**, *56*, 5942−5946.
(29) Rao, R.; Sankar, K. U.; Sambaiah, K.; Lokesh, B. Differential scanning calorimetric studies on structured lipids from coconut oil triglycerides containing stearic acid. *Eur. Food Res. Technol.* **2001**, *212*, 334−343.
(30) Nor, A. L.; Embong, M. S.; Abdullah, A.; Oh, F. C. H. Characteristics and pertormance of some commercial shortenings. *J. Am. Oil Chem. Soc.* **1992**, *69*, 912−916.
(31) Che Man, Y. B.; Tan, C. P. Effects of natural and synthetic antioxidants on changes in refined, bleached, and deodorized palm olein during deep-fat frying of potato chips. *J. Am. Oil Chem. Soc.* **1999**, *76*, 331−339.
(32) Solís, J. A.; Hernandez, M. D.; Duran, M. D. Determination of the predominant polymorphic from of mango (Mangifere indica) almond fat by differential scanning calorimetry and X-ray diffraction. *Eur. J. Lipid Sci. Technol.* **2005**, *107*, 395−401.
(33) Adhikari, P.; Shin, J. A.; Lee, J. H.; Kim, H. R.; Kim, I. H.; Hong, S. T.; Lee, K. T. Crystallization, Physicochemical Properties, and Oxidative Stability of the Interesterified Hard Fat from Rice Bran Oil, Fully Hydrogenated Soybean Oil, and Coconut Oil through Lipase-Catalyzed Reaction. *Food Bioprocess Tech.* **2012**, *5*, 2474−2487.
(34) Hartel, R. W. *Crystalization in foods*; Aspen Publishers: Gaithersburg, Germany, 2001.
(35) Arifin, N.; Peng, K. S.; Long, K.; Ping, T. C.; Yusoff, M. S. A. Y.; Aini, L. I.; Ming, L. O. Relationship between textural properties and sensory qualities of cookies made from medium-and long-chain triacylglycerol-enriched margarines. *J. Sci. Food Agric.* **2012**, *90*, 943−948.

estimated by inserting a preheated thermometer. When the thermometer was preheated to 65 and 78 °C, the temperature remained steady in the respective samples (165 and 198 kJ energy), the two lowest levels (settings) on the microwave oven. The amount of energy required to produce the corresponding temperature rise in the samples from room temperature (20 °C) is accounted for by an approximate 0.024% absorption of the total input energy, assuming the specific heat of the sample to be equal to that of water.

Cell Culture. Vero cells and Human Embryonic Kidney 293 cells (HEK293) were maintained in DMEM containing 10% fetal bovine serum (FBS) and 100 units/mL of both penicillin and streptomycin. Cells were trypsinized when ready to harvest.

Generation of Adenoviral Vectors That Express the GFP Gene. To visualize the effect of Shiga toxin on living cells, we measured changes in green fluorescent protein (GFP) expression levels. GFP gene was isolated from the Green Lantern vector (BRL) by digestion with the *Not I* restriction enzyme. The 750-bp fragment was purified from the gel using a Qiagen kit and was subcloned into the *Not I* site of the adenoviral shuttle plasmid between the Cytomegalovirus immediate-early promoter (CMV) and the polyadenylation signal from bovine growth hormone. The plasmid pJM17 containing the full length of the adenovirus genome including a 4.4-kb sequence of antibiotics resistance gene were cotransfected in HEK293 cells with the shuttle plasmid containing the GFP gene flanked by the adenovirus E1 sequences. After 10 days, the cytopathic effect appeared, and the transfected cells became round and detached from the plate. The cells were then analyzed by fluorescence microscopy to detect GFP gene expression. Individual plaques of Ad-GFP were amplified.[1,2]

Plaque Assays for Purification and Titration of the Adenovirus. Plaque assays depend on the ability of the adenovirus to propagate in HEK293 cells. Six 35-mm tissue culture plates were seeded with HEK293 cells. The cells were incubated at 37 °C in a 5% CO2 incubator until they were 90% confluent. Serial dilutions were made in the DMEM supplemented with 2% FBS. The diluted virus was added to the cells. After 2 h, the medium was removed and replaced with the Modified Eagle's medium (MEM) and 1% seaplaque agarose (FMC). The agar overlay was added to keep the virus localized after the cells had lysed. After 5 days, plaques were visible, and after 7 days, they were counted for titer determination.

Quantifying Stx2 Activity. Vero cells were plated on black 96-well plates (Greiner 655090 obtained from Sigma) at 1×10^4 cells in 100 μL of medium per well. Cells were incubated overnight to allow time for cells to attach to the plate. Spiked samples were added to each well, and the plates were then incubated for 48 h at 37 °C in a 5% CO2 incubator. The cells were then transduced with Ad-GFP at a multiplicity of infection (MOI) of 100 for 48 h. The medium was removed, and the cells were washed three times with pH 7.4 phosphate-buffered saline (PBS). Quantification of fluorescence emission by the cells expressing GFP was measured using a 528/20 nm emission filter and 485/20 nm excitation filter in a Synergy HT Multi-Detection Microplate Reader (BioTek, Winooki, VT, USA).

Visualized Stx2 by Gel Electrophoresis after Exposure to Microwaves. The electrophoresis equipment, buffers, gels, and SeeBlue Plus2 Protein Standard were purchased from Invitrogen (Carlsbad, CA, USA). Samples of Stx2 in phosphate-buffered saline (PBS, pH 7.4) were exposed to 165 and 198 kJ microwave treatments. The cooled Stx2 samples (2 μg) were then separated by sodium dodecyl sulfate polyacrylamide gel electrophoresis (SDS-PAGE) using 4−12% NuPAGE Novex Bis-Tris mini gels following the manufacturer's protocol. To visualize proteins directly after gel electrophoresis, the gels were stained with Coomassie Blue G-250 (Bio-Rad, Hercules, CA, USA).

Statistical Analysis. Statistical analysis was performed with SigmaStat 3.5 for Windows (Systat Software, San Jose, CA, USA). Multiple comparisons among transduced treated cells were made. One-way analysis of variance (ANOVA) was used to compare transduced treated cells (containing increasing concentrations of toxin or milk) to transduced untreated cells. The experiments were repeated at least three times, and results with $P < 0.05$ were considered statistically significant.

RESULTS

Low Level of Microwave Energy Does Not Inactivate the Stx2 Toxin in Milk. To test whether microwave heating inactivates the Stx2 toxin produced by toxigenic *E. coli*, we generated adenoviral vectors that encode and express the green fluorescent protein (GFP) gene (Ad-GFP) and used the GFP fluorescent intensity in transduced Vero cells for quantitative measurement of biological effects and cell viability. Reduced fluorescent intensity of the cells is the result of inhibition of protein synthesis by the toxin and is compared with cells starved in phosphate-buffered saline (PBS, pH 7.4) that lacks essential nutrients. Samples of milk spiked with Stx2 were tested for Stx2 activity after exposure to 165 or 198 kJ microwave treatments. Figure 1 shows that the toxin was

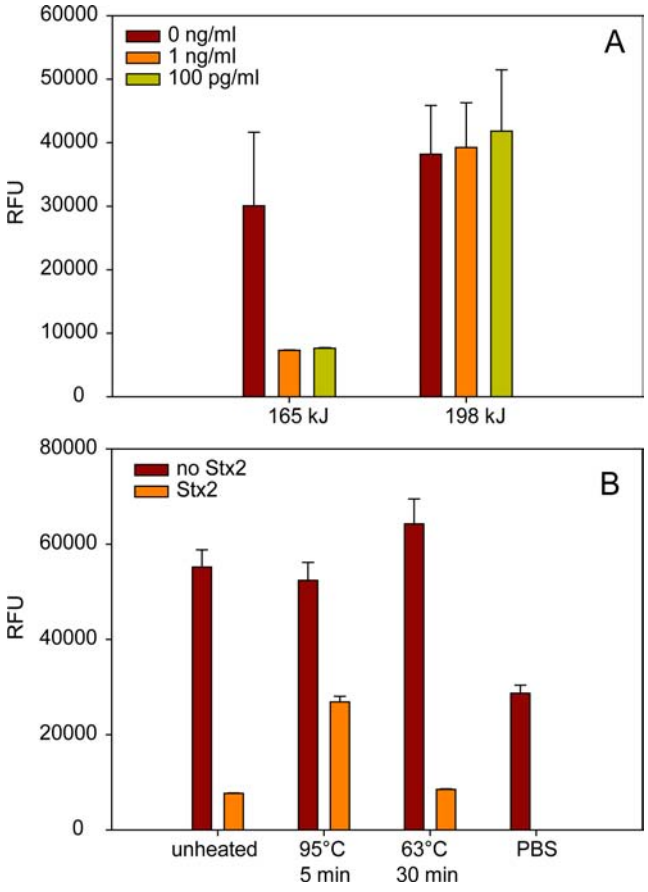

Figure 1. Microwave heating at 165 kJ does not reduce Shiga toxin inhibition of GFP expression. (A) Milk was spiked with 1 ng/mL or 100 pg/mL of Shiga toxin and treated with a microwave energy of 165 or 198 kJ. (B) Unheated milk containing Stx2 (1 ng/mL) was thermally treated at 95 °C for 5 min or pasteurized at 63 °C for 30 min. PBS buffer was used as a control, representing medium devoid of essential nutrients. Five microliters of spiked milk with 95 μL of medium was added to Vero cells. GFP expression was quantified fluorometrically after 48 h of incubation with the treated samples. Error bars represent standard errors.

inactivated neither by the low microwave radiation heating at 165 kJ nor by heat pasteurization. However, thermal heating at 95 °C for 5 min and the higher level of microwave radiation did reduce the activity of the toxin.

Degradation of Stx2 after Exposure to Microwave Treatment. Our results showed that heating of Stx2 with microwaves at 165 kJ did not inactivate the toxin. However,

exposure to the higher energy level of 198 kJ did inactivate the toxin. We then used SDS-PAGE to analyze the effect of exposure to the microwave treatment on Stx2 A and B subunits. As shown in Figure 2, microwave heating at 165 kJ did not

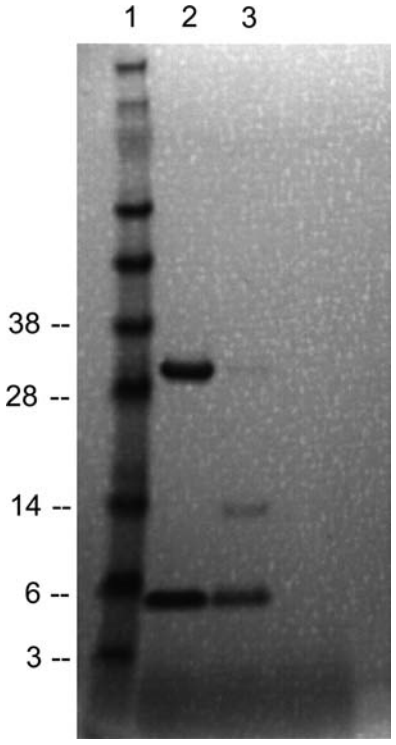

Figure 2. SDS-PAGE gel comparison of Stx2 samples (2 μg) treated at three microwave energy levels. The gel (NuPAGE Novex Bis Tris 4–12%) was stained with coomassie. Lane 1 shows the protein standard; lane 2, Stx2 treated at 165 kJ; lane 3, Stx2 treated at 198 kJ.

degrade the toxin. However, the microwave energy level of 198 kJ did degrade Stx2 and cut the A subunit into smaller sizes, with one fragment equal to a molecular weight of about 14 kD.

Microwave Heating at 198 kJ Destroys the Nutritional Value of Vero Cell Culture Medium. Our results showed that, under the tested conditions, Stx2 is inactivated by microwave heating at 198 kJ. To test whether microwave heating has the potential to reduce or destroy nutrients in culture medium used to grow the Vero cells, we quantitatively measured the biological effects of microwave energy on the cell culture medium. As shown in Figure 3, heating of the cell culture medium with a microwave energy of 165 kJ increased the cellular GFP fluorescent intensity comparable to that of the control untreated culture medium. Exposure to the higher energy level of 198 kJ resulted in decreased GFP fluorescent intensity. The intensity was reduced to the same level as exhibited by the PBS medium devoid of essential nutrients or the medium treated overnight at 100 °C. These results suggest that microwave heating at an energy level of >165 kJ caused a loss of the nutritional value of the growth medium, as indicated by its inability to support the growth of Vero cells.

These results were further confirmed by quantifying the fluorescent product of the cleaved substrate (glycyl-phenyl-alanyl-amino fluorocoumarin, GF-AFC) (Figure 4). This fluorogenic substrate enters cells and is cleaved by the protease activity of live cells, releasing AFC and generating a fluorescent signal proportional to the number of living cells. By contrast,

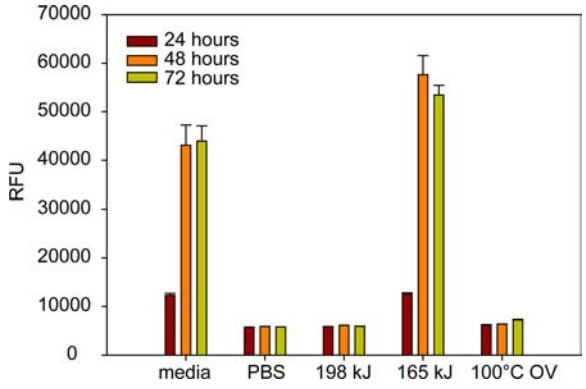

Figure 3. Microwave heating reduces the nutritional value of the cell culture medium as measured by reduced GFP expression in Vero cells. Samples of cell culture medium were treated with microwave energy at 198 or 165 kJ or by overnight heating at 100 °C. Untreated or treated medium or PBS was added to Vero cells. After incubation of treated culture medium for 24, 48, or 72 h with transduced Vero cells, GFP expression was quantified fluorometrically. Error bars represent standard errors. Note that the cell culture medium was microwaved in these experiments.

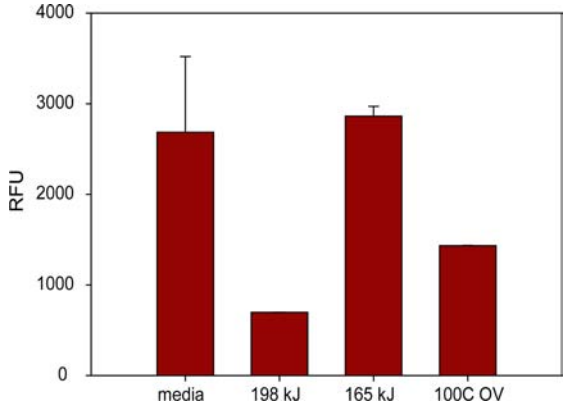

Figure 4. Microwave heating at energies of 198 kJ or higher lowers the nutrient value of the cell culture medium. Samples of cell culture medium were treated with microwave energy at 198 or 165 kJ or by overnight heating at 100 °C and then incubated for 72 h with Vero cells, followed by cleavage of the peptide GF-AFC by the live cell protease, releasing AFC and generating a fluorescent signal. The resultant fluorescence was measured by a fluorescence plate reader (excitation at 355 nm and emission at 523 nm). Error bars represent standard errors.

cells with compromised or disrupted cell membranes (i.e., dead cells) lose their protease activity and are unable to cleave the GF-AFC substrate. The absence of a fluorescent product usually formed in normal growing cells suggests that the cells have lost their viability. Figure 3 confirms by a second independent assay that medium treated at the higher levels of microwave energy or by overnight heating at 100 °C had a reduced ability to maintain the viability of the cells

DISCUSSION

Kindle et al.[5] found that microwave heating reduced the activities of *Pseudomonas aeruginosa*, *E. coli*, *Enterobacter sakazakii*, *Klebsiella pneumoniae*, *Staphylococcus aureus*, *Candida albicans*, *Mycobacterium terrae*, and bacteria in poliomyelitis vaccine suspended in five milk-type infant formulas. In another study, Santos Ferreira et al.[6] found that microwave heating of

dx.doi.org/10.1021/jf500278a | J. Agric. Food Chem. 2014, 62, 3301–3305

contaminated human milk prevented transmission of Chagas disease in mice caused by the protozoan *Trypanosoma cruzi* trypomastigotes.

The cited results indicate that pasteurization and microwave heating can be used to eliminate pathogenic bacteria such as *E. coli* from contaminated milk and milk-based products. There seem to be no reported studies on the effect of microwave heating on the biological activity of Stx2 or any other toxin in milk. Because high levels (306 ng/mL in milk and 452 ng/mL in meat)[7−9] of Shiga toxin have been observed in foods inoculated with *E. coli*, there is a need for such studies.

It has been reported that a malfunction at a milk production plant, prior to pasteurization, contributed to an outbreak of hemolytic uremic syndrome that was linked to drinking the subsequently pasteurized milk in which no live bacteria were found.[10] This finding suggests that the toxin produced and secreted by the bacteria was not inactivated by pasteurization and might be responsible for the illness

We previously reported that oral ingestion of Stx2 toxin alone without *E. coli* bacteria that produce the toxin causes histopathological changes in kidney, spleen, and thymus tissues and mortality in mice.[1] This finding demonstrated the need for new approaches to inactivate both the bacteria and the toxin produced by the bacteria. None of the cited studies examined the use of microwave radiation to inactivate Stx2 and other toxins produced by bacteria, although they do report effects beyond the mere elimination of the microbial pathogen.

In principle, microwave-induced inactivation of the toxin can occur by at least two pathways: (1) changes in the native integrity to a denatured form might inactivate the protein toxin by preventing molecular interaction with cell-membrane receptor sites of their host Vero cells and (b) the protein toxin with an AB5 structure in which five subunits are attached to a straight chain can undergo degradation (cleavage) to smaller fragments.

Figure 2 shows that the toxin seems to undergo degradation into smaller fragments and that the extent of degradation increases with the energy of the microwaves from 165 to 198 kJ. These results imply that the high-energy microwave radiation has the potential to protect consumers against adverse effects of Stx2 and possibly other toxins in contaminated water, milk, and possibly other foods. In the present study, we demonstrated that exposure of the milk solution to a higher level of microwave heating or to 95 °C for 5 min reduced Stx2 activity. In additional experiments, we found that heating reconstituted fat-free milk internally by higher microwave energy also inactivates Stx2 in milk. The use of microwave heating to inactivate the Shiga toxin complements published studies on the inhibition of the toxin's biological activity by naturally occurring compounds, reviewed in Friedman and Rasooly.[11] Exposure of food to microwave cooking is a much simpler process than the use of wet chemistry to inhibit the biological activity of Shiga and possibly other microbial and plant toxins that contaminate food.[12]

We also observed that the microwave heating destroyed the nutritional value of the culture medium used to grow the Vero cells. Our findings with the Shiga toxin and culture medium suggest the need to determine in detail the impact of microwave cooking on susceptible essential nutrients.

Finally, allthugh it is difficult to translate our results in culture medium and in milk to other food categories exposed to microwave radiation, the reported high susceptibility of vitamin C (ascorbic acid)[4,12,13] and vitamin B_1 (thiamin)[14,15] in different foods to microwave-cooking-induced destruction suggests that microwave destruction of these vitamins is a likely cause of the observed loss of nutritional value in the culture medium used to grow the Vero cells.

AUTHOR INFORMATION

Corresponding Author

*Tel.: 510-559-6478. Fax: 510-559-6429. E-mail: reuven.rasooly@ars.usda.gov.

Notes

The authors declare no competing financial interest.

ACKNOWLEDGMENTS

We thank Daphne Tamar and Sharon Abigail for helpful suggestions.

REFERENCES

(1) Rasooly, R.; Do, P. M.; Griffey, S. M.; Vilches-Moure, J. G.; Friedman, M. Ingested Shiga toxin 2 (Stx2) causes histopathological changes in kidney, spleen and thymus tissues and mortality in mice. *J. Agric. Food Chem.* **2010**, *58*, 9281−9286.

(2) Rasooly, R.; Do, P. M.; Levin, C. E.; Friedman, M. Inhibition of Shiga toxin 2 (Stx2) in apple juices and its resistance to pasteurization. *J. Food Sci.* **2010**, *75*, M296−M301.

(3) Kakisu, E.; Abraham, A. G.; Farinati, C. T.; Ibarra, C.; De Antoni, G. L. *Lactobacillus plantarum* isolated from kefir protects Vero cells from cytotoxicity by type-II Shiga toxin from *Escherichia coli* O157:H7. *J. Dairy Res.* **2013**, *80*, 64−71.

(4) Chandrasekaran, S.; Ramanathan, S.; Basak, T. Microwave food processing-A review. *Food Res. Int.* **2013**, *52*, 243−261.

(5) Kindle, G.; Busse, A.; Kampa, D.; Meyer-König, U.; Daschner, F. D. Killing activity of microwaves in milk. *J. Hosp. Infect.* **1996**, *33*, 273−278.

(6) Santos Ferreira, C.; Amato Neto, V.; Gakiya, E.; Bezerra, R. C.; Rodríguez Alarcón, R. S. Microwave treatment of human milk to prevent transmission of Chagas disease. *Rev. Inst. Med. Trop. Sao Paulo* **2003**, *45*, 41−42.

(7) Weeratna, R. D.; Doyle, M. P. Detection and production of verotoxin 1 of *Escherichia coli* O157:H7 in food. *Appl. Environ. Microbiol.* **1991**, *57*, 2951−2955.

(8) Cobbold, R. N.; Davis, M. A.; Rice, D. H.; Szymanski, M.; Tarr, P. I.; Besser, T. E.; Hancock, D. D. Associations between bovine, human, and raw milk, and beef isolates of non-O157 Shiga toxigenic *Escherichia coli* within a restricted geographic area of the United States. *J. Food Prot.* **2008**, *71*, 1023−1027.

(9) Farrokh, C.; Jordan, K.; Auvray, F.; Glass, K.; Oppegaard, H.; Raynaud, S.; Thevenot, D.; Condron, R.; De Reu, K.; Govaris, A.; Heggum, K.; Heyndrickx, M.; Hummerjohann, J.; Lindsay, D.; Miszczycha, S.; Moussiegt, S.; Verstraete, K.; Cerf, O. Review of Shiga-toxin-producing *Escherichia coli* (STEC) and their significance in dairy production. *Int. J. Food Microbiol.* **2013**, *162*, 190−212.

(10) Goh, S.; Newman, C.; Knowles, M.; Bolton, F. J.; Hollyoak, V.; Richards, S.; Daley, P.; Counter, D.; Smith, H. R.; Keppie, N. *E. coli* O157 phage type 21/28 outbreak in North Cumbria associated with pasteurized milk. *Epidemiol. Infect.* **2002**, *129*, 451−457.

(11) Friedman, M.; Rasooly, R. Review of the inhibition of biological activities of food-related selected toxins by natural compounds. *Toxins* **2013**, *5*, 743−775.

(12) Galgano, F.; Favati, F.; Caruso, M.; Pietrafesa, A.; Natella, B. The influence of processing and preservation on the retention of health-promoting compounds in broccoli. *J. Food Sci.* **2007**, *72*, S130−135.

(13) Friedman, M.; Gumbmann, M. R.; Ziderman, I. I. Nutritional value and safety in mice of proteins and their admixtures with carbohydrates and vitamin C after heating. *J. Nutr.* **1987**, *117*, 508−518.

(14) Khatoon, N.; Prakash, J. Nutritional quality of microwave-cooked and pressure-cooked legumes. *Int. J. Food Sci. Nutr.* **2004**, *55*, 441−448.
(15) Khatoon, N.; Prakash, J. Nutritional quality of microwave and pressure cooked rice (*Oryza sativa*) varieties. *Food Sci. Tech. Int.* **2006**, *12*, 297−305.

Table 1. Data for Linearity, Limit of Detection (LOD), Limit of Quantification (LOQ), and Recovery for Phenolics Determination by HPLC Technique (n = 15)

compounds	detection	range (μg/mL)	r^{2a}	LOD (μg/mL)	LOQ (μg/mL)	recovery (%)
gallic acid	270	0.020−40	0.998	0.005	0.020	97.2
hydroxybenzoic acid	270	0.015−40	0.997	0.004	0.015	96.8
caffeic acid	280	0.065−40	0.999	0.016	0.065	98.5
benzoic acid	270	0.065−40	0.996	0.016	0.065	93.7
salicylic acid	290	0.179−35	0.992	0.045	0.179	90.5
syryngic acid	270	0.028−40	0.999	0.007	0.028	98.6
chlorogenic acid	270	0.028−50	0.998	0.007	0.028	97.5
sinapinic acid	280	0.219−40	0.997	0.055	0.219	96.1
o-coumaric acid	290	0.035−45	0.999	0.010	0.038	98.4
p-coumaric acid	290	0.022−50	0.999	0.005	0.022	99.1
ferulic acid	290	0.040−50	0.998	0.010	0.040	96.8
daidzein	335	0.063−20	0.997	0.016	0.063	89.9
quercetin	360	0.047−35	0.998	0.012	0.047	92.3
naringenin	290	0.016−50	0.998	0.004	0.016	96.8
catechin	280	0.096−40	0.995	0.024	0.096	90.5

[a] r_2 = coefficient of determininationn.

stages. Special emphasis was placed on the nutritional quality of sprouts, including protein and starch contents, and their potential bioavailability.

MATERIAL AND METHODS

Chemicals. Ferrozine (3-(2-pyridyl)-5,6-bis(4-phenylsulfonic acid)-1,2,4-triazine), ABTS (2,2-diphenyl-1-picrylhydrazyl), α-amylase, pancreatin, pepsin, bile extract, Folin−Ciocalteau reagent, linoleic acid, ammonium thiocyanate, pepsin, chymotrypsin, and phenolic standards linoleic acid were purchased from Sigma-Aldrich Co. (Poznan, Poland). All other chemicals were of analytical grade.

Materials. Lentil (*Lens culinaris* Medik.) seeds var. Tina were purchased from the Horticulture and Seed Enterprises PNOS S.A. in Ozarów Mazowiecki, Poland.

Germination. Seeds were sterilized in 1% (v/v) sodium hypochloride for 10 min, then drained, and washed with distilled water until they reached neutral pH. They were placed in distilled water and soaked for 6 h at 25 °C. Seeds were dark germinated 6 days, at 25 °C, in a growth chamber on Petri dishes (φ 125 mm) lined with absorbent paper (approximately 150 seeds per dish). Seedlings were watered with 5 mL of Milli-Q water daily.

Elicitation. For the experiments, 2-day-old sprouts were incubated for 1 h at 4 and 40 °C (TC and TH, respectively). Temperatures for treatments were selected according to previous screening studies (sprouts vigor, phenolics content, and antiradical potential). Plates were transferred to the climatic chamber, discovered, and incubated for 1 h at appropriate temperature. After that, sprouts were cultivated under standard conditions (see the section Germination). Sprout samples were gently collected, weighed (fresh mass), rapidly frozen, and kept in polyethylene bags at −20 °C. For each treatment, three replicates were taken for analysis.

Flour Preparation. Sprouts were dried in a forced-air oven at 50 °C for 12 h to moisture content < 10%.[8] After that, sprouts were ground in a labor mill and sieved (60 mesh). Sprout flours were stored at 4 °C.

Growth Analysis. In order to determine the influence of elicitation on the vigor of the sprouts, the growth factor was proposed. The growth factor was defined as an amount of fresh weight (in grams) obtained on the second, third, fourth, and sixth days of germination from 1 g of dormant seeds.

Phenolic Content and Antioxidant Activities. *Extract Preparation.* Lentil flours (0.2 g) were extracted three times with 4 mL of acetone/water/hydrochloric acid (70:29:1, v/v/v). After centrifugation (10 min, 6800 relative centrifugal force (rcf)) fractions were collected, combined, and used for further analysis.

Phenolic Analysis. *Determination of Total Phenolic Compounds.* The amount of total phenolics (TPC) was determined using Folin−Ciocalteau reagent. [16] The amount of total phenolics was calculated as a gallic acid equivalent (GAE) in milligrams per gram of dry mass (DW).

Determination of Flavonoid Content. Total flavonoid content (TFC) was determined according to the method described by Lamaison and Carnat.[17] Total flavonoid content was calculated as a quercetin equivalent (QE) in milligrams per gram of DW.

Determination of Condensed Tannins Content. Condensed tannin content (CTC) was determined according to the method described by Sun et al.[18] CTC was calculated as a (+)-catechin equivalent (CE) in milligrams per gram of DW.

Quantitative−Qualitative Analysis of Phenolic. Samples were analyzed with a Varian ProStar high-performance liquid chromatrography (HPLC) system separation module (Varian, Palo Alto, CA, USA) equipped with Varian ChromSpher C18 reverse phase column (250 mm × 4.6 mm) and ProStar DAD detector. The column thermostat was set at 40 °C. The mobile phase consisted of 4.5% acetic acid (solvent A) and 50% acetonitrile (solvent B), and a flow rate of 0.8 mL min^{-1} was used. At the end of the gradient, the column was washed with 50% acetonitrile and equilibrated to the initial condition for 10 min. The gradient elution was used as follows: 0 min, 92% A; 30 min, 70% A; 45 min, 60% A; 80 min, 60% A; 82 min, 0% A; 85 min, 0% A; 86 min, 92% A; and 90 min, 92% A. Detection was carried out at 270 and 370 nm. Spectrum analysis and a comparison of their retention times with those of the standard compounds identified the phenolics in a sample. Quantitative determinations were carried out with the external standard calculation, using calibration curves of the standards. Detailed information concerning method validation is presented in Table 1. Phenolics were expressed in micrograms per gram of DM. [3]

Antioxidant Aactivities. *Antiradical Activity (ABTS).* The experiments were carried out using an improved ABTS decolorization assay.[19] Free radical scavenging ability was expressed as Trolox equivalent (TE) in millimoles per gram of DW.

Reducing Power. Reducing power (RP) was determined by the method of Oyaizu.[20] RP was expressed as Trolox equivalent in millimoles per gram of DW.

Metal Chelating Activity. Chelating power (CHP) was determined by the method of Guo and co-workers.[21] CHP was expressed as ethylenediaminetetraacetic acid (EDTA) equivalent in milligrams per gram of DW.

Inhibition of Linoleic Acid Peroxidation. The inhibition of the hemoglobin-catalyzed peroxidation of linoleic acid (LPI) was determined.[22] The activity was expressed as quercetin equivalent (Q) in milligrams per gram of DW.

Total Antioxidant Capacity Index. Four complementary antioxidant methods were intergraded to obtain the total antioxidant

dx.doi.org/10.1021/jf403923x | J. Agric. Food Chem. 2014, 62, 3306−3313

capacity index (AI). [10] The index may be useful for evaluation the total antioxidant potential of sprouts from different germination conditions with respect to control. The AI was calculated as the sum of relative activities (RA) for each antioxidant chemical method divided by the number of methods (n).

$$AI = \Sigma RA_{(n)}/n$$

RA was calculated as follows:

$$RA = Ax/Ac$$

where Ax = activity of modified sprouts for the method and Ac = activity of control sprouts determined for the method.

Soluble Protein Content. A 500 mg sample was twice extracted with 5 mL of 0.5 M NaCl solution in 0.05 M Tris-Hcl buffer, pH 7.0, at 4 °C for 2 h. After centrifugation (10 min, 6800 rcf) fractions were collected, combined, and used for further analysis. Total protein contents were determined with the Lowry method,[23] using bovine serum albumin as the standard protein.

Nonprotein Nitrogen Content. A 100 mg sample was twice extracted with 5 mL of 10% ethanol (v\v) at 4 °C for 2 h. After centrifugation (10 min, 6800 rcf) fractions were collected, combined, and used for further analysis. Nonprotein nitrogen was determined with 2,4,6-trinitrobenzene sulfonic acid (TNBS) according to the methods described by Habeeb,[24] using L-leucine as the standard.

Total Starch Content. The total starch (TS) content was determined after dispersion of the starch.[25] The glucose content was determined by using the standard dinitrosalicylic acid (DNSA) method.[26] Total starch was calculated as glucose × 0.9. The free reducing sugar content of the samples was determined in order to correct the obtained total starch values. The sucrose content of the samples was also determined in order to correct the obtained total starch values. The samples dispersed in sodium acetate buffer, pH 5.0, were treated with 200 μL of (10 mg in 1 mL of 0.4 M sodium acetate buffer, pH 5.0) invertase (EC 3.2.1.26; 300 U mg^{-1}) for 30 min at 37 °C. After centrifugation, reducing sugars were analyzed in the supernatants using the DNS reagent.

Digestion in Vitro. Simulated mastication and gastrointestinal digestion was performed according to Świeca and co-workers.[27]

In Vitro Protein digestibility. The *in vitro* protein digestibility was evaluated on the basis of the total soluble protein content and the content of protein determined after digestion *in vitro*.[10]

$$PD/\% = 100 - [(Pr/Pt \times 100]$$

where PD = *in vitro* digestibility of the protein, Pt = total protein content, and Pr = content of proteins after *in vitro* digestion.

In Vitro Starch Digestibility. The *in vitro* digestibility of starch was evaluated on the basis of total starch content (TS) and resistant starch (RS) determined after digestion *in vitro*.

Resistant and Potentially Bioavailable Starch Content. The resistant (RS) and potentially bioavailable starch (AS) content was analyzed on the basis of results obtained after simulated gastrointestinal digestion. After centrifugation (3000g, 15 min) and removal of supernatant, the pellet was dispersed with 2 M KOH, hydrolyzed with amyloglucosidase, and then liberated glucose was quantified, as described above, for total starch (TS, 2.8). RS was calculated as glucose × 0.9. AS content was calculated as the difference between TS and RS.

In Vitro Starch Digestion Rate and Expected Glycemic Index. The digestion kinetics and expected glycemic index (eGI) of the lentil sprouts were calculated in accordance with the procedure established by Goni and co-workers.[25] eGI was calculated using the equation proposed by Granfeldt and co-workers:[28] eGI = 8.198 + 0.862HI. The hydrolysis index (HI) was calculated on the basis of the starch hydrolysis curve (0−180 min) as the percentage of total glucose released over 180 min in comparison to that released from white bread over the same duration.

Hydrolase Inhibitors Activity. *Trypsin Inhibitors Activity.* A 100 mg sample was extracted with 4 mL of 0.05 M phosphate buffer, pH 7.6, at 4 °C for 2 h. The trypsin inhibitor activity (TIA) was determined using α-*N*-benzoyl-DL-arginine-*p*-nitroanilidehydrochloride (BAPNA) as the substrate.[29] TIA was expressed as trypsin inhibitor units per milligram of DW sample. One trypsin unit was defined as the increase by 0.01 absorbance units at 410 nm of the reaction mixture.

Chymotrypsin Inhibitors Activity. A 100 mg sample was extracted with 4 mL of 0.05 M phosphate buffer pH 7.6 at 4 °C for 2 h. Chymotrypsin inhibitor activity (CIA) was determined using sodium beznzylo-DL-tyrosine-*p*-nitroanilide (BTpNA) as the substrate.[30] CIA was expressed as chymotrypsin inhibitor units per milligram of DW sample. One chymotrypsin unit was defined as the increase by 0.01 absorbance units at 410 nm of the reaction mixture.

α-Amylase Inhibitors Activity. For extraction, 100 mg (DW) of lentil sprouts was suspended in 4 mL of 50 mM phosphate buffer, pH 7.6, then stirred for 2 h at 4 °C, and centrifuged at 3000g for 60 min. α-Amylase inhibitor (αAI) activity was measured according to the method described by Alonso and co-workers. [6] One inhibitory unit was defined as the amount of αAI that completely inhibited one enzyme unit (the amount of α-amylase which realized 1 μmol of reducing groups/(1 min at 40 °C) in the reaction conditions).

Statistic Analysis. All experimental results were mean ± standard deviation (SD) of three parallel experiments. Two-way analysis of variance (ANOVA and Tukeỳs posthoc test) was used to compare groups within different elicitors. α values < 0.05 were regarded as significant.

RESULTS

Diverse biological effects of legumes food are commonly considered in terms of phenolic content. In the light of this, increasing of the antioxidant potential by phenolics overproduction in lentil sprouts was performed using natural plant stress response pathways. Sprouts metabolism was induced by incubation of 2-day-old sprouts at low (4 °C, TC and high 40 °C, TH) temperature. Since the aim of the study was to determine the influence of temperature treatments, the results obtained for elicited sprouts were always compared to those obtained for control sprouts from the corresponding day of germination.

One of the most important factors during trials aimed to overproduce secondary metabolites by elicitation is a negative influence of stressed factors on plant growth and yield. Generally, in our studies growth conditions did not influence negatively on fresh mass yield (Table 2). Extracts obtained from sprouts at different stages of germination (control and elicited) were preliminarily studied for their phenolics content (Table 2). Sprouts obtained by elicitation were characterized by elevated content of condensed tannins, flavonoids, and total phenolics. A small reduction of flavonoids content (about 6% in comparison to control) was only found for 6-day-old sprouts induced at 4 °C. Induction at 40 °C most effectively increased the flavonoids content in the sprouts; in comparison to the control condition, their amounts were higher by about 28%, 43%, and 49% for 3-, 4-, and 6-day-old sprouts, respectively. We have previously demonstrated that growth conditions affected significantly the qualitative and quantitative changes in polyphenols profiles of sprouts;[3,4,7,14] thus, a further, precise analysis was performed. An exemplary profile of lentil sprouts phenolics is presented in Figure 1. In comparison to control, during growth of elicited sprouts an increase of salicylic and chlorogenic acids content was observed. Both treatments reduced also the content of syringic acid in sprouts; its level was lower by about 88%, 84%, and 52% in the third, fourth, and sixth 230 days of cultivation, respectively. Additionally, in 3-, 4-, and 6-day-old sprouts determined amounts of caffeic and *p*-coumaric acids (except *p*-coumaric acid content in 6-day-old TH sprouts) were significantly lower than those found for control sprouts. Both treatments caused significant changes of flavonoids fractions. Surprisingly, the

Table 2. Effect of Different Sprouting Conditions on Yield and Phenolics Composition of Lentil Sprouts[a]

		cultivation conditions[b]		
	time of germination (days)	C	TC	TH
total phenolics (mg/(g of DW))	2	19.8 ± 0.12a		
	3	19.8 ± 0.30a	21.2 ± 0.66bc	20.1 ± 0.34ab
	4	19.9 ± 0.19a	21.2 ± 1.00bc	21.7 ± 0.49bc
	6	19.4 ± 0.17a	21.6 ± 0.11c	23.7 ± 0.87d
total flavonoids (mg/(g of DW))	2	1.84 ± 0.04c		
	3	1.87 ± 0.03c	2.10 ± 0.06d	2.39 ± 0.05e
	4	1.71 ± 0.10bc	1.77 ± 0.08bc	2.44 ± 0.02e
	6	1.68 ± 0.06b	1.58 ± 0.02a	2.50 ± 0.07e
condensed tannins (mg/(g of DW))	2	6.06 ± 0.16f		
	3	5.63 ± 0.24f	5.82 ± 0.08ef	5.73 ± 0.08ef
	4	4.94 ± 0.12bc	5.26 ± 0.04d	5.25 ± 0.22cde
	6	4.33 ± 0.01a	4.80 ± 0.03b	4.57 ± 0.31a
growth factor (g)	2	2.51 ± 0.07b		
	3	2.79 ± 0.01 cd	2.70 ± 0.00c	2.29 ± 0.10a
	4	3.11 ± 0.15e	3.02 ± 0.18de	3.19 ± 0.15 e
	6	3.96 ± 0.10f	4.23 ± 0.07g	4.08 ± 0.11fg

[a]Means in rows, for the respective components followed by different small letters are significantly different at $\alpha = 0.05$. [b]C, control; TC, sprouts induced at 4 °C; TH, sprouts induced at 40 °C.

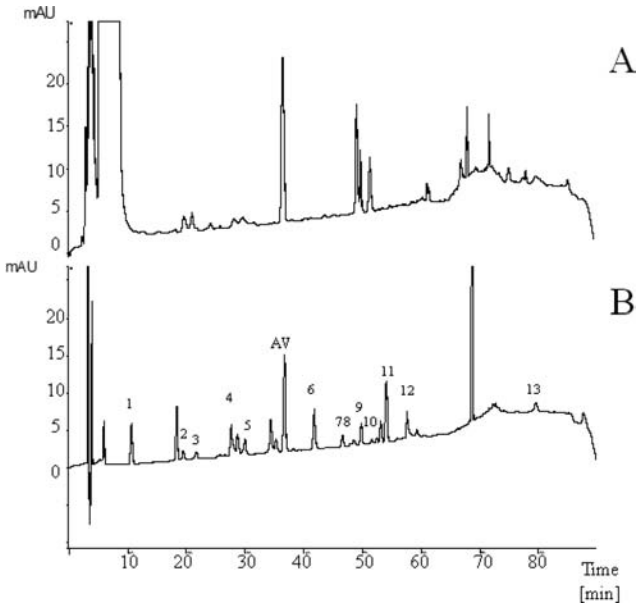

Figure 1. HPLC–DAD elution profile (270 nm) of standard and lentil samples ((A) 2-day-old sprouts; (B) standard): (1) hydroxybenzoic acid, (2) (+)-catechin, (3) vanillic acid, (4) chlorogenic acid, (5) syringic acid, (6) *p*-coumaric, (7) salicylic acid, (8) ferulic acid, (9) sinapinic acid, (10) *o*-coumaric acid, (11) daidzein, (12) quercetin, (13) naringenin, and (AV) internal standard. For details, see Materials and Methods.

levels of daidzein in elicited sprouts were lower than those determined for the control. It should be also noted that treated sprouts were characterized by significantly higher levels of (+)-catechin (Table 3). Phenolic compounds were determined by both spectrophotometric and HPLC techniques. Spectrophotometric methods are less precise (with respect to HPLC); however, they allow for better visualization of the effect of elicitation (changes are more visible). On the other hand, more accurate qualitative and quantitative data provided by HPLC technique coupled with diode array detection (DAD) technique allow to speculate about biological process taking place in the stressed plants, e.g., synthesis of the lignin precursors and changes in the phenylpropanoid metabolism such as synthesis of different classes of flavonoids.

In order to analyze the effect of elicitation and subsequent changes in the sprouts phenolics profile on the antioxidant capacities, four methods based on different modes of antioxidant action were used. The general trend of free radical scavenging, lipid preventing, and reducing properties in elicited lentil sprouts showed that induction significantly improved these activities (except the radical scavenging ability of 3-day-old sprouts). It is shown in Table 4 that temperature treatments caused a significant increase of radical scavenging ability of 4- and 6-day-old sprouts. Between elicited sprouts, the highest reducing power was determined on day 6 for sprouts induced at 40 °C (0.43 mmol of TE/(g of DW)), while the lowest, in those obtained on day 3 in those elicited at 4 °C (0.35 mmol of TE/(g of DW)). These parameters were higher than those determined for the respective control sprouts by 19% and 34%, respectively. It should be noted that, in comparison with samples cultivated under control conditions, sprouts obtained by induction at 40 °C (effect was not observed in the case of induction at 4 °C) were characterized by high chelating power; for 3-, 4-, and 6-day-old sprouts its activity was about 2-fold higher. Both studied modifications of sprouting (TH, TC) effectively elevated the ability to prevent lipids against oxidation. The best results were obtained on day 3, a 3.3- and 4-fold increase for TH and TC, respectively. Complementary antioxidant methods were intergraded to obtain the total antioxidant capacity index. All of the studied conditions significantly improved the nutraceutical value of sprouts. The highest antioxidant potentials were obtained for 6-day-old sprouts (2.25 and 3.11 for TC and TH, respectively) (Table 4).

Nowadays, one of the main areas of research is the search for new food products that in spite of nutritional quality also possess natural ingredients with biological activity. [1] Here it is presented that the induction of sprouts at 4 and 40 °C has allowed us to obtain a low-processed food with significantly enhanced antioxidant potential. Since elicitation may in some cases negatively influence nutrients content, we also placed a special emphasis on the nutritional quality of the sprouts.

On germination in control conditions, only a slight reduction in protein content was observed (Table 5). Elicitation by both

dx.doi.org/10.1021/jf403923x | J. Agric. Food Chem. 2014, 62, 3306–3313

Table 3. Effect of Different Sprouting Conditions on Phenolics Composition of Lentil Sprouts[a,b]

		Compounds (μg/ g DW)														
Time of germination [day]	Cultivation conditions	gallic acid	hydroxy-benzoic acid	caffeic acid	benzoic acid	salicylic acid	syryngic acid	chlorogenic acid	sinapinic acid	*o*-coumaric acid	*p*-coumaric acid	ferulic acid	daidzein	quercetin	naringenin	(+) catechin
2	C	4.45 ±0.31c	16.9 ±0.40a	17.2 ±2.02d	11.2 ±2.93b	8.65 ±0.30a	3.06 ±0.74b	44.4 ±4.42b	13.1 ±0.81b	12.4 ±2.25bc	61.4 ±3.41c	6.77 ±0.80ab	0.49 ±0.11b	2.38 ±0.11c	7.70 ±0.33c	161.5 ±3.80d
3	C	2.03 ±0.54a	17.7 ±0.93ab	4.63 ±0.20c	3.96 ±1.85a	11.0 ±0.73b	15.2 ±0.61f	40.2 ±3.9b	15.9 ±0.9c	14.2 ±0.55d	80.8 ±6.53e	9.11 ±1.3bc	2.40 ±0.15f	1.48 ±0.11a	7.17 ±0.52c	149.5 ±4.91c
	TC	4.09 ±0.40c	17.5 ±0.09ab	1.84 ±0.12a	4.85 ±0.41a	17.2 ±0.95d	1.95 ±0.29a	56.6 ±5.13b	14.4 ±0.20b	13.7 ±1.75cd	47.4 ±5.70b	7.99 ±0.40b	0.43 ±0.31b	4.00 ±0.09e	10.50 ±0.45e	181.4 ±5.36f
	TH	2.81 ±0.32b	16.7 ±0.42ab	2.95 ±0.35b	9.89 ±1.59b	15.9 ±0.87d	8.47 ±0.47d	61.4 ±1.96b	15.4 ±4.70bcd	7.00 ±0.14a	34.7 ±3.98a	7.86 ±1.56ac	0.29 ±0.02a	1.43 ±0.02a	4.36 ±0.42b	185.9 ±3.33f
4	C	2.20 ±0.13a	17.8 ±0.81abc	3.92 ±0.32c	74.80 ±4.16g	13.7 ±0.14c	14.2 ±0.33f	43.5 ±0.34b	18.4 ±1.76d	7.9 ±1.08a	76.7 ±5.96e	8.49 ±0.92b	4.95 ±0.11g	1.95 ±0.1 4b	8.04 ±0.1d	93.7 ±4.59b
	TC	4.11 ±0.01c	18.5 ±0.03c	2.39 ±0.24ab	55.9 ±3.00e	20.4 ±0.04e	2.10 ±0.10b	63.3 ±2.00cd	16.9 ±0.00d	17.1 ±0.03e	64.9 ±0.00c	8.21 ±0.05c	1.78 ±0.01e	3.15 ±0.20d	12.38 ±0.23f	169.2 ±5.61e
	TH	2.00 ±0.27a	17.9 ±0.29b	2.92 ±0.15b	34.5 ±0.95d	19.3 ±1.16e	5.28 ±0.56c	70.1 ±4.36e	15.4 ±4.77bcd	6.87 ±2.46a	66.9 ±0.60d	7.11 ±1.33ac	1.28 ±0.12d	3.21 ±0.69de	5.17 ±0.37b	175.4 ±3.40e
6	C	3.96 ±0.35c	21.7 ±0.21e	17.2 ±2.63d	67.3 ±1.61f	20.8 ±1.61e	10.9 ±0.27e	18.1 ±4.56a	17.4 ±1.48d	10.5 ±0.96b	111.9 ±6.91f	9.32 ±1.92bc	6.49 ±0.84h	2.49 ±0.13c	8.85 ±0.19d	63.9 ±2.21a
	TC	1.87 ±0.26a	18.2 ±2.36abcd	2.70 ±0.78ab	28.1 ±2.69c	30.5 ±2.01f	5.19 ±0.26c	84.5 ±8.13f	8.52 ±1.06a	21.7 ±1.28f	76.3 ±3.97e	6.10 ±0.03a	1.06 ±0.10cd	2.74 ±0.05c	6.63 ±4.69b	142.6 ±4.63c
	TH	2.74 ±0.26b	19.0 ±1.08d	2.94 ±0.08b	36.2 ±1.28d	27.7 ±0.59	5.17 ±0.11c	69.9 ±3.03def	9.02 ±0.68a	13.1 ±2.23bcd	134.1 ±1.67g	6.82 ±0.21a	0.83 ±0.17c	2.72 ±0.85cd	2.95 ±0.12a	153.7 ±4.93d

[a]Means, in columns, for the respective components followed by different small letters are significantly different at $\alpha = 0.05$. [b]C, control; TC, sprouts induced at 4 °C; TH, sprouts induced at 40 °C.

Table 4. Effect of Different Sprouting Conditions on Antioxidant Activity of Lentil Sprouts[a]

		cultivation conditions[b]		
	time of germination (days)	C	TC	TH
radical scavenging ability (mmol of TE/(g of DW))	2	5.75 ± 0.44e		
	3	3.69 ± 0.59bcd	3.63 ± 0.00bc	4.11 ± 1.76cde
	4	2.23 ± 0.25ac	4.56 ± 0.51de	4.64 ± 0.69de
	6	2.76 ± 0.19ac	3.88 ± 0.66bcd	4.20 ± 0.71d
reducing power (mmol of TE/(g of DW))	2	0.27 ± 0.02a		
	3	0.29 ± 0.02a	0.35 ± 0.04bcd	0.36 ± 0.00c
	4	0.30 ± 0.02ab	0.39 ± 0.03cde	0.38 ± 0.02de
	6	0.32 ± 0.01b	0.38 ± 0.01d	0.43 ± 0.02e
chelating power (mg of EDTA/(g of DW))	2	0.20 ± 0.03bc		
	3	0.23 ± 0.05bcd	0.15 ± 0.04b	0.45 ± 0.03f
	4	0.24 ± 0.03 cd	0.27 ± 0.02d	0.46 ± 0.03f
	6	0.17 ± 0.01b	0.07 ± 0.02a	0.38 ± 0.02e
inhibition of lipids peroxidation (mg of Q/(g of DW))	2	3.19 ± 0.34b		
	3	2.81 ± 0.27b	11.3 ± 0.34g	9.42 ± 0.47f
	4	4.54 ± 0.34c	7.55 ± 0.19d	7.13 ± 0.23d
	6	1.17 ± 0.17a	6.90 ± 0.43d	8.21 ± 0.32e
relative antioxidant index	3	1	1.80	1.93
	4	1	1.47	1.63
	6	1	2.25	3.11

[a]Means, in rows, for the respective activities followed by different small letters are significantly different at $\alpha = 0.05$. [b]C, control; TC, sprouts induced at 4 °C; TH, sprouts induced at 40 °C.

temperature stresses of 2-day-old sprouts caused a significant decrease in protein content only in 4- and 6-day-old sprouts: however, it did not affect protein digestibility. The processes of elicitation were associated with significant changes in the nonprotein nitrogen content. The highest levels of free amino acids and peptides were determined for 6-day-old sprouts elicited at 40 °C—95.1 mg/(g of DW) (increase by 25% in comparison to control sprouts). It should be noted that the used modification of sprouting caused a significant elevation of activity of trypsin and chymotrypsin inhibitors but, as was mentioned before, treatments had no significant effects on protein digestibility (Table 5).

Elicitation of sprouts influenced also starch degradation during sprouting (Table 6). In comparison to control (sprouts from corresponding days of germination), levels of total starch in 3-day-old sprouts elicited at 40 °C and 4-day-old sprouts elicited at 4 °C were significantly lower. Treatment at 4 °C caused a significant increase of potentially bioavailable starch and eGI value in 3-day-old sprouts. On the other hand treatment at 40 °C caused a significant decrease of resistant starch content in sprouts; with respect to control sprouts from corresponding days of germination its content was lower by about 15% and 18% for 3- and 4-day-old sprouts, respectively. Between elicited sprouts, the highest eGI was determined for 3-day-old sprouts induced at 4 °C (76.7; elevation by 13% in comparison to control 3-day-old sprouts), whereas the lowest was for 4-day-old sprouts induced at 40 °C (59.8; reduction by

dx.doi.org/10.1021/jf403923x | J. Agric. Food Chem. 2014, 62, 3306−3313

Table 5. Effect of Thermal Stress on Nonprotein Nitrogen and Protein Content, Protein Digestibility, and Protease Inhibitor Activities in Sprouts[a]

time of germination (days)	cultivation conditions[b]	protein (mg/(g of DW))	nonprotein nitrogen (mg/(g of DW))	protein digestibility (%)	trypsin inhibitor activity (U/(mg of DW))	chymotrypsin inhibitor activity (U/(mg of DW))
2	C	253 ± 2.85d	27.6 ± 2.65a	79.5 ± 1.98f	4.34 ± 0.36a	0.49 ± 0.04b
3	C	253 ± 1.45d	34.5 ± 1.76b	75.2 ± 4.56def	4.30 ± 0.26a	0.36 ± 0.07a
	TC	260 ± 3.87e	49.9 ± 2.89c	78.2 ± 1.23e	6.35 ± 0.40 cd	0.78 ± 0.00 cd
	TH	254 ± 2.22de	34.1 ± 1.04b	72.9 ± 0.99 cd	7.94 ± 0.24e	0.88 ± 0.02de
4	C	246 ± 1.98c	56.4 ± 4.23d	70.5 ± 1.23bcd	4.02 ± 0.25a	0.49 ± 0.08b
	TC	227 ± 4.32b	56.8 ± 1.65d	72.8 ± 1.98bcd	6.48 ± 0.11d	0.67 ± 0.02c
	TH	227 ± 2.99b	54.3 ± 2.78d	66.9 ± 2.56ab	5.26 ± 0.55bc	0.93 ± 0.13d
6	C	243 ± 1.87c	77.0 ± 2.99e	66.5 ± 2.03a	4.50 ± 0.23c	0.72 ± 0.05c
	TC	213 ± 4.01a	92.7 ± 1.72f	63.1 ± 3.56a	6.09 ± 0.15b	0.83 ± 0.09d
	TH	221 ± 0.99b	95.1 ± 4.78f	64.2 ± 0.45a	4.84 ± 0.86ab	0.79 ± 0.28cde

[a]Means, in columns, for the respective components or activities followed by different small letters are significantly different at $\alpha = 0.05$. [b]C, control; TC, sprouts induced at 4 °C; TH, sprouts induced at 40 °C.

Table 6. Effect of Thermal Stress on Starch Content and Digestibility, Expected Glycemic Index (eGI), and α-Amylase Inhibitor Activities[a]

time (day)	cultivation conditions[b]	total starch (mg/(g of DW)	bioavailable starch (mg/(g of DW))	resistant starch (mg/(g of DW)	eGI	starch digestibility (%)	α-amylase inhibitor activity (AiU/(g of DW))
2		273 ± 0.55 cd	159 ± 4.98b	114 ± 3.07f	59.0a	60.7 ± 1.37b	61.5 ± 8.15bc
3	C	282 ± 4.33ed	177 ± 3.25c	105 ± 0.25e	67.6b	62.8 ± 0.15b	59.8 ± 5.50bc
	TC	302 ± 13.8f	201 ± 1.33e	101 ± 3.18c	76.7d	67.3 ± 0.44c	33.9 ± 2.00a
	TH	259 ± 7.43b	162 ± 3.31b	96.6 ± 0.13b	66.9b	62.6 ± 1.12b	77.8 ± 17.1c
4	C	270 ± 1.25bc	164 ± 7.11bc	107 ± 2.93e	71.6c	60.5 ± 1.27b	33.7 ± 20.0a
	TC	222 ± 4.15a	113 ± 4.44a	109 ± 2.42ef	59.8a	51.0 ± 2.69a	51.9 ± 14.5abc
	TH	264 ± 19.9b	177 ± 2.67c	86.8 ± 2.80a	70.0c	67.1 ± 1.43c	74.9 ± 3.47c
6	C	301 ± 8.15f	201 ± 1.32e	100 ± 3.12 cd	64.5b	66.8 ± 1.94c	35.4 ± 10.6a
	TC	306 ± 3.60f	184 ± 4.87d	123 ± 5.33g	65.5b	67.7 ± 1.18c	279 ± 39.5d
	TH	299 ± 12.87fe	201 ± 9.11de	95.6 ± 6.63abc	65.8b	59.9 ± 2.21b	227 ± 29.9d

[a]Means, in columns, for the respective components or activities followed by different small letters are significantly different at $\alpha = 0.05$. [b]C, control; TC, sprouts induced at 4 °C; TH, sprouts induced at 40 °C.

about 16% in comparison to control 4-day-old sprouts). It should be mentioned that both treatments (except 3-day-old TC sprouts) caused an increase of α-amylase inhibitors activity in sprouts; however only in cases of 4-day-old TC and 6-day-old TH sprouts may this fact be linked with reduction of starch digestibility. In the others cases there was no simple relationship between eGI values, α-amylase inhibitor activity, starch digestibility, and resistant starch content (Table 6).

DISCUSSION

Modern communities are strictly focused on consumption of functional and direct food with desired properties; thus, there is need for search new tools that may be useful in designing such products. In recent years, food legumes have attracted a great deal of attention due to their functional components and health-promoting effects in relation to the prevention of chronic diseases including cardiovascular diseases, obesity, diabetes, inflammation, and cancer. [1] The role of germination as a method affecting the quality of food is well-documented.[3,4,8,27,31] The gradual reduction in phenolic content and the antioxidant potential of lentil sprouts during germination confirmed by previous studies fully justifies the use of elicitation in order to improve the nutraceutical properties of sprouts.[3,4,7,8,31] A significant statistical reduction was also observed in the total phenolic, tannin, and flavonoids contents of black soybeans;[2] soybeans, lentil, and alfalfa;[9] and cowpea, lentil, chickpea, and green gram[8] due to the effect of germination. Losses may result from leaching into the soak water and binding of polyphenols with other organic substances such as carbohydrate or protein. [32] On germination, protein, carbohydrates, and minerals become more bioavailable and bioaccessible.[3,9,10,27] In this study the gradual reduction of protein content and digestibility was also determined. On the third and fourth days of germination a significant decrease of total starch content and digestibility was observed. These data agree with the findings of Ghavidel and Prakash for the germinated green gram, cowpea, lentil, and chickpea.[8] Similar results were also obtained by Urbano and co-workers during germination of lentil.[33]

Changes of nutritional and nutraceutical potential occurring during sprouting depend on process conditions.[3,5,14] Additionally, sprouting conditions can have important effects on the composition of secondary metabolites with potential prohealth properties.[5] Although we did not investigate the mechanism of phenolic compound stimulation by temperature stress, previous studies have shown that most phenolic compounds are generated by the phenylpropanoid pathway, which is stimulated by biotic and abiotic stress.[5,12,34] In response to stress, plants induce endogenous plant hormones, which, in turn, induce enzymes involved in the phenylpropanoid pathway, including phenylalanine ammonia lyase (PAL), thereby resulting in the accumulation of phenolic compounds.[11,34,36] In comparison to control, during growth of elicited sprouts an increase of chlorogenic acid and (+)-catechin content was observed. However, chlorogenic acid was probably synthesized *de novo*; in the case of (+)-catechin some additional factors, such as the

dx.doi.org/10.1021/jf403923x | J. Agric. Food Chem. 2014, 62, 3306−3313

rate of condensed tanins degradation and/or the activation of endogenous enzymes (e.g., hydroxylases and polyphenoloxydases), played an important role.[3,8] Additionally, higher levels of *p*-coumaric acid in treated sprouts might be involved in overproduction of coumaryl-CoA, a key compound in flavonoids biosynthesis.[5,37] This statement may be also supported by the fact that elicited sprouts contained higher amounts of quercetin. An increase of cell barrier precursors such as *p*-coumaric, ferulic, and syringic acids was also observed that may be linked with cross-talk response on stress conditions.[36] Finally, an increased level of salicylic acid content in sprouts induced by heat and cold shocks may confirm the appearance of stress and the role of this compound in the signal transduction pathway.[34,38] Induction of sprouts metabolism by low and high temperature and subsequent elevation of phenolics was translated into an increase of antioxidant potential. Up to now, there are some reports concerning improvement of the nutraceutical potential of sprouts by elicitation. An increase in the free radical scavenging properties of dark germinated mung bean sprouts using natural elicitors, such as fish protein hydrolysates, lactoferrin, and oregano extract, is reported.[13] Also, Feng and co-workers [39] obtained a significant elevation in the antioxidant potential of black soybean sprouts by treatment with components of fungal cell walls. In studies of Oh and Rajashekar [40] chilling and high light intensity during growth of radish and alfalfa sprouts caused qualitative and quantitative changes in phenolic profiles and antioxidant activities. The effect of salinity stress on the nutritional quality of buckwheat sprouts was also studied.[41] A cited researcher observed an increase in phenolic compounds, carotenoids, and antioxidant capacity in the sprouts compared with the control. In the light of our results and cited studies, it may be stated that elicitation has been demonstrated to be a useful method for improving the antioxidant potential of low-processed foods.

Because modification of the growth (elicitation with abiotic and biotic factors) often has a negative impact on the sprouts growth and nutritional quality of food (content and bioaccessibility of nutrition and increased activity of hydrolases inhibitors), an evaluation of the influence of treatments was performed. In recent literature there are only a few reports concerning the influence of elicitation on the nutritional quality of sprouts.[10,27] A decrease in the protein content and subsequent elevation of the nonprotein nitrogen fraction may be explained by induction of proteolytic systems in response to stress conditions.[8,11,35] As had been reported by previous studies (cross-talk stress response theory), [36] a slight elevation of protease inhibitors activity was observed; however there was not any strong influence. Changes in total starch content in elicited sprouts may be due to modification of seedling metabolism in response to stress conditions, especially with the increased demand for energy needed to produce secondary metabolites. [11] Generally, growth conditions used to modify sprouts metabolism allow one to obtain product with a significantly enhanced phenolics content and antioxidant capacity. What is important is that modification did not affect negatively the growth and nutritional quality of the sprouts. In the light of epidemiological studies these kinds of sprouts (with enhanced antioxidant potential and lowered glycemic index) may be a predisposed product for specific consumers and consist of a useful tool for creating healthy eating habits.

AUTHOR INFORMATION

Corresponding Author

*Tel.: + 48-81-4623327. Fax: +48-81-4623324. E-mail: michal.swieca@up.lublin.pl.

Notes

The authors declare no competing financial interest.

REFERENCES

(1) Zhao, J. Nutraceuticals, nutritional therapy, phytonutrients, and phytotherapy for improvement of human health: A perspective on plant biotechnology application. *Recent Pat. Biotechnol.* **2007**, *1*, 75−97.

(2) Lin, P.-Y.; Lai, H.-M. Bioactive compounds in legumes and their germinated products. *J. Agric. Food Chem.* **2006**, *54* (11), 3807−3814.

(3) Świeca, M.; Gawlik-Dziki, U.; Kowalczyk, D.; Złotek, U. Impact of germination time and type of illumination on the antioxidant compounds and antioxidant capacity of *Lens culinaris* sprouts. *Sci. Hortic. (Amsterdam, Neth.)* **2012**, *140*, 87−95.

(4) Świeca, M.; Gawlik-Dziki, U.; Jakubczyk, A. Impact of seedling cultivation density on the growth and some nutraceutical properties of ready-to-eat lentil (*Lens culinaris*) sprouts. *Acta Sci. Pol., Hortorum Cultus* **2013**, *12* (4), 19−29.

(5) Shetty, K. Role of proline-linked pentose phosphate pathway in biosynthesis of plant phenolics for functional food and environmental applications: A review. *Process Biochem.* **2004**, *39* (7), 789−804.

(6) Alonso, R.; Aguirre, A.; Marzo, F. Effects of extrusion and traditional processing methods on antinutrients and in vitro digestibility of protein and starch in faba and kidney beans. *Food Chem.* **2000**, *68*, 159−165.

(7) Gawlik-Dziki, U.; Jezyna, M.; Świeca, M.; Dziki, D.; Baraniak, B.; Czyz, J. Effect of bioaccessibility of phenolic compounds on in vitro anticancer activity of broccoli sprouts. *Food Res. Int.* **2012**, *49*, 469−476.

(8) Ghavidel, R. A.; Prakash, J. The impact of germination and dehulling on nutrients, antinutrients, in vitro iron and calcium bioavailability and in vitro starch and protein digestibility of some legume seed. *Food Sci. Technol.* **2007**, *40*, 1292−1299.

(9) Cevallos-Casals, B. A.; Cisneros-Zevallos, L. Impact of germination on phenolic content and antioxidant activity of 13 edible seed species. *Food Chem.* **2010**, *119* (4), 1485−1490.

(10) Świeca, M.; Baraniak, B. Influence of elicitation with, H_2O_2 on phenolics content, antioxidant potential and nutritional quality of *Lens culinaris* sprouts. *J. Sci. Food Agric.* **2014**, *94* (3), 489−496.

(11) Zhao, J.; Lawrence, C. D.; Verpoorte, R. Elicitor signal transduction leading to production of plant secondary metabolites. *Biotechnol. Adv.* **2005**, *23*, 283−333.

(12) Dixon, R. A.; Paiva, N. L. Stress-induced phenylopropanoid metabolism. *Plant Cell* **1995**, *7*, 1085−1097.

(13) Randhir, R.; Lin, Y.-T.; Shetty, K. Stimulation of phenolics, antioxidant and antimicrobial activities in dark germinated mung bean sprouts in response to peptide and phytochemical elicitors. *Process Biochem.* **2004**, *39*, 637−646.

(14) Gawlik-Dziki, U.; Świeca, M.; Dziki, D.; Sugier, D. Improvement of nutraceutical value of broccoli sprouts by natural elicitors. *Acta Sci. Pol., Hortorum Cultus.* **2013**, *12* (1), 129−140.

(15) Khattak, A. B.; Zeb, A.; Khan, M.; Bibi, N.; Khalil, S. A.; Khattak, I. M. S. Influence of germination techniques on phytic acid and polyphenols content of chickpea (*Cicer arietinum* L) sprouts. *Food Chem.* **2007**, *104*, 1074−1079.

(16) Singleton, V. L.; Orthofer, R.; Lamuela-Raventos, R. M. Analysis of total phenols and other oxidation substrates and antioxidants by means of Folin-Ciocalteu reagent. *Methods Enzymol.* **1974**, *299*, 152−178.

(17) Lamaison, J. L. C.; Carnat, A. Teneurs en principaux flavonoids des fleurs de Crataegeus monogyna Jacq et de Crataegeus laevigata (Poiret D. C) en fonction de la vegetation. *Pharm. Acta Helv.* **1990**, *65*, 315−320.

(18) Sun, B.; Ricardo-Da-Silva, J. M.; Spranger, I. Critical factors of vanillin assay for catechins and proanthocyanidins. *J. Agric. Food Chem.* **1998**, *46*, 4267−4274.
(19) Re, R.; Pellegrini, N.; Proteggente, A.; Pannala, A.; Yang, M.; Rice-Evans, C. Antioxidant activity applying an improved ABTS radical cation decolorization assay. *Free Radicals Biol. Med.* **1999**, *26* (9−10), 1231−1237.
(20) Oyaizu, M. Studies on products of browning reaction—Antioxidative activities of products of browning reaction prepared from glucosamine. *Jpn. J. Nutr.* **1986**, *44*, 307−315.
(21) Guo, J.-T.; Lee, H.-L.; Chiang, S.-H.; Lin, H.-I.; Chang, C.-Y. Antioxidant properties of the extracts from different parts of broccoli in Taiwan. *J. Food Drug Anal.* **2001**, *9* (2), 96−101.
(22) Groupy, P.; Vulcain, E.; Caris-Veyrat, C.; Dangles, O. Dietary antioxidants as inhibitors of the heme-induced peroxidation of linoleic acid: Mechanism of action and synergism. *Free Radicals Biol. Med.* **2007**, *43*, 933−943.
(23) Lowry, O. H.; Rosebrough, N. J.; Farr, L.; Randall, R. J. Protein measurement with the Folin phenol reagent. *J. Biol. Chem.* **1951**, *193*, 265−275.
(24) Habeeb, A. Determination of free amino groups in proteins by trinitrobenzenosulfonic acid. *Anal. Biochem.* **1966**, *14*, 328−336.
(25) Goni, I.; Garcia-Alonso, A.; Saura-Calixto, F. A starch hydrolysis procedure to estimate glycemic index. *Nutr. Res.* **1997**, *17*, 427−437.
(26) Miller, G. L. Use of dinitrosalicylic acid reagent for determination of reducing sugar. *Anal. Chem.* **1959**, *31* (3), 426−428.
(27) Świeca, M.; Gawlik-Dziki, U.; Baraniak, B. In vitro digestibility and starch content, predicted glycemic index and potential in vitro antidiabetic effect of lentil sprouts obtained by different germination techniques. *Food Chem.* **2013**, *138* (2−3), 1414−1420.
(28) Granfeldt, Y.; Björck, I.; Drews, A.; Tovar, J. An in vitro procedure based on chewing to predict metabolic responses to starch in cereal and legume products. *Eur. J. Clin. Nutr.* **1992**, *46*, 649−660.
(29) Kakade, M. L.; Rackis, J. L.; McGhee, J. E.; Puski, G. Determination of trypsin inhibitor activity of soy bean products: A collaborative analysis of an improved procedure. *Cereal Chem.* **1974**, *51*, 376−382.
(30) Sathe, S. K.; Salunkhe, D. K. Studies on trypsin and chymotrypsin inhibitory activities, hemagglutinating activity, and sugars in the Great Northern beans (*Phaseolus vulgaris* L). *J. Food Sci.* **1981**, *46*, 626−629.
(31) Fernandez-Orozco, R.; Frias, J.; Zielinski, H.; Piskula, M. K.; Kozlowska, H.; Vidal-Valverde, C. Kinetic study of the antioxidant compounds and antioxidant capacity germination of *Vigna radiata* cv. emmerald, *Glycine max* cv. jutro and *Glycine* 419 *max* cv. Merit. *Food Chem.* **2008**, *111* (3), 622−630.
(32) Khandelwal, S.; Udipi, S. A.; Ghugre, P. Polyphenols and tannins in Indian pulses: effect of soaking, germination and pressure cooking. *Food Res. Int.* **2010**, *43* (2), 526−530.
(33) Urbano, G.; Lopez-Jurado, M.; Hernandez, J.; Fernandez, M.; Moren, M. C.; Frias, J.; Dıaz-Pollan, C.; Prodanov, M.; Vidal-Valverde, C. Nutritional assessment of raw, heated and germination lentils. *J. Agric. Food Chem.* **1995**, *43*, 1871−1877.
(34) Shinozaki, K.; Yamaguchi-Shinozaki, K. In *Molecular responses to cold, drought, heat and salt stress in higher plants*; Shinozaki, K., Yamaguchi-Shinozaki, K. R. G., Eds.; Landes: Austin, TX, USA, 1999. .
(35) Kosová, K.; Vítámvás, P.; Prášil, I. T.; Renaut, J. Plant proteome changes under abiotic stress—Contribution of proteomics studies to understanding plant stress response. *J. Proteomics* **2011**, *74* (8), 1301−1322.
(36) Fujita, M.; Fujita, Y.; Noutoshi, Y.; Takahashi, F.; Narusaka, Y.; Yamaguchi-Shinozaki, K.; Shinozaki, K. Crosstalk between abiotic and biotic stress responses: A current view from the points of convergence in the stress signaling networks. *Curr. Opin. Plant Biol.* **2006**, *9* (4), 436−442.
(37) Winkel-Shirley, B. Biosynthesis of flavonoids and effects of stress. *Curr. Opin. Plant Biol.* **2002**, *5*, 218−223.
(38) Shulaev, V.; Cortes, D.; Miller, G.; Mittler, R. Metabolomics for plant stress response. *Physiol. Plant.* **2008**, *132* (2), 199−208.
(39) Feng, S.; Song, L.; Lee, Y. K.; Huang, D. The effects of fungal stress on the antioxidant contents of black soybeans under germination. *J. Agric. Food Chem.* **2010**, *58* (23), 12491−12496.
(40) Oh, M.-M.; Rajeshekar, C. B. Antioxidant content of edible sprouts: Effect of environmental shocks. *J. Sci. Food Agric.* **2009**, *89*, 2221−2227.
(41) Lim, J.-H.; Park, K.-J.; Kim, B.-K.; Jeong, J.-W.; Kim, H.-J. Effect of salinity stress on phenolic compounds and carotenoids in buckwheat (*Fagopyrum esculentum* M.) sprout. *Food Chem.* **2012**, *135*, 1065−1070.

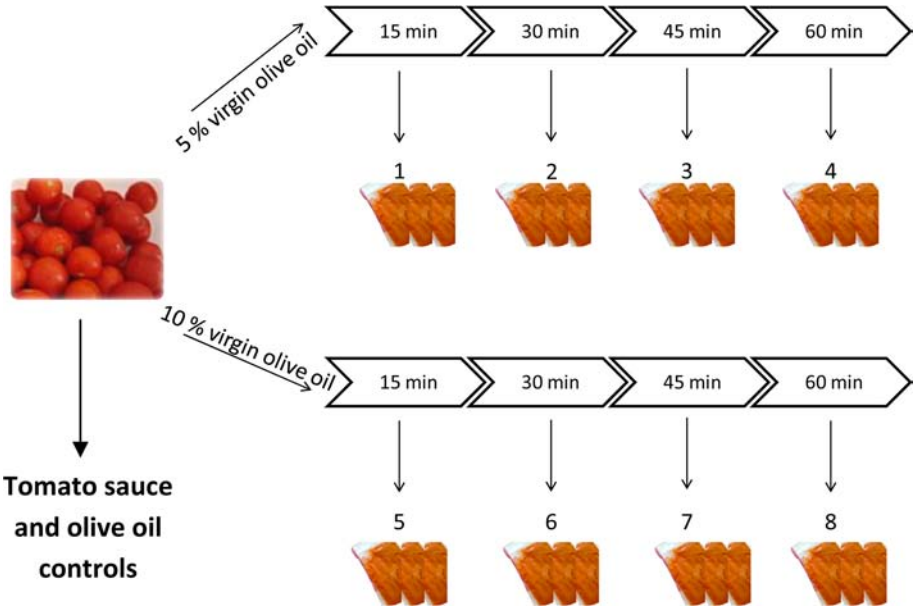

Figure 1. Diagram flowchart of the processes.

Table 1. Levels of Polyphenols in Tomato Sauce Control

chlorogenic acid (μg/g FW)	caffeic acid (μg/g FW)	ferulic acid (μg/g FW)	*p*-coumaric acid (μg/g FW)	protocatechuic acid (μg/g FW)	quercetin (μg/g FW)	rutin (μg/g FW)	naringenin (μg/g FW)	tyrosol (μg/g FW)	hydroxytyrosol (μg/g FW)
2.61 ± 0.03	2.55 ± 0.06	7.05 ± 0.43	0.15 ± 0.03	1.19 ± 0.08	3.02 ± 0.12	28.30 ± 0.41	4.97 ± 0.39	BDL[a]	BDL

[a]BDL: below detection limit.

Table 2. Levels of Polyphenols in VOO

chlorogenic acid (μg/g FW)	caffeic acid (μg/g FW)	ferulic acid (μg/g FW)	*p*-coumaric acid (μg/g FW)	protocatechuic acid (μg/g FW)	quercetin (μg/g FW)	rutin (μg/g FW)	naringenin (μg/g FW)	tyrosol (μg/g FW)	hydroxytyrosol (μg/g FW)
BDL[a]	BDL	0.41 ± 0.03	BDL	BDL	BDL	BDL	BDL	12.13 ± 0.67	8.15 ± 0.44

[a]BDL: below detection limit.

the study. VOO was kindly furnished by Manuel Heredia Halcón (Cortijo de la Suerte Alta, Albendin-Baena-Cordoba). The tomato sauces were prepared following a regular home cooking process at the Torribera Campus, University of Barcelona (Barcelona, Spain). Tomatoes were washed, chopped in a breaker unit, weighed, and crushed with a Thermomix. Two variables were evaluated: VOO addition at two different concentrations and thermal treatment time. The VOO (5 and 10% of oil, w/w) was added to the chopped tomatoes, and the mixture was cooked at 95−96 °C for 15, 30, 45, or 60 min. The tomato sauces were aliquoted and stored in vacuum bags at −20 °C until the day of the analysis. A 4 × 2 mixed-level factorial design was performed, involving a total of 8 randomized runs. For the reproducibility, each process was evaluated three times (Figure 1). The phenolic profile of tomato sauce control without addition of VOO and the content of polyphenols in VOO are reported in Tables 1 and 2.

Extraction and Analysis of Polyphenols. *Extraction of Polyphenols from Tomato Sauces.* Extraction and analysis of each replicate of the treatment was carried out in triplicate in a darkened room with a red safety light to prevent analyte oxidation, following the procedure of Vallverdu-Queralt et al.[13] with some modifications.

Tomato sauces (0.5 g) were weighed and homogenized with 80% ethanol in Milli-Q water (4 mL); the homogenate was sonicated for 5 min and centrifuged (4000 rpm at 4 °C) for 15 min. The supernatant was transferred into a flask and extraction was repeated. Both supernatants were combined and evaporated under nitrogen flow; finally, the residue was reconstituted up to 2 mL with Milli-Q water containing 0.1% of formic acid and filtered through a 0.45-μm polytetrafluoroethylene (PTFE) filter from Waters (Milford, USA) into an insert-amber vial.

Solid phase extraction (SPE) was carried out to eliminate interferences such as ascorbic acid, amino acids, and reducing sugars. For this purpose, Oasis MAX cartridges with 30 mg of mixed-mode anion-exchange and reversed-phase sorbent from Waters (Milford, USA) were used following the procedure of Vallverdu-Queralt et al.[14] The eluted fractions were evaporated under nitrogen flow and the residue was reconstituted up to 500 μL with Milli-Q water containing 0.1% formic acid and filtered through a 0.45-μm PTFE filter into an insert-amber vial for HPLC analysis.

Extraction of Polyphenols from VOO. The extraction of phenolic compounds from VOO was performed following the procedure previously described by García-Villalba et al.[15] Briefly, diol cartridges Supelclean LC-Diol (500 mg, 3 mL) from Sigma (Madrid, Spain) were placed in a SPE vacuum manifold and conditioned passing 5 mL of methanol and subsequently 5 mL of *n*-hexane without vacuum. About 3 g of VOO was accurately weighted and then thoroughly mixed with 3 mL of *n*-hexane and loaded onto the SPE cartridge under vacuum. The cartridge was then washed with 5 mL of *n*-hexane to remove the nonpolar fraction of the oil and then dried with nitrogen to remove the *n*-hexane. Finally, the phenolic compounds were eluted with 10 mL methanol under vacuum and the eluate was evaporated to dryness. The dried residue was then reconstituted in 1 mL of methanol/water (7:3, v/v) and filtered through a 0.45-μm PTFE filter for HPLC analysis.

Analysis of Polyphenols. Liquid chromatography coupled to electrospray ionization tandem mass spectrometry (HPLC−ESI-MS/

dx.doi.org/10.1021/jf500416n | J. Agric. Food Chem. 2014, 62, 3314−3320

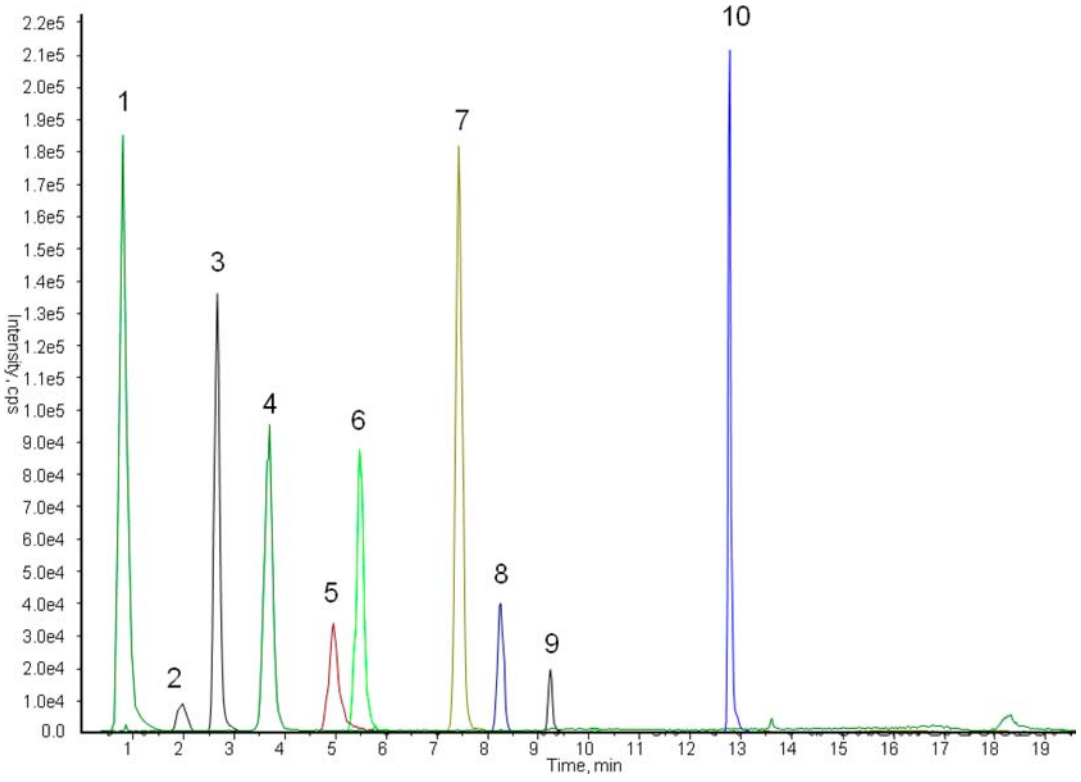

Figure 2. HPLC Chromatogram of tomato sauce treated during 15 min at 5% of VOO. 1. Hydroxytyrosol; 2. tyrosol; 3. protocatechuic acid; 4. chlorogenic acid; 5. caffeic acid; 6. *p*-coumaric acid; 7. rutin; 8. ferulic acid; 9. quercetin; 10. naringenin.

MS) was used to evaluate the content of flavonols, flavanones, and hydroxycinnamic acids in VOO and tomato sauces following the procedure of Vallverdu-Queralt et al.[13]

Liquid chromatography was performed with an Agilent series 1100 HPLC instrument (Agilent, Waldbronn, Germany) equipped with a quaternary pump, an autosampler, and a column oven set to 30 °C. A Luna C_{18} column 50 × 2.0 mm i.d., 5 μm (Phenomenex, Torrance, CA, USA) was used. The injection volume was 20 μL and the flow rate was 0.4 mL/min. Mobile phase consisted of Milli-Q water containing 0.5% acetic acid (A) and acetonitrile (B). Separation was carried out in 15 min under the following conditions: 0 min, 5% B; 10 min, 18% B; 13 min, 100% B; 14 min, 100% B; 15 min, 5% B. The column was equilibrated for 5 min prior to each analysis.

An API 3000 (PE Sciex, Concord, ON, Canada) triple quadrupole mass spectrometer equipped with a Turbo Ionspray source in negative-ion mode was used to obtain MS/MS data. Turbo Ionspray source settings were as follows: capillary voltage, −3500 V; nebulizer gas (N_2), 10 au (arbitrary units); curtain gas (N_2), 12 au; collision gas (N_2), 4 au; focusing potential, −200 V; entrance potential, −10 V; drying gas (N_2), heated to 400 °C and introduced to a flow rate of 6000 cm^3/min. The declustering potential and collision energy were optimized for each compound by infusion experiments: individual standard solutions (10 μg/mL) dissolved in 50:50 (v/v) mobile phase were infused at a constant flow rate of 5 μL/min using a model syringe pump (Harvard Apparatus, Holliston, MA, USA). Full-scan data acquisition was performed scanning from m/z 100 to 800 in profile mode and using a cycle time of 2 s with a step size of 0.1 u and a pause between each scan of 2 ms. For quantification purposes, data were collected in the multiple reaction monitoring (MRM) mode, tracking the transition of parent and product ions specific for each compound.

Quantification of polyphenols was performed by the internal standard method. Polyphenols were quantified related to their corresponding standard and results were expressed as μg/g fresh weight (FW).

Antioxidant Capacity. The antioxidant capacity of tomato sauces was measured using $ABTS^+$ and DPPH assays.[12]

$ABTS^+$ assay. One mM Trolox (antioxidant standard) was prepared in methanol once a week. Working standards were prepared daily by diluting 1 mM Trolox with methanol.

An $ABTS^+$ radical cation was prepared by passing a 5 mM aqueous stock solution of ABTS (in methanol) through manganese dioxide powder. Excess manganese dioxide was filtered through a 0.45-μm filter PTFE (Waters). Before analysis, the solution was diluted in methanol pH 7.4 to give an absorbance at 734 nm of 1.0 ± 0.1, and preincubated in ice. Then, 245 μL of $ABTS^+$ solution was added to 5 μL of Trolox or to tomato extracts and the solutions were stirred for 30 s. The absorbance was recorded continuously every 30 s with a UV/vis Multiskan Spectrum spectrophotometer from Thermo Fisher Scientific (San Jose, CA, USA) for 1 h and methanol blanks were run in each assay.

The working range for Trolox (final concentration 0−750 μM) was based on triplicate determinations and consisted of plotting the absorbance as a percentage of the absorbance of the uninhibited radical cation (blank). The activities of the tomato extracts were assessed at four different concentrations within the range of the dose−response curve. Each sample was analyzed in triplicate at each concentration. Results were expressed as mmol Trolox equivalent (TE)/100 g FW.

DPPH Assay. Antioxidant capacity was also studied by evaluating the free radical-scavenging effect on the DPPH radical. Solutions of known Trolox concentrations were used for calibration. Five μL of tomato extracts or Trolox was mixed with 250 μL of methanolic DPPH (0.025 g/L). The homogenate was shaken vigorously and kept in darkness for 30 min. Absorption of the samples was measured on a UV/vis Thermo Multiskan Spectrum spectrophotometer at 515 nm. The percentage of inhibition of the DPPH was calculated and plotted as a function of the concentration of Trolox for the standard reference data. The final DPPH values were calculated using a regression equation between the Trolox concentration and the percentage of DPPH inhibition and results were expressed as mmol TE/100 g FW.

Statistical Treatments. Treatments of tomato sauces were carried out in triplicate and each replicate was analyzed three times. Significance of the results and statistical differences were analyzed

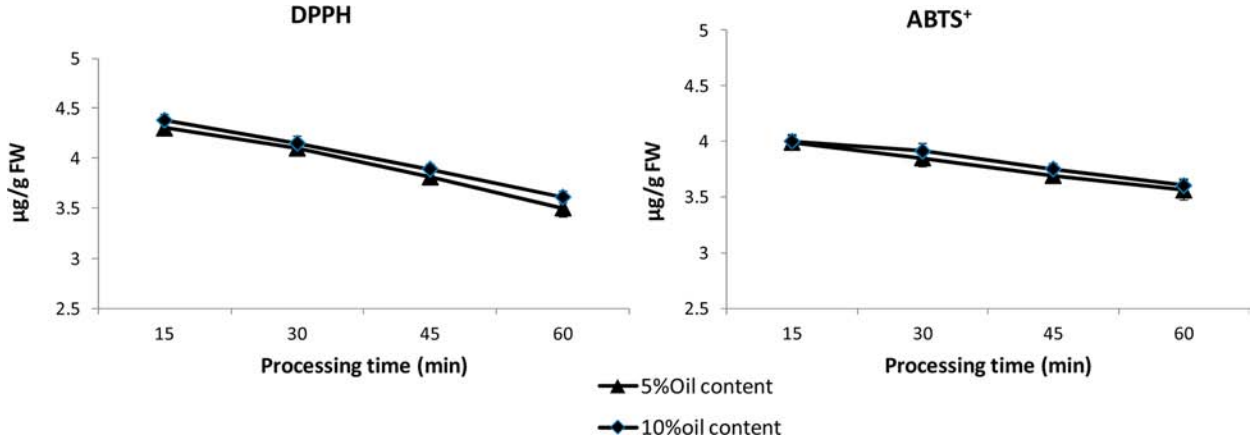

Figure 3. Changes in antioxidant capacity during processing time.

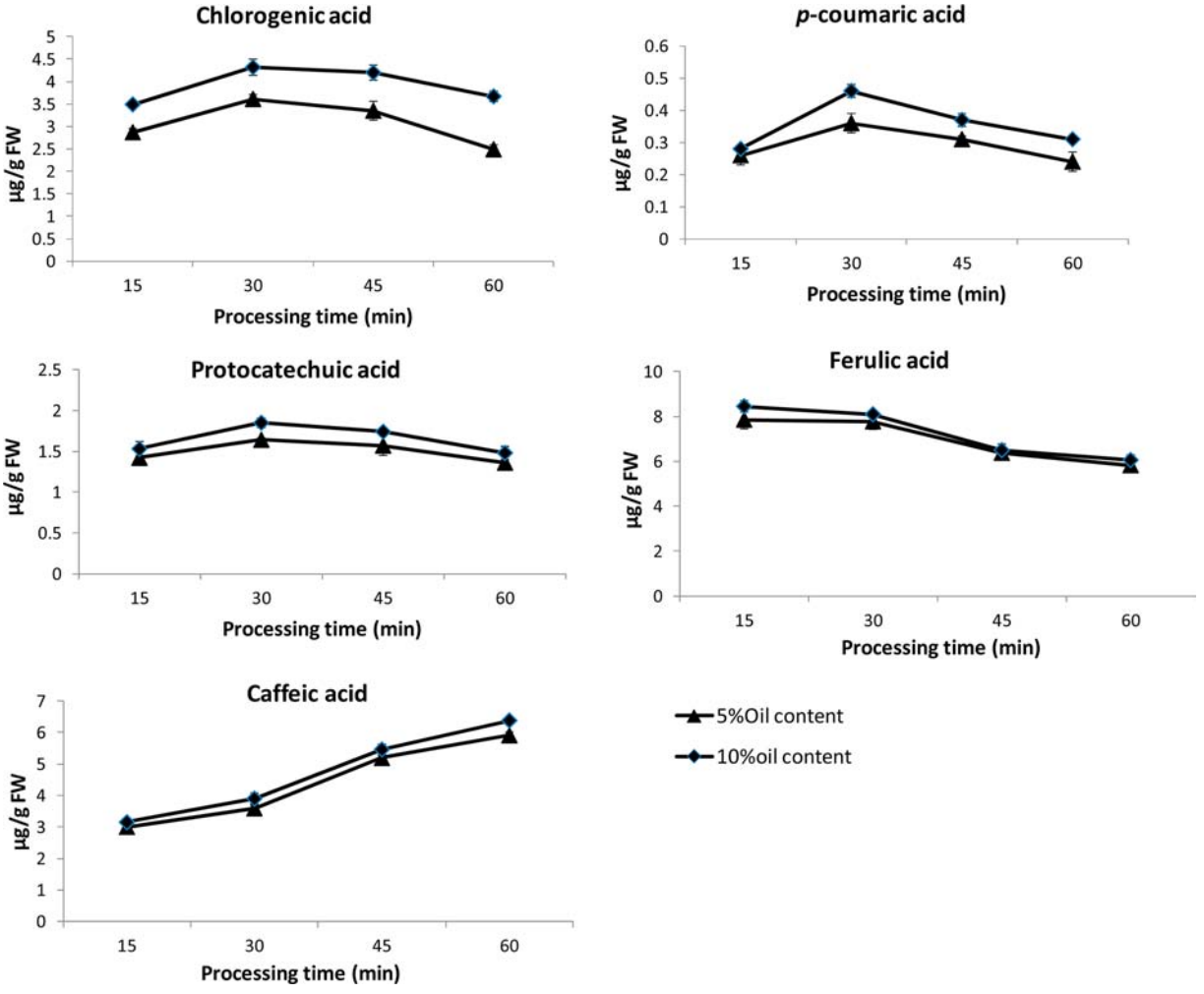

Figure 4. Changes in hydroxycinnamic and phenolic acids during processing time.

using Statgraphics plus v. 5.1 software (Manugistics, Inc., Rockville, MA, USA). Data were analyzed by multifactor analysis of variance and a Duncan multiple range test was applied to determine differences among means, with a significance level of $P = 0.05$.

RESULTS AND DISCUSSION

Changes in Antioxidant Capacity during Processing Time. It has been reported that some labile antioxidants are degraded during food processing, but other studies have shown that industrial-scale processing of tomatoes involving heat treatments may increase the levels of some bound antioxidants.[16,17] Figure 2 shows a chromatogram of tomato sauce treated during 15 min at 5% of VOO. Our analysis of antioxidant capacity showed that from 15 to 60 min of cooking, the level of antioxidants measured by the DPPH assay decreased from 4.3 to 3.5 μg/g FW in sauces containing 5% VOO and from 4.4 to 3.6 μg/g FW in sauces containing 10% extra VOO (Figure 3). The same pattern was observed in the

dx.doi.org/10.1021/jf500416n | J. Agric. Food Chem. 2014, 62, 3314−3320

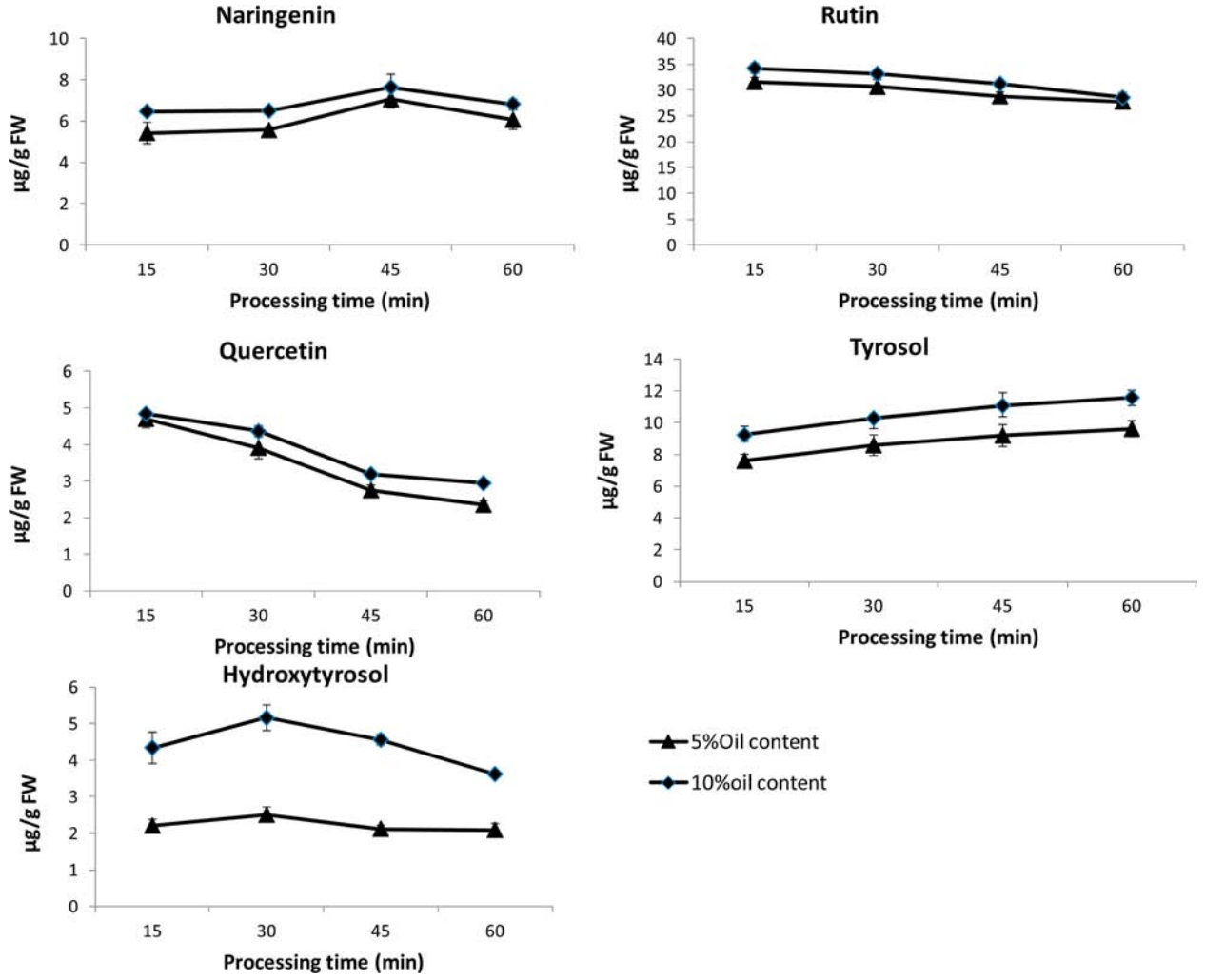

Figure 5. Changes in flavonols, flavanones, and other phenols.

ABTS$^+$ assay. Thermal processing of sauces might be expected to have an effect on heat-labile and oxidizable compounds. However, Dewanto et al.[18] reported that total polyphenols did not change during tomato processing.

The phenolic profile of tomato sauce control without addition of VOO and the content of polyphenols in VOO are reported in Tables 1 and 2. For all polyphenols, levels in tomato sauce control are lower than in samples containing 5% or 10% VOO (Figures 4 and 5). Probably, VOO enhances the extractability of phenolic compounds.[5] Moreover, tomato sauces with 5 and 10% VOO contain tyrosol and hydroxytyrosol due to the addition of VOO. It has previously been reported that the addition of olive oil to tomato sauces enriches meals with other polyphenols not present in tomatoes such as tyrosol and hydroxytyrosol.[3,6,7]

Changes in Hydroxycinnamic and Phenolic Acids during Processing Time. In our study, hydroxycinnamic and phenolic acids were also analyzed (Figure 4). *p*-Coumaric, protocatechuic, and chlorogenic acids achieved their maximum levels (0.3−4 μg/g FW) at 30 min of cooking, regardless of the amount of VOO added (5 or 10%) and then decreased slightly (at 45 and 60 min) (Figure 4). Higher levels of these compounds were found when sauces were supplemented with 10% rather than 5% of VOO. For example, at 30 min of cooking, sauces with 10% of VOO contained 4 μg/g FW of chlorogenic acid, whereas in those containing 5% of VOO, levels of chlorogenic acid were 3 μg/g FW (Figure 4). The same behavior was exhibited by protocatechuic and *p*-coumaric acids. The food matrix containing phenolic compounds plays a crucial role in determining their accessibility and bioavailability from food.[5] Thus, higher amounts of VOO could promote the extraction of phenolic compounds from tomato, leading to a higher phenolic content in the sauce.

Through the catalytic oxidation process, hydroxycinnamic acids can undergo oxidation to reactive *O*-quinones, which can interact with NH_2 and SH groups of amino acids.[19] However, in this work caffeic acid increased from 3 to 6 μg/g FW at 15−60 min of thermal treatment, irrespective of the amount of VOO added (5 or 10%) (Figure 4). It has been reported that air-drying tomatoes at 80 °C increases the number of free hydroxyl phenol groups owing to the hydrolysis of flavonoid glycosides and/or the release of cell wall polyphenols.[20] The 2-fold increase in caffeic acid we observed is in accordance with the results of Re et al.,[21] who reported a similar effect of heat treatment. In contrast, it should be noted that we observed the maximum concentration of ferulic acid at 15 min, after which it decreased slightly (at 30, 45, and 60 min). Values for ferulic acid at 15 min were 7.8 μg/g FW and 8.4 μg/g FW in sauces containing 5% and 10% of VOO, respectively (Figure 4). The addition of 10% of VOO slightly increased the amount of all

studied polyphenols, supporting the likelihood that olive oil added in the culinary process is an important factor increasing phenolic extractability.[5]

Changes in Flavonols, Flavanones, and Other Phenols. On the basis of average yearly consumption, red tomatoes contain 15 μg/g FW of flavonoids, determined as aglycones, according to the USDA flavonoid database. Naringenin (45%) is reported to be the main flavonoid in tomatoes, followed by quercetin (39%), myricetin (10%), and kaempferol (5%).[22] Other studies report rutin as the main flavonoid in several tomato cultivars.[14,22] In our work, rutin was the dominant flavonol in all the treatments, followed by naringenin. Naringenin contents increased slightly from 5.4 μg/g FW at 15 min of cooking to 6 μg/g FW at 45 min when sauces contained 5% of VOO. The same pattern was observed in sauces containing 10% olive oil. Longer cooking periods of up to 60 min resulted in a decrease in naringenin, irrespective of the content of added VOO (5 or 10%) (Figure 5). Our results are in accordance with Re et al.,[21] who analyzed the effects of three different methods for processing tomato sauces. The effect of processing on naringenin could be attributed to the formation of reactive quinones and the extensive oxidation process created during thermal processing.[23]

Similarly, rutin decreased from 35 μg/g FW in sauces cooked for 15 min with 5% of VOO to 28.5 μg/g FW after 60 min of cooking. The same pattern was observed in sauces containing 10% of VOO, with rutin decreasing from 30 to 27 μg/g FW during the thermal treatment (Figure 5). Capanoglu et al.[24] found that rutin decreased after heat treatments of up to 80 °C. These results are in agreement with those described previously.[25]

Quercetin decreased more abruptly during the cooking process than rutin, being reduced from 5 to 3 μg/g FW in sauces containing 5% VOO and from 4.7 to 2.30 μg/g FW in sauces containing 10% VOO (Figure 5). The acceleration of quercetin and rutin degradation may be caused by reactive oxygen species that are captured by flavonols. During thermal processing the flavonols are able to transfer one or two hydrogen atoms, forming quinonoid structures, which leads to the formation of quinones.[26] In the case of rutin, the 3-hydroxy-function at the *C*-ring is blocked by a sugar moiety, whereas in quercetin it remains unoccupied, thus explaining the higher stability of rutin toward oxidation.[27] Naringenin and rutin levels were slightly increased by the addition of 10% of VOO, once again suggesting that oil added in the culinary process may enhance the extractability of phenolic compounds from food.[5]

Finally, tyrosol and hydroxytyrosol from tomato sauces were also evaluated. Hydroxytyrosol increased during the cooking process from 15 to 30 min, decreasing thereafter (at 45 and 60 min), whereas tyrosol continued to increase slightly throughout (at 15, 30, 45, and 60 min) (Figure 5). These results are in line with those of Cheikhousman et al.,[28] who reported that during thermal oxidation hydroxytyrosol derivatives are the first antioxidants to be lost, which means they are the first compounds to be oxidized, while tyrosol derivatives seem to be the most stable compounds. This observed pattern is also in agreement with the high antioxidant activity of hydroxytyrosol and its secoiridoid derivatives in VOO compared with tyrosol derivatives.[29] Polyphenols from VOO are effective stabilizers of alpha-tocopherol during heating, thus contributing to the nutritional value of cooked foods.[30] The addition of VOO (5 or 10%) clearly enhanced the levels of both tyrosol and hydroxytyrosol, since both compounds are the main phenolic acids in VOO.[31]

In summary, in this work the effects of cooking time (15, 30, 45, and 60 min) and the amount of added VOO (5 and 10%) on the phenolic profile of tomato sauces were evaluated using HPLC−MS/MS. As a general pattern, the longer the cooking process, the greater the decrease in levels of polyphenols and antioxidants, with the exception of caffeic acid and tyrosol. However, during thermal treatments, free hydroxyl phenol groups may increase due to the hydrolysis of flavonoid glycosides and/or the release of cell wall polyphenols. Tomato sauces prepared with a higher percentage of VOO contained higher levels of polyphenols. Thus, the use of VOO in the culinary process may increase the range of phenolic compounds in the meal, and can also enhance phenolic bioavailability. There is not an increase in the antioxidant capacity with the oil addition, however, this does not mean that the functional capacity or the nutritional properties of these sauces with virgin olive oil have not increased; since a previous human intervention study from our group (data not yet published) demonstrated that the addition of refined oil in tomato sauce increased the antinflammatory properties of the sauce.

AUTHOR INFORMATION

Corresponding Author

*Telephone: +34-934034843. Fax: +34-934035931. e-mail: lamuela@ub.edu.

Funding

The authors express their gratitude to CICYT(AGL2010-22319-C03), from the Spanish Ministry of Science and Innovation (MICINN) for financial support and to the CIBERobn, that is an initiative from the Instituto de Salud Carlos III, Spain.

Notes

The authors declare no competing financial interest.

REFERENCES

(1) Cassidy, A. n.; Mukamal, K. J.; Liu, L.; Franz, M.; Eliassen, A. H.; Rimm, E. B. High anthocyanin intake is associated with a reduced risk of myocardial infarction in young and middle-aged women. *Circulation* **2013**, *127* (2), 188−196.

(2) Kay, C. D.; Hooper, L.; Kroon, P. A.; Rimm, E. B.; Cassidy, A. n. Relative impact of flavonoid composition, dose and structure on vascular function: A systematic review of randomised controlled trials of flavonoid-rich food products. *Mol. Nutr. Food Res.* **2012**, *56* (11), 1605−1616.

(3) Martin-Pelaez, S.; Covas, M. I.; Fito, M.; Kusar, A.; Pravst, I. Health effects of olive oil polyphenols: Recent advances and possibilities for the use of health claims. *Mol. Nutr. Food Res.* **2013**, *57* (5), 760−771.

(4) Visioli, F.; Galli, C. Olive oil phenols and their potential effects on human health. *J. Agric. Food Chem.* **1998**, *46* (10), 4292−4296.

(5) Tulipani, S.; Martínez-Huélamo, M.; Rotchés-Ribalta, M.; Estruch, R.; Ferrer, E.; Andres-Lacueva, C.; Illan, M.; Lamuela-Raventós, R. M. Oil matrix effects on plasma exposure and urinary excretion of phenolic compounds from tomato sauces: Evidence from a human pilot study. *Food Chem.* **2011**, *130*, 581−590.

(6) Torre-Carbot, K.; Jauregui, O.; Gimeno, E.; Castellote, A. I.; Lamuela-Raventos, R. M.; Lopez-Sabater, M. C. Characterization and quantification of phenolic compounds in olive oils by solid-phase extraction, HPLC-DAD, and HPLC-MS/MS. *J. Agric. Food Chem.* **2005**, *53* (11), 4331−4340.

(7) Miro-Casas, E.; Covas, M. I.; Fito, M.; Farre-Albadalejo, M.; Marrugat, J.; de la Torre, R. Tyrosol and hydroxytyrosol are absorbed

from moderate and sustained doses of virgin olive oil in humans. *Eur. J. Clin. Nutr.* **2003**, *57* (1), 186−190.
(8) Sharma, S. K.; LeMaguer, M. Lycopene in tomatoes and tomato pulp fraction. *Ital. J. Food Sci.* **1996**, *8* (2), 107−113.
(9) Goula, A. M.; Adamopoulos, K. G.; Chatzitakis, P. C.; Nikas, V. A. Prediction of lycopene degradation during a drying process of tomato pulp. *J. Food Eng.* **2006**, *74* (1), 37−46.
(10) Vallverdu-Queralt, A.; Medina-Remon, A.; Casals-Ribes, I.; Andres-Lacueva, C.; Waterhouse, A. L.; Lamuela-Raventos, R. M. Effect of tomato industrial processing on phenolic profile and hydrophilic antioxidant capacity. *LWT−Food Sci. Technol.* **2012**, *47* (1), 154−160.
(11) Chang, C. H.; Liu, Y. C. Study on lycopene and antioxidant contents variations in tomatoes under air-drying process. *J Food Sci.* **2007**, *72* (9), E532−E540.
(12) Vallverdú-Queralt, A.; Medina-Remón, A.; Andres-Lacueva, C.; Lamuela-Raventos, R. M. Changes in phenolic profile and antioxidant activity during production of diced tomatoes. *Food Chem.* **2011**, *126* (4), 1700−1707.
(13) Vallverdú-Queralt, A.; Rinaldi de Alvarenga, J. F.; Estruch, R.; Lamuela-Raventos, R. M. Bioactive compounds present in the Mediterranean sofrito. *Food Chem.* **2013**, *141*, 3366−3372.
(14) Vallverdu-Queralt, A.; Medina-Remon, A.; Martinez-Huelamo, M.; Jauregui, O.; Andres-Lacueva, C.; Lamuela-Raventos, R. M. Phenolic profile and hydrophilic antioxidant capacity as chemotaxonomic markers of tomato varieties. *J. Agric. Food Chem.* **2011**, *59* (8), 3994−4001.
(15) Garcia-Villalba, R.; Carrasco-Pancorbo, A.; Oliveras-Ferraros, C.; Vazquez-Martin, A.; Menendez, J. A.; Segura-Carretero, A. Characterization and quantification of phenolic compounds of extra-virgin olive oils with anticancer properties by a rapid and resolutive LC-ESI-TOF MS method. *J. Pharm. Biomed. Anal.* **2010**, *51*, 416−429.
(16) Abushita, A. A.; Daood, H. G.; Biacs, P. A. Change in carotenoids and antioxidant vitamins in tomato as a function of varietal and technological factors. *J. Agric. Food Chem.* **2000**, *48* (6), 2075−2081.
(17) Dewanto, V.; Wu, X.; Adom, K. K.; Liu, R. H. Thermal processing enhances the nutritional value of tomatoes by increasing total antioxidant activity. *J. Agric. Food Chem.* **2002**, *50* (10), 3010−3014.
(18) Dewanto, V.; Wu, X.; Adom, K. K.; Liu, R. H. Thermal processing enhances the nutritional value of tomatoes by increasing total antioxidant activity. *J. Agric. Food Chem.* **2002**, *50* (10), 3010−3014.
(19) Friedman, M. Dietary impact of food processing. *Annu. Rev. Nutr* **1992**, *12*, 119−137.
(20) Lavelli, V.; Hippeli, S.; Peri, C.; Elstner, E. F. Evaluation of radical scavenging activity of fresh and air-dried tomatoes by three model reactions. *J. Agric. Food Chem.* **1999**, *47* (9), 3826−3831.
(21) Re, R.; Bramley, P. M.; Rice-Evans, C. Effects of food processing on flavonoids and lycopene status in a Mediterranean tomato variety. *Free Radical Res.* **2002**, *36* (7), 803−810.
(22) Slimestad, R.; Fossen, T.; Verheul, M. J. The flavonoids of tomatoes. *J. Agric. Food Chem.* **2008**, *56* (7), 2436−2441.
(23) Singleton, V. L. Oxygen with phenols and related reactions in musts, wines, and model systems - Observations and practical implications. *Am. J. Enol. Vitic.* **1987**, *38* (1), 69−77.
(24) Capanoglu, E.; Beekwilder, J.; Boyacioglu, D.; Hall, R.; de Vos, R. Changes in antioxidant and metabolite profiles during production of tomato paste. *J. Agric. Food Chem.* **2008**, *56* (3), 964−973.
(25) Lavelli, V.; Peri, C.; Rizzolo, A. Antioxidant activity of tomato products as studied by model reactions using xanthine oxidase, myeloperoxidase, and copper-induced lipid peroxidation. *J. Agric. Food Chem.* **2000**, *48* (5), 1442−1448.
(26) Hvattum, E.; Ekeberg, D. Study of the collision-induced radical cleavage of flavonoid glycosides using negative electrospray ionization tandem quadrupole mass spectrometry. *J. Mass Spectrom.* **2003**, *38* (1), 43−49.
(27) Makris, D. P.; Rossiter, J. T. Heat-induced, metal-catalyzed oxidative degradation of quercetin and rutin (quercetin 3-O-rhamnosylglucoside) in aqueous model systems. *J. Agric. Food Chem.* **2000**, *48* (9), 3830−3838.
(28) Cheikhousman, R.; Zude, M.; Bouveresse, D. R.; Léger, C.; Rutledge, D.; Birlouez-Aragon, I. s. Fluorescence spectroscopy for monitoring deterioration of extra virgin olive oil during heating. *Anal. Bioanal. Chem.* **2005**, *382* (6), 1438−1443.
(29) Baldioli, M.; Servili, M.; Perretti, G.; Montedoro, G. F. Antioxidant activity of tocopherols and phenolic compounds of virgin olive oil. *J. Am. Oil Chem. Soc.* **1996**, *73* (11), 1589−1593.
(30) Pellegrini, N.; Visioli, F.; Buratti, S.; Brighenti, F. Direct analysis of total antioxidant activity of olive oil and studies on the influence of heating. *J. Agric. Food Chem.* **2001**, *49* (5), 2532−2538.
(31) Carrasco-Pancorbo, A. a.; Cerretani, L.; Bendini, A.; Segura-Carretero, A.; Lercker, G.; Fernández-Gutiérrez, A. Evaluation of the influence of thermal oxidation on the phenolic composition and on the antioxidant activity of extra-virgin olive oils. *J. Agric. Food Chem.* **2007**, *55* (12), 4771−4780.

Table 1. Structures of the Major Dietary Groups of Flavonoids and a Few Examples

Group	Structure	Example (frequently found)
Flavones	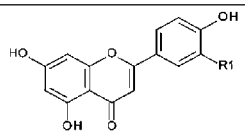	Apigenin (R1=H); Luteolin (R1=OH)
Flavonols	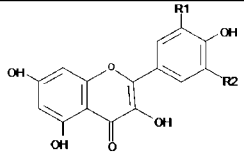	Quercetin (R1=OH, R2= H); Kaempferol (R1=H, R2= H); Myricetin (R1=OH, R2= OH); Isorhamnetin (R1=OMe, R2= H).
Flavanones	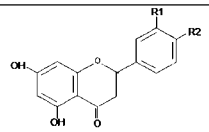	Hesperetin (R1=OH, R2= OMe), Naringenin (R1=H, R2= OH),
Isoflavones	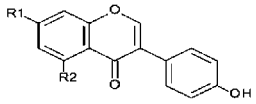	Genistein (R1=OH, R2= OH), Daidzein (R1=OH, R2= H), Glycitein (R1=OH, R2= H)
Flavan-3-ols	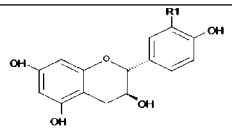	Catechin (R1= OH)
Anthocyanidins	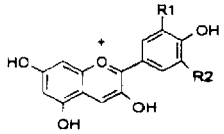	Cyanidin (R1= OH, R2= H); Delphinidin (R1= OH, R2= OH); Malvidin (R1= OMe, R2= OMe); Petunidin (R1= OMe, R2= OH)

formation flavonoid metabolites that may or may not have similar effects in vivo as their precursors. Hence, it makes sense to investigate related compounds (with different substituent patterns) in vitro to shed light on the influence of structural changes introduced during metabolism.[21]

Antioxidants are also used as additives to different compounds to prolong their life span.[22,23] Sectors of industry with interest in antioxidants include the food industry, but also plastics and rubber, gas and fuel, lubricants, adhesives, and cosmetics. Increased interest in obtaining products from renewable resources in these sectors (e.g., oils that are more oxidation prone when derived from renewables) has led to a growing market.[24] For industrial use it is important that the antioxidant can be dissolved together with the target compound and also that its action will proceed over a significant time span, keeping sufficient stability.

The antioxidizing power of flavonoids is along with other physicochemical characteristics (i.e., stability and solubility) important for function and depends on the substituents that decorate the flavonoid backbone. The focus of this paper is to review the influence of some major substituents occurring naturally, or as a consequence of in vitro modifications, in different subclasses of flavonoids (especially focusing on hydroxyl groups and their modification by glycosylation and acylation). This is followed by a discussion of current knowledge of the influence of these substituent groups in relation to their application, including methodologies to measure antioxidizing properties, solubility, and stability. Finally, current attempts to modify substituent patterns in vitro by biotechnological methods are reviewed.

OVERVIEW OF NATURAL FLAVONOIDS AND THEIR SUBSTITUENTS

Flavonoids are classified according to chemical structure, and their functionality depends on this structure including the relative orientation of different substituent groups on the molecule.[25] As flavonoids have attracted the attention of researchers in various areas (ranging from chemistry to biology, pharmaceutical sciences, and medicine), they have been named by diverse criteria. The numbers of subclasses vary, depending on the classification system used. On the basis of the backbone structure the IUPAC nomenclature recommends classification of the flavonoids into flavones, isoflavan, and neoflavone (Figure 1).[26] However, in the literature flavonoids have been divided into many groups, which are not all correct; thus, to avoid the confusion about nomenclature IUPAC is running a project called "Recommendations on Nomenclature of Flavonoids" (www.iupac.org). The classification that we find most sensible is the one shown in Table 1, which is built on the major dietary components, named as flavones, flavonols, flavanones, isoflavones, flavan-3-ols, and anthocyanidins. Other minor groups of flavonoids include chalcones,

dx.doi.org/10.1021/jf405570u | J. Agric. Food Chem. 2014, 62, 3321−3333

Table 2. Overview of Generally Occurring Flavonoid Glycosides and Acyls in Nature

subclass of flavonoids	position	monosaccharide	disaccharide	acyl group
flavones	5, 6, 7, 2′, 4′	glucose, galactose, xylose, rhamnose, arabinose, mannose	gentiobiose, rutinose, cellobiose, diglucose, dirhamnose	2-methylbutyric acid, 3-hydroxy-3-methylglutaric acid, acylated sugar
flavonols	3, 7, 5, 4′	glucose, rhamnose, xylose	rutinose,	isovaleric, vinylpropionic acid, acylated sugar
flavanones	5, 6, 7, 4′	glucose, rhamnose, galactose, fucose, arabinose	rhamnose-glucose	acylated sugar, *p*-coumaroyl
flavanonols	3, 7	glucose, rhamnose, arabinose	rhamnose-galactose	acylated sugar, isobutyric acid
isoflavons	7	glucose	not reported	malonic acid
flavan-3-ols (catechin)	7	glucose	not reported	
anthocyanidins	2, 3, 4, 5, 6, 7, 3′, 5′	glucose, galactose, rhamnose, xylose	sophorose, rutinose, sambubiose, robinobiose, gentiobiose	*p*-coumaric acid, caffeic acid, malonic acid, ferulic acid, sinapic acid

dihydrochalcones, dihydroflavonols, flavan-3,4-diols, coumarins, and aurones.[27]

The exact structure of flavonoids varies broadly within the different classes as a result of substitutions, and in plants the various substituent groups include, for example, OH groups, O- and C-methyl groups; methylenedioxy groups; O- and C-prenylation; furano, pyrano, and aromatic substitution; esterification, sulfation, and chlorination.[28−30] There are also many flavonoids available in nature in oligomeric forms, and one example is the tannins widely found in tea.[31]

Glycosyl groups (furanose and pyranose groups) are common in flavonoids and are connected via either O- or C-glycosylation. In the *C*-glycosides (found, e.g., in rice and cereals) the glycosyl group is linked to an aglycone carbon, usually at the C6- or C8-position.[32] More commonly, substitutions in flavonoids occur via reactions with the hydroxyl groups of the aglycone backbone, and *O*-glycosides are examples of this. The wide structural variation among flavonoid glycosides is thus influenced by several factors including linkage, number and nature of the sugars, and the hydroxylation pattern of the aglycone, which in turn determines the position of O-glycosylation. In nature, C-linked glycosylation is mostly found in the flavone group. In general, dicots or higher families have a tendency to accumulate flavone *O*-glycosides, whereas phylogenetically more primitive families such as ferns or gymnosperms produce more flavonol *O*-glycosides.[30,33] The O-glycosylated flavonoids are due to bioavailability frequently selected for analysis of potential effects on antioxidizing capacity, involving, for example, enzymatic modification trials in vitro (discussed below). A list stating the type and position of the O-linked glycosides and acyl groups of various types of flavonoids is given in Table 2. The substituents are affecting not only the antioxidizing properties but also the stability and solubility of the compounds. In the coming section we start by focusing attention on the antioxidizing capacity, including methods to obtain this on naturally occurring and differently substituted flavonoids.

MEASURING THE ANTIOXIDIZING PROPERTIES

The capacity of an antioxidant has, according to Biedrzycka and Amarowics,[34] been defined by Rice-Evans et al.[9] and is determined by (i) its reactivity as a hydrogen- or electron-donating agent (depending on its reduction potential), (ii) the fate of the resulting radical (controlled by the capacity to stabilize and delocalize the unpaired electron), (iii) the reactivity with other antioxidants, and (iv) the transition metal-chelating potential.

Antioxidizing (or reducing) properties can be displayed as either antioxidant activity or capacity. Antioxidant activity is molecule specific and can be described as a "rate constant of a reaction between a specific antioxidant and a specific oxidant", whereas antioxidant capacity measures "the amount (in moles) of a given free radical scavenged by a defined sample".[35] Measurements of antioxidant capacity can hence, depending on sample composition, yield scavenging ability either of an individual antioxidant or of the combined action of a mixture of antioxidants.

Flavonoids are known to be efficient scavengers of free radicals, such as $OH^{\bullet}$, $O_2^{\bullet}$, and $LOO^{\bullet}$ (lipid peroxide radicals).[9] Their potential as antioxidants is predicted by their reducing properties as hydrogen- or electron-donating agents, and evaluation is made using a variety of antioxidant assays, with different strengths and limitations. It is also difficult to compare data from investigations that use different methods, and thus it is recommendable to use a combination of assays. For this purpose, it is advisable to pick methods that are validated, standardized, and widely reported. A number of such methods are summarized in Table 3, along with a brief description of the analysis principle for the respective method. These methods, for example, include oxygen radical absorbance capacity (ORAC), Trolox equivalent antioxidant capacity (TEAC), 2,2-diphenyl-1-picrylhydrazyl (DPPH), ferric reducing antioxidant power (FRAP), cyclic voltammetry total reducing capacity (CV), Folin−Ciocalteu reducing capacity (FC), cupric reducing antioxidant capacity (CUPRAC), and total radical-trapping antioxidant parameter (TRAP).

Antioxidant assays can mainly be divided into one of the two groups: hydrogen atom transfer (HAT)-based assays[52] or electron transfer (ET)-based assays (see Table 3). HAT-based assays measure the capacity of an antioxidant to quench free radicals by hydrogen atom donation, and the majority involve a competitive reaction scheme. In these assays, thermal decomposition of azo-compounds generates peroxyl radicals, resulting in competition between the antioxidant and the substrate.[40] ET-based assays measure the ability of a potential antioxidant to transfer one electron to reduce any compound (which could be metals, carbonyls, and radicals). In principle, ET-based assays measure the capacity of an antioxidant to reduce an oxidant probe that changes color upon reduction[40] according to the following scheme:

$$\text{probe (oxidant)} + \text{antioxidant} \rightarrow \text{reduced probe} + \text{oxidized antioxidant}$$

Table 3. In Vitro Antioxidant Capacity Assays

	assays by hydrogen atom transfer reactions		assays by electron-transfer reaction					
method	ORAC[a]	TRAP[b]	TEAC[c]	DPPH[d]	CUPRAC[e]	FRAP[f]	CV[g]	FC[h]
probe	AAPH[i] (peroxyl radical generator)	AAPH[i] (peroxyl radical generator)	$ABTS^{\bullet+}$ radical[j]	$DPPH^{\bullet}$ radical[d]	bis(neocuproine) copper(-II) cation	ferric 2,4,6-tripyridyl-s-triazine complex		tungstate−molybdate complexes
principle of measurement	fluorescence decay along time due to oxidation of probe is inhibited by antioxidants	oxygen consumption	$ABTS^{\bullet+}$ radical cation[j] is reduced by antioxidants, causing absorbance decrease at 414 or 734 nm	$DPPH^{\bullet}$ radical[d] reduce causing absorbance decrease at 520 nm	bis(neocuproine) copper(-II) cation is reduced by antioxidants, causing absorbance decrease at 450 nm	ferric 2,4,6-tripyridyl-s-triazine complex is reduced by antioxidants causing absorbance increased at 595 nm	intensity of anodic current is increased due to oxidation of antioxidant compounds at the surface of the electrode	tungstate−molybdate complexes are reduced by antioxidants, causing absorbance increase at 750 nm
technique	fluorometric	oxygen electrode	spectrophotometric	spectrophotometric	spectrophoto-metric	spectrophotometric	electrochemical cell	spectrophotometric
quantification	net AUC[k] expressed as Trolox equivalents	lag time expressed as Trolox equivalents	Trolox equivalents	EC_{50}[l], Trolox equivalents	Trolox equivalents	ferrous ions equivalents	oxidation potential ($E_{1/2}$), intensity of the anodic current (I_a), area under the anodic wave (S)	gallic acid equivalents
references	36−38	36, 39	36, 40, 41	42	36, 43−48	36, 49	36, 50	36, 51

[a]ORAC, oxygen radical absorbance capacity. [b]TRAP, total radical-trappping antioxidant parameter. [c]TEAC, Trolox equivalent antioxidant capacity. [d]DPPH, 2,2-diphenyl-1-picrylhydrazyl. [e]CUPRAC, cupric reducing antioxidant capacity. [f]FRAP, ferric reducing antioxidant power. [g]CV, cyclic voltammetry total reducing capacity. [h]FC, Folin−Ciocalteu reducing capacity. [i]AAPH, 2,2′-azobis(2-amidinopropane) dihydrochloride. [j]$ABTS^{\bullet+}$, 2,2′-azinobis(3-ethylbenzothiazoline-6-sulfonic acid) radical cation. [k]AUC, area under the curve that represents the analytical property monitored along time. [l]EC_{50}, efficient concentration.

dx.doi.org/10.1021/jf405570u | J. Agric. Food Chem. 2014, 62, 3321−3333

After completion (no more change in color), the degree of color change is proportional to the concentration of antioxidant.[40]

ANTIOXIDANT CAPACITIES OF DIFFERENTLY SUBSTITUTED FLAVONOIDS

Structures of A-, B-, and C-Rings and Their Hydroxylation. The phenolic groups of flavonoids (B-ring, Figures 1 and 2) supply readily available H-atoms ensuring that the

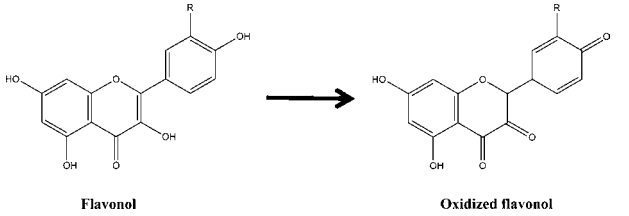

Figure 2. Structures of flavonols and their oxidized forms. R = OH, quercetin; R = H, kaempferol.

radicals produced can be delocalized over the flavonoid structure.[53] During the radical scavenging reaction, the flavonoid molecule donates a hydrogen atom to the reacting radical,[54] as shown in Figure 2. The flavonoid free radical formed in the reaction is more stable than the ROS that donates the electron due to the delocalization of the electron in the benzene ring (A-ring, Figures 1 and 2).

In vitro experiments have shown that substituents on the molecule affect the scavenging capability. Important for high antioxidizing capacity are the number and arrangement of hydroxyl groups on the aromatic backbone (A-, B-, and C-rings)[55−57] (Figure 3). Hydroxyls on the B-ring are important for the hydrogen-donating capacity. An *o*-dihydroxy group (catechol group) gives higher stability to the radical structure and takes part in electron delocalization[58] (Figure 3A). A

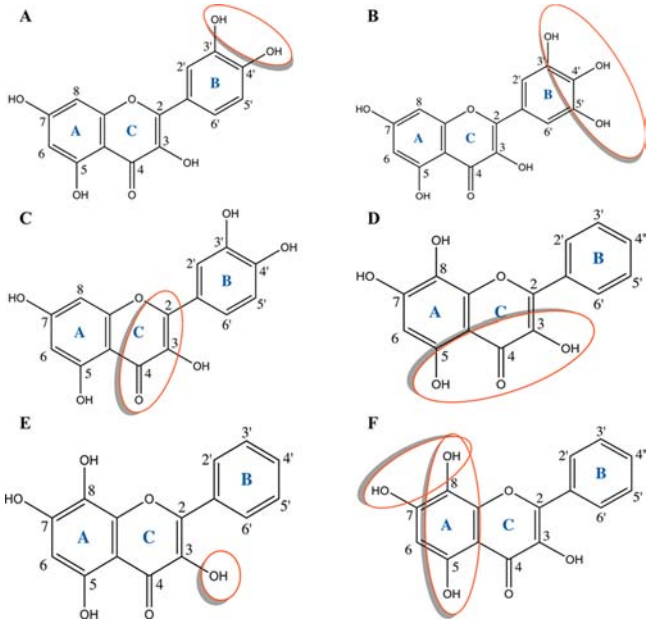

Figure 3. Basic structural features that characterize antioxidant functionality in polyphenols. Areas circled in red show features that are critical for efficient antioxidant function. Letters A, B, and C denote the ring structures of the flavonoid moiety.

pyrogallol group (hydroxyl groups at the 3′-, 4′-, and 5′-positions on the B-ring) enhances antioxidant capacity compared to flavonoids with single hydroxyl groups in ring B[59] (Figure 3B). Electron delocalization from ring B is promoted by a C-2, C-3 double bond combined with the 4-oxo function in the pyran ring (C-ring),[58] which also contributes to the antioxidant capacity (Figure 3C). In line with this, measurements using the TEAC assay (Table 3) show that quercetin presents enhanced antioxidant capacity compared to catechin[60] (see Table 1 for structures). The 3- and 5-OH groups (in the A- and C-rings, respectively) neighboring the 4-oxo function of the C-ring (Figure 3D) also promote high antioxidant capacity.[61] The presence of a free 3-OH group (Figure 3E) seems important as further modification (e.g., 3-glycosylation) leads to reduction of antioxidizing capacity.[55,62] In the A-ring, pairwise hydroxyl substitutions involving position 5 or 8 promote high antioxidant capacity. This is true for both 5,8- and 7,8-hydroxylation (Figure 3F), whereas corresponding groups at the 5,7-positions had little influence. A single 7-hydroxyl also had little effect, whereas a single 5-hydroxyl group (next to the 4-oxo function) increased antioxidant capacity.[63,64]

Following these criteria, a structure−antioxidant capacity relationship of flavonoids (quercetin > quercetin-3-*O*-rutinoside > kaempferol > luteolin) was proposed by Brown et al.[65] Quercetin (Table 1) has all requirements to exercise effective antioxidant function, mainly due to the presence of both a catechol group in the B-ring and a 3-hydroxyl group in the C-ring. Several studies[66,67] have also reported that flavanones with hydrogenated C-2 and C-3 (Table 1) are in principle inactive, indicating the importance of the double bond between C-2 and C-3 (Figure 3C), whereas luteolin (with the C-2, C-3 double bond and a 3′,4′-dihydroxyl group) has relatively high capacity.[66] The antioxidizing capacity of the anthocyanin molecule (with a structurally different C-ring, Table 1) is, however, high and in the same range as that of quercetin. The high capacity of the anthocyanin molecule has been attributed to its electron delocalization ability combined with its ability to form resonance structures upon changes in pH. The completely conjugated structure of anthocyanin allows electron delocalization, resulting in very stable radicals, which from this perspective is favorable.[59,68] Moreover, the positively charged oxygen atom in the C-ring makes it a better hydrogen-donating antioxidant compared to oligomeric proanthocyanidins and other flavonoids.[69]

Clearly, the antioxidant capacity of flavonoids is related to a combination of these chemical and structural elements. Generally, the higher degree of hydroxyl groups present in the flavonoid ring, the stronger the free radical scavenging will be. It is also apparent that hydroxyl groups of flavonoids are frequently sites of further modification, modulating antioxidant capacity by glycosylation, methylation, or, more rarely, acylation or sulfation.

Glycosylation Decreases Antioxidant Capacity. Most flavonoids are glycosylated in nature, and the position and nature of the sugar substituents are species specific.[70] Glycosylated flavonoids generally show decreased antioxidant capacity compared to the corresponding aglycones,[71] but glycosylation also modulates parameters, for example, solubility and stability, as discussed below. Zielinska et al.[72] determined antioxidant properties of quercetin and its glucosides from onion by the CV assay (Table 3) and showed that highest antioxidant capacity was obtained using the aglycone. The order of the antioxidant capacity was quercetin > quercetin-3-

dx.doi.org/10.1021/jf405570u | J. Agric. Food Chem. 2014, 62, 3321−3333

O-glucoside > quercetin-4′-*O*-glucoside > quercetin-3,4′-*O*-diglucoside. These results are in agreement with a report by Rice-Evans et al.[55] indicating that the antioxidant properties of quercetin glucosides were most affected by glycosylation of the hydroxyl group in the catechol group of the B-ring.

Plumb et al.[73] have also reported that antioxidant capacities of flavonol glycosides from tea decreased as the number of glycosidic moieties increased. Besides the total number of glycosidic moieties, the type of glycosylation (O- or C-) and the position and structure of the sugar play important roles. C-Glycosylation in the A-ring was in this case shown to decrease antioxidant capacity,[74] and this effect may be caused by the properties of the sugar molecule. Flavonoid glycosidic moieties occur most frequently as *O*-glycosides at the 3- or 7-position. The 7-glycoside (in ring A) resulted in a more pronounced decrease of capacity than 3-glycosylation in the C-ring.[75] Obviously, the presence of substituents also affects the bioavailability (uptake) of flavonoids by changing the solubility in hydrophilic solvents.

Acylation Is Mostly Investigated after in Vitro Modification. A way to improve the hydrophobic nature of flavonoids is, for example, to connect fatty acids to the hydroxyls by esterification. Acylated flavonoids may occur in natural sources (Table 2), but these modifications are not as common as glycosylation and do normally not encompass long hydrophobic molecules. In this field, in vitro acylation of flavonoids by fatty acids has been made and the effect of these substitutions on antioxidant capacity monitored (see also enzymatic modification, below). Hydroxyl groups on the sugar of a flavonoid glycoside (and not the backbone) are common targets for acylation and generally lead to reduced antioxidant capacity, although the results appear to be dependent on the model assay chosen to measure the resulting antioxidizing capacity. Acylation of quercetin-3-rutinoside via glucose with lauric acid (*n*-dodecanoic acid), more so than palmitic acid (hexadecanoic acid), negatively influenced overall metal chelation when compared to unesterified quercetin-3-*O*-rutinoside.[76] Acylation of the glucoside in quercetin-3-*O*-glucoside with fatty acids esters by Salem et al.,[77] on the other hand, resulted in the enhanced scavenging capacity of the quercetin-3-*O*-glucoside-ester against ABTS radicals but decreased it against DPPH and the superoxide radical. Furthermore, quercetin-3-*O*-glucoside esters exhibited an antioxidant capacity that depended on the acyl chain length, where the antioxidant capacity decreased with increasing acyl chain length.

Other Substituents. Methylation and sulfation of the free hydroxyl groups are examples of other substitutions, and these follow the trends seen for glycosylation and acylation in generally reducing antioxidant capacity. Rimbach et al.[78] studied the effect of sulfation and found that genistein-4′-sulfate was a less efficient antioxidant than genistein and genistein-4′,7-disulfate even less efficient. This indicates that sulfation masks important hydroxyl groups of the isoflavone molecule and decreases the antioxidant capacity of the resulting compound.

O-Methylated quercetin is also an example of a less potent peroxyl radical scavenger than unsubstituted quercetin, and several studies have reported that steric effects perturb the planarity of O-methylation, which may induce the suppression of antioxidant capacity.[75,79] Investigations, mainly using assays based on DPPH or ABTS (Table 3), have shown that the B-ring is especially sensitive to the position of methoxyl groups. Reduction of the antioxidant capacity was seen for 2′-*O*-methyl/4′,6′-hydroxy substitution in the B ring, whereas 2′,6′-hydroxy/4′-*O*-methyl substitution resulted in a lower effect.[80] Zima et al.[81] also showed that *O*-dihydroxy substitution of the flavanone B ring resulted in higher capacity than methoxylated compounds or compounds with para-located hydroxyl groups. Accordingly, reduction of antioxidant capacity by methylation depends on a combination of free hydroxyl groups and the position of methoxyl groups in the flavonoid.

Antioxidizing Effects Also Depend on the Chosen Model System. It is apparent that the antioxidant capacity of flavonoids has been studied in many different model systems to gain insights on structure−antioxidant capacity relationships and that the choice of assay system (depending on its mechanism) may affect the result obtained. In a recent study performed by Ishimoto et al.,[52] antioxidative properties of five typical flavonoids were assessed (kaempferol, quercetin, myricetin, isorhamnetin, and quercetin-3-glucuronide, Table 1) by the ORAC assay (Table 3). Despite previous findings that an increase in the number of hydroxyl groups in the B ring of a flavonol is generally correlated with an increase in antioxidative capacity, it was found that the ORAC level for kaempferol (with one hydroxyl group in the B-ring) was 1.5-fold higher than that of quercetin and myricetin (with two and three hydroxyl groups in their respective B-rings). It was also shown that the ORAC score of quercetin was comparable to the scores of both its methylated metabolite (isorhamnetin) and its 3-*O*-glucuronide.[52] In the same study, the ORAC score of (−)-epigallocatechin gallate was 1.5 times lower than that of its methylated metabolite, (−)-epigallocatechin 3-*O*-(3″-O-methyl)-gallate. On the other hand, (+)-catechin and (−)-epicatechin both showed remarkable antioxidative capacity (ORAC levels of 9.0 and 10.0 mol Trolox equiv/mol) compared to all 3′- and 4′-*O*-methyl-(+)-catechins and 3′- and 4′-*O*-methyl-(−)-epicatechins (ORAC values in the range of 5.7−6.5 mol Trolox equiv/mol). This shows that the scavenging ability depends not only on the structure of the antioxidant (discussed above) but also on the target molecule chosen to monitor oxidation.

In conclusion, antioxidant capacities are dependent on many specific structural features, of which one is the number and/or position of free hydroxyl groups of flavonoids. It is, however, also important to note that the choice of model system for measuring antioxidant capacity influences the results. Antioxidant assays differ from each other in terms of reaction mechanisms, oxidant and target/probed species, reaction conditions, and the form in which results are expressed.[36] Therefore, it is prudent to use more than one type of antioxidant assay and also consider the relevance of the assay in relation to putative use of the assayed molecule.

STABILITY AND SOLUBILITY ARE OTHER IMPORTANT PROPERTIES MODIFIED BY FLAVONOID SUBSTITUENTS

Most studies involving flavonoids have focused on the antioxidizing capacity. There are, however, other properties of importance, especially for use and selection of antioxidants for applied purposes. Such properties include the stability and solubility of the molecules. With increased industrial interest for use of antioxidants, the choice of antioxidant for a certain application will be dependent on both the possibility to dissolve the antioxidant and the possibility to prolong the shelf life of the antioxidant or of product compounds to which the antioxidant is added.

Substituents (such as the *O*-glycosyl groups connected to the hydroxyl groups in the flavonoids) not only regulate the antioxidizing capacity but also influence both the stability and solubility of the molecules. Although less attention has been given to these factors, they are important for successful use. Glycosylation frequently occurs in natural flavonoids and, in addition, both glycosylation and acylation have been done in vitro, to tune naturally occurring antioxidants to more desired properties for applied use. The effect of glycosylation and acylation on both stability and solubility is thus reviewed according to our current knowledge in the field.

Effect of Glycosylation on Stability. Relatively little information is available on the effect of glycosylation on the stability of flavonoid molecules. A few examples are however found where glycosylation has been shown to contribute to stability. For example, Buchner et al. measured the changes in concentration of rutin (also called quercetin-3-*O*-rutinoside or sophorin) and quercetin, in aqueous solution at 100 °C with air perfusion, and the results showed that rutin had higher stability compared to quercetin.[82] In another study of metal-catalyzed oxidative degradation, rutin and quercetin were dissolved in phosphate buffer containing Fe^{2+} and Cu^{2+}. It was also found that rutin had a slower degradation rate by monitoring the concentration changes during the degradation process.[83] Other oxidation studies (e.g., oxidation by peroxidase) of rutin and quercetin also reached the same conclusion.[84] In the study by Buchner et al.,[82] both quercetin and rutin were degraded in aqueous solutions at pH 5 and 8. Again, and at both conditions, the degradation of quercetin seemed to be much faster compared to that of rutin.

Rutin is glycosylated at a single point involving a disaccharide linked to the 3-OH on the quercetin C-ring. The stability of flavonoids is, however, also influenced by the number of glycosylated hydroxyl groups. As an example, studies have shown that boiling in water at 100 °C caused a greater decrease in quercetin-4′-glucoside content than in the content of quercetin-3,4′-diglucoside,[85,86] making the diglucoside more stable than the monoglucoside. The degradation was successive, and, for example, quercetin diglucosides almost completely broke down to aglycone via the monoglucose derivative by hydrolytic enzymes.[87−89]

Acylation Can Further Promote Stability. Although the mechanism is not known, the introduction of acyl groups has also been shown to enhance the thermostability of flavonoids. In Ishihara and Nakajima's study, in vitro monoacylation of quercetin-3-glucoside via a glucoside hydroxyl with nine different aromatic carboxylic acids all improved the thermostability and light-resistivity of the resulting flavonoids.[90] It was suggested that the reason for the improved stability by acylation might be that the intra- and intermolecular interactions, between the flavonoid skeleton and the aromatic ring in the acyl moiety, would prevent the degradation of the molecule.[90] A similar observation was reported by Fossen et al.[91] that complex anthocyanins such as petanin, which contains one aromatic acyl group, showed higher color intensity and stability than cyanidin-3-glucoside at pH 4.0−8.1.

In conclusion, the addition of the above substituents increased the stability of flavonoids. The additional sugar or acyl moiety could protect the aglycone from degradation to some extent, although so far there are no studies available to confirm the mechanism behind this.

Effect of Glycosylation on Solubility. Solubility is another important parameter that will determine whether it is possible to utilize an antioxidant as an additive. Solubility in oils can be desired to prevent oxidation,[92] and in addition solubility in water has previously been shown to improve the uptake of flavonoids supplied in the diet.[93] There is, however, very limited data on direct measurement of solubility of differently substituted flavonoids, like, for example, comparisons of glycosylated and nonglycosylated compounds. Moreover, some solubility data were obtained by comparing extraction[94] or chromatography data,[95] which makes it difficult to compare the solubility between different studies. Octanol−water distribution constant (log K_{ow}) values are related to water solubility, and such values can be used as index values for comparing the hydrophilicity of the flavonoids.[96,97] Frequently, available comparisons, however, report water solubility at a given temperature for different flavonoid compounds.

The presence of a sugar moiety usually increases the solubility of the flavonoids in water solutions. For example, quercetin has a low solubility in water at 25 °C (about 0.92 g/L).[98] Glycosylated quercetin[99] as well as other glycosylated flavonols[94] was reported to have considerably enhanced water solubility compared to the corresponding aglycone, although it is difficult to find exact numbers on the improvement from the literature. In the study of Chen et al.[94] it is reported that the higher solubility in water of glycosylated flavonols led to improved extraction yields. There was, however, no quantitative measurement of the solubility of the flavonols in the above studies. The position of the sugar moiety and the number of the bound sugars also play important roles. For example, the solubility of quercetin-3,4′-diglucoside, quercetin-3-glucoside, and quercetin-4′-glucoside in water solution decreases in the same order.[96,97] On the other hand, glycosylation will decrease the lipophilicity of the flavonoid aglycones. The review by Chebil et al., for example, shows that the solubility of rutin (quercetin-3-rutinoside) and isoquercitrin (quercetin-3-glucoside) was decreased in acetone and acetonitrile as compared to the solubility of the aglycone quercetin.[100]

Effect of Acylation on Solubility. If an increased lipophilicity is desired, acylation, particularly with long-chain fatty acids or vinyl esters from C4 to C18 in length, increases the solubility of flavonoids in organic solvent, that is, reflecting the lipophilicity of the flavonoids.[76,101] Such reactions have been done in vitro predominantly as enzymatic biotranformations. Another example is the use of aromatic acids such as hydroxycinnamic acids in acylation reactions, which have been shown to decrease the solubility of anthocyanins in cell cultures, which are hydrophilic environments.[95] However, acylation with small inorganic acids such as sulfuric acid instead increases the solubility of quercetin in water solution.[95] Therefore, it is reasonable to assume that acylation with hydrophilic acids will increase the hydrophilicity of the targeted flavonoids and vice versa.

All in all, although there are not so many studies comparing the absolute solubility data, this is very important in future flavonoid research. Existing literature data support the conclusion that the solubility of flavonoids is affected by the hydrophilicity of the additional moiety either through glycosylation or acylation. Adding hydrophilic groups will increase the hydrophilicity of the flavonoid; for example, glycosylation will increase the solubility of flavonoids in aqueous solution, whereas acylation will increase or decrease the solubility of flavonoids in aqueous solution by adding hydrophilic or hydrophobic acyl groups. Therefore, by choosing an appropriate method, it is possible to modify the solubility of

Table 4. Enzymatic Glycosylation of Flavonoids Using Glycoside Hydrolases

source	enzyme	donor	acceptor	product	reference
Aspergillus niger	cellulase	4NP-Fuc	catechin	catechin 4-β-D-fucopyranoside	112
Bacillus stearothermophilus	α-D-glucosidase	maltose	catechin	catechin 7-α-D-glucopyranoside catechin 5-α-D-glucopyranoside	112
Bacillus sp.	α-amylase	dextrin	catechin	catechin 7-α-D-maltoside catechin 5-α-D-maltoside	112
Leuconostoc mesenteroides	glucansucrase	sucrose	luteolin	luteolin-3′-α-D-glucopyranoside luteolin-4′-α-D-glucopyranoside	123
Leuconostoc mesenteroides	glucansucrase	sucrose	quercetin	quercetin-3′-α-D-glucopyranosides quercetin-4′α-D-glucopyranosides	123
Leuconostoc mesenteroides	glucansucrase	sucrose	myricetin	myricetin-3′-α-D-glucopyranoside myricetin-4′-α- D-glucopyranoside	123
Pencillium decumbens	cellulase	maltose	quercetin	quercetin-3-rutinoside	94
Humicola insolens	synthase Cel7B_E197S	α-glycosyl fluoride	luteolin	luteolin-5-α-D-glycosyl	119

flavonoid in vitro according to the need of the study, which of course, as described above, will also affect the antioxidant properties of the compounds. Enzymes are typically used to make selective modifications on flavonoids, and below some efforts in this field will be shown.

ENZYMATIC METHODS FOR IN VITRO MODIFICATION OF FLAVONOIDS

The use of enzymes and microorganisms has by the European Commission been identified as a key enabling technology in replacing nonrenewable chemicals and materials with renewable alternatives,[102−104] and for the purpose of flavonoid modification, enzymes classified as hydrolases (EC 3.*x*.*x*.*x*) are biocatalysts of special interest. Hydrolases can, depending on the reaction conditions, catalyze both hydrolysis and synthesis reactions and thus modify the content of glycosyl groups (using glycoside hydrolases (EC 3.2.1.*x*)[105]) or acyl groups (using lipases or carboxyl esterases (EC 3.1.1.*x*)[100]) in flavonoids in biotransformation reactions. These biotransformations may affect both the antioxidative power and the physicochemical properties of the target molecule, and the benefits of in vitro modification of flavonoid structures using enzymes include production possibilities in amounts that make bioavailability trials as well as proper investigations of physicochemical properties of designed molecules possible. In addition, novel compounds can be created, thus increasing the natural flavonoid diversity in the laboratory.[92,106−108] When it comes to practical use of flavonoids in pharmaceuticals, cosmetics, food, or other industrial applications, the relatively low solubility and stability in lipids or water (dependent on the molecule chosen), can also be improved by designed modifications,[109,110] avoiding current limitations.

Enzymatic Acylation Frequently Requires Glycosylated Acceptor Flavonoids. The enzymes most commonly used for in vitro modification to date are lipases, which have successfully been used to acylate flavonoids, using different esters (transesterification) and organic acids (direct esterification) as acyl donors, that, depending on the selected donor, can favor solubility of the product in lipids. Most lipases, however, require glycosylated flavonoid acceptor molecules for function, and they selectively acylate hydroxyl groups on glycosides and do not modify free hydroxyls on the flavonoid aglycone. Efforts in this field using lipases and carboxyl esterases (also including the protease subtilisin) have been carefully reviewed by Chebil and co-workers,[97] and it was shown that among the enzymes thus far used, it was only lipase PS from *Pseudomonas cepacia* (now renamed *Burkholderia cepacia*)[90,100] and carboxyl esterases from *Streptomyces rochei* and *Aspergillus niger*[100,111] that successfully acylated hydroxyls on a nonglycosylated phenolic antioxidant acceptor, which in both reported cases was catechin. A limited number of donor molecules were tried for these enzymes and were for lipase PS restricted to vinyl acetate (an ester of fossil origin), whereas for the carboxyl esterases a short series of esters were used, including ethyl acetate, ethyl propionate, phenyl propionate, and phenyl butyrate.[90,100,111]

Most commonly, free or immobilized forms of lipase B from *Candida antarctica* (CalB) have been used in various synthetic approaches for acylation of glycosylated flavonoids, using a range of donor molecules via both direct esterification and transesterification. The reaction conditions are largely influencing the yield, and immobilized CalB clearly showed the best conversion at water activities close to zero. The observed conversion yields vary largely between different studies, using different acyl donors. Different vinyl esters are relatively commonly used for this purpose[100] and, for example, the synthetic reaction in the production of 6-*O*-((+) catechin 7-*O*-α-D-glucopyranoside) cinnamate from vinylcinnamate reached a yield of 70%.[112] Among acyl donors tested in reactions involving CAL-B to obtain products with increased solubility in lipids, high conversion yields have in some cases been reported using fatty acid donors with carbon chains up to C18. For example, 71% yield has been noted in rutin palmitate synthesis using palmitic acid (C16:0) as donor in reactions using the immobilized form of CAL-B (Novozym435).[113]

From the available literature it can also be seen that the enzymes are to a certain extent regioselective. For example, CAL-B has by different authors been reported to prefer either the primary alcohol (C6-OH)[114] or the secondary alcohol at C4-OH[115] of the sugar for the acylation reaction. Most papers indicate monoacylation, but for isoquercitrin (quercetin-3-glucoside) diacylation on C6-OH and C3-OH has also been shown.[100]

Glycosides Can Be both Removed and Added by Glycoside Hydrolases. The hydrophilicity of flavonoids can also be varied by changes in the glycosidic group content. Glycoside hydrolases (GH) either catalyze hydrolysis or transglycosylation of glycosidic groups, and are in nature taking part in processes such as (i) degradation and assimilation of exogenous glycosides, (ii) recycling/remodeling of cellular components, or (iii) modification of biological activity of free glycosides.[104,116] These activities can of course also be utilized in vitro to deglycosylate flavonoids, for example, using thermostable β-glucosidase,[117] as well as to selectively glycosylate flavonoid molecules. The relationship between hydrolytic or transglycosylation activity varies between different enzymes and different GH families and can be modulated if the right conditions are found in the reaction, such as high sugar concentration and controlled water activity. Compared to the use of lipases, rather limited attempts have thus far been made in this field, but interest is increasing, and in addition to the use of natural enzymes, some nucleophile-mutated variants for improved performance have also been constructed and analyzed.[118,119] A problem encountered is that glycoside hydrolases require higher water activity (generally $a_w > 0.6$) than lipases,[120,121] whereas many flavonoid aglycones have low solubility in water.

Successful trials are summarized in Table 4 and include the use of a cellulase from *Aspergillus niger* and an α-amylase from a *Bacillus* sp., in reactions with 4-nitrophenyl-α-L-fucoside (4NP-Fuc) as sugar donor molecules and catechin aglycone as acceptor molecule. Although successful, the yields achieved under the conditions used were not so high, up to 26%.[112]

Attempts have also been made to optimize the conditions for glycosylation of the flavonoids. Quercetin glycosylation trials at various temperatures, pH values, solvents, and substrates using a *Penicillium decumbens* cellulase (40−60 °C, pH 6−7, 30−60% ethanol/water v/v) were made with glucose or maltose as the glycosyl donor. In this case, conversions up to 30% were reached.[122] Later, the same cellulase was used to assist in extractions of flavonoid compounds in mild solvents such as ethanol/water followed by transglycosylation of flavonoids, converting them into more polar molecules, but the highest transglycosylation yield was only 27% and was achieved using maltose and isorhamnetin.[94]

To overcome low glycosylation yields, an enzyme with higher natural transglycosylation activity, a glucansucrase from *Leuconostoc mesenteroides*, was used for glucosylation carried out in aqueous/organic solvents to improve flavonoid solubility. Conversion yields did, however, not improve so much, but varied depending on the flavonoid used, resulting in a conversion to glycosylated forms (Table 4) of luteolin (8%), quercetin (4%), and significantly higher for myricetin (49%).[123] In addition, using this enzyme, an α-linked glucoside (quercetin-α-D-glucopyranoside) not occurring in natural isolates was obtained.[124]

A new approach to glycosylate flavonoids is to use GHs, mutated in the catalytic nucleophile, so-called glycosynthases, to switch the enzyme mechanism to synthesis only. This methodology is established for oligosaccharide synthesis but has seldom been used for the modification of flavonoids. As the nucleophile of the enzyme is replaced, this approach requires that either fluorinated sugars or external nucleophiles are available in the reaction mixture.[125,126] In Yang et al.,[119] a high-throughput mass spectrometry-based method was used to assay biocatalysts and substrates for glycosynthesis, demonstrating that finding the right donor and acceptor is crucial for the glycosynthesis reactions. The glycosynthase Cel7B_E197S from *Humicola insolens* was found to catalyze the reaction, transferring an α-glycosyl fluoride (LacF) into the flavonoid, forming a glycosidic bond with a specificity for position 4′ and 6-linked OH groups on the flavonoid, with a rather high glycosylation yield (75−95%) compared to previous attempts using glycosidases and glycosyltransferases.[127] In addition, fair yields (up to 40%) were obtained using a glycosynthase of *Thermotoga neapolitana* β-glucosidase 3B, using a monoglucosylated quercetin as substrate in reactions obtaining the diglucoside, but required a second mutation in the active site for function.[128]

In summary, flavonoids are natural antioxidants, and they are getting more attention being molecules from renewable resources that can be utilized as additives in many types of products, ranging from food and pharmaceuticals to cosmetics and eventually larger scale industrial products. To efficiently use and select the antioxidants, a detailed understanding of the interplay between their activity, stability, and solubility is greatly aiding selection of suitable candidates. Substituents connected to their hydroxyl groups definitely have a role in the determination of these properties, and enzymatic routes to modify such substituents and properties are likely to play a role in future modification of natural flavonoids for more selective applications.

AUTHOR INFORMATION

Corresponding Author

*(M.P.) E-mail: Merichel.Plaza@chem.lu.se, merichelpla@gmail.com. Phone: +46 765855167. Fax: +46 46 222 82 09.

Funding

We acknowledge financial support from the Swedish Research Council Formas for funding the SuReTech research collaboration (229-2009-1527). T.P., K.Z.G.A., and E.N.K. also acknowledge support from the FP7 framework program AMYLOMICS. C.T. acknowledges the Swedish Research Council for funding (2010-333).

Notes

The authors declare no competing financial interest.

REFERENCES

(1) Transparency market research, Antioxidants Market − Global Industry Analysis, Market Size, Market Share, Growth and Forecast, 2012−2018, http://www.transparencymarketresearch.com/antioxidants-market.html#sthash.VtcXD4kh.dpuf (accessed Nov 8, 2013),

(2) Ghosh, D.; Scheepens, A. Vascular action of polyphenols. *Mol. Nutr. Food Res.* **2009**, *53*, 322−331.

(3) Cohen, S. D.; Kennedy, J. A. Plant metabolism and the environment: implications for managing phenolics. *Crit. Rev. Food Sci.* **2010**, *50*, 620−643.

(4) Van Dorsten, F. A.; Grun, C. H.; Van Velzen, E. J. J.; Jacobs, D. M.; Draijer, R.; Van Duynhoven, J. P. M. The metabolic fate of red

wine and grape juice polyphenols in humans assessed by metabolomics. *Mol. Nutr. Food Res.* **2010**, *54*, 897−908.
(5) Bennick, A. Interaction of plant polyphenols with salivary proteins. *Crit. Rev. Oral Biol. Med.* **2002**, *13*, 184−196.
(6) Scalbert, A.; Manach, C.; Morand, C.; Rémésy, C.; Jiménez, L. Dietary polyphenols and the prevention of diseases. *Crit. Rev. Food Sci. Nutr.* **2005**, *45*, 287−306.
(7) Ekman, A.; Campos, M.; Lindahl, S.; Co, M.; Börjesson, P.; Nordberg Karlsson, E.; Turner, C. Bioresource utilisation by sustainable technologies in new value-added biorefinery concepts − two case studies from food and forest industry. *J. Cleaner Prod.* **2013**, *57*, 46−58.
(8) Harborne, J. B.; Simmonds, N. W. In *Biochemistry of Phenolic Compounds*; Harborne, J., Ed.; Academic Press: New York, 1964; pp 77−127.
(9) Rice-Evans, C. A.; Miller, N. J.; Paganga, G. Antioxidant properties of phenolic compounds. *Trends Plant Sci.* **1997**, *2*, 152−159.
(10) Blokhina, O.; Virolainen, E.; Fagerstedt, K. V. Antioxidants, oxidative damage and oxygen deprivation stress: a review. *Ann. Bot.* **2003**, *91*, 179−194.
(11) Benthsath, A.; Rusznnyak, S.; Szent-György, A. In *Flavonoids in Health and Disease*; Dekker: New York, 1936; pp 137−161.
(12) Hollman, P. C. H.; Cassidy, A.; Comte, B.; Heinonen, M.; Richelle, M.; Richling, E.; Serafini, M.; Scalbert, A.; Sies, H.; Vidry, S. The biological relevance of direct antioxidant effects of polyphenols for cardiovascular health in humans is not established. *J. Nutr.* **2011**, *141*, 989S−1009S.
(13) Dhalla, N. S.; Temsah, R. M.; Netticadan, T. Role of oxidative stress in cardiovascular diseases. *J. Hypertens.* **2000**, *18*, 655−673.
(14) Mezzetti, A.; Cipollone, F.; Cuccurullo, F. Oxidative stress and cardiovascular complications in diabetes: isoprostanes as new markers on an old paradigm. *Cardiovasc. Res.* **2000**, *47*, 475−488.
(15) Sayre, L. M.; Smith, M. A.; Perry, G. Chemistry and biochemistry of oxidative stress in neurodegenerative disease. *Curr. Med. Chem.* **2001**, *8*, 721−738.
(16) Miulescu, R. D.; Dănoiu, S.; Purcărea, V.; Ionescu-Tîrgovişe, C. Factors that may influence the risk of cancer in diabetes. *Farmacia* **2012**, *60*, 602−614.
(17) Chiurchiù, V.; MacCarrone, M. Chronic inflammatory disorders and their redox control: from molecular mechanisms to therapeutic opportunities. *Antioxid. Redox Signal.* **2011**, *15*, 2605−2641.
(18) Ursini, F.; Maiorino, M.; Morazzoni, P.; Roveri, A.; Pifferi, G. A novel antioxidant flavonoid (IdB 1031) affecting molecular mechanisms of cellular activation. *Free Radical Biol. Med.* **1994**, *16*, 547−553.
(19) Middleton, E., Jr.; Kandaswami, C.; Theoharides, T. C. The effects of plant flavonoids on mammalian cells: Implications for inflammation, heart disease, and cancer. *Pharmacol. Rev.* **2000**, *52*, 673−751.
(20) Zhan, C. D.; Sindhu, R. K.; Pang, J.; Ehdaie, A.; Vaziri, N. D. Superoxide dismutase,catalase and glutathione peroxidase in the spontaneously hypertensive rat kidney: effect of antioxidant-rich diet. *J. Hypertens.* **2004**, *22*, 2025−2033.
(21) Hollman, P. C. H.; Katan, M. B. Absorption metabolism and health effects of dietary flavonoids in man. *Biomed. Pharmacother.* **1997**, *51*, 305−310.
(22) García-Jiménez, J. F.; Valencia, M. C.; Capitán-Vallvey, L. F. Simultaneous determination of antioxidants, preservatives and sweetener additives in food and cosmetics by flow injection analysis coupled to a monolithic column. *Anal. Chim. Acta* **2007**, *594*, 226−233.
(23) Chaithongdee, D.; Chutmanop, J.; Srinophakun, P. Effect of antioxidants and additives on the oxidation stability of Jatropha biodiesel. *Nat. Sci.* **2010**, *44*, 243−250.
(24) Ceresana, Market Study: Antioxidants, http://www.ceresana.com/en/market-studies/additives/antioxidants/ (accessed Nov 9, 2013).
(25) Cody, V. Crystal and molecular structures of flavonoids. *Prog. Clin. Biol. Res.* **1988**, *280*, 29−44.
(26) IUPAC. *Compendium of Chemical Terminology (the "Gold Book")*, 2nd ed.; compiled by McNaught, A. D., Wilkinson, A.; Blackwell Scientific Publications: Oxford, UK, 1997; XML on-line corrected version http://goldbook.iupac.org (2006) created by Nic, M., Jirat, J., Kosata, B.; updates compiled by Jenkins, A. ; ISBN 0-9678550-9-8; DOI:10.1351/goldbook.
(27) Del Rio, D.; Rodriguez-Mateos, A.; Spencer, J. P. E.; Tognolini, M.; Borges, G.; Crozier, A. Dietary (poly)phenolics in human health: structures, bioavailability, and evidence of protective effects against chronic diseases. *Antioxid. Redox Signal.* **2013**, *18*, 1818−1892.
(28) Harborne, J. B. Nature, distribution and function of plant flavonoids. *Prog. Clin. Biol. Res.* **1986**, *213*, 15−24.
(29) Harborne, J. B. Flavonoids in the environment: structure-activity relationships. *Prog. Clin. Biol. Res.* **1988**, *280*, 17−27.
(30) Quideau, S. Flavonoids. Chemistry, biochemistry and applications. *Angew. Chem., Int. Ed.* **2006**, *45*, 6786−6787.
(31) Brune, M.; Rossander, L.; Hallberg, L. Iron absorption and phenolic compounds: importance of different phenolic structures. *Eur. J. Clin. Nutr.* **1989**, *43*, 547−557.
(32) de Rijke, E.; Out, P.; Niessen, W. M.; Ariese, F.; Gooijer, C.; Brinkman, U. A. Analytical separation and detection methods for flavonoids. *J. Chromatogr., A* **2006**, *1112*, 31−63.
(33) Harborne, J. B.; Williams, C. A. Advances in flavonoid research since 1992. *Phytochemistry* **2000**, *55*, 481−504.
(34) Biedrzycka, E.; Amarovics, R. Diet and health: apple polyphenols as antioxidants. *Food Rev. Int.* **2008**, *24*, 235−251.
(35) MacDonald-Wicks, L. K.; Wood, L. G.; Garg, M. L. Methodology for the determination of biological antioxidant capacity in vitro: a review. *J. Sci. Food Agric.* **2006**, *86*, 2046−2056.
(36) Magalhaes, L. M.; Segundo, M. A.; Reis, S.; Lima, J. L. Methodological aspects about in vitro evaluation of antioxidant properties. *Anal. Chim. Acta* **2008**, *613*, 1−19.
(37) Cao, G.; Verdon, C. P.; Wu, A. H. B.; Wang, H.; Prior, R. L. Automated-assay of oxygen radical absorbency capacity with the cobas fara − II. *Clin. Chem.* **1995**, *41*, 1738−1744.
(38) Ou, B. X.; Huang, D. J.; Hampsch-Woodill, M.; Flanagan, J. A.; Deemer, E. K. Analysis of antioxidant activities of common vegetables employing oxygen radical absorbance capacity (ORAC) and ferric reducing antioxidant power (FRAP) assays: a comparative study. *J. Agric. Food Chem.* **2002**, *50*, 3122−3128.
(39) Somogyi, A.; Rosta, K.; Pusztai, P.; Tulassay, Z.; Nagy, G. Antioxidant measurements. Physiological. *Physiol. Meas.* **2007**, *28*, R41−R55.
(40) Huang, D. J.; Ou, B. X.; Prior, R. L. The chemistry behind antioxidant capacity assays. *J. Agric. Food Chem.* **2005**, *53*, 1841−1856.
(41) Dai, J.; Mumper, R. J. Plant phenolics: Extraction, analysis and their anatioxidant and anticancer properties. *Molecules* **2010**, *15*, 7313−7352.
(42) Brandwilliams, W.; Cuvelier, M. E.; Berset, C. Use of a free-radical method to evaluate antioxidant activity. *Food Sci. Technol.−LWT* **1995**, *28*, 25−30.
(43) Beer, C.; Myers, R. A.; Sorenson, J. H.; Bucci, L. R. Comprehensive comparison of the antioxidant activity of fruits and vegetables based on typical serving sizes from common methods. *Curr. Top. Nutraceut. Res.* **2004**, *2*, 227−250.
(44) Boga, M.; Hacibekiroglu, I.; Kolak, U. Antioxidant and anticholinesterase activities of eleven edible plants. *Pharm. Biol.* **2011**, *49*, 290−295.
(45) Cronin, J. R. Comparing antioxidant values with the ORAC method. *Alternat. Complement. Ther.* **2004**, *10*, 167−170.
(46) Gülçin, I. Antioxidant activity of food constituents: an overview. *Arch. Toxicol.* **2012**, *86*, 345−391.
(47) Triantis, T.; Stelakis, A.; Dimotikali, D.; Papadopoulos, K. Investigations on the antioxidant activity of fruit and vegetable aqueous extracts on superoxide radical anion using chemiluminescence technique.s. *Anal. Chim. Acta* **2005**, *536*, 101−105.
(48) Zujko, M. E.; Witkowska, A. M. Antioxidant potential and polyphenol content of selected food. *Int. J. Food Prop.* **2011**, *14*, 300−308.

(49) Benzie, I. F. F.; Strain, J. J. The ferric reducing ability of plasma (FRAP) as a measure of "antioxidant power": the FRAP assay. *Anal. Biochem.* **1996**, *239*, 70−76.
(50) Magalhaes, L. M.; Segundo, M. A.; Reis, S.; Lima, J. L. F. C. Methodological aspects about in vitro evaluation of antioxidant properties. *Anal. Chim. Acta* **2008**, *613*, 1−19.
(51) Singleton, V. L.; Rossi, J. A. Colorimetry of total phenolics with phosphomolybdic and phosphotungstic acid reagents. *Am. J. Enol. Vitic.* **1965**, *16*, 144−147.
(52) Ishimoto, H.; Tai, A.; Yoshimura, M.; Amakura, Y.; Yoshida, T.; Hatano, T.; Ito, H. Antioxidative properties of functional polyphenols and their metabolites assessed by an ORAC assay. *Biosci., Biotechnol., Biochem.* **2012**, *76*, 395−399.
(53) Burda, S.; Oleszek, W. Antioxidant and antiradical activities of flavonoids. *J. Agric. Food Chem.* **2001**, *49*, 2774−2779.
(54) Jacob, J. K.; Tiwari, K.; Correa-Betanzo, J.; Misran, A.; Chandrasekaran, R.; Paliyath, G. Biochemical basis for functioanl ingredient design from fruits. *Annu. Rev. Food Rechnol.* **2012**, *3*, 79−104.
(55) Rice Evans, C. A.; Miller, N. J.; Paganga, G. Structure-antioxidant activity relationships of flavonoids and phenolic acids. *Free Radical Biol. Med.* **1996**, *20*, 933−956.
(56) Chen, Z. Y.; Chan, P. T.; Ho, K. Y.; Fung, K. P.; Wang, J. Antioxidant activity of natural flavonoids is governed by number and location of their aromatic hydroxyl groups. *Chem. Phys. Lipids* **1996**, *79*, 157−163.
(57) Cao, G. H.; Sofic, E.; Prior, R. L. Antioxidant and prooxidant behavior of flavonoids: structure-activity relationships. *Free Radical Biol. Med.* **1997**, *22*, 749−760.
(58) Bors, W.; Heller, W.; Michel, C.; Saran, M. Flavonoids as antioxidants: determination of radical-scavenging efficiencies. *Methods Enzymol.* **1990**, *186*, 343−355.
(59) Van Acker, S. A. B. E.; Van Den Berg, D. J.; Tromp, M. N. J. L.; Griffioen, D. H.; Van Bennekom, W. P.; Van Der Vijgh, W. J. F.; Bast, A. Structural aspects of antioxidant activity of flavonoids. *Free Radical Biol. Med.* **1996**, *20*, 331−342.
(60) Salah, N.; Miller, N. J.; Paganga, G.; Tijburg, L.; Bolwell, G. P.; Rice-Evans, C. Polyphenolic flavanols as scavengers of aqueous phase radicals and as chain-breaking antioxidants. *Arch. Biochem. Biophys.* **1995**, *322*, 339−346.
(61) Bors, W.; Michel, C. Chemistry of the antioxidant effect of polyphenols. *Ann. N.Y. Acad. Sci.* **2002**, *957*, 57−69.
(62) Villano, D.; Fernandez-Pachon, M. S.; Troncoso, A. M.; Garcia-Parrilla, M. C. Comparison of antioxidant activity of wine phenolic compounds and metabolites in vitro. *Anal. Chim. Acta* **2005**, *538*, 391−398.
(63) Hu, J. P.; Calomme, M.; Lasure, A.; Debruyne, T.; Pieters, L.; Vlietinck, A.; Vandenberghe, D. A. Structure−activity relationship of flavonoids with superoxide scavenging activity. *Biol. Trace Elem. Res.* **1995**, *47*, 327−331.
(64) Wei, H. C.; Bowen, R.; Cai, Q. Y.; Barnes, S.; Wang, Y. Antioxidant and antipromotional effects of the soybean isoflavone genistein. *Proc. Soc. Exp. Biol. Med.* **1995**, *208*, 124−130.
(65) Brown, J. E.; Khodr, H.; Hider, R. C.; Rice-Evans, C. A. Structural dependence of flavonoid interactions with Cu^{2+} ions: implications for their antioxidant properties. *Biochem. J.* **1998**, *330*, 1173−1178.
(66) Furusawa, M.; Tanaka, T.; Ito, T.; Nishikawa, A.; Yamazaki, N.; Nakaya, K.; Matsuura, N.; Tsuchita, H.; Nagayama, M.; Iinuma, M. Antioxidant activity of hydroxyflavonoids. *J. Health Sci.* **2005**, *5*, 376−378.
(67) de Martino, L.; Mencherini, T.; Mancini, E.; Aquino, R. P.; de Almeida, L. F. R.; de Feo, V. In vitro phytotoxicity and antioxidant activity of selected flavonoids. *Int. J. Mol. Sci.* **2012**, *13*, 5406−5419.
(68) Kähkönen, M. P.; Heinonen, M. Antioxidant activity of anthocyanins and their aglycons. *J. Agric. Food Chem.* **2003**, *51*, 628−633.
(69) Kong, J. M.; Chia, L. S.; Goh, N. K.; Chia, T. F.; Brouillard, R. Analysis and biological activities of anthocyanins. *Phytochemistry* **2003**, *64*, 923−933.
(70) Williamson, G.; Plumb, G.; Garcia-Conesa, M. Glycosylation, esterification, and polymerization of flavonoids and hydroxycinnamates: effects on antioxidant properties. In *Plant Polyphenols 2*; Gross, G., Hemingway, R., Yoshida, T., Branham, S., Eds.; Springer: New York, 1999; Vol. 66, pp 483−494.
(71) Ben Sghaier, M.; Skandrani, I.; Nasr, N.; Franca, M. G. D.; Chekir-Ghedira, L.; Ghedira, K. Flavonoids and sesquiterpenes from *Tecurium ramosissimum* promote antiproliferation of human cancer cells and enhance antioxidant activity: a structure-activity relationship study. *Environ. Toxicol. Pharm.* **2011**, *32*, 336−348.
(72) Zielinska, D.; Wiczkowski, W.; Piskula, M. K. Determination of the relative contribution of quercetin and its glucosides to the antioxidant capacity of onion by cyclic voltammetry and spectrophotometric methods. *J. Agric. Food Chem.* **2008**, *56*, 3524−3531.
(73) Plumb, G. W.; Price, K. R.; Williamson, G. Antioxidant properties of flavonol glycosides from tea. *Redox Rep.* **1999**, *4*, 13−16.
(74) Mora, A.; Paya, M.; Rios, J. L.; Alcaraz, M. J. Structure-activity relationships of polymethoxyflavones and other flavonoids as inhibitors of non-enzymic lipid peroxidation. *Biochem. Pharm.* **1990**, *40*, 793−797.
(75) Heim, K. E.; Tagliaferro, A. R.; Bobilya, D. J. Flavonoid antioxidants: chemistry, metabolism and structure-activity relationships. *J. Nutr. Biochem.* **2002**, *13*, 572−584.
(76) Lue, B. M.; Nielsen, N. S.; Jacobsen, C.; Hellgren, L.; Guo, Z.; Xu, X. Antioxidant properties of modified rutin esters by DPPH, reducing power, iron chelation and human low density lipoprotein assays. *Food Chem.* **2010**, *123*, 221−230.
(77) Salem, J. H.; Humeau, C.; Chevalot, I.; Harscoat-Schiavo, C.; Vanderesse, R.; Blanchard, F.; Fick, M. Effect of acyl donor chain length on isoquercitrin acylation and biological activities of corresponding esters. *Process Biochem.* **2010**, *45*, 382−389.
(78) Rimbach, G.; Weinberg, P. D.; de Pascual-Teresa, S.; Alonso, M. G.; Ewins, B. A.; Turner, R.; Minihane, A. M.; Botting, N.; Fairley, B.; Matsugo, S.; Uchida, Y.; Cassidy, A. Sulfation of genistein alters its antioxidant properties and its effect on platelet aggregation and monocyte and endothelial function. *Biochim. Biophys. Acta−Gen. Subj.* **2004**, *1670*, 229−237.
(79) Dugas, A. J., Jr.; Castañeda-Acosta, J.; Bonin, G. C.; Price, K. L.; Fischer, N. H.; Winston, G. W. Evaluation of the total peroxyl radical-scavenging capacity of flavonoids: structure-activity relationships. *J. Nat. Prod.* **2000**, *63*, 327−331.
(80) Mathiesen, L.; Malterud, K. E.; Sund, R. B. Hydrogen bond formation as basis for radical scavenging activity: a structure-activity study of C-methylated dihydrochalcones from *Myrica gale* and structurally related acetophenones. *Free Radical Biol. Med.* **1996**, *22*, 307−311.
(81) Zima, A.; Hošek, J.; Treml, J.; Muselík, J.; Suchý, P.; Pražanová, G.; Lopes, A.; Žemlička, M. Antiradical and cytoprotective activities of several C-geranyl-substituted flavanones from *Paulownia tomentosa* fruit. *Molecules* **2010**, *15*, 6035−6049.
(82) Buchner, N.; Krumbein, A.; Rohn, S.; Kroh, L. W. Effect of thermal processing on the flavonols rutin and quercetin. *Rapid Commun. Mass Spectrom.* **2006**, *20*, 3229−3235.
(83) Makris, D. P.; Rossiter, J. T. Heat-induced, metal-catalyzed oxidative degradation of quercetin and rutin (quercetin 3-*O*-rhamnosylglucoside) in aqueous model systems. *J. Agric. Food Chem.* **2000**, *48*, 3830−3838.
(84) Takahama, U. Spectrophotometric study on the oxidation of rutin by horseradish peroxidase and characteristics of the oxidized products. *Biochim. Biophys. Acta−Gen. Subj.* **1986**, *882*, 445−451.
(85) Makris, D. P.; Rossiter, J. T. Domestic processing of onion bulbs (*Allium cepa*) and asparagus spears (*Asparagus officinalis*): effect on flavonol content and antioxidant status. *J. Agric. Food Chem.* **2001**, *49*, 3216−3222.

(86) Lombard, K.; Peffley, E.; Geoffriau, E.; Thompson, L.; Herring, A. Quercetin in onion (*Allium cepa* L.) after heat-treatment simulating home preparation. *J. Food Compos. Anal.* **2005**, *18*, 571−581.
(87) Lindahl, S.; Ekman, A.; Khan, S.; Wennerberg, C.; Börjesson, P.; Sjöberg, P. J. R.; Nordberg Karlsson, E.; Turner, C. Exploring the possibilities to use a thermostable mutant of *β*-glucosidase for rapid hydrolysis of quercetin glucosides in hot water. *Green Chem.* **2010**, *12*, 159−168.
(88) Rhodes, M. J. C.; Price, K. R. Analytical problems in the study of flavonoid compounds in onions. *Food Chem.* **1996**, *57*, 113−117.
(89) Price, K. R.; Rhodes, M. J. C. Analysis of the major flavonol glycosides present in four varieties of onion (*Allium cepa*) and changes in composition resulting from autolysis. *J. Sci. Food Agric.* **1997**, *74*, 331−339.
(90) Ishihara, K.; Nakajima, N. Structural aspects of acylated plant pigments: stabilization of flavonoid glucosides and interpretation of their functions. *J. Mol. Catal. B: Enzym.* **2003**, *23*, 411−417.
(91) Fossen, T.; Cabrita, L.; Andersen, O. M. Colour and stability of pure anthocyanins influenced by pH including the alkaline region. *Food Chem.* **1998**, *63*, 435−440.
(92) Viskupicova, J.; Danihelova, M.; Ondrejovic, M.; Liptaj, T.; Sturdik, E. Lipophilic rutin derivatives for antioxidant protection of oil-based foods. *Food Chem.* **2010**, *123*, 45−50.
(93) Hollman, P. C.; de Vries, J. H.; van Leeuwen, S. D.; Mengelers, M. J.; Katan, M. B. Absorption of dietary quercetin glycosides and quercetin in healthy ileostomy volunteers. *Am. J. Clin. Nutr.* **1995**, *62*, 1276−1282.
(94) Chen, S.; Xing, X.-H.; Huang, J.-J.; Xu, M. S. Enzyme-assisted extraction of flavonoids from *Ginkgo biloba* leaves: improvement effect of flavonol transglycosylation catalyzed by *Penicillium decumbens* cellulase. *Enzyme Microb. Technol.* **2011**, *48*, 100−105.
(95) Gläßgen, W.; Seitz, H. Acylation of anthocyanins with hydroxycinnamic acids via 1-*O*-acylglucosides by protein preparations from cell cultures of *Daucus carota* L. *Planta* **1992**, *186*, 582−585.
(96) Murota, K.; Shimizu, S.; Chujo, H.; Moon, J. H.; Terao, J. Efficiency of absorption and metabolic conversion of quercetin and its glucosides in human intestinal cell line Caco-2. *Arch. Biochem. Biophys.* **2000**, *384*, 391−397.
(97) Rothwell, J. A.; Day, A. J.; Morgan, M. R. A. Experimental determination of octanol−water partition coefficients of quercetin and related flavonoids. *J. Agric. Food Chem.* **2005**, *53*, 4355−4360.
(98) Razmara, R. S.; Daneshfar, A.; Sahraei, R. Solubility of quercetin in water + methanol and water + ethanol from (292.8 to 333.8) K. *J. Chem. Eng. Data* **2010**, *55*, 3934−3936.
(99) Calias, P.; Galanopoulos, T.; Maxwell, M.; Khayat, A.; Graves, D.; Antoniades, H. N.; d'Alarcao, M. Synthesis of inositol 2-phosphate-quercetin conjugates. *Carbohydr. Res.* **1996**, *292*, 83−90.
(100) Chebil, L.; Humeau, C.; Falcimaigne, A.; Engasser, J. M.; Ghoul, M. Enzymatic acylation of flavonoids. *Process Biochem.* **2006**, *41*, 2237−2251.
(101) Lue, B. M.; Guo, Z.; Xu, X. Effect of room temperature ionic liquid structure on the enzymatic acylation of flavonoids. *Process Biochem.* **2010**, *45*, 1375−1382.
(102) Blumer-Schuette, S. E.; Kataeva, I.; Westpheling, J.; Adams, M. W.; Kelly, R. M. Extremely thermophilic microorganisms for biomass conversion: status and prospects. *Curr. Opin. Biotechnol.* **2008**, *19*, 210−217.
(103) Commission of the European Communities. Communication from the Commission to the Eurpean Parliament, the Council, the European Economic AND Social Committee and the Committee of the Regions. Preparing for our future: Developing a common strategy for key enabling technologies in the EU, 2009; pp 1−11.
(104) Turner, P.; Mamo, G.; Nordberg Karlsson, E. *Microb. Cell Fact.* **2007**, *6*, 9−32.
(105) Ara, K. Z. G.; Khan, S.; Kulkarni, T.; Pozzo, T.; Nordberg Karlsson, E. In *Advances in Enzyme Biotechnology*; Shukla, P., Pletschke, B., Eds.; Springer: Dordrecht, The Netherlands, 2014; in press, ISBN 978-81-322-1093-1.
(106) Riva, S. Enzymatic modification of the sugar moieties of natural glycosides. *J. Mol. Catal. B: Enzym.* **2002**, *19*−*20*, 43−54.
(107) Wang, A.; Zhang, F.; Huang, L.; Yin, X.; Li, H.; Wang, Q.; Zeng, Z.; Xie, T. New progress in biocatalysis and biotransformation of flavonoids. *J. Med. Plant Res.* **2010**, *4*, 847−856.
(108) Bernhardt, P.; O'Connor, S. E. Opportunities for enzyme engineering in natural product biosynthesis. *Curr. Opin. Chem. Biol.* **2009**, *13*, 35−42.
(109) Smith, A. J.; Kavuru, P.; Wojtas, L.; Zaworotko, M. J.; Shytle, R. D. Cocrystals of quercetin with improved solubility and oral bioavailability. *Mol. Pharm.* **2011**, *8*, 1867−1876.
(110) Xiao, M.; Shao, Y.; Yan, W.; Zhang, Z. Measurement and correlation of solubilities of apigenin and apigenin 7-*O*-rhamnosylglucoside in seven solvents at different temperatures. *J. Chem. Thermodyn.* **2011**, *43*, 240−243.
(111) Sakai, M.; Suzuki, M.; Nanjo, F.; Hara, Y. 3-O-acylated catechins and methods of producing same. EP 0618203, 1994.
(112) Gao, C.; Mayon, P.; MacManus, D. A.; Vulfson, E. N. Novel enzymatic approach to the synthesis of flavonoid glycosides and their esters. *Biotechnol. Bioeng.* **2000**, *71*, 235−243.
(113) Ardhaoui, M.; Falcimaigne, A.; Engasser, J. M.; Moussou, P.; Pauly, G.; Ghoul, M. Acylation of natural flavonoids using lipase of *Candida antarctica* as biocatalyst. *J. Mol. Catal. B: Enzym.* **2004**, *29*, 63−67.
(114) Danieli, B.; Luisetti, M.; Sampognaro, G.; Carrea, G.; Riva, S. Regioselective catalysed by acylation of polyhydroxylated natural compounds *Candida antarctica* lipase B (Novozym 435) in organic solvents. *J. Mol. Catal. B: Enzym.* **1997**, *3*, 193−201.
(115) Ardhaoui, M.; Falcimaigne, A.; Ognier, S.; Engasser, J. M.; Moussou, P.; Pauly, G.; Ghoul, M. Effect of acyl donor chain length and substitutions pattern on the enzymatic acylation of flavonoids. *J. Biotechnol.* **2004**, *110*, 265−271.
(116) Faure, D. The family-3 glycoside hydrolases: from housekeeping functions to host-microbe interactions. *Appl. Environ. Microbiol.* **2002**, *68*, 1485−1490.
(117) Khan, S.; Pozzo, T.; Megyeri, M.; Lindahl, S.; Sundin, A.; Turner, C.; Nordberg Karlsson, E. Aglycone specificity of *Thermotoga neapolitana β*-glucosidase 1A modified by mutagenesis, leading to increased catalytic efficiency in quercetin-3-glucoside hydrolysis. *BMC Biochem.* **2011**, 12−11.
(118) Pozzo, T.; Plaza, M.; Romero-García, J.; Faijes, M.; Nordberg Karlsson, E.; Planas, A. Glycosynthases from *Thermotoga neapolitana β*-glucosidase 1A: a comparison of *α*-glucosyl fluoride reactions with reactions using exogenous nucleophile. *J. Mol. Catal. B: Enzym.* **2014**, accepted.
(119) Yang, M.; Davies, G. J.; Davis, B. G. A glycosynthase catalyst for the synthesis of flavonoid glycosides. *Ange. Chem. Int. Ed.* **2007**, *46*, 3885−3888.
(120) Hansson, T.; Andersson, M.; Adlercreutz, P. Influence of water activity on the competition between *β*-glucosidase-catalysed transglycosylation and hydrolysis in aqueous hexanol. *Enzym. Microb. Technol.* **2001**, *29*, 527−534.
(121) Ljunger, G.; Adlercreutz, P.; Mattiasson, B. Enzymic synthesis of octyl-*β*-glucoside in octanol at controlled water activity. *Enzym. Microb. Technol.* **1994**, *16*, 751−755.
(122) Xu, M. S.; Luo, M. F.; Xing, X. H.; Chen, H. Z. Characteristics of quercetin transglycosidation catalysed by *Penicillium decumbens* glycosidase. *Food Bioprod. Process.* **2006**, *84*, 237−241.
(123) Bertrand, A.; Morel, S.; Lefoulon, F.; Monsan, P.; Remaud-Simeon, M. *Leuconostoc mesenteroides* glucansucrase synthesis of flavonoid glucosides by acceptor reactions in aqueous-organic solvents. *Carbohydr. Res.* **2006**, *341*, 855−863.
(124) Moon, Y. H.; Lee, J. H.; Jhon, D. Y.; Jun, W. J.; Kang, S. S.; Sim, J.; Choi, H.; Moon, J. H.; Kim, D. Synthesis and characterization of novel quercetin-*α*-D-glucopyranosides using glucansucrase from *Leuconostoc mesenteroides*. *Enzym. Microb. Technol.* **2007**, *40*, 1124−1129.

(125) Cobucci-Ponzano, B.; Strazzulli, A.; Rossi, M.; Moracci, M. Glycosynthases in biocatalysis. *Adv. Synth. Catal.* **2011**, *353*, 2284−2300.
(126) Perez, X.; Faijes, M.; Planas, A. Artificial mixed-linked *β*-glucans produced by glycosynthase-catalyzed polymerization: tuning morphology and degree of polymerization. *Biomacromolecules* **2011**, *12*, 494−501.
(127) Williams, S. J.; Withers, S. G. Glycosyl fluorides in enzymatic reactions. *Carbohydr. Res.* **2000**, *327*, 27−46.
(128) Pozzo, T. *Thermostable Glycosidases and Glycosynthases as Biocatalysts in Green Chemistry Applications*. Doctoral thesis, Lund University, 2012; ISBN 978-91-89627-91-8.

PFAAs, whereas foliage/root concentration factors were lowest, and it was concluded that sorption to root surface tissue was the major uptake mechanism for the long-chain PFAAs. Recently some more mechanistic uptake studies have been published, investigating the influence of abiotic parameters, such as pH values or temperature,[36,37] and investigating the influence of metabolic inhibitors on the uptake.[38] These studies have been conducted with maize and wheat plants. Although these studies provide some initial insights into plant uptake of PFAAs from soil, there is still limited mechanistic understanding of the uptake, how it is influenced by the properties of the PFAAs and the characteristics of the plants, and how the PFAAs are distributed between different plant tissues.

The goal of the present study was to investigate the uptake of PFAAs and their distribution in different plant parts. To that end three crops were grown hydroponically in a greenhouse. A hydroponic system was used so that the water uptake could be readily monitored and the bioavailable concentrations of the PFAAs in the root zone could be directly measured. Further advantages are the controlled supply of nutrients, which together with the controlled light conditions ensures an optimal growth. A limitation of hydroponic studies is that they do not include the effect of soil on modulating chemical availability. A further drawback is that the nutrient solution has to be renewed regularly, which can lead to variability in exposure concentration for surface active chemicals such as PFAAs.

The crops were chosen to represent a variety of physiology. Tomato is a fruit-bearing crop of economic importance. Zucchini is another fruit-bearing crop belonging to the family of Cucurbitaceae, which has been shown to have a unique capability to transfer some hydrophobic organic contaminants from roots to shoots.[39,40] Cabbage is an important crop of which part of the leaves (the cabbage head) is eaten, and leaves were hypothesized to be a plant tissue that would amass high concentrations of short-chain PFAAs. A set of 11 perfluorinated carboxylic acids (PFCAs; carbon chain length from C4 to C14) and 3 perfluorinated alkyl sulfonates (PFSAs; C4, C6, and C8) was selected to provide a broad foundation for assessing the influence of chemical properties on PFAA uptake and distribution. When harvested, the plants were divided into roots, stems, leaves, and edible parts (tomatoes, zucchinis, and cabbage heads) to explore PFAA distribution within the plant. In tomato and zucchini, the stem tissue was further divided into the main stem (called "stem") and the tissue connecting the main stem to the leaves ("twigs") to provide more spatial resolution in the study to the transport of the PFAAs from the roots to the above-ground plant parts.

MATERIALS AND METHODS

Chemical Reagents and Laboratory Materials. All chemicals used in this study were of the highest quality and purity available. The abbreviations, suppliers, and purities of the chemicals can be found in Table S1 of the Supporting Information (SI).

Materials used for extraction and cleanup of the samples included Florisil SPE cartridges (1000 mg, 6 mL) from Applied Separations (Allentown, PA, USA), Oasis WAX 3 cm^3 SPE cartridges (60 mg) from Waters (Wexford, Ireland), and Supelclean ENVI-Carb 120/140 from Supelco (Bellefonte, PA, USA). Polypropylene (PP) tubes (50 and 15 mL) with screw caps were purchased from Sarstedt (Nümbrecht, Germany); PP vials (2.0 and 0.3 mL) were purchased from VWR International (Amsterdam, The Netherlands). Acrodisc LC13 GHP Pall 0.2 μm filters were obtained from Pall Corp. (Port Washington, NY, USA). The 10 L PP buckets were acquired from Harcotom (Purmerend, The Netherlands).

Plant Culture and Exposure Experiments. The uptake study was performed in a greenhouse (14 h of light). The plants were pregrown in soil until the seed leaves (cotyledons) were fully developed (BBCH stage 10). The soil was carefully washed off before the plants were transferred to the hydroponic system, where only the roots of the plants were exposed to the nutrient solution. The system is described in more detail in our previous study.[35] Tomato (*Solanum lycopersicum* var. Moneymaker) plants were grown in hydroponic solutions with nominal concentrations of 10, 100, 1000 and 10000 ng/L for each PFAA. Because the highest spiked concentration for tomatoes resulted in very high concentrations in plant parts, the zucchini (*Cucurbita pepo* var. Black Beauty) and cabbage (*Brassica oleracea* convar. *capitata* var. *alba*) plants were exposed to 10, 100, 500, and 1000 ng/L. For each plant a 10 L bucket was filled with 8 L of Hoaglands nutrient solution (see Table S2 in the SI for composition) and spiked with 100 μL/L of the respective PFAA stock solution. Six replicates per concentration were used for cabbage and tomato, whereas only four replicates could be used for zucchini due to their size. Two plants of each species were grown in unspiked nutrient solution as blank controls, and two pots without plants were used for evaporation measurements.

The plants were randomly distributed in the greenhouse room, and plant growth and water uptake were determined by weighing. The zucchini and tomato plants eventually grew too big to be moved, so no new randomization of the plant distribution was possible from then on. Furthermore, the tomato plants grew too big to be supported by the available equipment and had to be cut back from time to time. Secondary shoots were continuously removed as well. Thus, for tomato only the lower plant parts were analyzed. Pruning of tomato side shoots is a common practice and was done as soon as the secondary shoots were noticeable. The trimming of the top part of the plants was necessary and done for all plants at the same height, so that individual differences between plants were minimized. In total, the cutoff biomass for each plant was much less than the total biomass of the plants at the end of the experiment. We do not expect that the pruning and trimming had an influence on the uptake of PFAAs.

During the experiment the nutrient solution needed to be renewed several times due to the water uptake of the plants. This was done by replacing the buckets with new buckets containing freshly prepared spiked nutrient solution. Differences between the uptake of water and the uptake of PFAAs meant that the PFAA concentrations changed somewhat during the experiment. With decreasing water levels in the buckets, the PFAA concentrations in the solutions can significantly increase. We describe below how we dealt with these complications. On average, the tomato plants took up 46.7 L of the nutrient solution, the cabbage plants 24.6 L, and the zucchini plants 41.4 L.

Tomato and zucchini fruits were harvested when they were ripe. Other plant parts were collected for analysis only after the experiment was stopped. Cabbage plants were divided into roots, stem, leaves, and head. Tomato and zucchini plants were divided into roots, stem, twigs, leaves, and fruits. Table S3 in the SI lists start and end dates of the growth experiment as well as dates of renewal of the nutrient solution and harvest dates of tomato and zucchini fruits. Samples were stored at −20 °C until extraction. No differences in plant growth were observed between the different spiking levels, and there were no visible effects of the compounds on the plant health (discoloring, spots). Not all of the cabbages survived until the end of the experiment, but at least three plants of each concentration survived. In total, 7 of 26 cabbage plants were lost. Cabbage survival was independent of the spiked concentration, and fatalities were most likely caused by the temperature in the greenhouse. The optimal temperature range for cabbage is between 15 and 20 °C. Temperatures above 25 °C, which were experienced for several days during the cabbage growth phase, can lead to inhibited growth and dropping of the outer leaves, which was observed for all cabbage plants in the experiment.

Extraction. After the plant samples had been washed with demineralized water, the material was dried superficially and homogenized with a household blender (Braun Multiquick MX

2050). The extraction method used is based on the method of Vestergren et al.,[41] which is a modification of the method published by Hansen et al.[42] Briefly, 10 g of the homogenate was weighed in a 50 mL PP tube and spiked with mass-labeled surrogate standards. After 5 mL of 0.4 M NaOH solution was added and vortex-mixed, the samples were left in the refrigerator overnight to allow the internal standards to distribute in the plant matrix. Next, 4 mL of 0.5 M TBA solution and 5 mL of a carbonate buffer (0.25 M Na_2CO_3/$NaHCO_3$) were added to the samples and thoroughly mixed. After the addition of 10 mL of MTBE and vortex-mixing for 1 min, the samples were sonicated for 10 min. Phase separation was achieved by centrifuging for 10 min at 3000 rpm. The MTBE phase was transferred to a new 50 mL PP tube and the extraction repeated two times. The extracts were combined and concentrated to approximately 2 mL using a Rapidvap (Labconco Corp., Kansas City, MO, USA). Florisil SPE-cartridges were prepared with 1 g sodium sulfate on top and conditioned with 10 mL MeOH and 10 mL MTBE before they were loaded with the extract. The elution of the nonpolar matrix was done with 10 mL of MTBE before the target compounds were washed off the cartridge with 10 mL of MeOH/MTBE (30:70, v/v). This extract was again evaporated with the Rapidvap to 1 mL final volume. An additional cleanup step following the Powley method with ENVI-Carb was added when the final extract was still strongly colored.[43]

Nutrient solution samples were extracted with Oasis WAX-SPE cartridges, except the samples from the 10 μg/L variant for tomato, which were directly injected. Between 20 and 150 mL of sample, depending on the nominal concentration, were spiked with internal standards and passed through the cartridges, which had been conditioned with 2 mL of 0.1% NH_4OH in MeOH (v/v) and 3 mL of H_2O. The loading speed was set to not exceed 2 drops per second. After the loaded cartridges had been washed with MeOH/H_2O (40:60, v/v), they were dried under vacuum before the PFAAs were eluted two times with 500 μL of 2% NH_4OH in MeOH (v/v).

All final extracts were passed through an Acrodisc LC 13 GHP Pall nylon filter into 2 mL PP vials and stored at 4 °C until analysis.

Analysis. The analysis was performed on an HPLC system (LC-20AD XR pump, SIL-20A autosampler, and SCL-10A VP system controller, Shimadzu, Kyoto, Japan) coupled with a tandem mass spectrometer (4000 QTrap, Applied Biosystems, Toronto, Canada). The HPLC was equipped with a precolumn (Pathfinder 300 PS-C_{18} column; i.d., 4.6 mm; length, 50 mm; particle diameter, 3 μm; Shimadzu, Duisburg, Germany) prior to the injection valve to remove potential background contamination. An ACE 3 C18-300 column (i.d., 2.1 mm; length, 150 mm; particle diameter, 3 μm; Advanced Chromatography Technologies, Aberdeen, Scotland) was used for separation and maintained at 30 °C. The mass spectrometer was equipped with an electrospray ionization interface, operating in the negative ionization mode, and was run in the scheduled MRM mode.

The purified extracts were diluted 1:1 with H_2O prior to analysis to match the initial composition of the mobile phase of the HPLC. A volume of 20 μL was injected. The mobile phase consisted of two eluents, A (40:60 MeOH/H_2O, v/v) and B (95:5 MeOH/H_2O; v/v; both with 2 mM ammonium acetate). The gradient used for separation and the mass transitions as well as other mass spectrometer settings can be found in the Supporting Information. Raw data were processed with Analyst software 1.5 (Applied Biosystems).

Quality Assurance and Control. Repeated extraction of a sample showed that the standard deviation of the concentrations between extractions was <10% for all analytes (n = 5, see Table S5 in the SI). Consequently, the samples were extracted once and injected in duplicate.

The concentrations were quantified using a 12-point calibration with fitted correlation lines that had an R^2 value of >0.99 for all analytes (no weighting was applied).

Our laboratory also participated successfully in various interlaboratory studies (see, e.g., ref 44). For further information on quality assurance and quality control measures, see also our previous study.[35]

In this study the average recovery of the internal standards was between 48% (PFBA) and 97% (PFDoA). Recoveries were determined by comparison with matrix extracts spiked with mass-labeled standards prior to injection. Interestingly, some matrices affected the signal of the compounds quite intensively. Cabbage head and zucchini roots, for example, reduced the PFBA signal by up to 80%. Signal enhancement on the other hand was at most 12%. See Tables S6 and S7 in the Supporting Information for detailed information on recoveries and matrix effects for all compounds and all matrices.

Limits of quantification (LoQs) (Table S8 in the SI) were calculated on the basis of the lowest validated calibration standard (signal to noise ratio ≥ 10). The LoQ was derived from the analyte mass injected scaled up to an extract volume of 1 mL and divided by the average extracted sample quantity for the matrix. Method blanks were prepared repeatedly with the same extraction procedure as the samples, but showed no quantifiable contamination. Solvent blanks were injected every 10 injections to check for contamination from the LC system and for memory effects, but no contamination or memory effects were observed.

Background concentrations were taken from plants growing in nonspiked nutrient solution (n = 2) and used to correct the PFAA concentrations found in spiked experiments by subtraction. Any resulting concentrations below the LoQ were neglected.

The nonbranched (further referred to as "linear PFOS (L-PFOS)") and branched isomers of PFOS were quantified separately, assuming equal response factors for branched and nonbranched isomers. Branched isomers for other PFAAs were also observed but were not quantified.

Data Analysis. Uptake factors calculated from the data were evaluated for outliers using box plots with SigmaPlot (Systat Software, Inc., Chicago, IL. USA). Outliers and values below the LoQ were not included in data interpretation. Statistical analysis of the data was performed using IBM SPSS 21 (IBM, Armonk, NY, USA). One-way analysis of variance (ANOVA) in combination with the Tukey test was conducted to assess the significance of differences between spiking levels and plant species. t tests were performed to evaluate the differences between compounds. All statements regarding differences in this study are based on a significance level of $p < 0.05$.

RESULTS AND DISCUSSION

Because there is no evidence for microbial, physical, or any other degradation of PFAAs, we consider the breakdown of the PFAAs to have been negligible in all matrices analyzed.

PFAA Concentrations in Nutrient Solution. With increasing water uptake the nutrient solution in the hydroponic system was depleted. When there was only a small volume left, high PFAA concentrations were measured that frequently exceeded the nominal spiked concentrations. There are two possible explanations. (I) As described in our previous study[35] and also shown by Reth et al.,[45] PFAAs accumulate at the air−water interface. This has been observed to be particularly pronounced for long-chain PFAAs. When only a small volume of water was left in the bucket, it was not possible to avoid sampling some surface water. This would have led to sampling of PFAAs that had accumulated at the water−air interface, which may have resulted in elevated concentrations in the sample. (II) The plants may take up water more efficiently than they take up PFAAs. This would have resulted in an enrichment of the compounds in the water and thus higher concentrations with time.

For the tomato, zucchini, and cabbage plants, the nutrient solution volumes at the time of sampling went down to a minimum of 113 mL. To calculate uptake factors, we determined average PFAA concentrations in the bulk solution that the plants had been exposed to during the entire period of exposure. To interpolate the concentrations in time and between pots, the following equations were used to calculate the nominal and bulk PFAA concentrations for each day:

$$C_{\mathrm{nom}(t)} = \frac{(C_{\mathrm{nom}(t-1)} \times V_{(t-1)}) - ((V_{(t-1)} - V_{(t)} - V_{\mathrm{evap}}) \times f \times C_{\mathrm{bulk}(t-1)}}{V_{(t)}} \quad (1)$$

$$C_{\mathrm{bulk}(t)} = \frac{C_{\mathrm{nom}(t)} \times V_{(t)}}{V_{(t)} + K \times A \times 1000000} \quad (2)$$

f is the effectiveness of the plant's uptake of the PFAA with the nutrient solution, K is the interface to bulk solution partition coefficient (m), V is the volume of nutrient solution (m^3), and A is the area of the air/nutrient solution interface in the bucket (m^2). The average bulk concentrations in the spike control pots were used as the initial values of C_{bulk} and (together with the nominal concentrations and A) to calculate K. For each PFAA and plant species, f was then fitted against the amount of PFAA taken up by the plant (i.e., f was chosen such that the median quotient of the predicted and measured mass of the PFAA in the plant was equal to 1). For tomato, where the total amount of PFAA taken up was not measured, we estimated the total amount by using the concentrations for the lower plant parts also for the mid and top plant parts. The resulting values for f for tomato were similar to the ones for cabbage and zucchini. The water concentrations calculated for the sampling days were quite close to the measured water concentrations. The daily concentrations estimated in this manner were used to calculate average bulk concentrations weighted with the water volume transpired by the plants. These bulk concentrations were employed to calculate plant tissue concentration factors (see below).

Roots. The PFAA uptake in the roots was assessed using the root concentration factor (RCF). The RCF was defined as the ratio between the concentration of a compound in roots and its bulk concentration in the nutrient solution to which the roots were exposed:[46]

$$\mathrm{RCF} = \frac{\text{concn in root (ng/g FW)}}{\text{concn in nutrient solution (ng/mL)}} \quad (3)$$

Over a broad concentration range, a linear relationship between exposure concentration and uptake of PFAAs was observed by Stahl et al.[30] and in our previous study.[35] We therefore averaged the RCFs from the different exposure concentrations. If the ANOVA–Tukey test showed that the RCF from a given exposure concentration was significantly different from all other exposure concentrations, then this value was excluded from the calculation of the mean RCF. For tomato, PFDoA, PFTrA, and PFTeA had significantly lower RCFs at the highest spiking level tested (10000 ng/L). This was not observed for cabbage and zucchini, which may be due to the lower maximum spiking level tested (1000 ng/L). We also observed lower RCF values for long-chain PFCAs (especially PFDoA, PFTrA, and PFTeA) in the 10000 ng/L spiking level in our lettuce study, where we concluded that the nonlinear uptake was caused by the nonlinear adsorption of the compounds to the root surface.[35] For cabbage the lowest spiking concentration resulted in significantly higher RCFs for PFOA, PFNA, PFDA, and Br-PFOS than for the other spiking concentrations. For zucchini the RCF for PFDA was significantly higher for the lowest spiking level than for other spiking levels. We have no explanation for these observations.

The RCFs for the PFCAs generally increased markedly with increasing chain length between PFBA and PFUnA and were quite similar for PFUnA through PFTeA (Figure 1). The RCFs for the PFSAs generally increased with increasing chain length

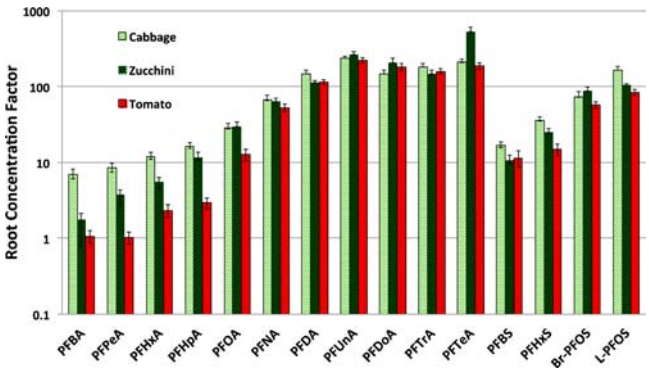

Figure 1. Root concentration factors (RCFs) for cabbage, zucchini, and tomato [(ng g^{-1})/(ng mL^{-1})]. The mean RCFs from each spiking level were averaged, whereby outliers were excluded (see text). Note the logarithmic scale. The error bars denote the standard error.

for all species. Different measures of hydrophobicity also increase with increasing chain length (SI Table S14), suggesting that the magnitude of root uptake may be determined by the hydrophobicity of the PFAA. However, for PFCAs with C > 11 the RCFs do not increase further, and hydrophobicity factors are not available for PFTrA and PFTeA, so it cannot be said with certainty that the root uptake is related to the hydrophobicity alone. The relationship between RCF and PFAA chain length is very similar to the relationship observed for lettuce in our previous study. The most pronounced difference is that lettuce showed a minimum RCF for PFHxA, whereas the three species studied here did not.

For the lettuce study we discussed two mechanisms for root uptake: sorption to the tissue between the root surface and the Casparian strip and uptake across the Casparian strip into vascular root tissue. We concluded that for lettuce sorption to root surface tissue is the dominant process for root uptake of the long-chain PFCAs, whereas for the short-chain PFCAs and PFSAs uptake across the Casparian strip into the vascular root tissue might be equally or more relevant.[35] Further support for this explanation can be found in the results presented below, which show that the stem concentration factors (SCFs) of PFDA are more than an order of magnitude less than the RCFs, even though PFDA has leaf concentration factors that are comparable to the short-chain PFCAs. Should uptake across the Casparian strip into vascular root tissue be the primary root uptake mechanism, one would expect the RCF and SCF to be similar if the vascular tissue in the roots and stem had similar sorption capacities for PFDA. The fact that the SCF is much smaller suggests that the sorption capacity of the root vascular tissue must be much greater than the sorption capacity of the stem vascular tissue or that sorption to the tissue between the root surface and the Casparian strip is an important root uptake mechanism for PFDA.

Above-ground Plant Parts. The distribution of PFAAs in the plant was assessed using various concentration factors. Concentration factors for each plant part (stem, leaves, twigs for tomato and zucchini, and edible parts) relative to the nutrient solution were calculated in the same way as the RCF and named analogously stem concentration factor (SCF), leaf concentration factor (LCF), twig concentration factor (TCF), and edible part concentration factor (ECF). Additionally,

concentration factors between plant parts (e.g., edible part/stem) were calculated to obtain insight into the translocation of the compounds within the plants.

Stem. All species had SCFs >1 for most of the compounds with the exceptions of PFBA, PFTrA, and PFTeA for zucchini and PFHpA, PFTrA, and PFBS for cabbage. The SCF for PFTeA for cabbage could not be calculated because the concentrations in the stem were below the LoQ (Figure 2). SCF values >1 denote an accumulation in the stem. The SCF values were in general much lower than the RCF values.

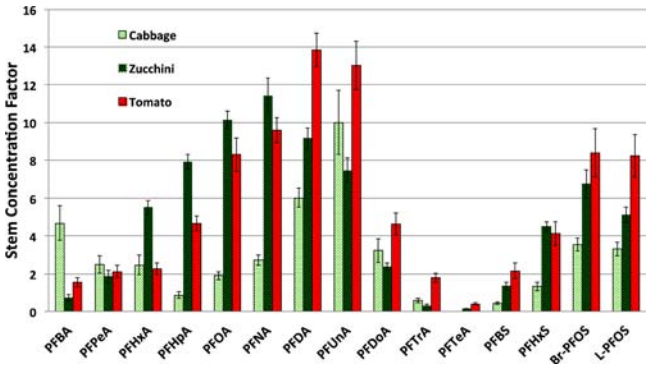

Figure 2. Stem concentration factors (SCFs) for cabbage, zucchini, and tomato [[(ng g^{-1})/(ng mL^{-1})]. The mean SCFs from each spiking level were averaged. The error bars denote the standard error.

The magnitude of the SCF is expected to depend largely on (I) the amount of PFAA being delivered by the transpiration stream from the roots and (II) the balance between retention of the PFAA in stem tissue versus further translocation with the transpiration stream to twigs and leaves. Lower SCFs were observed for the short-chain PFAAs (Figure 2). An explanation could be that the short-chain PFAAs do not partition as strongly into the stem tissue as their longer chain analogues. This could result in them not being retained in the stem tissue to the same extent, but rather being translocated further into other plant tissues. The higher SCF values of the C8−C11 PFAAs on the other hand can likely be explained by comparatively stronger sorption of the compounds on the stem tissue, resulting in stronger retention in the stem tissue and less translocation to twigs and leaves. An increase in organic matter/water partition coefficients with increasing PFAA chain length has been reported, for example, for sediment.[47] Also, experimentally determined hydrophobicity factors as well as modeled K_{OW} values have been observed to increase with increasing chain length[48,49] (SI Table S14). Therefore, it is not surprising that longer chain compounds are more retained in the stem tissue than short-chain compounds.

All three plant species showed a sharp decrease of the SCF for PFCAs with a chain length longer than C11. This is an indication that the translocation of these chemicals through the roots is considerably less efficient. One explanation could be restrictions on the ability of long-chain PFCAs to cross the Casparian strip. Another could be stronger partitioning of the long-chain PFCAs out of the xylem into the vascular tissue of the roots (see discussion under Roots above).

The low SCFs for the long-chain PFCAs also strengthen the argument for sorption to surface tissue being the dominant root uptake mechanism for these substances. Whereas the long-chain PFCAs had very low SCFs, they had the highest RCFs. Consequently, only a very small portion of the long-chain PFCAs in the roots was translocated to the stem.

Twigs. Twigs are present only in tomato and zucchini, because the leaves of cabbage grow directly on the stem. The twigs of zucchini are actually elongated leaf stalks (petioles), but because of their size they were analyzed separately from the leaf. The relationship between TCF and PFAA chain length was quite similar to the pattern observed for SCF, with the exception of PFBA and PFBS for tomato, where TCFs were much higher than SCFs (SI Figure S2). Furthermore, the twig/stem concentration factors (SI Figure S3) were close to 1 for most of the PFAAs with the notable exceptions of PFBA (3.3 in zucchini and 4.0 in tomato) and PFBS (4.0 in tomato). The explanations given for the SCFs can also be applied here.

Leaves. The LCFs were >1 in all plant species for all PFAAs except the long-chain PFCAs (Figure 3). This shows that all

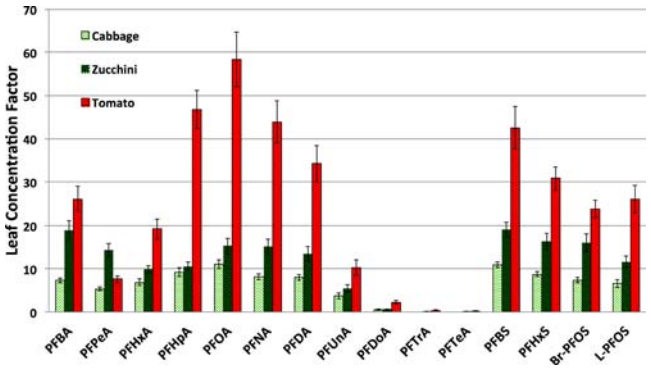

Figure 3. Leaf concentration factors (LCFs) for cabbage, zucchini, and tomato [[(ng g^{-1})/(ng mL^{-1})]. The mean LCFs from each spiking level were averaged. The error bars denote the standard error.

three plant species translocate all PFAAs except the long-chain PFCAs to the leaves and accumulate them there. One remarkable feature of these results is the similarity in the LCF values in a given plant for all compounds except the PFCAs >C10. The LCF values vary by a factor of <2 in both cabbage and zucchini. This indicates that the efficiency of these two plants at transferring the chemicals from nutrient solution to the leaves is relatively independent of the physical chemical properties within the property range bracketed by PFBA and PFDA/PFOS. Tomato shows a slightly different pattern with a maximum for PFOA and a pronounced minimum for PFPeA. The much lower LCF values for the PFCAs >C10 for all plants, despite their high RCF values (Figure 1), suggest that these substances are not transported effectively from the roots to the leaves. This was already indicated by the SCF and TCF results.

There were systematic differences in the LCFs between the plants; for zucchini and tomato they were on average 4.02 and 1.78 times higher, respectively, than for cabbage (with the exception of PFPeA in tomato). Factors that could influence the LCF include the amount of water transpired (higher transpiration would be expected to increase LCF) and leaf biomass (a high leaf biomass would tend to decrease LCF). However, no correlation could be found between LCFs and transpiration volumes, leaf biomass, or the quotient of these two parameters. The LCF is the result of more complex interactions among different plant tissues. More mechanistic insight into this is provided later.

Compared with the concentration factors of the other above-ground parts of the plants, the leaves show the highest

concentration factors for most of the compounds. The mass distributions of the chemicals between the different plant tissues show that of the above-ground tissues, the leaves also store the largest mass of all of the PFAAs (with the exception of PFPeA in tomato, Table 1 and Tables S9/S10 in the SI). This

Table 1. Mass Distribution of PFAAs in Different Tissues of Tomato Plants, Expressed as Percent of the Total Amount of PFAA Taken up by the Plant[a]

	Roots	Stem	Twig	Leaf	Fruit
PFBA	3%	4%	10%	43%	40%
PFPeA	5%	8%	7%	20%	60%
PFHxA	12%	8%	9%	42%	30%
PFHpA	12%	8%	9%	67%	4%
PFOA	29%	7%	9%	53%	1%
PFNA	56%	5%	7%	32%	0%
PFDA	72%	5%	5%	17%	0%
PFUnA	88%	4%	4%	5%	0%
PFDoA	90%	5%	3%	2%	0%
PFTrA	96%	2%	1%	1%	0%
PFTeA	98%	1%	0%	1%	0%
PFBS	21%	4%	9%	65%	1%
PFHxS	38%	5%	7%	49%	0%
Br-PFOS	68%	6%	5%	21%	0%
L-PFOS	71%	5%	4%	19%	0%

[a]Values shown are averages from all plants.

can be explained by the transpiration occurring in the leaves. The PFAAs are translocated to the leaves in the transpiration stream; there the water transpires and the PFAAs remain as residues in the leaves, where they accumulate.

Edible Part. In the edible part (i.e., cabbage head and tomato and zucchini fruits), no concentrations were detected above the LOQ for the long-chain PFCAs (C12−C14), not even at the highest tested exposure concentration (Table S11 in the SI). Consequently, no uptake factors could be calculated for these compounds.

The ECFs (Figure 4) were highest for the short-chain PFCAs and decrease with increasing chain length. Zucchini fruits were

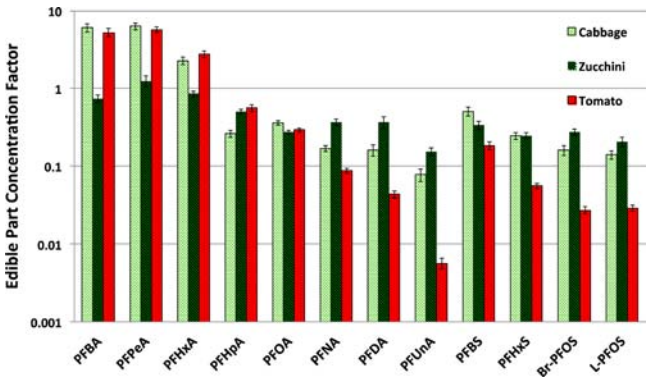

Figure 4. Edible part concentration factors (ECFs) for cabbage, zucchini, and tomato [[(ng g^{-1})/(ng mL^{-1})]. The mean ECFs from each spiking level were averaged. The error bars denote the standard error. Note the logarithmic scale.

far less contaminated than tomato fruits or cabbage heads. Thus, the exceptional ability of zucchini to accumulate some organic compounds such as polychlorinated dibenzo-*p*-dioxins (PCDDs) from soil[39] or water[40,50] was not observed for PFAAs.

The edible part/leaf transfer factors provide insight into the processes governing PFAA accumulation in the edible parts. Transpiration is low in fruits and in the cabbage head (which is tightly packed in leaves). The material for their development is provided by the phloem sap, which is produced in the leaves. It is thus to be expected that PFAAs will reach the fruits primarily via phloem sap. The efficiency of the leaf to fruit transfer of PFAAs can be assessed using the edible part/leaf transfer factor. All values were <1 in all cases (SI Figure S5), with values close to 1 for PFBA and PFPeA for cabbage and tomato. Because these two compounds sorb very little and transpiration is low from the edible parts, values close to 1 can be expected. The edible part/leaf transfer factor was similar for most compounds in zucchini and cabbage. For tomato it decreased exponentially with increasing chain length, and the difference between PFBA and PFUnA amounted to >3 orders of magnitude. A possible explanation for the different transport in the phloem sap is differences in the phloem sap composition, for example, different proteins.

Transpiration Stream Concentration Factor. The transpiration stream concentration factor (TSCF) describes the translocation potential of compounds from roots to aerial plant parts. Normally the TSCF is the concentration of the chemical in the transpiration stream divided by concentration in soil pore water.[46,51] Because direct measurement of the concentration in the transpiration stream was not possible, we estimated the TSCF by dividing the mass of the PFAAs in the aerial plant parts by the PFAA concentration in the nutrient solution multiplied by the volume of water transpired by the plant:

$$\text{TSCF} = [\text{concn in foliage (ng/g)} \times \text{foliage wt (g)}]/[\text{concn in nutrient solution (ng/mL)} \times \text{water transpired (mL)}] \quad (4)$$

Estimating the TSCF in this manner requires the assumptions that the compounds are not degraded in the plant, no chemical elimination from the plant occurs (e.g., loss of the compounds from the leaves to the atmosphere or back to the roots), and there is no other uptake pathway than through the roots (i.e., no atmospheric deposition). Due to the high persistence of the PFAAs and the low concentrations of the PFAAs in the above-ground parts of the control plants (no spiking with PFAAs of the nutrient solution), these assumptions are reasonable.

The TSCF values for cabbage, zucchini, and tomato thus calculated ranged between 0.05 and 0.23, with much lower values for the C12−C14 PFCAs (Figure 5). The TSCF values are relatively similar between compounds (generally a factor of <2) and between plant species (generally a factor of <2.5). There is, nevertheless, a consistent pattern in the TSCF values between the plants, with zucchini having significantly lower TSCF values than the other two tested species for all compounds except PFDoA. Because the TSCF was always <1, the transfer from the nutrient solution to the vegetative parts of the plants was inhibited. The pattern over chain length is similar for all three plant species and shows a minimum for PFHxA and a maximum for PFOA. This is also comparable to the pattern for lettuce from our previous study, with the difference that markedly higher values were measured for PFBA and the long-chain PFCAs (C > 10) in lettuce.

There is no consistent trend with the carbon chain length of the compounds, and there is no correlation between TSCF and

dx.doi.org/10.1021/jf500674j | J. Agric. Food Chem. 2014, 62, 3334−3342

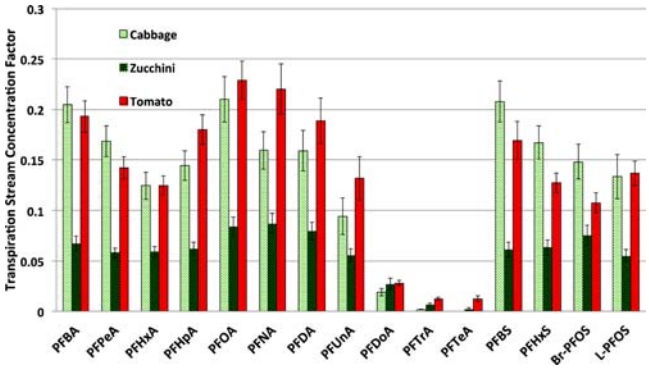

Figure 5. Transpiration stream concentration factors (TSCFs) for cabbage, zucchini, and tomato. The mean RCFs from each spiking level were averaged. The error bars denote the standard error.

measures of hydrophobicity such as log K_{OW} or log D_{OW} (SI Table S14). Briggs et al. reported that the TSCFs of nonionized chemicals depend on their log K_{OW} values and found the highest TSCF for compounds with a log K_{OW} of around 2.[51] As we discussed in our previous study,[35] PFAAs do not fit this model, as the PFAAs with a log K_{OW} around 2 show the lowest TSCF values, with the exception of the long-chain PFCAs.

Recently, Krippner et al.[37] reported a small influence of pH on the uptake of PFDA in maize roots, but found no influence of pH for C4−C9 PFCAs, PFBS, PFHxS, or PFOS. Due to very low pK_a values of PFAAs,[52] the compounds are in their ionic form at environmentally relevant pH levels. All plants in this study were grown in nutrient solutions with the same pH, so that interspecies differences cannot be explained by the influence of the pH.

Differences between Functional Groups and Isomers. To assess the influence of the PFAA functional group on PFAA uptake from soil and distribution in plants, PFBS was compared to PFPeA, PFHxS to PFHpA, and L-PFOS to PFNA, because these are pairs of compounds with the same length of perfluorinated carbon chain. Furthermore, branched and linear PFOS were compared to provide insight into the uptake of different isomers.

All PFSAs had significantly higher RCFs than the PFCAs with the same number of fluorinated carbon atoms by a factor of about 2−3. This shows that the uptake or adsorption is not only governed by the length of the fluorinated C chain, but rather by a combination of chain length and functional group. Higgins et al. came to similar conclusions when investigating the sorption of PFAAs to soils.[47] They found that the sorption of sulfonates was stronger than that of the carboxylic analogues. The higher RCFs for PFSAs correspond to higher values of several measures of hydrophobicity. The modeled log K_{OW}, as well as the experimentally determined log k_0 and log $P^{0'}$ (see Table S14 in the SI) are generally higher for the PFSAs than for their carboxylic analogues. However, this does not apply for the log D_{OW} values of the compounds.

In contrast, there were few significant differences in the TSCF between the PFSAs and the corresponding PFCAs. This suggests that the functional group had a minor influence on the uptake of the chemical into the root vascular tissue. Consequently, the stronger contribution of the sulfonate functional group to the RCF noted above is likely due to its contribution to a higher sorption to root surface tissue.

The transfer from leaves to the edible part was significantly higher for PFPeA and PFHpA than for the corresponding PFSAs. No difference was found between PFNA and L-PFOS.

A preference for the root uptake of the linear PFOS over the branched PFOS was also found for all species, but the difference was significant for only cabbage and tomato (Figure 1). This might be attributable to the smaller molecular volume of Br-PFOS resulting in lower root surface tissue/water sorption coefficients. However, no significant difference between branched and linear PFOS was found for the TSCF or the edible part/leaf concentration factor.

Clearly, some elements of the root uptake of PFAAs and their distribution in plants are influenced by the PFAA's functional group as well as its chain length.

Implications for Human Exposure. PFAA concentrations in the edible part were relatively low. The European Food Safety Authority (EFSA) has defined tolerable daily intake values (TDIs) for PFOA and PFOS of 1500 and 150 ng/kg body weight, respectively.[53] PFOA and PFOS concentrations in the edible parts of plants grown in the 1 μg/L exposure concentration did not exceed 0.5 and 0.2 ng/g fresh weight, respectively. Thus, to exceed the TDI for PFOA and PFOS, a person weighing 70 kg would need to eat around 210 and 50 kg, respectively, of these contaminated crops daily, which is of course impossible. The concentrations of the short-chain PFCAs were higher than the PFOA concentrations by up to a factor of ∼23 in cabbage and tomato and a factor of ∼5 in zucchini. Although no TDIs for these compounds exist, their toxicity is reported to be lower than for PFOA.[54] Because the concentrations of the most abundant PFAAs in tap and surface water are usually in the lower nanogram per liter range,[18] hydroponically grown crops generally should not be a danger to human health. However, should plants be exposed to much higher concentrations in soil or nutrient solution due to severe contamination, it is conceivable that TDI values could be exceeded and a risk for human health could occur.

All edible part/leaf transfer factors were <1 in all cases (see above and Figure S5 in the SI), which indicates that leafy crops with open leaves, such as spinach or some lettuce varieties, accumulate higher amounts in the edible part than fruit-bearing crops. Thus, leafy crops pose a higher risk for human exposure.

Mechanistic Description. The results of the present study can be summarized in the following simple mechanistic description of plant uptake of PFAAs from soil or nutrient solution and their distribution in plant tissue. PFAAs are taken up by the roots via the transpiration stream. With the exception of long-chain PFCAs (C > 10), their concentration in the transpiration stream entering the stem is ∼15% of the concentration in the nutrient solution. The majority of the PFAAs that enter the stem are carried with the transpiration stream to the leaves, where the transpiration of the water results in local accumulation of PFAAs. From the leaves, all PFAAs with the exception of long-chain PFCAs (C > 11) are transported via the phloem sap to the fruit and storage organs. Less PFAA accumulates in the fruit than in the leaves, which can in part be explained by the lower transpiration rate from fruits. There are species-specific differences in the effectiveness of this transfer: In cabbage and zucchini the effectiveness is similar both across chemicals and between species, whereas in tomato there is a pronounced decrease in transfer effectiveness with increasing chain length of the PFAAs. For the roots, there is a second accumulation mechanism in addition to the uptake with the transpiration stream, namely, sorption to root surface

tissue, which is especially important for the long-chain PFAAs. There was great consistency in this picture of PFAA uptake and distribution among the three plants studied here as well as the lettuce from the earlier study, the most notable difference being that lettuce also translocated long-chain PFCAs (C11−C14) to the above-ground plant parts.

This mechanistic description is plausible on the basis of the current understanding of contaminant behavior in plants and PFAA properties. However, it is based on controlled laboratory experiments in hydroponic solutions. Its applicability to plants growing in soil under field conditions needs to be demonstrated. The soil-related studies found in the literature do not provide enough information to calculate pore-water concentrations. Consequently, we believe that further experimental work is required to further develop our understanding of soil to plant transfer of PFAAs.

■ ASSOCIATED CONTENT

Supporting Information

Additional graphics and tables as mentioned. This material is available free of charge via the Internet at http://pubs.acs.org.

■ AUTHOR INFORMATION

Corresponding Author

*E-mail: W.P.deVoogt@uva.nl.

Funding

This study is part of the EU Project PERFOOD (KBBE-227525), and the financial support of the European Union is gratefully acknowledged.

Notes

The authors declare no competing financial interest.

■ ACKNOWLEDGMENTS

We thank Ludek Tikovsky for his help in the greenhouse.

■ REFERENCES

(1) de Voogt, P.; Saez, M. Analytical chemistry of perfluoroalkylated substances. *TrAC−Trends Anal. Chem.* **2006**, *25* (4), 326−342.

(2) Kissa, E. *Fluorinated Surfactants and Repellents*, 2nd ed.; Dekker: New York, 2001; Vol. 97, p 615.

(3) Liu, J. X.; Avendano, S. M. Microbial degradation of polyfluoroalkyl chemicals in the environment: a review. *Environ. Int.* **2013**, *61*, 98−114.

(4) Giesy, J. P.; Kannan, K. Global distribution of perfluorooctane sulfonate in wildlife. *Environ. Sci. Technol.* **2001**, *35* (7), 1339−1342.

(5) Giesy, J. P.; Kannan, K. Perfluorochemical surfactants in the environment. *Environ. Sci. Technol.* **2002**, *36* (7), 146A−152A.

(6) Prevedouros, K.; Cousins, I. T.; Buck, R. C.; Korzeniowski, S. H. Sources, fate and transport of perfluorocarboxylates. *Environ. Sci. Technol.* **2006**, *40* (1), 32−44.

(7) Barbarossa, A.; Masetti, R.; Gazzotti, T.; Zama, D.; Astolfi, A.; Veyrand, B.; Pession, A.; Pagliuca, G. Perfluoroalkyl substances in human milk: a first survey in Italy. *Environ. Int.* **2013**, *51*, 27−30.

(8) Karrman, A.; Domingo, J. L.; Llebaria, X.; Nadal, M.; Bigas, E.; van Bavel, B.; Lindstrom, G. Biomonitoring perfluorinated compounds in Catalonia, Spain: concentrations and trends in human liver and milk samples. *Environ. Sci. Pollut. Res.* **2010**, *17* (3), 750−758.

(9) Volkel, W.; Genzel-Boroviczeny, O.; Demmelmair, H.; Gebauer, C.; Koletzko, B.; Twardella, D.; Raab, U.; Fromme, H. Perfluorooctane sulphonate (PFOS) and perfluorooctanoic acid (PFOA) in human breast milk: results of a pilot study. *Int. J. Hyg. Environ. Health.* **2008**, *211* (3−4), 440−446.

(10) Antignac, J.-P.; Veyrand, B.; Kadar, H.; Marchand, P.; Oleko, A.; Le Bizec, B.; Vandentorren, S. Occurrence of perfluorinated alkylated substances in breast milk of French women and relation with socio-demographical and clinical parameters: results of the ELFE pilot study. *Chemosphere* **2013**, *91* (6), 802−808.

(11) Lau, C.; Anitole, K.; Hodes, C.; Lai, D.; Pfahles-Hutchens, A.; Seed, J. Perfluoroalkyl acids: a review of monitoring and toxicological findings. *Toxicol. Sci.* **2007**, *99* (2), 366−394.

(12) Saikat, S.; Kreis, I.; Davies, B.; Bridgman, S.; Kamanyire, R. The impact of PFOS on health in the general population: a review. *Environ. Sci.: Processes Impacts* **2013**, *15* (2), 329−335.

(13) Domingo, J. L. Health risks of dietary exposure to perfluorinated compounds. *Environ. Int.* **2012**, *40*, 187−195.

(14) D'Hollander, W.; de Voogt, P.; De Coen, W.; Bervoets, L. Perfluorinated substances in human food and other sources of human exposure. *Rev. Environ. Contamin. Toxicol.* **2010**, *208*, 179−215.

(15) Fromme, H.; Tittlemier, S. A.; Volkel, W.; Wilhelm, M.; Twardella, D. Perfluorinated compounds − exposure assessment for the general population in Western countries. *Int. J. Hyg. Environ. Health* **2009**, *212* (3), 239−270.

(16) Noorlander, C. W.; van Leeuwen, S. P. J.; Biesebeek, J. D. T.; Mengelers, M. J. B.; Zeilmaker, M. J. Levels of perfluorinated compounds in food and dietary intake of PFOS and PFOA in The Netherlands. *J. Agric. Food Chem.* **2011**, *59* (13), 7496−7505.

(17) Domingo, J. L.; Jogsten, I. E.; Eriksson, U.; Martorell, I.; Perello, G.; Nadal, M.; van Bavel, B. Human dietary exposure to perfluoroalkyl substances in Catalonia, Spain. Temporal trend. *Food Chem.* **2012**, *135* (3), 1575−1582.

(18) Eschauzier, C.; de Voogt, P.; Brauch, H.-J.; Lange, F. Polyfluorinated chemicals in European surface waters, ground- and drinking waters. In *Polyfluorinated Chemicals and Transformation Products*; Knepper, T. P., Lange, F. T., Eds.; Springer: Berlin, Germany, 2012; Vol. 17, pp 73−102.

(19) Ericson, I.; Domingo, J. L.; Nadal, M.; Bigas, E.; Llebaria, X.; van Bavel, B.; Lindstrom, G. Levels of perfluorinated chemicals in municipal drinking water from Catalonia, Spain. *Arch. Environ. Contam. Toxicol.* **2009**, *57* (4), 631−638.

(20) Skutlarek, D.; Exner, M.; Farber, H. Perfluorinated surfactants in surface and drinking waters. *Environ. Sci. Pollut. Res.* **2006**, *13* (5), 299−307.

(21) Haug, L. S.; Thomsen, C.; Brantsaeter, A. L.; Kvalem, H. E.; Haugen, M.; Becher, G.; Alexander, J.; Meltzer, H. M.; Knutsen, H. K. Diet and particularly seafood are major sources of perfluorinated compounds in humans. *Environ. Int.* **2010**, *36* (7), 772−778.

(22) Moody, C. A.; Martin, J. W.; Kwan, W. C.; Muir, D. C. G.; Mabury, S. C. Monitoring perfluorinated surfactants in biota and surface water samples following an accidental release of fire-fighting foam into Etohicoke Creek. *Environ. Sci. Technol.* **2002**, *36* (4), 545−551.

(23) Houde, M.; De Silva, A. O.; Muir, D. C. G.; Letcher, R. J. Monitoring of perfluorinated compounds in aquatic biota: an updated review. *Environ. Sci. Technol.* **2011**, *45* (19), 7962−7973.

(24) Ericson, I.; Marti-Cid, R.; Nadal, M.; Van Bavel, B.; Lindstrom, G.; Domingo, J. L. Human exposure to perfluorinated chemicals through the diet: intake of perfluorinated compounds in foods from the Catalan (Spain) market. *J. Agric. Food Chem.* **2008**, *56* (5), 1787−1794.

(25) Gem, M. *Fluorinated Chemicals: UK Dietary Intakes*; Food Standards Agency: London, UK, 2006.

(26) Herzke, D.; Huber, S.; Bervoets, L.; D'Hollander, W.; Hajslova, J.; Pulkrabova, J.; Brambilla, G.; Filippis, S.; Klenow, S.; Heinemeyer, G.; de Voogt, P. Perfluorinated alkylated substances in vegetables collected in four European countries; occurrence and human exposure estimations. *Environ. Sci. Pollut. Res.* **2013**, 1−10.

(27) Klenow, S.; Heinemeyer, G.; Brambilla, G.; Dellatte, E.; Herzke, D.; de Voogt, P. Dietary exposure to selected perfluoroalkyl acids (PFAAs) in four European regions. *Food Addit. Contam. Part A−Chem.* **2013**, *30* (12), 2141−2151.

(28) Kowalczyk, J.; Ehlers, S.; Oberhausen, A.; Tischer, M.; Fuerst, P.; Schafft, H.; Lahrssen-Wiederholt, M. Absorption, distribution, and milk secretion of the perfluoroalkyl acids PFBS, PFHxS, PFOS, and

PFOA by dairy cows fed naturally contaminated feed. *J. Agric. Food Chem.* **2013**, *61* (12), 2903−2912.
(29) van Asselt, E. D.; Kowalczyk, J.; van Eijkeren, J. C. H.; Zeilmaker, M. J.; Ehlers, S.; Furst, P.; Lahrssen-Wiederholt, M.; van der Fels-Klerx, H. J. Transfer of perfluorooctane sulfonic acid (PFOS) from contaminated feed to dairy milk. *Food Chem.* **2013**, *141* (2), 1489−1495.
(30) Stahl, T.; Heyn, J.; Thiele, H.; Huther, J.; Failing, K.; Georgii, S.; Brunn, H. Carryover of perfluorooctanoic acid (PFOA) and perfluorooctane sulfonate (PFOS) from soil to plants. *Arch. Environ. Contam. Toxicol.* **2009**, *57* (2), 289−298.
(31) Lechner, M.; Knapp, H. Carryover of perfluorooctanoic acid (PFOA) and perfluorooctane sulfonate (PFOS) from soil to plant and distribution to the different plant compartments studied in cultures of carrots (*Daucus carota* ssp. sativus), potatoes (*Solanum tuberosum*), and cucumbers (*Cucumis sativus*). *J. Agric. Food Chem.* **2011**, *59* (20), 11011−11018.
(32) Yoo, H.; Washington, J. W.; Jenkins, T. M.; Ellington, J. J. Quantitative determination of perfluorochemicals and fluorotelomer alcohols in plants from biosolid-amended fields using LC/MS/MS and GC/MS. *Environ. Sci. Technol.* **2011**, *45* (19), 7985−7990.
(33) Stahl, T.; Riebe, R. A.; Falk, S.; Failing, K.; Brunn, H. Long-term lysimeter experiment to investigate the leaching of perfluoroalkyl substances (PFASs) and the carry-over from soil to plants: results of a pilot study. *J. Agric. Food Chem.* **2013**, *61* (8), 1784−1793.
(34) Wen, B.; Li, L.; Zhang, H.; Ma, Y.; Shan, X.-Q.; Zhang, S. Field study on the uptake and translocation of perfluoroalkyl acids (PFAAs) by wheat (*Triticum aestivum* L.) grown in biosolids-amended soils. *Environ. Pollut. (Barking, Essex: 1987)* **2014**, *184*, 547−554.
(35) Felizeter, S.; McLachlan, M. S.; de Voogt, P. Uptake of perfluorinated alkyl acids by hydroponically grown lettuce (*Lactuca sativa*). *Environ. Sci. Technol.* **2012**, *46* (21), 11735−11743.
(36) Zhao, H.; Guan, Y.; Zhang, G.; Zhang, Z.; Tan, F.; Quan, X.; Chen, J. Uptake of perfluorooctane sulfonate (PFOS) by wheat (*Triticum aestivum* L.) plant. *Chemosphere* **2013**, *91* (2), 139−144.
(37) Krippner, J.; Brunn, H.; Falk, S.; Georgii, S.; Schubert, S.; Stahl, T. Effects of chain length and pH on the uptake and distribution of perfluoroalkyl substances in maize (*Zea mays*). *Chemosphere* **2014**, *94*, 85−90.
(38) Wen, B.; Li, L. F.; Liu, Y.; Zhang, H. N.; Hu, X. Y.; Shan, X. Q.; Zhang, S. Z. Mechanistic studies of perfluorooctane sulfonate, perfluorooctanoic acid uptake by maize (*Zea mays* L. cv. TY2). *Plant Soil* **2013**, *370* (1−2), 345−354.
(39) Huelster, A.; Mueller, J. F.; Marschner, H. Soil-plant transfer of polychlorinated dibenzo-*p*-dioxins and dibenzofurans to vegetables of the cucumber family (Cucurbitaceae). *Environ. Sci. Technol.* **1994**, *28* (6), 1110−1115.
(40) Gent, M. P. N.; White, J. C.; Parrish, Z. D.; Isleyen, M.; Eitzer, B. D.; Mattina, M. I. Uptake and translocation of *p,p′*-dichlorodiphenyldichloroethylene supplied in hydroponics solution to Cucurbita. *Environ. Toxicol. Chem.* **2007**, *26* (12), 2467−2475.
(41) Vestergren, R.; Ullah, S.; Cousins, I. T.; Berger, U. A matrix effect-free method for reliable quantification of perfluoroalkyl carboxylic acids and perfluoroalkane sulfonic acids at low parts per trillion levels in dietary samples. *J. Chromatogr., A* **2012**, *1237*, 64−71.
(42) Hansen, K.; Clemen, L. A.; Ellefson, M.; Johnson, H. Compound-specific, quantitative characterization of organic fluorochemicals in biological matrices. *Environ. Sci. Technol.* **2001**, *35*, 766−770.
(43) Powley, C. R.; George, S. W.; Ryan, T. W.; Buck, R. C. Matrix effect-free analytical methods for determination of perfluorinated carboxylic acids in environmental matrixes. *Anal. Chem.* **2005**, *77* (19), 6353−6358.
(44) Weiss, J. M.; van der Veen, I.; van Leeuwen, S. P. J.; Cofino, W.; Crum, S.; de Boer, J. Analytical improvements shown over four interlaboratory studies of perfluoroalkyl substances in environmental and food samples. *TrAC−Trends Anal. Chem.* **2013**, *43*, 204−216.
(45) Reth, M.; Berger, U.; Broman, D.; Cousins, I. T.; Nilsson, E. D.; McLachlan, M. S. Water-to-air transfer of perfluorinated carboxylates and sulfonates in a sea spray simulator. *Environ. Chem.* **2011**, *8* (4), 381−388.
(46) Trapp, S. Modelling uptake into roots and subsequent translocation of neutral and ionisable organic compounds. *Pest Manage. Sci.* **2000**, *56*, 767−778.
(47) Higgins, C. P.; Luthy, R. G. Sorption of perfluorinated surfactants on sediments. *Environ. Sci. Technol.* **2006**, *40* (23), 7251−7256.
(48) Arp, H. P. H.; Niederer, C.; Goss, K. U. Predicting the partitioning behavior of various highly fluorinated compounds. *Environ. Sci. Technol.* **2006**, *40* (23), 7298−7304.
(49) de Voogt, P.; Zurano, L.; Sern, P.; Haftka, J. J. H. Experimental hydrophobicity parameters of perfluorinated alkylated substances from reversed-phase high-performance liquid chromatography. *Environ. Chem.* **2012**, *9* (6), 564−570.
(50) Zhang, H. J.; Chen, J. P.; Ni, Y. W.; Zhang, Q.; Zhao, L. Uptake by roots and translocation to shoots of polychlorinated dibenzo-*p*-dioxins and dibenzofurans in typical crop plants. *Chemosphere* **2009**, *76* (6), 740−746.
(51) Briggs, G. G.; Bromilow, R. H.; Evans, A. A. Relationships between lipophilicity and root uptake and translocation of non-ionized chemicals by barley. *Pestic. Sci.* **1982**, *13* (5), 495−504.
(52) Steinle-Darling, E.; Reinhard, M. Nanofiltration for trace organic contaminent removal: structure, solution, and membrane fouling effects on the rejection of perfluorochemicals. *Environ. Sci. Technol.* **2008**, *42* (14), 5292−5297.
(53) EFSA. Opinion of the Scientific Panel on Contaminants in the Food Chain on perfluorooctane sulfonate (PFOS), perfluorooctanoic acid (PFOA) and their salts. *EFSA J.* **2008**, *653*, 5−131.
(54) Renner, R. The long and the short of perfluorinated replacements. *Environ. Sci. Technol.* **2006**, *40* (1), 12−13.

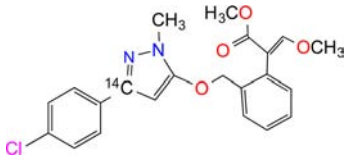

Figure 1. Chemical structure of SYP-3343.

performance liquid chromatography−liquid scintillation counting (HPLC−LSC) and thin-layer chromatography−isotope imaging (TLC−IIA) data indicated that both the radiochemical and chemical purities of the fungicide were over 98% and its specific activity was 5.042 ± 0.076 mCi/mmol.[17,18] 2,5-Diphenyloxazole (PPO) and 1,4-dis-[2′-(5′-phenyloxazolyl)]-benzene (POPOP) were of scintillation grade, purchased from Acros Organics (Geel, Belgium), and were used to prepare the scintillation cocktails as below: scintillation cocktail I, PPO (7.0 g) and POPOP (0.5 g) dissolved in a mixture of dimethyl benzene (650 mL) and glycol ether (350 mL); scintillation cocktail II, PPO (7.0 g) and POPOP (0.5 g) dissolved in a mixture of dimethyl benzene (600 mL), glycolether (225 mL), and ethanolamine (175 mL). The other chemical solvents were all analytical-grade.

Soil Preparation. Three representative soils were collected from the surface layers (0−20 cm) of agricultural regions in different areas of China, none of which had been previously applied with SYP-3343. The physical and chemical properties of these soils were shown in Table 1. The soil samples were air-dried, mixed, and sieved through a 1 mm sieve. The basic properties were determined using the standard methods.[19]

To examine the influence of soil microbes on ER, BR, and mineralization of SYP-3343, a subsample of loamy soil was sterilized through irradiation by Cobalt-60 at an absorbed dose of 6 kGy/100 g of soil.

Incubation and Treatments. The ^{14}C-labeled SYP-3343 was employed to determine the dynamic characteristics of SYP-3343 in soils. The incubation procedures were based on OECD guideline 307.[20] Briefly, after 300 g of soil sample (dry weight) was adjusted to a water holding capacity (WHC) of approximately 40% by adding distilled water, samples were pre-incubated in a dark cultivation cabinet at 25 ± 1 °C for 14 days to help the microbes adapt to the environmental change. An appropriate volume of the prepared ^{14}C-SYP-3343 in methanol solution (~7.4 × 10^5 Bq/sample) was added to each sample slowly. The treated samples were thoroughly mixed and placed in a fume hood to completely remove the methanol. Distilled water was added to readjust the soil moisture to about 60% WHC. The samples were incubated independently in the dark at 25 ± 1 °C under a continuous airflow. During the course of cultivation, moisture was maintained at 60% WHC using the weighing method. Each incubated flask was connected to a series of small flasks (see Figure S1 of the Supporting Information). First, two flasks (30 mL, 5.0 M NaOH) were set for scrubbing the inlet CO_2, while the following distilled water flask was used for maintaining constant soil moisture. Besides, the 1.0 M H_2SO_4 and glycol traps were used for absorbing volatile agents, and last two 5.0 M NaOH traps were set for trapping the released $^{14}CO_2$. At different time intervals (0, 5, 10, 20, 30, 45, 60, 75, and 100 days after treatment), the treated soils (10 g, dry weight) were sampled (three replicates) to subject the following extractions. The sterilized soil sample was analyzed under the same protocol, but all procedures were performed in a sterile environment.

^{14}C ER Analysis. The soil samples were extracted using four solvents (50 mL) in sequence, 0.01 M $CaCl_2$, acetonitrile/water (9:1, v/v), methanol, and dichloromethane, by shaking for 24 h and followed by centrifugation at 4000 rpm for 10 min, corresponding to the similar method reported by Mordaunt et al.[21] Subsequently, additional one or two extracting processes were conducted using methanol until no radioactivity could be detected in the extracts. After these exhaustive solvent extractions, the radioactivity of each supernatant was measured by a liquid scintillation counter (LSC, Wallac-1414, Wallac Co., Turku, Finland) using scintillation cocktail I.

Dissipation of Parent Compound Analysis. ER extracts were combined and concentrated on the vacuumed rotary evaporator (Eyela SB-1000, Eyela, Tokyo, Japan) at 37 °C, then recovered in 10 mL of methanol (chromatographic grade), and further condensed to 1.0 mL. The final extracts were passed through a 0.22 μm filter for HPLC analysis. A 20 μL aliquot of the final sample was injected into a Waters 2695 system (Waters 2998 photodiode array detector, Waters, Milford, MA) with a Diamonsil C_{18} column (5 μm, 250 × 4.6 mm, Dikama Technologies, Lake Forrest, CA). The column temperature was 28 ± 1 °C. The mobile phase was composed of A (methanol + 0.1% ethylic acid) and B (H_2O + 0.1% ethylic acid). The elution process was carried out under a gradient elution [A/B (%): 20:80 for 0 min, 75:25 for 20 min, 75:25 for 60 min, 100:0 for 65 min, 100:0 for 70 min, 0:100 for 75 min, 20:80 for 80 min] at a flow rate of 1.0 mL/min. A standard sample was used to confirm the retention time of the parent SYP-3343. Aliquots of the eluent were collected in a 20 mL glass scintillation vial at 1 min intervals. A total of 10 mL of scintillation cocktail I was added to each collected eluent for the radioactivity measurement by LSC.

^{14}C-BR Analysis. After 4−6 shaking extraction steps, the remaining soil pellets were placed in tubes and put inside the fume hood overnight to remove the residual solvent. The samples were then thoroughly mixed, and 0.5 g of soil was used for combustion with a biological oxidizer (OX-600, R.J. Harvey Instrument Corp., Hilldale, NJ). The oxidation procedure was held on for 4 min at 900 °C for combustion and 680 °C for catalysis, using scintillation cocktail II to absorb $^{14}CO_2$. The recovery efficiency of this procedure was more than 91.3%, measured by comparing the combustion of ^{14}C-SYP-3343 with a known radioactivity.

Mineralization Analysis. The measurement of mineralization was conducted by forcing air through the sample for 1.5 h/day to remove CO_2, which could be absorbed by two flasks of NaOH solution during the whole experimental period. This solution was changed every 5 days and stored in a refrigerator (4 °C) for further use of the radioactivity measurement. The two traps were combined and adjusted to a defined volume with distilled water. Then, a 1.0 mL aliquot was drawn, and its radioactivity was measured with 10 mL of scintillation cocktail I.

Statistical Analysis. The dissipation of parent ^{14}C-SYP-3343 was analyzed using the first-order regression model $C_t = C_0 \exp(-kt)$, where C_0 is the initial quantity, C_t is the quantity at time t, and k is the degradation constant. The half-life ($t_{1/2}$) value was calculated as ln 2/k.

All of the experiments were conducted in triplicate, and the standard deviations (mean ± standard deviation) presented in the text were calculated from the repeated measurements. Statistical analysis by one-way analysis of variance (ANOVA) was performed with SPSS 20.0 (IBM Corporation, Armonk, NY).

RESULTS AND DISCUSSION

Total ^{14}C Material Mass Balance. The total recovered ^{14}C was calculated as the sum of ^{14}C in continuous extraction steps,

Table 1. Basic Physical and Physicochemical Properties of the Selected Soils

number	soil type	pH	OM[a] (%)	CEC[b] (mequiv 100 g^{-1})	silt (%)	sand (%)	clay (%)
S1	coastal soil	8.23	1.23	11.77	31.32	26.32	42.36
S2	loamy soil	6.95	2.11	10.65	36.32	20.98	42.70
S3	red soil	5.53	2.65	8.93	33.25	21.01	45.75

[a]OM = organic matter. [b]CEC = cation-exchange capacity.

dx.doi.org/10.1021/jf500392d | J. Agric. Food Chem. 2014, 62, 3343−3347

BR, and CO_2 in mineralization after treatment. The total ^{14}C material mass balance was calculated by the total recovered ^{14}C to the initial added ^{14}C, ranging from 95.8 ± 2.9 to 103.5 ± 3.7% (n = 3) in the four tested soils. The high ^{14}C recoveries indicated that the procedure used for measuring the different residues was feasible.

Formation of the ER and Degradation of the Parent Compound. The decrease of ER over the incubation period was shown in Figure 2. In the initial 10 days of incubation, ER

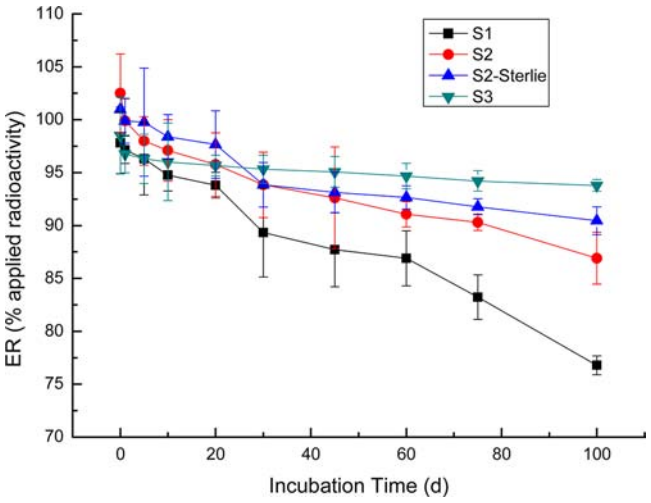

Figure 2. ER of SYP-3343 in aerobic soils (bars represent ±standard error of the mean).

was detected up to about 95% after the four extraction steps. A significant decrease of ER was observed in the coastal soil (S1); after incubation for 100 days, the ER ratio was determined to be 76.79 ± 1.89%. However, the ER level was almost constant in the red soil (S3), showing no significant decrease within the incubation time (p > 0.05), approximately 93.79 ± 3.55%, at the end of the incubation. In addition, ER in the sterilized loamy soil S2 (S2-sterile) was 90.45 ± 1.32%, which was slightly higher than ER in non-sterilized S2 (86.91 ± 2.45%), indicating that soil microbes may promote the dissipation of ER. However, only an inconspicuous decrease of ER in S3, from 98.5 ± 3.63 to 93.79 ± 3.55%, was observed over the incubation period. The ER levels in three tested soils were S1 < S2 < S2-sterile < S3. Possibly, the time dependence of the ER decrease can be attributed to the transformation into BR and mineralization to CO_2. Because of the high extraction rate, it may have potential harm to the downstream farm or water through irrigation. The above findings implied the specific type of soil needed to be considered for the use of fungicide in the context of environmentally friendly usage.

Radioactivity analysis after HPLC fractionation showed that the degradation of SYP-3343 was in accordance with the bi-exponential equation (r^2 > 0.90; see Table S1 of the Supporting Information). The remaining parent compound was 17.8 ± 1.62, 39.2 ± 1.19, 65.5 ± 4.52, and 56.6 ± 1.58% of the applied amount in S1, S2, S2-sterile, and S3 at the end of incubation, respectively (Figure 3), which suggested that the degradation of SYP-3343 in S1 was fastest compared to S2, S2-sterile, and S3. A previous study found that the half-life of SYP-3343 in soil under field conditions was only 2.6−2.7 days.[22] However, the half-lives in the four-treated soils ranged from 43.8 to 169.0 days under lab conditions (see Table S1 of the Supporting

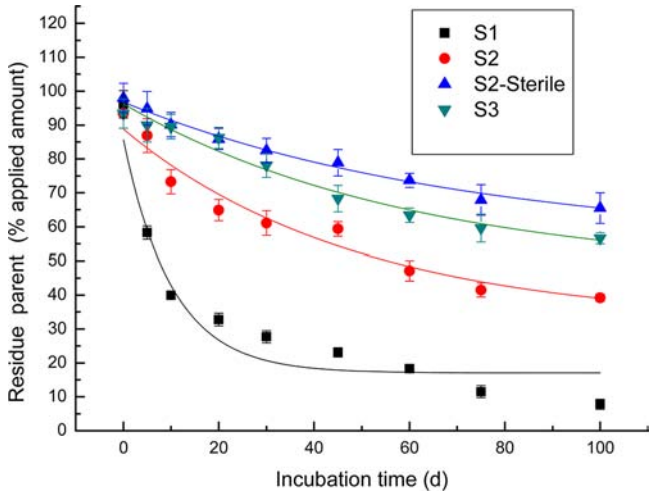

Figure 3. Dissipation of parent SYP-3343 in aerobic soils (bars represent ±standard error of the mean).

Information), which indicated that the degradation rates of SYP-3343 might be attributed to both the soil properties and its surroundings, such as pH, organic matter (OM), cation-exchange capacity (CEC), soil particles, temperature, and soil moisture. It is noteworthy that the half-life of the sterile S2 was about 2 times longer than the non-sterile S2 (169.0 versus 80.6 days), suggesting that microbes played an important role in its degradation. In S3, it has a calculated half-life of 123.7 days that exceeded the total incubation time. In general, degradation of parent SYP-3343 followed the order of S1 > S2 > S3 > S2-sterile. Previous studies showed that many chemicals (e.g., naproxen and carbamazepine) under different soil conditions had different rates of degradation.[23] Thus, it was likely to infer that soil enzymes, microbes, and sediments could selectively influence the performance of chemicals in soil.[24] The long-term dissipation may cause a potential hazard because of the accumulation in the future.

Formation of BRs. In the risk assessment of pesticides, BR is always used in the description of dissipation kinetics.[25] The BR fraction after 30 days of treatment treated with SYP-3343 increased rapidly in S1 and S2, but in the S2-sterile soil, no significant increase of BR was observed (p > 0.05). Furthermore, the BR in S3 was found to increase slightly until 1.73% at the end of incubation, which was much lower than those in S1 and S2. The formation of BR of many pesticides has been reported to be mediated by pH and CEC.[11] S3 has a low pH and CEC that may contribute to its low binding affinity. After 45 days of incubation, a significant difference between S2 and S2-sterile was observed (p < 0.01), indicating that soil microbes could affect the formation of BR. As shown in Figure 4, after incubation of 100 days, the BR followed the order of S1 (alkaline soil, 12.4%) > S2 (neutral soil, 9.9%) > S2-sterile (6.0%) > S3 (acid soil, 1.7%). These results demonstrated that SYP-3343 could be absorbed in the soil and increase with time. Therefore, the BR level reported here, which is much lower than 70%, satisfied the non-accumulation uniform principles demonstrated in laboratory tests.[13] The formation of BR was accompanied by degradation, which was also found in other chemicals, such as nonylphenol.[26]

Mineralization. It could be seen from Figure 5 that the mineralization of SYP-3343 increased gradually with time in the tested soils, indicating that the pyrazole ring could be gradually

dx.doi.org/10.1021/jf500392d | J. Agric. Food Chem. 2014, 62, 3343−3347

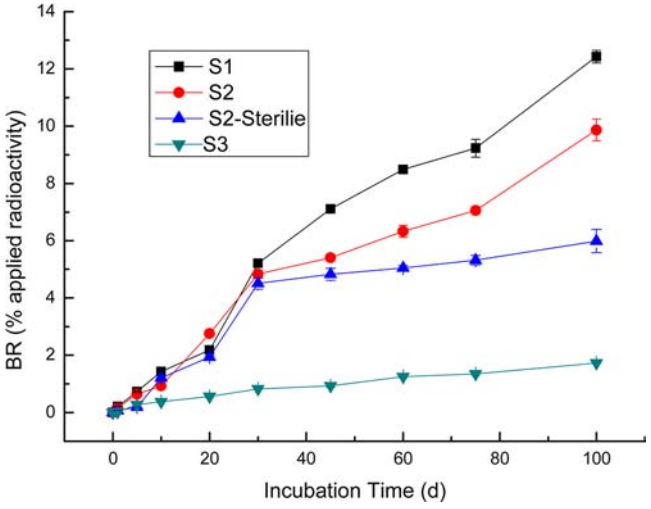

Figure 4. BR of SYP-3343 in aerobic soils (bars represent ±standard error of the mean).

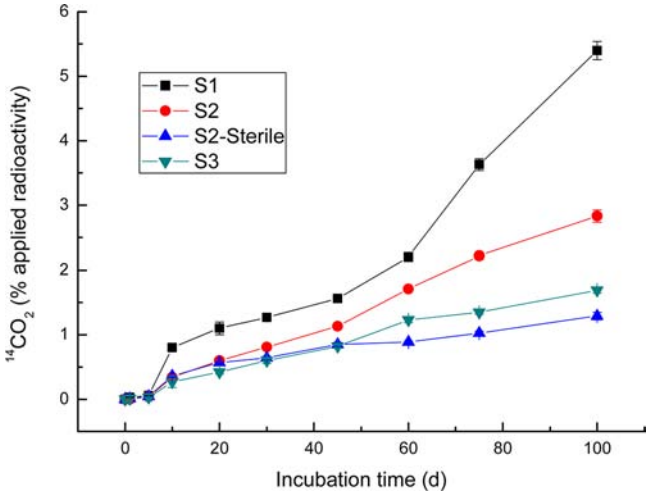

Figure 5. Mineralization of SYP-3343 in aerobic soils (Bars represent ±standard error of the mean).

opened under the present experimental conditions. The ratio of SYP-3343 mineralized to $^{14}CO_2$ was only 0.03−0.06% after 5 days of incubation. Despite the differences in soil properties, the mineralization ratio was lower than 5.4% in all treatments, suggesting that the cleavage of the pyrazole ring was difficult, so that the parent compound or metabolites of SYP-3343 might remain in aerobic soils for a prolonged period. After 100 days of incubation, the mineralization followed the pattern: S1 > S2 > S3 > S2-sterile.

A mineralization ratio of 2.83% was obtained in S2, which was about 2.5 times larger than that in S2-sterile (Figure 5). These findings indicated that soil microbes played an important role in SYP-3343 mineralization. Generally, the degree of mineralization can be affected by microbes and soil properties. A similar phenomenon was observed in the pesticide ZJ0273.[27] Because mineralization is regarded as one of the detoxification pathways, the above results indicated that SYP-3343 was not prone to degrade completely and might remain in soil as either the parent compound or a mixture of the parent compound and metabolites. Although it fits the non-accumulative principle stated by the Commission of the European Communities, it is not recommended to use in red soil. The potential toxicity of itself or its metabolites should deserve more attention. Therefore, more effective data should be acquired in the future for its environmentally friendly use.

■ ASSOCIATED CONTENT

Supporting Information

Incubation setup (Figure S1) and first-order rate constants (k), half-lives ($t_{1/2}$), and coefficients of determination (r^2) describing dissipation of the SYP-3343 parent compound in different soils (Table S1). This material is available free of charge via the Internet at http://pubs.acs.org.

■ AUTHOR INFORMATION

Corresponding Authors

*E-mail: qfye@zju.edu.cn.
*E-mail: dingxch@zju.edu.cn.

Funding

This work was financially supported by the special fund for Agro-scientific Research in the Public Interest (201103007), the Fundamental Research Funds for the Central Universities (2013FZA6011), and the Project of Science Technology Department of Zhejiang Province (2010R50033). Xun-Yue Liu thanks the Chinese Scholarship Council (CSC) for financial support.

Notes

The authors declare no competing financial interest.

■ REFERENCES

(1) Bhuniya, A. K.; Marik, R.; Banerjee, S. K. Biochemical effects of carbaryl on assimilating enzymes of cyanobacteria nostocmuscorum. *Bull. Environ. Contam. Toxicol.* **1994**, *l52*, 886−892.
(2) Jeyaratnam, J. Acute pesticide poising: A major global health problem. *World Health Stat. Q.* **1990**, *43* (3), 139−144.
(3) Katan, J.; Fuhremann, T. W.; Lichtenstein, E. P. Binding of [^{14}C] parathion in soil: A reassessment of pesticide persistence. *Science* **1976**, *193*, 891−893.
(4) Frank, R.; Braun, H. E.; Clegg, B. S. Survey of farm wells for pesticides, Ontario, Canada, 1986 and 1987. *Bull. Environ. Contam. Toxicol.* **1990**, *44*, 410−419.
(5) Bagchi, D.; Bagchi, M.; Hassoun, E. A.; Stohs, S. J. In vitro and in vivo generation of reactive oxygen species, DNA damage and lactate dehydrogenase leakage by selected pesticides. *Toxicology* **1995**, *104* (1−3), 129−140.
(6) Banerjee, B. D.; Seth, V.; Bhattacharya, A.; Pasha, S. T.; Chakraborty, A. K. Biochemical effects of some pesticides on lipid peroxidation and free-radical scavengers. *Toxicol. Lett.* **1999**, *107*, 33−37.
(7) Fent, G.; Hein, W. J.; Moendel, M. J.; Kubiak, R. Fate of the herbicide ^{14}C-terbuthylazinein Brazilian soils under various climatic conditions. *Chemosphere* **2003**, *51*, 735−746.
(8) Langenbach, T.; Schroll, R.; Scheunert, I. Fate of the herbicide ^{14}C-terbuthylazine in Brazilian soils under various climatic conditions. *Chemosphere* **2001**, *45* (3), 387−398.
(9) Jablonowski, N. D.; Linden, A.; Köppchen, S.; Thiele, B.; Hofmann, D.; Mittelstaedt, W.; Pütz, T.; Burauel, P. Long-term persistence of vaious ^{14}C-labeled pesticides in soils. *Environ. Pollut.* **2012**, *168*, 29−36.
(10) Khan, S. U.; Hamilton, H. A. Extractable and bound (nonextractable) residues of prometryn and its metabolites in an organic soil. *J. Agric. Food Chem.* **1980**, *28*, 126−132.
(11) Gevao, B.; Semple, K. T.; Jones, K. C. Bound pesticide residues in soils: A review. *Environ. Pollut.* **2000**, *108*, 3−14.
(12) Liu, J.; Wang, Y. F.; Jiang, B. Q.; Wang, L. H.; Chen, J. Q.; Guo, H. Y.; Ji, R. Degradation, metabolism, and bound-residue formation

and release of tetrabromobisphenol A in soil during sequential anoxic−oxic incubation. *Environ. Sci. Technol.* **2013**, *47*, 8348−8354.
(13) Commission of the European Communities (CEC). *Directive 97/57, Establishing Annex VI (Uniform Principles to Directive 91/414*; CEC, Directorate General for Agriculture, DG VI B II-1-Brussels: Brussels, Belgium, 1997.
(14) Sauter, H.; Steglich, W.; Anke, T. Strobilurins: Evolution of a new class of active substances. *Angew. Chem., Int. Ed.* **1999**, *38* (10), 1328−1349.
(15) Li, M.; Liu, C. L.; Yang, J. C.; Zhang, J. B.; Li, Z. N.; Zhang, H.; Li, Z. M. Synthesis and biological activity of new (*E*)-α-(methoxyimino)benzeneacetate derivatives containing a substituted pyrazole ring. *J. Agric. Food Chem.* **2010**, *58*, 2664−2667.
(16) Wang, L.; Li, B. J.; Xiang, W. S.; Shi, Y. X.; Liu, C. L. Control effects of pyraoxystrobin on cucumber powdery mildew. *Agrochemicals* **2008**, *47* (5), 378−380 (in Chinese).
(17) Li, M.; Li, L.; Liu, C. L.; Li, Z. M.; Li, Z. N.; Shi, N. G. *Proc. 7th Chin. Annu. Meet. Innovative Pestic.* **2009**, 242−246.
(18) Liu, X. Y.; Ye, Q. F.; Kan, D. L.; Zhang, Z.; Ding, X. C. Synthesis of carbon-14 labeled pyraoxystrobin, a novel fungicide. *J. Labelled Compd. Radiopharm.* **2011**, *54*, 780−782.
(19) Nelson, D. W.; Sommers, L. Chemical and microbiological properties. In *Methods of Soil Analysis, Part 2*; Page, A. L., Eds.; American Society of Agronomy: Madison, WI, 1982; pp 539−579.
(20) Organization for Economic Co-operation and Development (OECD). Aerobic and anaerobic transformation in soil, no. 307. *OECD Guidelines for the Testing of Chemicals*; OECD: Paris, France, 2002.
(21) Gee, G. W.; Bauder, W. Partical-size analysis. Physical and mineralogical methods. In *Methods of Soil Analysis, Part 1*; Klute, A., Eds.; Soil Science Society of America: Madison, WI, 1986; pp 383−412.
(22) Liu, Y. P.; Sun, H. B.; Zeng, F. J.; Liu, J. M.; Xu, Y. L.; Wang, S. W. Study on residual dynamics of SYP-3343 in cucumber and soil. *Guangdong Agric. Sci.* **2010**, *9*, 46−47 (in Chinese).
(23) Lin, K.; Gan, J. Sorption and degradation of wastewater-associated non-steroidal anti-inflammatory drugs and antibiotic in soils. *Chemosphere* **2011**, *83*, 240−246.
(24) Li, J. Y.; Dodgen, L.; Ye, Q. F.; Gan, J. Degradation kinetics and metabolites of carbamazepine in soil. *Environ. Sci. Technol.* **2013**, *47*, 3678−3684.
(25) Barriuso, E.; Benoit, P.; Dubus, I. Formation of pesticide nonextractable (bound) residues in soil: Magnitude, controlling factors and reversibility. *Environ. Sci. Technol.* **2008**, *42*, 1845−1854.
(26) Liu, J.; Shan, J.; Jiang, B. Q.; Wang, L. H.; Yu, B.; Chen, J. Q.; Guo, H. Y.; Ji, R. Degradation and bound-residue formation of nonylphenol in red soil and the effects of ammonium. *Environ. Pollut.* **2014**, *186*, 83−89.
(27) Wang, W.; Ye, Q. F.; Ding, W.; Han, A. L.; Wang, H. Y.; Lu, L.; Gan, J. Influence of soil factors on the dissipation of a new pyrimidynyloxybenzoic herbicide ZJ0273. *J. Agric. Food Chem.* **2010**, *58*, 3062−3067.

■ NOTE ADDED AFTER ASAP PUBLICATION

There was a mistake in the chemical name for SYP-3343 ((*E*)-2-(2-((3-(4-chlorophenyl)-1-methyl-1*H*-pyrazole-5-yloxy)methyl)phenyl)-3-methoxyacrylate) in the first sentence of the formula in the abstract, and incorrect reference citations in the first and second paragraph of the Materials and Methods section of the version of this article published April 2, 2014. The correct version published April 16, 2014.

Mesoporous molecular sieves have attracted significant attention especially in their application in catalysis. Among the mesoporous silica materials, SBA-15 silica is emerged as a promising catalyst support in heterogeneous catalysis owing to its well-ordered structure, nanosized channel, large surface area, and sufficient silanol group for surface modification.[20] The immobilization of organic base groups on the surface of the mesoporous material by grafting or co-condensation can be recognized as a promising approach to create efficient solid base catalysts with improved catalytic properties as compared to conventional homogeneous catalysts.[20−22] This approach can allow the catalyst to be separated easily from the reaction mixture with no wastewater originating from the catalyst neutralization step.

TBD (1,5,7-triazabicyclo[4.4.0]dec-5-ene) is a strong bicyclic guanidine base (pK_b = 25) widely utilized as a homogeneous base catalyst for various chemical reactions.[23] Mesoporous silica materials could be organically functionalized through grafting reactions in which the organic base is anchored onto the surface of the pores with the preservation of a pore host structure. Kalita et al. covalently grafted TBD onto MCM-41 nanoparticles and proved that the TBD-functionalized MCM-41 material is efficient for Michael-addition reactions under solvent-free conditions.[24] However, this kind of heterogeneous base catalysts is seldom used for the CIE reaction.[19] Due to the increased interest and demand for practical application, the environmentally friendly benign and easy-separable solid base catalysts are highly desirable. In the present contribution, for the purpose of providing a highly efficient and green procedure for the interesterification reaction, the guanidine base TBD was covalently bound onto the surface of the mesoporous SBA-15 silica to form the heterogeneous catalyst SBA-15-pr-TBD. Thereafter, this hybrid organic−inorganic material was tested for the interesterification of tributyrin and methyl stearate in solvent-free system for the production of LCSL. For this purpose, the TBD base was previously linked to 1,3-glycidyloxypropyl-trimethoxysilane by nucleophilic addition to the epoxide moiety. The resulting TBD-organosilane compound was then anchored to the mesoporous SBA-15 silica by reaction of the trimethoxysilyl group with the surface silanol. The as-prepared solid base catalyst was characterized by using small-angle X-ray scattering (SAXS), Fourier transform infrared (FT-IR) spectra, thermo gravimetric analysis (TG-DTA), scanning electron microscopy (SEM), transmission electron microscopy (TEM), nitrogen adsorption−desorption and elemental analysis techniques. By using this solid base catalyst, the LCSL was produced in a solvent-free system by interesterification of tributyrin and methyl stearate in a batch reactor. The TAG compositions of the interesterified products were determined by high-performance liquid chromatography (HPLC). Moreover, the interesterification parameters, including the molar ratio of substrate, reaction temperature, reaction time, and reusability of the solid catalyst were investigated systematically in the present investigation.

MATERIALS AND METHODS

Materials. Tributyrin (≥98%) and methyl stearate (≥98%) were obtained from Sinopharm Chemical Reagent Corporation (Sanghai, China). Pluronic copolymer P123 ($EO_{20}PO_{70}EO_{20}$, average molecular weight was 5800), 1,3-glycidyloxypropyl-trimethoxysilane (≥99.8%), 1,5,7-Triazabicyclo[4.4.0]dec-5-ene (TBD, ≥98%) and tetraethylorthosilicate (TEOS, ≥98%) were purchased from Sigma-Aldrich. All the other materials used were of either analytical or chromatographical grades.

Catalyst Preparation. Mesoporous silica SBA-15 was prepared according to a hydrothermal approach using Pluronic P123 triblock copolymer as a template under acidic conditions.[20] In a typical synthesis, 10 g of Pluronic copolymer P123 was first dissolved in 75 mL of double distilled water and 300 mL of 2 mol/L HCl solution at room temperature, and then stirred at 313 K until a homogeneous solution was obtained. Thereafter, 21 g of tetraethylorthosilicate (TEOS) was added under stirring to the P123 solution, and the stirring was continued for 24 h at 40 °C. Subsequently, the solution was taken in a Teflon-lined autoclave and heated at 100 °C for 48 h. After cooling to room temperature, the solid product was filtered, then washed thoroughly with deionized water, and finally dried in air at room temperature. The SBA-15 powder was obtained by calcining the material in air at 550 °C for 6 h to remove the template. The mesoporous SBA-15 silica was used as a support material for preparation of the solid catalyst.

The organic base TBD can be allowed to immobilize onto the surface of SBA-15 silica through the condensation reactions of TBD-organosilane with the surface silanol group. Initially, the TBD-organosilane was prepared by the reaction of 1,3-glycidyloxypropyl-trimethoxysilane with TBD base. Typically, 0.6 g of TBD was added to a solution of 1,3-glycidyloxypropyl-trimethoxysilane (4 mL) in dry DMF (10 mL), and after this the resulting mixture was continued to stir for 48 h at room temperature under nitrogen atmosphere. Thereafter, the solution was poured into a flask containing dry toluene (15 mL) and SBA-15 (1.2 g, previously heated at 350 °C for 10 h), after which the mixture was refluxed for 48 h under nitrogen atmosphere. The solid base catalyst thus obtained was filtered under vacuum, washed carefully with toluene and methanol, and extracted with a Soxhlet apparatus for 24 h using a 1/1 diethyl ether/methylene chloride mixture. Finally the solid catalyst was dried at 60 °C for 12 h under vacuum prior to use.

Catalyst Characterization. Small-angle X-ray scattering (SAXS) measurements were performed on a Bruker AXS Nanostar instrument with the Cu Kα radiation using an acceleration voltage of 40 kV and a current of 30 mA. Fourier transform infrared spectroscopy (FT-IR) was recorded for functional group detection in the 400−4000 cm^{-1} range on a Shimadzu IR-Prestige-21 spectrometer using the usual KBr pellet method.

Thermogravimetric measurements (TG-DTA) were conducted on a TA Instrument TG 2050 thermogravimetric analyzer with a heating speed of 20 °C/min under air atmosphere with a flow rate of 100 mL/min. Scanning electron microscope (SEM) measurements were carried out with a field-emission microscope (JEOL, JSM-6390LV) using an accelerating voltage of 15 kV. Transmission electronic microscopy (TEM) images were taken using a JSM-6390LV transmission electronic microscopy at an accelerating voltage of 200 kV.

The elemental analysis for carbon, hydrogen and nitrogen contents of the samples to measure the TBD loading in the solid catalyst were carried out on a Carlo-Erba 1106 elemental analyzer.

The textural properties of the solid catalysts were measured by nitrogen adsorption−desorption isotherm method at liquid nitrogen temperature (−196 °C) using a Quantachrome NOVA 1000e instrument. The specific surface area was calculated by using the Brunauer−Emmett−Teller (BET) method. The total pore volume and the pore size distribution were assessed according to the Barrett−Joyner−Halenda (BJH) method based on the adsorption isotherm.

Interesterification Procedures. A certain amount of tributyrin and methyl stearate mixture was charged into a 50 mL round-bottom flask. After raw materials were melted absolutely and dried under reduced pressure at 80 °C, the CIE reaction was carried out in solvent-free system by the addition of 1.5 wt % of TBD-functionalized SBA-15 silica as a catalyst. The interesterification of tributyrin with methyl stearate was allowed to proceed under reduced pressure at 80 °C in a water bath with magnetic stirring (~750 rpm). After completion of the reaction, the interesterified product was filtered, and then employed for subsequent analysis.

Analyses of TAG Composition. Reversed-phase high-performance liquid chromatography (HPLC) was used to determine the TAG composition of the interesterified product. A commercially packed Genesis C18 HPLC column (15 cm length × 4.6 mm) was used to separate the TAGs. The protocol employed for the mobile phase involved linear elution gradients for a dichloromethane/acetonitrile (HPLC grade) system from 35% acetonitrile increasing to 55% dichloromethane in 45 min. The mobile phase flow rate was 1.2 mL/min. The column temperature was held at 40 °C. The TAG species were detected by an Alltech 500eVaporative light scattering detector. Individual peaks were identified tentatively according to Han et al.[5] HPLC analysis was run in duplicate for each sample of the interesterified product.

RESULTS AND DISCUSSION

Catalyst Characterization. Surface functionalization has been employed to prepare TBD-functionalized mesoporous SBA-15 material. The TBD base can be covalently tethered onto the framework surface of the mesoporous SBA-15 silica due to the presence of silanol groups, which can form strong chemical bonds with TBD-containing organosilane precursors.[22] In the present study, the solid base catalyst was prepared by two steps. The TBD base was first reacted with 3-trimethoxysilylpropoxymethyloxirane in anhydrous DMF to afford a TBD-containing organosilane by nucleophilic addition of TBD to the epoxide moiety. Then, in the second step, the resulting solution was allowed to react with the SBA-15 silica forming the solid base catalyst. The obtained solid catalyst was identified by FT-IR spectroscopy, SAXS, TG-DTA analysis, nitrogen adsorption−desorption, and elemental analysis techniques.

Figure 1 shows the SAXS patterns of SBA-15 silica and functionalized SBA-15 silica. The SAXS pattern of siliceous

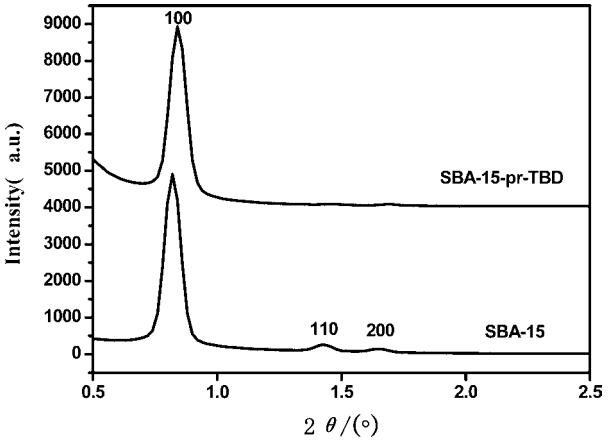

Figure 1. Small angle X-ray photoelectron spectroscopy patterns for samples: (a) SBA-15 and (b) SBA-15-pr-TBD.

SBA-15 exhibited an intense peak at 0.91° corresponding to the (100) reflection, and two low-intensity peaks at 1.56° and 1.76° that could be indexed as (110) and (200) reflections.[19,25] The (100) reflection was characteristic for p6mn symmetry, evidencing the formation of a well formed uniform hexagonal lattice.[24] For the functionalized SBA-15 material, the (100) peak was also observed in the SAXS pattern, however the (110) and (200) peaks were not clearly registered as evident from Figure 1. This observation suggested that the long-range ordering of the mesoporous structure remained unaltered even after incorporation of TBD into the SBA-15 silica. No obvious peak for (110) and (200) reflection was detected mostly likely owing to the decrease in the scattering contrast between the SBA-15 support walls and the filled pores with the organic moieties, which showed that the organic component was embedded into the channel of the support.[24−26] Moreover, the (100) peak of the functionalized SBA-15 silica was shown to shift to higher 2-theta value, revealing the reduction of pore size because of the incorporation of organic components into the pore channel of the support.[27] By drawing on the results, the ordered meso-structure of the siliceous SBA-15 is preserved after the incorporation of organic groups.

Figure 2 represents the FT-IR spectra of SBA-15 silica and SBA-15-pr-TBD sample. In the case of nonfunctionalized SBA-

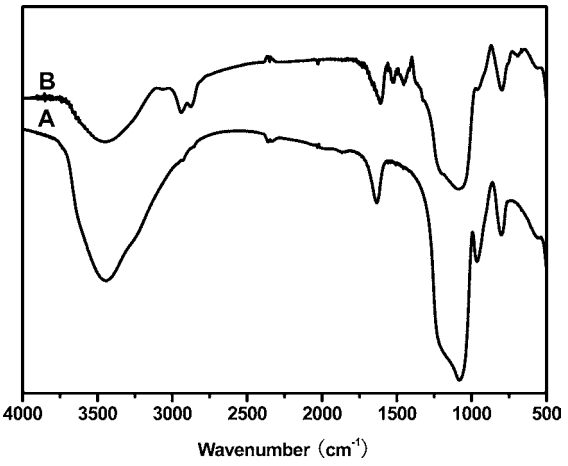

Figure 2. Fourier transform infrared spectra for samples. (a) SBA-15 and (b) SBA-15-pr-TBD.

15 silica, there was a broad IR absorption band centered at 3460 cm^{-1} mostly ascribed to the stretching vibration of framework hydroxyl groups and adsorbed water molecules, and the peak located at 1635 cm^{-1} was principally attributable to the bending mode of adsorbed water present in the SBA-15 material.[25] Moreover, a weak band in the mid-infrared region at 950 cm^{-1} for the SBA-15 support could be mainly responsible for Si−OH groups in SBA-15 silica.[27] Besides, three characteristic absorption bands around 1080 cm^{-1}, 780 cm^{-1}, and 470 cm^{-1} were the typical vibration modes of mesoporous framework Si−O−Si attributed to the condensed silica net in the samples.[27,28] By comparing the IR spectrum of the TBD-functionalized SBA-15 material, the IR characteristic peaks of surface hydroxyl groups at 3460 and 950 cm^{-1} were observed to decrease significantly in intensity after the organofunctionalization, thereby suggesting that the surface hydroxyl groups reacted with the anchored functional groups to form the functionalized SBA-15 material. In comparison with the SBA-15 support, new IR absorption bands at 2942 and 2876 cm^{-1} due to the CH_2 asymmetric and symmetric vibration respectively were appeared for the SBA-15-pr-TBD sample.[24,25] Additionally, the characteristic peaks at 1587 and 675 cm^{-1} for the TBD-functionalized SBA-15 material could be ascribed to the C═N stretching vibration and N−H bending vibration of TBD,[18,24] and these IR peaks were not found in the IR spectrum of the nonfunctionalized SBA-15 silica. On the basis of the results, the TBD has been successfully anchored on the surface of the SBA-15 material.

The thermal behavior of SBA-15-pr-TBD is illustrated in Figure 3. As indicated in this figure, the small amount of mass

dx.doi.org/10.1021/jf405434a | J. Agric. Food Chem. 2014, 62, 3348−3355

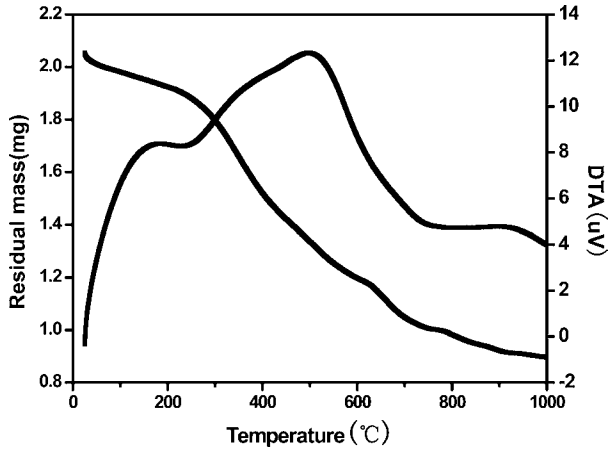

Figure 3. Thermo gravimetric curves of SBA-15-pr-TBD catalyst.

loss (about 8.7%) below 200 °C could be apparently originated from the removal of physically adsorbed water. Meanwhile, an endothermic event between 0 and 200 °C was also observed in the DTA curve. With further increasing the temperature, as shown in Figure 3, a significant mass loss in the temperature range of 200−750 °C (about 54.2%) and a strong endothermic event at about 500 °C were appeared. This main mass loss could be principally ascribed to the thermal decomposition of the organic moieties in the solid base catalyst. On the basis of the mass loss (200−750 °C), the amount of functional groups bound on the SBA-15 material could be estimated to be 2.23 mmol/g. Beyond a temperature of 750 °C, almost no obvious mass loss in the TG curve could be observed, revealing that the tethered organic moiety was decomposed totally at this temperature.

SEM techniques can be employed to study the morphology feature of the SBA-15-pr-TBD catalyst. The typical SEM micrograph of SBA-15-pr-TBD sample is shown in Figure 4. As can be seen, the SBA-15 silica displayed curved faceted and smooth rods based on elongated wheat-like macrostructures in SEM images.[19,24] The TBD-functionalized SBA-15 silica exhibited a similar wheat-like morphology to the non-functionalized SBA-15 silica. No significant variation in the surface morphology occurred after the modification of SBA-15 silica except that the domains were more densely packed.

The morphology property of the solid base catalyst was also characterized by TEM techniques. The TEM images of SBA-15 silica and TBD-functionalized SBA-15 silica are shown in Figure 5. The TEM images confirmed the presence of a honeycomb-like hexagonal array through the material for SBA-15 silica and TBD-functionalized SBA-15 silica.[25] The slight change in TEM image was observed after the functionalization of SBA-15 silica, thus implying that the incorporation of TBD into the SBA-15 silica does not destroy the mesopore structure of SBA-15 silica. This result is in good agreement with the other characterization technique results.

The C, H and N elemental analysis results for the solid base catalyst are summarized in Table 1. According to the results, the loading amount of TBD on the SBA-15 silica was calculated to be 2.35 mmol/g, which is in line with the result obtained from TG-DTA measurements.

The nitrogen adsorption−desorption isotherms of SBA-15 silica and SBA-15-pr-TBD catalyst are presented in Figure 6. For the two samples, the adsorption isotherm could be classed as type IV isotherm with H1-type hysteresis loop according to IUPAC classification, which was the typical behaviors of highly ordered mesoporous molecular sieves with narrow pore size distributions.[25,27] Moreover, the adsorption branch of isotherm displayed a sharp inflection at a relative pressure of about 0.65. This is characteristic of capillary condensation with uniform pore dimensions and high-ordering of the material. This phenomenon suggested that after the functionalization with the organic base the SBA-15 material could still maintain its mesoporous structure.

The textural properties of the samples are listed in Table 2. BET surface area and pore-size distribution were calculated using nitrogen adsorption at −196 °C. For pure SBA-15 silica, the mean pore size calculated from the N_2 adsorption−desorption isotherm was 6.65 nm, and the measured surface area and pore volume were determined to be 807 m^2/g and 1.25 cm^3/g, respectively, which are in accordance with the value reported in the literature.[19,24] As indicated in Table 2, for the SBA-15-pr-TBD catalyst, a surface area of 312 m^2/g and a pore volume of 0.43 cm^3/g were determined, and the pore size distribution was narrow with a mean pore diameter of 4.45 nm. Obviously, the SBA-15-pr-TBD catalyst showed some loss of surface area and a pronounced reduction in pore volume and pore diameter after the organofunctionalization, implying that the organic base was incorporated into the SBA-15 support. The decrease of these parameters upon the functionalization of SBA-15 silica could be expected since the partial filling of functionalized TBD base inside the mesopores would increase the average wall thickness, thus decreasing the pore diameter and BET surface area. Although such a change in the textural

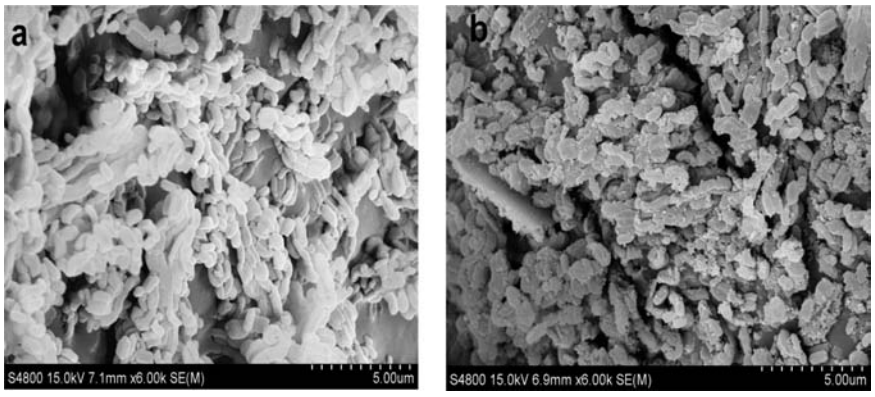

Figure 4. Scanning electron microscopy images of samples: (a) SBA-15 and (b) SBA-15-pr-TBD.

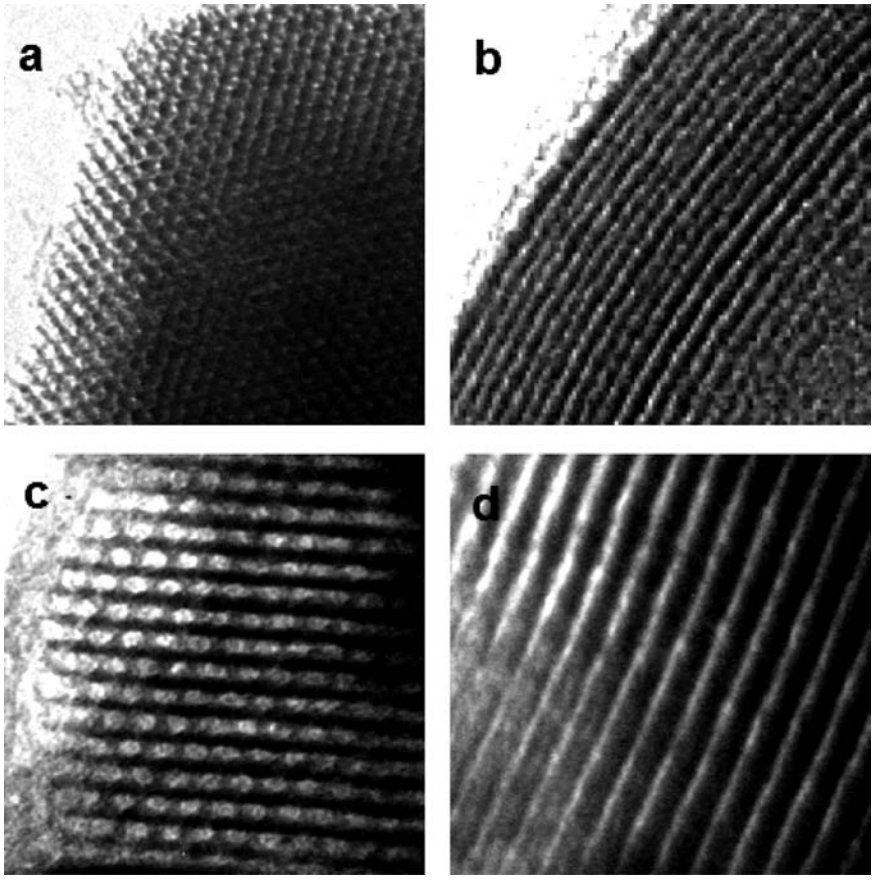

Figure 5. Transmission electron microscopy images of samples: (a) SBA-15 in top view; (b) SBA-15 in side view; (c) SBA-15-pr-TBD in top view; (d) SBA-15-pr-TBD in side view.

Table 1. Results for C, H, and N Elemental Analysis

sample	C (wt %)	H (wt %)	N (wt %)
SBA-15	NF[a]	NF[a]	NF[a]
SBA-15-pr-NR_3OH	16.92	2.85	1.76

[a]NF stands for not found.

properties, the functionalized SBA-15 silica still remained the typical mesoporous structure after the organofunctionalization reaction.

Influence of Interesterification Parameters. In the present study, the interesterification can substantially alter the TAG profiles of the starting oil blend, and the LCSL is produced by the interesterification of tributyrin and methyl stearate. The interesterified product was characterized by the combination of short-chain and long-chain acyl residues into a triacylglycerol structure. As shown in Figure 7, two new types of TAGs (SSL and SLL) were produced, representing the incorporation of stearoyl groups into the new type of TAGs. By varying the fatty acid composition and the ratio of SSL/SLL, the properties of the LCSL product can be improved accordingly.

As expected, there was no catalytic activity for the interesterification reaction to be observed for the SBA-15 support. However, after incorporation of TBD into the support, the SBA-15-pr-TBD catalyst displayed comparable activities toward the reaction. Figure 8 shows the TAG compositions on the solid base catalyst as a function of reaction time. At a reaction time of 0.5 h, the interesterified product contained 46.5% of SSL, 37.8% of SLL, and 3.4% of LLL (triacylglycerol that contains three long-chain acyl residues), suggesting that the interesterification proceeded smoothly by using the solid base catalyst. As indicated in Figure 7, the content of SLL was increased obviously with the reaction time in the first 1 h, and the increase became very slow beyond 1 h. However, upon prolonging the reaction time to 5 h, the content of SSL was gradually decreased and then remained almost constant beyond the reaction duration of 5 h. As observed, the LCSL content was shown to increase with increasing the reaction time from 0.5 to 1 h, and no remarkable alteration was found between 1 and 3 h. However, there was a decrease trend in the LCSL content beyond 3 h. In light of the results, it can be concluded that the suitable reaction time required for obtaining a good LCSL yield is 1 h.

Reaction temperature is another variable that can affect the interesterification reaction. The effect of reaction temperature on the interesterification reaction was investigated, and the results are illustrated in Figure 9. In absence of any solvent, the reaction temperature needs to be above the melting point of methyl stearate (38 °C), so that the interesterification reaction can be conducted by using the solid catalyst. As seen in Figure 8, when the reaction temperature was increased from 50 to 80 °C, the SLL content also increased from 33.7 to 47.3%. However, with subsequent increase in reaction temperature, the SLL content was dropped slightly. Besides, the SSL content was shown to decrease as the reaction temperature was increased from 50 to 80 °C, but no further variation in SSL content was observed beyond 80 °C. Moreover, the LCSL content of the interesterified product was gradually increased to 91.5% with

dx.doi.org/10.1021/jf405434a | J. Agric. Food Chem. 2014, 62, 3348−3355

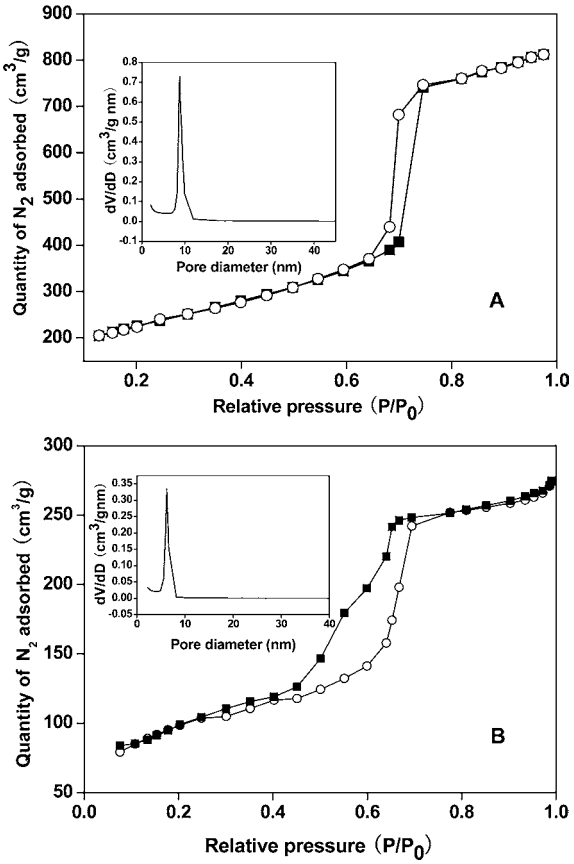

Figure 6. Nitrogen adsorption/desorption isotherms and pore size distribution profiles of samples: (a) SBA-15 and (b) SBA-15-pr-TBD.

Table 2. Textual Characteristics of SBA-15 and SBA-15-pr-NR_3OH Catalyst

sample	S_{BET} [a] (m^2/g)	V_p [b] (cm^3/g)	D_{BJH} [c] (nm)
SBA-15	807	1.25	6.65
SBA-15-pr-NR_3OH	312	0.43	4.45

[a]BET surface area. [b]Pore volume. [c]Average pore diameter from BJH desorption.

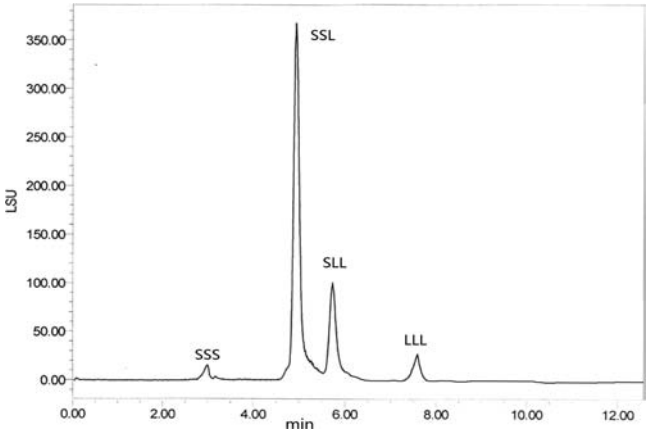

Figure 7. High performance liquid chromatography for the triacylglycerol compositions of the interesterified product. SSS, Tributyrin; SSL, triacylglycerol that contains two short-chain and one long-chain acyl residues; SLL, triacylglycerol that two long-chain and one short-chain acyl residues; LLL, triacylglycerol that contains three long-chain acyl residues.

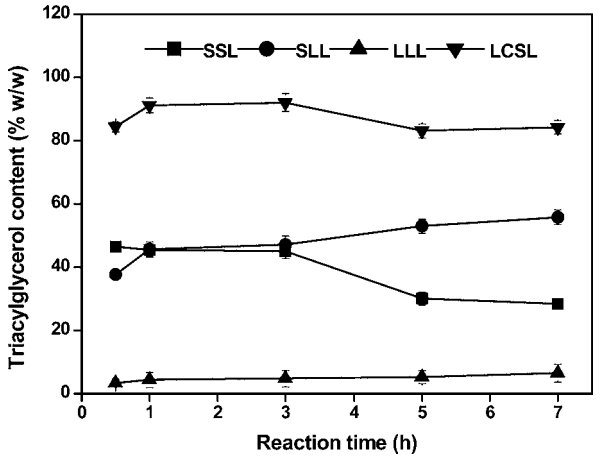

Figure 8. Evolution of the triacylglycerol distribution with reaction time during the interesterification reaction. Reaction conditions: methyl stearate/tributyrin molar ratio 2:1, reaction temperature 80 °C. SSL, triacylglycerol that contains two short-chain and one long-chain acyl residues; SLL, triacylglycerol that two long-chain and one short-chain acyl residues; LLL, triacylglycerol that contains three long-chain acyl residues; LCSL, low-calorie structured lipid.

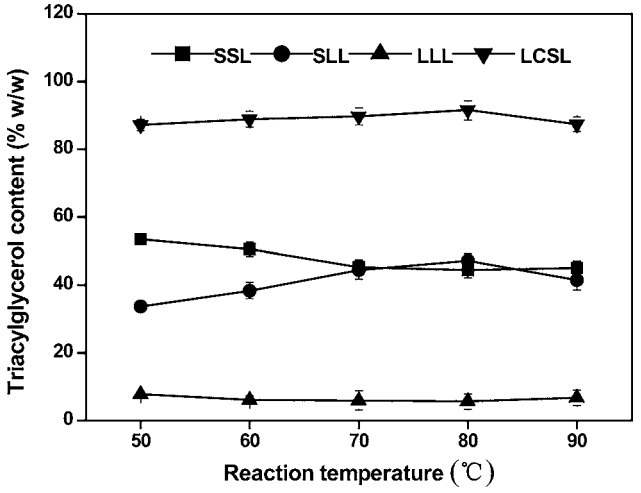

Figure 9. Evolution of the triacylglycerol distribution with reaction temperature during the interesterification reaction. Reaction conditions: methyl stearate/tributyrin molar ratio 2:1, reaction time 1 h. SSL, triacylglycerol that contains two short-chain and one long-chain acyl residues; SLL, triacylglycerol that two long-chain and one short-chain acyl residues; LLL, triacylglycerol that contains three long-chain acyl residues; LCSL, low-calorie structured lipid.

increasing the reaction temperature to 80 °C, and thereafter was diminished slightly at a temperature of 90 °C. Accordingly, in the present investigation, the proper temperature for the interesterification reaction is 80 °C.

The interesterification reaction is generally employed to produce structured lipids that have the improved functionality by rearranging the fatty acids on the glycerol backbone. For different mixtures of substrates, the interesterification was carried out by using the solid catalyst at a temperature of 80 °C. As shown in Figure 10, for all the experimental trials involving a variety of molar ratios of methyl stearate to tributyrin, the rapid depletion of tributyrin species occurred affording new SSL and SLL of TAGs simultaneously. With increasing methyl stearate/tributyrin molar ratio to 2:1, the content of SLL triacylglycerol in the interesterified product increased, while the SSL content

dx.doi.org/10.1021/jf405434a | J. Agric. Food Chem. 2014, 62, 3348−3355

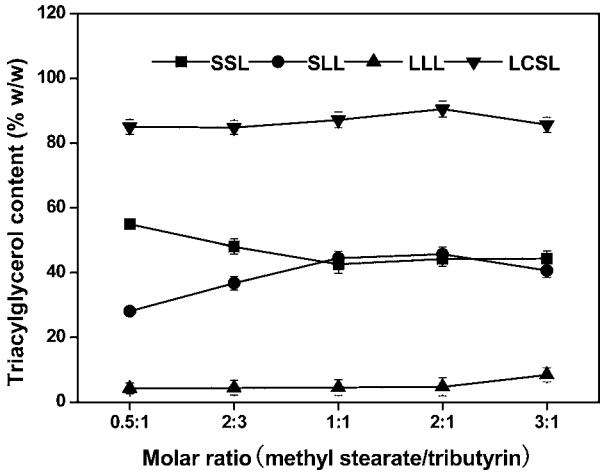

Figure 10. Evolution of the triacylglycerol distribution with tributyrin/methyl stearate ratio during the interesterification reaction. Reaction conditions: reaction temperature 80 °C, reaction time 1 h. SSL, triacylglycerol that contains two short-chain and one long-chain acyl residues; SLL, triacylglycerol that two long-chain and one short-chain acyl residues; LLL, triacylglycerol that contains three long-chain acyl residues; LCSL, low-calorie structured lipid.

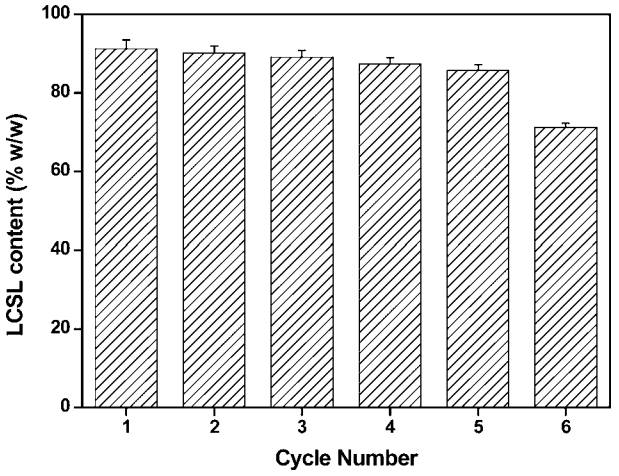

Figure 11. Low-calorie structured lipid content of the interesterified product over several catalyst cycles. Reaction conditions: methyl stearate/tributyrin molar ratio 2:1, reaction temperature 80 °C, reaction time 1 h. LCSL, low-calorie structured lipid.

diminished. In this case, with higher methyl stearate/tributyrin molar ratio than 2:1, the SLL content was declined slightly and the SSL content remained nearly constant. In all of these trials, the LLL triacylglycerol was observed to increase on increasing the methyl stearate/tributyrin molar ratio. From Figure 9, it was observed that the content of LCSL was initially ascended from 84.7 to 91.5% with the increase in methyl stearate/tributyrin molar ratio from 0.5:1 to 2:1. However, beyond the molar ratio of 2:1, the lower content of LCSL was observed. Given the present results, the appropriate molar ratio of methyl stearate to tributyrin is found to be 2:1, with the LCSL content of 91.5%.

Reusability of the Catalyst. The reusability is an important aspect to evaluate the feasibility of a heterogeneous catalyst for its application in industrial processes, which makes it economic and preferable over homogeneous one. In order to study the catalyst reusability, consecutive reaction runs were carried out using the SBA-15-pr-TBD catalyst. At the end of the interesterification, the catalyst was recovered by filtration, washed with cyclohexane and ethanol, and dried at 120 °C overnight in a vacuum oven. The recovered catalyst was used for the next cycle, and this process was repeated for several times under the optimized reaction conditions as described above. The experimental results are illustrated in Figure 11. It was indicated that the LCSL yield was almost kept stable without significant loss of its catalytic activity (91.5% in the first cycle versus 85.8% in the fifth cycle) for up to five times of use, thus indicating the good stability of the catalyst. However, the catalytic activity was obviously decreased as the catalyst was used more than five times, mostly owing to the accumulation of impurities on the catalyst surface.

In light of the aforementioned results, a heterogeneous catalyst, SBA-15-pr-TBD, was prepared by reactions of TBD-organosilane with the mesoporous SBA-15 material. By using this solid base catalyst, the interesterification between tributyrin and methyl stearate in a solvent-free system was performed for the production of LCSL. All the characterization results indicated the successful anchoring of organic base TBD on the framework channel of mesoporous SBA-15 materials. After the functionalization of SBA-15 silica, the ordered mesoporous structure remained almost unchanged, which was favorable for improving the contact between the catalytically active component and reactants. Further, the solid catalyst is applicable to the interesterification reaction as a stable and highly active catalyst. Over this catalyst, the LCSL, composed of stearic acid and butyric acid, was successfully prepared in a heterogeneous manner. In the previous work, Han et al. reported that the interesterification of tributyrin and methyl stearate was conducted using a commercially immobilized lipase, Lipozyme RM IM.[5] Compared to the immobilized lipase, the SBA-15-pr-TBD catalyst shows higher activities for the interesterification reaction owing to the shorter reaction time employed and lower catalyst loading.

AUTHOR INFORMATION

Corresponding Author

*E-mail: xwenlei@163.com. Phone: +86 371 67756302. Fax: +86 371 67756718.

Funding

This work was financially supported by research grants from the National Natural Science Foundation of China (Project No. 21276066), the Plan for Scientific Innovation Talent of Henan Province (144200510006) and the Program for Innovative Research Team in Universities of Henan Province in China (2012IRTSTHN009).

Notes

The authors declare no competing financial interest

ABBREVIATIONS USED

BET, Brunauer−Emmett−Teller; BJH, Barrett−Joyner−Halenda; CIE, chemical interesterification; DMF, *N*,*N*-dimethylformamide; EIE, enzymatic interesterification; FT-IR, Fourier transform infrared; HPLC, high-performance liquid chromatography; LCSL, low-calorie structured lipid; LLL, triacylglycerol that contains three long-chain acyl residues; SAXS, small-angle X-ray scattering; SEM, scanning electron microscopy; SSL, triacylglycerol that contains two short-chain and one long-chain acyl residues; SLL, triacylglycerol that two long-chain and one short-chain acyl residues; TAG, triacylglycerol; TBD, 1,5,7-triazabicyclo[4.4.0]dec-5-ene; TEM, transmission electron

microscopy; TEOS, tetraethylorthosilicate; TG-DTA, thermo gravimetric analysis; TLC, thin-layer chromatography

REFERENCES

(1) Lee, J. H.; Akoh, C. C.; Himmelsbach, D. S.; Lee, K. T. Preparation of interesterified plastic fats from fats and oils free of *trans* fatty acid. *J. Agric. Food Chem.* **2008**, *56*, 4039−4046.

(2) Xu, X. Production of specific-structured triacylglycerols by lipase-catalyzed reactions: a review. *Eur. J. Lipid Sci. Techol.* **2000**, *102*, 287−303.

(3) Yang, T.; Fruekilde, M. B.; Xu, X. Suppression of acyl migration in enzymatic production of structured lipids through temperature programming. *Food Chem.* **2005**, *92*, 101−107.

(4) Smith, R. E.; Finley, J. W.; Leveille, G. A. Overview of SALATRIM: a family of low-calorie fats. *J. Agric. Food Chem.* **1994**, *42*, 432−434.

(5) Han, L.; Xu, Z.; Huang, J.; Meng, Z.; Liu, Y.; Wang, X. Enzymatically catalyzed synthesis of low-calorie structured lipid in a solvent-free system: optimization by response surface methodology. *J. Agric. Food Chem.* **2011**, *59*, 12635−12642.

(6) Jeyarani, T.; Reddy, S. Y. Effect of enzymatic interesterification on physicochemical properties of mahua oil and kokum fat blend. *Food Chem.* **2010**, *123*, 249−253.

(7) Zou, X.; Huang, J.; Jin, Q.; Liu, Y.; Song, Z.; Wang, X. Lipase-catalyzed preparation of human milk fat substitutes from palm stearin in a solvent-free system. *J. Agric. Food Chem.* **2011**, *59*, 6055−6063.

(8) Xu, X.; Skands, A. R. H.; Høy, C. E.; Mu, H.; Balchen, S.; Adler-Nissen, J. Production of specific-structured lipids by enzymatic interesterification: Elucidation of acyl migration by response surface design. *J. Am. Oil Chem. Soc.* **1988**, *75*, 1179−1186.

(9) Ribeiro, A. P. B.; Grimaldi, R.; Gioielli, L. A.; Goncalves, L. A. G. Zero trans fats from soybean oil and fully hydrogenated soybean oil: physico-chemical properties and food applications. *Food Res. Int.* **2009**, *42*, 401−410.

(10) Meng, Z.; Liu, Y.; Shan, L.; Jin, Q.; Wang, X. Reduction of graininess formation in beef tallow-based plastic fats by chemical interesterification of beef tallow and canola oil. *J. Am. Oil Chem. Soc.* **2010**, *87*, 1435−1442.

(11) Raquel, C.; Véronique, G.; Roland, V.; Wim, D. G. Chemical and enzymatic interesterification of a blend of palm stearin: soybean oil for low *trans*-margarine formulation. *J. Am. Oil Chem. Soc.* **2009**, *86*, 681−697.

(12) Soares, F.A.S.D.M.; da Silva, R. C.; da Silva, C. G.; Lourenco, M. B.; Soares, D. F.; Gioielli, L. A. Effects of chemical interesterification on physicochemical properties of blends of palm stearin and palm olein. *Food Res. Int.* **2009**, *42*, 1287−1294.

(13) Semwal, S.; Arora, A. K.; Badoni, R. P.; Tuli, D. K. Biodiesel production using heterogeneous catalysts. *Bioresour. Technol.* **2011**, *102*, 2151−2161.

(14) Xie, W.; Huang, X.; Li, H. Soybean oil methyl esters preparation using NaX zeolites loaded with KOH as a heterogeneous catalyst. *Bioresour. Technol.* **2007**, *98*, 936−939.

(15) Yang, Z.; Xie, W. Soybean oil transesterification over zinc oxide modified with alkali earth metals. *Fuel Process. Technol.* **2007**, *88*, 631−638.

(16) Abdullah, A. Z.; Razali, N.; Lee, K. T. Optimization of mesoporous K/SBA-15 catalyzed transesterification of palm oil using response surface methodology. *Fuel Process. Technol.* **2009**, *90*, 958−964.

(17) Schuchardt, U.; Sercheli, R.; Vargas, R. M. Transesterification of vegetable oils: A review. *J. Braz. Chem. Soc.* **1998**, *9*, 199−210.

(18) Schuchardt, U.; Vargas, R. M.; Gelbard, G. Transesterification of soybean oil catalyzed by alkylguanidines heterogenized on different substituted polystyrenes. *J. Mol. Catal. A: Chem.* **1996**, *109*, 37−44.

(19) Xie, W.; Qi, C. Interesterification of soybean oil and lard blends catalyzed by SBA-15-pr-NR_3OH as a heterogeneous base catalyst. *J. Agric. Food Chem.* **2013**, *61*, 3373−3381.

(20) Yue, M.; Sun, L.; Cao, Y.; Wang, Z.; Wang, Y.; Yu, Q.; Zhu, J. Promoting the CO_2 adsorption in the amine-containing SBA-15 by hydroxyl group. *Microporous Mesoporous Mater.* **2008**, *114*, 74−81.

(21) Bhange, P.; Bhange, D. S.; Pradhan, S.; Ramaswamy, V. Direct synthesis of well-ordered mesoporous Al-SBA-15 and its correlation with the catalytic activity. *Appl. Catal. A: Gen.* **2011**, *400*, 176−184.

(22) Melero, J. A.; Bautista, L. F.; Morales, G.; Iglesias, J.; Sánchez-Vázquez, R. Biodiesel production from crude palm oil using sulfonic acid-modified mesostructured catalysts. *Chem. Eng. J.* **2010**, *161*, 323−331.

(23) Schroeder, G.; Leska, B.; Jarczewski, A.; Nowak-Wydra, B.; Brzezinski, B. FTIR, NMR and kinetic studies of proton transfer reactions from nitro-substituted diarylmethanes to N-bases with guanidine character. *J. Mol. Struct.* **1995**, *344*, 77−88.

(24) Kalita, P.; Kumar, R. Immobilization of 1,5,7-triazabicyclo[4.4.0]dec-5-ene over mesoporous materials: an efficient catalyst for Michael-addition reactions under solvent-free condition. *Appl. Catal. A: Gen.* **2011**, *397*, 250−258.

(25) Çıtak, A.; Erdem, B.; Erdem, S.; Öksüzoğlu, R. M. Synthesis, characterization and catalytic behavior of functionalized mesoporous SBA-15 with various organo-silanes. *J. Colloid Interface Sci.* **2012**, *369*, 160−163.

(26) Srivastava, R. An efficient, eco-friendly process for aldol and Michael reactions of trimethylsilyl enolate over organic base-functionalized SBA-15 catalysts. *J. Mol. Catal. A: Chem.* **2007**, *246*, 146−152.

(27) Prasetyanto, S. E. A.; Park, S. E. Synthesis of short-channeled amino-functionalized SBA-15 and its beneficial applications in base-catalyzed reactions. *Appl. Catal. A: Gen.* **2008**, *350*, 244−251.

(28) Yuan, C.; Huang, Z.; Chen, J. Basic ionic liquid supported on mesoporous SBA-15: An efficient heterogeneous catalyst for epoxidation of olefins with H_2O_2 as oxidant. *Catal. Commun.* **2012**, *24*, 56−60.

days before heading and up to 12 times after heading in each year. Sampling involved harvesting the whole plant about 15 cm above the soil, and the harvested biomass was separated into two parts: stems and leaves, and the heads. Only the heads were sampled in 2012, because the concentration in the stem plus leaf component was quite low in 2011 (see the Results). Sampling was done in triplicate. These samples were used to determine the FUM concentration. Details of the analysis are provided in the section Quantitative Analysis of FUMs.

Field Experiment 2: Differences in the FUM Concentration among Sites . We used the rice cultivar Yumeaoba in this experiment. Yumeaoba was cultivated at three sites in 2011 and 2012: the same experimental paddy field at NILGS that we used in field experiment 1, a farmer's paddy field in Ohtawara, Tochigi Prefecture, and a farmer's paddy field in Kumagaya, Saitama Prefecture. The sampling method was the same as in field experiment 1, but we did not use true replication at Ohtawara and Kumagaya; sampling was done in triplicate within the same field.

Isolation of FUM-Producing Fungi. Isolation of FUM-producing fungi was carried out in 2011. To isolate the fungi, we placed 3 to 5 cm samples of the leaf and stem or head tissues on plates of potato dextrose agar medium (PDA, Nissui Pharmaceutical Co. Ltd., Tokyo, Japan) containing 500 mg/L of streptomycin sulfate (Wako Pure Chemical Industries Co. Ltd., Osaka, Japan) and 500 mg/L of pentachloronitrobenzene (Tokyo Chemical Industry Co., Ltd., Tokyo, Japan). The plates were incubated at 25 °C in the dark for 5 to 7 days, and the fungi present in the cultures were picked up and transferred into water agar medium. A single isolate was obtained from each sample, except for one sample that contained two or more *Fusarium* species. We then isolated individual fungal spores and incubated them on PDA for 5 to 7 days in the dark at 25 °C. The colonies on PDA were used in subsequent FUM-production experiments and for identification to the species level.

FUM-Production Experiment Using the Isolated Fungi. We incubated the isolates in the dark on 1 g of corn grits in 1 mL of sterilized water at 25 °C for 7 days. We used noninoculated corn grits as a control. We then added 10 mL of methanol/water solution (3:1 v/v) to the incubated corn grits, homogenized the sample by stirring using a glass rod, and then set it aside overnight. We used 5 mL of the supernatant for our quantitative analysis of the FUM concentration. If the FUM concentration was greater than 1 mg/kg of the corn grits, we defined the isolate as a FUM-producing fungus.

Identification of *Fusarium* Species. We extracted total genomic DNA from the *Fusarium* isolates, as described previously.[14] We amplified part of the gene for translation elongation factor 1-α (EF-1α) by means of the polymerase chain reaction (PCR) using the primer pair EF-1H/EF-2T, following the method of O'Donnell.[15] We chose this gene because previous research[15] showed that it was capable of distinguishing among *Fusarium* species and between these species and other organisms. Purified PCR products were sequenced with an ABI Prism 3100 automated sequencer (Applied Biosystems, Foster City, CA) according to the manufacturer's instructions. The sequence data were compared with data in the DNA Data Bank of Japan (http://www.ddbj.nig.ac.jp/) by using the BLAST program.

Greenhouse Experiment: Inoculation with FUM-Producing Fungi. We used the cultivars Natsuaoba and Yumeaoba in this experiment. The greenhouse was kept at 25 °C under natural illumination. Seeds were germinated and then transplanted at a density of one plant per container into plastic containers (L 374 mm, W 254 mm, H 232 mm) filled with soil (Suitou-baido, Kantou-nousan Co. Ltd., Nasushiobara, Tochigi, Japan). We then added 3.5 g of inorganic fertilizer (14−14−14) to each container. We grew the seedlings for 40 days and then added an additional 2.5 g of the same fertilizer to each container as a top dressing.

We created a total of three treatments per cultivar in this experiment: control plants maintained in a separate greenhouse, noninoculated plants grown beside inoculated plants (hereafter, NBI plants), and inoculated plants. Triplicate measurements were collected from each treatment.

The inoculated plants were treated as follows: At 3 and 10 days after heading, we sprayed 50 mL of the spore solution from a height of about 50 cm above the rice plants to inoculate the head. After spraying, we covered the rice seedlings with a plastic bag for 12 h. The spore solution was prepared as follows: Isolates of *Fusarium fujikuroi* MO409[14] were grown on plates containing V-8 juice agar: 200 mL of V8 juice (Campbell Soup Company, Camden, NJ), 3 g of $CaCO_3$, and 15 g of agar/L. The plates were illuminated for 12 h with ultraviolet and violet light (FL15BLB lamps; Toshiba, Japan) and then left for 12 h in the dark, with both treatments at 25 °C. We incubated the solution in this manner for 14 days and then added 2 mL of sterile purified water to the plates. We then mixed the agar into the water and transferred the mixture into sterile purified water. After observing the spore density under a microscope, we adjusted the spore density to 1.0×10^5 cells/mL to produce the spore solution.

At 30 days after heading (the yellow-ripe stage) and 55 days after heading (the full-ripe stage), we harvested the plants at a height of 15 cm above the ground and divided them into two parts (stems plus leaves versus the heads).

Quantitative Analysis of FUMs. FUMs in the rice plants were quantitatively analyzed using the method described in our previous report[14,16] The fresh plant samples were dried in a forced-air oven at 65 °C for 48 h so that all concentrations could be expressed per unit dry weight. The dried samples were ground in a cutting mill (ZM200; Retsch GmbH, Haan, Germany) to pass through a 1 mm screen. We then added 30 mL of a methanol and water solution (3:1 v/v) to 2 g of each dried, ground sample.

We preconditioned an anion-exchange column (Bond Elut SAX; Varian Technologies, Palo Alto, CA) by washing it with 10 mL of a water and methanol solution (1:3 v/v); we then loaded the column with 10 mL of the supernatant from the sample solution and eluted the sample with 14 mL of methanol containing 10 mL/L acetic acid. The eluate was concentrated to 1 mL in vacuo and injected into a liquid chromatography−tandem mass spectrometry (LC/MS/MS) system (ACQUITY TQD UPLC; Waters, Milford, MA). The LC/MS/MS conditions were as follows: column, ACQUITY UPLC BEH C18 (2.1 mm ×50 mm, 1.7 μm; Waters); oven temperature, 40 °C; solvents, 1 mL/L aqueous formic acid/acetonitrile; running conditions, 0 to 3 min at 3/1 (v/v), a linear gradient for 3 to 4 min from 3/1 to 9/11; retention times of 2.8 min for $FUMB_1$ and 3.6 min for $FUMB_2$; monitored ions (ESI Positive), m/z 722.5 > 334.5 for $FUMB_1$, m/z 706.6 > 336.5 for $FUMB_2$; and confirmed ions, m/z 722.5 > 352.5 for $FUMB_1$, m/z 706.6 > 318.4 for $FUMB_2$.

The efficiency of FUM recovery from rice flour with a known FUM concentration (100 ng/g) was 108.2% ($FUMB_1$) and

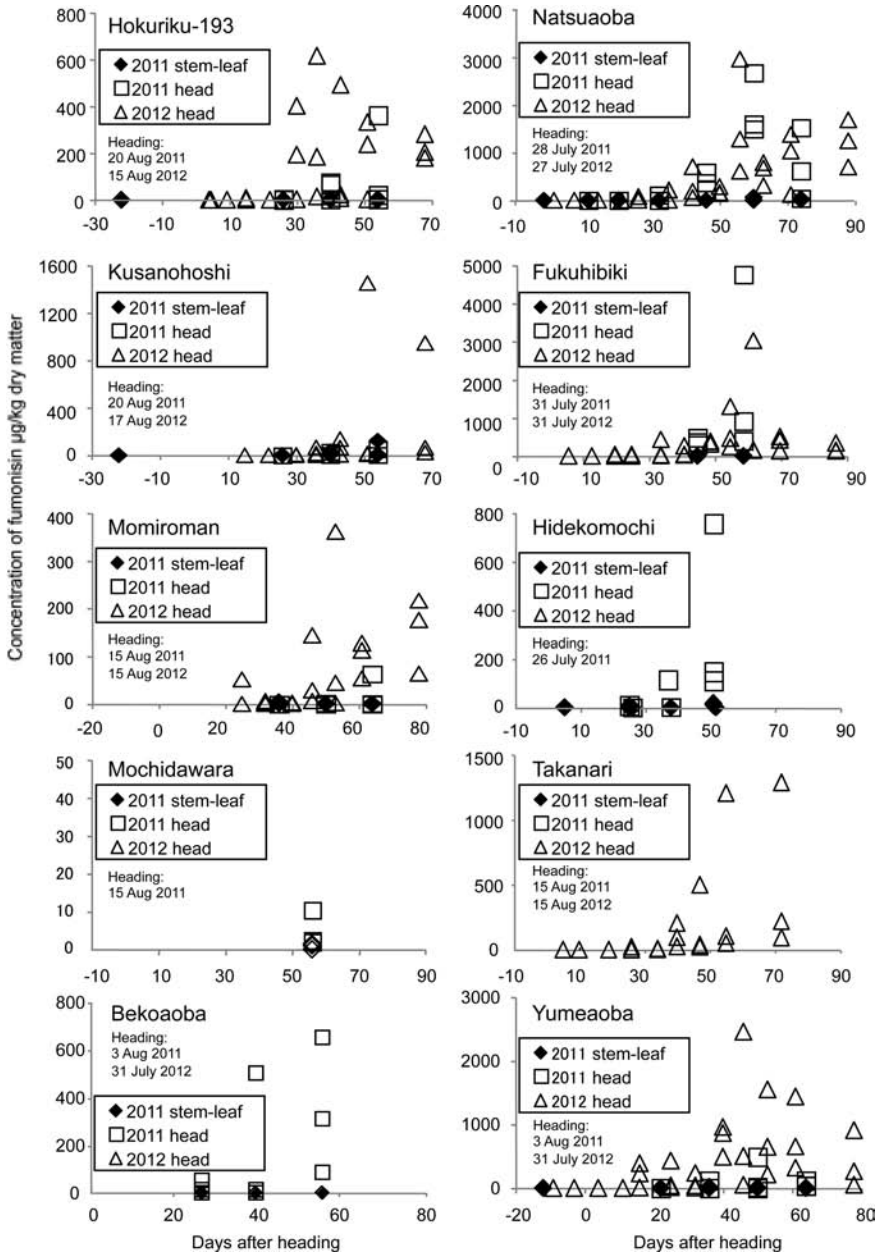

Figure 1. Changes in the fumonisin (FUM) concentration in the 10 cultivars during cultivation in field experiment 1 at the NILGS site. FUM concentrations represent the total ($FUMB_1$ + $FUMB_2$) content. Note that the *y*-axis scale differs among the graphs.

91.5% ($FUMB_2$), with a relative standard deviation (n = 3) of 2.6% ($FUMB_1$) and 4.5% ($FUMB_2$). The calibration curve had good linearity (>0.999) in the range of 0 to 5000 ng/mL for $FUMB_1$ and $FUMB_2$. The limit of quantification (LOQ) was 1 μg/kg DM ($FUMB_1$, $FUMB_2$). Values below the LOQ were treated as not detected. The total FUM concentration was defined as the sum of the concentrations of $FUMB_1$ and $FUMB_2$.

Statistical Analysis. To enhance the homoscedasticity that is required for performing ANOVA, we log-transformed the average FUM concentrations as ln(average +0.5w), where w is the maximum discrete width of the average. [17] To compare the cultivars, we analyzed the transformed averages using an unbalanced ANOVA in which the year (2011 and 2012) and the experimental plots (1, 2, and 3) were treated as blocks. When the ANOVA produced a significant result, we tested for differences among the cultivars in the FUM concentration using Tukey's HSD test.

To compare cultivation sites, we analyzed the log-transformed averages using an unbalanced one-way ANOVA in which the numbers of replicates were 3, 1, and 1 for the NILGS, Ohtawara, and Kumagaya sites, respectively. When the ANOVA produced a significant result, we tested for differences among the sites using Tukey's HSD test.

To compare the FUM concentrations among the inoculation treatments, we tested for treatment × cultivar interactions using Tukey's HSD test, because we suspected the existence of interactions.

To compare the FUM concentrations among the inoculation treatments, we tested the mean for treatment × cultivar combinations using Tukey's HSD test, because we suspected the existence of interactions. We calculated the mean using the log-transformed values of $FUMB_1$ + $FUMB_2$.

RESULTS

Changes in the FUM Concentration during Cultivation and Differences among the Cultivars. Figure 1 summarizes the changes during the growing season in the FUM concentrations in the rice plants of the cultivars grown at NILGS in 2011 and 2012. Table 1 summarizes the mean FUM concentration in the heads of each cultivar. Fukuhibiki had a significantly higher FUM concentration than Kusanohoshi, Momiroman, and Mochidawara. Bekoaoba and Natsuaoba had a significantly higher FUM concentration than Momiroman and Mochidawara. The other cultivars did not differ significantly.

Table 1. Mean Fumonisin (FUM) Concentrations in the 10 Cultivars Cultivated in Experiment 1[a]

cultivar	mean (±SE)[b]		
Fukuhibiki	6.150	(±0.529)	a
Bekoaoba	5.922	(±0.778)	ab
Natsuaoba	5.873	(±0.529)	ab
Hidekomochi	5.201	(±0.778)	abc
Yumeaoba	4.920	(±0.529)	abc
Hokuriku-193	4.102	(±0.529)	abc
Takanari	4.014	(±0.778)	abc
Kusanohoshi	3.480	(±0.529)	bc
Momiroman	2.741	(±0.529)	c
Mochidawara	1.976	(±0.778)	c

[a]Means represent log-transformed values, as described in the text. [b]Means followed by different letters differ significantly ($P < 0.05$, Tukey's HSD test).

The FUM concentrations in the stems and leaves of Hokuriku-193, Kusanohoshi, Fukuhibiki, and Momiroman were less than 10 μg/kg DM. The FUM concentration in stems and leaves of Hidekomochi at 40 days after heading were around 15 μg/kg DM (Figure 1). The FUM concentrations in stems and leaves of Natsuaoba were slightly higher than those in the other cultivars, reaching a maximum of 60 μg/kg DM.

In the heads, the FUM concentrations in all cultivars 30 days after heading were less than 10 μg/kg DM. However, by 40 days after heading, the FUM concentration in Natsuaoba, Fukuhibiki, Bekoaoba, and Hidekomochi began to increase. The FUM concentration reached its maximum around 50 to 70 days after heading, except for an earlier range of dates for Hokuriku-193 (40 to 60 days). Although the maximum concentration differed among the cultivars, the trend did not differ. The FUM concentration was greater than 100 μg/kg in Fukuhibiki, Bekoaoba, Natsuaoba, and Yumeaoba, although there was high variation among the replicates. For example, the FUM concentration in Natsuaoba at 56 days after heading ranged from less than 1000 μg/kg DM to more than 3000 μg/kg DM in 2012. Similarly, the FUM concentrations in Yumeaoba heads at this time ranged from less than 500 μg/kg DM to more than 2000 μg/kg DM.

Differences among the Sites in FUM Concentration. Figure 2 summarizes the FUM concentrations in Yumeaoba in the two paddy fields in Ohtawara and Kumagaya in 2011 and 2012. The result at NILGS is shown in the graph for Yumeaoba in Figure 1. Table 2 summarizes the statistical results. As in experiment 1, the maximum concentration was reached between 50 and 70 days after heading in both years and at both sites. In addition, the concentrations differed by more than 100% among the sites, and the NILGS site had a significantly higher mean concentration than the Kumagaya site. At the Ohtawara site, the maximum FUM concentration was 193 μg/kg DM. At the Kumagaya site, the maximum concentration was 113 μg/kg DM. The FUM concentration at Kumagaya was particularly low (<10 μg/kg) in 2012 until 90 days after heading, and in no sample was the concentration larger than 20 μg/kg DM.

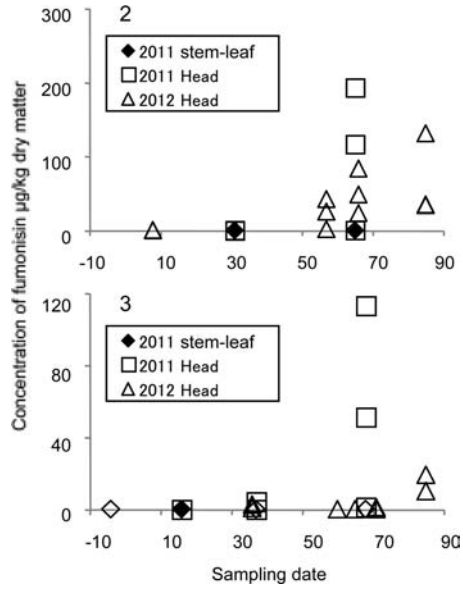

Figure 2. Differences in the FUM concentration between the two farm rice paddy sites. Values are the total FUM concentration ($FUMB_1$ + $FUMB_2$); the sampling date represents the number of days after heading. Upper (2): Ohtawara. Bottom (3): Kumagaya. Results for NILGS are shown in the graph for Yumeaoba in Figure 1. Note that the *y*-axis scale differs between the graphs.

Table 2. Differences in the Mean FUM Concentrations in Yumeaoba among the Three Field Sites[a]

location	mean (±SE)[b]		
NILGS	5.928	(±0.258)	a
Ohtawara	3.709	(±0.447)	ab
Kumagaya	2.272	(±0.447)	b

[a]Values are the log-transformed means (see the text for details). [b]Means followed by different letters differ significantly ($P < 0.05$, Tukey's HSD test).

Isolation and Identification of the FUM-Producing Fungi. We obtained 49 *Fusarium* isolates that were confirmed to produce FUM in the FUM production experiment. For these isolates, we obtained almost the full length of the EF-1α gene. We compared the sequences with those in the FUSARIUM-ID database (http://isolate.fusariumdb.org)[18,19] and calculated their similarities with two standard accessions (DQ790494 for *F. fujikuroi* and AF160280 for *F. proliferatum*). Of the 49 isolates, 48 had lengths of 638 to 640 bp and similarities of 99.2 to 99.7% with *F. fujikuroi*, whereas one had a length of 646 bp and 98.9% similarity with *F. proliferatum*. On the basis of these results, we identified the former isolates as *F. fujikuroi* and the latter as *F. proliferatum*.

We obtained the following numbers of isolates for the cultivars: 14 for Yumeaoba, 8 for Momiroman, 7 for Natsuaoba, 5 for Fukuhibiki, 5 for Hidekomochi, 4 for Hokuriku-193, 4 for Kusanohoshi, 1 for Bekoaoba, and 1 for Mochidawara. We obtained 31 isolates from the heads and 18 from the leaves and stems. The number of isolates also varied as a function of the

dx.doi.org/10.1021/jf405358h | J. Agric. Food Chem. 2014, 62, 3356−3362

number of days after heading: 1 at 0−10 days, 6 at 11 to 30 days, 20 at 31 to 51 days, and 22 at 51−74 days. The number of isolates also differed among the cultivation sites: 45 at NILGS, 3 at Ohtawara, and 1 at Kumagaya. We obtained FUM-producing *Fusarium* isolates from 9 of the 10 cultivars, excluding Takanari, and we isolated these fungi both from the stems and from the leaves and heads. The fungi were present from shortly after heading (7 days) to the end of the study period (74 days after heading), but the isolation frequency was greatest at 51 days after heading, with no distinction between the plant parts.

FUM-Producing Fungi in the Greenhouse. Figure 3 shows the results of the greenhouse inoculation experiment. At the yellow-ripe and full-ripe stages, the FUM concentrations in the stems and leaves of Natsuaoba and Yumeaoba ranged from undetectable to 5 μg/kg DM. The stem and leaf values were generally lower than the corresponding head values in both cultivars and were always lower in the inoculated plants. At the yellow-ripe stage, the FUM concentrations in the heads of the control and NBI plants were undetectable, whereas the inoculated heads of Natsuaoba and Yumeaoba had concentrations of 18 and 19 μg/kg DM, respectively. The inoculated plants had significantly higher concentrations than those in the other treatments in both cultivars. At the full-ripe stage, the FUM concentrations in the heads of the control and NBI plants were undetectable or very low, whereas the heads of the inoculated Natsuaoba and Yumeaoba plants had concentrations of 660 and 240 μg/kg DM, respectively, which were significantly higher than those in the other treatments.

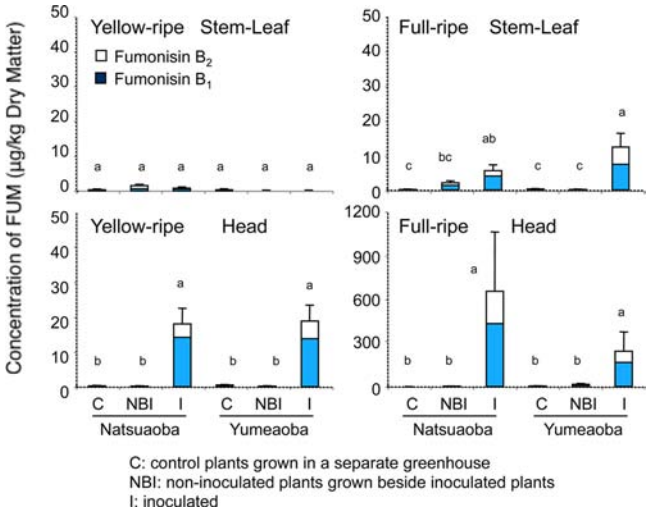

Figure 3. FUM concentrations in the greenhouse inoculation experiment; values are the total concentration of FUM ($FUMB_1$ + $FUMB_2$). Sample times were 30 days after heading for the yellow-ripe stage and 55 days after heading for the full-ripe stage. Values in each panel labeled with different letters differ significantly (Tukey's HSD test, $P < 0.05$). Values are means ± SE ($n = 3$) and were calculated using the log-transformed values of $FUMB_1$ + $FUMB_2$, as described in the text. Treatments: C, control plants grown in a separate greenhouse; NBI, noninoculated plants grown beside inoculated plants; I, inoculated plants. Note that the *y*-axis scale differs among the graphs.

DISCUSSION

In field experiment 1, the FUM concentrations in the heads of almost all cultivars started to increase by around 30 days after heading (the yellow-ripe stage) and became much higher than those in the stems and leaves by around 50 days after heading, which is near the full-ripe stage (Figure 1). This trend was similar for all cultivars, although the magnitudes of the increase differed among the cultivars. The reason for this pattern is currently unclear. Feng et al.[20] reported that deoxynivalenol production by *F. graminearum* increased greatly when sucrose, 1-kestose, and nystose were used as a carbon source in vitro. The increased FUM concentration in rice heads may similarly be a response to changes in some nutritional component in these tissues. Several cultivars differed significantly in their FUM concentration (Table 1). The FUM concentration tended to be higher in early maturing cultivars and low in late-maturing cultivars. The reason for this may relate to the cultivation time, a difference in the nutritional composition of the plants, or some other unknown cause. In corn, a similar difference in the mycotoxin concentration was observed among cultivars. [21] In future research, it will be necessary to determine the reasons for these differences, because they may support efforts to control the FUM concentration by means of appropriate cultivar selection.

In field experiment 2, we found that the FUM concentration was higher in the heads than in the stems and leaves for all cultivars at all sites. The FUM concentration in the heads increased greatly by 40 to 60 days after heading at all sites (Figure 1 and 2). This confirms the results in field experiment 1 (Figure 1). The FUM concentration in the heads grown at NILGS was significantly higher than that in the heads grown at Kumagaya (Table 2). This suggests that the FUM concentration was influenced by the cultivation environment. However, we did not obtain sufficient data on the cultivation methods and conditions at the three field sites to hypothesize about which cultivation-related factors might be responsible for these differences.

The isolated FUM-producing fungi were almost all *F. fujikuroi* (48 of 49 isolates). At NILGS, many *F. fujikuroi* isolates were obtained 31 days after heading. In contrast, at Kumagaya, we found few FUM-producing fungi, and the FUM concentration was significantly lower than at NILGS (Table 2). This may reflect differences among the sites in the inoculum levels. FUM-producing fungi were isolated from almost all cultivars, and the FUM concentrations differed among the cultivars. These fungi were also isolated from the stems and leaves, although the FUM concentrations were quite low compared with those in the heads. As we noted earlier, these differences may have resulted from differences in the nutrient compositions of the parts of the host plants, but this hypothesis must be confirmed in future research.

In the greenhouse inoculation experiment, the FUM concentration was substantially higher in the heads of inoculated plants than in the stems and leaves (Figure 3), especially at the full-ripe stage. This confirms the results of the two field experiments (Figures 1 and 2). The FUM concentration in the control and NBI heads did not increase until the full-ripe stage, even in NBI plants grown beside inoculated plants. On the other hand, the FUM concentration in the heads of inoculated plants increased rapidly after the yellow-ripe stage. These results suggest that inoculation of the plants 3 to 10 days after heading caused infection and greatly increased the FUM concentration in the rice heads between the yellow-ripe and full-ripe stages. In the field experiments, the isolation frequency was lower before the yellow-ripe stage than at the full-ripe stage. However, in the greenhouse experiment,

the presence of FUM-producing fungi just after the heading stage appears to be important for the increased FUM concentration. Yoshida et al. [22] reported that the most effective fungicide application for barley was at the anther-extrusion stage. Although crops likely differ in the optimal infection stage, it seems likely that the mycotoxin concentration in the *Poaceae* is strongly related to the time of infection. In other words, to control FUM concentrations in rice plants, it will be necessary to control infection by FUM-producing fungi just after the heading stage.

In summary, our results show that the FUM concentration in the heads of rice plants was substantially higher than that in the stems and leaves. In general, by around 30 to 40 days after heading (the yellow-ripe stage or late yellow-ripe stage), the FUM concentration began to increase and reached its maximum 50 to 70 days after heading (the full-ripe stage). The FUM concentration differed among the cultivars. Even within a cultivar, the FUM concentration varied widely among the three sites. Infection by FUM-producing fungi just after heading increased the FUM concentration in rice heads starting at the yellow-ripe stage.

These results suggest that control of FUM levels in forage rice can potentially be achieved by selecting cultivars in which infection produces a low FUM concentration by controlling FUM-producing fungi just after the heading stage by the application of appropriate fungicides and by obtaining a better understanding of the cultural factors that affect infection by the fungi and its subsequent growth.

AUTHOR INFORMATION

Corresponding Author

*E-mail: uegaki@affrc.go.jp. Fax: +81-28-736-6629. Tel.: +81-28-737-7804.

Present Address

[⊥]NARO Institute of Livestock and Grassland Science, Ikenodai 2, Tsukuba, Ibaraki, Japan, Fax: +81-29-838-8587, Tel: +81-29-838-8292.

Funding

This study was supported by the "Mycotoxins in Self-Sufficient Feed Production" project of NARO.

Notes

The authors declare no competing financial interest.

ACKNOWLEDGMENTS

The LC/MS/MS system was provided by the NARO Institute of Floricultural Science. We thank Dr. Koji Nakagome, a senior researcher at the NARO Tohoku Agricultural Research Center (current address: NARO Western Region Agricultural Research Center), and Dr. Kiyoyuki Miura, a senior researcher at the NARO Institute of Agricultural Research Center, who provided seeds for the cultivars used in this study. We also thank Ms. Miwa Shiomizu and Ms. Megumi Ezure for their technical contributions to our research.

ABBREVIATIONS USED

C, control plants grown in a separate greenhouse; DM, dry matter; EF-1α, translation elongation factor 1-α; FUM, fumonisin; $FUMB_1$ and $FUMB_2$, fumonisins B_1 and B_2; I, inoculated plants; LC/MS/MS, liquid chromatography–tandem mass spectrometry; LOQ, limit of quantification; NBI, noninoculated plants grown beside inoculated plants; NILGS, National Agriculture and Food Research Organization (NARO) Institute of Livestock and Grassland Science; PCR, polymerase chain reaction; PDA, potato dextrose agar

REFERENCES

(1) Ueno, Y.; Aoyama, S.; Sugiura, Y.; Wang, D.; Lee, U.; Hirooka, E.; Hara, S.; Karki, T.; Chen, G.; Yu, S. A limited survey of fumonisins in corn and corn-based products in Asian countries. *Mycotoxin Res.* **1993**, *9*, 27–34.

(2) Desjardins, A. E.; Plattner, R. D.; Nelson, P. E. Production of fumonisin B_1 and moniliformin by *Gibberella fujikuroi* from rice from various geographic areas. *Appl. Environ. Microbiol.* **1997**, *63*, 1838–1842.

(3) Binder, E. M.; Tan, L. M.; Chin, L. J. Worldwide occurrence of mycotoxins in commodities, feeds and feed ingredients. *Anim. Feed Sci. Technol.* **2007**, *137*, 265–282.

(4) Placinta, C. M.; D'Mello, J. P. F.; Macdonald, A. M. C. A review of worldwide contamination of cereal grains and animal feed with *Fusarium* mycotoxins. *Anim. Feed Sci. Technol.* **1999**, *31*, 21–37.

(5) Aoyama, K.; Ishikuro, E. Fumonisin contamination of feeds in Japan. *Mycotoxins* **2007**, *57*, 11–16 (In Japanese with English summary)..

(6) Gelderblom, W. C. A.; Sewram, V.; Shephard, G. A.; Snijman, P. W.; Tenza, K.; van der Westhuizen, L.; Vleggaar, R. Structure and natural occurrence of stereoisomers of the fumonisin B series mycotoxins. *J. Agric. Food Chem.* **2007**, *55*, 4388–4394.

(7) Voss, K. A.; Smith, G. W.; Haschek, M. W. Fumonisins: toxicokinetics, mechanism of action and toxicity. *Anim. Feed Sci. Technol.* **2007**, *137*, 299–325.

(8) Stockmann-Juvala, H.; Savolaonen, K. A review of the toxic effect and mechanisms of action of fumonisin B_1. *Hum. Exp. Toxicol.* **2008**, *27*, 799–809.

(9) Konishi, R.; Sugiyama, K. The risk assessment of mycotoxins and its international trends. *Food Hygiene Safety Sci.* **2008**, *49*, 1–10 (In Japanese.).

(10) MAFF. List of hazardous chemical substances prioritized for risk management. Ministry of Agriculture, Forestry and Fisheries, Japan. URL (http://www.maff.go.jp/j/syouan/seisaku/risk_analysis/priority/chemical.html) (accessed February 27, 2014)

(11) Yoshida, N. Production of self supplied feed in paddy field for sustainable animal husbandry. *Jpn. Soc. Grassl. Sci.* **2012**, *58*, 32–36 (In Japanese with English summary)..

(12) Kushiro, M.; Zheng, Y.; Nagata, R.; Nakagawa, H.; Nagashima, H. Limited surveillance of fumonisins in brown rice and wheat harvested in Japan. *J. Food Prot.* **2009**, *72*, 1327–1331.

(13) Abbas, H. K.; Cartwright, R. D.; Shier, W. T.; Abouzied, M. M.; Bird, C. B.; Rice, L. G.; Ross, P. F.; Sciumbato, G. L.; Meredith, F. I. Natural occurrence of fumonisins in rice with Fusarium sheath rot disease. *Plant Dis.* **1998**, *82*, 22–25.

(14) Uegaki, R.; Kobayashi, H.; Tohno, M.; Tsukiboshi, T. Identification of mycotoxin-producing *Fusarium* spp. isolated from corn and the changes in concentration of fumonisin during the cultivation period. *Grassl. Sci.* **2012**, *58*, 121–126.

(15) O'Donnell, K. Molecular phylogeny of the *Nectria haematococca–Fusarium solani* species complex. *Mycologia* **2000**, *92*, 919–938.

(16) Uegaki, R.; Kobayashi, H.; Inoue, H.; Tohno, M.; Tsukiboshi, T. Changes of fumonisin production in rice grain during ensiling. *Anim. Sci. J.* **2012**, *84*, 48–53.

(17) Yamamura, K. Transformation using $(x + 0.5)$ to stabilize the variance of populations. *Res. Popul. Ecol.* **1999**, *41*, 229–234.

(18) Funnell-Harris, D. L.; Pedersen, J. F. Presence of *Fusarium* spp. in air and soil associated with sorghum fields. *Plant Dis.* **2011**, *95*, 648–656.

(19) Geiser, D. M.; del Mar Jimenez-Gasco, M.; Kang, S.; Makalowska, I.; Veeraraghavan, N.; Ward, T. J.; Zhang, N.; Kuldua, G. A.; O'Donnell, K. FUSARIUM-id v. 1.0: a DNA sequence database for identifying *Fusarium*. *Eur. J. Plant Pathol.* **2004**, *110*, 473–479.

(20) Feng, J.; Kawakami, A.; Nakajima, T. Effects of different carbon sources on trichothecene production and *Tri* gene expression by

Fusarium graminearum in liquid culture. *FEMS Microbiol. Lett.* **2008**, *285*, 212−219.

(21) Uozumi, S.; Ashida, N.; Owari, T.; Sato, H.; Araki, T.; Ishiyama, T.; Matsuzawa, T.; Tohno, E.; Deguchi, S.; Uchino, H. Differences in resistance to corn ear rot and mycotoxin accumulation between cultivars of silage corn. *Jpn. J. Grassl. Sci.* **2013**, *59*, 98−104 (In Japanese with English summary)..

(22) Yoshida, M.; Nakajima, T.; Tomimura, K.; Suzuki, F.; Arai, M.; Miyasaka, A. Effect of the timing of fungicide application on fusarium head blight and mycotoxin accumulation in closed-flowering barley. *Plant Dis.* **2012**, *96*, 1164−1170.

fermentation broth of the biocontrol fungal strain *S. lamellicola* BCP. In addition, the in vitro and in vivo activities of the ethyl acetate layer and pure compounds were evaluated against phytopathogenic bacteria.

MATERIALS AND METHODS

Organisms and Culture Conditions. The following seven phytopathogenic bacterial strains were used for the antibacterial bioassay: *Acidovorax konjaci*, the causal agent of bacterial blight of konjac; *Agrobacterium tumefaciens*, the causal agent of crown gall disease; *Burkholderia glumae*, the causal agent of bacterial grain rot of rice; *Pectobacterium carotovorum* subsp. *carotovorum*, the causal agent of bacterial soft rot of potato; *Pseudomonas syringae* pv *lachrymans*, the causal agent of cucumber angular leaf spot; *R. solanacearum*, the causal agent of tomato bacterial wilt; and *Xanthomonas euvesicatoria*, the causal agent of pepper bacterial spot. All strains were grown on nutrient agar (NA) (Becton, Dickinson and Co., Sparks, MD, USA) and nutrient broth (NB), except *R. solanacearum*, which was grown in tryptone soy agar (TSA) (Becton, Dickinson and Co.) and tryptone soy broth (TSB) (Becton, Dickinson and Co.). *X. euvesicatoria* was cultured aerobically at 25 °C for 18−36 h, and the remaining strains were cultured aerobically at 30 °C for 18−36 h.

Isolation of Antibacterial Substances. Strain BCP was cultured on potato dextrose broth (PDB) medium (Becton, Dickinson and Co.) on a rotary shaker at 150 rpm and at 25 °C for 10 days as described previously by Kim et al.[4] The broth culture (10 L) was centrifuged at 10000*g* for 10 min. The obtained supernatant was mixed with an equal volume of acetone and incubated in a fume hood for 24 h. The precipitates were filtered out using filter paper, and the filtrate was concentrated under a vacuum to remove the acetone. The aqueous layer was then partitioned twice with equal volumes of ethyl acetate (EtOAc). The EtOAc layers were pooled and concentrated in a rotary evaporator at 40 °C to remove the organic solvent. The EtOAc concentrate (2.5 g) showed strong activity against *R. solanacearum* as determined by a disk diffusion assay.[4] The EtOAc concentrate was subjected to chromatography on a silica gel column [100 g of Kiesel gel 60 (230−400 mesh; E. Merck, Darmstadt, Germany), 3.4 cm × 40 cm, packed with EtOAc/methanol (MeOH) (9:1, v/v)] with successive elution with mixtures of EtOAc/MeOH/water (W) (80:10:2, v/v/v, 200 mL), EtOAc/MeOH/W (80:10:5, v/v/v, 200 mL), EtOAc/MeOH/W/acetic acid (80/10/8/1, v/v/v/v, 500 mL), and dichloromethane (DCM/MeOH/W (60:40:10, v/v/v, 500 mL), yielding 15 fractions, ABE 1−15. The fractions were monitored using thin-layer chromatography (TLC) (Kiesel gel 60GF 254, 0.25-mm layer thickness; E. Merck) with the developing solvent EtOAc/MeOH/W/acetic acid (80:10:8:1, v/v/v/v). The fractions were also assayed in vitro for growth inhibition of *R. solanacearum*. The active fractions ABE 5−8 displayed a similar pattern of primary components based on the TLC analysis and were pooled and further purified repeatedly using preparative HPLC (SCL-10A VP; Shimadzu Co., Kyoto, Japan) with a Capcell Pak C18 UG120 Å (5 μm, 20 mm × 250 mm; Shiseido Co., Tokyo, Japan). The combined fraction (460 mg) was eluted with a linear gradient from 45% MeOH to 100% MeOH for 30 min and then maintained at 100% MeOH for 10 min. The eluent (6.5 mL/min) was monitored at 204, 215, and 254 nm. Two compounds, **1** (85 mg) and **2** (23 mg), were isolated to purity by repeated preparative HPLC. Compound **3** (12 mg) was purified from fraction ABE 13 by preparative TLC (Kiesel gel 60GF 254, 0.5 mm layer thickness; E. Merck) with the developing solvent EtOAc/MeOH/W/acetic acid (80:10:8:1, v/v/v/v).

Degradative products of **1** were prepared by directed lactonization of fatty acids in the structure of **1** (12 mg), with the catalysis of 0.1 N HCl in CH_3CN (2 mL of a mixture of 1 mL of 0.1 HCl aq + 1 mL of CH_3CN). The reaction was performed at 80 °C for 2 h. The product was monitored by TLC with hexane/EtOAc (1:3, v/v) as the developing solvent. After working up the reaction, the nonpolar product was extracted twice with 1 mL of a mixture of EtOAc and hexane (3:1, v/v). The organic layers were pooled and concentrated under an N_2 stream at 40 °C until dryness. The residue was separated by preparative TLC using a mixture of hexane/EtOAc (1:3, v/v) to yield 4.2 mg of compound **4** and 5 mg of compound **5**.

The aqueous layer was concentrated to dryness and redissolved in 0.2 mL of 2 N HCl in a 7 mL screw-top vial. The vial was heated to 100 °C for 4 h to hydrolyze the sugar moiety. After hydrolysis, the mixture of products was divided into two parts. One portion was partitioned with DCM to remove the nonpolar impurities, and the aqueous layer was evaporated off under an N_2 stream. The residue was dissolved in MeOH and analyzed by TLC using DCM/MeOH/W (6:4:1, v/v/v) and was compared with authentic monosaccharides. The second portion was neutralized with $NaHCO_3$ and dried under an N_2 stream. The residue was acetylated with 0.2 mL of acetic anhydride/pyridine (1:1, v/v) at 100 °C for 45 min. After the acetylation reaction, the mixture of acetic anhydride/pyridine was removed under an N_2 stream. The residue containing the acetylated monosaccharide was dissolved into 0.2 mL of 2% $CuSO_4$ in water and partitioned twice with 0.5 mL of EtOAc. The EtOAc layers were pooled and dried under a nitrogen stream. The residue obtained after drying was dissolved in 50 μL of chloroform for GC-MS analysis. Authentic samples of glucose, rhamnose, mannose, galactose, and sorbitol (0.5 mg each) were also acetylated. The acetylated monosaccharides were analyzed by GC-MS on an SP2330 column (30 m × 0.32 mm i.d.; 0.25 μm film thickness; Supelco, Inc., Bellefonte, PA, USA) using He as the carrier gas with a temperature program of 120 °C (2 min) to 230 °C (5 °C min^{-1}) maintained for 12 min.

Structure Determination of Antibacterial Substances. The optical rotations of the purified compounds in MeOH were recorded on a JASCO J-20 automatic recording spectropolarimeter using a 1 cm path-length cell. The chemical structures were determined by mass and nuclear magnetic resonance (NMR) spectroscopy. Fast atom bombardment (FAB) analysis was performed with a glycerol matrix and Ar as the bombarding gas using a high-resolution mass spectrometer (JMS-AX505; JEOL Ltd., Tokyo, Japan). The electrospray ionization mass spectra (ESI-MS) of the purified compounds were recorded on an MSD1100 single-quadrupole mass spectrometer equipped with an ESI (Hewlett-Packard Co., Palo Alto, CA, USA). ^1H and ^{13}C NMR, COSY, HMQC, and HMBC spectra were recorded in CD_3OD (E. Merck) with a Bruker AMX-500 spectrometer (Bruker Analytische Messtechnik Gmbh, Rheinstetten, Germany).[7] The spectra were referenced to either tetramethylsilane (TMS) (^1H) or solvent signals (^{13}C). The coupling constants are reported in hertz. The chemical structures of the purified substances were analyzed on the basis of the MS and NMR spectral data and comparisons to reported values in the literature.

In Vitro Antibacterial Assay against Phytopathogenic Bacteria. An in vitro antibacterial assay was performed in 96-well microtiter plates based on a modification of the broth microdilution method.[8,9] The *R. solanacearum* strain was incubated in TSB medium, and the other bacteria were incubated in NB medium. The stock solutions of pure compounds dissolved in MeOH were diluted 100-fold with the proper growth medium for each strain and tested at final concentrations ranging from 0.39 to 100 μg/mL. Bacterial suspensions (50 μL) of each strain with an inoculum of 2 × 10^6 cells/mL were added to the wells containing 50 μL of 2-fold serially diluted pure compounds in the proper growth medium for a final volume of 100 μL in each well. The negative controls were treated with 1% MeOH, which corresponds to the highest concentration. The blank wells were prepared with culture medium containing pure compounds at the same test concentrations. The dilutions were prepared with three replicates, and the experiments were performed a minimum of three times. The inoculated plates were incubated at 30 °C, except for *X. euvesicatoria* at 25 °C, for 18−48 h after shaking at 300 rpm for 20 min on a microplate shaker. The optical density (OD) of each well was measured using a microplate reader (Bio-Rad, Benchmark Plus, USA) at 600 nm. The growth inhibition of each dilution was determined using the formula[9]

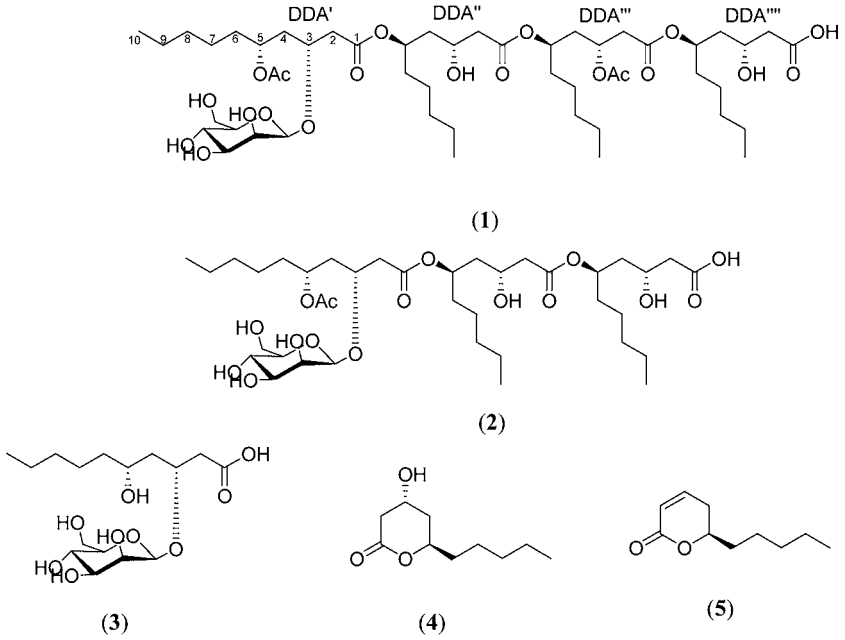

Figure 1. Chemical structures of the compounds isolated from the ethyl acetate layer of the *Simplicillium lamellicola* BCP broth. **1**, halymecin F; **2**, halymecin G; **3**, (3*R*,5*R*)-3-*O*-*β*-D-mannosyl-3,5-dihydroxydecanoic acid; **4**, (+)-(3*R*,5*R*)-3-hydroxydecan-5-olide; **5**, (−)-massoia lactone; DDA, 3, 5-dihydroxydecanoic acid.

$$\%\ \text{inhibition} = 100 \times [1 - \text{OD of treated well} / \text{OD of negative control well}]$$

where OD values of the negative control well and the OD of the treated well were corrected with the OD of the blank wells corresponding to each concentration. The IC_{50} values were derived from Probit analysis of the concentration−response data, with serially diluted concentrations of the pure compounds.

Disease Control Efficacy of the Ethyl Acetate Layer of *S. lamellicola* BCP against Tomato Bacterial Wilt. To evaluate the disease control efficacy of the EtOAc extract of *S. lamellicola* BCP culture broth against tomato bacterial wilt caused by *R. solanacearum* SL1944 (race 1, biovar 4),[10,11] 3-week-old tomato plants at the 4−5-true-leaf stage of 'Seokwang' were used. The plants were grown in vinyl pots with a volume of 170 mL in a greenhouse and were then transplanted into vinyl pots with a diameter of 7 cm (one plant per pot). Three different amounts of the EtOAc layer, 50, 100, and 200 mg, were dissolved in 2 mL of MeOH and then poured into 98 mL of distilled water containing 250 μg/mL Tween-20 to obtain test concentrations of 500, 1000, and 2000 μg/mL. *R. solanacearum* was cultured on TSA Petri dishes at 30 °C for 48 h and were subsequently washed twice from the dishes with sterile distilled water. The inoculum suspension was adjusted to an optical density OD_{600} of 0.1 (approximately 1.5×10^8 cells/mL) using sterile distilled water. The 20 mL aliquots of three EtOAc extract solutions were evenly applied to the soil of each pot. After 3 h, *R. solanacearum* was inoculated by applying 20 mL of the inoculum suspensions into the soil. The second treatment with the EtOAc layer was performed 5 days after the first treatment. Streptomycin sulfate (SM), a bactericidal antibiotic with a broad activity against both Gram-negative and Gram-positive bacteria, was used as a positive control at a concentration of 200 μg/mL. Pots treated with water containing Tween-20 (250 μg/mL) and MeOH (2%) served as the negative controls (CK). The plants were maintained in a controlled climate at 30 °C with a relative humidity of 70−80%. The disease severity was recorded on a scale of 0−5 as described by Winstead and Kelman.[12] The following scales were used: 0 = no symptoms, 1 = one leaf partially wilted, 2 = one to two leaves wilted, 3 = two to three leaves wilted, 4 = four or more leaves wilted, and 5 = death of the entire plant. The pots were arranged as a randomized complete block with five replicates per treatment. The experiment was repeated three times. The control value was calculated using the following formula: control value (%) = 100 × (disease severity of control − disease severity of treatment)/disease severity of control.

Statistical Analysis. The data obtained in this study were evaluated by one-way ANOVA, and the significance of the treatments was determined by Tukey's HSD for multiple comparisons ($P \leq 0.05$). The IC_{50} values were calculated on the basis of Probit analysis using WINPEPI software version 11.4.[13]

RESULTS AND DISCUSSION

This study focused on the identification of antibacterial metabolites produced by the biocontrol agent *S. lamellicola* BCP and the in vitro and in vivo activities of these compounds against phytopathogenic bacteria to identify either alternatives to currently used crop protection agents or lead compounds to synthesize derivatives with enhanced activities or environmental friendliness. The *S. lamellicola* BCP strain, previously identified as *A. strictum* BCP on the basis of morphological characteristics, was developed as a microbial fungicide for the control of various plant diseases, such as tomato gray mold and rice blast.[5,6] However, in the present study, we identified the strain as *S. lamellicola* BCP on the basis of sequence analysis of the 28S rRNA gene and ITS regions (Figures S1 and S2 in the Supporting Information). In addition, we found that the microbial fungicide also effectively suppressed the development of tomato bacterial wilt in fields. We previously reported that the antagonistic fungus produces verlamelin as an antifungal metabolite.[4] However, the metabolite did not show any antibacterial activity. Therefore, in this study, we characterized the antibacterial metabolites produced by *S. lamellicola* BCP.

Characterization of Substances from the Culture Broth of *S. lamellicola* BCP. When investigating the bioactivities of the EtOAc extract from the *S. lamellicola* BCP culture broth, we found that the EtOAc layer significantly inhibited the growth of *R. solanacearum* and also contained trimers and tetramers of (3*R*,5*R*)-3,5-dihydroxydecanoic acids (DDA) as the primary metabolites. Using bioassay-guided

dx.doi.org/10.1021/jf500361e | J. Agric. Food Chem. 2014, 62, 3363−3370

fractionation, the antibacterial metabolites were isolated from the EtOAc layer by various chromatographic methods.

Compound **1**, a main component (Figure 1) ($[\alpha]^{20}_{D}$ −11.9°; *c* 0.27, MeOH), was obtained as a colorless oil, and its molecular formula is $C_{50}H_{88}O_{20}$ as determined by FAB-MS ($[M + Na]^+$ 1032) and ESI-MS ($[M + Na]^+$ 1031.6) data. The FAB-MS and positive ESI-MS data (Figure 2) of **1** exhibited

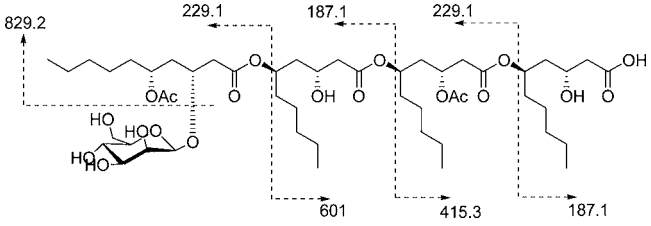

Figure 2. Fragmentation of halymecin F (**1**) ($C_{50}H_{88}O_{20}$, quasi-molecular ion peak *m/z* 1031.6 $[M + Na]^+$) generated by ESI-MS.

significant fragment peaks at *m/z* 829.2 $[M + H - 180]^+$, *m/z* 601 $[M + H - 180 - C_{12}H_{20}O_4]^+$, *m/z* 583 $[601 - H_2O]^+$, *m/z* 523 $[583 - 60]^+$, *m/z* 415.3 $[C_{22}H_{39}O_7]^+$, *m/z* 355.3 $[C_{22}H_{39}O_7 - 60]^+$, *m/z* 229.1 $[C_{12}H_{21}O_4]^+$, and *m/z* 187.1 $[C_{10}H_{19}O_3]^+$. Hydrolysis of **1** after lactonization yielded a hydrolysate containing a monosaccharide moiety. TLC analysis revealed that the sugar moiety is D-mannose on the basis of comparison to the authentic compound. GC-MS analysis of the acetylated product of the hydrolysate also confirmed the presence of pentaacetyl-β-D-mannose. These data suggest that **1** contains β-D-mannose, two acetyl groups (two losses of 60 in the MS spectrum), and $C_{10}H_{19}O_3$ units. The ^{1}H NMR spectrum of **1** (Table 1) displayed signals corresponding to four terminal methyl groups at δ 0.89 (12H, t, *J* = 7.01), two acetyl groups at δ 2.01 (3H, s) and 2.02 (3H, s), an anomeric proton at δ 4.61 (1H, brs), and a region of protons of oxygenated carbons. The ^{13}C NMR spectrum of **1** revealed the presence of 1 anomeric carbon at δ 101.18, 13 oxygenated carbons from δ 62.97 to δ 78.28, 6 carbonyl groups in the range of δ 172.47−173.63, and the methyl carbons of 2 acetyl groups at δ 21.24 (Table 1). On the basis of analysis of the COSY and HMQC spectra, assignment of the β-D-mannose moiety was verified. The proton spin system of the H1−H6 of each fatty acid was determined by COSY, and the position of the carbonyl group was determined by a cross peak between the methylene protons of the C-2 and the carbon of the carbonyl group. The long-range correlations of H-3 (δ 4.21, DDA′) with an anomeric carbon (101.18) on the HMBC spectrum demonstrated that the β-D-mannose moiety was situated at the C-3 of DDA′. The linkage of the C-5 with an acetyl group was deduced from cross peaks between the protons of the acetyl group and the C-4 (δ 39.84), C-5 (δ 72.78), and C-6 (δ 35.41) in the HMBC spectrum and the fragment peak at *m/z* 602 on the FAB-MS spectrum. The ester linkages between the carbonyl carbons with the C-5 in the remaining fatty acid chains were also deduced from the HMBC data. Furthermore, the HMBC data led to the assignment of the other acetyl group at the C-3 of DDA‴. The lactonization of **1** produced a known δ-lactone (**4**), which was identified as 3-hydroxydecan-5-olide. Its carbon chiral centers were determined as (3*R*, 5*R*) on the basis of the ^{1}H and ^{13}C NMR spectra and optical rotary power. A review of the literature and a comparison of the spectral data of **1** with mannosyl lipids suggested that the structure of **1** was a tetramer of 3,5-dihydrodecanoyl and that its structure was similar to that of halymecin B,[14] except for an additional acetyl group attached to the C-5 of DDA′. Compound **1** was named halymecin F, and its chemical structure is presented in Figure 1.

Compound **2** ($[\alpha]^{20}_{D}$ −8.99°; *c* 0.2, MeOH) was named halymecin G. Its molecular formula is $C_{38}H_{68}O_{16}$ as determined from the quasi-molecular ion peaks at *m/z* $[M + Na]^+$ 803.2 and *m/z* $[M - H]^-$ 779.7 in positive and negative ESI-MS spectra, respectively. These data suggest that **2** lacks one acetyl group and a DDA compared to **1**. The positive-FAB-MS spectrum of **2** showed significant fragment peaks at *m/z* 601 $[M + H - 180]^+$, *m/z* 373 $[C_{20}H_{37}O_6]^+$, and *m/z* 187.1 $[C_{10}H_{19}O_3]^+$. The fragmentation of 373 indicated a dimer of two DDA units without an acetyl group, and these data suggest that compound **2** is a partial structure of **1** and has an acetyl group located at DDA′. The ^{1}H and ^{13}C NMR spectra of **2** showed the presence of one acetyl group, one mannosyl moiety, four carbonyl carbons, and three terminal methyl groups. The location of the mannose moiety is at the C-3 of DDA′ via glycosidic linkage as determined by the HMBC correlation peaks at H-1 (4.61, mannose) with a carbon signal at 74.94. The stereochemical analysis for the DDAs of **2** was also performed as described for **1**, and the chemically degraded product was determined to be (3*R*,5*R*)-3-hydroxydecan-5-olide. Analysis of the 1D-NMR spectroscopic data and interpretation of the HMBC and HSQC allowed us to assign all signals of **2** and identified the compound as a monoacetate trimer of DDA units (Table 1 and Figure 1). Compound **2** was named halymecin G.

Compound **3** ($[\alpha]^{20}_{D}$ −2.9°; *c* 0.176, MeOH) has the molecular formula $C_{16}H_{30}O_9$ as determined by ESI-MS ($[M + Na]^+$ 389.2 and $[M - H]^-$ 365.4). The negative-ESI-MS spectrum of **3** showed a fragment peak at *m/z* 179.2 $[C_{10}H_{19}O_3 - H_2O]^+$, indicating a dehydrated DDA. The ^{1}H NMR spectrum of **3** exhibited a singlet of the anomeric proton H-1 (mannose) at δ 4.66 and a terminal methyl group at δ 0.91. The ^{13}C NMR spectrum had 16 carbon signals, including 6 carbons belonging to a β-D-mannose moiety and 10 carbons for one DDA. The position of the glycosidic linkage of the mannosyl and DDA was also determined by the HMBC analysis. Finally, compound **3** was identified as (3*R*,5*R*)-3-*O*-β-D-mannosyl-3,5-dihydroxydecanoic acid, and its NMR data and structure are presented in Table 1 and Figure 1.

δ-Lactones **4** and **5** were identified as (+)-(3*R*,5*R*)-3-hydroxy-decan-5-olide (EI-MS *m/z* 168 $[M - H_2O]^+$, $C_{10}H_{18}O_3$; $[\alpha]^{20}_{D}$ +39.9°; *c* 0.05, CH_2Cl_2), and (−)-massoia lactone (EI-MS *m/z* 168 $[M]^+$, $C_{10}H_{16}O_2$; $[\alpha]^{20}_{D}$ −65.9°; *c* 0.2, CH_2Cl_2),[15,16] respectively, on the basis of the analysis of the EI-MS, GC-MS, and 1D-NMR data (Figure 1; Table S1 and Figure S3 in the Supporting Information). In a previous study, compounds **4** and **5** were found as biologically active δ-lactones and were chemically synthesized from streptenol A. Optical rotary powers (**4**, $[\alpha]^{20}_{D}$ +36.9°; *c* 0.92, CH_2Cl_2; **5**, $[\alpha]^{20}_{D}$ −112.5°; *c* 1 $CHCl_3$) and MS and 1D-NMR data of these synthesized compounds were reported by Romeyke et al.[15] Although compounds **4** and **5** are chemically degraded products of compounds **1**−**3**, their presence in the EtOAc layer of the *S. lamellicola* BCP culture broth was also confirmed with TLC and GC-MS.

Halymecins were previously reported to be tetramers and trimers of (3*R*,5*R*)-3,5-dihydroxydecanoic acid isolated from *Fusarium* spp. and *Exophiala pisciphila*. All of the microorganism resources were collected from marine algae and sponges,[14,17] whereas *S. lamellicola* BCP was isolated as a

Table 1. ^{1}H and ^{13}C NMR (500 MHz) Data of Compounds 1−3 in Methanol-d_4[a]

	1		2		3	
position	^{13}C[b]	^{1}H	^{13}C[b]	^{1}H	^{13}C	^{1}H
mannose						
1′	101.18	4.61 brs	101.23	4.61 brs	100.7	4.66 brs
2′	72.76	3.83 m	72.70	3.83 m	72.71	3.87 m
3′	75.27	3.44 m	75.25	3.43 m	75.21	3.44 m
4′	68.56	3.53 m	68.60	3.52 m	68.55	3.53 m
5′	78.27	3.22 m	78.29	3.2 m	78.44	3.22 m
6′	62.97	3.71 m; 3.82 m	62.99	3.69 m; 3.83 m	62.93	3.69 m; 3.84 m
DDA′[c]						
1	173.06		173.14		173.06	
2	41.83	2.57 m; 2.85 m	42.10	2.36 m; 2.48 m	37.76	2.76 m; 2.84 m
3	74.93	4.21 m	74.94	4.17 m	78.01	4.67 m
4	39.84	1.74−1.92 m	39.82	1.82−1.91 m	36.63	1.64−1.73 m
5	72.84	5.03 m	72.80	5.03 m	70.83	4.40 m
6	35.41b	1.60 brs	35.39b	1.59 brs	33.75	1.62 brs
7	25.97c	1.31 brs	25.94c	1.29 brs	25.65	1.34 brs
8	32.83d	1.31 brs	32.79d	1.29 brs	32.77	1.34 brs
9	23.71e	1.31 brs	23.62	1.29 brs	23.61	1.34 brs
10	14.44f	0.89 t (7.01)	14.42	0.89 t (7.06)	14.41	0.91 t (6.9)
*CH_3*CO[d]	21.24	2.02 s	21.29	2.02 s		
CH_3*CO*	172.61		172.65			
DDA″						
1	172.47		173.06			
2	40.76	2.43−2.49 m	43.19	2.38−2.48 m		
3	66.77a	4.09 m	66.76a	3.54 m		
4	42.11	1.72−1.78 m	42.22	1.72−1.79 m		
5	73.71	5.05 m	73.13	5.07 m		
6	35.10b	1.61 brs	35.11b	1.59 brs		
7	25.91c	1.31 brs	25.94c	1.29 brs		
8	32.78d	1.31 brs	32.79d	1.29 brs		
9	23.60e	1.31 brs	23.62	1.29 brs		
10	14.37	0.89 t (7.01)	14.42	0.89 t (7.06)		
DDA‴						
1	172.63		175.69			
2	43.57	2.48−2.51 m	43.55	2.38−2.48 m		
3	70.02	5.28 m	66.85a	3.54 m		
4	39.30	1.81 m	42.36	1.72−1.79 m		
5	72.61	4.93 m	72.86	5.04 m		
6	35.14b	1.61 brs	35.11b	1.59 brs		
7	25.91c	1.31 brs	25.94c	1.29 brs		
8	32.82d	1.31 brs	32.79d	1.29 brs		
9	23.66e	1.31 brs	23.62	1.29 brs		
10	14.40f	0.89 t (7.01)	14.42	0.89 t (7.06)		
*CH_3*CO	21.24	2.01 s				
CH_3*CO*	172.47					
DDA‴″						
1	173.16					
2	43.55	2.43−2.48 m				
3	66.82a	4.09 m				
4	42.37	1.72−1.78 m				
5	72.84	5.03 m				
6	35.06b	1.61 brs				
7	25.91c	1.31 brs				
8	32.72d	1.31 brs				
9	23.59e	1.31 brs				
10	14.36f	0.89 t (7.01)				

[a]The chemical shifts (δ) are in ppm from TSM. The coupling constant J values (in hertzz) are given in parentheses. All assignments are based on the COSY, HMQC, and HMBC experiments. [b]Assignments followed by the same letters (a−f) in the same column may be interchangeable. [c]DDA, 3,5-dihydroxydecanoic acid. [d]CH_3CO, acetyl group

dx.doi.org/10.1021/jf500361e | J. Agric. Food Chem. 2014, 62, 3363−3370

Table 2. Antibacterial Activity of the Isolated Compounds against the Growth of Seven Phytopathogenic Bacteria

name	IC_{50} (95% CI)[a]		
	1	2	3
A. konjaci	22.5(8.5−59.9)	>100	>100
A. tumefaciens	1.58 (0.91−2.74)	1.49 (0.18−2.95)	24.8 (16.9−36.4)
B. glumae	33.2 (18.9−58.4)	>100	NI[b]
P. carotovora subsp. *carotovora*	>100	>100	NI
P. syringae pv *lachrymans*	>100	>100	>100
R. solanacearum	73.8 (41.4−106.1)	75.8 (44.3−107.4)	>100
X. euvesicatoria	72.1 (40.6−103.6)	>100	>100

[a]The antibacterial activity is expressed as the IC_{50} (concentration causing 50% growth inhibition) as determined by the broth microdilution method. Growth inhibition was observed 2 days after treatment. 95% CI, 95% confidence interval. [b]No inhibition.

mycoparasite of *B. cinerea*. The present study identifies compounds **1**−**3** for the first time.

Antibacterial Activity. The in vitro antibacterial activity of compounds **1**−**3** was tested in 96-well microtiter plates, and the results are presented in Table 2. Compound **1** displayed a broad spectrum and strong antibacterial activity compared to compounds **2** and **3**. Compound **1** caused growth inhibition of all seven phytopathogenic bacteria and was highly active against *A. konjaci*, *A. tumefaciens*, and *B. glumae*, with IC_{50} values of 25.5, 1.58, and 33.2 μg/mL, respectively. *R. solanacearum* (IC_{50} 73.8 μg/mL) and *X. euvesicatoria* (IC_{50} 72.1 μg/mL) were moderately sensitive to compound **1**. However, *P. carotovora* subsp. *carotovora* and *P. syringae* pv *lachrymans* were highly tolerant to this compound. Compound **2** also affected the cell growth of all bacteria tested. It effectively inhibited the growth of *A. tumefaciens* with an IC_{50} value of 1.49 μg/mL. *R. solanacearum* growth was inhibited by compound **2**, with an IC_{50} value of 75.8 μg/mL. Compound **3** caused good growth inhibition of *A. tumefaciens*, but had no effect against *B. glumae* and *P. carotovora* subsp. *carotovora*. Of the three compounds, compound **1** showed the strongest antibacterial activity against the phytopathogenic bacteria tested.

The EtOAc extract from the *S. lamellicola* BCP broth was evaluated for in vivo antibacterial activity against *R. solanacearum* on 3-week-old tomato seedlings (Figure 3). The extract suppressed the development of bacterial wilt in a dose-dependent manner. *R. solanacearum* caused severe wilting damage on seedlings treated with distilled water and 500 μg/mL EtOAc extract 9 days after inoculation (Figure 3B). However, the EtOAc extract at concentrations of 1000 and 2000 μg/mL displayed strong control efficacies of 85 and 100%, respectively, against *R. solanacearum* 9 days after inoculation. These disease control efficacies were higher than that of streptomycin sulfate (200 μg/mL). These results suggest that the EtOAc extract and the fermentation broth of *S. lamellicola* BCP may be used as a natural bactericide to control tomato bacterial wilt.

Biocontrol provides an alternative to the use of synthetic agrochemicals and is used as part of an overall integrated plant disease management program. Several filamentous fungal species are known mycoparasites against various phytopathogenic fungi.[18−20] The biocontrol mechanism is most likely due to the action of cell wall degradative enzymes and secondary metabolites.[21−23] In addition, the microorganisms that produce microbial polyesters (polyhydroxyalkanoates) have long been considered important in various sectors, such as the food, pharmaceutical, cosmetic, fragrance, flavor, and biofuel industries.[17]

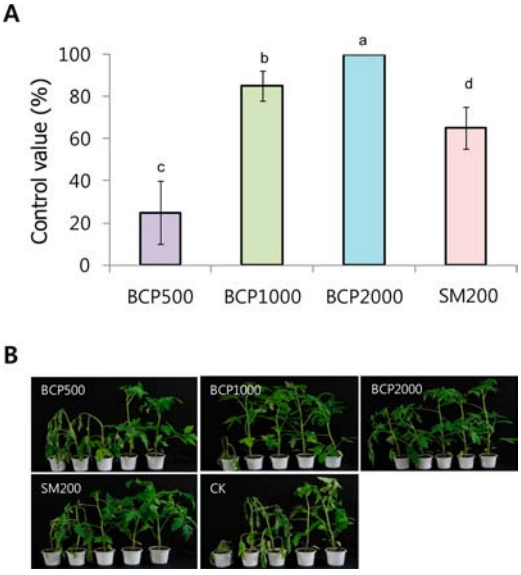

Figure 3. Control efficacy of the ethyl acetate layer of the *Simplicillium lamellicola* BCP culture broth in reducing wilting disease severity caused by *Ralstonia solanacearum* on tomato seedlings (A) and the treated plants 9 days after inoculation (B). BCP500, 500 μg/mL; BCP1000, 1000 μg/mL; and BCP2000, 2000 μg/mL, ethyl acetate extracts from the *S. lamellicola* BCP culture broth; ST200, 200 μg/mL of streptomycin sulfate; CK, untreated control. Each value represents the mean ± standard deviation of three experiments with five replicates each. Means (±SD) followed by the same letters above the bars are not significantly different (P = 0.05) in a Tukey's HSD test.

S. lamellicola BCP was reported to be a biocontrol fungus with good efficacy against *B. cinerea* and *M. grisea*.[5,6] *S. lamellicola* was previously known as *Cephalosporium lamellicola* and *Verticillium lamellicola*, which exhibited mycoparasitic interactions with phytopathogenic fungi causing rust diseases.[20,24] The strain BCP was also reported to produce verlamelin that significantly suppressed tomato late blight caused by *P. infestans*, wheat leaf rust caused by *P. recondita*, and barley powdery mildew caused by *B. graminis* f. sp. *hordei*.[4,25] In the present study, we demonstrated that *S. lamellicola* BCP produces different antimicrobial metabolites and may be considered a producer of polyesters of (3*R*,5*R*)-3,5-dihydroxydecanoic acid.

For the antimicrobial activities of substances containing (3*R*,5*R*)-3,5-dihydroxydecanoic acid, verbalactone isolated from the plant roots of *Verbascum undulatum* exhibited moderate antibacterial activity against *Salmonella enteritidis*, *Staphylococcus aureus*, and *S. epidermidis*.[26] Only a few tetramers and trimers of (3*R*,5*R*)-3,5-dihydroxydecanoic acid from three fungal strains

have previously been reported. Halymecins A, B, and C were isolated from *Fusarium* spp. FE-71-1, and halymecins D and E were isolated from *Acremonium* spp. FK-N30. Of these compounds, halymecin A is a tetramer of DDA and causes growth inhibition of bacteria, such as *Enterococcus faecium*, *Klebsiella pneumoniae*, and *Proteus vulgaris*. Halymecin A also showed strong antimicroalgal and cytotoxic activities.[14] Exophilin A was reported to be a trimer of (3*R*,5*R*)-3,5-dihydroxydecanoic acid isolated from *Exophiala pisciphila* NI10102. The trimer displayed antimicrobial activity against some Gram-positive bacterial strains, such as *Enterococcus faecium* and *Staphylococcus aureus*.[17] In our study, the mannosyl lipids halymecin F (**1**), halymecin G (**2**), and (3*R*,5*R*)-3-*O*-*β*-D-mannosyl-3,5-dihydroxydecanoic acid (**3**) were novel mannosyl lipids isolated from *S. lamellicola* BCP with antibacterial activities against phytopathogenic bacteria.

In addition, we successfully isolated and confirmed the presence of massoia lactone (**5**), an active metabolite member of the *Trichoderma* family,[23] in the culture broth of *S. lamellicola* BCP. Massoia lactone represents a minor component of the crude extracts of various *Trichoderma* spp., including *Trichoderma viride*. This compound was patented because it controls *B. cinerea* and *Phytopthora* species.[22] The role of *Trichoderma* antimicrobial metabolites in biocontrol remains unclear. Some of these compounds may be the major contributor to biocontrol activity for a certain strain but not for other strains.[21] The presence of massoia lactone (**5**) in *S. lamellicola* BCP suggests a relationship between the biocontrol mechanism of the strain and *Trichoderma* species. Our findings confirmed the production of mannosyl lipids **1**−**3** and massoia lactone from *S. lamellicola* BCP and the antibacterial activities of the novel mannosyl lipids against phytopathogenic bacteria. This strain may be considered a producer of polyesters of (3*R*,5*R*)-3,5-dihydroxydecanoic acid. The presence of the three novel mannosyl lipids in the fermentation broth cultures of *S. lamellicola* BCP was demonstrated in this study. Furthermore, the in vivo activities of the EtOAc extract against tomato bacterial wilt in a climate-controlled room and disease control of the microbial biopesticide Acre against tomato bacterial wilt in fields were also elucidated. These results suggest that *S. lamellicola* BCP and its mannosyl lipids could be used to control plant diseases caused by phytopathogenic bacteria.

■ ASSOCIATED CONTENT

Ⓢ Supporting Information

NMR spectral data and EI-MS spectrum of compound **4**, in vivo antifungal activity of ABE, and neighbor-joining trees based on sequence analysis of the 28S rRNA gene and ITS regions. This material is available free of charge via the Internet at http://pubs.acs.org.

■ AUTHOR INFORMATION

Corresponding Author

*(J.-C.K.) Phone: +82-42-860-7436. Fax: +82-42-861-4913. E-mail: kjinc@krict.re.kr.

Funding

This study was performed with support from the Cooperative Research Program for Agricultural Science and Technology Development (Project PJ010207022014), Rural Development Administration, Republic of Korea.

Notes

The authors declare no competing financial interest.

■ REFERENCES

(1) Hedin, P. A. New concepts and trends in pesticide chemistry. *J. Agric. Food Chem.* **1982**, *30*, 201−215.
(2) Vidhyasekaran, P. *Concise Encyclopedia of Plant Pathology*; Food Products Press: New York, 2004.
(3) Copping, L. G.; Duke, S. O. Natural products that have been used commercially as crop protection agents. *Pest Manage. Sci.* **2007**, *63*, 524−554.
(4) Kim, J.-C.; Choi, G. J.; Kim, H. J.; Kim, H. T.; Ahn, J. W.; Cho, K. Y. Verlamelin, an antifungal compound produced by a mycoparasite *Acremonium strictum*. *Plant Pathology J.* **2002**, *18*, 102−105.
(5) Choi, G. J.; Kim, J.-C.; Jang, K. S.; Nam, M. H.; Lee, S. W.; Kim, H.-T. Biocontrol activity of *Acremonium strictum* BCP against *Botrytis* diseases. *Plant Pathology J.* **2009**, *25*, 165−171.
(6) Choi, G. J.; Kim, J.-C.; Jang, K. S.; Cho, K.-Y.; Kim, H.-T. Mycoparasitism of *Acremonium strictum* BCP on *Botrytis cinerea*, the gray mold pathogen. *J. Microbiol. Biotechnol.* **2008**, *18*, 167−170.
(7) Yoon, M.-Y.; Choi, N. H.; Min, B. S.; Choi, G. J.; Choi, Y. H.; Jang, K. S.; Han, S. S.; Cha, B.; Kim, J.-C. Potent *in vivo* antifungal activity against powdery mildews of pregnane glycosides from the roots of *Cynanchum wilfordii*. *J. Agric. Food Chem.* **2011**, *59*, 12210−12216.
(8) Patton, T.; Barrett, J.; Brennan, J.; Moran, N. Use of a spectrophotometric bioassay for determination of microbial sensitivity to manuka honey. *J. Microbiol. Methods* **2006**, *64*, 84−95.
(9) De La Fuente, R.; Sonawane, N. D.; Arumainayagam, D.; Verkman, A. S. Small molecules with antimicrobial activity against *E. coli* and *P. aeruginosa* identified by high-throughput screening. *Br. J. Pharmacol.* **2006**, *149*, 551−559.
(10) Lee, H. J.; Jo, E. J.; Kim, N. H.; Chae, Y.; Lee, S. W. Disease responses of tomato pure lines against *Ralstonia solanacearum* strains from Korea and susceptibility at high temperature. *Res. Plant Dis.* **2011**, *17*, 326−333.
(11) Vu, T. T.; Kim, J.-C.; Choi, Y. H.; Choi, G. J.; Jang, K. S.; Choi, T. H.; Yoon, T. M.; Lee, S.-W. Effect of gallotannins derived from *Sedum takesimense* on tomato bacterial wilt. *Plant Dis.* **2013**, *97*, 1593−1598.
(12) Winstead, N. N.; Kelman, A. Inoculation techniques for evaluating resistance to *Pseudomonas solanacearum*. *Phytopathology* **1952**, *42*, 628−634.
(13) Abramson, J. H. WINPEPI (PEPI-for-Windows): computer programs for epidemiologists. *Epidemiol. Perspect. Innovations* **2004**, *1*, 6.
(14) Chen, C.; Imamura, N.; Nishijima, M.; Adachi, K.; Sakai, M.; Sano, H. Halymecins, new antimicroalgal substances produced by fungi isolated from marine algae. *J. Antibiot.* **1996**, *49*, 998−1005.
(15) Romeyke, Y.; Keller, M.; Kluge, H.; Grabley, S.; Hammann, P. Secondary metabolites by chemical screening − 13. Enantioselective synthesis of *δ*-lactones from streptenola, achiral building block from streptomyces. *Tetrahedron* **1991**, *47*, 3335−3346.
(16) Satō, T. Synthesis of optically active forms of the *δ*-lactone of 3,5-dihydroxydecanoic acid. *Can. J. Chem.* **1987**, *65*, 2732−2733.
(17) Doshida, J.; Hasegawa, H.; Onuki, H.; Shimidzu, N. Exophilin A, a new antibiotic from a marine microorganism *Exophiala pisciphila*. *J. Antibiot.* **1996**, *49*, 1105−1109.
(18) John, R. P.; Tyagi, R. D.; Prevost, D.; Brar, S. K.; Pouleur, S.; Surampalli, R. Y. Mycoparasitic *Trichodema viride* as a biocontrol agent against *Fusarium oxysporum* f. sp. *adzuki* and *Pythium arrhenomanes* and as a growth promoter of soybean. *Crop Prot.* **2010**, *29*, 1452−1459.
(19) Romero, D.; Rivera, M. E.; Cazorla, F. M.; Vicente, A. D.; Perez-Garcia, A. Effect of mycoparasitic fungi on the development of *Spaerotheca fusca* in melon leaves. *Mycol. Res.* **2003**, *107*, 64−71.
(20) Ward, N. A.; Robertson, C. L.; Vhanda, A. K.; Schneider, R. W. Effects of *Simplicillium lanosonivieum* on *Phakopsora pachyrhizi*, the soybean rust pathogen, and its use as a biological control agent. *Phytopathology* **2012**, *102*, 749−760.

(21) Harman, G. E.; Howell, C. R.; Viterbo, A.; Chet, I.; Lorito, M. *Trichoderma* species − opportunistic, avirulent plant symbionts. *Nat. Rev. Microbiol.* **2004**, *2*, 43−56.
(22) Hill, R. A.; Cutler, H. G.; Parker, S. R. Use of massoialactone for inhibition of fungal growth. U.S. Patent 6060507, 2000.
(23) Reino, J.; Guerrero, R.; Hernández-Galán, R.; Collado, I. Secondary metabolites from species of the biocontrol agent *Trichoderma*. *Phytochem. Rev.* **2008**, *7*, 89−123.
(24) Steenberg, T.; Humber, R. A. Entomopathogenic potential of *Verticillium* and *Acremonium* species (Deuteromycotina: Hyphomycetes). *J. Invertebr. Pathol.* **1999**, *73*, 309−314.
(25) Rowin, G. L.; Miller, J. E.; Albers-Schonberg, G.; Onishi, J. C.; Davis, D.; Dulaney, E. L. Verlamelin, a new antifungal agent. *J. Antibiot.* **1986**, *39*, 1772−1775.
(26) Magiatis, P.; Spanakis, D.; Mitaku, S.; Tsitsa, E.; Mentis, A.; Harvala, C. Verbalactone, a new macrocyclic dimer lactone from the roots of *Verbascum undulatum* with antibacterial activity. *J. Nat. Prod.* **2001**, *64*, 1093−1094.

extraction of different components from various sources.[16−19] Sonication involves the generation of sound waves that trigger extremely high alterations in pressure, leading to the formation of cavitation bubbles that damage the plant matrix and release extractive compounds.[16,20] The use of sonication in the release of nonextractable phenolics has not been widely investigated, more so the combination of sonication and alkaline hydrolysis.

Therefore, the aim of this study was to investigate the use of sonication and the combination of sonication and alkaline hydrolysis in the release of nonextractable phenolics from cauliflower waste. The yield of total nonextractable phenolics compared to the extractable fraction was also investigated. Different factors, such as sonication time, NaOH concentration, and temperature, were optimized to yield the highest total nonextractable phenolic content. Thereafter, the phenolic composition of the nonextractable fraction was characterized and quantified using advanced LC-MS techniques. Furthermore, the nonextractable phenolic compositions of the blade and petiole parts were also individually evaluated.

MATERIALS AND METHODS

Reagents. Kaempferol, quercetin, and ferulic, *p*-coumaric, gallic, and sinapic acids were purchased from Sigma (St. Louis, MO, USA). U(H)PLC-MS grade methanol and formic acid were acquired from Biosolve (Valkenswaard, The Netherlands). Analytical grade methanol used for extraction, HCl, and NaOH were purchased from VWR International (Leuven, Belgium).

Conventional Extraction of EP and Collection of Residues Containing NEP. Cauliflower (*Brassica oleracea* L. var. *botrytis*) wastes were obtained in a field in Ieper (Belgium) during harvest (July 2012), stored at −20 °C, and lyophilized. Dried leaves were ground and homogenized using a stirrer. Extraction was based on the method of Gonzales et al.[11] Briefly, approximately 2 g of leaves was placed in 50 mL tubes and homogenized with 15 mL of methanol at 10000 rpm using an ultraturrax for 45 s. The tubes were then placed on ice for 15 s. The mixture was centrifuged at 13000*g* for 10 min at 4 °C. The residue was re-extracted with 80% MeOH using the same procedure. After removal of the supernatant, the residue was dried under vacuum and stored at −20 °C until further analysis. Concurrently, blade and petiole parts were also manually separated and extracted separately. Extractions and analyses were done in triplicate.

Measurement of Total Phenolic Content (TPC). TPC was analyzed using the Folin−Ciocalteu method[21] with slight modifications and expressed as milligrams of gallic acid equivalents (GAE). Briefly, 50 μL of sample, 100 μL of Folin−Ciocalteu reagent, and 1.2 mL of distilled water were mixed in a 2 mL cuvette. After 5 min, 150 μL of 20% sodium carbonate was added and the mixture was incubated for 2 h in the dark. TPC was then measured at 760 nm. Calibration curves were drawn using gallic acid with R^2 values of >0.98. All analyses were performed in triplicates.

Alkaline Hydrolysis and Choice of Solvent on the Total Phenolic Content of Residues. Prior to optimization of the alkaline hydrolysis conditions, the choice of a suitable solvent and the effect of sonication were investigated. For this, a method previously used for the release of bound procyanidin from cranberry pomace by alkaline hydrolysis was employed.[7] Briefly, 0.1 g of residue was hydrolyzed using 2 mL of 2 M NaOH for 15 min at 60 °C in a screw-capped test tube previously flushed with nitrogen. The samples were then neutralized using 2 M HCl and extracted twice with different solvents for 2 min under vortex. Extraction solvents used were 4 mL of either methanol, acetone, or ethyl acetate (all containing 0.1% formic acid). The tubes were centrifuged for 10 min at 10000*g* and 4 °C. Extraction was done twice, and the supernatants were pooled and standardized to 20 mL using the corresponding solvents. Because methanol extracted significantly more phenolics, based on TPC, than ethyl acetate and acetone (results not shown), methanol was used as the extraction solvent for all other subsequent analyses.

Effect of Sonication and Combination with Alkaline Hydrolysis (Sonicated Alkaline Hydrolysis). The effect of sonication on the release of nonextractable phenolics was tested by mixing 0.1 g of residue with 20 mL of methanol in a sonicated bath for 15 min at 60 °C previously flushed with nitrogen. The ultrasonic extraction procedure was performed in an Elmasonic S60H unit with a frequency of 37 kHz and a nominal power of 180 W. The dimensions of the bath were 300 mm (W)/150 mm (D)/150 mm (H), and it was filled with 2 L of water. The suspension was centrifuged at 10000*g* at 4 °C for 10 min. The supernatant was kept for analysis.

Subsequently, the effect of combining alkaline hydrolysis and sonication was tested by sonicating a mixture of 0.1 g of residue with 2 mL of 2 M NaOH at 60 °C for 15 min. The phenolic content was extracted with methanol, as described above. Therefore, three setups were made: (1) alkaline hydrolysis, (2) ultrasound-assisted extraction, and (3) combined alkaline hydrolysis and sonicated extraction. Because sonicated alkaline hydrolysis significantly increased the TPC, optimization of this treatment was performed.

Optimization of the Sonicated Alkaline Treatment of the Residue. The conditions for sonicated alkaline hydrolysis were optimized to increase the TPC of the extract. Hydrolysis experiments were performed using a 3^3 factorial design comprising three different temperatures (40, 60, 80 °C), NaOH concentrations (1, 2, 4 M), and sonication time (15, 30, 45 min). Each treatment consisted of one temperature, one NaOH concentration, and one sonication time, thus 27 treatments in total. The analysis was performed in triplicates. Therefore, 0.1 g of residue was placed in each of 81 screw-capped test tubes, and these were hydrolyzed under various conditions as described in Table 1 and extracted as earlier described. Extracts are henceforth referred to as NEP solution.

Table 1. Treatment Conditions for Sonicated Alkaline Hydrolysis Treatment Optimization

temp (°C)	NaOH concn (M)	sonication time (min)
40	1	15
60	2	30
80	4	45

Solid Phase Extraction (SPE). A 1 mL aliquot of the NEP solution was diluted in 20 mL of 0.1% (v/v) formic acid (in ultrapure water) and loaded into a preconditioned C18 SPE cartridge (500 mg/4 mL) (Davison Discover Science, Deerfield, IL, USA). Preconditioning was done by loading the column with 2 × 3 mL of methanol and 2 × 3 mL of water, which was allowed to stand for at least 2 min for every solvent, prior to use. After sample loading, the cartridge was washed with 5 mL of 0.1% (v/v) formic acid and the phenolic compounds were recovered using 3 mL of methanol containing 0.1% (v/v) formic acid. The samples were then dried using nitrogen and redissolved in 1 mL of 10% methanol (0.1% v/v formic acid) prior to LC-MS analysis.

Identification of Compounds Using U(H)PLC-ESI-MS and Quantification by U(H)PLC-DAD. LC-MS analysis was performed with a Waters Acquity UPLC system (Waters Corp., Milford, MA, USA) connected to a Synapt HDMS TOF mass spectrometer (Waters Corp.). Chromatographic separation was done on a Waters Acquity BEHC18 column (2.1 mm × 150 mm, 1.7 μm particle size) attached to a Waters VanGuard precolumn (2.1 mm × 5 mm) using gradient elution. The mobile phase was composed of (A) water containing 0.1% (v/v) formic acid and (B) methanol containing 0.1% (v/v) formic acid. The column temperature was maintained at 40 °C, whereas the temperature of the autosampler was held at 10 °C. Five microliters of sample was injected, and a flow rate of 250 μL/min was applied during the gradient elution. The elution program was as follows: 0 min, 10% B; 0−6 min, 0−20% B linear; 6−12 min, 20% B isocratic; 12−13 min, 20−30% B linear; 13−23 min, 30−50% B linear; 23−30 min, 50−90% B linear; 30−35 min, 90% isocratic; 35−40 min, 90−10% B linear; and 40−45 min, 10% B isocratic. The eluent was then directed to the mass spectrometer equipped with an electrospray

dx.doi.org/10.1021/jf500835q | J. Agric. Food Chem. 2014, 62, 3371−3376

ionization (ESI) source. Data were acquired in continuum negative ionization in V-mode. Source parameters for the MS were set as follows: capillary voltage, 2 kV; sampling cone voltage, 40 V; extraction cone voltage, 4 V; source temperature, 150 °C; desolvation temperature, 350 °C; cone gas flow rate, 50 L/h; desolvation gas flow rate, 550 L/h. Collision energies were set at 6 V for low energy and 45 V for high energy. Mass range was set at 100−1500 Da with a scan speed of 0.2 s per scan using MassLynx software 4.1 (Waters Corp.). Structural characterization of the phenolic compounds, especially flavonoids, was based on an earlier published method.[11]

Quantification was done using a Thermo Dionex Ultimate 3000 U(H)PLC (ThermoScientific, Landsmeer, The Netherlands) equipped with a diode array detector at 280 and 330 nm using authentic standards. Column specifications as well as gradient elution are the same as described above. The content of flavonoid glycosides was quantified using their aglycone equivalents, kaempferol for kaempferol glycosides and quercetin for quercetin glycosides, whereas phenolic acids were quantified using authentic standards. Table 2 shows the R^2 values, limits of detection (LOD), and limits of quantification (LOQ) of the standards used. LOD and LOD were calculated using the equations

Table 2. Standards Used for the Quantification of Phenolics

	slope	intercept	R^2	LOD (ppm)	LOQ (ppm)
kaempferol	0.91	0.85	0.98	3.83	12.77
quercetin	0.96	−0.24	0.99	1.51	5.03
caffeic acid	2.20	0.76	0.99	0.85	2.82
coumaric acid	4.50	1.12	0.99	0.57	1.91
ferulic acid	2.36	0.35	0.99	0.33	1.09
synapic acid	0.65	0.28	0.99	0.83	2.77

$$\text{LOD} = 3\left(\frac{Sbl}{S}\right) \text{ and } \text{LOQ} = 10\left(\frac{Sbl}{S}\right) \quad (1)$$

where Sbl is the standard error of the intercept and S is the slope of the respective calibration curves as calculated using the LINEST function.

Statistical Analysis. Data were analyzed using one-way ANOVA using SPSS v.21 (IBM, Chicago, IL, USA). Differences were considered significant when $p < 0.05$. Differences between means (posthoc) were determined using the Tukey test.

RESULTS AND DISCUSSION

Figure 1 shows the TPC of the cauliflower waste after conventional extraction (EP), the residue following alkaline hydrolysis (60 °C, 2 M NaOH for 30 min), sonicated extraction, and sonicated alkaline hydrolysis. The TPC of the EP fraction was 6.1 ± 0.05 mg GAE/g dry waste. However, as shown, the residue left after conventional solvent extraction of the cauliflower waste contained a considerable amount of phenolics, which the current literature may have missed, regardless of the method employed. Sonication alone of the residue yielded the lowest TPC (1.5 ± 0.12 mg GAE/g dry waste). Alkaline hydrolysis, on the other hand, released significantly higher amounts of phenolics from the plant matrix (6.5 ± 0.27 mg GAE/g dry waste). However, this content is ever more significantly ($p < 0.05$) increased by the combination of sonication and alkaline hydrolysis (7.3 ± 0.17 mg GAE/g dry waste). The amount of NEP therefore comprises more than half of the total phenolic content, meaning that NEP is actually more than EP in terms of content.

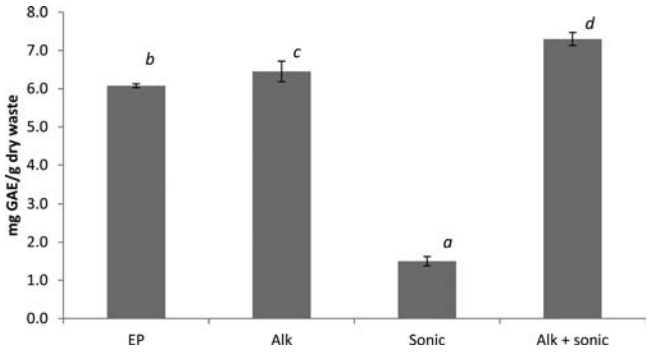

Figure 1. Total phenolic content of cauliflower waste (mg GAE/g dry waste) following conventional solvent extraction (EP), alkaline hydrolysis (Alk), sonicated extraction (Sonic), and sonicated alkaline hydrolysis (Alk+sonic). Different letters above bars indicate statistical difference ($p < 0.05$).

The results reveal that alkaline hydrolysis may not necessarily liberate all bound phenolic compounds in a short time span. Increasing the incubation time, however, may induce oxidation and loss of target compounds. Therefore, other techniques to increase yield without increasing temperature and incubation time are necessary.[7] In this study, it was shown that using ultrasonication along with alkaline hydrolysis serves as an effective method in increasing the yield of nonextractable phenolics. Ultrasonication, as earlier mentioned, damages the plant matrix, which increases the surface area of the sample. This probably allows the sodium hydroxide to react more efficiently in the matrix to break ester linkages and release the phenolic compounds. Although the use of sonication has been described as an effective method of extracting cellular content to liberate phenolics from various plant matrices,[17−19] its ability to break linkages that attach phenolics from other macromolecules has not been well described in the literature. Therefore, combining sonication and alkaline hydrolysis seems to be a logical method. It must be considered that ultrasonication causes an increase in temperature due to the shear forces generated. Therefore, the sonication was performed in a temperature-controlled sonic bath, and the temperature was manually adjusted whenever necessary. Because sonicated alkaline hydrolysis yielded higher TPC, the effects of temperature, NaOH concentration, and sonication time were investigated.

Figure 2 shows the 3D plot of the TPC as affected by time, NaOH concentration, and temperature. The ANOVA statistics are shown in Table 3. Accordingly, there are significant differences among treatments and also significant interactions among the different parameters, except for the interaction between NaOH concentration and sonication time. A significant interaction is noted when temperature is considered, which denotes the importance of this parameter. Looking at the

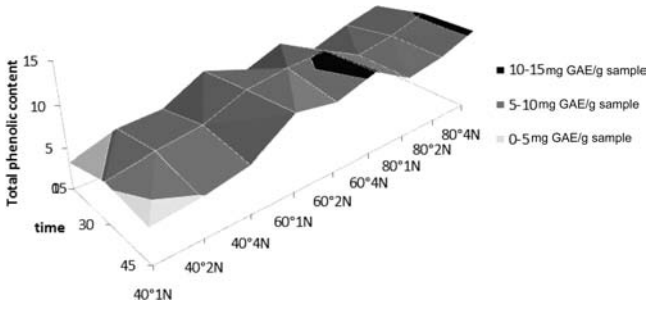

Figure 2. Optimization of sonicated alkaline hydrolysis treatment of residue after conventional solvent extraction.

dx.doi.org/10.1021/jf500835q | J. Agric. Food Chem. 2014, 62, 3371−3376

Table 3. Analysis of Variance for Total Phenolic Content under Sonicated Alkaline Hydrolysis Extraction

source	df	*F*	signif
temp	2	313.38	<0.001
M	2	60.698	<0.001
min	2	53.908	<0.001
temp × M	4	10.443	<0.001
temp × min	4	3.966	<0.001
M × min	4	0.993	0.420
temp × M × min	8	2.391	0.028

effect of temperature alone, it was observed that TPCs at 60 and 80 °C are not significantly different from each other, but are both significantly higher than at 40 °C. With regard to process efficiency, 60 °C is preferred over 80 °C. Also, it was observed that at 60 °C, TPCs of 30 and 45 min of sonication were similar and are significantly higher than at 15 min. Finally, TPCs of 2 and 4 M were similar and are both significantly higher than at 1 M NaOH concentration. Therefore, the optimal conditions for the release of NEP from cauliflower waste were 60 °C and 2 M NaOH for 30 min under sonication. In the end, the TPC of the NEP solution was found to be 9.82 ± 0.82 mg GAE/g dry residue or around 7.3 mg GAE/g dry waste sample. With TPC of the EP fraction added, the waste material therefore contained 13.4 mg GAE/g dry waste, of which around 45% is extractable and 55% is nonextractable.

To gain a better understanding on the nonextractable phenolics from cauliflower waste, the extract after sonicated alkaline hydrolysis was passed through a C18 SPE column to remove the salts and prepare it for U(H)PLC analysis and phenolic content identification using a mass spectrometer. Figure 3 shows the U(H)PLC-DAD of the cauliflower waste

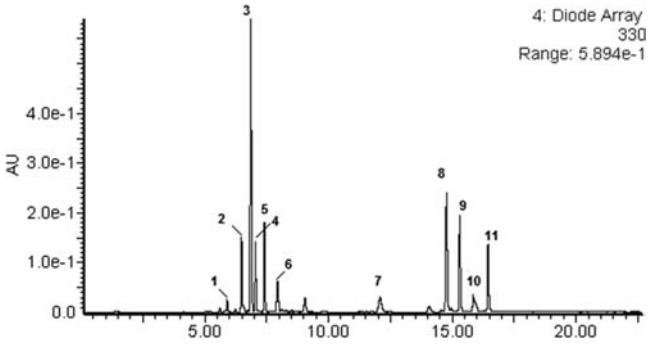

Figure 3. U(H)PLC-DAD chromatogram of cauliflower waste nonextractable phenolics (see Table 4 for peak identities).

NEP solution. Structural characterization and MS characteristics of flavonoid glycosides were described in a previous experiment on the EP fraction.[11] The occurrence of similar compounds in the NEP solution was detected by comparing their masses and retention times after LC-ESI and LC-DAD analysis. Table 4 shows the list of phenolics identified in the NEP solution as well as their content.

As shown, NEP is composed dominantly by flavonoid glycosides that are also found in the EP fraction. Kaempferol-3-*O*-diglucoside-7-*O*-glucoside is the most abundant flavonoid present in the NEP fraction (2.4 ± 0.1 mg/g dry waste), whereas sinapic acid (1.1 ± 0.0 mg/g dry waste) was the most abundant phenolic acid. It should be noted, however, that because the process involved alkaline hydrolysis, the analysis is limited to the fact that acylated flavonoid glycosides may also be present in the NEP fraction but cannot be determined. This is because alkaline hydrolysis also cleaves the ester linkage between the phenolic acid and the flavonoid glycoside.[12] Also, because phenolic acid glucosides are linked via an ester linkage, which is also degraded in alkaline conditions,[22] the occurrence of glucosidic forms of phenolic acids cannot be seen. Therefore, although phenolic acids and flavonoid glycosides may be isolated from the NEP fraction, the fact that they may actually come from the same parent molecule, for example, kaempferol-feruloyl-glycoside, or the occurrence of phenolic acid glucosides, such as feruloyl-glucoside, cannot be determined with this current method.

The high amounts of phenolic acids found in the NEP fraction are in agreement with previously reported data on the edible parts of *Brassica* species, wherein a marked increase in yield of phenolic acids was found after alkaline hydrolysis of residue left after conventional solvent extraction.[14,15,23,24] Indeed, phenolic acids are able to bind to macromolecules, such as fibers and other oligosaccharides, which hamper their extractability using conventional solvent extraction methods.

To investigate the distribution of these phenolic compounds within the waste stream, the waste was divided into blade, which constitutes the green leafy part, and petiole, which constitutes the major vein of the leaf. As shown in Table 5, the blades contain significantly higher amounts of phenolics than the petioles. Furthermore, the phenolic compositions of blades and petioles are found to be somewhat different. Greater variety and higher amounts of flavonoid glucosides and phenolic acids were extracted from the blade part than from the petiole. However, there seems to be a higher ratio of nonextractable phenolic acids in the petioles (relative to phenolic content) than in the blades. The most abundant phenolic compound from the blade is kaempferol-3-*O*-diglucoside-7-*O*-glucoside (4.51 ± 0.0 mg/g dry blade powder), whereas sinapic acid (0.29 ± 0.0 mg/g dry petiole powder) dominated the nonextractable phenolic content of the petioles. In total, 74% of the phenolic composition of the blades is composed of flavonoid glucosides. Conversely, most of the nonextractable phenolics in the petioles are phenolic acids, especially sinapic and ferulic acids, which comprised 57% of the phenolic content. This distribution could be due to the fact that phenolic acids are generally found to be bound to fibers and cell walls,[14] which are higher in the petioles than in the leaves. Whereas the linkage of phenolic acids in cell wall components has been largely observed, especially in *Brassica* species,[14,23,24] little is known about nonextractable flavonoids. Bound flavonoids have been characterized from pepper,[25] *Euphorbia*,[26] and other plants. An in-depth study on the tissue distribution of flavonoids in *Ligustrum vulgare* revealed that flavonoids, such as kaempferol and quercetin glucosides, are attached to lipid bilayers or noncovalently bound to proteins in the leaves.[27] Therefore, considering that studies of bound phenolics from *Brassica* have been done by first isolating the cell walls, information regarding flavonoids bound to membrane and membrane proteins may have been missed.

In conclusion, although no new compounds were found compared to the extractable fraction, the study showed that there are higher amounts of valuable health-promoting compounds from cauliflower waste than what is currently described in the literature. Results of this study may help food engineers and agriculturists devise methods for the scale-up extraction of these compounds for use in the agri-food industry.

Table 4. Phenolic Profile of Nonextractable Phenolics from Cauliflower Waste

peak	identity	rt (min)	m/z values MS	m/z values MS^E	λ_{max} (nm)	content[a] (μg/g dry waste)
1	quercetin-3-*O*-diglucoside-7-*O*-glucoside	6.04	787.1895	787, 625, 462, 300	254, 348	94 ± 0
2	kaempferol-3-*O*-triglucoside-7-*O*-glucoside	6.7	933.3650	933, 771, 446, 284	265, 348	520 ± 28
3	kaempferol-3-*O*-diglucoside-7-*O*-glucoside	6.9	771.2859	771, 609, 285	265, 346	2485 ± 166
4	kaempferol-3-*O*-triglucoside-7-*O*-diglucoside	7.08	1095.343	1095, 771, 609, 284	268 331	429 ± 16
5	kaempferol-3-*O*-diglucoside-7-*O*-diglucoside	7.45	933.3425	933, 609, 285	265, 345	550 ± 21
6	caffeic acid	7.96	179.0562	179, 135	216, 323	24 ± 4
7	coumaric acid	12.25	163.0603	163, 119	218, 309	39 ± 2
8	ferulic acid	14.97	193.0848	193, 134	223, 323	451 ± 19
9	sinapic acid	15.52	223.0974	223, 208	222 323	1071 ± 45
10	kaempferol-3-*O*-triglucoside	15.90	771.1885	771, 284	267, 346	134 ± 17
11	kaempferol-3-*O*-diglucoside	16.60	609.1251	609, 284	265, 346	479 ± 35

[a]Content of individual phenolics was based on calibration curve of their respective aglycone equivalent expressed as μg phenolic/g dry waste.

Table 5. Distribution Nonextractable Phenolics in the Cauliflower Waste

compound	content[a] blade	content[a] petiole
total phenolic content (TPC)	6109 ± 1045[b]	940 ± 16c
quercetin-3-*O*-diglucoside-7-*O*-glucoside	123 ± 5	54 ± 3
kaempferol-3-*O*-triglucoside-7-*O*-glucoside	1160 ± 23	nd[b]
kaempferol-3-*O*-diglucoside-7-*O*-glucoside	4513 ± 45	98 ± 10
kaempferol-3-*O*-triglucoside-7-*O*-diglucoside	1036 ± 20	69 ± 6
kaempferol-3-*O*-diglucoside-7-*O*-diglucoside	786 ± 14	18 ± 5
caffeic acid	37 ± 2	nd
coumaric acid	6.6 ± 0	nd
ferulic acid	720 ± 10	45 ± 18
sinapic acid	2266 ± 34	279 ± 38
kaempferol-3-*O*-triglucoside	267 ± 11	nd
kaempferol-3-*O*-diglucoside	591 ± 25	nd
total flavonoid glucosides	8478 ± 79	240 ± 23
total phenolic acids	3030 ± 43	324 ± 55

[a]Total phenolic content expressed as μg GAE/g dry waste; content of individual phenolics was based on calibration curve of their respective aglycone equivalent expressed as μg phenolic/g dry blade or petiole. Different letters of the TPC indicate statistical difference ($p < 0.01$). [b]nd, not detected.

AUTHOR INFORMATION

Corresponding Author

*(J.V.C.) E-mail: john.vancamp@ugent.be. Phone: +32-(0)9 264 62 08.

Funding

We thank the Special Research Fund (BOF) of Ghent University and the Hercules Project (AUGE028 and AUGE014) for financial support.

Notes

The authors declare no competing financial interest.

ACKNOWLEDGMENTS

Special thanks go to Sofie Coelus, Hanne Vanhoutte, and Geert Goeminne for their contributions in the execution of this work.

ABBREVIATIONS USED

GAE, gallic acid equivalents; U(H)PLC, ultra(high)-pressure liquid chromatography; MS, mass spectrometry; NEP, nonextractable phenolics; ESI, electrospray ionization; DAD, diode array detector; TPC, total phenolic content

REFERENCES

(1) Saura-Calixto, F. Concept and health-related properties of nonextractable polyphenols: the missing dietary polyphenols. *J. Agric. Food Chem.* **2012**, *60*, 11195−11200.

(2) Arranz, S.; Saura-Calixto, F.; Shaha, S.; Kroon, P. A. High contents of nonextractable polyphenols in fruits suggest that polyphenol contents of plant foods have been underestimated. *J. Agric. Food Chem.* **2009**, *57*, 7298−7303.

(3) Perez-Jimenez, J.; Saura-Calixto, F. Literature data may underestimate the actual antioxidant capacity of cereals. *J. Agric. Food Chem.* **2005**, *53*, 5036−5040.

(4) Pérez-Jiménez, J.; Torres, J. L. Analysis of nonextractable phenolic compounds in foods: the current state of the art. *J. Agric. Food Chem.* **2011**, *59*, 12713−12724.

(5) Arranz, S.; Silván, J. M.; Saura-Calixto, F. Nonextractable polyphenols, usually ignored, are the major part of dietary polyphenols: a study on the Spanish diet. *Mol. Nutr. Food Res.* **2010**, *54*, 1646−1658.

(6) Bonoli, M.; Verardo, V.; Marconi, E.; Caboni, M. F. Antioxidant phenols in barley (*Hordeum vulgare* L.) flour: comparative spectrophotometric study among extraction methods of free and bound phenolic compounds. *J. Agric. Food Chem.* **2004**, *52*, 5195−5200.

(7) White, B. L.; Howard, L. R.; Prior, R. L. Release of bound procyanidins from cranberry pomace by alkaline hydrolysis. *J. Agric. Food Chem.* **2010**, *58*, 7572−7579.

(8) Albishi, T.; John, J. A.; Al-Khalifa, A. S.; Shahidi, F. Phenolic content and antioxidant activities of selected potato varieties and their processing by-products. *J. Funct. Foods* **2013**, *5*, 590−600.

(9) Tow, W. W.; Premier, R.; Jing, H.; Ajlouni, S. Antioxidant and antiproliferation effects of extractable and nonextractable polyphenols isolated from apple waste using different extraction methods. *J. Food Sci.* **2011**, *76*, T163−T172.

(10) Cartea, M. E.; Francisco, M.; Soengas, P.; Velasco, P. Phenolic compounds in *Brassica* vegetables. *Molecules* **2010**, *16*, 251−280.

(11) Gonzales, G. B.; Raes, K.; Coelus, S.; Struijs, K.; Smagghe, G.; Van Camp, J. Ultra(high)-pressure liquid chromatography-electrospray ionization-time-of-flight-ion mobility-high definition mass spectrometry for the rapid identification and structural characterization of flavonoid glycosides from cauliflower waste. *J. Chromatogr., A* **2014**, *1323*, 39−48.

(12) Llorach, R.; Gil-Izquierdo, A.; Ferreres, F.; Tomás-Barberán, F. A. HPLC-DAD-MS/MS ESI characterization of unusual highly glycosylated acylated flavonoids from cauliflower (*Brassica oleracea* L. var. *botrytis*) agroindustrial byproducts. *J. Agric. Food Chem.* **2003**, *51*, 3895−3899.

(13) Llorach, R.; Espín, J. C.; Tomás-Barberán, F. A.; Ferreres, F. Valorization of cauliflower (*Brassica oleracea* L. var. *botrytis*) by-products as a source of antioxidant phenolics. *J. Agric. Food Chem.* **2003**, *51*, 2181−2187.
(14) Harbaum, B.; Hubbermann, E. M.; Zhu, Z.; Schwarz, K. Free and bound phenolic compounds in leaves of pak choi (*Brassica campestris* L. ssp. *chinensis* var. *communis*) and Chinese leaf mustard (*Brassica juncea* Coss). *Food Chem.* **2008**, *110*, 838−846.
(15) Frolov, A.; Henning, A.; Böttcher, C.; Tissier, A.; Strack, D. An UPLC-MS/MS method for the simultaneous identification and quantitation of cell wall phenolics in *Brassica napus* seeds. *J. Agric. Food Chem.* **2012**, *61*, 1219−1227.
(16) Kuo, C.-H.; Chen, B.-Y.; Liu, Y.-C.; Chang, C.-M.; Deng, T.-S.; Chen, J.-H.; Shieh, C.-J. Optimized ultrasound-assisted extraction of phenolic compounds from *Polygonum cuspidatum*. *Molecules* **2013**, *19*, 67−77.
(17) Muñiz-Márquez, D. B.; Martínez-Ávila, G. C.; Wong-Paz, J. E.; Belmares-Cerda, R.; Rodríguez-Herrera, R.; Aguilar, C. N. Ultrasound-assisted extraction of phenolic compounds from *Laurus nobilis* L. and their antioxidant activity. *Ultrason. Sonochem.* **2013**, *20*, 1149−1154.
(18) Izadifar, Z. Ultrasound pretreatment of wheat dried distiller's grain (DDG) for extraction of phenolic compounds. *Ultrason. Sonochem.* **2013**, *20*, 1359−1369.
(19) Golmohamadi, A.; Möller, G.; Powers, J.; Nindo, C. Effect of ultrasound frequency on antioxidant activity, total phenolic and anthocyanin content of red raspberry puree. *Ultrason. Sonochem.* **2013**, *20*, 1316−1323.
(20) Horžić, D.; Jambrak, A.; Belščak-Cvitanović, A.; Komes, D.; Lelas, V. Comparison of conventional and ultrasound assisted extraction techniques of yellow tea and bioactive composition of obtained extracts. *Food Bioprocess. Technol.* **2012**, *5*, 2858−2870.
(21) Singleton, V. L.; Orthofer, R.; Lamuela-Raventos, R. M. Analysis of total phenols and other oxidation substrates and antioxidants by means of Folin-Ciocalteu reagent. In *Oxidants and Antioxidants, Part A*; Packer, L., Ed.; Elsevier Academic Press: San Diego, CA, USA, 1999; Vol. 299, pp 152−178.
(22) Mattila, P.; Hellström, J. Phenolic acids in potatoes, vegetables, and some of their products. *J. Food Compos. Anal.* **2007**, *20*, 152−160.
(23) Ayaz, F. A.; Hayırlıoglu-Ayaz, S.; Alpay-Karaoglu, S.; Grúz, J.; Valentová, K.; Ulrichová, J.; Strnad, M. Phenolic acid contents of kale (*Brassica oleraceae* L. var. *acephala* DC.) extracts and their antioxidant and antibacterial activities. *Food Chem.* **2008**, *107*, 19−25.
(24) Liu, Q.; Wu, L.; Pu, H.; Li, C.; Hu, Q. Profile and distribution of soluble and insoluble phenolics in Chinese rapeseed (*Brassica napus*). *Food Chem.* **2012**, *135*, 616−622.
(25) Lee, Y.; Howard, L. R.; Villalón, B. Flavonoids and antioxidant activity of fresh pepper (*Capsicum annuum*) cultivars. *J. Food Sci.* **1995**, *60*, 473−476.
(26) Singh, G.; Kumar, P. Phytochemical study and screening for antimicrobial activity of flavonoids of *Euphorbia hirta*. *Int. J. Appl. Basic Med. Res.* **2013**, *3*, 111−116.
(27) Agati, G.; Stefano, G.; Biricolti, S.; Tattini, M. Mesophyll distribution of 'antioxidant' flavonoid glycosides in Ligustrum vulgare leaves under contrasting sunlight irradiance. *Ann. Bot.* **2009**, *104*, 853−861.

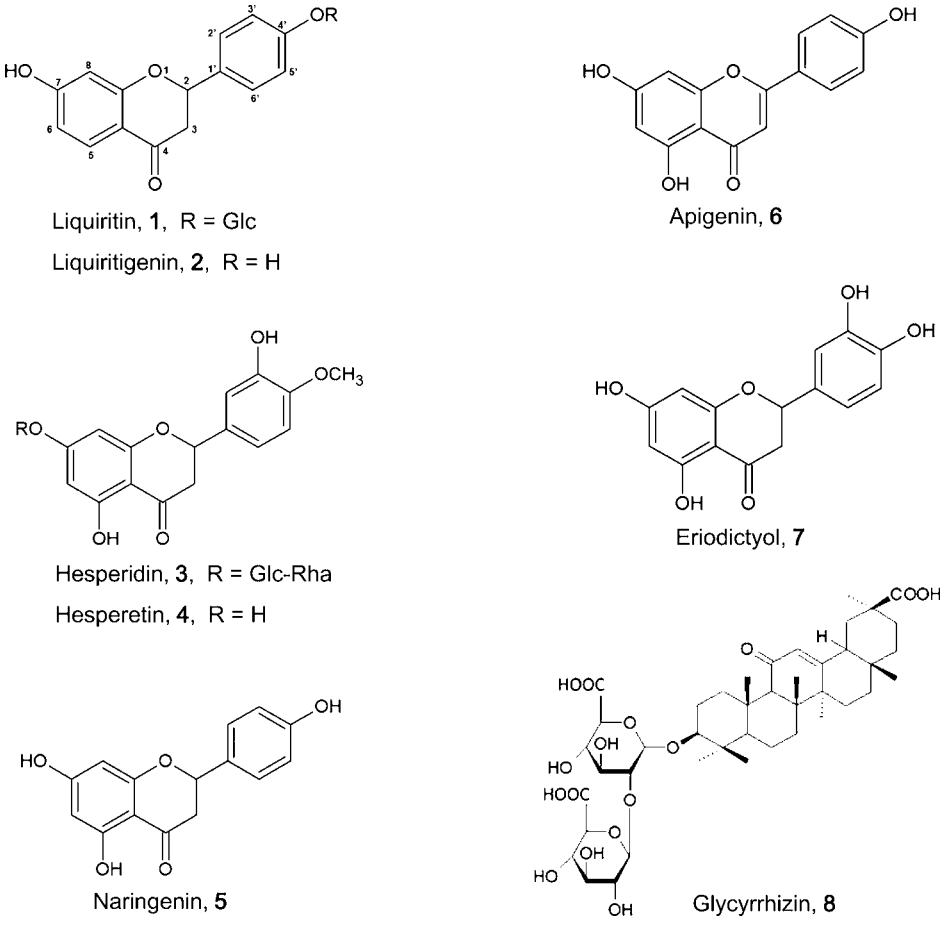

Figure 1. Structures of liquiritin, glycyrrhizin, and structurally related compounds.

supplements were purchased from a commercial market in Japan. Freund's complete and incomplete adjuvants, polyethylene glycol (PEG), and horseradish peroxidase (HRP)-labeled anti-mouse IgG (Fc specific) were obtained from Sigma (Steinheim, Germany). All other chemicals were standard commercial products of analytical grade.

Preparation of the Sample and Standard Solutions. Dried licorice root powder (100 mg) was extracted six times with 1.2 mL of methanol (MeOH) containing 0.1% NH_4OH with sonication for 20 min and centrifugation at 9000*g* for 2 min. The combined supernatant was evaporated with N_2 gas, and the residue was dissolved in 1.0 mL of MeOH containing 0.1% NH_4OH. The prepared extract solution was filtered using a 0.45 μm Cosmonice W filter unit (Nacalai Tesque, Kyoto, Japan) and was used as the sample solution. Solid licorice products such as candies and food supplements were dissolved in 10 mL of H_2O and then lyophilized. Freeze-dried licorice powder (200 mg) was extracted six times with 2.0 mL of MeOH containing 0.1% NH_4OH. The rest of the freeze-dried licorice powder procedure was the same as that followed for the dried licorice root powder. ELISA was used to analyze liquid samples such as beverages, beer, and soy sauce without any pretreatments.

Liquiritin was accurately weighed and dissolved in MeOH to prepare a 5 mg/mL stock solution. Several concentrations of liquiritin standard solutions were prepared by the serial dilution method (0.10, 0.20, 0.39, 0.78, 1.56, 3.13, 6.25, 12.5, 25, 50, and 100 μg/mL as liquiritin standard) using 20% MeOH. These samples and standard solutions were used for ELISA analysis.

Synthesis of Antigen–Carrier Protein Conjugates. Liquiritin–carrier protein conjugates were synthesized using a model based on the periodate oxidation method.[21] Liquiritin (5.0 mg) was dissolved in 0.4 mL of MeOH, and the solution was added dropwise to a sodium periodate (5.0 mg)/H_2O (0.4 mL) solution. Next, the mixture was stirred at room temperature for 30 min. After the oxidative reaction, KLH (5.0 mg) was added to 50 mM carbonate buffer (0.8 mL; pH 9.6) and was stirred at room temperature for 6 h. The oxidation reaction mixture was dialyzed against H_2O at 4 °C for 2 days and then lyophilized. Mice were then immunized with the liquiritin–KLH conjugate (3.6 mg), whereas the liquiritin–HSA conjugate (7.5 mg), which was prepared using the same method as for the liquiritin–KLH conjugate, was used for ELISA.

Analysis of the Liquiritin–Carrier Protein Conjugate by Matrix-Assisted Laser Desorption/Ionization Time-of-Flight Mass Spectrometry (MALDI-TOF MS). A previous study described how the hapten liquiritin–HSA conjugate was determined by MALDI-TOF.[26] Liquiritin–HSA conjugate (1–10 pmol) was mixed with a 10^3-fold molar excess of sinapinic acid in an aqueous solution containing 0.15% (v/v) trifluoroacetic acid. The mixture was subjected to a JEOL mass spectrometer (JMS) time-of-flight (TOF) mass monitor and irradiated with an N_2 laser (337 nm, 150 ns plus). The ion formed by each pulse was accelerated by a 20 kV potential into a 2.0 m evacuated tube.

Immunization, Hybridization, and Purification of mAb. All procedures and animal care were approved (approval no. 50) by the Committee on Ethics of Animal Experiments, Faculty of Pharmaceutical Sciences, Nagasaki International University; the procedures were conducted according to the Guidelines for Animal Experiments of the Faculty of Pharmaceutical Sciences, Nagasaki International University.

BALB/c male mice (6 weeks old) were intraperitoneally injected with the liquiritin–KLH solution four times. The first immunization was a 1:1 emulsion in Freund's complete adjuvant (0.5 mL, 50 μg of liquiritin–KLH). Two weeks later, a second immunization was repeated with the same amount of antigen, but the liquiritin–KLH solution was emulsified in Freund's incomplete adjuvant. After 2 weeks, a third immunization was administered, which consisted of

liquiritin–KLH (100 μg) dissolved in 0.5 mL of phosphate-buffered saline (PBS). The fourth and final immunization was repeated according to the method of the third immunization. Three days after the fourth immunization, immune splenocytes were exenterated and fused to a hypoxanthine–aminopterin–thymidine (HAT)-sensitive mouse myeloma cell line (SP2/0) using the PEG method. After HAT selection, the 2F8 hybridoma cell line secreting anti-liquiritin mAbs was cloned using a limited dilution method. The 2F8 hybridoma cell line was cultured at 37 °C under 5% CO_2 atmosphere in enriched RPMI1640–Dulbecco's–Ham's F12 medium containing 10% fetal bovine serum.

The mAbs that were prepared from the 2F8 hybridoma cell line were purified using a Protein G FF column (GE Healthcare UK Ltd., Amersham, UK). The cultured medium containing IgG (400 mL) was loaded into the column and was eluted with 100 mM citrate buffer (pH 2.7). The eluted IgG solution was adjusted to pH 7.0 with 1 M Tris-HCl buffer (pH 9.0) and then dialyzed against H_2O at 4 °C for 2 days. After lyophilization, anti-liquiritin mAb (7.52 mg) was obtained.

Direct ELISA. Liquiritin–HSA conjugate and other proteins (100 μL, 1 μg/mL) were dissolved in a 50 mM carbonate buffer (pH 9.6), loaded into a 96-well immunoplate, and incubated for 1 h. The plate was washed three times with PBS containing 0.05% Tween 20 (PBST). The plate was treated with 300 μL of PBS containing 5% skimmed milk (SPBS) for 1 h to reduce nonspecific reactions. After blocking, the plate was washed with PBST three times, and it was then reacted with 100 μL of anti-liquiritin mAb for 1 h. The plate was washed with PBST three times and incubated with 100 μL of a 1000-fold diluted HRP-labeled anti-mouse IgG solution for 1 h. After three washings of the plate with PBST, 100 μL of substrate solution of 0.1 M citrate buffer (pH 4.0) containing 0.003% (v/v) H_2O_2 and 0.3 mg/mL ABTS was added to each well and incubated for 20 min. The absorbance was measured with an Immuno Mini NJ-2300 microplate reader (Nalge Nunc, Roskilde, Denmark) at 405 nm. All reactions were conducted at 37 °C.

Competitive ELISA. Liquiritin–HSA (100 μL, 1 μg/mL) was dissolved in a 50 mM carbonate buffer (pH 9.6) and was loaded onto the 96-well immunoplate, which was then treated with 300 μL of SPBS to reduce nonspecific reactions. Fifty microliters of various liquiritin concentrations or samples dissolved in 20% MeOH solution were incubated with 50 μL of anti-liquiritin mAb solution (105.5 ng/mL) for 1 h. After three washings with PBST, the plate was then reacted with 100 μL of HRP-labeled anti-mouse IgG solution for 1 h. The plate was washed three times with PBST, and 100 μL of ABTS solution was added to each well and incubated for 20 min. Absorbance was recorded at 405 nm by a microplate reader. The glycyrrhizin contents in various foods containing licorice were determined by following a previously described method.[22]

Recovery Experiments. Various amounts of liquiritin standards (25, 50, and 100 μg) were spiked into dried licorice root powder (10 mg). Spiked samples were extracted six times with MeOH containing 0.1% NH_4OH under sonication, and the combined supernatant was evaporated with N_2 gas. The residue was dissolved in 1.0 mL of MeOH containing 0.1% NH_4OH and was filtered using a Cosmonice Filter W. The recovery experiment was performed by using a competitive ELISA.

The recovery of spiked liquiritin was calculated as follows:

$$\text{recovery (\%)} = \frac{\text{measured amount of liquiritin} - 298.07}{\text{spiked amount}} \times 100$$

The amount of liquiritin in the unspiked sample was determined to be 298.07 (μg) in dried licorice root powder (10 mg) by HPLC. For each level, three samples were analyzed.

Determination of Liquiritin Concentration by HPLC. Analytical HPLC was performed using the LC-8020 model III (Tosoh Co. Ltd., Tokyo, Japan). The column used was a 150 mm × 4.6 mm i.d., 3 μm, TSK gel ODS-100Z (Tosoh Co. Ltd.) at room temperature. The mobile phase was water/acetonitrile/acetic acid (82:18:1, by volume), and the flow rate was 0.7 mL/min. UV absorbance detection at 280 nm was used; in this case, the retention time of liquiritin was 14.6 min.

RESULTS AND DISCUSSION

Direct Determination of the Hapten–Carrier Protein Conjugate by MALDI-TOF MS Analysis. We evaluated the hapten number of liquiritin–HSA conjugate by MALDI-TOF MS analysis. A broad peak coinciding with the liquiritin–HSA conjugate was detected around m/z 68500 (data not shown). This result and the molecular weight of approximately 66400 for HSA revealed that the calculated value of the liquiritin component (MW = 418.4) was 4.83, indicating that at least four molecules of liquiritin were coupled with one molecule of HSA. Thus, the prepared liquiritin–HSA conjugate was suitable for use in ELISA by comparing these results to those of a previous study.[27]

The mAb was tested against liquiritin using a liquiritin–bovine serum albumin (BSA) conjugate as an immunogen. However, a suitable and specific mAb for liquiritin could not be obtained. Because the maximum molecular weight that can be detected by MALDI-TOF MS analysis is 260,000, determining the hapten liquiritin–KLH conjugate number using the MALDI-TOF MS system was impossible because the molecular weight of KLH is about 800,000. Thus, the liquiritin–KLH conjugate was prepared using the same procedure as for the liquiritin–HSA conjugate and was used as an immunogen for the anti-liquiritin mAb production without determination of the hapten liquiritin–KLH conjugate number.

Production and Characterization of Anti-liquiritin mAb. The immune splenocytes were fused with SP2/0 myeloma cells by using an established procedure in this laboratory. The 2F8 hybridoma cell line that produced mAb reactive to liquiritin was obtained and classified as IgG2a, which has a κ light chain.

The reactivity of anti-liquiritin mAbs was tested against the liquiritin–HSA conjugate and various proteins such as HSA, BSA, ovalbumin (OVA), and KLH with various anti-liquiritin mAb concentrations (Figure 2). Anti-liquiritin mAb did not recognize the HSA, BSA, OVA, and KLH carrier proteins; however, it specifically recognized the liquiritin portions in the liquiritin–HSA conjugate molecule. Furthermore, the absorbance, which was approximately 1.0, was obtained under the

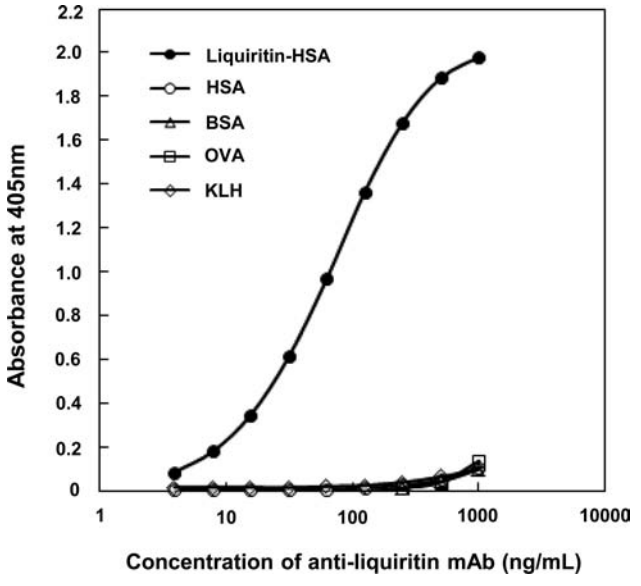

Figure 2. Reactivity of anti-liquiritin mAb against liquiritin–HSA conjugate and various proteins.

dx.doi.org/10.1021/jf404731z | J. Agric. Food Chem. 2014, 62, 3377–3383

antibody concentration (105.5 ng/mL) selected for competitive ELISA.

Assay Sensitivity and Specificity. The assay sensitivity was validated by using anti-liquiritin mAb with competitive ELISA. After incubation of anti-liquiritin mAb with competing liquiritin antigens, any mAb binding free liquiritin was washed out from the ELISA plate. The mAb binding to the liquiritin−HSA conjugate was bound to an enzyme-labeled secondary antibody and reacted to the substrate solution. Under these conditions, the full measuring range of the assay extended from 0.39 to 25 μg/mL (0.93−59.75 μM), as indicated in Figure 3.

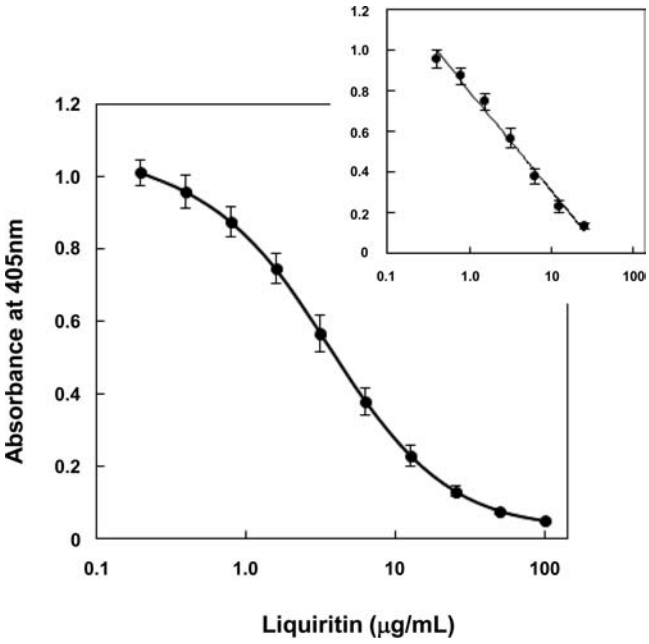

Figure 3. Calibration curve of liquiritin using anti-liquiritin mAb by competitive ELISA.

The cross-reactivities (CRs) of the anti-liquiritin mAb against the structurally related compounds were checked for the evaluation of assay specificity using competitive ELISA. The CRs were calculated and indicated as IC_{50} (μM).

$$IC_{50}\ (\mu M) = \text{concn}\ (\mu M)\ \text{of liquiritin or various structurally related compds yielding}\ A/A_0 = 50\%$$

A is the absorbance in the presence of the test compound, and A_0 is the absorbance in the absence of the test compound.

As indicated in Table 1, the mAb showed that the CRs against hesperetin (IC_{50} = 17.83 μM), liquiritigenin (IC_{50} = 33.09 μM), and naringenin (IC_{50} = 79.41 μM) have a flavanone molecular skeleton (Figure 1). On the other hand, flavones such as flavonols, flavanone, flavanols, isoflavonoids, flavonoid glycosides, and other tested compounds were not recognized by the anti-liquiritin mAb (Table 1). Thus, the hypothesis that the mAb simultaneously recognized the hydroxyl group at the C7 position and the hydrogen at C2 position as essential functions (Figure 1) was formulated.

The anti-liquiritin mAb that was obtained was comparatively recognized by liquiritigenin, and the ELISA that used the anti-liquiritin mAb performed in a linear range from 1.56 to 50 μg/mL (6.09−195.12 μM) for liquiritigenin (date not shown). Thus, the CR against liquiritigenin may have been an unexpected advantage from this experiment because an ELISA can now be developed for aglycone liquiritigenin using the anti-liquiritin mAb. A previous study developed an ELISA system for the aglycone of baicalin, baicalein, using anti-baicalin mAb, which had lower CRs against baicalein.[28]

Table 1. Cross-Reactivities of Anti-liquiritin mAb against Various Compounds

compound	classification	IC_{50} (μM)
liquiritin	flavanone glycoside	8.60
liquiritigenin	flavanone	33.09
hesperetin	flavonoid glycoside	17.83
hesperidin	flavanone	>100
(±)-naringenin	flavanone	79.41
(±)-eriodictyol	flavanone	>100
apigenin	flavone	>100
luteolin	flavone	>100
myricetin	flavonol	>100
quercetin	flavonol	>100
fisetin	flavonol	>100
kaempferol	flavonol	>100
isorhamnetin	flavonol	>100
(−)-epigallocatechin	flavanol	>100
(−)-epicatechin	flavanol	>100
daidzein	isoflavonoid	>100
rutin	flavonoid glycoside	>100
glycyrrhizin	triterpenoid	>100
3-monoglucuronyl-glycyrrhetic acid	triterpenoid	>100
glycyrrhetic acid	triterpenoid	>100
saikosaponin a	triterpenoid	>100
ginsenoside Rb1	triterpenoid	>100
peaoniflorin	monoterpenoid	>100

Assay Variation. The intra-assay (well-to-well) and inter-assay (plate-to-plate) variations were measured with a competitive ELISA because reproducibility and precision are important criteria for an immunoassay. The maximum relative standard deviations (RSDs) of intra-assay and interassay were 4.08 and 5.46%, respectively (Table 2). These results showed that competitive ELISA was accurate and precise for liquiritin.

Table 2. Validations among ELISA Runs for the Analysis of Liquiritin

	CV[a] (%)	
liquiritin (μg/mL)	intra-assay	interassay
0	0.60	3.49
0.39	1.81	1.25
0.78	4.08	1.23
1.56	2.71	3.29
3.13	1.73	4.29
6.25	0.95	3.20
12.50	1.12	5.22
25.00	0.62	5.46

[a]Data are mean ± SD for three replicate wells and three plates for each concentration within one plate from three consecutive days.

Recovery of Liquiritin by Competitive ELISA in Spiked Samples. The recovery experiment confirmed the accuracy of this assay system. Various amounts of liquiritin (25−100 μg) were added to the dried powder licorice root, and the amount of liquiritin was measured by competitive ELISA. The recovery was calculated, and the rates were between 100.9 and 103.7% with low RSD values (0.10−4.02%) as indicated in Table 3.

These results show that an ELISA using the anti-liquiritin mAb can be routinely used for phytochemical investigations involving crude plant extracts.

Table 3. Recovery of Liquiritin Determined by ELISA in Spiked Samples

spiked level (μg)	measured amount[a] (μg)	RSD[b] (%)	recovery[c] (%)
25	323.71 ± 0.31	0.10	102.6
50	348.50 ± 14.00	4.02	100.9
100	401.75 ± 14.12	3.51	103.7

[a]Data are mean ± SD from triplicate analyses for each sample. [b]Relative standard deviation. [c]Recovery (%) = (measured amount − 298.07)/spiked amount × 100.

Correlation of Liquiritin Contents in Licorice Roots Determined by ELISA and HPLC. To confirm the correlation results of liquiritin determination between ELISA and HPLC, the contents of liquiritin in various licorice roots using ELISA and HPLC were also analyzed. The concentrations of liquiritin, as determined by ELISA, were 0.95 ± 0.03, 3.11 ± 0.08, 1.34 ± 0.01, 0.17 ± 0.01, 0.78 ± 0.04, and 2.12 ± 0.08 g/kg dry weight root for samples 1, 2, 3, 4, 5, and 6, respectively. These values and HPLC liquiritin concentrations (concentrations were 0.92 ± 0.01, 3.02 ± 0.10, 1.39 ± 0.06, 0.20 ± 0.01, 0.94 ± 0.02, and 2.73 ± 0.01 g/kg dry weight root for samples 1, 2, 3, 4, 5, and 6, respectively) were similar. The correlation coefficient (R^2) between the analytical value of liquiritin from the ELISA and that from HPLC was 0.948 (Figure 4). This high correlation

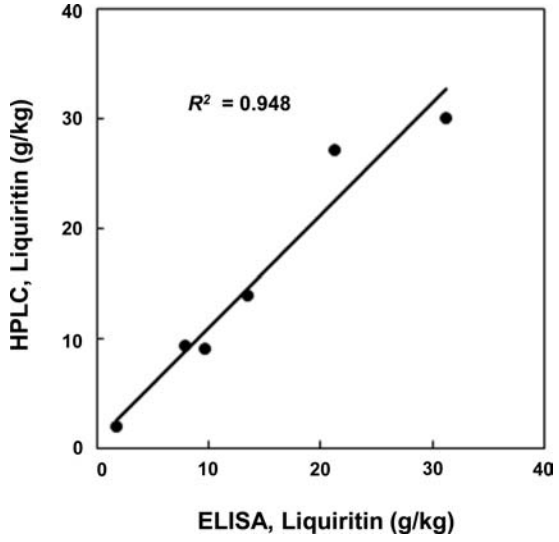

Figure 4. Correlative relationship of liquiritin contents in various licorice roots between the ELISA and HPLC.

indicates that the developed ELISA system could be useful in determining liquiritin in licorice crude extracts without any complicated pretreatments and without the influence of liquiritigenin on this assay system. Furthermore, competitive ELISA was at least 20 times more sensitive for liquiritin than compared with HPLC under the study conditions.

Determination of Liquiritin and Glycyrrhizin in Various Licorice Products for Quality Control Demonstrated by ELISA. Table 4 shows the quantitative analysis results of ELISA for liquiritin and glycyrrhizin in licorice root (Japanese Pharmacopoeia grade) and various foods and drinks

Table 4. Liquiritin and Glycyrrhizin Contents in Various Licorice Products Determined by ELISA[a]

	contents (g/kg)		
sample	liquiritin	glycyrrhizin	glycyrrhizin/liquiritin[b]
licorice root (JP grade)	27.15 ± 2.22	46.03 ± 3.93	1.70
	contents (g/kg)		
solid sample	liquiritin	glycyrrhizin	glycyrrhizin/liquiritin[b]
food suppl 1	1.18 ± 0.07	6.24 ± 0.56	5.29
food suppl 2	1.67 ± 0.09	0.02 ± 0.00	0.01
candy	tr[c]	0.07 ± 0.00	
	contents (mg/L)		
liquid sample	liquiritin	glycyrrhizin	glycyrrhizin/liquiritin[b]
soy sauce 1	214.45 ± 14.60	93.55 ± 6.22	0.44
soy sauce 2	249.41 ± 7.96	24.94 ± 0.58	0.10
soy sauce 3	235.46 ± 4.46	166.22 ± 1.73	0.71
soy sauce 4	272.99 ± 9.43	71.37 ± 2.47	0.26
soy sauce 5	226.70 ± 3.13	128.00 ± 2.16	0.56
soy sauce 6	124.82 ± 8.02	96.12 ± 2.98	0.77
beverage 1	tr	1.31 ± 0.07	
beverage 2	0.30 ± 0.01	8.78 ± 0.09	29.27
beer	tr	1.06 ± 0.09	

[a]Data are mean ± SD from triplicate analyses for each sample. [b]Glycyrrhizin/liquiritin = glycyrrhizin contents/liquiritin contents. [c]tr, trace (LOD ≤ tr ≤ LOQ).

including licorice. In a previous study, HPLC was most frequently used for liquiritin and/or glycyrrhizin analysis in numerous licorice roots that were used in traditional Chinese/Korean medicine.[14−17,29] Previously, glycyrrhizin and flavonoid concentrations including liquiritin in *Glycyrrhiza* species were determined by HPLC,[30] and licorice roots were applied to the glycyrrhizin ELISA system for quality control.[22] The quality control using both liquiritin and glycyrrhizin ELISA systems was not reported; thus, in this study the quality control of the licorice products was demonstrated by ELISA systems using the anti-liquiritin mAb and anti-glycyrrhizin mAb, respectively.

The calculated glycyrrhizin/liquiritin rate varied from 0.01 to 29.27 in all licorice products except for candies, beverages, and beer, as indicated in Table 4. Japanese Pharmacopoeia (JP) grade licorice root had a glycyrrhizin/liquiritin value of 1.70 that was obtained by ELISA. The difference of the glycyrrhizin/liquiritin value may be caused by the quality of the licorice plants because the liquiritin and glycyrrhizin components fluctuated with collection year and cultivation environment.[31] Furthermore, different licorice processing techniques and various preparation methods of licorice products could have affected the amount of glycyrrhizin/liquiritin in the licorice. Therefore, determining the amount of liquiritin in the licorice plants and products was necessary for quality control just as glycyrrhizin analysis of the Japanese Pharmacopoeia was regulated and reported by previous studies.[19,23−25,32]

Because licorice is used worldwide as a natural sweetener for food, it is an important herbal plant.[1] Liquiritin is one of the major flavonoid glycosides in licorice and is employed as a quality control marker for licorice in foods and phytochemical products because it has a variety of pharmacological activities.[2−8] Various analytical methods that have used chromatography have been reported;[14−17,29] however, an antibody-based immunochemical assay system has not been established for liquiritin in licorice plants and products.

In this study, an established 2F8 hybridoma cell line secreted mAb reactive to liquiritin, and an ELISA system using anti-liquiritin mAb was developed. Validation of ELISA confirmed its sensitivity, reproducibility, and accuracy from various validation experiments, and a correlation coefficient (R^2) of 0.948 was obtained between the ELISA and HPLC methods. The newly established immunochemical approach compared with instrumental analysis such as HPLC uses less organic solvent and is a cleaner analytical system; thus, the new immunochemical approach is better for the environment. Furthermore, an advantage of the developed ELISA system is that it can be directly applied to impure samples such as crude extracts and licorice products because complicated pretreatments are not necessary for the new system. These results show that ELISA can be a simple, fast, and convenient high-throughput analysis for numerous licorice samples and may apply to a small amount of analytical target samples.

In conclusion, the ELISA that was established in this study is a very useful technique for samples with many impurities such as crude extracts from the licorice root and its final products including functional foods that contain several hundred components. Moreover, the ELISA system can be useful for analyzing liquiritin in the manner that glycyrrhizin was analyzed in phytochemical products and medicine. There have been no previous papers indicating an immunoassay system for liquiritin; thus, this is the first time that an immunoassay system for liquiritin has been developed.

AUTHOR INFORMATION

Corresponding Author

*(Y.S.) Phone: 81-956-20-5653. Fax: 81-956-20-5740. E-mail: shoyama@niu.ac.jp.

Funding

This research was supported by faculties of Health Management and Pharmaceutical Sciences, Nagasaki International University. This work was also supported in part by the Laboratory for Medicinal Plant Cultivation (Saga, Japan).

Notes

The authors declare no competing financial interest.

REFERENCES

(1) Isao, K. Licorice root. A natural sweetener and an important ingredient in Chinese medicine. *Pure Appl. Chem.* **2002**, *74*, 1189−1198.

(2) Kim, Y. M.; Kim, T. H.; Kim, Y. W.; Yang, Y. M.; Ryu da, H.; Hwang, S. J.; Lee, J. R.; Kim, S. C.; Kim, S. G. Inhibition of liver X receptor-α-dependent hepatic steatosis by isoliquiritigenin, a licorice antioxidant flavonoid, as mediated by JNK1 inhibition. *Free Radical Biol. Med.* **2010**, *49*, 1722−1734.

(3) Xie, Y. C.; Dong, X. W.; Wu, X. M.; Yan, X. F.; Xie, Q. M. Inhibitory effects of flavonoids extracted from licorice on lipopolysaccharide-induced acute pulmonary inflammation in mice. *Int. Immunopharmacol.* **2009**, *9*, 194−200.

(4) Zhu, L.; Wei, H.; Wu, Y.; Yang, S.; Xiao, L.; Zhang, J.; Peng, B. Licorice isoliquiritigenin suppresses RANKL-induced osteoclastogenesis in vitro and prevents inflammatory bone loss in vivo. *Int. J. Biochem. Cell Biol.* **2012**, *44*, 1139−1152.

(5) Liu, Y.; Xie, S.; Wang, Y.; Luo, K.; Wang, Y.; Cai, Y. Liquiritigenin inhibits tumor growth and vascularization in a mouse model of HeLa cells. *Molecules* **2012**, *17*, 7206−7216.

(6) Jayaprakasam, B.; Doddaga, S.; Wang, R.; Holmes, D.; Goldfarb, J.; Li, X. M. Licorice flavonoids inhibit eotaxin-1 secretion by human fetal lung fibroblasts in vitro. *J. Agric. Food Chem.* **2009**, *57*, 820−825.

(7) Sun, Y. X.; Tang, Y.; Wu, A. L.; Liu, T.; Dai, X. L.; Zheng, Q. S.; Wang, Z. B. Neuroprotective effect of liquiritin against focal cerebral ischemia/reperfusion in mice via its antioxidant and antiapoptosis properties. *J. Asian Nat. Prod. Res.* **2010**, *12*, 1051−1060.

(8) Chen, Z. A.; Wang, J. L.; Liu, R. T.; Ren, J. P.; Wen, L. Q.; Chen, X. J.; Bian, G. X. Liquiritin potentiate neurite outgrowth induced by nerve growth factor in PC12 cells. *Cytotechnology* **2009**, *60*, 125−132.

(9) Ohtsuki, K.; Ishida, N. Inhibitory effect of glycyrrhizin on polypeptide phosporylation by polypeptide-dependent protein kinase (Kinase P) invitro. *Biochem. Biophys. Res. Commun.* **1988**, *157*, 597−604.

(10) Doll, R.; Hill, I. D.; Hutton, C.; Underwood, D. L. Clinical trial of a triterpenoid liquorice compound in gastric and duodenal ulcer. *Lancet* **1962**, *2*, 793−796.

(11) Pompei, R.; Flore, O.; Marccialis, M. A.; Pani, A.; Loddo, B. Glycyrrhizic acid inhibits virus growth and inactivates virus particles. *Nature* **1979**, *281*, 689−690.

(12) Kuroyanagi, T.; Saito, M. Effect of prednisolone and glycyrrhizin on passive transfer of experimental allergic encephalomyelitis. *Jpn. J. Allergol.* **1966**, *15*, 67−74.

(13) Fujita, H.; Sakurai, T.; Toyoshima, S. Studies on the regulation by drug against experimental hepatitis (1). *Pharmacometrics* **1978**, *16*, 637−645.

(14) Okamura, N.; Miki, H.; Orii, H.; Masaoka, Y.; Yamashita, S.; Kobayashi, H.; Yagi, A. Simultaneous high-performance liquid chromatographic determination of puerarin, daidzin, paeoniflorin, liquiritin, cinnamic acid, cinnamaldehyde and glycyrrhizin in Kampo medicines. *J. Pharm. Biomed. Anal.* **1999**, *19*, 603−612.

(15) Wu, Y. P.; Meng, X. S.; Bao, Y. R.; Wang, S.; Kang, T. G. Simultaneous quantitative determination of nine active chemical compositions in traditional Chinese medicine glycyrrhiza by RP-HPLC with full-time five-wavelength fusion method. *Am. J. Chin. Med.* **2013**, *41*, 211−219.

(16) Zhang, H.; Chen, S.; Qin, F.; Huang, X.; Ren, P.; Gu, X. Simultaneous determination of 12 chemical constituents in the traditional Chinese medicinal prescription Xiao-Yao-San-Jia-Wei by HPLC coupled with photodiode array detection. *J. Pharm. Biomed. Anal.* **2008**, *48*, 1462−1466.

(17) Seo, C. S.; Lee, M. Y.; Lim, H. S.; Kim, S. J.; Ha, H.; Lee, J. A.; Shin, H. K. Determination of 5-hydroxymethyl-2-furfural, albiflorin, paeoniflorin, liquiritin, ferulic acid, nodakenin, and glycyrrhizin by HPLC-PDA, and evaluation of the cytotoxicity of Palmul-tang, a traditional Korean herbal medicine. *Arch. Pharm. Res.* **2012**, *35*, 101−108.

(18) Wang, Y.; Yao, Y.; An, R.; You, L.; Wang, X. Simultaneous determination of puerarin, daidzein, baicalin, wogonoside and liquiritin of GegenQinlian decoction in rat plasma by ultra-performance liquid chromatography-mass spectrometry. *J. Chromatogr., B* **2009**, *877*, 1820−1826.

(19) Chen, X. J.; Zhao, J.; Meng, Q.; Li, S. P.; Wang, Y. T. Simultaneous determination of five flavonoids in licorice using pressurized liquid extraction and capillary electrochromatography coupled with peak suppression diode array detection. *J. Chromatogr., A* **2009**, *1216*, 7329−7335.

(20) Sakamoto, S.; Pongkitwitoon, B.; Nakahara, H.; Shibata, O.; Syoyama, Y.; Tanaka, H.; Morimoto, S. Fluobodies against bioactive natural products and their application in fluorescence-linked immunosorbent assay. *Antibodies* **2012**, *1*, 239−258.

(21) Tanaka, H.; Syoyama, Y. Formation of a monoclonal antibody against glycyrrhizin and development of an ELISA. *Biol. Pharm. Bull.* **1998**, *21*, 1391−1393.

(22) Shan, S.; Tanaka, H.; Shoyama, Y. Enzyme-linked immunosorbent assay for glycyrrhizin using anti-glycyrrhizin monoclonal antibody and an eastern blotting technique for glucuronides of glycyrrhetic acid. *Anal. Chem.* **2001**, *73*, 5784−5790.

(23) Spinks, E. A.; Fenwick, G. R. The determination of glycyrrhizin in selected UK liquorice products. *Food Addit Contam.* **1990**, *7*, 769−778.

(24) Sabbioni, C.; Ferranti, A.; Bugamelli, F.; Forti, G. C.; Raggi, M. A. Simultaneous HPLC analysis, with isocratic elution, of glycyrrhizin and glycyrrhetic acid in liquorice roots and confectionery products. *Phytochem. Anal.* **2006**, *17*, 25−31.
(25) Kvasnicka, F.; Voldrich, M.; Vyhnálek, J. Determination of glycyrrhizin in liqueurs by on-line coupled capillary isotachophoresis with capillary zone electrophoresis. *J. Chromatogr., A* **2007**, *1169*, 239−242.
(26) Xuan, L.-J.; Tanaka, H.; Morimoto, S.; Shoyama, Y.; Akanuma, H.; Muraoka, K. Determination of 1,5-anhydro-glucitol-carrier protein conjugates by matrix-assisted laser desorption/ionization tof mass spectrometry and antibody formation. *Spectroscopy* **2000**, *14*, 85−92.
(27) Morinaga, O.; Nakajima, S.; Tanaka, H.; Shoyama, Y. Production of monoclonal antibodies against a major purgative component, sennoside B, their characterization and use in ELISA. *Analyst* **2001**, *126*, 1372−1376.
(28) Kido, K.; Morinaga, O.; Shoyama, Y.; Tanaka, H. Quick analysis of baicalin in Scutellariae Radix by enzyme-linked immunosorbent assay using a monoclonal antibody. *Talanta* **2008**, *77*, 346−350.
(29) Kojoma, M.; Hayashi, S.; Shibata, T.; Yamamoto, Y.; Sekizaki, H. Variation of glycyrrhizin and liquiritin contents within a population of 5-year-old licorice (*Glycyrrhiza uralensis*) plants culti vated under the same conditions. *Biol. Pharm. Bull.* **2011**, *34*, 1334−1337.
(30) Kondo, K.; Shiba, M.; Nakamura, R.; Morota, T.; Shoyama, Y. Constituent properties of licorices derived from *Glycyrrhiza uralensis*, *G. glabra*, or *G. inflata* identified by genetic information. *Biol. Pharm. Bull.* **2007**, *30*, 1271−1277.
(31) Zhu, S.; Sugiyama, R.; Batkhuu, J.; Sanchir, C.; Zou, K.; Komatsu, K. Survey of Glycyrrhizae Radix resources in Mongolia: chemical assessment of the underground part of *Glycyrrhiza uralensis* and comparison with Chinese Glycyrrhizea Radix. *J. Nat. Med.* **2009**, *63*, 137−146.
(32) *The Japanese Pharmacopoeia*, 16th ed.; HirokawaShoten: Tokyo, Japan, 2011; pp D-158−D-170.

adapted to a microplate method[20] for the determination of proline in biological fluids. More recently, an isatin method for the determination of proline in grape juice was reported.[21] This method was robust for the analysis of end of fermentation samples and table wines and was linear over the concentration range 0−200 mg/L. However, the method involves an evaporation step and, as a result, interference from sugar concentrations >60 g/L was such that proline concentrations were considerably underestimated in grape juice.

The purpose of this study, therefore, was to revisit both methods to devise a simpler spectrophotometric method without the need for evaporation, as in the isatin method cited above, or the extraction step required with traditional ninhydrin methods. The final method developed is based on the ninhydrin reaction in strongly acidic conditions under which other amino acids do not interfere. Furthermore, relative volumes and the solvents were selected such that the need to extract the derived reaction product is obviated. The method was validated statistically, and results for 13 grape juice samples were compared with the HPLC−ninhydrin method for amino acid analysis. It was then applied to the determination of proline accumulation in microvine berries at all stages of development from fruit set to maturity.

MATERIALS AND METHODS

Reagents and Chemicals. All chemicals were of analytical grade or better, and freshly distilled water stored in a glass container was used for all experiments. Methanol, ethanol, dimethyl sulfoxide, glucose, and acetic, tartaric, malic, and formic acids were obtained from Carlo Erba, Val de Reuil, France. Individual amino acids (Ala, Asn, Arg, Asp, GABA, Glu, Glm, Ile, Leu, Lys, Met, Pro, Ser, Thr, Val) were obtained from Sigma-Aldrich (St Quentin-Fallavier, France). Isatin and ninhydrin were obtained from Fluka, France. Malvidin-3-glucoside was obtained from ExtraSynthèse, France.

Solutions. A synthetic grape juice was prepared containing 200 g/L glucose, 6 g/L malic acid, 8 g/L tartaric acid, and, for studies for the potential interference by anthocyanins, 250 mg/L malvidin 3-glucoside.

Stock solutions of 1 g/L of each of the amino acids were prepared in 0.1 M HCl and stored at −20 °C when not in use. Standard solutions of proline were prepared by serial dilution of the stock solution. A working mixture was prepared in water or synthetic grape solution containing typical concentrations of the principal grape amino acids: Ala, Asn, Glm, Ser, GABA, 100 mg/L; Arg, 500 mg/L; Asp and Glu, 150 mg/L; and 10 mg/L of the other amino acids.

Plant Material. The ML1 microvine that was used in this study shows a dwarf stature and produces inflorescences all along the main axes in the place of tendrils. This phenotype has been proposed as a new model for research in grapevine genetics and ecophysiology.[22−24] To study the proline accumulation pattern in berries of these plants, 10 plants were grown under controlled conditions in climate chambers under constant day/night temperatures (30/22 °C) for 3 months. All reproductive organs along the main axes from berry set to maturity were successively sampled within 2 h and immediately frozen in liquid nitrogen.

Determination of Proline by the Ninhydrin Method. Ground sample powder was diluted 5-fold with deionized water and frozen at −20 °C until analysis. Reconstituted samples were thawed and centrifuged at 3000*g* at 4 °C for 10 min. The supernatant was further diluted (5−20 times depending on the stage of development); 750 μL of the diluted sample was added to the same volume of formic acid and vortex-mixed for 2 min. A 750 μL aliquot of ninhydrin 3% in dimethyl sulfoxide (freshly prepared daily) was then added, and following vortex mixing, the reaction mixture was heated at 100 °C in a heating block for 15 min. The absorbance at 520 nm of the resultant salmon pink reaction product was then read on a Biochrom (UK) Libra S12 spectrophotometer. Concentrations were calculated by interpolation on a linear regression curve in the concentration range of 2.5−15 mg/L.

Validation. Calibration standards at five concentration points (2.5, 5, 7.5, 10, and 15 mg/L) were prepared in diluted (1 in 5) synthetic grape juice spiked with the analyte mixture. Standard calibration curves were obtained from unweighted least-squares linear regression analysis of the data. The slope and intercept of the calibration graphs were determined through linear regression of the absorbance versus concentration plot. Individual absorbances were then interpolated on the calibration graphs to determine the found (back-calculated) concentrations. The quality of fit was determined using back-calculated-to-nominal concentrations, and the "lack of fit" test was used to confirm the linearity of the method. Within-day and between-day precision and accuracy of the method were determined by carrying out replicate analyses of the calibration standards. Repeatability was determined by preparing and analyzing each calibration standard four times within a single day (i.e., 20 standards in total) under the same operating conditions. The intermediate precision was determined by carrying out the same operations over 4 days under different operating conditions (different reagents and materials). The precision was given by mean relative standard deviation of the absorbance values, and the accuracy of the method was evaluated as 100 × [mean found concentration/nominal concentration]. The method was cross-validated by comparing the results obtained by this method with those obtained for the same samples by the classic HPLC post-column derivatization with ninhydrin method.

Sugar and Organic Acid Analysis. Hexoses (glucose and fructose) and organic acids (malic, tartaric, citric, and shikimic acid) were determined in a single HPLC injection. The same (5-fold diluted) samples as were used for proline were further diluted 20-fold with 4.375 μM acetate as internal standard. To avoid potassium bitartrate precipitation, 1 mL of diluted sample was mixed with 0.18 g of Sigma Amberlite IR-120 Plus and agitated in a rotary shaker for at least 10 h before centrifugation (13000 rpm for 10 min). The supernatant was transferred into HPLC vials before injection on an Aminex HPX87H column eluted in isocratic conditions (0.05 mL min^{-1}, 60 °C, H_2SO_4).[25] Organic acids were detected at 210 nm with a Waters 2487 dual absorbance detector (Waters Corp., Milford, MA, USA). A refractive index detector Kontron 475 (Kontron Instruments, Rossdorf, Germany) was used to determine fructose and glucose concentrations. Concentrations were calculated according to a previously described method.[26]

RESULTS AND DISCUSSION

Method Development. Boctor[27] demonstrated that the reaction between isatin and proline is suitable to quantitatively determine proline in a protein hydrolysate and biological fluids. It is a highly specific color reagent for proline, forming a blue derivative, pyrrole blue. The technique adopted in this study was as previously described.[21] A 50 mg/L standard (100 μL) was diluted with citrate buffer (0.5 M, pH 4.1, 100 μL). Then 250 μL of a 0.075% (w/v) solution of isatin in acetone (250 μL) and ethanol (500 μL) was added. The tubes were evaporated to dryness in a heating block at 100 °C. The blue proline−isatin residue obtained was dissolved in aqueous 3 mL of acetone/water (2:1, v/v) and the absorbance of the resulting solution measured at 595 nm. This resulted in an absorbance reading of 0.37. Different permutations on the relative volumes and concentration of isatin (increasing to 0.3%) were investigated to obtain an increase in absorbance. However, the results proved inconclusive; it appeared that different absorbance values were obtained depending on the length of time it took the solvents to evaporate in the heating block, and it was difficult to obtain repeatable readings. Furthermore, when applied to real grape juice samples, absorbance reading were <0.1, and so it was concluded that the method would not be sufficiently sensitive for the intended purpose.

dx.doi.org/10.1021/jf404627n | J. Agric. Food Chem. 2014, 62, 3384−3389

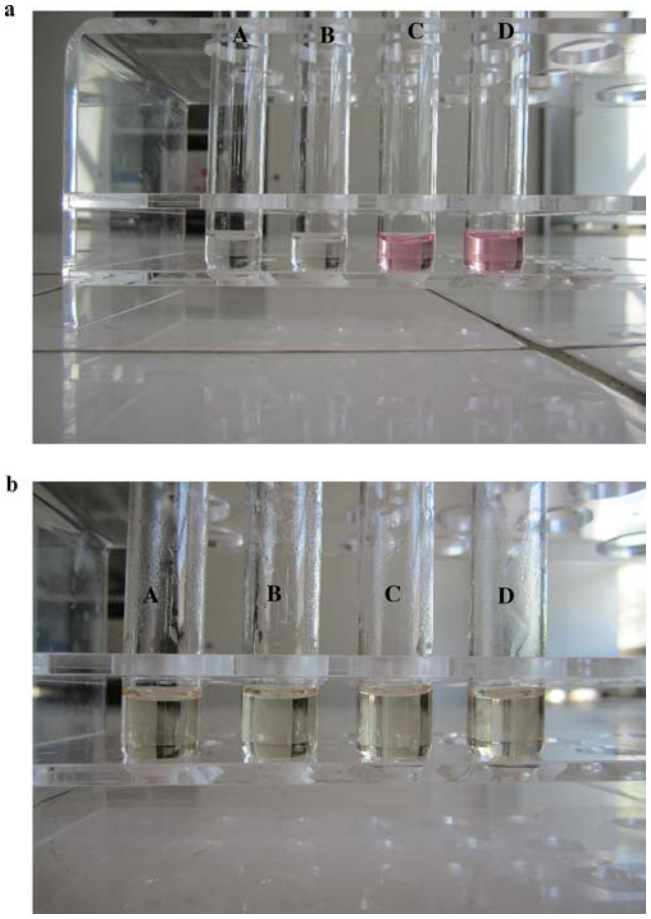

Figure 1. (a) White (A,B) and red (C, D) proline-free synthetic grape juice following dilution and the addition of formic acid. (b) The same solutions following the addition of ninhydrin in dimethyl sulfoxide and heating for 15 min at 100 °C.

The reaction of ninhydrin with primary amino groups to form the purple dye known as Ruhemann's purple was discovered by Siegfried Ruhemann in 1910[28] and has been extensively used in amino acid analysis in a multitude of areas. Upon heating in an alkaline medium with substances containing primary amino groups ($-NH_2$), ninhydrin yields a product with a stable deep blue-violet color, with maximum absorption at about 570 nm. Under the same conditions, proline and hydroxyproline yield a yellow color. In 1952, Chinard[29] reported that at acidic pH, ninhydrin forms a red product with proline. A similar assay was described by Bates,[30] and it became the standard method for many laboratories to determine proline. In this context, the determination is performed according to the modification of the Bates method in which the formed derivative is extracted from the acid aqueous solution with toluene and measured at 520 nm. Wallrauch[31] found that the use of ethyl acetate to extract the color produced by the acidic ninhydrin reaction was necessary for highly colored juices with low proline content. Ough[32] proposed an improved procedure to analyze proline in grape juice and wine in which the extraction step was replaced by a dilution during cooling with water/isopropanol. No significant interferences from other amino acids were found in amounts normally present in these matrices. A further variation on that method was applied to the determination of proline in orange juice,[33] and a similar approach was adopted in the present study, in which dimethyl sulfoxide was used as a solvent for ninhydrin. The challenge that remained was to ensure that the highly water-insoluble reaction product remained in solution to obviate the need for extraction or further dilution. Therefore, the relative volumes of sample, formic acid, and 3% ninhydrin reagent in dimethyl sulfoxide, in addition to the concentration range, were optimized for this purpose. The final operating conditions are given under Materials and Methods. Initial experiments with proline in the concentration range of 50−100 mg/L resulted in a pink precipitate in a solution of the same color. The concentration range was reduced to the low milligrams per liter (2.5−15 mg/L) range, which provided a linear absorbance response as a function of concentration. The developed method, which requires neither extraction nor

Table 1. Repeatability (Intraday Precision) and Recovery Data

concn (mg/L)	mean Abs[a]	SD[b]	CV (%)	mean AF[c] (mg/L)	nominal AF (% diff)	recovery (%)
day 1						
2.5	0.218	0.004	1.6	2.43	2.94	97.1
5	0.393	0.006	1.6	5.29	−5.71	105.7
7.5	0.564	0.030	5.3	8.08	−7.67	107.7
10	0.704	0.008	1.1	10.36	−3.63	103.6
15	1.023	0.016	1.6	15.57	−3.78	103.8
R^2	0.998	0.001	0.1			
day 2						
2.5	0.209	0.002	0.9	2.48	0.78	99.2
5	0.376	0.015	4.1	5.10	−1.95	101.9
7.5	0.535	0.015	2.7	7.58	−1.04	101.0
10	0.695	0.023	3.3	10.08	−0.78	100.8
15	1.014	0.036	3.5	15.05	−0.36	100.4
R^2	0.998					
day 3						
2.5	0.201	0.004	1.8	2.67	−6.94	106.9
5	0.360	0.006	1.7	5.01	−0.30	100.3
7.5	0.520	0.009	1.7	7.39	1.48	98.5
10	0.686	0.011	1.6	9.83	1.66	98.3
15	1.048	0.015	1.4	15.18	−1.21	101.2
R^2	0.999					
day 4						
2.5	0.207	0.011	5.6	2.56	−2.46	102.4
5	0.363	0.008	2.1	4.97	0.54	99.4
7.5	0.528	0.031	5.9	7.51	−0.15	100.1
10	0.714	0.026	3.6	10.37	−3.73	103.7
15	1.011	0.054	5.3	14.94	0.41	99.6
R^2	0.999					

[a]Mean absorbance, $n = 4$. [b]Standard deviation. [c]AF, amount found by interpolation.

Table 2. Intermediate (Interday Precision)

concn (mg/L)	mean Abs[a]	SD	CV (%)
2.5	0.209	0.008	3.6
5	0.374	0.013	3.4
7.5	0.527	0.018	3.4
10	0.701	0.019	2.6
15	1.031	0.021	2.0
slope	0.066		
intercept	0.042		
R^2	1.000		

[a]Mean absorbance, $n = 16$.

dx.doi.org/10.1021/jf404627n | J. Agric. Food Chem. 2014, 62, 3384−3389

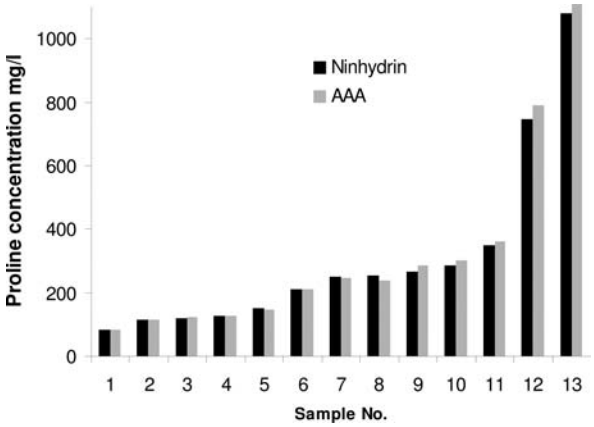

Figure 2. Histogram of proline concentrations obtained by using the proposed method and by using amino acid analysis.

dilution of the reaction product, was fully validated and a systematic study of matrix interferences is reported.

Interference Study. Different authors have reported various sources of interferences with the proline−ninhydrin assay, including high concentrations of sugars[34] and diverse amino acids.

Potential Interference from Sugars and Other Grape Juice Components. The sensitivity of the present method is such that the grape juice samples are diluted from 5- to 20-fold, resulting in final sugar concentrations of 10−40 g/L, concentrations that have not been reported to interfere with the assay. However, to verify this, a stock solution of 300 mg/L proline was prepared in synthetic grape juice (composition given under Materials and Methods). This solution was diluted 1 in 20, analyzed according to the developed method, and compared with an aqueous proline solution at 15 mg/L. Measured against blanks of synthetic grape juice or water, respectively, and subjected to the same reaction, the absorbances (n = 5) were not significantly different between the two groups. In all cases the blank (Supporting Information Supplemental Figure 1) is a pale yellow color with an absorbance of approximately 0.03.

Potential Interference from Other Amino Acids. Certain basic amino acids, such as ornithine, were reported by Chinard[29] to give colored products when heated with ninhydrin at low pH. With the exception of proline, the other commonly naturally occurring amino acids did not react significantly under these conditions. Given that in the grapevine, levels of these amino acids are substantially lower than those of proline, interference by these amino acids is likely to be negligible. Nonetheless, a mixture of amino acids at concentrations typical of grape juice was prepared in synthetic grape juice, diluted 20-fold with distilled water, and subjected to the assay. The result (Supporting Information Supplemental Figure 2) is a pale yellow solution, which gave an absorbance comparable to that of blank synthetic grape juice at approximately 0.03. It may thus be concluded that the other amino acids at typical grape juice concentrations do not interfere with proline determination by this assay.

Potential Interference by Anthocyanins. A potentially serious interference in this assay arises from anthocyanins (which strongly absorb at 520 nm) in red grape juice, an issue that as not been addressed in previous papers. Even diluted 20-fold, once formic acid is added to the grape juice sample, the intensely colored cation flavinium form of the anthocyanins is generated, thus increasing the intensity of the red color of the sample. Initially, carbon black was used with considerable success to remove the coloring matter, but it was found also to remove an unacceptably high amount (>10%) of proline. This observation is borne out in the literature.[35] Other adsorbents such as PVPP were found to be less effective in removing the coloring matter or also removed some proline, although to a lesser extent than carbon black. Another approach adopted was to evaluate the extent of interference by anthocyanins in the assay as it had been observed that the pink-purple color of the sample before the addition of the ninhydrin and heating transformed into the characteristic salmon pink of the proline−ninhydrin adduct after heating (Supporting Information Supplemental Figure 1).

Therefore, malvidin-3-glucoside was added to blank synthetic grape juice at a concentration of 250 mg/L; following 20-fold dilution and addition of formic acid, one sample was heated with ninhydrin in dimethyl sulfoxide and another with dimethyl sulfoxide only. The latter sample retained its color, whereas the color of the former was transformed to a pale yellow, the same color as is obtained with the blank (Figure 1). It therefore appears that ninhydrin reacts with anthocyanins in such a manner as to render them colorless. This reaction has not previously been reported in the literature and is currently under further investigation.

Validation. Calibration standards at five concentration points (2.5, 5, 7.5, 10, and 15 mg/L) were prepared in diluted

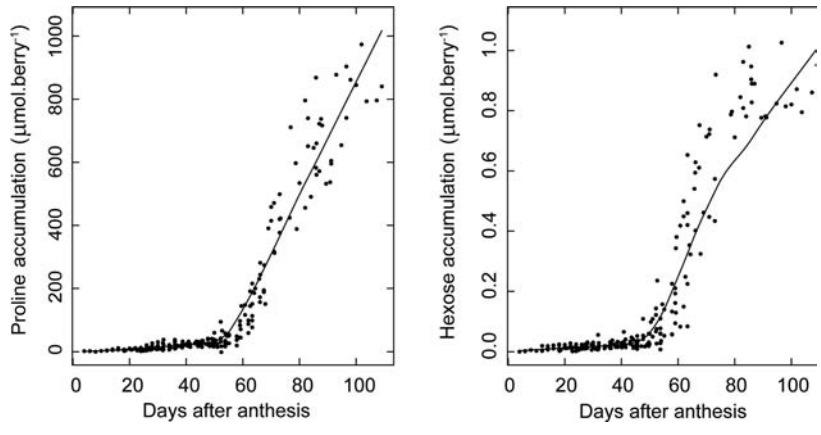

Figure 3. Proline and sugar accumulation in microvine berries. Lines are LOESS fits.

dx.doi.org/10.1021/jf404627n | J. Agric. Food Chem. 2014, 62, 3384−3389

(1 in 20) synthetic grape juice spiked with the analyte mixture. The repeatability or intraday precision is presented in Table 1. As may be seen, the intraday precision varies from <2% RSD to a maximum of 5.9%. The "lack of fit" test showed no significant deviation from linearity; the bias, calculated as the sum of the residuals (nominal − back-calculated concentration) was nonsignificant (t test P = 20.23%). Linear regression of the back-calculated-to-nominal concentrations provided a slope of 1.0013 and an intercept of −0.049. The accuracy of the method was evaluated as 100 × (mean found concentration/nominal concentration) as may be seen from Table 1, and percent difference between the nominal and back-calculated concentrations was in general <5%. The intermediate (interday) precision is presented in Table 2, and RSD values range from 2.03 to 3.59%. Although the limit of detection was not determined, it may be estimated at 1 mg/L given that 2.5 mg/L gives an absorbance of >0.2 and the blank (sample replaced by water) absorbance is 0.03.

Results obtained by this method for 13 grape juice samples were compared with those obtained for the same samples on a dedicated amino acid analyzer. Figure 2 shows a histogram of the values obtained by the two methods; the agreement is close (r = 0.99), thus adding further evidence of the utility of this new high-throughput method for the determination of proline in grapevine samples.

Application. As part of a cross-disciplinary project[36] to characterize the transcriptome and to map physiological and biochemical characteristics of the microvine berry, this method was applied to study the accumulation pattern of proline and compare it to those encountered in field-grown perennial macrovines.

The DRCF (dwarf, rapid cycling, and continuous flowering) microvine phenotype, discovered by Franks et al. in 2002,[37] shows dwarf stature and produces inflorescenes all along the main axes in place of tendrils. It has been demonstrated that this new material is suitable for genetic research[38] and can be grown under confined conditions in climate chambers.[23] The sugar content of DRCF berries was determined as described under Material and Methods.

As may be seen in Figure 3, both the proline and sugar accumulation patterns are similar to those encountered for classical field-grown vines. In fact, proline concentrations at close to maturity (approximately 1 mmol hexoses (g FW)$^{-1}$) were of the same order of magnitude as commonly found in other *Vitis vinifera* varieties (0.688 μmol (g FW)$^{-1}$ for Riesling up to 1794 μmol (g FW)$^{-1}$ for Cabernet Sauvigon).[39] Furthermore, this parallel between the accumulation of sugars and proline was also reported in the above reference, and the authors even suggested that the accumulation of proline may be a result of increased osmotic pressure arising from increased sugar concentration on the basis of the fact that proline is known to exercise an osmoprotective effect.

Given the reliability, precision, and ease of operation of this method, it could be envisaged for use in high-throughput analysis, such as in studies into the response of the grapevines (or indeed other fruiting plants and trees) to climate change, irrigation, N fertilization, etc. It could also be useful in screening fruit populations for adaptation to abiotic stress and, with appropriate extraction methods, in the analysis of proline accumulation in other plant parts.

■ ASSOCIATED CONTENT

Supporting Information

Supplemental Figures 1 and 2. This material is available free of charge via the Internet at http://pubs.acs.org.

■ AUTHOR INFORMATION

Corresponding Author

*E-mail: mary.kelly@univ-montp1.fr.

Funding

This work was partly funded by the Durativis program, which is supported by the Agence Nationale de la Recherche (ANR), the Comité National Interprofessionnel des Vins d'appellation d'origine (CNIV), and the foundation Jean Poupelain (Javrezac, Cognac).

Notes

The authors declare no competing financial interest.

■ ACKNOWLEDGMENTS

We thank Erick Casalta (UMR SPO, Montpellier, France) for the providing grape juice samples and results of proline analysis by amino acid analysis.

■ REFERENCES

(1) Rhodes, D.; Handa, S.; Bressan, R. A. Metabolic changes associated with adaptation of plant cells to water stress. *Plant Physiol.* **1986**, *82*, 890−903.

(2) Delauney, A. J.; Verma, D. P. S. Proline biosynthesis and osmoregulation in plants. *Plant J.* **1993**, *4*, 215−223.

(3) Kavi Kishor, P. B.; Sangam, S.; Amrutha, R. N.; Laxmi, P. S.; Naidu, K. R.; Rao, K. R. S. S.; Rao, S.; Reddy, K. J.; Theriappan, P.; Sreenivasulu, N. Regulation of proline biosynthesis, degradation, uptake and transport in higher plants: its implications in plant growth and abiotic stress tolerance. *Curr. Sci.* **2005**, *88*, 424−438.

(4) Verbruggen, N.; Hermans, C. Proline accumulation in plants: a review. *Amino Acids* **2008**, *35*, 753−759.

(5) Ahmad, I.; Wainwright, S. J.; Stewart, G. R. The solute and water relations of *Agrostis stolonifera* ecotypes differing in their salt tolerance. *New Phytol.* **1981**, *87*, 615−629.

(6) Fougere, F.; Le Rudulier, D.; Streeter, J. G. Effects of salt stress on amino acid, organic acid, and carbohydrate composition of roots, bacteroids, and cytosol of alfalfa *Medicago sativa* L. *Plant Physiol.* **1991**, *96*, 1228−1236.

(7) Armengaud, P.; Thiery, L.; Buhot, N.; Grenier-De March, G.; Savouré, A. Transcriptional regulation of proline biosynthesis in *Medicago truncatula* reveals developmental and environmental specific features. *Physiol. Plant.* **2004**, *120*, 442−450.

(8) Echeverria, M.; Sannazzaro, A. I.; Ruiz, O. A.; Menéndez, A. B. Modulatory effects of and on plant proline and polyamine levels during early plant response of to salinity. *Plant Soil* **2013**, *364*, 69−79.

(9) Newton, R. J.; Sen, S.; Puryear, J. D. Free proline changes in *Pinus taeda* L. callus in response to drought stress. *Tree Physiol.* **1986**, *1*, 325−332.

(10) Yamada, M.; Morishita, H.; Urano, K.; Shiozaki, N.; Yamaguchi-Shinozaki, K.; Shinozaki, K.; Yoshiba, Y. Effects of free proline accumulation in petunias under drought stress. *J. Exp. Bot.* **2005**, *56*, 1975−1981.

(11) Meon, S.; Fisher, J. M.; Wallace, H. R. Changes in free proline following infection of plants with either *Meloidogyne javanica* or *Agrobacterium tumefaciens*. *Physiol. Plant Pathol.* **1978**, *12*, 251−256.

(12) Fabro, G.; Kovács, I.; Pavet, V.; Szabados, L.; Alvarez, M. E. Proline accumulation and AtP5CS2 gene activation are induced by plant−pathogen incompatible interactions in *Arabidopsis*. *Mol. Plant−Microbe Interact.* **2004**, *17*, 343−350.

(13) Samuel, D.; Ganesh, G.; Yang, P.-W.; Chang, M.-M.; Wang, S.-L.; Hwang, K.-C.; Yu, C.; Jayaraman, G.; Kumar, T. K. S.; Trivedi, V.

D.; Chang, D.-K. Proline inhibits aggregation during protein refolding. *Protein Sci.* **2000**, *92*, 344−352.
(14) Sharma, S. S.; Schat, H.; Vooijs, R. In vitro alleviation of heavy metalinduced enzyme inhibition by proline. *Phytochemistry* **1998**, *49*, 1531−1535.
(15) Saradhi, P. P.; Alia Arora, A. S.; Prasad, K. V. S. K. Proline accumulates in plants exposed to UV radiation and protects them against UV induced peroxidation. *Biochem. Biophys. Res. Commun.* **1995**, *209*, 1−5.
(16) Smirnoff, N.; Cumbes, Q. J. Hydroxyl radical scavenging activity of compatible solutes. *Phytochemistry* **1989**, *28*, 1057−1060.
(17) Dukes, B. C.; Butzke, C. E. Rapid determination of primary amino acids in grape juice using an *o*-phthaldialdehyde/*N*-acetyl-L-cysteine spectrophotometric assay. *Am. J. Enol. Vitic.* **1998**, *49*, 125−134.
(18) Abrahám, E.; Hourton-Cabassa, C.; Erdei, L.; Szabados, L. Methods for determination of proline in plants. *Methods Mol. Biol.* **2010**, *639*, 317−331.
(19) Elliott, R. J.; Gardner, D. L. Proline determination with isatin in the presence of amino acids. *Anal. Biochem.* **1976**, *70*, 268−273.
(20) Grainger, D. J.; Aitken, S. A microtitre format assay for proline in human serum or plasma. *Clin. Chim. Acta* **2004**, *343*, 113−118.
(21) Long, D.; Wilkinson, K. L.; Poole, K.; Taylor, D. K.; Warren, T.; Astorga, A. M.; Jiranek, V. Rapid method for proline determination in grape juice and wine. *J. Agric. Food Chem.* **2012**, *60*, 4259−4264.
(22) Boss, P. K.; Thomas, M. R. Association of dwarfism and floral induction with a grape 'green revolution' mutation. *Nature* **2002**, *416*, 847−850.
(23) Rienth, M.; Dauzat, M.; Pellegrino, A.; Lopez, G.; Torresgosa, L.; Romieu, C. First observations of the microvine development under 100% LED light emitting diodes illumination. *Vitis* **2012**, *514*, 167−173.
(24) Chaïb, J.; Torregrosa, L.; Mackenzie, D.; Corena, P.; Bouquet, A.; Thomas, M. R. The grape microvine − a model system for rapid forward and reverse genetics of grapevines. *Plant J.* **2010**, *626*, 1083−1092.
(25) Schneider, A.; Gerbi, V.; Redoglia, M. A rapid HPLC method for separation and determination of major organic acids in grape musts and wine. *Am. J. Enol. Vitic.* **1987**, *38*, 151−155.
(26) Eyegghe-Bickong, H. A.; Alexandersson, E. O.; Gouws, L. M.; Young, P. R.; Vivier, M. A. Optimisation of an HPLC method for the simultaneous quantification of the major sugars and organic acids in grapevine berries. *J. Chromatogr., B* **2012**, *885−886*, 43−49.
(27) Boctor, F. N. An improved method for colorimetric determination of proline with isatin. *Anal. Biochem.* **1971**, *43*, 66−70.
(28) Ruhemann, S. Cyclic di- and tri-ketones. *Trans. Chem. Soc.* **1910**, *97*, 1438−1449.
(29) Chinard, F. P. Photometric estimation of proline and ornithine. *J. Biol. Chem.* **1952**, *199*, 91−95.
(30) Bates, S.; Waldren, R. P.; Teare, I. D. Rapid determination of free proline for water-stress studies. *Plant Soil* **1973**, *39*, 205−207.
(31) Wallrauch, S. Determination of proline in fruit juices, significance for the estimation. *Fluess. Obst* **1976**, *45*, 430−437.
(32) Ough, C. S. Rapid determination of proline in grapes and wines. *Food Sci.* **1969**, *34*, 228−230.
(33) Ting, S. V.; Rouseff, R. L. *Proc. Fla. State Hortic. Soc.* **1979**, *92*, 143−145.
(34) Magné, C.; Larher, F. High sugar content of extracts interferes with colorimetric determination of amino acids and free proline. *Anal. Biochem.* **1992**, *2001*, 115−118.
(35) Kuznetsova, E. S.; Ul'yanov, A. V.; Buryak, A. K. Molecular statistical calculations of the adsorption of proline and its hydroxy derivatives on graphitized thermal carbon black. *Russ. J. Phys. Chem. A* **2009**, *83*, 542−546.
(36) Rienth, M.; Torregrosa, L.; Kelly, M.; Luchaire, N.; Pellegrino, A.; Grimplet, J.; Romieu, C. Is transcriptomic regulation of berry development more important at night than during the day? *PLoS One* **2014**, DOI: 10.1371/journal.pone.0088844.
(37) Franks, T.; Botta, R.; Thomas, M. R.; Franks, J. Chimerism in grapevines: implications for cultivar identity, ancestry and genetic improvement. *Theor. Appl. Genet.* **2002**, *104*, 192−199.
(38) Peng, J.; Richards, D. E.; Hartley, N. M.; Murphy, G. P.; Devos, K. M.; Flintham, J. E.; Beales, J.; Fish, L. J.; Worland, A. J.; Pelica, F.; Sudhakar, D.; Christou, P.; Snape, J. W.; Gale, M. D.; Harberd, N. P. Green revolution genes encode mutant gibberellin response modulators. *Nature* **1999**, *400*, 256−261.
(39) Stines, A. P.; Grubb, J.; Gockowiak, H.; Henschke, P. A.; Høj, P. B.; van Heeswijck, R.. Proline and arginine accumulation in developing berries of *Vitis vinifera* L. in Australian vineyards: influence of vine cultivar, berry maturity and tissue type. *Aust. J. Grape Wine Res.* **2000**, *6*, 150−158.

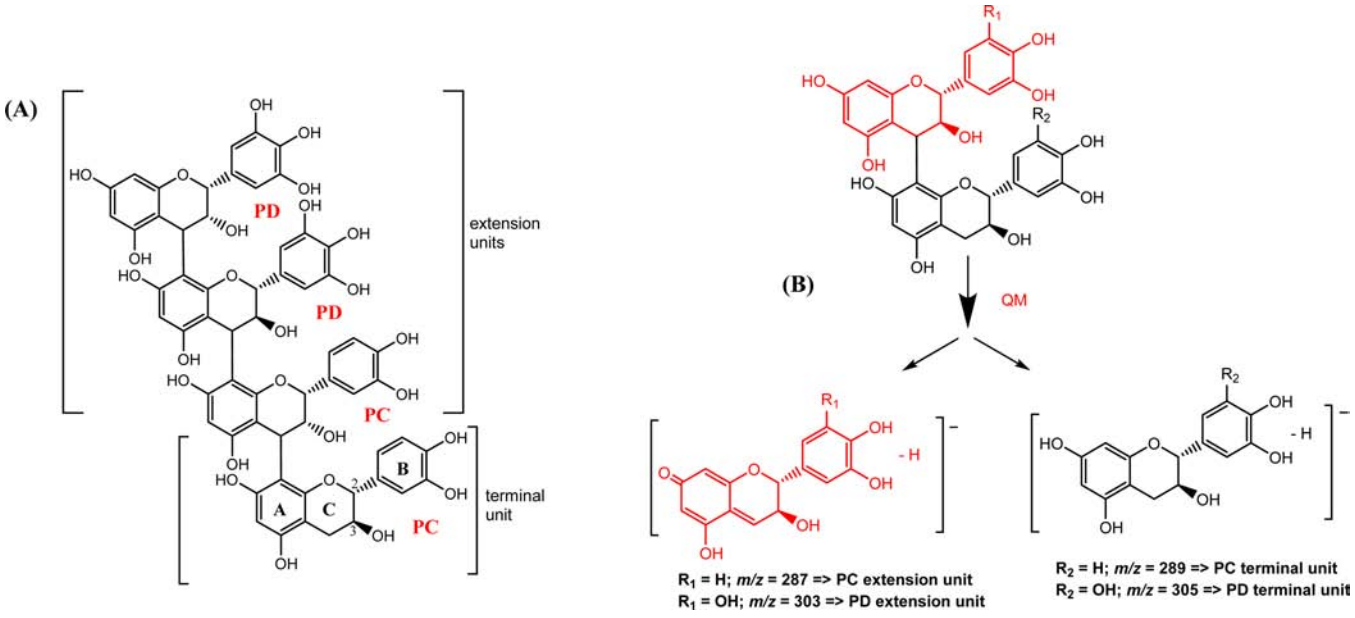

Figure 1. Model structure of a proanthocyanidin tetramer containing two prodelphinidin (PD) and two procyanidin (PC) units (A) and quinone methide fragmentation of proanthocyanidin dimer in negative ion mode ESI-MS (B).

relatively large amounts of plant tissue, in the range of hundreds of milligrams, for analysis.[17−19]

The development in LC-MS/MS instruments has been vast in recent years,[20−22] and the use of ultraperformance liquid chromatography combined with a mass spectrometer (UPLC-MS/MS) is becoming common also in proanthocyanidin studies.[23] UPLC enables rapid chromatography of different kinds of proanthocyanidin oligomers, whereas MS/MS fragments compounds into proanthocyanidin-specific precursor and product ions for detection with multiple reaction monitoring (MRM) methods. Specific fragmentations, that is, compound-specific methods, have been widely used for the identification and quantitation of relatively small proanthocyanidin oligomers.[23−25] However, no compound-specific methods have been reported for larger oligomers or proanthocyanidin polymers as the limit has been with tetramers.[23−26] Furthermore, to our knowledge, no group-specific method for the qualitative and quantitative determination of all proanthocyanidin sizes in plant samples has been reported. The present study explored the potential of UPLC combined with a triple-quadrupole mass spectrometer (TQ-MS) for the rapid qualitative and quantitative analyses of proanthocyanidins. Our main interest was in establishing a fast, sensitive, and selective method for the analysis of the two most common proanthocyanidin types: procyanidins and prodelphinidins.

MATERIALS AND METHODS

Chemicals and Reagents. LC-MS grade acetonitrile used in the UPLC analyses was from Sigma-Aldrich (Steinheim, Germany). Formic acid was from VWR (Helsinki, Finland). Water was purified with a Millipore Synergy water purification system (Merck KGaA, Darmstadt, Germany). Catechin was from Sigma (Sigma Chemical Co., St. Louis, MO, USA) and epigallocatechin from ExtraSynthese (Genay, France).

Materials. Pure compounds gallocatechin gallate, proanthocyanidin dimers and trimers, mixture of oligomers, and mixture of polymers (not fractions 1-F−13-F) used in optimization of cone voltages and collision energies were produced as described in Karonen et al.[17] Proanthocyanidin fractions 1-F−13-F were extracted from different plant materials with 70% aqueous acetone and subjected to Sephadex LH-20 column chromatography. F1 fractions were eluted with acetone/water (30:70, v/v) and F2 fractions with acetone/water (50:50, v/v). The procyanidin proportions of the fractions varied from 1 to 95% and the mDP from 2 to 14 (by thiolysis). The plant materials, fractions, and results from thiolysis are listed in Table 1.

Thiolysis. Thiolysis was carried out as described in Gea et al.[18]

HCl-Butanol Assay. A 0.1 mL aqueous solution of fractions 5F−13F (0.5 mg/mL) was added to 0.5 mL of a freshly prepared mixture of 1-butanol/hydrochloric acid (95:5 v/v) in 1.5 mL Eppendorf tubes. Tubes were locked with Eppendorf tube locks and vigorously mixed by hand. After mixing, tubes were placed in an oven at 95 °C for 2.5 h. Tubes were then cooled to room temperature, and the absorbance at 550 nm was measured using a Multiskan Ascent microplate photometer (Thermo Fisher Scientific, Shanghai, China). Standard curves were constructed using known concentrations of procyanidin-rich sample 1-F2 and prodelphinidin-rich sample 9-F2 in H_2O. Dilution range was from 5.0 to 0.1 mg/mL. Five replicates of each sample were run. Because the HCl-butanol assay measures only total proanthocyanidins and cannot separate procyanidins from prodelphinidins, the results were calculated by using the average calibration curve obtained from procyanidin and prodelphinidin standards separately.

UPLC-MS/MS Analysis. Sample analysis was carried out with an Acquity UPLC system (Waters Corp., Milford, MA, USA) coupled with a Xevo TQ triple-quadrupole mass spectrometer (Waters Corp., Milford, MA, USA). The UPLC system consisted of a sample manager, a binary solvent manager, a column, and a diode array detector. The column used was a 100 mm × 2.1 mm i.d., 1.7 μm, Acquity UPLC BEH Phenyl column (Waters Corp., Wexford, Ireland). The flow rate of the eluent was 0.5 mL/min. The elution profile used two solvents, acetonitrile (A) and 0.1% aqueous formic acid (B): 0−0.5 min, 0.1% A in B; 0.5−5.0 min, 0.1−30% A in B (linear gradient); 5.0−6.0 min, 30−35% A in B (linear gradient); 6.0−9.5 min, column wash and stabilization. UV and MS data were collected from 0 to 6 min. Negative ionization mode was used for MS analyses. ESI conditions were as follows: capillary voltage, 2.4 kV; desolvation temperature, 650 °C; source temperature, 150 °C; desolvation and cone gas (N_2), 1000 and 100 L/h, respectively; and collision gas, argon. Catechin (1 μg/mL) was used to monitor the stability of the ionization efficiency of the mass spectrometer.

Optimization of Cone Voltages and Collision Energies. When optimizing the cone voltages and the collision energies for the selected compounds and fractions, aqueous solutions of different proantho-

dx.doi.org/10.1021/jf500745y | J. Agric. Food Chem. 2014, 62, 3390−3399

Table 1. Plant Materials and Fractions Used in the Present Work[a]

sample	plant species	% PC	mDP
1-F1	*Onobrychis viciifolia* (sainfoin: Nova var.), leaves	28	6
1-F2	*Onobrychis viciifolia* (sainfoin: Nova var.), leaves	18	12
2-F1	*Lotus corniculatus* (birdsfoot trefoil: Rodeo var.), leaves	79	4
2-F2	*Lotus corniculatus* (birdsfoot trefoil: Rodeo var.), leaves	68	11
3-F1	*Lotus uliginosus* (big trefoil: ARS-1221 var.), leaves	31	4
3-F1b	*Lotus uliginosus* (big trefoil: ARS-1221 var.), leaves	26	7
3-F2	*Lotus uliginosus* (big trefoil: ARS-1221 var.), leaves	25	11
4-F1	*Securigera varia* (crownvetch: Emerald var.), leaves	12	11
4-F2	*Securigera varia* (crownvetch: Emerald var.), leaves	18	14
5-F1	*Salix caprea* (goat willow), leaves	94	2
5-F2	*Salix caprea* (goat willow), leaves	95	5
6-F1	*Coryllus avellana* (hazelnut), pericarp membrane	82	5
6-F2	*Coryllus avellana* (hazelnut), pericarp membrane	79	9
7-F1	*Salix caprea* (goat willow), twigs	84	2
7-F2	*Salix caprea* (goat willow), twigs	79	5
8-F1	*Pinus sylvestris* L. (scots pine tree), inner bark	85	2
8-F2	*Pinus sylvestris* L. (scots pine tree), inner bark	91	7
9-F1	*Onobrychis viciifolia* (sainfoin; Esparsette var.), whole plant	28	3
9-F2	*Onobrychis viciifolia* (sainfoin; Esparsette var.), whole plant	35	9
10-F1	*Salix babylonica* (weeping willow), catkins	75	3
10-F2	*Salix babylonica* (weeping willow), catkins	67	8
11-F1	*Ribes rubrum* (red currant), leaves	14	5
11-F2	*Ribes rubrum* (red currant), leaves	10	10
12-F1	*Ribes nigrum* (black currant), leaves	6	3
12-F2	*Ribes nigrum* (black currant), leaves	6	7
13-F1	*Trifolium repens* (white clover), flowers	2	2
13-F2	*Trifolium repens* (white clover), flowers	1	9

[a]F1 fractions were eluted with acetone/water (30:70; v/v) and F2 fractions with acetone/water (50:50; v/v); sample 3-F1 was passed through the Sephadex column twice; F1b after the second Sephadex purification. % PC, procyanidin concentration from total proanthocyanidin concentration as percent by thiolysis; mDP, mean degree of polymerization by thiolysis.

cyanidins were directly infused into the ESI source with a syringe pump at a flow rate of 5−40 μL/min. The concentrations of the aqueous proanthocyanidin solutions were 40 μg/mL for pure compounds and 2 mg/mL for proanthocyanidin-rich fractions. The ranges of cone voltage and collision energy varied between 10 and 170 V and between 5 and 50 eV, respectively.

Calibration Curves for Procyanidin and Prodelphinidin Contents. Solutions for calibration curves were produced from stock solutions (1.0 mg/mL) of procyanidin-rich sample 5-F2 (procyanidin content = 95%, determined by thiolysis) and prodelphinidin-rich sample 13-F2 (prodelphinidin content = 98%, determined by thiolysis) by dilution with acetonitrile/water (20:80, v/v). The dilution range was from 1.0 to 0.01 mg/mL.

Limit of Detection, Limit of Quantitation, and Linearity. Procyanidin and prodelphinidin dimers were used for determination of the limit of detection (LOD) and limit of quantitation (LOQ) for the presented MRM method at signal-to-noise ratios (S/N) >3 and >10, respectively. Dilution series were prepared from stock solutions of 40 μg/mL and diluted with H_2O. The dilution range was from 40 μg/mL to 0.019 ng/mL. Three replicates of each sample were run.

RESULTS AND DISCUSSION

Optimization of the MRM Methods. On the basis of the quinone methide cleavage theory (Figure 1B), both terminal and extension units of procyanidins and prodelphinidins yield different fragments,[4,27,28] and it was hypothesized that it would be possible to develop separate MRM methods for the specific detection of these fragments. To optimize MRM methods for the qualitative and quantitative analyses of procyanidin and prodelphinidin units of proanthocyanidins, direct flow injection experiments of the reference compounds were performed in both positive-ion and negative-ion modes. The reference compounds consisted of different proanthocyanidin monomers and oligomers, as well as semipurified mixtures of proanthocyanidin oligomers and polymers (fractions 1-F1−4-F2) (Table 1). Negative mode was superior to positive mode in terms of sensitivity, particularly for the terminal units (Figure 2) and, thus, negative-ion mode was selected to be used in the MRM methods.

As previously reported,[4,27,29,30] both procyanidin and prodelphinidin units of proanthocyanidins yielded two different types of ions in the collision-induced MS analysis depending on whether they represented the extension or terminal units of the

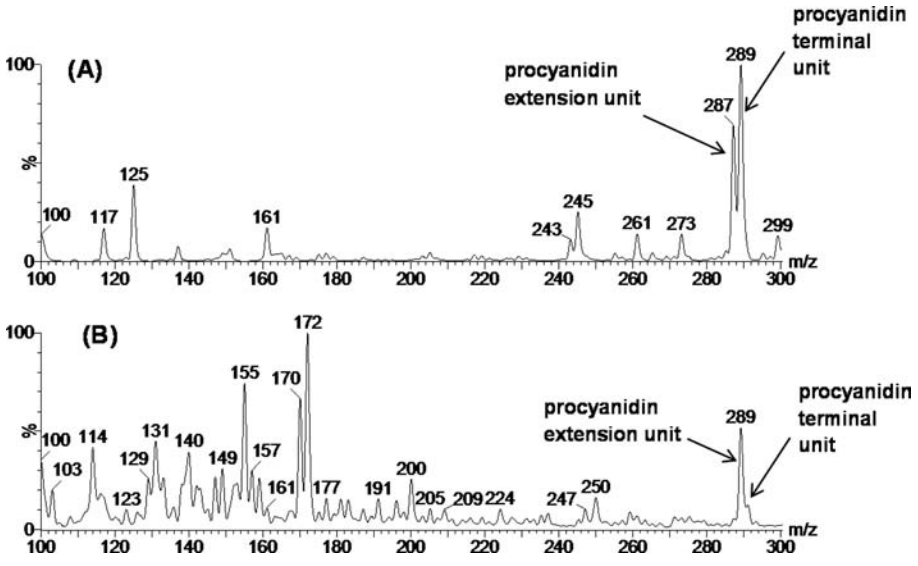

Figure 2. Detection of extension and terminal units of procyanidin trimer with negative-ion mode (A) and positive-ion mode (B).

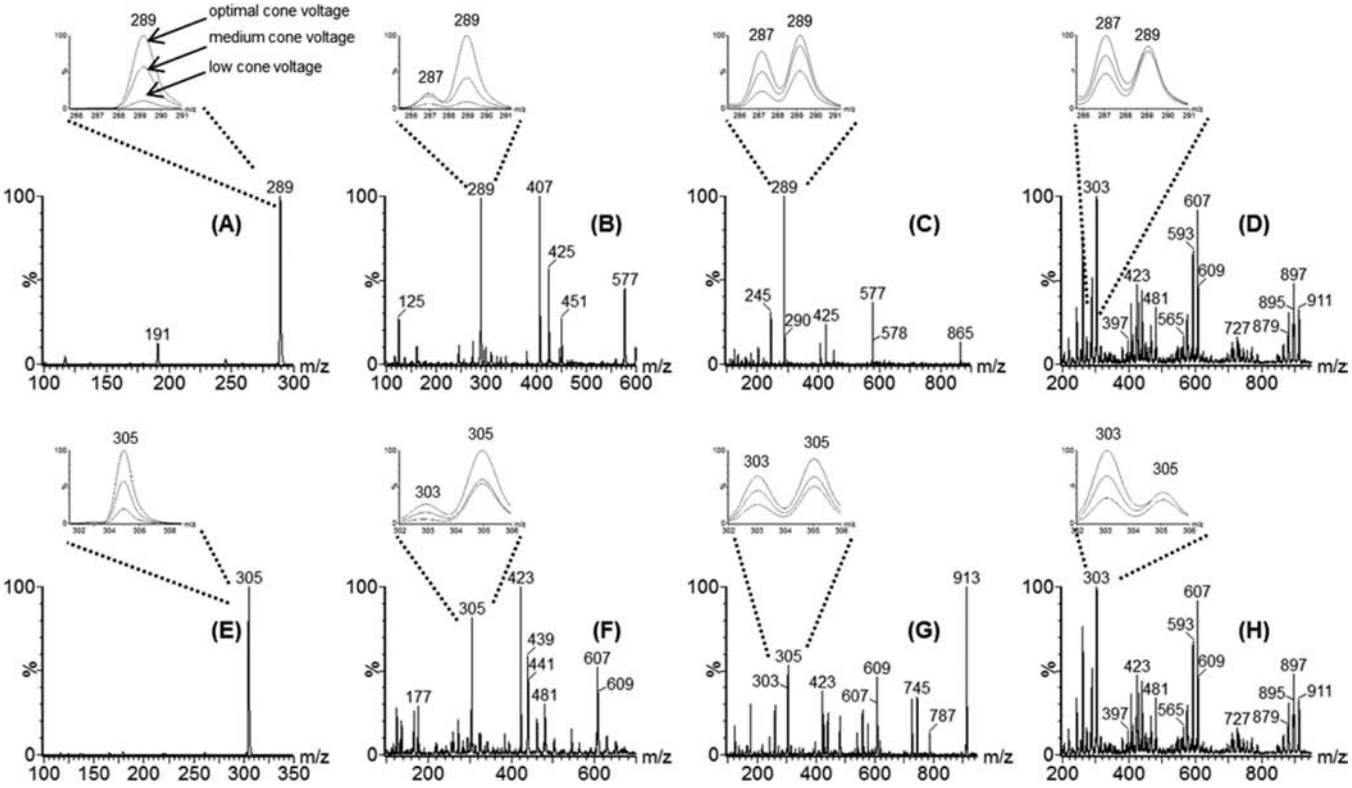

Figure 3. Mass spectra of proanthocyanidin monomers, dimers, trimers, and polymers obtained by in-source fragmentation: (A) catechin; (B) procyanidin dimer; (C) procyanidin trimer; (D) sample 1-F2; (E) epigallocatechin; (F) prodelphinidin dimer; (G) prodelphinidin trimer; (H) sample 1-F2. The insets show how the intensities of the extension units (m/z 287 and 303) and terminal units (m/z 289 and 305) change due to shifts in cone voltage. See Table 1 for fraction identities.

corresponding proanthocyanidin molecule (Figure 1B). For procyanidins the characteristic ions formed via quinone methide cleavage were m/z 287 and 289 and for prodelphinidins m/z 303 and 305, respectively. Also, ions formed by retro-Diels–Alder and heterocyclic ring fission mechanisms were detected at low intensity, but because these do not give specific information of proanthocyanidin extension and terminal units, they were not included in the MRM development section.

Figure 3 shows a comparison of the mass spectra of monomeric, dimeric, and trimeric procyanidins and prodelphinidins and oligomeric procyanidin/prodelphinidin mixture (sample 1-F2) with direct flow infusion into the MS. The zoomed m/z areas present results obtained with low, medium, and optimal cone voltages. In all cases the optimal cone voltage resulted in highest response and, correspondingly, the low cone voltage in lowest response. Catechin and epigallocatechin monomers yielded only ions at m/z 289 and 305, respectively. The other proanthocyanidin samples yielded ions at both m/z 287 and 289 for procyanidins and m/z 303 and 305 for prodelphinidins. The intensity of ions at m/z 287 and 303 increased as the degree of polymerization of the proanthocyanidin molecule increased, suggesting that the intensity of these ions in MS analysis was related to the number of extension units present in the original proanthocyanidin structure.

The cone voltage optimization experiments revealed that the larger the proanthocyanidin, the higher the cone voltage required to produce maximal ion intensities for the proanthocyanidin fragments. For monomers the optimal cone voltage was 30 V for ions at m/z 289 and 305. For dimers the optimal cone voltages were 50, 60, 60, and 55 V for ions m/z 287, 289, 303, and 305, respectively. Similar cone voltages have been also previously proposed for these fragmentations of the proanthocyanidin dimers and trimers.[31] For the proanthocyanidin fractions containing both oligomers and polymers, the optimal cone voltages ranged from 100 to 150 V. In general, the optimal cone voltage required for prodelphinidins was higher than that for procyanidins and higher for extension units (ions at m/z 287 and 303) than for terminal units (ions at m/z 289 and 305). These results indicate differences in the collision-induced dissociation of different types of proanthocyanidin molecules and that high energy is required to fragment as many extension units as possible.

The results from these experiments suggested that a single cone voltage cannot be used for the optimal detection of all types of proanthocyanidins. Therefore, the choice of an optimal cone voltage is not straightforward; the ideal cone voltage is highly dependent upon the size, composition, and structure of the analytes of interest. For example, when only small proanthocyanidins are studied, increasing the cone voltages beyond the optimum induces fragmentation before the ions enter the mass filter, resulting in a decrease in sensitivity. In contrast, when proanthocyanidin oligomers and polymers are studied, use of a too low cone voltage would lead to poor fragmentation of the original molecule and thus low sensitivity for the detection of the terminal and especially extension units. This in turn would cause underestimation of the concentrations of the oligomers and polymers.

Enhanced selectivity and sensitivity of the method is achieved by collision energies separately optimized for product ions of the specific procyanidin and prodelphinidin units. Such an approach allows the accurate qualitative and quantitative

Table 2. Cone Voltages and Collision Energies in the New MRM Method for the Detection of Procyanidin (PC) and Prodelphinidin (PD) Terminal and Extension Units

unit	precursor ion (m/z)	CV[a] 1 (V)	CV 2 (V)	CV 3 (V)	CV 4 (V)	CV 5 (V)	CV 6 (V)	fragment ion (m/z)	collision energy (eV)
PC extension unit	287	30	50	75	85	110	140	125	15
PC terminal unit	289	30	50	75	85	110	140	245	15
PD extension unit	303	30	55	80	110	130	150	125	20
PD terminal unit	305	30	55	80	110	130	150	125	20

[a]CV, cone voltage.

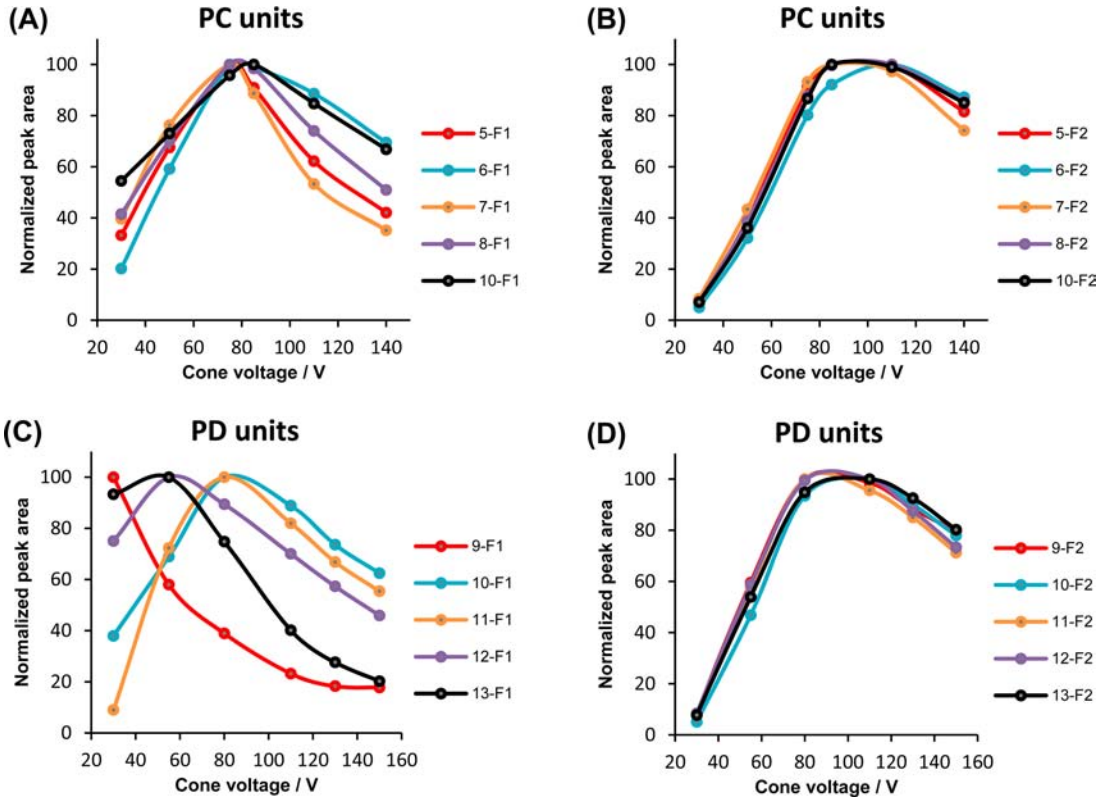

Figure 4. Normalized peak areas from the MRM chromatograms of procyanidin (PC) units (sum of procyanidin terminal and extension units) and prodelphinidin (PD) units (sum of prodelphinidin terminal and extension units) obtained with F1 fractions containing smaller proanthocyanidins (A, C) and F2 fractions containing larger proanthocyanidins (B, D). See Table 1 for fraction identities.

analyses of complex proanthocyanidins directly from plant crude extracts. In contrast to identifying optimal cone voltages, the choice of optimal collision energy was straightforward. The product ions produced from the ions derived from terminal and extension units always had the same optimal collision energy. The optimal collision energy for both transitions m/z 287 → 125 and 289 → 245 was 15 eV. For both transitions of m/z 303 → 125 and 305 → 125 the optimal collision energy was 20 eV. On the basis of the results from cone voltage and collision energy optimizations, one MRM method containing six different cone voltages for each terminal and extension unit ion and one optimal collision energy for the accumulation of the unit-specific product ions was developed (Table 2).

In previous studies, cone voltages and collision energies have been used for the optimization of separate MRM methods for small proanthocyanidin oligomers[32,32−36] and for studying the fragmentation patterns of proanthocyanidins.[22,37,38] No compound-specific MRM methods have been reported for larger proanthocyanidin oligomers or polymers as the limit has been with tetramers.[23−25,31] This highlights the novelty of our approach: to our knowledge, no previous study has used UPLC-MS/MS with a range of cone voltages and optimized collision energies for the detection of extension and terminal units and thus for the detection of total oligomeric and polymeric proanthocyanidins.

Effect of Optimized Cone Voltages and Sample Composition on Peak Areas. After optimization of MRMs, the new method was rigorously tested with an independent set of 18 structurally diverse proanthocyanidin fractions (5-F1−13-F2) prepared from nine plant species; the proportion of procyanidin units in these fractions ranged from 1 to 95% and mDP ranged from 2 to 10 (Table 1). Figure 4 shows the normalized peak areas for all 18 proanthocyanidin fractions plotted as a function of cone voltage. For better visual clarity, peak areas (a sum of terminal and extension units) for procyanidin-derived ions are shown for only the five procyanidin-richest fractions in Figure 4A,B. Similarly, peak areas (a sum of terminal and extension units) for prodelphinidin-derived ions are shown for the five prodelphinidin-richest fractions in Figure 4C,D.

For every F1 fraction, the largest procyanidin peak areas were detected with 75−80 V (Figure 4A). However, the profiles of

dx.doi.org/10.1021/jf500745y | J. Agric. Food Chem. 2014, 62, 3390−3399

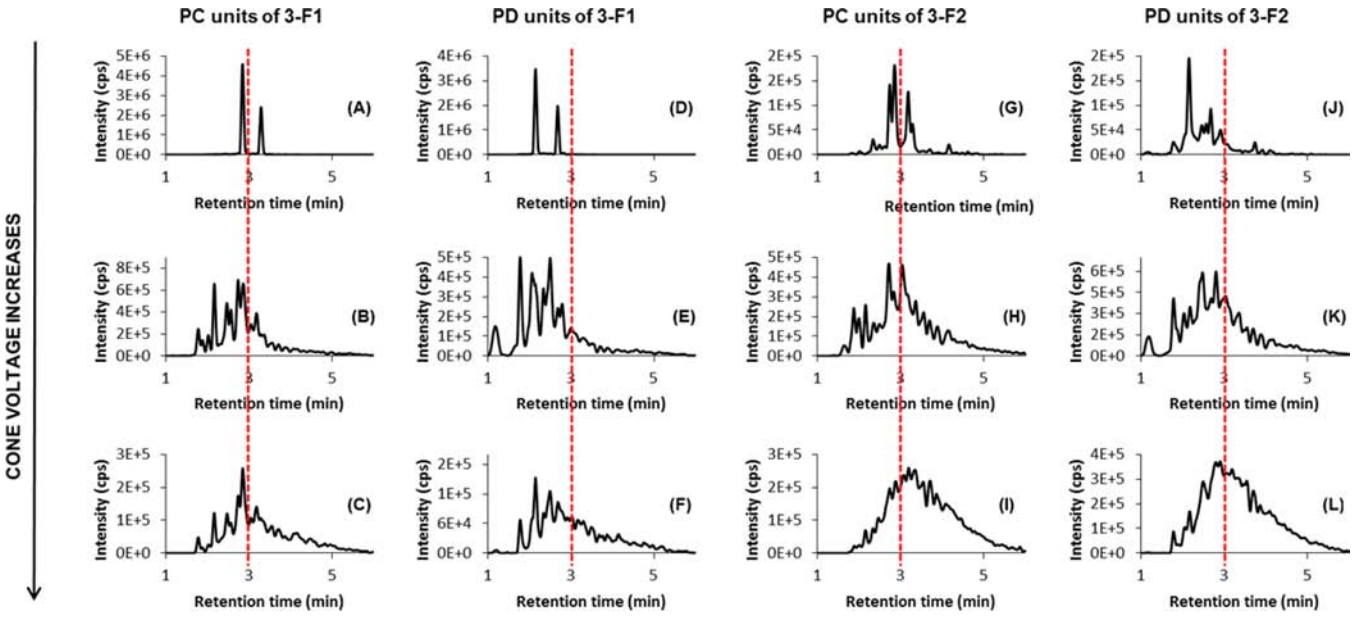

Figure 5. MRM chromatograms of procyanidin (PC) and prodelphinidin (PD) units for samples 3-F1 and 3-F2 (see Table 1) obtained with cone voltages of 30 V (A, D, G, J), 80 V (B, E, H, K), and 140 V (C, F, I, L).

the plots differed a little. In general, when the cone voltage increased beyond the optimal, the peak areas decreased more rapidly with samples having low mDP. This is in agreement with the earlier findings showing that smaller proanthocyanidins require lower cone voltages for their optimal detection.[31] In contrast, the procyanidin response of the larger proanthocyanidins of the F2 fractions did not significantly decrease even though the cone voltage was increased from 80 to 140 V (Figure 4B). This again confirmed the presence of larger proanthocyanidins in these samples.

The plots for prodelphinidin-richest F1 fractions were the most diverse compared to all other fractions (Figure 4C). The mDP values from thiolysis ranged from two to five and a qualitative comparison of the chromatograms revealed differences in the prodelphinidin composition of these fractions (data not shown). For example, fractions 9-F1 and 10-F1 both had an mDP of 3, but the prodelphinidin profiles differed. Detection with low cone voltage suggested that the 9-F1 sample contained a lot of monomers, which caused the sharp decrease in peak area with increasing cone voltage. The 10-F1 sample had a lot of oligomers in addition to monomers, and this explained the increasing peak area with increasing cone voltage. Similarly to the procyanidin detection (Figure 4B), the prodelphinidin-richest F2 fractions showed largest peak areas with cone voltages of 80−100 V. Also, the profiles of the two plots were similar (Figure 4B,D). The similarity among the F2 fractions was due to the absence of smaller proanthocyanidins, as these eluted generally in F1 fractions. Again, these results suggested that the developed MRM method is able to reveal whether the analyzed sample contains mainly small or large proanthocyanidins.

Qualitative Comparison of the MRM Chromatograms. The number of proanthocyanidin isomers increases with increasing degree of polymerization.[39] As a result, proanthocyanidin samples with high mDP generate a large unresolved hump in RP-LC.[40−43] However, a qualitative comparison of the chromatograms showed that higher cone voltages caused a shift in the detected proanthocyanidin hump to the right, that is, to later retention times and larger proanthocyanidins. When the chromatograms obtained with cone voltages of 30, 80, and 140 V are compared, a clear shift in the detected hump can be seen for both procyanidins (Figure 5A−C,G−I) and prodelphinidins (Figure 5D−F,J−L). A vertical line is shown that crosses the *x*-axis at 3 min to highlight these shifts. The lowest cone voltage detected mainly monomers and some smaller oligomers that are witnessed as sharp chromatographic peaks. Higher cone voltages also detected the proanthocyanidin hump characteristic for larger oligomers and polymers. In general, prodelphinidins eluted at earlier retention times than corresponding procyanidins. This can be seen when the chromatogram pairs A and D, B and E, C and F, G and J, H and K, and I and L in Figure 5 are compared. The elution time of compounds from reverse phase columns tends to be inversely related to their polarity; thus, shorter retention times of prodelphinidins would be expected because of their greater polarity associated with more extensive hydroxylation of the B-ring.[44]

In addition to the distribution of procyanidins and prodelphinidins along the chromatographic hump, the distribution of procyanidin and prodelphinidin extension and terminal units can be investigated by examining their MRM chromatograms. For example, the MRM chromatograms of extension units and terminal units of samples 1-F2 and 2-F2 are presented in Figure 6. To focus mainly on larger oligomers and polymers, MRM chromatograms with a cone voltage of 140 V were compared. In the 1-F2 sample, the MRM chromatographic hump of procyanidin extension units eluted later than prodelphinidin extension units and procyanidin and prodelphinidin terminal units (Figure 6A). This suggests that procyanidin extension units were most abundant in late-eluting proanthocyanidin molecules. It could also be seen that the chromatographic hump of terminal prodelphinidin units eluted earlier than terminal procyanidin units. This indicates that prodelphinidin terminal units were most abundant in earlier eluting proanthocyanidin molecules. In contrast, the shape of the chromatographic hump of procyanidin terminal units suggests that they were distributed fairly evenly among the proanthocyanidins. In contrast to the 1-F2 sample, the 2-F2

dx.doi.org/10.1021/jf500745y | J. Agric. Food Chem. 2014, 62, 3390−3399

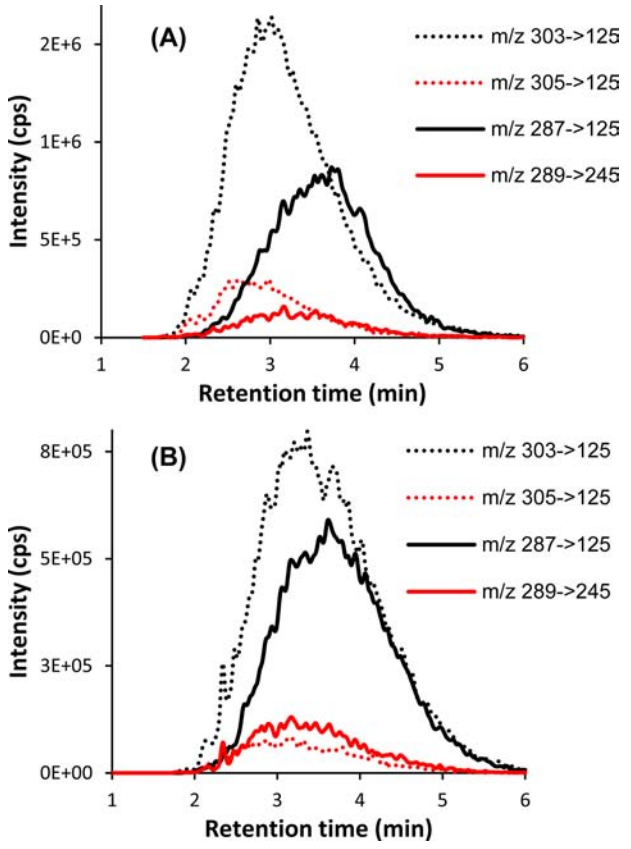

Figure 6. MRM chromatograms of procyanidin extension units (m/z 287 → 125), procyanidin terminal units (m/z 289 → 245), prodelphinidin extension units (m/z 303 → 125), and prodelphinidin terminal units (m/z 305→ 125) for samples 1-F2 (A) and 2-F2 (B). See Table 1 for fraction identities.

sample (Figure 6B) had a more uniform distribution of all procyanidin and prodelphinidin terminal and extension units, which would indicate a relatively homogeneous distribution of these units in the proanthocyanidins of this particular sample. The same kind of comparisons can be made at lower cone voltages to provide information on how the extension and terminal units of procyanidin and prodelphinidin are distributed across smaller oligomeric proanthocyanidins.

Determination of Proanthocyanidin Contents and Procyanidin/Prodelphinidin Ratios. To determine the total content of proanthocyanidins and procyanidin/prodelphinidin ratios, calibration curves were produced for the developed MRM method with pure procyanidins (fraction 5-F2) and pure prodelphinidins (fraction 13-F2). The five highest cone voltages were used for detection, and resulting peak areas were summed. The lowest cone voltage was not used to avoid monomer detection, because they are not classified as proanthocyanidins. These calibration curves were then used for estimation of procyanidin and prodelphinidin concentrations in all 18 proanthocyanidin fractions (5-F1−13-F2). The resulting proanthocyanidin contents were compared to proanthocyanidin contents estimated by thiolysis and HCl-butanol assay. Procyanidin/prodelphinidin ratios were then compared to procyanidin/prodelphinidin ratios estimated by thiolysis. A good correlation for proanthocyanidin contents with both thiolysis (R^2 = 0.82) and HCl-butanol assay (R^2 = 0.86) was achieved as was an excellent agreement for procyanidin/prodelphinidin ratios between the thiolysis and MRM results (R^2 = 0.98). These results suggest that our MRM approach allows both qualitative and quantitative analyses of complex proanthocyanidins directly from plant extracts.

Estimating the Mean Degree of Polymerization. On the basis of the quinone methide cleavage theory[4,27] (Figure 1B), it was hypothesized that an equation could be empirically developed to calculate the mDP of proanthocyanidins from total peak areas obtained for procyanidin and prodelphinidin extension and terminal units. A preliminary equation using estimated coefficients for each MRM transition was developed by comparing the thiolysis and MRM results from the 18 procyanidin- and prodelphinidin-rich fractions (5-F1−13-F2). Initially equations were developed individually for each cone voltage, but finally only one equation was developed by using the total peak area from the five highest cone voltages: 50, 75, 85, 110, and 140 V for procyanidins and 55, 80, 110, 130, and 150 V for prodelphinidins. The lowest cone voltage (30 V) was not used to avoid detection of monomers because monomers cause underestimation of the mDP. The resulting equation is as follows:

$$\mathrm{mDP} = \frac{0.37A_{287} + 0.42A_{289} + 2.15A_{303} + 0.68A_{305}}{0.42A_{289} + 0.68A_{305}}$$

A_{287}, A_{289}, A_{303}, and A_{305} are the sums of peak areas determined from MRM chromatograms of procyanidin extension units (m/z 287 → 125), procyanidin terminal units (m/z 289 → 245), prodelphinidin extension units (m/z 303 → 125), and prodelphinidin terminal units (m/z 305→ 125), respectively, with the five highest cone voltages (Table 2). The coefficients of the four ions differ due to the differing propensities of procyanidin/prodelphinidin extension and terminal units to undergo ionization. It should be noted that ionization coefficients could differ among UPLC-MS/MS instruments. Therefore, the correct ionization coefficients should be individually checked for each instrument. When this is done, the samples used should cover a wide range of proanthocyanidin types with various features (procyanidin/prodelphinidin ratio, mDP). In this study, 18 was a sufficient number of varying proanthocyanidin samples for adjusting these coefficients.

For the 18 samples used in the calibration, the mDPs estimated by the equation were naturally related (R^2 = 0.94) to results obtained by thiolysis. The equation was then independently tested with nine additional proanthocyanidin-rich fractions (1-F1−4-F2) to prove that it functions well also with other independent samples (R^2 = 0.90). Together these 27 fractions represented a diverse set of proanthocyanidins, with mDP values ranging from 2 to 15 and compositions varying from 95% procyanidin to 99% prodelphinidin. Therefore, these results indicated that the developed MRM method accompanied by this equation can reliably estimate the mDP of a wide variety of proanthocyanidins.

Previously, thiolysis and phloroglucinolysis have been the most commonly used tools for achieving information of proanthocyanidin content, procyanidin/prodelphinidin distribution, and mDP from plant extracts.[2,13−17] However, in these methods, proanthocyanidins are cleaved into monomer units before analysis, and all information of the individual oligomers and polymers is lost. Therefore, these methods lack the possibility to characterize the original oligomer and polymer fingerprint. In the presented UPLC-MS/MS method, the proanthocyanidin fragmentation takes place after the chromato-

graphic step, and therefore it is possible to estimate how the different proanthocyanidins, in terms of their procyanidin and prodelphinidin composition and mDP, are distributed along the chromatographic hump typically produced by large proanthocyanidin oligomers and polymers. Another advantage of the presented UPLC-MS/MS method is its sensitivity. It can be used to analyze samples produced from as little as 1 mg of plant powder, whereas thiolysis and phloroglucinolysis typically require relatively large amounts of plant tissue, in the range of hundreds of milligrams, for analysis.[17−19]

Repeatability of the UPLC-MS/MS Mthod. The repeatability of the method was determined using Student's *t* test at the 95% confidence interval. Five replicates of nine different proanthocyanidin fractions (1-F1−4-F2) were analyzed with the MRM method containing six different cone voltages and one optimal collision energy for each terminal and extension unit (Table 2). Results were presented as confidence intervals of the sums of peak areas obtained with different cone voltages and concentrations for procyanidins and prodelphinidins, procyanidin/prodelphinidin ratios, and mDP values. The procyanidin and prodelphinidin concentrations were calculated as milligrams per gram in fractions and procyanidin/prodelphinidin ratios as percent procyanidin. The relative standard deviation (RSD) for all nine samples with five replicates was determined from these results. The results showed that the quantitative determination of procyanidins is generally slightly less accurate than that for prodelphinidins (RSD = 3.5 and 2.1%, respectively). The RSDs for procyanidin/prodelphinidin ratio and mDP were small (0.6 and 1.4%, respectively), which demonstrates the pronounced reliability of this method for these qualitative measurements.

Limit of Detection, Limit of Quantitation, and Linearity. LOD, LOQ, and linearity were determined with the presented method for procyanidin and prodelphinidin dimers. LOD for procyanidin dimer was 16 ng/mL, whereas LOQ was 23 ng/mL. For prodelphinidin dimer, the corresponding values were 170 and 190 ng/mL, respectively. There was a difference in the efficiency of detection of procyanidin terminal and extension units; procyanidin terminal units were detected at 8 times lower concentration than the extension units. For prodelphinidins the difference was smaller; prodelphinidin terminal units were detected at 2 times lower concentration than prodelphinidin extension units. The linear areas were 0.04−2.5 μg/mL for procyanidins and 0.5−10 μg/mL for prodelphinidins. However, because the methodology presented is group-specific, that is, it is used for the analysis of the total amount of proanthocyanidins, values determined with pure dimers do not truly illustrate the limits of the method. Depending on the analyzed samples, different types of proanthocyanidins are detected from very small concentrations, whereas other proanthocyanidins can be detected only from more concentrated samples. In this study, it was not possible to determine the limits of detection of all possible individual proanthocyanidin compounds, and this will have to wait until pure oligomers and polymers of procyanidin and prodelphinidin compounds become available.

Use of the Method for Proanthocyanidin Characterization. Plants produce complex and often heterogeneous mixtures of procyanidins and prodelphinidins and, apart from small oligomers, it is practically impossible to purify large procyanidin and prodelphinidin oligomers or polymers individually.[6,14,45] For this reason the current research utilized a mixture of oligo- and polymeric quantitation standards that were chosen on the basis of their procyanidin and prodelphinidin purities. Naturally, the best quantitation results are expected with proanthocyanidin standards that are isolated from the very same species that is investigated for its proanthocyanidin content. This approach lowers the risk of utilization of wrong types of quantitation standards, but is too laborious with investigations that include hundreds of species, for example. In such cases, our MRM method offers a practical solution to significantly narrow the need for hundreds of standards.

We have used the method for the analysis of crude extracts of over 1000 plant species and found that the MRM chromatographic proanthocyanidin profiles (chromatographic fingerprint of the procyanidin and prodelphinidin extension and terminal units) (Figure 6) are not different with all of the species. Instead, it is possible to find several species clusters that share similar proanthocyanidin profiles (Salminen, unpublished observations). Thus, it would be sufficient to isolate one well-characterized proanthocyanidin standard per a given species cluster as proanthocyanidin fingerprints do not differ significantly within the cluster. Such an approach would allow the production of a library of proanthocyanidin standards, and each time the most correct standard could be chosen for any new plant species that was analyzed for its proanthocyanidin fingerprint during the 10 min analysis with the developed MRM method.

The present method can be used for both qualitative and quantitative analyses of complex proanthocyanidins directly from plant crude extracts. Instead of time-consuming degradation required by thiolysis or phloroglucinolysis, the present method describes in-source fragmentation of the UPLC-separated proanthocyanidin molecules by cone voltages optimized for terminal and extension units of procyanidins and prodelphinidins. UPLC enables rapid chromatography of different kinds of proanthocyanidins, whereas TQ-MS fragments compounds into proanthocyanidin-specific precursor and product ions for detection with MRM methods. The selective nature of the method enables the estimation of both the procyanidin/prodelphinidin ratio and mDP for the proanthocyanidins during the 10 min MS/MS analysis. Furthermore, because the proanthocyanidin fragmentation takes place after the chromatographic step, it is possible to estimate how the different proanthocyanidins in terms of their procyanidin and prodelphinidin composition and mDP are distributed along the chromatographic hump typically produced by large proanthocyanidin polymers. The UPLC-MS/MS method is able to handle 140 extracts, produced from as little as 1 mg of plant powder, in a day, and it offers a user-friendly, robust, and fast addition to the chemistry tools currently used for the qualitative and quantitative screening of large numbers of proanthocyanidin-containing plants for their bioactive proanthocyanidin types and content.

■ ASSOCIATED CONTENT

Ⓢ Supporting Information

UPLC traces of the fractions used in the present work (Figure S1−S7). HCl-butanol calibration curves used for quantitation of proanthocyanidin contents in the present work (Figure S8). UPLC-MS/MS calibration curves used for quantitation of procyanidins and prodelphinidins in the present work (Figure S9). Cone voltage optimization plots for the accumulation of precursor ions presenting procyanidin and prodelphinidin extension and terminal units (Figure S10). Collision energy

optimization plots for the accumulation of product ions presenting procyanidin and prodelphinidin extension and terminal units (Figure S11). Correlations between proanthocyanidin content determined by the MRM and thiolysis and MRM and HCl-butanol methods, correlation between procyanidin percentage of total proanthocyanidin content and correlation between mean degree of polymerization determined by the MRM and thiolysis methods for proanthocyanidin-rich fractions used in the present work (Figure S12). The effect of cone voltage to the peak areas of fractions 1-F1 to 13-F2 (Figure S13). Repeatability data of the presented MRM method determined with the Student's *t* test at 95% confidence interval (Table S1). This material is available free of charge via the Internet at http://pubs.acs.org.

AUTHOR INFORMATION

Corresponding Author

*(M.T.E.) Phone: +358 2 333 6755. E-mail: marica.engstrom@utu.fi.

Funding

This study was supported by Turku University Foundation, Academy of Finland (Grant 258992 to J.P.S.), the University of Turku Graduate School (UTUGS), an EU Marie Curie Initial Training Network (PITN-GA-2011-289377, "LegumePlus"), and an ARS Specific Cooperative Agreement with University of Reading (58-3655-0-155F). The Strategic Research Grant (Ecological Interactions) enabled the use of the UPLC-MS/MS instrument.

Notes

The authors declare no competing financial interest.

ACKNOWLEDGMENTS

We thank Aina Ramsay, Ron Brown, Jorma Kim, Milla Leppä, and Jaana Liimatainen for help with sample purification. We acknolwedge Jeff Ahern for checking the English language and Maarit Karonen, Nicolas Baert, Anne Koivuniemi, Honorata Ropiak, and Jere Koira for general help and discussion.

ABBREVIATIONS USED

UPLC, ultrahigh-performance liquid chromatography; TQ-MS, triple-quadrupole mass spectrometer; MRM, multiple reaction monitoring; mDP, mean degree of polymerization; ESI, electrospray ionization; LOD, limit of detection; LOD, limit of quantitation; S/N, signal-to-noise ratio; RSD, relative standard error

REFERENCES

(1) Haslam, E. Proanthocyanidins. In *Plant Polyphenols: Vegetable Tannins Revisited*; Cambridge University Press: Cambridge, UK, 1989; pp 14−79.

(2) Hemingway, R. W. Structural variation in proanthocyanidins and their derivatives. In *Chemistry and Significance of Condensed Tannins*; Hemingway, R. W., Karchesy, J. J., Eds.; Plenum Press: New York, 1989; pp 83−107.

(3) Porter, L. J. Tannins. In *Methods in Plant Biochemistry*; Dey, P. M., Harborne, J. B., Eds.; Academic Press: New York, 1989; Vol. 1, pp 389−419.

(4) Gu, L.; Kelm, M. A.; Hammerstone, J. F.; Beecher, G.; Holden, J.; Haytowitz, D.; Prior, R. L. Screening of foods containing proanthocyanidins and their structural characterization using LC-MS/MS and thiolytic degradation. *J. Agric. Food Chem.* **2003**, *51*, 7513−7521.

(5) Dixon, R. A.; Xie, D.-Y.; Sharma, S. B. Proanthocyanidins− a final frontier in flavonoid research? *New Phytol.* **2005**, *165*, 9−28.

(6) Mueller-Harvey, I. Unravelling the conundrum of tannins in animal nutrition and health. *J. Sci. Food Agric.* **2006**, *86*, 2010−2037.

(7) Hoste, H.; Jackson, F.; Athanasiadou, S.; Thamsborg, S. M.; Hoskin, S. O. The effects of tannin-rich plants on parasitic nematodes in ruminants. *Trends Parasitol.* **2006**, *22*, 253−261.

(8) Brunet, S.; Jackson, F.; Hoste, H. Effects of sainfoin (*Onobrychis viciifolia*) extract and monomers of condensed tannins on the association of abomasal nematode larvae with fundic explants. *Int. J. Parasitol.* **2008**, *38*, 783−790.

(9) Novobilský, A.; Mueller-Harvey, I.; Thamsborg, S. M. Condensed tannins act against cattle nematodes. *Vet. Parasitol.* **2011**, *182*, 213−220.

(10) Novobilský, A.; Stringano, E.; Carbonero, C. H.; Smith, L. M. J.; Enemark, H. L.; Mueller-Harvey, I.; Thamsborg, S. M. *In vitro* effects of extracts and purified tannins of sainfoin (*Onobrychis viciifolia*) against two cattle nematodes. *Vet. Parasitol.* **2013**, *196*, 532−537.

(11) Molan, A. L.; Waghorn, G. C.; Min, B. R.; McNabb, W. C. The effect of condensed tannins from seven herbages on *Trichostrongylus colubriformis* larval migration *in vitro*. *Folia Parasitol.* **2000**, *47*, 39−44.

(12) Manolaraki, F.; Sotiraki, S.; Skampardonis, V.; Volanis, M.; Stefanakis, A.; Hoste, H. Anthelmintic activity of some Mediterranean browse plants against parasitic nematodes. *Parasitology* **2010**, *137*, 685−696.

(13) Cheynier, V.; Fulcrand, H. Analysis of polymeric proanthocyanidins and complex polyphenols. In *Methods in Polyphenol Analysis*; Santos-Buelga, C., Williamson, G., Eds.; Royal Society of Chemistry: Cambridge, UK, 2003; pp 284−313.

(14) Hümmer, W.; Schreier, P. Analysis of proanthocyanidins. *Mol. Nutr. Food Res.* **2008**, *52*, 1381−1398.

(15) Gu, L. Analysis methods of proanthocyanidins. In *Analysis of Antioxidant-Rich Phytochemicals*; Xu, Z., Howard, L. R., Eds.; Wiley-Blackwell: Oxford, UK, 2012; pp 247−274.

(16) Thompson, R. S.; Jacques, D.; Haslam, E.; Tanner, R. J. N. Plant proanthocyanidins. Part I. Introduction; the isolation, structure, and distribution in nature of plant procyanidins. *J. Chem. Soc., Perkin Trans. 1* **1972**, *11*, 1387−1399.

(17) Karonen, M.; Leikas, A.; Loponen, J.; Sinkkonen, J.; Ossipov, V.; Pihlaja, K. Reversed-phase HPLC-ESI/MS analysis of birch leaf proanthocyanidins after their acidic degradation in the presence of nucleophiles. *Phytochem. Anal.* **2007**, *18*, 378−386.

(18) Gea, A.; Stringano, E.; Brown, R. H.; Mueller-Harvey, I. In situ analysis and structural elucidation of sainfoin (*Onobrychis viciifolia*) tannins for high-throughput germplasm screening. *J. Agric. Food Chem.* **2011**, *59*, 495−503.

(19) Hellström, J. K.; Törrönen, A. R.; Mattila, P. H. Proanthocyanidins in common food products of plant origin. *J. Agric. Food Chem.* **2009**, *57*, 7899−7906.

(20) Guillarme, D.; Schappler, J.; Rudaz, S.; Veuthey, J.-L. Coupling ultra-high-pressure liquid chromathography with mass spectrometry. *Trends Anal. Chem.* **2010**, *29*, 15−27.

(21) Motilva, M.-J.; Serra, A.; Macià, A. Analysis of food polyphenols by ultra high-performance liquid chromatography coupled to mass spectrometry: an overview. *J. Chromatogr., A* **2013**, *1292*, 66−82.

(22) Rodriguez-Aller, M.; Gurny, R.; Veuthey, J.-L.; Guillarme, D. Coupling ultra high-pressure liquid chromatography with mass spectrometry: constraints and possible applications. *J. Chromatogr., A* **2013**, *1292*, 2−18.

(23) Valls, J.; Millán, S.; Martí, M. P.; Borràs, E.; Arola, L. Advanced separation methods of food anthocyanins, isoflavones and flavanols. *J. Chromatogr., A* **2009**, *1216*, 7143−7172.

(24) Prasain, J. K.; Wang, C.-C.; Barnes, S. Mass spectrometric methods for the determination of flavonoids in biological samples. *Free Radical Biol. Med.* **2004**, *37*, 1324−1350.

(25) Prasain, J. K.; Barnes, S. Uptake and metabolism of dietary proanthocyanidins. In *Polyphenols in Human Health and Disease*; Watson, R. R., Preedy, V. R., Zibadi, S., Eds.; Academic Press: London, UK, 2014; Vol. 1, pp 553−560.

(26) Benavides, A.; Montoro, P.; Bassarello, C.; Piacente, S.; Pizza, C. Catechin derivatives in *Jatropha macrantha* stems: characterisation and LC/ESI/MS/MS quali-quantitative analysis. *J. Pharm. Biomed. Anal.* **2006**, *40*, 639−647.
(27) Friedrich, W.; Eberhardt, A.; Galensa, R. Investigation of proanthocyanidins by HPLC with electrospray ionization mass spectrometry. *Eur. Food Res. Technol.* **2000**, *211*, 56−64.
(28) Mari, A.; Eletto, D.; Pizza, C.; Montoro, P.; Piacente, S. Integrated mass spectrometry approach to profile proanthocyanidins occurring in food supplements: analysis of *Potentilla erecta* L. rhizomes. *Food Chem.* **2013**, *141*, 4171−4178.
(29) Flamini, R. Recent applications of mass spectrometry in the study of grape and wine polyphenols. *ISRN Spectrosc.* **2013**, *2013*, 1−45, article ID 813563; http://dx.doi.org/10.1155/2013/813563 (accessed Jan 9, 2014).
(30) Rebello, L. P. G.; Lago-Vanzela, E. S.; Barcia, M. T.; Ramos, A. M.; Stringheta, P. C.; Da-Silva, R.; Castillo-Muñoz, N.; Gómez-Alonso, S.; Hermosín-Gutiérrez, I. Phenolic composition of the berry parts of hybrid grape cultivar BRS Violeta (BRS Rubea × IAC 1398-21) using HPLC-DAD-ESI-MS/MS. *Food Res. Int.* **2013**, *54*, 354−366.
(31) Zywicki, B.; Reemtsma, T.; Jekel, M. Analysis of commercial vegetable tanning agents by reversed-phase liquid chromatography−electrospray ionization−tandem mass spectrometry and its application to wastewater. *J. Chromatogr., A* **2002**, *970*, 191−200.
(32) Monagas, M.; Garrido, I.; Lebrón-Aguilar, R.; Bartolomé, B.; Gómez-Cordovés, M. C. Almond (*Prunus dulcis* (Mill.) D.A. Webb) skins as a potential source of bioactive polyphenols. *J. Agric. Food Chem.* **2007**, *55*, 8498−8507.
(33) Touriño, S.; Fuguet, E.; Jáuregui, O.; Saura-Calixto, F.; Cascante, M.; Torres, J. L. High-resolution liquid chromatography/electrospray ionization time-of-flight mass spectrometry combined with liquid chromatography/electrospray ionization tandem mass spectrometry to identify polyphenols from grape antioxidant dietary fiber. *Rapid Commun. Mass Spectrom.* **2008**, *22*, 3489−3500.
(34) Callemien, D.; Collin, S. Use of RP-HPLC-ESI (−)-MS/MS to differentiate various proanthocyanidin isomers in lager beer extracts. *J. Am. Soc. Brew. Chem.* **2008**, *66*, 109−115.
(35) Monagas, M.; Garrido, I.; Lebrón-Aguilar, R.; Gómez-Cordovés, M. C.; Rybarczyk, A.; Amarowicz, R.; Bartolomé, B. Comparative flavan-3-ol profile and antioxidant capacity of roasted peanut, hazelnut, and almond skins. *J. Agric. Food Chem.* **2009**, *57*, 10590−10599.
(36) Fraser, K.; Harrison, S. J.; Lane, G. A.; Otter, D. E.; Hemar, Y.; Quek, S.-Y.; Rasmussen, S. HPLC−MS/MS profiling of proanthocyanidins in teas: a comparative study. *J. Food Compos. Anal.* **2012**, *26*, 43−51.
(37) Sarnoski, P. J.; Johnson, J. V.; Reed, K. A.; Tanko, J. M.; O'Keefe, S. F. Separation and characterisation of proanthocyanidins in Virginia type peanut skins by LC−MS^n. *Food Chem.* **2012**, *131*, 927−939.
(38) Ojwang, L. O.; Yang, L.; Dykes, L.; Awika, J. Proanthocyanidin profile of cowpea (*Vigna unguiculata*) reveals catechin-*O*-glucoside as the dominant compound. *Food Chem.* **2013**, *139*, 35−43.
(39) Wilson, E. L. High-pressure liquid chromatography of apple juice phenolic compounds. *J. Sci. Food Agric.* **1981**, *32*, 257−264.
(40) Guyot, S.; Doco, T.; Souquet, J.-M.; Moutounet, M.; Drilleau, J.-F. Characterization of highly polymerized procyanidins in cider apple (*Malus sylvestris* var. *kermerrien*) skin and pulp. *Phytochemistry* **1997**, *44*, 351−357.
(41) Roux, E. L.; Doco, T.; Sarni-Manchado, P.; Lozano, Y.; Cheynier, V. A-type proanthocyanidins from pericarp of *Litchi sinensis*. *Phytochemistry* **1998**, *48*, 1251−1258.
(42) Adamson, G. E.; Lazarus, S. A.; Mitchell, A. E.; Prior, R. L.; Cao, G.; Jacobs, P. H.; Kremers, B. G.; Hammerstone, J. F.; Rucker, R. B.; Ritter, K. A.; Schmitz, H. H. HPLC method for the quantification of procyanidins in cocoa and chocolate samples and correlation to total antioxidant capacity. *J. Agric. Food Chem.* **1999**, *47*, 4184−4188.
(43) Karonen, M.; Loponen, J.; Ossipov, V.; Pihlaja, K. Analysis of procyanidins in pine bark with reversed-phase and normal-phase high-performance liquid chromatography-electrospray ionization mass spectrometry. *Anal. Chim. Acta* **2004**, *522*, 105−112.
(44) Koupai-Abyazani, M. R.; McCallum, J.; Bohm, B. A. Identification of the constituent flavanoid units in sainfoin proanthocyanidins by reverse-phase liquid chromatography. *J. Chromatogr.* **1992**, *594*, 117−123.
(45) Santos-Buelga, C.; Scalbert, A. Proanthocyanidins and tannin-like compounds − nature, occurrence, dietary intake and effects on nutrition and health. *J. Sci. Food Agric.* **2000**, *80*, 1094−1117.

method[20] avoided the introduction of EOF reverse additives (such as cetyltrimethylammonium chloride and cetyltrimethylammonium bromide) in the background electrolyte (BGE), which made the BGE simple and the baseline steady and smooth and further improved the repeatability and detection. In our lab, we also prepared a trimethylamine amination polychloromethyl styrene nanolatex (TMAPL) and TMAPL-coated capillary column (ccc-TMAPL; Figure 1), and it has

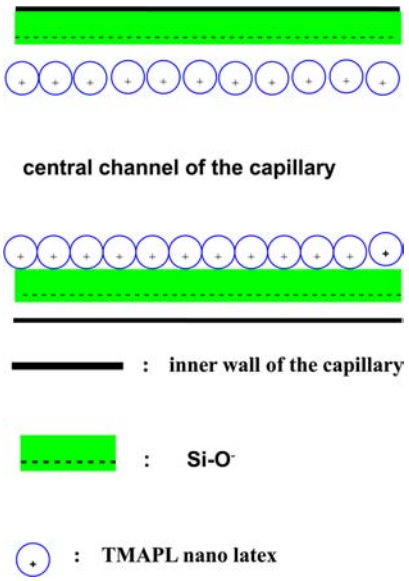

Figure 1. Schematic representation of the coating of the ccc-TMAPL.

been successfully applied for bromate analysis by OT-CEC.[36] Built on this success, we have in the present work crafted two major aims as follows: (i) to validate the practicability of the ccc-TMAPL and (ii) to develop an OT-CEC method for the analysis of nitrites and nitrates in hams and sausages.

MATERIALS AND METHODS

Reagents and Apparatus. Unless specified otherwise, all chemicals were of analytical reagent grade and obtained from Beijing Chemical Factory (Beijing, China). Thiourea was used as a neutral marker to measure the EOF and purchased from the Tianjin Dingshengxin Chemical Industry Limited Company (Tianjin, China). Water was purified using a Milli-Q water purification system (Millipore Corporation, Bedford, MA). The ham and sausage samples (made in different food factories in China) were purchased from the local supermarket. Their production dates were between May 2013 and June 2013, and they were kept in a refrigerating cabinet at 4 °C in the supermarket. All of solutions were degassed prior to use and filtered through a 0.22 μm membrane filter. Stock solutions (1 mg/mL) of $NaNO_3$ and $NaNO_2$ were prepared in deionized water. Quantification of samples was made using calibration curves of both nitrate and nitrite at the final concentrations of 10, 25, 50, 100, and 200 μg mL^{-1}. Each determination was performed in triplicate.

All experiments were performed on an Agilent CE system fitted with a diode-array detector and ChemStation software (Agilent Technologies, Waldbronn, Germany). The apparent pH was measured using a pH meter (Shanghai Weiye Factory, Shanghai, China). The dimensions of the bare fused-silica capillaries (Yongnian Optical Fiber Corporation, Hebei, China) were an inner diameter of 50 μm and a length of 50 cm (41.5 cm to the detection window). The ccc-TMAPL (Figure 1) is of 50 μm inner diameter and 50 cm length (41.5 cm to the detection window) coated with flushing TMAPL nanolatex through the bare fused-silica capillary. The preparation procedures of the ccc-TMAPL are the same as mentioned in our previous work[36] by introducing TMAPL nanoparticles into a treated bare fused-silica capillary 3 times, respectively. The nanoparticles will be coated onto the inner wall surface of the capillary by the electrostatic absorption interaction. The ccc-TMAPL has been characterized by infrared spectrum and EOF values. The absorptions at 1400 and 1637 cm^{-1} are observed and associated with the C−N and benzene ring stretching vibrations, respectively. Its EOF values are reversed and steady at ca. $-16.81 \pm 0.83 \times 10^{-5}$ cm^2 V^{-1} s^{-1} with pH 7.30−8.03. These results indicate that TMAPL has been successfully coated onto the inner wall of the capillary.

Electrophoretic Procedures. Before the electrophoretic procedure, the ccc-TMAPL was flushed with water for 30 min. After each separation run, the ccc-TMAPL was flushed with water for 3 min and running buffer solution for another 3 min to re-equilibrate the ccc-TMAPL. It is noteworthy that, to ensure reproducibility and accuracy of the determination, the buffer solution was changed after every 7−8 runs. All separation runs were undertaken at 25 °C. The separation voltage was −20 kV, and injections were performed hydrostatically using an applied pressure of 50 mbar for 3 s. Under the detection at 235 nm, the EOF (thiourea as marker) was determined when the buffer solution was 20 mM Tris and 12 mM $HClO_4$ with pH 8.03.

Sample Pretreatment. For sample preparation, similar procedures,[6] with a slight modification, were applied to extract nitrites and nitrates and deproteinized. A total of 100 g of the minced ham and/or sausage was mixed with deionized water (8 mL) and 1 g of activated charcoal in a 10 mL volumetric flask. Nitrites and nitrates were ultrasonically extracted for 30 min, and the volumetric flask was shaken 1 time per 5 min. Then, the volumetric flask was incubated in a warm water bath at 75 °C for 5 min, and then the liquid was tranferred to a 25 mL volumetric flask. the aforementioned extraction was repeated twice. About 20 mL of collected liquid was diluted 3 times to 25 mL with 5 mL of acetonitrile, and a portion (10 mL) was centrifuged for 15 min at 1000 revolutions/min. Then, 5 mL of supernatant was taken out and filtered through a 0.22 μm membrane filter before use.

RESULTS AND DISCUSSION

Condition Choice for Separation of Nitrite and Nitrate by OT-CEC. As reported in our previous work,[36] the ccc-

Table 1. Effect of Different $HClO_4$ Concentrations and pH Values on Rs and Theoretical Plates

concentration of $HClO_4$ in BGE (mmol L^{-1})	Rs (NO_3^-/NO_2^-)	theoretical plate (plates/m)	
		nitrate	nitrite
13.0 (pH 8.01)	1.54	16210	31163
13.5 (pH 7.87)	1.66	28821	58441
14.0 (pH 7.76)	1.24	30145	48652
14.5 (pH 7.62)			
15.5 (pH 7.33)			

Table 2. Rs and Theoretical Plates under Different Separation Voltages

separation voltage (kV)	Rs (NO_3^-/NO_2^-)	theoretical plate (plates/m)	
		nitrate	nitrite
−15	1.57	27674	49718
−20	1.66	28821	58441
−25	1.65	25076	42777

TMAPL possesses good separation selectivity for nitrites and nitrates because of the additional chromatographic interaction between the TMAPL coating and target analytes, which is similar to that observed in the published literature.[22] Using the usual Tris−$HClO_4$ buffer system[22,37] (ClO_4^- with high

Table 3. Recovery Results with OT-CEC

anion	amount detected for number 1 ham (mg kg^{-1})	amount spiked (μg mL^{-1})	total amount found (μg mL^{-1})	recovery (%)	RSD (%) interday migration time (n = 3)	RSD (%) interday peak area (n = 3)
nitrate	undetected out	20	18.64	93.2	1.0	1.3
			19.12	95.6		
			18.82	94.1		
		50	51.11	102.2	1.9	1.9
			48.54	97.1		
			48.42	96.8		
nitrite	10.22	20	29.64	97.1	2.0	3.5
			29.25	95.2		
			30.72	102.5		
		50	61.73	103.0	1.2	3.2
			58.54	96.6		
			57.46	94.5		

Table 4. Comparison of the Determination Results of Nitrites and Nitrates in Real Samples by the Developed OT-CEC and the Referenced IC Method[a]

sample	analyte	average content by OT-CEC (μg g^{-1}; n = 3)	average content by IC[a] (μg g^{-1}; n = 3)
number 1 ham	nitrate		
	nitrite	10.40 ± 0.36	10.19 ± 0.24
number 2 ham	nitrate	86.88 ± 0.45	87.02 ± 0.32
	nitrite	16.95 ± 0.25	16.68 ± 0.34
number 3 ham	nitrate		
	nitrite	30.50 ± 0.52	30.33 ± 0.44
number 4 ham	nitrate	18.71 ± 0.50	18.67 ± 0.41
	nitrite	39.26 ± 0.57	39.03 ± 0.37
number 5 ham	nitrate	17.68 ± 0.41	17.91 ± 0.27
	nitrite	20.70 ± 0.29	20.64 ± 0.32
number 6 ham	nitrate	12.77 ± 0.46	12.92 ± 0.34
	nitrite	20.50 ± 0.52	20.28 ± 0.36
number 1 sausage	nitrate	20.71 ± 0.34	20.56 ± 0.28
	nitrite	16.74 ± 0.47	16.49 ± 0.32
number 2 sausage	nitrate		
	nitrite	16.25 ± 0.32	16.41 ± 0.18
number 3 sausage	nitrate	16.71 ± 0.35	16.62 ± 0.26
	nitrite	34.60 ± 0.34	34.93 ± 0.28
number 4 sausage	nitrate		
	nitrite	35.07 ± 0.23	35.27 ± 0.35
number 5 sausage	nitrate	13.11 ± 0.13	13.24 ± 0.12
	nitrite	57.43 ± 0.52	57.26 ± 0.32
number 6 sausage	nitrate	31.36 ± 0.46	31.80 ± 0.32
	nitrite	12.60 ± 0.42	12.47 ± 0.14

[a]The IC method[40] was used with an IonPac AS9-HC anion-exchange column (250 × 4 mm inner diameter, 13 μm).

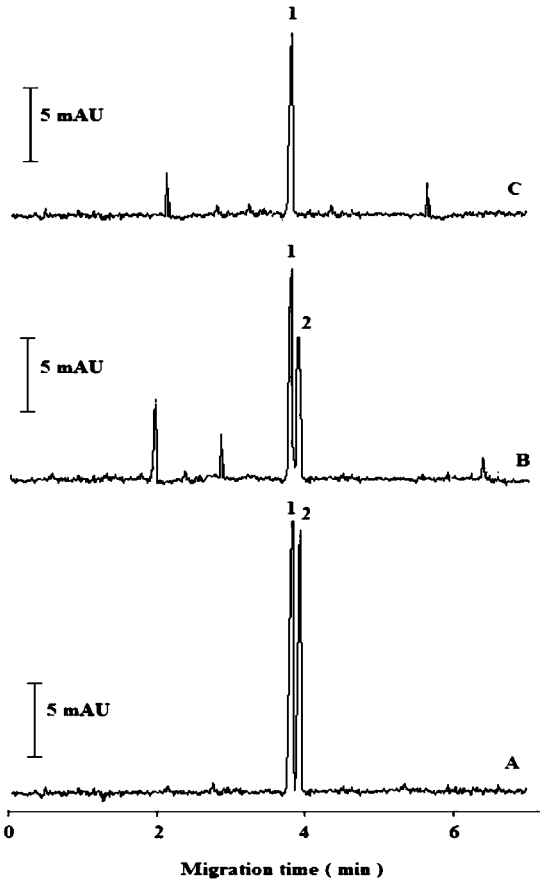

Figure 2. Typical electrochromatograms of (A) standard of nitrite and nitrate, (B) number 6 ham and (C) number 2 sausage samples. Conditions: column, 50 μm × 50 cm (effective length of 41.5 cm) ccc-TMAP; BGE, 20 mmol L^{-1} Tris + 13.5 mmol L^{-1} $HClO_4$ (pH 7.87); separation voltage, −20 kV; sample injection, 50 mbar × 3 s; detected wavelength, 214 nm; and temperature, 25 °C. Peaks: 1, nitrite; 2, nitrate.

eluotropic strength as a competing anion to elute nitrites and nitrates), the separations of nitrite and nitrate with different $HClO_4$ concentrations (13.0, 13.5, 14 0.0, 14.5, and 15.5 mmol L^{-1}) in BGE were carried out. The resolutions (Rs) and theoretical plates for both nitrites and nitrates were calculated and listed in Table 1. From Table 1, the larger Rs and higher theoretical plates could be obtained using 20 mmol L^{-1} Tris + 13.5 mmol L^{-1} $HClO_4$ (pH 7.87) as BGE of OT-CEC. It is noteworthy that the weakly acidic and basic buffers (pH < 8) are preferential for avoiding the TMAPL coating destroyed, which ensured the stability of EOF. The EOF values of about $-16.81 \pm 0.83 \times 10^{-5}$ cm^2 V^{-1} s^{-1} with pH 7.30−8.03[34] and about $-15.02 \pm 0.71 \times 10^{-5}$ cm^2 V^{-1} s^{-1} with pH 4.70−6.85 were obtained, which showed the reversal and steady EOFs. At the same time, the baselines with coated columns[14,20] are smoother than those by the CZE method without coated columns.[17,38] At the same time, the coating was removed by flushing 0.1 mmol L^{-1} NaOH solution and EOF will change to

dx.doi.org/10.1021/jf500020w | J. Agric. Food Chem. 2014, 62, 3400−3404

the normal positive value. This result implies that TMAPL is coated on the capillary based on the electrostatic absorption.

In the CE method, separation voltage can greatly affect migration time, Joule heat, Rs, and column efficiency. The separations, theoretical plates, and Rs (Table 2) for nitrites and nitrates were obtained under different separation voltages at −15, −20, and −25 kV. Using separation voltage at −20 kV, both nitrite and nitrate were baseline-resolved, and their theoretical plates and Rs were better than those at −15 and −25 kV.

Taking the migration time, Rs, and column efficiency into consideration, −20 kV of separation voltage and 20 mmol L^{-1} Tris + 13.5 mmol L^{-1} $HClO_4$ (pH 7.87) BGE were optimized for the separation of nitrites and nitrates.

Methodology. Under the optimized conditions, the standard solutions of both nitrites and nitrates (10, 25, 50, 100, and 200 μg mL^{-1} for each) were injected and performed by OT-CEC. Their regression equations (peak area y against concentration x) were obtained as follows:

for nitrate

$$y = 0.6756x - 0.1778 \quad (n = 5;\ R^2 = 0.9915)$$

for nitrite

$$y = 0.6585x - 0.1667 \quad (n = 5;\ R^2 = 0.9967)$$

The limits of detection (LODs) for nitrate and nitrite were found to be 3.5 and 4.2 μg mL^{-1} by calculating a sinal-to-noise ratio of 3. These LODs allow for nitrates and nitrites in hams and sausages to be detected out at their limits of quantitation (LOQs) of ca. 0.89 and 1.05 μg g^{-1}, respectively. These LOQs were similar to those by the reported CE method.[17]

To evaluate the accuracy of the method, the recoveries (Table 3) for both nitrites and nitrates were investigated by adding standard nitrites and nitrates to the number 1 ham sample (100 g) to prepare the test samples. It can be seen from Table 3 that the relative standard deviations (RSDs) of the migration times and peak area were less than 2.0 and 3.5%, respectively. The recoveries were between 94 and 103%. It implies that the developed OT-CEC was accurate and reproducible.

Application. Using the above method, the contents of nitrites and nitrates in ham and sausage samples were carried out. The determination results were listed in Table 4, and the typical electrochromatograms of the ham and sausage samples were represented in Figure 2. From Table 4, nitrites and/or nitrates were found ranging from 10 to 40 mg kg^{-1} in most samples. They are safe for the consumers. However, the contents of nitrites in number 5 sausage and nitrates in number 2 ham were exceeded by their maximum residue limit (MRL) of 50 μg g^{-1} in meat products.[39] Both of them should be prohibited on sale. It is noteworthy that the determination results of nitrites and nitrates in the real samples were coincident by the developed OT-CEC and the referenced ion chromatographic (IC) method.[40] It displays that the proposed OT-CEC is an accurate and practical method for the determination of nitrites and nitrates in foodstuffs.

In conclusion, a new and practical method for the separation and determination of nitrites and nitrates in hams and sausages was developed by OT-CEC using ccc-TMAPL as the column. The method was simple as a result of avoiding the introduction of an EOF reverse additive (such as CTAC and CTAB) in BGE while featuring good repeatability and accuracy. The results demonstrated that the ccc-TMAPL was of stability, and the developed method was suitable for the analysis of trace hazardous anions, nitrites, and nitrates. It would promise to be a practical application in the field of food safety analysis.

AUTHOR INFORMATION

Corresponding Authors

*E-mail: yuajuan@zzu.edu.cn.

*Telephone: 86-371-67763224. E-mail: zsszz@126.com.

Funding

The authors acknowledge the support of the National Science Foundation (NSF) of China (21077095 and 21275133).

Notes

The authors declare no competing financial interest.

ACKNOWLEDGMENTS

The authors thank Professor Aimin Liu of Georgia State University for assistance with editing the text.

REFERENCES

(1) Armenteros, M.; Aristoy, M. C.; Toldrá, F. Evolution of nitrate and nitrite during the processing of dry-cured ham with partial replacement of NaCl by other chloride salts. *Meat Sci.* **2012**, *91* (3), 378−381.

(2) Greer, F. R.; Shannon, M. Infant methaemoglobinaemia: The role of dietary nitrate. *Pediatrics* **2005**, *116* (3), 784−786.

(3) del Pilar García-Santos, M.; González-Mancebo, S.; Hernández-Benito, J.; Calle, E.; Casado, J. Reactivity of amino acids in nitrosation reactions and its relation to the alkylating potential of their products. *J. Am. Chem. Soc.* **2002**, *124* (10), 2177−2182.

(4) Pleissner, D.; Wimmer, R.; Eriksen, N. T. Quantification of amino acids in fermentation media by isocratic HPLC analysis of their α-hydroxy acid derivatives. *Anal. Chem.* **2011**, *83*, 175−181.

(5) Mitacek, E. J.; Brunnemann, K. D.; Suttajit, M.; Caplan, L. S.; Gagna, C. E.; Bhothisuwan, K. Geographic distribution of liver and stomach cancers in Thailand in relation to estimated dietary intake of nitrate, nitrite, and nitrosodimethylamine. *Nutr. Cancer* **2008**, *60* (2), 196−203.

(6) Ferreira, I. M.; Silva, S. Quantification of residual nitrite and nitrate in ham by reverse-phase high performance liquid chromatography/diode array detector. *Talanta* **2008**, *74* (5), 1598−1602.

(7) China National Standards Commission. Determination of nitrite and nitrate in foods. *Chinese National Food Safety Standard, GB 5009.33-2010*; China National Standards Commission: Beijing, China, 2010.

(8) Walters, C. L.; Gillatt, P. N.; Palmer, R. C.; Smith, P. L. R. A rapid method for the determination of nitrate and nitrite by chemiluminescence. *Food Addit. Contam., Part A* **1987**, *4* (2), 133−140.

(9) Nagaraj, P.; Prakash, J. S.; Shivakumar, A.; Shrestha, A. K. Sensitive spectrophotometric methods for the assessment of nitrite in water sample. *Environ. Monit. Assess.* **2008**, *147* (1−3), 235−241.

(10) Bintoro, V. P.; Cantin-Esnault, D.; Alary, J. A survey of nitrate contents in Indonesian milk by enzymic analysis. *Food Addit. Contam., Part A* **1996**, *13*, 77−87.

(11) Sousa, A. L.; Santos, W. J. R.; Luz, R. C. S.; Damos, F. S.; Kubota, L. T.; Tanaka, A. A.; Tanaka, S. M. C. N. Amperometric sensor for nitrite based on copper tetrasulphonated phthalocyanine immobilized with poly-L-lysine film. *Talanta* **2008**, *75*, 333−338.

(12) Xian, H.; Wang, P.; Zhou, Y.; Lu, Q.; Wu, S.; Li, Y.; Wang, L. Electrochemical determination of nitrite via covalent immobilization of a single-walled carbon nanotubes and single stranded deoxyribonucleic acid nanocomposite on a glassy carbon electrode. *Microchim. Acta* **2010**, *171* (1−2), 63−69.

(13) Ito, K.; Takayama, Y.; Makabe, N.; Mitsui, R.; Hirokawa, T. Ion chromatography for determination of nitrite and nitrate in seawater using monolithic ODS columns. *J. Chromatogr., A* **2005**, *1083*, 63−67.

(14) Zuo, Y. G.; Wang, C. J.; Thuan, V. Simultaneous determination of nitrite and nitrate in dew, rain, snow and lake water samples by ion-pair high-performance liquid chromatography. *Talanta* **2006**, *70*, 281−285.
(15) Dennis, M. J.; Key, P. E.; Papworth, T.; Pointer, M.; Massey, R. C. The determination of nitrate and nitrite in cured meat by HPLC/UV. *Food Addit. Contam., Part A* **1990**, *7* (4), 455−461.
(16) Oztekin, N.; Nutku, M. S.; Erim, F. B. Simultaneous determination of nitrite and nitrate in meat products and vegetables by capillary electrophoresis. *Food Chem.* **2002**, *76*, 103−106.
(17) Merusi, C.; Corradini, C.; Cavazza, A.; Borromei, M.; Salvadeo, P. Determination of nitrates, nitrites and oxalates in food products by capillary electrophoresis with pH-dependent electroosmotic flow reversal. *Food Chem.* **2010**, *120* (2), 615−620.
(18) Erdogan, B. Y.; Onar, A. N. Determination of nitrates, nitrites and oxalates in kale and sultana pea by capillary electrophoresis. *J. Anim. Vet. Adv.* **2011**, *10* (15), 2051−2057.
(19) Borties, P. N.; Scherman, E.; Dziedzic, L. Analysis of nitrite and nitrate in biological fluids by capillary electrophoresis. *Clin. Biochem.* **1999**, *32* (1), 9−14.
(20) Gáspár, A.; Juhász, P.; Bágyi, K. Application of capillary zone electrophoresis to the analysis and to a stability study of nitrite and nitrate in saliva. *J. Chromatogr., A* **2005**, *1065* (2), 327−331.
(21) Wang, X.; Masschelein, E.; Hespel, P.; Adams, E.; Van Schepdae, A. Simultaneous determination of nitrite and nitrate in human plasma by on-capillary preconcentration with field-amplified sample stacking. *Electrophoresis* **2012**, *33*, 402−405.
(22) Breadmore, M. C.; Macka, M.; Avdalovic, N.; Haddad, P. R. Open-tubular ion-exchange capillary electrochromatography of inorganic anions. *Analyst* **2000**, *125*, 1235−1241.
(23) Yan, C.; Schaufelberger, D.; Erni, F. Electrochromatography and micro high-performance liquid chromatography with 320 μm I.D. packed columns. *J. Chromatogr., A* **1994**, *670*, 15−23.
(24) Beate, B.; Edgar, G.; Ernst, B. Evaluation of the parameters determining the performance of electrochromatography in packed capillary. *J. Chromatogr., A* **1995**, *716*, 207−213.
(25) Wu, R. A.; Zou, H. F.; Ye, M. L.; Lei, Z. D.; Ni, J. Y. Capillary electrochromatography for separation of peptides driven with electrophoretic mobility on monolithic column. *Anal. Chem.* **2001**, *73*, 4918−4923.
(26) Ye, F. G.; Xie, Z. H. Monolithic silica columns with mixed mode of hydrophilic interaction and weak anion-exchange stationary phase for pressurized capillary electrochromatography. *Electrophoresis* **2006**, *27*, 3373−3380.
(27) Ye, F. G.; Wang, H. S.; Huang, A. J.; Zhao, S. L.; Ye, F.; Wang, H.; Huang, B.; Zhao, S. Maleopimaric acid anhydride-bonded silica monolith as chiral stationary phase for separations of phenylthiocarbamyl amino acids by CEC. *Electrophoresis* **2010**, *31*, 1488−1492.
(28) Wang, Z. X.; Chen, Y.; Yuan, H. S.; Huang, Z. T.; Liu, G. Q. Preparation and characterization of calixarene-coated capillaries for capillary electrophoresis. *Electrophoresis* **2000**, *21*, 1620−1624.
(29) Zeng, Z. R.; Xie, C. H.; Li, H. B.; Han, H. M.; Chen, Y. Open-tubular capillary electrochromatography using capillary columns chemically bonded with the new host molecules calix[6]crown, calix[6]arene. *Electrophoresis* **2002**, *23*, 1272−1278.
(30) Malik, A. Advances in sol-gel based columns for capillary electrochromatography: Sol-gel open-tubular columns. *Electrophoresis* **2002**, *23*, 3973−3992.
(31) Hu, K.; Tian, Y. L.; Yang, H.; Zhang, J. Q.; Xie, J.; Ye, B. X.; Wu, Y. J.; Zhang, S. S. Preparation and characterization of *p-tert*-butylcalix[4]arene modified sol-gel column for open-tubular capillary electrochromatography. *J. Liq. Chromatogr. Relat. Technol.* **2009**, *32*, 2627−2641.
(32) Wu, X. J.; Liu, H. X.; Liu, H.; Zhang, S. S.; Haddad, P. R. Preparation and characterization of *p-tert*-butylcalix[8]arene bonded capillaries for open-tubular capillary electrochromatography. *Anal. Chim. Acta* **2003**, *478*, 191−197.
(33) Zhang, S. S.; Macka, M.; Haddad, P. R. Preparation and characterisation of dual-layer latex-coated columns for open-tubular capillary electrochromatographic preconcentration of cations combined in-line with their separation by capillary electrophoresis. *Electrophoresis* **2006**, *27*, 1069−1077.
(34) Hutchinson, J. P.; Hilder, E. F.; Macka, M.; Avdalovic, N.; Haddad, P. R. Preparation and characterisation of anion-exchange latex-coated silica monoliths for capillary electrochromatography. *J. Chromatogr., A* **2006**, *1109*, 10−18.
(35) Hutchinson, J. P.; Hilder, E. F.; Shellie, R. A.; Smith, J. A.; Haddad, P. R. Towards high capacity latex-coated porous polymer monoliths as ion-exchange stationary phases. *Analyst* **2006**, *131*, 215−221.
(36) Guo, Y.; Xu, F.; Meng, L.; Tang, W.; Xia, Y.; Wu, Y.; Zhang, S. S. Preparation and application of trimethylamine amination polychloromethyl styrene nano-latex coated capillary column for the determination of bromate by field-amplified sample stacking open-tubular capillary electrochromatography. *Electrophoresis* **2013**, *34*, 1312−1318.
(37) Yang, H.; Zhang, R.; Lu, Y.; Ye, B.; Wu, Y.; Zhang, S. S. Separation and determination of calixarenes and related derivatives by capillary zone electrophoresis using acetonitrile as a modifier. *Chromatographia* **2008**, *68*, 123−127.
(38) Yokota, K.; Fukushi, K.; Ishio, N.; Sasayama, N.; Nakayama, Y.; Takeda, S.; Wakida, S. Capillary zone electrophoretic determination of iodide in seawater using transient isotachophoresis with artificial seawater as the background electrolyte. *Electrophoresis* **2003**, *24*, 2244−2251.
(39) European Union (EU). E249−E252. *European Parliament and Council Directive, No 95/2/EC*; EU: Brussels, Belgium, 1995.
(40) Iammarino, M.; Di Taranto, A.; Cristino, M. Endogenous levels of nitrites and nitrates in wide consumption foodstuffs: Results of five years of official controls and monitoring. *Food Chem.* **2013**, *40* (4), 763−771.

Scheme 1. Structure of Probe 1 and Sensing Mechanisms for CN^- and HSO_3^-

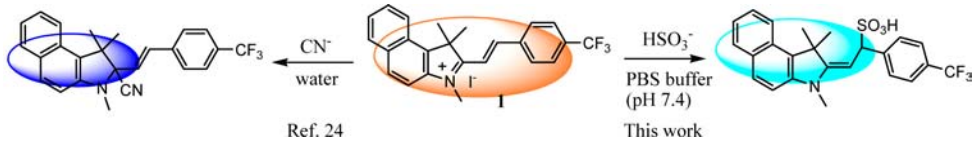

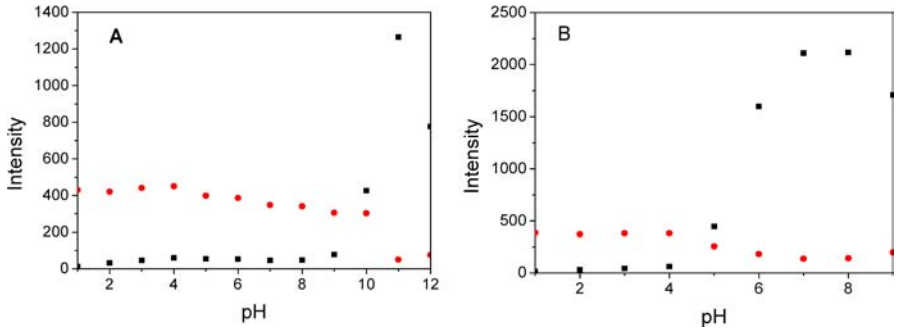

Figure 1. Fluorescent intensity of **1** (10 μM) in the absence (A) and presence (B) of HSO_3^- (10 μM): black squares, emission intensity at 465 nm; red dots, emission intensity at 571 nm. λ_{ex} = 400 nm. Slits: 5 nm/5 nm.

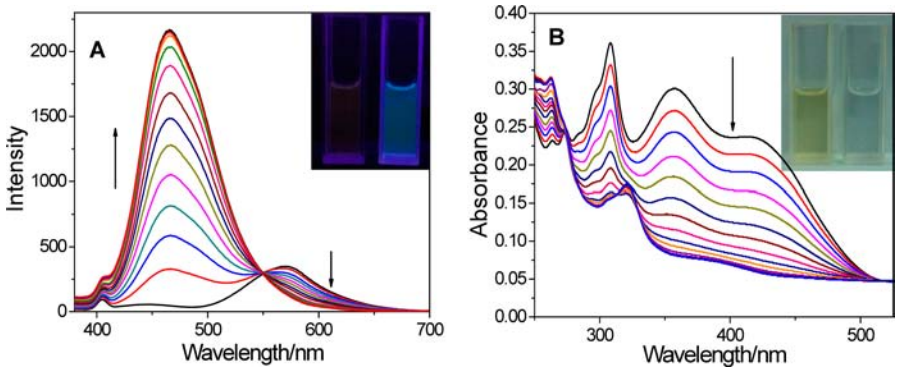

Figure 2. (A) Fluorescence spectra of **1** (10 μM) in PBS buffer (pH 7.4, 10 mM) obtained upon titration with HSO_3^-. (Inset) Photograph of **1** solution (10 μM) upon irradiation under UV light (365 nm) in the absence or presence of HSO_3^- (10 μM). λ_{ex} = 400 nm. Slits: 5 nm/5 nm. (B) Absorption spectra of **1** (20 μM) in PBS buffer (pH 7.4, 10 mM) obtained upon titration with HSO_3^-. (Inset) Photograph of **1** solution (20 μM) in the absence or presence of HSO_3^- (10 μM). The equivalents of HSO_3^- were varied in the following order: 0, 0.1, 0.2, 0.3, 0.4, 0.5, 0.6, 0.7, 0.8, 0.9, 1.0, 1.5, 2.0, 3.0, and 5.0.

addition reaction on the basis of our previous study,[20] and the interrupted π-conjugation led to the emission of 2-methylene benzo[*e*]indoline recovery at 465 nm. Thus, two well-separated emission peaks before and after the HSO_3^- addition could be obtained ($\Delta\lambda$ = 106 nm). Treatment with HSO_3^- resulted in an obvious color change in the test papers stained by probe **1**. Moreover, probe **1** could determine the HSO_3^- level in real sugar samples with good recovery.

MATERIALS AND METHODS

General Methods. All reagents and solvent were purchased from commercial sources and used without further purification, if not otherwise stated. All reactions were carried out on the magnetic stirrers, and their reaction process was monitored by thin layer chromatography (TLC). Absorption and fluorescence spectra were taken on a Shimadzu UV-1800 spectrophotometer and a Hitachi F-2700 fluorescence spectrometer, respectively. ^{1}H NMR and ^{13}C NMR measurements were recorded at 600 and 150 MHz on a Bruker Avance 600 MHz spectrometer. Dimethyl sulfoxide (DMSO-d_6) was solvent, and tetramethylsilane (TMS) was used as internal standard. ESIMS were taken on a Fourier transform ion cyclotron resonance mass spectroscopy (Varian 7.0T).

Preparation of Probe 1. Probe **1** were prepared according to the method we reported previously by a simple one-step reaction of 4-trifluoromethylbenzaldehyde in ethanol solution.[26] 1,2,3,3-Tetramethylbenz[*e*]indolium iodide (1.05 g, 3 mmol) was dissolved in ethanol (5 mL), then 4-trifluoromethylbenzaldehyde (0.52 g, 3 mmol) was added, and the reaction mixture was heated at reflux for 12 h. Then the reaction mixture was cooled to room temperature, and the precipitate was collected by filtration, washed with cold ethanol, and dried in vacuo. Probe **1** was obtained as an orange solid in 80% yield (1.2 g). ^{1}H NMR (600 MHz, DMSO-d_6): δ 8.50 (d, J = 16.6, 2H), 8.44 (d, J = 8.4, 2H), 8.38 (d, J = 8.1, 1H), 8.32 (d, J = 8.9, 1H), 8.25 (d, J = 8.1, 1H), 7.96 (d, J = 7.9, 2H), 7.84 (m, 2H), 7.77 (m, 1H), 4.32 (s, 3H), 2.03 (s, 6H). ^{13}C NMR (150 MHz, DMSO-d_6): δ 186.0, 152.5, 142.8, 142.1, 141.7, 136.8, 134.4, 134.0, 133.4, 131.9, 130.8, 130.0, 129.3, 126.7, 118.9, 116.9, 57.6, 39.2, 28.1. HRMS (ESI): calcd for $[M]^+$ 380.1621, found 380.1627.

RESULTS AND DISCUSSION

Probe **1** was easily synthesized in a one-step reaction by using 1,2,3,3-tetramethylbenz[*e*]indolium iodide and 4-trifluoromethylbenzaldehyde in ethanol. The synthetic route and the purification were simple. The total yield was 68%. The structure

dx.doi.org/10.1021/jf5004539 | J. Agric. Food Chem. 2014, 62, 3405−3409

of probe **1** was characterized via ^{1}H, ^{13}C NMR, and ESIMS (Figures S1−S3 in the Supporting Information).

As expected, probe **1** possessed good water solubility. The reaction media, pH value, and response time were investigated to optimize the sensing conditions. The fluorescent spectral response of **1** (10 μM) in the absence and presence of HSO_3^- (10 μM) at different pH values was evaluated as shown in Figure 1. The probe was stable in a pH range of 1−8 and displayed the best response for HSO_3^- in the physiological pH region. Thus, the PBS buffer solution (pH 7.4, 10 mM) was selected for the spectral studies. Time-dependent modulations in the fluorescence of the probe (10 μM) in the presence of HSO_3^- (1, 5, and 10 μM) suggested that the reaction could be completed within 90 s in the experimental conditions (Figure S4 in the Supporting Information). Thus, the detection was delayed for 90 s to ensure the reaction between **1** and HSO_3^- accomplished completely.

The fluorescence spectra of probe **1** (10 μM) after addition of various amounts of HSO_3^- (0−50 μM) are shown in Figure 2A. Probe **1** exhibits an emission at 571 nm, which was attributed to the large π-conjugation. The addition of HSO_3^- resulted in a gradual decrease in emission at 571 nm and an increase in emission at 465 nm, which corresponds to the 2-methylenebenzo[*e*]indoline moiety. A well-defined isoemissive point at 550 nm was also observed. The ratiometric change in fluorescence intensity indicated that the addition reaction between **1** and HSO_3^- interrupted the π-conjugation, and the fluorescence of 2-methylenebenzo[*e*]indoline was recovered. Accordingly, the fluorescence color changed from orange to cyan. The ratio of the emission intensities at 465 and 571 nm (I_{465}/I_{571}) was enhanced with the addition of HSO_3^- and became constant when the amount of HSO_3^- added reached 1 equiv (10 μM), which suggests a 1:1 binding stoichiometry between **1** and HSO_3^- (Figure S5 in the Supporting Information). The ratio value increased by >120-fold (from 0.12 to 15.4). To our knowledge, the notable fluorescent spectral change caused by 0.1 equiv of HSO_3^- (1 μM) and obtaining the maximal spectral signal with 1 equiv of HSO_3^- (10 μM) were impressive and unprecedented compared with those of many reported HSO_3^- probes. In similar conditions, the ratio changes produced an excellent linear function with HSO_3^- concentration between 0 and 10 μM (Figure S6 in the Supporting Information), and the detection limit for HSO_3^- was 5.6×10^{-9} M (R^2 = 0.9935). The absorption spectrum of probe **1** (20 μM) showed two strong bands at 310 and 360 nm (Figure 2B). The decrease in band intensity upon the addition of HSO_3^- also suggests that the π-conjugation was broken. This phenomenon leads to a solution color change from yellow to colorless. The noticeable color change indicates that HSO_3^- can be detected with the naked eye by using probe **1**.

The ratiometric sensing selectivity of probe **1** for HSO_3^- was further examined in PBS buffer (pH 7.4, 10 mM) as shown in Figure 3. Among the added representative anions, including HS^-, CN^-, F^-, Cl^-, Br^-, I^-, AcO^-, ClO_4^-, NO_3^-, N_3^-, SO_4^{2-}, HSO_4^{2-}, SCN^-, PO_4^{3-}, $H_2PO_4^-$, and HPO_4^{2-} (100 equiv, respectively), only HS^- caused an intensity change because of the 1,2-addition reaction with a fluorescent color change from orange to colorless. The other anions did not induce any significant fluorescence change, and the I_{465}/I_{571} values varied in a limited range between 0.15 and 1.2. By contrast, treatment of **1** with HSO_3^- resulted in an obvious ratiometric fluorescent response. Probe **1** was originally synthesized to detect CN^- in water, and the pH value of the solution changed from 7.2 to 9.4

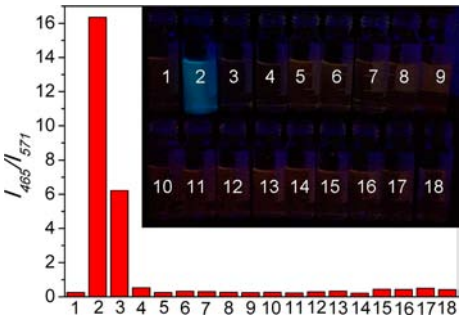

Figure 3. Emission ratio I_{465}/I_{571} of **1** (10 μM) in PBS buffer (pH 7.4, 10 mM) in the presence of various species. λ_{ex} = 400 nm. Slits: 5 nm/5 nm. (Inset) Corresponding fluorescent color changes under a handle UV lamp (365 nm): 1, probe alone; 2, HSO_3^- (10 μM); 3, HS^-; 4, CN^-; 5, F^-; 6, Cl^-; 7, Br^-; 8, I^-; 9, AcO^-; 10, ClO_4^-; 11, NO_3^-; 12, N_3^-; 13, SO_4^{2-}; 14, HSO_4^-; 15, SCN^-; 16, PO_4^{3-}; 17, HPO_4^{3-}; 18, $H_2PO_4^{3-}$ (3−27, 1000 μM).

with the addition of CN^-. However, the constant neutral pH condition suppressed the necleophilic addition of CN^- to **1** as the protonation of CN^- [p*K*a (HCN) = 9.2].[30,31] Competition experiments of probe **1** were also ascertained by various species mentioned previously in the same environment. The signaling of **1** toward HSO_3^- (1 equiv) was not affected by the presence of 100 equiv of coexisting species (Figure S7 in the Supporting Information). The phenomenon suggests that probe **1** could be used as an efficient signaling probe for HSO_3^- in aqueous media.

There was no spectral change when HSO_3^- was added to the solution of 1,2,3,3-tetramethylbenz[*e*]indolium iodide because of the steric effect. Hence, we proposed a 1,4-addition reaction occurred between **1** and HSO_3^- rather than a 1,2-addition reaction, and ^{1}H NMR analysis was carried out to demonstrate the proposed addition mechanism (Figure 4). After HSO_3^- was

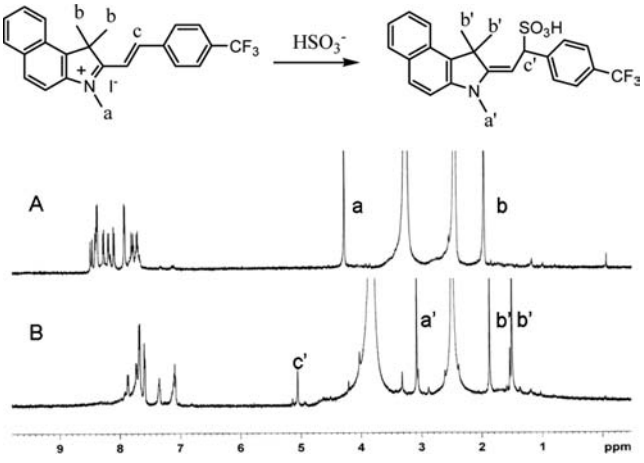

Figure 4. ^{1}H NMR spectral change of **1** (3×10^{-3} M) in the absence (A) and presence of 1 equiv of $NaHSO_3$ (B) in DMSO-d_6/D_2O = 9:1 (v/v).

added into the solution of **1**, all of the ^{1}H NMR signals shifted upfield because the nucleophilic attack of HSO_3^- toward C-4 disturbed the π-conjugation and weakened its electron-withdrawing characteristic. The proton signal (H^a, at δ 4.34) of the methyl group connected with N^+ was significantly shifted upfield to δ 3.05. The proton signal (H^b, at δ 2.03) of the two methyl groups was also shifted upfield and divided into two

dx.doi.org/10.1021/jf5004539 | J. Agric. Food Chem. 2014, 62, 3405−3409

single signals ($H^{b'}$, at δ 1.87 and 1.48), which become nonequivalent after the formation of **1**−SO_3H. Moreover, the proton signal (H^c, at δ 7.7−8.5) appeared at δ 5.05 after the HSO_3^- addition. Furthermore, the formation of **1**−SO_3H was further confirmed via mass spectrometry analysis, where the peak at m/z 460.1193 (calcd 460.1200) corresponding to $[M + SO_3]^-$ was clearly observed (Figure S8 in the Supporting Information).

To demonstrate the practical application of probe **1** for the detection of HSO_3^-, a preliminary paper test strip system was developed, as shown in Figure 5. After the neutral filter papers had been dipped into the solution of probe **1** (10 μM) and dried, yellow emission test papers were obtained under UV light (365 nm). When the various anion solutions (0.1 M) were dripped onto the test paper, only HSO_3^- induced a fluorescent color change from yellow to cyan. Although HS^- and CN^- also caused color changes from yellow to blue, they could be easily distinguished by the naked eye.

Figure 5. Photographs of the test paper exposure to various species under UV light (365 nm): 1, probe alone; 2, HSO_3^- (10 μM); 3, HS^-; 4, CN^-; 5, F^-; 6, Cl^-; 7, Br^-; 8, I^-; 9, AcO^-; 10, ClO_4^-; 11, NO_3^-; 12, N_3^-; 13, SO_4^{2-}; 14, HSO_4^-; 15, SCN^-; 16, PO_4^{3-}; 17, HPO_4^{3-}; 18, $H_2PO_4^{3-}$.

Finally, probe **1** was used to detect HSO_3^- in real samples. Granulated sugar, soft sugar, and crystal sugar purchased from a supermarket were used in the sample analysis. Sample solution was prepared by dissolving 5.0 g of sugar in deionized water and diluting to 10 mL. Aliquots of the sugar solution were added directly to the PBS buffer (pH 7.4, 10 mM) containing **1** (10 μM), and the emission intensities at 465 and 571 nm were recorded. Table 1 shows that probe **1** was able to determine HSO_3^- concentration in sugar with good recovery. The HSO_3^- levels in these samples were calculated to be 17.21, 10.70, and 14.58 mg/kg, respectively. To validate the accuracy of the method, we detected these sugar samples by a titration method,[32] and equivalent results were obtained as shown in Table 2.

Table 1. Results for the Determination of HSO_3^- in Various Samples

sample	HSO_3^- level (μmol/L)	added (μmol/L)	found (μmol/L)	recovery (%)
granulated sugar	4.13	3	7.26	101.8
		5	9.21	100.8
soft sugar	2.57	3	5.49	98.6
		5	7.48	98.8
crystal sugar	3.50	3	6.32	97.2
		5	8.24	97.0

Table 2. Results of This Method Compared with a Titration Method for HSO_3^- from Sugar Samples

sample	titration method (mg/kg)	this method (mg/kg)
granulated sugar	17.5	17.21
soft sugar	10.1	10.70
crystal sugar	14.3	14.58

In summary, a ratiometric fluorescent probe for HSO_3^- was introduced. The probe showed high selectivity and sensitivity to HSO_3^- in aqueous media with a short response time. The sensing mechanism was based on the 1,4-addition, which was confirmed via ^1H NMR titration and HRMS studies. Moreover, a simple test paper prepared using probe **1** for the rapid monitoring of HSO_3^- was developed, which could be used as a convenient signaling tool for HSO_3^- determination in chemical analyses. The aqueous solution of probe **1** could also be used to determine HSO_3^- levels in sugar samples.

■ ASSOCIATED CONTENT

Ⓢ Supporting Information

NMR, MS, and other fluorescence spectra. This material is available free of charge via the Internet at http://pubs.acs.org.

■ AUTHOR INFORMATION

Corresponding Author

*(L.D.) Fax: (+86)351-6018564. E-mail: duanlian@tyut.edu.cn.

Funding

This work was supported by the National Natural Science Foundation of China (21301126), Shanxi Province Science Foundation for Youths (2013021009-3), and Youth Foundation of Taiyuan University of Technology (2012L018 and 2012L062).

Notes

The authors declare no competing financial interest.

■ REFERENCES

(1) McFeeters, R. F. Use and removal of sulfite by conversion to sulfate in the preservation of salt-free cucumbers. *J. Food Prot.* **1998**, *61*, 885−890.

(2) Yang, X.; Guo, X.; Zhao, Y. Novel spectrofluorimetric method for the determination of sulfite with rhodamine B hydrazide in a micellar medium. *Anal. Chim. Acta* **2002**, *456*, 121−128.

(3) Fazio, T.; Warner, C. R. A review of sulphites in foods: analytical methodology and reported findings. *Food Addit. Contam.* **1990**, *7*, 433−454.

(4) Meng, Z. Q.; Qin, G. H.; Zhang, B.; Bai, J. L. DNA damaging effects of sulfur dioxide derivatives in cells from various organs of mice. *Mutagenesis* **2004**, *19*, 465−468.

(5) Shi, X. Generation of SO_3^- and OH radicals in SO_3^{2-} reactions with inorganic environmental pollutants and its implications to SO_3^{2-} toxicity. *J. Inorg. Biochem.* **1994**, *56*, 155−165.

(6) White granulated sugar GB317-2006, General Administration of Quality Supervision, Inspection and Quarantine of the People's Republic of China, 2006.

(7) Choi, M. G.; Hwang, J.; Eor, S.; Chang, S. K. Chromogenic and fluorogenic signaling of sulfite by selective deprotection of resorufin levulinate. *Org. Lett.* **2010**, *12*, 5624−5627.

(8) Gu, X.; Liu, C.; Zhu, Y.-C.; Zhu, Y. Z. A boron-dipyrromethene-based fluorescent probe for colorimetric and ratiometric detection of sulfite. *J. Agric. Food Chem.* **2011**, *59*, 11935−11939.

(9) Chen, S.; Hou, P.; Wang, H.; Song, X. A highly sulfite-selective ratiometric fluorescent probe based on ESIPT. *RSC Adv.* **2012**, *2*, 10869−10873.

(10) Chen, K.; Guo, Y.; Lu, Z.; Yang, B.; Shi, Z. Novel coumarin-based fluorescent probe for selective detection of bisulfite anion in water. *Chin. J. Chem.* **2010**, *28*, 55−60.
(11) Yang, X. F.; Zhao, M.; Wang, G. A rhodamine-based fluorescent probe selective for bisulfite anion in aqueous ethanol media. *Sens. Actuators B* **2011**, *152*, 8−13.
(12) Sun, Y. Q.; Wang, P.; Liu, J.; Zhang, J.; Guo, W. A fluorescent turn-on probe for bisulfite based on hydrogen bond-inhibited C═N isomerization mechanism. *Analyst* **2012**, *137*, 3430−3433.
(13) Yang, Y.; Huo, F.; Zhang, J.; Xie, Z.; Chao, J.; Yin, C.; Tong, H.; Liu, D.; Jin, S.; Cheng, F.; Yan, X. A novel coumarin-based fluorescent probe for selective detection of bissulfite anions in water and sugar samples. *Sens. Actuators B* **2012**, *166−167*, 665−670.
(14) Wang, G.; Qi, H.; Yang, X. F. A ratiometric fluorescent probe for bisulphate anion, employing intramolecular charge transfer. *Luminescence* **2013**, *28*, 97−101.
(15) Cheng, X.; Jia, H.; Feng, J.; Qin, J.; Li, Z. "Reactive" probe for hydrogen sulfite: good ratiometric response and bioimaging application. *Sens. Actuators B* **2013**, *184*, 274−280.
(16) Sun, Y.-Q.; Liu, J.; Zhang, J.; Yang, T.; Guo, W. Fluorescent probe for biological gas SO_2 derivatives bisulfite and sulfite. *Chem. Commun.* **2013**, *49*, 2637−2639.
(17) Wu, M.-Y.; He, T.; Li, K.; Wu, M.-B.; Huang, Z.; Yu, X.-Q. A real-time colorimetric and ratiometric fluorescent probe for sulfite. *Analyst* **2013**, *138*, 3018−3025.
(18) Tian, H.; Qian, J.; Sun, Q.; Bai, H.; Zhang, W. Colorimetric and ratiometric fluorescent detection of sulfite in water via cationic surfactant-promoted addition of sulfite to *α,β*-unsaturated ketone. *Anal. Chim. Acta* **2013**, *788*, 165−170.
(19) Wu, M.-Y.; Li, K.; Li, C.-Y.; Hou, J.-T.; Yu, X.-Q. A water-soluble near-infrared probe for colorimetric and ratiometric sensing of SO_2 derivatives in living cells. *Chem. Commun.* **2014**, *50*, 183−185.
(20) Sun, Y.; Fan, S.; Zhang, S.; Zhao, D.; Duan, L.; Li, R. A fluorescent turn-on probe based on benzo[*e*]indolium for bisulfite through 1,4-addition reaction. *Sens. Actuators B* **2014**, *193*, 173−177.
(21) Niu, L. Y.; Guan, Y. S.; Chen, Y. Z.; Wu, L. Z.; Tung, C. H.; Yang, Q. Z. BODIPY-based ratiometric fluorescent sensor for highly selective detection of glutathione over cysteine and homocysteine. *J. Am. Chem. Soc.* **2012**, *134*, 18928−18931.
(22) O' Neil, E. J.; Smith, B. D. Anion recognition using dimetallic coordination complexes. *Coord. Chem. Rev.* **2006**, *250*, 3068−3080.
(23) Niu, H.-T.; Jiang, X.; He, J.; Cheng, J.-P. Cyanine dye-based chromofluorescent probe for highly sensitive and selective detection of cyanide in water. *Tetrahedron Lett.* **2009**, *50*, 6668−6671.
(24) Lv, X.; Liu, J.; Liu, Y.; Zhao, Y.; Sun, Y. Q.; Wang, P.; Guo, W. Ratiometric fluorescence detection of cyanide based on a hybrid coumarin−hemicyanine dye: the large emission shift and the high selectivity. *Chem. Commun.* **2011**, *47*, 12843−12845.
(25) Huang, X.; Gu, X.; Zhang, G.; Zhang, D. A highly selective fluorescence turn-on detection of cyanide based on the aggregation of tetraphenylethylene molecules induced by chemical reaction. *Chem. Commun.* **2012**, *48*, 12195−12197.
(26) Sun, Y.; Fan, S.; Zhao, D.; Duan, L.; Li, R. A ratiometric fluorescent probe based on benzo[*e*]indolium for cyanide ion in water. *Sens. Actuators B* **2013**, *185*, 638−643.
(27) Sun, Y.; Fan, S.; Zhao, D.; Duan, L.; Li, R. A fluorescent turn-on probe based on benzo[*e*]indolium for cyanide ion in water with high selectivity. *J. Fluoresc.* **2013**, *23*, 1255−1261.
(28) Chen, Y.; Zhu, C.; Yang, Z.; Chen, J.; He, Y.; Jiao, Y.; He, W.; Qiu, L.; Cen, J.; Guo, Z. A ratiometric fluorescent probe for rapid detection of hydrogen sulfide in mitochondria. *Angew. Chem., Int. Ed.* **2013**, *52*, 1688−1691.
(29) Chang, J.; Lu, Y.; He, S.; Liu, C.; Zhao, L.; Zeng, X. Efficient fluorescent chemosensors for HSO_4^- based on a strategy of anion-induced rotation-displaced H-aggregates. *Chem. Commun.* **2013**, *49*, 6259−6261.
(30) Shiraishi, Y.; Adachi, K.; Itoh, M.; Hiral, T. Spiropyran as a selective, sensitive, and reproducible cyanide anion receptor. *Org. Lett.* **2009**, *11*, 3482−3485.
(31) Shiraishi, Y.; Sumiya, S.; Hiral, T. Highly sensitive cyanide anion detection with a coumarin−spiropyran conjugate as a fluorescent receptor. *Chem. Commun.* **2011**, *47*, 4953−4955.
(32) Liu, S.; Jiang, T.; Luo, P.; Song, Y.; Tao, Y.; Tan, F.; Ni, H. Fast detection for SO_2 in white granulate sugar and crystal sugar. *Food Sci. Technol.* **2013**, *38*, 312−314 (in Chinese).

Apoptosis is a highly regulated programmed cell death process that eliminates dysfunctional cells from the body by self-degradation.[6] Apoptosis can be triggered in a cell through either the extrinsic pathway or the intrinsic pathway. The extrinsic pathway is initiated through the stimulation of transmembrane death receptors such as Fas receptors, located on the cell membrane.[7] In contrast, the intrinsic pathway of apoptosis is driven by a mitochondria- mediated death signaling cascade through the release of death signal factors, and these two apoptotic pathways are executed mainly by a class of cysteine proteases known as caspases.[8]

During apoptosis, engagement of the mitochondrial pathway involves mitochondrial membrane permeabilization (MMP), which depends on activation, translocation, and oligomerization of multidomain Bcl-2 family proteins such as Bax or Bak. MMP triggers the release of cytochrome *c* and other apoptogenic proteins into the cytosol followed by the activation of caspase cascades, which eventually results in poly(ADP-ribose) polymerase (PARP) cleavage and apoptosis.[9] Besides, MMP induces apoptosis through altering the levels of expression of Bcl-2 family proteins.[10] PARP are critical to DNA repair and apoptosis signaling, and play an important role in various mechanisms of cellular stress.[7,8]

Apoptosis can also occur via the caspase-independent apoptotic pathway in which apoptosis-inducing factor (APIF) plays a key role.[11,12] APIF protein is normally confined to mitochondria and is released by cleavage of calpains upon apoptotic stimulation.[13,14] The truncated form of APIF protein acts as a pro-apoptotic mediator, which translocates first from mitochondria into the cytosol followed by entry into the nucleus, where it promotes chromatin condensation and DNA degradation.[15,16]

Codium decorticatum is a dark green alga belonging to the family Codiales, and it is commonly found in the Gulf of Mannar region, India. Thus far, there has been no report on the biological properties of glycoprotein (GLP) from seaweeds. Hence, in the present study, GLP from *C. decorticatum* was extracted, purified, and investigated for its cytotoxicity potential on human breast cancer (MDA-MB-231) cells against normal (HBL-100) breast epithelial cells that served as control. Also, the apoptotic effect of GLP through activation of intrinsic signaling cascade pathway in MDA-MB-231 breast cancer cells was evaluated with respect to the expression of mitochondrial membrane proteins, ROS generation and cleavage of PARP, and up- and downstream events of bcl-2 family genes.

MATERIALS AND METHODS

Materials and Chemicals. Toluidine Blue O and ammonium sulfate were purchased from SRL Chemicals, Mumbai, India. Q-Sepharose anionic exchanger, Dulbecco's minimal essential medium (DMEM), penicillin, streptomycin, 2′,7′-dichlorofluorescein-diacetate (DCFH-DA), DAPI stain, Acridine orange (AO), ethidium bromide (EtBr), and propidium iodide (PI) were purchased from Sigma Aldrich, USA. Dialysis membrane (MWCO 12−14 kDa) and methyl thiazol tetrazolium salt were purchased from HiMedia, India. Coomassie Brilliant Blue (CBB) stain, periodic acid−Schiff (PAS) stainm and medium-range protein marker (14.3−97.4 kDa) for SDS-PAGE were purchased from Genei, India. Fetal bovine serum was purchased from Gibco, Inc., USA. LDH assay kit was procured from Cayman Chemicals, USA. cDNA synthesis kit (SuPrimeScript RT Master Mix, catalog no. SR2000) was purchased from GeNetBio. Primary antibodies against cytochrome *c* and caspase 3 were purchased from Santa Cruz Biotechnology, Inc. (Santa Cruz, CA, USA). Anti-PARP antibody was procured from Pharmingen, San Diego, CA, USA. Antibody against β-actin was purchased from Bio-World (St. Louis Park, MN, USA). Horseradish peroxidase-conjugated secondary antibodies were purchased from Jackson Immuno Research (West Grove, PA, USA). All other reagents and chemicals were of the highest purity grade.

Extraction and Purification of GLP from *C. decorticatum*. The collection of fresh and healthy *C. decorticatum* specimens was made between December 2011 and January 2012 during low tide at the depth of 1−3 m along the coast of Kilakarai, Gulf of Mannar, Tamil Nadu, India. The collected algae were washed with seawater and distilled water. The fresh thallus of the alga was powdered with liquid nitrogen and stored at −80 °C until used. One hundred and fifty grams of powder was added to 1 L of 0.05 mM phosphate buffer (pH 7.2) and dispersed for 6 h with constant stirring at 4 °C followed by filtration using cheesecloth to remove insoluble debris. Furthermore, the sample was centrifuged at 12500 rpm for 20 min to remove insoluble matter. The supernatant was saturated with 20% followed by 70% ammonium sulfate and centrifuged at 12000 rpm for 20 min to obtain pellets, which were dissolved and dialyzed against 0.05 M phosphate buffer at pH 7.2. The dialyzed sample was loaded onto Q-Sepharose anionic exchange column (30 cm × 2.5 cm) and washed with 0.05 M phosphate buffer at pH 7.2. The sample was eluted serially with 50 mL of 50, 100, 150, 200, 300, 400, 500, and 700 mM NaCl in the same buffer with a flow rate of 2.0 mL/min. Fractions of 5 mL volume were collected and read at 280 and 490 nm using a UV−vis spectrophotometer (DU-40 spectrophotometer, Beckman, USA) for identification of protein- and carbohydrate-rich fractions, respectively. Furthermore, GLP-rich fractions showing the presence of GLP band by CBB and PAS staining methods on sodium dodecyl sulfate−polyacrylamide gel electrophoresis (SDS-PAGE) were collected, pooled, dialyzed against the same buffer, lyophilized (Vir Tis FTS systems, Warminster, PA, USA), and stored in vials at 4 °C for further use (Scheme 1). The purity of the GLP fraction from anion

Scheme 1. Extraction and Purification Process of Glycoprotein from *C. decorticatum*

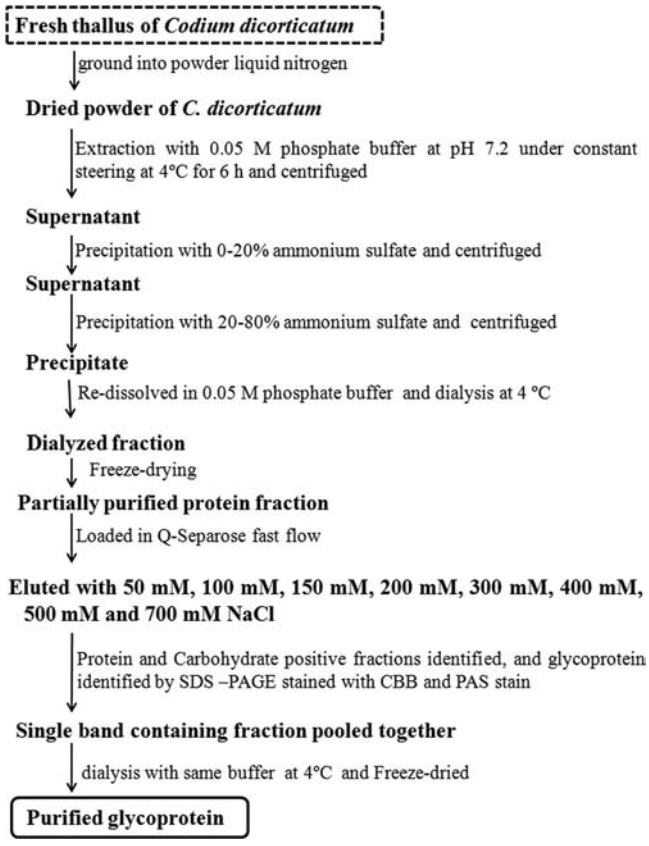

exchange chromatography was analyzed by the presence of a single band detected with CBB staining (for protein) and PAS staining (for polysaccharides) on SDS-PAGE. Besides, Toluidine Blue O staining was employed for the detection of polysaccharides resolved in agarose gel by electrophoresis.

Cell Culture and Maintenance. The selected cell lines of human MDA-MB-231 and HBL-100 cells were obtained from National Centre for Cells Science (NCCS), Pune, India. Detailed culture conditions are provided in the Supporting Information.

Cell Proliferation Assay. Cell proliferation was analyzed by 3-(4,5-dimethylthiazol-2-yl)-2,5-diphenyl-tetrazolium bromide (MTT) assay, as described by Mosmann.[17] Briefly, exponentially growing MDA-MB-231 and HBL-100 cells (1×10^4 cells/mL) were seeded in 96-well plates in a final volume of 100 μL/well and were treated with 10 μL of test sample (GLP) in FCS-free complete medium at various concentrations (5−100 μg/mL) for 48 h. One hundred microliters of MTT (5 mg/mL) was added to treated cells, and the plates were incubated at 37 °C for 4 h. The supernatant was aspirated, and 100 μL of dimethyl sulfoxide (DMSO) was added to each well to dissolve the Formosan crystals. Absorbance was measured at 620 nm using a 96-well microplate reader (THERMO Multiskan, USA), and the inhibitory concentrations (IC_{25}, IC_{50}, and IC_{75}) were determined for GLP causing reduction in cell viability. The percentage of cell survival was calculated using the following formula:

$$\text{cytotoxicity (\%)} = (\text{mean exptl absorbance} / \text{mean control absorbance}) \times 100$$

The control wells were not treated with GLP.

Lactate Dehydrogenase (LDH) Assay. The LDH assay was performed with an LDH colorimetric assay kit using an ELISA reader according to the manufacturer's protocol. Detailed experimental conditions are provided in the Supporting Information.

Determination of Apoptosis Induction and Cell Death. The induction of apoptosis by GLP-treated cells was analyzed by AO/EtBr staining. Detailed conditions for this method are provided in the Supporting Information.

Fluorescent Microscopic Studies on Chromatin Condensation. The condensation of chromatin and nuclear fragmentation in GLP-treated cells were analyzed by DAPI staining. Detailed conditions are provided in the Supporting Information.

Measurement of ROS Generation. 2′,7′-Dichlorofluorescein-diacetate (DCFH-DA) can be deacetylated by intracellular esterase to nonfluorescent DCFH, which can be oxidized by ROS, resulting in the formation of fluorescent compound 2′,7′-dichloroflorescein (DCF). The fluorescence intensity of DCF is proportional to the amount of ROS produced by the cells. After seeding of 5×10^5 cells/well to a 6-well plate, the cells were treated with GLP for 24 h in dose-dependent concentrations. Subsequently, cells were washed once with ice-cold PBS and incubated with DCFH-DA (50 μM final concentration) at 37 °C for 30 min in the dark. Then, the cells were washed twice and maintained in 1 mL of PBS. ROS generation was assessed using a fluorescence microscope (Nikon Eclipse, Inc., Japan) at excitation and emission wavelengths of 488 and 530 nm, respectively, and the mean fluorescence intensity of DCF was evaluated.

Determination of $\Delta\Psi_m$ by Flow Cytometry. MDA-MB-231 cells (1×10^5/mL) were seeded in a 6-well plate containing complete medium and allowed to attach for 24 h. The cells were treated with GLP for 24 h in dose-dependent concentrations and harvested. The medium was removed, and the adherent cells were trypsinized. The cells were pelleted by centrifugation at 2000 rpm for 10 min followed by resuspension with 1 mL of Rhodamine 123 (Rh 123; 5 μg/mL in methanol) for 30 min at 37 °C in dark, washed with PBS twice, and resuspended in PBS. Then, Rh 123-stained cells were fixed with 4% paraformaldehyde for 10 min. Finally, the cells were washed with methanol and analyzed for change in $\Delta\Psi_m$ using BD FACS caliber (FL-1 detector with 530 nm band-pass filter). Data were analyzed using Cell Quest Pro 6.0 software (BD Biosciences, San Jose, CA, USA).

Cell Cycle Analysis. Measurement of cellular DNA content and distribution of cells for cell cycle analysis were carried out by flow cytometry. Detailed experimental conditions are provided in the Supporting Information.

Semiquantitative Reverse Transcription PCR (RT-PCR) for Mitochondrial Gene Expression. RT-PCR was performed to determine changes in the expression of bax, bcl-2, and internal control β-actin genes. TriZol reagent was used to isolate total RNA and reverse transcribed. Briefly, the cDNA was synthesized using a cDNA synthesis kit and amplified according to the manufacturer's protocol in a 25 μL reaction mixture containing random primer pairs (1.0 μL): 10× buffer (5.0 μL), cDNA (2.0 μg), 25 mM/L MgCl (3.0 μL), 10 mM/L dNTPs (1.0 μL), and Taq polymerase (2.5 units). Amplification cycles consisted of denaturation at 94 °C for 1 min, primer annealing at 57 °C for 45 s, and extension at 72 °C for 45 s, for a total of 30 cycles followed by a final extension at 72 °C for 10 min. The following primer sequences were used for amplification: (a) bax gene, forward 5′-TTTGCTTCAGGGTTTCATCC-3′ and reverse 5′-CAGTTGAAGTTGCCGTCAGA-3′; (b) bcl-2 gene, forward 5′-CATCCATTATAAGCTGTCGCA-3′ and reverse 5′-TGCCGG-TTCAGGTACTCAGT-3′; and (c) β-actin, forward 5′-GTTGCT-ATCCAGGCTGTGC-3′ and reverse 5′-GCATCCTGTCGGCAA-TGC-3′. The PCR products were electrophoresed and visualized by transillumination system (Alpha Innotech Image viewer 6.0.0, Japan).

Analysis of Expression of Mitochondrial Membrane Proteins by Western Blot. Cells (1×10^6 cells/well) were transferred to a culture dish (100 mm × 20 mm) for 24 h; the cells were treated for 24 h with GLP in dose-dependent concentration, harvested, and washed twice with ice-cold PBS. Subsequently, a 1.5 mL microfuge tube containing cell extract was centrifuged at 2500 rpm for 5 min to discard the supernatant. Treated cells were washed in PBS and lysed in 100 μL of buffer containing 50 mM Tris-HCl (pH 8.0), 150 mM NaCl, 1% Triton X-100, 1 mM phenylmethanesulfonyl fluoride, 10 μg/mL pepstatin, and 10 μg/mL leupeptin. After 20 min, extracts were centrifuged at 12000 rpm for 10 min at 4 °C, and the supernatants were stored at −80 °C until further use. Proteins (30 μg/lane) were separated using 10% SDS-PAGE and transferred to PVDF membranes. The membranes were blocked in TBST solution containing 5% (w/v) nonfat milk for 2 h, followed by overnight incubation at 4 °C with primary antibodies such as cytochrome *c*, caspase 9, caspase 3, and β-actin. After being washed with TBST buffer, the membranes were incubated for 1 h with the secondary antibody, horseradish peroxidase-conjugated goat anti-rabbit IgG. Antibody-bound proteins were detected using enhanced chemiluminescence reagents. Blots were washed with washing buffer and incubated with secondary antibodies conjugated with horseradish peroxidase for 1 h at room temperature.

Poly(ADP-ribose) Polymerase (PARP) Cleavage Analysis. Protein samples (50 μg) in nuclear fractions were resolved on 7.5% SDS-PAGE gels and transferred to nitrocellulose membranes. The membranes were blocked overnight with BSA solution (5% bovine serum albumin in PBS) and 0.1% Tween 20 at 4 °C and thereafter incubated with anti-PARP antibody (1:2000). The immune complexes were visualized as described for immune-blot analysis.

Statistical Analysis. All of the experiments were done in triplicates, and the experiments were repeated at least three times. The statistical software SPSS version 17.0 (SPSS Inc., Chicago, IL, USA) was used for analysis. *p* values were determined using Student's *t* test; (*) $p \leq 0.05$ and (**) $p \leq 0.01$ were considered statistically significant.

RESULTS

Extraction and Purification of GLP from *C. decorticatum*. The crude extract from *C. decorticatum* was precipitated with 20 and 70% ammonium sulfate fractionation, and the precipitate of the 70% ammonium sulfate saturated fraction was subjected to dialysis. The dialyzed sample was loaded onto the Q-Sepharose anion exchange column chromatograph and fractions were collected. A total of 80 fractions were collected and the content of protein and carbohydrate was determined

for each fraction. Eight GLP-rich fractions (Figure 1A), eluted with 500 mM NaCl solution, were identified, and each fraction

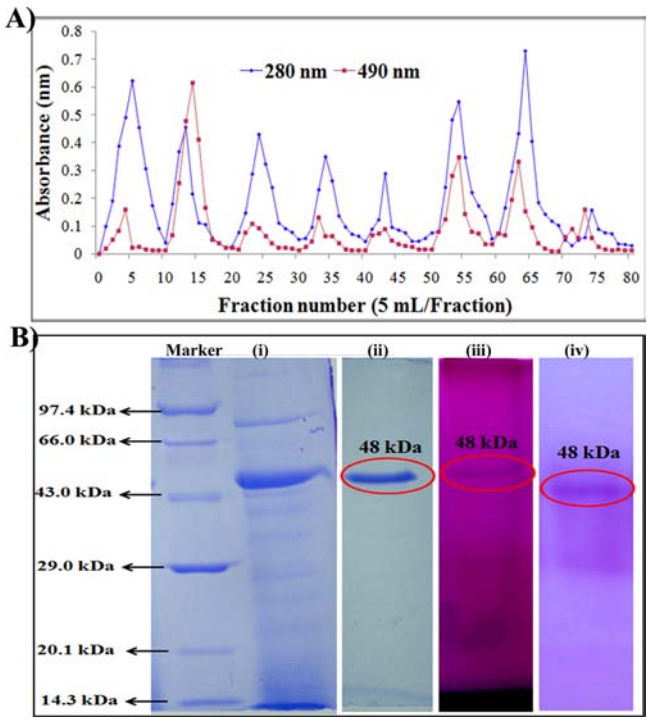

Figure 1. (A) Elution profile of crude GLP-rich extract on Q-Sepharose Fast Flow chromatography. (B) Electrophoretic analysis of GLP from *C. decorticatum*. CBB staining reveals (i) GLP-rich crude fraction and (ii) purified GLP by SDS-PAGE; PAS staining shows (iii) purified GLP by SDS-PAGE; Toluidine Blue staining shows (iv) purified GLP by agarose gel electrophoresis.

was again checked for purity by SDS-PAGE stained with CBB and PAS for protein and GLP, respectively. Among the 8eight fractions, six were homogeneous and were pooled, dialyzed, and lyophilized. We confirmed the presence of a GLP band having the molecular mass of ~48 kDa (Figure 1B). The yield of the purified GLP was found to be 195 mg (0.13%) from 150 g of dried extract of *C. decorticatum*, and the contents of carbohydrate and protein in GLP were found to be 36.24 and 63.76%, respectively. The detailed process of extraction and purification of GLP is depicted in Scheme 1.

GLP Reduces Cell Viability and Causes Membrane Damage. To investigate the effects of apoptotic cell death induced by GLP, MDA-MB-231 and HBL-100 cells were treated with GLP at different dose levels for 24 h and subjected to MTT assay. Results showed that MDA-MB-231 cells exhibited strong growth inhibitory effects when compared to HBL-100 cells (Supporting Information Figure S2). We evaluated the effect of GLP upon cell viability and plasma membrane damage of normal cell lines against untreated controls (Supporting Information Figure S2; Figure 2A,B). The cytotoxicities of GLP in dose-dependent concentration for MDA-MB-231 and HBL-100 cells were found to be 75 ± 0.23 μg/mL (IC_{25}), 55 ± 0.32 μg/mL (IC_{50}), and 30 ± 0.43 μg/mL (IC_{75}) and 90 ± 0.57 μg/mL (IC_{25}), 80 ± 0.48 μg/mL (IC_{50}), and 60 ± 0.26 μg/mL (IC_{75}), respectively (Figure 2A).

The extent of cell membrane damage of GLP-treated MDA-MB-231 cells at dose-dependent concentrations in 24 h was measured by LDH release assay (Figure 2B). The percentage of added LDH protein either absorbed or inactivated by dose-dependent concentrations in 24 h is shown in Figure 2B. The figure shows that the release of LDH was greater when the cells were treated with increasing concentrations of GLP.

In addition, direct observation using an inverted microscope revealed numerous morphological changes in MDA-MB-231 cells treated with GLP (data not shown). There are no significant cytotoxic effects of GLP in normal HBL-100 cells; hence, additional apoptotic parameters were performed only for cancer cells. In MDA-MB-231 cells, chromatin condensation, loss of nuclear construction, and formation of apoptosis bodies appeared in a dose-dependent manner after GLP treatment. To examine whether GLP inhibits the proliferation of MDA-MB-231 cells by inducing apoptosis, cells were investigated by nuclear DAPI staining (Figure 2C). The GLP-treated cells exhibited typical morphological features of apoptosis with nuclear fragmentation, whereas control (untreated) cells did not show these features.

Detection of Apoptosis Induction and Cell Death by AO/EtBr and DAPI Staining. Using fluorescence microscopy, necrotic and apoptotic cells were distinguished on the basis of overall cell morphology and cell membrane integrity. Upon staining with AO/EtBr, apoptotic cells containing apoptotic bodies and necrotic cells were observed as orange and red, respectively, whereas untreated MDA-MB-231 cells were found to exhibit green fluorescence with the absence of morphological changes (Figure 3). However, morphological changes as well as the induction of apoptosis in these cells were detected after treatment with GLP at dose-dependent concentrations for a period of 24 h, and the percentage of apoptotic induction is depicted in Figure 3.

DAPI is also known to form fluorescent complexes with double-stranded DNA and is useful in finding the apoptotic condensed nuclei. The 80−90% confluent MDA-MB-231 cells were seeded in 24-well plates and exposed to GLP for 24 h. The morphology and the condensed nuclei chromatins were observed in the cells using a fluorescence microscope after cell fixation. Apoptotic nuclei were identified by the reduced nuclear size and gathering of condensed chromatin at the periphery of the nuclear membrane besides the fragmented morphology of nuclear bodies (Figure 2C).

GLP Increases Intracellular ROS Level in MDA-MB-231 Cells. ROS play a central role in the regulation of cellular apoptosis. We examined the effect of GLP in intracellular ROS generation due to increase in $\Delta\Psi_m$ loss that could mediate intrinsic apoptotic signaling pathways (Figure 4). ROS scavenger DCFH-DA was used to confirm the role of ROS in GLP-induced apoptosis. The results showed that there was a reduction of $DCFH_2$ into DCF through esterase activity due to the release of peroxidase cytochrome *c* in the cytosol leading to increased production of ROS in GLP-treated MDA-MB-231 cells (Figure 4A,B) when compared to untreated cells (data not shown). After exposure of MDA-MB-231 cells to 75 ± 0.23 μg/mL (IC_{25}), 55 ± 0.32 μg/mL (IC_{50}), and 30 ± 0.43 μg/mL (IC_{75}) GLP for 24 h in a dose-dependent manner with untreated control cells, the ROS levels in these cells were measured as 21 ± 4.76, 43 ± 6.60, 62 ± 4.30, and 76.04 ± 5.34%, respectively (Figure 4B). The production of ROS is increased in a dose-dependent manner in GLP-treated MDA-MB-231 cells (Figure 4A,C). These data suggested that ROS generation is required for $\Delta\Psi_m$ loss and subsequent induction of intrinsic apoptotic signaling pathways in GLP-treated MDA-MB-231 cells.

dx.doi.org/10.1021/jf405329e | J. Agric. Food Chem. 2014, 62, 3410−3421

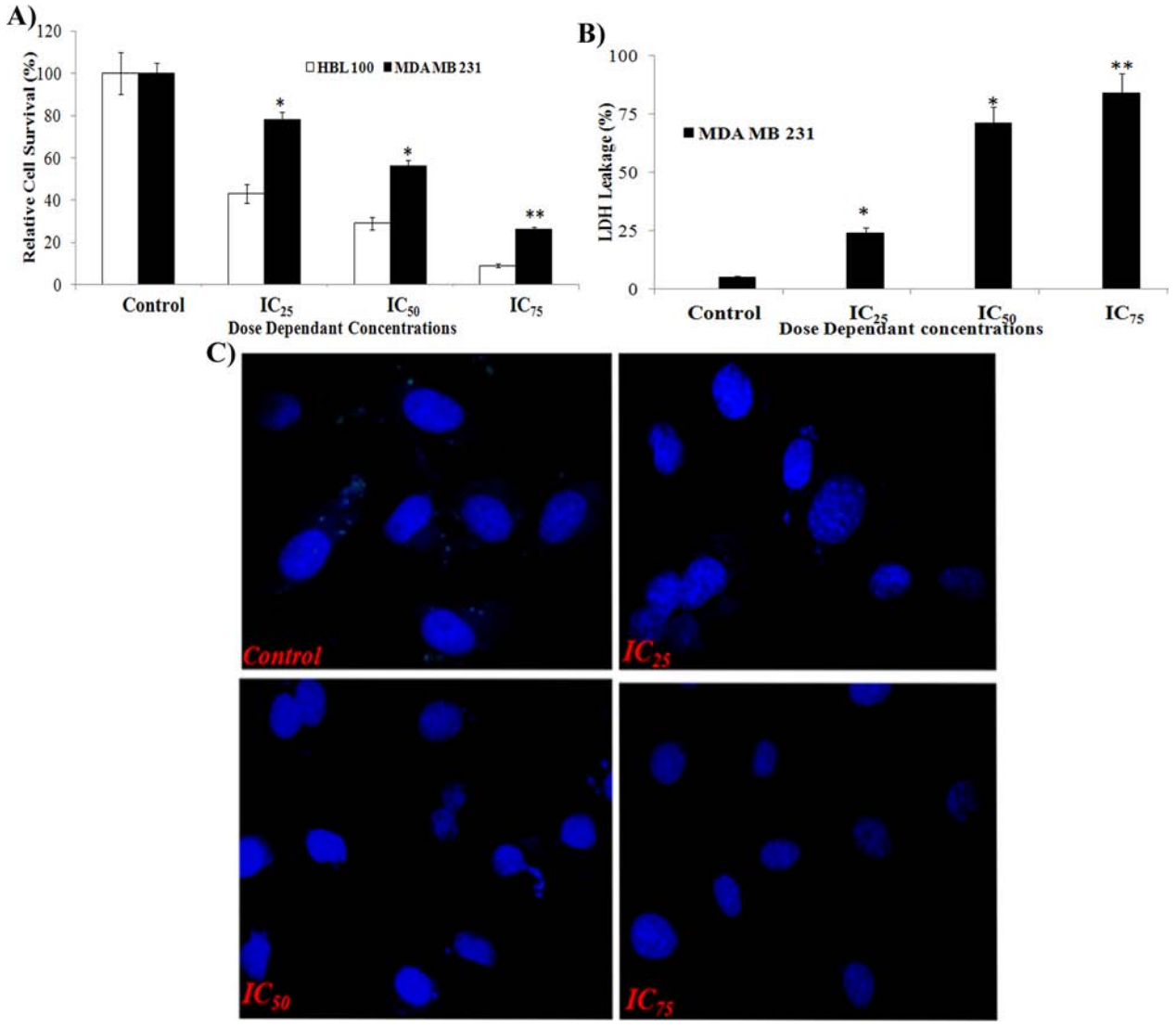

Figure 2. (A) GLP-induced cytotoxicity in MDA-MB-231 and HBL-100 cells treated with dose-dependent concentrations of GLP for 24 h in triplicates. (B) Plasma membrane damage of MDA-MB-231 breast cancer cells was assessed by LDH assay. (∗) $p \leq 0.05$ and (∗∗) $p \leq 0.01$, compared with untreated cells (control groups). (C) Effects of GLP on nuclear fragmentations in MDA-MB-231 cells by DAPI staining. Intensely stained condensed apoptotic nuclei bodies besides nuclear change and relocations were observed in GLP-treated cells by fluorescence microscope (400× magnification).

GLP Triggers Mitochondria-Dependent Apoptosis. To investigate the molecular mechanism of GLP-induced apoptosis, we examined the effect of GLP on mitochondrial function in MDA-MB-231 cells using Rh 123 fluorescence staining. Treatment with increasing concentrations of GLP induced a dose-dependent loss of $\Delta\Psi_m$ (Figure 5A). In addition, we found the dose-dependent release of cytochrome *c* from mitochondria into the cytosol, which was associated with changes in the ratio of expression of bcl-2/bax. These data reveal that GLP could cause mitochondrial dysfunction in MDA-MB-231 cells. The role of GLP in intracellular $\Delta\Psi_m$ dysfunction and the subsequent induction of mitochondria-mediated intrinsic apoptotic signaling pathways in MDA-MB-231 cells were evaluated by FACS analysis. The results showed that the loss of $\Delta\Psi_m$ increased in a dose-dependent manner in cells treated with GLP for 24 h, and this resulted in induction of intrinsic apoptotic signaling pathway in the cells (Figure 5B,C).

GLP Promotes G_2/M Arrest in MBA-MB-231 Cells. To understand the cell death mechanism, GLP was evaluated for its effect on cell cycle and induction of apoptosis in cancer cells by flow cytometry. The results on cell cycle analysis for untreated control cells and GLP-treated cells with dose-dependent concentrations are depicted in Figure 6A. From the figure, it was observed that there was a significant increase in cells at sub-G_0 as well as G_2/M phases (∗∗, $p \leq 0.01$). The cells at G_0/G_1 phase decreased significantly (∗, $p \leq 0.05$), whereas those at S phase did not change significantly (Figure 6B). The study findings revealed the effect of GLP on the accumulation of cells in G_2/M phase accompanied by cell cycle arrest (Figure 6). It was shown that GLP arrested the growth of cancer MDA-MB-231 cells in G_2/M phase. This suggested that GLP might act as a G_0/G_1 checkpoint that controlled the progression of cells from G_1 to S phase and thereby prevented the replication of DNA. These results suggested that the GLP delayed cell cycle progression by arresting cells in the G_2/M phase of cell cycle, resulting in apoptosis.

Expression of bcl-2 Family Genes, Attenuation of MMP, Loss of $\Delta\Psi_m$, and Induction of Apoptosis. As

dx.doi.org/10.1021/jf405329e | J. Agric. Food Chem. 2014, 62, 3410−3421

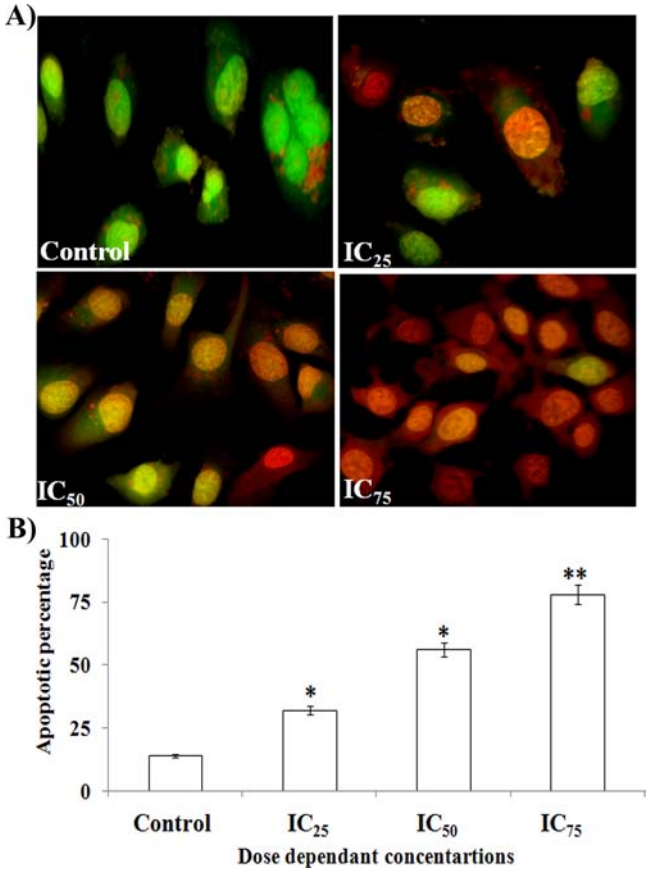

Figure 3. (A) Images of fluorescent microscopic analysis of GLP-induced apoptosis in MDA-MB-231 cells stained with AO/EtBr. Viable cells are shown in green, necrotic cells in red, and apoptotic cells in orange. (B) Graph shows apoptotic cells (%) after treating MDA-MB-231 cells with GLP. (*) $p \leq 0.05$ and (**) $p \leq 0.01$, compared with untreated cells (control groups).

shown in Figure 7A, an additional experiment was carried out to elucidate whether GLP-induced apoptosis is associated with the expression of bcl-2 family member genes such as bax and bcl-2. Cells were exposed to dose-dependent concentrations of GLP for 24 h with untreated control cells, and the expression profile of pro-apoptotic bax and anti-apoptotic bcl-2 family genes in response to dose-dependent manner was elucidated (Figure 7A). The gene expression profiles in GLP-induced apoptosis of MDA-MB-231 cells were further confirmed by investigating with densitometry calculations (Figure 7B). As shown in Figure 7B, exposure of cells to dose-dependent concentrations led to change in the expression of mitochondrial pro-apoptotic and anti-apoptotic genes. Furthermore, we investigated the role of mitochondria in GLP-induced apoptosis of MDA-MB-231 cells by measuring Rh 123 dye retention. As shown in Figure 7B, MDA-MB-231 cells treated with GLP exhibited a significant reduction in mitochondria dysfunction in a dose-dependent manner.

GLP Induces Apoptosis through a Caspase 3-Dependent Pathway. The mitochondrial pathway is one of the major apoptotic pathways, which is often related to the loss of $\Delta\Psi_m$. The release of cytochrome *c* from mitochondria to cytosol is the limiting factor in the mitochondrial pathway, and the loss of $\Delta\Psi_m$ has been suggested to cause the release of cytochrome *c*. Here, we investigated the activation of caspases and the subsequent proteolytic cleavage of PARP proteins in MDA-MB-231 cells by Western blotting. Western blot analysis suggested that GLP treatment with dose-dependent concentrations led to a significant increase in caspase 3, caspase 9, and PARP proteins (Figure 8A and B). The release of cytochrome *c* (14 kDa) could initiate apoptosis via the mitochondrial pathway by activation of caspase 9 and caspase 3, and cleavage of PARP. 37/35 kDa caspase 9, upon cleavage, was converted to active caspase 9 having the molecular weight of 17 kDa. The molecular weight of PARP before and after cleavage was 116 and 89 kDa, respectively (Figure. 8). After MDA-MB-231 cells were treated with GLP in dose dependent concentration for 24 h, the release of cytochrome *c* increased in a concentration-corresponding manner (Figure 8). The ratios for densitometric values of expression of cytochrome *c*/*β*-actin, caspase 9/*β*-actin, caspase 3/*β*-actin, and PARP/*β*-actin for control and cancer cells were also calculated (Figure 8B). These results suggested that GLP induced caspase 3-dependent apoptosis in MDA-MB-231 cells.

DISCUSSION

Cancer is one of the most common diseases that threaten human life. Unfortunately, the drugs used for cancer therapy are toxic and affect not only cancer cells but also normal cells. Thus, finding novel, effective, and nontoxic compounds from natural sources is important now more than ever before. Induction of apoptosis has been the target mechanism for cancer treatments, and DNA fragmentation is a marker of cell death. There have been limited studies on cytotoxic effects and apoptotic induction activities of GLP specifically against cancer cells;[18] however, there are no reports of GLP from green seaweeds having antiproliferative activities toward cancer cells.[19] Studies report that oral consumption of seaweeds significantly decreases the incidence of carcinogenesis in vivo.[5] Hence, we attempted to isolate and purify GLP from green seaweed *C. decorticatum* and evaluated its cytotoxic activities and antiproliferative mechanisms by induction of apoptosis using an in vitro cancer cell line model.

In Figure 1, purified GLP from *C. decorticatum* was shown as a single band on SDS-PAGE with a molecular mass of about 48 kDa consisting carbohydrate (36.24%) and protein (63.76%) moieties. The gels stained with Schiff's reagent and CBB reagent confirmed it as glycoprotein (GLP).

To elucidate clearly the specificity of GLP toward cancer cells, the cytotoxic effect of GLP on MDA-MB-231 cells was compared with normal breast HBL-100 cells. GLP of the study, with its inhibitory concentrations on cancer cells, produced no toxicity or variations in proliferative effects in HBL-100 cells as evidenced by MTT assay. Our data regarding MTT assay, LDH assay, and nuclear fragmentation were consistent, and these results suggested that GLP could penetrate test cancer cells (MDA-MB-231) and destroy plasma membrane integrity, which consequently caused apoptosis in the cells and LDH leakage (Figure 2B). The LDH assay was found to be susceptible to interference from particle adsorption or protein inactivation. The exact mechanism could not be determined by our experiments because both could cause a decrease in the measurable LDH protein, resulting in a false indication of a nontoxic response. There was a reduction in the measurable LDH content with increasing dose-dependent concentrations of GLP until a seemingly steady state condition was observed. The amount of LDH reduction was also affected by the concentration of GLP in 24 h. Han et al.[14] found indications of LDH binding to titanium dioxide nanoparticles during cell

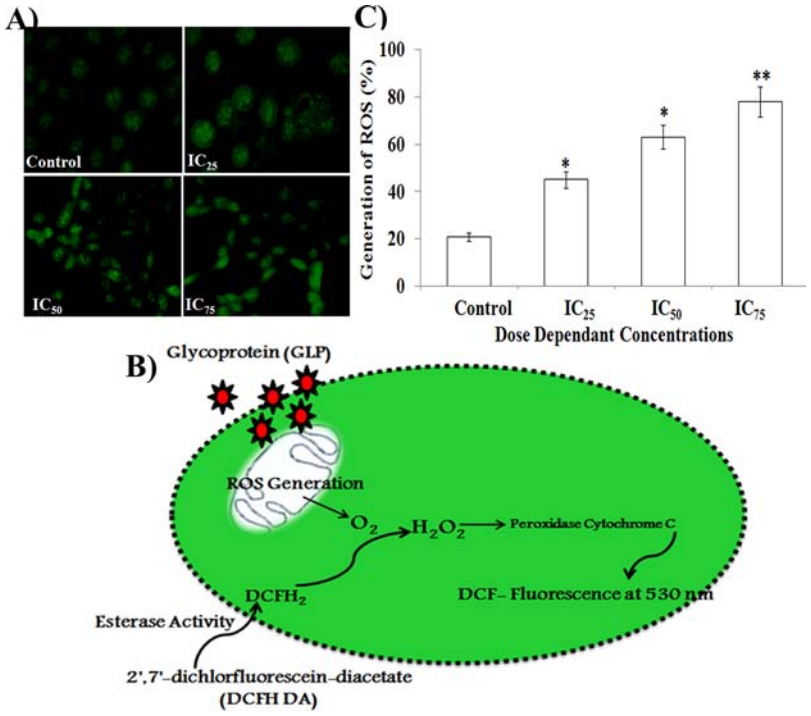

Figure 4. (A) Fluorescence microscopy at 530 nm (400× magnification) shows the effect of GLP on ROS generation due to change in $\Delta\Psi_m$ of MDA-MB-231 cells. (B) Schematic representation of mechanism involved in ROS production from cancer cells treated with GLP. The scheme provided was prepared on the basis of our study according to the report of Curtin et al.[48] (C) Release of ROS (%) from GLP-treated MDA-MB-231 cells with the dose-dependent concentrations of GLP for 24 h. (∗) $p \leq 0.05$ and (∗∗) $p \leq 0.01$, compared with untreated cells (control groups).

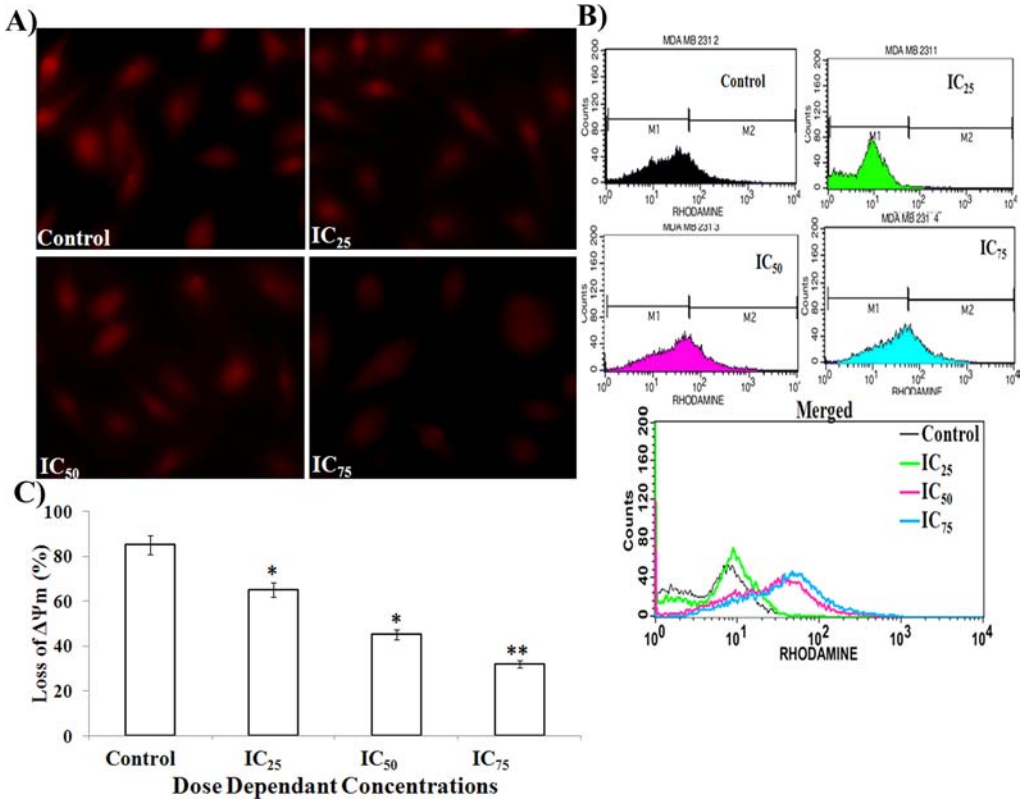

Figure 5. (A) Fluorescence microscopy studies using Rh 123 on the effect of dose-dependent concentrations of GLP in induction of mitochondria-mediated apoptosis in MDA-MB-231 cells via changes in $\Delta\Psi_m$ at 530 nm (400× magnification). (B) Flow cytometry analysis using Rh 123 on the effect of dose-dependent concentrations of GLP in induction of mitochondria-mediated apoptosis in MDA-MB-231 cells via changes in $\Delta\Psi_m$. (C) $\Delta\Psi_m$ loss (%) in GLP-treated MDA-MB-231 cells by flow cytometry. (∗) $p \leq 0.05$ and (∗∗) $p \leq 0.01$, compared with untreated cells (control groups).

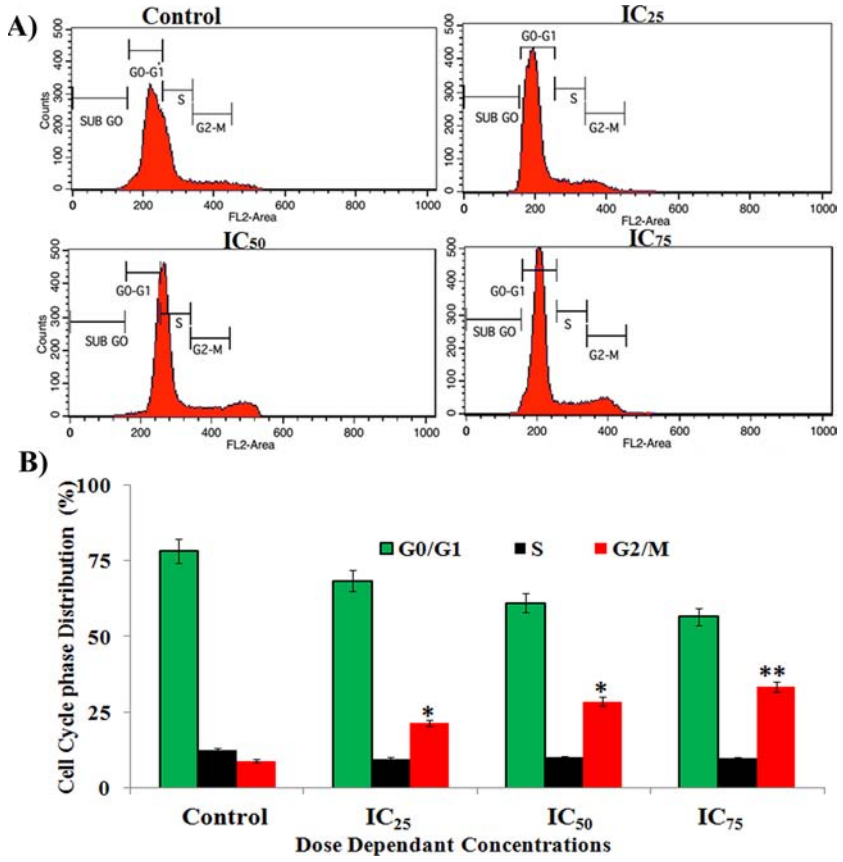

Figure 6. (A) GLP treated MDA-MB-231 cells stained with PI for cell cycle analysis by flow cytometry. Panels indicate the occurrence of cells in each phase of the cell cycle. (B) Data on cell cycle distribution represent the percentage of cell death in the total population. Experiments were performed in duplicates. Data show percentage of live cells in each phase of the cell cycle (G_0/G1, S, and G_2/M). A dose-dependent increase in the percentage of cell death was observed in G_2/M cycle. (∗) $p \leq 0.05$ and (∗∗) $p \leq 0.01$, compared with untreated cells (control groups).

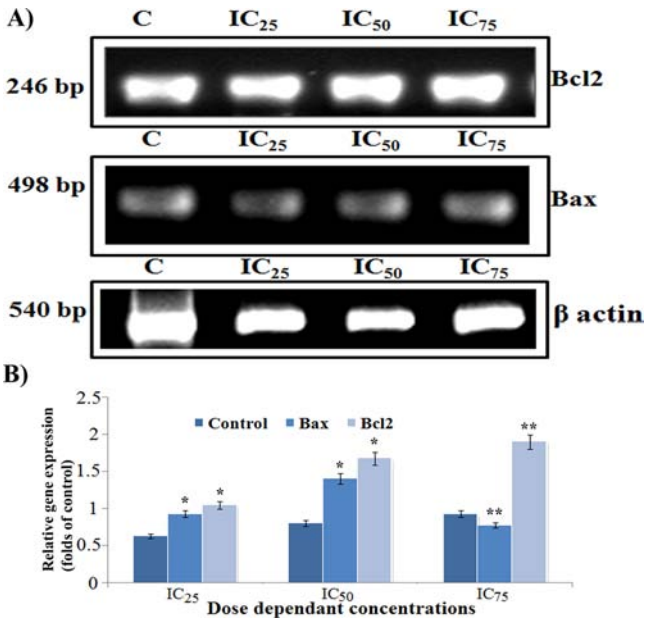

Figure 7. (A) RT-PCR studies on down-regulation of bax and up-regulation of bcl-2 genes induced by GLP in MDA-MB-231 cells. The events are associated with changes in the levels of $\Delta\Psi_m$ loss. β-Actin gene was used as an internal loading control for RT-PCR analysis. (B) Densitometry analysis of RT-PCR of intrinsic apoptotic related gene expression of GLP treated cells. (∗) $p \leq 0.05$ and (∗∗) $p \leq 0.01$, compared with untreated cells (control groups).

exposure but did not confirm with cell-free measurements of LDH absorption. The differences between our results and those of other groups may be due to the presence of other proteins or biological compounds that affect LDH absorption to particles.[14] Our measurements were performed with pure GLP in PBS with adherent cells, whereas other studies used different media or had the additional presence of intracellular proteins and cell debris generated during cell exposure.

The present study showed that after exposure to the GLP, MDA-MB-231 cells displayed typical apoptotic appearances such as nuclei condensation, cell shrinkage, and apoptotic bodies along with accumulation of a sub-G_1 cell cycle population, substantiating the activation of an intrinsic apoptotic pathway in cancer cells.[18−22] Although the caspase activation occurred in MDA-MB-231 cells, an increase in the expression of pro-apoptotic bcl-2 member genes resulted in nuclear translocation of APIF, which could be due to loss of $\Delta\Psi_m$.[23]

GLP induced apoptosis and cell death via cell cycle arrest in human breast cancer cell lines and not in normal cells. Results from Figure 2A clearly show that GLP induced cytotoxicity and reduced cell viability in breast cancer cell lines through induction of G_2/M phase arrest. It was reported that cell cycle control represents a major regulatory mechanism for cell growth,[24] wherein anticancer agents can play a role in blocking the progression of cell cycle, and development of new cancer therapeutics can be promising with this approach.[25,26] Cell cycle progression is partly controlled by a family of protein

dx.doi.org/10.1021/jf405329e | J. Agric. Food Chem. 2014, 62, 3410−3421

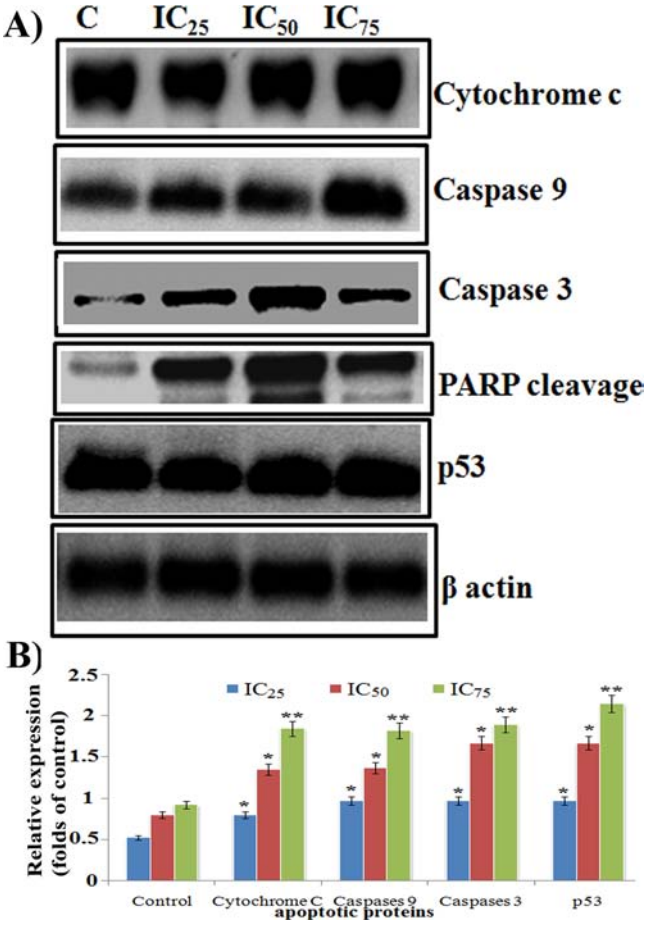

Figure 8. (A) Effect of GLP on activation of caspases, cleavage of PARP, release of cytochrome *c*, and $\Delta\Psi_m$ loss was evaluated by Western blotting and densitometry. Activities of caspases are indicated in percentage against unstimulated cells. Percentage of apoptotic population is represented on the basis of densitometry profile compared with its internal control *β*-actin. (B) Densitometry analysis of intrinsic apoptotic related protein expression of MDA-MB-231 cells treated with GLP. (∗) $p \leq 0.05$ and (∗∗) $p \leq 0.01$, compared with untreated cells (control groups).

kinase complexes in eukaryotic cells including cyclin-dependent kinases (CDKs) and their activating partners, the cyclins.[27] Together, these results suggested that GLP delayed cell cycle progression by arresting cells in the G_2/M phase of the cell cycle, resulting in significant induction of apoptosis.

Mitochondrial characteristics, such as mitochondrial mass, mitochondrial DNA, MMP, oxygen/glucose consumption, ROS, and ATP,[28,29] can aid in understanding the differences between sensitive and resistant cancer cells. An increasing number of studies have suggested that the function and integrity of mitochondria may affect the viability, proliferation/division, cytotoxic resistance, and hypoxic tolerance of cells. Hence, properties of mitochondria of cancer cells might become the basis of designing chemotherapeutic agents for effective cancer treatment. Mitochondrial targets such as (i) mitochondrial permeability transition, (ii) outer membrane permeabilization, and (iii) mitochondrial metabolism and metabolic reprogramming[30,31] have been recognized for developing potential strategies to overcome chemotherapeutic resistance. It is well-known that an increase in intracellular ROS can lead to apoptosis. On the other hand, a decrease of ROS can also ruin the stability of mitochondria, which is followed by a loss of $\Delta\Psi_m$, release of cytochrome *c* into cytosol, and activation of the caspase cascade.[32,33] To support this standpoint, GLP could be employed to circumvent cancer resistance due to its ability to target the hyperpolarized mitochondria.

Mitochondrial membrane dysfunction and the release of pro-apoptotic factors from the intermembrane space are controlled by Bcl-2 members.[34] The intrinsic mitochondrial-dependent pathway involves the disruption of outer mitochondrial membrane integrity that was followed by the reduction in MMP and the release of cytochrome *c* and other pro-apoptotic molecules from the mitochondria to the cytosol.[35] Additionally, the bcl-2 family genes and proteins are the essential regulators of apoptosis through controlling mitochondrial permeability.[36] A low concentration of ROS is important in redox balance and cell proliferation.[37] However, excessive ROS accumulation induces protein oxidation, lipid peroxidation, and DNA damage in cells, followed by cell death or apoptosis. It was reported that phenolic acids provoked ROS generation in HepG2 cells and IMR-32 cells.[38,39] Our results also showed that GLP could induce ROS generation in MDA-MB-231 cells. Furthermore, pretreatment of ROS significantly blocked GLP-induced cell death, confirming the involvement of ROS in this process. It has been demonstrated that ROS-mediated apoptosis is modulated by Akt and MAPK signaling pathways in HepG2 cells and U-937 cells, respectively.[38,39] Therefore we hypothesized that ROS might play a key role in regulating intrinsic apoptotic signaling pathways in GLP-induced apoptosis, which was substantiated in the present study by Western blotting and semiquantitative RT-PCR analysis of expression of apoptotic proteins and bcl-2 family genes, respectively (Figures 4−8).

The caspase cascade is a key pathway in the apoptotic signal transduction. Caspases include two types of subfamilies: upstream initiator caspases such as caspase 9, which are involved in regulatory events, and downstream effector caspase such as caspases 3 and 6, which correspond to the change in cell morphological events and to the cleavage on nuclear protein, PARP.[28,40] Thus, the increased activity of caspases in cells may enhance the risk of apoptosis. The present study showed that the treatment of cancer cells by GLP markedly elevated the activity of cytochrome *c*, caspase 9, and caspase 3, suggesting the activation of both upstream and downstream caspase cascades in these cells. Following caspase activation, an increasing number of proteins including PARP are degraded or cleaved,[36,37,41−46] which consequently promotes nuclear condensation and cell shrinkage, resulting in cell death. The results of our present study revealed that GLP activated caspase cascades and promoted the release of apoptotic factors to facilitate apoptosis in the cancer cells (Figure 8). The involvement of PARP in DNA repair is based on an earlier observation that the activity of this enzyme is increased several hundred-fold following DNA damage.[41,47] Many insights into possible functions of PARP in different biological processes were obtained from in vitro experiments employing NAD^+ analogues as inhibitors of poly(ADP-ribosylation) (e.g., nicotinamide, benzamide, and their derivatives).[47] These findings were further supported by PARP inhibition in intact MDA-MB-231 cells (Figure 8). Inhibition of PARP activity has been shown to protect cells from undergoing apoptosis.[42−46]

In summary, this study focused on the potential of a purified glycoprotein (GLP) from *C. decorticatum* for inducing apoptosis in human breast cancer MDA-MB-231 cells. GLP inhibited the growth of cancer cells when they were treated

Scheme 2. Proposed Schematic Diagram of GLP-Mediated Apoptosis in MDA-MB-231 Cells[a]

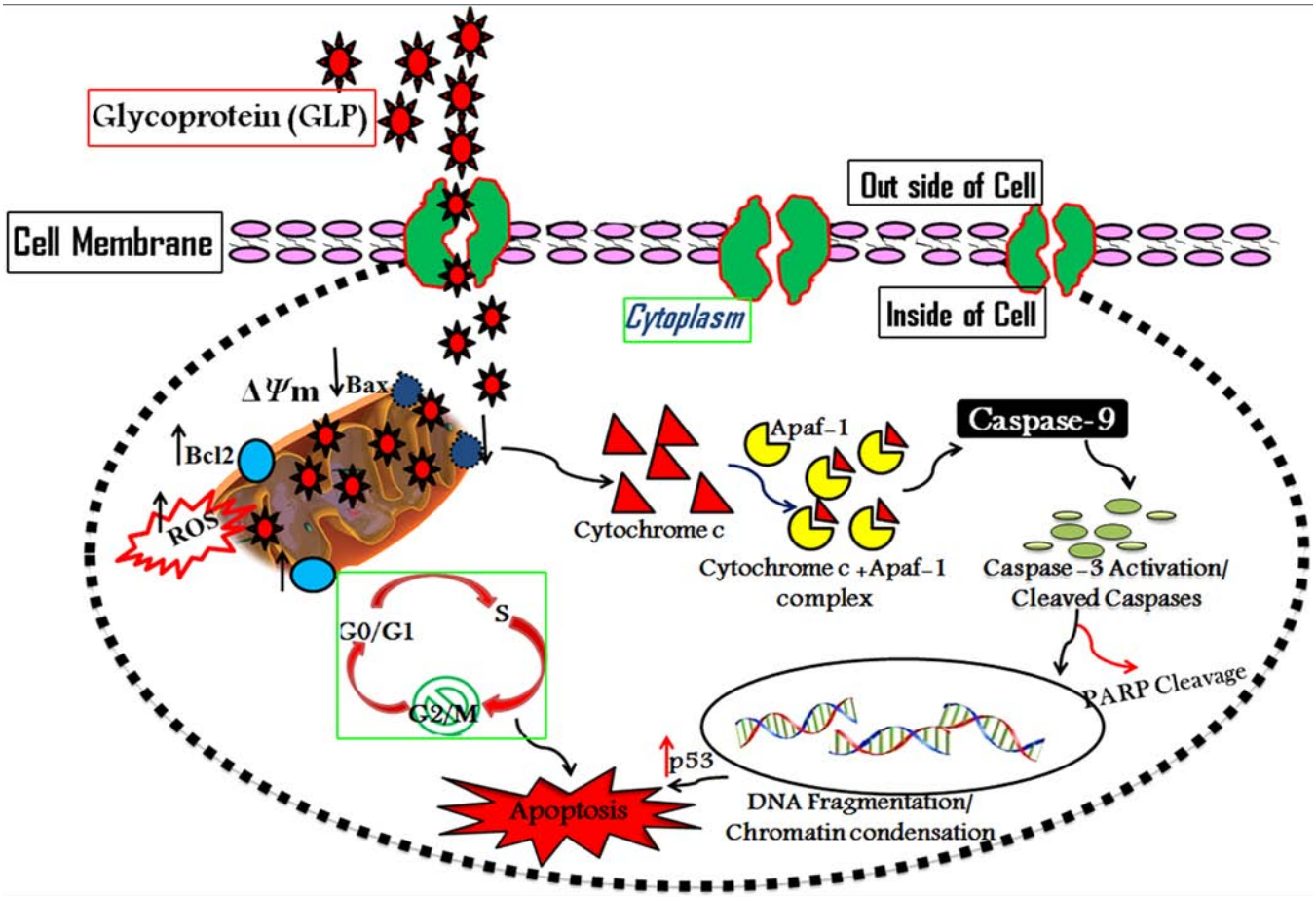

[a]GLP induces ROS generation, which promotes $\Delta\Psi_m$ loss and intrinsic apoptotic signaling pathways resulting in changes in the expression levels of bax/bcl-2. This leads to mitochondrial dysfunction and caspase 3 activation. Finally, GLP induces PARP cleavage and apoptosis in MDA-MB-231 cells via G_2/M cell cycle arrest, which mediates the nuclear damage of the cells.

with dose-dependent concentrations of GLP for 24 h. Observation of morphological changes in GLP-treated cancer cells suggested that apoptosis was induced in these cells, which was further confirmed by PARP cleavage (Figure 8). We also showed that mitochondria played a central role in the apoptotic induction process, and the mitochondria destabilization involves formation of ROS, release of cytochrome *c*, and activation of multiple caspases in MDA-MB-231 cells treated with GLP. GLP regulated mitochondrial membrane protein expression for the induction of intrinsic apoptotic pathway by causing G_2/M phase cell cycle arrest and halting cell cycle progression. Besides, it induced apoptosis through ROS generation from mitochondrial membranes of cancer cells and caused $\Delta\Psi_m$ stress, resulting in mitochondrial dysfunction. A schematic model depicting the actions of GLP is presented in Scheme 2. Our results supported the emerging picture of GLP from biological sources, especially from *C. decorticatum*, with respect to their therapeutic potential to treat breast cancers.

■ ASSOCIATED CONTENT

Supporting Information

Details of experimental conditions for cell culture and maintenance, lactate dehydrogenase (LDH) assay, determination of apoptosis induction and cell death by AO/EtBr staining, fluorescent microscopic studies on chromatin condensation by DAPI staining, cell cycle analysis by FACS, and results of cell viability of normal and cancer cells (Figure S2). This material is available free of charge via the Internet at http://pubs.acs.org.

■ AUTHOR INFORMATION

Corresponding Authors

*(R.T.) Phone: +91-8807293688. E-mail: thangam1985@yahoo.co.in.

*(V.S.) +91-9976619607. E-mail: veeraperumalsuresh@gmail.com.

*(S.K.) Phone +91-9486252052. Fax: +91-4222425706. E-mail: skperiyaruniv@gmail.com, sk_protein@buc.edu.in.

*(J.S.) E-mail: jays66@gmail.com.

Author Contributions

‖R.T. and D.S. equally contributed.

Notes

The authors declare no competing financial interest.

■ REFERENCES

(1) Okada, H.; Mak, T. W. Pathways of apoptotic and non-apoptotic death in tumour cells. *Nat. Rev. Cancer* **2004**, *4*, 592−603.

(2) Suresh, V.; Anbazhagan, C.; Thangam, R.; Senthilkumar, D.; Senthilkumar, N.; Kannan, S.; Rengasamy, R.; Palani, P. Stabilization of mitochondrial and microsomal function of fucoidan from *Sargassum*

plagiophyllum in diethylnitrosamine induced hepatocarcinogenesis. *Carbohydr. Polym.* **2013**, *92*, 1377−1385.
(3) Mohamed, S.; Hashim, S. N.; Rahman, A. H. Seaweeds: a sustainable functional food for complementary and alternative therapy. *Trends Food Sci. Technol.* **2012**, *23*, 83−96.
(4) Go, H.; Hwang, H. J.; Nam, T. J. Glycoprotein extraction from *Laminaria japonica* promotes IEC-6 cell proliferation. *Int. J. Mol. Med.* **2009**, *24*, 819−824.
(5) Sheu, J. H.; Huang, S. Y.; Duh, C. Y. Cytotoxic oxygenated desmosterols of the red alga *Galaxaura marginata*. *J. Nat. Prod.* **1996**, *59*, 23−26.
(6) Ashkenazi, A.; Dixit, V. M. Death receptors: signaling and modulation. *Science* **1998**, *281*, 1305−1308.
(7) Ashkenazi, A. Targeting death and decoy receptors of the tumour-necrosis factor super family. *Nat. Rev. Cancer* **2002**, *2*, 420−430.
(8) Susin, S. A.; Lorenzo, H. K.; Zamzami, N.; Marzo, I.; Snow, B. E.; Brothers, G. M.; Mangion, J.; Jacotot, E.; Costantini, P.; Loeffler, M.; Larochette, N.; Goodlett, D. R.; Aebersold, R.; Siderovski, D. P.; Penninger, J. M.; Kroemer, G. Molecular characterization of mitochondrial apoptosis-inducing factor. *Nature* **1999**, *397*, 441−446.
(9) Gatenby, R. A.; Gillies, R. J. Why do cancers have high aerobic glycolysis? *Nat. Rev. Cancer* **2004**, *4*, 891−899.
(10) Moubarak, R. S.; Yuste, V. J.; Artus, C.; Bouharrour, A.; Greer, P. A.; Menissier-de Murcia, J.; Susin, S. A. Sequential activation of poly(ADP-ribose) polymerase 1, calpains, and Bax is essential in apoptosis-inducing factor-mediated programmed necrosis. *Mol. Cell. Biol.* **2007**, *27*, 4844−4862.
(11) Fulda, S.; Galluzzi, L.; Kroemer, G. Targeting mitochondria for cancer therapy. *Nat. Rev. Drug Discovery* **2011**, *9*, 447−464.
(12) Er, E.; Oliver, L.; Cartron, P. F.; Juin, P.; Manon, S.; Vallette, F. M. Mitochondria as the target of the pro-apoptotic protein Bax. *Biochim. Biophys. Acta, Bioenerg.* **2006**, *1757*, 1301−1311.
(13) Wu, M.; Xu, L. G.; Li, X.; Zhai, Z.; Shu, H. B. AMID, an apoptosis-inducing factor-homologous mitochondrion-associated protein, induces caspase-independent apoptosis. *J. Biol. Chem.* **2002**, *277*, 25617−25623.
(14) Han, X.; Gelein, R.; Corson, N.; Wade-Mercer, P.; Jiang, J.; Biswas, P.; Finkelstein, J. N.; Elder, A.; Oberdörster, G. Validation of an LDH assay for assessing nanoparticle toxicity. *Toxicology* **2011**, *287*, 99−104.
(15) U.K. Department for Environment, Food and Rural Affairs. Characterising the potential risks posed by engineered nanoparticles, London, 2006.
(16) Ohiro, Y.; Garkavtsev, I.; Kobayashi, S.; Sreekumar, K. R.; Nantz, R.; Higashikubo, B. T.; Duffy, S. L.; Higashikubo, R.; Usheva, A.; Gius, D.; Kley, N.; Horikoshi, N. A. Novel p53-inducible apoptogenic gene, PRG3, encodes a homologue of the apoptosis-inducing factor (AIF). *FEBS Lett.* **2002**, *524*, 163−171.
(17) Mosmann, T. Rapid colorimetric assay for cellular growth and survival: application to proliferation and cytotoxicity assays. *J. Immunol. Methods* **1983**, *65*, 55−63.
(18) Sun, H. K.; Lee, S. J.; Lim, K. T. Cytotoxic effect of glycoprotein isolated from *Solanum nigrum* L. through the inhibition of hydroxyl radical-induced DNA-binding activities of NF-κB in HT-29 cells. *Environ. Toxicol. Pharmacol.* **2004**, *17*, 45−54.
(19) Jung, S. J.; Lim, K. T. Apoptosis induced by glycoprotein (150-kDa) isolated from *Solanum nigrum* L. is not related to intracellular reactive oxygen species (ROS) in HCT-116 cells. *Cancer Chemother. Pharmacol.* **2006**, *57*, 507−516.
(20) Barlow, P.; Clouter-Baker, A.; Donaldson, K.; Maccallum, J.; Stone, V. Carbon black nanoparticles induce type II epithelial cells to release chemotaxins for alveolar macrophages. *Part. Fibre Toxicol.* **2005**, *2*, 11−23.
(21) Hurt, R. H.; Monthioux, M.; Kane, A. Toxicology of carbon nanomaterials: status, trends, and perspectives on the special issue. *Carbon* **2006**, *44*, 1028−1033.
(22) Chung, I. M.; Kim, M. Y.; Park, S. D.; Park, W. H.; Moon, H. I. *In vitro* evaluation of the antiplasmodial activity of *Dendropanax morbifera* against chloroquine-sensitive strains of *Plasmodium falciparum*. *Phytother. Res.* **2009**, *23*, 1634−1637.
(23) Jeong, H. W.; Han, D. C.; Son, K. H.; Han, M. Y.; Lim, J. S.; Ha, J. H.; Lee, C. W.; Kim, H. M.; Kim, H. C.; Kwon, B. M. Antitumor effect of the cinnamaldehyde derivative CB403 through the arrest of cell cycle progression in the G2/M phase. *Biochem. Pharmacol.* **2003**, *65*, 1343−1350.
(24) Buolamwini, J. K. Cell cycle molecular targets in novel anticancer drug discovery. *Curr. Pharm. Des.* **2000**, *6*, 379−392.
(25) McDonald, E. R.; El-Deiry, W. S. Cell cycle control as a basis for cancer drug development (review). *Int. J. Oncol.* **2000**, *16*, 871−886.
(26) Malumbres, M.; Barbacid, M. Mammalian cyclin-dependent kinases. *Trends Biochem. Sci.* **2005**, *30*, 630−641.
(27) Bonnet, S.; Archer, S. L.; Allalunis-Turner, J.; Haromy, A.; Beaulieu, C.; Thompson, R.; Lee, C. T.; Lopaschuk, G. D.; Puttagunta, L.; Harry, G.; Hashimoto, K.; Porter, C. J.; Andrade, M. A.; Thebaud, B.; Michelakis, E. D. A mitochondria-K^+ channel axis is suppressed in cancer and its normalization promotes apoptosis and inhibits cancer growth. *Cancer Cell* **2007**, *11*, 37−51.
(28) Ye, X. Q.; Li, Q.; Wang, G. H.; Sun, F. F.; Huang, G. J.; Bian, X. W.; Yu, S. C.; Qian, G. S. Mitochondrial and energy metabolism-related properties as novel indicators of lung cancer stem cells. *Int. J. Cancer* **2011**, *129*, 820−831.
(29) Fulda, S.; Galluzzi, L.; Kroemer, G. Targeting mitochondria for cancer therapy. *Nat. Rev. Drug Discovery* **2011**, *9*, 447−464.
(30) Don, A. S.; Hogg, P. J. Mitochondria as cancer drug targets. *Trends Mol. Med.* **2004**, *10*, 372−378.
(31) Zhang, J. Y.; Wu, H. Y.; Xia, X. K.; Liang, Y. J.; Yan, Y. Y.; She, Z. G.; Lin, Y. C.; Fu, L. W. Anthracenedione derivative 1403P-3 induces apoptosis in KB and KBv200 cells via reactive oxygen species-independent mitochondrial pathway and death receptor pathway. *Cancer Biol. Ther.* **2007**, *6*, 1413−1421.
(32) Wang, X. H.; Jia, D. Z.; Liang, Y. J.; Yan, S. L.; Ding, Y.; Chen, L. M.; Shi, Z.; Zeng, M. S.; Liu, G. F.; Fu, L. W. Lgf-YL-9 induces apoptosis in human epidermoid carcinoma KB cells and multidrug resistant KBv200 cells via reactive oxygen species-independent mitochondrial pathway. *Cancer Lett.* **2007**, *249*, 256−270.
(33) Green, D. R.; Evan, G. I. A matter of life and death. *Cancer Cell* **2002**, *1*, 19−30.
(34) Gross, A.; McDonnell, J. M.; Korsmeyer, S. J. BCL-2 family members and the mitochondria in apoptosis. *Genes Dev.* **1999**, *13*, 1899−1911.
(35) Martinou, J. C.; Green, D. R. Breaking the mitochondrial barrier. *Nat. Rev. Mol. Cell Biol.* **2001**, *2*, 63−67.
(36) Sauer, H.; Wartenberg, M.; Hescheler, J. Reactive oxygen species as intracellular messengers during cell growth and differentiation. *Cell. Physiol. Biochem.* **2001**, *11*, 173−186.
(37) Mallis, R. J.; Buss, J.; Thomas, J. A. Oxidative modification of H-ras: S-thiolation and S-nitrosylation of reactive cysteines. *Biochem. J.* **2001**, *355*, 145−153.
(38) Lee, Y. S. Role of NADPH oxidase-mediated generation of reactive oxygen species in the mechanism of apoptosis induced by phenolic acids in HepG2 human hepatoma cells. *Arch. Pharm. Res. (Seoul)* **2005**, *28*, 1183−1189.
(39) Ranger, A. M.; Malynn, B. A.; Korsmeyer, S. J. Mouse models of cell death. *Nat. Genet.* **2001**, *28*, 113−118.
(40) Wu, J.; Suzuki, H.; Zhou, Y. W.; Liu, W.; Yoshihara, M.; Kato, M.; Akhand, A. A.; Hayakawa, A.; Takeuchi, K.; Hossain, K.; Kurosawa, M.; Nakashima, I. Cepharanthine activates caspases and induces apoptosis in Jurkat and K562 human leukemia cell lines. *J. Cell. Biochem.* **2001**, *82*, 200−214.
(41) Benjamin, R. C.; Gill, D. M. ADP-ribosylation in mammalian cell ghosts. Dependence of poly(ADP-ribose) synthesis on strand breakage in DNA. *J. Biol. Chem.* **1980**, *255*, 10493−10501.
(42) Green, D. R.; Reed, J. C. Mitochondria and apoptosis. *Science* **1998**, *281*, 1309−1312.
(43) Tong, W. M.; Cortes, U.; Wang, Z. Poly(ADP-ribose) polymerasea guardian angel protecting the genome and suppressing tumorigenesis. *Biochim. Biophys. Acta* **2001**, *1552*, 27−37.

(44) Shall, S.; de Murcia, G. Poly(ADP-ribose) polymerase-1 what have we learned from the deficient mouse model? *Mutat. Res.* **2000**, *460*, 1−15.
(45) Uchida, K.; Hanai, S.; Ishikawa, K.; Ozawa, Y.; Uchida, M.; Sugimura, T.; Miwa, M. Cloning of cDNA encoding *Drosophila* poly(ADP-ribose) polymerase leucine zipper in the auto-modification domain. *Proc. Natl. Acad. Sci. U.S.A.* **1993**, *90*, 3481−3485.
(46) Masutani, M.; Nozaki, T.; Hitomi, Y.; Ikejima, M.; Nagasaki, K.; de Prati, A. C.; Kurata, S.; Natori, S.; Sugimura, T.; Esumi, H. Cloning and functional expression of poly(ADP-ribose) polymerase cDNA from *Sarcophaga peregrine*. *Eur. J. Biochem.* **1994**, *200*, 607−614.
(47) Susin, S. A.; Lorenzo, H. K.; Zamzami, N.; Marzo, I.; Snow, B. E.; Brothers, G. M.; Mangion, J.; Jacotot, E.; Costantini, P.; Loeffler, M.; Larochette, N.; Goodlett, D. R.; Aebersold, R.; Siderovski, D. P.; Penninger, J. M.; Kroemer, G. Molecular characterization of mitochondrial apoptosis-inducing factor. *Nature* **1999**, *397*, 441−446.
(48) Curtin, J. F.; Donovan, M.; Cotter, T. G. Regulation and measurement of oxidative stress in apoptosis. *J. Immunol. Methods* **2002**, *265*, 49−72.

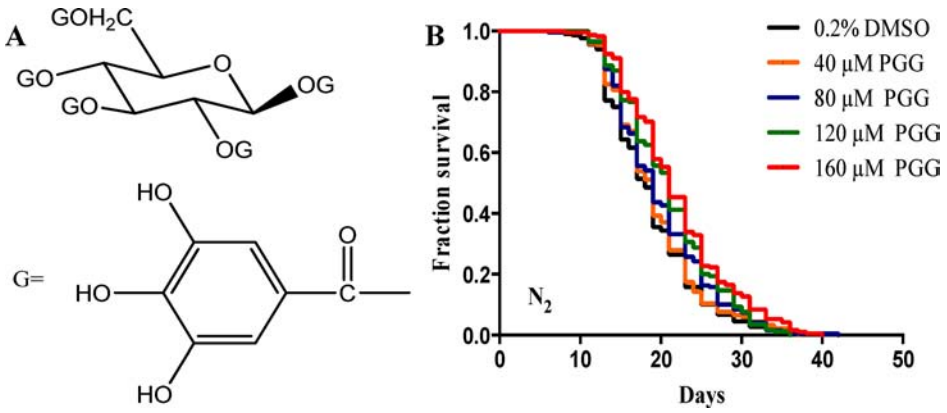

Figure 1. Effect of PGG treatment on the median lifespan of *C. elegans*. (A) Chemical structure of PGG. (B) Survival curves of wild-type (N_2) worms raised at 20 °C on the plates containing either 0.2% DMSO (control) or final concentrations of PGG (40, 80, 120, or 160 μM). The survival curves treated with 120 or 160 μM PGG were significantly different by the Log-rank test ($P < 0.05$). Four independent trials were performed.

(ad1116), *sir-2.1(ok434)*, *mev-1(kn1)*, *isp-1(qm150)*, and *clk-1(qm30)*. (The properties of the mutants are provided in Supporting Information.) All nematodes used in the study were supplied by the Caenorhabditis Genetics Center (CGC, University of Minnesota, Minneapolis, MN, USA).

Preparation of Treatment Plates. PGG (the chemical structure was presented in Figure 1A) was isolated from Eucalyptus leaves in our lab and was identified by comparing its nuclear magnetic resonance (^{1}H NMR and ^{13}C NMR) data with the reported literature.[12] PGG stock solution (80 mM in 100% DMSO) was diluted to the proper concentration. Then 5 μL of solution was added to 95 μL of *Escherischia coli* OP50, and the mixture was seeded onto the NGM plate (35 × 10 mm) and remained dry. To avoid autoxidation and polymerization of PGG, we analyzed the extraction of mixture with HPLC after it was seeded and found that there was a peak in the extraction that was identical with that of PGG. So PGG did not change before the treatment (the HPLC and MS of the PGG are provided in Supporting Information, Figures S1 and S2). The treatment plates contained different doses (final concentrations: 40, 80, 120, and 160 μM in 0.2% DMSO, respectively) of PGG or control solvent (0.2% DMSO).

Lifespan Assay. Lifespan analysis was performed by the same assay for all strains. If not stated otherwise, eggs isolated with hypochlorite (bleached with 5% sodium hypochlorite and 2.5 M sodium hydroxide) were transferred to the treatment plates and maintained at 20 °C in a temperature-controlled incubator. Synchronization was performed at L_4 larvae stage, and age synchronized young L_4 larvae (20 worms per plate and total of 3 plates per treatment) were then transferred to fresh treatment plates. During the reproductive period, these worms were transferred daily to new treatment plates and thereafter about every other day.

Live and dead *C. elegans* were counted daily (starting from the first day of hatching) until all individuals were dead. Nematodes that failed to respond to a gentle touch were scored as dead. Nematodes suffering from hatching of embryos within the adult hermaphrodite prior to eggs being laid (a so-called 'internal hatch') and those who escaped from the NGM agar were censored. Experiments were always performed in parallel with a control group. In the experiments assessing life span, reproduction, and pharyngeal pumping, treatments started from hatching unless otherwise stated.

Reproduction Assay. This assay was performed according to the previously reported method.[13] Wild-type *C. elegans* (10 individuals, 2 worms per plate) were shifted to fresh plates every day during the reproduction day, and the plates with eggs were left at 20 °C for 24 h to allow eggs to hatch. The number of progeny of each worm was counted at the L_4 stage to verify that eggs were hatched. Assay for each experiment was performed triplicates.

Pharynx Pumping Rate. Pharyngeal pumping was recorded on days 5, 10, and 15. Nematodes (10 individuals) were randomly selected, and the pumping assay was performed on NGM agar plate at room temperature. The number of their pharyngeal contractions was counted for 30 s.[13] All pumping rates were measured on a lawn of OP50 bacteria. The assay was repeated thrice with 10 worms per assay.

Age Pigments Fluorescence Spectroscopy. Fluorescence intensities of age pigments were measured as described.[13] Wild-type worms were raised from eggs on plates as in the lifespan assays. On days 5, 10, and 15 of life, 50 *C. elegans* were transferred to 50 μL of 10 mM NaN_3 solution in a single well of a 96-well white FluoroNunc plate. The 96-well plate was scanned in a spectrofluorimeter (Fluorolog-3, JobinYvon Inc., Edison NJ, USA). The fluorescence peak intensities of age pigments were obtained by scanning through the range of excitation wavelengths from 280 to 410 nm and an emission wavelength of 430 nm.

Locomotion Assay. *C. elegans* were raised from eggs similar to the lifespan assays. On days 5, 10, and 15, a total of 40 worms with or without PGG treatment were measured for body bend rate in liquid. Briefly, each time 4 worms were placed in 20 μL of M9 buffer on a glass slide. The locomotion of the worms was recorded by video for 30 s using a Qimaging Rotera-XR digital camera attached to a dissecting microscope and streamplx imaging software (ver. 3. 17. 2, NorPix Inc., Montreal, Quebec, Canada). Body bends in each frame of the 30 s film were analyzed by CeleST software. The assay was repeated three times with 40 worms per assay.[13]

Thermotolerance Assay. The thermotolerance assay was performed with hermaphrodites at 20 °C as for the aging assay. The adult worms with and without PGG treatment were shifted from 20 to 35 °C on day 4. Survivals were scored every hour after the temperature shift. Worms that died from desiccation on the sides of the plate were excluded.[3]

Accumulation of Reactive Oxygen Species (ROS). Accumulation of ROS was determined according to a modified protocol.[14] H_2DCF-DA (2,7-dichlorodihydrofluorescein diacetate) is a membrane-permeable compound and is converted to H_2-DCF when entering the cells of the worm. This nonfluorescent probe would be oxidized by ROS to yield the fluorescent dye DCF. Briefly, the worms were maintained and treated as in the lifespan method. After treatment with PGG or control for 96 h, worms were placed on a NGM plate to remove the bacteria three times. Then 80 worms were transferred to 50 μL of M9 buffer in a 96-well plate. In the meantime, 50 μL of fresh 100 μM H_2-DCF-DA solution in M9 buffer (100 mM stock solution in DMSO) was pipetted to the well (final concentration was 50 μM). On each plate, a control well containing H_2-DCF-DA without worms was included. Emission fluorescence intensity at 528 nm with excitation at 485 was recorded every 15 min for 12 h at 25 °C using a Synergy HT multimode microplate reader (Bio Tek Instruments Inc., Winooski City, VT, USA). The results are presented as means ± SD of relative fluorescence units (RFU) of three independent experiments with 240 individual worms in total.

Quantification of GFP-Labeled SOD-3 Expression. The GFP of the transgenic strain CF1553 {muIs84 [pAD76 (*sod-3*::gfp)]} can

dx.doi.org/10.1021/jf500210p | J. Agric. Food Chem. 2014, 62, 3422−3431

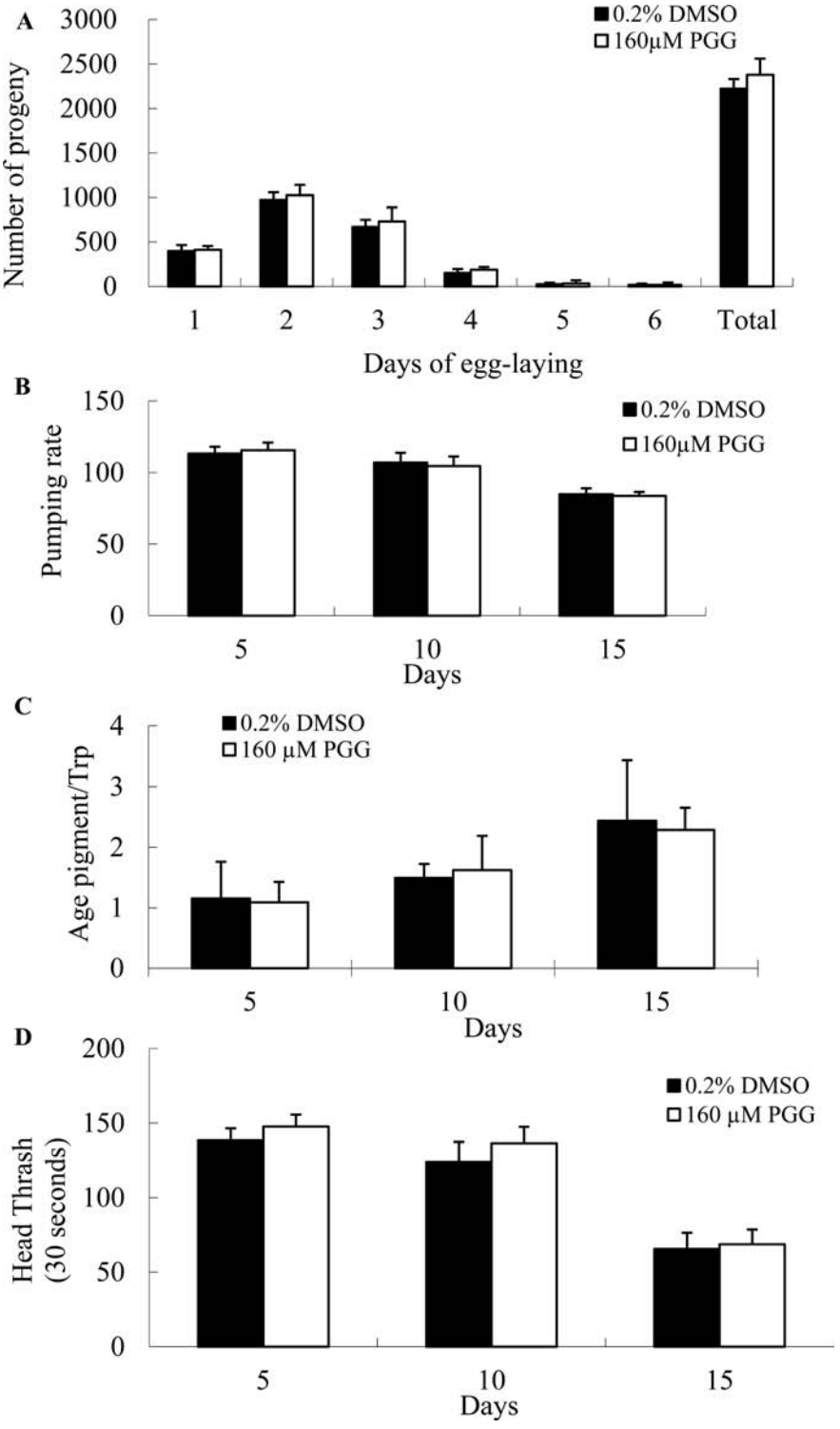

Figure 2. Physiological functions experiments were performed with wild-type worms raised from eggs on plates containing either 0.2% DMSO (control) or 160 μM PGG at 20 °C. (A) Wild-type worms (10 individuals, 2 worms per plate) were shifted to fresh plates every day during the reproduction day, and the plates with eggs were left at 20 °C for 24 h to allow eggs to hatch. The number of progeny of each worm was counted after the eggs were developed to the L_4 stage at 20 °C. (B) The number of their pharynx contractions was counted for 30 s. All pumping rates were measured on a lawn of OP50 bacteria. The assay was repeated thrice with 10 worms per assay. (C) Wild-type worms were transferred to 50 μL of 10 mM NaN_3 solution in a single well of a 96-well white FluoroNunc plate on days 5, 10, and 15. The peak age pigments fluorescence intensity was scanned through a range of excitation wavelengths from 280 to 410 nm and an emission wavelength of 430 nm. (D) The locomotion of 4 worms placed in 20 μL of M9 buffer on a glass slide was recorded by video for 30 s on days 5, 10, and 15. The number of head thrash in each frame of the 30 s film for worms was analyzed by CeleST software.

be induced by many environmental stresses, especially oxidative stress, and the expression of reporter GFP can reflect the level of *sod*-3.[15] Worms were raised from eggs on plates as in the lifespan assays until day 5 of life. The level of GFP was measured using an in vivo

dx.doi.org/10.1021/jf500210p | J. Agric. Food Chem. 2014, 62, 3422−3431

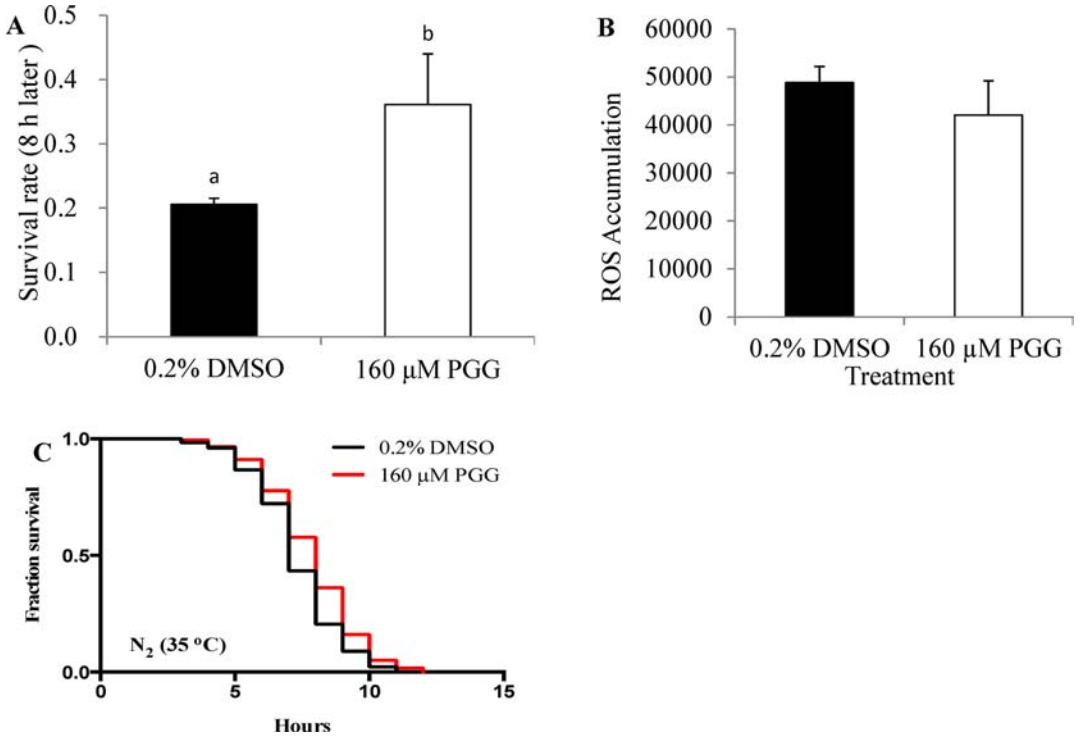

Figure 3. Effect of PGG treatment on thermal resistance and ROS accumulation. (A) Survival rates after being treated for 8 h after the worms were shifted from 20 to 35 °C on day 4. The different letters in the column denoted values that were significantly different ($p < 0.05$). (B) After treatment with PGG or control for 96 h, worms were placed on a NGM plate to remove the bacteria three times. Then 80 worms were transferred to 50 μL of M9 buffer in a 96-well plate and mixed with 50 μL of fresh 100 μM H_2-DCF-DA (final concentration, 50 μM). Emission fluorescence intensity at 528 nm with excitation at 485 was recorded every 15 min for 12 h at 25 °C. (C) Survival curve of worms after the worms were shifted from 20 to 35 °C on day 4.

spectrofluorometer (Fluorolog-3, Jobin Yvon Inc., Edison, NJ, USA). The results are the average fluorescence intensity levels of three independent trials.

Statistical Analysis. All results were presented as mean ± SD (n = 3). Assays for each experiment were performed three or four times. Log-rank (Mantel-Cox) tests were performed to analyze the survival curve using Graph Pad Prism version 5.00 for Windows (GraphPad Software, Inc., San Diega, CA, USA). One-way analysis of Variance (ANOVA) was performed using SPSS software (SPSS Inc., Chicago, IL, USA).

RESULTS AND DISCUSSION

Effect of PGG Treatment on the Median Lifespan of *C. elegans*. To address the concern about the stability of the *C. elegans* system used, first, the anti-aging effect of resveratrol (100 μM) (National Institutes for Food and Drug Control, Beijing, China) was investigated because of its widely anti-aging effect across diverse species including *C. elegans* and well-known mechanism of action.[8,16] We found that worms raised on 100 μM resveratrol not only manifested a significant survival curve ($P < 0.0001$ by the Log-rank test) but also showed a 13.2% increase in median lifespan (20.0 ± 1.0 days with resveratrol treatment vs 17.7 ± 0.6 days with control) ($p < 0.05$, ANOVA) (The survival curve for resveratrol is provided in Supporting Information, Figure S3), which was consistent with the results (approximately14%) obtained from the literature.[8] These results indicated the determination of lifespan in *C. elegans* in our lab was stable and comparable. So we continued to analyze the anti-aging effect of PGG with high cellular antioxidant activity in *C. elegans*.[12] To understand comprehensively the anti-aging effect, four different concentrations of PGG ranging from 40 to 160 μM were tested. The treatment of the wide-type worm started from embryo till death. We found that different concentrations of PGG had different performances. Of the four concentrations, worms raised on 160 μM PGG not only manifested a significant survival curve (Figure 1B) ($P < 0.0001$ by the Log-rank test) but also had a median lifespan of 21.5 ± 2.4 days with maximum lifespan of 40 days and increased by 18% ($p < 0.05$, ANOVA) in median lifespan. Worms treated with 40, 80, and 120 μM PGG did not show a significant increase in median lifespan, but their treatment showed a slightly increasing trend in median lifespan (4%, 3%, and 11% increase for 40, 80, and 120 μM PGG, respectively). Furthermore, worms cultured on 120 μM PGG displayed a significant different right-shifted survival curve ($P = 0.0010$ by the Log-rank test) when compared with the control, and the survival curve of 120 μM PGG was continuously above that of control (Figure 1B). Although worms treated with 120 μM PGG did not show significant increase in median lifespan, it was more effective than control in the survival curve.

Taken together, these findings indicated that PGG supplementation could prolong median lifespan in *C. elegans*, and the optimal concentration was observed at 160 μM PGG (increased by 18% in median lifespan) during the tested concentrations. Therefore, 160 μM PGG was chosen for further study.

Effect of PGG Treatment on Physiological Functions of *C. elegans*. The decline of physiological functions such as self-fertile reproduction, pharyngeal pumping, age pigments, and locomotion happened in the aging process. To determine whether PGG caused side effects on the physiological functions at the optimal concentration, we analyzed those physiological function changes under PGG treatment. First, it is critical to

dx.doi.org/10.1021/jf500210p | J. Agric. Food Chem. 2014, 62, 3422−3431

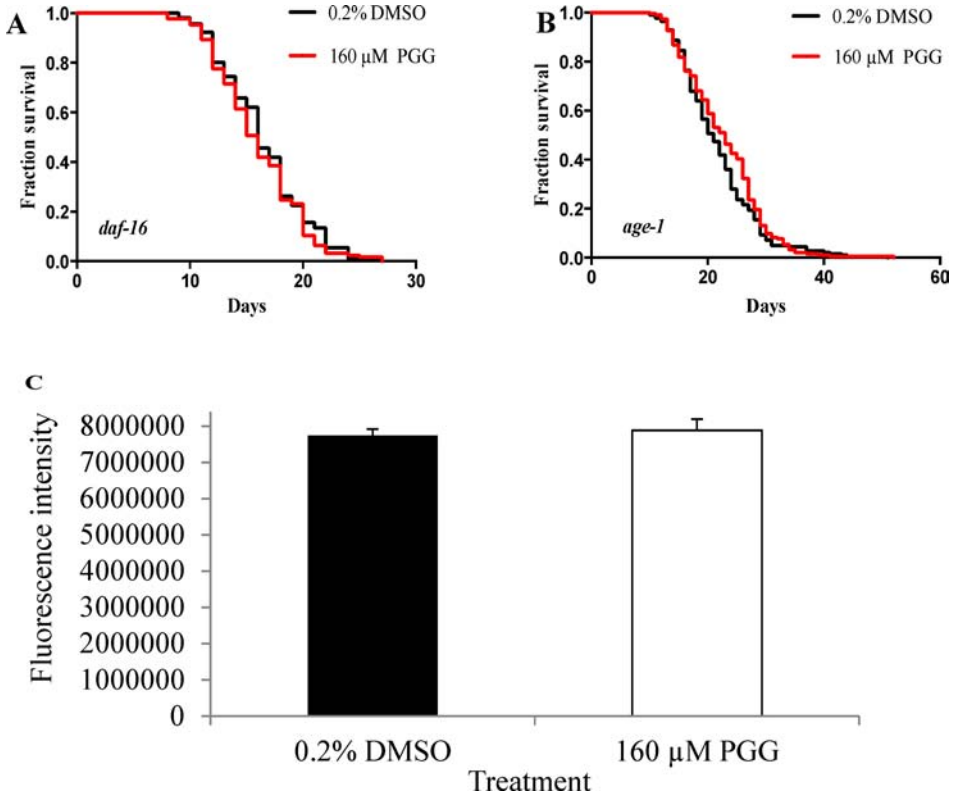

Figure 4. Effect of IIS pathway on the longevity extension induced by PGG. (A) Survival curves of *daf-16(mgDf50)* (Log-rank test, $P = 0.2774$). (B) Survival curves of *age-1(hx546)* (Log-rank test, $P = 0.0003$). (C) Worms of transgenic strain CF1553 [muIs84 [pAD76 (sod-3::gfp)]] were raised from eggs on plates as in the lifespan assays until day 5 of life. The level of expression of GFP in the transgenic strain was measured using an in vivo spectrofluorometer. The results are the average fluorescence intensity levels of three independent trials.

investigate progeny production because a few mechanisms that extend the longevity have an impact on it.[17] We recorded the effect of PGG treatment on the progeny production daily to investigate whether PGG suppressed or delayed it. Worms cultured on medium containing 160 μM PGG showed neither slowed reproduction nor reduced total progeny production. These results demonstrated that median lifespan extension induced by PGG treatment was not obtained by suppressing or delaying progeny production (Figure 2A).

One well-conserved feature of aging is the decline of pharyngeal pumping, which is rhythmic contraction in the neuromuscular organ.[18] We investigated whether PGG had an effect on pharyngeal pumping rate on days 5, 10, and 15. We found that pharyngeal pumping decreased with age, but PGG treatment did not affect the pharyngeal pumping rate in the three stages (Figure 2B). So the possibility that PGG extended lifespan by reducing food intake that results into dietary restriction could be ruled out.

Age pigments contain both intracellular and extracellular age-related, fluorescent material and include advanced glycation end-products and lipofuscin, a heterogeneous mix of oxidized and cross-linked molecules (proteins, lipids, and carbohydrates) that accumulate in intestinal lysosomes.[19] We measured the accumulation of age pigments in worms with PGG treatment in order to see the effect of PGG on the aging process. As shown in Figure 2C, age pigment fluorescence levels did not significantly lower or increase when the worms were cultured on 160 μM PGG at three stages. Therefore, PGG-induced lifespan extension was not associated with any significant change in the accumulation of age pigments .

Locomotion ability declines on solid and liquid media with increasing age, which is correlated with the level of muscle deterioration.[18] To determine whether PGG can enhance lifespan by extending locomotory ability, we tested the effect of the PGG treatment on the swimming vigor, defined as head thrash per unit time in a liquid environment, at early, middle, and late life stages (on days 5, 10, and 15, respectively). We found that head thrash of the worms declined with the increasing day and PGG treatment did not significantly change the swimming rates at the three stages (Figure 2D). These findings indicated PGG neither caused detrimental effects in locomotory ability nor increased swimming in a liquid environment.

To summarize, PGG treatment prolonged the median lifespan without causing obvious defect in physiological functions including fertility, pharyngeal pumping rate, age pigments, and locomotion ability. So we continued to gain insight into the related mechanisms.

Effect of PGG Treatment on Thermal Resistance and ROS Accumulation. Longevity extension is generally related with elevated survival under the conditions of stress.[20] To exploit whether PGG enhanced heat stress resistance, worms treated with or without compound were shifted from 20 to 35 °C on day 4. The survival rates after 8 h at 35 °C were increased significantly by PGG treatment (increasd from 21% to 36%) (Figure 3A). Compared with the control, the group with PGG treatment showed a significantly different survival curve ($P = 0.016$ by the Log-rank test) (Figure 3C). The findings suggested that PGG supplementation could act

dx.doi.org/10.1021/jf500210p | J. Agric. Food Chem. 2014, 62, 3422−3431

protectively under the thermal stress and enhance resistance to heat shock in *C. elegans*.

According to the free-radical theory of aging, an excess of reactive oxygen species (ROS) is responsible for the process of aging and the lifespan extension is associated with damage caused by ROS.[21] Therefore, we measured the effect of PGG on the intracellular amount of ROS. The accumulation of ROS was measured using H2DCF-DA, which is converted to the fluorescent dye DCF intracellularly. In states of exposure to PGG for 96 h, the reduction of ROS accumulation induced by PGG was not significantly different (Figure 3B). Strikingly, PGG showed high antioxidant activity in both chemical-based and cell-based assays[12] but did not exhibit the ROS scavenging activity in *C. elegans*. In fact, many factors and processes such as uptake, metabolism, and interaction need to be considered if the antioxidant activity needs to take effect in the whole organism. The reason for the failure in ROS scavenging ability could be that the antioxidant property of PGG was not sufficient to reduce the accumulation of ROS in *C. elegans* or the bioavailability of PGG was low in *C. elegans*.

Effect of PGG on Median Lifespan of Mutants Involved with the IIS Pathway. The insulin/IGF signaling (IIS) pathway is well-known to be a central controller of longevity in *C. elegans* regulated via the phosphorylation situation of the transcription factor DAF-16.[22] PGG could interact with DAF-2 (the proteins encoded by *daf-2*),[11] the only homologue of insulin receptor in the *C. elegans*, which could reduce their activity and result in lifespan extension through triggering the IIS pathway. To clarify this possibility, we tested a *daf-16(mgDf50)* null mutant strain cultured on 160 μM PGG and found that PGG did not increase the median lifespan of the *daf-16* mutant [16.7 days for the *daf-16(mgDf50)*] null mutant vs 17.3 days with PGG treatment (Figure 4A and Table 1). This finding suggested that PGG could extend median lifespan by acting through a mechanism that is dependent on DAF-16/FOXO. Next, to further understand the genetic requirement for the IIS pathway in the action, we tested the effect of long-lived *age-1(hx546)* mutants treated with PGG. Interestingly, worms cultured on 160 μM PGG displayed a significantly different survival curve compared with *daf-16(mgDf50)* mutant (the control), but PGG did not extend the median lifespan of *age-1(hx546)* (Figure 4B and Table 1). These findings suggested that PGG could be dependent on *daf-16(mgDf50)* and *age-1(hx546)* to increase median lifespan.

Considering that DAF-16 nuclear localization affects lifespan in the IIS pathway and *sod-3* is one of the DAF-16 direct target genes and encodes a Fe/Mn superoxide dismutase, we tested the effect of PGG on the fluorescence intensity in worms of the transgenic strain CF1553, which is SOD-3::GFP reporter gene expression.[15] However, the PGG-treated group did not demonstrate significant change in fluorescence intensity of the transgenic CF1553 on day 5 (Figure 4C). These results suggested that although *age-1* and *daf-16* were necessary for PGG-mediated median lifespan extension, the whole IIS pathway could not be a direct target of PGG. The possibility of this phenomenon was that PGG could act on another pathway that involved with *daf-16* and *age-1*. It has been proven that multiple interaction partners are necessary for proper DAF-16 activity.[23]

Effect of PGG on Median Lifespan of Mutants Involved with Dietary Restriction and the Sir-2.1 Pathway. The other well-known mechanism considered could be dietary restriction.[5] PGG also has the tannins' common characteristics of binding proteins by forming hydrogen and ionic bonds,[11] which would inhibit digestive enzymes and cause effects that are similar to a dietary restriction. Therefore, to test whether PGG extended the lifespan by acting through dietary restriction, the effect of PGG on the lifespan of the *eat-2(ad1116)* mutant was investigated, which is a long-lived mutant and a genetic model for dietary restriction due to decreased pharyngeal pumping in *C. elegans*.[5] PGG did not increase the median lifespan of the *eat-2(ad1116)* mutant (Figure 5A and Table 1). This indicated that PGG was depend on *eat-2(ad1116)*, which could be consistent with the model that PGG acts by stimulating the DR pathway. However, one feature of dietary restriction in *C. elegans* is a reduction of total number of progeny or an extended period of progeny production.[17] We found that PGG did not change the progeny production. To summarize, the results suggested that PGG did not act exactly through DR to increase median lifespan.

Given the genetic indication that dietary restriction (DR) was involved with the mechanism and the botanical polyphenol antioxidant resveratrol, a DR mimetic, extends the lifespan by stimulating the activity of *sir-2.1*, which encodes a histone deacetylase-like protein that integrates metabolic situation with lifespan,[24] we accordingly hypothesized that *sir-2.1* might be also involved into the mechanism of action of PGG-mediated longevity because of the common properties of polyphenol and antioxidant. Given that possibility, we tested PGG effects on the *sir-2.1(ok434)* mutant. We found PGG did not extend the lifespan of a *sir-2.1* null mutant (Figure 5B and Table 1).

Table 1. Genetic Requirement for Lifespan Extension Induced by PGG

genotype	treatment	median lifespan[a] (mean ± SD) (days)	maximum lifespan[a] (mean ± SD) (days)	genetic requirement
daf-16	0.2% DMSO	16.7 ± 1.2	24.0 ± 0.0	yes
	160 μM PGG	17.3 ± 1.2	23.3 ± 1.2	
age-1	0.2% DMSO	21.0 ± 1.8	44.8 ± 4.3	yes
	160 μM PGG	23.0 ± 3.2	37.8 ± 9.6	
eat-2	0.2% DMSO	21.3 ± 1.5	36.7 ± 5.5	yes
	160 μM PGG	22.7 ± 2.5	36.0 ± 2.0	
sir-2.1	0.2% DMSO	20.0 ± 0.0	29.3 ± 3.8	yes
	160 μM PGG	20.0 ± 0.0	31.7 ± 5.0	
isp-1	0.2% DMSO	23.0 ± 0.0	38.0 ± 3.5	yes
	160 μM PGG	21.0 ± 2.0	39.3 ± 1.2	
mev-1	0.2% DMSO	12.7 ± 1.0	18.5 ± 2.9	no
	160 μM PGG	**14.3 ± 1.2***	19.7 ± 0.8	
clk-1	0.2% DMSO	17.7 ± 1.5	36.0 ± 4.6	no
	160 μM PGG	**23.0 ± 2.6***	37.3 ± 3.2	

[a]The median lifespan is the time at which fraction survival equals 50%. The maximum lifespan is the time at which fraction survival equals 0%. The data was analyzed by One way-ANOVA analysis (SPSS 13), and and asterisk (*) designates significantly different values ($p < 0.05$).

dx.doi.org/10.1021/jf500210p | J. Agric. Food Chem. 2014, 62, 3422−3431

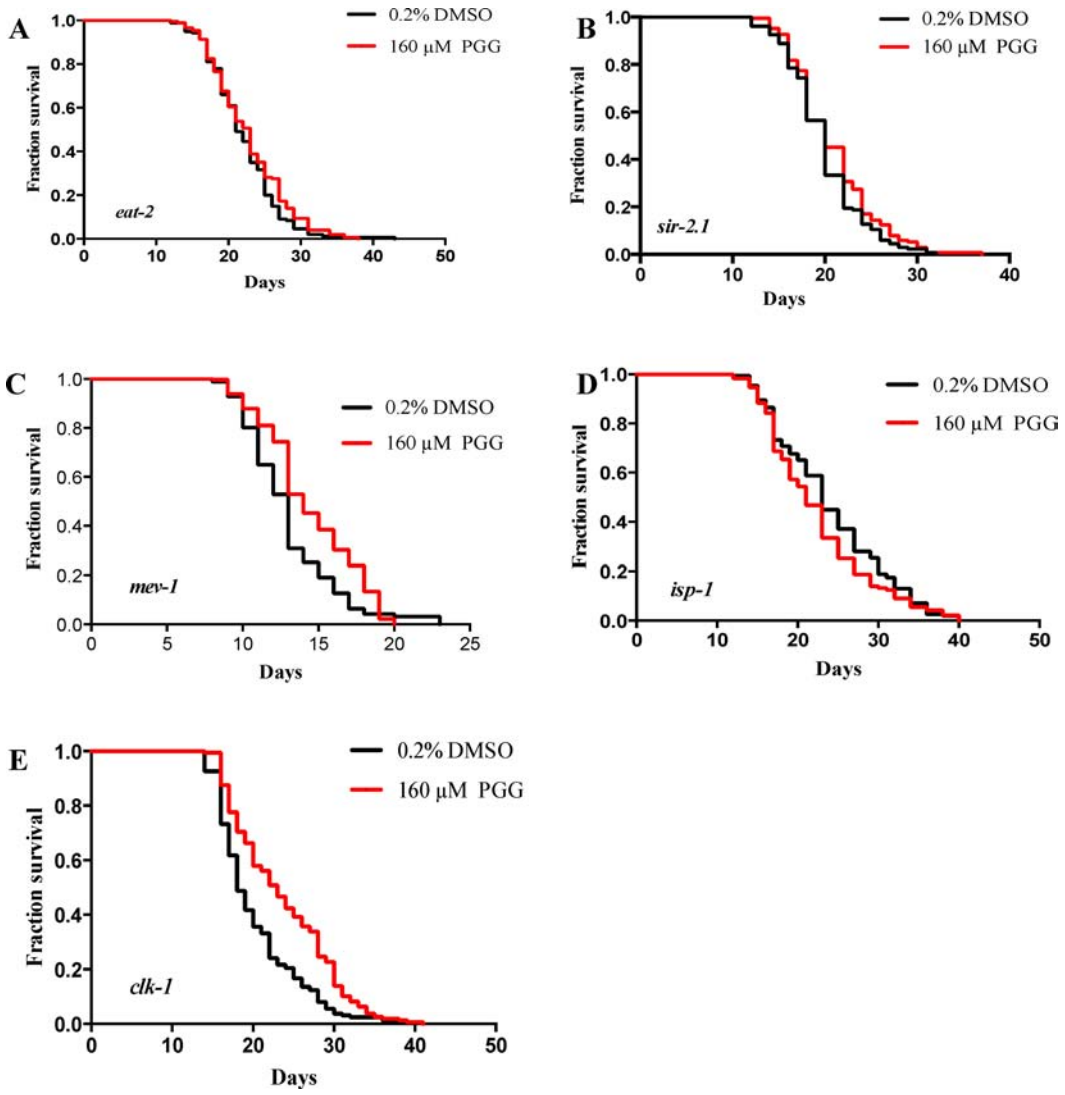

Figure 5. Survival curves of mutants raised at 20 °C on plates containing 0.2% DMSO (control) or 160 μM PGG. (A) The *P*-value for *eat-2(ad1116)* was 0.1010 (Log-rank test). (B) The *P*-value for *sir-2.1(ok434)* was 0.0702 (Log-rank test). (C) The *P*-value for *mev-1(kn1)* was <0.0001 (Log-rank test). (D) The *P*-value for *isp-1(qm150)* was 0.0730 (Log-rank test). (E) The *P*-value for *clk-1(qm30)* was <0.0001 (Log-rank test).

However, lifespan extension by resveratrol is mediated by *sir-2.1* and is independent on the insulin/IGF pathway.[25] The finding indicated that PGG acted differently from resveratrol, but Sir-2.1 signaling was part of the mechanism that increased the longevity induced by PGG.

Effect of PGG on Median Lifespan of Mutants Involved with Mitochondrial Electron Transport Chain Pathway. Oxidative stress is a factor of aging,[21] and ROS is mainly generated from mitochondrial metabolism.[26] Gene-encoded components in mitochondrial transport chains are identified to alter levels of oxidative stress in *C. elegans*.[26] So we wanted to elucidate whether mitochondrial function was the underlying mechanism of the lifespan extension. First, we observed the lifespan of the *mev-1(kn1)* mutant, which strain has a defect in the succinate dehydrogenase cytochrome *b* large subunit in the complex II of the mitochondrial electron transport chain. We found that PGG increased significantly the lifespan of the *mev-1(kn1)* mutant (Figure 5C and Table 1). Strikingly, PGG did not reduce internal reactive oxygen species (ROS) but prolonged the lifespan of mutant *mev-1*, which is hypersensitive to oxidative stress. The results indicated that PGG might act independently of MEV-1, but the lifespan extension for *mev-1(kn1)* might not be attributed to a direct antioxidative property of PGG. According to report, supernumerary apoptosis also contributed to the shortened lifespan of *mev-1*.[27] Like the coenzyme Q_{10}, PGG may prolong the longevity of *mev-1* mutant by lowering apoptosis.[10]

The mutation in iron sulfur protein (*isp-1*) resulted in low oxygen consumption, insensitivity to ROS, and long longevity. The *isp-1* gene encodes a component of mitochondrial complex III, which accepts electrons and protons from mitochondrial complexes I and II.[26] We found that *isp-1(qm150)* mutant with PGG treatment did not exhibit median lifespan extension (Figure 5D and Table 1), which indicated PGG might act dependently on ISP-1.

The gene *clk-1* encodes a demethoxyubiquinone hydroxylase that is necessary for the biosynthesis of ubiquinone (coenzyme Q_{10}). The long-lived *clk-1(qm30)* mutant is deficient in the endogenous form of coenzyme Q_{10}, which is responsible for the carrying of electron and protons from mitochondrial complexes I and II to complex III.[28] To test whether other mitochondrial function mutants were important for the extension benefit, we

dx.doi.org/10.1021/jf500210p | J. Agric. Food Chem. 2014, 62, 3422−3431

measured the lifespan effect on *clk-1*. We found that the median lifespan in *clk-1* mutant treated with PGG increased by 30% compared to the control (Figure 5E and Table 1)m which suggested that PGG might act independently of CLK-1.

Taken together, PGG treatment acted independently on MEV-1 and CLK-1 but acted dependently on ISP-1. The mitochondrial electron transport chain was partially involved with the PGG-mediated longevity extension.

Model of Action for the Longevity Extension Mechanism Mediated by PGG. A variety of genetic, environmental, and pharmacological treatments affect the lifespan. We will discuss how the PGG treatment extended the lifespan of *C. elegans*. First, there is a hormesis hypothesis that exposure to low-level toxic stress would result in a protective stress reaction and lifespan extension, which indicates that hormesis can slow down aging.[29] The mechanism of action for lifespan extension induced by tannin acid, one of the hydrolyzable tannins, was involved with a hormesis effect.[30] However, there was little possibility that the mechanism of action for PGG was consistent with the hormesis effect because even the low concentration treatments (40, 80, and 120 μM) did not show significant increase in median lifespan, the different concentration of PGG treatments also showed increase trend in lifespan, and 120 μM PGG displayed a significant different survival curve. What is more, 160 μM PGG did not show an obvious defect in physiological function. Further experiments at higher concentrations are needed to totally rule out this possibility. Second, there are physiological processes that promote a short lifespan, and inhibiting these processes can result in a longevity extension. Age pigments and ROS promoting aging were generated during the aging process.[19] Since PGG treatment did not reduce the accumulation of age pigments and ROS, we can rule out this possibility that PGG treatment extends the lifespan by lowering the accumulation of age pigments and ROS, but there is a possibility that PGG treatment directly or indirectly binds and decreases the activity of specific protein that inhibits longevity. Third, there is trade-off between reproduction and longevity. According to Kirkwood's "disposable soma theory", the energy for required lifespan extension is diverted from reproduction.[31] This explanation is unlikely to be considered for PGG treatment because PGG did not reduce reproduction. Fourth, longevity extension is generally related with elevated survival under the conditions of stress.[20] We found that PGG supplementation can enhance resistance to heat stress in *C. elegans*, So the longevity extension of PGG could be attributed to its protective effect under heat stress.

Finally, except for those factors, many genetic manipulations and pathways are known to influence aging, including insulin/IGF-1 signaling, caloric restriction signaling, and mitochondrial respiration. First, our results showed PGG increased neither the median lifespan of the *daf-16* or *age-1* mutants nor the fluorescence intensity of SOD-3. Those results indicated that although *age-1* and *daf-16* were necessary for PGG-mediated median lifespan extension, the IIS pathway might not be a direct target of PGG. Here, we came up with two explanations for that. The first explanation is that PGG or its metabolite directly binds one of the targets that function downstream of DAF-16. The second explanation is that the effect of PGG on the median lifespan of *age-1* and *daf-16* mutants reflects the toxicity of combining the mutation and the drug treatment. So the IIS pathway seemed not sufficient to explain PGG-mediated longevity. It has been proven that multiple interaction partners are necessary for proper DAF-16 activity.[23] Second, according to our current results, EAT-2 and Sir-2.1 in the DR mimetic pathway were also involved in the mechanism of action of lifespan extension induced by PGG but did not affect fecundity or pharyngeal pumping rate. According to report,[32] SIR-2.1 acts in parallel to the insulin-like pathway to regulate DAF-16 in a manner dependent on 14-3-3 proteins during stress and extended lifespan. So *sir-2.1* might act through DAF-16 in PGG-mediated longevity extension. We also found that the mitochondrial electron transport chain became partly involved in the PGG-mediated longevity extension. PGG treatment acted independently of MEV-1 and CLK-1 but acted dependently of ISP-1.

In summary, the insulin/IGF-1 signaling pathway, caloric restriction, mitochondrial metabolism, and Sir-2.1 signaling pathways could partly be involved with the specific mechanisms of action for PGG in lifespan. This finding is in agreement with the report that PGG shows a variety of biological activities through multiple mechanisms.[11] So we propose that the general model of action for PGG in longevity extension is that PGG or its metabolite likely binds one or more targets that function downstream of DAF-16 and EAT-2. The targets likely act through the ISP-1 pathway and trigger a series of events that elevate stress resistance and extend longevity (Figure 6).

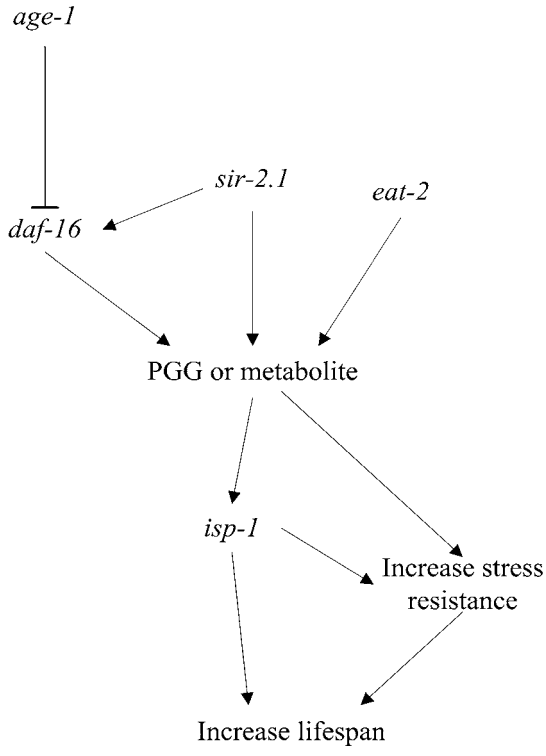

Figure 6. Model of action of the longevity extension mediated by PGG. PGG likely bound one or more targets that function downstream of DAF-16 and EAT-2. The targets likely acted through the ISP-1 pathway and triggered a series of events that elevated stress resistance and extended longevity.

Compared with the single-target therapeutics, multitarget therapeutics regulate multiple nodes of the disease network simultaneously and shows a synergistic effect and are unlikely to induce resistance, providing optimal clinical use.[33] Thus, there is a general agreement that molecules interfering simultaneously with multiple targets might be more effective

than single-target agents, and scientists have recently proposed that a new generation of drugs, able to inhibit more than one pathway, would probably play a major role.[34] So our results provide the first insights into the mechanism of longevity extension mediated by PGG in *C. elegans*, which might be developed into a novel multitarget drug for promoting healthy aging.

In conclusion, the lifespan and resistance under acute heat stress for *C. elegans* were improved without causing obviously adverse effects on physiological functions including reproduction, pharyngeal pumping rate, age pigments accumulation, and swimming ability. These significant findings indicated that the IIS pathway, dietary restriction, Sir-2.1 signaling, and mitochondrial electron transport chain could partly be involved with lifespan extension mediated by PGG and PGG could target multiple longevity mechanisms to extend lifespan. One possible mode of action drawn from our findings was that PGG or its metabolite likely bound one or more targets that functioned downstream of DAF-16 and EAT-2, and the targets likely acted through the ISP-1 pathway and triggered a series of events that elevated stress resistance and extended longevity. Our results provided the first insights into the mechanism of longevity extension mediated by PGG in *C. elegans*, which may be exploited in novel multitarget therapeutics for prolonging lifespan.

■ ASSOCIATED CONTENT

Ⓢ Supporting Information

This material is available free of charge via the Internet at http://pubs.acs.org.

■ AUTHOR INFORMATION

Corresponding Authors

*Phone: 732-445-7182. Fax: 732-445-7192. E-mail: driscoll@dls.rutgers.edu.

*Phone: +86-20-85286234. Fax: +86-20-85286234. E-mail: caoyong2181@scau.edu.cn.

*Phone: 848-932-5514. Fax: 732-932-6776. E-mail: qhuang@aesop.rutgers.edu.

Notes

The authors declare no competing financial interest.

■ ACKNOWLEDGMENTS

The first author is grateful for financial support of China Scholarship Council. *C. elegans* strains were provided by the *Caenorhabditis* Genetics Center at University of Minnesota. This research was supported by the special research projects for public welfare forestry public welfare from State Forestry Administration of the People's Republic of China (201104003-03) and the National Natural Science Foundation of the People's Republic of China (31100433).

■ ABBREVIATIONS

ABTS, 2,2′-azino-bis(3-ethylbenzothiazoline-6-sulfonic acid); *C. elegans*, *Caenorhabditis elegans*; DMSO, dimethyl sulfoxide; DPPH, 2,2-diphenyl-1-picrylhydrazyl; DR, dietary restriction; H_2DCF-DA, 2,7-dichlorodihydrofluorescein diacetate; HepG2, human hepatocellular liver carcinoma cell line; IIS, insulin/insulin-like growth factor signaling; mol, molar; NGM, nematode growth medium; NMR, nuclear magnetic resonance; OP50, *Escherichia coli* strain OP50; RFU, relative fluorescence units; PGG, pentagalloyl glucose (1,2,3,4,6-penta-*O*-galloyl-*β*-D-glucose); ROS, reactive oxygen species

■ REFERENCES

(1) Finch, C. E.; Pike, M. C.; Witten, M. Slow mortality rate accelerations during aging in some animals approximate that of humans. *Science* **1990**, *249*, 902−905.

(2) Pan, M. H.; Lai, C. S.; Tsai, M. L.; Wu, J. C.; Ho, C. T. Molecular mechanisms for anti-aging by natural dietary compounds. *Mol. Nutr. Food Res.* **2012**, *56*, 88−115.

(3) Honda, Y.; Tanaka, M.; Honda, S. Trehalose extends longevity in the nematode *Caenorhabditis elegans*. *Aging Cell* **2010**, *9*, 558−569.

(4) Kenyon, C.; Chang, J.; Gensch, E.; Rudner, A.; Tabtiang, R. A *C. elegans* mutant that lives twice as long as wild type. *Nature* **1993**, *366*, 461−464.

(5) Lakowski, B.; Hekimi, S. The genetics of caloric restriction in *Caenorhabditis elegans*. *Proc. Natl. Acad. Sci. U.S.A.* **1998**, *95*, 13091−13096.

(6) Cohen, E. Countering neurodegeneration by reducing the activity of the insulin/IGF signaling pathway: Current knowledge and future prospects. *Exp. Gerontol.* **2011**, *46*, 124−128.

(7) Kaletta, T.; Hengartner, M. O. Finding function in novel targets: *C. elegans* as a model organism. *Nat. Rev. Drug Discovery* **2006**, *5*, 387−399.

(8) Greer, E. L.; Brunet, A. Different dietary restriction regimens extend lifespan by both independent and overlapping genetic pathways in *C. elegans*. *Aging Cell* **2009**, *8*, 113−127.

(9) Abbas, S.; Wink, M. Epigallocatechin gallate from green tea (*Camellia sinensis*) increases lifespan and stress resistance in *Caenorhabditis elegans*. *Planta Med.* **2009**, *75*, 216−221.

(10) Ishii, N.; Senoo-Matsuda, N.; Miyake, K.; Yasuda, K.; Ishii, T.; Hartman, P. S.; Furukawa, S. CoenzymeQ_{10} can prolong *C. elegans* lifespan by lowering oxidative stress. *Mech. Aging Dev.* **2004**, *125*, 41−46.

(11) Zhang, J.; Li, L.; Kim, S. H.; Hagerman, A. E.; Lü, J. Anti-cancer, anti-diabetic and other pharmacologic and biological activities of penta-galloyl-glucose. *Pharm. Res.* **2009**, *26*, 2066−2080.

(12) Chen, Y.; Wang, J.; Ou, Y.; Chen, H.; Xiao, S.; Liu, G.; Cao, Y.; Huang, Q. Cellular antioxidant activities of polyphenols isolated from Eucalyptus leaves (*Eucalyptus grandis*× *Eucalyptus urophylla GL9*). *J. Funct. Foods* **2014**, DOI: 10.1016/j.jff.2013.12.003.

(13) Onken, B.; Driscoll, M. Metformin induces a dietary restriction-like state and the oxidative stress response to extend *C. elegans* Healthspan via AMPK, LKB1, and SKN-1. *PLoS One* **2010**, *5*, e8758.

(14) Kampkotter, A.; Nkwonkam, C. G.; Zurawski, R. F.; Timpel, C.; Chovolou, Y.; Watjen, W.; Kahl, R. Investigations of protective effects of the flavonoids quercetin and rutin on stress resistance in the model organism. *Caenorhabditis elegans*. *Toxicology* **2007**, *234*, 113−123.

(15) Libina, N.; Berman, J. R.; Kenyon, C. Tissue-specific activities of *C. elegans* DAF-16 in the regulation of lifespan. *Cell* **2003**, *115*, 489−502.

(16) Chung, J. H.; Manganiello, V.; Dyck, J. R. Resveratrol as a calorie restriction mimetic: therapeutic implications. *Trends Cell Biol.* **2012**, *22*, 546−554.

(17) Yamawaki, T. M.; Arantes-Oliveira, N.; Berman, J. R.; Zhang, P.; Kenyon, C. Distinct activities of the germline and somatic reproductive tissues in the regulation of *Caenorhabditis elegans*' longevity. *Genetics* **2008**, *178*, 513−526.

(18) Hosono, R.; Sato, Y.; Aizawa, S.-I.; Mitsui, Y. Age-dependent changes in mobility and separation of the nematode *Caenorhabditis elegans*. *Exp. Gerontol.* **1980**, *15*, 285−289.

(19) Gerstbrein, B.; Stamatas, G.; Kollias, N.; Driscoll, M. In vivo spectrofluorimetry reveals endogenous biomarkers that report healthspan and dietary restriction in *Caenorhabditis elegans*. *Aging Cell* **2005**, *4*, 127−137.

(20) Lithgow, G. J.; White, T. M.; Melov, S.; Johnson, T. E. Thermotolerance and extended life-span conferred by single-gene mutations and induced by thermal stress. *Proc. Natl. Acad. Sci. U.S.A.* **1995**, *92*, 7540−7544.

(21) Harman, D. *Aging: A Theory Based on Free Radical and Radiation Chemistry*; University of California Radiation Laboratory: Berkeley, CA, 1955; pp 298−300.
(22) Lin, K.; Hsin, H.; Libina, N.; Kenyon, C. Regulation of the *Caenorhabditis elegans* longevity protein DAF-16 by insulin/IGF-1 and germline signaling. *Nat. Genet.* **2001**, *28*, 139−145.
(23) Landis, J. N.; Murphy, C. T. Integration of diverse inputs in the regulation of *Caenorhabditis elegans* DAF-16/FOXO. *Dev. Dyn.* **2010**, *239*, 1405−1412.
(24) Park, S.-J.; Ahmad, F.; Philp, A.; Baar, K.; Williams, T.; Luo, H.; Ke, H.; Rehmann, H.; Taussig, R.; Brown, A. L. Resveratrol ameliorates aging-related metabolic phenotypes by inhibiting cAMP phosphodiesterases. *Cell* **2012**, *148*, 421−433.
(25) Viswanathan, M.; Kim, S. K.; Berdichevsky, A.; Guarente, L. A role for SIR-2.1 regulation of ER stress response genes in determining *C. elegans* life span. *Dev. Cell* **2005**, *9*, 605−615.
(26) Murakami, S.; Murakami, H. The effects of aging and oxidative stress on learning behavior in *C. elegans*. *Neurobiol. Aging* **2005**, *26*, 899−905.
(27) Senoo-Matsuda, N.; Hartman, P. S.; Akatsuka, A.; Yoshimura, S.; Ishii, N. A complex II defect affects mitochondrial structure, leading to ced-3-and ced-4-dependent apoptosis and aging. *J. Biol. Chem.* **2003**, *278*, 22031−22036.
(28) Miyadera, H.; Amino, H.; Hiraishi, A.; Taka, H.; Murayama, K.; Miyoshi, H.; Sakamoto, K.; Ishii, N.; Hekimi, S.; Kita, K. Altered quinone biosynthesis in the long-lived *clk-1* mutants of *Caenorhabditis elegans*. *J. Biol. Chem.* **2001**, *276*, 7713−7716.
(29) Rattan, S. I. Aging, anti-aging, and hormesis. *Mech. Aging Dev.* **2004**, *125*, 285−289.
(30) Saul, N.; Pietsch, K.; Menzel, R.; Stürzenbaum, S. R.; Steinberg, C. E. The longevity effect of tannic acid in *Caenorhabditis elegans*: disposable soma meets hormesis. *J. Gerontol., Ser. A* **2010**, *65*, 626−635.
(31) Kirkwood, T. B.; Rose, M. R. Evolution of senescence: late survival sacrificed for reproduction. *Phil. Trans. R. Soc. London, B* **1991**, *332*, 15−24.
(32) Berdichevsky, A.; Viswanathan, M.; Horvitz, H. R.; Guarente, L. *C. elegans* SIR-2.1 interacts with 14-3-3 proteins to activate DAF-16 and extend life span. *Cell* **2006**, *125*, 1165−1177.
(33) Espinoza-Fonseca, L M. The benefits of the multi-target approach in drug design and discovery. *Bioorg. Med. Chem.* **2006**, *14*, 896−897.
(34) Boran, A D; Iyengar, R. Systems approaches to polypharmacology and drug discovery. *Curr. Opin. Drug Discovery Dev.* **2010**, *13*, 297−309.

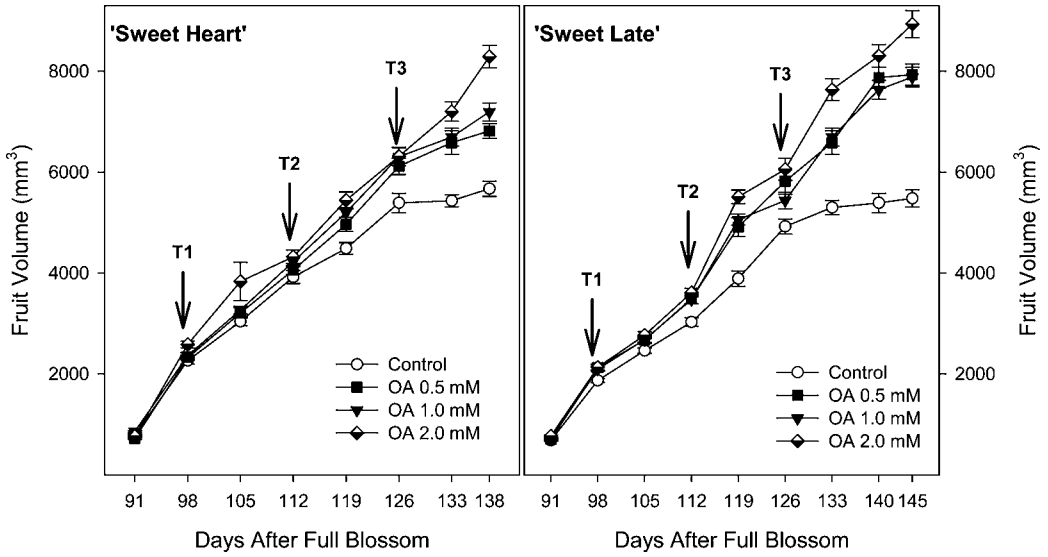

Figure 1. Fruit volume (mm^3) during on-tree fruit development of 'Sweet Heart' and 'Sweet Late' sweet cherry cultivars treated with oxalic acid (OA, 0.5, 1.0, or 2.0 mM) at 98, 112, and 126 days after full blossom (T1, T2, and T3). Data are the mean ± SE.

Spain). Freshly prepared solutions (containing 0.5% Tween 20) were foliar sprayed with a mechanical mist sprayer and repeated at three dates of the growth cycle: T1 (at pit hardening, 98 days after full blossom, DAFB), T2 (initial color changes, 112 DAFB), and T3 (onset of ripening, 126 DAFB). These dates corresponded to key events in the fruit developmental process, according to previous experiments.[3] Before T1 treatment, 20 fruits were labeled around the equatorial perimeter of each tree, in which fruit growth was followed by measuring polar, suture, and cheek diameters, and then fruit volume was calculated as previously reported.[3] On a weekly basis, from 1 week before the T1 treatment to commercial harvesting, 20 fruits (similar to those labeled) for each tree (or replicate) were picked for further analytical determinations: fruit firmness, color, total soluble solids (TSS), and total acidity (TA). In addition, the content of bioactive compounds (total phenolics and total anthocyanins) and total antioxidant activity were determined in fruits from control and 2.0 mM OA treated trees. In these fruits, the individual contents of anthocyanins, flavonols, and chlorogenic acid derivatives were measured at the last sampling date (commercial harvest). At the time of harvesting, 100 cherries from each tree, cultivar, and treatment were randomly picked for determining the fruit weight.

Ripening Parameters. Color was determined in each cheek of 20 fruits from each replicate by using a Minolta colorimeter (CRC200, Minolta Camera Co., Japan), using the CIELab coordinates and expressed as a^*/b^* index. Fruit firmness was determined independently in 20 fruits of each replicate using a TX-XT2i texture analyzer (Stable Microsystems, Godalming, UK) interfaced to a personal computer, with a flat steel plate mounted on the machine. For each fruit, the cheek diameter was measured, and then a force that achieved a 3% deformation of the fruit diameter was applied. Results were expressed as the force−deformation ratio (N mm^{-1}) and were the mean ± SE. After that, the 20 fruits of each sample were cut in small pieces to obtain a homogeneous sample for each replicate. TSS were determined in duplicate in the juice obtained from 5 g of each sample with a digital refractometer Atago PR-101 (Atago Co. Ltd., Tokyo, Japan) at 20 °C and expressed as grams per 100 g (mean ± SE). Total acidity (TA) was determined in duplicate in the same juice by automatic titration (785 DMP Titrino, Metrohm) with 0.1 N NaOH up to pH 8.1, using 1 mL of diluted juice in 25 mL of distilled H_2O, and results (mean ± SE) were expressed as grams of malic acid equivalent per 100 g of fresh weight.

Total Antioxidant Activity (TAA) Determination. TAA was quantified in duplicate in each sample as previously described.[10] Briefly, 5 g was homogenized in 5 mL of 50 mM sodium phosphate buffer, pH 7.8, and 3 mL of ethyl acetate and then centrifuged at 10000*g* for 15 min at 4 °C. The upper fraction was used for total antioxidant activity due to lipophilic compounds (L-TAA) and the lower fraction for total antioxidant activity due to hydrophilic compounds (H-TAA). In both cases, TAA was determined using the enzymatic system composed of the chromophore 2,2′-azinobis(3-ethylbenzothiazoline-6-sulfonic acid) diammonium salt (ABTS), the horseradish peroxidase enzyme (HRP), and its oxidant substrate (hydrogen peroxide, H_2O_2), in which $ABTS^{\bullet+}$ radicals are generated and monitored at 730 nm. The reaction mixture contained 2 mM ABTS, 15 μM H_2O_2, and 25 μM HRP in 50 mM sodium phosphate buffer (pH 7.8) in a total volume of 1 mL. The decrease in absorbance after adding the extract was proportional to the TAA of the sample. A calibration curve was performed with Trolox ((*R*)-(+)-6-hydroxy-2,5,7,8-tetramethylchroman-2-carboxylic acid) (0−20 nmol) from Sigma (Madrid, Spain), and results are expressed as milligrams of Trolox equivalent per 100 g of fresh weight.

Bioactive Compound Determination. Total phenolics were extracted according to the Tomás-Barberán et al. protocol[20] using water/methanol (2:8) containing 2 mM NaF (to inactivate polyphenol oxidase activity and prevent phenolic degradation) and quantified in duplicate using the Folin−Ciocalteu reagent, and results (mean ± SE) were expressed as milligrams of gallic acid equivalent per 100 g of fresh weight. Total anthocyanins were determined according to the method of García-Viguera et al.[21] adapted as previously reported[10] and calculated as cyanidin 3-glucoside equivalent (molar absorption coefficient of 23900 L cm^{-1} mol^{-1} and molecular weight of 449.2 g mol^{-1}), and results were expressed as milligrams per 100 g of fresh weight and were the mean ± SE. For individual phenolic compounds, the protocol described by Gironés-Vilaplana et al. was followed.[22] Briefly, lyophilized samples (100 mg) were mixed with 1 mL of methanol/formic acid/water (25:1:24, v/v/v), vortexed, sonicated in an ultrasonic bath for 60 min, and centrifuged at 10500*g* for 5 min. The supernatant was filtered through a 0.45 μm PVDF filter (Millex HV13, Millipore, Bedford, MA, USA) and used for HPLC analysis. The HPLC system was equipped with a Luna C18 column (25 cm × 0.46 cm i.d., 5 μm particle size; Phenomenex, Macclesfield, UK) with a C18 security guard (4.0 × 3.0 mm) cartridge system (Phenomenex). Water/formic acid (99:5, v/v) and acetonitrile were used as mobile phases A and B, respectively, with a flow rate of 1 mL/min. The linear gradient started with 8% of solvent B, reaching 15% of solvent B at 25 min, 22% at 55, and 40% at 60 min, which was maintained up to 70 min. The injection volume was 20 μL. Chromatograms were recorded at 280, 320, 360, and 520 nm. Different phenolics were characterized by chromatographic comparison with analytical standards as well as quantified by the absorbance of their corresponding peaks.

dx.doi.org/10.1021/jf500224g | J. Agric. Food Chem. 2014, 62, 3432−3437

Table 1. Quality Parameters of 'Sweet Heart' and 'Sweet Late' Sweet Cherry Cultivars at Harvest As Affected by Oxalic Acid (OA) Treatments[a]

	cultivar	control	OA (0.5 mM)	OA (1.0 mM)	OA (2.0 mM)
fruit weight (g)	'Sweet Heart'	6.77 ± 0.13 a	7.73 ± 0.25 b	7.94 ± 0.24 b	8.02 ± 0.12 bc
	'Sweet Late'	6.62 ± 0.14 a	7.89 ± 0.15 b	8.14 ± 0.26 b	8.64 ± 0.32 c
firmness (N mm^{-1})	'Sweet Heart'	3.09 ± 0.09 a	3.44 ± 0.09 b	3.66 ± 0.11 c	3.70 ± 0.11 c
	'Sweet Late'	2.61 ± 0.09 a	2.84 ± 0.10 b	2.96 ± 0.10 b	3.54 ± 0.07 c
color (a^*/b^*)	'Sweet Heart'	2.82 ± 0.09 a	3.02 ± 0.07 b	3.10 ± 0.12 b	3.21 ± 0.10 bc
	'Sweet Late'	3.19 ± 0.11 a	3.44 ± 0.10 b	3.34 ± 0.16 b	3.46 ± 0.14 b
TSS (g 100 g^{-1})	'Sweet Heart'	19.95 ± 0.09 a	19.40 ± 0.11 a	20.75 ± 0.35 b	20.88 ± 0.08 b
	'Sweet Late'	19.05 ± 0.20 a	19.43 ± 0.21 a	19.60 ± 0.12 ab	19.88 ± 0.18 ba
TA (g 100 g^{-1})	'Sweet Heart'	1.50 ± 0.01 a	1.59 ± 0.05 b	1.63 ± 0.02 b	1.59 ± 0.04 b
	'Sweet Late'	1.35 ± 0.01 a	1.41 ± 0.04 b	1.42 ± 0.02 b	1.54 ± 0.02 c

[a]Data are the mean ± SE. Different letters within a row show significant differences at $p < 0.05$.

Hydroxycinnamic derivatives, *p*-coumaroylquinic acid, and hydroxybenzoic acid were characterized by chromatographic comparison according to previous reports based on retention time and UV−vis spectra.[20] Anthocyanin standards (cyanidin 3-glucoside, cyanidin 3-rutinoside, and pelargonidin 3-rutinoside) were purchased from Polyphenols SA (Sandnes, Norway). Anthocyanins were quantified as cyanidin 3-*O*-glucoside at 520 nm, cinnamic acids as 5-*O*-caffeoylquinic acid at 320 nm, and flavonols as quercetin 3-*O*-rutinoside at 360 nm and expressed as milligrams per 100 g of fresh weight (mean ± SE).

Statistical Analysis. Data for the analytical determinations were subjected to analysis of variance (ANOVA). Sources of variation were days after full blossom and treatment or just treatment for individual anthocyanins, flavonols, and chlorogenic acid derivatives. Mean comparisons were performed using Tukey's HSD test to examine if differences were significant at $P < 0.05$. Linear regressions were performed between phenolic and anthocyanin concentrations, as well as among total phenolics and H-TAA, taking into account data from cultivars, treatments, and all sampling dates. All analyses were performed with SPSS software package v. 12.0 for Windows.

RESULTS AND DISCUSSION

Sweet Cherry Growth and Ripening Parameters. Fruit growth (measured as fruit volume) increased sharply from 91 DAFB until 126 and 133 DAFB in control fruit from 'Sweet Heart' and 'Sweet Late' cultivars, respectively, the increase being lower from this time to commercial maturity stage (Figure 1). However, in cherries from OA-treated trees the increase in fruit volume continued until the last sampling date, the highest fruit volume being reached with OA treatment at 2.0 mM in both sweet cherry cultivars. The effect of OA treatments on increasing fruit growth was also evident in the final fruit weight at the last sampling date, with values of 6.77 ± 0.13 and 6.62 ± 0.14 g for control fruits of 'Sweet Heart' and 'Sweet Late' cultivars, respectively, and significantly higher in cherries from OA-treated trees, ca. 8 and 8.5 g with 2.0 mM OA for 'Sweet Heart' and 'Sweet Late', respectively (Table 1).

Texture is one of the most important attributes in sweet cherry, and it is often used for quality assessment, although there are considerable genotypic differences.[3] Fruit firmness decreased sharply as fruit weight increased (data not shown), which simply reflects cell enlargement during fruit growth, whereas softening in the last days of on-tree fruit ripening has been attributed to cell wall modification, mainly due to increases in β-galactosidase activity.[3,23] However, fruit firmness at commercial ripening stage was significantly higher in cherries from OA-treated trees than in controls, especially with the 2.0 mM dose (Table 1). In plum and sweet cherry, postharvest treatments with OA decreased softening during storage as compared to control fruits, due to reduced activities of polygalacturonase and pectin methylesterase enzymes, leading to less pectin degradation and in turn to maintenance of fruit firmness,[13,19] which could be also reduced by preharvest OA treatments. In addition, the formation of oxalate-insoluble pectin could occur as a result of OA treatment, leading to a slowing of the softening process during on-tree ripening. In previous papers, it has been shown that the color parameter ratio a^*/b^* is a good index to describe the ripening process in sweet cherry, because it showed both a continuous increase until the last sampling date and important differences among cultivars.[3] Values at harvest of a^*/b^* index in 'Sweet Heart' and 'Sweet Late' cultivars were significantly higher in fruits from OA-treated trees than from controls, independent of the applied OA dose, showing a deeper red color in treated fruits than in controls (Table 1). In addition, TA and TSS were also increased in cherry fruits as a consequence of OA treatments, which could be attributed to an increase of net photosynthesis in OA-treated trees, this effect being also responsible for the higher fruit size and weight of cherries from treated trees as compared with those from control ones. In this sense, it has been reported that postharvest OA treatment of jujube fruit increased the abundance of three photosynthesis-related proteins, RuBisCO activase, RuBisCO large subunit-binding protein subunit β, and PSII oxygen-evolving complex protein.[15]

Postharvest OA treatment delayed the ripening process in climacteric fruits, such as mango,[12] plum,[13] banana,[24] and jujube fruit,[15] through inhibition of ethylene production. Although sweet cherry is a nonclimacteric fruit, postharvest OA treatments have been also effective in delaying the ripening process and maintaining fruit quality during storage, as well as in pomegranate, another nonclimacteric fruit.[16] However, in this experiment no effect of preharvest OA treatments was observed on the ripening process of sweet cherry, and fruits from control and treated trees were harvested on the same date.

Bioactive Compounds and Total Antioxidant Activity. Because the main effect of OA treatments on improving fruit quality parameters was obtained with the 2 mM dose, the content of bioactive compounds and antioxidant activity were

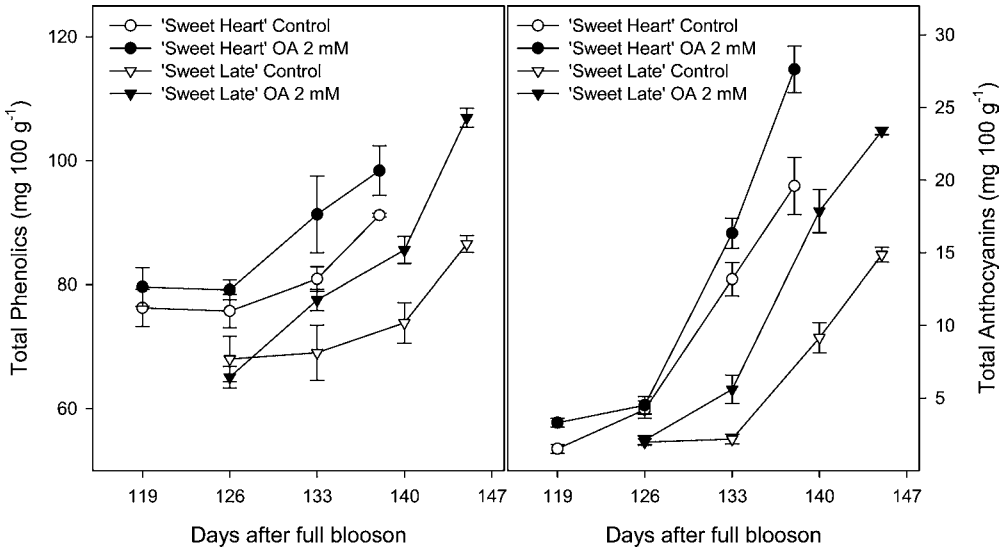

Figure 2. Total phenolics and total anthocyanins during on-tree fruit development in 'Sweet Heart' and 'Sweet Late' sweet cherry cultivars treated with oxalic acid (OA) at 2.0 mM, at 98, 112, and 126 days after full blossom. Data are the mean ± SE.

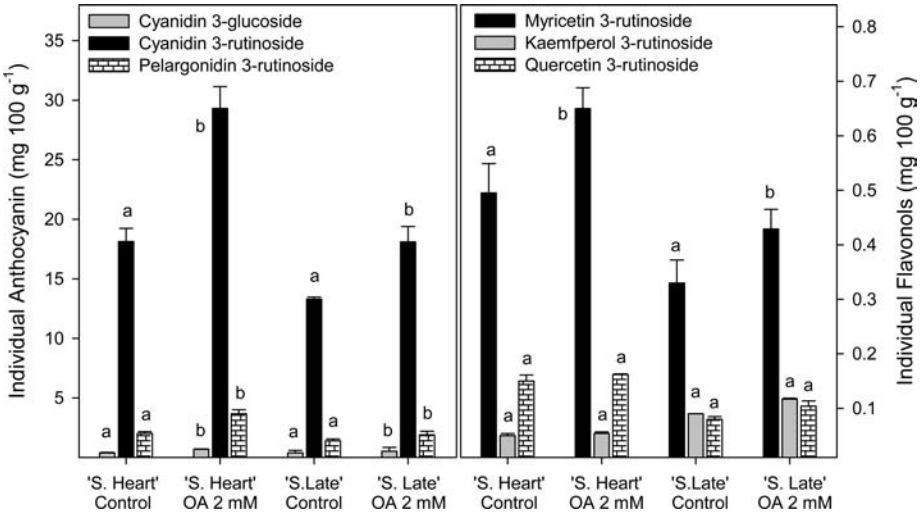

Figure 3. Individual anthocyanins and flavonols at commercial harvest in 'Sweet Heart' and 'Sweet Late' sweet cherry cultivars treated with oxalic acid (OA, 2.0 mM) at 98, 112, and 126 days after full blossom. Data are the mean ± SE. Bars with different letters show significant differences between control and treated fruits for each cultivar and individual compounds.

analyzed in cherries from control and 2 mM OA-treated trees. Total phenolics and anthocyanin concentrations increased sharply during the last 2 weeks of fruit ripening on-tree, although these values were higher in sweet cherries from OA-treated trees than in those from controls, for both cultivars (Figure 2). Accordingly, a significant increase in total phenolics as a consequence of postharvest OA treatment was also found during cold storage in sweet cherry,[19] as well as during storage at room temperature in the peel of banana[25] and mango[26] fruits, which was related to induced resistance against pathogenic attack. However, the mechanism behind how the OA treatment affects the phenolic content at molecular levels is still not completely known and deserves further research. On the contrary, in 'Damili' plum, postharvest OA treatment delayed the increase of anthocyanin content that occurred in control fruits during storage, attributed to a lower activity of phenylalanine ammonia-lyase (PAL), the key enzyme involved in the biosynthesis of anthocyanins.[13] However, in this fruit, the flesh reddening is associated with senescence and chilling injury symptoms, whereas in sweet cherry the accumulation of anthocyanins during development on-tree is a normal process of fruit ripening.[3] In addition, a close relationship was found between total phenolic and total anthocyanin concentrations ($y = 0.68x - 45.3$; $r^2 = 0.812$), taking into account data for both cultivars, treatments, and sampling dates, showing that in these sweet cherry cultivars anthocyanins are the main phenolic compounds, according to previous studies in other cherry cultivars.[10,27]

The predominant anthocyanin in both cherry cultivars was cyanidin 3-rutinoside followed by pelargonidin 3-rutinoside and cyanidin 3-glucoside, according to previous studies in other cherry cultivars,[8,10,27,28] and all of them were significantly higher in OA-treated than in control cherries at the last harvest sampling date (Figure 3). The individual flavonols were found at low concentrations, the main of them being myricetin 3-rutinoside in both sweet cherry cultivars, followed by quercetin 3-rutinoside and kaempferol 3-rutinoside, and all of them were significantly increased by OA treatment (Figure 3). Accord-

ingly, the main chlorogenic acid derivatives, neochlorogenic acid and chlorogenic acid, were also increased by OA treatment, whereas hydroxycinnamic derivative, *p*-coumaroylquinic acid, hydroxybenzoic acid, caffeic acid, and ferulic acid were found at low concentrations, without significant differences between cherries from control and treated trees (Figure 4). The

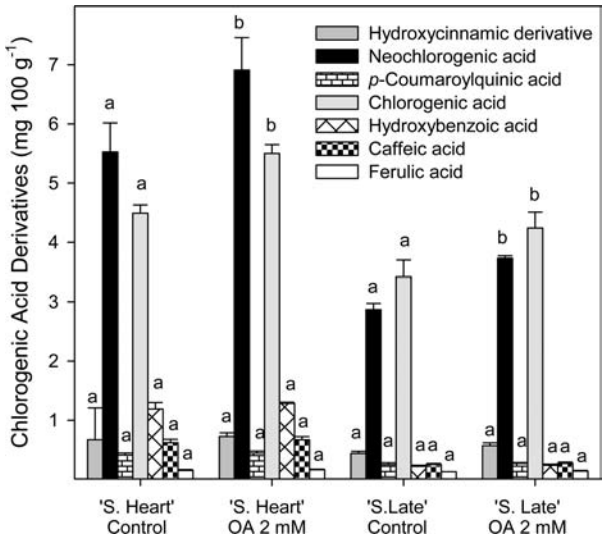

Figure 4. Individual phenolic acid derivatives at commercial harvest in 'Sweet Heart' and 'Sweet Late' sweet cherry cultivars treated with oxalic acid (OA, 2.0 mM) at 98, 112, and 126 days after full blossom. Data are the mean ± SE. Bars with different letters show significant differences between control and treated fruits for each cultivar and individual compounds.

flavonols and phenolic acid profile found in these cherry cultivars differed from previous results for other ones. Thus, for instance, in 'Lapins', 'Burlat', and 'Sylvia' cultivars *p*-coumaric acid derivatives were the main phenolic acids, together with chlorogenic and neochlorogenic acids,[2] and quercetin 3-rutinoside was the main flavonol in the 'Lapins' cultivar, which also varied depending on the cherry rootstock.[29]

TAA was measured in hydrophilic (H-TAA) and lipophilic (L-TAA) fractions separately, because early reports demonstrated that the contribution of L-TAA was about 20−30% of the TAA in a wide range of sweet cherry cultivars.[3] In 'Sweet Heart' and 'Sweet Late' cultivars H-TAA and L-TAA increased during fruit ripening on-tree, although the levels were significantly higher in fruits from OA-treated trees than in controls, especially for H-TAA (Figure 5). High correlation was found between total phenolic and H-TAA ($y = 2.16x - 95.9$; $r^2 = 0.687$), which is in agreement with previous papers reporting that phenolic compounds are the main hydrophilic compounds responsible for the antioxidant capacity of sweet cherry[2,3,10] and its health beneficial effects, such as the inhibition of human cancer cell proliferation.[31] Nevertheless, ascorbic acid is another hydrophilic compound that can also contribute to this antioxidant activity.[7] Accordingly, antioxidant activity due to phenolic compounds increased in banana peel as a consequence of postharvest OA treatment.[25] In addition, postharvest OA treatment of peach[14] and mango[18] fruits increased activities of the antioxidant enzymes superoxide dismutase, catalase, peroxidase, ascorbate peroxidase, and polyphenol oxidase. These antioxidant enzymes, together with the antioxidant compounds (phenolics, carotenoids, and ascorbic acid), are involved in scavenging free radicals and reactive oxygen species, which are generated during ripening and senescence.[30] Thus, preharvest OA treatment could also increase the antioxidant ability against oxidative damage and account for the beneficial effect of reducing cherry quality deterioration during postharvest storage.

In summary, results show for the first time that the application of the natural compound OA as preharvest treatment increased fruit size and other parameters related to sweet cherry fruit quality, such as firmness and color, but did not affect the normal ripening process on-tree. In addition, at harvest the content of bioactive phenolics, including anthocyanins, flavonols, and chlorogenic acid derivatives, and H-TAA and L-TAA were significantly higher in fruits from treated trees than in control fruits. Thus, OA preharvest treatment could be a natural and useful tool to improve the

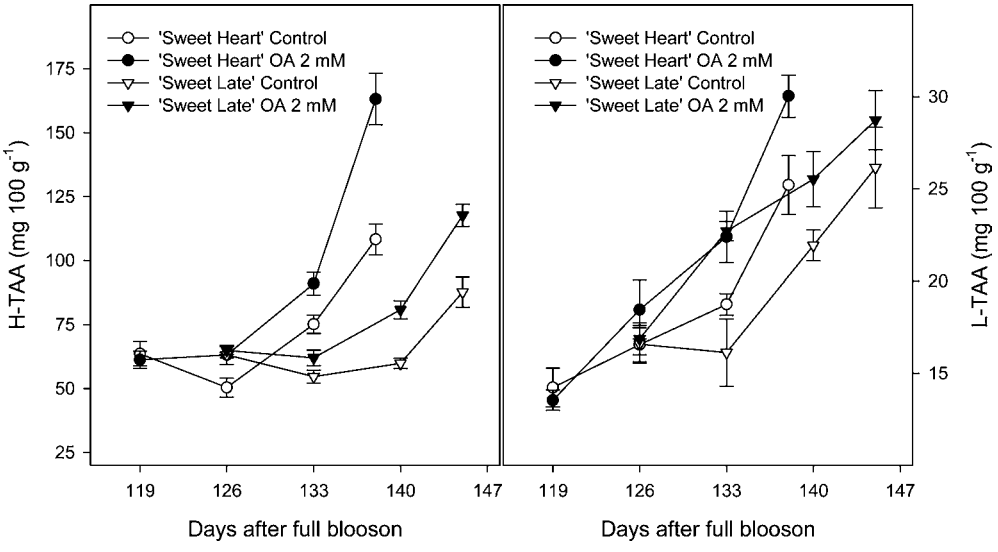

Figure 5. Changes in hydrophilic (H-TAA) and lipophilic total antioxidant activity (L-TAA) during on-tree fruit development in sweet cherry 'Sweet Heart' and 'Sweet Late' sweet cherry cultivars treated with oxalic acid (OA, 2.0 mM) at 98, 112, and 126 days after full blossom. Data are the mean ± SE.

dx.doi.org/10.1021/jf500224g | J. Agric. Food Chem. 2014, 62, 3432−3437

reported health-beneficial properties of sweet cherry consumption.

AUTHOR INFORMATION

Corresponding Author

*(M.S.) Fax: 34-96-6749678; E-mail: m.serrano@umh.es.

Funding

This work has been funded by the Spanish Ministry of Economy and Competitiveness through Project AGL2012-35402/ALI and by the European Commission with FEDER funds.

Notes

The authors declare no competing financial interest.

ACKNOWLEDGMENTS

We thank Finca Toli Frutas, S.L., for permission to use their plots, for provision of the cherries, and for the technical support received.

REFERENCES

(1) Muskovics, G.; Felföldi, J.; Kovács, E.; Perlaki, R.; Kállay, T. Changes in physical properties during fruit ripening of Hungarian sweet cherry (*Prunus avium* L.) cultivars. *Postharvest Biol. Technol.* **2006**, *4*, 56−63.

(2) Usenik, V.; Fabčič, J.; Štampar, F. Sugars, organic acids, phenolic composition and antioxidant activity of sweet cherry (*Prunus avium* L.). *Food Chem.* **2008**, *107*, 185−192.

(3) Díaz-Mula, H. M.; Castillo, S.; Martínez-Romero, D.; Valero, D.; Zapata, P. J.; Guillén, F.; Serrano, M. Organoleptic, nutritive and functional properties of sweet cherry as affected by cultivar and ripening stage. *Food Sci. Technol. Int.* **2009**, *15*, 535−543.

(4) Valero, D.; Serrano, M. *Postharvest Biology and Technology for Preserving Fruit Quality*; CRC Press/Taylor & Francis: Boca Raton, FL, USA, 2010.

(5) McCune, L. M.; Kubota, C.; Stendell-Hollins, N. R.; Thomson, C. A. Cherries and heatlh: a review. *Crit. Rev. Food Sci. Nutr.* **2011**, *51*, 1−12.

(6) Delgado, J.; Del Pilar Terrón, M.; Garrido, M.; Barriga, C.; Paredes, S. D.; Espino, J.; Rodríguez, A. B. Systemic inflammatory load in young and old ringdoves is modulated by consumption of a Jerte Valley cherry-based product. *J. Med. Food* **2012**, *15*, 707−712.

(7) Serrano, M.; Guillén, F.; Martínez-Romero, D.; Castillo, S.; Valero, D. Chemical constituents and antioxidant activity of sweet cherry at different ripening stages. *J. Agric. Food Chem.* **2005**, *53*, 2741−2745.

(8) Gonçalves, B.; Silva, A. P.; Moutinho-Pereia, J.; Bacelar, E.; Rosa, E.; Meyer, A. S. Effect of ripeness and postharvest storage on the evolution of color and anthocyanins in cherries (*Prunus avium* L.). *Food Chem.* **2007**, *103*, 976−984.

(9) Kim, D. O.; Heo, H. J.; Kim, Y. J.; Yang, H. S.; Lee, C. Y. Sweet and sour cherry and their protective effects on neuronal cells. *J. Agric. Food Chem.* **2005**, *53*, 9921−9927.

(10) Serrano, M.; Díaz-Mula, H.; Zapata, P. J.; Castillo, S.; Guillén, F.; Martínez-Romero, D.; Valverde, J. M.; Valero, D. Maturity stage at harvest determines the fruit quality and antioxidant potential after storage of sweet cherry cultivars. *J. Agric. Food Chem.* **2009**, *57*, 3240−3246.

(11) Zheng, X.; Jing, G.; Liu, Y.; Jiang, T.; Jiang, Y.; Li, J. Expression of expansin gene, MiExpA1, and activity of galactosidase and polygalacturonase in mango fruit as affected by oxalic acid during storage at room temperature. *Food Chem.* **2012**, *132*, 849−854.

(12) Zheng, X.; Tian, S.; Gidley, M. J.; Yue, H.; Li, B. Effects of exogenous oxalic acid on ripening and decay incidence in mango fruit during storage at room temperature. *Postharvest Biol. Technol.* **2007**, *45*, 281−284.

(13) Wu, F.; Zhang, D.; Zhang, H.; Jiang, G.; Su, X.; Qu, H.; Jiang, Y.; Duan, X. Physiological and biochemical response of harvested plum fruit to oxalic acid during ripening or shelf-life. *Food Res. Int.* **2011**, *44*, 1299−1305.

(14) Zheng, X.; Tian, S.; Meng, X.; Li, B. Physiological and biochemical response in peach fruit to oxalic acid treatment during storage at room temperature. *Food Chem.* **2007**, *104*, 156−162.

(15) Wang, Q.; Lai, T.; Qin, G.; Tian, S. Response of jujube fruits to exogenous oxalic acid treatment based on proteomic analysis. *Plant Cell Physiol.* **2009**, *50*, 230−242.

(16) Sayyari, M.; Valero, D.; Babalar, M.; Kalantari, S.; Zapata, P. J.; Serrano, M. Prestorage oxalic acid treatment maintained visual quality, bioactive compounds, and antioxidant potential of pomegranate after long-term storage at 2 °C. *J. Agric. Food Chem.* **2010**, *58*, 6804−6808.

(17) Zheng, X.; Tian, S. Effect of oxalic acid on control of postharvest browning of litchi fruit. *Food Chem.* **2006**, *96*, 519−523.

(18) Ding, Z. S.; Tian, S. P.; Zheng, X. L.; Zhou, Z. W.; Xu, Y. Responses of reactive oxygen metabolism and quality in mango fruit to exogenous oxalic acid or salicylic acid under chilling temperature stress. *Phyiol. Plant.* **2007**, *130*, 112−121.

(19) Valero, D.; Díaz-Mula, H. M.; Zapata, P. J.; Castillo, S.; Guillén, F.; Martínez-Romero, D.; Serrano, M. Postharvest treatments with salicylic acid, acetylsalicylic acid or oxalic acid delayed ripening and enhanced bioactive compounds and antioxidant capacity in sweet cherry. *J. Agric. Food Chem.* **2011**, *59*, 5483−5489.

(20) Tomás-Barberán, F. A.; Gil, M. I.; Cremin, P.; Waterhouse, A. L.; Hess-Pierce, B.; Kader, A. A. HPLC-DAD-ESIMS analysis of phenolic compounds in nectarines, peaches, and plums. *J. Agric. Food Chem.* **2001**, *49*, 4748−4760.

(21) García-Viguera, C.; Zafrilla, P.; Romero, F.; Abellá, P.; Artés, F.; Tomás-Barberán, F. A. Color stability of strawberry jam as affected by cultivar and storage temperature. *J. Food Sci.* **1999**, *64*, 243−247.

(22) Gironés-Vilaplana, A.; Villaño, D.; Moreno, D. A.; García-Viguera, C. New isotonic drinks with antioxidant and biological activities from berries (Maqui, Açaí and Blackthorn) and lemon juice. *Int. J. Food Sci. Nutr.* **2013**, *64*, 897−906.

(23) Gerardi, C.; Blando, F.; Santino, A.; Zacheo, G. Purification and characterisation of a β-glucosidase abundantly expressed in ripe sweet cherry (*Prunus avium* L.) fruit. *Plant Sci.* **2001**, *160*, 795−805.

(24) Huang, H.; Jing, G.; Guo, L.; Zhang, D.; Yang, B.; Duan, X.; Ashraf, M.; Jiang, Y. Effect of oxalic acid on ripening attributes of banana fruit during storage. *Postharvest Biol. Technol.* **2013**, *84*, 22−27.

(25) Zheng, X.; Ye, L.; Jiang, T.; Jing, G.; Li, J. Limiting the deterioration of mango fruit during storage at room temperature by oxalate treatment. *Food Chem.* **2012**, *130*, 279−285.

(26) Huang, H.; Zhu, Q.; Zhang, Z.; Yang, B.; Duan, X.; Jiang, Y. Effect of oxalic acid on antibrowning of banana (*Musa* spp., AAA group, cv. 'Brazil') fruit during storage. *Sci. Hortic.* **2013**, *160*, 208−212.

(27) Mozetič, B.; Simčič, M.; Trebše, P. Anthocyanins and hidroxycinnamic acids of Lambert Compact cherries (*Prunus avium* L.) after cold storage and 1-methylcyclorpoene treatments. *Food Chem.* **2006**, *97*, 302−309.

(28) Sharma, M.; Jacob, J. K.; Subramanian, J.; Paliyath, G. Hexanal and 1-MCP treatments for enhancing the shelf life and quality of sweet cherry (*Prunus avium* L.). *Sci. Hortic.* **2010**, *125*, 239−247.

(29) Jakobek, L.; Šeruga, M.; Voća, S.; Šindrak, Z.; Dobričević, N. Flavonol and phenolic acid composition of sweet cherries (cv. Lapins) produced on six different vegetative rootstocks. *Sci. Hortic.* **2009**, *123*, 23−28.

(30) Hodges, D. M.; Lester, G. E.; Munro, K. D.; Toivonen, P. M. A. Oxidative stress: importance for postharvest quality. *HortScience* **2004**, *39*, 924−929.

(31) Serra, A. T.; Duarte, R. O.; Bronze, M. R.; Duarte, C. M. M. Identification of bioactive response in traditional cherries from Portugal. *Food Chem.* **2011**, *125*, 318−325.

through oxidiation of lactose with bromine under mild conditions. Since then, many chemical, electrocatalytic,[30−32] and microbial or enzymatic processes[33,34] for the production of lactobionic acid have been investigated. The major application of lactobionic acid is its use as a constituent in solutions that stabilize organs before transplantation. This is based on the excellent metal-chelating properties of the acid which reduce the oxidative damages, caused by certain metal ions, to tissues during the storage and preservation of organs.[35] Additionally, the acid is also used for the stabilization of interferon preparations or for the improvement of solubility of macrolide antibiotics such as erythromycin.[36] Furthermore, lactobionic acid can have its utility as a biodegradable cobuilder in washing powder, which can contain up to 40% lactobionic acid.[37] The fatty acid derivatives of lactobionic acid can be used as biosurfactants. Lactobionic acid could have several possible applications in food technology. These include improvement in the taste perception of sour, elimination of bitterness, flavor enhancement, preservation of aroma freshness, and reduction of souring and ripening time of cheese and yogurt products.[38] Moreover, its mineral salt complexes are used for the fortification of functional drinks with essential minerals,[39] and its addition to functional food might be useful for its presumed prebiotic effect.[40]

T. clypeatus produces large quantities of endo-1,4-β-glucanase, β-glucosidase, and CDH in cellulose-containing medium.[41,42] The fungus was reported to be the highest producer of CDH.[42] In the present investigation, several agro-industrial byproducts were tested as substrates for CDH production by *T. clypeatus* (CDHtc) during shake-flask fermentations and the suitability of TKP was evaluated to stimulate CDH production in a 5 L stirred-tank fermenter.

MATERIALS AND METHODS

Microorganism. The stock cultures of *T. clypeatus* were maintained in PDA slants (20% potato extract, 2% dextrose, and 1.5% agar, pH 7.0) at 4 °C. Mycelia were transferred to fresh PDA slants for growth at 30 °C for 5 days. These slants were then stored at 4 °C for use in inoculum preparation.

Agro-residues. Corncob, coconut coir, rice husk, wheat bran, ground nut shell, sugar cane bagasse, sawdust (from *Tectona grandis*), and TKP were collected from the local markets of Kolkata, India. Various media constituents including malt extract, yeast extract, peptone, and other salts including buffer components were purchased from Hi-Media, Bombay, India. Fine chemicals including 2,6-dichlorophenol indophenol (DCIP), cellobiose, and other analytical reagents were obtained from Sigma-Aldrich, USA.

Substrate Preparation. The substrates were washed thoroughly in distilled water and dried at 50 °C until use. Corncob, coconut coir, ground nut shell, and bagasse were crushed to a fine powder in a grinder and sieved (mesh size BSS 30) to get a homogeneous powder (diameter of particles <5 mm). The powdered agro-residue samples were used as the starting material for further experiments. The moisture content of the dried biomasses was around 2%.

Preparation of Inoculums. Five-day-old mycelia of *T. clypeatus* from PDA slants were transferred to 100 mL of MYG liquid medium (1% malt extract, 0.4% yeast extract, and 1% glucose) in 500 mL polypropylene flasks with two 1 cm diameter glass beads and incubated at 30 °C for 5 days under constant shaking of 150 rpm. The fragmented mycelial culture (1% v/v ∼ 0.018% w/v unless or otherwise specified) was used as the inoculum for CDHtc production.

Cultural Conditions for CDH Production. The basic media for CDHtc contained 1.0% cellulose or agro-residues as and where specified, 0.15% KH_2PO_4, 0.037% $CaCl_2{\cdot}2H_2O$, 0.03% $ZnSO_4$, 0.05% $MgSO_4$, 0.05% H_3BO_3, 0.0036% $MnCl_2$, 0.0032% Na_2MoO_4, and 2.2% $NH_4H_2PO_4$. The pH values of the media were adjusted to 7.0 before autoclaving. Yeast extract (0.2%) and peptone (0.2%) were added in the medium as and where mentioned. The fungus was cultured for up to 17 days at 30 °C under constant shaking of 150 rpm. Aliquots of the culture filtrate were collected at 1 day intervals and clarified by centrifugation at 21000*g* for 30 min to determine the enzyme activities. The culture medium was adjusted to its original volume with fresh medium after each collection.

Enzyme Production in 5 L Stirred-Tank Bioreactor. Large-scale enzyme production was carried out in a 5 L benchtop stirred-tank bioreactor (BioFlo 3000, New Brunswick Scientific Co., Inc., New Brunswick, NJ, USA). The fermenter was equipped with an automatic computerized control system (Bio Command Software, New Brunswick Scientific Co.) for temperature, aeration, agitation, and pH. The temperature was maintained at 30 °C. Air was supplied at a continuous rate of 1.0 vvm. Agitation was limited to 150 rpm. The initial pH of the medium was adjusted to 7.0 before sterilization, and no pH control was imposed during growth. Dow Corning silicon antifoam (0.2% v/v) was used to check the frothing during the fermentation. Samples were withdrawn after every 24 h during 12 days of fermentation and centrifuged at 21000*g* for 30 min. The supernatants thus obtained were used as enzyme solutions for the assays.

Enzyme Activity Assay. CDHtc activity was measured by following the decrease in absorbance of DCIP for 5 min at 520 nm, pH 5.0, and 25 °C with a Shimadzu UV−vis spectrophotometer (model 1700).[43] The reaction mixture (1 mL) contained 20 mM cellobiose, 0.3 mM DCIP, 100 mM sodium acetate buffer (pH 5.0), and enzyme solution. One unit (U) of enzyme activity was defined as the amount of enzyme that reduced 1 μmol of DCIP per minute under the experimental conditions. All results presented are the mean of five replicates. The error bars in the figures indicate standard deviations.

Measurement of Mycelial Growth. Mycelial growth was measured by determining the glucosamine concentration after acid hydrolysis of mycelia following the method of Desgranges et al.[44] Mycelia after growth were collected through centrifugation at 21000*g* for 30 min and washed repeatedly to remove the media remaining with the mycelial pellets. Subsequently, the samples were freeze-dried and treated with 10 mL of 10 M HCl for 16 h at 20 °C. Hydrolysis was completed by autoclaving the acid-hydrolyzed mycelia at 121 °C for 2 h after the total volume of the incubation mixture had been adjusted to 50 mL with the addition of distilled water. The concentration of glucosamine−HCl released after hydrolysis of the mycelia was measured colorimetrically according to the method of Nilsson and Bjurman.[45]

Measurement of Crystallinity. The crystallinity of the agro-residue samples was determined by using a wide-angle X-ray diffractometer. The samples were transferred to the glass sample holder and analyzed under plateau conditions. The radiation was generated at a voltage of 40 kV and a current of 40 mA. The scan scope was set between 7° and 40° with a step size of 0.02°. Holding time was 1 s. The crystallinity index along with the intensity of the main crystalline plane (002) and the amorphous fraction was calculated using the intensity at ∼18°of 2θ for amorphous fraction and maximum intensity of (002) plane at ∼22.5° of 2θ for crystalline fraction as described by Segal et al.[46] and Sasmal et al.[47]

$$\mathrm{CRI} = \frac{(I_{002} - I_{\mathrm{amor}})}{I_{002}} \times 100 \quad (1)$$

CRI = crystallinity index, I_{002} = intensity at 22.5°, and I_{amor} = intensity at 18°.

Fourier Transform Infrared Spectroscopy (FTIR) Study. FTIR is accomplished to provide accurate predictions of the chemical composition of lignocellulosic biomass as minimal sample preparation is required and very small quantities of agro-residue sample (2 mg) can be analyzed when compared to conventional gravimetric techniques, for which several grams are required.[48] An FTIR spectrum contains information on the fundamental vibrations and has more separation between similar signals, for example, hydroxyls for carbohydrate isomers.[49]

Table 1. Crystallinity Index and Structural Components of Biomasses

biomass	crystallinity (%)	cellulose (%)	hemicellulose (%)	lignin (%)	ash (%)
coconut coir	47.42 ± 0.8	43 ± 0.5	12 ± 0.6	32.5 ± 0.2	1.5 ± 0.4
corncob	27.79 ± 0.2	38.2 ± 0.2	24.6 ± 0.8	28.6 ± 0.5	3.9 ± 0.2
ground nut shell	50.04 ± 0.6	34.2 ± 0.2	17.4 ± 0.5	31.4 ± 0.4	4.5 ± 0.1
rice husk	40.14 ± 0.2	30.8 ± 0.4	24.1 ± 0.4	14.4 ± 0.5	23.6 ± 0.3
sugar cane bagasse	56.83 ± 0.5	42.8 ± 0.2	25.3 ± 0.7	14.5 ± 0.7	2.1 ± 0.2
teak wood	49.27 ± 0.3	41.7 ± 0.7	16 ± 0.6	34 ± 0.4	1.8 ± 0.1
wheat bran	29.61 ± 0.5	11.2 ± 0.5	28.5 ± 0.2	4.2 ± 0.5	4.6 ± 0.2
TKP	18.37 ± 0.8	22.87 ± 0.8	20.12 ± 0.8	41.6 ± 0.2	0.39 ± 0.3
cellulose	84.28 ± 0.1				

FTIR study of the subjected agro-residue samples was carried out by dispersing the dried (50 °C for 24 h) powdered samples (2 mg) of the fibers of biomass on IR grade potassium bromide (200 mg). Diffuse reflection method of FTIR analyses was performed using a Shimazdu spectrophotometer (IR Affinity-1). All of the spectra were obtained using the Happ-Genzel apodization function, a resolution of 4 cm^{-1}, and an interval of 1 cm^{-1}, and 64 scans were performed for each background and sample spectra, respectively. The reproducibility of the spectra of all the samples was verified on three sample preparations, from 64 scans with a resolution of 4 cm^{-1}. FTIR spectra were interpreted following the characteristic bands for all functional groups as reported in the literature. The assignments of bands to structural components (as determined by other researchers) are provided in the results.

RESULTS AND DISCUSSION

XRD and FTIR Analyses of the Agro-residues. The degree of crystallinity depends on the molecular arrangement of

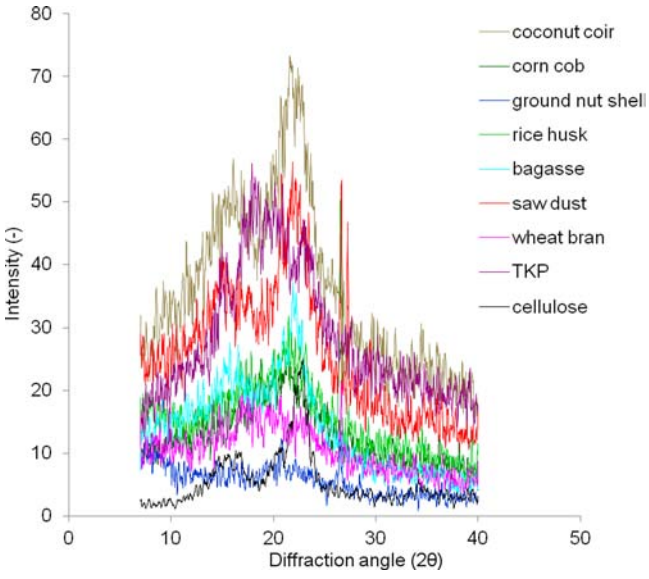

Figure 1. X-ray diffraction analysis of agro-residues.

lignin, cellulose, and hemicellulose content. The maximum crystallinity was observed in sugar cane (56.83%) and least in TKP (18.37%) as shown in Table 1, obtained from the XRD graph (Figure 1). The least crystallinity index of TKP manifests the highly amorphous nature of this substrate comparative to other agro-residues, which favors the growth of micro-organisms.[50]

The fingerprints of FTIR are illustrated in Figure 2. FTIR spectroscopy has been widely used for both quantitative and qualitative determinations of wood density,[51] chemical

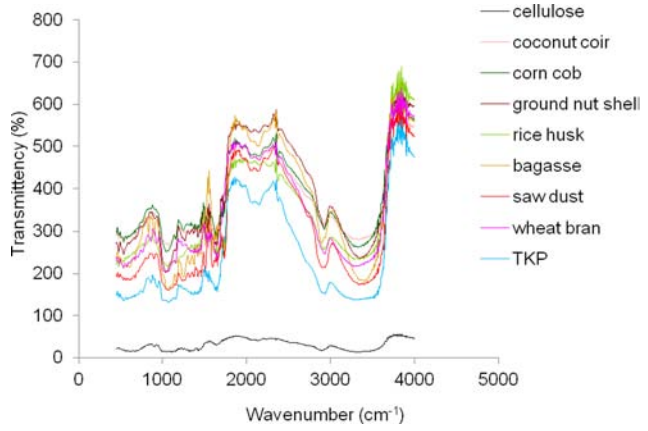

Figure 2. FTIR analysis of all tested agro-residue samples.

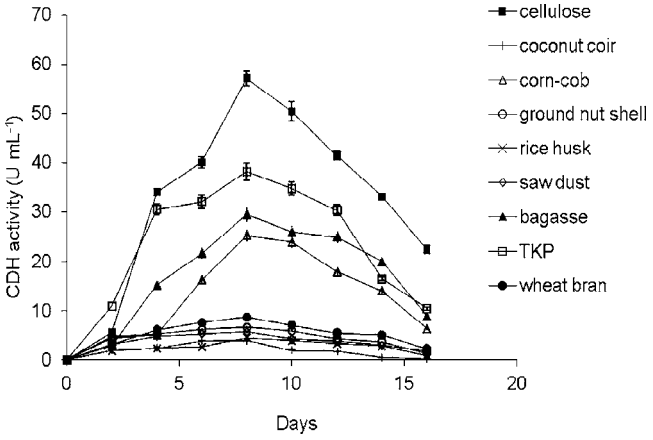

Figure 3. CDHtc production with 1% of different agro-residues in the media: (■) cellulose; (+) coconut coir; (Δ) corncob; (○) ground nut shell; (×) rice husk; (◇) sawdust; (□) TKP; (●) wheat bran; (▲) bagasse. (Reaction conditions: biomass load = 1%, pH 7.0, temperature = 30 °C, RPM = 150.)

constituents,[49] and lignin distribution.[52] As the major component of all the agro-residues are cellulose based, the observed FTIR spectra can be ascribed mainly to these components, that is, cellulose, hemicellulose, and lignin. Lignin is a complex polymer of aromatic coniferyl, coumaryl, and sinapyl alcohols, which can be described by the fingerprints near 1700 cm^{-1} for unconjugated and 1650 cm^{-1} for conjugated carbonyl compounds.[53,54] The maximum intensity in this region signifies the presence of lignin.[55] The present study shows that TKP has less intensity in all of the regions mentioned above, which signifies that it contains lesser amounts of lignin and other chemical constituents. Results

dx.doi.org/10.1021/jf405278y | J. Agric. Food Chem. 2014, 62, 3438−3445

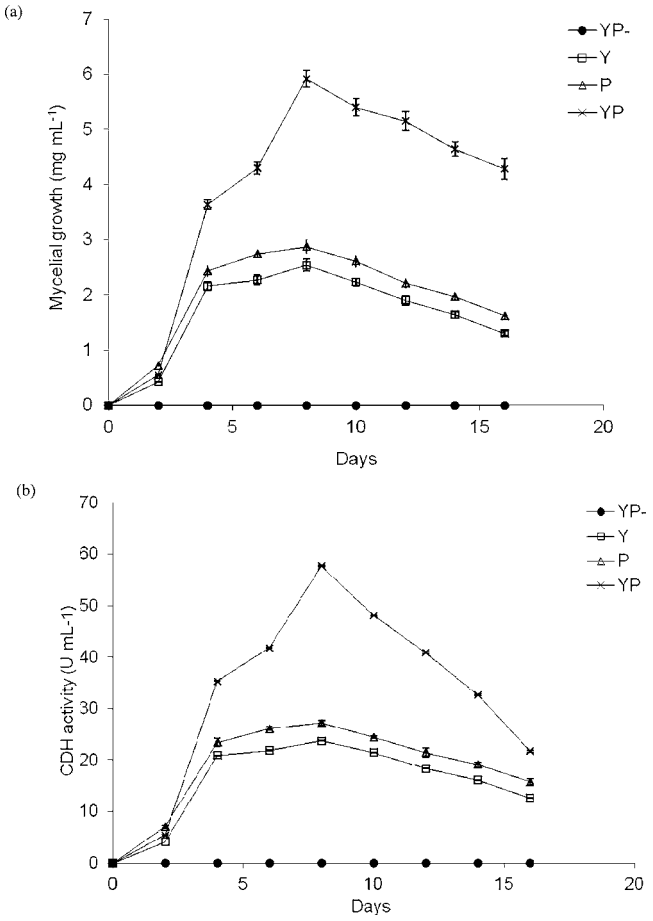

Figure 4. Effects of addition of yeast extract or peptone in cellulose medium on CDHtc production: (a) mycelial growth; (b) CDHtc production; (●) YP-, yeast extract or peptone absent; (□) Y, yeast extract present; (△) P, peptone present; (×) YP, yeast extract and peptone present.

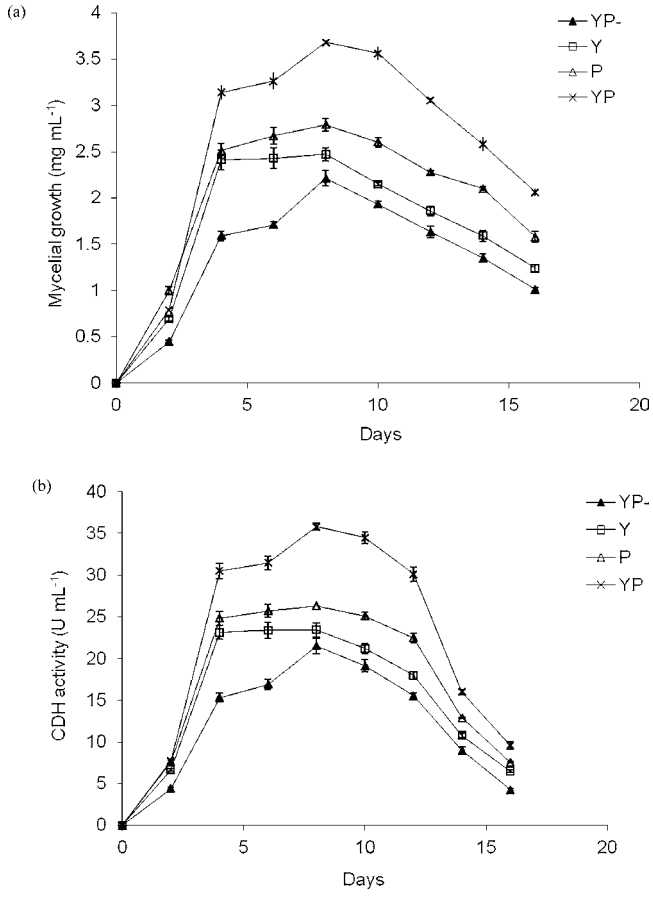

Figure 5. Effects of addition of yeast extract or peptone in TKP medium on CDHtc production: (a) mycelial growth; (b) CDHtc production; (▲) YP-, yeast extract or peptone absent; (□) Y, yeast extract present; (△) P, peptone present; YP (×) yeast extract and peptone present.

also reveal the amorphous nature of TKP through crystallography and FTIR profile, which demonstrate the fitness of its candidacy as a lignocellulosic feedstock for fermentation process.

CDHtc Production in Shake-Flasks Using the Agro-residues. *T. clypeatus* produces 55.88 U mL^{-1} CDH, which is estimated to be highest among all reported species.[41] Initially, we investigated the effect of different agro-residues on CDHtc production in shake-flask fermentations by replacing cellulose with these cheap substrates. Agro-residues (1% each) such as corncob (25.29 U mL^{-1}) and bagasse (29.5 U mL^{-1}) were found to be good substrates of CDHtc. However, among all of the tested agro-residues, TKP gave maximum enzyme yield. However, the yield was ∼67% of that obtained in the cellulose-containing medium (Figure 3). TKP is one of the cheapest gums available in India. The chemical constituents of TKP include (% w/w) carbohydrate (73.68), protein (14.38), ash (3.28), and moisture (8.67).[56] The carbohydrate part is composed of a (1→4)-β-D-glucan backbone substituted with α-D-xylopyranoside and β-D-galactopyranosyl (1→2)-α-D-xylopyranose linked (1→6) to glucose residues in the side chain.[57] The rich carbohydrate content of TKP also proves to be a good supplement to cellulose for CDHtc production under submerged conditions.

It was observed that carbon sources, such as yeast extract, casein hydrolysate, or other gluconeogenic amino acids, directly related to the citric acid cycle allowed secretion of endo-1,4-β-glucanase by *T. clypeatus* in cellulose medium.[41] The authors suggested that in *T. clypeatus* a negative regulation was mediated by the carbon catabolic product(s) that regulated growth as well as secretion of endo-1,4-β-glucanase. Similar results were observed for obtaining CDHtc in cellulose medium, where addition of yeast extract or peptone was found to be essential for growth and CDHtc production in the extracellular medium (Figure 4). The combined effect of yeast extract and peptone is more impressive than their individual effects. The mycelial growth was increased by 2−2.3 times (Figure 4a), whereas production of CDH was almost 2.4−2.5 times more when both yeast extract and peptone were added in cellulose medium, respectively (Figure 4b). The need for both yeast extract and peptone is unavoidable in cellulose medium; however, it was observed that when TKP was used as a substrate, the need for both of these costly ingredients can be avoided for CDHtc production. The yield of CDH was improved ∼2.6 times only after the addition of yeast extract and peptone along with TKP. Therefore, the presence of yeast extract or peptone was not necessary to induce CDHtc secretion in TKP-containing medium (Figure 5). The result indicated the possible presence of some compound(s) in the substrate that restricted the carbon catabolic rates similar to the

dx.doi.org/10.1021/jf405278y | J. Agric. Food Chem. 2014, 62, 3438−3445

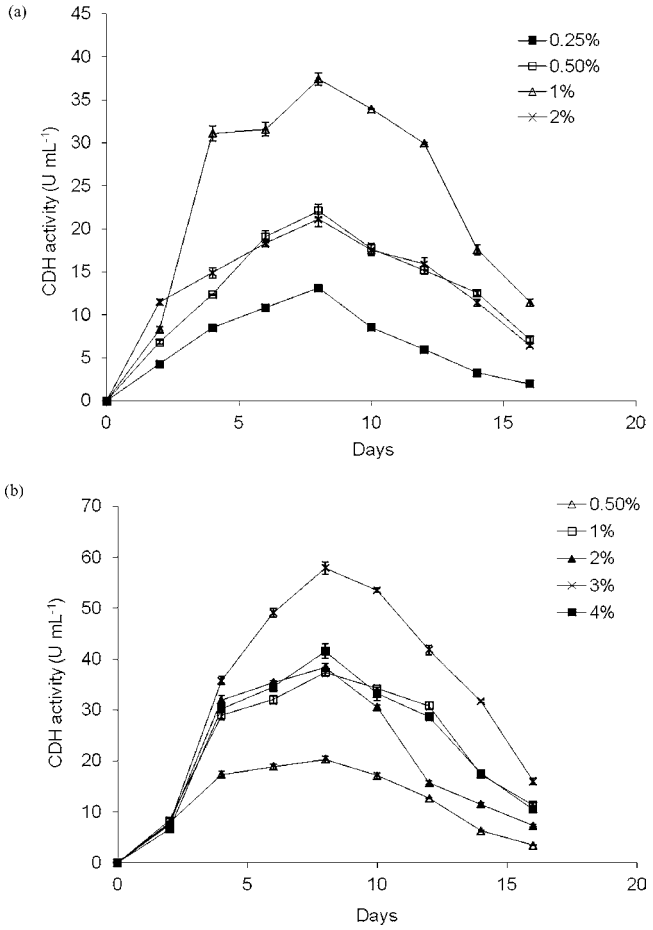

Figure 6. CDHtc production in TKP medium: (a) enzyme production in 1% TKP with variation of inoculum concentration ((■) 0.25%, (□) 0.50%, (△) 1.0%, (×) 2.0%); (b) enzyme production with 1% inoculum using different concentrations of TKP ((△) 0.50%, (□) 1%, (▲) 2%, (×) 3%, (■) 4%).

Table 2. Specific Growth and Biomass Production of *T. clypeatus* at Different TKP Concentrations

	TKP concentration				
	0.5%	1%	2%	3%	4%
r (h^{-1})	0.0242	0.0249	0.0251	0.0257	0.0279
K (mg mL^{-1})	6.2	6.58	7.17	7.13	6.2

findings of Mukherjee et al.[41] The higher yield of CDHtc in the presence of yeast extract or peptone with TKP might be due to the high rate of mycelial growth (Figure 5b) as observed earlier by Saha et al.[42]

In shake-flask cultures, the yield of CDHtc increased with the increase in inoculum concentration, and maximum enzyme activity (37.42 U mL^{-1}) was observed in the presence of 0.018% inoculum (w/v) in 1% TKP-containing medium (Figure 6a). However, with further increase in inoculum concentration, the enzyme production decreased possibly due to the depletion of media nutrients, which might result in lower metabolic rates.

CDHtc production increased with higher concentrations of TKP in shake-flask cultures with 1% (v/v) inoculum. The yield of enzyme was not improved further with the increase in inoculum concentration (Figure 6a). Maximum enzyme production (57.9 U mL^{-1}) occurred on the eighth day of

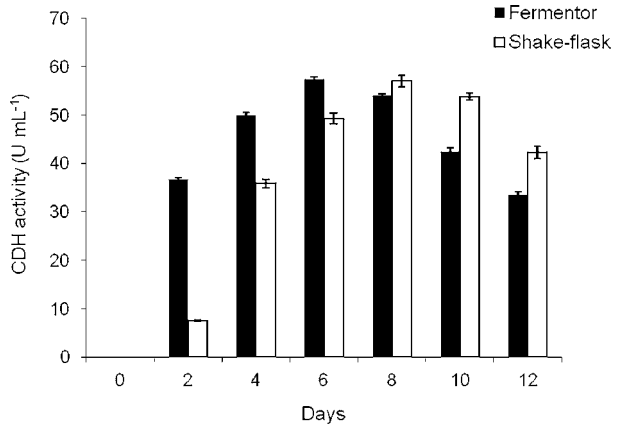

Figure 7. Comparison of CDHtc production in fermenter and shake-flask cultures: (black bars) enzyme activity in fermenter; (white bars) enzyme activity in shake-flask cultures.

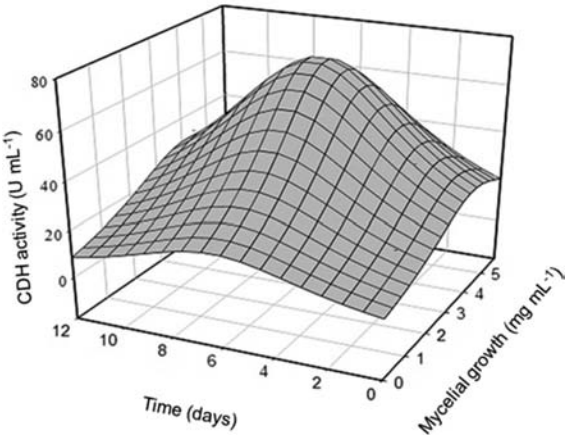

Figure 8. Time profile of CDH production and mycellial growth using TKP as the substrate.

Table 3. Statistical Analysis of the Model

coefficient	value	std error	t	p
a	72.027	14.722	4.893	0.0012
b	2.696	0.577	4.668	0.0016
c	4.742	0.894	5.303	0.0007

Table 4. ANOVA Results of the Model

	DF	SS	MS	F	p
regression	4	3030.959	757.74	57.411	<0.0001
residual	8	105.588	13.199		
total	12	3136.547	261.379		

fermentation in 3% TKP medium (Figure 6b). However, on the same day, with 4% TKP concentration, the enzyme yield was lower (41.53 U mL^{-1}) compared to that obtained using 3% TKP, with 1% (v/v) inoculum, possibly due to the enhanced viscosity (apparent viscosity was reached 0.8−14 cP at a shear rate range of 10−400 s^{-1}) of the media that led to poor aeration during fermentation (the DO level reached 4.5%). The agro-residue at 5% concentration could not be used in shake-flask cultures because the medium density was too high to carry out submerged fermentations.

It has been observed that there is a definite relationship between fungal growth and CDH production by *T. clypeatus* in

dx.doi.org/10.1021/jf405278y | J. Agric. Food Chem. 2014, 62, 3438−3445

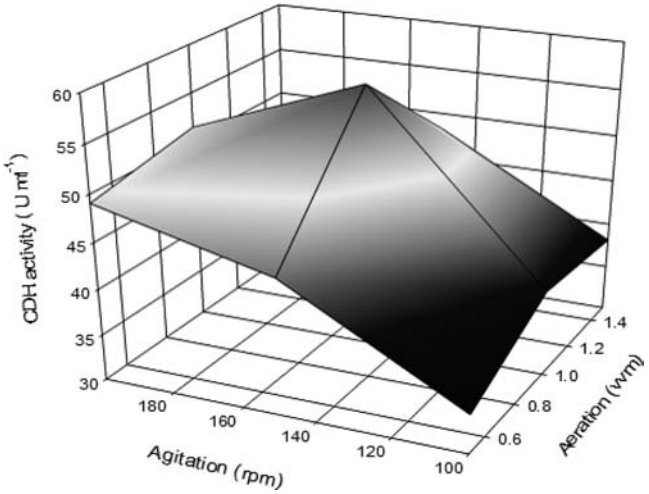

Figure 9. Surface plot for the enzyme activity (CDH U mL^{-1}) as a function of aeration (vvm) and agitation (rpm) after fermentation.

both cellulose and TKP media, where the enzyme production was directly proportional to the growth of the organism (Figures 4 and 5).

Modeling of Biomass Production. The modeling of biomass production at variable concentrations of principle carbon source (TKP) was studied. The logistic equation was used to describe the rate of biomass changes, that is, production of biomass as a function of biomass alone. The logistic model used in this study is described in eq 1

$$X = \frac{K}{1 + C\exp(-rt)} \quad (1)$$

where C = constant.

The equation described in this study is already proven for the microbial growth prediction[58] and has been widely used for describing the growth of microorganisms, too.[59,60] The phase of death is not considered in the logistic model.

By differentiating eq 1 we get eq 2

$$\frac{dX}{dt} = rX\left(1 - \frac{X}{K}\right) \quad (2)$$

where X = amount of mycelia (mg mL^{-1}), r = specific growth rate, K = carrying capacity, and t = time. The values of r and K were determined at different TKP concentrations that are shown in Table 2.

CDHtc Production in a 5 L Bioreactor. Large-scale production of CDH has been restricted to only a few organisms. Schmidhalter and Canevascini[61] cultured the brown-rot fungus *Coniophora puteana* in bioreactors with working volumes of 1.8 and 6 L. The authors found that maximum production of CDH occurred when the fungus was grown with amorphous cellulose. Baminger et al.[62] carried out laboratory fermentation of *Sclerotium rolfsii* in a 20 L stirred-tank bioreactor with a working volume of 15 L with cellulose as the carbon source, which yielded 7400 U mL^{-1} of cytochrome *c* reducing activity and 7500 U mL^{-1} of DCIP reducing activity in the extracellular medium after 130 h of cultivation. Raices et al.[63] investigated the induction of CDH and cellobiose quinone oxidoreductase (CBQ) in *Phanerochaete chrysosporium*. The fungus was grown in a 10 L automatic bioreactor with cellobiose as carbon source. Ludwig et al.[64] studied the production of CDH from *Trametes pubescens* and *Trametes villosa* in a 20 L laboratory bioreactor with 15 L of medium containing cellulose and yeast extract. The maximum enzyme activities for DCIP reduction (1450 U L^{-1}) and cytochrome *c* reduction (1600 U L^{-1}) were reached after 150 h of cultivation of *T. pubescens*. The cultivation of *T. villosa* yielded DCIP reducing activity of 830 U L^{-1} and cytochrome *c* activity of 680 U L^{-1} in the extracellular medium after 173 h of cultivation. Zamocky et al.[65] studied the production of the heterologous protein CDH from *Myriococcum thermophilum* in the methylotrophic yeast *Pichia pastoris* in a bioreactor. After optimization of the various process parameters, CDHtc production was monitored in a 5 L fermenter with 4 L of medium containing 3% TKP and 1% inoculum (v/v). Yield of the enzyme (57.4 U mL^{-1}) in the bioreactor (Figure 7) was almost similar to that observed in shake-flask fermentation (57.05 U mL^{-1}). However, the optimum day for the enzyme production in the bioreactor shifted to the sixth day compared to the shake-flask fermentations (Figure 7). The calculated correlation coefficients between CDHtc yield and biomass production in the fermenter showed that these two parameters correlated well. The value of the coefficient was ~0.94. The novelty of the paper relies on the report of highest large-scale CDH production of 57400 U L^{-1} using the cheap agro-residue TKP. These findings suggest that a laborious and expensive technique such as heterologous protein expression would not be needed to achieve CDH production on an industrial scale. Furthermore, we found that by total replacement of cellulose, yeast extract, and peptone, *T. clypeatus* in the presence of TKP produces ~2.6 times less CDH, which is appreciable when compared to the reduced production cost by ~2 times.

The viscosity and dissolved oxygen profile in the 5 L bioreactor were also examined thoroughly. The apparent viscosity reached 0.8−28 cP at a shear rate range of 10−400 s^{-1}. The proper aeration in the bioreactor led to improved enzyme production as well as the viscosity of the broth, which was quite difficult to obtain in the shake flask. The time profile of enzyme production is depicted in Figure 8. The three-dimensional graph shows a nonlinear pattern with respect to growth of biomass and time. It was observed that the enzyme production reached maximum at the exponential phase of biomass growth. The production of enzyme declined after the 12th day of the fermentation process possibly due to the lack of nutrients in the medium. Therefore, the modeling study considered the data up to 12 days only. This phenomenon can be explained mathematically by eq 3

$$z = \frac{a}{\left[1 + \left(\frac{x - x_0}{b}\right)^2\right]\left[1 + \left(\frac{y - y_0}{c}\right)^2\right]} \quad (3)$$

where z= CDH activity (U mL^{-1}), x = mycelial growth (mg mL^{-1}), y = fermentation time (days), and a, b, and c = constants.

The values of the constants were determined as a = 72.027, b = 2.696, and c = 4.742 (Table 3). An analysis of variance (ANOVA) was carried out to investigate the robustness of the model (Table 4). The Fisher ratio (F value; Table 4) was found to be quite higher (p value <0.0001) than the corresponding calculated value, which shows that the model was statistically significant.

Effects of aeration and agitation on enzyme production were also studied. Agitation speed was varied from 100 to 200 rpm and aeration rate from 0.5 to 1.5 vvm (volume of air sparged per volume of broth per minute). According to the results from

dx.doi.org/10.1021/jf405278y | J. Agric. Food Chem. 2014, 62, 3438−3445

the experimental design, as depicted from Figure 9, the enzyme production was influenced by both aeration and agitation. Merely increasing both parameters such as agitation speed beyond 150 rpm and aeration >1 vvm does not improve the production much.

AUTHOR INFORMATION

Corresponding Author

*(T.S.) Phone: +91-98 3018 6877, +91-94 7730 0821. Fax: +91-033-2582-8282. E-mail: sahatanima@yahoo.co.in, sahatanima@klyuniv.ac.in.

Author Contributions

‖T.S. and S.S. have contributed equally to the paper.

Funding

University Grants Commission (UGC), New Delhi, India, is acknowledged by T.S. for funding the project. The DST-PURSE Program at University of Kalyani is also acknowledged for financial aid.

Notes

The authors declare no competing financial interest.

ACKNOWLEDGMENTS

The Council of Scientific and Industrial Research (CSIR), New Delhi, India, is gratefully acknowledged for the laboratory facilities. T.S. acknowledges Dr. Mina Mukherjee (Ex-Scientist, Indian Institute of Chemical Biology, Kolkata, India) for her constant encouragement, support in manuscript preparation, and laboratory facilities.

ABBREVIATIONS USED

CDH, cellobiose dehydrogenase; CDHtc, cellobiose dehydrogenase from *Termitomyces clypeatus*; TKP, tamarind kernel powder; PDA, potato dextrose agar; FTIR, Fourier transform infrared spectroscopy; XRD, X-ray diffraction; DCIP, 2,6-dichlorophenol indophenol; MYG, malt extract, yeast extract, glucose; CRI, crystallinity index; DO, dissolved oxygen

REFERENCES

(1) Sandhu, S. K.; Oberoi, H. S.; Babbar, N.; Miglani, K.; Chadha, B. S.; Nanda, D. K. Two-stage statistical medium optimization for augmented cellulase production via solid-state fermentation by newly isolated *Aspergillus niger* HN-1 and application of crude cellulase consortium in hydrolysis of rice straw. *J. Agric. Food Chem.* **2013**, *61*, 12653−12661.

(2) Díaz, A. B.; Alvarado, O.; de Ory, I.; Caro, I.; Blandino, A. Valorization of grape pomace and orange peels: Improved production of hydrolytic enzymes for the clarification of orange juice. *Food Bioprod. Process.* **2013**, *91*, 580−586.

(3) da Silva Delabona, P.; Pirota, R. D. P. B.; Codima, C. A.; Tremacoldi, C. R.; Rodrigues, A.; Farinas, C. S. Using Amazon forest fungi and agricultural residues as a strategy to produce cellulolytic enzymes. *Biomass Bioenergy* **2012**, *37*, 243−250.

(4) Sasmal, S.; Goud, V. V.; Mohanty, K. Determination of salutary parameters to facilitate bio-energy production from three uncommon biomasses using thermogravimetric analysis. *J. Therm. Anal. Calorim.* **2013**, *111*, 1649−1655.

(5) Gassara, F.; Brar, S. K.; Tyagi, R. D.; Verma, M.; Surampalli, R. Y. Screening of agro-industrial wastes to produce ligninolytic enzymes by *Phanerochaete chrysosporium*. *Biochem. Eng. J.* **2010**, *49*, 388−394.

(6) Goyal, P.; Kumar, V.; Sharma, P. Carboxymethylation of tamarind kernel powder. *Carbohydr. Polym.* **2007**, *69*, 251−255.

(7) Menon, V.; Prakash, G.; Rao, M. Enzymatic hydrolysis and ethanol production using xyloglucanase and *Debaromyces hansenii* from tamarind kernel powder: galactoxyloglucan predominant hemicellulose. *J. Biotechnol.* **2010**, *148*, 233−239.

(8) Sandford, P. A. U.S. Patent 4,429,121, 1984.

(9) Babu, G. V.; Gowrisankar, V.; Himasankar, K.; Murthy, K. V. Studies on the applicability of tamarind kernel powder as a carrier in the dissolution enhancement of poorly water soluble drug, celecoxib. *Boll. Chim. Farm.* **2003**, *142*, 76−82.

(10) Pal, S.; Sen, G.; Mishra, S.; Dey, R. K.; Jha, U. Carboxymethyl tamarind: synthesis, characterization and its application as novel drug-delivery agent. *J. Appl. Polym. Sci.* **2008**, *110*, 392−400.

(11) Kaur, G.; Jain, S.; Tiwary, A. K. Chitosan-carboxymethyl tamarind kernel powder interpolymer complexation: investigations for colon drug delivery. *Sci. Pharm.* **2010**, *78*, 57−78.

(12) Sarkar, P. B.; Mazumdar, A. K. Composition of tamarind seed kernel powder. *J. Text. Inst.* **1952**, T453−T454.

(13) Jana, S.; Lakshman, D.; Sen, K. K.; Basu, S. K. Development and evaluation of epichlorohydrin cross-linked mucoadhesive patches of tamarind seed polysaccharide for buccal application. *Int. J. Pharm. Sci. Drug Res.* **2010**, *2*, 193−198.

(14) Kumar, C. S.; Bhattacharya, S. Tamarind seed: properties, processing and utilization. *Crit Rev. Food Sci. Nutr.* **2008**, *48*, 1−20.

(15) Gupta, V.; Singh, A. V.; Sindal, R. S.; Gupta, D. K.; Shashikala. Synthesis and application of new 2-amino ethyl ether of tamarind kernel powder as ion-exchanger. *Asian J. Chem.* **2004**, *16*, 1540−1544.

(16) Gupta, V.; Agarwal, J.; Purohit, M. V. Adsorption studies of Cu(II) from aqueous medium by tamarind kernel powder. *Res. J. Chem. Environ.* **2007**, *11*, 40−43.

(17) Gupta, V.; Sharma, M.; Jaya; Parag. Synthesis and application of secondary amine derivative of tamarind. *J. Ultra Chem.* **2007**, *3*, 201−204.

(18) Gupta, V.; Sharma, M. Adsorption analysis of Cr(VI) by natural polymer tamarind kernel powder (TKP) in aqueous medium. *Res. J. Chem. Environ.* **2010**, *14*, 41−45.

(19) Singh, A. V.; Sharma, N. K. Synthesis and characterization of an ion exchanger based on tamarind kernel powder and its application for removal of some metal ions from industrial effluents. *Toxicol. Environ. Chem.* **2011**, *93*, 1897−1907.

(20) Shanthi, S.; Mahalakshmi, T. Studies on the removal of Malachite Green and Methylene Blue dyes from aqueous solutions of their binary mixture by adsorbtion over commercial activated carbon and tamarind kernel powder. *Int. J. Res. Pharm. Chem.* **2012**, *2*, 289−298.

(21) Viswanathan, R.; Jagadeesh Babu, P. E. Studies on the production of pectinase from tamarind kernel powder by submerged fermentation using *Aspergillus* species, and optimization of medium using design expert. *Chem. Biochem. Eng. Q.* **2008**, *22*, 481−489.

(22) Jagadeesh Babu, P. E.; Viswanathan, R. Studies on the effect of pH, temperature and metal ions on the production of pectinase from tamarind kernel powder by submerged fermentation using *Aspergillus foetidus* (NCIM 505). *Asia−Pac. J. Chem. Eng.* **2010**, *5*, 396−400.

(23) Chatterjee, R.; Majumder, K.; Sengupta, S. Tamarind kernel powder co-induces xylanase and cellulase production during submerged fermentation of *Termitomyces clypeatus*. *Biotechnol. Bioproc. Engg.* **2010**, *15*, 854−861.

(24) Bao, W.; Renganathan, V. Cellobiose oxidase of *Phanerochaete chrysosporium* enhances crystalline cellulose degradation by cellulases. *FEBS Lett.* **1992**, *302*, 77−80.

(25) Duarte, J. C.; Costa-Ferreira, M.; Sena-Martins, G. Cellobiose dehydrogenase. Possible roles and importance for pulp and paper biotechnology. *Bioresour. Technol.* **1999**, *68*, 43−48.

(26) Henriksson, G.; Johansson, G.; Pettersson, G. A critical review of cellobiose dehydrogenases. *J. Biotechnol.* **2000**, *78*, 93−113.

(27) Baminger, U.; Ludwig, R.; Galhaup, C.; Leitner, C.; Kulbe, K. D.; Haltrich, D. Continuous enzymatic regeneration of redox mediators used in biotransformation reactions employing flavoproteins. *J. Mol. Catal. B: Enzym.* **2001**, *11*, 541−550.

(28) Ludwig, R.; Ozga, M.; Zamocky, M.; Peterbauer, C.; Kulbe, K. D.; Haltrich, D. Continuous enzymatic regeneration of electron acceptors used by flavoenzymes: cellobiose dehydrogenase-catalyzed

production of lactobionic acid as an example. *Biocatal. Biotransf.* **2004**, *22*, 97−104.
(29) Fischer, E.; Meyer, J. Oxydation des Milchzuckers. *Ber. Dt. Chem. Ges.* **1889**, *23*, 361−364.
(30) Druliolle, H.; Kokoh, K. B.; Beden, B. Selective oxidation of lactose to lactobionic acid on lead-adatoms modified platinum electrodes in Na_2CO_3 + $NaHCO_3$ buffered medium. *J. Electroanal. Chem.* **1995**, *385*, 77−83.
(31) Magariello, E. R. Production of lactobionic acid and its delta-lactone. U.S. Patent 2746916, 1956.
(32) Sen Gupta, M. L.; Bhattacharya, N.; Basu, U. P. Preparation of calcium lactobionate by electrolytic oxidation of lactose: part I − oxidation in electrolytic cell using stationary electrodes. *Indian J. Technol.* **1967**, *5*, 152−154.
(33) Meiberg, J. B. M.; Bruinenberg, P. M.; Sloots, B. A process for the fermentative oxidation of reducing disaccharides. EP 0384534, 1990.
(34) Satory, M.; Furlinger, M.; Haltrich, D.; Kulbe, K. D.; Pittner, F.; Nidetzky, B. Continuous enzymatic production of lactobionic acid using glucose-fructose oxidoreductase in an ultrafiltration membrane reactor. *Biotechnol. Lett.* **1997**, *19*, 1205−1208.
(35) Southard, J. H.; Belzer, F. O. Organ preservation. *Annu. Rev. Med.* **1995**, *46*, 235−247.
(36) Shi, L.; Wang, X.; Pan, J. Stability of erythromycin lactobionate in five intravenous infusions. *Zhongguo Yaoxue Zazhi* **1989**, *24*, 217−218.
(37) Gerling, K. G.; Wilke, D. Washing or detergent composition containing lactobionic acid or lactobionic acid salts. U.S. Patent 5069808, 1991.
(38) Gerling, K. G. Large scale production of lactobionic acid − use and new applications. *Int. Dairy Fed.* **1998**, *9804*, 251−261.
(39) Toshiaki, S.; Shuichi, Y.; Seiichiro, A.; Sakanori, S. Mineral absorption promoters containing lactobionic acid. JPO 07277991, 1995.
(40) Toshiaki, S.; Shuichi, Y.; Tomoko, K.; Sakanori, S. Bifidus factors containing lactobionic acid. JPO 07277990, 1995.
(41) Mukherjee, M.; Khowala, S.; Ghosh, A. K.; Sengupta, S. Regulation of endo-1,4-β-glucanase secretion from *Termitomyces clypeatus* by carbon catabolic product(s). *Folia Microbiol.* **1995**, *40*, 475−480.
(42) Saha, T.; Ghosh, D.; Mukherjee, S.; Bose, S.; Mukherjee, M. Cellobiose dehydrogenase production by the mycelial culture of the mushroom *Termitomyces clypeatus*. *Process Biochem.* **2008**, *43*, 634−641.
(43) Karapetyan, K. N.; Fedorova, T. V.; Vasil'chenko, L. G.; Ludwig, R.; Haltrich, D.; Rabinovich, M. L. Properties of neutral cellobiose dehydrogenase from the ascomycete *Chaetomium* sp. INBI 2-26 (−) and comparison with basidiomycetous cellobiose dehydrogenase. *J. Biotechnol.* **2006**, *121*, 34−48.
(44) Desgranges, C.; Vergoignan, C.; Georges, M.; Durand, A. Biomass estimation in solid state fermentation. Part I. Manual biochemical methods. *Appl. Microbiol. Biotechnol.* **1991**, *35*, 200−205.
(45) Nilsson, K.; Bjurman, J. Chitin as an indicator of the biomass of two wood decay fungi in relation to temperature, incubation time, and media composition. *Can. J. Microbiol.* **1998**, *44*, 575−581.
(46) Segal, L.; Creely, J. J.; Martin, A. E., Jr.; Conrad, C. M. An empirical method for estimating the degree of crystallinity of native cellulose using the X-ray diffractometer. *Textile Res. J.* **1959**, *29*, 786−794.
(47) Sasmal, S.; Goud, V. V.; Mohanty, K. Optimisation of the acid catalysed pretreatment of areca nut husk fibre using the Taguchi design method. *Biosyst. Eng.* **2011**, *110*, 465−472.
(48) Pandey, K. K.; Pitman, A. J. FTIR studies of the changes in wood chemistry following decay by brown-rot and white-rot fungi. *Int. Biodeter. Biodegrad.* **2003**, *52*, 151−160.
(49) Kelley, S. S.; Rowell, R. M.; Davis, M.; Jurich, C. K.; Ibach, R. Rapid analysis of the chemical composition of agricultural fibers using near infrared spectroscopy and pyrolysis molecular beam mass spectrometry. *Biomass Bioenergy* **2004**, *27*, 77−88.
(50) Ahmed, I. N.; Santoso, S. P.; Tran-Nguyen, P. L.; Huynh, L. H.; Ismadji, S.; Ju, Y. H. Impact of pretreatments on morphology and enzymatic saccharification of shedding bark of *Melaleuca leucadendron*. *Bioresour. Technol.* **2013**, *139*, 410−414.
(51) Meder, R.; Gallagher, S.; Mackie, K. L.; Böhler, H.; Meglen, R. R. Rapid determination of the chemical composition and density of *Pinus radiata* by PLS modeling of transmission and diffuse reflectance FTIR spectra. *Holzforschung* **1999**, *53*, 261−266.
(52) Rana, R.; Langenfeld-Heyser, R.; Finkeldey, R.; Polle, A. FTIR spectroscopy, chemical and histochemical characterisation of wood and lignin of five tropical timber wood species of the family of Dipterocarpaceae. *Wood Sci. Technol.* **2010**, *44*, 225−242.
(53) Guimarães, J. L.; Frollini, E.; da Silva, C. G.; Wypych, F.; Satyanarayana, K. G. Characterization of banana, sugarcane bagasse and sponge gourd fibers of Brazil. *Ind. Crop. Prod.* **2009**, *30*, 407−415.
(54) Sasmal, S.; Goud, V. V.; Mohanty, K. Characterization of biomasses available in the region of north-east India for production of biofuels. *Biomass Bioenergy* **2012**, *45*, 212−220.
(55) Kuhad, R. C.; Gupta, R.; Khasa, Y. P.; Singh, A. Bioethanol production from *Lantana camara* (red sage): pretreatment, saccharification and fermentation. *Bioresour. Technol.* **2010**, *101*, 8348−8354.
(56) Marathe, R. M.; Annapure, U. S.; Singhal, R. S.; Kulkarni, P. R. Gelling behaviour of polyose from tamarind kernel polysaccharide. *Food Hydrocolloids* **2002**, *16*, 423−426.
(57) Glicksman, M., Ed. Tamarind seed gum. In *Food Hydrocolloids*; CRC Press: Boca Raton, FL, USA, 1996; pp 191−202.
(58) Speers, R. A.; Rogers, P.; Smith, B. Non-linear modeling of industrial brewing fermentation. *J. Inst. Brew.* **2003**, *109*, 229−235.
(59) Pandey, A.; Soccol, C. R.; Mitchell, D. New developments in solid state fermentation: I − bioprocesses and products. *Process Biochem.* **2000**, *35*, 1153−1169.
(60) García-Ochoa, F.; Casas, J. A. Unstructured kinetic model for sophoro lipid production by *Candida bombicola*. *Enzyme Microb. Technol.* **1999**, *25*, 613−621.
(61) Schmidhalter, D. R.; Canevascini, G. Characterization of the cellulolytic enzyme system from the brown-rot fungus *Coniophora puteana*. *Appl. Microbiol. Biotechnol.* **1992**, *37*, 431−436.
(62) Baminger, U.; Subramaniam, S. S.; Renganathan, V.; Haltrich, D. Purification and characterization of cellobiose dehydrogenase from the plant pathogen *Sclerotium* (*Athelia*) *rolfsii*. *Appl. Environ. Microbiol.* **2001**, *67*, 1766−1774.
(63) Raices, M.; Montesino, R.; Cremata, J.; Garcia, B.; Perdomo, W.; Szabo, I.; Henriksson, G.; Hallberg, B. M.; Pettersson, G.; Johansson, G. Cellobiose quinone oxidoreductase from the white rot fungus *Phanerochaete chrysosporium* is produced by intracellular proteolysis of cellobiose dehydrogenase. *Biochim. Biophys. Acta* **2002**, *1576*, 15−22.
(64) Ludwig, R.; Salamon, A.; Varga, J.; Zamocky, M.; Peterbauer, C. K.; Kulbe, K. D.; Haltrich, D. Characterisation of cellobiose dehydrogenases from the white-rot fungi *Trametes pubescens* and *Trametes villosa*. *Appl. Microbiol. Biotechnol.* **2004**, *64*, 213−222.
(65) Zamocky, M.; Schumann, C.; Sygmund, C.; O'Callaghan, J.; Dobson, A. D. W.; Ludwig, R.; Haltrich, D.; Peterbauer, C. K. Cloning, sequence analysis and heterologous expression in *Pichia pastoris* of a gene encoding a thermostable cellobiose dehydrogenase from *Myriococcum thermophilum*. *Protein Express. Purif.* **2008**, *59*, 258−265.

MATERIALS AND METHODS

Materials. α-Cellulose (DP 900), DMSO, IPA, and DBU were purchased from Sigma-Aldrich Co. (Guangzhou, China), and CTA was purchased from Acros Organics (Morris Town, NJ, USA). Other chemicals were supplied by Guangzhou Chemical Reagent Factory (Guangzhou, China). All chemicals were of analytical reagent grade and directly used as received without further purification.

Cellulose Acetylation. The acetylation of cellulose was carried out under mild conditions in DMSO by using IPA as acetylation reagent and DBU as catalyst. α-Cellulose (0.5 g) was suspended in DMSO (10 mL) in a 50 mL vial. The mixture was agitated for 15 min at room temperature for cellulose dispersing and swelling. Then, 5 mL of IPA and 1.5 mL of DBU were added into the cellulose suspension, and the obtained yellow mixture was put in an oil bath at 70−130 °C for cellulose acetylation with magnetic agitation for 3−12 h. After the required time, the resulting dark brown mixture was poured into 750 mL of a mixture of distilled water and ethanol (2:1, v/v). The precipitates formed were filtered out and thoroughly washed with 750 mL of ethanol (three times). The residues were dried overnight under vacuum at 60 °C.

DS Determination by Titration. The DS of CA was determined by titration according to the published procedure[22,23] with some modifications. Dried and well-pulverized sample (0.5 ± 0.0001 g) was added into 75% ethanol (20 mL) in a flask and stirred at 60 °C for 30 min. Then, 20 mL of standard 0.5 M NaOH solution was added into the mixture and stirred at 60 °C for another 30 min. To guarantee the saponification of acetates, the mixture was stirred at room temperature for 72 h. The blank was run under the same conditions without the addition of CA. After the required time, the excess alkali was titrated with standard 0.5 M HCl with phenolphthalein as an indicator. Then, another 1 mL of standard HCl (0.5 M) was added and stirred overnight. The excess acid was back-titrated with standard 0.5 M NaOH solution to the phenolphthalein end-point. The DS was calculated according to the equations

$$m = [(A - B)N_b - (C - D)N_a] \times 43/W \quad (1)$$

$$DS = (162 \times m)/(43 - 42 \times m) \quad (2)$$

where m (g) is the content of acetyl group, DS is the average number of acetyl groups attached to an anhydroglucose unit (AGU) in cellulose, A (mL) is the total volume of standard NaOH solution added into the samples, B (mL) is the total volume of standard NaOH solution added into the blank, N_b (mol/mL) is the molarity of the standard NaOH solution, C (mL) is the total volume of standard HCl added into the samples, D (mL) is the total volume of standard HCl added into the blank, N_a (mol/mL) is the molarity of the standard HCl, W (g) is the weight of sample analyzed, 43 (g/mol) is the molar mass of an acetyl group, 162 (g/mol) is the molar mass of an AGU, and 42 (g/mol) is the net increase of the mass of an AGU for each acetyl substituted.

FT-IR. FT-IR spectra of unmodified cellulose and CA were recorded on a spectrophotometer (Tensor 27, Bruker, Germany) using a KBr disk containing 1% sample in the range of 4000−400 cm^{-1} at a resolution of 2 cm^{-1}. To remove the present moisture, the following modified procedure was adopted according to the earlier studies.[24−26] A small amount of sample, previously dried at 105 °C for >10 h, was ground for 2−10 min in a grinder (Mikro-Dismembrator S, Sartorius, Germany). KBr, previously dried at 105 °C for >10 h, was mixed with the ground sample with a ratio of sample to KBr of 1:100 (w/w). The mixture was ground for 2 min and further dried overnight in an oven at 105 °C. The dried mixtures were cooled in desiccators and measured on the FT-IR spectrophotometer as soon as possible after removal from the desiccators. The blank experiment without sample was done from KBr pellet as a reference.

^{1}H NMR and ^{13}C NMR. The ^{1}H NMR and ^{13}C NMR spectra were recorded on a Bruker AVIII HD 600 spectrometer (Germany). The ^{1}H NMR spectra were recorded at 298.0 K from the dried samples (10−15 mg) dissolved in 0.5 mL of DMSO-d_6 and a drop of trifluoroacetic acid-d. The detailed collecting and processing parameters for the ^{1}H NMR analysis were as follows: number of scans, 16; receiver gain, 69; acquisition time, 2.7263 s; relaxation delay, 1.0 s; pulse width, 11.0 s; spectrometer frequency, 600.17 MHz; and spectral width, 12019.2 Hz. For ^{13}C NMR analysis, dried samples (25−40 mg) were dissolved in 0.7 mL of DMSO-d_6, and the spectra were recorded at 353.1 K to obtain improved spectral resolution and an acceptable signal-to-noise ratio. The detailed collecting and processing parameters were as follows: number of scans, 10000; receiver gain, 187; acquisition time, 0.9088 s; relaxation delay, 2.0 s; pulse width, 12.0 s; spectrometer frequency, 150.91 MHz; and spectral width, 36057.7 Hz.

The DS values of CA were also calculated on the basis of the ^{1}H NMR analysis according to eq 3[27−29]

$$DS = 7 \times I_{(CH_3,H)}/[3 \times I_{(AGU,H)}] \quad (3)$$

where $I_{(CH_3, H)}$ is the integration of the resonances assigned to methyl protons of acetyl group ($\delta \sim 1.70$−2.20), 7 and 3 are the amounts of protons in the glucose ring and acetyl group, respectively, and $I_{(AGU, H)}$ is the integration of the resonances assigned to protons of the glucose ring ($\delta \sim 2.8$−5.5).

Intrinsic Viscosity. For each acetylated sample, a solution in DMSO at the concentration of 2 g/L was prepared. Experimental determination of intrinsic viscosity was carried out by counting the efflux time of the solvent and sample solution in an Ubbelohde viscometer (0.01203 mm capillary). Before each measurement, the viscometer was immersed in a thermostatic bath (PTI-TV 2000/AKV, Germany) at 25 ± 0.01 °C for 20 min to stabilize the temperature.

RESULTS AND DISCUSSION

Cellulose Acetylation. DS of CA determined by titration is shown in Table 1. As shown in Table 1, cellulose acetylation was successfully performed in DMSO with DBU as a catalyst and IPA as an acetylation reagent. The schematic DBU-mediated acetylation of cellulose is shown in Figure 1, and the proposed catalytic mechanism of DBU for cellulose acetylation is illustrated in Figure 2. In the cellulose acetylation, DBU acts as an acyl transfer agent. The nucleophilic nitrogen in the DBU molecule attacks the electron-deficient carbon of the acetyl group in IPA and gives rise to cleavage of the C−O bond and the formation of N-acetylated intermediate **2**. This intermediate can react with the hydroxyl group of cellulose **1**, resulting in the

Table 1. Conditions and Results of the Acetylation of Cellulose with IPA Catalyzed with DBU in DMSO

	acetylation conditions		DS[a]	
sample	time (h)	temp (°C)	DS_1	DS_2
1	3	70	1.81	1.87
2	3	90	2.10	2.12
3	3	110	2.68	2.71
4	3	130	2.90	2.88
5	6	70	2.14	2.18
6	6	90	2.39	2.40
7	6	110	2.98	2.98
8	6	130	2.96	2.95
9	9	70	2.17	2.20
10	9	90	2.74	2.71
11	9	110	2.96	2.95
12	9	130	2.99	2.95
13	12	70	2.20	2.20
14	12	90	2.93	2.88
15	12	110	2.99	2.99
16	12	130	2.99	2.95

[a]DS_1, calculated by titration; DS_2, calculated by ^{1}H NMR.

dx.doi.org/10.1021/jf5002233 | J. Agric. Food Chem. 2014, 62, 3446−3452

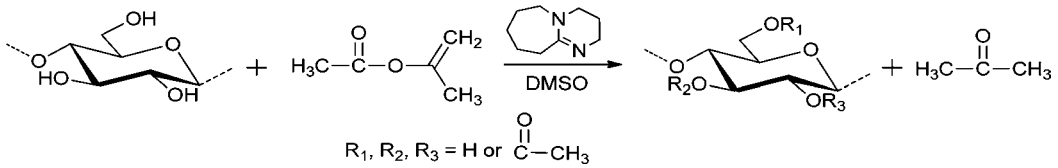

Figure 1. Acetylation reaction of cellulose with IPA using DBU as a catalyst in DMSO.

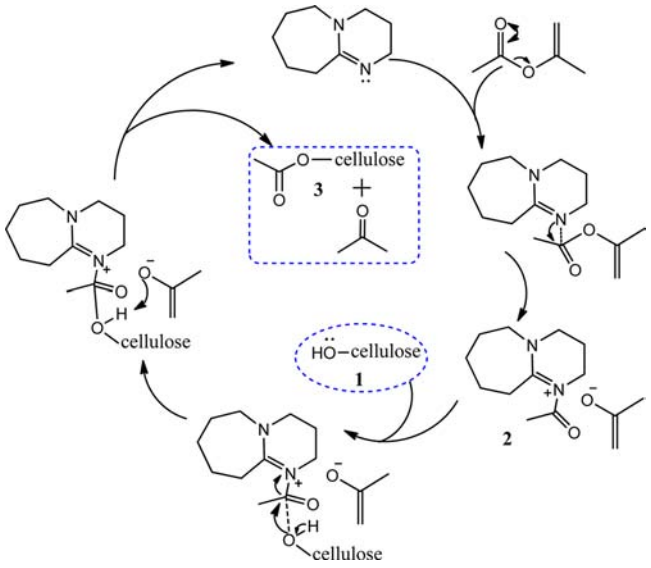

Figure 2. Proposed catalytic mechanism of DBU for cellulose acetylation.

formation of the desired CA **3** and byproduct acetone after deprotonation and isomerization. DBU enters into the next cycle of catalyzed reaction to perform the cellulose acetylation. As shown in Table 1, the DBU-catalyzed acetylation was very efficient. CA with DS > 2.0 was easily obtained under the selected conditions, which was probably due to the high catalytic activity of DBU. Per-O-acetylation was achieved within 3 h at 130 °C, within 6 h at 110 °C, and in 9 h at 90 °C, indicating increased acetylation with higher reaction temperature. In addition, reaction time had a positive effect on acetylation. At 70 °C, DS of CA reached 1.81 within 3 h, 2.14 within 6 h, 2.17 with 9 h, and 2.20 in 12 h; similarly, at 90 °C, DS was 2.10, 2.39, 2.74, and 2.93 at 3, 6, 9, and 12 h, respectively. Clearly, the influence of reaction time on DS at 70 °C was less than that at 90 °C, which was probably due to the low activity of DBU-catalyzed transesterification of cellulose in DMSO at low temperature. At higher temperature, cellulose per-O-acetylation was readily achieved to produce CTA with DS 2.90−2.99. Compared with the traditional methods to produce CTA, this procedure exhibits noticeable advantages. DMSO and unreacted IPA can be recycled and reused after the removal of water, ethanol, and byproduct acetone, which is easily achieved by simple evaporation under reduced pressure. Ethanol used in the procedure could also be recycled. More importantly, the modification conditions in this procedure are very mild, without any acidic reagents, avoiding the degradation of cellulose macromolecules and equipment corrosion. This very mild procedure is promising for the production of cellulose-based biocomposites in many fields.

The solubility of the prepared CA was also studied in common organic solvents including DMSO, chloroform, methylene chloride, acetone, THF, and DMF, and the results are shown in Table 2. As expected, CA prepared in DMSO followed by precipitation in ethanol is still soluble in DMSO.

Table 2. Solubility of CA Determined at a Concentration of 2 g/100 mL

sample	DS_1[a]	DMSO	$CHCl_3$	CH_2Cl_2	acetone	THF	DMF
1	1.81	++[b]	+[c]	+	−[d]	−	+
2	2.10	++	+	+	−	−	+
3	2.68	++	+	+	−	−	++
4	2.90	++	++	+	−	−	++
5	2.14	++	+	+	−	−	+
6	2.39	++	+	+	−	−	++
7	2.98	++	++	+	−	−	++
8	2.96	++	++	+	−	−	++
9	2.17	++	+	+	−	−	+
10	2.74	++	++	+	−	−	++
11	2.96	++	++	+	−	−	++
12	2.99	++	++	+	−	−	++
13	2.20	++	+	+	−	−	++
14	2.93	++	++	+	−	−	++
15	2.99	++	++	+	−	−	++
16	2.99	++	++	+	−	−	++

[a]DS_1, calculated by titration. [b]++, soluble. [c]+, swelling. [d]−, insoluble.

Meanwhile, the solubility of CA samples in chloroform, methylene chloride, and DMF is similar to the results reported in previous studies.[12,30] CA with DS ranging from 2.0 to 2.7 was reported to be soluble in acetone.[13] However, in the present study, CA with DS ranging from 1.81 to 2.99 was insoluble in acetone, which was probably due to the high DP of cellulose in this study. The similarly different solubility of CA with increased molecular weight was also reported, and the results showed that the dissolution of CA in acetone was achieved with a molecular weight of $<10^5$, whereas it failed when this value was exceeded.[31] THF could dissolve CA with DS 1.5−2.77.[12] However, in the present study CA samples were insoluble in THF, similar to acetone, due to the relatively high DP of the original cellulose.

FT-IR. Figure 3 illustrates the FT-IR spectra of unmodified α-cellulose, the prepared CA samples 1, 6, and 12 in Table 1, and the commercial CTA. In comparison with that in α-cellulose, the intensity of the band at 3440 cm^{-1} for O−H stretching significantly decreased in the prepared CA samples and the commercial CTA, which was obviously due to acetylation of hydroxyl groups in cellulose. Moreover, the bands at 1750 cm^{-1} for C═O stretching, 1380 cm^{-1} for C—H bending, and 1235 cm^{-1} for the symmetric stretching of C—O in ester noticeably increased after acetylation, indicating the attachment of an acetyl group onto cellulose macromolecules. The intensities of these three important bands increased from sample 1 to sample 6 and to sample 12, corresponding to the increased DS in Table 1. Compared with the commercial CTA, sample 12 exhibited a similar FT-IR spectrum with the same

dx.doi.org/10.1021/jf5002233 | J. Agric. Food Chem. 2014, 62, 3446−3452

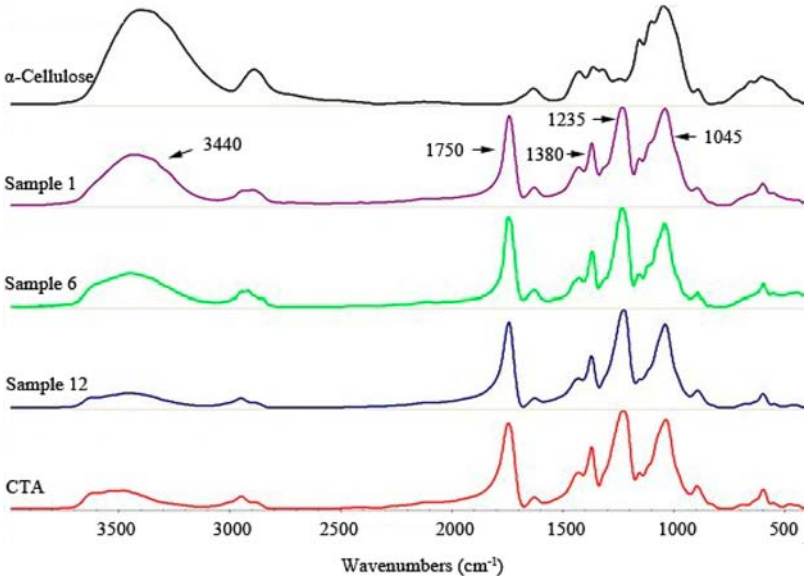

Figure 3. FT-IR spectra of α-cellulose, the prepared CA samples 1 (DS 1.81), 6 (DS 2.39), and 12 (DS 2.99), and the commercial CTA.

characteristic bands and similar intensities, suggesting the achievement of per-O-acetylation of sample 12.

FT-IR analysis also provides a method to comparatively evaluate the DS of CA on the basis of the ratio of the height of the peak at 3440 cm^{-1} for hydroxyl stretching to the integrated area of the absorbance at 1750 cm^{-1} assigned to carbonyl stretching.[32] As shown in Table 3, the ratio significantly decreased from acetylated cellulose sample 1 to sample 6 and to sample 12, which was consistent with the increased DS in Table 1. In addition, sample 12 had a similar ratio to commercial CTA, indicating the successful preparation of the per-O-acetylated cellulose under the selected conditions.

Table 3. Ratio of OH (Peak Height) over C═O (Peak Area) for Samples Collected under Given Conditions Calculated from the FT-IR Spectra

sample	DS_1[a]	$A_{C=O}$[b]	H_{OH}[c]	$H_{OH}/A_{C=O} \times 10^3$
1	1.81	36.23	0.29	8.00
6	2.39	54.60	0.29	5.31
12	2.99	51.95	0.10	1.92
CTA[d]	>2.97	48.28	0.10	2.07

[a]DS_1, calculated by titration. [b]Area of the band at 1735 cm^{-1} for C═O stretching. [c]Height of the band at 3440 cm^{-1} for OH stretching. [d]Commercial CTA with OH group <1%.

^{1}H NMR and ^{13}C NMR. ^{1}H NMR is a common method to determine the DS of modified cellulose. In the present study, DS of CA samples was also determined by ^{1}H NMR, and the results are listed in Table 1. The DS values from ^{1}H NMR without any pretreatment (perdeuteroacetylation or perpropionylation) are reliable and time-saving compared with those determined by titration. However, the absorbed water in DMSO exhibits the signals in the range of the protons from AGU units, resulting in the interference of DS determination by ^{1}H NMR, even far different from those by titration. In this paper, a drop of trifluoroacetic acid-*d* was added to remove the interference from water.[27,28] According to Table 1, the DS values from ^{1}H NMR were very close to those determined by titration, confirming the achievement of CA with high DS under the transesterification procedure.

Figure 4 illustrates the ^{13}C NMR spectra of partially acetylated (sample 5) and per-O-acetylated cellulose (sample 11). The carbon signals at 103.2, 99.4, 80.3, 75.8, 70.3−73.4, and 62.3 ppm are attributed to C-1, C-1_s (hydroxyl group of C-2 is substituted), C-4, C-4_s (hydroxyl group of C-3 is substituted), the combined C-2, C-3, and C-5, and C-6_s (hydroxyl group of C-6 is substituted) of AGU, respectively. Comparatively, the carbon signals for C-1 and C-4 in partially acetylated cellulose sample 5 disappeared in per-O-acetylated cellulose sample 11, indicating the complete substitution of hydroxyl groups at C-2, C-3, and C-6 positions. In addition, the strong signals at about 20 and 170 ppm are assigned to the carbons from methyl (C-7) and carbonyl (C-8) in the acetyl group attached onto cellulose, indicating the occurrence of DBU-catalyzed transesterification in DMSO. Detailed information on signals at about 170 ppm provided more support to acetylation, as shown in the upper left corner inset in Figure 4. Theoretically, each kind of AGU unit with hydroxyl groups substituted at different positions is present in the partially acetylated cellulose, and the marginally different signals assigned to the attached carbonyl carbons give the complicated spectrum of partially acetylated cellulose.[33−35] As shown in the upper left corner inset in Figure 4, sample 5 exhibited a more complicated spectrum than sample 11, which provided clearly resolved peaks of carbonyl carbons due to high DS. Clearly, the well-resolved carbonyl carbon signals confirmed the per-O-acetylation of sample 11. On the basis of the NMR analyses, the acetylation reaction occurs under the selected conditions and per-O-acetylation is confirmed.

Intrinsic Viscosity. Intrinsic viscosity of polymers measured in solution provides insight into molecular structure. According to the single-point method,[36] the intrinsic viscosity is calculated using the relationships

$$[\eta] = \sqrt{2(\eta_{sp} - \ln(\eta_r))}/c \quad (4)$$

$$\eta_{sp} = \eta_r - 1 \quad (5)$$

$$\eta_r = t/t_0 \quad (6)$$

dx.doi.org/10.1021/jf5002233 | J. Agric. Food Chem. 2014, 62, 3446−3452

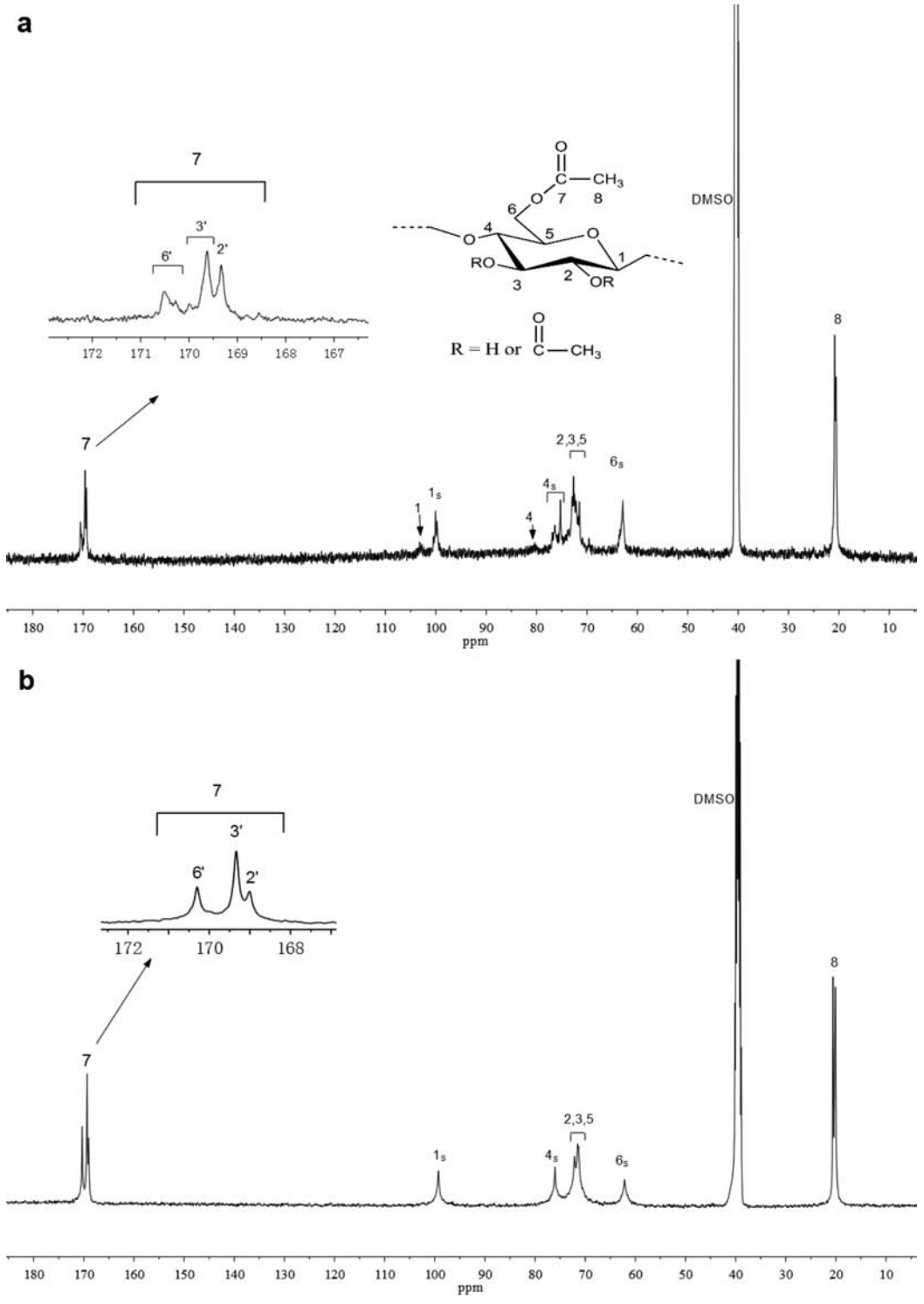

Figure 4. ^{13}C NMR spectra of sample 5 (a, DS 2.14) and sample 11 (b, DS 2.96).

where $[\eta]$ is the intrinsic viscosity, η_r is the relative viscosity, η_{sp} is the specific viscosity, c is the concentration of the solution, and t and t_0 are the solution and solvent efflux times, respectively.

On the basis of these equations, the intrinsic viscosity of a polymer in solution at a certain concentration could be determined from the efflux time of the solution and the solvent. According to the Mark−Houwink−Sakurada equation, the relationship between the intrinsic viscosity of a polymer solution and the molecular weight of the polymer is provided as

$$[\eta] = K(\overline{M}_v)^a \quad (7)$$

where K and a are constants relative to the type of polymer and solvent at a given temperature.

It is suggested from eq 7 that the changes of the molecular weight of polymers can be inferred from the varied intrinsic viscosity of polymer solution. The intrinsic viscosity of the dilute solution of cellulose and cellulose derivatives depends primarily upon the molecular weight of the cellulose materials.[37] Therefore, although the constants K and a are

dx.doi.org/10.1021/jf5002233 | J. Agric. Food Chem. 2014, 62, 3446−3452

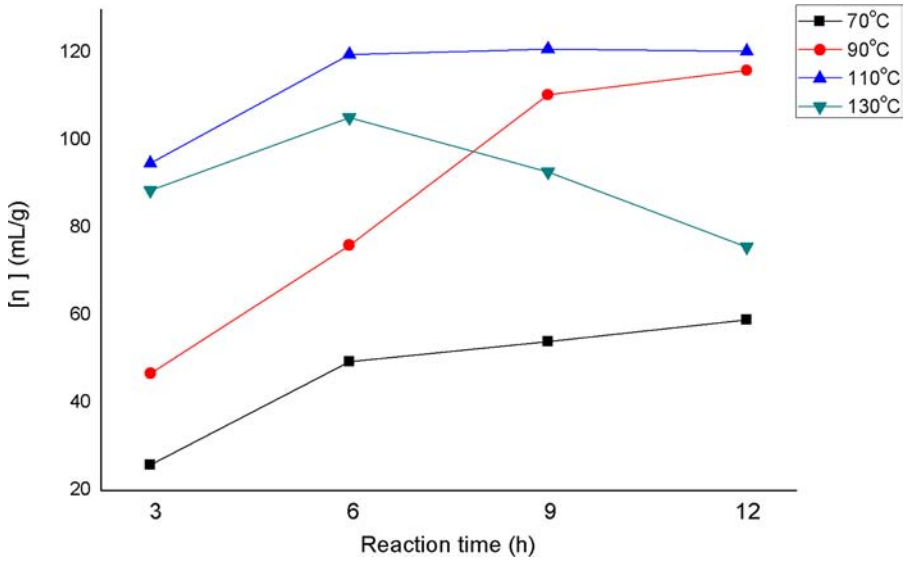

Figure 5. Intrinsic viscosity of CA solution in DMSO.

not proposed for CA in DMSO, the changes of the molecular weight of acetylated cellulose are still implied from the varied intrinsic viscosity of the dilute CA solution in DMSO. As shown in Figure 5, an increase of the intrinsic viscosity was clearly observed with the increased reaction time from 3 to 12 h at 70−90 °C and from 3 to 6 h at 110−130 °C, corresponding to the increased DS in Table 1. Similarly, the intrinsic viscosity of CA solution in DMSO was almost stable at 110 °C from 6 to 12 h, in agreement with the stable and highest DS of per-O-acetylated cellulose, confirming the degradation of cellulose does not occur during the mild transesterification of cellulose in DMSO below 110 °C with IPA as acetylating reagent and DBU as catalyst. However, at higher temperature (130 °C) and long reaction time (6−12 h), the intrinsic viscosity unexpectedly decreased. Considering the almost stable DS in Table 1, this decrease was attributed to the degradation of cellulose macromolecule at relatively mild condition (130 °C for 6−12 h). On the basis of these findings, it was suggested that the degradation of cellulose during acetylation under the selected conditions did not occur at low temperature (70−110 °C) and did occur at high temperature (130 °C) over a long reaction time (6−12 h).

In conclusion, the per-O-acetylation of cellulose was achieved in DMSO with IPA as acetylating reagent and DBU as catalyst. Titration, FT-IR, ^{1}H NMR, and ^{13}C NMR analyses provided evidence of cellulose per-O-acetylation. The degradation of cellulose did not occur at low temperature (70−110 °C) due to the mild conditions of the transesterification reaction. However, the degradation did occur at higher temperature (130 °C) over a long time (6−12 h).

AUTHOR INFORMATION

Corresponding Author

*(C.-F.L.) Phone: 86-20-87111735. Fax: 86-20-87111861. E-mail: chfliu@scut.edu.cn.

Funding

This work was financially supported by the National Natural Science Foundation of China (31170550), the Program for New Century Excellent Talents in University (NCET-11-0154), and the Fundamental Research Funds for the Central Universities.

Notes

The authors declare no competing financial interest.

REFERENCES

(1) Cao, Y.; Wu, J.; Zhang, J.; Li, H. Q.; Zhang, Y.; He, J. S. Room temperature ionic liquids (RTILs): a new and versatile platform for cellulose processing and derivatization. *Chem. Eng. J.* **2009**, *147*, 13−21.

(2) Miyamoto, T.; Sato, Y.; Shibata, T.; Tanahashi, M.; Inagaki, H. ^{13}C-NMR spectral studies on the distribution of substituents in water-soluble cellulose acetate. *J. Polym. Sci., Polym. Chem.* **1985**, *23*, 1373−1381.

(3) Duus, J. O.; Gotfredsen, C. H.; Bock, K. Carbohydrate structural determination by NMR spectroscopy: modern methods and limitations. *Chem. Rev.* **2000**, *100*, 4589−4614.

(4) Potluri, V. K.; Xu, J.; Enick, R.; Beckman, E.; Hamilton, A. D. Peracetylated sugar derivatives show high solubility in liquid and supercritical carbon dioxide. *Org. Lett.* **2002**, *4*, 2333−2335.

(5) Puls, J.; Wilson, S.; Hölter, D. Degradation of cellulose acetate-based materials: a review. *J. Polym. Environ.* **2011**, *19*, 152−165.

(6) Sata, H.; Murayama, M.; Shimamoto, S. Properties and applications of cellulose triacetate film. *Macromol. Symp.* **2004**, *208*, 323−333.

(7) Yip, N. Y.; Tiraferri, A.; Phillip, W. A.; Schiffman, J. D.; Elimelech, M. High performance thin-film composite forward osmosis membrane. *Environ. Sci. Technol.* **2010**, *44*, 3812−3818.

(8) Wei, J.; Qiu, C.; Tang, C. Y.; Wang, R.; Fane, A. G. Synthesis and characterization of flat-sheet thin film composite forward osmosis membranes. *J. Membr. Sci.* **2011**, *372*, 292−302.

(9) Heinze, T.; Liebert, T. Chemical characteristics of cellulose acetate. *Macromol. Symp.* **2004**, *208*, 167−237.

(10) Tosh, B.; Saikia, C. N.; Dass, N. N. Homogeneous esterification of cellulose in the lithium chloride−*N*,*N*-dimethylacetamide solvent system: effect of temperature and catalyst. *Carbohydr. Res.* **2000**, *327*, 345−352.

(11) Morgado, D.; Rodrigues, B.; Almeida, E.; Seoud, O.; Frollini, E. Bio-based films from linter cellulose and its acetates: formation and properties. *Materials* **2013**, *6*, 2410−2435.

(12) Ass, B. A. P.; Frollini, E.; Heinze, T. Studies on the homogeneous acetylation of cellulose in the novel solvent dimethyl sulfoxide/tetrabutylammonium fluoride trihydrate. *Macromol. Biosci.* **2004**, *4*, 1008−1013.

(13) Wu, J.; Zhang, J.; Zhang, H.; He, J.; Ren, Q.; Guo, M. Homogeneous acetylation of cellulose in a new ionic liquid. *Biomacromolecules* **2004**, *5*, 266−268.

(14) Abbott, A. P.; Bell, T. J.; Handa, S.; Stoddart, B. O-Acetylation of cellulose and monosaccharides using a zinc based ionic liquid. *Green Chem.* **2005**, *7*, 705−707.
(15) Zhu, S.; Wu, Y.; Chen, Q.; Yu, Z.; Wang, C.; Jin, S.; Ding, Y.; Wu, G. Dissolution of cellulose with ionic liquids and its application: a mini-review. *Green Chem.* **2006**, *8*, 325−327.
(16) Granstrom, M.; Kavakka, J.; King, A.; Majoinen, J.; Makela, V.; Helaja, J.; Hietala, S.; Virtanen, T.; Maunu, S. L.; Argyropoulos, D. S.; Kilpelainen, I. Tosylation and acylation of cellulose in 1-allyl-3-methylimidazolium chloride. *Cellulose* **2008**, *15*, 481−488.
(17) Schuchardt, U.; Sercheli, R.; Vargas, R. M. Transesterification of vegetable oils: a review. *J. Brazil. Chem. Soc.* **1998**, *9*, 199−210.
(18) Birman, V. B.; Li, X.; Han, Z. Nonaromatic amidine derivatives as acylation catalysts. *Org. Lett.* **2007**, *9*, 37−40.
(19) Scebach, D.; Thaler, A.; Blaser, D.; Ko, S. Y. Transesterifications with 1,8-diazabicyclo[5.4.0]undec-7-ene/lithium bromide (DBU/LiBr) − also applicable to cleavage of peptides from resins in merrifleld syntheses. *Helv. Chim. Acta* **1991**, *74*, 1102−1118.
(20) Ghosh, N. DBU (1,8-diazabicyclo[5.4.0]undec-7-ene) − a nucleophillic base. *Synlett* **2004**, 574−575.
(21) Ji, L.; Qian, C.; Chen, X. Z. Lewis basic ionic liquid as an efficient and facile catalyst for acetylation of alcohols, phenols, and amines under solvent-free conditions. *Monatsh. Chem.* **2013**, *144*, 369−374.
(22) Yuan, H.; Nishiyama, Y.; Kuga, S. Surface esterification of cellulose by vapor-phase treatment with trifluoroacetic anhydride. *Cellulose* **2005**, *12*, 543−549.
(23) Sanchez-Rivera, M. M.; Almanza-Benitez, S.; Bello-Perez, L. A.; Mendez-Montealvo, G.; Nunez-Santiago, M. C.; Rodriguez-Ambriz, S. L.; Gutierrez-Meraz, F. Acetylation of banana (*Musa paradisiaca* L.) and corn (*Zea mays* L.) starches using a microwave heating procedure and iodine as catalyst: II. Rheological and structural studies. *Carbohydr. Polym.* **2013**, *92*, 1256−1261.
(24) Van de Velde, K.; Kiekens, P. Structure analysis and degree of substitution of chitin, chitosan and dibutyrylchitin by FT-IR spectroscopy and solid state ^{13}C NMR. *Carbohydr. Polym.* **2004**, *58*, 409−416.
(25) Kim, D.-Y.; Nishiyama, Y.; Kuga, S. Surface acetylation of bacterial cellulose. *Cellulose* **2002**, *9*, 361−367.
(26) Sabnis, S.; Block, L. Improved infrared spectroscopic method for the analysis of degree of N-deacetylation of chitosan. *Polym. Bull.* **1997**, *39*, 67−71.
(27) Sun, X.; Lu, C.; Zhang, W.; Tian, D.; Zhang, X. Acetone-soluble cellulose acetate extracted from waste blended fabrics via ionic liquid catalyzed acetylation. *Carbohydr. Polym.* **2013**, *98*, 405−411.
(28) Ass, B. A. P.; Ciacco, G. T.; Frollini, E. Cellulose acetates from linters and sisal: correlation between synthesis conditions in DMAc/LiCl and product properties. *Bioresour. Technol.* **2006**, *97*, 1696−1702.
(29) Elomaa, M.; Asplund, T.; Soininen, P.; Laatikainen, R.; Peltonen, S.; Hyvärinen, S.; Urtti, A. Determination of the degree of substitution of acetylated starch by hydrolysis, ^{1}H NMR and TGA/IR. *Carbohydr. Polym.* **2004**, *57*, 261−267.
(30) Cao, Y.; Wu, J.; Meng, T.; Zhang, J.; He, J.; Li, H.; Zhang, Y. Acetone-soluble cellulose acetates prepared by one-step homogeneous acetylation of cornhusk cellulose in an ionic liquid 1-allyl-3-methylimidazolium chloride (AmimCl). *Carbohydr. Polym.* **2007**, *69*, 665−672.
(31) Cowie, J. M. G.; Maconnachie, A.; Ranson, R. J. Phase equilibria in cellulose acetate-acetone solutions. The effect of the degree of substitution and molecular weight on upper and lower critical solution temperatures. *Macromolecules* **1971**, *4*, 57−61.
(32) Samios, E.; Dart, R. K.; Dawkins, J. V. Preparation, characterization and biodegradation studies on cellulose acetates with varying degrees of substitution. *Polymer* **1997**, *38*, 3045−3054.
(33) Buchanan, C. M.; Edgar, K. J.; Hyatt, J. A.; Wilson, A. K. Preparation of cellulose [1-^{13}C]acetates and determination of monomer composition by NMR spectroscopy. *Macromolecules* **1991**, *24*, 3050−3059.
(34) Kowsaka, K.; Okajima, K.; Kamide, K. Determination of the distribution of the substituent group in cellulose acetate by full assignment of all carbonyl carbon peaks of ^{13}C{^{1}H} NMR spectra. *Polym. J.* **1988**, *20*, 827−836.
(35) Miyamoto, T.; Sato, Y.; Shibata, T.; Inagaki, H.; Tanahashi, M. ^{13}C nuclear magnetic resonance studies of cellulose acetate. *J. Polym. Sci., Polym. Chem.* **1984**, *22*, 2363−2370.
(36) Pamies, R.; Hernández Cifre, J.; del Carmen López Martínez, M.; García de la Torre, J. Determination of intrinsic viscosities of macromolecules and nanoparticles. Comparison of single-point and dilution procedures. *Colloid Polym. Sci.* **2008**, *286*, 1223−1231.
(37) González-Labrada, E.; Gray, D. Viscosity measurements of dilute aqueous suspensions of cellulose nanocrystals using a rolling ball viscometer. *Cellulose* **2012**, *19*, 1557−1565.

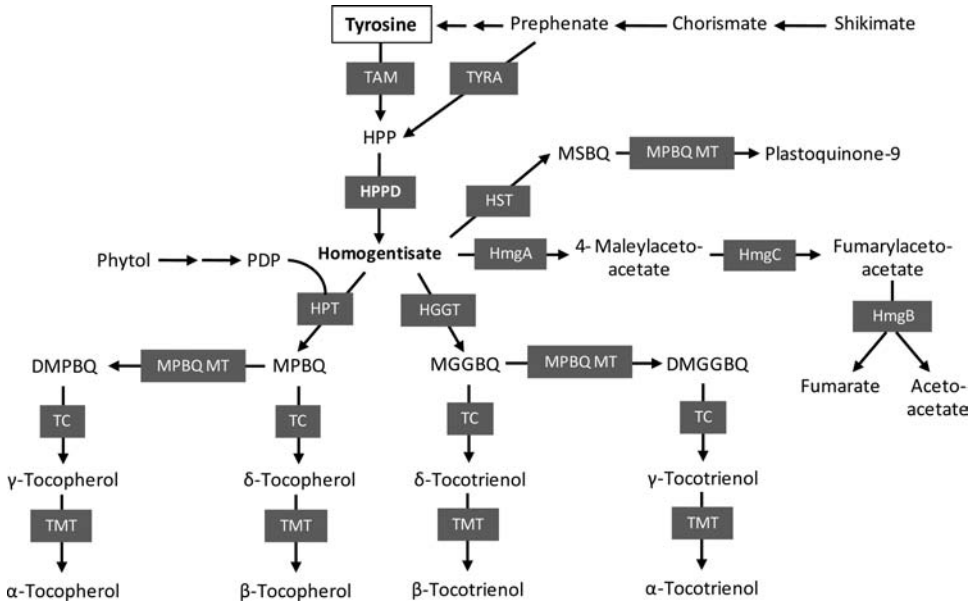

Figure 2. Tyrosine catabolic pathway. DMGGBQ, 2,3-dimethyl-5-geranylgeranyl-1,4-benzoquinone; DMPBQ, 2,3-dimethyl-5-phytyl-1,4-benzoquinone; HGGT, homogentisate geranylgeranyl transferase; HmgA, homogentisate dioxygenase; HmgB, fumarylacetoacetate hydrolase; HmgC, maleylacetoacetate isomerase; HPP, 4-hydroxyphenylpyruvate; HPPD, *p*-hydroxyphenylpyruvate dioxygenase; HPT, homogentisate phytyltransferase; HST, homogentisate solanyltransferase; MGGBQ, 2-methyl-6-geranylgeranyl-1,4-benzoquinone; MPBQ, 2-methyl-6-phytyl-1,4-benzoquinone; MPBQ MT, MPBQ methyltransferase; MSBQ, 2-methyl-6-solanyl-1,4-benzoquinone; PDP, phytyldiphosphate; TAM, L-tyrosine aminotransferase; TC, tocopherol cyclase; TMT, tocopherol methyltransferase; TYRA, bifunctional chorismate mutase-prephenate.

water deficit,[16,17] and crop management practices such as seeding rate, row spacing, and planting date.[8]

Syngenta has genetically modified soybean (*Glycine max* (L.) Merr.) to express an *hppd* gene derived from oat (*Avena sativa* L.). This gene, designated *avhppd-03,* encodes a *p*-hydroxyphenylpyruvate dioxygenase isozyme (AvHPPD-03) that has >99.7% sequence identity with the HPPD isozyme from *A. sativa*. In comparison with the endogenous soybean HPPD, the AvHPPD-03 isozyme from oat has reduced binding affinity for mesotrione, a herbicide that inhibits HPPD. The *avhppd-03* gene is linked to a constitutive promoter that expresses AvHPPD-03 at a higher level than the wildtype soybean *hppd*. Expression of *avhppd-03* in soybean plants confers a mesotrione tolerance phenotype. Syngenta has produced three mesotrione-tolerant soybean events (SYHT04R, SYHT06W, and SYHT0H2) and has evaluated the effect of expression of *avhppd-03* on tocochromanol levels in seeds from these events grown under field conditions in two consecutive years.

MATERIALS AND METHODS

Production of Seed Samples. During 2009 and 2010, three soybean events expressing *avhppd-03* and the corresponding non-transgenic, near-isogenic control variety 'Jack'[18] (maturity group 2.9) were grown according to local agronomic practices in the United States. The field trials were conducted at six locations (in Nebraska, Ohio, Michigan, Arkansas, Missouri, and Iowa) in 2009 and at eight locations [in Nebraska, Missouri, Iowa, Illinois (2), North Carolina, Pennsylvania, and Indiana] in 2010. One event (SYHT04R) was grown in both years, and the other two events (SYHT06W, SYHT0H2) were each grown in one year (2009 or 2010, respectively). To establish a range of natural variability, six nontransgenic precommercial Syngenta soybean reference varieties (maturity groups 2.3−3.5) were also grown at the same locations in the same years.

At each location, two entries of each transgenic soybean event, the corresponding control soybean, and the reference varieties were grown in a randomized complete block design with four replicate plots for each entry. In each trial, one entry of each transgenic soybean event was treated with mesotrione herbicide (0.1 kg active ingredient per hectare) at the V3−V5 growth stage.[19] The other transgenic entry was not treated with mesotrione. All entries within a trial were treated with maintenance chemicals as needed for optimum plant health.

Seed samples were obtained from 30 randomly selected plants from each plot after plants reached full maturity (R8 stage).[19] Representative subsamples were finely ground on dry ice and maintained at approximately −20 °C until they were analyzed.

Quantitation of Tocopherol and Tocotrienol Levels in Soybean Seed. The levels of tocopherols and tocotrienols in the seed were determined by Covance Laboratories, Inc. (Madison, WI, USA) using validated methods based on literature references. Representative aliquots from the homogeneous samples were analyzed in a random order. Following quantitation of the tocochromanols, all results were converted to equivalent units of dry weight based on the moisture content of the seed samples.

Tocopherols. To release vitamin E, the aliquots (approximately 6 g) were saponified to break down any fat. The saponified mixture was extracted with diethyl ether, evaporated to near dryness, and diluted to a volume of 2 mL in hexane. The levels of *α*-, *β*-, *γ*-, and *δ*-tocopherols were quantitated by high-performance liquid chromatography (HPLC) using fluorescence detection (excitation, 292 nm; emission, 325 nm). HPLC was performed with the following parameters: a silica column (ES Ind. Chromegabond Diol 3 μm 60 Å, 15 cm × 4.0 mm), guard column (Diol, 12.5 mm × 4.6 mm, 4 μm packing), flow rate of 1.0 mL/min, run time of 20 min, and injection volume of 15 μL, with mobile phase A [3% tetrahydrofuran (THF), 0.05% glacial acetic acid (HOAc) in iso-octane] and mobile phase B (30% THF, 0.05% HOAc in iso-octane).[20−22]

Tocotrienols. Aliquots (approximately 2 g) were treated with sodium bicarbonate and sodium ascorbate to buffer the solution. Pyrogallol (4 mL) was added as an antioxidant. The samples were extracted with 8 mL of 2,2,4-trimethylpentane (iso-octane), and dimethyl sulfoxide (4 mL) was added to increase extraction efficiency. Methanolic sulfuric acid solution (3.33 N) was added to further break down the sample matrix. Additional iso-octane (8 mL) was added to aid in phase separation. The samples were centrifuged, and the *α*-, *β*-, *γ*-, and *δ*-tocotrienols in the supernatant were quantitated by HPLC and fluorescence detection (excitation, 292 nm; emission, 325 nm). The HPLC was performed with

dx.doi.org/10.1021/jf4048995 | J. Agric. Food Chem. 2014, 62, 3453−3457

Table 1. Tocopherol Levels[a] in Three Field-Grown *avhppd-03*-Expressing Soybean Events

line	N	statistic	α-tocopherol	β-tocopherol	γ-tocopherol	δ-tocopherol
			2009 Trials			
SYHT04R	24	mean	–[b]	–	178	**128***[c]
		range	<LOQ–36.4[d]	<LOQ–9.17	26.1–270	45.1–172
SYHT04R+[e]	24	mean	–	–	**187***	**133***
		range	<LOQ–33.3	<LOQ–7.60	37.2–268	62.5–166
control for SYHT04R	24	mean	–	–	164	84.0
		range	<LOQ–26.3	<LOQ	41.5–233	43.5–113
SYHT06W	28	mean	–	–	**202***	**125***
		range	<LOQ–25.0	<LOQ	56.1–308	78.3–167
SYHT06W+	28	mean	–	–	**206***	**128***
		range	<LOQ–25.9	<LOQ	72.2–297	91.8–170
control for SYHT06W	28	mean	–	–	171	79.3
		range	<LOQ–29.4	<LOQ	25.7–249	30.5–106
ref varieties	143	mean	–	–	151	92.5
		range	<LOQ–32.4	<LOQ–8.81	13.7–242	22.3–149
			2010 Trials			
SYHT04R	32	mean	26.9	–	**229***	**105***
		range	10.6–79.4	<LOQ–6.86	185–276	56.6–141
SYHT04R+	32	mean	27.8	–	**233***	**102***
		range	11.0–72.8	<LOQ–6.58	188–278	59.7–143
SYHT0H2	31	mean	**22.8***	–	**226***	**78.9***
		range	9.96–62.8	<LOQ	183–268	51.8–107
SYHT0H2+	32	mean	24.1	–	**214***	**76.0***
		range	10.2–55.2	<LOQ	163–261	41.6–107
control for all events	32	mean	25.8	<LOQ	201	61.1
		range	9.34–60.5	<LOQ	154–244	31.2–84.5
ref varieties	192	mean	29.5	–	175	68.7
		range	11.5–77.1	<LOQ–7.79	127–236	32.0–112

[a]Tocopherol levels given as micrograms per gram seed dry weight. [b]When some values were <LOQ means could not be calculated (shown as –). [c]Bold values and asterisks indicate significant differences between the transgenic soybean and the control soybean ($p < 0.05$). [d]The limit of quantitation (LOQ) for all tocopherols was 5.3–7.3 μg/g DW, varying with the moisture content of the sample. [e]Crop treated with mesotrione herbicide indicated with +.

the following parameters: a silica column (ES Ind. Chromegabond Diol 3 μm 60 Å, 15 cm × 4.0 mm), flow rate of 1.0 mL/min, run time of 30 min, and injection volume of 60 μL, with mobile phase A (3% THF, 0.05% HOAc in iso-octane) and mobile phase B (30% THF, 0.05% HOAc in iso-octane).[21,23−25]

Statistical Comparisons. The data for the quantifiable tocopherols were subjected to analysis of variance (ANOVA) using the following mixed model:

$$Y_{ijk} = U + T_i + L_j + B(L)_{jk} + LT_{ij} + e_{ijk}$$

In this model, Y_{ijk} is the observed response for entry i at location j block k, U is the overall mean, T_i is the entry effect, L_j is the location effect, $B(L)_{jk}$ is the effect of block within location, LT_{ij} is the location-by-entry interaction effect, and e_{ijk} is the residual error. Entry was regarded as a fixed effect, whereas the effects of location, block within location, and location-by-entry interaction were regarded as random.

The statistical significance of the differences in levels of α-, γ-, and δ-tocopherols were assessed using t tests for comparisons between the control soybean and each of the transgenic soybean lines and between the control soybean and each of the transgenic soybean lines treated with mesotrione. Significance was based on an α level of 0.05. No statistical comparisons were performed for β-tocopherol or any tocotrienols because the levels were below the limit of quantitation in most or all samples.

RESULTS AND DISCUSSION

Levels of α-tocopherol, the isoform with the highest vitamin E activity in humans,[26] were variable across the three events, and most differences observed in the comparisons of the transgenic soybean and the control soybean were small and not statistically significant. The only statistically significant change in the level of α-tocopherol observed was a 12% decrease in the 2010-grown SYHT0H2 soybean that was not treated with mesotrione [22.8 μg per gram seed dry weight (μg/g DW)] when compared with the control soybean (25.8 μg/g seed DW). The levels of β-tocopherol, and all tocotrienols (data not shown), were either below, or only slightly above, the limit of quantitation.

Increased seed γ-tocopherol and δ-tocopherol levels were consistently observed in *avhppd*-03-expressing soybean events. In seed produced from field trials in both years, levels of these two vitamin E isoforms were statistically higher in all three *avhppd*-03-expressing soybean events compared with levels in the near-isogenic, nontransgenic control soybean (Table 1). Mean levels of γ-tocopherol increased by as much as 21% (1.2-fold) in the SYHT06W soybean treated with mesotrione herbicide (206 μg/g seed DW) when compared with the control soybean (171 μg/g seed DW). Mean levels of δ-tocopherol increased by as much as 72% (1.7-fold) in the SYHT04R soybean (105 μg/g seed DW) when compared with the control soybean (61.1 μg/g seed DW) (Table 2).

These findings were expected because they are consistent with reports that overexpression of HPPD in plants resulted in increased tocochromanol content.[6,27,28] The observed increases in the levels of the γ and δ isoforms, without corresponding increases in the α and β isoforms, are consistent with previous

Table 2. Increases in γ- and δ-Tocopherol Levels in Three *avhppd-03*-Expressing Soybean Events

	γ-tocopherol		δ-tocopherol	
line	Δ%[a]	Δ-fold[b]	Δ%	Δ-fold
2009 Trials				
SYHT04R	9	1.1	52	1.5
SYHT04R+[c]	14	1.1	58	1.6
SYHT06W	18	1.2	58	1.6
SYHT06W+	21	1.2	62	1.6
2010 Trials				
SYHT04R	14	1.1	72	1.7
SYHT04R+	16	1.2	67	1.7
SYHT0H2	12	1.1	30	1.3
SYHT0H2+	7	1.1	25	1.3

[a]Δ% = percent increase when compared to control, calculated as (transgenic − control)/control × 100). [b]Δ-fold difference based on comparison of means (transgenic mean/control mean). [c]Crop treated with mesotrione herbicide indicated with +.

hypotheses that tocopherol methyltransferase (TMT) is a rate-limiting enzyme in the tocopherol biosynthetic pathway.[29,30]

When comparisons between transgenic soybean and the corresponding nontransgenic comparators are considered, the inherent natural variability of tocochromanols in soybean is pertinent. Within a single crop season, levels of γ-tocopherol in the control soybean grown in this study varied by almost 10-fold. The tocopherol contents of the six soybean reference varieties were also quite variable, with levels of γ-tocopherol varying by almost 18-fold and levels of δ-tocopherol varying by nearly 7-fold within a single year. Because the six varieties represented a very limited range of maturity groups (from 2.3 to 3.5), it would be expected that the wider range of 13 soybean maturity groups grown globally across latitudes and under significantly variable cultivation practices, would exhibit a greater range in tocochromanol levels.

Although statistically significant increases in γ- and δ-tocopherol were observed in the three *avhppd-03*-expressing soybean events, these absolute differences (<2-fold, Table 2) in concentration were quite small when viewed in the context of the existing natural variability of soybean tocopherol levels. For α-tocopherol, the most biologically active tocopherol for humans, the International Life Sciences Institute crop composition database[31] reports a 32-fold range of variability in conventional soybean seed. Under high-temperature conditions at different developmental stages of two soybean cultivars, Chennupati et al. reported α-tocopherol concentrations increased by as much as 7-fold (752%), γ-tocopherol decreased by an average of 34%, and δ-tocopherol decreased by 74%.[15] In 89 Brazilian soybean cultivars grown across multiple locations, Carrao-Panizzi and Erhan reported a 16-fold difference in α-tocopherol levels, an 11-fold difference in β-tocopherol levels, a 4-fold difference in γ-tocopherol levels, and a 3-fold difference in δ-tocopherol levels among the cultivars, and within a single cultivar grown at 15 locations, variability of nearly 8-fold was observed.[17]

HPPD activity also appears to be one of the key factors influencing the production of tocopherols, as evidenced by reports of increased tocopherol levels in *Arabidopsis* (*Arabidopsis thaliana*),[6,27,28] tobacco (*Nicotiana tabacum*),[32,33] canola (*Brassica napus* L.),[6] and soybean (*Glycine max* L.)[6] engineered with additional *hppd* genes.

The high degree of natural variability for soybean tocopherol levels is well documented and corresponds with global food standards. Variability of up to 39-fold is observed in the Codex Alimentarius standard for soybean oil (Table 3).[34]

Table 3. Codex Alimentarius Standard Ranges for Tocopherol Levels in Soybean Oil (Codex Alimentarius Commission 2001)

tocopherol	standard range (mg/kg)	fold range
α-tocopherol	9−352	39-fold
β-tocopherol	undetectable (<1)−36	∼36-fold
γ-tocopherol	89−2307	26-fold
δ-tocopherol	154−932	6-fold

As noted by the Institute of Medicine Food and Nutrition Board, no adverse consequences in humans or laboratory animals have been documented from eating high dietary vitamin E obtained from food.[26] The only reports of adverse consequences in humans have been in studies in which vitamin E as α-tocopherol was given as supplements.[35] However, a greater public health problem for most Americans is the inadequate intake of vitamin E relative to recommendations.[36,37] Food sources of vitamin E are largely from vegetable oils, and soybean oil is particularly rich in γ-tocopherol.[38] However, the processing of soybeans to generate vegetable oil involves cooking and a distillation process that removes much of the vitamin E.[39] Commercially, the vitamin E is added back to protect the soybean oil or is used to make vitamin E supplements. It should be noted that there are beneficial effects of dietary non-α-tocopherols, specifically γ-tocopherol,[40] especially with regard to cancer.[41] Thus, the slight increases in some forms of tocopherol in these transgenic soybean events expressing an oat *hppd* gene may have a slight benefit but, given the processing of soybeans, are unlikely to have a material impact on human nutrition with regard to soybean oil and its vitamin E concentrations.

AUTHOR INFORMATION

Corresponding Author

*(C.K.) E-mail: catherine.kramer@syngenta.com. Phone: (919) 281-7284. Fax: (919) 281-2222.

Notes

[†]Analytical work conducted at Covance Laboratories, Inc., 3301 Kinsman Blvd., Madison, WI 53704, USA.

The authors declare no competing financial interest.

ACKNOWLEDGMENTS

We thank Covance Laboratories (Madison, WI, USA) for performing the analytical determination of tocochromanol content in the soybean samples and Keith Ward (Syngenta, Ltd., Bracknell, UK) for performing the statistical analyses.

ABBREVIATIONS USED

HGA, homogentisate; HOAc, glacial acetic acid; HPLC, high-perfomance liquid chromatography; ANOVA, analysis of variance; THF, tetrahydrofuran; TMT, tocopherol methyltransferase; HPPD, *p*-hydroxyphenylpyruvate dioxygenase

REFERENCES

(1) Arias-Barrau, E.; Olivera, E. R.; Luengo, J. M.; Fernández, C.; Galán, B.; García, J. L.; Díaz, E.; Miñambres, B. The homogentisate pathway: a central catabolic pathway involved in the degradation of L-phenylalanine, L-tyrosine, and 3-hydroxyphenylacetate in *Pseudomonas putida*. *J. Bacteriol.* **2004**, *186*, 5062−5077.

(2) DellaPenna, D.; Pogson, B. J. Vitamin synthesis in plants: tocopherols and carotenoids. *Annu. Rev. Plant Biol.* **2006**, *57*, 11−38.
(3) Moran, G. R. 4-Hydroxyphenylpyruvate dioxygenase. *Arch. Biochem. Biophys.* **2005**, *433*, 117−128.
(4) Zbierzak, A. M.; Kanwischer, M.; Wille, C.; Vidi, P. A.; Giavalisco, P.; Lohmann, A.; Briesen, I.; Porfirova, S.; Bréhélin, C.; Kessler, F.; Dörmann, P. Intersection of the tocopherol and plastoquinol metabolic pathways at the plastoglobule. *Biochem. J.* **2010**, *425*, 389−399.
(5) DellaPenna, D. A decade of progress in understanding vitamin E synthesis in plants. *J. Plant Physiol.* **2005**, *162*, 729−737.
(6) Karunanandaa, B.; Qi, Q.; Hao, M.; Baszis, S.; Jensen, P. K.; Wong, Y.-H. H.; Jiang, J.; Venkatramesh, M.; Gruys, K. J.; Moshiri, F.; Post-Beittenmiller, D.; Weiss, J. D.; Valentin, H. E. Metabolically engineered oilseed crops with enhanced seed tocopherol. *Metab. Eng.* **2005**, *7*, 384−400.
(7) Lushchak, V. I.; Semchuk, N. M. Tocopherol biosynthesis: chemistry, regulation and effects of environmental factors. *Acta Physiol. Plant* **2012**, *34*, 1607−1628.
(8) Seguin, P.; Tremblay, G.; Pageau, D.; Liu, W. Soybean tocopherol concentrations are affected by crop management. *J. Agric. Food Chem.* **2010**, *58*, 5495−5501.
(9) Rani, A.; Kumar, V.; Verma, S. K.; Shakya, A. K.; Chauhan, G. S. Tocopherol content and profile of soybean: genotypic variability and correlation studies. *J. Am. Oil Chem. Soc.* **2007**, *84*, 377−383.
(10) Ujiie, A.; Yamada, T.; Fujimoto, K.; Endo, Y.; Kitamura, K. Identification of soybean varieties with high α-tocopherol content. *Breed. Sci.* **2005**, *55*, 123−125.
(11) Almonor, G. O.; Fenner, G. P.; Wilson, R. F. Temperature effects on tocopherol composition in soybeans with genetically improved oil quality. *J. Am. Oil Chem. Soc.* **1998**, *75*, 591−596.
(12) Dolde, D.; Vlahakis, C.; Hazebroek, J. Tocopherols in breeding lines and effects of planting location, fatty acid composition, and temperature during development. *J. Am. Oil Chem. Soc.* **1999**, *76*, 349−355.
(13) Britz, S. J.; Kremer, D. F.; Kenworthy, W. J. Tocopherols in soybean seeds: genetic variation and environmental effects in field-grown crops. *J. Am. Oil Chem. Soc.* **2008**, *85*, 931−936.
(14) Carrerra, C.; Martinez, M. J.; Dardanelli, J.; Balzarini, M. Environmental variation and correlation of seed components in nontransgenic soybeans: protein, oil, unsaturated fatty acids, tocopherols, and isoflavones. *Crop Sci.* **2011**, *51*, 800−809.
(15) Chennupati, P.; Seguin, P.; Liu, W. Effects of high temperature stress at different development stages on soybean isoflavone and tocopherol concentrations. *J. Agric. Food Chem.* **2011**, *59*, 13081−13088.
(16) Britz, S. J.; Kremer, D. F. Warm temperatures or drought during seed maturation increase free α-tocopherol in seeds of soybean (*Glycine max* [L.] Merr.). *J. Agric. Food Chem.* **2002**, *50*, 6058−6063.
(17) Carrão-Panizzi, M. C.; Erhan, S. Z. Environmental and genetic variation of soybean tocopherol content under Brazilian growing conditions. *J. Am. Oil Chem. Soc.* **2007**, *84*, 921−928.
(18) Nickell, C. D.; Noel, G. R.; Thomas, D. J.; Waller, R. Registration of 'Jack' soybean. *Crop Sci.* **1990**, *30*, 1365−1365.
(19) Pederson, P. *Soybean Growth and Development*; Iowa State University, University Extension: Ames, IA, USA, 2009; 28 pp.
(20) Speek, A. J.; Schijver, J.; Schreurs, W. H. P. Vitamin E composition of some seed oils as determined by high-performance liquid chromatography with fluorometric detection. *J. Food Sci.* **1985**, *50*, 121−124.
(21) Cort, W. M.; Vicente, T. S.; Waysek, E. H.; Williams, B. D. Vitamin E content of feedstuffs determined by high-performance liquid chromatographic fluorescence. *J. Agric. Food Chem.* **1983**, *31*, 1330−1333.
(22) McMurray, C. H.; Blanchflower, W. J.; Rice, D. A. Influence of extraction techniques on determination of α-tocopherol in animal feedstuffs. *J. Assoc. Off. Anal. Chem.* **1980**, *63*, 1258−1261.
(23) Franke, A. A.; Murphy, S. P.; Lacey, R.; Custer, L. J. Tocopherol and tocotrienol levels of foods consumed in Hawaii. *J. Agric. Food Chem.* **2007**, *55*, 769−778.
(24) United States Pharmacopeia and National Formulary. USP 32-NF 27. Oil- and water-soluble vitamins with minerals tablets. United States Pharmacopeia Convention: Rockville, MD, USA, 2009; Vol. 1, p 1090.
(25) United States Pharmacopeia and National Formulary. USP 34-NF 29. Oil- and water-soluble vitamins with minerals tablets. United States Pharmacopeia Convention: Rockville, MD, USA, 2011; Vol. 1, p 1323.
(26) Institute of Medicine Food and Nutrition Board. In *DRI Dietary Reference Intakes for Vitamin C, Vitamin E, Selenium, and Carotenoids*; National Academy Press: Washington, DC, USA, 2000; 506 pp.
(27) Matringe, M.; Sailland, A.; Pelissier, B.; Rolland, A.; Zink, O. *p*-Hydroxyphenylpyruvate dioxygenase inhibitor-resistant plants. *Pest Manage. Sci.* **2005**, *61*, 269−276.
(28) Tsegaye, Y.; Shintani, D. K.; DellaPenna, D. Overexpression of the enzyme *p*-hydroxyphenylpyruvate dioxygenase in arabidopsis and its relation to tocopherol biosynthesis. *Plant Physiol. Biochem.* **2002**, *40*, 913−920.
(29) Shintani, D.; DellaPenna, D. Elevating the vitamin E content of plants through metabolic engineering. *Science* **1998**, *282*, 2098−2100.
(30) Collakova, E.; DellaPenna, D. Homogentisate phytyltransferase activity is limiting for tocopherol biosynthesis in arabidopsis. *Plant Physiol.* **2003**, *131*, 632−642.
(31) ILSI. International Life Sciences Institute Crop Composition Database, v. 4.2. https://www.cropcomposition.org; search parameters: crop type = "SOYBEAN," tissue type = "SEED", crop year = "All", country = "All", and regions = "All" (accessed Sept 12, 2013).
(32) Falk, J.; Andersen, G.; Kernebeck, B.; Krupinska, K. Constitutive overexpression of barley 4-hydroxyphenylpyruvate dioxygenase in tobacco results in elevation of the vitamin E content in seeds but not in leaves. *FEBS Lett.* **2003**, *540*, 35−40.
(33) Rippert, P.; Scimemi, C.; Dubald, M.; Matringe, M. Engineering plant shikimate pathway for production of tocotrienol and improving herbicide resistance. *Plant Physiol.* **2004**, *134*, 92−100.
(34) Codex Alimentarius Commission Codex Standard for Named Vegetable Oils, CODEX STAN 210-1999. In *The CODEX Alimentarius*, 2nd ed.; World Health Organization Joint FAO/WHO Food Standards Programme: Rome, Italy, 2011; Vol. 8, 16 pp; http://www.fao.org/DOCREP/004/Y2774E/Y2774E00.HTM (accessed Sept 16, 2013).
(35) Bjelakovic, G.; Nikolova, D.; Gluud, L. L.; Simonetti, R. G.; Gluud, C. Antioxidant supplements for prevention of mortality in healthy participants and patients with various diseases. *Cochrane Database Syst. Rev.* **2012**, *3*, CD007176.
(36) Maras, J. E.; Bermudez, O. I.; Qiao, N.; Bakun, P. J.; Boody-Alter, E. L.; Tucker, K. L. Intake of α-tocopherol is limited among US adults. *J. Am. Diet. Assoc.* **2004**, *104*, 567−575.
(37) Lebold, K. M.; Ang, A.; Traber, M. G.; Arab, L. Urinary α-carboxyethyl hydroxychroman can be used as a predictor of α-tocopherol adequacy, as demonstrated in the Energetics Study. *Am. J. Clin. Nutr.* **2012**, *96*, 801−809.
(38) Traber, M. G. Vitamin E. In *Present Knowledge in Nutrition*; Erdman, J., Macdonald, I., Zeisel, S., Eds.; ILSI Press: Washington, DC, USA, 2012: pp 214−229.
(39) Ito, V. M.; Batistella, C. B.; Maciel, M. R.; Maciel Filho, R. Optimization of tocopherol concentration process from soybean oil deodorized distillate using response surface methodology. *Appl. Biochem. Biotechnol.* **2007**, *136−140*, 885−896.
(40) Wiser, J.; Alexis, N. E.; Jiang, Q.; Wu, W.; Robinette, C.; Roubey, R.; Peden, D. B. In vivo γ-tocopherol supplementation decreases systemic oxidative stress and cytokine responses of human monocytes in normal and asthmatic subjects. *Free Radical Biol. Med.* **2008**, *45*, 40−49.
(41) Yang, C. S.; Suh, N. Cancer prevention by different forms of tocopherols. *Top. Curr. Chem.* **2013**, *329*, 21−33.

flavonoids including apigenin, catechin, daidzein, diosmin, epicatechin, eriodictyol, genistein, hesperetin, hesperidin, isorhamnetin, kamempferol, luteolin, morin, myricetin, naringenin, naringin, neohesperidin, quercetin, quercitrin, and rutin used for phenolic composition analysis were purchased from Sigma Co. (St. Louis, MO, USA). Proanthocyanidin A2 was prepared as reported previously.[11] LPS, glutamine, Griess reagent [1% sulfanilamide, 0.1% *N*-(1-naphthyl)-ethylenediamine dihydrochloride, and 2.5% phosphoric acid), ethylenediaminetetraacetic acid (EDTA), phenylmethanesulfonyl fluoride (PMSF), phosphate-buffered saline (PBS), sodium chloride (NaCl), sodium nitrite ($NaNO_2$), Triton X-100, and Tris were obtained from Sigma Co. (St. Louis, MO, USA). RPMI-1640 medium, fetal bovine serum (FBS), and penicillin-streptomycin-amphotericin (PSA) were purchased from Gibco/Invitrogen Co. (Carlsbad, CA, USA). Enzyme immunoassay (EIA) kits for determination of TNF-α, IL-1β, and IL-6 were purchased from Invitrogen Co. (Carlsbad, CA, USA). An EIA kit for PGE2 assay was purchased from Cayman Chemical (Ann Arbor, MI, USA). A lactic dehydrogenase (LDH) assay kit was purchased from Bioassay Systems (Hayward, CA, USA). A Cell Counting Kit-8 (CCK-8) was purchased from Enzo Life Sciences Inc. (Farmingdale, NY, USA). The specific antibodies for iNOS, COX-2, phosphorylated IκBα (P-IκBα), IκBα, p50, p38, JAK2, phosphorylated JAK2 (P-JAK1/2), STAT1, phosphorylated STAT1 (P-STAT1), STAT3, phosphorylated STAT3 (P-STAT3), poly-(ADP ribose) polymerase (PARP), and β-actin were purchased from GeneTex Inc. (Irvine, CA, USA). IκB kinase (IKK) α/β, phosphorylated IKKα (Ser180)/IKKβ (Ser181) (P-IKKα/β), c-Jun NH_2-terminal protein kinase 1/2 (JNK1/2), phosphorylated JNK1/2 (P-JNK1/2), phosphorylated ERK1/2 (P-ERK1/2), and phosphorylated p38 (P-p38) were purchased from Santa Cruz Biotechnology Inc. (Santa Cruz, CA, USA). p65 and ERK1/2 were purchased from Spring Bioscience, Inc. (Danvers, MA, USA). Horseradish peroxidase-conjugated antigoat or antirabbit IgG was purchased from Bio-Rad Laboratories, Inc. (Hercules, CA, USA). A nuclear extraction kit (AY2002) was purchased from Panomics, Inc. (Redwood City, CA, USA).

Preparation of LFEE. Fresh litchi flowers gathered from a farm in Taichung, Taiwan (March 2012) were lyophilized with a freeze-dryer (Vastech Scientific Co., Ltd., Taipei, Taiwan). The samples were extracted with ethanol (1/20, g/mL) for 24 h in the dark. After the mixture had been filtered, the solvent was evaporated to dryness on a rotary evaporator (Panchun Scientific Co., Kaohsiung, Taiwan). The extract was then stored at −80 °C in an airtight bottle before use in experiments.

Determination of Phytochemicals in LFEE. The extract (5 mg) was dissolved in MeOH (20 mL) for high-performance liquid chromatography (HPLC) analysis. The determination of flavonoid and phenolic acid was performed based on the report of Chen et al.:[4] stationary phase, Hypersil GOLD C_{18} column (250 × 4.6 mm, 5 μm; Thermo Fisher Scientific Inc., Fairlawn, NJ, USA); mobile phase, MeOH (solvent A) and 9% CH_3COOH prepared with dd H_2O (solvent B) (conditions: 0−5 min, increase from 5% to 17% A; 5−25 min, maintain at 17% A; 25−40 min, increase from 17% to 31% A; 40−76 min, maintain at 31% A; 76−80 min, increase from 31% to 40% A; 80−120 min, maintain at 40% A); flow rate, 0.8 mL/min; detection, 210−650 nm. Proanthocyanidins were determined according to the method of Hwang et al.:[6] stationary phase, Hypersil GOLD C_{18} column (250 mm × 4.6 mm i.d., 5 μm); mobile phase, ACN (solvent A) and 2% CH_3COOH prepared with dd H_2O (solvent B) (conditions: 0−5 min, increase from 10% to 20% A; 10−13 min, increase from 20% to 30% A; 13−15 min, increase from 30% to 100% A; 15−20 min, maintain at 100% A); flow rate, 1 mL/min. The analytical equipment included a PrimeLine Gradient model 500G HPLC pump system (Analytical Scientific Instruments, Inc., El Sobrante, CA, USA), an S-3210 photodiode-array (PDA) detector (Schambeck SFD GmbH, Bad Honnef, Germany), and a Thermo Finnigan LCQ classic quadrupole ion trap HPLC−mass spectrometry (MS) system (Gentech, Arcade, NY, USA) equipped with an electrospray ionization (ESI) source (positive-ion mode). The HPLC−MS instrument was used to determine mass spectra recorded from m/z 50 to 1000 with the following conditions: nebulizer pressure, 70 psi; capillary temperature, 200 °C; dry gas flow, 11 L/min; electrospray voltage of the ion source, 3000 V; capillary exit, −159 V; skimmer, 40 V.

Cell Line. Murine macrophage RAW264.7 cells obtained from the American Type Culture Collection (ATCC, Manassas, VA, USA) were cultured in RPMI-1640 medium supplemented with 10% heat-inactivated FBS and 1% PSA. The cells were incubated in a Thermo Scientific Forma Direct-Heat CO_2 Incubator (Thermo Fisher Scientific Inc., Mississauga, ON, USA) (37 °C, 5% CO_2).

Cell Viability Assay. CCK-8 was used for the cell viability assay. The kit contained WST-8 [2-(2-methoxy-4-nitrophenyl)-3-(4-nitrophenyl)-5-(2,4-disulfophenyl)-2H-tetrazolium, monosodium salt], which can be reduced by dehydrogenase in the cell and produces an orange-colored formazan that is soluble in tissue culture medium. The level of the formazan dye is proportional to the number of living cells.[12] RAW264.7 cells were plated at a density of 1×10^6 cells/well into 24-well plates, preincubated for 1 h with various concentrations (0, 0.1, 0.2, 0.3, 0.4, and 0.5 mg/mL) of LFEE (dissolved in EtOH), and stimulated with or without 1 μg/mL of LPS for 24 h at 37 °C in the CO_2 incubator. The EtOH concentration in each well was 0.0475% (v/v), which was the final concentration after the LFEE/ethanol solution had been diluted with PBS. After treatment, the CCK-8 solution (10 μL) was added to each well, and the mixture was incubated for 2 h at 37 °C. The absorbance at 450/595 nm was read using a microplate reader (Multiskan Spectrum, Thermo Scientific Co., Vantaa, Finland). The absorption from the control cells was set as 100% cell viability.

LDH Assay. LDH released from damaged cells was determined according to the method of Haslam et al.[13] RAW264.7 cells were plated at a density of 1×10^6 cells/well into 24-well plates, preincubated for 1 h with various concentrations (0, 0.1, 0.2, 0.3, 0.4, and 0.5 mg/mL) of LFEE (dissolved in EtOH), and stimulated with or without 1 μg/mL of LPS for 24 h at 37 °C in the CO_2 incubator. The EtOH concentration in each well was 0.0475% (v/v). After treatment, the 24-well culture plates were centrifuged at 300g for 5 min, and 50 μL of supernatant was transferred from each well to clear flat-bottom 96-well plates. LDH assay reagent (100 μL) was then added to each well of the 96-well plates and incubated for 30 min in the dark. After the addition of 15 μL of 1 N HCl, the absorbance at 450/595 nm was read using a microplate reader (Multiskan Spectrum, Thermo Scientific Co., Vantaa, Finland). Culture medium wells (no cells, blank) and control well cells treated with Triton X-100 (total lysis) were also assayed. Results are expressed as percentages of the maximum LDH release in the total lysis and sample wells.

Determination of Nitrite, PGE2, and Pro-Inflammatory Cytokines. RAW264.7 cells were plated at a density of 1×10^6 cells/well in 24-well plates, pretreated with various concentrations (0, 0.1, 0.2, and 0.3 mg/mL) of LFEE (dissolved in EtOH), and stimulated with or without 1 μg/mL of LPS for 24 h at 37 °C in the CO_2 incubator. The EtOH concentration in each well was 0.0475% (v/v). NO levels in the cultured medium were determined as nitrite using Griess reagent.[14] Each cultured medium (supernatant, 100 μL) was mixed with Griess reagent (100 μL) and incubated for 10 min. The absorbance of the mixture was read at 540 nm using a microplate reader. The nitrite levels were calculated with a standard curve developed using $NaNO_2$. The levels of $PGE2_2$ and pro-inflammatory cytokines (TNF-α, IL-1β, and IL-6) in the cultured medium (supernatant) were determined with an enzyme-linked immunosorbent assay (ELISA) in accordance with the manufacturer's protocols. The absorbances of $PGE2_2$ and the cytokines were measured at 412 and 450/650 nm, respectively, with a microplate reader.

Preparation of Nuclear Extracts. Nuclear−cytoplasmic fractionation was conducted using NE-PER Nuclear and Cytoplasmic Extraction Reagent kits (Thermo Fisher Scientific Inc., Rockford, IL, USA) according to the manufacturer's protocol. The samples were incubated with rocking at 4 °C for 15 min and centrifuged for 5 min at 12000*g*. The protein concentration of the supernatant was determined with a Bicinchoninic Acid protein assay kit (Thermo Fisher Scientific Inc., Rockford, IL, USA).

Western Blotting Analysis. Western blotting analysis was performed based on the report of Jung et al.[15] RAW264.7 cells were plated at a density of 1×10^6 cells/well in 24-well plates, pretreated with various concentrations (0, 0.1, 0.2, and 0.3 mg/mL) of LFEE (dissolved in EtOH), and stimulated with or without 1 μg/mL of LPS for 24 h at 37 °C in the CO_2 incubator. The EtOH concentration in each well was 0.0475% (v/v). Subsequently, the cells were washed with PBS, collected, suspended in the lysis buffer [150 mM NaCl, 10 mM Tris (pH 7.5), 5 mM EDTA, 1% Triton X-100] with protease inhibitors (1 μg/mL leupeptin and 100 μg/mL PMSF), and centrifuged at 12000*g* for 20 min at 4 °C to yield cell lysates. The protein levels were measured with a protein assay kit (Bio-Rad Laboratories, Inc., Hercules, CA, USA). The proteins (RAW264.7 lysates) were separated with 10% sodium dodecyl sulfate (SDS) polyacrylamide gels and transferred to poly(vinylidene difluoride) (PVDF) membranes (New Life Science Products, Inc., Boston, MA, USA). The membranes were then blocked in Tris-buffered saline (TBS)/Tween 20 solution with 5% nonfat dry milk and incubated sequentially with primary antibody and horseradish peroxidase-conjugated antigoat or antirabbit IgG (Bio-Rad Laboratories, Inc., Hercules, CA, USA). The protein bands were visualized with an enhanced chemiluminescence (ECL) system (Amersham Biosciences, Piscataway, NJ, USA), and their densities were quantified using Alpha Imager 2200 software (Alpha Innotech Co., San Leandro, CA, USA).

Statistical Analysis. All assays were performed in triplicate, and the mean values were calculated. The data were subjected to analysis of variance (ANOVA), and Duncan's multiple range tests were used to assess differences between means. Significant differences were concluded at a level of $p < 0.05$.

RESULTS

Flavonoids, Phenolic Acids, and Proanthocyanidin A2 in LFEE. Five flavanoids [total amount, 102.73 ± 5.50 mg/g of dried extract (mg/gDE)], including epicatechin (78.77 ± 4.21 mg/gDE), rutin (19.05 ± 1.02 mg/gDE), naringin (0.39 ± 0.01 mg/gDE), quercitrin (2.22 ± 0.12 mg/gDE), and neohesperidin (2.30 ± 0.14 mg/gDE), and nine phenolic acids (total amount, 60.31 ± 4.52 mg/gDE), including gallic acid (0.25 ± 0.01 mg/gDE), gentisic acid (32.14 ± 2.72 mg/gDE), chlorogenic acid (2.32 ± 0.08 mg/gDE), vanillic acid (0.60 ± 0.04 mg/gDE), *p*-coumaric acid (0.17 ± 0.01 mg/gDE), ferulic acid (18.25 ± 1.37 mg/gDE), sinapic acid (4.64 ± 0.20 mg/gDE), syringic acid (0.88 ± 0.04 mg/gDE), and *p*-anisic acid (1.06 ± 0.05 mg/gDE), were identified in LFEE. In addition, proanthocyanidin A2 (the major proanthocyanidin) was present in the extract at a level of 79.31 ± 2.95 mg/gDE. LFEE was then dissolved in EtOH to estimate its anti-inflammatory activity with LPS-stimulated RAW264.7 cells.

Viability and LDH Release of RAW264.7 Cells Treated with LFEE. The EtOH concentration in the medium of RAW264.7 cells (47.5 μL of EtOH in 100 mL of medium) provided good dissolution ability for LFEE. Also, it did not influence the assay of the anti-inflammatory activity of LFEE. The CCK-8 assay showed that an LPS concentration of 1 μg/mL and/or an LFEE concentration of less than 0.4 mg/mL did not significantly change RAW264.7 cell proliferation. Similar results were seen in the LDH assay; an LPS concentration of 1 μg/mL and/or an LFEE concentration of less than 0.4 mg/mL did not significantly impair RAW264.7 cells (data not shown). Therefore, LFEE concentrations of 0, 0.1, 0.2, and 0.3 mg/mL were used in this investigation.

Effects of LFEE on LPS-Stimulated Productions of Nitrite, PGE2, and Pro-Inflammatory Cytokines and Protein Expressions of iNOS and COX-2 in RAW264.7 Cells. Figure 1 shows that LPS stimulation substantially increased the productions of nitrite, $PGE2_2$, and pro-inflammatory cytokines (IL-1β, IL-6, and TNF-α) in RAW264.7 cells. When the cells were pretreated with LFEE, the levels of LPS-induced nitrite, $PGE2_2$, IL-1β, IL-6, and TNF-α were lowered significantly, especially for the cells pretreated with 0.3 mg/mL LFEE.

For the Western blot analysis, Figure 2 shows that LPS highly induced the expressions of iNOS and COX-2 in RAW264.7 cells; nevertheless, their expressions were decreased significantly when the cells were pretreated with LFEE. The higher the LFEE concentration, the greater the suppressive effect. The reduction of the expressions of iNOS and COX-2 responded to the downregulation of the productions of NO and $PGE2_2$.

Effects of LFEE on LPS-Induced IKKα/β Phosphorylation and Translocation of NF-κB p50/p65 Subunits in RAW264.7 Cells. Figure 3 shows that LPS treatment caused the translocation of cytoplasmic p50 and p65 to the nucleus. Following LFEE pretreatment, the levels of translocated p50 and p65 were decreased significantly. The results demonstrated that LFEE-mediated suppression of the production of pro-inflammatory mediators is regulated by the NF-κB pathway in LPS-stimulated RAW264.7 cells.

Upon LPS stimulation, IKK α/β phosphorylation was greatly increased in RAW264.7 cells. However, this increase was lowered significantly when the cells were pretreated with LFEE.

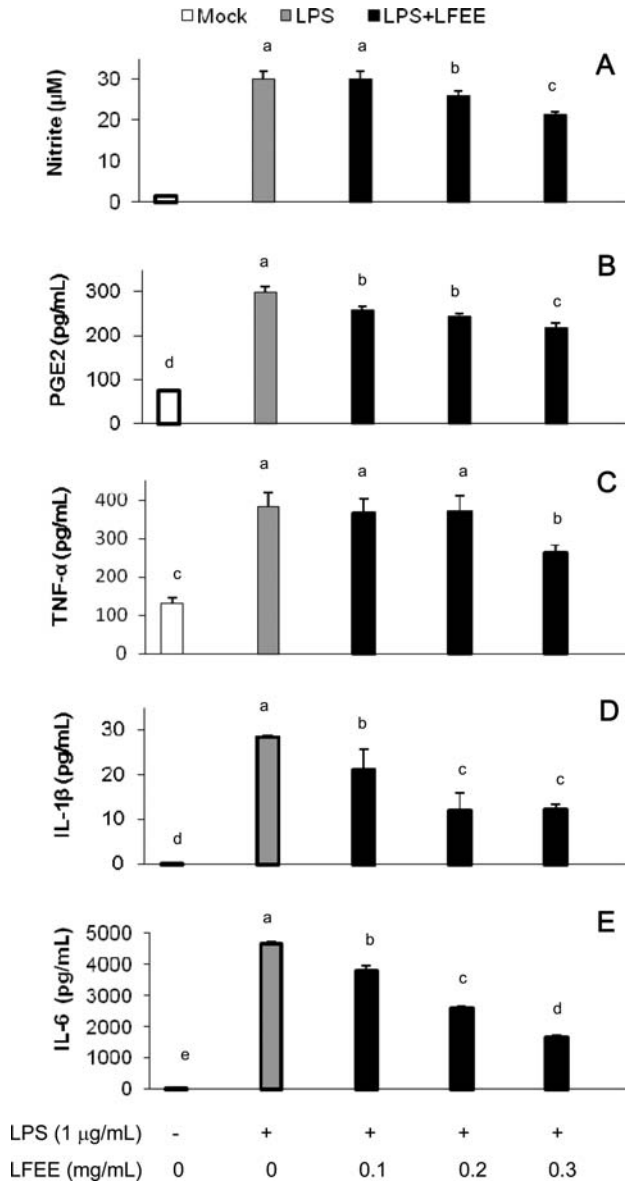

Figure 1. Effects of LFEE on LPS-stimulated productions of NO, PGE2, IL-1β, IL-6, and TNF-α in RAW264.7 cells. The cells plated in 24-well plates (1×10^6 cells/well) were pretreated with various concentrations (0−0.3 mg/mL) of LFEE for 1 h and then stimulated with or without (mock) LPS (1 μg/mL) for 24 h. The cultured media were used for assays. The level of (A) nitrite was determined through Griess reagent to evaluate NO production. The levels of (B) PGE2, (C) TNF-α, (D) IL-1β, and (E) IL-6 were measured by ELISA. Each value is expressed as mean ± SD (n = 3). Means with different letters are significantly different at the level of $p < 0.05$.

Therefore, LFEE suppression of NF-κB activation was caused by reducing the phosphorylation of the IKK complex.

Effects of LFEE on LPS-Induced Phosphorylation of Mitogen-Activated Protein Kinases (MAPKs) in RAW264.7 Cells. Figure 4 shows that MAPKs including JNK, p38, and ERK were markedly activated by LPS in RAW264.7 cells. LFEE pretreatment significantly lowered ERK phosphorylation in a dose-dependent manner; nevertheless, phosphorylated JNK and p38 did not show a significant decrease. Therefore, ERK inactivation is responsible for the LFEE-mediated suppression of the productions of pro-inflammatory mediators in LPS-stimulated RAW264.7 cells.

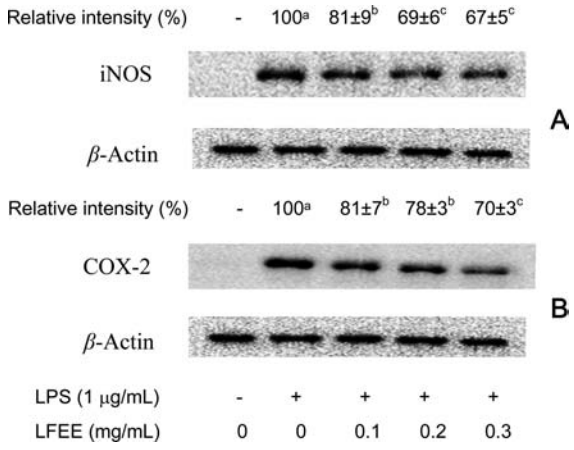

Figure 2. Effects of LFEE on LPS-stimulated protein expressions of iNOS and COX-2 in RAW264.7 cells. The cells were pretreated with various concentrations (0−0.3 mg/mL) of LFEE for 1 h and then stimulated with or without LPS (1 μg/mL) for 24 h. Protein levels of (A) iNOS and (B) COX-2 were measured by Western blot; the signals of iNOS and COX-2 were normalized to the β-actin signal. Each data point represents the mean ± SD of three independent experiments and is expressed as the percentage of the culture treated with LPS alone. Means with different letters are significantly different at the level of $p < 0.05$.

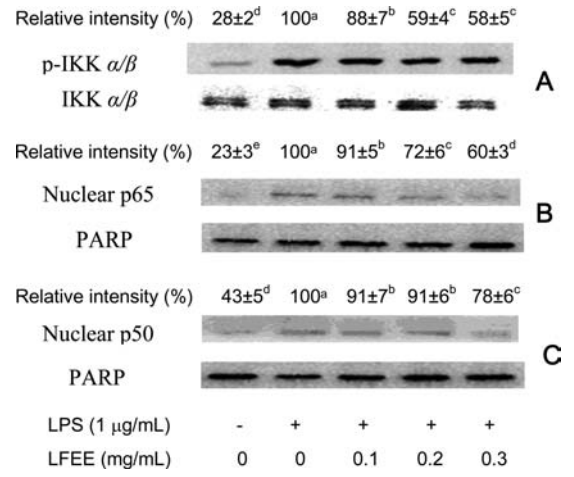

Figure 3. Effects of LFEE on LPS-induced phosphorylation of IκB IKKα/β and NF-κB p50 and p65 subunits in RAW264.7 cells. The cells were pretreated with various concentrations (0−0.3 mg/mL) of LFEE for 1 h and then stimulated with or without LPS (1 μg/mL) for 24 h. The levels of (A) phosphorylation of IKKα/β and IKKα/β were measured with Western blot; the ratios of immunointensity between phosphorylated IKKα/β and IKKα/β are shown. The levels of (B,C) nuclear translocation of NF-κB (B) p50 and (C) p65 subunits were measured with Western blot; each of their signals was normalized to the β-actin signal. Each data point represents the mean ± SD of three independent experiments and is expressed as the percentage of the culture treated with LPS alone. Means with different letters are significantly different at the level of $p < 0.05$.

Effects of LFEE on LPS-Induced Phosphorylation of JAK2, STAT1, and STAT3 in RAW264.7 Cells. Figure 5 shows that the expressions of phosphorylation of STAT1 and STAT3 could be significantly increased in RAW264.7 cells through LPS stimulation. When the cells were pretreated with a higher concentration of LFEE, a greater reduction of STAT3 activation, but not STAT1 activation, could be observed.

dx.doi.org/10.1021/jf5003705 | J. Agric. Food Chem. 2014, 62, 3458−3465

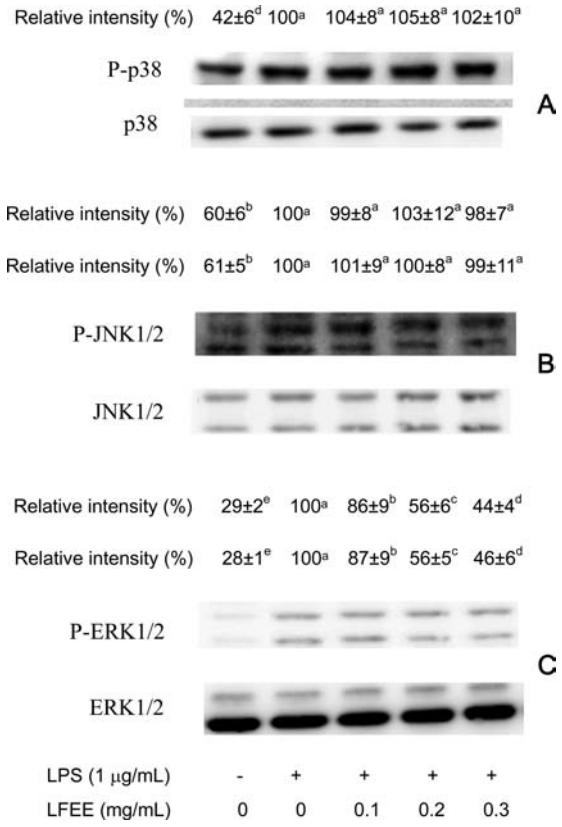

Figure 4. Effects of LFEE on LPS-activated MAPKs in RAW264.7 cells. The cells were pretreated with various concentrations (0−0.3 mg/mL) of LFEE for 1 h and then stimulated with or without LPS (1 μg/mL) for 24 h. The levels of total or phosphorylated (A) p38, (B) JNK1/2, and (C) ERK1/2 were measured with Western blot; the ratios of immunointensity between the MAPKs and the phosphorylated MAPKs are shown. Each data point represents the mean ± SD of three independent experiments and is expressed as the percentage of the culture treated with LPS alone. Means with different letters are significantly different at the level of $p < 0.05$.

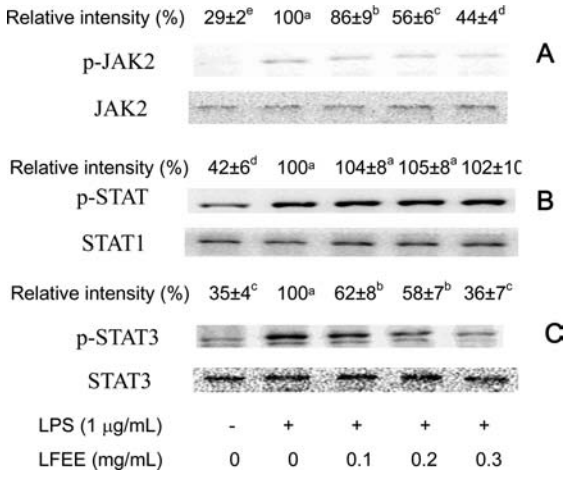

Figure 5. Effects of LFEE on LPS-activated JAK2 and STATs in RAW264.7 cells. The cells were pretreated with various concentrations (0−0.3 mg/mL) of LFEE for 1 h and then stimulated with or without LPS (1 μg/mL) for 24 h. The levels of total or phosphorylated (A) JAK2, (B) STAT1, and (C) STAT3 were measured with Western blot; the ratios of immunointensity between JAK2 and phosphorylated JAK2 and between the STATs and the phosphorylated STATs are shown. Each data point represents the mean ± SD of three independent experiments and expressed as the percentage of the culture treated with LPS alone. Means with different letters are significantly different at the level of $p < 0.05$.

Therefore, STAT3 inactivation should be associated with the anti-inflammatory effect of LFEE.

Similarly, LPS stimulation significantly increased JAK2 phosphorylation in RAW264.7 cells. LFEE addition caused a dose-dependent decrease of JAK2 activation. Therefore, LFEE cessation of STAT3 activation is caused by attenuating JAK2 activation.

DISCUSSION

During inflammation, excess levels of NO, $PGE2_2$, and cytokines (IL-1β, IL-6, and TNF-α) are induced by activated inflammatory cells (e.g., eosinophils, macrophages, mononuclear phagocytes, neutrophils). This leads to the damaging of cells and tissues and the activation of macrophages in inflammation-associated diseases (e.g., rheumatoid arthritis, chronic hepatitis).[14] Macrophages play an important role in regulating several immunopathological conditions and inducing overexpression of the pro-inflammatory mediators of the inflammatory process.[14]

Throughout the inflammatory processes, iNOS and COX-2 expressions are notably increased and promote the generations of NO and $PGE2_2$, respectively. Thus, inhibition of NO and $PGE2_2$ production could be an important marker for anti-inflammatory effects.[16] NF-κB plays a principle role in regulating the expressions of COX-2 and iNOS by the transcription factor. It exists in the cytoplasm as inactive heterodimers composed of the p50 and p65 subunits that are bound to the inhibitor of κB (IκB). Upon inflammatory stimulation including LPS, IκB kinase (IKK) is activated, after which IκB ubiquitination and degradation is induced. NF-κB is then free to translocate from the cytosol to the nucleus, where it promotes transcription of target genes and further induces the transcription of pro-inflammatory mediators, such as iNOS, COX-2, TNF-α, and cytokines.[17−20] Kim et al.[18] indicated that many anti-inflammatory agents exhibit their potencies by suppressing NF-κB signaling.

Ho et al.[8] found that logan aqueous and ethanolic extracts contain abundant levels of phenolic compounds that can suppress LPS-induced iNOS expression as well as NO production in RAW264.7 cells. These extracts can also inhibit $PGE2_2$ generation. Hu and Kitts[21] reported that ethanolic extracts of dandelion (*Taraxacum officinale*) flower with caffeic acid, chlorogenic acid, luteolin, and luteolin-7-O-glucoside suppress the expressions of iNOS and COX-2 and the productions of NO and $PGE2_2$ in LPS-activated RAW264.7 cells. Choi et al.[22] demonstrated that ethanolic extract of *Inula japonica* (Inulae Flos) flower inhibits LPS-stimulated iNOS expression, NO production, and release of pro-inflammatory cytokines (TNF-α and IL-6) through the downregulation of NF-κB activation in RAW264.7 cells. Jung et al.[17] found that methanolic extracts of *Panax notoginseng* flower significantly inhibit the expressions of iNOS and COX-2 as well as the productions of NO and $PGE2_2$ in LPS-stimulated RAW264.7 cells. The extract also significantly inhibits the production of TNF-α and IL-1β. The molecular mechanism of the extract-mediated attenuation in RAW264.7 cells has a close relationship to the suppression of the translocation of NF-κB p65 subunit into the nucleus.

dx.doi.org/10.1021/jf5003705 | J. Agric. Food Chem. 2014, 62, 3458−3465

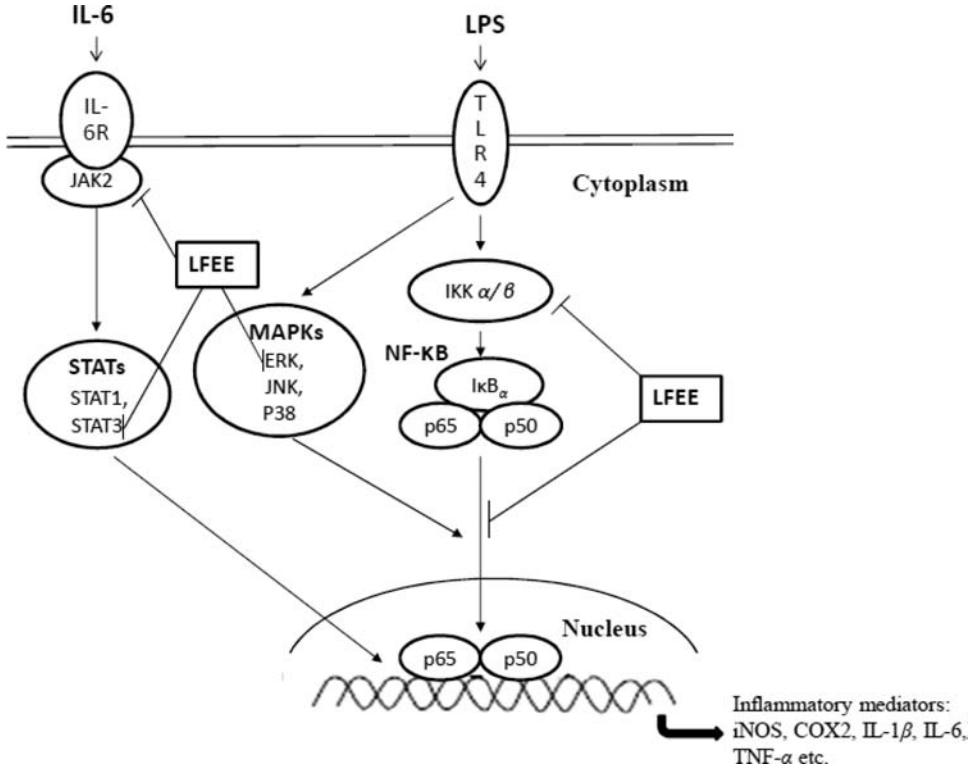

Figure 6. Possible role of LFEE in the production of LPS-stimulated pro-inflammatory mediators in RAW264.7 cells.

Our study showed that LFEE downregulates the expressions of iNOS and COX-2 as well as the productions of NO and $PGE2_2$ in LPS-stimulated RAW264.7 cells (Figures 1 and 2). In addition, LFEE could also lower the secretions of pro-inflammatory cytokines, TNF-α, IL-1β, and IL-6 (Figure 1). The molecular mechanism of LFEE-mediated attenuation in the RAW264.7 cells was closely related to suppression of IκB kinase activation followed by inhibition of the translocation of NF-κB p50/p65 subunits into the nucleus (Figure 3). These results suggest that LFEE suppresses the expression of pro-inflammatory mediators by downregulating the NF-κB pathway in stimulated macrophages.

MAPKs including ERK, JNK, and p38 are a group of signaling molecules. They also appear to play a crucial role in inflammatory processes.[23] Kaminska[24] indicated that LPS could stimulate MAPK cascades and the pathways leading to activation of NF-κB. Upon MAPK activation, transcription factors present in the cytoplasm or nucleus are phosphorylated, leading to target gene expression resulting in a biological response. Reports[25−27] have indicated that MAPK pathways are involved in LPS-induced iNOS and COX-2 expression in macrophages.

Choi et al.[22] reported that LPS-stimulated RAW264.7 cells cause phosphorylation of ERK, JNK, and p38; nevertheless, ERK and p38 phosphorylation could be significantly inhibited through treatment with the ethanolic extract of the *Inula japonica* (Inulae Flos) flower. Jung et al.[17] reported that the methanolic extract of *Panax notoginseng* flower suppresses the phosphorylation of ERK1/2 and JNK and slightly decreases the phosphorylation of p38 in LPS-stimulated RAW264.7 cells.

In agreement with previous investigations, ERK, JNK, and p38 could be phosphorylated remarkably as the RAW264.7 cells were stimulated with LPS. Treatment with LFEE was observed to significantly lower ERK phosphorylation in the LPS-stimulated RAW264.7 cells (Figure 4). The results suggest that blocking of the ERK pathway is involved in the suppression of LPS-stimulated NF-κB bound by LFEE in RAW264.7 cells.

IL-6 provokes a broad range of cellular and physiological responses, including immune response and inflammation. IL-6 could use the JAK/STAT signaling pathway for signal transduction.[28] IL-6 signaling is initiated by binding to its receptor subunit IL-6R (IL-6-binding α-subunit receptor), which subsequently transduces a signal that activates intracytoplasmic JAKs. The activated JAKs could transduce the intracellular signal by further phosphorylating and activating STATs. The activated STATs could translocate to the nucleus, where they activate NF-κB.[29] Ichikawa et al.[30] demonstrated that LPS could induce the activation of the STAT pathway, leading to a significant production of pro-inflammatory mediators in RAW264.7 cells.

To the best of our knowledge, no reports regarding the suppression of pro-inflammatory responses in macrophages by flower extract with a focus on STAT signaling have been published. In this study, we found that LFEE could decrease IL-6 secretion, which might lead to further lowering of the activation of JAK2 and STAT3 but not STAT1 in LPS-induced 264.7 cells. The results illustrate that blocking the STAT cascade is another important mechanism contributing to the anti-inflammatory activity of LFEE in macrophages.

Our investigation found that the molecular mechanism for LFEE-mediated attenuation of LPS-induced inflammatory responses in RAW264.7 cells correlates with downregulation of IKK α/β phosphorylation, thus inhibiting p50 and p65 subunits translocation into the nucleus. Furthermore, LFEE inhibits the LPS-induced activation of ERK as well as JAK2/STAT3. The results are summarized in Figure 6.

dx.doi.org/10.1021/jf5003705 | J. Agric. Food Chem. 2014, 62, 3458−3465

LFEE was found to contain abundant phenolic components including five flavanoids (epicatechin, rutin, naringin, quercitrin, and neohesperidin), nine phenolic acids (gallic acid, gentisic acid, chlorogenic acid, vanillic acid, *p*-coumaric acid, ferulic acid, sinapic acid, syringic acid, and *p*-anisic acid), and proanthocyanidin A2. Our previous results[11] also showed that proanthocyanidin A2 and epicatechin are the two major compounds responsible for the antioxidation activity of LFEE. Ho et al.[8] indicated that proanthocyanidin A2 is the key anti-inflammatory component in the longan flower extract. Bellik et al.[31] reported that gallic acid, ferulic acid, coumaric acid, and rutin have anti-inflammatory effects. They are also found in the LFEE. Therefore, these compounds should contribute to the anti-inflammatory activity of LFEE. Through evaluation of the LFEE anti-inflammatory effect with LPS-mediated RAW264.7 macrophages, remarkable suppression of the protein expressions of iNOS and COX-2; the productions of NO and PGE2; and the secretions of IL-1β, IL-6, and TNF-α was found. The results demonstrated that LFEE modulates inflammatory processes through the inactivation of NF-κB, ERK, and JAK2/STAT3. Litchi flower should have the potential to be exploited as a functional food for anti-inflammation activity.

AUTHOR INFORMATION

Corresponding Author

*Tel.: +886-4-24730022 ext. 11868. Fax: +886-4-2324189. E-mail: jtlin@csmu.edu.tw.

Funding

This research was supported by the National Science Council, Taiwan (Project NSC 101-2313-B-040-009-MY3).

Notes

The authors declare no competing financial interest.

ACKNOWLEDGMENTS

The authors thank Dr. Bernard A. Schwetz for carefully reading the manuscript and for helpful discussions that improved the article quality.

REFERENCES

(1) Rivera-López, J.; Ordorica-Falomir, C.; Wesche-Ebeling, P. Changes in anthocyanin concentration in Lychee (*Litchi chinensis* Sonn.) pericarp during maturation. *Food Chem.* **1999**, *65*, 195−200.

(2) Salunke, D. K.; Desai, B. *Postharvest Biotechnology of Fruits*; CRC Press: Boca Raton, FL, 1984; Vol. *II*, pp 77−80.

(3) Liu, S. C.; Lin, J. T.; Wang, C. K.; Chen, H. Y.; Yang, D. J. Antioxidant properties of various solvent extracts from lychee (*Litchi chinenesis* Sonn.) flowers. *Food Chem.* **2009**, *114*, 577−581.

(4) Chen, Y. C.; Lin, J. T.; Liu, S. C.; Lu, P. S.; Yang, D. J. Composition of flavonoids and phenolic acids in lychee (*Litchi chinensis* Sonn.) flower extracts and their antioxidant capacities estimated with human LDL, erythrocyte and blood models. *J. Food Sci.* **2011**, *76*, C724−C728.

(5) Yang, D. J.; Chang, Y. Y.; Hsu, C. L.; Liu, C. W.; Wang, Y.; Chen, Y. C. Protective effect of a litchi (*Litchi chinensis* Sonn.)-flower-water-extract on cardiovascular health in a high-fat/cholesterol-dietary hamsters. *Food Chem.* **2010**, *119*, 1457−1464.

(6) Hwang, Z. Y.; Lin, J. T.; Liu, S. C.; Hu, C. C.; Shyu, Y. S.; Yang, D. J. Protective role of litchi (*Litchi chinensis* Sonn.) flower extract against cadmium- and lead-induced cytotoxicity and transforming growth factor β1-stimulated expression of smooth muscle α-actin estimated with rat liver cell lines. *J. Funct. Foods* **2013**, *5*, 698−705.

(7) Wu, Y. S.; Chiu, C. H.; Yang, D. J.; Lin, Y. L.; Tseng, J. K.; Chen, Y. C. Inhibitory effects of litchi (*Litchi chinensis* Sonn.) flower-water extracts on lipase activity and diet-induced obesity. *J. Funct. Foods* **2013**, *5*, 923−929.

(8) Ho, S. C.; Hwang, L. S.; Shen, Y. J.; Lin, C. C. Suppressive effect of a proanthocyanidin-rich extract from longan (*Dimocarpus longan* Lour.) flowers on nitric oxide production in LPS-stimulated macrophage cells. *J. Agric. Food Chem.* **2007**, *55*, 10664−10670.

(9) Tanko, Y.; Kamba, B.; Saleh, M. I. A.; Musa, K. Y.; Mohammed, A. Anti-nociceptive and anti-inflammatory activities of ethanolic flower extract of *Newbouldia laevis* in mice and rats. *Int. J. Appl. Res. Nat. Prod.* **2008**, *1*, 13−19.

(10) Yadav, Y.; Mohanty, P. K.; Kasture, S. B. Anti-inflammatory activity of hydroalcoholic extract of *Quisqualis indica* Linn. flower in rats. *Int. J. Pharm. Life Sci.* **2012**, *2*, 977−981.

(11) Yang, D. J.; Chang, Y. Z.; Chen, Y. C.; Liu, S. C.; Hsu, C. H.; Lin, J. T. Antioxidant effect and active components of litchi (*Litchi chinensis* Sonn.) flower. *Food Chem. Toxicol.* **2012**, *50*, 3056−3061.

(12) Ishiyama, M.; Miyazono, Y.; Sasamoto, K.; Ohkura, Y.; Ueno, K. A highly water-soluble disulfonated tetrazolium salt as a chromogenic indicator for NADH as well as cell viability. *Talanta* **1997**, *44*, 1299−1305.

(13) Haslam, G.; Wyatt, D.; Kitos, P. A. Estimating the number of viable animal cells in multi-well cultures based on their lactate dehydrogenase activities. *Cytotechnology* **2000**, *32*, 63−75.

(14) Yoon, W. J.; Ham, Y. M.; Kim, S. S.; Yoo, B. S.; Moon, J. Y.; Baik, J. S.; Lee, N. H.; Hyun, C. G. Suppression of pro-inflammatory cytokines, iNOS, and COX-2 expression by brown algae *Sargassum micracanthum* in RAW264.7 macrophages. *EurAsian J. BioSci.* **2009**, *3*, 130−143.

(15) Jung, H. W.; Seo, U. K.; Kim, J. H.; Leem, K. H.; Park, Y. K. Flower extract of *Panax notoginseng* attenuates lipopolysaccharide-induced inflammatory response via blocking of NF-κB signaling pathway in murine macrophages. *J. Ethnopharmacol.* **2009**, *122*, 313−319.

(16) Huang, N.; Hauck, C.; Yum, M. Y.; Rizshsky, L.; Widrlechner, M. P.; McCoy, J. A.; Murphy, P. A.; Dixon, P. M.; Nikolau, B. J.; Birt, D. F. Rosmarinic acid in *Prunella vulgaris* ethanol extract inhibits lipopolysaccharide-induced prostaglandin E2 and nitric oxide in RAW264.7 mouse macrophages. *J. Agric. Food Chem.* **2009**, *57*, 10579−10589.

(17) Jung, W. K.; Heo, S. J.; Jeon, Y. J.; Lee, C. M.; Park, Y. M.; Byun, H. G.; Choi, Y. H.; Park, S. G.; Choi, I. W. Inhibitory effects and molecular mechanism of dieckol isolated from marine brown alga on COX-2 and iNOS in microglial cells. *J. Agric. Food Chem.* **2009**, *57*, 4439−4446.

(18) Kim, H. G.; Shrestha, B.; Lim, S. Y.; Yoon, D. H.; Chang, W. C.; Shin, D. J.; Han, S. K.; Park, S. M.; Park, J. H.; Park, H. I.; Sung, J. M.; Jang, Y.; Chung, N.; Hwang, K. C.; Kim, T. W. Cordycepin inhibits lipopolysaccharide-induced inflammation by the suppression of NF-κB through Akt and p38 inhibition in RAW 264.7 macrophage cells. *Eur. J. Pharmacol.* **2006**, *545*, 192−199.

(19) Lau, F. C.; Joseph, J. A.; McDonald, W.; Kalt, W. Attenuation of iNOS and COX2 by blueberry polyphenols is mediated through the suppression of NF-κB activation. *J. Funct. Foods* **2009**, *1*, 274−283.

(20) Tak, P. P.; Firestein, G. S. NF-κB: A key role in inflammatory diseases. *J. Clin. Invest.* **2001**, *107*, 7−11.

(21) Hu, C.; Kitts, D. D. Luteolin and luteolin-7-O-glucoside from dandelion flower suppress iNOS and COX-2 in RAW264.7 cells. *Mol. Cell. Biochem.* **2004**, *265*, 107−113.

(22) Choi, J. H.; Park, Y. N.; Li, Y.; Jin, M. H.; Lee, J.; Lee, Y.; Son, J. K.; Chang, H. W.; Lee, E. Flowers of Inula japonica attenuate inflammatory responses. *Immune Network* **2010**, *10*, 145−152.

(23) Yang, D. J.; Lin, J. T.; Chen, Y. C.; Liu, S. C.; Lu, F. J.; Chang, T. J.; Wang, M.; Lin, H. W.; Chang, Y. Y. Suppressive effect of carotenoid extract of *Dunaliella salina* alga on production of LPS-stimulated pro-inflammatory mediators in RAW264.7 cells via NF-κB and JNK inactivation. *J. Funct. Foods* **2013**, *5*, 607−615.

(24) Kaminska, B. MAPK signalling pathways as molecular targets for anti-inflammatory therapy—From molecular mechanisms to therapeutic benefits. *Biochim. Biophys. Acta* **2005**, *1754*, 253−262.

(25) Chen, B. C.; Chen, Y. H.; Lin, W. W. Involvement of p38 mitogen-activated protein kinase in lipopolysaccharide-induced iNOS and COX-2 expression in J774 macrophages. *Immunology* **1999**, *97*, 124−129.
(26) Guha, M.; Mackman, N. LPS induction of gene expression in humanmonocytes. *Cell. Signalling* **2001**, *13*, 85−94.
(27) Tang, W.; Chen, L. H.; Daun, H.; Ho, C. T.; Pan, M. H. Inhibitory effects of hexahydro-*β*-acids in LPS-stimulated murine macrophage. *J. Funct. Foods* **2011**, *3*, 215−222.
(28) Ladenburger, A.; Seehase, M.; Kramer, B. W.; Thomas, W.; Wirbelauer, J.; Speer, C. P.; Kunzmann, S. Glucocorticoids potentiate IL-6-induced SP-B expression in H441 cells by enhancing the JAK-STAT signaling pathway. *Am. J. Physiol. Lung Cell. Mol. Physiol.* **2010**, *299*, L578−L584.
(29) Hou, T.; Tieu, B. C.; Ray, S.; Recinos, A.; Cui, R.; Tilton, R. G.; Brasier, A. R. Roles of IL-6-gp130 signaling in vascular Inflammation. *Curr. Cardiol. Rev.* **2008**, *4*, 179−192.
(30) Ichikawa, T.; Li, J.; Nagarkatti, P.; Nagarkatti, M.; Hofseth, L. J.; Windust, A.; Cui, T. American ginseng preferentially suppresses STAT/iNOS signaling in activated macrophages. *J. Ethnopharmacol.* **2009**, *125*, 145−150.
(31) Bellik, Y.; Boukraâ, L.; Alzahrani, H. A.; Bakhotmah, B. A.; Abdellah, F.; Hammoudi, S. M.; Iguer-Ouada, M. Molecular mechanism underlying anti-inflammatory and anti-allergic activities of phytochemicals: An update. *Molecules* **2013**, *18*, 322−353.

between the intake of wine and death resulting from coronary heart disease.[16] Since then, a lot of different targets have been found to be influenced by resveratrol treatment.[17,18] Previous studies showed that red wine polyphenols contribute to improvements in endothelial dysfunction and ultimately reduce the blood pressure and associated cardiac and vascular diseases.[19,20] Our previous studies have shown that resveratrol can protect cerebrovascular endothelial cells from oxLDL-induced apoptotic insults through Lox-1 receptor-mediated signal-transducing events.[21,22] But to date, much less is known about the effects of the consumption of red wine on high-fat diet-influenced BBB damage and subsequent neuronal damage. Therefore, in this study, we attempted to evaluate the effects of resveratrol on high-fat diet-induced disruption of the BBB and its possible mechanisms.

MATERIALS AND METHODS

Chemicals. Resveratrol, Evans blue dye, sodium pentobarbital, methanol, and Triton-X were purchased from Sigma (St. Louis, MO, USA). The purity of resveratrol used in this study was 99%. Acetone and ethanol were bought from Mallinckrodt Baker (Paris, KY, USA). Phosphate-buffered saline buffer (PBS) was prepared by mixing 0.14 M sodium chloride, 2.6 mM potassium chloride, 8 mM sodium phosphate, and 1.5 mM potassium phosphate. Sodium chloride, potassium chloride, sodium phosphate, and potassium phosphate were purchased from Sigma.

Animals. All procedures were performed according to the National Institutes of Health Guidelines for the Use of Laboratory Animals and approved by the Institutional Animal Care and Use Committee of Taipei Medical University, Taipei, Taiwan. Male ICR mice weighing 20−25 g were purchased from the Animal Center of the College of Medicine, National Taiwan University, Taipei, Taiwan. Before the experiments began, mice were allowed to acclimatize for 1 week in their animal quarters with air conditioning and an automatically controlled photoperiod of 12 h of light daily. Animals were allowed free access to rodent laboratory chow (Purina Mills, St. Louis, MO, USA).

Experimental Design. Animals were randomly divided into (1) normal diet-, (2) normal diet + resveratrol-, (3) high-fat diet-, and (4) high-fat diet + resveratrol-treated groups. The normal standard diet contained 5.1% fat (unsaturated fatty acids), 23.5% protein, and 50.3% complex carbohydrates. The composition of the high-fat diet included 20.1% fat (saturated fatty acids), 18.3% protein, and 51.2% carbohydrates. Our previous studies have shown that resveratrol at 10 μM can protect cerebrovascular endothelial cells from oxLDL-induced apoptotic insults.[21,22] Provinciali et al. reported that when a mouse drank 1 mg/L resveratrol daily, the serum concentrations of resveratrol were about 4 μM.[23] Thus, in the present study, resveratrol was dissolved in methanol and diluted with tap water to a concentration of 2.5 mg/L. The respective dose of resveratrol daily exposed to a mouse was 0.4 mg/kg body weight. Mice were administered a high-fat diet and resveratrol for 8 weeks. Control animals received 0.02% ethanol. The tap water with resveratrol was refreshed every day. The amounts of water and food consumed and the body weights were measured. At the end of the experiments, animals were sacrificed. Blood samples were collected and centrifuged to obtain serum. The brains were removed, weighed, and collected.

Analysis of Serum Cholesterol and LDL. After drug treatment, ICR mice were sacrificed and the blood was collected. Serum fractions were prepared by centrifugation of blood samples. Levels of serum total cholesterol, triglycerides, and high-density lipoprotein (HDL) were measured according to commercial kits provided by Randox Laboratories (Crumlin, Ireland, UK). Amounts of LDL were calculated by the formula LDL = total cholesterol − triglycerides/5 − HDL.

Assays of the BBB Integrity. Integrity of the BBB was analyzed by assessing extravasation of Evans blue dye according to a previously described method.[24] Briefly, after drug treatment, 0.1 mL of Evans blue dye (2%) was intravenously injected and allowed to circulate for 1 h. Subsequently, mice were intraperitoneally anesthetized with 80 mg sodium pentobarbital per kg body weight and perfused with PBS until a colorless perfusion fluid was obtained from the right atrium. Then, the brains were removed, weighed, and photographed for colorimetric blue signals.

Confocal Microscopic Analysis of Evans Blue Dye. To further determine the effects of resveratrol and a high-fat diet on the BBB integrity, a confocal microscopic analysis of Evans blue was carried out as described previously.[25] Briefly, after drug treatment, Evans blue dye was intravenously injected into mice. Following perfusion, the brain tissues were removed and sliced for the analysis of fluorescent signals excited by Evans blue in the brains using a confocal laser scanning microscope (model FV500, Olympus, Tokyo, Japan). Images were acquired and quantified using FLUOVIEW 4.0 software (Olympus).

Confocal Microscopic Analyses of Occludin and ZO-1 Polymerization, Factor VIII, and Activated Caspase-3. Polymerization of occludin and ZO-1 in brain tissues was recognized by specific antibodies, and these were visualized using confocal microscopy following a previously described method.[12] Briefly, after drug administration, brain tissues were removed, collected, and sliced. Tissues were fixed with a fixing reagent (acetone/methanol, 1:1) at −20 °C for 10 min. Following rehydration, the brains were incubated with 0.2% Triton X-100 at room temperature for 15 min. Rabbit polyclonal antibodies used in this study were respectively generated against human occludin and ZO-1 proteins (Invitrogen, Carlsbad, CA, USA). Immunodetection of occludin and ZO-1 in mouse brain tissues was carried out at 4 °C overnight. After washing, slices were sequentially reacted with the second antibodies and biotin-SP-conjugated AffiniPure goat antirabbit immunoglobulin G (IgG) (Jackson ImmunoResearch, West Grove, PA, USA) at room temperature for 1 h. After washing, the third antibody with Cy3-conjugated streptavidin (Jackson ImmunoResearch) was added to the brain slices and reacted at room temperature for 30 min. Localization of the BBB in brain tissues was recognized using an antibody against factor VIII protein (BioGenex, San Francisco, CA, USA). Activated caspase-3 was immunodetected using a polyclonal antibody against human cleaved caspase-3 (Cell Signaling Technology, Danvers, MA, USA). A confocal laser scanning microscope (Olympus) was utilized for sample observation. The excitation wavelength was set to 568 nm, while a 585-nm long-pass filter was used to collect the emitted light. Images were acquired and quantified using FLUOVIEW software (Olympus).

Immunodetection of Occludin and ZO-1. After drug treatment, the brains were removed and homogenized with lysis buffer (50 mM Tris-HCl (pH 7.4), 150 mM NaCl, 1 mM EGTA, 1% NP-40 supplemented with 1 mM PMSF, 1 μM aprotinin, 1 μM leupeptin, 1 mM Na_2VO_4, and 1 mM NaF). Protein concentrations were quantified using a bicinchonic acid protein assay kit (Pierce, Rockford, IL, USA). Proteins

(50 μg/well) were subjected to sodium dodecyl sulfate polyacrylamide gel electrophoresis (SDS-PAGE), and transferred to nitrocellulose membranes as described previously.[21] Membranes were blocked with 5% nonfat milk at 37 °C for 1 h. Occludin and ZO-1 proteins were immunodetected using polyclonal antibodies (Invitrogen). β-Actin was immunodetected using a mouse monoclonal antibody against mouse β-actin (Sigma) as an internal control. Intensities of the immunoreactive protein bands were determined using an UVIDOCMW vers. 99.03 digital imaging system (UVtec, Cambridge, UK).

Terminal Deoxynucleotidyl Transferase dUTP Nick End Labeling (TUNEL) Assay. A TUNEL assay was performed using the In Situ Cell Death Detection Kit (Roche Diagnostics, Mannheim, Germany), following the manufacturer's instructions. In brief, brain sections were fixed in 4% paraformaldehyde for 20 min and incubated with 0.1% Triton X-100 for 10 min. A TUNEL labeling reaction with fluorescein-conjugated dUTP was carried out at 37 °C for 60 min. These samples were then double-stained with a monoclonal antibody that specifically recognizes a vertebrate nervous system- and neuron-specific nuclear protein (NeuN; Millipore, Billerica, MA, USA) and endothelium-specific factor VIII, and observed under a confocal microscope (Olympus) as described previously.[22]

Statistical Analyses. The statistical significance of differences between the control and drug-treated groups was evaluated using Student's *t*-test, and differences were considered statistically significant at p values of <0.05. Differences between resveratrol- and high-fat diet-treated animals were considered significant when the p value of Duncan's multiple-range test was <0.05. Statistical analysis between groups over time was carried out by a two-way analysis of variance (ANOVA).

RESULTS

Resveratrol Alleviates High-Fat Diet-Induced Alterations Of Body Weights and Amounts of Total Cholesterol and LDL. After consuming a high-fat diet for more than 3 weeks, the body weight of ICR mice significantly increased (Table 1). Resveratrol did not change the body weights of control or high-fat diet-treated animals. Administration of both resveratrol and a high-fat diet did not affect the ratio of brain weight to body weight (data not shown). Administration of a high-fat diet to mice for 8 weeks caused a significant 54% increase in the level of serum total cholesterol (Figure 1A). Resveratrol alone decreased serum cholesterol levels by 16%. Simultaneously, the high-fat diet-augmented serum total cholesterol was reduced by 18% after resveratrol administration (Figure 1A). The high-fat diet caused a 2.2-fold increase in the amount of serum LDL (Figure 1B). Resveratrol did not affect the basal level of LDL but significantly decreased the high-fat diet-caused enhancement of serum LDL by 33%.

Resveratrol Protects Against High-Fat Diet-Induced Breakage of the BBB. An assay of the BBB integrity showed that Evans blue dye did not pass through the BBB in control mice (Figure 2A, top-left panel). After exposure to a high-fat diet for 8 weeks, the integrity of the BBB was disrupted, such that Evans blue dye passed the barrier and appeared in brain tissues (bottom-left panel). Resveratrol did not affect the permeability of the BBB (top-right panel), but obviously protected against high-fat diet-induced breakage of the BBB (bottom-right panel).

The resveratrol-involved protection against high-fat diet-induced insults to the BBB was further confirmed by confocal microscopy (Figure 2B). Evans blue dye was not detected in control brain slices. Meanwhile, when exposed to a high-fat diet for 8 weeks, Evans blue dye penetrated the BBB and then was observed in cerebral cortex. Resveratrol did not affect the permeability of the BBB, but prevented high-fat diet-caused damage (Figure 2B). The intensities of fluorescent signals were quantified and analyzed (Figure 2C). Treatment of ICR mice with a high-fat diet increased the signals of Evans blue dye in brain slices by 22-fold. However, exposure to resveratrol caused a significant 88% decrease in high-fat diet-induced BBB breakage (Figure 2C).

High-Fat Diet and Resveratrol Did Not Cause Death of Cerebrovascular Endothelial Cells. The localization and structure of the BBB were recognized by immunodetecting endothelium-specific factor VIII as analyzed by confocal microscopy (Figure 3). In control brain slices, factor VIII-recognizing cerebrovascular endothelial cells were observed. However, administration of neither a high-fat diet, resveratrol, nor a combination of resveratrol and the high-fat diet caused the death of cerebrovascular endothelial cells (Figure 3).

Resveratrol Attenuates High-Fat Diet-Induced Interruption of the Tight Junction Proteins, Occludi, and ZO-1 but Does Not Affect Their Protein Syntheses. Mechanisms of resveratrol-involved protection against high-fat diet-induced breakage of the BBB were determined by immunodetection of occludin and ZO-1, two typical tight junction proteins (Figure 4). In control mice, continuous occludin polymers were observed (Figure 4A). However, after administration of a

Table 1. Effects of Resveratrol (Res) and a High-Fat Diet (HFD) on the Body Weights of Mice[a]

	body weight (g)			
time (weeks)	control	Res	HFD	Res+HFD
0	24.33 ± 0.54	24.33 ± 0.54	24.33 ± 0.54	24.33 ± 0.54
1	29.51 ± 1.17	29.69 ± 1.19	29.80 ± 1.16	30.52 ± 0.92
2	33.97 ± 1.07	34.46 ± 1.09	34.99 ± 1.27	35.53 ± 0.84
3	36.21 ± 1.01	36.09 ± 1.09	38.04 ± 1.48*	37.49 ± 0.96
4	37.92 ± 0.98	37.90 ± 1.39	39.99 ± 1.57*	39.55 ± 0.86*
5	38.94 ± 0.95	39.51 ± 1.30	42.01 ± 1.73*	41.01 ± 1.04*
6	40.16 ± 1.06	39.82 ± 1.21	43.83 ± 1.88*	41.09 ± 0.79*
7	40.94 ± 1.16	41.21 ± 1.33	44.50 ± 2.20*	43.88 ± 1.43*
8	41.50 ± 1.44	40.69 ± 1.18	44.6s7 ± 2.11*	44.51 ± 1.78*

[a]Male ICR mice were treated with the control normal diet, resveratrol (Res), the HFD, and a combination of Res and the HFD for 8 weeks. Body weights were measured and statistically analyzed. Each value represents the mean ± SEM for $n = 6$. The asterisk symbol, *, indicates that the values significantly ($p < 0.05$) differ from the respective control group.

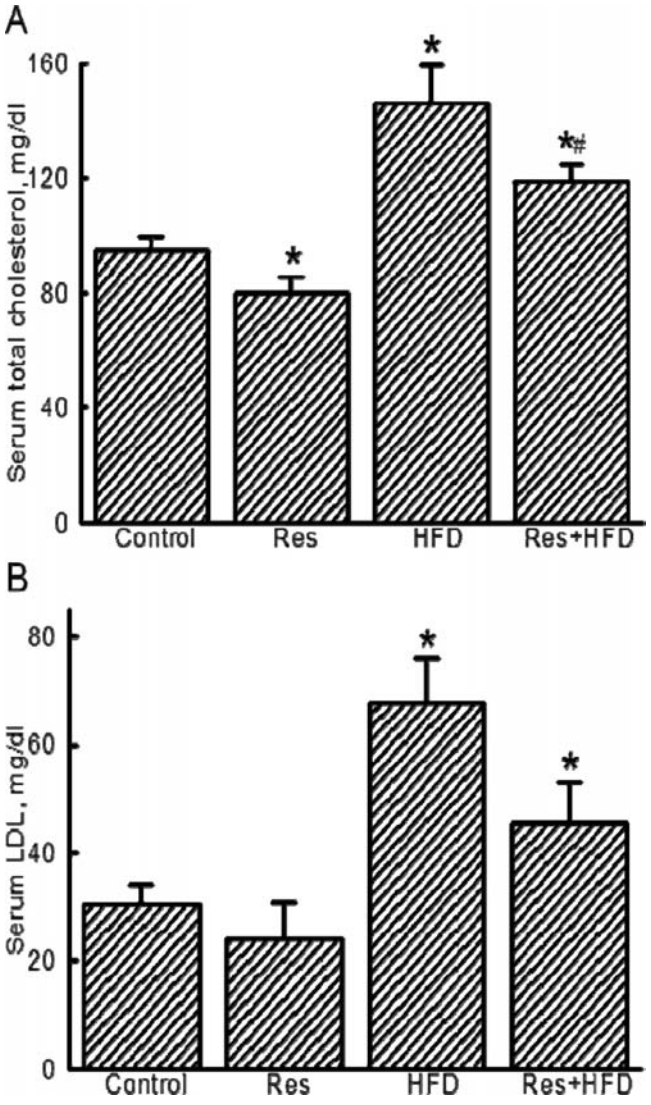

Figure 1. Effects of resveratrol (Res) on high-fat diet (HFD)-induced enhancement of serum total cholesterol and LDL. Male ICR mice were fed the control normal diet, Res, an HFD, and a combination of Res and the HFD for 8 weeks. After drug treatment, animals were sacrificed, and the blood was collected for analyses of total cholesterol (A) and LDL (B). Each value represents the mean ± SEM for $n = 6$. The asterisk and number symbols, * and #, indicate that values significantly ($p < 0.05$) differ from the respective control and HFD-treated groups.

high-fat diet, the occludin-formed polymers were disrupted into discontinuous spots. Resveratrol did not affect occludin polymerization, but lessened high-fat diet-caused disruption of the tight junction structure (Figure 4A). Similarly, continuous and uniform ZO-1 polymers were observed in control mouse brains (Figure 4B). After exposure to a high-fat diet for 8 weeks, the structure of ZO-1 polymerization was interrupted. Resveratrol did not change the ZO-1 tight junctions, but alleviated high-fat diet-caused breakage of ZO-1 polymerization (Figure 4B).

The intensities of the fluorescent signals presented in Figure 4A, B were quantified and statistically analyzed, and are presented in Table 2. Our data reveal that administration of a high-fat diet to mice for 8 weeks decreased polymerization of occludin and ZO-1 by 48% and 45%, respectively. Resveratrol did not alter the tight junctions constructed by occludin and ZO-1. However, cotreatment with resveratrol and a high-fat diet completely lowered the diet-induced breakage of occludin and ZO-1 tight junctions (Table 2).

To further determine the possible mechanisms of resveratrol-engaged preclusion of high-fat diet-caused rupture of occludin and ZO-1 tight junctions, immunoblot analyses were carried out (Figure 4C, D). Occludin and ZO-1 were immunodetected in control mouse brains (Figure 4C, top-two panels, lane 1). Resveratrol did not affect the contents of these two junction proteins in brain tissues (lane 2). After treatment with a high-fat diet and a combination of resveratrol and the high-fat diet for 8 weeks, the amounts of occludin and ZO-1 were not affected (lanes 3 and 4). Levels of β-actin were immunodetected as the internal controls (Figure 4C, bottom panel). These immunoreactive protein bands were quantified and analyzed (Figure 4D). Administration of neither resveratrol, a high-fat diet, nor a combination of resveratrol and the high-fat diet affected the contents of occludin or ZO-1 in brain tissues.

Resveratrol Defends Against High-Fat Diet-Induced Caspase-3 Activation and DNA Fragmentation of Brain Neurons. The protection by resveratrol against high-fat diet-induced insults to brain neurons was evaluated by analyzing activated caspase-3 and damage to genomic DNA (Figure 5). Brain neurons are specifically recognized by NeuN. Exposure of mice to a high-fat diet for 8 weeks increased the levels of cleaved caspase-3 in brain tissues (Figure 5A). Resveratrol did not affect caspase-3 activation. However, following cotreatment with resveratrol, the high-fat diet-caused caspase-3 activation obviously decreased (Figure 5A). Data from the TUNEL assay revealed high-fat diet-induced DNA fragmentation of brain neurons (Figure 5B). Resveratrol did not lead to DNA damage but obviously lowered high-fat diet-caused fragmentation of genomic DNA in brain neurons.

■ DISCUSSION

The cardioprotective effects of resveratrol, a constituent of red wine, are widely accepted, but its roles in the cerebral BBB are not well understood. This study showed that exposure of ICR mice to a high-fat diet for 8 weeks elevated the levels of serum total cholesterol and LDL, and body weight, but resveratrol significantly lowered such augmentations. At the same time, resveratrol protected the BBB from high-fat diet-induced interruption. The BBB is an important barricade situated in cerebral capillaries to maintain the homeostasis of the cerebral microenvironment.[9] Dysfunction of the BBB leads to profound and irreversible injuries to brain neurons.[25] In parallel with injuries to the BBB, this study showed that a high-fat diet induced insults to brain neurons. However, resveratrol decreased such damage. Therefore, the data presented in this study show that resveratrol can protect against high-fat diet-induced breakage of the BBB and consequently attenuate damage to brain neurons caused by this diet.

After exposure to resveratrol for 8 weeks, the high-fat diet-caused increase in body weight significantly decreased. Resveratrol can disturb the adipocyte life cycle via inhibiting adipogenesis or inducing apoptosis.[26] Accordingly, resveratrol possibly decreases the body weight through interfering with the adipocyte life cycle. Simultaneously, this study demonstrated that the high-fat diet-caused enhancements of serum total cholesterol and LDL were significantly reduced by resveratrol. As critical indicators of obesity, the augmentation of total cholesterol and LDL indicates the potential induction of tissue/cell damage.[27] In obese rats, long-term administration of resveratrol was reported to reduce the blood pressure through

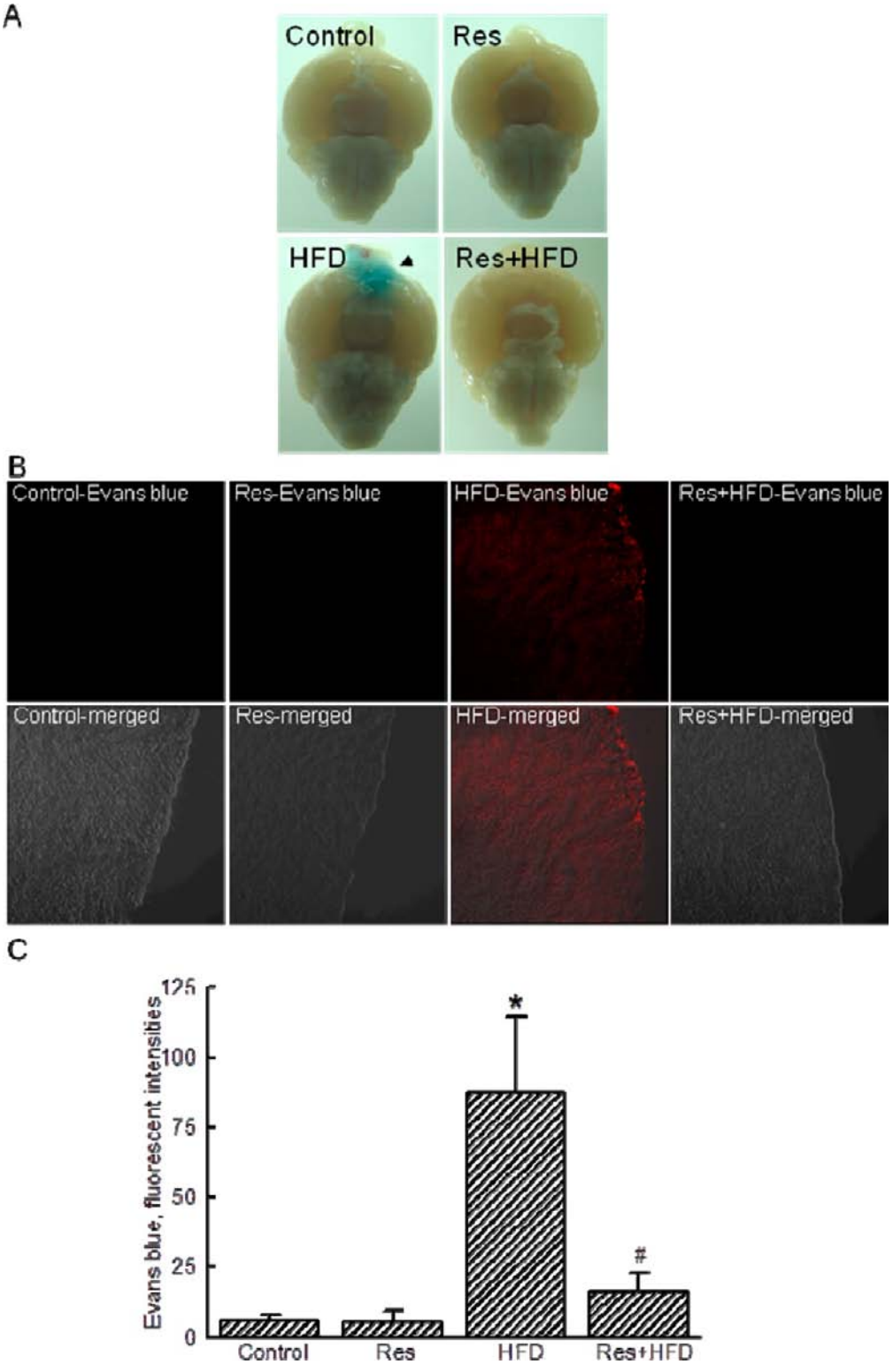

Figure 2. Effects of resveratrol (Res) on high-fat diet (HFD)-induced extravasation of Evans blue dye through the blood-brain barrier. Mice were fed the normal diet, Res, HFD, and a combination of Res and HFD for 8 weeks. After drug treatment, Evans blue dye was intravenously injected into animals and allowed to circulate for 1 h. Following reperfusion to wash out the dye in the vessels, mice were sacrificed and the brains were collected and photographed (A). Evans blue dye in brain slices was analyzed using confocal microscopy (B). Intensities of the fluorescent signals were quantified and statistically analyzed (C). Each value represents the mean ± SEM for $n = 6$. The asterisk and number symbols, * and #, indicate that values significantly ($p < 0.05$) differed from the respective control and HFD-treated groups. Magnification of confocal images: 600×.

decreasing total cholesterol levels.[28] LDL and its oxidized derivative, oxLDL, can induce pathophysiological conditions in various tissues and cells.[29] Reductions in the levels of total cholesterol and LDL can partially explain the potential of resveratrol to improve the health and survival of animals on a high-calorie diet.

dx.doi.org/10.1021/jf403286w | J. Agric. Food Chem. 2014, 62, 3466−3475

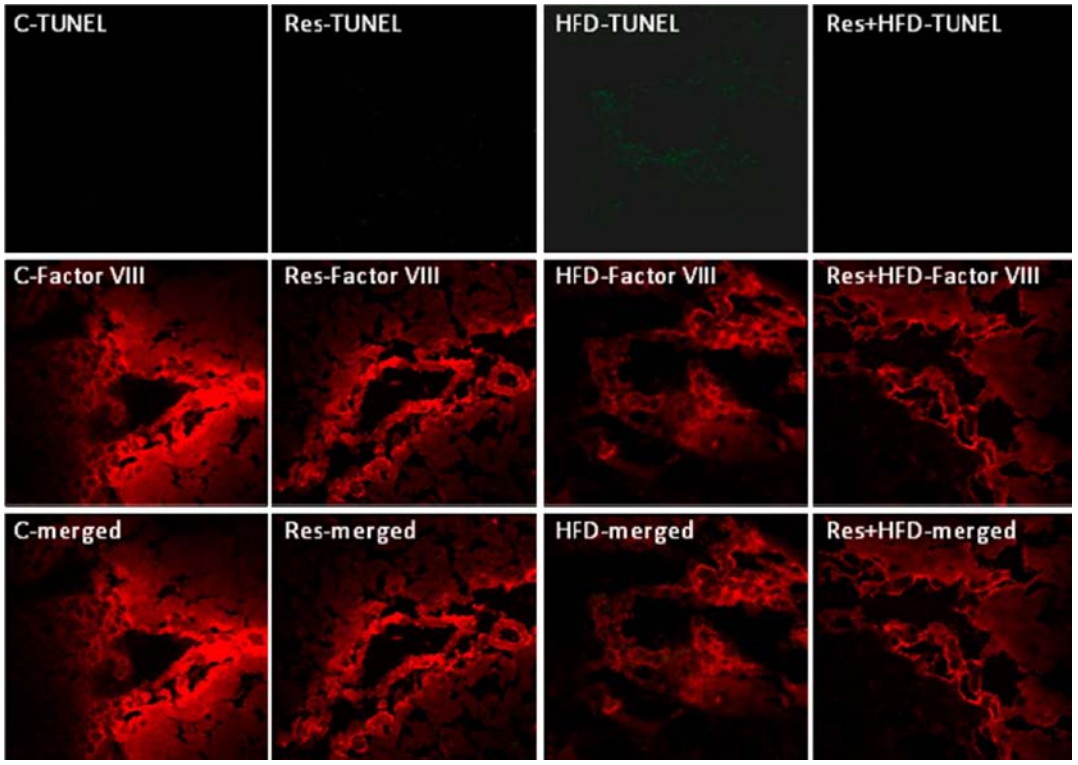

Figure 3. Effects of resveratrol (Res) and a high-fat diet (HFD) on distribution of cerebrovascular endothelial cells. Mice were fed the normal diet (C), Res, HFD, and a combination of Res and HFD for 8 weeks. After drug treatment, the brain tissues were frozen and sliced. TUNEL assays were performed and analyzed by confocal microscopy (top panels). Levels of factor VIII, an endothelium-specific protein, were immunodetected and analyzed by confocal microscopy (middle panels). The merged signals are also presented (bottom panels). Magnification of confocal images: 600×.

Many epidemiologic studies showed that elevated total cholesterol and LDL are possible risk factors for ischemic stroke.[30] In a hamster model, red wine, dealcoholized red wine, and especially grape juice inhibited atherosclerosis.[31] A previous study also reported that treatment with red wine can protect against oxidative stress and enhanced antioxidant enzyme activities in the brain and kidneys of rats fed a hyperlipidemic diet.[32] This study showed that mice fed a high-fat diet for 8 weeks exhibited hypercholesterolemia and increased circulating LDL levels, but oral intake of resveratrol simultaneously improved such elevation. High-fat diet-induced hypercholesterolemia is associated with endothelial dysfunction in cerebral arterioles which subsequently promotes the development of atherosclerosis and pathological changes in the CNS.[7,8] Therefore, resveratrol may lessen high-fat diet-induced cerebral diseases such as ischemic stroke.

The BBB is a complex structure acting essentially as a selective barrier for maintaining the cerebral microenvironment, and the main components responsible for the barrier properties are the tight junctions.[9,10] Disruption of tight junctions by drugs or disease is a destructive change that leads to impaired integrity of the BBB, thus compromising brain functions.[10,11] Ghribi et al. reported that hypercholesterolemia compromises the BBB in rabbits fed a cholesterol-enriched diet for 7 months.[33] Our present study further showed that exposure of ICR mice to a high-fat diet for 8 weeks induced hypercholesterolemia and simultaneously increased the extravasation of Evans blue dye. The appearance of Evans blue dye in brain tissues after intravenous perfusion and reperfusion indicates breakage of the BBB.[34] Our data suggest that a high-fat diet might contribute to the pathogenesis of brain-related diseases such as ischemia or Alzheimer's disease by virtue of its ability to disrupt the BBB integrity. However, resveratrol administration can alleviate the high-fat diet-caused damage to the BBB and brain neurons.

Table 2. Quantification of the Fluorescent Intensities Presented in Figure 4A, B[a]

	occludin (fluorescent intensity)	ZO-1 (fluorescent intensity)
control	398 ± 11	323 ± 14
Res	428 ± 163	313 ± 40
HFD	207 ± 10*	179 ± 20*
Res+HFD	303 ± 101	283 ± 28#

[a]Male ICR mice were treated with resveratrol (Res), a high-fat diet (HFD), and a combination of Res and the HFD for 8 weeks. Tight junction proteins were immunodetected and analyzed by confocal microscopy. Intensities of immunoreacted fluorescent signals were quantified and analyzed. Each value represents the mean ± SEM for $n = 6$. The asterisk and number symbols, * and #, indicate that the values significantly ($p < 0.05$) differ from the respective control and HFD-treated groups.

Cerebrovascular endothelial cells are major components of the BBB.[9] Our previous study demonstrated that oxLDL induces apoptotic insults to cerebrovascular endothelial cells,[12] and such insults are attenuated by resveratrol (data not shown). The data presented in this study further reveal that resveratrol can lower high-fat diet-augmented LDL levels. LDL is easily oxidized into oxLDL at the moieties of apolipoprotein B and lipids.[29] Thus, resveratrol may decrease high-fat diet-induced apoptotic insults to cerebrovascular endothelial cells and then protect against BBB damage. In addition, astrocytes and pericytes are two cell components of the BBB.[9] Our preliminary results showed that oxLDL could induce apoptosis of astrocytes.

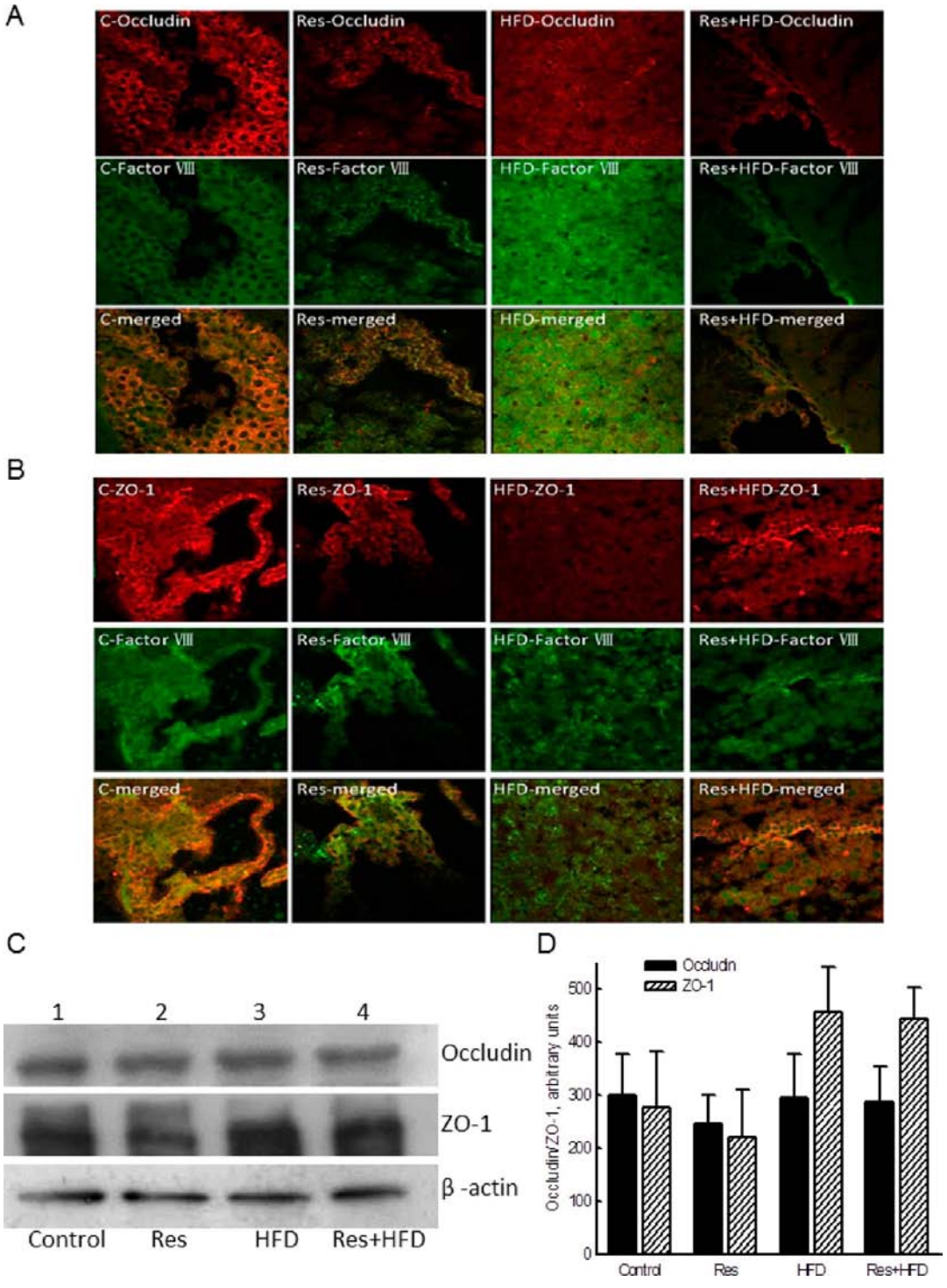

Figure 4. Effects of resveratrol (Res) on high-fat diet (HFD)-induced disruption of occludin and ZO-1 tight junctions and their protein levels. Mice were fed the normal diet, Res, HFD, and a combination of Res and HFD for 8 weeks. After drug treatment, the brain tissues were frozen and sliced. Occludin- and ZO-1-formed tight junctions were immunodetected and analyzed by confocal microscopy (A, B). Intensities of the fluorescent signals were quantified and statistically analyzed, and are presented in Table 2. Total proteins from animals were prepared for immunodetection of occludin and ZO-1 (C, top two panels). Levels of β-actin were detected as the internal standard (bottom panel). These protein bands were quantified and analyzed (D). Each value represents the mean ± SEM for $n = 6$. C, control. Magnification of confocal images: 600×.

Nevertheless, treatment of astrocytes with resveratrol lowered oxLDL-induced damage. A previous study reported that exposure of diabetic rats to a high-fat diet decreased number of retinal pericytes.[35] Interestingly, Kim et al. demonstrated the protective effects of resveratrol against diabetes-induced pericyte loss in mouse retinas.[36] Hence, astrocytes and pericytes may also contribute to resveratrol-involved protection of the BBB against high-fat diet-induced injuries. However, studies about interaction of resveratrol with cerebrovascular pericytes are limited. In our lab, the effects of resveratrol and high-fat diet on astrocytes and pericytes will be further examined.

dx.doi.org/10.1021/jf403286w | J. Agric. Food Chem. 2014, 62, 3466−3475

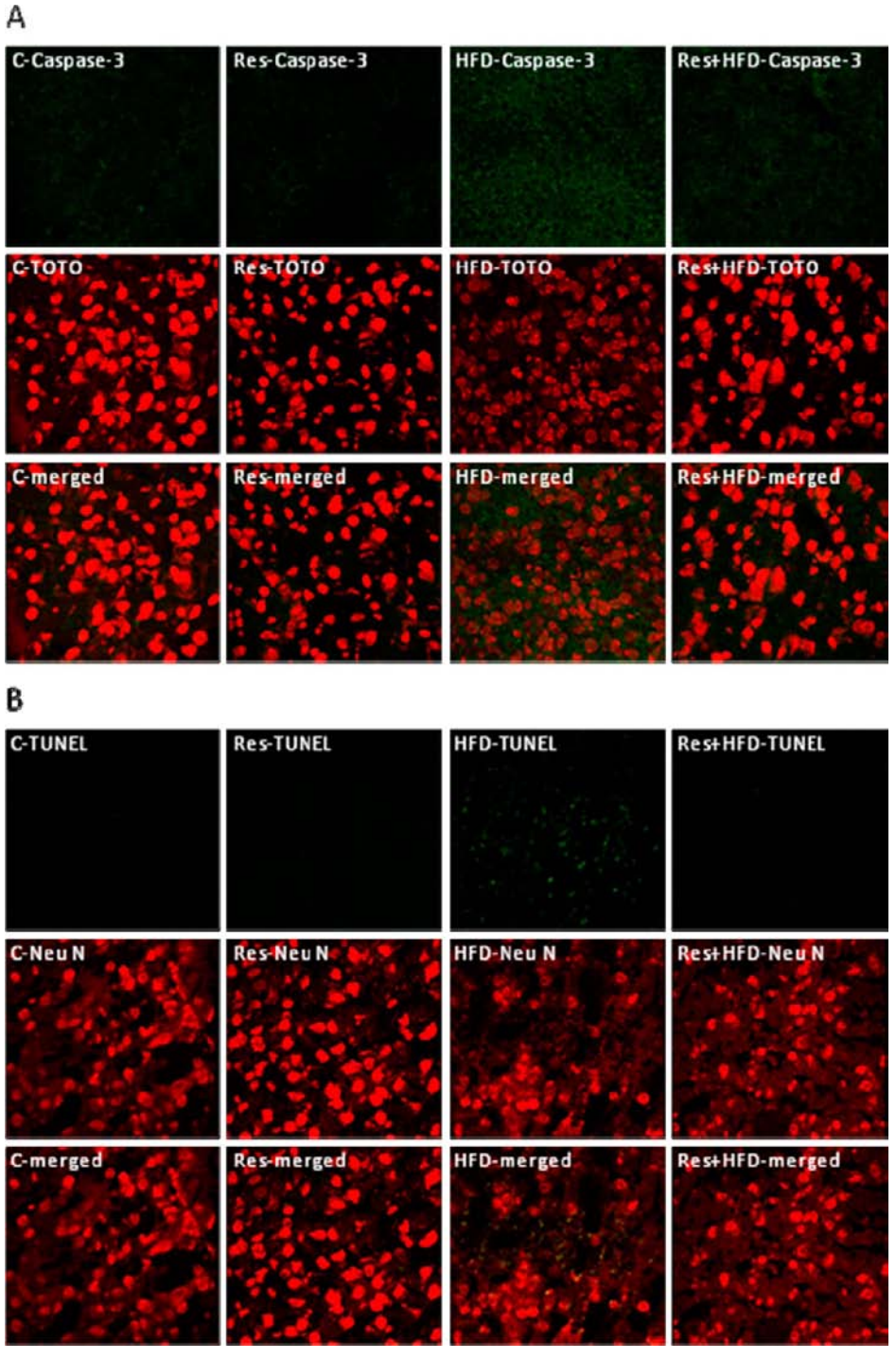

Figure 5. Effects of resveratrol (Res) on high-fat diet (HFD)-induced damage to brain neurons. Mice were fed the normal diet, Res, HFD, and a combination of Res and HFD for 8 weeks. After drug treatment, the brain tissues were frozen and sliced. Levels of activated caspase-3 were immunodetected and analyzed by confocal microscopy (A). TUNEL assays were executed and analyzed by confocal microscopy (B). Brain neurons are specifically recognized by NeuN. Magnification of confocal images: 600×.

Occludin and ZO-1 are two typical tight junction proteins which comprise the BBB.[9,21] Our results reveal that resveratrol could ease the high-fat diet-caused interruption of occludin and ZO-1 tight junctions. However, immunoblotting analyses showed no effect of resveratrol and a high-fat diet on the contents of occludin and ZO-1 in mouse brains. Cytoskeleton and cellular adenosine triphosphate (ATP) have been reported to participate in construction of the tight junction barrier.[37,38] Our previous study showed that oxLDL induced disruption of cytoskeleton polymerization and ATP synthesis in cerebrovascular endothelial cells, but treatment with resveratrol lessened such injuries.[21] As a result, one possible reason that resveratrol could ameliorate high-fat diet-induced disturbance of occludin and ZO-1 tight junctions may occur through promoting cytoskeleton construction and energy production. Taken together, resveratrol possibly protects the BBB against high-fat diet-induced breakage through suppression of damage to cerebrovascular endothelial cells and polymerization of occludin and ZO-1.

dx.doi.org/10.1021/jf403286w | J. Agric. Food Chem. 2014, 62, 3466−3475

Latour et al. reported that early BBB breakdown precedes neuronal damage in human focal brain ischemia.[39] After exposure to resveratrol for 8 weeks, the high-fat diet-caused caspase-3 activation and DNA fragmentation simultaneously decreased. Caspase-3 activation and DNA fragmentation are two important characteristics of cells undergoing apoptosis.[12,22] Thus, resveratrol protects brain neurons against high-fat diet-induced neuronal damage via an antiapoptotic mechanism. Studzinski et al. showed that consumption of a Western diet for 4 weeks significantly elevated cerebral oxidative stress and induced brain damage.[40] Resveratrol has efficient antioxidant activity to scavenge lipid hydroperoxyl free radicals.[18,21] Such antioxidant properties, at least in part, protect neuronal cells from high-fat diet-induced damage. Dysfunction of the BBB is recognized as a critical cause of brain neuron injuries.[22,24] Therefore, resveratrol can defend against high-fat diet-induced injuries of brain neurons through lessening the breakage of the BBB.

In conclusion, this study showed that a high-fat diet increased the body weight and serum levels of total cholesterol and LDL, but resveratrol significantly decreased such augmentations. The high-fat diet-induced interruption of the BBB integrity decreased after resveratrol administration. Resveratrol attenuated high-fat diet-caused breakage of the BBB through improving polymerization of occludin and ZO-1. Consequently, the high-fat diet-induced caspase-3 activation and DNA fragmentation were alleviated by resveratrol. Therefore, we suggest that long-term administration of resveratrol can protect against high-fat diet-caused disruption of the BBB through activating polymerization of occludin and ZO-1, and attenuates apoptotic injuries to brain neurons by dietary fat.

AUTHOR INFORMATION

Corresponding Author

*Phone: + 886-2-27361661 ext. 3222. Fax: +886-2-86621119. E-mail: rmchen@tmu.edu.tw.

Notes

The authors declare no competing financial interest.

ACKNOWLEDGMENTS

This study was supported by Wan-Fang Hospital (100swf08; 99-wf-eva-13), the Ministry of Health and Welfare (MOHW103-TD-B-111-01), and the National Science Council (NSC101-2314-B-038-003-MY3), Taipei, Taiwan. We express their gratitude to Ms. Yi-Ling Lin, Dai-Er Li, and Xin-Yu Qin for their technical support and data collection for these experiments.

REFERENCES

(1) Tsai, T. Y.; Chu, L. H.; Lee, C. L.; Pan, T. M. Atherosclerosis-preventing activity of lactic acid bacteria-fermented milk-soymilk supplemented with *Momordica charantia*. *J. Agric. Food Chem.* **2009**, *57*, 2065−2071.

(2) Wilde, D. W.; Massey, K. D.; Walker, G. K.; Vollmer, A.; Grekin, R. J. High-fat diet elevates blood pressure and cerebrovascular muscle Ca^{2+} current. *Hypertension* **2000**, *35*, 832−837.

(3) Allen, C. L.; Bayraktutan, U. Risk factors for ischaemic stroke. *Int. J. Stroke* **2005**, *3*, 105−116.

(4) Glass, C. K.; Witztum, J. L. Atherosclerosis: The road ahead. *Cell* **2001**, *104*, 503−516.

(5) Wang, D.; Wei, X.; Yan, X.; Jin, T.; Ling, W. Protocatechuic acid, a metabolite of anthocyanins, inhibits monocyte adhesion and reduces atherosclerosis in apolipoprotein E-deficient mice. *J. Agric. Food Chem.* **2010**, *58*, 12722−12728.

(6) Hansson, G. K. Inflammation, atherosclerosis, and coronary artery disease. *N. Engl. J. Med.* **2005**, *352*, 1685−1695.

(7) Kitayama, J.; Faraci, F. M.; Lentz, S. R.; Heistad, D. D. Cerebral vascular dysfunction during hypercholesterolemia. *Stroke* **2007**, *38*, 2136−2141.

(8) Hall, W. L. Dietary saturated and unsaturated fats as determinants of blood pressure and vascular function. *Nutr. Res. Rev.* **2009**, *22*, 18−38.

(9) Wolburg, H.; Lippoldt, A. Tight junctions of the blood-brain barrier: Development, composition and regulation. *Vasc. Pharmacol.* **2002**, *38*, 323−337.

(10) Huber, J. D.; Egleton, R. D.; Davis, T. P. Molecular physiology and pathophysiology of tight junctions in the blood-brain barrier. *Trends Neurosci.* **2001**, *24*, 719−725.

(11) Hawkins, B. T.; Davis, T. P. The blood-brain barrier/neurovascular unit in health and disease. *Pharmacol. Rev.* **2005**, *57*, 173−185.

(12) Chen, T. G.; Chen, T. L.; Chang, H. C.; Tai, Y. T.; Cherng, Y. G.; Chang, Y. T.; Chen, R. M. Oxidized low-density lipoprotein induces apoptotic insults to mouse cerebral endothelial cells via a bax-mitochondria-caspase protease pathway. *Toxicol. Appl. Pharmacol.* **2007**, *219*, 42−53.

(13) Mulder, M.; Blokland, A.; Van den Berg, D. J.; Schulten, H.; Bakker, A. H. F.; Terwel, D.; Honig, W.; de Kloet, E. R.; Havekes, L. M.; Steinbusch, H. W. M.; de Lange, E. C. M. Apolipoprotein E protects against neuropathology induced by a high-fat diet and maintains the integrity of the blood-brain barrier during aging. *Lab. Invest.* **2001**, *81*, 953−960.

(14) Mato, M.; Ookawara, S.; Sakamoto, A.; Aikawa, E.; Ogawa, T.; Mitsuhashi, U.; Masuzawa, T.; Suzuki, H.; Honda, M.; Yazaki, Y.; Watanabe, E.; Luoma, J.; Yla-Herttuala, S.; Fraser, I.; Gordon, S.; Kodama, T. Involvement of specific macrophage-lineage cells surrounding arterioles in barrier and scavenger function in brain cortex. *Proc. Natl. Acad. Sci., U. S. A.* **1996**, *93*, 3269−3274.

(15) Baur, J. A.; Sinclair, D. A. Therapeutic potential of resveratrol: The in vivo evidence. *Nat. Rev. Drug Discovery* **2006**, *5*, 493−506.

(16) Dell'Agli, M.; Busciala, A.; Bosisio, E. Vascular effects of wine polyphenols. *Cardiovasc. Res.* **2004**, *63*, 593−602.

(17) Perez-Vizcaino, F.; Duarte, J.; Andriantsitohaina, R. Endothelial function and cardiovascular disease: Effects of quercetin and wine polyphenols. *Free Radical Res.* **2006**, *40*, 1054−1065.

(18) Rossi, L.; Mazzitelli, S.; Arciello, M.; Capo, C. R.; Rotilio, G. Benefits from dietary polyphenols for brain aging and Alzheimer's disease. *Neurochem. Res.* **2008**, *33*, 2390−2400.

(19) Andriambeloson, E.; Kleschyov, A. L.; Muller, B.; Beretz, A.; Stoclet, J. C.; Andriantsitohaina, R. Nitric oxide production and endothelium-dependent vasorelaxation induced by wine polyphenols in rat aorta. *Br. J. Pharmacol.* **1997**, *120*, 1053−1058.

(20) Leikert, J. F.; Rathel, T. R.; Wohlfart, P.; Cheynier, V.; Vollmar, A. M.; Dirsch, V. M. Red wine polyphenols enhance endothelial nitric oxide synthase expression and subsequent nitric oxide release from endothelial cells. *Circulation* **2002**, *106*, 1614−1617.

(21) Lin, Y. L.; Chang, H. C.; Chen, T. L.; Chang, J. H.; Chiu, W. T.; Lin, J. W.; Chen, R. M. Resveratrol protects against oxidized LDL-induced breakage of the blood-brain barrier by lessening disruption of tight junctions and apoptotic insults to mouse cerebrovascular endothelial cells. *J. Nutr.* **2010**, *140*, 2187−2192.

(22) Chang, H. C.; Chen, T. G.; Tai, Y. T.; Chen, J. T.; Chen, R. M. Resveratrol attenuates oxidized LDL-evoked Lox-1 signaling and consequently protects against apoptotic insults to cerebrovascular endothelial cells. *J. Cereb. Blood Flow Metab.* **2011**, *31*, 842−854.

(23) Provinciali, M.; Re, F.; Donnini, A.; Orlando, F.; Bartozzi, B.; Di Stasio, G.; Smorlesi, A. Effect of Resveratrol on the development of spontaneous mammary tumors in HER-2/neu transgenic mice. *Int. J. Cancer* **2005**, *115*, 36−45.

(24) Aoki, T.; Sumii, T.; Mori, T.; Wang, X.; Lo, E. H. Blood-brain barrier disruption and matrix metalloproteinase-9 expression during reperfusion injury: Mechanical versus embolic focal ischemia in spontaneously hypertensive rats. *Stroke* **2002**, *33*, 2711−2717.

(25) Hawkins, B. T.; Egleton, R. D. Fluorescence imaging of blood-brain barrier disruption. *J. Neurosci. Methods* **2006**, *151*, 262−267.
(26) Rayalam, S.; Della-Fera, M. A.; Baile, C. A. Phytochemicals and regulation of the adipocyte life cycle. *J. Nutr. Biochem.* **2008**, *19*, 717−726.
(27) Poobalan, A.; Aucott, L.; Smith, W. C.; Avenell, A.; Jung, R.; Broom, J. Effects of weight loss in overweight/obese individuals and long-term lipid outcomes-A systematic review. *Obesity Rev.* **2004**, *5*, 43−50.
(28) Rivera, L.; Moron, R.; Zarzuelo, A.; Galisteo, M. Long-term resveratrol administration reduces metabolic disturbances and lowers blood pressure in obese Zucker rats. *Biochem. Pharmacol.* **2009**, *77*, 1053−1063.
(29) Matsuura, E.; Hughes, G. R.; Khamashta, M. A. Oxidation of LDL and its clinical implication. *Autoimmun. Rev.* **2008**, *7*, 558−566.
(30) Navi, B. B.; Segal, A. Z. The role of cholesterol and statins in stroke. *Curr. Cardiol. Rep.* **2009**, *11*, 4−11.
(31) Vinson, J. A.; Teufel, K.; Wu, N. Red wine, dealcoholized red wine, and especially grape juice, inhibit atherosclerosis in a hamster model. *Atherosclerosis* **2001**, *156*, 67−72.
(32) Montilla, P.; Espejo, I.; Munoz, M. C.; Bujalance, I.; Muñoz-Castañeda, J. R.; Tunez, I. Protective effect of red wine on oxidative stress and antioxidant enzyme activities in the brain and kidney induced by feeding high cholesterol in rats. *Clin. Nutr.* **2006**, *25*, 146−153.
(33) Ghribi, O.; Golovko, M. Y.; Larsen, B.; Schrag, M.; Murphy, E. J. Deposition of iron and beta-amyloid plaques is associated with cortical cellular damage in rabbits fed with long-term cholesterol-enriched diets. *J. Neurochem.* **2006**, *99*, 438−449.
(34) del Valle, J.; Camins, A.; Pallas, M.; Vilaplana, J.; Pelegrí, C. A new method for determining blood-brain barrier integrity based on intracardiac perfusion of an Evans Blue-Hoechst cocktail. *J. Neurosci. Methods* **2008**, *174*, 42−49.
(35) Mancini, J. E.; Ortiz, G.; Croxatto, J. O.; Gallo, J. E. Retinal upregulation of inflammatory and proangiogenic markers in a model of neonatal diabetic rats fed on a high-fat-diet. *BMC Ophthalmol.* **2013**, *Apr 15*, 13−14.
(36) Kim, Y. H.; Kim, Y. S.; Roh, G. S.; Choi, W. S.; Cho, G. J. Resveratrol blocks diabetes-induced early vascular lesions and vascular endothelial growth factor induction in mouse retinas. *Acta Ophthalmol.* **2012**, *90*, e31−e37.
(37) Yap, A. S.; Manley, S. W. Microtubule integrity is essential for apical polarization and epithelial morphogenesis in the thyroid. *Cell Motil. Cytoskeleton* **2001**, *48*, 201−212.
(38) Cavanaugh, K. J., Jr.; Oswari, J.; Margulies, S. S. Role of stretch on tight junction structure in alveolar epithelial cells. *Am. J. Respir. Cell Mol. Biol.* **2001**, *25*, 584−591.
(39) Latour, L. L.; Kang, D. W.; Ezzeddine, M. A.; Chalela, J. A.; Warach, S. Early blood-brain barrier disruption in human focal brain ischemia. *Ann. Neurol.* **2004**, *56*, 468−477.
(40) Studzinski, C. M.; Li, F.; Bruce-Keller, A. J.; Fernandez-Kim, S. O.; Zhang, L.; Weidner, A. M.; Markesbery, W. R.; Murphy, M. P.; Keller, J. N. Effects of short-term Western diet on cerebral oxidative stress and diabetes related factors in APP x PS1 knock-in mice. *J. Neurochem.* **2009**, *108*, 860−866.

and elucidate the processes involved. Recent studies by Upreti et al. have characterized some of the photoinduced degradation products of monatin,[27] but more rigorous investigation of the mechanisms is required to fully understand the degradation pathways of monatin and the conditions under which this occurs. We postulated that monatin may undergo photodegradation pathways similar to those recently elucidated for the structurally related amino acid tryptophan and its derivatives.[29−31] We report here on studies carried out to examine the mechanisms of monatin degradation and the factors that influence these processes.

MATERIALS AND METHODS

(2*R*,4*R*)-Monatin salt (Na) was supplied by Cargill Ltd. (Wayzata, MN, USA). Hydrogen peroxide, 30% solution, iron(II) sulfate heptahydrate were supplied by Merck (Darmstadt, Germany). Catalase (bovine liver), citric acid, deuterium oxide (97%), xylenol orange tetrasodium salt, Rose Bengal, trisodium citrate dehydrate were supplied by Sigma-Aldrich (Castle Hill, NSW, Australia). All water (H_2O) was filtered to Nanopure quality using a four-stage Milli-Q system (Millipore, North Ryde, Australia)). Sulfuric acid, 95−98% (~18 M), was from Ajax Finechem (Sydney, NSW, Australia). Syringe filters (0.45 μm, 33 mm diameter) were from Sartorius (Dandenong South, VIC, Australia). Disposable plastic cuvettes (0.5−2.0 mL, 1 cm path length) were from Interpath (West Heidelberg, VIC, Australia).

Composition of Mock Beverage Solutions. Standard beverage solutions consisted of monatin (0.005%, 170 μM), sodium benzoate (0.015%, 1 mM), citric acid (0.16%, 8.3 mM), and trisodium citrate (0.02%, 680 μM) in Nanopure water or deuterium oxide (D_2O) with the pH/pD adjusted to 3.0. Variations are discussed as appropriate in the text.

Photooxidation Apparatus. Beverage samples were illuminated using a light box (Medlite, Sydney, Australia) fitted with a circular 32 W daylight fluorescence tube (FCL32D; 1890 lm; NEC, Tokyo, Japan) and opaque diffuser. The samples were placed a fixed distance from the illumination source to receive a standardized light exposure of 7.5 W m^{-2} (equivalent to 3000 Lux; for lamp profile see Supporting Information Figure 1A). Light doses were calibrated using a Stellarnet spectrometer (Comet-SL-3C-50, Warsash Scientific, Redfern, NSW, Australia).

Oxidation of Monatin with Singlet Oxygen. Singlet oxygen-mediated photooxidation of monatin beverage solutions was achieved using a modification of a previous method.[32,33] Briefly, Rose Bengal (10 μM) was added to the standard monatin beverage solutions (as above). The samples were kept at 21 °C and bubbled with compressed air during illumination for up to 15 min with visible light (820 W m^{-2} equivalent to 250 000 Lux; for lamp profile see Supporting Information Figure 1B) from an AV2050 slide projector (Kodak, Box Hill, VIC, Australia).

Columns and Mobile Phases Used for Liquid Chromatography. Chromatographic separations were carried out on an Acquity HSS T3 UHPLC column (2.1 × 100 mm; 1.8 μm pore size; Waters, Rydalmere, NSW, Australia) using gradients (as specified below) of solvent A (10 mM ammonium formate, with 0.1% formic acid in water) and solvent B (10% acetonitrile in methanol).

Quantification of Monatin Oxidation Products by UHPLC with UV or Accurate Mass QTOF Detection. UHPLC of monatin and its reaction products was carried out with a column temperature of 45 °C and a mobile phase (0.6 mL min^{-1}) consisting of a gradient (see above for buffer compositions) as follows: 5% solvent B and 95% solvent A for 1.5 min with a linear increase to 12% solvent B over the next 2 min and a further increase to 35% solvent B over the next 5.5 min. The column was then washed by increasing to 95% solvent B over 2 min, holding at 95% B for 1 min, before decreasing to 5% B over 0.1 min, with 1.9 min reequilibration prior to the next injection. Samples were filtered with centrifugal filters (MF 0.2 μm; Pall Nanosep, Somersby, NSW, Australia) to remove particulate matter prior to analysis and placed in glass HPLC vials. Quantification of monatin and its products was carried out (at 280 nm) using a Shimadzu Nexera UHPLC system (Shimadzu, South Rydalmere, NSW, Australia) following 2 μL injections. Monatin eluted at 5.07 min, and the corresponding monatin lactone (lactone) at 4.33 min. Peak areas were determined using Lab Solutions 5.32 SP1 (Shimadzu).

Accurate mass and MS/MS analyses of monatin products (20 μL sample injections) were carried out using an Agilent 1290 UHPLC system (Agilent Technologies, Santa Clara, CA, USA) coupled to an Agilent 6530 QTOF instrument (Agilent Technologies) operating in both positive and negative ionization modes with an Agilent Jet Stream electrospray source. The QTOF spectrometer was operated under the following conditions: source gas temperature of 350 °C, drying gas flow of 10 L/min, nebulizer gas pressure of 20 psig, sheath gas temperature of 385 °C, sheath gas flow of 12 L/min, VCap of 3000 V, and a fragmentor voltage of 125 V. Ultrahigh purity nitrogen was used as the collision gas for MS/MS experiments.

Analysis of Monatin Oxidation Products by LC−MS/MS. A Thermo LCQ Deca XP MAX Plus (Thermo Fisher, North Ryde, NSW, Australia) ion-trap instrument coupled to a Finnigan Surveyor HPLC (Thermo Fisher) system was used with electrospray ionization in positive ion mode. Samples were held at 10 °C prior to injection (20 μL), before separation at 40 °C at a flow rate of 100 μL min^{-1}. Compounds were eluted using the following gradient: 100% solvent A for 10 min, then a linear increase to 40% B over 20 min, followed by a rapid increase to 100% B over 5 min, a 5 min wash with 100% B, before returning to 100% A over 2 min and reequilibration with solvent A for 18 min, to give a total run time of 70 min. The electrospray needle was held at 4.5 kV. Helium was used as the collision gas, and nitrogen was used as the sheath and sweep gas set to 70 and 30 arbitrary units, respectively. The temperature of the heated capillary was 250 °C. Selective ion monitoring (SIM) detection was carried out with an isolation width of ±1 mass unit from the specified m/z values as required, with collision energies of 28 or 35%.

Quantification of Peroxides by the FOX Assay. Peroxides were quantified using a modified FOX assay, with data reported as H_2O_2 equivalents as the reaction stoichiometry for monatin-derived peroxides with the FOX reagent is unknown.[34] The FOX reagent was prepared from xylenol orange (3,3-bis[*N*,*N*-bis(carboxylmethyl)amino-methyl]-*o*-cresolsulfonephthalein, Na^+ salt), sulfuric acid, and iron(II) sulfate (5 mM, 0.5 M, and 5 mM, respectively). Organic peroxide levels were determined after treatment (15 min) of samples with catalase (50 μL of a 1 mg mL^{-1} solution) to remove H_2O_2 before addition of the FOX reagent. Previous studies have verified that organic peroxides are not affected by catalase.[33,35]

Sample Concentration for UHPLC and LC−MS/MS Analysis. Photolyzed monatin standard beverage samples were concentrated as necessary using the following procedure. Ten milliliters of solution was treated overnight with washed Chelex 100 resin (BioRad, Gladesville, NSW, Australia) to remove trace metal ions. The supernatant was removed, and 1 mL aliquots were dried by vacuum centrifugation (18 h). Dried samples were reconstituted in 100 μL of Nanopure water (giving a 10-fold concentration of the sample) before filtering using 0.2 μm centrifugal filters. Samples were kept at <10 °C prior to analysis.

Statistical Analyses. Data are reported as mean ± standard error of the mean (SEM) from three or more independent experiments. Statistical analyses were performed using GraphPad Prism 5 (GraphPad Software, San Diego, CA; http://www.graphpad.com) using two-way ANOVA with Bonferroni's post hoc test. Significance was taken as $p < 0.05$.

RESULTS

Time Course and Treatment Studies. *Monatin Degradation in the Presence of Light.* Because previous studies have provided evidence of monatin degradation on exposure to UV/visible light,[25,27] initial experiments quantified monatin photodegradation under a variety of conditions. Mock beverage solutions of monatin [0.005% (170 μM); pH 3 in citrate buffer; see Materials and Methods] were illuminated by fluorescent light (7.5 W m^{-2}) in colorless, transparent PET bottles using a light

box. Samples were removed at regular time points, stored at −20 °C, and analyzed by UHPLC (see Supporting Information Figure 2 for example traces). The parent monatin peak decreased in intensity with increasing photolysis time (Figure 1A), with ∼27% loss observed after 14 days and ∼76% by 50 days.

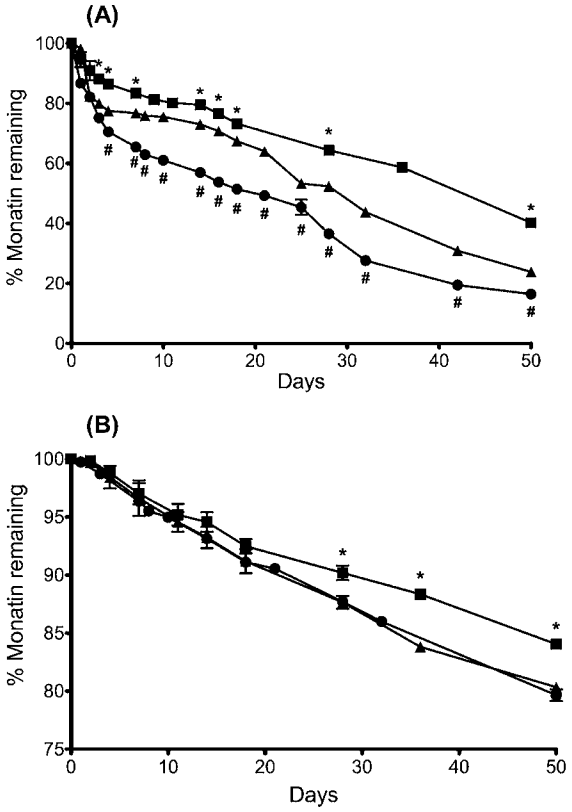

Figure 1. Monatin loss over time: (A) following illumination with a fluorescent light source (7.5 W m^{-2}) and (B) following incubation in the dark (note difference in vertical axis scale between A and B). The mock beverage samples (170 μM monatin) were prepared in H_2O control (▲), D_2O (●) or Chelex-treated (■) citrate buffers (pH 3). Values are shown as mean ± SEM (N = 3 replicates). # Statistically significant from control (P < 0.05). * Chelex treatment significantly different from D_2O and control (P < 0.05).

To investigate whether $^1O_2$ plays a role in monatin photodegradation, beverage solutions were prepared with D_2O in place of H_2O, as the decay rate of $^1O_2$ is slowed in D_2O,[36,37] thereby promoting $^1O_2$-mediated processes. Photolysis of monatin solutions in D_2O enhanced monatin loss, with ∼43% of the parent lost after 14 days, and ∼84% by 50 days (Figure 1A).

The involvement of metal ions (via possible interaction with dissolved O_2 or peroxides; see eqs 1−4[38]) was probed by treating either the citrate buffer prior to preparation of the monatin solutions, or the monatin solutions once generated, with Chelex 100 resin to remove adventitious metal ions. Photolysis of these Chelex-treated samples resulted in significantly less parent monatin loss compared with those prepared in untreated buffer. The data obtained with both Chelex treatments were identical, with ∼20% monatin lost after 14 days, and ∼60% after 50 days (Figure 1A; data for Chelex-treated preformed monatin solutions not shown).

$$[\text{monatin}] + Fe^{3+} \rightarrow Fe^{2+} + [\text{monatin}]^{+\bullet} \quad (1)$$

$$Fe^{2+} + O_2 \rightarrow Fe^{3+} + O_2^{-\bullet} \quad (2)$$

$$2O_2^{-\bullet} \rightarrow O_2 + H_2O_2 \quad (3)$$

$$H_2O_2 + Fe^{2+} \rightarrow Fe^{3+} + HO^- + HO^{\bullet} \quad (4)$$

Degradation of Monatin in the Absence of Light. Identical mock beverage solutions to those described above were kept in the dark for 50 days. Monatin degradation was much slower in the absence of light than in its presence, with samples prepared in control (H_2O) or D_2O buffers losing ∼7% of parent monatin after 14 days (and ∼20% after 50 days), whereas in Chelex-treated samples, ∼6% and ∼16% of monatin was lost after 14 and 50 days, respectively (Figure 1B).

Effect of Chelating Agents and Added Transition Metal Ions. The protective effect of Chelex pretreatment is consistent with a role for metal ions in monatin degradation, irrespective of the presence of light. Thus, experiments were repeated with either added metal ion chelators or added metal ions to identify species that might be involved. EDTA (a nonspecific metal chelator, 50 μM) or desferrioxamine (a specific iron chelator, 50 μM) was added to standard mixtures and illuminated for 14 days. Controls were prepared with untreated or Chelex-treated citrate buffer (control). After 14 days, the control samples had lost ∼31% monatin, compared with ∼24%, ∼21%, and ∼20% for the samples prepared with EDTA, desferrioxamine, and Chelex-treated buffer, respectively (Figure 2A). The similar levels of monatin loss observed with each of these treatments are consistent with trace metal ions, particularly iron ions, playing a role in monatin degradation.

For experiments with added metal ions, Fe_2SO_4 (100 nM or 50 μM) or $CuCl_2$ (50 μM) were added to Chelex-treated mock beverage solutions. The samples were illuminated (or kept in the dark) for 14 days together with control samples without any metal ion additions. After 14 days, Chelex-treated samples had lost ∼20% monatin, whereas with Fe_2SO_4, a greater loss that was dose-dependent (∼28% with 100 nM and ∼89% with 50 μM Fe_2SO_4; Figure 2B) was observed. Samples supplemented with $CuCl_2$ (50 μM) lost only ∼14% of monatin, less than that observed in the controls. The loss of monatin in nonilluminated samples was much less than in the photodegraded samples, but the pattern of monatin loss followed that in the illuminated samples [8% (control), 6% ($CuCl_2$), 9% (100 nM Fe_2SO_4), and 16% (50 μM Fe_2SO_4)].

Characterization of Intermediates. In addition to monatin loss during light exposure, UHPLC analysis demonstrated growth of a peak at 4.33 min. This peak reached maximal intensity after a few days before declining at longer times. This peak is assigned to monatin lactone [**3**], which is in equilibrium with parent monatin (Scheme 2).[10,23,24] The extent of lactonization versus oxidation was assessed by comparing peak areas. The rapid loss of monatin during the initial photolysis period (Figure 2) was mirrored by an increase in lactone. From comparison of the peak areas, it is estimated that ∼60% of the initial monatin loss (corresponding to ∼15% of the total monatin present) arises from lactone formation. From here on, "total indole" is used to refer to the total of monatin and lactone (calculated assuming an identical extinction coefficient for both compounds; data not shown).

Photooxidation of Trp [**2**] gives Trp peroxides as major initial products; these undergo photodegradation on extended illumination.[29] Thus, the ferrous xylenol orange (FOX) assay [34] was used to measure the formation of H_2O_2 or monatin

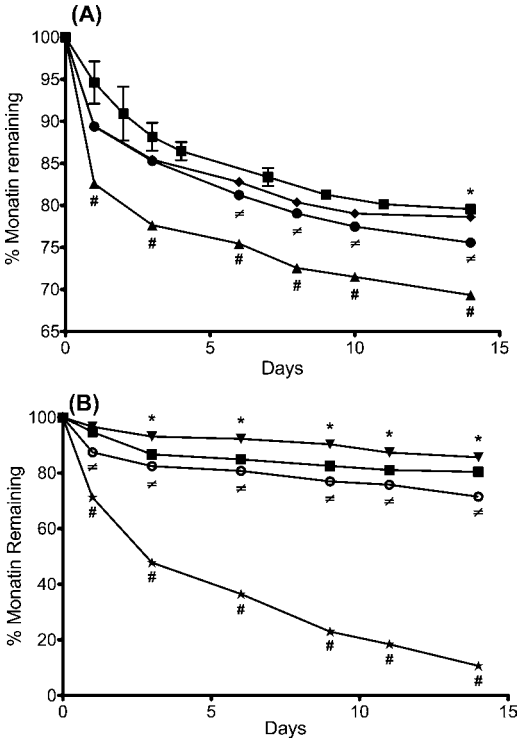

Figure 2. The effect of metal ion chelators on monatin loss in illuminated mock beverage solutions (7.5 W m^{-2}). (A) Mock beverage solutions were treated with different metal chelators (untreated buffer control (▲), desferrioxamine (50 μM; ♦), EDTA (50 μM; ●), and Chelex-treated buffer (■). # Statistically significant to control (P < 0.05). * Chelex and desferrioxamine treatments significantly different from EDTA and control (P < 0.05). ≠ EDTA treatment significantly different from other treatments (B) Mock beverage samples prepared with Chelex-treated buffer (■) were spiked with $CuCl_2$ (50 μM;▼), Fe_2SO_4 [100 nM (○), or 50 μM (★)]. # Treatments statistically significant to spiked Fe_2SO_4 [50 μM] (P < 0.05). ≠ Samples with added Fe_2SO_4 [100 nM] significantly different from other treatments. * Samples with added $CuCl_2$ [50 μM] significantly different from all other treatments (P < 0.05). All values are shown as mean ± SEM (N = 3 replicates). Note the difference in the y-axis scale between A and B.

Scheme 2. Intramolecular Rearrangement Reactions of Monatin [1] To Form the Monatin Lactone [3] and Lactam [4]

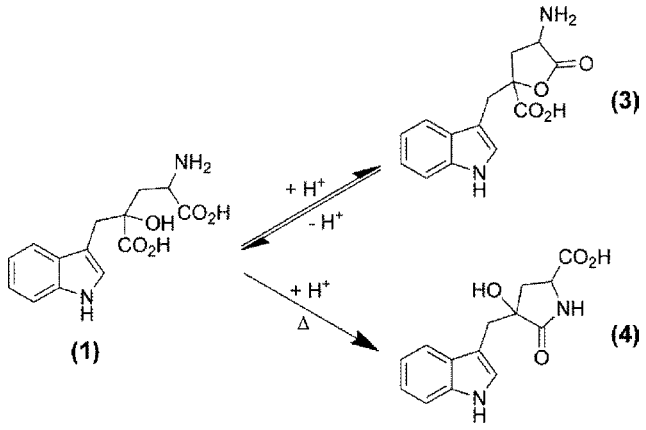

peroxides in light-exposed standard beverage solutions of monatin prepared with H_2O-, D_2O-, or Chelex-treated citrate buffers. Pretreatment of the samples with catalase prior to the assay allowed the proportion of H_2O_2 versus monatin-derived peroxides to be assessed (as catalase does not remove organic peroxides[33,35]).

An increase in total peroxide levels over ~30 days of illumination was observed in all cases, after which peroxide levels started to decrease (Figure 3). Catalase pretreatment

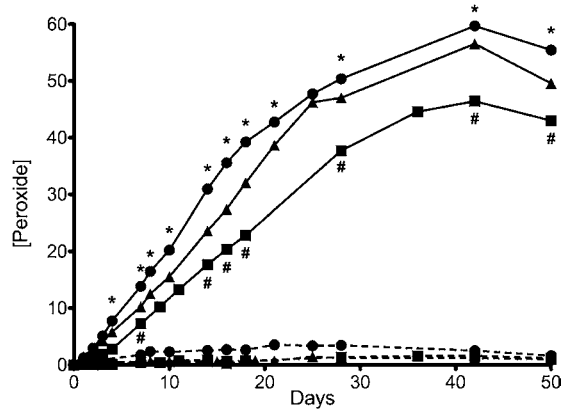

Figure 3. Concentration (μM) of all peroxides (solid lines) or organic peroxides (dashed lines) generated following illumination (7.5 W m^{-2}) of monatin beverage solutions prepared with H_2O control (▲), D_2O (●), or Chelex-treated (■) buffers. Values are shown as mean ± SEM (N = 3 replicates). # Statistically significant to Chelex-treated buffers (P < 0.05). * D_2O significantly different from H_2O control and Chelex-treated (P < 0.05). Organic peroxide concentrations were statistically different when compared with the total peroxide concentrations at all illumination times (P < 0.05).

showed that the majority of the detected peroxide(s) was H_2O_2 (>40 μM), with lower, but significant, levels (≤4 μM) of monatin peroxides. The peroxide levels achieved in D_2O buffer were higher (up to 60 μM) than in samples made up using H_2O or Chelex-treated buffer (57 and 46 μM, respectively) after 42 days of illumination (Figure 3). The corresponding peroxide levels in samples kept in the dark were significantly lower (<5 μM total and <1 μM monatin peroxides), indicating that photochemical processes account for much of their production. In the absence of light, the proportion of organic peroxides generated (~20%) was much higher, and Chelex treatment of the buffer had a much smaller, but still significant, protective effect (data not shown).

Peroxide concentrations in metal ion spiked solutions of monatin (see above) were also assessed. Illuminated samples containing Fe_2SO_4 (50 μM) exhibited a significant increase in peroxide levels (total, 12 μM; organic, 8 μM) after 1 day of incubation, but no further increase at longer time points. In contrast, nonspiked samples showed a linear increase over 14 days that reached 11 μM total peroxides and <1 μM organic peroxide. Samples spiked with 50 μM $CuCl_2$ generated lower levels of peroxides (3 μM total, 1 μM organic). In the absence of light, the corresponding Chelex-treated and $CuCl_2$-spiked samples accumulated <2 μM total peroxides over 14 days, whereas in the 50 μM Fe_2SO_4-spiked samples, significant accumulation of predominantly organic peroxides (9 μM) occurred. The effect of EDTA and desferroxamine on peroxide formation could not be assessed because these compounds interfere with the FOX assay.

Peroxide Formation in Monatin Solutions Exposed to a Singlet Oxygen-Generating System. The experiments with D_2O buffers suggest a role for $^1O_2$ in monatin photodegradation, consistent with the peroxide formation observed on Trp [2]

dx.doi.org/10.1021/jf404198w | J. Agric. Food Chem. 2014, 62, 3476−3487

exposed to $^1O_2$.[29] The role of $^1O_2$ in monatin-derived peroxide formation was examined by adding Rose Bengal (RB; 10 μM) to mock beverage samples of monatin prepared in H_2O or D_2O citrate buffer (pH 3) and subsequently exposing these materials to light. The samples (together with controls without RB) were bubbled with air and photolyzed with a slide projector (820 W m^{-2}). The peroxide levels in the samples containing RB increased significantly over 15 min of photolysis (Figure 4A), with >70% of the peroxides attributed to organic (presumed to be monatin-derived) species. In the absence of RB, insignificant levels of peroxide were detected. In identical experiments in D_2O citrate buffer, elevated peroxide levels were detected (Figure 4A), consistent with $^1O_2$ being the primary oxidant in this system.

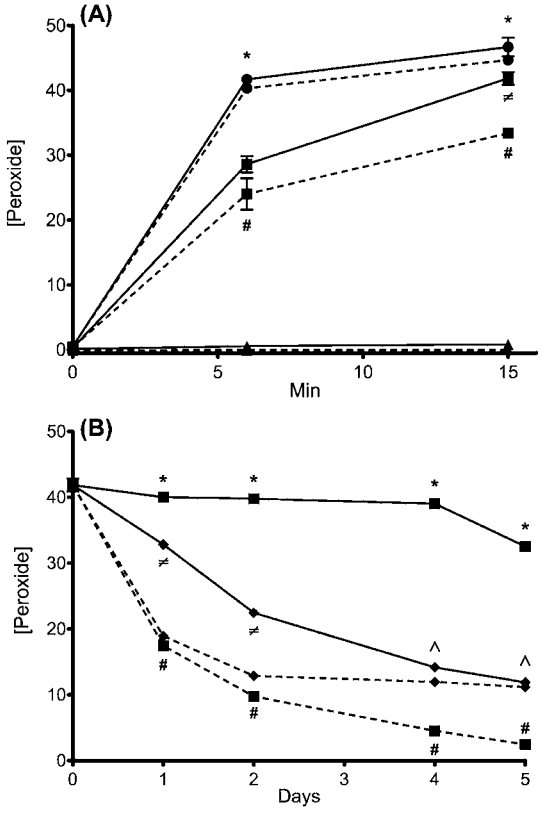

Figure 4. (A) Concentration (μM) of total peroxide (solid lines) or organic peroxide (dashed lines) formed in Rose Bengal photosensitized beverage solutions of monatin on photolysis with a slide projector (820 W m^{-2}) for 15 min. Control H_2O (▲), Rose Bengal in D_2O buffers (●), Rose Bengal in H_2O buffers (■). # Statistically significant to Rose Bengal in H_2O buffer ($P < 0.05$). ≠ Total peroxides for Rose Bengal in H_2O buffers significantly different from other treatments. * Both total and organic peroxides for Rose Bengal in D_2O buffer significantly different from all other treatments ($P < 0.05$). Control samples were statistically significant throughout ($P < 0.05$). (B) Stability of organic peroxides generated by Rose Bengal/light/O_2/monatin photolysis to thermal- (■) or Fe_2SO_4 (40 μM; ♦)-stimulated decay in the dark over a period of 5 days (total peroxide, solid lines; organic peroxide, dashed lines). # Statistically significant to thermal decomposition of organic peroxides ($P < 0.05$). ≠ Total peroxide decomposition with added Fe_2SO_4 [40 μM] significantly different from other treatments.^ Levels of organic and total peroxides exposed to Fe_2SO_4 [40 μM] significantly different from other treatments. * Total peroxides in thermally exposed samples significantly different from all other treatments ($P < 0.05$). Values are shown as mean ± SEM ($N = 3$ replicates, with error bars being smaller than the symbol in some cases).

The thermal stability (in the dark) of the (monatin-derived) organic peroxides was monitored for 5 days following photolysis. Parallel experiments with Fe_2SO_4 (40 μM) added to stimulate peroxide decay were also carried out, as with Trp-derived peroxides in which concomitant radical formation occurred.[29] For the untreated (no added Fe_2SO_4) samples, the total peroxide levels remained relatively constant over 5 days (Figure 4B), but the organic peroxide levels dropped to ∼33% of the initial concentration (44 μM) (Figure 4B). Addition of Fe^{2+} promoted both total and organic peroxide decay (Figure 4B), with the rate of peroxide decay less in samples in D_2O compared with samples in H_2O (data not shown).

LC−MS Analysis of Parent Monatin and Monatin Lactone. LC−MS analysis of control, nonilluminated samples of monatin exhibited a strong peak at ∼35.8 min in the UV (280 nm) detection channel. The full mass spectrum of this peak had an intense ion with m/z 293.3, consistent with (protonated) parent monatin ([**1**]; $[monatin+H]^+$). The identity of this peak was confirmed by selective ion monitoring (SIM) of the m/z 293.3 ion (Figure 5A), with the fragmentation spectrum (Table 1) consistent with that for monatin.[27] The chromatograms of nonilluminated monatin also contained a weaker peak (∼ 3% of the monatin peak detected at 280 nm) at ∼33.5 min. This peak had m/z 275.3 and fragmented (Figure 5B, Table 1) in a manner consistent with monatin lactone [**3**] as described previously.[27]

Photolysis of monatin solutions in the presence or absence of metal ions resulted in a time-dependent loss of the monatin and lactone peaks, with numerous new peaks detected using UV detection at 280 nm. In previous studies examining photooxidation of Trp [**2**], multiple products containing one or two incorporated oxygen atoms were detected (Scheme 3, refs 29−31), and Upreti et al. have reported the incorporation of a single oxygen atom to generate a 2-hydroxyindole derivative ([**12**], Scheme 4) after short-wavelength UV photolysis.[27] The identity of these oxygenated products was examined by LC−MS/MS analysis.

LC−MS/MS Analysis of $[M + 16 + H]^+$ Monatin Photoproducts. Selective ion monitoring of m/z 309.3 (corresponding to the mass of monooxygenated monatin) revealed three new peaks whose intensities increased with photolysis time. Two of these peaks eluted at early times (∼8.1 and ∼11.2 min; Figure 5C,D) with fragmentation patterns (Figure 6A,B, Table 1) similar to those reported by Upreti et al. for 2-hydroxymonatin [**12**].[27] Interestingly, although the fragment ion masses were the same for the $[monatin + 16 + H]^+$ species at ∼8.1 and ∼11.2 min, the intensity of the fragment ion with m/z 272.9 (corresponding to loss of two H_2O, Table 1) was greater for the peak eluting at ∼11.2 min. This was also observed previously for Trp photooxidation products (Scheme 3; cis and trans isomers of [**7**]); thus, the two monooxygenated monatin-derived species detected at early elution times have been assigned to the cis and trans isomers of the 3α-hydroxypyrolloindole derivatives [**13**] of monatin that arise through cyclization of the α-amino group onto the oxidized indole ring (see Scheme 4).[29−31] In monatin, ring closure could potentially occur via a γ-carbon OH group, so experiments were carried out with indole-3-lactic acid instead of Trp [**2**] (in which a hydroxyl replaces the α-amino group). These studies indicate that ring closure via the OH group occurs less readily than with the α-amino group of Trp [**2**] (data not shown). The fragmentation spectra for the $[monatin + 16 + H]^+$ species at ∼8.1 and ∼11.2 min support predominant ring closure via the α-amino group because fragment ions consistent with the loss of H_2O (m/z 291.1) and $2H_2O$ (m/z 272.9), but not NH_3

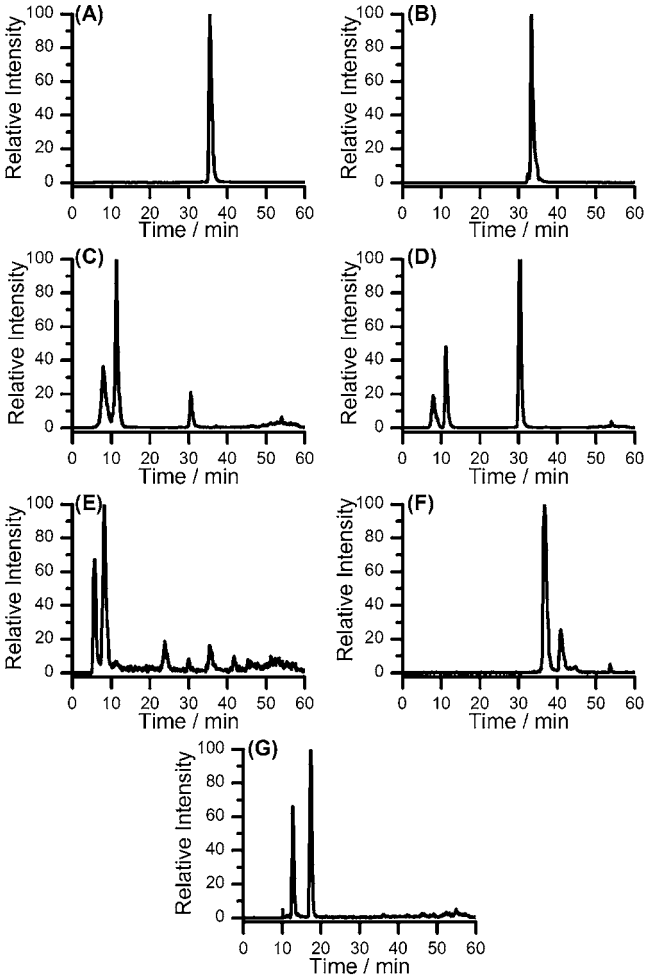

Figure 5. Selected ion chromatograms obtained from samples (concentrated 10-fold) photo-oxidized (7.5 W m^{-2}) for 14 days (unless otherwise stated) for (A) monatin (m/z 293.3 → full scan), (B) monatin lactone (m/z 275.3 → 158.1), (C) monatin alcohols (m/z 309.3 → full scan) in the absence of added Fe^{2+}, (D) monatin alcohols (m/z 309.3 → full scan) in the presence of 100 nM Fe^{2+}, (E) cyclized monatin diols (m/z 325.3 → 306.9; retention times, 5.7 and 8.1 min) in the absence of added Fe^{2+}, (F) *N*-formylkynurenine derivative of monatin (m/z 325.3 → 297.1; retention time, 36.6 min) in the presence of 100 nM Fe^{2+} and (G) cyclized monatin peroxides (m/z 325.3 → full scan; retention times, 12.7 and 17.3 min) formed by 10 μM Rose Bengal photosensitization.

(m/z 292.1) or NH_3 + H_2O (m/z 274.1), are detected, suggesting that the α-amino group is no longer free but contained in the heterocycle.

The third peak with m/z 309.3 eluted at ∼31.2 min (Figure 5C) and was more abundant when the samples were spiked with 100 nM Fe^{2+} (Figure 5, D vs C). This species yielded an intense fragment ion with m/z 291.0 (consistent with loss of H_2O), with only one other weak fragment ion (intensity <2% of the m/z 291.0 fragment; Table 1). This peak appears to correspond to the keto/enol equilibrium mixture of 2-hydroxymonatin (Scheme 4, [**12**]) reported previously,[27] although using different elution methods makes direct comparison impossible. This assignment is also consistent with a late eluting $[M + 16 + H]^+$ peak observed from photooxidized Trp, which was assigned to 3-hydroxy-Trp ([**5**], Scheme 3).[29]

LC−MS/MS Analysis of [M + 32 + H]$^+$ Monatin Photoproducts. The formation of dioxygenated monatin products was investigated by SIM of m/z 325.3 ions. Two peaks were detected at ∼5.7 and ∼8.1 min (Figure 5E) in samples with or without Fe^{2+} present, although their presence was favored by the absence of metal ions. In more heavily oxidized samples, a later-eluting peak of the same mass was detected at ∼36.6 min (Figure 5F). Low-intensity peaks were also detected at ∼23.4, ∼27.0, and ∼41.8 min, but their low abundance precluded further analysis.

The fragmentation spectra for the two early-eluting peaks are very similar, with only small differences in the relative intensities of the fragment ions (Table 1, Figure 6C,D). The two main fragment ions (Table 1) are consistent with consecutive loss of two H_2O molecules from the dioxygenated monatin. The other major fragment ion (m/z 146.1) has been reported previously for 2-hydroxymonatin and assigned to a fragment consisting of a monooxygenated indole ring.[27] This common indole-derived fragment was also detected for dioxygenated Trp products assigned to dioxindolylalanine [**8**], cyclized 3α-dihydroxypyrolloindoles [**9**], and cyclized 3α-hydroperoxypyrolloindoles [**10**] formed on $^1O_2$-mediated oxidation of Trp (Scheme 3).[29−31,39] Weak fragment ions were also detected for the peaks eluting at ∼5.7 and ∼8.1 min (Table 1), but as with the monooxygenated monatin products and dioxygenated Trp products ([**8**, **9**], Scheme 3), the relative fragment ion intensities varied.[29−31,39] These dioxygenated monatin peaks were thermally stable and have been assigned to the monatin derivatives ([**15**, **16**], Scheme 4) of the dioxyindolylalanine [**8**] and cyclized diol [**9**] species characterized previously with Trp (Scheme 3) rather than peroxides (which would be thermally unstable). The predominant form of these ring tautomers in acidic solutions is likely to be the dioxyindolyl species [**15**] (cf. data in ref 39), rather than the cyclized diol [**16**], which is favored at alkaline pH.[40]

The dioxygenated peak detected at ∼36.6 min has a markedly different fragmentation pattern (Figure 6G, Table 1) from the earlier eluting peaks. It is suggested, by comparison with free Trp,[29−31] that this product is the monatin equivalent ([**17**], Scheme 4) of *N*-formylkynurenine ([**11**], Scheme 3) in which addition of two oxygen atoms results in pyrrole ring cleavage.

LC−MS/MS Analysis of Oxygenated Monatin Products Formed by Rose Bengal-Mediated Photooxidation. Because many of the monatin products appear to be similar to those detected from $^1O_2$-mediated oxidation of Trp, oxidation of monatin with RB and light was examined. LC−MS/MS of these samples revealed many of the mono- and dioxygenated species that were observed in the direct photodegradation studies, but over different time frames and concentrations.

Analysis of samples by SIM immediately after photolysis (or following prolonged storage at −20 °C) showed two dioxygenated monatin products (m/z 325.3) (Figure 5G) that were not observed in the direct photolysis studies (Figure 5E). These species eluted at ∼12.7 and ∼17.3 min but were absent (or detected at much lower levels) in samples stored at 22 °C for up to 5 days or after addition of 40 μM Fe^{2+}. This thermal instability suggests that these are the cis and trans isomers of the monatin analogues ([**18**], Scheme 4) of the cyclized 3α-hydroperoxypyrolloindole species ([**10**], Scheme 3) detected with Trp (i.e., monatin peroxides). The fragmentation spectra (Figure 6E,F, Table 1) support these assignments, with each exhibiting a fragment ion at m/z 291.0 corresponding to loss of H_2O_2 (34 mass units). Numerous other fragment ions were detected (Figure 6E,F, Table 1), but as with the corresponding alcohols, variations in the fragment ion intensities between the two species are consistent with an assignment to the cis and trans isomers of the cyclized peroxides [**18**]. Decomposition of these peroxides resulted in an increased concentration of the pair of

dx.doi.org/10.1021/jf404198w | J. Agric. Food Chem. 2014, 62, 3476−3487

Table 1. Summary of LC−MS/MS Data for the Compounds Detected in Mock Beverage Samples of Monatin Following Photodegradation and Photosensitization Studies[a]

$[M + H]^+$ m/z	RT/ min	fragment ions (assignments of neutral losses)	assignment
293.3	36.1	257.0 ($-2H_2O$), 274.9 ($-H_2O$), 158.2 (−135), 230.1 (−63), 247.0 (−CO, $-H_2O$)	monatin [**1**]
275.3	33.5	158.1 (−117), 229.0 (−CO, $-H_2O$)	monatin lactone [**3**]
		Monooxygenated Products	
309.3	8.1	291.1($-H_2O$), 244.9 (−CO, $-2H_2O$), 272.9 ($-2H_2O$)	cyclized monatin C3-alcohol [**13**/**14**]
309.3	11.2	291.1($-H_2O$), 244.9 (−CO, $-2H_2O$), 272.9 ($-2H_2O$)	cyclized monatin C3-alcohol [**13**/**14**]
309.3	31.2	291.1($-H_2O$), 244.9 (−CO, $-2H_2O$)	monatin C2-alcohol [**12**]
		Dioxygenated Products	
325.3	5.7	306.9($-H_2O$), 288.8 ($-2H_2O$), 146.1(−179), 260.8(−CO, $-2H_2O$), 278.9 (−CO, $-H_2O$), 242.9 (−CO, $-3H_2O$), 270.8 ($-3H_2O$), 245.9 (−78), 227.9 (−97)	cyclized monatin C2,C3-diol [**16**]
325.3	8.1	306.9($-H_2O$), 288.8 ($-2H_2O$), 146.1(−179), 260.8(−CO, $-2H_2O$), 245.9 (−78), 278.9 (−CO, $-H_2O$)	cyclized monatin C2,C3-diol [**16**]
325.3	12.7	190.0 (−135), 246.0 (−79), 263.0 (−62), 271.0 (−54), 261.0 (−CO, $-2H_2O$), 228.0 (−97), 216.0 (−109), 306.9 ($-H_2O$), 170.0 (−155), 288.9 (−36), 148.1 (−177), 291.0 ($-H_2O_2$), 132.2 (−193)	cyclized monatin C3-peroxide [**18**]
325.3	17.3	190.0 (−135), 271.0 (−54), 246.0 (−79), 228.0 (−97), 263.0 (−62), 261.0 (−CO, $-2H_2O$), 291.0 ($-H_2O_2$), 148.1 (−177), 170.0 (−155), 200.0 (−125), 132.2 (−193)	cyclized monatin C3-peroxide [**18**]
325.3	36.6	297.1(−CO), 263.1(−62), 307.1($-H_2O$)	monatin derivative of *N*-formylkynurenine [**17**]
		Other Photoproducts	
227.1	11.8	peak too weak for reliable MS/MS analysis	unknown
227.1[b]	32.6	183.2 ($-CO_2$), 209.1 ($-H_2O$), 156.2 (−71)	unknown
241.1[c]	29.9	223.1 ($-H_2O$), 195.0 ($-H_2O$, −CO)	potentially structure [**19**]
243.2[d]	46.0	MS^2: 215.2 (−CO) MS^3 of 215.2 fragment: 197.1 (−CO, $-H_2O$), 169.1 (−2CO, $-H_2O$)	2-(2-formamidophenyl) isonicotinic acid (2-2-FAPINA) [**20**]
263.2[e]	31.7	MS^2: 246.0 ($-NH_3$) MS^3 of 246.0 fragment: 228.0 ($-NH_3$, $-H_2O$), 200.1 ($-NH_3$, $-H_2O$, −CO), 132.1 (−131)	unknown
263.2[f]	40.3	no fragment ions detected	indigo [**21**]

[a]Fragment ions are listed in order of decreasing intensity, with assignments or mass differences of neutral losses in parentheses. High accuracy QTOF and UHPLC−MS/MS analysis of some photoproducts was also carried out, and the data are summarized in the following footnotes. [b]$[M + H]^+$ = 227.0821, $[M- H]^-$ = 225.0675, predicted chemical formula $C_{13}H_{10}N_2O_2$, fragment ions (+ve ion), m/z 183.0914 ($-CO_2$), 209.0710 ($-H_2O$), 156.0808 ($-C_2HNO_2$). [c]$[M + H]^+$ = 241.0618, $[M- H]^-$ = 239.0475, predicted chemical formula $C_{13}H_8N_2O_3$, peak was of insufficient intensity for accurate mass MS/MS. [d]$[M + H]^+$ = 243.0773, $[M- H]^-$ = 241.0631, predicted chemical formula $C_{13}H_{10}N_2O_3$, fragment ions (+ve ion), m/z 215.0819 (−CO). [e]$[M + H]^+$ = 263.1036, $[M- H]^-$ = 261.0889, predicted chemical formula $C_{13}H_{14}N_2O_4$, fragment ions (+ve ion), m/z 200.0703 ($-CH_5NO_2$), 132.0440 ($-C_8H_5NO$). [f]$[M + H]^+$ = 263.0823, predicted chemical formula $C_{16}H_{10}N_2O_2$.

Scheme 3. Summary of the Photooxidized Products Previously Identified for Trp [2].[29−31,39]

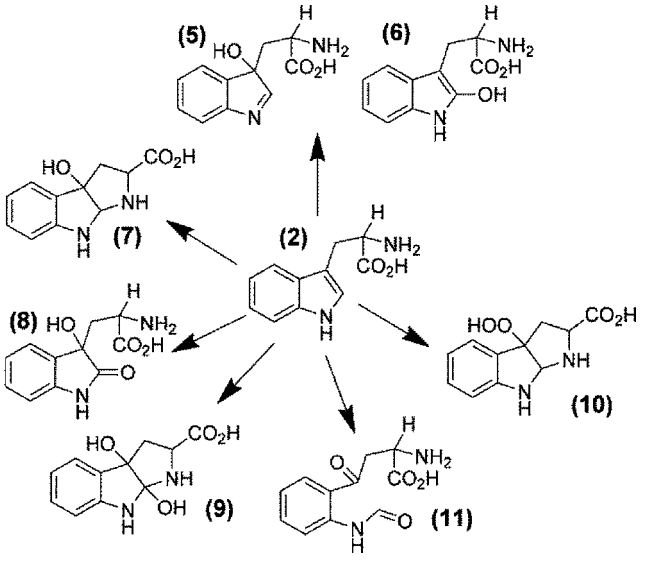

monooxygenated monatin species (m/z 309.3) at ∼8.1 and ∼11.2 min, consistent with peroxide decomposition to the corresponding alcohols [**14**]. The m/z 309.3 peak observed at ∼31.2 min in the direct photolysis experiments (i.e., 7.5 W m^{-2}, no RB) was much less intense with RB oxidation (data not shown). This suggests different mechanism(s) of formation of the three mono-oxygenated monatin species (m/z 309.3), with the early eluting, ring-closed species (8.1 and 11.2 min, [**14**]) generated primarily by $^1O_2$ reactions, whereas the 2-hydroxyindole product [**12**] eluting at ∼31.2 min may be generated primarily by radical pathways.

LC−MS/MS Analysis of Other Monatin Photoproducts. In addition to the above mono- and dioxygenated monatin products, LC−MS/MS studies identified multiple other product peaks with m/z 227.1, 241.1, 243.1, and 263.1 (Table 1) on photolysis of monatin; SIM studies of these masses are discussed in order of increasing m/z below.

A new peak (m/z 227.1) eluted at ∼32.6 min (Supporting Information Figure 3A, Table 1) whose intensity increased after 14 days of photolysis and was further enhanced when samples were spiked with 10 μM Fe^{2+}. A much weaker intensity peak (m/z 227.1) was also detected at 11.8 min (Supporting Information Figure 3A, Table 1), but this was detected only upon photolysis of Fe^{2+}-spiked samples. The identities of these products have not been determined unequivocally, but accurate mass (QTOF) measurements (Table 1 footnote) for the ∼32.6 min peak are consistent with a formula of $C_{13}H_{10}N_2O_2$ (cf. $C_{14}H_{16}N_2O_5$ for monatin). The low carbon−hydrogen ratio for this species is

Scheme 4. Proposed Degradation Mechanisms of Monatin [1][a]

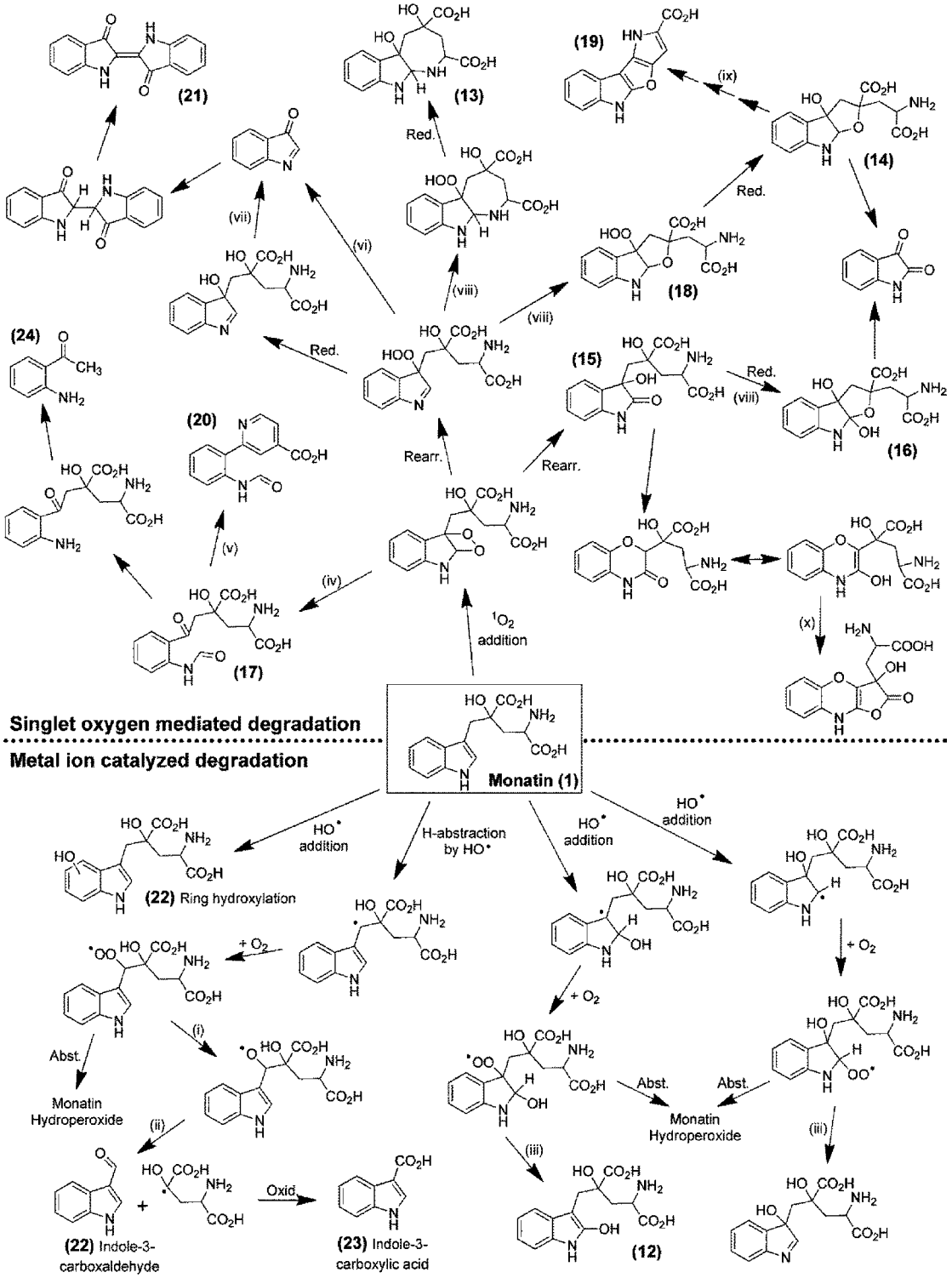

[a]Key to abbreviations: Abst., hydrogen atom abstraction; Red., reduction; Oxid., oxidation; Rearr., rearrangement. (i) Via dimerization to unstable tetroxide with O_2 elimination or hydroperoxide formation followed by one electron reduction. (ii) β-Scission. (iii) Elimination of $HO_2^\bullet$ to generate H_2O_2. (iv) Oxidative ring-opening. (v) Cyclization, H_2O elimination, and aromatization. (vi) Via alkoxyl radical and β-scission. (vii) Side chain cleavage. (viii) Ring closure. (ix) Multiple steps, incl. ring closure, decarboxylation, dehydration and aromatization. (x) Lactone formation with the proximal carboxylic acid.

consistent with a cyclized, aromatized structure. Although accurate mass UHPLC–MS/MS (Table 1 footnote) data was obtained, no structural assignment is possible. The other peak with m/z 227.2 that eluted at ~11.8 min was too weak for accurate mass and MS/MS analysis.

A product peak with m/z 241.1 eluted at 29.9 min (Supporting Information Figure 3B, Table 1), which increased in intensity on

dx.doi.org/10.1021/jf404198w | J. Agric. Food Chem. 2014, 62, 3476–3487

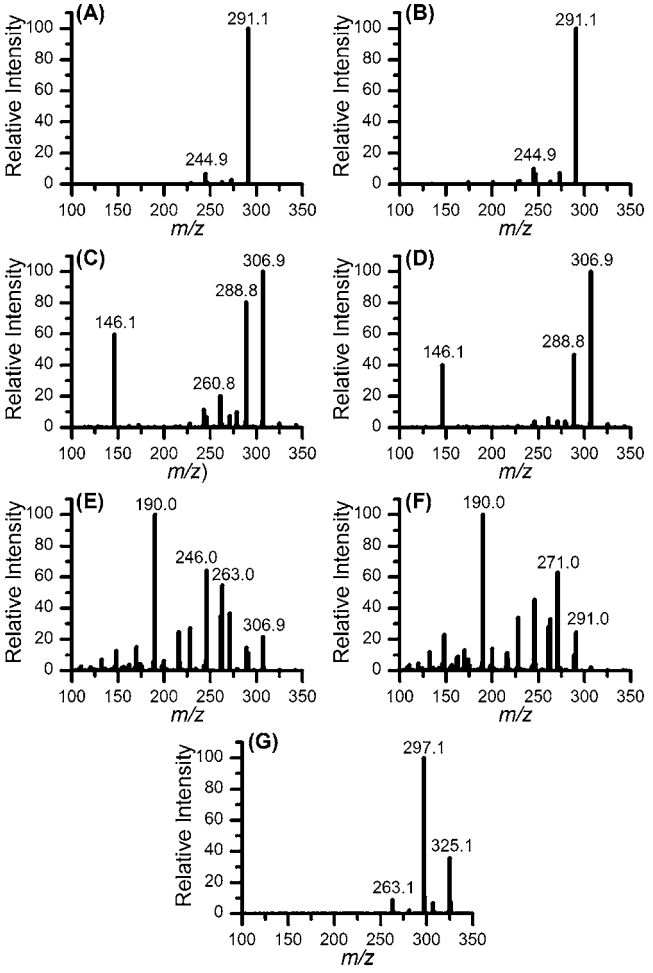

Figure 6. MS/MS spectra for mono- and dioxygenated products of monatin obtained from samples exposed to illumination (7.5 W m^{-2}) for 14 days in Chelex-treated buffer and subsequently concentrated 10-fold (except where otherwise stated). (A, B) cyclized monatin alcohols (m/z 309.3) eluting at 8.1 and 11.2 min, (C, D) cyclized monatin diols (m/z 325.3) eluting at 5.7 and 8.1 min, (E, F) cyclized monatin peroxides (m/z 325.3) eluting at 12.7 and 17.3 min (formed by photosensitization with Rose Bengal), and (G) *N*-formylkynurenine derivative of monatin (m/z 325.3) eluting at 36.6 min detected in samples with 100 nM Fe^{2+} added to sample.

exposure to light and spiking with Fe^{2+}. LC−MS/MS data (Table 1) show facile loss of H_2O and CO, and accurate mass QTOF analysis (Table 1 footnote) gave a chemical composition of $C_{13}H_8N_2O_3$. These data are consistent with an assignment to an extensively cyclized, unsaturated structure ([**19**], Scheme 4), which may arise via the cyclized peroxide structures ([**18**], Scheme 4).

Several low-intensity peaks with m/z 243.2 were detected from 25 to 40 min, but they were too weak to characterize. In addition, a relatively intense peak (m/z 243.2, ∼46.0 min; Supporting Information Figure 3C, Table 1) eluted ∼10 min after parent monatin. The peak intensity was dependent on photolysis time and the presence of Fe^{2+}. QTOF analysis (Table 1 footnote) gives a formula of $C_{13}H_{10}N_2O_3$ for the uncharged molecule, and accurate mass UHPLC−MS/MS suggested facile loss of CO (Table 1 footnote). LC−MS^3 experiments demonstrated sequential loss of H_2O and CO from the m/z 215.2 fragment ion (Table 1). This peak was assigned to 2-(2-formamidophenyl)isonicotinic acid (2-2-FAPINA; [**20**], Scheme 4) as previously;[27] this species is proposed to form via the ring-opened, oxidized monatin derivative [**17**], equivalent to *N*-formylkynurenine [**11**] in Trp oxidation (Scheme 3).

Two peaks with m/z 263.2 eluted at ∼31.7 and ∼40.3 min (Supporting Information Figure 3D, Table 1). The ∼31.7 min peak intensity increased with photolysis and/or spiking with Fe^{2+} (10 μM); the weaker peak at 40.3 min was observed only on illumination of Fe^{2+} spiked samples. QTOF analysis (Table 1 footnote) indicated formulae of $C_{13}H_{14}N_2O_4$ and $C_{16}H_{10}N_2O_2$ respectively. Accurate mass UHPLC−MS/MS (Table 1 footnote) data suggest, but do not prove, that the latter species is a dimeric indigo-like species (e.g., [**21**], Scheme 4). The earlier eluting species could not be characterized.

Authentic samples of previously reported monatin degradation products[25,27] or other feasible products (see Scheme 4), including indole-3-carboxaldehyde (m/z 146.2; [**22**]), 3-indole acetic acid (m/z 176.2), indole-3-carboxylic acid (m/z 162.2; [**23**]), 3-methyl-indole (skatole; m/z 132.2), and 2-amino-acetophenone (m/z 136.2; [**24**]) were monitored by SIM. All of these materials were readily detected, except indole-3-carboxylic acid and skatole that ionize poorly. None of these materials were detected in the photolyzed samples, either with or without 10 μM Fe^{2+}. However, upon 10-fold concentration of photo-oxidized samples, indole-3-carboxaldehyde (also known as 3-formylindole) was detected by selective reaction monitoring of the m/z 146.2 → m/z 118.2 fragmentation (due to loss of CO), consistent with a previous report.[27]

The formation of low yield products was investigated by exposing monatin samples to light (7.5 W m^{-2}) for up to 3 months. When these samples were concentrated ∼10-fold by vacuum centrifugation, several new peaks (m/z 225.2 (28.7 min), 291.1 (11.2, 28.1, 30.7, 32.4, 34.1, 37.4 min), 343.0 (27.6 min), and 363.0 (25.6 min)) were observed by full-scan LC−MS. These peaks were verified by LC−MS/MS and most readily lost H_2O (−18 m/z), CO (−28 m/z), or both H_2O and CO (−46 m/z); however, these species could not be characterized by accurate mass (QTOF or UHPLC−MS/MS) measurements because of their low abundance even in heavily oxidized, concentrated samples.

DISCUSSION

The data described above and those from previous studies,[25,27,28] including one using high-intensity simulated sunlight,[27] demonstrate that monatin degrades in mock beverage solutions over extended illumination periods. The results obtained in the current study show that the rate and extent of monatin consumption varies significantly, depending on the conditions employed, and that multiple mechanisms and intermediates are involved. A considerable proportion (76%) of monatin was lost in samples prepared in a standard citrate (mock beverage) buffer that was exposed to standard fluorescent light illumination (7.5 W m^{-2}) for 50 days. In the current studies, a (relatively low level) fluorescent light source was used to provide a model relevant to commercial storage and vending situations. A previous study employed a sun-test chamber that was equivalent to 4 days of direct sun exposure in the Arizona desert.[27] With our milder conditions, much of the monatin lost over the initial few days arises from intramolecular rearrangement to the corresponding lactone ([**3**], Scheme 2), with ∼15% of the initial monatin converted to the lactone over the first 14 days of photolysis and ∼10% converted to oxidation products. This lactonization is associated with a loss in sweetness,[41] but it does not appear to lead to unpleasant flavors or aromas. This suggests that the major

loss of sweetness and the development of negative taste and sensory effects in mock monatin beverage solutions arise from alternative oxidative processes.

In parallel experiments with citrate buffer prepared using D_2O in place of H_2O, an enhanced rate of photodecomposition was observed with up to 84% of monatin consumed by day 50. This suggests a major role for $^1O_2$ in the photodegradation because D_2O enhances the lifetime of $^1O_2$ and thereby enhances damage.[31,32] A key role for species generated by light is confirmed by studies using samples kept in the dark, in which the rate of monatin loss was markedly reduced, but not entirely eliminated. The loss of monatin in the dark demonstrates that non-light-induced reactions also lead to monatin degradation, but at a slower rate. Significantly, there was no difference in monatin degradation between samples prepared in D_2O or H_2O citrate buffer in the dark; thus, $^1O_2$ plays a major role only in light-exposed samples. It is proposed that in the initial stages of the reaction, $^1O_2$ arises from (inefficient) photosensitization reactions mediated by the indole ring; however, once indole ring degradation has commenced, either via the mediation of $^1O_2$ or radicals, more efficient photosensitizers are formed, such as *N*-formylkynurenine, kynurenine, and indigo derivatives (Scheme 4), that are more efficient photosensitizers of $^1O_2$ and drive further oxidation.[42,43]

Given the data implicating $^1O_2$ in light-induced monatin degradation, photooxidation induced by a RB/light/O_2 system was examined because this gives high levels of $^1O_2$. High yields of monatin peroxides were formed as well as multiple downstream products, with the peroxide yields further increased when the experiments were carried out in D_2O (cf. refs 31, 32). The monatin peroxides were long-lived in the absence of light and metal ions, but their decay was enhanced by the deliberate addition of Fe^{2+}. By analogy with $^1O_2$-generated Trp, His, and Tyr peroxides,[29,32,33] it is likely that Fe^{2+}-mediated reduction of monatin peroxides results in the formation of monatin radicals that contribute to photoinduced monatin degradation.

Significant levels of H_2O_2 and organic peroxides were detected in the mock beverage samples illuminated with a fluorescent light source (7.5 W m^{-2}) in the absence of RB, suggesting that peroxides are key intermediates, because the levels of these materials and the rate of monatin loss were enhanced by D_2O. At least some of the H_2O_2 formation appears to arise via $^1O_2$-mediated reactions, with this postulated to occur via elimination from endo- or hydroperoxide intermediates. The peroxide levels detected in the illuminated samples were significantly higher than those present in the dark controls, consistent with the greater rate of degradation upon light exposure and the mediation of these species.

The removal of trace transition metal ions (by pretreating buffers with Chelex 100-resin) significantly attenuated monatin degradation. Furthermore, the peroxide levels detected in Chelex-treated buffer samples were much lower than in nontreated buffers. These data suggest that transition metal ions also play a key role in monatin degradation, both in illuminated and nonilluminated samples. This hypothesis is supported by addition of the metal ion chelators EDTA and desferrioxamine, which had an effect on monatin stability that was similar to treatment with Chelex resin. Conversely, spiking of Chelex-treated mock beverage samples with Fe^{2+} led to enhanced rates of monatin loss, with this dependent on the added Fe^{2+} concentration. These data implicate Fe^{2+} in monatin degradation under mock beverage conditions in both nonilluminated and illuminated samples, particularly because equivalent samples spiked with Cu^{2+} (instead of Fe^{2+}) exhibited *less* monatin degradation than nonspiked controls. This effect may be due to light absorption by the Cu^{2+} ions. A role for Fe^{2+} in monatin degradation is further supported by the enhanced initial rate of total and organic peroxide formation in the spiked samples. This effect was lost over longer times, probably because of Fe^{2+}-catalyzed degradation of the peroxides (eqs 1−4), with these secondary reactions contributing to the overall extent of monatin degradation.

The mechanistic insight into monatin degradation provided by the data obtained, together with the product analyses outlined here and elsewhere,[25−28] has allowed a scheme to be proposed that accounts for the observed products and processes known to affect monatin degradation (Scheme 4). This scheme also indicates a pathway through which direct UV photolysis can initiate (or enhance) monatin photodegradation, because it is well established that direct (short-wavelength) UV absorption by Trp can result in photoionization to yield a radical cation that can deprotonate to give a neutral indolyl radical or a radical at the β-carbon (i.e., at the methylene $-CH_2-$ linking the indole ring to the amino acid backbone).[42,43] Analogous reactions with monatin would provide pathways to δ-carbon and indolyl radicals proposed as intermediates on the pathway to indole-3-carboxaldehyde [**22**] and indole-3-carboxylic acid [**23**] formation. Because these direct photoionization reactions occur primarily with short-wavelength UV light, this proposed mechanism would account for the lower levels of indole-3-carboxaldehyde [**22**] and indole-3-carboxylic acid [**23**] (and associated off-flavors and aromas) detected in the current study compared with those reported previously[25,27] in which light sources with greater output at shorter wavelengths were employed. These observations indicate a potential route through which the formation of undesired materials might be mitigated.

In summary, the current studies have provided a detailed mechanistic analysis and rationale for the photodegradation of the high-potency sweetener monatin under simulated acidic beverage conditions (mock lemon/lime systems). These studies demonstrate that both photooxidation reactions and metal ions contribute to monatin degradation, with these two pathways being synergistic. The product profiles determined by UHPLC and LC−MS/MS are consistent with a role for both $^1O_2$- and radical-mediated pathways in the presence of light, and primarily metal-ion catalyzed, radical-mediated pathways in the absence of light. In both cases, peroxides (either H_2O_2 or monatin-derived) are likely to be key intermediates. The conditions used here represent typical storage and vending conditions for beverages, providing a mechanism-based approach to optimize monatin-containing beverage compositions with prolonged shelf lives. Strategies to minimize these degradation pathways have also been investigated (Storkey et al., unpublished results).

■ ASSOCIATED CONTENT

Supporting Information

Three figures (spectral profiles, UHPLC chromatograms, and ion chromatograms). This material is available free of charge via the Internet at http://pubs.acs.org.

■ AUTHOR INFORMATION

Corresponding Author

*Phone: +61 2 8208 8900. Fax: +61 2 9565 5584. E-mail: daviesm@hri.org.au.

Author Contributions

‡C.S. and D.I.P. contributed equally.

Funding

This research was funded by Cargill, Inc.

Notes

The authors declare no competing financial interest.

■ ACKNOWLEDGMENTS

M.J.D. is supported by an Australian Research Council Professorial Fellowship through the ARC Discovery Program (DP0988311) and an Australian Research Council Centre of Excellence grant (ARC Centre of Excellence for Free Radical Chemistry and Biotechnology, CE0561607).

■ ABBREVIATIONS:

FOX assay, ferrous oxidation-xylenol orange; HPLC, high performance liquid chromatography; LC−MS/MS, liquid chromatography coupled with tandem mass spectrometry; MS/MS, tandem mass spectrometry; QTOF, quadrupole time-of-flight; RB, Rose Bengal; SIM, single ion monitoring; UHPLC, ultrahigh performance liquid chromatography

■ REFERENCES

(1) Schulze, M. B.; Manson, J. A. E.; Ludwig, D. S.; Colditz, G. A.; Stampfer, M. J.; Willett, W. C.; Hu, F. B. Sugar-sweetened beverages, weight gain, and incidence of type 2 diabetes in young and middle-aged women. *J. Am. Med. Assoc.* **2004**, *292*, 927−934.

(2) Malik, V. S.; Schulze, M. B.; Hu, F. B. Intake of sugar-sweetened beverages and weight gain: a systematic review. *Am. J. Clin. Nutr.* **2006**, *84*, 274−288.

(3) Vartanian, L. R.; Schwartz, M. B.; Brownell, K. D. Effects of soft drink consumption on nutrition and health: a systematic review and meta-analysis. *Am. J. Public Health* **2007**, *97*, 667−675.

(4) Bukowiecki, L. J.; Lupien, J.; Follea, N.; Jahjah, L. Effects of sucrose, caffeine, and cola beverages on obesity, cold resistance, and adipose tissue cellularity. *Am. J. Physiol. Regul. Integr. Compar. Physiol.* **1983**, *244*, R500−R507.

(5) Stanhope, K. L.; Havel, P. J. Endocrine and metabolic effects of consuming beverages sweetened with fructose, glucose, sucrose, or high-fructose corn syrup. *Am. J. Clin. Nutr.* **2008**, *88*, 1733S−1737S.

(6) Berkey, C. S.; Rockett, H. R. H.; Field, A. E.; Gillman, M. W.; Colditz, G. A. Sugar-added beverages and adolescent weight change. *Obesity* **2004**, *12*, 778−788.

(7) Marshall, T. A.; Levy, S. M.; Broffitt, B.; Warren, J. J.; Eichenberger-Gilmore, J. M.; Burns, T. L.; Stumbo, P. J. Dental caries and beverage consumption in young children. *Pediatrics* **2003**, *112*, E184−E191.

(8) Dhingra, R.; Sullivan, L.; Jacques, P. F.; Wang, T. J.; Fox, C. S.; Meigs, J. B.; D'Agostino, R. B.; Gaziano, J. M.; Vasan, R. S. Soft drink consumption and risk of developing cardiometabolic risk factors and the metabolic syndrome in middle-aged adults in the community. *Circulation* **2007**, *116*, 480−488.

(9) Duffy, V. B.; Anderson, G. Position of the American Dietetic Association: use of nutritive and nonnutritive sweeteners. *J. Am. Diet. Assoc.* **1998**, *98*, 580−587.

(10) Vleggaar, R.; Ackerman, L. G. J.; Steyn, P. S. Structure elucidation of monatin, a high-intensity sweetener isolated from the plant *Schlerochiton ilicifolius*. *J. Chem. Soc., Perkin Trans. 1* **1992**, 3095−3098.

(11) Fry, J. C.; Yurttas, N.; Biermann, K. L.; Lindley, M. G.; Goulson, M. J. The sweetness concentration-response of (*R,R*)-monatin, a naturally occurring high-potency sweetener. *J. Food. Sci.* **2012**, *77*, S362−4.

(12) Bassoli, A.; Borgonovo, G.; Morini, G. Lost and found in sweeteners: forgotten molecules and unsolved problems in the chemistry of sweet compounds. *Flavour Fragr. J.* **2011**, *26*, 269−273.

(13) Kim, N. C.; Kinghorn, A. D. Highly sweet compounds of plant origin. *Arch. Pharm. Res.* **2002**, *25*, 725−46.

(14) Buddoo, S.; Rousseau, A. L.; Gordon, G. E. R. Production of monatin enantiomers. Patent WO/2009/044245, 2009.

(15) Abraham, T. W.; Cameron, D. C.; Goulson, M. J.; Hicks, P. M.; Lindley, M. G.; McFarlan, S. C.; Millis, J. R.; Rosazza, J.; Zhao, L.; Weiner, D. P. Beverage compositions comprising monatin and methods of making same. Patent US/2005/0106305, 2005.

(16) Hicks, P. M. Monatin tabletop sweetener compositions and methods of making same. Patent WO/2005/014839, 2005.

(17) Amino, Y.; Hirasawa, K. Organic amine salts of glutamic acid derivatives and their application. Patent US/2009/7612214, 2009.

(18) Brazeau, B. J.; Burke, E.; DeSouza, M.; Gort, S. J.; Hicks, P. M.; Kollmann, S. R.; Luginbuhl, P.; McFarlan, S. C.; Richardson, T.; Sanchez-Riera, F. A.; Solheid, C.; Weiner, D. P.; Zhao, L. Polypeptides and biosynthetic pathways for the production of stereoisomers of monatin and their precursors. Patent EP2010650, 2009.

(19) Hicks, P. M.; McFarlan, S. C.; Abraham, T. W.; Cameron, D. C.; Millis, J. R.; Rosazza, J.; Zhao, L.; Weiner, D. P. Polypeptides and biosynthetic pathways for the production of monatin and its precursors. Patent US/2009/7572607, 2009.

(20) Brady, D.; Steenkamp, L. H.; Rousseau, A. L.; Buddoo, S.; Steenkamp, P. A. Production of monatin enantiomers. Patent US/2011/8003361, 2011.

(21) Brady, D.; Steenkamp, L. H.; Rousseau, A. L.; Buddoo, S.; Steenkamp, P. A. Production of monatin enantiomers. Patent WO/2009/044244, 2009.

(22) Rousseau, A. L.; Buddoo, S. R.; Gordon, G. E. R.; Beemadu, S.; Kupi, B. G.; Lepuru, M. J.; Maumela, M. C.; Parsoo, A.; Sibiya, D. M.; Brady, D. Scale-up of a chemo-biocatalytic route to (2*R*,4*R*)- and (2*S*,4*S*)-monatin. *Org. Process Res. Dev.* **2011**, *15*, 249−257.

(23) Bassoli, A.; Borgonovo, G.; Busnelli, G.; Morini, G.; Drew, M. G. B. Monatin and its stereoisomers: chemoenzymatic synthesis and taste properties. *Eur. J. Org. Chem.* **2005**, 1652−1658.

(24) Nakamura, K.; Baker, T. J.; Goodman, M. Total synthesis of monatin. *Org. Lett.* **2000**, *2*, 2967−2970.

(25) Evans, J. C.; Goulson, M. J. Shelf stable monatin sweetened beverage. Patent WO/2010/138513, 2010.

(26) Mori, K. Sweetener composition. Patent US/2006/0083695, 2006.

(27) Upreti, M.; Somayajula, K. V.; Milanowski, D. J.; Kowalenko, P.; Mocek, U.; San Miguel, R.; Prakash, I. Photostability study of natural high-potency sweetener Monatin in a model beverage system and characterization of the degradation products. *Food Chem.* **2012**, *131*, 413−421.

(28) Roy, G. M. Beverage composition and method of reducing degradation of monatin. Patent WO/2010/036576, 2010.

(29) Gracanin, M.; Hawkins, C. L.; Pattison, D. I.; Davies, M. J. Singlet oxygen-mediated amino acid and protein oxidation: formation of tryptophan peroxides and decomposition products. *Free Radic. Biol. Med.* **2009**, *47*, 92−102.

(30) Ronsein, G. E.; de Oliveira, M. C.; de Medeiros, M. H.; Di Mascio, P. Characterization of O_2 ($^1\Delta_g$)-derived oxidation products of tryptophan: a combination of tandem mass spectrometry analyses and isotopic labeling studies. *J. Am. Soc. Mass Spectrom.* **2009**, *20*, 188−197.

(31) Ronsein, G. E.; Oliveira, M. C.; Miyamoto, S.; Medeiros, M. H.; Di Mascio, P. Tryptophan oxidation by singlet molecular oxygen [O_2 ($^1\Delta_g$)]: mechanistic studies using ^{18}O-labeled hydroperoxides, mass spectrometry, and light emission measurements. *Chem. Res. Toxicol.* **2008**, *21*, 1271−1283.

(32) Agon, V. V.; Bubb, W. A.; Wright, A.; Hawkins, C. L.; Davies, M. J. Sensitizer-mediated photooxidation of histidine residues: evidence for the formation of reactive side-chain peroxides. *Free Radic. Biol. Med.* **2006**, *40*, 698−710.

(33) Wright, A.; Bubb, W. A.; Hawkins, C. L.; Davies, M. J. Singlet oxygen-mediated protein oxidation: evidence for the formation of reactive side-chain peroxides on tyrosine residues. *Photochem. Photobiol.* **2002**, *76*, 35−46.

(34) Hawkins, C. L.; Morgan, P. E.; Davies, M. J. Quantification of protein modification by oxidants. *Free Radic. Biol. Med.* **2009**, *46*, 965−988.

(35) Morgan, P. E.; Dean, R. T.; Davies, M. J. Inhibition of glyceraldehyde-3-phosphate dehydrogenase by peptide and protein peroxides generated by singlet oxygen attack. *Eur. J. Biochem.* **2002**, *269*, 1916−1925.
(36) Kim, J.; Rodriguez, M. E.; Guo, M.; Kenney, M. E.; Oleinick, N. L.; Anderson, V. E. Oxidative modification of cytochrome *c* by singlet oxygen. *Free Radic. Biol. Med.* **2008**, *44*, 1700−11.
(37) Gay, C.; Collins, J.; Gebicki, J. M. Hydroperoxide assay with the ferric-xylenol orange complex. *Anal. Biochem.* **1999**, *273*, 149−155.
(38) Halliwell, B.; Gutteridge, J. M. C. *Free Radicals in Biology and Medicine*, 4th ed.; Oxford University Press: Oxford, 2007; pp 1−704.
(39) Ronsein, G. E.; de Oliveira, M. C.; de Medeiros, M. H.; Di Mascio, P. Mechanism of dioxindolylalanine formation by singlet molecular oxygen-mediated oxidation of tryptophan residues. *Photochem. Photobiol. Sci.* **2011**, *10*, 1727−30.
(40) Bond, A. M.; Tucker, D. J.; Qing, Z.; Rivett, D. E. Determination of the redox-active forms of oxindolylalanine and peptides of kynurenine on the basis of electrochemical studies at mercury electrodes in aqueous media. *J. Electroanal. Chem.* **1991**, *315*, 125−141.
(41) Ikeda, R.; Kogiso, K.; Nakamura, K., Loss of sweetness of monatin with lactamization. In *Proceedings of the 4th International Peptide Symposium*, Wilce, J., Ed. **2007**, pp. 1−4.
(42) Creed, D. The photophysics and photochemistry of the near-UV absorbing amino acids. I. Tryptophan and its simple derivatives. *Photochem. Photobiol.* **1984**, *39*, 537−562.
(43) Pattison, D. I.; Rahmanto, A. S.; Davies, M. J. Photo-oxidation of proteins. *Photochem. Photobiol. Sci.* **2012**, *11*, 38−53.

Table 1. Maturity and Quality Attributes of 'October Sun' and 'Jesca' Peaches at Harvest and after 5 Days at 20 °C[a]

parameter	'October Sun'				'Jesca'			
	harvest		harvest + 5 days		harvest		harvest + 5 days	
wt (g)	209.1	a	197.3	b	210.9	a	202.6	ab
diameter (cm)	7.82	a	7.60	a	7.89	a	7.75	a
fruit surface[b] (cm^2)	192.1	a	181.5	a	195.6	a	188.7	a
ethylene production ($\mu L\ kg^{-1}\ h^{-1}$)	0.38	c	0.77	c	4.71	b	6.72	a
respiration rate (mL $CO_2\ kg^{-1}\ h^{-1}$)	229.3	b	164.6	c	251.9	ab	283.6	a
firmness (N)	49.0	a	5.5	c	37.1	b	8.7	c
wt loss (%)			5.6	a			3.9	a
SSC (°Brix)	12.8	ab	13.2	a	12.3	b	13.1	a
TA ($g\ L^{-1}$)	8.1	a	7.1	a	5.4	b	5.3	b
SSC/TA ratio	1.6	b	1.9	b	2.3	a	2.5	a
hue (deg)	49.2	c	50.5	c	87.0	a	81.6	b
lightness (L^*)	47.8	d	50.2	c	70.2	a	67.8	b

[a]Values represent means of 15 or 3 (ethylene and CO_2 production) replicates. Mean values followed by a different letter within the same row are significantly different at $P \leq 0.05$ (LSD test). [b]Total surface was estimated from the average diameter of each fruit assuming a spherical shape.

(September 7 and October 7, respectively) from a commercial orchard located in Alguaire, in the area of Lleida (northeastern Spain), at marketable maturity according to the usual indices in the producing area. Uniform, defect-free samples were selected and transported directly to the laboratory, where they were kept at 20 °C for 5 days to simulate commercial shelf life.

Standard quality parameters were determined on 15 fruits per each cultivar and analysis date. Fruit firmness (N) was measured on opposite sides of each fruit using a hand-held Effegi penetrometer (model FT 327; Milan, Italy) equipped with an 8 mm diameter tip. The weight of 15 fruits was assessed at harvest and 5 days thereafter to determine weight loss (%). Soluble solids content (SSC) and titratable acidity (TA) were assessed in juice pressed from the whole fruit. SSC was determined with a digital hand-held refractometer (Atago, Tokyo, Japan), and results were expressed as °Brix. For TA determination, 10 mL of juice was diluted in 10 mL of distilled water and titrated with 0.1 M NaOH to pH 8.1; results are given as grams of malic acid per liter. Skin color was determined at two opposite equatorial points of 15 fruits using a portable tristimulus colorimeter (Chroma Meter CR-200, Minolta Corp., Osaka, Japan), with CIE D_{65} illuminant and 8 mm aperture diameter. Lightness (L^*) values were recorded, and hue angle was calculated from a^* and b^* parameters as arctg b^*/a^*.

For the assessment of ethylene production and respiration rates, three fruits per each cultivar were kept individually in 3 L glass jars, continuously aerated with humidified air at a rate of 1.5 L h^{-1}. Gas samples (1 mL) of the effluent air were taken with a syringe and injected into a gas chromatograph (model 6890N; Agilent Technologies, Madrid, Spain) equipped with a flame ionization detector and an alumina column (1.5 m × 3 mm). Analyses were conducted isothermally at 100 °C, with N_2 as the carrier gas, in the presence of air and H_2 (45, 400, and 45 mL min^{-1}, respectively). The injector and detector were held at 120 and 180 °C, correspondingly, and results are expressed as microliters per kilogram per hour. Respiration was determined as CO_2 production by directly connecting the effluent air from each jar to an infrared gas analyzer (Sensotran S.L., El Prat de Llobregat, Spain). Results are given as milligrams of CO_2 per kilogram per hour).

Chemical Standards and Reagents. The reagents and standards used for the analysis of cuticular components were supplied by Sigma-Aldrich (Steinheim, Germany). All standards used were of analytical grade.

Cuticle Isolation. Skin samples were taken at harvest and 5 days thereafter, and cuticles were isolated and analyzed as described below. Exocarp segments were excised from the cheek region of five fruits using a cork borer (13 mm i.d.). Twelve skin disks were so obtained from each individual fruit. Cuticular membranes (CM) were isolated enzymatically by incubation at 37 °C in 0.2% (w/v) cellulase and 100 U mL^{-1} pectinase in 50 mM citrate buffer (pH 4.0) until no more material was released, in the presence of 1 mM NaN_3 to prevent microbial growth. After isolation, CM were washed in citrate buffer (50 mM, pH 4.0) at 37 °C once or twice every day until no material was left in suspension, thoroughly rinsed in distilled water,[11] dried at 40 °C, and kept in hermetically capped vials until used. The mass of CM was determined gravimetrically and expressed per unit of fruit surface ($\mu g\ cm^{-2}$) as well as on a total surface basis (mg per fruit).

Extraction and Analysis of Cuticular Wax Compounds. Waxes were recovered from the 60 dry CM disks (79.64 cm^2/sample) obtained in each case. CM samples were dewaxed by shaking in $CHCl_3$ (1 mg of sample mL^{-1}) for 24 h at 25 °C, followed by incubation (15 min) in an ultrasonic bath. This dewaxing procedure was repeated three times. After filtration, the chloroform extracts were pooled and concentrated using a rotary evaporator at 50 °C and the waxes transferred to a preweighed vial, dried under N_2 until complete dryness, and weighed in a microbalance for calculation of total wax yield ($\mu g\ cm^{-2}$). Free hydroxyl and carboxyl groups were converted respectively into their trimethylsilyl (TMSi) ethers and esters by derivatizing with *N*,*O*-bis(trimethylsilyl)trifluoroacetamide (BSTFA) in pyridine (2:1, v/v) for 15 min at 100 °C.

After derivatization, eicosane (C_{20}) and dotriacontane (C_{32}) were added to wax samples as internal standards, and the mixtures were injected (1 μL) in on-column mode into a gas chromatography−mass spectrometry (GC-MS) system for compound identification. GC equipment (Agilent 6890N) coupled with a quadrupole mass selective detector (Agilent 5973N) was used for these analyses, equipped with a capillary column (BPX5, 30 m × 0.25 mm, 0.25 μm; SGE Europe Ltd., Milton Keynes, UK). Wax compounds were identified by comparing their retention indices with those of standards and their identities then confirmed by matching their electron ionization mass spectra (EI-MS) (70 eV, m/z 50−700) with those from the NIST 08 MS library. The oven was set at 50 °C (2 min), and the temperature was raised initially at 40 °C min^{-1} to 200 °C, kept at 200 °C for 2 min, raised again at 3 °C min^{-1} to 310 °C, and then kept constant at 310 °C for 30 min. Helium was used as the carrier gas (2 mL min^{-1}). Quantitative determination of wax compounds was carried out under the same chromatographic conditions using a GC system equipped with a flame ionization detector (FID).

Extraction and Analysis of Cutin Monomers. Samples (10 mg) of dewaxed cuticular membranes (DCM) were hydrolyzed in 3 mL of 1 M HCl in 100% MeOH and esterified in the same solvent for 2 h at 80 °C. After cooling, 2 mL of saturated NaCl was added to the methanolysate. The cutin monomers were extracted three times in 2 mL of hexane for 10 min, followed by thorough mixing and centrifugation at 20 °C. The monomer extracts were combined and evaporated to dryness in a N_2 steam. Cutin yields were determined gravimetrically as micrograms per square centimeter. Dry cutin samples were derivatized with BSTFA for 15 min at 100 °C, and then heptadecanoate (C_{17}) and tricosanoate (C_{23}) were added as

dx.doi.org/10.1021/jf5003528 | J. Agric. Food Chem. 2014, 62, 3488−3495

Table 2. Total Amount of Cuticle Recovered and Wax, Cutin, and Cutan Yields Obtained from 'October Sun' and 'Jesca' Peaches at Harvest and after 5 Days at 20 °C[a]

	'October Sun'				'Jesca'			
	harvest		harvest + 5 days		harvest		harvest + 5 days	
cuticle amount[b] (mg)	120.0		127.3		108.3		137.1	
cuticle yield (μg cm^{-2})	1506.8	ab	1598.4	ab	1359.9	b	1721.5	a
cuticle yield (mg/fruit)	289.5	ab	290.1	ab	266.0	b	324.8	a
wax yield (μg cm^{-2})	518.3	ab	549.8	ab	425.6	b	676.5	a
wax yield (mg/fruit)	99.6	b	99.8	b	83.2	c	127.7	a
cutin yield (μg cm^{-2})	164.2	ab	188.6	a	111.5	b	187.6	a
cutin yield (mg/fruit)	31.5	ab	34.2	a	21.8	b	35.4	a
cutan yield[c] (μg cm^{-2})	824.2	bc	859.9	a	822.7	c	857.3	ab
cutan yield[c] (mg/fruit)	158.3	a	156.1	a	160.9	a	161.8	a
wax (%)	34.4	ab	34.4	ab	31.3	b	39.3	a
cutin (%)	10.9	a	11.8	a	8.2	b	10.9	a
cutan[c] (%)	54.7	ab	53.8	ab	60.5	a	49.8	b

[a]Yields represent means of three replicates. Mean values followed by a different letter within the same row are significantly different at $P \leq 0.05$ (LSD test). [b]Recovered from 60 skin disks (12 disks × 5 fruit), corresponding in total to 79.64 cm^2. [c]Cutan yields were taken as the nonhydrolyzable residue remaining after cutin extraction.

internal standards, and the mixtures were injected (1 μL) to GC-FID for quantitative determination.

Cutin compounds were identified from their EI-MS spectra (70 eV, m/z 50−700) after GC-MS analysis using the same GC-MS system as described in the previous section. The oven was set and held at 50 °C for 2 min, and then the temperature was raised to 250 °C at 10 °C min^{-1}, kept at 250 °C for 1 min, raised again at 3 °C min^{-1} to 310 °C, and kept at that temperature for 20 min. The same chromatographic conditions were used for quantitative determination of cutin compounds by GC-FID.

Statistical Analysis. A multifactorial design with cultivar and days after harvest as factors was used to statistically analyze the results. All data were tested by analysis of variance (ANOVA) with the Minitab 16 program package, and means were separated by Fisher's LSD test at $P \leq 0.05$.

RESULTS AND DISCUSSION

The standard indicators of physiological and commercial maturity were determined at harvest. The values for these parameters (Table 1) were generally within the recommended ranges for this species in the producing area, showing that fruits were picked at a suitable maturity stage. Fruit size and firmness at harvest were above the minimum requirements for commercialization (≥70 mm and >30 N, respectively), and SSC values were around 12−13%, which in peach are associated with high consumer acceptance scores.[12] In both cultivars, fruit firmness decreased sharply 5 days after harvest, this loss being somewhat less dramatic for 'Jesca' samples. Although TA levels in 'October Sun' peaches were a bit higher than recommended for these fruits (4−7 g L^{-1}), acidity declined after the fruit had been kept at 20 °C for 5 days. Differences in hue and lightness of fruit surface reflect the different typologies of the two genotypes selected for this study, 'October Sun' and 'Jesca' being, respectively, a yellow-fleshed cultivar displaying 100% red skin and a yellow-skinned variety. Ethylene production rates by 'Jesca' fruit were approximately 10-fold those by 'October Sun' samples, but respiration rates were similar in both cases.

Fruit lost some weight after the simulated commercial period at 20 °C, although this loss was significant only in 'October Sun' samples (Table 1). Despite weight loss, fruit diameter and total surface did not show significant differences in comparison with those at harvest. These data were used to express cuticle amounts obtained from fruit skin on a whole fruit basis. The absolute amount of cuticle recovered from the 60 skin disks (roughly 80 cm^2 in total) was higher in 'October Sun' than in 'Jesca' (120 vs 108 mg, respectively) (Table 2). When these amounts were expressed per unit surface area (μg cm^{-2}) and per total fruit surface (mg fruit^{-1}), differences were not significant. However, whereas cuticle yields remained unchanged in 'October Sun' fruit after being kept for 5 days at 20 °C, a significant increase was found in 'Jesca' samples (Table 2), which suggests cuticle thickening in these fruit after harvest. The same trend was observed for total wax and cutin, yields after 5 days at 20 °C remaining at similar levels in 'October Sun' but increasing in 'Jesca' in comparison with those at commercial harvest, in both absolute (mass per surface unit and mass per total surface) and relative (%) terms. Because total fruit surface did not change significantly after the shelf-life period (Table 1), this observation possibly reflects active cuticle deposition taking place during that time.

Wax percentages in cuticles of 'October Sun' and 'Jesca' fruit at harvest were similar and represented around 34 and 31% of total cuticle recovered, respectively (Table 2). In contrast, cutin percentage at harvest was significantly higher in 'October Sun' than in 'Jesca' cuticles (11 vs 8%). We are aware of only one previously published study on peach fruit cuticle, in which cuticles of the 'Calrico' cultivar were found to be composed of 27% waxes and 23% cutin.[2] Trichomes were removed and analyzed separately, and found to contain lower percentages of wax (15%) and cutin (19%). However, the detailed composition of these cuticular fractions was not reported. Therefore, in this work we extracted and analyzed waxes and cutin monomers from cuticles isolated from peach fruit.

Wax Composition of Peach Fruit Cuticles. Compositional analysis of cuticular waxes of 'October Sun' and 'Jesca' fruit revealed that, despite being composed of similar chemical families, cultivar-related differences exist in the abundance of particular compounds. The main wax type in quantitative terms was triterpenoid acids, which agrees with observations for sweet cherry fruit (Belge et al., unpublished data),[13,14] the only stone fruit species for which detailed information on cuticle waxes is available. Significant differences in the total content of triterpenoid acids in cuticular waxes of fruit at harvest were found between both cultivars, levels being higher in 'October

Table 3. Wax Constituents (Relative Percent) Identified in Cuticles of 'October Sun' and 'Jesca' Peaches at Harvest and after 5 Days at 20 °C[a]

	'October Sun'				'Jesca'			
compound family	harvest		harvest + 5 days		harvest		harvest + 5 days	
triterpenes	**51.916**	**a**	**51.080**	**a**	**44.053**	**b**	**40.886**	**c**
oleanolic acid	22.728	a	21.495	b	17.208	c	16.184	c
ursolic acid	29.188	a	29.585	a	26.845	b	24.703	c
alkanes	**16.510**	**c**	**16.505**	**c**	**29.403**	**a**	**27.691**	**b**
dodecane (C12)	0.006	b	0.008	b	0.041	a	0.006	b
tridecane (C13)	0.008	b	0.006	b	0.042	a	0.004	b
tetradecane (C14)	0.007	a	0.004	b	0.003	b	0.004	b
pentadecane (C15)	0.003	a	nd		0.002	b	0.004	a
hexadecane (C16)	0.004	a	0.004	a	0.004	a	0.003	a
heptadecane (C17)	0.004	a	0.003	a	0.003	a	nd	
octadecane (C18)	0.006	b	0.007	ab	0.006	b	0.008	a
nonadecane (C19)	0.011	b	0.035	b	0.035	b	0.080	a
henicosane (C21)	0.049	c	0.122	c	0.305	b	0.575	a
docosane (C22)	0.034	b	0.038	b	0.042	b	0.060	a
tricosane (C23)	2.561	c	3.138	c	9.541	a	9.050	a
tetracosane (C24)	0.282	c	0.491	c	0.635	a	0.612	ab
pentacosane (C25)	4.608	c	4.582	c	9.025	a	7.849	a
hexacosane (C26)	0.246	a	0.244	a	0.213	c	0.234	c
heptacosane (C27)	3.614	c	3.361	c	5.315	a	5.084	a
octacosane (C28)	0.267	a	0.258a	a	0.237	b	0.262	a
nonacosane (C29)	3.954	a	3.504	b	3.515	b	3.418	b
triacontane (C30)	0.146	a	0.139	b	0.110	d	0.122	c
hentriacontane (C31)	0.699	a	0.560	b	0.328	c	0.316	c
fatty acids	**8.270**	**b**	**10.255**	**b**	**10.220**	**b**	**12.668**	**a**
C12:0	0.013	b	0.011	b	0.015	a	0.011	b
C14:0	0.036	b	0.047	a	0.046	a	0.042	b
C15:0	0.006	d	0.008	c	0.013	b	0.015	a
C16:0	2.165	b	2.724	a	2.470	ab	2.746	a
C17:0	0.013	c	0.015	b	0.018	a	0.017	a
C18:0	1.094	ab	1.240	a	0.749	b	1.342	a
C18:1 (9)	2.630	ab	2.343	b	2.348	b	2.856	a
C18:2 (9, 12)	2.299	c	3.855	b	4.557	ab	5.629	a
trans-C18:2 (9,12)	0.015	a	0.012	ab	0.006	c	0.010	b
phytosterols	**2.052**	**a**	**1.562**	**b**	**0.897**	**c**	**0.963**	**c**
campesterol	1.622	a	1.152	b	0.483	c	0.648	c
β-sitosterol	0.430	a	0.410	a	0.414	a	0.315	b
fatty alcohols	**2.559**	**b**	**2.656**	**a**	**2.584**	**b**	**2.577**	**b**
tricosanol (C23)	1.080	b	1.173	a	1.181	a	1.206	a
tetracosanol (C24)	0.489	b	0.413	c	0.643	a	0.559	b
hexacosanol (C26)	0.122	a	0.108	a	0.054	b	0.063	b
octacosanol (C28)	0.487	b	0.566	a	0.436	b	0.444	b
triacontanol (C30)	0.382	a	0.396	a	0.271	c	0.305	b
identified wax	**81.307**	**c**	**82.058**	**c**	**87.157**	**a**	**84.786**	**b**
unidentified	**18.693**	**a**	**17.942**	**a**	**12.843**	**c**	**15.214**	**b**

[a]Values represent means of three replicates (nd, nondetectable). Mean values followed by a different letter within the same row are significantly different at $P \leq 0.05$ (LSD test).

Sun' (52%) than in 'Jesca' (44%). Substantial amounts of ursolic and oleanoic acids were detected in both cases (Table 3). However, although ursolic acid has been consistently found to be largely dominant among the triterpenoid components of sweet cherry waxes (ranging from 47 to 60% of total waxes depending on the cultivar considered) (Belge et al., unpublished data),[13,14] amount differences with oleanoic acid, the second triterpene in quantitative terms, were moderate in both peach genotypes studied herein, particularly in 'October Sun' samples (Table 3). Ursolic acid percentages over total cuticular waxes in 'October Sun' and 'Jesca' were approximately 29 and 27% at harvest, whereas those of oleanoic acid were around 23 and 17%, correspondingly. The amount of total triterpenes was maintained in 'October Sun' samples along the simulated commercial life subsequent to harvest, both in relative (Table 3) and absolute (Figure 1) terms. In contrast, the absolute amount of total triterpenes (μg cm^{-2}) increased significantly in 'Jesca' fruit after harvest (Figure 1), which indicates that triterpenes must have been actively synthesized during the shelf-life period. However, triterpene synthesis was apparently not intense enough to keep pace with higher cuticle

dx.doi.org/10.1021/jf5003528 | J. Agric. Food Chem. 2014, 62, 3488−3495

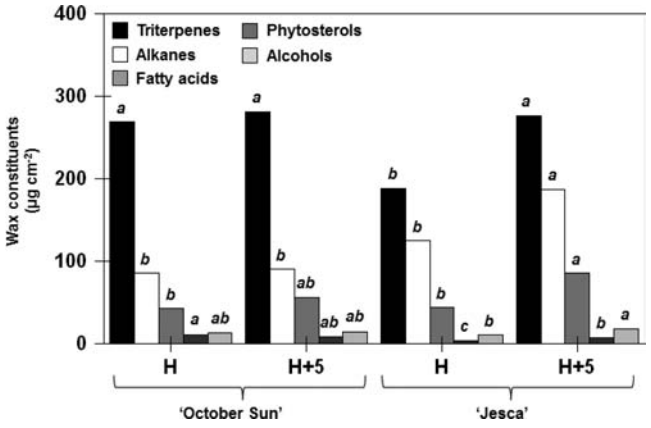

Figure 1. Amount (μg cm^{-2}) of the main families of wax constituents identified in cuticles of 'October Sun' and 'Jesca' peaches at harvest (H) and after 5 days at 20 °C (H+5). For each type of wax constituent, values bearing different letters are significantly different at $P \leq 0.05$ (LSD test).

yields (Table 2), resulting in a significantly decreased percentage of total triterpenes over total waxes (Table 3).

Alkanes were the second most important type of wax components in quantitative terms, also in accordance with observations for sweet cherry (Belge et al., unpublished data).[13,14] Yet, cuticular waxes of the nonmelting 'Calrico' peach were reported recently to contain as much as 76% of *n*-alkanes,[2] thus standing for the main group of wax components. Although the percentage of total alkanes detected herein was much lower, 'Jesca' cuticles were remarkably richer in this type of wax compound than those obtained from 'October Sun' fruit (roughly 29 vs 16% at harvest, correspondingly), which shows substantial cultivar-to-cultivar variability. In most published studies on composition of fruit cuticles, *n*-nonacosane (C_{29}) and/or *n*-hentriacontane (C_{31}) have been reported to be the main alkanes in cuticular waxes.[1] This is in contrast with data shown herein for peach fruit. Although important amounts of *n*-nonacosane (3−4%) were indeed detected in cuticular waxes of both cultivars, the predominant alkanes were *n*-tricosane (C_{23}), *n*-pentacosane (C_{25}), and *n*-heptacosane (C_{27}), which in 'Jesca' accounted together for almost 24% of total waxes at harvest, even though levels in 'October Sun' were lower (roughly 11%) (Table 3). Cultivar-related differences were also observed in relation to the evolution of total alkanes after harvest, which remained unchanged in 'October Sun' in both absolute (Figure 1) and relative (Table 3) terms. In contrast, a significant decline in alkane percentage over total waxes was observed for 'Jesca' after 5 days at 20 °C. However, alkane biosynthesis must have taken place after harvest, because the amount per surface area unit (μg cm^{-2}) increased significantly (Figure 1), hence contributing to the observed increment in cuticle yields (Table 2).

Cuticular wax constituents of both peach cultivars also included substantial amounts of fatty acids, particularly of those of the C_{18} type (Table 3). Linoleic acid was prominent among this type of wax components, followed by oleic and stearic acids. Cuticular waxes of fruit assessed were also rich in the C_{16}-type palmitic acid. Generally speaking, the percentage of fatty acids in cuticular waxes, as well as their total amount per unit of surface area (Figure 1), showed an increasing trend during the shelf-life period at 20 °C, although some variability was found for particular compounds (Table 3).

Cuticles of 'October Sun' fruit were richer in phytosterols than those of 'Jesca', both in relative (Table 3) and absolute (Figure 1) terms. This difference was due to a higher content of campesterol, because the percentages of β-sitosterol were similar in both cases. With regard to alcohols, the percentage over total waxes and the amount per surface unit at harvest were similar in both cultivars. However, cultivar-related differences were observed in the specific composition of this type of wax constituents: whereas 'Jesca' was richer in tricosanol (C_{23}) and tetracosanol (C_{24}), cuticles of 'October Sun' contained higher percentages of hexacosanol (C_{26}) and triacontanol (C_{30}).

The data thus indicate the existence of significant differences in the percentage of particular families of wax constituents in the fruit cuticles of both peach cultivars considered in this study. Whereas 'October Sun' fruits were richer in triterpenoid acids and phytosterols, 'Jesca' cuticles contained a higher percentage of alkanes (Table 3). The possible relationship of these differences with the postharvest performance of each particular genotype deserves further attention. For instance, it has been suggested that the waterproofing properties of fruit cuticles are defined primarily by the *n*-alkane components,[15] because the presence of amorphous waxes such as triterpenoids would impair the transpiration barrier function of cuticles.[16] Accordingly, dehydration rates in pepper fruit correlated inversely with the ratio of alkanes to triterpenoids plus sterols.[17] The composition data obtained herein indicate that this ratio was 0.31 in 'October Sun' and 0.65 in 'Jesca' at commercial harvest, which agrees with lower weight loss in the latter after 5 days at 20 °C (5.6 vs 3.9%, respectively) (Table 1).

The data also indicate that postharvest modifications in the composition of cuticular waxes were more intense in 'Jesca' than in 'October Sun' fruits. For 'October Sun', no significant changes were found after the simulated shelf-life period in the total amount of the main families of wax constituents in terms of mass per surface unit (Figure 1) and, for the quantitatively main types of compounds (triterpenes, alkanes, and acids), also not in relative terms (Table 3). In contrast, the percentage of fatty acids over total waxes increased significantly in 'Jesca' fruit after the same period, whereas that of triterpenes and alkanes decreased (Table 3). However, the absolute amount of all types of wax compounds identified herein increased significantly (Figure 1), indicating active biosynthesis in this cultivar after harvest, which must have accounted for augmented cuticle yields in these fruits (Table 2).

Cutin Composition of Peach Fruit Cuticles. Although significant differences were found at harvest between both cultivars in the relative (%) amount of cutin recovered from fruit cuticles, the total amounts of cutin were similar when expressed in terms of mass per surface unit and per total surface (Table 2). Detailed analysis of cutin monomer composition revealed that the cutin fraction of 'October Sun' and 'Jesca' peach fruit at harvest maturity was composed mainly of C_{18} monomers (54.7 and 57.1%, respectively), comprising mono-carboxylic, α,ω-dicarboxylic, and ω-hydroxylated acids (Table 4). The most abundant of these C_{18} constituents were 18-hydroxyoleic acid, oleic acid, linoleic acid, 1,18-oleic diacid, and 18-hydroxylinoleic acid. In turn, palmitoleic acid predominated among the C_{16}-type monomers. This contrasts with findings on sweet cherry fruit, another *Prunus* species, in which, conversely, undetectable or very low levels of palmitoleic acid could be found in cutin, hexadecane-1,16-dioic acid (Belge et al., unpublished data) or 9,16-dihydroxypalmitic acid[14] being the

Table 4. Cutin Constituents (Relative Percent) Identified in Cuticles of 'October Sun' and 'Jesca' Peaches at Harvest and after 5 Days at 20 °C[a]

	'October Sun'				'Jesca'			
compound family	harvest		harvest + 5 days		harvest		harvest + 5 days	
alkan-1-oic acids	**29.276**	**c**	**29.703**	**c**	**34.355**	**b**	**36.618**	**a**
C14:0	0.052	b	0.118	a	0.134	a	0.169	a
C15:0	0.049	c	0.107	b	0.169	a	0.139	ab
C16:1 (9)	6.082	c	6.284	c	7.187	b	7.470	a
C18:1 (9)	10.557	a	8.923	b	9.906	ab	10.630	a
C18:2 (9, 12)	5.713	c	7.441	b	11.638	a	12.682	a
C20:0	1.624	a	1.496	b	0.238	c	0.266	c
C22:0	4.779	a	4.584	b	4.767	a	4.870	a
C26:0	0.420	ab	0.489	a	0.316	c	0.392	bc
C28:0	nd		0.261	a	nd		nd	
alkan-2-oic acids	**1.960**	**b**	**2.400**	**a**	**1.808**	**b**	**1.645**	**b**
C18:0	1.724	b	2.236	a	1.681	b	1.645	b
C22:0	0.236	a	0.164	ab	0.127	b	nd	
α,ω-dicarboxylic acids	**11.383**	**a**	**11.541**	**a**	**9.991**	**b**	**9.133**	**c**
1,16-dioic C_{16}	1.991	a	1.988	a	1.724	b	1.696	b
1,18-dioic $C_{18:1}$	9.392	a	9.553	a	8.267	b	7.437	c
hydroxyacids	**30.173**	**a**	**29.850**	**a**	**28.330**	**b**	**26.695**	**c**
2-OH $C_{14:0}$	2.553	a	2.380	a	1.795	b	2.430	a
16-OH $C_{16:0}$	0.282	b	0.253	b	0.952	a	0.421	b
18-OH $C_{18:1}$	20.149	a	19.968	a	17.580	b	15.985	c
18-OH $C_{18:2}$	7.189	c	7.249	c	8.003	a	7.859	b
alkanes	**3.061**	**c**	**3.305**	**ab**	**3.438**	**a**	**3.182**	**c**
hexadecane (C16)	0.658	a	0.658	a	0.440	c	0.462	b
nonadecane (C19)	0.283	d	0.290	c	0.302	b	0.311	a
icosane (C20)	nd		0.112	a	nd		nd	
docosane (C22)	0.411	d	0.437	c	0.720	a	0.689	b
tricosane (C23)	0.471	a	0.296	b	0.270	b	0.374	ab
tetracosane (C24)	0.564	a	0.553	b	0.459	c	0.461	c
hexacosane (C26)	0.279	b	0.591	ab	0.754	a	0.410	b
octacosane (C28)	0.395	b	0.368	b	0.493	a	0.475	a
fatty alcohols	**0.692**	**c**	**0.887**	**bc**	**0.913**	**b**	**1.146**	**a**
octadecanol (C18)	nd		0.186	a	nd		nd	
tetracosanol (C24)	0.692	c	0.701	c	0.778	b	0.889	a
hexacosanol (C26)	nd		nd		0.134	b	0.257	a
identified cutin	**76.546**	**c**	**77.686**	**b**	**78.834**	**a**	**78.417**	**ab**
unidentified	**23.454**	**a**	**22.314**	**b**	**21.166**	**c**	**21.583**	**bc**

[a]Values represent means of three replicates (nd, nondetectable). Mean values followed by a different letter within the same row are significantly different at $P \leq 0.05$ (LSD test).

predominant C_{16}-type monomers, depending on the cultivar considered. Although currently available information on the specific composition of fruit cuticles is limited, published studies indicate that substantial variability exists among species or even cultivars,[1] meaning that there is ample opportunity for further research.

Only minor quantitative differences in cutin composition were found at harvest between both cultivars considered, whereas the main types of constituent compounds were the same. Cutin of 'October Sun' fruit was richer in dicarboxylic and hydroxylated acids, whereas that of 'Jesca' peaches displayed higher percentages of monocarboxylic acids, alkanes, and alcohols (Table 4). Dicarboxylic and ω-hydroxyacids have been suggested to be important for the formation and cross-linking of the cutin polymers,[18,19] which might account partially for lower total amounts of cutin in cuticles isolated from 'Jesca' fruit (Table 2).

However, results revealed a different evolution of particular compounds after harvest for each of the peach genotypes assessed. The percentages of particular cutin monomer types in 'October Sun' cuticles showed limited changes after shelf life at 20 °C, the only significant variation observed being restricted to an increase in total alkanes, expressed both as the percentage over total cutin (Table 4) and as micrograms per square centimeter of surface area (Figure 2), even though unchanged or even declining levels could also be found for individual compounds. Contrarily, the amount of all of the identified types of cutin monomers increased significantly after harvest when expressed per unit of surface area (Figure 2), which indicates that the involved biochemical pathways were up-regulated during that period. Yet, owing to augmented cuticle yields (Table 2), the amounts of some of these families of cutin compounds were lower than at harvest when expressed as a percentage (Table 4), suggesting that not all of the related processes were enhanced to the same extent.

In conclusion, the composition of cuticular waxes and cutin monomers in cuticles isolated from peach fruit was characterized for the first time in both a melting and a

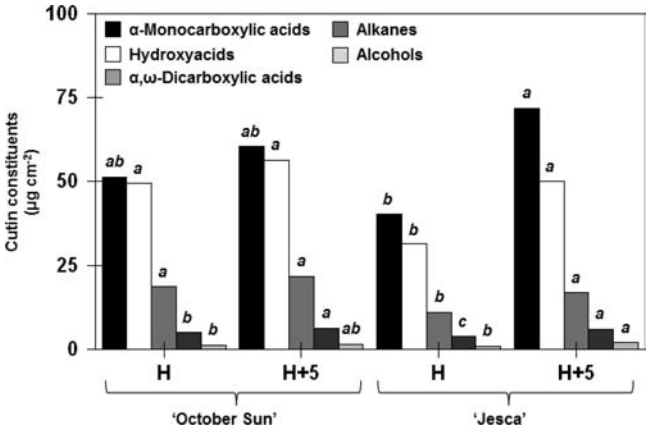

Figure 2. Amount (μg cm^{-2}) of the main types of cutin monomers identified in cuticles of 'October Sun' and 'Jesca' peaches at harvest (H) and after 5 days at 20 °C (H+5). For each type of cutin monomer, values bearing different letters are significantly different at $P \leq 0.05$ (LSD test).

nonmelting cultivar. The triterpenoid ursolic and oleanoic acids and the alkanes *n*-tricosane and *n*-pentacosane were quantitatively prominent among the wax compounds identified, whereas cutin composition was dominated by the C_{18} monomer type. Some quantitative differences in the abundance of particular components were observed between the cuticles isolated from 'October Sun' and 'Jesca' peaches at harvest, but postharvest modifications in cuticle composition were more intense in 'Jesca'. The question arises whether this aspect may relate to the different ethylene production rates observed in each case (Table 1). A few published studies have provided evidence that the composition of cuticular waxes may be an ethylene-associated attribute in some fruit species. For example, 1-MCP treatment of 'Red Fuji', 'Autumn Gold', and 'Royal Gala' apples largely attenuated the quantitative changes observed after long-term cold storage in the contents of particular wax constituents required for the formation of cuticular wax crystals.[20,21] Accordingly, ethylene treatment of 'Navelate' orange fruit increased the content of epicuticular waxes and caused surface structural changes during shelf life at 22 °C.[22] To the best of our knowledge, this is the first study characterizing the composition of the cuticle of peach fruit and describing the changes therein after harvest. Further work focusing on these modifications in response to different factors will be required for a deeper understanding of the physiological consequences of these compositional changes and of their influence on quality attributes of peach fruit.

AUTHOR INFORMATION

Corresponding Author

*(I.L.) E-mail: lara@quimica.udl.cat. Phone: +34 973 702526.

Funding

B.B. is the recipient of a FI-DGR grant from AGAUR (Generalitat de Catalunya). This work was supported through the AGL2010-14801/ALI project, funded by the Ministerio de Ciencia e Innovación (MICINN) of Spain.

Notes

The authors declare no competing financial interest.

ACKNOWLEDGMENTS

Fruit samples were provided by F. Guàrdia (CEFRUCO S.C.C.L., Alguaire).

REFERENCES

(1) Lara, I.; Belge, B.; Goulao, L. F. The fruit cuticle as a modulator of postharvest quality. *Postharvest Biol. Technol.* **2014**, *87*, 103−112.
(2) Fernández, V.; Khayet, M.; Montero-Prado, P.; Heredia-Guerrero, J. A.; Liakopoulos, G.; Karabourniotis, G.; del Río, V.; Domínguez, E.; Tacchini, I.; Nerín, C.; Val, J.; Heredia, A. New insights into the properties of pubescent surfaces: peach fruit as a model. *Plant Physiol.* **2011**, *156*, 2098−2108.
(3) Fishman, M. L.; Levaj, B.; Gillespie, D.; Scorza, R. Changes in the physicochemical properties of peach fruit pectin during on-tree ripening and storage. *J. Am. Soc. Hortic. Sci.* **1993**, *118*, 343−349.
(4) Lurie, S.; Crisosto, C. H. Chilling injury in peach and nectarine. *Postharvest Biol. Technol.* **2005**, *37*, 195−208.
(5) Lin, T. T.; Pitt, R. E. Rheology of apple and potato tissue as affected by cell turgor pressure. *J. Texture Stud.* **1986**, *17*, 291−313.
(6) Heyes, J. A.; Sealey, D. F. Textural changes during nectarine (*Prunus persica*) development and ripening. *Sci. Hortic.* **1996**, *65*, 49−58.
(7) Saladié, M.; Matas, A. J.; Isaacson, T.; Jenks, M. A.; Goodwin, S. M.; Niklas, K. J.; Xiaolin, R.; Labavitch, J. M.; Shackel, K. A.; Fernie, A. R.; Lytovchenko, A.; O'Neill, M. A.; Watkins, C. B.; Rose, J. K. C. A reevaluation of the key factors that influence tomato fruit softening and integrity. *Plant Physiol.* **2007**, *144*, 1012−1028.
(8) Paniagua, A. C.; East, A. R.; Hindmarsh, J. P.; Heyes, J. A. Moisture loss is the major cause of firmness change during postharvest storage of blueberry. *Postharvest Biol. Technol.* **2013**, *79*, 13−19.
(9) Edelmann, H. G.; Neinhuis, C.; Bargel, H. Influence of hydration and temperature on the rheological properties of plant cuticles and their impact on plant organ integrity. *J. Plant Growth Regul.* **2005**, *24*, 116−126.
(10) Matas, A. J.; López-Casado, G.; Cuartero, J.; Heredia, A. Relative humidity and temperature modify the mechanical properties of isolated tomato fruit cuticles. *Am. J. Bot.* **2005**, *92*, 462−468.
(11) Schönherr, J.; Riederer, M. Plant cuticles sorb lipophilic compounds during enzymatic isolation. *Plant Cell Environ.* **1986**, *9*, 459−466.
(12) Crisosto, C. H.; Crisosto, G.; Bowerman, E. Understanding consumer acceptance of peach, nectarine and plum cultivars. *Acta Hortic.* **2003**, *604*, 115−119.
(13) Markley, K. S.; Sando, C. E. The wax-like constituents of the cuticle of the cherry, *Prunus avium* L. *J. Biol. Chem.* **1937**, *119*, 641−645.
(14) Peschel, S.; Franke, R.; Schreiber, L.; Knoche, M. Composition of the cuticle of developing sweet cherry fruit. *Phytochemistry* **2007**, *68*, 1017−1025.
(15) Vogg, G.; Fischer, S.; Leide, J.; Emmanuel, E.; Jetter, R.; Levy, A. A.; Riederer, M. Tomato fruit cuticular waxes and their effect on transpiration barrier properties: functional characterization of a mutant deficient in a very-long-chain fatty acid β-ketoacyl-CoA synthase. *J. Exp. Bot.* **2004**, *55*, 1404−1410.
(16) Isaacson, T.; Kosma, D. K.; Matas, A. J.; Buda, G. J.; He, Y.; Yu, B.; Pravitasari, A.; Batteas, J. D.; Stark, R. E.; Jenks, M. A.; Rose, J. K. C. Cutin deficiency in the tomato fruit cuticle consistently affects resistance to microbial infection and biomechanical properties, but not transpirational water loss. *Plant J.* **2009**, *60*, 363−377.
(17) Parsons, E. P.; Popopvsky, S.; Lohrey, G. T.; Lü, S.; Alkalai-Tuvia, S.; Perzelan, Y.; Paran, I.; Fallik, E.; Jenks, M. A. Fruit cuticle lipid composition and fruit post-harvest water loss in an advanced backcross generation of pepper (*Capsicum* sp.). *Physiol. Plant.* **2012**, *146*, 15−25.
(18) Bonaventure, G.; Beisson, F.; Ohlrogge, J.; Pollard, M. Analysis of the aliphatic monomer composition of polyesters associated with *Arabidopsis* epidermis: occurrence of octadeca-*cis*-6,*cis*-9-diene-1,18-dioate as the major component. *Plant J.* **2004**, *40*, 920−930.

(19) Pollard, M.; Beisson, F.; Li, Y.; Ohlrogge, J. B. Building lipid barriers: biosynthesis of cutin and suberin. *Trends Plant Sci.* **2008**, *13*, 236−246.
(20) Dong, X.; Rao, J.; Huber, D. J.; Chang, X.; Xin, F. Wax composition of 'Red Fuji' apple fruit during development and during storage after 1-methylcyclopropane treatment. *Hortic. Environ. Biotechnol.* **2012**, *53*, 288−297.
(21) Curry, E. Effects of 1-MCP applied postharvest on epicuticular wax of apples (*Malus domestica* Borkh.) during storage. *J. Sci. Food Agric.* **2008**, *88*, 996−1006.
(22) Cajuste, J. F.; González-Candelas, L.; Veyrat, A.; García-Breijo, F. J.; Reig-Armiñana, J.; Lafuente, M. T. Epicuticular wax content and morphology as related to ethylene and storage performance of 'Navelate' orange fruit. *Postharvest Biol. Technol.* **2010**, *55*, 29−35.

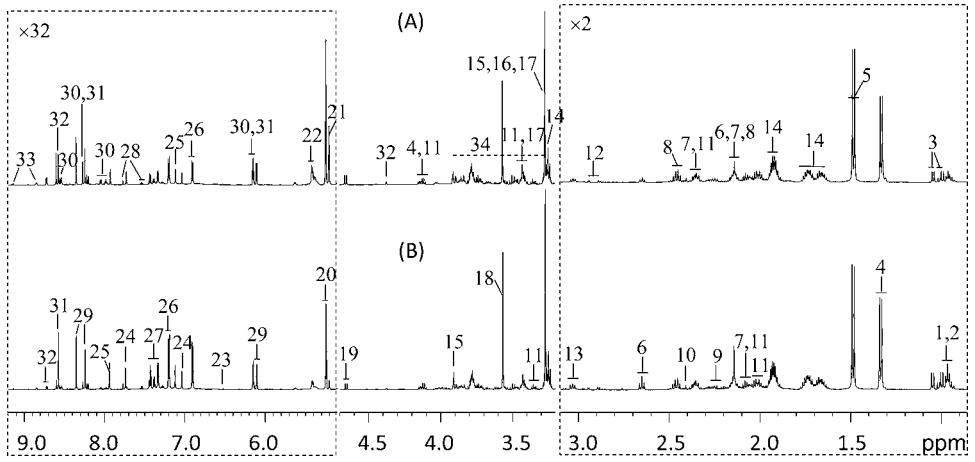

Figure 1. Representative 600 MHz ^{1}H NMR spectra of muscle extracts from WG (A) and SG (B). The dotted regions were vertically expanded 32 and 2 times, respectively. Resonance assignments are given in Supplementary Table S1 in the Supporting Information. Peaks: 1, isoleucine; 2, leucine; 3, valine; 4, lactate; 5, alanine; 6, methionine; 7, glutamate; 8, glutamine; 9, α-aminoadipate; 10, succinate; 11, proline; 12, asparagine; 13, lysine; 14, arginine; 15, betaine; 16, trimethylamine-*N*-oxide; 17, taurine; 18, glycine; 19, β-glucose; 20, α-glucose; 21, trehalose; 22, maltose; 23, fumarate; 24, histamine; 25, histidine; 26, tyrosine; 27, phenylalanine; 28, tryptophan; 29, inosine; 30, adenosine triphosphate; 31, adenosine diphosphate; 32, 2-pyridinemethanol; 33, trigonelline; 34, sugar and amino acids.

spectroscopy in conjunction with high-throughput data analysis. Our aims are to understand (1) the metabolic phenotype modulation in crabs responding to low-salinity exposure and (2) the physiological advantages caused by low-salinity training.

MATERIALS AND METHODS

Chemicals and Reagents. Methanol, sodium chloride, $K_2HPO_4\cdot 3H_2O$, and $NaH_2PO_4\cdot 2H_2O$ (all of analytical grade) were purchased from Sinopharm Chemical Co., Ltd. (Shanghai, China), and sodium azide was bought from Fuchen Chemical Reagent Co. (Tianjin, China). Sodium 3-trimethylsilyl [2,2,3,3-$^2D_4$]propionate (TSP-d_4) and deuterated water (D_2O, 99.9% D) were obtained from Cambridge Isotope Laboratories, Inc. (Tewksbury, MA, USA).

Animals and Sample Treatment. Larvae of *P. trituberculatus* (about 3.0 g) from a commercial farm in Xiangshan, China, were put into a salinity of 4‰ for 72 h for natural selection. The surviving individuals were collected and named the screened group (SG). The larvae crabs having no experience in low salinity were named the wild group (WG). All of the crabs were fed frozen fish once daily at 5:00–6:00 p.m. For the low-salinity tolerance study, 30 SG crabs and 30 WG crabs with average weight of 65.3 ± 5.2 g per individual were exposed to 4‰ salinity stress. Six crabs of each group were sacrificed following the sample collection at time points of 0, 12, 24, 48, and 72 h, respectively. The muscle tissue of each crab was immediately collected, homogenized, and snap-frozen in liquid nitrogen and stored at −80 °C until metabonomic analysis.

Metabolite Extraction of Crab Muscle. Each of the muscle samples (200 mg) was homogenized in 1 mL of ice-cold H_2O/methanol (1:2 v/v) extraction solution followed by sonification on wet ice for 150 cycles with each cycle consisting of a 2 s sonication and a 2 s break. Supernatant for each sample was collected respectively after 10 min of centrifugation (12000 rpm, 4 °C). The remaining solid residues of each sample were further extracted once using the above extraction procedure. After centrifugation for 10 min (12000 rpm and 4 °C), the resultant two supernatants were combined and lyophilized following removal of methanol in vacuo. The extracts were then reconstituted into 600 μL of phosphate buffer (0.1 M K_2HPO_4/NaH_2PO_4, 0.1% NaN_3, 0.005% TSP, 100% D_2O, pH 7.4). Following centrifugation, 550 μL of the supernatant from each extract was transferred into a 5 mm NMR tube for NMR analysis.

NMR Spectroscopic Analysis. All of ^{1}H NMR spectra of muscle extracts were acquired at 298 K on a Bruker Avance III 600 MHz spectrometer, operating at 600.13 MHz for ^{1}H equipped with an inverse cryogenic probe (Bruker Biospin, Germany). For all of the extracts, a standard water-suppressed ^{1}H NMR spectrum named NOESYGPPR1D pulse sequence (recycle delay−G_1−90°−t_1−90°−t_m−G_2−90°−acquisition) was recorded with recycle delay of 2 s, t_1 of 3 ms and t_m of 100 ms. Meanwhile, the 90° pulse length was adjusted to approximately 10 μs, and 64 transients were collected into 32 K data points for each spectrum with a spectral width of 20 ppm.

For NMR signal assignment purposes, a series of two-dimensional NMR spectra were acquired for selected samples and processed according to a previously reported method, including ^{1}H−^{1}H correlation spectroscopy (COSY), ^{1}H−^{1}H total correlation spectroscopy (TOCSY), ^{1}H−^{13}C heteronuclear single-quantum correlation (HSQC), and ^{1}H−^{13}C heteronuclear multiple-bond correlation spectra (HMBC).[26,27]

NMR Data Processing and Multivariate Data Analysis. All free induction decays were multiplied by an exponential function with a line-broadening factor of 1 Hz and zero-filled to 128 K prior to Fourier transformation. After manual phase- and baseline correction with the chemical shift referenced to TSP as δ 0.00, all ^{1}H NMR spectra (δ 0.7–9.5) without residual water signals δ 4.70–5.15 were integrated into regions with equal widths of 0.004 ppm (2.4 Hz). All of the integral regions were normalized to wet weight of muscle for each spectrum to compensate for the overall concentration differences prior to the multivariate data analysis.

Multivariate data analysis was performed with the software package SIMCA-P$^+$ (12.0, Umetrics, Umea, Sweden). Principal component analysis (PCA) was carried out using the mean-centered NMR data to obtain an overview of group clustering and search for possible outliers. Subsequently, orthogonal projection to latent structure discriminant analysis (OPLS-DA) was conducted with six-fold cross-validation using the unit-variance scaled NMR data as *X*-matrix and the group information as *Y*-matrix. All OPLS-DA models were validated by CV-ANOVA approach with $p < 0.05$ as the significant level.[28] The coefficient plots of OPLS-DA models were displayed to show changed metabolites at different post-treatment time points in both WG and SG crabs against their levels at 0 h. A cutoff value of 0.755 was used in the present study, and the metabolites with $r > 0.755$ or $r < -0.755$ were considered to be statistically significant ($p < 0.05$).

Univariate Data Analysis. The selected metabolites with significant difference at different time points of post-treatment obtained from multivariate data analysis were further analyzed with Student's *t* test (if criteria met) or nonparametric tests. The concentration of these metabolites was calculated by the integral of least-overlapping NMR signals for those metabolites as described previously,[29] using SPSS 13.0 software (SPSS, Chicago, IL, USA). To illustrate the dynamic metabolite changes induced by low-salinity

dx.doi.org/10.1021/jf405668a | J. Agric. Food Chem. 2014, 62, 3496−3503

challenge, the ratio for metabolite concentrations in both WG and SG crabs at different time points of post-treatment were also calculated as previously described[20,30] in the form of $(C_T - C_0)/C_0$, where C_T denotes the concentration of metabolite at the time point of post-treatment and C_0 denotes the concentration of metabolite at 0 h.

RESULTS

Metabolites in the Crab Muscle Extracts. Figure 1 shows representative 600 MHz ^{1}H NMR spectra of muscle extracts obtained from WG and SG crabs. Both ^{1}H and ^{13}C NMR resonances for detectable metabolites were assigned according to the published results[25] and further confirmed by a series of 2D NMR spectra including COSY, TOCSY, HSQC, and HMBC. The detectable metabolites of muscle extracts include a range of amino acids, sugars, carboxylic acids, trimethylamine-*N*-oxide (TMAO), betaine, and nucleotides (Supporting Information Table S1). To obtain more details on the metabolite alterations induced by low-salinity stress, multivariate data analysis and univariate data analysis were conducted on these NMR data.

Metabolite Alterations Induced by Low-Salinity Exposure. To summarize the similarities and differences between low-salinity-induced metabolic phenotypes in WG and SG crabs, the mean PCA metabolic trajectories for each crab group were plotted in the first two principal components (Figure 2). Clearly, both WG and SG crabs presented a similar

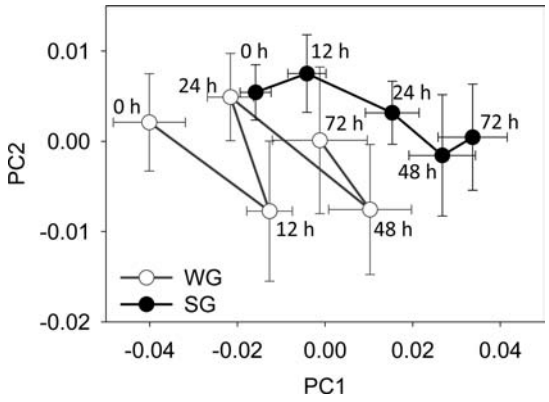

Figure 2. PCA trajectories generated from muscle extract profiles obtained from WG and SG as a function of low-salinity exposure.

tendency of metabolic alteration in response to low-salinity stress. However, the metabolic responses of SG crabs to low-salinity stress exhibited a more direct shift of metabolic profiles than WG crabs during the 72 h treatment.

The PCA scores plots of the ^{1}H NMR spectral data also revealed a clear difference of metabonome at each time point of post-treatment compared to 0 h in both WG and SG crabs (Supporting Information Figure S1). The metabolite alterations in WG and SG induced by low salinity were extracted using OPLS-DA models with R^2X and Q^2, which indicate the quality of these models. The validity of each OPLS-DA model was further evaluated with the CV-ANOVA approach ($p < 0.05$). OPLS-DA loadings plots were obtained to show the metabolites in muscle extracts from WG and SG crabs exposed to low salinity at different time points of 12, 24, 48, and 72 h against their levels of 0 h, respectively. Although the Q^2 of each OPLS-DA model in our present study was >0.5, only two of the models for SG passed the rigorous test of CV-ANOVA. These two models and their corresponding OPLS-DA coefficient plots are illustrated in Figure 3. The dynamic changes of representative metabolites in two *P. trituberculatus* strains exposed to low salinity at different time points of post-treatment are shown in Figure 4. Their corresponding correlation coefficients, which are above the cutoff value, 0.755, are listed in Table S2 in the Supporting Information.

To ensure the reliability of the obtained results, the selected metabolites were further studied using univariate data analysis. Our results showed that most alterations in the metabolite levels were in agreement with those from multivariate data analysis. Interestingly, the alterations of some metabolites previously shown to be nonsignificant in multivariate data analysis presented a significant difference at the level of $p < 0.05$. As an example, an increase in the ATP levels of WG crabs was significant from 2.05 ± 0.54 mg/g crab muscle at 0 h to 4.97 ± 1.47 mg/g crab muscle at 12 h ($p = 0.003$), 5.67 ± 1.37 mg/g crab muscle at 48 h ($p = 0.001$), and 3.76 ± 0.79 mg/g crab muscle at 72 h ($p = 0.001$) (Table 1 and Table S3 in the Supporting Information). Moreover, a significant elevation in the ATP levels of SG crabs was also observed from 2.49 ± 0.17 mg/g crab muscle at 0 h to 4.75 ± 1.17 mg/g crab muscle at 12 h ($p = 0.001$) and 3.42 ± 0.43 mg/g crab muscle at 24 h ($p = 0.001$) based on the univariate data analysis.

For WG crabs, 12 h of low-salinity exposure resulted in significantly reduced levels of inosine and a range of amino acids, including valine, isoleucine, leucine, alanine, histidine, and glutamine, accompanied by drastically elevated levels of trigonelline and ATP. The 24 h low-salinity challenge merely led to significantly decreased levels of succinate and inosine, as well as more amino acids including valine, isoleucine, leucine, alanine, methionine, glutamate, glutamine, lysine, histidine, tyrosine, and phenylalanine. When WG crabs were exposed to low salinity for 48 h, the levels of trigonelline, TMAO, and ATP were markedly increased, whereas the levels of valine, isoleucine, leucine, alanine, glutamine, histidine, and inosine were greatly decreased. At 72 h, crabs presented dramatically elevated metabolites including inosine, 2-pyridinemethanol (2-PM), trigonelline, TMAO, and ATP along with significantly reduced metabolites including valine, leucine, alanine, methionine, and glutamine at all time points of low-salinity treatment. Conversely, low salinity caused more extensive alterations of metabolites in SG crabs relative to WG crabs. At 12 h, the levels of alanine, histidine, and inosine were significantly decreased, whereas the levels of 2-PM, trigonelline, and ATP were remarkably increased in the low-salinity-exposed SG crabs. At 24 h, SG crabs exhibited a significant decrease in the levels of inosine and a range of amino acids including valine, isoleucine, leucine, alanine, methionine, glutamate, glutamine, succinate, lysine, histidine, tyrosine, and phenylalanine accompanied with a dramatic increase in the levels of 2-PM and ATP. Similar changes of metabolites occurred at 48 h, but trigonelline and TMAO were significantly elevated instead of glutamate, lysine, and succinate, for which significant alterations were detected in 24 h low-salinity-exposed SG crabs. At 72 h, a significant elevation in the levels of 2-PM, trigonelline, and TMAO was observed in low-salinity-exposed SG crabs, together with a remarkable decline in the levels of a range of amino acids, including valine, isoleucine, leucine, alanine, methionine, glutamate, glutamine, histidine, tyrosine, and phenylalanine.

The dynamic metabolite changes due to low-salinity exposure by calculating the concentration changes for those metabolites with significant differences (Table 1) are illustrated in Figure 5. A range of amino acids responded vigorously after

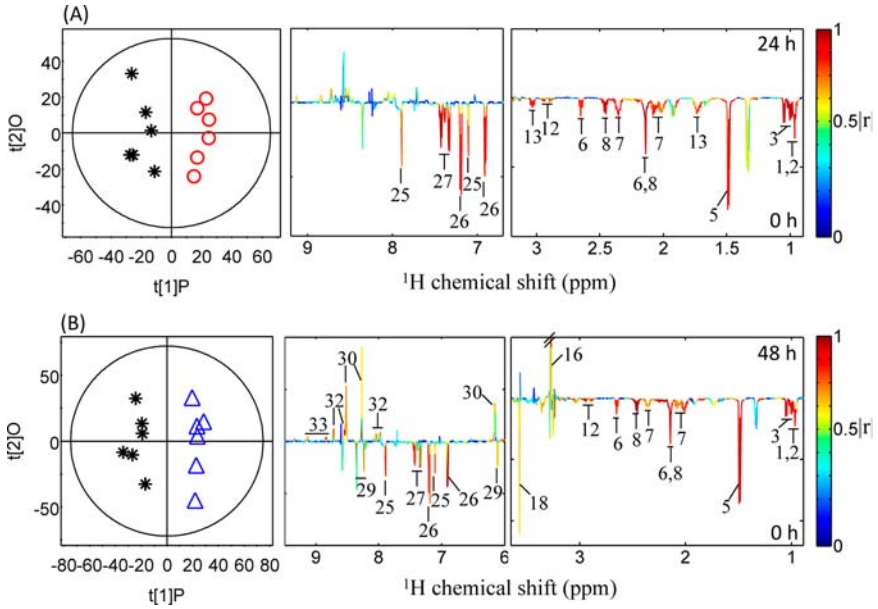

Figure 3. OPLS-DA scores plots (left) and corresponding color-coded correlation coefficient loadings plots (right) generated by comparisons between muscle extract spectra of SG at 0 h (black star) and those from SG exposed to low salinity at the time points of 24 h (red circle) and 48 h (blue open triangle), respectively. These models are cross-validated with CV-ANOVA, $p = 1.60 \times 10^{-2}$ and $p = 6.59 \times 10^{-3}$, respectively. Metabolite keys to the numbers are shown in Figure 1 and the Supporting Information Table S1.

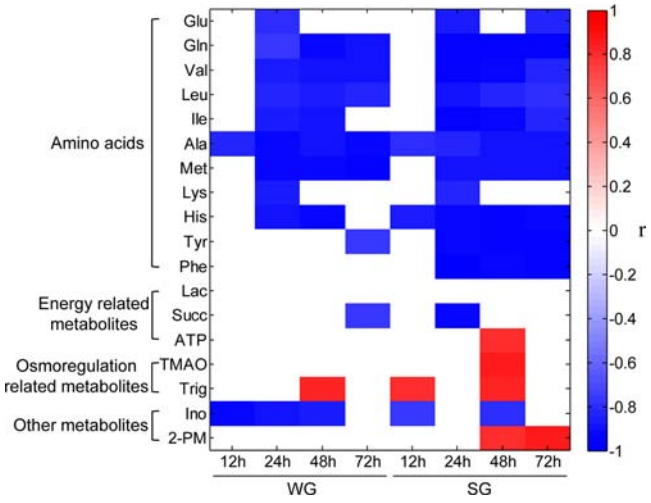

Figure 4. Dynamic alterations of key muscle extract metabolites in response to low-salinity exposure to WG (left) and SG (right). The color indicates a correction coefficient as scaled on the right-hand side. The warm colors (e.g., red) denote an increase in the level of metabolites at the time points of 12, 24, 48, and 72 h against the level of 0 h exposed to low salinity, respectively, and the cool colors (e.g., blue) indicate a decrease. Glu, glutamate; Gln, glutamine; Val, valine; Leu, leucine; Ile, isoleucine; Ala, alanine; Met, methionine; Lys; lysine; His, histidine; Tyr, tyrosine; Phe, phenylalanine; Lac, lactate; Succ, succinate; ATP, adenosine triphosphate; TMAO, trimethylamine-*N*-oxide; Trig, trigonelline; Ino, inosine; 2-PM, 2-pyridinemethanol.

low-salinity exposure. For example, the levels of valine, leucine, alanine, and glutamine declined throughout the post-treatment in WG crabs. Different from these amino acids, the inosine level fluctuated with a 47% decrease before the first 48 h of low-salinity challenge and a 35% increase at 72 h for both WG and SG crabs. In addition, the level of ATP dramatically increased about 180% at 48 h against the level of 0 h in both WG and SG crabs. Interestingly, we noted that the concentration ratio of 2-PM changed significantly in SG crabs throughout low-salinity exposure with the highest increase up to 170% at 48 h of low-salinity exposure against the level of 0 h, whereas it changed dramatically at 72 h in WG crabs. It is also worthwhile noting that the level of trigonelline increased for 35−67% in SG crabs but only 4−37% in WG crabs after low-salinity exposure.

DISCUSSION

This study showed the dynamic metabolic responses of two *P. trituberculatus* strains to low-salinity stress. We found that low-salinity exposure resulted in essential metabolic changes involving many pathways including osmoregulation, gluconeogenesis, and energy production (Figure 6). The SG crabs presented a quicker metabolic modulation in response to low-salinity exposure compared to WG crabs. Such differential characterization might result from low-salinity training, which determines their different abilities to adapt and acclimate to low salinity.

Osmotic Rebalancing. In this study, we observed a significant elevation in the level of TMAO in both WG and SG crabs after 48 h of low-salinity stress (Figure 3; Table 1). It has been well documented that TMAO functions as a ubiquitous compatible osmolyte in marine crustraceans.[31] Our observations suggest that low-salinity stress can cause a disturbance in the osmotic homeostasis in two crab groups. TMAO accumulation may contribute to the rebalance of the osmotic equilibrium. Moreover, a significant elevation in the trigonelline (nicotinic acid betaine) level compared to controls was also observed in muscle tissue extracts of WG and SG crabs exposed to low salinity (Figure 3; Table 1). This quaternary ammonium compound is a methylated product of nicotinic acid (vitamin B_3)[32] and has been reported to function as a compatible osmolyte or an osmoprotectant on enzymes when animals and plants are subjected to salinity and water deficit stress.[33−38] Interestingly, the increased trigonelline accumulation has been found in muscle tissue extracts of green shore crab *Carcinus maenas* exposed to the two highest seawater CO_2

dx.doi.org/10.1021/jf405668a | J. Agric. Food Chem. 2014, 62, 3496−3503

Table 1. Content of Selected Muscle Extract Metabolites for the Wild Group (WG) and Screened Group (SG) Crabs Exposed to Low Salinity at Different Time Points of Exposure

	WG, mean ± SD[a] (mg/g)				
component	0 h	12 h	24 h	48 h	72 h
glutamate	4.88 ± 0.93	4.61 ± 0.95	3.03 ± 0.69*	5.19 ± 1.57	3.58 ± 1.47
glutamine	4.83 ± 1.25	3.50 ± 0.61*	2.21 ± 0.62**	2.01 ± 0.87**	2.40 ± 0.55**
valine	1.87 ± 0.80	0.84 ± 0.30*	0.61 ± 0.23**	0.77 ± 0.12*	0.97 ± 0.37*
leucine	4.70 ± 1.95	2.31 ± 1.00*	1.79 ± 0.71**	2.19 ± 0.45*	2.50 ± 0.96*
isoleucine	1.05 ± 0.44	0.54 ± 0.30*	0.39 ± 0.20*	0.52 ± 0.12*	0.71 ± 0.36
alanine	9.55 ± 2.66	4.58 ± 1.02**	4.49 ± 0.99**	4.73 ± 1.26**	4.56 ± 1.03**
methionine	2.21 ± 0.68	1.52 ± 0.49	1.38 ± 0.32*	1.65 ± 0.25	1.40 ± 0.43*
lysine	2.67 ± 1.09	1.52 ± 1.19	1.24 ± 0.58*	1.95 ± 0.61	2.30 ± 0.86
histidine	0.49 ± 0.14	0.26 ± 0.20*	0.21 ± 0.09**	0.27 ± 0.06**	0.36 ± 0.11
tyrosine	1.30 ± 0.46	1.03 ± 0.36	0.74 ± 0.37*	0.95 ± 0.22	0.85 ± 0.41
phenylalanine	0.94 ± 0.40	0.68 ± 0.44	0.47 ± 0.23*	0.59 ± 0.16	0.71 ± 0.43
lactate	5.20 ± 2.93	5.18 ± 1.78	2.70 ± 2.16	7.70 ± 3.16	6.44 ± 5.21
succinate	0.23 ± 0.06	0.21 ± 0.04	0.16 ± 0.04*	0.23 ± 0.04	0.19 ± 0.02
ATP[b]	2.05 ± 0.54	4.97 ± 1.47**	2.69 ± 0.60	5.67 ± 1.37**	3.76 ± 0.79**
TMAO	3.76 ± 1.19	4.80 ± 1.20	3.19 ± 0.35	7.26 ± 2.38*	5.76 ± 1.17*
trigonelline	0.05 ± 0.01	0.08 ± 0.02*	0.05 ± 0.01	0.10 ± 0.03**	0.12 ± 0.03**
inosine	1.05 ± 0.27	0.17 ± 0.08***	0.37 ± 0.08***	0.55 ± 0.24**	1.44 ± 0.25*
2-PM	1.63 ± 0.47	1.83 ± 0.59	1.69 ± 0.33	2.03 ± 0.61	2.23 ± 0.45*
	SG, mean ± SD[a] (mg/g)				
component	0 h	12 h	24 h	48 h	72 h
glutamate	5.47 ± 1.66	4.76 ± 1.96	2.32 ± 0.67**	4.84 ± 1.43	2.74 ± 0.34**
glutamine	3.44 ± 0.67	2.60 ± 1.34	1.58 ± 0.49***	1.86 ± 0.29***	2.04 ± 0.38**
valine	1.36 ± 0.47	1.06 ± 0.68	0.37 ± 0.12**	0.51 ± 0.14**	0.59 ± 0.19**
leucine	3.45 ± 1.08	2.83 ± 1.75	1.09 ± 0.31**	1.56 ± 0.43**	1.61 ± 0.54**
isoleucine	0.71 ± 0.19	0.71 ± 0.49	0.23 ± 0.06**	0.36 ± 0.09**	0.42 ± 0.13**
alanine	8.10 ± 1.43	5.15 ± 0.80**	3.76 ± 0.81***	4.40 ± 0.81***	3.20 ± 1.07***
methionine	2.49 ± 0.70	2.27 ± 1.18	1.03 ± 0.32**	1.31 ± 0.52**	1.06 ± 0.35**
lysine	1.95 ± 0.74	1.38 ± 0.53	0.84 ± 0.16**	1.72 ± 0.31	1.64 ± 0.43
histidine	0.38 ± 0.11	0.19 ± 0.08**	0.14 ± 0.05**	0.22 ± 0.05**	0.22 ± 0.05**
tyrosine	1.26 ± 0.21	1.58 ± 1.16	0.50 ± 0.22***	0.69 ± 0.31**	0.57 ± 0.16***
phenylalanine	0.78 ± 0.15	0.92 ± 0.72	0.31 ± 0.09***	0.45 ± 0.16**	0.42 ± 0.12***
lactate	6.10 ± 2.78	4.55 ± 3.02	3.88 ± 2.49	7.11 ± 3.41	4.31 ± 4.18
succinate	0.19 ± 0.03	0.21 ± 0.05	0.13 ± 0.02**	0.23 ± 0.03	0.17 ± 0.03
ATP	2.49 ± 0.17	4.75 ± 1.17**	3.42 ± 0.43**	6.92 ± 1.25***	3.54 ± 1.54
TMAO	4.55 ± 0.34	5.28 ± 0.77	4.62 ± 0.57	7.61 ± 0.79***	6.55 ± 1.04**
trigonelline	0.05 ± 0.01	0.11 ± 0.05*	0.08 ± 0.03	0.12 ± 0.05**	0.10 ± 0.02***
inosine	1.02 ± 0.27	0.43 ± 0.20**	0.47 ± 0.23**	0.46 ± 0.18**	1.51 ± 0.48
2-PM	1.31 ± 0.24	2.18 ± 0.45**	1.76 ± 0.39*	2.41 ± 0.68*	2.18 ± 0.38**

[a]Average concentration and standard deviation (mean ± SD, mg/g crab muscle) were obtained from six parallel samples. Significance when compared with 0 h: *, $p < 0.05$; **, $p < 0.01$; ***, $p < 0.001$. [b]ATP, adenosine triphosphate; TMAO, trimethylamine-*N*-oxide; 2-PM, 2-pyridinemethanol.

levels.[39] Taken together, trigonelline may play a role in rebalancing the osmotic pressures for low-salinity adaptation and acclimation of *P. trituberculatus*. This osmotic rebalance is also supported by a previous study in which membrane fluidity, lipid composition, fatty acid concentration, and intra/extracellular ion concentration were significantly changed in estuarine mud crabs in response to salinity stress.[40] It is further supported by another previous investigation on increased level of total phospholipids of posterior gills when crab *Eriocheir sinensis* was acclimated in a low-salinity challenge.[41]

In addition, we note that low-salinity-trained SG crabs contain a higher concentration of TMAO than WG crabs, especially highlighted at 24 h with an approximate 45% higher than that in SG crabs (Table 1). Such difference in the TMAO concentration between two crab groups might result from the low-salinity training. It is possible that SG crabs can obtain far-reaching metabolic alterations and gain swifter response to low salinity than WG crabs. In fact, a PCA trajectory plot (Figure 2) clearly indicates the distinctive feature of metabolite alterations in SG crabs. It also implies a trend of metabolic changes in WG crabs toward SG crabs. Our observations are in broad agreement with previous findings in which heat hardening accelerates the reestablishment of metabolite homeostasis in *Drosophila melanogaster*.[42]

Gluconeogenesis from Amino Acids and Energy Accumulation. Another prominent finding is a rise in the ATP level in the crab muscle after low-salinity stress (Figure 3; Table 1). Consistently, an increase in energy production for ion transportation has been observed in *Callinectes sapidus* and *Callinectes similis* exposed to low salinity.[43] ATP can be produced by three main pathways including glycolysis, respiration, and β-oxidation. In glycolysis, glucose is metabo-

dx.doi.org/10.1021/jf405668a | J. Agric. Food Chem. 2014, 62, 3496−3503

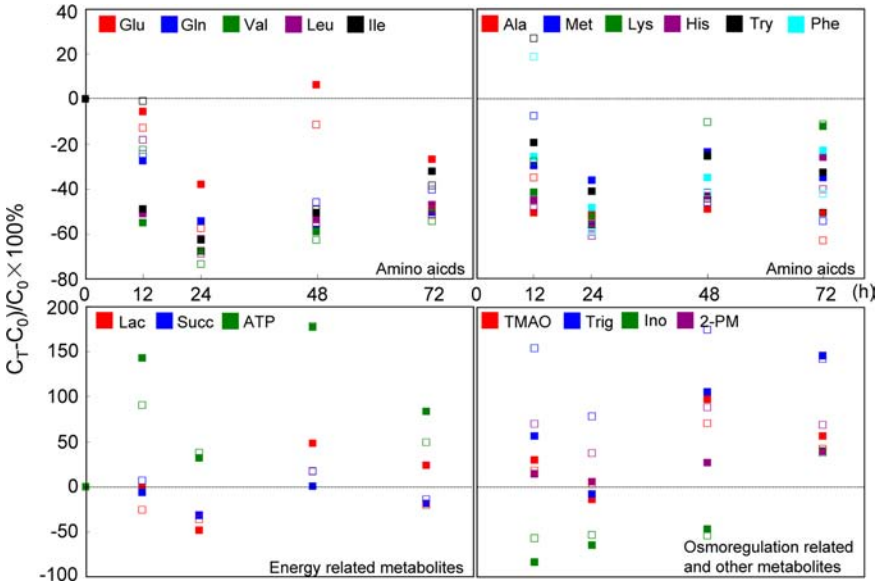

Figure 5. Dynamic changes of muscle metabolites as a function of low-salinity stress. The empty symbols represent SG crabs, whereas the solid ones represent WG crabs.

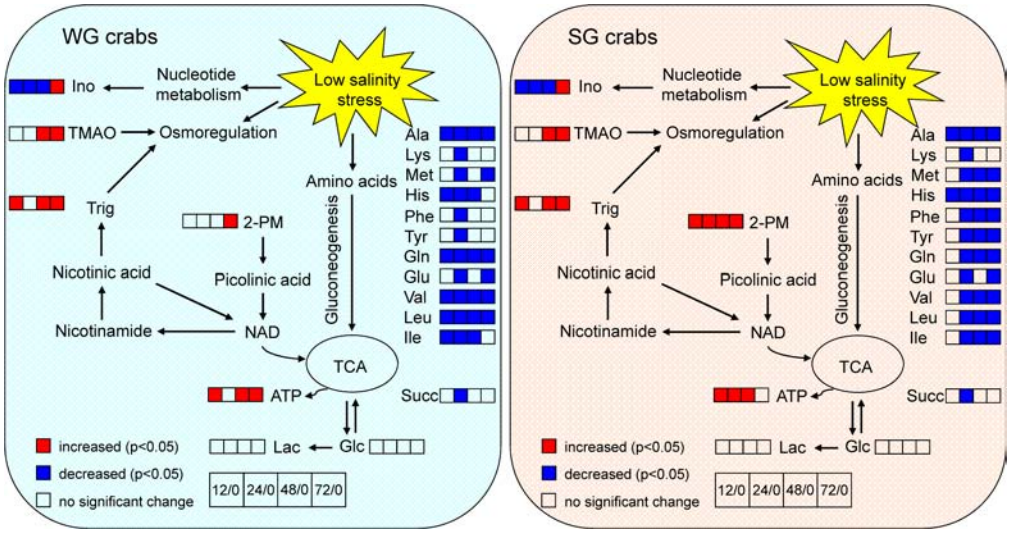

Figure 6. Summary of dynamic metabolic responses of WG and SG crabs to low-salinity exposure. Metabolites with red or blue boxes represent significant increases or decreases in levels, respectively, at the significance level of $p < 0.05$ at this time point against the level at 0 h. NAD, nicotinamide adenine dinucleotide; TCA, tricarboxylic acid.

lized to pyruvate and the latter is a substrate for the tricarboxylic acid (TCA) cycle and anaerobic respiration. Intriguingly, no significant alteration in the levels of glucose was caused by low salinity in crabs in this study. However, we noted a pronounced depletion of the amino acid pool in low-salinity-exposed crabs, which has also been observed in crab muscle and hepatopancreas responding to low-salinity challenge.[15] It is known that most amino acids are glucogenic amino acids, which can be converted into glucose through gluconeogenesis, thus likely replenishing the consumption of glucose in the ATP production in our study. This notion is consistent with previous findings of enhanced production of glucose by gluconeogenesis in the hepatopancreas of crab *Chasmagnathus granulata* in response to low-salinity challenge.[44] Moreover, gluconeogenesis promotion is concomitant with the decreased level of succinate (Table 1),[23] which is also in agreement with our observation in low-salinity-stressed crabs. However, we cannot exclude the responsibility of β-oxidation of fatty acid for the elevated level of ATP due to low salinity because lipids seem to be the major source of energy in crustaceans[45] and have previously been found significantly lower in gill and muscle of crabs subjected to hypo-osmotic stress.[16,45]

Similarly to the TMAO alteration, the more significantly accumulated ATP and depleted amino acid pool in SG crabs relative to WG crabs indicate low-salinity training enabled crabs to develop an ability for more extensive metabolic modulation (Table 1).

Other Metabolic Changes. The inosine was noted to be markedly decreased in both WG and SG crabs during the first 48 h of low-salinity challenge but remarkably increased at 72 h. This nucleotide is involved in the nucleotide metabolism. The significant fluctuation in the inosine levels may result from the altered NAD cycle activity induced by low salinity.

dx.doi.org/10.1021/jf405668a | J. Agric. Food Chem. 2014, 62, 3496−3503

In addition, we observed a significant 2-PM accumulation in crabs during the low-salinity exposure. Importantly, a faster rise occurred in SG crabs than in WG crabs (Table 1; Figure 5), implying a role during the response of crabs to low salinity. 2-PM is a picolinic acid-related compound that has a growth-simulating effect in rats.[46] It has also been shown to improve the immune system and induce apoptosis in HL-60 cells.[47,48] However, little information exists on the physiological function of 2-PM in marine crustraceans. Future studies should determine the positive role of 2-PM in crabs responding to low salinity.

In this study, we found that the dominant metabolites in crab muscle comprise amino acids, sugars, carboxylic acids, betaine, TMAO, trigonelline, and nucleotides. The strategy of metabolic modulation of *P. trituberculatus* in response to low salinity includes osmotic rebalancing, enhanced gluconeogenesis from amino acids, and energy accumulation. These metabolic adaptions were manifested in the accumulation of TMAO, ATP, 2-PM, and trigonelline and in the depletion of the amino acid pool as well as in the fluctuation of inosine levels. This lends to support to the fact that low-salinity training accelerates the response of crabs to low-salinity stress. These findings provide a comprehensive insight into the mechanisms of metabolic modulation in *P. trituberculatus* in response to low salinity. Our work also highlights the approach of NMR-based metabonomics in conjunction with multivariate data analysis and univariate data analysis in understanding the strategy of metabolic phenotype modulation against stressors.

■ ASSOCIATED CONTENT

Supporting Information

Additional figure and tables as cited in the text. This material is available free of charge via the Internet at http://pubs.acs.org.

■ AUTHOR INFORMATION

Corresponding Author

*(C.W.) Phone: +86-(0)574-87600356. Fax: +86-(0)27-87600356. E-mail: wangchunlin@nbu.edu.cn.

Author Contributions

‖Y.Y. and Y.A. contributed equally to this work.

Funding

Financial support was received from the National High Technology Research and Development Program of China (No. 2012AA10A409), National Natural Science Foundation of China (No. 41106123), Zhejiang Major Special Program of Breeding (2012C12907-3, 2012C12907-9), Scientific Research Fund of Zhejiang Provincial Education Department (No. Z201121258), Public Interest Program of Zhejiang Province (2013C31032), Ningbo Innovative Program of Agriculture (2012C92010), National Sparking Plan Project (2013GA7010022013, GA701041), the major program of Ningbo (2013C11017), Ningbo Agricultural Technologies R&D Project (2012C10027) Program for Science and Technology Innovative Research Team of Ningbo (No. 2011B81003), and K C Wong Magana Fund in Ningbo University.

Notes

The authors declare no competing financial interest.

■ ABBREVIATIONS USED

NMR, nuclear magnetic resonance; TSP, sodium 3-trimethylsilyl [2,2,3,3-$^2D_4$]propionate; D_2O, deuterated water; SG, screened group; WG, wild group; TMAO, trimethylamine-*N*-oxide; ATP, adenosine triphosphate; 2-PM, 2-pyridinemethanol; COSY, $^1H-^1H$ correlation spectroscopy; TOCSY, $^1H-^1H$ total correlation spectroscopy; HMBC, $^1H-^{13}C$ heteronuclear multiple-bond correlation; HSQC, $^1H-^{13}C$ heteronuclear signal-quantum correlation; PCA, principal component analysis; OPLS-DA, orthogonal projection to latent structure discriminant analysis; TCA, tricarboxylic acid

■ REFERENCES

(1) Sun, Y. Y.; Yan, M.; Sun, J. J. Larval development of the swimming crab, *Portunus trituberculatus*. *J. Fish. Chin.* **1984**, *8*, 219–226.

(2) Lawal-Are, A. O.; Kusemiju, K. Effect of salinity on survival and growth of blue crab, *Callinectes amnicola* from Lagos Lagoon, Nigeria. *J. Environ. Biol.* **2010**, *31*, 461–464.

(3) Minagawa, M. Effects of salinity of survival, feeding, and development of larvae of the red frog crab *Ranina ranina*. *Nippon Suisan Gakkaishi* **1992**, *58*, 1855–1860.

(4) Henry, R. P.; Gehnrich, S.; Weihrauch, D.; Towle, D. W. Salinity-mediated carbonic anhydrase induction in the gills of the euryhaline green crab, *Carcinus maenas*. *Comp. Biochem. Physiol. A–Mol. Integr. Physiol.* **2003**, *136*, 243–258.

(5) Xu, Q. H.; Liu, Y. Gene expression profiles of the swimming crab *Portunus trituberculatus* exposed to salinity stress. *Mar. Biol.* **2011**, *158*, 2161–2172.

(6) Henry, R. P.; Thomason, K. L.; Towle, D. W. Quantitative changes in branchial carbonic anhydrase activity and expression in the euryhaline green crab, *Carcinus maenas*, in response to low salinity exposure. *J. Exp. Zool. Part A* **2006**, *305A*, 842–850.

(7) Towle, D. W.; Henry, R. P.; Terwilliger, N. B. Microarray-detected changes in gene expression in gills of green crabs (*Carcinus maenas*) upon dilution of environmental salinity. *Comp. Biochem. Physiol. D–Genomics Proteomics* **2011**, *6*, 115–125.

(8) Narasimh, T.; Krishnam, R. V. Myosin ATPase activity in an estuarine decapod crustacean, *Scylla serrata*, as a function of salinity adaptation. *J. Gen. Physiol.* **1974**, *64*, A7–A8.

(9) Lovett, D. L.; Towle, D. W.; Faris, J. E. Salinity-sensitive alkaline phosphatase activity in gills of the blue crab, *Callinectes sapidus* Rathbun. *Comp. Biochem. Physiol. B–Biochem. Mol. Biol.* **1994**, *109*, 163–173.

(10) Pinoni, S. A.; Mananes, A. A. L. Alkaline phosphatase activity sensitive to environmental salinity and dopamine in muscle of the euryhaline crab *Cyrtograpsus angulatus*. *J. Exp. Mar. Biol. Ecol.* **2004**, *307*, 35–46.

(11) Pinoni, S. A.; Goldemberg, A. L.; Mananes, A. A. L. Alkaline phosphatase activities in muscle of the euryhaline crab *Chasmagnathus granulatus*: response to environmental salinity. *J. Exp. Mar. Biol. Ecol.* **2005**, *326*, 217–226.

(12) Zhang, X.-Y.; Zhang, M.-Z.; Zheng, C. J.; Liu, J.; Hu, H. J. Identification of two hsp90 genes from the marine crab, *Portunus trituberculatus* and their specific expression profiles under different environmental conditions. *Comp. Biochem. Physiol. C–Toxicol. Pharmacol.* **2009**, *150*, 465–473.

(13) Soledad Michiels, M.; Cristina Del Valle, J.; Lopez Mananes, A. A. Effect of environmental salinity and dopamine injections on key digestive enzymes in hepatopancreas of the euryhaline crab *Cyrtograpsus angulatus* (Decapoda: Brachyura: Varunidae). *Sci. Mar.* **2013**, *77*, 129–136.

(14) Krishnam, R. V.; Srihari, K. Changes in the excretory patterns of the fresh-water field crab *Paratelphusa hydrodromous* upon adaptation to higher salinities. *Mar. Biol.* **1973**, *21*, 341–348.

(15) Boone, W. R.; Claybrook, D. L. The effect of low salinity on amino acid metabolism in the tissues of the common mud crab, *Panopeus herbstii* (Milne-Edwards). *Comp. Biochem. Physiol. A–Physiol.* **1977**, *57*, 99–106.

(16) Pinoni, S. A.; Michiels, M. S.; Mananes, A. A. L. Phenotypic flexibility in response to environmental salinity in the euryhaline crab

Neohelice granulata from the mudflat and the saltmarsh of a SW coastal lagoon. *Mar. Biol.* **2013**, *160*, 2647−2661.
(17) Tang, H. R.; Wang, Y. L. Metabonomics: a revolution in progress. *Prog. Biochem. Biophys.* **2006**, *33*, 401−417.
(18) Straadt, I. K.; Young, J. F.; Bross, P.; Gregersen, N.; Oksbjerg, N.; Theil, P. K.; Bertram, H. C. NMR-based metabonomic investigation of heat stress in myotubes reveals a time-dependent change in the metabolites. *J. Agric. Food Chem.* **2010**, *58*, 6376−6386.
(19) Ye, Y.; Zhang, L.; Hao, F.; Zhang, J.; Wang, Y.; Tang, H. Global metabolomic responses of *Escherichia coli* to heat stress. *J. Proteome Res.* **2012**, *11*, 2559−2566.
(20) An, Y.; Xu, W.; Li, H.; Lei, H.; Zhang, L.; Hao, F.; Duan, Y.; Yan, X.; Zhao, Y.; Wu, J.; Wang, Y.; Tang, H. High-fat diet induces dynamic metabolic alterations in multiple biological matrices of rats. *J. Proteome Res.* **2013**, *12*, 3755−3768.
(21) Dong, F.; Zhang, L.; Hao, F.; Tang, H.; Wang, Y. Systemic responses of mice to dextran sulfate sodium-induced acute ulcerative colitis using ^{1}H NMR spectroscopy. *J. Proteome Res.* **2013**, *12*, 2958−2966.
(22) Dai, H.; Xiao, C. N.; Liu, H. B.; Tang, H. R. Combined NMR and LC-MS analysis reveals the metabonomic changes in *Salvia miltiorrhiza* Bunge induced by water depletion. *J. Proteome Res.* **2010**, *9*, 1460−1475.
(23) Zhang, J.; Zhang, Y.; Du, Y.; Chen, S.; Tang, H. Dynamic metabonomic responses of tobacco (*Nicotiana tabacum*) plants to salt stress. *J. Proteome Res.* **2011**, *10*, 1904−1914.
(24) Ye, Y. F.; Zhang, L. M.; Yang, R.; Luo, Q. J.; Chen, H. M.; Yan, X. J.; Tang, H. R. Metabolic phenotypes associated with high-temperature tolerance of *Porphyra haitanensis* strains. *J. Agric. Food Chem.* **2013**, *61*, 8356−8363.
(25) Ye, Y.; Zhang, L.; Tang, H.; Yan, X. Survey of nutrients and quality assessment of crab paste by ^{1}H NMR spectroscopy and multivariate data analysis. *Chin. Sci. Bull.* **2012**, *57*, 3353−3362.
(26) Xiao, C.; Dai, H.; Liu, H.; Wang, Y.; Tang, H. Revealing the metabonomic variation of rosemary extracts using ^{1}H NMR spectroscopy and multivariate data analysis. *J. Agric. Food Chem.* **2008**, *56*, 10142−10153.
(27) Dai, H.; Xiao, C. N.; Liu, H. B.; Hao, F. H.; Tang, H. R. Combined NMR and LC-DAD-MS analysis reveals comprehensive metabonomic variations for three phenotypic cultivars of *Salvia miltiorrhiza* bunge. *J. Proteome Res.* **2010**, *9*, 1565−1578.
(28) Eriksson, L.; Trygg, J.; Wold, S. CV-ANOVA for significance testing of PLS and OPLS (R) models. *J. Chemom.* **2008**, *22*, 594−600.
(29) Duan, Y.; An, Y.; Li, N.; Liu, B.; Wang, Y.; Tang, H. Multiple univariate data analysis reveals the inulin effects on the high-fat-diet induced metabolic alterations in rat myocardium and testicles in the preobesity state. *J. Proteome Res.* **2013**, *12*, 3480−3495.
(30) Xu, W.; Wu, J.; An, Y.; Xiao, C.; Hao, F.; Liu, H.; Wang, Y.; Tang, H. Streptozotocin-induced dynamic metabonomic changes in rat biofluids. *J. Proteome Res.* **2012**, *11*, 3423−3435.
(31) Yancey, P. H.; Blake, W. R.; Conley, J. Unusual organic osmolytes in deep-sea animals: adaptations to hydrostatic pressure and other perturbants. *Comp. Biochem. Physiol. A−Mol. Integr. Physiol.* **2002**, *133*, 667−676.
(32) Upmeier, B.; Gross, W.; Köster, S.; Barz, W. Purification and properties of *S*-adenosyl-L-methionine: nicotinic acid-*N*-methyltransferase from cell suspension cultures of *Glycine max* L. *Arch. Biochem. Biophys.* **1988**, *262*, 445−454.
(33) Wood, A. J. Comparison of salt-induced osmotic adjustment and trigonelline accumulation in two soybean cultivars. *Biol Plant.* **1990**, *42*, 389−394.
(34) Cho, Y.; Lightfoot, D. A.; Wood, A. J. Trigonelline concentrations in salt stressed leaves of cultivated *Glycine max*. *Phytochemistry* **1999**, *52*, 1235−1238.
(35) Rajasekaran, L. R.; Aspinall, D.; Jones, G. P.; Paleg, L. G. Stress metabolism IX: effect of salt stress on trigonelline accumulation in tomato. *Can. J. Plant Sci.* **2001**, *81*, 487−498.
(36) Minorsky, P. V. Trigonelline: a diverse regulator in plants. *Plant Physiol.* **2002**, *128*, 7−8.
(37) Suzuki-Yamamoto, M.; Mimura, T.; Ashihara, H. Effect of short-term salt stress on the metabolic profiles of pyrimidine, purine and pyridine nucleotides in cultured cells of the mangrove tree, *Bruguiera sexangula*. *Physiol. Plant.* **2006**, *128*, 405−414.
(38) Lee, G.; Carrow, R. N.; Duncan, R. R.; Eiteman, M. A.; Rieger, M. W. Synthesis of organic osmolytes and salt tolerance mechanisms in *Paspalum vaginatum*. *Environ. Exp. Bot.* **2008**, *63*, 19−27.
(39) Hammer, K. M.; Pedersen, S. A.; Størseth, T. R. Elevated seawater levels of CO_2 change the metabolic fingerprint of tissues and hemolymph from the green shore crab *Carcinus maenas*. *Comp. Biochem. Physiol.* **2012**, *7*, 292−302.
(40) Bhoite, S.; Roy, R. Role of membrane lipid in osmoregulatory processes during salinity adaptation: a study with chloride cell of mud crab *Scylla serrata*. *Mar. Freshw. Behav. Physiol.* **2013**, *46*, 287−300.
(41) Chapelle, S.; Dandrifosse, G.; Zwingelstein, G. Metabolism of phospholipids of anterior or posterior gills of the crab *Eriocheir sinensis* M. EDW, during the adaptation of this animal to media of various salinities. *Int. J. Biochem.* **1976**, *7*, 343−351.
(42) Malmendal, A.; Overgaard, J.; Bundy, J. G.; Sorensen, J. G.; Nielsen, N. C.; Loeschcke, V.; Holmstrup, M. Metabolomic profiling of heat stress: hardening and recovery of homeostasis in *Drosophila*. *Am. J. Physiol. Regul. Integr. Comp. Physiol.* **2006**, *291*, R205−R212.
(43) Piller, S.; Henry, R.; Doeller, J.; Kraus, D. A comparison of the gill physiology of two euryhaline crab species, *Callinectes sapidus* and *Callinectes similis*: energy production, transport-related enzymes and osmoregulation as a function of acclimation salinity. *J. Exp.Biol.* **1995**, *198*, 349−358.
(44) Oliveira, G. T.; da Silva, R. S. M. Hepatopancreas gluconeogenesis during hyposmotic stress in crabs *Chasmagnathus granulata* maintained on high-protein or carbohydrate-rich diets. *Comp. Biochem. Physiol. B−Biochem. Mol. Biol.* **2000**, *127*, 375−381.
(45) Luvizotto-Santos, R.; Lee, J. T.; Branco, Z. P.; Bianchini, A.; Nery, L. E. M. Lipids as energy source during salinity acclimation in the euryhaline crab *Chasmagnathus granulata* Dana, 1851 (Crustacea-Grapsidae). *J. Exp. Zool. Part A* **2003**, *295A*, 200−205.
(46) Evans, G. W.; Johnson, E. C. Growth stimulating effect of picolinic acid added to rat diets. *Proc. Soc. Exp. Biol. Med.* **1980**, *165*, 457−461.
(47) Melillo, G.; Cox, G. W.; Radzioch, D.; Varesio, L. Picolinic acid, a catabolite of L-tryptophan, is a costimulus for the induction of reactive nitrogen intermediate production in murine macrophages. *J. Immunol.* **1993**, *150*, 4031−4040.
(48) Ogata, S.; Inoue, K.; Iwata, K.; Okumura, K.; Taguchi, H. Apoptosis induced by picolinic acid-related compounds in HL-60 cells. *Biosci., Biotechnol., Biochem.* **2001**, *65*, 2337−2339.

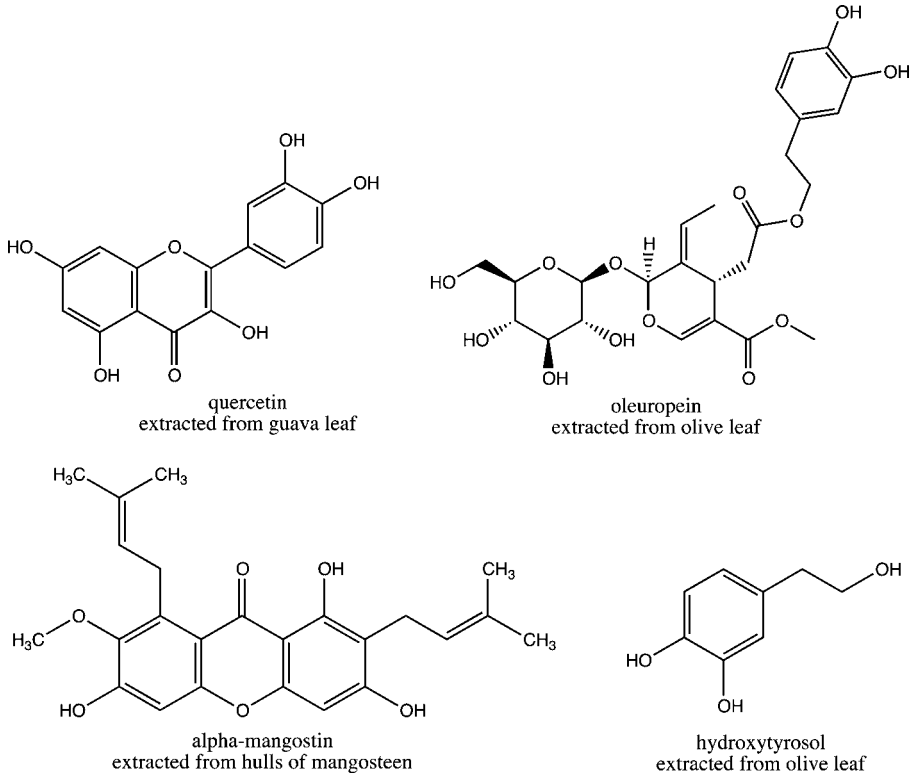

Figure 1. Chemical structures of polyphenols that have been extracted and isolated and found to effectively inhibit adipogenesis via in vitro test on 3T3-L1 preadipocyte cells.

icals that exhibit antioxidant and anti-inflammatory capabilities are also present in the less studied components of the fruits, which includes the rinds, seeds, peels, flowers, and leaves of the fruit. In this paper, the role of these aforementioned components in altering the obesity pathophysiology will be reviewed. Following this, the need for the development of effective fruit waste processing/recycling techniques to effectively tap the maximum potential of tropical fruit waste components as future potential therapeutics will be addressed.

POTENTIAL OF TROPICAL FRUIT WASTE COMPONENTS AS ANTIOBESITY SUPPLEMENTARY TREATMENT

Multiple studies have shown that phytochemical compounds present in tropical fruits possess the ability to inhibit adipogenesis and essentially may offer a suitable therapy against obesity.[7,16,17] These phytochemicals could work as fatty acid synthase (FAS) inhibitors, preventing the formation of fatty acids and their accumulation in the body.[18] Alternatively, they may inhibit the differentiation of preadipocytes to adipocytes (adipogenesis).[10,19,20] Tropical fruits are rich in a diverse array of bioactive phytochemicals that can do so.[21,22] Among the bioactive phytochemical compounds in tropical fruits, quercetin[20] and hydroxytyrosol and oleuropein[16] (Figure 1) are some of the well-known polyphenols that have been identified and found to effectively inhibit adipogenesis in vitro, via the different mechanistic pathways mentioned. Interestingly, these bioactive phytochemicals have recently been discovered to be present in the inedible or waste components of the tropical fruit parts.[17,23,24] In addition, a series of comparative studies have found that the extracts of these "fruit waste components" have higher polyphenol content than the main flesh, thereby making them a potentially more prospective therapeutic source for further studies.[19,25,26]

Ideally, with enough studies to support their antiobesity capabilities, the idea of utilizing these waste components as potential therapeutics will not only help to supplement more alternatives for antiobesity treatment but also potentially reduce environmental concern as this simultaneously offers a solution to reduce landfill waste problems as well.

TROPICAL FRUIT WASTE COMPONENTS AND THEIR BIODEFENSIVE POTENTIAL AS ANTIOBESITY THERAPEUTICS

Different components of tropical fruit wastes, mainly the seeds, flowers, and leaves as well as rinds, have been found to successfully regulate lipid accumulation. This section introduces these previous discoveries brought by the scientific community in the pursuit of novel phytochemical-based antiobesity therapeutics. Various methods have been developed to identify and analyze the qualitative and quantitative occurrence of bioactive compounds in the fruit waste extracts (Table 1) such as normal phase silica gel column chromatography, reversed phase high-performance liquid chromatography (HPLC), liquid chromatography–mass spectrometry (LC-MS), HPLC-linked with photodiode array detector (HPLC-PDA), and the sophisticated methods involving electrospray ionization tandem mass spectrometry (ESI-MS).

Seeds. Although some seeds may be edible such as those of corn and nuts, the majority of the tropical fruit seeds are inedible and are often discarded after consumption of the fruit. Phytochemicals present within these seeds have been found to exhibit properties that are capable of preventing oxidative stress, a process linked to being overweight and to the onset of diseases including diabetes.[17]

dx.doi.org/10.1021/jf5007352 | J. Agric. Food Chem. 2014, 62, 3505−3516

Table 1. Major Phenolic Compounds Identified in the Respective Fruit Waste Extracts That May Be Responsible for the Overall Biological Activity Observed in the Respective Experimental Model

fruit component	name of fruit	major compounds identified	method used for identification	biological activity	study design	ref
seed	avocado (*Persea americana* Mill)	protocatechuic acid	HPLC-PDA	hypolipidemic effect (antiobesity)	in vivo model, 8−10-week-old adult male CD-1 mice with an average weight of 28 ± 2 g	17
		procyanidin	HPLC-ESI-MS	antioxidant capacities	in vitro oxygen radical absorbance capacity (ORAC) assay, DPPH assay	27
		catechin, hydroxycinnamic acids, procyanidin	Waters Acquity UPLC	antioxidant	in vitro ABTS assay, DPPH assay	28
	Hunteria umbellata	alkaloids, flavonoids, saponins identification	coloration tests	antiobesity and antihyperlipidemic effects	in vivo olive oil-induced and Triton-induced hyperlipidemic rats	29, 31, 32
	bishop's weed (*Ammi majus*)	furocoumarins: xanthotoxin, isopimpinellin, (+)-oxypeucedanin	HPLC	antihyperlipidemic, antiinflammatory, analgesic	in vivo albino rats	36
	prickly pear (*Opuntia joconostle*)	quercetin, rutin, catechin	HPLC-PDA	hypolipidemic effect (antiobesity)	in vivo model, 8-week-old CD-1 mice mean weight 28 ± 2 g	39
		4-hydroxybenzoic acid, chlorogenic acid, protocatechuic acid	HPLC-PDA	antioxidants		7
flowers	pomegranate (*Punica granatum* L.)	oleanolic, gallic, ursolic	HPLC	hypolipidemic (antiobesity), anti-hyperglycaemic, anti-inflammation	in vivo high fat diet-induced hyperlipidemia (HDF) mice and Zucker diabetic fatty	41
	longan (*Dimocarpus longons* L.)	gentisic acid, epicatechin, ferulic acid	HPLC-PDA	hypolipidemic effect (antiobesity)	in vivo Sprague−Dawley (SD) rats, 9 weeks old	23
leaves	mango (*Mangifera indica* L.)	foliamangiferosides A, iriflophenone-3-*C*-β-glucoside, maclurin-3-*C*-β-D-glucoside, mangiferin	column chromatography, HPLC (isolated)	antiobesity	in vitro 3T3-L1 preadipocyte cells	54
	olive (*Olea europaea*)	oleuropein, hydroxytyrosol	HPLC	antiobesity	in vitro 3T3-L1 preadipocyte cells	16
		oleuropein, hydroxytyrosol, luteolin, luteolin-4-*O*-β-D-glucopyranoside, luteolin-7-*O*-β-D-glucopyranoside	LC/DAD/ESI-MS	AGE end-products (diabetes treatment)	in vitro experimental model	55
	guava (*Psidium guajva*)	quercetin-3-*O*-(6-feruloyl)-β-D-galactopyranoside (QFG), quercetin	column chromatography, octadecylsilyl silica gel (0DS) HPLC	antiobesity, antioxidant	in vitro 3T3-L1 preadipocyte cells	20
	amla (*Emblica officinalis*)	ellagic acid, gallic acid, ascorbic acid, tannins emblicannin A and B, kaemferol, rutin, kaempferol-3-*O*-glucoside	HPLC	antioxidant and antidiabetic capacities	in vivo streptozotocin-induced diabetic rats	69−71
	papaya (*Carica papaya*)	no isolation/identification of bioactive compounds	not applicable	hypoglycemic effect	in vivo streptozotocin induced diabetic rats	68
rind/peel	mangosteen (*Garcina mangostana*)	α-mangostin	column chromatography	antiobesity	in vitro 3T3-L1 preadipocyte cells	18
		α-mangostin, β-mangostin, γ-mangostin, 9-hydroxycalabaxanthone, garcinone E, 1,5-dihydroxy-3-methoxy-2-(3-methylbuten-1-yl)-9*H*-xanthen-9-one, 1,3/7-trihydroxyxanthone, 2,4,6,7-tetrahydroxyxanthone, 3,4,5,30-tetrahydroxybenzophenone, 2,4,6,30,50-pentahydroxybenzophenone, neosmitilbin, epicatechin, egonol	column chromatography	FAS inhibitor (antiobesity treatment)	FAS inhibitory activity (assay, spectrophtometer absorbance at 340 nm)	63

dx.doi.org/10.1021/jf5007352 | J. Agric. Food Chem. 2014, 62, 3505−3516

Table 1. continued

fruit component	name of fruit	major compounds identified	method used for identification	biological activity	study design	ref
	small oranges (*Citrus sunki*)	polymethoxyflavonones (PMFs), namely, tangeretin and nobiletin	HPLC	antiobesity	in vivo high-fat diet-induced obese mice and in vitro 3T3-L1 adipocyte cells	79
	pomelo (*Citrus grandis*)	presence of flavanoids detected	coloration of flavanoids	antiobesity, prevent metabolic disorders	in vivo high-fat diet-induced metabolic disorders in C57BL/6 mice	82
	mango (*Mangifera indica* L.) Irwin & Nam Doc	no isolation/identification of bioactive compounds	not applicable	antiobesity	test three different cultivars on in vitro 3T3-L1 preadipocyte cells	19

Avocado Seeds (Persea americana Mill). Avocado seeds (*P. americana* Mill) have been found to contain elevated levels of phenolic compounds and exhibit antioxidant properties.[17,27] The seed, which is inedible, represents the majority bulk of the fruit that is often discarded. In an experimental study conducted by Gu et al. on a variety of avocado cultivars, it was found that seeds contained the highest antioxidant capacities, phenolic content, and procyanidins, whereas the pulp had the lowest. A series of compounds were identified in peels and seeds using a normal-phase HPLC-ESI-MS analytical technique including catechin, epicatechin, A- and B-type dimers, trimers, tetramers, pentamers, and hexamers. On the basis of the close correlations and further in vitro analysis between the total phenolic content in the avocado and the antioxidant capacities, the study concluded that procyanidins were the major phenolic compounds that contributed to this effect.[27]

In a separate in vivo experimental model reported by Pahua-Ramos et al. using a hypercholesterolemia mouse, treatment with avocado seed flour (ASF) was reported to drastically reduce the levels of total cholesterol, low-density lipoprotein cholesterol (LDL-C), and atherogenic index. This effect could be attributed to the phenolic content, antioxidant activity, and/or dietary and crude fiber content of the seed. Further analysis of the chemical composition of the ASF using HPLC-PDA found that protocatechuic acid was the major phenolic compound identified in ASF to contribute to the overall hypolipidemic effect on the in vivo model.[17] Such differences in the major phenolic compounds contributing to the different bioactive effects on experimental models as reported by the above studies highlight the wide array of potential therapeutic capabilities that avocado seeds may possess.

The various chemical compositions of phytochemical compounds identified in avocado seeds as reported by Rodriguez-Carpena et al. that include catechins (sum of catechin and epicatechin), hydroxycinnamic acids (*p*-hydroxybenzoic, protocatechuic, vanillic, syringic, and gallic), and procyanidins[28] implied that therapeutic effects exhibited by avocado seed extracts in both in vivo and in vitro experimental model could be due to a collective effect of several phenolic compounds acting together. This further suggests that a study involving the isolation of such compounds from these seed extracts, and testing its individual effects on various biological activities would therefore be useful to understand this phenomenon. The overall in vitro and in vivo experimental models have indicated how avocado seeds, typically regarded as industrial wastes during avocado processing, do have therapeutic properties that can potentially be exploited as a future source of alternative remedy. Phenolic compounds present within the seed have been hypothesized to be responsible for the antioxidant capacities and hypolipidemic effect observed. However, studies involving the isolation of the individual bioactive compounds on the overall lipid regulation effect are still understudied.

Hunteria umbellata (HU) Seeds. Traditionally, *HU* seeds have been widely used for the local management of obesity, diabetes, and hyperlipidemia among the Nigerian folk medicine community.[29,30] Understanding the dearth of scientific reports on the therapeutic potential of this plant, particularly in the management of obesity and hyperlipidemia, Adeneye et al. investigated its respective effects via in vivo experimental models (i.e., rats). These rats included normal, olive-induced hyperlipidemic, and Triton-induced hyperlipidemic rats. In their study, they found that with dose-dependent dosage of

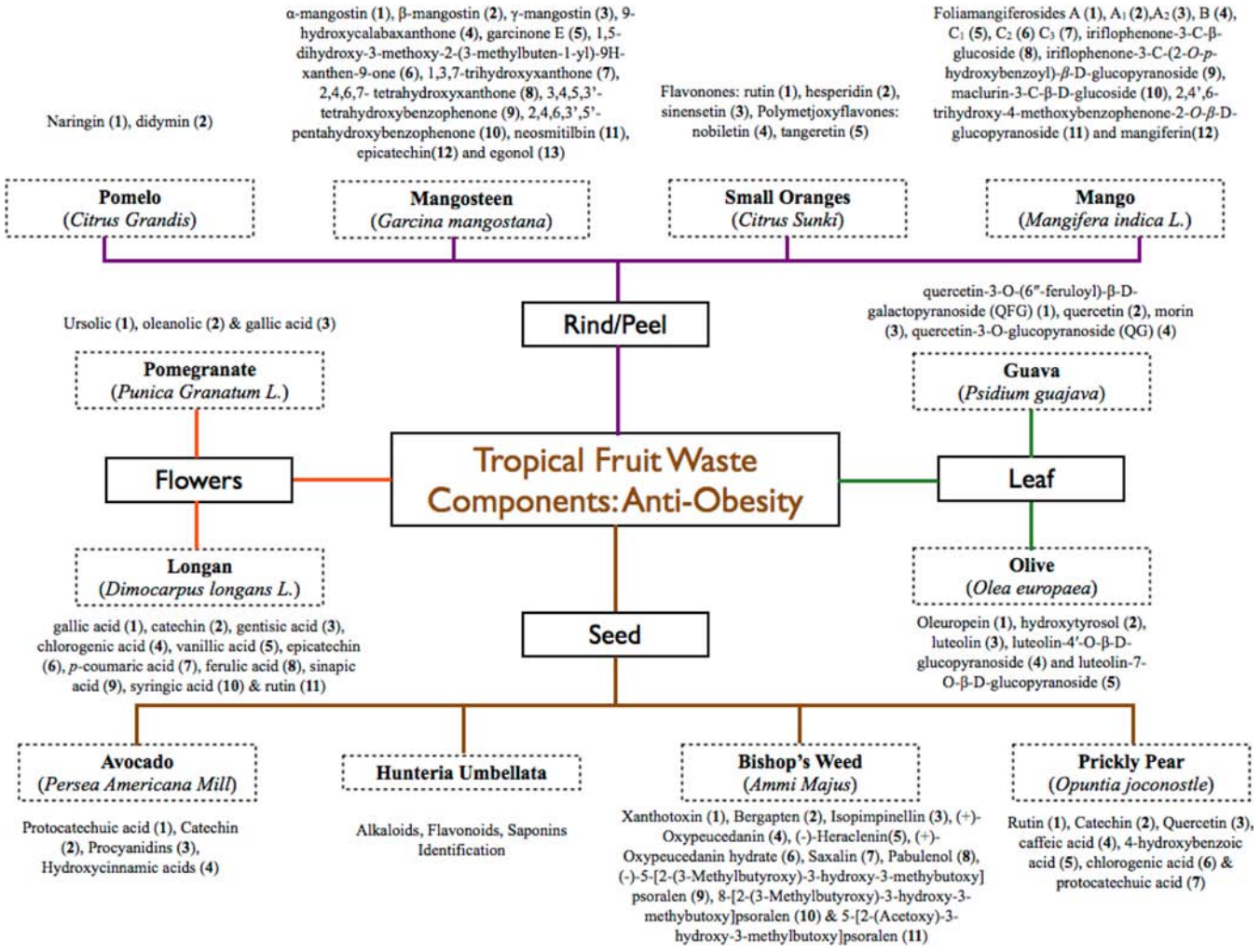

Figure 2. Summary of some examples of tropical fruit waste components that have been experimentally found to possess special properties in their extract that may potentially be used to treat obesity and its associated diseases through its ability to regulate lipid accumulation in living cells.

aqueous seed extract *HU*, reductions of weight gain pattern and levels of serum lipids, adiposity (measured using Lee's index), and coronary artery risk index (represents the ratio of LDL-c to HDL-c and antherogenic indices (AI), ratio of total cholesterol to HDL-c) were observed. Their assessment of the histopathological effect of hepatic fatty degeneration on the test rat's liver further revealed the biochemical evidence of the antihypertriglyceridemic and hypocholesterolemic activities of *HU*.[31] With prior identification of primary phytochemical compounds present in the extract that mainly consist of alkaloids, flavonoids, and saponins,[29,32] the author concluded that the antiobesity and antihyperlipidemic effects observed were likely mediated via inhibition of intestinal lipid absorption and de novo triglyceride and cholesterol biosynthesis. This conclusion was collectively made in close reference to several other studies done by Schoenfelder et al. as well as Han et al. that highlight phytocomponents', such as saponins', capacity to increase intestinal absorption of dietary lipid bioactivity, respectively.[33,34] The isolation of bioactive compounds from this crude seed extract, however, has yet to be done.

Bishop's Weed (Ammi majus) Seeds. Among some of the lesser known species would be *A. majus* that is typically grown in Egypt. The initial study of this species of seed was inspired from its common use in folk medicine to treat various ailments such as vitiligo.[35] Koriem et al. used an in vivo experimental model, particularly on albino rats, to evaluate the antihyperlipidemic, anti-inflammatory, and analgesic as well as antipyretic activities of the extract. In their study, they discovered that the administration of alcoholic *A. majus* seed extract resulted in a significant decrease in concentrations of cholesterol, triglycerides, and LDL as well as an increase in HDL in a dose-dependent manner. The aforementioned results therefore suggested positive antihyperlipidemic, anti-inflammatory, analgesic, and antipyretic effects of the seed extract.[36] Although the study did not isolate the chemical compounds responsible for the respective effects mentioned, 12 furocoumarins that may be responsible for the aforementioned effects were identified. The identification of these 12 furocoumarins (Figure 2) was in line with several other studies previously done on the same species.[37,38] Further studies involving the isolation of the furocoumarins along with other compounds is required to further investigate the mechanistic angle of the respective effects addressed.

Prickly Pear Seeds (Opuntia joconostle). The prickly pear (*O. joconostle*) is a species in the cactus family, Cactaceae, that grows widely in North American deserts, mainly in the southwestern part of the United States, Mexico, and Canada. High antioxidant activities of different parts of prickly pear have been reported (62.96% in pericarp, 42.27% in mesocarp, and 51.70% in endocarp) and are related to phenolic and flavonoid

composition.[7] This content was found to be especially higher in seeds than in peel (23-fold), mesocarp (34-fold), and endocarp (47-fold).[39] Clinical studies have reported that consumption of the *O. joconostle* pericarp may reduce glucose and cholesterol levels and modify LDL-C levels in patients with both type 1 and 2 diabetes.[7] In addition to these papers, a study reporting the influence of the *O. jocostle* seed methanolic extract on the plasma lipid profile in mouse models showed that the seed extract was also able to prevent an increase in total cholesterol, LDL-C, triglyceride level, and atherogenic index. Of the seven polyphenol compounds identified in the fruit component via the HPLC-PDA analytical system (Figure 2), the study concluded that the observable effects were believed to be caused by the flavonoids present in the seed, specifically quercetin, rutin, and catechin. It possibly occurs through the up-regulation of LDL receptor expression and inhibition of hepatic lipid synthesis and lipoprotein secretion, thereby enhancing cholesterol elimination through bile acids.[40]

Overall, the ability of the methanolic extract of prickly pear seeds to exhibit hypolipidemic activity with no apparent toxic manifestations suggests that this could be an ideal supplement to short-term hypercholesterolemia treatment. Such seed extracts from *P. americana*, *H. umbellata*, *A. majus*, and *O. joconostle* could potentially be used as future antiobesity therapeutics in the long run with the development of a proper processing and extraction technique for these seed components.

Flowers. The flower is a structure specialized for sexual reproduction. Many flowers have evolved traits such as brightly colored petals and attractive chemical scents to attract pollinators. In addition to facilitating the reproduction of flowering plants, the polyphenols, flavonoids, and anthocyanin present in flowers have recently been discovered to potentially exhibit medicinal properties.[41,42] We could gain much from exploring and tapping the antiobesity potential of the phytochemicals that flowers contain as some studies have shown.

Pomegranate Flower (Punica granatum L.). The pomegranate (*P. granatum* L.) is considered to be one of the oldest known edible fruits and is the symbol of abundance and prosperity in some cultures. The pomegranate has been known to be a fruit of multiple health purposes for many centuries. Recently, there has been scientific evidence suggesting the therapeutic activity observed in pomegranate such as antiatherogenic, antioxidant, anticarcinogenic, and anti-inflammatory effects.[41,43,44] These beneficial effects were attributed to the antioxidative properties of pomegranate phenolic compounds, such as tannins and anthocyanin, present in its fruit components.[44]

A series of in vivo and in vitro experimental models using pomegranate flower (PGF) extract have been found to result in hypoglycemic, hypolipidemic, and anti-inflammatory effects in type 2 diabetes, obesity, and related cardiovascular diseases based on its modulation of PPARα- and/or PPARγ-mediated gene transcription. It is hypothesized in a review by Li et al. that the components present in PGF extract were able to promote a dual function activating both PPARα and PPARγ that accounts for the desired bioactivity required for treatment of diseases such as type 2 diabetes and obesity.[45] The biologically active components that have been identified in PGF extract via HPLC methods[46] include gallic, ursolic, and oleanolic acids. In a study done by Jang et al., commercially obtained gallic acid was seen to effectively an exhibit hypolipidemic effect on high fat diet-induced hyperlipidemia mice.[47] Ursolic and oleanolic acids are two triterpenoids that have long been recognized to have significant medicinal properties to the extent that these compounds have been isolated, treated, and marketed in countries such as China as an oral drug for human liver disorders as early as the 1980s.[48] The possible mechanisms for the pharmacological effects and the prospects for these two compounds exhibiting antihyperlipidemia, antitumor activity, and anti-inflammation have also been discussed by Liu et al., suggesting that the presence of these two compounds identified in PGF makes it a potentially useful source not just for antiobesity but other associated diseases as well.[49]

In close relation to this, an in vivo experimental model study of Zucker diabetic fatty (ZDF) rats conducted by Li et al. showed that the administration of PGF extracts was able to exert a protective effect, preventing the increase in blood glucose level, total cholesterol, triglycerides, LDL-C, and lipid peroxidation levels of infected mice.[41,42] This phenomenon could be explained by the ability of the bioactive components present within PFG extract to enhance the expression of PPARα and acyl-CoA oxidase (ACO) mRNAs as observed in the liver-derived HepG2 cell line.[41] These series of studies thereby highlighted the ability of PGF to ameliorate obesity via a varied series of mechanistic pathways that essentially leads to the decrease of lipid accumulation in liver.

Longan Flower (Dimocarpus longans Lour.). Longan (*D. longans* Lour.) is a tropical tree that produces edible fruit which is widely grown in Myanmar through southern China and Southeast Asia. Unpollinated longan flowers are generally regarded as disposable byproducts. Yang et al. have identified several phenolic acids and flavonoids present in longan flower water extract (LFWE) via HPLC methods running against several commercially available phenolic acid and flavonoid standards, of which gentisic acid, epicatechin, and ferulic acid were among the major compounds identified. The study went on to investigate the effects of administration of LFWE on 9-week-old Sprague−Dawley hypercaloric rats. It was found that LFWE was able to lower the liver cholesterol and triglyceride levels as well as inhibit pancreatic lipase activities by up-regulation of LDL-receptor and PPARα mRNA expression. It was also found to have lowered the rate of lipid biosynthesis via the down-regulation of sterol regulatory element binding protein-1c (SREBP-1c), a critical transcription factor that stimulates several lipogenic enzymes involved in fatty acid biosynthesis, as well as fatty acid synthase (FAS) gene expression.[23]

This observation is further supported by a series of other studies highlighting the similar ability of naturally occurring polyphenols contributing to similar effects.[50,51] Overall, Yang et al. have shown the ability of LFWE to result in antiobesity and hypolipidemic effects via a combined effect of decreased exogenous lipid absorption, normalization of hepatic PPARα gene expression, suppression of pancreatic activity and SREBP-1c and FAS gene expression, and higher fecal triglyceride. Hsieh and colleagues have also demonstrated the role of epicatechin as the major component in longan flowers that promotes antioxidant effects on cells.[52] These series of studies have shown a collectible amount of findings, which significantly indicated the ability of longan flowers to be used as future therapeutics against not just obesity but also a series of other associated diseases.

Leaves. Leaves are organs of the plants where photosynthesis takes place by which captured solar energy is converted into useful chemical energy, which liberates oxygen required for

respiration by living organisms. Besides the photosynthetic roles, leaves also serve as a chemical energy storage point for plants. Tapping this knowledge, several studies have been done to investigate the efficacy of phytochemical compounds present in leaves as potential therapeutics for obesity.

Mango Leaves (Mangifera indica L.). Mango leaves (*M. indica* L.) have proven to be beneficial in alleviating diabetes and inhibiting triglyceride accumulation in 3T3-L1 cells. It is thus a prospective candidate for such tropical fruit waste component to be recycled and used as potential therapeutics for related diseases, namely, diabetes and obesity. In a study conducted by Kumar et al., mangiferin, a bioactive phytochemical component, was extracted and isolated from stem bark of *M. indica* and subjected to a glucose utilization test with 3T3-L1 cells. The results showed that treatment of the 3T3-L1 cells with mangiferin increased the glucose utilization in a dose-dependent manner.[53] Zhang et al. isolated 12 active fractions, as highlighted in Figure 2, via ordinary and reversed phase silica gel column chromatography as well as HPLC from *M. indica* L. leaf extracts and tested each compound against 3T3-L1 cells to monitor their respective effects on gene expression. The study indicated that of the 12 compounds (summarized in Figure 2), foliamangiferoside A, iriflophenone-3-*C*-β-glucoside, iriflophenone-3-*C*-(2-*O*-*p*-hydroxybenzoyl)-β-D-glucopyranoside, maclurin-3-*C*-β-D-glucoside, and mangiferin were able to significantly suppress the accumulation of triglyceride in mature 3T3-L1 cells and inhibit the expression of genes including SREBP1c, FAS, and hormone-sensitive lipase (HSL), all associated with triglyceride biosynthesis.[54]

Olive Leaves (Olea europaea). Several studies have suggested that oleuropein and hydroxytyrosol present in *O. europaea* leaves are the key antioxidants responsible for preventing LDL oxidation and protecting cells against numerous diseases.[55−57] Oleuropein is a principal phenolic compound in olive leaves, which can produce other bioactive substances such as hydroxytyrosol upon hydrolysis. Drira et al. obtained these bioactive compounds commercially to study their respective in vitro inhibition activity on adipocyte differentiation using 3T3-L1 preadipocyte cells. The results showed that oleuropein and hydroxytyrosol dose-dependently suppressed intracellular triglyceride accumulation during adipocyte differentiation without effect on cell viability. PPARγ, C/EBPα, and SREBP-1c transcription factors and their downstream targets (GLUT4, CD36, and FASN), all of which are adipogenesis-related genes, were down-regulated after treatment by oleuropein and hydroxytyrosol. In addition, a flow cytometry study also revealed that both polyphenols were able to inhibit the division of 3T3-L1 preadipocytes during mitotic clonal expansion and cause cell cycle delay. This combinative effect of the bioactive compounds extracted and isolated from olive leaves was observed to collectively result in an overall reduction of lipid accumulation in 3T3-L1 cells and thus regulate the size of fat cells, giving them potential as useful obesity-preventive additives to foods and drinks.[16]

In addition, besides oleuropein and hydroxytyrosol, among other phenolic compounds that were identified in the most recent study conducted by Kontogianni et al. via liquid chromatography−ultraviolet−visible (UV−vis) diode array coupled to electrospray ionization multistage mass spectrometry (LC/DAD/ESI-MS) were luteolin, luteolin-4′-*O*-β-D-glucopyranoside, and luteolin-7-*O*-β-D-glucopyranoside. These compounds were assigned as potent advanced glycation end product (AGE) inhibitors, which may potentially be useful for treatments for associated diseases that include diabetes.[58,59]

Guava Leaves (Psidium guajava). Guava (*P. guajava*) leaves have been used as traditional medicine for various kinds of diseases over centuries.[60] The rich content of antioxidants, antibacterial agents, anti-inflammatory agents, and tannins present in *P. guajava* leaves makes it a medicinally useful tool for traditional remedy. In a recent study, Yang et al. reported that quercetin-3-*O*-(6″-feruloyl)-β-D-galactopyranoside (QFG), an active compound isolated and extracted from *P. guajava* via octadecylsilyl silica gel (ODS) HPLC, has suppressive effects on adipogenesis in 3T3-L1 preadipocytes through down-regulation of PPARγ and C/EBPα expression.[20]

Quercetin is a typical flavonoid proven to play a pivotal role in the prevention of obesity[61,62] and is abundant in guava leaves. It was extracted and its suppressive effects on adipogenesis were compared with QFG. The efficacy of the two respective compounds was analyzed via Oil Red O staining[63] and triglyceride assay. It was found that QFG inhibited adipogenesis in a dose- and time-dependent manner and exerted a stronger suppressive effect than quercetin in all setups. Both mRNA and protein expressions of the key adipogenic transcriptional factors, PPARγ and C/EBPα, were inhibited by QFG. These series of results suggest that both QFG and quercetin present in *P. guajava* leaves were able to effectively suppress adipogenesis.[20] In a separate study, it was also found that quercetin was able to inhibit adipogenesis in 3T3-L1 preadipocytes by adenosine monophosphate kinase (AMPK) and mitogen-activated protein kinase (MAPK) pathways and that the combination of quercetin and resveratrol enhanced the inhibition.[62,64]

Essentially, these series of studies showing the therapeutic capabilities of the major bioactive components identified in guava leaves have certainly shown the potential of such fruit waste components to be used as alternative sources of remedy.

Potential Antidiabetic Properties of Tropical Fruit Leaves. Although this review mainly highlights the key tropical fruits that have been discovered to exhibit antiobesity potential, a series of related diseases that often can be associated with obesity cannot be neglected. A commonly related disease that can be linked with obesity is type 2 diabetes. A review by Kahn et al. discussed how obesity subsequently leads to an increased risk of developing insulin resistance and, consequently, type 2 diabetes. As mentioned, "in obese individuals, adipose tissue releases increased amounts of non-esterified fatty acids, glycerol, hormones, pro-inflammatory cytokines and other factors that are involved in the development of insulin resistance. When insulin resistance is accompanied by dysfunction of pancreatic islet β-cells, failure to control blood glucose levels results. Abnormalities in β-cell function are therefore critical in defining the risk and development of type 2 diabetes."[65]

Understanding how obesity can lead to diabetes via several underlying mechanisms, we will then discuss some examples of tropical fruit leaf components that have been found to exhibit antidiabetic activity. To name some examples, the amla and papaya leaves will be discussed in the following section. There have yet to be studies done on the same component exhibiting antiobesity effects.

Papaya Leaves (Carica papaya). Traditionally, papaya leaves have been widely used in Mexican folk medicine to treat diabetes and inflammation as well as diarrhea.[66,67] In a study done by Juárez-Rojop et al. the hypoglycemic effect of the

aqueous extract of *C. papaya* leaves in streptozotocin-induced diabetic rats was evaluated. It was found that the administration of this extract was able to significantly reduce the blood glucose level in diabetic rats and decrease cholesterol and triacylglycerol as well as amino-transferase blood levels. Additionally, the cell size preservation observed under histological reference of the diabetic rat's pancreas further suggested the ability of *C. papaya* aqueous extract to help in islet regeneration. In the liver histopathological examination, it was further revealed that the aqueous extract was able to prevent hepatocyte disruption, as well as accumulation of glycogen and lipids. On the basis of the collective data gathered from their study, the author confirmed the hypoglycemic effect of *C. papaya* leaves and their ability to prevent further disruption produced by diabetes.[68] However, admittedly, the lack of studies investigating the implicated phytochemical constituents and the exact mechanism of action responsible for the overall positive activity mentioned has yet to be addressed.

Amla Leaves (Emblica officinalis). In traditional Indian medicine, all parts of *E. officinalis* Gaertn. plant including the fruit, seed, leaves, root, bark. and flowers are used in various herbal preparations for the treatment of diabetes mellitus and chronic diarrhea and as an anti-inflammatory and antipyretic. In a study conducted by Nain et al. using in vivo streptozotocin-induced diabetic rats as an experimental model, they discovered that the extract of leaves of *E. officinalis* Gaertn. (HMELEO) was able to effectively normalize the impaired antioxidant status in streptozotocin-induced diabetic rats in a dose-dependent manner. In addition to this, its ability to exert rapid protective effects against lipid peroxidation by scavenging free radicals thereby contributes to the overall reduction in the risk of diabetic complications.[69] Although the study did not isolate or identify the phytochemicals that were responsible for the observed bioactivity, the author cross-linked with a series of previous studies of the same species suggesting that ellagic acid, gallic acid, ascorbic acid, tannins emblicannin A and B, and tannoids kaempferol, kaempferol-3-*O*-glucoside, and rutin may be the bioactive compounds.[70,71]

Rind/Peel. The outer covering of a fruit is known as the peel or rind. However, there is a subtle difference between the rind and the peel. The rind generally is harder and thicker, whereas the peel/skin is generally thin and soft. Rinds, peels, and skins of fruits contain several phytochemicals that can help maintain good health, which is evident in several studies.[18,19,24,72]

Mangosteen Rind (Garcina mangostana). A potentially useful tropical fruit rind that has shown to exhibit antiobesity potentials would be that of the *G. mangostana* fruit. The fruit hulls of *G. mangostana*, just like *P. guajava* leaves, have long been used throughout Southeast Asia as a medical plant for a wide variety of treatments.[73] Modern research has identified and isolated 13 phenolic compounds from the hulls of *G. mangostana* by column chromatography, which are α-mangostin, β-mangostin, γ-mangostin, 9-hydroxycalabaxanthone, garcinone E, 1,5-dihydroxy-3-methoxy-2-(3-methylbut-en-1-yl)-9*H*-xanthen-9-one, 1,3,7-trihydroxyxanthone, 2,4,6,7-tetrahydroxyxanthone, 3,4,5,3′-tetrahydroxybenzophenone, 2,4,6,3′,5′-pentahydroxybenzophenone, neosmitilbin, epicatechin, and egonol.[74]

In an experiment done by Quan et al., it was discovered that among the 13 phenolic compounds isolated,[74] α-mangostin induced apoptosis and suppressed differentiation of 3T3-L1 cells through inhibition of fatty acid synthase (FAS). Further Oil Red O staining tests showed that it was able to prevent the intracellular lipid accumulation of the differentiating adipocytes and that it stimulated fat cell breakdown in the mature adipocytes.[18] Loftus et al. highlighted how central inhibition of FAS suppressed food intake and led to dramatic weight loss in mice.[75] It is believed that natural sources of nutraceuticals that are capable of reducing FAS activity or expression levels may be useful for the supplementary treatment of obesity. Among the 13 phenolic compounds present in the hulls of *G. mangostana* (Figure 2), it was found that phenolic constituents containing the conjugated system of phenyl and carbonyl, especially xanthones and benzophenones, particularly α-mangostin, γ-mangostin, garcinone E, and 2,4,6,3′,5′-pentahydroxybenzophenone, exhibited the strongest inhibitory activity of FAS.[74]

These series of findings suggesting the ability of isolated components extracted from the hulls of mangosteen fruit, namely, α-mangostin, to induce apoptosis of 3T3-L1 preadipocytes that consequently suppressed lipid accumulation as well as α-mangostin, γ-mangostin, garcinone E, and 2,4,6,3′,5′-pentahydroxybenzophenone exhibiting strong inhibitory activity of FAS, certainly highlights the great potential of this fruit component to be exploited and used to treat obesity.

Citrus Genus Peel (C. sunki, C. reticulata, C. grandis, C. aurantifolia). Over the past years, a series of studies have been done on the *Citrus* family. Whereas the flesh itself has been widely known to contain antioxidants and weight -loss properties,[76] the peels of a few species were recently discovered to exhibit a wide range of biological activities, including antioxidative, antihypertension, antihyperglycemia, and anti-obesity effects.[77−79] Among the species identified include the peels of *C. sunki*, *C. ichangenesis*, and *C. grandis*. These potentially health-promoting effects observed from the citrus components have been ascribed to the bioactive compounds present such as flavanoids, coumarins, polyphenols, limonoids, and alkaloids.

The immature *C. sunki* peel extract as recently discussed by Kang et al. was found to exhibit antiobesity effects by β-oxidation and lipolysis in adipose tissue.[77] The study was based on an in vivo experimental model of which controlled dosage of *C. sunki* extract was administered to high fat diet-induced obese mice, and their respective liver, epididymal tissue, and perirenal adipose tissue were regularly monitored. Protein expressions of the related pathways were then investigated by obtaining the total RNA from the respective adipose tissue of mice and in vitro 3T3-L1 adipocyte cells, via reverse transcription polymerase chain reaction (RT-PCR). The collective data were sufficient for the author to conclude that the peel of *C. sunki* had an antiobesity effect. However, although no phytochemicals were isolated in the study, polymethoxyflavonones (PMFs), namely, tangeretin and nobiletin, were identified in the extract and deduced to be the possible bioactive compounds that mediate the antiobesity effect.[77,80]

In a research study done by Ding et al., they made a similar observation in *C. grandis*, more commonly known as the pomelo, peels. Using an in vivo experimental model of obese C57BL/6 mice induced with a high-fat diet (HFD), they found that the peel crude extract was able to block the body weight gain and lower the blood glucose level, serum total cholesterol, liver lipid levels, and serum insulin levels as well as improve glucose tolerance and insulin resistance. Further effects of the extract on various gene expressions were also investigated using quantitative RT-PCR via extraction of total RNA from mouse tissues. Interestingly, despite the lack of identification of

bioactive compounds[81] presented in their study, Ding et al. brought up several differences in bioactivity of *C. grandis* originating from different cultivars.[82] This observation, therefore, illustrated an important fact as to how agronomic factors, such as environmental factors and varied conditions, may affect the overall bioactivity and antioxidant capacity of the fruit.

Mango Peel (Mangifera indica L.). *M. indica* L. is a tropical fruit that is rich in a diverse array of bioactive phytochemicals. There is a growing body of evidence that links phytochemicals with the inhibition of adipogenesis and protection against obesity. In particular, Taing et al. carried out an experiment demonstrating not only the effect of the mango peel extract on adipogenesis in 3T3-L1 cells but also how the differences in phytochemical quantity and composition between species of the same fruit can exhibit different adipogenesis inhibition efficiencies.[19]

Methanol extracts of peel and flesh from three archetypal mango cultivars, Irwin, Nam Doc Mai, and Kensington Pride, were assessed for their effects on the 3T3-L1 preadipocyte cell line model of adipogenesis, respectively. Whereas the flesh from all three cultivars was ineffective, two of the peel extracts, namely, Irwin and Nam Doc Mai, inhibited adipogenesis. This observation was further analyzed, and it was concluded that differences in phytochemical composition between mango cultivars may influence their effectiveness in inhibiting adipogenesis and that specific components within the phenolic content make a major contribution to its overall antiadipogenic effects. The studies further showed that the inhibition of adipogenesis occurred possibly through the inhibition of mitotic clonal expansion, mediated by pathways similar to those of the red grape component resveratrol.[83] Essentially, regardless of the different efficiencies, the ability of *M. indica* L. to promote positive inhibition effects toward adipogenesis puts forth another fruit waste component as a potential tropical fruit source to treat obesity.

In general, several studies of various tropical fruit components and their respective observed biological activities have certainly highlighted the potential benefits that may result when they are used as supplements for the treatment of obesity, along with its related diseases such as diabetes. The study of mango peels originating from various cultivars, as discussed by Taing et al., exhibiting varied effects on the overall biological activity suggests that the chemical composition present in fruits may differ, even if they are from the same species. The environmental factor, weather conditions, amount of nutrition, and the overall agricultural technique used to grow these fruits will essentially determine the primary composition of the fruit components. Ideally, then, before the agronomic approaches can be developed to alter the agricultural conditions leading to an effective yield of fruit components consisting of highly bioactive phytochemicals, the actual bioactive phytochemicals have to first be determined. This would therefore require further isolation and elucidation of the active compounds responsible for the overall respective antihyperlipidemic, anti-inflammatory, hypoglycemic, and antiobesity effects as addressed previously.

Although the isolation and effective separation process of various chemicals from the fruit waste components may be time-consuming, it is absolutely necessary for the effective development of this field. The presence of more advanced analytical devices such as the prep-HPLC, supercritical fluid extraction technique, and LC-MS, for instance, will definitely help to facilitate this research. The subsequent steps would therefore require further elucidation of chemical structure for the novel bioactive phytochemicals. As for the existing/current bioactive chemicals identified, further investigation is required so that absolute confirmation of its respective bioactive capacity proposed can be done.

PHYTOCHEMICALS RESPONSIBLE FOR THE RESPECTIVE BIOACTIVITY

Polyphenols are often associated as the component responsible for antioxidant effects commonly observed in natural products.[84,85] Therefore, this would also suggest that if a fruit component exhibits high antioxidant capacity, it effectively means that there is a high presence of polyphenols in the fruit component. In addition to this, polyphenols have also been found in several studies to be responsible for the positive antiobesity effect as established by Wang et al.[86] In relation to the commonly suggested "high antioxidant capacity in natural components reflecting higher potential to treat disease" phenomenon, a comparative study recently published by Al-Mansoub et al. on antihyperlipidemic and antioxidant effects of *Garcinia atroviridis* showed an interesting observation that suggests otherwise. In their study, they revealed that the aqueous extract was observed to contain fewer polyphenols than the methanolic extract but reflected a stronger bioactivity (antihyperlipidemic effect). This finding further suggested that there were other compounds besides polyphenols that were involved, leading to the overall efficacy of the bioactivity observed.[87]

From the collection of major compounds identified in the series of studies as summarized in Table 1, we have found that the bioactive phytochemicals recommended were not necessarily polyphenols. In promegranate flowers, for instance, the major compounds identified were oleanolic acid and ursolic acid,[41] whereas in the bishop's weed, the main components identified as exhibiting antiobesity activities were the furocoumarins. Among some of the other nonpolyphenols were the polymethoxyflavonones (PMFs) found in *C. sunki* and flavonoids in *C. grandis* and *H. umbellata*.[31,77,82] Therefore, the independent role of polyphenols in inducing positive antiobesity effects was questioned. How these phytochemicals were proposed in the studies to effectively result in the reduction of lipid accumulation at the adipocytes, a characteristic of antiobesity properties, differed from one component to another. Could it be a combinatorial effect with other compounds mentioned? Do they share a similar lipid accumulation inhibition mechanism as polyphenols?

Although the exact role of the bioactive compounds in the overall inhibition of lipid accumulation has yet to be determined, various studies have shown the different possible mechanisms that these compounds may play. On the basis of the mechanistic analysis of how the respective major bioactive compounds identified play a role in the overall positive antiobesity effect, it was observed that each compound reacts differently from one another, regardless of its class (i.e., polyphenols or flavonoids or PMFs). Typically, this boils down to the different set of genetic expressions that these compounds affect, which gradually leads to the overall antiobesity effect observed in the end. Between the polyphenols identified in olive leaves and mango leaves, for instance, the oleuropein and hydroxtyrosol in olives were found to prevent 3T3-L1 adipocyte differentiation via the inhibition of the mitotic clonal expansion and down-regulation of the adipogenesis-related genes, namely, PPARγ, C/EBPα, and SREBP-1c,[16] whereas the

foliamangiferoside A, iriflophenone-3-*C*-β-glucoside, and mangiferin found in mango leaves were found to result in the same effect but via the down-regulation or inhibition of the FAS and hormone-sensitive lipase (HSL) gene expression.[54] In *C. sunki* peel extract, where the major compounds identified were mainly flavonoids, it was found that the observed antiobesity effect proceeded via elevated β-oxidation and lipolysis in adipose tissue. This was deduced from a series of results that included the crude extract's ability to increase AMPK and ACC phosphorylation in mature 3T3-L1 adipocytes.[77]

We therefore conclude that there is indeed no one mechanism that is used to find the cure to obesity. Many scientists used different models in identifying antiobesity capacity, some of which use the in vivo experimental model, whereas others use the in vitro assay, typically 3T3-L1 adipocyte cells. There is, however, no specific right or wrong answer to this phenomenon. The mechanisms by which these bioactive compounds proceed to sequentially result in an overall positive antiobesity effect vary from one fruit component to another. The roles of the specific bioactive phytochemicals, mainly the polyphenols, flavonoids, and furocoumarins, in the overall mechanism have yet to be established. More research, particularly in the area of isolation, identification, and elucidation of bioactive compounds, has to be done. Subsequently, crystallization of these compounds can then proceed, in order for computational modeling to be generated to further investigate how these respective bioactive compounds play an essential role in the overall mechanism (such as adipogenesis), that leads to the positive antiobesity effect, initially observed in vivo.

Following this, only then can the in vivo as well as clinical studies, using the isolated bioactive phytochemicals, be facilitated to support the therapeutic roles of fruit waste components in the overall effect of obesity treatment. Such results may then push for further development of new agronomic approaches, implementing new technological innovation to cultivate tropical fruit parts enriched in a specifically desired composition of phytochemicals and, at the same time, an effective large-scale processing technique of specific tropical fruit wastes can be strategized.

DEVELOPMENT OF EFFECTIVE FRUIT WASTE PROCESSING/RECYCLING TECHNIQUES AND AGRONOMIC ADVANCES

In the pursuit of finding an alternative means to combat obesity using natural sources, studies of fruit waste components have been done, and they have appeared to be prospective sources of remedy due to their high bioactivity and lesser tendency of inducing detrimental side effects. Although more elaborate studies have to be done specifically on the isolation and elucidation of compounds responsible for their respective bioactivity, as addressed earlier in the review, there are a few other challenges that have to be dealt with. To effectively tap the maximum potential of tropical fruit waste components as future therapeutics, an effective large-scale processing technique for these waste components has to be designed. Other relevant factors include finding the right places and equipment to store these components to prevent them from decaying, intricate engineering of large-scale extraction techniques to take up only the desired materials, and implementing necessary agronomic advances to utilize and develop new technological innovations to cultivate crops containing high useful phytochemical compositions.

FUTURE OF TROPICAL FRUIT WASTE COMPONENTS

Tropical fruit waste components, as discussed in this review, have various bioactive components with health benefits. The combination of these effects rendered by the reported tropical fruit "waste components" is crucial to prevent the development of complex pathophysiology of obesity and diabetes. The extraction of these components and in-depth study of their effects on the various genetic expression using in vitro and in vivo test models, as addressed in this paper, have shown clear evidence of the positive effects that these bioactive phytochemicals possess. This essentially suggests the potential use of such components as future therapies to further supplement antiobesity treatments. In addition, as these components originate from natural sources, the likelihood of these extracts being toxic and detrimental is decreased.[9]

Further studies involving the isolation of bioactive compounds from tropical fruit waste components and the elaboration of a mechanistic approach toward the overall lipid regulation in cells is, however, still necessary for further advances in the development of these waste components. The exact structural roles of the bioactive phytochemicals in the overall antiobesity mechanism have to be further looked into, of which some of the studies may encompass the need for chemical crystallization and computer modeling. In addition, further large-scale defined basic and clinical studies are critical to determine optimal dietary regimens to achieve the desired beneficial health effects. Ultimately, only with enough positive and reliable relevant data can the commercial use of these tropical fruit waste components as future therapeutics be advocated.

AUTHOR INFORMATION

Corresponding Author

*E-mail: zhangdw@ntu.edu.sg.

Author Contributions

‖K.L. and H.L.T. contributed equally to this work.

Notes

The authors declare no competing financial interest.

REFERENCES

(1) Basu, S.; Millett, C. Social epidemiology of hypertension in middle-income countries: determinants of prevalence, diagnosis, reatment, and control in he WHO SAGE study. *Hypertension* **2013**, *62* (1), 18−26.

(2) Malnick, S. D. H.; Knobler, H. The medical complications of obesity. *QJM* **2006**, *99* (9), 565−579.

(3) Hossain, P.; Kawar, B.; El Nahas, M. Obesity and diabetes in he developing world — a growing challenge. *New Engl. J. Med.* **2007**, *356* (3), 213−215.

(4) Young, J. B. Diabetes, obesity, and heart failure: the new pandemic. *Methodist Debakey Cardiovasc J.* **2010**, *6* (2), 20−26.

(5) Fleming, J. W.; McClendon, K. S.; Riche, D. M. New obesity agents: lorcaserin and phentermine/topiramate. *Ann. Pharmacother.* **2013**, *47* (7−8), 1007−1016.

(6) Padwal, R.; et al. Bariatric surgery: a systematic review and network meta-analysis of randomized rials. *Obesity Rev.* **2011**, *12* (8), 602−621.

(7) Osorio-Esquivel, O.; et al. Antihyperlipidemic effect of methanolic extract from *Opuntia joconostle* seeds in mice fed a hypercholesterolemic diet. *Plant Foods Hum. Nutr.* **2012**, *67* (4), 365−370.

(8) Fogari, R.; Zoppi, A. Effect of antihypertensive agents on quality of life in the elderly. *Drugs Aging* **2004**, *21* (6), 377−393.

(9) Ji, H.-F.; Li, X.-J.; Zhang, H.-Y. Natural products and drug discovery. Can thousands of years of ancient medical knowledge lead us to new and powerful drug combinations in the fight against cancer and dementia? *EMBO Rep.* **2009**, *10* (3), 194−200.
(10) Lu, K.; et al. Scutellarin from *Scutellaria baicalensis* suppresses adipogenesis by upregulating PPARα in 3T3-L1 cells. *J. Nat. Prod.* **2013**, *76* (4), 672−678.
(11) Trujillo, M. E.; Scherer, P. E. Adipose issue-derived factors: impact on health and disease. *Endocrine Rev.* **2006**, *27* (7), 762−778.
(12) Farmer, S. R. Transcriptional control of adipocyte formation. *Cell Metab.* **2006**, *4* (4), 263−273.
(13) White, U. A.; Stephens, J. M. Transcriptional factors that promote formation of white adipose tissue. *Mol. Cell. Endocrinol.* **2010**, *318* (1−2), 10−14.
(14) Evans, R. M.; Barish, G. D.; Wang, Y. X. PPARs and he complex journey to obesity. *Nat. Med.* **2004**, *10* (4), 355−361.
(15) Devalaraja, S.; Jain, S.; Yadav, H. Exotic fruits as herapeutic complements for diabetes, obesity and metabolic syndrome. *Food Res. Int.* **2011**, *44* (7), 1856−1865.
(16) Drira, R.; Chen, S.; Sakamoto, K. Oleuropein and hydroxytyrosol inhibit adipocyte differentiation in 3 3-L1 cells. *Life Sci.* **2011**, *89* (19−20), 708−716.
(17) Pahua-Ramos, M.; et al. Hypolipidemic effect of avocado (*Persea americana* Mill) seed in a hypercholesterolemic mouse model. *Plant Foods Hum. Nutr.* **2012**, *67* (1), 10−16.
(18) Quan, X.; et al. α-Mangostin induces apoptosis and suppresses differentiation of 3T3-L1 cells via inhibiting fatty acid synthase. *PLoS One* **2012**, *7* (3), e33376.
(19) Taing, M. W.; et al. Mango fruit peel and flesh extracts affect adipogenesis in 3T3-L1 cells. *Food Funct.* **2012**, *3* (8), 828−836.
(20) Yang, L.; et al. Suppressive effects of quercetin-3-*O*-(6″-feruloyl)-β-D-galactopyranoside on adipogenesis in 3T3-L1 preadipocytes through down-regulation of PPARγ and C/EBPα expression. *Phytother. Res.* **2012**, *26* (3), 438−444.
(21) González-Castejón, M.; Rodriguez-Casado, A. Dietary phytochemicals and their potential effects on obesity: a review. *Pharmacol. Res.* **2011**, *64* (5), 438−455.
(22) Andersen, C.; et al. Phytochemicals and adipogenesis. *BioFactors* **2010**, *36* (6), 415−422.
(23) Yang, D. J.; et al. Antiobesity and hypolipidemic effects of polyphenol-rich longan (*Dimocarpus longans* Lour.) flower water extract in hypercaloric-dietary rats. *J. Agric. Food Chem.* **2010**, *58* (3), 2020−2027.
(24) Wu, G.; et al. Dietary supplementation with watermelon pomace juice enhances arginine availability and ameliorates the metabolic syndrome in Zucker diabetic fatty rats. *J. Nutr.* **2007**, *137* (12), 2680−2685.
(25) Daud, N. H.; et al. Mango extracts and the mango component mangiferin promote endothelial cell migration. *J. Agric. Food Chem.* **2010**, *58* (8), 5181−5186.
(26) Wilkinson, A. S.; et al. Bioactivity of mango flesh and peel extracts on peroxisome proliferator-activated receptor γ[PPARγ] activation and MCF-7 cell proliferation: fraction and fruit variability. *J. Food Sci.* **2011**, *76* (1), H11−H18.
(27) Wang, W.; Bostic, R.; Gu, L. Antioxidant capacities, procyanidins and pigments in avocados of different strains and cultivars. *Food Chem.* **2010**, *122* (4), 1193−1198.
(28) Rodríguez-Carpena, J. G.; et al. Avocado (*Persea americana* Mill.) phenolics, in vitro antioxidant and antimicrobial activities, and inhibition of lipid and protein oxidation in porcine patties. *J. Agric. Food Chem.* **2011**, *59* (10), 5625−5635.
(29) Adeneye, A. A.; Adeyemi, O. O. Hypoglycaemic effects of the aqueous seed extract of *Hunteria umbellata* in normal and glucose- and nicotine-induced hyperglycaemic rats. *Int. J. Appl. Res. Nat. Prod.* **2009**, *2*, 9−18.
(30) Falodun, A.; Nworgu, Z. A. M.; Ikponmwonsa, M. O. Phytochemical components of *Hunteria umbellata* (K. Schum) and its effect on isolated non-pregnant rat uterus in oestrus. *Pakistani J. Pharm. Sci.* **2006**, *19*, 256−258.
(31) Adeneye, A. A.; Adeyemi, O. O.; Agbajeb, E. O. Anti-obesity and antihyperlipidaemic effect of *Hunteria umbellata* seed extract in experimental hyperlipidaemia. *J. Ethnopharmacol.* **2010**, *130*, 307−314.
(32) Ibeh, I. N.; Idu, M.; Ejimadu, I. M. Toxicological assessment of 'Abeere' seed *Hunteria umbellata* K. Schum (Apocynaceae). *Biociencia* **2007**, *15*, 4−7.
(33) Schoenfelder, T.; Pich, C. T.; Geremia, R.; Avila, S.; Daminella, E. N.; Pedrosa, R. C.; Tiol, J. Antihyperlipidaemic effect of *Casearia sylvestris* methanolic extract. *Fitoterapia* **2008**, *79*, 465−467.
(34) Han, L. K.; Kimura, Y.; Kawashima, M.; Takaku, T.; Taniyama, T.; Hayashi, T.; Zheng, Y. N.; Okuda, H. Anti-obesity effects in rodents of dietary easaponin, a lipase inhibitor. *Int. J. Obesity Relat. Metab. Disorders* **2001**, *25*, 1459−1464.
(35) El Moftey, A. M. A preliminary clinical report on the treatment of leucoderma with *Ammi majus* Linn. *J. R. Egypt. Med. Assoc.* **1948**, *31* (8), 561−665.
(36) Koriem, K. M. M.; Megahed, A. G.; Zahran, H. A.; Arbid, M. S. Evaluation of the antihyperlipidemic, anti-inflammatory, analgesic, and antipyretic activities of ethanolic extract of *Ammi majus* seeds in albino rats and mice. *Int. J. Toxicol.* **2012**, *31*, 294.
(37) Ivie, G. W. Linear furocoumarins (psoralens) from the seed of Texas *Ammi majus* L. (bishop's weed). *J. Agric. Food Chem.* **1978**, *26* (6), 1394−1403.
(38) Pokrovskii, O. I.; Markoliya, A. A.; Lepeshkin, F. D.; Kuvykin, I. V.; Parenago, O. O.; Gonchukov, S. A. Extraction of linear furocoumarins from *Ammi majus* seeds by means of supercritical fluid extraction and supercritical fluid chromatography. *Russ. J. Phys. Chem. B* **2009**, *3* (8), 1165−1171.
(39) Osorio-Esquivel, O.; et al. Phenolics, betacyanins and antioxidant activity in *Opuntia joconostle* fruits. *Food Res. Int.* **2011**, *44* (7), 2160−2168.
(40) Chumark, P.; et al. The in vitro and ex vivo antioxidant properties, hypolipidaemic and antiatherosclerotic activities of water extract of *Moringa oleifera* Lam. leaves. *J. Ethnopharmacol.* **2008**, *116* (3), 439−446.
(41) Xu, K. Z.-Y.; et al. Pomegranate flower ameliorates fatty liver in an animal model of type 2 diabetes and obesity. *J. Ethnopharmacol.* **2009**, *123* (2), 280−287.
(42) Al-Muammar, M. N.; Khan, F. Obesity: the preventive role of the pomegranate (*Punica granatum*). *Nutrition (Burbank, Los Angeles County, Calif.)* **2012**, *28* (6), 595−604.
(43) Adhami, V. M.; et al. Oral infusion of pomegranate fruit extract inhibits prostate carcinogenesis in the TRAMP model. *Carcinogenesis* **2012**, *33* (3), 644−651.
(44) Faria, A.; Calhau, C. The bioactivity of pomegranate: impact on health and disease. *Crit. Rev. Food Sci. Nutr.* **2011**, *51* (7), 626−634.
(45) Li, Y.; et al. Pomegranate flower: a unique raditional antidiabetic medicine with dual PPAR-α/-γ activator properties. *Diabetes, Obesity Metab.* **2008**, *10* (1), 10−17.
(46) Huang, H.; Peng, G.; Kota, B. P.; Li, G. Q.; Yamahara, J.; Roufogalis, B. D.; Li, Y. Anti-diabetic action of *Punica granatum* flower extract: activation of PPAR-γ and identification of an active component. *Toxicol. Appl. Pharmacol.* **2005**, *207*, 160−169.
(47) Jang, A.; et al. Comparison of hypolipidemic activity of synthetic gallic acid−linoleic acid ester with mixture of gallic acid and linoleic acid, gallic acid, and linoleic acid on high-fat diet induced obesity in C57BL/6 Cr Slc mice. *Chem.−Biol. Interact.* **2008**, *174* (2), 109−117.
(48) Yao, Z. C. Effects of oleanolic acid on experimental liver injury and herapeutic value in human hepatitis. *Tradit. Med. Hunan Med. Inst.* **1977**, *8*, 32−37.
(49) Liu, J. Pharmacology of oleanolic acid and ursolic acid. *J. Ethnopharmacol.* **1995**, *49* (2), 57−68.
(50) He, Q.; Lv, Y.; Yao, K. Effects of tea polyphenols on the activities of R-amylase, pepsin, trypsin and lipase. *Food Chem.* **2006**, *101*, 1178−1182.
(51) Sugiyama, H.; Akazome, Y.; Shoji, T.; Yamaguchi, A.; Yasue, M.; Kanda, T.; Ohtake, Y. Oligomeric procyanidins in apple polyphenol are main active components for inhibition of pancreatic lipase and triglyceride absorption. *J. Agric. Food Chem.* **2008**, *55*, 4606−4609.

(52) Hsieh, M. C.; Shen, Y. J.; Kuo, Y. H.; Hwang, L. S. Antioxidative activity and active components of longan (*Dimocarpus longan* Lour.) flower extracts. *J. Agric. Food Chem.* **2008**, *56*, 7010−7016.
(53) Kumar, B. D.; et al. Effect of mangiferin and mahanimbine on glucose utilization in 3T3-L1 cells. *Pharmacogn. Mag.* **2013**, *9* (33), 72−75.
(54) Zhang, Y.; et al. Identification of benzophenone *C*-glucosides from mango tree leaves and their inhibitory effect on triglyceride accumulation in 3T3-L1 adipocytes. *J. Agric. Food Chem.* **2011**, *59* (21), 11526−11533.
(55) Al-Azzawie, H. F.; Alhamdani, M.-S. S. Hypoglycemic and antioxidant effect of oleuropein in alloxan-diabetic rabbits. *Life Sci.* **2006**, *78* (12), 1371−1377.
(56) Han, J.; et al. Anti-proliferative and apoptotic effects of oleuropein and hydroxytyrosol on human breast cancer MCF-7 cells. *Cytotechnology* **2009**, *59* (1), 45−53.
(57) Santiago-Mora, R.; et al. Oleuropein enhances osteoblastogenesis and inhibits adipogenesis: the effect on differentiation in stem cells derived from bone marrow. *Osteoporosis Int.* **2011**, *22* (2), 675−684.
(58) Vassiliki, G.; Kontogianni, P. C.; Margianni, E.; Lamari, F. N.; Gerothanassis, I. P.; Andreas, G. Z. Olive leaf extracts are a natural source of advanced glycation end product inhibitors. *J. Med. Food* **2013**, *16* (9), 817−822.
(59) Takeuchi, M.; Yamagishi, S.; Iwaki, M.; Nakamura, K.; Imaizumi, T. Advanced glycation end product (age) inhibitors and their therapeutic implications in diseases. *Int. J. Clin. Pharmacol. Res.* **2004**, *24*, 95−101.
(60) Gutiérrez, R. M. P.; Mitchell, S.; Solis, R. V. *Psidium guajava*: a review of its traditional uses, phytochemistry and pharmacology. *J. Ethnopharmacol.* **2008**, *117* (1), 1−27.
(61) Hui-xing, W.; X, F. L.; Rong, L.; et al. Study on anti-oxidative components from leaves of *Psidium guajava*. *Chinese Tradit. Herbal Drugs* **2010**, *41*, 276−282.
(62) Ahn, J.; Lee, H.; Kim, S.; et al. The anti-obesity effect of quercetin is mediated by the AMPK and MAPK signaling pathways. *Biochem. Biophys. Res. Commun.* **2008**, *373*, 545−549.
(63) Novikoff, A. B.; et al. Organelle relationships in cultured 3T3-L1 preadipocytes. *J. Cell Biol.* **1980**, *87* (1), 180−196.
(64) Yang, J. Y.; Della-Fera, M. A.; Rayalam, S.; Ambati, S.; et al. Enhanced inhibition of adipogenesis and induction of apoptosis in 3T3-L1 adipocytes with combinations of resveratrol and quercetin. *Life Sci.* **2008**, *82*, 1032−1039.
(65) Kahn, S. E.; Hull, R. L.; Utzschneider, K. M. Mechanisms linking obesity to insulin resistance and type 2 diabetes. *Nature* **2006**, *444*, 840−846.
(66) Corral-Aguayo, R. D.; Yahia, E. M.; Carrillo-López, A.; González-Aguilar, G. Correlation between some nutritional components and the total antioxidant capacity measured with six different assays in eight horticultural crops. *J. Agric. Food Chem.* **2008**, *56*, 10498−10504.
(67) Chávez-Quintal, P.; González-Flores, T.; Rodríguez-Buenfil, I.; Gallegos-Tintoré, S. Antifungal activity in ethanolic extracts of *Carica papaya* L. cv. Maradolleaves and seeds. *Indian J. Microbiol* **2011**, *51*, 54−60.
(68) Juárez-Rojop, I. E.; Díaz-Zagoya, J. C.; Ble-Castillo, J. C.; Miranda-Osorio, P. H.; Castell-Rodríguez, A. E.; Tovilla-Zárate, C. A.; Rodríguez-Hernández, A.; Aguilar-Mariscal, H.; Ramón-Frías, T.; Bermúdez-Ocaña, D. Y. Hypoglycemic effect of *Carica papaya* leaves in streptozotocin-induced diabetic rats. *BMC Complement. Altern. Med.* **2012**, *12*, 236.
(69) Nain, P.; et al. Antidiabetic and antioxidant potential of *Emblica officinalis* Gaertn. leaves extract in streptozotocin-induced type-2 diabetes mellitus (T2DM) rats. *J. Ethnopharmacol.* **2012**, *142* (1), 65−71.
(70) Duke, J. A. *Handbook of Phytochemical Constituents of GRAS Herbs and Other Economic Plants*; CRC Press: Boca Raton, FL, USA, 1992.
(71) Thakur, R. S.; Puri, H. S.; Husain, A. *Major Medicinal Plants of India*; Central Institute of Medicinal and Aromatic Plants: Lucknow, India, 1989; pp 78−81.
(72) Thitilertdecha, N.; et al. Identification of major phenolic compounds from *Nephelium lappaceum* L. and their antioxidant activities. *Molecules* **2010**, *15* (3), 1453−1465.
(73) Pedraza-Chaverri, J.; et al. Medicinal properties of mangosteen (*Garcinia mangostana*). *Food Chem. Toxicol.* **2008**, *46* (10), 3227−3239.
(74) Jiang, H. Z.; et al. Fatty acid synthase inhibitors of phenolic constituents isolated from *Garcinia mangostana*. *Bioorg. Med. Chem. Lett.* **2010**, *20* (20), 6045−6047.
(75) Loftus, T. M.; Jaworsky, D. E.; Frehywot, G. L.; Townsend, C. A.; Ronnett, G. V.; Lane, M. D.; Kuhajda, F. P. Reduced food intake and body weight in mice treated with fatty acid synthase inhibitors. *Science* **2000**, *288*, 2379.
(76) Haaz, S.; Fontaine, K. R.; Cutter, G.; Limdi, N.; Perumean-Chaney, S.; Allison, D. B. *Citrus aurantium* and synephrine alkaloids in the treatment of overweight and obesity: an update. *Obesity Rev.* **2008**, *7*, 79−88.
(77) Kang, S. H.; Shin, H. S.; Kim, H. M.; Hong, Y. S.; Yoon, S. A.; et al. Immature *Citrus sunki* peel extract exhibits anti-obesity effects by β-oxidation and lipolysis in high-fat diet-induced mice. *Biol. Pharm. Bull.* **2012**, *35*, 223−230.
(78) Ono, E.; Inoue, J.; Hashidume, T.; Shimizu, M.; Sato, R. Anti-obesity and anti-hyperglycemic effects of the dietary citrus limonoid nomilin in mice fed a high-fat diet. *Biochem. Biophys. Res. Commun.* **2011**, *410*, 677−681.
(79) Shin, H.-S.; Kang, S.-I.; Ko, H.-C.; Kim, H.-M.; Hong, Y.-S.; et al. Anti-inflammatory effect of the immature peel extract of *Jinkyool* (*Citrus sunki* Hort. ex Tanaka). *Food Sci. Biotechnol.* **2011**, *20*, 1235−1241.
(80) Kurowska, E. M.; Manthey, J. A. Hypolipidemic effects and absorption of citrus polymethoxylated flavones in hamsters with diet-induced hypercholesterolemia. *J. Agric. Food Chem.* **2004**, *52* (10), 2879−2886.
(81) Zarina, Z.; Tan, S. Y. Determination of flavonoids in *Citrus grandis* (pomelo) peels and their inhibition activity on lipid peroxidation in fish tissue. *Int. Food Res. J.* **2012**, *20* (1), 313−317.
(82) Ding, X.; et al. Extracts of pomelo peels prevent high-fat diet-induced metabolic disorders in C57BL/6 mice through activating the PPARα and GLUT4 pathway. *PLoS One* **2013**, *8* (10), e77915.
(83) Gerhart-Hines, Z.; et al. Metabolic control of muscle mitochondrial function and fatty acid oxidation through SIRT1/PGC-1α. *EMBO J.* **2007**, *26* (7), 1913−1923.
(84) Santhakumar, A. B.; Bulmer, A. C.; Singh, I. A review of the mechanisms and effectiveness of dietary polyphenols in reducing oxidative stress and thrombotic risk. *J. Hum. Nutr. Diet.* **2014**, *27* (1), 1−21.
(85) Scalbert, A.; Johnson, I. T.; Saltmarsh, M. Polyphenols: antioxidants and beyond 1, 2, 3. *Am. J. Clin. Nutr.* **2005**, *81*, 2155−2175.
(86) Wang, S.; et al. Novel insights of dietary polyphenols and obesity. *J. Nutr. Biochem.* **2014**, *25* (1), 1−18.
(87) Al-Mansoub, M. A.; Asmawi, M. Z.; Murugaiyah, V. Effect of extraction solvents and plant parts used on the antihyperlipidemic and antioxidant effects of *Garcinia atroviridis*: a comparative study. *J. Sci. Food Agric.* **2013**, DOI: 10.1002/jsfa.6456.

Table 1. Primers Used in This Work

name	sequence*
ureABC-F	GTTCGGACGCACTGCGATGG
ureABC-R	CGTAATGATTTCGACCTTCG
ureG-F	TGTGGTCGCCGCGATGCACG
ureG-R	CATGGACGTCGATCGCACGT
PS1	GTGTAGGCTGGAGCTGCTTC
PS2	CATATGAATATCCTCCTTAG
Delta ureABC-F	GCTGTGGTTGAATTGACGTGTTGAACGGAAGAGATTTCGCGTGTAGGCTGGAGCTGCTTC
Delta ureABC-R	AAACCGTCCCCGGACAGGCTCCGGGGACCGGGGCGCTATTCATATGAATATCCTCCTTAG
Delta ureG-F	GGGTCCTGGCTTTCGCCAGGACGACGATAGGAAAGAATCAGTGTAGGCTGGAGCTGCTTC
Delta ureG-R	GTTAACGGCGGAAAACCCCTGTGCCAAGTCGTCGCGTTCGCATATGAATATCCTCCTTAG

*Underlined sequences refer to PS1 and PS2.

defense was postulated.[15] Consistent with a role in defense, eSBU and jack bean seed urease display insecticidal effects, in part due to the action of a subpeptide released by cathepsin-type proteases in the gut of susceptible insects.[7,8]

Soybean expresses a second urease, the tissue-ubiquitous urease (uSBU), essential for assimilation of urea, either endogenously generated or environmentally available. uSBU is encoded by *Eu4* (Glyma11g37250), which is expressed in all tissues examined, including callus and the developing embryo.[11,16] Loss of uSBU activity leads to accumulation of urea in seeds and in leaves to the extent that leaf tips become necrotic,[14] a trait also observed in soybean plants deprived of nickel,[17] a component of the urease active site. Endogenous urea is produced by arginase action, for example, during mobilization of seed protein reserves.[18] Consistent with a general role of ureases in defense, uSBU-suppressed soybean plants showed increased susceptibility to fungal infection.[19]

Few, if any, studies have addressed the involvement of urease in the symbiosis of nitrogen-fixing bacteria and their host plants. In light of the now recognized multifunctionality of ureases,[7,20] the main objective of this study was to test the hypothesis that both plant and bacterial enzymes are involved in communication between the soybean plant and its symbiont *B. japonicum*.

MATERIALS AND METHODS

Plant Material. Seeds of *Glycine max* (L.) Merr cv. Williams 82 were commercially available (Missouri Seed Foundation). Soybean double mutant *eu1-a,eu4* (in the Williams 82 background) has a lesion in the *eu1* gene and is null for synthesis of eSBU protein[12,21] and transcript.[11] The *eu-1* allele was orignally termed *eu1-sun* (seed urease-null[11]) and is here termed *eu1-a*, consistent with designation of alleles of other soybean urease loci.[13] The second lesion is a missense alteration in the *eu4* gene, resulting in inactive ubiquitous urease.[16,22] Two homozygous double mutant strains were employed—both contained the same *eu1-a* null allele[11] but differed in the *eu4* allele (*aj3* vs *aj6*), each containing a unique single base missense mutation inactivating the ubiquitous urease.[16]

Bacterial Strains and Culture Conditions. *B. japonicum* strain USDA110 was routinely maintained on HM salts medium[23] supplemented with 0.5% yeast extract at 28 °C with shaking (200 rpm). When necessary, antibiotics were supplied at 150 $\mu g \cdot mL^{-1}$ (kanamycin) and 30 $\mu g \cdot mL^{-1}$ (chloramphenicol). *Escherichia coli* strains were cultured on Luria−Bertani medium at 37 °C.

Construction of B. japonicum Urease Mutants. Primers used in this work are described in Table 1. To generate mutants, the genes of interest were amplified with primers ureABC-F and ureABC-R or ureG-F and ureG-R. Polymerase chain reaction (PCR) products contained the full sequence of the genes of interest in addition to about 400 bp 5′ and 3′ flanking sequence. The PCR products were inserted into the suicide vector pKnockout,[24] generating PKO Ω−URE. A kanamycin cassette from pHP45 Ω−Km[25] was amplified with primers PS1 and PS2, and then, this product was used as the template for another PCR with primers Delta ureABC-F/R and Delta ureG-F/R, generating pKO Ω−URE−Km. These primers added to the kanamycin gene 40 base pairs identical to regions flanking the genes of interest. This construct was transferred from *E. coli* DH5α to *B. japonicum* USDA110 by triparental conjugation with the helper plasmid pRK2073.[26] Deletion mutant recombinants were selected by kanamycin resistance and confirmed as described in the Results section.

Canavalia ensiformis Urease (JBU). Urease type C-III from jack bean (Sigma−Aldrich) was used in all experiments. The protein (hexameric form, M_r = 540 kDa) was solubilized in 20 mM sodium phosphate buffer, pH 7.0.

Soybean Embryo-Specific Urease. eSBU was purified as described[27] from soybean flour (Sigma−Aldrich) and dialyzed against 20 mM phosphate buffer, pH 7.0 prior to use.

Soybean Ubiquitous Urease. Cells of *E. coli* BL21-RIL:pGEX-4T-2 containing the full length cDNA encoding the uSBU[28] were grown in 2xYT medium (16 $g \cdot L^{-1}$ tryptone, 10 $g \cdot L^{-1}$ yeast extract, 5 $g \cdot L^{-1}$ sodium chloride, pH 7.0) containing ampicillin (150 $\mu g \cdot mL^{-1}$) and chloramphenicol (40 $\mu g \cdot mL^{-1}$) and maintained at 37 °C with shaking (200 rpm). When the culture reached 0.7 OD_{600}, the expression of uSBU fused to glutathione S-transferase at its N terminus (GST-uSBU) was induced by adding 0.55 mM IPTG, keeping the culture at 24 °C with shaking (200 rpm) for 15 h. Bacteria were collected by centrifugation, suspended in phosphate-buffered saline (PBS, 140 mM NaCl, 2.7 mM KCl, 10 mM Na_2HPO_4, 1.8 mM KH_2PO_4, pH 7.3), and subjected to lysis by ultrasound. After centrifugation at 60 000*g* for 25 min, the supernatant was passed through a 0.45 μm membrane, and the filtrate was applied onto a Glutathione Sepharose 4B (GE Healthcare) column. Retained GST-uSBU was eluted with 10 mM reduced glutathione in 50 mM Tris−HCl, pH 8.0. The GST protein (not fused to uSBU) was used as a control and was obtained from *E. coli* BL21:pGEX-4T-2 grown in 2xYT medium supplemented with 150 $\mu g \cdot mL^{-1}$ ampicillin and maintained at 37 °C with shaking (200 rpm). When the culture reached 0.7 OD_{600}, expression of GST was induced by adding 1 mM IPTG, and the culture was maintained at 37 °C for 3 h with shaking (200 rpm). Purification of GST was performed by affinity chromatography as described above.

Urease Activity. The phenol-nitroprusside colorimetric determination of ammonia[29] was used to determine urease activity in soybean tissues and nodules. One unit of urease activity was defined as the amount of enzyme that produces 1 μmol of ammonia per minute at 37 °C. Alternatively, urease activity in whole cells or tissue samples was semiquantitatively evaluated in a weakly buffered urea solution containing a pH indicator. Samples were incubated in 1 mL of 100 mM urea, 1 mM EDTA, 10 mM KPO_4, pH 7.0, and 5 $mg \cdot L^{-1}$ cresol red and kept at room temperature. Urease-positive samples turned the solution sequentially from yellow to pink to vermillion[30] in a time frame dependent on urease level.

Urease Inactivation. JBU and eSBU were inactivated by treatment with *p*-hydroxy-mercurybenzoate (Sigma−Aldrich), as previously described.[27] Excess inhibitor was removed by extensive dialysis against

20 mM phosphate buffer, pH 7.0. In one set of experiments, urease-inhibited soybean plants were obtained by adding 100 μM phenylphosphorodiamidate (PPD) (Sigma–Aldrich) to the plant nutrient solution.[31] PPD is an analogue of urea that binds to the urease active site.[32]

Chemotaxis Assays. *B. japonicum* chemotaxis was assayed as described[33] with minor modifications, using a 48-well Boyden chamber (Neuroprobe Microchemotaxis System, Gaithersburg, MD) with 2 μm PVP-free polycarbonate filters. Chemotactic stimulation was tested in 50 μL containing 9 μM of one of the following: GST-uSBU, eSBU, JBU, soybean genistein (Sigma–Aldrich), lectins (Sigma–Aldrich) from *Phaseolus vulgaris*, *G. max*, and *C. ensiformis*, or bovine serum albumin (BSA). Individual putative attractants, diluted with 20 mM phosphate buffer, pH 7.0, were added to the top wells of the Boyden chamber. *B. japonicum* cells suspended in saline solution (10^6 cells·mL^{-1}) were added (28 μL) to the bottom chamber wells and incubated 60 min at room temperature, after which bacterial cells in the top wells were collected and plated counting of colony-forming units (CFUs).

Plant Growth and Inoculation. Soybean seeds were surface sterilized and germinated as described.[34] After 48 h, seedlings were inoculated with isogenic *B. japonicum* USDA110 urease-positive or urease-negative mutants for 30 min and then planted in autoclaved Leonard jars[35] containing a 1:1:1 mixture of vermiculite/perlite/sand supplied with a nitrogen-free plant nutrient solution.[36] During growth, sterile nutrient solution was added to the lower reservoir as needed. Plants were maintained in growth chambers at 28 °C and 16 h light. Nodules were harvested from the roots 16–42 d after planting and kept frozen at −80 °C until use.

Leghemoglobin Content. Nodules were transferred to 2 mL tubes containing a 5 mm steel ball. PBS was added, and nodules were macerated and homogenized in a TissueLyser system (Qiagen) with pulses of 3 min at a frequency of 30 Hz. Samples were subjected to two cycles of centrifugation, first at 3000*g* for 10 min and the second at 18 000*g* for 20 min. Leghemoglobin content (mg·mg^{-1} protein) in the second supernatant was estimated by absorbance at 410 nm and an extinction coefficient[37] of 33.9 × 10^3 L·mol^{-1}·cm^{-1}.

Protein Determination. The protein content of samples was determined by their absorbance at 280 nm or alternatively by the Coomassie dye method[38] using BSA as the standard.

Electron Microscopy. Nodule samples were fixed in 25% glutaraldehyde in 0.1 M phosphate buffer (pH 7.0) for 1 h at room temperature and then kept at 4 °C for 16 h. Samples were then washed with three changes of 0.1 M phosphate buffer and postfixed in 2.0% osmium tetroxide for 1 h. Samples were again washed with buffer as above before being dehydrated through 30%, 50%, 70%, 95%, and 100% acetone. The tissues were then embedded stepwise in Epon resin. For polymerization, the material was kept at 60 °C for 72 h. The resulting blocks of embedded biofilm were sectioned in an ultramicrotome (Leica Ultracut UCT) with a diamond knife at a thickness of 800 nm and stained with aqueous toluidine blue and 1% basic fuchsin. Ultrathin sections (100 nm thick) were prepared using the same ultramicrotome and post contrasted with uranyl acetate and lead citrate. Samples were visualized under a transmission electron microscope (Philips model EM208S, Center of Electron Microscopy and Microanalysis, Universidade Luterana do Brasil, Canoas, RS).

Statistical Analysis. Data were evaluated using "one-way" ANOVA followed by the *t* test of Bonferroni or Tukey. A *p* value less than 0.05 was considered statistically significant. All analyzes were performed using GraphPad Prism software (version 5.0 for Windows).

RESULTS

Construction of *B. japonicum* Mutants. To examine the role of ureases in the interaction between soybean and *B. japonicum*, two mutants of *B. japonicum* were constructed. The mutant strain Δ*ureABC* is deleted in the three urease structural genes thus lacking urease protein. The mutant strain Δ*ureG* has a deletion of the gene encoding the accessory protein UreG, which participates in the assembly of the protein metallocenter, thus producing an enzymatically inactive apoenzyme, with no Ni^{2+} in its active site.[39] The approach used for construction of the mutants consists of inserting the gene that confers resistance to kanamycin via homologous recombination in regions flanking the target genes into the genome of *B. japonicum*. Mutants were confirmed by PCR (Figure 1) employing genomic primers

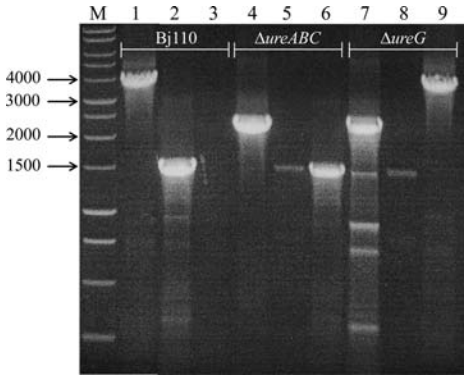

Figure 1. Validation of mutants by PCR. Genomic DNA from wild-type *B. japonicum* USDA110 (Bj110) and deletion mutants (Δ*ureABC* and Δ*ureG*) was subjected to PCR with specific primers. (1) Intact ureABC, (2) intact *ureG*, (3) Can^r, (4) interruption of *ureABC* by Can^r, (5) Can^r, (6) intact *ureG*, (7) interruption of *ureG* by Can^r, (8) Can^r, (9) intact *ureABC*.

flanking the putative insert and by the absence of ureolytic activity. In the PCR amplifications, the sizes of *ureABC* and *ureG* fragments in Bj110 are 3814 and 1491 bp, respectively. Homologous recombination in the regions flanking the genes of interest promotes the insertion of the kanamycin resistance gene (Can^r). Thus, in the genomic PCR amplifications, Δ*ureABC* generates a fragment of 2212 bp, while no change is seen in *ureG*. In turn, from the DNA of mutant Δ*ureG*, a fragment of 2287 bp is amplified without change in *ureABC*.

To verify the ureolytic activity, 1 mL of stationary-phase bacterial cells were collected by centrifugation and suspended in a solution containing weakly buffered 100 mM urea and pH indicator cresol red (Materials and Methods). Alkalinization of the medium by urea hydrolysis induced a color change of the pH indicator after 2 h at room temperature by wild-type bacterium Bj110. Mutants Δ*ureG* and Δ*ureABC* showed no ureolytic activity, since after incubation the medium kept the original yellow color for at least 16 h (Figure S1, Supporting Information). Lack of urease was further confirmed by the lack of growth of the mutant bacteria on minimal medium containing urea as the sole nitrogen source (data not shown).

Chemotaxis toward Plant Ureases. Plant ureases were found to be strongly chemotactic to *B. japonicum*. JBU, eSBU, and recombinant GST-uSBU induced chemotaxis of *B. japonicum* in the 0.1–9 μM concentration range. Figure 2 shows that increasing concentrations of JBU and GST-uSBU were accompanied by an increase in the CFUs of *B. japonicum* recovered in the upper compartment of the Boyden chamber. While recombinant GST-uSBU is fused to GST, recombinant GST alone induced a much weaker chemotaxis. The GST response peaked at 0.5 μM, whereas chemotaxis increased steadily up to 9 μM GST-uSBU.

It was shown previously that GST-uSBU is not active enzymatically,[28] most likely due to lack of incorporation of Ni into the urease active site by the *E. coli* host, lacking urease accessory proteins. The contribution of the ureolytic activity to chemotaxis was evaluated by testing enzymatically active plant

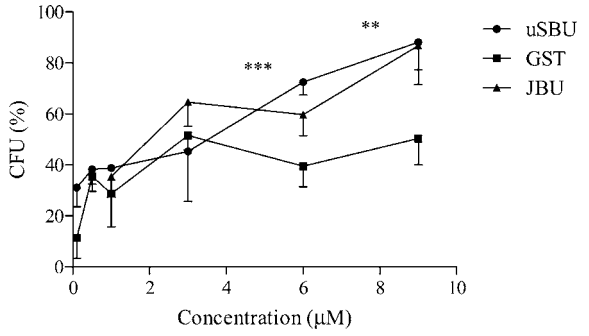

Figure 2. Response curve of *B. japonicum* to various concentrations of soybean ubiquitous urease (uSBU), jack bean urease (JBU), and glutathione-S-transferase (GST). The experiment was performed in a Boyden chamber containing 10^6 cells·mL^{-1} of Bj110 in the lower wells and different concentrations of uSBU or GST (control) in the upper wells. After 1 h at room temperature, the cells that migrated to the upper wells of the chamber were collected and plated for CFU counts. The points represent the mean ± SD of triplicates. Points marked with ** ($p < 0.01$) or *** ($p < 0.001$) were significantly different compared to control at the same dose by the Bonferroni test.

ureases eSBU and JBU before and after treatment with *p*-hydroxymercuribenzoate (*p*-HMB), an irreversible inhibitor of urease catalytic activity.[27] Ureases (3 μM) were added to the upper compartment of the Boyden chamber, and no significant differences were observed in their chemotactic effect, regardless of their ureolytic activities (Figure 3). Chemotaxis assays with

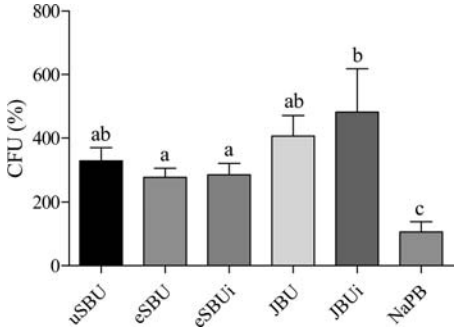

Figure 3. Effect of ureolytic activity in the chemotaxis of *B. japonicum* to plant ureases. Ureases were incubated at 4 °C for 16 h with 50 mM *p*-hydroxymercuribenzoate (*p*-HMB). Excess inhibitor was removed by dialysis prior to testing. All proteins were tested at a concentration of 3 μM. After 1 h at room temperature, the cells that migrated to the upper compartment of the chamber were collected and plated for CFU counts. (eSBU) soybean embryo-specific urease, (eSBUi) inactivated eSBU, (JBU) *C. ensiformis* urease, (JBUi) inactivated JBU, (uSBU) soybean recombinant ubiquitous urease. Bars represent the mean ± SD of triplicates.

mutants of *B. japonicum* indicated that the absence of the urease protein (Δ*ureABC*) or of its ureolytic activity (Δ*ureG*) in the bacteria did not alter their attraction to uSBU, as illustrated in Figure 4.

Finally, we compared the response of *B. japonicum* cells to the chemotactic effect of nonurease proteins (BSA, GST, and the lectins PHA-L from *P. vulgaris*, soybean agglutinin SBA, and jack bean concanavalin A) and the soybean flavonoid genistein. It can be observed in Figure 5 that soybean or jack bean ureases were the most potent chemotactic stimuli compared to the other tested compounds, followed by plant lectins. GST and BSA also

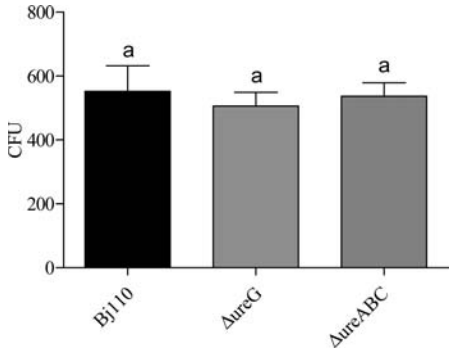

Figure 4. Chemotactic response of wild-type and urease deficient *B. japonicum* to uSBU. The experiment was performed in a Boyden chamber containing 10^6 cells·mL^{-1} of bacteria in the lower wells and 9 μM uSBU in the upper wells. After 1 h at room temperature, the cells that migrated to the upper wells of the Boyden chamber were recovered and plated for CFU counts. Bars represent the mean ± SD of six replicates.

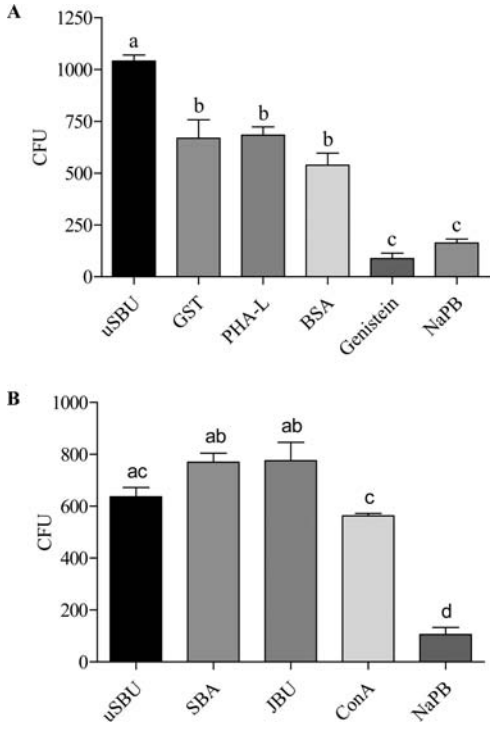

Figure 5. (A) Chemotactic response of *B. japonicum* USDA110 induced by 9 μM of the following: ubiquitous recombinant urease soybean (uSBU), the GST fusion protein, a lectin from *P. vulgaris* (PHA-L), bovine serum albumin (BSA), and genistein from soybean. (B) Chemotactic response of *B. japonicum* USDA110 induced by 9 μM ubiquitous recombinant urease soybean (uSBU), soybean lectin (SBA), *C. ensiformis* urease (JBU), and *C. ensiformis* lectin (ConA). Sodium phosphate buffer (NaPB, 20 mM) was used as a control. After 1 h at room temperature, the cells that migrated to the upper compartment of the Boyden chamber were recovered and plated for CFU counts. Columns with the same letter do not differ by the Tukey test ($p > 0.05$).

induced migration of *B. japonicum* but were significantly less chemotactic than ureases. Genistein was a very poor attractant.

Assays of Nodule Properties. To evaluate the role of plant and bacterial ureases in nodulation and nitrogen fixation, wild-type and urease-negative soybean were inoculated with wild-type and urease-negative *B. japonicum* mutants in all possible

dx.doi.org/10.1021/jf5000612 | J. Agric. Food Chem. 2014, 62, 3517−3524

combinations. The number and fresh weight of nodules were determined 21 d after inoculation.

Wild-type plants showed a higher number of nodules when compared to mutant plants, regardless of the inoculated bacterial strain (Figure 6A). However, there was a marked increase in the size of nodules in mutant plants *eu1-a,eu4*, again regardless of the inoculated strain. No differences were seen in the total fresh mass of nodules per plant (Figure 6B).

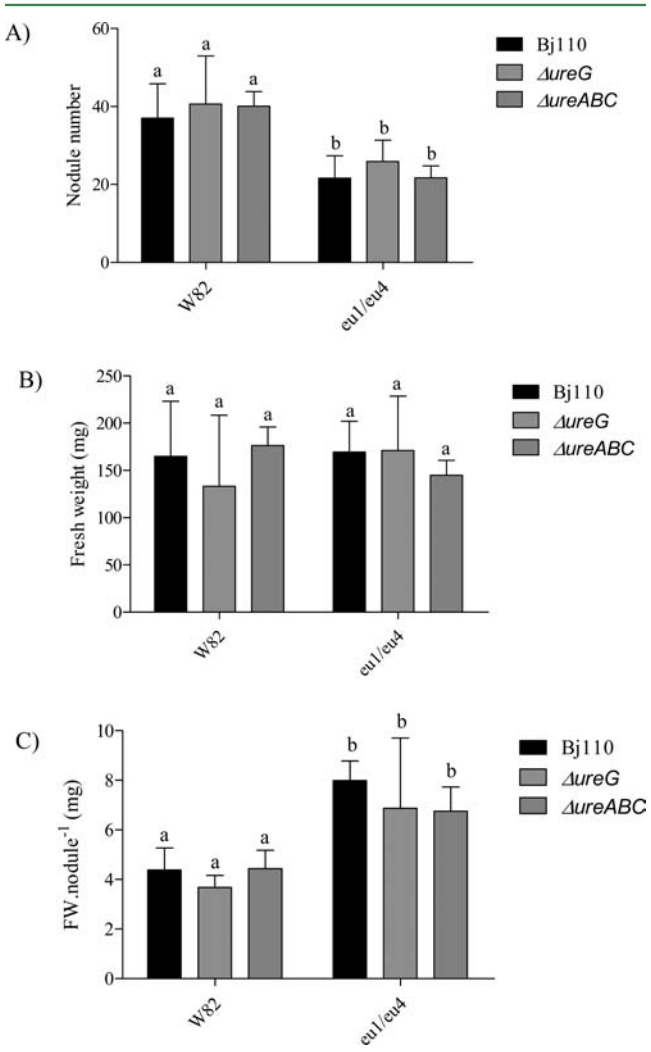

Figure 6. Wild-type soybean plants (W82) and a mutant deficient in embryo-specific and ubiquitous ureases (eu1/eu4) were inoculated with *B. japonicum* wild-type (Bj110), with a mutant strain that produces an apourease (Δ*ureG*), or a mutant strain that does not produce urease (Δ*ureABC*). Nodule number and weight were assessed 21 d after inoculation. (A) Number of nodules per plant. (B) Total fresh weight of nodules per plant. (C) Ratio between the total fresh weight of nodules and the number of nodules. Bars represent the mean of five Leonard pots, each containing 2−3 plants. Bars with the same letter do not differ by the Tukey test ($p > 0.05$).

To evaluate the importance of urease enzyme activity during soybean nodulation by *B. japonicum*, we used the urease inhibitor PPD, an analogue of urea that binds to the active site of the enzyme.[32] Wild-type soybean seedlings were inoculated with wild-type *B. japonicum* as described in Materials and Methods, and 100 μM PPD was added to the nutrient solution in the Leonard jars. Inhibition was maintained throughout the experimental period. Plants were analyzed 21 d after inoculation by counting and weighing the nodules formed. At the end of the experiment, urease activity was measured in extracts of leaves and nodules, confirming the inhibition of the enzyme by PPD (data not shown). Still, no differences were observed either in the number or fresh weight of nodules of PPD-treated urease-inhibited plants (data not shown).

Nodule Analysis by Optical and Transmission Electron Microscopies. Nodules of wild-type and *eu1-a,eu4* plants collected 35 d after inoculation with the *B. japonicum* wild-type strain were analyzed by optical and transmission electron microscopies. No alterations in architecture and histological organization of the nodules in the urease-deficient plants were observed (Figure S2, Supporting Information).

Leghemoglobin (LegHb) Content. The amount of LegHb in the supernatant of nodule macerates was estimated at times from 16 to 42 d after inoculation. As can be observed in Figure 7 (and Table S1, Supporting Information), the accumulation of LegHb from wild-type and mutant plants followed the same trend, regardless of the inoculant bacterial strain. Wild-type plants had lower nodule LegHb content at day 16, and it rose rapidly, peaking at 21 d after inoculation. On the other hand, nodules from mutant plants had a higher level of LegHb at 16 d after inoculation compared to wild-type but were slower to reach the maximal LegHb content, observed only at 35 d after inoculation (Figure 7). The altered pattern of accumulation of LegHb in *eu1-a,eu4* plants suggests that lesions in the structural genes of both soybean ureases, resulting in the absence of eSBU and in an inactivated uSBU, somehow compromised the symbiosis between the plant and the bacterium, delaying the LegHb peak from 21 d in the wild plant to about 35 d after inoculation.

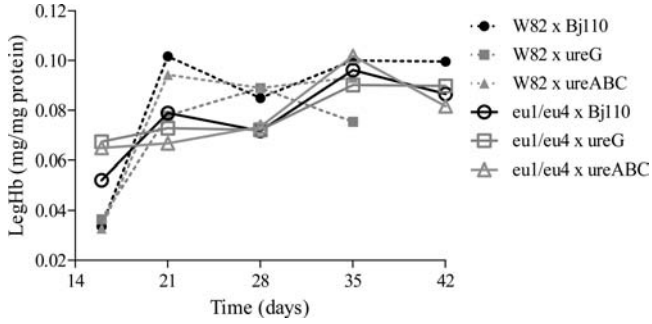

Figure 7. Leghemoglobin (LegHb) content of nodules versus time postinoculation. Wild-type (W82) and mutant (eu1/eu4) soybean plants were inoculated with wild-type *B. japonicum* (Bj110), with a mutant strain that produces an apourease (Δ*ureG*) or with a mutant strain that does not produce urease (Δ*ureABC*). LegHb content was measured by absorbance at 410 nm in extracts of nodules collected from 16 up to 42 d after inoculation. Each point is the average of three to six replicates.

DISCUSSION

Ureases have highly conserved structures and very similar catalytic mechanisms, reflective of their conservation throughout evolution.[40] In microorganisms, urease activity is involved in the assimilation of urea nitrogen, in pathogenicity in animals and humans, and in the metabolism of ruminants.[7] On the other hand, the physiological role(s) of this enzyme in plants is(are) still a matter of debate.[1,7] Addressing this question with in vivo studies using urease-deficient organisms may help to advance our understanding of the biological properties of this enzyme.

dx.doi.org/10.1021/jf5000612 | J. Agric. Food Chem. 2014, 62, 3517−3524

Here, we investigated the hypothesis that ureases from soybean and/or *B. japonicum* could be involved in the signaling between plant and bacterium—a concept originally suggested by the common platelet aggregation properties of plant ureases and the urease of the soil bacterium, *Bacillus pasteurii*.[41] Previous results from our group with canatoxin,[42] an isoform of jack bean urease, and *Helicobacter pylori* urease[33] have shown that these proteins are chemotactic to neutrophils and other proinflammatory cells. Considering these data, we evaluated a possible chemotactic activity of SBU toward *B. japonicum*. Our results showed that *B. japonicum* cells are attracted to SBU isoforms and to JBU and that this response is independent of urease enzymatic activity or the urease status of the bacteria. Thus, plant ureases exert chemotaxis in bacteria, as well as in eukaryotic cells such as neutrophils and monocytes.

High molecular-weight components in root exudates, which include lectins,[43] can affect symbiosis between plants and nodule bacteria. Plant lectins are known to act as chemoattractants and to promote adhesion of rhizobia to root hairs, enhancing the symbiotic properties of root nodule bacteria. Not all steps of lectin−rhizobia interaction are species-specific.[44] Accordingly, here, *B. japonicum* migrated toward different legume lectins. As reported previously,[45] genistein behaved as a weak attractant to *B. japonicum*.

Chemotaxis induced by ureases is also not species-specific, as jack bean urease also attracted *B. japonicum*, and in the same micromolar concentration range observed for lectins. It is not known if ureases are present in root exudates. However, it is plausible to think of a gradient of urease originating from death/shedding of root (or root cap) cells, with concentrations decreasing with distance from roots. Chemotaxis of *B. japonicum* toward soybean urease may be indirectly implicated in the nodulation process, directing the bacteria toward the roots. On the other hand, GST and BSA stimulated chemotaxis of *B. japonicum* similarly to soybean lectin. Previously, Sytnikov et al.[46] reported that incubating *B. japonicum* with the nonplant protein human serum albumin (at 0.4 μM), resulted in soybean plants with increased nodule nitrogen-fixing activity.

The Boyden chamber allowed easy assay of migration after 1 h of simultaneous exposure to multiple attractants, within the same time frame as the Pfeffer's capillary tube method.[47] Both methods are much faster than the swarm plate assay,[48] for which migration is measured after 48 h. Only the bacteria that crossed the 0.2 μm filter and were recovered in the liquid medium in the opposite chamber were plated for CFU analysis.

To the best of our knowledge, there are very few published studies that evaluated the role of ureases in the symbiosis between plants and microorganisms. Toffanin and co-workers[49] used a *Rhizobium leguminosarum* strain mutated in the *ureE* gene to show that urease activity is not important for biological nitrogen fixation in pea. This mutation prevents the proper formation of the urease active site, since in the absence of accessory protein UreE, there is no incorporation of Ni^{2+} into the apoenzyme.[39] However, this mutation does not affect the synthesis of apoenzyme(s), which could be contributing to the process of nodulation independently of ureolytic activity.

In our study, we used urease-deficient mutants of soybean as well as *B. japonicum*. In agreement with the study by Toffanin and co-workers,[49] who concluded that the urease of *R. leguminosarum* was not implicated in nodulation, our data showed that neither *B. japonicum* apo-urease (in Δ*ureG*) nor active *B. japonicum* urease affected nodulation in soybean.

In contrast, we showed that in *eu1-a,eu4* soybean plants, nodulation by *B. japonicum* is compromised, yielding higher mass nodules in a reduced number with no gross alteration in morphology. This double mutant does not synthetize eSBU (*eu1* null allele[11]) and produces an enzymatically inactive uSBU.[16] Two missense point mutations *eu4* alleles have been described (G468E in the *aj3*/*aj3* allele and R201C in the *aj6*/*aj6* allele, now termed *eu4-a* and *eu4-b*, respectively[16]). Both changes are radical as all bacterial, fungal, and plant urease sequences showing significant alignments with uSBU have the wild-type Arg201 and Gly468 residues at these positions. Modeling of either mutated uSBU showed that the affected amino acids occur at different points of the surface of the protein likely contributing contacts at the interfaces of the urease trimer. Thus, both amino acids are probably important for maintaining urease structure and/or function.[16] It has been shown that leaves of *eu4*(*aj3*) plants produce 40% the wild-type urease antigen,[22] consistent with instability of the mutant uSBU in *eu4*(*aj3*).

It can be argued that mutagenesis to derive the *eu4* mutation resulted in an altered genetic background, influencing nodule size and number. Arguing against a "background" effect on nodule size/number, we employed two different *eu1-a,eu4* double mutants, each with a different *eu4* mutant allele and hence each derived from a separate mutagenic event.

Torisky and Polacco reported that the eSBU is abundant in roots of 4 d old soybean plantlets, both in the wild-type Williams 82 or in the *eu4*(*aj3*) mutant plant, with specific activities at the root/shoot junction region of about 1500 and 3000 units per milligram of protein, respectively.[10] In roots of 4 d old *eu1-a*/*eu1-a* plants, which produce only uSBU, the specific urease activity reached 20 units per milligram of protein. The eSBU found in the young radicles is derived from the cotyledons, and its levels in the roots decline as the plant grows, but 5% of the 4 d value still remains after the third week of development.[10] In our work, *B. japonicum* was inoculated in soybean seedlings 48 h after germination. Thus, the deleterious effects we observed in the double mutant *eu1-a,eu4* plants could be due to the absence of the eSBU in the initial phase of root development, or reflect the presence of a mutated uSBU, or be a sum of both traits. We did not measure the content of urease protein in the roots of the double mutants *eu1-a,eu4* plants.

We assessed the ability of nodules to fix nitrogen by quantifying LegHb. The presence of this protein in the nodules is connected to nitrogenase activity, which is extremely sensitive to O_2; a function of LegHb is to maintain a low O_2 environment inside the nodules.[50] Hence, the LegHb content is an indirect measure of nitrogenase activity and hence total biological nitrogen fixation at a given developmental stage.

The time course of LegHb accumulation was altered in nodules of soybean *eu1-a,eu4* plants. Mutation in both plant urease genes delayed the LegHb peak from 21 d in the wild plant to 35 d in mutant plants, independent of the bacterial strain, implicating a role of the plant ureases in the soybean−*B. japonicum* symbiosis.

In previous studies[31], we observed no changes in total protein content or ureides in inoculated soybean plants, treated or not treated with PPD. Accordingly, we reported here that the nodulation process was also not affected in inoculated wild-type soybean plants grown in the presence of PPD. These results indicate that any possible role of urease on nodulation would be independent of ureolytic activity, either from the plant or from the bacterial enzymes.

Taken together, our results show that a deficiency (quantitative and/or qualitative) of soybean ureases alters the physiology of the nodules with consequent changes in nitrogen fixation. In addition, altered urease levels/structure may potentially interfere with chemotactic signals triggered by soybean plants in the rhizosphere. None of these processes apparently involves the bacterial urease.

The data shown here represent a new approach in studies of ureases. The multifunctionality of this protein and the lack of consensus about its physiological function(s) make it important to develop studies that go beyond considering urease as solely a ureolytic enzyme, expanding information to understand the conservation of this macromolecule during evolution and its presence in the most diverse organisms.

■ ASSOCIATED CONTENT

Supporting Information

Figures showing the ureolytic activity of wild-type and urease mutants of *B. japonicum* and transmission electron micrographs of nitrogen-fixating nodules from soybean plants; table showing LegHb content of soybean nodules. This material is available free of charge via the Internet at http://pubs.acs.org.

■ AUTHOR INFORMATION

Corresponding Authors

*(C.R.C.) Phone: +55 51 3308 7606; fax: +55 51 3308 7003; e-mail: celia.carlini@pq.cnpq.br or ccarlini@ufrgs.br.

*(J.C.P.) Phone: (573) 882-4846; fax: (573) 882-5635; e-mail: polaccoj@missouri.edu.

Present Address

[∇]C. R. Carlini: Instituto do Cérebro (InsCer, Pontifícia Universidade Católica do Rio Grande do Sul (PUCRS), Av. Ipiranga 6690, Porto Alegre, RS CEP 90610-000, Brazil.

Author Contributions

[○]These authors share senior authorship.

Author Contributions

M.M.-S., M.P.B., and S.B.P. produced soybean ureases and collected data on chemotaxis, nodulation, and leghemoglobin; W.F. constructed *B. japonicum* mutants; K.N.S., D.W.E., and G.S. helped to design nodulation and leghemoglobin experiments; J.P.C. developed the mutant soybean lines; J.C.P. and C.R.C. conceived and supervised all phases of the work.

Funding

This work was financed by the Brazilian agencies Coordenadoria de Aperfeiçoamento de Pessoal de Nível Superior (CAPES), Conselho Nacional de Desenvolvimento Científico e Tecnológico (CNPq), and Fundação de Apoio à Pesquisa do Estado do Rio Grande do Sul (FAPERGS).

Notes

The authors declare no competing financial interest.

■ ACKNOWLEDGMENTS

The authors acknowledge Rodrigo Ligabue-Braun for the drawing of the Table of Contents graphic.

■ ABBREVIATIONS USED

BNF, biological nitrogen fixation; eSBU, embryo-specific urease; uSBU, soybean ubiquitous urease; JBU, jack bean urease; PCR, polymerase chain reaction; GST, gluthatione-S-transferase; PBS, phosphate-buffered saline; PPD, phenylphosphoro-diamidate; CFUs, colony-forming units; *p*-HMB, *p*-hydroxymercuribenzoate; SBA, soybean agglutinin; BSA, bovine serum albumin; LegHb, leghemoglobin

■ REFERENCES

(1) Witte, C. P. Urea metabolism in plants. *Plant Sci.* **2011**, *180*, 431−438.

(2) Giovannini, C.; Garcia-Mina, J. M.; Ciavatta, C.; Marzadori, C. Ureic nitrogen transformation in multi-layer soil columns treated with urease and nitrification inhibitors. *J. Agric. Food Chem.* **2009**, *57*, 4883−4887.

(3) Hirel, B.; Le Gouis, J.; Ney, B.; Gallais, A. The challenge of improving nitrogen use efficiency in crop plants: Towards a more central role for genetic variability and quantitative genetics within integrated approaches. *J. Exp. Bot.* **2007**, *58*, 2369−2387.

(4) Bais, H. P.; Weir, T. L.; Perry, L. G.; Gilroy, S.; Vivanco, J. M. The role of root exudates in rhizosphere interations with plants and other organisms. *Annu. Rev. Plant Biol.* **2006**, *57*, 233−266.

(5) Loh, J.; Stacey, G. Nodulation gene regulation in *Bradyrhizobium japonicum*: A unique integration of global regulatory circuits. *Appl. Environ. Microbiol.* **2003**, *69*, 10−17.

(6) Oldroyd, G. E. D.; Downie, J. M. Coordinating nodule morphogenesis with rhizobial infection in legumes. *Annu. Rev. Plant Biol.* **2008**, *59*, 519−546.

(7) Carlini, C. R.; Polacco, J. C. Toxic properties of urease. *Crop Sci.* **2008**, *48*, 1665−1672.

(8) Staniscuaski, F.; Carlini, C. R. Plant ureases and related peptides: Understanding their entomotoxic properties. *Toxins* **2012**, *4*, 55−67.

(9) Menegassi, A.; Wassermann, G. E.; Olivera-Severo, D.; Becker-Ritt, A. B.; Martinelli, A. H.; Feder, V.; Carlini, C. R. Urease from cotton (*Gossypium hirsutum*) seeds: Isolation, physicochemical characterization, and antifungal properties of the protein. *J. Agric. Food Chem.* **2008**, *56*, 4399−4405.

(10) Torisky, R. S.; Polacco, J. C. Soybean roots retain the seed urease isozyme synthesized during embryo development. *Plant Physiol.* **1990**, *94*, 681−689.

(11) Torisky, R. S.; Griffin, J. D.; Yenofsky, R. L.; Polacco, J. C. A single gene (Eu4) encodes the tissue-ubiquitous urease of soybean. *Mol. Gen. Genet.* **1994**, *242*, 404−414.

(12) Meyer-Bothling, L. E.; Polacco, J. C. Mutational analysis of the embryo-specific urease locus of soybean. *Mol. Gen. Genet.* **1987**, *209*, 439−444.

(13) Polacco, J. C.; Hyten, D. L.; Medeiros-Silva, M.; Sleper, D. A.; Bilyeu, K. D. Mutational analysis of the major soybean UreF paralogue involved in urease activation. *J. Exp. Bot.* **2011**, *62*, 3599−3608.

(14) Stebbins, N.; Holland, M. A.; Cianzio, S. R.; Polacco, J. C. Genetic tests of the roles of the embryonic ureases of soybean. *Plant Physiol.* **1991**, *97*, 1004−1010.

(15) Polacco, J. C.; Holland, M. A. Roles of urease in plant cells. *Int. Rev. Cytol.* **1993**, *145*, 65−103.

(16) Goldraij, A.; Beamer, L. J.; Polacco, J. C. Interallelic complementation at the ubiquitous urease coding locus of soybean. *Plant Physiol.* **2003**, *132*, 1801−1810.

(17) Eskew, D. L.; Welch, R. M.; Cary, E. E. Nickel: An essential micronutrient for legumes and possibly all higher-plants. *Science* **1983**, *222*, 621−623.

(18) Goldraij, A.; Polacco, J. C. Arginase is inoperative in developing soybean embryos. *Plant Physiol.* **1999**, *119*, 297−303.

(19) Wiebke-Strohm, B.; Pasquali, G.; Margis-Pinheiro, M.; Bencke, M.; Bucker-Neto, L.; Becker-Ritt, A. B.; Martinelli, A. H. S.; Rechenmacher, C.; Polacco, J. C.; Stolf, R.; Marcelino, F. C.; Abdelnoor, R. V.; Homrich, M. S.; Del Ponte, E. M.; Carlini, C. R.; De Carvalho, M.; Bodanese-Zanettini, M. H. Ubiquitous urease affects soybean susceptibility to fungi. *Plant Mol. Biol.* **2012**, *79*, 75−87.

(20) Real-Guerra, R.; Staniscuaski, F.; Carlini, C. R. Soybean urease: Over a hundred years of knowledge. In *A Comprehensive Survey of International Soybean Research − Genetics, Physiology, Agronomy and Nitrogen Relationships*; Board, J. E., Ed.; InTech: Rijeka, Croatia, 2013; pp 317−340.

(21) Polacco, J. C.; Winkler, R. G. Soybean leaf urease: A seed enzyme? *Plant Physiol.* **1984**, *74*, 800−803.
(22) Polacco, J. C.; Judd, A. K.; Dybing, J. K.; Cianzio, S. R. A new mutant class of soybean lacks urease in leaves but not in leaf-derived callus or in roots. *Mol. Gen. Genet.* **1989**, *217*, 257−262.
(23) Cole, M. A.; Elkan, G. H. Multiple antibiotic-resistance in *Rhizobium japonicum*. *Appl. Environ. Microbiol.* **1979**, *37*, 867−870.
(24) Windgassen, M.; Urban, A.; Jaeger, K. E. Rapid gene inactivation in *Pseudomonas aeruginosa*. *FEMS Microbiol. Lett.* **2000**, *193*, 201−205.
(25) Fellay, R.; Frey, J.; Krisch, H. Interposon mutagenesis of soil and water bacteria: A family of DNA fragments designed for invitro insertional mutagenesis of gram-negative bacteria. *Gene* **1987**, *52*, 147−154.
(26) Leong, S. A.; Ditta, G. S.; Helinski, D. R. Heme-biosynthesis in *Rhizobium*. Identification of a cloned gene coding for δ-aminolevulinic-acid synthetase from *Rhizobium meliloti*. *J. Biol. Chem.* **1982**, *257*, 8724−8730.
(27) Follmer, C.; Real-Guerra, R.; Wasserman, G. E.; Olivera-Severo, D.; Carlini, C. R. Jackbean, soybean and *Bacillus pasteurii* ureases: Biological effects unrelated to ureolytic activity. *Eur. J. Biochem.* **2004**, *271*, 1357−1363.
(28) Martinelli, A. H. S. Expressão da urease ubíqua de soja em *Escherichia coli*. Dissertation, Universidade Federal do Rio Grande do Sul, Porto Alegre, RS, Brazil, 2007.
(29) Weatherburn, M. W. Phenol-hypochlorite reaction for determination of ammonia. *Anal. Chem.* **1967**, *39*, 971−974.
(30) Meyer-Bothling, L. E.; Polacco, J. C.; Cianzio, S. R. Pleiotropic soybean mutants defective in both urease isozymes. *Mol. Gen. Genet.* **1987**, *209*, 432−438.
(31) Todd, C. D.; Polacco, J. C. Soybean cultivars 'Williams 82' and 'Maple Arrow' produce both urea and ammonia during ureide degradation. *J. Exp. Bot.* **2004**, *55*, 867−877.
(32) Benini, S.; Rypniewski, W. R.; Wilson, K. S.; Miletti, S.; Ciurli, S.; Mangani, S. A new proposal for urease mechanism based on the crystal structures of the native and inhibited enzyme from *Bacillus pasteurii*: Why urea hydrolysis costs two nickels. *Structure* **1999**, *7*, 205−216.
(33) Uberti, A. F.; Olivera-Severo, D.; Wassermann, G. E.; Scopel-Guerra, A.; Moraes, J. A.; Barcellos-de-Souza, P.; Barja-Fidalgo, C.; Carlini, C. R. Pro-inflammatory properties and neutrophil activation by *Helicobacter pylori* urease. *Toxicon* **2013**, *69*, 240−249.
(34) Shah, R.; Emerich, D. W. Isocitrate dehydrogenase of *Bradyrhizobium japonicum* is not required for symbiotic nitrogen fixation with soybean. *J. Bacteriol.* **2006**, *188*, 7600−7608.
(35) Leonard, L. T. A simple assembly for use in the testing of cultures of rhizobia. *J. Bacteriol.* **1943**, *45*, 523−525.
(36) Broughton, W. J.; Dilworth, M. J. Control of leghaemoglobin synthesis in snake beans. *Biochem. J.* **1971**, *125*, 1075−1080.
(37) Appleby, C. A.; Bergersen, F. J. Preparation and experimental use of leghemoglobin. In *Methods for Evaluating Biological Nitrogen Fixation*; Bergersen, F. J., Ed.; Wiley: New York, 1980; pp 315−335.
(38) Bradford, M. M. A rapid and sensitive method for the quantitation of microgram quantities of protein utilizing the principle of protein-dye binding. *Anal. Biochem.* **1976**, *72*, 248−254.
(39) Zambelli, B.; Musiani, F.; Benini, S.; Ciurli, S. Chemistry of Ni^{2+} in urease: Sensing, trafficking, and catalysis. *Acc. Chem. Res.* **2011**, *44*, 520−530.
(40) Ligabue-Braun, R.; Andreis, F. C.; Verli, H.; Carlini, C. R. 3-to-1: Unraveling structural transitions in ureases. *Naturwissenschaften* **2013**, *100*, 459−467.
(41) Olivera-Severo, D.; Wassermann, G. E.; Carlini, C. R. *Bacillus pasteurii* urease shares with plant ureases the ability to induce aggregation of blood platelets. *Arch. Biochem. Biophys.* **2006**, *452*, 149−155.
(42) Barja-Fidalgo, C.; Carlini, C. R.; Guimaraes, J. A.; Flores, C. A.; Cunha, F. Q.; Ferreira, S. H. Role of resident macrophages in canatoxin-induced in vivo neutrophil migration. *Inflammation* **1992**, *16*, 1−12.
(43) Halverson, L. J.; Stacey, G. Effect of lectin on nodulation by wild-type *Bradyrhizobium japonicum* and a nodulation-defective mutant. *Appl. Environ. Microbiol.* **1986**, *51*, 753−760.
(44) Baimiev, A. K.; Gubaidullin, I. I.; Baimiev, A. K.; Chemeris, A. V. The effects of natural and hybrid lectins on the legume-rhizobium interactions. *Appl. Biochem. Microbiol.* **2009**, *45*, 74−80.
(45) Barbour, W. M.; Hattermann, D. R.; Stacey, G. Chemotaxis of *Bradyrhizobium japonicum* to soybean exudates. *Appl. Environ. Microbiol.* **1991**, *57*, 2635−2639.
(46) Sytnikov, D. M.; Kirizii, D. A.; Malichenko, S. M.; Kots, S. Y. Productivity of soybean-rhizobium symbiosis after modification of root nodule bacteria activity with exogenous proteins. *Russ. J. Plant Physiol.* **2007**, *54*, 366−372.
(47) Adler, J. Method for measuring chemotaxis and use of method to determine optimum conditions for chemotaxis by *Escherichia coli*. *J. Gen. Microbiol.* **1973**, *74*, 77−91.
(48) Bergman, K.; Gulashhoffee, M.; Hovestadt, R. E.; Larosiliere, R. C.; Ronco, P. G.; Su, L. Physiology of behavioral mutants of *Rhizobium meliloti*: Evidence for a dual chemotaxis pathway. *J. Bacteriol.* **1988**, *170*, 3249−3254.
(49) Toffanin, A.; Cadahia, E.; Imperial, J.; Ruiz-Argueso, T.; Palacios, J. M. Characterization of the urease gene cluster from *Rhizobium leguminosarum* bv. viciae. *Arch. Microbiol.* **2002**, *177*, 290−298.
(50) Downie, J. A. Legume haemoglobins: Symbiotic nitrogen fixation needs bloody nodules. *Curr. Biol.* **2005**, *15*, R196−R198.

Table 1. Bioactivity of Crude Extracts of Fungal Strains HJS 1929−1942[a] against Selected Fungal and Bacterial Strains after 55 Days (Strain 1937) or 41 Days (All Others)[b]

	Colletotrichum fioriniae	*Pichia anomala*	*Saccharomyces cerevisiae*	*Bacillus subtilis*	*Escherichia coli*
Microcyclospora					
M. malicola 1929	6.25	300	>300	>300	>300
M. malicola 1930	25	>300	>300	150	>300
M. malicola 1931	25	>300	>300	>300	>300
M. malicola 1932	12.5	>300	>300	>300	>300
M. pomicola 1933	12.5	>300	>300	150	>300
M. pomicola 1934	6.25	300	>300	150	>300
M. tardicrescens 1935	12.5	>300	>300	300	>300
M. tardicrescens 1936	12.5	>300	>300	>300	>300
Microcyclosporella					
M. mali 1937	25	>300	>300	>300	>300
M. mali 1939	25	>300	>300	>300	>300
M. mali 1940	50	>300	>300	>300	>300
M. mali 1942	6.25	>300	>300	>300	>300

[a]Culture collection of H. J. Schroers, Agricultural Institute of Slovenia. [b]Values are given as minimal inhibitory concentration (MIC) of the crude extract.

Dickinson, Difco, USA), 5 g of yeast extract (Biolife, Italy), 15 g of technical agar (Biolife, Italy)]. Colony plugs of SBFS fungi were placed at a distance of 15 mm from the edge of a 90 mm diameter plastic Petri dish. Following incubation for 4 days in darkness at 23 °C, aqueous conidial suspensions of *C. fioriniae* were placed in the colony center by needle point inoculation. Negative control plates consisted of needle point inoculated *C. fioriniae* colonies. The dual culture plates were incubated at 23 °C in the dark. The inhibitory effect of *M. tardicrescens* was measured and described after 7, 8, 10, 12, and 14 days of incubation. The assay was replicated three times per SBFS strain. The percentage inhibition of mycelial growth (PIMG) was determined according to the method of Lahlali and Hijri:[11] PIMG = $100 \times (R_1 - R_2)/R_1$, where R_1 was the radial colony growth of *C. fioriniae* in control plates and R_2 the inhibited radial colony growth of *C. fioriniae* in dual culture plates toward the colony of *M. tardicrescens* (mm). Mean values were then calculated from three replicates.

Bioactivity-Guided Fractionation. The effect of methanolic SBFS fungal extracts (prepared by extraction of the agar plates with 20 mL of methanol for 20 min and subsequent filtration of the methanol and its evaporation in vacuo) was tested on the growth of *C. fioriniae* and *Mucor hiemalis* in agar diffusion assays using 10 mL of MYC medium [10 g/L phytone peptone; 10 g of glucose; 11.9 g of Hepes (Carl Roth, Germany), 18 g/L agar (BD) (Bacto, USA)] poured into 90 mm Petri dishes as the base layer. After solidification, 5 mL of MYC medium prepared with 9 g/L agar (BD) (Bacto, USA) together with 5 mL of conidial suspension from *C. fioriniae* and *M. hiemalis* (1×10^6 conidia/mL) was poured onto the base layer. Test substances were applied as methanolic solutions (50 μL, 1 mg/mL) on sterile filter disks of 10 mm diameter (Schleicher & Schuell), allowed to dry, and placed onto the surface of the agar plates. After incubation (25 °C for 48 h), the zone diameter (mm) of the growth inhibition was determined.

Cultivation of *Microcyclospora tardicrescens* Strain 1936 and Preparation of Crude Extracts for Preparative HPLC. Six colony plugs of *M. tardicrescens* strain 1936 were excised from 10-day-old PDA incubated at 23 °C, transferred to 100 mL of YMG medium[7] in 250 mL Erlenmeyer flasks, and incubated at 23 °C on a rotary shaker with 140 rpm for 10 days. Fungal mycelium and culture fluid were then transferred to CYA plates (30 replicates, ca. 3 mL of fungal culture per plate) and incubated for 10 days at 23 °C in darkness. The fungal biomass was lyophilized with the entire agar plates and extracted two times with 1300 mL of methanol for 30 min in an ultrasonic bath at 40 °C. The liquid extracts were filtered through a paper, combined, and evaporated to dryness. The crude extract was then partitioned between 300 mL of water and 300 mL of ethyl acetate (J. T. Baker, Germany). Whereas the aqueous phase was discarded because of lack of bioactivity, the bioactive organic phase was analyzed by ESIMS before fractionation by preparative HPLC.

Isolation of 1 and 2. The crude extract was fractionated by preparative RP HPLC. A 250 × 21 mm i.d., 5 μm, VP Nucleodur C18 Gravity (Macherey-Nagel, Düren, Germany) column was utilized, and an acetonitrile−water gradient with 0.5% HCOOH, 20−100% MeCN in 30 min, and flow = 20 mL/min provided 4.2 mg of **1**, 1.1 mg of **2**, and 2.4 mg of a mixture of **1** and **2**, all with strong antifungal activity. **1** eluted at 16.8−17.8 min, and **2** eluted at 16.4−17.2 min. Silica gel HPLC with a 250 × 20 mm, 7 μm, Nucleosil 100 Å column (Knauer, Berlin, Germany) and isocratic conditions (97% dichloromethane, 3% methanol, flow = 20 mL/min) yielded 5.5 mg of **1** and 3.2 mg of **2**. **1** eluted at 3.8−5.8 min, and **2** eluted at 7.7−10.2 min.

Trichothecolone Acetate (1). ^{1}H (700 MHz, chloroform-*d*) and ^{13}C (175 MHz, chloroform-*d*) NMR spectroscopic data are shown in Table 3; ESI-MS, *m*/*z* 307.1 [M + H$^+$]; HRESIMS (*m*/*z*) found 307.1536 [M + H$^+$], calcd for $C_{17}H_{23}O_5$ 307.1540. Spectroscopic and spectrometric data are in good agreement with the literature.[12,13]

7-Hydroxytrichothecolone Acetate (2). **2** was obtained as a white amorphous powder; $[\alpha]^D_{25}$ = +34 (*c* 0.2, MeOH); UV (MeOH) λ_{max} (log ε) 226 (3.82); IR (KBr) ν_{max} 3450, 2963, 2926, 1737, 1685, 1261, 1243, 1081, 1034, 968, 802 cm^{-1}; ^{1}H (700 MHz, chloroform-*d*) and ^{13}C (175 MHz, chloroform-*d*) NMR spectroscopic data are shown in Table 3; ESIMS *m*/*z* 323.1 [M + H$^+$]; HRESIMS *m*/*z* 323.1481 [M + H$^+$] (calcd for $C_{17}H_{23}O_6$, 323.1489).

Biological Assays for Evaluation of Antimicrobial and Cytotoxic Activities. Biological assays were performed as previously described.[14] The compounds were tested against the bacteria *Bacillus subtilis* DSM 10, *Escherichia coli* DSM 1116, and *Staphylococcus aureus* DSM 346 and the fungi *Colletotrichum fioriniae* HJS 2018, *Pichia anomala* DSM 6766, *Candida albicans* DSM 1665, and *Saccharomyces cerevisiae* DSM 1333. The concentration of the purified compounds was tested at 100, 50, 25, 12.5, 6.25, 3.13, 1.56, and 0.78 μg/mL. The criterion of the minimal inhibitory concentration (MIC) was defined as the lowest concentration showing no visible bacterial or fungal growth after 24 h of incubation.

RESULTS AND DISCUSSION

Isolation of Strains and Co-Cultivation. Eleven strains (Table 1) were significantly antagonistic to fungal growth in dual culture and were chosen for further studies. Extracts of liquid cultures of all of these strains showed antifungal activity against *Colletotrichum fioriniae* with MIC values between 6.3 and 50 μg/mL (Table 1). Some of them were also active against *P. anomala* and *B. subtilis*. *Microcyclospora tardicrescens*

strain 1936 inhibited the colony growth of *C. fioriniae* by 46% after 7 days of incubation and by 55% after 14 days (Table 2; Figure 1) and was selected for scale-up and preparative chromatography. An extract from cultivation of strain 1936 on 30 agar plates was processed by a bioassay-guided fractionation strategy using *C. fioriniae* as indicator organism. Fractionation of the crude extract by reverse phase HPLC resulted in an active fraction that consisted of a mixture of two bioactive metabolites according to HPLC-MS analyses. Subsequent silica gel HPLC resulted in the isolation of both metabolites (**1** and **2**) as white powders.

Table 2. In Vitro Inhibition of Colony Growth of *Colletotrichum fioriniae* in Dual Culture with Antagonistic *Microcyclospora tardicrescens* Strain 1936 on Czapek Yeast Agar

incubation time (days)	inhibited radial colony growth[a] (mm)	radial colony growth in control plate[a] (mm)	growth inhibition percentage of *C. fioriniae*[a]
7	11.7	21.7	46.1
8	12.3	22.7	45.3
10	12.7	27.0	53.0
12	15.3	33.7	54.6
14	17.0	38.0	55.3

[a]Means of three replicates.

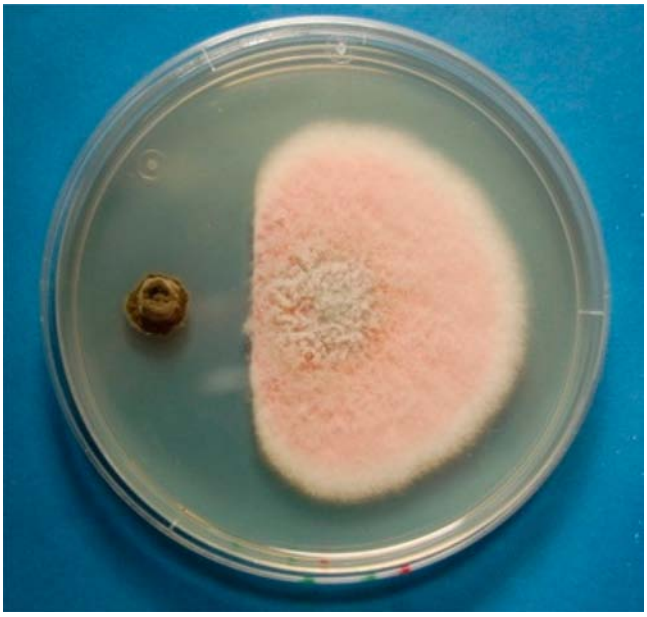

Figure 1. *Microcyclospora tardicrescens* strain 1936 (left) inhibiting the colony growth of *Colletotrichum fioriniae* (right) after 10 days of dual culture incubation on Czapek yeast agar at 23 °C.

HRESIMS revealed the molecular formula of $C_{17}H_{22}O_5$ for compound **1**. The ^{1}H and ^{13}C NMR spectra (Table 3) indicated the presence of four methyl groups, one sp^2 olefinic carbon, one quaternary sp^2 carbon, three sp^3 quaternary carbons, one of which connected to oxygen, three oxygen-bearing methines, three methylenes, and two carbonyls. COSY and HMBC NMR data provided the characteristic structure of 12,13-epoxytrichothec-9-en-8-ones and identified the metabolite as the known trichothecolone acetate (Figure 2).[12,13]

Table 3. ^{13}C NMR (175 MHz) and ^{1}H NMR (700 MHz) Data of Metabolites 1 and 2 in $CDCl_3$

	1		2	
position[a]	δ_C	δ_H (J_{HH} in Hz)	δ_C	δ_H (J_{HH} in Hz)
2	79.5	3.93 (m)	80.1	3.99 (d, 4.8)
3	36.8	2.61 (dd, 15.6, 1.4)	36.6	2.55 (dd, 15.4; 7.9)
		2.08 (m)		2.14 (m)
4	73.9	5.52 (dd, 7.9; 3.7)	73.9	5.48 (dd, 7.9; 4.1)
5	48.9		49.7	
6	43.7		48.2	
7	42.1	2.88 (dd, 15.3; 1.0)	74.4	4.81 (s)
		2.30 (dd, 15.3; 1.4)		
8	198.6		200.1	
9	138.2		135.5	
10	137.0	6.48 (dd, 5.9; 1.5)	137.7	6.51 (d, 5.8)
11	70.1	3.93 (m)	70.8	4.06 (d, 5.8)
12	65.4		65.0	
13	47.5	3,15 (d, 4.0)	46.6	3.17 (d, 4.0)
		2.86 (d, 4.0)		3.15 (d, 4.0)
14	5.6	0.72 (s)	6.9	1.00 (s)
15	18.4	1.06 (s)	11.9	0.95 (s)
16	15.4	1.83 (s)	14.7	1.89 (s)
17	170.9		170.6	
18	21.1	2.10 (s)	20.7	2.11 (s)
7-OH				3.72 (s)

[a]Assignments confirmed by 2D COSY, HSQC, and HMBC experiments.

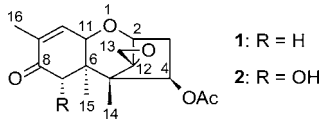

Figure 2. Chemical structures of **1** and **2** isolated from *M. tardicrescens* strain 1936.

For compound **2**, HRESIMS gave the molecular formula $C_{17}H_{22}O_6$. The molecular formula, together with an absorption at 3450 cm^{-1} in the IR spectrum, indicated that **2** is a hydroxylated derivative of **1**. Furthermore, the ^{1}H and ^{13}C NMR spectra of **2** (Table 3) resembled those of **1** with the exception of the absence of a methylene signal for 7-H_2 (δ_C 42.1; δ_H 2.88 and 2.30). Instead of the aforementioned methylene signal, an oxygenated methine (δ_C 74.4, δ_H 4.81) was observed together with a broad singlet at 3.72 ppm; the absence of an HSQC connection of this signal revealed it to be connected to an oxygen atom. The methine gave HMBC correlations (Figure 3) to C-5, C-6, C-8, C-9, C-11, and C-15 and the hydroxyl group to C-6, C-7 and C-8. Thus, the more polar metabolite **2** was identified as 7-hydroxytrichothecolone acetate. The stereochemistry (Figure 4) of the additional chiral center of **2** was assigned by interpretation of the ROESY spectrum in conjunction with the known stereochemistry of trichothecolone acetate (**1**).[15] In the ROESY spectrum 7-OH correlated with 13-H_2, whereas 7-H showed correlations to 14-H_3 and 15-H_3. These observations were confirmed by a 1D NOESY experiment irradiating at the shifts of 7-H and 7-OH. Thus, an *S*-configuration can be deduced for C-7.

Trichothecenes are a family of over 200 toxins with a common tricyclic 12,13-epoxytrichothec-9-ene core structure.[16,17] The trichothecenes are agriculturally important mycotoxins that present a potential threat to animal and

dx.doi.org/10.1021/jf500153d | J. Agric. Food Chem. 2014, 62, 3525−3530

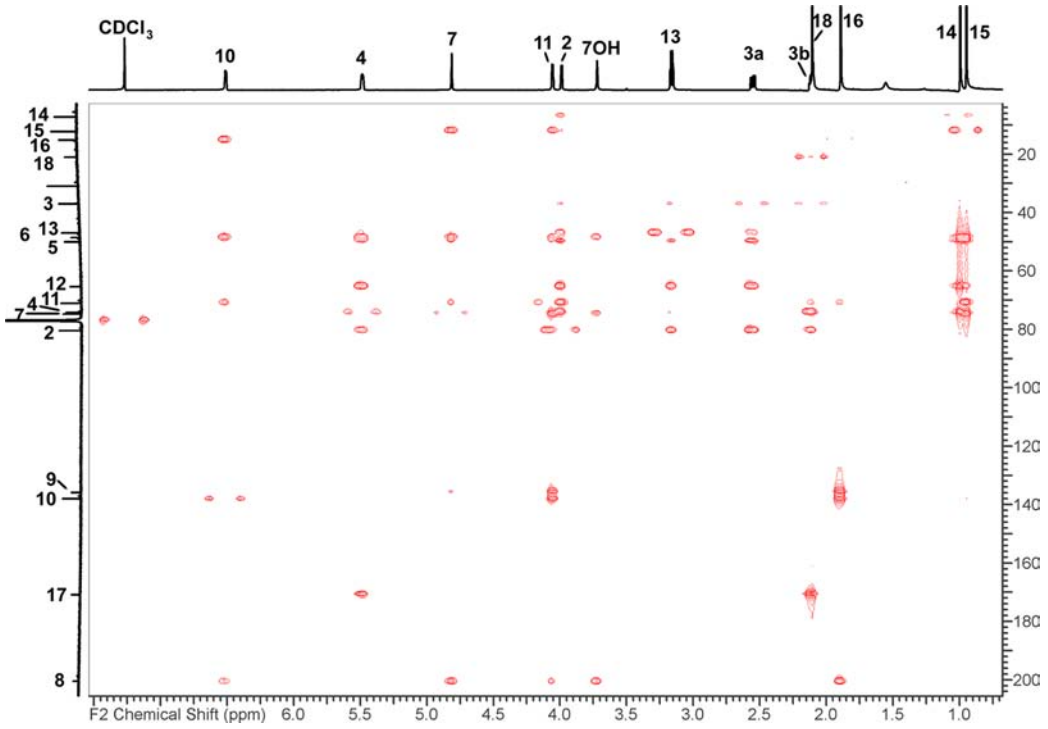

Figure 3. HMBC NMR (700 MHz, $CDCl_3$) spectrum of (*S*)-7-hydroxytrichothecolone acetate (**2**).

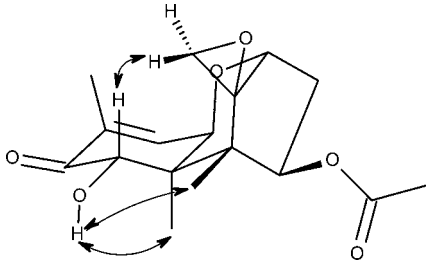

Figure 4. Selected NOE correlations indicating the configuration of **2**.

human health throughout the world.[17] This large family of toxins is produced by fungi in genera, such as *Fusarium*, *Myrothecium*, *Trichoderma*, *Trichothecium*, and *Stachybotrys* (and the compounds we have isolated are actually most similar to some metabolites from *Trichothecium*).[18] Those genera all belong to the order Hypocreales, whereas the SBFS fungi studied belong to the Capnodiales. It should be interesting to compare the biosynthesis gene clusters for trichothecenes in *M. tardicrescens* with those of the above-mentioned fungi. However, this was beyond the scope of the present study and would afford extensive work using methods of molecular biology. The only capnodialean fungus previously reported to produce trichothecenes is *Peltaster fructicola*. Among other compounds, this species produced trichothecolone acetate (**1**), which showed antifungal properties in vitro against *Botryosphaeria* causing bitter rot.[5] The here-reported rediscovery of **1** from *M. tardicrescens* strain 1936 indicates that trichothecenes might occur more widely in the Capnodiales or other related SBFS fungi. However, retrospective analysis of the extracts of strain 1935, another representative of *M. tardicrescens*, and of the other 70 isolated strains by HPLC-MS using pure compounds of **1** and **2** as internal standards did not yet result in the discovery of another trichothecene producer.

The bioactivity of **1** and **2** was evaluated by determining their MIC against a broad test panel of bacteria and fungi (Table 4).

Table 4. Antifungal Activity of Compounds 1 and 2 from *M. tardicrescens* Strain 1936 against Selected Fungal and Bacterial Strains (as Minimum Inhibitory Concentration, MIC, in μg/mL after 24 h)[a]

	strain			
compound	*Colletotrichum fioriniae*	*Pichia anomala*	*Candida albicans*	*Saccharomyces cerevisiae*
trichothecolone acetate (**1**)	6.25	50	50	6.25
7-hydroxy-trichothecolone acetate (**2**)	12.5	50	100	12.5

[a]The bacteria *Bacillus subtilis*, *Escherichia coli*, and *Staphylococcus aureus* were also tested but proved insensitive up to 100 μg/mL.

Compounds **1** and **2** showed no activity against the bacteria *Bacillus subtilis*, *Escherichia coli*, and *Staphylococcus aureus* but moderate activity against *Colletotrichum fioriniae* and *Saccharomyces cerevisiae* besides weak activity against *Pichia anomala* and *Candida albicans*. In a proliferation assay against the mouse fibroblast cell line L-929, strong cytotoxic effects were determined for both **1** (IC_{50} = 0.08 μg/mL) and **2** (IC_{50} = 0.17 μg/mL). All of these effects can be explained by the well-known inhibitory activity of eukaryotic protein synthesis.[16,17] However, the biological role of the observed trichothecenes for SBFS fungi in nature remains elusive. They could inhibit competitor SBFS fungi occupying the same ecological niche or plant pathogenic microorganisms that colonize the exocarps before fruit invasion. However, trichothecenes are known to act also as phytotoxins and may present plant pathogen virulence factors in the SBFS/fruit system.

To demonstrate a possible role of **1** and **2** in vivo, we cultivated *M. tardicrescens* 1936 on apple skin. Unfortunately, we could not detect either **1** or **2** due to strong contamination by wax in the extracts, which precluded their straightforward detection by analytical HPLC. A scale-up procedure and semipreparative HPLC separation prior to detection seems necessary to obtain more conclusive results. Therefore, we cannot assess the extension of a potential hazard resulting from trichothecene mycotoxins produced by SBFS fungi. However, the fact that juxtaposing colonies of different SBFS fungi are frequently separated from each other indicates that bioactive metabolites may be released on or into the fruit exocarp. SBFS are obviously well-adapted to epiphytically colonize fruit exocarps, whereas they are not known as fruit-destroying disease agents. Plants may profit mutualistically from the release of small amounts of toxic components, tolerated by the plant but inhibiting the development of other pathogenic agents.

Our results indicate that SBFS fungi are able to produce secondary metabolites with a wide spectrum of antibacterial and antifungal activities. The exploration of these substances might be suited as pharmaceuticals or in agriculture. Certainly, they will help us to understand the complex relationship between the different SBFS fungi and their plant hosts. Evaluation of the other strains listed in Table 1 is presently ongoing, and we expect to isolate further non-trichothecene bioactive compounds that may have some practical utility.

■ ASSOCIATED CONTENT

Ⓢ Supporting Information

HPLC-ESIMS and ^{1}H and ^{13}C NMR spectra of compounds **1** and **2**, and COSY, ROESY, HSQC, and HMBC spectra of **2**. This material is available free of charge via the Internet at http://pubs.acs.org.

■ AUTHOR INFORMATION

Corresponding Author

*(M.S.) Phone: +49 531 6181-4240. Fax: +49 531 6181 9499. E-mail: marc.stadler@helmholtz-hzi.de.

Author Contributions

Structure determination of chemical compounds and manuscript preparation was done by F.S. Underlying hypotheses of the study are those of A.M., who found the bioactivity in the first place and helped isolate the active principles as a guest Ph.D. student in the laboratories of M.S.

Funding

Financial support by COST Action FA1103 for a short time scientific mission (STSM) to A.M. for visiting the HZI in Braunschweig in 2012 and conducting the analytical experiments is gratefully acknowledged. The Slovenian Research Agency (ARRS) supported this work by a Young Researcher Grant, 1000-09-310214, to A.M.

Notes

The authors declare no competing financial interest.

■ ACKNOWLEDGMENTS

We thank our colleagues Wera Collisi and Bettina Hinkelmann for conducting the bioassays, Christel Kakoschke for recording NMR spectra, and Philine Wotsch for expert technical assistance in the mycological laboratory at HZI. For measurements of HPLC-MS data we are grateful to Aileen Teichmann and Heinrich Steinmetz.

■ ABBREVIATIONS USED

SBFS, sooty blotch flyspeck; PDA, potato dextrose agar; CYA, Czapek yeast agar; PIMG, percentage inhibition of mycelial growth; RP HPLC, reverse phase high-performance liquid chromatography; UPLC-DAD, ultraperformance liquid chromatography coupled with diode array detector; HR ESI-TOF-MS, high-resolution electrospray ionization coupled time-of-flight mass spectrometry; ITMS, ion trap mass spectrometry; MIC, minimum inhibitory concentration

■ REFERENCES

(1) Williamson, S. M.; Turner, S. B. Sooty blotch and flyspeck of apple: etiology, biology, and control. *Plant Dis.* **2000**, *84*, 714−724.

(2) Gleason, M. L.; Batzer, J. C.; Sun, G. Y.; Zhang, R.; Díaz Arias, M. M.; Sutton, T. B.; Crous, P. W.; Ivanović, M.; McManus, P. S.; Cooley, D. R.; Mayr, U.; Weber, R. W. S.; Yoder, K. S.; Del Ponte, E. M.; Biggs, A. R.; Oertel, B. A new view of sooty blotch and flyspeck. *Plant Dis.* **2011**, *95*, 368−383.

(3) Williamson, S. M.; Hodges, C. S.; Sutton, T. B. Re-examination of *Peltaster fructicola*, a member of the apple sooty blotch complex. *Mycologia* **2004**, *96*, 885−890.

(4) Johnson, E. M.; Sutton, T. B.; Hodges, C. S. Etiology of apple sooty blotch disease in North Carolina. *Phytopathology* **1997**, *87*, 88−95.

(5) Venkatasubbaiah, P.; Sutton, T. B.; Chilton, W. S. The structure and biological properties of secondary metabolites produced by *Peltaster fructicola*, a fungus associated with apple sooty blotch disease. *Plant Dis.* **1995**, *79*, 1157−1160.

(6) Chomnunti, P.; Hongsanan, S.; Aguirre-Hudson, B.; Qing, T.; Peršoh, D.; Dhami, M. K.; Alias, S. A.; Xu, J.; Liu, J.; Stadler, M.; Hyde, K. D. The sooty moulds. *Fungal Divers.* **2014**, DOI: 10.1007/s13225-014-0278-5.

(7) Thongbai, B.; Surup, F.; Mohr, K.; Kuhnert, E.; Hyde, K. D.; Stadler, M. Gymnopalynes A and B − chloropropynyl-isocoumarin antibiotics from cultures of the basidiomycete *Gymnopus* sp. *J. Nat. Prod.* **2013**, *76*, 2141−2144.

(8) Frank, J.; Crous, P. W.; Groenewald, J. Z.; Oertel, B.; Hyde, K. D.; Phengsintham, P.; Schroers, H.-J. *Microcyclospora* and *Microcyclosporella*: novel genera accommodating epiphytic fungi causing sooty blotch on apple. *Persoonia* **2010**, *24*, 93−105.

(9) Batzer, J. C.; Arias, M. M.; Harrington, T. C.; Gleason, M. L.; Groenewald, J. Z.; Crous, P. W. Four species of *Zygophiala* (Schizothyriaceae, Capnodiales) are associated with the sooty blotch and flyspeck complex on apple. *Mycologia* **2008**, *100*, 246−258.

(10) Hinton, M. J.; Parry, D. W. Screening selected fungi for antagonism towards *Pseudocercosporella herpotrichoides* (Fron) Deighton, the cause of eyespot disease of cereals. *Biocontrol Sci.Technol.* **1993**, *3*, 13−19.

(11) Lahlali, R.; Hijri, M. Screening, identifcation and evaluation of potential biocontrol fungal endophytes against *Rhizoctonia solani* AG3 on potato plants. *FEMS Microbiol. Lett.* **2010**, *311*, 152−159.

(12) Ghosal, S.; Chakrabarti, D. K.; Srivastava, A. K.; Srivastava, R. S. Toxic 12,13-epoxytrichothecenes from anise fruits infected with *Trichothecium roseum*. *J. Agric. Food Chem.* **1982**, *30*, 106−109.

(13) Schumacher, R.; Gutzwiller, J.; Tamm, C. 2*β*,13-Oxidoapotrichothecane: Synthese, chemische und physikalische Eigenschaften. *Helv. Chim. Acta* **1971**, *54*, 2080−2093.

(14) Surup, F.; Mohr, K. I.; Jansen, R.; Stadler, M. Cohaerins G.-K., azaphilone pigments from *Annulohypoxylon cohaerens* and absolute stereochemistry of cohaerins C-K. *Phytochemistry* **2013**, *95*, 252−258.

(15) Xu, X.-J.; Li, X.-L.; Cheng, J.-L.; Zhao, J.-H. 8-{[(*E*)-3-(2-Chloro-phenyl)acrylo-yloxy]imino}-12,13-epoxytrichethec-9-en-4-yl (*E*)-3-(2-chlorophenyl)acrylate. *Acta Crystallogr., Sect. E: Struct. Rep. Online* **2011**, *67*, o2834.

(16) McCormick, S. P.; Stanley, A. M.; Stover, N.; Alexander, N. J. Trichothecenes: from simple to complex mycotoxins. *Toxins* **2011**, *3*, 802−814.

(17) Li, Y.; Wang, Z.; Beier, R. C.; Shen, J.; De Smet, D.; De Saeger, S.; Zhang, S. T-2 Toxin, a trichothecene mycotoxin: review of toxicity, metabolism, and analytical methods. *J. Agric. Food Chem.* **2011**, *59*, 3441−3453.
(18) Laatsch, H., Ed. *AntiBase 2012 The Natural Compound Identifier*; Wiley-VCH Verlag: Weinheim, Germany, update 2012.

intervals, the samples were analyzed directly by liquid scintillation counting (LSC) to determine the total test substance related amounts in each sample to account for mass balance. Applied test substance recovery was quantitative in all reaction samples.

For high-temperature reactions, each test vessel was filled, leaving a small headspace to allow for expansion during heat treatment, with ca. 12 mL of sterile buffer containing the test substance. The test vessels were capped and heat-treated at either 90, 100, or 120 °C for short durations (<1 h) as is customary for such regulatory studies. Samples incubated at 90 °C were placed in a water bath. Samples incubated at 100 and 120 °C were placed in an oven maintained at constant temperature.

Sample Analysis. Test solutions were subjected to HPLC analysis to investigate the nature of the products formed, and identities of the products were established by a comparison of the HPLC retention times as well as by mass spectroscopy. The following equipment was used for these experiments: a Waters/Micromass Q-TOF micromass spectrometer operating MassLynx software (version 4.0, S.P. 2), an Agilent UV detector, and an Agilent 1100 liquid chromatograph. Radiodetection was performed by means of a Packard 505TR radioactivity flow detector and Flo-One software. The column employed was a Luna C_{18}, 150 mm × 4.6 mm, 5 μm (Phenomenex) with a guard column: Securiguard C_{18}, 3.0 × 4.0 mm (Phenomenex). HPLC analysis was conducted at ambient temperature. Mobile phases A (0.1% formic acid in Milli-Q water) and B (0.1% formic acid in acetonitrile) were used for a gradient, which started at 60% A and gradually decreased to 0% A, with balance as solvent B over 20 min. Solvent flow rate was 1 mL/min, and injection volumes for the analysis solutions were in the 10−200 μL range. The UV detector used in tandem was set for detection at 254 nm. Mass spectral analysis conducted for confirmation of various components was in positive ion mode with electrospray ionization. Various settings for the mass spectrometer were as follows: capillary voltage, 3500 V; sample cone, 25 V; extraction cone, 0.8 V; source temperature, 80 °C; and desolvation temperature, 150 °C.

Product Identification. The hydrolysis reaction components were easily identified initially on the basis of the HPLC retention times. A few chromatograms included in Figure 4 illustrate the main hydrolysis

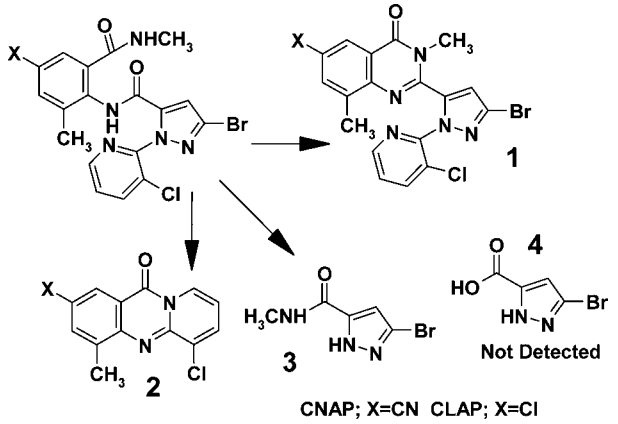

Figure 2. Degradation reactions of chlorantraniliprole and cyantraniliprole under hydrolysis conditions.

components. Analysis of typical CNAP hydrolysis samples showed two radiocarbon-containing peaks at 8.1 and 16.3 min. These peaks were coincident with peaks at 7.8 and 16 min in the UV chromatogram and at 8 and 16.1 min in the TIC from mass spectrometer detection. Unchanged CNAP in the hydrolysis samples was identified by comparing the retention time of the radioactive peak near 8 min with that of an authentic standard. LC-MS analysis was performed on selected samples to confirm the product identity as CNAP. The background-subtracted full-scan spectrum of the peak at 8 min in the TIC matched that of the CNAP reference standard with a major ion cluster at m/z 473, 475, and 477 and a small fragment at m/z 284, 286,

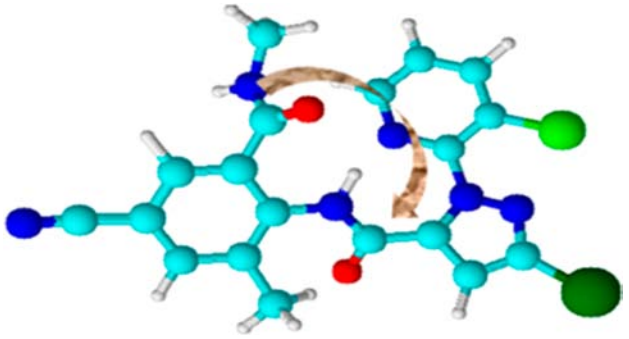

Figure 3. Intramolecular juxtaposition of amide functionality.

and 288. The three-ion clusters reflected the isotopes due to one Br and one Cl atom present in the molecule. HPLC cochromatography with authentic standards and mass spectral analysis confirmed this component as CNAP.

Degradate **1** from CNAP was identified using HPLC by comparing the retention time of the radioactive peak with that of an authentic standard. The background-subtracted full-scan spectrum of the peak at 16.1 min in the TIC was in good agreement with that of degradate **1** reference standard, and a molecular ion cluster at m/z 455, 457, and 459 further verified its identity.

High-temperature hydrolysis showed two additional components in small amounts. A component detected only in the PC-labeled samples accounted for 5−8% of the applied radioactivity (AR) in high-temperature hydrolysis samples. LC-MS analysis showed ions at m/z 204 and 206 in the background-subtracted full-scan spectrum of the TIC at 13.7 min. This spectrum was in good agreement with the reference standard of degradate **3**. Another component was a minor product in CN-labeled CNAP samples, which accounted for about 5% of product mixture. LC-MS confirmed that the molecular ion cluster present at m/z 270 and 272 was in good agreement with the reference standard of degradate **2**, as was the HPLC retention time.

Degradation products were identified for CLAP in a manner similar to those described above for CNAP. Identification of CLAP degradates **1**−**3** was also confirmed via HPLC and mass spectral methods. Chromatographic as well as mass spectrum information on CLAP has been reported previously[6] in connection with another study and does not need repetition here.

Determination of Rate Constants. Optimization of kinetics and rate constant calculations was conducted by setting up a first-order kinetics model in ModelMaker (software purchased from apbenson.com). The model, which is represented in the graphic below, illustrates CNAP degrading to degradate **1** and to all other products (denoted as sink). The rate constants for each transformation were iteratively optimized on the basis of the observed percent of each component at various sampling intervals. Because degradation to **1** was the main product in most of the experiments, the rate constant associated with process F2 was found to be a very small number or manually set to a very small value to mimic essentially no transformation. Whenever possible, it too was allowed to optimize in the cases when minor products accounted for a meaningful portion (approximately 5%) of degradation. Rate constants generated using this software program are summarized in Table 1, and the optimized decline/formation curves are illustrated in Figure 5. (Dots in Figure 5 represent the observed data; all observed amounts are expressed as percent of applied radioactivity, abbreviated %AR.)

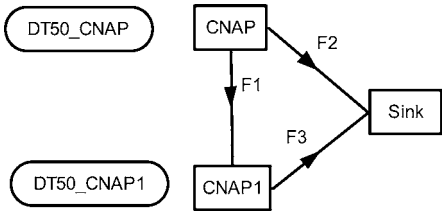

dx.doi.org/10.1021/jf500671w | J. Agric. Food Chem. 2014, 62, 3531−3536

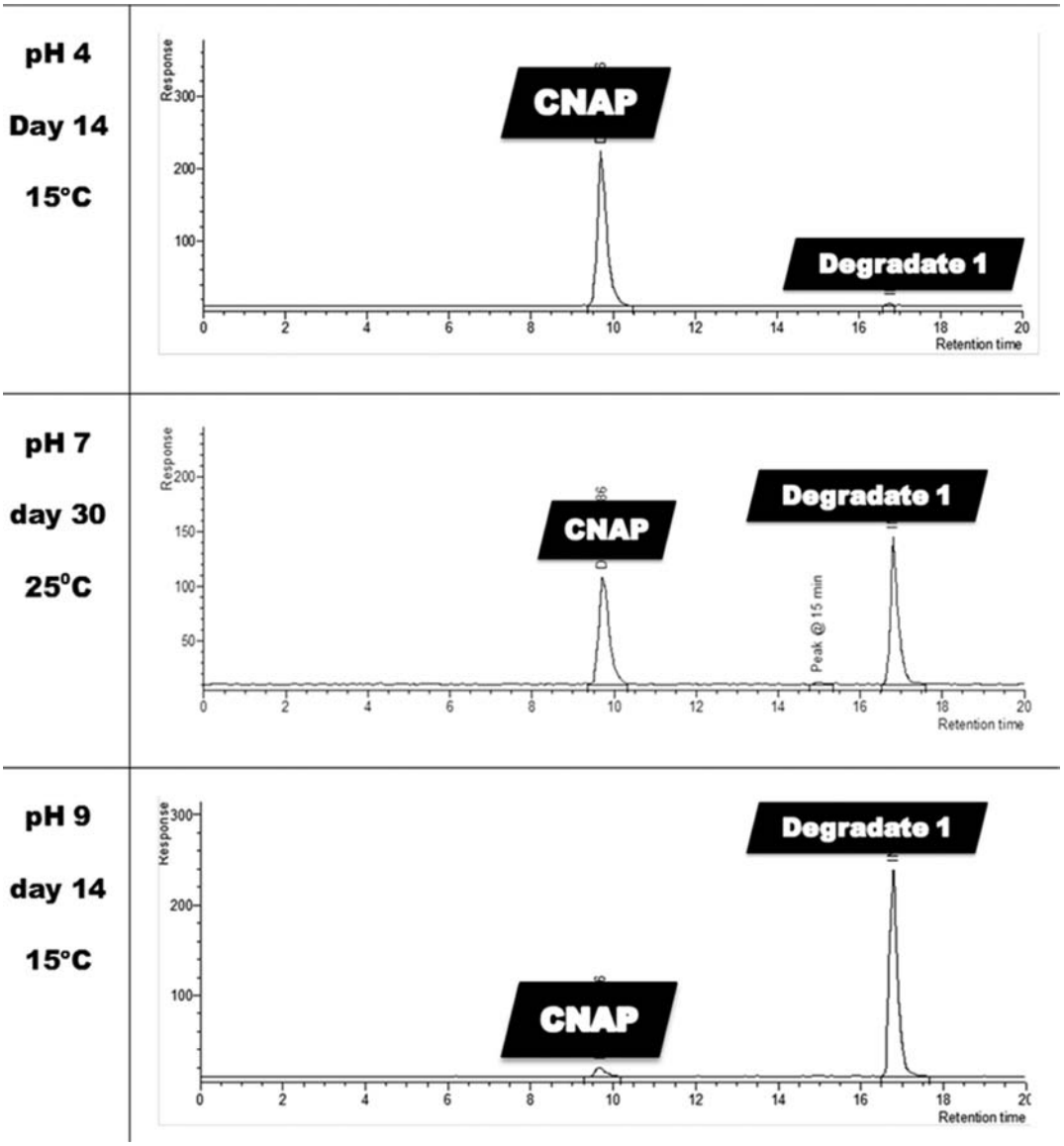

Figure 4. Sample chromatograms for cyantraniliprole hydrolysis.

Table 1. Rate Constants and DT_{50} Values for CNAP and CLAP

compd	pH	T (°C)	DT_{50} (days)	k (day^{-1})	T (°K)	E_{act} (kcal/mol)
CNAP	4	15	365	0.0019	288	
CNAP	4	25	210	0.0033	298	16.6
CNAP	4	35	55	0.0126	308	
CNAP	7	15	126	0.0055	288	
CNAP	7	25	30	0.0229	298	24.9
CNAP	7	35	8	0.0923	308	
CNAP	9	15	3.10	0.2234	288	
CNAP	9	25	0.85	0.8152	298	14.9
CNAP	9	35	0.58	1.203	308	
CLAP	9	15	50	0.0138	288	
CLAP	9	25	10	0.069	298	26.9
CLAP	9	50	0.3	2.264	323	

In some cases, particularly at pH 9, it was apparent that some hydrolytic conversion of the test compound had taken place at time 0 during the short interval between dosing and analysis. To more accurately treat these data for kinetics analysis, the amount of degradate **1** observed at time 0 was added back to the observed amount of parent compound, and the amount of this degradate was treated as 0%.

For calculation of thermodynamic parameters, the linear form of the Arrhenius equation (eq 1) was fitted to the data (plots of ln k vs $1/T$, shown in Figure 6), using the trend line feature in Microsoft Excel. The slope of the line was used to calculate the activation energy using (eq 2).

$$\ln k = [(-E_a/R) \times (1/T)] + \ln A \quad (1)$$

k = degradation rate constant (day^{-1}), E_a = activation energy (cal/mol), R = gas constant (1.987 cal/mol·K), T = temperature (K), and A = constant.

$$\text{slope} = -E_a/R \text{ or } E_a = \text{slope} \times R \quad (2)$$

RESULTS AND DISCUSSION

The material balance of radioactivity for all test samples was within the range of 96−103.5% of the total applied quantity, which demonstrated that the observed products accounted for

dx.doi.org/10.1021/jf500671w | J. Agric. Food Chem. 2014, 62, 3531−3536

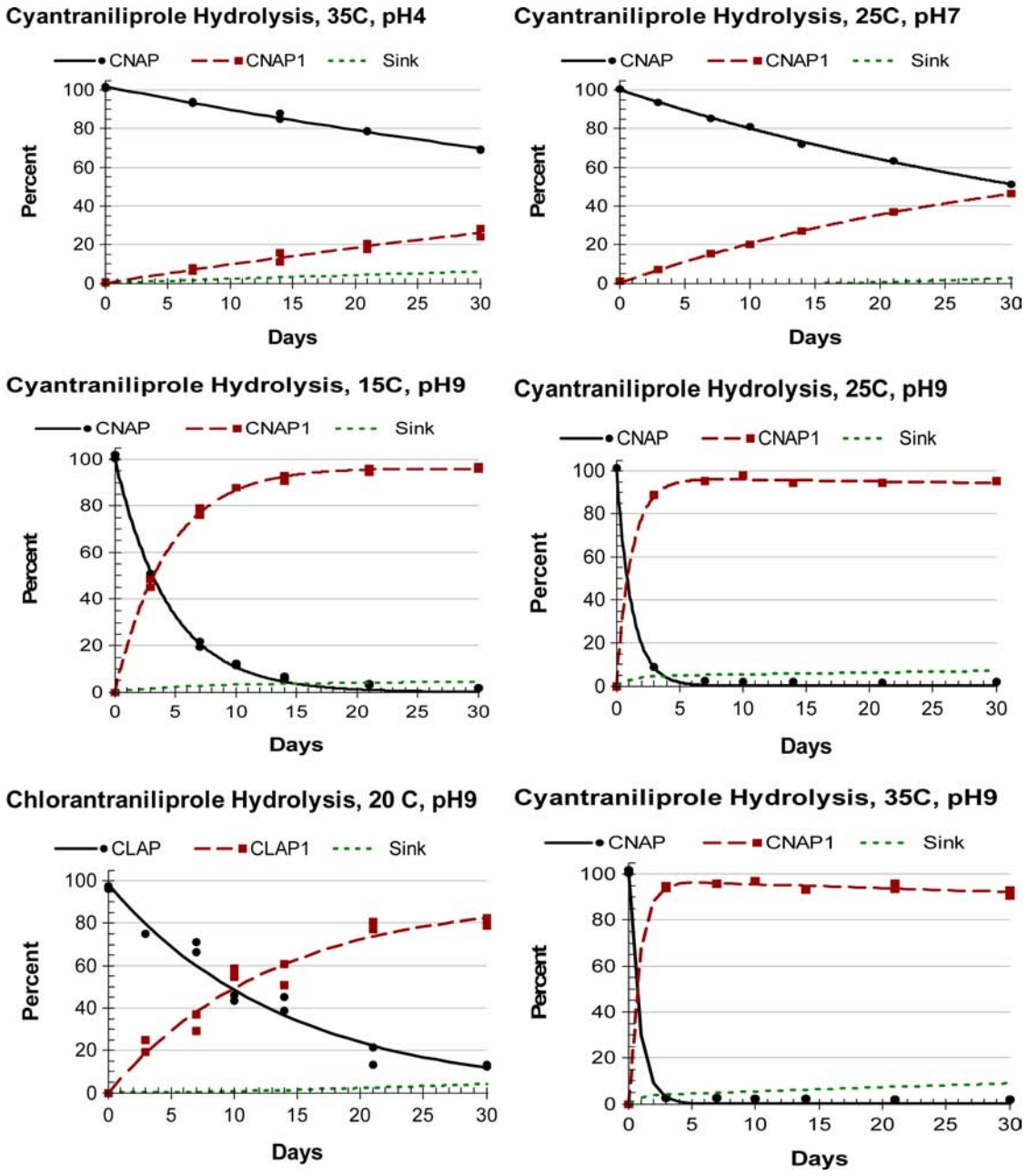

Figure 5. Cyantraniliprole and chlorantraniliprole hydrolysis in various pH buffers.

the entire applied material. The products observed were analogous for both compounds, as they are outlined in Figure 2, and were the only products observed in these experiments.

For both CLAP and CNAP hydrolysis experiments at all pH values, the main hydrolysis product, which accounted for the largest amount in the reaction mixtures, was a result of cyclodehydration, identified as degradate **1**. For CNAP, the hydrolysis was slow at pH 4 with minimal amounts of degradate **1**, especially at lower temperatures. Only 1.4−2.7% of degradate **1** was observed at 15 °C after 30 days, and its percentage increased to 8% at 25 °C and up to 28% at 35 °C. Transformation of CNAP at 35 °C and pH 4 is illustrated in Figure 5. Once the solution pH was increased to pH 7, the formation of degradate **1** from CNAP further increased at each temperature, as compared to pH 4 results, and the maximum amounts observed after 30 days were 16, 49, and 88% at 15, 25, and 35 °C, respectively. At pH 9, the reaction was quite rapid and transformation of CNAP to **1** was nearly quantitative, even at 15 °C. Degradate **1** accounted for 96−98% within the 30 day period at all three temperatures and pH 9. The transformation, as expected, proceeded at the fastest rate at the higher temperatures of 35 °C, and the parent compound disappeared entirely by day 5. Products **2** and **3** were not encountered in a meaningful proportion. Only at the higher temperature were ∼1−3% of additional products noted, and they were identified as degradates **2** and **3**, on the basis of the similarity of the HPLC retention times.

In short-exposure−high-temperature experiments for CNAP, conducted at 90−120 °C, the primary product observed was again identified as the cyclization product degradate **1** (maximum 14% AR); however, the additional pathway that leads to products **2** and **3** started to become competitive. Hydrolysis was most pronounced at pH 5 (100 °C), due to the

dx.doi.org/10.1021/jf500671w | J. Agric. Food Chem. 2014, 62, 3531−3536

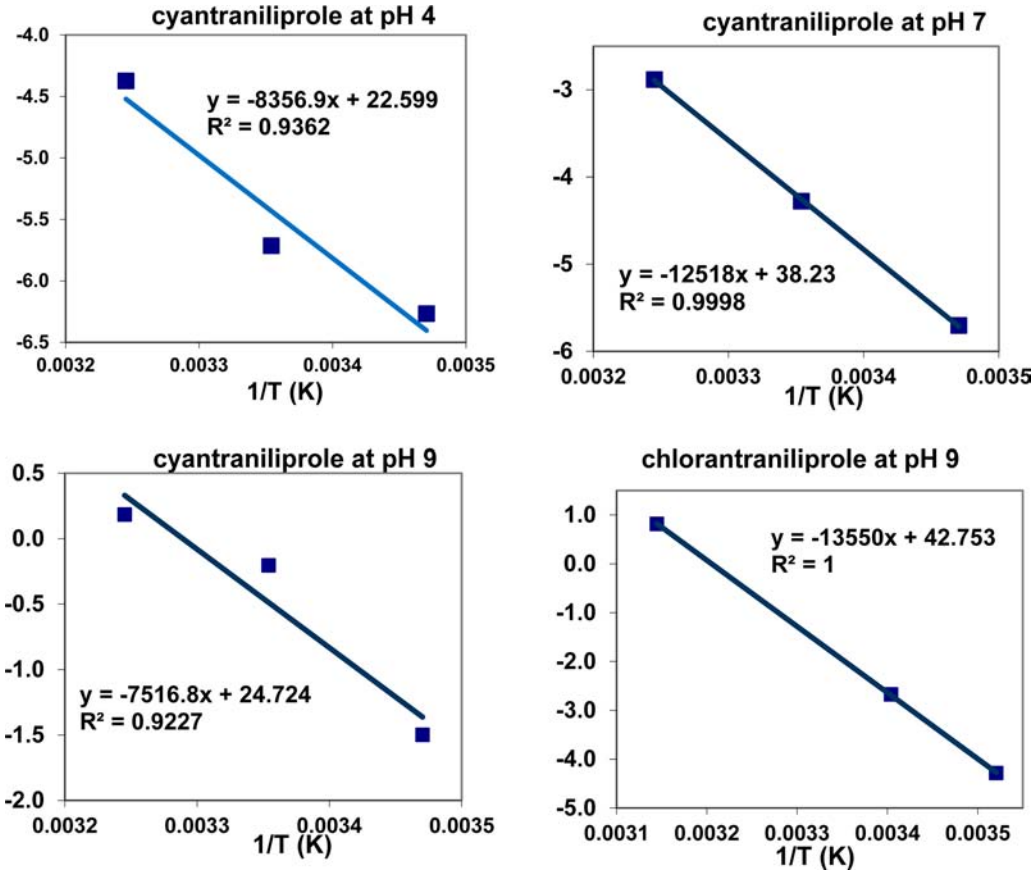

Figure 6. Arrhenius plots (ln k vs $1/T$).

longer incubation time (60 min), and in addition to degradate **1**, two additional components observed were identified as degradate **3** (maximum 5.8% AR) in PC-labeled samples and degradate **2** (maximum 9.7% AR) in CN-labeled samples.

In comparison with CNAP, CLAP was considerably slower in all hydrolytic transformations, including its conversion to degradate **1**. Virtually no degradation was noted at pH 4 and 7 for CLAP. Only at pH 9 did conversion to degradate **1** warrant further scrutiny, and increasing degradate amounts were found with rising reaction temperatures. Slower degradation of CLAP as compared with CNAP is obvious from the illustration in Figure 5. Similarly high temperature transformations, leading to additional degradates **2** and **3**, were also noted for CLAP at 90−120 °C, but with lower conversion into each of these degradates. Compounds **2** and **3** were observed only in the BC and PC-labeled experiments, respectively. In all of these experiments, any free carboxylic acids resulting from hydrolysis of any of the amides were notably absent.

Transformation data under various conditions of temperature and pH, for both CNAP and CLAP, to degradate **1** were used to model the kinetics of this transformation and to obtain the rate constants for this reaction. The rate data are summarized in Table 1 and also illustrated in the kinetics plots for selected experiments in Figure 5. Formation of degradates **2** and **3** was captured by the sink term used in kinetics modeling. A comparison of rate constants at pH 9 for CLAP and CNAP indicated that conversion to degradate **1** was nearly 15-fold faster for the latter compound. Arrhenius plots for both compounds and for each pH are illustrated in Figure 6. The activation energy, E_a, for CNAP was calculated as 16.6, 24.9, and 14.9 kcal/mol for pH 4, 7, and 9, respectively.

In all cases, the main product observed (degradate **1**) was clearly a result of cyclization with concomitant loss of water. A reaction carried out in water and leading to loss of water was somewhat counterintuitive, but not unprecedented. Weddige[8] had reported that attempted recrystallization of similar diamides in alkaline ethanol led to the isolation of the cyclized molecules instead of the diamides. Errede[9] postulated that hydrogen bonding with the solvents used in this reaction had a strong influence on the course of cyclization reaction. Errede further reported that the presence of water, and not anhydrous solvents, facilitated cyclodehydration. Therefore, observation of predominantly cyclodehydration in aqueous buffers was not a unique phenomenon in our experiments. An examination of the structure, as depicted in Figure 3, underscores that the benzamide nitrogen is well-positioned for initial cyclization via a nucleophilic attack onto the pyrazole carbonyl; this reversible reaction can easily happen in any media. In our view, it is the elimination of water, which leads to a stable quinazolinone ring, that has a strong pH dependence. This is also the reaction that is amenable to a significant substituent (X) effect. The initial cyclization leading to intermediate **1A** could, in principle, be catalyzed by an acid or base, which explains decreased E_{act} under both acidic and neutral conditions. Once this intermediate is generated, dehydration by protonating the "OH" reaction receives more pronounced acceleration via proton abstraction in intermediate **1A** (Figure 7), followed by expulsion of OH. This proton abstraction on "NH" located in the para position to substituent X explains the pH effect on the reaction rate. The proton abstraction from NH, which is strongly influenced by the nature of substituent X, explains a 15-fold faster reaction of CNAP versus CLAP. The

dx.doi.org/10.1021/jf500671w | J. Agric. Food Chem. 2014, 62, 3531−3536

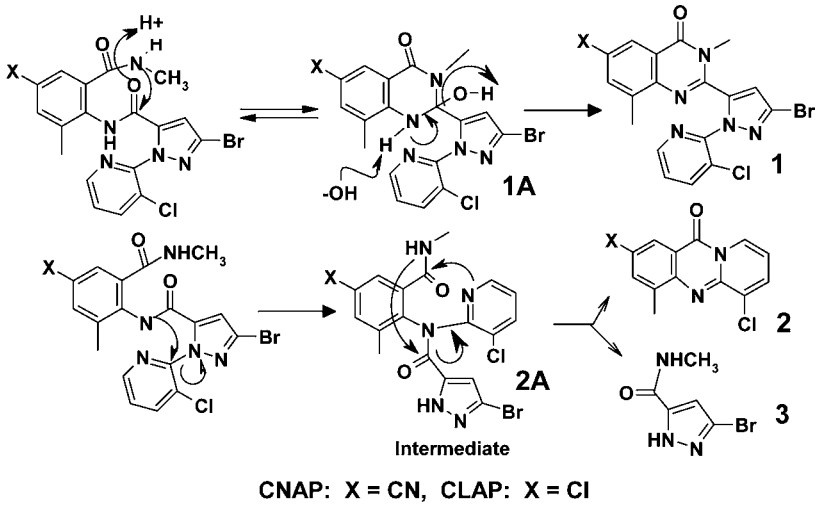

Figure 7. Mechanism of formation of degradates **1**, **2**, and **3**.

inductive effect of CN versus Cl (0.56 for CN vs 0.46 for Cl[11]) partly explains the ease of proton abstraction in CNAP. Resonance effect contribution from CN substituent undoubtedly assists this process further. The energy of activation (E_{act}) for this reaction is significantly lower (14.9 kcal/m) at pH 9 for CNAP and much lower than E_{act} for CLAP (26.9 kcal/m). The pK_a for CNAP, 8.8, versus 10.8 for CLAP, is also possibly due to the ease of amide deprotonation in CNAP.

Equally interesting was the formation of minor products (**2** and **3**) at high temperatures, which are formed via an entirely different intramolecular rearrangement. A pseudo Smiles rearrangement involving migration of nitrogen accounts for initial transformation into intermediate **2A**. E_{act} associated with such a reaction is considerably higher[10] than the values we calculated for transformation into degradate **1**, which is the reason this reaction makes a significant contribution only at high temperatures. Formation of the intermediate **2A** also requires ionization of the same amide N−H bond, which explains why even this reaction was more prominent for CNAP as compared to CLAP. Intermediate **2A** (Figure 7) has been not only observed but also isolated as a stable entity in some structurally related compounds. Subsequently, formation of degradates **2** and **3** occurs via intramolecular reorganization of the structure in which the transfer of CH_3NH occurs in concert with a nucleophilic attack by pyridine−nitrogen onto the amide−carbonyl, leading to molecular fission into the two degradates. A transition state associated with this reaction has been previously illustrated[6] in the papers from our laboratories. In conclusion, hydrolytic degradation of CLAP and CNAP led to some unusual products, all due to intramolecular reactions rather than typical hydrolytic degradation of the amides. The ease of conversion of these compounds to degradate **1** in aqueous media also makes it a prominent metabolite in environmental as well as plant and animal studies.

AUTHOR INFORMATION

Notes

The authors declare no competing financial interest.

ACKNOWLEDGMENTS

Contributions of Suzanne Singles, Ralph Warren, and Kalumbu Malikani are gratefully acknowledged.

REFERENCES

(1) Selby, T. P.; Lahm, G. P.; Stevenson, T. M.; Hughes, K. A.; Cordova, D.; Annan, B.; Barry, J. D.; Benner, E. A.; Curries, M. J.; Pahutski, T. F. *Bioorg. Med. Chem. Lett.* **2013**, *23*, 6341−6345.

(2) Lahm, G. P.; Stevenson, T. M.; Selby, T. P.; Freudenberger, J. H.; Cordova, D.; Flexner, L.; Bellin, C. A.; Dubas, C. M.; Smith, B. K.; Hughes, K. A.; Hollingshaus, J. G.; Clark, C. E.; Benner, E. A. *Bioorg. Med. Chem. Lett.* **2007**, *17*, 6274−6279.

(3) Cordova, D.; Benner, E. A.; Sacher, M. D.; Rauh, J. J.; Sopa, J. S.; Lahm, G. P.; Selby, T. P.; Stevenson, T. M.; Flexner, L.; Gutteridge, S.; Rhoades, D. F.; Wu, L.; Smith, R. M.; Tao, Y. *Pestic. Biochem. Physiol.* **2006**, *84*, 196−214.

(4) Lahm, G. P.; Cordova, D.; Barry, J. D. *Bioorg. Med. Chem.* **2009**, *17*, 4127−4133.

(5) Gaddamiddi, V.; Scott, M. T.; Swain, S. R.; Macpherson, D.; Lowrie, C. J. *Agric. Food Chem.* **2011**, *59*, 1316−1323.

(6) Gaddamiddi, V.; Zimmerman, W. T.; Ponte, M.; Ruzo, L. *J. Agric. Food Chem.* **2011**, *59*, 9424−9432.

(7) Lavtizar, V.; van Gestel, C. A. M.; Dolenc, D.; Trebse, P. *Chemosphere* **2013**.

(8) Weddige, A. *J. Prakt. Chem.* **1887**, *36*, 141.

(9) Errede, L. A.; Martinucci, P. D.; McBrady, J. J. *J. Org. Chem.* **1980**, *45*, 3009−3017.

(10) Dey, C.; Katayev, D.; Ylijoki, K. E. O.; Kundig, E. P. *Chem. Commun.* **2012**, *48*, 10957−10959.

(11) Hine, J. *Structural Effects on Equilibria in Organic Chemistry*; Wiley-Interscience: Hoboken, NJ, USA, 1975.

reliable differentiation of bitter and sweet fennel is beneficial for pharmaceutical quality control, because both fennel types are included in the European Pharmacopoeia and possess different applications in the food and pharmaceutical industries.[17−19] Therefore, the aim of this work was to develop new rapid and easy to perform analytical methods based on vibrational spectroscopy techniques (IR, NIR, and Raman) allowing a reliable discrimination of different wild fennel chemotypes occurring in nature. Furthermore, it was aimed to determine simultaneously the individual content of valuable substances in fennel fruits without the necessity of performing any sample preparation.

In this context a new chemotype of fennel, the essential oil of which is dominated by the phenylpropanoid γ-asarone, was discovered for the first time and characterized by GC-MS, nuclear magnetic resonance (NMR), and IR spectroscopy.

MATERIALS AND METHODS

Chemicals. Pure standard substances (*trans*-anethole, α-pinene, *p*-cymene, limonene, fenchone, estragole, anisaldehyde, α-asarone, and β-asarone, all >98%; myrcene, 95%; γ-terpinene, 97%) were purchased as analytical standards for terpene analysis or GC reference from Roth (Karlsruhe, Germany) and Sigma-Aldrich (Taufkirchen, Germany), respectively. All other reagents were of analytical grade and used without further purification.

Plant Material. Fruits of different fennel accessions were provided by the Institute of Plant Genetics and Crop Plant Research in Gatersleben (IPK) and of the Federal Plant Variety Office in Dachwig (Germany). For further botanical description (as far as obtainable) see Table 1.

Table 1. Notation and Botanical Description of the 10 Considered Fennel Accessions

	source		
notation	IPK	Federal Plant Variety Office	botanical description/origin
cv. Berfena		X	*Foeniculum vulgare* Mill. subsp. *vulgare* var. *vulgare* (Mill.)
cv. Chumen		X	*Foeniculum vulgare* Mill. subsp. *vulgare* var. *dulce* (Mill.), Germany
cv. Feniks		X	*Foeniculum vulgare* Mill. subsp. *vulgare* var. *dulce* (Mill.), Germany
FOE 16	X		*Foeniculum vulgare* Mill., Vacratot, Hungary
FOE 18	X		*Foeniculum vulgare* Mill. subsp. *vulgare* var. *azoricum* (Mill.) Thell., Spain
FOE 25	X		*Foeniculum vulgare* Mill., Gyancourt, France
FOE 43	X		*Foeniculum vulgare* Mill. subsp. *vulgare* var. *dulce* (Mill.) Batt., Georgian Republic
FOE 48	X		*Foeniculum* sp., Leicester, UK
FOE 86	X		*Foeniculum vulgare* Mill., Lisbon, Portugal
FOE 87	X		*Foeniculum vulgare* Mill., Lisbon, Portugal

Reference GC-FID and GC-MS Analyses. Approximately 200 mg of air-dried fennel fruits was homogenized in 10 mL of CCl_4 with an Ultra Turrax T25 blender for 1 min. Each accession was extracted twice, and the individual extracts were subsequently analyzed after centrifugation (4 min at 2415 *g*) by gas chromatography−flame ionization detection (GC-FID) using an Agilent gas chromatograph 6890N, fitted with an HP-5 column (50 m ×x 0.32 mm i.d., film thickness = 0.52 μm). This GC instrument is routinely used for essential oil analysis and continuously validated with external standards. Hence, no repeat determination was performed and each sample was investigated once. Detector and injector temperatures were set at 280 and 250 °C, respectively. The following oven temperature program was used: heating from 80 to 220 °C at a rate of 8 °C/min. This final temperature was held for 10 min. Carrier gas was hydrogen with a constant flow rate of 1 mL/min (split = 1:20). GC-MS analyses of the fennel extracts were performed using an Agilent MSD 5972/HP 5890 series II, equipped with a 30 m × 0.25 mm i.d., 0.5 μm, HP-5MS column. Column temperature was programmed from 60 to 120 °C at a rate of 3 °C/min, increased to 220 °C at 8 °C/min, and held for 10 min. Carrier gas was helium with a constant flow rate of 1.1 mL/min and a split of 1:10. Injector and detector temperatures were set at 250 and 280 °C, respectively. The ionization energy was set at 70 eV. Identification of the detected compounds was based on their relative retention times and their mass spectra in comparison with those observed for the above-mentioned pure standard substances. The other compounds were tentatively identified by using the NBS75K and Wiley 138 library databases of the GC-MS system. The percentage composition of the volatile fraction was computed from the GC peak areas according to the 100% method without using any correction factors. Identification and structural determination of γ-asarone were performed on the basis of the MS fragmentation patterns compared to authenticated standards (α- and β-asarone).

For further analysis, the essential oil of FOE 87 was obtained by hydrodistillation of approximately 2 g of fennel fruits.

Vibrational Spectroscopic Measurements. Besides the above-mentioned terpenoid standards and the intact fennel fruits, also solvent extracts of fennel fruits were investigated by Raman and ATR-FTIR spectroscopy. These extracts were produced following the protocol described under Reference GC-FID and GC-MS Analyses.

ATR-FTIR Spectroscopy. MIR spectra of intact fennel fruits, CCl_4 solvent extracts, and pure standards were recorded in the wavenumber range from 4000 to 375 cm^{-1} with a portable ATR diamond crystal infrared spectrometer (Alpha, Bruker Optics GmbH, Ettlingen, Germany). Approximately 5−10 mg of the standards was placed on the surface of the diamond crystal and directly measured. One hundred microliters of the solvent extracts was applied dropwise on the diamond crystal, and the spectra were recorded after evaporation of the solvent (observation of the disappearing CCl_4 absorption bands). Intact fennel fruits were measured under gently pressure with the interior side directed to the crystal, keeping the pressure constant for all measurements and avoiding damage to the fruits. All spectra were composed of 32 scans with a spectral resolution of 4 cm^{-1}. Each sample was measured triply, and the resulting triplicates were finally averaged and used for later chemometric calculations.

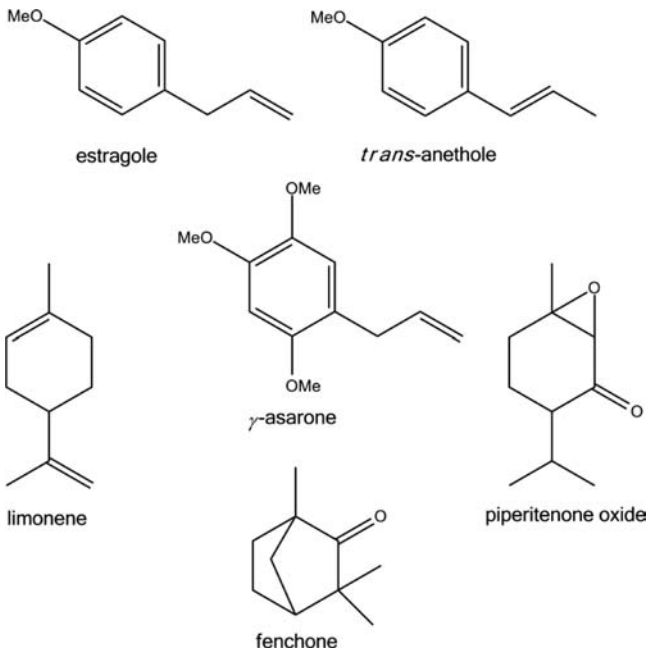

Figure 1. Molecular structures of most valuable volatiles detected in the analyzed fennel fruits.

Table 2. Gas Chromatographic Composition (Mean GC Peak Area Percentages for Each Component) of the Investigated Fennel Accessions and Their Classification into Chemotypes[a]

sample ID	fenchone	estragole	*trans*-anethole	piperitenone oxide	γ-asarone	anisaldehyde	limonene	α-pinene	myrcene	*p*-cymene	γ-terpinene	terpinolene	β-phellandrene	methyleugenol	not identified	chemotype
cv. Berfena	24.7	2.2	52.8	nd	nd	1.8	2.7	5.9	1.1	0.4	nd	nd	nd	nd	8.4	anethole[1]
FOE 16/03	25.3	2.3	54.9	nd	nd	1.3	3.1	4.3	1.0	0.9	nd	nd	nd	nd	6.9	anethole[1]
FOE 18/11	6.3	2.8	73.0	nd	nd	nd	11.2	1.7	nd	0.2	nd	nd	nd	nd	4.9	anethole[1]
FOE 25/10	0.3	nd	nd	28.7	nd	nd	47.2	0.6	0.9	1.5	10.6	5.6	nd	nd	4.7	piperitenone oxide[1,3,5]
FOE 43/02	33.2	53.8	0.2	nd	nd	nd	3.9	2.6	1.8	1.3	nd	nd	nd	nd	3.2	estragole[1]
FOE 48/03	35.1	44.7	nd	nd	nd	nd	3.8	7.5	2.2	0.7	nd	nd	nd	nd	6.1	estragole[1,5]
FOE 86/99	9.2	nd	nd	nd	66.0	nd	1.6	15.3	1.2	nd	nd	nd	2.3	nd	4.6	γ-asarone
FOE 87/99	8.9	nd	nd	nd	68.6	nd	1.8	11.4	1.2	nd	nd	nd	2.6	1.8	3.8	γ-asarone
cv. Chumen	7.8	2.9	76.4	nd	nd	nd	3.4	3.9	0.7	0.3	nd	nd	nd	nd	4.6	anethole[1,5]
cv. Feniks	10.0	3.1	75.5	nd	nd	nd	4.3	2.8	1.0	0.5	nd	nd	nd	nd	2.9	anethole[1,5]

[a]nd, not detectable.

Figure 2. Mass spectra of α-asarone (top) and β-asarone (middle) standards and of the main component in the volatile fraction of FOE 87 identified as γ-asarone (bottom).

Identification and structural determination of γ-asarone were performed by comparing the ATR-FTIR spectrum of purified γ-asarone with the α- and β-asarone standard. Pure γ-asarone was obtained by thin layer chromatography (TLC) of the extract of accession FOE 87 prepared for GC-MS. TLC was performed at TLC-aluminum sheets coated with silica gel 60 F254 (layer thickness of 0.2 mm) obtained from Merck KGaA, Darmstadt, Germany. As mobile phase a solvent mixture of chloroform and hexane at the volume ratio of 3:1 was used. The relatively low amount of purified γ-asarone was completely used for ATR-FTIR analyses.

dx.doi.org/10.1021/jf405752x | J. Agric. Food Chem. 2014, 62, 3537−3547

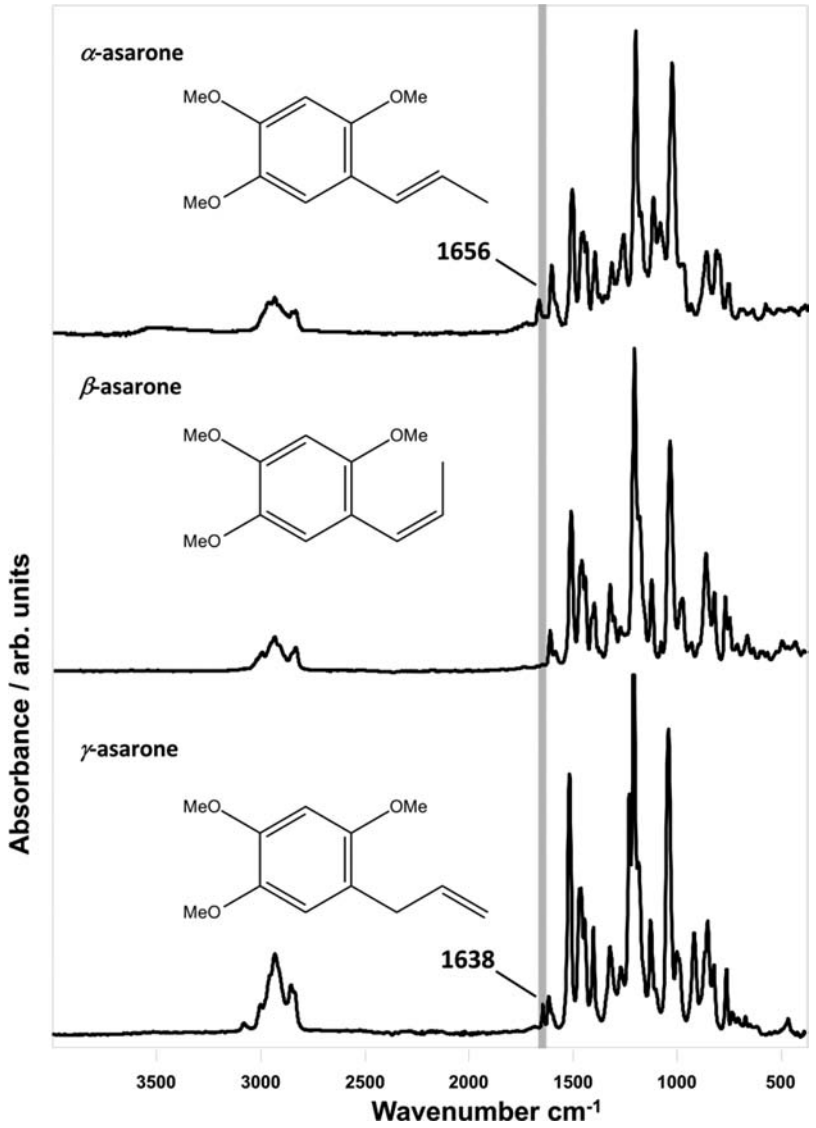

Figure 3. ATR-FTIR spectra of α-asarone (top) and β-asarone (middle) standards and of the main component in the volatile fraction of FOE 87 identified as γ-asarone (bottom).

NIR Spectroscopy. NIR analyses were performed in the range from 12500 to 3600 cm^{-1} with a spectral resolution of 8 cm^{-1} on an FT-NIR spectrometer (Multi Purpose Analyzer, Bruker Optics). Approximately 0.5 g of fennel fruits was loosely packed in glass cuvettes, and the resulting spectra were collected during 32 scans; the raw spectra were corrected for the effects resulting from scatter and baseline drift using the weighted multiplicative scatter correction algorithm (WMSC) of the OPUS 6.5 software (Bruker GmbH, Germany). Each sample was analyzed with three-fold repetition followed by averaging of the triplicates. Averaged spectra were exclusively used for the subsequent chemometric evaluation.

FT-Raman Spectroscopy. Raman spectra were recorded on a Bruker RFS 100S with a diode-pumped Nd:YAG laser, emitting at 1064 nm, and a germanium detector cooled with liquid nitrogen. All spectra were measured with a resolution of 4 cm^{-1} in the range from 4000 to 100 cm^{-1} with a laser power of 500 mW supplied by a focused laser spot size of 100 μm in diameter. The fennel extracts were directly measured in solution in glass vials and the spectra were accumulated from 64 scans. As far as the samples were measured in liquid solution, no measurement replications were performed, and each sample was analyzed only once.

Because of high fluorescence appearance at lower laser energy and burning of the sample by increasing energy, it was unfortunately not possible to obtain meaningful Raman spectra of the fennel fruits. Hence, only the extracts were analyzed by Raman spectroscopy.

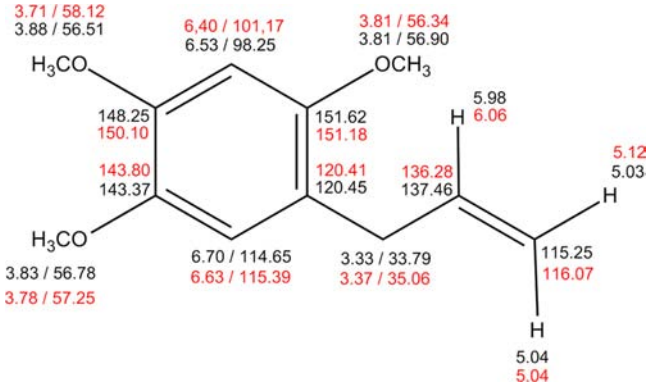

Figure 4. Chemical shifts of the ^{1}H and ^{13}C NMR spectra from the postulated γ-asarone structure and the calculated theoretical shifts (red) obtained from ACD software (Advanced Chemistry Development Inc., Toronto, Canada).

^{1}H and ^{13}C NMR Spectroscopy. Because of the relatively high concentration of the unknown phenylpropanoid structure in the essential oil of FOE 86 and FOE 87, the crude essential oil of FOE 87, obtained by hydrodistillation, was redissolved in deuterated chloroform

dx.doi.org/10.1021/jf405752x | J. Agric. Food Chem. 2014, 62, 3537−3547

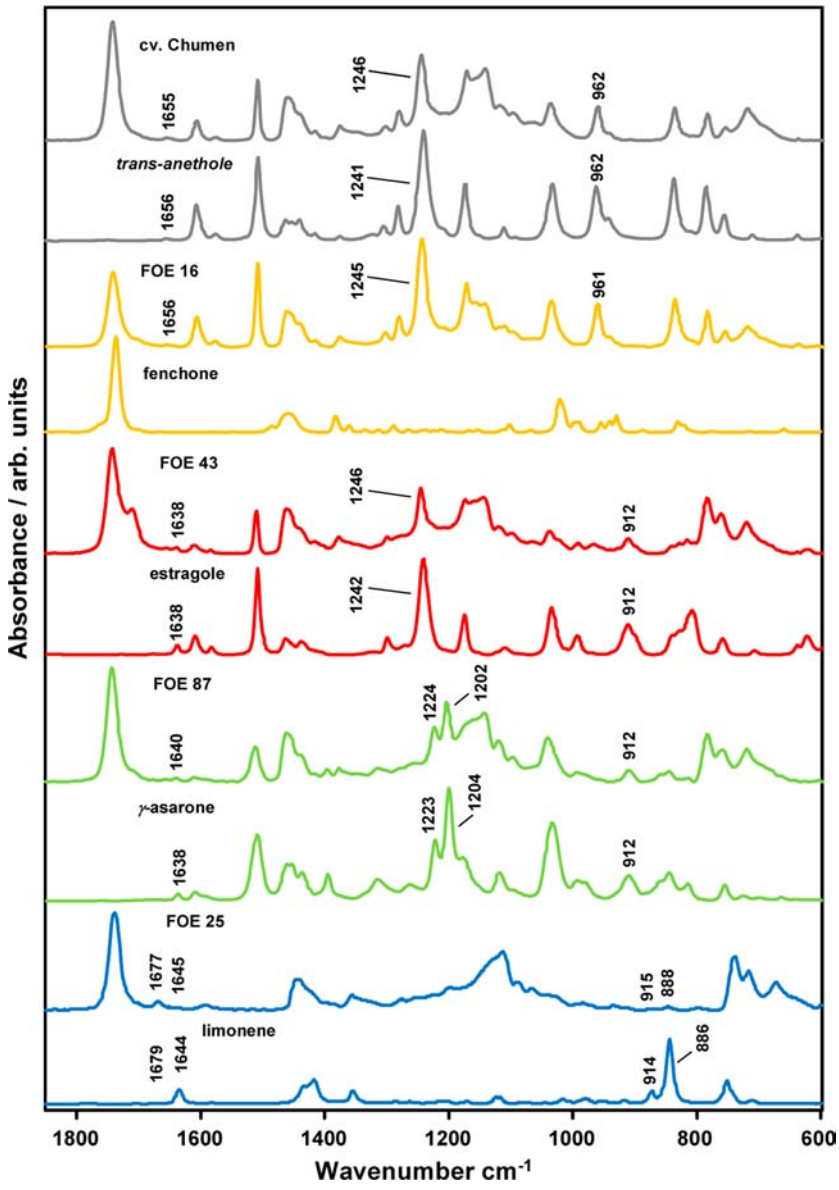

Figure 5. ATR-FTIR spectra obtained from CCl_4 extracts of different fennel genotypes and the corresponding standards for the most valuable components in the volatile fraction.

($CDCl_3$, Deutero GmbH, Germany) and investigated by ^1H and ^{13}C NMR without previous purification.

The ^1H NMR (200 MHz) and the ^{13}C spectrum (50 MHz) were recorded on a Varian Gemini 2000), both at 298 K. The chemical shifts, δ, are given in parts per million. The solvent signals of $CDCl_3$ were used for internal calibration and appeared at δ 7.26 (^1H) and δ 77.16 (^{13}C), respectively.

Additionally, the ^{13}C spectrum of γ-asarone was calculated using ADS software (Advanced Chemistry Development Inc., Toronto, ON, Canada), and the theoretical signals were compared to the experimentally determined results.

Chemometrics. For estimating the variability of the samples, hierarchical cluster analysis (Ward's algorithm) was applied under usage of the instrument software OPUS 6.5 (Bruker, Germany).

Relevant spectral ranges were determined by comparison of sample spectra with those of appropriate standards and by principal component analysis (PCA).

RESULTS AND DISCUSSION

The molecular structures of the most important volatile substances occurring in the analyzed fennel fruits are presented in Figure 1, whereas Table 2 shows the mean values for the most important volatile components as determined by GC-FID.

As can be seen in Table 2, each genotype shows an individual metabolic profile in the volatile fraction and can be classified into different groups according to its main component(s).

Except accession FOE 25, all considered fennel fruits contained fenchone in the concentration range between 6.29 and 35.08% in the solvent extracts and are dominated by at least one phenylpropanoid species as the main component, either *trans*-anethole or estragole.

In contrast, the CCl_4 extract of FOE 25 is dominated by nearly 47% of limonene and 29% of piperitenone oxide. The identification of piperitenone oxide has already been performed earlier by Badoc et al. on the basis of GC–high resolution MS data using the same fennel subspecies (*F. vulgare* sp. *piperitum*, Table 1).[3] Accordingly, this accession is assigned to the piperitenone/piperitenone oxide chemotype.[3,5]

Identification of a New Fennel Chemotype and Structural Evaluation of γ-Asarone. Two other accessions,

dx.doi.org/10.1021/jf405752x | J. Agric. Food Chem. 2014, 62, 3537−3547

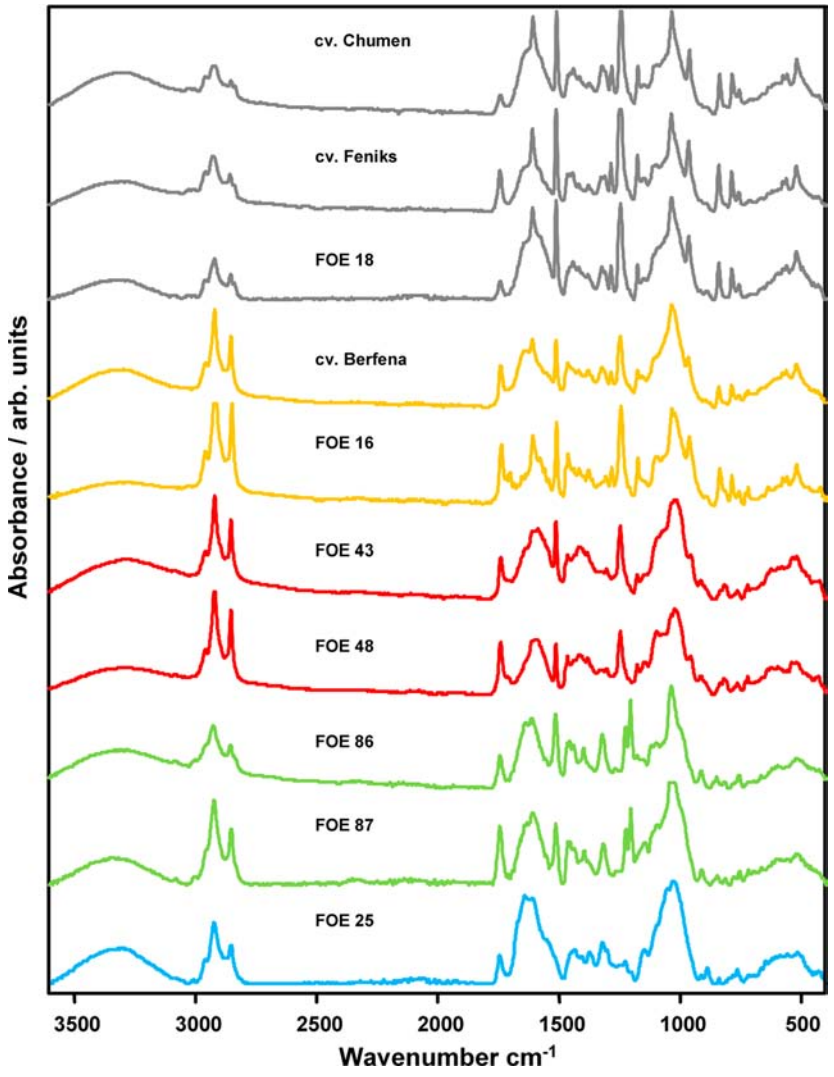

Figure 6. ATR-FTIR spectra obtained from the fruits of different fennel genotypes.

FOE 86 and FOE 87, also contain high amounts of a phenylpropanoid substance, but neither estragole nor *trans*-anethole could be detected in these samples by GC-MS or vibrational spectroscopy. Nevertheless, the MS data clearly showed a structural relationship to estragole and *trans*-anethole, but indicates a higher substitution of the aromatic ring system with three methoxy groups (Figure 2).

The molecular ion M^+ with m/z 208 indicates three methoxy groups as substituents at the aromatic ring. Comparison of the mass spectra of α- and β-asarone standards with those of the unknown component in FOE 86 and FOE 87 shows a higher fragment at m/z 177 $(M - 31)^+$ for the extract (Figure 2, bottom). This is caused by the higher fragmentation tendency of the ring system at the methoxy groups (-31 m/z) in the extract compared to α- and β-asarone. With the conjugated side chain in α- and β-asarone, fragmentation appears more at the C3 substituent as shown in the relatively low intensity of fragment m/z 177 (Figure 2, top and middle).

The corresponding ATR-FTIR spectrum additionally showed an allylic character of the aliphatic C═C double bond similar to that of estragole (Figure 3).

Hence, under usage of GC-MS and ATR-FTIR and in comparison to α- and β-asarone as commercially available standards, the structure of the unknown compound was proposed as γ-asarone (Figure 1), which is already known to be present in the essential oil of various plant species and for its fungitoxic and antibacterial activity.[20−22]

The *cis*−*trans* isomers α-asarone and β-asarone themselves could be excluded as the unknown phenylpropanoid, as the results from ATR-FTIR clearly manifest the allyl substituent at the aromatic ring.

To prove the suggestion of the γ-asarone structure, ^{1}H and ^{13}C NMR experiments of the pure essential oil of FOE 87 were performed. Because of the relatively high concentration of this compound of about 70% in the essential oil fraction, no prior purification step was performed.

Figure 4 presents the results from ^{1}H and ^{13}C NMR as well as from the theoretical calculation of the ^{13}C NMR spectrum. Besides the very good correlation of theoretical and experimental data, the signal assignment is in good accordance with NMR data for γ-asarone described in the literature.[23]

The occurrence of γ-asarone in *F. vulgare*, representing nearly 70% of the essential oil of accessions FOE 86 and FOE 87, is described here for the first time. This is why we introduce the name "γ-asarone type" for this new fennel chemotype.

Spectroscopic Analysis. Generally, all vibrational spectroscopy methods applied in this study are useful for rapid and reliable discrimination of the described fennel chemotypes.

dx.doi.org/10.1021/jf405752x | J. Agric. Food Chem. 2014, 62, 3537−3547

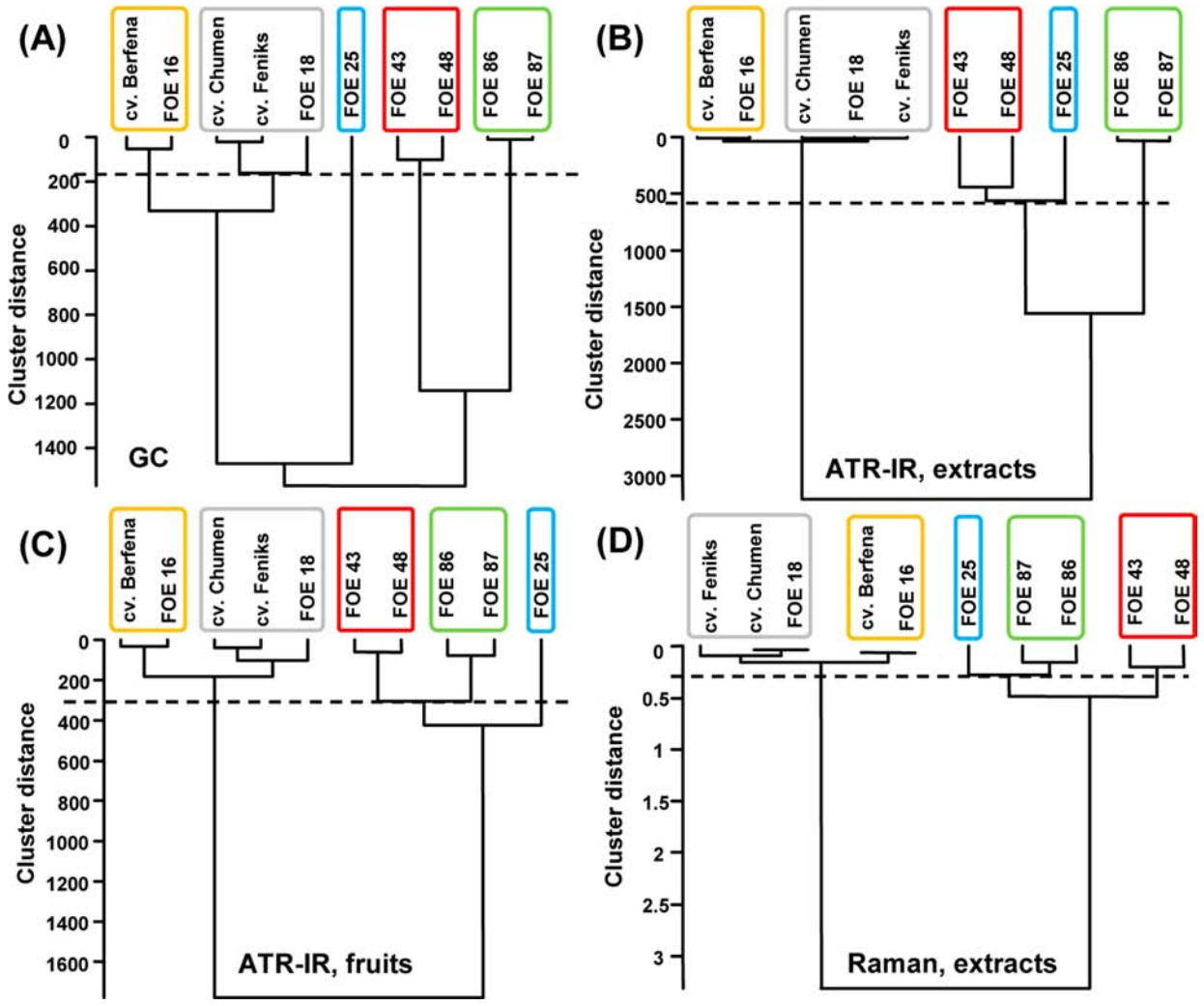

Figure 7. Hierarchical cluster analysis of 10 different fennel accessions based on the GC-FID data (A), the ATR-FTIR spectra of the CCl_4 extracts (B), the ATR-FTIR spectra of the intact fruits (C), and the Raman spectra of the CCl_4 extracts (D). The dashed line marks the lowest level of complete discrimination of the individual clusters.

For NIR, only intact fruits were analyzed because of the small available amounts of solvent extracts. For ATR-FTIR the extracts as well as the intact fruits were evaluated, whereas for Raman only the extracts were analyzed (see FT-Raman Spectroscopy). High fluorescence appearance in the spectra along with burning of the sample under the applied laser energy made it impossible to obtain meaningful Raman spectra with the used spectrometer.

ATR-FTIR Spectroscopy. As presented in Table 2, all fennel accessions contain higher amounts of a ketone (fenchone or piperitenone oxide) and an unsaturated phenylpropanoid substance. The high IR activity of the C═O bond resulting in strong signals in the ATR spectra of the extracts as well as the fennel fruits made it nearly impossible to distinguish the different fennel chemotypes on the basis of their fenchone/piperitenone oxide content. Figure 5 shows the ATR spectra of the individual fennel extracts in the fingerprint region from 1850 to 600 cm^{-1} and the corresponding reference compounds for the main volatile components.

In nearly all fennel accessions the strong $\nu_{C=O}$ absorption band around 1742 cm^{-1} dominates the spectrum in the fingerprint region even if the concentration of the corresponding carbonyls (fenchone/piperitenone oxide) in sum averages only 7.75% (cv. Chumen). As a consequence, the strong IR activity of this polar bond with its high dipole moment makes it impossible to distinguish the different genotypes on the level of their fenchone/piperitenon oxide concentration.

Besides the ketone function, the phenylpropanoids as well as the terpenoids differ only in their carbon structure and the presence and number of methoxy groups.

As can be easily seen when the MIR spectra of the extracts are compared with those of the pure standards, *trans*-anethole and estragole can be distinguished only by the signals resulting from the nonaromatic C═C double bond. Because of the resonance effect in *trans*-anethole, the signals for $\nu_{C=C}$ (1656 cm^{-1}) and γ_{CH} (962 cm^{-1}) are shifted hypsochromically to higher wavenumbers, compared to estragole ($\nu_{C=C}$ at 1638 cm^{-1} and γ_{CH} at 912 cm^{-1}) and γ-asarone ($\nu_{C=C}$ at 1640 cm^{-1} and γ_{CH} at 912 cm^{-1}).

For the two isolated double bonds in limonene the corresponding signals are $\nu_{C=C}$ at 1679 and 1644 cm^{-1} as well as γ_{CH} at 914 and 886 cm^{-1}.

For the differentiation of estragole and γ-asarone the wavenumber range from 1200 to 1130 cm^{-1}, showing the asymmetric and symmetric valence vibrations ν_{C-O-C} from the different methoxy groups, proved to be suitable.

dx.doi.org/10.1021/jf405752x | J. Agric. Food Chem. 2014, 62, 3537−3547

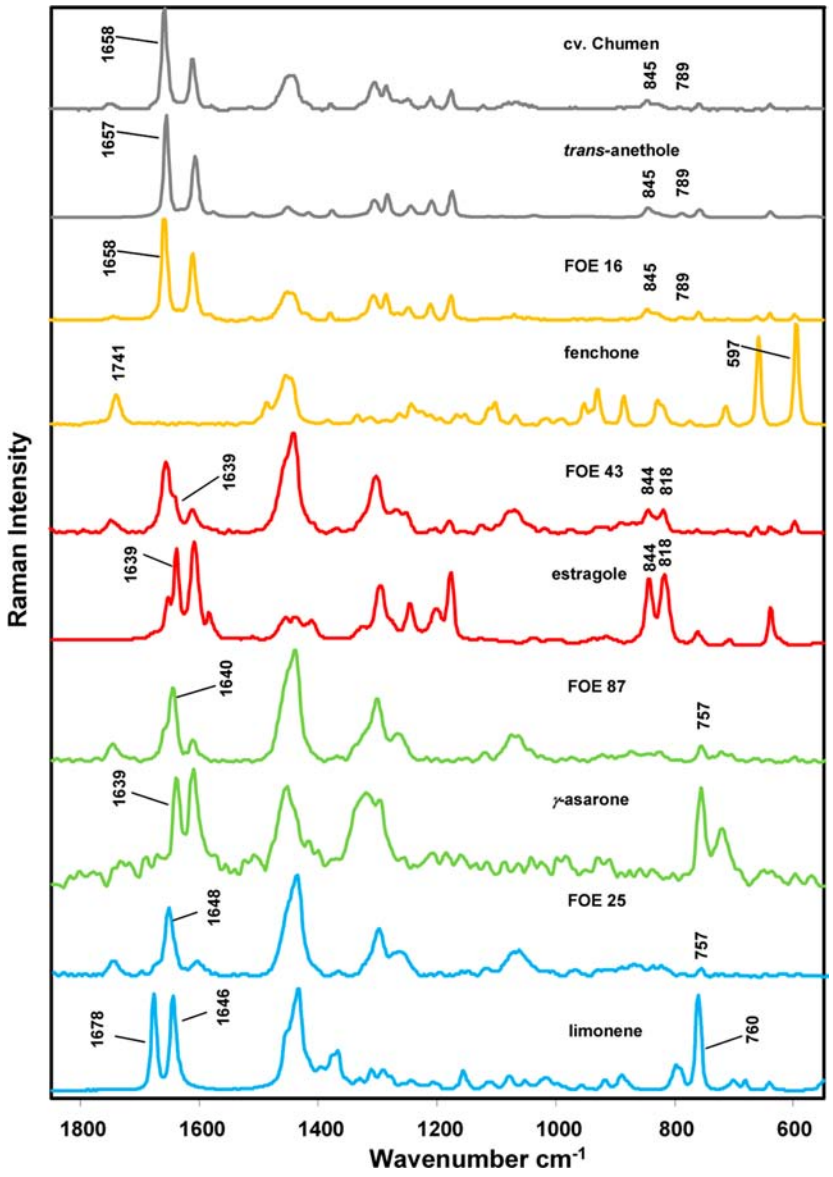

Figure 8. Raman spectra of CCl_4 extracts from different fennel genotypes and the corresponding standards for the most valuable components in the volatile fraction.

Despite the relatively weak IR activity of the C═C double bonds, cluster analysis on the basis of the above-mentioned spectral ranges results in a successful differentiation and classification of the four considered fennel chemotypes, even for the intact fennel fruits, the spectra of which are dominated by matrix signals from starch, lipids, and water (Figure 6).

Figure 7 shows the hierarchical cluster analysis of all fennel accessions investigated in this study according to the GC-FID data (A), compared to the ATR-FTIR spectra of the fennel extracts (B) and the intact fruits (C), as well as the Raman spectra of the extracts (D, discussed later).

According to the qualitative and quantitative composition of their volatile fraction, the 10 considered fennel genotypes can be classified into 4 chemotypes: the *trans*-anethole type with accessions cv. Berfena, FOE 16, FOE 18, cv. Chumen, and cv. Feniks; the estragole type with FOE 43 and FOE 48; the γ-asarone type with FOE 86 and FOE 87; and the piperitenone oxide type FOE 25, shown in Figure 7A.

The same classification is obtained by ATR-FTIR for both the fruits and the extract (Figure 7B,C). The only difference is the subgrouping of FOE 25, which is pooled together with the estragole type and the γ-asarone type in a larger cluster for ATR-FTIR and with the *trans*-anethole type for GC. This might be easily explained by the absence or very low concentration of *trans*-anethole in FOE 25, the estragole type, and the γ-asarone type.

Additionally, for the fruits and the extracts, a strict separation of sweet and bitter fennel, as demanded by the European Pharmacopoeia, can be observed between the cluster of the *trans*-anethole chemotype. The two accessions, cv. Berfena and FOE 16, contain much more than 15% of fenchone and simultaneously a content of *trans*-anethole of about 60%. In contrast, cv. Chumen, cv. Feniks, and FOE 18 show a fenchone content between 6 and 10% going along with concentrations of *trans*-anethole of 73% and higher. The slightly lower values for *trans*-anethole, as demanded by the European Pharmacopoeia, is a consequence of the solvent extraction used in this work instead of water steam distillation.

dx.doi.org/10.1021/jf405752x | J. Agric. Food Chem. 2014, 62, 3537−3547

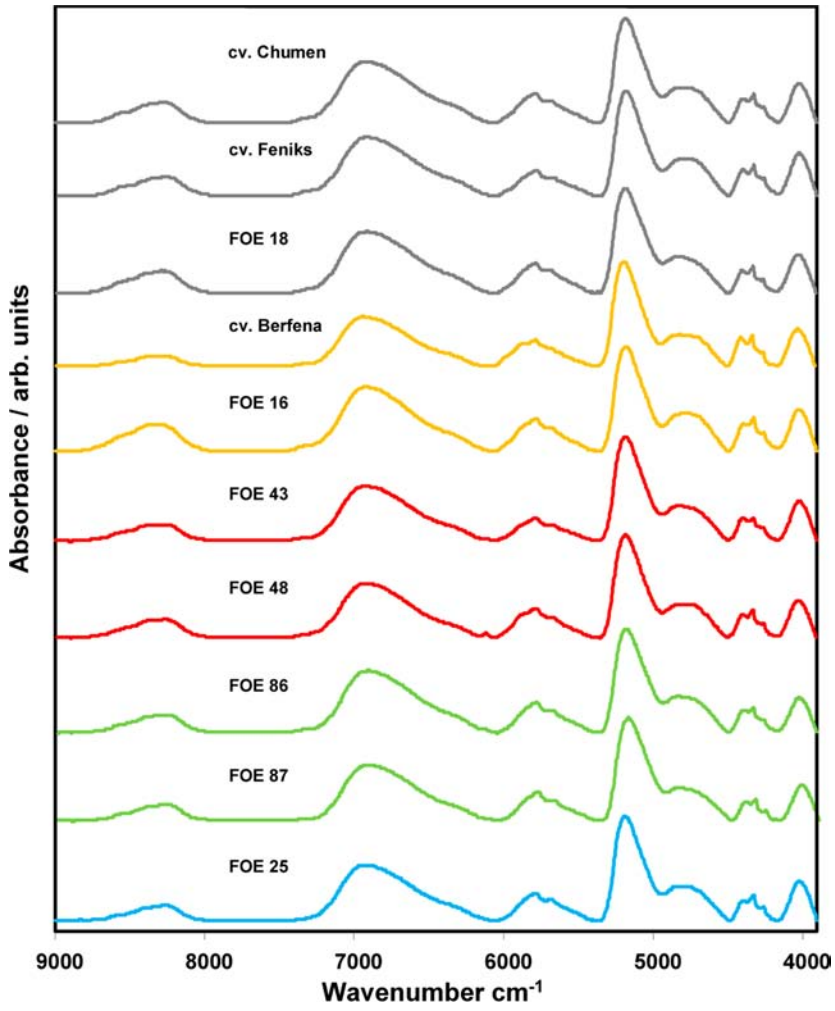

Figure 9. NIR spectra of intact fennel fruits from different fennel genotypes.

Hence, the ATR-FTIR technique offers for both the extracts and the intact fruits a fast tool for the discrimination of different fennel chemotypes according to the chemical profile of their volatile fraction and additionally allows a fast differentiation of sweet and bitter fennel within one chemotype, the *trans*-anethole type.

Raman Spectroscopy. The principle of Raman spectroscopy is the changing polarizability of a bond through the absorption of light. Therefore, structures with unsaturated carbon bonds, especially when conjugated, are highly Raman active.

Because the most significant differences in the structure of the essential oil components are the number and connectivity of C═C double bonds, one can expect an unambiguous classification of the fennel accessions by Raman spectroscopy. Figure 8 presents the Raman spectra of fennel extracts from five representative genotypes in the fingerprint region from 1800 to 550 cm^{-1} compared to the corresponding standards of the main components in the volatile fraction.

As already mentioned for ATR-FTIR, the main differences in the spectra are due to the vibrations of the C═C double bond in the side chain. The conjugation of this bond with the aromatic ring system in *trans*-anethole results in a hypsochromic shift of $\nu_{C=C}$ to 1658 cm^{-1} compared to estragole with its isolated C═C and $\nu_{C=C}$ at 1638 cm^{-1}. Limonene is determined by its γ_{CH} at 760 cm^{-1}. According to previous work, the vibration at 597 cm^{-1} was set as a marker band for fenchone because no other main component shows any significant signal at this spectral range.[10]

On the basis of these marker bands hierarchical cluster analysis was performed resulting in a classification of the fennel extracts according to their chemotype as shown in Figure 7D.

According to the results from ATR-FTIR, the same grouping of the fennel genotypes according to their main components in the volatile fraction is obtained. The first criterion for the clustering (cluster distance around 3.5) is the nature of the C═C double bond in the side chain resulting in one cluster containing the *trans*-anethole type (conjugated C═C, $\nu_{C=C}$ to 1658 cm^{-1}) and one containing the estragole type, γ-asarone type, and piperitenone oxide type (isolated C═C in estragole, γ-asarone, and limonene).

The next classification at a cluster distance of 0.5 separates the estragole type from the γ-asarone type and the piperitenone oxide type due to the contents of fenchone (597 cm^{-1}). The same attribute separates the "sweet" fennel from the "bitter" fennel in the cluster of the *trans*-anethole- type (cluster distance around 0.2). Finally, discrimination between FOE 25 and FOE 86/FOE 87, the piperitenone oxide type, and γ-asarone type results on the basis of the limonene content and its marker band γ_{CH} at 760 cm^{-1}.

In conclusion, the results obtained in this study show that Raman spectroscopy allows a fast and precise discrimination of different fennel chemotypes according to their chemical

dx.doi.org/10.1021/jf405752x | J. Agric. Food Chem. 2014, 62, 3537−3547

composition even on the level of a single spectrum. As already presented for ATR-FTIR, Raman spectroscopy is also a suitable tool to distinguish between sweet and bitter fennel without application of time-consuming chromatography.

NIR Spectroscopy. NIRS has been established for years as a fast and nondestructive method for qualitative and quantitative evaluation of numerous primary and secondary metabolites directly in plant material.[12,24−26]

A few years ago our group already developed a reliable quantification protocol for the determination of valuable essential oil components directly in intact fennel fruits, presenting NIRS as a promising tool for the chemotaxonomical characterization of the considered fennel chemotypes.[16] According to former studies performed on basil, oregano, and thyme, the NIR spectra of the analyzed fennel fruits are dominated by overtones or different combinations of C−H stretching and bending vibrations occurring between 4000 and 9000 cm^{-1}. As shown in Figure 9, the NIR spectra of the fruits obviously show no significant differences.

As the essential oil composition structurally differs only in comparatively narrow ranges, the similarity of the NIR spectra is evident. Nevertheless, even those small variations can be sufficient for a successful interpretation by applying chemometric algorithms.

Figure 10 presents a cluster analysis based on NIR spectral data resulting in a strict separation of all four fennel chemotypes

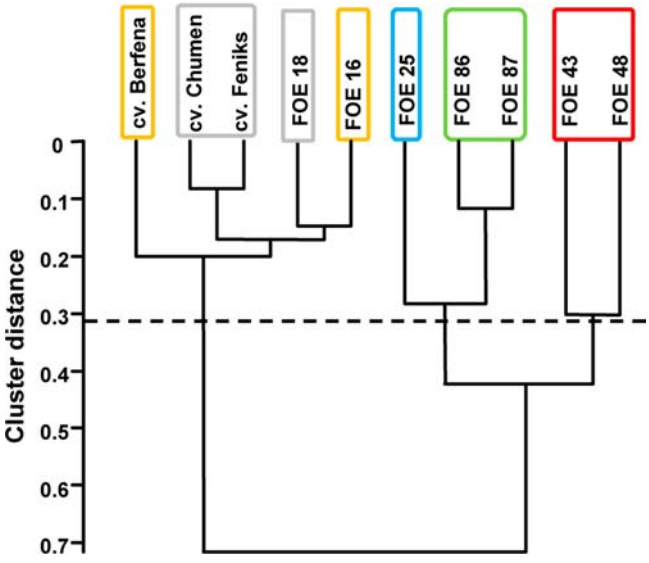

Figure 10. Hierarchical cluster analysis of 10 different fennel accessions based on the NIR spectra of the intact fruits.

in the same manner as described for Raman and ATR-FTIR spectroscopy. The considered spectral ranges are restricted to combination vibrations and the first and second overtones of C−H and C−C (4100−4650, 6000−6250, and 8200−9000 cm^{-1}). Only the discrimination of sweet and bitter fennel is not sufficiently obtained when this NIRS method is applied.

Nevertheless, NIRS offers a fast and easy way to distinguish different fennel chemotypes on the base of their main essential oil components directly in intact fruits. An indirect discrimination of sweet and bitter fennel can be obtained by the verified prediction of the *trans*-anethole and fenchone contents by NIRS, published by Steuer and Schulz.[16] Furthermore, the special advantage of NIRS measurements over mid-IR or Raman spectroscopy is that analyzed samples are more representative with regard to their sample presentation technique and sample quantity (approximately 0.5 g of the fennel fruits is put into glass cuvettes, resulting in a "sample layer" of about 15 mm thickness with a penetration depth of the NIR beam of several millimeters). This guarantees improved sample homogeneity compared to the two other vibrational spectroscopy techniques.

AUTHOR INFORMATION

Corresponding Author

*(H.S.) E-mail: Hartwig.Schulz@jki.bund.de. Phone: +49 30/8304 2500. Fax: +49 30/8304 2503.

Funding

We gratefully acknowledge the financial support obtained from the Deutsche Forschungsgemeinschaft (DFG) in Bonn, Germany (Project Schu 566/14-1).

Notes

The authors declare no competing financial interest.

ACKNOWLEDGMENTS

We thank Bärbel Zeiger for her support in sample preparation and GC-MS analysis, as well as Dr. Andreas Börner and Dr. Ulrike Lohwasser (Genebank of IPK Gatersleben, Germany) for providing the plant material.

ABBREVIATIONS USED

ATR-FTIR, attenuated total reflectance Fourier transform infrared; NIR, near-infrared; FT-Raman, Fourier transform Raman spectroscopy; GC, gas chromatography; GC-MS, gas chromatography−mass spectrometry; GC-FID, gas chromatography−flame ionization detection; FT-NIR, Fourier transform near-infrared; NMR, nuclear magnetic resonance spectroscopy; WMSC, weighted multiplicative scatter correction; PCA, principal component analysis; ppm, parts per million

REFERENCES

(1) Bernath, J.; Nemeth, E. Chemical systematization of the genus *Foeniculum* Mill. based on the accumulation and qualitative differentiation of the essential oil. *Nat. Prod. Commun.* **2007**, *2*, 309−314.

(2) Parzinger, R. Fenchel, Unterschiede der beiden offizinellen Varietäten. *Dtsch. Apoth. Ztg.* **1996**, *136* (7), 27−28.

(3) Badoc, A.; Deffieux, G.; Lamarti, A.; Bourgeois, G.; Carde, J. Essential oil of *Foeniculum vulgare* Mill. (fennel) subsp. *piperitum* (Ucria) Cout. fruit. *J. Essent. Oil Res.* **1994**, *6*, 333−336.

(4) Bernath, J.; Nemeth, E.; Kattaa, A.; Hethelyi, E. Morphological and chemical evaluation of fennel (*Foeniculum vulgare* Mill.) populations of different origin. *J. Essent. Oil Res.* **1996**, *8*, 247−253.

(5) Krüger, H.; Hammer, K. Chemotypes of fennel (*Foeniculum vulgare* Mill.). *J. Essent. Oil Res.* **1999**, *11*, 79−82.

(6) *Food Chemical Codex FCC*, 9th ed.; United States Pharmacopeia, 2013.

(7) Stahl, E.; Jork, H. Chemische Rassen bei Arzneipflanzen 1. Mitt.: Untersuchung der Kulturvarietäten Europäischer Petersilienherkünfte. *Arch. Pharm. Ber. Dtsch. Pharm. Ges.* **1964**, *297*, 273−281.

(8) Baranska, M.; Schulz, H.; Rösch, P.; Strehle, M. A.; Popp, J. Identification of secondary metabolites in medicinal and spice plants by NIR-FT-Raman microspectroscopic mapping. *Analyst* **2004**, *129*, 926−930.

(9) Daferera, D. J.; Tarantilis, P. A.; Polissiou, M. G. Characterization of essential oils from *Lamiaceae* species by Fourier transform Raman spectroscopy. *J. Agric. Food Chem.* **2002**, *50*, 5503−5507.

(10) Strehle, M. A.; Rösch, P.; Baranska, M.; Schulz, H.; Popp, J. On the way to a quality control of the essential oil of fennel by means of Raman spectroscopy. *Biopolymers* **2005**, *77*, 44−52.
(11) Baranska, M.; Schulz, H.; Krüger, H.; Quilitzsch, R. Chemotaxonomy of aromatic plants of the genus *Origanum* via vibrational spectroscopy. *Anal. Bioanal. Chem.* **2005**, *381*, 1241−1247.
(12) Schulz, H.; Schrader, B.; Quilitzsch, R.; Pfeffer, S.; Krüger, H. Rapid classification of basil chemotypes by various vibrational spectroscopy methods. *J. Agric. Food Chem.* **2003**, *51*, 2475−2481.
(13) Rösch, P.; Kiefer, W.; Popp, J. Chemotaxonomy of mints of genus *Mentha* by applying Raman spectroscopy. *Biopolymers* **2002**, *67*, 358−361.
(14) Schulz, H.; Schrader, B.; Quilitzsch, R.; Steuer, B. Quantitative analysis of various citrus oils by ATR/FT-IR and NIR-FT Raman spectroscopy. *Appl. Spectrosc.* **2002**, *56*, 117−124.
(15) Schulz, H.; Quilitzsch, R.; Krüger, H. Rapid evaluation and quantitative analysis of thyme, oregano and chamomile essential oils by ATR-IR and NIR spectroscopy. *J. Mol. Struct.* **2003**, *661*, 299−306.
(16) Steuer, B.; Schulz, H. Near-infrared analysis of fennel (*Foeniculum vulgare* Miller) on different spectrometers − basic considerations for a reliable network. *Phytochem. Anal.* **2003**, *14*, 285−289.
(17) *Foeniculum vulgare* Mill. ssp. *vulgare* var. *vulgare*. In *Ph. Eur. European Pharmacopoeia 7.0*, Grundwerk 2011; Deutscher Apotheker Verlag: Stuttgart, Germany, 2011; p 1713.
(18) *Foeniculum vulgare* Mill. ssp. *vulgare* var. *dulce* (Mill.) Thell. In *Ph. Eur. European Pharmacopoeia 7.0*, Grundwerk 2011; Deutscher Apotheker Verlag: Stuttgart, Germany, 2011; p 1714.
(19) Bitterfenchelöl *Foeniculum amari fructus aetheroleum*. In *Ph. Eur. European Pharmacopoeia*, Grundwerk 2011; Deutscher Apotheker Verlag: Stuttgart, Germany, 2011; p 1658.
(20) Brophy, J.; Goldsack, R.; Punruckvong, A.; Forster, P. I; Fookes, C. Essential oils of the genus *Crowea* (Rutaceae). *J. Essent. Oil Res.* **1997**, *9*, 401−409.
(21) Geda, A. A stereochemical approach to antibacterial activity of steam volatile ethers. *J. Med. Aromat. Plant Sci.* **2000**, *22*−*23*, 190−191.
(22) Varma, J.; Tripathi, M.; Ram, V. J.; Pandey, V. B.; Dubey, N. K. *g*-Asarone − the fungitoxic principle of the essential oil of *Caesulia axillaris*. *World J. Microbiol. Biotechnol.* **2002**, *18*, 277−279.
(23) Santos, B. V. D.; da-Cunha, E. V. L; Chaves, M. C. D.; Gray, A. I. Phenylalkanoids from *Piper marginatum*. *Phytochemistry* **1998**, *49*, 1381−1384.
(24) Schulz, H.; Drews, H.; Krüger, H. Rapid NIRS determination of quality parameters in leaves and isolated essential oils of *Mentha* species. *J. Essent. Oil Res.* **1999**, *11*, 185−190.
(25) Krähmer, A.; Gudi, G.; Weiher, N.; Gierus, M.; Schütze, W.; Schulz, H. Characterization and quantification of secondary metabolite profiles in leaves of red and white clover species by NIR and ATR-IR spectroscopy. *Vib. Spectrosc.* **2013**, *68*, 96−103.
(26) Krüger, H.; Schulz, H. Analytical techniques for medicinal and aromatic plants. *Stewart Postharvest Rev.* **2007**, *3* (4), 1−12.

the lipid bilayer significantly and that insertion of each terpene in the bilayer is driven by a different balance of entropy and enthalpy, determined by the functional groups present on the terpene.[19]

One of the common antimicrobial monoterpenes found in several EOs is α-pinene. The strained four-membered ring of α-pinene is very reactive and makes it prone to opening and skeletal rearrangements.[20,21] In addition to research about the antimicrobial activity of monoterpenes/monoterpenoids, there has been some recent work by Wilderman and colleagues that has shown that (+)-α-pinene (**1a**) is a potent P_{450} 2B inhibitor.[22] With microbes becoming increasingly resistant to known antibiotics, it is imperative to develop drugs that are active against the next generation of microbes. Both enantiomers of α-pinene are readily available, and hence it is an excellent starting material for synthesizing a variety of functionally and skeletally altered α-pinene derivatives. In this study, we investigate the structure−antimicrobial activity relationship for both (+)- and (−)-α-pinene and the corresponding derivatives. Antimicrobial activity was assessed on four test microorganisms (*Staphylococcus aureus*, *Micrococcus luteus*, *Escherichia coli*, and *Candida albicans*) using a bioautographic assay.[23,24] This bioassay gave good reproducibility. Lastly, membrane fatty acid composition of the test microorganisms was determined by fatty acid methyl ester (FAME) analysis.

MATERIALS AND METHODS

Chemicals. Silica gel 60 Å 70−230 or 230−400 mesh ASTM from Sigma-Aldrich was used for gravity column chromatography. TLC plates containing silica on aluminum/glass with a fluorescent indicator (254 nm), starting materials (+)-α-pinene 98% and (−)-α-pinene 98%, lithium aluminum hydride (LAH) powder, and all ACS grade solvents were purchased from Sigma-Aldrich and used as such. Chlorosulfonylisocyanate (CSI) 98+% was purchased from Acros Organics. IR spectra were recorded on a Perkin-Elmer FTIR 1600 series in CH_2Cl_2 solution, and ^1H and ^{13}C NMR spectra were recorded on a JEOL Eclipse 300 MHz NMR spectrometer in $CDCl_3$. Synthesized compounds were >95% pure as verified by ^1H NMR and were purified by chromatography, recrystallization, or trituration. Modified experimental procedures[25] for **9a**, **10a**, **11a**, **12a**, **13a**, and **14a** are provided in the Supporting Information along with the ^1H NMR and ^{13}C NMR spectra of the synthesized compounds.

Microorganisms and Culture Media. Three of the microorganisms used in this study (*M. luteus*, *E. coli*, and *S. aureus*) were clinical isolates and were received as a gift from Katherine Greiner, Associate Professor of the Medical Technology Program at Marist College; *C. albicans* (ATCC 90294) was purchased from Sigma. The bacterial cultures were subcultured in Luria−Bertani (LB) medium, and the yeast was subcultured in Sabaraud (SAB) at 37 °C for 12−14 h (*M. luteus* was grown at 25 °C for 60−72 h) at 135 rpm. The optical density of the culture was measured with a UV−vis Beckman 650 spectrophotometer at 600 nm (OD_{600} = 1 corresponds to approximately 10^9 cells/mL).[26] Culture media were autoclaved at 120 °C for 20 min.

Bioautographic Assay. The antimicrobial activity of the nine compounds synthesized was evaluated against four test microorganisms (Gram-positive bacteria *S. aureus* and *M. luteus*, Gram-negative bacterium *E. coli*, and unicellular fungus *C. albicans*) by bioautographic assay using a modified published procedure.[23,27] Each TLC glass plate was divided into 20 equal squares. Stock solution of each of the compound was made (1 mg/10 μL of dichloromethane), and 25 μL of this solution was spotted (2.5 mg of the compound), making sure that all of the spots were close to 3 mm in diameter. The positive control used was Sigma A5955 (antibiotic−antimycotic solution comprising penicillin G (100,000 units/mL), streptomycin sulfate (10 mg/mL), and amphotericin B (25 μg/mL)), and the negative control used was dichloromethane. The log phase microbes were sprayed on the TLC plates (∼7−10 mL) ensuring that the plates were evenly wet, followed by a spray of (∼7−10 mL) half-strength LB agar (maintained in a water bath at ∼55 °C). Each plate was placed on cork supports in a humid chamber (made by placing wet paper towels in plastic containers) in an incubator at 37 °C (25 °C for *M. luteus*) for 12−18 h to allow the bacteria to grow.[23] A freshly prepared aqueous solution (5 mg/mL) of (3-(4,5-dimethylthiazol-2yl)-2,5-diphenyltetrazolium bromide) (MTT) was sprayed (1−2 mL) on the plate covered with bacteria, and the plate was put back in a humid chamber at the appropriate temperature for 4−5 h or until the purple color appeared. Actively growing microbes convert MTT (yellow) to formazan (purple). Zones of inhibition appear white against a purple background.

Microbial Growth Inhibition Measurements. The inhibition diameter was taken as an average of four measurements per TLC plate. The diameter of each inhibition zone was further determined in four different directions (0°, 45°, 90°, and 135°) as described in the literature.[27,28] The bioassay for each compound was done in triplicate.

Statistical Analysis. Data were statistically evaluated using one-way ANOVA, followed by a post hoc Newman−Keuls multiple-comparison test. The values were expressed as the mean ± SD and considered significant at $p \leq 0.05$.

FAME Analysis. Bacterial and yeast cultures were grown, and fatty acids were extracted using the methods described by Sasser.[29] Extracts were analyzed using an Agilent 6890N gas chromatograph with an Agilent Ultra 2 column. Sherlock Microbial ID system version 4.5 was used to analyze the data.

RESULTS AND DISCUSSION

Investigation of this approach began with the synthesis of α-pinene derivatives using modified literature procedures.[20,25] Treatment of (+)-α-pinene (**1a**) with chlorosulfonylisocyanate furnished the β-lactam *N*-sulfonyl chloride **9a** in 64% yield as a single stereoisomer (Scheme 1). The N−S bond was

Scheme 1. Synthetic Modifications of α-Pinene

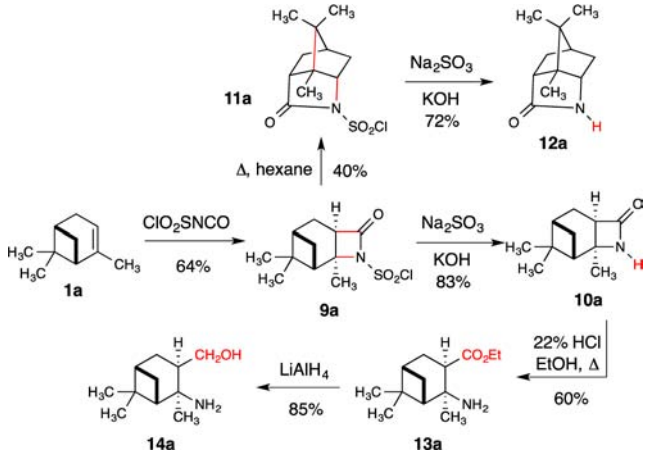

subsequently cleaved using sodium sulfite to give H-β-lactam **10a** in an 83% yield. Alternatively, rearrangement of the α-pinene skeleton by refluxing lactam **9a** in hexanes provided the γ-lactam *N*-sulfonyl chloride **11a** in modest yield (40%). The sulfonyl group of γ-lactam **11a** was cleaved as above to yield H-γ-lactam **12a** in 72% yield. Finally, opening of the β-lactam with ethanol under acidic conditions provided ethyl ester **13a** in 60% yield. Ester **13a** was reduced with lithium aluminum hydride to provide amino alcohol **14a** in 85% yield.

dx.doi.org/10.1021/jf403586t | J. Agric. Food Chem. 2014, 62, 3548−3552

Additionally, the corresponding enantiomers of the β-lactam **10a**, amino ester **13a**, and amino alcohol **14a** were synthesized using the same route except beginning with (−)-α-pinene (**1b**).

Most common antimicrobial agents in use are those containing the β-lactam ring.[30] Such antibiotics are known to work on bacteria via two mechanisms that target the cell wall synthesis.[31] A Cambridge database-based study correlates biological activity in β-lactams with Woodward and Cohen structural parameters.[32] It should be noted that well-known antibiotic β-lactams have a tertiary nitrogen in the β-lactam ring, whereas the α-pinene-based β-lactams **10a** and **10b** have a secondary nitrogen. Because lactams **10a** and **10b** are derived from α-pinene, we assume that they will also interact in the membrane like other pinene derivatives, although the antimicrobial activity of these compounds via inhibition of cell wall synthesis cannot be ruled out. The antimicrobial results are shown in Figures 1 and 2. β-Lactam **10b** is more

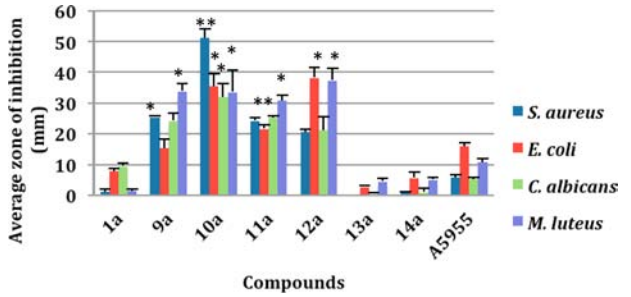

Figure 1. Antimicrobial activity of (*R*)-(+)-α-pinene (**1a**) and its derivatives: β-lactam **10a**, β-lactam *N*-sulfonyl chloride **9a**, γ-lactam **12a**, γ-lactam *N*-sulfonyl chloride **11a**, amino ester **13a**, and amino alcohol **14a**. (∗) $P < 0.05$ and (∗∗) $P < 0.01$, compared to **1a** at the corresponding time. The antimicrobial potential of **13a** and **14a** was found to be not significant compared to **1a** at the corresponding time.

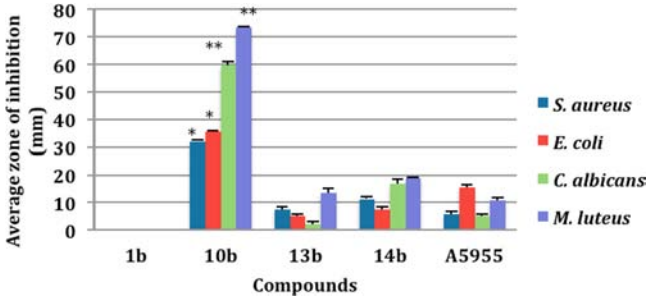

Figure 2. Antimicrobial activity of (*S*)-(−)-α-pinene (**1b**) and its derivatives, β-lactam**10b**, amino ester**13b**, and amino alcohol**14b**. (∗)$P < 0.05$ and (∗∗) $P < 0.01$, compared to **1b** at the corresponding time.

antimicrobial than **10a** toward *M. luteus* and *C. albicans*, whereas lactam **10a** shows greater antimicrobial activity toward *S. aureus*. Lastly, N−H lactams **10a** and **10b** show similar zones of inhibition toward *E. coli*. It should be noted that both β-lactams have greatly enhanced antimicrobial activity toward all four test microorganisms in comparison to the starting materials, (+)- and (−)-α-pinene, respectively. β-Lactam **10a** (as compared to its starting material (+)-α-pinene **1a**) showed an approximately 43-fold increase in antimicrobial activity toward *S. aureus*, a 22-fold increase toward *M. luteus*, a 4.5-fold increase toward *E. coli*, and a nearly 3.5-fold increase toward *C. albicans*. Similarly, β-lactam **10b** (as compared to its starting material (−)-α-pinene **1b**) showed an approximately 32-fold increase in antimicrobial activity toward *S. aureus*, a 73-fold increase toward *M. luteus*, a 35-fold increase toward *E. coli*, and a 60-fold increase toward *C. albicans*.

We next examined the differences in antimicrobial potential between β-lactam (**10a**) and γ-lactam (**12a**) derived from (+)-α-pinene (**1a**) (Figure 1). Overall, β-lactam **10a** showed a stronger antimicrobial activity than γ-lactam **12a**. Although *M. luteus* and *S. aureus* are both Gram-positive bacteria, there is a statistically significant difference in antimicrobial activity of **10a** and **12a** toward *S. aureus*. Compound **10a** shows more than twice the area of inhibition with *S. aureus* compared to **12a** but similar antimicrobial activity toward *M. luteus*. Lactam **12a** showed the largest zones of inhibition for *E. coli* (Gram-negative) and *M. luteus* (Gram-positive). Compound **12a** is half as effective toward *C. albicans* and *S. aureus* as compared to *M. luteus* and *E. coli*. β-Lactam-containing antibiotics, such as penicillin G, are effective against Gram-positive bacteria, but not as effective against Gram-negative bacteria, whereas ampicillin and amoxicillin are effective against both Gram-positive and Gram-negative bacteria.[33] γ-Lactam **12a** is effective against both Gram-positive and Gram-negative bacteria, but its activity is found to be less than that of β-lactam **10a**. Lower antimicrobial activity of γ-lactam in comparison to β-lactam can partly be attributed to the ring strain found in the latter. γ-Lactam contains a five-membered ring, which is more stable than the four-membered ring found in a β-lactam. Due to the ring strain present in β-lactam, it is prone to opening by nucleophilic addition.[21] Stronger intramolecular hydrogen bonding is known to exist in γ-lactams, which may also contribute to its lower antimicrobial activity.[34] The bioassay shows that the two *N*-sulfonyl chlorides of β-lactam and γ-lactam (**9a** and **11a**, respectively) have similar antimicrobial activity.

Earlier studies have shown that introducing a single alcoholic (or amino functional group) in the α-pinene nucleus increases the antimicrobial activity, compared to the antimicrobial activity of (+)-α-pinene derivatives having other functional groups.[27] It is speculated that the presence of the alcoholic or amino functional group makes the compound more water-soluble and thereby helps it transverse the polar cell wall.[35−37] This allows the compound to reach the site of action, the microbial membrane, in greater concentration and hence permeate it more efficiently.[35−37] Therefore, we chose to synthesize amino ester **13a** and amino alcohol **14a** to determine if adding both the alcoholic and amino functions to the α-pinene nucleus will make the compound more antimicrobial than when only one of the two functional groups is present. Consequently, we synthesized two pairs of enantiomeric compounds (**13a** and **13b**; **14a** and **14b**). Overall, amino alcohol **14a** was found to be less antimicrobial than the starting material (**1a**) (Figure 1). Amino alcohol **14b** shows antimicrobial activity toward all four microorganisms used in the study (Figure 2) and by comparison is more antimicrobial than the starting material (**1b**), which under the test conditions did not exhibit any antimicrobial activity. However, the differences in antimicrobial activity of the two amino alcohols **14a** and **14b** were found to be statistically not significant. Both **14a** and **14b** were less antimicrobial than the previously evaluated (1*R*,2*R*,3*R*,5*S*)-(−)-iso-pinocampheol or (1*R*,2*R*,3*R*,5*S*)-(−)-iso-pinocampheylamine.[27] Lastly, ester **13b** was found to be more antimicrobial than the starting material (**1b**) (Figure 2). Conversely, ester **13a** displayed less antimicrobial activity

Table 1. Major Membrane Fatty Acids of the Four Microorganisms Used in the Study[a]

S. aureus		*M. luteus*		*E. coli*		*C. albicans*	
FA	%	FA	%	FA	%	FA	%
15:0 ANTEISO	43.67	15:0 ANTEISO	84.04	16:00	30.34	18:1 cis 9 (w9)	39.18
17:0 ANTEISO	11.81	17:0 ANTEISO	4.92	17:0 cyclo	20.82	18:2 cis 9,12/18:0a	29.57
15:0 ISO	11.19			18:1 w7c	16.30	16:00	13.80
18:00	10.06			12:0 ALDE	9.18	16:1 cis 9 (w7)	12.59
				14:0 3OH/16:1 ISO 1	9.08		

[a]Percentage composition reported as an average of two runs.

toward the four microorganisms in comparison to (**1a**); however, statistically the difference is not significant.

The antimicrobial potential of the enantiomeric starting materials (**1a** and **1b**) and β-lactams (**10a** and **10b**) is significantly different from each other not only toward various microorganisms used in this study but also in their extent of antimicrobial activity, whereas the antimicrobial potential of the amino esters (**13a** and **13b**) and amino alcohols (**14a** and **14b**) derived from the corresponding α-pinenes is found to be not significant as compared to their respective starting materials. Because the amino alcohols (**14a** and **14b**) have both hydroxyl as well as the amino functional groups, it is expected that these enantiomers will have much greater antimicrobial activity than α-pinene derivatives containing either of the two functional groups. This, however, was not the case. A possible explanation for this could be that amino alcohols and amino esters are known to form strong intramolecular hydrogen bonds due to the formation of a six-membered ring.[38,39] It is known that intramolecular hydrogen bonding affects the physical properties such as solubility of molecules.[40] Therefore, H-bonding capacity (inter versus intra) directly would affect the water solubility of a compound. The strong intramolecular hydrogen bonding in the amino alcohols (**14a** and **14b**) as well as the amino esters (**13a** and **13b**) would lower the water solubility of these compounds and hence might prevent these compounds from crossing the polar cell wall to reach the site of action, the cell membrane.[35−37] Structural features (carbon skeleton and functional groups) being the same, additional factors such as chirality and the capacity to hydrogen bond (intramolecular H-bonding seems to lower it, and intermolecular H-bonding seems to increase it) play an important role in determining the antimicrobial activity of this class of compounds.

Skeletally modified α-pinene derivatives studied were **9a**, **10a**, **10b**, **11a**, **11b**, and **12a**. All of these skeletally modified derivatives were much more antimicrobial than their corresponding starting material (+)-α-pinene **1a** and (−)-α-pinene **1b**, indicating that the carbon skeleton affects the antimicrobial activity. Functional groups present also affect antimicrobial activity. The starting materials (+)-α-pinene **1a** and (−)-α-pinene **1b** have alkene functionality that was converted to amino ester (**13a**, **13b**) amino alcohol (**14a**, **14b**), lactams (**10a**, **10b**, **12a**,) and lactam *N*-sulfonyl chloride (**9a**, **11a**,**11b**). Of the various functional groups evaluated, lactams proved to be the most antimicrobial followed by lactam *N*-sulfonyl chlorides. It also matters which enantiomer was used to synthesize a particular derivative (derived from (+)-α-pinene versus (−)-α-pinene). Of the two starting materials, (+)- and (−)-α-pinene, only (+)-α-pinene was found to be antimicrobial against all four test microorganisms at the reported concentration. However, derivatives obtained from (−)-α-pinene proved to be more antimicrobial than their mirror images obtained from the (+)-enantiomer. Although additional derivatives would have to be synthesized and evaluated to make a conclusive inference, our results suggest that derivatives of the most antimicrobial compound may not necessarily be more antimicrobial.

FAME results of the membrane composition of the test microbes (Table 1) show that the membrane composition of the four test microorganisms is very different and no linear relationship can be seen between a particular lipid and antimicrobial activity of the compounds evaluated in this study. Despite that, there is one interesting result from the FAME analysis. For all of the pinene derivatives (**10b**, **13b**, and **14b**) obtained from (−) α-pinene, *M. luteus* seemed to be the most susceptible microorganism. For the pinene derivatives obtained from the (+)-α-pinene, *M. luteus* seems to be the most susceptible microorganism for the two *N*-sulfonyl chlorides of β-lactam and γ-lactam. The membrane composition of *M. luteus* (Table 1) is unique and is mainly composed of 15:0 ANTEISO fatty acid (∼84%). The other three microorganisms have a spread of different membrane fatty acids.

■ ASSOCIATED CONTENT

Ⓢ Supporting Information

Additional experimental details. This material is available free of charge via the Internet at http://pubs.acs.org.

■ AUTHOR INFORMATION

Corresponding Author

*(P.D.) E-mail: dharp@newpaltz.edu. Phone: 845-257-3797. Fax: 845 257-3791.

Present Addresses

△(P.C.) Department of Pharmacology and Physiology, University of Rochester Medical Center, 601 Elmwood Ave., Box 711, Rochester, NY 14642, USA.

○(D.T.C.) Department of Chemistry, Weinberg College of Arts and Sciences, 2145 Sheridan Rd., Northwestern University, Evanston, IL 60208, USA.

▽(T.S.-L.) Soft Genetics, 100 Oakwood Place, State College, PA 16803, USA.

□(P.K.R.) Department of NMR, All India Institute of Medical Sciences, New Delhi 110029, India.

Funding

SURE, AYURE, and Research and Creative grants, SUNY New Paltz.

Notes

The authors declare no competing financial interest.

■ REFERENCES

(1) Chowdhury, S.; Nishteswar, K. Role of volatile oil of natural source in the cosmetics and health care industries. *Pharma Sci. Monit.* **2013**, *4*, 3738−3750.

(2) Maškovic, P.; Radojkovic, M.; Ristic, M.; Slavica, S. Studies on the antimicrobial and antioxidant activity and chemical composition of the essential oils of *Kitaibelia vitifolia*. *Nat. Prod. Comm.* **2013**, *8*, 667−670.
(3) Bozin, B.; Mimica-Dukic, N.; Samojlik, I.; Jovin, E. J. Antimicrobial and antioxidant properties of rosemary and sage (*Rosmarinus officinalis* L. and *Salvia officinalis* L., Lamiaceae) essential oils. *J. Agric. Food Chem.* **2007**, *55*, 7879−7885.
(4) Iscan, G.; Kirimer, N.; Kurkcuoglu, M.; Baser, K. H. C.; Demirci, F. Antimicrobial screening of *Mentha piperita* essential oils. *J. Agric. Food Chem.* **2002**, *50*, 3943−3946.
(5) Dadalioglu, I.; Evrendilek, G. A. Chemical compositions and antibacterial effects of essential oils of Turkish oregano (*Origanum minutiflorum*), bay laurel (*Laurus nobilis*), Spanish lavender (*Lavandula stoechas* L.), and fennel (*Foeniculum vulgare*) on common foodborne pathogens. *J. Agric. Food Chem.* **2004**, *52*, 8255−8260.
(6) Daferera, D.; Ziogas, B. N.; Polissiou, M. G. GC-MS analysis of essential oils from some Greek aromatic plants and their fungitoxicity on *Penicillum digitatum*. *J. Agric. Food Chem.* **2000**, *48*, 2576−2581.
(7) Lis-Balchin, M. Aromatherapy with essential oils. In *Handbook of Essential Oils*; CRC Press: Boca Raton, FL, USA, 2009; pp 549−736
(8) Irshad, M.; Rehman, H.; Shahid, M.; Aziz, S.; Ghous, T. Antioxidant, antimicrobial and phytotoxic activities of essential oil of *Angelica glauca*. *Asian J. Chem.* **2011**, *23*, 1947−1951.
(9) Cardile, V.; Russo, A.; Formisano, C.; Rigano, D.; Senatore, F.; Arnold, N. A.; Piozzi, F. Essential oils of *Salvia bracteata* and *Salvia rubifolia* from Lebanon: chemical composition, antimicrobial activity and inhibitory effect on human melanoma cells. *J. Ethnopharmacol.* **2009**, *126*, 265−272.
(10) Sharma, A.; Mann, A. S.; Gajbhiye, V.; Kharya, M. D. Phytochemical profile of *boswellia serrata*: an overview. *Pharmacogn. Rev.* **2007**, *1*, 137−142.
(11) Öztürk, M.; Duru, M. E.; Aydoğmuş-Öztürk, F.; Harmandar, M.; Mahlıçlı, M.; Kolak, U.; Ulubelen, A. GC-MS analysis and antimicrobial activity of essential oil of *Stachys cretica* subsp. *smyrnae*. *Nat. Prod. Commun.* **2009**, *4*, 109−114.
(12) Kiran, C. R.; Chakka, A. K.; Amma, K. P. P.; Menon, A. N.; Kumar, M. M. S.; Venugopalan, V. V. Influence of cultivar and maturity at harvest on the essential oil composition, oleoresin and [6]-gingerol contents in fresh ginger from northeast India. *J. Agric. Food Chem.* **2013**, *61*, 4145−4154.
(13) Sikkema, J.; Poolman, B.; Konings, W. N.; de Bont, J. A. Effects of the membrane action of tetralin on the functional and structural properties of artificial and bacterial membranes. *J. Bacteriol.* **1992**, *174*, 2986−2992.
(14) Sikkema, J.; de Bont, J. A.; Poolman, B. Interactions of cyclic hydrocarbons with biological membranes. *J. Biol. Chem.* **1994**, *269*, 8022−8028.
(15) Griffin, S. G.; Wyllie, S. G.; Markham, J. L. Antimicrobially active terpenes cause K^+ leakage in *E. coli* cells. *J. Essent. Oil Res.* **2005**, *17*, 686−690.
(16) Pasqua, R. D.; Betts, G.; Hoskins, N.; Edwards, M.; Ercolini, D.; Mauriello, G. Membrane toxicity of antimicrobial compounds from essential oils. *J. Agric. Food Chem.* **2007**, *55*, 4863−4870.
(17) Helander, I. M.; Alakomi, H.-L.; Latva-Kala, K.; Mattila-Sandholm, T.; Pol, I.; Smid, E. J.; Gorris, L. G. M.; von Wright, A. Characterization of the action of selected essential oil components on Gram-negative bacteria. *J. Agric. Food Chem.* **1998**, *46*, 3590−3595.
(18) Trombetta, D.; Castelli, F.; Sarpietro, M. G.; Venuti, V.; Cristani, M.; Daniele, C.; Saija, A.; Mazzanti, G.; Bisignano, G. Mechanisms of antibacterial action of three monoterpenes. *Antimicrob. Agents Chemother.* **2005**, *49*, 2474−2478.
(19) Witzke, S.; Duelund, L.; Kongsted, J.; Petersen, M.; Mouritsen, O. G.; Khandelia, H. Inclusion of terpenoid plant extracts in lipid bilayers investigated by molecular dynamics simulations. *J. Phys. Chem. B* **2010**, *114*, 15825−15831.
(20) Sasaki, T.; Eguchi, S.; Yamada, H. Reactions of isoprenoids. XVIII. Reactions of chlorosulfonyl isocyanate with bicyclic monoterpene olefins. Novel isomerization of 1-chlorosulfonyl-2-azetidinone. *J. Org. Chem.* **1973**, *38*, 679−686.
(21) Kamath, A.; Ojima, I. Advances in the chemistry of β-lactam and its medicinal applications. *Tetrahedron* **2012**, *68*, 10640−10664.
(22) Wilderman, P. R.; Shah, M. B.; Jang, H.-H.; Stout, C. D.; Halpert, J. R. Structural and thermodynamic basis of (+)-α-pinene binding to human cytochrome P450 2B6. *J. Am. Chem. Soc.* **2013**, *135*, 10433−10440.
(23) Rios, J. L.; Recio, M. C.; Villar, A. Screening methods for natural products with antimicrobial activity: a review of the literature. *J. Ethnopharmacol.* **1988**, *23*, 127−149.
(24) Brantner, A. H. Influence of various parameters on the evaluation of antibacterial compounds by the bioautographic tlc assay. *Pharm. Pharmacol. Lett.* **1997**, *4*, 152−154.
(25) Szakonyi, Z.; Martinek, T.; Hetényi, A.; Fülöp, F. Synthesis and transformations of enantiomeric 1,2-disubstituted monoterpene derivatives. *Tetrahedron: Asymmetry* **2000**, *11*, 4571−4579.
(26) Sambrook, J.; Russell, D. *Molecular Cloning*; CSHL Press: Cold Spring Harbor, NY, USA, 2001; Vol. 1, p 117.
(27) Dhar, P.; Ayala, U.; Andarge, E.; Morisseau, S.; Snyder-Leiby, T. Study of the structural changes on the antimicrobial activity of [3.1.1.]-bicyclics. *J. Essent. Oil Res.* **2004**, *16*, 612−616.
(28) Nieva Moreno, M. I.; Isla, M. I.; Cudmani, N. G.; Vattuone, M. A.; Sampietro, A. R. Screening of antibacterial activity of Amalcha del Valle (Tucumán, Argentina) propolis. *J. Ethnopharmacol.* **1999**, *68*, 97−102.
(29) Sasser, M. *Microbial Identification by Gas Chromatographic Analysis of Fatty Acid Methyl Esters (GC-FAME)*; MIDI Tehnical Note 101; MIDI Inc.: Newark, DE, USA, 2009; 6 pp.
(30) Georg, G. I. *The Organic Chemistry of β-Lactams*; VCH: New York, 1992; and references cited therein..
(31) Joumana, N. S.-K.; George, F. A. Recent developments in β lactamases and extended spectrum β lactamases. *BMJ* **2003**, *327*, 1209.
(32) Nangia, A.; Biradha, K.; Desiraju, G. R. Correlation of biological activity in β-lactam antibiotics with Woodward and Cohen structural parameters − a Cambridge database study. *J. Chem. Soc., Perkin Trans. 2* **1996**, *5*, 943−53.
(33) Neu, H. C. Antimicrobial activity and human pharmacology of amoxicillin. *J. Infect. Dis.* **1974**, *129*, S123−S131.
(34) Dobrowolski, J. C.; Sadlej, J.; Mazurek, A. P. Why are g- and d-less active than b-lactams? An *ab initio* study. *Pol. J. Chem.* **2001**, *75*, 1277−1286.
(35) Gallucci, M. N.; Oliva, M.; Casero, C.; Dambolena, J.; Luna, A.; Zygadlo, J.; Demo, M. Antimicrobial combined action of terpenes against the food-borne microorganisms *Escherichia coli*, *Staphyloccus aureus*, and *Bacillus cereus*. *Flavour Fragrance J.* **2009**, *24*, 348−354.
(36) Griffin, S. G.; Wyllie, S. G.; Markham, J. L.; Leach, D. N. The role of structure and molecular properties of terpenoids in determining their antimicrobial activity. *Flavour Fragrance J.* **1999**, *14*, 322−332.
(37) Knobloch, K.; Pauli, A.; Iberl, B.; Weigand, H.; Weis, N. Antibacterial and antifungal properties of essential oil components. *J. Essent. Oil Res.* **1989**, *1*, 119−128.
(38) Freedman, H. H. Intramolecular H-bonds. I. A spectroscopic study of the hydrogen bond between hydroxyl and nitrogen. *J. Am. Chem. Soc.* **1961**, *83*, 2900−2905.
(39) Mulla, S.; Jose, C. I. Intramolecular hydrogen bonding and intermolecular association of amino alcohols. *J. Chem. Soc., Faraday Trans. 1* **1986**, *82*, 691−706.
(40) Kuhn, B.; Mohr, P.; Stahl, M. Intra molecular hydrogen bonding in medicinal chemistry. *J. Med. Chem.* **2010**, *53*, 2601−2611.

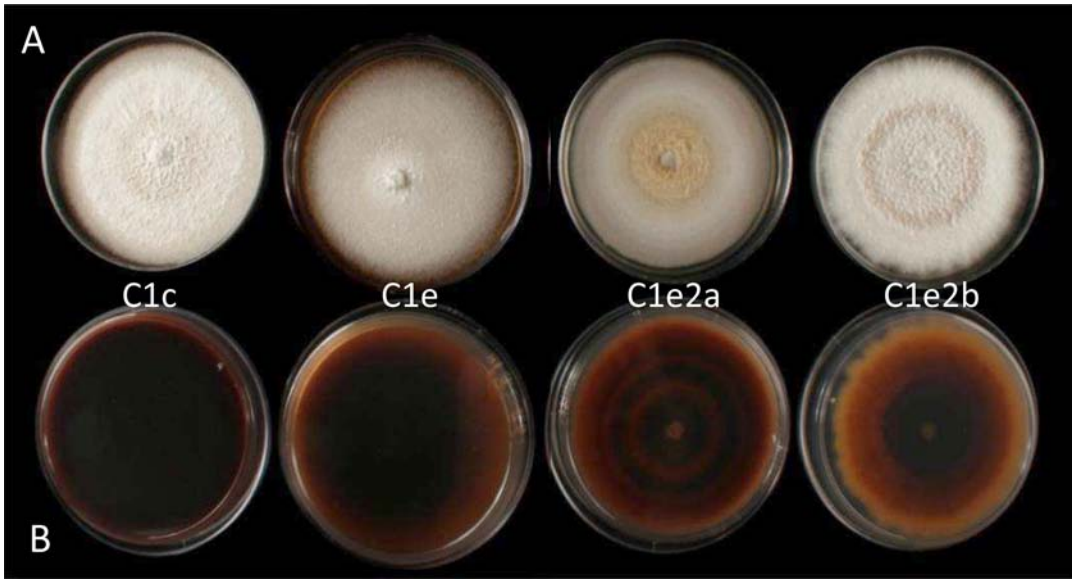

Figure 1. Morphological variants of *Edenia gomezpompae*: (A) colony appearance on potato dextrose agar (PDA) after 14 days at 25 °C; (B) reverse of culture showing typical reddish-brown pigmentation.

Fermentations of Morphological Variants of *E. gomezpompae*. Each morphological variant of *E. gomezpompae* (C1c, C1e, C1e2a, and C1e2b) was cultured in Fernbach flasks (2800 mL), each containing 1200 mL of potato dextrose broth (PDB). Each flask was inoculated with three 1 cm^2 agar plugs taken from a stock culture of *E. gomezpompae* on PDA maintained at 28 °C. Flask cultures were incubated under static conditions at 28 °C and a 12:12 h light−dark photoperiod with a T12 30 W fluorescent light (Phillips, Chihuahua, Mexico) for 90 days.

Extraction of Phytotoxins Produced by *E. gomezpompae*. At the end of fermentation, whole broth was filtered through cheesecloth to separate the culture medium from the mycelium. The culture medium (Med) was subsequently extracted with CH_2Cl_2 (equal volume × 5) and EtOAc (equal volume × 5). Both organic phases were combined and filtered over anhydrous Na_2SO_4 and concentrated in vacuo to yield 169 mg (C1c Med), 242 mg (C1e Med), 342 mg (C1e2a Med), and 149 mg (C1e2b Med) of a reddish solid. The mycelium (Myc) was macerated with 2 L of CH_2Cl_2 (× 5) and 2 L of EtOAc (× 5). The combined organic phases were filtered over anhydrous Na_2SO_4 and concentrated in vacuo to yield 821 mg (C1c Myc), 979 mg (C1e Myc), 2086 mg (C1e2a Myc), and 1901 mg (C1e2b Myc) of a reddish solid.

Isolation of Phytotoxic Compounds from *E. gomezpompae*. The combined phytotoxic extracts of morphological variants from *E. gomezpompae* (~5 g) were subjected to column chromatography on silica gel (630 g) eluting with a gradient of *n*-hexane/CH_2Cl_2 (100:0 to 0:100) and CH_2Cl_2/MeOH (99.9:0.1 to 50:50). From this chromatography, 241 fractions (200 mL each) were obtained. Fifteen fractions, F-I−F-XV, were pooled according to TLC analysis.

Bioactivity in a Petri dish bioassay showed 10 active pools (FIII−FXII). From primary fractions V (313 mg) and VII (188 mg) eluted with low-polarity *n*-hexane/CH_2Cl_2 (6:4), the known palmarumycins CP_2 (**6**) and CP_{17} (**3**) were isolated, respectively; then, they were purified by successive recrystallizations from CH_2Cl_2. The yields from this process included 128 mg of **6** and 31 mg of **3**. From fraction VIII (365.5 mg) eluted with *n*-hexane/CH_2Cl_2 (2:8) was isolated preussomerin EG_1 (**7**). After exhaustive washing with an *n*-hexane/dichloromethane mixture (1:1), as well as recrystallization from CH_2Cl_2/MeOH (99:1), 75 mg of compound **7** was obtained. Active fraction IX (111.7 mg) eluted with 100% CH_2Cl_2 was purified by successive preparative TLC (CH_2Cl_2 × 2) to yield preussomerin EG_4 (**4**) (25.9 mg) and an additional 26 mg of **7**. Fraction X (467 mg), eluted with CH_2Cl_2/MeOH (99:1), was chromatographed on a silica gel (135 g) column, eluting with a gradient of *n*-hexane/CH_2Cl_2 (50:50 to 0:100) and CH_2Cl_2/MeOH (99.9:0.1 to 50:50). Thirteen secondary fractions were obtained (F-X1−F-X13). Fraction X-9 (140 mg), eluted with CH_2Cl_2/MeOH (99:1), was further resolved by extensive preparative TLC (*n*-hexane/acetone 80:20) to yield 6.8 mg of ergosta-4,6,8(14),22-tetraen-3-one (**5**), 24 mg of preussomerin EG_3 (**9**), 6 mg of palmarumycin EG_1 (**1**), and 16.6 mg of palmarumycin CP_{19} (**2**). Primary fraction XI (870 mg), eluted with CH_2Cl_2/MeOH (98:2), was rechromatographed on a silica gel (149 g) column, eluting with a gradient of CH_2Cl_2/MeOH mixtures (99.9:0.1 to 50:50). Twelve secondary fractions were obtained (F-XI1−F-XI12). From secondary fraction XI-5 (186 mg), eluted with CH_2Cl_2/MeOH (98:2), preussomerin EG_2 (**8**) (12.1 mg) spontaneously crystallized, and after successive recrystallizations from CH_2Cl_2/MeOH (9:1), 9.5 mg of preussomerin EG_2 (**8**) was obtained. Finally, extensive TLC (*n*-hexane/acetone 80:20 × 2) of fraction XI-2 (8.5 mg) yielded an additional 3.0 mg of palmarumycin CP_{19} (**2**) (Figure 2).

Phytogrowth-Inhibitory Bioassays. The phytogrowth inhibitory activity of organic extracts from four morphological variants of *E. gomezpompae* and pure compounds was evaluated on seed germination, root elongation, and seedling respiration of two dicotyledonous species, *Amaranthus hypochondriacus* Amaranthaceae (amaranth) and *Solanum lycopersicum* var. *lycopersicum* (Solanaceae) (Italian tomato; pomodoro), and one monocotyledonous plant, *Echinochloa crus-galli*; Poaceae (barnyardgrass). Amaranth seeds were purchased at a local market in Tulyehualco in Mexico Federal District, and the tomato seeds were purchased at Semillas Berentsen, S.A. de C.V. in Celaya, Guanajuato State, whereas barnyardgrass seeds were collected from plants grown at the Instituto de Ecología (UNAM) greenhouse.

Bioassays to test the phytotoxic effects of the organic extracts of culture media and mycelia from morphological variants of *E. gomezpompae* on seedling growth were evaluated using a Petri dish bioassay.[3,4] The pure compound and organic extracts were evaluated at 50, 100, and 200 μg/mL by dilution in agar (1%). Each treatment was added to sterile agar in 6 cm Petri dishes prior to its solidification (~40 °C). Pure agar (1%) was used as negative control and agar with Rival [glyphosate: *N*-(phosphonomethyl)glycine] (Monsanto, Sao Paulo, Brazil) at 50, 100, and 200 μg/mL as positive control. Thirty seeds of each test plant were sown directly onto the agar of each Petri dish following a complete randomized design with four replications per treatment. The number of seeds used for each experiment was selected so that appreciable change in O_2 uptake could be detected. Petri dishes were wrapped in Parafilm foil and randomly placed in a germination cabinet under conditions of darkness at 27 °C. Seed germination, root

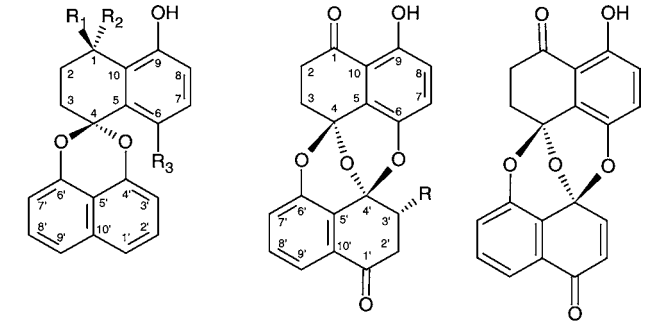

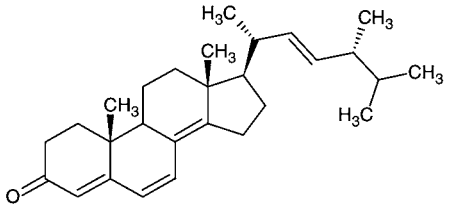

Figure 2. Structures of phytotoxic compounds isolated from the endophytic fungus *Edenia gomezpompae*.

elongation, and seedling respiration were measured 24 h after treatment for *A. hypochondriacus*, 48 h after treatment for *E. crus-galli*, and 72 h after treatment for *S. lycopersicum*.[3]

Seed respiration was measured polarographically as oxygen uptake during the germination process with a Clark-type electrode connected to a YSI 5300A biological oxygen monitor. The seedlings were transferred into a glass chamber containing 4 mL of air-saturated deionized water at 27 °C. Oxygen uptake, in the presence of different concentrations of organic extracts and pure compounds, was measured during 3 min. The requirement for oxygen was plotted as a percentage of the control at 100%.[4]

Isolation of Intact Mitochondria. Mitochondria were obtained by employing a modification of the proposed protocol by Rödinger et al.[5] One hundred and twenty grams of fresh green and turgid spinach leaves were washed with distilled water; then the central rib and the apex were removed. Afterward, they were fragmented into pieces and soaked in 200 mL of an extraction buffer (0.45 M sucrose, 15 mM MOPS, 1.5 mM EGTA, adjusting the pH to 7.4 with KOH and adding 0.6% PVP immediately prior to its use, 0.2% BSA, 10 mM DTT, and 0.2 mM PMSF). All of these were blended in a blender in five 5 s periods for each at maximal speed. Then, the homogenate was filtered through a six-layer cloth filter and centrifuged at 9000 rpm for 5 min. The pellet was discarded and the supernatant centrifuged at 16000 rpm for 10 min. The supernatant was again discarded, and the pellet that contained mitochondria was resuspended with a fine brush in 2 mL of washing buffer (0.3 M sucrose, 10 mM MOPS, 1 mM EGTA, adjusting the pH 7.2 with KOH and adding 0.2 M PMSF immediately prior to its use). Later, this suspension was placed in tubes containing Percoll concentration gradients. The gradient was previously prepared with 6 mL of 45, 25, and 5% of Percoll and 0.3 M sucrose buffer, 10 mM MOPS, pH 7.2, with KOH. The suspension was centrifuged for 45 min at 12800 rpm. Then, the intact mitochondria formed a plug, which was recovered on the 45% fraction of Percoll. This plug was added to 15 mL of resuspension buffer (0.3 M mannitol, 10 mM MOPS, 1 mM EDTA). The matrix was pH adjusted to 7.4 with KOH by adding 0.1% BSA immediately prior to its use and centrifuged during 15 min at 12800 rpm; finally, the pellet was resuspended in the buffer, and resuspension buffer was added in sufficient quantity to obtain 10 μg protein/μL (about 6 mL). The entire isolation process was carried out at 4 °C. Protein concentration was determined according to the method of Bradford.[6]

Once the mitochondria were isolated from the intact mitochondria suspension, 500 μL was transferred into a glass chamber. Oxygen consumption for the mitochondria at 27 °C was measured every 5 s for 3 min using a Clark-type electrode connected to a YSI 5300A biological oxygen monitor. The extracts were evaluated at 100 and 200 μg/mL, and the pure compounds were tested at 200 μg/mL. Only 2,4-dinitrophenol, used as positive control, was tested within the 10−800 μM concentration range. Linear regression analysis of the decreasing oxygen concentration in each extract or pure compound quantitatively determined oxygen consumption for the sample.

HPLC Analysis for Monitoring Secondary Metabolites Profile of the Extracts of Morphological Variants. HPLC analyses were performed on an Alliance 2695 system equipped with a model 2996 photodiode array detector (Waters, Milford, MA, USA). Analytical HPLC was performed using a reversed phase column (Atlantis C_{18}, 5 μm × 150 mm × 4.6 mm i.d.), at room temperature with a flow rate of 0.6−1 mL/min. The samples were filtered through a 0.4 μm nylon filter before HPLC analysis. Control of the equipment, data acquisition, and processing and management of chromatographic information were performed by the Empower 2.0 software program (Waters). The chromatograms were overlapped and colors added by using Gimp ver. 2.8.8 software, but no modifications were made in scale proportions.

Five milligrams of organic extracts from culture medium and mycelium of each morphological variant was taken and dissolved in 1 mL of acetonitrile. After filtering, they were analyzed by reversed phase HPLC using a gradient system starting with MeCN/H_2O, 80:20, to 100% MeCN for 0−30 min with a flow rate of 0.6 mL/min and maintaining this up to 40 min, with a flow rate of 1 mL/min. A known amount of an authentic pure sample of each compound was analyzed, and its retention time and peak size were determined. Retention times (t_R) of preussomerin and palmarumycin peaks were detected at wavelengths of 225 nm: **8** (t_R 13.9 min), **1** (t_R 17.4 min), **9** (t_R 18.0 min), **4** (t_R 18.6 min), **7** (t_R 19.5 min), **2**, **3** (t_R 20.1 min), and **6** (t_R 23.3 min).

Statistical Analysis. Experimental results concerning the effect of culture media and the mycelia extracts from morphological variants of *E. gomezpompae* and pure compounds on phytogrowth inhibitory activity and intact mitochondrial oxygen consumption were analyzed by analysis of variance (ANOVA) and Tukey statistical tests[7] utilizing GraphPad Prism ver. 5.01 statistical computer software (GraphPad software, La Jolla, CA, USA). The IC_{50} value (50% inhibitory concentration) for each activity was calculated by Probit analysis[8] based on the average percentage of inhibition obtained at each concentration of the different treatments. Data are represented as mean ± standard deviation (SD). A P value of ≤0.05 (*) was employed to indicate statistical significance.

Palmarumycin EG_1 (1). Colorless solid powder, mp 230 °C (decomp); $[\alpha]^{25}_D$ = −14 (c 0.1, $CHCl_3$); UV λ_{max} (log ε) 328.5 (3.3), 325.5 (3.13), 314.5 (3.46), 310.6 (3.42), 300.5 (3.58), 296 (3.54), 288 (3.58), 255 (2.82), 226.5 (4.38), 212.6 (4.16); IR t_{max} (KBr) 3453, 3063, 1608, 1468, 1409, 1376, 1264, 1053 cm^{-1}; ^1H and ^{13}C NMR, see Table 2; EIMS m/z 350 [M^+ (19)], 318 (100), 301 (7), 300 (7), 273 (7), 175 (7), 160 (24), 144 (7), 131 (8), 115 (5); HRMS m/z 350.11540 (calcd for $C_{21}H_{18}O_5$ 350.11542).

Preussomerin EG_4 (4). Yellowish amorphous solid, mp 242.1−246.0 °C; UV λ_{max} (log ε) 360 (3.65), 332 (3.47), 315 (3.56), 281 (3.12), 258 (4.17), 243.5 (4.01), 220 (4.48) nm; IR t_{max} (KBr) 3434, 3085, 1690, 1642, 1593, 1473, 1365, 1331, 1291, 1230 cm^{-1}; ^1H and ^{13}C NMR, see Table 3; ESIMS m/z 350 [M^+ (100)], 332 (7), 305 (4), 192 (9), 176 (82), 174 (34), 175 (19), 147 (8), 120 (4), 91 (4), 77 (4), 55 (5); HRMS m/z 350.0788 (calcd for $C_{20}H_{14}O_6$, 350.0790).

X-ray Crystallographic Analysis of Palmarumicyns CP_{19} (2) and CP_{17} (3). Colorless crystals of dimension 0.36 × 0.18 × 0.2 mm and yellow prisms of dimension 0.30 × 0.20 × 0.20 mm were obtained from slow evaporation of CH_2Cl_2 solution, for CP_{19} (**2**) and CP_{17} (**3**), with empirical formulas $C_{21}H_{18}O_4$ and $C_{20}H_{14}O_5$ and M_r = 334.35 and M_r = 334.31, respectively. CP_{19} (**2**) crystallized in monoclinic $P2_1$ (no.

dx.doi.org/10.1021/jf500965k | J. Agric. Food Chem. 2014, 62, 3553−3562

4) and CP_{17} (**3**) crystallized in triclinic system, P-1 (no. 2). The cell dimensions for CP_{19} (**2**) were a = 12.927(3) Å, b = 7.925(2) Å, c = 17.046(4) Å, α = 90°, β = 109.883(3)°, γ = 90°, V = 1642.2(7) Å^3, Z = 4, D_{calcd} = 1.352 Mg/m^3, mμ 0.093 mm^{-1}, and F(000) = 704, and those for CP_{17} (**3**) were a = 8.5101(6) Å, b = 12.8482(9) Å, c = 15.1746(10) Å, α = 66.0760(10)°, β = 83.5180(10)°, γ = 89.6990(10)°, V = 1505.44(18) Å^3, Z = 4, D_{calcd} = 1.475 Mg/m^3, mμ 0.107 mm^{-1}, and F(000) = 696. Temperature = 298(2) K. Both compounds were irradiated with Mo Kα radiation (λ = 0.71073 Å) on the Bruker Smart APEX diffractometer with AXS CCD area detector using a SMART program.[17] The data reduction was performed with the SAINT program.[9] Totals of 12965 and 12393 reflections were collected, of which 6016 (R_{int} = 0.0644) and 5289 (R_{int} = 0.0324) were independent, respectively. The structures were solved by direct methods and refined using full-matrix least-squares on F^2 using the programs SHELXS[10] and SHELXL,[10] respectively. The ORTEP-3[11] program was used to prepare the figures. Two crystallographic independent molecules were found in the unit cell in both compounds. The final values S = 0.846, R1 = 0.545 and wR2 = 0.0884 were based on 3304 reflections observed, 459 parameters for CP_{19} (**2**), and S = 0.865, R1 = 0.0362, and wR2 = 0.0728 were based on 5289 reflections observed, 463 parameters for CP_{17} (**3**). The largest different peak and hole were 0.400 and −0.148 e Å^{-3} and 0.147 and −0.162 e Å^{-3}, respectively.

RESULTS AND DISCUSSION

Morphological Variants of *E. gomezpompae*. The endophytic fungus *E. gomezpompae* was obtained from the leaves of *C. acuminata* collected at the Ecological Reserve "Eden"; four isolates of this species corresponding to strains C1c, C1e, C1e2a, and C1e2b were obtained. The differences in macroscopic characteristics exhibited by these strains were significant (Figure 1). However, microscopic characteristics and molecular studies revealed they were from the same species;[1] therefore, they were morphological variants of *E. gomezpompae* (isolate C1c). The morphological characteristics of microorganisms can be affected during antagonistic interspecific interactions due to their phenotypic plasticity, that is, the ability of a single genotype to produce more than one alternative form of morphology, physiological state, and/or behavior in response to environmental conditions.[12] Therefore, it is important to study whether the biological activity is modified by the morphological variants of the fungus, particularly because many secondary metabolites of fungal origin are of economic value due to their many and diverse biological activities.

In this context, we investigated the phytotoxic properties of the culture media and mycelia organic extracts of four morphological variants of *E. gomezpompae* as well as those of their pure compounds. The strains were grown under static conditions on PDB. In these conditions the mycelia of the fungi were developed better. The culture media and the mycelia were extracted with CH_2Cl_2 and EtOAc. The initial phytotoxic activity of the resulting extracts was evaluated on seed germination, root elongation, and seedling respiration of *A. hypochondriacus*, *S. lycopersicum*, and *E. crus-galli* using a Petri dish bioassay. According to the results summarized in Table 1, all extracts inhibited seed germination, root elongation, and seedling respiration of the three target species in a concentration-dependent manner (data not shown). The extracts from culture media were more phytotoxic than the mycelia extracts, showing IC_{50} values of <200 μg/mL. The extracts of morphological variant C1c showed the highest phytotoxic potential.

Isolation of Phytotoxic Compounds Produced by *E. gomezpompae*. TLC and HPLC chromatograms of the morphological variant extracts exhibited similar profiles. Therefore, the extracts were combined and fractionated by column chromatography for chemical analysis. This process led to the isolation of compounds **1**−**9**, including two new naphthoquinone spiroketals, namely, palmarumycin EG_1 (**1**) and a preussomerin EG_4 (**4**), which were characterized by extensive spectroscopic methods. In addition, known preussomerins EG_1−EG_3 (**7**−**9**) and palmarumycins CP_{19} (**2**), CP_{17} (**3**), and CP_2 (**6**) and the ergosta-4,6,8(14),22-tetraen-3-one (**5**) were obtained (Figure 2). Compounds **2**, **3**, and **5** are new to this species. Compounds **6**−**9** were identified by comparison with authentic samples;[2] compounds **2**,[2] **3**,[13,14] and **5**[15,16] were identified from their IR and ^{1}H NMR spectroscopic data. These were identical to those previously described in the literature.

Structural Elucidation of Compounds 1 and 4. *Palmarumycin EG_1 (**1**).* The molecular formula was established

Table 1. Phytogrowth-Inhibitory Activity of the Organic Extract from Morphological Variants of *Edenia gomezpompae* on the Germination, Root Elongation, and Seedling Respiration of *Amaranthus hypochondriacus*, *Solanum lycopersicum*, and *Echinochloa crus-galli*

		IC_{50} (μg/mL)		
organic extract[a]	seed	germination	root growth	respiration
C1c Myc	*A. hypochondriacus*	>200	>200	>200
	S. lycopersicum	128.7	53	96.8
	E. crus-galli	112.5	197.8	66.9
C1c Med	*A. hypochondriacus*	>200	82.5	161.5
	S. lycopersicum	194.5	109.9	147.3
	E. crus-galli	>200	15.1	56.9
C1e Myc	*A. hypochondriacus*	>200	>200	>200
	S. lycopersicum	>200	>200	>200
	E. crus-galli	>200	>200	>200
C1e Med	*A. hypochondriacus*	>200	112.2	147.9
	S. lycopersicum	>200	173.5	152.3
	E. crus-galli	143.8	88.67	55.9
C1e2a Myc	*A. hypochondriacus*	>200	>200	>200
	S. lycopersicum	>200	>200	>200
	E. crus-galli	>200	>200	>200
C1e2a Med	*A. hypochondriacus*	>200	>200	>200
	S. lycopersicum	>200	>200	>200
	E. crus-galli	>200	>200	>200
C1e2b Myc	*A. hypochondriacus*	>200	>200	>200
	S. lycopersicum	>200	>200	139.1
	E. crus-galli	>200	>200	>200
C1e2b Med	*A. hypochondriacus*	>200	127.7	132.5
	S. lycopersicum	144.1	131.8	>200
	E. crus-galli	187.2	198.2	197.8
Rival	*A. hypochondriacus*	>200	115.5	114.1
	S. lycopersicum	>200	105.7	83.5
	E. crus-galli	>200	94.9	84.9

[a]Rival = glyphosate, *N*-(phosphonomethyl) glycine (positive control); Med, culture medium; Myc, mycelium.

dx.doi.org/10.1021/jf500965k | J. Agric. Food Chem. 2014, 62, 3553−3562

Table 2. NMR Spectroscopic Data for Palmarumycin EG_1 (1) (500 MHz for ^1H and 125 MHz for ^{13}C)

position	δ_C	DEPT mult	δ_H (mult, J in Hz)	HMBC H→C	NOESY
1	75.5	CH	4.85 (1H, pseudo t dd, 6.0, 7.5)	C-2, -3, -5, -9, -10, OCH_3	3, 2a, CH_3O-1, OH-9
2	27.2	CH_2	1.98 m	C-1, -3, -4,	2b, 3
			2.42 m	C-1, -3, -4, -10	2a, 3
3	22.5	CH_2	2.13 m	C-1, -2, -4, -5	1, 2a, 2b, CH_3O-1
4	102.5	C			
5	122.1	C			
6	149.5	C			
7	119.2	CH	6.94 (1H, d, 9.0)	C-6, -9, -10	
8	120.0	CH	6.96 (1H, d, 9.0)	C-6, -9, -10	
9	149.4	C			
10	119.5	C			
1′	121.2	CH	7.56 (1H, dd, 1.0, 7.5)	C-3′, -4′, -5′, -10′	2′, 3′
2′	127.5	CH	7.46 (1H, dd, 7.5, 7.5)	C-3′, -4′, -10′	1′, 3′
3′	110.4	CH	7.00 (1H, dd, 1.0, 7.5)	C-1′, -4′, -5′	2′, 1′
4′	146.5	C			
5′	113.8	C			
6′	147.1	C			
7′	110.5	CH	7.02 (1H, dd, 1.0, 7.5)	C-5′, -6′, -9′	8′, 9′
8′	127.6	CH	7.47 (1H, dd, 7.5, 8.5)	C-6′, -7′, -10′	7′, 9′
9′	121.6	CH	7.57 (1H, dd, 1.0, 8.5)	C-5′, -6′, -7′, -10′	8′, 7′
10′	134.2	C			
OH-6			7.57 (1H, s)	C-6, -7	
OH-9			7.03 (1H, s)	C-8, -9	1, CH_3O-1
CH_3O-1	54.2	CH_3	3.48 (3H, s)	C-1	1, 3, OH-9

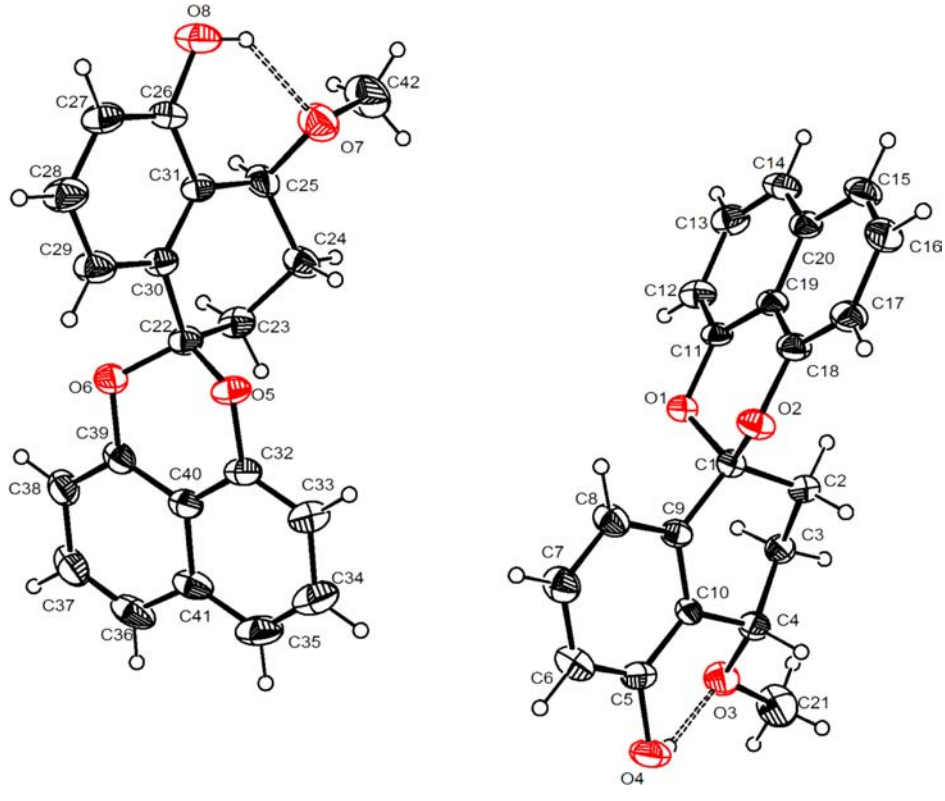

Figure 3. X-ray crystal structure of palmarumicyn CP_{19} (2).

as $C_{21}H_{18}O_5$ (13 unsaturations) by HRMS. The IR spectrum displayed the absorption bands indicative of the presence of hydroxyl (3453 cm^{-1}) and aromatic groups (1608 cm^{-1}). ^1H and ^{13}C NMR spectra suggested that the molecule was a deoxypreussomerin type of compound related to palmarumycin CP_{19} (2). The 1,8-dihydroxynaphthalene ring system and the substitution pattern in the nonaromatic ring in both molecules were identical, but the third aromatic ring was different. Thus, the two exchangeable singlets D_2O at δ 7.57 (OH-6) and 7.03 (OH-9), plus the AB-spin system at δ 6.94 (d, J = 9.0 Hz; H-7) and 6.96 (d, J = 9.0 Hz; H-8) in the ^1H NMR spectrum indicated the presence of a *p*-hydroquinone fragment in the

dx.doi.org/10.1021/jf500965k | J. Agric. Food Chem. 2014, 62, 3553−3562

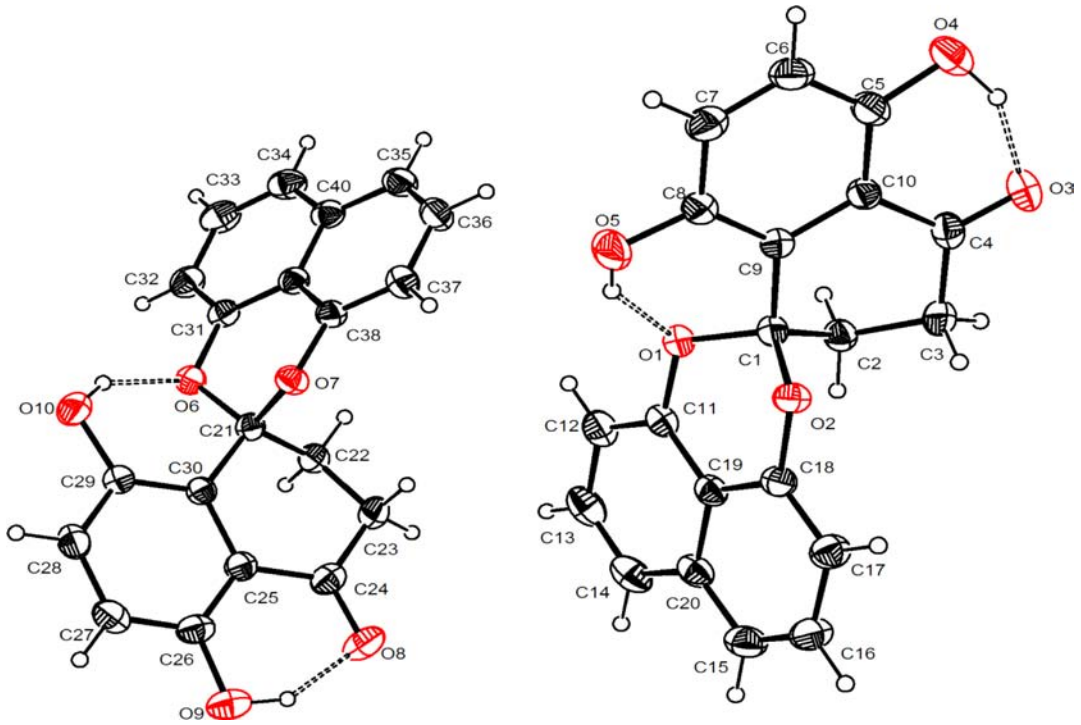

Figure 4. X-ray crystal structure of palmarumicyn CP_{17} (**3**).

Table 3. NMR Spectroscopic Data for Preussomerin EG_4 (4) (500 MHz for ^1H and 125 MHz for ^{13}C)

position	δ_C	mult DEPT	δ_H (mult, J in Hz)	HMBC H→C	NOESY
1	202.2	C			
2a	33.7	CH_2	2.90 (1H, ddd, 19.5, 5.5, 2.0)	C-1, -3, -4, -10	2b, 3a, 3b
2b			3.36 (1H, ddd, 19.5, 13.5, 5.5)	C-1, -3, -4	2a, 3a, 3b
3a	32.7	CH_2	2.50 (1H, ddd, 13.5, 13.5, 5.5)	C-1, -2, -4, -5, -6, -6′	2a, 2b, 3b,
3b			2.71 (1H, ddd, 13.5, 5.5, 2.0)		2a, 2b, 3a
4	93.3	C			
5	120.0	C			
6	141.4	C			
7	126.0	CH	7.03 (1H, d, 9.5)	C-4, -5, -6, -9, -10	8
8	120.6	CH	6.91 (1H, d, 9.5)	C-5, -6, -7, -9, -10	7, OH-9
9	157.2	C			
10	113.0	C			
1′	195.8	C			
2a′	33.8	CH_2	2.86 (1H, ddd, 19.0, 5.5, 2.0)	C-1′, -3′, -4′, -10′	2b′, 3a′, 3b′
2b′			3.28 (1H, ddd, 19.0, 13.5, 5.5)	C-1′, -3′, -4′	2a′, 3a′, 3b′
3a′	32.8	CH_2	2.46 (1H, ddd, 13.5, 13.5, 5.5)	C-1′, -2′, -4′, -5′, -6, -6′	2a′, 2b′, 3b′
3b′			2.74 (1H, ddd, 13.5, 5.5, 2.0)	C-1′, -2′, -4′, -5′, -6, -6′	2a′, 2b′, 3a′
4′	93.3	C			
5′	122.5	C			
6′	149.4	C			
7′	120.5	CH	7.62 (1H, dd, 1.0, 8.0)	C-4′, -5′, -6′, -8′, -9′, -10′	8′, 9
8′	130.8	CH	7.39 (1H, dd, 8.0, 8.0)	C-5′, -6′, -7′, -9′, -10′	7′, 9′
9′	121.4	CH	7.07 (1H, dd, 1.0, 8.0)	C-4′, -5′, -6′, -7′, -8′, -10′	8′, 7′
10′	130.9	C			
OH-9			11.69 (1H, s)	C-1, -7, -8, -9, -10	8

molecule. Signals at δ 149.5 and 149.4 in the ^{13}C NMR confirmed this assignment. Furthermore, the correlations observed in the NOESY and HMBC spectra supported the presence of the hydroxyl groups at C-6 and C-9 of the palmarumycin skeleton (Table 2). The signals and coupling pattern in the ^1H NMR spectrum for the oxymethine (δ 4.85, H-1, pseudo-t dd, J = 6.0, 7.5 Hz) and methoxy groups (s, δ_H 3.48) were similar to those of palmarumycin CP_{19} (**2**), suggesting that **1** was its 6-hydroxy analogue; the HMBC and $^1H-^1H$ NOESY data (Table 2), as well as the mass fragments at m/z 318 and 160 were assignable to hydrobenzoquinone and 1,8-dihydroxynaphthalene subunits, respectively, were consistent with this structural proposal. Finally the negative value of

dx.doi.org/10.1021/jf500965k | J. Agric. Food Chem. 2014, 62, 3553−3562

the specific optical rotation led us to propose the same *S* absolute configuration at C-1 as for **2**.[14,17,18]

Palmarumycins CP_{19} (**2**) and CP_{17} (**3**) were previously described by Martínez-Luis et al. as new metabolites from *Edenia* sp. obtained from the leaves of *Petrea volubilis* L.[14] The spectroscopic and spectrometric properties of both compounds were identical to those reported. In the present study, however, we confirmed the structural assignments of **2** and **3** by single-crystal diffraction X-ray analysis (Figures 3 and 4).

Preussomerin EG_4 (4). Mass spectrometric analysis of preussomerin EG_4 (**4**) gave a molecular ion at *m/z* 350 ($C_{20}H_{14}O_6$, 14 unsaturations), thus differing from preussomerin EG_1 (**7**) by 2 mass units. The infrared spectrum of **4** showed absorption bands for a conjugated carbonyl at 1642 cm^{-1}. As with compound **7**, the NMR spectrum contained resonances for 1,2,3-trisubstituted and 1,2,3,4-tetrasubstituted aromatic rings. The most obvious differences in the spectra (Table 3) were the absence of the two vinyl signals (δ_C/δ_H 133.27/6.56 and 141.24/7.17) for the *cis*-olefinic nuclei of preussomerin EG_1 (**7**).[2] Instead, the ^1H NMR spectrum of **4** displayed four self-coupled aliphatic protons in the upfield region of the spectrum between δ 2.50 (H-2′) and 3.36 (H-3′), which were correlated with the signals at δ 33.8 and 32.8, respectively, in the HSQC experiment. Two conjugated carbonyls appearing at δ_C 195.8 and 202.2 were also detected in the ^{13}C NMR spectrum, which were assigned to C-1′ and C-1, respectively, on the basis of the observed HMBC correlations (Table 3). The other HMBC and NOESY correlations summarized in Table 3, as well as the mass fragments at *m/z* 174, 175, and 176 observed in the MS spectrum, were in agreement with structure **4** for the new natural product,[19] which was given the common name of preussomerin EG_4.

Phytogrowth-Inhibitory Activity of the Natural Compounds. Natural products **2**–**9** were evaluated for their ability to inhibit the seed germination, root elongation, and seedling respiration of *A. hypochondriacus*, *S. lycopersicum*, and *E. crus-galli*. Figure 5 depicts the phytotoxic effect of the isolate compounds at 100 μg/mL. The results are expressed as inhibition percentages. In general, the compounds tested exhibited a significant phytotoxic effect and were more potent as germination and root elongation inhibitors than as seedling respiration inhibitors (Figure 5). All eight compounds reduced the germination of the three target species. Compounds **4** and **7**–**9** at 100 μg/mL inhibited germination by >50%, being more potent than the positive control Rival (glyphosate) (Figure 5A). Compounds **2**, **8**, and **9** were more active as root elongation inhibitors (>50%) of *A. hypochondriacus* and *E. crus-galli*. Only compound **8** significantly inhibited (>50%) the root elongation of three species (Figure 5B). On the other hand, the compounds tested also significantly inhibited the seedling respiration of *S. lycopersicum*. The phytotoxic activity was comparable to that of the positive control. Only compound **2** significantly inhibited the oxygen consumption of three seedlings, and compounds **4** and **7** also significantly inhibited the seedling respiration of *S. lycopersicum* and *E. crus-galli* (Figure 5C). In summary, all compounds inhibited seed germination, root elongation, and seedling respiration of the three target species in a concentration-dependent manner. Table 4 summarizes the phytotoxic effect of the isolate compounds expressed as IC_{50} values. The IC_{50} values confirm that, in general, compounds **2**–**9** were more potent as germination and root elongation inhibitors than as seedling respiration inhibitors.

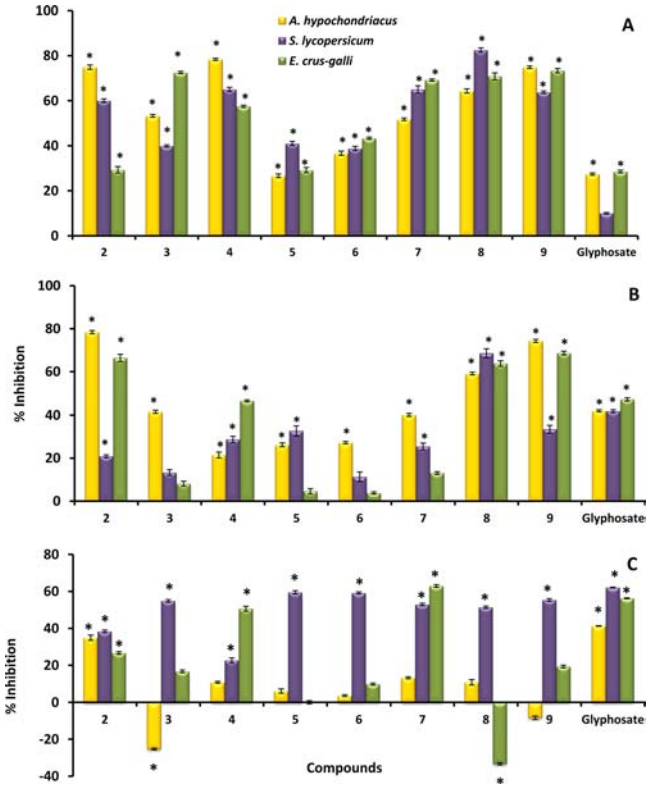

Figure 5. Phytotoxic effect of bioactive compounds (100 μg/mL) isolated from endophytic fungus *Edenia gomezpompae* on (A) seed germination, (B) root elongation, and (C) seedling respiration of *Amaranthus hypochondriacus*, *Solanum lycopersicum*, and *Echinochloa crus- galli*. Palmarumycins CP_{19} (**2**) and CP_{17} (**3**), preussomerin EG_4 (**4**), ergosta-4,6,8(14),22-tetraen-3-one (**5**), palmarumycin CP_2 (**6**), and preussomerins EG_1 (**7**), EG (**8**), and EG_3 (**9**). A positive value represents inhibition; a negative value represents stimulation. Vertical bars represent SD, $n = 4$; (∗)$P < 0.05$.

Mitochondrial Oxygen Consumption. In an attempt to discover potential herbicidal agents with an effect on respiration, the phytotoxic extracts from morphological variants of *E. gomezpompae* and pure compounds were further evaluated for their capacity to inhibit mitochondrial respiration in intact mitochondria isolated from spinach. In general, the extracts demonstrated significant inhibition in the mitochondrial respiratory chain at the highest test concentration of 200 μg/mL (Figure 6). However, the inhibitory effect was low. Both organic extracts of morphological variant C1e2a and the mycelium extracts of morphological variants C1e were most active on mitochondrial respiration, inhibiting its activity by approximately 40%. It is noteworthy that extracts of morphological variant C1e2a were the least phytotoxic on the three plants tested (IC_{50} values of >200 μg/mL); however, these were the extracts with the greatest effect on mitochondrial oxygen consumption, indicating the presence of the phytotoxic compounds.

Furthermore, oxygen consumption in intact mitochondria was significantly inhibited by compounds **2**–**9**; however the effect was lower than that of the positive control. In general, preussomerins were more active than palmarumycins. Preussomerins EG_4 (**4**) and EG_1 (**7**) and palmarumycins CP_{17} (**3**) and CP_2 (**6**) were more active, inhibiting 34, 26, 17, and 26%, respectively (Figure 6).

Table 4. Phytogrowth-Inhibitory Activity of Isolated Compounds from *Edenia gomezpompae* on the Germination, Root Elongation, and Seedling Respiration of *Amaranthus hypochondriacus*, *Solanum lycopersicum*, and *Echinochloa crus-galli*

		IC_{50} (μM)		
compd[a]	seed	germination	root growth	seedling respiration
2	*A. hypochondriacus*	194.0	180.8	416.5
	S. lycopersicum	240.4	>598.8	378.7
	E. crus-galli	516.2	213.5	531.7
3	*A. hypochondriacus*	272.1	342.5	594.6
	S. lycopersicum	378.4	>598.8	238.0
	E. crus-galli	206.6	471.3	>598.8
4	*A. hypochondriacus*	179.4	330.6	>571.4
	S. lycopersicum	214.6	478.0	>571.4
	E. crus-galli	237.1	279.1	264.9
5	*A. hypochondriacus*	466.0	465.1	>510.2
	S. lycopersicum	429.6	337.2	204.3
	E. crus-galli	285.7	276.0	>510.2
6	*A. hypochondriacus*	397.2	562.0	>628.9
	S. lycopersicum	347.2	>628.9	272.0
	E. crus-galli	380.5	>628.9	>628.9
7	*A. hypochondriacus*	271.8	300.0	>574.7
	S. lycopersicum	216.1	534.8	277.3
	E. crus-galli	207.8	>574.7	216.9
8	*A. hypochondriacus*	208.2	225.7	>546.5
	S. lycopersicum	168.6	199.7	259.0
	E. crus-galli	183.3	214.2	>546.5
9	*A. hypochondriacus*	170.5	166.6	>526.3
	S. lycopersicum	198.4	355.8	240.5
	E. crus-galli	182.1	195.8	>526.3
Rival	*A. hypochondriacus*	>1183.4	683.4	675.1
	S. lycopersicum	>1183.4	625.4	494.1
	E. crus-galli	>1183.4	561.5	502. 4

[a]Rival = glyphosate, *N*-(phosphonomethyl) glycine (positive control).

HPLC Analysis of Secondary Metabolites Production from Extracts of Morphological Variants. Preussomerin and palmarumycin contents in morphological variants of *E. gomezpompae* were analyzed by HPLC (Figure 7). The chromatographic profiles showed that the four variants showed differences in the concentration of the major components (Table 5). These results could be due to the phenotypic plasticity of *E. gomezpompae*; accordingly, each phenotype, with different morphology and different biological activity, exhibited also important differences in chemical compound production.

The highest activity on mitochondrial respiration of culture broth extracts of morphological variants C1e and C1e2a could be associated with the presence of many peaks in the chromatographic region from 0 to 7 min, which should be further investigated. On the other hand, the highest activity against seed germination, root elongation, and seedling respiration of C1c, C1e, and C1e2b culture media extracts

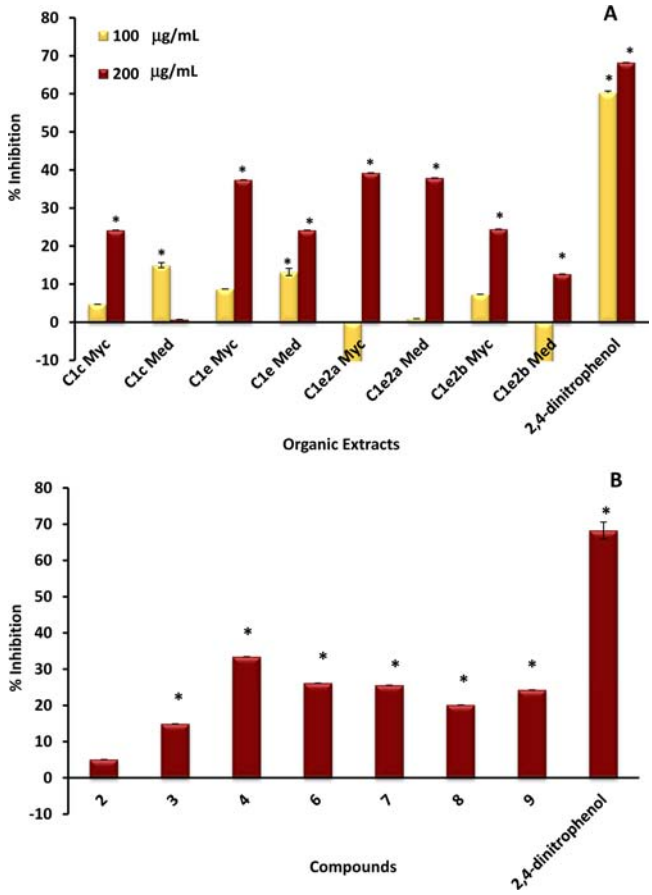

Figure 6. Inhibitory activity of the organic extract (100 and 200 μg/mL) from (A) morphological variants of *Edenia gomezpompae* and (B) phytotoxic compounds (200 μg/mL) on mitochondrial oxygen consumption on intact mitochondria isolated from spinach. Palmarumycins CP_{19} (**2**) and CP_{17} (**3**), preussomerin EG_4 (**4**), palmarumycin CP_2 (**6**), and preussomerins EG_1 (**7**), EG (**8**), and EG_3 (**9**). A positive value represents inhibition; a negative value represents stimulation. Vertical bars represent SD, $n = 4$; (*) $P < 0.05$.

can be associated with the presence in high amounts of preussomerin EG_3 (**8**), and the highest inhibitory activity of C1c of mycelium extracts was associated with the highest abundance of palmarumycin CP_2 (**6**)

Because all components detected in each variant were active, they are of possible benefit for the plant species hosting the fungus in its natural habit. The endophytic fungi generally exist harmlessly within their host, but under different conditions they could be facultative pathogens.[20] On the other hand, the secondary metabolites produced by endophytic fungi play a role in vivo and are important for numerous metabolic interactions between fungi and their plant hosts, such as signaling and regulation of the symbiosis.[21,22] Some may also serve in the overall biology of the plant, especially as it relates to insects and disease, as well as other environmental stresses including drought tolerance.[23−25] One of the important roles of endophytic fungi is to initiate the biological degradation of dead or dying plant hosts, which is necessary for nutrient recycling.[26] As a result, it is possible that the phytotoxins produced by *E. gomezpompae* are involved in the role in plant host defense and/or in the biological degradation of dead or dying plant hosts.

dx.doi.org/10.1021/jf500965k | J. Agric. Food Chem. 2014, 62, 3553−3562

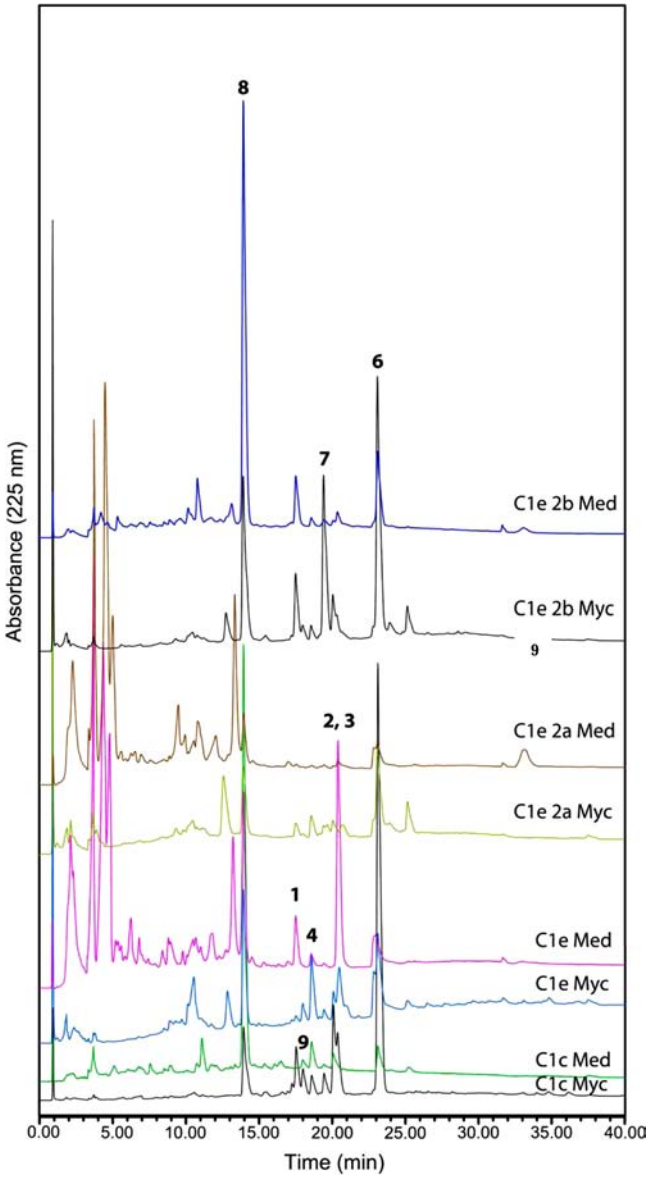

Figure 7. HPLC profiles of preussomerins and palmarumycins present in organic extract from morphological variants of *E. gomezpompae* in static liquid culture fermentation at 225 nm. Palmarumycins EG_1 (**1**), CP_{19} (**2**), and CP_{17} (**3**), preussomerin EG_4 (**4**), palmarumycin CP_2 (**6**), and preussomerins EG_1 (**7**), EG (**8**), and EG_3 (**9**).

Table 5. HPLC Analysis of Preussomerins and Palmarumycins Present in Organic Extract from Morphological Variants of *E. gomezpompae*

morphological variant[a]	compds detected	major compds (% area)
C1c Myc	**1**, **2**, **3**, **4**, **6**, **7**, **8**, **9**	**6** (54.6), **3** (9.1), **8** (8.6), **1** (7.3)
C1c Med	**1**, **3**, **4**, **6**, **7**, **8**, **9**	**8** (62.4), **6** (8.7), **3** (8.5)
C1e Myc	**2**, **3**, **4**, **6**, **8**	**8** (29.8), **6** (25.6), **4** (16.0)
C1e Med	**1**, **3**, **4**, **6**, **8**	**3** (38.8), **8** (22.9), **1** (8.3)
C1e2a Myc	**1**, **2**, **3**, **4**, **6**, **7**, **8**, **9**	**8** (20.4), **6** (32.3)
C1e2a Med	**6**, **8**	**8** (14), **6** (12)
C1e2b Myc	**1**, **2**, **3**, **4**, **6**, **7**, **8**, **9**	**6** (32.4), **8** (20.1), **7** (19.6), **1** (7.3)
C1e2b Med	**1**, **2**, **3**, **4**, **6**, **7**, **8**, **9**	**8** (63.2), **6** (14.5), **1** (8.6)

[a]Med, culture medium; Myc, mycelium.

In summary, naphthoquinone spiroketals **2**–**8** biosynthesized by four morphological variants of *E. gomezpompae* possess phytotoxic properties against seed germination, root elongation, and seedling respiration of two dicotyledon species, *A. hypochondriacus* and *S. lycopersicum*, and one monocotyledon plant, *E. crus-galli*, and a slight effect on the respiration of intact mitochondria. According to these results, further studies will be carried out to better understand the mechanism of action associated with the phytotoxic effects of the organic extracts and selected phytotoxins produced by *E. gomezpompae*. In particular, preussomerins EG_4 (**4**) and EG_1 (**7**) and palmarumycins CP_{17} (**3**) and CP_2 (**6**) will be considered for exploration in the immediate future on the basis of their inhibitory effect on oxygen consumption in intact mitochondria.

■ ASSOCIATED CONTENT

Ⓢ Supporting Information

Bioassays to test the phytotoxic effects of isolated compounds from morphological variants of *E. gomezpompae* on the germination, root elongation, and seedling respiration of *A. hypochondriacus*, *S. lycopersicum*, and *E. crus-galli* were evaluated at 50, 100, and 200 μg/mL. This material is available free of charge via the Internet at http://pubs.acs.org. Crystallographic data for palmarumycins CP_{19} (**2**) and CP_{17} (**3**) reported in this paper have been deposited at the Cambridge Crystallographic Data Centre (CCDC) as supplementary publications CCDC 967944 and CCDC 96794, respectively. Copies of the data can be obtained, free of charge, from http://www.ccdc.cam.ac.uk/data_request/cif.

■ AUTHOR INFORMATION

Corresponding Author

*(M.L.M.-R.) Phone: + 52 (55) 56 22 44 32. Fax: + 52 (55) 56 16 22 17. E-mail: mlmacias@unam.mx, mamaciasr@gmail.com.

Funding

This work was supported by Grants CONACyT 81017 and 179194.

Notes

The authors declare no competing financial interest.

■ ACKNOWLEDGMENTS

We thank Dr. Ana Luisa Anaya Lang and Q.A. Blanca Estela Hernández-Bautista from Instituto de Ecología, UNAM, for their valuable support during the development of this research. We are also grateful to Beatriz Quiroz, Héctor Ríos, Elizabeth Huerta, Ma. de los Ángeles Peña, Isabel Chávez, Luis Velasco-Ibarra, Javier Pérez Flores, and Rocío Patiño from Instituto de Química, UNAM, for recording NMR, MS IR, and UV spectra. We are also grateful to Carmen Loyola from Instituto de Biología, UNAM, for her valuable help with the photographic work and to Jordi Muria González for his help in HPLC analyses.

■ REFERENCES

(1) González, M. C.; Anaya, A. L.; Glenn, A. E.; Saucedo-García, A.; Macías-Rubalcava, M. L.; Hanlin, R. T. A new endophytic ascomycete from El Eden Ecological Reserve, Quintana Roo, Mexico. *Mycotaxon* **2007**, *101*, 251–260.

(2) Macías-Rubalcava, M. L.; Hernández-Bautista, B. E.; Jiménez-Estrada, M.; González-Villaseñor, M. C.; Glenn, A. E.; Hanlin, R. T.; Saucedo-García, A.; Muria-González, J. M.; Hernández-Ortega, S.; Anaya, A. L. Naphthoquinone spiroketal with allelochemical activity

from the newly discovered endophytic fungus *Edenia gomezpompae*. *Phytochemistry* **2008**, *69*, 1185−1196.
(3) Macías-Rubalcava, M. L.; Hernández-Bautista, B. E.; Oropeza, F.; Duarte, G.; González, C.; Glenn, A. E.; Hanlin, R. T.; Anaya, A. Allelochemical effects of volatile compounds and organic extracts from *Muscodor yucatanensis*, a tropical endophytic fungus from *Bursera simaruba*. *J. Chem. Ecol.* **2010**, *36*, 1122−1131.
(4) Céspedes, C. L.; Calderón, J. S.; Salazar, J. R.; Lotina-Hennsen, B.; Segura, R. Plantgrowth inhibitory activity of cedrelanolide from *Cedrela salvadorensis*. *J. Chem. Ecol.* **2001**, *27*, 137−149.
(5) Rödiger, A.; Baudisch, B.; Klösgen, R. B. Simultaneous isolation of intact mitochondria and chloroplasts from a single pulping of plant tissue. *J. Plant Physiol.* **2009**, *167*, 620−624.
(6) Bradford, M. M. A rapid and sensitive method for the quantitation of microgram quantities of protein utilizing the principle of protein-dye binding. *Anal. Biochem.* **1976**, *7*, 248−254.
(7) Mead, R.; Curnow, R. N.; Hasted, A. M. Statistical methods. In *Agriculture and Experimental Biology*, 3rd ed.; Chapman and Hall, CRC: Boca Raton, FL, USA, 2002.
(8) Zar, J. H. *Biostatistical Analysis*; Prentice Hall: Upper Saddle River, NJ, USA, 2007.
(9) Bruker. *SAINT & SMART Program*; Bruker AXS Inc.: Madison, WI, USA, 2007.
(10) Sheldrick, G. M. A short history of SHELX. *Acta Crystallogr.* **2008**, *A64*, 112−122.
(11) Farrugia, L. J. ORTEP-3. *J. Appl. Crystallogr.* **2012**, *45*, 849−854.
(12) West-Eberhard, M. J. Phenotypic plasticity and the origins of diversity. *Annu. Rev. Ecol. Evol. Syst.* **1989**, *20*, 249−278.
(13) Martínez-Luis, S.; Della-Togna, G.; Coley, P. D.; Kursar, T. A.; Gerwick, W. H.; Cubilla-Rios, L. Antileishmanial constituents of the Panamanian endophytic fungus *Edenia* sp. *J. Nat. Prod.* **2008**, *71*, 2011−2014.
(14) Martínez-Luis, S.; Cherigo, L.; Spadafora, C.; Gerwick, W. H.; Cubilla-Rios, L. Additional anti-leishmanial constituents of the Panamanian endophytic fungus *Edenia* sp. *Rev. Latinoam. Quim.* **2009**, *37*, 104−114.
(15) Tanaka, N.; Hosoi, K. I.; Tanaka, D.; Takahashi, M. Photochemical reaction of ergosta-4,6,8(14),22-tetraen-3-one. *Chem. Pharm. Bull.* **1996**, *44*, 843−846.
(16) Lee, W. Y.; Park, Y.; Anh, J. K.; Park, S. Y.; Lee, H. J. Cytotoxic activity of ergosta-4,6,8(14),22-tetraen-3-one from the sclerotia of *Polyporus umbellatus*. *Bull. Korean Chem. Soc.* **2005**, *26*, 1464−1466.
(17) Sakemi, S.; Inagaki, T.; Kaneda, K.; Hirai, H.; Iwata, E.; Sakakibara, T.; Yamauchi, Y.; Norcia, M.; Wondrack, L. M.; Sutcliffe, J. A.; Kojima, N. CJ-12,371 and CJ-12,372, two novel DNA gyrase inhibitors fermentation, isolation, structural elucidation and biological activities. *J. Antibiot.* **1995**, *48*, 134−142.
(18) Barrett, A. G. M.; Blaney, F.; Campbell, A. D.; Hamprecht, D.; Meyer, T.; White, A. J. P.; Witty, D.; Williams, D. J. Unified route to the palmarumycin and preussomerin natural products enantioselective synthesis of (−)-preussomerin G. *J. Org. Chem.* **2002**, *67*, 2735−2750.
(19) Singh, S. B.; Zink, D. L.; Liesch, J. M.; Ball, R. G.; Goetz, M. A.; Bolessa, E. A.; Giacobbe, R. A.; Silverman, K. C.; Bills, G. F.; Pelaez, F.; Cascales, C.; Gibbs, J. B.; Lingham, R. B. Preussomerins and deoxypreussomerins: novel inhibitors of ras farnesyl-protein transferase. *J. Org. Chem.* **1994**, *59*, 6296−6302.
(20) Stone, J. K.; Bacon, C. W.; White, J. F., Jr. An overview of endophytic microbes: endophytism defined. In *Microbial Endophytes*; Bacon, C. W., White, J. F., Jr., Eds.; Dekker: New York, 2000; pp 3−30.
(21) Gunatilaka, A. A. L. Natural products from plant-associated microorganisms: distribution, structural diversity, bioactivity, and implications of their occurrence. *J. Nat. Prod.* **2006**, *69*, 509−26.
(22) Kusari, S.; Spiteller, M. Are we ready for industrial production of bioactive plant secondary metabolites utilizing endophytes? *Nat. Prod. Rep.* **2011**, *28*, 1203−7.
(23) Schulz, B.; Boyle, C. The endophytic continuum. *Microbiol. Res.* **2005**, *109*, 661−686.
(24) Rodriguez, R. J.; White, J. F.; Arnold, A. E.; Redman, R. S. Fungal endophytes: diversity and functional roles. *New Phytol.* **2009**, *182*, 314−30.
(25) Gao, F. K.; Dai, C. C.; Liu, X. Z. Mechanisms of fungal endophytes in plant protection against pathogens. *Afr. J. Microbiol. Res.* **2010**, *4*, 1346−1351.
(26) Strobel, G. A. Microbial gifts from rain forests. *Can. J. Plant Pathol.* **2002**, *24*, 14−20.

Table 1. Composition of the Experimental Diets (g/kg)

ingredient	control diet	soy peptides (SP) diet
casein	140.0	70.0
SP	–	70.0
L-cystein	1.8	1.8
constarch	465.7	465.7
α-constarch	155.0	155.0
sucrose	100.0	100.0
soybean oil	40.0	40.0
cellulose	50.0	50.0
mineral mixture[a]	35.0	35.0
vitamin mixture[b]	10.0	10.0
choline bitartrate	2.5	2.5
tert-butylhydroquinone	0.008	0.008

[a]Mineral mixture, AIN-93 M (Oriental Yeast Corp., Tokyo, Japan). [b]Vitamin mixture, AIN-93 (Oriental Yeast Corp., Tokyo, Japan).

control (n = 8) and (4) SAMR1 SP (n = 8). The control group was fed a normal AIN-93 M diet (Oriental Yeast, Tokyo, Japan) and the SP group was fed a SP diet containing 7% (w/w) SP (Table 1). The mice were allowed free access to the diet and tap water. Food intake and body weight were measured once a week. After 26 weeks, all mice were tested in the Morris water maze and then sacrificed. The brain was rapidly excised and quickly put on ice. These tissues were soaked in RNA later (Sigma-Aldrich, St. Louis, MO) and RIPA lysis buffer (Santa Cruz Biotechnology, Santa Cruz, CA) for RNA isolation and Western blot, respectively, and then stored at −80 °C until use.

Morris Water Maze for Cognitive Testing. Spatial learning and memory of animals were tested in a Morris water maze.[17] A circular plastic pool (diameter, 120 cm; height, 50 cm) was filled with water kept at 25 ± 1 °C. An escape platform (diameter, 11 cm) was hidden 1 cm below the surface of water on a fixed location in the pool. On training trials, the mice were given four trials per session for 7 subsequent days in the presence of the platform, each trial having a ceiling time of 60 s and a trial interval of approximately 20 s. When mice found the platform, they were allowed to stay on it for 20 s. The mice that did not find the platform within 60 s were placed on the platform for 20 s at the end of trial. One day after the last training trial sessions, mice were subjected to a probe trial session in which the platform was removed from the pool. The mice were allowed to swim for 120 s to search for it. Escape latency time (the first time that the mice crossed the former platform) and time in target quadrant (time searching the pool quadrant where the platform had been) were recorded and analyzed by an overhead camera and ANY-maze video tracking system software (Stoelting Co., Wood Dale, IL).

RNA Isolation. Total RNA was isolated from the tissues of each mouse using RNAiso Plus (TaKaRa Bio, Shiga, Japan) according to the manufacturer's instructions. Briefly, brain tissues were homogenized in RNAiso Plus. Total RNA was extracted with the phenol-chloroform method, followed by isopropyl alcohol precipitation and ethanol washing. cDNA was synthesized using a Rever Tra Ace qPCR RT kit (Toyobo, Osaka, Japan) according to the manufacturer's instructions.

Real-Time PCR Quantification. Quantification of relative gene expression was performed by real-time quantitative PCR, using a StepOne Real-time PCR System (Applied BioSystems, Foster City, CA). Real-time PCR was carried out using the Kapa SYBR Fast qPCR kit (Kapa Biosystems, Woburn, MA). Quantitative PCR was carried out using the thermal cycling program, which consisted of one cycle at 95 °C for 3 min, 40 three-segment cycles (95 °C for 3 s and 60 °C for 20 s), and a final dissociation cycle (95 °C for 15 s and stepwise increase from 60 to 95 °C). To normalize the amount of total RNA present in each reaction, β-actin was used as an internal standard, and the expression in the experimental group was expressed as folds of SAMP8 controls using the comparative Ct method. The primer sequences were as follows: NGF: 5′-CAAGCGTTGACAACAGATGA-3′ (forward) and 5′-CAGCCTCTTCTTGTAGCCTTCC-3′ (reverse), BDNF: 5′-GCGGCAGATAAAAAGACTGC-3′ (forward) and 5′-CTTATGAATCGCCAGCCAAT-3′ (reverse), NT-3: 5′-TTTCTCGCTTATCTCCGTGGCATCC-3′ (forward) and 5′-GGCAGGGTGCTCTGGTAATTTTCCT-3′ (reverse), SIRT1: 5′-TGACCGATGGACTCCTCACT-3′ (forward) and 5′-ACAATCTGCCACAGCGTCAT-3′ (reverse), and β-actin: 5′-GCGGCAAAGACAAGAAAAAG-3′ (forward) and 5′-GAAGTGGTCCTCCCAGTCAT-3′ (reverse).

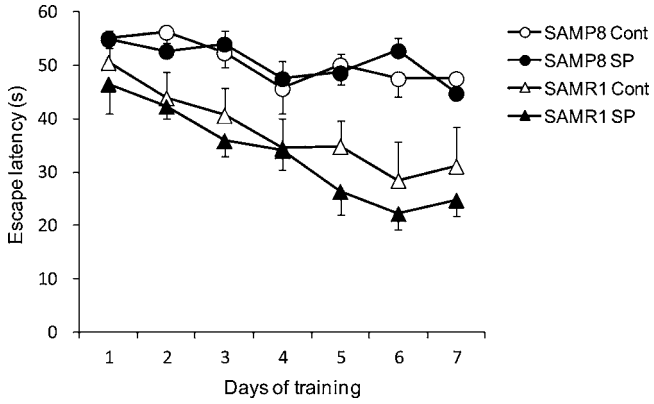

Figure 1. Effect of soy peptides (SP) oral administration for 26 weeks on spatial learning and memory ability during the training trial sessions of the Morris water maze performance in SAMP8 and SAMR1 mice. Escape latency was used as a measure of spatial leaning in the platform task. Data are expressed as means ± SEM.

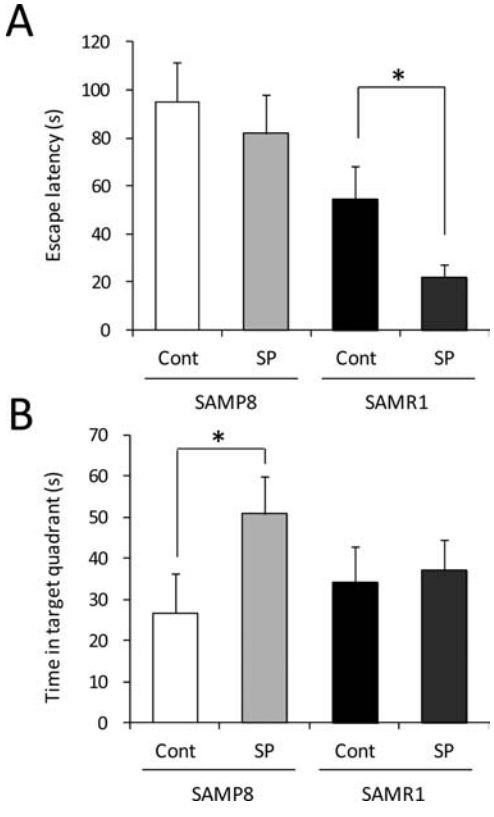

Figure 2. Effect of SP oral administration for 26 weeks on spatial learning and memory ability during the probe trial session of the Morris water maze performance in SAMP8 and SAMR1 mice. (A) Escape latency and (B) time in target quadrant were used as a measure of spatial leaning in the hidden platform task. Data are expressed as means ± SEM *p < 0.05: significantly different from control.

Western Blotting Analysis. The brain tissues were homogenized in RIPA lysis buffer according to standard procedures and centrifuged

dx.doi.org/10.1021/jf405416s | J. Agric. Food Chem. 2014, 62, 3563−3569

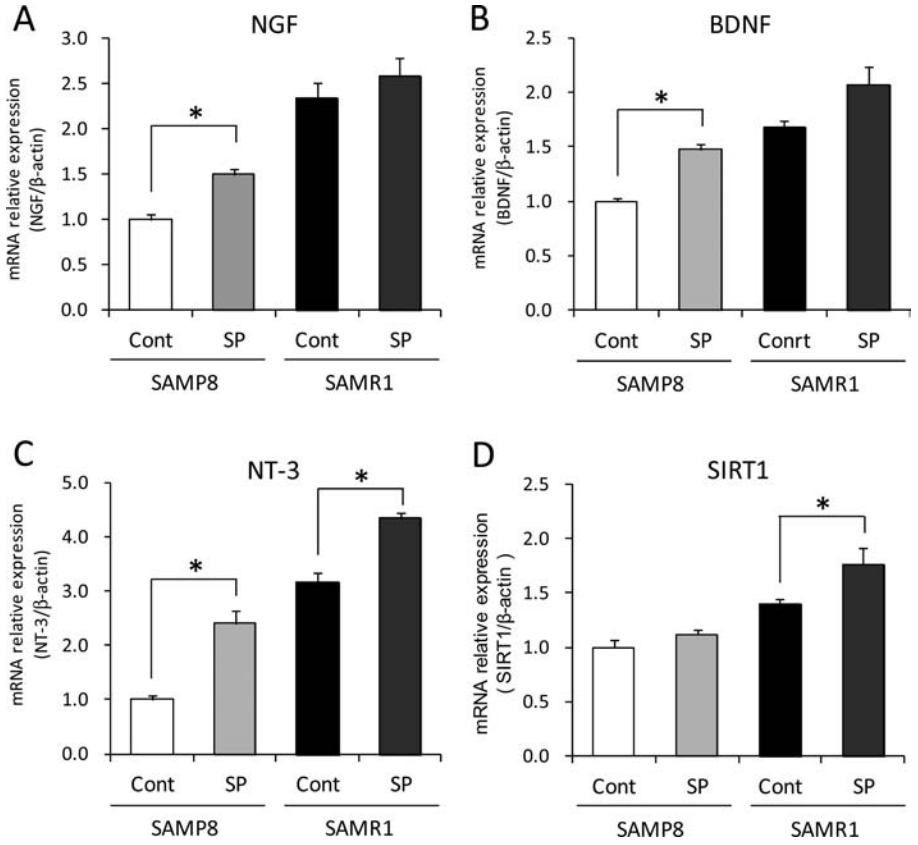

Figure 3. Effect of SP oral administration on mRNA expressions of (A) NGF, (B) BDNF, (C) NT-3, and (D) SIRT1 in the brain from SAMP8 and SAMR1 mice. Data are expressed as means ± SEM *$p < 0.05$: significantly different from control.

at 12 000 rpm for 10 min at 4 °C. The supernatants were collected and protein concentration was determined using the BCA protein assay with bovine serum albumin as standard. Levels of NGF, BDNF, NT-3, CREB, and Ser-133 phosphorylated CREB, extracellular-regulated kinase1/2 (ERK1/2), and Thr-185/Tyr-187 phosphorylated ERK1/2 were analyzed by Western Blot. Briefly, protein samples (12.5 μg) were electrophoresed on 15% polyacrylamide gels and blotted onto polyvinylidene fluoride membranes (Clear Blot Membrane-P; ATTO, Tokyo, Japan). Blots were incubated with antibodies against NGF (1:500, Abcam, Cambridge, MA), BDNF (1:1000, Sigma-Aldrich), NT-3 (1:250, Abcam), CREB (1:750, Abcam), Ser-133 phosphorylated CREB (1:500, Abcam), ERK1/2 (1:500, Enzo Life Sciences, Farmingdale, NY), phosphorylated ERK1/2 (1:1000, Enzo), and β-actin (1:5000, Sigma-Aldrich), followed by antirabbit IgG horseradish peroxidase-conjugate (1:5000, Anaspec, San Jose, CA). Chemiluminescence detection was performed using Pierce Western blotting substrate (Thermo Scientific, Rockford, IL) and AE-9300 Ez-Capture (ATTO). β-Actin was used as an internal control for Western Blot.

Immunostaining. The harvested brains were washed once in cold PBS to remove blood and fixed with 30% paraformaldehyde. The tissues were embedded in paraffin and sectioned at a thickness of 6 μm. Following blocking with 10% goat serum in PBS containing 0.1% Tween 20, the sections were incubated with antibody against NT-3 (1:750, Abcam, Cambridge, MA). After rinsing six times with 0.1% BSA in PBS, samples were further incubated the secondary antibody, Alexa Fluor 488 goat antirabbit IgG (H&L) (1:1000, Abcam). After rinsing six times with 0.1% BSA in PBS, the sections were mounted with immunoselect antifading mounting medium DAPI (Dianova, Hamburg, Germany). We acquired images with an EVOS fluorescence microscope (EVOS fl; Advanced Microscopy Group, Bothell, WA).

Statistical Analysis. Data are presented as mean ± SEM the training session data in Morris water maze were analyzed by two-way ANOVA and the other data were analyzed with Student *t* test. A level of $p < 0.05$ was considered significant.

RESULTS

SAMP8 and SAMR1 were fed control or SP for 26 weeks from 16 weeks of age. Dietary food intake and weight gain did not differ among groups throughout the experiments (data not shown). The Morris water maze test was performed to investigate the effects of a prolonged consumption of SP on the decline in spatial memory and learning abilities of SAMP8 and SAMR1. The probe trial was performed the day after completing the 7-day training trial. In the Morris water-maze training session, SAMR1 rapidly learned the location of the platform, whereas SAMP8 had longer escape latency on every test days compared to SAMR1 (Figure 1). No significant decrease in escape latency was observed between control and SP-fed groups of SAMP8. In contrast, the escape latency of SP-fed SAMR1 mice was shortened compared to that of control mice; however, there was no statistical difference. In the probe trial, the escape latency of SP-fed SAMP8 and SAMR1 mice was faster than that of their controls (Figure 2A). Statistically significant decrease in escape latency was observed in the SP-fed SAMR1 groups. On the other hand, SP-fed SAMP8 mice spent significantly more time in the target quadrant as compared to control mice (Figure 2B).

We next examined whether SP feeding can modulate the expression of neurotrophic and longevity factors in the brain (Figure 3). The mRNA expression of NGF, BDNF, and NT-3 in SAMP8 and SAMR1 mice was up-regulated by SP feeding. Among them, a statistical significant increase of NT-3 expression was found in both SP-fed groups of SAMP8 and SAMR1. On the other hand, an increase in the mRNA expression of SIRT1 was observed in the SP-fed SAMR1, but not SP-fed SAMP8.

dx.doi.org/10.1021/jf405416s | J. Agric. Food Chem. 2014, 62, 3563−3569

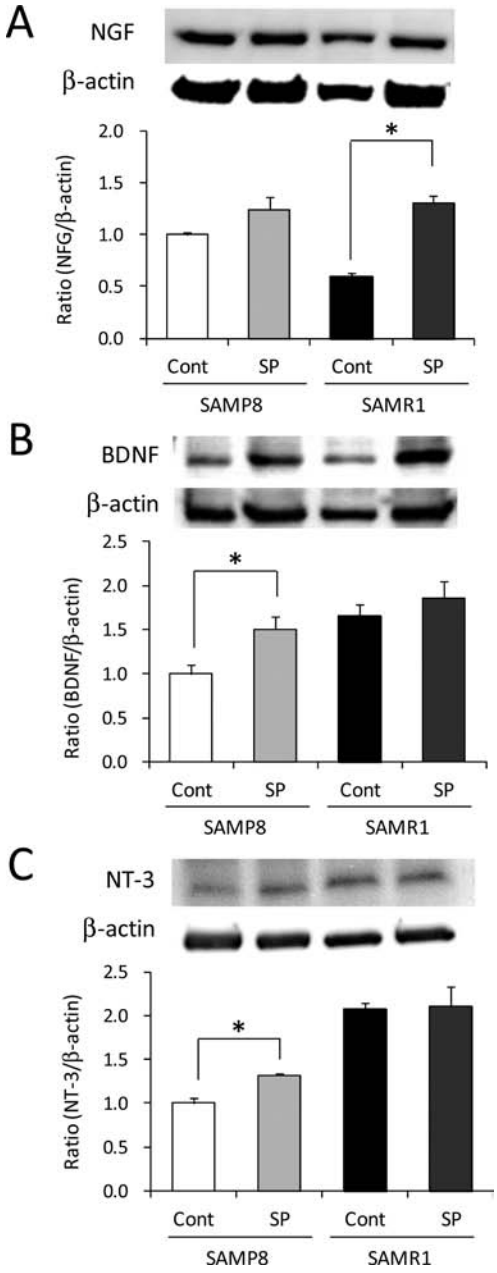

Figure 4. Effect of SP oral administration on protein level of NGF, BDNF, and NT-3 in the brain of SAMP8 and SAMR1 mice. (A) Representative images of Western blotting. (B) Densitometric quantification of band intensities. Data are expressed as means ± SEM $*p < 0.05$: significantly different from control.

The protein levels of NGF, BDNF, and NT-3 in the brain was analyzed using Western blotting (Figure 4). There was a significant increase in BDNF and NT-3 protein levels of SP-fed SAMP8 group compared to control group, whereas no increase was observed in SP-fed SAMR1 group. In contrast, a significant increase in the NGF protein level was observed in SP-fed SAMR1, but not SP-fed SAMP8. Since the hippocampus is important for many aspects of learning and memory, the localization of NT-3 in the hippocampus was examined using immunostaining followed by fluorescence microscopy (Figure 5). NT-3 protein expression was confirmed in the hippocampus of SAMP8 mice. Further, the phosphorylated level of transcription factor CREB in brain was examined to demonstrate whether

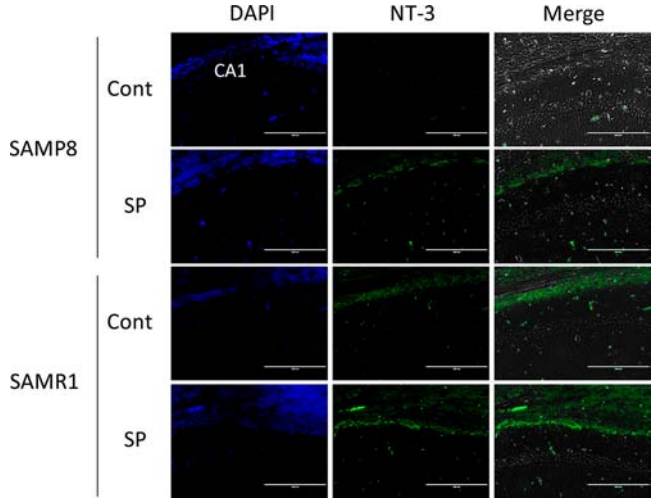

Figure 5. Localization of NT-3 in the hippocampus containing the CA1 layer was examined using immunostaining. Scale bar: 100 μm.

CREB activation occurs (Figure 6). A significant increase in the phosphorylated CREB was observed in the brain of SP-fed SAMP8 group compared with the control group. The phosphorylated ERK1/2 of SP-fed SAMP8 group was increased compared with that of the control group, although this was not statistically significant.

DISCUSSION

Recently, much attention has been focused on a potential neuromodulatory functions and brain protective properties of naturally occurring compounds. Our study demonstrated that the SP-fed mice improved spatial learning and memory when compared with the control mice. The interesting finding of the present study is the significant up-regulation of neurotrophic factors such as NGF, BDNF, and NT-3, which promote neurogenesis, neurodifferentiation, neuroprotection, and neuroplasticity.[18] NT-3 is widely distributed throughout both the peripheral and central nervous system[19] and plays a crucial role in the promotion of neuronal survival and nerve fiber outgrowth and in the enhancement of regeneration of damaged nerve.[20] Thus, the NT-3 enhancement in the brain is a potential therapeutic strategy for preventing age-related cognitive decline. Generally, BDNF exerts multiple cellular functions, including the protective effects on crucial neuronal circuitry involved in Alzheimer's disease (AD).[21] Previous studies have been demonstrated that Ginkgolide B inhibits Aβ (25−35)-induced apoptosis in hippoicampal neurons via up-regulation of BDNF expression.[22] Further, resveratrol treatment enhanced the generation of newborn neurons in dentate gyrus and restored the decreased hippocampal BDNF level significantly in prenatally stressed rat brain.[23] The present study suggests that it is possible to use SPs to prevent degenerative neurological disorders of aging because SPs have minor side effects. It is well-known that the dysregulation of adult neurogenesis progresses in AD patients and in various AD model mice.[24,25] Thus, neurotrophic agents may have therapeutic potential for prevention and treatment of AD.

This study showed that SP administration resulted in an increased SIRT1 expression level of SAMR1 mice. Sirtuin activity has been shown to play a significant role in promoting longevity, preventing disease and increasing cell survival.[26] Thus, the up-regulation of SIRT1 might contribute to the protective effect on cognitive decline in SP-fed SAMR1.

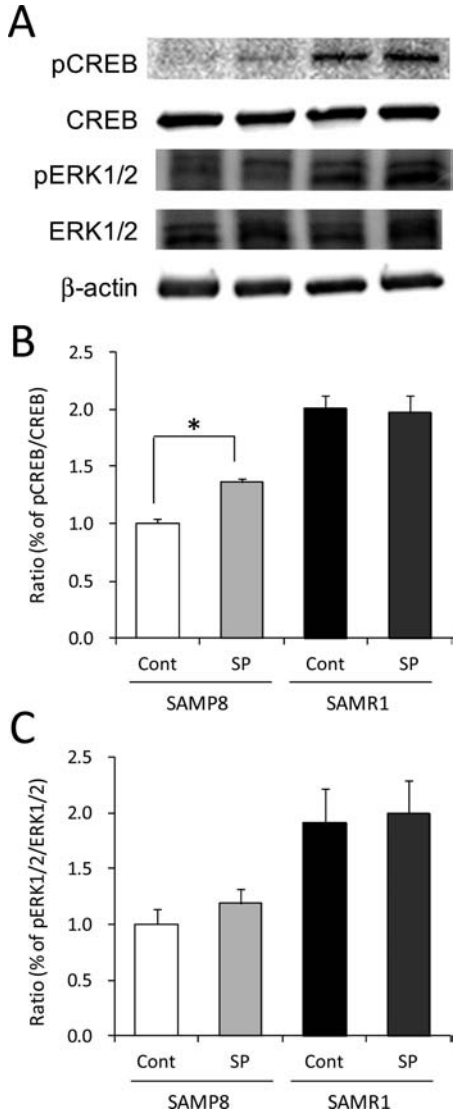

Figure 6. Effect of SP oral administration on protein level of phosphorylated CREB and ERK1/2 in the brain from SAMP8 and SAMR1 mice. Data are expressed as means ± SEM $*p < 0.05$: significantly different from control.

Porquet et al.[9] have demonstrated that SIRT1 activation by long-term dietary resveratrol not only reduces cognitive impairment but also increases mean life expectancy and maximal life span in SAMP8 and SAMR1. During our experiment, there were no deaths in SAMR1 mice; however, the up-regulation of SIRT1 expression by dietary SP may affect the longevity of SAMR1 mice.

Neurotrophic factors termed neurotrophins (NGF, BDNF, NT-3, and NT-4/5) play an important role in the growth and survival of neurons. CREB is a transcription factor implicated in the control of adaptive neuronal responses and the regulation of neurotrophic genes.[27,28] This study suggests that increased gene expression of NGF, BDNF, and NT-3 observed in SP-fed SAMP8 group was accompanied by activation of CREB-dependent pathways. The induction of neurotrophic factors by SP feeding could contribute to a protective effect on cognitive decline in SAMP8. Recent work suggests that the trans-activation of CREB was mainly caused by the mitogen-activated protein kinase/extracellular-regulated kinase (MAPK/ERK), which plays an important role in long-term synaptic plasticity and memory formation.[29,30] However, no significant increase in phosphorylated ERK protein levels was observed in this study. A number of kinases, including protein kinase A protein kinase C, and AKT, are also known to be phosphorylate and activate CREB.[31] Therefore, it seems that another signaling pathway exists in the activation of CREB by SP feeding. Further investigation is needed to explore the signal transduction cascade to induce the neurotrophic factors in the SP-fed SAMP8 group.

In the experiment of water maze task, no significant difference in escape latency was observed between control and SP-fed groups in the training session in both SAMP8 and SAMR1. However, a significant difference was observed in the probe trials in escape latency of SAMR1 and in time in target quadrant of SAMP8. This discrepancy is caused by a difference of the time-limit between training session and probe trials, which were 60 and 120 s, respectively. In particular, since SAMP8 at 42 weeks were not quick in movement, they needed more time compared to SAMR1. Therefore, it is considered that the measurement of time in the target quadrant is suitable to evaluate the spatial learning and memory ability of SAMP8. Taking these results into consideration, our data support that the SP feeding could affect the memory function of both SAMP8 and SAMR1.

In the present study, we used SAMP8 mice as a model of age-related cognition disorder and SAMR1 mice as normal aging control mice. Indeed, SAMP8 showed not only greater decline in performance in the Morris water maze but also decreased expression levels of neurotrophic factors. A significant increase of SIRT1 mRNA was found in only SP-fed SAMR1, while a significant increase of pCREB was found in only SP-fed SAMP8. These results suggest that the working point of SP feeding in SAMP8 is different from that of SAMR1. It is reasonable to assume that this difference was caused by different gene expression profiles of receptors and coregulators.

The SP used in this study was composed mainly di- and tripeptides, and this peptide mixture have been reported to increase the serum levels of amino acids more rapidly than the original soy proteins or an amino acid mixture of equivalent composition.[32] It was also shown that short-term oral intake of SP increases neuroactive amino acids such as the neurotransmitter L-glutamate, its precursor L-glutamine, the neuromodulator D-asparatate, and branched-chain amino acids such as L-valine, L-leucine, and L-isoleucine.[33] Generally, dipeptides and tripeptides are absorbed by small intestinal cells in peptide form using the PepT1 peptide transporter and hydrolyzed by cellular enzymes and the resultant amino acids are transported across the serosal membrane. Taking these results into consideration, it appears possible that neuroactive amino acids produced from the SP exhibit an effective nutraceutical for promoting brain function. The mechanism for oligopeptide transport in the intestinal tract is not fully understood; however, Shimizu et al. demonstrated that antihypertensive tripeptide VPP transpiorted across human intestinal epithelial cells monolayers via the paracellular route, which is a nondegradation pathway.[34] It is possible that the intact dipeptides directly contribute to the induction of neurotrophic factors. Further studies are needed to determine the mechanism of action and identify the active sequence of peptides.

In conclusion, the present study has demonstrated that SPs have the potential for the prevention of cognitive impairment via the neurotrophic effects in SAMP8 mice. These results indicated that SP may play an important role for the prevention of age-related cognitive decline and neurodegenerative diseases such as AD.

AUTHOR INFORMATION

Corresponding Author

*Tel & Fax: +81-265-77-1609. E-mail: snakamu@shinshu-u.ac.jp.

Notes

The authors declare no competing financial interest.

ABBREVIATIONS USED

AD, Alzheimer's disease; BDNF, brain-derived neurotrophic factor; CREB, cAMP response element binding protein; ERK, extracellular-regulated kinase; MAPK, mitogen-activated protein kinase; NGF, neuron growth factor; NT-3, neurotrophin-3; SAMP8, senescence-accelerated mice prone 8; SAMR1, senescence-accelerated resistant mouse 1; SIRT1, Sirtuin 1; SP, soy peptides

REFERENCES

(1) Fusco, D.; Colloca, G.; Monaco, M. R. L.; Cesari, M. Effects of antioxidant supplementation on the aging process. *Clin. Interv. Aging* **2007**, *2*, 377−387.

(2) Ferrari, C. K. Functional foods and physical activities in health promotion of aging people. *Maturitas* **2007**, *58*, 327−339.

(3) Takeda, T. Senescence-accelerated mouse (SAM): A biogerontological resource in aging research. *Neurobiol. Aging.* **1999**, *20*, 105−110.

(4) Chen, G. H.; Wang, Y. J.; Wang, X. M.; Zhou, J. N. Accelerated senescence prone mouse-8 shows early onset of deficits in spatial learning and memory in the radial six-arm water maze. *Physiol. Behav.* **2004**, *82*, 883−890.

(5) Wu, A.; Ying, Z.; Gomez-Pinilla, F. Docosahexaenoic acid dietary supplementation enhances the effects of exercise on synaptic plasticity and cognition. *Neuroscience* **2008**, *155*, 751−759.

(6) Zhao, H. F.; Li, Q.; Zhang, Z. F.; Pei, X. R.; Wang, J. B.; Li, Y. Long-term ginsenoside consumption prevents memory loss in aged SAMP8 mice by decreasing oxidative stress and up-regulating the plasticity-related proteins in hippocampus. *Brain Res.* **2009**, *1256*, 111−122.

(7) Li, Q.; Zhao, H. F.; Zhang, Z. F.; Liu, Z. G.; Pei, X. R.; Wang, J. B.; Li, Y. Long-term green tea catechin administration prevents spatial learning and memory impairment in senescence-accelerated mouse prone-8 mice by decreasing a beta(1−42) oligomers and upregulating synaptic plasticity-related proteins in the hippocampus. *Neuroscience* **2009**, *163*, 741−749.

(8) Gomez-Pinilla, F.; Huie, J. R.; Ying, Z.; Ferguson, A. R.; Crown, E. D.; Baumbauer, K. M.; Edgerton, V. R.; Grau, J. W. BDNF and learning: Evidence that instrumental training promotes learning within the spinal cord by up-regulating BDNF expression. *Neuroscience* **2007**, *148*, 893−906.

(9) Porquet, D.; Casadesus, G.; Bayod, S.; Vicente, A.; Canudas, A. M.; Vilaplana, J.; Pelegri, C.; Sanfeliu, C.; Camins, A.; Pallas, M.; del Valle, J. Dietary resveratrol prevents Alzheimer's markers and increases life span in SAMP8. *Age* **2013**, *35*, 1851−1865.

(10) Yokozawa, T.; Lee, Y. A.; Zhao, Q.; Matsumoto, K.; Cho, E. J. Persimmon oligomeric proanthocyanidins extend life span of senescence-accelerated mice. *J. Med. Food* **2009**, *12*, 1199−1205.

(11) Inoue, N.; Nagao, K.; Sakata, K.; Yamano, N.; Gunawardena, P. E.; Han, S. Y.; Matsui, T.; Nakamori, T.; Furuta, H.; Takamatsu, K.; Yanagita, T. Screening of soy protein-derived hypotriglyceridemic di-peptides in vitro and in vivo. *Lipids. Health Dis.* **2011**, *10*, 1−10.

(12) Matsui, T.; Zhu, X. L.; Shiraishi, K.; Ueki, T.; Noda, Y.; Matsumoto, K. Antihypertensive effect of salt-free soy sauce, a new fermented seasoning, in spontaneously hypertensive rats. *J. Food Sci.* **2010**, *75*, H129−134.

(13) Matemu, A. O.; Nakamura, K.; Kayahara, H.; Murasawa, H.; Katayama, S.; Nakamura, S. Enhanced antiviral activity of soybean beta-conglycinin-derived peptides by acylation with saturated fatty acids. *J. Food Sci.* **2011**, *76*, M299−304.

(14) Young, D.; Ibuki, M.; Nakamori, T.; Fan, M.; Mine, Y. Soy-derived di- and tripeptides alleviate colon and ileum inflammation in pigs with dextran sodium sulfate-induced colitis. *J. Nutr.* **2012**, *142*, 363−368.

(15) Maebuchi, M.; Kishi, Y.; Koikeda, T.; Furuya, S. Soy peptide dietary supplementation increases serum dopamine level and improves cognitive dysfunction in subjects with mild cognitive impairment. *Jpn. Pharmacol. Ther.* **2013**, *41*, 67−73.

(16) Yimit, D.; Hoxur, P.; Amat, N.; Uchikawa, K.; Yamaguchi, N. Effects of soybean peptide on immune function, brain function, and neurochemistry in healthy volunteers. *Nutrition* **2012**, *28*, 154−159.

(17) Morris, R. Developments of a water-maze procedure for studying spatial learning in the rat. *J. Neurosci. Methods* **1984**, *11*, 47−60.

(18) Huang, E. J.; Reichardt, L. F. Neurotrophins: roles in neuronal development and function. *Annu. Rev. Neurosci.* **2001**, *24*, 677.

(19) Frade, J. M.; Bovolenta, P.; Rodríguez-Tébar, A. Neurotrophins and other growth factors in the generation of retinal neurons. *Microsc. Res. Tech.* **1999**, *45*, 243−251.

(20) Bartkowska, K.; Turlejski, K.; Djavadian, R. L. Neurotrophins and their receptors in early development of the mammalian nervous system. *Acta Neurobiol. Exp. (Wars)* **2010**, *70*, 454−467.

(21) Nagahara, A. H.; Merrill, D. A.; Coppola, G.; Tsukada, S.; Schroeder, B. E.; Shaked, G. M.; Wang, L.; Blesch, A.; Kim, A.; Conner, J. M.; Rockenstein, E.; Chao, M. V.; Koo, E. H.; Geschwind, D.; Masliah, E.; Chiba, A. A.; Tuszynski, M. H. Neuroprotective effects of brain-derived neurotrophic factor in rodent and primate models of Alzheimer's disease. *Nat. Med.* **2009**, *15*, 331−337.

(22) Xiao, Q.; Wang, C.; Li, J.; Hou, Q.; Li, J.; Ma, J.; Wang, W.; Wang, Z. Ginkgolide B protects hippocampal neurons from apoptosis induced by beta-amyloid 25−35 partly via up-regulation of brain-derived neurotrophic factor. *Eur. J. Pharmacol.* **2010**, *647*, 48−54.

(23) Madhyastha, S.; Sekhar, S.; Rao, G. Resveratrol improves postnatal hippocampal neurogenesis and brain derived neurotrophic factor in prenatally stressed rats. *Int. J. Dev. Neurosci.* **2013**, *31*, 580−585.

(24) Demars, M.; Hu, Y. S.; Gadadhar, A.; Lazarov, O. Impaired neurogenesis is an early event in the etiology of familial Alzheimer's disease in transgenic mice. *J. Neurosci. Res.* **2010**, *88*, 2103−2117.

(25) Jin, K.; Peel, A. L.; Mao, X. O.; Xie, L.; Cottrell, B. A.; Henshall, D. C.; Greenberg, D. A. Increased hippocampal neurogenesis in Alzheimer's disease. *Proc. Natl. Acad. Sci. U.S.A.* **2004**, *101*, 343−347.

(26) Dali-Youcef, N.; Lagouge, M.; Froelich, S.; Koehl, C.; Schoonjans, K.; Auwerx, J. Sirtuins: the 'magnificent seven', function, metabolism and longevity. *Ann. Med.* **2007**, *39*, 335−345.

(27) Riccio, A.; Pierchala, B. A.; Ciarallo, C. L.; Ginty, D. D. An NGF-TrkA-mediated retrograde signal to transcription factor CREB in sympathetic neurons. *Science* **1997**, *277*, 1097−1100.

(28) Tao, X.; Finkbeiner, S.; Arnold, D. B.; Shaywitz, A. J.; Greenberg, M. E. Ca^{2+} influx regulates *BDNF* transcription by a CREB family transcription factor-dependent mechanism. *Neuron* **1998**, *20*, 709−726.

(29) English, J. D.; Sweatt, J. D. A requirement for the mitogen-activated protein kinase cascade in hippocampal long term potentiation. *J. Biol. Chem.* **1997**, *272*, 19103−19106.

(30) Impey, S.; Obrietan, K.; Storm, D. R. Making new connections: Role of ERK MAP kinase signaling in neuronal plasticity. *Neuron* **1999**, *23*, 11−14.

(31) Kandel, E. R. The molecular biology of memory: cAMP, PKA, CRE, CREB-1, CREB-2, and CPEB. *Mol. Brain* **2012**, *5*, 14.

(32) Maebuchi, M.; Samoto, M.; Kohno, M.; Ito, R.; Koikeda, T.; Hirotsuka, M.; Nakabou, Y. Improvement in the intestinal absorption of soy protein by enzymatic digestion to oligopeptide in healthy adult men. *Food Sci. Technol. Res.* **2007**, *13*, 45−53.

(33) Esaki, K.; Kokido, T.; Ohmori, T.; Tsukino, M.; Ohshima, T.; Furuya, S. Soy Peptide Ingestion Increases Neuroactive Amino Acids

in the Adult Brain of Wild-Type and Genetically Engineered Serine-Deficient Mice. *J. Nutr. Food Sci.* **2011**, *1*, 1−6.
(34) Satake, M.; Enjoh, M.; Nakamura, Y.; Takano, T.; Kawamura, Y.; Arai, S.; Shimizu, M. Transepithelial transport of the bioactive tripeptide, Val-Pro-Pro, in human intestinal Caco-2 cell monolayers. *Biosci. Biotechnol. Biochem.* **2002**, *66*, 378−384.

feeding species-rich herbage on BH of the major FAs.[8,14] Only one study emanates the effect that single plant species have on BH of major FAs[13] but to the authors' knowledge, studies on the importance of feeding regimen for BH of major FAs in single plant species to minimize BH rate of beneficial PUFAs are missing.

The aim of the present study was to elucidate the effect of (i) feeding either TMR, pure grass, or species-rich silage on BH rate of ALA and LA, (ii) study differences in BH rate of ALA and LA in single plant species, and (iii) whether BH rates of ALA and LA in single plant species depend on the feeding regimen of the donor cow.

MATERIALS AND METHODS

Treatment of the Donor Cows. Three lactating Holstein cows (weight, 573 ± 43 kg; daily milk yield, 30 ± 4 kg), fitted with ruminal cannulas, were housed in tie stalls. The experiment was carried out at Aarhus University, Department of Animal Sciences, Denmark, and was carried out in accordance with the Danish Ministry of Justice Law No. 1306 (November 23, 2007) on animal experiments and care of experimental animals. The cows were subject to three different diets. Each dietary treatment lasted three coherent weeks with one daily feeding at 3:45 p.m. The normal diet of the cows in the research facility was a traditional total mixed ration (19.0% starch, 18.1% crude protein, and 4.1% crude fat on DM basis) composed of (% of DM) 35 corn silage, 31 grass clover silage, 14 barley, 9 rapeseed, 9 soybean meal, and 2 vitamin and mineral mixture. The TMR was chosen to represent BH in a traditional conventional feeding regimen. After 21 days, the diet was changed to herb silage acquired from a local farmer (HERB) (0.19% starch, 14.1% crude protein, and 3.9% crude fat on DM basis). The silage was composed of 10 different species with the following botanical composition (% of kg sown mixture): 24 salad burnet (*Poterium sangusisorba*), 12 chicory (*Cihorium intybus*), 12 caraway (*Carum carvi*), 12 birdsfoot trefoil (*Lotus corniculatus*), 12 English plantain (*Plantago lanceolata*), 11 alfalfa (*Meticago sativa*), 8 white meliot (*Melilotus officinalis*), 5 borago (*Borago officinalis*), 2 yarrow (*Achillea millefolium*), and 2 red clover (*Trifolium pratense*). Finally, the cows were switched to a diet composed of pure perennial ryegrass (*Lolium perenne*) silage grown on the research facility (GRASS) (0.93% starch, 15.5% crude protein, and 3.5% crude fat on DM basis). To maximize diet effects, concentrate was not added to the HERB or to the GRASS diet. One cow had to be taken out of the experiment in the second week on the pure ryegrass feeding due to disease, resulting in only two replicas in the GRASS feeding period.

Design of the in Vitro Experiment. Five single plant species in three replicas (alfalfa (*M. sativa*), birdsfoot trefoil (*L. corniculatus*), chicory (*C. intybus*), English plantain (*P. lanceolata*), salad burnet (*P. sangusisorba*)) and a clover grass mixture (% of DM) (80 white clover (*Trifolium repens*) and 20 perennial ryegrass (*Lolium perenne*)) were investigated. Cultivation, handling, and chemical composition of the herbs and the clover mixture are described elsewhere.[19,20] The five plant species were chosen because they already are commonly used in seed mixture for pasture on Danish organic farms and have shown persistence in regrowth after cutting.

Rumen fluids were collected at day 21 in each of the three feeding periods at 7 a.m. Rumen fluids were filtered through double-layered cheesecloth and then immediately transferred separately under anaerobe conditions to the laboratory in sealed and preheated vacuum flasks. Twenty-two milliliters of the strained rumen fluid was transferred to 60 mL tubes. Prior to the transfer of the rumen fluid, 1 g of freeze-dried plant species and 22 mL of buffer solution were added to the tubes. The buffer was prepared according to the method of McDougall.[18] The lid of the tube was punctured with an injection needle and then equipped with a syringe to allow gas escape from the tubes without compromising the anaerobic environment. Incubations were stopped at 0, 2, 4, 6, 12, 24, and 30 h by placing test tubes containing buffered rumen fluid and plant materials in an ice slurry. The complete samples were freeze-dried and stored at −20 °C until further analysis.

Throughout the experiment, the pH value was followed in samples of the buffered rumen fluid with the added material of alfalfa and birdsfoot trefoil. Over the experimental period the pH value decreased on an average by 1.0 unit. The lowest pH value after 30 h was observed in TMR fluids (0 and 30 h; pH 6.7 and 5.9, respectively). The pH values after 0 and 30 h in HERB samples were 7.9 and 6.2, respectively, and in GRASS samples, 7.1 and 6.2, respectively.

Fatty Acid Analysis. Lipids were extracted in a mixture of chloroform and methanol according to the method of Bligh and Dyer[21] after acidification by boiling in 3 mol/L of HCl for 1 h, and FA were converted into methyl esters (FAME) as described by Jensen.[22] Lipids were quantified as FA methyl ester according to Jensen and Nielsen[23] with small adjustments to the temperature program. Briefly, 250 mg of the freeze-dried samples was weighed in culture tubes and extracted with 4 mL of chloroform containing C17:0 (heptadecanoic acid, Sigma-Alrich, St. Louis, MO, USA) as internal standard, 3 mL of methanol, and 1.5 mL of distilled water. The extracts were centrifuged for 10 min at 3000*g*. After extraction, 1 mL of the extracts was transferred to new culture tubes, evaporated to exact dryness under a stream of N_2, and then methylated. Fatty acids were methylated with 0.8 mL of NaOH in methanol (0.5 M), sealed with Ar, and placed at 100 °C for 15 min. After cooling, 1 mL of boron trifluoride was added, and tubes were sealed with Ar and placed at 100 °C for 45 min. FA methyl esters were then extracted with 1 mL of heptane and analyzed with a gas chromatograph (Hewlett-Packard 6890 series, Agilent Technologies, Palo Alto, CA, USA) equipped with an automatic column injector (Hewlet Packard 7673), a capillary column of 30 m × 0.32 mm i.d., 0.25 μm thickness (Omegawax 320; Supelco, Sigma-Aldrich), and a flame ionization detector. The initial temperature was set at 170 °C, and then the temperature was raised to 200 °C at the rate of 2 °C/min. The 200 °C was held for 5 min and finally raised to 220 °C at the rate 5 °C/min. Fatty acids were identified by comparison of retention times with external standards (GLC-68C, Nu-Prep-Check, Elysian, MN, USA). Four to five peaks eluted between the peaks of C18:1n-9 and C18:2n-6 contributing to approximately 5% of total FA composition. These peaks were most likely different C18:1 isomers, but we were not able to identify these peaks.

Twenty-two samples (representing the whole incubation time from 0 to 30 h) were processed without internal standard to secure the applicability of C17:0 as internal standard. Chromatograms of samples processed without addition of internal standard showed that naturally occurring C17:0 contributed with an area of <0.5% of the area from the added 5 mg of C17:0. The contribution of naturally occurring C17:0 therefore could be neglected.

Kinetic Calculations. According to the Michaelis−Menten equation

$$V = V_{max} \times \frac{[s]}{k_M + [s]}$$

a Hanes plot is a straight line. The results determined in the in vitro BH experiment were analyzed by linear regression according to the Hanes plot as the time ($[s]$, hours) against the time divided by the amount of ALA or LA disappeared or C18:0 formed (hour/g/kg DM).

V_{max} (g FA/kg DM) was calculated as the reciprocal slope, and K_M (hour) was calculated as the intercept multiplied by V_{max} and is the time for 50% reduction in ALA and LA concentration or 50% increase in C18:0 formation. For ALA and LA their initial concentrations were subtracted from the concentration at the time when incubation was stopped (e.g., time = 0 h subtracted from time = 2, 4, 6, 12, 24, and 30 h), giving the total sum of products from the BH at the given time. Rumen BH is a complex system, where formation of the different intermediates can originate from isomerization, desaturation, or hydrolysation along the different BH pathways,[24] and therefore modeling of intermediates is difficult. In the current study modeling of the intermediate C18:1*t*11 was attempted under the assumption that the concentration would increase over time as a result of BH. The

Table 1. Initial Fatty Acid Content (Grams FA per Kilogram DM) in Single Plant Species

	plant species[a]							
	salad burnet	clover grass	chicory	birdsfoot trefoil	alfalfa	plantain	SE	significance (P value)
total FA	15.8bc	18.2b	14.9bc	22.8a	12.4c	14.1bc	1.49	0.003
C14:0	0.47c	0.60b	0.30e	0.84a	0.52cb	0.43c	0.03	<0.001
C16:0	1.91	3.84	3.67	4.27	3.50	2.78	0.77	0.438
C18:0	0.68a	0.61b	0.26e	0.43d	0.51c	0.28e	0.03	<0.001
C18:1n-9	0.68b	1.00a	0.45c	0.51bc	0.46bc	0.56b	0.03	<0.001
C18:2n-6	3.22b	3.25b	3.44b	4.00a	2.60c	3.34b	0.14	0.006
C18:3n-3	8.26b	8.37b	6.56c	12.3a	4.49d	6.44c	0.28	<0.001

[a]Means within a row with different letters indicate significant differences ($P \leq 0.05$).

Table 2. Fatty Acid Content and Proportion of Selected Fatty Acids in Buffered Rumen Fluid before Incubation

	donor cow diet[a]				
	TMR	HERB	GRASS	SE	significance (P value)
total FA (g/kg DM)	0.43a	0.38ab	0.20±b	0.05	<0.005
FA composition (g FA/100 g FAME)					
C14:0	2.88b	5.77a	2.13b	0.35	<0.001
C16:0	19.1c	26.8a	22.9b	0.93	<0.001
C16:1n-9	0.43b	0.95a	<0.001c	0.18	<0.001
C18:0	54.1a	43.7b	55.3a	2.56	<0.001
C18:1*t*11	4.33a	2.64b	1.47b	0.66	0.0068
C18:1n-9	6.00a	3.17b	3.29b	0.44	<0.001
C18:2n-6	6.21a	5.50b	4.38b	0.71	<0.001
C18:3n-3	2.09b	6.28a	5.25a	1.12	0.003

[a]Means within a row with different letters indicate significant differences ($P \leq 0.05$).

Table 3. Effect of Diet on K_m and V_{max} for C18:3n-3, C18:2n-6, C18:0, and C18:1*t*11

	fatty acid[a]							
	C18:3n-3		C18:2n-6		C18:0		C18:1*t*11[b]	
diet	K_m (h)	V_{max} (g FA/kg DM)	K_m (h)	V_{max} (g FA/kg DM)	K_m (h)	V_{max} (g FA/kg DM)	K_m (h)	V_{max} (g FA/kg DM)
TMR	0.77b	1.44a	1.30c	0.79a	1.01b	3.83a	1.05b	0.085
HERB	3.16a	0.67b	4.72b	0.27b	2.79a	1.58c	2.95a	0.134
GRASS	3.31a	0.71b	6.71a	0.26b	1.88c	2.24b	1.59b	0.120
SE	0.24	0.31	0.57	0.05	0.24	0.18	0.31	0.03
significance (P value)	<0.001	<0.001	<0.001	<0.001	<0.001	<0.001	<0.001	0.449

[a]Means within a column with different letters indicate significant differences ($P \leq 0.05$). [b]To be considered as apparent appearance due to the complexity of formation of BH intermediates.

results are to be considered as the apparent appearance of C18:1*t*11 for the reasons stated above.

Statistics. Statistical analysis was carried out using the PROC MIXED procedures in the SAS package, ver. 9.2, with diet, single species, and the interactions between diet and single species as fixed effects. The effect of cow was tested, but no significance was found, and so cow was included as a random effect in the final model. Differences in mean treatment effects were tested using the PDIFF command. The general model used was

$$Y_{ij} = \mu + D_i + S_j + (D \times S)_{ij} + C_{ijk} + e_{ijk}$$

where μ is the overall mean, D_i and S_j are the fixed effects of diet$_i$ and single species$_j$, $(D \times S)_{ij}$ is the interaction between diet$_i$ and single species$_j$, C_{ijk} is the random effect of cow, and e_{ijk} is the residual error. Random effects were assumed to be normally distributed with a mean value of 0 and constant variance, $C_{ijk} \sim N(0, \sigma_C^2)$ and $e_{ijk} \sim N(0, \sigma^2)$. Significance was accepted at $P \leq 0.05$.

RESULTS

Fatty Acid Content in Single Species. Total FA content in the herb species varied from 12.4 g/kg DM in alfalfa to 22.8 g/kg DM in birdsfoot trefoil (Table 1). ALA was the dominating FA in all species with LA or C16:0 as the second dominating FA. Following the content of total FA, the lowest contents of ALA and LA were seen in alfalfa (4.49 and 2.60 g/kg DM, respectively), and the highest contents were seen in birdsfoot trefoil (12.3 and 4.00 g/kg DM, respectively).

Fatty Acid Composition of Rumen Fluid. The initial FA profile differed between the diets (Table 2). The sum of ALA and LA was highest in the HERB and GRASS diets, although the LA content was highest in the TMR diet. The accumulation of intermediates of BH, represented by C18:1*t*11, was highest in the rumen fluid from the TMR diet, whereas no differences were seen between the HERB and GRASS diets. CLA was detected in only trace amounts and could not be used to highlight further differences in intermediates of BH. The end product of rumen BH C18:0 was found to be similar in rumen fluid from the TMR and GRASS diets, whereas it was significantly lower in rumen fluid from the HERB diet.

Effect of the Donor Cows' Diet on Biohydrogenation Rate. Biohydrogenation of ALA and LA occurred at a faster rate in rumen fluid from cows fed TMR diet compared to

dx.doi.org/10.1021/jf405552m | J. Agric. Food Chem. 2014, 62, 3570−3576

Table 4. Effect of Species on K_m and V_{max} for C18:3n-3, C18:2n-6, C18:0, and C18:1*t*11

	fatty acid[a]							
	C18:3n-3		C18:2n-6		C18:0		C18:1*t*11[b]	
species	K_m (h)	V_{max} (g FA/kg DM)	K_m (h)	V_{max} (g FA/kg DM)	K_m (h)	V_{max} (g FA/kg DM)	K_m (h)	V_{max} (g FA/kg DM)
salad burnet	2.67	0.75c	5.37	0.26c	1.43bc	2.19bc	0.95c	0.06
clover grass	2.31	0.99b	5.21	0.53ab	1.97ab	2.59ab	3.46a	0.11
chicory	2.24	0.94b	4.09	0.55a	2.30a	2.83a	1.11c	0.08
birdsfoot trefoil	1.83	1.59a	2.87	0.60a	2.62a	2.84a	2.30b	0.098
alfalfa	3.16	0.60d	5.04	0.40abc	0.87c	2.02c	2.17b	0.092
plantain	2.26	0.74c	2.69	0.30c	2.17a	2.73a	1.21bc	0.23
SE	0.36	0.05	0.87	0.08	0.23	0.28	0.39	0.04
significance (P value)	0.161	<0.001	0.119	0.019	<0.001	0.005	<0.001	0.099

[a]Means within a column with different letters indicate significant differences ($P \leq 0.05$). [b]To be considered as apparent appearance due to the complexity of formation of BH intermediates.

HERB or GRASS diets, indicated by low K_M and high V_{max} values in the TMR group ($P < 0.001$) (Table 3). In accordance with the BH pattern for ALA and LA, the TMR diet also showed the fastest formation of C18:0 shown by a low K_M value and a high V_{max} value ($P < 0.001$). The apparent appearance of C18:1*t*11 was fastest in the TMR diet compared to both GRASS and HERB diets as shown by the lower K_M values ($P < 0.001$), but V_{max} was numerically highest in the HERB diet.

Effect of Species on Biohydrogenation Rate. Salad burnet and alfalfa differentiated from the other species, as they showed the lowest BH rate of ALA and LA, indicated by the lowest V_{max} values ($P < 0.001$ and $P = 0.019$, respectively) and also the lowest K_M values for the formation of C18:0 ($P < 0.001$) (Table 4). Birdsfoot trefoil showed the highest BH rate of both ALA and LA. Plantain had numerically lower V_{max} values for ALA and LA than alfalfa, but the formation of C18:0 was significantly higher ($P < 0.05$). Apparent formation of C18:1*t*11 revealed differences when compared to BH patterns for formation of C18:0 in the single plant species, as salad burnet and chicory seemed to have the lowest apparent formation rate of C18:1*t*11. The highest apparent formation rate seemed to occur in plantain, which was one of the species with the lowest BH rate of ALA and LA (Figure 1), although the K_M value for C18:1*t*11 was highest in the clover grass mixture ($P < 0.001$).

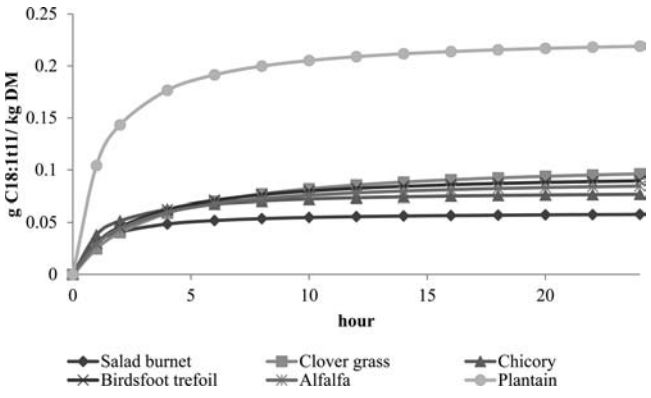

Figure 1. Apparent appearance of C18:1*t*11 in single species. Although only K_M was found significantly different between species, data modeled according to Michaelis–Menten kinetics highlight these differences between plant species.

Effect of Diet and Species Interaction on Biohydrogenation Rate of ALA. A significant interaction between diet and species was seen for K_M for ALA ($P = 0.005$). Only alfalfa seemed to react differently when compared to the general effect of diets, as the highest K_M value for alfalfa was seen in the GRASS diet compared to both TMR and HERB diets (6.36, 0.72, and 2.41, respectively, $P = 0.005$); this implies a lower BH of ALA in the GRASS diet (Figure 2) . No significant effect of

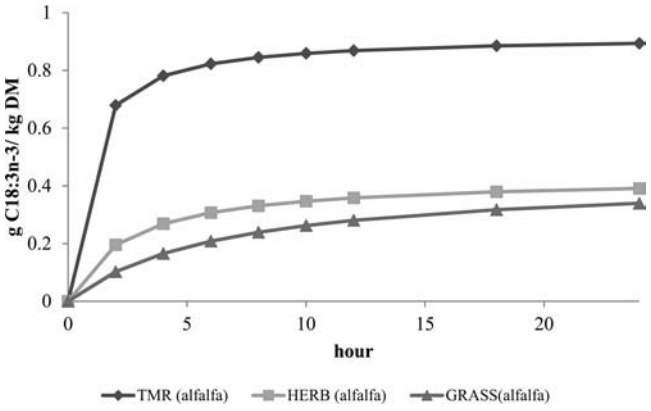

Figure 2. Effect of interaction between diet and plant species for disappearance of C18:3n-3 in alfalfa in rumen fluid from TMR, GRASS, and HERB fed donor cows modeled according to Michaelis–Menten kinetics. The effect of interaction between diet and plant species was seen only for K_M values of C18:3n-3 ($P = 0.005$), and only alfalfa behaved differently compared to the general effect seen for diet.

interaction between diet and species was seen for LA, C18:0, or C18:1*t*11 for either K_M ($P = 0.66$, $P = 0.08$, and $P = 0.33$, respectively) or V_{max} ($P = 0.24$, $P = 0.77$, and $P = 0.81$, respectively).

Michaelis–Menten Kinetics. Application of Michaelis–Menten kinetics to model rumen BH of C18 FAs showed high regression values (R^2) for the fitted Hanes plots and were on average 0.972, 0.933, 0.965, and 0.968 and for ALA, LA, C18:0, and C18:1*t*11, respectively (data not shown). The R^2 for ALA ranged from 0.734 (data for alfalfa in rumen fluid from GRASS-fed donor cows) to 0.997 for LA from 0.649 (data for salad burnet in rumen fluid from HERB-fed donor cows) to 0.997. For C18:0, R^2 ranged from 0.840 (data for birdsfoot trefoil in rumen fluid from GRASS-fed donor cows) to 0.998.

DISCUSSION

Effect of Diet on Rumen Fluid FA Profile and Biohydrogenation. One of the hypotheses for the higher content of ALA and LA in milk from cows grazing alpine pasture or fed species-rich silages is that the feeding regimens would lead to reduced BH of PUFAs. Thus, accumulation of ALA and LA in the rumen fluid should occur compared to feeding pure ryegrass.[14] As seen in other studies, when ryegrass and species-rich herbage were compared,[2,14] no differences in ALA and LA rumen content between the HERB or GRASS diets were seen. Thus, this indicates that accumulation of PUFAs in the rumen cannot solely explain differences in milk ALA and LA contents when species-rich herbages and clover or ryegrass grass herbages[2,9] are compared.

It has been speculated that species-rich herbages could contain secondary plant metabolites that would inhibit normal BH pattern and thus lead to accumulation of BH intermediates such as C18:1*t*11.[24] As a consequence, this would reduce the production of C18:0 in the rumen. Although the content of C18:0 was higher in the GRASS rumen fluid compared to the HERB fluid, the contents of C18:1*t*11 were not different between the HERB and GRASS diets. One of the major BH intermediates of LA, c9*t*12 CLA, was detected in only trace amounts in a few samples and could not be used to detect differences in rumen BH. Nevertheless, the significantly lower content of C18:0 in HERB rumen fluid suggests some alterations in rumen BH in HERB diet compared to both GRASS and TMR diets. Further identification of unidentified peaks that occurred in the present study would probably have helped to emphasize these alterations.

In the present study, rumen fluid from cows on the TMR diet had a significantly higher content of LA than rumen fluid from cows fed the HERB and GRASS diets. A high content of LA is shown to be more toxic than C18:1 isomers to bacteria cells responsible for conversion of LA to C18:1*t*11.[25] The slow and low apparent appearance of C18:1*t*11 and fast formation of C18:0 from the TMR diet in the in vitro batches indicates such possible effects of the TMR diet on the rumen bacterial cultures compared to both HERB and GRASS diets, as the apparent appearance of C18:1*t*11 was similar in the HERB and GRASS diets. The supplies of energy and fermentable carbohydrates for the microbes are also higher on the TMR diet than on the HERB and GRASS diets and possibly provide better bacteria growth. Combined with a numerically lower pH value and thus more hydrogen available for BH, this could contribute to optimized conditions for BH in the rumen and could be one explanatory factor for a higher BH rate in the TMR diet.

Effect of Species on Biohydrogenation. The single plant species differ in chemical composition,[20] and these factors could therefore influence the BH rate. Optimal conditions for BH would among others include supply of energy and protein as well as content of secondary metabolites in single plant species to the bacterial cultures responsible for BH.

Clear differences in BH were seen between the investigated species. Although the K_M values were significantly different only for the end BH product, C18:0, alfalfa and salad burnet continuously showed the lowest BH of ALA and LA, whereas the fastest BH occurred in birdsfoot trefoil. An interesting factor is that alfalfa had the lowest and birdsfoot trefoil the highest content of both ALA and LA, and if only the disappearance of PUFA were investigated, the initial content of single FAs could possibly interfere with the results; however, as these differences are taken into consideration when using the model, the initial FA content cannot explain the differences in BH in these two species from the Fabacea family. Apparent recovery of ALA from feed to milk is also reported to improve when feeding alfalfa compared to feeding grass and a grass clover mixture,[26] which supports our findings with a slow and low BH of ALA in alfalfa when added as single species to in vitro cultures. To the authors' knowledge only one study has looked into the effect of single species on rumen BH, and the differences seen in BH could not be based on simple family classification as well.[13] Therefore, it seems family classification cannot explain the differences seen in the present study.

In recent years evidence for the inhibitory effects of tannins on rumen BH has been shown,[12,27] which has been linked to possible changes in the microbial and protozoa communities.[28] Birdsfoot trefoil is known to contain tannins[29] and in theory should have shown reduced BH of ALA and LA, but was in fact the species with the highest BH of both ALA and LA. On the other hand, alfalfa does not contain considerable amounts of tannins[30] and was one of the single species with the slowest BH of both ALA and LA. The other species with one of the slowest BH of ALA and LA was salad burnet, which is also known to contain tannins.[31] Although different tannins in single plant species could affect rumen BH differently, the content of tannins does not seem to be the only explanatory factor for reduced rumen BH caused by single plant species.

Chemical composition and digestibility of the plants species used in the present in vitro study differed considerably.[20] However, it seems that these differences do not explain the effect on rumen BH of salad burnet, plantain, and alfalfa, but instead further emphasize the complexity of rumen BH as species.

Although BH of ALA and LA was reduced in alfalfa and salad burnet, C18:0 was formed rapdily in the two plant species, too, especially in alfalfa. This could mean that the reaction responsible for the formation of C18:0 saturates faster in alfalfa and salad burnet than in the other species, reducing the conversion of ALA and LA to their respective BH intermediates, as indicated by the high K_M and low V_{max} values. The fact that different species seems to affect the rumen BH pathway differently[4,13] is supported by different apparent formation rates of C18:1*t*11 in the present study; birdsfoot trefoil was not different from alfalfa, although V_{max} values for ALA were significantly different between the two plant species. Plantain, on the other hand, seemed to accelerate the apparent appearance of C18:1*t*11, although it was one of the species showing the slowest BH of both ALA and LA. Plantain is a species with high values of phenolic acids[32] as is salad burnet,[31] and they had the highest and lowest apparent appearance of C18:1*t*11, respectively. This again highlights the complexity in the mechanism affecting rumen BH.

To a certain extent the clover−grass mixture follows the pattern seen for salad burnet. No single cultures of the white clover and ryegrass were sown, and as season and harvest can affect the growth and nutritional composition of plants,[7,33] the clover−grass mixture cultivated under the same conditions as the other species was used. It has been shown that white clover increases milk content of ALA compared to grass[26] through increased passage rate or high content of ALA.[10,11] This could explain the similar BH rate of the clover−grass mixture and salad burnet. As white clover and ryegrass are very different, both physically and chemically,[26,34] it would have been interesting to investigate the effect of the single species on

rumen BH, but for reasons stated above this was not possible in the study presented here. The mixture, although predominately containing white clover, could possibly interact with the rumen microflora different from a single species. In the present study no clear correlation between single species trait and BH of ALA and LA was seen, and further studies are required to elucidate the differences in BH of ALA and LA observed between species.

The interaction between diet and species on BH of ALA offers another interesting aspect, especially as alfalfa was the only species behaving differently when the HERB and GRASS diets were compared. It has repeatedly been shown that a diet containing alfalfa has a positive effect on milk content of ALA.[10] Although alfalfa does not contain noticeable amounts of tannin, it has been shown to contain flavonoids,[35] which could have a specific impact on rumen BH. It has been shown that flavonoids alter rumen fermentation patterns,[36] but the cause of the surprising effect of alfalfa in the GRASS diet is not clear yet and warrants further studies.

AUTHOR INFORMATION

Corresponding Author

*(M.B.P.) E-mail: mbp@agrotech.dk. Phone: +45 8743 8441 Fax: +45 8743 8410.

Funding

This study was part of an industrial Ph.D. funded by the Danish Ministry of Science, Innovation, and Higher Education, AgroTech, Aarhus University, and Future Food Innovation.

Notes

The authors declare no competing financial interest.

ACKNOWLEDGMENTS

We thank M. Würtz Reeh and E. Lyng Pedersen for helping with the laboratory work.

REFERENCES

(1) Glasser, F.; Ferlay, A.; Chilliard, Y. Oilseed lipid supplements and fatty acid composition of cow milk: a meta-analysis. *J. Dairy Sci.* **2008**, *91*, 4687−4703.

(2) Lourenco, M.; Vlaeminck, B.; Bruinenberg, M.; Demeyer, D.; Fievez, V. Milk fatty acid composition and associated rumen lipolysis and fatty acid hydrogenation when feeding forages from intensively managed or semi-natural grasslands. *Anim. Res.* **2005**, *54*, 471−484.

(3) Collomb, M.; Butikofer, U.; Sieber, R.; Jeangros, B.; Bosset, J. O. Correlation between fatty acids in cows' milk fat produced in the Lowlands, Mountains and Highlands of Switzerland and botanical composition of the fodder. *Int. Dairy J.* **2002**, *12*, 661−666.

(4) Povolo, M.; Pelizzola, V.; Passolungo, L.; Biazzi, E.; Tava, A.; Contarini, G. Characterization of two Agrostis-Festuca Alpine pastures and their influence on cheese composition. *J. Agric. Food Chem.* **2013**, *61*, 447−455.

(5) Dewhurst, R. J.; Shingfield, K. J.; Lee, M. R. F.; Scollan, N. D. Indcreasing the concentrations of beneficial polyunsaturated fatty acids in milk produced by dairy cows in high-forage systems. *Anim. Feed Sci. Technol.* **2006**, *131*, 168−206.

(6) Leiber, F.; Kreuzer, M.; Nigg, D.; Wettstein, H. R.; Scheeder, M. R. L. A study on the causes for the elevated n-3 fatty acids in cows' milk of alpine origin. *Lipids* **2005**, *40*, 191−202.

(7) Clapham, W. M.; Foster, J. G.; Neel, J. P. S.; Fedders, J. M. Fatty acid composition of traditional and novel forages. *J. Agric. Food Chem.* **2005**, *53*, 10068−10073.

(8) Lourenco, M.; Van Ranst, G.; Vlaeminck, B.; De Smet, S.; Fievez, V. Influence of different dietary forages on the fatty acid composition of rumen digesta as well as ruminant meat and milk. *Anim. Feed Sci. Technol.* **2008**, *145*, 418−437.

(9) Petersen, M. B.; Soegaard, K.; Jensen, S. K. Herb feeding increases n-3 and n-6 fatty acids in cow milk. *Livest. Sci.* **2011**, *141*, 90−94.

(10) Chilliard, Y.; Glasser, F.; Ferlay, A.; Bernard, L.; Rouel, J.; Doreau, M. Diet, rumen biohydrogenation and nutritional quality of cow and goat milk fat. *J. Lipid Sci. Techol.* **2007**, *109*, 828−855.

(11) Dewhurst, R. J.; Evans, R. T.; Scollan, N. D.; Moorby, J. M.; Merry, R. J.; Wilkins, R. J. Comparison of grass and legume silages for milk production. 2. In vivo and in sacco evaluations of rumen function. *J. Dairy Sci.* **2003**, *86*, 2612−2621.

(12) Khiaosa-Ard, R.; Bryner, S. F.; Scheeder, M. R.; Wettstein, H. R.; Leiber, F.; Kreuzer, M.; Soliva, C. R. Evidence for the inhibition of the terminal step of ruminal α-linolenic acid biohydrogenation by condensed tannins. *J. Dairy Sci.* **2009**, *92*, 177−188.

(13) Jayanegara, A.; Kreuzer, M.; Leiber, F. Ruminal disappearance of polyunsaturated fatty acids and appearance of biohydrogenation products when incubating linseed oil with alpine forage plant species in vitro. *Livest. Prod. Sci.* **2012**, *147*, 104−112.

(14) Khiaosa-Ard, R.; Soliva, C. R.; Kreuzer, M.; Leiber, F. Influence of alpine forage either employed as donor cow's feed or as incubation substrate on in vitro ruminal fatty acid biohydrogenation. *Livest. Sci.* **2011**, *140*, 80−87.

(15) Povolo, M.; Pelizzola, V.; Lombardi, G.; Tava, A.; Contarini, G. Hydrocarbons and fatty acid composition of cheese as affected by the pasture vegetation type. *J. Agric. Food Chem.* **2012**, *60*, 299−308.

(16) Khiaosa-Ard, R.; Soliva, C. R.; Kreuzer, M.; Leiber, F. Effects of species-diverse high-alpine forage on in vitro ruminal fermentation when used as donor cow's feed or directly incubated. *Animal* **2012**, *11*, 1764−1773.

(17) Zened, A.; Troegeler-Meynadier, A.; Nicot, M. C.; Combes, S.; Cauquil, L.; Farizon, Y.; Enjalbert, F. Starch and oil in the donor cow diet and starch in substrate differently affect the in vitro ruminal biohydrogenation of linoleic and linolenic acids. *J. Dairy Sci.* **2011**, *94*, 5634−5645.

(18) McDougall, E. I. Studies on ruminant saliva. 1. The composition and output of sheep's saliva. *Biochem. J.* **1948**, *43*, 99.

(19) Elgersma, A.; Søegaard, K.; Jensen, S. K. Fatty acids, α-tocopherol, β-carotene and lutein contents in forage legumes, forbs and a grass-clover mixture. *J. Agric. Food Chem.* **2013**, *61*, 11913−11920.

(20) Elgersma, A.; Søegaard, K.; Jensen, S. K. Herbage dry-matter production and forage quality of three legumes and four non-leguminous forbs grown in single-species stands. *Grass Forage Sci.* **2013**, 1−12.

(21) Bligh, E. G.; Dyer, W. J. A rapid method of total lipid extraction and purification. *J. Biochem. Physiol.* **1959**, *37*, 911−917.

(22) Jensen, S. K. Improved Bligh and Dyer extraction procedure. *Lipid Technol.* **2008**, *20*, 280−281.

(23) Jensen, S. K.; Nielsen, K. N. Tocopherols, retinol, β-carotene and fatty acids in fat globule membrane and fat globule core in cows' milk. *J. Dairy Res.* **1996**, *63*, 565−574.

(24) Bauman, D. E.; Griinari, J. M. Regulation and nutritional manipulation of milk fat: low-fat milk syndrome. *Livest. Prod. Sci.* **2001**, *70*, 15−29.

(25) Choi, N.; Park, H. G.; Kim, J. H.; Hwang, H.; Kwon, K. H.; Yoon, J. A.; Kwon, E. G.; Chang, J.; Hwang, I. H.; Kim, Y. J. Characterizations of environmental factors in conjugated linoleic acid production by mixed rumen bacteria. *J. Agric. Food Chem.* **2009**, *57*, 9263−9267.

(26) Dewhurst, R. J.; Fisher, W. J.; Tweed, J. K. S.; Wilkins, R. J. Comparison of grass and legume silages for milk production. 1. Production responses with different levels of concentrate. *J. Dairy Sci.* **2003**, *86*, 2598−2611.

(27) Vasta, V.; Makkar, H. P. S.; Mele, M.; Priolo, A. Ruminal biohydrogenation as affected by tannins in vitro. *Br. J. Nutr.* **2009**, *102*, 82−92.

(28) Vasta, V.; Yanez-Ruiz, D. R.; Mele, M.; Serra, A.; Luciano, G.; Lanza, M.; Biondi, L.; Priolo, A. Bacterial and protozoal communities

and fatty acid profile in the rumen of sheep fed a diet containing added tannins. *Appl. Environ. Microbiol.* **2010**, *76*, 2549−2555.
(29) Marley, C.; Fychan, R.; Jones, R. Yield, persistency and chemical composition of *Lotus* species and varieties (birdsfoot trefoil and greater birdsfoot trefoil) when harvested for silage in the UK. *Grass Forage Sci.* **2006**, *61*, 134−145.
(30) Goplen, B.; Howarth, R.; Sarkar, S.; Lesins, K. A search for condensed tannins in annual and perennial species of *Medicago*, *Trigonella*, and *Onobrychis*. *Crop Sci.* **1980**, *20*, 801−804.
(31) Ayoub, N. Unique phenolic carboxylic acids from *Sanguisorba minor*. *Phytochemistry* **2003**, *63*, 433−436.
(32) Fraisse, D.; Carnat, A.; Viala, D.; Pradel, P.; Besle, J. M.; Coulon, J. B.; Felgines, C.; Lamaison, J. L. Polyphenolic composition of a permanent pasture: variations related to the period of harvesting. *J. Sci. Food Agric.* **2007**, *87*, 2427−2435.
(33) Boufaied, H.; Chouinard, P. Y.; Tremblay, G. F.; Petit, H. V.; Michaud, R.; Belanger, G. Fatty acids in forages. I. Factors affecting concentrations. *Can. J. Anim. Sci.* **2003**, *83*, 501−511.
(34) Søegaard, K.; Eriksen, J.; Askegaard, M. Herbs in grasslands − effect of slurry and grazing/cutting on species composition and nutritive value. *Grassland Sci. Eur.* **2008**, *13*, 200−202.
(35) Prati, S.; Baravelli, V.; Fabbri, D.; Schwarzinger, C.; Brandolini, V.; Maietti, A.; Tedeschi, P.; Bevenuti, S.; Macchia, M.; Bonetti, A.; Catizone, P.; Dinelli, G. Composition and content of seen flavonoids in forages and grain legume crops. *J. Sep. Sci.* **2007**, *30*, 491−501.
(36) Balcells, J.; Aris, A.; Serrano, A.; Seradj, A. R.; Crespo, J.; Devant, M. Effect of an extract of plant flavonoids (Bioflavex) on rumen fermentation and performance in herifers fed high-concentrate diets. *J. Anim. Sci.* **2012**, *90*, 4975−4984.

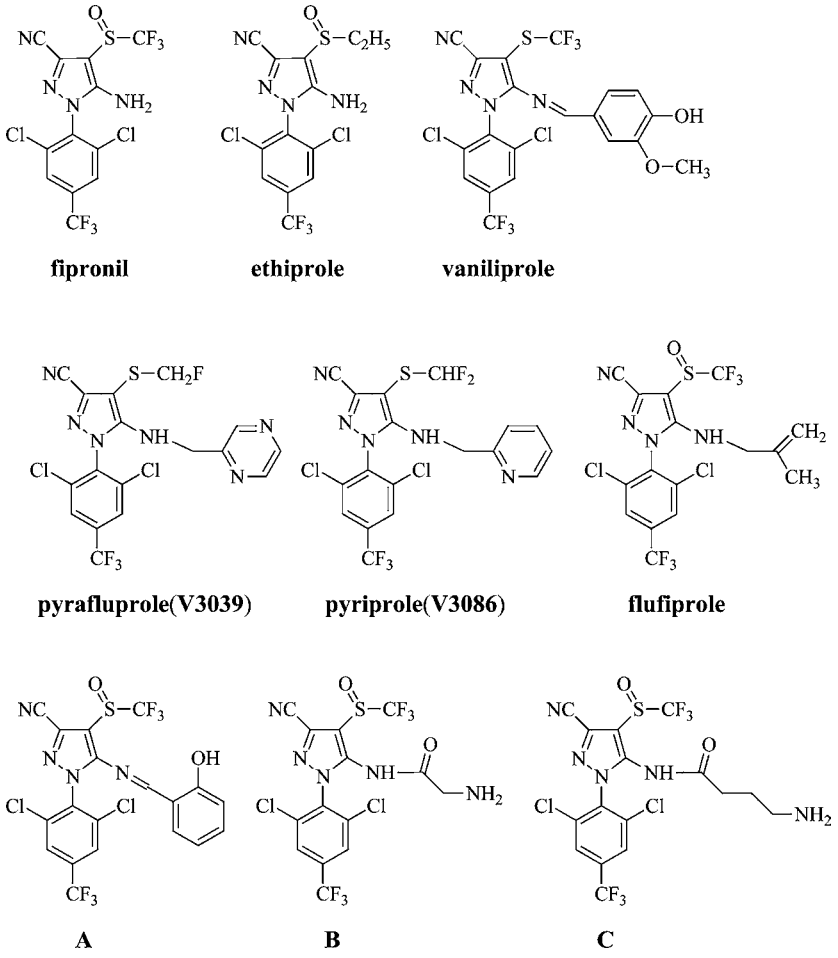

Figure 1. Structures of fipronil derivatives.

side effects due to the reduced ability to penetrate the blood–brain barrier.

To develop dual-target insecticides that act on $GABA_AR$ and nAChRs, we herein report the synthesis and structure–activity relationships (SARs) of phenyl pyrazole inner salts of fipronil derivatives (**1a–1g**) and phenyl pyrazole amido (hydantoin) derivatives (**2a–2d**). **1a–1g** compounds, containing the phenyl pyrazole structure of fipronil and quaternary ammonium structure, would probably act on the two targets $GABA_AR$ and nAChRs.[23−29]

MATERIALS AND METHODS

General. All melting points were obtained with a RY-1G melting point apparatus (Tianjin Tianguang Optical Instruments Co. Ltd., China) and are uncorrected. ^{1}H NMR and ^{13}C NMR spectra were recorded on a Bruker AVANCE 600 (600 MHz) or Bruker AC-P400Q instrument. ESI-MS was recorded on AccuTOF CS JMS-T100CS (JEOL), and EI-MS was recorded on DSQ (Thermo). EI-HRMS was recorded on MAT95XP (Thermo). ESI-HRMS was recorded on LTQ Orbitrap Elite (Thermo Fisher) or ESI-Q-TOF (Bruker Daltonics).

General Procedure for the Synthesis of Intermediate 2-Bromo-*N*-(3-cyano-1-(2,6-dichloro-4-(trifluoromethyl)phenyl)-4-(trifluoromethylsulfinyl)-1*H*-pyrazol-5-yl) Acetamide (Compound 1). Almost 98% fipronil (4.4 g, 0.01 mol) was dissolved in anhydrous tetrahydrofuran (40 mL), to which sodium hydride (0.8 g of 36% oil dispersion) was added three times below 0 °C under nitrogen and stirred below 10 °C. After 3 h, bromoacetyl bromide (7 mL) was added and stirred at room temperature for another 3 h. The reaction mixture was filtered and the filtrate evaporated in vacuo. The solid residue was purified by chromatography and eluted with petroleum ether/ethyl acetate (3:1, v/v) to give clear colorless crystals (mp 105–107 °C, yield = 72%). ^{1}H NMR ($CDCl_3$, 600 MHz) δ 9.22 (s, 1H, NH), 7.77 (s, 2H, ArH), 4.12 (s, 2H, CH_2); ^{13}C NMR (150 MHz, $CDCl_3$) δ 171.37, 164.07, 141.38, 136.03, 135.58, 134.80, 134.57, 134.36, 126.59, 126.57, 126.18, 109.64, 107.90, 26.63; ESI-MS, m/z (%) 559 $[M + H]^+$ (40), 581 $[M + Na]^+$ (100), 597 $[M + K]^+$ (28).

General Procedure for the Synthesis of Compounds 1a–1g. Compound **1** (3.00 g, 0.0054 mol) was dissolved in 15 mL of THF in a 150 mL round-bottom flask equipped with a magnetic stirrer and a calcium tube. Then 0.01 mol of tertiary amine or nitrogen heterocycles in 10 mL of THF was dropped into the solution and stirred for 2–4 h at room temperature. The reaction mixture was evaporated in vacuo. The residue was purified by chromatography eluting using ethyl acetate/methanol and afforded the desired products **1a–1g**.

*(3-Cyano-1-(2,6-dichloro-4-(trifluoromethyl)phenyl)-4-((trifluoromethyl)sulfinyl)-1H-pyrazol-5-yl) (2-(Trimethylammonio) acetyl)amide (**1a**).* Column chromatography (ethyl acetate/methanol = 7:1 → 6:1, v/v) afforded compound **1a** as a clear colorless crystal: mp 199–201 °C; yield = 89%. ^{1}H NMR (600 MHz, $(CD_3)_2CO$) δ 8.05 (s, 2H, ArH), 3.95 (d, 1H, J = 15.6 Hz, CH_2-1), 3.90 (d, 1H, J = 15.6 Hz, CH_2-2), 3.35 (s, 9H, 3 × CH_3); ^{13}C NMR (150 MHz, $(CD_3)_2CO$) δ 167.1, 152.6, 139.3, 136.8, 134.0, 133.8, 133.5, 128.8, 126.8, 126.6, 126.1, 124.3, 122.5, 113.6, 104.2, 68.8, 53.9; EI-MS, m/z (%) 535 $[M]^+$ (80); EI-HRMS for $C_{17}H_{13}Cl_2F_6N_5O_2S$ $[M]^+$, calcd 535.0066, found 535.0061.

*(3-Cyano-1-(2,6-dichloro-4-(trifluoromethyl)phenyl)-4-((trifluoromethyl)sulfinyl)-1H-pyrazol-5-yl) (2-(Triethylammonio)-acetyl)amide (**1b**).* Column chromatography (ethyl acetate/methanol = 8:1 → 6:1, v/v) afforded compound **1b** as a clear colorless crystal: mp 180–182 °C; yield = 75%. ^{1}H NMR (600 MHz, MeOD) δ 8.03 (s,

dx.doi.org/10.1021/jf405512e | J. Agric. Food Chem. 2014, 62, 3577–3583

2H, ArH), 4.82 (s, 2H, CH_2), 3.63−3.72 (m, 2H, CH_2), 3.37−3.41 (m, 4H, $2CH_2$), 1.14−1.17 (m, 9H, 3 × CH_3); ^{13}C NMR (150 MHz, $CDCl_3$) δ 167.5, 152.9, 139.3, 137.5, 137.4, 135.3, 135.1, 134.8, 134.6, 127.1, 127.1, 126.4, 124.6, 124.3, 122.8, 113.4, 104.9, 61.0, 54.7, 7.8; EI-MS, *m/z* (%) 577 $[M]^+$ (30); EI-HRMS for $C_{20}H_{19}O_2N_5Cl_2F_6S$ $[M]^+$, calcd 577.0535, found 577.0534. (The single crystal data are available from Cambridge Crystallographic Data Centre (CCDC 975075).)

*(3-Cyano-1-(2,6-dichloro-4-(trifluoromethyl)phenyl)-4-((trifluoromethyl)sulfinyl)-1H-pyrazol-5-yl) (2-(Tributylammonio)-acetyl)amide (**1c**).* Column chromatography (ethyl acetate/methanol = 10:1 → 7:1, v/v) afforded compound **1c** as a clear colorless crystal: mp 221−223 °C; yield = 54%. ^{1}H NMR (600 MHz, $(CD_3)_2SO$) δ 8.27 (s-like, 1H, ArH), 8.26 (s-like, 1H, ArH), 3.75 (d, 1H, *J* = 15.6 Hz, CH_2-1), 3.70 (d, 1H, *J* = 15.6 Hz, CH_2-2), 3.23−3.25 (m, 6H, 3 × CH_2), 1.45−1.49 (m, 6H, 3 × CH_2), 1.11−1.45 (m, 6H, 3 × CH_2) 1.11 (t, 9H, *J* = 7.2 Hz, 3 × CH_3); ^{13}C NMR (150 MHz, $(CD_3)_2SO$) δ 206.4, 166.6, 151.2, 137.7, 135.2, 135.1, 126.2, 125.3, 112.7, 60.6, 58.1, 30.6, 23.1, 19.1, 13.4; ESI-MS, *m/z* (%) 662 $[M + H]^+$ (80), 684 $[M + Na]^+$ (100); ESI-HRMS for $C_{27}H_{32}O_4N_5Cl_2F_6S$ $[M + HCOO]^-$, calcd 706.14617, found 706.14694.

*(3-Cyano-1-(2,6-dichloro-4-(trifluoromethyl)phenyl)-4-((trifluoromethyl)sulfinyl)-1H-pyrazol-5-yl) (2-(Quinolin-1-ium-1-yl)-acetyl)amide (**1d**).* Column chromatography (ethyl acetate/methanol = 12:1 → 10:1, v/v) afforded compound **1d** as a clear colorless crystal: mp 243−245 °C; yield = 83%. ^{1}H NMR (600 MHz, MeOD) δ 9.15 (dd, 1H, *J* = 6.0, 1.2 Hz, quinoline), 8.93 (d, 1H, *J* = 7.8 Hz, quinoline), 8.24 (d, 1H, *J* = 8.4 Hz, quinoline), 8.11−8.12 (m, 2H, quinoline), 7.97−7.94 (m, 2H, quinoline), 7.86 (d, 1H, *J* = 8.4 Hz, quinoline), 7.84 (d, 1H, *J* = 8.4 Hz, quinoline), 7.60 (d, 1H, *J* = 1.2 Hz, Ar-H), 7.57 (d, 1H, *J* = 1.8 Hz, Ar-H), 5.57 (d, 1H, *J* = 16.8 Hz, CH_2-1), 5.51 (d, 1H, *J* = 16.8 Hz, CH_2-2); ^{13}C NMR (150 MHz, MeOD) δ 169.2, 152.2, 151.0, 148.3, 140.4, 138.5, 136.8, 136.6, 131.4, 131.1, 130.8, 126.8, 126.5, 122.3, 120.2, 113.3, 62.7; ESI-MS, *m/z* (%) 606 $[M + H]^+$ (100), 628 $[M + Na]^+$ (70); ESI-HRMS for $C_{24}H_{14}O_3N_5Cl_2F_6S$ $[M + CH_3O]^-$, calcd 636.01041, found 636.01105.

*(3-Cyano-1-(2,6-dichloro-4-(trifluoromethyl)phenyl)-4-((trifluoromethyl)sulfinyl)-1H-pyrazol-5-yl) (2-(Pyridine-1-ium-1-yl)-acetyl)amide (**1e**).* Column chromatography (ethyl acetate/methanol = 9:1 → 7:1, v/v) afforded compound **1e** as a clear colorless crystal: mp 225−227 °C; yield = 81%. ^{1}H NMR (600 MHz, $(CD_3)_2SO$) δ 8.96 (s-like, 2H, pyridine), 8.63−8.64 (m, 1H, pyridine), 8.41−8.35 (m, 2H, pyridine), 8.14 (brs, 2H, benzene), 4.25 (brs, 2H, CH_2); ^{13}C NMR (150 MHz, $(CD_3)_2SO$) δ 146.3, 135.5, 134.9, 127.7, 127.5, 127.2, 126.9, 126.8, 125.5, 124.9, 124.6, 123.1, 121.2, 119.4, 111.0, 61.9; ESI-MS, *m/z* (%) 556 $[M + H]^+$ (100); ESI-HRMS for $C_{19}H_8O_2N_5Cl_2F_6S$ $[M - H]^-$, calcd 553.96854, found 553.96906.

*(3-Cyano-1-(2,6-dichloro-4-(trifluoromethyl)phenyl)-4-((trifluoromethyl)sulfinyl)-1H-pyrazol-5-yl) (2-(4-(Dimethylamino)-pyridine-1-ium-1-yl)acetyl)amide (**1f**).* Column chromatography (ethyl acetate/methanol = 8:1 → 7:1, v/v) afforded compound **1f** as a clear colorless crystal: mp 214−216 °C; yield = 62%. ^{1}H NMR (600 MHz, $(CD_3)_2SO$) δ 8.11 (s, 1H, Ar-H), 8.10 (s, 1H, Ar-H), 7.98 (d, 2H, *J* = 7.8 Hz, pyridine-H), 6.78 (d, 2H, *J* = 7.8 Hz, pyridine-H), 4.71 (d, 1H, *J* = 16.2 Hz, CH_2-1), 4.64 (d, 1H, *J* = 16.8 Hz, CH_2-2), 3.12 (s, 6H, 2 × NCH_3); ^{13}C NMR (150 MHz, $(CD_3)_2SO$) δ 169.6, 156.9, 155.4, 151.7, 143.0, 139.1, 137.5, 135.2, 135.0, 127.4, 125.6, 125.2, 125.0, 123.1, 121.3, 112.8, 106.9, 106.1, 60.5; ESI-MS, *m/z* (%) 599 $[M + H]^+$ (10); ESI-HRMS for $C_{22}H_{15}O_4N_6Cl_2F_6S$ $[M + HCOO]^-$, calcd 643.01622, found 643.01703.

*(3-Cyano-1-(2,6-dichloro-4-(trifluoromethyl)phenyl)-4-((trifluoromethyl)sulfinyl)-1H-pyrazol-5-yl) (2-(4-Methylpyridin-1-ium-1-yl)acetyl)amide (**1g**).* Column chromatography (ethyl acetate/methanol = 7:1 → 6:1, v/v) afforded compound **1g** as a clear colorless crystal: mp 208−210 °C; yield = 43%. ^{1}H NMR (600 MHz, $(CD_3)_2CO$) δ 8.97 (d, 2H, *J* = 6.6 Hz, pyridine-H), 8.05 (d, 2H, *J* = 6.0 Hz, pyridine-H), 8.00 (d, 2H, *J* = 0.6 Hz, Ar-H), 5.88 (d, 1H, *J* = 16.2 Hz, CH_2-1), 5.79 (d, 1H, *J* = 16.8 Hz, CH_2-2), 2.09 (s, 3H, CH_3); ^{13}C NMR (150 MHz, $(CD_3)_2CO$) δ 166.8, 161.0, 145.9, 137.3, 136.8, 136.5, 134.5, 128.7, 128.2, 127.2, 127.0, 126.0, 124.2, 122.4, 112.3, 63.4; ESI-MS, *m/z* (%) 569 $[M]^+$ (100); ESI-HRMS for $C_{20}H_{11}Cl_2F_6N_5O_2S$ $[M + H]^+$, calcd 569.9987, found 570.0012.

General Procedure for the Synthesis of Compounds 2a−2d. *N-(3-Cyano-1-(2,6-dichloro-4-(trifluoromethyl)phenyl)-4-((trifluoromethyl)sulfinyl)-1H-pyrazol-5-yl)-2-(2,4-dichlorophenoxy) Acetamide (**2a**).* 2,4-Dichlorophenoxyacetyl chloride was synthesized according to a method from the literature.[30] Almost 98% fipronil (4.4 g, 0.01 mol), triethylamine (0.013 mol), and *N*,*N*-dimethylaminopyridine (DMAP) (0.001 mol) dissolved in chloroform (15 mL) were added to 2,4-dichlorophenoxyacetic chloride (2.14 g, 0.009 mol). The reaction mixture was stirred at reflux temperature for about 3 h and monitored by TLC. After cooling to room temperature, the reaction mixture was filtered, and dichloromethane (20 mL) was added and washed with 1 M HCl (10 mL) and water (2 × 20 mL). The organic extracts were dried with anhydrous sodium sulfate and then evaporated in vacuo. The solid residue was purified by column chromatography by petroleum ether and ethyl acetate to give clear colorless crystals (yield = 46%): mp 161−163 °C. ^{1}H NMR (400 MHz, DMSO-d_6) δ 8.35, 8.31 (2H, s, $CF_3C_6H_2Cl_2$), 7.57 (1H, d, *J* = 2.0 Hz, 3-$C_6H_3Cl_2$), 7.34 (1H, dd, *J* = 2.0, 8.0 Hz, 5-$C_6H_3Cl_2$), 6.91 (1H, d, *J* = 8.0 Hz, 6-$C_6H_3Cl_2$), 4.90, 4.85 (2H, d, *J* = 16.0 Hz, CH_2); ESI-MS, *m/z* (%) 638 (100) $[M + H]^+$, 641 $[M + H + 2]^+$, 643 $[M + H + 4]^+$.

*N-(3-Cyano-1-(2,6-dichloro-4-(trifluoromethyl)phenyl)-4-((trifluoromethyl)sulfinyl)-1H-pyrazol-5-yl)-2-(2,4,5-trichlorophenoxy) Acetamide (**2b**).* Compound **2b** was synthesized according to the same method as used for **2a**. Compound **2b** was colorless crystals (yield = 34%): mp 147−149 °C. ^{1}H NMR (400 MHz, DMSO-d_6) δ 11.63 (1H, s, NH), 8.40, 8.36 (2H, s, $CF_3C_6H_2Cl_2$), 7.84, 7.25 (2H, s, 6,3-$C_6H_2Cl_3$), 4.98 (2H, s, CH_2); ESI-MS, *m/z* (%) 672 (100) $[M + H]^+$, 675 $[M + H + 2]^+$.

*N-((3-Cyano-1-(2,6-dichloro-4-(trifluoromethyl)phenyl)-4-((trifluoromethyl)sulfinyl)-1H-pyrazol-5-yl)carbamoyl)-2-(2,4-dichlorophenoxy) Acetamide (**2c**).* 2-(2,4-Dichlorophenoxy) acetamide and 2-(2,4-dichlorophenoxy) acetyl isocyanate was synthesized according to a method from the literature.[30] 2-(2,4-Dichlorophenoxy) acetyl isocyanate (2.5 g, 0.01 mol) was dissolved in anhydrous diethyl ether (50 mL), to which fipronil (4.4 g, 0.01 mol) dissolved in anhydrous diethyl ether (20 mL) was added below 0 °C, stirred at room temperature, and monitored by TLC. The reaction mixture was filtered and the filtrate evaporated in vacuo. The solid residue was purified by chromatography and eluted with petroleum ether/ethyl acetate to give colorless crystals (yield = 57%): mp 142−144 °C. 1H NMR (400 MHz, $CDCl_3$) δ 10.96, 8.94 (2H, s, 2NH), 7.86−7.83 (2H, s, $CF_3C_6H_2Cl_2$), 7.46 (1H, d, *J* = 2.2 Hz, 3-$C_6H_3Cl_2$), 7.27 (1H, dd, *J* = 2.2, 8.0 Hz, 5-$C_6H_3Cl_2$), 6.85 (1H, d, *J* = 8.0 Hz, 6-$C_6H_3Cl_2$), 4.64 (2H, s, CH_2); ESI-MS, *m/z* (%) 685 $[M + H + 4]^+$ (50), 684 $[M + H + 2]^+$ (100), 681 $[M + H]^+$ (80).

*N-((3-Cyano-1-(2,6-dichloro-4-(trifluoromethyl)phenyl)-4-((trifluoromethyl)sulfinyl)-1H-pyrazol-5-yl)carbamoyl)-2-(2,4,5- trichlorophenoxy) Acetamide (**2d**).* Compound **2d** was synthesized according to the same method as used for **2c**. Compound **2d** was colorless crystals (yield = 37%): mp 101−103 °C. ^{1}H NMR (400 MHz, $CDCl_3$) δ 10.87, 8.85 (2H, s, 2NH), 7.81, 7.78 (2H, s, $CF_3C_6H_2Cl_2$), 7.51 (1H, s, 6-$C_6H_2Cl_3$), 6.97 (1H, s, 3-$C_6H_2Cl_3$), 4.60 (2H, s, CH_2); ESI-MS, *m/z* (%) 717 $[M + H + 2]^+$ (100), 715 $[M + H]^+$ (60).

Bioactivity Assay against *Plutella xylostella*. *Rearing Methods for P. xylostella.* Healthy larvae of *P. xylostella* were collected from the experimental farm of Dongguan Agricultural Science Research Center, Guangdong, China, and were reared on Chinese cabbage (*Brassica rapa*) under cage conditions of 24−29 °C, 70−80% relative humidity, and photoperiod 16:8 h light/dark for the third-instar larvae.

Assessment of Bioactivity on P. xylostella. The bioactivities of phenyl pyrazole derivatives and fipronil against the third-instar larvae of *P. xylostella* were determined by the leaf disk-dipping assay. Leaves of Chinese cabbage grown in the greenhouse were collected, and disks (5.5 cm diameter) were punched from each leaf. The compounds were dissolved in acetone and suspended in distilled water containing Triton X-100. Leaf disks were dipped in each test solution for 30 s and allowed to dry for 2 h. The treated leaf disks were placed into Petri

Scheme 1. Synthesis of 1a−1g[a]

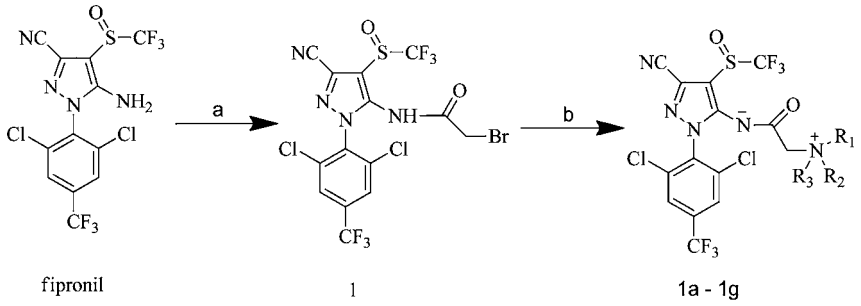

Comp.	$NR^1R^2R^3$
1a	trimethylamine
1b	triethylamine
1c	tri-n-butylamine
1d	quinoline
1e	pyridine
1f	*N*,*N*-dimethylpyridin-4-amine
1g	4-methylpyridine

[a]Reagents and conditions: (a) bromoacetyl bromide, NaH, THF; (b) tertiary amine or nitrogen heterocyclic compounds, THF.

Scheme 2. Synthesis of 2a−2d[a]

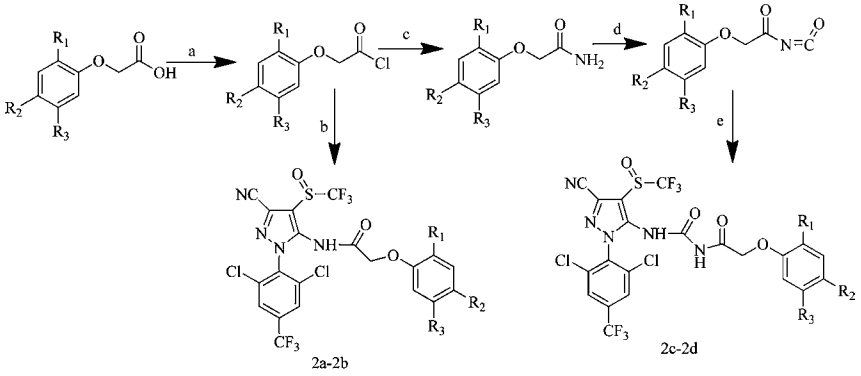

Comp.	R_1	R_2	R_3
2a	Cl	Cl	H
2b	Cl	Cl	Cl
2c	Cl	Cl	H
2d	Cl	Cl	Cl

[a]Reagents and conditions: (a) $SOCl_2$; (b) fipronil, triethylamine, DMAP, $CHCl_3$; (c) $NH_3{\cdot}H_2O$; (d) $(COCl)_2$, 1,2-dichloroethane; (e) fipronil, anhydrous diethyl ether.

dishes (9 cm diameter). Then, 10 *P. xylostella* larvae were introduced into each dish. Distilled water containing an acetone−Triton X-100 solution but not the test compound was used as the control. Petri dishes were kept in an incubator at 26 °C and 85% relative humidity under a photoperiod of 16:8 h light/dark. All treatments were replicated five times. Mortalities were determined 24 h after treatment. The death rate of each treatment group was confirmed. The LC_{50} value was calculated by the SPSS software.

Docking Study. The *Musca domestica* GABA receptor subunit sequence was obtained from the NCBI database (GenBank AAC23602.1). The sequence and structure of the nicotinic acetylcholine receptor (nAChR) were obtained from the RSCB protein data bank at 4 Å resolutions (PDB ID 2BG9). The amino acid sequence of the subunit was edited to remove the extracellular region and residues in the loop between transmembrane (TM) domains 3 and 4 (TM3−TM4 loop). Using the sequence analysis program above, sequence alignment was carried out. The sequence and structure of the nicotinic

dx.doi.org/10.1021/jf405512e | J. Agric. Food Chem. 2014, 62, 3577−3583

acetylcholine receptor (nAChR) were obtained from the RSCB protein data bank at 4 Å resolutions (PDB ID 3C79). The models of the transmembrane region of the GABA receptor subunit were built by homology modeling using the MODELER program with the default parameters. In the model building, we employed an optimization method involving conjugate gradients and molecular dynamics to minimize violations of the spatial restraints. All molecule modeling was done using Discovery Studio 2.5 on SGI workstation. The initial structures of these compounds were built and energetically minimized. To investigate how the insecticide anchored at the putative binding cavity, fipronil and phenyl pyrazole inner salts were docked into the ion channel pore formed by the second transmembrane segments of the homooligomeric receptor. Binding site interactions of compounds and AChBP are simulated with *Aplysia californica* AChBP on the basis of its structure cocrystallized with bound IMI (Protein Data Bank code 3C79). The A−E subunit interface of the AChBP−IMI complex is arbitrarily used for modeling because the homomeric AChBP pentamer has five identical binding pockets localized at subunit interfacial regions. The compound is docked into the ligand-binding pocket of IMI. All molecule dockings were done using the CDOCK program with the default parameters. The docking complexes were solvated in the water layer in a truncated octahedral periodic box. Then, the complexes were minimized using the molecular dynamics simulation.

RESULTS AND DISCUSSION

Synthesis. The synthesis of compounds **1a−1g** and **2a−2d** was outlined in Schemes 1 and 2. Fipronil was reacted with bromoacetyl bromide in the presence of sodium hydride to afford the key intermediate **1**. Compounds **1a−1g** were obtained via the reaction of intermediate **1** and tertiary amine or nitrogen heterocyclic compounds in the presence of tetrahydrofuran. Compounds **2a−2d** were obtained by using the classical methodology.

Table 1. 24 h Effect of Phenyl Pyrazole Inner Salts against Third-Instar Larvae of Diamondback Moth (*Plutella xyllostella* L.)

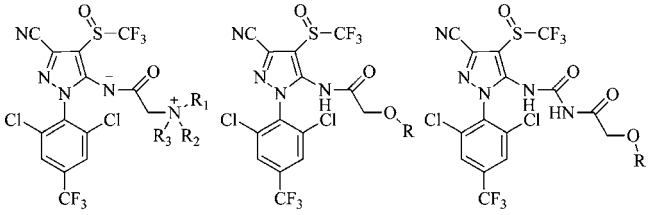

1a-1g **2a-2b** **2c-2d**

compd	$NR^1R^2R^3$ (R)	LC_{50} ($\mu g\ mL^{-1}$)	95% confidence interval of LC_{50} ($\mu g\ mL^{-1}$)
1a	trimethylamine	15.10	9.92−23.01
1b	triethylamine	20.84	13.61−31.92
1c	tri-*n*-butylamine	24.69	14.16−43.06
1d	quinoline	8.31	5.84−11.82
1e	pyridine	12.85	9.05−18.24
1f	*N*,*N*-dimethylpyridin-4-amine	24.71	14.73−41.46
1g	4-methylpyridine	18.55	12.57−27.38
2a	2,4-dichlorobenzene	58.58	26.78−128.15
2b	2,4,5-trichlorobenzene	56.00	28.71−109.26
2c	2,4-dichlorobenzene	153.52	17.68−1333.19
2d	2,4,5-trichlorobenzene	210.00	10.93−4034.25
fipronil		24.93	16.55−37.54

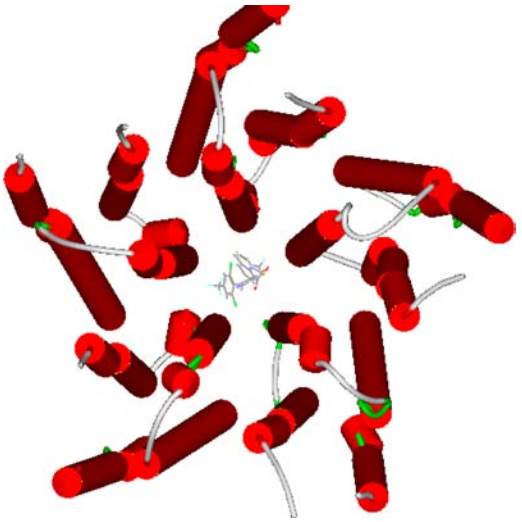

Figure 2. Model of compound **1d** in the $GABA_A$ receptor $\beta 3$ homopentamer binding site. It shows a model of the ion channel with five helices and compounds docked into the putative binding site, which it clearly fills to block the pore. Compounds interact with resides of TM2 and contact A2, T6, and L9 coinciding with mutation experiments.

Figure 3. Simulated binding site interactions of compound **1d** with the *Aplysia californica* AChBP structural surrogate of the extracellular domain of the nAChR. The structure of *Aplysia californica* AChBP cocrystallized with bound IMI (Protein Data Bank code 3C79) shows the binding site of IMI was located in the interface of the AChBP subunit. Simulated docking shows docking compounds in the same site formed $\pi-\pi$ stacking interactions and hydrogen bonding.

SAR. The preliminary insecticidal activities of compounds **1a−1g** and **2a−2d** were assessed by the leaf disk-dipping assay, and the results are listed in Table 1. Due to the low insecticidal activities of **2a−2d**, the SAR study does not include the compounds **2a−2d**.

For the alkyl quaternary ammonium **1a−1c**, the activities decreased from 15.10 $\mu g\ mL^{-1}$ (LC_{50} value, 24 h) to 24.69 $\mu g\ mL^{-1}$ (LC_{50} value, 24 h) against *P. xylostella*, respectively, whereas the bulk of R^1, R^2, and R^3 increased. The activity of compound **1a**, 15.10 $\mu g\ mL^{-1}$ (24 h LC_{50} value), was better than that of fipronil, 24.93 $\mu g\ mL^{-1}$ (24 h LC_{50} value), against *P. xylostella*, indicating that the steric hindrance of $NR^1R^2R^3$ is unfavorable for the insecticidal activity of the phenyl pyrazole inner salts.

dx.doi.org/10.1021/jf405512e | J. Agric. Food Chem. 2014, 62, 3577−3583

Compounds **1d**−**1g** are heterocyclic quaternary ammoniums. It is clear that the insecticidal activity obviously increased when the ring of $NR^1R^2R^3$ was enlarged. For instance, compounds **1d** (10-member bicyclic aromatic ring, 8.31 μg mL^{-1}, 24 h LC_{50} value) and **1e** (6-member ring, 12.85 μg mL^{-1}, 24 h LC_{50} value) have better activity than fipronil (24.93 μg mL^{-1}, 24 h LC_{50} value) against *P. xylostella*. This result is opposite to traditional agonists, as the increase of the bulk of R^1, R^2, and R^3 weakens the activity significantly.[31] This may confirm the effect of the unique heterocyclic quaternary ammonium conformation, possibly due to the influence of the size of cycle on the conformation. Therefore, an appropriate conformation is critical for the interaction between cationic nitrogen and receptor.

With the pyridine group considered to be the key pharmacophore in **1e**, compounds **1f** and **1g** were synthesized. The bioassay data on compounds **1e**, **1f**, and **1g** revealed that a large substituent at the 4-position of the 6-member $NR^1R^2R^3$ ring is not preferred. A substitution at the 4-position of the 6-member $NR^1R^2R^3$ ring is unfavorable for the insecticidal activity, and steric hindrance may weaken the activity. The bioactivity of compound **1f** ($NR^1R^2R^3$ = *N*,*N*-dimethylpyridin-4-amine) was similar to that of fipronil, but **1g** ($NR^1R^2R^3$ = 4-methylpyridine) was more active than fipronil with an insecticidal activity of 18.55 μg mL^{-1} (24 h LC_{50} value). These results suggested that the substituent at the 4-position of the 6-member $NR^1R^2R^3$ ring might bind to the receptor as an H-bond acceptor.

Furthermore, the influence of the substituted groups of the 4-pyridine ring on insecticidal activity was explored. As compared to compound **1e** (12.85 μg mL^{-1}, 24 h LC_{50} value) without any substituted group, the electron-donating group (**1f**, 4-$N(CH_3)_2$, 24.71 μg mL^{-1}, 24 h LC_{50} value, and **1g**, 4-CH_3, 18.55 μg mL^{-1}, 24 h LC_{50} value) at the 4-position was unfavorable for insecticidal activity.

Because of the special conformation of the heterocyclic quaternary ammonium structure, substitution at the 4-position of the pyridine ring was unfavorable for cooperative $\pi-\pi$ interaction.[32] This may confirm the effect of the special heterocyclic quaternary ammonium conformation.

On the contrary, **1e** with pyridine for $NR^1R^2R^3$ exhibited excellent insecticidal activity (12.85 μg mL^{-1}, 24 h LC_{50} value) and may have a special conformation to bind to receptors. Inspired by this result, we introduced quinoline to the fipronil molecule and obtained **1d** with a rather good insecticidal activity (**1d**, 8.31 μg mL^{-1}, 24 h LC_{50} value). The insecticidal potency of **1d** and **1e** indicated that a quinoline or pyridine ring at a proper position of $NR^1R^2R^3$ was preferred, which might contribute to affinity with a suitable conformation and/or hydrogen bonding and cooperative $\pi-\pi$ interaction.[33]

Docking Study. To clarify the binding mode of our synthesized phenyl pyrazole inner salts, compounds were docked in the active site of the $GABA_A$ receptor recombinant β3 homopentamer and the crystal structures of the acetylcholine binding protein (AChBP) (Figure 2).[34] The fipronil-related phenyl heterocyclic compounds were effective as noncompetitive antagonists to the housefly GABA receptor. Several observations suggest that the noncompetitive antagonists interact with the same position of the M2 transmembrane segment region on the cytoplasmic side [A]. As a channel blocker, the fipronil-related noncompetitive antagonists interact with the ion channel associated with the β3-homopentamer.

The structure of *A. californica* AChBP cocrystallized with bound IMI (Protein Data Bank code 3C79) shows the binding site of IMI was located in the interface of the AChBP subunit. Simulated docking shows docking compounds into the same site formed $\pi-\pi$ stacking interactions and hydrogen bonding (Figure 3).[35] The interaction was not the same with IMI.

In summary, by selecting phenyl pyrazole inner salts of fipronil derivatives as the lead compounds, a series of phenyl pyrazole inner salts were designed and synthesized to search for a new dual-target insecticide with low side effects. Extensive SAR studies revealed that a suitable $NR^1R^2R^3$ was critical for the insecticidal activity, which might be beneficial to expose the cationic nitrogen to bind to the receptor and possibly interact with the receptor via hydrogen bonding and cooperative $\pi-\pi$ interaction. More importantly, compound **1d**, a new type of quinoline quaternary ammonium salt, showed potent insecticidal activity, which would be very valuable for the further development of dual-target insecticides. The action mechanism of dual-target phenyl pyrazole inner salts deserves further study.

AUTHOR INFORMATION

Corresponding Author

*(Hanhong Xu) Tel.: +86-20-85285127; E-mail: hhxu@scau.edu.cn.

Funding

This research was supported by the National Natural Science Foundation of China (No. 31171871), the Guangdong Natural Science Foundation (No. S2011010001141), and the Research Foundation for Talented Scholars (No. (2010)79).

Notes

The authors declare no competing financial interest.

REFERENCES

(1) Moffat, A. S. New chemicals seek to outwit insect pests. *Science* **1993**, *261*, 550−551.

(2) Ikeda, T.; Zhao, X.; Nagata, K.; Kono, Y.; Shono, T.; Yeh, J. Z. Fipronil modulation of γ-aminobutyric acid (A) receptors in rat dorsal root ganglion neurons. *J. Pharmacol. Exp. Ther.* **2001**, *296*, 914−921.

(3) Hainzl, D.; Casida, J. E. Fipronil insecticide: novel photochemical desulfinylation with retention of neurotoxicity. *Proc. Natl. Acad. Sci. U.S.A.* **1996**, *93*, 12764−12767.

(4) Li, A.; Yang, Y.; Wu, S.; Li, C.; Wu, Y. Investigation of resistance mechanisms to fipronil in diamondback moth (Lepidoptera *Plutellidae*). *J. Econ. Entomol.* **2006**, *99*, 914−919.

(5) Kristensen, M.; Hansen, K. K.; Jensen, K. M. Cross-resistance between dieldrin and fipronil in German cockroach (Dictyoptera *Blattellidae*). *J. Econ. Entomol.* **2005**, *98*, 1305−1310.

(6) Tang, J.; Li, J.; Shao, Y.; Yang, B. J.; Liu, Z. W. Fipronil resistance in the white backed planthopper (*Sogatella furcifera*): possible resistance mechanisms and cross-resistance. *Pest Manage. Sci.* **2010**, *66*, 121−125.

(7) Ozoe, Y.; Yagi, K.; Nakamura, M.; Akamatsu, M.; Miyake, T.; Matsumura, F. Fipronil-related heterocyclic compounds: structure-activity relationships for interaction with γ-aminobutyric acid-and voltage-gated ion channels and insecticidal action. *Pestic. Biochem. Physiol.* **2000**, *66*, 92−104.

(8) Zhang, Y. B.; Zhang, Y. *New Progress of Pesticide in World* (in Chinese); Chemical Industry: Beijing, China, 2006; p 152.

(9) Peng, Y. Q.; Gao, C. F.; Ma, C. Y.; Mao, Y. X.; Shen, J. L. Risk assessment and genetic analysis of fipronil resistance and insecticide susceptibility in the small brown planthopper, *Laodelphax striatellus* (Homoptera: *Delphacidae*) (in Chinese). *Chin. J. Rice Sci.* **2009**, *23*, 645−652.

(10) Niu, H. T.; Luo, W. C.; Zong, J. P.; Wei, S. J.; Wang, H. Y.; Pan, Z. X. Realized heritability of resistance to butene-fipronil in

diamondback moth, *Plutella xylostella* (in Chinese). *Acta Phytophylacica Sinica* **2008**, *35*, 165−168.
(11) Jiang, D. X.; Lu, X. L.; Hu, S.; Zhang, X. B.; Xu, H. H. A new derivative of fipronil: effect of adding a glycinyl group to the 5-amine of pyrazole on phloem mobility and insecticidal activity. *Pestic. Biochem. Physiol.* **2009**, *95*, 126−130.
(12) Zheng, X. H.; Jiang, D. X.; Liu, Z. C.; Xu, H. H. Synthesis, characterization and bioactivity of fipronil derivatives as a lead for new insecticide. *Indian J. Chem. Technol.* **2010**, *17*, 215−219.
(13) Xu, H. H.; Jiang, D. X.; Hu, S.; Zhang, X. W.; Liu, Z. C.; Zheng, X. H. Fipronil-GABA conjugate − a phloem mobile insecticide against sucking insect. *4th Pan Pacific Conference on Pesticide Science*, Hawaii, USA; American Chemical Society: Washington DC, 2008; p 39.
(14) Xu, H. H.; Jiang, D. X.; Hu, S. Synthesis of guided pesticide and their biological activities. *11th IUPAC International Congress of Pesticide Chemistry*, Kobe, Japan; Pesticide Science Society of Japan: Tokyo, Japan, 2006; p 26.
(15) Guo, Y. S.; Guo, Z. R. Design of multiple targeted drugs (in Chinese). *Acta Pharm. Sinica* **2009**, *44*, 276−281.
(16) Guo, Z. R. Strategy of molecular drug design: dual-target drug design (in Chinese). *Acta Pharm. Sinica* **2009**, *44*, 209−218.
(17) Jones, A. K.; Sattelle, D. B. Diversity of insect nicotinic acetylcholine receptor subunits. *Adv. Exp. Med. Biol.* **2010**, *683*, 25−43.
(18) Kizawa, Y.; Takayanagi, I. Nicotinic stimulant, DMPP (1,1-dimethyl-4-phenylpiperazinium iodide) on the isolated bronchial smooth muscle preparation of guinea-pig. *Gen. Pharmacol.* **1984**, *15*, 149−150.
(19) Lippiello, P. M.; Fernandes, K. G. The binding of L-[^{3}H] nicotine to a single class of high affinity sites in rat brain membranes. *Mol. Pharmacol.* **1986**, *29*, 448−454.
(20) Romanelli, M. N.; Manetti, D.; Scapecchi, S.; Borea, P. A.; Dei, S.; Bartolini, A. Structure-affinity relationships of a unique nicotinic ligand: *N*(1)-dimethyl-*N*(4)-phenylpiperazinium iodide (DMPP). *J. Med. Chem.* **2001**, *44*, 3946−3955.
(21) Simsek, R.; Chang, F. J.; Lee, M.; Dukat, M.; Damaj, M. I.; Martin, B. R. Quaternary ammonium 3-(aminoethoxy)pyridines as antinociceptive agents. *Bioorg. Med. Chem. Lett.* **2003**, *13*, 2917−2920.
(22) Gündisch, D.; Andrä, M.; Munoz, L.; Tilotta, M. C. Synthesis and evaluation of phenylcarbamate derivatives as ligands for nicotinic acetylcholine receptors. *Bioorg. Med. Chem.* **2004**, *12*, 4953−4962.
(23) Toda, N.; Tago, K.; Marumoto, S.; Takami, K.; Ori, M.; Yamada, N. A conformational restriction approach to the development of dual inhibitors of acetylcholinesterase and serotonin transporter as potential agents for Alzheimer's disease. *Bioorg. Med. Chem.* **2003**, *11*, 4389−4415.
(24) Kogen, H.; Toda, N.; Tago, K.; Marumoto, S.; Takami, K.; Ori, M. Design and synthesis of dual inhibitors of acetylcholinesterase and serotonin transporter targeting potential agents for Alzheimer's disease. *Org. Lett.* **2002**, *4*, 3359−3362.
(25) Cavalli, A.; Bolognesi, M. L.; Minarini, A.; Rosini, M.; Tumiatti, V.; Recanatini, M. Multi-target-directed ligands to combat neurodegenerative diseases. *J. Med. Chem.* **2008**, *51*, 347−372.
(26) Meunier, B. Hybrid molecules with a dual mode of action: dream or reality? *Acc. Chem. Res.* **2008**, *41*, 69−77.
(27) Woo, L. W. L.; Bubert, C.; Purohit, A.; Potter, B. V. L. Hybrid dual aromatase-steroid sulfatase inhibitors with exquisite picomolar inhibitory activity. *ACS Med. Chem. Lett.* **2011**, *2*, 243−247.
(28) Wenzel, N. I.; Chavain, N.; Wang, Y.; Friebolin, W.; Maes, L.; Pradines, B. Antimalarial versus cytotoxic properties of dual drugs derived from 4-aminoquinolines and Mannich bases: interaction with DNA. *J. Med. Chem.* **2010**, *53*, 3214−3226.
(29) Detsi, A.; Bouloumbasi, D.; Prousis, K. C.; Koufaki, M.; Athanasellis, G.; Melagraki, G. Design and synthesis of novel quinolinone-3-aminoamides and their alpha-lipoic acid adducts as antioxidant and anti-inflammatory agents. *J. Med. Chem.* **2007**, *50*, 2450−2458.
(30) Liu, L.; Xue, S. J.; Bu, H. F.; Chen, L. Synthesis and biological activities of 2,4-dichlorophenoxyacetyl(thio)urea and *S*-(+)-3-methyl-2-(4-chlorophenyl) butyramide derivatives. *Chem. Res. Chinese Univ.* **2010**, *26*, 929−932.
(31) Lin, S. W.; Sun, Q.; Ge, Z. M.; Wang, X.; Ye, J.; Li, R. T. Synthesis and structure-analgesic activity relationships of a novel series of monospirocyclopiperazinium salts (MSPZ). *Bioorg. Med. Chem. Lett.* **2011**, *21*, 940−943.
(32) Ye, Z. J.; Xia, S.; Shao, X. H.; Cheng, J. G.; Xu, X. Y.; Xu, Z. P. Design, synthesis, crystal structure analysis, and insecticidal evaluation of phenylazoneonicotinoid. *J. Agric. Food Chem.* **2011**, *59*, 10615−10623.
(33) Wang, Y. L.; Cheng, J. G.; Qian, X. H.; Li, Z. Actions between neonicotinoids and key residues of insect nAChR based on an ab initio quantum chemistry study: hydrogen bonding and cooperative π-π interaction. *Bioorg. Med. Chem.* **2007**, *15*, 2624−2630.
(34) Chen, L.; Durkin, K. A.; Casida, J. E. Structural model for γ-aminobutyric acid receptor noncompetitive antagonist binding: widely diverse structures fit the same site. *Proc. Natl. Acad. Sci. U.S.A.* **2006**, *103*, 5185−5190.
(35) Ohno, I.; Tomizawa, M.; Durkin, K. A.; Casida, J. E.; Kagabu, S. Bis-neonicotinoid insecticides: observed and predicted binding interactions with the nicotinic receptor. *Bioorg. Med. Chem. Lett.* **2009**, *19*, 3449−3452.

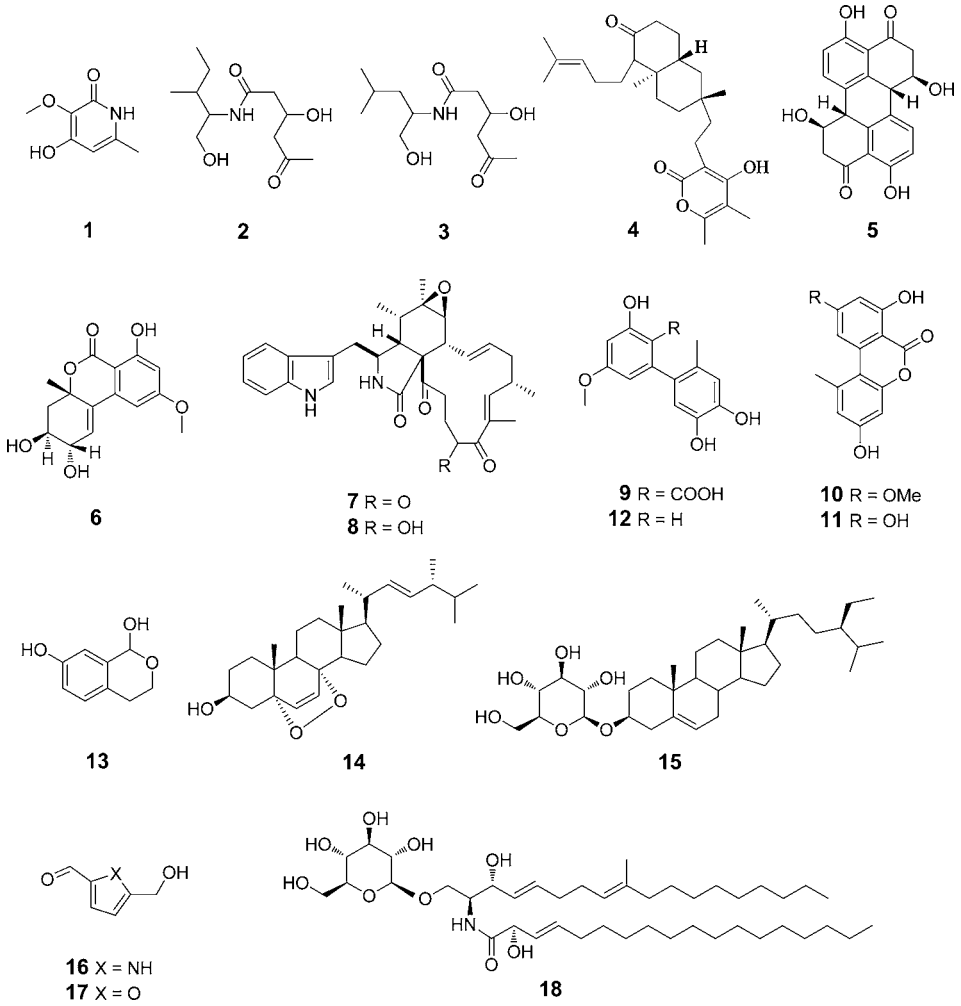

Figure 1. Structures of metabolites **1**–**18** isolated from *B. dothidea*.

Table 1. ^{1}H NMR (500 MHz) and ^{13}C NMR (125 MHz) Data for Compounds 1,[a] 2,[b] and 3[b]

	1		2		3	
	δ_H	δ_C	δ_H, multi (*J* in Hz)	δ_C	δ_H, multi (*J* in Hz)	δ_C
1		162.7 s		172.1 s		172.0 s
2		132.0 s	2.45, dd (14.9, 3.7)	42.3 t	2.43, dd (14.9, 3.6)	42.2 t
			2.36, dd (14.9, 7.7)		2.35, dd (14.9, 7.7)	
3		159.2 s	4.39, m	65.0 d	4.39, m	64.9 d
4	6.05, s	100.5 d	2.73, dd (17.5, 8.1)	49.1 t	2.73, dd (17.4, 8.1)	49.1 t
			2.67, dd (17.5, 4.3)		2.67, dd (17.5, 4.0)	
5		141.0 s		209.3 s		209.2 s
6	2.21, s	19.0 q	2.19, s	30.8 q	2.19, s	30.8 q
7	4.02, s	59.7 q				
1′			3.71, dd (11.1, 3.3)	63.5 t	3.67, d (10.4)	66.0 t
			3.59, dd (11.2, 6.8)		3.49, m	
2′			3.81, m	56.0 d	4.05, m	50.0 d
3′			1.60, m	35.7 d	1.34, m	40.0 t
4′			1.48, m	25.5 t	1.63, m	24.9 d
			1.13, m			
5′			0.88, d (7.4)	11.3 q	0.93, d (6.6)	23.0 q
6′			0.91, d (6.9)	15.5 q	0.89, d (6.6)	22.1 q
1′-OH			3.20, s		3.11, s	
3-OH	12.84, br s		4.25, s		4.18, s	
NH			6.52, d (8.5)		6.33, d (7.3)	

[a]In pyridine-d_5. [b]In $CDCl_3$.

dx.doi.org/10.1021/jf500054f | J. Agric. Food Chem. 2014, 62, 3584−3590

Fungal Material. The endophytic fungal strain KJ-1 was isolated from the symptomless tissue of stem bark of *M. azedarach* L., which was collected at Yangling, Shaanxi province, China, in August 2011. The species was identified on the basis of the phylogenetic taxonomy with sequence alignment of ITS and had a genetic closeness of 100% to the *B. dothidea* strain. This strain was defined as *B. dothidea* KJ-1 and was deposited at the College of Science, Northwest A&F University, China.

Fermentation and Cultivation. The producing strain was cultured on a plate of potato dextrose agar (PDA) medium at 28 ± 0.5 °C for 5 days. Then one piece (approximately 7 mm^2) of mycelium was inoculated aseptically to 50 mL Erlenmeyer flasks each containing 20 mL of PD liquid medium, and the seed liquids were incubated at 28 ± 0.5 °C for 3 days on a rotary shaker at 120 rpm. A suspension (100 μL) of the seed liquid was inoculated aseptically to 500 mL Erlenmeyer flasks each containing 60 g of rice and 90 mL of distilled water. There were 300 flasks in total, and the flask cultures were incubated at 28 ± 0.5 °C for 4 weeks.

Extraction and Isolation. Strain cultures were ultrasonically extracted three times with methanol (MeOH). The solvent was removed and dried under vacuum to yield a crude extract. The extract was dissolved in 90% MeOH/H_2O (4 L) and further extracted three times with petroleum ether, and the remaining layer was adjusted to 50% aqueous methanol and extracted by chloroform. The chloroform extract (60 g) was separated by silica gel CC with $CHCl_3$/MeOH (100:0 to 0:100) to provide four fractions.

Fraction 1 ($CHCl_3$) was separated by PTLC and repeated CC on silica gel, Sephadex LH-20, to yield compounds **4** (25 mg), **14** (6.5 mg), and **18** (85 mg). Fraction 2 ($CHCl_3$/MeOH = 50:1) was separated by repeated CC on silica gel, Sephadex LH-20, followed by purification with PTLC to yield compounds **5** (13 mg), **6** (12 mg), **10** (8.5 mg), **11** (9.5 mg), and **16** (2.5 mg). Fraction 3 ($CHCl_3$/MeOH = 20:1) was chromatographed over repeated CC on MCI gel, silica gel, Sephadex LH-20, and RP-C_{18} to yield compounds **1** (8 mg), **2** (9 mg), **3** (9 mg), **12** (90 mg), **13** (2.5 mg), and **17** (5 mg). Fraction 4 ($CHCl_3$/MeOH = 5:1) was separated by repeated CC on silica gel, Sephadex LH-20, and RP-C_{18} to yield compounds **7** (13 mg), **8** (13 mg), **9** (38 mg), and **15** (40 mg).

3-Hydroxy-2-methoxy-5-methylpyridin-2(1*H*)-one (1). Light orange crystal (MeOH); mp 272.5−273.1 °C; UV (MeOH) λ_{max} (log ε) = 207 (2.30), 285 nm (0.60); IR (KBr) ν_{max} = 3442, 3017, 2927, 1630, 1571, 1461, 1221 cm^{-1}; ^1H and ^{13}C NMR data are shown in Table 1; ESI-MS *m/z* 156.0 $[M + H]^+$; HR-ESI-MS *m/z* 156.0647 ($[M + H]^+$, $C_7H_{10}NO_3^+$; calcd 156.0655).

3-Hydroxy-*N*-(1-hydroxy-3-methylpentan-2-yl)-5-oxohexanamide (2). Colorless solid; $[\alpha]_D^{23}$ −6.33 (*c* 0.14, $CHCl_3$); IR (KBr) ν_{max} = 3373, 3315, 1695, 1651, 1558, 1360, 1281 cm^{-1}; ^1H and ^{13}C NMR data, see Table 1; ESI-MS *m/z* 245.81 $[M + H]^+$; HR-ESI-MS *m/z* 268.1507 ($[M + Na]^+$, $C_{12}H_{23}NaNO_4^+$; calcd 268.1519).

3-Hydroxy-*N*-(1-hydroxy-4-methylpentan-2-yl)-5-oxohexanamide (3). Colorless solid; $[\alpha]_D^{23}$ −4.51 (*c* 0.12, $CHCl_3$); IR (KBr) ν_{max} = 3325, 3278, 1707, 1657, 1575 cm^{-1}; ^1H and ^{13}C NMR data, see Table 1; ESI-MS *m/z* 267.98 $[M + Na]^+$; HR-ESI-MS *m/z* 268.1506 ($[M + Na]^+$, $C_{12}H_{23}NaNO_4^+$; calcd 268.1519).

Antifungal Bioassay. Metabolites were tested in vitro for the antifungal activity against four different phytopathogenic fungi: *Colletotrichum gloeosporiodes*, *Gibberella saubinetti*, *Botrytis cinerea*, and *Alternaria solani*. All of these phytopathogenic fungi tested were provided by the College of Plant Protection, Northwest A&F University, and were deposited at the College of Science, Northwest A&F University, China.

Antifungal activity was assessed by the microbroth dilution method in 96-well flat-microtiter plates using a potato dextrose (PD) medium.[12] Compounds were made up to 4 mM in DMSO. Two commercial fungicides, carbendazim and hymexazol (Aladdin Chemistry Co. Ltd.), together with toosendanin, the efficient pesticide from *M. azedarach* L., were used as positive controls. The solution of equal concentration of DMSO was used as a negative control. The fungi were incubated in the PD medium for 18−36 h at 28 ± 0.5 °C at 150 rpm, and spore concentrations of different microorganism were diluted to approximately 1 × 10^6 colony-forming units/mL (CFU/mL) with PD medium. In flat microtiter plates, tested compounds, fungal suspension, and sterile water were added to make up final concentrations of the compounds in the range of 1.57−200 μM. Each measurement consisted of three replicates. Cultures then grew in the dark at 28 ± 0.5 °C for 48 h. Minimum inhibitory concentrations (MICs) were inspected as the lowest concentrations in which no fungal growth could be observed.

Antibacterial Bioassay. Metabolites were tested in vitro for the antibacterial activity against four pathogenetic bacteria: *Escherichia coli*, *Bacillus subtilis*, *Staphyloccocus aureus*, and *Bacillus cereus*. All of these tested pathogenetic bacteria were deposited at the College of Science, Northwest A&F University, China.

Antibacterial activity was assessed by the microbroth dilution method in 96-well flat microtiter plates using a beef protein liquid (BP) medium.[12] Antibacterial activity was assessed according to the same procedure as antifungal bioassay. Streptomycin sulfate, ampicillin, and toosendanin were used as positive controls, and the solution of equal concentration of DMSO was used as a negative control. Cultures were grown for 24 h at 37 ± 0.5 °C in the dark without shaking, in a moist chamber.

1,1-Diphenyl-2-picrylhydrazyl (DPPH) Radical Scavenging Assay. A previously described method[13] was used to evaluate the radical scavenging capability of metabolites using DPPH. The reaction mixture (total volume = 4 mL), consisting of 1 mL of 0.2 mM DPPH in methanol and 3 mL of sample solution in methanol, was shaken vigorously and left to stand for 30 min in the dark; each measurement consisted of three replicates, and the absorbance was then measured at 517 nm. Tertiary butylhydroquinone (TBHQ) and vitamin C (V_C) were used as positive controls. Lower absorbance of the reaction mixture indicated higher free radical scavenging activity. The DPPH radical concentration was calculated using the equation

$$\text{DPPH scavenging effect (\%)} = (1 - A_1/A_0) \times 100\%$$

where A_0 and A_1 are the 517 nm absorption of the control and the absorption of the sample reaction mixture, respectively.

Brine Shrimp Bioassay. Metabolites were tested in vitro for the brine shrimp (*Artemia salina*) bioassay, processed according to the previously identified method.[12] The final concentrations of the tested compounds were 10, 50, and 100 μM. Toosendanin was used as the positive control, and DMSO as the negative control. The lethality of each concentration was recorded.

Cytotoxic Assay. In vitro cytotoxicity was assessed by using the SRB colorimetric assay.[14] Briefly, 100 μL of HCT116 cells containing 2.5 × 10^4 cells/mL was added to each well of the 96-well flat microtiter plates and allowed to attach for 24 h. Then the medium was replaced by fresh medium, and cells were incubated with various amounts of the test compounds. After incubation for an additional 72 h at 37 °C, sulforhodamine B solution 0.4% (w/v) in 1% acetic solution was added to each well, and then bound sulforhodamine B was subsequently solubilized with 10 mM Tris base (pH 10.0), and the absorbance was read at 560 nm using an Epoch microplate reader. Each measurement consisted of three replicates. The percentage of cell viability was calculated relative to control wells designated as 100% viable cells. The IC_{50} values were measured by sigmoidal fit using Origin 7.5 software.

X-ray Single-Crystal Diffraction. Crystals of compound **1** were grown in methanol at room temperature. Crystallographic data for **1** were collected on a SuperNova Eos diffractometer with graphite monochromatic Cu Kα radiation at 298(2) K. All calculations were performed using the SHELXL-97 program.[15] Crystallographic data and experimental details for structure are listed in Table S1 in the Supporting Information. Parameters in CIF format are available as Electronic Supplementary Publication from Cambridge Crystallographic Data Centre (CCDC978829). These data can be obtained from http://www.ccdc.cam.ac.uk/conts/retrieving.html.

RESULTS AND DISCUSSION

Structure Elucidation. Compound **1** was obtained as a light orange crystal, and its molecular formula was assigned as $C_7H_9NO_3$ on the basis of the pseudomolecular ion at *m/z* 156.0647 $[M + H]^+$ in HR-ESI-MS, requiring four degrees of unsaturation. The IR spectrum showed absorption for hydroxyl group and/or amide proton (3442 cm^{-1}) and a conjugated amide carbonyl group (1630 cm^{-1}). A strong UV absorption appeared at 285 nm, indicating that **1** contained a chromophoric moiety. The ^1H NMR spectra of **1** (Table 1) displayed the presence of one methyl (δ 2.21, s), one methoxyl (δ 4.02, s), and one double-bond proton (δ 6.05, s). The ^{13}C NMR and DEPT spectra of **1** (Table 1) revealed seven carbon signals, including one methyl (δ 19.0 q), one methoxyl (δ 59.7 q), one olefinic methine (δ 100.5 d), and four sp^2 quaternary carbons (including one oxygenated olefin at δ 159.2 and 132.0 (two oxygenated olefinic carbons), a trisubstituted olefin carbon (δ 141.0 s), and an amide carbonyl (δ 162.7 s)). The assignment of all ^1H and ^{13}C NMR signals for **1** was achieved by analysis of HSQC and HMBC spectral data. In the HMBC spectrum of **1**, correlations of H-4 (δ 6.05) with C-2, C-3, C-5, and C-6, H_3-6 with C-4, C-5, and H_3-7 to C-2 indicated locations of the methyl at C-5 (δ 141.0) and the methoxy group at C-2 (δ 132.0) in the molecule. This evidence suggests the existence of one 2-methoxy-3-hydroxypenta-2,4-diene moiety. Considering the molecular formula of **1**, the remaining carbonyl and secondary amino NH groups should form an amide −CONH− unit that was attached to C-2 and C-5, respectively. However, no correlations from NH to C-1, C-2, C-5, and C-6 in the HMBC spectrum were observed. From the above-mentioned data, the planar structure of **1** was deduced as shown in Figure 2a. X-ray single-crystal diffraction of **1** with Cu

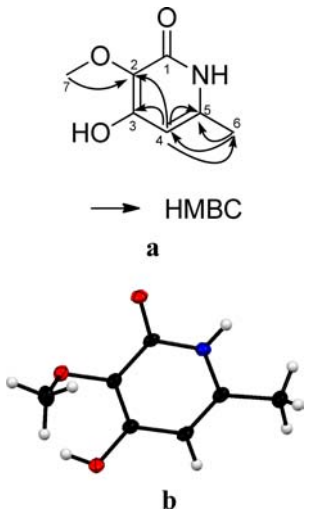

Figure 2. Key HMBC (**2a**) and ORTEP diagram (**2b**) of **1**.

Kα radiation confirmed the proposed structure (Figure 2b; for further details see Table S1 in the Supporting Information). Thus, the structure of **1** was elucidated as 3-hydroxy-2-methoxy-5-methylpyridin-2(1*H*)-one.

Compound **2** was obtained as a colorless solid and analyzed for the molecular formula $C_{12}H_{23}NO_4$ by HR-ESI-MS (*m/z* 268.1507 $[M + Na]^+$), requiring two degrees of unsaturation. The ^1H NMR and ^{13}C NMR spectra of **2** (Table 1) showed two aliphatic methyl doublets [δ_H 0.88 (3H, d, *J* = 7.4 Hz), 0.91 (3H, d, *J* = 6.9 Hz); δ_C 11.3 (q), 15.5 (q)], one methyl singlet [δ_H 2.19 (3H, s); δ_C 30.8 (q)], four aliphatic methylenes [δ_H 1.13 (1H, m, H-4′b), 1.48 (1H, m, H-4′a), 2.36 (1H, dd, *J* = 14.9, 7.7 Hz, H-2b), 2.45 (1H, dd, *J* = 14.9, 3.7, H-2a), 2.67 (1H, dd, *J* = 17.5, 4.3 Hz, H-4b), 2.73 (1H, dd, *J* = 17.5, 8.1 Hz, H-4a), 3.59 (1H, dd, *J* = 11.2, 6.8 Hz, H-1′b), 3.71 (1H, dd, *J* = 11.1, 3.3 Hz, H-1′a); δ_C 25.5 (t), 42.3 (t), 49.1 (t), 63.5 (t)], three aliphatic methines [δ_H 1.60 (1H, m), 3.81 (1H, m), 4.39 (1H, m); δ_C 35.7 (d), 56.0 (d), 65.0 (d)], two hydroxyls [δ_H 3.20, 4.25 (1H each, s)], one amide proton [δ_H 6.52 (1H, d, *J* = 8.5 Hz)], and two carbonyl carbons including an amide carbonyl one (δ_C 172.1) and a ketone carbonyl carbon (δ_C 209.3). The above evidence suggests that this compound is a short-chain fatty amide derivative. The correlations observed in the $^1H-^1H$ COSY and HSQC spectra of **2** indicate the presence of the following distinct spin systems: $HOCH_2-CH(NH)-CH(CH_3)-CH_2CH_3$ (C-1′ to C-5′), and $-CH_2CH(OH)CH_2-$ (C-4 to C-2). These data and HMBC correlations of NH/C-1, -2′, -3′, H-1′a/C-2′, -3′, H-2′/C-1, -1′, -3′, -4′, -6′, H-3′/C-4′, H-4′b/C-2′, -3′, -5′, -6′, H-6′/C-2′, -3′, -4′, H-2/C-1, -3, -4, H-4/C-2, -3, -5, and H-6/C-4 revealed a fatty amide of an isoleucinol and locations of a hydroxyl at C-3 and one ketone carbonyl group at C-5, as shown in Figure 3.

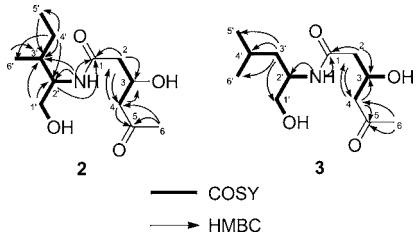

Figure 3. Key HMBC and $^1H-^1H$ COSY correlations of **2** and **3**.

These findings also confirmed the presence of an acyl residue, namely, 3-hydroxy-5-oxohexanoyl group ($CH_3COCH_2CH(OH)CH_2CO-$). Thus, the structure of **2** was determined to be 3-hydroxy-*N*-(1-hydroxy-3-methylpentan-2-yl)-5-oxohexanamide.

Compound **3** was obtained as a colorless solid. Its molecular formula was assigned as $C_{12}H_{23}NO_4$ on the basis of the molecular ion at *m/z* 268.1506 $[M + Na]^+$ in the HR-ESI-MS. Comparison of its ^1H and ^{13}C NMR spectra (Table 1) with those of **2** suggests that compound **3** had the same framework as **2**. A significant difference was that the aliphatic C-6′ methyl should be placed at C-4′ (δ_C 24.9 d) in **3** rather than at C-3′ (δ_C 35.7 d) as in **2**. The structure of **3** was further confirmed by analysis of $^1H-^1H$ COSY correlations of NH/H-2′, H-2′/H-1′, -3′, H-1′/1′-OH, H-4′/H-3′, -5′, -6′, H-3/H-2, 3-OH, -4, and the HMBC correlations of NH/C-1, -2′, H-3′/C-2′, -4′, -5′, -6′, H-4′/C-3′, -5′, -6′, H-2/C-1, -3, -4, H-4/C-2, -3, -5, H-6/C-4, -5 (Figure 3). Thus, the structure of **3** was elucidated as 3-hydroxy-*N*-(1-hydroxy-4-methylpentan-2-yl)-5-oxohexanamide, which possesses a leucinol unit. Although it can be searched in SciFinder, it is a new natural product, and this is the first report of its spectral data. Compounds **2** and **3** belong to a group of ceramides. Absolute stereochemistries of **2** and **3** remain undetermined due to limited amounts.

The structures of 15 known compounds were identified as pycnophorin (**4**),[16] stemphyperylenol (**5**),[17] altenuene (**6**),[18] chaetoglobosin C (**7**),[19,20] chaetoglobosin F (**8**),[20] altenusin (**9**),[21] djalonensone (**10**),[22] alternariol (**11**),[23,24] 5′-methoxy-6-methylbiphenyl-3,4,3′-triol (**12**),[14] 7-hydroxy-1-isochromanone

(**13**),[25] ergosterol peroxide (**14**),[26] β-sitosterol glucoside (**15**),[27] 5-(hydroxymethyl)-1*H*-pyrrole-2-carbaldehyde (**16**),[28] 5-hydroxymethylfurfural (**17**),[29] and cerebroside C (**18**)[30] by comparison of their spectroscopic data with those reported in the literature, including UV, IR, NMR, and MS data. To our knowledge, this is the first report of the isolation of these compounds from *B. dothidea* as endophytic fungus.

Interestingly, perylenequinone derivatives, for example, stemphyperylenol (**5**), have been previously reported from the genera *Alternaria*, *Stemphylium*, and *Talaromyces*.[31−34] Altenuene derivatives, for example, altenuene (**6**), have been reported from the genera *Alternaria*,[35−37] *Ulocladium*,[14] *Nigrospora*, and *Phialophora*.[38] In addition, alternariol analogues (**10** and **11**) have been previously reported from several genera of microorganisms,[36−43] especially from the common fungal genus *Alternaria*.[35] Chaetoglobosins (**7** and **8**) are a family of cytochalasans with a wide range of biological activities targeting cytoskeletal processes, which have been produced by several genera of microorganisms, especially by the common fungal genus *Chaetomium*.[44,45] According to previous investigations, alternariol and alternariol monomethyl ether were reported to have antimicrobial, cytotoxic, and antitumor activities,[35,36] and alternariol (**11**) showed antiviral effects against herpes simplex virus in vitro.[38] Some perylenequinone derivatives are phytotoxins and mutagenic.[46,47]

Antimicrobial Assays. Metabolites **1**−**18** were tested in vitro for antifungal activity against four phytopathogenic fungi: *Colletotrichum gloeosporiodes*, *Gibberella saubinetti*, *Botrytis cinerea*, and *Alternaria solani*. None of the tested compounds displayed any obvious antifungal activities against *C. gloeosporiodes* and *G. saubinetti* (Supporting Information Table S2). Compounds **4**, **5**, **7**, **10**, **11**, **15**, and **17** showed strong to moderate antifungal activities against *A. solani* (MICs of 1.57−25 μM) and did not have effects against *B. cinerea* (Table 2).

Table 2. Inhibitory Effects of Compounds 1−18 on Phytopathogenic Fungi[a]

	phytopathogenic fungi[a] (MIC, μM)	
compd	*B. cinerea*	*A. solani*
4	100	6.25
5	100	1.57
7	200	12.5
10	25	25
11	NA	12.5
12	NA	50
15	100	6.25
16	100	50
17	50	6.25
carbendazim	12.5	1.57
hymexazol	200	6.25
toosendanin	200	6.25

[a]NA, inactive. Compounds with no antifungal activity are not shown in the table.

Methylation of 5-OH in alternariol (**11**) resulted in diminished activity (MIC of 25 μM for djalonensone (**10**) vs MIC of 12.5 μM for **11**) to *A. solani*. Of these compounds, stemphyperylenol (**5**), with the lowest MIC value of 1.57 μM, had the best inhibition, which is comparable to that of the positive control, carbendazim (MIC of 1.57 μM), or better than those of hymexazol and toosendanin (MICs of 6.25 μM), indicating that it could be used as a fungicide or as a lead compound of new fungicides to *A. solani*. Compound **10** also displayed moderate antifungal activities against *B. cinerea* (MIC of 25 μM).

Compounds **1**−**18** were tested in vitro for their antibacterial activity against pathogenetic bacteria *Escherichia coli*, *Bacillus subtilis*, *Staphyloccocus aureus*, and *Bacillus cereus*, and the results are listed in Table S3 in the Supporting Information. The results showed that compound **4** mildly inhibited the growth of *B. subtilis* and *S. aureus* with both having MICs of 25 μM; the effects are much weaker than those of two positive controls, ampicillin and streptomycin sulfate, whereas the other compounds had weak activity (MICs of >50 μM).

DPPH Radical Scavenging Assay. Both compounds **9** and **12** showed marked DPPH radical scavenging activities with IC_{50} values of 17.6 ± 0.23 and 18.7 ± 0.18 μM, respectively, which are weaker than those of the positive controls TBHQ and Vc (IC_{50} of 10 μM). These results are in agreement with those reported by Wang et al.[14] Compounds **1** and **4** were found to be weak DPPH scavengers at concentrations of 50 μM, with scavenging rates of 22.5 and 30.9%, respectively, and the remaining metabolites showed no activity. From a comparison of the structures of compounds **6**, **10**, and **11** to compounds **9** and **12**, it can be found that opening of the middle ring can result in enhanced DPPH scavenging capacity.

Brine Shrimp Bioassay. Brine shrimp can be used as a convenient bioassay model for insecticidal activity.[48] Compounds **1**−**18** were evaluated for insecticidal activity, and brine shrimp lethality is shown in Table S4 in the Supporting Information. Among the compounds tested, compound **4** was found to show the best activity with lethality of 43.8% at a concentration of 100 μM, whereas the other compounds were inactive.

Cytotoxicity Bioassay. Compounds **1**−**18** were also evaluated in vitro against cancer cell line HCT116 by the sulforhodamine B (SRB) colorimetric assay, and the results are summarized in Table 3. Among them, compounds **5** and **6** exhibited the strongest cytotoxicity against HCT116 with an IC_{50} value of 3.13 μM, which is comparable to that of the positive control etoposide (IC_{50} of 2.13 μM), whereas compounds **4**, **8**, **9**, and **11** exhibited moderate activity (IC_{50} of 10−40 μM), and the remaining compounds were inactive (IC_{50} of >40 μM). These results indicate that compounds **5** and **6** could be promising lead compounds for the development of new antitumor drugs and need to be studied for their mechanisms of action.

Table 3. Cytotoxicity of Compounds 1−18 against Human Colorectal HCT 116 Cell Line[a]

compd	IC_{50}[a] (μM)	compd	IC_{50}[a] (μM)
1	>100	**11**	33.9
2	>100	**12**	73.4
3	>100	**13**	NA
4	21.4	**14**	72.3
5	3.13	**15**	NA
6	3.13	**16**	>100
7	>100	**17**	NA
8	26.5	**18**	NA
9	28.9		
10	NA	etoposide	2.13

[a]NA, inactive.

In recent years, many metabolites having plant protection have been identified from plant endophytes, such as ambuic

acid and phenazine-1-carboxylic acid.[49,50] In the present study, the secondary metabolites produced by the endophyte *B. dothidea* were found to have some antimicrobial and antioxidant activities. Stemphyperylenol (**5**) was found to display significant antifungal activity against *A. solani*. Altenusin (**9**) and 5′-methoxy-6-methylbiphenyl-3,4,3′-triol (**12**) showed marked DPPH radical scavenging activities. These bioactive metabolites in *B. dothidea* could protect the host plant against pathogenic attacks and oxidation stress in nature, which may play a defensive role.

■ ASSOCIATED CONTENT

Ⓢ Supporting Information

1D and 2D NMR, HR-ESI-MS spectra of compounds **1**−**3**, X-ray crystallographic data of **1**, and some bioassays results. This material is available free of charge via the Internet at http://pubs.acs.org.

■ AUTHOR INFORMATION

Corresponding Author

*(J.-M.G.) Phone: +86-29-87092515. E-mail: jinminggao@nwsuaf.edu.cn.

Author Contributions

‖J.X. and Q.Z. contributed equally to this work.

Funding

This work is supported by the Program for New Century Excellent Talents in University (NCET-05-0852).

Notes

The authors declare no competing financial interest.

■ REFERENCES

(1) Chandra, S. Endophytic fungi: novel sources of anticancer lead molecules. *Appl. Microbiol. Biotechnol.* **2012**, *95*, 47−59.

(2) Ebrahim, W.; Aly, A. H.; Mandi, A.; Totzke, F.; Kubbutat, M. H. G.; Wray, V.; Lin, W.-H.; Dai, H.; Proksch, P.; Kurtan, T.; Debbab, A. Decalactone derivatives from *Corynespora cassiicola*, an endophytic fungus of the mangrove plant *Laguncularia racemosa*. *Eur. J. Org. Chem.* **2012**, *18*, 3476−3484.

(3) Gao, J. M.; Yang, S. X.; Qin, J. C. Azaphilones: chemistry and biology. *Chem. Rev.* **2013**, *113*, 4755−4811.

(4) Schulz, B.; Boyle, C.; Draeger, S.; Römmert, A.-K.; Krohn, K. Endophytic fungi: a source of novel biologically active secondary metabolites. *Mycol. Res.* **2002**, *106*, 996−1004.

(5) Qin, J. C.; Zhang, Y. M.; Gao, J. M.; Bai, M. S.; Yang, S. X.; Laatsch, H.; Zhang, A. L. Bioactive metabolites produced by *Chaetomium globosum*, an endophytic fungus isolated from *Ginkgo biloba*. *Bioorg. Med. Chem. Lett.* **2009**, *19*, 1572−1574.

(6) Schulz, B.; Wanke, U.; Draeger, S.; Aust, H. J. Endophytes from herbaceous plants and shrubs: effectiveness of surface sterilization methods. *Mycol. Res.* **1993**, *97*, 1447−1450.

(7) Yang, S. X.; Xiao, J.; Laatsch, H.; Holstein, J. J.; Dittrich, B.; Zhang, Q.; Gao, J. M. Fusarimine, a novel polyketide isoquinoline alkaloid, from the endophytic fungus *Fusarium* sp. LN12, isolated from *Melia azedarach*. *Tetrahedron Lett.* **2012**, *53*, 6372−6375.

(8) Yang, S. X.; Gao, J. M.; Zhang, Q.; Laatsch, H. Toxic polyketides produced by *Fusarium* sp., an endophytic fungus isolated from *Melia azedarach*. *Bioorg. Med. Chem. Lett.* **2011**, *21*, 1887−1889.

(9) Fill, T. P.; Pereira, G. K.; dos Santos, R. G.; Rodrigues-Fo, E. Four additional meroterpenes produced by *Penicillium* sp. found in association with *Melia azedarach*. Possible biosynthetic intermediates to austin. *Z. Naturforsch.* **2007**, *62B*, 1035−1044.

(10) Geris dos Santos, R. M.; Rodrigues-Fo, E. Meroterpenes from *Penicillium* sp. found in association with *Melia azedarach*. *Phytochemistry* **2002**, *61*, 907−912.

(11) Zhang, Q.; Wang, S. Q.; Tang, H. Y.; Li, X. J.; Zhang, L.; Xiao, J.; Gao, Y. Q.; Zhang, A. L.; Gao, J. M. Potential allelopathic indole diketopiperazines produced by the plant endophytic *Aspergillus fumigatus* using the one strain-many compounds method. *J. Agric. Food Chem.* **2013**, *61*, 11447−11452.

(12) Li, X. J.; Zhang, Q.; Zhang, A. L.; Gao, J. M. Metabolites from *Aspergillus fumigatus*, an endophytic fungus associated with *Melia azedarach*, and their antifungal, antifeedant, and toxic activities. *J. Agric. Food Chem.* **2012**, *60*, 3424−3431.

(13) Wang, Q. X.; Bao, L.; Yang, X. L.; Guo, H.; Yang, R. N.; Ren, B.; Zhang, L. X.; Dai, H. Q.; Guo, L. D.; Liu, H. W. Polyketides with antimicrobial activity from the solid culture of an endolichenic fungus *Ulocladium* sp. *Fitoterapia* **2012**, *83*, 209−214.

(14) Skehan, P.; Storeng, R.; Scudiero, D.; Monks, A.; McMahon, J.; Vistica, D.; Warren, J. T.; Bokesch, H.; Kenney, S.; Boyd, M. R. New colorimetric cytotoxicity assay for anticancer-drug screening. *J. Natl. Cancer Inst.* **1990**, *82*, 1107−1112.

(15) Sheldrick, G. M. *SHELXTL-97 − A Program for Refining Crystal Structure*; University of Goettingen: Goettingen, Germany, 1997.

(16) Sassa, T.; Kato, H.; Kajiura, H. Isolation and structure of pycnophorin, a novel diterpene α-pyrone with antimicrobial activity, produced by phytopathogenic *Macrophoma kuwatsukai*. *Tetrahedron Lett.* **1986**, *27*, 2121−2124.

(17) Arnone, A.; Nasini, G.; Merlini, L.; Assante, G. Secondary mould metabolites. Part 16. Stemphyltoxins, new reduced perylenequinone metabolites from *Stemphylium botryosum* var. Lactucum. *J. Chem. Soc., Perkin Trans. 1* **1986**, 525−530.

(18) Bradburn, N.; Coker, R. D.; Blunden, G.; Turner, C. H.; Crabb, T. A. 5′-Epialtenuene and neoaltenuene, dibenzo-α-pyrones from *Alternaria alternata* cultured on rice. *Phytochemistry* **1994**, *35*, 665−669.

(19) Sekita, S.; Yoshihira, K.; Natori, S.; Kuwano, H. Chaetoglobosins, cytotoxic 10-(indol-3-yl)-[13] cytochalasans from *Chaetomium* spp. III. Structures of chaetoglobosins C, E, F, G, and J. *Chem. Pharm. Bull.* **1982**, *30*, 1629−1638.

(20) Sekita, S.; Yoshihira, K.; Natori, S. Chaetoglobosins, cytotoxic 10-(indol-3-yl)-[13] cytochalasans from *Chaetomium* spp. IV. ^{13}C-nuclear magnetic resonance spectra and their application to a biosynthetic study. *Chem. Pharm. Bull.* **1983**, *31*, 490−498.

(21) Singh, S. B.; Jayasuriya, H.; Dewey, R.; Polishook, J. D.; Dombrowski, A. W.; Zink, D. L.; Guan, Z.; Collado, J.; Platas, G.; Pelaez, F.; Felock, P. J.; Hazuda, D. J. Isolation, structure, and HIV-1 integrase inhibitory activity of structurally diverse fungal metabolites. *J. Ind. Microbiol. Biotechnol.* **2003**, *30*, 721−731.

(22) Onocha, P. A.; Okorie, D. A.; Connolly, J. D.; Roycroft, D. S. Monoterpene diol, iridoid glucoside and dibenzo-α-pyrone from *Anthocleista djalonensis*. *Phytochemistry* **1995**, *40*, 1183−1189.

(23) Qin, J. C.; Zhang, Y. M.; Hu, L.; Ma, Y. T.; Gao, J. M. Cytotoxic metabolites produced by *Alternaria* no. 28, an endophytic fungus isolated from *Ginkgo biloba*. *Nat. Prod. Commun.* **2009**, *4*, 1473−1476.

(24) Koch, K.; Podlech, J.; Pfeiffer, E.; Metzler, M. Total synthesis of alternariol. *J. Org. Chem.* **2005**, *70*, 3275−3276.

(25) Odasso, G.; Winters, G. Cyclic hydrazides. IV. Synthesis of 2-amino-3,4-dihydroisoquinolin-1(2*H*)-one. *Farmaco* **1978**, *33*, 148−155.

(26) Chen, Y. K.; Kuo, Y. H.; Chiang, B. H.; Lo, J. M.; Sheen, L. Y. Cytotoxic activities of 9,11-dehydroergosterol peroxide and ergosterol peroxide from the fermentation mycelia of *Ganoderma lucidum* cultivated in the medium containing leguminous plants on Hep 3B cells. *J. Agric. Food Chem.* **2009**, *57*, 5713−5719.

(27) Kojima, H.; Sato, N.; Hatano, A.; Ogura, H. Sterol glucosides from *Prunella vulgaris*. *Phytochemistry* **1990**, *29*, 2351−2355.

(28) Sudhakar, G.; Kadam, V. D.; Bayya, S.; Pranitha, G.; Jagadeesh, B. Total synthesis and stereochemical revision of acortatarins A and B. *Org. Lett.* **2011**, *13*, 5452−5455.

(29) Jogia, M. K.; Vakamoce, V.; Weavers, R. T. Synthesis of some furfural and syringic acid derivatives. *Aust. J. Chem.* **1985**, *38*, 1009−1016.

(30) Koga, J.; Yamauchi, T.; Shimura, M.; Ogawa, N.; Oshima, K.; Umemura, K.; Kikuchi, M.; Ogasawara, N. Cerebrosides A and C, sphingolipid elicitors of hypersensitive cell death and phytoalexin accumulation in rice plants. *J. Biol. Chem.* **1998**, *273*, 31985−31991.
(31) Gao, S. S.; Li, X. M.; Wang, B. G. Perylene derivatives produced by *Alternaria alternata*, an endophytic fungus isolated from *Laurencia* species. *Nat. Prod. Commun.* **2009**, *4*, 1477−1480.
(32) Davis, V. M.; Stack, M. E. Mutagenicity of stemphyltoxin III, a metabolite of *Alternaria alternata*. *Appl. Environ. Microbiol.* **1991**, *57*, 180−182.
(33) Arone, A.; Nasini, G. Secondary mould metabolites. Part 16. Stemphyltoxins, new reduced perylenequione metabolites from *Stermphylium botryosum* var. Lactucum. *J. Chem. Soc., Perkin Trans. 1* **1986**, 525−530.
(34) Liu, F.; Cai, X. L.; Yang, H.; Xia, X. K.; Guo, Z. Y.; Yuan, J.; Li, M. F.; She, Z. G.; Lin, Y. C. The bioactive metabolites of the mangrove endophytic fungus *Talaromyces* sp. ZH-154 isolated from *Kandelia candel* (L.) Druce. *Planta Med.* **2010**, *76*, 185−189.
(35) Aly, A. H.; Edrada-Ebel, R.; Indriani, I. D.; Wray, V.; Müller, W. E. G.; Totzke, F.; et al. Cytotoxic metabolites from the fungal endophyte *Alternaria* sp. and their subsequent detection in its host plant *Polygonum senegalense*. *J. Nat. Prod.* **2008**, *71*, 972−980.
(36) Kjer, J.; Wray, V.; Edrada-Ebel, R.; Ebel, R.; Pretsch, A.; Lin, W.; Proksch, P. Xanalteric acids I and II and related phenolic compounds from an endophytic *Alternaria* sp. isolated from the mangrove plant *Sonneratia alba*. *J. Nat. Prod.* **2009**, *72*, 2053−2057.
(37) Stack, M. E.; Mazzola, E. P.; Page, S. W.; Pohland, A. E.; Highet, R. J.; Tempesta, M. S.; Corley, D. G. Mutagenic perylenequinone metabolites of *Alternaria alternata*: altertoxins I, II and III. *J. Nat. Prod.* **1989**, *49*, 866−871.
(38) He, J. W.; Chen, G. D.; Gao, H.; Yang, F.; Li, X. X.; Peng, T.; Guo, L. D.; Yao, X. S. Heptaketides with antiviral activity from three endolichenic fungal strains *Nigrospora* sp., *Alternaria* sp. and *Phialophora* sp. *Fitoterapia* **2012**, *83*, 1087−1091.
(39) Matumoto, T.; Hosoya, T.; Shigemori, H. Palmariols A and B, two new chlorinated dibenzo-α-pyrones from Discomycete Lachnum palmae. *Heterocycles* **2010**, *81*, 1231−1237.
(40) Hussain, H.; Krohn, K.; Ullah, Z.; Draeger, S.; Schulz, B. Bioactive chemical constituents of two endophytic fungi. *Biochem. Syst. Ecol.* **2007**, *35*, 898−900.
(41) Zhang, H. W.; Huang, W. Y.; Song, Y. C.; Chen, J. R.; Tan, R. X. Four 6*H*-dibenzo[*b*,*d*]pyran-6-one derivatives produced by the endophyte *Cephalosporium acremonium* IFB-E007. *Helv. Chim. Acta* **2005**, *88*, 2861−2864.
(42) Dai, J. Q.; Krohn, K.; Flörke, U.; Gehle, D.; Aust, H. J.; Draeger, S.; Schulz, B.; Rheinheimer, J. Novel highly substituted biraryl ethers, phomosines D−G, isolated from the endophytic fungus *Phomopsis* sp. from *Adenocarpus foliolosus*. *Eur. J. Org. Chem.* **2005**, *23*, 5100−5105.
(43) Oyama, M.; Xu, Z. H.; Lee, K. H.; Spitzer, T. D.; Kitrinos, P.; Mcdonald, O. B.; Jones, R. R. J.; Garvey, E. P. Fungal metabolites as potent protein kinase inhibitors: identification of a novel metabolite and novel activities of known metabolites. *Lett. Drug. Des. Discovery* **2004**, *1*, 24−29.
(44) Zhang, Q.; Li, H. Q.; Zong, S. C.; Gao, J. M.; Zhang, A. L. Chemical and bioactive diversities of the genus *Chaetomium* secondary metabolites. *Mini Rev. Med. Chem.* **2012**, *12*, 127−148.
(45) Xue, M.; Zhang, Q.; Gao, J. M.; Li, H.; Tian, J. M.; Pescitelli, G. Chaetoglobosin V_b from endophytic *Chaetomium globosum*: absolute configuration of chaetoglobosins. *Chirality* **2012**, *24*, 668−674.
(46) Stack, M. E.; Prival, M. J. Mutagenicity of the *Alternaria* metabolites altertoxins I, II, and III. *Appl. Environ. Microbiol.* **1986**, *52*, 718−722.
(47) Hradil, C. M.; Hallock, Y. F.; Clardy, J.; Kenfield, D. S.; Strobel, G. Phytoxins from *Alternaria cassiae*. *Phytochemistry* **1989**, *28*, 73−75.
(48) Blizzard, T. A.; Ruby, C. L.; Mrozik, H.; Preiser, F. A.; Fisher, M. H. Brine shrimp (*Artemia salina*) as a convenient bioassay for avermectin analogs. *J. Antibiot. (Tokyo)* **1989**, *42*, 1304.
(49) Li, J.; Harper, J. K.; Grant, D. M.; Tombe, B. O.; Bashyal, B.; Hess, W.; Strobel, G. A. Ambuic acid, a highly functionalized cyclohexenone with antifungal activity from *Pestalotiopsis* spp. and *Monochaetia* sp. *Phytochemistry* **2001**, *56*, 463−468.
(50) Delaney, S. M.; Mavrodi, D. V.; Bonsall, R. F.; Thomashow, L. S. phzO, a gene for biosynthesis of 2-hydroxylated phenazine compounds in *Pseudomonas aureofaciens* 30-84. *J. Bacteriol.* **2001**, *183*, 318−327.

of their conjugates were investigated in relation to their protein structures. Because heat treatment and gastric digestion can affect the allergenic character, the immunoreactivity of PTT conjugates was assessed after these two treatments.

MATERIALS AND METHODS

Materials. Potato protein Solanic 206P (PTT ≈ 75%, PIs ≈ 25%) was kindly provided by Solanic (Foxhol, Ne). Potato galactan and endo-1−4-β-D-galactanase from *Aspergillus niger* were purchased from Megazyme (Wicklow, Ir). Furosine standard was purchased from Neosystem Laboratories (Strasbourg, Fr). Biogel P2 extra fine, Bradford reagent, and broad range SDS−PAGE standards were purchased from Bio-Rad (Philadelphia, PA). Four potato-sensitive human sera (Table SI-1, Supporting Information) were acquired from PlasmaLab (Everett, WA) (8.75−22.40 kU_A/1 potato specific IgE, ImmunoCAP; Pharmacia, Uppsala). Sera from nonallergic (no specific IgE) and dust-mite allergic (>100.00 kU_A/1 dust-mite specific IgE) individuals as controls were also obtained from PlasmaLab. All other chemicals were purchased from Sigma Chemical Co. (St. Louis, MO).

Preparation of Conjugates. PTT and PIs present in Solanic 206P were separated by ultrafiltration using a stirred ultrafiltration unit (Amicon system, Millipore, Billerica, MA) fitted with a 30 kDa molecular mass cut-off membrane. The SDS−PAGE gels (Figure SI-2, Supporting Information) of the purified PTT and PIs were analyzed using AlphaView Software (Cell Biosciences, Santa Clara, CA). The retentate recovered upon ultrafiltration was composed of 90% PTT, while the filtrate consisted of 95% protease inhibitors. The retentate and the filtrate containing PTT and PI-enriched extracts were freeze-dried separately. GOS (MW of 1,990.9 g/mol) were prepared from potato galactan using endo-(1−4)-β-D-galactanase from *A. niger* as described previously.[25] PTT or PIs and each of the galactose or GOS or galactan at the molar ratio of 1:9 were dissolved in 0.1% (w/v) of 0.05 M sodium phosphate buffer (pH 7.0). Protein−carbohydrate mixtures were lyophilized and incubated in sealed glass desiccators at 48 °C for 1 to 3 days under a controlled a_w value of 0.65 equilibrated with a saturated solution of potassium iodide. Control experiments (control PTT and PIs) were performed with selected proteins incubated under the same conditions in the absence of carbohydrates.

Determination of Glycation Extent of Potato Proteins with Selected Carbohydrates. To determine the extent of glycation of PTT and PIs, the percent blocked lysine was estimated from the total free amino content and the acid-generated furosine content, according to a modified method of Seo et al.[25] The free amino groups of native PTT and PIs were determined using a trinitrobenzene sulfonic acid (TNBS) assay. Then, 0.25 mL of 0.01% (v/v) TNBS was added to 0.5 mL of native protein solutions (10 mg/mL) in 0.1 M sodium bicarbonate buffer (pH 8.5). After 2 h of incubation at 37 °C, 0.25 mL of 10% (w/v) sodium dodecyl sulfate (SDS) and 0.125 mL of 1 M HCl were added to the mixtures to solubilize the protein and to avoid their precipitation. The assays were run in triplicate, and the standard curve was constructed using L-leucine. To estimate the ϵ-*N*-2-(furoylmethyl)-L-lysine (furosine), 500 μL of the 20 mg/mL of protein sample in water was hydrolyzed with 200 μL of 8 M HCl for 23 h at 110 °C capped under nitrogen. The hydrolyzed sample was cooled to room temperature and centrifuged at 13,000*g* for 15 min. The supernatant (500 μL) was applied to a previously activated Sep-Pak C18 cartridge (Waters Corp, Milford, MA). Furosine was eluted with 3 M HCl and evaporated until dryness under nitrogen. The sample was resolubilized in 200 μL of a water/acetonitrile/formic acid mixture (95:4.5:0.5, v/v/v) and analyzed through high-pressure liquid chromatography (HPLC). A Waters Bioseparations module and a photodiode array detector equipped with Empower 2 software for data collection were used. A sample volume of 20 μL was separated using a Waters Symmetry Shield RP8 3.5 μm (4.6 × 50 mm) column using an isocratic elution of 5 mM octanesulfonic acid in water/acetonitrile/formic acid mixture (79.8:20:0.2, v/v/v) for 20 min at a flow rate of 0.3 mL/min. The detection of furosine was performed at 280 nm. The calibration curve was constructed using a furosine standard. All assays were run in triplicate and injected with and without the internal standard. No furosine was detected in the control samples, nonincubated mixtures of protein and carbohydrate. The final percentage of blocked lysine was indirectly estimated from the total free amino content and furosine content using the following equation, considering that the Amadori compound, tagatosyllysine, formed during the Maillard reaction, generates about 42% furosine upon 8 M HCl hydrolysis.[26]

$$\text{Percent blocked lysine} = (1/0.42 \times \text{furosine}) \times 100/\text{total lysine} \quad (1)$$

Purification of Patatin Conjugates. Native PTT, incubated control PTT, as well as PTT/galactose, PTT/GOS, and PTT/galactan conjugates were subjected to ultrafiltration using a stirred ultrafiltration unit (Amicon system, Millipore) fitted with a 30 kDa or 300 kDa molecular mass cutoff membrane to remove the smaller Maillard reaction species and the unreacted saccharides present in the mixture. The retentates were collected for further analyses.

Simulated Gastric Digestion. Native PTT, incubated control PTT, and PTT conjugates were subjected to simulated gastric digestion according to the modified method of Moreno et al.[27] Proteins and glycoproteins (1 mg/mL) were solubilized in simulated gastric fluid (0.75 M NaCl, pH 2.5). To initiate the enzymatic digestion, porcine pepsin (7 mg/mL, ≥ 2,500 units/mg protein) was then added at a ratio of 1:50 (v/v). After the digestion was performed at 37 °C for 2 h, the pH was raised to 7.5 with 0.125 M ammonium carbonate. To simulate the duodenal environment, the following solutions were added: (1) 10 μL of the following bile salt mixture (0.025 M sodium taurocholate, 0.025 M sodium glycodeoxycholic acid, 0.4 M $CaCl_2$, and 0.5 M Bis−Tris) and (2) 6 μL of porcine trypsin (3 mg/mL, ≥ 6,000 units/mg protein) and 10 μL of bovine α-chymotrypsin (4.77 mg/mL, ≥ 39 units/mg protein). The samples were then incubated at 37 °C for 1 h. The reaction was stopped by heating the samples in boiling water for 5 min. The control without the incubation steps was prepared as the unhydrolyzed control, and the native PTT was used as the hydrolyzed control. All assays were done in triplicate.

The quantification of the digested species was performed with a Beckman HPLC (Beckman Coulter, Fuellerton, CA) system equipped with a programmable solvent module (model 126), a photodiode array detector and 32 Karat software for data collection. The separation was performed on a Zorbax SB-C8 (4.6 × 150 mm, 5 μm, Agilent Technologies, Mississauga, ON, Canada). The digested sample (20 μL) was injected in triplicate. The absorbance was measured at 214 nm. A linear gradient at a flow of 0.5 mL/min was used using water/acetonitrile/formic acid (90:10:0.1, mL/mL/mL) as solvent A and water/acetonitrile/formic acid (10:90:0.07, mL/mL/mL) as solvent B. The elution gradient was as follows: 1−45 min, 50% B; 45−50 min, 100% B; 50−55 min, 58% B; 55−60 min, 0% B; and 60−80 min, 0% B. The unhydrolyzed control was used as a standard to quantify the unhydrolyzed PTT in the samples.

$$\text{Percent protein digestion} = 100 - ((\text{the peak area of unhydrolyzed PTT over the peak area of the PTT control}) \times 100) \quad (2)$$

The samples were kept at −20 °C before the assessment of their immunoreactivity.

Determination of IgE-Immunoreactivity. Native PTT or PIs were diluted with PBS buffer containing 0.1% (v/v) Tween 20 (PBS-T) to reach a final concentration of 5.4 μg/mL, coated onto flat-bottomed high binding polystyrene Costar 3590 microtiter plates with 96 wells (50 μL per well, Corning, Tewksbury, MA), and incubated overnight at 4 °C. The sera pool or control serum (diluted 1:3 with 1% w/v BSA in PBS-T) was mixed with conjugates as inhibitor (0.0012000 μg/mL in 1% w/v BSA in PBS-T) at a ratio of 1:1 (v/v) and incubated overnight at 4 °C. As a positive control, a BSA solution (0.001−2000 μg/mL in 1% w/v BSA in PBS-T) was incubated with the antipotato sera pool. The pool was composed of sera from 4 subjects with high levels of specific IgE antibody to potato proteins (PlasmaLab). Human serum with specific IgE antibody to dust mites but none to potato proteins was used as the control. The microtiter plate coated with native proteins was

washed 3 times with 300 μL of PBS-T using a Biotek ELx405 microplate washer (Winooski, VT) and was blocked using 5% (w/v) BSA in PBS-T for 2 h at 25 °C. After washing 3 times with PBS-T, 50 μL of PTT conjugates and serum pool mixtures were added onto the PTT-coated microtiter plate. The plate was incubated at 25 °C for 2 h and washed with PBS-T three times. After incubation with 50 μL of anti-human IgE conjugated with horseradish peroxidase (1:2000 dilution with 1% w/v BSA in PBS-T) for 1 h at 25 °C, the plate was washed 3 times and developed with 50 μL of substrate solution (3,3′,5,5′-tetramethylbenzidine, TMB, Bioshop, Burlington, ON, Canada) at 25 °C for 15 min. The reaction was stopped by adding 50 μL of 0.5 M sulfuric acid solution. The absorbance was measured at 450 nm. The loss of the specific IgE binding ability of the patients' sera resulting from the conjugation of PTT with galactose/GOS/galactan was expressed as follows:

$$\text{Percent inhibition} = 100 - ((\text{absorbance of the glycated samples preincubated with sera pool}/\text{absorbance of positive control}) \times 100) \quad (3)$$

The experimental values were fitted to a four-parameter logistic equation using the SigmaPlot software from SPSS Inc. (Chicago, IL) and were subjected to normality (Shapiro-Wilk) and to constant variance tests to validate assumptions of one-way analysis of variance (ANOVA). IC_{50} was defined as the concentration of inhibitor at the inflection of the fitted curve. All assays were done in triplicate. p values ≤ 0.05 were considered to be statistically significant. To assess the effect of heat treatment, PTT and its conjugates (20 mg/mL) were incubated at 80 °C for 15 min before assessing their immunoreactivity.

Protein Primary Sequence Analysis. The primary sequence of PTT and its conjugates were analyzed through protein mass mapping, which consists of the tryptic hydrolysis of proteins followed by mass spectrometric analysis of the released peptides.

Tryptic Digestion. The digestion of PTT and its conjugates were performed on a MassPrep liquid handling robot (Micromass, Manchester, U.K.) according to the protocol of Shevchenko et al.[28] with modifications of Havlis et al.[29] The native PTT, the incubated control PTT, and the PTT conjugates (10 μL each; 1 μg/mL) were resolved by electrophoresis (Mini-Protean Tetra system, Bio-Rad) on Mini-Protean TGX precast gels (Bio-Rad). Proteins bands taken from the SDS–PAGE gel were reduced with 10 mM dithiothreitol and alkylated with 55 mM iodoacetamide. Trypsin digestion was performed using 105 mM of modified porcine trypsin (sequencing grade, Promega, Madison, WI) at 58 °C for 1 h. Digestion products were extracted using a formic acid/acetonitrile/water mixture (1:2:97, v/v/v) followed by a formic acid/acetonitrile/water mixtire (1:50:49, v/v/v). Recovered extracts were pooled, dried by vacuum centrifugation, resuspended into 10 μL of 0.1% (v/v) formic acid, and analyzed by mass spectrometry.

Mass Spectrometry. Peptide samples were separated by online reversed-phase (RP) nanoscale capillary liquid chromatography (nanoLC) and analyzed by electrospray–mass spectrometry (ES-MS/MS). Analyses were performed with a Thermo Surveyor MS pump connected to an LCQ Deca XP mass spectrometer (Thermo Electron, San Jose, CA) supplied with a nanoelectrospray ion source (Thermo Electron, San Jose, CA). Peptides were bound on a cap trap (Michrom Bioresources, Auburn, CA) at 10 μL/min after which chromatographic separation took place using a PicoFrit column BioBasic C18 (10 cm ×0.075 mm) (New Objective, Woburn, MA) set with a linear gradient from 2 to 50% of solvent B (acetonitrile and 0.1% v/v formic acid) for 30 min, at 200 nL/min (obtained by flow-splitting). Mass spectra were acquired using a data-dependent acquisition mode using Xcalibur software, version 1.2. Each full scan mass spectrum (400–2000 m/z) was followed by collision-induced dissociation of the three most intense ions. The dynamic exclusion (30 s exclusion duration) function was enabled, and the relative collisional fragmentation energy was set to 35%.

Database Searching. All MS/MS samples were analyzed using Mascot (Matrix Science, London, UK; version 2.4.1) and X! Tandem (The GPM, thegpm.org; version CYCLONE (2010.12.01.1)). X! Tandem was set up to search the UR12_5_SolanumTub_20120718 database (2615 entries) also assuming trypsin. Mascot was set up to search the UR12_5_SolanumTub_20120718 database assuming the digestion enzyme trypsin. Mascot and X! Tandem were searched with a fragment ion mass tolerance of 0.100 Da and a parent ion tolerance of 0.100 Da. Carbamidomethyl of cysteine was specified in Mascot and X! Tandem as a fixed modification. Dehydrated of the N-terminus, Glu→pyro-Glu of the N-terminus, ammonia-loss of the N-terminus, Gln→pyro-Glu of the N-terminus, deamidated of asparagine and glutamine, oxidation of methionine, and hex of lysine and arginine were specified in X! Tandem as variable modifications. Glu→pyro-Glu of the N-terminus, Gln→pyro-Glu of the N-terminus, deamidated of asparagine and glutamine, oxidation of methionine, hex of lysine and arginine, galactosyl of lysine, and galactosyl (R) of arginine were specified in Mascot as variable modifications.

Criteria for Protein Identification. Scaffold (version 3.6.2, Proteome Software Inc., Portland, OR) was used to validate MS/MS based peptide and protein identifications. Peptide identifications were accepted if they could be established at greater than 95.0% probability as specified by the Peptide Prophet algorithm.[30] Protein identifications were accepted if they could be established at greater than 95.0% probability and contained at least 2 identified peptides. Protein probabilities were assigned by the Protein Prophet algorithm.[31] Proteins that contained similar peptides and could not be differentiated based on MS/MS analysis alone were grouped to satisfy the principles of parsimony.

Secondary Structure Analysis. The secondary structure analysis of PTT and it conjugates was analyzed by Fourier transform infrared spectroscopy (FTIR). The samples were dissolved in ^2H_2O to achieve a final concentration of 100 mg protein/mL. Infrared spectra were recorded using a 8210 Nicolet FTIR spectrometer (Thermo Electron Corporation, Madison, WI) equipped with a deuterated triglycine sulfate (DTGS) detector. The spectrometer was continuously purged with dry air from Balston dryer (Balston, Haverhill, MA). The samples (9 μL) were placed between two CaF_2 windows separated by a 25 μm Teflon film spacer (Harrick Scientific, Pleasantville, NY). Each spectrum was obtained by coadding 256 scans to minimize the signal-to-noise ratio. Fourier self-deconvolution (FSD) in the amide I′ region was performed using Omnic 6.0 software (Thermo Electron Corporation, Madison, WI) applying a bandwidth of 40 cm^{-1} and a resolution enhancement parameter of 3. The curve fitting was performed by using Origin 8 (OriginLab, Northampton, MA). The Gaussian function was chosen to fit the overlapped peaks. The amide I′ region of PTT solution in ^2H_2O revealed five components upon deconvolution and curve-fitting. The band at 1628 cm^{-1} had been assigned to strongly bonded β-strands indicative of an aggregated strands type structure.[32] The remaining structures were assigned as follows: bands at 1637 ± 3.0 and 1675 ± 5.0 cm^{-1} as β-sheets, band at 1645 ± 4.0 cm^{-1} as random coils, bands at 165 ± 4.0 cm^{-1} as α-helices, and bands at 1671 ± 3.0 and 1689 ± 2.0 cm^{-1} as β-turns.[33]

Three-Dimensional Mapping. The FASTA format of amino acid sequence of PTT (accession number Q2MY50, UniProtKB) was submitted to Swissmodel.[34] This server used the template of SeMet Patatin (Protein Data Bank ID: 1OXW) for the prediction. The predicted model had a Q-MEAN Z-score, a useful measure for the description of the absolute quality of theoretical models, of −1.12, which indicates acceptable quality. The predicted model was viewed by Jmol.[35]

RESULTS AND DISCUSSION

Glycation Extent of Potato Proteins. Table 1 shows the percent blocked lysine of conjugates of PTT and PIs. As compared to GOS and galactan, higher levels of glycation of PTT and PIs with galactose were obtained with percent blocked lysine of 33.3 and 25.2%, respectively. These results are in agreement with other studies[36] in which the higher reactivity of monosaccharides was attributed to their higher proportion in the open-ring form and/or to their high affinity to the glycation sites of PTT.[37] The difference in the number of glycated residues between PTT and PIs can be explained by the different accessibilities of Lys ε-amino groups.[38] Indeed, there are 24

dx.doi.org/10.1021/jf5003073 | J. Agric. Food Chem. 2014, 62, 3591–3598

Table 1. Extent of Glycation of PTT and PIs with Selected Carbohydrates

conjugates	incubation time (days)	blocked lysine (%)[a]
PTT/galactose	1	33.3 (±0.5)
PTT/galactose	3	77.0 (±1.7)
PTT/GOS	3	4.0 (±0.0)
PTT/galactan	3	9.1 (±0.0)
PIs/galactose	1	25.2 (±0.0)
PIs/GOS	3	10.3 (±0.0)

[a]Experimental results are averages of triplicates. and the standard deviations are given.

and 10−14 reactive amino groups on PTT and on major PIs, respectively (accession numbers Q2MY50, P58514, Q41448, and P16348, UniProtKB). The higher percent blocked lysine of PTT is attributed to the high number of its more exposed Lys residues as compared to the PIs. However, the lower level of conjugation of potato proteins with GOS can be attributed to the high rate of the glycoxidation reaction of GOS competing with the glycation rate through the progress of the Maillard reaction.[39,40] The results also show that the percent level of blocked lysine of PTT (4%) upon glycation with GOS was lower as compared to that of PIs (10.3%). These results reveal the higher susceptibility of PTT to form protein aggregates upon the generation of protein cross-linking dicarbonyls through the glycoxidation/autoxidation of GOS,[39] therefore leading to the lower accessibility of the glycation sites as compared to PIs.

Effect of Glycation on the Immunoreactivity of PTT and PI Conjugates. To determine the allergenic potential of native and conjugated potato proteins, IgE binding activity of the native protein was investigated by an inhibition ELISA assay using a serum pool of four subjects with specific IgE to potato proteins. The sera from different donors were first tested individually against native PTT and protease inhibitors to confirm the extent of their immunoreactivity (data not shown). The sera were then pooled to obtain a more general immunoreactivity profile. The IgE's in the serum pool showed immunoreactivity to the patatin band (Sol t 1 allergen, Figure SI-3, Supporting Information) but also to some protease inhibitors (Sol t 2−4 allergen, Figure SI-3, Supporting Information). An anti-dust mite serum sample was used as a negative control. Figure 1A demonstrates a typical inhibition curve for the native PTT and the PTT conjugates. Control experiments performed with incubated PTT without carbohydrates demonstrated a decrease in the concentration required for half-maximal inhibition of IgE binding (IC_{50} of 0.82 μg/mL, $p < 0.01$) as compared to the native PTT (IC_{50} of 1.19 μg/mL, $p < 0.01$). This increase in IgE binding affinity of PTT upon incubation is attributed to a change in PTT structure, leading to a higher exposure of its epitopes. The IC_{50} of PTT/galactose and PTT/GOS conjugates were estimated to be 0.70−0.90 μg/mL (1−3 days incubation; $p < 0.01$) and 0.38 μg/mL ($p < 0.01$), respectively. These experimental findings reveal an increase in the level of IgE binding extent upon the glycation of PTT with galactose and GOS as compared to the native PTT. These results are attributed to an increased exposure of the epitopes and/or the formation of novel IgE-binding sites upon covalent modifications of PTT during glycation with small carbohydrates.[41,42] As compared to PTT/galactose conjugates formed upon 1 day of incubation, the slightly lower immunoreactivity obtained with PTT/galactose conjugates obtained upon 3 days of incubation indicates further structural changes due to extensive glycation leading to lower exposure of

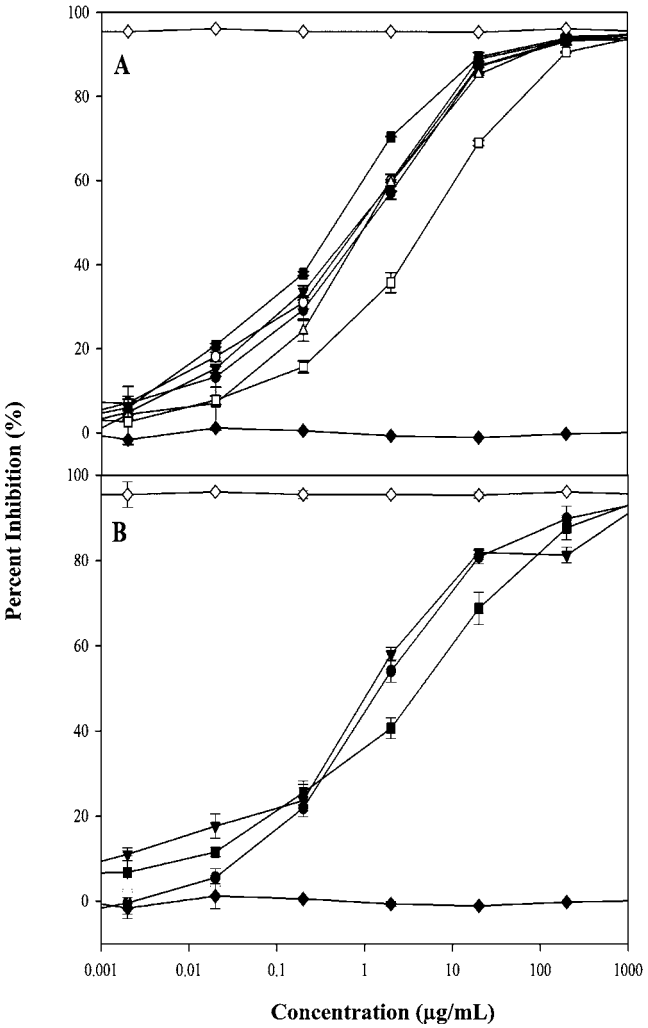

Figure 1. Effect of glycation on PTT and PI immunoreactivity obtained through inhibition ELISA: (A) PTT (●), incubated PTT (○), PTT/galactose conjugates (1-day) (▼), PTT/galactose conjugates (3-day) (Δ), PTT/GOS conjugates(■), PTT/galactan conjugates (□), positive control (♦), and negative control (◊). (B) PIs (●), PIs/galactose conjugates (▼), PIs/GOS conjugates (■), positive control (♦), and negative control (◊).

the epitopes. In contrast, lower immunoreactivity of ovalbumin after glycation with glucose was reported by Ma et al.[43] However, the results show that the glycation of PTT with galactan (IC_{50} of 5.49 μg/mL; $p < 0.01$) resulted in a significant decrease in the affinity for the specific IgE as compared to the native PTT (IC_{50} of 1.19 μg/mL, $p < 0.01$). Similarly, Aoki et al.[41] have reported a decrease in the IgE binding activity of a major allergen of Japanese cedar, Cry j 1, conjugated with galactomannan and attributed this decrease in immunoreactivity to the effectiveness of polysaccharide chains at masking the molecular surface epitopes of an allergen.

Control experiments performed with control incubated PIs without carbohydrates did not show any difference in IgE binding level compared to that of the native proteins (data not shown). Contrary to the results obtained with PTT (Figure 1A), the conjugation of PIs to carbohydrates resulted in lower immunoreactivity as compared to the native compound (IC_{50} of 1.11 μg/mL, $p < 0.01$), where the conjugation with GOS (IC_{50} of 5.17 μg/mL, $p < 0.01$) resulted in a higher decrease in immunoreactivity than that with galactose (IC_{50} of 1.21 μg/

dx.doi.org/10.1021/jf5003073 | J. Agric. Food Chem. 2014, 62, 3591−3598

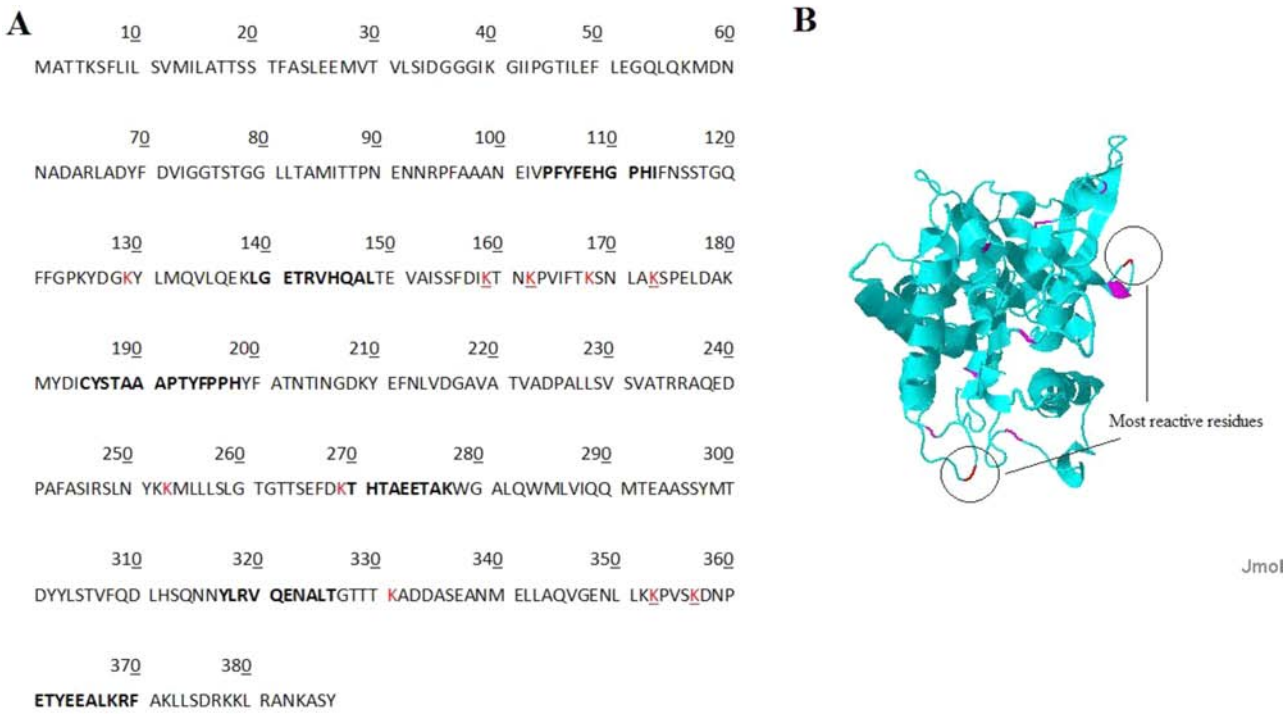

Figure 2. (A) Amino acid sequence of PTT glycated with galactose (red), glycated with GOS (red, underlined), and documented epitopes (bold). (B) Three-dimensional mapping of PTT with glycated residues (magenta) and the most reactive glycated residues (red).

mL, $p < 0.01$) (Figure 1B). It is likely that the conjugation of PIs to galactose or GOS resulted in epitope modification and/or to epitope shielding, thereby affecting the antigen−antibody recognition.[43] A decrease in the immunoreactivity of lysozyme was also obtained, in our previous study, upon its conjugation with galactose and GOS.[44]

The overall results emphasize that the immunoreactivity effect is allergen and carbohydrate dependent.[19] For further studies, PTT, being a heat-labile allergen, was selected to study the effects of the primary and secondary molecular modifications upon glycation and thermal treatment on immunoreactivity.

Location of Conjugated PTT Residues. To determine the conjugated residues on PTT, the skipped trypsin cleavage sites due to glycation of lysine residues and the increase in molecular weight of the digested peptides were identified by peptide mapping of conjugated PTT (Figure 2A). Table SI-4 in the Supporting Information summarizes the peptide masses identified through MS analysis. As expected, the highest number of glycated residues was found in PTT glycated with galactose, after one day of incubation, (Lys 129, 159, 162, 168, 173, 253, 269, 331, 353, and 357, in red) as compared to PTT glycated with GOS, after three days of incubation (Lys 159, 162, 173, 353, and 357, underlined in red) confirming the higher reactivity of the smaller carbohydrate compared to that of the larger one. The most reactive residues were Lys 159 and 357, which were found in the highest proportion in their conjugated state. The glycated residues did not overlap with the amino acid sequence of the epitopes previously identified in PTT (in bold),[45] which demonstrates that the direct blocking of these epitopes did not occur. This supports our inhibition ELISA findings where no decrease in the immunoreactivity of PTT was observed upon its conjugation with galactose (Figure 1A). On the contrary, the minor increase observed in the immunoreactivity might be explained by the conjugation of the carbohydrate to the residues that are found in close proximity to the documented epitopes, such as Lys 269 and 357, which could have resulted in an increased exposure of these epitopes. The three-dimensional mapping of the PTT (Figure 2B) demonstrated that the glycation sites (in magenta) were mostly found toward the termini of individual PTT secondary structures, such as the α-helix and β-sheet, which indicates a minimal change in the secondary structure due to glycation. The most reactive residues (in red) are very easily accessible according to the three-dimensional mapping of the native PTT.

Investigation of the Secondary Structure of PTT Conjugates. Table 2 shows the percent change in the secondary structure of the conjugates compared to that of the native PTT estimated through FTIR. The FTIR spectrum of native PTT shows the presence of 13.8% aggregated strands, 43.3% β-sheet, 9.2% β-turns, and 33.7% α-helix. The FTIR spectrum of the control incubated PTT showed negligible change (<1%) in the protein's secondary structure upon incubation at mild temperature of 48 °C. The results also show that the glycation with galactose had minimal effects on the secondary structure of PTT with 9.2, 43.1, 8.6, and 39.1% of aggregated strands, β-sheet, β-turn, and α-helix, respectively. These results confirm the high affinity of galactose to exposed glycation sites located at the

Table 2. Effect of Glycation on the Secondary Structures of PTT and Its Conjugates Obtained through FTIR[a]

PTT sample	α-helix (%)	β-sheets (%)	β-turns (%)	aggregated sheets (%)
PTT	33.75	43.27	9.16	13.82
incubated PTT	34.19	42.36	9.07	14.38
PTT/galactose	39.02	43.14	8.62	9.22
PTT/GOS	34.54	43.29	9.43	12.74
PTT/galactan	31.10	37.99	6.94	23.96

[a]Each spectrum was obtained by coadding 256 scans.

dx.doi.org/10.1021/jf5003073 | J. Agric. Food Chem. 2014, 62, 3591−3598

termini of PTT secondary structures (Figure 2B), leading to minimal secondary structural changes of PTT upon glycation. Similar low structural changes were exhibited by PTT/GOS conjugates with 12.7, 43.3, 9.4, and 34.6% of aggregated strands, β-sheet, β-turn, and α-helix, respectively. The most significant changes in the secondary structure of PTT were observed upon glycation with galactan with 24.0, 38.0, 6.9, and 31.1% of aggregated strands, β-sheet, β-turn, and α-helix, respectively; these results are due to the disruption of intermolecular noncovalent interactions that stabilize the secondary structure of PTT.[46] The significant structural changes observed in the PTT/galactan conjugates resulted in the burying of IgE specific epitopes between the protein molecules and to the subsequent decrease in IgE binding affinity.[47] Although relatively small, the changes in PTT secondary structure upon conjugation with the smaller carbohydrates induced an exposure of inner epitopes, leading to an increase in the immunoreactivity as observed in Figure 1A. Ma et al.[43] have reported that the increase in the immunoreactivity of the ovalbumin conjugated with glucose was due to the exposure of hydrophobic epitopes upon glycation.

Effect of Heat Treatment on the Immunoreactivity and the Secondary Structures of PTT Conjugates. The effect of heat treatment (80 °C for 15 min) on the immunoreactivity of native PTT and PTT conjugates was assessed (Table 3). The

Table 3. Effect of Heat Treatment on PTT Conjugates' Immunoreactivity Obtained through Competition ELISA[a]

		IC_{50} (μg/mL)[a]	
conjugates	incubation time (days)	nonheated	heated
PTT		1.19 (±0.11)	2.77 (±0.66)
incubated PTT	3	0.82 (±0.16)	2.64 (±0.28)
PTT/galactose	1	0.70 (±0.10)	0.98 (±0.65)
PTT/GOS	3	0.38 (±0.05)	0.03 (±0.01)
PTT/galactan	3	5.49 (±0.79)	0.81 (±0.05)

[a]IC_{50} is the concentration of PTT conjugates that produced 50% inhibition of antibody binding to the native PTT. All assays were done in triplicate. p values ≤0.05 were considered to be statistically significant.

heat treated native PTT demonstrated a significant decrease in the IgE binding affinity with an IC_{50} value of 2.77 μg/mL ($p < 0.01$) as compared to the nonheat treated PTT (IC_{50} value of 1.19 μg/mL ($p < 0.01$). Koppelman et al.[47] have obtained similar results to native PTT after heat treatment and attributed the decrease in the immunoreactivity to the hiding of the epitopes through their aggregation, caused by the exposure of hydrophobic regions of PTT during heat induced denaturation. However, the heat treatment did not affect the IgE binding affinity of PTT/galactose conjugates (IC_{50} of 0.98 μg/mL, $p < 0.01$). Contrary to PTT/galactose conjugates, an increase in the IgE binding affinity of PTT/GOS conjugates (IC_{50} of 0.03 μg/mL, $p < 0.01$) and of PTT/galactan conjugates (IC_{50} of 0.81 μg/mL, $p < 0.01$) were obtained after heat treatment. These results can be explained by an increase in the exposure of the epitopes after a partial protein unfolding and/or by the efficiency of longer carbohydrate chains (GOS, galactan) in preventing thermal protein aggregation upon glycation, leading to a better accessibility of the epitopes by IgE.[47] The increase in the immunoreactivity observed with the PTT conjugates are in direct contrast to the results obtained by Vissers et al.[48] where carbohydrate conjugated 2S albumins had lower IgE binding capacity after heat treatment.

To better understand the effect of the conformational changes on the immunoreactivity of PTT conjugates, the changes in secondary structures after heat treatment (Figure 3) were

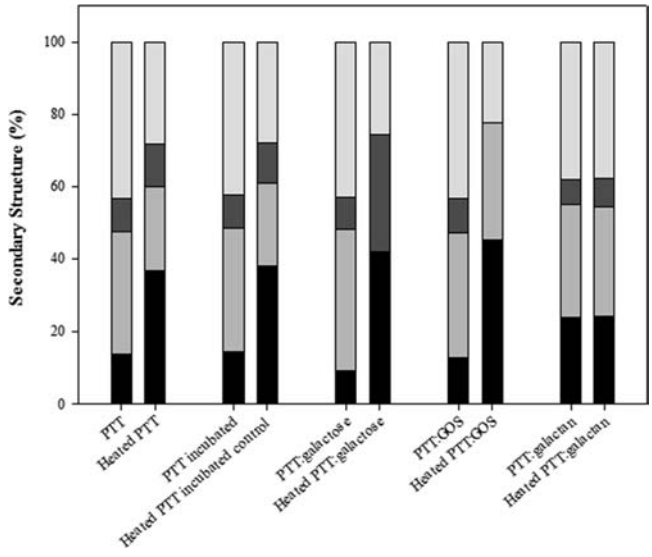

Figure 3. Effect of heat treatment on PTT and its conjugates' secondary structure obtained through FTIR: intermolecular β-sheet (black rectangle), α-helix (medium gray rectangle), β-turn (dark gray rectangle), and intramolecular β-sheet (light gray rectangle).

assessed. The results demonstrate that the partial unfolding of PTT and its conjugates upon heat treatment supports previous findings.[49] Indeed, an increase in the intermolecular β-sheets (>23.03%) after heat treatment was observed for PTT and its conjugates, except for PTT/galactan conjugates. These results confirm the strong tendency of native PTT and its conjugates with galactose and GOS to aggregate upon partial denaturation. Although the largest increase in the aggregated sheets was observed with PTT/galactose (32.67%) and PTT/GOS (32.45%) conjugates upon heat treatment, these changes did not lead to a decrease in the immunoreactivity of the conjugates, as observed with the native and the control PTT (Table 3). The major secondary structural changes observed with PTT/galactose and PTT/GOS conjugates were the complete loss of α-helices and β-turns, respectively; such structural modifications resulted in an increased exposure of the PTT epitopes, leading to an increase in the immunoreactivity of these conjugates even after aggregation (Table 3). On the contrary, galactan stabilizes PTT against heat denaturation with only 2.71% total change in the secondary structure. However, the relatively small change in the secondary structure resulted in an exposure of the hydrophobic epitopes. In addition, the lack of subsequent protein aggregation after exposure of the hydrophobic groups due to galactan conjugation resulted in a significant increase in immunoreactivity (Table 3).

Effect of Digestion on the Immunoreactivity of PTT Conjugates. The effect of in vitro simulated gastric digestion on the allergenic potential of native PTT and its conjugates was assessed by subjecting the samples to simulated gastric digestion before measuring their immunoreactivity by inhibition ELISA (Figure 4). The highest percent digestion was obtained with the native PTT (59.6%) as compared to PTT conjugates. The low percent digestion of PTT conjugates is explained by the fact that the cleavage site of one of the digestive enzymes, trypsin, is specific toward the Lys residues, which are involved in the

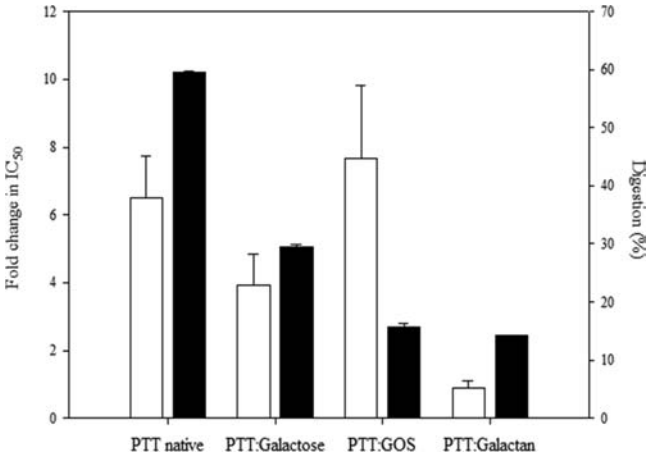

Figure 4. Effect of simulated gastric digestion on PTT conjugates' immunoreactivity: fold change in IC_{50} (white bar) and percent digestion (black bar).

conjugation reaction with carbohydrates. These results are in accordance with those reported by Jiménez-Saiz et al.[42] showing a decrease in ovalbumin conjugates' digestibility as a result of glycation. Nevertheless, as compared to PTT/galactose conjugates (29.5% degree of digestion), the higher resistance of PTT/GOS (15.7%) and PTT/galactan (14.2%) conjugates to digestion could be due to the large size of their carbohydrates moieties, shielding PTT proteolytic sites. The results (Figure 4) also show that the digestion resulted in a 6.51-fold decrease in the IgE binding affinity of native PTT as compared to the nondigested one; these experimental findings can be explained by the disruption of both conformational and sequential epitopes. Similarly, a decrease in the IgE binding affinity of PTT/galactose and PTT/GOS conjugates by 3.94- and 7.66-fold, respectively, was obtained upon digestion. In contrast, the IgE binding affinity of digested PTT/galactan conjugates remained unchanged compared to that of the undigested conjugates; this can be due to the large polysaccharide chains that have sterically blocked the disruption of the epitopes.[41] However, compared to the digested native PTT (IC_{50} of 7.75 μg/mL, $p < 0.01$), a higher retention in IgE binding was exhibited by digested PTT/galactose (IC_{50} of 2.76 μg/mL), PTT/GOS (IC_{50} of 2.91 μg/mL), and PTT/galactan conjugates (IC_{50} of 4.90 μg/mL). These high immunoreactivities of digested conjugates is due to their lower susceptibility to digestion, thereby preserving the integrity of IgE binding sites on conjugated PTT.

■ ASSOCIATED CONTENT

Supporting Information

Level of specific IgE found in the serum of donors characterized by ImmunoCAP; SDS−PAGE gel of isolated PTT and PIs through ultrafiltration; Western blot of potato proteins using the serum pool taken from four donors with specific IgE toward potato proteins; peptide composition of the tryptic hydrolysates of PTT and its PTT/galactose conjugates. This material is available free of charge via the Internet at http://pubs.acs.org.

■ AUTHOR INFORMATION

Corresponding Author

*Tel: +1-514-398-8666. Fax: +1-514-398-7977. E-mail: salwa.karboune@mcgill.ca.

Funding

We are grateful to The Natural Sciences and Engineering Research Council (NSERC) of Canada for financial support.

Notes

The authors declare no competing financial interest.

■ ACKNOWLEDGMENTS

We gratefully acknowledge Solanic (Avebe) for providing us with the potato proteins and the Proteomics Platform of the Quebec Genomics Center at the CHUQ Research Center for their help with the MS analysis and peptide identification.

■ ABBREVIATIONS USED

PTT, patatin; PIs, protease inhibitors; GOS, galactooligosaccharides; FTIR, Fourier transform infrared spectroscopy

■ REFERENCES

(1) Hefle, S. L.; Nordlee, J. A.; Taylor, S. L. Allergenic foods. *Crit. Rev. Food Sci. Nutr.* **1996**, *36*, S69−S89.

(2) Church, M. K.; Bradding, P.; Walls, A. F.; Okayama, Y. Mast Cells and Basophils. In *Allergy and Allergic Diseases*; Kay, A. B., Ed.; Blackwell: Oxford, U.K., 1997; pp 149−170.

(3) Wahl, R.; Lau, S.; Maasch, H. J.; Wahn, U. IgE mediated allergic reactions to potatoes. *Int. Arch. Allergy Immunol.* **1990**, *92*, 168−174.

(4) Ebner, C.; Hirschwehr, R.; Bauer, L.; Breiteneder, H.; Valenta, R.; Ebner, H.; Kraft, D.; Scheiner, O. Identification of allergens in fruits and vegetables: IgE cross-reactivities with the important birch pollen allergens Bet v 1 and Bet v 2 (birch profilin). *J. Allergy Clin. Immunol.* **1995**, *95*, 962−969.

(5) Iliev, D.; Wuthrich, B. Occupational protein contact dermatitis with type I allergy to different kinds of meat and vegetables. *Int. Arch. Occup. Environ. Health* **1998**, *71*, 289−292.

(6) Seppala, U.; Alenius, H.; Turjanmaa, K.; Reunala, T.; Palosuo, T.; Kalkkinen, N. Identification of patatin as a novel allergen for children with positive skin prick test responses to raw potato. *J. Allergy Clin. Immunol.* **1999**, *103*, 165−171.

(7) Castells, M. C.; Pascual, C.; Esteban, M. M.; Ojeda, J. A. Allergy to white potato. *J. Allergy Clin. Immunol.* **1986**, *78*, 1110−1114.

(8) Ralet, M.-C.; Gueguen, J. Les protéines de pomme de terre: composition, isolement et propriétés fonctionnelles. *Sci. Aliments* **1999**, *19*, 147−165.

(9) Shieber, A.; Stintzing, F. C.; Carle, R. By-products of plant food processing as a source of functional compounds. Recent developments. *Trends Food Sci. Technol.* **2001**, *12*, 401.

(10) Waglay, A.; Karboune, S.; Alli, I. Potato protein isolates: Recovery and characterization of their properties. *Food Chem.* **2014**, *142*, 373−382.

(11) Pots, A. M.; Gruppen, H.; Hessing, M.; van Boekel, M. A. J. S.; Voragen, A. G. J. Isolation ad characterization of patatin isoforms. *J. Agric. Food Chem.* **1999**, *47*, 4587−4592.

(12) Sun, Y.; Jiang, L.; Wei, D. Partial characterization, *in vitro* antioxidant and antiproliferative activities of patatin purified from potato fruit juice. *Food Funct.* **2013**, *4*, 1502−1511.

(13) Sharma, N.; Gruszewski, H. A.; Park, S.-W.; Holm, D. G.; Vivanco, J. M. Purification of an isoform of patatin with antimicrobial activity against *Phytophthora infestans*. *Plant Physiol. Biochem.* **2004**, *42*, 647−655.

(14) Deveaux-Gobert, V. Protéines de pommes de terre: vers de nouveaux axes de valorisation? *Cah. Agric.* **2008**, *17*, 407−411.

(15) Creusot, N.; Wierenga, P. A.; Laus, M. C.; Giuseppin, M. L. F.; Gruppen, H. Rheological properties of patatin gels compared with beta-lactoglobulin, ovalbumin, and glycinin. *J. Sci. Food Agric.* **2010**, *91*, 253−261.

(16) Seppala, U.; Majamaa, H.; Turjanmaa, K.; Helin, J.; Reunala, T.; Kalkkinen, N.; Palosuo, T. Identification of four novel potato (*Solanum tuberosum*) allergens belonging to the family of soybean trypsin inhibitors. *Allergy* **2001**, *56*, 619−626.

(17) Komarnytsky, S.; Cook, A.; Raskin, I. Potato protease inhibitors inhibit food intake and increase circulating cholecystokinin levels by a trypsin-dependent mechanism. *Int. J. Obes.* **2011**, *35*, 236−243.
(18) Giuseppin, M. L. F.; Nieuwenhuijzen, N. H.; Lambers, R. R.; Spelbrink, R. E. J. Non-astringent Protein Products. WO 2011/059330 A1, 2011.
(19) Taheri-Kafrani, A.; Gaudin, J.-C.; Rabesona, H.; Nioi, C.; Agarwal, D.; Drouet, M.; Chobert, J.-M.; Bordbar, A.-K.; Haertlé, T. Effects of heating and glycation of β-lactoglobulin on its recognition by IgE of sera from cow milk allergy patients. *J. Agric. Food Chem.* **2009**, *57*, 4974−4982.
(20) de Jongh, H. H. J.; Robles, C. L.; Timmerman, E.; Nordlee, J. A.; Lee, P.-W.; Baumert, J. L.; Hamilton, R. G.; Taylor, S. L.; Koppelman, S. J. Digestibility and IgE-binding of glycosylated codfish parvalbumin. *BioMed Res. Int.* **2013**, *2013*. DOI: 10.1155/2013/756789.
(21) Sathe, S. K.; Teuber, S. S.; Roux, K. H. Effects of food processing on the stability of food allergens. *Biotechnol. Adv.* **2005**, *23*, 423−429.
(22) Arita, K.; Babiker, E. E.; Azakami, H.; Kato, A. Effect of chemical and genetic attachment of polysaccharides to proteins on the production of IgG and IgE. *J. Agric. Food Chem.* **2001**, *49*, 2030−2036.
(23) Gruber, P.; Becker, W.-M.; Hofmann, T. Influence of the Maillard reaction on the allergenicity of rAra h 2, a recombinant major allergen from peanut (*Arachis hypogaea*), its major epitopes, and peanut agglutinin. *J. Agric. Food Chem.* **2005**, *53*, 2289−2296.
(24) Nakamura, A.; Watanabe, K.; Ojima, T.; Ahn, D.-H.; Saeki, H. Effect of Maillard reaction on allergenicity of scallop tropomyosin. *J. Agric. Food Chem.* **2005**, *53*, 2559−2564.
(25) Seo, S.; Karboune, S.; Yaylayan, V. A.; L'Hocine, L. Glycation of lysozyme with galactose, galactooligosaccharides and potato galactan through the Maillard reaction and optimization of the production of prebiotic glycoproteins. *Process Biochem.* **2012**, *47*, 297−304.
(26) Krause, R.; Knoll, K.; Henle, T. Studies on the formation of furosine and pyridosine during acid hydrolysis of different Amadori products. *Eur. Food Res. and Technol.* **2003**, *216*, 277−283.
(27) Moreno, F. J.; Quintanilla-Lopez, J. E.; Lebron-Aguilar, R.; Olano, A.; Sanz, M. L. Mass spectrometric characterization of glycated beta-lactoglobulin peptides derived from galacto-oligosaccharides surviving the in vitro gastrointestinal digestion. *J. Am. Soc. Mass Spectrom.* **2008**, *19*, 927−937.
(28) Shevchenko, A.; Wilm, M.; Vorm, O.; Mann, M. Mass spectrometric sequencing of proteins from silver-stained polyacrylamide gels. *Anal. Chem.* **1996**, *68*, 850−858.
(29) Havlis, J.; Thomas, H.; Sebela, M.; Shevchenko, A. Fast-response proteomics by accelerated in-gel digestion of proteins. *Anal. Chem.* **2003**, *75*, 1300−1306.
(30) Keller, A.; Nesvizhskii, A. I.; Kolker, E.; Aebersold, R. Empirical statistical model to estimate the accuracy of peptide identifications made by MS/MS and database search. *Anal. Chem.* **2002**, *74*, 5383−5392.
(31) Nesvizhskii, A. I.; Keller, A.; Kolker, E.; Aebersold, R. A statistical model for identifying proteins by tandem mass spectrometry. *Anal. Chem.* **2003**, *75*, 4646−58.
(32) Allain, A.-F.; Paquin, P.; Subirade, M. Relationship between conformation of beta-lactoglobulin in solution and gel states as revealed by attenuated total reflection fourier transform infrared spectroscopy. *Int. J. Biol. Macromol.* **1999**, *26*, 337−344.
(33) Kong, J.; Yu, S. Fourier transform infrared spectroscopic analysis of protein secondary structures. *Acta Biochim. Biophys. Sin.* **2007**, *39*, 549−559.
(34) Kiefer, F.; Arnold, K.; Künzli, M.; Bordoli, L.; Schwede, T. The SWISS-MODEL repository and associated resources. *Nucleic Acids Res.* **2009**, *37*, 387−392.
(35) Jmol: An Open-Source Java Viewer for Chemical Structures in 3D. http://www.jmol.org/.
(36) Oliver, C. M.; Melton, L. D.; Stanley, R. A. Glycation of caseinate by fructose and fructo-oligosaccharides during controlled heat treatment in the 'dry' state. *J. Sci. Food Agric.* **2006**, *86*, 722−731.
(37) ter Haar, R.; Schols, H. A.; Gruppen, H. Effect of saccharide structure and size on the degree of substitution and product diversity of α-lactalbumin glycated via the Maillard reaction. *J. Agric. Food Chem.* **2011**, *59*, 9378−9385.
(38) Jiménez-Castaño, L.; Villamiel, M.; López-Fandiño, R. Glycosylation of individual whey proteins by Maillard reaction using dextran of different molecular mass. *Food Hydrocolloids* **2007**, *21*, 433−443.
(39) Hollnagel, A.; Kroh, L. W. Degradation of oligosaccharides in nonenzymatic browning by formation of α-dicarbonyl compounds via a "Peeling off" mechanism. *J. Agric. Food Chem.* **2000**, *48*, 6219−6226.
(40) Yeboah, F. K.; Alli, I.; Yaylayan, V. A.; Konishi, Y.; Stefanowicz, P. Monitoring glycation of lysozyme by electrospray ionization mass spectrometry. *J. Agric. Food Chem.* **2000**, *48*, 2766−2774.
(41) Aoki, R.; Saito, A.; Azakami, H.; Kato, A. Effects of various saccharides on the masking of epitope sites and uptake in the gut of cedar allergen Cry j 1-saccharide conjugates by a naturally occurring Maillard reaction. *J. Agric. Food Chem.* **2010**, *58*, 7986−7990.
(42) Jiménez-Saiz, R.; Belloque, J.; Molina, E.; López- Fandiño, R. Human immunoglobulin E (IgE) binding to heated and glycated ovalbumin and ovomucoid before and after in vitro digestion. *J. Agric. Food Chem.* **2011**, *59*, 10044−10051.
(43) Ma, X. J.; Chen, H. B.; Gao, J. Y.; Hu, C. Q.; Li, X. Conformation affects the potential allergenicity of ovalbumin after heating and glycation. *Food Addit. Contam., Part A* **2013**, *30*, 1684−1692.
(44) Seo, S.; Karboune, S.; L'Hocine, L.; Yaylayan, V. Characterization of glycated lysozyme with galactose, galactooligosaccharides and galactan: Effect of glycation on structural and functional properties of conjugates. *LWT Food Sci. Technol.* **2013**, *53*, 44−53.
(45) Alibhai, M. F.; Astwood, J. D.; McWherter, C. A.; Sampson, H. A. Preparation of Deallergenized Proteins and Permuteins. WO 01/49834 A2, 2005.
(46) Povey, J. F.; Howard, M. J.; Williamson, R. A.; Smales, C. M. The effect of peptide glycation on local secondary structure. *J. Struct. Biol.* **2008**, *161*, 151−161.
(47) Koppelman, S. J.; van Koningsveld, G. A.; Knulst, A. C.; Gruppen, H.; Pigmans, I. G. A. J.; de Jongh, H. H. J. Effect of heat-induced aggregation on the IgE binding of patatin (*Sol t 1*) is dominated by other potato proteins. *J. Agric. Food Chem.* **2002**, *50*, 1562−1568.
(48) Vissers, Y. M.; Blanc, F.; Skov, P. S.; Johnson, P. E.; Rigby, N. M.; Przybylski-Nicaise, L.; Bernard, H.; Wal, J.-M.; Ballmer-Weber, B.; Zuidmeer-Jongejan, L.; Szepfalusi, Z.; Ruinemans-Koerts, J.; Jansen, A. P. H.; Savelkoul, H. F. J.; Wichers, H. J.; Mackie, A. R.; Mills, C. E. N.; Adel-Patient, K. Effect of heating and glycation on the allergenicity of 2S albumins (Ara h 2/6) from peanut. *PLoS One* **2011**, *6*, e23998.
(49) Pots, A. M.; De Jongh, H. H. J.; Gruppen, H.; Hamer, R. J.; Voragen, A. G. J. Heat-induced conformational changes of patatin, the major potato tuber protein. *Eur. J. Biochem.* **1998**, *252*, 66−72.

The present investigation attempts to develop an oral colon-targeted controlled-release system by an aqueous dispersion film coating process at low temperature. Starch was treated by a high-temperature−pressure reaction, enzymatic debranching, and retrogradation. The structural changes and the digestion resistibility were investigated. With the aqueous dispersion film coating technique, the formation of RS3 and the film coating could be achieved simultaneously. Thus, in this study, insulin-loaded microparticles coated with the in situ formed RS3 film were prepared, following optimization of the colon-targeting controlled-release property of the RS3 film-coated microparticles by in vitro experiments (i.e., under the conditions of simulated human GI tract). Furthermore, the in vivo effectiveness of the RS3 film-coated insulin-loaded microparticles was evaluated by tissue immunocytochemistry and in vivo insulin bioactivity studies in streptozotocin (STZ)-induced diabetic rats.

MATERIALS AND METHODS

Materials. High-amylose corn starch (Gelose 50, G50) was obtained from Penford (Australia). Pullulanase was of analytical grade and supplied by Yulibao Biology and Technology Co., Ltd. (Guangzhou, China). Termamyl α-amylase (120 KNU/g) from *Bacillus licheniformis* and Amyloglucosidase (300 AGU/g) from *Aspergillus niger* were purchased from Novo Nordisk Bioindustrials (Guangzhou, China). Microcrystalline cellulose was purchased from Anhui Shanhe Medicinal Accessary Material Co., Ltd. (Huainan, China). 5-Aminosalicylic acid (5-ASA) was supplied by Yuancheng Technology Development Co., Ltd. (Wuhan, China). Commercial long-acting insulin was purchased from Newprobe Bioscience and Technology Co., Ltd. (Beijing, China). Medicinal starch was supplied by Defeng Starch Sugar Co., Ltd. (Shunde District, Foshan, China). Pepsin, pancreatin, and STZ were purchased from Sigma-Aldrich Co. LLC (Santa Clara, CA, USA) and were of pharmaceutical grade. The rest of the chemical reagents were of analytical grade.

Preparation of RS. The preparation procedure used in this work was according to our earlier method of high-temperature−pressure and debranching treatment, which can increase the RS content of starch.[31] About 25 g of dry high-amylose corn starch was dispersed in 225 mL of water and cooked in a sealed pressure reactor (Parr 4545, Parr Instrument Co., USA) at 110 °C under the pressure of 12.4 MPa with stirring at 200 rpm for 30 min. Then, the gelatinized starch dispersion was cooled to 60 °C, and its pH value was adjusted to 5.0 using 10% (w/v) citric acid. Subsequently, different amounts of pullulanase were added to the reactor for debranching the starch molecules at 60 °C under atmospheric pressure with stirring at 20 rpm for 6 h. The debranched starch was cooked at 100 °C for 10 min to stop the enzymatic hydrolysis and then cooled and stored at 4 °C for 24 h (during which retrogradation happened). Then, parts of the retrograded starch pastes were spray-dried for the analysis of characteristics, and the other parts were diluted by purified water for the preparation of the RS3-based aqueous dispersions.

Digestion Resistibility and Structural Changes of the RS Samples. *Digestion Resistibility in the Upper GI Tract.* The RS content of the RS3 samples was determined by using method 991.43, total dietary fiber (TDF), of the Association of Official Analytical Chemists (AOAC) in in vitro model with Termamyl α-amylase and Amyloglucosidase.

Molecular Molar Mass (M_w) Analysis. The molecular molar mass (M_w) analysis was carried out by using a gel permeation chromatography (GPC) system coupled with a multiangle light scattering (MALS) detector and a refractive index (RI) detector. The GPC system consisted of a pump (1515, Waters, Milford, MA, USA), an autoinjector with a 0.1 mL loop (717, Waters), and a column (Sytyragel HMW7 GPC column, 7.8 × 300 mm, Waters). The MALS detector (632.8 nm, DAWN HELEOS, Wyatt Technology, Santa Barbara, CA, USA) and the RI detector (Optilab rex, Wyatt Technology) were connected to the column.

Fifty milligrams of starch was dispersed in 10 mL of dimethyl sulfoxide (DMSO) containing LiBr (50 mM) with heating in a boiling water bath for 1 h, followed by the shaking of the sample at 60 °C in the water bath for another 12 h. Before injection, the starch sample solutions were filtered using a membrane filter (5.0 μm LS, Millipore Corp., Bedford, MA, USA). The mobile phase used for GPC was DMSO (HPLC grade) containing LiBr (50 mM), which had been filtered through a 0.2 μm membrane filter (0.2 μm FG, Millipore Corp.) and degassed by ultrasound. The flow rate of the mobile phase was 0.7 mL/min; the column was maintained at 45 °C, and the detectors were maintained at 25 °C. The specific RI increment value (dn/dc) of starch in DMSO was found to be 0.074 mL/g.[32] The data were analyzed by the Astra 3.4 software program (Wyatt Technology).

X-ray Diffraction (XRD). Wide-angle X-ray powder diffraction analysis was performed using an X-ray diffractometer (X'Pert Prox, PANalytical, Eindhoven, The Netherlands) operating at 40 kV and 40 mA with Cu Kα radiation (λ = 0.1542 nm). The diffractograms of the RS3 samples were acquired at an angular range of 2θ from 4° to 40° with the step size of 0.033° and the counting time of 4 s for each step. The samples were sieved through 0.180 mm and equilibrated at 25 °C for 24 h prior to the analysis. The relative crystallinity of the samples was quantitatively estimated according to the method of Nara and Komiya.[33] A smooth curve connected with the constant peak baseline was computer-plotted on the diffraction. The ratio of the upper area (crystalline portion) to the total diffraction area (based on a linear baseline) was taken as the relative crystallinity with the software MDI Jade 6.0.

Small Angle X-ray Scatting (SAXS). SAXS measurements were performed on a SAXSess camera (Anton-Paar, Graz, Austria) using Cu Kα radiation (0.1542 nm wavelength) at 40 kV and 50 mA according to our previous studies.[31,34] The starch slurries with similar moisture content (60%, w/w) were prepared for this experiment and equilibrated at 26 °C for 24 h before the analysis. The samples were filled into a paste sample cell and fixed and placed in a TCS 120 temperature-controlled unit (Anton Paar) along the line-shaped X-ray beam in the evacuated camera housing. Each measurement was collected for 10 min. The 2D data were integrated into the 1D scattering function $I(q)$ as a function of the magnitude of the scattering vector q and normalized. The background and smeared intensity were removed using the SAXSquant 3.0 software program for further analysis.

If Bragg's law is applied, q is proportional to the inverse of the apparent periodic length d, as $d = 2\pi/q$. The surface/mass fractal structure can be obtained from the slope of the log−log SAXS graph according to the method of Suzuki, Chiba, and Yarno.[35] The scattering objects with a surface fractal dimension (D_s) are more compact than those with a mass fractal dimension (D_m).

Preparation of the RS3 Film-Coated Microparticles. Bioactive component-loaded microparticle cores (containing microcrystalline cellulose and starch in the ratio of 3:1 and the bioactive component in varied content) were obtained via extrusion−spheronization.[5] 5-ASA and insulin were chosen as model bioactive components, respectively. During the extrusion−spheronization, the temperature was kept at 5−10 °C to maintain the activity of the bioactive components.

Purified water was added into the retrograded starch pastes until starch-based aqueous dispersions (8%, w/w) were obtained. After homogenization by a high-pressure homogenizer (Panda Plus2000, Gea Niro Soavi, Italy), 1,2-propanediol was added into the dispersions, which were then stirred for 8 h by a magnetic stirrer. Thus, the RS3-based aqueous coating dispersions were obtained.

The bioactive component-loaded microparticle cores were coated using a bottom spray fluid bed coater (Mini-XYT; Xinyite Technology Co., Shenzhen, China) until the coated-film thickness of 5−30% (w/w) was achieved, which was representative of the dry weight gain of the microparticles.[5] The process parameters were as follows: inlet temperature at 45 ± 1 °C; temperature of the bioactive component-loaded microparticles at 30 ± 1 °C; spray rate of coating dispersion at 0.7−0.8 mL/min; atomization pressure at 0.15 MPa; and fluidization pressure at 0.15 MPa. After coating, the coated microparticles were further fluidized dried at 35 °C for different times.

Table 1. RS3 Samples and Their GPC-MALLS Parameters, Crystallinity, and SAXS Parameters

pullulanase activity (U/g)	RS content[a] (%)	M_w (g/mol)	R_g[a] (nm)	conformation	crystallinity (%)	α	D_s	D_m	A_q
0	10.4 ± 0.4^A	3.501×10^6 (2%[b])^A	85.0 (1%)^A	spherical	34.4	−3.82	2.18		0.1077
5	10.8 ± 0.7^A	1.463×10^6 (5%)^B	56.2 (1%)^B	spherical	37.2	−1.71		1.71	0.7190
10	15.6 ± 0.6^B	7.315×10^5 (2%)^C	47.5 (2%)^C	spherical	41.4	−1.81		1.87	0.7637
50	20.1 ± 0.7^C	3.271×10^5 (1%)^D	36.2 (3%)^D	spherical	45.6	−1.87		1.87	0.7681
100	34.3 ± 0.7^D	1.692×10^5 (3%)^E	33.8 (9%)^D	spherical	59.5	−2.06		2.06	0.8395
200	41.8 ± 0.8^E	3.067×10^4 (1%)^F	29.4 (5%)^E	spherical	62.7	−2.06		2.06	0.8420

[a]Values followed by the different upper case letters within a column differ significantly ($n = 3$, $P < 0.05$). [b]Precision of global fit.

In Vitro Release Testing and Related Morphological Observation. The bioactive component release tests were carried out using a dissolution rate test apparatus according to the USP23 dissolution method. The RS3 film coated microparticles were incubated in simulated gastric fluid (SGF) for the first 2 h, then in simulated intestinal fluid (SIF) for another 6 h, and afterward in simulated colonic fluid (SCF) for an additional 22 h, in sequence, all at 37 °C.[5,28,29] When the simulated digestive fluid was changed, the microparticles were filtered by filter paper under vacuum, washed with distilled water two times, and then put into the following simulated digestive fluid. At each of the predetermined time points, 5 mL of the tested sample was withdrawn and analyzed for the 5-ASA or insulin content by a UV spectrophotometer (Unico, UV-3802, Shanghai, China).

The morphological change of the RS3 film-coated microparticles during the release process in the simulated fluids was monitored by a scanning electronic microscope Hitachi S3700 (Tokyo, Japan).

In Vivo Release of Insulin from Microparticles after Oral Administration. The in vivo insulin bioactivity of the microparticles was evaluated using a STZ-induced diabetic animal model. STZ (40 mg/kg of rat) in 0.1 M citrate buffer (pH 4.5) was injected intraperitoneally into male Sprague−Dawley (SD) rats, each weighing 273 ± 12 g (Guangdong Animal Experimental Centre, Foshan, China). Two weeks after the STZ treatment, the fasting plasma glucose levels of the rats were monitored at 24 h after fasting. If two successive glucose levels of the rats were >7.8 mmol/L, the rats were diagnosed as having type II diabetes and were used for the in vivo insulin release studies.

Tissue Immunocytochemistry. The rats with type II diabetes were fasted with free access to water for 24 h before the study. The RS3 film-coated insulin-loaded microparticles were orally administered to the stomach via polyethylene tubing under light ether anesthesia. Insulin was dosed at 25 U/kg body weight. Dose selection was based on the expected pharmacodynamics of insulin. At certain times after their oral administration, the rats were sacrificed by cervical dislocation; the tissues of the stomach, small intestine, and colon were obtained, and the insulin distribution in the different parts of the rat GI tract were detected using the hematoxylin−eosin and immunohistochemical staining method. Formalin-fixed, paraffin-embedded tissue sections of the stomach, small intestine, and colon of the rats were used for immunohistochemical studies according to the protocol specified in the ImmunoCruz rat ABC staining kit (Santa Cruz Biotechnology, Inc.). The section slides were washed in xylene and hydrated in different concentrations of alcohol and then were pretreated with 3% H_2O_2 for 10 min and 5% nonimmune bovine serum albumin for 15 min to seal the compounds, which can result in nonspecific background brown color. The slides were incubated with the primary antibody against insulin at 4 °C for 12 h. A horseradish peroxidase-conjugated secondary antibody was applied to locate the primary antibody. The specimens were stained with diaminobenzidine chromogen and counterstained with hematoxylin. The presence of brown staining was considered to be a positive identification of insulin. An optical microscope was used to observe the images on the slides, and the images were analyzed by the Image-Pro Plus (IPP) software program.

Insulin Bioactivity. The type II diabetic rats were randomly divided into five groups (the average plasma glucose concentrations of the different groups differed by ≤2 mmol/L). Before the test, all of the rats were fasted for 12 h with free access to water. The insulin-loaded microparticles coated by RS3 film were orally administered to the stomach via polyethylene tubing under light ether anesthesia. Insulin was dosed at different dosages, that is, 15, 25, and 35 U/kg body weight, respectively. The group that was subcutaneously injected with 25 U/kg of commercial long-acting insulin was used as the positive control group and the diabetic group without insulin treatment was used as the negative control group. After insulin administration, the rats in all of the groups were allowed to eat freely. At predetermined time points, the plasma glucose concentrations of the rats were monitored by the glucose oxidase method. The relative pharmacodynamic bioactivity of insulin (F_{rel}%) was calculated using the equations

$$F_{rel} = \frac{\frac{[AUC_T]}{dose_T}}{\frac{[AUC_{iv}]}{dose_{iv}}} \times 100$$

$$AUC = \sum_{n=0}^{8} (t_{n+1} - t_n) \times \frac{(100 - P_n) + (100 - P_{n+1})}{2}$$

$$P_n\% = \frac{C_n}{C_0} \times 100$$

where C_n and t_n are the plasma glucose concentration (mmol/L) and monitored time (h) at the nth blood collection, respectively; P_n % is the relative plasma glucose level (% of initial plasma glucose concentration); AUC is the total area of all the trapeziums between every two neighboring points and the 100% horizontal line in the relative plasma glucose concentration−time profile; dose is the intake dosage of insulin; and the subscripts T and iv represent oral administration and subcutaneous injection, respectively.

For the analysis of plasma insulin concentrations, blood samples were centrifuged and subsequently determined by an enzyme immunoassay kit (BG Co., USA), and the relative insulin bioavailability (B_{rel}%) of the insulin-loaded microparticles coated with RS3 film after oral administration was calculated.[36]

Statistical Analysis. All data were subjected to statistical analysis using the SPASS 10.0 statistical package and were presented as mean ± standard deviation (±SD). Differences between groups were estimated by analysis of t test, and $P < 0.01$ was considered to indicate a statistically significant difference between two groups.

RESULTS AND DISCUSSION

Preparation and Characteristics of the RS3 Samples. *Preparation of the RS3 Samples.* As the delivery carrier for colon-specific controlled release system, the starch-based film coated to the surface of the microparticles loaded with bioactive components must have suitable digestion resistibility to realize the delivery of the microparticles targeting the colon. Thus, the digestion resistibility of the RS3 films with different molecular molar masses, formed by the aggregation of gelled starch molecules upon dehydration and drying during the aqueous dispersion coating process, was investigated. The gelled starch molecules with different molecular molar masses were obtained by the high-temperature−pressure and debranching treatment and the RS contents of the treated starch samples with different

dx.doi.org/10.1021/jf500472b | J. Agric. Food Chem. 2014, 62, 3599−3609

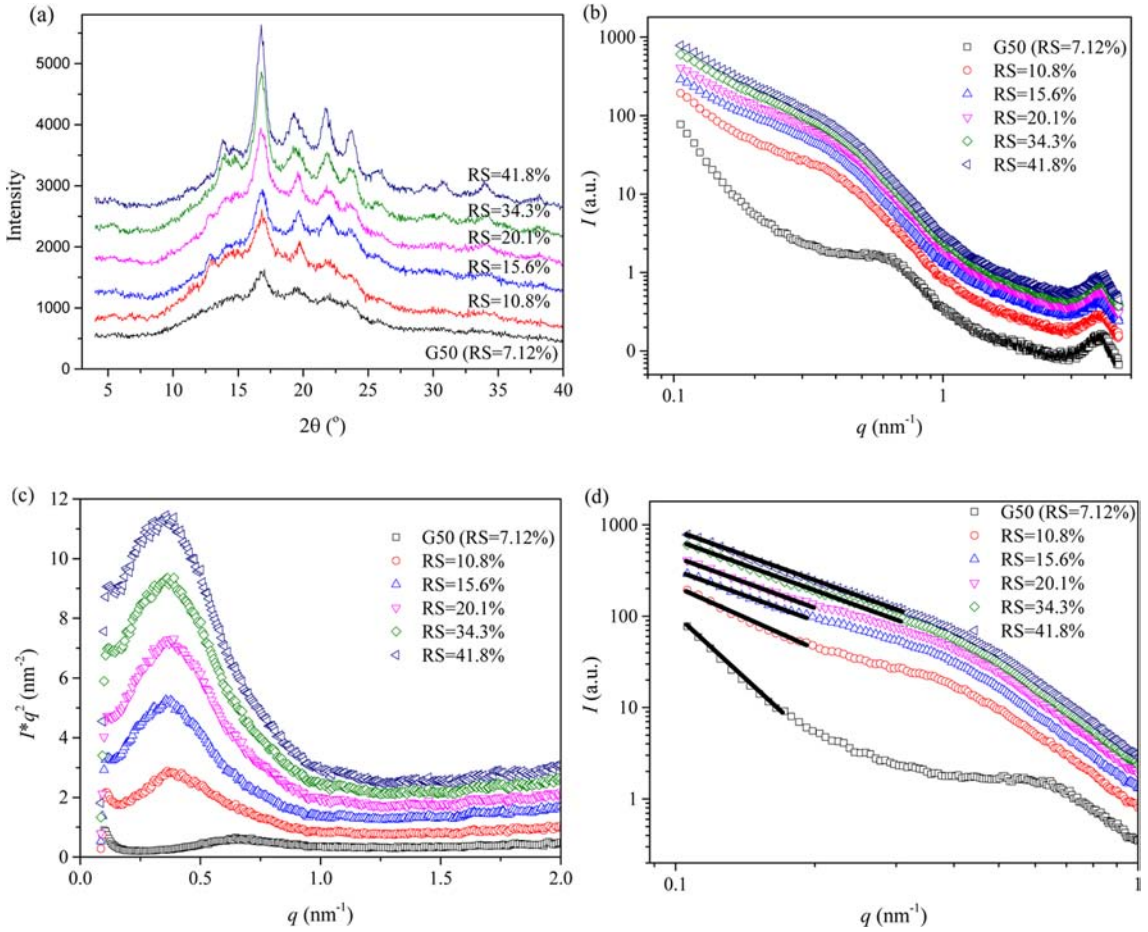

Figure 1. XRD patterns (a) and SAXS patterns of native G50 starch and the RS3 samples with different RS contents: (b) double-logarithmic SAXS patterns; (c) $I \times q^2 - q$ SAXS patterns; (d) double-logarithmic SAXS patterns in the range of $0.08 < q < 1$. The real lines show the relationship $I \sim q^{\alpha}$). All of the intensities are shifted along the ordinate to avoid overlapping of the symbols.

amounts of the debranching enzyme, pullulanase, are shown in Table 1.

A significant increase in the RS content, reaching a maximum value of 41.8%, was observed when the pullulanase content used in the treatment was increased to 200 U/g. Nevertheless, when the amount of pullulanase was increased to 300 U/g, the RS content was reduced to 33.7%, which indicated that a further increase in the amount of pullulanase reduced the RS content ($P < 0.05$). The high-temperature−pressure and debranching treatment with a suitable amount of pullulanase, followed by subsequent retrogradation and drying, could result in the degradation of starch molecules, and some of the degraded molecules of suitable molar mass could reassociate to form tightly packed ordered aggregations stabilized by hydrogen bonding, which were more difficult for starch enzymes to hydrolyze, leading to the formation of a higher amount of RS3. However, with a further increase in the amount of pullulanase, the starch molecules could be degraded further, and these molecules could not preferably form tightly packed ordered aggregations; thus, a decrease in the RS content was observed. The results here demonstrate that the digestion resistibility of starch could be improved by the high-temperature−pressure and debranching treatment and the following retrogradation and drying processes. Thus, the RS3 film with suitable digestion resistibility can be obtained through controlling the starch molecular molar mass during the preparation of starch-based aqueous coating dispersion and the subsequent aqueous dispersion coating process (where retrogradation and drying occur).

Weight-Average Molecular Molar Mass (M_w). After the high-temperature−pressure and debranching treatment, the M_w of native G50 starch was reduced from 3.501×10^6 to 1.463×10^6 g/mol when the RS content was 10.8% (Table 1). The M_w was further reduced to 3.271×10^5 g/mol when the RS content was 20.1% and to 3.067×10^4 g/mol when the RS content was 41.8%. This shows that the high-temperature−pressure and debranching treatment could result in a significant decrease in the M_w of starch ($P < 0.05$). The decrease in the R_g value with an increase in the RS content suggests that the starch molecular size became smaller after the high-temperature−pressure and debranching treatment, which is consistent with the results regarding the M_w. In addition, as seen from the results of the logM_w/log R_g, the conformation of molecules of the RS3 samples was spherical and was not changed with the varied RS content. Along with the RS contents of the samples after the treatment with pullulanase, it seems that the degraded starch molecules with $M_w = 3.067 \times 10^4$ g/mol should preferably form RS3 and the starch molecules with M_w below or above 3.067×10^4 g/mol could be easily digested by the enzyme.

Crystalline Structure. Figure 1a shows the wide-angle XRD spectra of native G50 starch and the RS3 samples with different RS contents, and the relative crystallinity values are shown in Table 1. It can be seen that the native G50 starch gives the strongest diffraction peak at around $2\theta = 17.0°$and a few small

dx.doi.org/10.1021/jf500472b | J. Agric. Food Chem. 2014, 62, 3599−3609

peaks at around 2θ values of 5.6°, 15.0°, 22.0°, 23.4°, and 26.0°, which are indicative of the B-type diffraction pattern, and one peak at 19.8°, which was related to the V-type diffraction pattern. Thus, native G50 starch presented a B+V-type diffraction pattern.[37,38] Comparaed with the XRD pattern of native G50 starch, RS3 samples with RS content between 10.8 and 20.1% showed a new diffraction peak at around 2θ = 13.0°, and this peak changed to about 14.0° as the RS content increased. These two peaks are also related to the B-type diffraction pattern. For the RS3 samples with RS content of 34.3 and 41.8% the peak at around 2θ = 26.0° became distinct as the RS content increased. Although the RS3 samples exhibit a similar B+V-type crystal form, most of the peak intensity was gradually strengthened with an increase in the RS content, which indicated that the starch molecules in RS3 samples can form better-crystallized B- and V-type crystals after the high-temperature−pressure and debranching treatment. The relative crystallinity sharply increased with an increase in the RS content. Particularly, when the RS content was 41.8%, the relative crystallinity reached 62.7%. Combined with the M_w data, it is concluded that the starch molecules with M_w = 3.067 × 10^4 g/mol tended to arrange and form the crystalline structure. These results indicate that the total amount of crystallinity should be one of the reasons for the enhanced starch resistibility against enzymatic digestion.

Lamellar Structure. Figure 1b shows the double-logarithmic SAXS patterns of native G50 starch and the RS3 samples. It can be seen from Figure 1b that native G50 starch had an apparent scattering peak at q = 0.65 nm^{-1}, which corresponds to a Bragg distance of about 9.7 nm and is considered due to the long-range periodicity occurring from the alternating crystalline and amorphous lamellar structure of the starch granule.[34,39−41] After the high-temperature−pressure and debranching treatment with the following retrogradation and drying processes, the peak at q = 0.65 nm^{-1} disappeared in the scattering patterns of the RS3 samples. Instead, there was a shoulder-like peak at q = 0.42 nm^{-1}, corresponding to a Bragg distance of about 14.9 nm, suggesting the formation of a new repeat aggregation structure with the repeat distance of about 14.9 nm.

The difference in the aggregation structure can cause a difference in the electron density, which influences the scattering intensity. The ordering of starch molecules can be quantified by calculating the area under the curve ($\int_0^\infty I(q)q^2 dq$) (Figure 1c). As the RS content increased, the integrated area (A_q) under the SAXS curve also increased (Table 1). During the high-temperature−pressure and debranching treatment with following retrogradation and drying processes, the starch molecules rearranged and aggregated. Thus, the molecular ordering in the aggregation structure of RS3 samples increased. These results indicate that the higher amount of starch molecular aggregation orders as a result of the newly formed repeat aggregation structure with the repeat thickness of about 14.9 nm contributed to the higher resistibility against enzymatic digestion of the RS3 starch samples.

Fractal Structure. As presented in the double-logarithmic SAXS patterns (Figure 1d), the solid lines show the relationship of $I \sim q^{-\alpha}$ and the fractal dimensions are shown in Table 1. It can be seen from Figure 1d and Table 1 that native G50 starch showed a surface fractal structure in the length scale of 36.5 < d < 59.3 nm and the D_s was close to 2.18. For the RS3 samples, a mass fractal structure in the length scale of 31.7 < d < 59.3 nm was shown, with the D_m increasing from 1.71 to 1.87 with an increase in the RS content from 10.8 to 20.1%. A further increase in the RS content from 34.3 to 41.8% would contribute to the formation of a mass fractal structure in the larger length scale of 20.3 < d < 59.3 nm with the D_m of 2.06. This suggests that the treatment contributed to an increase in the compactness of the scattering objects and the formation of the mass fractal structure in a larger scale range. On the basis of the fractal geometry, the D_m of the linear arrangement, the surface-like arrangement, and the regular arrangement (such as a cube or sphere) are 1, 2, and 3, respectively.[35] Thus, the arrangement of the scattering objects in these RS3 samples changed from the linear form to the surface-like form. Considering the RS contents, it is evident that the mass fractal structure in the larger length scale of 20.3 < d < 59.3 nm with a higher D_m value contributed to a higher RS content. The reason could be that some glucosidic bonds of the starch molecules were masked by the ordered aggregations of starch molecular chains in the scattering objects. Meanwhile, when the scattering objects became more compact with an increasing D_m value, it could be more difficult for the starch enzymes to attack the active sites of starch molecules of these scattering objects with a mass fractal structure.

In Vitro Insulin Release from the RS3 Film-Coated Microparticles. *In Vitro Release Behavior.* To optimize the colon-targeting release property of RS3 film, the RS3 film-coated microparticle delivery system was obtained using 5-ASA as the model bioactive compound and the effects of RS content, plasticizer content, film coating thickness, and heat treatment time after coating on the 5-ASA release behavior from the RS3 film-coated microparticles in the simulated human GI tract were investigated, and the results were presented in Figure 1S of the Supporting Information. On the basis of the optimization of the coating process for colon-targeting obtained from Figure 1S, the RS3 film-coated microparticles, in which insulin was loaded, were prepared using the RS3 film with the molecular molar mass of 3.067 × 10^4 g/mol (of which the RS content was 41.8%) as the coating material, with the 1,2-propanediol content being 10%, the coating thickness being 30%, and the time of heat treatment after coating being 8 h; the insulin release profiles are shown in Figure 2. It can be seen from the results that the RS3 film-coated microparticles showed a good colon targeting and release property. The cumulative release percentage of insulin was up to 25.31% within the first 8 h in the upper GI tract and then reached 80.66% at 30 h, suggesting that about 55% of insulin could be delivered to the SCF and

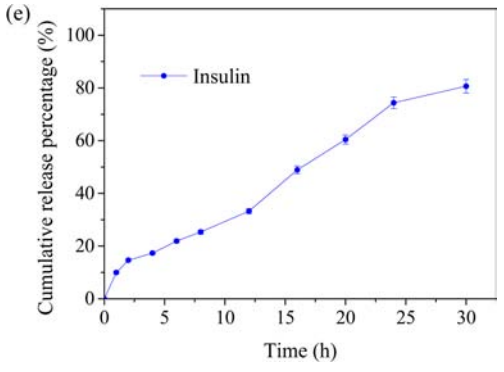

Figure 2. Insulin release from RS3 film-coated microparticles using the RS3 film with RS content of 41.8% as the coating material, with the 1,2-propanediol content being 10%, the coating thickness being 30%, and the time of heat treatment after coating being 8 h.

dx.doi.org/10.1021/jf500472b | J. Agric. Food Chem. 2014, 62, 3599−3609

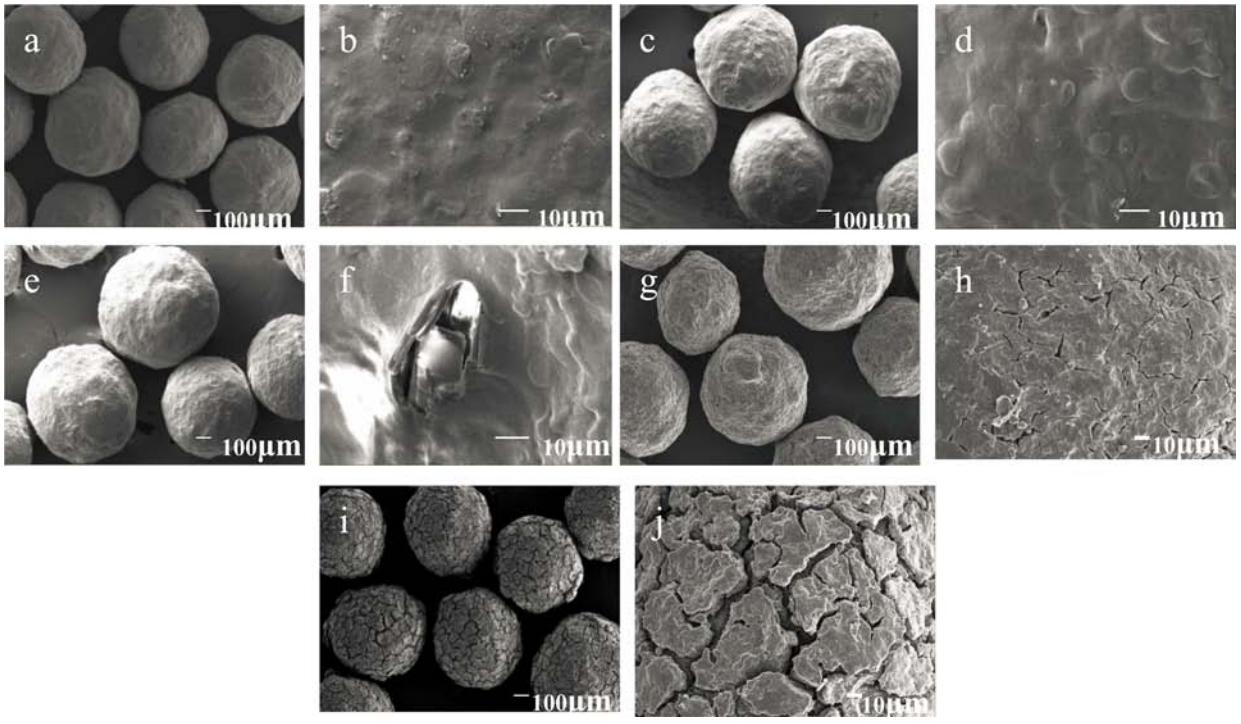

Figure 3. Surface change of RS3 film-coated microparticles during drug release: (a) microparticles, before release; (b) surface of microparticles, before release; (c) microparticles, after release for 2 h; (d) surface of microparticles, after release for 2 h; (e) microparticles, after release for 8 h; (f) surface of microparticles, after release for 8 h; (g) microparticles, after release for 24 h; (h) surface of microparticles, after release for 24 h; (i) microparticles, after release for 30 h; (j) surface of microparticles, after release for 30 h.

could be released sustainably from the RS3 film-coated microparticles in SCF.

Morphological Change of the RS3 Film-Coated Microparticles. To investigate the insulin release mechanism from RS3 film-coated microparticles in the simulated human GI tract, SEM was used to observe the coating film surface on the microparticles after incubation in SGF, SIF, and SCF for the specific periods. The insulin-loaded microparticles coated by the RS3 film under the optimization coating process were incubated in SGF, SIF, and SCF for the specific periods, and the results are shown in Figure 3. It is revealed that the surface morphology of the RS3 film-coated microparticles could be affected by the incubation time. From Figure 3a,b, it can be seen that the microparticles were rounded and the surface of the coated RS3 film showed no obvious change after 2 h in SGF (Figure 3c,d), suggesting that the film could resist the acid in SGF. Transferred to and immersed in SIF (pH 6.8) for another 6 h, the microparticles displayed a few small holes on their coated film. After 2 h in SGF and 6 h in SIF (Figure 3e,f), although a few small holes appeared, the film still kept its integrity, which showed the ability to resist the enzyme in SIF. The next immersion of the microparticles in SCF (pH 7.0) for another 16 h resulted in an increased amount of holes on the surface. After 24 h in these digestive fluids (2 h in SGF, 6 h in SIF, and 16 h in SCF, Figure 3g,h), more holes and cracks emerged and the integrity of the film was impaired. With the prolongation of soaking time (Figure 3i,j), the sizes of holes on the microparticle surfaces were even larger and cracks appeared, deepening toward the interior, suggesting that the coated RS3 film was almost disintegrated. It is shown that the RS3 film has good resistance to degradation by the acid and enzymes in the simulated upper GI tract. Therefore, the RS3 film exhibits a good colon-targeting property.

In Vivo Insulin Release from RS3-Film Coated Microparticles. *Distribution of Insulin in the GT Epithelial Tissues of Rats.* After testing the in vitro colon targeting behavior of the RS3-film coated microparticles, it was worthwhile to assess the in vivo behavior of formulation in terms of the residence time of formulation in different parts of the GI tract. By tissue slices and immunohistochemistry, the insulin release property of the RS3 film-coated microparticles in the type II diabetic model rats was studied. The images showing the insulin distribution in the GI epithelial tissues of rats after administration of the RS3 film-coated microparticles for different times are shown in Figure 4. Before administration, the immunohistochemical images displayed a blue background, indicating no positive insulin sign in the stomach, small intestine, and colon of the rats (Figure 4a–c). At 2 h after intragastric administration, there was a slight insulin positive sign (the brown part) in the stomach of rats (Figure 4d), which means a very small amount of insulin released in the stomach. Meanwhile an insulin positive sign was also observed in the small intestine (Figure 4e), which was due to the fact that part of the insulin released in the stomach had reached the small intestine and some of the insulin released from the microparticles reached the small intestine, although no positive sign was observed in the colon at this moment (Figure 4f). At 8 h after intragastric administration, although there was no insulin positive sign in the stomach, a strong insulin positive sign was shown in the small intestine (Figure 4g,h) and a slight insulin positive sign was reflected in the colon (Figure 4i). From 24 h after intragastric administration, the insulin positive sign concentrated in the colon, suggesting that the microparticles had reached the colon, where the insulin had been released from the microparticles (Figure 4l,o).

dx.doi.org/10.1021/jf500472b | J. Agric. Food Chem. 2014, 62, 3599–3609

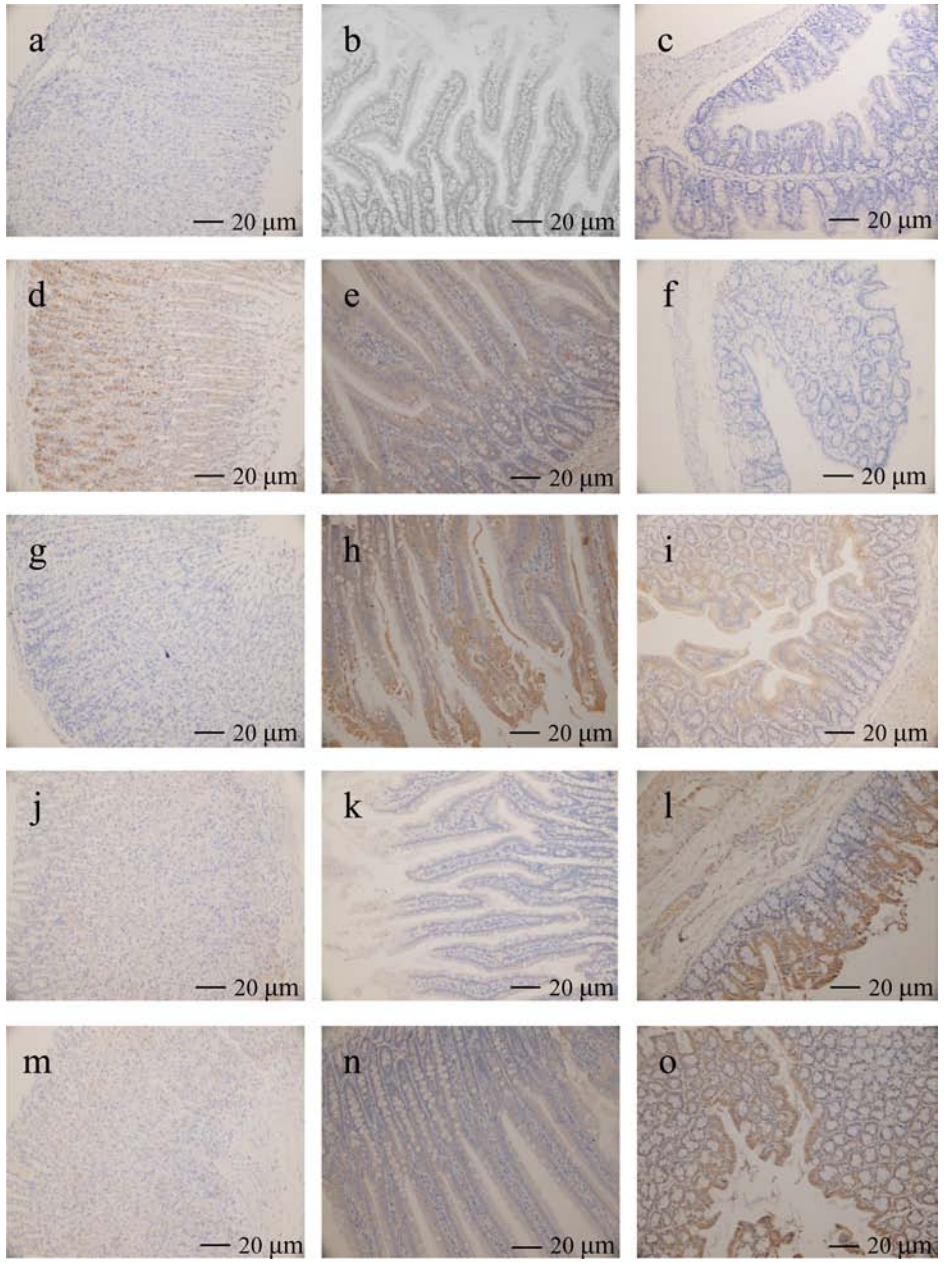

Figure 4. Insulin distribution in the gastrointestinal epithelial tissues of rats after administration of the RS3 film-coated microparticles for different times: (a) stomach, 0 h; (b) small intestine, 0 h; (c) colon, 0 h; (d) stomach, 2 h; (e) small intestine, 2 h; (f) colon, 2 h; (g) stomach, 8 h; (h) small intestine, 8 h; (i) colon, 8 h; (j) stomach, 24 h; (k) small intestine, 24 h; (l) colon, 24 h; (m) stomach, 30 h; (n) small intestine, 30 h; (o) colon, 30 h.

By the color image analytic system IPP, the optical density of insulin could be determined, and the result is shown in Table 2. Before administration, no insulin was determined in the stomach, small intestine, and colon of the rats. At 2 h after administration, a small amount of insulin was released in the stomach and small intestine. Then, the microparticles reached the small intestine and released insulin at 8 h, as shown by a high optical density of insulin determined in the small intestine and a slight optical density of insulin in the colon. At 24 h after administration, the optical density of insulin in the colon reached the highest value (0.57 ± 0.02). When the administration time reached 30 h, a low optical density of insulin was determined in the small intestine, but the optical density of insulin was maintained at a high level, indicating a

Table 2. Integrated Optical Density of Insulin in the Digestive Tract Tissues of Rats at Different Times after Administration

time (h)	stomach[a]	small intestine[a]	colon[a]
0			
2	0.21 ± 0.02	0.12 ± 0.01^{A}	
8		0.49 ± 0.03^{B}	0.16 ± 0.02^{A}
24		0.13 ± 0.01^{A}	0.57 ± 0.02^{C}
30		0.11 ± 0.01^{A}	0.40 ± 0.02^{B}

[a]Values are means ± SD of three determinations (n = 3). Values followed by different upper case letters within a column differ significantly (P < 0.05).

dx.doi.org/10.1021/jf500472b | J. Agric. Food Chem. 2014, 62, 3599−3609

Table 3. Plasma Glucose, Corresponding Plasma Insulin Concentrations at Different Postadministration Times, and Pharmacokinetic Parameters of Insulin in Diabetic Rats Following the Administration of Different Insulin Formulations (n = 6 for Each Group)[a]

		control group		insulin injected group (25 U/kg)		RS3 film-coated microparticles group (25 U/kg)	
		plasma glucose (mmol/L)	insulin (mIU/L)	plasma glucose (mmol/L)	insulin (mIU/L)	plasma glucose (mmol/L)	insulin (mIU/L)
C (mIU/L)	0	25.4 ± 1.1	18.52 ± 2.62	24.0 ± 1.5	20.65 ± 3.22	23.0 ± 0.9	21.90 ± 3.80
	2	26.4 ± 1.4	20.11 ± 1.78	19.5 ± 1.5*	39.06 ± 4.32*	18.7 ± 0.6*	40.60 ± 7.34*
	6	28.0 ± 1.2	19.81 ± 2.20	6.2 ± 0.5*	493.25 ± 34.54*	11.8 ± 0.7*#	196.80 ± 19.10*#
	8	22.8 ± 1.3	17.09 ± 3.54	5.3 ± 0.4*	524.17 ± 22.98*	7.2 ± 0.4*#	343.76 ± 18.73*#
	10	19.7 ± 0.8	15.35 ± 4.77	6.3 ± 0.4*	490.40 ± 56.34*	6.5 ± 0.5*	500.14 ± 27.89*
	12	20.9 ± 1.0	20.12 ± 2.23	3.4 ± 0.4*	667.79 ± 68.34*	5.6 ± 0.6*	530.23 ± 23.90*
	24	24.6 ± 0.9	29.90 ± 3.78	4.2 ± 0.5*	635.53 ± 34.44*	5.0 ± 0.6*	601.17 ± 29.79*
	26	28.0 ± 0.8	27.03 ± 5.90	17.0 ± 2.3*	67.72 ± 7.23*	6.9 ± 0.3*#	302.91 ± 11.8*#1
	30	27.1 ± 0.3	25.73 ± 4.69	21.6 ± 0.6*	39.56 ± 4.32	15.7 ± 0.6*#	128.81 ± 10.23*#
C_{max}(mIU/L)				667.79 ± 68.34		601.17 ± 29.79	
T_{max}(h)				12		24	
AUC (mIU·h/L)				13052.2 ± 20.5		11508.1 ± 18.6	
B_{rel} (%)				100		88.2 ± 1.2	

[a]Control, diabetic model control group without any treatment; C, plasma glucose concentration at different postadministration times; C_{max}, maximum plasma insulin concentration; T_{max}, time at which C_{max} is attained; AUC, area under the plasma concentration−time curve. *, means compared with those of the diabetic model control group (P < 0.01); #, means compared with those of the insulin injected group (P < 0.01).

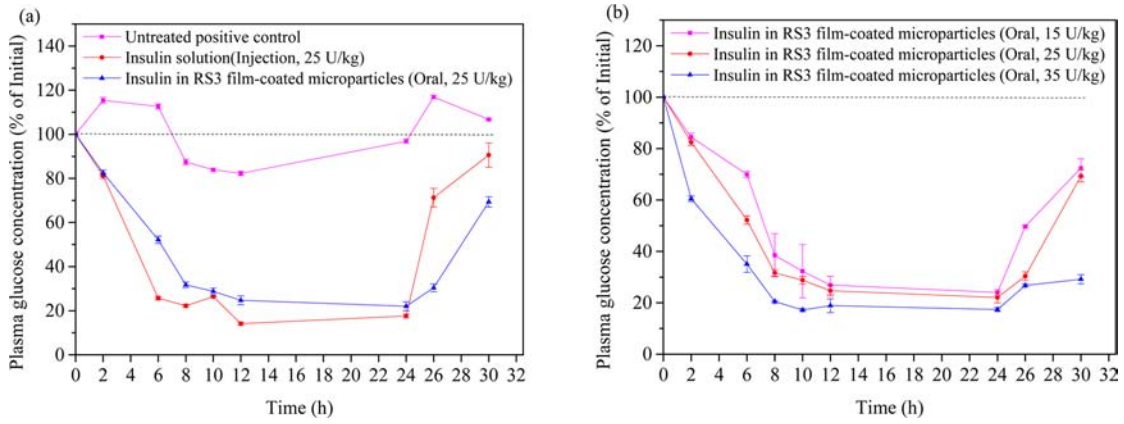

Figure 5. Relative plasma glucose concentration of the diabetic rats following (a) the administration of different insulin formulations and (b) the oral administration of different doses of insulin.

large amount of insulin released in the colon. These results showed that the RS3 film-coated microparticles could target insulin to the colon.

In Vivo Bioactivity of Insulin-Loaded RS3 Film-Coated Microparticles. In the treatment of diabetes mellitus, steadily decreasing the plasma glucose concentration is important to the patients. The fluctuation of plasma glucose concentration in the therapeutic process could make the patients suffer from glycopenia and glycemic excursion, which might lead to diabetic complications.[42] In this study, the plasma glucose concentration and corresponding plasma insulin concentration of the different type II diabetic rat groups with different treatments at different postadministration times were investigated, and the results are presented in Table 3.

It can be seen from Table 3 that the plasma glucose concentration of the type II diabetic rats (negative control group) without insulin treatment was higher (18.6−29.7 mmol/L) than those of the positive control group, subcutaneously injected with commercial long-acting insulin, and the test groups which were fed by the RS3 film-coated microparticles with the same insulin load through an oral route. Although theoretically endogenous insulin could still be produced in the type II diabetic rats, the plasma insulin concentration was too low to control the plasma glucose level. Therefore, the plasma glucose concentration of this group remained higher during the whole monitoring period (30 h).

For the insulin-injected (positive control) group, from 2 to 6 h after injection, there was a sharp increase (from 39.06 ± 4.32 to 493.25 ± 34.54 mU/L) in the plasma insulin concentration, accompanied by a sharp decrease (from 19.5 ± 1.5 to 6.2 ± 0.5 mmol/L) in the plasma glucose concentration. The percentage of decrease in the plasma glucose concentration was 74.2 ± 0.8% from the beginning (0 h) to 6 h (Figure 5a). Although a strong hypoglycemic effect was observed between 6 and 24 h after injection in the insulin-injected group rats (Figure 5a), a glycopenia (an abnormally low plasma glucose level of 3.4 ± 0.4 mmol/L) occurred at 12 h after injection when a maximum plasma insulin concentration of 667.79 ± 68.34 mU/L was reached. After that, the plasma glucose concentration experienced a rapid increase.

After the RS3 film-coated microparticles containing 25 U/kg insulin were orally administered, a high level of the plasma

dx.doi.org/10.1021/jf500472b | J. Agric. Food Chem. 2014, 62, 3599−3609

Table 4. Plasma Glucose Concentrations and Relative Bioavailability in the Different Groups with Different Dosages of Insulin in the RS3 Film-Coated Microparticles (n = 6 for Each Group)

		insulin dose*		
		15 U/kg	25 U/kg	35 U/kg
plasma glucose concentration (mmol/L) at different postadministration times (h)	0	23.7 ± 1.4	23.0 ± 0.9	25.9 ± 0.8
	2	20.1 ± 1.6	18.7 ± 0.6	15.7 ± 0.4*#
	6	16.6 ± 0.8	11.8 ± 0.7*	9.1 ± 1.2*#
	8	9.1 ± 2.0	7.2 ± 0.4*	5.3 ± 1.1*#
	10	7.6 ± 2.3	6.5 ± 0.5	4.5 ± 0.6*#
	12	6.4 ± 0.8	5.6 ± 0.6	4.9 ± 0.8
	24	5.7 ± 0.3	5.0 ± 0.6	4.5 ± 0.2
	26	11.8 ± 0.8	6.9 ± 0.3*	6.9 ± 0.3*
	30	17.2 ± 0.2	15.7 ± 0.6*	7.6 ± 0.7*#
AUC		1644.7 ± 74.0	1817.9 ± 30.5	2145.4 ± 23.8
F_{rel}(%)		88.2 ± 4.0	97.5 ± 1.6	115.1 ± 1.3

**, means compared with those of the low-dose group (P < 0.01); #, means compared with those of the medial-dose group (P < 0.01).

insulin concentration could be maintained from 6 h after oral administration as well; furthermore, for a longer period of time (up to 30 h) compared with the trend shown by the insulin-injected (positive control) group. A moderate hypoglycemic effect was observed at 6 h after oral administration but the plasma glucose concentration was still higher than that of the insulin-injected group at the same time. There was a 47.8 ± 1.6% decrease in the plasma glucose concentration from 0 to 6 h when the plasma insulin concentration was increased to 196.80 ± 19.10 mU/L (Figure 5a), indicating that some insulin released from the RS3 film-coated microparticles had entered the colon. At 8 h after oral administration, the plasma glucose concentration was decreased to 7.2 ± 0.4 mmol/L, and there was a 68.3 ± 1.3% decrease from the beginning (0 h) (Figure 5a). A significant hypoglycemic effect was shown from 8 to 26 h after oral administration of the RS3 film-coated insulin-loaded microparticles (Figure 5a). Although the plasma glucose concentration increased to 15.7 ± 0.6 mmol/L at 30 h after oral administration, it was still much lower than that of the insulin-injected group rats (21.6 ± 0.6 mmol/L). Furthermore, no glycopenia was observed between 8 and 26 h (total 18h) after oral administration and the hypoglycemic effect was slowly but steadily maintained for a long time (Figure 5a), suggesting that insulin could be well protected by the RS3 film-coated microparticles from the degradation by the various proteolytic enzymes in the upper digestive tract and therefore the colon-targeting controlled release of insulin was achieved. The results here show that the RS3 film-coated microparticles could target insulin to the colon and could maintain a sustainable release of insulin, which would not lead to hypoglycemia and glycemic excursion. Compared with that of the insulin-injected group, the relative insulin bioavailability (B_{rel}%) of the RS3 film-coated microparticles containing the same insulin dosage after oral administration was 88.2 ± 1.2% (Table 3), and the relative pharmacodynamic bioavailability (F_{rel}%) was as high as 97.5 ± 1.6% (Table 4).

Experiments were further carried out to investigate the effect of dosage of oral administration of the RS3 film-coated microparticles received by the type II diabetic model rats on the change in the plasma glucose concentration, and the results are shown in Table 4. The hypoglycemic effect was further increased by an increase in the dosage of oral administration. It can be seen that the plasma glucose concentration declined to a lower range (<8 mmol/L) at 10 h after oral administration of the low-dose microparticles and was kept within the lower range for another 14 h (seen from Figure 5b). The medial-dose group experienced a steady decrease in the plasma glucose concentration from 8 h after oral administration, which was a little more rapid than that of the low-dose group. In contrast to those of these two groups, the plasma glucose concentration of the high-dose group decreased more rapidly within 2−10 h after oral administration (P < 0.01) and kept within the lower range from 8 to 30 h (for a total of 22 h) (seen from Figure 5b). The maximum percentages of decrease in the plasma glucose concentration of the low-dose microparticles group, medial-dose group, and high-dose group were 76.0 ± 1.1, 78.0 ± 2.0, and 82.8 ± 0.6%, respectively (Figure 5b). These results indicate that the insulin plasma concentration was related to the dosage of administration. An increase in the dosage of oral administration of insulin could lead to a remarkable decrease in the plasma glucose level. Compared with the insulin-injected group, the relative pharmacodynamic bioactivities (F_{rel}%) of insulin in the high-dose microparticles group, medial-dose microparticles group, and low-dose microparticles group were 115.1 ± 1.3, 97.5 ± 1.6, and 88.2 ± 4.0%, respectively (Table 4). In conclusion, the RS3 film-coated microparticles can protect the insulin from enzymatic degradation in the upper digestive tract, prolong the insulin release time, and enhance the hypoglycemic effect. The plasma glucose concentration of the diabetic model rats was decreased steadily by using the RS3 film-coated microparticles for the delivery of insulin. Thus, this study demonstrates the potential of the RS3 film-coated microparticles for the colon-targeting delivery of insulin and other polypeptide or protein ingredients.

■ ASSOCIATED CONTENT

Ⓢ Supporting Information

Additional experimental details. This material is available free of charge via the Internet at http://pubs.acs.org.

■ AUTHOR INFORMATION

Corresponding Authors

*(L.C.) E-mail: felchen@scut.edu.cn.

*(X.L.) E-mail: xxlee@scut.edu.cn.

Funding

We acknowledge the National Natural Science Funds of China (No. 31271824, 31071503), the National Science and Technology Supporting Program Projects (2012BAD33B04), the Ministry of Education Special R&D Funds for the Doctoral

Disciplinary Stations in Universities (20120172110014), the Office of Education of Guangdong Province Science and Technology Innovation (Key) Projects in Universities (2012CXZD0006), the Ministry of Education Program for Supporting New Century Excellent Talents (NCET-12-0193), the Fundamental Research Funds for the Central Universities, SCUT (2013ZG0009), and CERS-China Equipment and Education Resources System (CERS-1-2).

Notes

The authors declare no competing financial interest.

REFERENCES

(1) Day, L.; Seymour, R. B.; Pitts, K. F.; Konczak, I.; Lundin, L. Incorporation of functional ingredients into foods. *Trends Food Sci. Technol.* **2009**, *20*, 388−395.

(2) Mills, S.; Stanton, C.; Hill, C.; Ross, R. New developments and applications of bacteriocins and peptides in foods. *Annu. Rev. Food Sci. Technol.* **2011**, *2*, 299−329.

(3) Hartmann, R.; Meisel, H. Food-derived peptides with biological activity: from research to food applications. *Curr. Opin. Biotechnol.* **2007**, *18*, 163−169.

(4) McClements, D. J.; Decker, E. A.; Park, Y.; Weiss, J. Structural design principles for delivery of bioactive components in nutraceuticals and functional foods. *Crit. Rev. Food Sci.* **2009**, *49*, 577−606.

(5) Pu, H. Y.; Chen, L.; Li, X. X.; Xie, F. W.; Yu, L.; Li, L. An oral colon-targeting controlled release system based on resistant starch acetate: synthetization, characterization, and preparation of film-coating pellets. *J. Agric. Food Chem.* **2011**, *59*, 5738−5745.

(6) Van den Mooter, G. Colon drug delivery. *Expert Opin. Drug Del.* **2006**, *3*, 111−125.

(7) Patel, M.; Shah, T.; Amin, A. Therapeutic opportunities in colon-specific drug-delivery systems. *Crit. Rev. Ther. Drug Carrier Syst.* **2007**, *24*, 147−202.

(8) Maroni, A.; Zema, L.; Del Curto, M. D.; Foppoli, A.; Gazzaniga, A. Oral colon delivery of insulin with the aid of functional adjuvants. *Adv. Drug Delivery Rev.* **2012**, *64*, 540−56.

(9) Hamman, J. H.; Enslin, G. M.; Kotze, A. F. Oral delivery of peptide drugs − barriers and developments. *Biodrugs* **2005**, *19*, 165−177.

(10) Lin, Y.; Chen, Q.; Luo, H. Preparation and characterization of *N*-(2-carboxybenzyl)chitosan as a potential pH-sensitive hydrogel for drug delivery. *Carbohydr. Res.* **2007**, *342*, 87−95.

(11) Said, A. E. A. Radiation synthesis of interpolymer polyelectrolyte complex and its application as a carrier for colon-specific drug delivery system. *Biomaterials* **2005**, *26*, 2733−2739.

(12) Freire, C.; Podczeck, F.; Veiga, F.; Sousa, J. Influence of the coating formulation on enzymatic digestibility and drug release from 5-aminosalicylic acid pellets coated with mixtures of high-amylose starch and Surelease (R) intended for colon-specific drug delivery. *Drug Dev. Ind. Pharm.* **2010**, *36*, 161−172.

(13) Patel, M. M.; Amin, A. F. Process, optimization and characterization of mebeverine hydrochloride loaded guar gum microspheres for irritable bowel syndrome. *Carbohydr. Polym.* **2011**, *86*, 536−545.

(14) Chambin, O.; Dupuis, G.; Champion, D.; Voilley, A.; Pourcelot, Y. Colon-specific drug delivery: influence of solution reticulation properties upon pectin beads performance. *Int. J. Pharm.* **2006**, *321*, 86−93.

(15) Liu, L. S.; Fishman, M. L.; Kost, J.; Hicks, K. B. Pectin-based systems for colon-specific drug delivery via oral route. *Biomaterials* **2003**, *24*, 3333−3343.

(16) Bayat, A.; Dorkoosh, F. A.; Dehpour, A. R.; Moezi, L.; Larijani, B.; Junginger, H. E.; Rafiee-Tehrani, M. Nanoparticles of quaternized chitosan derivatives as a carrier for colon delivery of insulin: ex vivo and in vivo studies. *Int. J. Pharm.* **2008**, *356*, 259−266.

(17) Del Curto, M. D.; Maroni, A.; Palugan, L.; Zema, L.; Gazzaniga, A.; Sangalli, M. E. Oral delivery system for two-pulse colonic release of protein drugs and protease inhibitor/absorption enhancer compounds. *J. Pharm. Sci.−U.S.* **2011**, *100*, 3251−3259.

(18) Akhgari, A.; Farahmand, F.; Garekani, H. A.; Sadeghi, F.; Vandamme, T. F. Permeability and swelling studies on free films containing inulin in combination with different polymethacrylates aimed for colonic drug delivery. *Eur. J. Pharm. Sci.* **2006**, *28*, 307−314.

(19) Singh, J.; Kaur, L.; McCarthy, O. J. Factors influencing the physico-chemical, morphological, thermal and rheological properties of some chemically modified starches for food applications − a review. *Food Hydrocolloids* **2007**, *21*, 1−22.

(20) BeMiller, J. N.; Whistler, R. L. *Starch: Chemistry and Technology*; Access Online via Elsevier: Amsterdam, The Netherlands, 2009.

(21) Chen, L.; Li, X.; Li, L.; Guo, S. Acetylated starch-based biodegradable materials with potential biomedical applications as drug delivery systems. *Curr. Appl. Phys.* **2007**, *7*, e90−e93.

(22) Sharma, A.; Yadav, B. S. Ritika, resistant starch: physiological roles and food applications. *Food Rev. Int.* **2008**, *24*, 193−234.

(23) Thompson, D. B. Strategies for the manufacture of resistant starch. *Trends Food Sci. Technol.* **2000**, *11*, 245−253.

(24) Fuentes-Zaragoza, E.; Sánchez-Zapata, E.; Sendra, E.; Sayas, E.; Navarro, C.; Fernández-López, J.; Pérez-Alvarez, J. A. Resistant starch as prebiotic: a review. *Starch/Staerke* **2011**, *63*, 406−415.

(25) Charalampopoulos, D.; Wang, R.; Pandiella, S. S.; Webb, C. Application of cereals and cereal components in functional foods: a review. *Int. J. Food Microbiol.* **2002**, *79*, 131−141.

(26) Fuentes-Zaragoza, E.; Riquelme-Navarrete, M.; Sánchez-Zapata, E.; Pérez-Álvarez, J. Resistant starch as functional ingredient: a review. *Food Res. Int.* **2010**, *43*, 931−942.

(27) Chen, L.; Li, X.; Pang, Y.; Li, L.; Zhang, X.; Yu, L. Resistant starch as a carrier for oral colon-targeting drug matrix system. *J. Mater. Sci.−Mater. Med.* **2007**, *18*, 2199−2203.

(28) Li, X. X.; Liu, P.; Chen, L.; Yu, L. Effect of resistant starch film properties on the colon-targeting release of drug from coated pellets. *J. Controlled Release* **2011**, *152*, E5−E7.

(29) Chen, L.; Pu, H. Y.; Li, X. X.; Yu, L. A novel oral colon-targeting drug delivery system based on resistant starch acetate. *J. Controlled Release* **2011**, *152*, E51−E52.

(30) Singh, J.; Dartois, A.; Kaur, L. Starch digestibility in food matrix: a review. *Trends Food Sci. Technol.* **2010**, *21*, 168−180.

(31) Zhang, B.; Chen, L.; Zhao, Y.; Li, X. Structure and enzymatic resistivity of debranched high temperature−pressure treated high-amylose corn starch. *J. Cereal Sci.* **2013**, *57*, 348−355.

(32) Millard, M. M.; Dintzis, F. R.; Willett, J. L.; Klavons, J. A. Light-scattering molecular weights and intrinsic viscosities of processed waxy maize starches in 90% dimethyl sulfoxide and H_2O. *Cereal Chem.* **1997**, *74*, 687−691.

(33) Nara, S.; Komiya, T. Studies on the relationship between water-saturated state and crystallinity by the diffraction method for moistened potato starch. *Starch* **2006**, *35*, 407−410.

(34) Zhu, J.; Li, L.; Chen, L.; Li, X. Study on supramolecular structural changes of ultrasonic treated potato starch granules. *Food Hydrocolloids* **2012**, *29*, 116−122.

(35) Suzuki, T.; Chiba, A.; Yarno, T. Interpretation of small angle X-ray scattering from starch on the basis of fractals. *Carbohydr. Polym.* **1997**, *34*, 357−363.

(36) Sonaje, K.; Chen, Y. J.; Chen, H. L.; Wey, S. P.; Juang, J. H.; Nguyen, H. N.; Hsu, C. W.; Lin, K. J.; Sung, H. W. Enteric-coated capsules filled with freeze-dried chitosan/poly(γ-glutamic acid) nanoparticles for oral insulin delivery. *Biomaterials* **2010**, *31*, 3384−3394.

(37) Rindlav, A.; Hulleman, S. H. D.; Gatenholm, P. Formation of starch films with varying crystallinity. *Carbohydr. Polym.* **1997**, *34*, 25−30.

(38) Shamai, K.; Bianco-Peled, H.; Shimoni, E. Polymorphism of resistant starch type III. *Carbohydr. Polym.* **2003**, *54*, 363−369.

(39) Cameron, R. E.; Donald, A. M. A small-angle X-ray scattering study of the annealing and gelatinization of starch. *Polymer* **1992**, *33*, 2628−2635.

(40) Cameron, R. E.; Donald, A. M. A small-angle X-ray scattering study of starch gelatinization in excess and limiting water. *J. Polym. Sci., Part B: Polym. Phys.* **1993**, *31*, 1197−1203.
(41) Jenkins, P. J.; Comerson, R. E.; Donald, A. M.; Bras, W.; Derbyshire, G. E.; Mant, G. R.; Ryan, A. J. In situ simultaneous small and wide angle X-ray scattering: a new technique to study starch gelatinization. *J. Polym. Sci., Part B: Polym. Phys.* **1994**, *32*, 1579−1583.
(42) Monnier, L.; Mas, E.; Ginet, C.; Michel, F.; Villon, L.; Cristol, J. P.; Colette, C. Activation of oxidative stress by acute glucose fluctuations compared with sustained chronic hyperglycemia in patients with type 2 diabetes. *JAMA−J. Am. Med. Assoc.* **2006**, *295*, 1681−1687.

and pest insects.[4] The breakdown products of glucosinolates include allyl isothiocyanate (AITC), allylcyanide, and 1-cyano-2-hydroxy-3-butene, which have also been proposed for fumigation of stored product pests because of the volatile nature of these compounds.[3] Oriental mustard, *B. juncea*, has been developed into a biopesticide that can control nematodes, a pest that leads to $78 billion U.S. in crop losses. AITC is the principal product formed from allylglucosinolate (sinigrin) that is found in *B. carinata*, *B. juncea*, and *B. napus*, with the highest concentrations found in the seeds of *B. juncea*. The seeds and bran or husk contain 5 and 2% sinigrin, respectively. Indian mustard, *B. juncea*, contains glucosinolates that were shown to reduce herbivore feeding and the associated damage to the plant.[14] The focus of the current project was to extract these known compounds for biopesticide use through an alternative process, thermochemical conversion.

Prior to this study, it was determined that many natural products, including glucosinolates, are stable at moderately high temperatures. Pyrolysis is the thermochemical process that can convert abundant agricultural biomass residues into gases, bio-oils, and char by heating under the absence of oxygen, and the products from pyrolysis are recognized as a CO_2-neutral alternative compared to fossil fuels.[15] The use of these end products includes fuels, chemicals, and fertilizers. Previous research by our group determined that pyrolysis products produced from a variety of crop residues are active as pesticides, and the chemical content was analyzed. Bio-oil from tobacco stalks and leaves,[15,16] tomato leaves and stalks,[17] coffee grounds,[18] and cellulose, hemicellulose, and lignin[19] had antimicrobial and insecticidal activity. The separation of the bio-oil components responsible for pesticidal activity has identified many small molecules, including phenols and their derivatives. However, these compounds may not be desirable for crop protection because of the broad toxic effects of phenol derivatives.[20]

For this reason, the current project focused on specific compounds and biomass with known pesticidal properties and applied pyrolysis as a unique method for separation and isolation. In the present study, dried straw from *B. napus*, *B. carinata*, and *B. juncea*, as a potential source of the known anti-herbivore compounds and as a source of other insecticide material, was converted by thermochemical means through the process of fast pyrolysis. The resulting bio-oils were evaluated as a source of material for pesticide use and then further fractionated to isolate the active compounds. The hypothesis of the project was that glucosinolates or isothiocyanates present in the Brassicaceae straw material would contribute to the insecticidal activity of extracts. In contrast, it was other compounds, including fatty acids, hexadecanoic and octadecanoic acids, that were isolated in the active fractions and determined to be potentially responsible for both acute toxicity and feeding deterrence.

MATERIALS AND METHODS

Biomass and Insects. The canola *B. napus* and mustard *B. juncea* and *B. carinata* straw were collected from Agriculture and Agri-Food Canada (AAFC), Saskatoon, Saskatchewan, Canada, research fields in October 2008 (batch 1). In 2010, *B. juncea* was collected from the same research fields to provide a second year of biomass for a comparison to the 2008 findings (batch 2). The field-dried straw was ground using a blender/mixing mill and sieved to a Sauter mean diameter of 60 μm for pyrolysis.

Colorado potato beetle (CPB), *Leptinotarsa decemlineata* Say (Coleoptera: Chrysomelidae), was maintained without exposure to insecticides for over 100 generations at the AAFC, London, Ontario, Canada, laboratory. The colony was reared at an average temperature of 25 °C, 50% relative humidity (RH), and a photoperiod of 16:8 light/dark on greenhouse grown potato plants (var. Kennebec).

Bioassay Method. A potato leaf disc bioassay was used to test the insecticidal activity of the original bio-oil, and extracts were prepared through aqueous and solvent separations or high-performance liquid chromatography (HPLC) fractionation. A 50 μL sample of bio-oil extract was spread on the top of a 4 cm diameter potato leaf disc, and a 100 μL sample of bio-oil extract was spread on the bottom of the leaf disc. All leaf discs were held in the fume hood for 20 min to ensure adequate drying before transferring the disc to a 4.25 cm Gelman Petri dish with a moistened (30 μL of water) filter paper to maintain humidity. Control leaf discs were treated with the same volume of reverse osmosis (RO) water or acetone as a check for the aqueous- or organic-phase bio-oil, respectively. Five first instar CPB larvae were placed on each leaf disc, and the Petri dishes were put into a holding chamber for 3 days (25 °C, 50% RH, and 16:8 light/dark). All trials were repeated 3 times. Mortality and leaf consumption was assessed at 24, 48, and 72 h. Fatty acid, octadecanoic and hexadecanoic acids, and methyl ester bioassays were conducted with similar volumes of each compound dissolved in acetone at 1 and 10 mg/mL concentrations and applied to potato leaf discs, as described above.

Pyrolysis and Bio-oil Preparation. The canola and mustard bio-oils were produced by pyrolysis at 300 and 500 °C. Bio-oil produced in the first batch was from all three *Brassica* species, while the second batch was only *B. juncea* bio-oil. Further purification of the aqueous fraction of the first batch mustard straw bio-oils focused on *B. juncea* bio-oil because of the greater quantities of dry *B. juncea* bio-oil available for testing. Pyrolysis was carried out using a fluidized-bed pilot plant with a 0.078 m diameter atmospheric fluidized-bed reactor, as described by Booker et al.[15] The dried, ground straw was injected into the reactor and produced vapors that exited at the top of the reactor and were collected in a bio-oil-condensing system consisting of a cyclonic condenser (aqueous and organic phases) immersed in chilled water and an electrostatic precipitator (ESP) that charged fine droplets escaping from the condenser and then used an electric field to collect them. The bio-oil collected from the condenser contains both polar and nonpolar compounds, while the ESP bio-oil is one-phase, which contains nonpolar compounds that dissolves in acetone. The condenser and ESP were weighed before and after each run to obtain an accurate liquid yield. The amount of bio-oil collected in the condenser and ESP was typically greater after 500 °C pyrolysis compared to 300 °C. The 500 °C pyrolysis of ground *B. juncea* straw, the condenser, and ESP yields were 24 and 14%, respectively, for a total yield of 38% (all reported yields are on a mass basis). Reducing the pyrolysis temperature to 300 °C decreased the condenser and ESP yields to 17 and 6%, respectively, for a total yield of 23%. The same reactor conditions yielded greater amounts of bio-oil when tobacco leaf and coffee grounds were pyrolyzed at 500 °C, a 43% yield,[15,18] and similar yields were obtained with tobacco leaf using a batch or slow pyrolysis.[21]

The bio-oil from the condenser was passed through a 9 cm diameter, qualitative filter paper (Whatman, U.K.) and then separated into aqueous and organic phases. Filtering removed solid material (char and other precipitates) that was not soluble in either water or organic solvent. All three phases (condenser aqueous and organic and ESP phases) were dried and then redissolved in either water (aqueous phase) or acetone (organic and ESP phases) to make a solution with a concentration of 30 or 50 mg/mL. The bioactivity was tested by the CPB–potato leaf dip bioassay.

Solvent Extraction. A selected bio-oil phase, 3 g, was separated by mixing equal parts water and dichloromethane (DCM) (the ratio of bio-oil/solvent was 1:50). A residue that did not dissolve in water, ethanol, methanol, or DCM was partially dissolved in acetone. When tested with the insect bioassay, no activity was observed with this layer. The original bio-oil phase, fraction A, was separated into the water phase, fraction B, and the DCM phase, fraction C (Figure 1). Fractions B and C were evaporated to dryness at 50 °C and redissolved with water (fraction B) and acetone (fraction C) to make a solution of 30

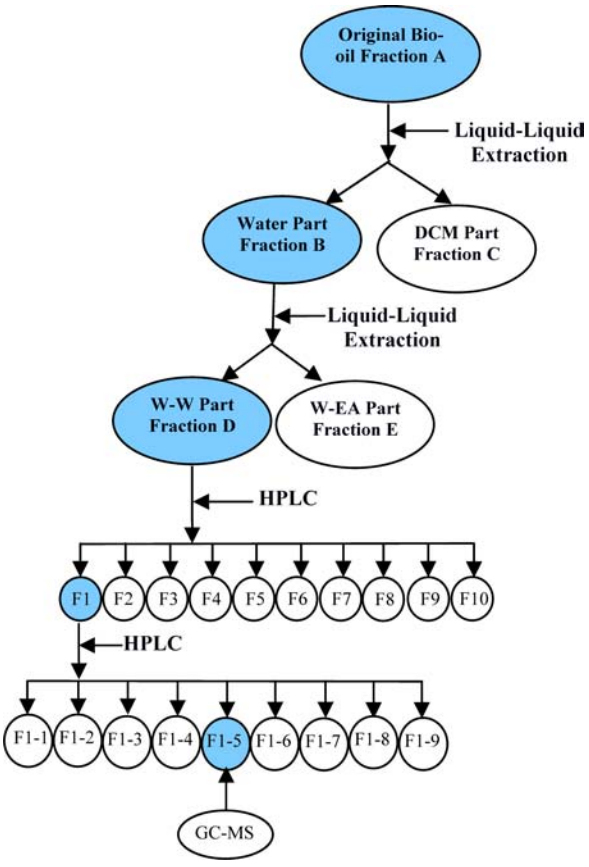

Figure 1. *Brassica* bio-oil purification diagram. All bio-oil phases and liquid−liquid separations colored blue indicate separations and fractions that caused high CPB larval mortality and/or feeding deterrence.

mg of dried B or C/mL, respectively, and the bioactivity was tested by the CPB−potato leaf disc bioassay.

The batch 1 bio-oil fraction B was further separated with water and ethyl acetate (EA) using equal parts of each (1:50 bio-oil/water−solvent) to create fraction D (water−water phase) and fraction E (water−EA phase). According to the bioassay results of these fractions, only fraction D was considered for further fractionation and purification. The second batch bio-oil fraction B was not separated by water−EA but freeze-dried at −80 °C overnight, and the final weight and concentration were calculated. Tests with the insect bioassay were performed with 30 and 50 mg/mL concentrations redissolved in water. The batch 2 aqueous fraction B for both the 300 and 500 °C bio-oils was measured in a preweighed vial and dried using a stream of nitrogen. The samples were redissolved in water to a concentration of 50 mg/mL and tested with the insect bioassay.

Gas Chromatography−Mass Spectrometry (GC−MS) Analysis. A HP 6890 Series gas chromatography system with a 5973 mass selective detector was used to analyze the various extracted bio-oil fractions. The experiments were performed on a HP-5MS, 30 m column, with an inner diameter of 0.25 mm and a film of 0.25 μm (Agilent Technologies). A 1 μL sample with a pulsed splitless injection at 25 psi until 0.5 min was followed by purge flow to split vent 40 mL/min at 1 m. The injector and auxiliary temperatures were maintained at 300 °C. The oven temperature began at 60 °C for 2 min, then was increased at 10 °C/min to 280 °C, and was held for 6 min. A mass/charge scan range of 50−300 at a rate of 2.98 scans/s was used.[16] The National Institute of Standards and Technology (NIST) 2008 library was used to identify the peaks found in the GC−MS chromatograms for the *Brassica* bio-oil liquid−liquid phases. A total of 10 standards were obtained to confirm the presence of the phenols previously found in bio-oil fractions.[16] These included phenol, 3-methylphenol, 4-methylphenol, 4-ethylphenol, 2-methylphenol, indole, D-limonene, 2,4-dimethylphenol, 3,4-dimethylphenol, and 2,3-dimethylphenol.

HPLC Fractionation and Isolation: Purification for Aqueous Fraction D. To further separate the chemical components in the batch 1 bio-oil fraction D, an Agilent 1200 Series HPLC was used with a Waters symmetry semi-preparative C18 column (7 μm, 7.8 × 300 mm). This HPLC instrument was equipped with a photodiode array detector and ChemStation software, which was used for the data acquisition and analysis. Injections (200 μL) were made using an Agilent 1200 autosampler. The binary mobile phase was composed of water and acetonitrile (AcN). The flow rate was kept constant at 3 mL/min for a total run time of 70 min. The system was run with the following gradient program: 100% water was run for 10 min, then linearly changed to 80% water/20% AcN over 10 min, then linearly changed to 50% water/50% AcN over 25 min, then linearly changed to 100% AcN over 5 min, where it was held for 10 min, and then brought back to 100% water in 1 min, where it was held for 9 min. The time-based trigger mode was used to collect 2 min fractions starting at 2 min. The concentration of fraction D was 30 mg/mL with 50 injections for a total of 10 mL of fraction D. The 34 fractions collected were combined into 10 subfractions based on chromatogram peak occurrences (Figure 1). All subfractions were evaporated to dryness, and then 10 mL of distilled water was added to redissolve samples for use in the leaf disc bioassay.

Purification of Aqueous Subfraction F1. According to the bioassay results, the most polar fraction, F1, was the most active. Further subfractionation was used to resolve the F1 compounds with the same semi-preparative column as above. Samples were run isocratically with 98% water/2% AcN for a total run time of 20 min. The injection volume was 100 μL, and 50 injections were run. Between 1 and 7 min, the flow rate was linearly decreased from 1 to 0.7 mL/min and held at 15 min. The trigger mode of the collector was peak-based (from 8.5 to 11 min) and time-based (from 11 to 15 min, with time slices of 1 min). The purification of F1 produced only five peaks, and nine fractions were collected (Figure 1). All fractions were evaporated to dryness, and 5 mL of water was added to redissolve for the bioassay. The insecticidal activity was found primarily in fraction 1-5 and partly in fraction 1-4.

Aqueous F1-5 Subfractionation. To isolate the individual peaks in fraction F1-5, a Water's amino semi-preparative column was used (Nova NH_2, 4 μm, 7.8 × 250 mm) to collect the F1-5 fractions. A 100 μL injection volume for a total of 40 injections was used, and the flow rate was 3 mL/min for a total run time of 26 min. The system was run with the following gradient program: 5% water/95% AcN isocratic for 3 min, then increased to 90% water/10% AcN at 15 min, and then brought back to 5% water/95% AcN in 1 min, where it was held for 10 min. The trigger mode of the fraction collector was peak-based (from 4 to 9 min, with the maximum peak duration of 1 min) and time-based (from 14 to 26 min, with time slices of 2 min). This purification of F1-5 with the same program produced four peaks collected over 10 fractions, which were dried and then redissolved into 4 mL of water.

GC−MS Analysis. The aqueous fractions collected from the amino semi-preparative column were analyzed using a 7890A GC system (5975C MSD, Agilent Technologies) with a HP-5MS, 30 m × 250 μm × 0.25 μm, column (Agilent). The oven temperature began at 70 °C for 5 min and then increased at 5 °C/min to 290 °C, where it was held for 10 min. A mass/charge scan range of 40−1050 was used at a rate of 1.49 scans/s. Samples were prepared by drying 20 μL of the 50 mg/mL bio-oils in GC vials and preparing a 1 mg/mL solution. The bio-oil solution was filtered using a 0.45 μm nylon CHROMSPEC filter, and 100 μL of the bio-oil solution was added to a GC vial, with 10 μL of 0.2 mg/mL ribitol being added. Solutions were dried with N_2 for 5 min and derivatized by adding 80 μL of methoxyamine hydrochloride (MOX, 20 mg/mL in pyridine, Sigma) to the vial and heating at 50 °C for 1.5 h in a heating block, after which 80 μL of *N*-methyl-*N*-trimethylsilyltrifluoroacetamide (MSTFA, Sigma) was added with heating at 50 °C for 0.5 h.

Fatty acid standards, hexadecanoic (palmitic) acid (Sigma) and octadecanoic (stearic) acid (Eastman Organic Chemicals), were dissolved in acetone at concentrations of 1, 5, 15, and 50 mg/L, and

100 μL of each standard solution was added to 1.5 mL amber GC vials. To each one of the vials containing the standard solutions, 10 μL of 0.2 mg/mL ribitol was added as an internal standard. Solutions were dried with N_2 for 5 min and derivatized as described above.

Statistical Analyses. Statistical analysis was undertaken using Graphpad Prism 5.01 software, and the log-transformed and arcsine-transformed data were subjected to the general linear model procedure to test the significant differences between individual fractions using two-way analysis of variation (ANOVA) and Bonferroni post-tests.

RESULTS AND DISCUSSION

Insecticide Bioassay-Guided Separation of *Brassica* Bio-oil. The CPB bioassay determined that the batch 1 mustard straw condenser bio-oil produced at 300 °C was more active than the oil produced at 500 °C, despite the higher yield at 500 °C (data not shown). To isolate and identify the more active components, the remaining tests focused only on the 300 °C bio-oil, where the condenser bio-oil was separated into aqueous and solvent phases and compared to the ESP solvent-soluble phase.

From the bioassay results, the aqueous bio-oil phases of all three *Brassica* species collected in the condenser were just as active as the ESP solvent phase because they all produced 100% CPB mortality after 72 h at the 30 mg/mL concentration. The condenser organic phase contained less active components because there was <20% mortality for the two mustard species bio-oils (Figure 2). On the basis of these results, further

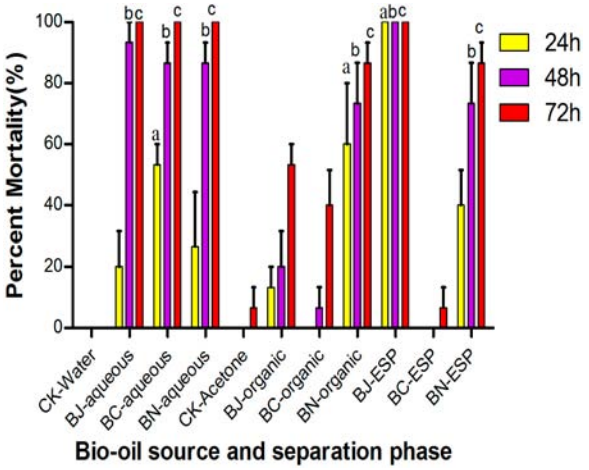

Figure 2. Percent mortality ± standard error for CPB larvae after 24, 48, and 72 h of exposure to condenser aqueous, organic, and ESP phases of *B. carinata* (BC), *B. juncea* (BJ), and *B. napus* (BN) bio-oil (30 mg/mL) produced with 300 °C pyrolysis in batch 1. Bars with a letter are significantly different ($p < 0.05$; a, b, and c for 24, 48, and 72 h, respectively) compared to control mortality at the same time.

examination focused on the aqueous *B. juncea* bio-oil phase (fraction A of Figure 1) produced in batches 1 and 2 because of its high availability. Fraction A was separated by liquid−liquid extraction with water and DCM and produced a water fraction (fraction B of Figure 1) and solvent fraction (fraction C of Figure 1). Both fractions B and C at 30 mg/mL produced significantly greater CPB mortality compared to controls after 48 h ($p < 0.05$) and reduced feeding at 24 h with relatively low mortality [degrees of freedom (df) = 14; $F = 34.1$; $p < 0.05$; Figure 3]. Fraction B was selected for further study because it produced 25% greater mortality at 30 mg/mL than fraction C (df = 14; $F = 5.1$; $p < 0.05$; Figure 3). Fraction B was further

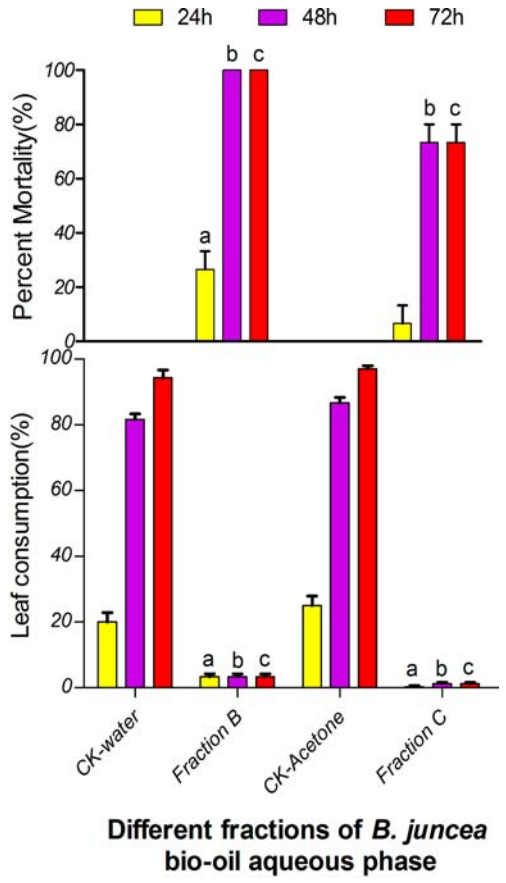

Figure 3. Percent mortality and percent leaf consumption ± standard error for CPB larvae after 24, 48, and 72 h of exposure to 3 and 30 mg/mL *B. juncea* aqueous (fraction B) and organic (fraction C) separations. Bars with a letter are significantly different ($p < 0.05$; a, b, and c for 24, 48, and 72 h, respectively) compared to control mortality and leaf consumption at the same time.

purified with water (fraction D dissolved in water) and EA (fraction E dissolved in acetone), and bioassays determined that fraction D produced 100% greater mortality at 30 mg/mL compared to fraction E (df = 16; $F = 7.3$; $p < 0.05$; Figure 4).

There was no significant difference in mortality for 30 mg/mL fraction E treatments compared to the solvent control ($p > 0.05$), but feeding was reduced at 48 h ($p < 0.001$; Figure 4). GC−MS analyses of the separated bio-oil phases for *B. juncea* batch 1 determined that fraction C contained phenols, such as 2-methoxyphenol and 2,6-dimethoxyphenol, while fraction E contained a large proportion of phenols, including catechin, *p*-dihydroxybenzene, and other benzene compounds (Table 1).

Hydroquinone, also present in fraction E, is one of several that may be considered genotoxic and mutagenic, and 1,2-benzenediol or catechol is a likely human and animal carcinogen.[20] In the redissolved condenser solid and the ESP bio-oil, phenol compounds were also predominant. All phenol derivatives are undesirable contaminants, and it would be best to avoid these types of compounds in a biopesticide because potential health and environmental problems could occur with the necessary concentrations required for insect control. Fraction D, the aqueous phase, did not contain phenol-related compounds but did contain 1,1-dimethylhydrazine, considered to be carcinogenic and a skin hazard.[20] However, this compound was not measured in the final aqueous fraction of batch 2 (Tables 2 and 3).

dx.doi.org/10.1021/jf500048t | J. Agric. Food Chem. 2014, 62, 3610−3618

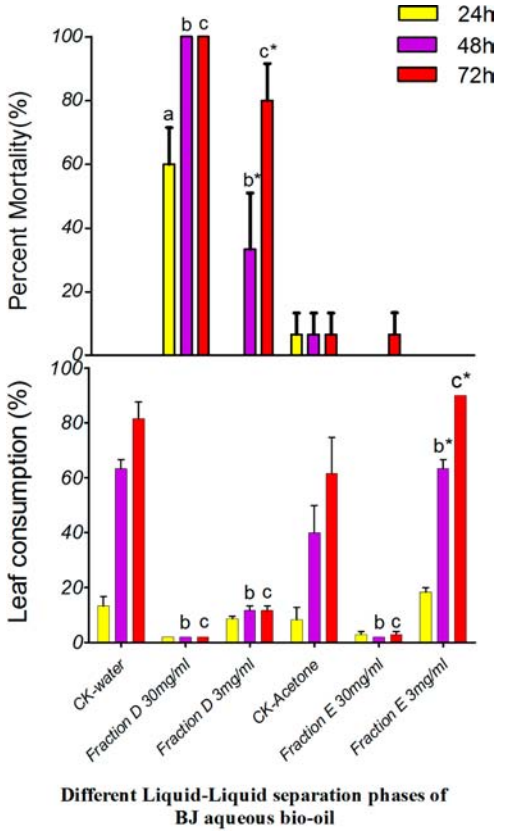

Figure 4. Percent mortality and percent leaf consumption ± standard error for CPB larvae after 24, 48, and 72 h of exposure to 3 and 30 mg/mL *B. juncea* aqueous–aqueous (fraction D) and aqueous–organic (fraction E) separations. Bars with a letter are significantly different ($p < 0.05$; a, b, and c for 24, 48, and 72 h, respectively) compared to control mortality and leaf consumption at the same time. Bars with an asterisk indicate a significant difference between treatments at the same time period within each separation phase (aqueous or solvent).

Table 1. GC–MS Analyses of Batch 1 Bio-oil Samples and Separated Fractions

sample (fraction)	compounds present in the highest concentration in samples from aqueous and solvent separated phases of the original bio-oil prepared from *B. juncea* straw
condensor liquid (fraction C)	2,6-dimethoxyphenol, 2-methoxyphenol, and 4-hydroxy-3,5-dimethoxybenzaldehyde
condensor liquid (fraction D)	1,1-dimethylhydrazine, 2-methylhexadecanal, and dimethyl sulfide
condensor liquid (fraction E)	1,2-benzenediol (catechol), hydroquinone, and 3-methoxy-1,2-benzenediol
condensor solid	2,6-dimethoxy-4-(2-propenyl)-phenol, 2,6-dimethoxyphenol, and 4-hydroxy-3,5-dimethoxybenzaldehyde
ESP	2,6-dimethoxyphenol (syringol), 2,6-dimethoxy-4-(2-propenyl)-phenol, and (*E*)-9-octadecenoic acid

In a previous work by our group,[16] much of the insecticidal and antimicrobial activities were associated with the solvent phase of the tobacco bio-oil, because of the presence of many phenol compounds, especially the dialkylated phenols. However, it was concluded that the observed pesticide activity of the bio-oil solvent fraction would require multiple combinations of the individual phenols or excessively high concentrations of individual compounds, and those phenols and their derivatives would be difficult to register because of their broad toxic effects.[20] In the present study, many similar compounds were found in the solvent phase of the *B. juncea* bio-oil collections, but fraction D did not contain these compounds, even though insecticidal activity was present. Therefore, the insecticidal activity associated with fraction D was pursued as a potential source of compounds other than phenols. Therefore, further research was conducted to isolate the active compounds and analyze for any known harmful chemicals within fraction D.

Table 2. GC–MS Characterization of Batch 2, 300 °C Bio-oil Aqueous Phase with a Quality Match of ≥80% by NIST 2007

peak	retention time (min)	area (%)	NIST assignment
1	11.42	1.29	L-(+)-lactic acid
2	11.91	1.93	glycolic acid
3	12.65	0.17	2-aminoethanethiol
4	17.67	2.29	1-hexadecanol
5	17.77	1.64	glycerol
6	19.37	0.40	glyceric acid
7	19.88	0.44	citraconic acid 1
8	22.78	1.32	threose 1
9	22.92	0.93	threose 2
10	27.96	0.31	ribose
11	33.44	0.14	D-(+)-altrose 1
12	36.60	0.36	palmitic acid
13	40.40	0.22	stearic acid

Table 3. GC–MS Characterization of Batch 2, 500 °C Bio-oil Aqueous Phase with a Quality Match of ≥80% by NIST 2007

peak	retention time (min)	area (%)	NIST assignment
a	10.68	0.23	2-hydroxypiridine
b	11.15	0.28	pyruvic acid
c	11.41	0.77	L-(+)-lactic acid
d	11.91	1.35	glycolic acid
e	17.66	1.28	1-hexadecanol
f	17.77	1.91	glycerol
g	19.37	0.23	glyceric acid
h	19.44	0.22	succinic acid
i	19.88	0.37	citraconic acid
j	22.92	0.61	threose 2
k	27.95	0.47	D-lixose 2
l	36.56	0.24	palmitic acid
m	40.37	0.24	steric acid

Insecticide Bioassay-Guided HPLC Fractionation of the *B. juncea* Aqueous Bio-oil Phase (Fraction D). To determine the active compounds in fraction D, further separation of the liquid–liquid phase of the *B. juncea* condenser bio-oil was accomplished by HPLC fractionation into 10 fractions. Subsequent bioassay results indicated that the most polar, fraction 1, collected between 2 and 4 min (Figure 5), produced the greatest mortality relative to the control and other nine fractions (df = 22; $F = 41.6$; $p < 0.05$; Figure 6).

Fraction 1 produced the same CPB mortality and reduced leaf consumption as the original aqueous phase (df = 22; $F = 25.5$; $p < 0.05$; Figure 6). The HPLC chromatogram for peak areas visible at 205 nm shows a number of partially resolved peaks within fraction 1 (Figure 5). To separate these peaks,

dx.doi.org/10.1021/jf500048t | J. Agric. Food Chem. 2014, 62, 3610–3618

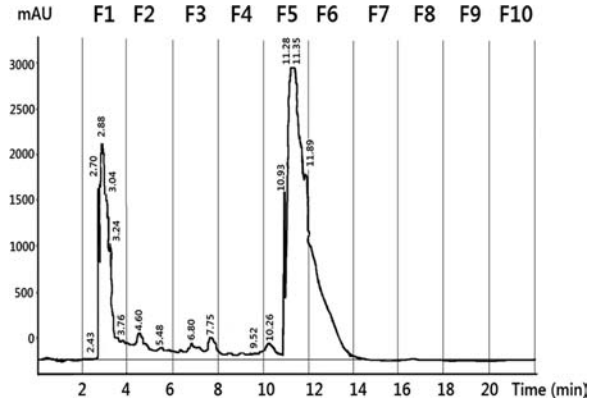

Figure 5. HPLC chromatogram showing *B. juncea* aqueous−aqueous (fraction D) subfractionation and active fraction 1.

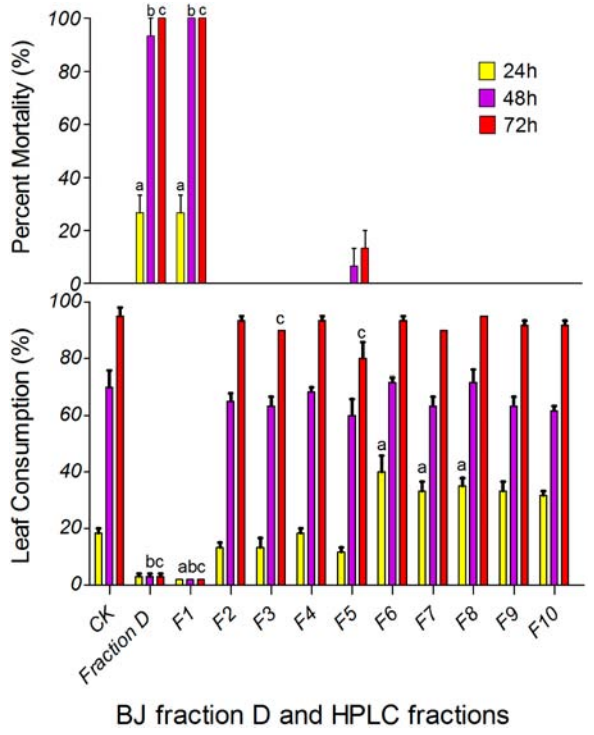

Figure 6. Percent mortality and percent leaf consumption ± standard error for CPB larvae after 24, 48, and 72 h of exposure to 10 HPLC fractions (F1−F10) of *B. juncea* aqueous−aqueous (fraction D) separation. Bars with a letter are significantly different ($p < 0.05$; a, b, and c for 24, 48, and 72 h, respectively) compared to control mortality and leaf consumption at the same time.

HPLC purification of fraction 1 (F1) was again used to isolate five peaks and nine subfractions were collected. Insecticidal activity was found primarily in subfraction 1-5 and partially in subfraction 1-4, where the 48 h CPB mortality was 53.33 and 20%, respectively (Figure 7). Again the subfraction activity was not significantly different from F1 after 72 h (df = 9 and 54; $F = 83.89$; $p > 0.05$).

Both subfractions 1-5 and 1-4 reduced leaf consumption to 5 and 13.3% after 48 h of treatment, respectively (Figure 7), an effect not significantly different to the activity demonstrated by F1 (df = 9 and 54; $F = 83.89$; $p > 0.05$). Further purification of F1-5 by HPLC using an amino column indicated the presence of four peaks, and a further 10 collections were made. The combined amino column fraction of F1-5 was analyzed using

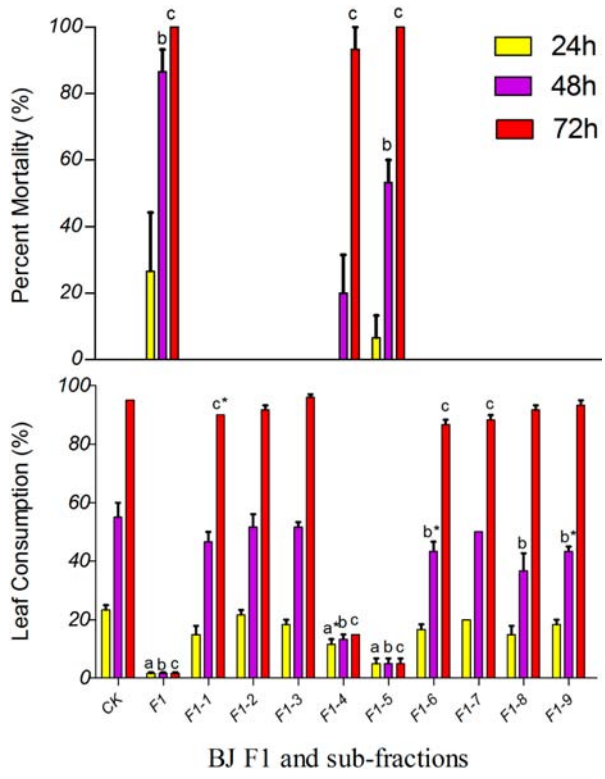

Figure 7. Percent mortality and percent leaf consumption ± standard error for CPB larvae after 24, 48, and 72 h of exposure to 10 HPLC subfractions of the *B. juncea* aqueous−aqueous (fraction D) F1 fraction. Bars with a letter are significantly different ($p < 0.05$; a, b, and c for 24, 48, and 72 h, respectively) compared to control mortality and leaf consumption at the same time. Bars with an asterisk indicate a significant difference between treatments at the same time period within each separation phase (aqueous or solvent).

the Agilent 7890A GC−MS, and three of the major peaks were identified as fatty acids, hexadecanoic and octadecanoic acids (palmitic and stearic acids, respectively), and monooctadecanoylglycerol based on the NIST 2008 (version 2.0.f) library match. Unfortunately, the concentration of each fatty acid could not be calculated; however, the batch 2 condenser aqueous samples prepared at 300 and 500 °C, as described in the Materials and Methods, were also determined to contain hexadecanoic and octadecanoic acids (panels A and B of Figure 8) among other compounds found in the 300 °C (Table 2) and 500 °C (Table 3) bio-oil aqueous fractions. These fractions were also found to have insecticidal activity at 50 mg/mL, significantly reducing leaf consumption relative to the controls (df = 3; $F = 110.6$; $p < 0.0001$; Figure 9). No difference in insecticidal activity was determined between the two temperature bio-oil fractions ($p > 0.05$), but the concentration of both fatty acids was 4−5-fold greater in the 500 °C aqueous bio-oil fraction relative to the 300 °C aqueous bio-oil fraction (254−309 versus 1023−1282 ppm). Similarly, there was no greater feeding repellency observed with the 500 °C aqueous fraction ($p > 0.05$; Figure 9). It was assumed that the fatty acids found in aqueous fractions from both 300 and 500 °C pyrolysis likely originated from the biomass and did not degrade during the pyrolysis process. However, because the concentration of both fatty acids was greater in the higher temperature bio-oil in batch 2, it is possible that these compounds are formed under pyrolysis conditions or released in greater amounts from the biomass. Unfortunately, this comparison could not be

dx.doi.org/10.1021/jf500048t | J. Agric. Food Chem. 2014, 62, 3610−3618

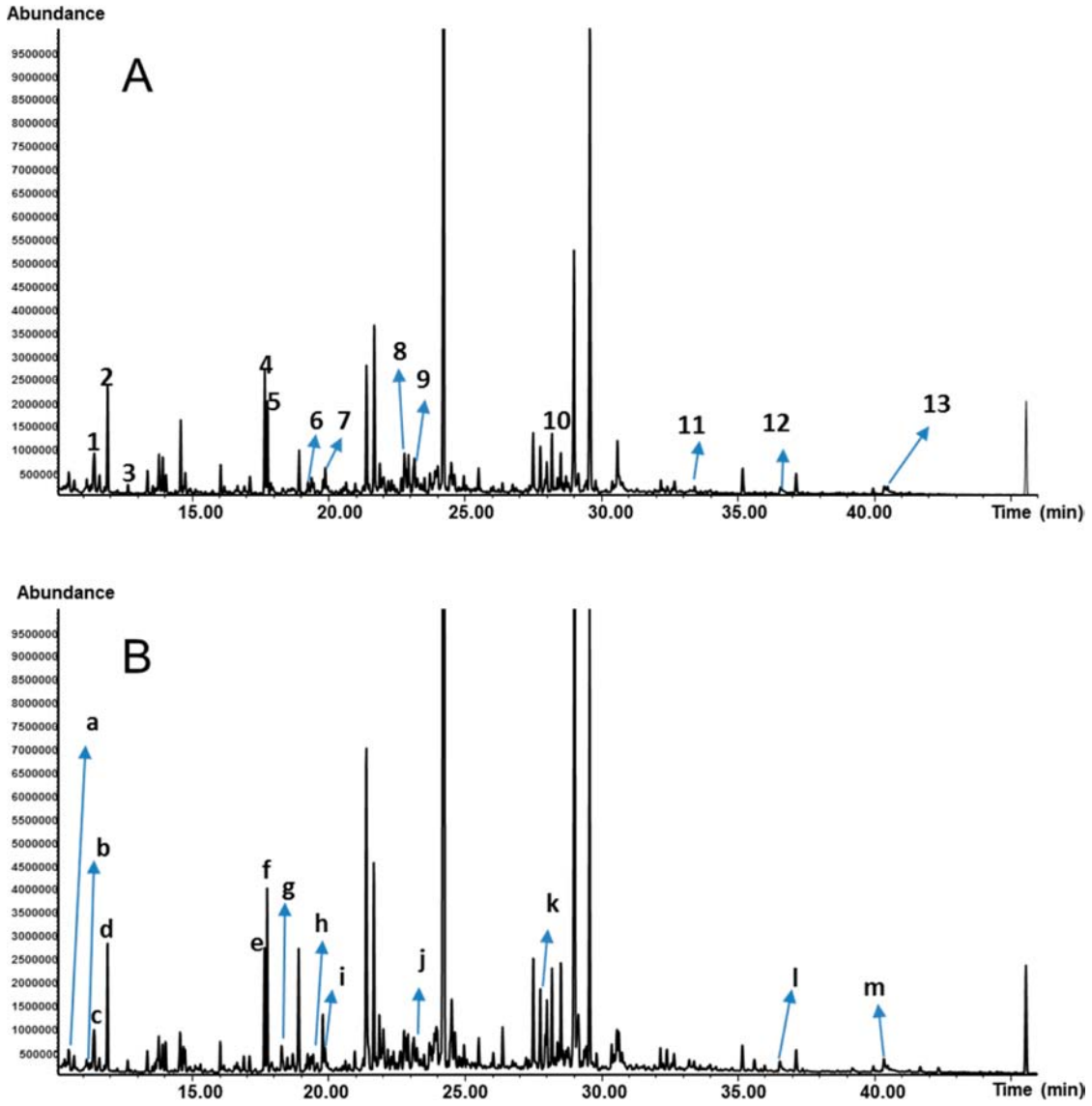

Figure 8. Total ion chromatogram (TIC) GC–MS, with 3× enhancement of the *B. Juncea* bio-oil aqueous phase: (A) fraction A produced at 300 °C pyrolysis and (B) fraction B produced at 500 °C pyrolysis (batch 2).

confirmed with the batch 1 bio-oil. Because there was no difference in the concentration between hexadecanoic or octadecanoic acids in the aqueous phase of the batch 2 condenser bio-oil at either pyrolysis temperature, this confirms that the relative amounts of each are similar under the same heating conditions. Shin et al.[22] found that octadecanoic acid was stable at 300 °C and up to 370 °C, but unsaturated fatty acids, such as oleic and linoleic acids, are less stable. This suggests that higher temperatures, such as 500 °C, would degrade fatty acids faster than 300 °C, but in this study, the short pyrolysis residence time in the bubbling-bed reactor may not be a sufficient exposure to degrade the compounds. Higher pyrolysis temperatures will create increasingly smaller compounds because the reaction breaks down large molecules present in the biomass to form gases and other compounds, such as phenols.

The presence of fatty acids in the aqueous fractions may explain the insecticidal activity, both toxicity and feeding deterrence. To confirm whether the fatty acids were active in the 1–10 mg/mL range, a bioassay with standards for both fatty acids and their respective methyl esters was used to measure the feeding deterrent effect. No significant effect on leaf consumption relative to controls was determined, even at the higher concentration ($p > 0.05$), except with the methyl ester of hexadecanoic acid at 10 mg/mL (df = 4; $F = 8.18$; $p < 0.005$; Figure 10).

Therefore, the two fatty acids are not solely responsible for the insecticidal activity observed with the batch 2 bio-oil but could have contributed to the activity observed with the aqueous bio-oil fractions generated in batch 1 (concentrations appeared higher but were not determined). Fatty acids have been documented to have insecticidal activity against a number of insect pests. As early as the 1850s, whale oil soap was found to be the cheapest and most effective insecticide for the rose chafer *Macrodactylus subspinosus*.[23] Since then, other fatty acids, such as oleic acid, lauric acid, etc., have been used to control a variety of insect pests over the years, as reviewed by Kabara.[23] More recent studies have documented that pure myristic acid at 50 $\mu g/\mu L$ produced 53% mortality with wheat weevil *Sotophilus granarius*, which were topically treated with 1 μL of solution per

dx.doi.org/10.1021/jf500048t | J. Agric. Food Chem. 2014, 62, 3610–3618

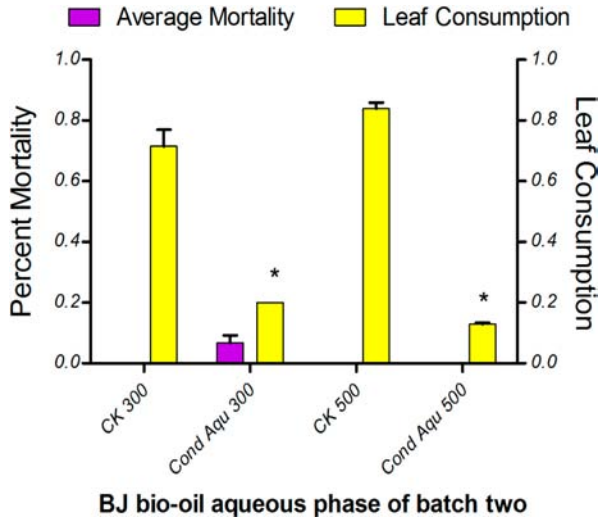

Figure 9. Percent mortality and percent leaf consumption ± standard error for CPB larvae after 72 h of exposure to 50 mg/mL *B. juncea* aqueous phase produced with 300 and 500 °C pyrolysis (batch 2). Bars with an asterisk are significantly different ($p < 0.001$) compared to respective control leaf consumption.

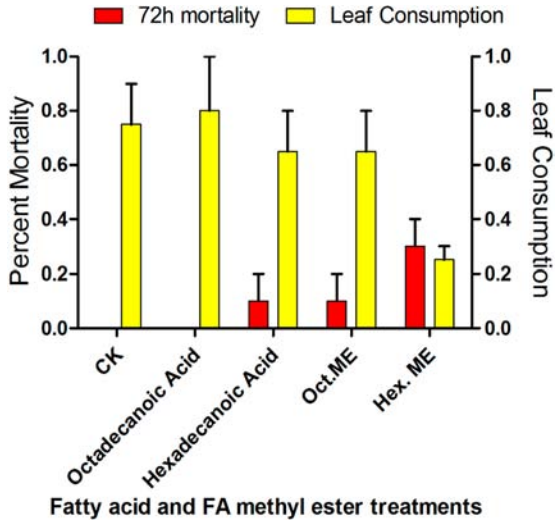

Figure 10. Percent mortality and percent leaf consumption ± standard error for CPB larvae after 72 h of exposure to 10 mg/mL hexadecanoic and octadecanoic acids and their methyl esters.

insect,[24] and that lauric acid achieved 100% mortality against cotton aphids *Aphis gossypii*, with a 0.5% (w/w) concentration.[25] In the latter case, the toxicity to the aphids was probably related to suffocation and/or desiccation through changes to the cuticle and cell permeability. Plant extracts that contain fatty acids with insecticidal activity include the Egyptian *Halocnemon strobilacium* (Chenopodiaceae).[26] The crude extract contained almost 70% fatty acids and their esters, with the largest proportion being oleic acid ester (38%) and octadecanoic acid (16%). Bioassays with individual fatty acids, linolenic and linoleic acids, were found to have similar larvicidal activity against the fall armyworm *Spodoptera frugiperda*.[27] Both linolenic and linoleic acids were found in the largest proportion in hexane extracts of *Ricinus communis* (Euphorbiaceae) leaves, 48 and 15%, respectively, while hexadecanoic and octadecanoic acids were lower (13 and 1.7%, respectively). However, as the work of Shin et al.[22] found, oleic and linoleic acids will not survive higher pyrolysis temperatures, perhaps suggesting that the hexadecanoic and octadecanoic acids would be the likely fatty acids to be found in the bio-oil. In the present study, hexadecanoic methyl ester was more active against the CPB than hexadecanoic acid or the octadecanoic methyl ester. The methyl esters of hexadecanoic acid were active against cabbage looper *Trichoplusia ni* as both toxins and repellents.[28] Herein, GC−MS analysis of the two aqueous fractions in both the 300 and 500 °C bio-oils identified many other compounds based on NIST 2008 library matches (Tables 2 and 3), a combination of which could synergize the activity of the fatty acids but was not tested. Sinigrin but not AITC was detected in most of the Soxhlet extracts of *B. carinata* seed, *B. juncea* straw, and the bio-oil aqueous phase for *B. juncea* (data not shown). However, sinigrin elutes later than fraction 1 with the HPLC method applied, and no insecticidal activity was associated with the fractions containing sinigrin; therefore, it is not responsible for the activity observed in fraction F1-5.

Conversion of the fatty acids isolated in the aqueous bio-oil fractions to methyl esters by esterification will provide a more valuable pesticide material. These interesting findings indicate that the polar phase (fraction D) of pyrolysis bio-oils is a promising use of agricultural residue biomass that can be converted by a thermochemical process. It has yet to be determined whether or not the fatty acid yield is affected by pyrolysis, because this would suggest whether the starting material is crucial to the final products. However, plant material that contains high levels of fatty acids to begin with affords a more promising source of biomass to extract these compounds for insecticidal application. Considering the possible toxic compounds produced during pyrolysis, any future pyrolysis bio-oil products should be tested for non-target and environmental toxicity prior to their recommendation for use in agriculture.

AUTHOR INFORMATION

Corresponding Author

*Telephone: 1-519-457-1470, ext. 281. Fax: 519-457-3997. E-mail: ian.scott@agr.gc.ca.

Notes

The authors declare no competing financial interest.

ACKNOWLEDGMENTS

The funding for this research was provided by the Shanxi Scholarship Council of China (2010064) and Agriculture and Agri-Food Canada (AAFC). The authors gratefully acknowledge the technical assistance of B. Pocs, D. MacArthur, and A. Majkrzak. Brassicacae straw samples were supplied by K. Falk, AAFC, Saskatoon, Saskatchewan, Canada, and partial funding was provided by Agricultural Bioproducts Innovation Program (ABIP), AAFC.

REFERENCES

(1) Hopkins, R. J.; van Dam, N. M.; van Loon, J. J. A. Role of glucosinolates in insect−plant relationships and multitrophic interactions. *Annu. Rev. Entomol.* **2009**, *54*, 57−83.

(2) United States Environmental Protection Agency (U.S. EPA). *Biopesticides Registration Action Document. Oriental Mustard Seed (OMS). PC Code 014921*; Office of Pesticide Programs, Biopesticides and Pollution Prevention Division, U.S. EPA: Washington, D.C., Dec 17, 2008; p 15.

(3) Tsao, R.; Yu, Q.; Friesen, I.; Potter, J.; Chia, M. Factors affecting the dissolution and degradation of oriental mustard-derived sinigrin

and allyl isothiocyanate in aqueous media. *J. Agric. Food Chem.* **2000**, *48*, 1898−1902.
(4) Yu, Q.; Tsao, R.; Chiba, M.; Potter, J. Selective nematicidal activity of allyl isothiocyanate. *J. Food Agric. Environ.* **2007**, *5*, 374−379.
(5) Agriculture and Agri-Food Canada (AAFC). *Profile. Canada's Mustard Seed Industry. Mustard Seed Statistics*; AAFC: Ottawa, Ontario, Canada, 2013; http://www.agr.gc.ca/eng/industry-markets-and-trade/statistics-and-market-information/by-product-sector/crops/pulses-and-special-crops-canadian-industry/mustard-seed/?id=1175116081724 (accessed Oct 29, 2013).
(6) Fenwick, G. R.; Heaney, R. K. Glucosinolates and their breakdown products in cruciferous crops, foods and feeding stuffs. *Food Chem.* **1983**, *11*, 249−271.
(7) Stefansson, B. R.; Hougen, F. W. Selection of rape plants (*Brassica napus*) with seed oil practically free from erucic acid. *Can. J. Plant Sci.* **1964**, *44*, 359−264.
(8) Cheeke, P. R.; Shull, L. R. *Natural Toxicants in Feeds and Poisonous Plants*; AVI Publishing Company, Inc.: Westport, CT, 1985; p 492.
(9) Canola Council of Canada. *Estimated Acreage and Percentage of HT and Conventional Canola*; Canola Council of Canada: Winnipeg, Manitoba, Canada, Dec 3, 2010; http://www.canolacouncil.org/markets-stats/statistics/estimated-acreage-and-percentage/ (accessed Oct 29, 2013).
(10) Canadian Grain Commission. *Quality of Western Canadian Mustard*; Canadian Grain Commission: Winnipeg, Manitoba, Canada, 2010; http://www.grainscanada.gc.ca/mustard-moutarde/harvest-recolte/2010/hqm10-qrm10-3-eng.html (accessed Oct 29, 2013).
(11) Taylor, D. C.; Falk, K. C.; Palmer, C. D.; Hammerlindl, J.; Babic, V.; Mietkiewska, E.; Jadhav, A.; Marillia, E.-F.; Francis, T.; Hoffman, T.; Giblin, E. M.; Katavic, V.; Keller, W. A. *Brassica carinata*—A new molecular farming platform for delivering bio-industrial oil feedstocks: Case studies of genetic modifications to improve very long-chain fatty acid and oil content in seeds. *Biofuels, Bioprod. Biorefin.* **2010**, *4*, 538−561.
(12) Pal, S.; Banik, S. P.; Khowala, S. Mustard stalk and straw: A new source for production of lignocellulolytic enzymes by the fungus *Termitomyces clypeatus* and as a substrate for saccharification. *Ind. Crops Prod.* **2013**, *41*, 283−288.
(13) Stamigna, C.; Chiaretti, D.; Chiaretti, E.; Prosini, P. P. Oil and furfural recovery from *Brassica carinata*. *Biomass Bioenergy* **2012**, *39*, 478−483.
(14) Mathur, V.; Ganta, S.; Raaijmakers, C. E.; Reddy, A. S.; Vet, L. E. M.; van Dam, N. M. Temporal dynamics of herbivore-induced responses in *Brassica juncea* and their effect on generalist and specialist herbivores. *Entomol. Exp. Appl.* **2011**, *139*, 215−225.
(15) Booker, C. J.; Bedmutha, R.; Vogel, T.; Gloor, A.; Xu, R.; Ferrante, L.; Yeung, K.K.-C.; Scott, I. M.; Conn, K. L.; Berruti, F.; Briens, C. Experimental investigations into the insecticidal, fungicidal, and bactericidal properties of pyrolysis bio-oil from tobacco leaves using a fluidized bed pilot plant. *Ind. Eng. Chem. Res.* **2010**, *49*, 10074−10079.
(16) Booker, C. J.; Bedmutha, R.; Scott, I. M.; Conn, K.; Berruti, F.; Briens, C.; Yeung, K.K.-C. Bioenergy II: characterization of pesticide properties of tobacco bio-oil. *Int. J. Chem. Reactor Eng.* **2010**, *8*, A26.
(17) Caceres, L. A.; McGarvey, B. D.; Scott, I. M.; Conn, K.; Berruti, F.; Briens, C.; Yeung, K. K. Pesticidal properties of tomato plant residue bio-oil. *2011 Pest Management Research Report—2011 Growing Season*; Agriculture and Agri-Food Canada (AAFC): Ottawa, Ontario, Canada, May 2012; pp 50−59, http://www.cps-cp.ca/publications.shtml.
(18) Bedmutha, R.; Booker, C. J.; Ferrante, L.; Briens, C.; Berruti, F.; Yeung, K.K.-C.; Scott, I.; Conn, K. Insecticidal and bactericidal characteristics of the bio-oil from the fast pyrolysis of coffee grounds. *J. Anal. Appl. Pyrolysis* **2011**, *90*, 224−231.
(19) Hossain, M. M.; Scott, I. M.; McGarvey, B. D.; Conn, K.; Ferrante, L.; Berruti, F.; Briens, C. Toxicity of lignin, cellulose and hemicellulose-pyrolyzed bio-oil combinations: Estimating pesticide resources. *J. Anal. Appl. Pyrolysis* **2013**, *99*, 211−216.
(20) International Agency for Research on Cancer (IARC). Re-evaluation of some organic chemicals, hydrazine and hydrogen peroxide. *IARC Monogr. Eval. Carcinog. Risks Hum.* **1999**, *71*, 1586.
(21) Hossain, M. M. New approaches to obtain pesticides from biomass pyrolysis. Master's Thesis, Department of Chemical and Biochemical Engineering, Faculty of Engineering, Western University, London, Ontario, Canada, 2011; p 95.
(22) Shin, H.-Y.; Ryu, J.-H.; Park, S.-Y.; Bae, S.-Y. Thermal stability of fatty acids in subcritical water. *J. Anal. Appl. Pyrolysis* **2012**, *98*, 250−253.
(23) Kabara, J. J. Fatty acids and esters as antimicrobial/insecticidal agents. In *Ecology and Metabolism of Plant Lipids*; Fuller, G., Nes, D., Eds.; American Chemical Society (ACS): Washington, D.C., 1987; ACS Symposium Series, Vol. *325*, Chapter 14, pp 220−238.
(24) Abay, G.; Altun, M.; Karakoc, O. C.; Gul, F.; Demirtas, I. Insecticidal activity of fatty acid-rich Turkish bryophyte extracts against *Sitophilus granarius* (Coleoptera: Curculionidae). *Comb. Chem. High Throughput Screening* **2013**, *16*, 806−816.
(25) Mohamad, S. F. S.; Mohamad, S.; Aziz, A. A. The susceptibility of aphids, *Aphis gossypii* Glover to lauric acid based natural pesticide. *Procedia Eng.* **2013**, *53*, 20−28.
(26) Abdallah, S. A.; Barakat, A. A.; Badawy, H. M. A.; Mansour, F. A.; Solimann, M. M. M. Toxicological and phytochemical studies of wild plant *Halocnemon strobilacium* crude extracts and their components against *Aphis craccivora* Koch. *J. Appl. Sci. Res.* **2009**, *5*, 699−705.
(27) Ramos-López, M. A.; González-Chávez, M. M.; Cárdenas-Ortega, N. C.; Zavala-Sánchez, M. A.; Pérez, G. S. Activity of the main fatty acid components of the hexane leaf extract of *Ricinus communis* against *Spodoptera frugiperda*. *Afr. J. Biotechnol.* **2012**, *11*, 4274−4278.
(28) Antonius, G. F.; Meyer, J. E.; Rogers, J. A.; Hu, Y.-H. Growing hot pepper for cabbage looper, *Trichoplsia ni* (Hübner), and spider mite, *Tetranychus urticae* (Koch) control. *J. Environ. Sci. Health, Part B* **2007**, *42*, 559−567.

Table 1. Chemical Composition of Bagasse after Pretreatment

	glucan (%)	xylan (%)	arabinan (%)	total lignin (%)	R_{glucan} (%)	R_{xylan} (%)	$R_{delignification}$ (%)	Y_{solid} (%)
Bref	40.9 (0.2)[a]	23.9 (0)[a]	1.5 (0)[a]	17.7 (3)[a]				
BN	56.1 (0.3)	22.4 (0.1)	1.7 (0)	6.4 (0.1)	83.4 (0.4)[a]	56.9 (0.3)[a]	78.0 (0.3)[a]	60.8 (2)[a]
BH	54.9 (0)	24.1 (0.1)	1.7 (0)	8.4 (0.3)	87.8 (0.1)	66.2 (0.3)	68.9 (1.1)	65.5 (1)
Bsxs	77.3 (0.4)	7.0 (0.01)	0.1 (0)	6.3 (1.1)	81.2 (0.6)	12.6 (0.01)	84.7 (2.7)	43 (2)

[a]The standard deviation is presented in parentheses.

perspective, and according to our knowledge hydrotropic pretreatment is an emerging technology.

MATERIALS AND METHODS

Materials. Sugar cane bagasse was obtained from Centro de Tecnologia Canavieira, Brazil. For removal of sucrose, bagasse was washed with tap water until the washing liquor was colorless and thereafter stored in a freezer room. Sodium hydroxide (NaOH), 30% hydrogen peroxide (H_2O_2), and sodium xylene sulfonate (SXS) with 90% purity as hydrotropic solvent were purchased from Fluka. Commercial enzymes cellulase (Celluclast 1.5 L) and β-glycosidase (Novozyme 188) were kindly supplied by VTT Technical Research Centre of Finland. The activities of the cellulase and the β-glycosidase were 75 FPU/mL and 5900 nkat/mL, respectively. All chemicals and enzymes were used as received without further purification.

Pretreatment Methods. *Dilute Alkaline Pretreatment.* Bagasse was treated by 0.2 g/g (substrate) NaOH at 60 °C in a water bath for 2 h. The liquid/solid ratio (w/w) was 10:1. After pretreatment, the residue of bagasse was washed until the pH was neutral.[25]

Sodium Hydroxide–Hydrogen Peroxide Pretreatment. Bagasse was treated by same dosage of NaOH as alkaline treatment together with 0.25 g/g (substrate) H_2O_2 in a 500 mL flask. The flask was put on a magnetic stirrer at 150 rpm for 24 h. To avoid decomposition of H_2O_2, the reaction was carried out in a dark place at room temperature. The liquor/wood ratio (w/w) was 10:1. Upon completion, the substrate was washed until neutral and then stored in a freezer.[26]

Hydrotropic Pretreatment. Bagasse was pretreated by 30% (w/v) SXS and 0.17% (w/v) formic acid in a revolving digester under the controlled temperature of 160 °C for 40 min; the liquor/wood ratio (w/w) was 10:1, and the initial pH was 3.5 ± 0.05. After pretreatment, the substrates were disintegrated and washed with 5% (w/w) NaOH solution and then washed by tap water until the washing liquor was colorless.

After pretreatments, all treated samples were collected and weighed for further analysis and tests.

Enzymatic Hydrolysis of Pretreated Samples. The pretreated samples were hydrolyzed by cellulase at a dosage of 20 FPU/g substrate together with 300 nkat β-glycosidase/g substrate at 50 °C in pH 5.0. Consistency was 20 mg/mL (w/v). Acetic acid buffer was used to modify the pH. The reaction time interval was 2, 6, 24, 48, and 72 h, respectively. The enzyme hydrolysis was ended by boiling for 10 min. After cooling with cold water, the hydrolysate was centrifuged at 1730*g* (3000 rpm) for 20 min. The supernatant was collected for sugar analysis.

Chemical Composition Analysis. The reference sample and pretreated samples were first extracted with acetone for 5 h in a Soxhlet device. The extractive free samples were used for chemical composition analysis. Glucan, xylan, and lignin content of untreated and pretreated biomass were determined following the NREL procedure for the determination of structural carbohydrates and lignin in biomass.[27] The loading yield after pretreatments (Y_{solid}), the recovered ratio of glucan or xylan ($R_{glucan/xylan}$), and the delignification rate ($R_{delignification}$) were calculated by the following formulas:

$$Y_{solid}\ (\%) = \frac{\text{pretreated biomass (g)}}{\text{original biomass (g)}} \times 100 \quad (1)$$

$$R_{glucan/xylan}\ (\%) = \frac{Y_{solid} \times C_{glucan/xylan\ of\ pretreated\ biomass}}{C_{glucan/xylan\ of\ original\ biomass}} \quad (2)$$

$$R_{delignification}\ (\%) = 1 - \frac{Y_{solid} \times C_{lignin\ of\ pretreated\ biomass}}{C_{lignin\ of\ original\ biomass}} \quad (3)$$

Glucan and xylan of both enzyme and sulfuric acid hydrolyzed pretreated samples (45 μm syringe film filtered) were detected by using a HPLC system (model 1200, Agilent, USA) equipped with a Bio-Rad Aminex HPX-87H column (300 mm × 7.8 mm) and refractive index detector. The column was operated at 55 °C with 0.005 mol/L H_2SO_4 solution as the mobile phase at a flow rate of 0.5 mL/min. Sample injection volume was 20 μL. Quantitative analysis was performed using a calibration with external standards of known concentrations. For each experiment on the pretreatments and the enzymatic hydrolysis, at least three replicates were made, and the average of the results was reported. The glucan and xylan yield after enzymatic hydrolysis was calculated on the basis of the glucan and xylan contents of the initial raw material.

Topochemical Characterization. Untreated and treated biomasses were evaluated with field emission scanning electron microscope (FE-SEM) LEO 1530 Gemini equipment. Samples were previously coated with carbon using a coating system equipped with a rotating base. Images were obtained with 500× and 15000 × magnifications.

X-ray spectroscopy (XPS) spectra were obtained with a Physical Electronics PHI Quantum 2000 ESCA instrument equipped with a monochromatic Al Kα X-ray source. Low-resolution spectra were measured in 3.5 min with a pass energy of 187 eV and high-resolution spectra of C_{1s} peak in 9 min using a pass energy of 23 eV. At least four different spots were measured on each sample. The O/C ratios were calculated from the low-resolution XPS spectra. Both acetone-extracted samples (Soxhlet, acetone/water mixture 9:1 (v/v), overnight) and unextracted samples after freeze-drying were analyzed. The surface coverage by lignin (S_{lig}), carbohydrates (S_{carb}), and extractives (S_{ext}) were calculated according to the following equations using the average O/C ratio value:[17,19,24]

$$S_{ext} = (O/C_{extracted} - O/C_{before\ extraction}) / (O/C_{extracted} - O/C_{extractives}) \times 100 \quad (4)$$

$$S_{lig} = (O/C_{extracted} - O/C_{carbohydrate}) / (O/C_{lignin} - O/C_{carbohydrate}) \times 100 \quad (5)$$

$$S_{carb} = 100 - S_{lig}\% \quad (6)$$

$$O/C_{carbohydrate} = 0.83, \quad O/C_{lignin} = 0.33, \quad O/C_{extractives} = 0.09$$

ATR-FTIR was used to analyze the samples after pretreatment. Small amounts of freeze-dried samples after pretreatment were placed on the diamond probe of Nicolet IS 50 FTIR (software OMNIC 7.3, wavenumbers in cm^{-1}). Thirty-six scans were acquired for each sample, recorded from 4000 to 400 cm^{-1}.

Time-of-flight secondary ion mass spectrometry (ToF-SIMS) analysis was performed with a Physical Electronics ToF-SIMS TRIFT II spectrometer on the pretreated and enzymatically

dx.doi.org/10.1021/jf500582w | J. Agric. Food Chem. 2014, 62, 3619−3625

hydrolyzed samples. All of the samples were freeze-dried after the acetone extraction. The instrument was equipped with a primary ion beam of $^{69}Ga^{+}$ liquid metal ion source and an electron flood gun for charge compensation. Positive secondary ions were detected using 25 kV acceleration voltage in 8 min. At least three measurements were done on each sample.

RESULTS AND DISCUSSION

Chemical Composition of Bagasse after Pretreatments. The chemical compositions of bagasse after dilute alkaline, alkaline peroxide, and hydrotropic pretreatments are given in Table 1. With dilute alkaline, alkaline peroxide, and hydrotropic pretreatments, the total amount of lignin in bagasse was reduced from the original 17.7 to 6.4, 8.4, and 6.3%, respectively. The pretreatment technology was applied before enzymatic hydrolysis process to overcome the limits for enzyme access to the polysaccharides, where cell wall lignin is one of the main causes of recalcitrance.[16,17] Lignin was removed as expected by all three of the used pretreatment methods, typically by hydrotropic pretreatment. Another significant difference was detected between the methods with regard to their impact on the bagasse carbohydrates. As shown in Table 1, hemicelluloses were less degraded by diluted alkaline and alkaline peroxide pretreatment than by hydrotropic pretreatment. However, hydrotropic pretreatment could remove both lignin and hemicelluloses. For instance, arabinan was almost totally degraded, and xylan was efficiently removed, whereas only slightly lower glucan was recovered in the hydrotropic process compared with other methods used (Table 1). As reported, acid pretreatment and steam explosion could also remove hemicelluloses, but acid pretreatment may cause equipment corrosion,[6] whereas steam explosion may require high capital cost, particularly for large-scale production.[8] Although alkali-based pretreatment can remove lignin, high capital cost in the chemical recovery system or wastewater treatment may be needed. Therefore, hydrotropic pretreatment was appropriate for removing xylose and lignin from bagasse, and it was an efficient technology to remove mainly hemicellulose in comparison with acid pretreatment and steam explosion. Certainly, more extensive studies of hydrotropic pretreatment (e.g., the optimization of pretreatment conditions, economic evaluation for overall process) for different feedstocks should be performed in the future. Furthermore, the recovery of lignin and xylan from hydrotropic pretreatment process can be a promising biorefinery application for producing high-value-added chemicals and biomaterials.[14,15]

Surface Chemical Composition after Pretreatment Analyzed by XPS. The elemental composition of the sample surfaces was investigated by XPS. The main constituents were carbon and oxygen. In the reference sample (Bref), additionally small amounts of N, Al, and Si were detected in the XPS low-resolution spectra. These were probably originated from the native constituents in sugar cane. In Table 2, the O/C ratios before and after sample extraction are given. As can be seen, the removal of carbon-rich material from the bagasse surface during pretreatments and, on the other hand, during the acetone extraction, is demonstrated by the increase of the O/C ratio. Furthermore, the surface coverage by lignin, carbohydrates, and extractives of bagasse after different pretreatment methods was gained from the XPS results (Table 2). After the pretreatments applied, the surface of bagasse samples contained more carbohydrates and less lignin than the reference sample. The surface coverage by lignin value of BN and Bsxs were on the same level. However, during alkaline pretreatment, together with lignin removal a notable amount of extractives was reduced from the fiber surface as well.

Table 2. Surface Chemical Composition of Bagasse after Pretreatment As Detected by XPS

sample	O/C_{ext}	O/C	S_{exts} (%)	S_{lig} (%)	S_{carb} (%)
Bref	0.68 (0.11)[a]	0.45 (0.03)[a]	38.1	31.0	69.0
BN	0.77 (0.06)	0.69 (0.03)	12.6	11.8	89.2
BH	0.84 (0.11)	0.63 (0.03)	28.6	0	100
Bsxs	0.77 (0.04)	0.61 (0.02)	24.7	11.3	89.7

[a]The standard deviation is presented in parentheses.

Table 2 also shows that the O/C value of BH after extraction was close to that of pure cellulose. However, this high O/C ratio was probably caused by oxidation of surface lignin and insertion of oxygen atoms to form carbonyl and carboxyl groups. According to the results shown in Table 1, the residual total lignin of BH was 8.4%, which was higher than that of BN and Bsxs, but the surface coverage by lignin for BN and Bsxs was >11%, whereas the BH had 0%. This was a limitation of the XPS method to assess detailed chemical changes in surface lignin. ATR-FTIR and ToF-SIMS spectrometry methods were applied here to complement XPS data.

ATR-FTIR of Bagasse after Pretreatment. The samples after pretreatment were measured by ATR-FTIR. The analysis depth of ATR-FTIR was from <200 nm to >1 μm, which was deeper than XPS (5−10 nm). The spectra are shown in Figure 1, and the bonding vibrations are summarized in Table 3.[5,10,25−32] The broad band from 3340 cm^{-1} has been reported as the O−H bond that could be found in carbohydrates and lignin, and for agriculture materials, the signal also possibly arises from the aliphatic fraction of waxes.[5,10] With the different pretreatment methods, this group did not obviously change. In Figure 1, 2896 cm^{-1} is the C—H bond in polysaccharides.[30] It was stronger in the pretreated bagasse samples. The signal at 1733 cm^{-1} is attributed to the C═O of acetyl groups in hemicellulose that was obviously shown in the untreated bagasse but not detected in BN, BH, or Bsxs samples, because of the removal of acetyl groups during pretreatment.[30] The

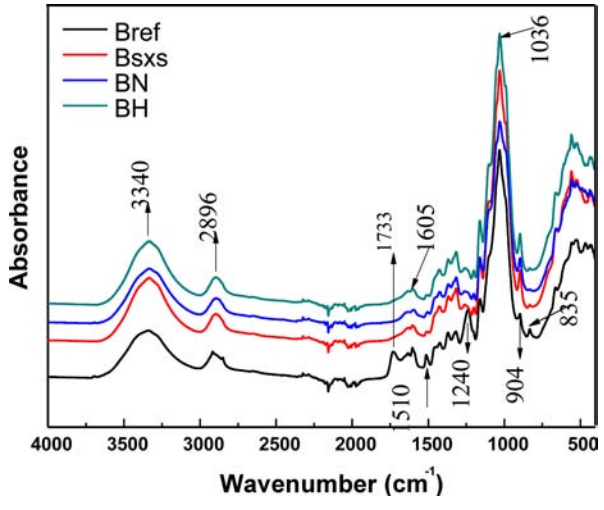

Figure 1. ATR-IR of bagasse after pretreatment. Bref, reference sample of sugar cane bagasse; Bsxs, hydrotropic pretreated sample; BN, alkaline pretreated sample; BH, alkaline peroxide pretreated sample.

Table 3. Chemical Bond Assignment of ATR-FTIR for Bagasse after Pretreatments

wavenumber (cm^{-1})	vibration	source
3340	O—H stretching	water/polysaccharides
2896	C—H (CH_2) stretching	polysaccharides
1730	C═O stretching	acetyl groups of hemicelluloses
1605	C—Ph aromatic ring	lignin
1510	C═C aromatic ring	lignin
1240	C—O	guaiacyl lignin
1036	C—O—C	polysaccharides
904	C—H deformation	lignin
835	C—H out of plane	*p*-coumaric ester groups

signals at 1605 and 1510 cm^{-1} were signs of lignin, and 1240 cm^{-1} was assigned to the aryl C−O bond from guaiacyl lignin, which existed only in untreated bagasse, indicating lignin dissolution during pretreatment.[28,31] The signal at 904 cm^{-1} was assigned as the β-glucosidic bond, which was stronger in the pretreated samples because of more carbohydrate on the fiber surface,[28] and this is in agreement with the results by XPS in Table 2. The signal at 835 cm^{-1} has been reported as the ester carbonyl signal of *p*-coumaric ester groups,[31] and it was detected only in the untreated sample.

Surface Morphology after Pretreatment. The surface morphology of bagasse samples after pretreatment was investigated by FE-SEM. In Figure 2a, the reference bagasse fiber was covered by some fragments, probably fibrils created by mechanical forces during the sugar cane squeeze stage in the sugar mill. The pits in the cell wall were shown in all samples at such high magnification, 15000×. Shrinkage trace was present on alkaline-treated fiber that proved the fiber swelling caused by alkaline pretreatment in Figure 2b. Alkaline treatment could swell wheat straw fiber, leading to the increase of the internal surface,[11] and the same action to sugar cane bagasse was found. After alkaline peroxide pretreatment, some substances formed spider web-like structures covering the fiber surface in Figure 2c. A similar phenomenon was found on softwood fiber surface after mechanical refining treatment because of xylan released from the fiber wall readsorbing on the surface.[16] It was probably due to the high surface carbohydrates covering bagasse fiber, as detected by XPS (Table 2). These substances were probably released from the collapsed inner fiber wall, which is shown in Figure 2d. After hydrotropic pretreatment, the fibrils could be seen in Figure 2e. It seems that the surface cell wall was ripped off. Fibers were expanded and more pores exposed. The performance of the fiber digestibility improved by pretreatment cannot be sufficiently explained by the change of chemical composition only. The fiber structure features and cell wall damage created by the pretreatment procedure could assist the enhancement of the fiber accessibility for enzyme as well.[32,33] The factors affecting the fiber accessibility are complementing each other.

Enzymatic Hydrolysis of Pretreated Bagasse. After dilute alkaline, alkaline peroxide, and hydrotropic pretreatments, the glucan and xylan yields of bagasse were studied (Figures 3 and 4). The maximum glucan yields of bagasse samples BN, BH, and Bsxs were 78.3, 73, and 83.9%, respectively. The glucan yield achieved from low-temperature alkaline pretreatment at 60 °C for 2 h was better than that from the sodium hydroxide peroxide pretreatment at room temperature for 24 h. This was because of the lesser contents of lignin

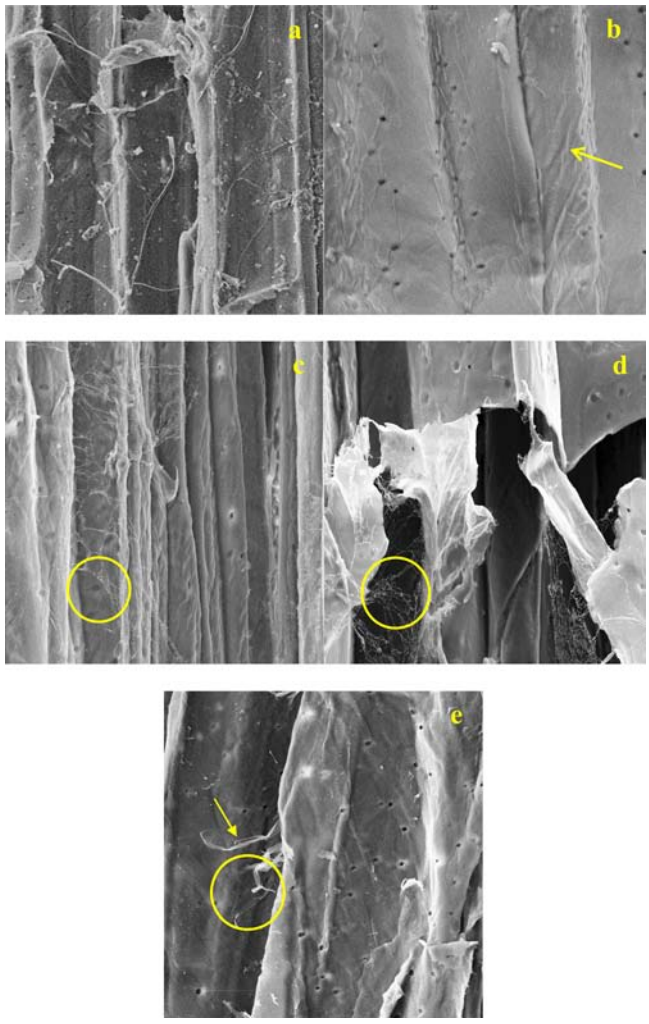

Figure 2. Morphology of bagasse after pretreatment (Bref (a), BN (b), BH(c, d), Bsxs (e)).

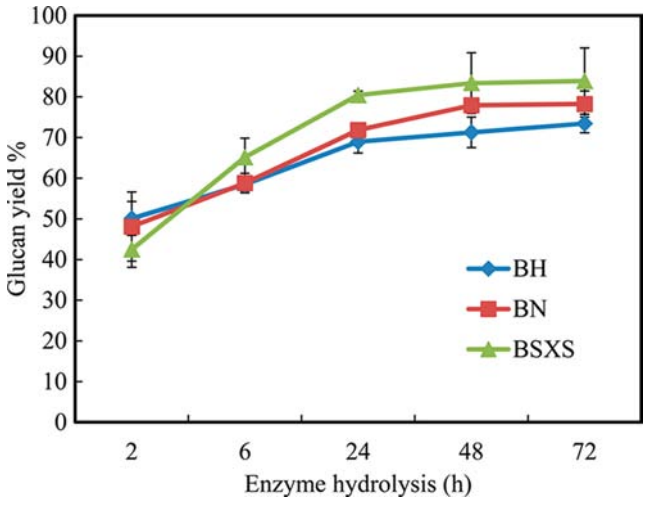

Figure 3. Glucan yield of bagasse after enzyme hydrolysis.

and hemicelluloses in BN (Table 1), as both lignin and hemicelluloses are key barriers for glucan conversion.[34] On the other hand, the surface distribution of lignin and xylan is also of critical importance for enzymatic hydrolysis.[17] According to the results in Figure 3, the highest glucan yield could be achieved

dx.doi.org/10.1021/jf500582w | J. Agric. Food Chem. 2014, 62, 3619−3625

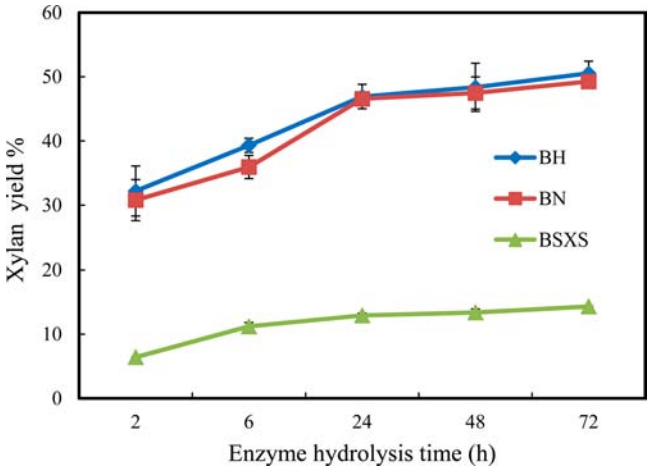

Figure 4. Xylan yield of bagasse after enzyme hydrolysis.

by hydrotropic pretreatment. This is due to the lower lignin and xylan content (Table 1) as well as the lesser surface coverage by lignin and xylan (Table 2) on bagasse fibers after hydrotropic pretreatment. Similar results were also reported for the pretreatment of common reed.[17] The low xylan yield for the case of hydrotropic pretreatment (Figure 4) was because of the low xylan recovery (Table 1). Therefore, on the basis of the results obtained, it could be concluded that among the studied pretreatment techniques, the hydrotropic method was the most efficient one to significantly improve the glucan conversion for bagasse.

Surface Chemical Characterization by ToF-SIMS. The surface chemical composition and the component distribution on the outermost surface of bagasse after alkaline, sodium hydrogen peroxide, and hydrotropic pretreatments were studied by TOF-SIMS. Samples after the following enzymatic hydrolysis were investigated also. The surface sensitivity and specificity of ToF-SIMS is 1−3 nm. Thus, ToF-SIMS can provide more detailed information on surface chemical compositions.[16,35] Sugar monomers from hexosans (cellulose, mannan, galactan) were identified by ToF-SIMS spectrum at m/z 127 and 145 and from pentosans at m/z 115 and 133. In ToF-SIMS, lignin gives the characteristic mass fragments m/z 107 and 121 from the *p*-hydroxyphenyl (H) unit, m/z 137 and 151 from the guaiacyl (G) unit, m/z 167 and 181 from the syringyl (S) unit,[36] and m/z 77 and 91 from the general aromatic ring.[21,37]

In Figure 5, the mass region m/z 100−200 of the alkaline hydrogen peroxide and hydrotropic pretreated samples is displayed as well as the same after enzymatic hydrolysis. In general, in the pretreated samples the sugar monomer fragments were clearly seen in the spectra. After the enzymatic hydrolysis again, the lignin peaks were visually more evident in

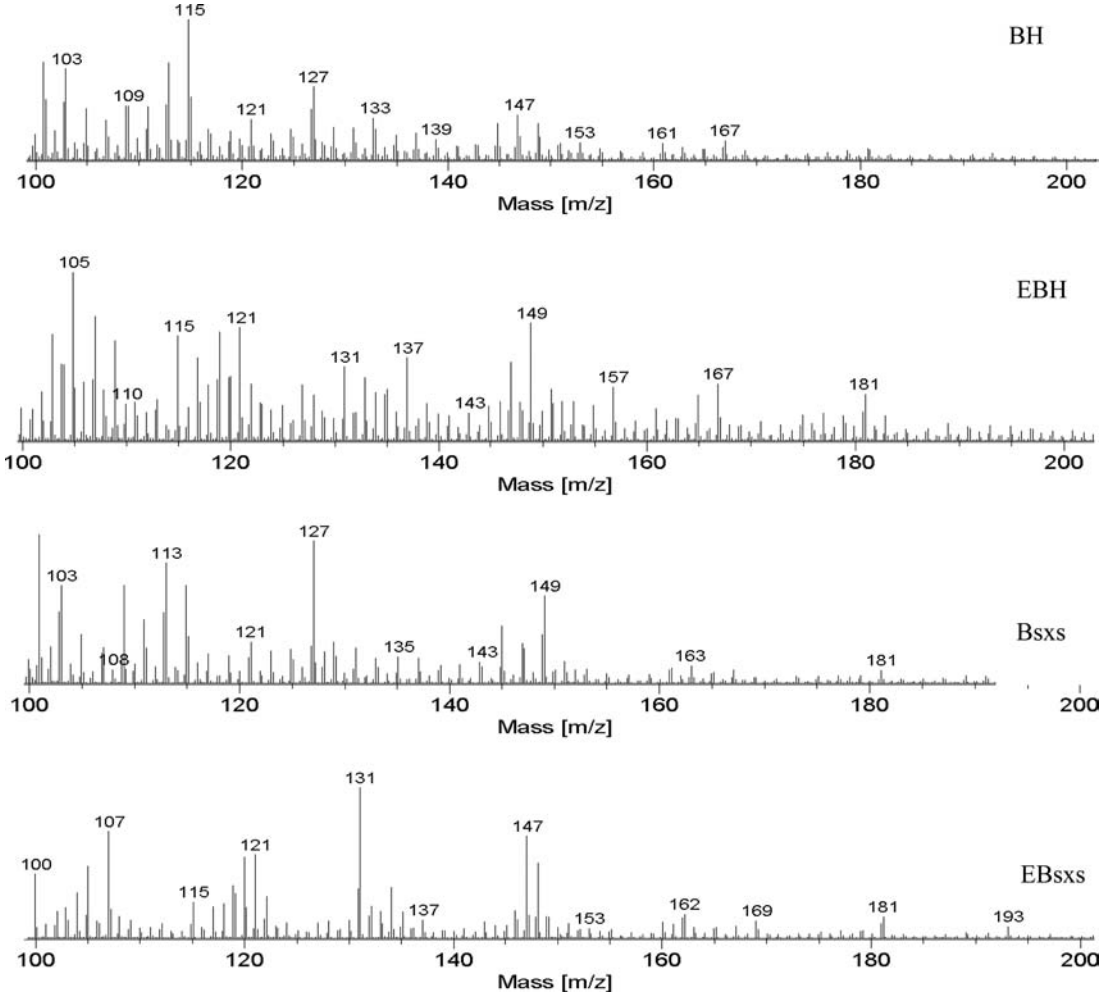

Figure 5. Positive ion ToF-SIMS spectra of BH, EBH, Bsxs, and EBsxs in the mass range m/z 100−200.

dx.doi.org/10.1021/jf500582w | J. Agric. Food Chem. 2014, 62, 3619−3625

the spectra. This was verified when the peak intensities were compared numerically.

The relative peak intensities of the characteristic mass peaks of carbohydrates and lignin were calculated (Table 4). The bagasse samples after both pretreatment and enzyme hydrolysis were studied in Table 4. The increasing ratio between carbohydrate and lignin peak intensities reflects lignin reduction on the fiber surface. After hydrotropic pretreatment, the ratio value between carbohydrates and lignin was increased about 3 times compared with the reference. This supports the finding that lignin on the surface was profusely removed by hydrotropic pretreatment (Table 2). The peak intensities of hexose monomer fragments and pentose monomer fragments in the ToF-SIMS spectra were also compared (Table 4). For that, the peak intensities were normalized individually by the total counts in the spectrum. After the hydrotropic pretreatment, the ratio value of hexose to total was raised to 4 times compared to the reference. Hexose of bagasse is mainly from cellulose that contains glucose according to the results shown in Table 1. Results from ToF-SIMS are in good agreement with XPS in Table 2. After enzymatic hydrolysis, the ratio value of carbohydrates to lignin was decreased following the hydrolyzation and removal of carbohydrates from the sample surfaces. This was not detected in the reference sample. It can be seen as a clear indication of the impact of the pretreatments on the hydrolysis efficiency by reducing the biomass recalcitrance. The value had no large difference between the different pretreatment methods. Hexose and pentose ratios follow the same trend. Especially for the hydrotropic pretreated bagasse, the hexose ratio was reduced from 4.8 to 0.8. Most of the glucose was hydrolyzed by hydrotropic pretreatment. In the case of BH and BN, xylan hydrolysis was also contributing to the decreasing ratio between carbohydrates and lignin. Thus, ToF-SIMS also demonstrated the high efficiency of hydrotropic pretreatment on delignification and enzyme saccharification.

Table 4. Ratio of the Peak Intensities of the Characteristic Mass Peaks of Carbohydrates and Lignin between Bagasse (B) Samples after Pretreatment and Enzymatic Hydrolysis (E) in ToF-SIMS

sample	carbohydrates/lignin	hexose/total × 10^3	pentose/total × 10^3
Bref	0.67 (0.07)[a]	1.1 (0.3)[a]	1.7 (0.6)[a]
BN	1.09 (0.51)	2.3 (1.4)	3.1 (1.8)
BH	1.27 (0.48)	2.6 (1.1)	3.1 (1.8)
Bsxs	1.82 (0.43)	4.8 (1.3)	3.7 (0.7)
EBref	1.02 (0.27)	3.1 (0.7)	2.7 (0.2)
EBN	0.36 (0.01)	0.7 (0.1)	1.2 (0.1)
EBH	0.47 (0.04)	0.6 (0.3)	1.0 (0.4)
EBsxs	0.48 (0.12)	0.8 (0.3)	2.2 (0.9)

[a]The standard deviation is presented in parentheses.

Overall, the bulk chemical composition, surface chemical distribution, and fiber morphology are correlated and should be considered together for comprehensive understanding of the mechanism of pretreatment to accelerate enzymatic hydrolysis. The glucan yield of sugar cane bagasse by enzymatic hydrolysis was advanced by mildly alkaline and alkaline hydroxide pretreatments at room temperature. A much better improvement was achieved with hydrotropic pretreatment through lignin removal and change in surface distribution. Typically for hydrotropic pretreatment, in addition to delignification, xylan was significantly removed. The surface morphology features after hydrotropic pretreatment also benefit enzyme access to fibers. A new biorefinery platform combining production of cellulosic ethanol and recovery of lignin and xylan can be developed on the basis of our results.

AUTHOR INFORMATION

Corresponding Authors

*(H.M.) E-mail: hmou@abo.fi.

*(P.F.) E-mail: pfardim@abo.fi,

Notes

The authors declare no competing financial interest.

ACKNOWLEDGMENTS

We thank Top Analytica Ltd. for providing surface analytical instruments.The enzymes were kindly supplied from VTT Technical Research Centre of Finland.

ABBREVIATIONS USED

Bref, sugar cane bagasse reference sample; BH, alkaline peroxide pretreated sugar cane bagasse sample; BN, alkaline pretreated sugar cane bagasse sample; Bsxs, hydrotropic pretreated bagasse sample; SXS, sodium xylenesulfonate; XPS, X-ray electron xpectroscopy; ATR-FTIR, attenuated total reflectance-infrared spectra; ToF-SIMS, time of flight secondary ion mass spectrometry; FE-SEM, field emission-scanning electron microscope; S_{ext}, surface coverage by extractives; S_{lig}, surface coverage by lignin; S_{carb}, surface coverage by carbohydrates

REFERENCES

(1) Rocha, G. J. M.; Gonçalves, A. R.; Oliveira, B. R.; Olivares, E. G.; Rossell, C. E. V. Steam explosion pretreatment reproduction and alkaline delignification reactions performed on a pilot scale with sugarcane bagasse for bioethanol production. *Ind. Crops Prod.* **2012**, *35*, 274−279.

(2) Hoareau, W.; Trindade, W. G.; Siegmund, B.; Castellan, A.; Frollini, E. Sugarcane bagasse and curaua lignins oxidized by chlorine dioxide and reacted with furfuryl alcohol: characterization and stability. *Polym. Degrad. Stab.* **2004**, *86*, 567−576.

(3) Pereira, P. H. F.; Voorwald, H. C. J.; Cioffi, M. O. H.; Mulinari, D. R.; Luz, S. M. D.; Silva, M. L. C. P. D. Sugarcane bagasse pulping and bleaching thermal and chemical characterization. *BioResources* **2000**, *6* (3), 2471−2482.

(4) Pandey, A.; Soccol, C. R.; Nigam, P.; Soccol, V. T. Biotechnological potential of agro-industrial residues. I: Sugarcane bagasse. *Bioresour. Technol.* **2000**, *74* (1), 69−80.

(5) Corrales, R. C. N. R.; Mendes, F. M. T.; Perrone, C. C.; Anna, C. S.; Souza, W.; Abud, Y.; Bon, E. P.S.; Ferreira-Leitão, V. Structural evaluation of sugar cane bagasse steam pretreated in the presence of CO_2 and SO_2. *Biotechnol. Biofuels* **2012**, *5*, 36.

(6) Chen, W. H.; Ye, S. C.; Sheen, H. K. Hydrolysis characteristics of sugarcane bagasse pretreated by dilute acid solution in a microwave irradiation environment. *Appl. Energy* **2012**, *93*, 237−244.

(7) Rabelo, S. C.; Fonseca, N. A. A.; Andrade, R. R.; Filho, R. M.; Costa, A. C. Ethanol production from enzymatic hydrolysis of sugarcane bagasse pretreated with lime and alkaline hydrogen peroxide. *Biotechnol. Bioeng.* **2011**, *35* (7), 2600−2607.

(8) Rocha, G. J. M.; Gonçalves, A. R.; Oliveira, B. R.; Olivares, E. G.; Rossell, C. E. V. Steam explosion pretreatment reproduction and alkaline delignification reactions performed on a pilot scale with sugarcane bagasse for bioethanol production. *Ind. Crops Prod.* **2012**, *35*, 274−279.

(9) Laser, M.; Schulman, D.; Allen, S. G.; Lichwa, J.; Antal, M. J., Jr.; Lynd, L. R. A comparison of liquid hot water and steam pretreatments

of sugarcane bagasse for bioconversion to ethanol. *Bioresour. Technol.* **2002**, *81* (1), 33−44.
(10) Shen, J.; Liu, Z.; Li, J.; Niu, J. Wettability changes of wheat straw treated with chemicals and enzymes. *J. For. Res.* **2011**, *22* (1), 107−110.
(11) Jackson, M. G. The alkali treatment of straws. *Anim. Feed. Sci. Technol.* **1977**, *2*, 105−130.
(12) Costa, J. A.; Júnior, J. E. M.; Gonçalves, L. R. B.; Rocha, M. V. P. Alkaline hydrogen peroxide pretreatment of cashew apple bagasse for ethanol production: study of parameters. *Bioresour. Technol.* **2013**, *139*, 249−256.
(13) Mishima, D.; Tateda, M.; Ike, M.; Fujita, M. Comparative study on chemical pretreatments to accelerate enzymatic hydrolysis of aquatic macrophyte biomass used in water purification processes. *Bioresour. Technol.* **2006**, *97*, 2166−2172.
(14) Procter, A. R. Review of hydrotropic pulping. *Pulp Pap. Mag. Can.* **1971**, *72* (8), 67−74.
(15) Gabov, K.; Fardim, P.; da Silva Júnior, F. G. Hydrotropic fractionation of birch wood into cellulose and lignin: a new step towards green biorefinery. *BioResources* **2013**, *8* (3), 3518−3531.
(16) Mou, H.; Iamazaki, E.; Zhan, H.; Orblin, E.; Fardim, P. Advanced studies on the topochemistry of softwood fibers in low-consistency refining as analyzed by FE-SEM, XPS, and ToF-SIMS. *BioResources* **2013**, *8* (2), 2325−2336.
(17) Mou, H.; Heikkiläa, E.; Fardim, P. Topochemistry of alkaline, alkaline-peroxide and hydrotropic pretreatments of common reed to enhance enzymatic hydrolysis efficiency. *Bioresour. Technol.* **2013**, *150*, 36−41.
(18) Korpinen, R.; Fardim, P. Lignin extraction from wood biomass by a hydrotropic solution. *Papel* **2009**, *70* (5), 69−82.
(19) Ström, G.; Carlsson, J. Wettability of kraft pulps − effects of surface composition and oxygen plasma treatment. *Adhes. Sci. Technol.* **1992**, *6*, 745−761.
(20) Fardim, P.; Durán, N. Modification of fibre surfaces during pulping and refining as analysed by SEM, XPS and ToF-SIMS. *Colloids Surf., A* **2003**, *223*, 263−276.
(21) Koljonen, K.; Österberg, M.; Johansson, L. S.; Stenius, P. Surface chemistry and morphology of different mechanical pulps determined by ESCA and AFM. *Colloids Surf., A* **2003**, *228*, 143−158.
(22) Kangas, H.; Suurnäkki, A.; Kleen, M. Modification of the surface chemistry of TMP with enzymes. *Nord. Pulp Pap. Res. J.* **2007**, *22* (4), 415−423.
(23) Tokareva, E.; Fardim, P.; Pranovich, A.; Fagerholm, H. P.; Daniel, G.; Holmbom, B. Imaging of wood tissue by ToF-SIMS: critical evaluation and development of sample preparation techniques. *Appl. Surf. Sci.* **2007**, *253*, 7569−7577.
(24) Laine, J.; Stenius, P.; Carlsson, G.; Ström, G. Surface characterization of unbleached kraft pulps by means of ESCA. *Cellulose* **1994**, *1*, 145−160.
(25) Wu, L.; Arakane, M.; Ike, M.; Wada, M.; Takai, T.; Gau, M.; Tokuyasu, K. Low temperature alkali pretreatment for improving enzymatic digestibility of sweet sorghum bagasse for ethanol production. *Bioresour. Technol.* **2011**, *102*, 4793−4799.
(26) Cao, W.; Sun, C.; Liu, R.; Yin, R.; Wu, X. Comparison of the effects of five pretreatment methods on enhancing the enzymatic digestibility and ethanol production from sweet sorghum bagasse. *Bioresour. Technol.* **2012**, *111*, 215−221.
(27) Sluiter, A.; Hames, B.; Ruiz, R.; Scarlata, C.; Sluiter, J.; Templeton, D.; Crocker, D. *Determination of Structural Carbohydrates and Lignin in Biomass*; Technical Report NREL/TP510-42618; National Renewable Energy Laboratory: Golden, CO, USA, 2011
(28) Sun, R.; Lawther, J. M.; Banks, W. B. Influence of alkaline pretreatments on the cell wall components of wheat straw. *Ind. Crops Prod.* **1995**, *4* (2), 127−145.
(29) Guo, D. L.; Lou, S. B.; Lou, R.; Yin, X.; Yang, Q. Effect of organic bound Na groups on pyrolysis and CO_2-gasification of alkaline lignin. *BioResources* **2011**, *6* (4), 4145−4157.
(30) Pereira, P. H. F.; Voorwald, H. C. J.; Cioffi, M. O. H.; Mulinari, D. R.; Luz, S. M. D.; Silva, M. L. C. P. D. Sugarcane bagasse pulping and bleaching: thermal and chemical characterization. *BioResources* **2011**, *6* (3), 2471−2482.
(31) Derkacheva, O.; Sukhov, D. Investigation of lignins by FTIR spectroscopy. *Macromol. Symp.* **2008**, *265*, 61−68.
(32) Fan, L. T.; Gharpuray, M. M.; Lee, Y.-H. In *Cellulose Hydrolysis Biotechnology Monographs*; Springer: Berlin, Germany, 1987; Vol. 3, p 57.
(33) Donohoe, B. S.; Vinzant, T. B.; Elander, R. T.; Pallapolu, V. R.; Lee, Y. Y. Surface and ultrastracuture characterization of raw and pretreated switchgrass. *Bioresour. Technol.* **2011**, *102* (24), 11097−11104.
(34) Leu, S. Y.; Zhu, J. Y. Substrate-related factors affecting enzymatic saccharification of lignocelluloses: our recent understanding. *Bioenergy Res.* **2013**, *6*, 405−415.
(35) Mou, H. Y.; Li, B.; Heikkilä, E.; Iamazaki, E.; Zhan, H.; Fardim, P. Low consistency refining of *Eucalyptus* pulp: effects on surface chemistry and interaction with FWAs. *BioResources* **2013**, *8* (4), 5995−6013.
(36) Saito, K.; Kato, T.; Tsuji, Y.; Fukushima, K. Identifying the characteristic secondary ions of lignin polymer using ToF-SIMS. *Biomacromolecules* **2005**, *6*, 678−683.
(37) Goacher, R. E.; Edwards, E. A.; Yakunin, A. F.; Mims, C. A.; Master, E. R. Application of time-of-flight-secondary ion mass spectrometry for the detection of enzyme activity on solid wood substrates. *Anal. Chem.* **2012**, *84* (10), 4443−4451.

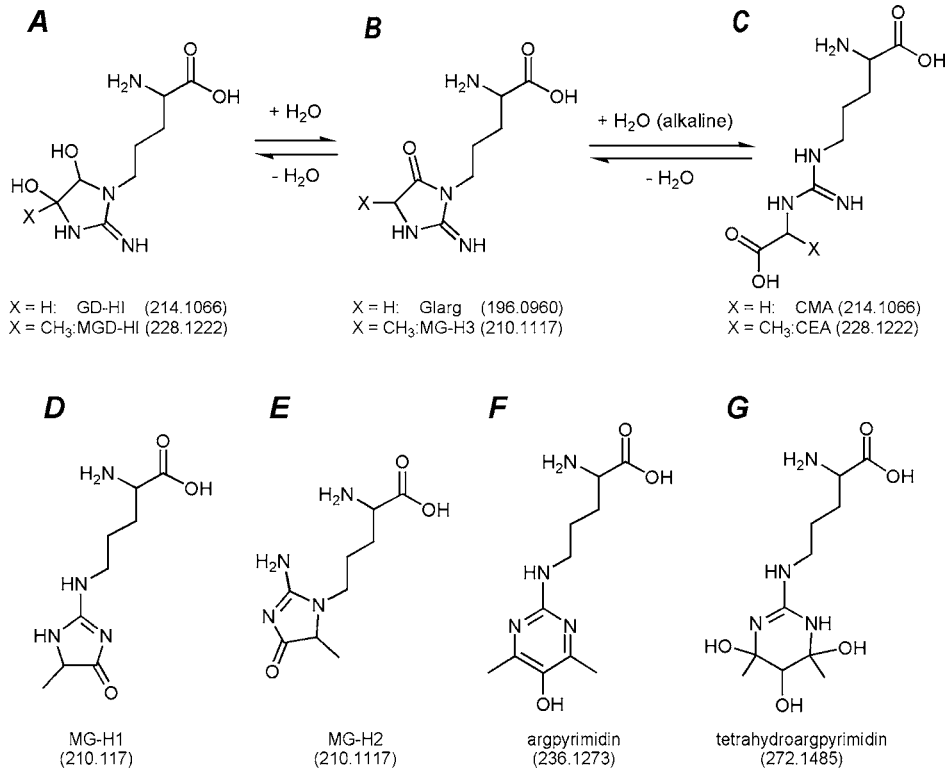

Figure 1. Structures and mass increments of glyoxal- (A, B) and methylglyoxal-derived (C−G) arginine-AGEs: Glarg (A), CMA (B), MG-H1 (C), MG-H2 (D), MG-H3 (E), CEA (F), and argpyrimidine (G).

their formation and degradation was studied for a period of 4 h. Additionally, the effects of reactive oxygen species (ROS) and nearby amino acid residues were evaluated.

MATERIALS AND METHODS

Chemicals. Suppliers and their products were as follows: Iris Biotech GmbH (Marktredwitz, Germany): 9-fluorenylmethoxycarbonyl (Fmoc-) rink amide AM resin and Fmoc-L-Arg(Pbf)−OH (peptide synthesis grade); ORPEGEN Pharma (Heidelberg, Germany): all other Fmoc-protected L-amino acids (peptide synthesis grade); Biosolve (Valkenswaard, Netherlands): *N,N′*-dimethylformamide (DMF, ≥99.8%), piperidine (≥99.5%), and dichloromethane (DCM, ≥99.9%); Carl Roth GmbH & Co KG (Karlsruhe, Germany): trifluoroacetic acid (TFA, 99.9%), α-D-glucose hydrate (≥99.5%), potassium hydrogen phosphate (≥99%), and potassium dihydrogen phosphate (≥99%); VWR International GmbH (Dresden, Germany): diethyl ether (100%) and acetonitrile (≥99.9%). All other chemicals were purchased from Sigma-Aldrich Chemie GmbH (Taufkirchen, Germany). Water was purified in-house (resistance 18 mΩ/cm) on a PureLab Ultra Analytic System (ELGA Lab Water, Celle, Germany).

Peptide Synthesis. Peptides Ac-ASGAGSARASGXASA-NH_2 with X = Ala (1), X = His (2), and X = Glu (3) were synthesized on a multiple peptide synthesizer Syro2000 (MultiSynTech GmbH, Witten, Germany) by Fmoc/*tert*-butyl-chemistry using eight equivalents (equiv) of Fmoc-amino acid derivatives (or acetic acid for N-terminal acetylation) activated with DIC/HOBt in DMF.[23] Peptides were cleaved with TFA at RT (2 h), precipitated with diethyl ether, and purified by RP-HPLC using formic acid or TFA (0.1% v/v) in water (eluent A) and 60% (v/v) aqueous acetonitrile (eluent B) using a gradient slope of 1% eluent B/min. The peptides were aliquoted (32 nmol) in 1.5-mL safe lock tubes (Eppendorf AG, Hamburg, Germany), dried under vacuum, and stored at −20 °C.

In vitro Glycation Reactions with Model Peptides. Peptide aliquots were reconstituted in potassium phosphate buffer (0.1 mol/L, pH 7.4, 0.1 mL) containing iron(II) sulfate (0, 18, or 590 μmol/L) and ascorbic acid (0, 60, or 1200 μmol/L), and incubated (95 °C, up to 4 h) under continuous shaking (450 rpm) in the absence or presence of D-glucose (25 mmol/L). Incubations were stopped by addition of aqueous EDTA (6 mmol/L, 10 μL) on ice and stored at −80 °C.

RP-HPLC-ESI-QqTOF-MS and MS/MS. Samples corresponding to an initial amount of 90 pmol peptide were separated on a Aqua C_{18}-column using a HPLC 1100 system (Agilent Technologies, Böblingen, Germany) consisting of a binary gradient pump (G1312A), online micro degasser (G1379A) and Marathon autosampler (10 μL full loop injection, Spark Holland B.V., Emmen, Netherlands). Eluents A and B were water and acetonitrile, respectively, containing formic acid (0.1%, v/v). Elution was achieved by isocratic conditions (3% eluent B, 5 min) followed by two consecutive linear gradients to 40% (3 min) and 95% eluent B (23 min) using a flow rate of 220 μL/min. LC-MS/MS relied on a shallower gradient (from 4% to 30% eluent B in 4 min and then to 37% eluent B in 14 min). The ESI-QqTOF-MS was equipped with a TurboIon Spray source (QSTAR Pulsar I; AB Sciex, Darmstadt, Germany) and operated in positive ion mode using the Analyst QS 1.0 software (AB Sciex, Darmstadt, Germany). Ion spray voltage and declustering potential were set to 5000 and 50 V, respectively. Curtain, nebulizing, and drying gases were set to 30 psig. The ion source was held at 450 °C. Spectra were acquired with automatically adjusted pulsing frequency and 1 s accumulation time. Collision-induced dissociation (CID) MS/MS experiments relied on low Q1 resolution, collision potentials of 40−70 V, and nitrogen as collision gas (5 psig). In MS mode the instrument was calibrated with a mixture of glycine, sucrose, and maltoheptaose (250 μmol/L each, 60%, v/v aq. acetonitrile) using the $[MH + Gly]^+$ ions of sucrose (m/z 418.1555) and maltoheptaose (m/z 1228.4196). Calibration of the tandem mass spectra relied on y_1- (m/z 175.195) and y_{11}-ions (m/z 1285.545) of the doubly protonated [Glu-1] fibrinogen peptide 1. Relative quantification was performed by integration of extracted ion chromatograms (XICs, ± 0.1 m/z-units) at specific retention times.

dx.doi.org/10.1021/jf4050183 | J. Agric. Food Chem. 2014, 62, 3626−3635

RESULTS

Identification of Arginine-Derived Glycation Products. When peptide **1** was incubated with D-glucose and $Fe(II)SO_4$ at 95 °C, a total of eight peptide products with lower or higher masses than the original peptide were detected by RP-HPLC-ESI-QqTOF-MS already after 15 min of exposure time (Table 1). Reaction products were numbered in their elution order and identified by their exact m/z values and tandem mass spectra (Table 1 and Figure 2). The tandem mass spectra typically displayed intense signals of the b-ion series indicating that the mass shift was located at Arg8, while in some cases it was deduced from the exact mass shift of a peptide fragment (Supporting Information (SI) Figure S-1). The increment masses revealed three glyoxal- (Glarg, GD-HI, and CMA) and two methylglyoxal-derived modifications (MG-H and MGD-HI) as well as ornithine (loss of urea). Furthermore, two signals with m/z-values corresponding to an argpyrimidine-modified peptide were detected at different retention times (Table 1). Neither cross-linked products (dimers) nor oxidized arginine residues, such as hydroxy-arginine or glutamate-5-semialdehyde, were observed.[24]

Some modified peptides displayed characteristic fragment ions that further supported the deduced structures. Glarg- (**1-2**) and MG-H-containing peptides (**1-7**, Figures 2B and SI S-1B) as well as the corresponding hydrated forms (**1-3** and **1-8**, respectively) displayed signals at m/z 152.1 and 166.1. Most likely, these signals were related to the arginine immonium ion (Im, m/z 129.1) and represented the corresponding Im-NH_3 fragment (m/z 112.1) containing Glarg and MG-H moieties (mass shifts of 40 and 54 m/z-units, respectively). If this assumption is correct, then the signals would represent hydroimidazolinone and dihydroxyimidazolidine and thus confirm **1-3** and **1-8** as glyoxal- and methylglyoxal-derived dihydroxy-imidazolidines (GD-HI and MGD-HI), respectively (Table 1, Figure 1). As the MG-H-modified peptide eluted in one peak in RPC using different eluent compositions (SI Figure S-2), it remains open, if it was a single MG-H-modified peptide or a mixture of different MG-H-versions. Based on the absence of the signal at m/z 152.1 in the tandem mass spectrum of peptide **1-5**, this analyte was annotated as CMA (Table 1).

Table 1. Retention Times, Precise Masses, and Arginine-Derived AGE-Modified Peptides Identified during the Incubation of Peptide 1 with D-Glucose (25 mmol/L) in the Presence of $Fe(II)SO_4$ (18 μmol/L)

no.	t_R (min)	m/z^a $[M + 2H]^{2+}$	Δm^b	residue in position 8	mass accuracy (ppm)
1	18.6	616.831 ± 0.006	+0.00	arginine	46.2
1-1	18.3	595.802 ± 0.002	−42.06	ornithine	17.4
1-2	18.5	636.805 ± 0.003	+39.95	Glarg	7.9
1-3	18.5	645.816 ± 0.002	+57.97	GD-HI	16.7
1-4	18.5	656.801 ± 0.003	+79.94	argpyrimidine	22.3
1-5	18.8	645.817 ± 0.001	+57.98	CMA	18.2
1-6	18.8	656.803 ± 0.002	+79.94	argpyrimidine	19.2
1-7	19.0	643.821 ± 0.017	+53.98	MG-H	20.9
1-8	19.0	652.818 ± 0.002	+71.97	MGD-HI	7.5

[a]Average m/z-value and standard deviation recorded during different experiments. [b]Modification-specific mass shift relative to the increment mass of an arginine residue.

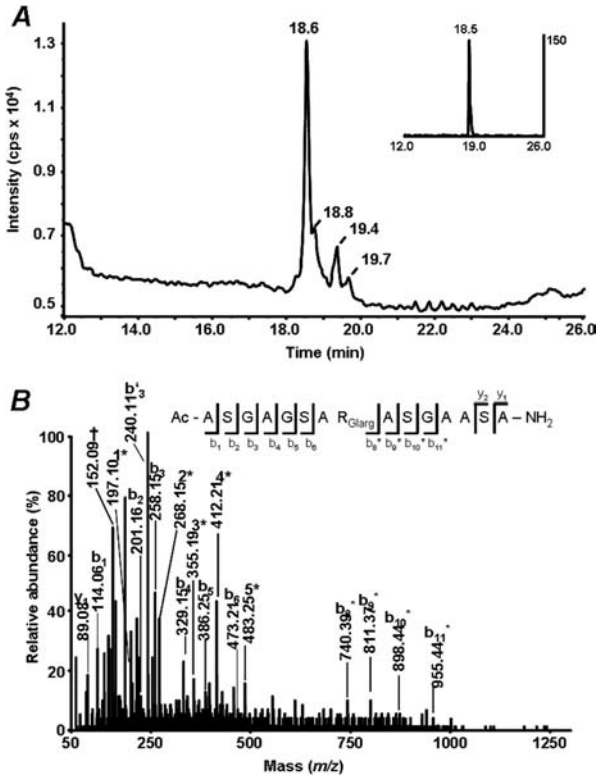

Figure 2. Total ion current chromatogram (A), extracted ion chromatogram (m/z 636.8 ± 0.1; small insert), and tandem mass spectrum of the precursor ion at m/z 636.8 (B) representing Glarg-containing peptide $ASGAGSAR_{Glarg}ASGAASA$.

CEA was neither detected here nor in any of the other incubation mixtures.

Kinetics of Arginine-Related AGEs. Unmodified peptide **1** was very stable when incubated with iron(II) sulfate (18 μmol/L, 95 °C). Basically no degradation products were detected by RPC-MS. The peak area, which was calculated from the XICs, decreased only to ∼86% after 4 h (t test: $p = 0.14$; Figure 3A). The degradation rate was significantly higher in the presence of D-glucose, with 46% of the initial peptide amount left after 1 h and only 5% after 4 h. Obviously, the peptide loss was related to glucose oxidation[25] yielding glyoxal- and methylglyoxal-derived AGEs or oxidative degradation of the peptide backbone.[26] As described above, the incubation yielded eight modified peptides in reasonable quantities (Table 1), which could be separated by RPC and MS and thus be quantified from their XICs. It should be noted that Arg-derived modifications with different gas phase basicity could influence the ionization properties of AGE-modified peptides significantly. Thus, only signal intensities of structurally related peptides can be used to estimate their relative quantities at different time points.

The detected amount of the GD-HI-modified peptide (**1-3**) increased for 45 min and decreased afterward almost to background level after 4 h (Figure 3B). The Glarg-peptide (**1-2**) quantity increased during the first hour and was basically stable within the error range afterward (Figure 3B). The same was true for the CMA-adduct (**1-5**). Considering the slow degradation of the unmodified peptide, it can be concluded that Glarg- or CMA-modified peptides were either not further produced after 1 h or they were immediately degraded upon formation.

dx.doi.org/10.1021/jf4050183 | J. Agric. Food Chem. 2014, 62, 3626−3635

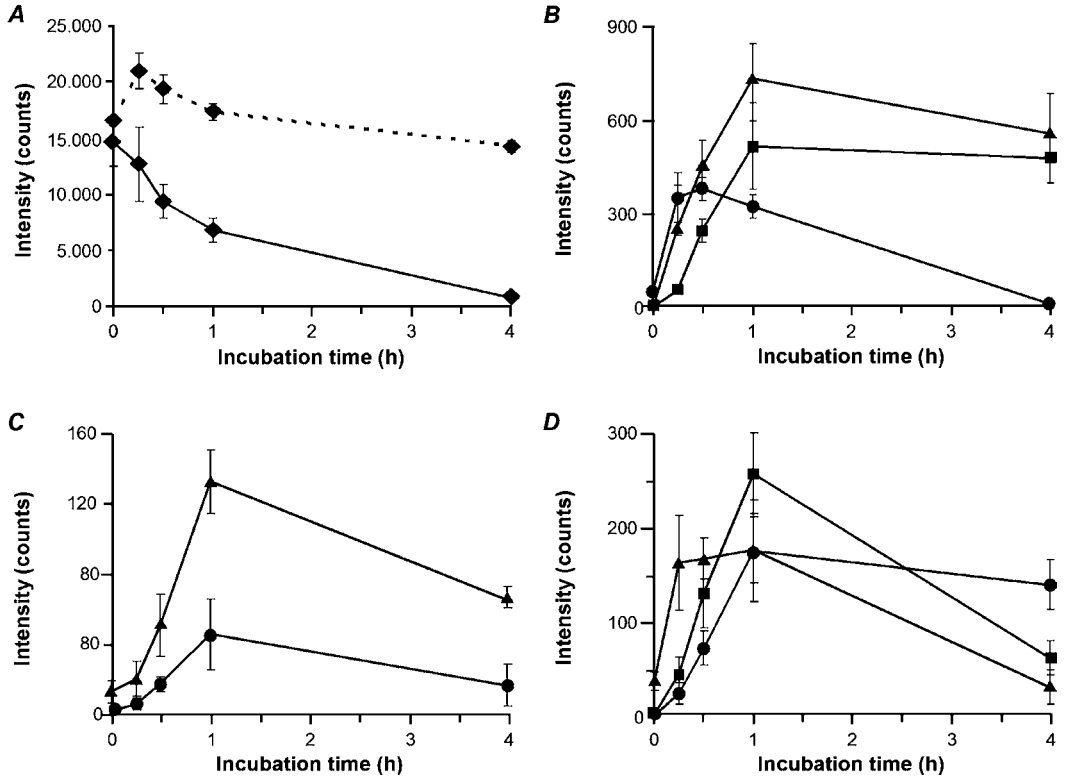

Figure 3. Degradation of peptide **1** (A, ♦) when incubated with (solid) and without (dotted) D-glucose (25 mmol/L) Fe(II)SO_4 (18 μmol/L) and formation of the detected AGE products (B–D). Aliquots were analyzed after 0, 15, 30, 60, and 240 min by RPC-ESI-QqTOF-MS in positive ion mode. Presented are the peak areas calculated by integrating the XICs of the doubly protonated quasimolecular ions ($\pm$0.10 m/z-units) containing a glyoxal-derived residue (B), i.e. Glarg (▲), GD-H1(●), and CMA (■), a methylglyoxal-derived residue (C), i.e. MG-H (▲) and MGD-H1 (●), or another reaction product (D), i.e. ornithine (■) and argpyrimidine (**1-4** ▲, **1-6** ●).

The two methylglyoxal-derived modifications, i.e. MG-H (**1-7**) and MGD-HI (**1-8**), showed similar kinetics as GD-HI with increasing amounts up to around 1 h and a decrease afterward (Figure 3B and C). The degradation rates from 1 to 4 h were slightly higher than that for the unmodified peptide (Figure 3), but lower than that for the GD-HI peptide. The signal intensities of the methylglyoxal-derived products were 10-fold lower than for the corresponding glyoxal-derived peptides.

The formation and degradation of the ornithine-containing peptide (**1-1**) resembled the kinetics for MG-H and to a lower extent that of Glarg (Figure 3D). Interestingly, the two products annotated as argpyrimidine (**1-4** and **1-6**) showed different kinetics with the earlier eluting compound being produced fast within the first 15 min, and then slightly increased up to 1 h before it slowly decreased. Peptide **1-6** increased continuously for 1 h and decreased 20% during the following 3 h period, which resembled the kinetics of GD-HI (Figure 3). Thus, the two products annotated as argpyrimidine must have different structures and should be formed and degraded by different reactions. Further studies are required to identify their stereochemical structures and origins.

Influence of Nearby Residues on Formation of Arg-Derived AGEs. Up to this point, only one inert peptide sequence was studied containing a single reactive arginine residue in position eight. Thus, we extended our study to two highly conserved peptides by substituting Ala-12 with His (peptide **2**) or Glu (peptide **3**). These peptides were incubated with glucose and iron sulfate in conditions identical to those described for the alanine-containing analogue. Peptide **3** was as stable as peptide **1** (~80%), whereas the content of peptide **2** decreased to 60% after 4 h incubation (SI Figure S-3). In the presence of glucose, all three peptides demonstrated very similar degradation kinetics and their amounts decreased to about 5% after 4 h.

Interestingly, the kinetics of all three glyoxal-derived products, i.e. Glarg (***i*-2**, *i* corresponds to the peptide number), GD-HI (***i*-3**), and CMA (***i*-5**) depended on the substitution in position 12 (Figure 4A–C). All three peptides showed very similar formation kinetics of Glarg and GD-HI during the first 30 min. The content of the Glarg-modified peptide **2** (Glu) decreased afterward and was near background levels at the end of the incubation period. The amounts of the corresponding Ala- and His-containing peptides increased further up to 60 min before they decreased slowly with the Glarg-modified peptide **3** being always present at high levels (Figure 4A). The GD-HI-modified products showed a similar profile, but here peptides **1** and **2** showed similar kinetics reaching the maximal amounts after 45 min, whereas the quantities of the GD-HI-modified peptide **3** increased further for the next 15 min and then decreased relatively fast afterward. Surprisingly, CMA-modified peptides showed a different behavior with peptide **3** forming very small amounts of the CMA-product, whereas peptide **2** was modified at higher levels than peptide **1** between 1 and 4 h (Figure 4C).

Unexpectedly, the substitutions had only minor effects on the kinetics of both methylglyoxal products (Figure 4D and E), although His might favor the formation of MG-H at the beginning. The only difference was seen for the MGD-HI-containing peptides in the last 3 h of the incubation period, when peptide **2** was degraded faster than peptide **3**. Thus, our

dx.doi.org/10.1021/jf4050183 | J. Agric. Food Chem. 2014, 62, 3626–3635

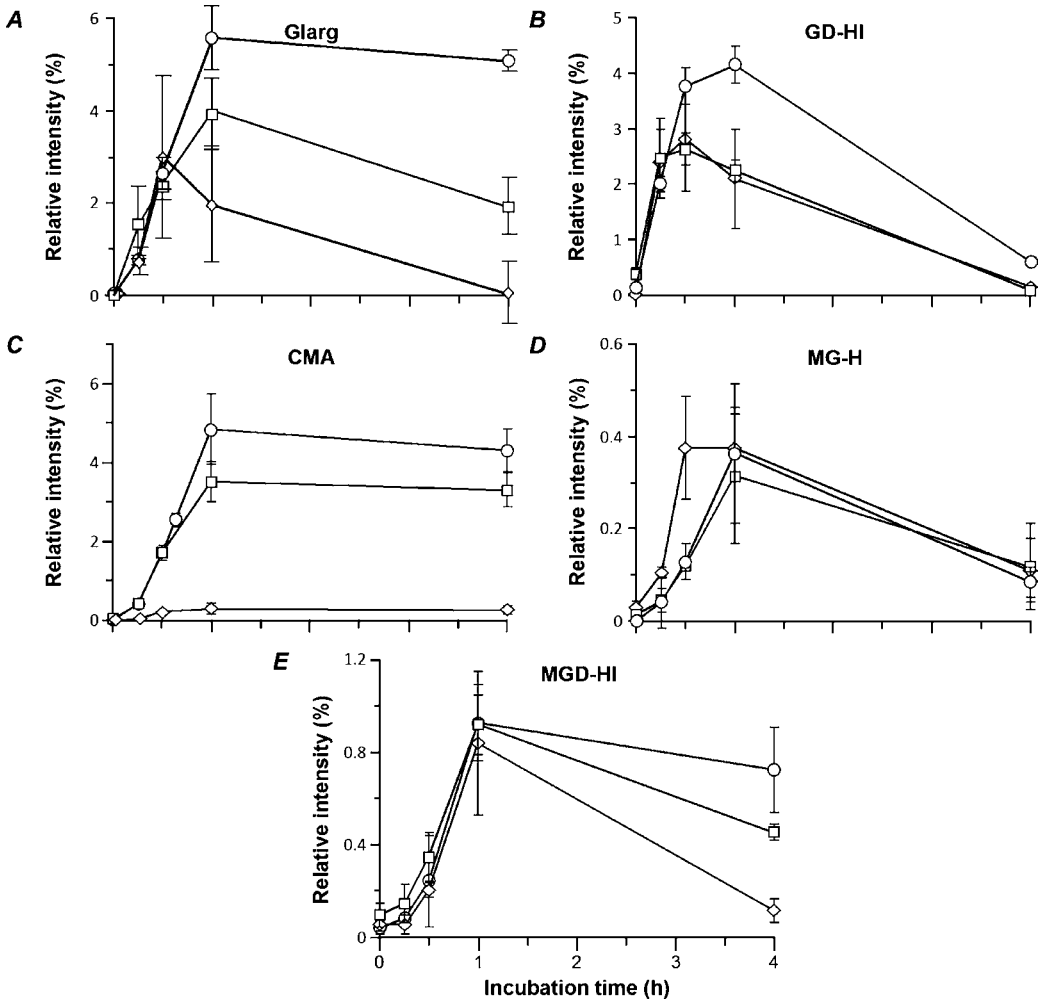

Figure 4. Formation and degradation curves of Glarg- (*i*-**2**, A; *i* denotes the peptide number), GD-HI- (*i*-**3**, B), CMA- (*i*-**6**, C), MG-H- (*i*-**8**, D), and MGD-HI-modified (*i*-**9**, E) peptides **1** (□), **2** (◊), and **3** (○). Peptides were incubated with D-glucose (25 mmol/L) and Fe(II)SO_4 (18 μmol/L) at 95 °C. Samples were analyzed by RPC-ESI-QqTOF-MS in positive ion mode after incubation periods of 0, 15, 30, 60, and 240 min. Intensities were calculated as peak areas by integrating the XICs (n = 3) of the doubly protonated quasimolecular ions (±0.10 m/z-units).

findings give support for stabilizing effect of His and a destabilizing effect of Glu on MGD-HI (Figure 4E).

Effect of ROS on the Formation and Degradation of Arginine-Derived AGEs. After analyzing the formation and degradation of AGEs under weak oxidation conditions (18 μmol/L Fe(II)SO_4), the influence of lower and higher iron(II)-concentrations as well as the presence of ascorbate at two different concentrations was tested for peptide **1**. Based on the above results the incubation period was reduced to 195 min, as the signals of all AGEs reached the highest intensities after about 1 h. Additionally, the incubation mixtures were analyzed at six time points within the first hour to describe the quantitative changes more precisely. In the absence of D-glucose, the unmodified peptide was degraded by approximately 50% within the first hour with only 5% left after 195 min of incubation. In the presence of D-glucose, the peptide was always degraded at very similar rates mostly independent of the Fe(II) and ascorbate concentrations. Higher Fe(II) concentrations appeared to favor the degradation slightly, whereas ascorbate accelerated it at low Fe(II) concentrations (3.3-fold molar access of ascorbate) and reduced it for high Fe(II) concentrations (2-fold molar access of ascorbate) (Figure 5A).

The Glarg-modified peptide (**1**-**2**) was obtained at around 20% lower quantities in the absence of iron(II) and approximately 70% higher quantities at high iron(II) concentrations relative to the original conditions. Addition of ascorbate significantly increased Glarg formation at low iron(II) concentration conditions, but decreased its formation at high iron(II) concentration (Figure 5B). The maximal amount of Glarg was detected in all samples after approximately 1 h. The GD-HI-modified peptide (**1**-**3**) showed basically a similar dependence on the iron(II) and ascorbate concentrations as the Glarg-containing peptide (Figure 5B and C) with the maximal product quantities obtained after 45 to 60 min. Afterward the peptide amounts decreased significantly and reached nearly identical levels at the end of the incubation period. Formation of the CMA-modified peptide (**1**-**5**) depended on the iron(II) and ascorbate concentrations as described above for Glarg and GD-HI. The highest levels were again obtained after 1 h. The degradation, however, depended on the presence of ascorbate. Without ascorbate the product amounts were stable from 60 to 195 min, whereas they decreased significantly in the presence of ascorbate (Figure 5D).

dx.doi.org/10.1021/jf4050183 | J. Agric. Food Chem. 2014, 62, 3626−3635

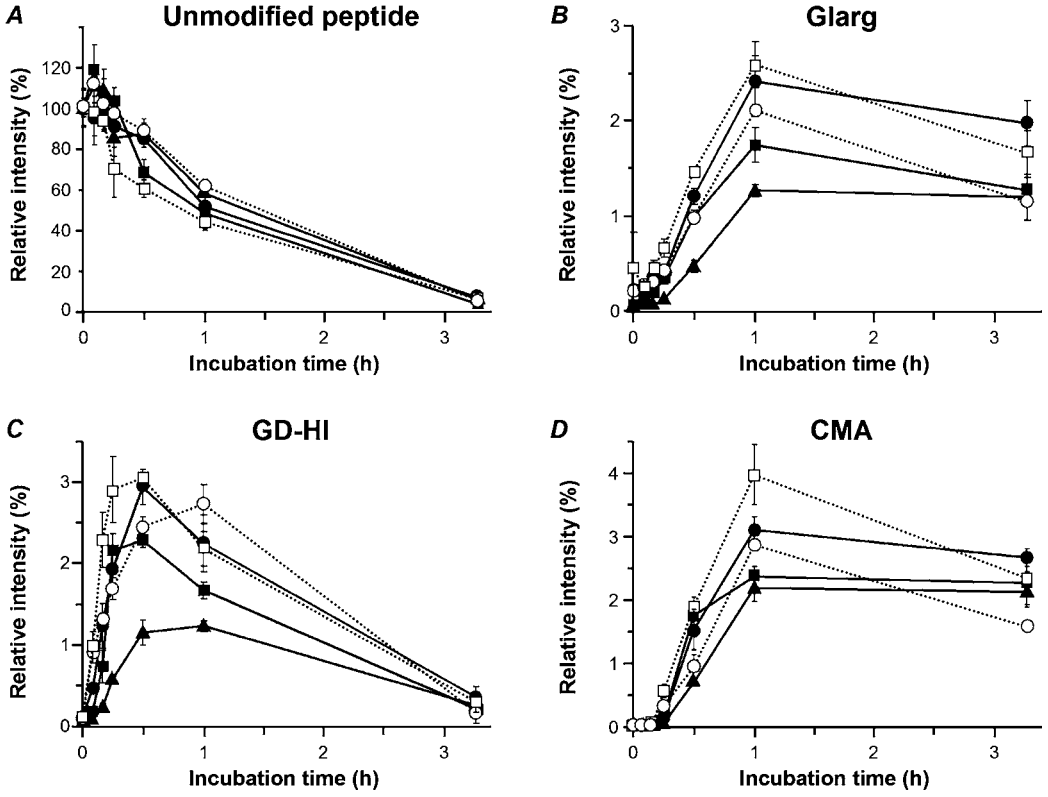

Figure 5. Time-course curves of unmodified (**1**, A), Glarg- (**1-2**, B), GD-HI- (**1-3**, C) and CMA-modified peptides (**1-5**, D) observed after incubation of peptide **1** with D-glucose and different concentrations of iron(II) and ascorbate. Peptide **1** was incubated at 95 °C with D-glucose (25 mmol/L) in phosphate buffer (▲) containing 18 μmol/L $Fe(II)SO_4$ (■), 590 μmol/L $Fe(II)SO_4$ (●), 18 μmol/L $Fe(II)SO_4$ and 60 μmol/L ascorbate (□), or 590 μmol/L $Fe(II)SO_4$ and 1.2 mmol/L ascorbate (○). Samples were analyzed by RPC-ESI-QqTOF-MS in a positive ion mode after incubation periods of 0, 5, 10, 15, 30, 60, and 195 min. Intensities were calculated as peak areas by integrating the XICs (n = 3) of the doubly protonated quasimolecular ions (±0.10 m/z-units).

DISCUSSION

Peptide Sequence and Incubation Conditions. To simplify the data analysis and to obtain mostly Arg-derived modifications at a single position, the peptide sequence consisted only of Ala, Gly, and Ser. These three amino acids are relatively inert against oxidation and do not react with intermediately formed aldehydes, such as glyoxal and methylglyoxal. At the same time they are relatively polar and thus guarantee a good solubility, even when the guanidino-group is transformed to a hydrophobic AGE. The only reactive groups would be the N-terminus, which could even be glycated, and the C-terminus. To avoid any degradation at the termini, these were blocked by acetylation and amidation, respectively. Additionally, Arg was flanked by two inert Ala-residues, which contain only a side-chain methyl-group that is unlikely to interfere sterically with reactions at the guanidino-group. Finally and very important for deducing AGE-modified peptides, the tandem mass spectra of model peptide Ac-ASGAGSARAS-GAASA-NH_2 (**1**) displayed an almost complete b-series at similar intensities all over the mass spectrum (SI Figure S-1A). Therefore, although proline would prevent ordered structures, it was excluded from the sequence, to avoid any influence on the fragmentation pattern and interference with modification-specific signals.[27]

The selected D-glucose concentration corresponded to the highest levels occurring in mammals,[28,29] which represent a good landmark for the maximal "natural" sugar load in protein-rich food. The iron(II) concentration was similar to the levels found in blood and tissue.[30]

Qualitative Analysis of Arg-Derived AGEs. The pattern of identified glyoxal-derived products (GD-HI, Glarg, and CMA) matched well to data reported previously for amino acids.[8] As we observed only one symmetrical chromatographic peak for MG-H (SI Figure S-4), it remains unclear if only one of the three reported MG-H-isomers was produced or several that were not resolved by RP-HPLC. At the amino acid level, this separation is achieved significantly easier than in a 15-residue-long peptide, where the relatively polar MG-H will only slightly contribute to the retention. Thus, further studies using shorter peptides are necessary to provide a better chromatographic separation.

Recently MGD-HI was proposed as an intermediate of MG formation using methylglyoxal and Boc-protected arginine.[22] This compound was indeed detected here and tentatively identified by its characteristic MS/MS fragmentation pattern. Most likely it is more stable within a peptide or protein sequence than at the amino acid level, which would indicate an influence of the α-carboxyl-group on the product stability.

In spite of ornithine not being considered as an AGE product, it is a well-known marker of Arg-related AGEs in proteins.[31] Here, we could show that Arg can lose urea at significant levels and that the obtained Orn is relatively quickly degraded afterward, most likely through glycation of its δ-amino group. Nevertheless, this possibility was not further investigated.

dx.doi.org/10.1021/jf4050183 | J. Agric. Food Chem. 2014, 62, 3626−3635

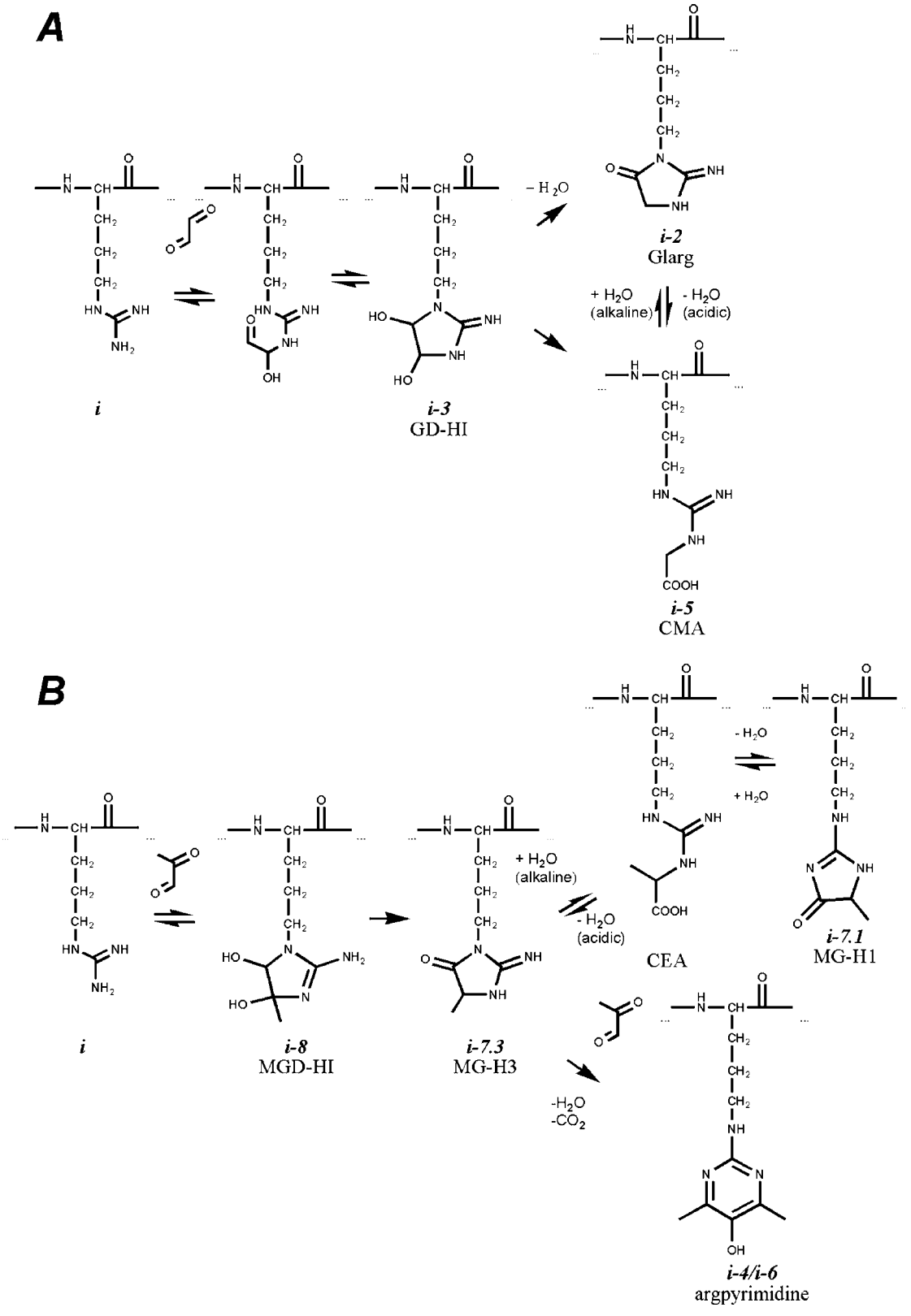

Figure 6. Proposed pathways of the formation of arginine-related peptide glyoxal- (A) and methylglyoxal- (B) derived glycation end-products.

The fragmentation patterns of AGE-containing peptides by CID displayed many internal fragment ions, which were not observed for the unmodified peptide and thus can be considered as characteristic for AGE-modified peptides containing hydroimidazolinone or dihydroxyimidazolidine groups (SI Figure S-1B–E and Table S-1). These signals likely originated from the nucleophilic attack of the imino nitrogen on a carbonyl C atom of the peptide backbone[32] These internal fragments and the immonium ions (Im-NH_3) distinguished isobaric dihydroxyimidazolidine from carboxymethylated or

dx.doi.org/10.1021/jf4050183 | J. Agric. Food Chem. 2014, 62, 3626–3635

carboxyethylated species. The patterns of these signals in the product ion mass spectra of GD-HI-modified peptide **1-3** (m/z 645.8) and the Glarg-modified peptide **1-2**, for example, were quite similar (SI Figures S-1C and S-2B, respectively). In contrast, the tandem mass spectrum of CMA-modified peptide **1-5** did not display any of these internal fragments (SI Table S-1). Thus, the increment mass of 214 m/z-units indicated CMA at position 8 (SI Figure S-1E).

The two weak signals at m/z 656.8 eluting at 18.5 and 18.8 min were annotated as argpyrimidine-containing peptides (**1-4** and **1-6**, Table 1), but the tandem mass spectra did not provide sufficiently intense signals to deduce their structures. Obviously, the low levels of methylglyoxal produced by oxidation of glucose reduced the probability that the guanidino group can react with two dicarbonyl molecules before the intermediate undergoes further modifications. This confirms earlier reports that the reaction of MG-H3 with a second methylglyoxal molecule requires high dicarbonyl concentrations and long incubation times at the amino acid level.[22] Our data collected under physiological conditions indicate, however, that these AGE-modifications will be produced at very low levels in vivo.

Mechanistic Considerations of AGE-Formation and Degradation. Although signal intensities in ESI-MS depend on many factors and are difficult to judge even for closely related sequences, several Arg-derived AGE modifications have closely related structures and properties, and thus show similar ionization properties in peptides. This was shown, for example, for the model peptide and its Glarg- and MG-H2-modified versions that were displayed in the mass spectra at very similar intensities (SI Figure S-5). Only the carboxyl groups of CMA and CEA should significantly weaken their ionization. For hydroimidazolone-related AGE-modifications, the relative signal intensities are expected to be closely dependent upon their concentrations (SI Figure S-4). Thus, it is possible to quantify not only the signal intensity of a given AGE-modification at different time points, but also the relative contents of chemically related products, i.e. Glarg, GD-HI, MG-H, MGD-HI, and argpyrimidine.

The Glarg-modified peptide **1-2** showed a degradation time curve identical to that of its dihydroxyimidazolidine precursor GD-HI (**1-3**), though at a higher intensity after 30 min (Figure 3B). The spectral intensities of the CMA-modified peptide **1-5** were just below those of **1-2**, but considering the suppressive effect of the negatively charged carboxyl-group of CMA, peptide **1-5** was probably present at significantly higher quantities than **1-2** (Glarg) and especially **1-3** (GD-HI). The delayed appearance of **1-5** (CMA) relative to **1-2** (Glarg) and the earlier degradation of **1-3** (GD-HI) might indicate that GD-HI is the precursor of Glarg, which is further processed to CMA. This assumption is in full agreement with a mechanism proposed by Glomb and Lang at the amino acid level.[8] The authors observed a 50% conversion of Glarg to CMA within 6 h at 37 °C. The higher temperatures applied here should accelerate the reaction around 60-fold considering that chemical reactions are typically accelerated 2-fold when increasing the reaction temperatures by 10 °C. Thus, hydrolytic cleavage of the hydroimidazolone ring of Glarg appears to be the dominant pathway of CMA formation, though the ring-opening reaction of GD-HI might represent a minor pathway (Figures 3B and 6A).

Methylglyoxal-derived products MG-H (peptide **1-7**) and MGD-HI (peptide **1-8**) showed the same time dependence as the above-discussed glyoxal-derived AGEs (Figure 3B and C), but their signal intensities and thus their quantities were around 5−10 times lower than those for Glarg and GD-HI, respectively. This difference can be explained by the higher glyoxal concentrations in comparison to methylglyoxal during glucose degradation.[33] Therefore, a lesser amount of MG-H was produced than Glarg during the first 15 min (Figure 2C). The degradation of Glarg and MG-H occurred at similar rates indicating that they are equally stable and their spectral decrease results mostly from peptide degradation. The same appears to be true for MGD-HI and GD-HI (Figure 3B and C).

The mechanisms of hydroimidazolinone formation and degradation were comprehensively evaluated by incubating Boc-Arg-OH with methylglyoxal.[22] The authors proposed the formation of MG-H3 through a dihydroxy-imidazolidine precursor, but could not detect it. This intermediate was, however, detected in tryptic digests of human plasma treated with methylglyoxal in vitro,[34] indicating, in line with our findings, that MGD-HI is more stable in peptides and proteins than in Boc-Arg-OH. At neutral pH MG-H3, its hydrolysis product CEA, and MG-H1 form an equilibrium.[22] As we detected only MG-H, the CEA-product was present at significantly lower levels (below the detection limit) indicating that the equilibrium was shifted to the most stable product MG-H1. This would also explain why we detected only a single MG-H peak, corresponding to MG-H1 whereas MG-H3 was below the detection limit. Alternatively, MG-H3 could be further processed, for example to argpyrimidine. In this case analogue **1-7** would also correspond to MG-H1. This could be clarified by NMR, but NMR spectroscopy requires considerably larger amounts of samples. This was not further investigated, as the functional effects of MG-H do not appear to depend upon the isomer.

The increasing amounts of the Orn-containing peptide confirm the proposed equilibrium between AGE formation and cleavage,[31] which may involve a ring-opening reaction with a subsequent nucleophilic attack of the guanidine nitrogen on the β-C atoms of CMA or CEA. Among the two products annotated as argpyrimidine, only **1-6** accumulated over time as reported previously for Boc-Arg-OH at 37 °C.[22] The intensities of argpyrimidine and MG-H pseudomolecular ions were quite similar, though glucose is slowly degraded to methylglyoxal under the applied conditions.[33] Assuming similar ionization efficiencies for both peptides, our findings indicate that argpyrimidine but not CEA was the main product of MG-H transformation. Thus, the detected hydroimidazolone was presumably MG-H3, which reacted more or less quantitatively with a second methylglyoxal molecule to yield argpyrimidine (peptide **1-6**). Based on the kinetics of **1-6** and **1-7** it can be concluded that either (i) MG-H is not the only precursor of argpyrimidine, or (ii) at least one relatively stable MG-H-derived intermediate of argpyrimidine formation exists though not detected here (Figure 6B).

Neighbor Group Effect. In vitro and in vivo data indicate that basic and acidic residues in the *i+4* position (nearest side chain in an α-helix) modulate both Schiff base formation and Amadori-rearrangement[35,36] whereas such neighbor group effects have not been investigated for Arg-derived AGE-modifications. Thus, we studied the influence of Glu- and His-substitutions at position 12 (*i+4* relative to Arg-8). As the basic or acidic residue altered the ionization efficiencies relative to the original peptide, the peak areas were normalized to the preincubation peak area of each peptide (SI Figure S-3).

dx.doi.org/10.1021/jf4050183 | J. Agric. Food Chem. 2014, 62, 3626−3635

His substitution yielded higher Glarg quantities, while the negatively charged Glu reduced them (Figure 4A). Both observations can be explained by the proton-catalyzed formation of Glarg.[8] The protonated His residue should favor this reaction whereas the deprotonated Glu residue would disfavor it. This His effect was also obtained for GD-HI-modified peptide 3 (Figure 4B). Considering additionally the kinetics of the Glarg-containing peptides (Figure 4A), Glu most likely suppressed the dehydration process of GD-HI accompanied by Glarg formation (Figure 6A). Remarkably, the basic and acidic residues did not affect the rate of GD-HI formation. Hence, the stabilizing effect that prevents degradation of Glarg- and CMA-containing peptides might be more important than the catalytic effect. Interestingly, this stabilization was also observed for MGD-HI, but not for its direct product MG-H (Figure 4E and D, respectively).

The presence of Glu drastically reduced the quantities of CMA (Figure 4C), most likely by forming an ion pair with Glarg. This would increase the electron density of the hydroimidazolone ring in position C-5 and thus reduce the strength of the nucleophilic addition of a hydroxide, the reaction of which initiates the bond cleavage between C_4 and C_5 to convert Glarg into CMA. Additionally, the negative charge of the carboxylate might also prevent the nucleophilic attack of the hydroxide.

Variation of Oxidation Conditions. As the initially chosen incubation conditions yielded dominantly glyoxal-derived AGEs (peptides **1**-**2**, **1**-**3**, and **1**-**5**), the oxidation conditions were varied assuming that ROS production levels might influence peptide degradation rates and AGE patterns. Thus, the H_2O_2-driven Fenton reaction[37] was studied for trace, low, and high iron(II) concentrations, and enhanced by ascorbate-mediated Fe(III) reduction.[38,39]

The higher peptide degradation rates observed for low additive concentrations (Figure 5A) may indicate a dual role of ascorbate with pro-oxidative effects at low concentrations and antioxidative properties at high concentrations.[38] Expectedly, the opposite effects were obtained for the AGE modifications (Figure 5B–D). Most probably, iron(II) had a pro-oxidative effect by accelerating metal-catalyzed autoxidation of glucose and thus favored the production of α-dicarbonyls (glyoxal and methylglyoxal),[25] whereas ascorbate had only a low influence. Remarkably, GD-HI (**1**-**3**) was produced much faster than Glarg (**1**-**2**) and CMA (**1**-**3**), which both showed similar formation rates. This correlates to the reportedly faster glucose oxidation caused by higher ROS quantities[25] and thus higher levels of glyoxal. Remarkably, both Glarg- and CMA-containing peptides were stable in the absence of iron(II) and only slowly degraded in the presence of iron(II). The addition of ascorbate increased the degradation of both peptides strongly, very similar to that of GD-HI that was very labile under all conditions.

Our observations clearly indicate that glycoxidation is a relatively fast process with many products already formed after short periods of elevated temperatures. Whereas the peptides were relatively stable in the absence of sugars when heated under air atmosphere, the addition of D-glucose drastically accelerated peptide degradation including the formation of seven different AGE products, a process that was even more pronounced in the presence of low iron(II) concentrations, a condition characteristic to commercial meat products. Hence, cooking of protein-rich food in the presence of sugars can produce presumably toxic compounds within a few minutes. It should be noted, however, that the content of these AGE-modified peptides decreased for longer heating periods, although it is unclear if only the peptide was further degraded leading to a heterogeneous mixture of small peptides and amino acids not detectable by RPC-ESI-MS or if the AGE modification itself was eliminated along with cleavage of the peptide chain. Since this issue remains to be answered to evaluate the potential toxicity of AGEs produced during cooking, further research is needed to characterize the formation and degradation of peptide- and protein-related AGEs using conditions more closely mimicking household food cooking protocols.

■ ASSOCIATED CONTENT

Supporting Information

Table S-1, Modification-specific internal fragment ions of peptide 1; Figure S-1, Tandem mass spectra of the unmodified peptide 1 and its AGE-modified products; Figure S-2, Initial peak areas of peptides 1, 2, and 3 calculated from XICs; Figure S-3, Stability of peptides 1 to 3 at 95 °C; Figure S-4, Reversed-phase and extracted ion chromatograms of peptide 1; Figure S-5, Signal intensities of peptide H-AGSARASGFA-NH_2 and related AGEs. This material is available free of charge via the Internet at http://pubs.acs.org.

■ AUTHOR INFORMATION

Corresponding Author

*Tel: +49 (0) 341 9731330. Fax: +49 (0) 341 9731339. E-mail: hoffmann@chemie.uni-leipzig.de.

Author Contributions

†Authors A.F. and R.S. contributed equally in the manuscript.

Notes

The authors declare no competing financial interest.

■ ACKNOWLEDGMENTS

Financial support from the "Deutsche Forschungsgemeinschaft" (DFG, HO-2222/7-1), the European Fund for Regional Structure Development (EFRE, European Union and Free State Saxony), the "Bundesministerium für Bildung and Forschung" (BMBF), and a stipend to U.G. provided by the Ernst Schering Foundation is gratefully acknowledged.

■ REFERENCES

(1) Ulrich, P.; Cerami, A. Protein glycation, diabetes, and aging. *Recent Prog. Horm. Res.* **2001**, *56*, 1–21.

(2) Hodge, J. E. The Amadori rearrangement. *Adv. Carbohydr. Chem.* **1955**, *10*, 169–205.

(3) Heyns, K.; Noack, H. Die Umsetzung von D-Fructose mit L-Lysine und L-Arginin und deren Beziehung zu nichtenzymatischen Bräunungsreaktionen. *Chem. Ber.* **1962**, *95*, 720–727.

(4) Grillo, M. A.; Colombatto, S. Advanced glycation end-products (AGEs): involvement in aging and in neurodegenerative diseases. *Amino Acids* **2008**, *35*, 29–36.

(5) Betts, M. J.; Russell, R. B. Amino acid properties and consequences of substitutions. In *Bioinformatics for Geneticists*; Barnes, M. R., Gray, I. C., Eds.; John Wiley & Sons, Ltd: New York, 2003; pp 289–316.

(6) Ahmed, N.; Thornalley, P. J.; Dawczynski, J.; Franke, S.; Strobel, J.; Stein, G.; Haik, G. M. Methylglyoxal-derived hydroimidazolone advanced glycation end-products of human lens proteins. *Invest. Ophthalmol. Vis. Sci.* **2003**, *44* (12), 5287–5292.

(7) Schwarzenbolz, U.; Henle, T.; Haeßner, R.; Klostermeyer, H. On the reaction of glyoxal with proteins. *Z. Lebensm. Unters. Forsch. A* **1997**, *205*, 121–124.

(8) Glomb, M. A.; Lang, G. Isolation and characterization of glyoxal-arginine modifications. *J. Agric. Food Chem.* **2001**, *49* (3), 1493−1501.
(9) Henle, T.; Walter, A. W.; Haeßner, R.; Klostermeyer, H. Detection and identification of a protein-bound imidazolone resulting from the reaction of arginine residues and methylglyoxal. *Z. Lebensm. Unters. Forsch.* **1994**, *199*, 55−58.
(10) Ahmed, N.; Argirov, O. K.; Minhas, H. S.; Cordeiro, C. A.; Thornalley, P. J. Assay of advanced glycation endproducts (AGEs): Surveying AGEs by chromatographic assay with derivatization by 6-aminoquinolyl-N-hydroxysuccinimidyl-carbamate and application to N^{ε}-carboxymethyl-lysine- and N^{ε}-(1-carboxyethyl)lysine-modified albumin. *Biochem. J.* **2002**, *364* (Pt 1), 1−14.
(11) Gruber, P.; Hofmann, T. Chemoselective synthesis of peptides containing major advanced glycation end-products of lysine and arginine. *J. Pept. Res.* **2005**, *66* (3), 111−124.
(12) Shipanova, I. N.; Glomb, M. A.; Nagaraj, R. H. Protein modification by methylglyoxal: Chemical nature and synthetic mechanism of a major fluorescent adduct. *Arch. Biochem. Biophys.* **1997**, *344* (1), 29−36.
(13) Oya, T.; Hattori, N.; Mizuno, Y.; Miyata, S.; Maeda, S.; Osawa, T.; Uchida, K. Methylglyoxal modification of protein. Chemical and immunochemical characterization of methylglyoxal-arginine adducts. *J. Biol. Chem.* **1999**, *274* (26), 18492−18502.
(14) Henle, T. Protein-bound advanced glycation end-products (AGEs) as bioactive amino acid derivatives in foods. *Amino Acids* **2005**, *29* (4), 313−322.
(15) Ahmed, N.; Thornalley, P. J. Advanced glycation endproducts: What is their relevance to diabetic complications? *Diabetes, Obes. Metab.* **2007**, *9* (3), 233−245.
(16) Price, C. L.; Knight, S. C. Advanced glycation: A novel outlook on atherosclerosis. *Curr. Pharm. Des.* **2007**, *13* (36), 3681−3687.
(17) Thornalley, P. J.; Rabbani, N. Highlights and hotspots of protein glycation in end-stage renal disease. *Semin. Dial.* **2009**, *22* (4), 400−404.
(18) Ahmed, N.; Thornalley, P. J.; Dawczynski, J.; Franke, S.; Strobel, J.; Stein, G.; Haik, G. M. Methylglyoxal-derived hydroimidazolone advanced glycation end-products of human lens proteins. *Invest. Ophthalmol. Vis. Sci.* **2003**, *44* (12), 5287−5292.
(19) Koschinsky, T.; He, C. J.; Mitsuhashi, T.; Bucala, R.; Liu, C.; Buenting, C.; Heitmann, K.; Vlassara, H. Orally absorbed reactive glycation products (glycotoxins): An environmental risk factor in diabetic nephropathy. *Proc. Natl. Acad. Sci. U. S. A* **1997**, *94* (12), 6474−6479.
(20) Goh, S. Y.; Cooper, M. E. Clinical Review: The role of advanced glycation end products in progression and complications of diabetes. *J. Clin. Endocrinol. Metab.* **2008**, *93*, 1143−1152.
(21) Schmidt, A. M.; Stern, D. M. RAGE: A new target for the prevention and treatment of the vascular and inflammatory complications of diabetes. *Trends Endocrinol. Metab.* **2000**, *11* (9), 368−375.
(22) Klopfer, A.; Spanneberg, R.; Glomb, M. A. Formation of arginine modifications in a model system of N^{α}-tert-butoxycarbonyl (Boc)-arginine with methylglyoxal. *J. Agric. Food Chem.* **2011**, *59* (1), 394−401.
(23) Rich, D. H.; Singh, J. The Carbodiimide Method. In *The Peptides*; Gross, E., Meinenhofer, J., Eds.; Academic Press: New York, 1979; pp 241−261.
(24) Amici, A.; Levine, R. L.; Tsai, L.; Stadtman, E. R. Conversion of amino acid residues in proteins and amino acid homopolymers to carbonyl derivatives by metal-catalyzed oxidation reactions. *J. Biol. Chem.* **1989**, *264* (6), 3341−3346.
(25) Wolff, S. P.; Dean, R. T. Glucose autoxidation and protein modification. The potential role of "autoxidative glycosylation" in diabetes. *Biochem. J.* **1987**, *245* (1), 243−250.
(26) Berlett, B. S.; Stadtman, E. R. Protein oxidation in aging, disease, and oxidative stress. *J. Biol. Chem.* **1997**, *272* (33), 20313−20316.
(27) Papayannopoulos, I. A. The interpretation of collision-induced dissociation tandem mass spectra of peptides. *Mass Spectrom. Rev.* **1995**, *14*, 49−73.
(28) Fox, A.; Eastwood, C.; Gentry, C.; Manning, D.; Urban, L. Critical evaluation of the streptozotocin model of painful diabetic neuropathy in the rat. *Pain* **1999**, *81* (3), 307−316.
(29) Shimomura, I.; Bashmakov, Y.; Ikemoto, S.; Horton, J. D.; Brown, M. S.; Goldstein, J. L. Insulin selectively increases SREBP-1c mRNA in the livers of rats with streptozotocin-induced diabetes. *Proc. Natl. Acad. Sci. U. S. A* **1999**, *96* (24), 13656−13661.
(30) Jacobs, A.; Miller, F.; Worwood, M.; Beamish, M. R.; Wardrop, C. A. Ferritin in the serum of normal subjects and patients with iron deficiency and iron overload. *Br. Med. J.* **1972**, *4* (5834), 206−208.
(31) Sell, D. R.; Monnier, V. M. Conversion of arginine into ornithine by advanced glycation in senescent human collagen and lens crystallins. *J. Biol. Chem.* **2004**, *279* (52), 54173−54184.
(32) Bythell, B. J.; Csonka, I. P.; Suhai, S.; Barofsky, D. F.; Paizs, B. Gas-phase structure and fragmentation pathways of singly protonated peptides with N-terminal arginine. *J. Phys. Chem. B* **2010**, *114* (46), 15092−15105.
(33) Phillips, S. A.; Thornalley, P. J. The formation of methylglyoxal from triose phosphates. Investigation using a specific assay for methylglyoxal. *Eur. J. Biochem.* **1993**, *212* (1), 101−105.
(34) Kimzey, M. J. Identification, characterization, and quantification of dicarbonyl adducts in the plasma proteome in type-2 diabetes. Doctoral Dissertation. The University of Arizona, Department of Pharmaceutical Sciences: Tucson, AZ, 2011.
(35) Venkatraman, J.; Aggarwal, K.; Balaram, P. Helical peptide models for protein glycation: Proximity effects in catalysis of the Amadori rearrangement. *Chem. Biol.* **2001**, *8* (7), 611−625.
(36) Zhang, Q.; Monroe, M. E.; Schepmoes, A. A.; Clauss, T. R.; Gritsenko, M. A.; Meng, D.; Petyuk, V. A.; Smith, R. D.; Metz, T. O. Comprehensive identification of glycated peptides and their glycation motifs in plasma and erythrocytes of control and diabetic subjects. *J. Proteome Res.* **2011**, *10* (7), 3076−3088.
(37) Jomova, K.; Vondrakova, D.; Lawson, M.; Valko, M. Metals, oxidative stress and neurodegenerative disorders. *Mol. Cell. Biochem.* **2010**, *345* (1−2), 91−104.
(38) Buettner, G. R.; Jurkiewicz, B. A. Catalytic metals, ascorbate and free radicals: combinations to avoid. *Radiat. Res.* **1996**, *145* (5), 532−541.
(39) Bollineni, R. C.; Fedorova, M.; Hoffmann, R. Identification of carbonylated peptides by tandem mass spectrometry using a precursor ion-like scan in negative ion mode. *J. Proteomics* **2011**, *74* (11), 2351−2359.

Table 1. Protein, Lipid, and Amylose Contents, Average Particle Size, Relative Crystallinity (XRD), and Short-Range Order (FTIR) of Native and Alkali-Treated Starches[a]

samples	protein content (%)	lipid content (%)	amylose content (%)	average particle size (μm)	XRD crystallinity (%)	FTIR 1045/1022 ratio
native starch	0.46 ± 0.02 d	0.59 ± 0.03 c	27.1 ± 0.8 a	21.1 ± 0.02 a	32.7	0.658
0.1% 1W	0.34 ± 0.07 c	0.38 ± 0.02 b	27.9 ± 0.7 a	21.1 ± 0.02 a	31.6	0.650
0.1% 2W	0.30 ± 0.02 bc	0.36 ± 0.05 b	27.7 ± 0.5 a	21.1 ± 0.10 a	31.4	0.651
0.1% 3W	0.31 ± 0.04 bc	0.35 ± 0.04 b	27.4 ± 0.7 a	21.2 ± 0.10 a	31.5	0.649
0.25% 1W	0.26 ± 0.06 ab	0.28 ± 0.01 a	26.9 ± 0.6 a	24.6 ± 0.03 b	31.4	0.648
0.25% 2W	0.25 ± 0.05 ab	0.26 ± 0.02 a	27.4 ± 1.0 a	25.8 ± 0.04 c	31.4	0.649
0.25% 3W	0.20 ± 0.02 a	0.25 ± 0.03 a	26.8 ± 0.6 a	25.5 ± 0.04 c	31.5	0.647

[a]XRD and FTIR calculations are within SD of 2%. Values are the mean ± SD. Values with the same letters in the same column are not significantly different ($p < 0.05$).

addition on the properties of starch seems to be very important. In this study, we aimed at determining the effect of alkali treatment on functionality and *in vitro* enzymic digestibility of bread wheat starch. The information obtained will be very useful in understanding the effect of NaOH addition on the quality and nutrition of starchy food products.

EXPERIMENTAL SECTION

Materials. Beijing 0045 is a leading hard wheat variety in the northern China plain region. Sound grains harvested in 2011−2012 season were provided by the Institute of Crop Science, Chinese Academy of Agricultural Science. Dried wheat grains were tempered and milled into flour using a Buhler Experimental Mill (Buhler Bros, Uzwil, Switzerland), with the flour yield of 75%. Starch was isolated from wheat flour using a dough ball method.[21]

Preparation of Alkali-Treated Starch. Alkali-treated starch was prepared according to Wang and Copeland,[22] with minor modifications. Three lots of wheat starch (10 g, dry weight) were each suspended in 100 mL of 0.025 and 0.0625 M NaOH solution. After incubation at 30 °C for 1, 2, and 3 weeks with intermittent shaking by hand to resuspend the starch granules, the slurry was filtered through Whatman No. 1 filter paper with suction. The starch cake was washed with distilled water until the pH value of the filtrate was 7 and then washed twice with water-free ethanol. The resulting alkali-treated starch was dried overnight at room temperature.

Protein and Lipid Contents. The nitrogen content of starch samples was determined by standard Kjeldahl methodology. The protein content (%) was then calculated from protein (%) = nitrogen (%) × 6.25. The lipid content of starches was determined gravimetrically after extraction with ether at 60−70 °C for 6−8 h.

Apparent Amylose Content. The apparent amylose content was determined by the iodine binding colorimetric method.[23]

Starch Crystallinity. Starch crystallinity was measured using a Panalytical X'Pert Pro X-ray diffractometer (PANalytical, Eindhoven, Netherlands) with a Co Kα source (λ = 0.1789 nm) operating at 45 kV and 35 mA. The detailed operating conditions and sample treatment before measurement were described elsewhere.[24] The relative crystallinity was quantitatively estimated as a ratio of the crystalline area to the total area between 4 and 40° (2θ) using the Origin software (version 7.5, Microcal, Inc., Northampton, MA).

Fourier Transform Infrared (FTIR) Spectroscopy. The infrared (IR) spectra were obtained with a Bruker Tensor 27 FTIR scanner (Bruker, Germany). The starch samples were mixed with KBr powder in a weight ratio of 1:150 and then ground finely. The resulting fine powders were pressed into the transparent round tablets and tested by the transmission method. The sample holder with KBr was used for the background spectra, and 64 co-added scans were taken for each sample from 4000 to 400 cm^{-1} at a resolution of 4 cm^{-1}. The samples were dried at 105 °C for 12 h before analysis to avoid interference by moisture. The ratio of absorbance at 1045 to that at 1022 cm^{-1} was calculated to represent the short-range ordered structure of starch.[25]

Granule Morphology. Native and alkali-treated starches were fixed onto the surface of double-sided, carbon-coated adhesive tape attached to an aluminum stub. The mounted starch samples were coated with gold prior to imaging in a scanning electron microscope (SU1510, Hitachi High-Technologies Corporation, Tokyo, Japan). The accelerating voltage was 10.0 kV.

Particle Size Distribution. The particle size distribution of native and alkali-treated starch granules was measured using laser light scattering (Mastersizer X, Malvern, U.K.). A polydisperse mode of analysis and a 300 mm lens were used. The starch was evenly dispersed in deionized water with magnetic agitation to attain an obscuration of 20−30%. The measurements were performed in duplicate. The median volume-based diameter was used to represent the average particle size.

Swelling Power and Starch Solubility. Swelling power (SP) and starch solubility (SS) of native and alkali-treated starches were determined in triplicate according to the method described elsewhere.[26]

Thermal Analysis. Thermal transition analysis of starch samples was made using a differential scanning calorimeter (DSC 200 F3, NETZSCH, Selb, Germany) equipped with a thermal analysis data station and data recording software. The operating conditions and definitions of thermal transition parameters were described elsewhere.[27]

Pasting Properties. The pasting profiles were analyzed using a Newport Scientific rapid visco analyzer 4 (RVA-4) (Newport Scientific, Warriewood, New South Wales, Australia). Starch slurries containing 8% (w/w) starch (dry weight) in a total weight of 28 g were held at 50 °C for 1 min before heating at a rate of 6 °C/min to 95 °C, holding at 95 °C for 5 min, then cooling at a rate of 6 °C/min to 50 °C, and held at 50 °C for 2 min. The speed of the mixing paddle was 960 rpm for the first 10 s and then 160 rpm for the remainder of the experiment. Peak viscosity (PV), viscosity at trough [also known as minimum viscosity (MV)], and final viscosity (FV) were recorded, and breakdown (BD, which is PV minus MV) and setback (SB, which is FV minus MV) were calculated using the Thermocline software provided with the instrument.

***In Vitro* Starch Digestibility.** *In vitro* starch digestibility was determined by a modified Englyst et al. procedure.[28] Amylase solution was prepared by suspending 1.3 g of porcine pancreatic α-amylase (28 units/mg, Sigma A3176) in 11.9 mL of water at 37 °C with magnetic stirring for 10 min. The mixture was centrifuged (1500*g* for 10 min) and 0.1 mL of amyloglucosidase (3260 units/mL, Megazyme) was added to 8 mL of the supernatant. Starch (100 mg) was dispersed in 4 mL of 0.1 M sodium acetate buffer (pH 5.2), and after adding 1 mL of the freshly prepared enzyme solution, the mixture was incubated at 37 °C with magnetic stirring (260 rpm). Aliquots (0.1 mL) were taken at intervals and mixed with 0.9 mL of 95% ethanol. The glucose released was measured by the glucose oxidase−peroxidase reagent (Megazyme). Starch classifications based on the rate of hydrolysis were rapidly digested starch (RDS, digested within 20 min), slowly digested starch (SDS, digested between 20 and 120 min), and resistant starch (RS, undigested starch after 120 min).

Statistical Analysis. All experiments were conducted at least twice, and the results were reported as the mean values and standard deviations (SDs). In the case of X-ray diffraction (XRD) and FTIR, only one measurement was performed. Analysis of variance (ANOVA) by Duncan's test ($p < 0.05$) was conducted using the SPSS 10.0 statistical software program (SPSS, Inc., Chicago, IL).

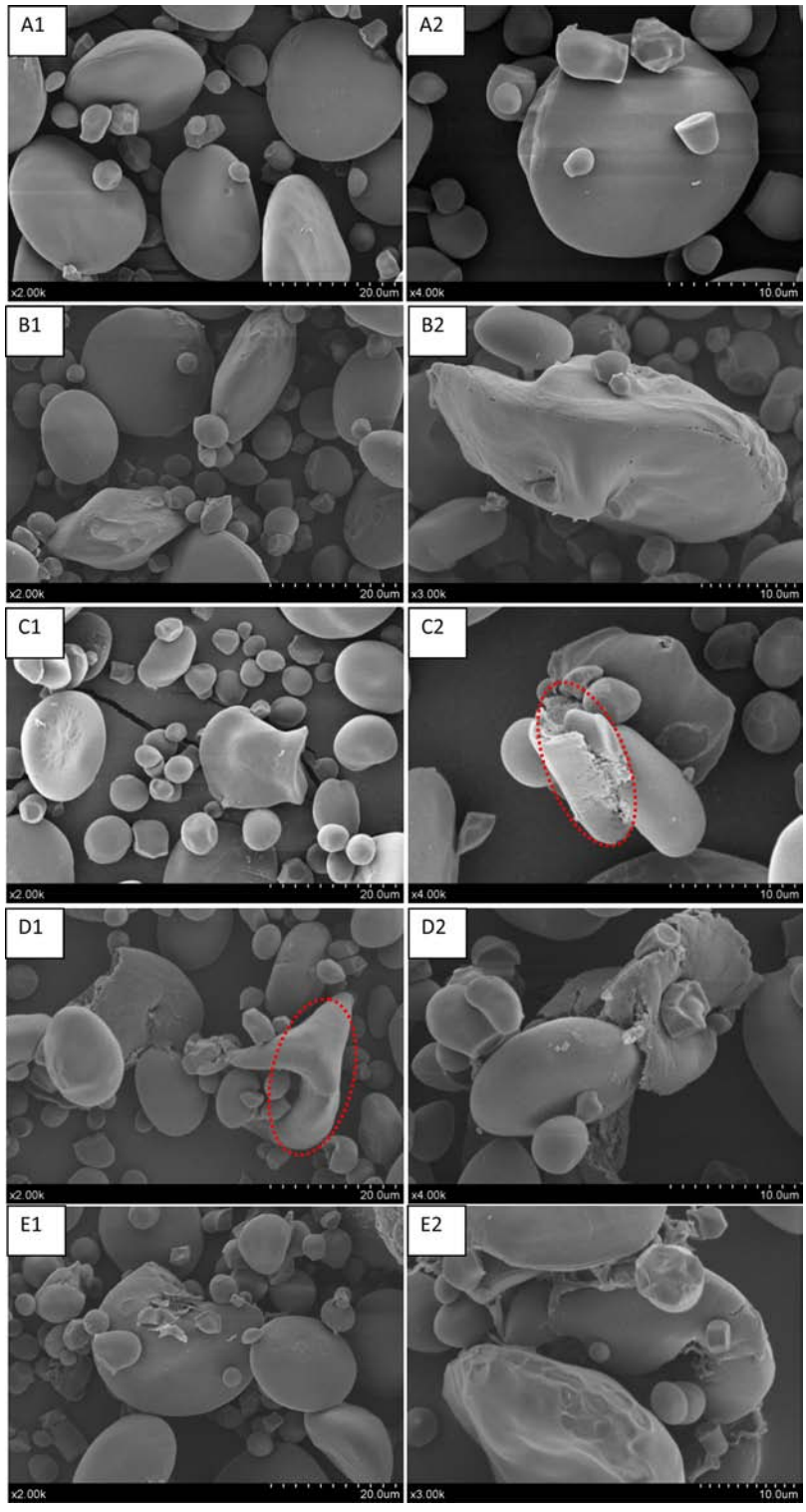

Figure 1. continued

dx.doi.org/10.1021/jf500249w | *J. Agric. Food Chem.* 2014, 62, 3636−3643

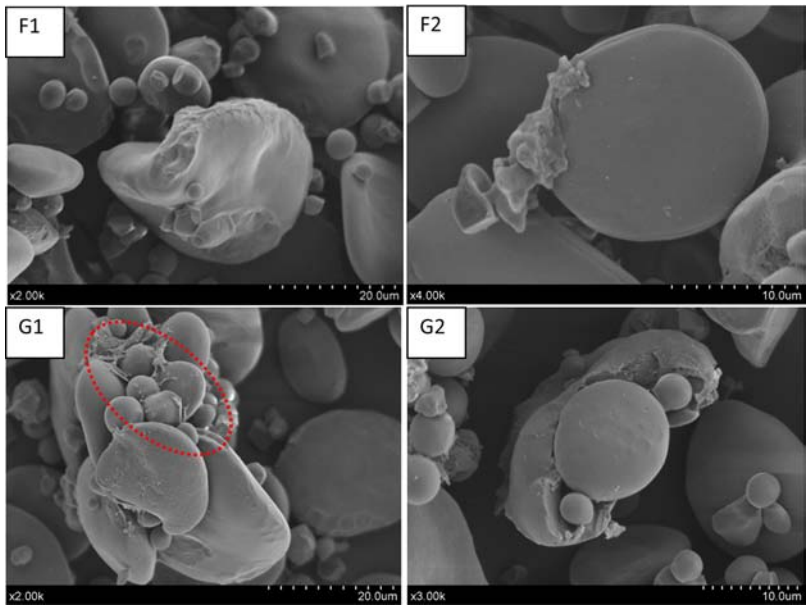

Figure 1. SEM photographs of native and alkali-treated wheat starch granules: (A1 and A2) native starch, (B1 and B2) 0.1% NaOH for 1 week, (C1 and C2) 0.1% NaOH for 2 weeks, (D1 and D2) 0.1% NaOH for 3 weeks, (E1 and E2) 0.25% NaOH for 1 week, (F1 and F2) 0.25% NaOH for 2 weeks, and (G1 and G2) 0.25% NaOH for 3 weeks.

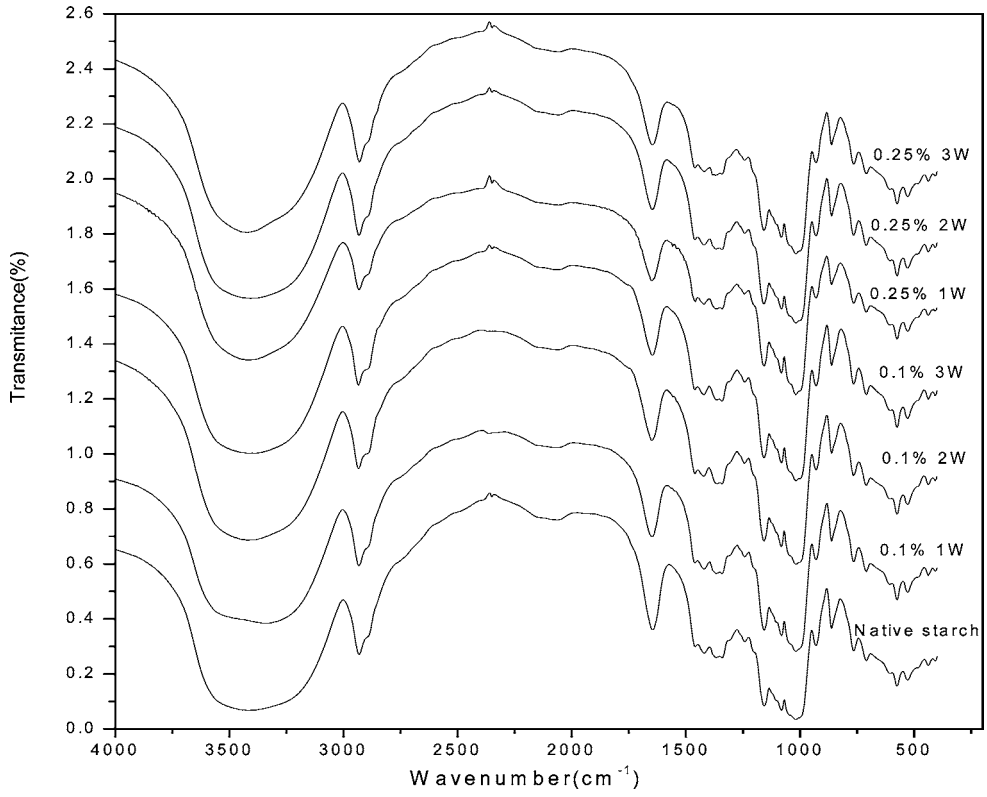

Figure 2. FTIR spectra of native and alkali-treated wheat starches.

RESULTS

Protein, Lipid, and Amylose Contents. Native wheat starch had a protein content of 0.46%, which was decreased significantly by alkali treatments (Table 1). After 0.1% NaOH treatment, the protein content decreased to 0.30−0.34%. The protein content decreased further when starch was treated with 0.25% NaOH. No significant differences were observed in the protein content of starches treated for different times. The lipid content decreased from 0.59% for native starch to 0.25% for starch treated with 0.25% NaOH for 3 weeks. Similarly, no significant differences were noted in the lipid content of starches treated for different times. The amylose content of native wheat starch was 27.1%, which remained essentially unchanged after alkali treatment.

Starch Granule Morphology and Particle Size Distribution. Native wheat starch was observed to be composed of

dx.doi.org/10.1021/jf500249w | J. Agric. Food Chem. 2014, 62, 3636−3643

two populations of granules, namely, large A-type granules and small B-type granules (Figure 1). The surface of granules was largely smooth, with some grooves or indentations. After 0.1% NaOH treatment, some starch granules were observed to be deformed or roughened on the surface (panel D1 of Figure 1). A very small proportion of granules was observed to be disrupted (panels C2 and D2 of Figure 1). These changes became more obvious after longer exposure to the alkali or after treatment with 0.25% NaOH. Some starch granules appeared to adhere to form some aggregates or agglomerates (panel G1 of Figure 1). In contrast, the large A-type granules were subjected to more severe damage than the small B-type granules. Native wheat starch had an average granule size of 21.1 μm. The 0.1% NaOH treatment did not cause significant changes in the average granule size. However, the average granule size increased significantly to about 25.0 μm after 0.25% NaOH treatment (Table 1).

FTIR of Native and Alkali-Treated Starches. The FTIR spectrum of native wheat starch is presented in Figure 2. The characteristic peaks at 3380 and 2930 cm^{-1} were attributed to the vibration of O−H stretching and the C−H deformation of the glucose unit, respectively. The absorbance at 1643 cm^{-1} was assigned to the vibration of O−H stretching of water absorbed in the amorphous regions of starch. There were three characteristic peaks occurring between 1019 and 1065 cm^{-1}, which were assigned to the vibration of C−O stretching. The peak at 1019 cm^{-1} was ascribed to the vibration of C−O−H deformation. Absorbances at 1080 and 1156 cm^{-1} were assigned to the coupling of C−O, C−C, and O−H bond stretching and bending and asymmetrical stretching of the C−O−C glycosidic bond.[25,29] Alkali treatment did not greatly alter the FTIR spectra of starch samples. However, there was a small decrease in the absorbance ratio at 1045 and 1022 cm^{-1} after alkali treatment (Table 1), from 0.658 for native starch to 0.647 for starch treated with 0.25% NaOH for 3 week.

XRD. Native wheat starch presented a characteristic XRD pattern of A-type polymorphs (Figure 3), with the diffraction

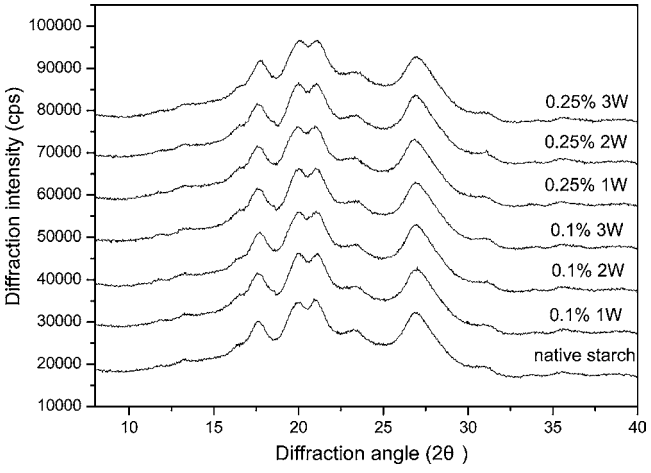

Figure 3. XRD patterns of native and alkali-treated wheat starches.

peaks occurring at 2θ 17.7°, 20.1°, 21.1°, and 26.9°. Alkali treatment did not change the polymorphic forms of wheat starch. The relative crystallinity of native wheat starch granules was about 32.7%, which slightly decreased to about 31.4−31.6% after alkali treatment (Table 1).

Swelling Power and Starch Solubility. Native wheat starch granules had a swelling power of 11.4 g/g, which increased significantly to 13.0−14.0 g/g after alkali treatment (Table 2). No significant differences were observed between alkali-treated starches. Likewise, alkali treatment resulted in the significant increase in starch solubility from 10.9% for native starch to 22.1% for starch treated with 0.25% NaOH for 3 weeks. The degree of increase varied with treatment time and NaOH concentration.

Thermal Transition. The thermal transition profiles of native and alkali-treated starches are presented in Figure 4, and the corresponding parameters are summarized in Table 2. The onset (T_o), peak (T_p), and conclusion (T_c) temperatures of wheat starch were 57.3, 61.7, and 66.1 °C, respectively. The enthalpy change (ΔH) was 9.3 J/g (Table 2). Alkali treatment resulted in the significant increase in T_o, T_p, and T_c of wheat starch. For example, T_o, T_p, and T_c increased to 61.7, 64.9, and 68.7 °C for starch treated with 0.25% NaOH for 3 weeks. Starch treated with 0.25% NaOH showed a greater increase in thermal transition temperatures than starch treated with 0.1% NaOH. For starch treated with 0.1% NaOH, longer treatment resulted in the greater increase in the thermal transition temperatures. However, no significant differences were observed between starches treated with 0.25% NaOH. The thermal transition temperature range ($T_c - T_o$) decreased from 8.8 °C for native starch to 7.0 °C for starch treated with 0.25% NaOH for 3 weeks, but the enthalpy change did not change significantly after alkali treatment.

Pasting Properties. The pasting profiles and parameters of wheat starch before and after alkali treatment are summarized in Figure 5 and Table 3, respectively. Alkali treatment increased breakdown viscosity and setback viscosity but decreased trough viscosity and pasting temperature. The 0.25% NaOH treatment decreased trough viscosity of wheat starch more greatly than the 0.1% NaOH treatment. However, the 0.1% NaOH treatment increased breakdown viscosity and setback viscosity of wheat starch more significantly than the 0.25% NaOH treatment. Alkali treatment significantly decreased the pasting temperature from 89.6 to 67.4 °C, with no significant differences being observed between alkali-treated starches. In contrast to the above pasting parameters, the peak and final viscosities were affected by alkali treatment in different ways. For example, the peak and final viscosities were increased after 0.1% NaOH treatment but decreased after 0.25% NaOH treatment.

***In Vitro* Enzymatic Digestibility.** The proportions of RDS, SDS, and RS in wheat starch were changed after alkali treatment (Table 4). Alkali treatment increased the RDS and SDS contents of starch granules significantly, with the latter being increased more greatly from 13.6% in native starch to 34.5% in starch treated with 0.25% NaOH for 2 weeks. Significant differences were noted in RDS and SDS contents between alkali-treated starches. In contrast to RDS and SDS, the RS content was decreased significantly from 69.9% in native starch to 45.2% in starch treated with 0.25% NaOH for 2 weeks. Likewise, significant differences were observed in the RS content between alkali-treated starches.

DISCUSSION

Effect of the Alkali Treatment on the Structure of Wheat Starch Granules. Alkali treatment decreased the protein and lipid contents of wheat starch significantly. Similar observations have also been reported with starches treated with alkali solution[13] and SDS buffer[7] or washed with alkali solution in starch extraction.[30−33] The decreased protein and lipid contents of alkali-treated starch could be attributed to the solubilization of surface starch granule-associated proteins and lipids as internal

Table 2. Swelling Power, Starch Solubility, and Thermal Transition Parameters of Native and Alkali-Treated Starches[a]

samples	SP (g/g)	SS (%)	T_o (°C)	T_p (°C)	T_c (°C)	$T_c - T_o$ (°C)	ΔH (J/g)
native starch	11.4 ± 0.1 a	10.9 ± 0.9 a	57.3 ± 0.1 a	61.7 ± 0.2 a	66.1 ± 0.1 a	8.8 ± 0.2 a	9.3 ± 0.6 a
0.1% 1W	13.6 ± 0.1 c	21.5 ± 0.6 d	58.7 ± 0.2 b	62.8 ± 0.0 b	67.4 ± 0.1 b	8.7 ± 0.1 a	10.7 ± 0.7 a
0.1% 2W	14.1 ± 0.5 d	19.2 ± 0.2 b	59.2 ± 0.1 b	63.4 ± 0.1 c	67.5 ± 0.1 b	8.3 ± 0.3 ab	9.8 ± 0.8 a
0.1% 3W	13.4 ± 0.2 bc	20.8 ± 1.2 cd	60.0 ± 0.1 c	63.8 ± 0.1 c	67.9 ± 0.2 bc	7.9 ± 0.2 b	10.4 ± 1.5 a
0.25% W	13.1 ± 0.1 bc	19.9 ± 0.1 bc	61.2 ± 0.1 d	64.5 ± 0.2 d	68.6 ± 0.5 c	7.4 ± 0.1 bc	9.8 ± 0.3 a
0.25% 2W	13.0 ± 0.8 b	21.4 ± 0.6 d	61.5 ± 0.5 d	64.8 ± 0.5 d	68.9 ± 0.9 c	7.4 ± 0.4 bc	9.6 ± 0.6 a
0.25% 3W	13.1 ± 0.1 bc	22.1 ± 0.3 d	61.7 ± 0.1 d	64.9 ± 0.1 d	68.7 ± 0.2 c	7.0 ± 0.1 c	10.5 ± 0.3 a

[a]Values are the mean ± SD. Values with the same letters in the same column are not significantly different ($p < 0.05$).

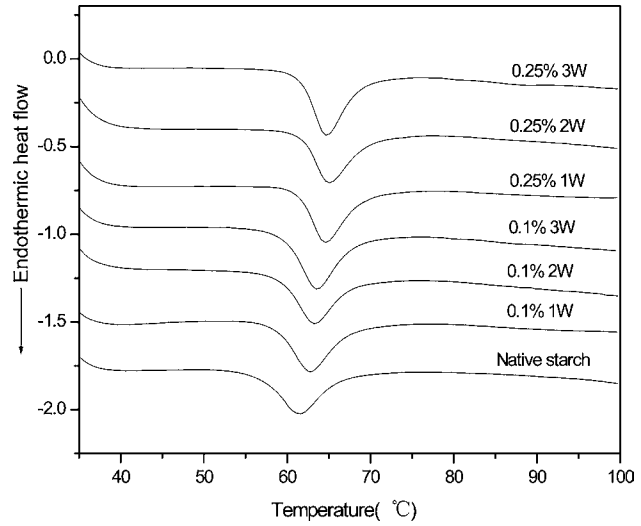

Figure 4. DSC thermograms of native and alkali-treated starches.

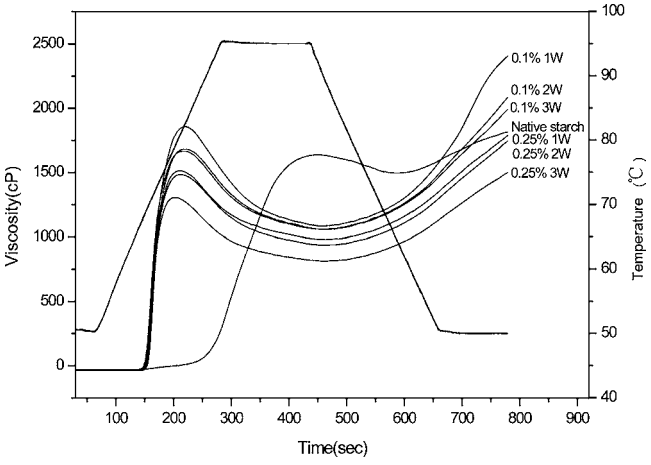

Figure 5. Pasting profiles of native and alkali-treated starches.

Table 4. Proportion of RDS, SDS, and RS in Native and Alkali-Treated Starches[a]

samples	RDS (%)	SDS (%)	RS (%)
native starch	16.5 ± 1.6 a	13.6 ± 1.7 a	69.9 ± 9.1 d
0.1% 1W	19.9 ± 1.0 b	28.8 ± 0.5 b	51.3 ± 0.5 c
0.1% 2W	19.3 ± 1.6 b	28.9 ± 2.4 b	51.8 ± 1.2 c
0.1% 3W	19.2 ± 2.0 b	31.2 ± 0.7 bc	49.6 ± 1.2 bc
0.25% 1W	19.7 ± 1.4 b	32.9 ± 3.0 c	47.4 ± 0.6 b
0.25% 2W	20.3 ± 2.4 bc	34.5 ± 2.1 d	45.2 ± 0.3 a
0.25% 3W	21.2 ± 1.3 c	33.3 ± 0.2 c	45.5 ± 0.1 a

[a]Values are the mean ± SD. Values with the same letters in the same column are not significantly different ($p < 0.05$).

proteins, and lipids are hardly extracted from the ungelatinized starch granules.[34] Alkali treatment did not change the amylose content of wheat starch significantly, indicating that leaching or degradation of amylose molecules did not occur during treatment. In previous studies, alkali treatment has been shown to decrease the amylose content of pea starch granules[22] or sago, corn, and potato starch granules.[13] The effect of alkali treatment on pea starch granules was regarded as being analogous to a limited form of gelatinization.[22] In this study, the alkali-induced gelatinization of wheat starch granules could be too limited to render the leaching or degradation of amylose molecules.

Alkali treatment resulted in the deformation, disruption, or coalescence of wheat starch granules, as was also noted for alkali-treated pea, sago, corn, and potato starches[13,22,35] or alkali-washed rice and pinhão starches.[30−32] The obvious morphological changes, such as disruption and coalescence, of starch granules after 0.25% NaOH treatment could result from the small swelling of wheat starch granules during alkali treatment, as evidenced by the small increase in the average particle size. The swelling of starch granules was proposed to mainly occur at amorphous growth rings and lamellae, with little effect on high-density crystalline lamellae.[32] As a result, the relative proportion of amorphous to crystalline regions increased, consistent with the observed small decrease in relative crystallinity and absorbance ratios from 1045 to 1022 cm^{-1} of alkali-treated starches. The

Table 3. Pasting Parameters of Native and Alkali-Treated Starches[a]

samples	PV (cP)	TV (cP)	BD (cP)	FV (cP)	SB (cP)	PT (°C)
native starch	1610 ± 42 bc	1314 ± 63 d	297 ± 21 a	1814 ± 79 b	501 ± 16 a	89.6 ± 1.2 b
0.1% 1W	1858 ± 50 d	1085 ± 18 c	773 ± 32 d	2406 ± 8 d	1321 ± 11 g	67.5 ± 0.8 a
0.1% 2W	1666 ± 54 c	1061 ± 29 bc	606 ± 25 c	2085 ± 23 c	1024 ± 6 f	67.4 ± 0.6 a
0.1% 3W	1683 ± 55 c	1059 ± 37 bc	625 ± 18 c	1990 ± 51 c	932 ± 13 e	68.2 ± 0.5 a
0.25% 1W	1514 ± 86 b	980 ± 47 b	535 ± 39 b	1788 ± 82 b	809 ± 35 d	68.3 ± 0.5 a
0.25% 2W	1363 ± 43 a	886 ± 30 a	477 ± 13 b	1616 ± 38 a	730 ± 8 c	68.7 ± 0.8 a
0.25% 3W	1304 ± 45 a	814 ± 22 a	491 ± 23 b	1500 ± 41 a	687 ± 19 b	68.7 ± 0.9 a

[a]Values are the mean ± SD. Values with the same letters in the same column are not significantly different ($p < 0.05$).

dx.doi.org/10.1021/jf500249w | J. Agric. Food Chem. 2014, 62, 3636−3643

decreased crystallinity of alkali-treated starch was also observed with pea,[22] pinhão,[32] and rice[30] starches.

Effect of the Alkali Treatment on Starch Functionality. Swelling power and starch solubility of the wheat starch were increased greatly by the alkali treatment. The considerable increase in swelling power of alkali-treated wheat starch could be attributed to the partial removal of surface proteins and lipids, which were considered to inhibit the swelling of starch granules. Similar results were also reported by other researchers.[7,10,11] In other studies, the observed increase in swelling power of alkali-treated corn and potato starches was attributed to the reduction of restraining effects of amylose in the amorphous regions, allowing for the granules to swell more freely.[13,35] Upon heating in excess water, alkali-treated starch granules were visually observed to form a more transparent and softer paste, which was poured out in a small amount with supernatant during the swelling power test. The separated paste in the supernatant was taken as solubilized starch, hence resulting in the large increase in starch solubility.

Alkali treatment increased the thermal transition temperatures of wheat starch but decreased the temperature range. Higher DSC transition temperatures are thought to be associated with a higher degree of crystallinity or more ordered crystalline structure, which makes the granules more resistant to be gelatinized. Because there was a small decrease in relative crystallinity, the increased gelatinization temperature and decreased temperature range indicated that the stability and homogeneity of the crystal structure of alkali-treated starch was enhanced in comparison to that of native starch. In addition to the solubilization of surface proteins and lipids, the annealing of starch granules during alkali treatment may also occur, which leads to the increased stability and homogeneity of the crystal structure.[36] The enthalpy change was little changed by alkali treatment, consistent with the slight decrease in the relative crystallinity of starch granules. Previous studies have shown that the effect of alkali treatment on the starch thermal transition varies with the alkali concentration, treatment period, and starch sources.[13,22,35]

Alkali treatment with 0.1% NaOH significantly increased the peak viscosity, with 1 week treatment leading to the greatest increase. The increase in peak viscosity is consistent with the increased swelling power of alkali-treated starches. In contrast, 0.25% NaOH treatment resulted in the decreased peak viscosity of wheat starch, with three week treatment causing the greatest decrease. The decrease in peak viscosity of alkali-treated starches with 0.25% NaOH seemed to be inconsistent with the increased swelling power. After treatment with 0.25% NaOH, starch granules were assumed to be more fragile to destruction (or amylopectin molecules more vulnerable to degradation), especially when heated under the shear forces.[22] The decreased peak viscosity after 0.25% NaOH treatment was indicative of the degradation of amylopectin molecules during RVA heating under shear forces. The degradation of amylopectin molecules was further corroborated by the decreased trough viscosity and increased breakdown viscosity of alkali-treated starches. The setback viscosity is thought to result from the rearrangement of amylose molecules that have leached from swollen starch granules during cooling and is indicative of the retrogradation tendency of starch.[37] The increased setback viscosity of alkali-treated starch indicated the faster retrogradation of starch paste. Alkali treatment decreased the pasting temperature by about 12 °C, indicating that alkali-treated starch has a more rapid swelling tendency than native starch. Alkali treatment has been shown to influence the pasting properties of starches in different ways, depending upon the alkali concentration, treatment period, temperature, and starch sources.[11,13,22,35]

Effect of the Alkali Treatment on Starch *in Vitro* Digestibility. Alkali treatment greatly decreased the RS content and increased the RDS and SDS contents, indicating the increased digestibility of wheat starch after alkali treatment. The increased digestibility of alkali-treated starch could be attributed to factors such as the removal of some surface proteins, roughening on the granule surface, disruption of starch granules, or increased amorphous regions in starch granules. The digestion of native starch granules is a very complex process consisting of the diffusion of the enzymes into the substrate, adsorption of enzymes to the substrate, and hydrolytic event.[38−40] Of these processes, the diffusion of α-amylase into the substrate is considered as a key step of hydrolysis. The presence of some surface non-starchy substances, such as proteins and lipids, can limit the rate of enzymatic hydrolysis by reducing the diffusion of enzymes into the granules and blocking the adsorption site of the substrate.[9,19] Removal of surface proteins and lipids after alkali treatment could greatly accelerate the penetration of enzymes into the granules and absorption of enzymes to its substrate, therefore increasing the digestibility of alkali-treated starch. In addition, roughening on the granule surface or granule disruption could also enhance the accessibility of enzymes to starch, hence increase the enzymatic digestibility. With the easy penetration of enzymes into alkali-treated starch granules, the resistant part of starch is more accessible for amylase to digest than that of native starch granules, leading to the decreased RS content.

In summary, alkali treatment can remove the proteins and lipids (mostly from the surface) from starch granules without significantly affecting the internal crystalline structure of starch. In contrast, the functionality of starch granules was altered greatly by alkali treatment. The swelling power and starch solubility were increased greatly by alkali treatment. However, the alkali treatment effect on properties of thermal transition and pasting varied with the concentration of NaOH and treatment period. The *in vitro* digestibility of starch granules was increased significantly by alkali treatment, as evidenced by the increased RDS and SDS contents and decreased RS content. The alkali-induced changes in functionality and *in vitro* digestibility of wheat starch granules could be predominantly attributed to the removal of surface proteins and lipids, but the alterations to granular morphology and small swelling of amorphous regions may also be taken into account. Our results clearly indicated that alkali treatment can be taken to be an important modification method to modify the quality and nutritional properties of starchy food products.

AUTHOR INFORMATION

Corresponding Authors

*E-mail: sjwang@tust.edu.cn.

*E-mail: s.wang@tust.edu.cn.

Funding

Shujun Wang gratefully acknowledges the financial support from the National Natural Science Foundation of China (31371720) and the Natural Science Foundation of Tianjin (13JCYBJC38100). Shujun Wang also greatly appreciates the financial support of Haihe River Scholar Program (000050401) from Tianjin University of Science and Technology.

Notes

The authors declare no competing financial interest.

REFERENCES

(1) Tetlow, I. J. Starch biosynthesis in developing seeds. *Seed Sci. Res.* **2011**, *21*, 5−32.

(2) Pérez, S.; Bertoft, E. The molecular structures of starch components and their contribution to the architecture of starch granules: A comprehensive review. *Starch/Staerke* **2010**, *62*, 389−420.

(3) Wang, S. J.; Copeland, L. Effect of acid hydrolysis on starch structure and functionality: A review. *Crit. Rev. Food Sci. Nutr.* **2012**, DOI: 10.1080/10408398.2012.684551.

(4) Copeland, L.; Blazek, J.; Salman, H.; Tang, M. C. M. Form and function of starch granules. *Food Hydrocolloids* **2009**, *23*, 1527−1534.

(5) Wang, S. J.; Copeland, L. Molecular disassembly of starch granules during gelatinization and its effect on starch digestibility: A review. *Food Funct.* **2013**, *4*, 1564−1580.

(6) Baldwin, P. M. Starch granule-associated proteins and polypeptides: A review. *Starch/Staerke* **2001**, *53*, 475−503.

(7) Debet, M. R.; Gidley, M. J. Three classes of starch granule swelling: Influence of surface proteins and lipids. *Carbohydr. Polym.* **2006**, *64*, 452−465.

(8) Morrison, W. R. Starch lipids and how they relate to starch granule structure and functionality. *Cereal Foods World* **1995**, *40*, 437−446.

(9) Svihus, B.; Uhlen, A. K.; Harstad, O. M. Effect of starch granule structure, associated components and processing on nutritive value of cereal starch: A review. *Anim. Feed Sci. Technol.* **2005**, *122*, 303−320.

(10) Tester, R. F.; Morrison, W. R. Swelling and gelatinization of cereal starches. I. Effects of amylopectin, amylose, and lipids. *Cereal Chem.* **1990**, *67*, 551−557.

(11) Chan, H.-T.; Bhat, R.; Karim, A. A. Effects of sodium dodecyle sulphate and sonication treatment on physicochemical properties of starch. *Food Chem.* **2010**, *120*, 703−709.

(12) Radhika, G. S.; Moorthy, S. N. Effect of sodium dodecyl sulphate on the physicochemical, thermal and pasting properties of cassava starch. *Starch/Staerke* **2008**, *60*, 87−96.

(13) Nor Nadiha, M. Z.; Fazilah, A.; Bhat, R.; Karim, A. A. Comparative susceptibilities of sago, potato and corn starches to alkali treatment. *Food Chem.* **2010**, *121*, 1053−1059.

(14) Chan, H. T.; Fazilah, A.; Bhat, R.; Leh, C. P.; Karim, A. A. Effect of deproteinization on degree of oxidation of ozonated starch. *Food Hydrocolloids* **2012**, *26*, 339−343.

(15) Brand-Miller, J. Glycemic load and chronic disease. *Nutr. Rev.* **2003**, *61*, S49−S55.

(16) Willett, W.; Manson, J.; Liu, S. M. Glycaemic index, glycaemic load, and risk of type 2 diabetes. *Am. J. Clin. Nutr.* **2002**, *76*, 274S−280S.

(17) Zhang, G.; Hamaker, B. R. Slowly digestible starch: Concept, mechanism, and proposed extended glycemic index. *Crit. Rev. Food Sci. Nutr.* **2009**, *49*, 852−867.

(18) Singh, J.; Dartois, A.; Kaur, L. Starch digestibility in food matrix: A review. *Trends Food Sci. Technol.* **2010**, *21*, 168−180.

(19) Oates, C. G. Towards an understanding of starch granule structure and hydrolysis. *Trends Food Sci. Technol.* **1997**, *8*, 375−382.

(20) Williamson, G.; Belshaw, N. J.; Self, D. J.; Noel, T. R.; Ring, S. G.; Cairns, P.; Morris, V. J.; Clark, S. A.; Parker, M. L. Hydrolysis of A- and B-type crystalline polymorphs of starch by α-amylase, β-amylase and glucoamylase 1. *Carbohydr. Polym.* **1992**, *18*, 179−187.

(21) Finnie, S. M.; Jeannotte, R.; Morris, C. F.; Giroux, M. J.; Faubion, J. M. Variation in polar lipids located on the surface of wheat starch. *J. Cereal Sci.* **2010**, *51*, 73−80.

(22) Wang, S.; Copeland, L. Effect of alkali treatment on structure and function of pea starch granules. *Food Chem.* **2012**, *135*, 1635−1642.

(23) Williams, P. C.; Kuzina, F. D.; Hlynka, I. A rapid calorimetric procedure for estimating the amylose content of starches and flours. *Cereal Chem.* **1970**, *47*, 411−420.

(24) Wang, S. J.; Yu, J. L.; Zhu, Q. H.; Yu, J. G.; Jin, F. M. Granular structure and allomorph position in C-type Chinese yam starch granule revealed by SEM, ^{13}C CP/MAS NMR and XRD. *Food Hydrocolloids* **2009**, *23*, 426−433.

(25) van Soest, J. J. G.; Tournois, H.; de Wit, D.; Vliegenthart, J. F. G. Short-range structure in (partially) crystalline potato starch determined with attenuated total reflectance Fourier-transform IR spectroscopy. *Carbohydr. Res.* **1995**, *279*, 201−214.

(26) Wang, S. J.; Copeland, L. New insight into loss of swelling power and pasting profiles of acid-hydrolysed starch granules. *Starch/Staerke* **2012**, *64*, 538−544.

(27) Wang, S.; Copeland, L. Phase transitions of pea starch over a wide range of water content. *J. Agric. Food Chem.* **2012**, *60*, 6439−6446.

(28) Englyst, H. N.; Kingman, S. M.; Cummings, J. H. Classification and measurement of nutritionally important starch fractions. *Eur. J. Clin. Nutr.* **1992**, *46*, S33−S50.

(29) Kizil, R.; Irudayaraj, J.; Seetharaman, K. Characterization of irradiated starches by using FT-Raman and FTIR spectroscopy. *J. Agric. Food Chem.* **2002**, *50*, 3912−3918.

(30) Cardoso, M. B.; Putaux, J.-L.; Samion, D.; Silveira, N. P. Influence of alkali concentration on the deproteinization and/or gelatinization of rice starch. *Carbohydr. Polym.* **2007**, *70*, 160−165.

(31) Cardoso, M. B.; Samios, D.; Silveira, N. P. Study of protein detection and ultrastructure of Brazilian rice starch during alkaline extraction. *Starch/Staerke* **2006**, *58*, 345−352.

(32) Thys, R. C. S.; Westfahl, H.; Norena, C. P. Z.; Marczak, L. D. F.; Silveira, N. P.; Cardoso, M. B. Effect of alkaline treatment on ultrastructure of C-type starch granules. *Biomacromolecules* **2008**, *9*, 1894−1901.

(33) Han, X.; Hamaker, B. R. Partial leaching of granule-associated proteins from rice starch during alkaline extraction and subsequent gelatinization. *Starch/Staerke* **2002**, *54*, 454−460.

(34) Wang, S. J.; Hassani, M. E.; Crossett, B.; Copeland, L. Extraction and identification of internal granule proteins from waxy wheat starch. *Starch/Staerke* **2013**, *65*, 186−190.

(35) Karim, A. A.; Nor Nadiha, M. Z.; Chen, F. K.; Phuah, Y. P.; Chui, Y. M.; Fazilah, A. Pasting and retrogradation properties of alkali-treated sago (*Metroxylon sagu*) starch. *Food Hydrocolloids* **2008**, *22*, 1048−1053.

(36) Wang, S. J.; Jin, F. M.; Yu, J. G. Pea starch annealing: New insights. *Food Bioprocess Technol.* **2013**, *6*, 3564−3575.

(37) Karim, A. A.; Norziah, M. H.; Seow, C. C. Methods for the study of starch retrogradation. *Food Chem.* **2000**, *71*, 9−36.

(38) Colonna, P.; Leloup, V.; Buleon, A. Limiting factors of starch hydrolysis. *Eur. J. Clin. Nutr.* **1992**, *46*, S17−32.

(39) Mahasukhonthachat, K.; Sopade, P. A.; Gidley, M. J. Kinetics of starch digestion in sorghum as affected by particle size. *J. Food Eng.* **2010**, *96*, 18−28.

(40) Htoon, A.; Shrestha, A. K.; Flanagan, B. M.; Lopez-Rubio, A.; Birds, A. R.; Gilbert, E. P.; Gidley, M. J. Effects of processing high amylose maize starches under controlled conditions on structural organization and amylase digestibility. *Carbohydr. Polym.* **2010**, *22*, 236−245.

Table 1. Summary of the Physicochemical Properties of the Four Insecticides Studied

Pesticides	Acetamiprid	Methomyl	Deltamethrin	Chlorpyrifos
Family	neonicotinoid	carbamate	pyrethroid	Organophosphate
Structure	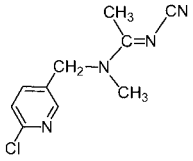	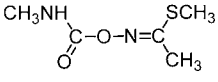	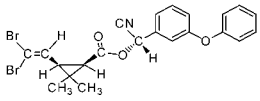	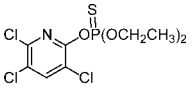
Mol. wt.	222.7	162.2	505.2	350.6
Solubility in water mg/L (25 C)	4,250	57,900	<0.0002	1.4
V.P. (mPa)	<1E-3	0.72	1.24E-5	2.7
K_{OW} logP	0.80	0.093	4.6	4.7
Mode of action	Systemic, contact, stomach	Systemic, contact, stomach	Contact and stomach action	Contact, stomach, respiratory

with acetone, acetonitrile, or methanol. Stock solutions were diluted with proper solvent to make standard solutions in the range of 0.01−5 mg/L to prepare calibration curves. All of the solvents were of pesticide grade (TEDIA, USA) or analytical grade and purchased from Merck Co. (Darmstadt, Germany). Anhydrous Na_2SO_4 was purchased from Merck (Taipei, Taiwan). Commercial acetamiprid 20% SP, chlorpyrifos 22.5% EC, deltamethrin 2.4% SC, and methomyl 40% SP were purchased from Great Victory Chemical, Xinnong, Bayer, and Du Pont, respectively, Taiwan.

Extraction Procedures. A 20 g portion of vegetable sample was weighed in a glass jar of a blender and homogenized with 60 mL of acetone for 1 min. The macerate was then filtered under vacuum through a funnel using Advantec no. 2 filter paper (Toyo Roshi Kaisha, Japan). The volume of filtrate was adjusted to 100 mL with the same solution. For cabbage and Chinese cabbage before solid phase extraction (SPE), a 10 mL portion of filtrate solvent was transferred into a separatory funnel and partitioned twice with 50/30 mL of ethyl acetate. The organic phase was collected, filtered through 20 g of anhydrous Na_2SO_4, and evaporated to dryness under reduced pressure. For all vegetables, the residue was dissolved in 3.5 mL of a solution of *n*-hexane/acetone (90:10, v/v) and loaded to the Florisil (1000 mg/6 mL, JT Baker) cartridge (×2) for SPE. The combined cartridges were previously conditioned with 10 mL of *n*-hexane, followed by sample loading and collecting with 3.5 + 7 mL of *n*-hexane/acetone (90:10, v/v) and collecting with 8 mL of *n*-hexane/acetone (50:50, v/v) after washing with 10 mL of *n*-hexane/acetone (90:10, v/v). The combined eluents were evaporated to dryness under nitrogen and reconstituted to 2 mL of acetonitrile for GC/μ-ECD analysis to determine acetamiprid, chlorpyrifos, and deltamethrin. A 1 mL portion of acetonitrile was reconstituted to methanol for the HPLC-FLD (OPA post reaction) analysis to determine methomyl.

GC/μ-ECD. An Agilent 6890 (Taipei, Taiwan Ltd.) gas chromatograph equipped with a 63Ni μ-electron-capture detector (μ-ECD) and a fused silica capillary column DB-608 (30 m × 0.25 mm i.d., 0.25 μm film thickness) was used. The operating conditions were as follows: initial temperature, 200 °C (5 min), increased at 10 °C min^{-1} to 220 °C for 2 min and increased at 20 °C min^{-1} to 280 °C for 10 min; injector temperature, 270 °C; N_2 carrier gas; column average linear velocity (μ = 40 cm/s) operated in the splitless mode; injection volume, 1 μL; detector temperature, 300 °C; makeup gas, N_2. Identification of acetamiprid, chlorpyrifos, and deltamethrin was carried out by comparing their individual retention times on GC/μ-ECD. The amounts of standards in the test solution were calculated from the peak areas. If the amount corresponding to the peak areas was larger than that of the maximum amount from the calibration curve, the test solutions were diluted to an appropriate concentration.

HPLC with Postcolumn Derivatization and Fluorescence Detection (FLD). The system consisted of an Agilent model 1100 HPLC quaternary pump, a model G1313A autoinjector, and a model G1321A fluorescence detector. All runs were acquired and processed using the Agilent ChemStation software. Chromatographic separations were carried out on a Merck LiChroCart 250 × 4.0 mm i.d. cartridge column, packed with LiChrosphere 100 RP select B (5 μm), in conjunction with a 4.0 × 4.0 mm i.d. guard column, packed with LiChrosorb 100 RP-18. Isocratic analysis was performed with a methanol/water (60:40) mobile phase at a flow rate of 0.8 mL min^{-1}. The postcolumn reaction system consisted of a Pickering PCX 5000 postcolumn reaction module. The first pump added a 0.05 M NaOH solution through a vortex mixing chamber (1.2 μL volume) to the column eluent. Hydrolysis took place in a PTFE knitted tube (5.1 m × 0.25 mm i.d.; 1.0 mL volume), kept at a temperature of 100 °C. After the hydrolysis reaction coil, *o*-phthalaldehyde/thiofluor reagent (0.05 M) was added through the second mixing chamber. The flow rate of both reaction solutions was 0.3 mL min^{-1}. The excitation and emission wavelengths for fluorescence detection were 330 and 460 nm, respectively.

Recovery Test. The specificity of the analytical method was confirmed by analysis of blank vegetable samples in triplicate and by processing through the extraction procedures described above. No interference peak was observed on the chromatograms from the blank samples. The accuracy and precision of the analytical method were confirmed by the recovery test of acetamiprid, chlorpyrifos, deltamethrin, and methomyl.

Field Experiments. The field experiments on head lettuce (*Lactuca sativa* L. var. *capitata* L.), cabbage (*B. oleracea* Linn. var. *capitata* DC.), Chinese cabbage (*B. pekinensis* Skeels), and broccoli (*B. oleracea* var. *italica*) were conducted in a field in Changhua, Taiwan, from September 15, 2008, to January 14, 2009. The experimental design was a split-plot arrangement of a randomized complete block with three replicates. The tank mix of acetamiprid 20% SP, chlorpyrifos 22.5% EC, deltamethrin 2.4% SC, and methomyl 40% SP was applied at the recommended (label) dose (0.2, 1.5, 1.0, and 0.8

dx.doi.org/10.1021/jf405555w | J. Agric. Food Chem. 2014, 62, 3644−3648

Table 2. Mean Recoveries (R) and Relative Standard Deviations (RSD) of Acetamiprid, Chlorpyrifos, Deltamethrin, and Methomyl in Four Vegetables

		cabbage		Chinese cabbage		head lettuce		broccoli	
pesticide	spike levels, n = 3 (ppm)	% R	% RSD	% R	% RSD	% R	% RSD	% R	% RSD
acetamiprid	0.125	75.9	1.1	77.4	4.5	89.2	1.5	80.9	5.9
	0.25	76.9	3.0	91.4	2.6	90.0	2.7	85.8	4.8
	0.5	76.3	2.9	80.9	3.9	90.9	2.3	82.3	0.9
chlorpyrifos	0.25	77.4	0.7	78.1	5.2	80.1	4.2	83.1	6.7
	0.5	82.4	0.3	81.3	2.7	84.1	1.2	83.8	2.6
	1	84.1	0.2	80.2	2.2	82.7	1.9	81.9	1.3
deltamethrin	0.25	72.3	1.5	76.3	5.0	90.8	3.5	85.9	9.6
	0.5	83.9	1.6	83.1	2.6	92.1	1.5	85.7	3.2
	1	82.5	1.4	77.8	3.2	100.8	1.3	80.4	4.2
methomyl	0.25	83.5	0.4	86.2	9.5	109.0	3.4	86.4	2.1
	0.5	80.5	2.0	88.4	5.2	97.0	4.6	94.2	3.7
	1	83.4	1.7	93.8	5.2	92.6	1.1	84.8	0.3

L/ha) and at 2 times the rates (0.4, 3.0, 2.0, and 1.6 L/ha), respectively. They were applied with a hand-driven knapsack sprayer. One application was conducted at 65 days (for Chinese cabbage and head lettuce), 80 days (for cabbage), and 98 days (for broccoli) after seeding of the respective vegetables.

Sampling and Storage. Sample (12 plants at least) collection was initiated 2−3 h after foliar application of a tank mix of four pesticides. The process of collection was repeated at 3, 6, 9, 12, 15, 18, and 21 days afterward to determine the residues of four pesticides in/on vegetable samples. Meteorological conditions were continuously recorded. During the period of pesticide application and sampling, daily total rainfall amounts ranged from 0 to 18.7 mm/day. The minimum and maximum temperatures were 10.1 and 31.1 °C, respectively. The stability of pesticides in vegetable samples during frozen storage was evaluated using 20 g aliquots of blank vegetable samples. The prepared blank samples in triplicate were spiked at levels of 0.25, 0.5, and 1 ppm (μg/g) of the four pesticides. The residues in blank samples were determined as described above.

RESULTS AND DISCUSSION

Recoveries of Pesticides. The recoveries of analytical methods were 72.3−109.0% (levels, 0.125−1.0 mg/kg; RSD, 0.3−9.6%; n = 3) for the residue determination of four insecticides on head lettuce, broccoli, cabbage, and Chinese cabbage. Limits of quantification (defined as a signal-to-noise ratio >10) were 0.01 mg/kg (Table 2).

Comparative Dissipation of Pesticides on Vegetables. Residues of four pesticides in/on four vegetable samples collected after pesticide application at double doses are shown in Figure 1−4. Whereas the initial deposits of all pesticides on head lettuce were higher than those of the other three crops at 0 days after application, the residues on all crops dissipated with time. On the four vegetables, acetamiprid residues declined to less than the tolerance (MRL), 2.0 mg/kg, at the recommended preharvest interval (PHI, 6−12 days, Figure 1). On head lettuce and broccoli, the concentrations of chlorpyrifos and deltamethrin were still higher than the tolerance at the PHI of 6−10 days (Figures 2 and 3). Only on the head lettuce were the residues of methomyl higher than 0.7 mg/kg at 6 days after application (Figure 4). Ripley et al. compared the residues of pesticides on different vegetables. The residues of five of the nine pesticides applied to cabbage, Chinese cabbage, and bok choi did not differ significantly from 3 to 14 days after application, but the

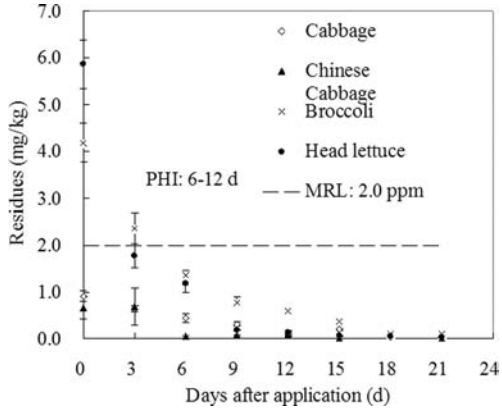

Figure 1. Dissipation of acetamiprid in different wrapped leaf vegetables treated with higher doses. MRL: standards for pesticide residue limits of acetamiprid in the four vegetables, Food and Drug Administration, Ministry of Health and Welfare, Taiwan.

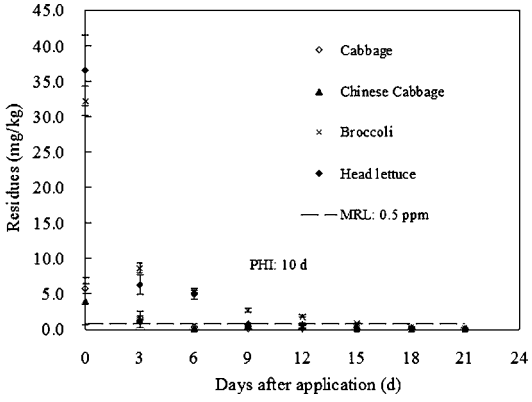

Figure 2. Dissipation of chlorpyrifos in different wrapped leaf vegetables treated with higher doses. MRL: standards for pesticide residue limits of chlorpyrifos in the four vegetables, Food and Drug Administration, Ministry of Health and Welfare, Taiwan.

residues of cypermethrin and three fungicides were significantly higher on Chinese cabbage and bok choi.[8] Residues were generally significantly higher on bok choi than on the other cultivars.[8] Ripley et al. found that structure significantly affects

dx.doi.org/10.1021/jf405555w | J. Agric. Food Chem. 2014, 62, 3644−3648

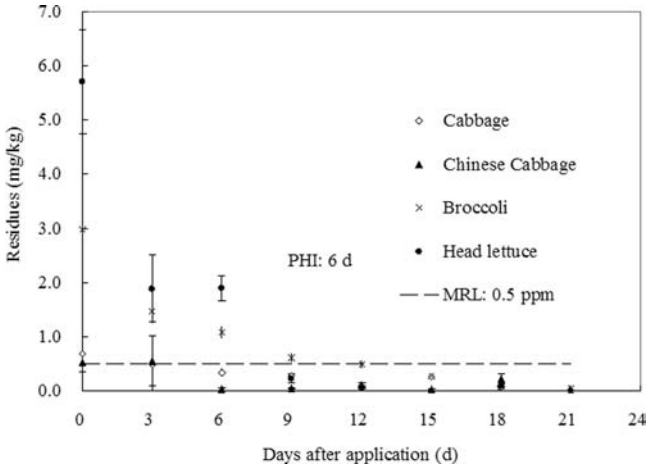

Figure 3. Dissipation of deltamethrin in different wrapped leaf vegetables treated with higher doses. MRL: standards for pesticide residue limits of deltamethrin in the four vegetables, Food and Drug Administration, Ministry of Health and Welfare, Taiwan.

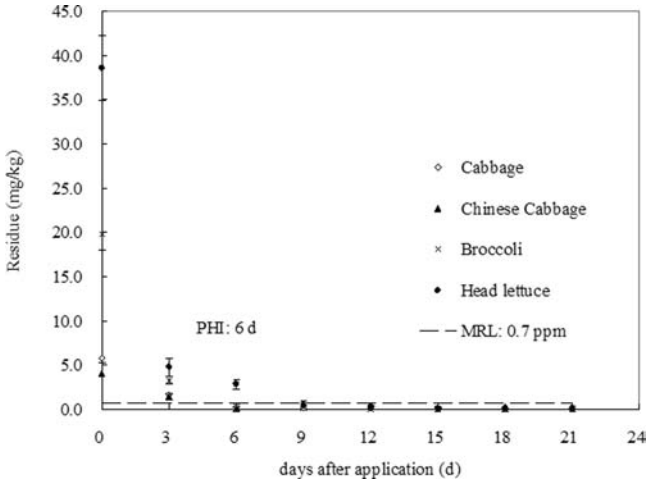

Figure 4. Dissipation of methomyl in different wrapped leaf vegetables treated with higher doses. MRL: standards for pesticide residue limits of methomyl in the four vegetables, Food and Drug Administration, Ministry of Health and Welfare, Taiwan.

residue deposit and dissipation of pesticides on vegetables because of the higher exposed surface area-to-mass ratios; leafier crops had higher residue concentrations than head varieties.[8] Their results showed that different PHIs might be necessary to achieve established MRLs for the different cultivars.[8] Zhang et al. evaluated multiresidual dynamics of the pesticides in the spring (*B. oleracea* L. var. *capitata*) and autumn (*B. chinensis* L.) cabbages.[5,6] Their results showed that the pesticide residues were closely related with the times and dosages of application and the weather after spraying.[5,6] Raina and Raina studied the dissipation of chlorpyriphos on cauliflower following pesticide applications and recommend a safe preharvest interval of 6 days.[9]

Lots of variations of residue levels on different crops have been reported. Wang et al. studied pyrimorph residues in tomatoes and cucumbers and showed relatively similar dissipation rates, with half-lives of 5.8−7.7 days in tomatoes and 5.7−7.1 days in cucumbers.[10] Fujita et al. considered the difference in the relative distribution of acetamiprid and cypermethrin between cabbage and grapes might be due to the influence of various factors such as differences in crop species, plant cultivation methods, and physicochemical properties of the pesticides.[7] They found that the variability factors in the residue levels of both pesticides in cabbage were clearly higher than those in grapes.[7] Yu et al. reported that both the hermetic environment of a greenhouse and season affected dissipation rates of chlorpyrifos on pakchoi (leafy vegetable).[11] They found that chlorpyrifos declined more rapidly outside than inside the greenhouse.[11] Lozowicka et al. monitored the presence of pesticide residues in broccoli, Brussels sprouts, cauliflower, and head and Chinese cabbages produced in northeastern Poland (2006−2009), which could not be considered a serious public health problem.[12]

The global food classification and crop group was revised by Codex and the International Crop Grouping Consulting Committee (ICGCC). Head lettuce was grouped within the leafy vegetables but not a member of bulb or cole vegetables according to the classification of Codex or ICGCC. Our results indicated that head lettuce contains higher residues than other vegetables. The major production of vegetables is cabbage in Taiwan. Residues of eight of the nine pesticides on head lettuce were lower than on the other lettuces 1 day after the last application.[8] There are significantly different residue potentials and cultivated behaviors between head lettuce and the other leafy lettuces, so that head lettuce is not suitable for grouping within the leafy vegetables with small leaves.[8]

The present study demonstrated that the initial deposits of all pesticides in head lettuce were higher than in broccoli, cabbage, and Chinese cabbage. The concentrations of some pesticides were still higher than MRLs at the PHIs if treated with higher doses.

Storage Stability. All treated samples in this study were stored frozen for no longer than 336 days between sampling and analysis. Fortified and unfortified samples were analyzed to evaluate the storage stability of insecticides in vegetable samples during storage at −20 ± 5 °C for up to 336 days. The results indicated that these insecticides were stable in samples under frozen condition for up to 336 days.

AUTHOR INFORMATION

Corresponding Author

*(M.-F.C.) Phone:+886-918-262605. E-mail mfchen99@nfu.edu.tw.

Notes

The authors declare no competing financial interest.

ACKNOWLEDGMENTS

We thank Dr. G. C. Li (former director of Taiwan Agricultural Chemicals and Toxic Substances Research Institute, gcli@tactri.gov.tw) for his valuable suggestions. We also thank the workers at the Taiwan Agricultural Chemicals and Toxic Substances Research Institute for their cooperation in the field experiments.

REFERENCES

(1) Food and Drug Administration, Ministry of Health and Welfare. *Classification of Crops for the Pesticide Residue Limits in Foods*; Standards for Pesticide Residue Limits in Foods. Taiwan; http://www.fda.gov.tw/EN/law.aspx, amended Sept 26, 2013 (accessed Sept 30, 2013).

(2) Tomlin, C. D. S. *A World Compendium, The Pesticide Manual*, 14th ed.; British Crop Production Council: Surrey, UK, 2006.

(3) Codex Classification of Foods and Animal Feeds. *Pesticide Residues in Food*; Codex Alimentarius, Joint FAO/WHO Food

Standards Programme; FAO/WHO: Rome, Italy, 1993; Vol. 2, pp 147−157.
(4) Chen, M. F.; Chien, H. P.; Wong, S. S.; Li, G. C. Dissipation of the fungicide azoxystrobin in Brassica vegetables. *Plant Prot. Bull.* **2004**, *46*, 123−130.
(5) Zhang, Z. Y.; Zhang, C. Z.; Liu, X. J.; Hong, X. Y. Dynamics of pesticide residues in the autumn Chinese cabbage (*Brassica chinensis* L.) grown in open fields. *Pest Manage. Sci.* **2006**, *62*, 350−355.
(6) Zhang, Z. Y.; Liu, X. J.; Yu, X. Y.; Zhang, C. Z.; Honga, X. Y. Pesticide residues in the spring cabbage (*Brassica oleracea* L. var. *capitata*) grown in open field. *Food Control* **2007**, *18*, 723−730.
(7) Fujita, M.; Yajima, T.; Iijima, K.; Sato, K. Comparison of the variability in the levels of pesticide residue observed in Japanese cabbage and grape units. *J. Agric. Food Chem.* **2012**, *60*, 1516−21.
(8) Ripley, B. D.; Ritcey, G. M.; Harris, C. R.; Denommé, M. A.; Lissemore, L. I. Comparative persistence of pesticides on selected cultivars of specialty vegetables. *J. Agric. Food Chem.* **2003**, *51*, 1328−35.
(9) Raina, A.; Raina, M. Dissipation of chlorpyriphos on cauliflower (*Brassica oleracea* L. var. *botrytis*). *Pestic. Res. J.* **2008**, *20*, 263−265.
(10) Wang, J.; Zhao, L.; Li, X.; Jiang, Y.; Li, N.; Qin, Z.; Pan, C. Residue dynamic of pyrimorph on tomatoes, cucumbers and soil under greenhouse trails. *Bull. Environ. Contam. Toxicol.* **2011**, *86*, 326−330.
(11) Yu, Y.-L.; Fang, H.; Wang, X.; Yu, J.-Q.; Fan, D.-F. Dissipation of chlorpyrifos on pakchoi inside and outside greenhouse. *J. Environ. Sci.* **2005**, *17*, 503−505.
(12) Lozowicka, B.; Jankowska, M.; Kaczyński, P. Pesticide residues in Brassica vegetables and exposure assessment of consumers. *Food Control* **2012**, *25*, 561−575.

International Forum, organized for the first time this year, brought interesting topics and comparisons between regulatory enforcement and monitoring approaches from different countries.

The papers included in this special section of the *Journal of Agricultural and Food Chemistry* are a good representation of the topics discussed at the 2013 NACRW and should provide an invitation to the future meetings, including the next one, which will be held July 20−23, 2014, at the TradeWinds in St. Pete Beach, FL, USA. Please come to learn, discuss, and network with your colleagues and take advantage of the many opportunities that this friendly event has to offer!

Katerina Mastovska*

2013 NACRW Program Committee Chair, Covance Laboratories, Nutritional Chemistry and Food Safety, 3301 Kinsman Boulevard, Madison, Wisconsin 53704, United States

AUTHOR INFORMATION

Corresponding Author

*E-mail: katerina.mastovska@covance.com.

Notes

The authors declare no competing financial interest.

Table 1. Overview of Compounds Analyzed by LC-MS/MS[a]

	methods and compounds	cone voltage (V)	transition 1 *	CE 1 (eV)	transition 2	CE 2 (eV)
LC-MS/MS Multiresidue (ES+)						
(a)	2-aminoflubendazole (ES)	28	256 → 123	22	256 → 95	38
(a)	cimetidine (ES)	40	253 → 159	14	253 → 117	16
(a)	ciprofloxacin (IS)	40	332 → 314	18	332 → 288	14
(a)	codeine (ES)	52	300 → 199	26	300 → 215	22
(a)	danofloxacin (IS)	12	358 → 340	20	358 → 255	36
(a)	decoquinate (ES)	70	418 → 204	30	418 → 372	14
(a)	diclofenac (IS)	98	214 → 179	28	214 → 151	32
(a)	difloxacin (IS)	14	400 → 356	18	400 → 382	20
(a)	dipyridamole (ES)	40	505 → 385	38	505 → 429	40
(a)	doxycycline (IS)	20	445 → 154	26	445 → 428	14
(a)	enrofloxacin (IS)	40	360 → 316	16	360 → 342	20
(a)	erythromycin (IS)	40	734 → 158	26	734 → 576	16
(a)	flubendazole (IS)	40	314 → 282	15	314 → 123	25
(a)	gliclazide (ES)	40	324 → 110	18	324 → 127	18
(a)	irbestan (ES)	40	429 → 207	22	429 → 195	20
(a)	lasalocid (ES)	52	613 → 377	38	613 → 577	30
(a)	lincomycin (IS)	30	407 → 126	20	407 → 359	16
(a)	maduramycin (ES)	50	939 → 877	44	939 → 895	52
(a)	mebeverine (ES)	40	430 → 121	16	430 → 149	6
(a)	mefenamic acid (ES)	22	242 → 224	16	242 → 209	26
(a)	sulfasalazine (ES)	36	399 → 223	28	399 → 381	16
(a)	sulfadiazine (IS)	42	251 → 156	14	251 → 108	20
(a)	tilmicosin (ES)	40	870 → 174	42	870 → 697	36
(a)	yrimethoprim (ES)	60	291 → 230	22	291 → 261	22
(b)	cvefalexin (ES)	26	348 → 158	4	348 → 174	10
(b)	chlorhexidine (ES)	40	505 → 184	24	505 → 336	16
(b)	chlortetracycline (IS)	28	479 → 444	20	479 → 462	14
(b)	dicyclanil (ES)	48	191 → 150	14	191 → 109	24
(b)	florfenicol amine (ES)	20	248 → 230	12	248 → 130	20
(b)	flucloxacillin (ES)	22	454 → 160	10	454 → 114	36
(b)	quinine (ES)	48	325 → 160	26	325 → 307	22
(b)	robenidine hydrochloride (ES)	58	334 → 138	24	334 → 155	18
(b)	salinomycin sodium (ES)	86	774 → 431	48	774 → 531	44
(b)	tetracycline (IS)	40	445 → 410	16	445 → 154	26
(b)	toltrazuril sulfoxide (ES)	42	442 → 373	18	442 → 233	26
(b)	tramadol (ES)	30	264 → 246	8	264 → 121	28
Aminoglycosides and Related Compounds (ESI+)						
(c)	apramycin (ES)	50	540 → 378	15		
(c)	dihydrostreptomycin (ES)	50	584 → 263	20	584 → 221	40
(c)	gentamicin C1 (ES)	50	478 → 157	20		
(c)	gentamicin C1a (ES)	50	450 → 160	20		
(c)	gentamicin C2 + C2a (ES)	50	464 → 160	15		
(c)	kanamycin A (ES)	50	485 → 163	20		
(c)	neomycin B (ES)	50	615 → 161	30		
(c)	paromomycin (ES)	50	616 → 163	35		
(c)	spectinomycin (ES)	90	333 → 189	20		
(c)	streptomycin (ES)	125	582 → 263	25	582 → 221	30
Coccidiostats (ESI+)						
(a)	diclazuril (IS)	30	405 → 334	20	407 → 336	20
(a)	dinitrocarbanilide (IS)	30	301 → 137	15	301 → 107	45
(a)	lasalocid (ES)	30	613 → 577	33	613 → 377	44
(a)	maduramycin (ES)	30	940 → 878	35	940 → 896	45
(a)	monensin (ES)	30	693 → 675	40	693 → 461	55
(a)	narasin (ES)	30	787 → 431	52	787 → 531	47
(a)	salinomycin (ES)	30	774 → 431	51	774 → 531	42

dx.doi.org/10.1021/jf4052418 | J. Agric. Food Chem. 2014, 62, 3651−3659

Table 1. continued

	methods and compounds	cone voltage (V)	transition 1 *	CE 1 (eV)	transition 2	CE 2 (eV)
Parabens (ESI−)						
(a)	butyl paraben (ES)	50	193 → 92	22	193 → 136	16
(a)	benzyl paraben (ES)	42	227 → 92	22	227 → 136	16
(a)	ethyl paraben (ES)	46	165 → 92	20	165 → 136	14
(a)	methyl paraben (IS)	52	151 → 92	20	151 → 136	12
(a)	isobutyl paraben (ES)	54	193 → 92	22	193 → 136	16
(a)	isopropyl paraben (ES)	54	179 → 92	22	179 → 136	16
(a)	propyl paraben (ES)	40	179 → 92	22	179 → 136	14

[a]IS, internally standardized; ES, externally standardized; *, transition 1 used for quantification. Compounds were overspiked at (a) 1 ng/g, (b) 5 ng/g, or (c) 10 ng/g.

compounds, which have been used extensively as fragrance fixatives in PCPs, are also recognized as common contaminants in the environment, especially in water.[10] Previous concern arising from the use and persistence of nitro musks has led to restrictions on their use, and in recent times these compounds have been replaced by polycyclic musks, in particular galaxolide and tonalide. These are reported to account for around 90% of polycyclic musk usage in Europe during the past decade,[15] but there is only limited information on their occurrence in the environment and their potential uptake into food.

MATERIALS AND METHODS

Prioritization. The scope of the prioritization undertaken was dependent on the food type and contaminant group of interest. Usage information was used to identify the most used HPs and VMs in the United Kingdom (UK), whereas appropriate usage data for PCPs could not be identified and, therefore, compound identification was based on expert opinion. Prioritizations were performed for nine different scenarios: HPs and PCPs in leaf crops, root crops, fish, and offal and VMs in leaf crops, root crops, fish, offal, and mushrooms. For example, the prioritization of HPs in leaf crops considered usage, adsorption to sewage sludge, sludge application to land, irrigation of contaminated surface waters, and subsequent uptake into root and translocation to leaves.[16,17] The prioritization of VMs in farmed fish considered the potential surface water concentrations resulting from the treatment of intensively reared and pasture animals[18] and the subsequent theoretical fish steady-state plasma concentration.[19] Once the individual prioritizations were complete, the list was then finalized, taking into account the availability of methods for the analysis of the top-ranked compounds. The list of compounds analyzed by liquid chromatography−tandem mass spectrometry (LC-MS/MS) is given in Table 1. Also, six musk compounds (cashmeran, celestolide, galaxolide, tonalide, musk-xylene, and musk-ketone) were included in the study and analyzed by gas chromatography (GC)−high resolution (HR) MS.

Reagents. HP, VM, and PCP standards were obtained from Qmx Laboratories (Thaxted, UK), Toronto Research (Toronto, Canada), Witega (Berlin, Germany), or Sigma-Aldrich (Gillingham, UK). Thirteen labeled analogues were used in this study: difloxacin-d_3, ciprofloxacin-d_8, enrofloxacin-d_5, flubendazole-d_3, and dinitrocarbanilide-d_8, purchased from Witega; ^{13}C-erythromycin-d_3, danofloxacin-d_3, lincomycin-d_3, sulfadiazine-d_4, and tetracycline-d_6, obtained from Toronto Research; diclofenac-d_4 and ^{13}C-PCB77 from Cambridge Isotope Laboratories (Tewksbury, MA, USA); and ^{13}C methyl paraben from Fluka (Gillingham, UK).

Oxalic acid, glacial acetic acid, anhydrous sodium sulfate, aluminum oxide, sodium chloride, potassium phosphate monobasic, heptafluorobutyric acid (HFBA), and BakerBond CBX (500 mg, 6 mL) cartridges were acquired from Fisher Scientific (Loughborough, UK). Ethylenediaminetetraacetic acid (EDTA) disodium salt and trichloroacetic acid were purchased from Alfa Aesar (Heysham, UK). UPLC grade methanol, acetonitrile, and formic acid were obtained from Biosolve (Greyhound Chromatography, UK). Chromasolv acetonitrile and methanol, and magnesium sulfate, were purchased from Sigma-Aldrich. Doubly distilled grade dichloromethane, *n*-hexane, and ethyl acetate were acquired from Rathburn Chemicals (Walkerburn, UK). Polytetrafluoroethylene (PTFE, 0.22 μm) filters were obtained from QMX Laboratories. Dispersive solid-phase extraction (SPE) sorbents (Bondesil C_{18}, NH_2, and PSA) were supplied by Agilent (Wokingham, UK). Ultrapure water (18.2 MΩ cm) was obtained using a Purelab ultrapure water system (ELGA Purelab, UK).

Sampling. Approximately 400 individual food/crop samples were collected for analysis. Sample preparation (including compositing and separation of component plant parts) produced around 200 samples for analysis. Samples were homogenized under cryogenic conditions using dry ice to minimize any loss of analytes. After cryogenic homogenization, the subsamples requiring screening for musk compounds were freeze-dried.

Fish and Shrimp. A total of 30 samples of fish were collected from fish farms downstream of large urban sewage treatment effluent release points or from catchments close to areas of intensive livestock production. In addition, 21 samples of fish and 32 samples of shrimp imported from countries in Southeast Asia were also analyzed because of frequent detection of residues and reports issued by the EU Rapid Alert System for Food and Feed (RASFF). Fish were filleted, and the muscle including the subcutaneous fat was retained for analysis; the head, tail, and gut contents were not analyzed.

Mushrooms. A total of 33 mushroom samples were collected from retail sources (sample origins labeled as UK, Ireland, or China) and growers in England. Mushroom samples (*Agaricus bisporus*) cultivated using compost from the two main commercial suppliers in the UK were obtained. The mushroom samples collected in the early stages of the study were brushed and rinsed (tap water) to remove compost adhering to the surface. A number of mushroom samples collected during the later stages in the study were peeled and destalked prior to extraction and these parts analyzed separately. In addition to mushrooms, associated compost material was also collected.

Bovine Offal. Samples of bovine liver and bovine kidney were collected from abattoirs located in areas where the uptake of VMs or HPs and PCPs was considered a possibility: either rural areas associated with intensive livestock production or locations near major conurbations in the UK, respectively. Slices of kidney (typically 100 g) from 105 individual animals and slices of liver (typically 100 g) from another 95 individual animals were collected. On receipt at the laboratory the tissues were combined (5 samples representing 5 different animals, collected on the same day from the same abattoir) to produce a total of 40 composited samples (21 kidney and 19 liver) for analysis. This approach was employed to increase the chance of detecting residues because a greater number of animals would ultimately be tested.

Root and Foliage Crops. A total of 22 samples of sugar beet, oilseed rape, and wheat were analyzed. Sugar beet leaves and roots were analyzed separately. Similarly, the stalks and heads of wheat were separated and treated as individual samples. For oilseed rape the oilseeds were separated from the foliage. These crops were collected from fields that had received applications of animal manures (pig slurry or cattle manure) or biosolids just before the sampled crop was sown.

Table 2. Overview of Commodities and Compounds Classes Tested

	multiresidue	aminoglycosides	parabens	coccidiostats	musks
imported fish	yes		yes		yes
imported shrimp	yes		yes		yes
trout	yes		yes		yes
mushrooms	yes	yes		yes	
offal	yes				yes
plant crops	yes				yes

Sample Preparation. *Multianalyte/Multiclass Method.* The extraction method was based on the acetonitrile water extraction method described elsewhere.[20] Briefly, cryogenically milled analytical portions (5 g) of the samples were spiked with 12 available deuterated/^{13}C-labeled analogues. Water (2−5 mL depending on the sample) was added and the extraction performed using 1% oxalic acid in acetonitrile (15 mL). Anhydrous sodium sulfate (5 g) was added to reduce the water content prior to a cleanup step using dispersive solid-phase extraction (dSPE) with C18 and primary−secondary amine (PSA) to reduce the matrix coextractives. Finally, an aliquot (3 mL) of the extract was evaporated and reconstituted with acetonitrile/water (1:1, 1 mL). The final solvent composition was selected as a compromise between sufficient analyte solubility and acceptable chromatographic peak shapes for early-eluting polar compounds. All extracts were filtered through 0.22 μm PTFE filters.

In the case of kidney and liver, 1% acetic acid in acetonitrile (instead of oxalic acid) was used because this modifier resulted in lower amounts of coextractives.

Parabens. Cryogenically comminuted samples (5 g) spiked with ^{13}C-labeled methyl paraben were extracted with acetonitrile (10 mL). Magnesium sulfate (2 g) was added to reduce the volume of water in the final extract. Resultant extracts were purified by means of dSPE using C_{18} and PSA. Finally, an aliquot (4 mL) of the extract was concentrated to give a final volume of 1 mL in a mixture acetonitrile/water (1:1). All extracts were filtered through 0.22 μm PTFE filters.

Coccidiostats. Cryogenically milled mushroom samples (5 g), spiked with dinitrocarbanilide-d_8, were extracted with 1% acetic acid in acetonitrile (15 mL). Anhydrous sodium sulfate (5 g) was added to reduce the volume of water, prior to dSPE cleanup with C_{18} and NH_2. Finally, an aliquot (3 mL) of the cleaned up extract was evaporated and reconstituted with acetonitrile/water (3:1). All extracts were filtered through 0.22 μm PTFE filters.

Aminoglycosides. Aminoglycoside residues were extracted from mushroom samples using a phosphate (20 mM KH_2PO_4) and EDTA (0.4 mM Na_2EDTA) buffer containing trichloroacetic acid (2%) to precipitate proteins. The extract was then neutralized and cleaned up using a weak cation exchange solid-phase extraction cartridge (BakerBond CBX, 500 mg), which was eluted with 10% acetic acid in methanol (3 mL). The methanolic eluate was evaporated and reconstituted in an aqueous solution of an ion-pair reagent (400 μL of 20 mM HFBA).

Musks. An aliquot (10 g) of the freeze-dried sample was homogenized with a mixture of dichloromethane/hexane (40:60, 30 mL) and placed in an ultrasonic bath for 30 min at 40 °C. The extract was cooled, filtered through anhydrous sodium sulfate, and then concentrated to ∼0.5 mL. The concentrated extract was purified on activated alumina (6 g) previously washed with hexane (100 mL) followed by ethyl acetate/hexane (1:10), before elution of musks with ethyl acetate/hexane (1:2) and ethyl acetate. The extracts were concentrated to ∼250 μL with the addition of ^{13}C-labeled PCB77 internal standard. For some matrices, in particular kidneys, the final extracts were allowed to stand refrigerated, overnight/ and were then centrifuged to remove any solid material (e.g., salts) that may have precipitated, prior to analysis.

Analytical Approach. Due to the diversity of samples analyzed and because individual samples, even of the same sample type, can exhibit different suppression effects, a sample "overspiking" approach (single-point standard addition) was employed to assess the validity of each individual LC-MS/MS commodity−analyte result. In this approach each sample was analyzed twice, once without addition of analyte and once following addition of a known amount of analyte (typically equivalent to 1−10 ng/g in the sample, see Table 1). This enabled the detection of the analyte at the spiked concentration to be verified for each individual sample.

Analyte concentrations were quantified against matrix-matched calibration standards. The calibration curve typically comprised five concentration levels prepared using a single sample known to be blank and of the type relevant to the sample batch. Blanks were subject to the same procedures as the samples and were spiked with the corresponding standards and internal standards at the end of the extraction and immediately before the evaporation step. Internal calibration was used for a selected number of compounds; others were quantified by external standardization (Table 1).

Analytical standard solutions of each of the six musks were serially diluted in *n*-nonane and used to produce calibration standards for the quantification. The linearity of measurement with target musk compounds normalized to ^{13}C-PCB77 was confirmed over a range corresponding to <0.2−50 ng/g. An in-house reference material (fortified pike tissue) was run with each batch of samples analyzed. Results for these were in agreement with fortified values.

Determination Conditions. The analytical methods developed in this study included a multianalyte/multiclass procedure for the determination of 36 different VM and HP compounds and separate chemical-class specific methods for the determination of 10 aminoglycosides, 7 coccidiostats, 7 parabens, and 6 musks. Table 2 gives an overview of the combination of commodities and compound classes tested. Table 1 summarizes the ionization modes (positive or negative), capillary voltages, collision energies, and the transitions included in the LC-MS/MS methods. The method for the analysis of aminoglycosides included only one MS/MS transition for most of the compounds to optimize the response of the primary transition for the purpose of screening. Any samples found to contain potential residues of aminoglycosides would require further analysis.

Multianalyte/Multiclass Analysis. As well as parabens and coccidiostats, determinations were performed by ultraperformance liquid chromatography−electrospray (UPLC-ESI)-MS/MS using an Acquity UPLC-Xevo TQ-S system (Waters, Manchester, UK). Instrument conditions were typically within the following values: capillary voltage between 1 and 2.5 kV (the ESI source was operated in the negative mode for parabens and in positive mode for all other compounds), desolvation temperature and gas flow were 500 °C and 1000 L/h, respectively. The cone gas flow was maintained at 150 L/h and the source temperature set at 150 °C.

Aminoglycosides. Analyses were performed by high-performance liquid chromatography (HPLC)-ESI-MS/MS (Alliance 2695-Quattro Ultima, Waters). Instrumental conditions were the following: capillary voltage, 3 kV (ESI source operated in positive mode); desolvation temperature and gas flow, 300 °C and 741 L/h, respectively. The cone gas flow was mantained at 108 L/h and the source temperature set at 120 °C.

Chromatographic Conditions. *Multianalyte/Multiclass Method.* Separation of analytes was achieved using a Phenomenex Kinetex XB-C18 (100 × 2.1 mm, 2.6 μm) column maintained at 40 °C and gradient elution using (A) 0.1% formic acid in water and (B) 0.1% formic acid in methanol/acetonitrile (1:1). The gradient program was as follows: 95% A (0−0.2 min), 5% A (3.0−6.6 min), 95% A (6.7−8.0 min). The flow rate during the separation was set at 0.4 mL/min, but increased to 0.5 mL/min between 3.6 and 7.5 min to minimize the

dx.doi.org/10.1021/jf4052418 | J. Agric. Food Chem. 2014, 62, 3651−3659

time required to clean the column after elution of the analytes. The injection volume was 3 μL.

Parabens. Target compounds were separated using a Phenomenex Kinetex XB-C18 (100 × 2.1 mm, 2.6 μm) column maintained at 40 °C using gradient elution with (A) 1 mM ammonium acetate in water and (B) 1 mM ammonium acetate in methanol. The gradient program was as follows: 60% A (0−0.2 min), 45% A (2.5−4.9 min), 5% A (5.1−6.1 min), 60% A (6.3−7.8 min). The mobile phase flow used was 0.4 mL/min, and the injection volume was 1 μL.

Coccidiostats. The chromatographic separation was achieved using a Waters Acquity CSH phenyl-hexyl column (100 × 2.1 mm, 1.7 μm) maintained at 40 °C and gradient elution using (A) 0.1% formic acid in water and (B) 0.1% formic acid in methanol/acetonitrile (1:1). The gradient program was as follows: 95% A (0−0.2 min), 60% A (1 min), 5% A (3.0−5.6 min), 95% A (5.7−7 min). The mobile phase flow was set at 0.4 mL/min (0.5−0.6 mL/min from 3.5 to 5.7 min), and the injection volume was 1 μL.

Aminoglycosides. Aminoglycosides were separated using a Phenomenex Gemini C_{18} (100 × 2 mm, 3 μm) column maintained at 30 °C using a ternary gradient with water (A), acetonitrile (B), and 100 mM HFBA aqueous solution (C). The gradient was the following: 75% A, 5% B, 20% C (0−0.5 min); 20% A, 60% B, 20% C (1 min); 10% A, 70% B, 20% C (12 min); 0% A, 80% B, 20% C (12.1−15.0 min); 75% A, 5% B, 20% C (15.1 min). The injection volume was 30 μL and the flow rate set at 0.25 mL/min.

Musks. Musk determinations were performed using a Micromass Autospec high-resolution mass spectrometer coupled to an Agilent 6890N gas chromatograph fitted with an Agilent J&W DB-5 MS fused silica capillary column (60 m × 0.25 mm i.d., 0.25 μm film thickness) and a programmable temperature vaporisation (PTV) injector operated in constant flow (∼1 mL/min helium) mode. The mass spectrometer was operated in electron ionization (EI) mode at a mass resolution of ∼10000 (at 10% peak height). Two ions were monitored in the selected ion monitoring (SIM) mode: *m/z* 206.1671, 191.1436 (cashmeran); *m/z* 244.1827, 229.1592 (celestolide); *m/z* 258.1984, 243.1749 (galaxolide); *m/z* 258.1984, 243.1749 (tonalide); *m/z* 282.0726, 297.0961 (musk-xylene); and *m/z* 279.0981, 294.1216 (musk-ketone). An acceleration voltage of 7 kV was used in conjunction with an electron energy of 32−37 eV and a trap current of 450 μA. The GC-MS interface was set to 280 °C.

Samples (5 μL) were injected into the PTV injector at 60 °C. The PTV injector program consisted of a 3 min isothermal period at 60 °C followed by heating at 12 °C/s to 320 °C, for 10 min, then at 12 °C/s to 340 °C to the end of the run. The chromatographic separation was achieved using the following temperature program: isothermal period at 60 °C (5 min), 24 °C/min to 160 °C for 2 min, 3 °C/min to 250 °C, and 5 °C/min to 300 °C for 3 min.

RESULTS AND DISCUSSION

Validation. Validation of the LC-MS/MS methods was based on an overspiking approach in an attempt to counter matrix effects from the complex samples analyzed. This approach, which we refer to as sample overspike validation, involved analysis of all samples without spiking and with overspiking at 1−5 ng/g (10 ng/g in the case of aminoglycosides).

This overspiking approach demonstrated whether or not the response obtained for each analyte in each sample was acceptable. Recoveries were calculated against matrix-matched calibration standards prepared from blank samples. With the exception of aminoglycosides, linearity was typically confirmed over a range corresponding from 0.2 to 5 ng/g for LC-MS/MS compounds spiked at 1 and 1.0−25 ng/g for compounds spiked at 5 ng/g (see Table 1). For aminoglycosides, the calibration curves were linear over the range 1−20 ng/g. As expected, the recoveries were more variable than those obtained with the usual approach to validation (spiking a single matrix in a single batch), but were considered to provide a more realistic assessment of method performance. In total, >6500 recovery determinations were carried out to support the validity of the methods used.

The assessment of the results from the multiresidue method for the samples of fish and shrimp overspiked at 1 ng/g (24 analytes) and 5 ng/g (12 analytes) demonstrated that the method was fit for the purpose. The majority of recoveries were in the range of 60−120%, and associated relative standard deviations (RSDs) were generally <20%. The method did not produce reliable results and/or the response was insufficient for cefalexin, chlorhexidine, florfenicol amine, sulfasalazine, and tramadol. For the analysis of both imported fish and shrimp, enrofloxacin, chlortetracycline, and flucloxacillin suffered from irreproducible calibration. The analyte responses in mushroom were generally not as good as in fish, but most of the recoveries were in the range of 53−107% with associated RSDs between 8 and 33%. Florfenicol amine and chlorhexidine gave no detectable response at any of the concentrations (up to 10 ng/g) tested, possibly because of suppression of the response by matrix coextractives. In the case of liver samples, the majority of recoveries were in the range of 57−104% with associated RSDs below 29%. For kidney composite samples recoveries were generally between 50 and 127% with associated RSDs below 23%. Oilseed rape proved to be the most challenging plant crop matrix. Ten compounds that were detected in other matrices (e.g., sugar beet) could not be reported in oilseed rape due to lack of sufficient selectivity or sensitivity. For sugar beet samples (roots and leaves) recoveries ranged from 52 to 135%, excluding salinomycin and quinine. Recoveries for wheat heads and stalks were quite similar and above 50% with the exception of salinomycin and with RSD <20% excluding chlortetracycline and robenidine.

The collated recovery results for parabens in fish and shrimp were in the range of 79−125% with associated RSDs in the range of 4−23%. In the case of coccidiostats in mushrooms, recoveries were in the 41−106% range with associated RSDs below 13% except for diclazuril, which was more variable.

During an initial validation using matrix-extracted calibration (spikes before extraction), 10 aminoglycosides were detected at 2−5 ng/g in mushroom samples with recoveries in the range of 98−127% with associated RSDs in the range of 7−20%. Unfortunately, the response of the LC-MS/MS could not be maintained during the analysis of sample batches, presumably because of differences in matrix effects, and thus the reporting limits had to be raised. This is one of the reasons why we opted for the overspiking approach to ensure the validity of the data generated in each batch. The collated recovery results for seven aminoglycosides from the overspiking of each individual mushroom samples at 10 ng/g were in the 58−85% range with associated RSDs in the range of 9−20% For neomycin B low and variable recoveries were observed, but the response was sufficient to screen samples, especially as the overspike was detected in all cases. Streptomycin and spectinomycin were not detected at the highest spiking concentration (10 ng/g), and hence no results were obtained for these two compounds.

The linearity of measurement with target musk compounds normalized to ^{13}C-PCB77 was confirmed over a range corresponding to <0.2−50 ng/g. The analytical recoveries were typically in the range of 50−100%, but musk-xylene, which is more labile, generally gave lower recoveries (typically 30−46%). Measurement precision determined using a fish

Table 3. Interbatch Validation (Percent Recovery and RSD Percent) of the LC-MS/MS Method for the Analysis of Analytes Detected[a]

compound	Iinternal standard	spike (ng/g)	imported shrimp [32]	imported fish [21]	UK trout [30]	mushrooms [25]	composite liver samples [19]	composite kidney samples [21]
decoquinate		1	73 ± 13	107 ± 17	65 ± 15	68 ± 14	78 ± 11	67 ± 18
diclofenac	yes	1	101 ± 18	126 ± 21	101 ± 15	101 ± 10	89 ± 27	97 ± 15
enrofloxacin	yes	1	*	*	93 ± 12	90 ± 16#	88 ± 10	90 ± 11
lincomycin	yes	1	67 ± 32	57 ± 10	98 ± 10	70 ± 32	87 ± 16	94 ± 16
methyl paraben	yes	1	125 ± 15	117 ± 13	99 ± 23	–	–	–
propyl paraben		1	89 ± 9	79 ± 5	86 ± 16	–	–	–
tilmicosin		1	65 ± 18	43 ± 16	64 ± 55	73 ± 11	95 ± 19	81 ± 15
trimethoprim		1	69 ± 15	69 ± 12	59 ± 13	81 ± 16	66 ± 9	72 ± 4

[a]Number of samples analyzed is presented in square brackets; 25 different mushroom samples, caps and stalks/peelings analyzed separately for 16 samples; #, calculated on the basis of 30 recovery measurements; *, calibration issues; –, compound not required.

matrix was found to be in the range of 13–21% (RSD) except for cashmeran, which was higher at 30%.

The recoveries for analyte–sample combinations found to contain incurred residues are presented in Table 3. The reporting limits for analytes determined by LC-MS/MS across the different matrices are presented in Table 4. The reporting limits for musk compounds were found to be as low as 0.01–0.02 ng/g but typically higher, around 0.15 ng/g, for galaxolide and tonalide, reflecting their widespread environmental presence and much greater current use.

Table 4. Overview of LC-MS/MS Reporting Limits for the Several Compounds Tested across the Different Matrices

	no. of compounds at a reporting limit of			
	0.2 ng/g	0.5–1 ng/g	1–5 ng/g	insufficient S/N[a]
trout	32	12		2
imported fish	25	10		5
imported shrimp	28	9	2	2
mushrooms	17	15	8	5
wheat		22	11	2
oilseed rape		17	9	3
sugar beet		24	10	2
liver	19	12	1	3
kidney	18	13	2	3

[a]S/N, signal-to-noise ratio.

Study Findings. A summary of the residues found in the different matrices analyzed are presented in Table 5. Results indicate that the uptake of target chemicals was limited, and the residues detected were mostly at low nanograms per gram concentrations. Some differences observed between samples were related to the country of origin and sampling location.

Fish and Shrimp. Samples of trout from the UK contained up to eight different contaminants, whereas fish and shrimp from Southeast Asia were found to contain up to five of the targeted analytes. Methyl paraben (MeP) was found in the concentration range of 0.6–2.8 ng/g in 23 samples (77%) of UK trout and propyl paraben (PrP) in 19 samples (63%) at concentrations in the range of 0.4–1.3 ng/g. By contrast, these compounds were detected at lower concentrations in fish and shrimp imported from Southeast Asia. Because parabens are approved for use as food preservatives,[14] the low concentrations detected in this study are not likely to give cause for concern to regulators. Initially, it was thought that the results could reflect the difference in usage of these compounds in Southeast Asia and the UK; however, Ramaswamy et al.[21] detected MeP, PrP,

Table 5. Overview of Residues Found in the Selected Commodities[a]

	residues (ng/g)					
compound	UK trout	imported fish	imported shrimp	mushrooms	composite liver samples	composite kidney samples
decoquinate					0.4, 0.5 (11)	0.5 (5)
diclofenac					0.2 (11)	
enrofloxacin		0.3–5.1i (100)	1.3i, 4.7i (6)			
lincomycin			1.1 (3)			
tilmicosin					0.3, 7.9i (11)	
trimethoprim				0.07–0.7i (72)		
methyl paraben	0.6–2.8 (77)		0.4–5.0i (25)			
propyl paraben	0.4–1.3 (63)		7.3i (3)			
cashmeran	0.1–2.8 (47)	0.1, 0.2 (20)			0.1–0.3 (58)	
celestolide	0.1–0.9 (97)	0.01 (30)			0.01–0.1i (21)	0.02 (14)
galaxolide	1.6–50.3 (80)	1.1 (10)			0.8–2.3 (37)	0.9–2.5i (28)
musk-xylene	0.03–0.7 (80)	0.02–0.06 (40)	0.04, 0.06 (20)		0.05–0.1 (53)	
musk-ketone	0.04–2.0 (77)	0.01–0.03 (50)	0.02i (10)			
tonalide	0.7–34.3 (97)	0.1–0.3 (60)			0.4–1.2 (16)	0.2–0.4 (43)

[a]Range of found concentrations, with the percentage of samples containing residues above reporting limit given in parentheses; i, indicative value (residue concentration outside calibration range or calibration issues). Number of samples analyzed for musk compounds were UK trout (29), imported fish (10), imported shrimp (10), liver (17), and kidney (18).

and ethyl paraben (EtP) compounds in >90% of the analyzed samples at concentrations up to 3600 ng/g (MeP) in different species from Manila Bay in The Philippines, which suggests that the occurrence of these chemicals in fish is scenario-related.

MeP and PrP (as well as EtP) are the most commonly found paraben species in the environment.[11−13] MeP and PrP occur in raw wastewater at concentrations up to 10 and 2.8 μg/L, respectively.[13] However, their elimination rates at wastewater treatment plants have been reported to be high, and thus very low levels are found in effluent samples.[21,22] This may explain why low concentrations of parabens were found in fish samples obtained from fish farms located downstream of wastewater treatment plants compared to other scenarios (Table 6).

Residues of enrofloxacin (0.3−5.1 ng/g), a fluoroquinolone antibiotic, were detected in 21 samples (100%) of fish and in 2 samples (6%) of shrimp (1.3 and 4.7 ng/g) from Southeast Asia. By contrast, no residues of enrofloxacin were detected in UK trout, but this is not surprising because enrofloxacin is not authorized for use on fish in the UK. One sample of shrimp from Bangladesh contained a residue of lincomycin at 1.10 ng/g.

The results obtained for enrofloxacin are in general agreement with reports in the literature. He et al.[23] reported the occurrence of selected fluoroquinolones (norfloxacin, ciprofloxacin, and enrofloxacin) in fish collected from two marine aquaculture regions of the Pearl River Delta in China. The presence of this fluoroquinolone in farmed shrimp from Vietnam has also been reported in recent years.[24]

Residues of musk compounds occurred at higher concentrations (up to 50 ng/g) and higher frequency (100%) in trout collected in the UK compared to imported fish from Southeast Asia, for which 70% of the samples contained residues of up to 0.3 ng/g. Shrimp imported from Southeast Asia showed considerably lower occurrence and were found to contain only musk-xylene at 0.04 and 0.06 ng/g in two samples and musk-ketone at 0.02 ng/g in one sample. The highest concentrations of galaxolide and tonalide occurred in fish collected from fish farms located downstream of large urban sewage treatment effluent release points in the UK (Table 6). As only one species of freshwater fish (trout) was investigated, species selective uptake cannot be ruled out. However, other studies on contaminants in freshwater fish indicate a greater dependence of contaminant occurrence on local pollution levels. The occurrence of the individual musk compounds in fish and shrimp confirms the potential for human dietary exposure and may also indicate the chronology and magnitude of usage. "Older" compounds such as musk-xylene and musk-ketone, which are no longer used, were either not detected or occurred at a much lower frequency than polycyclic musk compounds such as galaxolide and tonalide. The use of these is more recent, accounting for >90% of polycyclic musk usage.[15] Similarly, the lower occurrence of cashmeran and celestolide may reflect their decreasing usage.

Mushrooms. Residues of trimethoprim, which is used as a potentiator for sulfonamide antibiotics, were detected at approximately 0.07−0.73 ng/g in 18 (72%) mushroom samples both in mushroom caps and in peelings/stalks at similar concentrations, indicating that occurrence was not due to surface contamination. Identification of trimethoprim was based on the ratio of two transitions in the sample compared to the ratios in a matrix-matched standard. Selected samples were reanalyzed using a different column and including an

Table 6. Overview of All Residues Detected at or above the Reporting Limits in Samples of Fish and Shrimp[a]

sample ID	scenario	MeP	PrP	cashmeran	celestolide	galaxolide	tonalide	musk-xylene	musk-ketone	enrofloxacin	lincomycin
trout samples (UK)	VMs, cattle and pig culture, UK	0.9−2.1 (6)	0.4−0.7 (2)	0.3−0.4i (2)	0.1−0.3 (5)	13.7−13.6 (3)	1.5−5.4 (5)	0.03−0.07 (5)	0.04−0.18i (5)		
	VMs, pig culture, UK	0.6−0.8 (4)	0.4−1.3 (6)	0.1−0.2 (3)	0.1−0.2 (9)	1.6−14.7 (6)	0.7−3.7 (9)	0.04−0.1 (4)	0.08−0.09 (2)		
	downstream STP, UK	0.6−2.8 (13)	0.4−1.0 (11)	0.2−2.8i (8)	0.1−0.9 (15)	1.9−50.3 (15)	2.9−34.3 (15)	0.1i−0.7 (15)	0.2−2.0 (15)		
imported farmed fish	Vietnam			0.1−0.2i (2)	0.01	1.1 (1)	0.1−0.3 (6)	0.02−0.06 (4)	0.01−0.03 (5)	0.3−5.1i (21)	
imported farmed shrimp	Vietnam	0.5−5.0 (3)	7.3i (1)					0.04−0.06 (2)	0.02i (1)	1.3i−4.7i (2)	
	India	0.4−0.7i (3)									
	Bangladesh										1.1 (1)
	Thailand	0.8i−0.9i (2)									

[a]Range of found concentrations (expressed in ng/g), with the number of samples containing residues above the reporting limit given in parentheses; i, indicative value (residues concentration outside calibration range or calibration issues); SA, standard addition; STP, sewage treatment plant.

dx.doi.org/10.1021/jf4052418 | J. Agric. Food Chem. 2014, 62, 3651−3659

additional third transition in the method to provide more confidence on the identification of these very low level residues. Additional evidence of identification of trimethoprim for some samples was also provided by MS/MS with measurement of the fragment ions at 35000 resolution (Thermo Scientific Orbitrap technology). Although trimethoprim was not detected in the selected compost samples analyzed (possibly due to deficiencies of the extraction method for compost), the relatively consistent concentration of trimethoprim throughout the mushroom does suggest possible uptake. Further analysis of the compost using improved methodology is required to attempt to detect residues and thus provide further evidence for possible uptake.

No residues of aminoglycosides were detected in mushrooms at or above 5 ng/g. The method of analysis was particularly problematic for compost. Without reliable detection of aminoglycosides in mushroom litter, it is difficult to conclude that no uptake occurred.

Samples of mushroom compost prepared from chicken litter were screened for veterinary drugs by LC-ToFMS. The mushroom compost matrix proved to be difficult, binding analytes to give rise to low recovery or causing matrix suppression and chemical interference in LC-MS. No residues of the sulfonamides sought were detected in the compost, but this could have been as a result of poor extraction with the methods employed. Residues of coccidiostats were detected in selected composts at estimated concentrations up to 60 ng/g DNC, 54 ng/g monensin, and 1 ng/g narasin. At this point, it was decided to screen the mushroom samples for a number of coccidiostats not included in the priority list. Although a specific method for the analysis of coccidiostats was employed, the recovery of coccidiostats spiked into the compost matrix were variable and <40%, indicating that the extraction efficiency for incurred residues is likely to be poor. Hence, further investigation using a more appropriate method is required to be able to provide a more definitive conclusion. No residues of coccidiostats were detected in any of the mushroom samples analyzed. Strong binding to the compost could explain why there was no bioavailability of these compounds.

Bovine Offal. Composite liver and kidney samples contained up to five different residues. Residues of decoquinate (0.4 and 0.5 ng/g), diclofenac (0.2 and 0.2 ng/g), and tilmicosin (0.3 and around 7.9 ng/g) were found in composite samples of liver. Decoquinate at 0.5 ng/g was also found in one composite sample of kidney.

Diclofenac, decoquinate, and tilmicosin are all approved for use in cattle in the UK; therefore, it is impossible to differentiate whether the residues detected in the bovine liver and kidney samples were a result of normal medication or indirect exposure through the contamination of food and/or drinking water.

Musk residues found in offal samples were at much lower concentrations than those detected in fish samples. In liver samples, galaxolide showed the highest concentrations (0.8−2.3 ng/g in seven composite samples) followed by tonalide (0.4−1.2 ng/g in three composite samples). Residues of cashmeran, celestolide, and musk-xylene were not detected (LOD−0.3 ng/g) in any samples of liver. Musk-ketone was not detected in any of the composite samples. In the case of kidney, neither musk-xylene, musk-ketone, nor cashmeran was detected in composite samples. As for liver samples, the highest residue concentrations corresponded to galaxolide (0.9−~2.5 ng/g) followed by tonalide (0.2−0.4 ng/g) and celestolide (three samples contained 0.02 ng/g).

Root and Foliage Crops. The only residues detected in crops were musk compounds. Residues of all six musks were detected at or above respective reporting limits in wheat samples with concentrations up to 4.5 ng/g. Two of three samples of sugar beet leaves contained cashmeran at 0.2 ng/g. None of the three samples of sugar beet roots analyzed contained musk compounds at detectable concentrations. This may suggest contamination of foliage, either by aerial deposition or from surface contact with contaminated soil, but the reasoning can only be tentative given the low number of samples analyzed.

Hu et al.[25] systematically evaluated the occurrence and potential uptake of 10 veterinary antibiotics by crops (radish, rape, celery, and coriander) in fields amended with manure in northern China. Uptake in different crops was variable. Radish leaves were found to contain nine antibiotics at concentrations between 0.1 and 57 ng/g, whereas in roots three compounds were detected: oxytetracycline at 8.3 ng/g, sulfadoxine at 0.1−0.4 ng/g, and lincomycin at 1.5−3.9 ng/g. Across all of the crops in this study the highest concentrations were found in leaves followed by stems and roots. In our study only a limited number of plant crop samples were analyzed. Musk residues were detected in sugar beet leaves but not in the roots (data based only on three samples). Because sugar beet roots, compared to radish, are relatively large, any low-concentration residues may have been further diluted by growth of the root. Crop samples were collected from fields that had received biosolid or slurry/manure applications. No attempt was made to confirm whether these materials contained any of the analytes of interest; therefore, the lack of detection does not necessarily represent a lack of uptake, but could indicate the soil improvers did not include the contaminants in the first place.

AUTHOR INFORMATION

Corresponding Author

*(R.J.F.) E-mail: richard.fussell@fera.gsi.gov.uk. Phone: 0044 (0)1904 462445.

Funding

We acknowledge the U.K. Food Standards Agency for funding the work (FS241004). M.G.L. acknowledges her funding through a postdoctoral contract by the Spanish Ministry of Education, Culture and Sport (National Programme for Human Resources Mobility R&D and Innovation 2008-2011).

Notes

The authors declare no competing financial interest.

ACKNOWLEDGMENTS

We acknowledge the support from the farms, fish farms, mushroom growers, and abattoirs that allowed sample collection from their establishments. Moreover, we thank Jonathan Hulland (Centre for Environment, Fisheries and Aquaculture Science), Tim Burch (Anglian Water Ltd.), and Gemma Forrest (Food Standards Agency) for their assistance with site identification and sample collection. In addition, we thank the many analysts at Fera who also contributed to sample preparation and analysis, particularly Daniel Kneale, Melissa Bowen, Alyson Moore, Melanie Holland, Mike Hetmanski, Frankie Smith, James Jowett, and Lewis Hutchinson.

REFERENCES

(1) Ternes, T. A. Occurrence of drugs in German sewage treatment plants and rivers. *Water Res.* **1998**, *32*, 3245−3260.

(2) Petrovic, M.; Gonzalez, S.; Barcelo, D. Analysis and removal of emerging contaminants in wastewater and drinking water. *Trends Anal. Chem.* **2003**, *22*, 685−696.
(3) Broekaert, N.; Daeseleure, E.; Delezie, E.; Vandecasteele, B.; De Beer, T.; Van Poucke, C. Can the use of coccidiostats in poultry breeding lead to residues in vegetables? An experimental study. *J. Agric. Food Chem.* **2012**, *60*, 12411−12418.
(4) Boxall, A. B. A.; Johnson, P.; Smith, E. J.; Sinclair, C. J.; Stutt, E.; Levy, L. S. Uptake of veterinary medicines from soil into plants. *J. Agric. Food Chem.* **2006**, *54*, 2288−2297.
(5) Lillenberg, M.; Litvin, S. V.; Nei, L.; Roasto, M.; Sepp, K. Enrofloxacin and ciprofloxacin uptake by plants from soil. *Agron. Res.* **2010**, *8*, 807−814.
(6) Van Peteghem, C.; Van Poucke, C.; Broekaert, N.; Daeseleire, E.; Delezie, E.; Vandecasteele, B. Experimental study: uptake of coccidiostats in vegetables. Question number EFSA-Q-2010-00862, 2012; available at http://www.efsa.europa.eu/en/supporting/pub/273e.htm (last accessed Oct 2013).
(7) Kang, D. H. K.; Gupta, S.; Rosen, C.; Fritz, V.; Singh, A.; Chander, Y.; Murray, H.; Rohwer, C. Antibiotic uptake by vegetable crops from manure-applied soils. *J. Agric. Food Chem.* **2013**, *61*, 9992−10001.
(8) Boxall, A. B. A.; Tiede, K.; Bryning, G.; Bevan, R.; Tam, C.; Levy, L. S. Desk-based study of current knowledge on veterinary medicines in drinking water and estimation of potential levels. Report ref. DWI 70/2/235, 2011; available at http://dwi.defra.gov.uk/research/completed-research/reports/dwi70-2-235.pdf (last accessed Oct 2013).
(9) Watts, C.; Maycock D.; Crane, M.; Fawell, J.; Goslan, E. Desk-based review of current knowledge on pharmaceuticals in drinking water and estimation of potential levels. Report ref. DWI, 70/2/213, 2007; available at http://dwi.defra.gov.uk/research/completed-research/reports/dwi70-2-213.pdf (last accessed Oct 2013).
(10) Rimkus, G. G. Polycyclic musk fragrances in the aquatic environment. *Toxicol. Lett.* **1999**, *111*, 37−56.
(11) Nieto, A.; Borrull, F.; Marce, R. M.; Pocurrull, E. Determination of personal care products in sewage sludge by pressurized liquid extraction and ultra-high performance liquid chromatography−tandem mass spectrometry. *J. Chromatogr., A* **2009**, *1216*, 5619−5625.
(12) Canosa, P.; Rodriguez, I.; Rubi, E.; Cela, R. Determination of parabens and triclosan in Indoor dust using matrix solid-phase dispersion and gas chromatography with tandem mass spectrometry. *Anal. Chem.* **2007**, *79*, 1675−1681.
(13) Gonzalez-Mariño, I.; Quintana, J. B.; Rodriguez, I.; Cela, R. Evaluation of the occurrence and biodegradation of parabens and halogenated by-products in wastewater by accurate mass liquid chromatography-quadrupole-time-of-flight-mass spectrometry (LC-QTOF-MS). *Water Res.* **2011**, *45*, 6770−6780.
(14) European Parliament and Council Directive No. 95/2/EC. *Off. J. Eur. Communities* **1995**, *L61*, 1−40.
(15) HERA. Polycyclic musks AHTN and HHCB. Human and environmental risk assessment on ingredients of household cleaning products. Environmental Section, version 2; Human and environmental risk assessment; Brussels, Belgium, 2004; available at http://www.heraproject.com/files/28-E-36551E10-F8EF-E807-E4199B9BB0076A9F.pdf (last accessed Jan 2014).
(16) Duarte-Davidson, R.; Jones, K. C. Screening the environmental fate of organic contaminants in sewage sludge applied to agricultural soils: II. The potential for transfers to plants and grazing animals. *Sci. Total Environ.* **1996**, *185*, 59−70.
(17) Technical Guidance Document on Risk Assessment in support of Commission Directive 93/67/EEC on Risk Assessment for new and notified substances, Commission Regulation (EC) No. 1488/94 on Risk Assessment for existing substances, Directive 98/8/EC of the European Parliament and Council concerning the placing of biocidal products on the market, Part II, European Commission, Luxembourg, 2003; available at http://echa.europa.eu/documents/10162/16960216/tgdpart2_2ed_en.pdf (last accessed Oct 2013).
(18) Revised guideline on environmental impact assessment for veterinary medicinal products, European Medicines Agency, London, UK, 2008. Doc. Ref. EMEA/CVMP/ERA/418282/2005; available at http://www.ema.europa.eu/docs/en_GB/document_library/Scientific_guideline/2009/10/WC500004389.pdf (last accessed Oct 2013).
(19) Brown, J. N.; Paxeus, N.; Forlin, L.; Larsson, D. G. J. Variations in bioconcentration of human pharmaceuticals from sewage effluents into fish blood plasma. *Environ. Toxicol. Pharm.* **2007**, *24*, 267−274.
(20) Tarbin, J. A.; Fussell, R. J. Metabolite profiling using liquid chromatography/quadrupole time-of-flight mass spectrometry for the identification of a suitable marker and target matrix of griseofulvin use in bovines. *Rapid Commun. Mass Spectrom.* **2013**, *27*, 1287−1293.
(21) Ramaswamy, B. R.; Kim, J.-W.; Isobe, T.; Chang, K.-H.; Amano, A.; Miller, T. W.; Siringan, F. P.; Tanabe, S. Determination of preservative and antimicrobial compounds in fish from Manila Bay, Philippines using ultra high performance liquid chromatography tandem mass spectrometry, and assessment of human dietary exposure. *J. Hazard. Mater.* **2011**, *192*, 1739−1745.
(22) Lee, H.-B.; Peart, T. E.; Svoboda, M. L. Determination of endocrine-disrupting phenols, acidic pharmaceuticals, and personal-care products in sewage by solid-phase extraction and gas chromatography−mass spectrometry. *J. Chromatogr., A* **2005**, *1094*, 122−129.
(23) He, X. T.; Wang, Z. H.; Nie, X. P.; Yang, Y. F.; Pan, D. B.; Leung, A. O. W.; Cheng, Z.; Yang, Y. T.; Li, K. B.; Chen, K. C. Residues of fluoroquinolones in marine aquaculture environment of the Pearl River Delta, South China. *Geochem. Health* **2012**, *34*, 323−335.
(24) Seafish (2011); available at http://www.seafish.org/industry-support/legislation/updates/news/japan-finds-enrofloxacin-in-vietnamese-shrimp (last accessed Oct 2013).
(25) Hu, X.; Zhou, Q.; Luo, Y. Occurrence and source analysis of typical veterinary antibiotics in manure, soil, vegetables and groundwater from organic vegetable bases, northern China. *Environ. Pollut.* **2010**, *158*, 2992−2998.

Table 1. List of Compounds with Formulas, Mass, Precursor Ion *m/z*, Retention Time, and Screening Limits of Detection in Milk

compounds	formula	mass	precursor ion (m/z)[a]	RT (min)	estimated screening LOD in milk (ng/mL)[b]	screening results at 10 ng/mL (X/20, %RSD)[c]
Aminoglycosides						
amikacin	$C_{22}H_{43}N_5O_{13}$	585.28574	586.2930	0.8	NA[d]	
apramycin	$C_{21}H_{41}N_5O_{11}$	539.28026	540.2875	0.76	NA	
dihydrostreptomycin	$C_{21}H_{41}N_7O_{12}$	583.28132	584.2886	0.93	>100	
gentamicin C1	$C_{21}H_{43}N_5O_7$	477.31625	478.3235	0.8	1000	
gentamicin C1A	$C_{19}H_{39}N_5O_7$	449.28495	450.2922	0.8	>1000	
gentamicin C2	$C_{20}H_{41}N_5O_7$	463.30060	464.3079	0.8	>1000	
kanamycin	$C_{18}H_{36}N_4O_{11}$	484.23806	485.2453	0.8	NA	
kanamycin B	$C_{18}H_{37}N_5O_{10}$	483.25404	484.2613	0.8	>100	
neomycin	$C_{23}H_{46}N_6O_{13}$	614.31229	615.3196	0.8	500	
netilmicin	$C_{21}H_{41}N_5O_7$	475.30006	476.3079	0.8	NA	
spectinomycin	$C_{14}H_{24}N_2O_7$	332.15835	333.1656	0.9	NA	
streptomycin	$C_{21}H_{39}N_7O_{12}$	581.26567	582.2729	0.8	NA	
Avermectins						
abamectin	$C_{48}H_{72}O_{14}$	872.49221	895.4814[e]	17.8	>1000	
doramectin	$C_{50}H_{74}O_{14}$	898.50786	921.4971[e]	18.2	>1000	
emamectin B1a	$C_{49}H_{75}NO_{13}$	885.52384	886.5311	14.4	1000	
eprinomectin B1a	$C_{50}H_{75}NO_{14}$	913.51876	936.5080[e]	17.5	>1000	
ivermectin B1a	$C_{48}H_{74}O_{14}$	874.50786	897.4970[e]	18.9	>1000	
moxidectin	$C_{37}H_{53}NO_8$	639.37712	662.3663[e]	18.0	>1000	
selemectin	$C_{43}H_{63}NO_{11}$	769.44011	770.4474	18.7	>1000	
Benzimidazoles						
albendazole	$C_{12}H_{15}N_3O_2S$	265.08850	266.0958	10.6	10	20 (43%)
fenbendazole	$C_{15}H_{13}N_3O_2S$	299.07285	300.0801	12.6	100	
oxibendazole	$C_{12}H_{15}N_3O_3$	249.11134	250.1186	8.7	5	20 (27%)
thiabendazole	$C_{10}H_7N_3S$	201.03607	202.0433	5.6	5[f]	
β-Agonists						
clenbuterol	$C_{12}H_{18}Cl_2N_2O$	276.07962	277.0869	7.3	5	20 (14%)
ractopamine	$C_{18}H_{23}NO_3$	301.16779	302.1751	6.5	10	20 (14%)
salbutamol	$C_{13}H_{21}NO_3$	239.15214	240.1594	3.7	10[g]	NA
zilpaterol	$C_{14}H_{19}N_3O_2$	261.14773	262.1550	3.7	10	19 (28%)
β-Lactams						
amoxicillin	$C_{16}H_{19}N_3O_5S$	365.10454	366.1118	3.0	>100	
ampicillin	$C_{16}H_{19}N_3O_4S$	349.10963	350.1169	5.8	<5[f]	
benzylpenicilloic acid	$C_{16}H_{20}N_2O_5S$	352.10929	353.1166	9.2	NA	
cloxacillin	$C_{19}H_{18}ClN_3O_5S$	435.06557	436.0728	13.2	10[f]	
dicloxacillin	$C_{19}H_{17}Cl_2N_3O_5S$	469.02660	470.0339	14.4	>200	
oxocillin	$C_{19}H_{19}N_3O_5S$	401.10454	402.1118	12.9	100	
penillic acid	$C_{16}H_{18}N_2O_4S$	334.09873	335.1060	7.2	<5[f]	
penicillin G	$C_{16}H_{18}N_2O_4S$	334.09873	335.1060	11.2	NA	
penicillin V	$C_{16}H_{18}N_2O_5S$	350.09364	351.1009	12.3	100	
penilloic acid	$C_{15}H_{20}N_2O_3S$	308.11946	309.1267	11	NA	
sulbactam	$C_8H_{11}NO_5S$	233.03579	234.0431	5.6	1000[g]	
ticarcillin	$C_{15}H_{16}N_2O_6S_2$	384.04498	385.0523	9.8	100	
Cephalosporins						
cefadroxil	$C_{16}H_{17}N_3O_5S$	363.08889	364.0962	5	500	
cefalonium	$C_{20}H_{18}N_4O_5S_2$	458.07186	459.0791	6.9	>1000	
cefapirin (cephapirin)	$C_{17}H_{17}N_3O_6S_2$	423.05588	424.0632	5.2	20[f]	
cefoperazone	$C_{25}H_{27}N_9O_8S_2$	645.14240	646.1497	9.4	>1000	
cefotaxime	$C_{16}H_{17}N_5O_7S_2$	455.05694	456.0642	7.4	10	15 (28%)
cefoxitin	$C_{16}H_{17}N_5O_7S_2$	455.05694	456.0642	ND[h]	NA	
cefquinome	$C_{23}H_{24}N_6O_5S_2$	528.12496	529.1322	6.4	10	4 (21%)
ceftiofur	$C_{19}H_{17}N_5O_7S_3$	523.02905	524.0363	10.1	100	
ceftriaxone	$C_{18}H_{18}N_8O_7S_3$	554.04606	555.0533	7.0	>1000	
cefuroxime	$C_{16}H_{16}N_4O_8S$	424.06888	447.0581[e]	8.8	1000	
cephalothin (cefalotin)	$C_{16}H_{16}N_2O_6S_2$	396.04498	419.0342[e]	11.0	500	
cephradine (cefradine)	$C_{16}H_{19}N_3O_4S$	349.10963	350.1169	6.6	10	20 (15%)
desacetylcephapirin	$C_{15}H_{15}N_3O_5S_2$	381.04531	382.0526	2.3	NA	

dx.doi.org/10.1021/jf405321w | J. Agric. Food Chem. 2014, 62, 3660−3674

Table 1. continued

compounds	formula	mass	precursor ion (m/z)[a]	RT (min)	estimated screening LOD in milk (ng/mL)[b]	screening results at 10 ng/mL (X/20, %RSD)[c]
Cephalosporins						
desacetylcephapirin dehydrated	$C_{15}H_{13}N_3O_4S_2$	363.03475	364.0420	1.6	NA	
Dyes						
brilliant green	$C_{27}H_{32}N_2$	384.25655	385.2638	14.9	NA	
crystal violet	$C_{25}H_{30}N_3$	372.24397	372.2434	13.6	NA	
leucocrystal violet	$C_{25}H_{31}N_3$	373.25180	374.2591	7.8	NA	
leucomalachite green	$C_{23}H_{26}N_2$	330.20960	331.2169	11.8	NA	
malachite green	$C_{23}H_{25}N_2$	329.20177	329.2012	12.2	NA	
methylene blue	$C_{16}H_{17}N_3S$	283.11432	284.1216	8.6	NA	
Flukacides						
bithionol	$C_{12}H_6C_{l4}O_2S$	353.88426	352.8770[i]	16.9	500	
clorsulon	$C_8H_8Cl_3N_3O_4S_2$	378.90218	377.8949[i]	10.8	10	NA
closantel	$C_{22}H_{14}Cl_2I_2N_2O_2$	661.85217	660.8449[i]	17.8	>1000	
niclosamide	$C_{13}H_8Cl_2N_2O_4$	325.98611	324.9788[i]	16.5	>1000	
nitroxinil	$C_7H_3IN_2O_3$	289.91883	288.9116[i]	13.1	NA	
oxyclozanide	$C_{13}H_6Cl_5NO_3$	398.87903	397.8718[i]	16.2	20	
rafoxanide	$C_{19}H_{11}Cl_2I_2NO_3$	624.82053	623.8133[i]	18.2	500	
Ionophores						
lasalocid A	$C_{34}H_{54}O_8$	590.38187	613.3711[e]	20.5	NA	
monensin	$C_{36}H_{62}O_{11}$	670.42921	693.4184[e]	19.6	NA	
narasin	$C_{43}H_{72}O_{11}$	764.50746	787.4967[e]	17.7	NA	
nigericin	$C_{40}H_{68}O_{11}$	724.47616	747.4654[e]	19.8	NA	
salinomycin	$C_{42}H_{70}O_{11}$	750.49181	773.4810[e]	17.4	NA	
Lincosamides						
clindamycin	$C_{18}H_{33}ClN_2O_5S$	424.17987	425.1871	8.4	5	20 (16%)
lincomycin	$C_{18}H_{34}N_2O_6S$	406.21376	407.2210	5.1	5	20 (15%)
pirlimycin	$C_{17}H_{31}ClN_2O_5S$	410.16422	411.1715	8.1	5	20 (19%)
Macrolides						
clarithromycin	$C_{38}H_{69}NO_{13}$	747.47689	748.4842	10.6	20[g]	19 (53%)
desacetyl troleandomycin	$C_{39}H_{65}NO_{14}$	771.44051	772.4478	11.3	100	
erythromycin A	$C_{37}H_{67}NO_{13}$	733.46124	734.4685	9.3	10	
erythromycin anhydrate	$C_{37}H_{65}NO_{12}$	715.45068	716.4580	10.1	5[f]	
josamycin	$C_{42}H_{69}NO_{15}$	827.46672	828.4740	11.5	100	
natamycin	$C_{33}H_{47}NO_{13}$	665.30474	666.3120	10.1	>100	
roxithromycin	$C_{41}H_{76}N_2O_{15}$	836.52457	837.5318	11.1	100	
spiramycin	$C_{43}H_{74}N_2O_{14}$	842.51401	843.5213	7.9	100	
tilmicosin	$C_{46}H_{80}N_2O_{13}$	868.56604	869.5733/435.2905[j]	8.2	10[f]	
tulathromycin	$C_{41}H_{79}N_3O_{12}$	805.56638	806.5737	6.6	100	
tylosin A	$C_{46}H_{77}NO_{17}$	915.51915	916.5264	9.8	<5[f]	
tylosin B (desmycosin)	$C_{39}H_{65}NO_{14}$	771.44051	772.4478	9.4	NA	
Miscellaneous						
acepromazine	$C_{19}H_{22}N_2OS$	326.14528	327.1526	10.3	5	12 (57%)
acetaminophen	$C_8H_9NO_2$	151.06333	152.0706	4.4	NA	
α-zearalenol	$C_{18}H_{24}O_5$	320.16237	321.1697	13.5	>100	
amprolium	$C_{14}H_{18}N_4$	242.15315	243.1604	1.4	NA	
caffeine	$C_8H_{10}N_4O_2$	194.08038	195.0877	6.3	NA	
clavulanate	$C_8H_9NO_5$	199.04807	200.0553/198.0408[i]	ND	NA	
clopidol	$C_7H_7Cl_2NO$	190.99047	191.9977	6.2	5	20 (20%)
decoquinate	$C_{24}H_{35}NO_5$	417.25152	418.2588	17.1	>1000	
detomidine	$C_{12}H_{14}N_2$	186.11570	187.1230	8.1	5	20 (12%)
dexamethasone	$C_{22}H_{29}FO_5$	392.19990	393.2072	12	NA	
diclazuril	$C_{17}H_9Cl_3N_4O_2$	405.97911	404.9718[i]	15.9	NA	
diminazene	$C_{14}H_{15}N_7$	281.13889	282.1462	4.9	100	
ethopabate	$C_{12}H_{15}NO_4$	237.10011	238.1074	9.9	10	20 (28%)
fumagillin	$C_{26}H_{34}O_7$	458.23045	481.2197[e]	16	NA	
halofuginone	$C_{16}H_{17}ClBrN_3O_3$	413.01418	414.0215	8.4	5	20 (17%)
imidocarb	$C_{19}H_{20}N_6O$	348.16986	349.1771	5.6	5	20 (44%)
ketamine	$C_{13}H_{16}ClNO$	237.09204	238.0993	6.9	5	20 (20%)
ketoconazole	$C_{26}H_{28}Cl_2N_4O_4$	530.14876	531.1560	10.6	10[g]	18 (27%)

dx.doi.org/10.1021/jf405321w | J. Agric. Food Chem. 2014, 62, 3660−3674

Table 1. continued

compounds	formula	mass	precursor ion (m/z)[a]	RT (min)	estimated screening LOD in milk (ng/mL)[b]	screening results at 10 ng/mL (X/20, %RSD)[c]
Miscellaneous						
levamisole	$C_{11}H_{12}N_2S$	204.07212	205.0794	5.4	20	
lidocaine	$C_{14}H_{22}N_2O$	234.17321	235.1805	6.3	5	20 (26%)
maduramicin	$C_{47}H_{80}O_{17}$	916.53955	939.5288[e]	21	1000	
melamine	$C_3H_6N_6$	126.06539	127.0727	1.1	NA	
nicarbazin (4,4′-dinitrocarbanilide)	$C_{13}H_{10}N_4O_5$	302.06512	301.0578[i]	15.5	100	
novobiocin	$C_{31}H_{36}N_2O_{11}$	612.23191	613.2392	16.3	>1000	
ormetoprim	$C_{14}H_{18}N_4O_2$	274.14298	275.1503	6.8	5	20 (12%)
progesterone	$C_{21}H_{30}O_2$	314.22458	315.2319	16.5	NA	
pyrimethamine	$C_{12}H_{13}ClN_4$	248.08287	249.0902	8.6	5	20 (19%)
rifampin	$C_{48}H_{58}N_4O_{12}$	882.40512	883.4124	ND	NA	
robenidine	$C_{15}H_{13}Cl_2N_5$	333.05480	334.0621	12	>100	
tiamulin	$C_{28}H_{47}NO_4S$	493.32258	494.3299	10.6	5	20 (70%)
toltrazuril	$C_{18}H_{14}F_3N_3O_4S$	425.06571	424.0584[i]	16.1	>100	
trichlormethiazide	$C_8H_8Cl_3N_3O_4S_2$	378.90218	377.8949[i]	10.4	10	NA
trimethoprim	$C_{14}H_{18}N_4O_3$	290.13789	291.1452	5.8	5	20 (16%)
tripelennamine	$C_{16}H_{21}N_3$	255.17355	256.1808	6.9	<5[f]	
virginiamycin M1	$C_{28}H_{35}N_3O_7$	525.24750	526.2547	12.5	10[f]	
virginiamycin S1	$C_{43}H_{49}N_7O_{10}$	823.35409	824.3614	15.2	>100	
xylazine	$C_{12}H_{16}N_2S$	220.10342	221.1107	7.1	5	20 (14%)
Nitromidazoles						
dimetridazole	$C_5H_7N_3O_2$	141.05383	142.0611	5.3	5	20 (18%)
metronidazole	$C_6H_9N_3O_3$	171.06439	172.0717	4.3	20	
metronidazole hydroxide	$C_6H_9N_3O_4$	187.05931	188.0666	3.3	NA	
ornidazole	$C_7H_{10}ClN_3O_3$	219.04107	220.0483	7.8	NA	
ronidazole	$C_6H_8N_4O_4$	200.05455	201.0618/223.0438[e]	5.4	NA	
tindazole	$C_8H_{13}N_3O_4S$	247.06268	248.0700	6.9	NA	
NSAIDs						
flunixin	$C_{14}H_{11}F_3N_2O_2$	296.07726	297.0845	13.8	5	20 (32%)
phenylbutazone	$C_{19}H_{20}N_2O_2$	308.15248	309.1598	15.9	200	
flunixin hydroxide	$C_{14}H_{11}F_3N_2O_3$	312.07218	313.0795	12.9	<5[f]	
carprofen	$C_{15}H_{12}ClNO_2$	273.05566	274.0629/272.0484[i]	15.3	>200	
diclofenac	$C_{14}H_{11}Cl_2NO_2$	295.01668	296.0240	15.7	>200	
ketoprofen	$C_{16}H_{14}O_3$	254.09429	255.1016	13.6	100	
mefenamic acid	$C_{15}H_{15}NO_2$	241.11028	242.1176/240.1030[i]	16.2	>200	
naproxen	$C_{14}H_{14}O_3$	230.09429	231.1016	13.7	200	
niflumic acid	$C_{13}H_9F_3N_2O_2$	282.06161	283.0689/281.0543[i]	15.6	10	NA
suxibuzone	$C_{24}H_{26}N_2O_6$	438.17909	439.1864	15.4	200	
Peptides						
bacitracin A	$C_{66}H_{103}N_{17}O_{16}S$	1421.74894	1422.7562/711.8817[j]	8.3	>500[f]	
colistin B−polymix E2	$C_{52}H_{98}N_{16}O_{13}$	1154.74993	1177.7391[e]	6.1	NA	
colistin B−polymix E1	$C_{53}H_{100}N_{16}O_{13}$	1168.76558	1191.7548[e]	6.6	NA	
vancomycin	$C_{66}H_{75}Cl_2N_9O_{24}$	1447.43020	724.7224[j]	5.4	>100	
Phenicols						
chloramphenicol	$C_{11}H_{12}Cl_2N_2O_5$	322.01233	321.0051[i]	9.8	5	20 (29%)
chloramphenicol-d_5	$C_{11}H_7D_5Cl_2N_2O_5$	327.04371	326.0364[i]	9.8	NA	
florfenicol	$C_{12}H_{14}Cl_2FNO_4S$	357.00046	355.9932[i]	9.2	10	20 (23%)
thiamphenicol	$C_{12}H_{15}Cl_2NO_5S$	355.00480	353.9975[i]	7.2	5	20 (29%)
florfenicol amine	$C_{10}H_{14}FNO_3S$	247.06784	248.0751	1.5	100	
Quinolones						
ciprofloxacin	$C_{17}H_{18}FN_3O_3$	331.13322	332.1405	6.4	<5[f]	
danofloxacin	$C_{19}H_{20}FN_3O_3$	357.14887	358.1561	6.8	5	20 (14%)
desethylene ciprofloxacin	$C_{15}H_{16}FN_3O_3$	305.11757	306.1248	6.2	NA	
desethylene enrofloxacin	$C_{17}H_{20}FN_3O_3$	333.14887	334.1561	6.4	NA	
difloxacin	$C_{21}H_{19}F_2N_3O_3$	399.13945	400.1467	7.4	5	20 (30%)
enofloxacin (enoxacin)	$C_{15}H_{17}FN_4O_3$	320.12847	321.1357	6.6	5	20 (21%)
enrofloxacin	$C_{19}H_{22}FN_3O_3$	359.16452	360.1718	6.8	5	20 (34%)
fleroxacin	$C_{17}H_{18}F_3N_3O_3$	369.13003	370.1373	7.0	5	20 (25%)

dx.doi.org/10.1021/jf405321w | J. Agric. Food Chem. 2014, 62, 3660−3674

Table 1. continued

compounds	formula	mass	precursor ion (m/z)[a]	RT (min)	estimated screening LOD in milk (ng/mL)[b]	screening results at 10 ng/mL (X/20, %RSD)[c]
Quinolones						
flumequine	$C_{14}H_{12}FNO_3$	261.08012	262.0874	11.8	10	20 (34%)
gatifloxacin	$C_{19}H_{22}FN_3O_4$	375.15943	376.1667	7.7	5	20 (30%)
lomefloxacin	$C_{17}H_{19}F_2N_3O_3$	351.13945	352.1467	6.7	5	20 (27%)
marbofloxacin	$C_{17}H_{19}FN_4O_4$	362.13903	363.1463	6.6	10	20 (22%)
moxifloxacin	$C_{21}H_{24}FN_3O_4$	401.17508	402.1824	8.3	10	20 (41%)
nadifloxacin	$C_{19}H_{21}FN_2O_4$	360.14854	361.1558	11.7	100[g]	
nalidixic acid	$C_{12}H_{12}N_2O_3$	232.08479	233.0921	11.4	20[g]	20 (39%)
norfloxacin	$C_{16}H_{18}FN_3O_3$	319.13322	320.1405	6.3	10	20 (23%)
ofloxacin (racemic mix)	$C_{18}H_{20}FN_3O_4$	361.14378	362.1511	6.4	5	20 (33%)
orbifloxacin	$C_{19}H_{20}F_3N_3O_3$	395.14568	396.1530	7.5	5	20 (26%)
oxociprofloxacin	$C_{17}H_{16}FN_3O_4$	345.11248	346.1198	9.3	NA	
oxolinic acid	$C_{13}H_{11}NO_5$	261.06372	262.0710	9.8	5	20 (32%)
pazufloxacin	$C_{16}H_{15}FN_2O_4$	318.10159	319.1089	7.0	10	20 (23%)
pefloxacin	$C_{17}H_{20}FN_3O_3$	333.14887	334.1561	6.4	5	19 (32%)
pipemidic acid	$C_{14}H_{17}N_5O_3$	303.13314	304.1404	6.3	5	20 (43%)
piromidic acid	$C_{14}H_{16}N_4O_3$	288.12224	289.1295	13.2	10[g]	20 (54%)
prulifloxacin	$C_{21}H_{20}FN_3O_6S$	461.10568	462.1130	9.3	NA	
sarafloxacin	$C_{20}H_{17}F_2N_3O_3$	385.12380	386.1311	7.2	<5[f]	
sparfloxacin	$C_{19}H_{22}F_2N_4O_3$	392.16600	393.1733	7.4	5	20 (35%)
Sulfonamides						
dapsone	$C_{12}H_{12}N_2O_2S$	248.06195	249.0692	9.2	5	20 (21%)
sulfabenzamide	$C_{13}H_{12}N_2O_3S$	276.05686	277.0641	10.6	5	18 (29%)
sulfacetamide	$C_8H_{10}N_2O_3S$	214.04121	215.0485	5.5	20	
sulfachloropyridazine	$C_{10}H_9ClN_4O_2S$	284.01347	285.0208	8.5	<5[f]	
sulfadiazine	$C_{10}H_{10}N_4O_2S$	250.05245	251.0597	5.5	5[f]	
sulfadimethoxine	$C_{12}H_{14}N_4O_4S$	310.07358	311.0809	10.3	<5[f]	
sulfadoxine	$C_{12}H_{14}N_4O_4S$	310.07358	311.0809	9.4	5	20 (23%)
sulfaguanidine	$C_7H_{10}N_4O_2S$	214.05245	215.0597	2	10	0
sulfamerazine	$C_{11}H_{12}N_4O_2S$	264.06810	265.0754	6.3	10[f]	
sulfameter(sulfametoxydiazine)	$C_{11}H_{12}N_4O_3S$	280.06301	281.0703	7.9	10	
sulfamethazine (sulfadimidine)	$C_{12}H_{14}N_4O_2S$	278.08375	279.0910	7.3	5[f]	
sulfamethazine−lactose adduct	$C_{24}H_{34}N_4O_{12}S$	602.18939	603.1967	4.8	NA	
sulfamethoxazole	$C_{10}H_{11}N_3O_3S$	253.05211	254.0594	8.8	5	20 (25%)
sulfamethoxypyridazine	$C_{11}H_{12}N_4O_3S$	280.06301	281.0703	8.6	5	20 (23%)
sulfamonomethoxine	$C_{11}H_{12}N_4O_3S$	280.06301	281.0703	7.9	10	20 (24%)
sulfanilamide	$C_6H_8N_2O_2S$	172.03065	173.0379	2.5	>100	
sulfanitran	$C_{14}H_{13}N_3O_5S$	335.05759	336.0649	12.5	100	
sulfaphenazole	$C_{15}H_{14}N_4O_2S$	314.08375	315.0910	11	10	19 (30%)
sulfapyridine	$C_{11}H_{11}N_3O_2S$	249.05720	250.0645	6.2	10[f]	
sulfaquinoxaline	$C_{14}H_{12}N_4O_2S$	300.06810	301.0754	10.3	<5[f]	
sulfathiazole	$C_9H_9N_3O_2S_2$	255.01362	256.0209	6.0	5[f]	
sulfisoxazole	$C_{11}H_{13}N_3O_3S$	267.06776	268.0750	10	5	20 (36%)
*N*4-acetyl-sulfamethazine	$C_{14}H_{16}N_4O_3S$	320.09431	321.1016	7.4	NA	
Tetracyclines						
4-epi-tetracycline	$C_{22}H_{24}N_2O_8$	444.15327	445.1605	6.5	20	
chlortetracycline	$C_{22}H_{23}ClN_2O_8$	478.11429	479.1216	7.8	10[f]	
demeclocycline	$C_{21}H_{21}ClN_2O_8$	464.09864	465.1059	7.6	>100	
doxycycline	$C_{22}H_{24}N_2O_8$	444.15327	445.1605	8.2	10[f]	
oxytetracycline	$C_{22}H_{24}N_2O_9$	460.14818	461.1555	6.3	10[f]	
tetracycline	$C_{22}H_{24}N_2O_8$	444.15327	445.1605	6.6	10[f]	

[a]$[MH]^+$ unless otherwise indicated. [b]At estimated screening limit of detection (LOD), analyte is found in all three replicates. [c]Number of times compound found at 10 ng/mL in 20 fortified milk samples (% relative standard deviation of those replicates). [d]NA = not analyzed. [e]$[MNa]^+$ [f]From previously published work.[1] [g]Not found in all three replicates at LOD, but found in replicates at lower levels. [h]ND = not detected. [i]$[M - H]^-$. [j]$[MH_2]^{2+}$.

data that can be evaluated later to look for additional nontargeted compounds.

Another reason to collect exact mass data for a large number of compounds is that elemental compositions for product ions can be proposed using a combination of measured exact

dx.doi.org/10.1021/jf405321w | J. Agric. Food Chem. 2014, 62, 3660−3674

masses, isotope patterns, predictive fragmentation pathways, and published literature. The compiled data will be useful for the development of future veterinary drug residue methods regardless of the MS platform (e.g., Orbitrap or triple quadrupole) that is utilized. This paper describes the collection and evaluation of measured exact mass data for approximately 200 veterinary drugs obtained using a LC Q-TOF MS. In addition, determining how well the compounds of interest chromatograph and are extracted from a matrix with a given analytical method is important when implementing these procedures to analyze regulatory samples. The performance of many of these compounds through the milk screening extraction procedure described earlier[1] was evaluated, and these results are also reported.

MATERIALS AND METHODS

Reagents and Consumables. Solvents used to prepare standard stock solutions (methanol and dimethylformamide (DMF)) were HPLC grade purchased from EMD Chemicals (Billerica, MA). The water, acetonitrile, and formic acid used to prepare the LC mobile phase were LC-MS grade (Fisher Optima, Fair Lawn, NJ). Formic acid solution (0.1% v/v) was prepared by pipetting 1.0 mL of formic acid into a 1000 mL graduated cylinder and diluting to mark with water. Amicon Ultra centrifugal filters (0.5 mL, 3000 Da molecular weight cutoff, no. UFC500396) were purchased from Millipore Corp. (Bedford, MA). LC column was YMC ODS-AQ, 120 Å, 2 mm × 100 mm, 3 μm, no. 50−874−228 (Fisher Scientific, Houston, TX).

Standard Preparation. The majority of standards used in this study were purchased from Sigma Aldrich (St. Louis, MO). Several other compounds were already being used in our laboratory for regulatory residue methods, and these were primarily purchased from U.S. Pharmacopeia (Rockville, MD). A few of the less common compounds were purchased from alternative sources such as LKT (St. Paul, MN) and Waco (Richmond, VA). Individual stock solutions were prepared for all compounds at a concentration of approximately 100 μg/mL (ranging from ∼50 to 200 μg/mL) in methanol depending on solubility and amount of standard available. If not soluble in methanol, the standards were dissolved in water or DMF. Mixed working standards were made by diluting an appropriate volume (after correcting for purity and any counterion) of stock standards to 10 mL with either methanol or water to give a final concentration of 1000 ng/mL. Then serial dilutions were prepared with 0.1% formic acid at concentrations of 100, 10, and 1 ng/mL for LC Q-TOF MS analysis.

LC Q-TOF MS Parameters. The LC Q-TOF MS was operated using the conditions described earlier.[1] Briefly, the instrument was an Agilent (Santa Clara, CA) quadrupole time-of-flight (Q-TOF) 6530 mass spectrometer coupled to an Agilent 1290 liquid chromatograph. Electrospray ionization with Agilent Jet Stream Technology was utilized. The time-of-flight MS was calibrated daily. Typical resolution values obtained during calibration were 9000 (m/z 322) and 15000 (m/z 1522) full width half-maximum. A reference mass solution was continuously introduced along with the LC stream for accurate mass calibration at a flow rate of ∼0.005 mL/min using a stand-alone LC pump with a flow of 0.5 mL/min and a 100:1 splitter (Agilent no. G1607-60000). Reference masses at m/z 121.05087 (purine) and m/z 922.00980 (hexakis(1*H*,1*H*,3*H*-tetrafluoropropoxy) phosphazine) were used for positive ion; m/z 112.985587 (trifluoroacetate) and 966.000725 (formate adduct of hexakis(1*H*,1*H*,3*H*-tetrafluoropropoxy) phosphazine) were used for negative ion.

The following parameters were used for the MS source: fragmentor (150 V), nozzle (250 V), Vcap (4000 V), drying gas (11 L/min, N_2), sheath gas (11 L/min, N_2). The TOF (MS^1 only) data acquisition rate was 4 GHz (to m/z 1700) and the actual scan range was m/z 100−1200 at a rate of 1.08 spectra/s. Data were collected in both centroid and profile modes. In general, to minimize processing time only centroid data were evaluated, but profile data could be used to better distinguish coeluting isobaric compounds if needed. Compounds that ionized in the negative ion mode were analyzed separately using a different acquisition program. The MS source parameters were as above for negative ion except that the Vcap and nozzle voltages were 2000 and 200 V, respectively.

The LC program was also consistent with previous work[1] using an YMC ODS-AQ column with gradient of 0.1% formic acid and acetonitrile as follows: 5% acetonitrile for 2 min, ramp 5−50% acetonitrile over 10 min, hold at 50% acetonitrile for 1 min, ramp 50−100% acetonitrile over 3 min, hold at 100% acetonitrile for 2 min. The flow rate was 250 μL/min, and the column was maintained at room temperature (22 ± 1 °C). A postequilibration time of 3 min was used. Injections of 10 μL were made with a 3 s 50:50 methanol:water needle wash. For most analytes, the column was held at 100% acetonitrile for the 2 min described above for a total analysis time of 18 min. However, some compounds being investigated did not elute in that time frame, so an additional 4 min of 100% acetonitrile can be added to the chromatographic program to make an extended LC program that is 23 min long.

Once retention times and precursor ions (MH^+, $M - H^-$, or MNa^+) were established, MS/MS data were collected at three different collision energies (CEs) for each compound. The formula "[3 × (mass/100)] + 10" is suggested by Agilent to calculate a reasonable CE for compounds using their acquisition software and was used here; data were also collected at approximately 10 V higher and lower than that value. Medium isolation width (4 m/z) and 200 ms/spectrum were used to collect product ion spectra. These spectra, along with retention time information, were added to the in-house database using the Agilent *Personal Compound Database Library* software.

Solvent Standard Analysis. For the initial analysis, compounds were randomly mixed according to the order in which they were prepared (mixtures of 4−10 analytes). These mixed solvent standard solutions were prepared at concentrations of 100, 10, and 1 ng/mL and analyzed. Compounds that had been characterized and documented previously[1,11] were not reanalyzed, but those data are also shown in Table 1.

Milk Samples. Several brands of pasteurized whole milk were purchased from local retail stores. After testing to ensure that this milk did not contain any analytes, it was used for negative control and was fortified with target compounds. Incurred (raw) milk obtained from the Food and Drug Administration's Center for Veterinary Medicine was also used. Milk was aliquoted (1.0 mL) into 15 mL centrifuge tubes and frozen (−40 °C) until needed.

Extraction of Milk Samples. Analytes were fortified into milk and extracted using the method published earlier[1] and briefly described here. Acetonitrile (1.0 mL) was added to 1.0 mL of milk, and the sample was vortex mixed for 20 s and then centrifuged at 3250 rcf (× *g*) and 4 °C for 20 min. A 1.0 mL aliquot of the resulting supernatant was transferred to a 16 mm × 150 mm disposable glass tube containing 0.5 mL of 0.1% formic acid. Using a Turbo-vap set at 40 °C with nitrogen (10−15 psi), the solvent was evaporated until the volume was slightly less than 0.5 mL. The sample may be quite cloudy at this point. Sample cleanup was performed with 3000 Da molecular weight cutoff centrifuge filters that were first prewashed by adding 0.5 mL of 0.1% formic acid to the filters and centrifuging at 17000 rcf (× *g*) for 5 min. The extracts were added to the cutoff filters, and the volume was adjusted as needed to ∼0.5 mL with 0.1% formic acid. The samples were centrifuged at 17000 rcf (× *g*) for 15 min, and then the filtered extracts were transferred to LC vials (polypropylene with conical insert for low volume) for analysis.

Fortification and Validation Protocol. For the fortification experiments, analytes were generally grouped by class (e.g., sulfonamides, quinolones, macrolides) and mixed fortification standards were prepared at 1000 ng/mL using methanol or water. Milk was fortified at levels varying from 5 to 100 ng/mL by adding an appropriate volume of the mixed fortification standard. For example, to fortify 1 mL of milk at 10 ng/mL, 10 μL of the 1000 ng/mL mixed fortification standard was added. Samples for each level were prepared in triplicate and analyzed by using both TOF (MS^1) and MS/MS acquisition programs. For some compounds that performed poorly, a higher concentration fortification standard was made at 10000 ng/mL (10 μg/mL) and added to the milk, for a final fortification level of

dx.doi.org/10.1021/jf405321w | J. Agric. Food Chem. 2014, 62, 3660−3674

500−1000 ng/mL. For analytes that performed well in initial testing (~60 new compounds were detected at 10 ng/mL or lower), additional validation samples (n = 20) were prepared by fortifying milk at 10 ng/mL. Three different sources of milk (retail organic whole (n = 6), retail nonorganic whole (n = 6), and raw (n = 8)) were used for this part of the method validation. Nonfortified samples from each source of milk were also analyzed as negative controls. The number of false negatives and the precision of the analyte response (MS^1 only) at the 10 ng/mL fortification level were determined from this expanded sample set.

Data Analysis. The TOF data were evaluated against a database of compounds compiled in-house for their possible veterinary drug application (n = 267). Using Agilent's MassHunter *Find by Formula* algorithm, data files were compared to the database using search windows of 10 ppm and a 1 min retention time for ions corresponding to $[M + H]^+$, $[M - H]^-$, or $[M + Na]^+$. Mass accuracy errors were obtained by comparing experimental data to potential matching compounds in the database. The MS/MS data were processed by manually extracting narrow window (10 ppm) product ion scans. Product ion spectra from the resulting extracted ion chromatograms were evaluated by comparing mass assignments to theoretical values.

RESULTS AND DISCUSSION

Analysis of Solvent Standards. Our laboratory has an in-house database that contains formulas and exact mass data for 267 veterinary drugs. Approximately 200 of these analytes were included in this study and are listed in Tables 1 and 3. The remaining are minor components of mixtures (e.g., eprinomectin B1b) or drug metabolites for which no standards were available. Although this database may change over time when new compounds are added or more analytical standards become available, this paper describes the process and impact of adding additional data (retention time, product ions, and method performance information) to exact mass data when applying this technology to regulatory food analyses. With very few exceptions, all of the compounds analyzed by this LC QTOF MS method were detected. Many analytes could be detected at levels down to 1 ng/mL using the *Find by Formula* software program; others were found only at concentrations of 100 or 10 ng/mL. A list of the compounds analyzed, their formulas, neutral masses, and precursor ions are given in Table 1. Most were detected as the protonated molecules with a measured mass within 2 ppm of the theoretical values. Some compounds, including ionophores such as monensin, formed sodium adducts; others were detected only in negative ion mode. For a few analytes, degradation products were observed, in addition to or instead of, the expected parent compound. This has been documented previously for penicillin G and macrolides.[1,5,13,14] In another example, troleandomycin should have a formula of $C_{41}H_{67}NO_{15}$ with a protonated molecule at m/z 814.4583. Instead, only m/z 772.4478 was observed, indicating degradation by loss of an acetyl group to form desacetyl troleandomycin, a compound isobaric with desmycosin which is a degradation product of tylosin. Others[15] have observed this as well, listing the expected precursor ion of troleandomycin as m/z 772.5.

The observed retention times for these compounds are also listed in Table 1. The retention times remained fairly stable over time (well within the 1 min time window) regardless of whether analyzing solvent standards or milk extracts, with instrument maintenance, and with LC column replacement. Some nonpolar compounds, including the avermectins, required an extended chromatographic program to elute from the LC column. Although the retention times generated will be specific to this column and mobile phase gradient, the relative polarities of these compounds as measured by elution times on a reversed-phase LC column should still be useful to others.

Using Experimental Data to Rule out False Detects. Using the *Find by Formula* algorithm and only measured exact mass data (no retention time matching required) resulted in many false detects in milk samples, even when being compared to a relatively small (n = 267) database of compounds. This is in part due to the need to set the mass window relatively wide (10 ppm) for the initial screen. We have previously shown that when using instruments with medium (10−15K) resolution, interfering matrix components can cause shifts in mass accuracy.[1] Table 2 shows an increase in false negatives, especially at lower residue levels, when the mass window is narrowed to 5 ppm.

Table 2. Percent False Negatives for Milk Fortified with Sulfadimethoxine, Oxytetracycline, Penicillin G, and Erythromycin

fortification level[a] (ng/mL)	5 ppm window (%)	10 ppm window (%)
20	13	3
10	27	10

[a] N = 60 at each level (5 samples × 3 replicate injections × 4 residues).

The use of a relatively wide mass window can lead to the apparent detection of compounds that are not actually present (false detects that could lead to the reporting of false positives), especially when sample extracts are not very clean because rapid generic extraction procedures are used. In some cases using the *Find by Formula* program, the ^{13}C (M + 1) isotope ion of a matrix component will match the m/z of a compound in the database when screening with a wide m/z window. Others have also observed this phenomenon.[9,12] An example of this is shown in Figure 1, where moxidectin was "detected" even though the ion correlating with the protonated molecule of moxidectin (m/z 640.3844) is part of an isotope pattern for an ion at nominal m/z 639. Analysis of an actual standard of moxidectin shows a peak at a much later retention time, with MNa^+ as the primary ion. There can also be ubiquitous impurities, either from matrix or instrument background, that are isobaric with known analytes. Figure 2 shows a false detect for netilimicin in a milk extract. The mass accuracy (<5 ppm) and isotope pattern indicate a reasonable match for this compound. But because netilimicin is an aminoglycoside, it is not expected to elute in the middle of the gradient program with good chromatographic peak shape. However, until an actual standard of this compound could be obtained and was observed to elute with the solvent front as expected, it could not be completely ruled out. The product ion spectrum of netilimicin also does not match that obtained from the impurity (data not shown).

By adding retention time and product ion data for most compounds in the database, the analysis of samples becomes much more efficient as many false detects can be ruled out quickly based initially on retention time matching followed by product ion comparison if needed. Data files from milk sample extracts (N = 120; 40 samples injected in triplicate) were evaluated against the veterinary drug database with and without retention time matching. When retention time matching was included, significantly fewer compounds (average of 3) were detected as compared to when only accurate mass was used (average of 30 compounds "found" in each data file). Instrument companies are also aware of these issues, and in

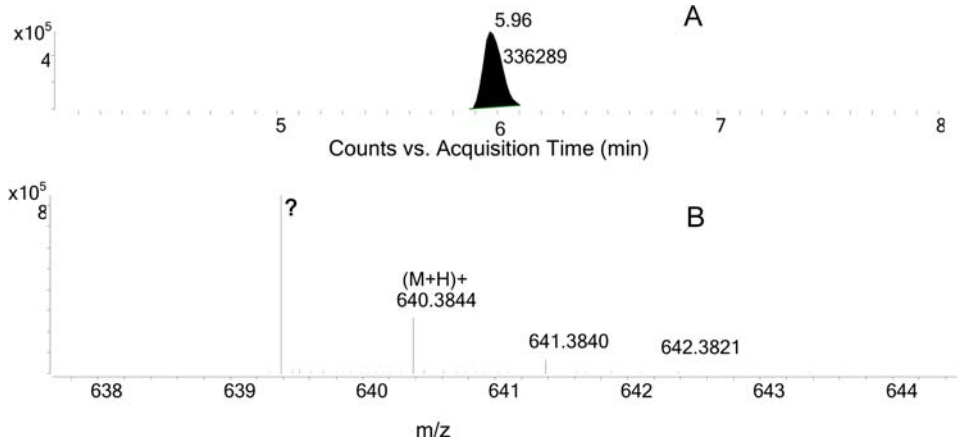

Figure 1. False detection of moxidectin. Extracted ion chromatogram in milk extract with 10 ppm window for MH^+ (m/z 640.3844) gives reasonable chromatographic peak (A), but inspection of the MH^+ spectral pattern (B) shows this ion is ^{13}C isotope peak of another (matrix) compound.

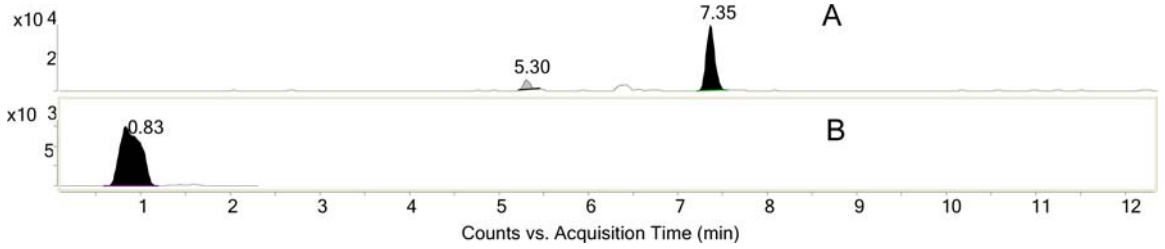

Figure 2. False detection of netilimicin. Extracted ion chromatogram in milk extract with 10 ppm window for MH^+ (m/z 476.3079) gives reasonable chromatographic peak (A), but analysis of a 100 ng/mL standard of netilimicin (B) indicates analyte has very different retention time.

addition to improving their software data mining capabilities, they are developing "turn-key kits" for residue analysis. For example, Waters Corp. is marketing the *UNIFI* package[16] for pesticide analysis which includes standard mixes, chromatographic columns, methods, and databases that include retention times and product ion spectra specific to their methodology. Agilent has recently developed a similar kit for residues including veterinary drugs, hormones, and many pesticides.[17]

Detection of Analytes in Milk Extracts. Ideally, the compounds that are detected with the LC Q-TOF MS instrumental method could also be reliably monitored in milk using this method. To determine the actual ability of this method to detect analytes of interest in this matrix, varying levels of these compounds were fortified into control milk samples that were then extracted. A majority (56%) of the analytes tested in milk extracts could be successfully detected using the *Find by Formula* program at levels of 10 ng/mL or lower (see Table 1 and Figure 3). At fortification levels of 100 ng/mL, over 70% of analytes could be detected. The estimated screening limit of detection is defined as the level at which an analyte was found in all three replicate injections. For a few analytes (noted in Table 1), the compound was found in only two of the replicates at the level of detection but was also found in at least one replicate at a lower level of fortification. Analytes that had been previously validated for the milk screening method were not reanalyzed. This initial set of 25 compounds had tolerance or safe levels in the United States. So although the majority of the data for these analytes were collected for samples fortified at that "1X" level, some experiments were performed to determine the limits of detection in milk. These results were published previously[1] but are also included in Table 1 for comparison.

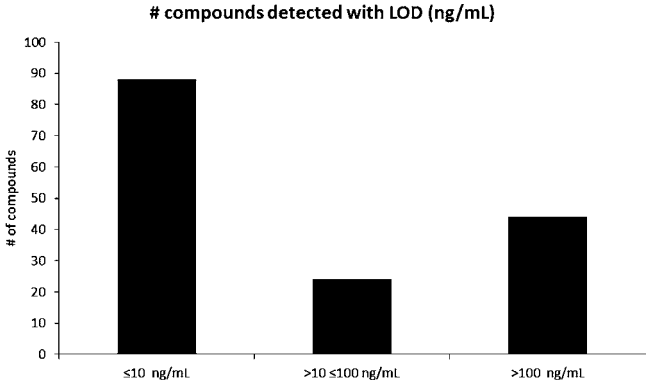

Figure 3. Screening LODs (ng/mL) for analytes in milk. LOD is defined as the fortification level at which an analyte is found. A total of 156 compounds were tested.

For most new analytes that could be detected at 5−10 ng/mL in the initial experiments, additional replicates (n = 20) using three different sources of milk fortified at 10 ng/mL were prepared and analyzed. The majority of analytes in this validation were detected in all 20 replicates (or >90%) using *Find by Formula* analysis of the MS^1 data. The few exceptions were acepromazine and sulfaguanidine, as well as two cephalosporins. In addition, the variance of the signal from analytes in milk fortified at 10 ng/mL is also documented in Table 1. In general, the relative standard deviation for the analytes tested at this level was 20−25%. Given the fact that the final extract volume was not meticulously controlled and internal standards were not used, this type of variance is reasonable and acceptable for this type of screening method. Some residues, especially those with a lower response and

dx.doi.org/10.1021/jf405321w | J. Agric. Food Chem. 2014, 62, 3660−3674

Table 3. Proposed Elemental Formulas and Exact Masses for Product Ions Detected for Veterinary Drugs

compd (reference)	precursor (±)	*m/z*	product ion 1[a]	*m/z*	product ion 2	*m/z*	product ion 3	*m/z*
Aminoglycosides[20,23]								
amikacin	$C_{22}H_{44}N_5O_{13}^+$	586.2930	$C_{16}H_{33}N_4O_9^+$	425.2242	$C_{10}H_{22}N_3O_5^{+b}$	264.1554	$C_6H_{15}N_2O_3^{+b}$	163.1077
apramycin	$C_{21}H_{42}N_5O_{11}^+$	540.2875	$C_{15}H_{28}N_3O_8^+$	378.1871	$C_9H_{17}N_2O_4^+$	217.1183		
dihydrostreptomycin	$C_{21}H_{42}N_7O_{12}^+$	584.2886	$C_8H_{19}N_6O_4^+$	263.1462	$C_7H_{17}N_4O_4^+$	221.1244	$C_7H_{14}NO_4^{+b}$	176.0917
gentamicin C1	$C_{21}H_{44}N_5O_7^+$	478.3235	$C_8H_{17}N_2O^+$	157.1335	$C_{13}H_{28}N_3O_6^+$	322.1973		
gentamicin C1A	$C_{19}H_{40}N_5O_7^+$	450.2922	$C_7H_{14}NO_3^+$	160.0968	$C_{13}H_{28}N_3O_6^+$	322.1973		
gentamicin C2	$C_{20}H_{42}N_5O_7^+$	464.3079	$C_7H_{14}NO_3^+$	160.0968	$C_{13}H_{28}N_3O_6^+$	322.1973		
kanamycin	$C_{18}H_{37}N_4O_{11}^+$	485.2453	$C_6H_{15}N_2O_3^+$	163.1077	$C_{12}H_{26}N_3O_7^+$	324.1765		
neomycin B	$C_{23}H_{47}N_6O_{13}^+$	615.3196	$C_{17}H_{35}N_4O_{10}^+$	455.2348	$C_{11}H_{21}N_2O_7^+$	293.1343	$C_6H_{13}N_2O_3^+$	161.0921
netilmicin	$C_{21}H_{42}N_5O_7^+$	476.3079	$C_{14}H_{27}N_4O_3^+$	299.2078	$C_8H_{19}N_2O_3^+$	191.1390	$C_6H_{10}NO^{+b}$	112.0757
spectinomycin	$C_{14}H_{25}N_2O_7^+$	333.1656	$C_{13}H_{20}NO_7^{+b}$	302.1234	$C_7H_{10}NO_2^+$	140.0706	$C_8H_{17}N_2O_3^{+b}$	189.1234
streptomycin	$C_{21}H_{40}N_7O_{12}^+$	582.2729	$C_{14}H_{27}N_6O_8^+$	407.1885	$C_8H_{19}N_6O_4^+$	263.1463		
Benzimidazoles[4,27]								
albendazole	$C_{12}H_{16}N_3O_2S^+$	266.0958	$C_{11}H_{12}N_3OS^+$	234.0696	$C_8H_5N_3OS^+$	191.0148	$C_8H_5N_3O^+$	159.0427
fenbendazole	$C_{15}H_{14}N_3O_2S^+$	300.0801	$C_{14}H_{10}N_3OS^+$	268.0539	$C_8H_5N_3O^+$	159.0427		
oxibendazole	$C_{12}H_{16}N_3O_3^+$	250.1186	$C_{11}H_{12}N_3O_2^+$	218.0924	$C_8H_6N_3O_2^+$	176.0455	$C_7H_6N_3O^+$	148.0505
thiabendazole	$C_{10}H_8N_3S^+$	202.0433	$C_9H_7N_2S^+$	175.0324				
β-Agonists[28,29]								
clenbuterol	$C_{12}H_{19}Cl_2N_2O^+$	277.0869	$C_8H_9Cl_2N_2^+$	203.0137	$C_{12}H_{17}Cl_2N_2^+$	259.0763		
ractopamine	$C_{18}H_{24}NO_3^+$	302.1751	$C_8H_9O^+$	121.0648	$C_7H_7O^+$	107.0491	$C_{10}H_{14}NO^{+b}$	164.1070
salbutamol	$C_{13}H_{22}NO_3^+$	240.1594	$C_9H_{10}NO^+$	148.0757	$C_{13}H_{20}NO_2^+$	222.1489		
zilpaterol	$C_{14}H_{20}N_3O_2^+$	262.1550	$C_{14}H_{18}N_3O^+$	244.1444	$C_{11}H_{12}N_3O^+$	202.0975	$C_{11}H_9N_2O^+$	185.0709
β-Lactams[14,23,25,30]								
amoxicillin	$C_{16}H_{20}N_3O_5S^+$	366.1118	$C_4H_4NOS^+$	114.0008	$C_{16}H_{17}N_2O_5S^+$	349.0853	$C_{10}H_{10}NO_2S^+$	208.0427
ampicillin	$C_{16}H_{20}N_3O_4S^+$	350.1169	$C_7H_8N^+$	106.0651	$C_6H_{10}NO_2S^+$	160.0427		
benzylpenicilloic acid	$C_{16}H_{21}N_2O_5S^+$	353.1166	$C_{15}H_{21}N_2O_3S^+$	309.1267	$C_6H_{10}NO_2S^+$	160.0427	$C_7H_{12}NO_2S^+$	174.0583
cloxacillin	$C_{19}H_{19}ClN_3O_5S^+$	436.0728	$C_{13}H_{10}ClN_2O_3^+$	277.0374	$C_6H_{10}NO_2S^+$	160.0427		
dicloxacillin	$C_{19}H_{18}Cl_2N_3O_5S^+$	470.0339	$C_6H_{10}NO_2S^+$	160.0427	$C_{13}H_9Cl_2N_2O_3^+$	310.9985		
oxocillin	$C_{19}H_{20}N_3O_5S^+$	402.1118	$C_{13}H_{11}N_2O_3^{+b}$	243.0764	$C_6H_{10}NO_2S^{+b}$	160.0427	$C_5H_8NS^+$	114.0372
penillic acid	$C_{16}H_{19}N_2O_4S^+$	335.1060	$C_{15}H_{17}N_2O_2S^+$	289.1005	$C_{10}H_{10}NO_2^{+b}$	176.0706	$C_6H_{10}NS^+$	128.0528
penicillin G	$C_{16}H_{19}N_2O_4S^+$	335.1060	$C_6H_{10}NO_2S^{+b}$	160.0427	$C_{10}H_{10}NO_2^{+b}$	176.0706	$C_5H_8NS^+$	114.0372
penicillin V	$C_{16}H_{19}N_2O_5S^+$	351.1009	$C_6H_{10}NO_2S^{+b}$	160.0427	C_5H_8NS+	114.0372		
penilloic acid	$C_{15}H_{21}N_2O_3S^+$	309.1267	$C_7H_{12}NO_2S^+$	174.0583	$C_6H_{10}NS^+$	128.0528		
sulbactam	$C_8H_{12}NO_5S^+$	234.0431	$C_7H_{10}NO^+$	124.0757	$C_6H_{10}N^+$	96.0808		
ticarcillin	$C_{15}H_{17}N_2O_6S_2^+$	385.0523	$C_6H_{10}NO_2S^{+b}$	160.0427	$C_5H_8NS^+$	114.0372	$C_9H_8NO_4S^+$	226.0169
Cephalosporins[23,25,30,31]								
cefadroxil	$C_{16}H_{18}N_3O_5S^+$	364.0962	$C_4H_4NOS^+$	114.0008	$C_{10}H_{10}NO_2S^{+b}$	208.0427		
cefalonium	$C_{20}H_{19}N_4O_5S_2^+$	459.0791	$C_7H_6NOS^{+b}$	152.0165				
cefapirin (cephapirin)	$C_{17}H_{18}N_3O_6S_2^+$	424.0632	$C_{13}H_{14}N_3OS_2^{+b}$	292.0573	$C_7H_6NOS^+$	152.0165		
cefoperazone	$C_{25}H_{28}N_9O_8S_2^+$	646.1497	$C_6H_{11}N_2O_2^+$	143.0815	$C_{14}H_{16}N_3O_4^{+b}$	290.1135	$C_{19}H_{21}N_7O_5S^{+b}$	459.1319
cefotaxime	$C_{16}H_{18}N_5O_7S_2^+$	456.0642	$C_{12}H_{14}N_5O_2S_2^+$	324.0583	$C_7H_7N_2OS^+$	167.0274	$C_4H_3N_3S^+$	125.0042
cefquinome	$C_{23}H_{25}N_6O_5S_2^+$	529.1322	$C_9H_{12}N^+$	134.0964	$C_{14}H_{14}N_5O_5S_2^+$	396.0431		
ceftiofur	$C_{19}H_{18}N_5O_7S_3^+$	524.0363	$C_8H_9N_4O_3S^+$	241.0390	$C_4H_4N_3S^+$	126.0120	$C_{11}H_{11}NO_4S_2^+$	285.0124
ceftriaxone	$C_{18}H_{19}N_8O_7S_3^+$	555.0533	$C_{14}H_{14}N_5O_5S_2^+$	396.0431	$C_{12}H_{14}N_5O_2S_2^+$	324.0583	$C_7H_7N_2OS^+$	167.0274
cefuroxime	$C_{16}H_{16}N_4O_8SNa^+$	447.0581	$C_{11}H_{15}N_2O_7SNa^+$	342.0492	$C_5H_4N_4SNa^+$	175.0049	$C_{15}H_{13}N_3O_6SNa^+$	386.0417
cephalothin (cefalotin)	$C_{16}H_{16}N_2O_6S_2Na^+$	419.0342	$C_{14}H_{12}N_2O_4S_2Na^+$	359.0131	$C_{13}H_{12}N_2O_2S_2Na^+$	315.0232		
desacetylcephapirin	$C_{15}H_{16}N_3O_5S_2^+$	382.0526	$C_7H_6NOS^+$	152.0165	$C_5H_6NS^+$	112.0215	$C_{13}H_{14}N_3OS_2^+$	292.0573
Dyes[24,32]								
brilliant green	$C_{27}H_{33}N_2^+$	385.2638	$C_{24}H_{25}N_2^+$	341.2012	$C_{21}H_{17}N_2^+$	297.1386		
crystal violet	$C_{25}H_{30}N_3^+$	372.2434	$C_{24}H_{26}N_3^+$	356.2121	$C_{17}H_{19}N_2^+$	251.1543		
leucocrystal violet	$C_{25}H_{32}N_3^+$	374.2591	$C_{24}H_{28}N_3^+$	358.2278	$C_{16}H_{19}N_2^+$	239.1543	$C_{17}H_{21}N_2^+$	253.1699
leucomalachite green	$C_{23}H_{27}N_2^+$	331.2169	$C_{16}H_{19}N_2^+$	239.1543	$C_{14}H_{12}N^+$	194.0964	$C_{22}H_{23}N_2^+$	315.1856
malachite green	$C_{23}H_{25}N_2^+$	329.2012	$C_{22}H_{21}N_2^+$	313.1699	$C_{15}H_{14}N^+$	208.1121		
Flukacides[33]								
bithionol	$C_{12}H_5Cl_4O_2S^-$	352.8770	$C_6H_3Cl_2O^{-b}$	160.9566	$C_6H_2Cl_2OS^{-b}$	191.9209		
clorsulon	$C_8H_7Cl_3N_3O_4S_2^-$	377.8949	$C_8H_6Cl_2N_3O_4S_2^-$	341.9182	$C_8H_5ClN_3O_2S^{-b}$	241.9796		
closantel	$C_{22}H_{13}Cl_2I_2N_2O_2^-$	660.8449	I^{-b}	126.9050	$C_6H_3I_2O^-$	344.8279		
niclosamide	$C_{13}H_7Cl_2N_2O_4^-$	324.9788	$C_{13}H_6ClN_2O_4^{-b}$	289.0022	$C_6H_4ClN_2O_2^{-b}$	170.9967		
nitroxinil	$C_7H_2IN_2O_3$-	288.9116	I^{-c}	126.9050	$C_7H_2N_2O_3^{-b}$	162.0071		
oxyclozanide	$C_{13}H_5Cl_5NO_3^-$	397.8718	$C_{13}H_4Cl_4NO_3^-$	361.8951	$C_7H_2Cl_2NO_2^{-b}$	201.9468	$C_6H_4Cl_2NO^{-b}$	175.9675
rafoxanide	$C_{19}H_{10}Cl_2I_2NO_3^-$	623.8133	$C_6H_3I_2O^{-b}$	344.8279	I^{-b}	126.9050		

dx.doi.org/10.1021/jf405321w | J. Agric. Food Chem. 2014, 62, 3660−3674

Table 3. continued

compd (reference)	precursor (±)	*m/z*	product ion 1[a]	*m/z*	product ion 2	*m/z*	product ion 3	*m/z*
Ionophores[23]								
lasalocid A	$C_{34}H_{54}O_8Na^+$	613.3711	$C_{21}H_{38}O_4Na^+$	377.2662	$C_{34}H_{50}O_6Na^+$	577.3500	$C_{34}H_{52}O_7Na^+$	595.3605
monensin	$C_{36}H_{62}O_{11}Na^+$	693.4184	$C_{36}H_{60}O_{10}Na^+$	675.4079	$C_{25}H_{42}O_6Na^+$	461.2874		
maduramicin	$C_{47}H_{80}O_{17}Na^+$	939.5288	$C_{46}H_{78}O_{14}Na^+$	877.5284	$C_{35}H_{62}O_8Na^+$	633.4337		
narasin	$C_{43}H_{72}O_{11}Na^+$	787.4967	$C_{23}H_{36}O_6Na^+$	431.2404	$C_{29}H_{48}O_7Na^+$	531.3292	$C_{14}H_{24}O_4Na^+$	279.1567
nigericin Na	$C_{40}H_{68}O_{11}Na^+$	747.4654	$C_{40}H_{66}O_{10}Na^+$	729.4548	$C_{39}H_{68}O_9Na^+$	703.4756	$C_{28}H_{46}O_6Na^+$	501.3187
salinomycin	$C_{42}H_{70}O_{11}Na^+$	773.4810	$C_{23}H_{36}O_6Na^+$	431.2404	$C_{13}H_{22}O_4Na^+$	265.1410	$C_{29}H_{48}O_7Na^+$	531.3292
Lincosamides[25,34]								
clindamycin	$C_{18}H_{34}ClN_2O_5S^+$	425.1871	$C_8H_{16}N^+$	126.1277	$C_{17}H_{30}ClN_2O_5^+$	377.1838		
lincomycin	$C_{18}H_{35}N_2O_6S^+$	407.2210	$C_8H_{16}N^+$	126.1277	$C_{17}H_{31}N_2O_6^{+b}$	359.2177		
pirlimycin	$C_{17}H_{32}ClN_2O_5S^+$	411.1715	$C_7H_{14}N^+$	112.1121	$C_{16}H_{28}ClN_2O_5^+$	363.1681		
Macrolides[4,13,25,35,36]								
clarithromycin	$C_{38}H_{70}NO_{13}^+$	748.4842	$C_8H_{16}NO_2^+$	158.1176	$C_{30}H_{56}NO_{10}^+$	590.3899		
desacetyl troleandomycin	$C_{39}H_{66}NO_{14}^+$	772.4478	$C_8H_{16}NO_2^+$	158.1176	$C_{30}H_{52}NO_{10}^+$	586.3586		
erythromycin A	$C_{37}H_{68}NO_{13}^+$	734.4685	$C_8H_{16}NO_2^+$	158.1176	$C_{29}H_{54}NO_{10}^+$	576.3742	$C_5H_7O^+$	83.0491
erythromycin anhydrate	$C_{37}H_{66}NO_{12}^+$	716.4580	$C_8H_{16}NO_2^+$	158.1176	$C_{29}H_{48}NO_7^+$	522.3425		
josamycin	$C_{42}H_{70}NO_{15}^+$	828.4740	$C_8H_{16}NO_3^+$	174.1125	$C_{30}H_{50}NO_{11}^+$	600.3378		
natamycin	$C_{33}H_{48}NO_{13}^+$	666.3120	$C_{27}H_{31}O_7^+$	467.2064	$C_{16}H_{19}O_2^{+b}$	243.1380		
roxithromycin	$C_{41}H_{77}N_2O_{15}^+$	837.5318	$C_{33}H_{63}N_2O_{12}^+$	679.4376	$C_8H_{16}NO_2^{+b}$	158.1176		
spiramycin	$C_{43}H_{75}N_2O_{14}^+$	843.5213	$C_8H_{16}NO_3^{+b}$	174.1125	$C_{28}H_{46}NO_9^{+b}$	540.3167		
tilmicosin	$C_{46}H_{81}N_2O_{13}^+$	869.5733	$C_8H_{16}NO_3^+$	174.1125	$C_{38}H_{66}NO_{10}^{+b}$	696.4681	$C_{30}H_{52}NO_6^+$	522.3789
tulathromycin	$C_{41}H_{80}N_3O_{12}^+$	806.5737	$C_{29}H_{57}N_2O_9^+$	577.4059	$C_8H_{16}NO_2^{+b}$	158.1176		
tylosin A	$C_{46}H_{78}NO_{17}^+$	916.5264	$C_{39}H_{66}NO_{14}^+$	772.4478	$C_8H_{16}NO_3^+$	174.1125		
tylosin B (desmycosin)	$C_{39}H_{66}NO_{14}^+$	772.4478	$C_8H_{16}NO_3^+$	174.1125	$C_{30}H_{53}O_{11}^+$	589.3582		
Miscellaneous[4,22,25,27,37−40]								
acepromazine	$C_{19}H_{23}N_2OS^+$	327.1526	$C_5H_{12}N^{+b}$	86.0964	$C_3H_8N^{+b}$	58.0651		
acetaminophen	$C_8H_{10}NO_2^+$	152.0706	$C_6H_8NO^+$	110.0600	$C_6H_5O^+$	93.0335		
α-zearalenol	$C_{18}H_{25}O_5^+$	321.1697	$C_{10}H_5O_2^+$	157.0284				
amprolium	$C_{14}H_{19}N_4^+$	243.1604	$C_8H_{12}N_3^+$	150.1026	$C_6H_8N_3^+$	122.0713	$C_6H_8N^+$	94.0651
caffeine	$C_8H_{11}N_4O_2^+$	195.0877	$C_6H_8N_3O^+$	138.0662	$C_5H_8N_3^+$	110.0713		
clopidol	$C_7H_8Cl_2NO^+$	191.9977	$C_5H_6Cl^+$	101.0153	$C_4H_4Cl^{+b}$	86.9996		
decoquinate	$C_{24}H_{36}NO_5^+$	418.2588	$C_{22}H_{30}NO_4^+$	372.2169	$C_{12}H_{10}NO_4^+$	232.0604		
detomidine	$C_{12}H_{15}N_2^+$	187.1230	$C_4H_5N_2^{+b}$	81.0447	$C_3H_4N^{+b}$	54.0338		
dexamethasone	$C_{22}H_{30}FO_5^+$	393.2072	$C_{22}H_{27}O_4^+$	355.1904	$C_{14}H_{18}FO_2^{+b}$	237.1285	$C_{10}H_{11}O^{+b}$	147.0804
diclazuril	$C_{17}H_8Cl_3N_4O_2^-$	404.9718	$C_{15}H_7Cl_3N_3^-$	333.9711				
diminazene	$C_{14}H_{16}N_7^+$	282.1462	$C_{14}H_{16}N_5^+$	254.1400	$C_7H_7N_2^{+b}$	119.0604	$C_{14}H_{13}N_4^+$	237.1135
ethopabate	$C_{12}H_{16}NO_4^+$	238.1074	$C_7H_6NO_2^+$	136.0393	$C_9H_{10}NO_2^{+b}$	164.0706		
fumagillin	$C_{26}H_{34}O_7Na^+$	481.2197	$C_{16}H_{24}O_3Na^+$	287.1618				
halofuginone	$C_{16}H_{18}ClBrN_3O_3^+$	414.0215	$C_5H_{10}NO^+$	100.0757	$C_8H_{12}NO^+$	138.0913	$C_{16}H_{16}ClBrN_3O_2^+$	396.0109
imidocarb	$C_{19}H_{21}N_6O^+$	349.1771	$C_{10}H_{10}N_3O^+$	188.0818	$C_9H_{12}N_3^+$	162.1026		
ketamine	$C_{13}H_{17}ClNO^+$	238.0993	$C_7H_6Cl^+$	125.0153	$C_{11}H_{12}Cl^+$	179.0622		
ketoconazole	$C_{26}H_{29}Cl_2N_4O_4^+$	531.1560	$C_{24}H_{27}Cl_2N_4O_3^+$	489.1455	$C_4H_6N_2^+$	82.0525		
levamisole	$C_{11}H_{13}N_2S^+$	205.0794	$C_{10}H_{12}NS^+$	178.0685	$C_7H_7S^+$	123.0263	$C_7H_7^+$	91.0542
lidocaine	$C_{14}H_{23}N_2O^+$	235.1805	$C_5H_{12}N^+$	86.0964	$C_3H_8N^{+b}$	58.0651		
nicarbazin (as 4,4′ DNC)	$C_{13}H_9N_4O_5^-$	301.0578	$C_6H_5N_2O_2^{-b}$	137.0357	$C_6H_5NO^-$	107.0377		
novobiocin	$C_{31}H_{37}N_2O_{11}^+$	613.2392	$C_{12}H_{13}O_2^{+b}$	189.0910	$C_{22}H_{22}NO_6^+$	396.1442		
ormetoprim	$C_{14}H_{19}N_4O_2^+$	275.1503	$C_5H_7N_4^+$	123.0665	$C_{13}H_{15}N_4O_2^{+b}$	259.1190		
progesterone	$C_{21}H_{31}O_2^+$	315.2319	$C_6H_9O^+$	97.0648	$C_7H_9O^+$	109.0648	$C_{21}H_{29}O^+$	297.2213
pyrimethamine	$C_{12}H_{14}ClN_4^+$	249.0902	$C_{11}H_{10}ClN_4^+$	233.0589	$C_9H_6ClN_2^+$	177.0214		
robenidine	$C_{15}H_{14}Cl_2N_5^+$	334.0621	$C_7H_8ClN_2^+$	155.0371	$C_7H_5ClN^+$	138.0105		
tiamulin	$C_{28}H_{48}NO_4S^+$	494.3299	$C_8H_{18}NO_2S^+$	192.1053	$C_4H_7O_2S^+$	119.0161		
trichlormethiazide	$C_8H_7Cl_3N_3O_4S_2^-$	377.8949	$C_8H_5ClN_3O_2S^{-b}$	241.9796	$C_8H_5ClN_3O_4S_2^{-b}$	305.9415		
trimethoprim	$C_{14}H_{19}N_4O_3^+$	291.1452	$C_{12}H_{14}N_4O^+$	230.1162	$C_5H_7N_4^+$	123.0665		
tripelennamine	$C_{16}H_{22}N_3^+$	256.1808	$C_{14}H_{15}N_2^+$	211.1230	$C_7H_7^{+b}$	91.0542		
vancomycin	$C_{66}H_{77}Cl_2N_9O_{24}^{2+}$	724.7224	$C_7H_{14}NO_2^+$	144.1019	$C_5H_{10}NO^+$	100.0757		
virginiamycin M1	$C_{28}H_{36}N_3O_7^+$	526.2548	$C_{28}H_{34}N_3O_6^{+b}$	508.2442	$C_{19}H_{17}N_2O_4^{+b}$	337.1183		
virginiamycin S1	$C_{43}H_{50}N_7O_{10}^+$	824.3614	$C_{14}H_{16}N_3O_4^+$	290.1135	$C_{10}H_9N_2O_3^+$	205.0608	$C_{33}H_{39}N_6O_9^+$	663.2773
xylazine	$C_{12}H_{17}N_2S^+$	221.1107	$C_9H_{10}NS^+$	164.0528	$C_3H_8NS^+$	90.0372		
Nitromidazoles[37,41]								
dimetridazole	$C_5H_8N_3O_2^+$	142.0611	$C_5H_8N_2^+$	96.0682	$C_4H_5N_2^+$	81.0447	$C_3H_4N^{+b}$	54.0338
metronidazole	$C_6H_{10}N_3O_3^+$	172.0717	$C_4H_6N_3O_2^{+b}$	128.0455	$C_4H_6N_2^{+c}$	82.0525		
ornidazole	$C_7H_{11}ClN_3O_3^+$	220.0483	$C_4H_6N_3O_2^+$	128.0455	$C_4H_6N_2^+$	82.0525		
ronidazole	$C_6H_9N_4O_4^+$	201.0618	$C_5H_6N_3O_2^+$	140.0455	$C_3H_5N^{+b}$	55.0417		

dx.doi.org/10.1021/jf405321w | J. Agric. Food Chem. 2014, 62, 3660−3674

Table 3. continued

compd (reference)	precursor (±)	*m/z*	product ion 1[a]	*m/z*	product ion 2	*m/z*	product ion 3	*m/z*
Nitromidazoles[37,41]								
tindazole	$C_8H_{14}N_3O_4S^+$	248.0700	$C_4H_6N_3O_2^+$	128.0455	$C_4H_9O_2S^+$	121.0318	$C_4H_6N_2^{+b}$	82.0525
NSAIDs[25,42]								
carprofen	$C_{15}H_{13}ClNO_2^+$	274.0629	$C_{14}H_{11}ClN^+$	228.0575	$C_{14}H_{11}N^{+b}$	193.0886		
diclofenac	$C_{14}H_{12}Cl_2NO_2^+$	296.0240	$C_{13}H_{10}ClN^+$	215.0496	$C_{13}H_{10}Cl_2N^+$	250.0185	$C_{14}H_{10}Cl_2NO^+$	278.0134
flunixin	$C_{14}H_{12}F_3N_2O_2^+$	297.0845	$C_{14}H_{10}F_3N_2O^+$	279.0740	$C_{13}H_7F_3N_2O^+$	264.0505		
flunixin hydroxide	$C_{14}H_{12}F_3N_2O_3^+$	313.0795	$C_{14}H_{10}F_3N_2O_2^+$	295.0689	$C_{13}H_7F_3N_2O_2^+$	280.0454		
ketoprofen	$C_{16}H_{15}O_3^+$	255.1016	$C_{15}H_{13}O^+$	209.0961	$C_7H_5O^+$	105.0335		
mefenamic acid	$C_{15}H_{16}NO_2^+$	242.1176	$C_{15}H_{14}NO^+$	224.1070	$C_{14}H_{11}NO^+$	209.0835	$C_{13}H_{10}N^+$	180.0808
naproxen	$C_{14}H_{15}O_3^+$	231.1016	$C_{13}H_{13}O^+$	185.0961	$C_{12}H_{10}O^{+b}$	170.0726		
niflumic acid	$C_{13}H_{10}F_3N_2O_2^+$	283.0689	$C_{13}H_8F_3N_2O^+$	265.0583	$C_{13}H_7F_2N_2O^+$	245.0521		
phenylbutazone	$C_{19}H_{21}N_2O_2^+$	309.1598	$C_7H_6NO^{+b}$	120.0444	$C_{11}H_{14}N^+$	160.1121		
suxibuzone	$C_{24}H_{27}N_2O_6^+$	439.1864	$C_{19}H_{21}N_2O_2^+$	309.1598	$C_{16}H_{15}N_2O_2^+$	267.1128		
Phenicols[43,44]								
chloramphenicol	$C_{11}H_{11}Cl_2N_2O_5^-$	321.0051	$C_7H_6NO_3^-$	152.0353	$C_9H_6NO_3^-$	176.0353	$C_{10}H_{10}ClN_2O_4^-$	257.0335
florfenicol	$C_{12}H_{13}FCl_2NO_4S^-$	355.9932	$C_8H_9O_3S^-$	185.0278	$C_{12}H_{12}Cl_2NO_4S^-$	335.9870		
thiamphenicol	$C_{12}H_{14}Cl_2NO_5S^-$	353.9975	$C_8H_9O_3S^-$	185.0278	$C_{11}H_{13}ClNO_4S^-$	290.0259		
flofenicol amine	$C_{10}H_{15}FNO_3S^+$	248.0751	$C_{10}H_{13}FNO_2S^+$	230.0646	$C_9H_8N^+$	130.0651		
Quinolones[1,4,23−25,45]								
ciprofloxacin	$C_{17}H_{19}FN_3O_3^+$	332.1405	$C_{17}H_{17}FN_3O_2^+$	314.1299	$C_{16}H_{19}FN_3O^+$	288.1507	$C_{14}H_{14}FN_2O^+$	245.1085
danofloxacin	$C_{19}H_{21}FN_3O_3^+$	358.1561	$C_{19}H_{19}FN_3O_2^+$	340.1456	$C_{18}H_{21}FN_3O^{+b}$	314.1663		
desethylene ciprofloxacin	$C_{15}H_{17}FN_3O_3^+$	306.1248	$C_{15}H_{15}FN_3O_2^+$	288.1143	$C_{15}H_{14}N_3O_2^{+b}$	268.1081		
desethylene enrofloxacin	$C_{17}H_{21}FN_3O_3^+$	334.1561	$C_{17}H_{19}FN_3O_2^{+b}$	316.1456	$C_{17}H_{18}N_3O_2^+$	296.1394	$C_{13}H_{10}FN_2O_2^+$	245.0721
difloxacin	$C_{21}H_{20}F_2N_3O_3^+$	400.1467	$C_{20}H_{20}F_2N_3O^+$	356.1569	$C_{17}H_{13}F_2N_2O^+$	299.0990		
enofloxacin (enoxacin)	$C_{15}H_{18}FN_4O_3^+$	321.1357	$C_{15}H_{16}FN_4O_2^+$	303.1252				
enrofloxacin	$C_{19}H_{23}FN_3O_3^+$	360.1718	$C_{19}H_{21}FN_3O_2^+$	342.1612	$C_{18}H_{23}FN_3O^+$	316.1820	$C_{14}H_{14}FN_2O^+$	245.1085
fleroxacin	$C_{17}H_{19}F_3N_3O_3^+$	370.1373	$C_{16}H_{19}F_3N_3O^{+b}$	326.1475	$C_{13}H_{12}F_3N_2O^+$	269.0896		
flumequine	$C_{14}H_{13}FNO_3^+$	262.0874	$C_{14}H_{11}FNO_2^+$	244.0768	$C_{11}H_5FNO_2^+$	202.0299		
gatifloxacin	$C_{19}H_{23}FN_3O_4^+$	376.1667	$C_{18}H_{23}FN_3O_2^+$	332.1769	$C_{19}H_{21}FN_3O_3^+$	358.1561	$C_{16}H_{18}FN_2O_2^+$	289.1347
lomefloxacin	$C_{17}H_{20}F_2N_3O_3^+$	352.1467	$C_{14}H_{15}F_2N_2O^+$	265.1147	$C_{16}H_{20}F_2N_3O^{+b}$	308.1569		
marbofloxacin	$C_{17}H_{20}FN_4O_4^+$	363.1463	$C_4H_{10}N^+$	72.0808	$C_{15}H_{15}FN_3O_4^+$	320.1041		
moxifloxacin	$C_{21}H_{25}FN_3O_4^+$	402.1824	$C_{21}H_{23}FN_3O_3^+$	384.1718	$C_{14}H_{14}FN_2O_2^+$	261.1034		
nadifloxacin	$C_{19}H_{22}FN_2O_4^+$	361.1558	$C_{19}H_{20}FN_2O_3^+$	343.1452	$C_{14}H_{10}FN_2O_2^{+b}$	257.0721		
nalidixic acid	$C_{12}H_{13}N_2O_3^+$	233.0921	$C_{12}H_{11}N_2O_2^+$	215.0815	$C_{10}H_7N_2O_2^{+b}$	187.0502	$C_9H_7N_2O^+$	159.0553
norfloxacin	$C_{16}H_{19}FN_3O_3^+$	320.1405	$C_{16}H_{17}FN_3O_2^+$	302.1299	$C_{15}H_{19}FN_3O^+$	276.1507		
ofloxacin (racemic mix)	$C_{18}H_{21}FN_3O_4^+$	362.1511	$C_{17}H_{21}FN_3O_2^+$	318.1612	$C_{14}H_{14}FN_2O_2^+$	261.1034		
orbifloxacin	$C_{19}H_{21}F_3N_3O_3^+$	396.1530	$C_{18}H_{21}F_3N_3O^+$	352.1631	$C_{15}H_{14}F_3N_2O^+$	295.1053		
oxociprofloxacin	$C_{17}H_{17}FN_3O_4^+$	346.1198	$C_{17}H_{15}FN_3O_3^+$	328.1092	$C_{14}H_{10}FN_3O_3^+$	287.0701		
oxolinic acid	$C_{13}H_{12}NO_5^+$	262.0710	$C_{13}H_{10}NO_4^+$	244.0604	$C_{11}H_6NO_4^+$	216.0291		
pazufloxacin	$C_{16}H_{16}FN_2O_4^+$	319.1089	$C_{16}H_{13}FNO_4^+$	302.0823	$C_{15}H_{13}FNO_2^+$	258.0925		
pefloxacin	$C_{17}H_{21}FN_3O_3^+$	334.1561	$C_{17}H_{19}FN_3O_2^+$	316.1456	$C_{16}H_{21}FN_3O^+$	290.1663	$C_{13}H_{14}FN_2O^+$	233.1085
pipemidic acid	$C_{14}H_{18}N_5O_3^+$	304.1404	$C_{14}H_{16}N_5O_2^+$	286.1299	$C_{11}H_{13}N_4O^+$	217.1084		
piromidic acid	$C_{14}H_{17}N_4O_3^+$	289.1295	$C_{14}H_{15}N_4O_2^+$	271.1190	$C_{13}H_{17}N_4O^+$	245.1397		
prulifloxacin	$C_{21}H_{21}FN_3O_6S^+$	462.1130	$C_{21}H_{19}FN_3O_5S^{+b}$	444.1024	$C_{21}H_{18}N_3O_3^+$	360.1343		
sarafloxacin	$C_{20}H_{18}F_2N_3O_3^+$	386.1311	$C_{20}H_{16}F_2N_3O_2^+$	368.1205	$C_{19}H_{18}F_2N_3O^+$	342.1412	$C_{17}H_{13}F_2\ N_2O^+$	299.0990
sparfloxacin	$C_{19}H_{23}F_2N_4O_3^+$	393.1733	$C_{18}H_{23}F_2N_4O^+$	349.1834	$C_{15}H_{16}F_2N_3O^+$	292.1256		
Sulfonamides[46]								
dapsone	$C_{12}H_{13}N_2O_2S^+$	249.0692	$C_6H_6NO^+$	108.0444	$C_6H_6N^+$	92.0495	$C_6H_6NO_2S^+$	156.0114
sulfabenzamide	$C_{13}H_{13}N_2O_3S^+$	277.0641	$C_6H_6NO_2S^+$	156.0114	$C_6H_6NO^+$	108.0444	$C_6H_6N^+$	92.0495
sulfacetamide	$C_8H_{11}N_2O_3S^+$	215.0485	$C_6H_6NO_2S^{+b}$	156.0114	$C_6H_6NO^+$	108.0444	$C_6H_6N^{+b}$	92.0495
sulfadoxine	$C_{12}H_{15}N_4O_4S^+$	311.0809	$C_6H_6NO_2S^+$	156.0114	$C_6H_6NO^+$	108.0444	$C_6H_6N^+$	92.0495
sulfaguanidine	$C_7H_{11}N_4O_2S^+$	215.0597	$C_6H_6NO_2S^+$	156.0114	$C_6H_6NO^+$	108.0444	$C_6H_6N^+$	92.0495
sulfameter	$C_{11}H_{13}N_4O_3S^+$	281.0703	$C_6H_6NO^{+b}$	108.0444	$C_6H_6NO_2S^+$	156.0114	$C_6H_6N^{+b}$	92.0495
sulfamethoxypyridazine	$C_{11}H_{13}N_4O_3S^+$	281.0703	$C_6H_6NO_2S^+$	156.0114	$C_6H_6N^+$	92.0495	$C_5H_8N_3O^+$	126.0662
sulfamonomethoxine	$C_{11}H_{13}N_4O_3S^+$	281.0703	$C_6H_6NO^+$	108.0444	$C_6H_6NO_2S^+$	156.0114	$C_6H_6N^+$	92.0495
sulfanilamide	$C_6H_9N_2O_2S^+$	173.0379	$C_6H_7N^+$	93.0573	$C_5H_6^+$	66.0464		
sulfanitran	$C_{14}H_{14}N_3O_5S^+$	336.0649	$C_6H_6NO_2S^{+b}$	156.0114	$C_8H_8NO^{+b}$	134.0600	$C_6H_6NO^+$	108.0444
sulfaphenazole	$C_{15}H_{15}N_4O_2S^+$	315.0910	$C_9H_{10}N_3^{+b}$	160.0869	$C_9H_8N_3^+$	158.0713	$C_6H_6NO^{+b}$	108.0444
sulfisoxazole	$C_{11}H_{14}N_3O_3S^+$	268.0750	$^bC_6H_6NO_2S^+$	156.0114	$C_6H_6NO^+$	108.0444	$C_5H_9N_2O^+$	113.0709
*N*4-acetyl-sulfamethazine	$C_{14}H_{17}N_4O_3S^+$	321.1016	$C_6H_8N_3O_2S^+$	186.0332	$C_{14}H_{15}N_4O^+$	255.1240		
sulfachloropyridazine	$C_{10}H_{10}ClN_4O_2S^+$	285.0208	$C_6H_6NO_2S^+$	156.0114	$C_6H_6NO^+$	108.0444		
sulfadiazine	$C_{10}H_{11}N_4O_2S^+$	251.0597	$C_6H_6NO_2S^{+b}$	156.0114	$C_6H_6N^{+b}$	92.0495	$C_6H_6NO^{+b}$	108.0444
sulfadimethoxine	$C_{12}H_{15}N_4O_4S^+$	311.0809	$C_6H_6NO_2S^+$	156.0114	$C_6H_6NO^+$	108.0444	$C_6H_{10}N_3O_2^+$	156.0768

dx.doi.org/10.1021/jf405321w | J. Agric. Food Chem. 2014, 62, 3660−3674

Table 3. continued

compd (reference)	precursor (±)	*m/z*	product ion 1[a]	*m/z*	product ion 2	*m/z*	product ion 3	*m/z*
Sulfonamides[46]								
sulfamerazine	$C_{11}H_{13}N_4O_2S^+$	265.0754	$C_6H_6NO_2S^+$	156.0114	$C_6H_6N^{+b}$	92.0495	$C_6H_6NO^{+b}$	108.0444
sulfamethazine	$C_{12}H_{15}N_4O_2S^+$	279.0910	$C_6H_8N_3O_2S^+$	186.0332	$C_6H_6NO_2S^+$	156.0114	$C_6H_{10}N_3^{+b}$	124.0869
sulfamethazine −lactose	$C_{24}H_{35}N_4O_{12}S^+$	603.1967	$C_{18}H_{25}N_4O_7S^+$	441.1438	$C_{14}H_{17}N_4O_3S^+$	321.1016	$C_{12}H_{15}N_4O_2S^+$	279.0910
sulfamethoxazole	$C_{10}H_{12}N_3O_3S^+$	254.0594	$C_6H_6NO_2S^+$	156.0114	$C_6H_6NO^+$	108.0444	$C_6H_6N^{+b}$	92.0495
sulfapyridine	$C_{11}H_{12}N_3O_2S^+$	250.0645	$C_{11}H_{10}N_3^{+b}$	184.0869	$C_6H_6NO_2S^{+b}$	156.0114	$C_6H_6NO^{+b}$	108.0444
sulfaquinoxaline	$C_{14}H_{13}N_4O_2S^+$	301.0754	$C_6H_6NO_2S^+$	156.0114	$C_6H_6NO^+$	108.0444	$C_6H_6N^{+b}$	92.0495
sulfathiazole	$C_9H_{10}N_3O_2S_2^+$	256.0209	$C_6H_6NO_2S^+$	156.0114	$C_6H_6NO^+$	108.0444	$C_6H_6N^+$	92.0495
Tetracyclines[4,47,48]								
4-epi-Tetracycline	$C_{22}H_{25}N_2O_8^+$	445.1605	$C_{22}H_{20}NO_7^+$	410.1234	$C_7H_8NO_3^+$	154.0499		
chlortetracycline	$C_{22}H_{24}ClN_2O_8^+$	479.1216	$C_{22}H_{21}ClNO_8^+$	462.0950	$C_{22}H_{19}ClNO_7^+$	444.0845	$C_7H_8NO_3^{+b}$	154.0499
demeclocycline	$C_{21}H_{22}ClN_2O_8^+$	465.1059	$C_{21}H_{19}ClNO_8^+$	448.0794	$C_{21}H_{17}ClNO_7^+$	430.0688	$C_7H_8NO_3^+$	154.0499
doxycycline	$C_{22}H_{25}N_2O_8^+$	445.1605	$C_{22}H_{20}NO_7^+$	410.1234	$C_7H_8NO_3^+$	154.0499		
oxytetracycline	$C_{22}H_{25}N_2O_9^+$	461.1555	$C_{22}H_{20}NO_8^+$	426.1183	$C_7H_8NO_3^+$	154.0499		
tetracycline	$C_{22}H_{25}N_2O_8^+$	445.1605	$C_{22}H_{20}NO_7^+$	410.1234	$C_7H_8NO_3^+$	154.0499		

[a]Product ions listed in order of abundance (will depend on collision energy used). [b]Experimental exact mass for ion differed from the theoretical value listed in this table by 5−20 ppm. [c]Experimental exact mass for ion differed from the theoretical value listed in this table by more than 20 ppm.

larger molecules such as macrolides, showed more variability. This was also observed in the original method.[1]

Because this is an evaluation of a screening procedure, not a quantitative method, the recoveries for these analytes were not calculated. Only the ability of the method to reliably detect analytes at specific fortification levels was tested. This parallels work published previously to evaluate residue screening methods[7] and is consistent with FDA guidelines,[18] indicating qualitative broad-band screening methods should determine the minimum detectable concentration. In general, compounds with medium polarity (eluting between 4 and 12 min with this chromatographic program) performed well. For example, fluoroquinolones/quinolones, macrolides and lincomycins, many sulfonamides, and some *β*-lactams could be reliably detected in milk samples that had been fortified at low (≤10 ng/mL) levels.

On the other hand, some analytes were only detected at very high fortification levels or not at all. There are several possible reasons for this. One is simply that the analytes do not respond (ionize) very well and their levels of detection, even for solvent standards, are quite high. Many of the cephalosporin compounds fall into this category. Compounds that were not detected at all include rifampin, clavulanate, and cefoxitin. Another reason why analytes may not be detected in fortified milk samples is that they are not extracted or recovered from the milk matrix with this procedure. For example, the aminoglycosides are detected in solvent standard, but they are very polar and elute with the solvent front. It has been shown that while acetonitrile solvent extraction is effective for many veterinary drug residues, these compounds need a more polar extraction procedure.[19,20] Aminoglycosides were detected in milk samples that were fortified postextraction (endspike) using this LC Q-TOF MS method. For other analytes, such as avermectins, compounds were not observed in either extracted milk or in postfortified samples. This indicates that matrix effects (ion suppression) are severe for these analytes. This is not surprising as the sample cleanup is minimal with no defatting and these compounds typically elute very late in the chromatogram with 100% acetonitrile. Some compounds in the database that are not a concern in milk (ionophores, dyes) were not tested through the extraction method, but the experimental data obtained from analyzing solvent standards of these compounds is still useful to rule out false detects in milk samples.

The challenge of finding the best extraction for a wide variety of veterinary drug residues has been evaluated by others.[6,21,22] In a recent review, Berendsen et al.[21] discussed the advantages and disadvantages of several types of extraction procedures including SPE, dispersive SPE (QuEChERS), and simple solvent extraction. Their conclusions were that simple solvent extractions were often best because they did not discriminate against analytes, but success was not universal and matrix effects could be problematic. Others[5] have found that QuEChERS extraction procedure for veterinary drug screens using HRMS has worked well for many compounds, but others (aminoglycosides, *β*-lactams, tetracyclines) were excluded for poor performance. Also, Nacher-Mestre et al.[7] used a generic extraction for residues in feed and fish with minimal sample cleanup and found that many compounds could only be detected at 100 ng/g or not at all. This is consistent with what has been observed in this work. The results presented here indicate that this procedure may not be applicable to all veterinary drug residues. Therefore, it is important to note that while high resolution instruments allow us to monitor for more analytes, they should still not be considered "universal".

Proposed Identification of Product Ions. Product ion spectra were also collected from solvent standard mixes and milk extracts. Elemental composition of the product ions were proposed using the experimental *m/z* and generating formulas (using Agilent *Mass Hunter Formula Calculator Tool*) restraining the number and type of atoms to those found in the precursor ion. These data are shown in Table 3. When possible, these postulated ions were evaluated for reasonableness by generating structures using Agilent's *Molecular Structure Correlator* program and *ChemDraw* as well as comparing to fragmentation patterns in the published literature.[4,23−25] The experimental mass accuracy for the product ions from the analysis of 100 ng/mL solvent standards was within ±5 ppm of the value of the proposed structures unless otherwise noted in Table 3. More specific literature references identifying product ions for specific classes of compounds are also listed in Table 3.

In the literature, there is general consensus that at least one product ion is required to confirm the identity of analytes even when using measured exact mass data.[4,7,8,25,26] In some cases,

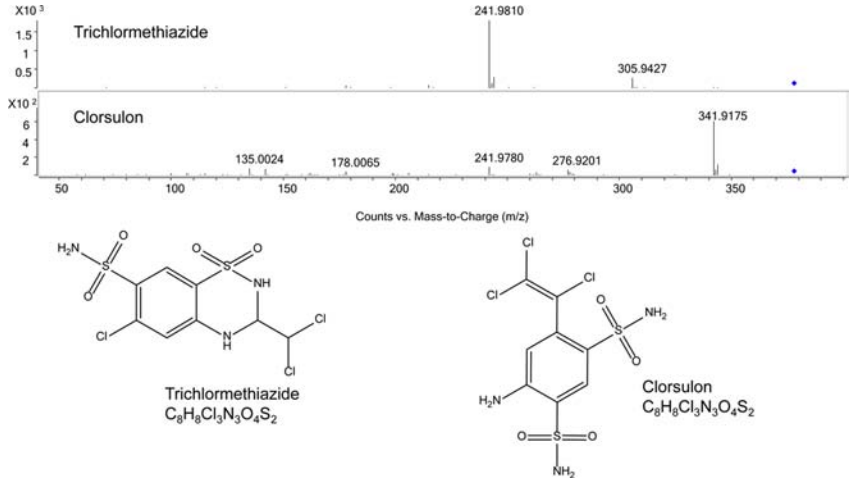

Figure 4. MS/MS spectra of isobaric compounds (m/z 377.8949). Solvent standard solutions (100 ng/mL) were analyzed using 20 V collision energy for both compounds.

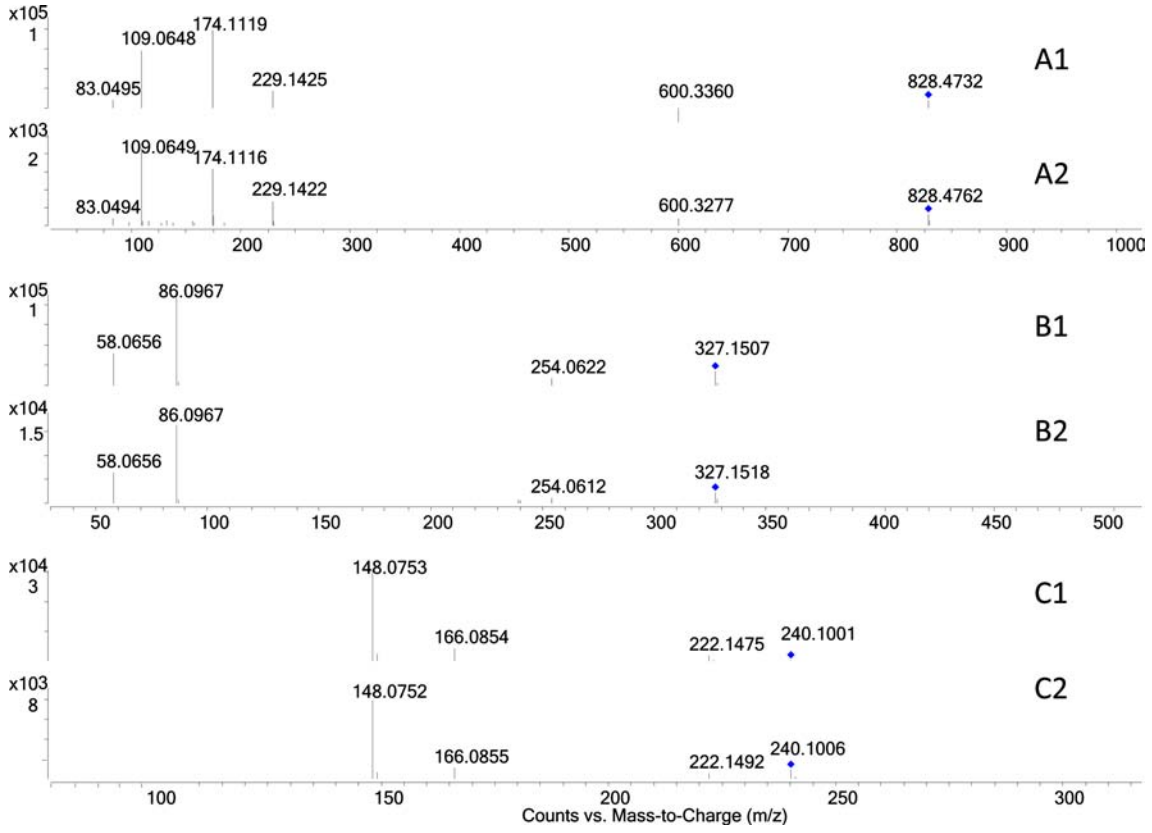

Figure 5. MS/MS spectra of josamycin (A), acepromazine (B), and salbutamol (C) in 100 ng/mL solvent solutions (1) and in extracts from milk fortified at 100 ng/mL (2).

unique MS/MS product ion spectra may be needed to distinguish between isomeric compounds. For example, clorsulon and trichlormethiazide are compounds that both have the formula $C_8H_8Cl_3N_3O_4S_2$, ionize in negative ion mode, and have very similar retention times. Figure 4 shows the structures and respective product ion spectra for these two compounds. For example, clorsulon has a large product ion at m/z 341.9175 corresponding to loss of HCl that is not present in the MS/MS spectrum of trichlormethiazide. We have previously shown[1] that product ion spectra were needed to identity desenrofloxacin, a metabolite of enrofloxacin, to distinguish it from another isomeric fluoroquinolone, pefloxacin.

Using the exact mass capability of this instrument to catalogue a database of potential fragment ions for a large number of analytes should prove very helpful for the development of veterinary drug residue MS methods in general, regardless of the specific platform. For example, a single-stage Orbitrap (Exactive) instrument does not have the ability to isolate a precursor ion prior to forming product ions. Using the information in Table 3 would give confidence that the product ions observed are directly related to the precursor

dx.doi.org/10.1021/jf405321w | J. Agric. Food Chem. 2014, 62, 3660−3674

ion of interest rather than produced from matrix components. In addition, it is also useful to identify product ion structures detected in a triple quadrupole multiple reaction monitoring experiment and this information is not always available in the literature.

Using the LC Q-TOF MS, it is also possible to evaluate the product ion spectra for analytes in milk samples. The development of criteria for the confirmation of identity using measured exact mass data is still in progress.[26] The data generated in this study indicate that the fortification level required to obtain an MS/MS spectrum with two or more product ions with mass accuracy within 5 ppm of the theoretical value is typically 2−5 times higher than the screening level of detection with this instrument. Examples of product ion spectra from solvent standards and milk extracts are shown in Figure 5. The fragment ions from compounds in the milk extracts have very similar measured exact mass (generally within 5 ppm) and relative intensity when compared to those from solvent standards.

In conclusion, the use of LC QTOF MS has the potential to greatly expand the scope of monitoring for contamination of food by veterinary drug residues. When searching accurate mass databases for low levels of residues in complex matrices, it is critical to overcome the challenge of not reporting false negatives while also avoiding an onerous number of false detects. This can be achieved by using adequately wide mass extraction windows combined with retention time matching to known standards. Using this method, data including retention times, as well as accurate mass measurements for precursor and product ions, have been collected for over 200 veterinary drugs for which standards are available. The screening limits of detection in milk for many of these compounds using a rapid extraction procedure have been determined. In addition to the 25 compounds that were initially included in this screening procedure, the method performance (number of false negatives, reproducibility) for approximately 60 additional compounds in milk fortified at the 10 ng/mL level was performed.

AUTHOR INFORMATION

Corresponding Author

*Phone: 303-236-3072. E-mail: sherri.turnipseed@fda.hhs.gov.

Notes

The authors declare no competing financial interest.

ACKNOWLEDGMENTS

We acknowledge Jon Wong of FDA/CFSAN and Selen Stromgren of FDA/ORA/ORS for technical collaboration as well as their help in obtaining veterinary drug standards.

REFERENCES

(1) Turnipseed, S. B.; Storey, J. M.; Clark, S. B.; Miller, K. Analysis of veterinary drugs and metabolites in milk using quadrupole time-of-flight liquid chromatography mass spectrometry. *J. Agric. Food Chem.* **2011**, *59*, 7569−7581.

(2) Peters, R. J. B.; Bolck, Y. J. C.; Rutgers, P.; Stolker, A. A. M.; Nielen, M. W. F. Multi-residue screening of veterinary drugs in egg, fish and meat using high resolution liquid chromatography accurate mass time-of-flight mass spectrometry. *J. Chromatogr., A* **2009**, *1216*, 8206−8216.

(3) Stolker, A. A. M.; Rutgers, P.; Oosterink, E.; Lasaroms, J. J. P.; Peters, R. J. B.; Van Rhijn, J. A.; Neilen, M. W. F. Comprehensive screening and quantification of veterinary drugs in milk using UPLC-ToF-MS. *Anal. Bioanal. Chem.* **2008**, *391*, 2309−2322.

(4) Romero-Gonzalez, R.; Aguilera-Luiz, M. D.; Plaza-Bolanos, P.; Garrido Frenich, A.; Martinez Vidal, J. L. Food contaminant analysis at high resolution mass spectrometry: application for the determination of veterinary drugs in milk. *J. Chromatogr., A* **2011**, *1218*, 9353−9365.

(5) Wang, J.; Leung, D. The challenges of developing a generic extraction procedure to analyze multi-class veterinary drug residues in milk and honey using ultra-high pressure liquid chromatography quadrupole time-of-flight mass spectrometry. *Drug Test. Anal.* **2012**, *4*, 103−111.

(6) Villar-Pulido, M.; Gilbert-Lopez, B.; Garcia-Reyes, J. F.; Martos, N. R.; Molina-Díaz, A. Multiclass detection and quantitation of antibiotics and veterinary drugs in shrimps by fast liquid chromatography time-of-flight mass spectrometry. *Talanta* **2011**, *85*, 1419−1427.

(7) Nacher-Mestre, J.; Ibanez, M.; Serrano, R.; Perez-Sanchez, J.; Hernandez, F. Qualitative screening of undesirable compounds from feeds to fish by liquid chromatoghy coupled to mass spectrometry. *J. Agric. Food Chem.* **2013**, *61*, 2077−2087.

(8) Leon, N.; Roca, M.; Igualada, C.; Martins, C. P. B.; Pastor, A.; Yusa, V. Wide-range screening of banned veterinary drugs in urine by ultra high liquid chromatography coupled to high-resolution mass spectrometry. *J. Chromatogr., A* **2012**, *1258*, 55−65.

(9) Kaufmann, A.; Butcher, P.; Maden, K.; Walker, S.; Widmer, M. Semi-targeted residue screening in complex matrices with liquid chromatography coupled to high resolution mass spectrometry: current possibilities and limitations. *Analyst* **2011**, *136*, 1898−1909.

(10) Gomez-Perez, M.; Plaza-Bolanos, P.; Romero-Gonzalez, R.; Martinez-Vidal, J. L.; Garrido Frenich, A. Comprehensive qualitative and quantitative determination of pesticides and veterinary drugs in honey using liquid-chromatography−Orbitrap high resolution mass spectrometry. *J. Chromatogr., A* **2012**, *1248*, 130−138.

(11) Turnipseed, S. B.; Clark, S. B.; Storey, J. M.; Carr, J. R. Analysis of veterinary drug residues in frog legs and other aquacultured species using liquid chromatography quadrupole time-of-flight mass spectrometry. *J. Agric. Food Chem.* **2012**, *60*, 4430−4439.

(12) Croley, T. R.; White, K. D.; Callahan, J. H.; Musser, S. M. The chromatographic role in high resolution mass spectrometry for non-targeted analysis. *J. Am. Soc. Mass Spectrom.* **2012**, *23*, 1569−1578.

(13) Wang, J.; Leung, D. Analyses of macrolide antibiotic residues in eggs, raw milk, and honey using both ultra-performance liquid chromatography/quadrupole time-of-flight mass spectrometry and high-performance liquid chromatography/tandem mass spectrometry. *Rapid Commun. Mass Spectrom.* **2007**, *21*, 3213−3222.

(14) Li, D.; Yang, M.; Hu, J.; Zhang, Y.; Chang, H.; Jin, F. Determination of penicillin G and its degradation products in a penicillin production wastewater treatment plant and the receiving river. *Water Res.* **2008**, *42*, 307−317.

(15) Tao, Y.; Yu, G.; Chen, D.; Pan, Y.; Wei, H.; Peng, D.; Huang, L.; Wang, Y.; Yuan, Z. Determination of 17 macrolide antibiotics and avermectins residues in meat with accelerated solvent extraction by liquid chromatography−tandem mass spectrometry. *J. Chromatogr., B* **2012**, *897*, 64−71.

(16) Roberts, D.; McCullagh, M.; Stead, S.; Cleland, G.; Shah, D.; Mullin, L.; Burgess, J. *A Novel Mass Screening Solution Incorporating the UNIFI Scientific Information System for the Routine Analysis of Pesticide Residues at Regulatory Limits in Food*; Waters: Milford, MA, 2012.

(17) *Agilent LC/MS Veterinary Drug Application Kits*; Agilent Technologies: Santa Clara, CA, 2014; http://www.chem.agilent.com/en-US/products-services/instruments-systems/mass-spectrometry/lc-ms-veterinary-drug-application-kits/Pages/default.aspx (accessed January 16, 2014).

(18) *Guidelines for the Validation of Chemical Methods for the FDA Foods Program*; U.S. Food and Drug Administration: Silver Spring, MD, 2012.

(19) Gaugain-Juhel, M.; Delepine, B.; Gautier, S.; Fourmond, M. P.; Guadin, V.; Hurtaud-Pessel, D.; Verdon, E.; Sanders, P. Validation of a liquid chromatography−tandem mass spectrometry screening method to monitor 58 antibiotics in milk: a qualitative approach. *Food Addit. Contam.* **2009**, *26*, 1459−1471.

(20) Lehotay, S. J.; Mastovska, K.; Lightfield, A. R.; Nunez, A.; Dutko, T.; Ng, C.; Bluhm, L. Rapid analysis of aminoglycoside antibiotics in bovine tissues using disposable pipette extraction and ultrahigh performance liquid chromatography−tandem mass spectrometry. *J. Chromatogr., A* **2013**, *1313*, 103−112.
(21) Berendsen, B. J. A.; Stolker, A. A. M.; Nielen, M. W. F. Selectivity in the sample preparation for the analysis of drug residues in products of animal origin using LC-MS. *Trends Anal. Chem* **2013**, *43*, 229−239.
(22) Van Poucke, C.; Dumoulin, F.; Van Peteghem, C. Detection of banned antibacterial growth promoters in animal feed by liquid chromatography−tandem mass spectrometry: optimisation of the extraction solvent by experimental design. *Anal. Chim. Acta* **2005**, *529*, 211−220.
(23) Gentili, A.; Perret, D.; Marchese, S. Liquid chromatography−tandem mass spectrometry for performing confirmatory analysis of veterinary drugs in animal-food products. *Trends Anal. Chem.* **2005**, *24*, 704−733.
(24) Li, H.; Kijak, P. J.; Turnipseed, S. B.; Cui, W. Analysis of veterinary drug residues in shrimp: a multi-class method by liquid chromatography−quadrupole ion trap mass spectrometry. *J. Chromatogr., B* **2006**, *836*, 22−38.
(25) Ferrer, I.; Thurman, E. M. Analysis of 100 pharmaceuticals and their degradates in water samples by liquid chromatography/quadrupole time-of-flight mass spectrometry. *J. Chromatogr., A* **2012**, *1259*, 148−157.
(26) U.S. Food and Drug Adminstration, Exact Mass Measurement Working Group. Personal Communication, 2014.
(27) De Ruyck, H.; Daeseleire, E.; De Ridder, H.; Van Renterghem, R. Development and validation of a liquid chromatographic−electrospray tandem mass spectrometric multiresidue method for anthelmintics in milk. *J. Chromatogr., A* **2002**, *976*, 181−194.
(28) Churchwell, M. I.; Holder, C. L.; Little, D.; Preece, S.; Smith, D. J.; Doerge, D. R. Liquid chromatography/electrospray tandem mass spectrometric analysis of incurred ractopamine residues in livestock tissues. *Rapid Commun. Mass Spectrom.* **2002**, *16*, 1261−1265.
(29) De Wasch, K.; De Brabander, H.; Courtheyn, D. LC-MS-MS to detect and identify four beta-agonists and quantify clenbuterol in liver. *Analyst* **1998**, *123*, 2701−2705.
(30) Heller, D. N.; Ngoh, M. A. Electrospray ionization and tandem ion trap mass spectrometry for the confirmation of seven beta-lactam antibiotics in bovine milk. *Rapid Commun. Mass Spectrom.* **1998**, *12*, 2031−2040.
(31) Berendsen, B. J. A.; Essers, M. L.; Mulder, P. P. J.; van Bruchem, G. D.; Lommen, A.; van Overbeek, W. M.; Stolker, A. A. M. Newly identified degradation products of ceftiofur and cephapirin impact the analytical approach for quantitative analysis of kidney. *J. Chromatogr., A* **2009**, *1216*, 8177−8186.
(32) Hurtaud-Pessel, D.; Couëdor, P.; Verdon, E. Liquid chromatography−tandem mass spectrometry method for the determination of dye residues in aquaculture products: development and validation. *J. Chromatogr., A* **2011**, *1218*, 1632−1645.
(33) Kinsella, B.; Lehotay, S. J.; Mastovska, K.; Lightfield, A. R.; Furey, A.; Danaher, M. New method for the analysis of flukicide and other anthelmintic residues in bovine milk and liver using liquid chromatography−tandem mass spectrometry. *Anal. Chim. Acta* **2009**, *637*, 196−207.
(34) Sin, D. W. M.; Ho, C.; Wong, Y. C.; Ho, S. K.; Ip, A. C. B. Simultaneous determination of lincomycin and virginiamycin M1 in swine muscle, liver and kidney by liquid chromatography−electrospray ionization tandem mass spectrometry. *Anal. Chim. Acta* **2004**, *517*, 39−45.
(35) Boner, P. L.; Gottschall, D. W.; Kim-Kang, H. Determination and confirmation of tulathromycin residues in bovine liver and porcine kidney via their common hydrolytic fragment using HPLC/tandem mass spectrometry. *J. AOAC Int.* **2011**, *94*, 436−445.
(36) Dubois, M.; Fluchard, D.; Sior, E.; Delahaut, P. Identification and quantification of five macrolide antibiotics in several tissues, eggs and milk by liquid chromatography−electrospray tandem mass spectrometry. *J. Chromatogr., B* **2001**, *753*, 189−202.
(37) Cronly, M.; Behan, P.; Foley, B.; Malone, E.; Earley, S.; Gallagher, M.; Shearan, P.; Regan, L. Development and validation of a rapid multi-class method for the confirmation of fourteen prohibited medicinal additives in pig and poultry compound feed by liquid chromatography−tandem mass spectrometry. *J. Pharm. Biomed. Anal* **2010**, *53*, 929−938.
(38) Gomez, M. J.; Petrovic, M.; Fernandez-Alba, A. R.; Barcelo, D. Determination of pharmaceuticals of various therapeutic classes by solid-phase extraction and liquid chromatography−tandem mass spectrometry analysis in hospital effluent wastewaters. *J. Chromatogr., A* **2006**, *1114*, 224−233.
(39) Korfmacher, W. A.; Freeman, J. P.; Hansen, E. B., Jr; Holder, C. L.; Getek, T. A. Characterization of the antihistamines tripelennamine, methapyrilene, and thenyldiamine and their *N*-oxides by thermospray mass spectrometry. *J. Anal. Toxicol.* **1989**, *13*, 94−96.
(40) Olejnik, M.; Szprengier-Juszkiewicz, T.; Jedziniak, P. Multi-residue confirmatory method for the determination of twelve coccidiostats in chicken liver using liquid chromatography tandem mass spectrometry. *J. Chromatogr., A* **2009**, *1216*, 8141−8148.
(41) Mottier, P.; Hure, I.; Gremaud, E.; Guy, P. A. Analysis of four 5-nitroimidazoles and their corresponding hydroxylated metabolites in egg, processed egg, and chicken meat by isotope dilution liquid chromatography tandem mass spectrometry. *J. Agric. Food Chem.* **2006**, *54*, 2018−2026.
(42) Boner, P. L.; Liu, D. D.; Feely, W. F.; Wisocky, M. J.; Wu, J. Determination and confirmation of 5-hydroxyflunixin in raw bovine milk using liquid chromatography tandem mass spectrometry. *J. Agric. Food Chem.* **2003**, *51*, 3753−3759.
(43) Hammack, W.; Carson, M. C.; Neuhaus, B. K.; Hurlbut, J. A.; Nochetto, C.; Stuart, J. S.; Youngs, K.; Ferbos, K.; Heller, D. N. Multilaboratory validation of a method to confirm chloramphenicol in shrimp and crabmeat by liquid chromatography−tandem mass spectrometry. *J. AOAC Int.* **2003**, *86*, 1135−1143.
(44) Turnipseed, S. B.; Roybal, J. E.; Pfenning, A. P.; Kijak, P. J. Use of liquid chromatography−ion trap mass spectrometry to screen and confirm drug residues in aquacultured products. *Anal. Chim. Acta* **2003**, *483*, 373−386.
(45) Paschoal, J.; Reyes, F.; Rath, S. Quantitation and identity confirmation of residues of quinolones in tilapia fillets by LC-ESI-MS-MS QToF. *Anal. Bioanal. Chem.* **2009**, *394*, 2213−2221.
(46) Samanidou, V. F.; Tolika, E. P.; Papadoyannis, I. N. Chromatographic residue analysis of sulfonamides in foodstuffs of animal origin. *Sep. Purif. Rev.* **2008**, *37*, 327−373.
(47) Jin, H.; Kumar, A. P.; Paik, D. H.; Ha, K. C.; Yoo, Y. J.; Lee, Y. I. Trace analysis of tetracycline antibiotics in human urine using UPLC-QToF mass spectrometry. *Microchem. J.* **2010**, *94*, 139−147.
(48) Vartanian, V. H.; Goolsby, B.; Brodbelt, J. S. Identification of tetracycline antibiotics by electrospray ionization in a quadrupole ion trap. *J. Am. Soc. Mass Spectrom.* **1998**, *9*, 1089−1098.

Table 1. Mass Spectrometry Settings for the LC-MS/MS System[a]

pesticide	first transition $m/z \rightarrow m/z$	DP	CE	CXP	second transition $m/z \rightarrow m/z$	DP	CE	CXP
amitraz	294.3 → 121.9	51	43	8	294.3 → 163.2	51	21	14
atrazine	216 → 174	66	25	12	218.1 → 176.1	51	25	10
azoxystrobin	404.2 → 329	46	41	18	404.2 → 344.1	46	35	20
boscalid	343.1 → 139.9	76	29	12	343.1 → 306.8	76	29	18
carbaryl	202.2 → 127.1	46	39	8	202.2 → 145.1	46	13	10
carbendazim	192.2 → 132	56	43	22	192.2 → 160.1	51	25	10
carboxin	236.1 → 143.1	46	23	8	236.1 → 87	46	35	14
chlorpyrifos-ethyl	351.9 → 200	61	25	1	351.9 → 97.1	61	53	4
clodinafop-propargyl	350.1 → 238.2	41	31	4	350.1 → 266.1	41	23	4
coumaphos	363 → 227	81	37	12	363 → 306.9	81	25	18
cyhalothrin-λ	467.1 → 225.1	51	23	12	467.1 → 450.1	51	15	6
dimethoate	230.1 → 124.9	46	29	10	230.1 → 170.9	46	21	14
epoxiconazole	330.1 → 121.1	51	29	8	330.1 → 75	51	101	6
hexythiazox	353.1 → 168	66	37	14	353.1 → 227.7	61	23	14
fenpropathrin	367.2 → 125.1	41	23	6	367.2 → 350.1	41	11	4
imidacloprid	256.1 → 175	51	19	10	256.1 → 209	51	21	12
iprodione	330.1 → 244.9	61	21	14	330.1 → 287.9	61	19	16
linuron	249 → 159.9	61	25	10	249 → 182	61	23	12
metalxyl	280.2 → 192.1	61	25	10	280.2 → 220.1	61	21	12
methomyl	163.1 → 105.9	46	15	18	163.1 → 107.1	46	11	8
methoxyfenozide	369.3 → 149.1	21	23	4	369.3 → 313.2	21	15	6
metolachlor	284.1 → 176.1	46	35	10	284.1 → 252	51	21	16
metribuzin	215.2 → 187.1	66	25	12	215.2 → 74.1	66	49	12
myclobutanil	289.2 → 125	61	49	8	289.2 → 70	61	37	12
omethoate	214.1 → 124.9	51	31	8	214.1 → 154.8	51	23	14
pirimicarb	239.2 → 182.1	51	23	12	239.2 → 72	51	37	12
profenofos	373.1 → 128.1	41	55	4	373.1 → 302.9	41	25	4
pyraclostrobin	388.1 → 163	51	35	14	388.1 → 194	51	19	16
tebuconazole	308.1 → 125	51	55	4	310.1 → 70	51	43	4
tebufenozide	353.3 → 133	16	25	4	353.3 → 297.2	16	15	4
tetraconazole	371.9 → 159	61	49	10	371.9 → 70	61	51	4
thiacloprid	253.1 → 126	41	29	4	255.1 → 128	41	27	4
thiamethoxam	292 → 131.9	26	29	4	292 → 181.2	26	29	4
thiodicarb	355 → 107.9	61	21	20	355 → 87.9	56	33	14
thiophanate-methyl	343.1 → 151	76	23	14	343.1 → 310.8	76	17	18
triflumuron	359.1 → 139	31	47	4	359.1 → 156.2	31	23	4

[a]DP, declustering potential; CE, collision energy; CXP, cell exit potential.

database[21] as well as on the basis of recent data concerning the usage and import of pesticides in Uruguay. This paper focuses on the validation of an analytical procedure for the determination of pesticide residues in beeswax, a peculiar matrix often containing high levels of incurred pesticides, as well as on the strategies applied to overcome the analytical difficulties found.

EXPERIMENTAL PROCEDURES

Chemicals and Standards. Acetonitrile and methanol of HPLC quality were from Merck (Darmstadt, Germany). Water was deionized in the laboratory using a Millipore (Billerica, MA, USA) Direct-Q 3 water purification system. Ammonium formate was purchased from Sigma-Aldrich (Steinheim, Germany). Magnesium sulfate anhydrous, reagent grade, was from Sigma-Aldrich (St. Louis, MO, USA), and formic acid p.a. (98−100%) was purchased from Merck. A solution of 5% formic acid (v/v) was prepared in acetonitrile. The bulk amino sorbent (Bondesil-PSA, 40 μm) was from Varian (Palo Alto, CA, USA). Analytical standards, ≥95% purity, were from Dr. Ehrenstorfer (Augsburg, Germany), Riedel-de Haen (Seelze, Germany), and LGC Promochem (Wesel, Germany). Stock standard solutions of 1 mg/mL were prepared, considering standard purity, by weighing individual analytical standards into flasks and dissolving and diluting them to accurate volume with acetonitrile using an automatic dispenser.

Working standard mixtures were prepared by appropriately diluting multiple stock solutions with acetonitrile using an automatic dispenser. The stock solutions of PCB 138 and chlorpyrifos D_{10}, which were employed as internal standards (ISTDs), were prepared in the same way as the pesticide stock standard solutions. An ISTD working mixture containing 20 μg/mL of each ISTD was also prepared in acetonitrile. The ISTD working mixture was mainly used for spiking the matrix prior to sample preparation in recovery experiments. An appropriate dilution of this ISTD solution to 2 μg/mL with acetonitrile was also prepared and was mainly used for the preparation of matrix-matched calibration standards. All solutions, except the ISTD working solution, were stored in the dark at 4 °C.

Apparatus. The automatic dispenser was an OPUS model (20 or 50 mL) from Hirschmann Laborgeräte (Eberstadt, Germany). A Repro high-precision sample divider from Bürkle (Bad Bellingen, Germany) was employed to portion the solids needed for dSPE.

GC×GC-TOF analysis was performed with a Pegasus 4D GC×GC/TOF-MS from Leco Corp. (St. Joseph, MI, USA). Sample injection volume was 3 μL with helium as carrier gas at a flow rate of 2 mL/min. The initial inlet temperature was set at 40 °C and increased after 0.6 min to 300 °C at a rate of 720 °C/min with a hold for 2 min and then decreased to 280 °C at the same rate with a hold for 5 min. The split valve remained open during the first 30 s following injection to allow

solvent evaporation at a flow rate of 20 mL/min and a pressure of 0.73 psi (solvent vent mode). After this 30 s period, the split valve was closed again (to transfer the analytes to the analytical column) and reopened at 2 min after injection. The first-dimension column was a DB-5MS (30.3 m, 0.25 mm i.d., 0.25 μm df). The temperature profile started at 80 °C, which was kept for 2 min and then ramped at 30 °C/min to 220 °C, then ramped again at 8 °C/min to 280 °C, and finally ramped at 20 °C/min to 300 °C with a hold for 10 min. The second-dimension column was a VF-17 ms (1.8 m, 0.1 mm i.d., 0.1 μm df), and the temperature profile was exactly the same as the first dimension only with a temperature offset of +30 °C. The second-dimension separation time was set to 4 s and controlled with an internal thermomodulator creating a hot/cold pulse. This instrument utilizes electron impact ionization (EI). The ion source temperature was set at 200 °C. The detector voltage was set at 1600 V and the filament bias at −70 V. The mass range collected was 70−550 amu with an acquisition rate of 200 spectra/s.

LC-MS/MS was performed with a Waters (Milford, MA, USA) Acquity UPLC system coupled to an API 4000 Qtrap MS/MS from Applied Biosystems (Foster City, CA, USA) run in the MS/MS mode. LC separation was performed on a Phenomenex (Torrance, CA, USA) Aqua 150 mm × 2 mm, 3 μm particle size, C18 column. The operation of the LC gradient involved the following two eluent components: (A) water/ammonium formate 5 mM; (B) methanol/ammonium formate 5 mM (%). It was run at 100 μL min^{-1} starting with 100% component A at injection time and gradually changing to 30% A (70% B) over 3 min, then to 15% A (85% B) over 3 min at 300 μL min^{-1}, followed by a shift to 10% A (90% B) over 3 min. This eluent composition was kept for 3 min and then shifted back to the starting conditions (100% component A) and kept there until 22 min after injection. The injection volume was 5 μL. MS/MS detection was performed in the multiple-reaction monitoring (MRM) mode using an ESI interface in the positive ion mode. The ionization voltage was 4500 V, the nebulizer gas was synthetic air at 70 psi, and the curtain gas was nitrogen at 30 psi. The solvent evaporation in the source was assisted by a drying gas (heated synthetic air at 425 °C/50 psi). Numerous experiments using solutions of the individual analytes were performed to determine the optimal MRM transitions, collision energies (CE), and declustering potentials (DP) for each individual compound. For this, the standard solutions were infused directly to the instrument by a syringe at constant flow. The MS/MS settings used in this study are listed in Table 1.

Methodology. Wax (2 ± 0.1 g) was weighed into a 50 mL centrifuge tube, 10 mL of acetonitrile was added, and the tube was closed and placed in a water bath at ∼80 °C. After the wax had melted, the tube was shaken vigorously for 10−15 s and placed back into the water bath to melt again. The procedure was repeated four times. Then, the tube was left to cool to room temperature and put into the freezer (−18 °C, for at least 2 h, e.g., overnight) for precipitation of the wax. An aliquot of the extract was transferred into a PP single-use centrifugation tube, which contained 25 mg of PSA primary−secondary amine (PSA) and 25 mg of C18 sorbent per milliliter of extract; the internal standard was added and the tube shaken vigorously for 30 s and centrifuged for 5 min at 3000 U/min. Finally, the cleaned extract was transferred into a screw-cap vial, and the pH was quickly lowered to ca. 5 by adding a 5% formic acid solution in acetonitrile (v/v) (10 μL/mL extract) and injected in LC-MS/MS and/or GC×GC-TOF.

Matrix-Matched Calibration and Recovery Calculations. Five-level matrix-matched calibration curves were constructed for matrix effects evaluation. Two-level calibrations within the dynamic range were performed for the evaluation of each recovery level: calibrant 1 at 60% and calibrant 2 at 120% of the aimed concentration of each level (0.01, 0.1, and 0.2 mg/kg). Calibration levels were prepared by adding the desired volume of appropriate dilution of working standard solutions to 1 mL of blank extract and equaling all of the final volumes within a batch (recoveries, blanks, and calibration vials) with acetonitrile. Recoveries were calculated as the percentage from the known added concentration of pesticides of the calculated concentration of the extract by interpolation.

RESULTS AND DISCUSSION

Impact of Sample Amount on Pesticide Residue Recoveries. The distribution of pesticides between the added acetonitrile and the liquefied beeswax phase depends on the volume ratio of the phases and the lipophilicity of the pesticides as reflected by their Log K_{OW} values. Increasing the beeswax phase volume will affect the partitioning equilibrium of the pesticides and consequently their recoveries, with lipophilic pesticides experiencing the highest losses. Influence of wax sample size was studied as follows: Different sample amounts of wax (0.5, 1, 1.5, 2, 3, 4, and 5 g) were spiked with 200 μL of a pesticide mixture containing 1 μg/mL of each pesticide dissolved in acetonitrile (0.2 μg of each pesticide) and immediately extracted according to the described procedure.

Figure 1 shows how the variation of the sample size affected the recoveries for some of the most lipophilic pesticides. As

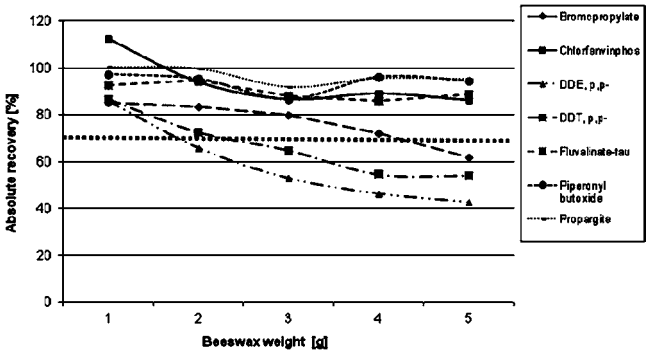

Figure 1. Influence of sample weight on pesticide recovery.

expected, pesticide recoveries decreased as the volume of the wax phase increased. The recovery drop was most pronounced for pesticides with strong lipophilic character such as DDT, DDE, and bromopropylate (Log K_{OW} values of 6.91, 6.36, and 5.4, respectively) that have a strong tendency to remain in the liquefied wax rather than to partition into the acetonitrile phase. On the basis of the results of this experiment, a ratio of 2 g of wax sample to 10 mL of acetonitrile was considered as a good compromise giving acceptable recoveries (70−120%) for almost all tested wax-relevant pesticides and a tolerable load of coextractives in the final extract of ca. 0.7 mg/mL, which corresponds to ca. 0.35% of the initial matrix weight employed for extraction (200 mg/mL). The same sample to acetonitrile ratio has been employed for the extraction of pesticide residues from vegetable oils.[20] The authors reported similar observations regarding the matrix load in the final extracts. It should be noted that when the ratio between wax and acetonitrile is kept constant, the recoveries achieved should be in principle highly reproducible, thus allowing for recovery-based result corrections with the help of suitable recovery factors derived from validation experiments.

Extractability of Incurred Residues Depending on Particle Size. The poor ability of acetonitrile to dissolve highly lipophilic compounds is, on the one hand, beneficial because it limits the amount of lipids (including waxes) dissolved in the raw and cleaned-up extract; on the other hand, it also considerably limits the accessibility of apolar pesticides incorporated in these lipids, which is the key to achieving good extraction yields and a broad scope method.

To demonstrate the importance of melting the wax to obtain optimal accessibility of residues enclosed in wax and to check

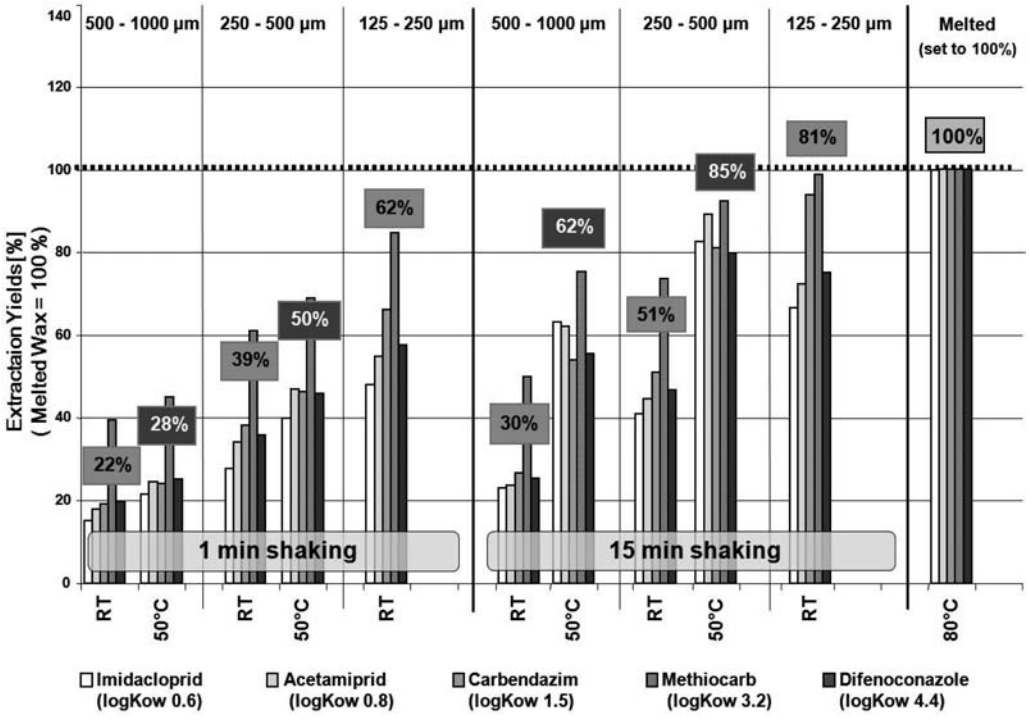

Figure 2. Impact of particle size (fractions 125−250, 250−500, and 500−1000 μm), temperature (room temperature, 50 and 80 °C), and shaking time (1 and 15 min) on the extraction yields of pesticides incorporated in beeswax. Results obtained when the wax was extracted at 80 °C (using the procedure described here) were set to 100%, n = 3, in each case. The percentage values in boxes indicate the average relative extraction yields of five wax-incorporated pesticides (imidacloprid, acetamiprid, carbendazim, methiocarb, and difenconazole).

how the comminution grade of wax affects extractability, a certain amount of beeswax was melted and spiked with a mixture of pesticides covering a broad polarity range at a level of ca. 0.1 mg/kg. By spiking the melted beeswax, a homogeneous residue distribution within it was ensured. Then, the spiked wax was deep frozen (−80 °C), intensively milled with a knife mill, adding some dry ice to keep it cold, and finally sieved into fractions (125−250, 250−500, and 500−1000 μm). Afterward, 2 g of each beeswax fraction was extracted for 1 or 15 min with acetonitrile without the addition of water. The extractions were conducted in triplicate at two different extraction temperatures: ambient (room temperature) and 50 °C. The results obtained for each pesticide as well as for all pesticides together were averaged. The results obtained when the wax was extracted at 80 °C (in melted condition as described under Methodology) were set to 100%. Figure 2 shows the results of this experiment, whic simultaneously demonstrates the positive effect of a good comminution grade (larger surface area) and of higher temperatures (better extraction kinetics and soaking of the wax) on the pesticide yields. Nevertheless, even for the finest wax fraction (125−250 μm) the average relative extraction yield at ambient temperature was only 81% compared to the yield at 80 °C, although the full volume of wax was available for potential partitioning losses at 80 °C as oposed to only the surface of the wax at ambient temperature. This experiment nicely demonstrates the difficulty of the extraction solvent to access residues incorporated in the wax and that decreasing particle size (i.e., increasing wax surface area) improves residue accessibility and thus extraction yields. Melting the wax ensured optimal accessibility to the residues via liquid−liquid partitioning.

Similar observations were made when a commercial beeswax containing incurred residues of τ-fluvalinate, piperonil butoxide, propargite, and coumaphos was extracted (results not shown here).

Comparison of Different Cleanup Possibilities. Beeswax is composed of a variety of highly lipophilic compounds such as esters of long-chain aliphatic alcohols with fatty acids or hydroxy-fatty acids, long-chain hydrocarbons, and trace levels of carotenoids. On the basis of their low solubility in acetonitrile, such highly lipophilic compounds are not expected to be present at remarkable levels in the final extracts. It is also expected that these compounds can be additionally removed to a large extent either by freezing-out (which further reduces their solubility, forcing them to precipitate) or via dispersive solid phase extraction (dSPE) using RP-C18 sorbents. Beeswax also contains a relatively more polar fraction of compounds that contains free long-chain fatty acids such as melissic and cerotic acid (that make ca. 12% of the beeswax), free hydroxy-fatty acids, and free aliphatic fatty alcohols. These compounds are still lipophilic enough to be removed to a certain degree via freeze-out or via dSPE using C18 sorbents but, in particular for the fatty acids, the cleanup approach of choice is dSPE with amino sorbents (such as PSA). Some of the polar pigments originated from the flowers visited by bees (e.g., anthocyanidines) can also be removed via dSPE.

Various experiments were conducted to study the extent to which beeswax coextractives can be removed via freeze-out and/or dSPE using C18 and/or PSA. The efficiency of cleanup was assessed on the basis of the remaining dry residue following extract evaporation but also by observing GC×GC-TOF chromatograms. Practical aspects, that is, the simplicity of the cleanup procedure, were also taken into account.

Following the first extraction step (2 g of wax + 10 mL of acetonitrile at 80 °C in a water bath), aliquots were taken from the initial extract and subjected to different cleanup procedures

Table 2. Extract Dry Residue Derived with Different Cleanup Procedures

	dry residue (mg) per mL of extract	compared to dry residue in raw extract (=100%)	compared to initial sample amount (200 mg/mL = 1000‰)
without cleanup (raw extract)	3.12	100	15.6
freeze-out 1 h	2.80	90	14.0
freeze-out 2 h	2.72	87	13.6
freeze-out 4 h	2.60	83	13.0
+3% H_2O freeze-out 1 h	2.75	88	13.7
+3% H_2O freeze-out 2 h	2.78	89	13.9
+6% H_2O freeze-out 2 h	2.60	83	13.0
+10% H_2O freeze-out 2 h	2.40	77	12.0
PSA (25 mg/mL)	1.16	37	4.3
PSA (50 mg/mL)	1.15	37	4.1
+ 3% H_2O PSA/$MgSO_4$ (25/150 mg/mL)	1.00	32	5.0
+ 6% H_2O PSA/$MgSO_4$ (25/150 mg/mL)	0.97	31	4.9
C18 (25 mg/mL)	2.65	85	13.3
C18 (50 mg/mL)	2.55	82	12.7
+ 3% H_2O C18/$MgSO_4$ (25/150 mg/mL)	2.40	77	12.0
+ 6% H_2O C18/$MgSO_4$ (25/150 mg/mL)	2.32	74	11.6
+ 10% H_2O C18/$MgSO_4$ (25/150 mg/mL)	2.17	70	10.9
+ 3% H_2O freeze-out 2 h/filtration/PSA/$MgSO_4$ (25/150 mg/mL)	0.80	26	4.0
PSA/C18 (25/25 mg/mL)	0.85	27	4.3
freeze-out/PSA (25 mg/mL)	0.77	25	3.8
freeze-out/PSA/C18 (25/25 mg/mL)	0.71	23	3.5

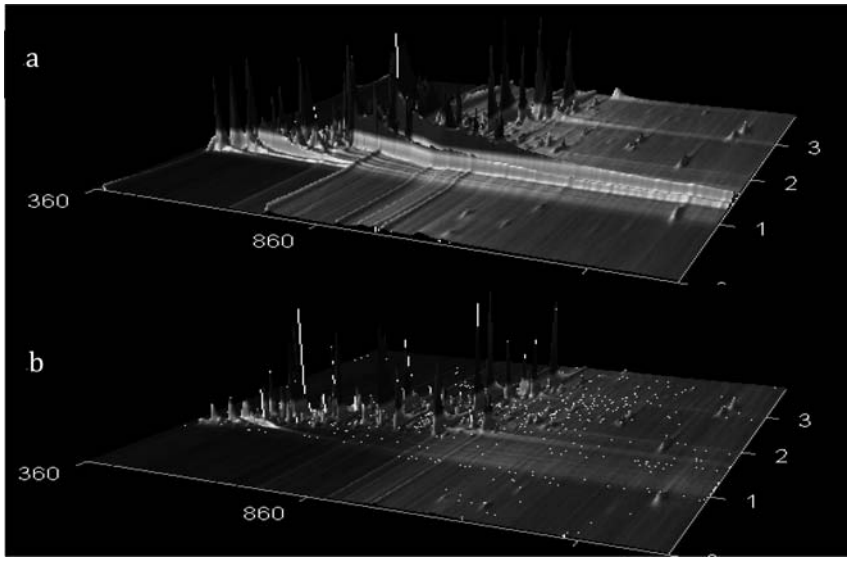

Figure 3. GC×GC-TOF plots of (a) raw extract (without cleanup) and (b) extract following dSPE with PSA.

as follows: (a) freeze-out (leave the aliquot for 1, 2, and 4 h in a freezer (−20 °C)); (b) dSPE with PSA (25 and 50 mg/mL); (c) dSPE with C18 (25 and 50 mg/mL); (d) freeze-out followed by dSPE with PSA (25 mg/mL); and (e) dSPE with PSA plus C18 (25 mg/mL each).

The influence of water addition to the raw extracts on the removal of coextractives during cleanup was also studied. A positive effect was expected in the removal of lipophilic compounds due to an increased polarity of the solvent and a negative effect regarding the efficiency of dSPE with PSA due to water interference with hydrogen bond formation between the amino groups of the sorbent and polar moieties of fatty acids or other coextracted matrix components. The following additional experiments involving water addition to the initial extract were conducted: (f) water addition (3, 6, and 10%) followed by freeze-out (1 and 2 h); (g) water addition (3, 6, and 10%) followed by dSPE with C18 (25 and 50 mg/mL); and (h) water addition (3 and 6%) followed by dSPE with PSA (25 mg/mL).

As can be seen in Table 2, dSPE using PSA removed the largest fraction of coextractives from the initial extracts (ca. 70−

dx.doi.org/10.1021/jf405771t | J. Agric. Food Chem. 2014, 62, 3675−3683

Table 3. Recoveries, RSDs, and LOQs of the Pesticides Analyzed by GC×GC-TOF (n = 5 Replicates)

	0.2 mg/kg		0.1 mg/kg					
	recovery (%)	RSD (%)	recovery (%)	RSD (%)	LOQ (mg/kg)	linear range (mg/kg)	linear correlation coefficient (r^2)	matrix effect (%)
bromopropylate[a]	83	4	102	9	0.1	0.025−1	0.992	139
chlorfenvinphos	91	10	80	6	0.1	0.25−1	0.998	15
p,p-DDE	61	21	73	4	0.1	0.025−1	0.98	144
p,p-DDT	103	3	108	17	0.1	0.025−1	0.995	127
diazinon	81	4	94	12	0.1	0.25−1	0.999	155
endosulfan α	120	10	158	18	0.2	0.25−1	0.999	245
endosulfan β	88	12	104	40	0.2	0.25−1	0.997	89
endosulfan sulfate	71	11	84	8	0.1	0.25−1	0.997	61
lindane	93	5	101	7	0.1	0.05−1	0.999	185
phorate	106	5	112	9	0.1	0.25−1	0.999	283
piperonyl butoxide[a]	95	1	102	10	0.1	0.025−1	0.999	79
propargite[a]	76	13	284	28	0.2	0.25−1	0.998	−32
trifluralin	79	13	85	16	0.1	0.25−1	0.999	188
τ-fluvalinate[a]						0.25−1	0.999	23

[a]Pesticide present as incurred residue in the beeswax sample used for spiking.

75% of the dry residue was removed). PSA effectively removed fatty acids that give large tailing peaks in GC as shown in Figure 3. Dispersive SPE using C18 sorbent and freeze-out proved to act similarly, both removing ca. 15−20% of the dry residue when no water was added and between 25 and 30% when water was added. Nevertheless, GC-MS/MS chromatograms looked similar for both treatments. Freeze-out is more difficult to handle than dSPE with C18 sorbent as it requires a filtration step through cotton, during which part of the precipitated lipids redissolve due to temperature increase. However, as it was observed that when the extract was allowed to cool to room temperature on the bench, wax precipitation was slowed, an additional freeze-out step to speed precipitation and increase repeatability was included. This is followed by dSPE with PSA sorbent and C18 sorbent, the latter serving the further reduction of lipids in the extract but not being absolutely necessary. For simplicity the freeze-out step was conducted in the extraction tube with the aliquot employed for dSPE being directly withdrawn from the cold vessel without any need for a tedious filtration step.

Cleanup with a combination of PSA and C18 (or freeze-out) is highly recommended to reduce the matrix coextractives introduced into the GC and LC system. Introduction of non-cleaned-up extracts would require shorter maintenance intervals and reduce the overall productivity, especially for GC systems.

Water addition was slightly beneficial in all experiments, helping to remove additional lipids, but the benefits did not justify the additional workload introduced by water addition and its subsequent removal with $MgSO_4$. Within this context the conditions described under Experimental Procedures were preferred. Two grams of wax was melted at 80 °C in a water bath and extracted with acetonitrile. The extracting solution was left to cool to room temperature and frozen out for at least 2 h (e.g., overnight). From the cold solution, an aliquot was subjected to dSPE cleanup using C18 and PSA sorbents (25 mg/mL). Following acidification with 5% formic acid in acetonitrile (10 μL/mL) and ISTD addition, the extracts were analyzed by GC×GC-TOF and LC-MS/MS.

Method Validation. After the optimal sample amount, particle size, and the best cleanup approach had been chosen, five replicates of spiked blanks of beeswax at different levels (0.1 and 0.2 mg/kg for GC×GC-TOF analysis and 0.01, 0.1, and 0.2 mg/kg for LC-QTrap analysis) were analyzed to assess accuracy (% recovery) and repeatability (% RSD) of the procedure.

In agreement with the analytical quality control procedures document by DG-SANCO,[22] the limits of quantification (LOQs) were considered as the lowest successfully validated levels, that is, the levels at which acceptable recoveries (70−120%) and RSDs (<20%) were achieved. LOQs would have been surely different if other spiking levels were chosen. Of course, LOQs will also depend on other factors such as the type of instrumentation used and its condition.

For GC×GC-TOF matrix-matched calibration was used, whereas for LC-MS/MS calibration curves were constructed using both solvent-based and matrix-matched standards at five concentration levels (0.001, 0.002, 0.01, 0.02, and 0.05 μg/mL, corresponding to 0.005, 0.01, 0.05, 0.1, and 0.25 mg/kg beeswax). GC×GC-TOF analysis was conducted using an ISTD, whereas no ISTD was used in LC-MS/MS.

The matrix effects were calculated as the percentage difference in the best-fit slopes of the matrix-matched calibration curves versus the respective best-fit slopes of the solvent calibration curves. The peak areas rather than the relative peak areas against the ISTD were used to avoid matrix effects on the ISTD that potentially affect the calculation.[23]

In GC×GC-TOF large and positive matrix effects were observed (Table 3) except for propargite, which presented a negative effect.

In LC-MS/MS matrix effects were quite pronounced and variable from analyte to analyte as shown in Table 4. This is explained by the fact that matrix effects depend on whether a target analyte coelutes with coextracted matrix components, affecting the yield of free analyte ions generated within the ESI-ion source and thus the detection signals. A dSPE cleanup of the raw wax extracts with PSA contributed in reducing to some extent the matrix effects of certain compounds (boscalid from −10 to −1; imidacloprid from −50 to 3; tebuconazole from −33 to 9; dimethoate from 20 to −2; carbaryl from −20 to 3; thiacloprid from −25 to 1). Similar observations were also previously made using extracts of other "difficult" commodities such as oranges.[24] When matrix effects remain strong, the use of matrix-matched calibration standards (prepared from extracts of blank matrix so far available) or the method of standard

Table 4. Percentage Recoveries, RSDs, and LOQs of the Pesticides Analyzed by LC-MS/MS (n = 5 Replicates)

	0.2 mg/kg		0.1 mg/kg		0.01 mg/kg					
	recovery (%)	RSD (%)	recovery (%)	RSD (%)	recovery (%)	RSD (%)	LOQ (mg/kg)	linear range (mg/kg)	linear correlation coefficient (r^2)	matrix effect (%)
amitraz	73	2	77	4	85	13	0.01	0.005−0.25	0.999	−2
atrazine	89	4	94	4	97	13	0.01	0.006−0.24	0.999	
azoxystrobin	110	3	111	4	112	14	0.01	0.005−0.25	0.997	24
boscalid	98	6	103	8	105	24	0.1	0.005−0.25	0.999	5
carbaryl[a]	104	4	111	5	165	6	0.1	0.005−0.25	0.995	4
carbaryl[b]					112	2				
carbendazim	72	4	78	6	100	15	0.01	0.005−0.25	0.999	32
carboxin	104	4	108	6	107	9	0.01	0.005−0.25	0.999	−6
chlorpyrifos-ethyl[a]	92	6	105	6	218	15	0.1	0.005−0.25	0.999	−13
clodinafop-propargyl	104	1	105	5	104	14	0.01	0.005−0.25	0.999	88
coumaphos[a]	144	3	229	4	1679	8		0.005−0.25	0.999	24
cyhalothrin-λ	92	16	100	9	not detectable		0.1	0.005−0.25	0.999	−23
dimethoate	102	6	106	6	107	7	0.01	0.005−0.25	0.997	2
epoxiconazole	94	4	106	7	not detectable		0.1	0.005−0.25	0.999	−33
fenpropathrin	95	7	102	11	159	15	0.1	0.006−0.24	0.997	
flutriafol	101	11	114	15	not detectable		0.1	0.005−0.25	0.998	−55
hexythiazox[a]	182	4	323	5	2800	3		0.005−0.25	0.999	−41
hexythiazox[b]					87	8				
imidacloprid	108	7	106	8	100	9	0.01	0.005−0.25	0.996	−0,1
iprodione	108	27	123	24	not detectable		0.2	0.005−0.25	0.997	−7
linuron	96	6	99	5	107	15	0.01	0.005−0.25	0.999	−41
metalaxyl	107	3	109	5	113	15	0.01	0.005−0.25	0.997	−20
methomyl	111	8	127	4	113	12	0.01	0.005−0.25	0.999	−21
methoxyfenozide[a]	107	4	111	5	146	7	0.1	0.005−0.25	0.999	−15
methoxyfenozide[b]					116	18				
metolachlor	96	3	103	2	120	17	0.01	0.005−0.25	0.999	−20
metribuzin	102	7	111	7	not detectable		0.1	0.005−0.25	0.999	−3
myclobutanil	106	5	102	10	123	14	0.1	0.005−0.25	0.998	−7
omethoate	96	11	104	8	111	6	0.01	0.005−0.25	0.992	−33
pendimethalin	81	19	83	19	not detectable		0.1	0.06−0.24	0.995	
pirimicarb	108	3	114	4	111	11	0.01	0.005−0.25	0.999	−10
profenofos	89	6	94	6	92	18	0.01	0.005−0.1	0.999	−32
pyraclostrobin	102	4	106	5	112	14	0.01	0.005−0.25	0.999	−33
tebuconazole	98	11	99	5	103	27	0.1	0.005−0.25	0.999	2
tebufenozide	96	4	99	5	104	15	0.01	0.005−0.25	0.998	−25
tetraconazole	103	7	104	6	111	23	0.1	0.005−0.25	0.996	−22
thiacloprid	113	7	120	5	108	18	0.01	0.005−0.25	0.999	−7
thiamethoxam	103	14	103	7	106	15	0.01	0.005−0.25	0.999	13
thiodicarb	90	5	85	7	107	12	0.01	0.005−0.25	0.999	−25
thiophanate-methyl	94	5	91	7	97	15	0.01	0.005−0.25	0.997	−22
triflumuron	91	5	98	10	104	12	0.01	0.005−0.25	0.999	−46

[a]Pesticides present as incurred residues in the beeswax sample used for spiking. [b]Recovery experiment at 0.01 in blank beeswax (Pharmacognosy collection).

additions is recommended to obtain reliable quantification.[22] Matrix coextractives in LC-MS/MS mainly cause signal suppression, whereas signal enhancement is typically observed in GC applications. This is due to the different mechanisms behind matrix effects in each case.[25,26] Matrix coextractives of beeswax behave as analyte protectants hampering pesticide degradation in the injector and along the chromatographic column, resulting in signal enhancement.

Recoveries of GC- and LC-amenable pesticides were in almost all cases between 70 and 120% with RSDs below 20% at least at one of the levels assayed (Tables 3 and 4). The exceptions were mainly due to the incurred residues found in the commercial beeswax that was used to conduct the recovery experiments. Some recovery experiments were repeated using as blank material all of the beeswax from the year 1932 that could be withdrawn from the Pharmacognosy collection of the Chemistry College of Universidad de la República, which did not contain pesticide residues. Recoveries could then be properly evaluated for carbaryl, hexythiazox, and methoxyfenozide at 0.01 mg/kg ranging from 87 to 116% and RSDs being below 18%, whereas chlorpyrifos could not be quantified at this low level. Coumaphos and τ-fluvalinate were studied at higher levels (0.2 and 0.1 mg/kg) because they are used directly inside the hive to protect bees from mites. Good results were obtained for τ-fluvalinate at the level of 0.2 mg/kg (102% recovery and 5% RSD) and for coumaphos at both levels (103 and 109%

dx.doi.org/10.1021/jf405771t | J. Agric. Food Chem. 2014, 62, 3675−3683

recoveries; 4 and 10% RSDs, respectively). With beeswax being a natural product, differences in composition between samples were expected. Table 5 shows validation data for a group of

Table 5. Percentage Recoveries and RSDs (n = 5) of a selected Group of Pesticides at 0.1 mg/kg in Different Samples Assayed

	commercial beeswax from Germany		commercial beeswax from Uruguay		beeswax from pharmacognosy collection	
	recovery (%)	RSD (%)	recovery (%)	RSD (%)	recovery (%)	RSD (%)
azoxystrobin	111	4	88	4	99	7
boscalid	103	8	76	6	107	7
carbaryl	111	5	84	3	93	4
chlorpyrifos-ethyl	105	6	77	6	94	11
dimethoate	106	6	86	3	94	10
imidacloprid	106	8	86	3	93	3
tebuconazole	99	5	77	1	78	10
thiacloprid	120	5	82	2	99	12
thiamethoxam	103	7	86	3	98	20

selected pesticides spiked onto three different beeswax samples (samples purchased in Germany and Uruguay and the wax from the Pharmacognosy museum). These data further demonstrate the suitability and ruggedness of the method for this complex matrix. The use of different beeswax samples with different incurred residues for analytical validation purposes is a useful tool not only to cross check the obtained results but also to broaden the scope of compounds that can be successfully validated. In summary, a simple variation of the QuEChERS method, involving extraction of wax at high temperatures (~80 °C) to enable liquid–liquid partitioning between the liquefied wax phase and acetonitrile followed by a simple freeze-out plus a dSPE step, proved to be effective for the multiresidue analysis of 51 pesticides in beeswax. Several critical aspects (sample weight, particle size, and different cleanup options) were studied in the course of method development. A comprehensive cleanup involving freeze-out and dSPE using PSA and C18 was shown to remove ca. 75% of the coextractives from the raw extract and ca. 99.6% of the initial wax. Quantitative analysis was accomplished by LC-MS/MS and GC×GC-TOF. Fifty-one pesticides proved to be accurately determined with the developed methodology. The method can be easily expanded to other pesticides that, although not included in the present study, could be found in beeswax samples produced in other environments or agricultural systems. Beeswax is a long-term "pollution reservoir" due to its particular physicochemical properties; it stores the pesticide residues to which the hive is exposed. Therefore, the analysis of this complex matrix will give relevant data on the sustainability of specific agroecosystems.

AUTHOR INFORMATION

Corresponding Author

*(H.H.) E-mail: heinzen@fq.edu.uy.

Notes

The authors declare no competing financial interest.

ACKNOWLEDGMENTS

CVUA Stuttgart, PEDECIBA Química, CSIC, and Facultad de Química (Universidad de la República) are greatly acknowledged.

ABBREVIATIONS USED

QuEChERS, quick, easy, cheap, effective, rugged, and safe; dSPE, dispersive solid phase extraction; LC-MS/MS, liquid chromatography–tandem mass spectrometry; GCxGC-TOF, two-dimensional gas chromatography–time of flight detection; RSD, relative standard deviation; PCB, polychlorinated biphenyl; ISTD, internal standard; MRM, multiple-reaction monitoring; ESI, electrospray ionization; PSA, primary and secondary amine

REFERENCES

(1) Schmidt, J. O.; Buchmann, S. L. Other products of the hive. In *The Hive and the Honey Bee*; Graham, J. M., Ed.; Dadant and Sons: Hamilton, IL, USA, 1992.

(2) Bargańska, Ż.; Namieśnik, J. Pesticide analysis of bee and bee product samples. *Crit. Rev. Anal. Chem.* **2010**, *40* (3), 159–171.

(3) Pareja, L.; Colazzo, M.; Pérez-Parada, A.; Niell, S.; Carrasco-Letelier, L.; Besil, N.; Cesio, M. V.; Heinzen, H. Detection of pesticides in active and depopulated beehives in Uruguay. *Int. J. Environ. Res. Public Health* **2011**, *8* (10), 3844–3858.

(4) Porrini, C.; Sabatini, A. G.; Girotti, S.; Ghini, S.; Medrzycki, P.; Grillenzoni, F.; Bortolotti, L.; Gattavecchia, E.; Celli, G. Honey bees and bee products as monitors of the environmental contamination. *Apiacta* **2003**, *38*, 63–70.

(5) Haarmann, T. Honey bees as indicators of radionuclide contamination. In *Honey Bees: Estimating the Environmental Impact of Chemicals*; CRC Press: Boca Raton, FL, USA, 2002; pp 132–150.

(6) Porrini, C.; Ghini, S.; Girotti, S.; Sabatini, A.; Celli, G.; Gattavecchia, E. Use of honey bees as bioindicators of environmental pollution in Italy. In *Honey Bees: Estimating the Environmental Impact of Chemicals*; CRC Press: Boca Raton, FL, USA, 2002; pp 186–247.

(7) Kezic, N.; Barisic, D.; Bromenshenk, J.; Vertacnik, A. The role of honey bees in environmental monitoring in Croatia. In *Honey Bees: Estimating the Environmental Impact of Chemicals*; CRC Press: Boca Raton, FL, USA, 2002; pp 160–185.

(8) Raeymaekers, B. A prospective biomonitoring campaign with honey bees in a district of Upper-Bavaria (Germany). *Environ. Monit. Assess.* **2006**, *116* (1), 233–243.

(9) Balayiannis, G.; Balayiannis, P. Bee honey as an environmental bioindicator of pesticides' occurrence in six agricultural areas of Greece. *Arch. Environ. Contam. Toxicol.* **2008**, *55* (3), 462–470.

(10) Adamczyk, S.; Lázaro, R.; Pérez-Arquillué, C.; Bayarri, S.; Herrera, A. Impact of the use of fluvalinate on different types of beeswax from Spanish hives. *Arch. Environ. Contam. Toxicol.* **2010**, *58* (3), 733–739.

(11) Adamczyk, S.; Lázaro, R.; Pérez-Arquillué, C.; Herrera, A. Determination of synthetic acaricides residues in beeswax by high-performance liquid chromatography with photodiode array detector. *Anal. Chim. Acta* **2007**, *581* (1), 95–101.

(12) Lodesani, M.; Costa, C.; Serra, G.; Colombo, R.; Sabatini, A. Acaricide residues in beeswax after conversion to organic beekeeping methods. *Apidologie* **2008**, *39* (3), 324–333.

(13) Martel, A.-C.; Zeggane, S.; Aurières, C.; Drajnudel, P.; Faucon, J.-P.; Aubert, M. Acaricide residues in honey and wax after treatment of honey bee colonies with Apivar® or Asuntol®50. *Apidologie* **2007**, *38* (6), 534–544.

(14) Bogdanov, S.; Kilchenmann, V.; Seiler, K.; Pfefferli, H.; Frey, T.; Roux, B.; Wenk, P.; Noser, J. Residues of *p*-dichlorobenzene in honey and beeswax. *J. Apic. Res.* **2004**, *43* (1), 14–16.

(15) Chauzat, M. P.; Faucon, J. P. Pesticide residues in beeswax samples collected from honey bee colonies (*Apis mellifera* L.) in France. *Pest Manage. Sci.* **2007**, *63* (11), 1100–1106.

(16) Johnson, R.; Ellis, M.; Mullin, C.; Frazier, M. Pesticides and honey bee toxicity – USA. *Apidologie* **2010**, *41* (3), 312–331.
(17) Jiménez, J. J.; Bernal, J. L.; Nozal, M. J. d.; Alonso, C. Liquid-liquid extraction followed by solid-phase extraction for the determination of lipophilic pesticides in beeswax by gas chromatography-electron-capture detection and matrix-matched calibration. *J. Chromatogr., A* **2004**, *1048* (1), 89–97.
(18) Fernández, M.; Picó, Y.; Mañes, J. Analytical methods for pesticide residue determination in bee products. *J. Food Prot.* **2002**, *65* (9), 1502–1511.
(19) Mullin, C. A.; Frazier, M.; Frazier, J. L.; Ashcraft, S.; Simonds, R.; vanEngelsdorp, D.; Pettis, J. S. High levels of miticides and agrochemicals in North American apiaries: implications for honey bee health. *PLoS One* **2010**, *5* (3), e9754.
(20) Anastassiades, M.; Tasdelen, B.; Scherbaum, E.; Stajnbaher, D. Recent developments in QuEChERS methodology for pesticide multiresidue analysis. In *Pesticide Chemistry: Crop Protection, Public Health, Environmental Safety*; Ohkawa, H., Miyagawa, H., Lee, P. W., Eds.; Wiley-VCH: Weinheim, Germany, 2007.
(21) CVUA Stuttgart, Pesticides Online website. http://www.pesticides-online.com (accessed Nov 30, 2013).
(22) DG-SANCO. Method Validation and Quality Control Procedures for Pesticide Residues Analysis in Food and Feed. Document SANCO/12495/2011, 2011.
(23) Koesukwiwat, U.; Lehotay, S. J.; Miao, S.; Leepipatpiboon, N. High throughput analysis of 150 pesticides in fruits and vegetables using QuEChERS and low-pressure gas chromatography-time-of-flight mass spectrometry. *J. Chromatogr., A* **2010**, *1217* (43), 6692–6703.
(24) Payá, P.; Anastassiades, M.; MacK, D.; Sigalova, I.; Tasdelen, B.; Oliva, J.; Barba, A. Analysis of pesticide residues using the quick easy cheap effective rugged and safe (QuEChERS) pesticide multiresidue method in combination with gas and liquid chromatography and tandem mass spectrometric detection. *Anal. Bioanal. Chem.* **2007**, *389* (6), 1697–1714.
(25) Kruve, A.; Künnapas, A.; Herodes, K.; Leito, I. Matrix effects in pesticide multi-residue analysis by liquid chromatography–mass spectrometry. *J. Chromatogr., A* **2008**, *1187* (1–2), 58–66.
(26) Maštovská, K.; Lehotay, S. J.; Anastassiades, M. Combination of analyte protectants to overcome matrix effects in routine GC analysis of pesticide residues in food matrixes. *Anal. Chem.* **2005**, *77* (24), 8129–8137.

Table 1. Pesticide Retention Times, Lowest Calibrated Level (LCL), Average Recoveries (n = 5), and Standard Deviations (SD) for Fortified Samples[a]

			spiking level			
	t_R (min)	LCL (ng/g)	1 ng/g	5 ng/g	50 ng/g	100 ng/g
alachlor	4.553	0.5	112 ± 14	116 ± 6	112 ± 6	103 ± 4
aldrin	4.825	0.5	70 ± 10	94 ± 13	108 ± 13	99 ± 5
α-BHC	4.13	0.5	94 ± 20	104 ± 8	109 ± 6	108 ± 7
atrazine	4.529	0.5	109 ± 10	103 ± 4	103 ± 1	102 ± 5
azinphos-ethyl	6.259	1	<LCL	70 ± 6	110 ± 5	94 ± 3
azinphos-methyl	6.124	1	<LCL	108 ± 12	90 ± 17	116 ± 6
β-BHC + lindane	4.23	0.5	<LCL	86 ± 6	98 ± 16	100 ± 8
bifenthrin	5.73	1	<LCL	116 ± 4	93 ± 6	99 ± 3
bromophos	4.86	0.5	117 ± 10	100 ± 8	98 ± 7	90 ± 8
bromophos-ethyl	5.032	0.5	117 ± 7	100 ± 7	89 ± 6	85 ± 1
bromopropylate	5.8	0.5	**148** ± 10	104 ± 8	93 ± 10	101 ± 3
bupirimate	5.192	5	<LCL	**127** ± 10	102 ± 19	103 ± 6
buprofezin	5.216	1	89 ± 13	103 ± 11	109 ± 17	114 ± 3
cadusafos	3.903	0.5	114 ± 9	113 ± 7	114 ± 18	112 ± 5
carbaryl	3.653	1	<LCL	83 ± 8	117 ± 15	84 ± 16
carbofuran	4.149	0.5	87 ± 12	111 ± 6	109 ± 6	86 ± 3
carbophenothion	5.496	1	**127** ± 6	113 ± 9	101 ± 14	97 ± 4
chinomethionat	5.11	1	<LCL	111 ± 21	96 ± 8	118 ± 4
chlorfenvinphos	4.928	0.5	**132** ± 6	106 ± 10	105 ± 9	118 ± 2
chlorothalonil	4.363	0.5	112 ± 6	**41 ± 17**	**12 ± 59**	**19 ± 184**
chlorpropham	3.95	0.5	102 ± 13	107 ± 7	100 ± 14	106 ± 4
chlorpyrifos	4.526	0.5	**131** ± 6	118 ± 6	96 ± 10	104 ± 1
chlorpyrifos-methyl	4.527	0.5	115 ± 15	108 ± 3	109 ± 9	96 ± 2
cis-chlordane	5.092	0.5	106 ± 9	114 ± 7	111 ± 4	97 ± 3
cis-nonachlor	5.425	0.5	88 ± 6	94 ± 13	98 ± 7	104 ± 5
cis-permethrin	6.381	1	<LCL	89 ± 15	99 ± 8	80 ± 5
coumaphos	6.493	1	<LCL	116 ± 24	112 ± 5	108 ± 4
cyanophos	4.259	0.5	106 ± 10	117 ± 7	105 ± 11	107 ± 3
cyfluthrin	6.706	1	<LCL	100 ± 21	99 ± 9	93 ± 5
cypermethrin	6.864	5	<LCL	77 ± 11	108 ± 4	100 ± 3
cyprodinil	4.903	0.5	112 ± 17	102 ± 14	96 ± 10	109 ± 3
δ-BHC + lindane	4.288	0.5	97 ± 19	75 ± 10	102 ± 3	101 ± 3
deltamethrin	7.999	1	<LCL	101 ± 13	97 ± 11	106 ± 5
demeton-s-methyl	3.883	0.5	104 ± 14	93 ± 6	117 ± 5	92 ± 7
demeton-s-methyl sulfone	4.648	1	<LCL	105 ± 16	112 ± 12	80 ± 12
diazinon	4.246	0.5	109 ± **25**	122 ± 3	103 ± 10	112 ± 3
dichlorfenthion	4.482	0.5	114 ± 14	110 ± 8	101 ± 3	93 ± 3
dicloran	4.182	0.5	97 ± 9	108 ± 4	112 ± 11	106 ± 3
dicrotophos	3.752	0.5	**52** ± 13	86 ± 10	83 ± 8	**67** ± 7
dieldrin	5.278	1	<LCL	87 ± 11	91 ± 6	87 ± 13
dimethoate	4.156	1	<LCL	112 ± 3	106 ± 7	97 ± 3
dioxathion	4.24	1	<LCL	117 ± 12	118 ± 9	81 ± 2
diphenylamine	3.673	1	<LCL	75 ± 9	100 ± 11	107 ± 4
disulfoton	3.883	1	<LCL	120 ± 2	104 ± 13	109 ± 3
disulfoton sulfone	5.08	0.5	**149** ± 8	112 ± 12	115 ± 15	112 ± 6
endosulfan sulfate	5.582	0.5	89 ± **23**	81 ± 18	104 ± 5	97 ± 5
endrin	5.358	1	**145** ± 17	105 ± 8	115 ± 10	74 ± 2
endrin ketone	5.86	0.5	116 ± 19	110 ± 9	98 ± 7	95 ± 5
EPN	5.799	1	<LCL	108 ± 5	98 ± 10	90 ± 4
esfenvalerate	7.52	1	<LCL	100 ± 12	75 ± 11	81 ± 10
ethalfluralin	3.898	0.5	114 ± 10	95 ± 13	113 ± 7	108 ± 8
ethion	5.348	1	<LCL	117 ± 3	103 ± 16	98 ± 3
ethoprophos	3.903	0.5	97 ± 9	111 ± 10	105 ± 5	109 ± 5
famphur	5.481	1	<LCL	114 ± 9	98 ± 9	113 ± 4
fenarimol	6.31	1	<LCL	111 ± 3	97 ± 13	87 ± 4
fenchlorphos	4.611	0.5	105 ± 7	99 ± 3	105 ± 8	95 ± 3
fenitrothion	4.666	0.5	116 ± 5	105 ± 6	98 ± 8	105 ± 2
fenpropathrin	5.789	1	<LCL	96 ± 17	89 ± 10	87 ± 5

dx.doi.org/10.1021/jf404389e | J. Agric. Food Chem. 2014, 62, 3684−3689

Table 1. continued

			spiking level			
	t_R (min)	LCL (ng/g)	1 ng/g	5 ng/g	50 ng/g	100 ng/g
fensulfothion	5.352	0.5	114 ± 9	103 ± 13	103 ± 5	108 ± 7
fenthion	4.76	0.5	102 ± 9	100 ± 6	106 ± 3	102 ± 1
fenthion sulfone	5.369	0.5	**127** ± 5	99 ± 9	107 ± 5	92 ± 4
fenvalerate	7.46	1	<LCL	95 ± 6	86 ± 4	112 ± 5
fipronil	4.9	1	<LCL	103 ± 6	106 ± 8	96 ± 3
flucythrinate	6.85	1	<LCL	73 ± 13	85 ± 2	101 ± 2
fluvalinate	7.434	1	<LCL	75 ± 13	86 ± 4	109 ± 4
fonofos	4.299	0.5	109 ± 16	117 ± 6	104 ± 4	115 ± 5
heptachlor	4.649	0.5	89 ± 11	83 ± 10	98 ± 4	90 ± 6
heptachlor epoxide	4.992	0.5	93 ± 17	106 ± 5	104 ± 9	100 ± 2
heptenophos	3.752	0.5	74 ± 24	96 ± 7	104 ± 11	77 ± 14
hexachlorobenzene	4.163	0.5	97 ± 20	97 ± 10	82 ± 2	88 ± 5
iprodione	5.787	5	<LCL	111 ± 18	92 ± 18	76 ± 5
isofenphos	4.91	0.5	**133** ± 12	119 ± 8	102 ± 7	99 ± 1
kresoxim-methyl	5.191	1	<LCL	115 ± 16	107 ± 11	119 ± 3
leptophos	6.021	1	<LCL	105 ± 18	95 ± 16	95 ± 6
malathion	4.675	1	**124** ± 10	70 ± 7	106 ± 6	106 ± 4
metalaxyl	4.579	0.5	**134** ± 12	79 ± 6	103 ± 4	97 ± 2
methacrifos	3.556	0.5	96 ± 16	110 ± 7	115 ± 10	107 ± 8
methidathion	5.05	1	<LCL	**126** ± 6	118 ± 3	101 ± 4
methiocarb	4.675	0.5	98 ± 11	107 ± 5	100 ± 13	108 ± 3
methoxychlor	5.814	1	<LCL	97 ± 4	101 ± 6	95 ± 7
methyl parathion	4.559	0.5	100 ± 10	100 ± 5	100 ± 11	91 ± 3
metolachlor	4.743	0.5	**122** ± 6	115 ± 6	101 ± 5	102 ± 1
metribuzin	4.522	0.5	119 ± 18	119 ± 8	106 ± 8	113 ± 1
mevinphos	3.387	0.5	85 ± 4	95 ± 7	99 ± 13	73 ± 16
mirex	6.281	0.5	116 ± 16	81 ± 12	75 ± 11	78 ± 8
myclobutanil	5.25	1	<LCL	117 ± 12	109 ± 17	104 ± 3
o,p′-DDD	5.245	1	<LCL	116 ± 9	103 ± 19	102 ± 3
o,p′-DDE	5.065	1	<LCL	92 ± 17	93 ± 16	102 ± 3
o,p′-DDT + *p,p′*-DDD	5.387	0.5	106 ± 11	105 ± 19	97 ± 13	97 ± 6
o-phenylphenol	3.673	1	<LCL	93 ± 9	120 ± 9	105 ± 9
oxadixyl	5.391	1	<LCL	115 ± 11	91 ± 17	93 ± 3
oxyfluorfen	5.177	1	<LCL	116 ± 9	95 ± 11	127 ± 2
p,p′-DDE	5.19	1	<LCL	98 ± 4	94 ± 5	107 ± 8
p,p′-DDT	5.56	0.5	97 ± 13	74 ± 12	81 ± 20	96 ± 3
parathion	4.776	0.5	86 ± 23	72 ± 17	108 ± 3	108 ± 2
penconazole	4.929	0.5	120 ± 13	99 ± 3	96 ± 7	107 ± 4
pendimethalin	4.895	0.5	116 ± 3	97 ± 7	87 ± 5	89 ± 2
pentachloroanisole	4.174	0.5	112 ± 11	104 ± 9	90 ± 3	94 ± 5
pentachlorothioanisole	4.752	0.5	90 ± 13	87 ± 4	74 ± 6	79 ± 4
phorate	4.057	0.5	114 ± 5	**121** ± 8	113 ± 5	116 ± 7
phosalone	6.005	1	<LCL	116 ± 6	99 ± 10	87 ± 3
phosmet	5.812	1	<LCL	116 ± 9	104 ± 7	110 ± 5
phosphamidon	4.276	0.5	**64** ± 18	106 ± 8	100 ± 5	82 ± 9
phthalimide	3.543	1	<LCL	**65** ± 19	108 ± 12	116 ± 3
piperonyl butoxide	5.588	1	<LCL	112 ± 4	93 ± 14	89 ± 3
pirimiphos-ethyl	4.797	0.5	108 ± 17	111 ± 5	97 ± 3	91 ± 1
pirimiphos-methyl	4.626	0.5	**122** ± 8	114 ± 5	106 ± 4	102 ± 1
procymidone	4.997	0.5	**137** ± 9	109 ± 7	97 ± 8	93 ± 2
profenophos	5.172	0.5	**125** ± 20	98 ± 9	99 ± 9	106 ± 11
propachlor	3.861	0.5	99 ± 5	110 ± 4	112 ± 7	110 ± 7
propazine	4.199	0.5	90 ± 3	113 ± 3	111 ± 8	107 ± 4
propetamphos	4.211	0.5	110 ± 18	105 ± 4	116 ± 6	112 ± 2
propham	3.484	0.5	113 ± 14	107 ± 5	113 ± 7	110 ± 8
propiconazole	5.6	1	118 ± **24**	120 ± 4	108 ± 7	90 ± 4
propoxur	3.834	0.5	82 ± 10	102 ± 9	114 ± 6	116 ± 8
propyzamide	4.268	0.5	118 ± 7	113 ± 1	111 ± 4	104 ± 1
pyrimethanil	4.314	0.5	109 ± 6	107 ± 4	95 ± 4	90 ± 1

dx.doi.org/10.1021/jf404389e | J. Agric. Food Chem. 2014, 62, 3684−3689

Table 1. continued

	t_R (min)	LCL (ng/g)	spiking level 1 ng/g	5 ng/g	50 ng/g	100 ng/g
quintozene	4.269	0.5	116 ± 15	103 ± 8	98 ± 5	96 ± 5
resmethrin	5.595	5	<LCL	82 ± 13	93 ± 13	84 ± 4
simazine	4.165	0.5	**135** ± 15	112 ± 18	99 ± **21**	106 ± 3
sulprofos	5.436	0.5	**139** ± 6	108 ± 10	103 ± 6	87 ± 2
tebuconazole	5.72	1	<LCL	87 ± 11	81 ± 9	72 ± 6
tecnazene	3.855	0.5	98 ± 7	102 ± 10	104 ± 4	100 ± 8
terbufos	4.256	0.5	112 ± 11	116 ± 7	99 ± 16	115 ± 4
terbutylazine	4.244	0.5	116 ± 10	113 ± 2	105 ± 10	91 ± 3
tetrachlorvinphos	5.055	0.5	**121** ± 8	**121** ± 3	96 ± 18	106 ± 7
tetraconazole	4.765	0.5	**132** ± 10	103 ± 2	79 ± 16	81 ± 3
tetradifon	5.983	1	<LCL	104 ± 8	95 ± 9	110 ± 5
tolclofos-methyl	4.566	0.5	113 ± 11	116 ± 7	100 ± 7	104 ± 1
trans-chlordane	5.149	1	<LCL	104 ± 15	97 ± 17	103 ± 13
trans-nonachlor	5.16	0.5	119 ± 22	108 ± 16	90 ± 10	100 ± 6
trans-permethrin	6.48	1	<LCL	78 ± 9	93 ± 14	91 ± 8
triadimefon	4.788	0.5	**127** ± 6	115 ± 3	93 ± 12	110 ± 2
triazophos	5.421	1	<LCL	115 ± 8	90 ± 19	98 ± 3
trifluralin	3.93	1	<LCL	112 ± 24	111 ± 13	99 ± **22**
vinclozolin	4.529	0.5	118 ± 16	113 ± 5	110 ± 4	105 ± 1
α-endosulfan	5.159	5	<LCL	102 ± 13	109 ± 8	112 ± 3
β-endosulfan	5.413	1	<LCL	103 ± 3	101 ± 10	117 ± 3
λ-cyhalothrin	6.063	1	<LCL	101 ± 6	111 ± 7	105 ± 5
4,4′-dichlorobenzophenone	4.838	0.5	113 ± 8	104 ± 4	96 ± 3	93 ± 2

[a]Recoveries <70% and >120% and SDs >20% are highlighted in bold.

Sep is a new commercially available sorbent based on zirconium oxide. Formic acid (88% purity) was obtained from Spectrum Quality Products Inc. (New Brunswick, NJ, USA). Standard Reference Materials (SRMs) 1974b (Organics in Mussel Tissue) and 1947 (Lake Michigan Fish Tissue) were purchased from the National Institute of Standards and Technology (NIST, Gaithersburg, MD, USA).

Approximately 1 kg filets of catfish muscle tissue were purchased from local food stores. Samples were homogenized with an Ultra-Turrax T25 homogenizer (Janke & Kunkel GmbH & Co., IKA Labortechnik, Wilmington, NC, USA) and stored in a −18 °C freezer. The average fat content of catfish muscle is 5.9% by weight,[2] and measured moisture content was 80%.

A standard mixture of pesticides at 20 μg/mL in 0.05% formic acid in MeCN was used as a spiking solution for 100 and 50 ng/g spiking levels, and a pesticide standard mixture at 500 ng/mL in 0.05% formic acid in MeCN was used for 5 and 1 ng/g spiking levels in the recovery experiments. A mixture of atrazine-d_5 and fenthion-d_6 at 10 μg/mL was prepared in 0.05% formic acid in MeCN.

Sample Preparation. The sample preparation was based on the unbuffered QuEChERS method with MeCN extraction and d-SPE with zirconium-based sorbent Z-Sep as previously described:[10] (1) weigh 10 g of homogenized sample into a 50 mL polypropylene centrifuge tube; (2) add 1000 ng of internal standards (ISTDs), yields 100 ng/mL; (3) add 10 mL of MeCN and vigorously shake by hand for 30 s; (4) pour the entire extract, including tissue, into another 50 mL centrifuge tube with 4 g of anh $MgSO_4$ and 1 g of NaCl; (5) shake vigorously for 1 min and centrifuge the tube for 2 min at 3250 rcf; (7) take 1 mL of the extract into a mini-cetrifuge 2 mL tube containing 50 mg of Z-Sep and 150 mg of anh $MgSO_4$; (8) shake the tube vigorously for 30 s and centrifuge for 2 min at 3250 rcf; (9) transfer 0.5 mL of the catfish extract into an autosampler vial for GC analysis. For a reagent blank sample, use 5 mL of DI water in place of a tissue. The equivalent tissue concentration per sample extract was 1 g/mL.

Low-Pressure Gas Chromatography/Tandem Mass Spectrometry (LP-GC/MS-MS). An Agilent (Little Falls, DE, USA) 7000B triple−quadrupole mass spectrometer (GC-MS/MS) with electron ionization (EI) high-sensitivity source was interfaced to an Agilent 7890A gas chromatograph operated in low-pressure vacuum outlet mode. The separation was achieved on a 15 m × 0.53 mm × 1 μm film thickness Rti-5 ms GC column connected to a 5 m × 0.18 mm noncoated guard column from Restek (Bellefonte, PA, USA). The calculated virtual column length used for the GC configuration was 5.5 m × 0.18 mm i.d. (vacuum outlet). Ultrahigh-purity helium (He) was used as a carrier gas at a 2 mL/min constant flow rate. At the transfer line the GC column was connected to a ∼17 cm × 0.53 mm i.d. phenyl-methyl deactivated guard column (Restek). Both connections were secured by Ultimate Union column connectors (Agilent). More details on the LP-GC-MS/MS can be found elsewhere.[11,12]

The GC oven temperature program was as follows: 70 °C held for 1.5 min, ramped at 80 °C/min to 180 °C, then ramped at 40 °C/min to 250 °C, followed by 70 °C/min to 290 °C, and held for 4.5 min. The total run time was 10 min. The MSD transfer line was at 250 °C, and the ion source was set at 320 °C. The QqQ collision gas was nitrogen at 1.5 mL/min, and quench gas was He at 2.25 mL/min. EI energy was −70 eV, quadrupole temperatures were set at 150 °C, and the solvent delay was at 2 min. An Agilent Multimode Inlet (MMI) was operated as a programmable temperature vaporizer with solvent vent mode of He flow at 50 mL/min with an injection volume of 5 μL. The MMI temperature program was 70 °C held for 0.31 min (at which point the vent was closed), then ramped to 420 °C at 320 °C/min, and held at 420 °C for the rest of the GC run.

Two multiple reaction monitoring (MRM) transitions and their ratios were used for identification as previously described.[13] The MRM method was divided into 13 time segments with a dwell time of 2.5 ms and the "wide" MS resolution.

Method Evaluation. Five replicates of fortified catfish samples were prepared for each spiking level (1, 5, 50, and 100 ng/g) as described under Sample Preparation. Each batch of samples included a reagent blank and a sample blank (the catfish sample spiked with internal standards only). Matrix-matched calibration standards at concentrations of 0.5, 1, 5, 10, 25, 50, 100, 250, and 400 ng/mL were used to calculate the recoveries of the pesticides. Fenthion-d_6 was used as an ISTD for pesticide quantification, and atrazine-d_5 was used as a back-up ISTD if needed. Method detection limits were determined as the pesticide's lowest calibrated levels (LCL). Visual inspection of

calibration curves and linear regression R^2 values ≥0.99 demonstrated linearity.

NIST standard reference materials (SRMs) 1974b (Organics in Mussel Tissue) and 1947 (Lake Michigan Fish Tissue) with certified/reference values for select pesticides were used to validate the method "trueness" (% accuracy vs the certified value). In the case of SRM 1974b, 10 g of material was extracted as described above. The equivalent tissue concentration per sample extract for SRM 1974b was 1 g/mL. In the case of SRM 1947, 5 g of material was used to prepare the extract, and the equivalent tissue concentration per sample extract was 0.5 g/mL. Five replicates of each SRM were analyzed in the experiment.

RESULTS AND DISCUSSION

In terms of sensitivity, the developed method provided relatively low detection limits −0.5−1 ng/g for all of the pesticides, except cypermethrin, α-endosulfan, iprodione, and resmethrin, for which the detection limits were 5 ng/g (see Table 1). Because the lowest tolerances for pesticides in food are established at 10 ng/g,[7] this method allows pesticide measurement even below tolerance levels and at environmentally relevant concentrations.

Four spiking levels were used to validate the method, and each level was tested in five replicates plus one reagent blank and one sample blank per batch. The calculated average recoveries and standard deviations for the five replicated catfish samples fortified at the four spiking levels are presented in Table 1. For the majority of pesticides, the recoveries were satisfactory, ranging from 70 to 120% for all spiking levels. Chlorothalonil showed highly variable recoveries, with 112% for the 1 ng/g spiking level, and 41, 12, and 19% for the 5, 50, and 100 ng/g spiking levels, respectively. For 21 pesticides, recoveries exceeded 120% (127−149%) at the spiking level close to their detection limit (Table 1, highlighted in bold). On the other hand, phosphamidon (64%) and dicrotophos (52%) recoveries were below 70% at the 1 ng/g spiking level. More uncertainties of quantification are observed at the lowest concentrations close to detection limits.

Method repeatability, expressed in standard deviation for five replicate samples, was satisfactory (<20%) for the majority of pesticides, with the exceptions of diazinon (25%), endosulfan sulfate (23%), and propiconazole (24%) for the 1 ng/g spiking level and simazine (21%) and trifluralin (22%) for the 50 and 100 ng/g spiking levels, respectively.

To show the accuracy of measurements of the developed method, the standard reference materials SRMs 1974b (Organics in Mussel Tissue) and 1947 (Lake Michigan Fish Tissue) with the certified/reference values for the selected pesticides were analyzed. Each SRM was prepared in five replicates as described under Sample Preparation. The measured values were in good agreement with certified values for both of the SRMs (see Tables 2 and 3). For SRM 1947, the average accuracy measured as a percent of the measured concentration versus the certified concentration was acceptable (71−118%) for all 15 pesticides except *trans*-chlordane (136%) and mirex (58%). Relative standard deviations (RSDs) were from 3 to 14%, indicating the method's acceptable repeatability.

For the SRM 1974b, the calculated accuracy for the 11 pesticides was 72−118% for all of the pestcides, except *o,p'*-DDT + *p,p*-DDD (45%) and heptachlor (133%). Heptachlor's certified concentration in SRM 1974B is 0.212 ng/g, which is below its detection limit (0.5 ng/g); however, heptachlor's amount was calculated at 0.282 ng/g in the SRM material. RSDs were acceptable for all pesticides: 4−12% in SRM 1974b.

Table 2. Determined Pesticide Concentrations (Wet Weight Basis) with the Method for SRM 1947, $n = 5$[a]

	certified/reference value (ng/g ± SD)	measured value (ng/g ± SD)	% accuracy (RSD, %)
hexachlorobenzene	7.48 ± 0.66	5.32 ± 0.27	71 (5)
α-HCH	1.06 ± 0.12	1.10 ± 0.15	104 (14)
heptachlor epoxide	13.4 ± 0.8	10.6 ± 0.9	79 (8)
cis-nonachlor	54.1 ± 7.3	49.8 ± 6.5	92 (13)
dieldrin	80.8 ± 3.8	80.8 ± 3.9	100 (5)
mirex	5.09 ± 0.73	2.94 ± 0.27	**58** (9)
o,p-DDE	3.39 ± 0.28	4.01 ± 0.12	118 (3)
p,p-DDE	720 ± 43	800 ± 34	111 (4)
o,p-DDD	3.31 ± 0.16	2.67 ± 0.36	81 (4)
o,p-DDT + *p,p*-DDD	61.6	53.6 ± 2.17	87 (4)
cis-chlordane	49 ± 5.5	53.7 ± 2.9	110 (6)
trans-chlordane	12.8 ± 1.2	17.4 ± 1.5	**136** (6)
trans-nonachlor	127 ± 6	96 ± 9	76 (9)
p,p-DDT	59.5 ± 6.7	57.6 ± 3.6	97 (6)

[a]Recoveries outside the acceptable range (70−120%) are highlighted in bold.

Table 3. Determined Pesticide Concentrations (Wet Weight Basis) with the Method for SRM 1974b, $n = 5$[a]

	certified/reference value (ng/g ± SD)	measured value (ng/g ± SD)	% accuracy (RSD, %)
heptachlor	0.212 ± 0.084	0.282 ± 0.014	**133** (5)
dieldrin	0.62 ± 0.13	0.44 ± 0.04	71 (9)
cis-nonachlor	0.64 ± 0.16	LCL = 1 ng/g	
o,p-DDT + *p,p*-DDD	4.234	1.917 ± 0.121	**45** (6)
o,p-DDE	0.336 ± 0.044	0.236 ± 0.015	71 (5)
p,p-DDE	4.15 ± 0.38	3.13 ± 0.13	75 (4)
o,p-DDD	1.09 ± 0.16	1.01 ± 0.05	92 (5)
cis-chlordane	1.36 ± 0.10	1.51 ± 0.11	111 (7)
trans-chlordane	1.14 ± 0.17	1.32 ± 0.15	115 (12)
trans-nonachlor	1.3 ± 0.14	1.36 ± 0.15	105 (11)

[a]Recoveries outside the acceptable range (70−120%) are highlighted in bold.

SRM 1974b is a mussel sample with total extractable organics (TEO) of 6.3%, which is close to the TEO determined for the catfish samples in this study (5.9%). On the other hand, SRM 1947 is a fish tissue with 10.4% extractable fat. The accuracy of the measurements, achieved by this method, in SRM 1947 with higher TEO, makes it applicable to fish/seafood samples with variable fat content.

Analysis of Catfish Samples from the Market. To demonstrate the applicability of the developed method to real-world samples, it was applied for the analysis of 20 catfish samples from different countries: United States, China, Vietnam, and Cambodia, purchased at supermarkets. Catfish samples were homogenized and prepared as described above. A reagent blank, replicate samples, a matrix spike sample, and SRM samples were included in each batch of samples for quality assurance/control purposes. Residues of dimethoate (ND−8.3 ng/g), hexachlorobenzene (ND−3.7 ng/g), β-BHC and lindane (ND−5.2 ng/g), *cis*-nonachlor (ND−0.6 ng/g), *trans*-nonachlor (ND−2.3 ng/g), chlorpyrifos (ND−2.8 ng/g), trifluralin (ND−35.2 ng/g), *p,p*-DDE (ND−0.8 ng/g), *p,p*-DDD (ND−4.8 ng/g), *o,p*-DDD (ND−1.2 ng/g), *o,p*-DDT and *p,p*-DDD (ND−7.2 ng/g), *cis*-chlordane (ND−2.3 ng/g),

dx.doi.org/10.1021/jf404389e | J. Agric. Food Chem. 2014, 62, 3684−3689

trans-chlordane (ND−1.1 ng/g), and α-BHC (ND−4.1 ng/g) were measured in catfish samples.

Some of the pesticides measured in catfish samples, including DDT and its metabolites DDE and DDD, lindane, hexachlorobenzene, and chlordane, are persistent organochlorine pollutants identified by the Stockholm Convention.[14] These pesticides were banned many years ago, but due to their persistence (for example, DDT's estimated half-life is 20−30 years),[15] they are still being detected today. α-BHC and trifluralin were the most frequently detected pesticide residues measured in fish samples (38% frequency of detection) in concentrations ranging from 1.7 to 4.1 ng/g (α-BHC) and from 1.4 to 35.2 ng/g (trifluralin). Trifluralin had the highest measured concentration among all of the pesticides (35.2 ng/g). Because there are no tolerances established for these pesticides in fish/catfish, it is unclear if the amounts measured in catfish in this study may cause any human health effects for people consuming these fish. For most commodities, such as barley, corn, and wheat, trifluralin's lowest tolerance is 50 ng/g, and the amounts measured in catfish in our study were below this value. For most of the pesticides in fruits and vegetables, the tolerances are established at 10 ng/g, and all of the pesticides in this study, with the exception of trifluralin, were measured in concentrations below 10 ng/g. Chronic exposure to low levels of pesticides, most of which are lipophilic and therefore may accumulate in human fat,[16] is another under investigated area. Therefore, monitoring of trace amounts of pesticides in the imported/exported food supply is important for consumer protection.

In conclusion, a simple and fast analytical method for the simultaneous determination of multiple pesticides was developed and validated. A QuEChERS-based extraction with MeCN allowed for fast and efficient extraction without coextracting significant amounts of fat and lipids. Cleanup with Z-Sep in d-SPE provided significant removal of coextractive materials[10] and excellent recoveries and acceptable SDs for the majority of selected pesticides, even at a low spiking level (1 ng/g), making the method applicable for analysis at environmentally relevant concentrations. The method is simple and fast; a batch of 10 homogenized samples can be prepared within 1 h by a single analyst, and LP-GC/MS-MS provides fast separation of analytes within 9 min. The calculated sample preparation cost is ≈$2.5/sample using bulk materials, and small amounts of organic solvent used for extraction lead to reduced solvent waste and minimal environmental impact. With low detection limits achieved by this method, it can be easily applicable to the analysis of pesticide residues at environmentally relevant concentrations, and the generated data on their occurrence may aid in future risk assessment and regulations.

AUTHOR INFORMATION

Corresponding Author

*E-mail: yelena.sapozhnikova@ars.usda.gov.

Notes

The authors declare no competing financial interest.

Disclaimer: Mention of trade names or commercial products in this publication is solely for the purpose of providing specific information and does not imply recommendation or endorsement by the U.S. Department of Agriculture.

ACKNOWLEDGMENTS

The technical assistance of Tawana Simons and Lucía Geis-Asteggiante is greatly appreciated. We thank Dr. Olga Shimelis (Supelco) for providing Z-Sep sorbent and Jennifer Cassidy and Dr. Kathleen Rajkowski for providing catfish samples.

REFERENCES

(1) USDA. National Agricultural Statistics Service. Catfish processing report, released Feb 21, 2012; http://usda01.library.cornell.edu/usda/nass/CatfProc//2010s/2012/CatfProc-02-21-2012.pdf (accessed July 12, 2012).

(2) USDA National Agricultural Library. Nutrient data laboratory; http://ndb.nal.usda.gov/ndb/foods/show/4673?qlookup=15234&fg=&format=&man=&lfacet=&max=25&new=1 (accessed June 20, 2012).

(3) Weaver, K. L.; Ivester, P.; Chilton, J. A.; Wilson, M. D.; Pandey, P.; Chilton, F. H. The content of favorable and unfavorable polyunsaturated fatty acids found in commonly eaten fish. *J. Am. Diet. Assoc.* **2008**, *108*, 1178−1185.

(4) NOAA Fisheries, Aquaculture, Seafood and Human Health; http://www.nmfs.noaa.gov/aquaculture/faqs/faq_seafood_health.html (accessed Aug 20, 2013).

(5) Cheng, D. X.; Yang, Z. Z.; Wang, X. T.; Sun, Y. Z.; Xu, X. B. Organochlorine pesticides in tissues of catfish (*Silurus asotus*) from Guanting reservoir, People's Republic of China. *Bull. Environ. Contam. Toxicol.* **2006**, *76*, 766−773.

(6) John, P. J.; Prakash, A. Bioaccumulation of pesticides on some organs of freshwater catfish *Mystus vittatus*. *Bull. Environ. Contam. Toxicol.* **2003**, *70*, 1013−1016.

(7) Code of Federal Regulations. Title 40 — protection of environment [40 cfr]. Part 180 — Tolerances and exemptions for pesticide chemical residues in food [40 cfr 180]; http://cfr.regstoday.com/40cfr180.aspx#40_CFR_180p342 (accessed Aug 23, 2013).

(8) Sapozhnikova, Y.; Liebert, D.; Wirth, E.; Fulton, M. Polycyclic musk fragrances in sediments and shrimp tissues. *Polycycl. Arom. Compd.* **2010**, *30*, 298−308.

(9) Saito, K.; Sjödin, A.; Sandau, C. D.; Davis, M. D.; Nakazawa, H.; Matsuki, Y.; Patterson, D. G., Jr. Development of a accelerated solvent extraction and gel permeation chromatography analytical method for measuring persistent organohalogen compounds in adipose and organ tissue analysis. *Chemosphere* **2004**, *57*, 373−381.

(10) Sapozhnikova, Y.; Lehotay, S. J. Multi-class, multi-residue analysis of pesticides, polychlorinated biphenyls, polycyclic aromatic hydrocarbons, polybrominated diphenyl ethers and novel flame retardants in fish using fast, low-pressure gas chromatography−tandem mass spectrometry. *Anal. Chim. Acta* **2013**, *758*, 80−92.

(11) Koesukwiwat, U.; Lehotay, S. J.; Miao, S.; Leepipatpiboon, N. High throughput analysis of 150 pesticides in fruits and vegetables using quechers and low-pressure gas chromatography-time-of-flight mass spectrometry. *J. Chromatogr., A* **2010**, *1217*, 6692−6703.

(12) Mastovska, K.; Hajslova, J.; Lehotay, S. J. Ruggedness and other performance characteristics of low-pressure gas chromatography-mass spectrometry for the fast analysis of multiple pesticide residues in food crops. *J. Chromatogr., A* **2004**, *1054*, 335−349.

(13) Koesukwiwat, U.; Lehotay, S. J.; Leepipatpiboon, N. Fast, low-pressure gas chromatography triple quadrupole tandem mass spectrometry for analysis of 150 pesticide residues in fruits and vegetables. *J. Chromatogr., A* **2011**, *1218*, 7039−7050.

(14) The Stockholm Convention on Persistent Organic Pollutants. United Nations environmental progamme; http://chm.pops.int/Convention/tabid/54/Default.aspx (accessed Aug 9, 2013).

(15) Dimond, J. B.; Owen, R. B. Long-term residue of DDT compounds in forest soils in Maine. *Environ. Pollut.* **1996**, *92*, 227−230.

(16) Sasaki, K.; Ishizaka, T.; Suzuki, T.; Takeda, M.; Uchiyama, M. Accumulation levels of organochlorine pesticides in human adipose tissue and blood. *Bull. Environ. Contam. Toxicol.* **1991**, *46*, 662−669.

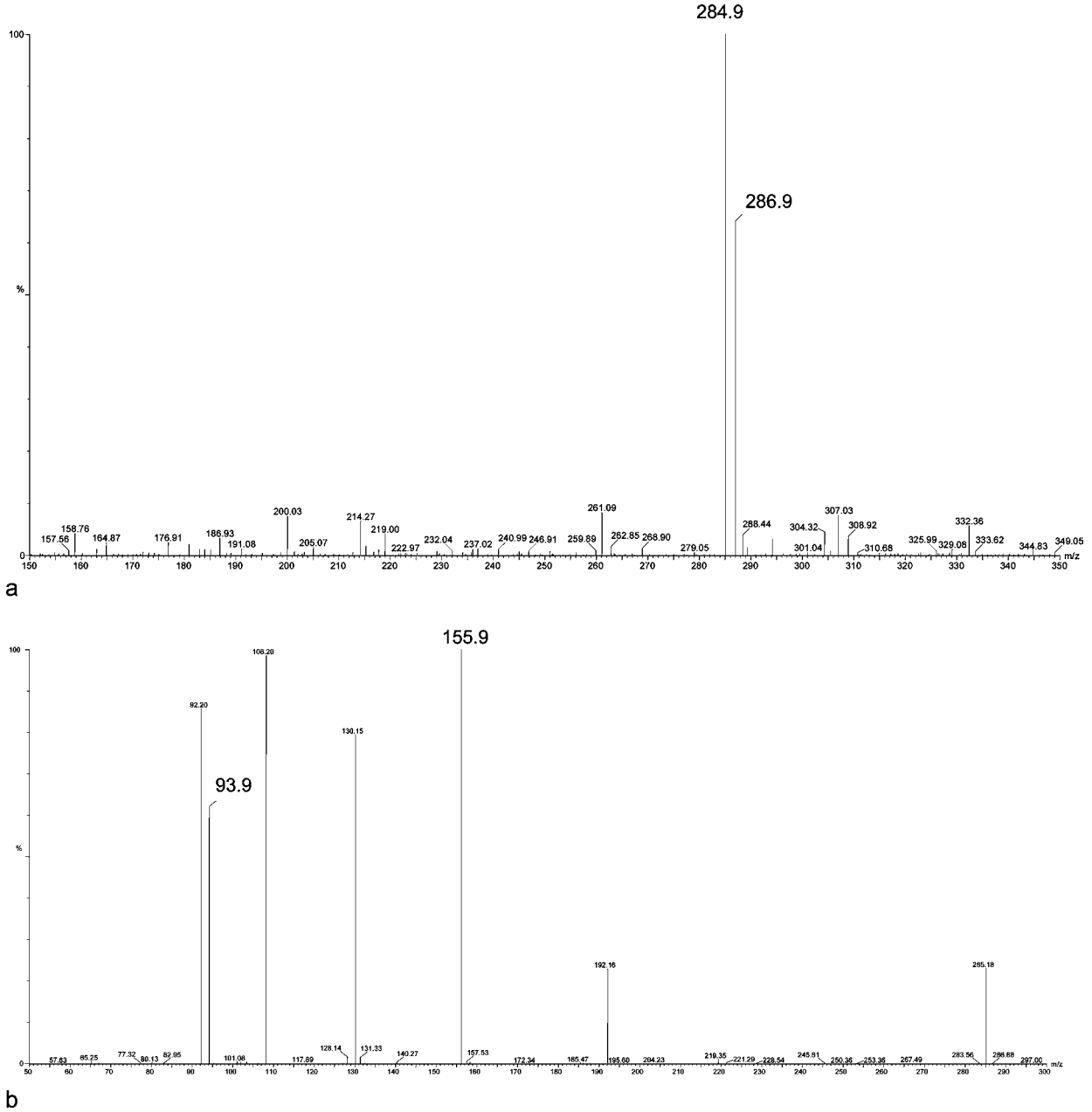

Figure 1. (a) Sulfaclozine full scan MS; (b) sulfaclozine MS/MS.

MATERIALS AND METHODS

Chemicals and Materials. Enrofloxacin (EFC), tilmicosin (TLS), trimethoprim (TMP), sulfaclozine (SCZ), sulfamethoxazole (SMX), and sulfaquinoxaline (SQX) standards were purchased from Sigma-Aldrich (St. Louis, MO, USA). Methanol and acetonitrile were purchased from J. T. Baker (Phillipsburgh, NJ, USA). NaCl was purchased from Fisher Scientific (Worcester, MA, USA). Nitrogen was purchased from Airgas (Malvern, PA, USA). All deionized water was prepared using a Barnstead Nanopure II (Dubuque, IA, USA). The large-capacity mixer was purchased from Glas-Col (Terre Haute, IN, USA). The 0.2 μm nylon filters were purchased from Whatman (Florham Park, NJ, USA). The TurboVap liquid concentrator was purchased from Biotage (Charlotte, NC, USA). The centrifuge was purchased from Thermo Scientific (Waltham, MA, USA). Disposable centrifuge tubes, monoject 3 mL luer lock syringes, autosampler vials, and Kuderna–Danish concentrator tubes were purchased from Krackeler Scientific (Albany, NY, USA).

Standard Preparation. All individual standard solutions were prepared by dissolving the appropriate amount of neat standard in methanol, and each stock standard was prepared to a 100 μg/mL solution. A 1 μg/mL mixed standard solution was prepared by mixing 1 mL of each of the six standards into 100 mL of methanol, which was further diluted to a 0.1 μg/mL solution. Five levels of matrix-matched working standards were prepared by diluting the 0.1 μg/mL mix solution with extracted matrix of antibiotic-free chicken jerky. A 15 ng/mL standard was prepared by adding 850 μL of matrix and 150 μL of 0.1 ug/mL mix solution. A 11.25 ng/mL standard was prepared by adding 100 μL of matrix and 300 μL of the 15 ng/mL standard. A 7.5 ng/mL standard was generated by adding 100 μL of matrix and 100 μL of 15 ng/mL standard. A 3.75 ng/mL standard was prepared by adding 300 μL of matrix and 100 μL of 15 ng/mL standard. A 1.5 ng/mL standard was prepared by adding 360 μL of matrix and 40 μL of 15 ng/mL standard.

Sample Preparation/Extraction. Each chicken jerky strip was designated a subsample of the container from which it was taken. The entire jerky treat strip was ground using a Retch grinding mill equipped with a 0.75 mm screen set at a speed of 12000 rpm. The ground sample

dx.doi.org/10.1021/jf405458m | J. Agric. Food Chem. 2014, 62, 3690−3696

Table 1. Instrument Conditions for MS/MS Analysis of Six Antibiotics[a]

analyte	MW	RT	transition	cone V	collision energy	dwell
enrofloxacin	359.4	3.10	360.0 → 316.3	40	20	0.1
			360.0 → 245.2	40	20	0.1
sulfaclozine	84.7	4.17	284.9 → 155.9	35	18	0.1
			284.9 → 93.9	35	15	0.1
sulfaquinoxaline	300.37	4.41	300.9 → 108.2	35	30	0.1
			300.9 → 156.1	35	15	0.1
trimethoprim	290.32	6.02	291.1 → 123	45	27	0.1
			291.1 → 230.1	45	25	0.1
tilmicosin	869.13	3.98	869.4 → 696.4	90	45	45
			869.4 → 174.1	90	45	0.1
sulfamethoxazole	253.28	3.49	253.9 → 156.1	35	15	0.1
			253.9 → 92.2	35	30	0.1

[a]All compounds ESI+, MRM.

was then placed in a 50 mL polypropylene centrifuge tube. To extract all six of the antibiotics, two extractions were used.

Extraction 1 (for the extraction of sulfamethoxazole, enrofloxacin, trimethoprim and tilmicosin): weigh 1.0 g of ground sample into a disposable 50 mL polyprolylene centrifuge tube and record the weight to 0.001 g; add spikes; add 5.0 mL of deionized water and mix using a mixer at high speed for 5 min; add 10 mL of acetonitrile and mix well using a mixer at high speed for 20 min; add 2 g of NaCl and mix well using a mixer for 5 min; centrifuge at 3000 rpm for 10 min; transfer a 5.0 mL aliquot of supernatant into a 10 mL graduated concentrator tube; concentrate to between 0.2 and 0.1 mL under nitrogen using a turbovap liquid concentrator; add deionized water to the 1.0 mL level and mix well using a mixer at high speed; filter through a 0.2 μm luer lock disk filter using a disposable monoject lock syringe directly into a 2 mL autosampler vial; analyze by UPLC-MS/MS.

Extraction 2 (for the extraction of sulfaclozine and sulfaquinoxaline): weigh 1.0 g of ground sample into a disposable 50 mL polyprolylene centrifuge tube and record the weight to 0.001 g; add spikes; add 5.0 mL of deionized water and mix using a mixer at high speed for 5 min; add 10 mL of acetonitrile and mix well using a mixer at high speed for 20 min; add 2 g of NaCl and mix well using a mixer for 5 min; centrifuge at 3000 rpm for 10 min; transfer a 5.0 mL aliquot of supernatant into a 10 mL graduated concentrator tube; concentrate to 0.3 mL under nitrogen using a turbovap liquid concentrator; add deionized water to the 1.0 mL level and mix well using a mixer at high speed; filter through a 0.2 μm luer lock disk filter using a disposable monoject lock syringe directly into a 2 mL autosampler vial; analyze by UPLC-MS/MS.

Method Validation. The method was validated by determining limits of detection and limits of quantitation and evaluating the results of various levels of spikes. The LOD was determined by obtaining a chicken jerky sample that was free of any of the antibiotics and spiking it at 1.0 ng/g in duplicate. The resulting response of each parent daughter transition was determined to be at least 3 times that of the accompanying noise. Additionally, the ratio of the quantitation ion to the qualifier ion was calculated and compared to that of the standard. The measured ratios of the sample must agree with that of the standard within 15% for an identification to be made. Also, the retention time of an analyte in a sample must match that of the standard within 5%. The LOQ was determined to be 3 times the LOD or 3.0 ng/g. Antibiotic-free chicken jerky was spiked at LOQ (1.0 ng/G), 5 × LOQ (15 ng/g), and 10 × LOQ (30 ng/g). Each spike level was extracted and analyzed three times, and recoveries were calculated.

UPLC-MS/MS Conditions. Liquid chromatographic separation was performed using a Water Acquity UPLC binary pump, column heater, in-line degasser, and autosampler. The UPLC system was coupled to a Waters Quattro Premier XE triple-quadrupole mass spectrometer. Samples were held at 15 °C in the autosampler. The analytical column was an Acquity BEH C18, 1.0 × 100 mm, with 1.7 μm particle size. Mobile phase A consisted of 0.15% acetic acid in deionized water, and mobile phase B was 0.15% acetic acid in acetonitrile. For method 1 (sulfaclozine and sulfquinoxaline) the initial UPLC conditions were 90% A and 10% B and were held constant for 2.0 min. From 2.0 to 8.2 min, the gradient was changed from 90% A−10% B to 2% A−98% B. At this point the mobile phase was returned to the initial conditions and held for 3.8 min. For method 2 (sulfamethoxazole, enrofloxacin, trimethoprim, and tilmicosin) the initial UPLC conditions were 96% A and 4% B and were constant for 2.0 min. From 2.0 to 8.2 min, the gradient was changed from 96% A−4% B to 2% A−98% B. At this point the mobile phase was returned to the initial conditions and held for 3.8 min. For both methods the flow rate was held at 0.13 mL/min, the injection volume was 10 μL, and the column was held at 65 °C throughout the chromatographic run.

RESULTS AND DISCUSSION

UPLC-MS/MS Conditions. Infusion experiments of all analytes yielded strong protonated molecular ions [M + 1] in full scan ESI. In all cases this ion was used as the precursor, and fragmentation produced at least two products. For confirmational purposes two product ions were chosen to monitor in multiple reaction monitoring (MRM) mode. Most product ions have been previously reported with the exception of sulfaclozine, which has not been studied extensively.[14,16,17,21] ESI+ ionization of sulfaclozine produced strong signals at m/z 284.9 along with the corresponding A + 2 isotope (Figure 1). Fragmentation of m/z 284.9 yields several products including m/z 93.9 and 155.9 (b). Both of these products have been previously reported for other sulfonamides, indicating a fragmentation pattern common to this class.[14,22] Although most analytes in this study generated several abundant fragmentation products, many times the matrix being studied can influence the choice. In the case of sulfaclozine, although 284.9 → 155.9 and 284.9 → 93.9 were not the most abundant products observed during infusion, they were affected to the least extent by the matrix after extraction. In a similar way two transitions were determined for sulfaquinoxaline, sulfamethoxazole, enrofloxacin, trimethoprim, and tilmicosin (Table 1).

Various chromatographic conditions were evaluated to optimize peak shape and signal strength. All six analytes

Table 2. Recovery Efficiencies for All Six Antibiotics in Chicken Jerky Treats

	ave % recovery (n = 3)						
	LOQ	5 × LOQ	10 × LOQ	overall % recovery av	correl coeff	20 point SD	20 point av
enrofloxacin	49.7	67.7	60.7	59.4	0.99748	12.84	49.3
sulfaclozine	125.0	92.3	95.0	104.1	0.99949	27.91	76.0
sulfaquinoxaline	125.3	81.0	96.3	100.9	0.99987	29.54	70.2
trimethoprim	54.7	55.7	59.7	56.7	0.99997	12.73	61.4
tilmicosin	67.3	94.0	100.3	87.2	0.99702	23.07	68.2
sulfamethoxazole	68.7	60.0	63.0	63.9	0.99628	20.26	64.7

performed best using a mobile phase of A = 0.15% acetic acid and B = 0.15% acetic acid in acetonitrile. Unfortunately, due to differences in water solubility, trimethoprim and tilmicosin produced optimal peak shape with initial conditions of A = 96%, whereas sulfaclozine, sulfaquinoxaline, sulfamethoxazole, and enrofloxacin performed best with mobile phase A beginning at 90%. Because of this, two injections were made per sample.

Sample Preparation and Extraction. This investigation into the possibility of an unknown contaminant was unusual in that it appeared not every animal that consumed the chicken jerky became ill. If the suspect products were the cause of the illnesses, this would mean that either not every one of these products contained the contaminant or that not every animal was susceptible to becoming ill from the contaminant. To minimize the possibility that hot spots of contamination would be diluted to the point of not being detectable, each chicken jerky treat was homogenized separately as opposed to many treats being homogenized and combined as one sample.

The use of acetonitrile led to good recovery of the six analytes; however, there were slight differences in recovery depending on the final concentration procedure. Sulfaclozine and sulfaquinoxaline were found to recover better when the final concentration step was ended at 0.3 mL, whereas the remaining analytes were extracted more efficiently when concentrated to between 0.2 and 0.1 mL.

Matrix-induced signal suppression was corrected with the use of matrix-matched external standards. This was accomplished by extracting chicken jerky that was found to be free of analytes and diluting the standard mix in the extract. A five-point curve was generated for each analyte from 1.5 to 15 ng/mL, and samples found to contain analytes greater than the highest level were diluted and reanalyzed.

Method Validation. The LOD for all analytes was determined to be 1.0 ng/g through spiking experiments. This is lowest concentration at which an analyte produces well-resolved peaks at least 3 times the signal-to-noise for both transitions and can pass the confirmation criteria. The confirmation criteria include matching the retention time of that of a standard within 5% and matching the ion ratio of a standard within 15%. Results of LOQ, 5 × LOQ, and 10 × LOQ spikes are presented in Table 2. Recovery efficiencies for all compounds were between 50 and 100%, although enrofloxacin and trimethoprim were below 60%. Efforts were made to improve these recovery efficiencies including extending the time the sample is mixed in acetonitrile and sonication during this step without success. The 20-point average recovery and standard deviation in Table 2 refers to the QC results that accompanied the last 20 sample sets analyzed. These results show somewhat lower recoveries and several standard deviations above 20%. This may be due to the variation in sample type as more products were analyzed for these compounds. A five-point matrix-matched external calibration curve was used for the quantification of all analytes. Good linearity was seen for all compounds, and acceptability was measured by correlation coefficient being >0.995 (Figure 2).

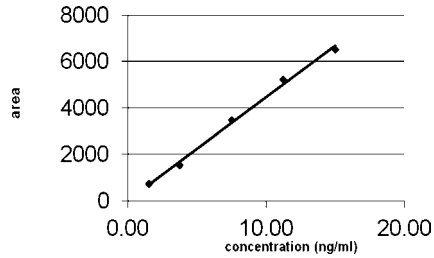

Figure 2. Sulfaclozine calibration curve.

Sample Results. Figure 3 shows typical chromatograms from each analyte found in a sample (a), a standard (b), and a blank chicken jerky (c). The selected transitions for all analytes provided well-resolved peaks and did not suffer from matrix interferences.

Chicken jerky dog treats are typically sold in bags containing from 10 to 60 individual treats. As previously described, each treat was individually ground using a Retch grinding mill and are given a sample number, which denotes it is one of a given number of treats from a given bag. In this way we can determine the homogeneity of antibiotic contamination and identify high and low concentrations of the analytes. A summary of the results is presented in Table 3. Over 800 samples of various types of dog treats have been analyzed using this method. The sample type with the most detections of antibiotics and the highest concentration of antibiotics is chicken jerky. Sulfaclozine was found the most frequently in this sample type (30% of samples) and was found at the highest concentration (2873 ng/g). Sulfaquinoxaline was the second most frequently detected antibiotic and is the only compound evaluated in this study with an FDA tolerance. The U.S. Code of Federal Regulations, Title 21 chapter I, section 556.685, indicates a 100 ng/g tolerance for sulfaquinoxaline in chicken. This tolerance was exceeded in several chicken jerky samples, with the highest concentration found at 828 ng/g. Sulfaclozine, sulfamethoxazole, enrofloxacin, trimethoprim, and tilmicosin are not allowed in chicken at any level. The chicken-based treats indicated in Table 3 refer to treats that contained ingredients other than chicken but seemed to have chicken as a main component. These treats had many fewer antibiotic detects as well as lower concentrations of analytes. Salmon- and duck-based treats had the lowest percentage of detects, with only sulfaquinoxaline detected in 3% of these samples.

Analyzing each jerky treat individually allowed for the observation of differences between each strip within one bag within each bag. Our analysis shows that some treats contain

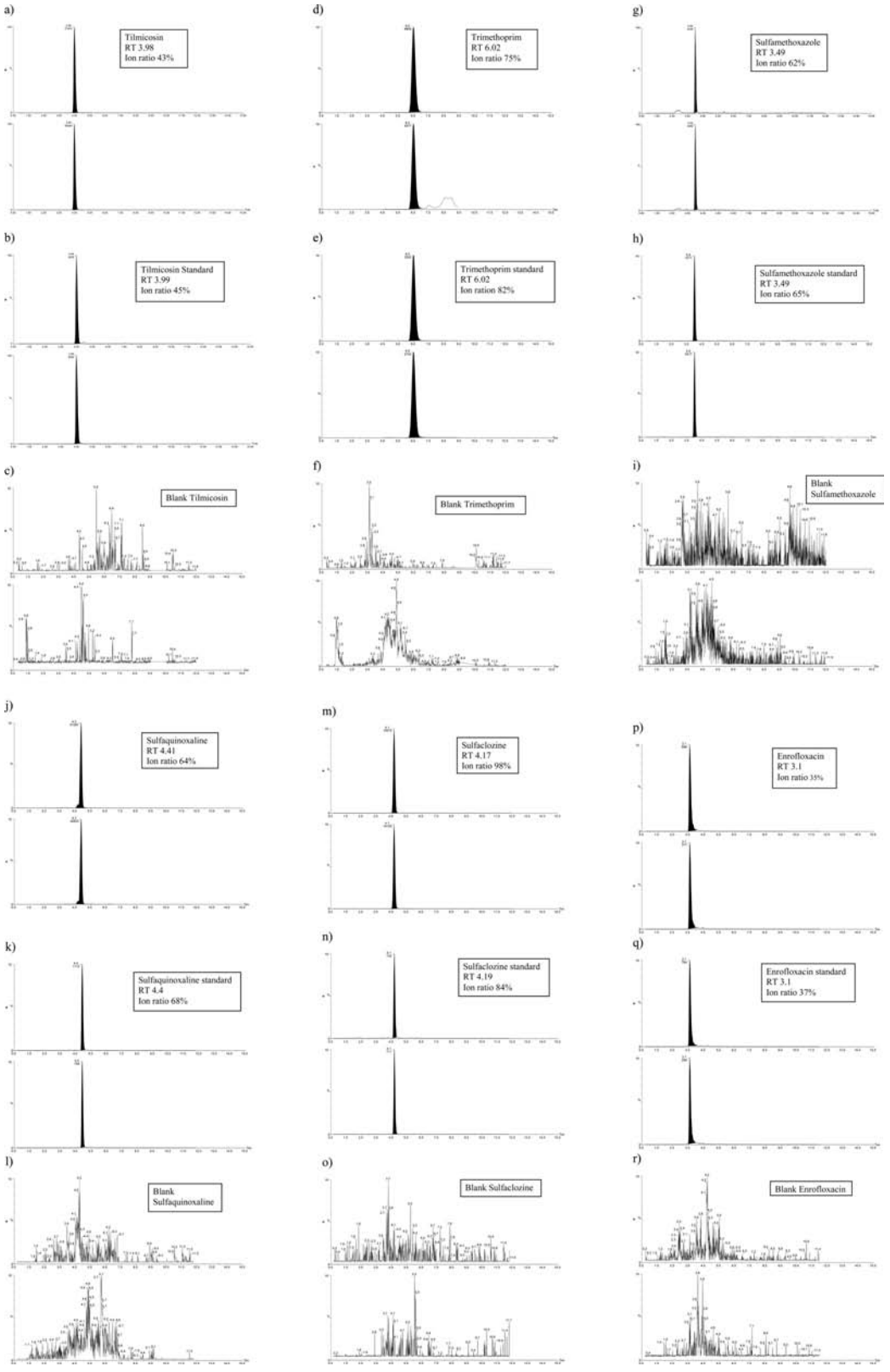

Figure 3. Chromatograms of incurred TLS (a), TLS standard (b), blank TLS (c), incurred TMP (d), TMP standard (e), blank TMP (f), incurred SMX (g), SMX standard (h), blank SMX (i), incurred SQX (j), SQX standard (k), blank SQX (l), incurred SCZ (m), SCZ standard (n), blank SCZ (o), incurred EFC (p), EFC standard (q), and blank EFC (r).

much higher levels of antibiotic residues than other treats from the same bag. Table 4 shows the results of two bags of chicken jerky treats where 10 treats were analyzed from bag 1 and 4 were analyzed from bag 2. Whereas tilmicosin was detected in all samples from this bag, the concentration found in treat 10 was >40 times higher than was found in the other 9 treats. Three antibiotics were detected in all four treats from bag 2; however, two of the four treats had 100 times as much sulfaclozine and

dx.doi.org/10.1021/jf405458m | J. Agric. Food Chem. 2014, 62, 3690−3696

Table 3. Analysis Results from 805 Dog Treat Samples

	no. of chicken jerky samples: 494			no. of chicken-based treats: 221			no. of salmon/duck-based treats: 90		
analyte	total >LOQ	highest concn (ng/g)	sample	total >LOQ	highest concn (ng/g)	sample	total >LOQ	highest concn (ng/g)	sample
sulfaclozine	147	2873.3	13c00286-2	11	20.67	13c00096-10	0	0	
sulfaquinoxaline	66	828	12c03337-2	3	6.41	13c00096-8	3	11.92	13c00287-1
enrofloxacin	23	132	12c02709-2	13	47.09	13c00096-7	0	0	
sulfamethoxazole	7	5.48	12c03248-6	0	0		0	0	
tilmicosin	49	483	12c03249-10	2	3.93	13c00096-4	0	0	
trimethoprim	0	<3		10	41	12c02249-1	0	0	

Table 4. Analysis Results of 10 Chicken Jerky Samples from Bag 1 and 4 Samples from Bag 2

bag 1			bag 2		
treat	analyte	concn (ng/g)	treat	analyte	concn (ng/g)
1	tilmicosin	9.9	1	sulfaclozine	3.5
2	tilmicosin	4.3		sulfaquinoxaline	7.5
3	tilmicosin	nd		sulfaquinoxaline	<3
4	tilmicosin	3.3			
5	tilmicosin	5.6	2	sulfaclozine	751
6	tilmicosin	8.5		sulfaquinoxaline	828
7	tilmicosin	<3		enrofloxacin	<3
8	tilmicosin	<3			
9	tilmicosin	nd	3	sulfaclozine	728
10	tilmicosin	438		sulfaquinoxaline	815
				enrofloxacin	<3
			4	sulfaclozine	12
				sulfaquinoxaline	12
				Enrofloxacin	<3

sulfaquinoxaline as the other two treats did. These differences indicate that there are hot spots of high concentrations of antibiotic residues within bags of treats. This illustrates the differences that can occur between individual pieces of a product of this type. Analyzing a small number of treats from a given bag or homogenizing all of the contents from a bag would not identify these differences or detect highly contaminated individual pieces.

A method for the detection of six antibiotics in chicken jerky treats was developed and applied to the analysis of retail samples. The analysis of >800 samples indicated that these antibiotics were consistently present in chicken jerky treats imported from China. In addition, the levels found were above the U.S. FDA tolerance. Whereas there is currently no evidence indicating the presence of these antibiotics is related to the illnesses and deaths of dogs, their presence in food or animal feed is not allowed in most countries including the United States, Canada, and the European Union.

AUTHOR INFORMATION

Corresponding Author

*(R.S.) Phone: (518) 457-8885. Fax: (518) 485-8097. E-mail: Robert.sheridan@agriculture.ny.gov.

Notes

The authors declare no competing financial interest.

REFERENCES

(1) U.S. Food and Drug Administration. www.fda.gov/animalveterinary/newsevents/cvmupdates/ucm280586.htm (accessed Oct 15, 2013).

(2) U.S. Food and Drug Administration. http://www.fda.gov/animalveterinary/safetyhealth/productsafetyinformation/ucm295445.htm (accessed Oct 15, 2013)

(3) Barbier, O.; Jacquillet, G.; Tauc, M.; Cougnon, M.; Poujeol, P. Effect of heavy metals on, and handling by, the kidney. *Nephron Physiol.* **2005**, *99*, 105−10.

(4) Izzedine, H.; Launay-Vacher, V.; Isnard-Bagnis, C.; Deray, G. Drug-induced Fanconi's syndrome. *Am. J. Kidney Dis.* **2003**, *41*, 292−309.

(5) Watanabe, T.; Yoshikawa, H.; Yamazaki, S.; Abe, Y.; Abe, T. Secondary renal Fanconi syndrome caused by valproate therapy. *Pediatr. Nephrol.* **2005**, *20*, 814−817.

(6) Chan, J.; Yang, A.; Kao, K.; Tarng, D. Acquired Fanconi syndrome induced by mixed Chinese herbs presenting as proximal muscle weakness. *J. Chin. Med. Assoc.* **2004**, *67*, 193−196.

(7) Kapitsinou, P. P.; Ansari, N. Acute renal failure in an AIDS patient on tenofovir: a case report. *J. Med. Case Rep.* 2008, *2*, http://www.jmedicalcasereports.com/content/2/1/94 (accessed Oct 15, 2013).

(8) Khosrokhavar, R.; Hosseini, M.; Amini, M.; Pirali-Hamedani, M.; Ghazi-Khansari, M.; Bakhtiarian, A. Validation of an analytical methodology for determination of oxytetracycline residue in milk by HPLC with UV detection. *Toxicol. Mech. Methods* **2008**, *18*, 351−354.

(9) Paige, J. C.; Tollefson, L.; Miller, M. A. Health implications of residues of veterinary drugs and chemicals in animal tissue. *Vet. Clin. North Am. Food Anim. Pract.* **1999**, *15*, 31−43.

(10) Al-Mustafa, Z.; Al-Ghamdi, M. Use of norfloxacin in poultry production in the eastern province of Saudi Arabia and its possible impact on public health. *Int. J. Environ. Health Res.* **2000**, *10*, 291−299.

(11) Apata, D. F. The emergence of antibiotics resistance and utilization of probiotics for poultry production. *Sci. J. Microbiol.* **2012**, *2*, 8−13.

(12) Randall, L. P.; Ridley, A. M.; Cooles, S. M.; Sharma, M.; Sayers, A. R.; Pumbwe, L.; Newell, D. G.; Piddock, L. J. V.; Woodward, M. J. Prevalance of multiple antibiotic resistance in 443 *Campylobacter* spp. isolated from humans and animals. *J. Antimicrob. Chemother.* **2003**, *52*, 507−510.

(13) Stobberingh, E.; van den Bogaard, A.; London, N.; Driessen, C.; Top, J.; Willems, R. Enterococci with glycopeptide resistance in turkeys, turkey farmers, turkey slaughterers, and (sub)urban residents in the south of The Netherlands: evidence for transmission of vancomycin resistance from animals to humans? *Antimicrob. Agents Chemother.* **1993**, *43*, 2215−2221.

(14) Yu, H.; Tao, Y.; Chen, D.; Wang, Y.; Huang, L.; Peng, D.; Dai, M.; Liu, Z.; Wang, X.; Yuan, Z. Development of a high performance liquid chromatography method and a liquid chromatography-tandem mass spectrometry method with the pressurized liquid extraction for the quantification and confirmation of sulfonamides in the foods of animal origin. *J. Chromatogr., B* **2001**, *879*, 2653−2662.

(15) Tang, H. P.; Ho, C.; Lai, S. S. High-throughput screening for multi-class veterinary drug residues in animal muscle using liquid chromatography/tandem mass spectrometry with on-line solid-phase extraction. *Rapid Commun. Mass Spectrom.* **2006**, *20*, 2565−2572.

(16) Wang, J. Determination of five macrolide antibiotic residues in honey by LC-ESI-MS and LC-ESI-MS/MS. *J. Agric. Food Chem.* **2004**, *52*, 171−181.

(17) Kiehl, D. E.; Kennington, A. S. Analysis of tilmicosin in swine liver extracts by liquid chromatography/atmospheric pressure chemical ionization mass spectrometry. *Rapid Commun. Mass Spectrom.* **1995**, *9*, 1297−1301.
(18) Herrera, M.; Ding, H.; McClanahan, R.; Owens, J. G.; Hunter, R. P. Quantitative determination of tilmicosin in canine serum by high performance liquid chromatography-tandem mass spectrometry. *J. Chromatogr., B* **2007**, *857*, 9−14.
(19) Dubois, M.; Fluchard, E.; Sior, E.; Delahaut, Ph. Identification and quantification of five macrolide antibiotics in several tissues, eggs and milk by liquid chromatography-electrospray tandem mass spectrometry. *J. Chromatogr., B* **2001**, *753*, 189−202.
(20) Wang, J.; Leung, D. Analyses of macrolide antibiotic residues in eggs, raw milk, and honey using both ultra-performance liquid chromatography/quadrupole time-of-flight mass spectrometry and high-performance liquid chromatography/tandem mass spectrometry. *Rapid Commun. Mass Spectrom.* **2007**, *21*, 3213−3222.
(21) Wei, R.; Ge, F.; Chen, M.; Wang, R. Occurrence of ciprofloxacin, enrofloxacin, florfenicol in animal wastewater and water resources. *J. Environ. Qual.* **2012**, *41*, 1481−1486.
(22) Hou, X.; Wu, Y.; Yang, T.; Du, X. Multi-walled carbon nanotubes-dispersive solid-phase extraction combined with liquid chromatography-tandem mass spectrometry for the analysis of 18 sulfonamides in pork. *J. Chromatogr., B* **2013**, *929*, 107−115.

extraction procedure detailed below. Calibration standards were prepared daily for each matrix type.

Samples. Apple samples from the 2013 growing season, which either had no wax coating or had a morpholine-free coating, were provided by local growers. Whole citrus samples from the 2012 and 2013 growing seasons were provided by the USDA-IR4 program and had no coatings. All samples at the Trace Analytical Laboratory (TAL, UC Davis, CA, USA) facility were homogenized in the presence of dry ice using a Blixer food processor (Robot-Coupe USA, Inc.). Each chopped sample was stored in a labeled jar (approximately 1 L), and a lined lid was loosely closed on top to allow the dry ice to sublime during storage at −20 °C. All samples at the Pacific Agricultural Laboratory (PAL, Portland, OR, USA) facility were homogenized fresh using a Blendtec high-speed blender.

Extraction. Fifteen grams of homogenized sample was weighed into a 50 mL polypropylene centrifuge tube, and water (1.4−2.4 mL) was added to yield 15 mL of total water based on moisture content of commodity.[11] The addition of water aids in the extraction of morpholine. Recovery samples were fortified at this point, and 15 mL of 1% acetic acid in methanol was added to the tube. A ceramic homogenizer was added to each tube and shaken vigorously for 1 min by hand or using a mechanical shaker at 1000 strokes/min (Geno/Grinder, model 2010, SPEX CertiPrep). Following extraction, the sample tubes were centrifuged at 4000 rpm for 5 min. The supernatant was poured off into clean culture tubes and stored at ∼5 °C prior to analysis. Typically, the extracts were stored for no more than 2 days. An aliquot of the extract was then diluted 1:5 with 20 mM ammonium formate in 60:40 water/MeCN (v/v, adjusted to pH 3.5 with formic acid) and filtered through a 0.2 μm PTFE syringe filter (VWR International) before it was submitted for LC-MS/MS analysis.

Sample Analysis. At the PAL facility, sample analysis was conducted using a Waters Acquity UHPLC system (binary) coupled to a Waters Xevo tandem mass spectrometer via electrospray ionization (ESI). The TAL facility utilized an Agilent 1200 series binary LC coupled to an Agilent 6430 tandem mass spectrometer equipped with ESI. See Table 1 for instrument-specific conditions.

Table 1. Mass Spectrometer Instrument Parameters

parameter	Waters Xevo	Agilent 6430
source temperature	150 °C	300 °C
desolvation temperature	450 °C	N/A
source gas flow (N_2)	800 L/h	11.5 L/min
cone/nebulizer gas flow (N_2)	5 L/h	50 psi
capillary voltage	1000 V	1000 V
collision gas	Ar (0.11 mL/min)	N_2 (8 mTorr)
morpholine primary transition	88.1 → 70.1[a]	88.1 → 70.1
morpholine secondary transition	88.1 → 42.1[b]	88.1 → 42.1
frag/collision energy (primary)	30/12	40/14
frag/collision energy (secondary)	30/12	40/22
ion ratio 42.1/70.1	20 ± 10%	40 ± 10%

[a]Proposed collision-induced dissociation: $[M + H]^+$ → loss of water (18). [b]Proposed collision-induced dissociation: $[M + H]^+$ → loss of $HOCH_2CH_3$ (46).

Chromatographic separation was accomplished with a SIELC Technologies hydrophilic interaction (HILIC) Primesep-A column (100 × 2.1 mm i.d., 5.0 μm particle size,). The PAL system utilized a column heater, which held the analytical column at 45 °C, whereas the TAL system was operated at ambient temperature (∼25 °C). The mobile phase was operated in isocratic mode with a composition of 20 mM ammonium formate in 60:40 water/MeCN (adjusted to pH 3.5 with formic acid) at 0.50 mL/min (TAL) and 0.55 mL/min (PAL). Following the completion of the analytical set, the column was flushed with 20 mM ammonium formate and then MeCN to remove accumulated matrix. Injection volume was 10 μL. Morpholine residues were quantified using a linear standard curve method with $1/x$ weighting. Typically, the primary transition was used for quantitation, and the secondary transition and ion ratio were used for compound confirmation.

Table 2. Morpholine Residue Recoveries (Percent) in Apples and Citrus

	fortification level[a]			
commodity	0.01 μg/g	0.04 μg/g	0.2 μg/g	calcd MDL[b] (μg/g)
TAL Testing Facility				
apple	104 ± 6	100 ± 2	107 ± 1	0.0018
orange	106 ± 5	101 ± 2	107 ± 3	0.0015
lemon	104 ± 3	102 ± 1	107 ± 1	0.0010
grapefruit	103 ± 3	102 ± 2	109 ± 2	0.0010
PAL Testing Facility				
apple	108 ± 13	104 ± 2	94 ± 4	0.0040
orange	92 ± 11	92 ± 2	92 ± 3	0.0034

[a]Replication for each fortification level, $n = 7$. [b]Calculated MDL: standard deviation at 0.01 μg/g fortification level × 3.143 (Student t_{99} $(n - 1)$).

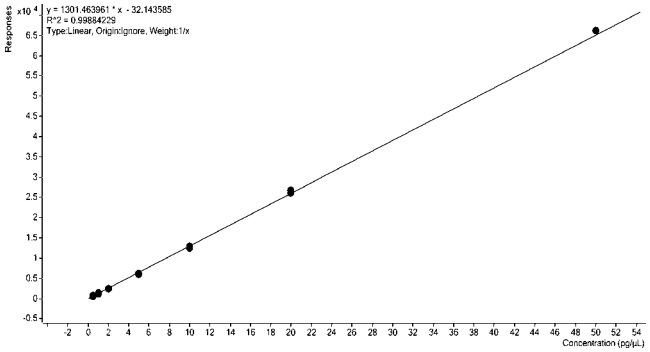

Figure 2. Example standard curve of apple matrix-matched calibration standards from Agilent 6430.

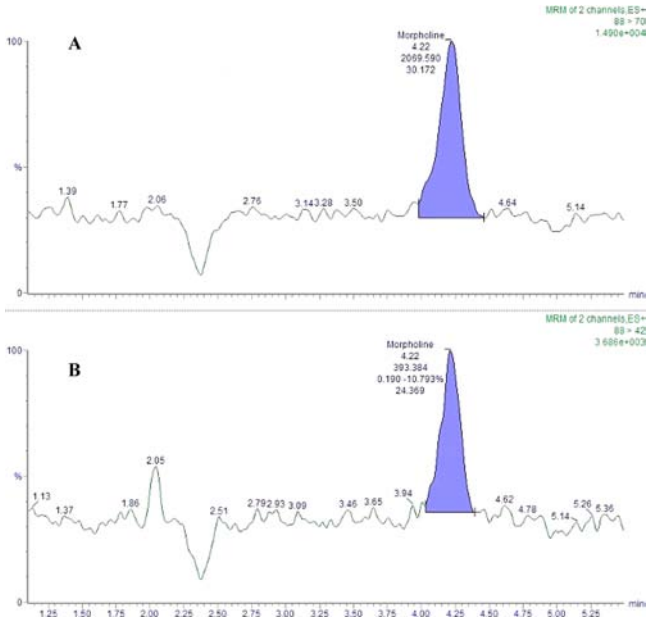

Figure 3. Extracted ion chromatograms of 1 pg/μL (equivalent to 0.01 μg/g) calibration standard from Waters Xevo: (A) MRM transition 88 → 70; (B) MRM transition 88 → 42.

RESULTS AND DISCUSSION

Method Development. During the initial phases of method development, one of the main goals was to have a very simple and rapid sample workup that could provide a target limit of quanititation (LOQ) of 0.01 μg/g. This target

dx.doi.org/10.1021/jf500734b | J. Agric. Food Chem. 2014, 62, 3697−3701

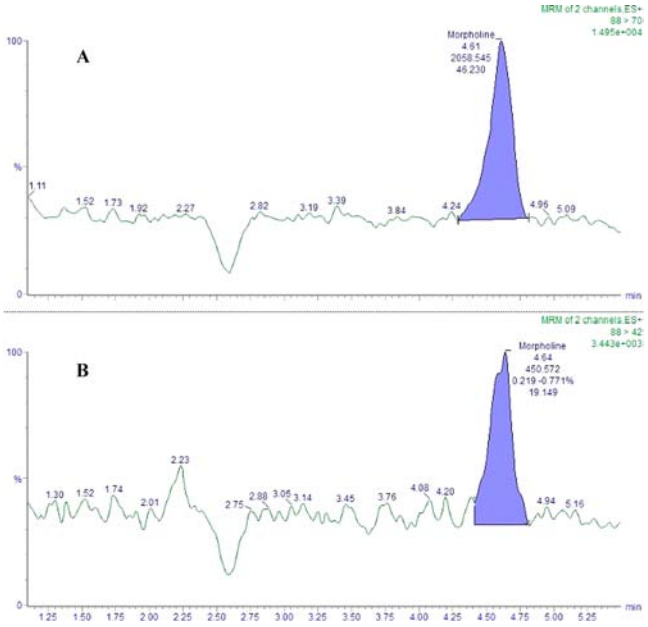

Figure 4. Extracted ion chromatograms of apple control sample fortified at 0.01 μg/g from Waters Xevo: (A) MRM transition 88 → 70; (B) MRM transition 88 → 42.

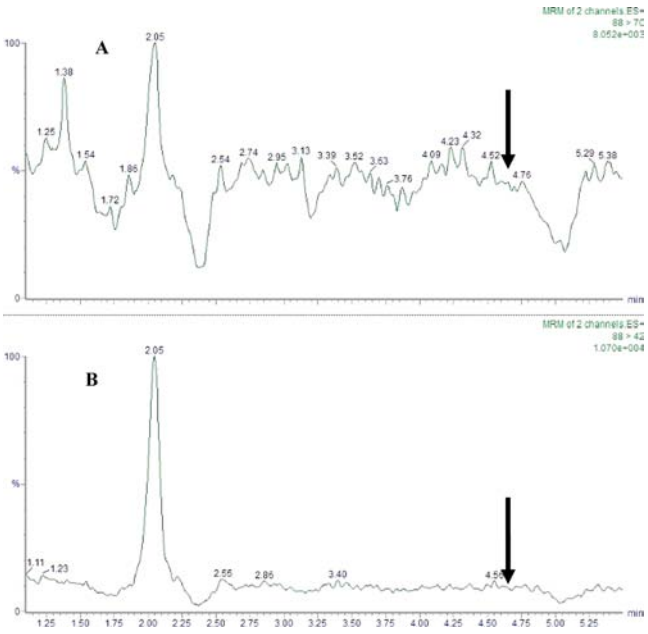

Figure 5. Extracted ion chromatograms of apple control sample from Waters Xevo: (A) MRM transition 88 → 70; (B) MRM transition 88 → 42.

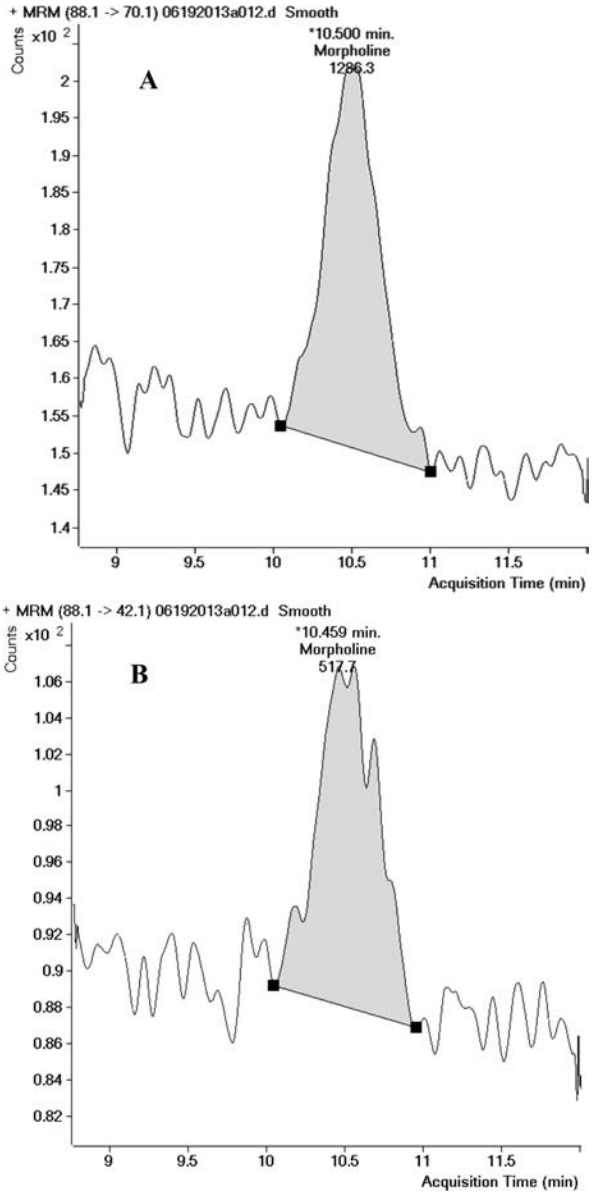

Figure 6. Extracted ion chromatograms of 1 pg/μL (equivalent to 0.01 μg/g) calibration standard from Agilent 6430: (A) MRM transition 88 → 70; (B) MRM transition 88 → 42.

was based on the default threshold which some governmental agencies, such as the EU, typically set at 0.01 μg/g on compounds that do not have established tolerances.[12] Another goal was to have a method that utilized a relatively small amount of solvent and did not require the use of expensive and often difficult to obtain labeled internal standards. Gros et al. reported an LC-MS/MS based method for the determination of morpholine on pineapples which was able to achieve an LOQ of 0.01 μg/g.[13] Although this method achieved the target LOQ, the procedure was not favorable as it required a dual solid phase extraction cartridge system, which adds additional time and cost to the analysis. An unpublished method by Anastassiades et al. described a procedure for very polar, non-QuEChERS-amenable compounds in foods that utilizes acidified methanol extraction and determination by LC-MS/MS.[14] This method met our needs in terms of simple and rapid sample workup but only showed recovery data on lime at 1.0 μg/g and extrapolated LOQs on apples and citrus at 0.01 μg/g.[14,15] We therefore adopted a similar extraction procedure utilizing acidified methanol as in the Anastassiades method as a starting point for our method development.

Initial attempts to run morpholine on a traditional reverse phase C_{18} column resulted in little to no retention and very poor peak shape under high-aqueous conditions. As morpholine has relatively high polarity, this observation was not unexpected. To improve retention and peak shape, a HILIC column was chosen. During early instrumental analysis fortified extracts were compared to external standards prepared in solvent to assess possible ion enhancement/suppression. It was

dx.doi.org/10.1021/jf500734b | J. Agric. Food Chem. 2014, 62, 3697−3701

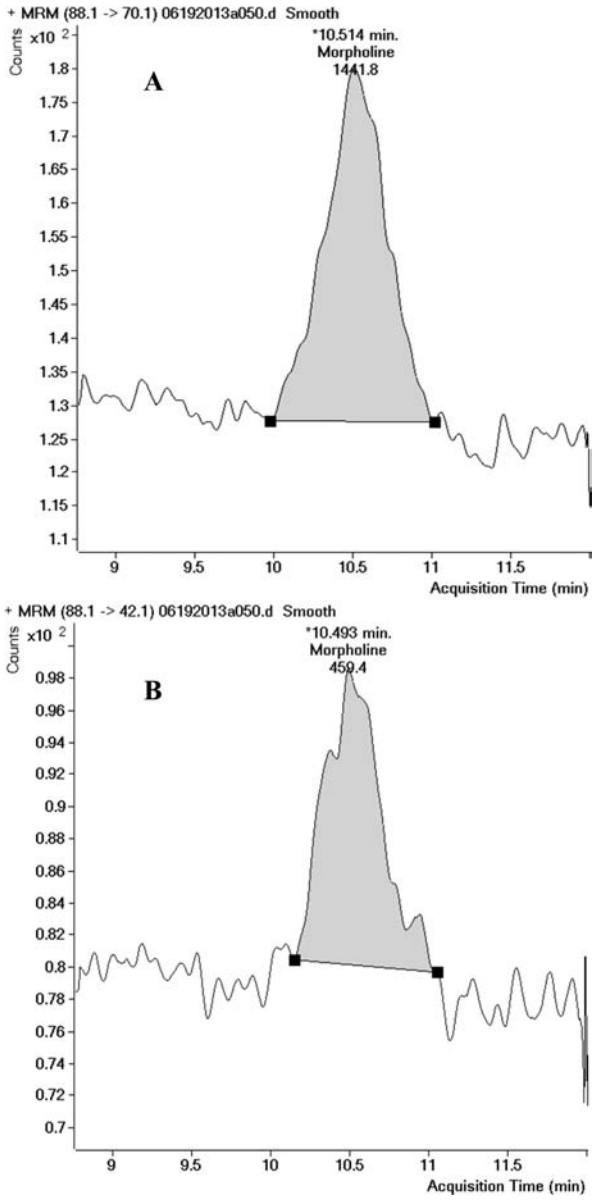

Figure 7. Extracted ion chromatograms of apple control sample fortified at 0.01 μg/g from Agilent 6430: (A) MRM transition 88 → 70; (B) MRM transition 88 → 42.

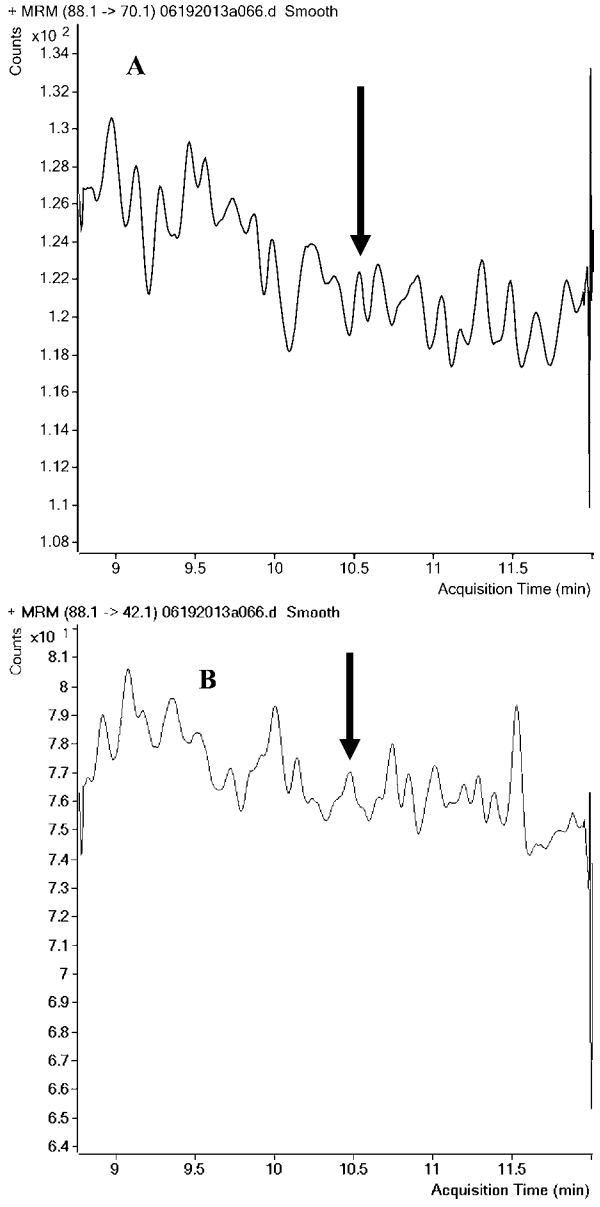

Figure 8. Extracted ion chromatograms of apple control sample from Agilent 6430: (A) MRM transition 88 → 70; (B) MRM transition 88 → 42.

observed that the response from the fortified extracts was suppressed >20% relative to the standard in solvent. As a result of these observations, the researchers chose to prepare matrix-matched standards for each crop type (apple and citrus) to correct the suppression effects.

Method Validation. In addition to the goals above, the method needed to be rugged and transferrable to other laboratories that may utilize instrumentation from different vendors (e.g., Agilent or Waters). Therefore, method validation was conducted at both the PAL and TAL facilities. All control samples used for the validation studies showed no significant morpholine residues for apple or citrus above the instrument limit of detection (LOD) of 0.3 pg/μL as defined by a S/N > 3. The LOQ was defined as 1 pg/μL (0.01 μg/g equivalent), which achieved a S/N > 10. Recovery data (Table 2) generated at the PAL facility for apples and oranges ranged from 84 to 120% over three levels of fortification (0.2, 0.04, and 0.01 μg/g) with all standard deviations ≤15% (n = 7 for each fortification level). The TAL facility produced recovery data for apples, oranges, lemons, and grapefruits that ranged from 97 to 112% over the same fortification levels listed above. As with the PAL data, good precision was observed at the TAL facility with all standard deviations ≤15% (n = 7 for each fortification level). Overall, the results from apple and orange method validation correlated very well between the two laboratories (Table 2). Lemons and grapefruits were also validated to assess the method on different types of citrus. As can been seen in Table 2, the results have excellent correlation to the results from the orange validation and suggest the method is suitable for citrus as a crop group. The coefficient of determination (R^2) for morpholine was ≥0.99 at both facilities. An example calibration curve can be seen in Figure 2. Typical chromatograms of standards and crop extracts can be seen in Figures 3−8 for both instruments. Retention time differences can be

dx.doi.org/10.1021/jf500734b | J. Agric. Food Chem. 2014, 62, 3697−3701

attributed to different flow rates, slight pH differences in the mobile phase preparation, and the usage of a column heater at the PAL facility.

As a result of the research conducted, a rapid, rugged, and selective method was developed for the screening of morpholine in apple and citrus fruits. With the method presented herein, 50 samples can be extracted in ∼4 h and analyzed by LC-MS/MS overnight.

AUTHOR INFORMATION

Corresponding Author

*(M.J.H.) Phone: (530) 752-2402. Fax: (530) 754-8556. E-mail: mjhengel@ucdavis.edu.

Notes

The authors declare no competing financial interest.

ACKNOWLEDGMENTS

We thank Mike Willett from Northwest Horticultural Council for his valued support of this project.

REFERENCES

(1) Noncitrus Fruits and Nuts 2011Summary. U.S. Department of Agriculture, National Agricultural Statistics Service, 2012; http://usda01.library.cornell.edu/usda/nass/NoncFruiNu//2010s/2012/NoncFruiNu-07-06-2012.pdf (accessed Sept 2013).

(2) Fresh Deciduous Fruit (Apples, Grapes, & Pears): World Markets and Trade. U.S. Department of Agriculture, Foreign Agricultural Service, 2013; http://usda01.library.cornell.edu/usda/current/decidwm/decidwm-06-21-2013.pdf (accessed Sept 2013).

(3) Citrus Fruits 2013 Summary. U.S. Department of Agriculture, National Agricultural Statistics Service, 2013; http://usda01.library.cornell.edu/usda/current/CitrFrui/CitrFrui-09-19-2013.pdf (accessed Sept 2013).

(4) Citrus: World Markets and Trade. U.S. Department of Agriculture, Foreign Agricultural Service, 2013; http://usda01.library.cornell.edu/usda/current/citruswm/citruswm-07-25-2013.pdf (accessed Sept 2013).

(5) Baldwin, E. A. *Edible Coatings for Fresh Fruits and Vegetables: Past, Present, And Future, Edible Coatings and Films to Improve Food Quality*; Krochta, J. M., Baldwin, E. A., Nisperos Carriedo, M. O., Eds.; Technomic Publishing, Lancaster, PA, USA, 1994; p 25.

(6) Code of Federal Regulation (CRF) Food and Drug Administration (FDA) 21CFR172.235; http://www.accessdata.fda.gov/scripts/cdrh/cfdocs/cfcfr/cfrsearch.cfm?fr=172.235 (accessed Feb 2014).

(7) European Union Food Additives Database; https://webgate.ec.europa.eu/sanco_foods/main/index.cfm (accessed Sept 2013).

(8) Willett, M. Northwest Horticultural Council, Yakima, WA, USA. Personal communication, 2013.

(9) Good Fruit Grower; http://www.goodfruit.com/Good-Fruit-Grower/March-15th-2012/EU-regulations-stifle-fruit-exports/ (accessed Sept 2013).

(10) National Organic Standards Board, Technical Advisory Panel Review of Morpholine, 2001; http://www.ams.usda.gov/AMSv1.0/getfile?dDocName=STELPRDC5067002 (accessed Sept 2013).

(11) *Pesticide Analytical Manual, Vol. I: Multiresidue Methods*, 3rd ed.; U.S. Food and Drug Administration: Washington, DC,, 1999; http://www.fda.gov/downloads/Food/FoodScienceResearch/ucm111500.pdf (accessed Sept 2013).

(12) European Union Pesticide Database; http://ec.europa.eu/sanco_pesticides/public/index.cfm?event=commodity.selection (accessed May 2010).

(13) Gros, P.; Matignon, F.; Plonevez, S. Determination of morpholine in fruits using LC-MS/MS. *Ann. Falsif. Expert. Chim. Toxicol.* **2011**, *974*, 17−22.

(14) Anastassiades, M.; Kolberg, D. I.; Mack, D.; Sigalova, I.; Roux, D.; Fügel, D. Quick method for the analysis of residues of highly polar pesticides in foods of plant origins involving simultaneous extraction with methanol and LC-MS/MS determination (QuPPe-method). *EU Reference Laboratories for Residues of Pesticides*, version 6, 2011; http://www.eurl-pesticides.eu (accessed Oct 2012).

(15) Anastassiades, M.; Kolberg, D. I.; Mack, D.; Wildgrube, C.; Sigalova, I.; Roux, D.; Fügel, D. Quick method for the analysis of residues of highly polar pesticides in foods of plant origins involving simultaneous extraction with methanol and LC-MS/MS determination (QuPPe-method). *EU Reference Laboratories for Residues of Pesticides*, version 7.1, 2013; http://www.crl-pesticides.eu/library/docs/srm/meth_QuPPe.pdf (accessed Nov 2013).

and DCBC.[6] The metabolites, however, are not well recovered from the ginseng matrix using this method.

Zoxamide, the parent compound, is well recovered from ginseng root by a modification of the commonly used multiresidue method known as the QuEChERS-based (for quick, easy, cheap, effective, rugged, safe) approach,[7] which has gained international popularity for its extraction efficiency and ease of use. However, the small acid metabolites of zoxamide (DCHB molecular weight 221.04 and DCBC molecular weight 235.02) were not well recovered from ginseng root through the aforementioned QuEChERS multiresidue approach during the initial recovery trials in this work. Residue analytical methods are required by the EPA to determine the parent compound and metabolites of significance to enforce tolerances.[8] The residue analytical method presented here is a miniaturized extraction that effectively recovered the small acid metabolites DCHB and DCBC as well as the zoxamide parent molecule and uses liquid chromatography coupled with tandem quadrupole mass spectrometry (UPLC-MS/MS). This method rivals the QuEChERS-based approach for its ease of use and rapid sample preparation time.

MATERIALS AND METHODS

Materials and Standards Preparation. Zoxamide and the zoxamide metabolite DCHB analytical standards, of 99.1 and 99.82% purity, respectively, were provided by the U.S. EPA National Pesticide Standard Repository. The zoxamide metabolite DCBC, of 98.8% purity, was provided by the U.S. Department of Agriculture Inter-Regional Research Project No. 4 (IR-4 Project, also referred to as the Minor Crop Pest Management Program). American ginseng root samples, untreated with pesticides, dried for 2 weeks at 35 °C, and finely homogenized using a Wiley mill, were also provided by the IR-4 Project. HPLC grade acetonitrile, ethyl acetate, toluene, and sodium hydroxide solution 40% were purchased from Fisher Scientific (Pittsburgh, PA, USA). Hydrochloric acid 37% ACS Reagent, reagent plus grade ≥99 glycine, and ammonium hydroxide solution 28−30% were purchased from Sigma-Aldrich (St. Louis, MO, USA). Supelclean ENVI-Carb SPE tubes, 0.5 g, 6 mL, were purchased from Supelco Analytical (Bellefonte, PA, USA). pH indicator strips (pH 0−2.5 and 0−14) were purchased from colorpHast (Gibbstown, NJ, USA). Eppendorf variable-volume (10−100 μL, 100−1000 μL) pipets were from Eppendorf AG (Hamburg, Germany), calibrated and certified.

Separate stock solution standards of zoxamide and metabolite DCBC were prepared by dissolving approximately 25 mg in 25.0 mL of acetonitrile for approximately 1.0 mg/mL standard concentrations. Intermediate dilutions were prepared by transferring 1.0 mL of the stock solutions to separate 100 mL volumetric flasks and diluting to volume with acetonitrile for concentrations of 10.1 μg/mL zoxamide and 10.9 μg/mL DCBC. The metabolite DCHB standard was prepared by dissolving approximately 10 mg in 25.0 mL of acetonitrile for a stock standard concentration of approximately 0.4 mg/mL. An intermediate dilution was prepared by transferring 2.5 mL of DCHB stock standard to a separate 100 mL volumetric flask and diluting to volume with acetonitrile for a concentration of 10.6 μg/mL. A second intermediate dilution (1.01 μg/mL) of zoxamide standard was prepared by transferring 0.5 mL of the 10.1 μg/mL standard and diluting to a final volume of 5.0 mL in acetonitrile. A mixed solvent standard, used to prepare the matrix-matched standards for quantitation and for fortification of untreated control ginseng extracts, was prepared by transferring 0.1 mL of the metabolite intermediate standards (10 μg/mL) and diluting to a final volume of 2.0 mL in acetonitrile for final concentrations of 532 ng/mL DCHB and 545 ng/mL DCBC. A second mixed standard, also used for the matrix-matched standards for quantitation and for fortification of control ginseng extracts, was prepared by transferring 0.040 mL of the zoxamide intermediate standard (1.01 μg/mL) and 0.113 and 0.110 mL of the metabolite intermediate standards (10 μg/mL) and diluting to a final volume of 2.0 mL in acetonitrile for a final concentration 20 ng/mL zoxamide and 600 ng/mL DCHB and DCBC. A standard of zoxamide, used for the matrix-matched standards and for fortification of control ginseng extracts, was prepared by transferring 0.044 mL of the zoxamide intermediate standard (1.01 μg/mL) and diluting to a final volume of 2.0 mL in acetonitrile for a final concentration of 22 ng/mL.

A 4 M NaOH solution was prepared by adding 10 mL of 10 M solution to a 25 mL volumetric flask and diluting to volume with Millipore water. The 1 M glycine buffer solution at pH 10 was prepared by dissolving 7.5 g of glycine with 60 mL of Millipore water in a 100 mL graduated cylinder, adding 3.5 mL of 4 M NaOH, and then diluting to 100 mL volume[9−12] with Millipore water.

Sample Preparation. A schematic of the extraction and cleanup procedure is shown in Figure 2. Dried, finely ground ginseng root (0.2 g) was weighed into a screw-capped polypropylene 15 mL centrifuge tube. Glycine buffer (1 M), pH 10 (2 mL), was added and vigorously vortexed for 30 s. Millipore water (2 mL) was added and shaken vigorously by hand for 1 min. Both 1 N HCl (0.8 mL) and 12 N HCl (0.2 mL) were added to the aqueous extract and vigorously shaken for 1 min. Four milliliters of ethyl acetate was added and the centrifuge tube vigorously shaken for 1 min and centrifuged (Jouan Inc.,

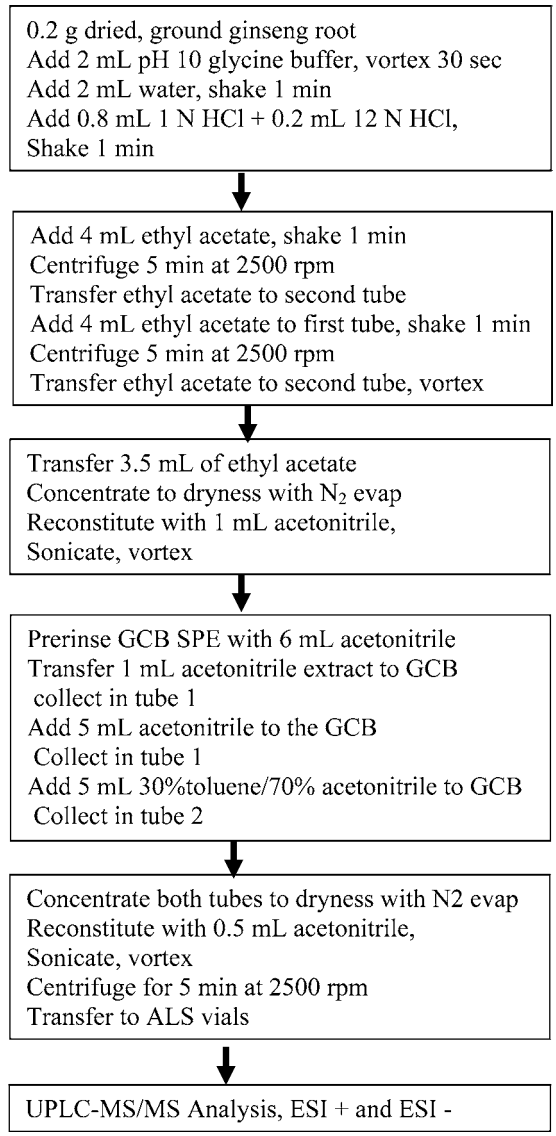

Figure 2. Flowchart of the method for the analysis of zoxamide and its metabolites (DCHB and DCBC) in dried ginseng powder.

Table 1. Analyte Name, Retention Time, Primary and Confirmatory Ion Transitions, and Molecular Formulas of Zoxamide and Its Metabolites

compd	mol formula	mol wt	retention time (min)	LOD (ng/g)	primary and confirmatory ion transitions (P/C ratio %)
zoxamide	$C_{14}H_{16}Cl_3NO_2$	336.64	5.45	6.7	**336**, 186.9, 158.8 (2.2)
DCHB	$C_8H_6Cl_2O_3$	221.04	1.14	71	**218.8**, 174.8, 144.8 (2.05)
DCBC	$C_8H_4Cl_2O_4$	235.02	0.5	73	**232.8**, 188.8, 152.8 (2.6), 108.8 (1.9)

Winchester, VA, USA) for 5 min at 2500 rpm at ambient temperature. The ethyl acetate layer (2 mL) was transferred to a second 15 mL centrifuge tube. Ethyl acetate (4 mL) was added to the first tube containing the ginseng and hand shaken again vigorously for 1 min and centrifuged for 5 min at 2500 rpm. The ethyl acetate layer (5−6 mL) was removed and added to the second tube (sum 7−7.5 mL) and vigorously vortexed for 10 s. A portion of the ethyl acetate extract (3.5 mL) was transferred to a third 15 mL tube and concentrated to dryness with nitrogen evaporation (N-EVAP, Organomation Associates, Inc., Berlin, MA, USA). Acetonitrile (1 mL) was added to the centrifuge tube, sonicated for 10 s, and vortexed for 10−15 s. A GCB SPE cartridge was prerinsed with acetonitrile to waste. The extract (1 mL) was transferred to the GCB and collected, without vacuum, in a 15 mL tube labeled fraction 1. Acetonitrile (5 mL) was added to the GCB and collected in the same tube. A solution of 30% toluene/70% acetonitrile (5 mL) was added to the GCB and collected in a second tube labeled fraction 2. Both tubes were concentrated to dryness using nitrogen evaporation. Acetonitrile (0.5 mL) was added to both tubes, vortexed for 15 s, sonicated for 15 s, and centrifuged for 5 min at 2500 rpm. The extracts were transferred to LC autosampler vials for UPLC-MS/MS analysis. Sample preparation time for a set of 6−10 samples is 45 min or less.

UPLC-MS/MS Analysis. A Waters Acquity ultraperformance liquid chromatograph (UPLC) was equipped with a Quattro Premier tandem quadrupole mass spectrometer and an Acquity HSS-T3 column (100 mm × 2.1 mm) of 1.8 μm particle size, all supplied by Waters (Milford, MA, USA), with a void volume of 0.24 mL[13] and a dwell volume of 0.090 mL. Reverse phase operating conditions were as follows: an injection volume of 5 μL at ambient column temperature; a flow rate of 0.3 mL/min using a mobile phase of acetonitrile, H_2O, and ammonium hydroxide prepared as two separate solutions: solvent A, 100% H_2O and 1 mM ammonium hydroxide (500 mL of H_2O + 34 μL of NH_4OH); solvent B, 100% ACN and 3.5 mM ammonium hydroxide (500 mL of H_2O + 120 μL of NH_4OH). The initial conditions were set at 100% solvent A for 2 min using a 0.3 mL/min flow rate; a linear gradient was programmed within 2 min to 10 + 90 (solvent A + solvent B), followed by a 2 min linear gradient to 30 + 70 (solvent A + solvent B) continuing at 0.3 mL/min, and a step back to 100% solvent A for a 3 min equilibration for a total analysis time of 10 min. The mass spectrometer was operated by switching between positive (ESI^+) and negative (ESI^-) electrospray ionization (interchannel delay of 0.020 s) in the multiple reagent monitoring (MRM) mode. The ion source temperature was 130 °C and the desolvation temperature 450 °C. The cone gas flow (high-purity compressed nitrogen) was 50 L/h, and the desolvation gas flow was 800 L/h of nitrogen gas. The collision cell gas was ultrahigh-purity argon with a flow of 0.3 mL/min. Two precursor/product ion transitions were monitored for each compound, and the sum of the areas of both the target ion and the confirmatory ion were used as the total response for quantitation. Analytes were further confirmed when MRM ion transition ratios were within ±20% (absolute) of the ratios in standards. The MRM ion transitions, cone voltages, and collision energies used were as follows: for zoxamide (ESI^+), 336.0 → 158.80 (30 V, 40 eV) and 336.0 → 186.9 (30 V, 20 eV); for DCHB (ESI^-), 218.8 → 144.6 (25 V, 14 eV) and 218.8 → 174.8 (25 V, 10 eV); for DCBC (ESI^-), 232.8 → 108.8 (10 V, 21 eV), 232.8 → 152.8 (10 V,14 eV), and 232.8 → 188.8 (10 V, 9 eV) (see Table 1). Because an external standard was used for quantitation, the retention times of the compound of interest in the standard and the same compound in the sample were ±0.1 min.

Fortification Studies. For all fortification studies, various amounts of spiking standards prepared in acetonitrile were added to 0.2 g test portions of dried control ginseng root in centrifuge tubes. The tubes containing fortified ginseng were vigorously vortexed to distribute the analytes through the ginseng test portions, and the tubes were uncapped to allow the acetonitrile solvent to evaporate prior to sample extraction. For quantification by external calibration, matrix-matched standards were used. Matrix-matched standards were prepared by extracting control ginseng samples (as described above under Sample Preparation including GCB cleanup) and then fortifying the dried extracts with the acetonitrile standards and adjusting the final volume to 0.5 mL with acetonitrile.

For LOD and LOQ fortification studies of DCHB and DCBC, appropriate amounts of a mixed spiking standard containing DCHB (532 μg/mL) and DCBC (545 μg/mL) were added to 0.2 g of ginseng for final concentrations of 0.071 and 0.216 μg/g for DCHB and 0.073 and 0.221 μg/g for DCBC. The matrix-matched standards were prepared at concentration levels of 14.4, 28.7, 86.2, and 172.5 ng/mL for DCHB and 14.7, 29.4, 88.3, and 176.5 ng/mL for DCBC.

For the LOD fortification study of zoxamide, an appropriate amount of a standard of zoxamide (22.4 ng/mL) was added to 0.2 g of ginseng to a final concentration of 0.007 μg/g. The matrix-matched standards were prepared at concentration levels of 0.605, 1.21, and 3.63 ng/mL for zoxamide.

For the fortification studies of the LOQ of zoxamide and 3× LOQ of DCHB and DCBC, a mixed spiking standard prepared in acetonitrile containing zoxamide (20 ng/mL), DCHB (600 ng/mL), and DCBC (600 ng/mL) was added to 0.2 g of ginseng to final concentrations of 0.020 μg/g (zoxamide) and 0.6 μg/g (DCHB and DCBC). The matrix-matched standards were prepared at concentration levels of 1.18, 3.53, 7.07, and 14.1 ng/mL for zoxamide and 35, 105, 210, and 420 ng/mL for DCHB and DCBC.

For the fortification studies of 10× LOQ of zoxamide and 30× LOQ of DCHB and DCBC, various amounts of the intermediate dilutions of 1.01 and 10 μg/mL were added directly to 0.2 g of ginseng to final concentrations of 0.2 μg/g (zoxamide) and 6.0 μg/g (DCHB and DCBC). The matrix-matched standards were prepared at concentration levels of 1.18, 3.53, 7.07, 14.1, 28.3, and 35.3 ng/mL for zoxamide and 35, 105, 210, 420, 830, and 1045 ng/mL for DCHB and DCBC.

Statistics and Calculations. Averages and standard deviations from fortification studies were determined using Microsoft Excel 2003. Linear regressions, correlation coefficients, and analyte concentrations from fortification studies for the UPLC-MS/MS were calculated with the Waters Target Lynx/Mass Lynx software version 4.1 using the sum of peak area responses of the primary ion transition and the confirmatory ion transition.

RESULTS AND DISCUSSION

Extraction Procedure. Recoveries of >90% have been reported for the parent molecule, zoxamide, from ginseng using an acetonitrile extraction of the QuEChERS approach,[2] but the acid metabolites are not well recovered from this matrix. Although a solution of 2% sodium bicarbonate in acetonitrile effectively extracts the metabolites from potato matrices,[6] this solution yielded recoveries of only 30−40% for the acid metabolites in ginseng during the initial recovery trials in this work. To effectively extract the metabolites of zoxamide from ginseng, several different aqueous solutions of various pH values, including glycine buffer solutions,[9−12] a sodium

dx.doi.org/10.1021/jf405403v | J. Agric. Food Chem. 2014, 62, 3702−3709

Table 2. Recoveries (Percent) of Zoxamide and Metabolites DCHB and DCBC Extracted from Dried Ginseng Powder Fortified at Three and Four Different Levels, Respectively

	zoxamide			DCHB			DCBC		
validation level (replicates)	spike level (μg/g)	% mean recovery	% RSD	spike level (μg/g)	% mean recovery	% RSD	spike level (μg/g)	% mean recovery	% RSD
LOD (3)	0.007	124	15	0.071	103	10	0.073	113	4
LOQ (5)	0.020	95	4	0.216	106	11	0.221	107	15
10× LOQ (3)	0.202	96	5						
3× LOQ (5)				0.600	86	12	0.600	95	12
30× LOQ (3)				6.0	96	6	6.0	105	10

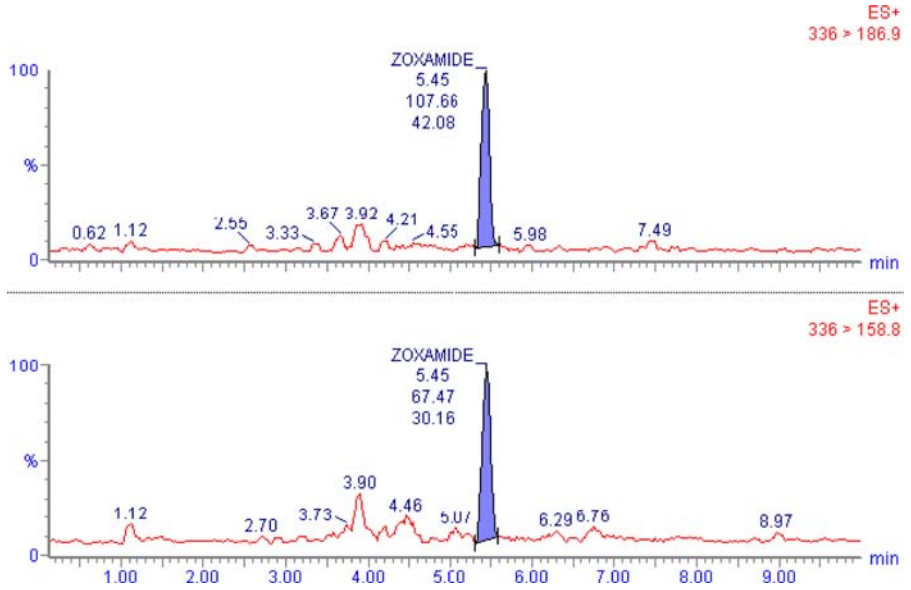

Figure 3. LC-MS/MS of ginseng root fortified with zoxamide at the LOQ of 0.020 ppm.

hydroxide solution, and a neutral acetonitrile/water solution, were evaluated. The results of these trials revealed that a glycine buffer solution (pH 10) effectively recovered both the parent molecule, zoxamide, and the metabolites DCBC and DCHB from the ginseng matrix with average recoveries >95 and >86%, respectively (Table 2).

The 2% sodium bicarbonate/acetonitrile method, which was developed for the extraction of the metabolites from potato,[6] yields poor recoveries of the metabolites from ginseng root and also required derivatization with diazomethane to methylate the metabolites to their methyl esters prior to GC determination. In the method presented here for ginseng root, derivatization with diazomethane is not required. The purified ginseng extract is directly injected into the LC-MS/MS without derivatization. Specifically, in this method, 0.2 g of ground, homogenized ginseng matrix is rendered alkaline with glycine buffer (pH 10) to extract the parent and metabolite molecules and then diluted with water. The solution is acidified with 1 N HCl to neutralize the acid metabolites and partitioned into ethyl acetate in preparation for LC analysis without the need for derivatization.

Initially during the development of the method, the aqueous ginseng extracts were centrifuged prior to partitioning with ethyl acetate. When the aqueous extracts were centrifuged and decanted from the ginseng solids and then partitioned with ethyl acetate, the recoveries of the metabolites DCHB and DCBC were acceptable, but the extraction efficiency of the parent molecule, zoxamide, resulted in low recoveries (30%). By partitioning the water/buffer−ginseng mixture with ethyl acetate in the presence of the ginseng solids, followed then by centrifugation, zoxamide recoveries were improved to >90% and the extraction efficiency of the metabolites remained the same.

A 3.5 mL aliquot of the 7.5 mL ethyl acetate extract is taken through cleanup for instrumental analysis. The remaining 3.5 mL portion of ethyl acetate extract is reserved for a potential second analysis if necessary. A simple solid phase extraction (SPE) cleanup method using graphitized carbon black (GCB) was used for the complete recovery of the analytes. Two fractions were collected through the GCB and injected separately. The first, 5 mL of acetonitrile, captures approximately 30% of the zoxamide analyte. The second fraction of 5 mL of toluene/acetonitrile, 30:70, captures the remaining 70% zoxamide and the metabolites DCHB and DCBC. Two fractions are used because the zoxamide response is affected by matrix coextractants and more coextractants are present in the second, toluene, fraction. To calculate zoxamide recovery, the levels of zoxamide found in the first and second fractions are summed. The advantages of the GCB cleanup are simplicity and speed. The final acetonitrile extract is centrifuged prior to instrumental analysis. Alternatively, filtration with syringe filters should be tested for suitability for the full recovery of the analytes.

Method Validation. Zoxamide and its metabolites, DCHB and DCBC, were analyzed using UPLC-MS/MS. Retention times, quantitation, confirmation, and regression coefficients of zoxamide were determined in the electrospray positive (ESI^+) mode and DCHB and DCBC were determined in the electrospray negative (ESI^-) mode. The extraction and

dx.doi.org/10.1021/jf405403v | J. Agric. Food Chem. 2014, 62, 3702−3709

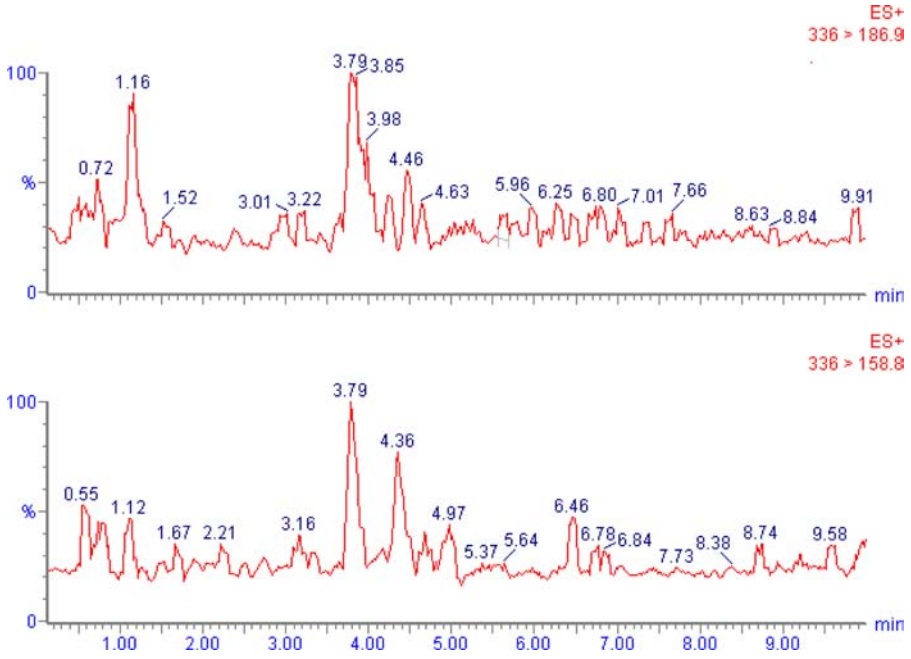

Figure 4. LC-MS/MS of ginseng root control in ES^+ at the retention time and transitions of zoxamide.

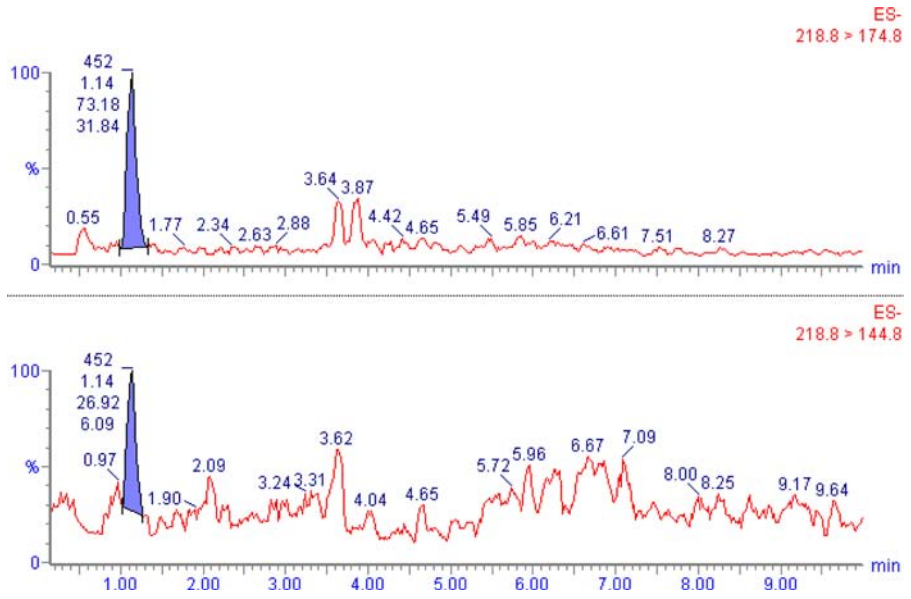

Figure 5. LC-MS/MS of ginseng root fortified with metabolite DCHB at the LOQ of 0.200 ppm.

instrumental analysis method was validated at three different fortification levels for zoxamide including replicates at the limit of detection (LOD), the limit of quantitation (LOQ), and 10× the LOQ. Four different levels were evaluated for the studied metabolites, DCBC and DCHB, including the limit of detection (LOD), the limit of quantitation (LOQ), and 3× and 10× the LOQ. The LOD was defined by the fortification level with a signal-to-noise of a minimum of 3:1, which was determined by the Mass Lynx software and is the standard deviation of the noise data in the monitored range, for both the primary and confirmatory ion transitions; the LOQ was defined by 3× the LOD. Table 2 lists the results of method validation. In general, the regression coefficients r^2 for the matrix-matched calibration curves of each analyte were as follows: zoxamide ranged from 0.986 to 0.998; DCHB, $r^2 > 0.995$; and DCBC, $r^2 > 0.988$. Figures 3, 5, and 7 show chromatograms of ginseng root extract fortified at the LOQ of 0.020 μg/g for zoxamide and 0.2 μg/g for DCHB and DCBC metabolites. The peak shapes are consistent and Gaussian with baseline separations. No significant background interfering peaks are observed in the control ginseng chromatograms shown in Figures 4, 6, and 8.

Instrumental Analysis. Weak acids, such as acetic acid and formic acid, are frequently used mobile phase modifiers that increase ionization of many analytes using positive ESI.[14] However, neither formic acid nor acetic acid improved the response of the acid metabolites, DCHB and DCBC, in the ESI^- mode. The neutral salts, ammonium formate and ammonium acetate, which are also commonly used modifiers in ESI^+ mode, also did not result in improved ionization of the zoxamide metabolites in ESI^- mode. The volatile base,

dx.doi.org/10.1021/jf405403v | J. Agric. Food Chem. 2014, 62, 3702−3709

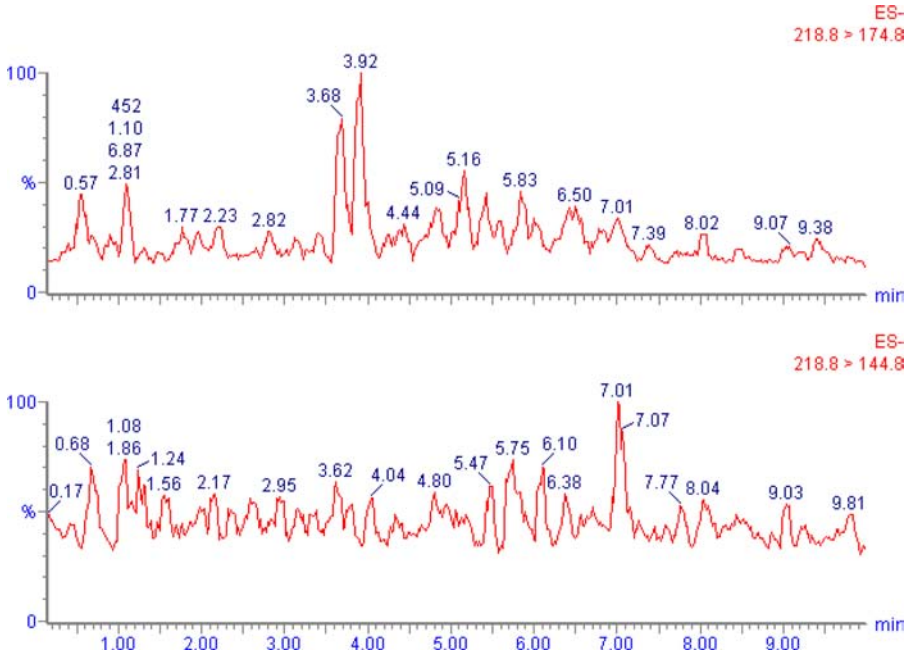

Figure 6. LC-MS/MS of ginseng root control in ES$^-$ at the retention time and transitions of DCHB.

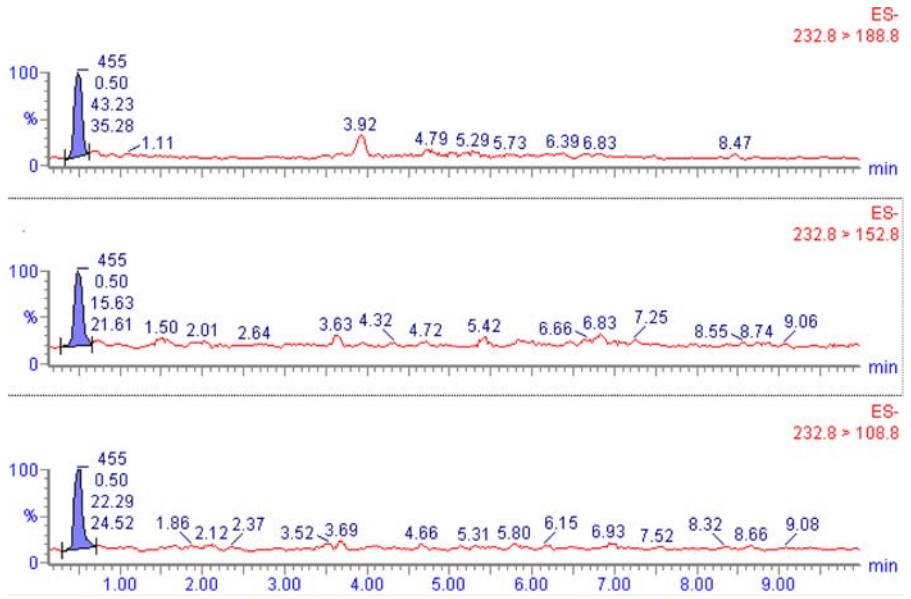

Figure 7. LC-MS/MS of ginseng root fortified with metabolite DCBC at the LOQ of 0.200 ppm.

ammonium hydroxide, resulted in the ionization of the small metabolite molecules DCBC and DCHB in the negative-ion mode ESI. A low concentration of 1 mM ammonium hydroxide in the aqueous mobile phase was sufficient for ionization in the ESI$^-$ mode, and higher molar concentrations did not improve ionization or detection limits.

Fortification Studies. The recoveries from fortification studies of zoxamide and the metabolites DCHB and DCBC, evaluated by UPLC-MS/MS and based on external calibration using ginseng root matched standards, are shown in Table 2. The dried, powdered ginseng was fortified with zoxamide to levels of 0.007, 0.020, and 0.202 μg/g; DCHB to levels of 0.071, 0.216, 0.600, and 6.0 μg/g; and DCBC to levels of 0.073, 0.221, 0.600, and 6.00 μg/g. The mean recovery ranges for zoxamide and the metabolites at the aforementioned levels were from 95 to 124% for zoxamide, from 86 to 106% for DCHB, and from 95 to 113% for DCBC.

Matrix Effects. The use of ginseng matrix-matched standards for quantitation instead of solvent standards was necessary because of pronounced matrix effects from ginseng extracts. Although there were no significant matrix interferences, the presence of the ginseng matrix reduced the signal by approximately 3× for DCHB, 4× for DCBC, and 6× for zoxamide. Although recoveries at the LOD of DCHB and DCBC were generally consistent using ginseng matrix standards, recoveries of zoxamide at the LOD of 0.007 μg/g were less consistent.

The challenge of the ginseng matrix was the efficient extraction of the metabolites of the parent molecule zoxamide. The miniaturized extraction presented here effectively recov-

dx.doi.org/10.1021/jf405403v | J. Agric. Food Chem. 2014, 62, 3702−3709

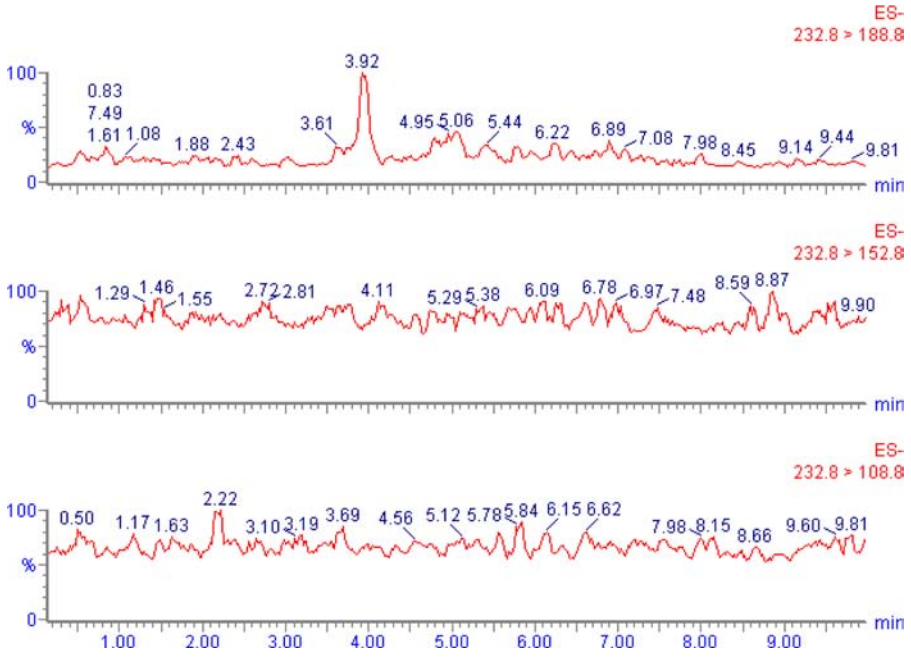

Figure 8. LC-MS/MS of ginseng root control in ES^- at the retention time and transitions of DCBC.

ered the acid metabolites 3,5-dichloro-4-hydroxymethyl benzoic acid and 3,5-dichloro-1,4-benzenedicarboxylic acid at a LOQ of 0.2 ppm as well as the parent, zoxamide, at a LOQ of 0.02 ppm from fortified ginseng root samples. The method uses a pH 10 1 M glycine buffer and also uses a simple graphitized carbon black cleanup and UPLC-MS/MS for quantitation. Unlike other single-analyte or specialized methods, this extraction method is simple and rapid. This analytical method is suitable for the EPA approved use of the fungicide zoxamide for ginseng root crops.

■ ASSOCIATED CONTENT

Supporting Information

Additional information about the dried control ginseng samples. This material is available free of charge via the Internet at http://pubs.acs.org.

■ AUTHOR INFORMATION

Corresponding Author

*E-mail: Podhorniak.Lynda@epa.gov.

Notes

The authors declare no competing financial interest.

■ ACKNOWLEDGMENTS

We thank the USDA IR-4 Project, especially Johannes Corley and Dan Kunkel, for providing ground ginseng roots for blanks used to prepare the matrix-matched standards and to fortify spiked samples and for providing analytical standards.

■ REFERENCES

(1) Method Validation and Quality Control Procedures for Pesticide Residues Analysis in Food and Feed, Document No. SANCO/12495/2011; pp 13, 24.

(2) Wong, J.; Hennessy, M.; Hayward, D.; Krynitsky, A.; Cassias, I.; Schenck, F. Analysis of organophosphorus pesticides in dried ground ginseng root by capillary gas chromatography-mass spectrometry and -flame photometric detection. *J. Agric. Food Chem.* **2007**, *55*, 1117−1128.

(3) 49110 Federal Register/Vol. 66, No. 187/Wednesday, Sept 26, 2001/Rules and Regulations, Environmental Protection Agency 40 CFR Part 180 [OPP-301176; FRL-6803-7] RIN 2070-AB78 Zoxamide 3,5-dichloro-*N*-(3-chloro-1-ethyl-1-methyl-2-oxopropyl)-4-methylbenzamide; Pesticide Tolerance; http://www.gpo.gov/fdsys/pkg/FR-2001-09-26/pdf/01-23640.pdf.

(4) European Commission Health and Consumer Protection Directorate-General Directorate E − Food Safety: plant health, animal health and welfare, international questions E1 − Plant health Zoxamide SANCO/10297/2003-Final. 4 February 2004 Appendix II End Points and Related Information 1. Toxicology and metabolism, 5 Aug 2003; p 9; http://ec.europa.eu/food/plant/protection/evaluation/newactive/zoxamide.pdf.

(5) National Library of Medicine HSDB Database TOXNET Toxicology Data Network; http://toxnet.nlm.nih.gov/cgi-bin/sis/search/a?dbs+hsdb:@term+@DOCNO+7278.

(6) Ipin Guo, I.; Kurilla, K.; Hofmann, C. Tolerance Enforcement Method for Parent RH-7281 and Its Two Acid Metabolites, RH-1452 and RH-1455, in Potato Peel Waste: Lab Project Number: 34-00-49, 2000; unpublished study prepared by Rohm and Haas Company; 85 pp; http://www.epa.gov/pesticides/methods/rammethods/2001_009M.pdf.

(7) Wong, J.; Hao, C.; Zhang, K.; Yang, P.; Banerjee, K.; Hayward, D.; Iftakhar, I.; Schreiber, A.; Tech, K.; Sack, C.; Smoker, M.; Chen, X.; Utture, S. C.; Oulkar, D. P. Development and interlaboratory validation of a QuEChERS-based liquid chromatography-tandem mass spectrometry method for multiresidue pesticide analysis. *J. Agric. Food Chem.* **2010**, *58*, 5897−5903.

(8) U.S. Environmental Protection Agency, Prevention, Pesticides and Toxic Substances (7101) EPA 712-C-96-174, Aug 1996; Residue Chemistry Test Guidelines OCSPP 860.1340, (b) (1) p 1, Residue Analytical Method; http://fedbbs.access.gpo.gov.

(9) Identification of Poisons and Toxins by GC/MS Food Safety and Inspection Service, Office of Public Health Science. U.S. Department of Agriculture Food Safety and Inspection Service, Office of Public Health Science, May 5, 2013; http://www.fsis.usda.gov/horses/CLG-TOX1.pdf.

(10) Crockett, D.; Lorrie Lin, L.; Mulligan, K. SOP No: FERN-CHE.0006.00, USFDA, ORA Forensic Chemistry Center, 2010; pp 1−21; unpublished.

(11) Mohan, C. *Buffers: A Guide for the Preparation and Use of Buffers in Biological Systems*; EMD Biosciences: Darmstadt, Germany, 2003, p 21.
(12) Mulligan, K. J. General Method to Examine Foods and Beverages for Volatile and Semi-volatile Contaminants Using Acidic and Basic Extraction with Capillary gas Chromatography − Mass Spectrometry. U.S. FDA SOP T021(004); Elexnet −FERN/FERN Methods and SOPs/Documents/Chemical/Interim Methods, 2006.
(13) http://www.chiralizer.com/colvol.htm.
(14) Wu, Z.; Gao, W.; Phelps, M. A.; Wu, D.; Miller, D. D.; Dalton, J. T. Favorable effects of weak acids on negative-ion electrospray ionization mass spectrometry. *Anal. Chem.* **2004**, *76* (3), 839−847.

Table 1. MRM Transitions and Other GC-MS/MS Parameters for the Compounds in Groups A and B

no.	pesticide	RT (min)	quantification transition[a]	confirmation transition[a]
		(A) Group A		
1	acetochlor	20.59	174.0→146.1 (10)	146.0→131.1 (10)
2	acrinathrin	32.05	207.8→181.1 (10)	181.0→152.0 (30)
3	alachlor	21.21	188.1→160.2 (10)	160.0→132.1 (10)
4	aldrin	19.89	262.9→192.9 (35)	254.9→220.0 (20)
5	anilofos	31.83	225.9→184.0 (10)	225.9→157.0 (10)
6	atrazine	17.89	214.9→200.2 (10)	214.9→58.1 (10)
7	azaconazole	28.39	217.0→173.1 (15)	219.0→175.0 (15)
8	benalaxyl	29.29	148.0→77.0 (10)	148.0→105.1 (10)
9	bendiocarb	15.61	166.0→151.1 (10)	126.0→52.1 (15)
10	benoxacor	20.26	120.1→65.1 (20)	258.9→120.1 (15)
11	α-BHC	15.30	216.9→181.1 (5)	181.0→145.0 (15)
12	β-BHC	17.51	216.9→181.1 (5)	181.0→145.0 (15)
13	δ-BHC	23.15	217.0→181.1 (5)	181.0→145.0 (15)
14	bifenox	31.64	189.1→126.0 (20)	340.9→309.9 (10)
15	bifenthrin	29.86	181.2→166.2 (10)	181.2→165.2 (10)
16	bitertanol	33.37	170.1→141.1 (10)	170.1→115.0 (10)
17	bromophos-ethyl	26.77	358.7→302.8 (15)	302.8→284.7 (15)
18	bupirimate	28.21	272.9→193.1 (10)	272.9→108.0 (10)
19	buprofezin	27.15	105.0→104.1 (10)	105.0→77.0 (10)
20	butachlor	26.25	188.1→160.2 (10)	176.1→147.1 (10)
21	cadusafos	13.91	158.8→97.0 (10)	158.8→131.0 (10)
22	carbaryl	23.76	144.0→115.1 (10)	144.0→116.1 (10)
23	carbofuran	17.88	164.2→149.1 (10)	149.1→121.1 (5)
24	chlordimeform	13.67	195.9→181.0 (5)	151.9→117.1 (10)
25	chlorfenapyr	29.13	136.9→102.0 (10)	246.9→227.0 (15)
26	chlorpyrifos-methyl	20.00	124.9→47.0 (15)	124.9→78.9 (10)
27	clodinafop-propargyl	29.45	266.0→91.0 (15)	238.0→130.0 (15)
28	coumaphos	34.81	210.0→182.0 (10)	361.9→109.0 (15)
29	cyanophos	19.56	242.9→109.0 (10)	124.9→47.0 (10)
30	cyflufenamid	27.95	118.1→90.0 (10)	118.1→89.0 (10)
31	cyfluthrin I	34.23	162.9→90.9 (10)	162.9→127.0 (10)
32	cyfluthrin II	34.52	162.9→90.9 (10)	162.9→127.0 (10)
33	cypermethrin IV	34.83	163.1→127.1 (10)	163.1→91.0 (10)
34	DCPA	22.92	298.9→221.0 (25)	300.9→223.0 (25)
35	*o,p′*-DDD	27.14	235.0→165.2 (20)	237.0→165.2 (20)
36	*o,p′*-DDE	24.73	246.0→176.2 (30)	248.0→176.2 (30)
37	*p,p′*-DDE	26.06	246.1→176.2 (30)	315.8→246.0 (15)
38	*o,p′*-DDT	27.54	235.0→165.2 (20)	237.0→165.2 (20)
39	DEF	26.47	169.0→57.1 (5)	202.0→147.0 (10)
40	deltamethrin	38.79	181.0→152.1 (10)	252.9→93.0 (15)
41	diazinon	16.71	137.1→84.0 (10)	137.1→54.0 (10)
42	dichlofenthion	19.12	278.9→222.9 (15)	222.9→204.9 (15)
43	dichlorvos	6.21	109.0→79.0 (5)	184.9→93.0 (10)
44	diclobutrazol	28.23	269.8→158.9 (20)	271.8→160.9 (15)
45	diclofop-methyl	29.57	253.0→162.1 (15)	339.9→252.9 (10)
46	dicloran	18.06	206.1→176.0 (10)	160.1→124.1 (10)
47	dieldrin	26.52	262.9→193.0 (35)	277.0→241.0 (5)
48	difenoconazole I	38.29	322.8→264.8 (15)	264.9→202.0 (20)
49	difenoconazole II	38.36	322.8→264.8 (15)	264.9→202.0 (20)
50	dimethipin	22.26	124.0→76.0 (5)	118.0→58.0 (5)
51	dimethoate	19.98	92.9→63.0 (10)	86.9→46.0 (15)
52	dimethylvinphos	24.17	294.9→108.9 (15)	296.9→108.9 (15)
53	diphenylamine	13.21	169.0→168.2 (15)	168.0→167.2 (15)
54	disulfoton	17.71	88.0→60.0 (5)	153.0→96.9 (10)
55	dithiopyr	22.02	353.9→306.0 (5)	305.9→286.1 (5)
56	edifenphos	29.60	172.9→109.0 (5)	108.9→65.1 (15)
57	EPN	31.22	169.0→141.1 (10)	169.0→77.1 (10)
58	fenitrothion	23.80	125.1→47.0 (10)	125.1→79.0 (10)
59	fludioxonil	30.60	248.0→182.1 (10)	248.0→154.1 (10)
60	fluvalinate-τ I	37.61	250.0→55.0 (40)	181.0→152.0 (10)

dx.doi.org/10.1021/jf405240j | J. Agric. Food Chem. 2014, 62, 3710−3725

Table 1. continued

no.	pesticide	RT (min)	quantification transition[a]	confirmation transition[a]
		(A) Group A		
61	fluvalinate-τ II	37.77	250.0→55.0 (40)	181.0→152.0 (10)
62	furathiocarb	31.16	163.1→135.1 (10)	163.1→107.1 (10)
63	iprobenfos	18.97	203.9→91.0 (5)	121.9→121.0 (15)
64	lindane	21.98	216.9→181.0 (5)	181.0→145.0 (15)
65	p,p'-DDD	28.53	235.0→165.2 (20)	237.0→165.2 (20)
66	p,p'-DDT	28.94	235.0→165.2 (20)	237.0→165.2 (20)
67	pentachloronitrobenzene	15.94	236.9→142.9 (10)	236.9→118.9 (10)
68	phorate	14.46	121.0→65.0 (10)	121.0→47.0 (10)
69	piperonyl butoxide	29.19	176.1→131.1 (10)	176.1→103.1 (10)
70	procymidone	26.84	96.0→67.1 (10)	96.0→53.1 (10)
71	pronamide	19.37	173.0→145.0 (15)	175.0→147.0 (15)
72	prothiofos	26.27	113.0→94.9 (10)	266.9→239.0 (5)
73	pyridaben	32.83	147.2→117.1 (10)	147.2→132.2 (10)
74	pyrimethanil	16.96	198.0→183.1 (10)	198.0→118.1 (10)
75	quinalphos	25.42	146.0→118.0 (10)	146.0→91.0 (10)
76	silafluofen	34.08	179.2→151.1 (10)	286.0→258.1 (10)
77	sulfotep	14.76	201.8→145.9 (10)	237.8→145.9 (10)
78	tebuconazole	30.81	250.0→125.0 (20)	125.0→89.0 (15)
79	tecnazene	11.88	260.9→203.0 (10)	214.9→179.0 (10)
80	*cis*-tefluthrin	16.97	177.1→127.1 (15)	197.0→141.1 (10)
81	terbacil	23.33	160.0→117.1 (5)	161.1→144.1 (10)
82	terbufos	16.37	230.9→129.0 (10)	230.9→175.0 (10)
83	tetraconazole	26.24	336.0→217.9 (20)	170.9→136.0 (10)
84	tetradifon	31.65	158.9→131.0 (10)	226.9→199.0 (15)
85	tolclofos-methyl	20.70	265.0→250.0 (10)	265.0→93.0 (10)
86	triadimefon	24.58	208.0→181.1 (10)	208.0→111.0 (10)
87	triadimenol	27.34	168.0→70.0 (10)	128.0→65.0 (25)
88	triallate	16.68	268.0→184.1 (20)	142.9→83.0 (15)
89	triazophos	29.89	161.2→134.2 (10)	161.2→106.1 (10)
90	trifloxystrobin	29.17	116.0→89.0 (15)	172.0→145.1 (15)
91	trifluralin	14.30	305.9→264.0 (5)	264.0→160.1 (15)
92	vinclozolin	21.67	187.0→124.0 (20)	197.9→145.0 (15)
		(B) Group B		
1	ametryn	21.45	227.0→58.1 (10)	185.0→170.0 (10)
2	benfluralin	14.43	292.0→264.0 (15)	292.0→206.0 (15)
3	butafenacil	35.05	331.0→180.0 (15)	180.0→124.0 (15)
4	cafenstrole	35.97	100.0→72.0 (15)	188.0→118.9 (15)
5	α-chlordane	25.70	271.9→236.9 (20)	372.9→265.9 (20)
6	γ-chlordane	25.39	271.7→236.9 (15)	372.8→265.8 (15)
7	chlorobenzilate	28.12	251.1→139.1 (15)	139.0→111.0 (15)
8	chlorpropham	14.62	153.0→125.0 (10)	153.0→90.0 (10)
9	chlorpyrifos	22.37	198.9.0→171.0 (15)	196.9→169.0 (15)
10	cloquintocet-mexyl	30.54	192.0→190.0 (10)	192.0→162.0 (10)
11	cyhalofop-butyl	32.13	256.2→120.0 (10)	120.1→91.0 (10)
12	cyprodinil	23.87	225.2→224.3 (20)	224.2→208.2 (20)
13	diflufenican	29.97	266.0→238.0 (15)	266.0→246.0 (15)
14	dimepiperate	24.57	119.0→91.0 (10)	118.0→117.0 (10)
15	dimethenamid	20.58	230.0→154.1 (10)	154.1→111.1 (10)
16	diphenamid	25.50	167.1→165.0 (10)	167.1→152.0 (10)
17	α-endosulfan	25.09	206.9→172.0 (15)	194.9→158.9 (15)
18	β-endosulfan	28.65	206.9→172.0 (15)	194.9→158.9 (15)
19	esprocarb	20.82	222.0→91.0 (15)	91.0→65.1 (15)
20	ethalfluralin	13.93	275.9→202.1 (10)	315.9→275.9 (10)
21	ethion	28.71	152.9→96.9 (15)	124.9→96.9 (15)
22	ethoprophos	13.13	157.9→97.0 (10)	157.9→114.0 (10)
23	etofenprox	33.79	163.0 → 135.1 (10)	163.0 → 107.1 (10)
24	etrimfos	17.82	181.0→153.1 (5)	168.0→153.1 (5)
25	fenarimol	32.59	219.0→107.0 (10)	251.0→139.0 (10)
26	fenobucarb	13.65	121.0→ 77.0 (10)	121.0→ 103.1 (10)
27	fenothiocarb	13.65	160.1→72.0 (15)	253.4→169.1 (10)

dx.doi.org/10.1021/jf405240j | J. Agric. Food Chem. 2014, 62, 3710−3725

Table 1. continued

no.	pesticide	RT (min)	quantification transition[a]	confirmation transition[a]
		(B) Group B		
28	fenoxycarb	26.14	255.2→186.2 (10)	186.2→158.2 (10)
29	fensulfothion	29.77	156.0→141.0 (15)	140.0→125.0 (15)
30	fenvalerate	36.56	167.0→125.1 (5)	208.9→141.1 (5)
31	fipronil	29.64	350.8→254.8 (20)	366.8→212.8 (20)
32	flamprop-methyl	28.35	105.0 → 77.1 (10)	105.0 → 51.1 (10)
33	flucythrinate	35.43	198.9→157.0 (10)	156.9→107.1 (10)
34	flumioxazin	38.70	354.0→325.9 (10)	354.0→107.0 (30)
35	fluquinconazole	33.73	340.0 → 298.0 (10)	108.0 → 57.0 (10)
36	flusilazole	28.52	233.0→165.0 (15)	233.0→91.0 (15)
37	flutolanil	28.51	173.0→145.1 (20)	280.9→173.0 (20)
38	fosthiazate I	26.17	195.0 → 103.0 (10)	195.0 → 60.0 (10)
39	fosthiazate II	26.27	195.0 → 103.0 (10)	195.0 → 60.0 (10)
40	halfenprox	33.38	265.0→117.0 (10)	262.9→169.0 (10)
41	isofenphos	25.47	212.9→121.0 (20)	212.9→185.0 (20)
42	isoprocarb	12.08	121.0→77.1 (5)	136.0→121.1 (5)
43	isoprothiolane	27.84	162.1→85.0 (20)	162.1→134.0 (20)
44	isoxathion	28.17	105.0→77.0 (15)	105.0 → 51.0 (10)
45	kresoxim-methyl	27.40	116.0→89.0 (15)	116.0→63.0 (15)
46	lactofen	32.66	343.8→222.9 (10)	343.8→299.9 (10)
47	malathion	23.69	126.9 → 99.0 (10)	172.9 → 99.0 (10)
48	mepronil	29.72	119.1→91.0 (15)	119.1→65.1 (15)
49	metalaxyl	22.25	234.0→146.1 (20)	220.0→192.1 (20)
50	methacrifos	10.16	207.9→180.1 (5)	124.9→47.1 (10)
51	methamidophos	7.51	141.0→95.0 (10)	95.0→79.0 (10)
52	methidathion	26.91	144.9→85.0 (15)	144.9→58.1 (15)
53	*p*,*p*′-methoxychlor	30.47	227.0 → 169.1 (10)	227.0 → 141.1 (10)
54	metolachlor	23.18	238.0→162.2 (10)	162.2→133.2 (10)
55	metominostrobin	27.66	191.2→160.2 (20)	196.2→77.1 (20)
56	mevinphos	9.49	127.0→109.0 (10)	127.0→95.0 (10)
57	molinate	10.13	126.2→55.1 (5)	126.2→83.1 (5)
58	myclobutanil	29.26	179.0→125.1 (15)	179.0→90.0 (15)
59	napropamide	27.18	128.0→72.0 (20)	128.0→100.0 (20)
60	nitrothal-isopropyl	23.94	236.0 → 194.1 (10)	194.0 → 148.1 (10)
61	oxadiazon	27.39	174.9→112.0 (15)	174.9→76.0 (15)
62	oxyfluorfen	28.37	252.0→196.0 (15)	252.0→146.0 (15)
63	paclobutrazol	27.68	236.0→125.0 (15)	125.1→89.0 (15)
64	parathion	24.73	290.9→109.0 (10)	138.9→109.0 (10)
65	parathion-methyl	22.56	262.9→109.0 (10)	125.0→47.0 (10)
66	penconazole	25.77	248.0→157.1 (10)	248.0→192.1 (10)
67	pendimethalin	24.80	251.8→162.2 (10)	251.8→161.1 (10)
68	phenthoate	25.70	274.0 → 121.0 (10)	274.0 → 125.0 (10)
69	permethrin	32.25	183.1→168.1 (15)	183.1→165.1 (15)
70	phenthoate	20.37	274.0→121.0 (20)	274.0→125.0 (20)
71	phosalone	31.22	182.0→111.0 (15)	182.0→102.0 (15)
72	piperophos	21.48	320.0→122.0 (10)	140.0→98.0 (10)
73	pirimiphos-methyl	27.16	290.0→125.0 (20)	232.9→151.0 (20)
74	prochloraz	34.49	180.0→138.0 (15)	195.9→96.9(15)
75	profenofos	26.97	338.8→268.7 (20)	207.9→63.0 (20)
76	promecarb	15.66	135.1→91.0 (15)	150.1→135.2 (15)
77	prometryn	21.27	226.0→184.0 (10)	199.0→184.1 (15)
78	propachlor	13.70	120.0→77.1 (5)	176.1→57.1 (5)
79	propargite	29.57	135.0→107.0 (15)	149.9→135.0 (15)
80	propazine	17.74	214.2→172.2 (10)	229.1→58.1 (10)
81	propham	9.47	136.9→93.0 (10)	119.0→91.0 (10)
82	propiconazole	29.71	172.9→109.0 (10)	172.9→145.0 (10)
83	propoxur	14.40	110.0→63.0 (5)	110.0→64.0 (5)
84	pyrazophos	32.50	221.0→193.0 (10)	232.0→204.0 (10)
85	pyributicarb	30.02	165.0→108.0 (10)	108.0→93.0 (10)
86	pyridaphenthion	31.30	340.0→199.0 (10)	204.0→203.0 (10)
87	pyrimidifen	34.78	184.1→169.1 (10)	186.0→171.1 (10)

dx.doi.org/10.1021/jf405240j | J. Agric. Food Chem. 2014, 62, 3710−3725

Table 1. continued

no.	pesticide	RT (min)	quantification transition[a]	confirmation transition[a]
		(B) Group B		
88	quinoclamine	25.00	207.0 → 172.1 (10)	209.0 → 172.1 (10)
89	quinoxyfen	28.78	271.9→237.1 (10)	237.0→208.0 (10)
90	ronnel	20.53	285.0→269.9 (15)	286.9→272.0 (15)
91	simeconazole	23.01	121.0 → 101.1 (10)	121.0 → 75.1 (10)
92	tebufenpyrad	30.28	332.9→171.0 (10)	275.9→171.0 (10)
93	terbutryn	22.01	241.1→170.2 (15)	185.0→170.0 (15)
94	thiazopyr	23.76	327.1→277.0 (10)	349.0→329.0 (10)

[a]Collision energy (eV) is given in parentheses.

introduced by Anastassiades and Lehotay et al. in 2003.[15,16] Its main advantage is comprehensiveness, being useful for the analysis of various pesticides. A great deal of literature suggests that better results are obtained by the QuEChERS method with efficient removal of matrix compounds and higher recoveries of pesticides with minimal solvent.[9,17−20] The first step of the QuEChERS method is to extract the analytes from samples with a small amount of acetonitrile, followed by liquid−liquid partition by salting-out with sodium chloride and magnesium sulfate. Then, a cleanup step is often carried out by mixing the acetonitrile extract with loose sorbents, which was based on reversed-dispersive solid phase extraction (r-DSPE) to absorb the interference substances in the matrices, rather than the analytes. In most cases, primary−secondary amine (PSA), graphitized carbon black (GCB), or C_{18} was used as r-DSPE sorbent to remove the interference substances in the matrix such as fatty acid compounds, pigments, sterols, and other nonpolar interfering substances.[21−23]

Carbon nanotubes (CNTs), first reported by Iijiama in 1991,[24] are interesting carbonaceous materials as new carbon-based nanomaterials. According to the carbon atom layers in the wall of the nanotubes, CNTs can be divided into single-walled carbon nanotubes (SWCNTs) and multiple-walled carbon nanotubes (MWCNTs). MWCNTs have been widely used as sorbent materials in inorganic elements, pollutants, and veterinary drugs.[25−27] In our previous study, MWCNTs were used as alternative reversed-dispersive solid phase extraction materials in pesticide multiresidue analysis with the QuEChERS method.[28,29] They were also mixed with other sorbents such as PSA and GCB for dispersive cleanup of acetonitrile extracts from tea samples.[30]

A more practical way to perform the r-DSPE method is to use cartridges (like most SPE cartridges) where the sample matrix compounds in the acetonitrile extraction interact with the sorbents.[31] In the work presented here, an r-DSPE cleanup method for tomato product extracts was developed using multiplug filtration cleanup (m-PFC) followed by gas chromatography−triple-quadruple tandem mass spectrometry (GC-MS/MS) analysis. The cartridges of m-PFC contained MWCNTs and anhydrous magnesium sulfate to efficiently clean up QuEChERS extracts prior to analysis. The proposed technique based on MWCNTs intends to adsorb the interfering substances in the matrices, rather than the analytes, and anhydrous magnesium sulfate could remove water from the extract. The m-PFC method is shown to be very rapid to perform without any solvent evaporation. It is expected to facilitate routine analyses of pesticides in fresh vegetable/fruit samples such as tomato and its processed products.

MATERIALS AND METHODS

Standards, Reagents, and Materials. Analytical standards of the pesticides in the study were provided by the Institute of the Control of Agrochemicals, Ministry of Agriculture, Peoples' Republic of China. The purities of the standard pesticides were from 95 to 99%. Stock solutions of 10 mg L^{-1} for pesticide mixtures were prepared in acetonitrile and stored at −20 °C. The working solutions were prepared daily. HPLC grade acetonitrile was obtained from Fisher Chemicals (Fair Lawn, NJ, USA). Analytical reagent grade anhydrous sodium chloride (NaCl) and magnesium sulfate ($MgSO_4$) were obtained from Sinopharm Chemical Reagent (Beijing, China). MWCNTs with average external diameters of 10−20 nm were provided by Tianjin Bonna-Agela Technologies Co., Ltd. (China). M-PFC tips were packed with 10 mg of MWCNTs and 150 mg of anhydrous magnesium sulfate with assistance from Tianjin Bonna-Agela Technologies.

GC-MS/MS Analytical Conditions. Determinations were performed using an Agilent 7000B triple-quadrupole mass spectrometer interfaced to an Agilent 7890A GC. An Agilent Technologies capillary column HP1701 MS analytical column (30 m × 250 μm × 0.25 μm film thickness) was used for GC separation, with helium (99.9999%) as carrier gas at a constant flow rate of 1.2 mL min^{-1}. The column temperature was initially at 80 °C (hold for 1 min), increased to 150 °C at a rate of 30 °C min^{-1} and then to 210 °C at a rate of 3 °C min^{-1}, and finally increased to 290 °C at a rate of 10 °C min^{-1}, holding for 12 min. The temperature of the injector port was 260 °C, and a volume of 1 μL was injected in splitless mode. The total running time was 43 min.

The mass spectrometer was operated in electron ionization mode (70 eV). Default instrument settings of collision gas flow of N_2 at 1.5 mL min^{-1} and He at 2.25 mL min^{-1} and quadrupole temperature of 150 °C were used in all MS/MS experiments. The detector voltage was automatically set by the instrument after automated MS/MS tuning, which was typically 1250 V. A full autotune of the mass spectrometer using the default parameters of the instrument was performed before each sequence. Agilent MassHunter was used for instrument control and data acquisition/processing. For the final multiple reaction monitoring (MRM) acquisition method, two ion transitions at the experimentally optimized collision energy (CE) were monitored for each analyte. Both pairs of the MRM transitions were used for confirmation analysis, which meets the EU Decision,[32] and the most sensitive transitions were selected for quantification analysis.

To obtain better separation efficiency, the 186 compounds were divided into two groups: groups A and B consisted of 92 and 94 compounds, respectively. Therefore, the 186 pesticides were detected by two GC-MS/MS analyses. Table 1 summarizes the optimized MS/MS conditions for the individual analytes and their typical retention times (RT) in groups A and B.

Sample Preparation. The tomato, tomato juice, and ketchup samples were obtained from a local supermarket, and tomato samples were homogenized with a blender for 1 min at room temperature. For recovery determination, the homogenized samples (10.0 ± 0.1 g) were spiked by the addition of the standard stock solutions at two concentration levels of 10 and 100 μg kg^{-1}. The spiked samples were set aside for 30 min before extraction.

An amount (10.0 ± 0.1 g) of ground tomato, tomato juice, or ketchup samples was weighed into a 50 mL centrifuge tube, and 10 mL of acetonitrile was added. The resulting solution was shaken by the vortex for 1 min. One gram of sodium chloride and 4 g of anhydrous magnesium sulfate were added for tomato and ketchup extracts, and 3 g of sodium chloride and 4 g of anhydrous magnesium sulfate were added for tomato juice extracts. The tube was cooled to room temperature in an ice−water bath immediately. The centrifuge tube was shaken vigorously for 1 min to prevent salt agglomeration before centrifugation at 3800 rpm for 5 min. The supernatant was used for further m-PFC.

M-PFC Procedures. A 1 mL aliquot of the initial extracts was used for extraction, which was introduced into a 2.0 mL microcentrifuge tube. The m-PFC procedure was carried out with a 2.0 mL syringe and an m-PFC tip. The sorbent in the tip was 10 mg of MWCNTs mixed with 150 mg of $MgSO_4$.

Schematic diagrams of an m-PFC tip and the procedures are shown in Figure 1. As shown in Figure 2, the syringe needle was kept under

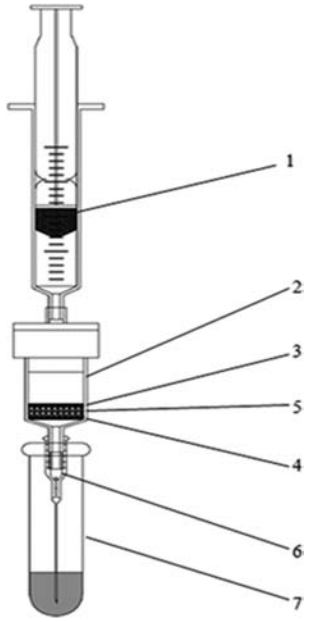

Figure 1. Schematic diagram of an m-PFC tip: 1, syringe; 2, column; 3, PE frits (upper); 4, PE frits (low); 5, MWCMNs (10 mg) and anhydrous magnesium sulfate (150 mg); 6, syringe needle; 7, 2.0 mL microcentrifuge tube.

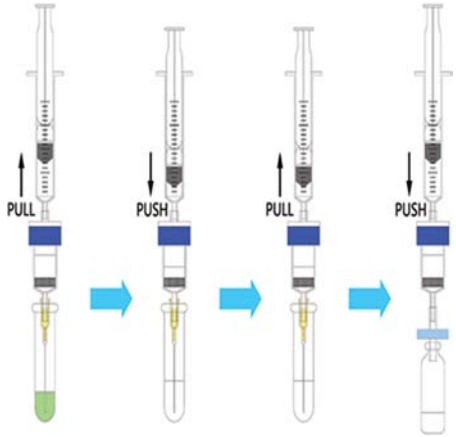

Figure 2. Schematic diagram of the rapid m-PFC method.

the surface of the extract, and then the syringe piston was pushed and pulled as follows: Step 1, pull the piston. All of the extracts were sucked into the m-PFC tip and filtered through the sorbent. Step 2, push the piston. All of the extracts were pressed into the microcentrifuge tube and filtered through the sorbent a second time. Step 3, repeat steps 1 and 2 twice. Step 4, remove the needle and press the extracts into an LC vial to carry out the chromatographic analysis. At the same time, the acetonitrile layer was filtered through a 0.22 μm filter membrane.

Method Performances. Three kinds of tomato products were selected for validation purposes: tomato, tomato juice, and ketchup. Validation data were obtained for each type of sample. The following parameters were determined during validation of the analytical method: linearity, limit of quantification (LOQ), limit of detection (LOD), accuracy, and precision. Linearity was studied using matrix-matched calibration by analyzing samples of tomato, tomato juice, and ketchup. The recovery and reproducibility experiments were carried out for each sample in five replicates at two fortification levels (10 and 100 μg kg^{-1}). The LODs were determined as the concentration of analyte giving a signal-to-noise ratio (S/N) of 3 for the target ion (the less intense transition); LOQs were determined as the concentration of analytes giving a S/N of 10 for the target ion (the less intense transition).

RESULTS AND DISCUSSION

Optimization of GC-MS/MS Conditions. Optimization of triple-quadrupole MS/MS was a rather demanding task because specific experimental conditions were required for each target compound to conduct analyses.[33] To find the retention times and the best resolution between the analyte peaks, preliminary experiments were carried out systematically in full scan mode using compound standard solutions.

A tandem mass detector has high selectivity and sensitivity and provides an effective solution. The relevant consideration included the choice of precursor ions, product ions, and optimization of collision energies for best response. The mass spectrometric parameters option was initially performed by full scan for the compounds. After that, the precursor ion for each analyte was selected, and then the collision energy voltages (potential on second quadrupole) were optimized to generate MS/MS product ions. The characteristic ion transition and collision energy for each compound during MRM acquisition are listed in Table 1. The collision energy was optimized for two selective ion transitions for every pesticide. Both pairs of MRM transitions were used for confirmation analysis, which meets the EU Decision,[32] and the most sensitive transitions were selected for quantification analysis.

Because of the large number of compounds to be detected, the 186 pesticides were divided into two groups and analyzed twice by GC-MS/MS. Groups A and B consisted of 92 and 94 compounds, respectively. The conditions of gas chromatography for the two groups were the same, but the MS/MS conditions were different due to the various pesticides. The developed method was highly selective with the monitoring of specific MRM of each analyte, which was essential to reduce the risk of false-positive results.

Extraction Procedure Optimization. In the original QuEChERS method, the amounts of acetonitrile and sodium chloride were 10 mL and 1 g per 10 g of sample, respectively. In our pre-experiments, the original QuEChERS extraction procedure with 1 g of sodium chloride and 10 mL of acetonitrile was used, and good recoveries (>70%) could be obtained for most pesticides in the matrices of tomato and ketchup. However, when it came to tomato juice, the recoveries for 82 pesticides (of the 186 pesticides) decreased below 60%, probably due to the high content of water in juice. To obtain better recoveries for tomato juice, different amounts of sodium

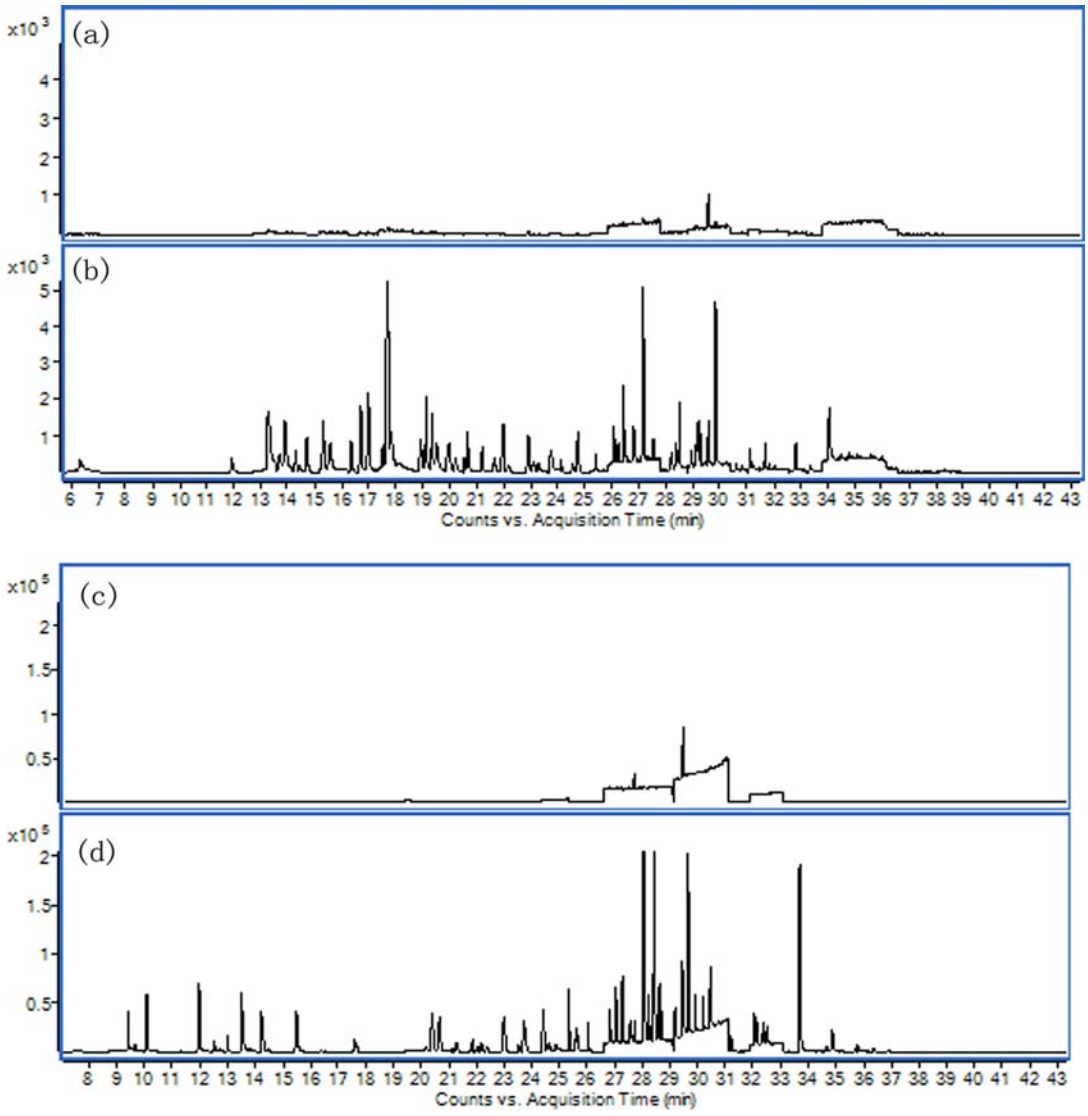

Figure 3. Chromatograms for tomato extracts after m-PFC: (a) total ion current (TIC) chromatogram for a typical blank sample of the target analytes in group A; (b) TIC chromatogram for a typical blank sample spiked at 10 μg kg^{-1} of the target analytes in group A; (c) TIC chromatogram for a typical blank sample of the target analytes in group B; (d) TIC chromatogram for a typical blank sample spiked at 10 μg kg^{-1} of the target analytes in group B.

chloride (1, 2, and 3 g) were employed and analyzed in triplicate at one calibration point (100 μg kg^{-1}). It was shown that the salting-out effect of 3 g of sodium chloride was notably higher in comparison with the other amounts, and the recoveries for most compounds were satisfactory and acceptable. Therefore, 3 g of sodium chloride was added for salting-out after acetonitrile extraction, which was employed as the optimum amount for the matrix of tomato juice in the study. The original QuEChERS extraction procedure (1 g of sodium chloride) was used for the other two matrices of tomato and ketchup.

M-PFC Process. The m-PFC process was performed to remove the sample matrix in the extract prior to chromatographic analysis. The removal of interference substances in the matrices is necessary to ensure reproducible peak intensities for quantitative analysis. The proposed cleanup method was based on the m-PFC procedure with the mixture of anhydrous magnesium sulfate and MWCNTs. Anhydrous magnesium sulfate was used to remove the water in the matrices, and MWCNTs were used to remove other interference substances such as fatty acids, pigments, and other matrix compounds.

In our previous study, we found that MWCNTs could be used as alternative r-DSPE materials in pesticide multiresidue analysis with the QuEChERS method.[28] The optimal amount of MWCNTs was 10 mg, which was suitable for cleanup. A smaller amount of MWCNTs (5 mg) could not obtain as good a cleanup performance as 10 mg of MWCNTs and 15 mg or more MWCNTs could lead to low recoveries (<70%) for most pesticides. In addition, the final samples processed by 10 mg of MWCNTs looked transparent in color. In this study, we used 10 mg of MWCNTs mixed with 150 mg of $MgSO_4$ as the sorbent, referred to the previous work. In most cases, the recoveries could meet the requirement of the pesticide residue analysis.

To obtain the best recovery and cleanup performance, the cycles of pulling and pushing during the m-PFC procedure were optimized. Better recoveries were achieved with one or two times of pulling and pushing, but the cleanup performance was not as good as three times, and there were more

Table 2. Calibration Curve Coefficients (R^2), LOQs (S/N Ratio of 10), and LODs (S/N Ratio of 3) for 186 Pesticides in Tomato, Tomato Juice, and Ketchup

	tomato			tomato juice			ketchup		
compound	R^2	LOQ ($\mu g\ kg^{-1}$)	LOD ($\mu g\ kg^{-1}$)	R^2	LOQ ($\mu g\ kg^{-1}$)	LOD ($\mu g\ kg^{-1}$)	R^2	LOQ ($\mu g\ kg^{-1}$)	LOD ($\mu g\ kg^{-1}$)
acetochlor	0.992	3	1	0.994	2	1	0.999	8	2
acrinathrin	0.977	3	1	0.998	1	0.2	0.998	4	1
alachlor	0.996	2	1	0.994	3	1	0.997	1	0.2
aldrin	0.997	3	1	0.983	7	2	0.996	10	3
ametryn	0.995	1	0.3	0.998	1	0.2	0.994	3	1
anilofos	0.998	4	1	0.993	1	0.2	0.998	1	0.2
atrazine	0.998	3	1	0.993	1	0.2	0.997	1	0.3
azaconazole	0.991	2	1	0.993	8	2	0.997	8	2
benalaxyl	0.997	4	1	0.995	1	0.3	0.997	4	1
bendiocarb	0.996	7	2	0.991	5	2	0.996	5	2
benfluralin	0.994	1	0.2	1.000	1	0.3	0.993	1	0.3
benoxacor	0.998	5	1	0.982	10	3	0.991	4	1
α-BHC	0.998	8	2	0.992	8	2	0.996	8	2
β-BHC	0.996	1	0.3	0.990	1	0.3	0.997	1	0.3
δ-BHC	0.997	2	1	0.993	1	0.2	0.997	1	0.3
bifenox	0.997	3	1	0.995	1	0.2	0.996	1	0.3
bifenthrin	0.998	1	0.3	0.996	2	1	0.997	1	0.2
bitertanol	0.990	8	2	0.997	1	0.2	0.997	1	0.2
bromophos-ethyl	0.990	2	1	0.994	1	0.4	0.997	1	0.3
bupirimate	0.997	1	0.3	0.996	1	0.3	0.998	1	0.2
buprofezin	0.996	6	2	0.992	4	1	0.985	4	1
butachlor	0.996	6	2	0.984	3	1	0.997	4	1
butafenacil	0.996	2	0.5	0.999	1	0.3	0.996	1	0.3
cadusafos	1.000	1	0.3	0.993	3	1	0.996	2	0.5
cafenstrole	0.994	7	2	0.991	5	1	0.982	3	1
carbaryl	0.993	2	1	0.993	1	0.3	0.959	1	0.3
carbofuran	0.996	2	1	0.990	1	0.2	0.994	1	0.2
α-chlordane	0.997	1	0.3	0.996	1	0.4	0.996	1	0.2
γ-chlordane	0.997	1	0.2	0.996	1	0.3	0.997	1	0.2
chlordimeform	0.999	8	2	0.999	3	1	0.997	2	1
chlorfenapyr	0.994	2	1	1.000	1	0.3	0.994	1	0.3
chlorobenzilate	0.996	1	0.4	0.995	1	0.3	0.997	1	0.3
chlorpropham	0.999	10	3	0.997	8	2	0.995	5	2
chlorpyrifos	0.997	1	0.2	0.996	1	0.4	0.995	3	1
chlorpyrifos-methyl	0.996	1	0.3	0.991	4	1	0.997	3	1
clodinafop-propargyl	0.991	7	2	0.999	1	0.4	0.996	2	1
cloquintocet-mexyl	0.996	3	1	0.995	1	0.4	0.997	1	0.3
coumaphos	0.992	3	1	0.999	1	0.2	0.995	1	0.4
cyanophos	0.997	1	0.3	0.991	2	1	0.997	2	1
cyflufenamid	0.976	6	2	0.958	4	1	0.998	7	2
cyfluthrin I	0.995	3	1	1.000	1	0.2	0.995	1	0.2
cyfluthrin II	0.997	10	3	0.991	3	1	0.994	10	3
cyhalofop-butyl	0.996	2	1	0.996	1	0.3	0.997	1	0.3
cypermethrin IV	0.996	3	1	0.984	4	1	0.996	6	2
cyprodinil	0.997	1	0.3	0.994	1	0.2	0.996	1	0.3
DCPA	0.997	4	1	0.990	1	0.2	0.997	2	0.5
o,p′-DDD	0.997	1	0.2	0.992	2	1	0.997	1	0.3
o,p′-DDE	0.996	1	0.3	0.992	1	0.3	0.997	1	0.3
p,p′-DDE	0.997	1	0.2	0.992	1	0.4	0.997	2	1
o,p′-DDT	0.993	2	1	0.990	1	0.3	0.997	1	0.2
DEF	0.991	3	1	0.989	1	0.4	0.997	2	0.5
deltamethrin	0.996	5	2	1.000	5	1	0.997	3	1
diazinon	0.998	2	1	0.992	3	1	0.996	1	0.3
dichlofenthion	0.997	3	1	0.991	1	0.3	0.997	1	0.3
dichlorvos	0.999	4	1	0.996	1	0.2	0.998	1	0.2
diclobutrazol	0.995	3	1	0.995	1	0.3	0.997	1	0.3
diclofop-methyl	0.999	6	2	0.997	3	1	0.997	1	0.4
dicloran	0.995	2	1	0.996	1	0.3	0.995	1	0.2

dx.doi.org/10.1021/jf405240j | J. Agric. Food Chem. 2014, 62, 3710−3725

Table 2. continued

compound	tomato			tomato juice			ketchup		
	R^2	LOQ (μg kg^{-1})	LOD (μg kg^{-1})	R^2	LOQ (μg kg^{-1})	LOD (μg kg^{-1})	R^2	LOQ (μg kg^{-1})	LOD (μg kg^{-1})
dieldrin	0.998	4	1	0.998	1	0.3	0.998	1	0.4
difenoconazole I	0.993	10	3	0.993	10	3	0.995	6	2
difenoconazole II	0.984	10	3	0.995	7	2	0.994	10	3
diflufenican	0.993	2	1	0.996	2	0.5	0.998	1	0.4
dimepiperate	0.989	4	1	0.991	2	1	0.991	4	1
dimethenamid	0.997	1	0.3	0.998	1	0.3	0.998	1	0.3
dimethipin	0.993	5	1	0.993	5	2	0.997	2	1
dimethoate	0.998	10	3	0.992	10	3	0.997	10	3
dimethylvinphos	0.997	10	3	0.999	10	3	0.997	8	2
diphenamid	1.000	8	2	0.996	8	2	0.997	10	3
diphenylamine	0.995	5	2	0.994	10	3	1.000	6	2
disulfoton	0.996	2	0.5	0.991	1	0.2	0.996	1	0.3
dithiopyr	0.997	10	3	0.996	8	2	0.998	8	2
edifenphos	0.998	8	2	0.992	10	3	0.997	8	2
α-endosulfan	0.998	10	3	0.989	10	3	0.957	10	3
β-endosulfan	0.998	10	3	0.997	10	3	0.995	10	3
EPN	0.991	6	2	1.000	3	1	0.984	2	1
esprocarb	0.996	1	0.2	0.999	1	0.3	0.996	1	0.3
ethalfluralin	0.998	2	1	1.000	1	0.3	0.993	1	0.3
ethion	0.993	3	1	0.997	6	2	0.997	2	1
ethoprophos	0.998	1	0.3	0.999	1	0.2	0.997	1	0.3
etofenprox	0.996	2	1	0.996	1	0.4	0.998	1	0.3
etrimfos	0.998	10	3	0.998	5	2	0.981	10	3
fenarimol	0.997	5	2	0.997	3	1	0.998	2	1
fenitrothion	0.998	8	2	0.993	10	3	0.996	10	3
fenobucarb	0.998	6	2	0.997	10	3	0.997	8	2
fenothiocarb	0.992	1	0.3	0.992	1	0.3	0.997	1	0.3
fenoxycarb	0.996	5	1	0.992	10	3	0.998	5	2
fensulfothion	0.994	10	3	0.994	5	1	0.990	5	2
fenvalerate	0.996	10	3	0.976	10	3	0.992	6	2
fipronil	0.994	10	3	0.991	5	1	1.000	5	2
flamprop-methyl	0.996	10	3	0.999	10	3	0.988	10	3
flucythrinate	0.995	5	1	0.997	5	2	0.993	1	0.4
fludioxonil	0.998	4	1	0.995	1	0.4	0.997	1	0.4
flumioxazin	0.985	10	3	0.990	10	3	0.998	10	3
fluquinconazole	0.967	3	1	0.993	2	1	0.993	1	0.3
flusilazole	0.982	2	1	0.997	2	1	0.998	1	0.4
flutolanil	0.995	3	1	0.995	1	0.3	0.997	1	0.2
fluvalinate-τ I	0.994	3	1	0.997	2	1	0.997	1	0.2
fluvalinate-τ II	0.996	4	1	0.999	1	0.4	0.997	1	0.2
fosthiazate I	0.998	10	3	0.996	4	1	0.997	4	1
fosthiazate II	0.998	10	3	0.996	4	1	0.974	3	1
furathiocarb	0.994	1	0.3	0.991	1	0.3	0.997	1	0.3
halfenprox	0.997	5	2	0.998	2	1	0.996	2	1
iprobenfos	0.995	1	0.3	0.991	1	0.4	0.996	1	0.3
isofenphos	0.959	1	0.3	0.992	2	0.5	0.996	1	0.3
isoprocarb	0.999	10	3	0.993	5	2	0.955	5	2
isoprothiolane	0.997	1	0.4	0.996	1	0.2	0.997	1	0.3
isoxathion	0.990	10	3	0.999	5	2	0.992	5	1
kresoxim-methyl	0.995	3	1	0.995	3	1	0.996	3	1
lactofen	1.000	4	1	0.999	4	1	0.996	2	1
lindane	0.988	2	0.5	0.090	4	1	0.997	2	1
malathion	0.974	10	3	1.000	10	3	0.991	10	3
mepronil	0.995	10	3	0.994	5	2	0.993	5	2
metalaxyl	0.997	1	0.2	0.995	1	0.2	0.997	1	0.2
methacrifos	0.997	1	0.3	0.998	1	0.3	0.997	1	0.3
methamidophos	0.980	10	3	1.000	10	3	0.995	10	3
methidathion	0.995	3	1	0.996	2	1	0.994	2	1
p,p'-methoxychlor	0.993	3	1	0.999	2	1	0.993	1	0.4

dx.doi.org/10.1021/jf405240j | J. Agric. Food Chem. 2014, 62, 3710−3725

Table 2. continued

	tomato			tomato juice			ketchup		
compound	R^2	LOQ (μg kg^{-1})	LOD (μg kg^{-1})	R^2	LOQ (μg kg^{-1})	LOD (μg kg^{-1})	R^2	LOQ (μg kg^{-1})	LOD (μg kg^{-1})
metolachlor	0.996	1	0.3	0.996	1	0.3	0.996	1	0.3
metominostrobin	0.997	5	2	0.989	3	1	0.999	2	1
mevinphos	1.000	6	2	0.995	3	1	0.997	2	1
molinate	0.997	5	1	0.998	6	2	0.997	6	2
myclobutanil	0.995	3	1	0.998	1	0.4	0.996	1	0.2
napropamide	0.996	10	3	0.990	5	2	0.991	5	2
nitrothal-isopropyl	0.994	1	0.2	0.997	1	0.2	0.992	1	0.3
oxadiazon	0.997	2	1	0.995	1	0.3	0.998	1	0.3
oxyfluorfen	0.994	5	2	0.997	5	2	0.992	5	2
p,p′-DDD	0.996	1	0.4	0.996	4	1	0.997	2	1
p,p′-DDT	0.993	2	1	0.997	1	0.4	0.996	1	0.3
paclobutrazol	0.995	3	1	0.993	3	1	0.996	1	0.2
parathion	0.995	3	1	0.996	1	0.4	0.986	1	0.4
parathion-methyl	0.996	1	0.3	0.997	2	1	0.996	1	0.2
penconazole	0.997	2	1	0.994	1	0.3	0.997	1	0.2
pendimethalin	0.990	1	0.3	0.999	1	0.2	0.992	1	0.3
pentachloronitrobenzene	0.995	8	2	0.991	5	2	0.997	5	2
permethrin	0.992	2	1	0.998	2	1	0.996	1	0.3
phenthoate	0.991	1	0.2	0.999	1	0.3	0.991	2	1
phenthoate	0.995	10	3	0.995	5	1	0.992	10	3
phorate	0.994	10	3	0.997	10	3	0.996	8	2
phosalone	0.998	1	0.2	0.998	1	0.3	0.993	1	0.3
piperonyl butoxide	0.997	1	0.3	0.995	2	0.5	0.997	1	0.2
piperophos	0.996	1	0.3	0.999	1	0.3	0.997	1	0.3
pirimiphos-methyl	0.997	10	3	0.996	5	2	0.998	5	2
prochloraz	0.990	10	3	0.997	10	3	0.998	10	3
procymidone	0.997	4	1	0.974	1	0.4	0.925	1	0.3
profenofos	0.998	4	1	0.995	4	1	0.995	1	0.4
promecarb	0.998	4	1	0.998	3	1	0.993	2	1
prometryn	0.988	1	0.3	0.995	1	0.3	0.994	2	1
pronamide	0.997	2	1	0.992	1	0.2	0.996	1	0.3
propachlor	0.998	1	0.4	1.000	2	1	0.998	3	1
propargite	0.990	8	2	0.966	10	3	0.982	10	3
propazine	0.998	2	1	0.998	1	0.2	0.997	1	0.2
propham	1.000	3	1	0.999	2	1	0.997	3	1
propiconazole	0.990	8	2	0.991	8	2	0.996	10	3
propoxur	0.996	2	1	0.992	1	0.4	0.993	1	0.4
prothiofos	0.996	1	0.3	0.990	2	0.5	0.992	1	0.3
pyrazophos	0.992	10	3	0.997	10	3	0.997	8	2
pyributicarb	0.996	2	1	0.997	2	0.5	0.996	2	1
pyridaben	0.998	6	2	0.994	4	1	0.996	8	2
pyridaphenthion	0.993	1	0.2	0.997	1	0.3	0.997	1	0.3
pyrimethanil	0.997	3	1	0.995	2	1	0.996	1	0.3
pyrimidifen	0.995	10	3	0.992	10	3	0.998	10	3
quinalphos	0.995	4	1	0.991	1	0.3	0.997	1	0.4
quinoclamine	0.971	2	1	0.998	2	1	0.991	1	0.4
quinoxyfen	0.997	2	1	0.996	1	0.3	0.997	2	1
ronnel	0.997	2	1	0.999	1	0.2	0.996	1	0.3
silafluofen	1.000	3	1	0.997	3	1	0.997	6	2
simeconazole	0.994	1	0.2	1.000	1	0.2	0.994	1	0.2
sulfotep	0.990	1	0.3	0.952	4	1	0.995	4	1
tebuconazole	0.998	4	1	0.997	5	1	0.997	5	2
tebufenpyrad	0.996	3	1	0.996	1	0.3	0.997	1	0.3
tecnazene	0.998	1	0.3	0.993	2	1	1.000	1	0.4
cis-tefluthrin	0.998	1	0.3	0.993	8	2	0.996	4	1
terbacil	0.994	8	2	0.990	5	1	0.997	3	1
terbufos	0.995	1	0.3	0.993	2	1	0.997	1	0.4
terbutryn	0.995	1	0.4	0.993	2	0.5	0.999	1	0.3
tetraconazole	0.998	2	1	0.994	2	1	0.998	1	0.4

dx.doi.org/10.1021/jf405240j | J. Agric. Food Chem. 2014, 62, 3710−3725

Table 2. continued

compound	tomato			tomato juice			ketchup		
	R^2	LOQ (μg kg^{-1})	LOD (μg kg^{-1})	R^2	LOQ (μg kg^{-1})	LOD (μg kg^{-1})	R^2	LOQ (μg kg^{-1})	LOD (μg kg^{-1})
tetradifon	0.999	7	2	0.996	10	3	0.997	8	2
thiazopyr	0.993	2	1	0.996	1	0.3	0.996	1	0.3
tolclofos-methyl	0.997	8	2	0.991	10	3	0.997	8	2
triadimefon	0.993	10	3	0.995	8	2	0.998	10	3
triadimenol	0.998	6	2	0.993	8	2	0.997	5	2
triallate	0.996	5	2	0.996	8	2	0.996	8	2
triazophos	0.992	5	2	0.991	10	3	0.997	10	3
trifloxystrobin	0.996	6	2	0.993	3	1	0.997	3	1
trifluralin	0.996	1	0.3	0.994	3	1	0.997	3	1
vinclozolin	0.996	10	3	0.993	10	3	0.997	8	2

chromatographic interferences when pulling and pushing one or two times. The recoveries for most compounds (expect eight compounds) were also acceptable when three times of pulling and pushing were used. In addition, four or more times were also tested, but there was no significant difference for the cleanup performance between three times and four times. As a result, three times of pulling and pushing was chosen as the optimized m-PFC procedure.

Figure 3 shows GC-MS/MS chromatograms of the blank tomato sample and the spiked sample after cleanup procedures using m-PFC, respectively. Little interference appeared in the chromatogram of samples. Finally, 10 mg of MWCNTs mixed with 150 mg of $MgSO_4$ (1 mL extract) was used for the m-PFC process in the further studies because acceptable recoveries and good cleanup performances were both obtained for most compounds.

Method Validation. The linearity of the method was tested using matrix-matched calibration solutions. As recommended in EU guidelines, in our study validation experiments were calculated using matrix-matched calibration standards for the more accurate results, excluding any influence produced by matrix effects. Calibration curves were constructed from calibration solutions in extracts of three kinds of matrices, tomato, tomato juice, and ketchup at five different concentrations in the range of 5−200 μg L^{-1} for all pesticides. The quantitative results of a detection method greatly depend on its calibration. As shown in Table 2, good linearity was found for most pesticides with coefficients of determination (R^2) better than 0.990.

As LODs and LOQs are matrix dependent, the proposed method was tested for extraction and determination of multiresidues in different kinds of matrices (tomato, tomato juice, and ketchup), which manifested various levels of LOD and LOQ. In this study, LODs and LOQs were calculated as the concentration giving signal-to-noise ratios of 3 (S/N = 3) and 10 (S/N = 10), respectively, which was analyzed by the MassHunter Workstation software qualitative analysis version B.03.01/build 3.1.346.0 and Microsoft Excel. As shown in Table 2, the LODs for these pesticides studied ranged from 0.2 to 3 μg kg^{-1} in the three matrices and the LOQs ranged from 1 to 10 μg kg^{-1}.

To study the accuracy and precision of the proposed method using GC-MS/MS analysis, three different sample matrices were spiked with standard pesticides at a low level (10 μg kg^{-1}) and a high level (100 μg kg^{-1}). The results of the average recoveries and relative standard deviations (RSDs) of pesticides spiked at the two levels are shown in Table 3. The recoveries of most pesticides were in the range from 70 to 137% (71−137% for tomato, 70−131% for tomato juice, and 70−130% for ketchup). RSDs were below 15% for most cases. However, low recoveries (<65%) were obtained for eight compounds (cyprodinil, diflufenican, prochloraz, pyrimidifen, quinoclamine, quinoxyfen, cyflufenamid, and pyrimethanil). The nature of these compounds is readily suggested by their chemical structures (Figure 4). It was found that all eight pesticides contained two rings at least or one benzoheterocycle. The recoveries for the eight compounds ranged from 20 to 65% and RSDs were>20% in some cases, which could not meet the requirements for the analysis of pesticides. By reducing the cycles of m-PFC procedure to one or two times of pulling and pushing, the recoveries of those compounds increased a little (by 5−15%) and RSDs were >15%, which still could not meet the requirements for the analysis of pesticides. As a result, the m-PFC based on the MWCNTs process might not be suitable for the analysis of those compounds containing many rings or benzoheterocycle. It is possible to incorporate an alternative sorbent to extract these compounds using m-PFC technology.

Real Samples Analysis. To evaluate the proposed method, it was applied to the analysis of real samples. It was used for the analysis of pesticide residues in 10 tomato, 5 tomato juice, and 5 ketchup samples, which were obtained from local markets and supermarkets in Beijing. All of the samples were extracted and analyzed as described under Materials and Methods. From the analytical results, chlorpyrifos (1.6−8.1 μg kg^{-1}), procymidone (17−51 μg kg^{-1}), flucythrinate (5.6−8.7 μg kg^{-1}), and metalaxyl (2.3−11.2 μg kg^{-1}) were detected in six tomato samples. Procymidone (2.5 μg kg^{-1}) was detected in one tomato juice sample. Chlorpyrifos residues were detected in one ketchup sample, with the concentration of 3.3 μg kg^{-1}.

A rapid and sensitive method for the analysis of multiresidues in tomato products has been developed using m-PFC technology combined with the QuEChERS method. The m-PFC process provided an effective method for cleanup of pesticide extracts from matrices. The cleanup procedure after extraction was focused on removing the interfering substances in the matrices, rather than extracting and isolating the analytes. In most cases, satisfactory recoveries of 70−130% were obtained with relative standard deviations of <15%. The sample cleanup process was achieved without any solvent evaporation or vortex or centrifugation procedure. The feasibility of rapid, high-throughput analysis of pesticides by performing the m-PFC process of acetonitrile extracts of tomato products in tens of seconds with no additional concentration and solvent exchange steps is demonstrated.

Table 3. Average Recoveries and Relative Standard Deviations (RSDs) at Two Spiked Levels in Tomato, Tomato Juice, and Ketchup

	average recovery (%) (RSD, %) (n = 5)					
	tomato		tomato juice		ketchup	
compound	10 μg kg^{-1}	100 μg kg^{-1}	10 μg kg^{-1}	100 μg kg^{-1}	10 μg kg^{-1}	100 μg kg^{-1}
acetochlor	101 (5)	96 (6)	106 (5)	100 (8)	93 (9)	91 (7)
acrinathrin	82 (6)	95 (10)	104 (5)	98 (13)	101 (8)	111 (6)
alachlor	101 (4)	100 (4)	107 (4)	98 (5)	99 (8)	93 (4)
aldrin	93 (12)	84 (5)	101 (1)	90 (9)	95 (7)	98 (2)
ametryn	105 (12)	80 (7)	107 (10)	85 (7)	102 (12)	96 (3)
anilofos	111 (6)	109 (8)	104 (6)	97 (8)	98 (7)	103 (6)
atrazine	96 (6)	111 (11)	108 (7)	112 (12)	102 (7)	106 (10)
azaconazole	103 (6)	113 (10)	101 (7)	119 (12)	95 (9)	110 (11)
benalaxyl	130 (7)	103 (10)	122 (4)	99 (7)	97 (7)	94 (4)
bendiocarb	100 (8)	103 (8)	107 (3)	120 (11)	117 (7)	106 (13)
benfluralin	82 (8)	95 (8)	96 (5)	74 (9)	89 (5)	73 (7)
benoxacor	102 (6)	103 (6)	110 (8)	99 (2)	105 (11)	112 (14)
α-BHC	95 (7)	92 (5)	108 (4)	79 (7)	96 (7)	80 (4)
β-BHC	94 (7)	90 (5)	108 (4)	80 (6)	97 (7)	85 (7)
δ-BHC	102 (5)	104 (5)	103 (4)	94 (8)	97 (8)	92 (9)
bifenox	98 (6)	109 (6)	111 (13)	89 (8)	115 (9)	98 (6)
bifenthrin	97 (5)	99 (4)	100 (6)	91 (6)	99 (7)	94 (2)
bitertanol	93 (9)	111 (7)	92 (8)	100 (6)	101 (10)	112 (8)
bromophos-ethyl	114 (9)	86 (3)	72 (5)	80 (4)	108 (7)	82 (7)
bupirimate	94 (6)	97 (12)	99 (5)	100 (7)	96 (5)	96 (4)
buprofezin	102 (6)	98 (10)	118 (4)	91 (7)	94 (7)	76 (3)
butachlor	119 (4)	101 (10)	117 (4)	96 (12)	84 (11)	93 (11)
butafenacil	109 (8)	102 (6)	101 (5)	98 (8)	88 (7)	100 (4)
cadusafos	97 (6)	105 (3)	106 (4)	88 (8)	98 (6)	96 (7)
cafenstrole	105 (14)	84 (7)	91 (3)	74 (8)	84 (11)	99 (7)
carbaryl	91 (6)	129 (15)	86 (14)	86 (8)	98 (8)	118 (9)
carbofuran	92 (7)	135 (10)	108 (10)	118 (12)	111 (9)	111 (11)
α-chlordane	91 (9)	77 (11)	95 (7)	81 (10)	91 (6)	76 (6)
γ-chlordane	88 (1)	87 (10)	101 (7)	81 (10)	87 (9)	78 (7)
chlordimeform	90 (3)	98 (6)	85 (4)	115 (15)	97 (5)	106 (10)
chlorfenapyr	72 (9)	113 (3)	126 (3)	100 (7)	103 (5)	97 (2)
chlorobenzilate	101 (5)	87 (5)	99 (6)	88 (9)	85 (7)	83 (5)
chlorpropham	83 (8)	113 (6)	94 (7)	83 (4)	85 (9)	83 (1)
chlorpyrifos	79(8)	96 (4)	77 (9)	76 (14)	71 (10)	82 (6)
chlorpyrifos-methyl	93 (8)	102 (8)	95 (5)	88 (14)	95 (9)	89 (9)
clodinafop-propargyl	132 (8)	94 (8)	115 (6)	94 (2)	104 (7)	106 (11)
cloquintocet-mexyl	78 (6)	78 (10)	71 (6)	84 (5)	71 (7)	71 (4)
coumaphos	89 (5)	85 (7)	88 (7)	81 (7)	91 (8)	81 (7)
cyanophos	102 (6)	95 (8)	105 (4)	103 (14)	98 (9)	99 (6)
cyflufenamid	**41 (23)**	**49 (13)**	**34 (22)**	**67 (22)**	**31 (19)**	**66 (24)**
cyfluthrin I	115 (8)	112 (6)	98 (11)	111 (5)	117 (11)	94 (9)
cyfluthrin II	116 (12)	85 (3)	99 (15)	84 (4)	118 (12)	100 (11)
cyhalofop-butyl	101 (7)	75 (8)	97 (6)	88 (7)	87 (6)	91 (4)
cypermethrin IV	104 (5)	86 (15)	102 (7)	89 (9)	99 (7)	101 (7)
cyprodinil	**35 (21)**	**27 (23)**	**48 (19)**	**41 (14)**	**60 (17)**	**63 (15)**
DCPA	101 (7)	101 (9)	105 (4)	88 (8)	97 (8)	92 (7)
o,p'-DDD	100 (7)	94 (7)	103 (4)	90 (2)	98 (7)	86 (5)
o,p'-DDE	96 (8)	89 (7)	101 (3)	86 (3)	96 (6)	83 (5)
p,p'-DDE	94 (8)	88 (6)	103 (3)	85 (4)	94 (6)	85 (6)
o,p'-DDT	97 (7)	93 (10)	99 (5)	84 (4)	99 (9)	90 (5)
DEF	85 (8)	94 (12)	95 (4)	88 (12)	99 (6)	89 (4)
deltamethrin	90 (8)	97 (6)	98 (6)	84 (5)	94 (9)	120 (4)
diazinon	96 (5)	96 (7)	105 (4)	97 (3)	97 (6)	92 (5)
dichlofenthion	90 (8)	94 (9)	97 (2)	84 (9)	95 (6)	84 (5)
dichlorvos	103 (7)	129 (7)	114 (6)	119 (10)	100 (7)	103 (14)
diclobutrazol	104 (13)	97 (15)	97 (5)	100 (8)	93 (10)	101 (5)
diclofop-methyl	110 (6)	93 (8)	101 (7)	90 (9)	98 (6)	95 (7)

dx.doi.org/10.1021/jf405240j | J. Agric. Food Chem. 2014, 62, 3710−3725

Table 3. continued

compound	average recovery (%) (RSD, %) (n = 5)					
	tomato		tomato juice		ketchup	
	10 μg kg^{-1}	100 μg kg^{-1}	10 μg kg^{-1}	100 μg kg^{-1}	10 μg kg^{-1}	100 μg kg^{-1}
dicloran	71 (8)	74 (6)	72 (9)	76 (10)	70 (12)	74 (9)
dieldrin	108 (9)	89 (3)	104 (6)	93 (8)	97 (7)	84 (4)
difenoconazole I	86 (5)	103 (6)	87 (5)	105 (9)	96 (13)	94 (3)
difenoconazole II	85 (8)	101 (5)	87 (5)	104 (2)	92 (4)	94 (3)
diflufenican	**41 (27)**	**54 (18)**	**55 (20)**	**35 (26)**	71 (8)	70 (5)
dimepiperate	99 (6)	87 (7)	100 (6)	88 (9)	82 (9)	80 (5)
dimethenamid	98 (5)	94 (7)	102 (6)	94 (10)	87 (5)	88 (4)
dimethipin	92 (3)	119 (5)	106 (4)	126 (12)	99 (7)	107 (9)
dimethoate	104 (11)	101 (8)	99 (5)	99 (4)	96 (8)	102 (11)
dimethylvinphos	103 (7)	116 (12)	102 (5)	90 (7)	98 (8)	102 (9)
diphenamid	108 (12)	88 (7)	102 (7)	98 (13)	86 (7)	97 (3)
diphenylamine	82 (8)	79 (7)	91 (8)	73 (13)	85 (10)	87 (10)
disulfoton	91 (9)	93 (7)	102 (4)	98 (5)	96 (6)	80 (5)
dithiopyr	98 (7)	102 (6)	103 (4)	95 (2)	98 (7)	96 (1)
edifenphos	106 (8)	104 (9)	96 (9)	89 (8)	96 (8)	92 (7)
α-endosulfan	91 (5)	83 (4)	113 (8)	82 (8)	110 (12)	81 (11)
β-endosulfan	106 (3)	83 (5)	104 (7)	85 (8)	94 (9)	79 (5)
EPN	78 (9)	90 (2)	77 (12)	82 (4)	84 (13)	112 (5)
esprocarb	95 (4)	81 (9)	100 (7)	80 (9)	86 (6)	80 (6)
ethalfluralin	86 (6)	87 (8)	100 (6)	82 (10)	87 (5)	73 (7)
ethion	104 (5)	88 (6)	110 (5)	85 (8)	90 (7)	84 (6)
ethoprophos	86 (6)	84 (9)	99 (6)	90 (9)	86 (6)	87 (4)
etofenprox	97 (8)	86 (4)	95 (7)	75 (10)	89 (7)	83 (6)
etrimfos	107 (6)	94 (4)	101 (10)	88 (9)	105 (7)	96 (9)
fenarimol	75 (7)	97 (4)	98 (5)	94 (6)	87 (5)	96 (3)
fenitrothion	110 (6)	103 (11)	99 (4)	90 (7)	100 (9)	97 (10)
fenobucarb	99 (9)	85 (10)	104 (7)	96 (8)	85 (6)	90 (4)
fenothiocarb	87 (7)	90 (5)	86 (6)	95 (9)	82 (6)	88 (4)
fenoxycarb	98 (4)	109 (10)	86 (6)	88 (7)	96 (10)	83 (3)
fensulfothion	104 (14)	101 (2)	104 (7)	99 (7)	81 (2)	103 (2)
fenvalerate	87 (8)	99 (7)	78 (7)	93 (6)	92 (5)	94 (3)
fipronil	71 (7)	96 (12)	115 (6)	103 (7)	83 (7)	99 (3)
flamprop-methyl	137 (14)	103 (5)	97 (4)	76 (5)	96 (12)	85 (5)
flucythrinate	106 (12)	118 (8)	105 (5)	85 (14)	91 (5)	125 (5)
fludioxonil	79 (5)	86 (10)	80 (11)	100 (8)	89 (12)	102 (8)
flumioxazin	78 (8)	102 (9)	76 (4)	88 (14)	72 (6)	112 (4)
fluquinconazole	96 (9)	89 (5)	94 (7)	86 (13)	89 (5)	99 (3)
flusilazole	103 (10)	98 (9)	98 (7)	91 (6)	85 (6)	96 (3)
flutolanil	108 (11)	115 (1)	102 (7)	96 (7)	87 (6)	97 (4)
fluvalinate-τ I	103 (9)	95 (9)	91 (5)	83 (3)	96 (8)	98 (4)
fluvalinate-τ II	71 (10)	88 (8)	81 (5)	84 (3)	78 (3)	98 (3)
fosthiazate I	111 (5)	123 (9)	99 (4)	127 (7)	89 (2)	105 (2)
fosthiazate II	111 (7)	107 (10)	108 (7)	127 (7)	88 (6)	105 (2)
furathiocarb	98 (8)	114 (8)	97 (7)	91 (7)	102 (7)	99 (5)
halfenprox	95 (13)	90 (9)	97 (5)	77 (9)	88 (5)	82 (6)
iprobenfos	99 (5)	108 (9)	102 (4)	95 (9)	99 (8)	89 (7)
isofenphos	96 (5)	96 (4)	101 (6)	76 (8)	87 (6)	82 (5)
isoprocarb	81 (10)	97 (11)	103 (7)	104 (10)	83 (3)	101 (3)
isoprothiolane	106 (8)	94 (3)	103 (6)	91 (8)	87 (7)	87 (4)
isoxathion	103 (5)	96 (3)	101 (6)	75 (5)	108 (14)	116 (3)
kresoxim-methyl	127 (10)	112 (4)	99 (6)	88 (8)	84 (6)	83 (5)
lactofen	104 (4)	113 (4)	113 (3)	99 (7)	94 (5)	93 (6)
lindane	98 (7)	102 (3)	107 (3)	111 (7)	99 (7)	90 (8)
malathion	80 (13)	97 (5)	75 (7)	72 (14)	105 (9)	73 (1)
mepronil	123 (12)	104 (4)	75 (12)	83 (8)	72 (14)	100 (4)
metalaxyl	102 (8)	100 (7)	102 (7)	108 (1)	86 (4)	107 (3)
methacrifos	84 (9)	92 (5)	98 (6)	87 (9)	87 (4)	88 (4)
methamidophos	73 (9)	99 (6)	82 (13)	88 (8)	109 (12)	83 (3)

dx.doi.org/10.1021/jf405240j | J. Agric. Food Chem. 2014, 62, 3710−3725

Table 3. continued

compound	average recovery (%) (RSD, %) (n = 5)					
	tomato		tomato juice		ketchup	
	10 μg kg^{-1}	100 μg kg^{-1}	10 μg kg^{-1}	100 μg kg^{-1}	10 μg kg^{-1}	100 μg kg^{-1}
methidathion	111 (10)	103 (6)	103 (7)	92 (9)	86 (6)	89 (4)
p,p′-methoxychlor	95 (7)	95 (2)	106 (8)	86 (9)	87 (8)	83 (6)
metolachlor	95 (4)	101 (8)	102 (7)	93 (10)	87 (7)	84 (5)
metominostrobin	86 (8)	125 (3)	102 (9)	104 (9)	86 (6)	100 (4)
mevinphos	88 (5)	107 (9)	100 (7)	75 (5)	85 (5)	113 (3)
molinate	82 (9)	93 (8)	96 (4)	82 (8)	81 (6)	81 (5)
myclobutanil	102 (12)	93 (9)	100 (5)	100 (6)	86 (6)	106 (3)
napropamide	108 (6)	81 (4)	91 (7)	93 (7)	84 (8)	92 (4)
nitrothal-isopropyl	90 (6)	88 (6)	95 (7)	79 (8)	83 (6)	80 (6)
oxadiazon	97 (4)	103 (4)	99 (5)	87 (9)	87 (6)	81 (5)
oxyfluorfen	78 (8)	110 (5)	107 (3)	91 (6)	84 (6)	88 (5)
p,p′-DDD	99 (7)	95 (9)	105 (5)	91 (12)	101 (7)	90 (5)
p,p′-DDT	99 (7)	98 (8)	102 (5)	86 (12)	102 (9)	95 (6)
paclobutrazol	116 (8)	97 (6)	99 (6)	97 (6)	86 (7)	102 (3)
parathion	95 (3)	94 (2)	99 (7)	82 (8)	86 (5)	82 (5)
parathion-methyl	101 (10)	96 (6)	103 (7)	88 (6)	86 (6)	89 (5)
penconazole	98 (8)	82 (7)	98 (7)	90 (8)	86 (5)	93 (3)
pendimethalin	89 (8)	88 (7)	95 (6)	75 (8)	87 (7)	77 (6)
pentachloronitrobenzene	80 (13)	75 (12)	82 (12)	73 (7)	99 (10)	78 (5)
permethrin	103 (12)	93 (13)	107 (6)	87 (8)	91 (5)	84 (5)
phenthoate	100 (6)	103 (3)	108 (8)	93 (9)	100 (3)	86 (6)
phenthoate	127 (13)	108 (2)	94 (9)	70 (7)	81 (7)	83 (5)
phorate	106 (9)	119 (7)	131 (12)	108 (11)	79 (4)	114 (2)
phosalone	96 (7)	103 (6)	98 (5)	90 (10)	100 (7)	94 (6)
piperonyl butoxide	105 (16)	92 (8)	103 (6)	91 (15)	89 (7)	87 (5)
piperophos	95 (7)	87 (5)	99 (7)	81 (7)	85 (7)	81 (5)
pirimiphos-methyl	78 (8)	79 (7)	91 (6)	88 (8)	84 (4)	80 (5)
prochloraz	73 (10)	75 (6)	**64 (16)**	**59 (15)**	**64 (14)**	67 (3)
procymidone	129 (11)	98 (7)	98 (12)	92 (12)	123 (11)	134 (4)
profenofos	97 (12)	96 (6)	98 (8)	78 (8)	89 (7)	81 (4)
promecarb	101 (8)	95 (11)	106 (6)	96 (8)	85 (5)	97 (4)
prometryn	102 (10)	87 (8)	98 (7)	78 (7)	130 (8)	84 (4)
pronamide	100 (7)	106 (6)	118 (6)	104 (6)	99 (8)	90 (8)
propachlor	90 (9)	95 (9)	101 (6)	95 (9)	85 (5)	91 (4)
propargite	76 (8)	97 (9)	83 (4)	78 (9)	78 (7)	88 (10)
propazine	95 (4)	87 (10)	99 (7)	96 (10)	90 (5)	94 (3)
propham	85 (7)	82 (7)	101 (8)	99 (10)	86 (5)	95 (4)
propiconazole	85 (13)	101 (10)	90 (12)	92 (7)	76 (7)	85 (5)
propoxur	93 (8)	94 (4)	107 (8)	103 (1)	86 (5)	117 (3)
prothiofos	111 (7)	82 (11)	90 (11)	94 (7)	104 (8)	92 (12)
pyrazophos	94 (4)	80 (5)	83 (4)	85 (6)	95 (4)	84 (5)
pyributicarb	105 (11)	98 (2)	100 (7)	85 (10)	87 (7)	81 (5)
pyridaben	77 (15)	103 (7)	84 (13)	95 (10)	98 (12)	93 (3)
pyridaphenthion	103 (10)	77 (5)	103 (6)	87 (7)	86 (7)	96 (3)
pyrimethanil	**39 (18)**	**40 (23)**	**52 (17)**	**61 (20)**	**48 (24)**	**59 (17)**
pyrimidifen	**36 (19)**	**33 (14)**	**48 (15)**	**46 (14)**	**55 (6)**	**62 (6)**
quinalphos	109 (6)	88 (11)	109 (6)	83 (4)	122 (6)	88 (5)
quinoclamine	**25 (12)**	**20 (18)**	**33 (12)**	**32 (16)**	**48 (9)**	**50 (12)**
quinoxyfen	**41 (16)**	**49 (10)**	**50 (16)**	**37 (15)**	**60 (16)**	**59 (19)**
ronnel	84 (7)	79 (5)	91 (7)	70 (9)	84 (5)	79 (6)
silafluofen	107 (4)	90 (6)	78 (14)	87 (8)	97 (8)	92 (3)
simeconazole	100 (11)	88 (12)	101 (6)	108 (6)	92 (5)	96 (5)
sulfotep	93 (8)	105 (5)	105 (5)	96 (13)	102 (7)	92 (11)
tebuconazole	94 (6)	97 (9)	90 (15)	97 (13)	89 (13)	96 (11)
tebufenpyrad	114 (10)	87 (4)	99 (7)	82 (8)	88 (5)	83 (5)
tecnazene	83 (8)	86 (9)	94 (2)	70 (14)	91 (6)	77 (4)
cis-tefluthrin	94 (10)	102 (7)	104 (3)	89 (6)	98 (6)	84 (3)
terbacil	107 (5)	106 (10)	106 (7)	108 (12)	98 (8)	104 (8)

dx.doi.org/10.1021/jf405240j | J. Agric. Food Chem. 2014, 62, 3710−3725

Table 3. continued

compound	average recovery (%) (RSD, %) (n = 5)					
	tomato		tomato juice		ketchup	
	10 μg kg^{-1}	100 μg kg^{-1}	10 μg kg^{-1}	100 μg kg^{-1}	10 μg kg^{-1}	100 μg kg^{-1}
terbufos	94 (8)	100 (5)	104 (5)	99 (4)	101 (7)	92 (6)
terbutryn	95 (8)	88 (10)	96 (6)	85 (7)	78 (8)	89 (4)
tetraconazole	98 (5)	112 (7)	105 (5)	106 (12)	96 (7)	104 (9)
tetradifon	91 (5)	95 (11)	97 (6)	88 (9)	78 (6)	86 (4)
thiazopyr	97 (4)	92 (10)	101 (8)	92 (10)	89 (6)	82 (5)
tolclofos-methyl	90 (8)	94 (7)	97 (4)	81 (8)	96 (7)	88 (5)
triadimefon	106 (5)	102 (12)	104 (4)	94 (3)	97 (8)	99 (6)
triadimenol	130 (11)	119 (13)	101 (5)	118 (12)	97 (9)	92 (7)
triallate	91 (8)	93 (6)	102 (3)	115 (8)	97 (5)	80 (4)
triazophos	97 (5)	100 (6)	96 (10)	94 (9)	100 (10)	100 (6)
trifloxystrobin	89 (8)	103 (12)	105 (5)	97 (5)	90 (4)	95 (3)
trifluralin	96 (4)	98 (7)	105 (4)	92 (8)	97 (8)	94 (4)
vinclozolin	101 (6)	102 (7)	106 (2)	90 (12)	96 (6)	89 (10)

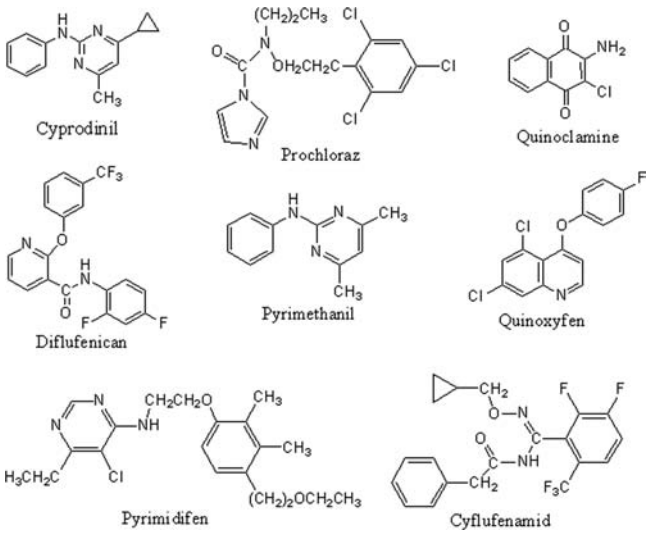

Figure 4. Chemical structures of eight compounds with low recoveries.

The validation parameters of the method in terms of analytical range, precision, recovery, and trueness showed that the proposed method meets the requirements for pesticide analysis. These findings are important for pesticide analysis at trace levels for sample cleanup. This method is expected to be widely applied for monitoring of pesticides at trace levels in the future for various agricultural commodities. The results confirm the feasibility of the proposed method, which can be easily implemented for routine testing and monitoring of pesticide residues in tomato products

AUTHOR INFORMATION

Corresponding Author

*(C.P.) E-mail: canpingp@cau.edu.cn. Fax: +86-10 62733620.

Funding

This work was supported by an instrumentation special project (no. 2013YQ510391) from the Chinese Ministry of Science and Technology and by the National Science Foundation for Fostering Talents in Basic Research of China (no. J1210064). We are grateful for the Guangxi Special Invited Scientist (2013) program in Agric-Environment and Agro-products Safety.

Notes

The authors declare no competing financial interest.

ABBREVIATIONS USED

SPE, solid-phase extraction; QuEChERS, quick, easy, cheap, effective, rugged, and safe; r-DSPE, reversed-dispersive solid phase extraction; MRL, maximum residue limit; PSA, primary−secondary amine; GCB, graphitized carbon black; CNTs, carbon nanotubes; SWCNTs, single-walled carbon nanotubes; MWCNTs, multiwalled carbon nanotubes; m-PFC, multiplug filtration cleanup; GC-MS/MS, gas chromatography−electrospray tandem mass spectrometry; MRM, multiple reaction monitoring; CE, collision energy; RT, retention time; LOQ, limit of quantification; LOD, limit of detection; RSD, relative standard deviations; S/N, signal-to-noise ratio

REFERENCES

(1) Engindeniz, S. Economic analysis of pesticide use on processing tomato growing: a case study for Turkey. *Crop Prot.* **2006**, *25*, 534−541.

(2) Gambacorta, G.; Faccia, M.; Lamacchia, C.; Di Luccia, A.; La Notte, E. Pesticide residues in tomato grown in open field. *Food Control* **2005**, *16*, 629−632.

(3) Giovannucci, E. Tomatoes, tomato-based products, lycopene, and cancer: review of the epidemiologic literature. *J. Natl. Cancer Inst.* **1999**, *91*, 317−331.

(4) Ravelo-Pérez, L. M.; Hernández-Borges, J.; Borges-Miquel, T. M.; Rodríguez-Delgado, M. Á. Pesticide analysis in tomatoes by solid-phase microextraction and micellar electrokinetic chromatography. *J. Chromatogr., A* **2008**, *1185*, 151−154.

(5) Watanabe, E.; Kobara, Y.; Baba, K.; Eun, H. Reduction of hazardous organic solvent in sample preparation for hydrophilic pesticide residues in agricultural products with conventional liquid chromatography. *J. Agric. Food Chem.* **2013**, *61*, 4792−4798.

(6) Bedendo, G. C.; Carasek, E. Simultaneous liquid−liquid microextraction and polypropylene microporous membrane solid-phase extraction of organochlorine pesticides in water, tomato and strawberry samples. *J. Chromatogr., A* **2010**, *1217*, 7−13.

(7) Xie, W.; Han, C.; Qian, Y.; Ding, H.; Chen, X.; Xi, J. Determination of neonicotinoid pesticides residues in agricultural samples by solid-phase extraction combined with liquid chromatography−tandem mass spectrometry. *J. Chromatogr., A* **2011**, *1218*, 4426−4433.

(8) Wan Ibrahim, W. A.; Veloo, K. V.; Sanagi, M. M. Novel sol−gel hybrid methyltrimethoxysilane−tetraethoxysilane as solid phase extraction sorbent for organophosphorus pesticides. *J. Chromatogr., A* **2012**, *1229*, 55−62.

(9) Kaewsuya, P.; Brewer, W. E.; Wong, J.; Morgan, S. L. Automated QuEChERS tips for analysis of pesticide residues in fruits and vegetables by GC-MS. *J. Agric. Food Chem.* **2013**, *61*, 2299−2314.
(10) Korba, K.; Pelit, L.; Pelit, F. O.; Özdokur, K. V.; Ertaş, H.; Eroğlu, A. E.; Ertaş, F. Preparation and characterization of sodium dodecyl sulphate doped polypyrrole solid phase micro extraction fiber and its application to endocrine disruptor pesticide analysis. *J. Chromatogr., B* **2013**, *929*, 90−96.
(11) Robinson, E. M.; Trumble, S. J.; Subedi, B.; Sanders, R.; Usenko, S. Selective pressurized liquid extraction of pesticides, polychlorinated biphenyls and polybrominated diphenyl ethers in a whale earplug (earwax): a novel method for analyzing organic contaminants in lipid-rich matrices. *J. Chromatogr., A* **2013**, *1319*, 14−20.
(12) Li, M.; Conlon, P.; Fiorenza, S.; Vitale, R. J.; Alvarez, P. J. J. Rapid analysis of 1,4-dioxane in groundwater by frozen micro-extraction with gas chromatography/mass spectrometry. *Ground Water Monit. Rem.* **2011**, *31*, 70−76.
(13) Asiabi, H.; Yamini, Y.; Moradi, M. Determination of sulfonylurea herbicides in soil samples via supercritical fluid extraction followed by nanostructured supramolecular solvent microextraction. *J. Supercrit. Fluid* **2013**, *84*, 20−28.
(14) Fontana, A. R.; Patil, S. H.; Banerjee, K.; Altamirano, J. C. Ultrasound-assisted emulsification microextraction for determination of 2,4,6-trichloroanisole in wine samples by gas chromatography tandem mass spectrometry. *J. Agric. Food Chem.* **2010**, *58*, 4576−4581.
(15) Anastassiades, M.; Maštovská, K.; Lehotay, S. J. Evaluation of analyte protectants to improve gas chromatographic analysis of pesticides. *J. Chromatogr., A* **2003**, *1015*, 163−184.
(16) Anastassiades, M.; Lehotay, S. J.; Stajnbaher, D.; Schenck, F. J. Fast and easy multiresidue method employing acetonitrile extraction/partitioning and "dispersive solid-phase extraction" for the determination of pesticide residues in produce. *J. AOAC Int.* **2003**, *86*, 412−431.
(17) Wang, J.; Chow, W.; Leung, D.; Chang, J. Application of ultrahigh-performance liquid chromatography and electrospray ionization quadrupole orbitrap high-resolution mass spectrometry for determination of 166 pesticides in fruits and vegetables. *J. Agric. Food Chem.* **2012**, *60*, 12088−12104.
(18) Li, Z.; Li, Y.; Liu, X.; Li, X.; Zhou, L.; Pan, C. Multiresidue analysis of 58 pesticides in bean products by disposable pipet extraction (DPX) cleanup and gas chromatography−mass spectrometry determination. *J. Agric. Food Chem.* **2012**, *60*, 4788−4798.
(19) Zhang, K.; Wong, J. W.; Yang, P.; Tech, K.; DiBenedetto, A. L.; Lee, N. S.; Hayward, D. G.; Makovi, C. M.; Krynitsky, A. J.; Banerjee, K.; Jao, L.; Dasgupta, S.; Smoker, M. S.; Simonds, R.; Schreiber, A. Multiresidue pesticide analysis of agricultural commodities using acetonitrile salt-out extraction, dispersive solid-phase sample clean-up, and high-performance liquid chromatography−tandem mass spectrometry. *J. Agric. Food Chem.* **2011**, *59*, 7636−7646.
(20) Nunez, O.; Gallart-Ayala, H.; Ferrer, I.; Moyano, E.; Galceran, M. T. Strategies for the multi-residue analysis of 100 pesticides by liquid chromatography−triple quadrupole mass spectrometry. *J. Chromatogr., A* **2012**, *1249*, 164−180.
(21) Lehotay, S. J.; Son, K. A.; Kwon, H.; Koesukwiwat, U.; Fu, W.; Mastovska, K.; Hoh, E.; Leepipatpiboon, N. Comparison of QuEChERS sample preparation methods for the analysis of pesticide residues in fruits and vegetables. *J. Chromatogr., A* **2010**, *1217*, 2548−2560.
(22) Shen, C.-y.; Cao, X.-w.; Shen, W.-j.; Jiang, Y.; Zhao, Z.-y.; Wu, B.; Yu, K.-y.; Liu, H.; Lian, H.-z. Determination of 17 pyrethroid residues in troublesome matrices by gas chromatography/mass spectrometry with negative chemical ionization. *Talanta* **2011**, *84*, 141−147.
(23) Gilbert-Lopez, B.; Garcia-Reyes, J. F.; Lozano, A.; Fernandez-Alba, A. R.; Molina-Díaz, A. Large-scale pesticide testing in olives by liquid chromatography−electrospray tandem mass spectrometry using two sample preparation methods based on matrix solid-phase dispersion and QuEChERS. *J. Chromatogr., A* **2010**, *1217*, 6022−6035.
(24) Iijima, S. Helical microtubules of graphitic carbon. *Nature* **1999**, *354*, 56−58.
(25) Zawisza, B.; Skorek, R.; Stankiewicz, G.; Sitko, R. Carbon nanotubes as a solid sorbent for the preconcentration of Cr, Mn, Fe, Co, Ni, Cu, Zn and Pb prior to wavelength-dispersive X-ray fluorescence spectrometry. *Talanta* **2012**, *99*, 918−923.
(26) Zhao, Q.; Wei, F.; Luo, Y.-B.; Ding, J.; Xiao, N.; Feng, Y.-Q. Rapid magnetic solid-phase extraction based on magnetic multiwalled carbon nanotubes for the determination of polycyclic aromatic hydrocarbons in edible oils. *J. Agric. Food Chem.* **2011**, *59*, 12794−12800.
(27) Du, X.-D.; Wu, Y.-L.; Yang, H.-J.; Yang, T. Simultaneous determination of 10 β2-agonists in swine urine using liquid chromatography−tandem mass spectrometry and multi-walled carbon nanotubes as a reversed dispersive solid phase extraction sorbent. *J. Chromatogr., A* **2012**, *1260*, 25−32.
(28) Zhao, P.; Wang, L.; Zhou, L.; Zhang, F.; Kang, S.; Pan, C. Multi-walled carbon nanotubes as alternative reversed-dispersive solid phase extraction materials in pesticide multi-residue analysis with QuEChERS method. *J. Chromatogr., A* **2012**, *1225*, 17−25.
(29) Zhao, P.; Wang, L.; Luo, J.; Li, J.; Pan, C. Determination of pesticide residues in complex matrices using multi-walled carbon nanotubes as reversed-dispersive solid-phase extraction sorbent. *J. Sep. Sci.* **2012**, *35*, 153−158.
(30) Zhao, P.; Wang, L.; Jiang, Y.; Zhang, F.; Pan, C. Dispersive cleanup of acetonitrile extracts of tea samples by mixed multiwalled carbon nanotubes, primary secondary amine, and graphitized carbon black sorbents. *J. Agric. Food Chem.* **2012**, *60*, 4026−4033.
(31) Guan, H.; Brewer, W. E.; Garris, S. T.; Morgan, S. L. Disposable pipette extraction for the analysis of pesticides in fruit and vegetables using gas chromatography/mass spectrometry. *J. Chromatogr., A* **2010**, *1217*, 1867−1874.
(32) European Council 2002/657/EC, implementing council directive 96/23/EC concerning the performance of analytical methods and the interpretation of results, 2002.
(33) Walorczyk, S. Development of a multi-residue screening method for the determination of pesticides in cereals and dry animal feed using gas chromatography−triple quadrupole tandem mass spectrometry. *J. Chromatogr., A* **2007**, *1165*, 200−212.

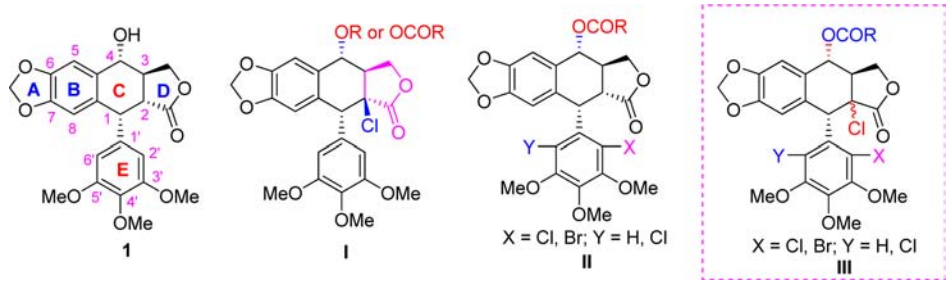

Figure 1. Chemical structures of podophyllotoxin (**1**) and its derivatives (**I**–**III**).

MATERIALS AND METHODS

General. All chemical reagents were commercially available, and solvents were purified with standard methods[31] before use. Analytical thin-layer chromatography (TLC) and preparative thin-layer chromatography (PTLC) were performed with silica gel plates using silica gel 60 GF_{254} (Qingdao Haiyang Chemical Co., Ltd. Qingdao, China), and the solvent system was a mixture of ethyl acetate and petroleum ether. Melting points were carried out on an XT-4 digital melting-point apparatus (Beijing Tech Instrument Co., Ltd., Beijing, China) and were uncorrected. Proton nuclear magnetic resonance spectra (^{1}H NMR) and carbon nuclear magnetic resonance spectra (^{13}C NMR) were recorded in $CDCl_3$ on a Bruker Avance 400 or 500 MHz instrument using tetramethylsilane (TMS) as the internal standard. High-resolution mass spectra (HR-MS) were carried out with an IonSpec 4.7 T FTMS instrument. 2′-Chloropodophyllotoxin (**2a**, 85% yield), 2′,6′-dichloropodophyllotoxin (**2b**, 90% yield), and 2′-bromopodophyllotoxin (**2c**, 85% yield) were prepared in the same way as in our previous paper.[30]

Stereoselective Synthesis of 2α-Chloro-2′(2′,6′)-(di)-halogenopicropodophyllotoxin Derivatives (5a–c). Two drops of phosphorus oxychloride were added to a solution of **2a**, **2b**, or **2c** (1.8 mmol) in dihydropyran (10 mL). Then the mixture was stirred at room temperature. After 2 h, the mixture was poured into ice-cold petroleum ether (100 mL) and vigorously stirred. The resulting solids were collected and dissolved in CH_2Cl_2 (50 mL). The corresponding solution was washed by water (25 mL × 2), dried over anhydrous Na_2SO_4, concentrated in vacuo, and purified by silica gel column chromatography to give products **3a** (89% yield), **3b** (78% yield), or **3c** (85% yield). To a solution of lithium diisopropylamide (LDA, 0.6 mmol) in dry tetrahydrofuran (THF, 5 mL) at −78 °C under N_2 was then added dropwise a solution of **3a**, **3b**, or **3c** (0.5 mmol) in dry THF (5 mL) for 10 min. After the addition, the reaction mixture was stirred for 15 min, and a solution of hexachloroethane (C_2Cl_6, 0.7 mmol) in dry THF (5 mL) was added dropwise for 10 min. Subsequently, the solution was allowed to warm slowly from −78 °C to the ambient temperature. When the reaction was complete according to TLC analysis, the solvent was removed and the residue was diluted by CH_2Cl_2 (50 mL). The corresponding solution was washed by water (25 mL), 0.5 N aqueous HCl (25 mL), and water (25 mL), dried over anhydrous Na_2SO_4, and concentrated under reduced pressure to give the residue, which was used directly for the next step without further purification. A solution of the above residue in concentrated HCl/THF (1:9, v/v, 10 mL) was stirred for 2 h and then adjusted a pH value of 5 by using 5% aqueous Na_2CO_3. After removal of THF, the mixture was extracted with CH_2Cl_2 (40 mL × 3), and the combined organic phase was washed by 5% aqueous Na_2CO_3 (20 mL) and brine (20 mL), dried over anhydrous Na_2SO_4, concentrated in vacuo, and purified by silica gel column chromatography to give **5a** (68% yield), **5b** (62% yield), or **5c** (71% yield).

*Data for **5a**:* white solid; mp = 183–184 °C; $[\alpha]^{20}_D$ = −83 (*c* 3.1 mg/mL, $CHCl_3$); ^{1}H NMR (400 MHz, $CDCl_3$) δ 7.07 (s, 1H, H-5), 6.74 (s, 1H, H-8), 6.62 (s, 1H, H-6′), 5.92 (dd, *J* = 5.2, 1.2 Hz, 2H, OCH_2O), 5.48 (s, 1H, H-1), 4.90 (d, *J* = 2.8 Hz, 1H, H-4), 4.81 (dd, *J* = 9.2, 4.8 Hz, 1H, H-11), 4.47 (d, *J* = 9.2 Hz, 1H, H-11), 3.93 (s, 3H, 3′-$OCHH_3$), 3.88 (s, 3H, 5′-$OCHH_3$), 3.73 (s, 3H, 4′-$OCHH_3$), 3.14–3.16 (m, 1H, H-3), 2.47 (s, 1H, OH); ^{13}C NMR (100 MHz, $CDCl_3$) δ 172.3, 152.1, 149.7, 148.7, 148.2, 142.5, 132.3, 129.7, 128.5, 121.5, 109.1, 107.4, 101.5, 73.5, 73.0, 67.0, 61.1, 61.0, 56.3, 50.7, 45.2; HRMS *m*/*z* calcd for $C_{22}H_{20}O_8Cl_2Na$ ([M + Na]$^+$) 505.0427, found 505.0428.

*Data for **5b**:* white solid; mp = 92–93 °C; $[\alpha]^{20}_D$ = −104 (*c* 3.9 mg/mL, $CHCl_3$); ^{1}H NMR (400 MHz, $CDCl_3$) δ 7.04 (s, 1H, H-5), 6.13 (s, 1H, H-8), 5.99 (s, 1H, H-1), 5.90 (dd, *J* = 7.2, 1.2 Hz, 2H, OCH_2O), 4.82 (dd, *J* = 8.8, 3.6 Hz, 1H, H-11), 4.62 (d, *J* = 9.2 Hz, 1H, H-11), 4.43 (d, *J* = 9.2 Hz, 1H, H-4), 3.98 (s, 3H, 3′-$OCHH_3$), 3.96 (s, 3H, 5′-$OCHH_3$), 3.82 (s, 3H, 4′-$OCHH_3$), 3.16 (dd, *J* = 9.6, 3.6 Hz, 1H, H-3), 1.58 (s, 1H, OH); ^{13}C NMR (100 MHz, $CDCl_3$) δ 173.3, 149.4, 148.9, 147.7, 147.5, 147.3, 134.2, 129.6, 127.4, 127.2, 125.9, 107.6, 104.7, 101.3, 70.8, 69.0, 65.6, 61.3, 61.2, 61.1, 50.8, 44.1; HRMS *m*/*z* calcd for $C_{22}H_{19}O_8Cl_3Na$ ([M + Na]$^+$) 539.0037, found 538.0051.

*Data for **5c**:* white solid; mp = 170–172 °C; $[\alpha]^{20}_D$ = −94 (*c* 3.4 mg/mL, $CHCl_3$); ^{1}H NMR (400 MHz, $CDCl_3$) δ 7.10 (s, 1H, H-5), 6.74 (s, 1H, H-8), 6.64 (s, 1H, H-6′), 5.91 (dd, *J* = 5.2, 1.2 Hz, 2H, OCH_2O), 5.56 (s, 1H, H-1), 4.89 (d, *J* = 2.8 Hz, 1H, H-4), 4.81 (dd, *J* = 9.2, 4.8 Hz, 1H, H-11), 4.47 (d, *J* = 9.2 Hz, 1H, H-11), 3.92 (s, 3H, 3′-$OCHH_3$), 3.88 (s, 3H, 5′-$OCHH_3$), 3.72 (s, 3H, 4′-$OCHH_3$), 3.14 (t, *J* = 4.0 Hz, 1H, H-3), 2.53 (s, 1H, OH); ^{13}C NMR (100 MHz, $CDCl_3$) δ 172.3, 152.8, 150.7, 148.6, 148.2, 142.4, 134.1, 129.8, 128.4, 113.1, 109.4, 108.9, 107.5, 101.5, 73.4, 73.1, 67.1, 61.0, 61.0, 56.4, 50.7, 47.8; HRMS *m*/*z* calcd for $C_{22}H_{20}O_8ClBrNa$ ([M + Na]$^+$) 548.9922, found 548.9906.

General Procedure for the Synthesis of 2α-Chloro-2′(2′,6′)-(di)halogenopicropodophyllotoxin Esters (6a–k, 7a–i, and 8a–h). A solution of compound **5a**, **5b**, or **5c** (0.15 mmol), the corresponding carboxylic acids RCO_2H (0.18 mmol), *N*,*N*′-dicyclohexylcarbodiimide (DCC, 0.18 mmol), and 4-*N*,*N*-dimethylaminopyridine (DMAP, 0.03 mmol) in dry CH_2Cl_2 (10 mL) was stirred at room temperature. When the reaction was complete as checked by TLC analysis, the solution of the mixture was diluted with CH_2Cl_2 (40 mL). Subsequently, the solution was washed by water (15 mL), 0.1 N aqueous HCl (25 mL), 5% aqueous Na_2CO_3 (25 mL), and brine (25 mL), dried over anhydrous Na_2SO_4, concentrated in vacuo, and purified by PTLC to give the target products **6a–k**, **7a–i**, and **8a–h**. The example data of **6a–c**, **7a–c**, and **8a–c** are shown as follows, whereas data of **6d–k**, **7d–i**, and **8d–h** can be found in the Supporting Information.

*Data for **6a**:* yield 82%; white solid; mp = 150–151 °C; $[\alpha]^{20}_D$ = −78 (*c* 3.5 mg/mL, $CHCl_3$); ^{1}H NMR (500 MHz, $CDCl_3$) δ 6.68 (s, 1H, H-5), 6.64 (s, 1H, H-8), 6.58 (s, 1H, H-6′), 5.93–5.95 (m, 3H, H-4, OCH_2O), 5.52 (s, 1H, H-1), 4.80–4.81 (m, 2H, H-11), 3.94 (s, 3H, 3′−$OCHH_3$), 3.88 (s, 3H, 5′-$OCHH_3$), 3.76 (s, 3H, 4′-$OCHH_3$), 2.97–2.98 (m, 1H, H-3), 2.16 (s, 3H, $COCH_3$); ^{13}C NMR (125 MHz, $CDCl_3$) δ 171.9, 170.6, 152.0, 149.9, 149.2, 148.2, 142.6, 132.1, 130.8, 123.9, 122.0, 108.8, 108.6, 108.3, 101.7, 75.1, 73.2, 66.8, 61.1, 61.1, 56.1, 49.3, 44.7, 21.1; HRMS *m*/*z* calcd for $C_{24}H_{22}O_9Cl_2Na$ ([M + Na]$^+$) 547.0533, found 547.0529.

*Data for **6b**:* yield 78%; white solid; mp = 179–180 °C; $[\alpha]^{20}_D$ = −80 (*c* 2.9 mg/mL, $CHCl_3$); ^{1}H NMR (400 MHz, $CDCl_3$) δ 6.67 (s, 1H, H-5), 6.62 (s, 1H, H-8), 6.57 (s, 1H, H-6′), 5.93–5.94 (m, 3H, OCH_2O, H-4), 5.51 (s, 1H, H-1), 4.80–4.81 (m, 2H, H-11), 3.93 (s, 3H, 3′-$OCHH_3$), 3.88 (s, 3H, 5′-$OCHH_3$), 3.75 (s, 3H, 4′-$OCHH_3$),

dx.doi.org/10.1021/jf405316w | J. Agric. Food Chem. 2014, 62, 3726–3733

Scheme 1. Synthetic Approach for 2α-Chloropicropodophyllotoxin Derivatives (5a−c) and 2β-Chloropodophyllotoxin Derivatives (5a′−c′)

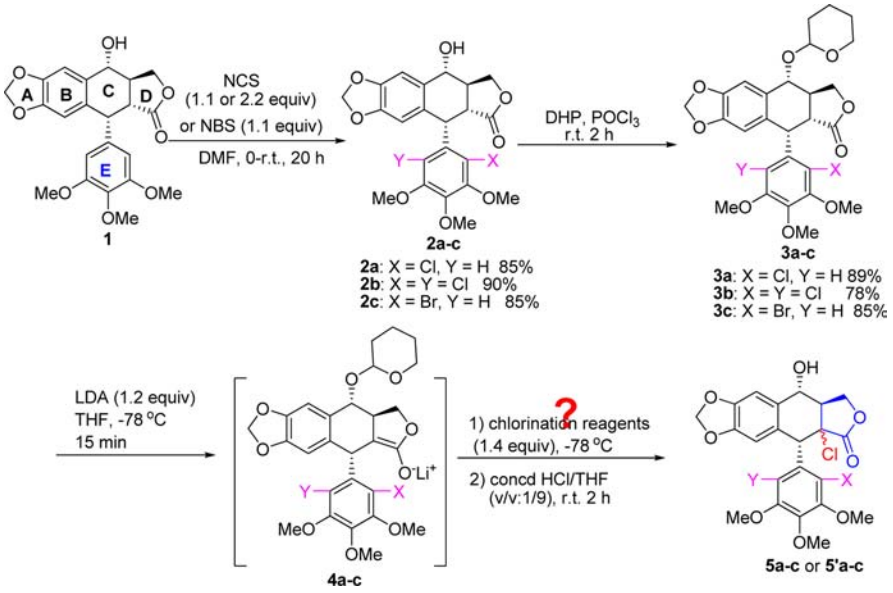

2.96−2.97 (m, 1H, H-3), 2.35−2.42 (m, 2H, CH_3CH_2), 1.20 (t, J = 7.6 Hz, 3H, CH_3CH_2); ^{13}C NMR (100 MHz, $CDCl_3$) δ 174.2, 171.9, 152.1, 150.0, 149.2, 148.2, 142.8, 132.2, 130.7, 124.2, 122.1, 108.8, 108.6, 108.5, 101.7, 74.9, 73.1, 66.8, 61.1, 61.1, 56.2, 49.4, 44.7, 27.5, 9.0; HRMS m/z calcd for $C_{25}H_{24}O_9Cl_2Na$ ([M + Na]$^+$) 561.0689, found 561.0691.

Data for ***6c:*** yield 77%; white solid; mp = 79−80 °C; $[\alpha]^{19}_D$ = −66 (c 3.6 mg/mL, $CHCl_3$); ^{1}H NMR (400 MHz, $CDCl_3$) δ 7.27−7.39 (m, 5H), 6.67 (s, 1H, H-5), 6.57 (s, 1H, H-8), 6.51 (s, 1H, H-6′), 5.93 (d, J = 1.2 Hz, 2H, OCH_2O), 5.89 (d, J = 3.2 Hz, 1H, H-4), 5.50 (s, 1H, H-1), 4.77−4.78 (m, 2H, H-11), 3.93 (s, 3H, 3′-$OCHH_3$), 3.89 (s, 3H, 5′-$OCHH_3$), 3.75 (s, 3H, 4′-$OCHH_3$), 3.67 (d, J = 6.8 Hz, 2H, $PhCH_2$), 2.99−3.00 (m, 1H, H-3); ^{13}C NMR (100 MHz, $CDCl_3$) δ 171.8, 171.6, 152.0, 150.0, 149.2, 148.2, 142.8, 132.6, 132.1, 130.6, 129.0, 128.9, 127.7, 123.9, 122.1, 108.7, 108.6, 108.4, 101.7, 75.5, 72.9, 66.7, 61.1, 61.1, 56.3, 49.2, 44.6, 41.1; HRMS m/z calcd for $C_{30}H_{26}O_9Cl_2Na$ ([M + Na]$^+$) 623.0846, found 623.0849.

Data for ***7a:*** yield 90%; white solid; mp = 92−93 °C; $[\alpha]^{20}_D$ = −86 (c 3.3 mg/mL, $CHCl_3$); ^{1}H NMR (400 MHz, $CDCl_3$) δ 6.51 (s, 1H, H-5), 6.23 (s, 1H, H-8), 6.07 (s, 1H, H-1), 5.92−5.93 (m, 3H, OCH_2O, H-4), 4.76−4.78 (m, 1H, H-11), 4.57−4.59 (m, 1H, H-11), 3.98 (s, 3H, 3′-$OCHH_3$), 3.96 (s, 3H, 5′-$OCHH_3$), 3.83 (s, 3H, 4′-$OCHH_3$), 3.39−3.41 (m, 1H, H-3), 2.24 (s, 3H, $COCH_3$); ^{13}C NMR (100 MHz, $CDCl_3$) δ 172.8, 171.1, 149.3, 148.9, 148.1, 147.6, 147.4, 133.3, 127.5, 125.9, 125.5, 107.8, 105.7, 101.5, 71.2, 70.9, 64.9, 61.3, 61.3, 61.2, 48.9, 44.1, 21.1; HRMS m/z calcd for $C_{24}H_{21}O_9Cl_3Na$ ([M + Na]$^+$) 581.0143, found 581.0150.

Data for ***7b:*** yield 61%; white solid; mp = 84−86 °C; $[\alpha]^{20}_D$ = −107 (c 2.8 mg/mL, $CHCl_3$); ^{1}H NMR (400 MHz, $CDCl_3$) δ 6.49 (s, 1H, H-5), 6.23 (s, 1H, H-8), 6.07 (s, 1H, H-1), 5.90−5.93 (m, 3H, OCH_2O, H-4), 4.75 (dd, J = 7.2, 3.2 Hz, 1H, H-11), 4.58 (d, J = 7.6 Hz, 1H, H-11), 3.98 (s, 3H, 3′-$OCHH_3$), 3.96 (s, 3H, 5′-$OCHH_3$), 3.83 (s, 3H, 4′-$OCHH_3$), 3.38 (dd, J = 5.6, 2.8 Hz, 1H, H-3), 2.49−2.52 (m, 2H, $COCH_2CH_3$), 1.23 (t, J = 6.0 Hz, 3H, $COCH_2CH_3$); ^{13}C NMR (100 MHz, $CDCl_3$) δ 174.4, 172.8, 149.3, 149.0, 148.1, 147.6, 147.4, 133.3, 127.5, 126.1, 125.5, 107.8, 105.8, 101.4, 71.3, 70.9, 65.0, 61.3, 61.2, 61.1, 49.1, 44.1, 27.7, 9.1; HRMS m/z calcd for $C_{25}H_{23}O_9Cl_3Na$ ([M + Na]$^+$) 595.0299, found 595.0300.

Data for ***7c:*** yield 71%; white solid; mp = 78−80 °C; $[\alpha]^{20}_D$ = −95 (c 2.8 mg/mL, $CHCl_3$); ^{1}H NMR (400 MHz, $CDCl_3$) δ 7.31−7.38 (m, 5H), 6.34 (s, 1H, H-5), 6.21 (s, 1H, H-8), 6.05 (s, 1H, H-1), 5.88 (dd, J = 10.0, 1.2 Hz, 2H, OCH_2O), 5.86 (d, J = 7.2 Hz, 1H, H-4), 4.65 (dd, J = 9.2, 4.0 Hz, 1H, H-11), 4.46 (d, J = 9.6 Hz, 1H, H-11), 3.97 (s, 3H, 3′-$OCHH_3$), 3.95 (s, 3H, 5′-$OCHH_3$), 3.83 (s, 3H, 4′-$OCHH_3$), 3.76 (s, 2H, $PhCH_2$), 3.31 (dd, J = 7.2, 3.6 Hz, 1H, H-3); ^{13}C NMR (100 MHz, $CDCl_3$) δ 172.7, 171.6, 149.2, 148.9, 148.1, 147.6, 147.3, 133.2, 133.1, 129.2, 128.8, 127.6, 127.5, 127.5, 125.8, 125.5, 107.7, 105.8, 101.4, 71.6, 71.1, 64.9, 61.3, 61.2, 61.1, 49.0, 44.1, 41.5; HRMS m/z calcd for $C_{30}H_{25}O_9Cl_3Na$ ([M + Na]$^+$) 657.0456, found 657.0424.

Data for ***8a:*** yield 95%; white solid; mp = 176−178 °C; $[\alpha]^{20}_D$ = −94 (c 3.4 mg/mL, $CHCl_3$); ^{1}H NMR (400 MHz, $CDCl_3$) δ 6.71 (s, 1H, H-5), 6.63 (s, 1H, H-8), 6.60 (s, 1H, H-6′), 5.93−5.95 (m, 3H, OCH_2O, H-4), 5.59 (s, 1H, H-1), 4.80−4.81 (m, 2H, H-11), 3.92 (s, 3H, 3′-$OCHH_3$), 3.88 (s, 3H, 5′-$OCHH_3$), 3.76 (s, 3H, 4′-$OCHH_3$), 2.97 (dd, J = 5.2, 2.8 Hz, 1H, H-3), 2.15 (s, 3H, $COCH_3$); ^{13}C NMR (100 MHz, $CDCl_3$) δ 171.9, 170.6, 152.7, 150.9, 149.2, 148.2, 142.6, 133.9, 130.9, 123.9, 113.7, 108.8, 108.7, 108.6, 101.7, 75.1, 73.1, 66.8, 61.1, 61.0, 56.2, 49.4, 47.3, 21.0; HRMS m/z calcd for $C_{24}H_{22}O_9ClBrNa$ ([M + Na]$^+$) 591.0028, found 591.0028.

Data for ***8b:*** yield 93%; white solid; mp = 169−170 °C; $[\alpha]^{20}_D$ = −83 (c 3.2 mg/mL, $CHCl_3$); ^{1}H NMR (400 MHz, $CDCl_3$) δ 6.71 (s, 1H, H-5), 6.62 (s, 1H, H-8), 6.60 (s, 1H, H-6′), 5.93−5.94 (m, 3H, OCH_2O, H-4), 5.59 (s, 1H, H-1), 4.80−4.81 (m, 2H, H-11), 3.92 (s, 3H, 3′-$OCHH_3$), 3.88 (s, 3H, 5′-$OCHH_3$), 3.75 (s, 3H, 4′-$OCHH_3$), 2.96−2.99 (m, 1H, H-3), 2.35 (q, J = 7.6 Hz, 2H, $COCH_2CH_3$), 1.20 (t, J = 7.6 Hz, 3H, $COCH_2CH_3$); ^{13}C NMR (100 MHz, $CDCl_3$) δ 174.2, 171.9, 152.7, 150.9, 149.2, 148.2, 142.7, 134.0, 130.8, 124.1, 113.7, 108.9, 108.7, 108.5, 101.7, 74.8, 73.1, 66.8, 61.1, 61.0, 56.2, 49.4, 47.2, 27.5, 9.0; HRMS m/z calcd for $C_{25}H_{24}O_9ClBrNa$ ([M + Na]$^+$) 605.0184, found 605.0169.

Data for ***8c:*** yield 98%; white solid; mp = 88−90 °C; $[\alpha]^{20}_D$ = −68 (c 3.6 mg/mL, $CHCl_3$); ^{1}H NMR (400 MHz, $CDCl_3$) δ 7.28−7.39 (m, 5H), 6.70 (s, 1H, H-5), 6.59 (s, 1H, H-8), 6.51 (s, 1H, H-6′), 5.94 (d, J = 0.8 Hz, 2H, OCH_2O), 5.88 (d, J = 3.2 Hz, 1H, H-4), 5.58 (s, 1H, H-1), 4.78−4.79 (m, 2H, H-11), 3.92 (s, 3H, 3′-$OCHH_3$), 3.88 (s, 3H, 5′-$OCHH_3$), 3.75 (s, 3H, 4′-$OCHH_3$), 3.67 (d, J = 7.2 Hz, 2H, $PhCH_2$), 2.99 (dd, J = 5.2, 3.2 Hz, 1H, H-3); ^{13}C NMR (100 MHz, $CDCl_3$) δ 171.8, 171.6, 152.7, 151.0, 149.2, 148.2, 142.7, 133.9, 132.6, 130.8, 129.0, 128.9, 127.7, 123.8, 113.8, 108.9, 108.6, 108.3, 101.7, 75.4, 72.9, 66.8, 61.09, 61.01, 56.3, 49.3, 47.2, 41.1; HRMS m/z calcd for $C_{30}H_{26}O_9ClBrNa$ ([M + Na]$^+$) 667.0341, found 667.0320.

Biological Assay. On the basis of the leaf-dipping method,[30] the biological activity of 2α-chloro-2′(2′,6′)-(di)-halogenopicropodophyllotoxin esters (**6a−k**, **7a−i**, and **8a−h**) was evaluated as the mortality rate values against *Mythimna separata* Walker. For each compound, 30 pre-third-instar larvae (10 larvae per

dx.doi.org/10.1021/jf405316w | J. Agric. Food Chem. 2014, 62, 3726−3733

Table 1. Investigation of 3a−c Reacting with Different Chlorination Reagents (La−d)

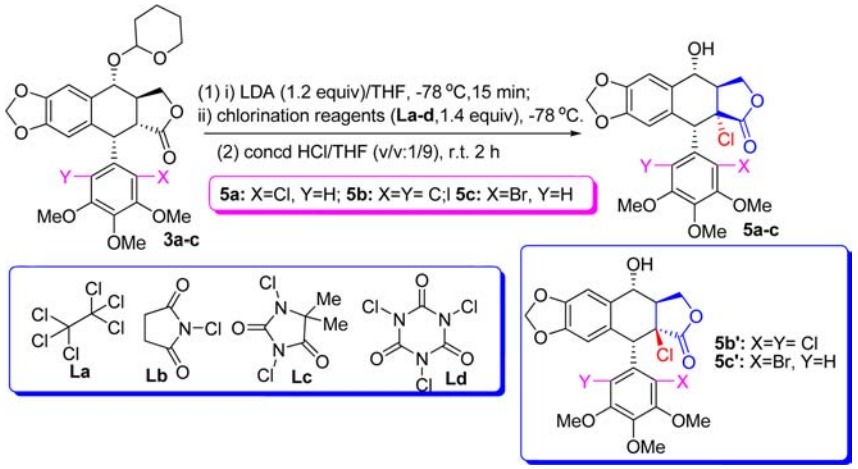

entry	compd	chlorination reagent	T (°C)	t (h)	isolated yield (%) of **5**
1	**3a**	**La**	−78 to 23	16	**5a** (68)
2	**3a**	**Lb**	−78 to −18	3.5	**5a** (56)
3	**3a**	**Lc**	−78 to −39	2	**5a** (66)
4	**3a**	**Ld**	−78 to 27	24	**5a** (0)
5	**3b**	**La**	−78 to 26	18	**5b** (62)
6	**3b**	**Lb**	−78 to −23	3	**5b** (45) + **5b′** (14)[a]
7	**3b**	**Lc**	−78 to −40	2	**5b** (49) + **5b′** (21)[a]
8	**3b**	**Ld**	−78 to 27	24	**5b** (0)
9	**3c**	**La**	−78 to 17	12	**5c** (71)
10	**3c**	**Lb**	−78 to −21	3	**5c** (13) + **5c′** (44)[a]
11	**3c**	**Lc**	−78 to −33	2.5	**5c** (45) + **5c′** (20)[a]
12	**3c**	**Ld**	−78 to 27	24	**5c** (0)

[a]Determined by ^{1}H NMR spectra.

group) were used. Acetone solutions of compounds **6a−k**, **7a−i**, and **8a−h** were prepared at the concentration of 1 mg/mL. Toosendanin was used as the positive control at 1 mg/mL. Fresh wheat leaves were dipped into the corresponding solution for 3 s, then taken out, and dried in a room. Leaves treated with acetone alone were used as a blank control group. Several treated leaves were kept in each dish (10 larvae were raised in each dish, and three dishes were used per treatment), which was then placed in a conditioned room (25 ± 2 °C, 65−80% relative humidity (RH), 12 h/12 h (light/dark) photoperiod). If the treated leaves were consumed, additional treated leaves were added to the dish. Forty-eight hours later, untreated fresh leaves were added to all dishes until adult emergence. The corrected mortality rate was assessed by the formula

$$\text{corrected mortality rate (\%)} = (T - C) \times 100/(100\% - C)$$

where T is the mortality rate in the tested compounds group and C is the mortality rate in the blank control group (T and C were expressed as percentages).

RESULTS AND DISCUSSION

Synthesis. As shown in Scheme 1, first, three halogenation products of **1** such as 2′-chloropodophyllotoxin (**2a**), 2′,6′-dichloropodophyllotoxin (**2b**), and 2′-bromopodophyllotoxin (**2c**) were smoothly prepared by the reaction of **1** with *N*-chlorosuccinimide (NCS) or *N*-bromosuccinimide (NBS).[30] Second, the 4-hydroxy group of **2a−c** was protected by a tetrahydropyranyl (THP) group in the presence of phosphorus oxychloride ($POCl_3$) and dihydropyran (DHP) to produce **3a−c**. Subsequently, as described in Table 1, compounds **3a−c** reacted with lithium diisopropylamide (LDA) at −78 °C via the intermediates **4a−c** (lithium enolates), followed by reaction with four different chlorination reagents, such as hexachloroethane (C_2Cl_6, **La**), NCS (**Lb**), 1,3-dichloro-5,5-dimethylhydantoin (**Lc**), and 1,3,5-trichloroisocyanuric acid (**Ld**), were investigated. The chlorination of **3a−c** with **La** stereoselectively afforded 2α-chloropicropodophyllotoxins (**5a−c**) in 62−71% yields (entries 1, 5, and 9), and the chlorination of **3a** with **La−c** stereoselectively gave **5a** in 56−68% yields (entries 1−3). Although chlorination of **3a** with **Lb** or **Lc** stereoselectively produced **5a**, chlorination of **3b** and **3c** with **Lb** or **Lc** gave mixtures of two isomers, **5b**/**5b′** (2β-chloro-2′,6′-dichloropodophyllotoxin) and **5c**/**5c′** (2β-chloro-2′-bromopodophyllotoxin) (entries 6, 7, 10, and 11), respectively. The ratio of **5b**/**5b′** or **5c**/**5c′** was determined by the corresponding ^{1}H NMR spectra (see the Supporting Information). However, chlorination of **3a−c** with **Ld** did not afford any products except the starting materials, even if the reaction time was prolonged to 24 h (entries 4, 8, and 12). Obviously, chlorination reagent **La** could be used to stereoselectively prepare **5a−c**. In our previous paper, we found when **1** reacted with **La** in the presence of LDA, 2β-chloropodophyllotoxin was stereoselectively obtained.[28,29] According to the above results, this suggested that besides their 2′-halogen-substituted E ring, stereoselective α-chlorination at the C-2 position of **3a−c** was also related to the chlorination reagents. The structures of **5a−c** were well characterized by ^{1}H NMR, ^{13}C NMR, HRMS, optical rotation, and mp. Moreover, the precise three-dimensional steric structures of **5b** and **5c** were further ascertained by single-crystal X-ray diffraction (Figures 2 and 3). This obviously demonstrated that the C-2 chlorine atoms of **5b** and **5c** were clearly present in α configuration. The configuration of **5a** was

dx.doi.org/10.1021/jf405316w | J. Agric. Food Chem. 2014, 62, 3726−3733

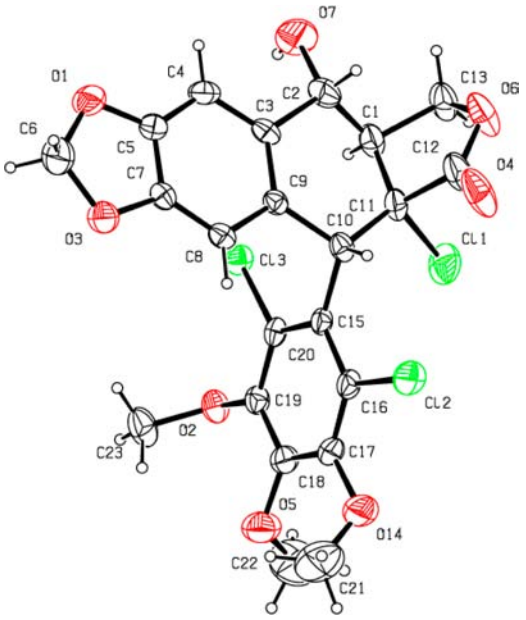

Figure 2. X-ray crystal structure of **5b**.

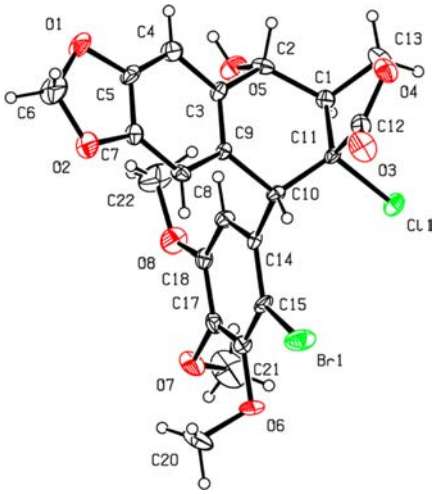

Figure 3. X-ray crystal structure of **5c**.

confirmed on the basis of the X-ray crystallography structure of its ester **6a** (see Figure 4), and the C-2 chlorine atom of **6a** adopted an α configuration. Therefore, the C-2 chlorine atom of **5a** should also adopt an α configuration. Finally, 2α-chloro-2′(2′,6′)-(di)halogenopicropodophyllotoxin esters (**6a**−**k**, **7a**−**i**, and **8a**−**h**) were afforded by reaction of **5a**, **5b**, or **5c** with the corresponding carboxylic acids (**9**) in the presence of *N*,*N*′-dicyclohexylcarbodiimide (DCC) and 4-*N*,*N*-dimethylaminopyridine (DMAP) (Scheme 2). The structures of the title compounds were identified by ^{1}H NMR, ^{13}C NMR, HRMS, optical rotation, and mp. Crystallographic data (excluding structure factors) for the structures of three compounds, **5b**, **5c**, and **6a**, have been deposited at the Cambridge Crystallographic Data Centre with Data CCDC 918889, 918888, and 918696, respectively. These data can be obtained free of charge from the CCDC [fax +44 (0)1223 336033 or e-mail deposit@ccdc.cam.ac.uk].

Insecticidal Activity. The insecticidal activity of novel 2α-chloro-2′(2′,6′)-(di)halogenopicropodophyllotoxin esters (**6a**−**k**, **7a**−**i**, and **8a**−**h**) against the pre-third-instar larvae of *M. separata* was tested by the leaf-dipping method at 1 mg/mL. Toosendanin was used as the positive control at the concentration of 1 mg/mL. In general, we found that the mortality rates of *M. separata* caused by these derivatives after 35 days were higher than those after 10 and 20 days in the same way as in our previous studies,[28−30,32] As described in Table 2, foe **6e**, for instance, the corrected mortality rates against *M. separata* after 10 and 20 days were 10 and 43.3%, respectively, but after 35 days, the mortality rate was increased to 66.7%, which was >6 times that after 10 days. Meanwhile, the

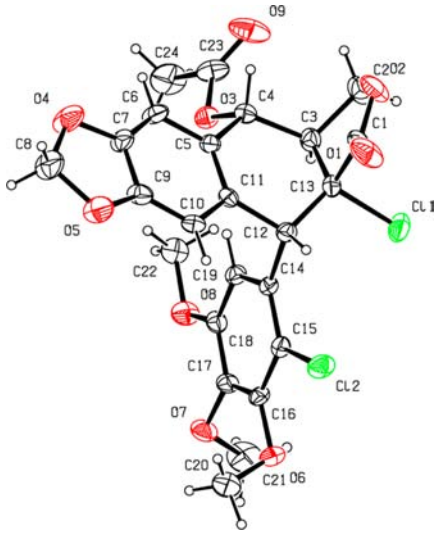

Figure 4. X-ray crystal structure of **6a**.

Scheme 2. Route for Synthesis of 2α-Chloro-2′(2′,6′)-(di)halogenopicropodophyllotoxin Esters (6a−k, 7a−i, and 8a−h)

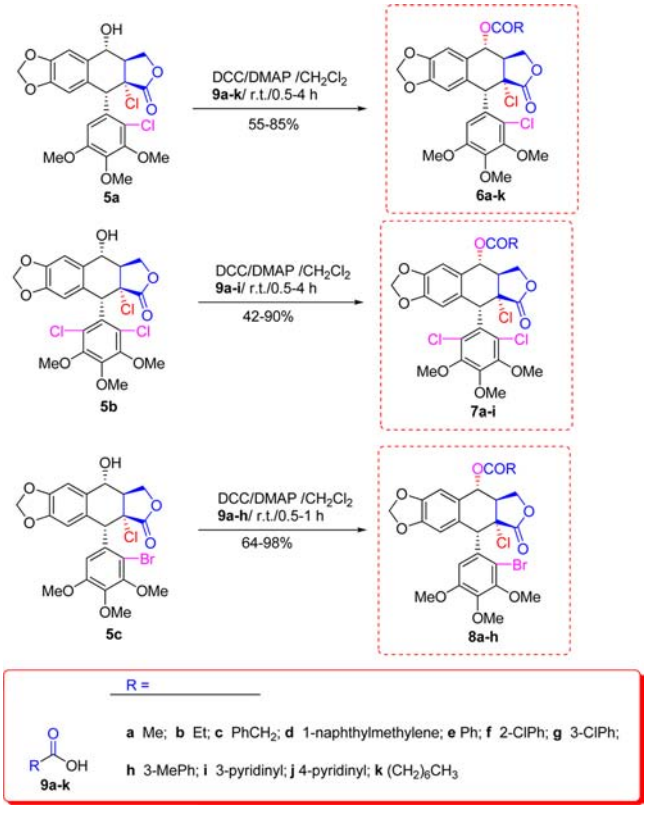

dx.doi.org/10.1021/jf405316w | J. Agric. Food Chem. 2014, 62, 3726−3733

Table 2. Insecticidal Activity of 2α-Chloro-2′(2′,6′)-(di)halogenopicropodophyllotoxin Esters (6a−k, 7a−i, and 8a−h) against the Pre-third-Instar Larvae of *M. separata* on Leaves Treated with a Concentration of 1 mg/mL

	corrected mortality rate (%)		
compd	10 days	20 days	35 days
1	6.7 ± 3.3	30.0 ± 0	37.0 ± 3.3
2a	10.0 ± 0	36.7 ± 3.3	51.9 ± 0
2b	10.0 ± 5.8	36.7 ± 3.3	55.6 ± 0
2c	0 ± 0	20.0 ± 5.8	48.1 ± 3.3
5a	16.7 ± 3.3	33.3 ± 3.3	48.1 ± 3.3
5b	10.0 ± 0	23.3 ± 3.3	33.3 ± 5.8
5c	10.0 ± 5.8	23.3 ± 3.3	51.9 ± 3.3
6a	6.7 ± 3.3	13.3 ± 3.3	37.0 ± 3.3
6b	10.0 ± 5.8	33.3 ± 6.7	40.7 ± 3.3
6c	13.3 ± 3.3	23.3 ± 3.3	25.9 ± 3.3
6d	16.7 ± 3.3	30.0 ± 0	44.4 ± 5.8
6e	10.0 ± 5.8	43.3 ± 3.3	66.7 ± 5.8
6f	3.3 ± 4.7	40.0 ± 0	55.6 ± 0
6g	3.3 ± 3.3	20.0 ± 0	48.1 ± 3.3
6h	6.7 ± 3.3	26.7 ± 3.3	37.0 ± 3.3
6i	10.0 ± 5.8	30.0 ± 0	44.4 ± 5.8
6j	13.3 ± 3.3	40.0 ± 5.8	48.1 ± 3.3
6k	0 ± 0	26.7 ± 3.3	40.7 ± 3.3
7a	6.7 ± 3.3	20.0 ± 0	33.3 ± 5.8
7b	0 ± 0	20.0 ± 0	37.0 ± 3.3
7c	10.0 ± 5.8	36.7 ± 3.3	55.6 ± 5.8
7d	10.0 ± 8.2	26.7 ± 3.3	37.0 ± 3.3
7e	10.0 ± 5.8	33.3 ± 3.3	44.4 ± 5.8
7f	6.7 ± 6.7	23.3 ± 3.3	44.4 ± 0
7g	0 ± 0	36.7 ± 3.3	51.9 ± 3.3
7h	16.7 ± 3.3	33.3 ± 3.3	40.7 ± 3.3
7i	6.7 ± 3.3	36.7 ± 3.3	40.7 ± 3.3
8a	10.0 ± 0	40.0 ± 5.8	44.4 ± 0
8b	6.7 ± 3.3	26.7 ± 3.3	44.4 ± 0
8c	10.0 ± 0	26.7 ± 3.3	33.3 ± 5.8
8d	13.3 ± 6.7	30.0 ± 0	40.7 ± 3.3
8e	3.3 ± 3.3	40.0 ± 0	44.4 ± 5.8
8f	6.7 ± 3.3	53.3 ± 3.3	63.0 ± 3.3
8g	13.3 ± 3.3	30.0 ± 0	48.1 ± 3.3
8h	6.7 ± 3.3	23.3 ± 3.3	51.9 ± 3.3
toosendanin[a]	6.7 ± 3.3	36.7 ± 3.3	51.9 ± 3.3

[a]Toosendanin was used as a positive control at 1 mg/mL.

symptoms of *M. separata* in the treated groups were characterized; for example, at the larval stage some larvae with slim and wrinkled bodies were dying due to feeding too much on treated leaves during the first 48 h (Figure 5), some larvae were molting to malformed pupae or dying during the pupation period (Figure 6), and malformed moths were appearing with imperfect wings (Figure 7).[28−30,32] According to the above symptoms, the tested compounds probably exhibited the antimolting hormone effect. As shown in Table 2, nine compounds, **2a**, **2b**, **5c**, **6e**, **6f**, **7c**, **7g**, **8f**, and **8h**, displayed insecticidal activity equal to or higher than that of toosendanin. Among all of the derivatives, especially compounds **6e** and **8f** exhibited the most potent insecticidal activity with final mortality rates >60%. As in our previous studies,[29,30] introduction of a chlorine or bromine atom at the C-2′ or C-2′ and C-6′ position on the E ring or at the C-2 position of podophyllotoxin could lead to the more potent compounds **2a−c**, **5a**, and **5c** than their precursor podophyllotoxin, except

Figure 5. Representative abnormal larvae pictures of **6f**, **7c**, **7g**, **8f**, and **8h** during the larval period (CK, blank control group).

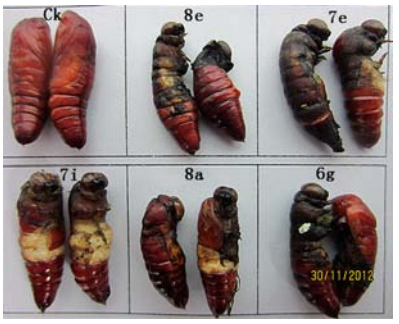

Figure 6. Representative malformed pupae pictures of **6g**, **7e**, **7i**, **8a**, and **8e** during the pupation period (CK, blank control group).

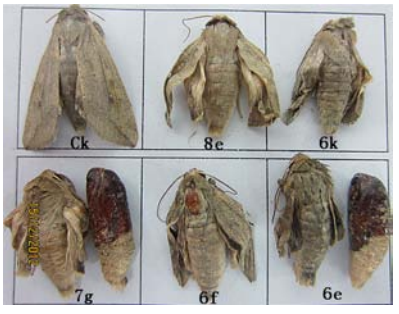

Figure 7. Representative malformed moth pictures of **6e**,**6f**,**6k**, **7g**, and **8e** during the emergence period (CK, blank control group).

5b. For 4α-(alkylacyl)oxy derivatives of **5a−c**, the effect of the length of their side chain at the C-4 position of the podophyllotoxin skeleton on the insecticidal activity was not very obvious (e.g., 37% for **6a**, 40.7% for **6b**, and 40.7% for **6k**; 33.3% for **7a** and 37% for **7b**; 44.4% for **8a** and 44.4% for **8b**). However, for 4α-(arylacyl)oxy derivatives of **5a**, introduction of the electron-withdrawing groups on their phenyl ring at the C-4 position of podophyllotoxin skeleton could lead to the potent compounds. For example, the final mortality rates of **6e** (R = Ph), **6f** (R = 2-ClPh), and **6g** (R = 3-ClPh) were 66.7, 55.6, and 48.1%, respectively, whereas the final mortality rate of **6h** (R = 3-MePh) was only 37%. For 4α-(arylacyl)oxy derivatives of **5c**, introduction of the electron-withdrawing or electron-denoting substituents on their phenyl ring at the C-4 position of podophyllotoxin skeleton could lead to the more potent compounds. For example, the final mortality rates of **8f** (R = 2-ClPh), **8g** (R = 3-ClPh), and **8h** (R = 3-MePh) were 63, 48.1, and 51.9%, respectively, whereas the final mortality rate of **8e** (R = Ph) was 44.4%. However, introduction of the (heterocyclylacyl)oxy group at the C-4 position of **5a** or **5b**

dx.doi.org/10.1021/jf405316w | J. Agric. Food Chem. 2014, 62, 3726−3733

could not afford the more potent compounds (e.g., 44.4% for **6i** and 48.1% for **6j**; 40.7% for **7i**). In our previous paper, we found that introduction of a (1-naphthylacetyl)oxy group at the C-4 position of the corresponding podophyllotoxin derivatives led to the more potent compounds,[29,30] but herein introduction of a (1-naphthylacetyl)oxy group at the C-4 position of **5a**−**c** did not result in the potent compounds. For example, the final mortality rates of **6d**, **7d**, and **8d** were only 44.4, 37, and 40.7%, respectively, so the insecticidal activity of **6d**, **7d**, and **8d** was also related to the chemical structures of their precursors.

In summary, a series of novel esters of 2α-chloro-2′(2′,6′)-(di)halogenopicropodophyllotoxin with modified C, D, and E rings of podophyllotoxin were prepared. In the meantime, an efficient method for the stereoselective α-chlorination at the C-2 position of 2′(2′,6′)-(di)halogenopodophyllotoxin derivatives in the presence of hexachloroethane (C_2Cl_6) was developed. Three steric structures of compounds **5b**, **5c**, and **6a** were determined by single-crystal X-ray diffraction. Their insecticidal activity was evaluated against pre-third-instar larvae of the oriental armyworm, *M. separata* (Walker), in vivo at a concentration of 1 mg/mL. This demonstrated that besides their 2′-halogen-substituted E ring, the stereoselective α-chlorination at the C-2 position of 2′(2′,6′)-(di)-halogenopodophyllotoxins was also related to the chlorination reagents. Among all of the derivatives, 2α-chloro-4α-(benzoyl)-oxy-2′-chloropicropodophyllotoxin (**6e**) and 2α-chloro-4α-(2-chlorophenylacyl)oxy-2′-bromopicropodophyllotoxin (**8f**) showed the most potent insecticidal activities with final mortality rates of >60%. For 4α-(alkylacyl)oxy derivatives of 2α-chloro-2′(2′,6′)-(di)halogenopicropodophyllotoxin, the effect of the length of their side chain at the C-4 position of podophyllotoxin skeleton on the insecticidal activity was not very obvious. For 4α-(arylacyl)oxy derivatives of 2α-chloro-2′-chloro/bromopicropodophyllotoxin, the electronic effect of the substituents on their phenyl ring at the C-4 position of podophyllotoxin skeleton on the insecticidal activity was observed.

■ ASSOCIATED CONTENT

Ⓢ Supporting Information

Data on ^{1}H NMR, ^{13}C NMR, optical rotation, and melting point for the target compounds. This material is available free of charge via the Internet at http://pubs.acs.org.

■ AUTHOR INFORMATION

Corresponding Author

*(H.X.) Phone: +86(0)29-87091952. Fax: +86(0)29-87091952. E-mail orgxuhui@nwsuaf.edu.cn.

Author Contributions

‖L.F. and Y.G. contributed equally to this work.

Funding

The present research was supported by the National Natural Science Foundation of China (No. 31071737,31171896) and Special Funds of Central Colleges Basic Scientific Research Operating Expenses (YQ2013008) to H.X.

Notes

The authors declare no competing financial interest.

■ REFERENCES

(1) Muralidharan, K.; Pasalu, I. C. Assessments of crop losses in rice ecosystems due to stem borer damage (Lepidoptera: Pyralidae). *Crop Prot.* **2006**, *25*, 409−417.

(2) Tabashnik, B. E.; Brevault, T.; Carriere, Y. Insect resistance to Bt crops: lessons from the first billion acres. *Nat. Biotechnol.* **2013**, *31*, 510−521.

(3) Santiago, R.; Butron, A.; Reid, L. M.; Arnason, J. T.; Sandoya, G.; Souto, X. C.; Malvar, R. A. Diferulate content of maize sheaths is associated with resistance to the Mediterranean corn borer *Sesamia nonagrioides* (Lepidoptera: Noctuidae). *J. Agric. Food Chem.* **2006**, *54*, 9140−9144.

(4) Padmaja, P. G.; Aruna, C.; Patil, J. V. Evidence of genetic transmission of antibiosis and antixenosis resistance of sorghum to the spotted stemborer, *Chilo partellus* (Lepidoptera: Pyralidae). *Crop Prot.* **2012**, *33*, 21−26.

(5) Kaur, P.; Dilawari, V. K. Inheritance of resistance to *Bacillus thuringiensis* Cry1Ac toxin in *Helicoverpa armigera* (Hubner) (Lepidoptera: Noctuidae) from India. *Pest Manage. Sci.* **2011**, *67*, 1294−1302.

(6) Edwards, K. T.; Caprio, M. A.; Allen, K. C.; Musser, F. R. Risk assessment for *Helicoverpa zea* (Lepidoptera: Noctuidae) resistance on dual-gene versus single-gene corn. *J. Econ. Entomol.* **2013**, *106*, 382−392.

(7) Xu, H. *Comments to "Insecticide resistance after silent spring"*; http://comments.sciencemag.org/content/10.1126/science.1226994, 2013.

(8) Wu, M.; Han, G. F.; Wang, Z. W.; Liu, Y. X.; Wang, Q. M. Synthesis and antiviral activities of antofine analogues with different C-6 substituent groups. *J. Agric. Food Chem.* **2013**, *61*, 1030−1035.

(9) Caboni, P.; Saba, M.; Tocco, G.; Casu, L.; Murgia, A.; Maxia, A.; Menkissoglu-Spiroudi, U.; Ntalli, N. Nematicidal activity of mint aqueous extracts against the root-knot nematode meloidogyne incognita. *J. Agric. Food Chem.* **2013**, *61*, 9784−9788.

(10) Lang, K. L.; Deagosto, E.; Zimmermann, L. A.; Machado, V. R.; Bernardes, L. S. C.; Schenkel, E. P.; Duran, F. J.; Palermo, J.; Rossini, C. Chemical modification produces species-specific changes in cucurbitacin antifeedant effect. *J. Agric. Food Chem.* **2013**, *61*, 5534−5539.

(11) Glazer, I.; Masaphy, S.; Marciano, P.; Bar-Ilan, I.; Holland, D.; Kerem, Z.; Amir, R. Partial identification of antifungal compounds from *Punica granatum* peel extracts. *J. Agric. Food Chem.* **2012**, *60*, 4841−4848.

(12) Stark, T. D.; Matsutomo, T.; Losch, S.; Boakye, P. A.; Balemba, O. B.; Pasilis, S. P.; Hofmann, T. Isolation and structure elucidation of highly antioxidative 3,8″-linked biflavanones and flavanone-C-glycosides from *Garcinia buchananii* bark. *J. Agric. Food Chem.* **2012**, *60*, 2053−2062.

(13) Lin, L.; Mulholland, N.; Wu, Q.; Beattie, D.; Huang, S.; Irwin, D.; Clough, J.; Gu, Y.; Yang, G. F. Synthesis and antifungal activity of novel sclerotiorin analogues. *J. Agric. Food Chem.* **2012**, *60*, 4480−4491.

(14) Sun, J.; Awakawa, T.; Noguchi, H.; Abe, I. Induced production of mycotoxins in an endophytic fungus from the medicinal plant *Datura stramonium* L. *Bioorg. Med. Chem. Lett.* **2012**, *22*, 6397−6400.

(15) Lv, M.; Xu, H. Recent advances in semisynthesis, biosynthesis, biological activities, mode of action, and structure-activity relationship of podophyllotoxins: an update (2008−2010). *Mini-Rev. Med. Chem.* **2011**, *11*, 901−909.

(16) Miyazawa, M.; Fukuyama, M.; Yoshio, K.; Kato, T.; Ishikawa, Y. Biologically active components against *Drosophila melanogaster* from *Podophyllum hexandrum*. *J. Agric. Food Chem.* **1999**, *47*, 5108−5110.

(17) Carpenter, C. D.; O'Neill, T.; Picot, N.; Johnson, J. A.; Robichaud, G. A.; Webster, D.; Gray, C. A. Anti-mycobacterial natural products from the Canadian medicinal plant *Juniperus communis*. *J. Ethnopharmacol.* **2012**, *143*, 695−700.

(18) Stadler, D.; Bach, T. Concise stereoselective synthesis of (−)-podophyllotoxin by an intermolecular iron(III)-catalyzed Friedel-Crafts alkylation. *Angew. Chem., Int. Ed.* **2008**, *47*, 7557−7559.

(19) Engelhardt, U.; Sarkar, A.; Linker, T. Efficient enantioselective total synthesis of (−) epipodophyllotoxin. *Angew. Chem., Int. Ed.* **2003**, *42*, 2487−2489.

(20) Reynolds, A. J.; Scott, A. J.; Turner, C. I.; Sherburn, M. S. The intramolecular carboxyarylation approach to podophyllotoxin. *J. Am. Chem. Soc.* **2003**, *125*, 12108−12109.
(21) Wu, Y.; Zhao, J.; Chen, J.; Pan, C.; Li, L.; Zhang, H. Sequential conjugate addition-allylation reactions: a concise total synthesis of (+)-podophyllotoxin. *Org. Lett.* **2009**, *11*, 597−600.
(22) Wu, Y.; Zhang, H.; Zhao, Y.; Zhao, J.; Chen, J.; Li, L. A new and efficient strategy for the synthesis of podophyllotoxin and its analogues. *Org. Lett.* **2007**, *9*, 1199−1202.
(23) Vitale, M.; Prestat, G.; Lopes, D.; Madec, D.; Kammerer, C.; Poli, G.; Girnita, L. New picropodophyllin analogs via palladium-catalyzed allylic alkylation−Hiyama cross-coupling sequences. *J. Org. Chem.* **2008**, *73*, 5795−5805.
(24) Ren, J.; Wu, L.; Xin, W. Q.; Chen, X.; Hu, K. Synthesis and biological evaluation of anticancer activity for novel 4*β*-amino oxadiazole derivatives of podophyllotoxin. *Bioorg. Med. Chem. Lett.* **2012**, *22*, 4778−4782.
(25) Chen, S. W.; Xiang, R.; Liu, J.; Tian, X. Synthesis and biological evaluation of novel conjugates of podophyllotoxin and 5-FU as antineoplastic agents. *Bioorg. Med. Chem.* **2009**, *17*, 3111−3117.
(26) Cappelletti, G.; Cartelli, D.; Peretto, B.; Ventura, M.; Riccioli, M.; Colombo, F.; Snaith, J. S.; Borrelli, S.; Passarella, D. Tubulin-guided dynamic combinatorial library of thiocolchicine-podophyllotoxin conjugates. *Tetrahedron* **2011**, *67*, 7354−7357.
(27) Passarella, D.; Peretto, B.; Yepes, R. B.; Cappelletti, G.; Cartelli, D.; Ronchi, C.; Snaith, J.; Fontana, G.; Danieli, B.; Borlak, J. Synthesis and biological evaluation of novel thiocolchicine-podophyllotoxin conjugates. *Eur. J. Med. Chem.* **2010**, *45*, 219−226.
(28) Xu, H.; Xiao, X.; Wang, Q. T. Natural products-based insecticidal agents 7. Semisynthesis and insecticidal activity of novel 4*α*-alkyloxy-2-chloropodophyllotoxin derivatives against *Mythimna separata* Walker in vivo. *Bioorg. Med. Chem. Lett.* **2010**, *20*, 5009−5012.
(29) Xu, H.; Xiao, X.; Zhao, X. F.; Guo, Y.; Yao, X. J. Unexpectedly convenient and stereoselective synthesis of 4*α*-acyloxy-2-chloropodophyllotoxins in the presence of $BF_3{\cdot}Et_2O$. *Bioorg. Med. Chem. Lett.* **2011**, *21*, 4008−4012.
(30) Che, Z.; Yu, X.; Zhi, X. Y.; Fan, L. L.; Xu, H. Synthesis of novel 4*α*-(acyloxy)-2′(2′,6′)-(di)halogenopodophyllotoxin derivatives as insecticidal agents. *J. Agric. Food Chem.* **2013**, *61*, 8148−8155.
(31) Perrin, D. D.; Armarego, W. L. F. *Purification of Laboratory Chemicals*, 3rd ed.; Pergamon Press: Oxford, UK, 1988.
(32) Wang, J. J.; Zhi, X. Y.; Yu, X.; Xu, H. Synthesis and insecticidal activity of new deoxypodophyllotoxin-based phenazine analogs against *Mythimna separata* Walker. *J. Agric. Food Chem.* **2013**, *61*, 6336−6343.

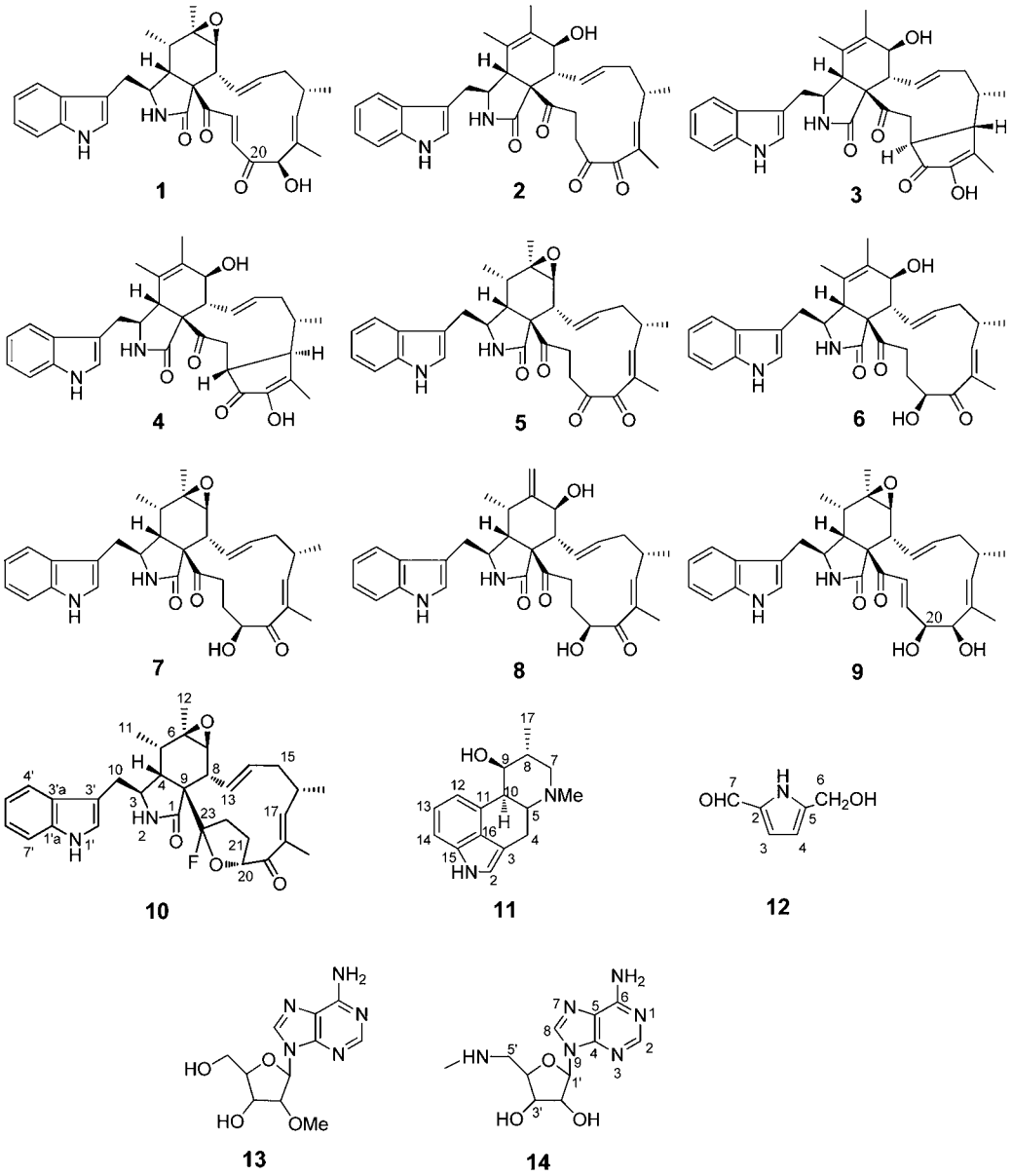

Figure 1. Structures of compounds **1**−**14**: chaetoglobosins A (**1**), G (**2**), V (**3**), V_b, (**4**), C (**5**), E (**6**), F (**7**), and F_{ex} (**8**); 20-dihydrochaetoglobosin A (**9**); and chaetoglobosin F_a (**10**), as well as fumigaclavine B (**11**), 5-(hydroxymethyl)-1*H*-pyrrole-2-carbaldehyde (**12**), 2′-*O*-methyladenosine (**13**), and 5′-deoxy-5′-methylamino-adenosine (**14**).

tetramethylsilane (TMS) or CF_3COOH as internal and external standards, respectively. Electrospray ionization mass spectrometry (ESI-MS) was obtained on a Bruker Esquire 6000 instrument, and high-resolution ESI-MS was recorded on a Thermo Fisher Scientific Q-TOF mass spectrometer.

Thin-layer chromatography (TLC) was performed on silica gel 60 F_{254} (Qingdao Marine Chemical Ltd.). Column chromatography (CC) was performed on MCI gel (75−150 mm, Mitsubishi Chemical Corp., Tokyo, Japan), 200−300 mesh silica gel (Qingdao Marine Chemical Factory, China), Sephadex LH-20 (Pharmacia), and RP-18 (Merck). Fractions were monitored by TLC, and spots were visualized by spraying with 5% H_2SO_4 in ethanol, followed by heating. All other chemicals used in this study were of analytical grade.

Five cytochalasans, chaetoglobosins A, G, V, V_b, and C (**1**−**5**), were isolated and identified previously from the cultures of *C. globosum*, an endophyte residing in the leaves of *G. biloba*, in three different media.[15−17]

Fungal Material. The fungal strain *C. globosum* was isolated from the sterilized leaves of *G. biloba*, a medicinal plant growing in Linyi, Shandong province, China, authenticated on the basis of morphological studies,[15] and has been deposited at the College of Science, Northwest A&F University.

Preparative Scale Culture. This fungus was grown on a sterilized moistened rice medium in Roux flasks (100 g/flask × 200) at 25 °C for 21 days to give green moldy rice.

Extraction and Isolation. The fungal cultures were ultrasonically extracted four times with MeOH. The solvent was removed under reduced pressure to give a crude extract. The extract was dissolved in 90% MeOH/H_2O (2 L) and treated four times with petroleum ether to give 0.5 g of residue. The remaining layer was adjusted to 50% aqueous methanol and partitioned with $CHCl_3$. The chloroform-soluble portion (20 g) was subjected to column chromatography on silica gel with $CHCl_3$/MeOH (100:1, 50:1, 20:1, 10:1) to give four fractions A−D.

Fraction A (4.5 g) was subjected to MCI column chromatography (CC) and Sephadex LH-20 ($CHCl_3$/MeOH 1:1), followed by purification with PTLC to yield compounds **5** (12 mg) and **7** (50 mg).

dx.doi.org/10.1021/jf500390h | *J. Agric. Food Chem.* 2014, 62, 3734−3741

Table 1. ^{1}H (500 MHz) and ^{13}C NMR (125 MHz) Data of Compounds 7 and 10[a]

	compound 7			compound 10[b]	
no.	δ_C[c]	δ_H (mult, J in Hz)[c]	δ_C[b]	δ_C (mult, J in Hz)	δ_H (mult, J in Hz)
1	173.64		175.23	174.21	
2		8.29 (1H, s)			9.13 (1H, s)
3	52.16	3.63 (1H, m)	53.39	53.71	4.20 (1H, m)
4	47.89	2.34 (1H, m)	48.36	50.45	2.72 (1H, m)
5	35.66	1.57 (1H, overlap)	37.03	36.91	2.14 (1H, m)
6	56.94		57.55	57.37	
7	61.22	2.64(1H, m)	62.45	62.62	3.00 (1H, m)
8	46.85	2.18 (1H, m)	49.80	45.79	3.02 (1H, m)
9	63.66		66.11	56.86 ($J_{C,F}$ = 28.8)	
10	29.88	1.57 (2H, overlap)	31.85	35.69	3.30 (1H, m, H-10a)
					3.20 (1H, m, H-10b)
11	12.11	0.61 (3H, d, 7.1)	12.85	13.99	1.16 (3H, d, 7.4)
12	19.13	1.09 (3H, s)	19.65	20.48	1.30 (3H, s)
13	128.52	6.33 (1H, m)	129.94	128.96	5.35 (1H, m)
14	132.85	5.17 (1H, dd, 14.4, 11.7)	133.61	133.77	7.02 (1H, dd, 15.3, 9.2)
15	40.20	1.97, 2.37 (2H, m)	41.01	41.23	2.04, 2.37 (2H, m)
16	32.80	2.75 (1H, m)	33.51	34.23	2.70 (1H, m)
17	147.71	6.19 (1H, d, 9.5)	148.47	153.30	6.73 (1H, d, 9.8)
18	134.97		135.84	130.75	
19	209.10		209.75	202.62	
20	70.29	4.58 (1H, m)	71.95	84.46	5.40 (1H, m)
21	32.74	2.58 (2H, m)	34.84	24.25	2.69 (1H, m, H-21a)
					2.21 (1H, m, H-21b)
22	36.41	2.11, 2.61 (2H, m)	38.07	36.23 ($J_{C,F}$ = 30.4)	2.36−2.45 (2H, m)
23	204.06		205.03	123.66 ($J_{C,F}$ = 224.7)	
1′		10.88 (1H, br s)			12.08 (1H, br s)
2′	124.27	7.09 (1H, s)	124.98	124.75	7.57 (1H, s)
3′	109.02		110.81	111.74	
3′a	127.52		128.51	128.30	
4′	117.92	7.43 (1H, d, 7.8)	118.91	118.80	7.94 (1H, d, 7.5)
5′	120.84	7.05 (1H, m)	121.95	122.08	7.36 (1H, m)
6′	118.42	6.97 (1H, m)	119.54	119.62	7.34 (1H, m)
7′	111.44	7.32 (1H, d, 8)	112.29	112.36	7.67 (1H, d, 7.5)
1′a	136.00		137.63	137.89	
16-Me	19.63	0.98 (3H, d, 6.5)	19.78	19.29	0.92 (3H, d, 6.7)
18-Me	11.98	1.69 (3H, s)	12.43	11.80	1.85 (3H, s)

[a]Assignments were aided by a combination of $^{1}H-^{1}H$ COSY, HSQC, and HMBC experiments. [b]Measured in C_5D_5N. [c]Measured in DMSO-d_6.

Fraction B (1.8 g) was applied to MCI CC using MeOH/H_2O (10:90−100:0) to provide fractions B1, B2, B3, and B4. Fraction B3 was subjected to Sephadex LH-20 ($CHCl_3$/ MeOH 1:1), then followed by silica gel with $CHCl_3$/acetone (8:2) and $CHCl_3$/MeOH (35:1) to give compounds **6** (18 mg) and **8** (10 mg).

Fraction C (6.1 g) was applied to MCI CC using MeOH/H_2O (10:90−100:0) to provide fractions C1, C2, C3, C4, and C5. Fraction C2 was purified by repeated CC on Sephadex LH-20 ($CHCl_3$/MeOH 1:1) and silica gel ($CHCl_3$/MeOH, 95:5; $CHCl_3$/acetone 1:1) to give compound **14** (4.7 mg). Fraction C4 was chromatographed over Sephadex LH-20 with MeOH and repeatedly purified by CC with $CHCl_3$/acetone (8:2) and CH_2Cl_2/MeOH (98:2) to give compound **9** (5 mg).

Fraction D (2.9 g) was purified by CC on MCI, Sephadex LH-20 (MeOH), and silica gel (petroleum ether/acetone, 1:1; $CHCl_3$/ acetone, 2:1; $CHCl_3$/MeOH, 10:1), to give compounds **11** (1.8 mg), **12** (10 mg), and **13** (4 mg).

*Chaetoglobosin F (**7**):* white amorphous powder; $[\alpha]_D^{15}$ = −67.5 (*c* 0.10 in $CHCl_3$) (lit.[12] $[\alpha]_D$ = −69.0 ($CHCl_3$)); ^{1}H and ^{13}C NMR data, see Table 1; ESI-MS (negative) *m*/*z* 529.17 $[M - H]^-$. These data were identical to those recorded in the literature.[4,19,20]

*Chaetoglobosin F_{ex} (**8**):* white amorphous powder; $[\alpha]_D^{15}$ = +62.5 (*c* 0.10 in $CHCl_3$) (lit.[5] $[\alpha]_D$ = +63.8 (MeOH)); ESI-MS (negative) *m*/*z* 529.17 $[M - H]^-$; ^{1}H and ^{13}C NMR (DMSO-d_6) data were identical to those recorded in the literature.[5]

*20-Dihydrochaetoglobosin A (**9**):* white amorphous powder; $[\alpha]_D^{15}$ = −56.2 (*c* 0.10 in $CHCl_3$) (lit.[5] $[\alpha]_D$ = −52.0 (MeOH)); ^{1}H NMR (500 MHz, DMSO-d_6) δ 10.84 (1H, s, H-2), 8.15 (1H, s, H-1′), 7.38 (1H, d, *J* = 7.9 Hz, H-4′), 7.31 (1H, d, *J* = 8.1 Hz, H-7′), 7.04 (1H, m, H-5′), 7.01 (1H, s, H-2′), 6.94 (1H, m, H-6′), 6.74 (1H, dd, *J* = 15.2, 3.3 Hz, H-21), 6.42 (1H, d, *J* = 15.1 Hz, H-22), 6.06 (1H, m, H-13), 5.10 (1H, m, H-14), 4.98 (1H, d, *J* = 4.5 Hz, 20-OH), 4.87 (1H, d, *J* = 5 Hz, 19-OH), 4.60 (1H, d, *J* = 9.9 Hz, H-17), 4.44 (1H, br s, H-20), 4.01(1H, br s, H-19), 3.62 (1H, m, H-3), 2.76 (1H, dd, *J* = 14.0, 5.2 Hz, H-10a), 2.66 (1H, d, *J* = 5.4 Hz, H-7), 2.32−2.42 (3H, m, H-4, 8, 10b), 2.52 (1H, m, overlap, H-16), 2.22 (1H, m, H-15a), 1.70 (2H, m, H-5, 15b), 1.63 (3H, s, 18-Me), 1.06 (3H, s, H-12), 0.88 (3H, d, *J* = 6.5 Hz, 16-Me), 0.52 (3H, d, *J* = 7.2 Hz, H-11); ^{13}C NMR (125 MHz, DMSO-d_6) δ 198.03 (C-23), 173.35 (C-1), 147.81 (C-21), 136.08 (C-1a′), 134.74 (C-14), 133.93 (C-18), 131.40 (C-17), 127.30 (C-3a′), 126.07 (C-13), 123.51 (C-5′), 123.10 (C-22), 120.92 (C-2′), 118.43 (C-6′), 117.95 (C-4′), 111.39 (C-7′), 109.78 (C-3′), 78.14 (C-19), 76.04 (C-20), 63.21 (C-9), 61.07 (C-7), 56.82 (C-6), 52.13 (C-3), 46.74 (C-8), 45.63 (C-4), 38.82 (C-15), 35.78 (C-5), 32.96 (C-10), 31.73 (C-16), 21.26 (16-Me), 19.01 (C-12), 13.58 (18-Me),

dx.doi.org/10.1021/jf500390h | J. Agric. Food Chem. 2014, 62, 3734−3741

12.02 (C-11); ESI-MS (negative) m/z 529.17 $[M - H]^-$. These data were identical to those recorded in the literature.[5,21]

Semisynthesis of Chaetoglobosin F_a (10).[22] To a solution of compound **7** (37 mg, 0.070 mmoL) in CH_2Cl_2 (2 mL) was added DAST (28 μL, 0.21 mmoL), and the mixture was stirred at room temperature for 1.5 h. Water (2 mL) was added to the solution, and the mixture was diluted with CH_2Cl_2 (30 mL). The solution was washed sequentially with water (2 × 15 mL) and brine (15 mL), dried over Na_2SO_4, and filtered, and the solvent was removed in vacuo. The residue was chromatographed over silica gel (petroleum ether/acetone 7:3) to give compound **10** (20 mg, 53.9%).

Chaetoglobosin F_a (10): white amorphous powder; $[\alpha]_D^{29} = -98.5$ (c 0.20 in $CHCl_3$); UV ($CHCl_3$) λ_{max} (log ε) = 227(3.55), 242 (3.74), 282 (3.40), 290 (3.30); ^{1}H and ^{13}C NMR data, see Table 1; IR (KBr) υ 3390, 2955, 2923, 1686, 1638, 1073 cm^{-1}; HR ESI-MS (negative) m/z 531.2656 $[M - H]^-$ (calcd for $C_{32}H_{36}N_2O_4F$, 531.2665).

Fumigaclavine B (11): white amorphous powder; ^{1}H NMR (500 MHz, CD_3OD) δ 7.13 (1H, d, J = 8.1 Hz, H-12), 7.09 (1H, m, H-13), 6.93 (1H, d, J = 6.9 Hz, H-14), 6.90 (1H, s, H-2), 4.54 (1H, m, H-9), 3.44 (1H, dd, J = 14, 4.3 Hz, H-4a), 3.21(1H, d, J = 10.2 Hz, H-7a), 2.95 (1H, dd, J = 11.4, 2.6 Hz, H-7b), 2.68 (1H, m, H-5), 2.64 (1H, m, H-4b), 2.63 (1H, H-10), 2.47 (3H, s, NMe), 2.16 (1H, m, H-8), 1.28 (3H, d, J = 7.4 Hz, H-17); ^{13}C NMR (125 MHz, CD_3OD) δ 135.39 (C-15), 130.53 (C-11), 123.52 (C-13), 123.52 (C-16), 119.25 (C-2), 113.92 (C-12), 109.51 (C-14), 109.51 (C-3), 69.62 (C-9), 62.39 (C-5), 58.36 (C-7), 43.89 (N-Me), 41.83 (C-10), 36.88 (C-8), 26.99 (C-4), 17.12 (C-17); ESI-MS (positive) m/z 257.0 $[M + H]^+$. These data were identical to those reported in the literature.[23]

5-(Hydroxymethyl)-1H-pyrrole-2-carbaldehyde (12): white amorphous powder; ^{1}H NMR (500 MHz, CD_3OD) δ 9.36 (1H, s, H-7), 6.98 (1H, d, J = 3.6 Hz, H-3), 6.26 (1H, d, J = 3.5 Hz, H-4), 4.60 (2H, s, H-6); ^{13}C NMR (125 MHz, CD_3OD) δ 180.59 (C-7), 143.38 (C-5), 133.95 (C-2), 123.42 (C-3), 110.41 (C-4), 57.84 (C-6); ESI-MS (negative) m/z 124.08 $[M - H]^-$. These data were identical to those described in the literature.[24]

2′-O-Methyladenosine (13): white amorphous powder; ^{1}H NMR (500 MHz, DMSO-d_6) δ 8.39 (1H, s, H-2), 8.14 (1H, s, H-8), 7.37 (2H, s, NH_2), 6.00 (1H, d, J = 5.97 Hz, H-1′), 4.34 (1H, m, H-3′), 4.33 (1H, m, H-2′), 3.98 (1H, m, H-4′), 3.67 (1H, m, H-5′), 3.30 (3H, s, OMe); ^{13}C NMR (125 MHz, DMSO-d_6) δ 156.20 (C-6), 152.56 (C-8), 149.01 (C-4), 139.72 (C-2), 119.28 (C-5), 86.47 (C-4′), 85.82 (C-2′), 82.45 (C-1′), 68.81 (C-3′), 61.51 (C-5′), 57.48 (C-OMe); ESI-MS (positive) m/z 282.04 $[M + H]^+$. These data were identical to those described in the literature.[25]

5′-Deoxy-5′-methylamino-adenosine (14): white amorphous powder; ^{1}H NMR (500 MHz, CD_3OD) δ 8.48 (1H, s, H-2), 8.40 (1H, s, H-8), 6.05 (1H, m, H-1′), 4.77 (1H, m, H-2′), 4.47 (1H, m, H-4′), 4.37 (1H, m, H-3′), 3.45 (1H, m, H-5′a), 3.20 (1H, m, H-5′b), 2.67 (3H, s, N−CH_3); ^{13}C NMR (125 MHz, CD_3OD) δ 153.37 (C-6), 150.87 (C-4), 146.42 (C-2), 144.83 (C-8), 121.76 (C-5), 91.23 (C-1′), 79.58 (C-4′), 75.79 (C-2′), 75.39 (C-3′), 57.91 (C-5′), 40.19 (N−CH_3); ESI-MS (positive) m/z 281.07 $[M + H]^+$. These data were identical to those described in the literature.[26]

Phytotoxicity Bioassay. Phytotoxicity was assayed by the method reported previously.[27,28] Briefly, radish seedlings were washed by running water for 120 min and then soaked in 0.3% $KMnO_4$ for 15 min and flushed to colorless. An acetone solution containing a sample at a defined concentration (200 or 50 ppm) was poured on two sheets of filter paper in a 12-well microplate. After removal of the solvent in vacuo, 200 μL of aseptic water was added on it. Radish seedlings of uniform shape and size were placed on the filter paper. In this experiment the seedlings were grown for 4 days at 25 °C under completely dark conditions. The inhibitory effects were observed after 96 h. Glyphosate was used as the positive control. Acetone served as a blank control. Each experiment was conducted three times and presented as the mean ± standard deviation of three replicates.

Cytotoxicity Bioassay. Cytotoxicity in vitro was assessed by the SRB colorimetric assay, which estimates cell number indirectly by measuring total basic amino acids of cultured cells.[29] Briefly, 100 μL aliquots of the exponentially growing HCT116 cells containing 2.5 × 10^4 cells/mL were added to each well of a 96-well flat-microtiter plate and cells allowed to attach for 24 h. Then the medium was replaced by fresh medium, and cells were incubated with various amounts of the test compound for an additional 72 h. Four replicate wells were used in each point in the experiments. After incubation at 37 °C, culture medium was moved, cells were fixed in situ with 100 μL aliquots of cold 10% trichloroacetic acid (TCA), and plates were incubated for 1 h at 4 °C. Thereafter, supernatant was discarded and plates were washed five times with distilled water and air-dried. Sulforhodamine B solution at 0.4% (w/v) in 1% acetic acid was added to each well, and plates were incubated for 20−30 min at room temperature. The unbound dye was removed by washing five times with 1% acetic acid, and plates were air-dried. Bound sulforhodamine B was subsequently solubilized with 10 mM Tris base, and the absorbance was read at 560 nm using an Epoch (Bio-Tek) microplate reader. The percentage of cell viability was calculated relative to control wells designated as 100% viable cells. All of the results were expressed as the mean ± standard deviation of triplicate determinations. The data analysis was performed using Origin 8.0 software.

RESULTS AND DISCUSSION

Cultivation, Isolation, and Structure Elucidation. The fungal strain was cultured in rice medium at 28 °C for 21 days. The extract of the culture was partitioned between chloroform and 50% MeOH/H_2O. The chloroform extract was repeatedly purified by RP-18 gel, silica gel, and Sephadex LH-20 CC to afford nine compounds. The structures of the known compounds were characterized by means of spectroscopic comparisons with literature data as chaetoglobosins C (**5**), E (**6**), F (**7**),[4,19,20] and F_{ex} (**8**),[5] 20-dihydrochaetoglobosin A (**9**),[5,21] fumigaclavine B (**11**),[23] 5-(hydroxymethyl)-1*H*-pyrrole-2-carbaldehyde (**12**),[24] 2′-*O*-methyladenosine (**13**),[25] and 5′-deoxy-5′-methylamino-adenosine (**14**) (Figure 1).[26]

Some of the isolated chaetoglobosins (A, C, E, and F) are well-known metabolites isolated from different fungal strains of *C. globosum*,[2] whereas 20-dihydrochaetoglobosin A (**9**), which was reported for the first time from the plant endophytic *C. globosum*, had been isolated before from *C. subaffine*.[5] A search of known *C. globosum* secondary metabolites from the CrossFire Beilstein database revealed that these four compounds, **11**−**14**, had not been previously described in *C. globosum*.

Semisynthesis of Chaetoglobosin F_a (10). Selective introduction of fluorine atom(s) to bioactive natural and unnatural products is of extreme interest in pharmaceutical research[30] because fluorine atom(s) are well-known as pharmacophore(s). (Diethylamino)sulfur trifluoride (DAST) is often used for the preparation of fluorinated compounds. This reagent can convert alcohols into fluorides or ketones into *gem*-difluoro compounds under quite mild conditions.[22,31] As a consequence, we made attempts to obtain 20-fluorochaetoglobosin F through treatment of chaetoglobosin F (**7**) with DAST (3 equiv) in dichloromethane at room temperature for 1.5 h; unexpectedly, however, this process failed to directly give 20-fluorinated product but provided 23-fluorinated product chaetoglobosin F_a (**10**) in 53.9% yield, which possesses an oxolane ring between C-20 and C-23, as shown in Scheme 1.

HR-ESIMS of compound **10** gave a pseudomolecular ion at m/z 531.2656 $[M - H]^-$ (calcd for $C_{32}H_{36}N_2O_4F$, 531.2665). These data, coupled with ^{13}C NMR spectroscopic data, established the molecular formula of **10** as $C_{32}H_{37}N_2O_4F$ (15 degrees of unsaturation), suggesting 2 amu more than the mass of chaetoglobosin F (**7**). The ^{1}H-decoupled ^{19}F NMR spectroscopic data also confirmed the existence of the fluorine atom (δ_F −100) in **10** (see Figure S3 in the Supporting

Scheme 1. Chemical Transformation of 7 into 10

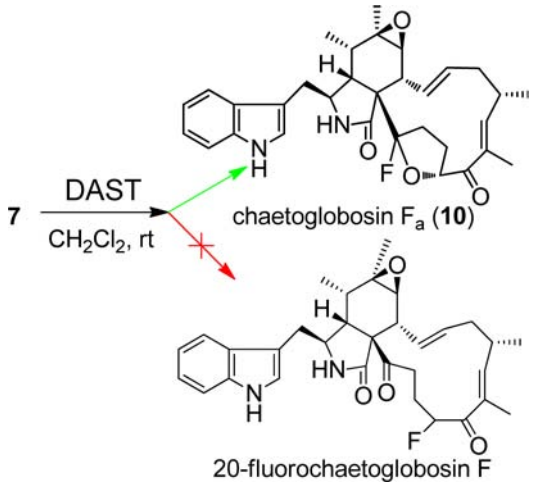

Information). The IR spectrum of **10** exhibited absorption bands at 3390 (NH and/or OH), 1686 (C═O), and 1638 (C═O) cm^{-1}. The ^{13}C NMR and DEPT spectra of **10** (Table 1) displayed 32 carbon signals, including 4 methyls, 4 sp^3 methylenes, 7 sp^3 and 8 sp^2 methines, 3 sp^3 and 4 sp^2 quaternary carbons, and 1 ketone carbon (δ_C 202.62), as well as an amide carbonyl (δ_C 174.21). The ^1H NMR spectrum of **10** showed the presence of an indole moiety, including 1,2-disubstituted benzene [δ_H 7.94 (t, J = 7.5 Hz, H-4′), 7.36 (m, H-5′), 7.34 (m, H-6′), and 7.67 (t, J = 7.5 Hz, H-7′)], an olefinic proton at δ_H 7.57 (H-2′), and a broad NH singlet at δ_H 12.08 (H-1′), along with the ^{13}C NMR spectrum, which gave six aromatic carbons at δ_C 137.89 (s, C-1′a), 128.30 (s, C-3′a), 119.62 (d, C-6′), 122.08 (d, C-5′), 118.80 (d, C-4′), and 112.36 (d, C-7′) and two olefinic carbons at δ_C 124.75 (d, C-2′) and 111.74 (s, C-3′). In addition, the ^1H NMR spectrum showed the presence of two tertiary methyls (δ_H 1.30, 1.85), two secondary methyls (δ_H 0.92, 1.16), three olefinic protons (δ_H 5.35, m; 6.73, d; 7.02, dd), and an amide proton (δ_H 9.13, s). Comparison of its ^{13}C NMR data with those of **7** revealed that an additional sp^3 quaternary carbon C-23 (δ_C 123.66) with a huge coupling constant ($J_{C,F}$ = 224.7 Hz) in **10** appeared and that a corresponding ketone carbon at δ_C 204.06 in **7** disappeared. Meanwhile, two carbons adjacent to C-23, an sp^3 methylene carbon C-22 signal (δ_C 36.23, $J_{C,F}$ = 30.4 Hz) and a quaternary carbon C-9 (δ_C 56.86, $J_{C,F}$ = 28.8 Hz), were also observed. These typical splitting patterns indicated that this fluorine atom was attached to C-23, as evidenced by HMBC correlations from H-21 and H-22 to C-23. The downfield chemical shift of sp^3 hybridized C-23 (δ_C 123.66) revealed the connection with the additional oxygen atom. Considering degrees of unsaturation, this molecule should contain an oxolane ring between C-20 and C-23. This deduction was supported by HMBC correlations of H-20 (δ_H 5.40) with C-23 and H-21 with C-20 as well as $^1H-^1H$ COSY correlations of H-20/H-21/H-22 (Figure 2). This gave rise to significant differences in the chemical shifts measured in C_5D_5N of C-17 to C-23 between **7** and **10** (Table 1). Finally, comprehensive $^1H-^1H$ COSY and HMBC analysis (Figure 2) allowed the complete assignment of the proton and carbon signals for **10** (see the Supporting Information).

Rearrangement reactions are sometimes observed in DAST fluorination.[32−34] For example, preparation of γ-fluorobutyrolactones from the reaction of γ-ketoacids with DAST was

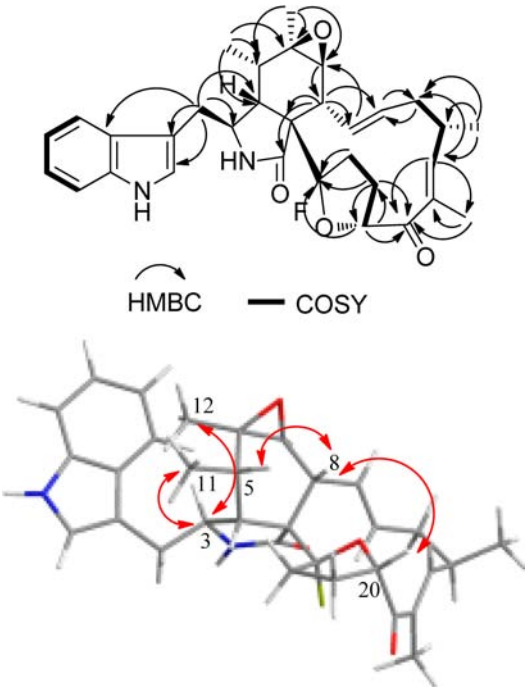

Figure 2. Key HMBC, $^1H-^1H$ COSY, and ROESY correlations in **10**.

reported by Chen et al.[34] In the current work, similarly, the mechanism of oxolane ring formation between C-20 and C-23 in **10** is postulated to occur via the pathway (Figure 3). The

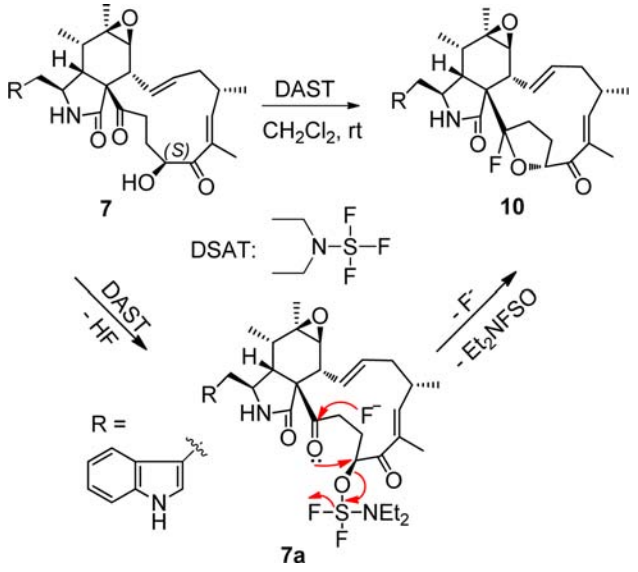

Figure 3. Potential mechanism of chemical transformation of compound **7** into **10**.

first step is the nucleophilic displacement of fluorine on sulfur by oxygen of the 20-OH accompanied by elimination of hydrogen fluoride to give the intermediate **7a**. Then, the addition of fluorine to C-23 of **7a** was accompanied by O-23 attached to C-20 from the backside and elimination of Et_2NFSO and F^-.[35,36] Consequently, an inversion of the configuration of C-20 in the resulting **10** took place, which was further confirmed by the cross-peak between H-8 and H-20 in the ROESY spectrum of **10** (Figure 2).

dx.doi.org/10.1021/jf500390h | J. Agric. Food Chem. 2014, 62, 3734−3741

The configuration of the core skeleton, 10-(indol-3-yl)-[13]cytochalasan, in these chaetoglobosins could be assigned on the basis of the biosynthesis with those of chaetoglobosin A (**1**)[21] as well as on a ROESY experiment. The absolute configuration of 20-dihydrochaetoglobosin A (**9**) was established previously by X-ray single-crystal analysis as 3*S*, 4*R*, 5*S*, 6*R*, 7*S*, 8*R*, 9*R*, 16*S*, 19*R*, and 20*S*,[21] so the absolute configuration of **7** was assigned as 3*S**, 4*R**, 5*S**, 6*R**, 7*S**, 8*R**, 9*R**, 16*S**, and 20*S**. The members of the chaetoglobosin family possess structures that are chirally dense at six (C-3, C-4, C-5, C-8, C-9, C-16) or eight vicinal positions (C-3, C-4, C-5, C-6, C-7, C-8, C-9, C-16) and one remote site (C-19/C-20). Interestingly, the sign of the rotation is not sensitive to the minor structural changes. For example, chaetoglobosin A (**1**), 20-dihydrochaetoglobosin A (**9**), and chaetoglobosin F_a (**10**) reported here and prochaetoglobosin I[21] all showed negative specific rotations, despite a large variance in structure at C-6, C-7, C-19, and C-20 and configuration at C-5 and C-8. In addition, the co-occurrence of these isolated metabolites **1**−**9** in the title fungus suggests that they shared the same biogenetic pathway, and biogenetic insights previously published[3,21] have suggested that the configuration at C-4, C-5, C-8, and C-9 is set via a stereospecific enzyme-mediated Diels−Alder reaction.[11,21] After several attempts, unfortunately, no good crystals suitable for X-ray analysis of chaetoglobosin F_a (**10**) were obtained because this compound is easily changeable in proton solvents. Consequently, the absolute stereochemistry of the new semisynthetic derivative **10** was proposed as 3*S**, 4*R**, 5*S**, 6*R**, 7*S**, 8*R**, 9*R**, 16*S**, and 20*R**. Thus, the total structure of **10** was elucidated as shown in Figure 1. It should be mentioned that the absolute configuration at the new chrial center C-23 of **10** remains undetermined.

Phytotoxic Activity of Selected Compounds. The phytotoxic effects of eight selected compounds **1**, **3**−**8** and **10**, except for **2** and **11**−**14** (due to insufficient samples) on radish seedlings were examined, and the results are listed in Table 2. Chaetoglobosin A (**1**) darkened the roots at two concentrations of 200 and 50 ppm, these results being consistent with those obtained with alfalfa seedlings,[27] and other compounds also showed similar inhibitory effects. At a low concentration of 50 ppm, compounds **1**, **3**−**8**, and **10** exhibited weak to strong phytotoxic activities against the roots with inhibition rates in the range of 26.4−67.5% and against hypocotyl elongation with inhibition rates ranging from 33.3 to 71.6% (except **10**). Among the tested compounds, at 50 ppm, inhibition rates of chaetoglobosins A (**1**), V (**3**), E, F, and F_{ex} (**6**−**8**) were >60% toward the roots, as active as positive control, glyphosate (63.5%); chaetoglobosins A (**1**), C, E, F, and F_{ex} (**5**−**8**) displayed phytotoxic activities to hypocotyls with inhibition rates of almost ≥60%, which were about 2-fold of the control. In comparison to **7**, its semisynthetic fluorinated derivative, chaetoglobosin F_a (**10**) weakly inhibited the root growth of the seedlings with 26.4 and 59.4% of inhibition at 50 and 200 ppm, respectively, but had no phytotoxicity to hypocotyls at either concentration. In addition, at low concentrations, >60% inhibition of chaetoglobosin V (**3**) on radish seedlings was >33−46% that of V_b (**4**). It seemed that the configurations of C-17 and C-21 in both molecules could influence phytotoxicity potency.

At 200 ppm, chaetoglobosins A (**1**) and C−F (**5**−**7**) exhibited phytotoxicity to roots with inhibition rates from 71.7 to 76%, which were slightly weaker than the control (81.5%). Meanwhile, chaetoglobosins A (**1**) and C−F (**5**−**7**) presented phytotoxic effects on hypocotyls with inhibition rates from 60.7 to 71.2%, almost as active as glyphosate (67.1%). These findings demonstrated that radish seedlings were highly sensitive to these tested chaetoglobosins at low concentrations but only slightly sensitive at high concentrations. It was interesting that the dose−response relationship of these tested compounds was not apparent in our bioassay.

Table 2. Inhibitory Effects of Compounds 1, 3−8, and 10 on the Growth of Radish Seedlings

		inhibition ratio[a] (%)	
compd	concn (ppm)	radish root	radish hypocotyl
1	200	74.0 ± 3.1	64.4 ± 3.0
	50	63.5 ± 3.8	60.0 ± 3.1
3	200	36.3 ± 2.8	55.1 ± 3.0
	50	62.3 ± 2.1	71.6 ± 2.8
4	200	65.2 ± 2.9	48.1 ± 2.8
	50	46.8 ± 4.3	33.3 ± 2.4
5	200	73.4 ± 2.9	71.2 ± 4.0
	50	50.0 ± 1.4	71.0 ± 3.8
6	200	76.0 ± 3.2	64.3 ± 4.1
	50	65.5 ± 2.5	69.0 ± 2.5
7	200	71.7 ± 2.9	60.7 ± 3.7
	50	67.5 ± 2.1	64.4 ± 2.4
8	200	67.0 ± 2.6	52.9 ± 2.49
	50	64.6 ± 2.3	57.9 ± 2.6
10	200	59.4 ± 2.3	2.5 ± 2.0
	50	26.4 ± 2.8	4.3 ± 2.8
glyphosate	200	81.5 ± 3.0	67.0 ± 2.3
	50	63.5 ± 3.2	33.9 ± 2.6

[a]Mean ± SD.

It has been proved that some chaetoglobosins have been found to be phytotoxic to different plants. Chaetoglobosin A (**1**) and its 19-*O*-acetylchaetoglobosin A, isolated from the culture of *Calonectria morganii*, inhibited the root and shoot growth of cresson seedlings;[37] chaetoglobosins A (**1**), C (**5**), and O, phytotoxic metabolites from *Cylindrocladium floridanum*, a causal fungus of alfalfa black rot disease, caused potent growth inhibition on alfalfa seedlings.[27] Furthermore, chaetoglobosin K showed growth-inhibiting effects on wheat coleoptiles, isolated from cultures of *Diplodia macrospora*, a corn pathogen causing ear and stalk rot.[38] This is the first report of phytotoxicity of these test chaetoglobosins to radish seedlings.

In Vitro Cytotoxic Evaluation of Compounds 1−10. All 10 chaetoglobosins (**1**−**10**) were evaluated for their cytotoxic activities against the HTC116 cell line except for chaetoglobosin C (**5**), which has low solubility in DMSO, and the results are presented in Table 3. Four of them, chaetoglobosins A (**1**) and F_{ex} (**8**), 20-dihydrochaetoglobosin A (**9**), and chaetoglobosin F_a (**10**), displayed high cytotoxic activity with IC_{50} values of 3.15, 4.43, 8.44, and 5.85 μM, respectively, as compared to the antitumoral drug etoposide (IC_{50} = 2.13 μM), whereas chaetoglobosins G (**2**), V (**3**), V_b (**4**), E (**6**), and F (**7**) were found to be weak (IC_{50} > 17 μM). Among them,

dx.doi.org/10.1021/jf500390h | J. Agric. Food Chem. 2014, 62, 3734−3741

Table 3. Cytotoxicity of Compounds 1−10 against Human Colorectal HCT116 Cell Line

compd	IC_{50} (μM)[a]	improve cytotoxicity	decrease cytotoxicity
1	3.15 ± 0.45	epoxide ring;[b] 20-carbonyl group	
2	65.6 ± 5.9		epoxide ring disappears[b]
3	29.5 ± 2.7	C-17/C-21 junction	epoxide ring disappears[b]
4	18.4 ± 2.0	C-17/C-21 junction	epoxide ring disappears[b]
5	nt[c]		
6	>100		epoxide ring disappears[b]
7	17.8 ± 1.9	epoxide ring[b]	20-OH
8	4.43 ± 0.52	double bond at C-6(12)	20-OH
9	8.44 ± 0.89	epoxide ring[b]	20-OH
10	5.85 ± 0.65	epoxide ring;[b] fluorine atom, furan ring	
etoposide	2.13 ± 0.45		

[a]Mean ± SD. [b]Epoxide ring at C-6/C-7. [c]Not tested.

chaetoglobosin A (**1**) was about 2.5 times more active than 20-dihydrochaetoglobosin A (**9**) on HCT116 cells, suggesting that reduction of the carbonyl group at C-20 lowered cytotoxicity. This deduction was consistent with that of chaetoglobosin G (**2**) (IC_{50} = 65.6 μM), showing higher toxicity than chaetoglobosin E (**6**) (IC_{50} > 100 μM), despite their lower toxicity. Chaetoglobosin F (**7**) exhibited much higher cytotoxic abilities than chaetoglobosin E (**6**), with IC_{50} values of 17.8 and >100 μM, respectively. These results suggested that the introduction of an epoxide ring at C6/C7 greatly improved cytotoxicity. Chaetoglobosin F_{ex} (**8**) (IC_{50} = 4.43 μM) showed much stronger cytotoxic effects than chaetoglobosin E (**6**), implying that the presence of a double bond at C6(12) was favorable for imparting cytotoxicity. Especially, chaetoglobosin F_a (**10**) (IC_{50} = 5.85 μM) was about 3 times more active than the parent **7** (IC_{50} = 17.8 μM) toward HCT116 cells. This indicated that the introduction of F and the formation of the furan ring in **10** could enhance activity. Chaetoglobosins V (**3**) and V_b (**4**), incorporating a five-membered ring between C-17 and C-21, were found to be weak, with IC_{50} values of 29.5 and 18.4 μM, respectively, but stronger than the parental compound **2** (IC_{50} = 65.6 μM), indicating the C-17/C-21 junction in both molecules appeared to improve toxicity. These findings suggested that an epoxide ring at C-6−C-7 or a double bond at C-6(12) is an important feature responsible for activity.

Reportedly, among chaetoglobosins is chaetoglobosin A (**1**), which has a unique inhibitory activity against actin polymerization in mammalian cells.[3] Chaetoglobosins displayed cytotoxicity on a panel of human cancer cell lines.[2,3,39,40] Chaetoglobosins A (**1**), C (**5**), E (**6**), and G (**2**) exhibited acute toxic effects against HeLa cells (IC_{50} = 3.2−20 μM).[20,41] Compound **1** possessed significant cytotoxicity against P388 murine leukemia cell line.[6] Compounds **5** and **2** showed cytotoxicities against human breast cancer (BC1) cell lines (IC_{50} = 6.27−20.0 μM).[10] Recently, chaetoglobosins C (**5**) and F (**7**) exhibited moderate cytotoxic activity against SKOV-3 cells (IC_{50} = 2−8 μM).[42] Chaetoglobosins A (**1**), G (**2**), V (**3**), C (**5**), E (**6**), F (**7**), and F_{ex} (**8**) exhibited moderate cytotoxic activities against four human cancer cell lines (KB, K562, MCF-7, and HepG2).[43] Compounds **1** and **5** presented significant growth inhibitory activity against the brine shrimp[15] and also had toxic effects to mouse and rat cells and chick embryos.[44,45] To our knowledge, this is the first report on the cytotoxicity of these chaetoglobosins to the HCT116 cell line.

In summary, in this study, nine known metabolites including chaetoglobosins C, E, F, and F_{ex}, and 20-dihydrochaetoglobosin A (**5**−**9**) and four known compounds (**11**−**14**) were identified from the solid culture of the endophytic *C. globosum*, and a new fluorinated chaetoglobosin, chaetoglobosin F_a (**10**), was semisynthesized from chaetoglobosin F. The phytotoxic compounds (**1**, **3**, and **6**−**8**) displayed marked phytotoxic activity against radish seedlings at 50 ppm, which were comparable to the positive control. Compounds **1** and **8**−**10** exhibited pronounced cytotoxicity against the HCT116 colon cancer cell, in contrast to the positive drug. The epoxide ring between C-6 and C-7 or the double bond at C-6(12) appeared to be important for cytotoxicity, and chaetoglobosin F_a (**10**) presented a markedly increased cytotoxicity but decreased phytotoxicity. On the basis of results in both bioassays, there was no relationship between cytotoxicity and phytotoxicity. The mechanisms of action of some bioactive compounds we have identified will need to be studied.

■ ASSOCIATED CONTENT

Ⓢ Supporting Information

1D and 2D NMR spectra of compound **10**. This material is available free of charge via the Internet at http://pubs.acs.org.

■ AUTHOR INFORMATION

Corresponding Author

*(J.-M.G.) Phone: +86-29-87092515. E-mail: jinminggao@nwsuaf.edu.cn.

Author Contributions

‖H.L. and J.X. contributed equally to this work.

Funding

This work was financially supported by the National Natural Science Foundation of China (31371886).

Notes

The authors declare no competing financial interest.

■ REFERENCES

(1) Cutler, H. G. *Biologically Active Natural Products from Fungi: Templates for Tomorrow's Pesticides*; Academic Press: New York, 1984; pp 153−170.

(2) Zhang, Q.; Li, H. Q.; Zong, S. C.; Gao, J. M.; Zhang, A. L. Chemical and bioactive diversities of the genus *Chaetomium* secondary metabolites. *Mini-Rev. Med. Chem.* **2012**, *12*, 127−148.

(3) Scherlach, K.; Boettger, D.; Remme, N.; Hertweck, C. The chemistry and biology of cytochalasans. *Nat. Prod. Rep.* **2010**, *27*, 869−886.

(4) Sekita, S.; Yoshihira, K.; Natori, S. Chaetoglobosins, cytotoxic 10-(indol-3-yl)-[13]cytochalasans from *Chaetomium* spp. IV. ^{13}C-Nuclear magnetic resonance spectra and their application to a biosynthetic study. *Chem. Pharm. Bull.* **1983**, *31*, 490−498.

(5) Oikawa, H.; Murakami, Y.; Ichihara, A. 20-Ketoreductase activity of chaetoglobosin A and prochaetoglobosins in a cell-free system of *Chaetomium subaffine* and the isolation of new chaetoglobosins. *Biosci., Biotechnol., Biochem.* **1993**, *57*, 628−631.

(6) Jiao, W.; Feng, Y.; Blunt, J. W.; Cole, A. L. J.; Munro, M. H. G. Chaetoglobosins Q, R, and T, Three further new metabolites from *Chaetomium globosum*. *J. Nat. Prod.* **2004**, *67*, 1722−1725.

(7) Ding, G.; Song, Y. C.; Chen, J. R.; Xu, C.; Ge, H. M.; Wang, X. T.; Tan, R. X. Chaetoglobosin U, a cytochalasan alkaloid from endophytic *Chaetomium globosum* IFB-E019. *J. Nat. Prod.* **2006**, *69*, 302−304.

(8) Cui, C. M.; Li, X. M.; Li, C. S.; Proksch, P.; Wang, B. G. Cytoglobosins A-G, cytochalasans from a marine-derived endophytic fungus, *Chaetomium globosum* QEN-14. *J. Nat. Prod.* **2010**, *73*, 729−733.
(9) Zhang, G.; Wang, F.; Qin, J.; Wang, D.; Zhang, J.; Zhang, Y.; Zhang, S.; Pan, H. Efficacy assessment of antifungal metabolites from *Chaetomium globosum* no. 05, a new biocontrol agent against *Setosphaeria turcica*. *Biol. Control* **2013**, *64*, 90−98.
(10) Thohinung, S.; Kanokmedhakul, S.; Kanokmedhakul, K.; Kukongviriyapan, V.; Tusskorn, O.; Soytong, K. Cytotoxic 10-(indol-3-yl)-[13]cytochalasans from the fungus *Chaetomium elatum* ChE01. *Arch. Pharm. Res.* **2010**, *33*, 1135−1141.
(11) Schumann, J.; Hertweck, C. Molecular basis of cytochalasan biosynthesis in fungi: gene cluster analysis and evidence for the involvement of a PKS-NRPS hybrid synthase by RNA silencing. *J. Am. Chem. Soc.* **2007**, *129*, 9564−9565.
(12) Sekita, S.; Yoshihira, K.; Natori, S.; Udagawa, S.; Sakabe, F.; Kurata, H.; Umeda, M. Chaetoglobosins, cytotoxic 10-(indol-3-yl)-[13]cytochalasans from *Chaetomium* spp. I. Production, isolation and some cytological effects of chaetoglobosins A−J. *Chem. Pharm. Bull.* **1982**, *30*, 1609−1617.
(13) Hu, Y.; Zhang, W.; Zhang, P.; Ruan, W.; Zhu, X. Nematicidal activity of chaetoglobosin A poduced by *Chaetomium globosum* NK102 against *Meloidogyne incognita*. *J. Agric. Food Chem.* **2013**, *61*, 41−46.
(14) Bode, H. B.; Bethe, B.; Höfs, R.; Zeeck, A. Big effects from small changes: possible ways to explore nature's chemical diversity. *ChemBioChem* **2002**, *3*, 619−627.
(15) Qin, J. C.; Zhang, Y. M.; Gao, J. M.; Bai, M. S.; Yang, S. X.; Laatsch, H.; Zhang, A. L. Bioactive metabolites produced by *Chaetomium globosum*, an endophytic fungus isolated from *Ginkgo biloba*. *Bioorg. Med. Chem. Lett.* **2009**, *19*, 1572−1574.
(16) Xue, M.; Zhang, Q.; Gao, J. M.; Li, H.; Tian, J. M.; Pescitelli, G. Chaetoglobosin Vb from endophytic *Chaetomium globosum*: absolute configuration of chaetoglobosins. *Chirality* **2012**, *24*, 668−674.
(17) Li, H. Q.; Li, X. J.; Wang, Y. L.; Zhang, Q.; Zhang, A. L.; Gao, J.-M.; Zhang, X.-C. Antifungal metabolites from *Chaetomium globosum*, an endophytic fungus in *Ginkgo biloba*. *Biochem. Syst. Ecol.* **2011**, *39*, 876−879.
(18) Gao, J. M.; Yang, S. X.; Qin, J. C. Azaphilones: chemistry and biology. *Chem. Rev.* **2013**, *113*, 4755−4811.
(19) Sekita, S.; Yoshihira, K.; Natori, S.; Kuwano, H. Structures of chaetoglobosins C, D, E, and F, cytotoxic indol-3-yl-[13]cytochalasans from *Chaetomium globosum*. *Tetrahedron Lett.* **1976**, *17*, 1351−1354.
(20) Sekita, S.; Yoshihira, K.; Natori, S.; Kuwano, H. Chaetoglobosins, cytotoxic 10-(indol-3-yl)-[13]cytochalasans from *Chaetomium* spp. III. Sructures of chaetoglobosins C, E, F, G, and J. *Chem. Pharm. Bull.* **1982**, *30*, 1629−1638.
(21) Ishiuchi, K.; Nakazawa, T.; Yagishita, F.; Mino, T.; Noguchi, H.; Hotta, K.; Watanabe, K. Combinatorial generation of complexity by redox enzymes in the chaetoglobosin A biosynthesis. *J. Am. Chem. Soc.* **2013**, *135*, 7371−7377.
(22) Hitotsuyanagi, Y.; Mitsui, K.; Fukaya, H.; Takeya, K. Fluorinated and rearranged gedunin derivatives. *Phytochem. Lett.* **2012**, *5*, 486−489.
(23) Bath, N. J.; Boaz, H. E.; KornfeId, E. C.; Chang, C. J.; Floss, H. G.; Hagaman, E. W.; Wenkert, E. Nuclear magnetic resonance spectral analysis of the ergot alkaloids. *J. Org. Chem.* **1974**, *39*, 1272−1276.
(24) Sudhakar, G.; Kadam, V. D.; Bayya, S.; Pranitha, G.; Jagadeesh, B. Total synthesis and stereochemical revision of acortatarins A and B. *Org. Lett.* **2011**, *13*, 5452−5455.
(25) Martínez-Montero, S.; Fernández, S.; Rodríguez-Pérez, T.; Sanghvi, Y. S.; Wen, K.; Gotor, V.; Ferrero, M. Improved synthesis and isolation of 2′-*O*-methyladenosine: effective and scalable enzymatic separation of 2′/3′-*O*-methyladenosine regioisomers. *Eur. J. Org. Chem.* **2009**, 3265−3271.
(26) Kuwada, K.; Kuramoto, M.; Utamura, M.; Matsushita, I.; Ishii, T. Isolation and structural elucidation of a growth stimulant for arbuscular mycorrhizal fungus from *Laminaria japonica* Areschoug. *J. Appl. Phycol.* **2006**, *18*, 795−800.
(27) Ichihara, A.; Katayama, K.; Teshima, H.; Oikawa, H.; Sakamura, S. Chaetoglobosin O and other phytotoxic metabolites from *Cylindrocladium floridanum*, a causal fungus of alfalfa black rot disease. *Biosci., Biotechnol., Biochem.* **1996**, *60*, 360−361.
(28) Zhang, Q.; Wang, S. Q.; Tang, H. Y.; Li, X. J.; Zhang, L.; Xiao, J.; Gao, Y. Q.; Tian, J. M.; Zhang, A. L.; Gao, J. M. Potential allelopathic indole diketopiperazines produced by the plant endophytic *Aspergillus fumigatus* using the one strain−many compounds method. *J. Agric. Food Chem.* **2013**, *61*, 11447−11452.
(29) Skehan, P.; Storeng, R.; Scudiero, D.; Monks, A.; McMahon, J.; Vistica, D.; Warren, J. T.; Bokesch, H.; Kenney, S.; Boyd, M. R. New colorimetric cytotoxicity assay for anticancer-drug screening. *J. Natl. Cancer Inst.* **1990**, *82*, 1107−1112.
(30) Purser, S.; Moore, P. R.; Swallow, S.; Gouverneur, V. Fluorine in medicinal chemistry. *Chem. Soc. Rev.* **2008**, *37*, 320−330.
(31) Boulton, K.; Cross, B. E. Synthesis of gem-difluoro derivatives of natural products by the reaction of ketones with diethylaminosulphur trifluoride. *J. Chem. Soc., Perkin Trans. 1* **1979**, 1354−1357.
(32) Chen, S. H.; Huang, S.; Wei, J. M.; Farina, V. Serendipitous synthesis of a cyclopropane-containing taxol analog via anchimeric participation of an unactivited angular methyl group. *J. Org. Chem.* **1993**, *58*, 4520−4521.
(33) Johnson, A. L. New reaction of (diethylamino)sulfur trifluoride: bis(diphenylmethyl) ethers as dehydration products of (diethylamino) sulfur trifluoride and diarylcarbinols. *J. Org. Chem.* **1992**, *57*, 5220−5222.
(34) Patrick, T. B.; Poon, Y. F. Preparation of fluorolactones from the reaction of γ-ketoacids with diethylaminosulfur trifluoride. *Tetrahedron Lett.* **1984**, *25*, 1019−1022.
(35) Defaye, J.; Gadelle, A.; Pedersen, C. The behavior of D-fructose and inulin towards anhydrous hydrogen fluoride. *Carbohydr. Res.* **1985**, *136*, 53−65.
(36) Defaye, J.; Gadelle, A.; Pedersen, C. The behavior of L-sorbose towards anhydrous hydrogen fluoride. *Carbohydr. Res.* **1986**, *152*, 89−98.
(37) Von Wallbrunn, C.; Luftmann, H.; Bergander, K.; Meinhardt, F. Phytotoxic chaetoglobosins are produced by the plant pathogen *Calonectria morganii* (anamorph *Cylindrocladium scoparium*). *J. Gen. Appl. Microbiol.* **2001**, *47*, 33−38.
(38) Cutler, H. G.; Crumley, F. G.; Cox, R. H.; Cole, R. J.; Dorner, J. W.; Springer, J. P.; Latterell, F. M.; Thean, J. E.; Rossi, A. E. Chaetoglobosin K: a new plant growth inhibitor and toxin from *Diplodia macrospora*. *J. Agric. Food Chem.* **1980**, *28*, 139−142.
(39) Umeda, M.; Ohtsubo, K.; Saito, M.; Sekita, S.; Yoshihira, K.; Natori, S.; Udagawa, S.; Sakabe, F.; Kurata, H. Cytotoxicity of new cytochalasans from *Chaetomium globosum*. *Experientia* **1975**, *31*, 435−438.
(40) Sekita, S.; Yoshihira, K.; Natori, S.; Kuwano, H. Structures of chaetoglobosin A and B, cytotoxic metabolites of *Chaetomium globosum*. *Tetrahedron Lett.* **1973**, *14*, 2109−2112.
(41) Sekita, S.; Yoshihira, K.; Natori, S.; Kuwano, H. Chaetoglobosins G, and J, cytotoxic indol-3-yl [13]-cytochalasans from *Chaetomium globosum*. *Tetrahedron Lett.* **1977**, *32*, 2771−2774.
(42) Kawahara, T.; Itoh, M.; Izumikawa, M.; Sakata, N.; Tsuchida, T.; Shin-Ya, K. New chaetoglobosin derivatives, MBJ-0038, MBJ-0039 and MBJ-0040, isolated from the fungus *Chaetomium* sp. f24230. *J. Antibiot.* **2013**, DOI: 10.1038/ja.2013.75.
(43) Zhang, J.; Ge, H. M.; Jiao, R. H.; Li, J.; Peng, H.; Wang, Y. R.; Wu, J. H.; Song, Y. C.; Tan, R. X. Cytotoxic chaetoglobosins from the endophyte *Chaetomium globosum*. *Planta. Med.* **2010**, *76*, 1910−1914.
(44) Ohtsubo, K.; Saito, M.; Sekita, S.; Yoshihira, K.; Natori, S. Acute toxic effects of chaetoglobosin A, a new cytochalasan compound produced by *Chaetomium globosum*, on mice and rats. *Jpn. J. Exp. Med.* **1978**, *48*, 105−110.
(45) Veselý, D.; Veselá, D.; Jelínek, R. *Penicillium aurantiogriseum* Dierckx produces chaetoglobosin A toxic to embryonic chickens. *Mycopathologia* **1995**, *132*, 31−33.

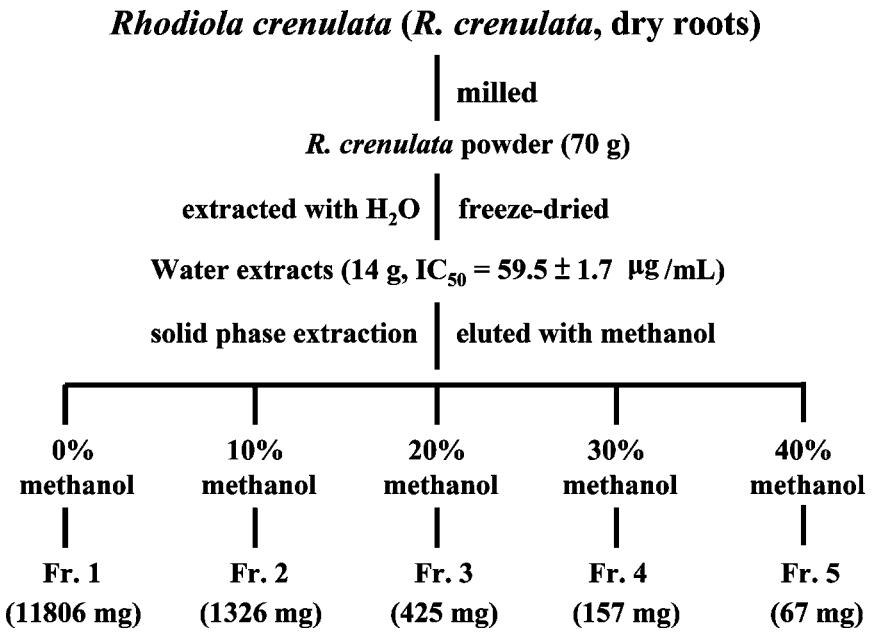

Figure 1. Scheme employed for the extraction of WE and its fractions from *R. crenulata*.

Taiwan) using DNA technology and the internal transcribed spacer sequence database. A total of 70 g of *R. crenulata* roots were milled using a laboratory-scale milling machine and extracted 3 times with distilled water (700 mL) at 30 °C. After 15 min of centrifugation at 12000g, the supernatant of collected samples were freeze-dried to yield the WE. The specimen was stored in the refrigerator (−20 °C) for further solid-phase extraction (SPE).

SPE Procedure. WE were redissolved in distilled water and underwent column chromatography on a vacuum manifold (Phenomenex, Torrance, CA) using SPE cartridges (6 mL/1000 mg, BAKERBOND octadecyl C18, J.T.Baker, Deventer, Netherlands). Each sample (50 mg) was chromatographed on a SPE cartridge. The sample was eluted with a stepwise method of 0, 10, 20, 30, and 40% methanol in distilled water. A total of five fractions, one for each methanol elution (20 mL), were collected. Samples were concentrated at 35 °C using a rotary evaporator and then freeze-dried. These five fractions (fractions 1−5) were then analyzed in the XO assay to assess the inhibitory activity.

HPLC Analysis of the WE of *R. crenulata* and Its Fractions. WE of *R. crenulata* and its fractions were dissolved in distilled water and subjected to column chromatography on the high-performance liquid chromatography (HPLC) system composed of a pump (PU-980, JASCO), a detector (UV-970, JASCO), and a C18 packed column (4.6 × 250 mm, 5 μm spherical, Dikma Technologies, Inc.). The mobile phase was solvent A (100% acetonitrile) and solvent B (ultrapure water). Elution conditions were as follows: 2−50% of A to B for 0−55 min (linear gradient) at a flow rate of 1 mL/min. The effluent was monitored through an optical absorption study carried out at 280 nm.

Isolation of Active Compounds from the WE of *R. crenulata*. WE and the fourth fraction (fraction 4) were redissolved in distilled water and subjected to column chromatography on the HPLC system composed of a pump (PU-980, JASCO), a detector (UV-970, JASCO) and a C18 packed column (4.6 × 250 mm, 5 μm spherical, Dikma Technologies, Inc.). The mobile phase was solvent A (100% acetonitrile) and solvent B (ultrapure water). Elution conditions for WE were as follows: 2−2% of A to B for 0−7 min and 2−30% A to B for 7−35 min (linear gradient). Elution conditions for fraction 4 were 14−14% A to B for 0−20 min and 14−18% A to B for 20−35 min (linear gradient). The elution began with solvent at a flow rate of 1 mL/min. The effluent was monitored through an optical absorption study carried out at 280 nm. The active compounds were then collected.

Identification of Purified Active Compounds. The chemical structures of the purified active compounds were identified by ultraviolet spectroscopy (UV, Hitachi, U-1900), Fourier transform infrared spectroscopy (FTIR, Bruker, Tensor27), polarity meter (PerkinElmer, 341), high-resolution electrospray ionization−TOF mass spectrometry (ESI−MS, BioTOF III; Bruker Daltonics, Inc., Billerica, MA), and nuclear magnetic resonance spectroscopy (NMR). NMR spectra, including ^{1}H, ^{13}C, distortionless enhancement by polarization transfer (DEPT), $^{1}H-^{1}H$ correlation spectroscopy (COSY), nuclear Overhauser effect spectrometry (NOESY), heteronuclear single-quantum coherence (HSQC), and heteronuclear multiple-bond correlation (HMBC), were recorded with a Bruker LC-SPE-NMR AVII 500 MHz spectrometer.[14]

Screening of Purified Active Compounds for XO Inhibitors. The XO inhibitory activity was assayed spectrophotometrically at 295 nm under aerobic conditions.[14] Absorbance (A) at 295 nm was measured using a UV spectrophotometer (U-1900, Hitachi High-Technologies Corporation, Minato-ku, Japan). The reaction mixture contained 200 mM sodium pyrophosphate buffer (pH 7.5), 100 μM xanthine, and 0.01 unit/mL of XO. The absorption rate at 295 nm indicates the formation of uric acid at 30 °C. The samples included WE and its five fractions (fractions 1−5), 4-HAP, B2−3′-*O*-gallate, salidroside, *p*-tyrosol, and allopurinol. Samples were dissolved directly in the buffer and incorporated into an enzyme assay to evaluate their inhibitory activities. Each sample was tested 3 times. The purified active compounds and allopurinol were tested for XO inhibitory activity at different concentrations (0−30 μM). The sample was dissolved directly in the buffer and incorporated into the enzyme assay to assess the inhibitory activity, and each sample was performed in triplicate. The inhibitory activity was determined by IC_{50}, which was obtained from percent inhibition calculated by

$$\text{percent inhibition (\%)} = [(A_{\text{without sample}} - A_{\text{with sample}})] \times 100\%/A_{\text{without sample}}$$

Lineweaver−Burk and Dixon Plots. To determine the mode of inhibition by 4-HAP and B2−3′-*O*-gallate, Lineweaver−Burk plot analysis was performed. This kinetics study was conducted in the absence and presence of inhibitors with varying concentrations of xanthine as the substrate. The initial velocity was expressed as the absorbance rate at 295 nm per 10 s in the assay. To determine the competitive inhibition constant (K_i) and uncompetitive inhibition constant (K_i'), Dixon plot analysis was performed. K_i is the

dx.doi.org/10.1021/jf5004094 | J. Agric. Food Chem. 2014, 62, 3742−3749

equilibrium constant for an inhibitor binding to XO, and K_i' is the equilibrium constant for an inhibitor binding to the XO−xanthine complex. The K_i and K_i' values of purified XO inhibitors were determined from the Dixon plot according to the method reported by Cornish-Bowden.[15] This kinetics study was carried out with varying concentrations of inhibitors and xanthine. The initial velocity was expressed as the absorbance rate at 295 nm per 10 s in the assay.

Statistical Analysis. Data were expressed as the mean ± standard deviation. The data were analyzed using the Statistical Package for the Social Sciences software (SPSS for Windows, version 10.0.7C, SPSS, Inc., Chicago, IL). Statistical significance among the treatments was determined by a one-way analysis of variation (ANOVA), followed by a Duncan's multiple range test. Three determinations for each treatment were made, and the significance level was set at $p < 0.05$.

RESULTS AND DISCUSSION

XO Inhibitory Activity of Fractionated Extracts of *R. crenulata*. The procedure for fractionation of the extracts of *R. crenulata* is shown in Figure 1. *R. crenulata* (70 g) was extracted with distilled water and freeze-dried to yield 14 g of WE, which displayed XO inhibitory activity (IC_{50} = 59.5 ± 1.7 μg/mL). The WE were then chromatographed on the SPE cartridges and eluted with varying concentrations of methanol. Finally, five fractions (fractions 1−5) were collected using a stepwise method of 0, 10, 20, 30, and 40% methanol in distilled water; the total yield of these fractions was 98.2%, and the yield of each fraction was 84.3, 9.4, 3.0, 1.1, and 0.4%, respectively. The IC_{50} values of WE and the associated fractions (fractions 1−5) were 59.5 ± 1.7, 862.2 ± 31.3, 524.2 ± 28.6, 94.7 ± 3.2, 16.1 ± 1.5, and 19.2 ± 1.8 μg/mL, respectively. Thus, we tested the inhibition of XO using WE and fractions at a final concentration of 0−60 μg/mL. Our results indicated that XO inhibition activity was 25.7% for WE and 2.8, 5.5, 17.2, 72.0, and 64.7% for fractions 1−5, respectively, at a concentration of 30 μg/mL (Figure 2). Among those fractions, the fourth

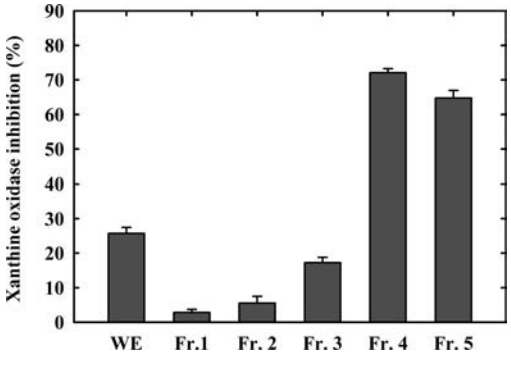

Figure 2. Inhibition of XO by the WE and its fractions at a final concentration of 30 μg/mL. Each value is represented as the mean ± standard deviation from triplicate measurements. WE, water extracts; Fr, fraction.

fraction (fraction 4) had the highest XO inhibitory activity (IC_{50} = 16.1 ± 1.5 μg/mL). Chen et al.[16] reported that the crude extracts of *Koelreuteria henryi*, *Prunus campanulata*, and *Rhodiola rosea* possessed strong XO inhibitory activity, with IC_{50} values of 91.8 ± 1.7, 64.6 ± 5.8, and 56.0 ± 1.0 μg/mL, respectively. These values indicate that the WE and fraction 4 would be plentiful sources of XO inhibitors.

HPLC Analysis of the WE and Its Fractions. To establish the fingerprint chromatogram of the WE and its five fractions, samples were analyzed by HPLC. The elution began with solvent at a flow rate of 1 mL/min, and a gradient elution from H_2O/acetonitrile (98:2) to H_2O/acetonitrile (50:50) over 55 min was performed to analyze these samples. The HPLC profile showed significant differences in the phytochemical patterns for each fraction. As shown in Figure 3, five major peaks were found in the WE at the elution times of 2−3, 5−7, 14−15, 21−22, and 23−24 min. Three peaks were found in fraction 1 at the elution times of 2−3, 5−7, and 14−15 min, while two peaks were found in fractions 2 and 3 at the elution times of 21−22 and 23−24 min. Furthermore, other minor peaks were found in fractions 3−5 at the elution time of 24−38 min. As previously mentioned, fractions 3−5 were used to inhibit XO at the concentration of 30 μg/mL, and the XO inhibitory activities were 17.2, 72.0, and 64.7%, respectively. Our results suggest that the peaks found in fraction 4 at the elution time of 24−38 min exhibit XO inhibitory properties.

Isolation and Identification of XO Inhibitors from *R. crenulata*. The WE and fraction 4 were analyzed and purified by HPLC (Figure 4). As shown in Figure 4A, a total 100 mg of WE was subjected to HPLC. Two major pure compounds (arrows, compounds **1** and **2**) were isolated, which were collected at the elution times of 21−22 and 23−24 min, respectively. The total yields of compounds **1** and **2** were 6.4 and 9.8 mg, respectively. Furthermore, a total of 157 mg of fraction 4 was then analyzed and purified by HPLC (Figure 4B). The individual peak was collected and used to inhibit XO. Consequently, two pure compounds (arrows, compounds **3** and **4**) were isolated and had XO inhibitory properties. These two compounds were collected at the elution times of 16−17 and 19−20 min, and the total yields of compounds **3** and **4** were 3.7 and 6.4 mg, respectively. Four purified compounds were analyzed using ESI−MS and NMR and were identified as salidroside, *p*-tyrosol, B2−3′-*O*-gallate, and 4-HAP. The following sections will focus on the spectral data of these compounds obtained from FTIR, UV, ESI−MS, and NMR.

Salidroside (Compound 1). Compound **1** was a white amorphous powder (Figure 4A), $[\alpha]_D^{20}$ −28.30° (*c* 0.00883, MeOH). UV (MeOH) λ_{max}, nm: 230, 273. IR ν_{max}: 3363, 2925, 2886, 1614, 1597, 1516, 1449, 1369, 1237, 1160, 1076, 1024. ESI−MS *m*/*z*: 323.1106 $[M + Na]^+$ (calculated for $C_{14}H_{20}O_7$). ^{1}H NMR (CD_3OD, 500 MHz) δ: 7.06 (2H, d, *J* = 8.4 Hz, H-2, 6), 6.69 (2H, d, *J* = 8.4 Hz, H-3, 5), 2.83 (1H, m, H-7), 4.03 (1H, m, H-8), 3.70 (1H, m, H-8), 4.29 (1H, d, *J* = 7.8 Hz, H-Glu.-1), 3.17 (1H, m, H-Glu.-2), 3.27 (1H, m, H-Glu.-3), 3.24 (1H, m, H-Glu.-4), 3.35 (1H, m, H-Glu.-5), 3.86 (1H, dd, *J* = 11.9, 2.0 Hz, H-Glu.-6), 3.66 (1H, dd, *J* = 11.9, 5.2 Hz, H-Glu.-6). ^{13}C NMR (CD_3OD, 125 MHz) δ: 130.9 (C-1), 131.1 (C-2, 6), 116.3 (C-3, 5), 157.0 (C-4), 36.6 (C-7), 72.3 (C-8), 104.6 (C-Glu.-1), 75.3 (C-Glu.-2), 78.1 (C-Glu.-3), 71.8 (C-Glu.-4), 78.3 (C-Glu.-5), 63.0 (C-Glu.-6). Compound **1** was identified as salidroside by direct comparison to commercial salidroside (Sigma Chemical Co., St. Louis, MO). On the basis of the data described above and the verified reference,[17] the structure of compound **1** was elucidated as salidroside. Yuan et al.[18] reported that salidroside exhibits antioxidant activity and a protective effect against furan-induced hepatocyte damage in mice.

***p*-Tyrosol (Compound 2).** Compound **2** was a white amorphous powder (Figure 4A). UV (MeOH) λ_{max}, nm: 223, 263. IR ν_{max}: 3386, 3141, 3024, 1598, 1510, 1452, 1363, 1230, 1105, 1051, 1015. ESI−MS *m*/*z*: 138 [M] (calculated for $C_8H_{10}O_2$). ^{1}H NMR (CD_3OD, 500 MHz) δ: 7.04 (2H, d, *J* = 8.6 Hz, H-2, 6), 6.71 (2H, d, *J* = 8.6 Hz, H-3, 5), 2.73 (2H, t,

dx.doi.org/10.1021/jf5004094 | J. Agric. Food Chem. 2014, 62, 3742−3749

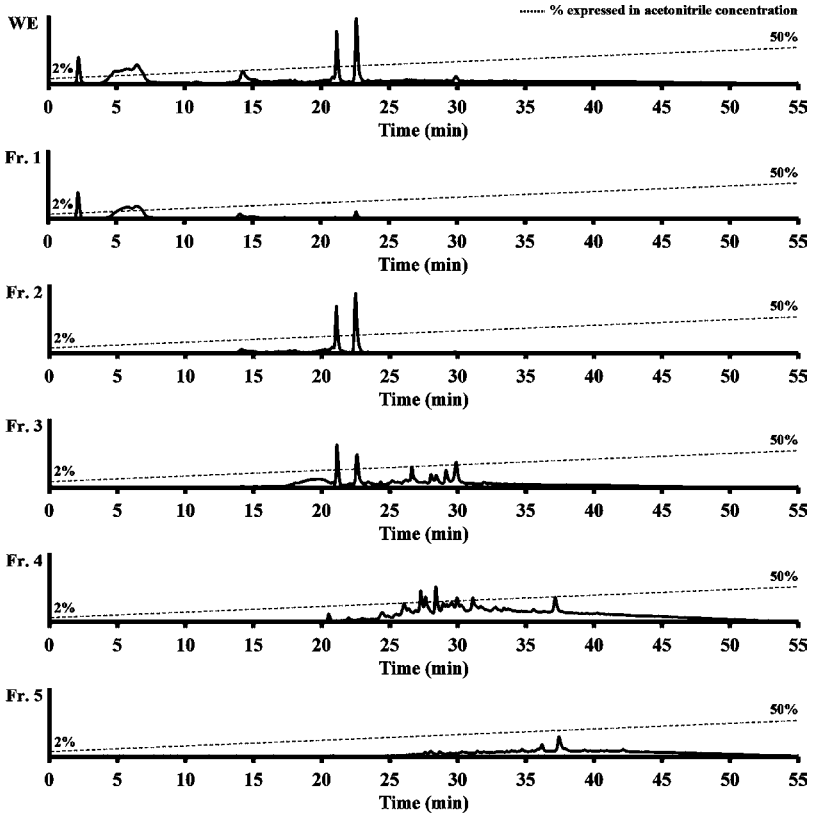

Figure 3. HPLC chromatograms of the WE and its fractions. Flow rate, 1.0 mL/min; UV detection, 280 nm. WE, water extracts; Fr, fraction.

Table 1. Structure, Molecular Weight, Molecular Formula, and IC_{50} Values of XO Inhibitors

Inhibitor	Structure	Molecular weight	Molecular formula	IC_{50} (μM)[a]
Allopurinol		136.11	$C_5H_4N_4O$	12.21 ± 0.27
4'-Hydroxyacetophenone (4-HAP)	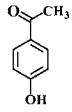	136.15	$C_8H_8O_2$	15.62 ± 1.19
Epicatechin-(4β,8)-epicatechin gallate (B2-3'-*O*-gallate)	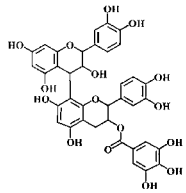	731.16	$C_{37}H_{30}O_{16}$	24.24 ± 1.80
p-Tyrosol	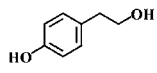	138.16	$C_8H_{10}O_2$	> 200
Salidroside	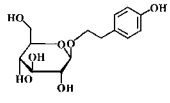	300.30	$C_{14}H_{20}O_7$	> 200

[a] IC_{50} values are expressed as the mean ± standard deviation.

dx.doi.org/10.1021/jf5004094 | J. Agric. Food Chem. 2014, 62, 3742−3749

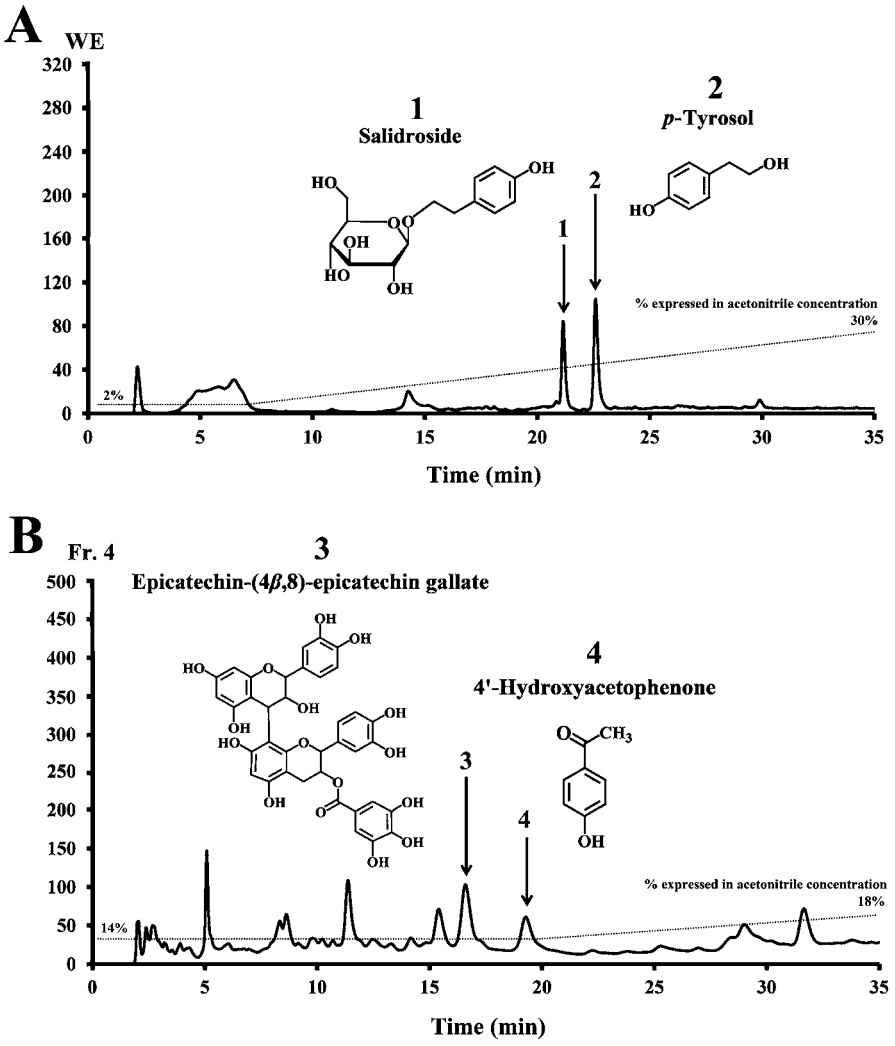

Figure 4. Isolation of active compounds from the (A) WE and (B) fraction 4. Arrow, active compounds; flow rate, 1.0 mL/min; UV detection, 280 nm.

J = 7.2 and 14.5 Hz, H-7), 3.70 (2H, t, J = 7.2 and 14.5 Hz, H-8). ^{13}C NMR (CD_3OD, 125 MHz) δ: 131.1 (C-1), 131.2 (C-2, 6), 116.3 (C-3, 5), 154.9 (C-4), 39.6 (C-7), 64.8 (C-8). Compound **2** was identified as *p*-tyrosol by direct comparison to commercial *p*-tyrosol (Sigma Chemical Co., St. Louis, MO). On the basis of the data described above and the verified reference,[19] the structure of compound **2** was elucidated as *p*-tyrosol. Dewapriya et al.[20] suggested that *p*-tyrosol has antioxidant activity and a protective effect against dopaminergic neuronal cell death in an *in vitro* model of Parkinson's disease.

B2−3′-*O*-Gallate (Compound 3). Compound **3** was a brown amorphous powder (Figure 4B), $[\alpha]_D^{20}$ −57.00° (*c* 0.00667, MeOH). UV (MeOH) λ_{max}, nm: 213, 228, 274. IR ν_{max}: 3321, 1690, 1609, 1520, 1448, 1370, 1284, 1235, 1156, 1099, 1039. ESI−MS m/z: 731.1615 $[M + H]^+$ (calculated for $C_{37}H_{30}O_{16}$). ^{1}H NMR (CD_3COCD_3, 500 MHz) δ: 5.26 (2H, s, H-2_U, 2_L), 4.06 (1H, s, H-3_U), 4.89 (1H, s, H-4_U), 6.03 (3H, m, H-6_U, 8_U, 6_L), 6.77 (3H, m, H-$2'_U$, $6'_U$, $5'_L$), 6.98 (1H, s, H-$5'_U$), 5.62 (1H, s, H-3_L), 2.98 (1H, d, J = 17.5 Hz, H-4_L), 3.13 (1H, dd, J = 17.1 and 4.4 Hz, H-4_L), 7.13 (3H, m, H-$2'_L$, $2''_L$, $6''_L$), 7.05 (1H, s, H-$6'_L$). ^{13}C NMR (CD_3COCD_3, 125 MHz) δ: 78.0 (C-2_U), 72.9 (C-3_U), 36.7 (C-4_U), 157.7 (C-5_U), 97.2 (C-6_U, 8_L), 158.2 (C-7_U), 96.3 (C-8_U), 158.2 (C-9_U), 107.9 (C-10_U), 132.5 (C-$1'_U$), 115.6 (C-$2'_U$), 145.3 (C-$3'_U$, $4'_U$, $3'_L$), 119.4 (C-$5'_U$), 119.1 (C-$6'_U$), 77.2 (C-2_L), 69.1 (C-3_L), 26.6 (C-4_L), 155.5 (C-5_L, 7_L), 95.8 (C-6_L), 156.0 (C-9_L), 99.6 (C-10_L), 131.2 (C-$1'_L$), 115.5 (C-$2'_L$), 145.2 (C-$4'_L$), 115.3 (C-$5'_L$), 114.7 (C-$6'_L$), 122.0 (C-$1''_L$), 110.2 (C-$2''_L$, $6''_L$), 145.7 (C-$3''_L$, $5''_L$), 138.7 (C-$4''_L$), 166.2 (C-$7''_L$). On the basis of the data described above and the verified reference,[21] the structure of compound **3** was elucidated as B2−3′-*O*-gallate. Lourenço et al.[22] reported that this compound has antioxidant activity and reduces the formation of UV-induced α-tocopheroxyl radicals.

4-HAP (Compound 4). Compound **4** was a white amorphous powder (Figure 4B). UV (MeOH) λ_{max}, nm: 222. IR ν_{max}: 3305, 1661, 1602, 1576, 1512, 1430, 1357, 1279, 1220, 1166, 1130, 1107, 1075, 1021. ESI−MS m/z: 136 [M] (calculated for $C_8H_8O_2$). ^{1}H NMR (CD_3OD, 400 MHz) δ: 7.88 (2H, d, J = 8.9 Hz, H-2, 6), 6.84 (2H, d, 2, J = 8.8 Hz, H-3, 5), 2.52 (3H, s, H-8). ^{13}C NMR (CD_3OD, 100 MHz) δ: 130.4 (C-1), 132.3 (C-2, 6), 116.4 (C-3, 5), 164.2 (C-4), 199.7 (C-7), 26.5 (C-8). Compound **4** was identified as 4-HAP by direct comparison to commercial 4-HAP (Sigma Chemical Co., St. Louis, MO). On the basis of the data described above and the verified reference,[23] the structure of compound **4** was elucidated as 4-HAP. Chen et al.[24] reported that 4-HAP exhibits antiallergic activities, and against β-hexosaminidase, it could release a marker of degranulation in rat basophilic leukemia (RBL)-2H3 cells.

dx.doi.org/10.1021/jf5004094 | J. Agric. Food Chem. 2014, 62, 3742−3749

XO Inhibitory Activity of 4-HAP, B2−3′-*O*-Gallate, Salidroside, *p*-Tyrosol, and Allopurinol. In the previous XO inhibitor studies, quercetin-3-*O*-rhamnopyranoside and luteolin isolated from *Acacia confusa* showed a strong inhibitory effect on XO, with IC_{50} values of 37.7 and 11.6 μM, respectively.[25] The inhibitory effects of 4-HAP, B2−3′-*O*-gallate, salidroside, *p*-tyrosol, and allopurinol on XO were tested at different concentrations. XO inhibition increased significantly with the addition of allopurinol ($p < 0.05$; Figure 5). When

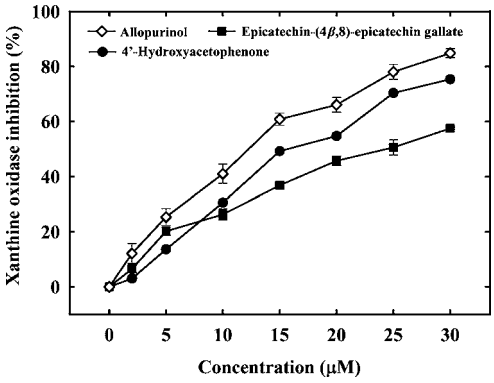

Figure 5. Inhibitory effects of allopurinol, B2−3′-*O*-gallate, and 4-HAP on XO. Each value is represented as the mean ± standard deviation from triplicate measurements.

15 μM of the inhibitor was added, the XO inhibition by allopurinol was 60.8%. Similar trends were also observed in the results for 4-HAP and B2−3′-*O*-gallate; they showed inhibitory effects on XO. When examining the inhibition of XO by 4-HAP at 25 μM and B2−3′-*O*-gallate at 30 μM, the XO inhibitory activities were 70.3 and 57.5%, respectively. 4-HAP and B2−3′-*O*-gallate showed remarkable inhibitory effects on XO ($p < 0.05$). However, we failed to observe any significant inhibitory effects on XO by salidroside or *p*-tyrosol at 30 μM (data not shown). As previously mentioned, five major peaks and one minor peak were found in the HPLC profile of WE (Figure 3). Salidroside and *p*-tyrosol indicated two major peaks in WE following elution times of 21−22 and 23−24 min, respectively. We observed that WE displayed XO inhibitory activity; however, the five major peaks in WE did not present significant inhibitory effects on XO, suggesting that the minor peak in WE at an elution time of 24−38 min exhibits XO. Nguyen et al.[26] reported that allopurinol is a substrate and a specific potent inhibitor of XO, but oxypurinol (1*H*-pyrazolo-[3,4-*d*]-pyrimidine-4,6-diol) is the basic functioning ingredient found in allopurinol. XO can catalyze the conversion of allopurinol into oxypurinol, and inhibition occurs mainly through direct substrate competition in the breakdown of purines. The XO inhibitory activities of purified salidroside, *p*-tyrosol, B2−3′-*O*-gallate, and 4-HAP from *R. crenulata* were evaluated and compared to that of allopurinol. The structure, molecular weight, molecular formula, and IC_{50} values of allopurinol, 4-HAP, B2−3′-*O*-gallate, *p*-tyrosol, and salidroside are shown in Table 1. Allopurinol, 4-HAP, and B2−3′-*O*-gallate showed strong inhibitory effects on XO, and the IC_{50} values of these compounds were 12.21 ± 0.27, 15.62 ± 1.19, and 24.24 ± 1.80 μM, respectively. This result indicated that 4-HAP and B2−3′-*O*-gallate have the potential to be XO inhibitors. However, the IC_{50} values of both salidroside and *p*-tyrosol were higher than 200 μM.

Modes of Inhibition of XO by B2−3′-*O*-gallate and 4-HAP. The 4-HAP and B2−3′-*O*-gallate were analyzed by Michaelis−Menten kinetic studies to determine their modes of inhibition of XO. In this study, the Michaelis constant (K_m) of XO was 5.33 ± 0.21 mM, which was similar to that reported by Tung et al.[27] They reported that the K_m value of XO was 21 μM. As shown in Figure 6, Lineweaver−Burk plots of B2−

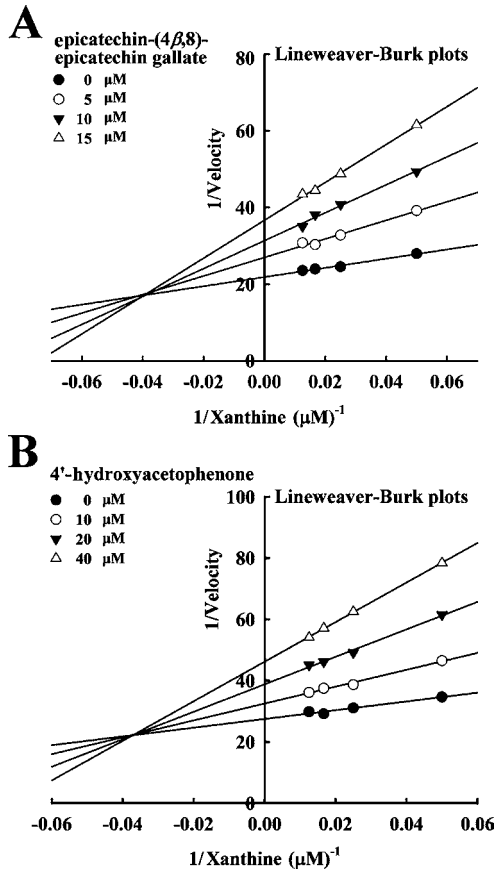

Figure 6. Lineweaver−Burk plots for the inhibition of XO by XO inhibitors with xanthine as the substrate: (A) B2−3′-*O*-gallate and (B) 4-HAP.

3′-*O*-gallate and 4-HAP were constructed. The Lineweaver−Burk plots of B2−3′-*O*-gallate (Figure 6A) and 4-HAP (Figure 6B) had no intersection on the *y* or *x* axis, indicating that the type of inhibition was a mixed-type mode. Therefore, the Lineweaver−Burk plots revealed that B2−3′-*O*-gallate and 4-HAP behaved as mixed-type inhibitors. Several mixed-type XO inhibitors have been reported. For example, a Lineweaver−Burk plot indicated that 3,4-dihydroxybenzoic acid isolated from the flowers of *Chrysanthemum sinense* appears to be a mixed-type inhibitor of XO.[26] Furthermore, Day et al.[28] reported that quercetin-3′-glucuronide showed mixed competitive inhibition of XO.

Dixon plots of B2−3′-*O*-gallate and 4-HAP on XO were also evaluated (Figure 7). The Dixon plots indicated that B2−3′-*O*-gallate (Figure 7A) and 4-HAP (Figure 7B) were mixed-type inhibitors of XO, and the values of K_i were 7.26 ± 0.38 and 8.45 ± 0.34 μM, respectively. Jiao et al.[29] reported that apigenin-4′-*O*-(2″-*O*-*p*-coumaroyl)-β-D-glucopyranoside purified from *Palhinhaea cernua* inhibits XO with mixed-type inhibition, with K_i and K_i' values of 14.35 and 93.68 μM, respectively. The K_i

dx.doi.org/10.1021/jf5004094 | J. Agric. Food Chem. 2014, 62, 3742−3749

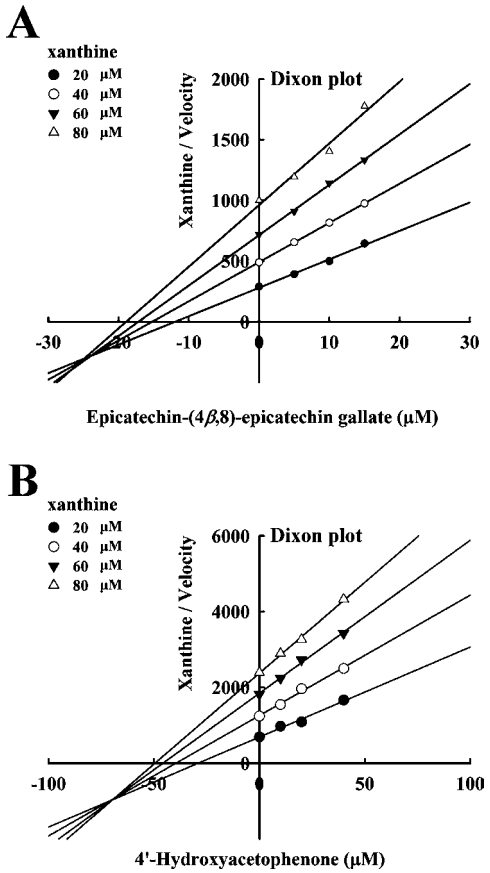

Figure 7. Dixon plots for the inhibition of XO by XO inhibitors with xanthine as the substrate: (A) B2−3′-*O*-gallate and (B) 4-HAP.

value of 4-HAP was higher than that of B2−3′-*O*-gallate. This indicated that B2−3′-*O*-gallate showed a higher binding affinity than 4-HAP to XO. Furthermore, the K_i' of B2−3′-*O*-gallate and 4-HAP were 24.43 ± 0.65 and 69.58 ± 1.13 μM, respectively. In addition, we noted that the values of K_i for B2−3′-*O*-gallate and 4-HAP were smaller than values of K_i'. As mentioned previously, K_i is the equilibrium constant for an inhibitor binding to XO, while K_i' is the equilibrium constant for inhibitor binding to the XO−xanthine complex. Cortés et al.[30] reported that, in the reversible mixed competitive inhibition, the values of K_i were smaller than the values of K_i'. This indicated that the binding affinity for the inhibitor−XO complex was higher than that for the inhibitor−XO−xanthine complex. Therefore, the inhibition kinetics study indicates that B2−3′-*O*-gallate and 4-HAP are mixed competitive inhibitors of XO. Although the binding sites and mechanisms of inhibition remain to be determined, the finding of mixed competitive inhibition of XO suggests that B2−3′-*O*-gallate and 4-HAP may bind to either XO or the XO−xanthine complex.

In summary, the WE of *R. crenulata* displayed XO inhibitory activity, and four active compounds, salidroside, *p*-tyrosol, B2−3′-*O*-gallate, and 4-HAP, were isolated from *R. crenulata*. Among these compounds, B2−3′-*O*-gallate and 4-HAP showed excellent XO inhibitory activity with a mixed competitive mode. Thus, B2−3′-*O*-gallate and 4-HAP have great potential to prevent hyperuricemia caused by XO. Therefore, our results suggest that B2−3′-*O*-gallate and 4-HAP could be adopted as candidates to treat gout, and further evaluation should be conducted with *in vivo* studies.

AUTHOR INFORMATION

Corresponding Author

*Telephone: +886-2-29052516. Fax: +886-2-29053622. E-mail: 075101@mail.fju.edu.tw.

Author Contributions

§Shih-Hsiung Wu and Jung-Feng Hsieh contributed equally to this work.

Funding

The authors thank the National Science Council (NSC 99-2313-B-030-001-MY3) for financial support.

Notes

The authors declare no competing financial interest.

ABBREVIATIONS USED

4-HAP, 4′-hydroxyacetophenone; B2−3′-*O*-gallate, epicatechin-(4β,8)-epicatechin gallate; IC_{50}, half maximal inhibitory concentration; K_i, inhibition constant; K_i', uncompetitive inhibition constant; K_m, Michaelis constant; NMR, nuclear magnetic resonance spectroscopy; SPE, solid-phase extraction; WE, water extracts; XO, xanthine oxidase

REFERENCES

(1) Unno, T.; Sugimoto, A.; Kakuda, T. Xanthine oxidase inhibitors from the leaves of *Lagerstroemia speciosa* (L.) Pers. *J. Ethnopharmacol.* **2004**, *93*, 391−395.

(2) Tung, Y. T.; Chang, S. T. Inhibition of xanthine oxidase by *Acacia confusa* extracts and their phytochemicals. *J. Agric. Food Chem.* **2010**, *58*, 781−786.

(3) Hammer, B.; Link, A.; Wagner, A.; Böhm, M. Hypersensitivity syndrome during therapy with allopurinol in asymptomatic hyperuricemia with a fatal outcome. *Dtsch. Med. Wochenschr.* **2001**, *26*, 1331−1334.

(4) Kong, L. D.; Cai, Y.; Huang, W. W.; Cheng, C. H.; Tan, R. X. Inhibition of xanthine oxidase by some Chinese medicinal plants used to treat gout. *J. Ethnopharmacol.* **2000**, *73*, 199−207.

(5) Flemmig, J.; Kuchta, K.; Arnhold, J.; Rauwald, H. W. *Olea europaea* leaf (Ph.Eur.) extract as well as several of its isolated phenolics inhibit the gout-related enzyme xanthine oxidase. *Phytomedicine* **2011**, *18*, 561−566.

(6) Ngoc, T. M.; Khoi, N. M.; Ha, D. T.; Nhiem, N. X.; Tai, B. H.; Don, D. V.; Luong, H. V.; Son, D. C.; Bae, K. Xanthine oxidase inhibitory activity of constituents of *Cinnamomum cassia* twigs. *Bioorg. Med. Chem. Lett.* **2012**, *22*, 4625−4628.

(7) Arimboor, R.; Rangan, M.; Aravind, S. G.; Arumughan, C. Tetrahydroamentoflavone (THA) from *Semecarpus anacardium* as a potent inhibitor of xanthine oxidase. *J. Ethnopharmacol.* **2011**, *133*, 1117−1120.

(8) Shen, C.; Jiang, L.; Gu, X.; Qiu, S.; Shen, X.; Yang, Q. Antioxidant compounds and antioxidant activity of *Rhodiola* drink. *Acad. Period. Farm. Prod. Process.* **2010**, *12*, 32−34.

(9) Chen, D.; Fan, J.; Wang, P.; Zhu, L.; Jin, Y.; Peng, Y.; Du, S. Isolation, identification and antioxidative capacity of water-soluble phenylpropanoid compounds from *Rhodiola crenulata*. *Food Chem.* **2012**, *134*, 2126−2133.

(10) Zhang, J.; Zhen, Y. F.; Ren, P. B. C.; Song, L. G.; Kong, W. N.; Shao, T. M.; Li, X.; Chai, X. Q. Salidroside attenuates β amyloid-induced cognitive deficits via modulating oxidative stress and inflammatory mediators in rat hippocampus. *Behav. Brain Res.* **2013**, *244*, 70−81.

(11) Wang, J.; Rong, X.; Li, W.; Yang, Y.; Yamahara, J.; Li, Y. *Rhodiola crenulata* root ameliorates derangements of glucose and lipid metabolism in a rat model of the metabolic syndrome and type 2 diabetes. *J. Ethnopharmacol.* **2012**, *142*, 782−788.

(12) Yang, Y. N.; Liu, Z. Z.; Feng, Z. M.; Jiang, J. S.; Zhang, P. C. Lignans from the root of *Rhodiola crenulata*. *J. Agric. Food Chem.* **2012**, *60*, 964−972.

(13) Sun, L.; Isaak, C. K.; Zhou, Y.; Petkau, J. C.; Karmin, O.; Liu, Y.; Siow, Y. L. Salidroside and tyrosol from *Rhodiola* protect H9c2 cells from ischemia/reperfusion-induced apoptosis. *Life Sci.* **2012**, *91*, 151−158.
(14) Hsieh, J. F.; Wu, S. H.; Yang, Y. L.; Choong, K. F.; Chen, S. T. The screening and characterization of 6-aminopurine-based xanthine oxidase inhibitors. *Bioorg. Med. Chem.* **2007**, *15*, 3450−3456.
(15) Cornish-Bowden, A. A simple graphical method for determining the inhibition constants of mixed, uncompetitive and non-competitive inhibitors. *Biochem. J.* **1974**, *137*, 143−144.
(16) Chen, C. H.; Chan, H. C.; Chu, Y. T.; Ho, H. Y.; Chen, P. Y.; Lee, T. H.; Lee, C. K. Antioxidant activity of some plant extracts towards xanthine oxidase, lipoxygenase and tyrosinase. *Molecules* **2009**, *14*, 2947−2958.
(17) Akita, H.; Kurashima, K.; Nakamura, T.; Kato, K. Chemo-enzymatic syntheses of naturally occurring β-glucosides. *Tetrahedron: Asymmetry* **1999**, *10*, 2429−2439.
(18) Yuan, Y.; Wu, S. J.; Liu, X.; Zhang, L. L. Antioxidant effect of salidroside and its protective effect against furan-induced hepatocyte damage in mice. *Food Funct.* **2013**, *4*, 763−769.
(19) Park, C. H.; Kim, K. H.; Lee, I. K.; Lee, S. Y.; Choi, S. U.; Lee, J. H.; Lee, K. R. Phenolic constituents of *Acorus gramineus*. *Arch. Pharm. Res.* **2011**, *34*, 1289−1296.
(20) Dewapriya, P.; Himaya, S. W.; Li, Y. X.; Kim, S. K. Tyrosol exerts a protective effect against dopaminergic neuronal cell death in *in vitro* model of Parkinson's disease. *Food Chem.* **2013**, *141*, 1147−1157.
(21) Saito, A.; Mizushina, Y.; Ikawa, H.; Yoshida, H.; Doi, Y.; Tanaka, A.; Nakajima, N. Systematic synthesis of galloyl-substituted procyanidin B1 and B2, and their ability of DPPH radical scavenging activity and inhibitory activity of DNA polymerases. *Bioorg. Med. Chem.* **2005**, *13*, 2759−2771.
(22) Lourenço, C. F.; Gago, B.; Barbosa, R. M.; de Freitas, V.; Laranjinha, J. LDL isolated from plasma-loaded red wine procyanidins resist lipid oxidation and tocopherol depletion. *J. Agric. Food Chem.* **2008**, *56*, 3798−3804.
(23) Vogl, M.; Kratzer, R.; Nidetzky, B.; Brecker, L. *Candida tenuis* xylose reductase catalysed reduction of acetophenones: The effect of ring-substituents on catalytic efficiency. *Org. Biomol. Chem.* **2011**, *9*, 5863−5870.
(24) Chen, H. J.; Shih, C. K.; Hsu, H. Y.; Chiang, W. Mast cell-dependent allergic responses are inhibited by ethanolic extract of adlay (*Coix lachryma-jobi* L. var. *ma-yuen* Stapf) testa. *J. Agric. Food Chem.* **2010**, *58*, 2596−2601.
(25) Hsieh, C. Y.; Chang, S. T. Antioxidant activities and xanthine oxidase inhibitory effects of phenolic phytochemicals from *Acacia confusa* twigs and branches. *J. Agric. Food Chem.* **2010**, *58*, 1578−1583.
(26) Nguyen, M. T.; Awale, S.; Tezuka, Y.; Ueda, J. Y.; Tran, Q. I.; Kadota, S. Xanthine oxidase inhibitors from the flowers of *Chrysanthemum sinense*. *Planta Med.* **2006**, *72*, 46−51.
(27) Tung, Y. T.; Hsu, C. A.; Chen, C. S.; Yang, S. C.; Huang, C. C.; Chang, S. T. Phytochemicals from *Acacia confusa* heartwood extracts reduce serum uric acid levels in oxonate-induced mice: Their potential use as xanthine oxidase inhibitors. *J. Agric. Food Chem.* **2010**, *58*, 9936−9941.
(28) Day, A. J.; Bao, Y.; Morgan, M. R.; Williamson, G. Conjugation position of quercetin glucuronides and effect on biological activity. *Free Radical Biol. Med.* **2000**, *29*, 1234−1243.
(29) Jiao, R. H.; Ge, H. M.; Shi, D. H.; Tan, R. X. An apigenin-derived xanthine oxidase inhibitor from *Palhinhaea cernua*. *J. Nat. Prod.* **2006**, *69*, 1089−1091.
(30) Cortés, A.; Cascante, M.; Cárdenas, M. L.; Cornish-Bowden, A. Relationships between inhibition constants, inhibitor concentrations for 50% inhibition and types of inhibition: New ways of analysing data. *Biochem. J.* **2001**, *357*, 263−268.

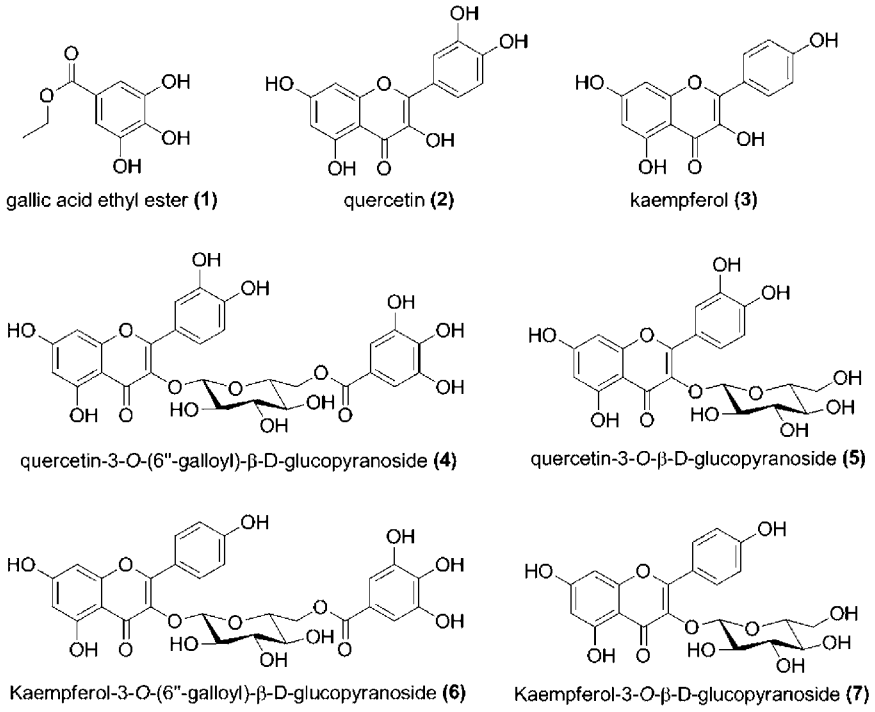

Figure 1. Chemical structure of flavones and flavone glycosides from *A. rossii*.

MATERIALS AND METHODS

Reagents and Materials. Reagents were obtained as follows: fetal bovine serum (FBS; Hyclone, South Logan, UT, USA), penicillin (Invitrogen, Carlsbad, CA, U.S.A.), Dulbecco's modified Eagle's medium (DMEM; Hyclone, South Logan, UT, U.S.A), antidinitrophenyl (DNP)-specific immunoglobulin E (IgE) (Sigma-Aldrich, St. Louis, MO, U.S.A.), DNP-bovine serum albumin (DNP-BSA, Sigma-Aldrich, St. Louis, MO, U.S.A.), PIPES (Sigma-Aldrich, St. Louis, MO, U.S.A.), PP2 (Sigma-Aldrich, St. Louis, MO, U.S.A.), and cyclooxygenase 2 (COX-2) antibody, 5-lipoxygenase (5-LO) antibody, phospho-Lyn (Tyr507) antibody, phospho-Syk (Tyr525/526) antibody, phospho-phospholipase C (PLC)γ (Tyr783) antibody, phospho-PKD/PKCμ (Ser916) antibody, phosphor-SAPK/JNK (Thr183/Tyr185) antibody, SAPK/JNK (Thr183/Tyr185) antibody, phospho-p44/42 MAPK antibody (Erk1/2), p44/42 MAPK (Erk1/2) antibody, phospho-p38 antibody, p38 antibody, and β-actin antibody (all from Cell Signaling Technology Inc., Danvers, MA, U.S.A.).

Plant Material. *A. rossii* was collected in Pyeongchang, Gangwon Province, Korea, in August 2010. A voucher specimen (DGR-012) was deposited at the Korea Institute of Science and Technology (KIST), Gangneung Institute. Extraction was performed by sonication using an RK158S ultrasonic bath (Bandelin, Germany).

Extraction and Isolation of Flavones and Flavone Glycosides from *A. rossii*. One kilogram of the dried aerial parts of *A. rossii* was extracted with 5 L of 95% ethanol at room temperature for 4 h and filtered through Whatman No. 1 filter paper (GE Healthcare Life Sciences, PA, U.S.A.). The filtrate was concentrated under reduced pessure by rotary evaporation at 40 °C, and 120 g of EtOH extract (ARE) was obtain. ARE (100 g) was sequentially partitioned into hexane (17.3 g), methylene chloride (7.3 g), ethyl acetate (12.3 g), butanol (29.1 g), and water portions (31.9 g) for β-hexosaminidase assay. Among ARE partitioned into other solvents, the ethyl acetate fraction (ARF) showed the highest inhibitory activity of mast cell degranulation (Figure S1 in Supporting Information [SI]); thus, a bioactivity-guided fractionation procedure was performed to obtain seven isolates. Ten grams of ARF was chromatographed on a silica gel column (Merck 230−400 mesh, 500 g, 5 cm diameter × 70 cm, Merck, Darmstadt, Germany) and successively eluted with a stepwise gradient of hexane/ethyl acetate [90:10 (3 L), 80:20 (2 L), 75:25 (2 L), 65:35 (2 L), 50:50 (2 L), 30:70 (2 L), 0:100 (1 L) by volume] to provide five fractions [ARF1 (168 mg), ARF2 (127 mg), ARF3 (150 mg), ARF4 (693 mg), ARF5 (790 mg)]. The subfractions were monitored by HPLC (Figure S2 in SI) and the ARF1−5 fractions showed similar inhibitory activity of β-hexosaminidase release (Figure S3 in SI). Isolation of flavone and flavone glycosides (Figure 1) from *A.rossii* was done as previously described.[14]

Cell Culture. RBL-2H3 cells obtained from the American Type Culture Collection (ATCC, Manassas, VA, USA) via the Korean Cell Line Bank (KCLB no. 22256, Seoul, Korea) were cultured in DMEM supplemented with 10% FBS and 100 U/mL penicillin. Cells were grown in 75 cm^2 culture flasks at 37 °C with 5% CO_2 in a humidified atmosphere.

Cell Viability Assay. Cell viability was checked using a 3-[4,5-dimethylthiazol-2-yl]-2,5-diphenyltetrazolium bromide (MTT) colorimetric assay (Sigma-Aldrich, St Louis, MO, U.S.A.). RBL-2H3 cells were grown in 24-well plates (2×10^5 cells/mL) for 24 h. After treating the cells with various concentrations of ARE for 6 h, the cells were washed and then treated with 200 μL MTT (0.5 mg/mL), and cells were incubated for an additional 4 h. Cells were then washed, and the insoluble formazan products were dissolved in 200 μL DMSO. Absorbance was measured by spectrophotometry at 550 nm using a microplate reader (Bio-Tek Instruments, Winooski, VT).

Measurement of Histamine and β-Hexosaminidase Release. RBL-2H3 cells were sensitized with 0.2 μg/mL monoclonal DNP-IgE. Cells were washed with modified PIPES buffer (25 mM PIPES, pH 7.2, 119 mM NaCl, 5 mM KCl, 0.4 mM $MgCl_2 \cdot 6H_2O$, 1 mM $CaCl_2$, 5.6 mM glucose, 40 mM NaOH and 0.1% BSA). Cells were treated with ARE or compounds **1**−**7** at the indicated concentrations for 1 h at 37 °C. After incubation, cells were challenged with 0.2 μg/mL DNP-BSA for 1 h at 37 °C. Histamine was then detected using an enzyme immunoassay kit (Oxford Biomedical Research, Rochester Hills, MI). Histamine release was expressed as a percentage of the total histamine produced by unstimulated cells. To determine β-hexosaminidase release, aliquots of supernatants and lysed pellets were transferred into 96-well plates. Samples were mixed with substrate solution (1 mM *p*-nitrophenyl *N*-acetyl-β-D-glucosamine in 0.05 M citrate buffer, pH 4.5) and incubated for 1 h at 37 °C. Reactions were terminated by the addition of 0.05 M sodium carbonate buffer, pH 10. Absorbance was measured by spectrophotometry at 405 nm.

dx.doi.org/10.1021/jf405486c | J. Agric. Food Chem. 2014, 62, 3750−3758

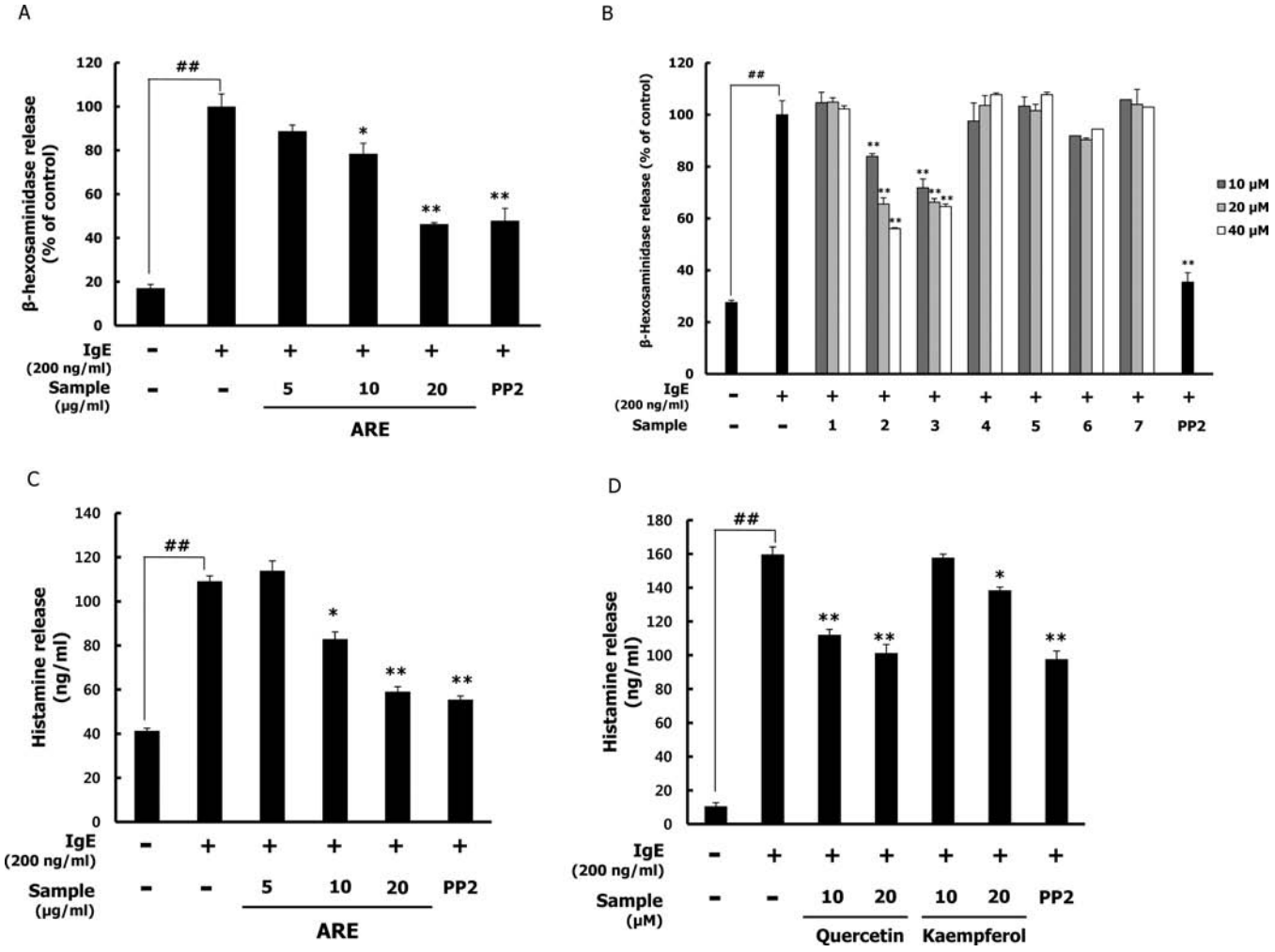

Figure 2. Effects of ARE, quercetin, and kaempferol on β-hexosaminidase and histamine release. (A) The degranulation was determined by measuring β-hexosaminidase release in DNP-IgE-sensitized RBL-2H3 cells. The RBL-2H3 cells were treated in the presence or absence of ARE (5, 10, or 20 μg/mL) for 1 h and then stimulated for 1 h with DNP-BSA. (B) The RBL-2H3 cells were treated in the presence or absence of gallic acid ethyl ester (1), quercetin (2), kaempferol (3), quercetin 3-*O*-(6″-galloyl)-β-D-glucopyranoside (4), quercetin 3-*O*-β-D-glucopyranoside (5), kaempferol 3-*O*-(6″-galloyl)-β-D-glucopyranoside (6), or kaempferol 3-*O*-β-D-glucopyranoside (7) (20 μM) for 1 h and then stimulated for 1 h with antigen. (C,D) Histamine release was determined with enzyme-linked immunosorbent assay kit. The RBL-2H3 cells were treated in the presence or absence of ARE (5, 10, or 20 μg/mL), quercetin (10 or 20 μM), or kaempferol (10 or 20 μM) for 1 h and then stimulated for 1 h with antigen. PP2 (10 μM) is a general Src-family kinase inhibitor. Results are expressed as the mean ± SD of three independent experiments. ($^{\#\#}p < 0.01$, $^{*}p < 0.05$, and $^{**}p < 0.01$).

Measurement of Prostaglandin E_2 and Leukotriene B_4. Cell culture medium was collected, and the secretions of prostaglandin E_2 (PGE_2) and leukotriene B_4 (LTB_4) were determined using competitive radioimmunoassay kits (R&D Systems, MN, U.S.A., and Cayman Chemical, MI, U.S.A., respectively) according to the manufacturers' protocol.

Measurement of Cytokine Release. IgE-sensitized RBL-2H3 cells were incubated with ARE, quercetin, and kaempferol (various concentrations) for 1 h and stimulated with DNP-BSA for 4 h. Interleukin (IL)-4 and tumor necrosis factor (TNF)-α concentrations in cell culture supernatants were measured using enzyme-linked immunosorbent assay kits (Abcam, UK).

Reverse Transcription-Polymerase Chain Reaction. (RT-PCR). RNA was extracted with Trizol reagent (Invitrogen) according to the manufacturer's protocol and quantified by spectrophotometry at 260 nm. The cDNA was synthesized in a 20 μL reaction containing 1 μg total RNA, oligo (dT), and reverse transcriptase premix (Elpis-Biotech., Inc., Taejeon, Korea). Reverse transcription (RT) was initiated at 70 °C for 5 min, followed by incubation at 42 °C for 60 min, and was terminated at 94 °C for 5 min. Amplification of the cDNA products (5 μL) by PCR was performed with a PCR premix (Elpis-Biotech) and the following primer pairs: TNF-α forward, 5′-CAA GGA GCA GAA GTT CCC AA-3′, and TNF-α reverse, 5′-CGG ACT CCG TGA TGT CTA AG-3′ (500 bp); IL-4 forward, 5′-ACC TTG CTG TCA CCC TGT TC-3′, and IL-4 reverse, 5′-TTG TGA GCG TGG ACT CAT TC-3′ (351 bp); COX-2 forward, 5′- TGA CTG TAC CCG GAC TGG AT-3′, and COX-2 reverse, 5′-CAT GGG AGT TGG GCA GTC AT-3′ (322 bp); 5-LO forward, 5′-TAC TCA TCA AGC GCT GCA CA-3′, and 5-LO reverse, 5′-TGG CCA AAA GCC AGT CGT AT-3′ (324 bp); β-actin forward, 5′-AGC CAT GTA CGT AGC CAT CC-3′, and β-actin reverse, 5′-TCT CAG CTG TGG TGG TGA AG-3′ (227 bp). Before PCR amplification, primers for cytokines and β-actin were denatured at 94 °C for 5 min. Amplification consisted of 28 cycles of denaturation at 94 °C for 30 s, annealing for 1 min (52 °C for IL-4; 55 °C for TNF-α and β-actin), and extension at 72 °C for 1 min, followed by a final 5 min extension at 72 °C. PCR was performed using a GeneAmp PCR System 9700 (Applied Biosystems, Foster City, CA, U.S.A.). PCR products were separated by 1.5% agarose gel electrophoresis and visualized by ethidium bromide staining and UV illumination. Densitometry was performed using DIG chemiluminescent film (volume of all markers/volume of β-actin).

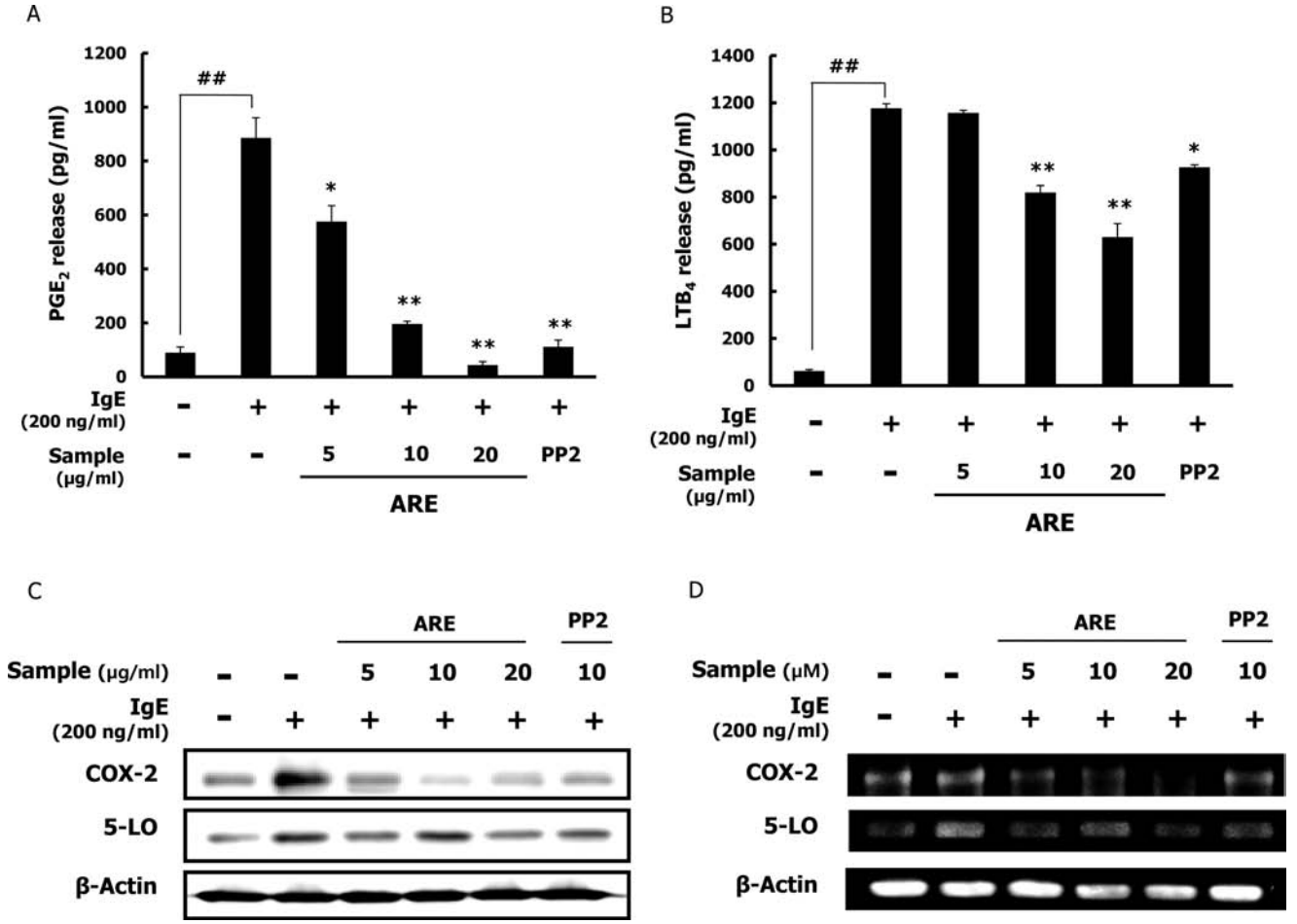

Figure 3. Effects of ARE on PGE_2 and LTB_4 secretion. RBL-2H3 cells were treated with ARE (5, 10, or 20 μg/mL) for 1 h and then stimulated for 4 h with antigen. (A,B) PGE_2 and LTB_4 secretion was determined by enzyme-linked immunosorbent assay kit. (C,D) COX-2 and 5-LO protein and mRNA level were determined with Western blot assay and RT-PCR, respectively. PP2 (10 μM) is a general Src-family kinase inhibitor. Results are expressed as the mean ± SD of three independent experiments. ($^{\#\#}p < 0.01$, $^{*}p < 0.05$, and $^{**}p < 0.01$).

Generation of Passive Cutaneous Anaphylaxis (PCA) in Mice. A 0.5 mg of DNP-IgE was injected subcutaneously into the left ears of 4-week-old male BALB/c mice, 24 h before antigen challenge. After IgE-sensitization, the mice were orally administered with ARE (100, 300 mg/kg) or cetirizine (20 mg/kg). After 60 min, the mice were intravenously injected with 250 μg of DNP-BSA in 250 μL of 1 × phosphate-buffered saline (PBS) containing Evans Blue (5 mg/mL). After 1 h, mice were euthanized and ear tissue was collected. The ear tissue absorbed dye was extracted overnight in 700 μL of formamide at 63 °C. The absorbance was measured at 620 nm to calculate dye concentration. Procedures used in this study were approved by the Animal Care and Use Committee of KIST.

Western Blot Analysis. RBL-2H3 cells were lysed in RIPA buffer containing protease inhibitors and then placed on ice for 10 min. Lysate protein concentrations were determined by Bradford protein assay (Bio-Rad Laboratories, Hercules, CA, U.S.A.). Equal amounts of protein (30 μg) were loaded in each sample, separated by 10% sodium dodecyl sulfate-polyacrylamide gel electrophoresis, and transferred to nitrocellulose membranes (Whatman GmbH, Dassel, Germany). Blotted membranes were blocked with 5% skimmed milk in Tris-buffered saline containing 0.1% Tween 20 for 1 h, and then incubated with primary antibodies for 16 h at 4 °C. After three washes in Tris-buffered saline containing 0.1% Tween 20, the membranes were incubated with horseradish peroxidase-linked secondary antibodies (Santa Cruz Biotechnology, Santa Cruz, CA, U.S.A.) for 2 h. Proteins were detected with enhanced chemoluminescence (Amersham Biosciences, Little Chalfont, UK) and visualized using an ECL Advanced system (GE Healthcare, Hatfield, UK).

Statistical Analysis. Each experiment was performed at least three times. Results are expressed as the mean ± standard deviation (SD). Vehicle (DMSO) and treated groups were compared by one-way analysis of variance followed by Scheffe's test (SPSS 17.0, Chicago, IL, USA). $^{\#\#}p < 0.01$, $^{*}p < 0.05$, and $^{**}p < 0.01$ were considered statistically significant. $^{\#\#}p < 0.01$ was compared with the control group (DNP-IgE treatment alone); $^{*}p < 0.05$, and $^{**}p < 0.01$ was compared with the DNP-IgE and DNP-BSA stimulated group.

RESULTS

Identification Flavone and Flavone Glycosides from *Aceriphyllum rossii*. Seven flavones and flavone glycosides were identified in *A. rossii* using LC−NMR/MS, including gallic acid ethyl ester, quercetin, kaempferol, quercetin 3-*O*-(6″-galloyl)-*β*-D-glucopyranoside (QGG), quercetin 3-*O*-*β*-D-glucopyranoside (QG), kaempferol 3-*O*-(6″-galloyl)-*β*-D-glucopyranoside (KGG), and kaempferol 3-*O*-*β*-D-glucopyranoside (KG) (Figure 1).

Cytotoxicity of Test Substances. The effect of ARE on RBL-2H3 cell viability was evaluated by colorimetric MTT assay. Treatment with ARE (5−20 μg/mL) had no effect on RBL-2H3 cell viability, and no cytotoxicity was observed (data not shown).

Inhibitory Effects of ARE and Flavones and Flavone Glycosides from *A. rossii* on *β*-hexosaminidase and Histamine Release in IgE-Stimulated RBL-2H3 Cells. To

dx.doi.org/10.1021/jf405486c | J. Agric. Food Chem. 2014, 62, 3750−3758

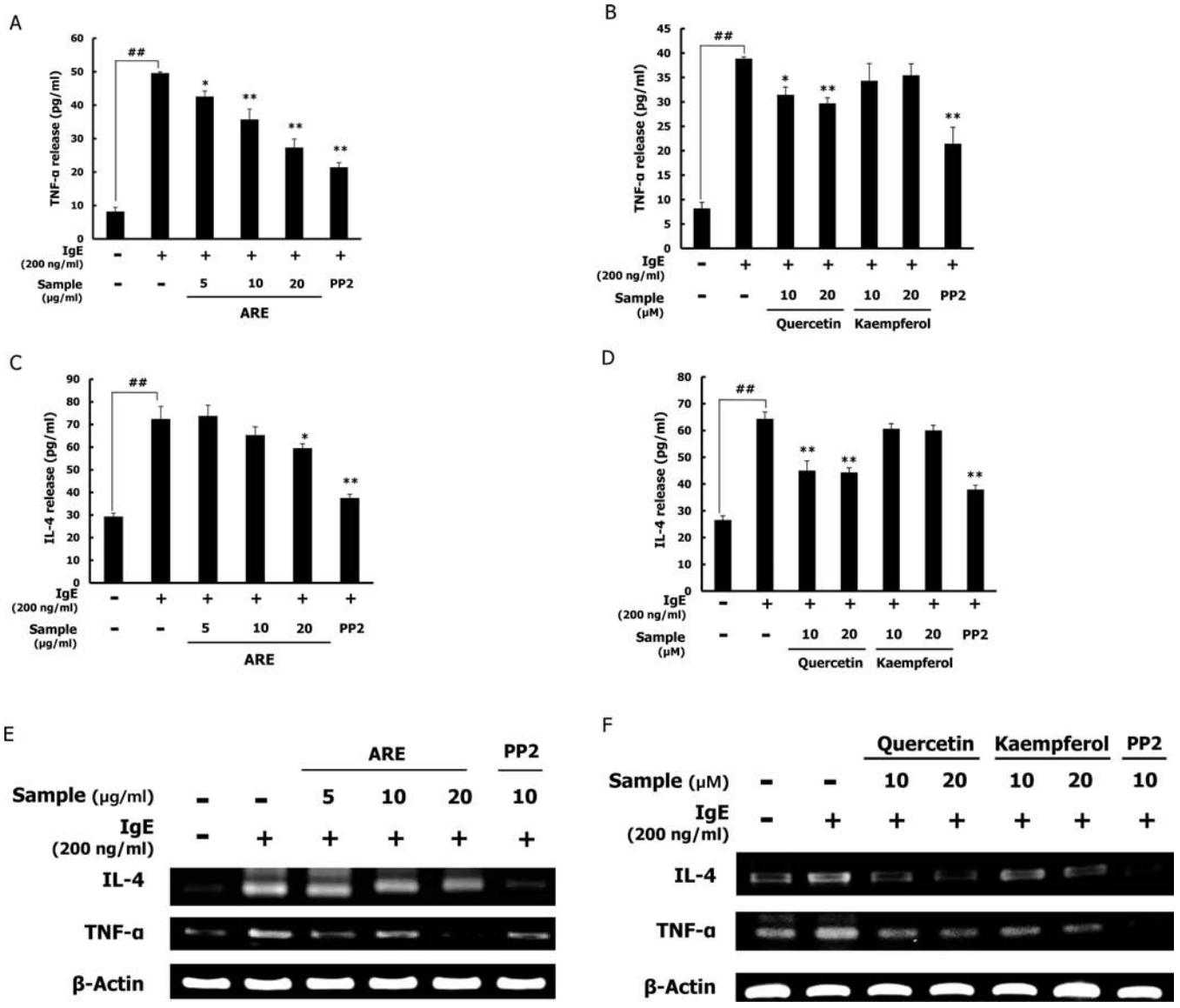

Figure 4. Effects of ARE, quercetin, and kaempferol on TNF-α and IL-4 production and expression. RBL-2H3 cells were treated with ARE, quercetin, and kaempferol for 1 h and then stimulated with DNP-BSA for 4 h. (A–D) TNF-α and IL-4 production was determined by enzyme-linked immunosorbent assay kit. (E,F) TNF-α and IL-4 mRNA levels were determined with RT-PCR. PP2 (10 μM) is a general Src-family kinase inhibitor. Results are expressed as the mean ± SD of three independent experiments. ($^{\#\#}p < 0.01$, $^{*}p < 0.05$, and $^{**}p < 0.01$).

determine the effect of ARE and its constituents on mast cell degranulation, its ability to inhibit the release of β-hexosaminidase was examined. ARE inhibited β-hexosaminidase release in RBL-2H3 cells treated with IgE at concentrations of 5, 10, and 20 μg/mL in a dose-dependent manner. At a concentration of 20 μM ARE, β-hexosaminidase release was inhibited by 46% (Figure 2A). In addition, quercetin and kaempferol inhibited the degranulation of DNP-BSA-stimulated RBL-2H3 cells to a greater degree than gallic acid ethyl ester, QGG, QG, KGG, or KG (Figure 2B). Therefore, further studies were performed using quercetin and kaempferol. The effect of ARE, quercetin, and kaempferol on histamine release was also evaluated to determine potential antiallergic activities. ARE, quercetin, and kaempferol inhibited histamine release in RBL-2H3 cells treated with IgE in a dose-dependent manner (C and D of Figure 2).

Inhibitory Effects of ARE on PGE_2 and LTB_4 Production and COX-2 and 5-LO Expression in IgE Stimulated RBL-2H3 Cells. The FcεRI receptor activates the arachidonate cascade in antigen-activated mast cells.[15] Thus, the effect of ARE on the production of proinflammatory lipid mediators (such as PGE_2 and LTB_4) was investigated. ARE significantly inhibited PGE_2 and LTB_4 secretion in IgE-stimulated RBL-2H3 cells in a dose-dependent manner. ARE (20 μM) inhibited PGE_2 and LTB_4 secretion by 5% and 53%, respectively (A and B of Figure 3). The effect of ARE on the expression of cyclooxygenase 2 (COX-2) and 5-lipoxygenase (5-LO), enzymes that produce PGs and LTs from arachidonic acid, was also evaluated by Western blot assay and RT-PCR. IgE treatment induced COX-2 and 5-LO protein and mRNA expression in RBL-2H3 cells. However, treatment with 5, 10, or 20 μg/mL of ARE attenuated the IgE-induced upregulation of COX-2 and 5-LO (C and D of Figure 3).

Inhibitory Effect of ARE, Quercetin, and Kaempferol on Proinflammatory Cytokine Production and Gene Expression in IgE Stimulated RBL-2H3 Cells. The

dx.doi.org/10.1021/jf405486c | J. Agric. Food Chem. 2014, 62, 3750–3758

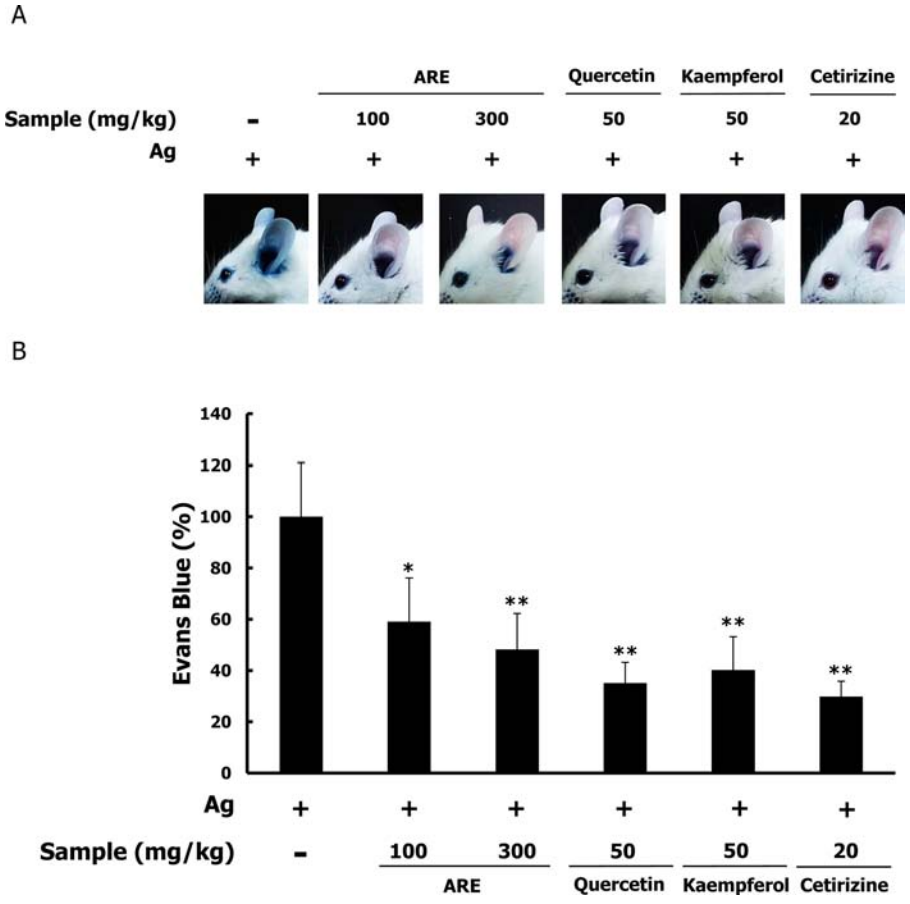

Figure 5. Effect of ARE, quercetin, and kaempferol on IgE-mediated passive cutaneous anaphylaxis (PCA). (A) ARE (100 or 300 mg/kg), quercetin (50 mg/kg), kaempferol (50 mg/kg), or cetrizine (20 mg/kg) was orally administered to mice for 1 h before IgE sensitization. Evans blue stained ears were photographed. (B) The ear absorbed dye was extracted with formamide. The quantification data is presented as % of IgE-stimulated control. Cetrizine (20 mg/kg) is an antihistamine reference drug. Results are expressed as the mean ± SD of three independent experiments. ($^{\#\#}p < 0.01$, $^{*}p < 0.05$, and $^{**}p < 0.01$).

proinflammatory cytokines, TNF-α and IL-4, are critical for allergic responses.[16] We therefore examined whether ARE, quercetin, and kaempferol regulate the production and mRNA expression of TNF-α and IL-4 in IgE-sensitized RBL-2H3 cells. As shown, ARE and quercetin inhibited both TNF-α and IL-4 production (A–D of Figure 4) and gene expression, while kaempferol did not affect production and expression of TNF-α and IL-4 (E and F of Figure 4).

Effect of ARE, Quercetin, and Kaempferol on Mast Cell-mediated PCA in Mice. PCA is widely used to determine local allergic reactions *in vivo*.[17] To investigate whether ARE, quercetin, and kaempferol inhibited allergic responses, we used a mast cell-dependent PCA model. IgE was injected subcutaneously into mouse ear tissue, followed by injection of DNP-BSA containing 5% Evans Blue. Oral administration of ARE, quercetin, and kaempferol inhibited the antigen-induced PCA response in a dose-dependent (Figures 5A and 5B). The inhibitory effect of ARE, quercetin, and kaempferol was similar to that of 20 mg/kg cetrazine,[18] a typical antihistamine drug, which was used as a positive control.

Effect of ARE, Quercetin, and Kaempferol on FcεRI Signaling in IgE Sensitized RBL-2H3 Cells. FcεRI signals through activation of Syk, Lyn, PKC, and PLCγ.[19] PP2, a general Src-family kinase inhibitor, markedly suppressed phosphorylation of Syk.[19] To investigate the mechanisms involved in ARE-, quercetin-, and kaempferol-mediated inhibition of degranulation, a number of intracellular signals were examined. DNP-BSA treatment of IgE-sensitized cells induced phosphorylation of Syk, PKD/PKCμ, and PLCγ at early time points, and this phosphorylation was reduced by treatment with ARE, quercetin, or kaempferol (A and B of Figure 6). During IgE-mediated activation of mast cells, three major subfamilies of MAPKs (extracellular signal-regulated kinase (ERK), c-Jun N-terminal kinase (JNK), and p38) can be activated, resulting in cytokine production.[20] To further identify the relevant downstream effectors that directly modulate cytokine production following ARE, quercetin, and kaempferol treatment, phosphorylation of ERK, JNK, and p38 was examined. IgE-induced phosphorylation of ERK, JNK, and p38 was inhibited by treatment with ARE, quercetin, or kaempferol (C and D of Figure 6).

■ DISCUSSION

Immediate-type hypersensitivity is initiated and amplified by inflammatory mediators (histamines, LTs, and PGs) and cytokines (TNF-α and IL-4) released from immune cells such as mast cells, eosinophils, and basophils. In particular, mast cells are crucial players in the regulation of allergic inflammatory responses due to their ability to produce proinflammatory mediators including histamines, PGE_2, and LTB_4.[21] A recent study in mast cell-deficient mice demonstrated that mast cell-derived mediators (histamines, cytokines,

dx.doi.org/10.1021/jf405486c | J. Agric. Food Chem. 2014, 62, 3750–3758

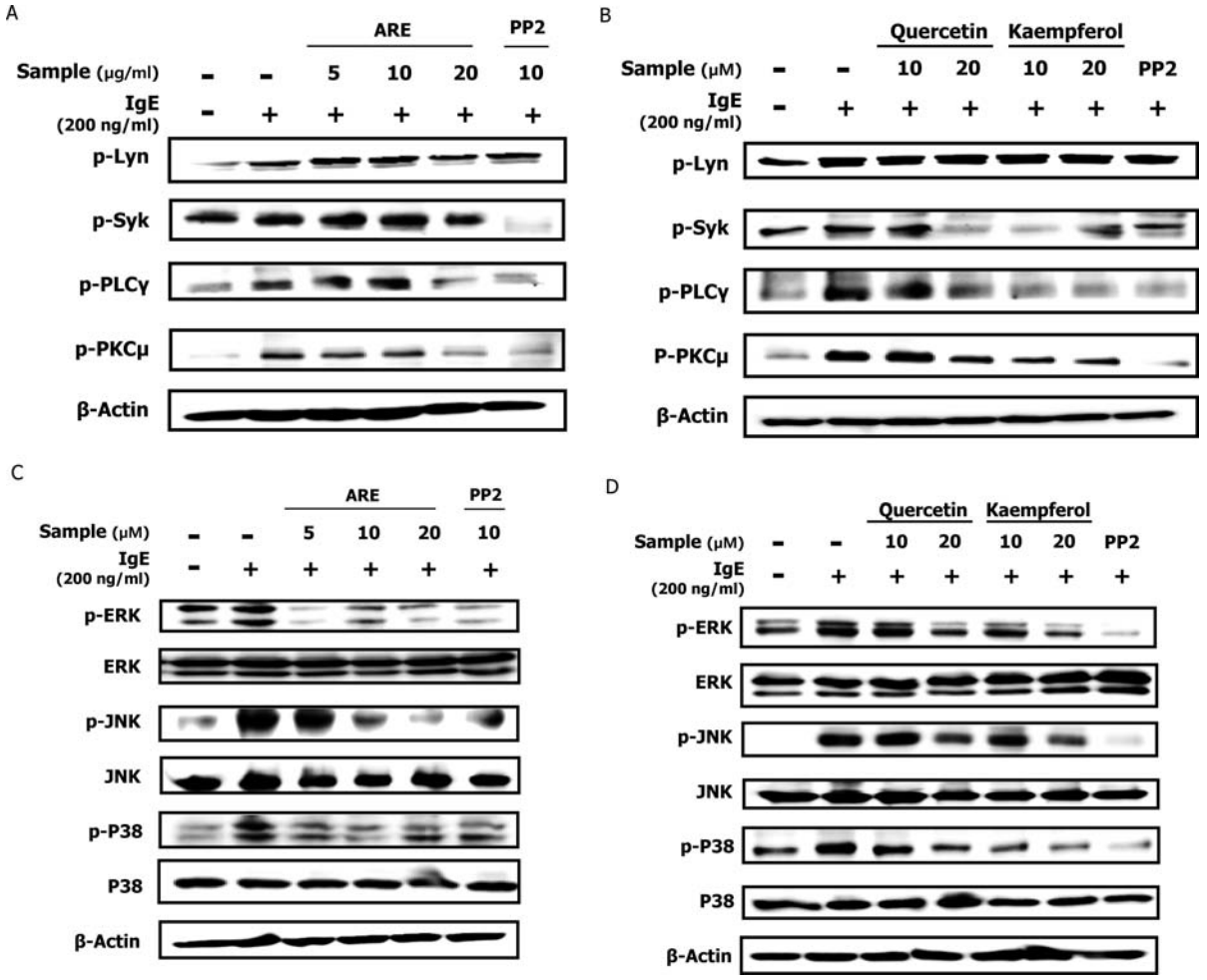

Figure 6. Effect of ARE, quercetin, and kaempferol on FcεRI Signaling. (A,B) RBL-2H3 cells were treated with ARE, quercetin, and kaempferol for 1 h and then stimulated with DNP-BSA for 10 min. Phosphorylation of Lyn, Syk, PLCγ, and PKD/PKCμ was determined with Western blot analysis. (C,D) RBL-2H3 cells were treated with ARE, quercetin, and kaempferol for 1 h and then stimulated with DNP-BSA for 30 min. Phosphorylation of JNK, ERK, and p38 was determined with Western blot analysis. PP2 (10 μM) is a general Src-family kinase inhibitor.

and proteases) play an important role during allergic inflammation.[22] Therefore, a number of studies have identified specific mediators of mast cell activation and have reported novel compounds targeting these inflammatory mediators.[3,23,24]

Quercetin and kaempferol are naturally occurring plant flavonoids found in many vegetables and fruits, and may possess anticancer, antioxidant, and anti-inflammatory properties.[25−27] Moreover, quercetin and kaempferol are also known to suppress various mediators of allergic responses. For example, quercetin, kaempferol, and several other flavonoids suppress degranulation by inhibiting β-hexosaminidase release and production of TNF-α and IL-4.[28] In addition, quercetin and kaempferol suppress IgE-mediated allergic inflammation in RBL-2H3 and Caco-2 cells.[29] However, the molecular mechanisms by which quercetin and kaempferol act on allergic disease are not fully understood. In the present study, we evaluated the inhibitory effects of ARE and its active compounds, quercetin and kaempferol, on allergic mediators in RBL-2H3 cells and in a murine PCA model.

Activation of FcεRI receptors present on mast cells through high affinity binding and aggregation of IgE initiates a signaling cascade that results in degranulation and secretion of inflammatory mediators, including histamine, lipid-derived mediators, and inflammatory cytokines.[30] We observed that ARE, quercetin, and kaempferol inhibited the release of both β-hexosaminidase (B and D of Figure 2) and histamine (C and E of Figure 2) in a dose-dependent manner. These results indicate that the antiallergic effects of ARE, quercetin, and kaempferol are due to the suppression of histamine release, known to cause vascular permeability, smooth-muscle contraction, and inflammation.

The FcεRI receptor signals through Lyn, Syk, and PLCγ to regulate degranulation.[16] The FcεRI receptor is a tetrameric complex, which binds IgE and initiates intracellular signaling to induce allergic responses. Activated FcεRI induces phosphorylation of Syk, which binds immunoreceptor tyrosine-based activation motifs (ITAMs) present on the FcεRI β and γ chains. In turn, Syk induces phosphorylation of PLCγ and PKC.[31] Notably, ARE, quercetin, and kaempferol also decreased the phosphorylation of Syk, PLCγ, and PKD/PKCμ (A and B of Figure 6). These results suggest that ARE, quercetin, and kaempferol may have antiallergic effects in antigen-induced mast cells, most likely by suppressing the activation of Syk, PLCγ, and PKC, and the consequent inhibition of mast cell degranulation.

ARE also reduced the secretion of the inflammatory mediators PGE_2 and LTB_4, which are arachidonic acid metabolites, via inhibition of the COX and LO pathways (A

dx.doi.org/10.1021/jf405486c | J. Agric. Food Chem. 2014, 62, 3750−3758

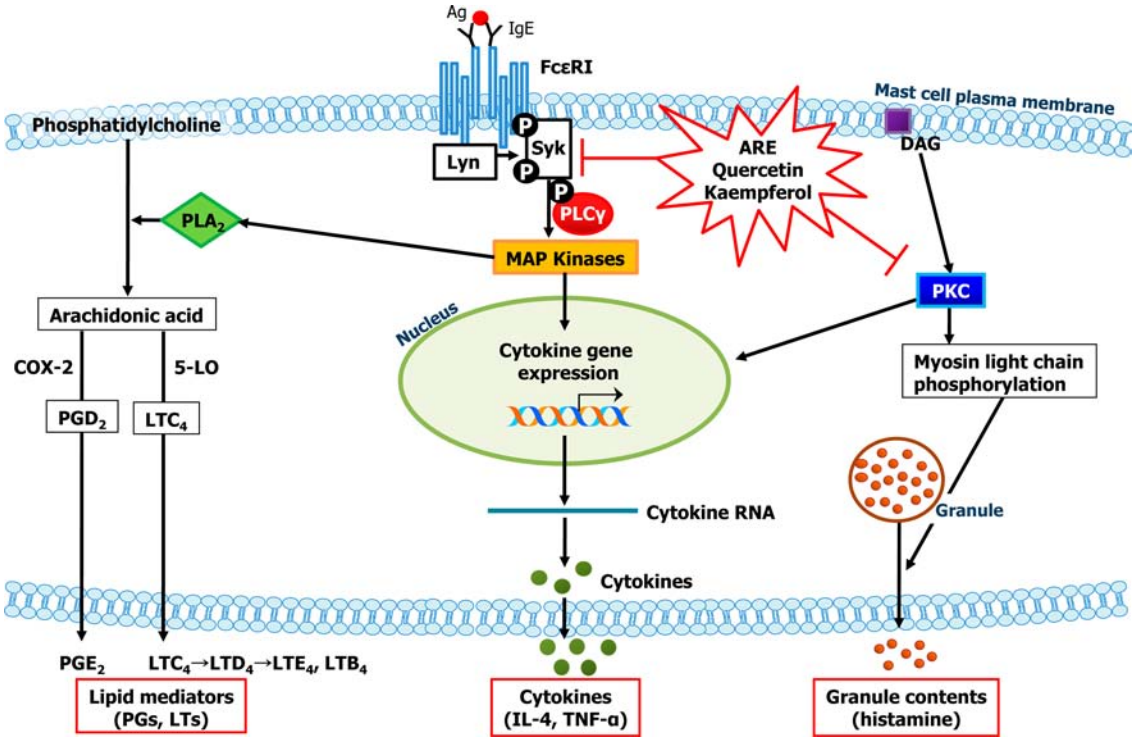

Figure 7. ARE, quercetin, and kaempferol inhibited FcεRI signaling pathways. The level of phosphorylated Syk proteins were reduced by ARE, quercetin, and kaempferol. ARE, quercetin, and kaempferol inhibited other downstream signaling molecules, including PKD/PKCμ and PLCγ. The activation of MAPKs were also suppressed by ARE, quercetin, and kaempferol.

and B of Figure 3).[32] Furthermore, ARE inhibited COX-2 and 5-LO expression, key enzymes in these pathways (C and D of Figure 3). These results indicate that ARE inhibits synthesis of inflammatory mediators by suppressing the COX and LO pathways.

We also found that ARE and quercetin significantly reduced both the production and mRNA expression of the proinflammatory cytokines TNF-α and IL-4 (Figure 4). TNF-α and IL-4 play a crucial role in triggering and sustaining allergic reactions in mast cells. IL-4 induces T-cell development and switches B-cells to the IgE isotype. TNF-α also activates physiological immune responses by promoting leukocyte infiltration and tissue fibrosis, and initiates cytokine-mediated inflammatory states via stimulation of cytokine production.[33] Although inflammation is a physiological defense mechanism against pathogens, overexpression of cytokines can also cause serious inflammatory diseases such as atopic dermatitis and asthma. The results suggest that these compounds may be useful for the treatment of allergic conditions.

MAPK pathways are a major therapeutic target in allergic disease.[34] Therefore, to investigate the mechanism by which ARE, quercetin, and kaempferol inhibit the activation of RBL-2H3 cells, MAPK (ERK, p38, and JNK) phosphorylation was evaluated. In this study, ARE, quercetin, and kaempferol inhibited IgE-induced phosphorylation of ERK, p38, and JNK, suggesting that these compounds attenuate mast cell activation by regulating MAPK signaling (C and D of Figure 6).

In conclusion, ARE and its active compounds, quercetin and kaempferol, inhibited degranulation and the release of histamine, lipid mediators, and proinflammatory cytokines in IgE-stimulated RBL-2H3 cells and had anti-inflammatory effects in a murine PCA model. ARE, quercetin, and kaempferol also inhibited downstream signaling from the FcεRI receptor by suppressing the phosphorylation of Syk, PLCγ, PKC, and MAPK, all of which mediate allergic responses in IgE-sensitized RBL-2H3 cells (Figure 7). These findings indicate that ARE, quercetin, and kaempferol may together be a useful therapeutic agent for preventing or treating IgE-mediated allergic diseases.

■ ASSOCIATED CONTENT

Supporting Information

This material is available free of charge via the Internet at http://pubs.acs.org.

■ AUTHOR INFORMATION

Corresponding Author

*E-mail: cwnho@kist.re.kr. Telephone: +82-33-650-3651. Fax: +82-33-650-3679.

Notes

The authors declare no competing financial interest.

■ ACKNOWLEDGMENTS

This work was supported by an intramural grant (2Z03850) from Korea Institute of Science and Technology, Gangneung Institute.

■ ABBREVIATIONS

DMSO, dimethyl sulfoxide; FcεRI, Fc receptor for IgE; IL, interleukin; MAPK, mitogen-activated protein kinases; RBL, rat basophilic leukemia; TNF, tumor necrosis factor; IgE, immunoglobulin E; PLC, phospholipase; protein kinase C, PKC; ERK, extracellular signal-regulated kinase; JNK, c-Jun N-terminal kinase; PGs, prostaglandins; LTs, leukotrienes; COX-2, cyclooxygenase 2; 5-LO, 5-lipoxygenase

REFERENCES

(1) Rosenwasser, L. J. Mechanisms of IgE Inflammation. *Curr. Allergy Asthma Rep.* **2011**, *11*, 178−183.

(2) Gilfillan, A. M.; Tkaczyk, C. Integrated signaling pathways for mast-cell activation. *Nat. Rev. Immunol.* **2006**, *6*, 218−230.

(3) Itoh, T.; Ohguchi, K.; Inuma, M.; Nozawa, Y.; Akao, Y. Inhibitory effects of polymethoxy flavones isolated from *Citrus reticulate* on degranulation in rat basophilic leukemia RBL-2H3: Enhanced inhibition by their combination. *Bioorg. Med. Chem.* **2008**, *16*, 7592−7598.

(4) Galli, S. J.; Tsai, M.; Piliponsky, A. M. The development of allergic inflammation. *Nature* **2008**, *454*, 445−454.

(5) Oppenheimer, J. J.; Casale, T. B. Next generation antihistamines: Therapeutic rationale, accomplishments and advances. *Expert Opin. Investig. Drugs.* **2002**, *11*, 807−817.

(6) Chan, B. C.; Hon, K. L.; Leung, P. C.; Sam, S. W.; Fung, K. P.; Lee, M. Y.; Lau, H. Y. Traditional Chinese medicine for atopic eczema: PentaHerbs formula suppresses inflammatory mediators release from mast cells. *J. Ethnopharmacol.* **2008**, *120*, 85−91.

(7) Ho-sub, L.; Kwan-Ha, P.; Kang-Beom, K.; Byeong-Sun, M.; Cheol-Min, S.; Yong-Seon, S.; Eun, A. S.; Young-suk, K.; Kang-Jeon, K.; Do-Gon, R. Anti-allergic activity of the *Sophorae radix* water extract in experimental animals. *Am. J. Chin. Med.* **2001**, *29*, 129−139.

(8) Knipping, K.; van Esch, E. C.; Wijering, S. C.; van der Heide, S.; Dubois, A. E.; Garssen, J. *In vitro* and *in vivo* anti-allergic effects of *Arctium lappa* L. *Exp. Biol. Med.* **2008**, *233*, 1469−1477.

(9) Lee, C. B. Illustrated Flora of Korea; Hyangmunsa: Seoul, Korea, 1989; p 409.

(10) Lee, W. C. Coloured Standard Illustrations of Korean Plants; Academybook: Seoul, Korea, 1996; p 152.

(11) Lee, Y. N. Flora of Korea; Kyohak Publishing Co., Ltd.: Seoul, Korea, 2002; p 280.

(12) Han, J.-T.; Kim, H.-Y.; Park, Y.-D.; Lee, Y.-H.; Lee, K.-R.; Kwon, B.-M.; Baek, N.-I. Aceriphyllic acid A, a new ACAT inhibitory triterpenoid, from *Aceriphyllum rossii*. *Planta Med.* **2002**, *68*, 558−561.

(13) Zheng, C. J.; Sohn, M. J.; Kim, K. Y.; Yu, H. E.; Kim, W. G. Olean-27-carboxylic acid-type triterpenes with potent antibacterial activity from *Aceriphyllum rossii*. *J. Agric. Food. Chem.* **2008**, *56*, 11752−11756.

(14) Han, J. T.; Bang, M. H.; Chun, O. K.; Kim, D. O.; Lee, C. Y.; Baek, N. I. Flavonol glycosides from the aerial parts of *Aceriphyllum rossii* and their antioxidant activities. *Arch. Pharm. Res.* **2004**, *27*, 390−395.

(15) Roth, K.; Chen, W. M.; Lin, T. J. Positive and negative regulatory mechanisms in high-affinity IgE receptor-mediated mast cell activation. *Arch. Immunol. Ther. Exp. (Warsz).* **2008**, *56*, 385−399.

(16) Theoharides, T. C.; Kalogeromitros, D. The critical role of mast cells in allergy and inflammation. *Ann. N.Y. Acad. Sci.* **2006**, *1088*, 78−99.

(17) Levy, L. Simultaneous passive cutaneous anaphylaxis and Arthus reactions in mouse, rat and guinea-pig. *Immunology* **1964**, *7*, 91−96.

(18) Chodaczek, G.; Bacsi, A.; Dharajiya, N.; Sur, S.; Hazra, T. K.; Boldogh, I. Ragweed pollen-mediated IgE-independent release of biogenic amines from mast cells via induction of mitochondrial dysfunction. *Mol. Immunol.* **2009**, *46*, 2505−2514.

(19) Lee, J. H.; Kim, J. W.; Ko, N. Y.; Mun, S. H.; Her, E.; Kim, B. K.; Han, J. W.; Lee, H. Y.; Beaven, M. A.; Kim, Y. M.; Choi, W. S. Curcumin, a constituent of curry, suppresses IgE-mediated allergic response and mast cell activation at the level of Syk. *J. Allergy Clin. Immunol.* **2008**, *121*, 1225−1231.

(20) Zhang, C.; Baumgartner, R. A.; Yamada, K.; Beaven, M. A. Mitogen-activated protein (MAP) kinase regulates production of tumor necrosis factor-α and release of arachidonic acid in mast cells: Indications of communication between p38 and p42 MAP kinases. *J. Biol. Chem.* **1997**, *272*, 13397−13402.

(21) Galli, S. J.; Kalesnikoff, J.; Grimbaldeston, M. A.; Piliponsky, A. M.; Williams, C. M.; Tsai, M. Mast cells as "tunable" effector and immunoregulatory cells: recent advances. *Annu. Rev. Immunol.* **2005**, *23*, 749−786.

(22) Wershil, B. K. Mast cell-deficient mice and intestinal biology. *Am. J. Physiol. Gastrointest. Liver Physiol.* **2000**, *278*, G343−G348.

(23) Tanifuji, S.; Aizu-Yokota, E.; Funakoshi-Tago, M.; Sonoda, Y.; Inoue, H.; Kasahara, T. Licochalcones suppress degranulation by decreasing the intracellular Ca^{2+} level and tyrosine phosphorylation of ERK in RBL-2H3 cells. *Int. Immunopharmacol.* **2010**, *10*, 769−776.

(24) Westcott, J. Y.; Wenzel, S. E.; Dreskin, S. C. Arachidonate-induced eicosanoid synthesis in RBL-2H3 cells: stimulation with antigen or A23187 induces prolonged activation of 5-lipoxygenase. *Biochim. Biophys. Acta* **1996**, *1303*, 74−81.

(25) Kang, J. W.; Kim, J. H.; Song, K.; Kim, S. H.; Yoon, J.-H.; Kim, K.-S. Kaempferol and quercetin, components of *Ginkgo biloba* extract (EGb 761), induce caspase-3-dependent apoptosis in oral cavity cancer cells. *Phytother. Res.* **2010**, *24*, S77−S82.

(26) Kanakis, C. D.; Tarantilis, P. A.; Polissiou, M. G.; Diamantoglou, S.; Tajmir-Riahi, H. A. DNA interaction with naturally occurring antioxidant flavonoids quercetin, kaempferol, and delphinidin. *J. Biomol. Struct. Dyn.* **2005**, *6*, 719−724.

(27) García-Mediavilla, V.; Crespo, I.; Collado, P. S.; Esteller, A.; Sánchez-Campos, S.; Tuñón, M. J.; González-Gallego, J. The anti-inflammatory flavones quercetin and kaempferol cause inhibition of inducible nitric oxide synthase, cyclooxygenase-2 and reactive C-protein, and down-regulation of the nuclear factor kappaB pathway in Chang Liver cells. *Eur. J. Pharmacol.* **2007**, *557*, 221−229.

(28) Mastuda, H.; Morikawa, T.; Ueda, K.; Managi, H.; Yoshikawa, M. Structural requirements of flavonoids for inhibition of antigen-Induced degranulation, TNF-alpha and IL-4 production from RBL-2H3 cells. *Bioorg. Med. Chem.* **2002**, *10*, 3123−3128.

(29) Lee, E. J.; Ji, G. E.; Sung, M. K. Quercetin and kaempferol suppress immunoglobulin E-mediated allergic inflammation in RBL-2H3 and Caco-2 cells. *Inflamm.Res.* **2010**, *10*, 847−854.

(30) Beaven, M. A.; Metzger, H. Signal transduction by Fc receptors: the Fc epsilon RI case. *Immunol. Today* **1993**, *14*, 222−226.

(31) Siraganian, R. P.; de Castro, R. O.; Barbu, E. A.; Zhang, J. Mast cell signaling: The role of protein tyrosine kinase Syk, its activation and screening methods for new pathway participants. *FEBS Lett.* **2010**, *584*, 4933−4940.

(32) Gonzalez-Periz, A.; Claria, J. New approaches to the modulation of the cyclooxygenase-2 and 5-lipoxygenase pathways. *Curr. Top. Med. Chem.* **2007**, *7*, 297−309.

(33) Bradding, P. Human mast cell cytokines. *Clin. Exp. Allergy* **1996**, *26*, 13−19.

(34) Abdel-Raheem, I. T.; Hide, I.; Yanase, Y.; Shigemoto-Mogami, Y.; Sakai, N.; Shirai, Y. Protein kinase C-alpha mediates TNF release process in RBL-2H3 mast cells. *Br. J. Pharmacol.* **2005**, *145*, 415−423.

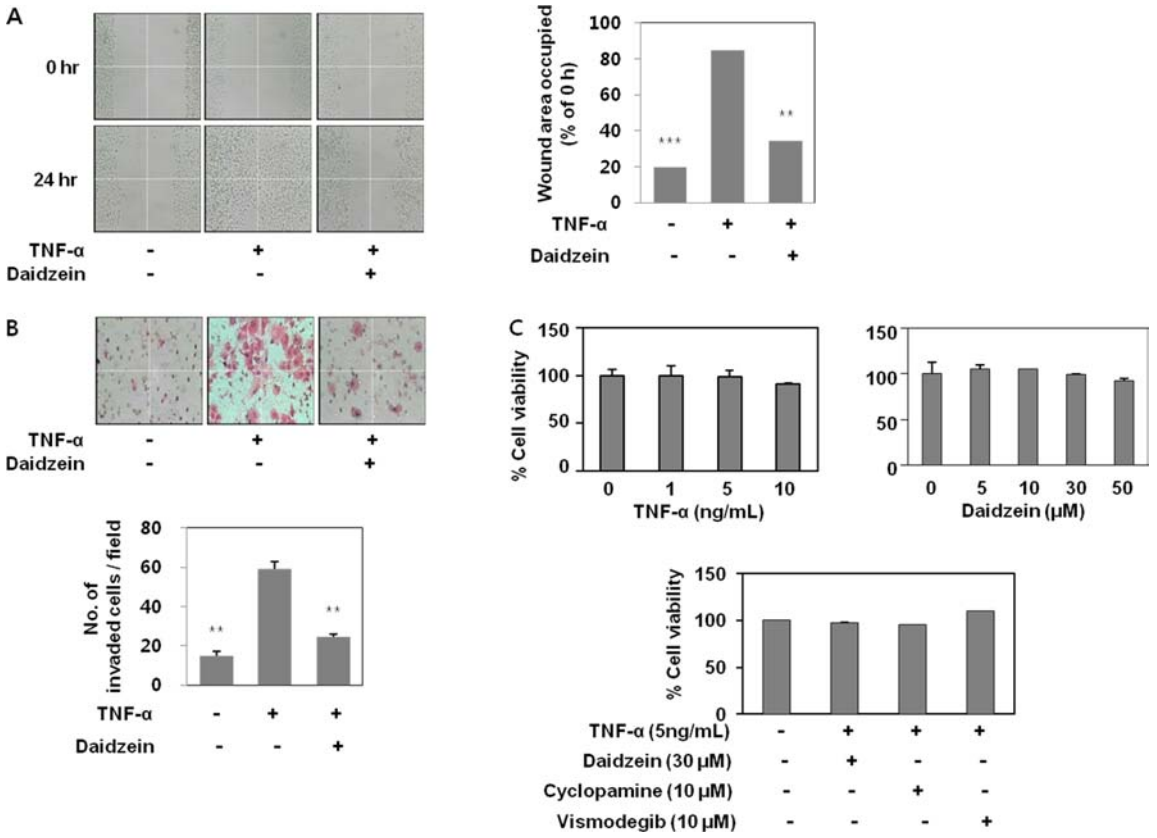

Figure 1. Effect of daidzein on TNF-α induced migration and invasion in MCF10DCIS.com human breast cancer cells. (A) Cells (5×10^5 cells/well in a 6-well plate) were treated with TNF-α (5 ng/mL) alone or together with daidzein (30 μM) for 24 h. Cell migration was assessed by light microscopy at 100× magnification and the number of cells at the injured area at 0 and 24 h was compared. (B) Cells (5×10^4 cells/well in a 24-well invasion chamber) were treated with TNF-α alone or together with daidzein for 24 h. Invasiveness was quantified by counting the number of cells that migrated to the lower side of the filter within randomly selected microscope fields. (C) Cells (5×10^3cells/well in a 96-well plate) were treated with TNF-α or daidzein alone at the indicated concentrations or cotreated TNF-α (5 ng/mL) with daidzein (30 μM), cyclopamine (10 μM), or vismodegib (10 μM) for 24 h. Cell viability was assessed with MTT assay. Values represent means ± SD $^{**}p < 0.01$, $^{***}p < 0.001$ compared to TNF-α treated cells.

MATERIALS AND METHODS

Reagents and Cell Culture. Daidzein and equol were purchased from Sigma (St. Louis, MO, USA), TNF-α from R&D Systems (Minneapolis, MN, USA), 6,7,4′-trihydroxyisoflavone from Indofine Chemical Company, Inc. (Hillsborough, NJ, USA), and vismodegib and cyclopamine from LC Laboratories (Woburn, MA, USA). MCF10DCIS.com human breast cancer cells were purchased from Asterand (Detroit, MI, USA) and cultured in DMEM/F12 (Life Technologies, Grand Island, NY, USA) supplemented with 5% horse serum, 1% HEPES, and 1% penicillin/streptomycin (Life Technologies) at 37 °C, 5% CO_2. Patched1 mutant (Ptch1(−/−)) embryonic fibroblasts (MEFs) were kindly provided by K. Anderson at Sloan Kettering Institute (New York, USA) and cultured in DMEM (Life Technologies, Grand Island, NY, USA) with 10% fetal bovine serum (FBS) and 1% penicillin/streptomycin (Life Technologies).

Cell Viability Assay. Cells were incubated with compounds at different concentrations for 24 h, and 200 μL of 3-(4,5-dimethylthiazol-2-yl)-2,5-diphenyltetrazolium bromide (MTT, Sigma) was added 4 h before harvest. Dark-blue formazan crystals were dissolved with DMSO, and absorbance was measured with an ELISA plate reader (Molecular Devices, Sunnyvale, CA, USA) at 570 nm. Cell growth was defined as the percentage of viable cells in comparison with the control.

RNA Extraction and Quantitative Real-Time PCR. Total cellular RNA was extracted using Trizol reagent (Life Technologies) and was reverse-transcribed to obtain cDNA using RevertAid First Strand cDNA Synthesis Kit (Thermo Scientific, Lafayette, CO, USA) in an Atlas Thermal Cycler (Astec, Fukuoka, Japan). The cDNA was amplified using 5× HOT FIREPol EvaGreen qPCR Mix Plus (Solis Biodyne, Tartu, Estonia) and the following primer sequences for Gli1, 5′-CCTTCTTCGCGAACGGTTT-3′ (forward) and 5′-GGGTGAAGGCTGCTCACGTA-3′ (reverse), and for GAPDH, 5′-CAATGCCAAGTATGACAT-3′ (forward) and 5′-CCTGTTAT-TATGGGGGTCTG-3′ (reverse). To detect MMP-2 and -9 mRNA expression levels, labeled TaqMan primers and TaqMan Fast Advanced Master Mix from Applied Biosystems (Foster City, CA, USA) were used, along with the ABI PRISM 7900 sequence detection system (Applied Biosystems). Results were normalized to GAPDH expression level, and relative quantitation was performed using the comparative $2^{-\Delta\Delta CT}$ method.

Protein Extraction. After treatment with a compound, cells were collected and washed with PBS. Total protein was extracted with radioimmunoprecipitation assay (RIPA) buffer (10 mM Tris-HCl, 5 mM EDTA, 150 mM NaCl, 1% Triton X-100, 1% sodium deoxycholate, 0.1% SDS, 0.1 mM Na_3VO_4, 1% phenylmethylsulfonyl fluoride, 1% protease inhibitor). Cytosolic and nuclear fractions were extracted using NE-PERTM Nuclear and cytoplasmic extraction reagents kit (Thermo Scientific) according to the manufacturer's instructions.

Western Blot Analysis. An equivalent amount of protein from cell lysates were resolved by 10% SDS-PAGE and transferred to polyvinylidene fluoride (PVDF, Millipore, Billerica, MA, USA) membranes which were probed with primary and secondary antibodies followed by chemiluminescence detection using EZ capture MG (ATTO, Tokyo, Japan). Primary antibodies used in this study were against Gli1, p-NFκB p65 (Ser536) (Cell Signaling Technology,

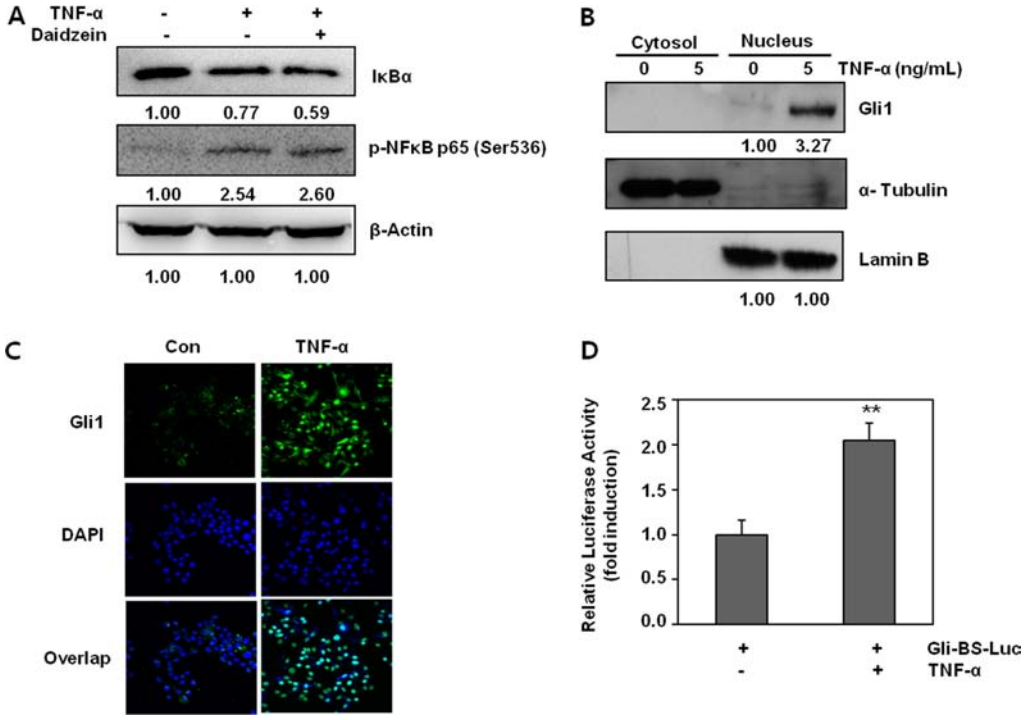

Figure 2. Effect of TNF-α on Hh signaling in MCF10DCIS.com human breast cancer cells. (A) Cells (7×10^5 cells in a 60 mm dish) were treated with TNF-α (5 ng/mL) alone or together with daidzein (30 μM) for 24 h. IκBα expression and NFκB p65 phosphorylation level at Ser 536 were determined by Western blotting. (B) Cytosolic and nuclear fractions of TNF-α treated cells were separated, and Gli1 nuclear translocation was determined by Western blotting. (C) Cells (2×10^5 cells/well in a glass bottom dish) treated with TNF-α were probed with anti-Gli1 antibody, with nuclei stained with DAPI, and cells were visualized by confocal microscopy. (D) Cells were transfected with 8X-Gli-BS-Luc and pCMV-β-gal vectors and treated with TNF-α. Relative luciferase activity from the Gli1 promoter was determined using a luminometer and normalized to β-galactosidase activity. $^{**}p < 0.001$ compared to the control.

Boston, MA, USA), IκBα, α-tubulin, lamin B, (Santa Cruz Biotechnology Inc., Santa Cruz, CA, USA), β-actin (Sigma, St. Louis, MO, USA). Horseradish peroxidase-conjugated secondary antibodies were purchased from Santa Cruz Biotechnology Inc. The blots were quantified using EZ West Lumi Plus (ATTO)

Confocal Microscopy. Cells were cultured in a glass bottom dish (MatTex, Ashland, MA, USA) and fixed with 4% paraformaldehyde in PBS 24 h after treatment with a compound. Cells were then treated with Gli1 antibody (1:100, Santa Cruz) and Alexa Fluor 488-conjugated secondary antibody (1:200, Life Technologies), and DAPI (Vector, Burlingame, CA, USA) was used to stain nuclei. Cells were visualized using a Nikon A1 confocal microscope (Nikon, Tokyo, Japan).

Transfection. Cells were transfected with 200 ng of Gli1 vector (pCMV-FLAG-mGli1 from Dr. Chi Chung Hui, University of Toronto) or Gli1 siRNA (200 nM, Bioneer, Daejeon, Korea) using FuGENE HD transfection reagent (Promega, Madison, WI, USA) in serum free medium. After 6 h, the treatment compound was added to the culture medium for 24 h. The expression of Gli1 protein was confirmed by Western blotting. Gli1 vector-transfected cells were seeded for the invasion assay.

Luciferase Assay. 8XGli-BS-Luc and pCMV-β-gal vectors were provided by Dr. Hiroshi Sasaki (RIKEN, Wako, Japan) and Dr. David Mangelsdorf (University of Texas Southwestern Medical School, Dallas, Texas), respectively. Cells were transfected with 200 ng of 8XGli1-BS-Luc and 50 ng of pCMV-β-gal using FuGENE HD transfection reagent in serum free medium. After 24 h, the culture medium was replaced and cells were treated with TNF-α (5 ng/mL) for 24 h. Cells were dissolved in 100 μL of reporter lysis buffer (Promega), and luciferase activity was determined using GLOMAX luminometer (Promega). Transcriptional activity was normalized to β-galactosidase activity.

Wound-Healing Cell Migration Assay. Cells were grown to confluence in six-well plates and then scratched with a pipet tip to create a gap. Wells were washed with PBS before adding fresh medium containing TNF-α (5 ng/mL) alone or with daidzein (30 μM). Cells were visualized under a light microscope (100× magnification) at 0 and 24 h. after treatment, and the relative wound area at these time points was calculated using Image Pro-plus 6.0 software (MediaCybernetics, Rockville, MD, USA).

Invasion Assay. The invasion assay was performed using Matrigel-coated invasion chambers (BD Biosciences, Bedford, MA, USA). The lower section was filled with 750 μL of culture medium containing 0.1% bovine serum albumin. Cells were placed in the upper section of the transwell plate in 500 μL of the same medium. After treatment with the compounds, cells in the lower and upper chambers were incubated for 24 h, fixed with methanol, and stained with hematoxylin and eosin for 10 and 5 min, respectively. After cells on the upper surface of the transwell plate were removed with a cotton swab, invading cells were observed under a light microscope, and cells in five randomly selected fields were counted.

Zymography Assay. The enzymatic activity of MMP-2 and -9 was determined by gelatin zymography. Conditioned medium was collected 24 h after treatment with a compound and was resolved by electrophoresis using a polyacrylamide gel containing 0.1% (w/v) gelatin. The gel was washed with 2.5% Triton X-100 to remove the SDS, rinsed with 50 mM Tris-HCl buffer (pH 7.6) containing 5 mM $CaCl_2$, 200 mM NaCl, and 0.02% Brij-35 (Merck, Darmstadt, Germany), and then incubated overnight at 37 °C. The following day, the gel was stained with 0.5% Coomassie Brilliant Blue R-250 (AMRESCO, Solon, OH, USA) solution containing 10% acetic acid and 20% methanol for 30 min, then destained with 7.5% acetic acid solution containing 10% methanol. The gelatinase activity was determined using EZ West Lumi Plus (ATTO).

Statistical Analysis. Data are presented as mean ± standard deviation (SD). Mean differences were assessed using the Student's *t*-test, and a *p*-value <0.05 was considered statistically significant.

dx.doi.org/10.1021/jf500231t | J. Agric. Food Chem. 2014, 62, 3759−3767

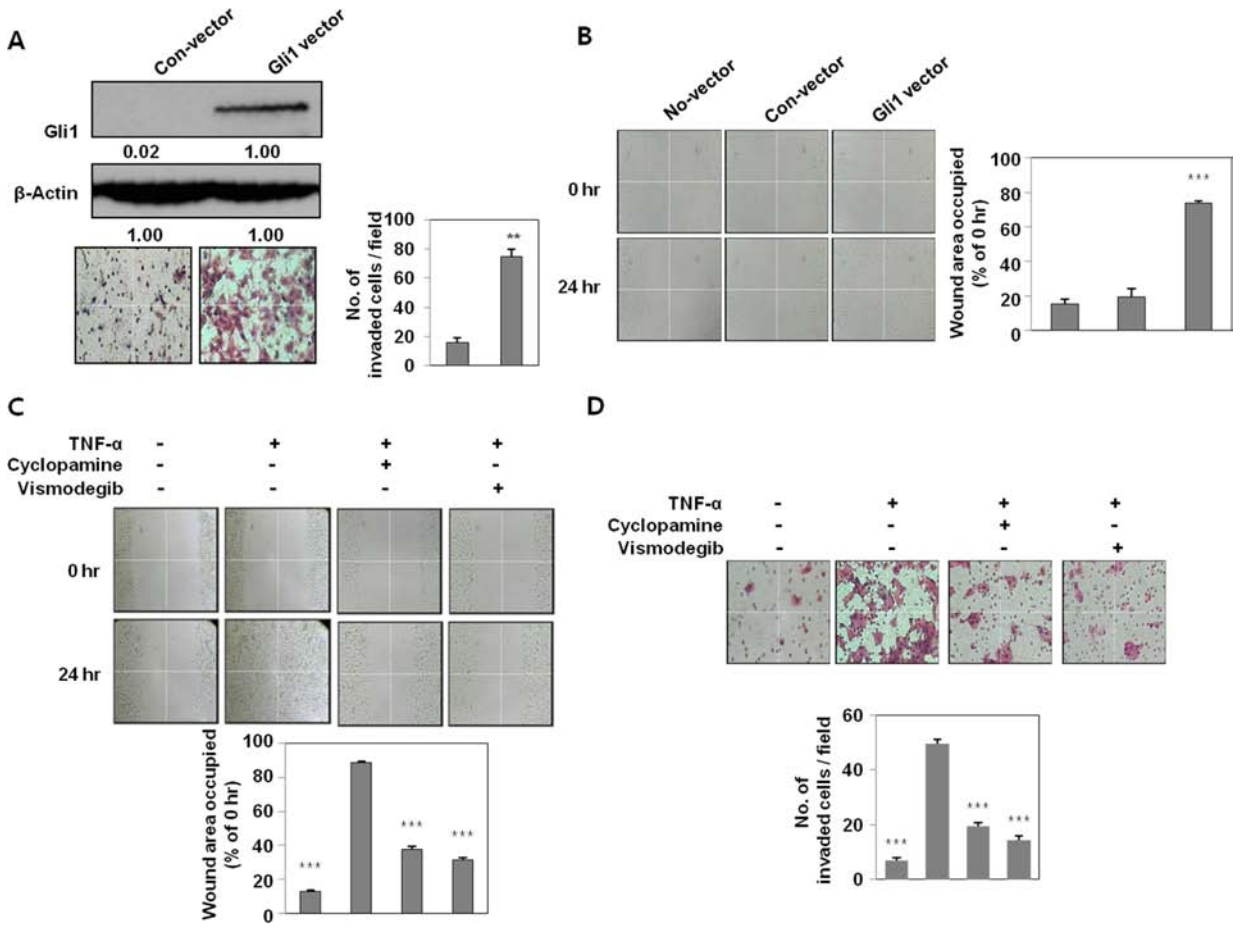

Figure 3. Effects of Gli1 overexpression on migration and invasion in MCF10DCIS.com human breast cancer cells. (A) Cells (7×10^5 cells in a 60 mm dish) were transfected with the pCMV-FLAG-mGli1 vector, and Gli1 overexpression was confirmed by Western blotting. (A) Invasion was determined by counting the number of invaded cells in the matrigel assay. Values represent means ± SD $^{**}p < 0.01$ compared to the control. (B) Cells were transfected with pCMV-FLAG-mGli1 vector, and the migration capabilities were determined by wound-healing assay. Values are means ± SD $^{***}p < 0.001$ compared to the control. (C) Migration was assessed in cells treated with TNF-α (5 ng/mL) alone or together with cyclopamine (10 μM) or vismodegib (10 μM) for 24 h. Values are means ± SD $^{***}p < 0.001$ compared to TNF-α treated group. (D) Cells (5×10^4 cells/well in a 24-well invasion chamber) were treated with TNF-α alone or together with cyclopamine or vismodegib for 24 h. Values represent means ± SD $^{***}p < 0.001$ compared to TNF-α treated group.

RESULTS

Daidzein Inhibits TNF-α Induced Cell Migration and Invasion in Estrogen Receptor (ER) Negative Basal-like MCF10DCIS.com Human Breast Cancer Cells. Because TNF-α is known to be involved in inducing cellular migration and invasion,[13,14] we first investigated whether daidzein can regulate them in MCF10DCIS.com cells. In a wound healing assay, the fraction of migrating cells increased from 19.5 to 84.9% upon treatment with TNF-α (5 ng/mL), which decreased to 34.6% in the presence of daidzein (30 μM, Figure 1A). The number of invading cells penetrating the artificial matrigel increased approximately 4-fold from 15 to 59 cells/field with TNF-α treatment, and daidzein (30 μM) significantly suppressed to near basal level, 25 cells/field (Figure 1B). To test whether TNF-α or daidzein may regulate the cell proliferation, the MTT assay was performed. The application of TNF-α and daidzein up to the concentrations of 10 ng/mL and 50 μM, as well as the cotreatment of TNF-α (5 ng/mL) with daidzein (30 μM), cyclopamine (10 μM), or vismodegib (10 μM), had no effects on cell viability. They also did not affect the cell viability.

TNF-α Activates the Hh Signaling Pathway in MCF10DCIS.com Human Breast Cancer Cells. The underlying mechanism of TNF-α on inducing invasion is reported to be through the NFκB signaling pathway.[13,14] Here, TNF-α treatment also induced the degradation of inhibitory κB-α (IκBα) and phosphorylation of NFκB p65 at Ser536. However, treatment with daidzein had no effect on IκBα expression and NFκB p65 phosphorylation (Figure 2A), indicating that daidzein inhibits cell migration and invasion via regulation of alternative pathways. Because it is reported that TNF-α activates the Hh signaling pathway in esophageal adenocarcinoma cells,[15] we examined whether TNF-α can modulate Hh signaling in MCF10DCIS.com breast cancer cells. As shown in Figure 2B, the treatment of TNF-α (5 ng/mL) induced the nuclear translocation of a Hh signaling mediator Gli1, which is confirmed by immunofluorescence staining (Figure 2C). Next, we performed the luciferase assay after transfecting 8X-Gli-BS-Luc to determine whether Gli1 transcriptional activity was correspondingly enhanced by TNF-α treatment. A 2-fold increase in Gli1-mediated transcription was observed in TNF-α treated cells compared to untreated control cells (Figure 2D). These results indicate that TNF-α activate the Hh/Gli1

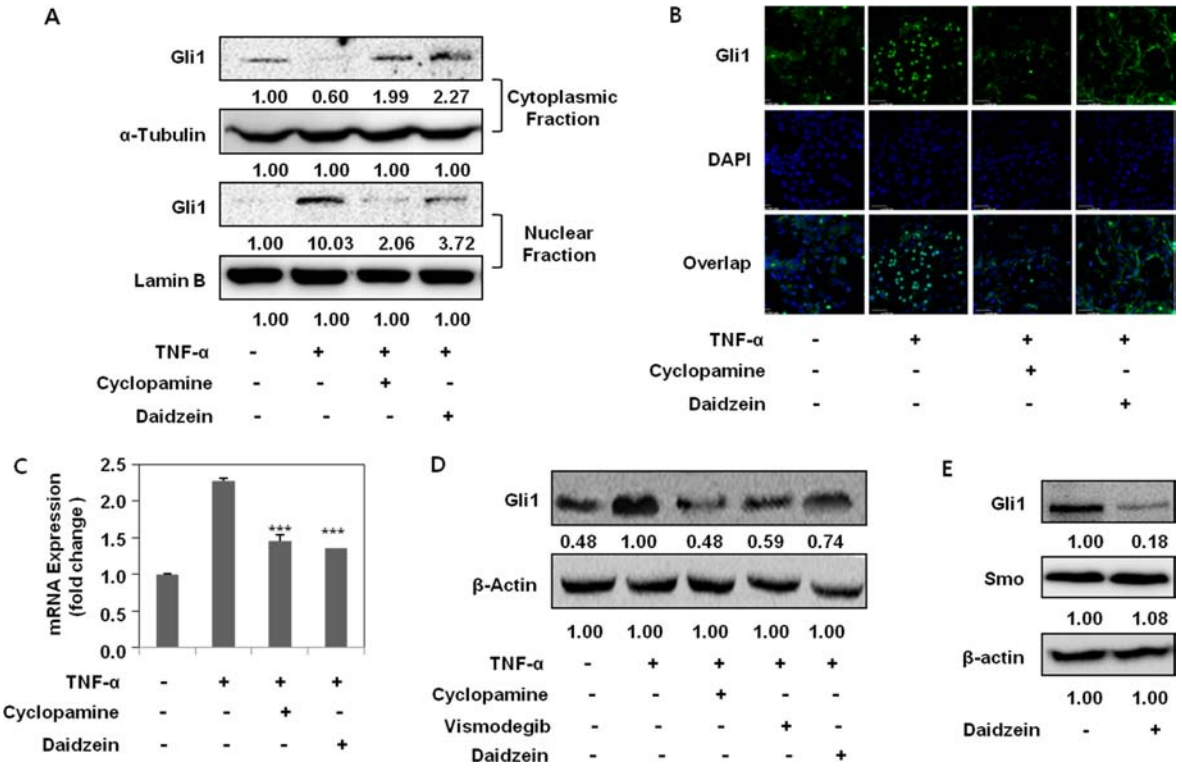

Figure 4. Effect of daidzein and Hh inhibitors on TNF-α induced Gli1 expression and translocation in MCF10DCIS.com human breast cancer cells and Ptch1(−/−) MEF cells fibroblast cells. (A) Cytosolic and nuclear fractions of cells treated with TNF-α (5 ng/mL) alone or together with daidzein (30 μM) or cyclopamine (10 μM) were separated, and Gli1 nuclear translocation was determined by Western blotting. (B) Cells (2×10^5 cells/well in a glass bottom dish) treated with TNF-α alone or together with daidzein or cyclopamine were probed with an antibody against Gli1, with nuclei stained with DAPI. Cells were visualized by confocal microscopy. (C) Cells (7×10^5 cells in a 60 mm dish) were treated with TNF-α alone or together with daidzein or cyclopamine for 12 h. Gli1 mRNA levels were analyzed by quantitative RT-PCR with GAPDH used as an internal control. Values represent means ± SD ***$p < 0.001$ compared to TNF-α treated cells. (D) Cells (7×10^5 cells in a 60 mm dish) were treated with TNF-α alone or together with daidzein (30 μM), cyclopamine, or vismodegib (10 μM) for 24 h. Gli1 protein expression was measured by Western blotting. (E) Cells (7×10^5 cells in a 60 mm dish) were treated with daidzein (30 μM) for 24 h in Ptch1(−/−) MEF cells, and the expression of Gli1 and Smo were determined.

signaling pathway in MCF10DCIS.com breast cancer cells through shifting subcellular localization of Gli1 into nucleus.

Gli1 Overexpression Induces the Cellular Invasion and Migration in MCF10DCIS.com Human Breast Cancer Cells. To examine the physiological role of Gli1 expression on the cellular invasiveness, the cells were transfected with a vector expressing full-length Gli1, and cell migration and invasion were assessed. The overexpression of Gli1 protein was confirmed by Western blotting (Figure 3A). Gli1 over-expresssion in MCF10DCIS.com cells exerted enhanced invasiveness compared to the control by increasing the invading cells from 4 cells/field to 33 cells/field (Figure 3A). In addition, the migration of the cells was enhanced from 15.2% to 73.5% (Figure 3B). Hh signaling inhibitors, cyclopamine and vismodegib, were tested to confirm the role of Hh signaling on the cellular invasion and migration. As shown in Figure 3C, both cyclopamine and vismodegib suppressed TNF-α induced cell migration from 98.9% to 36.7% and 33.3%, respectively, while invasiveness was reduced from 48 cells/field to 18 cells/field and 13 cells/field, respectively. Taken together, these findings strongly suggest that stimulation of migration and invasion in MCF10DCIS.com human breast cancer cells by TNF-α is at least in part through activation of Hh signaling.

Daidzein Blocks TNF-α Induced Gli1 Activation and Expression in MCF10DCIS.com Human Breast Cancer Cells. The studies showing that genistein can regulate Hh/Gli1 signaling in prostate cancer have been reported,[25,26] and we observed that Gli1 activation is highly linked to promoting the invasiveness of MCF10DCIS.com cells. Therefore, we determined the molecular regulatory mechanism of daidzein on Gli1 activity using the cytosolic/nuclear fractionation and confocal microscopy. As shown in Figure 4A,B, daidzein treatment at 30 μM suppressed the TNF-α induced translocation of Gli1 from the cytoplasm into the nucleus. The Hh signaling inhibitor, cyclopamine (10 μM), showed the similar inhibitory action in Gli1 nuclear translocation (Figure 4A,B). Because Gli1 is known as one of the Hh target genes,[27] we performed quantitative RT-PCR and Western blotting to check the expression level of Gli1. Daidzein, cyclopamine, and/or vismodegib significantly suppressed the mRNA and protein expression of Gli1 stimulated by TNF-α treatment (Figure 4C,D). In addition, daidzein significantly suppressed Gli1, but not Smoothened (Smo) protein expression in Ptch(−/−) cells, where Smo and Gli1 were overexpressed, suggesting that Gli1 in Hh signaling may be one of the molecular targets of daidzein in MCF10DCIS.com cells.

Daidzein Suppresses TNF-α Induced MMP-9 mRNA Expression and Its Enzymatic Activity in MCF10DCIS.-com Human Breast Cancer Cells. Tumor cell invasion is mainly derived from the enhanced activity of matrix metalloproteinases (MMPs), of which MMP-2 and -9 have been implicated in breast cancer progression.[28] Therefore, the effect

dx.doi.org/10.1021/jf500231t | J. Agric. Food Chem. 2014, 62, 3759−3767

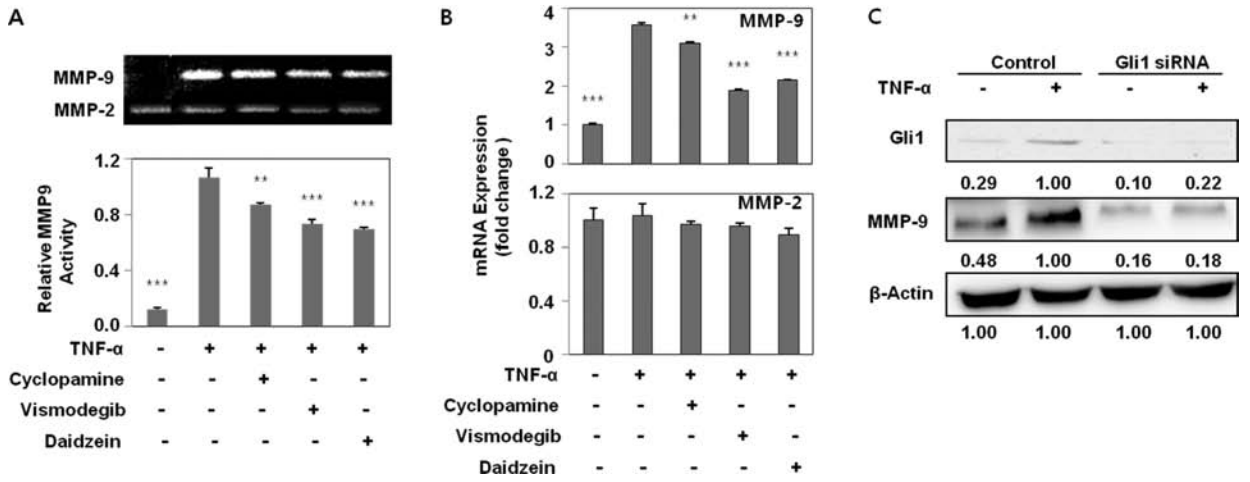

Figure 5. Effect of daidzein on TNF-α induced MMP-2 and -9 expression and activity in MCF10DCIS.com human breast cancer cells. (A,B) Cells (7×10^5 cells in a 60 mm dish) were treated with TNF-α (5 ng/mL) alone or together with daidzein (30 μM), cyclopamine (10 μM), or vismodegib (10 μM). (A) After 24 h, MMP enzymatic activity was determined by zymography. (B) After 12 h, MMP-2 and -9 mRNA expressions were determined by quantitative RT-PCR. Values are means ± SD $^{**}p < 0.01$, $^{***}p < 0.001$ compared to TNF-α treated cells. (C) Cells (7×10^5 cells in a 60 mm dish) were transfected with control siRNA and Gli1 siRNA as mentioned in Materials and Methods. After transfection, TNF-α (5 ng/mL) was treated and the protein expression of Gli1 and MMP-9 were determined.

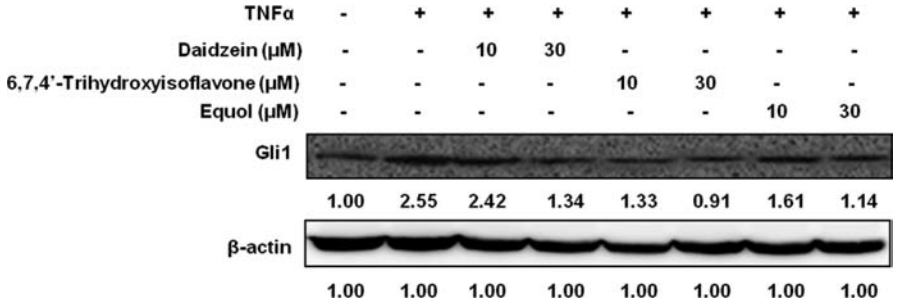

Figure 6. Effect of daidzein and its metabolites, 6,7,4′-trihydroxyisoflavone and equol, on TNF-α induced Gli1 expression in MCF10DCIS.com human breast cancer cells. Cells (7×10^5 cells in a 60 mm dish) were treated with TNF-α (5 ng/mL), alone or together with daidzein (10, 30 μM), 6,7,4′-trihydroxyisoflavone (10, 30 μM), or equol (10, 30 μM), and the protein expression of Gli1 was determined.

of TNF-α on the activity and expression of MMP-2 and -9 was assessed by zymography and quantitative RT-PCR, respectively. While TNF-α had little effect on MMP-2 activity and mRNA expression, MMP-9 activity was significantly suppressed by daidzein (30 μM), cyclopamine (10 μM), and vismodegib (10 μM) treatment (Figure 5A). In addition, TNF-α induced an upregulation of MMP-9 mRNA expression, and this effect was abrogated by daidzein and Hh signaling inhibitors (Figure 5B). To demonstrate the direct relationship between Gli1 and MMP-9 expression, we transfected Gli1 siRNA and checked the expression of MMP-9. As shown in Figure 5C, the enhanced expression of MMP-9 by TNF-α treatment was clearly abolished by inhibiting the expression of Gli1. These results indicate that TNF-α enhanced expression and enzymatic activity of MMP-9 through Hh/Gli1 signaling where the effects are significantly blocked by daidzein.

Daidzein Metabolites, 6,7,4′-Trihydroxyisoflavone and Equol, Reduce TNF-α Induced Gli1 Expression in MCF10DCIS.com Human Breast Cancer Cells. Daidzein is reported to be metabolized into equol by intestinal microflora and trihydroxyisoflavones by hepatic CYP enzymes.[29,30] To investigate in vivo physiological efficacy, we compared the effects of daidzein and its metabolites, 6,7,4′-trihydroxyisoflavone and equol, on inhibiting Gli1 expression. As shown in Figure 6, 6,7,4′-trihydroxyisoflavone and equol at 10 μM showed 48% and 37% suppression of TNF-α induced Gli1 expression, respectively, although daidzein did not exert the significant activity at the same concentration. This result indicates that in vivo metabolism of daidzein may enhance the physiological activities in regulating Hh signaling, which results in inhibiting the invasion and migration of mammary tumors.

■ DISCUSSION

Recent studies have demonstrated the regulatory effects of small botanical compounds on Hh signaling in different cancers.[25,26,31] Phytochemicals including genistein, curcumin, resveratrol, and others inhibited the proliferation of prostate cancer cells as well as tumor growth in transgenic adenocarcinoma of the mouse prostate (TRAMP) mice via modulation of Gli1 expression;[25] genistein was also shown to inhibit Hh signaling in prostate cancer cells, thereby suppressing their stem cell properties.[26] In breast cancer, cantharidin analogue, norcantharidin, suppressed Shh signaling, allowing cells to overcome multidrug resistance.[25,26,31] In the present study, application of nontoxic concentration of daidzein (30 μM, Figure 1C) significantly regulated Hh signaling by suppressing TNF-α induced Gli1 nuclear localization (Figure 4A,B) and genetic expressions into mRNA and protein (Figure 4C,D), resulting in the inhibition of TNF-α induced migration

and invasion (Figure 1A,B) in MCF10DCIS.com human breast cancer cells.

It was previously suggested that TNF-α enhances invasiveness in tumor cells by activating NF-κB signaling.[9,32] In breast cancer, an antimetastatic gene KiSS1 and costunolide identified from *Saussurea lappa* Clarke were both shown to inhibit MDA-MB-231 cell invasion stimulated by TNF-α through suppressing the NF-κB activation.[13,14] The present results confirmed that TNF-α enhanced migration and invasion in MCF10DCIS.com human breast cancer cells (Figure 1A,B), and promoted IκBα degradation, a key event for the activation of NF-κB signaling pathway (Figure 2A). Daidzein significantly suppressed TNF-α induced migration and invasion without affecting IκBα degradation and NFκB p65 phosphorylation (Figure 2A), suggesting that these effects were mediated through the regulating of an alternative pathway.

Hh signaling is known to play a crucial role in cell proliferation, differentiation, and organ patterning during embryogenesis and also in tumor initiation, progression, invasion, and metastasis during tumorigenesis.[18,27,33] In espophageal adenocarcinoma cells, TNF-α was shown to selectively activate Gli1.[15] The Hh signaling pathway is regulated by the secreted ligands such as Indian (Ihh), Desert (Dhh), and Sonic Hh (Shh) which can bind to its receptor, Patched1 (Ptch1). When Ptch1 is relieved by Hh ligand binding, Smo activates downstream intracellular signaling through zinc-finger transcriptional factors, Gli1, Gli2, and Gli3, and modulate the expression of target genes driving the development and maintenance of human cancers.[34] Dysregulation of the Hh signaling pathway, for instance by Gli overexpression, has been demonstrated to be critically involved in carcinogenesis. Ectopic expression of Gli1 or mutations resulting in overexpression of Gli1 was sufficient to induce the basal cell carcinoma,[35,36] while the loss of Gli1 function in Ptc1± mice showed significant reduction of medulloblastoma formation.[37] In addition, the involvement of Hh signaling via Gli family is reported in other malignancies such as colon and prostate cancers.[38,39] In this study, TNF-α enhanced the translocation of Gli1 into the nucleus (Figure 2B,C) and increased the transcriptional activity (Figure 2D), elucidating that TNF-α can activate the Hh signaling pathway in MCF10DCIS.com human breast cancer cells.

Several lines of evidence have demonstrated an association of aberrant Hh signaling with breast tumorigenesis.[40] Specifically, Gli1 was shown to be involved in regulating migration and invasion in estrogen independent breast cancer cells,[21,22] and the percentage of Gli1 nuclear translocation was correlated with the extent of the invasive phenotype.[20] In accordance with the previous studies, we found that the overexpression of Gli1 protein in ER negative MCF10DCIS.com cells significantly enhanced migration and invasion (Figure 3A,B). The Hh signaling inhibitors cyclopamine and vismodegib blocked the TNF-α induced migration and invasion (Figure 3C,D) and abolished the transcriptional activity through regulating the nuclear translocation of Gli1 and the expression of Hh signaling target genes (Figure 4). In addition, as one of the molecular targets of Hh signaling in tumor invasiveness and metastasis, MMP-9 was reported in gastric cancers.[41] We also found that knock-down of Gli1 using siRNA suppressed the expression of MMP-9 and abolished its expression induced by TNF-α (Figure 5C). These results strongly suggest that TNF-α enhance the invasiveness of MCF10DCIS.com human breast cancer cells through activating the Hh signaling pathway and enhancing the expression of MMP-9.

Isoflavones, which are naturally produced phytoestrogens, are reported to play a significant role in regulating the invasion in different cancers. For example, genistein and biochanin A decreased the invasive activity in U87MG human globlastoma cells,[42] and an isoflavan identified from licorice root, glabridin, suppressed migration, invasion, and angiogenesis by reducing integrin levels and inhibiting FAK/Src/AKT/Rho signaling in MDA-MB-231 cells.[43] In addition, genistein, daidzein, and a daidzein metabolite equol were reported to exert anti-invasive activity in DU145 prostate cancer cells[44] and in highly invasive MDA-MB-231 breast cancer cells by inhibiting the MMPs activity.[6,45] In line with the previous studies, we also found that treatment of daidzein and Hh signaling inhibitors significantly suppressed MMP-9 mRNA expression and its enzymatic activity without affecting MMP-2 (Figure 5A,B). These results suggest that MMP-9 regulated by daidzein could provide the mechanistic link between Hh signaling and breast cancer cell invasion.

It is also important to consider the in vivo metabolism of isoflavones. Intestinal microflora and liver CYP enzymes are known to metabolize the daidzein into equol and trihydroxyisoflavones, respectively,[29,30] indicating that daidzein, equol, and trihydroxyisoflavones can be present together in the blood system. Here, we found that daidzein metabolites, equol and 6,7,4′-trihydroxyisoflavone, exerted more significant activity in inhibiting TNF-α-induced Gli1 expression than daidzein (Figure 6), implying that we can expect the similar physiological effect of daidzein and its metabolites on regulation of in vivo invasion and migration in breast tumors.

To our best knowledge, the present study is the first report that TNF-α activated Hh signaling resulting in the stimulation of migration and invasion in ER-negative MCF10DCIS.com human mammary tumor cells which was effectively reversed by daidzein treatment. Although further studies are needed in order to understand the precise mechanisms in Hh signaling activation by TNF-α and identify the molecular targets of daidzien, the results we found may shed a new insight on the role of daidzein as possibly prevents from the mammary carcinogenesis, especially invasion and metastasis.

AUTHOR INFORMATION

Corresponding Author

*Phone: +82-31-670-3030. Fax: +82-31-675-4853. E-mail: hongjin@cau.ac.kr.

Author Contributions

[§]These authors contributed equally to this study.

Funding

This research was supported by Basic Science Research Program through the National Research Foundation of Korea (NRF) funded by the Ministry of Education, Science and Technology (2011-0013812) and by the Bio & Medical Technology Development Program of the National Research Foundation (NRF) funded by the Ministry of Science, ICT & Future Planning (2013M3A9C4078156).

Notes

The authors declare no competing financial interest.

ABBREVIATIONS USED

Hh, Hedgehog; Smo, Smoothened; Ptch1, Patched1; TNF-α, tumor necrosis factor-α; ER, estrogen receptor; MMP, matrix

metalloproteinase; NF-κB, nuclear factor-κB; mTOR, mechanistic target of rapamycin; DCIS, ductal carcinoma in situ; TRAMP, transgenic adenocarcinoma of the mouse prostate

REFERENCES

(1) Shu, X. O.; Zheng, Y.; Cai, H.; Gu, K.; Chen, Z.; Zheng, W.; Lu, W. Soy food intake and breast cancer survival. *JAMA, J. Am. Med. Assoc.* **2009**, *302*, 2437−2443.

(2) Ferlay, J.; Shin, H. R.; Bray, F.; Forman, D.; Mathers, C.; Parkin, D. M. Estimates of worldwide burden of cancer in 2008: GLOBOCAN 2008. *Int. J. Cancer* **2010**, *127*, 2893−2917.

(3) Banerjee, S.; Li, Y.; Wang, Z.; Sarkar, F. H. Multi-targeted therapy of cancer by genistein. *Cancer Lett.* **2008**, *269*, 226−242.

(4) Pugazhendhi, D.; Watson, K. A.; Mills, S.; Botting, N.; Pope, G. S.; Darbre, P. D. Effect of sulphation on the oestrogen agonist activity of the phytoestrogens genistein and daidzein in MCF-7 human breast cancer cells. *J. Endocrinol* **2008**, *197*, 503−515.

(5) Choi, E. J.; Kim, G. H. Antiproliferative activity of daidzein and genistein may be related to ERalpha/c-erbB-2 expression in human breast cancer cells. *Mol. Med. Rep.* **2013**, *7*, 781−784.

(6) Magee, P. J.; Allsopp, P.; Samaletdin, A.; Rowland, I. R. Daidzein, *R*-(+)equol and *S*-(−)equol inhibit the invasion of MDA-MB-231 breast cancer cells potentially via the down-regulation of matrix metalloproteinase-2. *Eur. J. Nutr.* **2013**, *53*, 345−350.

(7) Kessenbrock, K.; Plaks, V.; Werb, Z. Matrix metalloproteinases: regulators of the tumor microenvironment. *Cell* **2010**, *141*, 52−67.

(8) Mareel, M.; Constantino, S. Ecosystems of invasion and metastasis in mammary morphogenesis and cancer. *Int. J. Dev. Biol.* **2011**, *55*, 671−684.

(9) Balkwill, F. TNF-alpha in promotion and progression of cancer. *Cancer Metastasis Rev.* **2006**, *25*, 409−416.

(10) Balkwill, F. Tumor necrosis factor or tumor promoting factor? *Cytokine Growth Factor Rev.* **2002**, *13*, 135−141.

(11) Miles, D. W.; Happerfield, L. C.; Naylor, M. S.; Bobrow, L. G.; Rubens, R. D.; Balkwill, F. R. Expression of tumour necrosis factor (TNF alpha) and its receptors in benign and malignant breast tissue. *Int. J. Cancer* **1994**, *56*, 777−782.

(12) Hu, M.; Polyak, K. Molecular characterisation of the tumour microenvironment in breast cancer. *Eur. J. Cancer* **2008**, *44*, 2760−2765.

(13) Cho, S. G.; Li, D.; Stafford, L. J.; Luo, J.; Rodriguez-Villanueva, M.; Wang, Y.; Liu, M. KiSS1 suppresses TNFalpha-induced breast cancer cell invasion via an inhibition of RhoA-mediated NF-kappaB activation. *J. Cell Biochem.* **2009**, *107*, 1139−1149.

(14) Choi, Y. K.; Cho, S. G.; Woo, S. M.; Yun, Y. J.; Jo, J.; Kim, W.; Shin, Y. C.; Ko, S. G. *Saussurea lappa* Clarke-derived costunolide prevents TNF alpha-induced breast cancer cell migration and invasion by inhibiting NF-kappa B activity. *Evidence-Based Complementary Altern. Med.* **2013**, *2013*, 936257.

(15) Wang, Y.; Ding, Q.; Yen, C. J.; Xia, W.; Izzo, J. G.; Lang, J. Y.; Li, C. W.; Hsu, J. L.; Miller, S. A.; Wang, X.; Lee, D. F.; Hsu, J. M.; Huo, L.; Labaff, A. M.; Liu, D.; Huang, T. H.; Lai, C. C.; Tsai, F. J.; Chang, W. C.; Chen, C. H.; Wu, T. T.; Buttar, N. S.; Wang, K. K.; Wu, Y.; Wang, H.; Ajani, J.; Hung, M. C. The crosstalk of mTOR/S6K1 and Hedgehog pathways. *Cancer Cell* **2012**, *21*, 374−387.

(16) O'Toole, S. A.; Machalek, D. A.; Shearer, R. F.; Millar, E. K.; Nair, R.; Schofield, P.; McLeod, D.; Cooper, C. L.; McNeil, C. M.; McFarland, A.; Nguyen, A.; Ormandy, C. J.; Qiu, M. R.; Rabinovich, B.; Martelotto, L. G.; Vu, D.; Hannigan, G. E.; Musgrove, E. A.; Christ, D.; Sutherland, R. L.; Watkins, D. N.; Swarbrick, A. Hedgehog overexpression is associated with stromal interactions and predicts for poor outcome in breast cancer. *Cancer Res.* **2010**, *71*, 4002−4014.

(17) ten Haaf, A.; Bektas, N.; von Serenyi, S.; Losen, I.; Arweiler, E. C.; Hartmann, A.; Knuchel, R.; Dahl, E. Expression of the glioma-associated oncogene homolog (GLI) 1 in human breast cancer is associated with unfavourable overall survival. *BMC Cancer* **2009**, *9*, 298.

(18) Barakat, M. T.; Humke, E. W.; Scott, M. P. Learning from Jekyll to control Hyde: Hedgehog signaling in development and cancer. *Trends Mol. Med.* **2010**, *16*, 337−348.

(19) Kubo, M.; Nakamura, M.; Tasaki, A.; Yamanaka, N.; Nakashima, H.; Nomura, M.; Kuroki, S.; Katano, M. Hedgehog signaling pathway is a new therapeutic target for patients with breast cancer. *Cancer Res.* **2004**, *64*, 6071−6074.

(20) Souzaki, M.; Kubo, M.; Kai, M.; Kameda, C.; Tanaka, H.; Taguchi, T.; Tanaka, M.; Onishi, H.; Katano, M. Hedgehog signaling pathway mediates the progression of non-invasive breast cancer to invasive breast cancer. *Cancer Sci.* **2011**, *102*, 373−381.

(21) Kwon, Y. J.; Hurst, D. R.; Steg, A. D.; Yuan, K.; Vaidya, K. S.; Welch, D. R.; Frost, A. R. Gli1 enhances migration and invasion via up-regulation of MMP-11 and promotes metastasis in ERalpha negative breast cancer cell lines. *Clin. Exp. Metastasis* **2011**, *28*, 437−449.

(22) Thomas, Z. I.; Gibson, W.; Sexton, J. Z.; Aird, K. M.; Ingram, S. M.; Aldrich, A.; Lyerly, H. K.; Devi, G. R.; Williams, K. P. Targeting GLI1 expression in human inflammatory breast cancer cells enhances apoptosis and attenuates migration. *Br. J. Cancer* **2011**, *104*, 1575−1586.

(23) Li, Y.; Yang, W.; Yang, Q.; Zhou, S. Nuclear localization of GLI1 and elevated expression of FOXC2 in breast cancer is associated with the basal-like phenotype. *Histol. Histopathol.* **2012**, *27*, 475−484.

(24) Tao, Y.; Mao, J.; Zhang, Q.; Li, L. Overexpression of Hedgehog signaling molecules and its involvement in triple-negative breast cancer. *Oncol. Lett.* **2011**, *2*, 995−1001.

(25) Slusarz, A.; Shenouda, N. S.; Sakla, M. S.; Drenkhahn, S. K.; Narula, A. S.; MacDonald, R. S.; Besch-Williford, C. L.; Lubahn, D. B. Common botanical compounds inhibit the hedgehog signaling pathway in prostate cancer. *Cancer Res.* **2010**, *70*, 3382−3390.

(26) Zhang, L.; Li, L.; Jiao, M.; Wu, D.; Wu, K.; Li, X.; Zhu, G.; Yang, L.; Wang, X.; Hsieh, J. T.; He, D. Genistein inhibits the stemness properties of prostate cancer cells through targeting Hedgehog-Gli1 pathway. *Cancer Lett.* **2012**, *323*, 48−57.

(27) Katoh, Y.; Katoh, M. Hedgehog target genes: mechanisms of carcinogenesis induced by aberrant hedgehog signaling activation. *Curr. Mol. Med.* **2009**, *9*, 873−886.

(28) Ranogajec, I.; Jakic-Razumovic, J.; Puzovic, V.; Gabrilovac, J. Prognostic value of matrix metalloproteinase-2 (MMP-2), matrix metalloproteinase-9 (MMP-9) and aminopeptidase N/CD13 in breast cancer patients. *Med. Oncol* **2012**, *29*, 561−569.

(29) Kulling, S. E.; Honig, D. M.; Metzler, M. Oxidative metabolism of the soy isoflavones daidzein and genistein in humans in vitro and in vivo. *J. Agric. Food Chem.* **2001**, *49*, 3024−3033.

(30) Wang, X. L.; Hur, H. G.; Lee, J. H.; Kim, K. T.; Kim, S. I. Enantioselective synthesis of *S*-equol from dihydrodaidzein by a newly isolated anaerobic human intestinal bacterium. *Appl. Environ. Microbiol.* **2005**, *71*, 214−219.

(31) Chen, Y. J.; Kuo, C. D.; Chen, S. H.; Chen, W. J.; Huang, W. C.; Chao, K. S.; Liao, H. F. Small-molecule synthetic compound norcantharidin reverses multi-drug resistance by regulating Sonic hedgehog signaling in human breast cancer cells. *PLoS One* **2012**, *7*, e37006.

(32) Hagemann, T.; Robinson, S. C.; Schulz, M.; Trumper, L.; Balkwill, F. R.; Binder, C. Enhanced invasiveness of breast cancer cell lines upon co-cultivation with macrophages is due to TNF-alpha dependent up-regulation of matrix metalloproteases. *Carcinogenesis* **2004**, *25*, 1543−1549.

(33) Kasper, M.; Regl, G.; Frischauf, A. M.; Aberger, F. GLI transcription factors: mediators of oncogenic Hedgehog signalling. *Eur. J. Cancer* **2006**, *42*, 437−445.

(34) Cohen, M. M., Jr. The hedgehog signaling network. *Am. J. Med. Genet., Part A* **2003**, *123A*, 5−28.

(35) Dahmane, N.; Lee, J.; Robins, P.; Heller, P.; Ruiz i Altaba, A. Activation of the transcription factor Gli1 and the Sonic hedgehog signalling pathway in skin tumours. *Nature* **1997**, *389*, 876−881.

(36) Nilsson, M.; Unden, A. B.; Krause, D.; Malmqwist, U.; Raza, K.; Zaphiropoulos, P. G.; Toftgard, R. Induction of basal cell carcinomas

and trichoepitheliomas in mice overexpressing GLI-1. *Proc. Natl. Acad. Sci. U. S. A.* **2000**, *97*, 3438−3443.
(37) Kimura, H.; Stephen, D.; Joyner, A.; Curran, T. Gli1 is important for medulloblastoma formation in Ptc1± mice. *Oncogene* **2005**, *24*, 4026−4036.
(38) Agyeman, A.; Mazumdar, T.; Houghton, J. A. Regulation of DNA damage following termination of Hedgehog (HH) survival signaling at the level of the GLI genes in human colon cancer. *Oncotarget* **2012**, *3*, 854−868.
(39) Chen, M.; Carkner, R.; Buttyan, R. The hedgehog/Gli signaling paradigm in prostate cancer. *Expert Rev. Endocrinol. Metab.* **2011**, *6*, 453−467.
(40) Hatsell, S.; Frost, A. R. Hedgehog signaling in mammary gland development and breast cancer. *J. Mammary Gland Biol. Neoplasia* **2007**, *12*, 163−173.
(41) Yoo, Y. A.; Kang, M. H.; Lee, H. J.; Kim, B. H.; Park, J. K.; Kim, H. K.; Kim, J. S.; Oh, S. C. Sonic hedgehog pathway promotes metastasis and lymphangiogenesis via activation of Akt, EMT, and MMP-9 pathway in gastric cancer. *Cancer Res.* **2011**, *71*, 7061−7070.
(42) Puli, S.; Lai, J. C.; Bhushan, A. Inhibition of matrix degrading enzymes and invasion in human glioblastoma (U87MG) cells by isoflavones. *J. Neurooncol.* **2006**, *79*, 135−142.
(43) Hsu, Y. L.; Wu, L. Y.; Hou, M. F.; Tsai, E. M.; Lee, J. N.; Liang, H. L.; Jong, Y. J.; Hung, C. H.; Kuo, P. L. Glabridin, an isoflavan from licorice root, inhibits migration, invasion and angiogenesis of MDA-MB-231 human breast adenocarcinoma cells by inhibiting focal adhesion kinase/Rho signaling pathway. *Mol. Nutr. Food Res.* **2011**, *55*, 318−327.
(44) Zheng, W.; Zhang, Y.; Ma, D.; Shi, Y.; Liu, C.; Wang, P. (±)Equol inhibits invasion in prostate cancer DU145 cells possibly via down-regulation of matrix metalloproteinase-9, matrix metalloproteinase-2 and urokinase-type plasminogen activator by antioxidant activity. *J. Clin. Biochem. Nutr.* **2012**, *51*, 61−67.
(45) Kousidou, O. C.; Mitropoulou, T. N.; Roussidis, A. E.; Kletsas, D.; Theocharis, A. D.; Karamanos, N. K. Genistein suppresses the invasive potential of human breast cancer cells through transcriptional regulation of metalloproteinases and their tissue inhibitors. *Int. J. Oncol.* **2005**, *26*, 1101−1109.

but neither physical methods nor competitive binding studies were able to define a specific binding site.[16,19,20]

Further study of the interactions between a series of flavan-3-ols with HSA or BSA demonstrated a role for the galloyl ester D ring of the flavonoid (Figure 1a) in the formation of stable

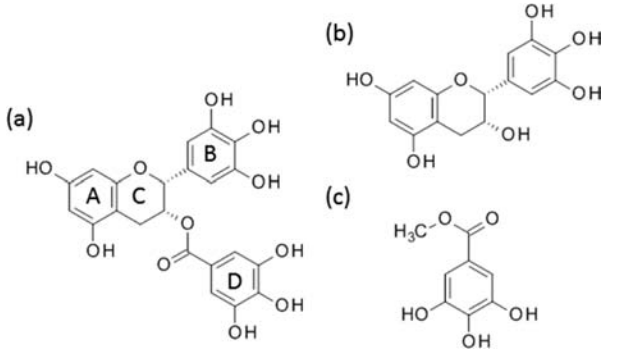

Figure 1. Structures of (a) epigallocatechin gallate (EGCg), (b) epigallocatechin (EGC), and (c) methyl gallate (MG). The A, B, C, and D rings of the flavan-3-ols are labeled in (a).

complexes.[18,20] These complexes could be covalently stabilized by reaction with cysteine or lysine residues.[12,17,21] Covalent modification of a specific cysteine residue by EGCg has been demonstrated for glyceraldehyde-3-phosphate dehydrogenase[22] but not for SA.

Only a few molecular docking studies have been performed for EGCg and SA. A docking study based on the crystal structure of HSA supports the experimental evidence for binding at both hydrophobic sites.[19] Docking studies with BSA have been hampered because the structure of the protein has not been available, but one study that used an amino acid sequence-based simulation for the BSA structure suggested preferred binding near Trp_{213}.[20] However, there is no strong experimental evidence for site-specific binding of BSA by EGCg.

In this study, we tested the model proposed by Skrt et al.[20] that describes a single binding site on BSA for EGCg. We used fluorescence, CD, and competitive binding studies to characterize the interaction and improved the molecular docking studies by using the recently established crystal structure for BSA.[15] Our data demonstrate that binding of EGCg induces a conformational change in BSA and requires the synergistic efforts of both the flavan-3-ol and galloyl moiety subunits. The former subunit binds to the entrance of the hydrophobic pocket, perhaps via covalent bonds, whereas the latter binds to the bottom mainly via hydrogen bonds. Our data provide insights into EGCg−SA interactions that are relevant to the human as well as the bovine protein.

MATERIALS AND METHODS

Materials. Bovine serum albumin (BSA) (fatty acid free, ≥96%), methyl gallate (MG), phenylbutazone (PB), and tolbutamide (TB) were purchased from Sigma-Aldrich Co. (St. Louis, MO, USA). EGCg (>95%) was provided by Lipton Tea Co. (Newark, NJ, USA). (−)-Epigallocatechin (EGC) (>95%) was purified from commercial tea (SilvaTeam, San Michele, Italy) by Sephadex LH20 column after tannase treatment and was characterized by HPLC and LC-MS (unpublished data). The chemical structures of the three phenolic compounds (EGCg, MG, EGC) are depicted in Figure 1.

All stock solutions were prepared by initially dissolving the compounds in water so there were no carrier solvent effects on ligand−protein interactions. BSA and EGCg concentrations were determined spectrophotometrically by their extinction coefficients (ε_{280} (BSA) = 43000 M^{-1} cm^{-1} and ε_{280}(EGCg) = 9700 M^{-1} cm^{-1}). Samples were diluted into 0.2 M sodium phosphate buffers (pH 3.0, 5.0, and 7.4) containing 0.1 M sodium chloride.

Fluorescence Spectroscopy and Quenching Constant Calculation. BSA was mixed with the desired amount of phenolic solution (EGC, EGCg, or MG), diluted to 5.0 mL and a final concentration of 3 μM protein with the appropriate phosphate buffer, vortexed for 10 s, immediately sparged with nitrogen for 20 min, and incubated for 1 h at 22 °C. The concentration of phenolic compound was varied from 0 to 25 μM in 5 μM increments. The stability of each phenolic compound under these conditions was checked by HPLC as described below.

The method of Soares et al.[23] was modified to evaluate the BSA fluorescence spectra between 290 and 500 nm with an LS55 luminescence spectrometer (PerkinElmer Inc., USA) with the excitation wavelength set at 280 nm. Slit widths for excitation and emission were 7.5 and 4.5 nm, respectively. Fluorescence intensity was corrected by eq 1 to compensate for the inner filter effect[24−26] due to sample absorbance at 280 and 350 nm.

$$F_{cor} = F_{obs} \times 10^{(Abs280+Abs350)/2} \quad (1)$$

F_{cor} and F_{obs} are, respectively, the corrected and observed fluorescence intensity. Abs280 and Abs350 represent the absorbances of samples in a 1 cm path length cell at the excitation and emission wavelengths. In this study, all fluorescence intensities were corrected prior to data analysis.

Fluorescence quenching is usually described by the Stern−Volmer equation (eq 2).[27] This classic model assumes that all fluorophores are equally accessible to the quencher.

$$F_0/F = 1 + K_{SV} \times [Q] = 1 + k_q \times \tau_0 \times [Q] \quad (2)$$

F_0 and F are the fluorescence intensities before and after the addition of the quencher, respectively. K_{SV} is the Stern−Volmer quenching constant, [Q] is the concentration of the quencher, k_q is the bimolecular quenching constant, and τ_0 is the native lifetime of the fluorophore. K_{SV} can thus be determined by linear regression of a plot of F_0/F against [Q].

Negative deviations from the Stern−Volmer equation are frequently found in the systems that have multiple fluorophores, such as BSA. The values of F_0/F, instead of increasing linearly with [Q] in the classic model, trend downward toward the x axis at high [Q], signifying differences in the accessibilities of fluorophores to the quencher.[27] The modified Stern−Volmer equation (eq 3) includes a factor for fractional accessibility f_a, allowing calculation for the modified SV constant K_a for systems with more than one fluorophore.

$$F_0/\Delta F = (1/(f_a \times K_a)) \times (1/[Q]) + 1/f_a \quad (3)$$

Time Domain Fluorescence Lifetime. Time-resolved fluorescence lifetime was measured with a TemPro 01 system (Horiba Jobin Yvon, USA), using a FluoroHub-B single-photon counting module with TBX detector. The excitation light (250 nm) was provided by a NanoLED light source, and the number of counts gathered in the channel of maximum intensity was 10000. The data were analyzed with CAS6 V6.6 decay analysis software. As BSA has two fluorophores with different lifetimes, eq 4 was used to describe the time-dependent decay of the biexponential fluorescence system.

$$F(t) = A + F_1 \times \exp(-t/\tau_1) + F_2 \times \exp(-t/\tau_2) \quad (4)$$

τ_1 and τ_2 are native fluorescence lifetimes for Trp_{134} and Trp_{213}, respectively, whereas F_1 and F_2 represent their relative amplitudes. Samples for the lifetime measurement were prepared in the same way as for the intensity measurements.

EGCg Stabilization and Competitive Binding. EGCg−SA interactions can be indirectly assessed by determining the BSA-mediated stabilization of EGCg.[12] We used that method to carry out competitive binding experiments between the drug PB or TB and EGCg. BSA (30 μM) was incubated at pH 7.4 with EGCg (25 μM)

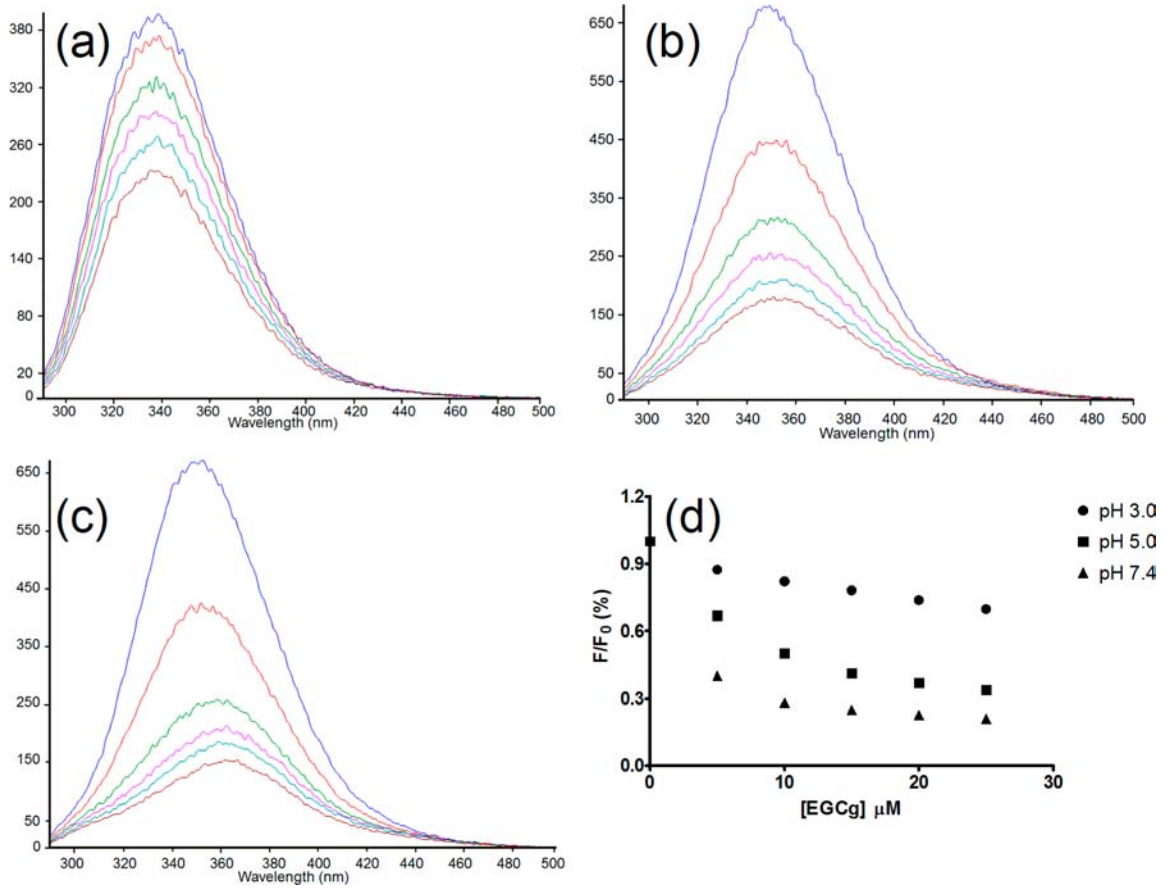

Figure 2. Quenching of 3 μM BSA by EGCg. Changes in the emission spectra of BSA were measured at (a) pH 3.0, (b) pH 5.0, and (c) pH 7.4. (d) The efficiencies of quenching were compared at pH 3.0 (●), 5.0 (■), and 7.4 (▲) by plotting the relative fluorescence intensity ($F/F_0 \times 100$) against EGCg concentration. All fluorescence intensities were corrected by eq 1 with a λ_{ex} = 280 nm and a λ_{em} = 350 nm, and the concentrations of EGCg were 0, 5, 10, 15, 20, and 25 μM.

and either PB or TB (0–900 μM) for 40 min at 37 °C before the amount of EGCg remaining was determined by high-performance liquid chromatography (HPLC) as described below. The amount of EGCg that remained in the samples at the end of the incubation was proportional to the amount of EGCg bound to the serum albumin.

HPLC Analysis. EGC, EGCg, and methyl gallate were quantitated with an Agilent 1100 series HPLC system equipped with a diode array detector (Agilent Technologies, USA). Separation was performed on a Zorbax Eclipse XD8 C8 column (5 μm, 4.6 × 150 mm i.d.) at a flow rate of 0.5 mL/min. Samples were eluted with a gradient of 0.1% trifluoroacetic acid in water (solvent A) and 0.13% trifluoroacetic acid in acetonitrile (solvent B) as follows: 0–10 min, 5% B; 10–20 min, 20% B; 20–30 min, 35% B; 30–34 min, 95% B. The elution profiles were recorded at 280 nm. Samples (10 μL) were injected into HPLC after filtration through 0.22 μm cellulose acetate spin filters. BSA solutions without EGCg were used as the background, and Agilent Chemstation A.09.03 software was used for peak integration.

Circular Dichroism Spectroscopy. The method of Nozaki et al.[28] was used in this study. A J-810 spectropolarimeter (Jasco Inc., Japan) was employed to collect CD spectra between 355 and 245 nm with a 1 mm path length cell. The system was purged with dry nitrogen gas during measurement at 298–301 K. CD spectra were built on accumulation of 12 cycles of scans with 0.5 nm data pitch, 1.0 nm bandwidth, 100 nm/min speed, and standard sensitivity.

All samples were prepared in 0.2 M sodium phosphate buffer at pH 7.4. The BSA concentration was 30 μM, whereas the concentrations of EGC, EGCg, and MG ranged from 0 to 200 μM. The spectrum of the buffer was subtracted from all samples to eliminate background noise. Induced CD spectra for BSA–EGCg samples (or EGC or MG) were obtained with eq 5.

$$\text{induced CD}_{\text{BSA-EGCg}} = \text{CD}_{\text{BSA-EGCg}} - (\text{CD}_{\text{BSA}} + \text{CD}_{\text{EGCg}}) \quad (5)$$

$\text{CD}_{\text{BSA-EGCg}}$ is the spectra of the BSA–EGCg sample, and CD_{BSA} and CD_{EGCg} represent the spectra of samples containing only BSA and EGCg.

Molecular Modeling. The crystal structure of BSA (code: 3 V03)[15] was downloaded from the Protein Data Bank. The 3D structure of EGCg (ChEBI:4806) was initially obtained from Chemical Entities of Biological Interest as a MOL file and converted afterward to a PDB file by OpenBabelGUI version 2.3.1. AutoDock Tool 4.2 v. 1.5.6rc3[29] was used to optimize both BSA and EGCg structures for docking experiments. For BSA, chain B and all water molecules were removed to produce a monomer structure. For EGCg, the structure was prepared by defaults setting with the gasteiger charges computed. Both BSA and EGCg structures had hydrogen atoms added.

The mechanism of the BSA–EGCg interaction was predicted on the molecular level with AutoDock Tool 4.2. The grid box was set up with 126 points in the *X*, *Y*, and *Z* dimensions, respectively. Each grid point had a spacing of 0.65 Å. Docking experiments were performed with default genetic algorithm parameters to generate 10 possible conformations with the lowest Gibbs free energy of binding.

RESULTS

Quenching of BSA Fluorescence Spectra by EGCg. Changes in pH affected the fluorescence spectrum of native BSA. At pH 3.0, the emission spectrum of BSA ranged from 290 to 480 nm with a maximum emission (λ_{em}) at 340 nm (Figure 2a). When the pH was increased to 5.0 or 7.4, the

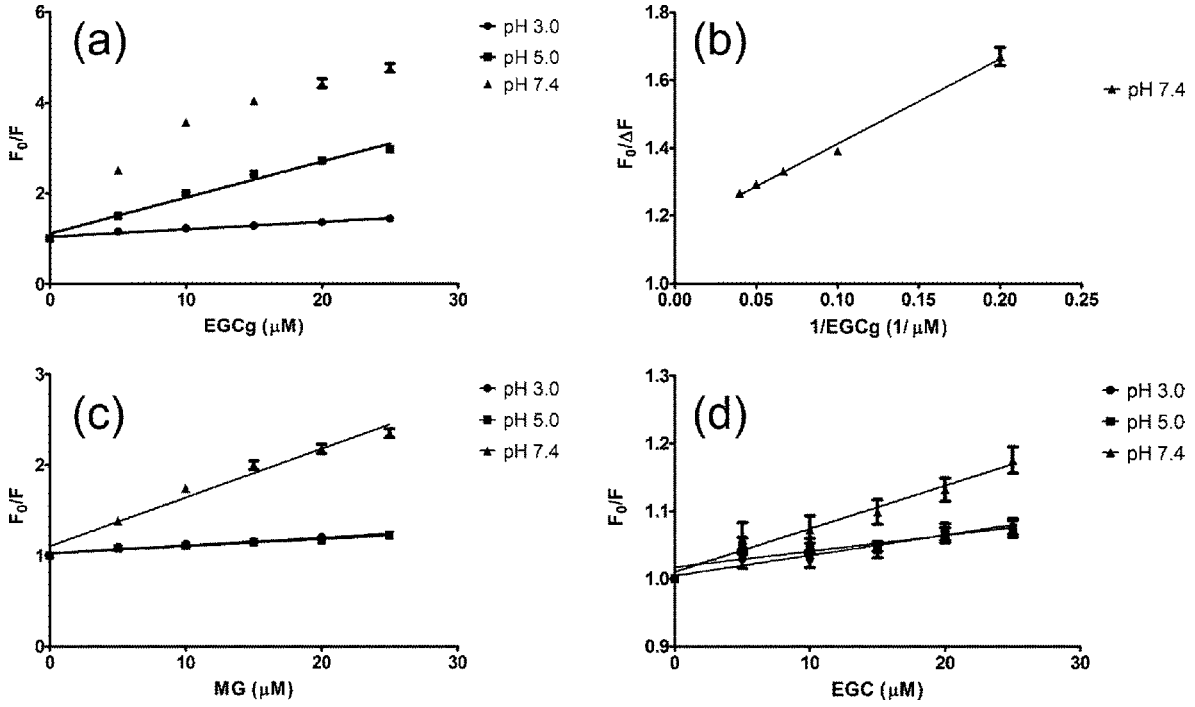

Figure 3. SV plots for the quenching of 3 μM BSA at pH 3.0 (●), pH 5.0 (■), and pH 7.4 (▲): (a) SV plots for EGCg-mediated quenching of BSA fluorescence; (b) modified SV plot for EGCg-mediated quenching of BSA fluorescence at pH 7.4; (c) SV plots for MG-mediated quenching of BSA fluorescence; (d) SV plots for EGC-mediated quenching of BSA fluorescence. All fluorescence intensities were corrected by eq 1 with a λ_{ex} = 280 nm and a λ_{em} = 350 nm, and the concentrations of EGCg were 0, 5, 10, 15, 20, and 25 μM.

spectrum was red-shifted to 280−500 nm with a λ_{em} at 350 nm (Figure 2b,c).

At all pH values tested, BSA fluorescence was affected by EGCg in a dose-dependent manner (Figure 2a−c). In acidic solutions (pH 3.0 and 5.0), addition of EGCg did not change the λ_{em} of BSA. However, λ_{em} was red-shifted from 350 to 365 nm at pH 7.4 when the EGCg concentration was increased from 0 to 25 μM. The efficacy of EGCg-induced quenching depended largely on the pH (Figure 2d). At pH 3.0, 25 μM EGCg quenched the BSA fluorescence to 68.4% of control value. At pH 5.0, the same concentration of EGCg brought the emission intensity down to 33.4% of control value. When the pH was increased to 7.4, only 20.7% of the control fluorescence remained in the presence of 25 μM EGCg.

The Stern−Volmer plots of EGCg-induced quenching of BSA fluorescence at pH 3.0 and 5.0 were linear, whereas at pH 7.4 the data were nonlinear, consistent with two fluorophores with different accessibilities[27] (Figure 3a). The data at pH 7.4 yielded a linear modified Stern−Volmer plot (Figure 3b). The Stern−Volmer constants (Table 1) were consistent with pH-dependent binding that is stronger at higher pH values.

Table 1. Stern−Volmer Constants Describing BSA Fluorescence Quenching by EGC, EGCg, or MG at pH 3.0, 5.0, and 7.4

	K_{SV} ($\times 10^4$ M^{-1})		
	pH 3.0	pH 5.0	pH 7.4
EGCg	1.6	8.0	461[a]
MG	0.85	0.81	5.4
EGC	0.30	0.23	0.64

[a]Estimated as K_a from modified SV plot.

Quenching of BSA Fluorescence Spectra by EGC or MG. MG did not quench as effectively as EGCg, but the pH dependence of quenching was similar to that of EGCg (Supporting Information Figure S1). The linear Stern−Volmer plots (Figure 3c) yielded K_{SV} values consistent with weaker interactions between BSA and MG compared to EGCg, but with a similar pH dependence (Table 1).

EGC was a very weak quencher under experimental conditions. After incubation with EGC, the spectra of BSA fluorescence were only slightly changed and the reduction of fluorescence intensity was small at λ_{em} (Supporting Information Figure S2). The linear SV plots (Figure 3d) yielded binding constants consistent with very weak, pH-independent interactions (Table 1).

BSA Fluorescence Lifetime. We used fluorescence lifetime to distinguish the effects of EGCg on Trp_{134}, a long-lifetime species, versus Trp_{213}, a short-lifetime species.[30,31] EGCg substantially diminished the fluorescence lifetime of Trp_{213} in a pH-dependent fashion, reducing the lifetime by about 50% at pH 5.0 or 7.4 (Table 2). At the same pH values, EGCg diminished the fluorescence lifetime of Trp_{134} about 15−25%

Table 2. Fluorescence Lifetime of Two Trp Residues in Bovine Serum Albumin in the Absence or Presence of 25 μM EGC, EGCg, or MG at pH 3.0, 5.0, and 7.4

	τ (ns)					
	pH 3.0		pH 5.0		pH 7.4	
	Trp_{134}	Trp_{213}	Trp_{134}	Trp_{213}	Trp_{134}	Trp_{213}
BSA	5.38	2.13	6.50	2.88	6.56	2.89
BSA + EGCg	5.24	1.86	5.49	1.43	4.92	1.34
BSA + MG	5.38	2.11	6.49	2.85	6.29	2.06
BSA + EGC	5.41	2.15	6.58	3.04	6.54	2.93

dx.doi.org/10.1021/jf500246m | J. Agric. Food Chem. 2014, 62, 3768−3775

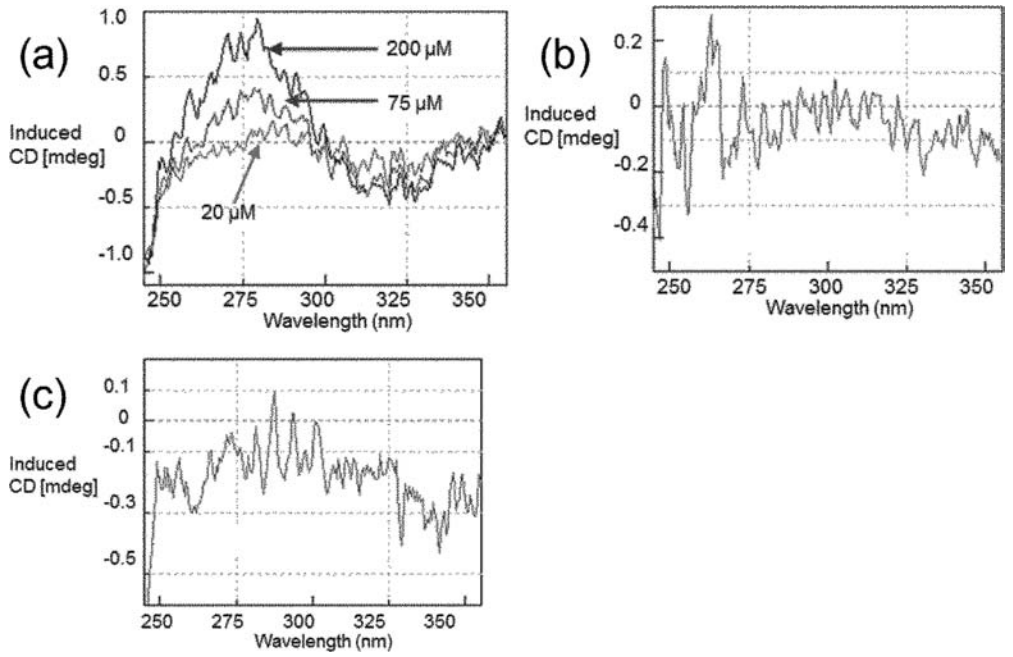

Figure 4. Induced CD spectra of 30 μM BSA in the presence of (a) EGCg, (b) EGC, and (c) MG. All induced CD spectra were obtained via eq 5. The concentrations of EGCg were 20, 75, and 200 μM, and the concentrations of EGC and MG were 200 μM.

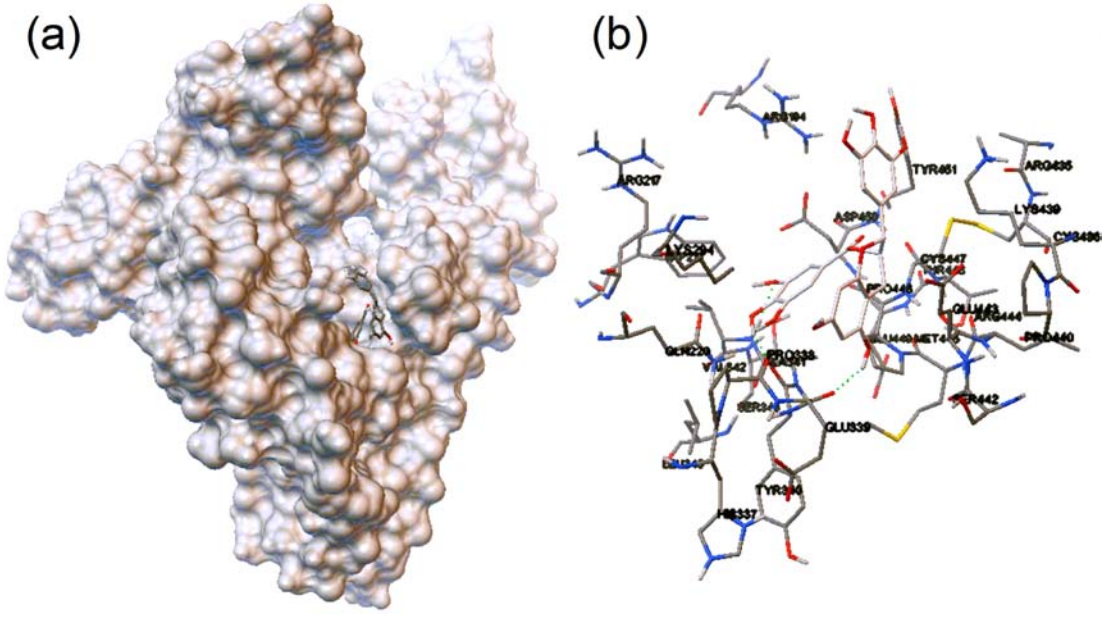

Figure 5. Docking simulation of EGCg for the hydrophobic pocket between subdomains IIA and IIIA of BSA: (a) complexation between BSA and EGCg; (b) amino residues involved in binding EGCg. The stick model indicates the involved amino acid residues and EGCg.

(Table 2). Methyl gallate diminished the lifetime of Trp_{213} only at pH 7.4 (30%), whereas EGC did not change the lifetime of either Trp at any pH (Table 2).

The bimolecular quenching constant k_q was estimated from the K_{SV} and the fluorescence lifetime data (eq 2) to distinguish static from dynamic binding. The upper limit of fluorescence lifetime is about 6 ns, so for the compounds we tested at pH 7.4, k_q ranges from about 10^{11} M^{-1} s^{-1} for EGC to about 10^{14} M^{-1} s^{-1} for EGCg.

Impact of Phenolics on the Conformation of BSA. In the presence of EGCg, the CD spectra of BSA were changed in a dose-dependent manner with positive amplitudes centering on 280 nm and negative amplitudes centering on 320 nm (Figure 4a). EGCg at 200 μM induced the largest change in the CD spectrum, giving ~0.8 mdeg at 280 nm and ~ −0.4 mdeg at 320 nm. MG or EGC did not significantly alter the conformation of BSA, as the amplitudes of the spectra fluctuated by only ~0.2 mdeg in the presence of 200 μM of either compound (Figure 4b,c).

EGCg Stabilization and Competitive Binding. In the absence of BSA, 29.2% of the EGCg remained after 40 min at pH 7.4, whereas with the addition of BSA 65.8% remained. We used the BSA-induced stabilization of EGCg as a surrogate for measuring binding of EGCg to BSA and did competitive

dx.doi.org/10.1021/jf500246m | J. Agric. Food Chem. 2014, 62, 3768−3775

binding assays with the drugs PB and TB. In competitive binding assays with 25 μM EGCg, the IC_{50} for PB was 450 μM, whereas that for TB was >900 μM (Supporting Information Figure S3).

Molecular Simulation of the Interaction between BSA and EGCg. The two docking models with the lowest free energies (−20.8 and −20.3 kJ mol^{-1}) put the Trp residues out of the effective quenching distance of EGCg. The molecular simulation with the next most favorable free energy (−17.9 kJ mol^{-1}) indicated that EGCg binds to the pocket between subdomains IIA and IIIA in the vicinity of Sudlow's site I. The galloyl moiety is projected toward the bottom, and the flavan-3-ol subunit is positioned in the entrance to the pocket (Figure 5a). The electrostatic interactions were weak between the protein−ligand pair, adding −0.46 kJ mol^{-1} to the binding energy, whereas van der Waals interactions, hydrogen bonds, and desolvation effects contributed −32.4 kJ mol^{-1}.

In this simulation model, the binding between EGCg and BSA consists of three hydrogen bonds and various hydrophobic interactions (Figure 5b). The hydrogen atom of the 3-hydroxyl group and the oxygen atom of the 4-hydroxyl group in the galloyl moiety (ring D, Figure 1a) and the hydrogen atom of the 5-hydroxyl group in ring A of the flavan-3-ol subunit of EGCg form hydrogen bonds with the atoms in the peptide backbone of Glu_{339}, Tyr_{340}, and Val_{342}. The simulation results suggest bond lengths of 2.2, 1.8, and 2.0 Å, respectively. EGCg interactions with other nearby amino acid residues, such as Trp_{134} and Pro_{446}, are dominated by van der Waals interactions and the hydrophobic effect. Electrostatic effects also contribute to EGCg binding, for example, by interactions between the electron-dense hydroxyl groups of the B and D rings with positively charged Arg_{194}, Lys_{294}, and Lys_{439}. The nitrogen atom of the Lys_{439} side chain is especially close to the oxygen atom of a B ring hydroxyl group (3.9 Å). In addition, the distance from the Trp_{213} residue to the galloyl moiety (6−10 Å) is shorter than the distance to the flavan-3-ol subunit (12−14 Å).

DISCUSSION

Our fluorescence studies demonstrated that EGCg interacts with BSA, with an apparent binding constant of about 4.6×10^{-5} M^{-1} at pH 7.4, similar to that obtained in other studies of EGCG−BSA interactions[20] and about 10-fold higher than that reported for EGCg−HSA.[18,19] However, the Stern−Volmer plot at pH 7.4 exhibited downward curvature, concave toward the x axis, at high EGCg concentrations. This phenomenon is often observed in systems with fluorophores that are unequally quenched due to their accessibility in the protein. Trp_{134}, which is responsible for 85% of the intrinsic fluorescence of BSA, is on the surface of the protein and is generally more accessible than Trp_{213}, which is buried in the hydrophobic pocket.[15,32] It has been proposed that EGCg binds near the buried Trp213 residue rather than at the surface-exposed Trp_{134},[20] and our data confirm that idea.

We used measurements of fluorescent lifetimes to more closely examine the binding site of EGCg. The two Trp residues can be distinguished by their fluorescent lifetimes, with lifetime of the surface Trp_{134} (around 5−6 ns) much longer than that of the buried Trp_{213} (around 2−3 ns) (Table 2). Fluorescence lifetime decay studies revealed large changes in the fluorescent lifetime of Trp_{213} induced by EGCg at pH 5 and 7 and demonstrate that EGCg does bind near this residue, deep in the hydrophobic pocket between domains IIA and IIIA. Our data support the binding site on BSA proposed by Skrt et al.[20] and demonstrate strong homology to binding with human serum albumin, which clearly involves the single, buried Trp_{214} on this protein.[18,19]

The pH dependence of the interaction between EGCg and BSA revealed by the magnitude of the fluorescence quenching is in accord with the importance of the hydrophobic pocket in the BSA−EGCg interaction. At pH 3.0, native BSA exhibits an expanded conformation by unfolding domains I and III,[14,33] disassembling the hydrophobic pocket and exposing Trp_{213} to a surface environment similar to that of Trp_{134}. EGCg-induced quenching effect was weak under this condition with small changes in the fluorescence lifetimes for both Trp residues, suggesting weak nonspecific binding. In addition, λ_{em} of the BSA fluorescence spectrum was neither red-shifted nor blue-shifted in the presence of EGCg, indicating a stable molecular environment around two Trp residues. When the pH is increased to 5.0 or 7.4, native BSA achieves its physiological conformation (or heart-shaped structure) with formation of the hydrophobic pocket,[14,33] and the affinity for EGCg increases, along with increased specific interaction at Trp_{213}. The λ_{em} of the BSA fluorescence spectrum was also gradually red-shifted with increasing EGCg concentration at pH 7.4 (Figure 2c), indicating possible changes in BSA conformation. We propose that EGCg specifically binds to BSA in the hydrophobic pocket between domains IIA and IIIA at physiological pH.

Our data demonstrate that both the flavan-3-ol and the galloyl group of EGCg are essential for site-specific, high-affinity binding. The apparent affinity of the flavan-3-ol EGC for BSA is only about 10^3 M^{-1}, slightly smaller than the value reported for several other flavan-3-ols in an earlier study.[23] The pH independence of EGC binding is consistent with non-specific interactions. MG has a somewhat higher affinity for BSA, and the pH dependence of the binding and the fluorescence lifetimes suggest that MG binds in the hydrophobic pocket near Trp_{213}. However, it binds an order of magnitude more weakly than EGCg. The CD spectra provide further evidence that EGCg binding requires both the flavan-3-ol and galloyl group. EGCg alters BSA conformation in a dose-dependent fashion, but neither MG nor EGC has this effect.

The molecular simulation model is consistent with our experimental work, demonstrating the favorable interaction of EGCg with the hydrophobic pocket of BSA. At pH 7.4, a positively charged microenvironment comprising Arg_{194}, Arg_{435}, Lys_{187}, Lys_{294}, and His_{438} is found at the entrance to the hydrophobic pocket, similar to that in human serum albumin.[19] These residues may be involved in the initial step of BSA−EGCg complexation by binding to the electron-dense B ring of the flavan-3-ol subunit.[22,34] In addition, the nitrogen atom of the Lys_{439} side chain is 3.9 Å from the oxygen atom in the B-ring hydroxyl group. Considering that the van der Waals radii of both nitrogen and oxygen atoms are about 1.6 Å,[35] it is plausible to assume that the distance between the surface of two atoms is <1 Å. Covalent binding to lysine has been invoked to explain the BSA-induced stabilization of EGCg,[12] and our data now suggest that the reaction might occur specifically between the B ring and Lys_{439} (Figure 5b). Covalent bonding in the hydrophobic pocket is supported by the values for the bimolecular quenching constant for the BSA−EGCg interaction, which were estimated to be 10^{14} $M^{-1}s^{-1}$ at pH 7.4, indicating static quenching typical of highly stable interaction such as covalent bonding. The B ring of EGCg is more reactive than the D ring,[17] providing additional indirect support for

covalent reaction as one component that stabilizes EGCg binding to BSA.

Although our model predicts that EGC binds in the neck of the pocket in a location similar to EGCg binding, our data showed that EGC binding was very weak and nonspecific. We speculate that in EGCg the galloyl ester is essential to position the flavan-3-ol for tight binding by its interaction at the base of the pocket. The model suggests that the critical role played by the galloyl moiety involves hydrogen bonds with the peptide backbone of two amino acids (Figure 5b), similar to the hydrogen bonds proposed by others.[18,20] Furthermore, the galloyl group appeared to rest between Arg_{217} and Asp_{450} in the bottom of the hydrophobic pocket, where it might disrupt a salt bridge and thus change the potential along the indole ring of Trp_{213}, leading to the red shift observed in the fluorescence spectra.[36]

Consistent with previous research,[11,12] our study showed that EGCg was stabilized by BSA at pH 7.4. We used that stabilization to monitor BSA−EGCg binding in competitive binding experiments with two drugs, PB and TB. The former binds Sudlow site I with an association constant of 6.2×10^5 M^{-1}, whereas the latter interacts more weakly and less specifically with BSA, binding to both Sudlow site I (8.7×10^4 M^{-1}) and Sudlow site II (0.81×10^4 M^{-1}).[37,38] PB effectively inhibited EGCg binding to BSA, consistent with our model in which EGCg binds to the hydrophobic pocket on BSA that overlaps with Sudlow site I. TB did not inhibit EGCg binding even at a 50-fold excess, supporting our model in which EGCg binds specifically and tightly in the hydrophobic pocket, not at other binding sites on BSA such as Sudlow II.

Our study indicated that EGCg binds selectively to the hydrophobic pocket on subdomains IIA and IIIA of BSA, overlapping with the Sudlow I binding site but also involving residues near Trp_{213} deep in the interior of the protein. The protein undergoes a slight conformational change upon polyphenol binding. The pH dependence of the binding is a consequence of the unfolding of BSA at low pH, destroying the hydrophobic pocket that is the EGCg binding site. The interaction requires both the flavan-3-ol and the galloyl moieties of the bioactive polyphenol and may involve site-specific covalent interaction at Lys_{439}. Lys_{195} occupies a position in the hydrophobic pocket of human SA that is similar to the position of Lys_{439} in BSA, leading us to suggest that it plays a similar role in stabilizing the HSA−EGCg interactions. Previous studies suggested a role for electrostatic binding at Lys_{195} in the interaction between human SA and EGCg,[19] but our model suggests covalent bond formation at this site. Formation of carbonyl groups on HSA during reaction with EGCg suggests that the reaction may involve Schiff base formation,[12] but direct evidence for that modification is not available. Further studies are needed to establish whether EGCg does covalently bind to a specific lysine residue in serum albumin and to further explore how SA−EGCg complexation controls both EGCg stability and redox reactivity in the bloodstream.

■ ASSOCIATED CONTENT

Supporting Information

Figures depicting additional fluorescence quenching data and competitive binding data. This material is available free of charge via the Internet at http://pubs.acs.org.

■ AUTHOR INFORMATION

Corresponding Author

*(A.E.H.) E-mail: hagermae@miamioh.edu. Phone: (513) 529-2827. Fax: (513) 529-5715.

Funding

Financial support was provided by USDA Specific Cooperative Agreement 58-1932-5-534 and by NIDDK R15DK069285 to A.E.H.

Notes

The authors declare no competing financial interest.

■ ACKNOWLEDGMENTS

We acknowledge Neil D. Danielson for the use of the LS55 luminescence spectrometer and C. Scott Hartley for the use of the TemPro 01 system.

■ ABBREVIATIONS USED

BSA, bovine serum albumin; CD, circular dichroism; EGC, (−)-epigallocatechin; EGCg, (−)-epigallocatechin-3-*O*-gallate; HPLC, high-performance liquid chromatography; MG, methyl gallate; PB, phenylbutazone; SV, Stern−Volmer; TB, tolbutamide

■ REFERENCES

(1) Weinreb, O.; Mandel, S.; Amit, T.; Youdim, M. B. H. Neurological mechanisms of green tea polyphenols in Alzheimer's and Parkinson's diseases. *J. Nutr. Biochem.* **2004**, *15*, 506−516.

(2) Velayutham, P.; Babu, A.; Liu, D. M. Green tea catechins and cardiovascular health: an update. *Curr. Med. Chem.* **2008**, *15*, 1840−1850.

(3) Setiawan, V. W.; Zhang, Z. F.; Yu, G. P.; Lu, Q. Y.; Li, Y. L.; Lu, M. L.; Wang, M. R.; Guo, C. H.; Yu, S. Z.; Kurtz, R. C.; Hsieh, C. C. Protective effect of green tea on the risks of chronic gastritis and stomach cancer. *Int. J. Cancer* **2001**, *92*, 600−604.

(4) Jagtap, S.; Meganathan, K.; Wagh, V.; Winkler, J.; Hescheler, J.; Sachinidis, A. Chemoprotective mechanism of the natural compounds, epigallocatechin-3-*O*-gallate, quercetin and curcumin against cancer and cardiovascular diseases. *Curr. Med. Chem.* **2009**, *16*, 1451−1462.

(5) Yang, C. S.; Hong, J. G. Prevention of chronic diseases by tea: Possible mechanisms and human relevance. *Annu. Rev. Nutr.* **2013**, *33*, 161−181.

(6) Singh, B. N.; Shankar, S.; Srivastava, R. K. Green tea catechin, epigallocatechin-3-gallate (EGCg): mechanisms, perspectives and clinical applications. *Biochem. Pharmacol.* **2011**, *82*, 1807−1821.

(7) Lambert, J. D.; Hong, J.; Lu, H.; Meng, X.; Lee, M.-J.; Yang, C. S. Bioavailabilities of tea polyphenols in humans and rodents. In *Protective Effects of Tea on Human Health*; Jain, N., Siddiqi, M., Weisburger, J., Eds.; Cabi Publishing: Wallingford, UK, 2006; pp 25−33.

(8) Tachibana, H.; Koga, K.; Fujimura, Y.; Yamada, K. A receptor for green tea polyphenol EGCg. *Nat. Struct. Mol. Biol.* **2004**, *11*, 380−381.

(9) Jovanovic, S. V.; Hara, Y.; Steenken, S.; Simic, M. G. Antioxidant potential of gallocatechins. A pulse radiolysis and laser photolysis study. *J. Am. Chem. Soc.* **1995**, *117*, 9881−9888.

(10) Zimeri, J.; Tong, C. Degradation kinetics of (−)-epigallocatechin gallate as a function of pH and dissolved oxygen in a liquid model system. *J. Food Sci.* **1999**, *64*, 753−758.

(11) Bae, M. J.; Ishii, T.; Minoda, K.; Kawada, Y.; Ichikawa, T.; Mori, T.; Kamihira, M.; Nakayama, T. Albumin stabilizes (−)-epigallocatechin gallate in human serum: binding capacity and antioxidant property. *Mol. Nutr. Food Res.* **2009**, *53*, 709−715.

(12) Ishii, T.; Ichikawa, T.; Minoda, K.; Kusaka, K.; Ito, S.; Suzuki, Y.; Akagawa, M.; Mochizuki, K.; Goda, T.; Nakayama, T. Human serum albumin as an antioxidant in the oxidation of (−)-epigallocatechin gallate: Participation of reversible covalent binding for interaction and stabilization. *Biosci., Biotechnol., Biochem.* **2011**, *75*, 100−106.

(13) Fanali, G.; di Masi, A.; Trezza, V.; Marino, M.; Fasano, M.; Ascenzi, P. Human serum albumin: from bench to bedside. *Mol. Asp. Med.* **2012**, *33*, 209−290.
(14) Kun, R.; Szekeres, M.; Dekany, I. Isothermal titration calorimetric studies of the pH induced conformational changes of bovine serum albumin. *J. Therm. Anal. Calorim.* **2009**, *96*, 1009−1017.
(15) Majorek, K. A.; Porebski, P. J.; Dayal, A.; Zimmerman, M. D.; Jablonska, K.; Stewart, A. J.; Chruszcz, M.; Minor, W. Structural and immunologic characterization of bovine, horse, and rabbit serum albumins. *Mol. Immunol.* **2012**, *52*, 174−182.
(16) Nozaki, A.; Hori, M.; Kimura, T.; Ito, H.; Hatano, T. Interaction of polyphenols with proteins: binding of (−)-epigallocatechin gallate to serum albumin, estimated by induced circular dichroism. *Chem. Pharm. Bull. (Tokyo)* **2009**, *57*, 224−228.
(17) Hagerman, A. E.; Dean, R. T.; Davies, M. J. Radical chemistry of epigallocatechin gallate and its relevance to protein damage. *Arch. Biochem. Biophys.* **2003**, *414*, 115−120.
(18) Trnkova, L.; Bousova, I.; Stankova, V.; Drsata, J. Study on the interaction of catechins with human serum albumin using spectroscopic and electrophoretic techniques. *J. Mol. Struct.* **2011**, *985*, 243−250.
(19) Maiti, T. K.; Ghosh, K. S.; Dasgupta, S. Interaction of (−)-epigallocatechin-3-gallate with human serum albumin: Fluorescence, fourier transform infrared, circular dichroism, and docking studies. *Proteins* **2006**, *64*, 355−362.
(20) Skrt, M.; Benedik, E.; Podlipnik, C.; Ulrih, N. P. Interactions of different polyphenols with bovine serum albumin using fluorescence quenching and molecular docking. *Food Chem.* **2012**, *135*, 2418−2424.
(21) Trombley, J. D.; Loegel, T. N.; Danielson, N. D.; Hagerman, A. E. Capillary electrophoresis methods for the determination of covalent polyphenol-protein complexes. *Anal. Bioanal. Chem.* **2011**, *401*, 1523−1529.
(22) Ishii, T.; Mori, T.; Tanaka, T.; Mizuno, D.; Yamaji, R.; Kumazawa, S.; Nakayama, T.; Akagawa, M. Covalent modification of proteins by green tea polyphenol (−)-epigallocatechin-3-gallate through autoxidation. *Free Radical Biol. Med.* **2008**, *45*, 1384−1394.
(23) Soares, S.; Mateus, N.; De Freitas, V. Interaction of different polyphenols with bovine serum albumin (BSA) and human salivary α-amylase (HSA) by fluorescence quenching. *J. Agric. Food Chem.* **2007**, *55*, 6726−6735.
(24) Kubista, M.; Sjoback, R.; Eriksson, S.; Albinsson, B. Experimental correction for the inner-filter effect in fluorescence-spectra. *Analyst* **1994**, *119*, 417−419.
(25) Ding, F.; Diao, J. X.; Sun, Y. Bioevaluation of human serum albumin-hesperidin bioconjugate: insight into protein vector function and conformation. *J. Agric. Food Chem.* **2012**, *60*, 7218−7228.
(26) Huang, Y.; Cui, L. J.; Wang, J. M.; Huo, K.; Chen, C.; Zhan, W. H.; Wang, Y. L. Interaction of aconitine with bovine serum albumin and effect of atropine sulphate and glycyrrhizic acid on the binding. *J. Lumin.* **2012**, *132*, 357−361.
(27) Lakowicz, J. R. *Principles of Fluorescence Spectroscopy*, 3rd ed.; Springer: New York, 2006.
(28) Nozaki, A.; Kimura, T.; Ito, H.; Hatano, T. Interaction of polyphenolic metabolites with human serum albumin: a circular dichroism study. *Chem. Pharm. Bull. (Tokyo)* **2009**, *57*, 1019−1023.
(29) Morris, G. M.; Huey, R.; Lindstrom, W.; Sanner, M. F.; Belew, R. K.; Goodsell, D. S.; Olson, A. J. Autodock4 and autodocktools4: automated docking with selective receptor flexibility. *J. Comput. Chem.* **2009**, *30*, 2785−2791.
(30) Patel, A. B.; Srivastava, S.; Phadke, R. S. Interaction of 7-hydroxy-8-(phenylazo) 1,3-naphthalenedisulfonate with bovine plasma albumin − spectroscopic studies. *J. Biol. Chem.* **1999**, *274*, 21755−21762.
(31) Tian, J. N. A.; Zhao, Y. C.; Liu, X. H.; Zhao, S. L. A steady-state and time-resolved fluorescence, circular dichroism study on the binding of myricetin to bovine serum albumin. *Luminescence* **2009**, *24*, 386−393.
(32) Militello, V.; Vetri, V.; Leone, M. Conformational changes involved in thermal aggregation processes of bovine serum albumin. *Biophys. Chem.* **2003**, *105*, 133−141.
(33) Peters, T. *All about Albumin: Biochemistry, Genetics and Medical Applications*; Academic Press: San Diego, CA, USA, 1996.
(34) Ishii, T.; Minoda, K.; Bae, M. J.; Mori, T.; Uekusa, Y.; Ichikawa, T.; Aihara, Y.; Furuta, T.; Wakimoto, T.; Kan, T.; Nakayama, T. Binding affinity of tea catechins for HSA: characterization by high-performance affinity chromatography with immobilized albumin column. *Mol. Nutr. Food Res.* **2010**, *54*, 816−822.
(35) Batsanov, S. S. Van der Waals radii of elements. *Inorg. Mater.* **2001**, *37*, 871−885.
(36) Vivian, J. T.; Callis, P. R. Mechanisms of tryptophan fluorescence shifts in proteins. *Biophys. J.* **2001**, *80*, 2093−2109.
(37) Ascenzi, P.; Bocedi, A.; Notari, S.; Menegatti, E.; Fasano, M. Heme impairs allosterically drug binding to human serum albumin sudlow's site I. *Biochem. Biophys. Res. Commun.* **2005**, *334*, 481−486.
(38) Joseph, K. S.; Anguizola, J.; Hage, D. S. Binding of tolbutamide to glycated human serum albumin. *J. Pharm. Biomed. Anal.* **2011**, *54*, 426−432.

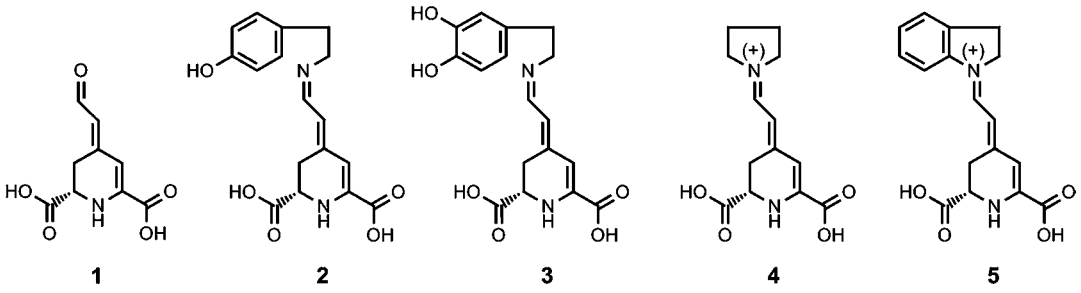

Figure 1. Structures for betalamic acid (**1**), the structural unit of betalains, and the derived pigments tyramine–betaxanthin (**2**), dopamine–betaxanthin (**3**), pyrrolidine–betaxanthin (**4**), and indoline–betacyanin (**5**).

betalamic acid and the amine groups present in the matrix surface, which can be displaced at mild conditions by the addition of amines. The novel material allows a one-step procedure for the formation of betaxanthins and betacyanins, thus significantly simplifying the process of obtaining semisynthetic betalains.

MATERIALS AND METHODS

Chemicals and Reagents. Red beet juice concentrate (B-50-WS) was purchased from CHR Hansen (Madrid, Spain). It is a liquid formulation obtained by squeezing out, concentrating, and pasteurizing the juice of beetroots, *B. vulgaris*. The starting matrix was Lewatit VP OC 1065 (surface area = 50 m^2/g), obtained from Sigma (Madrid, Spain). Solvents were from Merck (Madrid, Spain). HPLC grade acetonitrile was purchased from Labscan Ltd. (Dublin, Ireland). Other chemicals and reagents were obtained from Sigma (Madrid, Spain). Distilled water was purified using a Milli-Q system (Millipore, Bedford, MA, USA).

Development of the Betalamic Acid Support. Red beet juice concentrate was filtered by a 10 kDa ultrafiltration step (QuixStand System, GE Healthcare, Milwaukee, WI, USA). Betanin from this filtered solution was used as starting material. Basic hydrolysis (pH 11.4) of betanin in the presence of the starting matrix released betalamic acid (30 min, at room temperature) (**1**), which was then condensed with the primary amine present in the inorganic matrix after reaching pH 5.0. This bound betalamic acid to the surface of the support, which was then washed three times with 20 mM sodium acetate buffer, pH 5.0. The binding process was carried out in nitrogen atmosphere.

Semisynthesis of Betalains. For standard assays, the betalamic acid derivatized support (0.16 g) was incubated in a final volume of 0.5 mL with different amines, at the specified concentration, in 20 mM sodium acetate buffer, pH 5.0, or in 20 mM sodium phosphate buffer, pH 8.0, for tyramine. The reaction mixture for pyrrolidine–betaxanthin (**4**) and indoline–betacyanin (**5**) syntheses also contained 1.36 M sodium chloride to facilitate the release of the pigments from the support surface into the reaction medium. The formation of the corresponding betaxanthin or betacyanin was revealed by a characteristic deep yellow or violet color, respectively, in the reaction medium. After the indicated reaction time, an aliquot of 100 μL was removed for HPLC analysis. To analyze the formation of betalains with time, the reaction was scaled up to a final volume of 8 mL. The evolution of the reaction was monitored by HPLC analysis of the aliquots extracted at different times. For pH studies the reaction was carried out in 20 mM sodium acetate buffer (pH 3.5–5.5) or in 20 mM sodium phosphate buffer (pH 6.0–7.0). The buffer used for pH values >7.5 was 20 mM sodium borate.

Stability of the Betalamic Acid Support. The stability of the novel support was investigated by studying its capacity to synthesize betaxanthins as a function of storage time. Freshly made betalamic acid support (0.16 g) was incubated with 1.35 mM dopamine in 20 mM sodium acetate buffer, pH 5.0. An aliquot was taken after 40 min of reaction to analyze dopamine–betaxanthin (**3**) formation by HPLC. The betaxanthin concentration value obtained was considered as the starting capacity of synthesis. Then, the dopamine betaxanthin synthesis was performed with the support at different times throughout 6 months. Measurements were performed in triplicate, and mean and standard deviations were plotted. Relative synthetic activity was determined as the percentage of activity remaining after storage with respect to controls. Errors associated with the results provided were calculated on the basis of the residual standard deviations. The stability of the support was also studied by color assessment analysis. Color determinations of the immobilized betalamic acid support were made at 25 °C using a V-650 spectrophotometer equipped with an ISV-722 integrating sphere (Jasco Corp., Tokyo, Japan). The color parameters corresponded to the uniform CIELAB space (L^*, a^*, b^*, C^*, and $h°$) and were directly obtained from the apparatus software Spectra Manager version 2.07.[22]

Spectroscopy. A V-630 spectrophotometer (Jasco Corp., Tokyo, Japan), attached to a Tectron thermostatic bath (JP Selecta, Barcelona, Spain), was used for absorbance spectroscopy. For the quantitation of betalains, pigment concentration was evaluated by taking a molar extinction coefficient of ε = 48000/M/cm at 480 nm for betaxanthins and ε = 71000/M/cm at 524 nm for indoline–betacyanin.[7,23] Measurements were made in water at 25 °C.

HPLC Analysis. A Shimadzu LC-20AD apparatus (Kyoto, Japan) equipped with an SPD-M20A photodiode array detector (PDA) was used for analytical HPLC separations. Reversed phase chromatography was performed with a 250 × 4.6 mm Luna C-18(2) column packed with 5 μm particles (Phenomenex, Torrance, CA, USA). Gradients were formed with two solvents, A and B. Solvent A was H_2O with 0.05% trifluoroacetic acid (TFA); solvent B was acetonitrile with 0.05% TFA. A linear gradient was performed from 5 to 35% B for 35 min. The flow rate was 1 mL/min, operated at 25 °C. Injection volume was 20 μL.[24] All assays were performed in triplicate, and mean and standard deviations were plotted. Errors associated with the results provided were calculated on the basis of the residual standard deviations.

Scanning Electron Microscopy (SEM). Particle morphology was evaluated by SEM. Powders were attached to pieces of double-sided adhesive tape mounted on SEM stubs, coated with gold under vacuum using a SEM coating system by Bio-Rad Polaron Division and examined with a JSM-6100 (JEOL, Tokyo, Japan) scanning electron microscope operated at 15 kV. Images were analyzed using the open source image analysis software ImageJ (National Institutes of Health, NIH, Bethesda, MD, USA). Briefly, images were calibrated and, after that, an interactive measurement of the spheres was carried out. Micrographs were obtained with an Inca Oxford Image capture system (Oxford Instruments, Abingdon, UK).

RESULTS AND DISCUSSION

Development of a Betalamic Acid Derivatized Support. Betalamic acid (**1**) is the structural and bioactive unit of plant pigments betalains and the starting point for their formation both in vivo and in vitro. The production of individual compounds implies a purification of the acid, which leads to multistep procedures with low yields.[17,20,21] The aim of this work is the development of a novel support derivatized

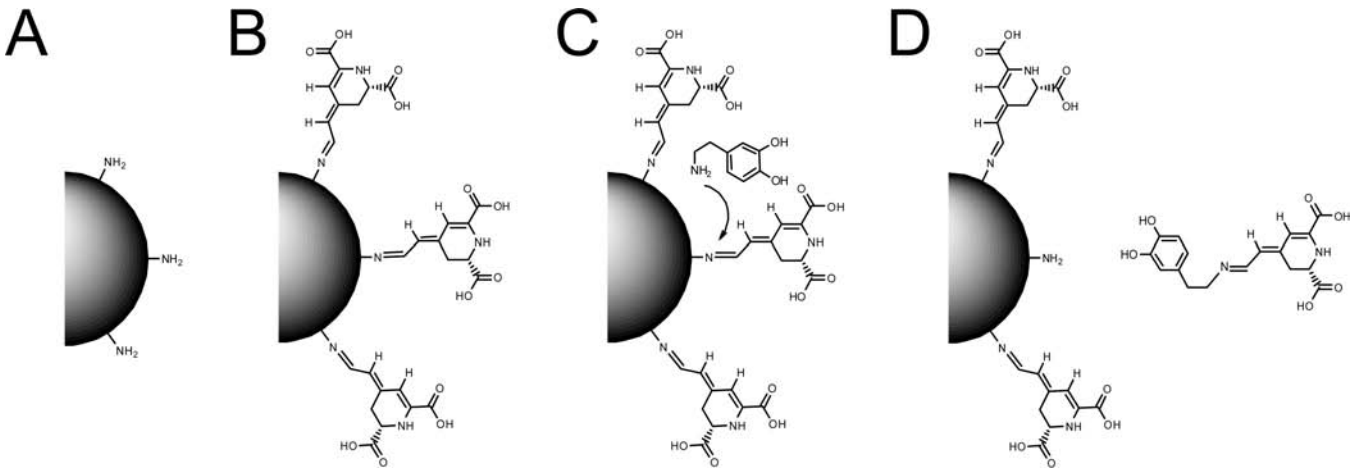

Figure 2. Schematic overview for the betalamic acid derivatized support and the surface reaction leading to pigment synthesis, exemplified for dopamine-derived betaxanthin (**3**): (A) starting material containing primary amine groups; (B) betalamic acid derivatized support; (C) amine attack to betalamic acid; (D) synthesis and concomitant release of the pigment.

with betalamic acid suitable for the synthesis of betalains. The basis of the proposed process is summarized in Figure 2.

First, betalamic acid is obtained in the presence of a resin that contains free primary amine groups. Given the reactivity of the aldehyde group of the acid, it was proposed that an imine would be formed with the amine of the support, thus causing the immobilization of betalamic acid to the resin. Betalamic acid was obtained by basic hydrolysis of purified betanin, the main pigment present in red beet root (*B. vulgaris*) extracts by the addition of ammonia.[21] Hydrolysis was carried out in the presence of the easily available cross-linked polystyrene resin VP OC 1065 (Lewatit), which contains primary amine groups, at room temperature and under nitrogen atmosphere. Under these experimental conditions betalamic acid was released from betanin. Neutralization with acetic acid was carried out after hydrolysis to promote the reaction of betalamic acid with the amines through a Schiff condensation reaction. This involved a change of color of the resin spheres from pale yellow to deep yellow, indicating the derivatization with betalamic acid. The resin was washed with 20 mM sodium acetate buffer, pH 5.0, until the washing solution was colorless. It was then allowed to dry at room temperature.

The binding reaction of betalamic acid to the matrix was confirmed by UV−vis spectrophotometry using an integrating sphere. This allowed the analysis of the color changes in the solid matrix. Figure 3A shows the spectrum obtained for the resin after betalamic acid reaction. The maximum wavelength was determined as λ_{max} 486 nm. Both the shape and maximum wavelength corresponded to the typical results of a betaxanthin, the yellow betalains formed by condensation of betalamic acid with simple amines.[7,23] Thus, the reaction between betalamic acid and the amine groups of the resin generated a solid support with the spectroscopic properties of a pseudobetaxanthin. The novel support was further characterized by SEM to analyze the effect of the treatment on the particle surface. Figure 3B shows a SEM microphotograph of the resin after betalamic acid immobilization. Particle analysis and sphericity were analogous to the results obtained for the resin without betalamic acid, indicating that the morphology of the resin was not altered by the immobilization process. Analysis of the particle morphology shows that the resin spheres possess a mean particle diameter of 0.59 ± 0.08 mm. SEM analysis also

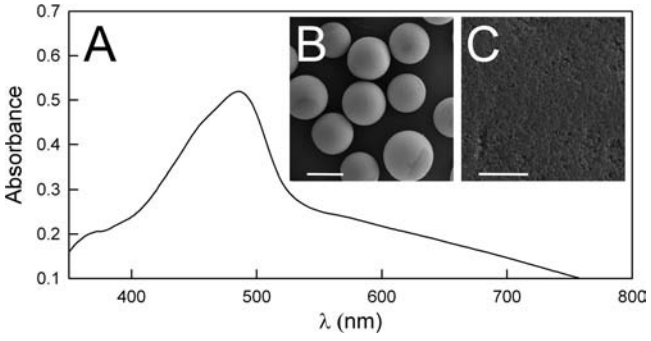

Figure 3. Spectroscopic and microscopic characterization of the betalamic acid derivatized support: (A) UV−vis spectrum for the solid matrix showing the characteristic spectrum for betaxanthins (spectrum was obtained with an integrating sphere after the subtraction of the spectrum for the basal absorbance of the starting matrix); (B) SEM image obtained for the spheres that constitute the novel matrix (scale bar = 500 μm); (C) closer SEM view showing the surface of the spheres (scale bar = 5 μm).

shows that the surface porosity of the spheres was not affected by the process (Figure 3C).

Thus, a matrix derivatized with betalamic acid was obtained for the first time. It is proposed that this support could be used for betalains synthesis simply by adding the selected amine. The reaction of betalamic with the amine would lead to the release of the pigment, as shown graphically in Figure 2.

Semisynthesis of Betalains. To test the concept of easy synthesis of betalains through the novel betalamic acid derivatized support, the resin was used for the production of different pigments. Four amines were selected as models to demonstrate this application: tyramine, dopamine, pyrrolidine, and indoline. The choice of tyramine and dopamine was based on the bioactive potential of their corresponding betaxanthins. Tyramine−betaxanthin (**2**) and dopamine−betaxanthin (**3**) possess high antioxidant and free radical scavenging activities due to the presence of phenolic hydroxyl groups (Figure 1).[25] They are natural pigments, also known by the trivial names miraxanthin III, and miraxanthin V, respectively, which were originally described in flowers of *Mirabilis jalapa* but are also present in the species *Celosia argentea* and *B. vulgaris* among others.[26−28] Structurally, these betaxanthins are derived from

primary amines and possess open structures. In contrast, pyrrolidine is a secondary amine, and the pigment derived (**4**) possesses a ring attached to the betalamic acid moiety while maintaining properties of a betaxanthin (Figure 1). Indoline is also a secondary amine and possesses the same ring of pyrrolidine plus an additional aromatic ring (Figure 1). This additional electron resonance system promotes a bathochromic shift in the absorbance spectrum, which makes the derived betalain violet. The indoline-derived pigment (**5**) is the simplest molecule with betacyanin properties and, thus, the betacyanin defining structure.[7]

When colorless solutions containing the individual model amines were added to the novel support, the solutions turned yellow in the case of tyramine, dopamine, and pyrrolidine and purple in the case of indoline. In contact with the support, the amines yielded the corresponding pigments through a Schiff condensation reaction with the aldehyde group of betalamic acid, thus releasing the synthesized betalain as postulated in Figure 2C. All pigments were characterized by HPLC-DAD, confirming the expected identity and the absence of additional coloring molecules. Retention times for tyramine-derived (**2**) and dopamine-derived (**3**) betaxanthins were 18.3 and 16.5 min, respectively, whereas for pyrrolidine-derived (**4**) and indoline-derived (**5**) betalains retention times were 15.2 and 23.6 min, respectively. The optimal experimental conditions for the novel synthesis on support were investigated by measuring the pigment generation by HPLC-DAD analysis of the solutions. Figure 4 shows the evolution of the synthesis reaction with time for each amine assayed at 25 °C. The temperature of 4 °C was also assayed in this study under the same conditions (data not shown). At this temperature the concentration of product obtained was lower than at 25 °C in all cases. Analysis of the time courses obtained at 25 °C determined the optimal times of reaction at this temperature, which varied depending on the amine used. The highest pyrrolidine-derived pigment (**4**) concentration was reached after only 4 min of reaction. For the rest of the compounds the estimated optimum reaction times were 20, 40, and 60 min for indoline-derived (**5**), dopamine-derived (**3**), and tyramine-derived (**2**) betalains, respectively. This variation may result from the different affinities of betalamic acid toward the amine groups of the support and the amines added in solution. This apparent affinity was greater for pyrrolidine. The existence of a maximum in all of the time courses presented indicates the existence of two processes taking place at the surface of the spheres. One is the synthesis and concomitant release of the pigments as discussed, causing the appearance of betalains in the medium immediately after the addition of the amines. The other is responsible for withdrawing the pigments obtained from the medium after their formation, so causing the decrease of concentration after synthesis in the solution. Pigment stability in the medium was confirmed by repetitive analysis of the pigment concentration after separation from the matrix, with no appreciable loss of the betalains (results not shown). Pigment concentration decreased only after the maximum times described above in the presence of the matrix, thus indicating an adsorption phenomenon. The nature of the adsorption process might be unspecific, but an electrostatic contribution was investigated. The addition of sodium chloride to the reaction mixture in the case of the pyrrolidine-derived betaxanthin (**4**) and the indoline-derived betacyanin (**5**) mitigated the electrostatic contribution of the positive charge of the pigments and facilitated the release of the resulting

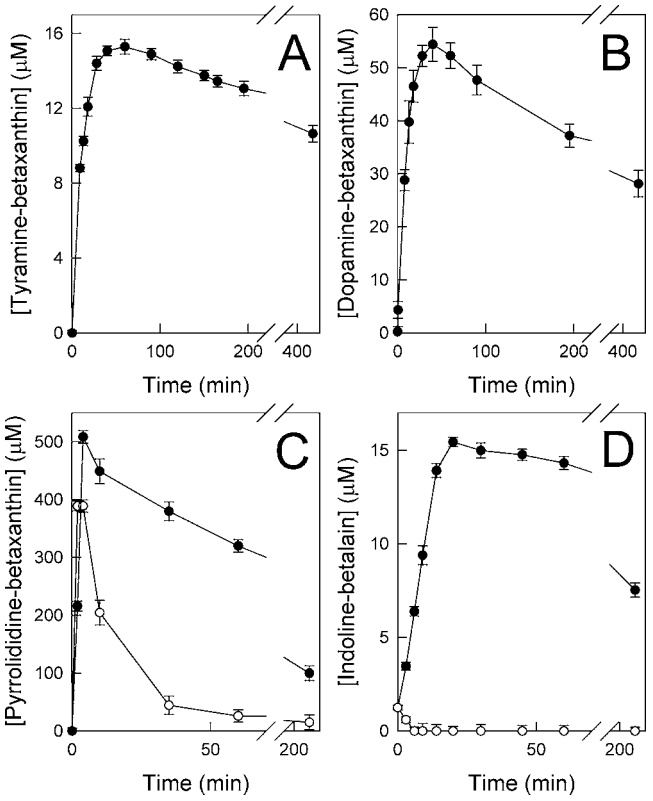

Figure 4. Time course for the evolution of pigment formation in reaction media containing the betalamic acid derivatized support at 25 °C and different amines; (A) tyramine, 0.85 M; (B) dopamine, 1.35 M; (C) pyrrolidine, 0.6 M; (D) indoline, at saturating concentration. In panels C and D, results are shown in the presence (●) and in the absence (○) of 1.36 M NaCl. Experimental conditions are detailed under Materials and Methods.

betalains from the resin surface into the solution (Figure 4C,D). This increased the amount of pigment obtained from the reaction on the novel material. An optimal concentration of 1.36 M NaCl was determined, with values below this causing a lower pigment release.

The effect of pH was also investigated in the pigment synthesis from the derivatized support. Figure 5 shows the results obtained when the pH of the amine-containing solution was varied from 3.5 to 9.0. Only in the case of dopamine was the range limited to 6.5 to avoid the catecholic substructure oxidation at higher pH values. Tyramine−betaxanthin (**2**) synthesis reached a maximum at pH 8.0 (Figure 5A), which was then selected for standard assays with this amine. However, as can be seen for the rest of amines, the pH variation did not significantly affect the synthesis. A pH of 5.0 was preferred to more alkaline values because of the higher stability of the compounds.[29,30]

Betalain synthesis was also dependent on the amine concentration. As shown in Figure 6, an increase in the concentrations of the amines resulted in a general increase in the formation and release of the derived betalains to the solution. However, the substrate concentration effect depended on the nature of each amine. Increasing concentrations of tyramine (Figure 6A) and dopamine (Figure 6B) led to a higher level of the derived betaxanthins in the solution. However, their concentrations could not be raised further because of the relatively low solubility of these compounds. In the case of pyrrolidine (Figure 6C), betaxanthin production

dx.doi.org/10.1021/jf500506y | J. Agric. Food Chem. 2014, 62, 3776−3782

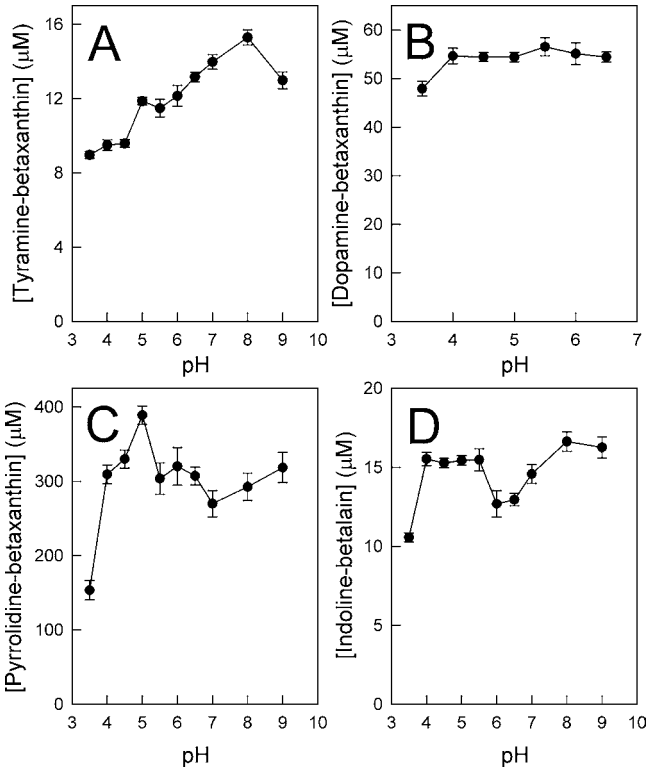

Figure 5. pH effect on the synthesis of betalains using the betalamic acid derivatized support and different amines: (A) tyramine, 0.85 M; (B) dopamine, 1.35 M; (C) pyrrolidine, 0.6 M; (D) indoline, at saturating concentration. The reaction was carried out in 20 mM sodium acetate buffer (pH 3.5−5.5), 20 mM sodium phosphate buffer (pH 6.0−7.0), or 20 mM sodium borate buffer (pH 8.0−9.0).

grew with increasing concentrations of the starting amine up to a maximum at 0.6 M. The scarce solubility of indoline in aqueous media prevented the study of the concentration effect, and this amine was always added to the reaction mixture at saturating concentration under the assay conditions.

From the above results it can be concluded that the optimization of the parameters which affect the novel one-step method for the easy synthesis of betalains should be made for each individual compound. Once optimized, the method allows a routine process to obtain individual compounds that significantly simplifies the previous methodology.[20,21] Betalamic acid obtained from red beet roots was previously used to obtain small amounts of betalain standards for pigment identification by its addition to amines after a process of hydrolysis and immediate partitioning steps with ethyl acetate followed by concentration and re-extraction prior to the synthesis reaction.[20] The combination of the hydrolysis and imine formation reactions in one merged procedure allowed higher amounts of betalains to be obtained but still required immediate purification steps with anionic exchange chromatography to avoid reversal of the reaction.[21] The methodology described here avoids the immediate purification steps and yields stable betalains in minutes, thus simplifying the process to obtain individual pigments. Figure 7 shows the use of the novel betalamic acid derivatized support as a matrix in chromatographic cartridges to speed the recovery of the pigments. The result is shown after the addition of the selected amines at the corresponding optimum concentration, pH, and reaction times determined above.

Stability of the Betalamic Acid Derivatized Support. The stability of betalamic acid after the resin derivatization was investigated by studying its capacity to synthesize betaxanthins as a function of storage time. As a control, a freshly prepared derivatized support was used to obtain dopamine−betaxanthin (**3**) as described above. The amount of betaxanthin obtained was considered to be the starting capacity of synthesis of the support. The synthesis reaction was repeated with the support at different times over 6 months. The support was stored at 4 °C in the absence of light. The results obtained for dopamine−betaxanthin (Figure 8) indicate that the resin retained approximately 50% of its potential after 6 months of storage. The loss of synthetic activity was pronounced during the first month, and from then on it remained practically stable in the production of the betaxanthin.

In addition, the stability of the derivatized support was evaluated by color assessment analysis of the resin. The changes in the appearance of the resin were quantitated by the results of the color CIELAB parameters, determined by spectrophotometry using an integrating sphere. Data were collected immediately after derivatization with betalamic acid. These results obtained for the freshly made support were compared to those found after 6 months of storage (Table 1). As can be seen, the a^* and b^* values decreased, indicating a loss in the red

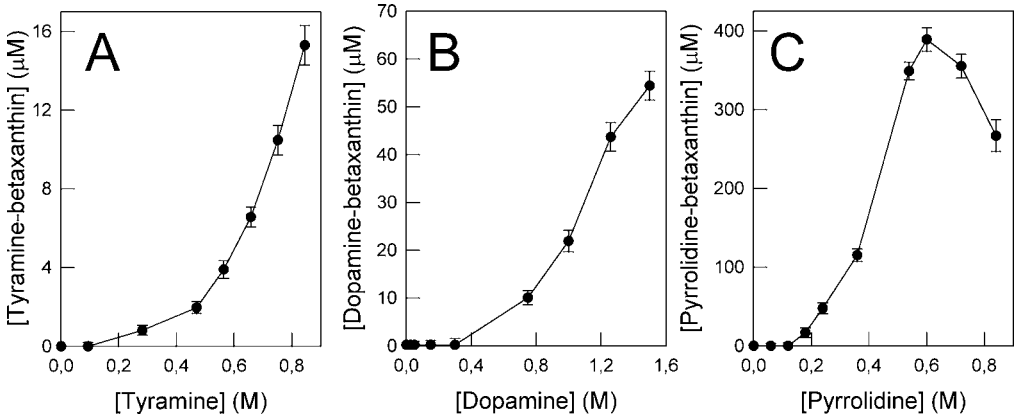

Figure 6. Effect of amine concentration on the formation of the betaxanthins derived from (A) tyramine, (B) dopamine, and (C) pyrrolidine. The reaction medium contained the derivatized support and the amine, at the specified concentration, in 20 mM sodium phosphate buffer, pH 8.0 (tyramine), or in 20 mM sodium acetate buffer, pH 5.0 (dopamine and pyrrolidine).

dx.doi.org/10.1021/jf500506y | J. Agric. Food Chem. 2014, 62, 3776−3782

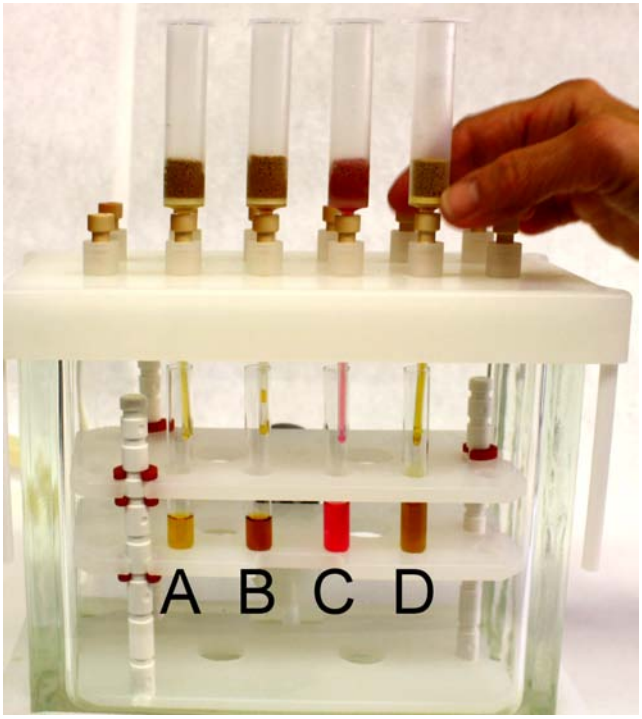

Figure 7. Application of the betalamic acid derivatized support to the synthesis of betalains in chromatographic cartridges. Solutions containing the individual pigments are obtained after the synthesis of (A) tyramine−betaxanthin (**2**), (B) dopamine−betaxanthin (**3**), (C) indoline-derived betacyanin (**5**), and (D) pyrrolidine−betaxanthin (**4**) under the optimized conditions.

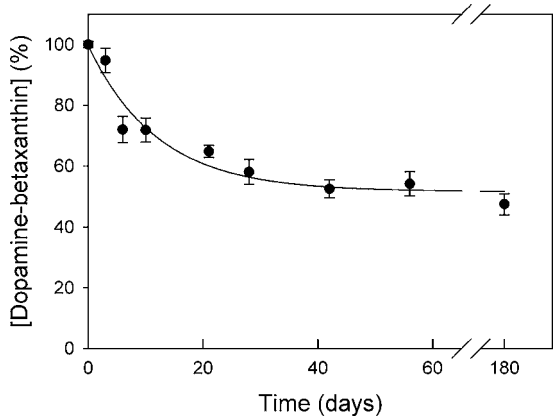

Figure 8. Effect of storage time on the capacity of the betalamic acid derivatized support to yield dopamine−betaxanthin (**3**). The optimized conditions were used for multiple assays during the indicated time.

Table 1. Color Analysis (CIELAB Parameters) for the Betalamic Acid Derivatized Support before and after a Period of 6 Months of Storage

	initial	6 months
a^*	7.18 ± 0.36	5.32 ± 0.11
b^*	32.52 ± 1.47	30.12 ± 1.01
L^*	63.25 ± 1.20	64.91 ± 1.05
$h°$	77.55 ± 0.08	79.98 ± 0.47
C^*	33.31 ± 1.51	30.59 ± 0.98
ΔE^*		3.46 ± 0.23

and yellow colors, respectively. This is probably due to a limited degradation of the pseudobetaxanthin formed, which possesses a maximum wavelength of λ_{max} 486 nm. This contributed to the change in hue angle ($h°$) and chroma (C^*). The L^* parameter was moderately increased, indicating that the color of the resin became lighter after the storage time. In conclusion, the color (a^*, b^*, $h°$), its intensity (C^*), and the lightness (L^*) of the derivatized support changed slightly after 6 months of storage, as confirmed by the value of ΔE^*. This parameter accounts for the color variation calculated with the differences between L^*, a^*, and b^* of the sample stored and the initial conditions. As can be seen, it was only slightly varied, indicating the stability of the betalamic acid resin.

The present work develops for the first time a support derivatized with the structural unit of betalains, betalamic acid. The novel material containing this natural molecule presents color properties of a pseudobetaxanthin and allows a procedure for the easy synthesis of individual betalains. The methodology is based on the addition of amines, which provokes the production of the corresponding derived pigments with the concomitant release from the matrix. The procedure is described in detail and provides a one-step method for the synthesis of betalains, thus considerably simplifying the previous methodologies. This tool opens up new perspectives in the research on betalains and may benefit current and future applications of the pigments.

AUTHOR INFORMATION

Corresponding Author

*(M.J.-A.) Phone: +34 868 884767. Fax: +34 868 884147. E-mail: mja@um.es.

Funding

This work was supported by the Ministerio de Ciencia e Innovación (MICINN, FEDER, Spain, Project AGL2011-25023) and by Fundación Séneca, Agencia de Ciencia y Tecnología de la Región de Murcia (Plan Regional de Ciencia y Tecnología 2007/2010, Programa de Ayudas a Grupos de Excelencia de la Región de Murcia). F.G.-H. has a contract with the Programa Ramón y Cajal (MICINN, FEDER, Spain).

Notes

The authors declare no competing financial interest.

REFERENCES

(1) Gandía-Herrero, F.; García-Carmona, F. Biosynthesis of betalains: yellow and violet plant pigments. *Trends Plant Sci.* **2013**, *18*, 334−343.

(2) Hempel, J.; Böhm, H. Betaxanthin pattern of hairy roots from *Beta vulgaris* var. *lutea* and its alteration by feeding of amino acids. *Phytochemistry* **1997**, *44*, 847−852.

(3) Osorio-Esquivel, O.; Ortiz-Moreno, A.; Álvarez, V. B.; Dorantes-Álvarez, L.; Giusti, M. M. Phenolics, betacyanins and antioxidant activity in *Opuntia joconostle* fruits. *Food Res. Int.* **2011**, *44*, 2160−2168.

(4) Svenson, J.; Smallfield, B. M.; Joyce, N. I.; Sanson, C. E.; Perry, N. B. Betalains in red and yellow varieties of the andean tuber crop ulluco (*Ullucus tuberosus*). *J. Agric. Food Chem.* **2008**, *56*, 7730−7737.

(5) Khan, M. I.; Harsha, P. S. C. S.; Giridhar, P.; Ravishankar, G. A. Pigment identification, nutritional composition, bioactivity, and in vitro cancer cell cytotoxicity of *Rivina humilis* L. berries, potential source of betalains. *LWT − Food Sci. Technol.* **2012**, *47*, 315−323.

(6) Cai, Y.; Sun, M.; Corke, H. Antioxidant activity of betalains from plants of the Amaranthaceae. *J. Agric. Food Chem.* **2003**, *51*, 2288−2294.

(7) Gandía-Herrero, F.; Escribano, J.; García-Carmona, F. Structural implications on color, fluorescence, and antiradical activity in betalains. *Planta* **2010**, *232*, 449−460.
(8) Wu, L. C.; Hsu, H. W.; Chen, Y. C.; Chiu, C. C.; Lin, Y. I.; Ho, J. A. A. Antioxidant and antiproliferative activities of red pitaya. *Food Chem.* **2006**, *95*, 319−327.
(9) Sreekanth, D.; Arunasree, M. K.; Roy, K. R.; Reddy, T. C.; Reddy, G. V.; Reddanna, P. Betanin, a betacyanin pigment purified from fruits of *Opuntia ficus-indica* induces apoptosis in human chronic myeloid leukemia cell line-K562. *Phytomedicine* **2007**, *14*, 739−746.
(10) Kapadia, G. J.; Azuine, M. A.; Sridhar, R.; Okuda, Y.; Tsuruta, A.; Ichiishi, E.; Mukainake, T.; Takasaki, M.; Konoshima, T.; Nishino, H.; Tokuda, H. Chemoprevention of DMBA-induced UV-B promoted, NOR-1-induced TPA promoted skin carcinogenesis, and DEN-induced phenobarbital promoted liver tumors in mice by extract of beetroot. *Pharmacol. Res.* **2003**, *47*, 141−148.
(11) Lechner, J. F.; Wang, L. S.; Rocha, C. M.; Larue, B.; Henry, C.; McIntyre, C. M.; Riedl, K. M.; Schwartz, S. J.; Stoner, G. D. Drinking water with red beetroot food color antagonizes esophageal carcinogenesis in *N*-nitrosomethylbenzylamine-treated rats. *J. Med. Food* **2010**, *13*, 733−739.
(12) Sandquist, C.; McHale, J. L. Improved efficiency of betanin-based dye-sensitized solar cells. *J. Photochem. Photobiol. A: Chem.* **2011**, *221*, 90−97.
(13) Calogero, G.; Yumb, J. H.; Sinopoli, A.; Di Marco, G.; Grätzel, M.; Nazeeruddin, M. K. Anthocyanins and betalains as light-harvesting pigments for dye-sensitized solar cells. *Sol. Energy* **2012**, *86*, 1563−1575.
(14) Gonçalves, L. C. P.; Tonelli, R. R.; Bagnaresi, P.; Mortara, R. A.; Ferreira, A. G.; Bastos, E. L. A nature-inspired betalainic probe for live-cell imaging of *Plasmodium*-infected erythrocytes. *PLoS One* **2013**, *8*, e53874.
(15) Gandía-Herrero, F.; García-Carmona, F.; Escribano, J. Floral fluorescence effect. *Nature* **2005**, *437*, 334−334.
(16) Gonçalves, L. C. P.; Da Silva, S. M.; DeRose, P. C.; Ando, R. A.; Bastos, E. L. Beetroot-pigment-derived colorimetric sensor for detection of calcium dipicolinate in bacterial spores. *PLoS One* **2013**, *8*, e73701.
(17) Büchi, G.; Fliri, H.; Shapiro, R. A synthesis of betalamic acid. *J. Org. Chem.* **1977**, *42*, 2192−2194.
(18) Wyler, H.; Wilcox, M. E.; Dreiding, A. S. Umwandlung eines Betacyans in ein Betaxanthin. Synthese von Indicaxanthin aus Betanin. *Helv. Chim. Acta* **1965**, *48*, 361−366.
(19) Huang, A. S.; von Elbe, J. H. Kinetics of the degradation and regeneration of betanine. *J. Food Sci.* **1985**, *50*, 1115−1120.
(20) Schliemann, W.; Kobayashi, N.; Strack, D. The decisive step in betaxanthin biosynthesis is a spontaneous reaction. *Plant Physiol.* **1999**, *119*, 1217−1232.
(21) Gandía-Herrero, F.; García-Carmona, F.; Escribano, J. Development of a protocol for the semi-synthesis and purification of betaxanthins. *Phytochem. Anal.* **2006**, *17*, 262−269.
(22) Gandía-Herrero, F.; Cabanes, J.; Escribano, J.; García-Carmona, F.; Jiménez-Atiénzar, M. Encapsulation of the most potent antioxidant betalains in edible matrixes as powders of different colors. *J. Agric. Food Chem.* **2013**, *61*, 4294−4302.
(23) Trezzini, G. F.; Zrÿd, J. P. Characterization of some natural and semisynthetic betaxanthins. *Phytochemistry* **1991**, *30*, 1901−1903.
(24) Gandía-Herrero, F.; García-Carmona, F.; Escribano, J. A novel method using high-performance liquid chromatography with fluorescence detection for the determination of betaxanthins. *J. Chromatogr., A* **2005**, *1078*, 83−89.
(25) Gandía-Herrero, F.; Escribano, J.; García-Carmona, F. The role of phenolic hydroxy groups in the free radical scavenging activity of betalains. *J. Nat. Prod.* **2009**, *72*, 1142−1146.
(26) Piattelli, M.; Minale, L.; Nicolaus, R. A. Betaxanthins from *Mirabilis jalapa* L. *Phytochemistry* **1965**, *4*, 817−823.
(27) Schliemann, W.; Cai, Y.; Degenkolb, T.; Schmidt, J.; Corke, H. Betalains of *Celosia argentea*. *Phytochemistry* **2001**, *58*, 159−165.
(28) Kugler, F.; Stintzing, F. C.; Carle, R. Identification of betalains from petioles of differently colored Swiss chard (*Beta vulgaris* L. ssp. *cicla* [L.] Alef. Cv. Bright lights) by high-performance liquid chromatography-electrospray ionization mass spectrometry. *J. Agric. Food Chem.* **2004**, *52*, 2975−2981.
(29) Pedreño, M. A.; Escribano, J. Correlation between antiradical activity and stability of betanine from *Beta vulgaris* L roots under different pH, temperature and light conditions. *J. Sci. Food Agric.* **2001**, *81*, 627−631.
(30) Cai, Y.; Sun, M.; Schliemann, W.; Corke, H. Chemical stability and colorant properties of betaxanthin pigments from *Celosia argentea*. *J. Agric. Food Chem.* **2001**, *49*, 4429−4435.

samples were ground and treated with ethanol to remove oligosaccharides. DEAE was purchased from Whatman International Ltd. (Kent, UK). Sephacryl S-400 was purchased from GE Healthcare (Uppsala, Sweden). Dextrans with different molecular weights and standard monosaccharides (arabinose, glucose, mannose, galactose, rhamnose, fucose, and xylose) were purchased from National Institute for the Control of Pharmaceutical and Biological Products (Beijing, China). Dihydrochloride (AAPH), 2,2′-azobis(2-amidinopropane), and *myo*-inositol were purchased from J&K Scientific (Beijing, China). Iron(III) chloride, 2,2-diphenyl-1-picrylhydrazyl radical (DPPH•), 6-hydroxy-2,5,7,8-tetramethylchroman-2-carboxylic acid (Trolox), fluorescein (FL), and dimethyl sulfoxide (DMSO) were obtained from Sigma-Aldrich (St. Louis, MO, USA). RAW 264.7 mouse macrophage was purchased from the Chinese Academy of Sciences (Shanghai, China). TRIzol reagent was bought from Invitrogen (Life Technologies, Carlsbad, CA, USA), whereas an IScript Advanced cDNA Synthesis kit was purchased from Bio-Rad (Bio-Rad Laboratories, Hercules, CA, USA). Lipopolysaccharide (LPS) from *Escherichia coli* 0111: B4 was obtained from Millipore (Millipore, MA, USA). All other reagents and chemicals were of the highest commercial grade and used without further purification.

Extraction, Isolation, and Purification of GPP-S. Ground *G. pentaphyllum* was extracted by distilled water and then decocted with 2% NaOH at 80 °C three times for 2 h for each time. The extracts were neutralized and combined after filtering and concentrated in a hot water bath. Hydrogen peroxide was added to remove the pigment at 60 °C for 6 h. The supernatant was then collected after centrifugation at 4500 rpm for 10 min and precipitated by adding 4 times volumes of ethanol. The crude polysaccharide of *G. pentaphyllum* was collected by centrifugation, followed by washing with ethanol and acetone, and finally dried with nitrogen.

The crude polysaccharide (500 mg) was dissolved in 6 mL of distilled water. After centrifugation, the supernatants were applied to a DEAE column (2.5 cm × 30 cm) and eluted with 0.6 M NaCl at a flow rate of 0.6 mL/min. Fractions were collected using an automatic fraction collector and examined with the phenol−sulfuric acid method. Each eluting peak was collected, concentrated, and loaded onto a column of Sephacryl S-400. The elutes were lyophilized to obtain the pure polysaccharide, named GPP-S.

Purity and Molecular Weight Determination. The purity and molecular weight of GPP-S were determined using an HPLC-ELSD (Shimadzu Technologies, Japan) with a gel filtration column (Shodex SUGAR KS-805, 8 mm i.d. × 300 mm, Showa Denko, Japan). The mobile phase was deionized water eluting at a flow rate of 1.0 mL/min for 30 min. The calibration curve was prepared with standard dextrans with different molecular weights (1800, 2500, 4600, 7100 and 2,000,000 Da). The mass of GPP-S was calculated by comparing the retention time of the standards.

Monosaccharide Composition Analysis. According to the method described previously,[15] GPP-S (5 mg) was incubated at 100 °C for 8 h after being dissolved in 1 mL of 2 M trifluoroacetic acid (TFA). The excess acid was removed by codistillation with 0.1% HCl−methanol. The residue was dissolved in 1 mL of distilled water ready for the following experiments.

Monosaccharide composition was analyzed according to a previously described procedure with minor modifications.[16] Each of the seven monosaccharide standards and the hydrolyzed polysaccharide were reacted with $NaBH_4$ at 65 °C for 1 h. The mixture was acetylated with pyridine and acetic anhydride at 100 °C for 2 h. Chloroform was used to extract the residues. The analysis was performed using an Agilent 7890A GC with a G4513 FID injector (Agilent Technologies, Palo Alto, CA, USA) equipped with an HP-5 capillary column (30 m × 0.32 mm, 0.25 μm). Injection volume was 1 μL. Oven temperature was first from 110 to 220 °C at 5 °C/min, held for 2 min, increased by 2 °C/min to 240 °C, held for 2 min, and then increased to a final temperature of 280 °C by 10 °C/min.

PMP derivatization of monosaccharides was performed according to a protocol described previously.[17] Briefly, 50 μL of seven standard monosaccharide mixtures or the hydrolyzed polysaccharide was mixed with 50 μL of NaOH (0.6 M), and then 50 μL of PMP methanol solution (0.5 M) was added to each sample. The mixture was allowed to react for 30 min at 70 °C, then cooled to room temperature, and neutralized with 100 μL of 0.3 M HCl. One milliliter of water was added to the solution, which was then extracted by chloroform (1.0 mL) three times. The aqueous layer was combined and centrifuged at 10000 rpm for 5 min. HPLC system equipment with a Zorbax Eclipse XDB-C18 column (250 mm × 4.6 mm, 5 μm, Agilent Technologies) was used to detect the PMP-labeled monosaccharide monitored by UV detector at 250 nm. The mobile phase was prepared by ammonium acetate solution (pH 5.5) and acetonitrile with a ratio of 78:22.

Infrared Spectral Analysis. The FT-IR spectrum was determined using a Fourier transform infrared spectrophotometer (Nicolet iN10 MX, Thermo Nicolet, USA) in the range of 4000−400 cm^{-1}. The sample was ground with spectroscopic grade potassium bromide (KBr) powder and pressed into 1 mm pellets for FT-IR measurements.

Methylation Analysis. Methylation analysis was performed according to the method of Needs and Selvendran with some modification.[18] Ten milligrams of GPP-S and NaOH (100 mg) were dissolved in 5 mL of DMSO. The mixture was methylated with 2 mL of methanol iodide with stirring. The completion of the methylation of GPP-S was confirmed by the disappearance of the OH band (3200−3700 cm^{-1}) in the IR spectrum. The methylated product was depolymerized in 3 mL of formic acid and further hydrolyzed by 2 M TFA (3 mL) at 100 °C for 3 h. After being reduced with sodium borohydride at 60 °C for 1 h, the methylated and hydrolyzed products of the GPP-S were acetylated with acetic anhydride and pyridine (1:1 molar ratio) for 1 h at 100 °C. The resulting product was washed with distilled water and dissolved in chloroform to be subjected to GC-MS analysis and identification according to the relative retention times and fragmentation patterns. The molar ratios of each residue were calibrated from peak areas and the response factor in GC.

NMR Spectroscopy. Polysaccharide was dissolved in D_2O. 1D and 2D spectra were recorded on a Bruker AV-500 MHz NMR spectrometer.

Oxygen Radical Absorbing Capacity (ORAC). The ORAC value was detected with fluorescein (FL) as the fluorescent probe using a Synergy 2 Multi-Mode Microplate Reader (BioTek, Winooski, VT, USA) according to a previously reported laboratory protocol.[19] Trolox was used as the standard. The initial reaction mixture contained 225 μL of 8.16×10^{-8} M FL and 30 μL of sample solution. After preheating at 37 °C for 20 min, 25 μL of 0.36 M AAPH was added into each reaction mixture. The reaction was measured every minute for 2 h. Excitation and emission wavelengths were 485 and 535 nm, respectively. Results were expressed as micromoles of trolox equivalents (TE) per gram of GPP-S.

DPPH• Radical Scavenging Capacity (RDSC). A laboratory protocol was used to determine the DPPH• radical scavenging capacity of the polysaccharide using a Synergy 2 Multi-Mode Microplate Reader (BioTek).[20] Briefly, each reaction mixture contained 100 μL of GPP-S, blank, or trolox standard and 100 μL of DPPH• solution. The absorbance of the reaction mixture was measured at 515 nm every minute for 1.5 h of reaction, and each sample was tested in triplicate. The RDSC was calculated using the area under the curve and reported as micromoles of TE per gram of GPP-S.

Hydroxyl Radical Scavenging Capacity (HOSC). The HOSC assay was conducted using FL as the fluorescent probe on a Synergy 2 Multi-Mode Microplate Reader (BioTek) according to a laboratory protocol reported previously.[21] FL solution was prepared in 75 mM sodium phosphate buffer (pH 7.4). The reaction mixture contained 170 μL of 9.28×10^{-8} M fluorescein, 30 μL of GPP-S or blank or standard, 40 μL of 0.199 M H_2O_2, and 60 μL of 3.43 M $FeCl_3$. The reaction was measured every minute for 6 h at ambient temperature, with the excitation wavelength at 485 nm and the emission wavelength at 528 nm. The results were expressed as micromoles of TE per gram of GPP-S.

Inhibition of IL-1β, IL-6, and COX-2 Gene Expressions in RAW 264.7 Mouse Macrophage Cells. GPP-S was dissolved in a known amount of DMSO and used for cell treatments. RAW 264.7 mouse macrophages were cultured in six-well plates overnight and reached 80% confluence. The cells were first treated with cell media

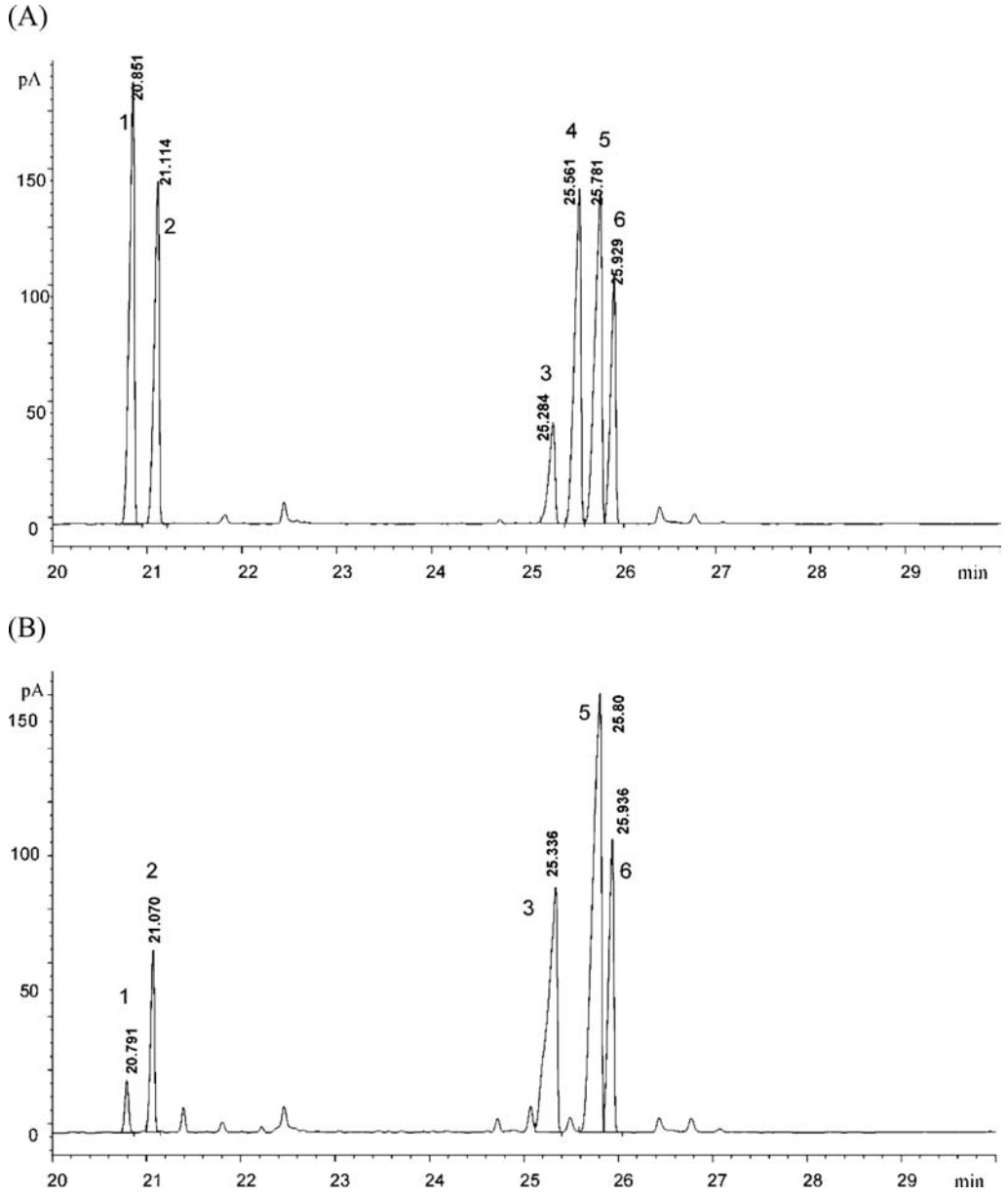

Figure 1. GC chromatograms of standard monosaccharides (A) and monosaccharide composition of GPP-S (B). Peaks: 1, rhamnose; 2, arabinose; 3, inositol; 4, mannose; 5, glucose; 6, galactose.

containing GPP-S for 24 h at 100 and 10 μg/mL concentrations. An initial concentration of 10 ng/mL of LPS was added into each well followed by incubation at 37 °C with 5% CO_2 for another 4 h. Then cells were collected for RNA isolation and real-time PCR analysis according to the previously published protocol.[22,23] After incubation, the TRIzol reagent was added for total RNA isolation, and the StrataScript First Strand complementary DNA Synthesis kit was used to reverse transcribe complementary DNA. Real-time PCR was performed using an ABI 7900HT Fast Real-Time PCR System (Applied Biosystems, Foster City, CA, USA) with an AB Power SYBR Green PCR Master Mix. The following amplification parameters were used for PCR: 50 °C for 2 min, 95 °C for 10 min, and 46 cycles of amplification at 95 °C for 15 s and at 60 °C for 1 min.

Statistical Analysis. Data were recorded as the mean ± SD for triplicate determinations. Tukey's test and one-way ANOVA were used to identify differences in means. Correlation was presented by a two-tailed Pearson's correlation test. Statistics were analyzed using SPSS for Windows (version rel. 10.0.5, 1999, SPSS Inc., Chicago, IL, USA). Statistical significance was declared at $P < 0.05$.

RESULTS AND DISCUSSION

Extraction and Purification of GPP-S. The crude polysaccharide was isolated from the alkaline extraction of tetraploid *G. pentaphyllum* with a yield of 5.07 g/100 g. After purification using DEAE and Sephacryl S-400 columns, GPP-S was obtained from the crude polysaccharides eluted by NaCl solution and distilled water, respectively. GPP-S showed a single sharp peak on the high-performance gel permeation chromatograph with a purity of 99.9% (Supporting Information Figure S1). No absorbance was detected at 260 or 280 nm in the UV spectrum, indicating that GPP-S was free of protein and nucleic acid.

Molecular Mass and Monosaccharide Composition of GPP-S. The average molecular mass of GPP-S was calculated as 1.2×10^6 Da on the basis of the standard curve of a series of standard dextran. According to the retention time showed in Figure 1 of alditol acetate derivatives of GPP-S hydrolysate in

dx.doi.org/10.1021/jf500438s | J. Agric. Food Chem. 2014, 62, 3783−3790

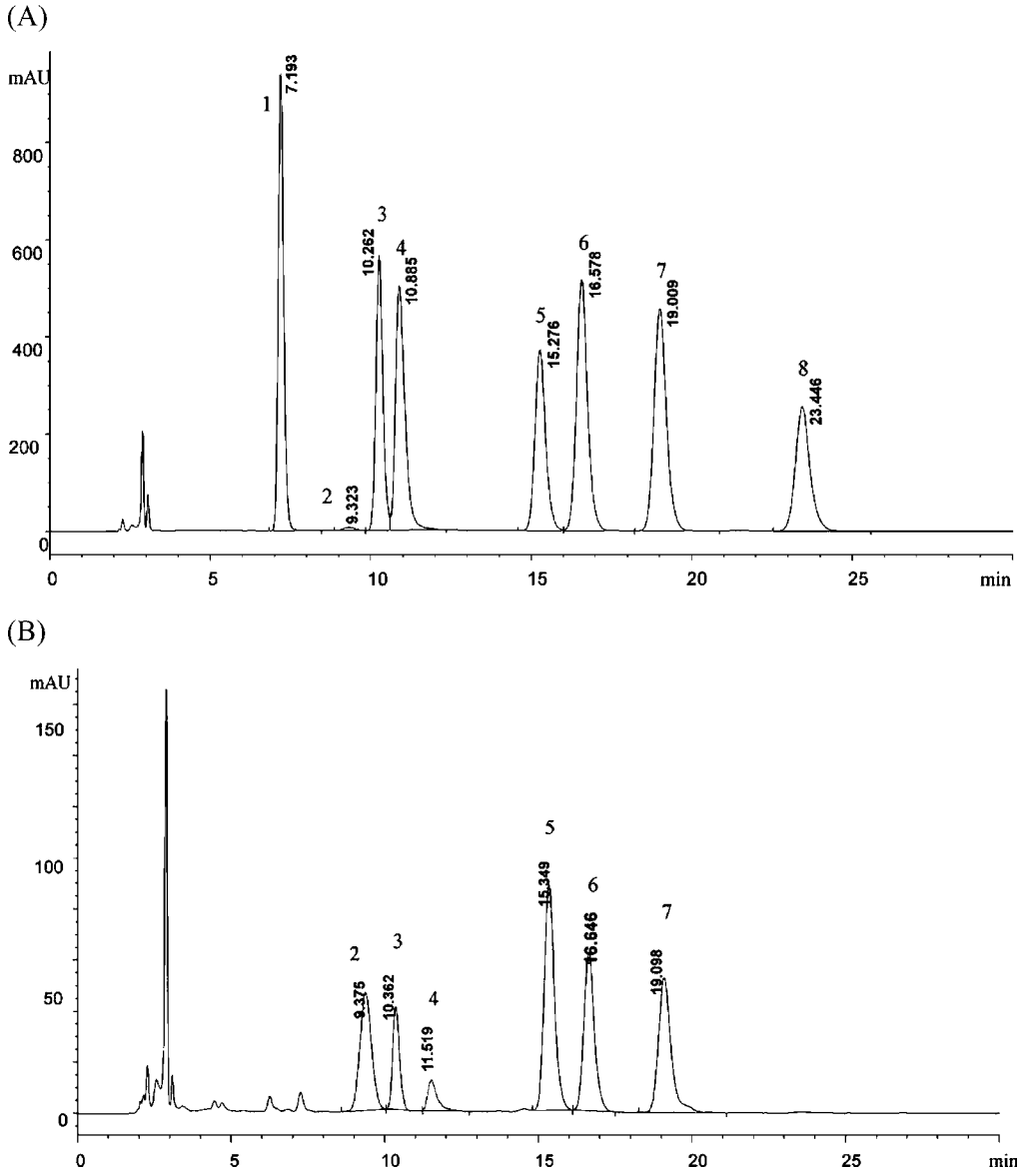

Figure 2. HPLC chromatograms of PMP derivatives of (A) seven standard monosaccharides and (B) GPP-S. Peaks: 1, mannose; 2, PMP; 3, rhamnose; 4, glucuronic acid; 5, glucose; 6, galactose; 7, arabinose; 8, fucose.

GC, GPP-S consisted of rhamnose, arabinose, glucose, and galactose with a molar ratio of 1.00:3.72:19.49:7.82. To further validate the GC analysis results, a PMP-HPLC analysis was carried out to determine the possible presence of uronic acid in GPP-S. As shown in Figure 2, GPP-S contained rhamnose, arabinose, glucose, galactose, and a small amount of glucuronic acid, which could prove the result of GC analysis. It needs to be pointed out that PMP derivatives were not stable, which made it difficult to accurately quantify the ratio of monosaccharides.

Structure Characterization of GPP-S. As shown in Figure 3, the IR spectrum of GPP-S displayed a broad stretching peak at 3346 cm^{-1}, which indicated the presence of hydroxyl groups. The weak peak at 2933 cm^{-1} was due to C−H stretching vibrations. Strong IR bands in the range of 1200−1030 cm^{-1} suggested the existence of C−O stretching vibrations of the pyranose rings.

Methylation analysis is widely used to determine the type of glucosidic bonds of polysaccharides.[24] After four methylations, the methylated polysaccharide was hydrolyzed and analyzed by GC-MS. As shown in Table 1, the four major peaks were identified as 2,3,6-tri-*O*-methylglucitol, 2,3-di-*O*-methylglucitol, 2,3,4-tri-*O*-methylgalactitol, and 2,3,4-tri-*O*-arabinitol with a molar ratio of 17.10:2.78:1.51:1.00. The results of methylation analysis indicated that the relative amount of (1→4,6)-linked glucose was 12.4%, suggesting that the backbone of GPP-S consisted of a (1→6)-linked branch every six residues.

The ^{1}H and ^{13}C NMR spectra of GPP-S are shown in Figure 4A,B. Four main signals from δ 95 to 105 were detected in the anomeric region. The anomeric proton signals (δ 5.41, 5.12, 5.14, and 5.28) and the anomeric carbon signals (δ 99.3, 101.1, 107.2, and 108.9) corresponded with H-1 and C-1 of four anomeric residues, including residue A as (1→4)-α-glucopyranose, residue B as (1→4,6)-α-glucopyranose, residue C as (1→6)-α-galactopyranose, and residue D as (1→)-α-arabinopyranose. All other carbon and proton signals are presented in Table 2 on the basis of the 1D and 2D NMR spectroscopy.[25−27] The signals of rhamnose residue were not detected in methylation and NMR analysis due to its low content. The HMBC spectra of GPP-S (Figure 4C) also showed the cross peak of H-1 and C-4 of residue A,

dx.doi.org/10.1021/jf500438s | J. Agric. Food Chem. 2014, 62, 3783−3790

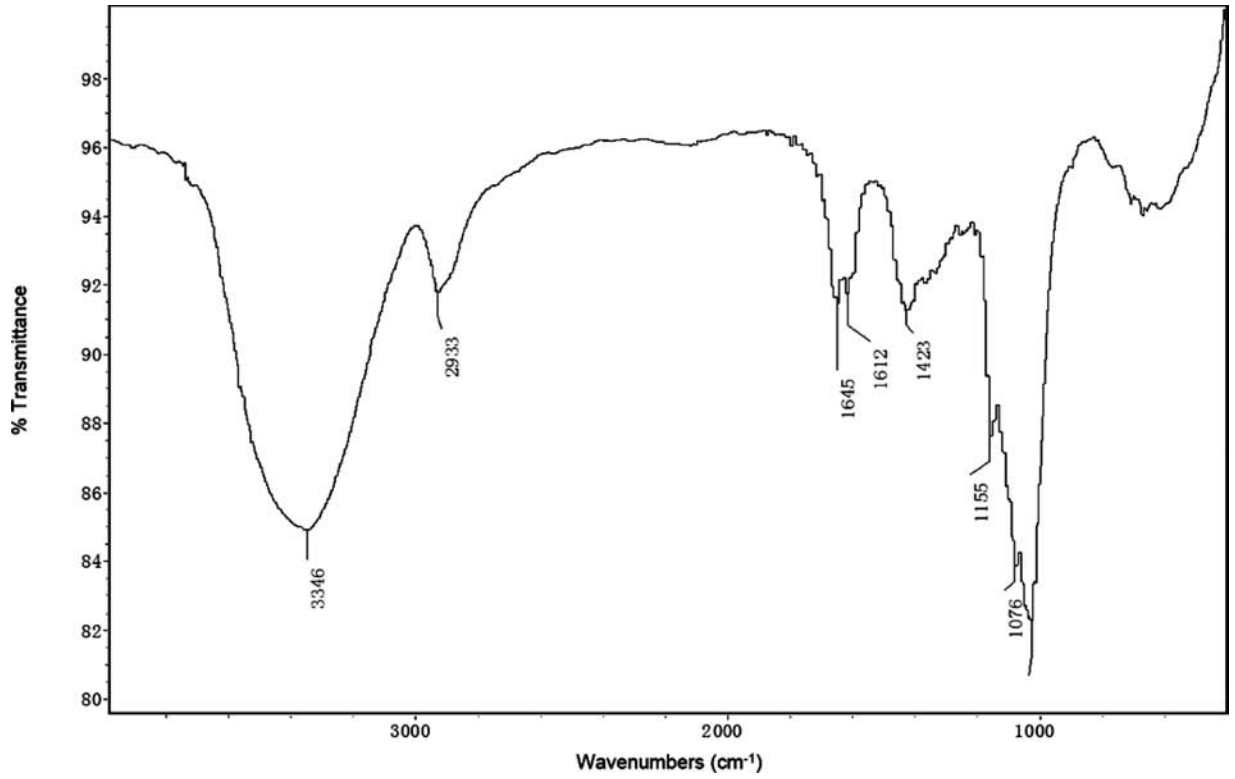

Figure 3. FT-IR spectrum of GPP-S.

Table 1. GC-MS Results of GPP-S

methylated sugar	retention time (min)	molar ratio	mass fragments (m/z)	linkage type
2,3,6-Me_3-Glc	13.64	17.1	43, 71, 87, 99, 101, 117, 129, 161, 173, 233	1,4-linked Glc
2,3-Me_2-Glc	15.23	2.78	43, 85, 101, 117, 142, 159, 201, 261	1,4,6-linked Glc
2,3,4-Me_3-Gal	12.3	1.51	45, 87, 101, 129, 161, 189, 233	1,6-linked Gal
2,3,4-Me_3-Ara	26.31	1.00	59, 87, 101, 117, 161	1-linked Ara

which suggested the linkage of two 1,4-α-Glcp residues. Both analyses of monosaccharide composition and methylation indicated that (1→4)-linked glucose was the residue at the largest amount, which formed the main structure of GPP-S. Cross peak A H1/B C4 and cross peak B H1/A C4 indicated that residue A was linked to residue B. Cross peak A H1/C C6 was observed in Figure 4C, which was possibly due to the linkage of residues A and C. No corresponding signal between residues B and C implied the branch residue linked only with 1,4-α-Glcp residues.

In summary, the structural analysis suggested that the backbone of GPP-S is (1→4)-linked glucose and (1→6)-linked galactose with a (1→4,6)-linked glucose branch every six residues. The predicted structure of GPP-S is shown in Figure 5.

Antioxidant Activity of GPP-S. The antioxidant ability of polysaccharides should be evaluated by different types of in vitro assays to avoid the influence of testing method on the antioxidant property estimation. Radical deactivation in the oxidation process has two major mechanisms, single electron transfer (SET) and hydrogen atom transfer (HAT). RDSC is a SET assay and measures the $DPPH^{\bullet}$ scavenging capacity of GPP-S. ORAC measures the oxygen radical absorbance capacity. HOSC evaluates the scavenging capacity against OH radical generated by the Fenton reaction of Fe(III) and peroxide. These two assays are based on the HAT mechanism. As shown in Figure 6, GPP-S showed the stronger scavenging capacity against $O_2^{\bullet -}$ radical and $HO^{\bullet}$ radical with ORAC and HOSC values of 28 and 19 μmol TE/g, respectively, whereas the $DPPH^{\bullet}$ radical scavenging capacity was 2 μmol TE/g. The results suggested that GPP-S may scavenge the radicals by both hydrogen atom or proton transfer mechanisms.

Effects of GPP-S on IL-1β, IL-6, and COX-2 mRNA expressions. Chronic inflammation is implicated in the pathogenesis of several chronic diseases including atherosclerosis, obesity, metabolic syndrome, diabetes, neurodegenerative diseases, and cancers.[28] The inhibitory effect of the pro-inflammatory

Table 2. ^{13}C and ^{1}H Chemical Shifts of GPP-S

	chemical shifts, δ					
sugar residue	C_1/H_1	C_2/H_2	C_3/H_3	C_4/H_4	C_5/H_5	C_6/H_6
(A) →4)-α-Glcp-(1→	99.3/5.41	76.6/3.67	73.8/4.05	72.9/3.73	70.9/3.86	60.2/3.85
(B) →4,6)-α-Glcp-(1→	101.1/5.12	76.0/4.15	74.5/3.75	76.6/3.87	71.1/3.67	69.1/3.44
(C) →6)-α-Glcp-(1→	108.9/5.28	81.0/4.25	77.4/3.98	71.2/3.66	69.5/3.70	70.7/3.86
(D) α-Ara-(1→	106.9/5.20	72.9/3.59	76.3/3.97	77.2/4.18	62.6/3.78	

dx.doi.org/10.1021/jf500438s | J. Agric. Food Chem. 2014, 62, 3783−3790

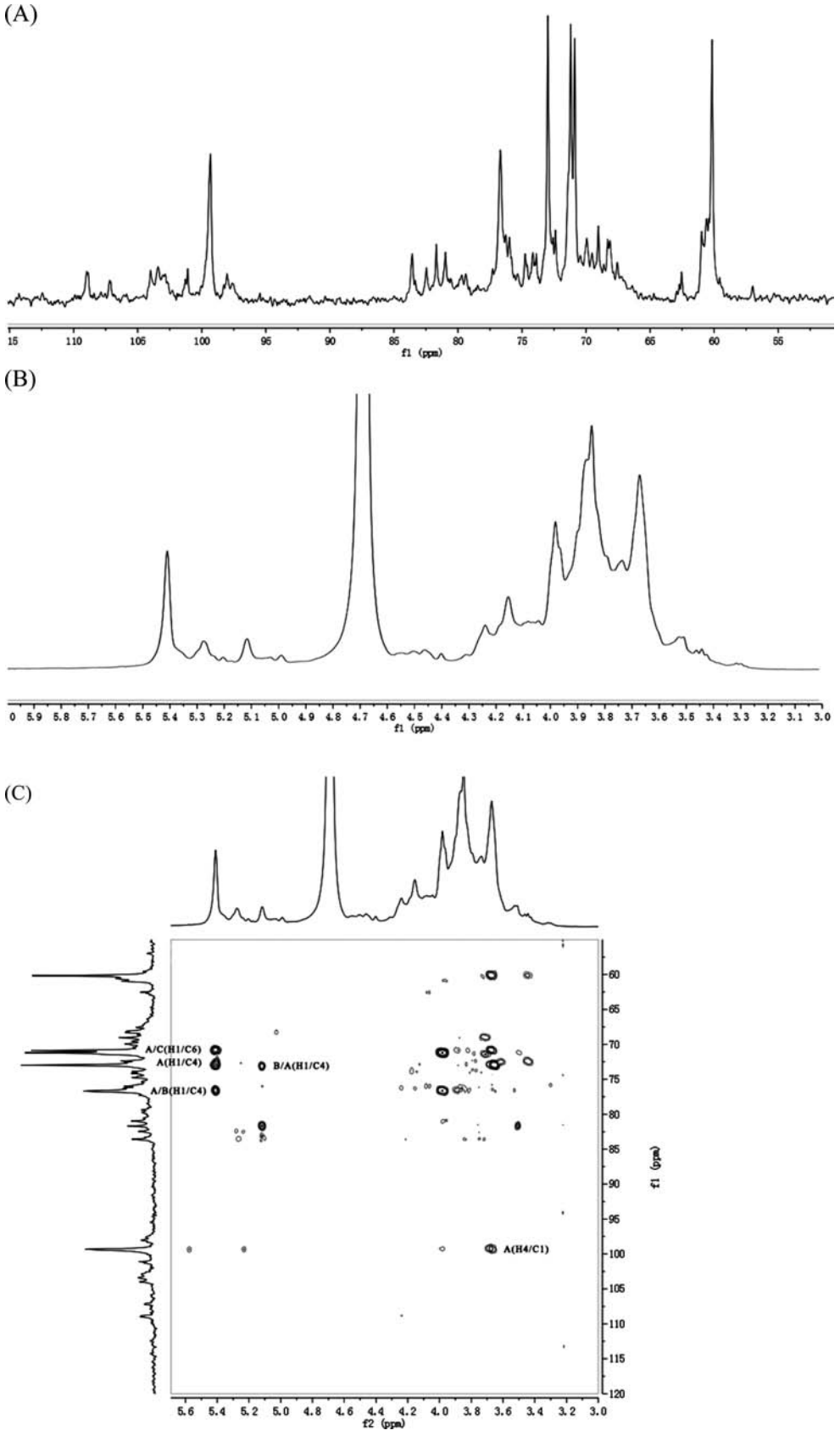

Figure 4. ^{13}C (A), ^{1}H (B), and HMBC (C) NMR spectra of GPP-S in D_2O solution at 30 °C.

cytokine genes expression of GPP-S was evaluated by measuring its ability to suppress the mRNA expressions of pro-inflammatory cytokines in RAW 264.7 mouse macrophage cells stimulated by LPS.

dx.doi.org/10.1021/jf500438s | J. Agric. Food Chem. 2014, 62, 3783−3790

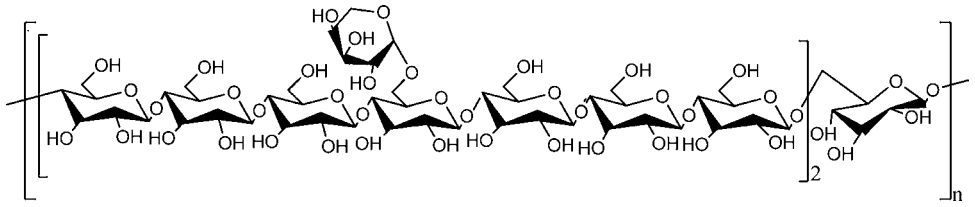

Figure 5. Possible repeating unit of GPP-S.

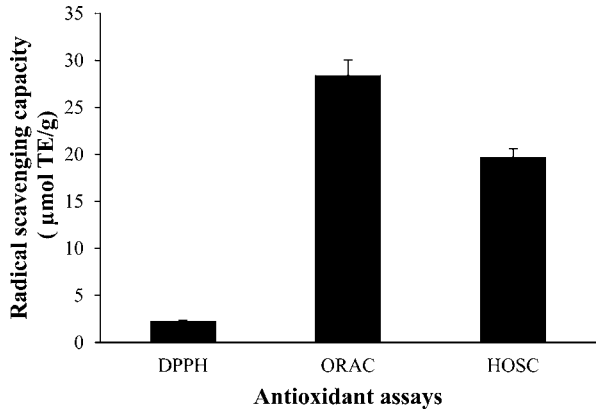

Figure 6. Antioxidant activities of GPP-S. Data are expressed as Trolox equivalents (TE) in μmol TE/g GPP-S. Antioxidant capacity was calculated using the area under the curve (AUC) against the Trolox standard. Vertical bars represent standard deviation (SD) for triplicate measurements.

The mRNA expression of IL-1β, IL-6, and COX-2 in the cells treated by 100 μg/mL GPP-S had 20.54, 82.15, and 41.75% reductions, respectively (Figure 7). The GPP-S of low concentration (10 μg/mL) showed significant suppression on IL-6 mRNA expression by 79.86% (Figure 7B), not suggesting a possible dose dependence. In conclusion, GPP-S exhibited significant inhibitory activity against mRNA expressions of the pro-inflammatory cytokine genes. Chronic inflammation involves the lining of blood vessels and many internal systems, which might contribute to the development of cancer, cardiovascular disease, diabetes, immune system decline, and other aging-associated health problems. The inflammatory process was often associated with oxidative stress and free radical damage. The antioxidant and potential anti-inflammatory activities of GPP-S implied that *G. pentaphyllum* could be used for a potential functional food ingredient to reduce the risk of chronic inflammatory diseases, warranting additional animal and human studies to further investigate and confirm the anti-inflammatory effects of GPP-S.

In summary, a novel alkaline-soluble polysaccharide (GPP-S), with a molecular mass of 1.2×10^6 Da, was isolated from tetraploid *G. pentaphyllum* Makino. It had a monosaccharide composition of rhamnose, arabinose, glucose, and galactose at a ratio of 1.00:3.72:19.49:7.82. The backbone of GPP-S is (1→4)-linked glucose and (1→6)-linked galactose with an occasional (1→4,6)-linked glucose, which terminated with 1-)-α-arabinose, glucuronic acid, and other monosaccharides.

In our previous research, two different kinds of polysaccharides, named GPP and GPP-TL, have been extracted by hot water from diploid and tetraploid *G. pentaphyllum* Makino, respectively.[15,29] Their molecular weights, monosaccharide compositions, and chemical structures were different from those of GPP-S, which led to the different antioxidant activities.

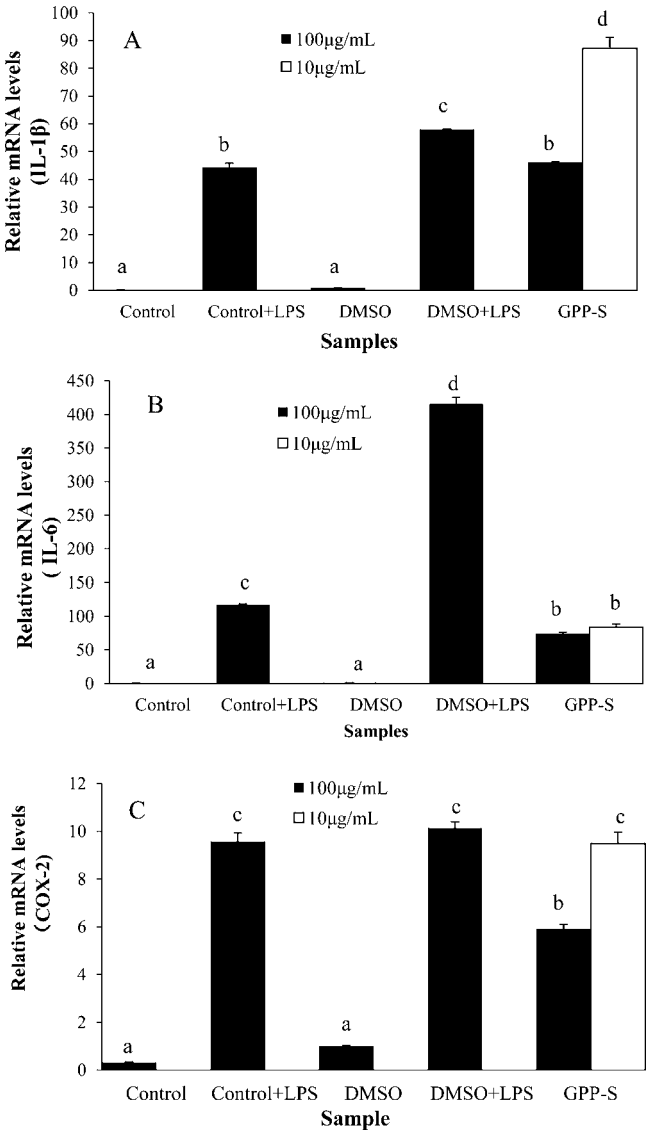

Figure 7. Effects of GPP-S on (A) IL-1β, (B) IL-6, and (C) COX-2 mRNA expressions in lipopolysaccharide (LPS)-stimulated RAW 264.7 mouse macrophage cells. DMSO was the vehicle. The solid and open bars represent initial GPP-S concentrations of 100 and 10 μg/mL, respectively. The vertical bars represent the standard deviation (n = 3) of each data point. Different letters represent significant differences ($P < 0.05$).

GPP-S showed higher scavenging ability against peroxide radicals than GPP and GPP-TL, whereas it had lower absorbance capacities for DPPH$^\bullet$ and HO$^\bullet$ than GPP and GPP-TL. In addition, GPP-S had significant inhibition of IL-1β, IL-6, and COX-2 gene expressions in RAW 264.7 mouse macrophage cells, suggesting its potential application in functional food and dietary supplement products.

dx.doi.org/10.1021/jf500438s | J. Agric. Food Chem. 2014, 62, 3783−3790

■ ASSOCIATED CONTENT

Supporting Information

Figure S1. Profile of GPP-S on a high-performance gel permeation chromatograph. Figure S2. H−H COSY NMR spectra of GPP-S. Figure S3. HSQC NMR spectra of GPP-S. This material is available free of charge via the Internet at http://pubs.acs.org.

■ AUTHOR INFORMATION

Corresponding Authors

*(Y.N.) Phone: (86)-21-34204538. E-mail: yugeniu@sjtu.edu.cn.
*(H.Z.) Phone: (86)-21-60877220. E-mail: zhanghua@sit.edu.cn.

Author Contributions

‖Y.N. and P.S. contributed equally to this work.

Funding

This research was supported by a Special Financial Grant and a General Grant from the Chinese Postdoctoral Science Foundation (Grants 2013T60450 and 2012M511098), a special fund for Agro-scientific Research in the Public Interest (Grant 201203069), SJTU 985-III disciplines platform and talent fund (Grants TS0414115001 and TS0320215001), and a grant from the Wilmar (Shanghai) Biotechnology Research & Development Center Co., Ltd.

Notes

The authors declare no competing financial interest.

■ REFERENCES

(1) Jiang, L. Y.; Qian, Z. Q.; Guo, Z. G.; Wang, C.; Zhao, G. F. Polyploid origins in *Gynostemma pentaphyllum* (Cucurbitaceae) inferred from multiple gene sequences. *Mol. Phylogenet. Evol.* **2009**, *52*, 183−191.

(2) Rujjanawate, C.; Kanjanapothi, D.; Amornlerdpison, D. The anti-gastric ulcer effect of *Gynostemma pentaphyllum* Makino. *Phytomedicine* **2004**, *11*, 431−435.

(3) Circosta, C.; Pasquale, R. D.; Occhiuto, F. Cardiovascular effects of the aqueous extract of *Gynostemma pentaphyllum* Makino. *Phytomedicine* **2005**, *12*, 638−643.

(4) Lin, C. C.; Huang, P. C.; Lin, J. M. Antioxidant and hepatoprotective effects of Anoectochillus formosanus and *Gynostemma pentaphyllum*. *Am. J. Chin. Med.* **2000**, *28*, 87−96.

(5) Aktan, F.; Henness, S.; Roufogalis, B. D.; Ammit, A. J. Gypenosides derived from *Gynostemma pentaphyllum* suppress NO synthesis in murine macrophages by inhibiting iNOS enzymatic activity and attenuating NF-KB-medicated iNOS protein expression. *Nitric Oxide* **2003**, *8*, 235−242.

(6) Attawish, A.; Chivapat, S.; Motohiro, T.; Hideki, M. Studies on interrelation of structure and anti-tumor effects of polysaccharides. *Carbohydr. Res.* **1981**, *92*, 115−129.

(7) Chen, T.; Li, B.; Li, Y.; Zhao, C.; Shen, J.; Zhang, H. Catalytic synthesis and antitumor activities of sulfated polysaccharide from *Gynostemma pentaphyllum* Makino. *Carbohydr. Polym.* **2011**, *83*, 554−560.

(8) Wang, Z. J.; Luo, D. H. Antioxidant activities of different fractions of polysaccharide purifies from *Gynostemma pentaphyllum* Makino. *Carbohydr. Polym.* **2007**, *68*, 54−58.

(9) Qian, X. H.; Wang, Y. X.; Tang, X. L. Effects of *Gynostemma pentaphyllum* Makino polysaccharide (PGP) on immunefuction. *J. China Pharm. Univ.* **1998**, *30*, 51−53.

(10) Chi, A. P.; Chen, J. P.; Wang, Z. Z.; Xiong, Z. Y.; Li, Q. X. Morphological and structural chatacterization of a polysaccharide from *Gynostemma pentaphyllum* Makino and its anti-exercise fatigue activity. *Carbohydr. Polym.* **2008**, *74*, 868−874.

(11) Parry, J.; Yu, L. L. Fatty acid cantent and antioxidant properties of cold-pressed black raspberry seed oil and meal. *Food Chem. Toxicol.* **2004**, *69*, 189−193.

(12) Polla, B. S.; Stubbe, H.; Kantengwa, S.; Maridonneau-Parini, I.; Jacquier, M. R. Differential induction of stress proteins and functional effeets of heat shock in human Phagoeytes. *Inflammation* **1995**, *19*, 363−378.

(13) Jiang, Y. H.; Jiang, X. L.; Wang, P.; Hu, X. K. In vitro antioxidant activities of water-soluble polysaccharide extracted from *Isaria farinosa* B05. *J. Food Biochem.* **2005**, *29*, 323−335.

(14) Ananthi, S.; Raghavendran, H. R. B.; Sunil, A. G.; Gayathri, V.; Ramakrishnan, G. V.; Vasanthi, H. R. *In vitro* antioxidant and *in vivo* anti-inflammatory potential of crude polysaccharide from *Turbinaria ornata* (brown alga). *Food Chem. Toxicol.* **2010**, *48*, 187−192.

(15) Niu, Y. G.; Yan, W.; Lv, J. L.; Yao, W. B.; Yu, L. L. Characterization of a novel polysaccharide from tetraploid *Gynostemma pentaphyllum* Makino. *J. Agric. Food Chem.* **2013**, *61*, 4882−4889.

(16) Fu, D. T.; Oneill, R. A. Monosaccharide composition analysis of oligosaccharides and glycoproteins by high-performance liquid chromatography. *Anal. Biochem.* **1995**, *227*, 377−384.

(17) Englyst, H. N.; Cumming, J. H. Simplified method for the measurement of tatal non-starch polysaccharides by gas-liquid chromatagraphy of constituent sugars as alditol acetates. *Analyst* **1984**, *109*, 937−942.

(18) Niu, Y. G.; Wang, H. Y.; Xie, Z. H.; Whent, M.; Gao, X. D.; Zhang, X.; Zou, S.; Yao, W. B.; Yu, L. L. Structural analysis and bioactivity of a polysaccharide from the roots of *Astragalus membranaceus* (Fisch) Bge. var. *mongolicus* (Bge.) Hsiao. *Food Chem.* **2011**, *128*, 620−626.

(19) Moore, J.; Hao, Z. G.; Zhou, K. Q.; Luther, M.; Costa, J.; Yu, L. L. Carotenoid, tocopherol, phenolic acid, and antioxidant properties of Maryland-grown soft wheat. *J. Agric. Food Chem.* **2005**, *53*, 6649−6657.

(20) Cheng, Z.; Moore, J.; Yu, L. L. High-throughput relative DPPH$^{\bullet}$ radical scavenging capacity assay. *J. Agric. Food Chem.* **2006**, *54*, 7429−7436.

(21) Moore, J.; Yin, J. J.; Yu, L. L. Novel fluorometric assay for hydroxyl radical scavenging capacity (HOSC) estimation. *J. Agric. Food Chem.* **2006**, *54*, 617−626.

(22) Huang, H. Q.; Cheng, Z. H.; Shi, H. M.; Xin, W. B.; Wang, T. T. Y.; Yu, L. L. Isolation and characterization of two flavonoids, engeletin and astilbin, from the leaves of *Engelhardia roxburghiana* and their potential anti-inflammatory properties. *J. Agric. Food Chem.* **2011**, *59*, 4562−4569.

(23) Trasino, S. E.; Kim, Y. S.; Wang, T. T. Y. Ligand, receptor, and cell type-dependent regulation of ABCA1 and ABCG1 mRNA in prostate cancer epithelial cells. *Mol. Cancer Ther.* **2009**, *8*, 1934−1945.

(24) Wang, Y. F.; Wei, X. L.; Jin, Z. Y. Structure analysis of a neutral polysaccharide isolated from green tea. *Food Res. Int.* **2009**, *42*, 739−745.

(25) Cui, S. W. *Food Carbohydrates: Chemistry, Physical Properties, and Applications*; Taylor & Francis Group/CRC Press: Boca Raton, FL, USA, 2005.

(26) Huang, Z.; Zhang, L. Chemical structures of water-soluble polysaccharides from *Rhizoma panacis* Japonici. *Carbohydr. Res.* **2009**, *344*, 1136−1140.

(27) Yu, R. M.; Yin, Y.; Yang, W.; Ma, W. L.; Yang, L.; Chen, X. J.; Zhang, Z.; Ye, B.; Song, L. Y. Structural elucidation and biological activity of a novel polysaccharide by alkaline extraction from cultured *Cordyceps militaris*. *Carbohydr. Polym.* **2009**, *75*, 166−171.

(28) Padilha, M. M.; Avila, A. A.; Sousa, P. J.; Cardoso, L. G.; Perazzo, F. F.; Carvalho, J. C. Anti-inflammatory activity of aqueous and alkaline extracts from mushrooms (*Agaricus blazei* Murill). *J. Med. Food* **2009**, *12*, 359−364.

(29) Wei, Y.; Niu, Y. G.; Lv, J. L.; Xie, Z. H.; Jin, L.; Yao, W. B.; Gao, X. D.; Yu, L. L. Characterization of a heteropolysaccharide isolated from diploid *Gynostemma pentaphyllum* Makino. *Carbohydr. Polym.* **2013**, *92*, 2111−2117.

through the liming effect.[9,13] In general, both pH and CEC of biochar influence the availability of nutrients to soil microbes and plants,[2] and soils amended with biochar or black carbon generally display higher CEC and SA than equivalent biochar-free soils.[3,14,15] Intensive studies showed biochar amendments increase soil pH and have significant consequent effects on plant growth.[9] On the other hand, some studies reported no or only slight changes in soil pH, CEC, and SA with biochar amendment, which is attributed to specific soil or biochar properties.[2,16] Detailed characterization of biochar is essential for forecasting and maximizing impacts of biochar amendment on soil properties.

Biochar properties have not yet been fully linked to production parameters, making the design of agronomic biochars a challenge.[3] Reasons for why this link does not yet exist may include the complexity of pyrolysis processes, which can be influenced by many factors. In addition, process parameters are difficult to control in large reactors, enhancing the complexity of biochar production processes and the heterogeneity of products.[2] Biochar properties can be assessed via a combination of rather simpler proxy-type analyses and advanced analytical techniques. Proxy-type analyses are therefore more practical also from a user standpoint as users may wish to mix various biochars for a homogeneous product. The International Biochar Initiative and a panel of experts have identified a proxy for the assessment of biochar stability,[17] and the characterization of other biochar properties will likely also rely on proxy-type analyses.

Robust assessment of biochar properties requires the existence of simple relationships, preferably linear, between production conditions or proxy measurements and complex properties. Several studies suggest that such simple relationships exist for critical chemical composition and surface property indicators. Increasing pyrolysis temperature has been reported to result in continuous increases in pH, CEC,[18] and SA.[19] However, not all studies agree with these findings. Surface area has been reported to reach a peak value and then decrease at higher HTT for both wood and wheat biochars.[20,21] Similarly, CEC has also been reported to display a localized maximum at midrange HTT.[22] Many studies use few biochar samples along a temperature continuum, and considerable uncertainty remains as to our ability to predict surface properties on the basis of biochar production methods. Here, our objective was to obtain detailed responses of selected biochar properties to HTT for three pyrolysis methods. For this, we used a ca. 15-point temperature series in slow pyrolysis of two feedstocks each as well as HTC hydrochars and flash carbonization biochars produced from the same feedstocks. This allowed us to obtain an extensive sample set for testing the hypothesis that surface properties follow simple relationships with HTT production conditions and can be predicted from chemical composition indicators.

MATERIALS AND METHODS

Carbonization. Three production methods were tested: slow pyrolysis, flash carbonization, and HTC treatment. Identical feedstocks were used for slow pyrolysis and HTC treatment: chaffed biomass of grass (*Miscanthus giganteus*) and corncob from maize (*Zea mays*) grown in Serbia (ZP Maize Hybrid 505). In addition to slow pyrolysis and HTC, flash carbonization was conducted on a batch of corncobs from Waimanalo Farm in Hawaii. In total, 34 biochars were produced (Table 1). In the present study, we used feedstock derived from plants using the C4 photosynthetic pathway, that is, miscanthus and maize. The C4 feedstock has a distinctive ^{13}C signature from that of soil organic matter, which we used in a parallel study on estimating the stability of biochar C structures in soil. Within the limited range of C4 feedstocks, miscanthus and corncob are good candidates for biochar production. Miscanthus is a high-yielding bioenergy crop requiring minimal soil preparation, and biochar prepared from it has potential for being a silicon fertilizer.[23] Corncob, in comparison, is a crop residue, which needs to be valorized and does not compete for land with food production.

Slow pyrolysis was performed in a muffle furnace at target temperatures ranging from 235 to 800 °C with a heating rate of 2.5 °C min^{-1}. Pyrolysis HTTs were selected to produce biochars containing a wide range of VM content. To aid the selection process, a set of preliminary analyses were conducted on the feedstocks using a thermogravimetric analyzer (SDT Q600, TA Instruments, New Castle, DE, USA). Fourteen miscanthus and 17 corncob biochars were generated through slow pyrolysis of chaffed miscanthus and corncobs cut into ca. 5 mm slices. A detailed procedure for the pyrolysis is provided by Wang et al.[24] Feedstock was dried at 105 °C for 24 h and

Table 1. Elemental Compositions of Corncob (CC) and Miscanthus (MS) Exposed to Hydrothermal Carbonization (HTC), Slow Pyrolysis (Slow), and Flash Carbonization (Flash) at Designated Highest Treatment Temperatures (HTT)[a]

feedstock-method	HTT (°C)	C (%)	N (%)	O (%)	H (%)
CC	105	47.7 (0.7)	0.4 (0.0)	56.5 (0.3)	6.5 (0.0)
CC-Flash	600	83.2 (1.0)	1.4 (0.1)	8.7 (0.2)	2.1 (0.1)
CC-HTC	230	59.9 (0.8)	0.4 (0.0)	40.7 (0.3)	6.0 (0.1)
CC-Slow		67.0 (0.6)	0.5 (0.0)	29.0 (0.2)	5.1 (0.1)
CC-Slow	377	74.1 (0.3)	0.6 (0.1)	20.6 (0.2)	4.5 (0.1)
CC-Slow	372	71.9 (0.8)	0.5 (0.0)	26.1 (0.5)	4.8 (0.1)
CC-Slow	369	74.2 (0.7)	0.6 (0.1)	23.3 (0.2)	4.6 (0.1)
CC-Slow	357	74.2 (1.0)	0.6 (0.0)	23.5 (0.1)	4.8 (0.1)
CC-Slow	386	76.2 (0.9)	0.7 (0.0)	20.6 (0.3)	4.2 (0.1)
CC-Slow	416	78.8 (1.2)	0.5 (0.0)	17.6 (0.2)	3.9 (0.1)
CC-Slow	440	80.1 (0.9)	0.6 (0.0)	15.0 (0.1)	3.5 (0.1)
CC-Slow	485	83.5 (0.7)	0.7 (0.0)	11.1 (0.3)	3.2 (0.1)
CC-Slow	562	86.8 (0.8)	0.8 (0.0)	9.1 (0.2)	2.7 (0.1)
CC-Slow	576	86.9 (0.8)	0.8 (0.0)	6.6 (0.3)	2.5 (0.1)
CC-Slow	687	90.1 (0.7)	1.0 (0.1)	4.8 (0.2)	1.8 (0.1)
CC-Slow	693	89.4 (0.4)	0.9 (0.1)	5.6 (0.1)	1.7 (0.1)
CC-Slow	796	91.5 (0.4)	1.0 (0.0)	4.6 (0.1)	1.0 (0.1)
MS	105	47.9 (0.9)	0.2 (0.0)	51.8 (0.5)	6.1 (0.1)
MS-HTC	230	62.2 (0.6)	0.2 (0.0)	35.4 (0.3)	5.6 (0.1)
MS-Slow	272	56.1 (1.5)	0.3 (0.0)	35.2 (0.1)	6.0 (0.1)
MS-Slow	235	46.1 (1.4)	0.3 (0.0)	40.1 (0.1)	5.4 (0.3)
MS-Slow	369	66.6 (0.7)	0.4 (0.0)	22.3 (0.5)	4.5 (0.1)
MS-Slow	385	67.7 (0.8)	0.4 (0.0)	19.7 (0.5)	4.1 (0.2)
MS-Slow	400	63.7 (1.4)	0.4 (0.0)	16.3 (0.3)	3.4 (0.1)
MS-Slow	406	70.9 (0.8)	0.4 (0.0)	17.2 (0.1)	3.8 (0.1)
MS-Slow	411	73.2 (1.8)	0.4 (0.0)	15.7 (0.3)	3.5 (0.1)
MS-Slow	406	72.0 (0.6)	0.4 (0.0)	18.9 (0.3)	4.2 (0.1)
MS-Slow	416	73.6 (2.1)	0.4 (0.0)	12.8 (0.3)	3.3 (0.1)
MS-Slow	442	73.6 (1.6)	0.4 (0.0)	12.1 (0.2)	3.1 (0.1)
MS-Slow	503	64.5 (4.1)	0.4 (0.1)	9.7 (0.3)	2.4 (0.2)
MS-Slow	464	75.3 (2.9)	0.5 (0.1)	11.2 (0.2)	3.1 (0.1)
MS-Slow	600	71.9 (3.3)	0.5 (0.1)	5.5 (0.5)	2.0 (0.1)
MS-Slow	590	77.3 (3.4)	0.5 (0.0)	6.8 (0.2)	2.2 (0.1)
MS-Slow	693	84.6 (2.1)	0.7 (0.1)	6.1 (0.3)	1.7 (0.1)
MS-Slow	682	75.6 (2.4)	0.6 (0.0)	5.0 (0.3)	1.5 (0.1)
MS-Slow	790	83.7 (1.6)	0.8 (0.1)	5.8 (0.2)	0.8 (0.1)

[a]Standard deviations are shown in parentheses for analytical replicates; $n = 5$ (C, H, and N) and $n = 3$ (O).

weighed prior to loading into a 1 L stainless steel retort. The retort, equipped with thermocouples placed at the center, bottom, side, and front, was then covered with a lid and placed into a furnace. The retort was purged for 1 h to create an inert atmosphere, and a constant flow of N_2 was maintained at 2 L min^{-1} during pyrolysis. After the desired final temperature was achieved, heat supply from the furnace was stopped and the sample cooled slowly to room temperature. To present a more representative sample history, we consistently reported measured HTTs from the average of the four thermocouples in the retort instead of set temperatures for the furnace. Exothermic reactions occurred during slow pyrolysis in the approximate temperature range of 250−400 °C, and actual HTTs measured by the thermocouples were higher than the set temperatures (Figure 1). As a result, few

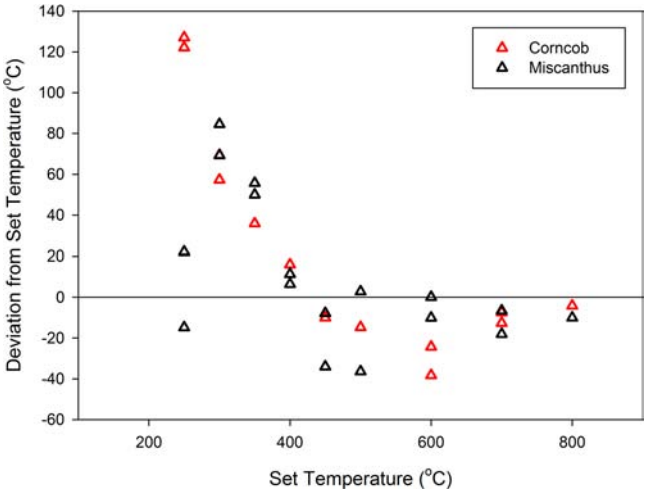

Figure 1. Deviation of measured highest treatment temperature (HTT) from oven set temperatures during slow pyrolysis.

samples are recorded at pyrolysis temperatures around 350 °C, at which the pyrolysis process is difficult to halt. At pyrolysis temperatures of ≥450 °C, measured HTTs in the retort did not exceed target values.

HTC treatment of corncob and miscanthus was performed in a 1 L steel autoclave (Anton Paar), immersed in water, and then heated at 230 °C for 6 h under autogenous pressure. After cooling, the autoclaves were opened, and the resultant hydrochar was removed from the aqueous dispersion by vacuum filtration. The resulting fine powder was dried at 40 °C. Because the hydrochar yield was not directly measured at the time of production, it was estimated from the literature[25] for the purpose of comparison.

Flash carbonization was performed on corncob to produce biochar according to the method of Antal et al.[26] The reaction lasted 20 min in a vessel pressurized to 0.8−3.4 MPa with air. Electric heating coils at the bottom of the pressure vessel ignited the lower portion of the biomass. After 360 s, compressed air was delivered to the top of the pressure vessel and flowed through the packed bed of feedstock to sustain the carbonization process. Pressure within the reactor was maintained at the specified range. After sufficient air was delivered to carbonize the corncob, air flow was halted and the reactor cooled overnight. The charcoal was removed from the reactor and allowed to equilibrate under a fume hood for 2 days.

All samples were crushed through a 2 mm sieve, and subsamples were subsequently ground for greater homogeneity with a ball mill for 3 min at 20 s^{-1} shaking frequency (MM 200, Retsch GmbH, Haan, Germany). The samples were stored in airtight bags until analyzed.

Physical and Chemical Analyses. Proximate analysis of the biomass feedstock was performed according to American Society for Testing and Materials (ASTM) methods E 871 and 872 with modifications as described by Wang et al.[24] In brief, ash content was determined according to ASTM method D 1102. The fixed carbon contents of the samples were calculated by difference between 100% and the sum of measured VM and ash contents. The VM content of the charcoal products was determined according to ASTM method D 1762-84 with the modification that samples were directly placed at the rear of a furnace for 6 min at 950 °C without preheating.[24]

Elemental composition (C, H, N) of the samples was determined on 50−100 mg samples by dry combustion using a Leco CHN1000 analyzer and coal reference material (Leco Corp., St. Joseph, MI, USA). Oxygen was determined on 2 mg samples dried at 90 °C with a TruSpec Makro analyzer and O add-on module (Leco Corp.). Results are reported on a dry weight basis. pH was determined in a biochar/water volume ratio of 1:10 using a combination Orion pH electrode (SA 720, Allometrics, Inc., Baton Rouge, LA, USA).

Potential CEC was determined by using a modified ammonium acetate compulsory displacement method. Soluble ions, which can constitute an artifact, were removed through five successive leachings of 0.5 g samples with 20 mL of deionized water. Preliminary analyses were conducted on the initial water leachates to determine the most important cations present following the method of Gaskin et al.[27] Analysis of the water leachates suggested that between 97 and 100% of the extractable/exchangeable cations were covered by five cations. After the removal of soluble ions with water, remaining cations were displaced using 50 mL of 1 M ammonium acetate buffered to pH 7. CEC was calculated by the sum of the cations Ca, Mg, K, and Na in the ammonium acetate percolate. H^+, determined by titration, was included when the pH was <7. Additional preliminary analyses involved CEC determination on a subset of samples exposed to pretreatment with acid. Acid washing is expected to remove carbonates, which may also interfere with the accurate determination of CEC. In this pretreatment, biochar−water mixtures were neutralized to pH 6.5 ± 0.02 by incremental additions of 0.5 M HCl and overnight shaking. The desired pH was obtained after 1 week, after which biochars were repeatedly washed until free of Cl^- as detected by $AgNO_3$ and dried at 50 °C for 5 days. Acid washing compared to only water leaching had little impact on the corncob biochar CEC, but it did reduce the miscanthus CEC by an average of 28%. Because the CEC of low-pH hydrochar was also reduced by 20% through acid washing, raising questions regarding the nature of the response, we chose a method that is less disruptive, namely, one without HCl washing.

Internal SA was measured using the Brunauer, Emmett, and Teller (BET) theory with N_2 as the adsorbate. Samples were dried at 106 °C for 90 min, milled, and then degassed in vacuum for 2 h at 120 or 150 °C: degassing temperature was chosen on the basis of sample HTT history. Measurements were performed on ca. 1 g samples on a NOVA 2000 (Quantachrome Instruments, Boynton Beach, FL, USA). The multipoint BET method was applied in the range of partial pressures of 0.05−0.30 P/P_0.

Statistics and Data Analysis. Multiple stepwise linear regressions and Spearman rank order correlations were performed with Sigmaplot version 11.0 (Systat Software Inc., San Jose, CA, USA).

RESULTS AND DISCUSSION

Yield and Proximate Analysis. Charcoal yield, VM content, and fixed carbon content changed nonlinearly in response to slow pyrolysis HTT (Figure 2). This type of nonlinear decrease in charcoal yield and VM and a corresponding increase in fixed carbon content are common biomass responses to increasing HTT.[5] Biochar yield and VM content responses to HTT were similar for the two feedstocks (Figure 2a,b). Eighty percent of VM loss occurred at 209−543 °C for corncob and at 241−509 °C for miscanthus. The VM contents of corncob and miscanthus feedstocks were similar, 81.1 and 78.0%, respectively. Despite the use of fairly similar C4 plants as feedstock, those being grass species of tropical origin, similar VM loss functions under pyrolysis were not necessarily obvious, as the two feedstocks differed somewhat in structural chemical composition. Our corncob and miscanthus feedstocks contained 13.8 and 21.3% lignin, respectively, as

dx.doi.org/10.1021/jf501139f | J. Agric. Food Chem. 2014, 62, 3791−3799

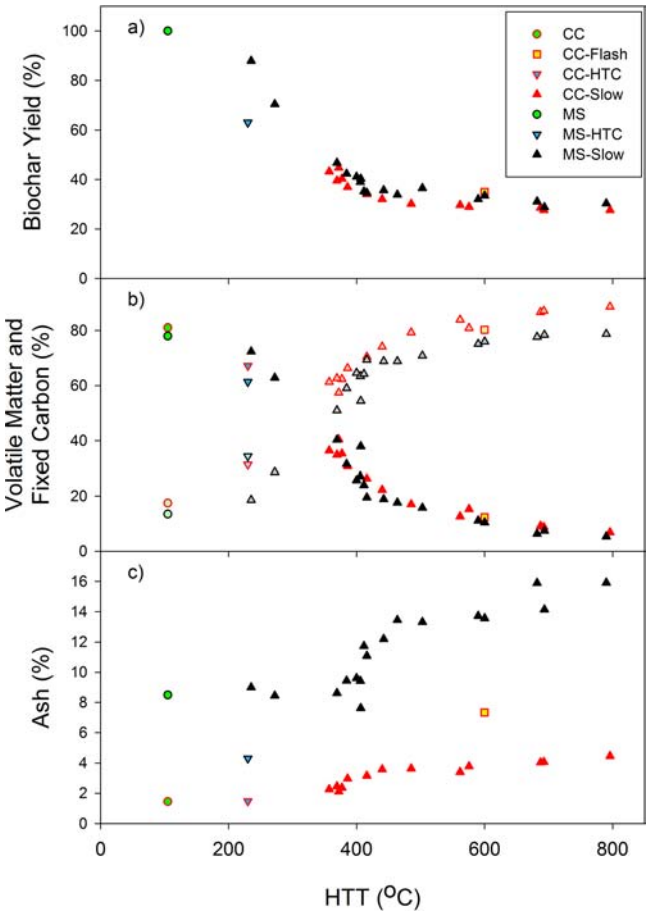

Figure 2. (a) Yield, (b) VM and fixed carbon (lighter fill) content, and (c) ash content as a function of highest treatment temperature (HTT) for corncob (CC), miscanthus (MS), and respective biochars produced through slow pyrolysis (Slow), flash carbonization (Flash), and hydrothermal carbonization (HTC). Reported biochar yield, VM, fixed carbon, and ash content are averages from three analytical replicates.

determined by advanced NMR investigations,[28] and these values are comparable to other reports of lignin in corncob and miscanthus: 14.7 and 23%, respectively.[19,29] Lignin content has been reported to affect biochar yield[30] due to the high C content of its constitutive polyphenol structure.[31] Additionally, mass loss during the pyrolysis process has been mainly attributed to degradation of cellulose at temperatures between 300 and 400 °C.[32] Our previous NMR investigations suggest that miscanthus had lower cellulose and hemicellulose contents than corncob but a higher degree of cellulose crystallinity.[28] Our results therefore suggest that the consistent biochar yield and VM contents obtained for grass-derived biochars hold across substantial variation in cellulose, hemicellulose, and lignin contents of feedstocks. The apparent absence of effect from variation in ash content and particle size would need to be confirmed with multiple grass feedstocks.

Hydrochars from HTC production displayed lower yield and VM content than slow pyrolysis biochars produced at similar HTT (Figure 2a,b). Although the hydrochars were produced at 230 °C, their VM and fixed C content were closer to those of 300 °C than of 250 °C slow pyrolysis biochars. On the basis of the amount of C recovered, Fuertes et al.[33] reported that 250 °C hydrochars are similar to slow pyrolysis biochars produced at nearly 400 °C. Our results confirm that HTC leads to a higher degree of carbonization than slow pyrolysis at comparable HTT. This is probably due to the reaction enhancement effects of pressure and the presence of water under HTC conditions. Flash carbonization HTT was not directly measured due to inhomogeneity within the reactor. The general relationship between VM and HTT for corncob (Figure 2b) suggests a production HTT for flash carbonization char between 520 and 640 °C. This temperature estimate is in the range of afterburner gas temperatures of the flash carbonizer.[34]

Ash in slow pyrolysis biochar became increasingly concentrated with increasing HTT (Figure 2c). Miscanthus hydrochar contained less ash than its feedstock, which is likely explained by mineral loss through the liquid phase during the HTC process. However, we did not observe a similar decrease in ash content for the corncob hydrochar, suggesting a feedstock-specific response. Contrasting trends in hydrochar ash content with different feedstocks were also found by Cao et al.[35] The ash content of feedstock used in flash carbonization was 6.3%, indicating that flash carbonization, like slow pyrolysis, leads to a concentration of ash. Only HTC produced a low-ash carbonization product.

Elemental Composition. Carbon and nitrogen were lost at a slower rate than oxygen and hydrogen during pyrolysis, resulting in their progressive concentration in the biochars with increasing pyrolysis HTT (Table 1). This effect has been well documented.[6] A Van Krevelen diagram relating H/C to O/C shows that the distribution of atomic ratios obtained from chars in this study was independent of feedstock and pyrolysis process (Figure 3). In our study, we directly measured O

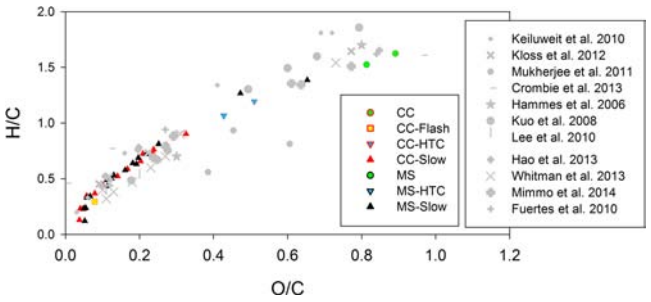

Figure 3. Van Krevelen diagram of samples analyzed in this study (in color) and literature values (gray) of grass feedstocks and biochars from 11 studies. Atomic ratios are averages from at least three analytical replicates.

contents, whereas most published studies report O values as calculated by subtracting the sum of C, H, N, and ash contents. Our measured values were more consistent than those we calculated by difference (data not shown), as the latter method combines the cumulative errors of all measurements. However, our O measurements for feedstocks were high, with O/C ratios between that of pure cellulose and sucrose. Despite the discrepancy at high O/C ratio, our atomic ratios obtained with measured O are remarkably consistent with literature values for grass-derived biochars obtained in 11 studies (Figure 3). It has been shown for biochars from a wide range of feedstocks that HTT plays a decisive role in causing the decrease in H/C and O/C ratios of produced biochar samples.[36] On the basis of the Van Krevelen plot, hydrochars and flash carbonization biochar appear equivalent to slow pyrolysis biochars produced at approximately 300 and 600 °C, respectively. This finding is

dx.doi.org/10.1021/jf501139f | J. Agric. Food Chem. 2014, 62, 3791−3799

consistent with the estimate of equivalent HTTs for chars from HTC and flash carbonization based on the relationship with VM. The independence of biochar elemental composition from feedstock and pyrolysis process is further confirmed by the consistent relationship between VM and molar ratios (Figure 4). Spokas[37] suggests that molar ratios encapsulate all

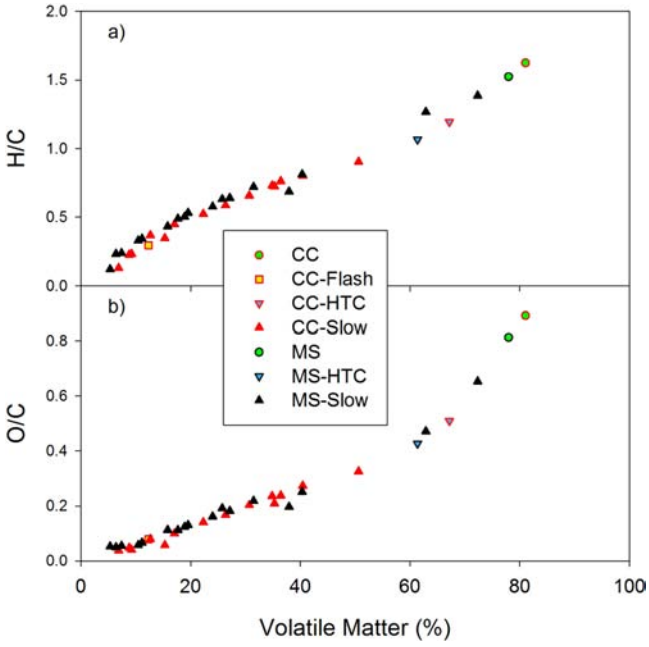

Figure 4. Atomic ratios (a) H/C and (b) O/C as a function of highest treatment temperature (HTT) for corncob (CC), miscanthus (MS), and respective biochars produced through slow pyrolysis (Slow), flash carbonization (Flash), and hydrothermal carbonization (HTC). Averages were obtained from at least three analytical replicates.

production parameters influencing carbonization. Other studies indicate that high-ash biochars such as those from food waste would require a combination of VM and atomic ratios for their characterization.[38] It has also been reported that H/C atomic ratios are not able to differentiate between the reactions occurring during HTC.[35] Our results suggest that both VM and atomic ratios can be used for characterizing the general charring history of grass-derived biochars. We further support the use of atomic ratios over volatile matter due to the stability of elemental composition measurements across studies as compared to proximate analysis.

Surface Property: pH. The pH of slow pyrolysis biochars increased with production HTT, reaching a plateau at approximately 450 °C (Figure 5a). Slow pyrolysis biochars produced above 450 °C had average pH that was 4.1 and 3.9 units higher than that of the corncob and miscanthus feedstocks, respectively. Flash carbonization biochar also had a pH that was 4.2 units above that of the feedstock. Our study shows that HTTs of 400−450 °C are sufficient for raising the biochar pH and producing C-rich biochar. Up to 7.6 pH unit increases have been shown in some biochars, with smaller increases in wood- and straw-derived biochars.[10] By contrast, HTC treatment significantly reduced the pH of the biomass by 1.3 and 2.4 units in corncob and miscanthus, respectively. Similar results were reported by Fuertes et al.,[33] who hypothesized that acidity in hydrochars may be due to a high content of carboxylic functional groups. The O/C atomic ratio, however, did not reflect the acidity of the hydrochars.

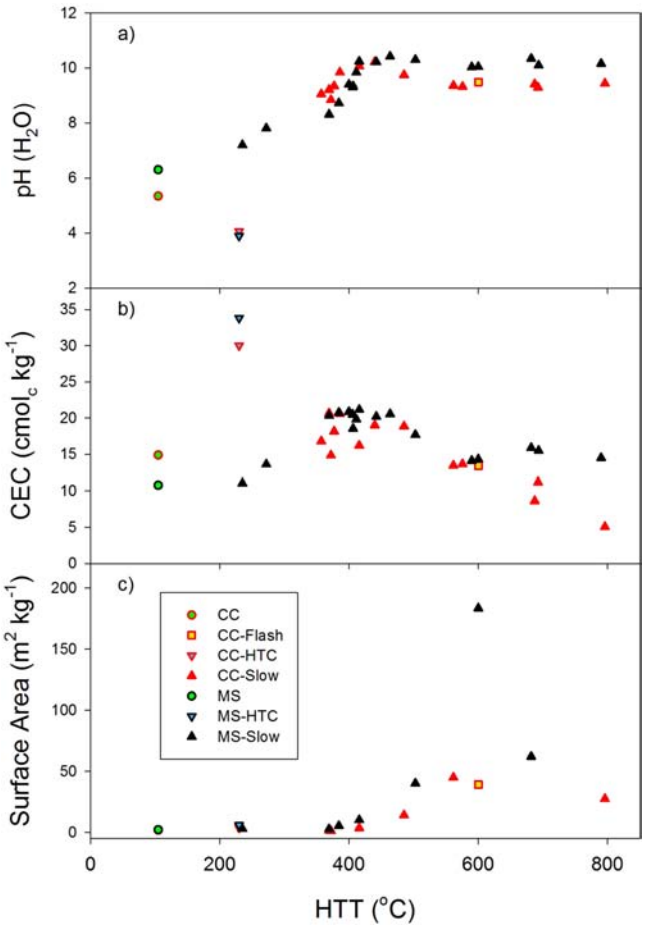

Figure 5. Surface properties (a) pH, (b) cation exchange capacity (CEC), and (c) surface area (SA), as a function of highest treatment temperature (HTT) for corncob (CC) and miscanthus (MS) and respective biochars produced through slow pyrolysis (Slow), flash carbonization (Flash), and hydrothermal carbonization (HTC). Analytical replicates, n, are (a) $n = 1$, (b) $n = 3$ for all with the exception of two points where $n = 1$ and 2, and (c) n = between 2 and 8.

A significant correlation was observed between pH and O/C ratio for the biochars in this study when hydrochars were excluded (Figure 6a, $R^2 = 0.854$). In addition, the pH was significantly correlated to VM across slow pyrolysis and flash carbonization biochars:

$$\text{pH} = 10.63 - (0.049 \times \text{VM}) \quad R^2 = 0.78 \qquad (1)$$

Alkalinity is caused by negatively charged organic groups, such as $-COO^-$ (carboxylate) and O^- (hydroxyl), and carbonates on the surface of biochar.[39] With increasing pyrolysis intensity, the number of acid functional groups (as carboxylic) decreases and the decrease is linearly correlated with the loss of volatile matter.[40] A decrease in surface acidic groups and a concomitant increase in surface basic groups with increasing HTT have been correlated to an increase in buffering capacity with HTT.[41] In addition to the decrease in acid functional groups, carbonates have been reported as a source of alkalinity for higher HTT biochars.[39] Here we obtained only a weak correlation between ash and pH (Table 2). Although we cannot exclude carbonate, the high correlation of pH with VM and corresponding weak correlation with ash content suggest that organic functional groups were the main determinant of the pH response with

dx.doi.org/10.1021/jf501139f | J. Agric. Food Chem. 2014, 62, 3791−3799

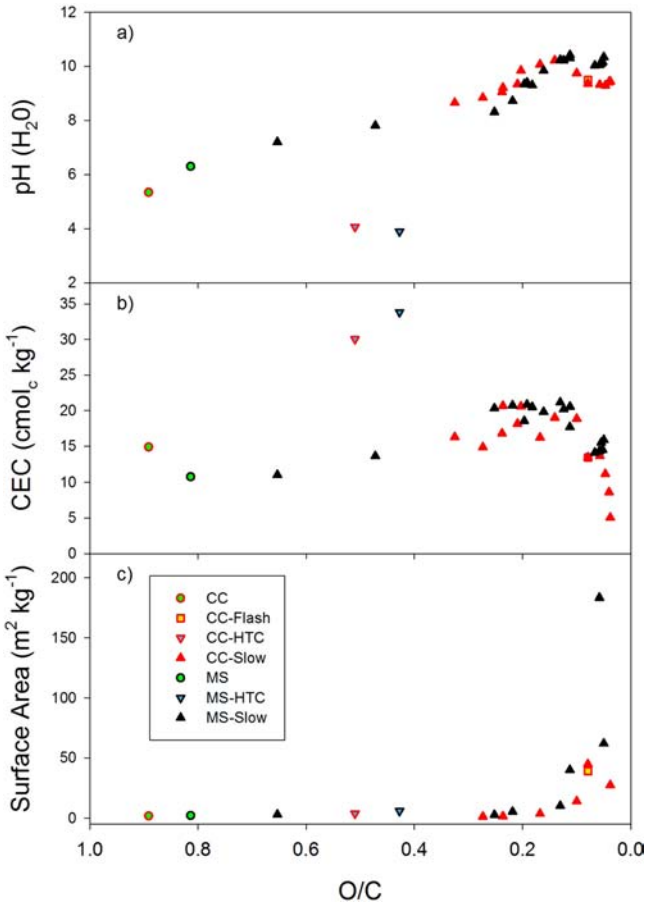

Figure 6. Surface properties (a) pH, (b) cation exchange capacity (CEC), and (c) surface area (SA) as a function of atomic ratio (O/C) for corncob (CC) and miscanthus (MS) and respective biochars produced through slow pyrolysis (Slow), flash carbonization (Flash), and hydrothermal carbonization (HTC). Analytical replicates, *n*, are (a) $n = 1$, (b) $n = 3$ for all with the exception of two points where $n = 1$ and 2, and (c) n = between 2 and 8.

HTT in slow pyrolysis biochars. Changes in pH as a function of the O/C ratio of slow pyrolysis biochars displayed a simple linear function, which did not fit the values of the hydrochars.

Surface Property: CEC. The CEC of both corncob and miscanthus slow pyrolysis biochars reached highest values at 350−475 °C (Figure 5b). The CEC of >450 °C biochars remained higher than that of feedstock for miscanthus while dropping substantially below for corncob. The lowest CEC was observed for the corncob sample pyrolyzed at 800 °C, suggesting that biochar CEC decreases with increasing HTT. Hydrochars displayed the highest CEC with an approximate doubling and tripling of CEC through HTC treatment of corncob and miscanthus, respectively. Flash carbonization, at an estimated 600 °C HTT, decreased the CEC of the feedstock only slightly, from 14.9 to 13.4 $cmol_c$ kg^{-1}.

Values of H/C and O/C atomic ratios in biochars are reported to be positively correlated to concentration in hydroxyl, carboxyl, and carbonyl groups and thereby to CEC.[25,42] Our HTC chars, however, had similar H/C and O/C values but higher CEC than low-HTT slow pyrolysis biochars. The higher CEC of our HTC chars was therefore not clearly reflected in these atomic ratios. The relationship we found between the atomic ratio O/C and CEC of both HTC and slow pyrolysis chars is presented in Figure 6b. Only at O/C ratios below 0.1 did we observe a marked reduction in CEC for corncob biochars. Simple correlations between CEC and other individual parameters were weak (Table 2), and the correlation between CEC and O/C excluding HTC was even weaker (R^2 = 0.012). We found that it is not possible to infer CEC on the basis of production parameters or chemical composition tested in this study and, therefore, could not confirm our initial hypothesis.

Changes in CEC have previously been explained by the presence of acid functional groups (AFGs).[43] Using various feedstocks, Wang et al.[44] found consistently lower CEC of biochars produced at 700 °C as compared to 500 °C and a correlating decrease in acid functional groups at the higher HTT. More specifically, Harvey and colleagues[22] observed an increase in −OH functional groups at or above 300 °C HTT and a loss of carboxylic groups at HTT above 500 °C. Although Mukherjee, Zimmerman, and Harris[40] found a correlation between VM and AFGs for 250, 400, and 650 °C chars, they also observed a lack of correlation between CEC and VM seen in our data set. They explained that not all AFGs can function as cation exchange sites and that HTT affects CEC more than it does AFGs. Especially because of the drastically different behavior of the hydrochars, our study suggests that the CEC response is difficult to predict over a wide range of temperatures because it is influenced by multiple factors with none clearly dominating.

Surface Property: SA. The surface area of biochar did not increase significantly until the raw feedstock was treated at HTT above 400 °C as shown in Figure 5c. The highest SA value of 183 m^2 g^{-1} was obtained through pyrolysis of miscanthus at 600 °C, this value being nearly 2 orders of magnitude higher than that of the feedstock. Biochar SA decreased at pyrolysis HTTs above 600 °C, corresponding to

Table 2. Correlation Coefficients from Spearman Rank Order Correlation[a]

	HTT	ash	VM	H/C	O/C	CEC	SA	pH
HTT	1							
ash	0.46**	1						
VM	−0.98***	−0.51**	1					
H/C	−0.99***	−0.47**	0.99***	1				
O/C	−0.99***	−0.46**	0.99***	0.99***	1			
CEC	−0.40*	−0.01	0.31	0.34*	0.34*	1		
SA	0.79***	0.58*	−0.83***	−0.81***	−0.82***	−0.12	1	
pH	0.71***	0.52***	−0.75***	−0.73***	−0.72***	0.04	0.61**	1

[a] *n* is the lowest number of samples of the two analyses: $n = 35$ for temp, $n = 18$ for SA, and $n = 36$ for all other analyses. ***, **, and * indicate respective significance levels of 0.001, 0.01, and 0.05.

O/C ratios below 0.2 (Figure 6c). HTC treatment did not increase SA, and this response is consistent with that of low-HTT slow pyrolysis biochars, both of which display high O/C ratios. The flash carbonization char exhibited a SA higher than most corncob chars in this study, and its SA appears to be similar to that of slow pyrolysis chars that underwent similar pyrolysis intensity.

Biochar SAs observed in this study are lower than values previously reported for corncob[45] and miscanthus[19] biochars of 300 and 400 $m^2 g^{-1}$. HTTs of 950 and 700 °C used to produce these respective biochars were also higher than those of the present study. Peak SA has been observed at HTTs between 650 and 850 °C for biochars from various feedstocks,[20] and HTTs >500 °C are needed to obtain significant increases in SA.[46] The increase in SA has been attributed mostly to the volatilization of organic compounds that otherwise clog pores,[42] similarly expressed in terms of loss of polar functional groups.[47] It has also been suggested that turbostratic structures harboring micropores develop through the growth of discontinuous graphene layers and that pore structures are destroyed at even higher temperatures when the turbostratic structures collapse into more organized graphite-like char.[48] Whereas HTT has been said to be the most important factor affecting SA,[49] the movement of volatiles away from char residues and the formation of cracks during pyrolysis are also influenced by carrier gas flow rate and other pyrolysis parameters involved with heat and mass transfer rates.[5,20] It is therefore not surprising that SA peaks and SA values at specific temperatures differ between studies, and although not all studies report a decrease in SA at higher HTT,[34,48] this effect might always be present if sufficiently high HTTs are applied. In our study, SA was poorly correlated to either VM content or O/C (Table 2), suggesting that the removal of VM from pores is not the only mechanism responsible for increased SA with increased HTT.

High SA, high CEC, and high pH are desirable properties of biochars for soil improvement. Here, as compared to feedstock, we increased SA by up to 2 orders of magnitude and pH by up to 4 units. In contrast, increases in CEC for slow pyrolysis remained modest irrespective of HTT. This finding suggests that designing a high-CEC biochar remains elusive, at least with the methods presently tested. This does not mean, however, that biochar transformations in soil cannot lead to improvement of soil CEC, as reported by Cheng et al.[43] Studies with wood-derived biochar suggested that concomitant increases in SA, CEC, and pH are obtained within a fairly narrow HTT range at around 400–450 °C.[18] Here, high SA was obtained only around 600 °C. This finding agrees with other grass-derived biochar studies which indicate that higher HTT is needed for obtaining high SA.[21] Proximate analysis and atomic ratios were poor predictors of SA and CEC, and our hypothesis that surface properties could be predicted from composition indicators was not confirmed. Specific production parameters appeared to have a significant impact on surface properties, indicating that specific analyses are necessary to identify and characterize high-SA biochars.

■ ASSOCIATED CONTENT

Supporting Information

Tables 1S and 2S. This material is available free of charge via the Internet at http://pubs.acs.org.

■ AUTHOR INFORMATION

Corresponding Author

*(A.B.) Phone: +47 954 79 226. E-mail: alice.budai@bioforsk.no.

Funding

Funding for the research was provided by the Research Council of Norway through the project "Advanced Techniques to Evaluate the Long-term Stability and Carbon Sequestration Potential of Different Types of Biochar", NFR197531.

Notes

The authors declare no competing financial interest.

■ ACKNOWLEDGMENTS

Hydrochar samples were prepared and provided by Markus Antonietti at the Max-Planck Institute for Colloids and Interfaces in Potsdam, Germany.

■ ABBREVIATIONS USED

VM, volatile matter; HTC, hydrothermal carbonization; CEC, cation exchange capacity; HTT, highest treatment temperature; SA, surface area

■ REFERENCES

(1) Lehmann, J.; Joseph, S. *Biochar for Environmental Management: An Introduction*; International Biochar Initiative: Westerville, OH, USA, 2009; pp 1–12.

(2) Spokas, K. A.; Cantrell, K. B.; Novak, J. M.; Archer, D. W.; Ippolito, J. A.; Collins, H. P.; Boateng, A. A.; Lima, I. M.; Lamb, M. C.; McAloon, A. J.; Lentz, R. D.; Nichols, K. A. Biochar: a synthesis of its agronomic impact beyond carbon sequestration. *J. Environ. Qual.* **2012**, *41*, 973–989.

(3) Manya, J. J. Pyrolysis for biochar purposes: a review to establish current knowledge gaps and research needs. *Environ. Sci. Technol.* **2012**, *46*, 7939–7954.

(4) Shafizadeh, F. The chemistry of pyrolysis and combustion. *Adv. Chem. Ser.* **1984**, *No. 207*, 491–529.

(5) Antal, M. J.; Gronli, M. The art, science, and technology of charcoal production. *Ind. Eng. Chem. Res.* **2003**, *42*, 1619–1640.

(6) Neves, D.; Thunman, H.; Matos, A.; Tarelho, L.; Gomez-Barea, A. Characterization and prediction of biomass pyrolysis products. *Prog. Energy Combust. Sci.* **2011**, *37*, 611–630.

(7) Lehmann, J.; Gaunt, J.; M, R. Bio-char sequestration in terrestrial ecosystems – a review. *Mitigation Adaptation Strategies Global Change* **2006**, *11*, 403–427.

(8) Glaser, B.; Lehmann, J.; Zech, W. Ameliorating physical and chemical properties of highly weathered soils in the tropics with charcoal – a review. *Biol. Fertil. Soils* **2002**, *35*, 219–230.

(9) Jeffery, S.; Verheijen, F. G. A.; van der Velde, M.; Bastos, A. C. A quantitative review of the effects of biochar application to soils on crop productivity using meta-analysis. *Agric. Ecosyst. Environ.* **2011**, *144*, 175–187.

(10) Ronsse, F.; van Hecke, S.; Dickinson, D.; Prins, W. Production and characterization of slow pyrolysis biochar: influence of feedstock type and pyrolysis conditions. *Global Change Biol. Bioenergy* **2013**, *5*, 104–115.

(11) Ippolito, J. A.; Laird, D. A.; Busscher, W. J. Environmental benefits of biochar. *J. Environ. Qual.* **2012**, *41*, 967–972.

(12) Ameloot, N.; Graber, E. R.; Verheijen, F. G. A.; De Neve, S. Interactions between biochar stability and soil organisms: review and research needs. *Eur. J. Soil Sci.* **2013**, *64*, 379–390.

(13) McCormack, S. A.; Ostle, N.; Bardgett, R. D.; Hopkins, D. W.; Vanbergen, A. J. Biochar in bioenergy cropping systems: impacts on soil faunal communities and linked ecosystem processes. *Global Change Biol. Bioenergy* **2013**, *5*, 81–95.

(14) Liang, B.; Lehmann, J.; Solomon, D.; Kinyangi, J.; Grossman, J.; O'Neill, B.; Skjemstad, J. O.; Thies, J.; Luizao, F. J.; Petersen, J.; Neves,

E. G. Black carbon increases cation exchange capacity in soils. *Soil Sci. Soc. Am. J.* **2006**, *70*, 1719−1730.
(15) Laird, D. A.; Fleming, P.; Davis, D. D.; Horton, R.; Wang, B. Q.; Karlen, D. L. Impact of biochar amendments on the quality of a typical Midwestern agricultural soil. *Geoderma* **2010**, *158*, 443−449.
(16) Van Zwieten, L.; Kimber, S.; Morris, S.; Chan, K. Y.; Downie, A.; Rust, J.; Joseph, S.; Cowie, A. Effects of biochar from slow pyrolysis of papermill waste on agronomic performance and soil fertility. *Plant Soil* **2010**, *327*, 235−246.
(17) Budai, A.; Zimmerman, A. R.; Cowie, A. L.; Webber, J. B. W.; Singh, B. P.; Glaser, B.; Masiello, C. A.; Andersson, D.; Shields, F.; Lehmann, J.; Camps Arbestain, M.; Williams, M.; Sohi, S.; Joseph, S. *Biochar Carbon Stability Test Method: An Assessment of Methods To Determine Biochar Carbon Stability*; International Biochar Initiative (IBI): Westerville, OH, USA, 2013.
(18) Lehmann, J. Bio-energy in the black. *Front. Ecol. Environ.* **2007**, *5*, 381−387.
(19) Lee, Y.; Eum, P. R. B.; Ryu, C.; Park, Y. K.; Jung, J. H.; Hyun, S. Characteristics of biochar produced from slow pyrolysis of Geodae-Uksae 1. *Bioresour. Technol.* **2013**, *130*, 345−350.
(20) Brown, R. A.; Kercher, A. K.; Nguyen, T. H.; Nagle, D. C.; Ball, W. P. Production and characterization of synthetic wood chars for use as surrogates for natural sorbents. *Org. Geochem.* **2006**, *37*, 321−333.
(21) Chun, Y.; Sheng, G. Y.; Chiou, C. T.; Xing, B. S. Compositions and sorptive properties of crop residue-derived chars. *Environ. Sci. Technol.* **2004**, *38*, 4649−4655.
(22) Harvey, O. R.; Herbert, B. E.; Kuo, L. J.; Louchouarn, P. Generalized two-dimensional perturbation correlation infrared spectroscopy reveals mechanisms for the development of surface charge and recalcitrance in plant-derived biochars. *Environ. Sci. Technol.* **2012**, *46*, 10641−10650.
(23) Houben, D.; Sonnet, P.; Cornelis, J. T. Biochar from miscanthus: a potential silicon fertilizer. *Plant Soil* **2014**, *374*, 871−882.
(24) Wang, L.; Trninic, M.; Skreiberg, O.; Gronli, M.; Considine, R.; Antal, M. J. Is elevated pressure required to achieve a high fixed-carbon yield of charcoal from biomass? Part 1: Round-robin results for three different corncob materials. *Energy Fuels* **2011**, *25*, 3251−3265.
(25) Wiedner, K.; Naisse, C.; Rumpel, C.; Pozzi, A.; Wieczorek, P.; Glaser, B. Chemical modification of biomass residues during hydrothermal carbonization − what makes the difference, temperature or feedstock? *Org. Geochem.* **2013**, *54*, 91−100.
(26) Antal, M. J.; Mochidzuki, K.; Paredes, L. S. Flash carbonization of biomass. *Ind. Eng. Chem. Res.* **2003**, *42*, 3690−3699.
(27) Gaskin, J. W.; Steiner, C.; Harris, K.; Das, K. C.; Bibens, B. Effect of low-temperature pyrolysis conditions on biochar for agricultural use. *Trans. ASABE* **2008**, *51*, 2061−2069.
(28) Calucci, L.; Rasse, D. P.; Forte, C. Solid-state nuclear magnetic resonance characterization of chars obtained from hydrothermal carbonization of corncob and miscanthus. *Energy Fuels* **2013**, *27*, 303−309.
(29) Vassilev, S. V.; Baxter, D.; Andersen, L. K.; Vassileva, C. G.; Morgan, T. J. An overview of the organic and inorganic phase composition of biomass. *Fuel* **2012**, *94*, 1−33.
(30) Demirbas, A. Effects of temperature and particle size on bio-char yield from pyrolysis of agricultural residues. *J. Anal. Appl. Pyrolysis* **2004**, *72*, 243−248.
(31) Antal, M. J.; Allen, S. G.; Dai, X. F.; Shimizu, B.; Tam, M. S.; Gronli, M. Attainment of the theoretical yield of carbon from biomass. *Ind. Eng. Chem. Res.* **2000**, *39*, 4024−4031.
(32) Ascough, P. L.; Bird, M. I.; Wormald, P.; Snape, C. E.; Apperley, D. Influence of production variables and starting material on charcoal stable isotopic and molecular characteristics. *Geochim. Cosmochim. Acta* **2008**, *72*, 6090−6102.
(33) Fuertes, A. B.; Arbestain, M. C.; Sevilla, M.; Macia-Agullo, J. A.; Fiol, S.; Lopez, R.; Smernik, R. J.; Aitkenhead, W. P.; Arce, F.; Macias, F. Chemical and structural properties of carbonaceous products obtained by pyrolysis and hydrothermal carbonisation of corn stover. *Aust. J. Soil Res.* **2010**, *48*, 618−626.
(34) Nunoura, T.; Wade, S. R.; Bourke, J. P.; Antal, M. J. Studies of the flash carbonization process. 1. Propagation of the flaming pyrolysis reaction and performance of a catalytic afterburner. *Ind. Eng. Chem. Res.* **2006**, *45*, 585−599.
(35) Cao, X.; Ro, K. S.; Libra, J. A.; Kammann, C. I.; Lima, I.; Berge, N.; Li, L.; Li, Y.; Chen, N.; Yang, J.; Deng, B.; Mao, J. Effects of biomass types and carbonization conditions on the chemical characteristics of hydrochars. *J. Agric. Food Chem.* **2013**, *61*, 9401−9411.
(36) Mukome, F. N. D.; Zhang, X. M.; Silva, L. C. R.; Six, J.; Parikh, S. J. Use of chemical and physical characteristics to investigate trends in biochar feedstocks. *J. Agric. Food Chem.* **2013**, *61*, 2196−2204.
(37) Spokas, K. A. Review of the stability of biochar in soils: predictability of O:C molar ratios. *Carbon Manage.* **2010**, *1*, 289−303.
(38) Enders, A.; Hanley, K.; Whitman, T.; Joseph, S.; Lehmann, J. Characterization of biochars to evaluate recalcitrance and agronomic performance. *Bioresour. Technol.* **2012**, *114*, 644−653.
(39) Yuan, J. H.; Xu, R. K.; Zhang, H. The forms of alkalis in the biochar produced from crop residues at different temperatures. *Bioresour. Technol.* **2011**, *102*, 3488−3497.
(40) Mukherjee, A.; Zimmerman, A. R.; Harris, W. Surface chemistry variations among a series of laboratory-produced biochars. *Geoderma* **2011**, *163*, 247−255.
(41) Al-Wabel, M. I.; Al-Omran, A.; El-Naggar, A. H.; Nadeem, M.; Usman, A. R. A. Pyrolysis temperature induced changes in characteristics and chemical composition of biochar produced from conocarpus wastes. *Bioresour. Technol.* **2013**, *131*, 374−379.
(42) Lee, J. W.; Kidder, M.; Evans, B. R.; Paik, S.; Buchanan, A. C.; Garten, C. T.; Brown, R. C. Characterization of biochars produced from cornstovers for soil amendment. *Environ. Sci. Technol.* **2010**, *44*, 7970−7974.
(43) Cheng, C. H.; Lehmann, J.; Thies, J. E.; Burton, S. D.; Engelhard, M. H. Oxidation of black carbon by biotic and abiotic processes. *Org. Geochem.* **2006**, *37*, 1477−1488.
(44) Wang, Y.; Hu, Y.; Zhao, X.; Wang, S.; Xing, G. Comparisons of biochar properties from wood material and crop residues at different temperatures and residence times. *Energy Fuels* **2013**, *27*, 5890−5899.
(45) Bourke, J.; Manley-Harris, M.; Fushimi, C.; Dowaki, K.; Nunoura, T.; Antal, M. J. Do all carbonized charcoals have the same chemical structure? 2. A model of the chemical structure of carbonized charcoal. *Ind. Eng. Chem. Res.* **2007**, *46*, 5954−5967.
(46) Kloss, S.; Zehetner, F.; Dellantonio, A.; Hamid, R.; Ottner, F.; Liedtke, V.; Schwanninger, M.; Gerzabek, M. H.; Soja, G. Characterization of slow pyrolysis biochars: effects of feedstocks and pyrolysis temperature on biochar properties. *J. Environ. Qual.* **2012**, *41*, 990−1000.
(47) Chen, B. L.; Zhou, D. D.; Zhu, L. Z. Transitional adsorption and partition of nonpolar and polar aromatic contaminants by biochars of pine needles with different pyrolytic temperatures. *Environ. Sci. Technol.* **2008**, *42*, 5137−5143.
(48) Keiluweit, M.; Nico, P. S.; Johnson, M. G.; Kleber, M. Dynamic molecular structure of plant biomass-derived black carbon (biochar). *Environ. Sci. Technol.* **2010**, *44*, 1247−1253.
(49) Lua, A. C.; Yang, T.; Guo, J. Effects of pyrolysis conditions on the properties of activated carbons prepared from pistachio-nut shells. *J. Anal. Appl. Pyrolysis* **2004**, *72*, 279−287.
(50) Crombie, K.; Masek, O.; Sohi, S. P.; Brownsort, P.; Cross, A. The effect of pyrolysis conditions on biochar stability as determined by three methods. *Global Change Biol. Bioenergy* **2013**, *5*, 122−131.
(51) Hammes, K.; Smernik, R. J.; Skjemstad, J. O.; Herzog, A.; Vogt, U. F.; Schmidt, M. W. I. Synthesis and characterisation of laboratory-charred grass straw (*Oryza sativa*) and chestnut wood (*Castanea sativa*) as reference materials for black carbon quantification. *Org. Geochem.* **2006**, *37*, 1629−1633.
(52) Kuo, L. J.; Herbert, B. E.; Louchouarn, P. Can levoglucosan be used to characterize and quantify char/charcoal black carbon in environmental media? *Org. Geochem.* **2008**, *39*, 1466−1478.

(53) Hao, F. H.; Zhao, X. C.; Ouyang, W.; Lin, C. Y.; Chen, S. Y.; Shan, Y. S.; Lai, X. H. Molecular structure of corncob-derived biochars and the mechanism of atrazine sorption. *Agron. J.* **2013**, *105*, 773−782.
(54) Mimmo, T.; Panzacchi, P.; Baratieri, M.; Davies, C. A.; Tonon, G. Effect of pyrolysis temperature on miscanthus (*Miscanthus* × *giganteus*) biochar physical, chemical and functional properties. *Biomass Bioenergy* **2014**, 10.1016/j.biombioe.2014.01.004.
(55) Whitman, T.; Hanley, K.; Enders, A.; Lehmann, J. Predicting pyrogenic organic matter mineralization from its initial properties and implications for carbon management. *Org. Geochem.* **2013**, *64*, 76−83.

just like the high solids effect, higher concentrations of dissolved solids lead to a decrease in the product yield. We used a pure microcrystalline cellulose substrate, Avicel, for the hydrolysis experiments to rule out other potential substrate-related inhibiting factors (lignin, hemicellulose) and focus on the liquid phase. The hydrolysis was furthermore run at 5% water insoluble solids to observe the impact of soluble compounds and not of a high solids content. The findings generated from this study remind us that enzymatic hydrolysis remains a biological process; enzyme performance is very sensitive to small changes in the external environment, which have to be accounted for during process design. This study is particularly relevant in industrial settings where hydrolysis is to be performed at high dry matter contents as soluble product accumulation is high in the liquid phase during hydrolysis[11] under these circumstances.

MATERIALS AND METHODS

Enzymatic Hydrolysis of Avicel with Novozymes Cellic CTec2. Fifty milligrams of Avicel was weighed in 2 mL screw-cap tubes and filled with diluted enzyme solution for a total water-insoluble solids loading of 5% w/w. The commercial cellulolytic enzyme mixture Cellic CTec2 from Novozymes A/S, Bagsværd, Denmark, was used in all studies. The mixture had a protein content of 161 mg/g, a filter paper activity of 120 FPU/g, and a β-glucosidase activity of 2731 U/g. The protein content was measured using the ninhydrin assay with BSA as the protein standard,[19] the filter paper activity was determined according to the method of Ghose,[20] and the β-glucosidase activity was measured using 5 mM *p*-nitrophenyl-β-D-glucopyranoside (Sigma-Aldrich) as substrate.[21] The enzymatic loading for all studies was 13 mg enzyme protein/g dry matter (approximately 10 FPU/g Avicel).

The hydrolysis of Avicel was performed in pure water as well as 50 mM citrate buffer at pH 4.8. Additionally, five soluble monosaccharides (glucose, galactose, mannose, fructose, and xylose) at 50, 270, 540, and 810 mM were used (in separate experiments) to spike the samples prior to hydrolysis. For the first four monosaccharides, the molar concentrations are equivalent to approximately 10, 50, 100, and 150 g/L mass concentration, respectively, that is, in or above the range of soluble glucose found during lignocellulose hydrolysis at high dry matter for an industrial setup.[11] The samples were spiked with glucose to study its effect as a hydrolysis end product; that is, product inhibition was expected. Galactose and mannose were chosen as they are stereoisomers of glucose but are not end products of hydrolysis. Xylose was used as it is one of the major monosaccharides found in biomass, and fructose, even though not a major component in biomass, is a structural isomer of glucose and is the most water-soluble of all monosaccharides. Samples were prepared in triplicates, and the hydrolysis was carried out using an incubator at 50 °C with an orbital shaker set at 150 rpm. Hydrolysis was run for 96 h.

Control samples (without enzyme) were prepared and analyzed for their sugar content at 15 min and at the end of hydrolysis to verify whether the sugars had degraded over time. The hydrolyses were terminated by centrifuging each sample at 13200*g* and 5 °C for 10 min and filtering through a 0.45 μm syringe filter (Millipore, Bedford, MA, USA). Filtrates were stored at −20 °C for further HPLC quantification.

Enzymatic Hydrolysis of Cellobiose with Novozymes Cellic CTec2. Fifty milligrams of D-cellobiose (Sigma-Aldrich, USA) was weighed in 2 mL screw-cap tubes and filled with diluted enzyme solution in 50 mM acetate buffer at pH 4.8 for a total dry matter content of 5% w/w. The enzymatic loading was 13 mg/g of cellobiose. Furthermore, 50, 270, 540, or 810 mM glucose or galactose was added. Samples were prepared in triplicates and incubated at 50 °C with an orbital shaker set at 150 rpm for 1 h. The hydrolysis was terminated by centrifugation and filtration as described above, followed by HPLC quantification.

Enzymatic Hydrolysis of Avicel and Cellobiose with Novozymes Cellic CTec2. Avicel hydrolysis samples were prepared as described above (5% water insoluble solids, 13 mg/g enzyme loading) in 50 mM acetate buffer at pH 4.8 and additional 50, 270, 540, and 810 mM glucose or galactose. At the end of 96 h, 200 μL of hydrolysate was removed from the sample and 200 μL of cellobiose (125 g/L in 50 mM acetate buffer) was introduced. The hydrolysate aliquots were centrifuged, filtered, and frozen as described above, whereas the original samples with freshly added cellobiose were incubated for 1 h further before termination of the hydrolysis and processed as described above, followed by HPLC quantification.

HPLC Sugar Quantification. D-Cellobiose, D-glucose, D-mannose, D-fructose, D-galactose, and D-xylose (standards obtained from Sigma-Aldrich, USA) were quantified with UltiMate 3000 HPLC (Dionex, Germany) equipped with a refractive index detector (Shodex, Japan). The separation was performed in a Phenomenex Resex ROA column at 80 °C with 5 mM H_2SO_4 as eluent at a flow rate of 0.6 mL/min. As mannose and xylose, plus fructose and galactose, have the same retention time of 11 min, with this column, their concentrations were separately quantified using their respective calibration standard curves. The results were analyzed using Chromeleon software from Dionex.

LF-NMR T_2 Relaxation. NMR measurements were performed on a Bruker mq20 minispec with a 0.47 T permanent magnet (equivalent to 20 MHz proton resonance frequency). The internal magnet temperature was 40 °C. T_2 values of hydrolysis solutions (before Avicel and cellulase addition) were measured using the CPMG pulse sequence. Each sample was run with 32 scans and a 5 s recycle delay containing 8000 points and a pulse separation of 1.2 ms between each scan. The obtained relaxation curves were analyzed using the inverse Laplace transformation method CONTIN,[22] where all solutions gave a single T_2 relaxation peak. The T_2 reported are thus the peak maxima positions of this peak.

Protein Adsorption Measurements. Fifty milligrams of Avicel was weighed in 2 mL screw-cap tubes and filled with diluted Novozymes Cellic CTec2 (10 FPU) for a total water-insoluble solids content of 5% w/w. The liquid fraction contained 50, 270, 540, or 810 mM glucose, galactose, mannose, or xylose. The samples were prepared in triplicates and incubated at 50 °C for 30 min to allow the protein to bind to the substrate. Avicel blanks without enzyme were run in parallel. To determine the free protein content in solution, diluted enzyme solutions without Avicel were also run in parallel. After incubation, the samples were centrifuged at 850*g* and 5 °C for 2 min, from which 400 μL of the supernatant was sampled. Two microliters of this supernatant was then analyzed for protein content on a Thermo Scientific NanoDrop 2000 spectrophotometer (Wilmington, DE, USA) at 280 nm UV wavelength absorption.

RESULTS AND DISCUSSION

Hydrolysis of Avicel at High Monosaccharide Concentrations. Solutions containing high concentrations of monosaccharides can decrease the mobility of free water and inhibit hydrolysis. Previous studies have indicated that high concentrations of glucose have an inhibitory effect on cellulase activity.[12,23,24] End products of hydrolysis, glucose and cellobiose, inhibit cellulases based on the classical definition of end-product inhibition.[25] However, as Xiao et al.[12] and Roberts et al.[14] have shown, the presence of other monosaccharides that are not end products of hydrolysis also decrease glucose yields. Figure 1 shows the glucose yield after 96 h for samples that were spiked with different monosaccharides. As expected, the yield decreased for all sugars studied as the initial monosaccharide concentration increased. Sugars at low concentration (50 mM) slightly boosted glucose production (especially galactose), but at higher concentrations (>270 mM) the yield decreased considerably compared to pure water.

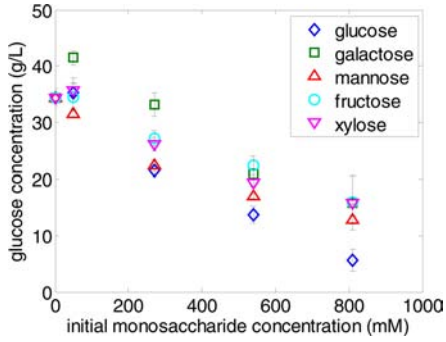

Figure 1. Hydrolysis of Avicel at 5% dry matter after 96 h spiked with glucose, xylose, galactose, fructose, or mannose from low to high concentrations of monosaccharides. Monosaccharides present at low concentrations seem to be beneficial to hydrolysis as there is a small boost in the product yield in some cases. At higher concentrations of sugars, however, they are detrimental to the cellulases as the yield keeps decreasing.

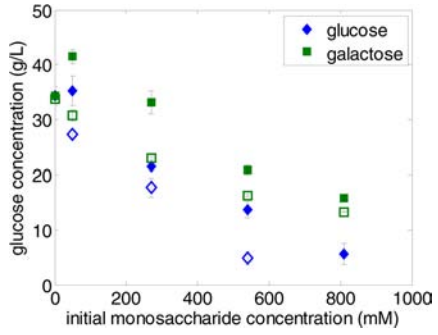

Figure 2. Glucose production after 96 h of Avicel hydrolysis in water (solid symbols) versus 50 mM acetate buffer (open symbols) with initial glucose or galactose spikes to determine additive effects between acetate and monosaccharide. Despite a more stable pH with a small added concentration of buffer, the additional presence of soluble salts at higher concentrations has a detrimental effect on the glucose yield.

Some of the sugar concentrations tested in Figure 1 are unrealistically high when compared to realistic biorefinery scenarios. For example, for hydrolysis of pretreated wheat straw at 30% dry matter content using Cellic CTec2, 95 g/L (approximately 527 mM) was the highest glucose concentration reported for a separate hydrolysis and fermentation process.[11] In a simultaneous hydrolysis and fermentation process, however, the glucose concentration will remain at <5 g/L (approximately 27 mM) as the yeast continuously ferments the glucose.[11]The study nevertheless illustrates the monosaccharide inhibition mechanisms at play.

The reasons for the increase in levels of hydrolysis at 50 mM monosaccharides are not fully understood, but it could be due to an improvement in protein stability.[16,26] At low concentrations of monosaccharide, these compounds are excluded from the protein hydration shell, but can play a role dictating the dynamic flexibility and biological activity of proteins,[27] protecting enzymes against inactivation, inhibition, and denaturation. With incremental additions of soluble compounds, these slowly will start interfering with the protein hydration shell in solution and eventually decrease enzyme performance.[27,28]

Whereas the pH fluctuations were around 4.80 ± 0.20 in all experiments shown in Figure 1, the cause of decreased glucose production had mainly to do with the presence of high sugar concentrations. As seen in Figure 2, performing the hydrolysis in 50 mM acetate buffer to stabilize the pH yields similar glucose concentrations as hydrolysis in pure water. With high concentrations of glucose or galactose in the liquid phase, however, the yield decreased compared to the hydrolysis performed in water.

Regardless of the monosaccharide structure, the general trend with increasing monosaccharides in the hydrolysate is that it is detrimental to the glucose yield of hydrolysis, which was shown by Roberts and co-workers[14] to be a mass transfer effect, the idea being that with the addition of glucose or mannose to the system, the water became more viscous, making it more difficult for the cellulases to diffuse into reaction sites. Although the mass transfer argument still holds, the experiments in this study show that the addition of the same amount of monosaccharides by weight (in the case of the C6 sugars) and by molar mass (all sugars including xylose) lower the cellulose conversion yield to different extents. At 810 mM sugars, for example, galactose and fructose give higher glucose hydrolysis yields than when having additional mannose in the hydrolysates. Thus, the saccharification rates must be limited by other factors aside from mass transfer and end-product (glucose) inhibition, which we suggest may have to do with the way each monosaccharide interacts with water. In this section, we look at three possibilities related to monosaccharide solutions: solubility, partial molar volume, and T_2 relaxation time.

Selig et al.[15] suggested that an increase in the amount of water-soluble species in the system can significantly inhibit cellulases. One can speculate that when soluble species form strong interactions with water to maintain their solubility, water has lower mobility and hydrolysis slows. In this case, it would mean that sugars which interact more with water in the solution should inhibit hydrolysis to a greater extent than those with weaker interactions. Therefore, we tested if the decrease in glucose yield could be linked to the water solubility of the monosaccharides, as more soluble monosaccharides would be expected to interact with fewer water molecules and hence produce higher glucose yields than the less soluble monosaccharides. Table 1 shows reported literature values[29,30] for the saturation point of sugars used in this study. Fructose is the most soluble sugar followed by xylose, glucose, mannose, and galactose. Whereas more soluble sugars interact with fewer water molecules in the system, our results show that despite galactose being the least soluble monosaccharide, it gave higher yields compared to the rest of the sugars. Therefore, the solubility of the monosaccharides cannot fully explain the recorded differences between hydrolysis yields.

Table 1. Sugar Saturation Points As Reported in the Literature

monosaccharide	solubility (g/L)
glucose	909
galactose	683
mannose	713
xylose	1250
fructose	3750

Another method of quantifying how much water monosaccharides take up in solution is the partial molar volume.[31] Experimental data from Shahidi et al.[32] showed larger partial molar volume for glucose followed by galactose, mannose,

dx.doi.org/10.1021/jf5012962 | J. Agric. Food Chem. 2014, 62, 3800−3805

fructose, and xylose at 25 °C. All of the C6 sugars studied contained the same number of hydroxyl groups capable of hydrogen bonding to the solvent, water. As xylose has one fewer hydroxyl group than the other sugars, it would be expected that its partial molar volume would be smaller. In this case, the strength of the solute−solvent interaction would be highly specific and dependent on the conformation of the monosaccharide in solution. Tait et al.[33] showed that monosaccharides with more equatorial groups tend to have higher partial molar volume, thus explaining why glucose (four equatorial OH groups in its open chain form) has a stronger interaction with water than mannose and galactose (both three equatorial OH groups) as it takes up more volume per mole in solution. Although this method sheds more light on the extent of inhibition caused by glucose despite its high solubility, it still does not fully explain why samples spiked with galactose consistently produced higher glucose yields despite the low solubility and high partial molar volume of galactose.

Lastly, we tested whether LF-NMR T_2 proton relaxation data could reveal differences in hydration behavior. Relaxation times depicted in Figure 3 show that galactose solutions have the highest free water mobilities (longest relaxation times) of all the monosaccharides, which correlate with the higher yields compared to the other sugars. The lower the relaxation time, the less overall free water in the system. At low concentrations of soluble molecules, the T_2 is very close to that of pure water (2696 ms). In fact, for samples with sugars that had higher T_2 than water, their cellulose conversions were actually higher than the hydrolysis performed in pure water. The trend with T_2, as discussed by Mora-Gutierrez and Baianu,[18] is that they decrease linearly as the concentration of dissolved solids increases because the average molecular distance between the solute becomes shorter.

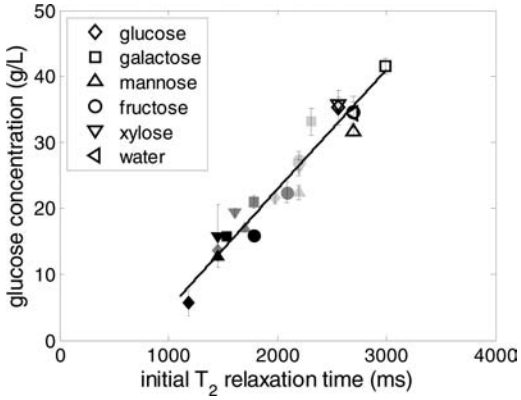

Figure 3. Initial T_2 of the liquid phase versus glucose production after 96 h of Avicel hydrolysis. Initial monosaccharide concentrations of 50 mM (open symbols), 270 mM (light gray symbols), 540 mM (dark gray symbols), or 810 mM (black symbols) show a linear correlation between the LF-NMR T_2 value and the concentration of glucose produced.

Correlations between the glucose hydrolysis yield and the T_2 of the hydrolysis liquid phase before saccharification are shown in Figure 3. At 50 mM dissolved solids, glucose yields are high regardless of which soluble molecules are present, and relaxation times have little significance over product yields. As the monosaccharide concentration increases, the relaxation time and glucose yield relationship becomes more linear, where solutions with lower free water availability produce lower glucose yields. Mora-Gutierrez and Baianu[18] give several explanations for the solution behavior under LF-NMR. Despite all C6 sugars possessing the same number of hydroxyl groups (potential solute hydration sites), their conformation in solution is different. As an example, glucose (aldo-sugar) mainly exists as two forms (α- and β-pyranose), whereas fructose (keto-sugar) has three (β-pyranose and α- and β-furanose). Therefore, the probability of forming H-bonds for fructose is lower as it is able to change to more conformations (i.e., water binding to glucose is stronger than to fructose). Our results indicate that the limitation of hydrolysis at higher monosaccharides content can be predicted by a LF-NMR T_2 measurement with a correlation coefficient of 0.94.

The way water is ordered around soluble compounds, based on solubility, partial molar volume, and water relaxation time data, has an effect on enzyme−substrate behavior and can be used to determine whether hydrolysis yields are affected. The degree of hydrolysis inhibition varied between different concentrations as well as chemical properties of the monosaccharides; for example, glucose and mannose are more inhibitory at high concentrations than galactose. Not only does the compound's solubility in water play a role but also does the overall water availability for hydrolysis.

Hydrolysis of Cellobiose at High Sugar Concentration. The saccharification results presented to this point have solely focused on glucose production. Cellobiose production has so far been neglected because, as shown in Table 2, in most cases it has been consumed by the β-glucosidases in the CTec2 mix. Its presence has been consistently below the detection limit for the HPLC (<0.5 g/L) except in the cases of glucose, galactose, and mannose at >270 mM. Despite the lack of a boiling step during the hydrolysis termination step, centrifuging at high speed followed by filtration and freezing yielded the same concentration of cellobiose and glucose when a boiling step was implemented (data not shown). Therefore, these results indicate that the cellulase components most inhibited by the high monosaccharide concentration are those acting on the insoluble substrate, that is, cellobiohydrolases and endoglucanases, and not the β-glucosidases. To investigate whether the cellobiose accumulation was an effect of low water availability or of end-product inhibition, two different experiments were performed: (1) hydrolysis of cellobiose for 1 h at 10 FPU with CTec2 (Figure 4a) and (2) hydrolysis of Avicel with additional cellobiose after 96 h (Figure 4b) to determine whether the cellobiose was still being hydrolyzed regardless of Avicel saccharification being at a standstill.

Table 2. Cellobiose Concentration (Grams per Liter) after 96 h of Hydrolysis of 50 g/L Avicel

	spike			
sugar	50 mM	270 mM	540 mM	810 mM
glucose	<0.5	0.91 ± 0.17	1.65 ± 0.18	3.63 ± 0.11
galactose	<0.5	0.95 ± 0.04	1.69 ± 0.03	2.23 ± 0.05
mannose	<0.5	1.18 ± 0.04	1.98 ± 0.05	2.60 ± 0.03
fructose	<0.5	<0.5	<0.5	<0.5
xylose	<0.5	<0.5	<0.5	<0.5

The data from Figure 4a show that the hydrolysis of cellobiose with CTec2 occurs regardless of the concentration of galactose but is inhibited in the presence of high concentrations of glucose. In other words, β-glucosidase is still active even at high concentrations of sugars, but undergoes end-product

dx.doi.org/10.1021/jf5012962 | J. Agric. Food Chem. 2014, 62, 3800−3805

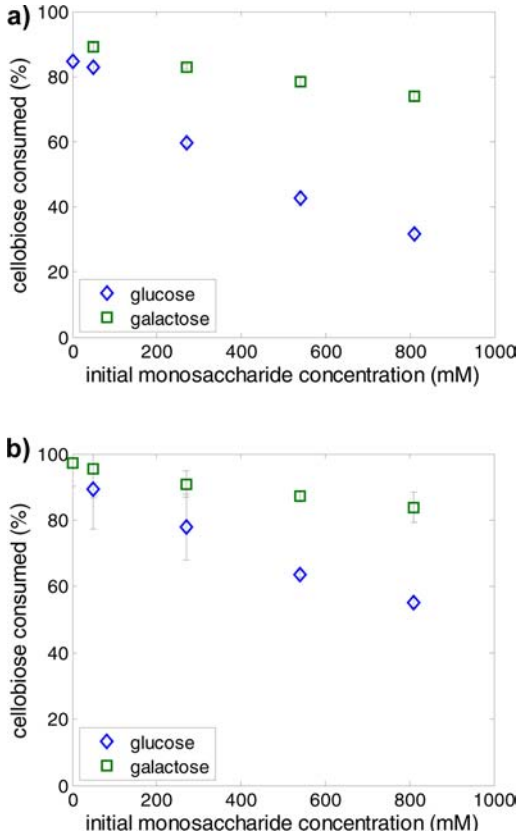

Figure 4. (a) Hydrolysis yield of 50 g/L cellobiose after incubation for 1 h with Cellic CTec2 in the presence of glucose or galactose. (b) Percentage of cellobiose consumed after the addition of 25 g/L cellobiose following Avicel hydrolysis after 96 h in the presence of glucose or galactose.

inhibition when the hydrolysates are spiked with glucose. In the case when cellobiose is added during conventional hydrolysis (Figure 4b), cellobiose is still being hydrolyzed by the β-glucosidases despite the cellobiohydrolases being inhibited in the presence of high concentrations of sugars, except glucose. Therefore, it is possible to predict hydrolysis yields based on LF-NMR T_2 measurements. However, end-product inhibition, observed only for the β-glucosidases, could not be correlated to relaxation data as it is an intrinsic property of the enzyme independent of the concentration of dissolved solids in solution.

Cellulase Adsorption at High Monosaccharide Concentration. One aspect of this study that has not been certain is whether a high concentration of sugars is preventing the cellulases from adsorbing to the substrate surface or depriving the cellulases from their biological activity. Previous work by Kumar and Wyman[34] showed that high concentrations of glucose prevented cellulase adsorption to the substrate; but it was not clear whether it was an inactivation of the catalytic domain and/or the binding domain or a combination of both. Furthermore, Kristensen et al.[9] showed that the increasing concentrations of glucose and cellobiose at high solids settings resulted in reduced enzyme adsorption, thereby potentially inhibiting the endoglucanase and cellobiohydrolase action. Binding kinetic studies are beyond the scope of this paper, but preliminary data (Figure 5) show that cellulase binding increases with increasing monosaccharide content (with the exception of glucose, for which binding to the substrate

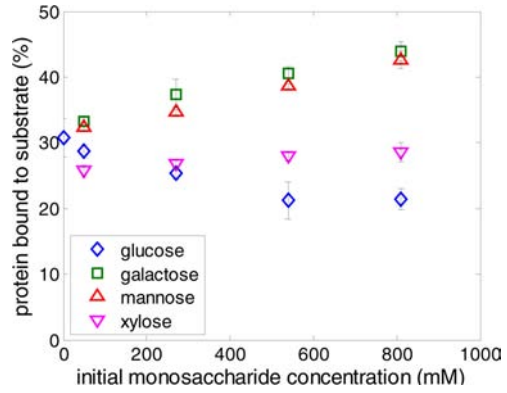

Figure 5. Percentage of protein bound to Avicel based on the protein adsorption at 280 nm of the hydrolysate liquid phase.

decreases). When high concentrations of glucose are present in the hydrolysates, both binding and activity of the cellulases are inhibited, whereas the other monosaccharides do not show a decrease in binding. These results imply that while binding is conducive to glucose production, a high binding affinity is no indication of high catalytic activity of the cellulases. There are two kinds of inhibition at play: the cellulase catalytic domain inhibition from the decrease in the free water availability for hydrolysis (all monosaccharides) and binding domain inhibition as well as end-product inhibition of the β-glucosidases (from glucose only). Monosaccharides in the hydrolysates could be seen as having a noncompetitive inhibition effect on the cellulases, where their presence disturbs the protein hydration shell and thereby affects cellulase performance.

The results obtained from this study are significant for hydrolysis carried out at high dry matter content, as there is limited free water availability and a high concentration of soluble end products. Similar to the case of the "high solids effect", where yields decrease as dry matter content increases, this study shows that yields also decrease as the dissolved solids content increases. In an industrial bioconversion setting, the additive effect of different sugars and soluble inhibitors can further decrease hydrolysis yields.

AUTHOR INFORMATION

Corresponding Author

*(C.C.H.) Phone: +45 3533 1500. Fax: +45 3533 1508. E-mail: chsi@ign.ku.dk.

Present Address

‡(H.J.) Department of Chemical and Biochemical Engineering, Technical University of Denmark, Søltofts Plads, Building 229, DK-2800 Kgs. Lyngby, Denmark.

Notes

The authors declare no competing financial interest.

ACKNOWLEDGMENTS

We thank Novozymes A/S, Denmark, for the Cellic CTec2 used in these studies. We also acknowledge Michael J. Selig and Dr. Katja S. Johansen for helpful comments and discussion on the manuscript.

ABBREVIATIONS USED

LF-NMR, low-field nuclear magnetic resonance; T_2, spin−spin relaxation time

REFERENCES

(1) Orts, W. J.; Holtman, K. M.; Seiber, J. N. Agricultural chemistry and bioenergy. *J. Agric. Food Chem.* **2008**, *56*, 3892−3899.

(2) Chen, L.; Fu, S. Enhanced cellulase hydrolysis of eucalyptus waste fibers from pulp mill by Tween 80-assisted ferric chloride pretreatment. *J. Agric. Food Chem.* **2013**, *61*, 3293−3300.

(3) Zhao, J.; Chen, H. Stimulation of cellulases by small phenolic compounds in pretreated stover. *J. Agric. Food Chem.* **2014**, *62*, 3223−3229.

(4) Mandels, M.; Reese, E. T. Inhibition of cellulases. *Annu. Rev. Phytopathol.* **1965**, *3*, 85−102.

(5) Mohagheghi, A.; Tucker, M.; Grohmann, K.; Wyman, C. High solids simultaneous saccharification and fermentation of pretreated wheat straw to ethanol. *Appl. Biochem. Biotechnol.* **1992**, *33*, 67−81.

(6) Jørgensen, H.; Vibe-Pedersen, J.; Larsen, J.; Felby, C. Liquefaction of lignocellulose at high-solids concentrations. *Biotechnol. Bioeng.* **2007**, *96*, 862−870.

(7) Huang, X.; Penner, M. H. Apparent substrate inhibition of the *Trichoderma reesei* cellulase system. *J. Agric. Food Chem.* **1991**, *39*, 2096−2100.

(8) Penner, M. H.; Liaw, E.-T. Kinetic consequences of high ratios of substrate to enzyme saccharification systems based on *Trichoderma* cellulase. In *Enzymatic Conversion of Biomass for Fuels Production*; Himmel, M. E., Baker, J. O., Overend, R. P., Eds.; ACS Symposium Series 566; American Chemical Society: Washington, DC, USA, 1994; pp 363−371.

(9) Kristensen, J. B.; Felby, C.; Jørgensen, H. Yield-determining factors in high-solids enzymatic hydrolysis of lignocellulose. *Biotechnol. Biofuels* **2009**, *2*, 11.

(10) Jørgensen, H.; Kristensen, J. B.; Felby, C. Enzymatic conversion of lignocellulose into fermentable sugars: challenges and opportunities. *Biofuels, Bioprod. Biorefin.* **2007**, *1*, 119−134.

(11) Cannella, D.; Jørgensen, H. Do new cellulolytic enzyme preparations affect the industrial strategies for high solids lignocellulosic ethanol production? *Biotechnol. Bioeng.* **2014**, *111*, 59−68.

(12) Xiao, Z.; Zhang, X.; Gregg, D. J.; Saddler, J. N. Effects of sugar inhibition on cellulases and β-glucosidase during enzymatic hydrolysis of softwood substrates. *Appl. Biochem. Biotechnol.* **2004**, *115*, 1115−1126.

(13) Hodge, D. B.; Karim, M. N.; Schell, D. J.; McMillan, J. D. Soluble and insoluble solids contributions to high-solids enzymatic hydrolysis of lignocellulose. *Bioresour. Technol.* **2008**, *99*, 8940−8948.

(14) Roberts, K. M.; Lavenson, D. M.; Tozzi, E. J.; McCarthy, M. J.; Jeoh, T. The effects of water interactions in cellulose suspensions on mass transfer and saccharification efficiency at high solids loadings. *Cellulose* **2011**, *18*, 759−773.

(15) Selig, M. J.; Hsieh, C.-W. C.; Thygesen, L. G.; Himmel, M. E.; Felby, C.; Decker, S. R. Considering water availability and the effect of solute concentration on high solids saccharification of lignocellulosic biomass. *Biotechnol. Prog.* **2012**, *28*, 1478−1490.

(16) Zaccai, G. The effect of water on protein dynamics. *Philos. Trans. R. Soc. London, B* **2004**, *359*, 1269−1275.

(17) Wilhm, J. L.; Dorris, T. C. Biological parameters for water quality criteria. *BioScience* **1968**, *18*, 477−481.

(18) Mora-Gutierrez, A.; Baianu, I. C. Proton NMR relaxation and viscosity measurements on solutions and suspensions of carbohydrates and starch from corn: the investigation of carbohydrate hydration and stereochemical and aggregation effects in relation to oxygen-17 and carbon-13 NMR data for carbohydrate solutions. *J. Agric. Food Chem.* **1989**, *37*, 1459−1465.

(19) Starcher, B. A ninhydrin-based assay to quantitate the total protein content of tissue samples. *Anal. Biochem.* **2001**, *292*, 125−129.

(20) Ghose, T. K. Measurement of cellulase activities. *Pure Appl. Chem.* **1987**, *59*, 257−268.

(21) Saha, B. C.; Bothast, R. J. Production, purification, and characterization of a highly glucose-tolerant novel β-glucosidase from *Candida peltata*. *Appl. Environ. Microbiol.* **1996**, *62*, 3165−3170.

(22) Provencher, S. W. CONTIN: a general purpose constrained regularization program for inverting noisy linear algebraic and integral equations. *Comput. Phys. Commun.* **1982**, *27*, 229−242.

(23) Stutzenberger, F.; Lintz, G. Hydrolysis products inhibit adsorption of *Trichoderma reesei* C30 cellulases to protein-extracted lucerne fibres. *Enzyme Microb. Technol.* **1986**, *8*, 341−344.

(24) Holtzapple, M.; Cognata, M.; Shu, Y.; Hendrickson, C. Inhibition of *Trichoderma reesei* cellulase by sugars and solvents. *Biotechnol. Bioeng.* **1990**, *36*, 275−287.

(25) Andrić, P.; Meyer, A. S.; Jensen, P. A.; Dam-Johansen, K. Reactor design for minimizing product inhibition during enzymatic lignocellulose hydrolysis: I. Significance and mechanism of cellobiose and glucose inhibition on cellulolytic enzymes. *Biotechnol. Adv.* **2010**, *28*, 308−324.

(26) Davis-Searles, P. R.; Saunders, A. J.; Erie, D. A.; Winzor, D. J.; Pielak, G. J. Interpreting the effects of small uncharged solutes on protein-folding equilibria. *Annu. Rev. Biophys. Biomol. Struct.* **2001**, *30*, 271−306.

(27) Grant, W. D. Life at low water activity. *Philos. Trans. R. Soc. London, B* **2004**, *359*, 1249−1267.

(28) Zaks, A.; Klibanov, A. M. The effect of water on enzyme action in organic media. *J. Biol. Chem.* **1988**, *263*, 8017−8021.

(29) *The Merck Index: An Encyclopedia of Chemicals, Drugs, and Biologicals*; online ed.; Merck & Co.: Whitehouse Station, NJ, USA, 2013.

(30) *Aldrich Catalog Handbook of Fine Chemicals*; Web ed.; Aldrich Chemical: Milwaukee, WI, USA, 2013.

(31) Franks, F.; Ravenhill, J. R.; Reid, D. S. Thermodynamic studies of dilute aqueous solutions of cyclic ethers and simple carbohydrates. *J. Solution Chem.* **1972**, *1*, 3−16.

(32) Shahidi, F.; Farrell, P. G.; Edward, J. T. Partial molar volumes of organic compounds in water. III. Carbohydrates. *J. Solution Chem.* **1976**, *5*, 807−816.

(33) Tait, M. J.; Suggett, A.; Franks, F.; Ablett, S.; Quickenden, P. A. Hydration of monosaccharides: a study by dielectric and nuclear magnetic relaxation. *J. Solution Chem.* **1972**, *1*, 131−151.

(34) Kumar, R.; Wyman, C. E. An improved method to directly estimate cellulase adsorption on biomass solids. *Enzyme Microb. Technol.* **2008**, *42*, 426−433.

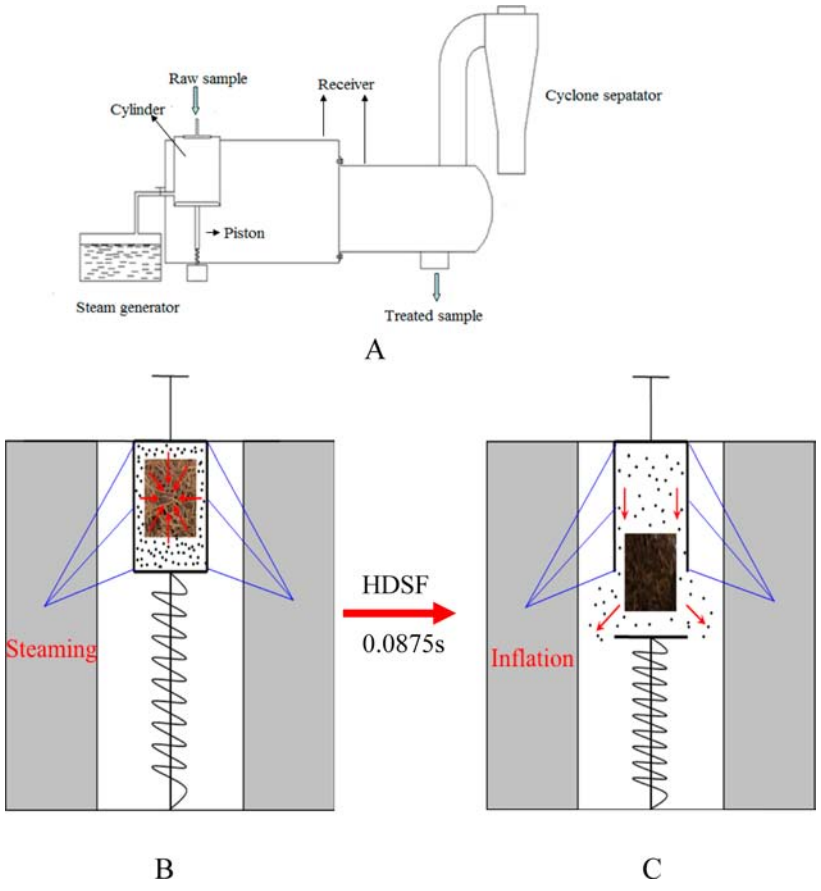

Figure 1. Illustration of the HDSF process. (A) The whole structure in catapult explosion mode is composed of a cylinder and piston. (B) In the steam pressurization phase, the two parts are tightly coupled. (C) During the explosion, the piston, driven by three pneumatic linear actuators and the kinetic energy of the steam and material, bursts out of the cylinder, a process that is equivalent to a vessel suddenly fracturing into two halves.

compare it with different extraction methods for extraction yield and efficiency, and to analyze the differences of chemical composition of extracts from raw and exploded samples.

MATERIALS AND METHODS

Pine (*Larix olgensis* Henry) Needles and Reagents. Pine (*Larix olgensis* Henry) needles collected from Jilin Province, China, were washed under tap water, drained and then, dried at 50 °C in a ventilated drying oven for 12 h to 5% moisture content. After drying, the sample was packed in paper bags and stored at room temperature (25 °C) in the dark. Standard of rutin (HPLC grade, ≥98%) was obtained from Sigma Chemical Company. Standards of quercetin, kaempferol, apigenin, and isorhamnetin (HPLC grade, ≥98%) were obtained from Shanghai Yuanye Biological Technology Co., Ltd.

HDSF Treatment. HDSF treatment was carried out in a batch apparatus (QBS-200B test-bed, Hebi right way bioenergy company, China) equipped with a 5 L reaction vessel. The diagram of the HDSF process is shown in Figure 1. The whole structure (Figure 1A) in catapult explosion mode is composed of a cylinder and a piston. In the steam pressurization phase, the two parts are coupled (Figure 1B). During the explosion, the piston, driven by three pneumatic linear actuators, bursts out of the cylinder, a process that is equivalent to a vessel suddenly fracturing into two halves (Figure 1C).[18] About 300 g of pine needles, soaked by water for 0.5−3.0 h, were put into the reactor, followed by HDSF treatment at a steam pressure of 0.5−2.0 MPa for 20−120 s, and finally termination by explosive decompression. The treated pine needles were collected and dried in a ventilated drying oven for 12 h at 50 °C. The dried sample contained 2.5% moisture content.

Flavonoids Extraction. The treated pine needles were extracted with 60% (v/v) ethanol solution at a solvent-to-solid ratio of 50 (mL/g) at 70 °C for 1.0 h. The solution was filtered through a 0.22 μm membrane filter. In the presence of sodium nitrite, flavonoids react with aluminum and form a chelating substance. The reaction product exhibits red-orange color by addition of sodium hydroxide solution. Therefore, the amount of total flavonoids was determined using a spectrophotometer.

Determination of Total Flavonoids. The determination of total flavonoids content was conducted using the method of Jia et al. with modification.[21] Extract solutions (1 mL) were added to a test tube containing 2 mL of 60% (v/v) ethanol solution. Sodium nitrite solution (5%, 0.5 mL) was added to the mixture and stood for 6 min, after which 0.5 mL of 10% aluminum chloride was added. After another 6 min, 1 mL of 60% ethanol solution was added and mixed, followed by 4 mL of 10% sodium hydroxide. The absorbance of the mixture at 510 nm was measured after 15 min in comparison to a standard curve that was prepared using rutin. The flavonoids contents were expressed as rutin equivalents mg/g dry weight.

Morphological Characterization. Scanning electron microscopy (SEM) analysis was performed with a Quanta 200 microscope (PHILI PS, Netherlands).

Kinetics of Flavonoids Extraction. A 1 g amount of sample and 50 mL of 60% (v/v) ethanol solution were used in all extraction experiments. For raw and steam-exploded pine needles, the samples were placed into a flask and heated at 70 °C in a water bath for 280 and 50 min, respectively. Ultrasound-assisted extraction was carried out using an ultrasonic bath of 40 kHz, a big and commonly used frequency in extraction. The sample was subjected to ultrasound treatment at 70 °C for 250 min. Microwave-assisted extraction was performed using a household microwave oven at 500 W. A 100 mL flask was exposed to microwave irradiation (irradiation cycle: 30 s of power-on, followed by 60 s of power-off) for 50 min. The extracts obtained from the aforementioned methods were filtered through a

dx.doi.org/10.1021/jf405412r | J. Agric. Food Chem. 2014, 62, 3806−3812

0.22 μm membrane filter, after which the amount of total flavonoids was determined using a spectrophotometer.

Sample Preparation for HPLC-DAD-ESI-MS Analysis. Raw and exploded pine needle samples (4.0 g) were extracted for 60 min with 160 mL of 60% (v/v) ethanol solution at 70 °C. The extracts were then filtered and centrifuged at 10 000 rpm for 20 min. The supernatant was concentrated to remove ethanol under reduced pressure and suspended in 25 mL of water. The resulting solution was extracted by 25 mL of petroleum ether and 25 mL of ethyl acetate consecutively and repeated three times. The ethyl acetate extract was dried and dissolved in 15 mL of 60% (v/v) ethanol solution. The solution was filtered through a 0.22 mm micropore membrane (Nylon-66; JinTeng, Tianjin of China) prior to LC/MS analysis. A 10 μL aliquot was introduced into the LC/MS instrument for analysis.

Instrumentation and Chromatographic Condition. The HPLC analyses were performed on a Hitachi series L-2000 HPLC instrument (Hitachi, Japan) equipped with a quaternary solvent delivery system, a diode-array detector, and a column compartment. Samples were separated on an Agilent Zorbax Sb-C18 column (5 μm, 4.6 mm × 250 mm). The mobile phase consisted of acetonitrile (A) and water containing 0.1% (v/v) formic acid (B). A gradient elution program was used as follows: 0−5 min, 15−20% A; 5−10 min, 20% A; 10−15 min, 20−15% A; 15−30 min, 15−25% A; 30−35 min, 25−30% A; 35−50 min, 30−35% A; 50−60 min, 35−40% A; 60−70 min, 40−100% A. The mobile phase flow rate was 1.0 mL/min. Spectral data were recorded using a diode-array detector over the wavelength range 200−600 nm, and the chromatogram was extracted at 370 nm. The column temperature was set at 30 °C.

The mass spectra were acquired using a Waters ZMD 4000 series SL ion trap mass spectrometer equipped with electrospray ionization (ESI) interface. Nitrogen (N_2) was used as the sheath and auxiliary gas, and helium (He) was used as the collision gas. The ESI-MS spectra were acquired in the positive ion mode recorded over a mass range of m/z 100−1500. Capillary voltage was 3.5 kV. The desolvent gas temperature was set at 350 °C with a gas flow rate of 500 L/h, and the nebulizing pressure was 35 psi.

Statistical Analysis. The data were presented as mean ± standard deviation (SD). Differences between the means of the individual groups were analyzed using the analysis of variance (ANOVA) procedure of Statistical Analysis System, SAS 16.0 (SAS Institute, Cary, NC, USA) with Duncan's multiple range tests. The significance of differences was defined at the $p < 0.05$ level.

RESULTS AND DISCUSSION

Effect of Steam Explosion on Extraction of Total Flavonoids. The effect of steam pressure on the yield of flavonoids extracted from pine needles is shown in Figure 2. The results show that the yield of extractable flavonoids from pine needles by HDSF pretreatment increased significantly. At a residence time of 60 s and an immersing time of 2.0 h, the yield of flavonoids increased with the increase of steam pressure from 0.5 to 1.5 MPa. However, there was no significant change at a steam pressure range 1.5−2.0 MPa. It is worth noting that the yield of flavonoids extracted from pine needles increased from 20.0 rutin equivalents mg/g before HDSF treatment to 50.8 rutin equivalents mg/g after 1.5 MPa HDSF treatment. This result is very important and promising for the employment of HDSF as an effective method for extraction of flavonoids from plant materials. Another noteworthy phenomenon is that, at higher pressures, which means at higher temperatures, the yield of flavonoids did not decrease significantly. This indicates that the flavonoids in pine needles could maintain stability at high temperatures of steam explosion for 60 s. This result is consistent with previous studies,[22] which reported that the flavonoids in sumac fruits could endure the high temperature of steam explosion for certain duration.

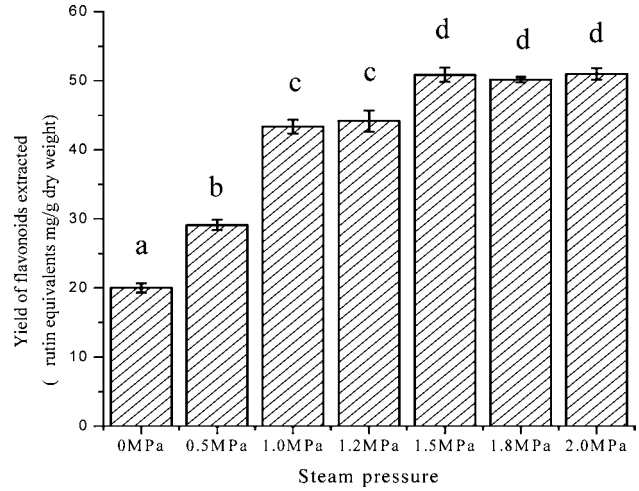

Figure 2. Effect of steam pressure on the yield of flavonoids extracted from pine needles at constant residence time (60 s) and soaking time (2.0 h). Extraction conditions: 60% ethanol, 50 mL/g, 70 °C, 1 h. Means with the different letters (a−d) are significantly different ($p < 0.05$) by Duncan's multiple range test.

As illustrated in Figure 3, residence time does not have a significant effect on the yield of flavonoids extracted from pine needles. This indicates that the most prominent factor in the action of HDSF is the kinetic energy produced by steam explosion rather than thermochemical reaction, which was also confirmed by Yu et al.[19] At residence times of 20, 60, and 80 s, the yield of flavonoids extracted increased overall with an increase in steaming time. The yield of flavonoids extracted reached its highest value of 48.8 rutin equivalents mg/g (dry pine needles) at a residence time of 80 s and a soaking time of 2.0 h. However, beyond 80 s, the yield decreased. HDSF is based on pressurization and forcing steam into fibrous tissues and cells of biomass, followed by rapidly releasing the pressure in an explosive decompression event.[18] The release of pressurized steam in an extremely short time could provide enough force to disrupt and unfold the compact structure of

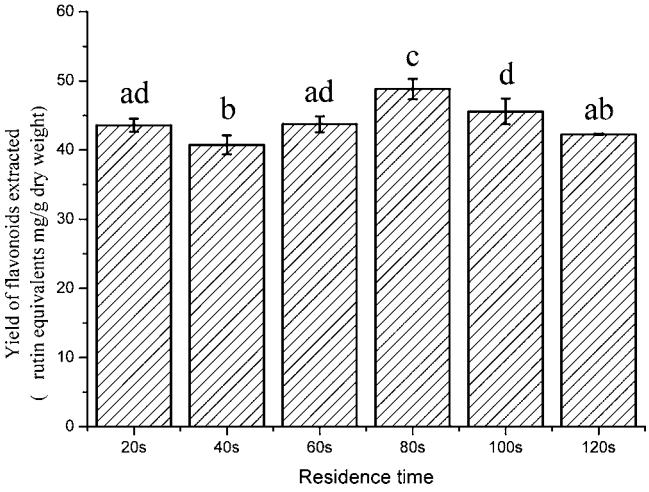

Figure 3. Effect of residence time on yield of flavonoids extracted from pine needles at constant steam pressure (1.2 MPa) and soaking time (2.0 h). Extraction conditions: 60% ethanol, 50 mL/g, 70 °C, 1 h. Means with the different letters (a−d) are significantly different ($p < 0.05$) by Duncan's multiple range test.

pine needles. Residence time (steaming time) affects the hydrolysis reaction. At a short residence time, the hydrolysis reaction did not progress enough, while at a long residence time, degraded compounds such as flavonoids were repolymerized into insoluble materials.

The effect of soaking times of 0, 0.5, 1.0, 1.5, 2.0, 2.5, and 3.0 h on the yield of extracted flavonoids was also studied. It can be seen in Figure 4 that the water content of the sample increased

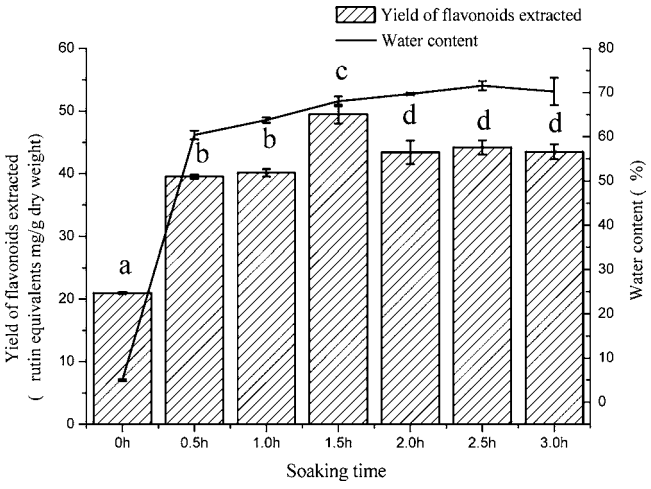

Figure 4. Effect of soaking time on yield of flavonoids extracted from pine needles at constant steam pressure (1.2 MPa) and residence time (60 s). Extraction conditions: 60% ethanol, 50 mL/g, 70 °C, 1 h. Means with the different letters (a–d) are significantly different ($p < 0.05$) by Duncan's multiple range test.

with the increase of soaking time in the first 1.5 h and then kept unchanged after 2.0 h. The yield of flavonoids reaches the maximum (49.5 rutin equivalents mg/g) at a water content of 64%. Soaking treatment followed by HDSF could greatly increase the yield of extracted flavonoids. Increased water content after soaking treatment made the hydrolysis reaction easier. In addition, Grous et al.[23] reported that steam explosion pretreatment significantly increased pore volume of the sample while oven-drying showed a reduction in available pore volume. Many stomata exist on the surface of pine needles, which results in limited pore volume in the dry state. Soaking treatment could increase the pore volume.

Researchers suggest that steam-explosion treatment efficiency is a result of several factors, including steam pressure, residence time, particle size, and moisture content.[24] High-pressure steams with a powerful seepage force will penetrate an organic tissue structure entirely. When a rapid enough decompression HDSF is triggered, most of the steam in the biomass will quickly expand and break free of the structure. This leads to disruption of the biomass internal structure by a mechanical shearing force. Residence time affects penetration and consequently softening degree of raw materials, thus affecting the disruption of internal structure of the biomass. Soaking treatment could increase the water content of pine needles. Overall, on the basis of the data in Figures 2–4, it shows that, in a certain range of steam pressure, residence time, and soaking time, the extraction yield of flavonoids from pine needles increases significantly by HDSF pretreatment.

Morphological Changes of Pine Needles Treated by HDSF. The effect of HDSF treatment on the morphology of pine needles is illustrated in Figure 5. SEM images of untreated (Figure 5A) and treated pine needles (Figure 5B, C) showed obvious morphological changes induced by HDSF treatment. Untreated pine needles still have structural integrity and a densely structured surface. This structure is not conducive for solvent extraction. It is interesting to note from Figure 5B that there are many pores on the surface of the pine needles, indicating the action of HDSF. When treated at 1.0 MPa, the pine needle structure was destroyed, and it changed into an amorphous state. HDSF treatment caused breakage and destruction of cell walls, leading to the formation of large cavities and intercellular spaces. When steam pressure was increased to 1.5 MPa, the pine needle structure was completely destroyed and changed from needlelike to particles. Micropores and smaller particles due to HDSF treatment were conducive for flavonoid extraction by increasing the specific surface area of the material. During the HDSF process, steam with a powerful seepage force penetrates the interior cells of pine needles. Upon an explosive decompression (within 0.0875 s), most of the steam in the pine needles will quickly expand and disrupt the internal structure, finally forming pores on the surface when the steam rushes out.

Comparisons of Different Extraction Methods for Extraction Yield and Extraction Efficiency of Flavonoids. The effect of extraction time on the yield of flavonoids extracted by four methods, namely, HDSF pretreatment, microwave-assisted, ultrasound-assisted, and solvent extraction is shown in Figure 6. For solvent extraction, the yield of flavonoids extracted reached a maximum of 22.7 rutin equivalents mg/g dry pine needles after 190 min. When the solvent extraction time was further increased, the yield did not increase. The yield of flavonoids extracted by ultrasound-assisted method was insignificantly higher (by 5.0 rutin equivalents mg/g) than that of solvent extraction, for the same extraction time. Ultrasound- assisted extraction took 220 min to reach a maximum yield of flavonoids (28.7 rutin equivalents mg/g). However, when the treatment time was extended, the yield decreased slightly. For microwave-assisted extraction, the yield of flavonoids increased rapidly with an increase in treatment time. It took 35 min to reach a maximum yield of 29.8 rutin equivalents mg/g flavonoids. Extraction by HDSF pretreatment resulted in huge benefits over the other three extraction methods. The yield of flavonoids extracted after explosion was greatly increased in comparison with the other three methods, for the same extraction time. In addition, extraction efficiency after explosion was higher than that of the other three methods. It took only 30 min to reach a maximum yield of 47.0 rutin equivalents mg/g. Some morphological changes, including production of smaller particles and expansion of micropores on pine needles, took place during HDSF treatment at 1.5 MPa. In addition, thick and dense wax layers were effectively removed by high-temperature steam in the HDSF pretreatment. Mass-transfer through the solid matrix is usually the rate-controlling step in food extractions.[22] Therefore, the extraction yield of flavonoids and the efficiency were greatly improved due to smaller particles and micropores caused by HDSF treatment as well as the removal of wax layers. The change in structure increased the specific surface area of pine needles, thereby increasing solvent accessibility.

Analysis by HPLC-DAD-ESI-MS. In order to investigate the effect of HDSF pretreatment on flavonoids from pine needles, the profile of raw extract and exploded pine needles was analyzed by high-performance liquid chromatography combined with photodiode-array detection and electrospray

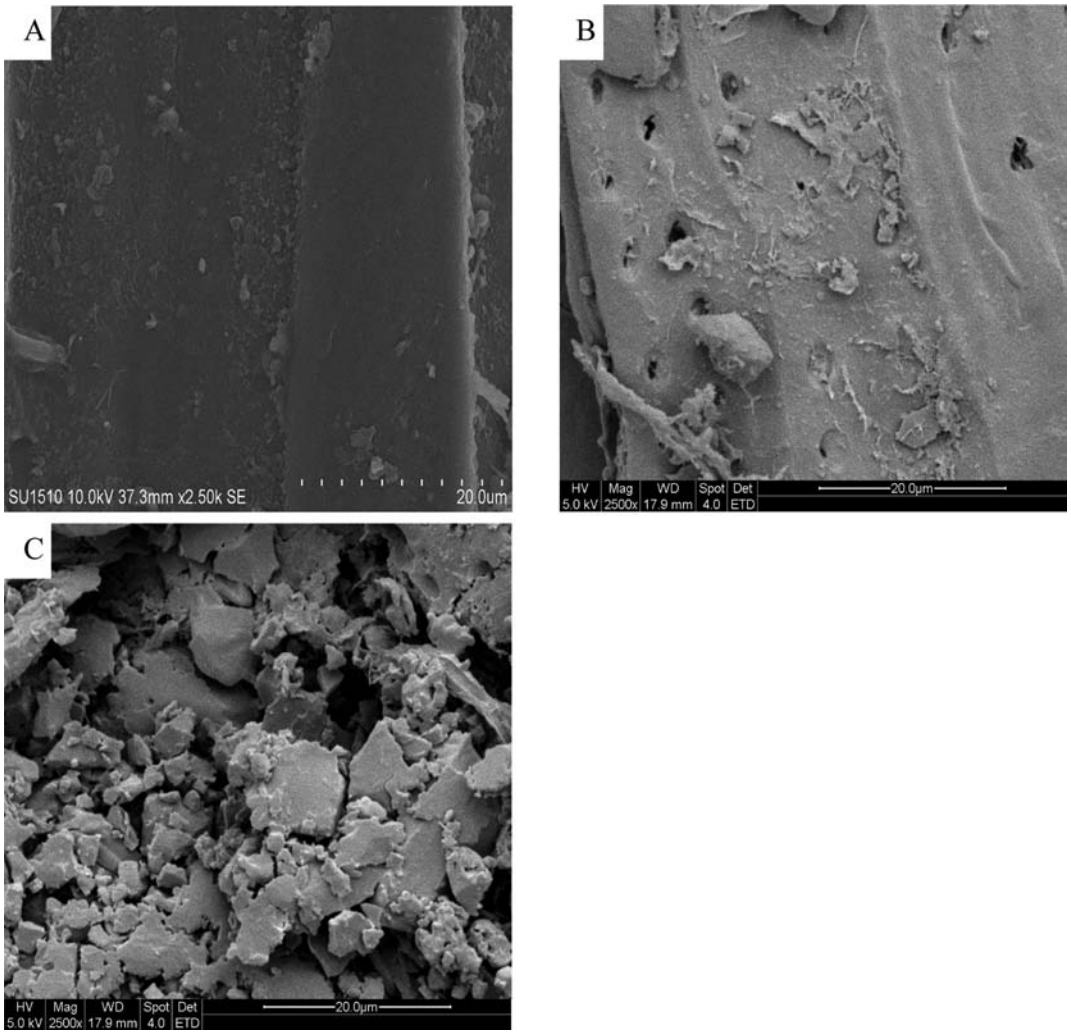

Figure 5. Scanning electron microcopy images of pine needles: (A) untreated pine needles (×2500), (B) treated pine needles (×2500) by HDSF at 1.0 MPa, and (C) treated pine needles (×2500) by HDSF at 1.5 MPa.

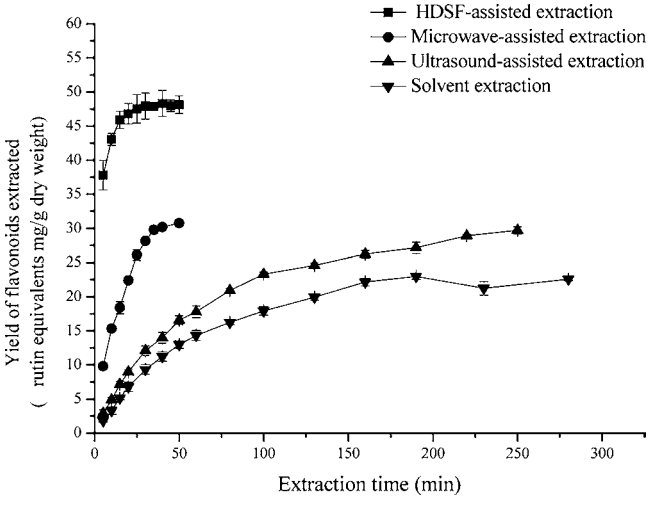

Figure 6. Effect of extraction time on yield of flavonoids extracted from pine needles.

ionization mass spectrometry (HPLC-DAD-ESI-MS). Figure 7 showed several peaks, and they were identified (Table 1). Among 11 major flavonoids, only 4 could be confirmed with authentic standards (peaks 8−11). Six were tentatively identified based on UV and MS spectral characteristics (peaks 1−3 and 5−7). Although the identity of peak 4 remained inconclusive, it was still identified as a kaempferol derivative. As shown in Figure 7, no significant differences between extracts from untreated and treated pine needles were observed at the qualitative level. However, the treated sample presented a much higher quantitative aglycone profile and lower glycosides profile in comparison with the untreated sample. The aglycones (peaks 8−11) extracted from treated pine needles were 3.17 times higher than that of untreated pine needles, while glycosides (peaks 1−7) were lower by 57% (in HPLC-DAD individuals' sum). This result indicates that the extract of treated pine needles by HDSF contain a higher proportion of flavonoid aglycone.

Flavonoids are polyphenolic compounds that can be divided into free, soluble esters or conjugates and insoluble bound forms.[25] Steam explosion could result in an increase in carboxyl and phenolic hydroxyl groups and a significant decrease in β-O-4 structures.[24] In addition, Gong et al.[25] reported that extraction yields of free phenolic acids and soluble conjugates increased sharply after steam explosion due to the hydrolysis of glycosidic linkages in hemicelluloses or celluloses and the β-O-4 ether bonds in lignin, as well as the ester and/or ether bonds between phenolic compounds, lignin, and carbohydrate. Thus,

dx.doi.org/10.1021/jf405412r | J. Agric. Food Chem. 2014, 62, 3806−3812

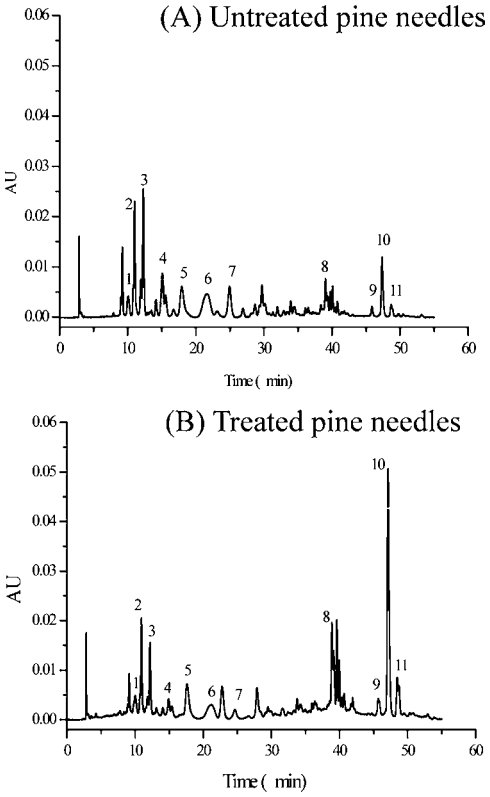

Figure 7. HPLC-DAD chromatograms of flavonoid extracts from (A) untreated pine needles and (B) treated pine needles at 360 nm. For peak identity, refer to Table 1.

HDSF pretreatment can successfully release insoluble bound flavonoids from pine needles. Also, it is well known that organic acids are formed under the combined effects of steam and high temperature during the steam explosion process. Steam explosion is an autohydrolytic process.[26] Therefore, soluble conjugates (flavonoid glycosides) could be hydrolyzed and converted into free aglycone under the effect of organic acids.

The absorption of flavonoids is the prerequisite for exerting diverse biological effects in the body. Although some flavonoid glycosides can be absorbed in the small intestines, it appears that, as a general rule, flavonoid glycosides are cleaved, either in the lumen or in the cells of the gut, before absorption.[27−29] Flavonoid aglycones are easier to be absorbed than glycoside due to improved solubility and smaller molecular weight. After HDSF treatment, the pine needle extract has a higher proportion of flavonoid aglycone. Moreover, the health food industry is now providing increasing numbers flavonoid aglycones as food supplements.[30] Therefore, HDSF is a practical pretreatment for extraction of flavonoids and conversion in healthy food and pharmaceutical industries.

In conclusion, the present study proposed an innovative pretreatment to assist the extraction of flavonoid compounds from pine (*Larix olgensis* Henry) needles by HDSF. The yield of total flavonoids extracted was 2.54-fold as that of the untreated sample after HDSF pretreated for 60 s at 1.5 MPa. This method led to higher extraction yield and extraction efficiency of flavonoids compared with microwave-assisted and ultrasound-assisted extraction. HDSF pretreatment caused the formation of large micropores on the pine needles and production of particles, as well as the hydrolysis of glycosides. The extract presented a much higher quantitative aglycone profile after HDSF pretreatment. HDSF was found to be effective for the extraction and conversion of flavonoids from pine (*Larix olgensis* Henry) needles.

AUTHOR INFORMATION

Corresponding Authors

*(R.Y.) yrj@jiangnan.edu.cn.

*(W.Z.) Phone/fax: +86 510 85919150; e-mail: zhaow@jiangnan.edu.cn.

Funding

The authors gratefully acknowledge the support by the Project of the National Natural Science Foundation of PR China (31271977).

Notes

The authors declare no competing financial interest.

REFERENCES

(1) Chung, S. K.; Sung, C. M.; Mee, S. L. Antioxidant, antimutagenic, and antitumor effects of pine needles (*Pinus densiflora*). *Nutr. Cancer* **2006**, *56*, 162−171.

(2) Zeng, W. C.; He, Q.; Sun, Q.; Zhong, K.; Gao, H. Antibacterial activity of water-soluble extract from pine needles of *Cedrus deodara*. *Int. J. Food Microbiol.* **2012**, *153*, 78−84.

Table 1. Characterization of Flavonoid Compounds of Pine Needles by HPLC-DAD-ESI-MS

						peak area	
no.	t_R (min)	λ_{max} (nm)	molecular weight	HPLC-ESI-MS (m/z)	identity	untreated pine needles	treated pine needles
1	9.99	271, 333 sh	578	579, 433, 415, 397, 337, 313, 271	apigenin-7-*O*-rhamnose-6-*C*-glucoside	38 178	41 177
2	10.93	269, 335	432	433, 415, 397, 379, 367, 343, 337, 283, 271	apigenin-6-*C*-glucoside	155 831	123 580
3	12.18	257, 285 sh, 350	464	465, 333, 303, 271, 227, 193, 149, 103	quercetin-3-*O*-glucoside	163 003	87 215
4	14.91	232, 265, 349	566	567, 435, 303, 287, 227	kaempferol derivative	67 932	10 181
5	17.61	266, 291 sh, 346	448	449, 287	kaempferol-3-*O*-glucoside	37 140	46 059
6	21.23	253, 350	508	509, 457, 419, 347, 317, 287, 149	3′,4′-dimethoxymyricetin-3-*O*-glucoside	50 476	21 924
7	24.65	232, 268, 284 sh, 338	432	433, 333, 271, 149	apigenin-7- *O*-glucoside	32 378	6637
8	38.85	256, 370	302	303, 287, 257, 236, 229	quercetin	57 036	101 499
9	45.87	241, 268, 323	270	271, 227, 177, 153, 147, 119	apigenin	5106	19 105
10	47.35	266, 322 sh, 367	286	287, 259, 153	kaempferol	91 724	459 224
11	48.68	253, 267 sh, 374	316	317, 287, 245, 227, 149	isorhamnetin	9011	99 807

(3) Yen, G. C.; Duh, P. D.; Huang, D. W.; Hsu, C. L.; Fu, T. Y.-C. Protective effect of pine (*Pinus morrisonicola* Hay.) needle on LDL oxidation and its anti-inflammatory action by modulation of iNOS and COX-2 expression in LPS-stimulated RAW 264.7 macrophages. *Food Chem. Toxicol.* **2008**, *46*, 175−185.
(4) Lee, S. H.; Lee, H. S.; Moon, H. C.; Kim, D. H.; Park, Y. S.; Hwang, B.; Lee, H. Y. The effect of α-pinene from *Pinus densiflora* S. and a polysaccharide from *Angelica gigas* Nakai on differentiation and proliferation of human embryonic stem cells. *Cytotechnology* **2005**, *49*, 87−94.
(5) Jung, M. J.; Chung, H. Y.; Choi, J. H.; Choi, J. S. Antioxidant principles from the needles of red pine, *Pinus densiflora*. *Phytother. Res.* **2003**, *17*, 1064−1068.
(6) Yamaguchi, L. F.; Vassao, D. J.; Kato, M. J.; Mascio, P. D. Biflavonoids from Brazilian pine *Araucaria angustifolia* as potentials protective agents against DNA damage and lipoperoxidation. *Phytochemistry* **2005**, *66*, 2238−2247.
(7) Liu, H. W. Effects of degreasing treatment with petroleum ether on extracting of flavonoids from *Coriandrum sativum* L. *J. Anhui Agric. Sci.* **2010**, *38*, 13699−13700.
(8) Chen, X. B.; Goodwin, S. M.; Boroff, V. L.; Liu, X. L.; Jenks, M. A. Cloning and characterization of the WAX2 gene of Arabidopsis involved in cuticle membrane and wax production. *Plant Cell* **2003**, *15*, 1170−1185.
(9) Zhang, J. Y.; Broeckling, C. D.; Blancaflor, E. B.; Sledge, M. K.; Sumner, L. W.; Wang, Z. Y. Overexpression of WXP1, a putative *Medicago truncatula* AP2 domain-containing transcription factor gene, increases cuticular wax accumulation and enhances drought tolerance in transgenic alfalfa (*Medicago sativa*). *Plant J.* **2005**, *42*, 689−707.
(10) Zhang, L.; Shan, Y.; Tang, K. J.; Putheti, R. Ultrasound-assisted extraction flavonoids from Lotus (*Nelumbo nuficera* Gaertn) leaf and evaluation of its anti-fatigue activity. *Int. J. Phys. Sci.* **2009**, *4*, 418−422.
(11) Xiao, W. H.; Han, L. J.; Shi, B. Microwave-assisted extraction of flavonoids from *Radix Astragali*. *Sep. Purif. Technol.* **2008**, *62*, 614−618.
(12) Amani, T.; David, A. R.; Elena, I.; Moktar, Z.; Anotonio, S. C.; Alberto, F. G. Optimization of microwave-assisted extraction for the characterization of olive leaf phenolic compounds by using HPLC-ESI-TOF-MS/IT-MS^2. *J. Agric. Food Chem.* **2012**, *60*, 791−798.
(13) Novak, I.; Janeiro, P.; Seruga, M.; Oliveira-Brett, A. M. Ultrasound extracted flavonoids from four varieties of Portuguese red grape skins determined by reverse-phase high-performance liquid chromatography with electrochemical detection. *Anal. Chim. Acta* **2008**, *630*, 107−115.
(14) Ghafoor, F.; Choi, Y. H.; Jeon, J. Y.; Jo, I. H. Optimization of ultrasound-assisted extraction of phenolic compounds, antioxidants, and anthocyanins from grape (*Vitis vinifera*) seeds. *J. Agric. Food Chem.* **2009**, *57*, 4988−4994.
(15) Galbe, M.; Zacchi, G. A review of the production of ethanol from softwood. *Appl. Microbiol Biot.* **2002**, *59*, 618−628.
(16) Wang, K.; Jiang, J. X.; Xu, F.; Sun, R. C. Effects of incubation time on the fractionation and characterization of lignin during steam explosion pretreatment. *Ind. Eng. Chem. Res.* **2012**, *51*, 2704−2713.
(17) Wang, H.; Srinivasan, R.; Yu, F.; Steele, P.; Li, Q.; Mitchell, B. Effect of acid, alkali, and steam explosion pretreatments on characteristics of bio-oil produced from pinewood. *Energy Fuels* **2011**, *25*, 3758−3764.
(18) Zhao, W.; Yang, R. J.; Zhang, Y. Q.; Wu, L. Sustainable and practical utilization of feather keratin by an innovative physicochemical pretreatment: high density steam flash-explosion. *Green Chem.* **2012**, *14*, 3352−3360.
(19) Yu, Z. D.; Zhang, B. L.; Yu, F. Q.; Xu, G. Z.; Song, A. D. A real explosion: The requirement of steam explosion pretreatment. *Bioresour. Technol.* **2012**, *121*, 335−341.
(20) Zhang, Y. P.; Zhao, W.; Yang, R. J.; Ahmed, M. A.; Hua, X.; Zhang, W. B.; Zhang, Y. Q. Preparation and functional properties of protein from heat-denatured soybean meal assisted by steam flash-explosion with dilute acid soaking. *J. Food Eng.* **2013**, *119*, 56−64.
(21) Jia, Z. S.; Tang, M. C.; Wu, J. M. The determination of flavonoids contents in mulberry and their scavenging effects on superoxide radicals. *Food Chem.* **1999**, *64*, 555−559.
(22) Chen, G. Z.; Chen, H. Z. Extraction and deglycosylation of flavonoids from sumac fruits using steam explosion. *Food Chem.* **2011**, *126*, 1934−1938.
(23) Grous, W. R.; Converse, A. O.; Grethlein, H. E. Effect of steam explosion pretreatment on pore size and enzymatic hydrolysis of poplar. *Enzyme Microb. Technol.* **1986**, *8*, 274−280.
(24) Raquel, M. S.; Ewellyn, A. C.; Ingrid, H.; Juan, C. V.; Orlando, J. R. Lignin changes after steam explosion and laccase-mediator treatment of eucalyptus wood chips. *J. Agric. Food Chem.* **2011**, *59*, 8761−8769.
(25) Gong, L. X.; Huang, L. L.; Zhang, Y. Effect of steam explosion treatment on barley bran phenolic compounds and antioxidant capacity. *J. Agric. Food Chem.* **2012**, *60*, 7177−7184.
(26) Talebnia, F.; Karakashev, D.; Angelidaki, I. Production of bioethanol from wheat straw: An overview on pretreatment, hydrolysis and fermentation. *Bioresour. Technol.* **2010**, *101*, 4744−4753.
(27) Spencer, J. P.; Chowrimootoo, G.; Choudhury, R.; Debnam, E. S.; Srai, S. K.; Rice, E. C. The small intestine can both absorb and glucuronidate luminal flavonoids. *FEBS Lett.* **1999**, *458*, 224−230.
(28) Wu, X.; Cao, G.; Prior, R. L. Absorption and metabolism of anthocyanins in elderly women after consumption of elderberry or blueberry. *J. Nutr.* **2002**, *132*, 1865−1871.
(29) Felgines, C.; Talavera, S.; Gonthier, M. P.; Texier, O.; Scalbert, A.; Lamaison, J. L. Strawberry anthocyanins are recovered in urine as glucuro- and sulfoconjugates in humans. *J. Nutr.* **2003**, *133*, 1296−1301.
(30) Walle, T. Absorption and metabolism of flavonoids. *Free Radical Biol. Med.* **2004**, *36*, 829−837.

utilized by several researchers to optimize various food processing methods such as fermentation,[26] milling,[27] extraction from vegetable matrices[28] and virgin olive oil mechanical extraction;[19] RSM has thus become one of the most popular optimization techniques in the field of food science.[29,30]

The objectives of this study were to systematically investigate the influence of temperature and oxygen concentration on the olive pastes belonging to four of the most important Italian olive cultivars during malaxation and to explore the best operative conditions for obtaining high quality EVOOs.

MATERIALS AND METHODS

Olives. In this research, olive drupes of Coratina, Peranzana, Itrana, and Ogliarola cultivars (cvs) were tested. Coratina and Ogliarola olive trees on a side and Peranzana by the other were planted in the Apulia Region, in the Province of Bari, and in the Province of Foggia, respectively. Instead, the growing area of Itrana olive trees was the Province of Latina (Lazio). All the cvs were harvested on the period October–November 2011 and the ripening stage of these olives, evaluated on the basis of the pigmentation index according to Pannelli et al.,[31] was 0.95. The olives have been processed within 48 h after harvesting.

Reference Compounds. The (*p*-hydroxyphenyl)ethanol (*p*-HPEA) was purchased from Fluka (Milan, Italy), while the 3,4-(dihydroxyphenyl)ethanol (3,4-DHPEA), produced by the Cayman Chemical Co. (Ann Arbor, MI, USA), was obtained from Cabru s.a.s. (Arcore, Milan, Italy). The dialdehydic forms of elenolic acid linked to 3,4-DHPEA and *p*-HPEA (3,4-DHPEA-EDA and *p*-HPEA-EDA, respectively), the isomer of oleuropein aglycon (3,4-DHPEA-EA), (+)-1-acetoxypinoresinol, and (+)-pinoresinol were extracted from virgin olive oil according to the method developed by Montedoro et al.[32] In this method the phenolic compounds were extracted from the extra virgin olive oil using a mixture of methanol/water (80:20 (v/v)); then, after solvent evaporation and a partial purification of the crude extract obtained from EVOO, the phenols were separated by semipreparative high performance liquid chromatography (HPLC) analysis. The HPLC separation was conducted using a Whatman Partisil 10 ODS-2 column (500 mm × 9.4 mm i.d.). The mobile phase was 0.2% acetic acid (pH 3.1) in water (A) and methanol (B), and the elution was performed at a flow rate of 6.5 mL/min. The total running time was 150 min, and the gradient changed as follows: the starting composition was 95% A/5% B, then the percentage of B was increased to 74% A/26% B in 2.5 min, 64% A/36% B in 4.5 min, and this percentage was maintained for 33 min, 61% A/39% B in 35 min, 0% A/100% B in 35 min, and this percentage was maintained for 20 min, returning at the end to the initial conditions (95% A/5% B) in 20 min. The phenols were detected using a diode array detector (DAD) at a wavelength of 278 nm.

The purity of these substances was tested by analytical HPLC,[33] and their chemical structures were verified by NMR using the same operating conditions reported in previous papers by recording ^{1}H and ^{13}C spectra.[32,34] Pure analytical standards of volatile compounds Fluka and Aldrich were purchased from Sigma-Aldrich (Milan, Italy).

Experimental Procedure. *Virgin Olive Oil Mechanical Extraction Process.* The experiments were conducted with an industrial plant using a TEM 200 system (Toscana Enologica Mori, Tavarnelle Val di Pesa, Florence, Italy) composed of a hammer mill, a malaxer with a gas controller system, and a working capacity of 200 kg of olives and a two-phase decanter; for the separation of olive oil, a UVPX 305 AGT 14 centrifuge (Alfa Laval S.p.A., Tavarnelle Val di Pesa, Florence, Italy) was used. The extraction was performed on a sample of 150 kg of olives, and malaxation was carried out for 40 min, a period commonly used in industrial plants, using a top-covered malaxing machine equipped with an O_2 valve and a Mettler-Toledo O_2 4100 sensor (Mettler-Toledo, Novate Milanese, Milan, Italy) for oxygen measurement.[35] The trials were performed at malaxing temperatures (ranging from 20 to 40 °C) and initial oxygen partial pressures in the headspace of the malaxer chamber (ranging from 21.3 to 101.3 kPa) according to a central composite circumscribed design (CCC; see Table 1 for the trial temperatures and oxygen partial pressures). The EVOO samples were filtered and stored in the dark at 13 °C until analyzed.

Table 1. Temperature and Oxygen Content According to a Central Composite Circumscribed Design Used in the Optimization Study of the Malaxation Process

trial	temp (°C)	oxygen content (kPa)
1	20	61.3
2	24	37.2
3	24	85.4
4	30	21.3
5	30	101.3
6	30	61.3
7	30	61.3
8	30	61.3
9	36	37.2
10	36	85.4
11	40	61.3

Analytical Methods. *Extraction and HPLC Analysis of the Phenolic Compounds of Virgin Olive Oils.* The extraction of EVOO phenolic compounds was performed in accordance with Montedoro et al.[36] The HPLC analyses of the phenolic extracts were conducted according to Selvaggini et al.[33] with a reversed-phase column using an Agilent Technologies system Model 1100 (Agilent Technologies, Santa Clara, CA, USA) which was composed of a vacuum degasser, a quaternary pump, an autosampler, a thermostated column compartment, a DAD, and a fluorescence detector (FLD). The C_{18} column used in this study was a Spherisorb ODS-1 250 mm × 4.6 mm with a particle size of 5 μm (Waters, Milford, MA, USA); the injected sample volume was 20 μL. The mobile phase was composed of 0.2% acetic acid (pH 3.1) in water (solvent A)/methanol (solvent B) at a flow rate of 1 mL/min and the gradient changed as follows: 95% A/5% B for 2 min, 75% A/25% B in 8 min, 60% A/40% B in 10 min, 50% A/50% B in 16 min, and 0% A/100% B in 14 min; this composition was maintained for 10 min and then returned to the initial conditions and equilibration in 13 min; the total running time was 73 min. Lignans were detected by using the FLD operated at an excitation wavelength of 280 nm and an emission of 339 nm; for the detection of all the other phenolic compounds a DAD was employed with the wavelength set at 278 nm.

Volatile Compounds Analysis. The evaluation and quantification of volatile compounds in EVOOs were done by headspace–solid phase microextraction (HS-SPME) followed by gas chromatography–mass spectrometry analysis (HS-SPME-GC/MS) according to Servili et al.[37] with few modifications.

For sampling the headspace volatile compounds, SPME was applied as follows: 3 g of EVOO were placed in a 10 mL vial and thermostated at 35 °C, then the SPME fiber (a 50/30 μm divinylbenzene/Carboxen/poly(dimethylsiloxane) (DVB/CAR/PDMS) with a length of 1 cm; StableFlex, Supelco, Inc., Bellefonte, PA, USA) was exposed to the vapor phase for 30 min to sample the volatile compounds. Afterward, the fiber was inserted into the GC injector set in splitless mode, using a splitless inlet liner of 0.75 mm i.d. for thermal desorption, where it was held for 10 min. All of the SPME operations were automated by using a Varian CP 8410 AutoInjector (Varian, Walnut Creek, CA, USA).

GC/MS Analysis. The analysis of the volatile compound sampled with SPME was conducted as reported in Servili et al.[37] with few modifications. A Varian 4000 GC/MS equipped with a 1079 universal capillary injector (Varian) was used. An Agilent J&W fused-silica capillary column was employed (DB-WAXetr, 50 m, 0.32 mm i.d., 1 μm film thickness; Agilent). The column was operated with helium at a constant flow rate of 1.7 mL/min maintained with an electronic flow controller (EFC). The GC oven heating program started at 35 °C. This temperature was maintained for 8 min, then increased to 45 °C at

a rate of 1.5 °C/min, increased to 150 °C at a rate of 3 °C/min, increased to 180 °C at a rate of 4 °C/min, and finally increased to 210 °C at a rate of 3.6 °C/min; this temperature was then held for 14.5 min. The total time of analysis was 80 min. The injector temperature was maintained at 250 °C; the temperature of the transfer line was fixed at 170 °C. The mass spectrometer was operated in the electron ionization (EI) mode at an ionization energy of 70 eV, with scanning in the mass range of m/z 25−350 amu at a scan rate of 0.79 s/scan and a trap set point temperature of 150 °C. The GC-MS was operated with the Varian MS Workstation Software, Version 6.6 (Varian). The volatile compounds were identified by comparison of their mass spectra and retention times with those of authentic reference compounds. Integration of all the chromatographic peaks was performed by choosing the three masses with the highest intensities among those specific for each compound, to selectively discriminate them from their nearest neighbors. The volatile compound results were calculated on the basis of the calibration curves for each compound and expressed in micrograms per kilogram of oil.[37]

Statistical Analysis. *Descriptive Statistics.* To show the variability of data were employed box and whisker plots, in which the lower and the upper edges of the box indicate the 25th and the 75th percentile, respectively; the line within the box shows the median while the whiskers designate the 10th and 90th percentiles. In addition, on the graphs, are reported two points representing the fifth and 95th percentiles. These plots were elaborated using the statistical software SigmaPlot version 12.3 (Systat Software, Inc., San Jose, CA, USA).

Principal Components Analysis. Principal component analysis (PCA) models were built to analyze the influence of processing parameters on the analytical data of EVOO. The SIMCA 13.0 chemometric package was used (Umetrics AB, Umeå, Sweden).

To perform multivariate statistical analysis, the analytical data were put in a matrix with the samples (n objects) in rows and the analytical parameters (k variables) in columns. The raw data were normalized, with the subtraction of the mean, and autoscaled, dividing these results by the standard deviation. The number of significant components was found by applying cross-validation. The results of PCA modeling are presented in graphical form.[38,39] First a PCA model with all data was built; then four SIMCA models, one for each cultivar studied in this work, were made for selecting a small number of variables (volatile and phenolic compounds), from among those with the highest absolute values of loadings, successively employed in the optimization study. When the distributions of these data were not normal (or Gaussian), the data were log-transformed.

Optimization by Response Surface Modeling. Response surface model (RSM) was obtained with the chemometric package MODDE. 9.1 (Umetrics AB).

To optimize the malaxation parameters in the mechanical extraction process, the original data (Y), phenols and volatile compounds chosen by previous PCA, were transformed into desirability functions (d_i), successfully used in RSM-based optimization when several response variables (several Y variables) are considered, so reducing the problem to the optimization of only one Y variable. d_i are dimensionless values, calculated using a linear transformation according to Derringer and Suich[40] with a small modification, so as to obtain desirabilities ranging between 0.1 and 1 using the following equation:

for phenolic and volatile compounds of EVOO that must be maximized:

$$d_i = \frac{0.9Y + 0.1Y_{max} - Y_{min}}{Y_{max} - Y_{min}}$$

for phenolic compounds of EVOO that must be minimized:

$$d_i = \frac{-0.9Y + Y_{max} - 0.1Y_{min}}{Y_{max} - Y_{min}}$$

Y_{min} and Y_{max} correspond to the minimum and the maximum variable values, respectively.

The overall desirability (D) was calculated as the geometric mean of the individual d_i values:

$$D = \sqrt[n]{d_1 d_2 \times \ldots \times d_n}$$

The partial least-squares analysis (PLS) was used to estimate the coefficients of the terms in the models.[41]

RESULTS AND DISCUSSION

The phenolic and volatile compounds of the EVOOs obtained in this study were determined according to the list given in Table 2.

Table 2. List of the Variables Evaluated in Extra Virgin Olive Oils

phenolic compounds	**alcohols**
hydroxytyrosol (3,4-DHPEA)	2-methyl-1-butanol
tyrosol (*p*-HPEA)	1-pentanol
3,4-DHPEA-EDA	1-hexanol
p-HPEA-EDA	1-heptanol
(+)-1-acetoxypinoresinol	1-octanol
(+)-pinoresinol	1-penten-3-ol
3,4-DHPEA-EA	(*E*)-2-penten-1-ol
total phenols	(*Z*)-2-penten-1-ol
	(*E*)-3-hexen-1-ol
volatile compounds	(*Z*)-3-hexen-1-ol
ketones	(*E*)-2-hexen-1-ol
3-pentanone	
1-penten-3-one	**esters**
	ethyl acetate
aldehydes	hexyl acetate
pentanal	(*Z*)-3-hexenyl acetate
hexanal	
octanal	**aromatic alcohols**
nonanal	benzyl alcohol
(*E*)-2-pentenal	phenylethyl alcohol
(*E,E*)-2,4-hexadienal	
2,4-hexadienal (i)	**sum of classes of volatile compounds**
(*Z*)-3-hexenal	sum of ketones
(*E*)-2-hexenal	sum of saturated aldehydes
(*E*)-2-heptenal	sum of C_6 unsaturated aldehydes
(*E*)-2-octenal	sum of saturated alcohols
	sum of C_5 unsaturated alcohols
phenols	sum of C_6 unsaturated alcohols
phenol	sum of esters

The results from the combinations of temperature and O_2 concentration applied during malaxation are shown, with respect to the phenolic compounds, as distributions in the box and whisker plots in Figure 1, while for volatile compounds the range and the average values contents are given in Table 3.

From Figure 1 can be evidenced a strong variation of the phenolic concentration among the cultivars and, in addition, the distribution of the values obtained with different malaxation conditions is cultivar-dependent (cvs Peranzana and Coratina by a side and cvs Ogliarola and Itrana by the other show similar trends). The main phenolic compounds in all the cultivars were the oleuropein and the ligstroside derivatives, while the lignans showed the lowest concentrations and the lowest variability with the operating extraction conditions. It is important to note

dx.doi.org/10.1021/jf405753c | J. Agric. Food Chem. 2014, 62, 3813−3822

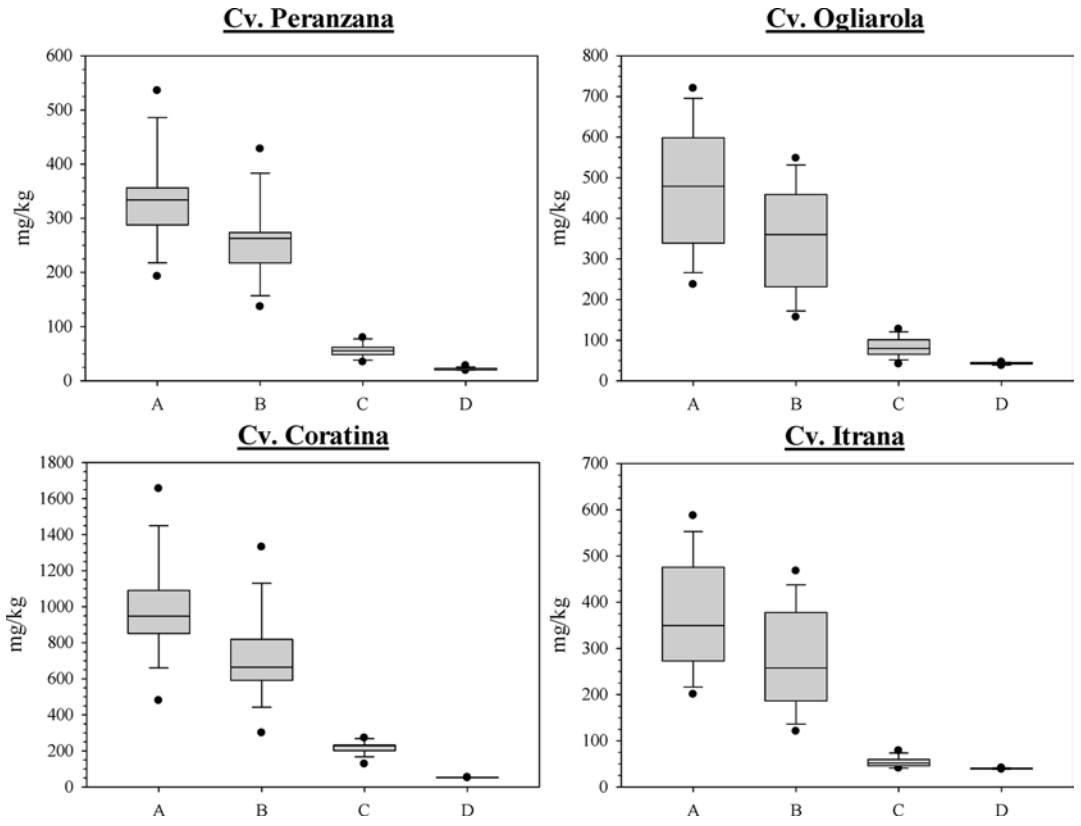

Figure 1. Box and whisker plots of total phenols (A), derivatives of oleuropein (B), derivatives of ligustroside (C), and lignans (D) evaluated on EVOOs obtained from four Italian olive cultivars in different malaxing conditions. (Limits in percentile: box = lower 25th, upper 75th; whiskers = lower 10th, upper 90th; points = lower fifth, upper 95th. The line within the box represents the median.)

Table 3. Range and Average Values (μg/kg) of Volatile Compounds Evaluated on EVOOs Obtained from Peranzana, Ogliarola, Coratina, and Itrana Cultivars in Different Malaxation Conditions

	cv. Peranzana		cv. Ogliarola		cv. Coratina		cv. Itrana	
	range	mean	range	mean	range	mean	range	mean
aldehydes								
pentanal	20–33	25	22–39	29	11–34	24	22–45	29
(*E*)-2-pentenal	120–186	149	66–114	92	66–134	102	116–352	254
hexanal	354–929	554	516–894	694	243–412	304	274–1,213	780
(*E*,*E*)-2,4-hexadienal	380–595	497	356–463	410	362–569	438	391–1,124	814
2,4-hexadienal (i)	164–258	215	182–230	207	180–286	219	176–461	347
(*Z*)-3-hexenal	236–303	275	301–501	413	322–439	377	302–891	595
(*E*)-2-hexenal	24,985–37,615	30,772	38,580–54,625	47,985	35,415–56,950	45,329	31,270–55,515	43,381
sum of C_6 unsaturated aldehydes	26,092–38,524	31,760	39,565–55,772	49,015	36,315–58,206	46,362	32,484–57,350	45,137
alcohols								
1-pentanol	13–26	19	11–19	15	11–20	15	28–78	44
(*E*)-2-penten-1-ol	29–47	37	16–43	31	28–47	38	27–68	49
(*Z*)-2-penten-1-ol	124–224	174	75–169	131	148–300	231	107–292	193
1-penten-3-ol	205–362	287	130–271	212	237–459	345	162–388	283
1-hexanol	659–1,891	1,025	779–1,211	934	607–1,925	1,000	1,543–4,340	2,859
(*E*)-3-hexen-1-ol	4–10	6	4–7	5	2–6	4	14–30	22
(*Z*)-3-hexen-1-ol	271–1,149	563	101–190	137	115–231	167	1,195–2,334	1,816
(*E*)-2-hexen-1-ol	1,028–3,667	1,899	2,053–3,463	2,585	1,425–2,557	2,031	2,556–5,487	3,743
sum of C_6 unsaturated alcohols	1,614–4,825	2,468	2,158–3,642	2,726	1,564–2,760	2,202	4,007–7,791	5,581
esters								
hexyl acetate	874–1,697	1,239	37–99	64	4–21	9	80–123	95
(*Z*)-3-hexenyl acetate	1,856–3,535	2,650	29–89	62	17–82	56	208–691	488
sum of esters	2,744–5,231	3,889	66–188	127	22–94	65	289–791	583

that the main contribution to the total phenols content was due to the oleuropein derivatives.

By the data analysis, the highest average value of total phenols was found in cv. Coratina (992 mg/kg) and the lowest in cv. Peranzana (337 mg/kg); the EVOOs obtained from cv.

dx.doi.org/10.1021/jf405753c | J. Agric. Food Chem. 2014, 62, 3813–3822

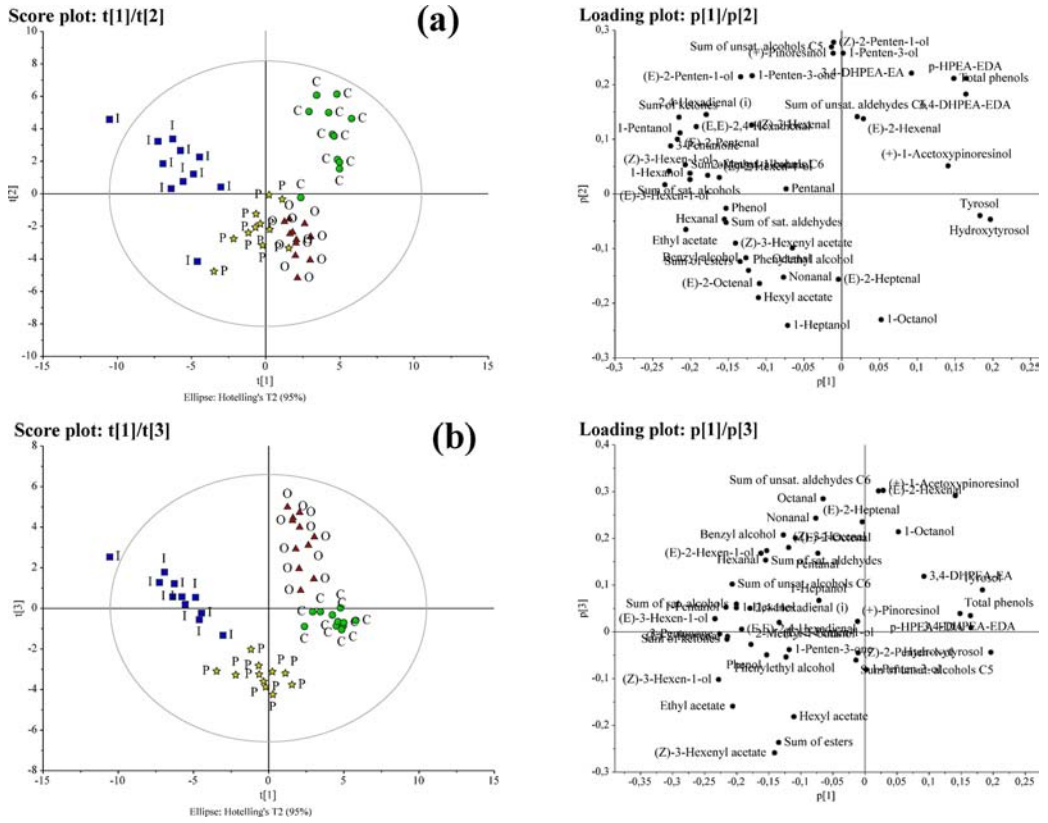

Figure 2. Score plot and loading plot of the first two principal components (a) and of the first and third components (b) of the PCA of EVOOs obtained from four Italian olive cultivars in different malaxation conditions. Abbreviations used: P = Peranzana; O = Ogliarola; C = Coratina; I = Itrana.

Itrana contained an average total phenols amount of 364 mg/kg, while that of cv. Ogliarola was 480 mg/kg. The phenolic variation among the cultivars, in agreement with the literature, indicates that genetic biodiversity is one of the most important parameters that affects the phenolic concentration in EVOOs.[1,2,42] So far, however, the impact on the bioactive phenols of the operative conditions of malaxation, such as O_2 concentration in the olive pastes and the processing temperature, was very strong in all the cultivars studied. This is demonstrated by the ranges of variability between the extreme values of the total phenols, corresponding to 1,241 mg/kg in cv. Coratina, 488 mg/kg in cv. Ogliarola, 387 mg/kg in cv. Itrana, and 351 mg/kg in cv. Peranzana.

High variability was observed also for the volatile compounds according to the cultivar and the operative conditions of malaxation, with the main variations found in the compounds, related to the lipoxygenase pathway, that include hexanal, (*E*)-2-hexenal, 1-hexanol, (*E*)-3-hexen-1-ol, (*Z*)-3-hexen-1-ol, and (*E*)-2-hexen-1-ol, together with esters such as hexyl acetate and (*Z*)-3-hexenyl acetate.

The significant differences in terms of cultivar impact in the C_6 unsaturated aldehydes show the lowest average value in cv. Peranzana (31,760 μg/kg) and the highest concentration in cv. Ogliarola (49,015 μg/kg); with regard to the C_6 unsaturated alcohols, these range between 2,202 and 5,581 μg/kg for the Coratina and the Itrana cvs, respectively. The most important variation in the volatile composition related to cultivar origin is, however, shown by the ester mean concentrations having the lowest value in cv. Coratina (65 μg/kg) and the highest in cv. Peranzana (3,889 μg/kg). All the classes of volatile compounds related to the EVOO flavor evaluated in this work are highly affected by the operative conditions. The maximum range of variability for the C_6 unsaturated aldehydes corresponding to 24,866 μg/kg was found in cv. Itrana; on the contrary, cv. Peranzana shows the minimum value with 12,432 μg/kg. The mean amounts of the C_6 unsaturated alcohols have the highest content in cv. Itrana (5,581 μg/kg), about twice the average amount of the other three cultivars; with respect to the range of variability for this class of compounds, cv. Itrana has the maximum value, 3,784 μg/kg, and cv. Coratina shows the minimum, with 1,196 μg/kg. Regarding the esters concentration, cv. Peranzana has the highest average value (3,889 μg/kg), about seven times the nearest value found in cv. Itrana, and even in this case the operative conditions of malaxation greatly affect their content: the maximum range of variability was found in cv. Peranzana, with 2,487 μg/kg, while the minimum value was found in cv. Coratina, with 72 μg/kg.

Multivariate statistical methods were used to better interpret all the data collected from the EVOO samples obtained by varying the combination of two malaxing parameters, the O_2 concentration in the olive pastes and the processing temperature, and to optimize these two variables. A PCA model was first built with the whole data set, which included the EVOOs evaluated for all four Italian cultivars studied using the list of compounds given in Table 2. The model, built with some variables log-transformed so as to obtain a distribution closer to a Gaussian, explains 93% of the total variance with seven significant principal components (37%, 22%, 15%, 9%, 5%, 3%, and 2%, respectively) and the results for the first two components are shown in Figure 2. A clear discrimination of

dx.doi.org/10.1021/jf405753c | J. Agric. Food Chem. 2014, 62, 3813−3822

the EVOOs in four clusters, corresponding to the olive cvs, is observed in the first three principal components, and in particular in the first component the oils most differentiated are Itrana (on the left side) and Coratina (on the right side), while in the second component there are the Coratina and Itrana EVOOs (on the upper side) opposite to the Peranzana and Ogliarola oils (Figure 2a). The loading plot in Figure 2a shows that the Itrana oils are characterized by higher concentration of ketones, C_6 saturated and unsaturated alcohols, (*E*)-2-pentenal, hexanal, and (*Z*)-3-hexenal; on the contrary, the Coratina EVOOs have a higher secoiridoids content, while Peranzana and Ogliarola EVOOs have lower contents of C_5 unsaturated alcohols and secoiridoids (in comparison with cv. Coratina) and higher concentrations of some saturated alcohols. In the score plot of the third component vs the first, there is a very good separation of Ogliarola (on the upper side) compared to Peranzana EVOOs and the former has higher levels of C_6 unsaturated aldehydes; on the other hand, Peranzana is very rich in esters (Figure 2b).

For the data set for each cultivar without the two lignans, due to very little differences in the samples, preliminary PCA models were built to establish the variables (with regard to the volatile compounds, those substances originated by the lipoxygenase pathway were chosen, significant in defining the flavor of EVOOs) that play an important role in the quality of this food product and that undergo the most variations under the different mechanical oil extraction conditions, temperature and oxygen concentration during malaxation, fixed with the CCC design (for a detailed description of these PCA models see the Supporting Information). For the RSM optimization, only a few analytical variables must be selected in order to define the overall desirability starting with the partial desirability functions (for the list of the variables chosen for each olive cultivar see Table 4).

The RSM models explain with two PLS components for all the cultivars analyzed 98%, 97%, 94%, and 85% of the total variance for Peranzana, Ogliarola, Coratina, and Itrana, respectively.

The results for Peranzana, given in Figure 3, show a response surface with a maximum located at about 33.5 °C and 54 kPa of oxygen. The most important effect is due to temperature, although oxygen also plays a significant role. For cv. Ogliarola, the surface shows a saddle shape and the best operative conditions can be found at the temperature of 32 °C and the lowest oxygen concentration (Figure 3); in this case, both temperature and oxygen are important in the optimization model. In the case of cv. Coratina, when transformed into desirability functions, due to very high concentration of the phenolic substances (for total phenols up to 1,690 mg/kg), a maximum total phenols value of 1,000 mg/kg was chosen for these compounds, and for secoiridoids proportional values to their original concentrations were calculated, above which the equation for the minimization of the desirability was used, because EVOOs with higher phenolic contents are unpleasant due to their bitter and pungent sensory notes.[43,44] The RSM model gave the best results with a temperature of 25 °C and an oxygen concentration of 21.3 kPa, even if in this case a high desirability function value can be obtained at a temperature of 36 °C and an oxygen concentration of 101.3 kPa with the two factors both influencing the model (Figure 4). The best malaxing conditions for cv. Itrana are a temperature of 33 °C and the lowest oxygen concentration, and as for cv. Coratina, very high response values were obtained at a temperature of 37 °C with the highest oxygen content; between the two factors now the temperature plays an important role in the modeling process (Figure 4).

Table 4. List of the Phenolic and Volatile Compounds Transformed into Desirability Function for Each Cultivar for the RSM

Peranzana	Ogliarola	Coratina	Itrana
3,4-DHPEA-EDA	3,4-DHPEA	3,4-DHPEA	3,4-DHPEA-EDA
p-HPEA-EDA	*p*-HPEA	*p*-HPEA	*p*-HPEA-EDA
3,4-DHPEA-EA	total phenols	3,4-DHPEA-EDA[a]	3,4-DHPEA-EA
(*Z*)-3-hexen-1-ol	hexanal	*p*-HPEA-EDA[a]	total phenols
hexanal	(*E*)-2-pentenal	3,4-DHPEA-EA[a]	hexanal
(*E*)-2-pentenal	(*E*)-2-hexenal	total phenols[a]	(*E*)-2-pentenal
(*E*)-2-hexenal	1-pentanol	hexanal	(*Z*)-3-hexenal
hexyl acetate	1-hexanol	(*E*)-2-pentenal	(*E*)-2-hexenal
(*E*)-2-hexen-1-ol	sum of C_5 unsaturated alcohols	(*E*)-2-hexenal	(*Z*)-3-hexen-1-ol
(*Z*)-3-hexenyl acetate	sum of C_6 unsaturated alcohols	(*Z*)-3-hexen-1-ol	(*E*)-2-hexen-1-ol
sum of saturated alcohols	sum of esters	(*E*)-2-hexen-1-ol	sum of C_5 unsaturated alcohols
sum of C_5 unsaturated alcohols		(*Z*)-3-hexenyl acetate	
		sum of C_5 unsaturated alcohols	

[a]Compounds maximized and minimized in the cv. Coratina (for details see the text).

The results of the optimization models show that the optimal malaxing conditions are strongly affected by genetic biodiversity. These results confirm, as found in previous works,[1,2,7,8,42] that cultivars have a significant impact on the chemical and biochemical characteristics of olive fruits and the EVOOs obtained from them. The total amount of phenols in the fruit and the activities of several endogenous enzymes that are involved in phenolic oxidation and aroma generation, such as polyphenoloxidases, peroxidases, and lipoxygenases, are influenced by the genetic origins of the cultivars. As a consequence, to obtain high quality EVOOs, the operative conditions of malaxation, such as the O_2 concentration in the pastes and the processing temperature, which both affect the activities of endogenous enzymes, must be optimized according to the cultivar. In this context it is very important to stress that the EVOOs obtained from Itrana and Peranzana among the cultivars studied, rich mainly in esters among the aromatic compounds, formed in the lipoxygenase pathway, but relatively poor in phenolic substances, show the highest malaxation temperatures for obtaining the maximum response values in the optimization models. The high temperatures (near 40 °C) reduce the activity of hydroperoxide lyase responsible for the formation of C_6 aldehydes and, consequently, of the other classes of compounds originated by these, but, at the same time, improving the cell wall degradation, due to the endogenous depolymerizing enzymes, and enhancing the solubility of these substances in the oils, they increase the release of phenols in the EVOOs and in the vegetation waters.[45,46] On the basis of these results, to improve the health and the sensory properties of EVOOs for cultivars poor in phenols and characterized by high

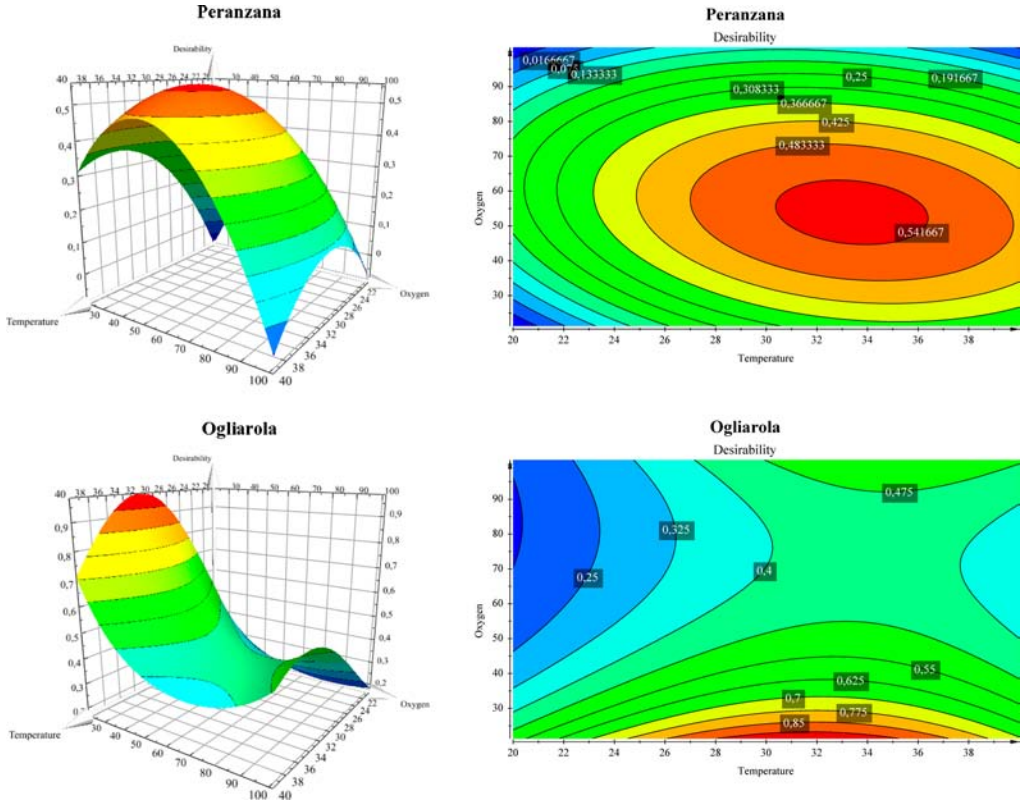

Figure 3. RSM and contour plots obtained in the PLS model built to optimize the temperature and oxygen concentration during malaxation in the Peranzana and Ogliarola cultivars.

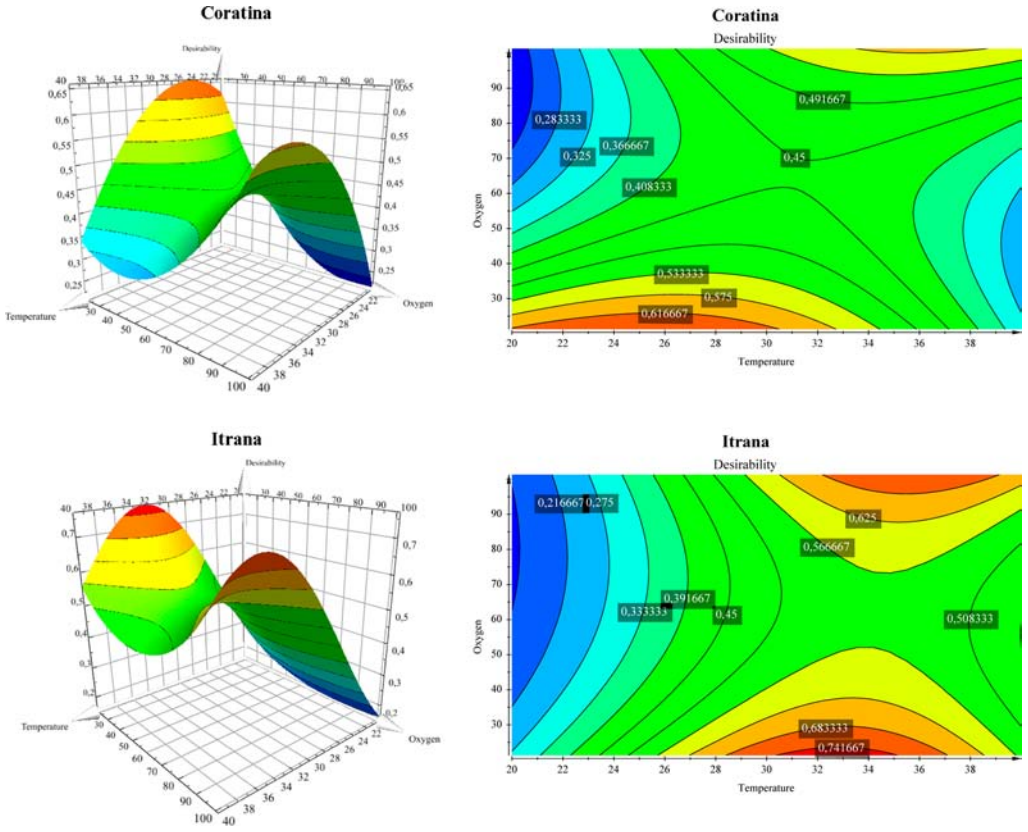

Figure 4. RSM and contour plots obtained using the PLS model built to optimize the temperature and oxygen concentration during malaxation in the Coratina and Itrana cultivars.

dx.doi.org/10.1021/jf405753c | J. Agric. Food Chem. 2014, 62, 3813−3822

LPO activity, the optimal malaxing conditions are obtained at temperatures ranging between 30 and 36 °C and low to mid O_2 concentrations. In this context the esters production seems to be increased by medium O_2 levels in the pastes, which is particularly apparent in cv. Peranzana, probably due to intense alcohol acetyltransferase activity, the last step in the lipoxygenase pathway formation of the volatile compounds. Cv. Coratina, on the contrary, which was characterized by the highest amount of phenols in the EVOOs,[33,47,48] shows that the operative conditions for obtaining the highest response value is located to quite low malaxation temperature of (25 °C) among the cultivars studied. Moreover, the results showed that the low O_2 amount in cv. Coratina seems to be in contrast with the reduction of the phenolic compounds content, which should be promoted in all cultivars extremely rich in these substances to improve the oil consumer acceptability by reducing the bitterness and the pungent sensory notes.[43,49] It is important to note, however, that this result has been obtained with the limit set at 1,000 mg/kg of total phenols content for obtaining pleasant EVOOs. Moreover, cv. Coratina is not only characterized by a high amount of phenols but, at the same time, shows a low polyphenoloxidase and peroxidase activity.[13] The low activity of these enzymes can explain why an increase of O_2 in the pastes produces a small reduction of the phenolic content in the oils, lower than that connected with the malaxing temperature; as a consequence, in cv. Coratina optimization model, low processing temperatures seem to be more important than high O_2 concentrations in the reduction of the phenolic compounds in the oils. This phenomenon could be explained by reduced activity of the depolymerizing enzymes in the pastes that decrease the release of phenols from the cell wall into the olive oil.

The optimization of the malaxing parameters of the four Italian cultivars conducted in this study pointed out the different results of the operative conditions, thus requiring specific investigations of the optimal setting for the oil mechanical extraction process for each individual cultivar due to the different influence of the temperature and oxygen concentration during malaxation. However, it is important to note that the malaxing parameters here investigated heavily modify the concentrations of both the phenolic and volatile compounds independently by olive cultivar.[10,14,15,19,50]

■ ASSOCIATED CONTENT

Supporting Information

Text describing PCA models, one for each cultivar, utilized to select the few analytical variables for the RSM optimization and figures showing score and loading plots of the first two principal components of the PCA models of EVOOs. This material is available free of charge via the Internet at http://pubs.acs.org.

■ AUTHOR INFORMATION

Corresponding Author

*Phone: +39 075 5857903. Fax: +39 075 5857916. E-mail: roberto.selvaggini@unipg.it.

Funding

This study was kindly supported by the Consorzio Olivicolo Italiano UNAPROL—Italy (Projects Reg. UE 1220/2011).

Notes

The authors declare no competing financial interest.

■ ACKNOWLEDGMENTS

We thank Michele Giglioni and Roberto Santibacci for their technical assistance during this study.

■ ABBREVIATIONS USED

RSM, response surface modeling (or response surface methodology); EVOOs, extra virgin olive oils; PPO, polyphenoloxidase; POD, peroxidase; LPO, lipoxygenase; CCD, central composite design; *p*-HPEA, (*p*-hydroxyphenyl)ethanol; 3,4-DHPEA, (3,4-dihydroxyphenyl)ethanol; 3,4-DHPEA-EDA, dialdehydic form of decarboxymethyl elenolic acid linked to (3,4-dihydroxyphenyl) ethanol; *p*-HPEA-EDA, dialdehydic form of decarboxymethyl elenolic acid linked to (*p*-hydroxypheny1)ethanol; 3,4-DHPEA-EA, isomer of the oleuropein aglycon; HPLC, high-performance liquid chromatography; DAD, diode array detector; NMR, nuclear magnetic resonance; CCC, central composite circumscribed design; FLD, fluorescence detector; HS-SPME-GC/MS, headspace−solid phase microextraction−gas chromatography−mass spectrometry; DVB/CAR/PDMS, divinylbenzene/carboxen/poly(dimethylsiloxane); EFC, electronic flow controller; PCA, principal component analysis; PLS, partial least-squares analysis

■ REFERENCES

(1) Servili, M.; Selvaggini, R.; Esposto, S.; Taticchi, A.; Montedoro, G.; Morozzi, G. Health and sensory properties of virgin olive oil hydrophilic phenols: Agronomic and technological aspects of production that affect their occurrence in the oil. *J. Chromatogr. A* **2004**, *1054*, 113−127.

(2) Angerosa, F.; Servili, M.; Selvaggini, R.; Taticchi, A.; Esposto, S.; Montedoro, G. Volatile compounds in virgin olive oil: Occurrence and their relationship with the quality. *J. Chromatogr. A* **2004**, *1054*, 17−31.

(3) Covas, M. I. Bioactive effects of olive oil phenolic compounds in humans: Reduction of heart disease factors and oxidative damage. *Inflammopharmacology* **2008**, *16*, 216−218.

(4) Gill, C. I. R.; Hashim, Y. Z. H.-Y.; Servili, M.; Rowland, I. Olive oil and its phenolic components and their effects on early- and late-stage events in carcinogenesis. In *Olives and olive oil in health and disease prevention*; Preedy, V. R., Watson, R. R., Eds.; Academic Press: Oxford, U.K., 2010; pp 1005−1012.

(5) Chiacchierini, E.; Mele, G.; Restuccia, D.; Vinci, G. Impact evaluation of innovative and sustainable extraction technologies on olive oil quality. *Trends Food Sci. Technol.* **2007**, *18*, 299−305.

(6) Obied, H. K.; Prenzler, P. D.; Ryan, D.; Servili, M.; Taticchi, A.; Esposto, S.; Robards, K. Biosynthesis and biotransformations of phenol-conjugated oleosidic secoiridoids from *Olea europaea* L. *Nat. Prod. Rep.* **2008**, *25*, 1167−1179.

(7) Inglese, P.; Famiani, F.; Galvano, F.; Servili, M.; Esposto, S.; Urbani, S. Factors affecting extra-virgin olive oil composition. *Hortic. Rev.* **2011**, *38*, 83−147.

(8) Vinha, A. F.; Ferreres, F.; Silva, B. M.; Valentão, P.; Gonçalves, A.; Pereira, J. A.; Oliveira, M. B.; Seabra, R. M.; Andrade, P. B. Phenolic profiles of Portuguese olive fruits (*Olea europaea* L.): Influences of cultivar and geographical origin. *Food Chem.* **2005**, *89*, 561−568.

(9) Servili, M.; Esposto, S.; Lodolini, E.; Selvaggini, R.; Taticchi, A.; Urbani, S.; Montedoro, G.; Serravalle, M.; Gucci, R. Irrigation effects on quality, phenolic composition, and selected volatiles of virgin olive oils cv. Leccino. *J. Agric. Food Chem.* **2007**, *55*, 6609−6618.

(10) Clodoveo, M. L. Malaxation: Influence on virgin olive oil quality. Past, present and future—An overview. *Trends Food Sci. Technol.* **2012**, *25*, 13−23.

(11) Servili, M.; Esposto, S.; Fabiani, R.; Urbani, S.; Taticchi, A.; Mariucci, F.; Montedoro, G. F. Phenolic compounds in olive oil:

Antioxidant, health and organoleptic activities according to their chemical structure. *Inflammopharmacology* **2009**, *17*, 76−84.
(12) García-Rodríguez, R.; Romero-Segura, C.; Sanz, C.; Sánchez-Ortiz, A.; Pérez, A. G. Role of polyphenol oxidase and peroxidase in shaping the phenolic profile of virgin olive oil. *Food Res. Int.* **2011**, *44*, 629−635.
(13) Servili, M.; Taticchi, A.; Esposto, S.; Urbani, S.; Selvaggini, R.; Montedoro, G. Effect of olive stoning on the volatile and phenolic composition of virgin olive oil. *J. Agric. Food Chem.* **2007**, *55*, 7028−7035.
(14) Servili, M.; Taticchi, A.; Esposto, S.; Urbani, S.; Selvaggini, R.; Montedoro, G. Influence of the decrease in oxygen during malaxation of olive paste on the composition of volatiles and phenolic compounds in virgin olive oil. *J. Agric. Food Chem.* **2008**, *56*, 10048−10055.
(15) Taticchi, A.; Esposto, S.; Veneziani, G.; Urbani, S.; Selvaggini, R.; Servili, M. The influence of the malaxation temperature on the activity of polyphenoloxidase and peroxidase and on the phenolic composition of virgin olive oil. *Food Chem.* **2013**, *136*, 975−983.
(16) Kalua, C. M.; Allen, M. S.; Bedgood, D. R., Jr.; Bishop, A. G.; Prenzler, P. D.; Robards, K. Olive oil volatile compounds, flavour development and quality: A critical review. *Food Chem.* **2007**, *100*, 273−286.
(17) Luaces, P.; Sanz, C.; Pérez, A. G. Thermal stability of lipoxygenase and hydroperoxide lyase from olive fruit and repercussion on olive oil aroma biosynthesis. *J. Agric. Food Chem.* **2007**, *55*, 6309−6313.
(18) Parenti, A.; Spugnoli, P.; Masella, P.; Calamai, L. The effect of malaxation temperature on the virgin olive oil phenolic profile under laboratory scale conditions. *Eur. J. Lipid Sci. Technol.* **2008**, *110*, 735−741.
(19) Servili, M.; Selvaggini, R.; Taticchi, A.; Esposto, S.; Montedoro, G. Volatile compounds and phenolic composition of virgin olive oil: Optimization of temperature and time of exposure of olive pastes to air contact during the mechanical extraction process. *J. Agric. Food Chem.* **2003**, *51*, 7980−7988.
(20) Migliorini, M.; Mugelli, M.; Cherubini, C.; Viti, P.; Zanoni, B. Influence of O_2 on the quality of virgin olive oil during malaxation. *J. Sci. Food Agric.* **2006**, *86*, 2140−2146.
(21) Mason, R. L.; Gunst, R. F.; Hess, J. L. Statistical design and analysis of experiments—With application to engineering and science, 2nd ed.; John Wiley & Sons: Hoboken, NJ, USA, 2003.
(22) Montgomery, D. C.; Runger, G. C.; Hubele, N. F. Engineering statistics, 5th ed.; John Wiley and Sons: Hoboken, NJ, USA, 2011.
(23) Vatsala, C. N.; Saxena, C. D.; Rao, P. H. Optimization of ingredients and process conditions for the preparation of puri using response surface methodology. *Int. J. Food Sci. Technol.* **2001**, *36*, 407−414.
(24) Bas, D.; Boyacı, I. H. Modeling and optimization II: Comparison of estimation capabilities of response surface methodology with artificial neural networks in a biochemical reaction. *J. Food Eng.* **2007**, *78*, 846−854.
(25) Tan, C.-H.; Ghazali, H. M.; Kuntom, A.; Tan, C.-P.; Ariffin, A. A. Extraction and physicochemical properties of low free fatty acid crude palm oil. *Food Chem.* **2009**, *113*, 645−650.
(26) Dhandhukia, P. C.; Thakkar, V. R. Response surface methodology to optimize the nutritional parameters for enhanced production of jasmonic acid by *Lasiodiplodia theobromae*. *J. Appl. Microbiol.* **2008**, *105*, 636−643.
(27) Ghodke, S. K.; Ananthanarayan, L.; Rodrigues, L. Use of response surface methodology to investigate the effects of milling conditions on damaged starch, dough stickiness and chapatti quality. *Food Chem.* **2009**, *112*, 1010−1015.
(28) Huang, W.; Li, Z.; Niu, H.; Li, D.; Zhang, J. Optimization of operating parameters for supercritical carbon dioxide extraction of lycopene by response surface methodology. *J. Food Eng.* **2008**, *89*, 298−302.
(29) Kong, K.-W.; Ismail, A. R.; Tan, S.-T.; Prasad, K. M. N.; Ismail, A. Response surface optimisation for the extraction of phenolics and flavonoids from a pink guava puree industrial by-product. *Int. J. Food Sci. Technol.* **2010**, *45*, 1739−1745.
(30) Gan, C.-Y.; Latiff, A. A. Optimisation of the solvent extraction of bioactive compounds from Parkia speciosa pod using response surface methodology. *Food Chem.* **2011**, *124*, 1277−1283.
(31) Pannelli, G.; Servili, M.; Selvaggini, R.; Baldioli, M.; Montedoro, G. F. Effect of agronomic and seasonal factors on olive (*Olea europaea* L.) production and on the qualitative characteristics of the oil. *Acta Hortic.* **1994**, *356*, 239−244.
(32) Montedoro, G.; Servili, M.; Baldioli, M.; Selvaggini, R.; Miniati, E.; Macchioni, A. Simple and hydrolyzable compounds in virgin olive oil. 3. Spectroscopic characterization of the secoiridoids derivatives. *J. Agric. Food Chem.* **1993**, *41*, 2228−2234.
(33) Selvaggini, R.; Servili, M.; Urbani, S.; Esposto, S.; Taticchi, A.; Montedoro, G. Evaluation of phenolic compounds in virgin olive oil by direct injection in high-performance liquid chromatography with fluorometric detection. *J. Agric. Food Chem.* **2006**, *54*, 2832−2838.
(34) Servili, M.; Baldioli, M.; Selvaggini, R.; Miniati, E.; Macchioni, A.; Montedoro, G. High-performance liquid chromatography evaluation of phenols in olive fruit, virgin olive oil, vegetation waters and pomace and 1D- and 2D-nuclear magnetic resonance characterization. *J. Am. Oil Chem. Soc.* **1999**, *76*, 873−882.
(35) Esposto, S.; Montedoro, G. F.; Selvaggini, R.; Riccò, I.; Taticchi, A.; Urbani, S.; Servili, M. Monitoring of virgin olive oil volatile compounds evolution during olive malaxation by an array of metal oxide sensors. *Food Chem.* **2009**, *113*, 345−350.
(36) Montedoro, G.; Servili, M.; Baldioli, M.; Miniati, E. Simple and hydrolyzable compounds in virgin olive oil. 1. Their extraction, separation and quantitative and semiquantitative evaluation by HPLC. *J. Agric. Food Chem.* **1992**, *40*, 1571−1576.
(37) Servili, M.; Selvaggini, R.; Taticchi, A.; Montedoro, G. F. Headspace composition of virgin olive oil evaluated by solid phase microextraction: Relationship with the oil sensory characteristics. In *Food Flavours and Chemistry: Advances of the New Millennium*; Spanier, A. M., Shahidi, F., Parliment, T. H., Mussinan, C., Ho, C.-T., Tratras Contis, E., Eds.; Royal Society of Chemistry: London, U.K., 2001; pp 236−247.
(38) Wold, S.; Albano, C.; Dunn, W. J.; Edlund, U.; Esbensen, K.; Geladi, P.; Hellberg, S.; Johansson, E.; Lindberg, W.; Sjöström, M. In *Chemometrics*; Kowalski, B., Ed.; Reidel: Dordrecht, The Netherlands, 1984; pp 17−96.
(39) Varmuza, K.; Filzmoser, P. *Introduction to multivariate statistical analysis in chemometrics*; CRC Press: Boca Raton, FL, USA, 2009.
(40) Derringer, G.; Suich, R. Simultaneous optimization of several response variables. *J. Qual. Technol.* **1980**, *12*, 214−219.
(41) Clementi, S.; Cruciani, G.; Giulietti, G.; Bertuccioli, M.; Rosi, I. Food quality optimization. *Food Qual. Prefer.* **1990**, *2*, 1−12.
(42) Gómez-Rico, A.; Fregapane, G.; Salvador, M. D. Effect of cultivar and ripening on minor components in Spanish olive fruits and their corresponding virgin olive oils. *Food Res. Int.* **2008**, *41*, 433−440.
(43) Andrewes, P.; Busch, J. L. H. C.; de Joode, T.; Groenewegen, A.; Alexandre, H. Sensory properties of virgin olive oil polyphenols: Identification of deacetoxy-ligstroside aglycon as a key contributor to pungency. *J. Agric. Food Chem.* **2003**, *51*, 1415−1420.
(44) Taticchi, A.; Esposto, S.; Servili, M. The basis of the sensory properties of virgin olive oil. In *Olive Oil Sensory Science*; Monteleone, E., Langstaff, S., Eds.; John Wiley & Sons: Oxford, U.K., 2014; pp 33−54.
(45) Vierhuis, E.; Servili, M.; Baldioli, M.; Schols, H. A.; Voragen, A. G. J.; Montedoro, G. F. Effect of enzyme treatment during the mechanical extraction of olive oil on phenolic compounds and polysaccharides. *J. Agric. Food Chem.* **2001**, *49*, 1218−1223.
(46) Esposto, S.; Veneziani, G.; Taticchi, A.; Selvaggini, R.; Urbani, S.; Di Maio, I.; Sordini, B.; Minnocci, A.; Sebastiani, L.; Servili, M. Flash thermal conditioning of olive pastes during the olive oil mechanical extraction process: Impact on the structural modifications of pastes and oil quality. *J. Agric. Food Chem.* **2013**, *61*, 4953−4960.

(47) Cicerale, S.; Conlan, X. A.; Sinclair, A. J.; Keast, R. S. J. Chemistry and health of olive oil phenolics. *Crit. Rev. Food Sci.* **2009**, *49*, 218−236.
(48) Favati, F.; Condelli, N.; Galgano, F.; Caruso, M. C. Extra virgin olive oil bitterness evaluation by sensory and chemical analyses. *Food Chem.* **2013**, *139*, 949−954.
(49) Gómez-Rico, A.; Inarejos-García, A. M.; Salvador, M. D.; Fregapane, G. Effect of malaxation conditions on phenol and volatile profiles in olive paste and the corresponding virgin olive oils (*Olea europaea* L. Cv. Cornicabra). *J. Agric. Food Chem.* **2009**, *57*, 3587−3595.
(50) Boselli, E.; Di Lecce, G.; Strabbioli, R.; Pieralisi, G.; Frega, N. G. Are virgin olive oils obtained below 27 °C better than those produced at higher temperatures? *LWT—Food Sci. Technol.* **2009**, *42*, 748−757.

Especially for the acid soil, which is deficient in N and P, fertilizing with N and P could enhance the yields and growth of tea leaves.[23]

Therefore, the aim of this study was to investigate whether different four fertilizing strategies (with exogenous Se, Zn, N, and P: Se + Zn, Se + Zn + N, Se + Zn + P, Se + Zn + N + P) could improve the element contents (Al, Mn, Se, and Zn) and functional component contents (total polyphenol, total free amino acid, tea polysaccharides, catechins, and caffeine) as well as the antioxidant activity in new and old tea leaves grown in a hilly red soil region.

MATERIALS AND METHODS

Chemicals and Reagents. A ferric reducing ability of plasma (FRAP) kit was purchased from Biyuntian Reagent Co. (Jiangsu). The standards (Se, Zn, Al, Mn) were purchased from National Institutes for Food and Drug Control (NIFDC), Beijing, China. 2,2-Diphenyl-1-picrylhydrazyl (DPPH) and the standards of epigallocatechin (EGC), catechin (CA), epigallocatechin gallate (EGCG), epicatechin (EC), caffeine (CAF), and theanine were purchased from Sigma (Steinheim, Germany). Methanol and acetonitrile were of high-performance liquid chromatography (HPLC) grade; HNO_3, $HClO_4$, and other chemicals were of guaranteed grade.

Plant Culture and Treatments. This study was conducted outdoors at Huangma country, Nanchang, China (28°20′ N, 116°01′ E). The pH of the planting soil was 5.4, and the organic matter, cation exchange capacity (CEC), total nitrogen, available phosphorus, available K, and total Al contents were 27.6 mg/kg, 11.24 cmol/kg, 0.87 g/kg, 1.32 mg/kg, 28.62 mg/kg, and 131 g/kg, respectively. Typical 30 years Fuding White tea (*C. sinensis* cv. Fuding-dabaicha) was chosen as the research object. One sample plot was divided into five parts, which had uniform size (3 m × 4 m) and spacing (3 m). A total of 30 tea plants were planted in two lines in each uniform size. Four kinds of fertilizing strategies (A, Se + Zn; B, Se + Zn + N; C, Se + Zn + P; D, Se + Zn + N + P) were compared, and the control group (CK) was regular fertilizer (H_2O).[24] Chemical reagents were resolved in water and then used to fertilize the soil. A total of 12 L of solution was used to irrigate 12 m^2 of soil at a time. Fertilization was done once a month for a year. Fertilizing strategy A (Se + Zn) was made up with 21.9 mg of Na_2SeO_3 and 2.53 g of $ZnSO_4{\cdot}7H_2O$ in 12 L of water and then used to irrigate 12 m^2 of soil. Fertilizing strategy B (Se + Zn + N) was made up with 21.9 mg of Na_2SeO_3, 2.53 g of $ZnSO_4{\cdot}7H_2O$, and 14.29 g of NH_4NO_3, respectively. Strategy C (Se + Zn + P) was made up with 21.9 mg of Na_2SeO_3, 2.53 g of $ZnSO_4{\cdot}7H_2O$, and 9.68 g of NaH_2PO_4, respectively. Strategy D (Se + Zn + N + P) was made up with 21.9 mg of Na_2SeO_3, 2.53 g of $ZnSO_4{\cdot}7H_2O$, 14.29 g of NH_4NO_3, and 9.68 g of NaH_2PO_4, respectively. Depending on the different fertilizing strategies, the total quantities of Se, Zn, N, and P were 8.33×10^{-1} mg/m^2, 3.33×10^{-2} g/m^2, 4.17×10^{-1} g/m^2, and 2.08×10^{-1} g/m^2, respectively. The solutions were fertilized to the soil under tea plant (in an area 30 cm away from each stem). Moreover, continuous sunny days (5 days or more) were chosen for fertilizing to avoid the loss of fertilizers. After being fertilized for a year (conducted in March 2011 and then fertilized once a month 12 times), new leaves (two leaves and a bud) and old leaves were collected in March 2012. The harvested tea leaves were washed with distilled water and dried, ground, and then stored at −80 °C before analysis.

Assay of Elements. The Zn, Al, and Mn contents were assessed by OPTIMA 5300DV ICP-AES (PerkinElmer, Santa Clara, CA, USA). The Se content was assessed by an AFS-230E AFS (Haiguang Co., Beijing, China). Briefly, 0.5 g of sample was assimilated with 10 mL of mixed acids (nitric acid/perchloric acid, 4:1, v/v) at 250 °C until the solution turned to colorless. Then the solution was filtered and diluted to 25 mL with ultrapure water.[25,26]

Total Free Amino Acids. In brief, 0.25 g of dried tea leaf powder and 50 mL of deionized hot water (80 °C) were mixed in a screw-capped test tube and kept in a water bath at the same temperature for 25 min. Then the tube was cooled to room temperature and centrifuged at 5000*g*/s for 5 min. The supernatant was filtered and diluted to 50 mL with ultrapure water.

One milliliter of tea diluted solution, 0.5 mL of phosphate buffer (PBS), and 0.5 mL of ninhydrin solution were mixed in a 25 mL volumetric flask and heated in a boiling water bath for 15 min. Then, the flask was cooled to room temperature, and the solution was diluted to 25 mL with distilled water. The absorbance of the diluted solution was measured at 570 nm by using an SP-1910UVPC UV spectrophotometer (Spectrum Instrument Co., Shanghai, China). Theanine (99%) was used as a standard, and the results were expressed as percent.[27]

Tea Polysaccharides. In brief, 0.25 g of dried tea leaf powder and 10 mL of 80% (v/v) ethanol were mixed and incubated in the water bath at 95 °C for 1 h. The ethanol was volatilized completely, and 25 mL of deionized water was added and heated in a boiling water bath for 1 h. After centrifugation (3200*g*/s, 10 min), the supernatant was diluted to 25 mL and used for analysis. One milliliter of the solution was mixed with 1.0 mL of phenol and homogenized. After 10 min, 5.0 mL of sulfuric acid was added and then set for 20 min. The absorbance was measured at 490 nm with an SP-1910UVPC UV spectrophotometer (Spectrum Instrument Co.). D-Glucose was used as standard, and the results were expressed as percent.[28,29]

Catechins and Caffeine. In brief, 0.25 g of sample and 2.5 mL of 70% (v/v) chromatographic grade methyl alcohol were mixed together and incubated in the water bath at 70 °C for 30 min. The mixture was centrifuged at 2450*g*/s for 10 min. The extraction was repeated twice, and the supernatants were combined and made up to 5.0 mL. The freshly prepared tea infusions from samples were filtered through 0.45 μm filters.[30]

To determine the catechins and caffeine contents, reverse phase high-performance liquid chromatography (RP-HPLC) was applied in the Agilent 1100 series (Agilent, Santa Clara, CA, USA). An Inertsil octadecylsilane (ODS) C_{18} column (4.6 mm i.d. × 250 mm, 5 μm, Shima, Kyoto, Japan) was used. The flow rate was set at 0.8 mL/min, and the column temperature was kept at 30 °C. The solvent compositions used were water with 0.1% formic acid (solvent A) and methanol (solvent B). The separation was checked by the spectra recorded using the diode array detector (DAD) and the ultraviolet (UV) detector set at 280 nm.[31] A dilution series of each standard (0.01−0.1 mg/mL) had been previously prepared for quantification.

Tea Polyphenols. The total phenolic content (TPC) was determined using the Folin−Ciocalteu procedure as described in International Standards Organisation (ISO) 14502-1:2005.[30] The sample was extracted by 50% (v/v) aqueous ethanol. The extraction was also used to measure the antioxidant activity. One milliliter of tea sample extraction was followed by 5 mL of 10% (v/v) Folin−Ciocalteu reagent and mixed. After 3 min, 4 mL of 20% Na_2CO_3 was added and reached a final volume of 10 mL with water. The mixture was left for 60 min at room temperature, and the absorbance was measured at 760 nm using an SP-1910UVPC UV spectrophotometer (Spectrum Instrument Co.). The result was expressed as percent.[32]

DPPH Radical-Scavenging Capacity. The DPPH assay is one of the most widely used methods to determine the antioxidant activity. The ethanolic DPPH solution (0.2 mmol/L, 2.0 mL) was used as control. The ethanolic DPPH solution was added to 2 mL of extract solution and then shaken vigorously. The samples were measured at 517 nm using an SP-1910UVPC UV spectrophotometer (Spectrum Instrument Co.) after being kept in a dark room for 30 min.[33]

Ferric Reducing Ability of Plasma (FRAP) Assay. The FRAP assay was carried out on the basis of the reduction of Fe^{3+}-TPTZ to Fe^{2+}-TPTZ. The working FRAP reagent was prepared by mixing 2,4,6-tripyridyl-*S*-triazine (TPTZ) dilution, TPTZ solution, and detective buffer in the ratio of 10:1:1 (v/v). About 5.0 μL of extracted solution (or 5.0 μL of deionized water as the blank) was added to 180 μL of fresh working FRAP reagent. After the solution had warmed to 37 °C for 3 min, the absorbance was read at 593 nm using a Varioskan Flash micro plant reader (Thermo, Waltham, MA, USA).[34,35] The results were expressed as $FeSO_4$ equivalent millimoles per gram. Different concentrations (0.15−1.5 mmo/L) of $FeSO_4$ solution were used as abscissa in the standard curve. $FeSO_4$ values were used as ordinate in

Table 1. Contents of Se, Zn, Al, and Mn in New and Old Leaves[a]

		element			
strategy		Se (μg/kg)	Zn (mg/kg)	Al (mg/kg)	Mn (mg/kg)
new leaves	A	0.171 ± 0.011b	32.285 ± 1.315bc	256.840 ± 15.247b	799.050 ± 0.014c
	B	0.208 ± 0.007c	34.235 ± 0.700c	253.797 ± 25.876b	747.658 ± 72.679c
	C	0.241 ± 0.008d	30.280 ± 0.311b	222.005 ± 7.715b	949.784 ± 1.038b
	D	0.228 ± 0.001d	31.032 ± 0.132b	243.549 ± 9.898b	833.388 ± 19.752bc
	CK	0.108 ± 0.004a	21.200 ± 1.131a	377.500 ± 14.142a	1797.000 ± 70.711a
old leaves	A	0.266 ± 0.003b	24.084 ± 0.122bc	2289.974 ± 264.571b	2108.818 ± 77.372cd
	B	0.396 ± 0.003c	28.284 ± 3.192c	1935.391 ± 22.079bc	1907.135 ± 107.193d
	C	0.444 ± 0.004e	20.073 ± 2.592b	1578.149 ± 10.072c	2575.110 ± 77.995b
	D	0.414 ± 0.003d	21.816 ± 2.875b	1626.053 ± 81.572c	2301.853 ± 74.749c
	CK	0.127 ± 0.006a	12.501 ± 0.001a	4937.500 ± 141.421a	3947.000 ± 141.421a

[a]Values represent the mean ± SD. Different letters in the same column indicate statistical difference ($p < 0.05$). A, B, C, and D represent four kinds of fertilization strategies, and CK was the control group.

Table 2. Contents of EGC, CA, CAF, EGCG, and EC[a] in New and Old Leaves[b]

		compound					
strategy		EGC (mg/g)	CA (mg/g)	EGCG (mg/g)	EC (mg/g)	total catechins(mg/g)	CAF (mg/g)
new leaves	A	5.981 ± 0.182b	1.257 ± 0.173ab	101.258 ± 1.698b	12.237 ± 0.479ab	120.703 ± 1.574b	50.116 ± 1.801ab
	B	6.047 ± 0.192b	1.315 ± 0.149ab	106.792 ± 1.939c	12.765 ± 0.482ab	126.919 ± 2.379c	56.684 ± 2.348c
	C	6.630 ± 0.168c	1.623 ± 0.174b	108.630 ± 2.131c	14.970 ± 1.346c	131.852 ± 3.819c	52.580 ± 1.559abc
	D	6.359 ± 0.201bc	1.484 ± 0.131b	108.053 ± 1.601c	13.644 ± 0.488bc	129.540 ± 1.042c	54.716 ± 2.127bc
	CK	5.420 ± 0.082a	0.964 ± 0.047a	81.278 ± 1.704a	11.165 ± 0.503a	98.827 ± 1.329a	48.512 ± 1.802a
old leaves	A	6.188 ± 0.059ab	1.119 ± 0.042ab	83.984 ± 1.438b	10.174 ± 0.579ab	101.465 ± 0.875b	23.732 ± 1.561ab
	B	6.259 ± 0.173bc	1.184 ± 0.168ab	84.637 ± 1.817b	10.642 ± 0.513abc	102.722 ± 1.990b	28.988 ± 2.216c
	C	6.912 ± 0.099d	1.328 ± 0.164b	86.607 ± 1.964b	12.504 ± 0.522c	107.351 ± 1.706b	24.020 ± 1.372ab
	D	6.653 ± 0.229cd	1.217 ± 0.158ab	85.300 ± 1.837b	11.542 ± 0.389bc	104.712 ± 2.613b	26.680 ± 2.348bc
	CK	5.767 ± 0.205a	0.926 ± 0.031a	62.336 ± 2.496a	9.026 ± 1.351a	78.055 ± 3.610a	21.008 ± 1.242a

[a]EGC, epigallocatechin; CA, catechin; EGCG, epigallocatechin gallate; EC, epicatechin; CAF, caffeine. [b]Values represent the mean ± SD. Different letters in the same column indicate the statistical difference ($p < 0.05$). A, B, C, and D represent four kinds of fertilized strategies, and CK was the control group.

the standard curves. Higher $FeSO_4$ values indicated higher ferric reducing power.

Reducing Power. One milliliter of extract solution was mixed with 2.5 mL of phosphate buffer (0.2 mol/L, pH 6.6) and 2.5 mL of potassium ferricyanide (1%, w/v). After incubation at 50 °C for 20 min, 1.0 mL of trichloroacetic acid (10%, w/v) was added to the mixture. The mixture was then shaken vigorously and centrifuged at 2450g/s for 10 min. After that, 2.5 mL of supernatant was mixed with 2.5 mL of distilled water and 0.5 mL of 0.1% ferric chloride. The absorbance was read at 700 nm using an SP-1910UVPC UV spectrophotometer (Spectrum Instrument Co.).[36] The results were expressed as the absorbance.

Statistical Analysis. Results were expressed as the mean ± SD of three independent extractions. Statistical comparisons were performed using the statistical software (SPSS 19.0) with analysis of variance (ANOVA). One-way ANOVA was used to compare the means. A level of probability at $p < 0.05$ was set as statistically significant.

RESULTS

Assay of Elements. The element contents (Se, Zn, Al, Mn) of tea leaves in the four treated groups (A–D) showed significant differences (Table 1). Compared with the control (group CK), the contents of Se and Zn in groups A–D were increased significantly ($p < 0.05$). On the other hand, the contents of Al and Mn were decreased significantly ($p < 0.05$).

Compared with the control group, the Se contents of both new and old leaves in the four treated groups were increased significantly with the order C > D > B > A > CK ($p < 0.05$). The highest Se contents were found in group C (new leaves, 0.241 μg/kg; old leaves, 0.444 μg/kg), which were much higher than those in group CK (new leaves, 0.108 μg/kg; old leaves, 0.127 μg/kg). The Zn content of new leaves in the four treated groups was higher than that in group CK, with the order B > A > D > C > CK, which was the same as the old leaves ($p < 0.05$). New leaves in group B (Se, Zn, and N treated) had the highest Zn content (34.235 mg/kg), which was 61.49% higher than group CK (21.200 mg/kg). However, the Zn contents of new leaves were higher than those in old leaves. For example, the Zn content of new leaves in group A was 32.285 mg/kg, whereas only 24.084 mg/kg Zn was found in old leaves.

The Al contents of both new and old leaves in the four treated groups were decreased significantly when compared with group CK, and the order was C < D < B < A < CK. Although the Al contents in groups A–D were significantly higher than that in group CK, no significant differences were observed in groups A–D (new leaves) and groups B–D (old leaves) ($p < 0.05$). The old leaves had consistently higher Al content than new leaves. For instance, the Al content of new leaves in group D was 243.549 mg/kg, which was only one-sixth that in old leaves (1626.053 mg/kg). By our management, the highest Se content as well as the lowest Al content (222.005 mg/kg) was found in group C (new leaves). Similarly, the Mn contents decreased significantly by new fertilizing strategies,

dx.doi.org/10.1021/jf5004286 | J. Agric. Food Chem. 2014, 62, 3823–3830

and the order was B < A < D < C < CK (Table 2). No significant differences were observed in groups A, B, and D (new leaves). However, group B had significant differences with groups C and D in old leaves ($p < 0.05$). The lowest Mn contents were found in group B (new leaves, 747.658 mg/kg; old leaves, 1907.135 mg/kg), followed by groups A (799.050 mg/kg), D (833.388 mg/kg), and C (949.784 mg/kg). Moreover, the highest Zn content as well as the lowest Mn content was found in group B (new leaves).

Total Free Amino Acid Content. The total free amino acid contents in both new and old leaves in four different treated groups were increased significantly, and the order was B > D > C > A > CK (Figure 1). In both new and old leaves, the total free amino acid contents in groups A–D were significantly higher than that in group CK ($p < 0.05$). The content of total free amino acids in new leaves was much higher than that in old leaves ($p < 0.05$). The highest total free amino acid content was found in group B (new leaves, 5.60%; old leaves, 2.90%), followed by groups D (5.48 and 2.51%, respectively), C (5.24 and 2.43%, respectively), A (5.01 and 2.27%, respectively), and CK (2.37 and 2.11%, respectively).

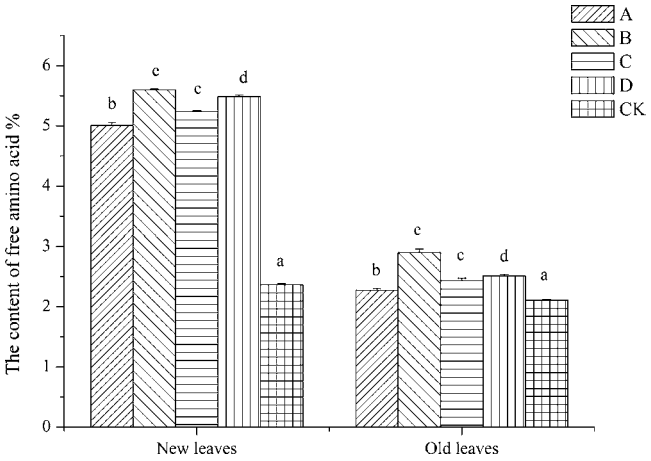

Figure 1. Contents of total free amino acids in new and old tea leaves. A, B, C, and D represent four kinds of fertilization strategies, and CK was the control group. Values represent the mean ± SD. Bars with the same letter above do not differ significantly. Different letters above the bars indicate statistical difference ($p < 0.05$).

Tea Polysaccharide Content. Using four different fertilizing strategies, the tea polysaccharide contents in both new and old leaves were significantly increased (Figure 2). The order was B > D > C > A > CK. There were significant differences among groups A, B, and C in new leaves and among groups A, B, and D in old leaves ($p < 0.05$). Furthermore, the polysaccharide contents in old leaves were much higher than that in new leaves (new leaves, 4.47%; old leaves, 5.80%). It was shown that group B had the highest tea polysaccharide content both in new leaves (4.47%) and in old leaves (5.80%), followed by groups D (4.11 and 5.37%, respectively) and C (3.87 and 5.09%, respectively). Group CK showed the lowest tea polysaccharide contents in new and old leaves (2.51 and 3.91%, respectively), which were 78.05 and 48.34% lower than those in group B.

Catechins and Caffeine Contents. Four catechins (EGC, CA, EGCG, and EC) were separated and analyzed in tea leaves (Figure 3). The total contents of catechins in new leaves were higher than those in old leaves (Table 2). The order was C > D > B > A > CK. For the total contents of catechins and EGCG, there were significant differences among groups A–D and CK in both new and old leaves ($p < 0.05$). However, there was no significant difference among groups B–D in new leaves or among groups A–D in old leaves ($p < 0.05$). For EGC, there were significant differences among groups A–D and CK in new leaves ($p < 0.05$). Groups C and D had significantly higher EC content than group CK in both new and old leaves ($p < 0.05$), which was the same as the catechin of CA. Group C showed the highest contents of EGC, CA, EGCG, and EC both in new leaves (6.630, 1.623, 108.630, and 14.970 mg/g, respectively) and in old leaves (6.912, 1.328, 86.607, and 12.504 mg/g, respectively). However, group CK showed the lowest contents of EGC, CA, EGCG, and EC in both new (5.420, 0.964, 81.278, and 11.165 mg/g, respectively) and old leaves (5.767, 0.926, 62.336, and 9.026 mg/g, respectively),

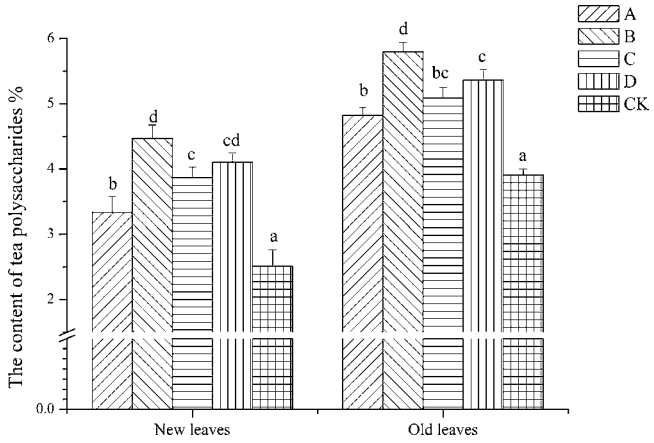

Figure 2. Contents of tea polysaccharides in new and old tea leaves. A, B, C, and D represent four kinds of fertilization strategies, and CK was the control group. Values represent the mean ± SD. Bars with the same letter do not differ significantly. Different letters indicate the statistical difference ($p < 0.05$).

The caffeine contents of both new and old leaves in four fertilizer-treated groups were higher than those in group CK, with the order B > D > C > A > CK. However, only groups B and D had significant difference with CK in new leaves, and only group B showed significant difference with CK in old leaves ($p < 0.05$). Group B showed the highest caffeine contents (56.684 mg/g in new leaves and 28.988 mg/g in old leaves), which were 16.85 and 37.99% higher, respectively, than those in group CK.

Tea Polyphenol Content. The total polyphenol contents of new leaves using four different fertilization strategies were higher than those in old leaves (Figure 4). Although all groups showed significant difference with CK in old leaves, only groups B–D had significant difference with CK in new leaves ($p < 0.05$). Group C showed the highest total polyphenol contents in new leaves and old leaves (28.29 and 27.74%, respectively), followed by groups D, B, A, and CK. The polyphenol contents in group CK were 26.62 and 25.35% in new leaves and old leaves, which were 6.27 and 9.43% lower than those in group C, respectively.

DPPH Radical-Scavenging Capacity. The orders of DPPH radical-scavenging capacities in both new leaves and old leaves were C > D > B > A > CK (Figure 5I). Although groups A–C showed significant difference with CK in new leaves, only group C had significant difference with groups A and D in old leaves ($p < 0.05$). New leaves showed higher

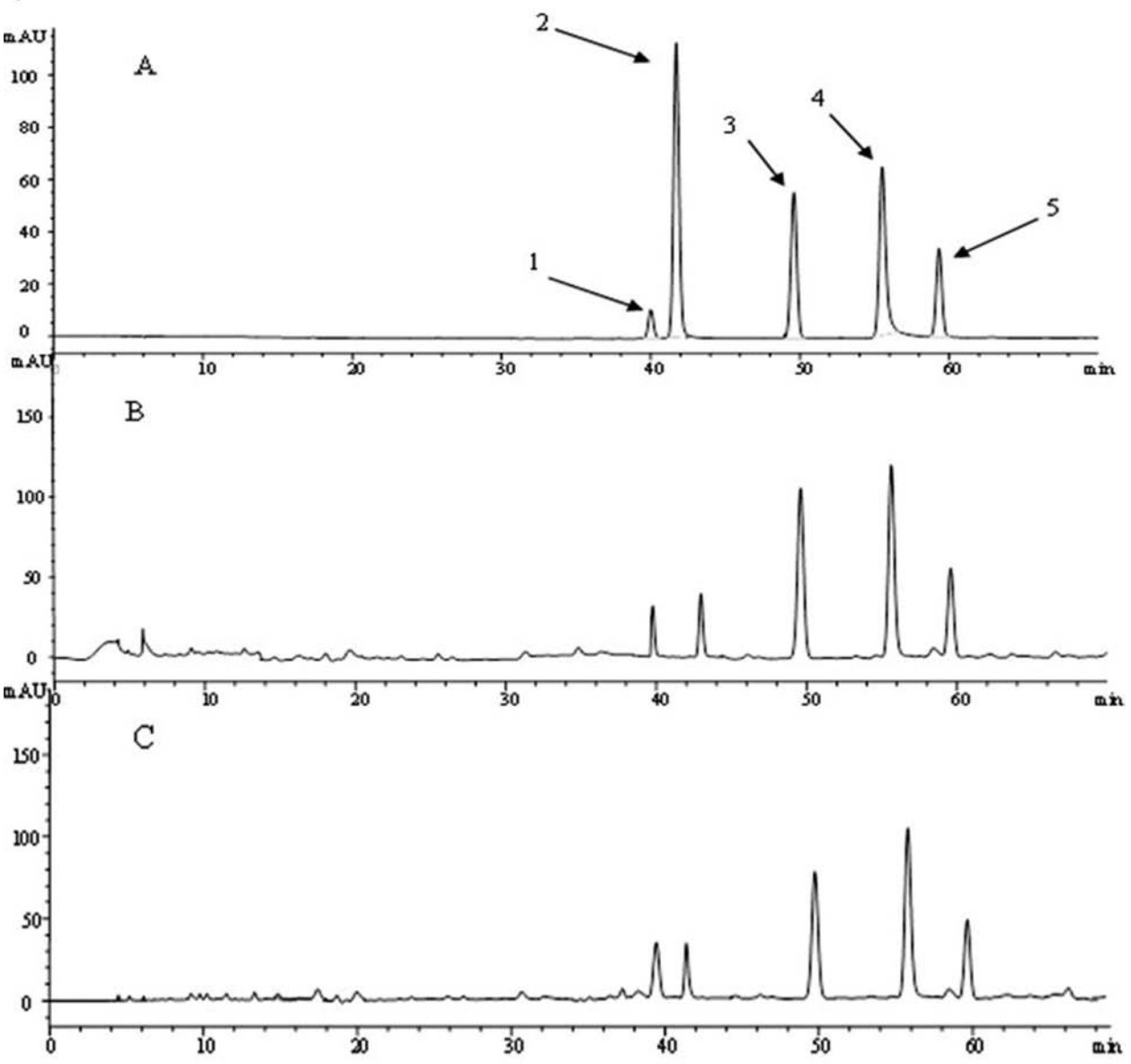

Figure 3. Mixed standards (A) and typical HPLC chromatogram of catechins and caffeine in new leaves (B) and old leaves (C). Numbers represent the different substances (1, catechins, EGC; 2, catechins, CA; 3, caffeine, CAF; 4, catechins, EGCG; 5, catechins, EC).

DPPH antioxidant activity than old leaves in all groups. The strongest DPPH antioxidant activity was found in group C (new leaves, 95.06%; old leaves, 89.65%), followed by groups D (93.22 and 85.48%, respectively) and B (91.59 and 84.43%, respectively). Nevertheless, the DPPH values in group CK were 15.70 and 11.60% (new and old leaves), which were much lower than those in other groups ($p < 0.05$).

FRAP Assay. Similarly, the order of FRAP values was C > B > D > A > CK in both new leaves and old leaves (Figure 5II). However, only groups B–D had significant difference with CK in both new or old leaves ($p < 0.05$). The FRAP values in new leaves were higher than those in old leaves (2.14% higher than old leaves). Among them, group C had the strongest FRAP values in both new and old leaves (3.81 and 3.73 mmol of $FeSO_4$/g, respectively), followed by groups B (3.76 and 3.71 mmol of $FeSO_4$/g, respectively) and D (3.71 and 3.68 mmol of $FeSO_4$/g, respectively). The weakest FRAP antioxidant activity was found in group CK, with values of 3.62 and 3.57 mmol of $FeSO_4$/g in new and old leaves, respectively.

Reducing Power. The reducing power in both new and old leaves from the strongest to weakest was C > D > B > A > CK (Figure 5III), which was similar to the DPPH and FRAP values. However, only group C showed significant difference with CK in new leaves, and groups C and D had significant difference with CK in old leaves ($p < 0.05$). Group C showed the strongest reducing power both in new leaves and old leaves (absorbance, 1.26 and 1.21, respectively), followed by groups D (1.23 and 1.20, respectively), B (1.22 and 1.18, respectively), and A (1.19 and 1.15, respectively). Group CK showed the lowest reducing power in both new (1.17) and old leaves (1.14). The reducing powers in new leaves (1.17–1.23) were higher than those in old leaves (1.14–1.20).

DISCUSSION

It was shown that the fertilizer P in red soil played a role in improving the content of Se in tea leaves. It was proven that P and Se had similar absorption sites in soil, which were

dx.doi.org/10.1021/jf5004286 | J. Agric. Food Chem. 2014, 62, 3823–3830

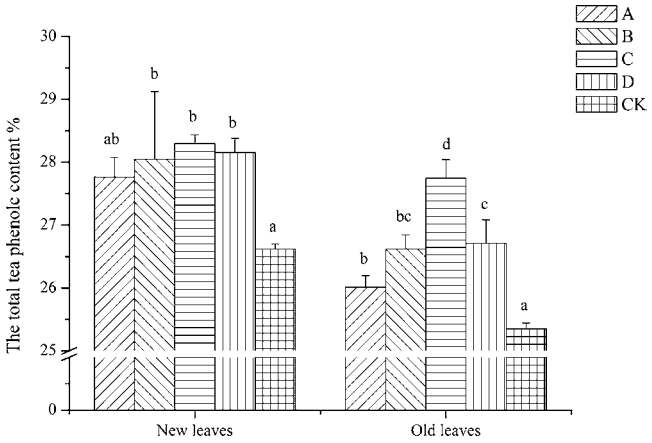

Figure 4. Contents of tea polyphenols in new and old tea leaves. A, B, C, and D represent four kinds of fertilization strategies, and CK was the control group. Values represent the mean ± SD. Bars with the same letter above do not differ significantly. Different letters indicate the statistical difference ($p < 0.05$).

competitively absorbed by soil.[35] Se showed preferential bonding with soil particle and therefore was hard to be absorbed by tea roots. Fertilizer P could exchange Se from the soil and made Se more easily absorbed by the tea plant.[37] Kopsell and Ekiza showed that the Se and Zn enriched soil could release more Se and Zn ions, which may be transferred to the tea leaves.[38,39] From our result, the content of Se in tea leaves was found to be negatively correlated with Al (Pearson's correlation coefficient, $r = -0.916$) (Table 1). It might be caused by the antagonistic effect of Se (obtain from fertilizer Se) and Al in the soil, which was less studied before. On the other hand, the content of Zn in tea leaves was negatively correlated with Mn ($r = -0.927$) in different fertilizer-treated groups, which might be caused by the competitive absorption of Zn (obtain from fertilizer Zn) and Mn in the soil.[40] Generally speaking, the four fertilizing strategies (with exogenetic N, P, Se, and Zn in soil) in our study were effective in enriching tea leaves with Se and Zn with low Al and Mn contents in an acid soil region.

It is interesting to note that fertilizer N in soil might help to increase the total amino acids in tea leaves (group B, 5.60%; blank group, 2.37%). N is necessary for the biosynthesis of amino acids, which could well explain that fertilization with N in soil contributed to the higher total amino acid contents in tea leaves. Moreover, the total amino acid content in new tea leaves was 92.97% higher than that in old leaves. The enzymes including glutamic-pyruvic transaminase (GTP), glutamate dehydrogenase (GLD), and amine oxidase were useful to the synthesis of amino acid. It was reported that the contents of these enzymes were much higher in new leaves than in old ones, which could help to increase the contents of amino acids in new tea leaves and therefore help the growth of the tea plant.[41]

Tea was mostly glycoconjugates, and the polysaccharide contents were increased significantly in the tea leaves fertilized with N. Fertilizer N in soil was found to be effective in the synthesis of chlorophyll, which could contribute to the carbon metabolism and help to enhance the tea polysaccharide contents.[42,43] The metabolism of old leaves was much slower, which might consume less carbohydrate and accumulate more polysaccharide. Therefore, the tea polysaccharide content in old leaves was higher than that in new leaves.

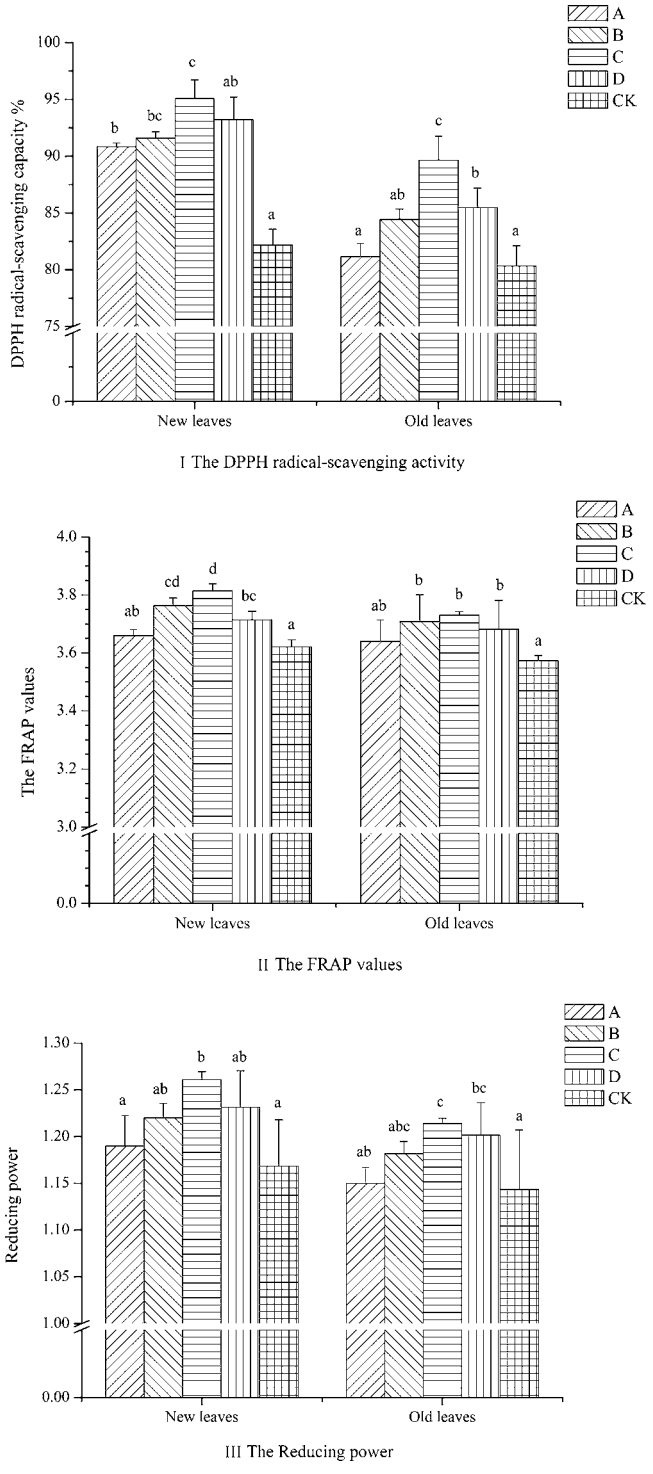

Figure 5. DPPH (I), FRAP (II), and reducing power (III) antioxidant activities in new and old tea leaves. A, B, C, and D represent four kinds of fertilization strategies, and CK was the control group. Values represent the mean ± SD. Bars with the same letter above do not differ significantly. Different letters indicate the statistical difference ($p < 0.05$).

Tea polyphenol is the major antioxidant substance in tea leaves.[44] The antioxidant activities showed good correlation with the tea total polyphenol content ($r = 0.910$). The tea leaves with higher polyphenol content also showed stronger antioxidant activities. It has been proven that P could synthesize to phenylalanine ammonia-lyase (PAL); it was very important

dx.doi.org/10.1021/jf5004286 | J. Agric. Food Chem. 2014, 62, 3823−3830

in generating the polyphenol in tea leaves.[22] Fertilizer P was therefore beneficial to increase the polyphenol content and antioxidant activity of tea leaves. It showed that the contents of EGCG in old tea leaves were lower than those in new leaves, which might be caused by the weaker activities of UDP-glucose:galloyl-1-*O*-*β*-D-glucosyl-transferase (UGGT) and epicatechin:1-*O*-galloyl-*β*-D-glucose *O*-galloyltransferase (ECGT) and the stronger galloylated catechin hydrolase (GCH) in old leaves.[45] Under the comprehensive works of these enzymes, EGCG was preferred to be hydrolyzed to EGC in old leaves. Moreover, the antioxidant and anticancer activities of EGCG was the strongest among different catechins.[46] It might also contribute to the greater antioxidant activities of new leaves with high EGCG contents. The tea leaves with higher content of Se also had stronger antioxidant activity. For example, the highest contents of Se (0.241 *μ*g/kg) and tea polyphenols (28.29%) as well as the greatest antioxidant activities (DPPH, 95.06%; FRAP, 3.81 mmol of $FeSO_4$/g; reducing power 1.26) were found in new leaves of group C. It was known that Se played an important part in the formation of GSH-Px, which was an important antioxidant enzyme in the body and helpful to improve the antioxidant activity. Elements N and P were also the most important substances to constitute the enzymes such as nitrate reductase (NR), adenosine triphosphate (ATP), and nicotinamide adenine dinucleotide phosphate (NADP), which could therefore improve the antioxidant activities in tea leaves.[23]

The Al and Mn contents in tea leaves were significantly decreased by our new fertilizing strategies (with exogenetic Se, Zn, N and P), the functional component (polyphenol, catechins, free amino acid, polysaccharide and caffeine) contents of the tea leaves planted in acid soil were increased and their antioxidant activity was also improved. The function improvement of the tea leaves could reduce the potential harm and enhance the healthcare effect in humans.

AUTHOR INFORMATION

Corresponding Authors

*(H.L.) Phone: +86 791 88314447-8226. Fax: 86 791 88304402. E-mail: lihongyan@ncu.edu.cn.

*(Z.-Y.D.) Phone/fax: +86 791 88304402. E-mail: zeyuandeng@hotmail.com.

Funding

This project was funded by the National Natural Science Funds of China (Grants 31301433 and 31060081), the China Postdoctoral Science Foundation funded project (Grant 2013M530306), and the Research Program of State Key Laboratory of Food Science and Technology (SKLF-TS-200921).

Notes

The authors declare no competing financial interest.

REFERENCES

(1) Sharangi, A. B. Medicinal and therapeutic potentialities of tea (*Camellia sinensis* L.). *Food Res. Int.* **2009**, *42*, 529−535.

(2) Serafini, M.; Ghiselli, A.; Ferro-Luzzi, A. In vivo antioxidant effect of green tea and black tea in man. *Eur. J. Clin. Nutr.* **1996**, *50* (1), 28−32.

(3) Nookabkaew, S.; Rangkadilok, N.; Satayavivad, J. Determination of trace elements in herbal tea products and their in fusions consumed in Thailand. *J. Agric. Food Chem.* **2006**, *54* (18), 6939−6944.

(4) Pohl, P.; Prusisz, B. Fractionation analysis of manganese and zinc in tea infusions by two-column solid phase extraction and flame atomic absorption spectrometry. *Food Chem.* **2007**, *102*, 1415−1424.

(5) Foy, C. D. Physiological effects of hydrogen, aluminum and manganese toxicities in acid soil. In *Soil Acidity and Liming*; American Society of Agronomy: Madison, WI, USA, 1984; Chapter 19, pp 57−97.

(6) Foy, C. D.; Chaney, R. L.; White, M. C. The physiology of metal toxicity in plants. *Annu. Rev. Plant Physiol.* **1978**, *29*, 511−566.

(7) Karak, T.; Bhagat, R. M. Trace elements in tea leaves, made tea and tea infusion. *Food Res. Int.* **2010**, *43*, 2234−2252.

(8) Moore, P. B.; Day, J. P.; Taylor, G. A.; Ferrier, I. N.; Fifield, L. K.; Edwardson, J. A. Absorption of aluminium-26 in Alzheimer's disease, measured using accelerator mass spectrometry. *Dement. Geriatr. Cogn. Disord.* **2000**, *11* (2), 66−69.

(9) Campbell, A.; Hamai, D.; Bondy, S. C. Differential toxicity of aluminum salts in human cell lines of neural origin: implications for neurodegeneration. *Neurotoxicology* **2001**, *22* (1), 63−71.

(10) Aschner, M.; Aschner, J. L. Manganese neurotoxicity: Cellular effects and blood-brain barrier transport. *Neurosci. Biobehav. Rev.* **1991**, *15* (3), 333−340.

(11) Zheng, W.; Liu, P.; Xu, G. Effect of aluminum on quality of tea plant (in Chinese). *Ecol. Environ.* **2006**, *15* (4), 822−826.

(12) Finley, J. W.; Ip, C.; Lisk, D. J.; Davis, C. D.; Hintze, K. J.; Whanger, P. D. Cancer − protective properties of high-selenium broccoli. *J. Agric. Food Chem.* **2001**, *49* (5), 2679−2683.

(13) Fang, Y.; Wang, L.; Xin, Z.; Zhao, L.; An, X.; Hu, Q. Effect of foliar application of zinc, selenium, and iron fertilizers on nutrients concentration and yield of rice grain in China. *J. Agric. Food Chem.* **2008**, *56* (6), 2079−2084.

(14) Ebert, R.; Jakob, F. Selenium deficiency as a putative risk factor for osteoporosis. *Int. Congr. Ser.* **2007**, *1297* (3), 158−164.

(15) McDaid, O.; Stewart-Knox, B.; Parr, H.; Simpson, E. Dietary zinc intake and sex differences in taste acuity in healthy young adults. *J. Hum. Nutr. Diet.* **2007**, *20* (2), 103−110.

(16) Shen, F. W.; Chen, H. W. Element composition of tea leaves and tea infusions and its Impact on health. *Bull. Environ. Contam. Toxicol.* **2008**, *80*, 300−304.

(17) Cabrera, C.; Giménez, R.; López, M. C. Determination of tea components with antioxidant activity. *J. Agric. Food Chem.* **2003**, *51* (15), 4427−4435.

(18) Sae-Lee, N.; Kerdchoechuen, O.; Laohakunjit, N. Chemical qualities and phenolic compounds of Assam tea after soil drench application of selenium and aluminium. *Plant Soil* **2012**, *356*, 381−393.

(19) Lombi, E.; Tearall, K. L.; Howarth, J. R.; Zhao, F. J.; Hawkesford, M. J.; McGrath, S. P. Influence of iron status on cadmium and zinc uptake by different ecotypes of the hyper-accumulator *Thlaspi caerulescens*. *Plant Physiol.* **2002**, *128*, 1359−1367.

(20) Mudau, N. F.; Soundy, P.; Du Toit, E. S. Plant growth and development of bush tea as affected by nitrogen, phosphorus and potassium nutrition. *HortScience* **2005**, *40* (6), 1898−1901.

(21) Venkatesan, S.; Ganapathy, M. N. K. Impact of nitrogen and potassium fertiliser application on quality of CTC teas. *Food Chem.* **2004**, *84* (3), 325−328.

(22) Lin, Z.; Qi, Y.; Chen, R.; Zhang, F.; Chen, L. Effects of phosphorus supply on the quality of green tea. *Food Chem.* **2012**, *130*, 908−914.

(23) Li, J.; Xia, J. G. Summary on nitrogen (N), phosphorus (P), potassium (K) and tea quality. *Chinese Agric. Sci. Bull.* **2005**, *21*, 62−65.

(24) Ma, R. X.; Wang, J. S.; Li, X. Z.; Liu, W. C. Effect of different NPK fertilizers cooperating application on yield and quality of high starch maize. *Appl. Mech. Mater.* **2012**, *214*, 423−429.

(25) Chen, L.; Yang, F.; Xu, J.; Hu, Y.; Hu, Q.; Zhang, Y.; Pan, G. Determination of selenium concentration of rice in China and effect of fertilization of selenite and selenate on selenium content of rice. *J. Agric. Food Chem.* **2002**, *50* (18), 5128−5130.

(26) Musa Özcan, M.; Ünver, A.; Uçar, T.; Arslan, D. Mineral content of some herbs and herbal teas by infusion and decoction. *Food Chem.* **2008**, *106*, 1120−1127.
(27) Shao, J. L.; Li, Q. W.; Dong, B. S.; Liu, H. C.; Shu, J. H. Determination of total free-amino acid in tea by nihydrin colorimetry. *China Food Addit.* **2008**, *2*, 162−165.
(28) Fu, B.; Xie, M.; Nie, S. Determination of tea polysaccharide contents. *Food Sci.* **2001**, *22*, 69−73.
(29) Dubois, M.; Gilles, K. A.; Hamilton, J. K.; Rebers, P. A.; Smith, F. Colorimetric method for determination of sugars and related substances. *Anal. Chem.* **1956**, *28* (3), 350−356.
(30) ISO 14502-1:2005. Determination of substances characteristic of green and black tea.
(31) Chen, Q.; Zhao, J.; Huang, X.; Zhang, H.; Liu, M. Simultaneous determination of total polyphenols and caffeine contents of green tea by near-infrared reflectance spectroscopy. *Microchem. J.* **2006**, *83* (1), 42−47.
(32) Rusak, G.; Komes, D.; Likić, S.; Horžić, D.; Kovač, M. Phenolic content and antioxidative capacity of green and white tea extracts depending on extraction conditions and the solvent used. *Food Chem.* **2008**, *110* (4), 852−858.
(33) Sheng, J. C.; Zhou, J.; Wang, L.; Xu, J.; Hu, Q. H. Antioxidant activity of ethanol and petroleum ether extracts from Brazilian propolis. *Eur. Food Res. Technol.* **2007**, *225* (2), 249−253.
(34) Benzie, I. F. F.; Strain, J. J. The ferric reducing ability of plasma (FRAP) as a measure of "antioxidant power": the FRAP assay. *Anal. Biochem.* **1996**, *239* (1), 70−76.
(35) Luo, J. G.; Li, L.; Kong, L. Y. Preparative separation of phenylpropenoid glycerides from the bulbs of *Lilium lancifolium* by high-speed counter-current chromatography and evaluation of antioxidant activities. *Food Chem.* **2012**, *131* (1), 1056−1062.
(36) Oyaizu, M. Studies on products of browning reaction. Antioxidative activities of products of browning reaction prepared from glucosamine. *Jpn. J. Nutr.* **1986**, *37*, 311−319.
(37) Liu, Q. Influences of application of phosphate paddy soil on absorption of selenium, calcium, zinc, and sulphur in rice. *Trace Elem. Sci.* **2003**, *10* (6), 20−24.
(38) Kopsell, D. A.; Randle, W. M. Selenate concentration affects selenium and sulfur uptake and accumulation by "Granex 33" onions. *J. Am. Soc. Hortic. Sci.* **1997**, *122* (5), 721−726.
(39) Ekiza, H.; Bagcia, S. A.; Kirala, A. S.; Ekerb, S.; Gültekina, I.; Alkanb, A.; Cakmakc, I. Effects of zinc fertilization and irrigation on grain yield and zinc concentration of various cereals grown in zinc-deficient calcareous soils. *J. Plant Nutr.* **1998**, *21* (10), 2245−2256.
(40) Li, Z. W.; Zhang, M.; Xu, G. S. Chemical speciation and bioavailability of Mn and Zn to tea in soils of the Fenghuangshan tea belt, east Guangdong. *J. Ecol. Rural Environ.* **2011**, *27* (5), 7−12.
(41) Deng, W. W.; Ogita, S.; Ashihara, H. Biosynthesis of theanine (γ-ethylamino-L-glutamic acid) in seedlings of *Camellia sinensis*. *Phytochem. Lett.* **2008**, *1* (2), 115−119.
(42) Huppe, H. C.; Turpin, D. H. Intergration of carbon and nitrogen metabolism in plant and algale cells. *Annu. Rev. Plant Physiol. Mol. Biol.* **1994**, *45*, 577−607.
(43) Klotz, L. K.; Campbell, L. G. Sucrose catabolism in developing roots of three beta vulgaris genotypes with different yield and sucrose accumulating capacities. *J. Sugar Beet Res.* **2004**, *41*, 73−88.
(44) Wan, X. Y. In *Biochemistry of Tea* (3); Agriculture Press: Beijing, China, 2003; pp 9−10, 18, 20.
(45) Niemetz, R.; Gross, G. G. Enzymology of gallotannin and ellagitannin biosynthesis. *Phytochemistry* **2005**, *66* (17), 2001−2011.
(46) Cabrera, C.; Artacho, R.; Giménez, R. Beneficial effects of green tea. *J. Am. Coll. Nutr.* **2006**, *25* (2), 79−99.

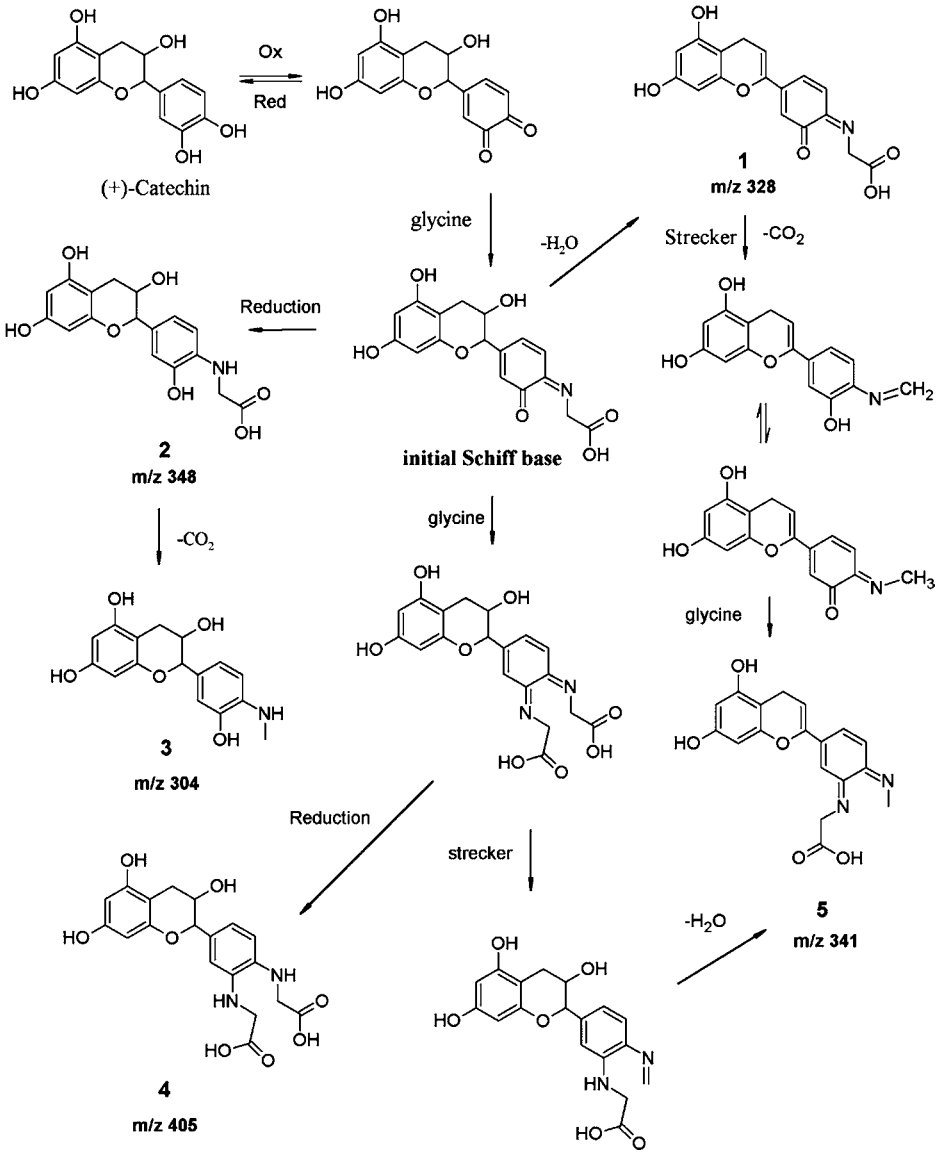

Figure 1. Proposed mechanism of (+)-catechin−glycine adduct formation. (For structures **1**, **2**, **3**, and **5** only one isomer is shown of two possible isomers.)

Table 1. Percent Incorporation of Labeled Glycine Atoms into Structures 1−5 Generated from Glycine/(+)-Catechin Model System

	[^{13}C-1]glycine					[^{13}C-2]glycine					[^{15}N]glycine			
structure	*m/z*	M	M + 1	M + 2	error[a] (ppm)	M	M + 1	M + 2	error[a] (ppm)	M	M + 1	M + 2	error[a] (ppm)
1	328	0	100	0	12	0	100	0	12	0	100	0	33
2	347	0	100	0	12	0	100	0	12	0	100	0	32
3	303	100	0	0	20	0	100	0	20	0	100	0	34
4	404	0	0	100	25	0	0	100	26	0	0	100	6.6
5	340	0	100	0	12	0	0	100	25	0	0	100	64

[a]Error in the calculation of molecular formulas with label incorporation.

from QTOF. Accurate mass analysis was performed with the aid of ChemCalc.[9] Structural identification was performed using AMDIS (v. 2.65) and NIST Standard Reference Databases (data v. NIST05 and software v. 2.0d) in addition to isotope-labeling data. Isotope-labeling studies were performed through replacing glycine with its labeled analogue [^{13}C-1]glycine or [^{13}C-2]glycine (99%) or [^{15}N]glycine (98%) in the model systems mentioned above. Furthermore, the MS/MS data were compared with previously reported[10] mass spectra of (+)-catechin. The correspondence of the peaks to those generated through labeling experiments was verified through matching their retention times on the Hypersil Gold PFP liquid chromatography column.

RESULTS AND DISCUSSION

Although the interaction of ring A of catechin with Maillard reaction intermediates such as 1,2-dicarbonyl compounds is well established,[1,2] the interaction of catechins with amino acids has not been observed or reported yet mainly due to the fact that

dx.doi.org/10.1021/jf5005989 | J. Agric. Food Chem. 2014, 62, 3831−3836

such studies have been conducted in the absence of air or under nitrogen and, in theory, an oxidation step is necessary to generate reactive *o*-quinonoidal moieties[8] for their interaction with amino acids. In this study, (+)-catechin hydrate was heated alone or in the presence of glycine under oxidative conditions (open flask), and the reaction mixtures were analyzed by high-resolution ESI TOF/MS. Comparison of the reaction profiles of the two systems has indicated the formation of new chromatographic peaks in the (+)-catechin hydrate/glycine model system having masses higher than that of (+)-catechin. Furthermore, isotope-labeling studies with [^{13}C-1]glycine, [^{13}C-2]glycine, and [^{15}N]-glycine indicated the incorporation of one or two glycine moieties in five of the adducts identified as shown in Figure 1 and Table 1 (structures **1**−**5**). Two of these adducts (**1** and **5**) underwent dehydration of ring C of (+)-catechin, and in the remaining three adducts (**2**, **3**, and **4**) ring C remained intact.

Interaction Pathways of Glycine with Oxidized B-Ring of Catechin. The ability of glycine to undergo either single- or double-addition reactions with 1,2-dicarbonyl compounds in general[11] and with *o*-quinonoidal moieties in particular has been observed previously.[8,12] Detailed analyses of the adducts listed in Table 1 and shown in Figure 1 have indicated that structure **1** (shown as one possible isomer) observed at m/z 328 corresponds to a single-addition product of glycine to an oxidized (+)-catechin with subsequent dehydration of ring C. Alternatively, the initial Schiff base adduct (see Figure 1) can either undergo reduction to generate structure **2** at m/z 348 or react with a second molecule of glycine and then undergo reduction, this time generating structure **4** at m/z 405. In turn, structure **2** can undergo decarboxylation to generate structure **3** at m/z 304. Finally, structure **1** can undergo Strecker decarboxylation followed by isomerization of ring B and addition of a second molecule of glycine to generate structure **5** at m/z 341. The high-resolution mass spectral data obtained (see Table 2) for structures **1**−**5** confirmed their elemental composition

Table 2. Calculated Elemental Composition of (+)-Catechin−Glycine Adducts

structure	m/z	M	elemental composition	error[a] (ppm)
(+)-catechin	291	291.0812	$C_{15}H_{14}O_6$	7.5
1	328	328.0755	$C_{17}H_{13}NO_6$	3.7
2	348	348.1015	$C_{17}H_{17}NO_7$	2.9
3	304	304.1123	$C_{16}H_{17}NO_5$	5.4
4	405	405.1216	$C_{19}H_{20}N_2O_8$	0.91
5	341	341.1072	$C_{18}H_{16}N_2O_5$	3.7

[a]Error in the calculation of elemental composition.

consistent with the proposed structures. In addition, the label incorporation data using [^{13}C-1]glycine, [^{13}C-2]glycine, and [^{15}N]glycine further supported the proposed structures (see Table 1).

MS/MS Analysis of (+)-Catechin−Glycine Adducts. To provide additional detailed evidence for the proposed structures, the characteristic ion fragmentation patterns previously reported for catechin[13] and for flavones and flavonols[14] were compared with those observed for structures **1**−**5**. In general, catechins undergo MS/MS fragmentations when exposed to collision energies >10 V through bond cleavages of the central ring C and generating fragments that retain either ring A or ring B moieties (see Figure 2). According to the accepted nomenclature rules, a fragment generated under positive ion mode and retaining the ring B moiety through cleavage of bonds 0 and 2 of the ring C

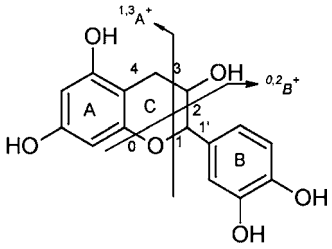

Figure 2. Nomenclature and C-ring bond cleavages in catechin.

could be designated fragment $^{0,2}B^+$ (see Figure 2). Such B^+ fragments could be used as diagnostic ions for the formation of amino acid adducts at ring B (in this case it was termed B_i^+, where i = 1, 2, 3, etc.) and A^+ fragments could be used to confirm the nature of adducts as originating from the catechin moiety. Among the five structures reported in Table 1 the adducts with nondehydrated C-rings (structures **2**−**4**) showed the characteristic A^+ and B^+ fragments of catechin and, on the other hand, the structures that underwent dehydration at the C-ring (**1** and **5**) showed only fragmentations originating from the amino acid moiety such as decarboxylation and Strecker type fragmentations (see Table 3). These observations are consistent with the fact

Table 3. Characteristic MS/MS Fragmentations Observed in Structures 1−5

structure	fragmenting moiety	fragmentation type	daughter ions[a]
1	amino acid	decarboxylation	283 (7.5)
		Strecker degradation	269 (60), 270 (10), 329 (20)
2	ring C	A^+	123 (30)
		B^+	226 (8), 180 (15), 196 (100), 150 (90)
3	ring C	A^+	123 (10)
		B^+	152 (100), 137 (25), 138 (75)
4	ring C	B^+	253 (100), 207 (10), 162 (10), 147 (15)
5	amino acid	decarboxylation	297 (65)
		Strecker degradation	282 (100), 283 (15), 342 (15)

[a]Relative intensities are reported in parentheses.

that A and B series ions result from bond cleavages of the intact ring C. Tables 4−8 show the major MS/MS fragments for structures **1**−**5** and their isotope incorporation patterns, and Figures 3−7 show the proposed fragmentation pathways (accurate mass analysis showed errors of <26 ppm for all

Table 4. MS/MS Data of m/z 328.0755 (Structure 1[a])

m/z	relative intensity (%)	elemental composition[b]	error (ppm)	label incorporation from glycine
328.0859	100	$C_{17}H_{14}NO_6$	12	1 × C-1; 1 × C-2; 1 × N
283.0839	7.5	$C_{16}H_{13}NO_4$	1.9	1 × C-2; 1 × N
270.0739	10	$C_{15}H_{12}NO_4$	10	1 × N
269.0710	60	$C_{15}H_{11}NO_4$	1.8	1 × N

[a]See Figure 1. [b]See Figure 3 for corresponding proposed structures.

dx.doi.org/10.1021/jf5005989 | J. Agric. Food Chem. 2014, 62, 3831−3836

Table 5. MS/MS Data of *m/z* 348.1015 (Structure 2[a])

m/z	relative intensity (%)	elemental composition[b]	error (ppm)	label incorporation from glycine
348.1091	5	$C_{17}H_{18}NO_7$	2.2	1 × C-1; 1 × C-2; 1 × N
226.0725	8	$C_{10}H_{12}NO_5$	4.2	1 × C-1; 1 × C-2; 1 × N
196.0633	100	$C_9H_{10}NO_4$	12	1 × C-1; 1 × C-2; 1 × N
180.0665	15	$C_9H_{10}NO_3$	2.4	1 × C-2; 1 × N
150.0562	90	$C_8H_8NO_2$	4.6	1 × C-2; 1 × N
147.0462	55	$C_9H_7O_2$	11	
123.0457	30	$C_7H_7O_2$	8.9	

[a]See Figure 1. [b]See Figure 4 for corresponding proposed structures of selected ions.

Table 6. MS/MS Data of *m/z* 304.1123 (Structure 3[a])

m/z	relative intensity (%)	elemental composition[b]	error (ppm)	label incorporation from glycine
304.1192	15	$C_{16}H_{18}NO_5$	2.3	1 × C-2; 1 × N
182.0804	5	$C_9H_{12}NO_3$	7.2	1 × C-2; 1 × N
152.0726	100	$C_8H_{10}NO_2$	9.5	1 × C-2; 1 × N
147.0462	15	$C_9H_7O_2$	11	
138.0556	75	$C_7H_8NO_2$	0.69	1 × N
137.0475	25	$C_7H_7NO_2^{\bullet}$	1.3	1 × N
123.0457	10	$C_7H_7O_2$	8.9	
109.0542	20	$C_6H_7NO^{\bullet}$	13	1 × N

[a]See Figure 1. [b]See Figure 5 for corresponding proposed structures of selected ions.

Table 7. MS/MS Data of *m/z* 405.1216 (Structure 4[a])

m/z	relative intensity (%)	elemental composition[b]	error (ppm)	label incorporation from glycine
405.1322	1	$C_{19}H_{21}N_2O_8$	25	2 × C-1; 2 × C-2; 2 × N
302.1061	20	$C_{16}H_{17}NO_5$	11	1 × C-2; 1 × N
254.0836	10	$C_{11}H_{13}N_2O_4O^{\bullet}$	26	2 × C-1; 2 × C-2; 2 × N
253.0831	100	$C_{11}H_{13}N_2O_5$	2.6	2 × C-1; 2 × C-2; 2 × N
207.0766	10	$C_{10}H_{11}N_2O_3$	1.7	1 × C-1; 2 × C-2; 2 × N
180.0665	10	$C_9H_{10}NO_3$	2	1 × C-2; 1 × N
162.0565	10	$C_9H_8NO_2$	6.1	1 × C-2; 1 × N
147.0462	15	$C_9H_8O_2$	11	

[a]See Figure 1. [b]See Figure 6 for corresponding proposed structures of selected ions.

Table 8. MS/MS Data of *m/z* 341.1072 (Structure 5[a])

m/z	relative intensity (%)	elemental composition[b]	error (ppm)	label incorporation from glycine
341.1109	70	$C_{18}H_{17}N_2O_5$	8.3	1 × C-1; 2 × C-2; 2 × N
297.1214	65	$C_{17}H_{16}N_2O_3$	8.5	2 × C-2; 2 × N
283.1059	15	$C_{16}H_{15}N_2O_3$	8.4	1 × C-2; 2 × N
282.1010	100	$C_{16}H_{14}N_2O_3$	1.9	1 × C-2; 2 × N

[a]See Figure 1. [b]See Figure 7 for corresponding proposed structures.

proposed structures). It is interesting to note that none of the structures exhibited the known retro-Diels–Alder reaction route of flavonoid fragmentation[14] to generate $^{1,3}A^+$ or $^{1,3}B^+$ fragments. In addition, as expected, the structures with a dehydrated C-ring,

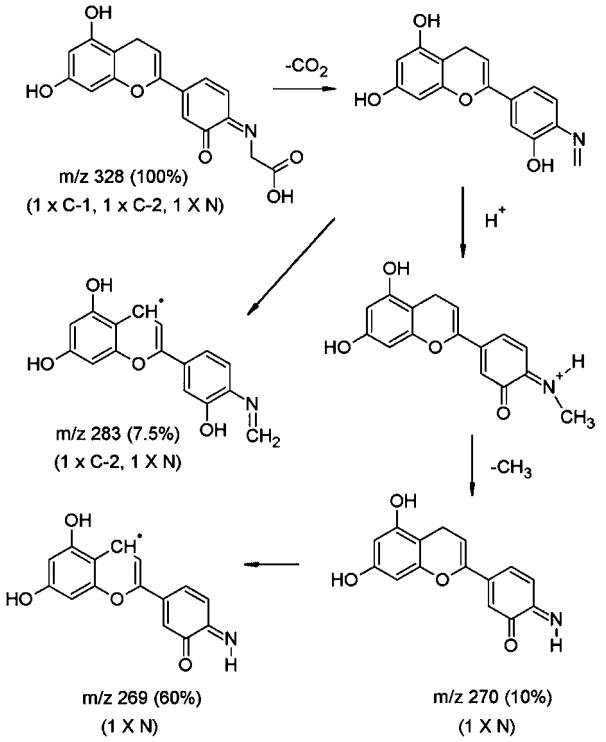

Figure 3. Proposed mass spectral fragments for structure **1**. Values in parentheses indicate the labeled atoms incorporated from glycine.

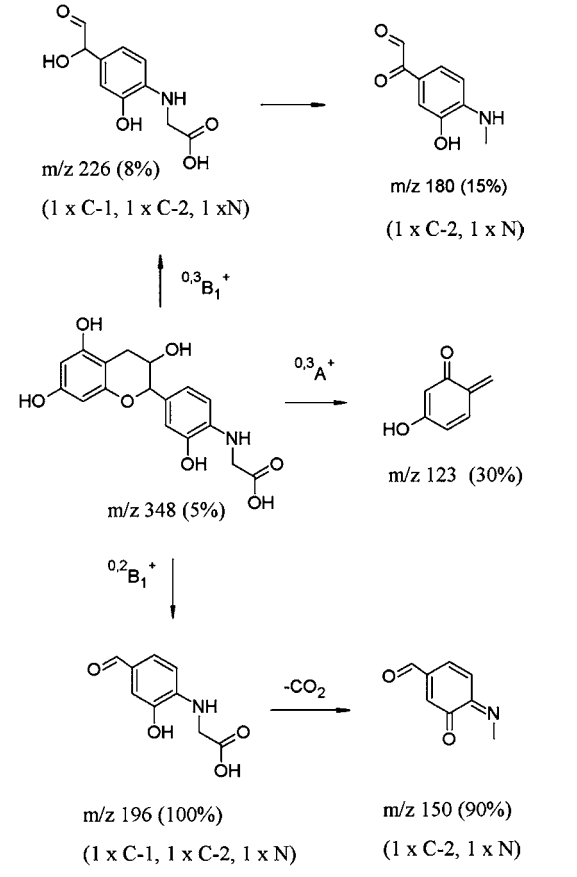

Figure 4. Proposed mass spectral fragments for structure **2**. Values in parentheses indicate the labeled atoms incorporated from glycine.

dx.doi.org/10.1021/jf5005989 | J. Agric. Food Chem. 2014, 62, 3831–3836

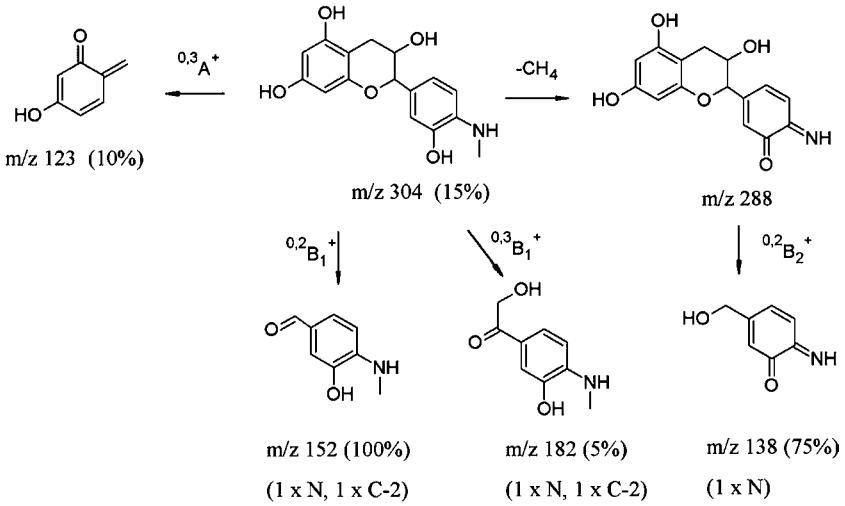

Figure 5. Proposed mass spectral fragments for structure **3**. Values in parentheses indicate the labeled atoms incorporated from glycine.

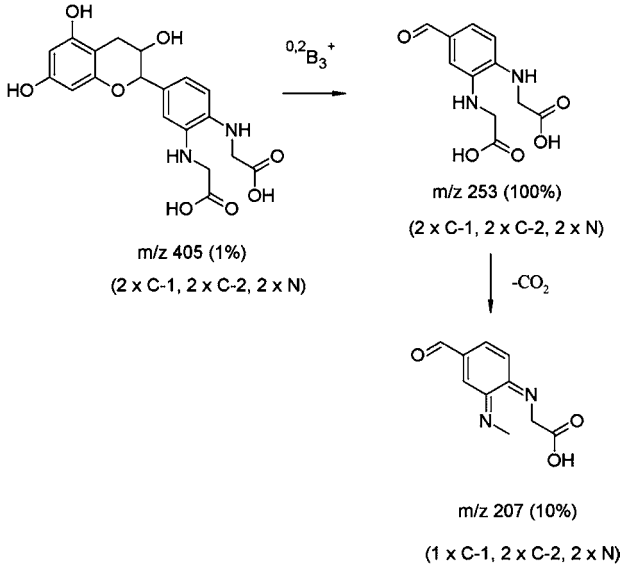

Figure 6. Proposed mass spectral fragments for structure **4**. Values in parentheses indicate the labeled atoms incorporated from glycine.

1 and **5**, did not show any of the characteristic fragmentations of catechins but exhibited fragmentations characteristic of amino acid derivatives (see Tables 4 and 8, as well as Figures 3 and 7).

Characteristic MS/MS Fragmentations of Structures 2, 3, and 4. Due to the presence of intact ring C in structures **2**, **3**, and **4**, it was not surprising to observe the characteristic fragmentations of catechin in these structures (see Figures 4−6 and Tables 5− 7). The fragmentations initiated through the cleavage of C-ring bonds can generate fragment ions retaining A- and B-ring moieties. In structures **2**, **3**, and **4** the $^{0,2}B^{+}$ series fragmentations generated base peaks at *m/z* 196, 152, and 253, respectively, and in general B series ions were found to predominate, allowing direct confirmation of the incorporation of glycine into ring B through isotope-labeling studies. Structures **2** and **3** also exhibited the A series fragmentations, further confirming the flavonoid origin of these structures. It is worth mentioning that the absence of the previously observed retro-Diels−Alder fragmentation pathway[14] could be due to the modifications in ring B structure induced by glycine.

Characteristic MS/MS Fragmentations of Structures 1 and 5. The dehydration of ring C in structures **1** and **5** precludes them from undergoing fragmentations initiated through the

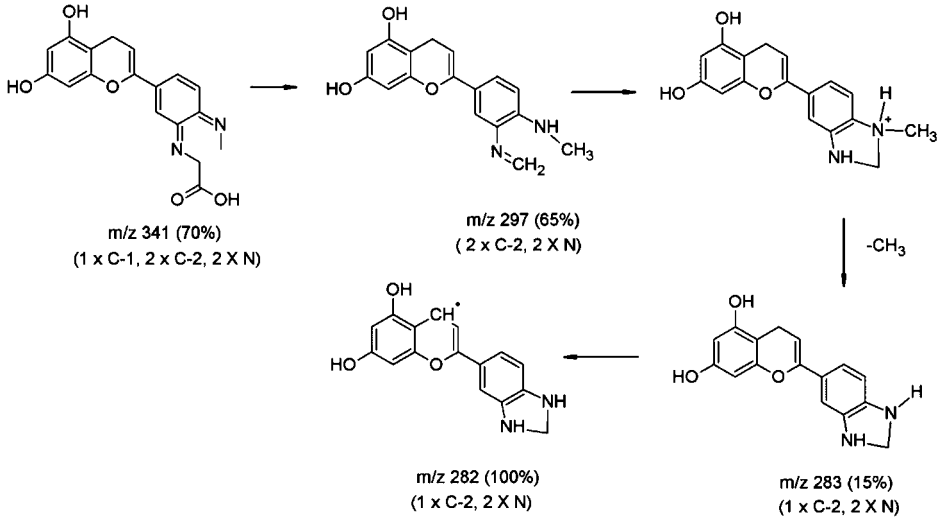

Figure 7. Proposed mass spectral fragments for structure **5**. Values in parentheses indicate the labeled atoms incorporated from glycine.

dx.doi.org/10.1021/jf5005989 | J. Agric. Food Chem. 2014, 62, 3831−3836

cleavage of C-ring bonds, and as a result they exhibit fragmentations initiated by the amino acid moiety such as decarboxylation and loss of alkyl groups of amino acids, preserving in these ions the integrity of rings A, B, and C (see Figures 3 and 7, as well as Tables 4 and 8). Interestingly, both structures **1** and **5** generated very stable 4*H*-chromen-4-yl radicals at *m*/*z* 269 and 282, respectively, as major radical ions in their MS/MS spectra. These radicals are stabilized through conjugation across both rings A and B. Formation of such radical cations under electrospray ionization conditions have been reported in the literature.[15]

It appears from the structural analysis of the products observed that the reaction of glycine and the oxidized form of catechin follows a pattern similar to that of other 1,2-dicarbonyls and leads to the formation of single- and double-addition products such as structures **2** and **4**. It seems the initial double Schiff base adduct on ring B is prone to reduction through disproportionation reaction coupled to catechin oxidation. Structures **2**, **3**, and **4** are such examples in which the oxidized moiety of catechin is reduced to its original oxidation state, and structures **1** and **5** represent examples of reaction products in which the reduced moiety is retained, most probably due to the additional stability gained through dehydration of the hydroxyl group in ring C. Formation of such nonvolatile (+)-catechin/amino acid adducts provides insight into how amino acids can have the potential of modifying the antioxidant properties of (+)-catechin through restoration of the oxidation state of ring B and how catechin-type structures interfere with the Maillard reaction in food through scavenging of amino acids.

AUTHOR INFORMATION

Corresponding Author

*(V.A.Y.) Phone: (514) 398-7918. Fax: (514) 398-7977. E-mail: varoujan.yaylayan@mcgill.ca.

Funding

We acknowledge funding for this research from the Natural Sciences and Engineering Research Council of Canada (NSERC).

Notes

The authors declare no competing financial interest.

REFERENCES

(1) Totlani, V. M.; Peterson, D. G. Influence of epicatechin reactions on the mechanisms of Maillard product formation in low moisture model systems. *J. Agric. Food Chem.* **2006**, *55*, 414−420.

(2) Totlani, V. M.; Peterson, D. G. Reactivity of epicatechin in aqueous glycine and glucose Maillard reaction models: quenching of C2, C3, and C4 sugar fragments. *J. Agric. Food Chem.* **2005**, *53*, 4130−4135.

(3) Colahan-Sederstrom, P. M.; Peterson, D. G. Inhibition of key aroma compound generated during ultrahigh-temperature processing of bovine milk via epicatechin addition. *J. Agric. Food Chem.* **2004**, *53*, 398−402.

(4) Noda, Y.; Peterson, D. G. Structure−reactivity relationships of flavan-3-ols on product generation in aqueous glucose/glycine model systems. *J. Agric. Food Chem.* **2007**, *55*, 3686−3691.

(5) Bin, Q.; Peterson, D. G.; Elias, R. J. Influence of phenolic compounds on the mechanisms of pyrazinium radical generation in the Maillard reaction. *J. Agric. Food Chem.* **2012**, *60*, 5482−5490.

(6) Zhu, N.; Huang, T.-C.; Yu, Y.; LaVoie, E. J.; Yang, C. S.; Ho, C.-T. Identification of oxidation products of (−)-epigallocatechin gallate and (−)-epigallocatechin with H_2O_2. *J. Agric. Food Chem.* **2000**, *48*, 979−981.

(7) Sang, S.; Tian, S.; Wang, H.; Stark, R. E.; Rosen, R. T.; Yang, C. S.; Ho, C.-T. Chemical studies of the antioxidant mechanism of tea catechins: radical reaction products of epicatechin with peroxyl radicals. *Bioorg. Med. Chem.* **2003**, *11*, 3371−3378.

(8) Guerra, P. V.; Yaylayan, V. A. Cyclocondensation of 2,3-butanedione in the presence of amino acids and formation of 4,5-dimethyl-1,2-phenylendiamine. *Food Chem.* **2013**, *141*, 4391−4396.

(9) Patiny, L.; Borel, A. ChemCalc: a building block for tomorrow's chemical infrastructure. *J. Chem. Inf. Model.* **2013**, *53*, 1223−1228.

(10) Horai, H.; Arita, M.; Kanaya, S.; Nihei, Y.; Ikeda, T.; Suwa, K.; Ojima, Y.; Tanaka, K.; Tanaka, S.; Aoshima, K.; Oda, Y.; Kakazu, Y.; Kusano, M.; Tohge, T.; Matsuda, F.; Sawada, Y.; Hirai, M. Y.; Nakanishi, H.; Ikeda, K.; Akimoto, N.; Maoka, T.; Takahashi, H.; Ara, T.; Sakurai, N.; Suzuki, H.; Shibata, D.; Neumann, S.; Iida, T.; Tanaka, K.; Funatsu, K.; Matsuura, F.; Soga, T.; Taguchi, R.; Saito, K.; Nishioka, T. MassBank: a public repository for sharing mass spectral data for life sciences. *J. Mass Spectrom.* **2010**, *45*, 703−714.

(11) Chu, F. L.; Sleno, L.; Yaylayan, V. A. Isotope labeling studies on the formation of multiple addition products of alanine in the pyrolysis residue of glucose/alanine mixtures by high-resolution ESI-TOF-MS. *J. Agric. Food Chem.* **2011**, *59*, 11629−11634.

(12) Guerra, P. V.; Yaylayan, V. A. Double Schiff base adducts of 2,3-butanedione with glycine: formation of pyrazine rings with the participation of amino acid carbon atoms. *J. Agric. Food Chem.* **2012**, *60*, 11440−11445.

(13) Cren-Olivé, C.; Déprez, S.; Lebrun, S.; Coddeville, B.; Rolando, C. Characterization of methylation site of monomethylflavan-3-ols by liquid chromatography/electrospray ionization tandem mass spectrometry. *Rapid Commun. Mass Spectrom.* **2000**, *14*, 2312−2319.

(14) Ma, Y. L.; Li, Q. M.; Van den Heuvel, H.; Claeys, M. Characterization of flavone and flavonol aglycones by collision-induced dissociation tandem mass spectrometry. *Rapid Commun. Mass Spectrom.* **1997**, *11*, 1357−1364.

(15) Meyer, S.; Metzger, J. Use of electrospray ionization mass spectrometry for the investigation of radical cation chain reactions in solution: detection of transient radical cations. *Anal. Bioanal. Chem.* **2003**, *377*, 1108−1114.

JOURNAL OF AGRICULTURAL AND FOOD CHEMISTRY

Addition/Correction

pubs.acs.org/JAFC

Correction to Free Radical Mediated Formation of 3-Monochloropropanediol (3-MCPD) Fatty Acid Diesters

Xiaowei Zhang, Boyan Gao[†], Fang Qin, Haiming Shi, Yuangrong Jiang, Xuebing Xu, and Liangli (Lucy) Yu*

J. Agric. Food Chem. **2013**, *61* (10), 2548−2555. DOI: 10.1021/jf305252q

Errors under Materials and Methods and the caption of Figure 1 are being corrected.

In the second paragraph under the side head ESR Determination of Radical Signals under Materials and Methods, the first sentence should read as follows: To determine the effect of thermal treatments on the generation of radicals, DSG solution (0.5 mg/mL in toluene) containing DMPO was kept at ambient temperature, 40, 60, and 80 °C, and DSG solution (0.5 mg/mL in xylene) containing DMPO was kept at 120 and 160 °C, respectively, for 20 min and measured for their ESR signals.

The caption of Figure 1 should read as follows: **Figure 1.** ESR spectra of 0.5 mg/mL of DSG dissolved in toluene with 20 mmol/L of DMPO kept at (A) ambient temperature after 20 min, (B) 40 °C after 20 min, (C) 60 °C after 20 min, and (D) 80 °C after 20 min and ESR spectra of 0.5 mg/mL of DSG dissolved in xylene with 20 mmol/L of DMPO kept at (E) 120 °C after 20 min and (F) 160 °C after 20 min. The *X*-axis is the magnetic field intensity, and the *Y*-axis is ESR signal intensity.

Published: April 16, 2014

ACS Publications © 2014 American Chemical Society

JOURNAL OF AGRICULTURAL AND FOOD CHEMISTRY

Addition/Correction

pubs.acs.org/JAFC

Correction to Investigation of Ethyl Radical Quenching by Phenolics and Thiols in Model Wine

Gal Y. Kreitman, V. Felipe Laurie, and Ryan J. Elias*

J. Agric. Food Chem. **2013**, *61* (3), 685−692. DOI: 10.1021/jf303880g

We reported that we collected the data in negative-ion mode, but all of the *m*/*z* values reported are based on positive mode. The error appears in Materials and Methods, under the subheading HPLC-MS Analysis of PBN/1-HER Spin Adducts, which should read as follows:

HPLC-MS Analysis of PBN/1-HER Spin Adducts. Samples were diluted 1:20 in Millipore water and filtered over polytetrafluoroethylene (PTFE) syringe tip filters (0.45 μm, 13 mm; Acrodisc, Ann Arbor, MI, USA). The HPLC system consisted of a binary pumping system (Shimadzu LC-10ADvp) with high-pressure mixing and sample introduction by means of a Shimadzu SIL 10ADvp autosampler. PBN/1-HER spin adducts were separated on a ZORBAX Eclipse Plus C18 column (4.6 × 150 mm, 5 μm; Agilent Technologies, Santa Clara, CA, USA). The mobile phase consisted of 0.1% v/v formic acid (A) and 0.1% v/v formic acid in methanol (B). PBN/1-HER adducts were eluted by gradient according to the following program: 0 min, 0% B; 0−5 min, 80% B; 5−18 min, 90% B; 18−22 min, 90% B; 22−23 min, 0% B; 23−26 min, 0% B.

Detection and quantification of spin adducts were achieved using a Waters Quattro micro-triple-quadrupole mass spectrometer (Waters Laboratory Informatics, Milford, MA, USA) coupled to the HPLC. Mass spectra were collected in positive-ion mode using electrospray ionization (ESI). ESI capillary spray was held at 0.50 kV. Cone source voltage was set to 60 V, and source temperature was set to 120 °C. Desolvation gas flow was 250 L/h. Selected ion monitoring mode was set to monitor ions with *m*/*z* of 178, 222, 223, 224, and 268, which correspond to unreacted PBN, oxidized PBN/1-HER adduct, radical PBN/1-HER adduct, reduced PBN/1-HER adduct, and PBN-HER biadduct, respectively (Figure 1). Due to the complexity of having pure standards for all of these adducts, their quantification was performed on the basis of raw areas.

Published: April 21, 2014

ACS Publications © 2014 American Chemical Society

by *Alan Crozier* from the University of Glasgow, United Kingdom, showed data obtained from a combination of animal and human studies on the bioavailability and biological effects of berry phenolics. Similarly, *Wilhelmina Kalt*, from Agriculture and Agri-Foods Canada, presented data on the bioavailability and absorption of anthocyanins, particularly in animal tissues, after long-term blueberry intake. Finally, *Maurizio Battino* from the Università Politecnica delle Marche, Italy, presented recent data on the effects of a one-month strawberry supplementation study on markers of cardiovascular risk and oxidative stress in human subjects.

Session 2, Berries and Cancer. The cancer chemopreventive effects of bioactive food components, including phenolic compounds found in berry fruits, continues to attract significant research and public attention.[4,5] In this session, *Laura Kresty* from the Medical College of Wisconsin, Milwaukee, WI, presented data on the ability of a standardized proanthocyanidin-rich cranberry extract to prevent esophageal adenocarcinoma, and the underlying mechanisms of activity, in a clinically relevant rodent model. *Christine Sardo* from the University of Arizona presented data from two human clinical studies. The first evaluated the effects of a freeze-dried black raspberry powder on postprandial measures of inflammation in overweight and obese male adults. The second evaluated pooled analyses of data obtained from two large phase II, double-blind, placebo-controlled clinical trials, to elucidate the role of plant-based foodstuffs on the recurrence of colorectal adenomas. *Ramesh Gupta* from the University of Louisville focused his talk on "berry colored compounds", namely, anthocyanins, from blueberries for the prevention and treatment of different forms of cancers including lung, breast, and cervical cancers.

Session 3, Berries and Aging. With a growing aging population in the United States and other developed countries, and a concomitant increase in age-related and neurodegenerative diseases, this research area on food bioactives, especially berries, is of significant scientific and public interest. *Barbara Shukitt-Hale* from the USDA-ARS Jean Mayer Center for Aging at Tufts University, Boston, MA, presented data from an ongoing three month intervention study to evaluate the effects of a freeze-dried blueberry powder, compared to a placebo, on cognition and motor function in healthy older adults (60−75 years of age). This human study is building on previous published data showing that blueberry supplementation improves motor and cognitive function in rodent models of aging. *Elizabeth Devore* from Brigham and Children's Hospital Harvard Medical School, Boston, MA, presented data from the Nurses' Health study whose participants were administered food frequency questionnaires every four years (starting in 1980), and cognitive function in 16010 participants, aged ca. 70 years and older, were measured at two-year intervals (starting in 1995−2001). Impressively, this study showed that long-term berry and flavonoid intake led to slower rates of cognitive decline in older adults. *Robert Krikorian* from the University of Cincinnati Academic Health Center, Cincinnati, OH, discussed initial findings from a human clinical study with berry fruit supplementation in the context of age-related memory decline. These data suggested that moderate-term berry fruit supplementation can improve cognitive performance and enhance cerebral function in humans.

Session 4, Berries and Metabolism. *Ronald Prior* from the Department of Food Science, University of Arkansas, Fayetteville, AR, presented data showing that, irrespective of the berry source, in this case, cranberry, blueberry, and black raspberry, common phenolic acids and their conjugates are excreted in the urine of rats. *Dragan Milenkovic* from the National Institute for Agricultural Research, France, presented data showing the inhibition of plaque development by anthocyanins (from bilberries) in an apolipoprotein-E deficient atherosclerosis mouse model. Finally, *Rosalia Simmen* from the University of Arkansas, Fayetteville, AR, discussed data suggesting that early nutritional exposure of a freeze-dried blueberry powder to pregnant and lactating dams results in favorable breast cancer outcomes in their female offsprings in a transgenic mouse model of human breast cancer.

Session 5, Berries and Heart Health. *Britt Burton-Freeman* from the Institute for Food Safety and Health, Illinois Institute of Technology, Bedford Park, IL, presented data discussing the positive effects of strawberry consumption on risk factors for diabetes and cardiovascular disease in human subjects. In addition, this discussion called for further investigation of the effects of berry consumption on different physiological states, in particular the postprandial state, to minimize imbalances in stress, which ultimately lead to various diseases. *Ana Rodriguez-Mateos* from the University of Reading, United Kingdom, presented data from three separate randomized, controlled, double-blind, crossover human intervention trials showing that blueberry polyphenol intake improves endothelial function in healthy men. Finally, *Howard Sesso* from Harvard University, Cambridge, MA, presented a review of epidemiological data obtained from large cohort studies including the Women's Health Study, the Nurse's Health Study, and the Health Professionals Follow-up Study indicating the positive effects of berry consumption on cardiovascular disease outcomes. This discussion raised the need for consideration of complementary data obtained from basic science, clinical, and epidemiologic studies to maximize statistical power and identify mechanistically relevant scientific aims to increase our insights on the role of berries on cardiovascular disease prevention.

Session 6, Berries and Gut Health/Gut Microbiota. This area of research continues to evolve at a rapid pace as it is now well-known that polyphenol gut microbiota metabolites exert biological effects that extend beyond the native compounds alone (see ref 5 and relevant papers cited therein for detailed discussion on this topic). *Jess Reed* from the Department of Animal Sciences, University of Wisconsin—Madison, Madison, WI, presented an overview of gut metabolism and the role that berry polyphenols play in gut health. *Dhanansayan Shanmuganayagam*, also from the University of Wisconsin—Madison, WI, presented data on the ability of cranberry proanthocyanidins to stimulate the mucosal immune system in a mouse model of elemental enteral nutrition-induced mucosal immune dysfunction. Finally, *Li Shu Wang* from the Department of Medicine, Medical College of Wisconsin, Milwaukee, WI, presented data from a human clinical study in colorectal cancer patients consuming black raspberry powder for 9 weeks. The data showed that black raspberry consumption resulted in modulation of enzymes associated with fatty acid metabolism, leading to decreased proliferation and inflammation in the colorectal cancer patients.

In conclusion, it is apparent that berry fruits have a positive impact on human health and disease risk reduction as was heard yet again at another very successful symposium. Given this research trajectory, I look forward with great anticipation to the new findings that will be presented in two years at the 2015

BHBS. Finally, I thank the *Journal of Agricultural and Food Chemistry*, all of the donors and participants of the 2013 BHBS symposium, and the authors who have contributed to the cluster of papers presented here.

Navindra P. Seeram*

Bioactive Botanical Research Laboratory, Department of Biomedical and Pharmaceutical Sciences, College of Pharmacy, University of Rhode Island, Kingston, Rhode Island 02881, United States

AUTHOR INFORMATION

Corresponding Author

*E-mail:nseeram@uri.edu.

Notes

The authors declare no competing financial interest.

REFERENCES

(1) Seeram, N. P. Berry fruits: compositional elements, biochemical activities and the impact of their intake on human health, performance and disease. *J. Agric. Food Chem.* **2008**, *56*, 627−629.

(2) Seeram, N. P. Recent trends and advances in berry health benefits research. *J. Agric. Food Chem.* **2010**, *58*, 3869−3870.

(3) Seeram, N. P. Emerging research supporting the positive effects of berries on human health and disease prevention. *J. Agric. Food Chem.* **2012**, *60*, 5685−5686.

(4) Tomás-Barberán, F. A.; Somoza, V.; Finley, J. Food bioactives research and the *Journal of Agricultural and Food Chemistry*. *J. Agric. Food Chem.* **2012**, *60*, 6641−6643.

(5) Tomás-Barberán, F. A.; Andrés-Lacueva, C. Polyphenols and health: current state and progress. *J. Agric. Food Chem.* **2012**, *60*, 8773−8775.

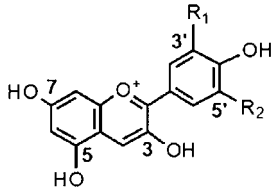

Anthocyanidin	R_1	R_2
Pelargonidin	H	H
Cyanidin	OH	H
Delphinidin	OH	OH
Peonidin	OCH_3	H
Petunidin	OCH_3	OH
Malvidin	OCH_3	OCH_3

Figure 1. Structures of the major berry anthocyanidins.

Oligomeric and polymeric proanthocyanidins have an additional chiral center at C-4 in the "upper" and "lower" units. Type B proanthocyanidins are formed from (+)-catechin and (−)-epicatechin by oxidative coupling between the C-4 of the "upper" monomer and the C-6 or C-8 of the adjacent "lower" or "extension" unit to create oligomers or polymers, and they are present in blueberries, for example. Type A proanthocyanidins have an additional ether bond between C-2 in the B-ring of one monomer and C-7 in the A-ring of the other monomer (Figure 2), and they are found in cranberries. Proanthocyanidins can occur as polymers of up to 50 units. Proanthocyanidins that consist exclusively of (epi)catechin units are called procyanidins and are the most abundant type of proanthocyanidins in plants.[9]

The nonflavonoids present in berries include hydroxycinnamates, such as the chlorogenic acids, of which 5-*O*-caffeoylquinic acid is the most widely distributed and which has been found in substantial amounts in blueberries.[11] Other hydroxycinnamates include ferulic acid and *p*-coumaric acid.[10] Berries can also contain phenolic acids, including gallic acid, whereas ellagic acid-based ellagitannins, such as sanguiin H-6 (Figure 2), have a much more widespread occurrence, being found in a diversity of berries including raspberries, strawberries, and blackberries. Stilbenes, such a resveratrol-3-*O*-glucoside (Figure 2), occur in some berries but typically in relatively small amounts.

EVIDENCE FROM EPIDEMIOLOGICAL STUDIES

Epidemiological studies suggest that the daily intake of berry flavonoids, in particular, anthocyanins, may have cardioprotective effects in humans.[4−7,12] The Iowa Women's Health prospective study followed nearly 35,000 postmenopausal women for 16 years and estimated the intake of seven flavonoid subclasses using the USDA database. The intake of anthocyanins was associated with a reduced risk of coronary heart disease (CHD) and CVD-related mortality.[7] This study also highlighted bran, apple, pear, chocolate, red wine, and strawberries as being the foods most likely to contribute significantly to reductions in disease risk. A more recent prospective study has found an inverse correlation between flavonoid intake and risk of death from CVD in a population of nearly 100,000 men and women of around 70 years of age.[6] In this study, a higher intake of flavonoids (512 vs 94 mg/day) was associated with an 18% lower risk of CVD death. In addition, anthocyanins, flavan-3-ols, flavonols, proanthocyanidins, and flavones were also associated with a 14−17% lower risk of CVD death.

Some data have been obtained with even younger populations, in particular, women, whose CVD risk increases significantly after menopause. A 2013 study found an association between higher anthocyanin intake and a 32% decrease in the risk of myocardial infarction (MI) in nearly 100,000 women 25−45 years of age, after a follow up period of 18 years.[4] For every 15 mg increase of anthocyanins in their diet, a 17% decrease in the risk of MI was observed. Strawberry

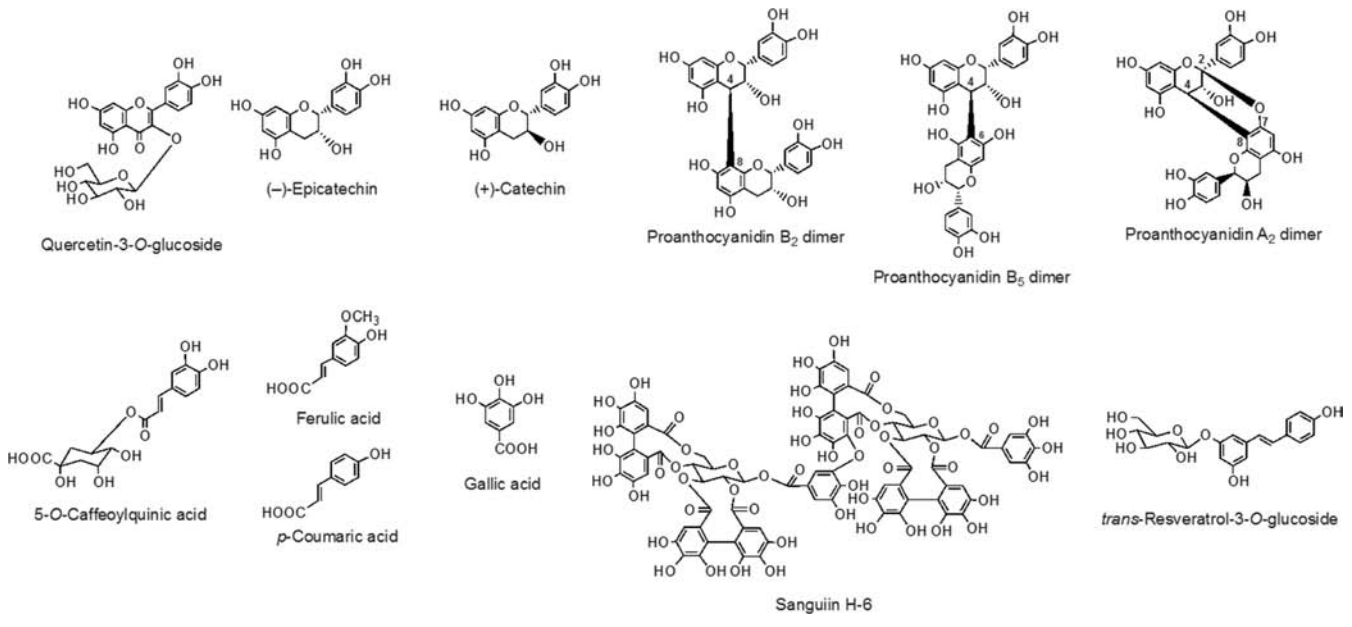

Figure 2. Structures of (poly)phenolic compounds occurring in berries.

dx.doi.org/10.1021/jf403757g | J. Agric. Food Chem. 2014, 62, 3842−3851

Table 1. Summary of Randomized Controlled Trials Investigating the Effect of Berry (Poly)phenols on Surrogate Markers of Cardiovascular Disease Risk

type of berry	population	days	BP	lipids	arterial stiffness	endothelial function	glucose	platelet	(poly)phenol content	fresh fruit or juice	absorption	double blind	ref
blueberries, freeze-dried	healthy	1	=		=	+			319−1791 mg TP,[l] 129−724 mg ACN,[a] 14−637 mg CA[b]	100−560 g	+	+	24
blueberries, frozen	healthy	1	=			=			727 mg TP,[l] 348 mg ACN,[a] 90 mg CA[b]	300 g	+	+	21
blueberries, fresh	smokers	21	=						nd[h]	250 g	−	+	22
blueberries, freeze-dried	CVD[d] risk	42	=	=	=	=	=		375 mg ACN,[a] 127 mg CA[b]	148 g	−	+	23
blueberries, freeze-dried	obese MS[g]	56	+	=			=		1624 mg TP,[l] 742 mg ACN[a]	350 g	−	−	20
blueberries, freeze-dried	obese	45	=	=			=		1462 mg TP,[l] 668 mg ACN[a]	≈280 g	−	+	19
bilberry/black currant ACN[a]	dyslipidemic	84	=	+			=		160 mg ACN[a]		−	+	36
bilberry/black currant ACN[a]	hyperchol[e]	90	+	+		+	=		320 mg ACN[a]		+	+	37
bilberry/black currant ACN[a]	hyperchol[e]	168	=	+					320 mg ACN[a]		−	+	47
bilberry/black currant ACN[a]	prehypertens[j]	28	=						640 mg ACN[a]		−	+	35
bilberry/black currant ACN[a]	prehypertens[j]	28	=	+			+		640 mg ACN[a]		+	+	52
chokeberry extract	MI[f]	45	+	=			=		215 mg TP,[l] 64 mg ACN[a]		−	+	25
cranberry juice	obese	28			=				400 mg TP,[l] 21 mg ACN[a]	500 mL	−	+	29
cranberry juice	MS[g]	56	=	=			=		458 mg TP,[l] 25 mg ACN[a]	480 mL	−	+	26
cranberry extract	T2D[k]	84	=	+			=		nd[h]		−	+	28
cranberry juice	healthy	14		=					2.1 mg ACN[a]	750 mL	−	+	49
cranberry extract	T2D[k]	84		=			=		nd[h]	240 mL	−	+	48
cranberry juice	CAD[c]	28	=	=	+	=			835 mg TP,[l] 94 mg ACN[a]	480 mL	−	+	27
strawberries, freeze-dried	obese	21	=	+			=		nd[h]	320 g	−	+	31
strawberries, freeze-dried	MS[g]	28	=	+					200 mg TP,[l] 154 mg ACN[a]	500 g	−	−	30
elderberry extract	healthy	14		=			=		40 mg ACN[a]	5 mL	+	+	38
elderberry extract	healthy postmen[i]	56	=	=			=	=	500 mg ACN[a]	25 g	+	+	32
black currant juice	healthy	1	=	=		=			204 mg TP,[l] 50 mg ACN[a]	250 mL	+	+	33
mixed berries, frozen	CVD[d] risk	56	+	+				+	835 mg TP,[l] 515 mg ACN[a]	160 g	+	−	34

[a]ACN, anthocyanins. [b]CA, chlorogenic acid. [c]CAD, coronary artery disease. [d]CVD, cardiovascular disease. [e]hyperchol, hypercholesterolemic. [f]MI, myocardial infarction. [g]MS, metabolic syndrome. [h]nd, not determined. [i]postmen, postmenopausal. [j]prehypertens, prehypertensive. [k]T2D, type 2 diabetes. [l]TP, total (poly)phenols.

dx.doi.org/10.1021/jf403757g | J. Agric. Food Chem. 2014, 62, 3842−3851

and blueberry intake also tended to be associated with a decrease in risk.

Cardiovascular health is determined by not only the absence of CVD but also the function of the cardiovascular system. A cross-sectional study investigated nearly 2000 women between 18 and 75 years old for 11 years and found an inverse correlation between a higher anthocyanin intake and lower arterial stiffness and central blood pressure.[12] An increase in the diet of 44 mg of anthocyanins/day was associated with a decrease in systolic BP of 3 mmHg and a decrease in pulse wave velocity (PWV) of 0.4 m/s. Interestingly, berries and red wine were also associated with a decrease in PWV. Furthermore, a large prospective study in men and women under 60 years of age that were followed up for 14 years also showed an association between a higher anthocyanin intake in their diets, mainly from strawberries and blueberries, and an 8% reduced risk of incident hypertension.[5]

Despite these encouraging data sets, there are several epidemiological studies that have found no relationship between berry flavonoid intake and cardiovascular risk.[13−17] Discrepancies between studies of this nature may be due to inadequacies in the ability of commonly used dietary intake questionnaires and food composition tables to accurately assess flavonoid intake in human populations or may even result from issues surrounding the nature of the human population studied with, for example, populations with a high baseline flavonoid intake showing no effect. To avoid such discrepancies, future observational studies must attempt to assess flavonoid intake via the analysis of reliable biomarkers of their intake in plasma, urine, or stool samples.

EVIDENCE FROM RANDOMIZED CONTROLLED TRIALS

Although epidemiological investigations are showing promising results regarding the potential role of berry (poly)phenols in cardiovascular health, as described in the previous section, to confirm if such observations are genuine and to build potential cause-and-effect relationships between berry (poly)phenols and clinically relevant end points of CVD risk, RCTs are necessary, as they are the most reliable method to investigate cause-and-effect relationships. In recent years, several such trials have been conducted, although many exhibit profound limitations. The most important limitations include lack of blinding, absence of proper controls, and lack of detailed compositional analysis of the foods that were tested. For example, to make inferences related to potential causal relationships between (poly)phenol intake and the clinical outcomes being assessed, a suitable control intervention is essential. Ideally, controls should be indistinguishable in taste and appearance from the intervention tested and accurately matched for micro- and macronutrient composition, including other potential bioactive compounds. So far, the basic understanding of berry (poly)phenol pharmacokinetics is incomplete, and to date the absorption and metabolism of many berry (poly)phenols have not been investigated. It is an important prerequisite to assess whether (poly)phenols, or more likely their metabolites, are indeed entering the circulatory system and may only then qualify for mediating the observed effects.

To date, no RCTs have investigated the effects of berry (poly)phenols on hard CVD end points, such as MI, or CVD mortality. However, there have been a number of short-term, small-scale, human intervention studies designed to test the effect of (poly)phenol-rich berries on prognostically validated surrogate markers of CVD risk, including hypertension, endothelial dysfunction, arterial stiffness, lipid metabolism, and platelet activation. In this section, we will discuss the most relevant human RCTs, in which at least one of these markers has been assessed.

Effects on Blood Pressure. Hypertension is a major risk factor for CVD and has been associated with the development of atherosclerosis and the progression of the disease.[18] Several studies have investigated changes in blood pressure after intake of blueberries,[19−24] chokeberries,[25] cranberries,[26−29] strawberries,[30,31] elderberries,[32] black currants,[33] mixed berries,[34] or purified anthocyanins[35−37] (Table 1). The length of these studies ranged from 1 to 90 days, and the study populations consisted mainly of people at risk or with CVD, but in a few studies healthy individuals were also tested.[21,24,32,33,38] From these investigations, only two double-blind RCTs, conducted with MI survivors and hypercholesterolemics, have shown improvements in blood pressure after berry consumption.[25,37] A 6 week supplementation with a chokeberry extract containing 64 mg of anthocyanins, 128 mg of procyanidins, and 23 mg of phenolic acids showed decreases in both systolic (SBP) and diastolic (DBP) blood pressure by 11 and 7.2 mmHg, respectively, in 44 MI survivors receiving statin therapy.[25] In another double-blind RCT, a decrease in SBP of 6.7 mmHg was observed in hypercholesteromic individuals after 12 weeks of daily consumption of 320 mg of berry anthocyanins in comparison to baseline values. However, when compared with the placebo group, the change in SBP was not significant.[37]

In addition, two single-blinded RCTs have reported changes in blood pressure.[20,34] Decreases in SBP of 6% and in DBP of 4% were observed after a 56 day supplementation with freeze-dried blueberries containing 1624 mg of total (poly)phenols and 742 mg of anthocyanins (equivalent to 350 g of fresh berries) by individuals with metabolic syndrome (MS).[20] Although smaller, significant reductions in blood pressure were also observed in the control group (decreases of 1.5 and 1.2% in SBP and DBP, respectively). The control intervention consisted of 950 mL of water per day, which was the same amount of water taken with the blueberry drink by the volunteers on the blueberry intervention arm. Another single-blinded study has shown a modest decrease in systolic blood pressure (1.2%) after an 8 week consumption of a mixture of bilberries, lingonberries, black currants, strawberry puree, and chokeberry and raspberry juice (837 mg of total (poly)phenols, 515 mg of anthocyanins) by a middle-aged population at risk of CVD.[34] The control used in this study was a mix of porridge, sugar water, and marmalade sweets. The results of those two studies should be interpreted with caution as these studies were not double-blinded, and controls were not macro- and micronutrient-matched to the berry intervention.

In most of the investigations mentioned above, blood pressure was not the primary outcome of the study. Furthermore, with one exception, none of the studies used 24 h ambulatory blood pressure, which is the gold standard technique for the measurement of blood pressure. In a double-blind crossover RCT, Hassellund and colleagues[35] investigated the effects of a 4 week supplementation of purified berry anthocyanins (2 × 320 mg) on sitting, supine, and 24 h ambulatory blood pressure in 27 healthy men with blood pressure >140/90 mmHg. No changes in sitting systolic blood pressure (primary end point), supine, or ambulatory blood

pressure after anthocyanin supplementation were observed in this study.

In summary, there is not enough evidence to support the involvement of berry (poly)phenols in lowering blood pressure. More controlled intervention studies in relevant populations over adequate time scales are required.

Effects on Endothelial Function. In the context of prognosis, endothelial dysfunction is an important process underlying the development and progression of atherosclerosis.[39] It is characterized by decreased bioactivity of nitric oxide and impaired flow-mediated vasodilation (FMD). Measurement of FMD of the brachial artery using high-resolution ultrasound is the most widely used validated method to assess endothelial function in humans.[40] Several studies have tested the effect of (poly)phenol-rich foods on FMD. The strongest evidence is the positive effects of flavan-3-ol-rich foods, such as cocoa or tea, on endothelial function after acute or short-term supplementation.[8,41] However, limited data exist regarding the effects of berry consumption on endothelial function (Table 1),[21,23,24,27,33,37] with only four RCT studies having investigated the effects of berry (poly)phenols on FMD.[24,27,37]

A recent double-blind crossover RCT conducted with healthy young men has shown significant improvements in FMD at 1, 2, and 6 h postconsumption of a wild blueberry drink containing 766−1791 mg of total (poly)phenols (310−724 mg of anthocyanins, 137−320 mg of procyanidins, and 273−637 mg of 5-*O*-caffeoylquinic acid).[24] The effects observed at 1−2 h were correlated with increases in plasma metabolites possibly derived from the metabolism and/or breakdown of anthocyanins and 5-*O*-caffeoylquinic acid, whereas the effects observed at 6 h were linked to gut microbial metabolites. A second crossover RCT, with a very similar population, investigated the intake dependency of blueberry (poly)phenols on FMD. This revealed that FMD increased with increasing intake from 319 to 766 mg of total (poly)phenols (129−310 mg of anthocyanins, 57−137 mg of procyanidins, 114−273 mg of 5-*O*-caffeoylquinic acid, equivalent to 100−240 g of fresh blueberries), after which FMD plateaued.[24] The effects on FMD observed are likely to be at least in part related to the anthocyanin content of blueberries, as in a crossover study with 12 hypercholesterolemic individuals, 1 and 2 h after acute consumption of a purified bilberry and black currant anthocyanin extract (320 mg of anthocyanins), FMD improved, by 2.7 and 1.8%, respectively, in parallel with the increases in plasma anthocyanin levels.[37] The magnitude of the changes in FMD were very similar to those obtained after consumption of blueberries (2.4 and 1.5% at 1 and 2 h, respectively). The short-term effects of anthocyanin consumption were also investigated in a parallel study with 150 hypercholesterolemic individuals, with a 2.8% increase in FMD observed after a 12 week supplementation.[37] Another study with cranberry juice failed to show an improvement on FMD after a 4 week supplementation by 44 CHD patients. However, an uncontrolled pilot study with 15 of these patients showed a 1% improvement in FMD 4 h after cranberry juice consumption.[27]

Some studies have used alternative techniques, such as peripheral artery tonometry (PAT) of the fingertips, to measure endothelial function. No changes were observed in acute endoPAT vascular function in healthy volunteers after consumption of 300 g of blueberries containing 348 mg of anthocyanins (1 h postconsumption).[21] Similarly, no changes in endoPAT were observed after a 6 week supplementation with a blueberry drink (375 mg of anthocyanins, 127 mg of 5-*O*-caffeoylquinic acid) by men at risk of CVD.[23] In another study, laser-Doppler iontophoresis was used to measure cutaneous perfusion microvascular function, with no improvements observed 2 h postconsumption of black currant juice by healthy volunteers.[33] More studies are needed to confirm that (poly)phenol-rich berries can improve endothelial function, in particular, over longer periods of time with healthy populations.

Effects on Arterial Stiffness. Arterial stiffness has been associated with the risk of CVD, and increased arterial stiffness is a recognized cardiovascular risk factor.[42−44] PWV, in particular, carotid−femoral PWV, is considered the most robust and reproducible method for measuring arterial stiffness.[43] A crossover RCT involving volunteers with coronary artery disease (CAD) showed a decrease in carotid−femoral PWV of 0.5 m/s after consumption of cranberry juice (835 mg of total (poly)phenols, 94 mg of anthocyanins) for 4 weeks.[27] In contrast, acute supplementation of a blueberry drink (766−1791 mg of total (poly)phenols, 310−724 mg of anthocyanins, 137−20 mg of procyanidins, 273−637 mg of 5-*O*-caffeoylquinic acid) had no effect on carotid−femoral PWV in healthy men.[24] Arguably, this suggests that chronic berry supplementation may be necessary to induce improvements in arterial stiffness in healthy young men.

Augmentation index (AI), another marker of arterial stiffness, has also been correlated with cardiovascular risk.[43,44] RCTs have found no changes in AI after a 4 week supplementation with cranberry juice (400 mg of total (poly)phenols, 21 mg of anthocyanins) by obese volunteers[23] and a 6 week supplementation with a blueberry drink (375 mg of anthocyanins, 127 mg of 5-*O*-caffeoylquinic acid) by subjects at risk of CVD.[29] To date, insufficient evidence exists to correlate berry (poly)phenol intake and improvements in arterial stiffness, although data from a well-conducted double-blind RCT with cranberry juice described above[12] and a cross-sectional study described in the epidemiology section,[27] in which a decrease in PWV was reported to be associated with a higher intake of anthocyanins in the diet and with berry intake, are promising.

Effects on Blood Lipids. Hypercholesterolemia is one of the major risk factors for the development of CVD. In particular, low-density lipoprotein-cholesterol, high-density lipoprotein-cholesterol, and total serum cholesterol levels (LDL-C, HDL-C, TC, respectively) have been related to cardiovascular risk.[45,46] The strongest evidence regarding the effect of berry (poly)phenols on blood lipids comes from studies conducted in dyslipidemic populations using purified bilberry and black currant anthocyanin extracts (Table 1). A 12 week study with bilberry and black currant anthocyanins (160 mg/day) involving 120 dyslipidemic subjects reported an increase of 14% in HDL-C and a decrease in LDL-C of 14%, with no changes in TC or triglycerides (TAG).[36] In a parallel study with a similar population of hypercholesterolemics, daily consumption of 320 mg of bilberry and black currant anthocyanins resulted in a 12% increase in HDL-C, a 10% decrease in LDL-C, and no changes in TC or TAG.[37] The same investigators also reported a 14% increase in HDL-C and a 10% decrease in LDL-C when the daily 320 mg anthocyanin intake by the same or similar populations was extended to 24 weeks.[47] This suggests that long-term berry consumption leads to sustained and clinically relevant improvement in blood lipids.

In addition to these studies with pure anthocyanins, several studies have shown that similar effects on blood lipids can be observed following berry supplementation (Table 1). A 3 week RCT with freeze-dried strawberries (equivalent to 320 g fresh weight) produced a decrease in TC of about 4% in obese individuals, with no changes in HDL-C, LDL-C, or TAG.[31] Unfortunately, the (poly)phenol content of the freeze-dried strawberries was not determined. The authors speculated that the 8 g of fiber in the intervention may have been partly responsible for the observed effects, as the control was matched for sugars, flavor, and color but not for fiber. A strength of this study is that the background diet was strictly controlled over the intervention, with all subjects following a controlled diet starting 1 week before initiation of the intervention and maintained during the 7 week supplementation period. However, no washout period between the intervention and the control arm was included, which may have confounding effects on the outcomes of the study due to potential carry-over effects. Another 4 week study with freeze-dried strawberry powder (equivalent to 500 g of fresh weight, 200 mg of total (poly)phenols, 154 mg of anthocyanins) in MS subjects produced 10 and 11% decreases in TC and LDL-C, respectively.[30] This RCT was single blinded as the control arm consisted of four cups of water, which was the amount of liquid ingested with the strawberry intervention. Thus, the control was not matched to the strawberry intervention for macro- and micronutrients.

With cranberry, decreases in LDL-C and TC were observed in 32 type 2 diabetics after daily consumption of 3 × 500 mg of an encapsulated cranberry extract over 12 weeks.[28] HDL-C and TAG did not differ between the intervention and control arms. Unfortunately, the (poly)phenol content of the intervention was not reported, so it is difficult to draw conclusions on the cause and effect relationship between the effects observed and the (poly)phenol amount ingested. In contrast to these findings, no changes were observed in three RCTs with cranberry interventions involving MS, type 2 diabetes, and healthy individuals,[26,48,49] or after black currant, blueberry, chokeberry, and elderberry supplementation in healthy individuals, subjects with CVD risk factors, and MI survivors (Table 1).[19,25,32,33,38] In a single-blinded study, a 5% increase in HDL-C was reported after 8 weeks' consumption of mixed berries (837 mg of total (poly)phenols, 515 mg of anthocyanins) by a middle-aged population at risk of CVD,[34] with no changes in TAG, TC, and LDL-C being observed.

Taken together, there is consistent evidence on the favorable effects of 12−24 week daily intake of 160−320 mg of anthocyanins on blood lipids in dyslipidemic individuals, and some evidence exists regarding improvements in obese/MS subjects after strawberry supplementation for 3−4 weeks. The potential beneficial effects of other berry (poly)phenols on blood lipids is at present unclear.

Effects on Platelet Aggregation. Another significant effect that has been attributed to (poly)phenols is the ability to inhibit platelet activation and, thus, the formation of blood clots, a key mechanism implicated in the pathophysiology of atherosclerosis. Platelets play an important role in the early stages of atherosclerosis and coronary thrombosis, and several studies have reported an inhibition of platelet activation after consumption of cocoa flavan-3-ols.[50,51] Only two RCTs have investigated the effect of berry (poly)phenol consumption on platelet activation and aggregation (Table 1). In a 12 week double-blind RCT, no changes were reported in platelet reactivity in response to stimulation to ADP and collagen after daily consumption of 500 mg of elderberry anthocyanins by healthy postmenopausal women.[32] In contrast, a single-blinded study has shown a decrease in platelet aggregation after consumption of mixed berries (837 mg of total (poly)phenols, 515 mg of anthocyanins) for 8 weeks by a middle-aged population at risk of CVD.[34] Berry consumption inhibited platelet function by 11% as measured with a platelet function analyzer using collagen and ADP as platelet activators. Double-blind RCTs are needed to confirm these interesting observations.

Effect on Blood Glucose Levels and Insulin Resistance. Most of the RCTs conducted with berries have reported no changes in serum glucose levels after cranberry, blueberry, strawberry, elderberry, chokeberry, or pure anthocyanin interventions (Table 1),[19,23,25,28,31,32,36,37,48] except for one study with 31 prehypertensive men who received a daily supplement of 640 mg of purified bilberry and black currant anthocyanins for a period of 1 month.[52]

One RCT produced an improvement in insulin sensitivity after consumption of a blueberry smoothie for 6 weeks (1462 mg of total (poly)phenols, 668 mg of anthocyanins) by obese, nondiabetic insulin-resistant individuals.[19] This study used the gold standard technique for the measurement of insulin sensitivity, the hyperinsulinemic−euglycemic clamp, and observed a 22% improvement in the blueberry group as compared with 5% in the control group. Two studies investigating insulin resistance in type 2 diabetics and dyslipidemics in a cranberry and purified anthocyanin intervention detected no changes in the homeostatic model of assessment of insulin resistance (HOMA-IR).[28,37] This is a less invasive, cheaper, and less labor intensive model for assessing insulin sensitivity, but it has certain limitations. More work is needed to investigate whether berry (poly)phenols can lower blood sugar and improve insulin resistance, with the potential of being therapeutic agents for the treatment of diabetes.

MECHANISMS OF ACTION

As well as providing evidence on the efficacy of berry (poly)phenols to improve cardiovascular risk surrogates, several RCTs have attempted to supply evidence for potential mechanisms of action. For example, Zhu et al.[37] reported an increase in serum cGMP in hypercholesterolemics after a 12 week supplementation with 320 mg of purified anthocyanins, and this was paralleled by increases in FMD ($r = 0.428$, $p < 0.05$). Importantly, when an intravenous infusion of L-*N*-monomethylarginine (L-NMMA), a competitive nitric oxide synthase (NOS) inhibitor, was given to six participants, the beneficial effects of the anthocyanins on FMD were abolished, and significant changes in hyperemic blood flow and blood pressure were observed between the anthocyanin and L-NMMA/anthocyanin interventions. This suggests that the mechanism of action of anthocyanins in the vasculature involves the nitric oxide/cGMP signaling pathway. It has recently been shown with healthy volunteers, 1, 2, and 6 h postconsumption, that blueberry-related increases in FMD were correlated with plasma levels of blueberry (poly)phenol metabolites and decreases in neutrophil NADPH oxidase activity.[24] The phenolic metabolites have a structure similar to the NADPH oxidase inhibitor apocynin (acetovanillone), and it has been proposed that in an in vitro model of endothelial cells they act as potent NAPDH oxidase inhibitors.[53] A decrease in

NADPH oxidase activity has previously been linked to alterations in nitric oxide levels via inhibition of superoxide production,[53,54] and the inhibition of NADPH oxidase activity has been proposed as the main mechanism mediating the short-term improvements in FMD observed after consumption of (−)-epicatechin.[55] These findings suggest that blueberry (poly)phenol metabolites may mediate improvements in endothelial function by increasing the bioavailability of nitric oxide via their potential to inhibit NAPDH-oxidase. However, further work is needed to confirm whether this is indeed the case.

In another study with purified berry anthocyanins in dyslipidemics, anthocyanins were shown to decrease the mass and activity of plasma cholesteryl ester transfer protein (CETP), a plasma protein that mediates the removal of cholesteryl ester HDL in exchange for a triglyceride molecule derived primarily from LDL, VLDL, or chylomicrons. The decreased levels of this protein have been suggested as a possible mechanism for the increase in HDL-C and decrease in LDL-C.[36] It was also found that changes in HDL-C correlated with the changes in CETP activity and that changes in LDL-C correlated with changes in CETP mass, whereas changes in cellular cholesterol efflux to serum positively correlated with changes in HDL-C. Thus, it is feasible to hypothesize that anthocyanins may act as CETP inhibitors.[36]

Numerous in vitro and animal studies have been conducted to investigate the mechanisms of action of berry (poly)phenols. Of note, many of these investigations using cell lines have made extensive use of berry extracts, (poly)phenolic aglycones, or sugar conjugates, at concentrations in the low micromolar to millimolar range. However, following ingestion, most berry (poly)phenolics appear in plasma not as the parent compound but as phase II metabolites, and their presence in the circulation after dietary intake rarely exceeds nanomolar concentrations. With in vivo studies, the same issues apply. When animal studies, such as human RCTs, are conducted, experimental design is of importance and should take into account factors such as a suitable control, characterized intervention, and blinding. Much of the in vivo mechanistic evidence comes from studies conducted with apoE deficient mice, a widely used animal model of accelerated atherosclerosis. Using this model, after a 20 week supplementation with a diet containing 1% freeze-dried blueberries, fewer atherosclerotic lesions were observed, with a decrease of 39% in the lesion area of the aortic sinus and a 58% decrease in the descending aorta.[56] These effects were independent of the blood lipid profile and the total plasma antioxidant capacity. Furthermore, four major antioxidant enzymes were up-regulated in blueberry-fed mice (superoxide dismutase (SOD) 1 and 2, glutathione reductase (GSR), and thioredoxin reductase 1), with the activities of SOD and GSR being higher in the liver and serum. An increase in hepatic SOD and GSR has also been reported together with an increase in plasma paraoxonase activity after intake of raspberry juice for 12 weeks by Syrian golden hamsters fed an atherogenic diet.[57] These studies suggest a potential mechanism of action for berries against atherosclerosis by inhibition of lipid peroxidation and enhancement of antioxidant defenses. Similarly, supplementation of apoE deficient mice with a 0.02% bilberry extract for 16 weeks inhibited plaque development.[58] Microarray analysis of the liver and the aorta of the animals after a 2 week supplementation with the bilberry extract indicated modulated gene expression, with respective changes in 2289 and 1261 genes involved in various cellular and molecular pathways such as cholesterol metabolism, inflammatory process and cell adhesion, oxidative stress, inflammation, angiogenesis, and transendothelial migration.[59,60] Another study with apoE deficient mice fed a 1% freeze-dried blueberry diet for 20 weeks reported that the supplement attenuated foam cell formation, which is an early stage of the development of atherosclerosis, by down-regulating the scavenger receptors SR-A and CD36, which are the major receptors responsible for the binding and uptake of modified LDL in macrophages.[61] (Poly)phenol colonic catabolites found in the serum of mice after blueberry consumption were also shown to inhibit mRNA expression and protein levels of pro-inflammatory cytokines TNF-α and IL-6, by reducing phosphorylation levels of MAPK JNK, p38, and Erk 1/2 in a murine macrophage cell line.[62] In a study using diabetic apoE deficient mice, supplementation with 0.2% cyanidin-3-*O*-glucoside for 6 weeks lowered the aortic lesion area by 45%, improved endothelium-dependent vasorelaxation, and increased the capacity of in vitro adhesion to fibronectin, migration, and tube formation of endothelial progenitor cells (EPCs).[63] The mechanism for these improvements involved higher phosphorylation levels of AMP-activated protein kinase Thr 172 and endothelial nitric oxide synthase Ser1177 in EPCs derived from the cyanidin-3-*O*-glucoside-treated diabetic mice compared with those in nondiabetic mice.

Physiologically relevant berry supplementations in different animal models, such as rats, Syrian golden hamsters, or pigs, have shown an array of beneficial effects such as reduced mortality after induced MI, inhibition of aortic lipid deposition, lowering of blood pressure, improvements in endothelium-dependent vasorelaxation, and decreases in plasma TC and LDL-C.[57,64−70] More efforts are needed to confirm the mechanisms that have been proposed to mediate the observed effects, using relevant in vivo models or in vitro models with circulating metabolites and microbial catabolites at biological concentrations.

SUMMARY

Although evidence for the cardiovascular benefits of berry (poly)phenols in humans is accumulating, their role in the prevention of CVD is, at present, unclear. Recent epidemiological studies have shown associations between higher berry flavonoid intake and lower risk of CVD, and a number of small-scale, human intervention studies have shed some light on the beneficial effects of various berry (poly)phenol-rich foods on surrogate markers of CVD risk. Whereas there is some evidence to suggest that acute and/or short-term consumption of berry (poly)phenols can have a positive effect on blood lipids or vascular function, the long-term effects of berry interventions are currently unknown, and RCTs with hard clinical end points are lacking. As a consequence, uncertainty remains regarding which specific (poly)phenols are directly responsible for beneficial actions in vivo, as berries contain not only anthocyanins but a diversity of (poly)phenolic compounds.[9] Investigations using pure anthocyanins are encouraging, suggesting that anthocyanins may be at least mediating part of the observed beneficial effects. Few studies have assessed the absorption and metabolism of berry (poly)phenols, which is a critical factor in establishing potential cause-and-effect relationships. More short- and long-term double-blind randomized studies, using well-characterized interventions and adequate controls and clinically relevant end points, are needed before conclusions can be drawn regarding their efficacy. The outcomes of such studies may help to elucidate the role of

berry (poly)phenols in the prevention of CVD risk and may be used to make specific dietary recommendations regarding berry consumption to the general population.

AUTHOR INFORMATION

Corresponding Author

*(A.R.-M.) Phone: +49-211-811-5893. E-mail: ana.rodriguez-mateos@med.uni-duesseldorf.de.

Notes

The authors declare no competing financial interest.

ABBREVIATIONS USED

AI, augmentation index; BP, blood pressure; CETP, cholesteryl ester transfer protein; cGMP, cyclic guanosine monophosphate; CHD, coronary heart disease; CVD, cardiovascular disease; DBP, diastolic blood pressure; FMD, flow-mediated dilation; GSR, glutathione reductase; HDL-C, high-density lipoprotein cholesterol; HOMA-IR, homeostatic model of assessment of insulin resistance; LDL-C, low-density lipoprotein cholesterol; L-NMMA, NG-monomethyl-L-arginine acetate; MI, myocardial infarction; MS, metabolic syndrome; PAT, peripheral arterial tonometry; PWV, pulse wave velocity; RCTs, randomized controlled trials; SBP, systolic blood pressure; SOD, superoxide dismutase; TAG, triacylglycerol; TC, total cholesterol; VLDL, very low density lipoproteins

REFERENCES

(1) Dauchet, L.; Czernichow, S.; Bertrais, S.; Blacher, J.; Galan, P.; Hercberg, S. Fruits and vegetables intake in the SU.VI.MAX study and systolic blood pressure change. *Arch. Mal. Coeur Vaiss.* **2006**, *99*, 669−673.

(2) He, F. J.; Nowson, C. A.; Lucas, M.; MacGregor, G. A. Increased consumption of fruit and vegetables is related to a reduced risk of coronary heart disease: meta-analysis of cohort studies. *J. Hum. Hypertens.* **2007**, *21*, 717−728.

(3) Joshipura, K. J.; Hu, F. B.; Manson, J. E.; Stampfer, M. J.; Rimm, E. B.; Speizer, F. E.; Colditz, G.; Ascherio, A.; Rosner, B.; Spiegelman, D.; Willett, W. C. The effect of fruit and vegetable intake on risk for coronary heart disease. *Ann. Intern. Med.* **2001**, *134*, 1106−1114.

(4) Cassidy, A.; Mukamal, K. J.; Liu, L.; Franz, M.; Eliassen, A. H.; Rimm, E. B. High anthocyanin intake is associated with a reduced risk of myocardial infarction in young and middle-aged women. *Circulation* **2013**, *127*, 188−196.

(5) Cassidy, A.; O'Reilly, E. J.; Kay, C.; Sampson, L.; Franz, M.; Forman, J. P.; Curhan, G.; Rimm, E. B. Habitual intake of flavonoid subclasses and incident hypertension in adults. *Am. J. Clin. Nutr.* **2011**, *93*, 338−347.

(6) McCullough, M. L.; Peterson, J. J.; Patel, R.; Jacques, P. F.; Shah, R.; Dwyer, J. T. Flavonoid intake and cardiovascular disease mortality in a prospective cohort of US adults. *Am. J. Clin. Nutr.* **2012**, *95*, 454−464.

(7) Mink, P. J.; Scrafford, C. G.; Barraj, L. M.; Harnack, L.; Hong, C. P.; Nettleton, J. A.; Jacobs, D. R., Jr. Flavonoid intake and cardiovascular disease mortality: a prospective study in postmenopausal women. *Am. J. Clin. Nutr.* **2007**, *85*, 895−909.

(8) Del Rio, D.; Rodriguez-Mateos, A.; Spencer, J. P.; Tognolini, M.; Borges, G.; Crozier, A. Dietary (poly)phenolics in human health: structures, bioavailability, and evidence of protective effects against chronic diseases. *Antioxid. Redox Signal.* **2013**, *18*, 1818−1892.

(9) Crozier, A.; Yokota, T.; Jaganath, I. B.; Marks, S.; Salthmarsh, M.; Clifford, M. N. Secondary metabolites as dietary components in plant-based foods and beverages. In *Plant Secondary Metabolites: Occurrence, Structure and Role in the Human Diet*; Crozier, A., Clifford, M. N., Ashihara, H., Eds.; Blackwell Publishing: Oxford, UK, 2006; pp 208−302.

(10) Taruscio, T. G.; Barney, D. L.; Exon, J. Content and profile of flavanoid and phenolic acid compounds in conjunction with the antioxidant capacity for a variety of northwest *Vaccinium* berries. *J. Agric. Food Chem.* **2004**, *52*, 3169−3176.

(11) Rodriguez-Mateos, A.; Cifuentes-Gomez, T.; Tabatabaee, S.; Lecras, C.; Spencer, J. P. Procyanidin, anthocyanin, and chlorogenic acid contents of highbush and lowbush blueberries. *J. Agric. Food Chem.* **2012**, *60*, 5772−5778.

(12) Jennings, A.; Welch, A. A.; Fairweather-Tait, S. J.; Kay, C.; Minihane, A. M.; Chowienczyk, P.; Jiang, B.; Cecelja, M.; Spector, T.; Macgregor, A.; Cassidy, A. Higher anthocyanin intake is associated with lower arterial stiffness and central blood pressure in women. *Am. J. Clin. Nutr.* **2012**, *96*, 781−788.

(13) Hertog, M. G.; Feskens, E. J.; Kromhout, D. Antioxidant flavonols and coronary heart disease risk. *Lancet* **1997**, *349*, 699.

(14) Lin, J.; Rexrode, K. M.; Hu, F.; Albert, C. M.; Chae, C. U.; Rimm, E. B.; Stampfer, M. J.; Manson, J. E. Dietary intakes of flavonols and flavones and coronary heart disease in US women. *Am. J. Epidemiol.* **2007**, *165*, 1305−1313.

(15) Rimm, E. B.; Katan, M. B.; Ascherio, A.; Stampfer, M. J.; Willett, W. C. Relation between intake of flavonoids and risk for coronary heart disease in male health professionals. *Ann. Intern. Med.* **1996**, *125*, 384−389.

(16) Sesso, H. D.; Gaziano, J. M.; Liu, S.; Buring, J. E. Flavonoid intake and the risk of cardiovascular disease in women. *Am. J. Clin. Nutr.* **2003**, *77*, 1400−1408.

(17) Cassidy, A.; Rimm, E. B.; O'Reilly, E. J.; Logroscino, G.; Kay, C.; Chiuve, S. E.; Rexrode, K. M. Dietary flavonoids and risk of stroke in women. *Stroke* **2012**, *43*, 946−951.

(18) Lenfant, C.; Chobanian, A. V.; Jones, D. W.; Roccella, E. J. Seventh report of the Joint National Committee on the Prevention, Detection, Evaluation, and Treatment of High Blood Pressure (JNC 7): resetting the hypertension sails. *Hypertension* **2003**, *41*, 1178−1179.

(19) Stull, A. J.; Cash, K. C.; Johnson, W. D.; Champagne, C. M.; Cefalu, W. T. Bioactives in blueberries improve insulin sensitivity in obese, insulin-resistant men and women. *J. Nutr.* **2010**, *140*, 1764−1768.

(20) Basu, A.; Du, M.; Leyva, M. J.; Sanchez, K.; Betts, N. M.; Wu, M.; Aston, C. E.; Lyons, T. J. Blueberries decrease cardiovascular risk factors in obese men and women with metabolic syndrome. *J. Nutr.* **2010**, *140*, 1582−1587.

(21) Del Bo, C.; Riso, P.; Campolo, J.; Moller, P.; Loft, S.; Klimis-Zacas, D.; Brambilla, A.; Rizzolo, A.; Porrini, M. A single portion of blueberry (*Vaccinium corymbosum* L.) improves protection against DNA damage but not vascular function in healthy male volunteers. *Nutr. Res. (N.Y.)* **2013**, *33*, 220−227.

(22) McAnulty, S. R.; McAnulty, L. S.; Morrow, J. D.; Khardouni, D.; Shooter, L.; Monk, J.; Gross, S.; Brown, V. Effect of daily fruit ingestion on angiotensin converting enzyme activity, blood pressure, and oxidative stress in chronic smokers. *Free Radical Res.* **2005**, *39*, 1241−1248.

(23) Riso, P.; Klimis-Zacas, D.; Del Bo, C.; Martini, D.; Campolo, J.; Vendrame, S.; Moller, P.; Loft, S.; De Maria, R.; Porrini, M. Effect of a wild blueberry (*Vaccinium angustifolium*) drink intervention on markers of oxidative stress, inflammation and endothelial function in humans with cardiovascular risk factors. *Eur. J. Nutr.* **2013**, *52*, 949−961.

(24) Rodriguez-Mateos, A.; Rendeiro, C.; Bergillos-Meca, T.; Tabatabaee, S.; George, T.; Heiss, C.; Spencer, J. P. Intake and time dependence of blueberry flavonoid-induced improvements in vascular function: a randomized, controlled, double-blind, crossover intervention study with mechanistic insights into biological activity *Am. J. Clin. Nutr.* **2013**, DOI: 10.3945/ajcn.113.066639,

(25) Naruszewicz, M.; Laniewska, I.; Millo, B.; Dluzniewski, M. Combination therapy of statin with flavonoids rich extract from chokeberry fruits enhanced reduction in cardiovascular risk markers in patients after myocardial infraction (MI). *Atherosclerosis* **2007**, *194*, e179−184.

(26) Basu, A.; Betts, N. M.; Ortiz, J.; Simmons, B.; Wu, M.; Lyons, T. J. Low-energy cranberry juice decreases lipid oxidation and increases plasma antioxidant capacity in women with metabolic syndrome. *Nutr. Res. (N.Y.)* **2011**, *31*, 190−196.
(27) Dohadwala, M. M.; Holbrook, M.; Hamburg, N. M.; Shenouda, S. M.; Chung, W. B.; Titas, M.; Kluge, M. A.; Wang, N.; Palmisano, J.; Milbury, P. E.; Blumberg, J. B.; Vita, J. A. Effects of cranberry juice consumption on vascular function in patients with coronary artery disease. *Am. J. Clin. Nutr.* **2011**, *93*, 934−940.
(28) Lee, I. T.; Chan, Y. C.; Lin, C. W.; Lee, W. J.; Sheu, W. H. Effect of cranberry extracts on lipid profiles in subjects with type 2 diabetes. *Diabetic Med.* **2008**, *25*, 1473−1477.
(29) Ruel, G.; Lapointe, A.; Pomerleau, S.; Couture, P.; Lemieux, S.; Lamarche, B.; Couillard, C. Evidence that cranberry juice may improve augmentation index in overweight men. *Nutr. Res. (N.Y.)* **2013**, *33*, 41−49.
(30) Basu, A.; Fu, D. X.; Wilkinson, M.; Simmons, B.; Wu, M.; Betts, N. M.; Du, M.; Lyons, T. J. Strawberries decrease atherosclerotic markers in subjects with metabolic syndrome. *Nutr. Res. (N.Y.)* **2010**, *30*, 462−469.
(31) Zunino, S. J.; Parelman, M. A.; Freytag, T. L.; Stephensen, C. B.; Kelley, D. S.; Mackey, B. E.; Woodhouse, L. R.; Bonnel, E. L. Effects of dietary strawberry powder on blood lipids and inflammatory markers in obese human subjects. *Br. J. Nutr.* **2012**, *108*, 900−909.
(32) Curtis, P. J.; Kroon, P. A.; aHollands, W. J.; Walls, R.; Jenkins, G.; Kay, C. D.; Cassidy, A. Cardiovascular disease risk biomarkers and liver and kidney function are not altered in postmenopausal women after ingesting an elderberry extract rich in anthocyanins for 12 weeks. *J. Nutr.* **2009**, *139*, 2266−2271.
(33) Jin, Y.; Alimbetov, D.; George, T.; Gordon, M. H.; Lovegrove, J. A. A randomised trial to investigate the effects of acute consumption of a blackcurrant juice drink on markers of vascular reactivity and bioavailability of anthocyanins in human subjects. *Eur. J. Clin. Nutr.* **2011**, *65*, 849−856.
(34) Erlund, I.; Koli, R.; Alfthan, G.; Marniemi, J.; Puukka, P.; Mustonen, P.; Mattila, P.; Jula, A. Favorable effects of berry consumption on platelet function, blood pressure, and HDL cholesterol. *Am. J. Clin. Nutr.* **2008**, *87*, 323−331.
(35) Hassellund, S. S.; Flaa, A.; Sandvik, L.; Kjeldsen, S. E.; Rostrup, M. Effects of anthocyanins on blood pressure and stress reactivity: a double-blind randomized placebo-controlled crossover study. *J. Hum. Hypertens.* **2012**, *26*, 396−404.
(36) Qin, Y.; Xia, M.; Ma, J.; Hao, Y.; Liu, J.; Mou, H.; Cao, L.; Ling, W. Anthocyanin supplementation improves serum LDL- and HDL-cholesterol concentrations associated with the inhibition of cholesteryl ester transfer protein in dyslipidemic subjects. *Am. J. Clin. Nutr.* **2009**, *90*, 485−492.
(37) Zhu, Y.; Xia, M.; Yang, Y.; Liu, F.; Li, Z.; Hao, Y.; Mi, M.; Jin, T.; Ling, W. Purified anthocyanin supplementation improves endothelial function via NO-cGMP activation in hypercholesterolemic individuals. *Clin. Chem.* **2011**, *57*, 1524−1533.
(38) Murkovic, M.; Abuja, P. M.; Bergmann, A. R.; Zirngast, A.; Adam, U.; Winklhofer-Roob, B. M.; Toplak, H. Effects of elderberry juice on fasting and postprandial serum lipids and low-density lipoprotein oxidation in healthy volunteers: a randomized, double-blind, placebo-controlled study. *Eur. J. Clin. Nutr.* **2004**, *58*, 244−249.
(39) Ribeiro, F.; Alves, A. J.; Teixeira, M.; Ribeiro, V.; Duarte, J. A.; Oliveira, J. Endothelial function and atherosclerosis: circulatory markers with clinical usefulness. *Rev. Port. Cardiol.* **2009**, *28*, 1121−1151.
(40) Corretti, M. C.; Anderson, T. J.; Benjamin, E. J.; Celermajer, D.; Charbonneau, F.; Creager, M. A.; Deanfield, J.; Drexler, H.; Gerhard-Herman, M.; Herrington, D.; Vallance, P.; Vita, J.; Vogel, R. Guidelines for the ultrasound assessment of endothelial-dependent flow-mediated vasodilation of the brachial artery: a report of the International Brachial Artery Reactivity Task Force. *J. Am. Coll. Cardiol.* **2002**, *39*, 257−265.
(41) Heiss, C.; Keen, C. L.; Kelm, M. Flavanols and cardiovascular disease prevention. *Eur. Heart J.* **2010**, *31*, 2583−2592.
(42) Vlachopoulos, C.; Aznaouridis, K.; Stefanadis, C. Prediction of cardiovascular events and all-cause mortality with arterial stiffness: a systematic review and meta-analysis. *J. Am. Coll. Cardiol.* **2010**, *55*, 1318−1327.
(43) Laurent, S.; Cockcroft, J.; Van Bortel, L.; Boutouyrie, P.; Giannattasio, C.; Hayoz, D.; Pannier, B.; Vlachopoulos, C.; Wilkinson, I.; Struijker-Boudier, H. Expert consensus document on arterial stiffness: methodological issues and clinical applications. *Eur. Heart J.* **2006**, *27*, 2588−2605.
(44) Nurnberger, J.; Keflioglu-Scheiber, A.; Opazo Saez, A. M.; Wenzel, R. R.; Philipp, T.; Schafers, R. F. Augmentation index is associated with cardiovascular risk. *J. Hypertens.* **2002**, *20*, 2407−2414.
(45) Cai, J.; Pajak, A.; Li, Y.; Shestov, D.; Davis, C. E.; Rywik, S.; Deev, A.; Tyroler, H. A. Total cholesterol and mortality in China, Poland, Russia, and the US. *Ann. Epidemiol.* **2004**, *14*, 399−408.
(46) Sharrett, A. R.; Ballantyne, C. M.; Coady, S. A.; Heiss, G.; Sorlie, P. D.; Catellier, D.; Patsch, W. Coronary heart disease prediction from lipoprotein cholesterol levels, triglycerides, lipoprotein(a), apolipoproteins A-I and B, and HDL density subfractions: The Atherosclerosis Risk in Communities (ARIC) Study. *Circulation* **2001**, *104*, 1108−1113.
(47) Zhu, Y.; Ling, W.; Guo, H.; Song, F.; Ye, Q.; Zou, T.; Li, D.; Zhang, Y.; Li, G.; Xiao, Y.; Liu, F.; Li, Z.; Shi, Z.; Yang, Y. Anti-inflammatory effect of purified dietary anthocyanin in adults with hypercholesterolemia: a randomized controlled trial. *Nutr. Metab. Cardiovasc. Dis.* **2013**, *23*, 843−849
(48) Chambers, B. K.; Camire, M. E. Can cranberry supplementation benefit adults with type 2 diabetes? *Diabetes Care* **2003**, *26*, 2695−2696.
(49) Duthie, S. J.; Jenkinson, A. M.; Crozier, A.; Mullen, W.; Pirie, L.; Kyle, J.; Yap, L. S.; Christen, P.; Duthie, G. G. The effects of cranberry juice consumption on antioxidant status and biomarkers relating to heart disease and cancer in healthy human volunteers. *Eur. J. Nutr.* **2006**, *45*, 113−122.
(50) Rein, D.; Paglieroni, T. G.; Wun, T.; Pearson, D. A.; Schmitz, H. H.; Gosselin, R.; Keen, C. L. Cocoa inhibits platelet activation and function. *Am. J. Clin. Nutr.* **2000**, *72*, 30−35.
(51) Holt, R. R.; Actis-Goretta, L.; Momma, T. Y.; Keen, C. L. Dietary flavanols and platelet reactivity. *J. Cardiovasc. Pharmacol.* **2006**, *47* (Suppl. 2), S187−S196 (discussion S206−S209).
(52) Hassellund, S. S.; Flaa, A.; Kjeldsen, S. E.; Seljeflot, I.; Karlsen, A.; Erlund, I.; Rostrup, M. Effects of anthocyanins on cardiovascular risk factors and inflammation in pre-hypertensive men: a double-blind randomized placebo-controlled crossover study. *J. Hum. Hypertens.* **2013**, *27*, 100−106.
(53) Steffen, Y.; Gruber, C.; Schewe, T.; Sies, H. Mono-O-methylated flavanols and other flavonoids as inhibitors of endothelial NADPH oxidase. *Arch. Biochem. Biophys.* **2008**, *469*, 209−219.
(54) Steffen, Y.; Schewe, T.; Sies, H. (−)-Epicatechin elevates nitric oxide in endothelial cells via inhibition of NADPH oxidase. *Biochem. Biophys. Res. Commun.* **2007**, *359*, 828−33.
(55) Schewe, T.; Steffen, Y.; Sies, H. How do dietary flavanols improve vascular function? A position paper. *Arch. Biochem. Biophys.* **2008**, *476*, 102−106.
(56) Wu, X.; Kang, J.; Xie, C.; Burris, R.; Ferguson, M. E.; Badger, T. M.; Nagarajan, S. Dietary blueberries attenuate atherosclerosis in apolipoprotein E-deficient mice by upregulating antioxidant enzyme expression. *J. Nutr* **2010**, *140*, 1628−1632.
(57) Suh, J. H.; Romain, C.; Gonzalez-Barrio, R.; Cristol, J. P.; Teissedre, P. L.; Crozier, A.; Rouanet, J. M. Raspberry juice consumption, oxidative stress and reduction of atherosclerosis risk factors in hypercholesterolemic golden Syrian hamsters. *Food Funct.* **2011**, *2*, 400−405.
(58) Mauray, A.; Milenkovic, D.; Besson, C.; Caccia, N.; Morand, C.; Michel, F.; Mazur, A.; Scalbert, A.; Felgines, C. Atheroprotective effects of bilberry extracts in apo E-deficient mice. *J. Agric. Food Chem.* **2009**, *57*, 11106−11111.
(59) Mauray, A.; Felgines, C.; Morand, C.; Mazur, A.; Scalbert, A.; Milenkovic, D. Nutrigenomic analysis of the protective effects of

bilberry anthocyanin-rich extract in apo E-deficient mice. *Genes Nutr.* **2010**, *5*, 343−353.
(60) Mauray, A.; Felgines, C.; Morand, C.; Mazur, A.; Scalbert, A.; Milenkovic, D. Bilberry anthocyanin-rich extract alters expression of genes related to atherosclerosis development in aorta of apo E-deficient mice. *Nutr. Metab. Cardiovasc. Dis.* **2012**, *22*, 72−80.
(61) Xie, C.; Kang, J.; Chen, J. R.; Lazarenko, O. P.; Ferguson, M. E.; Badger, T. M.; Nagarajan, S.; Wu, X. Lowbush blueberries inhibit scavenger receptors CD36 and SR-A expression and attenuate foam cell formation in ApoE-deficient mice. *Food Funct.* **2011**, *2*, 588−594.
(62) Xie, C.; Kang, J.; Chen, J. R.; Nagarajan, S.; Badger, T. M.; Wu, X. Phenolic acids are in vivo atheroprotective compounds appearing in the serum of rats after blueberry consumption. *J. Agric. Food Chem.* **2011**, *59*, 10381−10387.
(63) Zhang, Y.; Wang, X.; Wang, Y.; Liu, Y.; Xia, M. Supplementation of cyanidin-3-*O*-glucoside promotes endothelial repair and prevents enhanced atherogenesis in iabetic apolipoprotein E-deficient mice. *J. Nutr.* **2013**, *143*, 1248−1253.
(64) Ahmet, I.; Spangler, E.; Shukitt-Hale, B.; Joseph, J. A.; Ingram, D. K.; Talan, M. Survival and cardioprotective benefits of long-term blueberry enriched diet in dilated cardiomyopathy following myocardial infarction in rats. *PloS One* **2009**, *4*, e7975.
(65) Ahmet, I.; Spangler, E.; Shukitt-Hale, B.; Juhaszova, M.; Sollott, S. J.; Joseph, J. A.; Ingram, D. K.; Talan, M. Blueberry-enriched diet protects rat heart from ischemic damage. *PloS One* **2009**, *4*, e5954.
(66) Elks, C. M.; Reed, S. D.; Mariappan, N.; Shukitt-Hale, B.; Joseph, J. A.; Ingram, D. K.; Francis, J. A blueberry-enriched diet attenuates nephropathy in a rat model of hypertension via reduction in oxidative stress. *PloS One* **2011**, *6*, e24028.
(67) Kalt, W.; Foote, K.; Fillmore, S. A.; Lyon, M.; Van Lunen, T. A.; McRae, K. B. Effect of blueberry feeding on plasma lipids in pigs. *Br. J. Nutr.* **2008**, *100*, 70−78.
(68) Rodriguez-Mateos, A.; Ishisaka, A.; Mawatari, K.; Vidal-Diez, A.; Spencer, J. P.; Terao, J. Blueberry intervention improves vascular reactivity and lowers blood pressure in high-fat-, high-cholesterol-fed rats. *Br. J. Nutr.* **2012**, 1−9.
(69) Rouanet, J.-M.; Decorde, K.; Rio, D. D.; Auger, C.; Borges, G.; Cristol, J.-P.; Lean, M. E. J.; Crozier, A. Berry juices, teas, antioxidants and the prevention of atherosclerosis in hamsters. *Food Chem.* **2010**, *118*, 266−271.
(70) Shaughnessy, K. S.; Boswall, I. A.; Scanlan, A. P.; Gottschall-Pass, K. T.; Sweeney, M. I. Diets containing blueberry extract lower blood pressure in spontaneously hypertensive stroke-prone rats. *Nutr. Res. (N.Y.)* **2009**, *29*, 130−138.

by differences attributable to environmental conditions, ripeness at harvesting, and storage conditions. Additionally, the wide variety of structures and conjugates of (poly)phenols makes estimation in food substances extremely difficult, and therefore data on dietary intake are scarce. However, the recently developed and updated Phenol-Explorer database provides much useful information.[15] In a recent study by Pérez-Jiménez and co-workers,[16] daily consumption of total (poly)-phenols in a French population was estimated as 820 ± 335 mg/day (aglycone equivalents), which was similar to that previously observed in a Finnish cohort (863 ± 415 mg/day).[17] In both studies phenolic acids were the main (poly)phenols consumed, with intake in the Finnish cohort being twice that of the French cohort. The anthocyanin intake was reported to be marginally higher in the Finnish cohort than in the French at 47 ± 79 and 35 ± 29 mg/day (aglycone equivalents), respectively. The large variations evident in consumption likely reflect individual preferences, but it was not surprising that berries were a more prominent source of (poly)phenols in the Finnish diet than in the French.

Ileostomy feeding studies have demonstrated that substantial amounts of (poly)phenolic compounds in berries are not absorbed into circulation from the small intestine but rather pass into the large intestine where,[18,19] it is reasonable to infer, they come into direct contact with the colonic epithelium.[20,21] Moreover, the microbiota within the colon plays a key role in the fate of phytochemicals that are not absorbed in the small intestine. Once in the colon, berry (poly)phenolics are subject to the fermentative action of the microbiota, with catabolism giving rise to a diversity of phenolic acids.[19,22] Moreover, fermentable carbohydrates (fiber) present in whole foods such as berries might act in synergy with the mixture of (poly)phenols present in berries and contribute to their overall antigenotoxic activities, as these fermentable dietary fibers can beneficially modulate both the composition and metabolic output of the human gut microbiota.[23]

Several theories on the anticancer activity of (poly)phenols are supported by an expanse of data demonstrating the potential mechanisms involved. The most studied effects are those that modify proliferation and apoptosis, and these have been extensively reviewed elsewhere.[24] Other mechanisms responsible for the putative anticancer activity are still not fully understood but may include scavenging free radicals, induction of enzymes involved in metabolism of xenobiotics,[25] regulation of gene expression, and modulation of cellular signaling pathways including those involved in DNA damage detection and repair.

This review aims to assess the in vitro and in vivo evidence for anticancer activities for whole berries and berry extracts focusing particularly on the genoprotective element of these compounds.

DNA DAMAGE AND CANCER

DNA damage has a key role in cancer development. The initiating step in CRC development involves exposure to, or uptake of, carcinogens, resulting in permanent DNA damage. Considering the potentially toxic nature of the colon contents, it is not unsurprising that frequent mutations occur in colonic cells. Therefore, efficient DNA damage detection and repair mechanisms are present to prevent damage becoming a permanent sequence change. However, errors in detection and repair mechanisms may occasionally occur. Thus, reducing the frequency of DNA damage or enhancing the repair mechanisms may be a feasible explanation for the protective effects of berry (poly)phenols against initiation of CRC.

Unrepaired DNA damage can become incorporated into the genome as a permanent sequence change if the cell divides before the damage is repaired. For example, CRC is characterized by a multistep pathway involving sequential mutations and deletions of key oncogenes and tumor suppressor genes such as *APC*, K-*ras*, and *p53* in epithelial cells.[26] These genetic changes result in evasion of cell signaling pathways and cell cycle control points, leading to hyperproliferation, avoidance of apoptosis, and eventual invasion and metastasis. Under normal cellular conditions, reactive oxygen species (ROS) such as superoxide anions ($^{\bullet}O_2^-$) and hydroxyl radicals ($^{\bullet}OH^-$) are produced by endogenous metabolism and used by the cell to modulate biological processes; for example, the generation of ROS can lead to activation of receptors including G protein-coupled receptors, tyrosine, and serine/threonine kinases.[27] Downstream signaling components are stimulated as a response, and these include MAPK and protein kinase C, which are tightly regulated and are involved in proliferation, differentiation, cell survival, and apoptosis.[28] However, ROS production has also been implicated in sequential tumor development by a number of routes.[27] Reaction of ROS with DNA results in the formation of oxidized DNA bases, apurinic/apyrimidinic sites (AP sites), or DNA strand breaks. In particular, 8-oxo-7,8-dihydro-2′-deoxyguanosine (8-OHdG) is one of the most easily formed oxidative DNA lesions. Moreover, 8-OHdG can react with compounds such as peroxynitrate to produce further mutagenic lesions.[29]

ROS also react with phospholipids in the cell membrane and form lipid peroxidation products such as 4-hydroxynonenal, which in turn can react with DNA and to form cyclic-DNA adducts.[30] Other abundant lesions of oxidative DNA damage, which are also highly mutagenic, result from GC to TA transversions.[31]

ROS assault on cells in areas prone to DNA damage increases the probability that changes will go unrepaired and lead to conformational changes of the structure of DNA, rendering replication more difficult and error prone.[32,33] Furthermore, ROS may contribute toward carcinogenesis through differential regulation of cell signaling pathways. For example, modulation of MAPK, Jak/STAT, heat shock response, and PI3K/Akt pathways will affect gene expression, and, if activated, can in certain circumstances stimulate growth.[34,35] Given that STATs are generally associated with transcriptional activation, STAT-dependent transcriptional repression has also been reported.[36] Also, whereas activation of JNK signaling in response to a range of stress signals is generally thought to promote cell death or tumor suppression, there is evidence to suggest that JNK signaling may also be involved in the promotion of growth and the formation of tumors under certain circumstances.[37]

DNA damage from exogenous chemicals or radiation can have genotoxic activity and result in DNA modifications such as covalent bridging between bases as well as inducing single- and double-strand breaks. Therefore, cellular systems monitor the genome and repair DNA using different repair enzymes by removing damaged or incorrect sections of DNA and replacing them with the correct sequence. There are multiple different methods of DNA damage repair within the cell, including excision repair (for single-strand breaks), nonhomologous end joining and homologous recombination (for double-strand

Table 1. Effects of Berry Extracts or Berry Constituents on Models of DNA Damage and Scavenging Activity[a]

berry or berry constituent	colonocyte cell line	dose	end point	observation	protective/adverse effect	comment	ref
anthocyanin-rich fraction from *Vaccinium corymbosum* and *Vaccinium myrtilus*	Caco-2	0.5−50 μg/L	intracellular ROS levels, CAA assay	↓ in intracellular ROS by ∼40% after 0.5 μg/L and 1 h	+[b]	reduction of intracellular ROS at low concentrations of anthocyanin treatment	55
in vitro digested and in vitro fermented raspberry (*Rubus idaeus*), strawberry (*Fragaria* × *ananassa*) and black currant (*Ribes nigrum*) extracts	HT29	IVD = 3.125−50 μg/mL GAE	antigenotoxic activity, comet assay	↓ in strand breaks by ∼40% in all IVD berry extracts from 6.25 to 50 μg/mL after 24 h	+[b]	fermented, phenolic acid rich extracts cause a significant decrease in DNA damage and mutation frequency	64
		fermented = raspberry, 15.5 μg/mL; strawberry, 13.9 μg/mL; black currant, 12.4 μg/mL	mutation frequency assay	↓ in strand breaks by ∼30% in all fermented extracts after 24 h	+[b]		
				↓in RMF >50% in all IVD berry extracts after 24 h	+[b]		
				↓in RMF ∼40% in all fermented extracts after 24 h	+[b]		
anthocyanin-rich fraction from bilberry (*Vaccinium myrtilus*)	Caco-2	10−500 μg/mL	antigenotoxic activity, comet assay	↓ in strand breaks by ∼50% after in Caco-2 after 50 μg/mL and 24 h	+[b]	dose-dependent decrease in DNA damage and scavenging activity after anthocyanin treatment	54
	HT29		intracellular ROS levels, CAA assay	↓ in intracellular ROS by ∼30−40% in Caco-2 and HT29 after 250 μg/mL and 24 h	+[b]		
ursolic acid (UA)	Caco-2	5 μM or 10 μM	comet assay, endogenous and H_2O_2-induced DNA damage	both concentrations yielded ∼40% ↓ in strand breaks following 2 h of pre-incubation	+[b]	greater reduction in DNA damage after a short incubation period with UA; increase in BER activity	63
			base excision repair assay (BER) using enzyme 8-oxoguanine DNA glycosylase 1 (OGG1)	17% ↓ in strand breaks after 5 μM for 24 h			
				23.5% ↑ in BER activity, for Caco-2 cells pretreated (24 h) with UA			
quercetin	Caco-2	1 μM or 100 μM	comet assay, endogenous and H_2O_2-induced DNA damage	↓ in strand breaks by 42% at 1 μM and 57% at 100 μM	+[b]	quercetin shows antigenotoxic activity at low concentrations; enhanced DNA repair by modulation of DNA repair enzyme expression	62
				↑ mRNA expression of human 8-oxoguanine DNA glycosylase (hOGG1) at 0 and 4 h after H_2O_2 treatment			
ellagic acid		0−300 μM	modulation of $4E_2/CuCl_2$-induced oxidative DNA adducts	>60% ↓ of both unidentified oxidative adducts and 8-OHdG	+[b]	dose-dependent decrease in induced oxidative adducts after ellagic acid treatment	61
anthocyanin fraction from blackberry (*Rubus fruticosus*)	Caco-2	3.15−50 μg/mL	intracellular oxidation	dose-dependent ↓ in intracellular oxidation	+[b]	suggests anthocyanins protect by scavenging AAPH-induced peroxyl radicals generated within cells	53
				no ↓ in cell viability			
		0.8−25 μg/mL	oxidative cytotoxicity (CellTiter-Glo assay)	↓ cytotoxicity from 1.6 to 25 μg/mL	+[b]		
phenolics isolated from strawberries (*Fragaaria* × *ananassa*)		10 mg/mL	antioxidative ability, TEAC assay	three of the phenolics showed significant antioxidant capacity: cyanidin-3-glucoside (7156 μM Trolox/mg)	+[b]	isolation of the specific phenolics within strawberry extract has given a greater understanding on which compounds possess antioxidative capacity	52

dx.doi.org/10.1021/jf4050759 | J. Agric. Food Chem. 2014, 62, 3852−3866

Table 1. continued

berry or berry constituent	colonocyte cell line	dose	end point	observation	protective/ adverse effect	comment	ref
				pelargonidin (4922 μM Trolox/mg)			
				pelargonidin-3-rutinoside (5514 μM Trolox/mg)			
raspberry (*Rubus idaeus*) in vitro digested extract	HT29	0−50 μg/mL GAE	comet assay, endogenous and H_2O_2-induced DNA damage	↓ in H_2O_2 induced strand breaks by ∼50% from 3.125 to 50 μg/mL	+[b]	dose-dependent decrease in DNA damage after berry treatment	60
cyanidin	human colon epithelial cells (HCEC)	50 μM	comet assay, endogenous and H_2O_2-induced DNA damage	↓ strand breaks ∼39%	+[b]	all flavonoids significantly reduced oxidant-induced strand breakage	59
cyanidin-3-glucoside				↓ strand breaks ∼35%	+[b]		
quercetin				↓ strand breaks ∼30%	+[b]		
blackberry (*Rubus fruticosus*)		100 μL of juice extract	inhibition of ROS formation through direct scavenging	$OH^{\bullet} > H_2O_2 > O_2^{\bullet-} > {}^1O_2$	+[b]	scavenging activity varied with berry type and species of reactive oxygen	51
blueberry (*Vaccinium corymbosum*)				$H_2O_2 > O_2^{\bullet-} > OH^{\bullet} > {}^1O_2$	+[b]		
cranberry (*Vaccinium oxycoccos*)				$OH^{\bullet} > H_2O_2 > O_2^{\bullet-} > {}^1O_2$	+[b]		
raspberry (*Rubus idaeus*)				$OH^{\bullet} > H_2O_2 > O_2^{\bullet-} > {}^1O_2$	+[b]		
strawberry (*Fragaria* × *ananassa*)				$OH^{\bullet} > H_2O_2 > O_2^{\bullet-} > {}^1O_2$	+[b]		
quercetin	Caco-2	0−1 mM	comet assay, endogenous and H_2O_2-induced DNA damage	quercetin ↓ strand breaks by ∼50 and 65% after 0.5 and 18 h	+[b]	specific antigenotoxic activity against H_2O_2-induced strand breaks; no effect on oxidative base damage	58
myricetin				myricetin ↓ strand breaks at 1 mM	+[b]		
kaempferol				kaempferol and rutin, no effect	−		
rutin							

[a]GAE, gallic acid equivalents; ROS, reactive oxygen species; AAPH, 2,2′-azobis(2-methylpropanimidamide) dihydrochloride; NE, no effect; ↓, decrease; ↑, increase; 8-OHdG, 8-hydroxy-2′-deoxyguanosine; CAA, cellular antioxidant activity; IVD, in vitro digested; RMF, relative mutation frequency; TEAC, Trolox equivalent antioxidant capacity; UA, ursolic acid. [b]Significant result. +, protective effect; −, adverse effect.

dx.doi.org/10.1021/jf4050759 | J. Agric. Food Chem. 2014, 62, 3852−3866

breaks), and mismatch repair (for mismatched bases from DNA replication). However, if DNA damage goes undetected and unrepaired, this will become a mutation when the cell replicates.[38]

MEASUREMENT OF DNA DAMAGE

DNA damage can be determined in tissues and organs either by taking biopsies or by isolating exfoliated epithelial cells such as buccal, bladder, or intestinal cells. Systemic DNA damage is usually measured in peripheral blood mononuclear cells (PBMC) as they can be easily isolated from blood samples. In addition, they are believed to reflect DNA damage in other body tissues. Studies of DNA damage can be performed in vivo and ex vivo as well as in vitro. A recent study reported no genotoxic impact in human lymphocytes following exposure to radiofrequency electromagnetic field emission using four genotoxicity end points,[39] including the alkaline single-cell gel electrophoresis (comet) assay,[40] which is the most frequently applied assay to detect strand breaks and related events. The comet assay is applicable for a wide range of cell types and for in vivo and in vitro studies. It involves embedding a suspension of the target cells in agarose on a microscope slide, lysing the cells to liberate the DNA, and then treating under alkaline conditions, causing the DNA to unwind from sites of strand breakage. The slides are then subjected to electrophoresis, and DNA fragments induced by genotoxic agents migrate to the anode to form a comet "tail". The DNA is stained with a fluorescent dye and the proportion of damaged DNA in the tail assessed by image analysis. A modification to the procedure, in which enzymes that convert oxidized bases to strand breaks are added, allows oxidative DNA damage to be quantified. For example, the enzyme endonuclease III (EndoIII), which specifically nicks DNA at sites of oxidized pyrimidines, or alternatively formamidopyrimidine DNA glycosylase (FPG), which recognizes 8-oxoGua and other oxidized purines, can be added after lysis.[41]

Conversely, the combined use of fluorescence in situ hybridization (FISH)/comet assay allows for the detection of DNA damage/repair to specific genes. By combining these two well-established methods, the hybrid assay allows fragmented DNA to be separated from nonfragmented DNA, whereas the FISH element allows detection of specifically labeled DNA sequences of interest such as APC, Tp53, or KRAS.[42,43] The comet assay is widely regarded as a valuable tool for genotoxicity testing and biomonitoring of oxidative stress in humans,[44] and its applicability to cancer risk studies has been well discussed;[45,46] however, interlaboratory reproducibility remains an area for improvement.[47]

Systemic oxidative DNA damage can also be assessed by measurement of the formation of DNA adducts such as 8-hydroxy-2′-deoxyguanosine (8-OHdG, one of the predominant forms of free radical-induced oxidative lesions[48]) or by detection of lipid peroxidation products. 8-OHdG is commonly detected by HPLC with electrochemical detection or tandem MS or by GC-MS. Lipid peroxidation products in plasma or urine include hydroxyeicosatetraenoic acids (HETE), which are generally measured using HPLC with MS, chemiluminescence, or fluorescence detection.[49,50] It is interesting to note that there is evidence to suggestthat the enzymatic comet assay variant appears to be more accurate in the estimation of low background levels of oxidative damage than are the chromatographic methods.[44]

IN VITRO STUDIES

Multiple in vitro studies have assessed the anticancer activities of berry components, using cell models in attempts to represent the initiation stage of CRC. These studies have mainly assessed the efficacy of whole berry extracts, fractionated berry extracts, or purified/commercial berry components in a range of human colon cell lines. These studies are summarized in Table 1.

Berry (poly)phenols may exert potential anticancer effects by chelating redox active metals (such as iron) or by directly scavenging ROS [including hydrogen peroxide (H_2O_2), hydroxyl radicals ($^{\bullet}OH^{-}$), superoxide radicals ($^{\bullet}O_2^{-}$), and singlet oxygen ($^1O_2$)] by being effective electron donors to the ROS. ROS scavenging activity[51,52] and antioxidant capacity[53−55] in vitro vary with type of berry extract or isolated components of berries (Table 1). The scavenging activity of berry (poly)phenols in simple, cell-free antioxidant systems through the scavenging of free radicals is remarkably high compared to those of other standard antioxidants such as ascorbic acid and α-tocopherol.[51] However, although useful in assessing antioxidant potential, these chemical assays provide little in terms of mechanisms relating to biological activity. Modifications have included the use of simulated gastrointestinal digestion of fruits prior to testing: for example, cranberries mostly retained their antioxidant activity following digestion using cell-free (DPPH) and Caco-2-based assays, whereas blueberries lost 43% of their free radical scavenging activity.[56] The measurement of intracellular ROS levels is a simple method to assess efficacy in a cellular model, which has greater biological relevance with uptake, retention, and metabolism of antioxidant (poly)phenols under physiologically relevant conditions. Several authors have utilized this technique to demonstrate a reduction in intracellular chemically induced ROS upon addition of the peroxyl radical (AAPH) to induce oxidative damage and associated cytotoxicity in various colon cancer cells.[53−55] Although direct intracellular scavenging has been suggested as the mechanism for this decrease,[53,54] this may be an oversimplification of the mechanisms involved. It may be that berry (poly)phenols interact with cell receptors or enzymes resulting in altered cell redox status, which triggers redox-dependent reactions.[57] For example, Bornsek and colleagues[55] hypothesized that the level of antioxidant activity invoked was not consistent with the low concentration of berry (poly)phenols (0.5 μg/mL) and that a signaling cascade may be triggered, possibly through their binding to an extracellular receptor or acting as an intercellular secondary messenger, resulting in activation of endogenous antioxidant systems. This mechanism would result in the amplification of the signal, so that low levels of (poly)phenols would have greater efficacy.

Several in vitro studies have investigated the effects of berry (poly)phenols on H_2O_2-induced DNA strand breaks as a measure of genotoxicity and, overall, have shown a reduction in genotoxicity in response to berry extracts and isolated flavonoids[58−64] (Table 1). The suggested mechanisms responsible for this antigenotoxic activity have been described as increased antioxidant activity, enhanced DNA damage repair, or a combination of both. For example, this has been demonstrated with the flavonoid quercetin[62] and the pentacyclic triterpenoid acid ursolic acid,[63] which is found in some berry types. Both of these compounds, at physiologically relevant (colonic) concentrations (100 and 10 μM, respectively), have demonstrated potent antioxidant effects in Caco-2 cells through reducing levels of H_2O_2-induced DNA damage

and specific oxidized adducts (8-oxoG) as detected using the enzyme 8-oxoguanine DNA glycosylase 1 (OGG1) to specifically cleave DNA at these sites. Further analysis has revealed that pretreatment with ursolic acid prior to, but not following, exposure to oxidative insult enhanced the rate of repair of DNA strand breaks via base excision repair (BER),[63] possibly through up-regulation of the repair enzyme OGG1 as evidenced by Min and colleagues with quercetin.[62] However, earlier work did not detect changes in oxidative base damage with quercetin (50 μM), and Duthie et al.[58] concluded that quercetin may in fact act by stabilizing the DNA directly. Although the exact mechanism responsible is still unknown, it may be affected via augmentation of p53 in response to antioxidant molecules, leading to up-regulation of the DNA excision repair pathway.[65]

Although studies have shown the genoprotective effects of isolated components from berries,[54,58,59,62] few investigations have considered the effect of intestinal digestion and bacterial fermentation on (poly)phenols from whole berries, as would occur following human consumption. Post ingestion, the phytochemicals contained within berries undergo alterations in their structure, and possibly their function, because of the impact of the human digestive tract. We know, for instance, that substantial amounts of (poly)phenolic compounds in raspberries are not absorbed into circulation in the small intestine but pass into the large intestine[66,67] where, it is reasonable to infer, they come into direct contact with the colonic epithelium and exert beneficial effects. For example, Coates et al.[60] demonstrated a genoprotective effect in HT 29 cells for a raspberry extract that had undergone in vitro digestion. However, it is also clear that berry (poly)phenols are extensively metabolized to simpler phenolics by the colonic microbiota during passage through the large intestine,[67−69] and thus it seems reasonable to assume that the levels of intact berry (poly)phenols will decrease as they pass further through the colon, with a corresponding increase in microbiota-derived catabolites. Therefore, different parts of the proximal to distal colon will be exposed to different proportions of the original (poly)phenol components and their catabolites. Only a few studies have established that colonic catabolites of (poly)-phenols have bioactivities (at least in vitro) relevant to colon cancer.[64,70,71] We have previously demonstrated that in vitro digested and fermented raspberry, strawberry, and black currant extracts at physiological concentrations (<50 μg/mL gallic acid equiv) retained the ability to protect DNA from oxidative insult during the digestive and bacterial fermentation processes.[64] Additionally, individual phenolic compounds representative of bacterial catabolites, namely, tyrosol and 4′-hydroxyphenyl-acetic acid (5 and 10 μg/mL), offered protection against oxidative insult and reduced DNA damage to levels similar to that achieved by ursolic acid in a different study.[63] However, the level of reduction in strand breakage by individual phenolic acids was less pronounced than for the mixture of phenolics, as found in fermented berry extracts, suggesting that an additive or synergistic effect may enhance the protective effect against ROS. Similarly, Gimenez-Bastida et al.[72] reported that a mixture of ellagitannin metabolites, including urolithins A and B, improved the inflammatory response of colon fibroblasts CCD-18Co, significantly decreasing PGE(2), PAI-1, and IL8.

In conclusion, although these in vitro studies differ in choice of berry, (poly)phenolic compounds, and assays utilized, they demonstrate a consensus with respect to a protective effect for berries against ROS-induced DNA damage.

IN VIVO ANIMAL STUDIES

Following in vitro models, animal models enable the investigation of berry (poly)phenols in a living system, looking at the effects of berry extracts on different stages in colorectal carcinogenesis. In keeping with the theme of this review, studies investigating initiation (formation of aberrant crypt foci (ACF)) and markers of DNA damage including urinary 8-OHdG levels are included. For example, the Fischer 344 (F344) rat model is used to represent CRC development due to a histopathological resemblance to human CRC after azoxymethane (AOM) treatment, first forming ACF and then developing into adenomas, adenocarcinomas, and finally carcinomas.[73] ACF are early identifiable precancerous lesions present during the multistep pathway involved in CRC development in both humans and rodents.[73] Additional similarities include *APC* and *ras* gene mutations and induction of COX-2 gene expression, which occur after AOM treatment in F344 rats.[74] The $Apc^{Min/+}$ (multiple intestinal neoplasia) mouse model harbors a mutation in the *Apc* gene resulting in the spontaneous development of colorectal polyps and is utilized as a model of human familial adenomatous polyposis (FAP).[75] The effects of berry extracts and berry components on a range of end points in these animal models are summarized in Table 2.

Consumption of black currant juice effectively reduced levels of single-strand DNA breaks induced by oxidative insult in leucocytes from the circulating plasma of pigs, suggesting bioavailability of either parent (poly)phenols or perhaps, more plausibly, colonic catabolites, mediating genoprotective effects in vivo.[76] Although the mechanism still requires further elucidation, the lack of decrease in malondialdehyde (a marker of oxidative stress, produced by ROS in vivo) suggests that oxidative stress was not affected. Therefore, it is unlikely that berry (poly)phenolic compounds were acting as direct scavengers in this instance, but were instead mediating levels of DNA damage repair or detoxification enzymes. Indeed, the activation of detoxification enzymes was suggested as a possible mechanism by which grape juice protected against DNA adduct formation in the organs of mice treated with benzo(a)pyrene and dimethylbenzo(a)anthracene (heterocyclic amines produced by cooking food). A reduction in the activation of these carcinogens via decreased expression of phase I enzymes or by up-regulating the expression of phase II detoxification enzymes including glutathione-S-transferases (GSTs), which are involved in degrading and eliminating activated carcinogens, could be involved.[77]

One mechanism for protection against carcinogens is induction of enzymes involved in their metabolism, particularly the phase II enzymes (including GST), which protect against damage by activated electrophilic metabolites from phase I metabolism. GSTs, a large family of detoxification enzymes, deactivate carcinogens by conjugating them with endogenous glutathione, which also enhances their water solubility and thus their elimination.[78] A blueberry extract and cranberry juice have been shown to significantly induce hepatic GST levels in F344 rats treated with AOM, whereas a blackberry extract did not. However, the blackberry extract significantly inhibited ACF formation but failed to significantly induce GST.[79] Therefore, it is likely that different, as yet to be identified, mechanisms, working in parallel, are responsible for the total anticarcinogenic effects observed.

Table 2. Effects of Berry Extracts/Components in Animal Models of Colorectal Cancer[a]

berry or berry constituent	animal	dose and exposure	end point	observation	protective/adverse effect	comment	ref
black currant (*Ribes nigrum*) juice	pigs	A, black currant + linseed oil B, starch control C, linseed oil D, linseed + vitamin E	comet assay, DNA damage in leucocytes	↓ DNA in leucocytes by BC treatment	+[b]	black currant juice decreased DNA damage but was less effective than vitamin E treatment	76
			urinary excretion of malonaldehyde (MDA)	no effect on MDA excretion for BC	−		
blueberry (*Vaccinium corymbosum*) strawberry (*Fragaria* × *ananassa*) raspberry (*Rubus idaeus*) ellagic acid	CD-1 (F) mice	5% w/w of dehydrated berries or 400 ppm ellagic acid in diet 3 weeks	analysis of endogenous polar oxidative DNA adducts	↓ in oxidative adduct by ∼50% in mice supplemented by raspberry or ellagic acid	+[b]	reduction in oxidative adducts dependent on ellagic concentration low and moderate strawberry and blueberry showed no significant reduction	61
blueberry (*Vaccinium corymbosum*) blackberry (*Rubus fruticosus*) cranberry (*Vaccinium oxycoccus*) juice	F344 rats (M) with SC injections of AOM	5% fruit or 20% juice (final concn) 13 weeks	ACF	blueberry, blackberry, and cranberry juice ↓ ACF by 93, 85, and 77%, respectively	+[b]	treatment with whole berries and whole berry juice significantly ↓ the formation of ACF; increased GST activity may be a chemoprotective action of berries	79
			hepatic GST activity	↑ GST activity after blueberry and cranberry juice treatment but not blackberry	+[b]		
pterostilbene (PTER)	F334 rats (M) with SC injections of AOM	diet supplemented with PTER at 40 ppm 8 weeks	ACF	↓ ACF by 57%	+[b]	pterostilbene treatment ↓ ACF formation and inflammatory pathways in F344 rats	84
			PCNA	↓ in PCNA staining by ∼10%	+		
			iNOS	↓ expression of iNOS proteins	+		
			MUC2	↑ expression of MUC2	+		
bilberry (*Vaccinium myrtillus*) ARE chokeberry(*Aronis meloncarpa*) ARE grape (*Vitis vinifera*) ARE	F344 rats (M) with SC injection of AOM	3.85 g of monomeric anthocyanin/kg 14 weeks	ACF	↓ total number of ACF by 29, 26, and 27% for bilberry, chokeberry, and grape AREs	+	ARE treatment ↓ ACF incidence and ↓ number of large ACF for bilberry and chokeberry treatments as well as ↓ cell proliferation and ↓ expression of pro-inflammatory COX-2 gene expression	82
			PCNA	↓ colonic cell proliferation with bilberry and chokeberry	+		
			urinary 8-OHdG	no change in 8-OHdG levels	−		
			COX expression	↓ gene expression of COX-2 with bilberry and grape AREs	+		
Mirtoselect (extract from bilberry (*Vaccinium myrtilus*) and blueberry (*Vaccinium corymbosum*) containing 15 anthocyanins) cyanidin-3-glucoside (C3G)	*Apc* $^{Min/+}$ mice (M and F)	0.03, 0.1, and 0.3% w/w in diet 12 weeks	colon and SI tumor number	no change in colonic tumors; 30 and 45% ↓ in SI tumor number at 0.3% treatment for Mirtoselect and C3G; all doses ↓ SI tumor number	− +	↓ in tumor number in dose-dependent manner; purified C3G may be more effective but anthocyanin levels in Mirtoselect were lower than in purified C3G	83
			M_1dG levels	highly variable levels, no significant difference	−		
black raspberry (*Rubus occidentalis*) (BRB, freeze-dried)	F344 rats (M) with IP injections of AOM	0, 2.5, 5, and 10% w/w in diet 33 weeks	ACF	↓ in ACF with all treatments	+	significant ↓ in tumor number and a trend toward overall ↓ tumor burden after BRB treatment may be concentration dependent	81
			tumor number	↓ by 42, 45, and 71% for 2.5, 5, and 10% BRB treatment	+		
			tumor volume	↓ by 53% with 10% BRB	+ NS		
			tumor burden	↓ by 28, 42, and 75% for 2.5, 5 and 10% BRB treatment	+ NS		
			urinary 8-OHdG	↓ for all treatments	+		

dx.doi.org/10.1021/jf4050759 | J. Agric. Food Chem. 2014, 62, 3852−3866

Table 2. continued

[a] ↓, decrease; ↑, increase; 8-OHdG, 8-hydroxy-2′-deoxyguanosine; ACF, aberrant crypt foci; AOM, azoxymethane; ARE, anthocyanin-rich extract; F, female; GAE, gallic acid equivalents; GST, glutathione-S-transferase; IA, invasive adenocarcinoma; IP, intraperitoneal; NIA, noninvasive adenocarcinoma; M, male; M_1dG, malondialdehyde deoxyguanosine; NS, not significant; PCNA, proliferating cell nuclear antigen; SC, subcutaneous; SI, small intestine. [b]Significant result. +, protective effect; − adverse effect.

Urinary levels of 8-OHdG have been used as a biomarker for cancer risk as 8-OHdG is the base most readily formed by oxidative damage and, therefore being abundant, is the most suitable for measurements of changes in levels.[48] These base changes are promutagenic, and increased 8-OHdG levels can be assumed to reflect an increased risk of cancer.[80] Treatment with (poly)phenol-rich berry extracts demonstrated slightly contrasting results with respect to 8-OHdG levels in separate studies (Table 2). Urinary levels of 8-OHdG were diminished significantly in AOM-treated F344 rats fed black raspberries, reaching levels comparable with those of untreated control rats, suggesting an almost complete reduction in AOM-induced genotoxicity, which corresponded to a decrease in ACF and tumor number.[81] In contrast, no changes in urinary 8-OHdG levels were reported in F344 rats fed anthocyanin-rich extracts (AREs) from bilberry, chokeberry, and grape after AOM treatment; however, these extracts also reduced ACF.[82] Therefore, it is possible that (poly)phenol composition is an important factor in regulating DNA damage, as whole berry extracts were effective inhibitors of genotoxicity, whereas anthocyanin-rich extracts were not. Therefore, the reduction of ACF after berry treatment was not directly dependent on a decrease in genotoxicity, but the chemoprotection observed may be offered via several different mechanisms.

In the main, these studies have investigated whole extracts or juices[61,76−79,81−83] rather than individual components, such as pterostilbene,[84] as previous studies have demonstrated the potential synergistic or additive effect of several (poly)phenols; in addition, they are much more representative of the composition of ingested fruits. Following the consensus from the in vitro studies presented in this review, Boateng et al.[79] summarized data indicating that consumption of (poly)phenols as a food source may be of greater importance in protecting against initiation of colorectal cancer in vivo than consumption of higher levels of individual (poly)phenolic compounds.

Because inflammation undoubtedly plays a role in carcinogenesis, dysregulated activation of inducible enzymes, such as NADPH oxidase (NOX), inducible nitric oxide synthase (iNOS), and cyclooxygenase (COX)-2, may represent an important chemoprotective pathway for dietary phytochemicals as a number of dietary (poly)phenols have been reported to inhibit their activation.[85] Indeed, a recent paper by Serra and co-workers reported that anti-inflammatory activity of cyanidin-3-glucoside was in part mediated by inhibition of iNOS and Cox2 expression.[86] Furthermore, some animal studies have reported that a diet low in methoxylated pectin can increase MUC2 expression, leading to an increase in mucin production, which is considered to be protective.[87] In addition, black raspberry powder significantly reduced chronic inflammation and suppressed intestinal tumor formation in MUC 2−/− rats.[88] Unfortunately, extensive coverage of these areas is beyond the scope of this review, but the complementary role of other plant components is clearly an area of interest.

The use of animal models has confirmed the in vitro studies in that berry components have protective effects against chemically induced CRC in a living system. Although no two studies have looked at the same biomarkers to evaluate the mechanisms behind this anticancer activity, the results overall indicate that berry extracts or components are able to influence carcinogen metabolism and reduce levels of DNA adduct formation in animal models of CRC. The potential mechanisms responsible for this effect include reduction in levels of DNA damage and adduct formation through inhibition of phase I

enzymes and up-regulation of detoxification phase II enzymes, which may ultimately result in decreased levels of oxidative assault and fewer precancerous lesions, such as ACF.

HUMAN STUDIES

The task of assessing the anticancer effects of food constituents in humans is challenging[89−91] given that, for the most part, intervention studies rely on intermediate biomarkers, such as DNA damage, that are plausibly linked to cancer[92] in the absence of clinical trials using definitive end points such as cancer incidence or mortality. From a chemoprotective perspective, the antiproliferative effects of berries have previously been reviewed by Brown et al.,[24] and evidence suggests consistent effects across in vitro and animal models. Evidence is emerging from studies with CRC patients indicating that consumption of black raspberries decreases proliferation markers, improves inflammatory markers in colon tissue, results in demethylation of tumor suppressor genes, and causes modulation of other biomarkers of tumor development in the human colon and rectum.[93,94] The latter effects may be mediated in part through inhibition of DNA methyltransferase 1 (DNMT1).[95] In a pilot study in 25 CRC patients, a commercial bilberry extract (Mytocyan) significantly reduced the proliferation index (assessed by Ki67 staining) in biopsies of colorectal adenocarcinomas, although other cancer-related markers were unaffected.[96] Unlike for antiproliferative activity, no studies have yet assessed the antigenotoxic effects of berry consumption in CRC patients, although a recent study with CRC patients by Alotaibi et al.,[97] using lymphocyte samples treated in vitro with dietary (poly)phenols, reported a significant reduction in lymphocyte damage induced by oxaliplatin/satraplatin.

Although the experimental evidence discussed previously supports a role for berry consumption and decreased DNA damage, most of the human intervention studies below exclusively utilize biomarkers from surrogate tissue such as lymphocytes, measuring changes that are biologically relevant to cancer including modulation of phase II enzymes, adduct formation, and DNA damage in response to dietary intake of berry fruits.

Collectively, the consumption of berry fruits has been shown to exert protective effects against DNA damage in healthy populations (Table 3). For instance, a recent study by Del Bo et al.[98] reported that a single 300 g portion of blueberries significantly reduced (18%) exogenously induced oxidative damage (H_2O_2) in blood mononuclear cells 1 h post consumption. However, the effect was not maintained at 2 or 24 h post dose or for FPG sensitive sites. Similarly, the consumption of a wild blueberry drink for 6 weeks resulted in significant reductions in endogenously oxidized DNA damage (from 12.5 ± 5.6 to 9.6 ± 3.5%, $P < 0.01$) as well as exogenously induced oxidative damage (from 45.8 ± 7.9 to 37.2 ± 9.1%, $P < 0.01$) in blood mononuclear cells.[99] A larger study by Wilms et al.[100] reported similar findings for consumption of a mixed blueberry/apple drink daily for 4 weeks, with a 20% decrease ($p < 0.01$) in exogenously induced oxidative damage in lymphocytes. Antigenotoxicity activity in lymphocytes was also reported for consumption of a mixed berry juice (red grape, blackberry, sour cherry, black currant, and chokeberry) in a healthy population[101] and in a patient group under enhanced oxidative stress, over a 4 week period.[102] In both studies, the observed protective effect may have resulted from direct antioxidant effects as well as from enhancing the cellular antioxidant system as an increase in glutathione status was noted during the interventions. In a small parallel study, dried wolfberries (*Fructus barbarum* L.) were consumed (15 g/day) for 28 days, resulting in a slight but significant decrease DNA damage in buccal cells, in comparison to the control group.[103] Other studies that showed protection against oxidative DNA damage in lymphocytes with fruit juices include that of Riso et al.,[104] using blood orange juice, Park et al.,[105,106] using grape juice, and Bub et al.,[107] using a juice mixture containing boysenberries and blueberries providing 236 mg/day (poly)-phenols. In the Bub et al.[107] study, fruit juice intake for 2 weeks had no significant effect on DNA damage, but following a subsequent washout and a further 2 weeks of juice consumption, oxidative DNA damage was significantly decreased. This result suggests that (poly)phenols, and/or their metabolites/catabolites, may be acting not only via the mechanism of ROS scavenging but also by exerting an influence on the antioxidant defense system by modulating the activity of phase I and phase II enzymes that play a role in preventing DNA damage.

In humans, increased risk of CRC or incidence of tumors in the colonic mucosa has been associated with low GST activity, compared to higher GST activity in healthy individuals.[108] Human studies have shown that supplementation with berry (poly)phenol-rich drinks have had differing effects on GST activity (Table 3).[109,110] Over a short supplementation period (2 weeks) no change in GST activity was reported,[110] but over a longer period GST activity was increased.[109] This observed difference may be due to a time delay or a requirement for an accumulation of berry (poly)phenols to produce an effect, as evidenced by a decrease in levels of human GST protein (hGSTP1) at the beginning of supplementation followed by a significant increase in hGSTP1 levels toward the end of the supplementation.[109] Furthermore, Wilms and colleagues[100] reported that compared with wild types, polymorphisms in a range of phase I and II enzymes including Cyp1b1*5, COMT, and GSTT1 could affect how effectively an individual could protect against DNA damage in response to any intervention.

Some berry fruit interventions showed no protective effects on lymphocyte DNA damage, which could serve to highlight the importance of stratification with respect to susceptibility when the impact of dietary interventions is assessed. Such studies include the work of Carmen Ramirez-Tortosa et al.,[111] who gave a grape, cherry, blackberry, black currant, and raspberry juice mixture containing 224 mg/kg anthocyanins to elderly subjects for 2 weeks, and that of Moller et al.,[112] who used a black currant juice with 600 mg/L anthocyanins for 3 weeks. Moller et al.[112] ascribed the lack of effect to the very low DNA damage levels in the subjects at baseline. Whereas the studies by Bub et al.[107] and Wilms et al.[113] indicated an overall positive effect of berry interventions, the lack of a concurrent control group within the study design limits the conclusions that can be drawn. That the majority of, but not all, berry-based studies demonstrate significant antigenotoxic activity, is likely due as much to the well-documented diversity and variability in phytochemical content and composition of berries as to differences in study design or biological characteristics of the participants. An understanding of the comparative effectiveness of different berry polyphenols is relevant only if we improve our understanding of which components survive and are present in situ and which metabolites are formed.[114] In view of the impact that an individual's gut microbiota may have with respect to bioavailability and ultimately bioactivity of dietary phenols, the

Table 3. Effects of Supplementation of Berry Extracts/Components on Markers of Antigenotoxicity in Human Intervention Studies[a]

berry or berry constituent	subjects	dose and exposure	end point	observation	protective/adverse effect	comment	ref
blueberries (*Vaccinium corymbosum*)	18 healthy male volunteers	randomized crossover 1 × 25 g of freeze-dried blueberry powder (375 mg of ACNs) daily for 6 weeks, 6 week washout, placebo drink 6 weeks	comet assay, endogenous and H_2O_2-induced DNA damage and FPG sites	↓ in H_2O_2-induced DNA damage (18%) in MNBCs	+[b]	6 weeks of blueberry powder consumption induced a significant decrease in MNBC DNA damage	99
				↓ basal levels of DNA damage (30%) in MNBCs (oxidized FPG sites)	+[b]		
blueberries (*Vaccinium corymbosum*)	10 healthy male volunteers	randomized crossover 1 × 300 g of blueberries (348 mg of ACNs and 727 mg of total phenolics) or control jelly	comet assay, endogenous and H_2O_2-induced DNA damage and FPG sites	↓ in H_2O_2-induced DNA damage (18%) in MNBCs, 1 h post blueberry consumption (T1)	+[b]	overall minor antigenotoxic effects for blueberry consumption	98
				no effect H_2O_2-induced DNA damage T0, T2, T24	−		
				no change in FPG sites	−		
				no effect on basal levels of DNA damage T0, T1, T2, T24	−		
blueberry (*Vaccinium corymbosum*)/apple juice	168 healthy volunteers	blueberry/apple juice 1 L/day for 4 weeks containing 197 mg quercetin/L ascorbic acid 16 mg/L	comet assay, endogenous and H_2O_2-induced DNA damage ex vivo induced DNA adducts (BPDE); plasma antioxidant capacity, TEAC assay SNP genotyping	↓ in H_2O_2-induced DNA damage (20%) in lymphocytes	+[b]	4 weeks of blueberry/apple juice consumption induced a significant decrease in lymphocyte DNA damage and increased antioxidant status; study had no concurrent control group	100
				28% ex vivo induced DNA adducts (BPDE)	−[b]		
				2.5% in antioxidant activity	+[b]		
polyphenol-rich juices: A = aronia, blueberry (*Vaccinium corymbosum*) and boysenberry (*Rubus ursinus* × *idaeus*) B = green tea (*Camellia sinensis*), apricot (*Prunus armeniaca*) and lime (*Citrus aurantifolia*)	see Bub et al. [91]	see Bub et al. [91]	additional analysis on samples collected from Bub et al.[91]	↓ hGSTP1 protein levels after weeks 4 and 6 but ↑ levels at week 8	∓[b]	modulation of human GST protein after juice supplementation in leucocytes was not reflected in GST gene expression in leucocytes treated with juice in vitro; in vivo, however, GST proteins was related to ↓ DNA damage	109
			GST activity and DNA damage	↑ hGSTP1 levels correlate with ↓ levels of DNA damage	+[b]		
			gene expression of phase II enzymes from leucocytes treated with polyphenol-rich juice in vitro	no change in GST genes was observed in leucocytes in vitro but up-regulation of cyp P450 enzymes and sulfotransferase enzymes was observed for B but not for A	+[b]		
commercially available cranberry (*Vaccinium oxycoccos*) juice	20 healthy female volunteers	parallel study	antioxidant status of plasma	↑ with CJ compared to placebo	+[b]	CJ supplementation increased antioxidant status of blood due to vitamin C content of CJ, but did not ↓ endoge-	110

dx.doi.org/10.1021/jf4050759 | J. Agric. Food Chem. 2014, 62, 3852−3866

Table 3. continued

berry or berry constituent	subjects	dose and exposure	end point	observation	protective/adverse effect	comment	ref
		750 mL/day 2 weeks of cranberry (n = 11) or placebo juice (n = 9)	phase II enzyme activity	no difference in GSH-Px, CAT, or SOD activity	−	nous or induced DNA damage	
			urinary 8-OHdG endogenous and H_2O_2-induced DNA damage	no effect on 8-OHdG levels	−		
				no effect on endogenous or induced DNA damage in lymphocytes	−		
red mixed berry juice (red grape juice (40%), blackberry juice (20%), sour cherry juice (15%), black currant juice (15%), and elderberry juice (10%))	27 healthy male volunteers	parallel study	comet assay, endogenous and H_2O_2-induced DNA damage	↓ in H_2O_2-induced DNA damage in lymphocytes	+[b]	4 weeks of red mixed berry juice consumption induced a significant decrease in DNA damage in MNBCs	101
		700 mL of red berry juice pd for 4 weeks (n = 18)		↑ in reduced glutathione levels	+[b]		
		control juice for 4 weeks (n = 9)					
		3 week washout					
red mixed berry juice (red grape juice (40%), blackberry juice (20%), sour cherry juice (15%), black currant juice (15%), and elderberry juice (10%))	21 hemodialysis patients	parallel study	comet assay, endogenous and H_2O_2-induced DNA damage and (FPG sites)	↓ in H_2O_2 induced DNA damage in lymphocytes	+[b]	4 weeks of red mixed berry juice consumption induced a significant decrease in DNA damage in MNBCs	102
		200 mL/day red berry juice for 4 weeks (n = 18)		↑ in reduced glutathione levels	+[b]		
		control juice for 4 weeks (n = 9)					
		3 week washout					
blueberries (*Vaccinium corymbosun*)	16 healthy females volunteers	blueberry/apple juice 1 L/day for 4 weeks containing 34 mg quercetin/L	comet assay, endogenous and H_2O_2-induced DNA damage	↓ in H_2O_2 induced DNA damage (40%) in lymphocytes (p = 0.07)	+	4 weeks of blueberry/apple juice consumption induced a significant increase in antioxidant activity	113
		1.5 mg quercetin	plasma antioxidant capacity, TEAC assay	10% ↑ in antioxidant activity	+[b]	study had no concurrent control group	
				no effect in ex vivo induced DNA adducts (BPDE)			
black currant (*Ribes nigrum*) juice, anthocyanin drink	57 healthy volunteers	parallel study, 3 groups	comet assay, endogenous and H_2O_2-induced DNA damage and (Endo III sites, FPG sites)	no difference in DNA damage within MNBCs within any of the three groups	−	anthocyanin drink and black currant juice have shown no antigenotoxic effects	112
		(a) black currant juice (n = 18)		no change in Endo III sites	−	increase in FPG sites suggests an adverse effect, which is speculated to be due to excess vitamin C	
		(b) anthocyanin drink (n = 20)		↑ in FPG sensitive sites within the black currant juice group	−		
		(c) placebo (n = 19) for 3 weeks					
		daily dose was dependent upon body weight (475−1000 mL/day)					
polyphenol-rich juices	27 healthy male volunteers	crossover juice A or B	antioxidant status of plasma	↓ oxidative potential of plasma using TBARS measurement only	+[b]	a time delay was observed between juice intake and a measurable change in physiological function with both	107

dx.doi.org/10.1021/jf4050759 | J. Agric. Food Chem. 2014, 62, 3852−3866

Table 3. continued

berry or berry constituent	subjects	dose and exposure	end point	observation	protective/adverse effect	comment	ref
						A and B having a similar effect during the second period	
A = aronia, blueberry (*Vaccinium corymbosum*) and boysenberry (*Rubus ursinus* × *idaeus*)		weeks 1−2 run in	comet assay, endogenous and H_2O_2-induced DNA damage and (Endo III sites, FPG sites) immune status	no effect on strand breaks	−	no concurrent control group	
B = green tea (*Camellia sinensis*), apricot (*Prunus armeniaca*) and lime (*Citrus aurantifolia*)		weeks 3−4 juice A or B 330 mL/day		after second supplementation period with juice A or B ↓ in oxidized bases observed	+[b]		
		weeks 5−6 washout		both A and B IL-2 secretion	+[b]		
		weeks 7−8 juice B or A 330 mL/day					
		weeks 9−10 washout					

[a] ↓, decrease; ↑, increase; MNBC, mononuclear blood cells; BPDE, benzo(a)pyrene-diol-epoxide; Endo III, endonuclease III; FPG, formamidopyrimidine DNA glycosylase; TEAC, Trolox equivalent antioxidant capacity; SNP, single nucleotide polymorphism; TBARS, thiobarbituric acid reactive substances; GSH-Px, glutathione peroxidase; CAT, catalase; SOD, superoxide dismutas;. 8-OHdG, 8-hydroxy-2′-deoxyguanosine; GST, glutathione-*S*-transferase; hGSTP1, human glutathione-*S*-transferase P1 [b]Significant result. +, protective effect; − adverse effect.

importance of establishing an individual's (poly)phenol metabolizing phenotype or gut metabotype will become of increasing relevance in studies of colon cancer.[115,116]

To conclude, there is clearly extensive evidence from in vitro studies and animal models that berry extracts modulate biomarkers of DNA damage and that these effects may be potentially chemoprotective due to the role that oxidative damage likely plays in mutation rate and cancer risk. However, because the studies use berry extracts, it is difficult to determine which phytochemicals are responsible and whether for the most part the dose would be nutritionally achievable. Although the dietary intervention trials with berries are generally consistent and indicate a capacity to significantly decrease oxidative damage to DNA, they in themselves represent only weak evidence for anticarcinogenicity as they rely on surrogate putative markers for cancer risk. To understand the protective effects of berry consumption on colorectal cancer risk, future studies will need to be well controlled, using suitable and clinically relevant end points to support the tentative emerging evidence for a protective effect.

AUTHOR INFORMATION

Corresponding Author

*(C.I.R.G.) Phone: +44 (0) 28 70123181. Fax: +44 (0) 28 70122023. E-mail: C.Gill@ulster.ac.uk.

Funding

C.G. and A.C. acknowledge funding from the National Processed Raspberry Council. D.S. and G.McD. acknowledge funding from the following sources: Scottish Government Rural and Environment Science and Analytical Services Division, Climafruit (Interreg IVB), EUBerry (EU FP7 KBBE 2010 Grant 4265942), and BACHBERRY (EU FP7 KBBE 2013 Grant 613793)

Notes

The authors declare no competing financial interest.

REFERENCES

(1) Stewart, B. W., Kleihues, P., Eds. *World Cancer Report*; IARC Press: Lyon, France, 2003.

(2) Aune, D.; Chan, D. S.; Lau, R.; Vieira, R.; Greenwood, D. C.; Kampman, E.; Norat, T. Dietary fibre, whole grains, and risk of colorectal cancer: systematic review and dose-response meta-analysis of prospective studies. *BMJ* **2011**, *343*, d6617.

(3) Johnson, C. M.; Wei, C.; Ensor, J. E.; Smolenski, D. J.; Amos, C. I.; Levin, B.; Berry, D. A. Meta-analyses of colorectal cancer risk factors. *Cancer Causes Control* **2013**, *24*, 1207−1222.

(4) Deighton, N.; Brennan, R.; Finn, C.; Davies, H. V. Antioxidant properties of domesticated and wild *Rubus* species. *J. Sci. Food Agric.* **2000**, *80*, 1307−1313.

(5) Anttonen, M. J.; Karjalainen, R. O. Environmental and genetic variation of phenolic compounds in red raspberry. *J. Food Compos. Anal.* **2005**, *18*, 759−769.

(6) Mikulic-Petkovsek, M.; Schmitzer, V.; Slatnar, A.; Stampar, F.; Veberic, R. Composition of sugars, organic acids, and total phenolics in 25 wild or cultivated berry species. *J. Food Sci.* **2012**, *77*, C1064−1070.

(7) Castrejón, D. R.; Eichholz, I.; Rohn, S.; Kroh, L. W.; Huyskens-Keil, S. Phenolic profile and antioxidant activity of highbush blueberry (*Vaccinium corymbosum* L.) during fruit maturation and ripening. *Food Chem.* **2008**, *109*, 564−572.

(8) Häkkinen, S. H.; Kärenlampi, S. O.; Mykkänen, H. M.; Törrönen, A. R. Influence of domestic processing and storage on flavonol contents in berries. *J. Agric. Food Chem.* **2000**, *48*, 2960−2965.

(9) Connor, A. M.; Luby, J. J.; Hancock, J. F.; Berkheimer, S.; Hanson, E. J. Changes in fruit antioxidant activity among blueberry

cultivars during cold-temperature storage. *J. Agric. Food Chem.* **2002**, *50*, 893−898.
(10) Seeram, N. P. Berry fruits for cancer prevention: current status and future prospects. *J. Agric. Food Chem.* **2008**, *56*, 630−635.
(11) Seeram, N. P. Berries. In *Nutritional Oncology*, 2nd ed.; Heber, D., Blackburn, G., Go, V. L. W., Milner, J., Eds.; Academic Press: London, UK, 2006; pp 615−625.
(12) Liu, R. H. Health benefits of fruit and vegetables are from additive and synergistic combinations of phytochemicals. *Am. J. Clin. Nutr.* **2003**, *78*, 517S−520S.
(13) Crozier, A.; Jaganath, I. B.; Clifford, M. N. Dietary phenolics: chemistry, bioavailability and effects on health. *Nat. Prod. Rep.* **2009**, *26*, 1001−1043.
(14) Manach, C.; Scalbert, A.; Morand, C.; Rémésy, C.; Jiménez, L. Polyphenol: food sources and bioavailability. *Am. J. Clin. Nutr.* **2004**, *79*, 727−747.
(15) Rothwell, J. A.; Perez-Jimenez, J.; Neveu, V.; Medina-Remón, A.; M'hiri, N.; García-Lobato, P.; Manach, C.; Knox, C.; Eisner, R.; Wishart, D. S.; Scalbert, A. Phenol-Explorer 3.0: a major update of the Phenol-Explorer database to incorporate data on the effects of food processing on polyphenol content. *Database (Oxford)* **2013**, 2013:bat070, DOI: 10.1093/database/bat070.
(16) Pérez-Jiménez, J.; Fezeu, L.; Touvier, M.; Arnault, N.; Manach, C.; Hercberg, S.; Galan, P.; Scalbert, A. Dietary intake of 337 polyphenols in French adults. *Am. J. Clin. Nutr.* **2011**, *3*, 1220−1228.
(17) Ovaskainen, M. L.; Törrönen, R.; Koponen, J. M.; Sinkko, H.; Hellström, J.; Reinivuo, H.; Mattila, P. Dietary intake and major food sources of polyphenols in Finnish adults. *J. Nutr.* **2008**, *138*, 562−566.
(18) Gonzalez-Barrio, R.; Borges, G.; Mullen, W.; Crozier, A. Bioavailability of raspberry anthocyanins and ellagitannins following consumption of raspberries by healthy humans and subjects with an ileostomy. *J. Agric. Food Chem.* **2010**, *58*, 3933−3939.
(19) González-Barrio, R.; Edwards, C. A.; Crozier, A. Colonic catabolism of ellagitannins, ellagic acid and raspberry anthocyanins: in vivo and in vitro studies. *Drug Metab. Dispos.* **2011**, *39*, 1680−1688.
(20) Johnson, I. T. New approaches to the role of diet in the prevention of cancers in the alimentary tract. *Mutat. Res.* **2004**, *551*, 9−28.
(21) Del Rio, D.; Borges, G.; Crozier, A. Berry flavonoids and phenolics: bioavailability and evidence of protective effects. *Br. J. Nutr.* **2010**, *104* (Suppl. 3), S67−S90.
(22) Gill, C. I. R.; McDougall, G. J.; Glidewell, S.; Steward, D.; Tuohy, K.; Shen, Q.; Dobbin, A.; Boyd, A.; Brown, E. M.; Haldar, S.; Rowland, I. Profiling of phenols in human fecal water after raspberry supplementation. *J. Agric. Food Chem.* **2010**, *58*, 10389−10395.
(23) Tuohy, K. M.; Conterno, L.; Gasperotti, M.; Viola, R. Up-regulating the human intestinal microbiome using whole plant foods, polyphenols, and/or fiber. *J. Agric. Food Chem.* **2012**, *60*, 8776−8782.
(24) Brown, E. M.; Gill, C. I.; McDougall, G. J.; Stewart, D. Mechanisms underlying the anti-proliferative effects of berry components in in vitro models of colon cancer. *Curr. Pharm. Biotechnol.* **2012**, *13*, 200−209.
(25) Xiao, H.; Lüi, F.; Stewart, D.; Zhang, Y. Mechanisms underlying chemopreventive effects of flavonoids via multiple signalling nodes within Nrf2-ARE and AhR-XRE gene regulatory networks. *Curr. Chem. Biol.* **2013**, *7*, 2212−7968.
(26) Fearon, E. R.; Vogelstein, B. A genetic model for colorectal tumorigenesis. *Cell* **1990**, *61*, 759−767.
(27) Soobrattee, M. A.; Bahorun, T.; Aruom, O. I. Chemopreventive actions of polyphenolic compounds in cancer. *Biofactors* **2006**, *27*, 19−35.
(28) Kim, E. K.; Choi, E. J. Pathological roles of MAPK signalling pathways in human diseases. *Biochim. Biophys. Acta* **2010**, *1802*, 396−405.
(29) Friedberg, E. C.; Aguilera, A.; Gellert, M.; Hanawalt, P. C.; Hays, J. B.; Lehmann, A. R.; Lindahl, T.; Lowndes, N.; Sarasin, A.; Wood, R. D. DNA repair: from molecular mechanism to human disease. *DNA Repair* **2006**, *5*, 986−996.
(30) Winczura, A.; Zdżalik, D.; Tudek, B. Damage of DNA and proteins by major lipid peroxidation products in genome stability. *Free Radical Res.* **2012**, *46*, 442−459.
(31) Barnes, D. E.; Lindahl, T. Repair and genetic consequences of endogenous DNA base damage in mammalian cells. *Annu. Rev. Genet.* **2004**, *38*, 445−476.
(32) Halliwell, B.; Aruoma, O. I. DNA damage by oxygen-derived species. Its mechanism and measurement in mammalian systems. *FEBS Lett.* **1991**, *281*, 9−19.
(33) Dröge, W. Free radicals in the physiological control of cell function. *Physiol. Rev.* **2002**, *82*, 47−95.
(34) Osaki, M.; Oshimura, M.; Ito, H. PI3K-Akt pathway: its functions and alterations in human cancer. *Apoptosis* **2004**, *9*, 667−676.
(35) Horbinski, C.; Chu, C. T. Kinase signaling cascades in the mitochondrion: a matter of life or death. *Free Radical Biol. Med.* **2005**, *38*, 2−11.
(36) Aaronson, D. S.; Horvath, C. M. A road map for those who don't know JAK-STAT. *Science* **2002**, *31*, 1653−1655.
(37) Chen, F. JNK-induced apoptosis, compensatory growth, and cancer stem cells. *Cancer Res.* **2012**, *2*, 379−386.
(38) Aguilera, A.; Gómez-González, B. Genome instability: a mechanistic view of its causes and consequences. *Nat. Rev. Genet.* **2008**, *9*, 204−217.
(39) Waldmann, P.; Bohnenberger, S.; Greinert, R.; Hermann-Then, B.; Heselich, A.; Klug, S. J.; Koenig, J.; Kuhr, K.; Kuster, N.; Merker, M.; Murbach, M.; Pollet, D.; Schadenboeck, W.; Scheidemann-Wesp, U.; Schwab, B.; Volkmer, B.; Weyer, V.; Blettner, M. Influence of GSM signals on human peripheral lymphocytes: study of genotoxicity. *Radiat. Res.* **2013**, *179*, 243−253.
(40) Singh, N. P.; McCoy, M. T.; Tice, R. R.; Schneider, E. L. A simple technique for quantitation of low-levels of DNA damage in individual cells. *Exp. Cell Res.* **1998**, *175*, 184−191.
(41) Collins, A. R. The use of bacterial repair endonucleases in the Comet assay. *Methods Mol. Biol.* **2011**, *691*, 137−147.
(42) Glei, M.; Schaeferhenrich, A.; Claussen, U.; Kuechler, A.; Liehr, T.; Weise, A.; Marian, B.; Sendt, W.; Pool-Zobel, B. L. Comet fluorescence in situ hybridization analysis for oxidative stress-induced DNA damage in colon cancer relevant genes. *Toxicol. Sci.* **2007**, *96*, 279−284.
(43) Schlörmann, W.; Glei, M. Detection of DNA damage by comet fluorescence in situ hybridization. *Methods Mol. Biol.* **2012**, *920*, 91−100.
(44) Collins, A. R. Measuring oxidative damage to DNA and its repair with the comet assay. *Biochim. Biophys. Acta* **2014**, *1840*, 794−800.
(45) McKenna, D. J.; McKeown, S. R.; McKelvey-Martin, V. J. Potential use of the comet assay in the clinical management of cancer. *Mutagenesis* **2008**, *23*, 183−90.
(46) Clague, J.; Shao, L.; Lin, J.; Chang, S.; Zhu, Y.; Wang, W.; Wood, C. G.; Wu, X. Sensitivity to NNKOAc is associated with renal cancer risk. *Carcinogenesis* **2009**, *30*, 706−710.
(47) Ersson, C.; Møller, P.; Forchhammer, L.; Loft, S.; Azqueta, A.; Godschalk, R. W.; van Schooten, F. J.; Jones, G. D.; Higgins, J. A.; Cooke, M. S.; Mistry, V.; Karbaschi, M.; Phillips, D. H.; Sozeri, O.; Routledge, M. N.; Nelson-Smith, K.; Riso, P.; Porrini, M.; Matullo, G.; Allione, A.; Stepnik, M.; Ferlińska, M.; Teixeira, J. P.; Costa, S.; Corcuera, L. A.; López de Cerain, A.; Laffon, B.; Valdiglesias, V.; Collins, A. R.; Möller, L. An ECVAG inter-laboratory validation study of the comet assay: inter-laboratory and intra-laboratory variations of DNA strand breaks and FPG-sensitive sites in human mononuclear cells. *Mutagenesis* **2013**, *28*, 279−286.
(48) Valavanidis, A.; Vlachogianni, T.; Fiotakis, C. 8-Hydroxy-2′-deoxyguanosine (8-OHdG): a critical biomarker of oxidative stress and carcinogenesis. *J. Environ. Sci. Health C: Environ. Carcinog. Ecotoxicol. Rev.* **2009**, *27*, 120−139.
(49) Niki, E. Biomarkers of lipid peroxidation in clinical material. *Biochim. Biophys. Acta* **2014**, *1840*, 809−817.

(50) Yoshida, Y.; Umeno, A.; Shichiri, M. Lipid peroxidation biomarkers for evaluating oxidative stress and assessing antioxidant capacity in vivo. *J. Clin. Biochem. Nutr.* **2013**, *52*, 9−16.
(51) Wang, S. Y.; Jiao, H. Scavenging capacity of berry crops on superoxide radicals, hydrogen peroxide, hydroxyl radicals, and singlet oxygen. *J. Agric. Food Chem.* **2000**, *48*, 5677−5684.
(52) Zhang, Y.; Seeram, P.; Lee, R.; Fend, L.; Heber, D. Isolation and identification of strawberry phenolics with antioxidant and human cancer cell antiproliferative properties. *J. Agric. Food Chem.* **2008**, *56*, 670−675.
(53) Elisia, I.; Kitts, D. D. Anthocyanins inhibit peroxyl radical-induced apoptosis in Caco-2 cells. *Mol. Cell. Biochem.* **2008**, *312*, 139−45.
(54) Schantz, M.; Mohn, C.; Baum, M.; Richling, E. Antioxidative efficiency of an anthocyanin rich bilberry extract in the human colon tumour cell lines Caco-2 and HT-29. *J. Berry Res.* **2010**, *1*, 25−33.
(55) Bornsek, S. M.; Lovro, Z.; Polak, T.; Vanzo, A.; Ulrich, N. P.; Abram, V.; Tramer, F.; Passamonti, S. Bilberry and blueberry anthocyanins act as powerful intracellular antioxidants in mammalian cells. *Food Chem.* **2012**, *134*, 1878−1884.
(56) Slemmer, J. E.; Livingston-Thomas, J. M.; Gottschall-Pass, K. T.; Sweeney, M. I. Cranberries and wild blueberries treated with gastrointestinal enzymes positively modify glutathione mechanisms in Caco-2 cells in vitro. *J. Food Sci.* **2013**, *78*, H943−H947.
(57) Forman, H. J.; Torres, M.; Fukuto, J. Redox signaling. *Mol. Cell. Biochem.* **2002**, *234−235*, 49−62.
(58) Duthie, S. J.; Dobson, V. L. Dietary flavonoids protect human colonocyte DNA from oxidative attack in vitro. *Eur. J. Nutr.* **1999**, *38*, 28−34.
(59) Duthie, S. J.; Gardner, P. T.; Morrice, P. C.; Wood, S. G.; Pirie, L.; Bestwick, C. C.; Milne, L.; Duthie, G. G. DNA stability and lipid peroxidation in vitamin E-deficient rats in vivo and colon cells in vitro − modulation by the dietary anthocyanin, cyanidin-3-glycoside. *Eur. J. Nutr.* **2005**, *44*, 195−203.
(60) Coates, E. M.; Popa, G.; Gill, C. I.; McCann, M. J.; McDougall, G. J.; Stewart, D.; Rowland, I. Colon-available raspberry polyphenols exhibit anti-cancer effects on in vitro models of colon cancer. *J. Carcinog.* **2007**, *18*, 4−17.
(61) Aiyer, H. S.; Vadhanam, M. V.; Stoyanova, R.; Caprio, G. D.; Clapper, M. L.; Gupta, R. C. Dietary berries and ellagic acid prevent oxidative DNA damage and modulate expression of DNA repair genes. *Int. J. Mol. Sci.* **2008**, *9*, 327−341.
(62) Min, K.; Ebeler, S. E. Quercetin inhibits hydrogen peroxide-induce DNA damage and enhances DNA repair in Caco2-cells. *Food Toxicol.*. **2009**, *47*, 2716−2722.
(63) Ramos, A. A.; Pereira-Wilson, C.; Collins, A. R. Protective effects of ursolic acid and luteolin against oxidative DNA damage include enhancement of DNA repair in Caco-2 cells. *Mutat. Res.* **2010**, *692*, 6−11.
(64) Brown, E. M.; McDougall, G. J.; Stewart, D.; Pereira-Caro, G.; Gonzalez-Barrio, R.; Allsopp, P.; Magee, P.; Crozier, A.; Rowland, I.; Gill, C. I. Persistence of anticancer activity in berry extracts after simulated gastrointestinal digestion and colonic fermentation. *PLoS One* **2012**, *7*, 1−10.
(65) Seo, Y. R.; Fishel, M. L.; Amundson, S.; Kelley, M. R.; Smith, M. L. Implication of p53 in base excision DNA repair: in vivo evidence. *Oncogene* **2002**, *21*, 731−737.
(66) González-Barrio, R.; Borges, G.; Mullen, W.; Crozier, A. Bioavailability of anthocyanins and ellagitannins following consumption of raspberries by healthy humans and subjects with an ileostomy. *J. Agric. Food Chem.* **2010**, *58*, 3933−3939.
(67) González-Barrio, R.; Edwards, C. A.; Crozier, A. Colonic catabolism of ellagitannins, ellagic acid, and raspberry anthocyanins: in vivo and in vitro studies. *Drug Metab. Dispos.* **2011**, *39*, 1680−1688.
(68) Aura, A. M. Microbial metabolism of dietary phenolic compounds in the colon. *Phytochem. Rev.* **2008**, *7*, 407−429.
(69) Nurmi, T.; Mursu, J.; Heinone, M.; Nurmi, A.; Hiltunen, R.; Voutilainen, S. Metabolism of berry anthocyanins to phenolic acids in humans. *J. Agric. Food Chem.* **2009**, *57*, 2274−2281.
(70) Gao, K.; Xu, A.; Krul, C.; Venema, K.; Liu, Y.; Niu, Y.; Lu, J.; Bensoussan, L.; Seeram, N. P.; Heber, D.; Henning, S. M. Of the major phenolic acids formed during human microbial fermentation of tea, citrus, and soy flavonoid supplements, only 3,4-dihydroxyphenylacetic acid has antiproliferative activity. *J. Nutr.* **2006**, *136*, 52−57.
(71) Larossa, M.; Luceri, C.; Vivoli, E.; Pagliuca, C.; Lodovici, M.; Moneti, G.; Dolara, P. Polyphenol metabolites from colonic microbiota exert anti-inflammatory activity on different inflammation models. *Mol. Nutr. Food Res.* **2009**, *53*, 1044−1054.
(72) Giménez-Bastida, J. A.; Larrosa, M.; González-Sarrías, A.; Tomás-Barberán, F.; Espín, J. C.; García-Conesa, M. T. Intestinal ellagitannin metabolites ameliorate cytokine-induced inflammation and associated molecular markers in human colon fibroblasts. *J. Agric. Food Chem.* **2012**, *60*, 8866−8876.
(73) Raju, J. Azoxymethane-induced rat aberrant crypt foci: relevance in studying chemoprevention of colon cancer. *World J. Gastroenterol.* **2008**, *14*, 6632−6635.
(74) Shao, J.; Sheng, H.; Aramandla, R.; Pereira, M. A.; Lubet, R. A.; Hawk, E.; Grogan, L.; Kirsch, I. R.; Washington, M. K.; Beauchamp, R. D.; DuBois, R. N. Coordinate regulation of cyclooxygenase-2 and TGF-β1 in replication error-positive colon cancer and azoxymethane-induced rat colonic tumors. *Carcinogenesis* **1999**, *20*, 18−91.
(75) Su, L. K.; Kinzler, K. W.; Vogelstein, B.; Preisinger, A. C.; Moser, A. R.; Luongo, C.; Gould, K. A.; Dove, W. F. Multiple intestinal neoplasia caused by a mutation in the murine homolog of the APC gene. *Science* **1992**, *256*, 668−670.
(76) Salobir, J.; Zontar, T. P.; Levart, A.; Rezar, V. The comparison of black currant juice and vitamin E for the prevention of oxidative stress. *Int. J. Vitam. Nutr. Res.* **2010**, *80*, 5−11.
(77) Zhang, X.; Ishida, R.; Yuhara, Y.; Kamiya, T.; Hatano, T.; Okamoto, G.; Arimoto-Kobayashi, S. Anti-genotoxic activity of *Vitis coignetiae* Pulliat towards heterocyclic amines and isolation and identification of caftaric acid as an antimutagenic component of the juice. *Mutat. Res.* **2011**, *723*, 182−189.
(78) Kensler, T. W. Chemoprevention by inducers of carcinogen detoxification enzymes. *Environ. Health Perspect.* **1997**, *105*, 965−970.
(79) Boateng, J.; Verghese, M.; Shackelford, L.; Walker, L. T.; Khatiwada, J.; Ogutu, S.; Williams, D. S.; Jones, J.; Guyton, M.; Asiamah, D.; Henderson, F.; Grant, L.; DeBruce, M.; Johnson, A.; Washington, S.; Chawan, C. B. Selected fruits reduce azoxymethane (AOM)-induced aberrant crypt foci (ACF) in Fisher 344 male rats. *Food. Chem. Toxicol.* **2007**, *45*, 725−732.
(80) Kamiya, H. Mutagenicity of oxidized DNA precursors in living cells: roles of nucleotide pool sanitization and DNA repair enzymes, and translesion synthesis DNA polymerases. *Mutat. Res.* **2010**, *703*, 32−36.
(81) Harris, G. K.; Gupta, A.; Nines, R. G.; Kresty, L. A.; Habib, S. G.; Frankel, W. L.; LaPerle, K.; Gallaher, D. D.; Schwartz, S. J.; Stoner, G. D. Effects of lyophilized black raspberries on azoxymethane-induced colon cancer and 8-hydroxy-2′-deoxyguanosine levels in the Fischer 344 rat. *Nutr. Cancer* **2001**, *40*, 125−133.
(82) Lala, G.; Malik, M.; Zhao, C.; He, J.; Kwon, Y.; Giusti, M. M.; Magnuson, B. A. Anthocyanin-rich extracts inhibit multiple biomarkers of colon cancer in rats. *Nutr. Cancer* **2006**, *54*, 84−93.
(83) Cooke, D.; Schwarz, M.; Boocock, D.; Winterhalter, P.; Steward, W. P.; Gescher, A. J.; Marczylo, T. H. Effect of cyanidin-3-glucoside and an anthocyanin mixture from bilberry on adenoma development in the ApcMin mouse model of intestinal carcinogenesis − relationship with tissue anthocyanin levels. *Int. J. Cancer* **2006**, *119*, 2213−2220.
(84) Suh, N.; Paul, S.; Hao, X.; Simi, B.; Xiao, H.; Rimando, A. M.; Reddy, B. S. Pterostilbene, an active constituent of blueberries, suppresses aberrant crypt foci formation in the azoxymethane-induced colon carcinogenesis model in rats. *Clin.. Cancer Res.* **2007**, *13*, 350−355.
(85) Murakami, A.; Ohigashi, H. Targeting NOX, INOS and COX-2 in inflammatory cells: chemoprevention using food phytochemicals. *Int. J. Cancer* **2007**, *121*, 2357−2363.
(86) Serra, D.; Paixão, J.; Nunes, C.; Dinis, T. C.; Almeida, L. M. Cyanidin-3-glucoside suppresses cytokine-induced inflammatory re-

sponse in human intestinal cells: comparison with 5-aminosalicylic acid. *PLoS One* **2013**, *8*, e73001.
(87) Hino, S.; Sonoyama, K.; Bito, H.; Kawagishi, H.; Aoe, S.; Morita, T. Low-methoxyl pectin stimulates small intestinal mucin secretion irrespective of goblet cell proliferation and is characterized by jejunum Muc2 upregulation in rats. *Nutrition* **2013**, *143*, 34−40.
(88) Bi, X.; Fang, W.; Wang, L. S.; Stoner, G. D.; Yang, W. Black raspberries inhibit intestinal tumorigenesis in apc1638± and Muc2−/− mouse models of colorectal cancer. *Cancer Prev. Res.* **2010**, *3*, 1443−1450.
(89) Gill, C. I.; Rowland, I. R. Diet and cancer: assessing the risk. *Br. J. Nutr.* **2002**, *88*, S73−S87.
(90) Spencer, J. P.; Abd, E. l.; Mohsen, M. M.; Minihane, A. M.; Mathers, J. C. Biomarkers of the intake of dietary polyphenols: strengths, limitations and application in nutrition research. *Br. J. Nutr.* **2008**, *99*, 12−22.
(91) Del Rio, D.; Rodriguez-Mateos, A.; Spencer, J. P.; Tognolini, M.; Borges, G.; Crozier, A. Dietary (poly)phenolics in human health: structures, bioavailability, and evidence of protective effects against chronic diseases. *Antioxid. Redox Signal.* **2013**, *18*, 1818−1892.
(92) Pool-Zobel, B. L.; Dornacher, I.; Lambertz, R.; Knoll, M.; Seitz, H. K. Genetic damage and repair in human rectal cells for biomonitoring: sex differences, effects of alcohol exposure, and susceptibilities in comparison to peripheral blood lymphocytes. *Mutat. Res.* **2004**, *551*, 127−134.
(93) Wang, L. S.; Arnold, M.; Huang, Y. W.; Sardo, C.; Seguin, C.; Martin, E.; Huang, T. H.; Riedl, K.; Schwartz, S.; Frankel, W.; Pearl, D.; Xu, Y.; Winston, J., 3rd; Yang, G. Y.; Stoner, G. Modulation of genetic and epigenetic biomarkers of colorectal cancer in humans by black raspberries: a phase I pilot study. *Clin. Cancer Res.* **2011**, *17*, 598−610.
(94) Mentor-Marcel, R. A.; Bobe, G.; Sardo, C.; Wang, L. S.; Kuo, C. T.; Stoner, G.; Colburn, N. H. Plasma cytokines as potential response indicators to dietary freeze-dried black raspberries in colorectal cancer patients. *Nutr. Cancer* **2012**, *64*, 820−825.
(95) Wang, L. S.; Kuo, C. T.; Cho, S. J.; Seguin, C.; Siddiqui, J.; Stoner, K.; Weng, Y. I.; Huang, T. H.; Tichelaar, J.; Yearsley, M.; Stoner, G. D.; Huang, Y. W. Black raspberry-derived anthocyanins demethylate tumor suppressor genes through the inhibition of DNMT1 and DNMT3B in colon cancer cells. *Nutr. Cancer* **2013**, *65*, 118−125.
(96) Thomasset, S.; Berry, D. P.; Cai, H.; West, K.; Marczylo, T. H.; Marsden, D.; Brown, K.; Dennison, A.; Garcea, G.; Miller, A.; Hemingway, D.; Steward, W. P.; Gescher, A. J. Pilot study of oral anthocyanins for colorectal cancer chemoprevention. *Cancer Prev. Res.* **2009**, *2*, 625−633.
(97) Alotaibi, A.; Bhatnagar, P.; Najafzadeh, M.; Gupta, K. C.; Anderson, D. Tea phenols in bulk and nanoparticle form modify DNA damage in human lymphocytes from colon cancer patients and healthy individuals treated in vitro with platinum-based chemotherapeutic drugs. *Nanomedicine* **2013**, *8*, 389−401.
(98) Del Bo, C.; Riso, P.; Campolo, J.; Møller, P.; Loft, S.; Klimis-Zacas, D.; Brambilla, A.; Rizzolo, A.; Porrini, M. A single portion of blueberry (*Vaccinium corymbosum* L) improves protection against DNA damage but not vascular function in healthy male volunteers. *Nutr. Res. (N.Y.)* **2013**, *33*, 220−227.
(99) Riso, P.; Klimis-Zacas, D.; Del Bo, C.; Martini, D.; Campolo, J.; Vendrame, S.; Møller, P.; Loft, S.; De Maria, R.; Porrini, M. Effect of a wild blueberry (*Vaccinium angustifolium*) drink intervention on markers of oxidative stress, inflammation and endothelial function in humans with cardiovascular risk factors. *Eur. J. Nutr.* **2013**, *52*, 949−961.
(100) Wilms, L. C.; Boots, A. W.; de Boer, V. C.; Maas, L. M.; Pachen, D. M.; Gottschalk, R. W.; Ketelslegers, H. B.; Godschalk, R. W.; Haenen, G. R.; van Schooten, F. J.; Kleinjans, J. C. Impact of multiple genetic polymorphisms on effects of a 4-week blueberry juice intervention on ex vivo induced lymphocytic DNA damage in human volunteers. *Carcinogenesis* **2007**, *28*, 1800−1806.
(101) Weisel, T.; Baum, M.; Eisenbrand, G.; Dietrich, H.; Will, F.; Stockis, J. P.; Kulling, S.; Rüfer, C.; Johannes, C.; Janzowski, C. An anthocyanin/polyphenolic-rich fruit juice reduces oxidative DNA damage and increases glutathione level in healthy probands. *Biotechnol. J .* **2006**, *1*, 388−397.
(102) Spormann, T. M.; Albert, F. W.; Rath, T.; Dietrich, H.; Will, F.; Stockis, J. P.; Eisenbrand, G.; Janzowski, C. Anthocyanin/polyphenolic-rich fruit juice reduces oxidative cell damage in an intervention study with patients on hemodialysis. *Cancer Epidemiol. Biomarkers Prev.* **2008**, *17*, 3372−3380.
(103) Szeto, Y. T.; Benzie, I. F.; Collins, A. R.; Choi, S. W.; Cheng, C. Y.; Yow, C. M.; Tse, M. M. A buccal cell model comet assay: development and evaluation for human biomonitoring and nutritional studies. *Mutat. Res.* **2005**, *578*, 371−381.
(104) Riso, P.; Visioli, F.; Gardana, C.; Grande, S.; Brusamolino, A.; Galvano, F.; Galvano, G.; Porrini, M. Effects of blood orange juice intake on antioxidant bioavailability and on different markers related to oxidative stress. *J. Agric. Food Chem.* **2005**, *53*, 941−947.
(105) Park, Y. K.; Lee, S. H.; Park, E.; Kim, J. S.; Kang, M. H. Changes in antioxidant status, blood pressure, and lymphocyte DNA damage from grape juice supplementation. *Ann. N.Y. Acad. Sci.* **2009**, *1171*, 385−390.
(106) Park, Y. K.; Park, E.; Kim, J. S.; Kang, M. H. Daily grape juice consumption reduces oxidative DNA damage and plasma free radical levels in healthy Koreans. *Mutat. Res.* **2003**, *529*, 77−86.
(107) Bub, A.; Watzl, B.; Blockhaus, M.; Briviba, K.; Liegibel, U.; Müller, H.; Pool-Zobel, B. L.; Rechkemmer, G. Fruit juice consumption modulates antioxidative status, immune status and DNA damage. *J. Nutr. Biochem.* **2003**, *14*, 90−98.
(108) Grubben, M. J.; Nagengast, F. M.; Katan, M. B.; Peters, W. H. The glutathione biotransformation system and colorectal cancer risk in humans. *Scand. J. Gastroenterol.* **2001**, *234*, 68−76.
(109) Hofmann, T.; Liegibel, U.; Winterhalter, P.; Bub, A.; Rechkemmer, G.; Pool-Zobel, B. L. Intervention with polyphenol-rich fruit juices results in an elevation of glutathione *S*-transferase P1 (hGSTP1) protein expression in human leucocytes of healthy volunteers. *Mol. Nutr. Food Res.* **2006**, *50*, 1191−1200.
(110) Duthie, S. J.; Jenkinson, A. M.; Crozier, A.; Mullen, W.; Pirie, L.; Kyle, J.; Yap, L. S.; Christen, P.; Duthie, G. G. The effects of cranberry juice consumption on antioxidant status and biomarkers relating to heart disease and cancer in healthy human volunteers. *Eur. J. Nutr.* **2006**, *45*, 113−122.
(111) Carmen Ramirez-Tortosa, M.; García-Alonso, J.; Luisa Vidal-Guevara, M.; Quiles, J. L.; Jesús Periago, M.; Linde, J.; Dolores Mesa, M.; Ros, G.; Abellán, P.; Gil, A. Oxidative stress status in an institutionalised elderly group after the intake of a phenolic-rich dessert. *Br. J. Nutr.* **2004**, *91*, 943−950.
(112) Møller, P.; Loft, S.; Alfthan, G.; Freese, R. Oxidative DNA damage in circulating mononuclear blood cells after ingestion of blackcurrant juice or anthocyanin-rich drink. *Mutat. Res.* **2004**, *551*, 119−126.
(113) Wilms, L. C.; Hollman, P. C.; Boots, A. W.; Kleinjans, J. C. Protection by quercetin and quercetin-rich fruit juice against induction of oxidative DNA damage and formation of BPDE-DNA adducts in human lymphocytes. *Mutat. Res.* **2005**, *582*, 155−162.
(114) Del Rio, D.; Borges, G.; Crozier, A. Berry flavonoids and phenolics: bioavailability and evidence of protective effects. *Br. J. Nutr.* **2010**, *104* (Suppl. 3), S67−S90.
(115) van Duynhoven, J.; Vaughan, E. E.; Jacobs, D. M.; Kemperman, R.; van Velzen, E. J.; Gross, G.; Roger, L. C.; Possemiers, S.; Smilde, A. K.; Doré, J.; Westerhuis, J. A.; Van de Wiele, T. Metabolic fate of polyphenols in the human superorganism. *Proc. Natl. Acad. Sci. U.S.A.* **2011**, *108*, 4531−4538.
(116) Bolca, S.; Van de Wiele, T.; Possemiers, S. Gut metabotypes govern health effects of dietary polyphenols. *Curr. Opin. Biotechnol.* **2013**, *24*, 220−225.

Table 1. Nutrient Composition of Fresh Strawberries[a] (Adapted from U.S. Department of Agriculture[50])

proximates and carbohydrates		mineral content		vitamin content	
water (g)	90.95	calcium (mg)	16.00	vitamin C (mg)	58.80
energy (kcal)	32.00	iron (mg)	0.41	thiamin (mg)	0.02
protein (g)	0.67	magnesium (mg)	13.00	riboflavin (mg)	0.02
ash (g)	0.40	phosphorus (mg)	24.00	niacin (mg)	0.39
total lipid (g)	0.30	potassium (mg)	153.00	pantothenic acid (mg)	0.13
carbohydrate (g)	7.68	sodium (mg)	1.00	vitamin B_6 (mg)	0.05
sugars (g)	4.89	zinc (mg)	0.14	folate (μg)	24.00
sucrose (g)	0.47	copper (mg)	0.048	choline (mg)	5.70
glucose (g)	1.99	manganese (mg)	0.39	vitamin A, RAE (μg)	1.00
fructose (g)	2.44	selenium (μg)	0.40	lutein + zeaxanthin (μg)	26.00
dietary fiber (g)	2.00			vitamin E, α-tocopherol (mg)	0.29
				vitamin K, phylloquinone (μg)	2.20

[a]Amount in 100 g of strawberry.

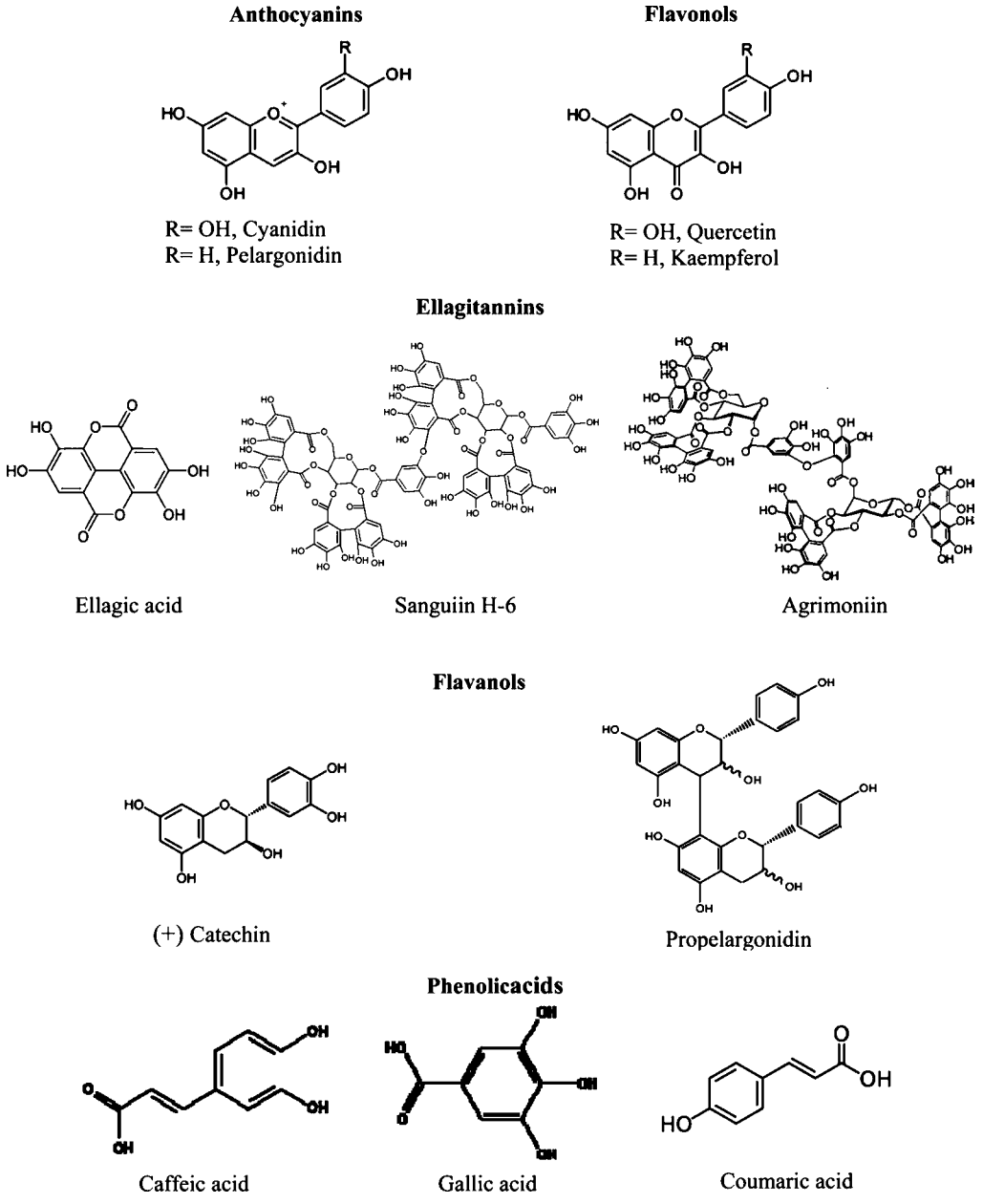

Figure 1. Chemical structures of the major polyphenolic compounds present in strawberries.

dx.doi.org/10.1021/jf405455n | J. Agric. Food Chem. 2014, 62, 3867−3876

Table 2. Concentrations of the Main Phenolic Compounds in Strawberries (Data Obtained from Aaby et al.[15])

group	compound	concentration (mg/100 g FW)
anthocyanins	cyanidin-3-glucoside	1.10
	pelargonidin-3-glucoside	25.30
	pelargonidin-3-rutinoside	1.10
	cyanidin-3-malonylglucoside	0.40
	pelargonidin-3-malonylglucoside	6.00
flavonols	quercetin glycosides	1.81
	kaempferol glycosides	0.84
flavan-3-ols	(+)-catechin	4.50
	proanthocyanidins	
	procyanidin dimers	9.10
	procyanidin trimers	7.90
ellagitannins	agrimoniin	8.80
	ellagic acid	0.52
ellagic acid glycosides	ellagic acid penthoside, ellagic acid deoxyhexoside, methylellagic acid deoxyhexoside	0.58
cinnamic acid conjugates	coumaroyl hexoses	5.40
	cinnamoyl glucose	5.00

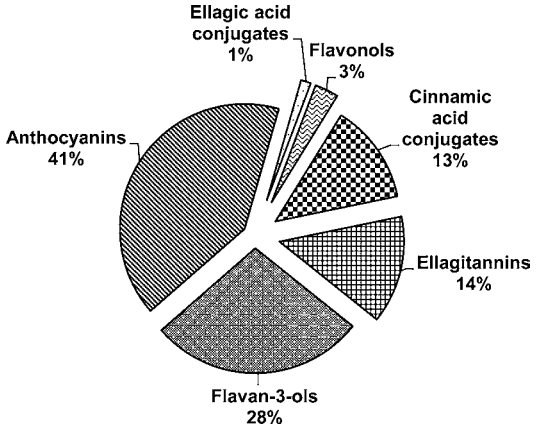

Figure 2. The most common phenolic compounds identified in strawberries. Data obtained from Aaby et al.[15]

important phenolic compounds present in strawberries and that the pelargonidin and cyanidin derivates are the most representative ones.[2,9,10,16] They have different properties (e.g., photoprotective, antioxidant, anti-inflammatory, anticarcinogenic, antimutagenic) and can also modulate enzymatic pathways; this is the way some of them may act in the prevention of oxidative stress-related diseases. Moreover, the daily intake of anthocyanins is very consistent and considered the most consumed group of phenolic compounds in the human diet: it has been estimated that the daily intake may reach 12.5 mg/day in the United States.[17]

Nowadays, it is known that fruit nutritional composition varies very considerably as a consequence of different pre- and postharvest factors, with the genetic background playing a major role in determining strawberry nutritional traits. For these reasons, breeding and biotechnological programs have focused their attention on ameliorating the productivity, aspect, shape, and firmness of the fruit, as well as its taste and aroma in different berry species. Only recently, strawberry nutritional value has been seriously studied and also requested as an added value by consumers, stimulating researchers to implement new breeding and biotechnological programs: for example, the increase of antioxidant compounds in commercial strawberries using wild germplasm as genetic material is a valid alternative to provide greater intake of healthy compounds even with a lower fruit consumption.[18,19] In this regard, only a few groups have demonstrated the correlation between the antioxidant and phenolic contents related to different genotypes, as well as the contribution of wild species to the bioactive compound contents in new genotypes.[20−22] These studies stressed the great importance of genetic background on antioxidant and chemical profiles of the strawberry. In fact, total antioxidant capacity and all classes of compounds tested, such as total phenols, flavonoids, anthocyanins, vitamin C, and folates, were significantly different according to their different genotypes. An online postcolumn antioxidant detection system adopted to evaluate the individual tribute of strawberry compounds to the total antioxidant capacity of the fruits also highlighted that vitamin C usually contributed >30% to the total antioxidant capacity in any cultivars and selections, whereas pelargonidin-3-glucoside contributed to the antioxidant capacity approximately 25% to nearly 40% of the eluting compounds depending on the cultivars tested.[20] Moreover, one of the advanced selections of the Marche Polytechnic University strawberry breeding program, obtained from a cross between a wild and cultivated species, was demonstrated as the most important genotype because of the highest total antioxidant capacity and total phenolic content, confirming once again the important role of the genetic background.

BIOAVAILABILITY AND METABOLISM OF PHENOLIC COMPOUNDS

In recent years it has become extremely important to comprehend the absorption, metabolism, and excretion of phenols after dietary intake, as proof of the possible disease-preventing and health-promoting effects of strawberry phenolic phytochemicals continues to pile up.

In general, most dietary phenols are assimilated in the intestine: indeed, after ingestion, flavonoids, in the form of glycoside conjugates, reach the brush border of the small intestine epithelial cells where they are hydrolyzed by lactase phloridizin hydrolase, leading to the release of aglycone, which is then enabled to pass into the same cells by passive diffusion as a result of its increased lipophilicity.[9,10,23,24] Another way by which glucoside conjugates are hydrolyzed is represented by a cytosolic β-glucosidase within the epithelial cells, after transportation of polar glucoside into the epithelial cells: it has been suggested that this can occur probably thanks to the active Na-dependent GLUT-1.[9,10,23,24] Aglycones resulting from this type of hydrolysis can suffer two different fates: (i) they can return into the lumen of the small intestine, possibly with the involvement of members of the ATP-binding family of transporters, or (ii) they can be processed in glucuronide, methylated metabolites, and/or sulfate, through the corresponding action of UDP-glucuronosyltransferases, catechol-*O*-methyltransferases, and sulfotransferases, and pass into the bloodstream.[9,10,23,24] They then quickly approach the liver: here, they can undergo phase II metabolism and pass to the systemic circulation; they can also move back to the small intestine thanks to bile excretion.

dx.doi.org/10.1021/jf405455n | J. Agric. Food Chem. 2014, 62, 3867−3876

All flavonoids that are not taken up in the small intestine pass into the colon and are processed by colonic microflora, which halve conjugating fractions; the resultant aglycones are transformed into phenolic acids and hydroxycinnamates that sometimes are assimilated, reaching the hepatic tissue; in the liver they can undergo phase II metabolism before being excreted in urine.[9,10,23,24]

Anthocyanins. Results from the few presently known investigations concerning anthocyanin bioavailability in humans demonstrate that these compounds are very exiguously absorbed: usually about 0.1% of the eaten amounts, or even less, has been found in urine within 24 h of consumption; lower concentrations have been detected in plasma.[9,10,23,24] The characteristics of both the anthocyanidin structure and the sugar moiety influence the limited absorption and excretion of anthocyanins. Indeed, anthocyanins do not seem to suffer wide metabolism to glucuronide derivates, unlike what happens to other flavonoids. In the stomach, the acid pH maintains anthocyanins in the stable flavylium cation form, so that a limited quantity can be quickly assimilated from the stomach after intake, through a mechanism which could implicate bilitranslocase.[9,10,23,24] The other part of anthocyanins reaches the small intestine, where they are converted into some neutral pH forms of anthocyanins: hemiketals, chalcones, and quinonoids. Such compounds appear to be just partially assimilated in the jejunum and undergo wide conjugation reactions, mostly in the liver but also in the kidney and in the intestine. Indeed, consistent quantities of ingested anthocyanins avoid absorption in the upper small intestine and pass into the colon, where they are exposed to a microbiota able to largely modify their molecular entity, breaking glycosidic linkages and heterocycle; colonic bacteria further convert the aglycones resulting from this process into smaller phenolic acids, such as protocatechuic acid for cyanidin-based anthocyanins or 4-hydroxybenzoic acid for pelargonidin-based anthocyanins.[9,10,23,24]

Ellagitannins. In the past decade, only a few studies have focused on the pharmacokinetics of dietary ellagitannins, especially after a single dose intake of red and black raspberries, walnuts, and pomegranate juice.[9,10,23,24] A complex picture emerged showing that ellagitannins are absorbed in the jejunum, where they are hydrolyzed to ellagic acid thanks to the neutral pH environment. Ellagic acid appears to be moved across the enterocyte apical membrane and rapidly transformed into methyl or dimethyl conjugated by catechol *o*-methyl transferase and presumably glucuronidated by UDP-glucuronosyltransferases. Afterward, ellagic acid metabolites undergo hepatic phase II biotransformations, producing a puzzling group of conjugated forms characterized by fast kinetics of plasma appearance and urinary excretion once they have entered the systemic circulation.[9,10,23,24]

In any case, within the intestinal lumen, most ellagitannins are subjected to microbiota transformation, resulting in the production of derivatives commonly known as urolithins (urolithins A−D). These metabolites are preferentially absorbed as their lipophilicity increases and, in the enterocyte and hepatocyte, further undergo phase II biotransformations, giving a combination of urolithin metabolites. For example, urolithin A 3-*O*-glucuronide and urolithin B 3-*O*-glucuronide are the major components found in plasma, whereas urolithin A and C glucuronides are present in urine.[9,10,23,24] Finally, it should be taken into account that the different colonic microbiota of different subjects are responsible for the consistent interindividual variability in the in vivo production of these metabolites, which makes the ellagitannin metabolism even more complex to explain.[23,24]

Proanthocyanidins. Results obtained in the few presently known investigations on the bioavailability of proanthocyanidins in the polymeric forms demonstrate that they are not absorbed to any degree.[23,24] Indeed, when they reach the large intestine unaltered, they are usually processed by colonic microbiota, leading to the production of an extensive range of phenolic acids such as 3-(3-hydroxyphenyl)propionic acid and 4-*O*-methylgallic acid; these metabolites pass into the circulatory system and are eliminated through the urine.[23,24] Only two investigations have found low levels of proanthocyanidin dimers in human plasma,[23,24] suggesting that polymerization greatly impairs intestinal absorption. According to this evidence, it is thought that the biological effects of proanthocyanidins are usually ascribed not to their direct action but to the activity of their metabolites, even though there is still little detailed information regarding this issue.

STRAWBERRY EFFECTS ON HUMAN HEALTH

Overcoming the Gap between in Vitro and in Vivo Studies. As known, polyphenols are among the most important and best known bioactive compounds present in fruits, especially berries. In the past few years, several investigations have been carried out to delineate the biological activity that these compounds exert in the maintenance of well-being and in the prevention of a huge variety of chronic pathologies (Table 3). Although berries are one of the most antioxidant-rich foods, and although the potential efficacy of polyphenols is currently receiving ample attention, most of the literature data are still obtained from in vitro studies. In this regard, one of the most interesting research areas focuses on the in vitro effects of polyphenols in skin well-being. Skin is always open to a diversity of chemical, genotoxic, and environmental agents that contribute to aging, disease, and carcinogenesis. A wide array of polyphenols from different dietary sources possess substantial skin protective effects, which has raised increasing interest in their systemic and topical applications for skin protection. Much of this interest concerns the antioxidant properties of polyphenols. A recent paper analyzed the in vitro protective capacity of an anthocyanin-rich strawberry extract on human dermal fibroblasts exposed to UV-A radiation.[2] UV-A radiation penetrates the dermis, causing oxidative damage by generating reactive oxygen species (ROS). In this study, incubation for 24 h with 0.5 mg/mL strawberry extracts led to photoprotective activity in human dermal fibroblasts subjected to UV-A radiation, with an increase in cellular viability and a decrease in DNA damage in a dose-responsive manner when compared to control cells. Yin et al.[3] obtained similar results: they found that 1 mg of quercitrin, a glycosylated form of quercitin, in mouse epidermal cells decreased ROS generation induced by UV-B irradiation and restored catalase expression and glutathione/glutathione disulfide ratio, leading to a reduction of oxidative DNA damage and apoptosis and to protection of the skin from inflammation. Likewise, another recent study[4] assessed the inhibitory effects of two powerful plant-based phenolic antioxidants (i.e., ferulic and caffeic acids) at different concentrations of 3.75, 7.5, 15, and 30 μM, on UV-A-induced cytotoxicity in human keratinocyte cells, evaluating the recovery of the antioxidant defense system. Results showed that ferulic and caffeic acids up-regulated activities and mRNA expression of catalase and

Table 3. Effects of Dietary Polyphenols

		effects	refs
UV	in vivo		
		decrease of intracellular ROS concentration	3, 5
		increase of antioxidant enzyme activities	3, 5
	in vitro		
		increase of cell viability	2
		reduction of DNA damage	2
		decrease of intracellular ROS concentration	3, 4
		increase of antioxidant enzyme activities	3, 4
		reduction of proinflammatory proteins	6, 7
		reduction of TNF-α	6, 7
aging	in vivo		
		increase of antioxidant defense	25, 26
		reduction of oxidative stress	25, 26
		increase of mitochondrial respiratory performance	25, 27
		decrease of age-related autophagy	27
gastric pathological conditions	in vivo		
		reduction of ulcer index	16
		decrease of gastric lipid peroxidation	16, 29, 30
		increase of antioxidant defense	16, 29, 30
		reduction of suppression of MMP-2 activity	30
		inhibition of phosphorylation of mitogen-activated protein kinases	30
	in vitro		
		decrease of gastric lipid peroxidation	30
		increase of antioxidant defense	30
		reduction of suppression of MMP-2 activity	30, 31
		inhibition of phosphorylation of mitogen-activated protein kinases	30, 31
cardiovascular disease	in vivo		
		reduction of inflammation	33, 36, 43
		inhibition of platelet aggregation	33, 37, 38
		improvement of endothelial function	35, 37, 38
		improvement of plasma lipid profile	33, 41, 42
		increase of LDL resistance to oxidation	37, 38, 42
		increase in plasma antioxidant capacity	32−34
		reduction of myocardial infarction risk	33, 37, 38
cancer	in vitro		
		demethylation of tumor suppressor genes	45, 46, 49
		induction of cell cycle arrest and apoptosis	45, 47, 48
		suppression of suppressing tumor	46

glutathione peroxidase as well as γ-glutamate cysteine ligase mRNA and glutathione concentrations in irradiated cells. However, many other recent studies[5−7] have shown new insights in the molecular mechanisms responsible for the healthful effects of polyphenols in skin application, beyond the antioxidant capacity. According to these findings, the potency of polyphenols to protect skin against harmful agents could be due to their capacity of altering signal transduction and epigenetic regulation of gene expression. For instance, green tea polyphenols,[5] quercetin,[6] and resveratrol[7] have shown an anti-inflamatory effect associated with the control of signal transduction, with the reduced expression of pro-inflammatory proteins (i.e., COX-2), inducible tumor necrosis factor-α (TNF-α), and nitric oxide synthase. These findings indicate that polyphenols may have protective effects on dermal cells in vitro, suggesting that these compounds could be helpful in protecting human dermal cells against several of the toxic agents to which the skin is frequently exposed.

Nevertheless, in vitro studies are often carried out in experimental conditions not comparable with the in vivo situation. Thus, it should be mandatory to endorse the potential health-promoting results of strawberry in vivo studies, especially in human studies. With these critical points taken into account, in recent years several studies have been carried out in vivo, in both physiological and pathological conditions, selecting strawberry varieties particularly rich in phytochemical compounds, mainly anthocyanins. For instance, in the feeding trial on rats we are currently carrying out in our laboratory, we are evaluating the possible role of strawberries in ameliorating the aging process.[25] In general, after 2 months of 15% strawberry consumption, a reduction of physiological oxidative damage has been observed at tissue, cellular, and subcellular levels as well as an enhancement in antioxidant biomarkers and an amelioration of lipid profile. A strawberry-enriched diet has also determined the reduction of oxidative stress in liver mitochondria, improving the animals' functionality and respiratory performance. These results agree with a recent feeding trial on old rats,[26] which demonstrated that the intake of polyphenols (75 mg/kg body weight) resulted in a decrease of ROS production, an enhancement of antioxidant defense, and the prevention of age-related mitochondrial respiratory impairment. Similarly, Laurent et al.[27] found that moderate oral supplementation of a red grape polyphenol extract improved the general antioxidant status of aged rats, increasing the biogenesis of mitochondria and decreasing age-dependent autophagy in gastrocnemius of the old animals. Interestingly, we obtained the same results when oxidative stress was induced by doxorubicin administration, a very toxic drug that alters DNA and produces free radicals at a very high rate. In particular, in the rat, strawberry supplementation seems to be able to give protection against oxidative injury induced by doxorubicin in plasma, lymphocytes, or liver at tissue, cellular, and subcellular levels. Our findings agree with the data obtained by Choi et al.,[28] who demonstrated that dietary supplementation with anthocyanin-rich bilberry extract (500 mg/kg body weight) was effective in reducing doxorubicin-induced oxidative damage and in improving antioxidant defense as well as in restoring hemoglobin levels and bone marrow cell and red blood cell counts, in both rats and mice. Again, another recent study[29] on rats showed that diet supplementation with grain rich in phenolic acids led to a decrease of oxidative status and of doxorubicin-induced liver inflammation and to a concomitant enhancement in antioxidant enzyme activities. These results confirm the possible health benefit of bioactive compounds in vivo against oxidative stress, also in physiological conditions characterized by a higher level of oxidative stress produced by aging or in pathological situations caused by the administration of oxidant agents.

Other in vivo studies[16,30] have recently shown that polyphenols may have a preventive function counteracting the progress of gastric ulcerations, erosions, and cancer. That is why an in vivo trial[16] on rats was carried out to examine the

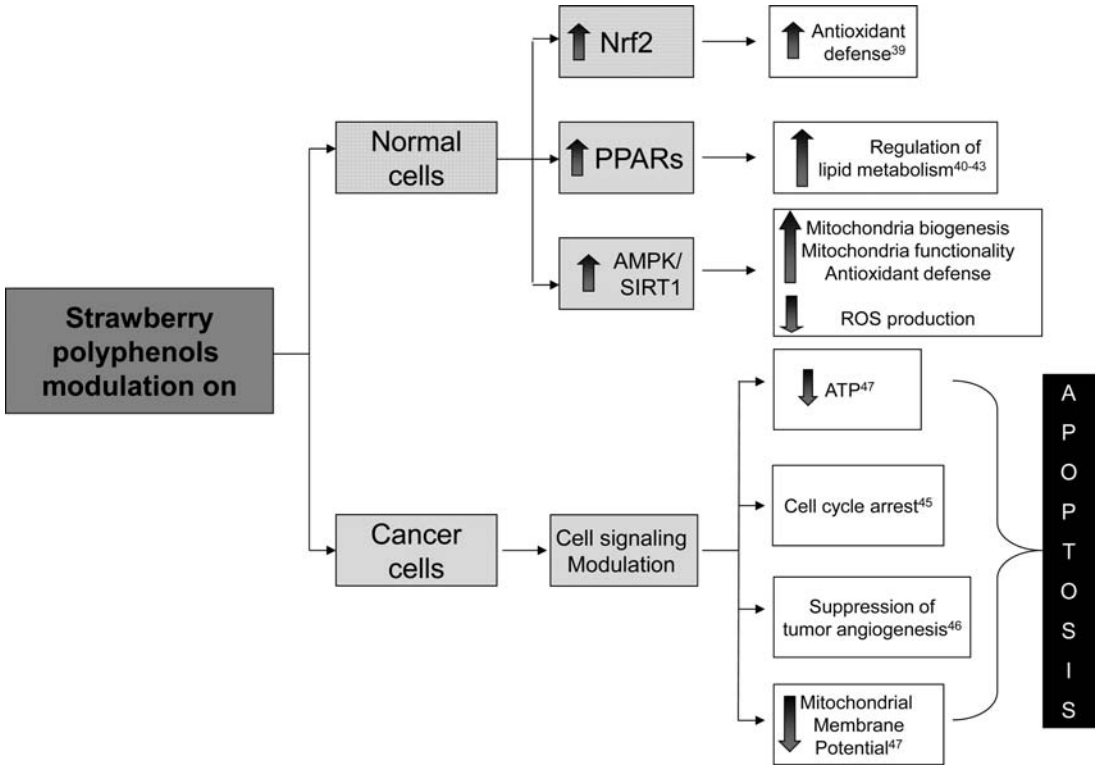

Figure 3. Mechanisms proposed for strawberry polyphenol modulation on normal and cancer cells. Abbreviations: Nrf2, nuclear factor-erythroid 2-related factor 2; PPARs, peroxisome proliferator-activated receptors; AMPK, 5′-adenosine monophosphate-activated protein kinase; Sirt1, sirtuin 1; ROS, reactive oxygen species; ATP, adenosine triphosphate.

strawberry protective and antioxidant effects toward ethanol-induced gastric mucosa damage. Strawberry consumption (40 mg/day/kg body weight) was able to protect against the deleterious role of ethanol, to significantly increase antioxidant enzyme activities, and to diminish, at the same time, gastric lipid peroxidation. Also, the percent of inhibition of ulcer index significantly correlated with total anthocyanin content. These results agree with those obtained in a recent study in rats,[30] where the administration of different concentrations of anthocyanins (5, 25, or 50 mg/kg body weight) from black rice bran was shown to significantly protect against gastric ulcer induced by a nonsteroidal anti-inflammatory drug, decreasing ROS levels and inhibiting lipid peroxidation, enhancing the antioxidant enzymes activities and attenuating the suppression of matrix metalloproteinase-2 (MMP-2) activity. Similarly, in another study[31] supplementation of different anthocyanin amounts (12.5, 25, 50, 100, or 200 μg/mL) exerted an anti-inflammatory effect in gastric epithelial cells infected by *Helicobacter pylori*, decreasing ROS concentration and inhibiting the phosphorylation of mitogen-activated protein kinases as well as the translocation of nuclear factor-κB. On the basis of this evidence, the potential of polyphenols could be taken into account for preventing/treating chronic subacute gastric lesions. The intake of a diet rich in bioactive compounds could prevent and/or ameliorate pathological states of the stomach as well as attenuate gastric mucosal damage, thereafter curing or diminishing ulcer formation, side effects of subacute chronic alcohol intake, nonsteroid anti-inflammatory-related gastritis, or *H. pylori* treatment.

The most significant outcomes of polyphenol supplementation in human studies[32−37] have addressed the possible variations in both cellular and plasma markers of antioxidant status in young and middle-aged subjects. In young healthy volunteers, total antioxidant capacity and vitamin C concentration in serum were significantly enhanced after the consumption of 300 g of strawberries (fresh fruit).[32] A concomitant decrease in oxidative biomarkers both in urine and in plasma was found after the consumption of 500 g of strawberries for 1 month.[33,34] Either oxidant-untreated or treated erythrocytes displayed improved protection to hemolysis as well as a highly reduced percentage of mortality and an increased proportion of metabolic activity in ex vivo mononuclear cells treated with H_2O_2 after consumption of 500 g of strawberries for 2 weeks.[35] Among the mechanisms of action implicated in the antioxidant effects of strawberry consumption, a reduction in DNA oxidative damage and an improvement of DNA repair capacity could be involved.

Nowadays, it is generally accepted that obesity and oxidative stress may be present at younger ages and persistent exposure to systemic inflammation could result in the onset and development of cardiovascular disease (CVD). Evidence suggests that the addition of polyphenol-rich foods in the diet may improve CVD risk factors, inhibiting inflammation and platelet aggregation and ameliorating endothelial function, plasma lipid profile, and free radical scavenging, thus increasing LDL resistance to oxidation. In overweight and obese children,[36] a short-term blueberry consumption, consisting of the weekly intake of 375 g of fresh blueberries during 8 weeks, resulted in enhanced antioxidant capacity of plasma and in a concomitant reduction of inflammation and oxidative stress markers, whereas in dyslipidemic subjects anthocyanin consumption[37] (about 160 mg twice daily for 12 weeks) was found to increase HDL-cholesterol concentrations and to decrease LDL-cholesterol concentrations and cholesteryl ester

transfer protein activity in plasma. Similarly, Cassidy et al.[38]demonstrated that, in young or middle-aged women, a reduced risk for myocardial infarction was associated with elevated anthocyanin intake. Another study[33] showed that the daily consumption of 500 g of strawberries for 1 month in young healthy volunteers was associated with a general improvement of the serum lipid profile of the subjects, through a reduction of total cholesterol, LDL-C, and triglyceride levels, indicating that some of the constituents of the fruit, such as vitamin C and anthocyanins, may favorably affect the plasma lipid profile. In this study, the intent was also to determine platelet basal activation in healthy subjects after strawberry consumption, as a preventive factor against CVD through a diet rich in antioxidants. Although the majority of platelets remained in the resting state after treatment, as expected, a significant decrease was found in the number of activated platelets during the strawberry supplementation period compared to baseline values, indicating a favorable effect of strawberry treatment on platelet function. Therefore, according to the data obtained in these studies, polyphenols seem to exert in vivo effects in the prevention of CVD risk, explaining in part the protective role of a diet abundant in vegetables and fruits in preventing CVD and other chronic diseases mediated by oxidative stress.

Effects beyond Antioxidant Capacity: 1. Possible Role in Chronic Metabolic Disorders. All of the beneficial effects that polyphenols exert in vivo on human health may not depend only on direct antioxidant properties. In fact, polyphenols are processed by the body as xenobiotics, stimulating the stress-related cell signaling pathways, which results in an increased expression of cytoprotective genes (Figure 3). Recently, it was found that polyphenols might increase gene transcription of nuclear factor-erythroid 2-related factor 2 (Nrf2), a transcription factor that binds to the antioxidant response element (ARE) and regulates enzymes involved in antioxidant functions or detoxification.[39] In this way, polyphenols may give antioxidant protection in an indirect way with the activation endogenous defense systems, mainly with the modulation of the expression of some antioxidant enzymes, and this fact may partly explain the increase in antioxidant enzymes found in in vivo studies.

Another important mechanism that should be taken into account besides the antioxidant capacity is the effect that polyphenols indirectly exert on peroxisome proliferator-activated receptors (PPARs), through Nrf2 activation.[40] PPARs are transcriptional factors that manage insulin sensitivity, glucose homeostasis, fatty acid oxidation, and lipid metabolism in general, so that their agonists are employed for treating metabolic syndrome, cardiovascular diseases, and hyperlipidemia. In this regard, a polyphenol-rich fraction from amla fruit (*Emblica officinalis* Gaertn.) in concentrations of 40 or 10 mg/kg body weight per day for 100 days was reported to improve age-related hypertriglyceridemia in young and old rats by stimulating liver PPARα expression,[41] whereas 1% of phenols and anthocyanins from cherries was found to decrease, in rat, hyperinsulinemia fasting blood glucose, hyperlipidemia, and fatty liver by enhancing hepatic PPARα mRNA and hepatic PPAR-α target acyl-CoA oxidase mRNA activity.[42] Similarly, the daily consumption of chokeberries (100 and 200 mg/kg body weight) led to a decrease in glycemia, cholesterol, LDL-cholesterol, triglycerides, and epididymal fat as well as to a reduction in plasma TNF-α and interleukin-6 levels and an up-regulation of the gene expression of PPARγ mRNA levels.[43] We also confirmed that a protracted consumption of strawberries is associated with a general improvement of the serum lipid profile in young subjects, through a reduction of total cholesterol, LDL-C, and triglyceride levels.[33] To summarize, polyphenols have different biological effects on metabolically active tissues, affecting insulin sensitivity, inflammation, lipid metabolism, and obesity, which could be switched on by PPAR activation, through Nrf2, reducing different phenotypic risk factors connected with the risk for type 2 diabetes and metabolic syndrome.

Finally, another possible mechanism to explain all of these polyphenol effects on health is the activation of the AMPk/SIRT1 (5′-adenosine monophosphate-activated protein kinase/sirtuin 1) signaling cascade that can lead to an increase in cellular metabolism, mitochondrial biogenesis and functionality, and antioxidant defense and to a concomitant decrease of ROS levels and inflammation. However, this is a new area of study that has begun to be investigated for elucidating the mechanisms and strawberry compounds implicated in these responses.

Effects beyond Antioxidant Capacity: 2. Possible Role in Cancer Prevention and Treatment. The fact that polyphenols extend their properties beyond antioxidation up to cell signaling modulation gives an interesting insight into their potential anticancer properties. In the past few years, polyphenol antioxidant capacity has been taken into account as one of the outstanding mechanisms of action in inhibiting mutagenesis and cancer initiation, by means of their capacity to scavenge ROS, activate antioxidant enzymes, prevent carcinogen-induced DNA adduct formation, enhance DNA repair, and reduce overall oxidative DNA injury[44] (Figure 3). Whereas antioxidation certainly has a pivotal function in polyphenols' anticancer effectiveness, several recent investigations have also supported their function as modulators of cellular processes connected with cancer growth: in vitro and in vivo evidence indicates in fact that phenolics may modulate cell signaling in the cancer cell by inhibiting proliferation of these cells through the demethylation of tumor suppressor genes,[45] inducing cell cycle arrest and apoptosis[45] and suppressing tumor angiogenesis.[46] A recent study[47] on PC-3 prostate cancer cells revealed that polyphenol-rich tea extracts at different concentrations (0.4, 0.8, 1.2, 1.6, or 2.0 mg/mL) inhibited cell proliferation, induced apoptosis, and provoked reduction of the mitochondrial membrane potential and ATP level decrease, whereas resveratrol metabolites (at 10, 20, and 30 μM) were reported to inhibit colon cancer cell growth and cause an accrual of cells in the S phase, inducing DNA damage and the apoptotic process.[48] Similarly, Link et al.[49] found that curcumin (7.5−10 μM) exerted chemopreventive effects, inducing DNA methylation at selected loci, rather than fully methylated sites in colorectal cancer cells, and that DNA methylation changes were obtained through analogous modifications in gene expression at either up- or down-regulated genes. Unfortunately, investigations devoted to the mechanisms underlying the anticancer efficacy of berry polyphenols are still limited. Recently, Wang et al.[45] reported that different concentrations of anthocyanins present in black raspberries canceled activity as well as protein expression of DNA methyltransferase enzymes, demethylated promoters of CDKN2A, and SFRP2, SFRP5, and WIF1 by inhibiting cell proliferation and inducing apoptosis in colorectal cancers. We are presently assaying the in vitro effects of strawberry polyphenols on a murine mammary cancer cell line N201/1A that expresses high levels of human epidermal growth

factor receptor 2 (HER-2) oncoprotein. HER2 expression in breast cancer has usually been considered an interesting therapeutic goal because it is frequently linked to an aggressive phenotype and poor prognosis. We have found that after strawberry treatment (corresponding to 2.5 μg of anthocyanins/mL), tumor cells that express the oncogene show higher levels of apoptosis at lower extract concentrations compared to tumor cells without the oncogene. This may mean that the N202/1A cells are more sensitive at lower extract concentrations, as demonstrated by the high apoptosis rate. Furthermore, strawberry treatment results in an increase in intracellular ROS and in an impairment of glycolysis and mitochondrial functionality in cells that express the oncogene compared to cells without the oncogene. Probably, there is a mechanism linked to the apoptotic pathway and cellular metabolism through the strawberry extract that can affect tumor cell viability, especially of the N202/1A cell line, which overexpresses the HER-2/*neu*oncogene. We obtained similar results also in an in vivo trial, on transgenic mice expressing the HER-2/*neu* oncogene (line FVB/N 233 neu-NT), supplemented for 4 months with 15% strawberries. A reduction of the number and size of metastases, as well as their propagation in the lung, was observed in animals fed strawberries compared to the control group. These findings lead to the conclusion that polyphenols, when investigated for their antitumoral effects, target distinct signaling mechanisms, therefore emphasizing the urgency of additional research to highlight the pathways involved in the anticancer effects of strawberries and to characterize the bioactive compounds that may play a fundamental role against cancer.

In conclusion, strawberry fruits possess a remarkable nutritional composition due to their high content of micronutrients such as folates, minerals, and vitamins, and are also a rich source of phenolic constituents. Currently, evidence on the biological activity of polyphenolic compounds is growing. Many mechanisms have been proposed to explain how polyphenols exert their biological protective effects, which, for several years, have been often ascribed mainly to their antioxidant capacity. However, this view is now challenged by recent findings, and more complex actions are being investigated. Recent findings have demonstrated that, besides antioxidant and anti-inflammatory capacities, phenolics may engage with cellular signaling flow, controlling the action of transcription factors and subsequently affecting the expression of those genes involved in cellular metabolism and cellular survival. Further in vivo investigations are required to translate the evidence obtained in vitro into actual outcomes in vivo and to understand the factors and mechanisms regulating the bioefficacy of strawberry phytochemicals.

AUTHOR INFORMATION

Corresponding Author

*(M.B.) Phone: +39 071 2204646. Fax: +39 071 2204123. E-mail: m.a.battino@univpm.it.

Notes

The authors declare no competing financial interest.

ACKNOWLEDGMENTS

We are indebted to M. Glebocki for extensive editing of the manuscript.

ABBREVIATIONS USED

Nrf2, nuclear factor-erythroid 2-related factor 2; AMPK, 5′-adenosine monophosphate-activated protein kinase; Sirt1, sirtuin1; CVD, cardiovascolar disease; MMP, matrix metalloproteinase; TNF-α, tumor necrosis factor-α; ARE, antioxidant response element; PPARs, peroxisome proliferator-activated receptors

REFERENCES

(1) Bach-Faig, A.; Berry, E. M.; Lairon, D.; Reguant, J.; Trichopoulou, A.; Dernini, S.; Medina, F. X.; Battino, M.; Belahsen, R.; Miranda, G.; Serra-Majem, L. Mediterranean Diet Foundation Expert Group. Mediterranean diet pyramid today. Science and cultural updates. *Public Health Nutr.* **2011**, *14*, 2274−2284.

(2) Giampieri, F.; Alvarez-Suarez, J. M.; Tulipani, S.; Gonzàles-Paramàs, A. M.; Santos-Buelga, C.; Bompadre, S.; Quiles, J. L.; Mezzetti, B.; Battino, M. Photoprotective potential of strawberry (*Fragaria* × *ananassa*) extract against UV-A irradiation damage on human fibroblasts. *J. Agric. Food Chem.* **2012**, *60*, 2322−2327.

(3) Yin, Y.; Li, W.; Son, Y. O.; Sun, L.; Lu, J.; Kim, D.; Wang, X.; Yao, H.; Wang, L.; Pratheeshkumar, P.; Hitron, A. J.; Luo, J.; Gao, N.; Shi, X.; Zhang, Z. Quercitrin protects skin from UVB-induced oxidative damage. *Toxicol. Appl. Pharmacol.* **2013**, *269*, 89−99.

(4) Pluemsamran, T.; Onkoksoong, T.; Panich, U. Caffeic acid and ferulic acid inhibit UVA-induced matrix metalloproteinase-1 through regulation of antioxidant defense system in keratinocyte HaCaT cells. *Photochem. Photobiol.* **2012**, *88*, 961−968.

(5) Rhodes, L. E.; Darby, G.; Massey, K. A.; Clarke, K. A.; Dew, T. P.; Farrar, M. D.; Bennett, S.; Watson, R. E.; Williamson, G.; Nicolaou, A. Oral green tea catechin metabolites are incorporated into human skin and protect against UV radiation-induced cutaneous inflammation in association with reduced production of pro-inflammatory eicosanoid 12-hydroxyeicosatetraenoic acid. *Br. J. Nutr.* **2013**, *28*, 1−10.

(6) Pastore, S.; Potapovich, A.; Lulli, D.; Fidanza, P.; Kostyuk, V.; De Luca, C.; Mikhalchik, E.; Korkina, L. Plant polyphenols regulate chemokine expression and tissue repair in human keratinocytes through interaction with cytoplasmic and nuclear components of epidermal growth factor receptor (EGFR) system. *Antioxid. Redox. Signal.* **2012**, *16*, 314−328.

(7) Pastore, S.; Lulli, D.; Potapovich, A. I.; Fidanza, P.; Kostyuk, V. A.; Dellambra, E.; de Luca, C.; Maurelli, R.; Korkina, L. G. Differential modulation of stress-inflammation responses by plant polyphenols in cultured normal human keratinocytes and immortalized HaCaT cells. *J. Dermatol. Sci.* **2011**, *63*, 104−114.

(8) Battino, M.; Beekwilder, J.; Denoyes-Rothan, B.; Laimer, M.; McDougall, G. J.; Mezzetti, B. Bioactive compounds in berries relevant to human health. *Nutr. Rev.* **2009**, *67*, S145−S150.

(9) Giampieri, F.; Alvarez-Suarez, J. M.; Mazzoni, L.; Romandini, S.; Bompadre, S.; Diamanti, J.; Capocasa, F.; Mezzetti, B.; Quiles, J. L.; Ferreiro, M. S.; Tulipani, S.; Battino, M. The potential impact of strawberry on human health. *Nat. Prod. Res.* **2013**, *27*, 448−455.

(10) Giampieri, F.; Tulipani, S.; Alvarez-Suarez, J. M.; Quiles, J. L.; Mezzetti, B.; Battino, M. The strawberry: composition, nutritional quality, and impact on human health. *Nutrition* **2012**, *28*, 9−19.

(11) Tulipani, S.; Mezzetti, B.; Battino, M. Impact of strawberries on human health: insight into marginally discussed bioactive compounds for the Mediterranean diet. *Public Health Nutr.* **2009**, *12*, 1656−1662.

(12) Niki, E. Antioxidant capacity: which capacity and how to assess it? *J. Berry Res.* **2011**, *1*, 169−176.

(13) Chiva-Blanch, G.; Visioli, F. Polyphenols and health: moving beyond antioxidants. *J. Berry Res.* **2012**, *2*, 63−71.

(14) Buendía, B.; Gil, M. I.; Tudela, J. A.; Gady, A. L.; Medina, J. J.; Soria, C.; López, J. M.; Tomás-Barberán, F. A. HPLC-MS analysis of proanthocyanidin oligomers and other phenolics in 15 strawberry cultivars. *J. Agric. Food Chem.* **2010**, *58*, 3916−3926.

(15) Aaby, K.; Mazur, S.; Nes, A.; Skrede, G. Phenolic compounds in strawberry (*Fragaria* × *ananassa* Duch.) fruits: composition in 27 cultivars and changes during ripening. *Food Chem.* **2012**, *132*, 86−97.

(16) Alvarez-Suarez, J. M.; Dekanski, D.; Ristic, S.; Radonjić, N. V.; Petronijević, N. D.; Giampieri, F.; Astolfi, P.; González-Paramás, A. M.; Santos-Buelga, C.; Tulipani, S.; Quiles, J. L.; Mezzetti, B.; Battino, M. Strawberry polyphenols attenuate ethanol-induced gastric lesion in rats by activation of antioxidant enzymes and attenuation of MDA increase. *PLoS One* **2011**, *6* (10), e25878.
(17) Wu, X.; Beecher, G. R.; Holden, J. M.; Haytowitz, D. B.; Gebhardt, S. E.; Prior, R. L. Concentrations of anthocyanins in common foods in the United States and estimation of normal consumption. *J. Agric. Food Chem.* **2006**, *54*, 4069−4075.
(18) Diamanti, J.; Capocasa, F.; Battino, M.; Mezzetti, B. Evaluation of *F.* × *ananassa* intra-specific and inter-specific back-crosses to generate new genetic material with increased fruit nutritional quality. *J. Berry Res.* **2010**, *1*, 103−114.
(19) Diamanti, J.; Capocasa, F.; Balducci, F.; Battino, M.; Hancock, J.; Mezzetti, B. Increasing strawberry fruit sensorial and nutritional quality using wild and cultivated germplasm. *PLoS One* **2012**, *7* (10), e46470.
(20) Tulipani, S.; Mezzetti, B.; Capocasa, F.; Bompadre, S.; Beekwilder, J.; Ric de Vos, C. H.; Capanoglu, E.; Bovy, A.; Battino, M. Antioxidants, phenolic compounds, and nutritional quality of different strawberry genotypes. *J. Agric. Food Chem.* **2008**, *56*, 696−704.
(21) Tulipani, S.; Marzaban, G.; Herndl, A.; Laimer, M.; Mezzetti, B.; Battino, M. Influence of environmental and genetic factors on health-related compounds in strawberry. *Food Chem.* **2011**, *124*, 906−913.
(22) Scalzo, J.; Battino, M.; Mezzetti, B. Breeding and biotechnology for improving berry nutritional quality. *Biofactors* **2005**, *23*, 1−8.
(23) Del Rio, D.; Borges, G.; Crozier, A. Berry flavonoids and phenolics: bioavailability and evidence of protective effects. *Br. J. Nutr.* **2010**, *104*, S67−S90.
(24) Del Rio, D.; Rodriguez-Mateos, A.; Spencer, J. P.; Tognolini, M.; Borges, G.; Crozier, A. Dietary (poly)phenolics in human health: structures, bioavailability, and evidence of protective effects against chronic diseases. *Antioxid. Redox Signal.* **2013**, *18*, 1818−1892.
(25) Giampieri, F.; Alvarez-Suarez, J. M.; Mazzoni, L.; Gasparrini, M.; Forbes-Hernandez, T. Y.; Mezzetti, B.; Battino, M. Strawberry enriched diet counteracts oxidative stress in plasma and liver of old rats and improves mitochondrial functionality. *Free Radical Biol. Med.* **2013**, *65*, S108.
(26) Charles, A. L.; Meyer, A.; Dal-Ros, S.; Auger, C.; Keller, N.; Ramamoorthy, T. G.; Zoll, J.; Metzger, D.; Schini-Kerth, V.; Geny, B. Polyphenols prevent ageing-related impairment in skeletal muscle mitochondrial function through decreased reactive oxygen species production. *Exp. Physiol.* **2013**, *98*, 536−545.
(27) Laurent, C.; Chabi, B.; Fouret, G.; Py, G.; Sairafi, B.; Elong, C.; Gaillet, S.; Cristol, J. P.; Coudray, C.; Feillet-Coudray, C. Polyphenols decreased liver NADPH oxidase activity, increased muscle mitochondrial biogenesis and decreased gastrocnemius age-dependent autophagy in aged rats. *Free Radical Res.* **2012**, *46*, 1140−1149.
(28) Choi, E. H.; Park, J. H.; Kim, M. K.; Chun, H. S. Alleviation of doxorubicin-induced toxicities by anthocyanin-rich bilberry (*Vaccinium myrtillus* L.) extract in rats and mice. *Biofactors* **2010**, *36*, 319−327.
(29) Benedetti, S.; Primiterra, M.; Tagliamonte, M. C.; Carnevali, A.; Gianotti, A.; Bordoni, A.; Canestrari, F. Counteraction of oxidative damage in the rat liver by an ancient grain (Kamut brand khorasan wheat). *Nutrition* **2012**, *28*, 436−441.
(30) Kim, S. J.; Park, Y. S.; Paik, H. D.; Chang, H. I. Effect of anthocyanins on expression of matrix metalloproteinase-2 in naproxen-induced gastric ulcers. *Br. J. Nutr.* **2011**, *106*, 1792−801.
(31) Kim, J. M.; Kim, K. M.; Park, E. H.; Seo, J. H.; Song, J. Y.; Shin, S. C.; Kang, H. L.; Lee, W. K.; Cho, M. J.; Rhee, K. H.; Youn, H. S.; Baik, S. C. Anthocyanins from black soybean inhibit *Helicobacter pylori*-induced inflammation in human gastric epithelial AGS cells. *Microbiol. Immunol.* **2013**, *57*, 366−373.
(32) Azzini, E.; Intorre, F.; Vitaglione, P.; Napolitano, A.; Foddai, M. S.; Durazzo, A.; Fumagalli, A.; Catasta, G.; Rossi, L.; Venneria, E.; Testa, M. F.; Raguzzini, A.; Palomba, L.; Fogliano, V.; Maiani, G. Absorption of strawberry phytochemicals and antioxidant status changes in humans. *J. Berry Res.* **2010**, *1*, 81−89.
(33) Alvarez-Suarez, J. M.; Giampieri, F.; Tulipani, S.; Casoli, T.; Di Stefano, G.; González-Paramás, A. M.; Santos-Buelga, C.; Busco, F.; Quiles, J. L.; Cordero, M. D.; Mezzetti, B.; Battino, M. One-month strawberry supplementation ameliorates cardiovascular risk, oxidative stress markers and platelets activation in humans. *J. Nutr. Biochem.* **2013**, DOI: 10.1016/j.jnutbio.2013.11.002.
(34) Tulipani, S.; Romandini, S.; Busco, F.; Bompadre, S.; Mezzetti, B.; Battino, M. Ascorbate, not urate, modulates the plasma antioxidant capacity after strawberry intake. *Food Chem.* **2009**, *117*, 181−188.
(35) Tulipani, S.; Armeni, T.; Giampieri, F.; Alvarez-Suarez, J. M.; González-Paramás, A. M.; Santos-Buelga, C.; Busco, F.; Principato, G.; Bompadre, S.; Quiles, J. L.; Mezzetti, B.; Battino, M. Strawberry intake increases blood fluid, erythrocyte and mononuclear cell defenses against oxidative challenge. *Food Chem.* **2104**, submitted for publication.
(36) Giongo, L.; Bozza, E.; Caciagli, P.; Valente, E.; Pasquazzo, M. S.; Pedrolli, C.; Iorio, E. L.; Costa, A. Short-term blueberry intake enhances biological antioxidant potential and modulates inflammation markers in overweight and obese children. *J. Berry Res.* **2011**, *1*, 147−158.
(37) Qin, Y.; Xia, M.; Ma, J.; Hao, Y.; Liu, J.; Mou, H.; Cao, L.; Ling, W. Anthocyanin supplementation improves serum LDL- and HDL-cholesterol concentrations associated with the inhibition of cholesteryl ester transfer protein in dyslipidemic subjects. *Am. J. Clin. Nutr.* **2009**, *90*, 485−492.
(38) Cassidy, A.; Mukamal, K. J.; Liu, L.; Franz, M.; Eliassen, A. H.; Rimm, E. B. High anthocyanin intake is associated with a reduced risk of myocardial infarction in young and middle-aged women. *Circulation* **2013**, *127*, 188−196.
(39) Na, H. K.; Surh, Y. J. Modulation of Nrf2-mediated antioxidant and detoxifying enzyme induction by the green tea polyphenol EGCG. *Food Chem. Toxicol.* **2008**, *46*, 1271−1278.
(40) Cho, H. Y.; Gladwell, W.; Wang, X.; Chorley, B.; Bell, D.; Reddy, S. P.; Kleeberger, S. R. Nrf2-regulated PPARγ expression is critical to protection against acute lung injury in ice. *Am. J. Respir. Crit. Care Med.* **2010**, *182*, 170−182.
(41) Yokozawa, T.; Kim, H. Y.; Kim, H. J.; Okubo, T.; Chu, D. C.; Juneja, L. R. Amla (*Emblica officinalis* Gaertn.) prevents dyslipidaemia and oxidative stress in the ageing process. *Br. J. Nutr.* **2007**, *97*, 1187−1195.
(42) Seymour, E. M.; Singer, A. A. M.; Kirakosyan, A.; Urcuyo-Llanes, D. E.; Kaufman, P. B.; Bolling, S. F. Altered hyperlipidemia, hepatic steatosis, and hepatic peroxisome proliferator-activated receptors in rats with intake of tart cherry. *J. Med. Food* **2008**, *11*, 252−259.
(43) Qin, B.; Anderson, R. A. An extract of chokeberry attenuates weight gain and modulates insulin, adipogenic and inflammatory signalling pathways in epididymal adipose tissue of rats fed a fructose-rich diet. *Br. J. Nutr.* **2012**, *108*, 581−587.
(44) Stoner, G. D.; Wang, L. S.; Casto, B. C. Laboratory and clinical studies of cancer chemoprevention by antioxidants in berries. *Carcinogenesis* **2008**, *29*, 1665−1674.
(45) Wang, L. S.; Kuo, C. T.; Cho, S J.; Seguin, C.; Siddiqui, J.; Stoner, K.; Weng, Y. I.; Huang, T. H.; Tichelaar, J.; Yearsley, M.; Stoner, G. D.; Huang, Y. W. Black raspberry-derived anthocyanins demethylate tumor suppressor genes through the inhibition of DNMT1 and DNMT3B in colon cancer cells. *Nutr. Cancer* **2013**, *65*, 118−125.
(46) Atalay, M.; Gordillo, G.; Roy, S.; Rovin, B.; Bagchi, D.; Bagchi, M.; Sen, C. K. Antiangiogenic property of edible berry in a model of hemangioma. *FEBS Lett.* **2003**, *544*, 252−257.
(47) Sun, S.; Pan, S.; Miao, A.; Ling, C.; Pang, S.; Tang, J.; Chen, D.; Zhao, C. Active extracts of black tea (*Camellia sinensis*) induce apoptosis of PC-3 prostate cancer cells via mitochondrial dysfunction. *Oncol. Rep.* **2013**, *30*, 763−772.
(48) Aires, V.; Limagne, E.; Cotte, A. K.; Latruffe, N.; Ghiringhelli, F.; Delmas, D. Resveratrol metabolites inhibit human metastatic colon

cancer cells progression and synergize with chemotherapeutic drugs to induce cell death. *Mol. Nutr. Food Res.* **2013**, *57*, 1170−1181.
(49) Link, A.; Balaguer, F.; Shen, Y.; Lozano, J. J.; Leung, H. C.; Boland, C. R.; Goel, A. Curcumin modulates DNA methylation in colorectal cancer cells. *PLoS One* **2013**, *8* (2), e57709.
(50) U.S. Department of Agriculture, Agriculture Research Service. USDA national nutrient for standard references, release 23, Fruits and fruit juices; 2010; pp 785−787; available at http://www.ars.usda.gov/Services/docs. htm?docid=8964 (accessed Jan 10, 2011).

major area of research emphasis in recent years. Fruits and vegetables contain a varied composition of bioactive compounds, many of which fall into the large family of compounds known as polyphenols. Early papers suggested that polyphenols were antinutritional components.[7] However, recent research supports the supposition that polyphenolic compounds have a strong potential to alter disease risk profiles in humans through their ability to modulate various biological pathways.[8−10]

In the past, polyphenols have been suggested to act as antioxidants in the body due to their ability to act as free radical quenchers or reducing agents. However, recent data derived from in vitro[11] and in vivo animal studies[12] suggest that they more likely alter disease risk profiles in humans through their ability to alter biological pathways via modulation of redox status, pathway signaling, and gene transcription in cells. Dietary polyphenols have been studied in a variety of clinical settings to determine whether these compounds impart health benefits.[13] The current evidence of protective effects of dietary polyphenols against chronic disease development has generated great interest from the beverage and nutritional supplements industry for the promotion and development of polyphenol-rich products.

Comprehensive reviews on the effect of high-pressure processing (HPP) on microbiological safety, quality, essential nutrients, and bioactive components are already presented by Barba et al., Barrett and Lloyd, Oms-Oliu et al., Gamlath and Wakeling, and Rastogi et al.[14−18] This review aims to complement those reviews by including the latest developments not included in or since publication of those papers (Table 1). Table 1 has summarized selective publications on the effects of HPP on the nutritional, microbiological, and physicochemical properties of fruit products.

TRADITIONAL PROCESSING OF FOODS AND BEVERAGES

Traditionally, the food industry has used thermal technologies to pasteurize and sterilize foods. Thermal processes are the established industry standard and involve subjecting foods/beverages to elevated temperatures for short periods of time with the goal of preventing growth of pathogenic microorganisms and spoilage-causing yeasts and molds to ensure safety over an extended shelf life. With the successful application of thermal processing, more people have access to a greater variety of safe foods and beverages. Although thermal processing is effective in inactivating detrimental microbiological intruders in foods and beverages, it can also destroy the functionality and flavors of many foods/beverages. For instance, reduced antiradical power values (as measured using 2,2-diphenyl-1-picrylhydrazyl radical (DPPH$^{\bullet}$) assay) were observed in strawberry purée samples treated with thermal processing when compared to unprocessed purée (reduced from 1.55 to 1.16 g/L^{-1}).[5] Increased processing temperatures can also significantly destroy heat-labile nutrients such as vitamins and bioactive phytochemicals. For example, Aaby et al. reported that exposure to relatively higher temperatures (75−80 °C) reduces the anthocyanin and total ascorbic acid content when strawberry is processed into purée.[19] In addition, thermal processing can also induce unintended formation of new compounds that may have unfavorable health effects or render the original compounds inactive.[20] Quality aspects related to flavor and color can also be compromised in thermally processed fruit juice concentrates such as strawberry concentrate stored at room temperature.[21]

CONSIDERATIONS FOR NEW PROCESSING TECHNIQUES

Currently, consumers have a greater appreciation for health-promoting properties of foods and demand foods and beverages that are fresher, nutrient dense, natural, additive-free, and minimally processed. Nonthermal food processing technologies have emerged as alternatives to thermal processing techniques to meet these consumer demands. HPP, light technologies (UV/pulsed UV), pulsed electric fields (PEF) treatment, and cold plasma are examples of nonthermal technologies. They are usually applied at (or below) room temperature and have minimal impact on the quality and freshness of food products,[22,23] including preserving nutrients and other health-promoting components. Klopotek et al. suggested that the reduction in total anthocyanins and hydrophilic antioxidant activity in strawberry beverages (nectar and juice) can be minimized if milder processing techniques are used instead of traditional thermal processing.[24]

The temperatures to which food products are exposed using advanced minimal processing techniques are relatively low and may be below pasteurization temperatures using conventional thermal processing.[25,26] For this reason, there is a tremendous potential for the production of superior quality products, especially with regard to higher nutrient content. Higher nutritive value is of no value, however, if the food is not safe. Hence, novel processing technologies that use temperatures below those used during thermal processing to enhance nutritional and other quality endpoints must also demonstrate the capability of inactivating microorganisms.[8,27,28] Research to optimize and validate novel processing conditions for different products will be of paramount importance for the industry in meeting consumer demands.

Research on processing technologies that retain freshlike appearance and high nutrient values in fruits has made tremendous progress in the past decade and will continue to develop in the future. In addition to enhancing nutrition and food safety, these novel technologies may reduce material, energy, and time costs.[29] Taste retention, shelf life extension, and fewer or no added chemical additives are also among the benefits touted, especially with HPP, making this a technology of great potential.

OVERVIEW OF THE HPP TECHNOLOGY

Among the nonthermal technologies, HPP is considered to be a promising technology for the food industry as it can result in the development of new shelf stable foods and/or extension of the shelf life of foods while preserving nutritional value and excellent organoleptic characteristics.[27,30] Therefore, food products treated with HPP have increasingly been introduced to the consumer market.[31] Formation of research consortiums across the globe and technological support from HPP manufacturing companies (Avure Technologies Inc., Elmhurst Research Inc., NC Hyperbaric, and many other established firms) have significantly contributed to the acceptance and implementation of HPP as a viable commercial alternative to thermal processing.

HPP can be used as an alternative processing method for fruit-based products while preserving the quality and nutritional properties of the products. Depending on the process temperature, HPP can be used for either pasteurization or sterilization of foods. In HPP, foods are subjected to high pressures by a hydraulic system in a pressure-sustainable

Table 1. Selected Examples of the Effects of HPP on Nutritional (Especially Bioactive Compounds), Microbiological, and Other Properties of Fruit Products

product	process conditions	effects on nutritional compounds including bioactives	effects on microorganisms	other effects (quality, physical properties, etc.)	ref
plum purée (cv. Crimson Globe, with red flesh and peel)	400, 500, and 600 MPa/1, 150, and 300 s	• slight reduction in anthocyanins and antioxidant activity after HPP, but no significant effect on total phenols	• inactivation of indigenous microorganisms (total aerobic mesophilic and psychrotrophic counts, and molds and yeasts) to undetected levels after HPP	• no significant changes in pH and soluble solid content after HPP • no sufficient inhibition of polyphenol oxidase (PPO) by HPP • significant enhancement of color: redness perception of treated purées	González-Cebrino et al.[47]
apricot nectars	300−500 MPa/5−20 min	• increased total and individual phenolics as a result of HPP, but no effect on total carotenoids and individual carotenes except for the treatment at 500 MPa/20 min, which increased total carotenoids and β-carotene		• significant activation of PPO and peroxidase (POD), but no change in the activity of pectinmethylesterase (PME) by HPP	Huang et al.[40]
fruit juice mixture (papaya, mango, orange)	300−500 MPa/5−15 min	• antioxidant compounds greatest with HPP at 300 MPa for 14 min			Carbonell-Capella et al.[71]
blueberry juice	200, 400, and 600 MPa/5, 9, and 15 min	• >92% vitamin C retention at all treatment intensities • increase in the total phenolic content mainly after HPP at 200 MPa for all treatment times • total and monomeric anthocyanin similar or higher than the value estimated for the fresh juice, being maximum at 400 MPa/15 min (16% increase) • no statistically different antioxidant capacity values for treatments at 200 MPa for 5−15 min in comparison with fresh juice • lowest values for total antioxidant capacity resulted from 400 MPa/15 min and 600 MPa for all times (8−16% reduction)		• no significant changes in pH and °Brix after HPP • no visually noticeable color changes after HPP	Barba et al.[23]
strawberry-based beverages formulated using milk vs water	200−800 MPa/1−15 min	• significant reduction of antioxidant capacity and flavonoid content by HTST pasteurization compared to HPP regardless of the matrix • potential protective effect of HPP (200−600 MPa) on antioxidant capacity that was not observed with HTST			Tadapaneni et al.[3]
avocado paste (*Persea americana* cv. Hass)	600 MPa/3 min	• significant increase (approximately 56%) in concentrations of total extractable carotenoids as a result of HPP • highest increases for individual carotenoids observed for neoxanthin-b (513%), followed by α-cryptoxanthin (312%), α-carotene (284%), β-cryptoxanthin (220%), β-carotene (107%), and lutein (40%); decrease in carotenoid levels during subsequent storage (40 days, 4 °C), but original carotenoid content was retained during product's shelf life (20 days) • decrease in ORAC values immediately after HPP followed by an increase during storage, indicating a minor contribution of the carotenoids to the total antioxidant capacity of the fruit			Jacobo-Velázquez and Hernández-Brenes[72]
blueberry juice	600 MPa/42 °C/5 min	• decrease <5% in ascorbic acid content compared with the untreated juice just after treatment • higher retention of ascorbic acid content during subsequent storage (56 days, 4 °C) in the HPP-treated juice in comparison with the untreated juice • better preservation of the antioxidant activity in the HPP-treated juice (21% loss) than in the untreated juice after 56 days at 4 °C		• slightly noticeable color changes (a^*, b^*, L, chroma, $h°$, and ΔE) after refrigerated storage in all juices	Barba et al.[22]

dx.doi.org/10.1021/jf404400q | J. Agric. Food Chem. 2014, 62, 3877−3885

Table 1. continued

product	process conditions	effects on nutritional compounds including bioactives	effects on microorganisms	other effects (quality, physical properties, etc.)	ref
nectarine (*Prunus persica* L.) purées	450 and 600 MPa/ 5 and 10 min	• highest carotenoid extractability by the lowest HPP treatment intensity and holding time (450 MPa/5 min), but no differences in individual or total carotenoid levels between the purées at the end of the storage (day 60) • highest polyphenol content after treatment and during storage achieved by HPP treatment at 600 MPa for 10 min • significantly higher total antioxidant activity in the purée treated at 450 MPa for 10 min than in untreated purée at day 0, but highest antioxidant activity at the end of the purée treated at 600 MPa for 10 min	• microorganisms' inactivation by HPP and microbial stability of the purées during subsequent refrigerated storage (up to 60 days) similar to those by conventional thermal pasteurization (85 °C/5 min)		García-Parra et al.[73]
orange juice–milk beverage	100–400 MPa/ 20–42 °C/2–9 min	• ascorbic acid retention >91% after HPP • significant increase in phenolic compounds at 100 MPa/7 min, and a nonsignificant decrease at 400 MPa/9 min • significantly higher total carotenoid content in the beverages treated at all pressures for 7 and 9 min than in the untreated beverage	• 5-log reduction of *Lactobacillus plantarum* CECT 220 after HPP treatment at 200 MPa for 5 min		Barba et al.[51]
cashew apple juice	250 and 400 MPa/25 °C/ 3, 5, and 7 min	• no change in ascorbic acid or hydrolyzable polyphenol content by HPP • higher soluble polyphenol contents in the juice pressurized for 3 and 5 min • no change in the antioxidant capacity by HPP measured by the ferric-reducing antioxidant power method, but an increased value in the juice treated at 250 MPa for 3 min when 2,2-diphenyl-1-picrylhydrazyl used		• no change in pH, acidity, and total soluble solids content by HPP	Queiroz et al.[74]
pomegranate juice	350–550 MPa/ 30, 90, and 150 s	• slight reduction in the antioxidant capacity during refrigerated storage • significant increase (between 3.38 and 11.99%) in the phenolic content at day 0 in the juice treated at 350 or 550 MPa	• reduction of the microbial load by around 4.0 logs and inhibition of the microbial populations below the detection limit during storage (4 °C/35 days) by HPP at 350 MPa for 150 s		Varela-Santos et al.[52]
peach (*Prunus persica*) juice	400–600 MPa/ 25 °C/5–25 min	• better preservation of L-ascorbic acid by HPP than by thermal processing		• activation of PPO and PME by 7.3 and 2.6% at 400 MPa, but significant inactivation of PPO and PME at 500 and 600 MPa • better preservation of color and sensory quality by HPP than by thermal processing	Rao et al.[75]
mango nectars	600 MPa/1 min (steam blanching used prior to HPP to inactive endogenous enzymes)	• no significant changes in the antioxidant capacity (FRAP assay), L-ascorbic acid, sodium erythorbate, total phenols, and total carotenoids after HPP (similar to the effects observed for HTST treatment at 110 °C for 8.6 s) • no significant changes in the antioxidant activity and antioxidant compounds of the nectars after 16 weeks storage of the treated product at 4 and 25 °C • more pronounced decreases in L-ascorbic acid and sodium erythorbate in the HPP-treated product than in the HTST-treated product during storage		• no significant changes in redness (a^*), yellowness (b^*), and browning degree (BD) after HPP (similar to the effects observed for HTST treatment at 110 °C for 8.6 s) • no significant change in the lightness (L^*) after HPP (unlike a significant decrease observed after HTST treatment) • significant changes in color and BD of the nectars after 16 weeks of storage of the treated product at 4 and 25 °C, with no significant differences between HPP- and HTST-treated products	Liu et al.[76]

dx.doi.org/10.1021/jf404400q | J. Agric. Food Chem. 2014, 62, 3877–3885

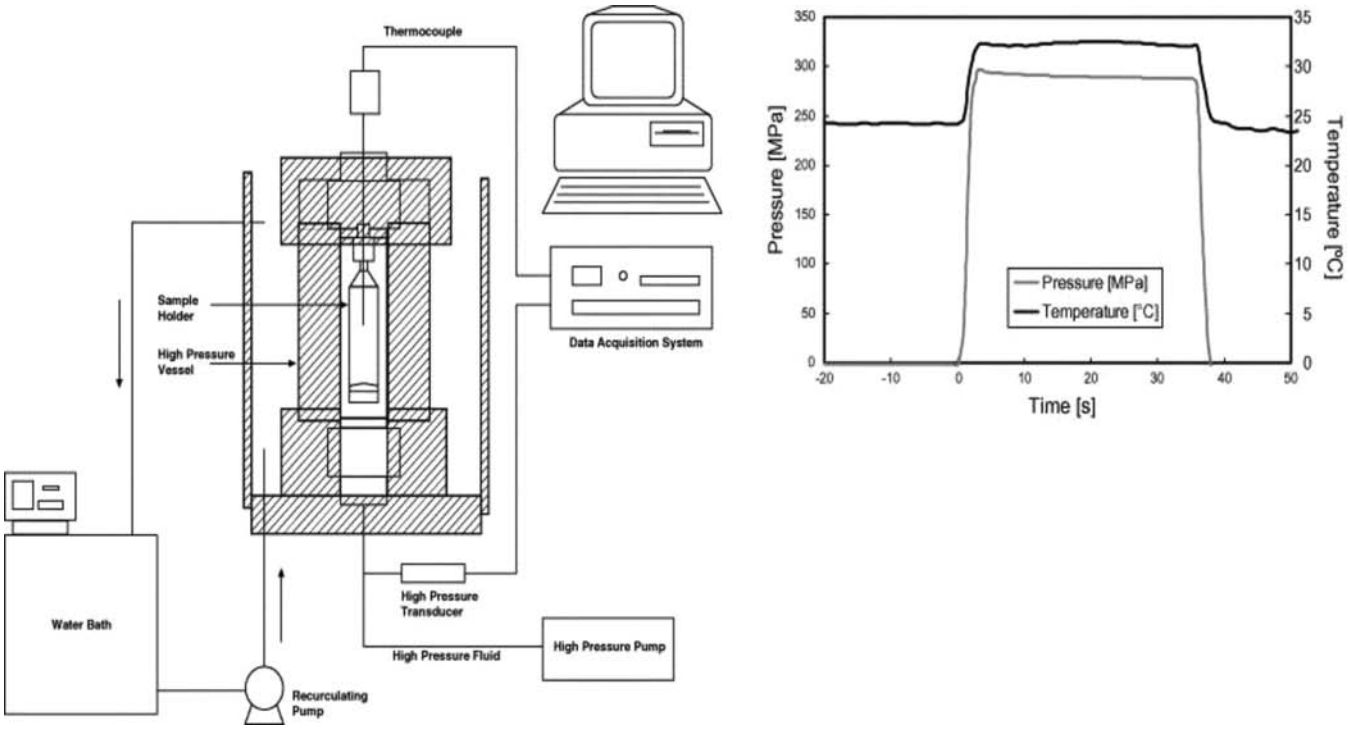

Figure 1. Schematic presentation of HPP assembly unit with time−temperature and pressure profiles of hydraulic medium in pressurized chamber. Reprinted with permission from ref 32. Copyright 2007 Elsevier.

cylinder, generally in the range of 400−800 MPa with a lower holding time at a lower temperature than thermal treatments[32] (Figure 1). At these elevated pressures, detrimental microorganisms are destroyed without degradation of flavor and nutrients.[33] Due to the reduced thermal stress, HPP retains the nutrients and quality of fresh fruits and vegetables better than traditional thermal treatments.[2,34,35]

In addition, HPP can either activate or inactivate enzymes depending upon the treatment pressure and temperature. HPP treatment at higher pressures and temperatures led to substantial inactivation of enzymes. For example, HPP (alone or in combination with moderate heat treatment) partially or substantially inactivated quality-degrading enzymes such as pectinmethylesterase (PME), polyphenol oxidase (PPO), polygalacturonase (PG), and peroxidase (POD) in fruits and fruit products and thus minimized quality losses during storage.[3,36−39] However, HPP treatment at lower pressures and temperatures can activate enzymes or have minimal effects on their activity. For instance, Huang et al. reported significant activation of PPO and POD and no change in the activity of PME in apricot nectars as a result of HPP treatment at 300−500 MPa for 5−20 min (started at ambient temperature). In contrast, a high-temperature−short-time (HTST) treatment at 110 °C for 8.6 s induced a complete inactivation of these enzymes.[40]

Minimal effects of HPP on the color of fruit products have been reported by a number of researchers. Huang et al. reported that the color of apricot nectars was closer to that of untreated apricot nectar after HPP treatment (300−500 MPa/5−20 min) than after HTST treatment (110 °C/8.6 s).[40] Patras et al. demonstrated that processing strawberry purée with HPP resulted in minor color (red) reductions in the fruit product compared to thermally processed purées.[5]

SAFETY ENHANCEMENT AND SPOILAGE CONTROL IN FRUIT PRODUCTS BY HPP

HPP can be used for cold pasteurization (in the operating range of 5−25 °C) of fruit products. For instance, fruit jams and juices are normally processed at pressures around 400 MPa or higher for 5−10 min at ≤20 °C. The treatment significantly reduces the number of spoilage microorganisms (such as yeasts and molds) and pathogens (such as *Escherichia coli* O157:H7 and *Salmonella* spp.).[36,41−44] The refrigerated shelf life of such products can be up to 30 days or longer, and they have superior sensory quality compared with those prepared in a conventional manner.[45] García-Parra et al. reported that the inactivation of microorganisms by HPP in nectarine (*Prunus persica* L.) purées and the microbial stability of the treated product during subsequent refrigerated storage (up to 60 days) were similar to those achieved by conventional thermal pasteurization (85 °C/5 min). These treatment conditions (600 MPa for 10 min) also resulted in higher polyphenol content.[46] Donsi et al. found no fungal growth in high-pressure-treated lemon juice (450 MPa for 2, 5, or 10 min), whereas control samples were spoiled by yeasts and filamentous fungi after 10 days.[36] They also reported that HPP had minimal effect on the constituents of the lemon juice and physicochemical properties.[36] In an another study, González-Cebrino et al. reported that indigenous microorganisms (total aerobic mesophilic and psychrotrophic counts, molds, and yeasts) in plum purée (cv. Crimson Globe, with red flesh and peel) were inactivated to undetected levels after HPP treatment at 400, 500, and 600 MPa for up to 300 s.[47]

Ascospores of yeasts and molds may show higher resistance to pressure as compared to the vegetative cells. For instance, Raso et al. reported a 5-log reduction of the vegetative cells of *Zygosaccharomyces bailii* (spoilage yeasts) in apple, orange, pineapple, cranberry, and grape juices by high-pressure

dx.doi.org/10.1021/jf404400q | J. Agric. Food Chem. 2014, 62, 3877−3885

treatment at 300 MPa for 5 min, whereas the same treatment resulted in only 0.5−1.0-log reduction of the yeast ascospore.[48] The resistance of the ascospores also depends upon the food matrix and water activity. Butz et al. achieved a 4.0-log and <1.0-log reductions of *Byssochlamys nivea* mold ascospores in grape juice and bilberry jam, respectively, after a 700 MPa treatment at 70 °C for 30 min.[49] The reduced inactivation of ascospores in jam is mainly due to the reduced water activity. Application of HPP at elevated process temperatures has also been effective in the inactivation of acidophilic, spore-forming spoilage bacteria, which is of major concern in the fruit juice industry. Ardia et al. reported a 6.0-log reduction of *Alicyclobacillus acidoterrestris* DMS 2498 spores in orange juice at 700 MPa (80 °C initial temperature) for 20 min.[50] Barba et al. reported a 5-log reduction of *Lactobacillus plantarum* CECT 220 in an orange juice−milk beverage after HPP treatment at 200 MPa for 5 min.[51] Varela-Santos et al. demonstrated that HPP treatment at 350 MPa for 150 s was sufficient to reduce the microbial load in pomegranate juice by around 4.0 logs and keep the microbial populations in the product below the detection limit during storage (4 °C/35 days).[52]

In a study conducted by our group, the efficacy of HPP (400 and 600 MPa) as a cold pasteurization technique for the inactivation of pathogenic bacteria in a formulated strawberry−blueberry-based beverage (20 g of freeze-dried powder from each and 25 g of sugar in 8 oz, pH 3.70) was demonstrated. *E. coli* O175:H7 (ENT C9490),[53] *Salmonella* Typhimurium (ATCC 14028), and *Listeria monocytogenes* (FRR W2542)[54] were subjected to high-pressure processing (initial temperature = 4 °C and final temperature = 22−25 °C). The data indicated an increase in the level of inactivation with increasing pressure or pressure holding time (Figure 2). *E. coli* O157:H7 appeared to be the most pressure-resistant pathogen among the three bacteria tested. At 400 MPa, a maximum 4-log reduction of this pathogen was achieved in the beverage after a 10 min pressure holding time. In contrast, the other two pathogens, *S.* Typhimurium and *L. monocytogenes*, were inactivated by 5.5−6.0 logs after a 400 MPa pressure treatment for 5 min (Figure 2A). A 5 min holding time was sufficient to inactivate the pressure-resistant *E. coli* O157:H7 in the beverage by 5.7 logs at 600 MPa (Figure 2B). A >5-log reduction was achieved for the other two pathogens at 600 MPa after a pressure holding time as short as 1 min (Figure 2B). This study demonstrated that a 600 MPa treatment for 5 min would be sufficient to achieve a 5-log reduction of the most resistant pathogens of public health concern in the product as mandated by the U.S. Food and Drug Administration[55] and produce a beverage as safe as the thermally pasteurized product (71.1 °C for 6 s).

IMPACT OF HPP ON BIOACTIVE COMPOUNDS IN FRUIT PRODUCTS

Several researchers have investigated the effects of HPP on the nutritional quality of foods, especially fruits and vegetables, and suggested that HPP could be an effective processing method for retaining health-promoting compounds such as polyphenolic compounds.[14,15,18,56] In contrast to losses of bioactive compounds in fruit juices due to thermal processing,[57] HPP offers the benefit of retaining nutritive value of juices without compromising food safety. Recent findings on the effect of high-pressure processing on bioactive components are summarized in Table 1. Matser et al. reported that sterilizing herbs and essential oils by HPP treatment preserved the heat-sensitive bioactive phytochemicals in comparison to

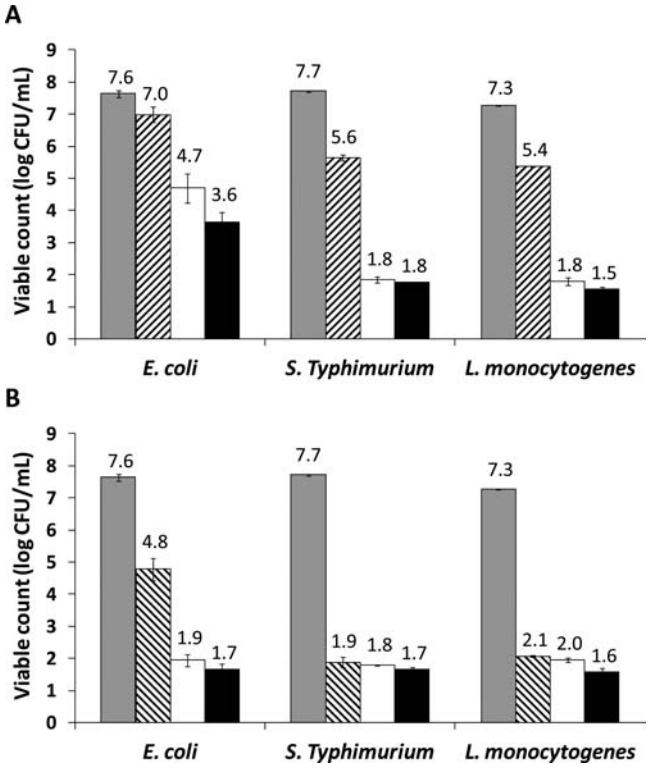

Figure 2. Viable counts of selected pathogenic bacteria (*Escherichia coli* O175:H7 (ENT C9490), *Salmonella* Typhimurium (ATCC 14028), and *Listeria monocytogenes* (FRR W2542)) inoculated in a formulated strawberry−blueberry-based beverage (pH 3.70) before treatment (gray bars) and after high-pressure treatment at 400 MPa (A) and 600 MPa (B) for 1 min (slashed bars), 5 min (white bars), and 10 min (black bars) (initial temperature = 4 °C). Bar graphs represent the mean viable counts of bacteria in the beverage obtained from two trials. Error bars indicate standard deviations, $n = 3$. Detection limit = 10 CFU/mL.

conventional retort process.[58] In a study investigating the total antioxidant capacity of reconstituted orange juice treated with different processing technologies, HPP-treated juice yielded higher total antioxidant retention under various storage conditions compared to conventional thermal pasteurization processing.[59] Other studies have indicated that the bioactive composition of strawberries is stable under pressures of 400−600 MPa, although there was a slight reduction in the anthocyanin content possibly due to interactions among flavonoid compounds under higher pressures.[60]

At the pressure of 600 MPa, total phenolics concentration in strawberry purée was increased by 9.8% and in a pressure range of 400−600 MPa the anthocyanin content was unaffected compared to thermal processing.[5] Researchers have shown that the extractability and potential bioaccessibility of compounds such as flavonols, carotenoids, and lycopene are improved with HPP.[61−63] However, the biological significance of high-pressure-processed fruit products, specifically as it relates to the bioavailability of nutrients and polyphenolic compounds, has not been studied.

The effect of food matrix may also affect the efficacy of HPP. Thermal versus HPP of strawberry-based beverages formulated using milk versus water showed that (1) the milk matrix alone (unprocessed) significantly the reduced antioxidant capacity and flavonoid content (i.e., anthocyanins and quercetin) of the beverages[3] and (2) processing with high temperatures

(pasteurization) significantly reduced the antioxidant capacity and flavonoid content compared to HPP regardless of the matrix. However, differential responses to HPP were evident depending on the matrix. Strawberry beverages without milk showed no significant difference in antioxidant capacity (as measured by oxygen radical absorbance capacity, ORAC) after HPP with pressures up to 600 MPa compared to unprocessed beverages, whereas applying higher pressures (700−800 MPa) resulted in significantly lower ORAC compared to unprocessed beverages. In contrast, beverages formulated with milk exhibited significantly higher ORAC values when treated with HPP up to 600 MPa compared to unprocessed beverages.[3] Measurements of antioxidant capacity by ferric reducing ability power (FRAP) showed that the strawberry beverage without milk had significantly lower FRAP values after HPP at all pressures tested (200−800 MPa). However, formulating the strawberry beverage with milk resulted in no change in FRAP after HPP compared to the unprocessed beverage.[3] Collectively, the data reveal an interaction of matrix and processing, suggesting a potential protective effect on antioxidant capacity with milk and HPP treatment that was not observed with HTST or water. Flavonoid composition decreased after the application of HPP (compared to the unprocessed beverages); however, reductions were modest compared to HTST processing and relatively stable until pressures of 700 and 800 MPa were applied. At higher pressures, reduced flavonoid concentrations were not different from those resulting from HTST.[3] Interestingly, the sensitivity of flavonoids to different pressures appeared to depend on the chemistry of the compound; for example, pelargonidin and quercetin linked to glucoside or malonylglucoside sugars were more stable at lower pressures than pelargonidin and quercetin compounds linked to rutinoside or coumaroylglucoside.[3]

Anthocyanins in fruit juices and purées (such as strawberry juice and purée, black currant juice, raspberry juice, and blackberry purée) have been reported to be stable to high-pressure treatment (up to 600 MPa) at ambient temperature.[5,19,64−66] Suthanthangjai et al. evaluated the effect of high-pressure treatment (200−800 MPa/18−22 °C/15 min) on anthocyanin in raspberry purée and observed the highest stability of the anthocyanin when the purée was pressurized at 200 or 800 MPa and stored at 4 °C.[67] Combined pressure and temperature treatment of blueberry juice resulted in a slightly faster degradation of total anthocyanins during storage as compared to heat treatments at ambient pressure.[67]

Ascorbic acid (vitamin C) is a heat-labile essential nutrient in fruits and vegetables. Canned fruit and vegetable products have lower ascorbic acid than fresh products.[4] Patras et al. reported that HPP treatment of strawberry purées resulted in a >90% retention of ascorbic acid, whereas significant losses of ascorbic acid were evident after thermal processing.[5] Polydera et al. reported greater retention of ascorbic acid in pressurized orange juice (500 MPa/35 °C/5 min) as compared to conventionally pasteurized juice (80 °C/30 s).[58,68,69] However, ascorbic acid content in orange juice was lower than that in untreated juice when pressurized (800 MPa/25 °C/1 min) and stored for >2 months at 4 or 37 °C.[58] These losses may be due in part to the length of storage. Fernandez Garcia et al. demonstrated that high-pressure treatment of orange juice and an orange−carrot−lemon juice product (500 or 800 MPa for 5 min) had no significant effect on the vitamin C content, antioxidant capacity, and sugar and carotene contents during storage for up to 21 days at 4 °C.[69] Retention of ascorbic acid was also found in strawberry nectar after high-pressure treatment at 500 MPa for 3 min at room temperature.[70]

Barba et al. studied the effects of HPP (600 MPa/42 °C/5 min) and PEF processing (36 kV/cm, 100 μs) on the quality and nutritional characteristics of blueberry juice. They observed a higher retention of ascorbic acid content (31% loss) and a better preservation of the antioxidant activity (21% loss) in the HPP-treated juice compared to the unprocessed and PEF-treated samples.[22] In another study, they found no statistical difference in the antioxidant capacity of blueberry juice treated at 200 MPa for 5−15 min compared to fresh juice.[23] However, the values were lowest after treatment at 400 MPa/15 min and 600 MPa/5−15 min.

HPP is among the emerging, novel, nonthermal technologies that present niche processing opportunities to commercial processors. Application of HPP to process fruit-based products has been shown to produce safe food and retain health-promoting bioactive compounds and other quality attributes compared to thermal processing. However, the biological importance of the retention of nutrients and bioactive phytochemical compounds imparted by HPP remains to be shown.

Overall, there is a critical need to deliver more opportunities to consumers to eat fruits and vegetables. HPP is poised to deliver on these opportunities by providing convenient, nutritionally improved products. In some cases, HPP may enhance the bioaccessibility of plant components, and therefore greater benefit may be afforded by the processed product. Due to the importance of diet (particularly fruits and vegetables) to health, there is no doubt that the field will continue to evolve.

AUTHOR INFORMATION

Corresponding Author

*(B.M.B.-F.) Phone: +1 (708) 341-7078. Fax: +1 (708) 563-1873. E-mail: bburton@iit.edu.

Notes

The authors declare no competing financial interest.

REFERENCES

(1) U.S. Department of Agriculture and U.S. Department of Health and Human Services. *Dietary Guidelines for Americans*, 7th ed.; U.S. Government Printing Office: Washington. DC, USA, 2010.

(2) FAO/WHO. Food Standards Program Codex Alimentarius Commission. *Codex Alimentarius*, 2nd ed.; FAO: Rome, Italy, 1994; Vol. 4.

(3) Tadapaneni, R. K.; Banaszewski, K.; Patazca, E.; Edirisinghe, I.; Cappozzo, J.; Jackson, L.; Burton-Freeman, B. Effect of high-pressure processing and milk on the anthocyanin composition and antioxidant capacity of strawberry-based beverages. *J. Agric. Food Chem.* **2012**, *60*, 5795−5802.

(4) Rickman, J. C.; Bruhn, C. M.; Barrett, D. M. Review: Nutritional comparison of fresh, frozen, and canned fruits and vegetables. Part I. Vitamins C and B and phenolic compounds. *J. Sci. Food Agric.* **2007**, *87*, 930−944.

(5) Patras, A.; Brunton, N. P.; Da Pieve, S.; Butler, F. Impact of high pressure processing on total antioxidant activity, phenolic, ascorbic acid, anthocyanin content and color of strawberry and blackberry purées. *Innovative Food Sci. Emerging Technol.* **2009**, *10*, 308−313.

(6) Kris-Etherton, P. M.; Hecker, K. D.; Bonanome, A.; Coval, S. M.; Binkoski, A. E.; Hilpert, K. F.; Griel, A. E.; Etherton, T. D. Bioactive compounds in foods: their role in the prevention of cardiovascular disease and cancer. *Am. J. Med.* **2002**, *13*, 71−88.

(7) Bravo, L. Polyphenols: chemistry, dietary sources, metabolism, and nutritional significance. *Nutr. Rev.* **1998**, *56*, 317−333.

(8) Burton-Freeman, B.; Linares, A.; Hyson, D.; Kappagoda, C. T. Strawberry modulates LDL oxidation and postprandial lipemia in

response to high-fat meal in overweight hyperlipidemic men and women. *J. Am. Coll. Nutr.* **2010**, *29*, 46−54.
(9) Ellis, C. L.; Edirisinghe, I.; Kappagoda, C. T; Burton-Freeman, B. M. Attenuation of meal induced inflammatory and thrombotic responses in overweight men and women after 6-week daily strawberry (*Fragaria*) intake. *J. Atheroscler. Thromb.* **2011**, *18*, 318−327.
(10) Edirisinghe, I.; Banaszewski, K.; Cappozzo, J.; Krishnankutty, S.; Ellis, C. L.; Tadapaneni, R. K.; Kappagoda, C. T.; Burton-Freeman, B. M. Strawberry anthocyanin and its association with postprandial inflammation and insulin. *Br. J. Nutr.* **2011**, *106*, 913−922.
(11) Vauzour, D.; Rodriguez-Mateos, A.; Corona, G.; Oruna-Concha, M. J.; Spencer, J. P. Polyphenols and human health: prevention of disease and mechanisms of action. *Nutrients* **2010**, *2*, 1106−1131.
(12) González-Gallego, J.; García-Mediavilla, M. V.; Sánchez-Campos, S.; Tuñón, M. J. Fruit polyphenols, immunity and inflammation. *Br. J. Nutr.* **2010**, *104*, S15−S27.
(13) Joseph, S.; Edirisinghe, I.; Burton-Freeman, B. Fruit polyphenols: a review of anti-inflammatory effects in humans. *Crit. Rev. Food Sci. Nutr.* **2014**, in press.
(14) Barba, F. J.; Esteve, M. J.; Frígola, A. High pressure treatment effect on physicochemical and nutritional properties of fluid foods during storage: a review. *Compr. Rev. Food Sci. Food Saf.* **2012**, *11*, 307−322.
(15) Barrett, D. M.; Lloyd, B. Advanced preservation methods and nutrient retention in fruits and vegetables. *J. Sci. Food Agric.* **2012**, *92*, 7−22.
(16) Oms-Oliu, G.; Odriozola-Serrano, I.; Martín-Belloso, O. The effects of non-thermal technologies on phytochemicals. In *Phytochemicals − A Global Perspective of Their Role in Nutrition and Health*; Rao, V., Ed.; InTech: Rijeka, Croatia, 2012; pp 107−126.
(17) Gamlath, S.; Wakeling, L. Trends in high pressure processing of foods: food quality and bioactive components. In *New Topics in Food Engineering*; Comeau, M. A., Ed.; Nova Science Publishers: Hauppauge, NY, USA, 2011; pp 121−149.
(18) Rastogi, N. K.; Raghavarao, K. S. M. S; Balasubramaniam, V. M.; Niranjan, K.; Knorr, D. Opportunities and challenges in high pressure processing of foods. *Crit. Rev. Food Sci. Nutr.* **2007**, *47*, 69−112.
(19) Aaby, K.; Wrolstad, R.; Ekeberg, D.; Skrede, G. Polyphenol composition and antioxidant activity in strawberry purées; impact of achene level and storage. *J. Agric. Food Chem.* **2007**, *55*, 5156−5166.
(20) van Boekel, M.; Fogliano, V.; Pellegrini, N.; Stanton, C.; Scholz, G.; Lalljie, S.; Somoza, V.; Knorr, D.; Jasti, P. R.; Eisenbrand, G. A review on the beneficial aspects of food processing. *Mol. Nutr. Food Res.* **2010**, *54*, 1215−1247.
(21) Lundahl, D. S.; McDaniel, M. R.; Wrolstad, R. E. Flavor, aroma, and compositional changes in strawberry juice concentrate stored at 20 °C. *J. Food Sci.* **1989**, *54*, 1255−1258.
(22) Barba, F. J.; Jäger, H.; Meneses, N.; Esteve, M. J.; Frígola, A.; Knorr, D. Evaluation of quality changes of blueberry juice during refrigerated storage after high-pressure and pulsed electric fields processing. *Innovative Food Sci. Emerging Technol.* **2012**, *14*, 18−24.
(23) Barba, F. J.; Esteve, M. J.; Frígola, A. Physicochemical and nutritional characteristics of blueberry juice after high pressure processing. *Food Res. Int.* **2013**, *50*, 545−549.
(24) Klopotek, F.; Otto, K.; Böhm, V. Processing strawberries to different products alters contents of vitamin C, total phenolics, total anthocyanins, and antioxidant capacity. *J. Agric. Food Chem.* **2005**, *53*, 5640−5646.
(25) Butz, P.; Tauscher, B. Emerging technologies: chemical aspects. *Food Res. Int.* **2002**, *35*, 279−284.
(26) Gerlach, D.; Alleborn, N.; Baars, A.; Delgado, A.; Moritz, J.; Knorr, D. Numerical simulations of pulsed electric fields for food preservation: a review. *Innovative Food Sci. Emerging Technol.* **2008**, *9*, 408−417.
(27) Buckow, R.; Chandry, P. S.; Ng, S. Y.; McAuley, C. M.; Swanson, B. G. Opportunities and challenges in pulsed electric field processing of dairy products. *Int. Dairy J.* **2014**, *34*, 199−212.
(28) Markland, S. M.; Kniel, K. E.; Setlow, P.; Hoover, D. G. Nonthermal inactivation of heterogeneous and superdormant spore populations of *Bacillus cereus* using ozone and high pressure processing. *Innovative Food Sci. Emerging Technol.* **2013**, *19*, 44−49.
(29) Oey, I.; Lille, M.; Loey, A. V.; Hendrickx, M. Effect of high-pressure processing on colour, texture and flavour of fruit-and vegetable-based food products: a review. *Trends Food Sci. Technol.* **2008**, *19*, 320−328.
(30) Farkas, D. F. High pressure processing pathways to commercialization. In *Nonthermal Processing Technologies for Foods*; Zhang, H. Q. Barbosa-Canovas, G. V., Balasubramaniam, V. M., Dunne, C. P., Farkas, D. F., Yuan, J. T., Eds.; IFT Press, Wiley-Blackwell: Chicago, IL, USA, 2011; pp 28−35.
(31) Hayashi, R. An overview of the use of high pressure in bioscience and biotechnology. In *High Pressure Bioscience and Biotechnology*; Hayashi, R., Balny, C., Eds.; Elsevier: Amsterdam, The Netherlands, 1996; Vol. 13, pp 1−6.
(32) Patazca, E.; Koutchma, T.; Balasubramaniam, V. M. Quasi-adiabatic temperature increase during high pressure processing of selected foods. *J. Food Eng.* **2007**, *80*, 199−205.
(33) Señorans, J.; Ibáñz, E.; Cifuentes, A. New trends in food processing. *Crit. Rev. Food Sci. Nutr.* **2003**, *43*, 507−526.
(34) Ludikhuyze, L.; Van Loey, A.; Smout, C.; Indrawati; Hendrickx, M. Effects of combined pressure and temperature on enzymes related to quality of fruits and vegetables: from kinetic information to process engineering aspects. *Crit. Rev. Food Sci. Nutr.* **2003**, *43*, 527−586.
(35) Sánchez-Moreno, C.; De Ancos, B.; Plaza, L.; Elez-Martínez, P.; Cano, M. P.Nutritional approaches and health-related properties of plant foods processed by high pressure and pulsed electric fields. *Crit. Rev. Food Sci. Nutr.* **2009**, *49*, 552−576.
(36) Donsi, G.; Ferrari, G.; di Matteo, M.; Bruno, M. C. High-pressure stabilization of lemon juice. *Ital. Food Beverage Technol.* **1998**, *14*, 14−16.
(37) Lambert, Y.; Demazeau, G.; Largeteau, A.; Bouvier, J. M. Changes in aromatic volatile composition of strawberry after high pressure treatment. *Food Chem.* **1999**, *67*, 7−16.
(38) Nienaber, U.; Shellhammer, T. H. High pressure processing of orange juice: combination treatments and a shelf life study. *J. Food Sci.* **2001**, *66*, 332−336.
(39) Phunchaisri, C.; Apichartsrangkoon, A. Effects of ultra-high pressure on biochemical and physical modification of lychee (*Litchi chinensis* Sonn.). *Food Chem.* **2005**, *93*, 57−64.
(40) Huang, W.; Bi, X.; Zhang, X.; Liao, X.; Hu, X.; Wu, J. Comparative study of enzymes, phenolics, carotenoids and color of apricot nectars treated by high hydrostatic pressure and high temperature short time. *Innovative Food Sci. Emerging Technol.* **2013**, *18*, 74−82.
(41) Linton, M.; McClements, J. M. J.; Patterson, M. F. Survival of *Escherichia coli* O157:H7 during storage in pressure-treated orange juice. *J. Food Prot.* **1999**, *62*, 1038−1040.
(42) Ramaswamy, H. S.; Riahi, E.; Idziak, E. High-pressure destruction kinetics of *E. coli* (29055) in apple juice. *J. Food Sci.* **2003**, *68*, 1750−1756.
(43) Bull, M. K.; Zerdin, K.; Howe, E.; Goicoeche, G.; Paramanandhan, P.; Stockman, R.; Sellahewa, J.; Szabo, E. A.; Johnson, R. L.; Stewart, C. M. The effect of high pressure processing on the microbial, physical and chemical properties of Valencia and Navel orange juice. *Innovative Food Sci. Emerging. Technol.* **2004**, *5*, 135−149.
(44) Tonello, C. Case studies on high-pressure processing of foods. In *Nonthermal Processing Technologies for Foods*; Zhang, H. Q., Barbosa-Canovas, G. V., Balasubramaniam, V. M., Dunne, C. P., Farkas, D. F., Yuan, J. T., Eds.; IFT Press, Wiley-Blackwell: Chicago, IL, USA, 2011; pp 36−50.
(45) Ludikhuyze, L.; Hendrickx, M. E. G. Effects of high pressure on chemical reactions related to food quality. In *Ultra High Pressure Treatments of Foods*; Hendrickx, M. E. G., Knorr, D., Eds.; Kluwer Academic/Plenum Publishers: New York, 2001; pp 167−188.
(46) González-Cebrino, F.; Durán, R.; Delgado-Adámez, J.; Contador, R.; Ramírez, R. Changes after high-pressure processing on physicochemical parameters, bioactive compounds, and polyphenol

oxidase activity of red flesh and peel plum purée. *Innovative Food Sci. Emerging Technol.* **2013**, *20*, 34−41.
(47) Raso, J.; Calderón, M. L.; Góngora, M.; Barbosa-Cánovas, G. V.; Swanson, B. G. Inactivation of *Zygosaccharomyces bailii* in fruit juices by heat, high hydrostatic pressure and pulsed electric fields. *J. Food Sci.* **1998**, *63*, 1042−1044.
(48) Butz, P.; Funtenberger, S.; Haberditzl, T.; Taischer, B. High pressure inactivation of *Byssochlamys nivea* ascospores and other heat resistant molds. *Lebensm. Wiss. Technol.* **1996**, *29*, 404−410.
(49) Ardia, A.; Knorr, D.; Ferrari, G.; Heinz, V. Kinetic studies on combined high-pressure and temperature inactivation of *Alicyclobacillus acidoterrestris* spores in orange juice. *Appl. Biotechnol. Food Sci. Pol.* **2003**, *1*, 169−173.
(50) Barba, F. J.; Cortés, C.; Esteve, M. J.; Frígola, A. Study of antioxidant capacity and quality parameters in an orange juice−milk beverage after high-pressure processing treatment. *Food Bioprocess Technol.* **2012**, *5*, 2222−2232.
(51) Varela-Santos, E.; Ochoa-Martinez, A.; Tabilo-Munizaga, G.; Reyes, J. E.; Pérez-Won, M.; Briones-Labarca, V.; Morales-Castro, J. Effect of high hydrostatic pressure (HHP) processing on physicochemical properties, bioactive compounds and shelf-life of pomegranate juice. *Innovative Food Sci. Emerging Technol.* **2012**, *13*, 13−22.
(52) Benito, A.; Ventoura, G.; Casadei, M.; Robinson, T.; Mackey, B. Variation in resistance of natural isolates of *Escherichia coli* O157 to high hydrostatic pressure, mild heat, and other stresses. *Appl. Environ. Microbiol.* **1999**, *65*, 1564−1569.
(53) Youart, A. M.; Huang, Y.; Stewart, C. M.; Kalinowski, R. M.; Legan, J. D. Modeling time to inactivation of *Listeria monocytogenes* in response to high pressure, sodium chloride, and sodium lactate. *J. Food Prot.* **2010**, *73*, 1793−1802.
(54) U.S. Food and Drug Administration. *Guidance for Industry: Juice HACCP Hazards and Controls Guidance*, 1st ed.; final guidance, 2004; http://www.fda.gov/Food/GuidanceComplianceRegulatoryInformation/GuidanceDocuments/Juice/ucm072557.htm.
(55) Altuner, E. M.; Tokuşoğlu, Ö. The effect of high hydrostatic pressure processing on the extraction, retention and stability of anthocyanins and flavonols contents of berry fruits and berry juices. *Int. J. Food Sci. Technol.* **2013**, *48*, 1991−1997.
(56) Wang, W.; Xu, S. Degradation kinetics of anthocyanins in blackberry juice and concentrate. *J. Food Eng.* **2007**, *82*, 271−275.
(57) Matser, A. M.; Krebbers, B.; Van Den Berg, R. W.; Bartels, P. V. Advantages of high pressure sterilization on quality of food products. *Trends Food Sci. Technol.* **2004**, *15*, 79−85.
(58) Polydera, A. C.; Stoforos, N. G.; Taoukis, P. S. The effect of storage on the antioxidant activity of reconstituted orange juice which had been pasteurized by high pressure or heat. *Int. J. Food Sci. Technol.* **2004**, *39*, 783−791.
(59) Tiwari, B. K.; O'Donnell, C. P.; Cullen, P. J. Effect of non-thermal processing technologies on the anthocyanin content of fruit juices. *Trends Food Sci. Technol.* **2009**, *20*, 137−145.
(60) McInerney, J. K.; Seccafien, C. A.; Stewart, C. M.; Bird, A. R. Effects of high pressure processing on antioxidant activity, and total carotenoid content and availability, in vegetables. *Innovative Food Sci. Emerging Technol.* **2007**, *8*, 543−548.
(61) Phunchaisri, C.; Apichartsrangkoon, A. Effects of ultra-high pressure on biochemical and physical modification of lychee (*Litchi chinensis* Sonn.). *Food Chem.* **2005**, *93*, 57−64.
(62) de Ancos, B.; Gonzalez, E.; Cano, P. Effect of high-pressure treatment on the carotenoid composition and the radical scavenging activity of persimmon fruit purées. *J. Agric. Food Chem.* **2000**, *48*, 3542−3548.
(63) Polydera, A. C.; Stoforos, N. G.; Taoukis, P. S. Comparative shelf life study and vitamin C loss kinetics in pasteurized and high pressure processed reconstituted orange juice. *J. Food Eng.* **2003**, *60*, 21−29.
(64) Zabetakis, I.; Leclerc, D.; Kajda, P. The effect of high hydrostatic pressure on the strawberry anthocyanins. *J. Agric. Food Chem.* **2000**, *48*, 2749−2754.
(65) Kouniaki, S.; Kajda, P.; Zabetakis, I. The effect of high hydrostatic pressure on anthocyanins and ascorbic acid in blackcurrants (*Ribes nigrum*). *Flavour Fragrance J.* **2004**, *19*, 281−286.
(66) Garcia-Palazon, A.; Suthanthangjai, W.; Kajda, P.; Zabetakis, I. The effects of high hydrostatic pressure on β-glucosidase, peroxidase and polyphenoloxidase in red raspberry (*Rubus idaeus*) and strawberry (*Fragaria* × *ananassa*). *Food Chem.* **2004**, *88*, 7−10.
(67) Suthanthangjai, W.; Kajdaa, P.; Zabetakis, I. The effect of high hydrostatic pressure on the anthocyanins of raspberry (*Rubus idaeus*). *Food Chem.* **2005**, *90*, 193−197.
(68) Polydera, A. C.; Stoforos, N. G.; Taoukis, P. S. Effect of high hydrostatic pressure treatment on post processing antioxidant activity of fresh navel orange juice. *Food Chem.* **2005**, *91*, 495−503.
(69) Fernandez Garcia, A.; Butz, P.; Bognar, A.; Tauscher, B. Antioxidative capacity, nutrient content and sensory quality of orange juice and an orange lemon carrot juice product after high-pressure treatment and storage in different packaging. *Eur. Food Res. Technol.* **2001**, *213*, 290−296.
(70) Rovere, P.; Carpi, G.; Gola, S.; Dall'Aglio, G.; Maggy, A. HPP strawberry products: an example of processing line. In *High Pressure Bioscience and Biotechnology*; Hayashi, R., Balny, C., Eds.; Elsevier Science: Amsterdam, The Netherlands, 1996; pp 445−450.
(71) Carbonell-Capella, J. M.; Barba, F. J.; Esteve, M. J.; Frígola, A. High pressure processing of fruit juice mixture sweetened with *Stevia rebaudiana* Bertoni: optimal retention of physical and nutritional quality. *Innovative Food Sci. Emerging Technol.* **2013**, *18*, 48−56.
(72) Jacobo-Velázquez, D. A.; Hernández-Brenes, C. Stability of avocado paste carotenoids as affected by high hydrostatic pressure processing and storage. *Innovative Food Sci. Emerging Technol.* **2012**, *16*, 121−128.
(73) García-Parra, J.; González-Cebrino, F.; Delgado, J.; Lozano, M.; Hernández, T.; Ramírez, R. Effect of thermal and high-pressure processing on the nutritional value and quality attributes of a nectarine purée with industrial origin during the refrigerated storage. *J. Food Sci.* **2011**, *76*, C618−C625.
(74) Queiroz, C.; Moreira, C. F. F.; Lavinas, F. C.; Lopes, M. L. M.; Fialho, E.; Valente-Mesquita, V. L. Effect of high hydrostatic pressure on phenolic compounds, ascorbic acid and antioxidant activity in cashew apple juice. *High Pressure Res.* **2010**, *30*, 507−513.
(75) Rao, L.; Guo, X.; Pang, X.; Tan, X.; Liao, X.; Wu, J. Enzyme activity and nutritional quality of peach (*Prunus persica*) juice: effect of high hydrostatic pressure. *Int. J. Food Properties* **2013**, in press.
(76) Liu, F.; Wang, Y.; Li, R.; Bi, X.; Liao, X. Effects of high hydrostatic pressure and high temperature short time on antioxidant activity, antioxidant compounds and color of mango nectars. *Innovative Food Sci. Emerging Technol.* **2014**, DOI: 10.1016/j.ifset.2013.09.015.

effect in mixed fruit/mixed dietary polyphenol formulation were included in this review. Four studies were not included due to mixed fruit preparations[45−47] or mixed polyphenol sources (i.e., berry plus tea).[48]

INFLAMMATION – GENERAL OVERVIEW

Inflammation is the normal, protective, and (usually) temporary response of the innate immune system to pathogens and injury. However, with recurrent stimuli or inefficient regulation, chronic inflammation ensues. Quantifiable inflammatory responses are characterized by the production of pro-inflammatory molecules and anti-inflammatory cytokines acting as signals between immune cells to coordinate the inflammatory response. Cytokines are immune-modulatory molecules that control the inflammatory response. Nuclear factor kappa B (NF-κB), a redox-sensitive transcription factor, is a central orchestrator of the inflammatory response. Once NF-κB is activated, it stimulates the expression of a number of genes including those responsible for the production of cytokines (i.e., tumor necrosis factor (TNF)-α, interleukin (IL)-6, IL-1β), chemokines (i.e., monocyte chemoattractant protein (MCP)-1), adipokines (i.e., leptin, adiponectin), cell adhesion molecules (i.e., E-selectin, P-selectin, soluble vascular cell adhesion molecule-1 (sVCAM-1), and soluble intercellular adhesion molecule-1 (sICAM-1)), and acute phase proteins (i.e., (hs) C-reactive protein (CRP), fibrinogen).[49] Other important mediators of inflammation include pattern recognition receptors (PRR) such as Toll-like receptors (TLRs) and kinases such as mitogen-activated protein kinase (MAPK) and c-Jun N-terminal kinases (JNK). The inflammatory response can be triggered by stimuli such as endotoxin (lipopolysaccharide from bacteria), viruses, and changes in levels of reactive oxygen species (ROS), cellular redox status, fatty acids, cytokines, growth factors, and carcinogens among others.

LIFESTYLE CONTRIBUTORS TO INFLAMMATION

In addition to classic inflammatory stimuli (i.e., bacteria), inflammatory stress can also result from excess body fat and poor diet. Obesity is well recognized as a chronic, low-grade inflammatory state. Hotamisligil et al. first reported a positive relationship between adipose mass and expression of the pro-inflammatory gene TNF-α.[50] Nowadays, it is well recognized that adipose tissue is much more than a static depot of fat but rather a dynamic secretory tissue that produces a large number of hormones and cytokines.[51] In obesity, morphological changes in adipocytes result in altered secretory responses favoring an inflammatory state. Expanding adipose tissue mass recruits macrophages that produce pro-inflammatory proteins such as TNF-α, IL-6, and MCP-1 contributing further to the pro-inflammatory state. Elevated circulating inflammatory proteins are observed in obesity and explain the critical link between obesity and the development of insulin resistance, type 2 diabetes, and CVD.[52]

In addition to excess body adiposity, excess energy intake and poor dietary composition typical of Western eating patterns promote acute (postprandial) as well as cumulative sustained inflammatory responses in both obese and normal weight individuals.[53−56] The postprandial period is a time of active oxidative metabolism and formation of ROS. Excess energy intake stimulates overproduction of ROS, resulting in metabolic oxidative stress and cellular redox imbalance. This change in a cell's redox status activates redox-sensitive signaling molecules, such as NF-κB, JNK, and other stress-signaling molecules, ultimately resulting in increased expression of genes, many of which are inflammation mediators.[6] Hence, elevations in inflammatory molecules in the postprandial state are often accompanied, and perhaps preceded by, increases in oxidative stress markers.

MEASURING INFLAMMATORY STATUS

Several biomarkers have been identified as appropriate indicators of inflammatory status in humans. Circulating concentrations of inflammatory molecules, such as acute phase proteins, cytokines, adipokines, and adhesion molecules, are the main measures used in research as well as in some clinical practices. Gene expression of transcription factors, receptors, and protein kinases in immune cells such as monocytes and macrophages help to identify mechanisms and pathways that are either stimulated or inhibited under varying conditions resulting in a particular inflammatory outcome. The various (pro-)inflammation markers that are measured in humans include the acute phase proteins (CRP, fibrinogen, serum amyloid A); cytokines and chemokines (TNF-α, IL-6, IL-1β, MCP-1); and adhesion molecules (E-selectin, P-selectin, sVCAM-1, sICAM-1). Anti-inflammatory markers that are measured and may be suppressed in inflammation include adiponectin and IL-10. Commonly measured molecular targets for assessing inflammation include suppressor of cytokine signaling (SOCS) and NF-κB.[57] In general, modulation of these responses, negatively or positively, acutely or sustained under the various circumstances is measurable. Healthy individuals define fluctuations within a "normal" range and demonstrate a relative homeostatic flexibility. Assessing the effects of nutrition/nutritional components on inflammation/inflammatory status has been suggested to include examining patterns of change in inflammatory markers against a reference range for "normal" or prevention of modulation induced by other factors (such as poor diet) and modulation from a less favorable range to a more favorable range.[58] Other effects may include modulation from outside the reference range back into the reference range or modulation from within the range to outside the range. Even with this background, the study of nutrition and inflammation in chronic diseases (NCD) development/prevention/management is relatively new. Continued attention to the field and reviews such as this will help advance knowledge and constructive design of future research.

BERRIES, ANTHOCYANINS, AND BIOLOGICAL EFFECTS

The botanical definition of a berry is different from the average consumer's definition of "berries" in the marketplace. Botanically, berries are defined simply as fleshy fruit produced from a single ovary.[59] In common English terms, "berries" are usually described as small edible fruits that are brightly colored in shades of red-blue-purple and do not have a pit, although they may contain seeds. Consumers typically identify strawberries, blueberries, blackberries, and raspberries as "berries", but only blueberries are true berries according to the scientific definition of a berry. Despite the incongruent definitions, one unifying trait among "berries" (with few exceptions) is that they contain anthocyanins, which are pigment polyphenol compounds that give them their distinctive color.

Anthocyanins constitute a significant percentage of berry polyphenols. Anthocyanins are a type of flavonoid; they are glycosylated polyhydroxy and polymethoxy derivatives of flavilium salts and possess a characteristic C6−C3−C6 carbon

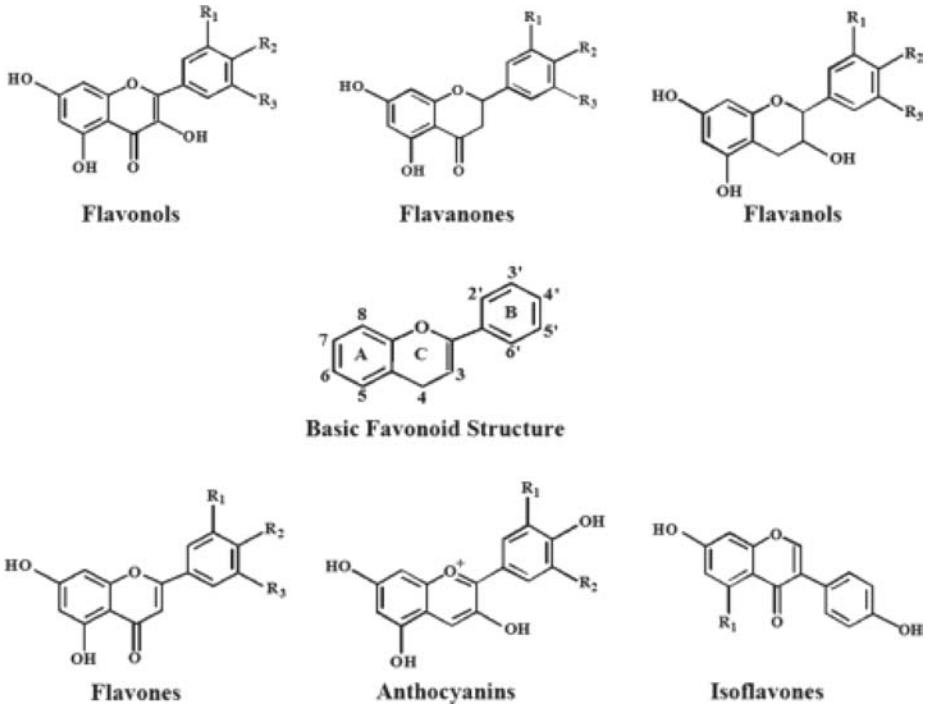

Figure 1. Molecular structures of berry flavonoids. Reprinted with permission from ref 61. Copyright 2009 Hindawi Publishing Co.

Table 1. Major Anthocyanin (Polyphenols) in Selected Berries

berry	botanical name	major anthocyanins	ref
bilberry	*Vaccinium myrtillus*	delphinidin-3-*O*-glucoside, cyanidin-3-*O*-glucoside, malvidin-3-*O*-glucoside	Määttä-Riihinen (2004)
black currant	*Ribes nigrum*	cyanidin-3-*O*-glucoside, -rutinoside; delphinidin-3-*O*-glucoside, -rutinoside	Kapasakalidis (2006)
black raspberry	*Rubus occidentalis*	cyanidin-3-*O*-glucoside, -2^G-xylosylrutinoside, -rutinoside	Wang (2009)
blueberry	*Vaccinium corymbosum*	delphinidin 3-*O*-galactoside, -arabinoside; malvidin 3-*O*-galactoside, petunidin 3-*O*-galactoside	Cho (2004)
chokeberry	*Aronia melanocarpa*	cyanidin-3-glucoside, -galactoside, -arabinoside; cyanidin-3-xyloside	Wu (2004)
cranberry	*Vaccinium macrocarpon*	peonidin 3-*O*-galactoside, -arabinoside; cyanidin 3-*O*-galactoside	Zheng (2003)
sea buckthorn berry	*Hippophae rhamnoides*	isorhamnetin-3-rutinoside, -galactoside, -glucoside; trace amounts of delphinidin, cyanidin, and peonidin	Mishra (2008)
strawberry	*Fragaria* × *ananassa*	pelargonidin; pelargonidin 3-*O*-glucoside; cyanidin 3-*O*-glucoside	Wang (2002)
wolfberry	*Lycium barbarum*	no documented anthocyanins	Potterat (2010)

structure (Figure 1).[60] The most commonly identified anthocyanins in berries are cyanidin, delphinidin, malvidin, pelargonidin, peonidin, and petunidin. In addition to anthocyanins, berries contain several other (poly)phenolic compounds that may contribute to their anti-inflammatory potential, such as flavonols, phenolic acids, proanthocyanidins, and ellagitannins. Anthocyanins are uniquely characterized by the presence of an oxonium ion on the C ring and are highly colored (Figure 1).[61] Selected details of the anthocyanin content of berries are presented in Table 1.

Estimates of anthocyanin intake vary widely within and between populations as does the composition of anthocyanin intake, which is based on food and beverage selection. In France, anthocyanin intake is estimated to be ~57 mg/day,[62] and in Finland, an average intake of 47 mg/day of anthocyanins has been estimated.[63] Wu et al. estimated that the daily consumption of anthocyanins in the United States in 2001−2002 from fruits, vegetables, and beverages was 12.5 mg/day.[64] Of the total anthocyanins consumed/day, almost 70% was accounted for by fruit intake (24 g of fruit contributing ~8.7 g of anthocyanins). Apples ('Red Delicious') dominated the percent of fruit intake (~50% of anthocyanin-containing fruit), yet apples contributed only 8% of anthocyanin intake. In contrast, berries were only ~13.5% of the fruit intake, but contributed ~56% of the fruit-derived anthocyanins. Americans currently eat about half the dietary recommendation for fruit (1 cup equivalent/day), and on the basis of these data, fruit variety, particularly of the red-blue-purple fruits, appears to be limited.[65,66]

Berry research has traditionally focused on their antioxidant properties. Berries (or their extracts) rank highly on in vitro antioxidant measures, such as oxygen radical absorbance capacity (ORAC) and ferric reducing antioxidant capacity (FRAP) analyses,[67−69] and have been shown in various in vitro assay systems to mitigate oxidative stress.[70−72] Polyphenols, including anthocyanins, have antioxidant capability; however, biologically, several studies suggest that their effects in vivo are not through antioxidant scavenging properties. Current dogma suggests polyphenols work via activation/inhibition of various cell signaling processes such as modulating kinase activity resulting in transcription factor activation (e.g., Nrf-2, NF-κB), altering receptor activation (PRR dimerization) as well as possible direct ligand activity (e.g., PPAR-γ).[73,74] Berry extracts and anthocyanin preparations have been shown in various in vitro and in vivo animal models to affect specific steps in cell

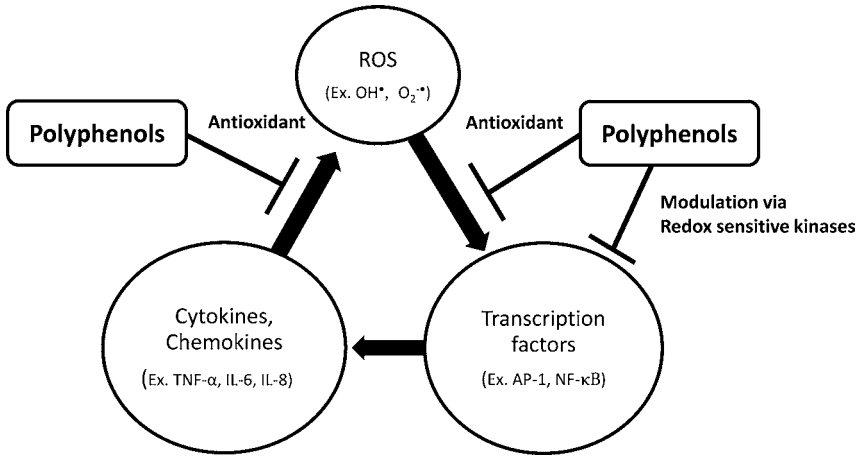

Figure 2. Schematic representation of link between antioxidative and anti-inflammatory potential of dietary polyphenols. ROS, reactive oxygen species; $OH^•$, hydroxyl radical; $O_2^{-•}$, superoxide radical; AP-1, activator protein-1; NF-κB, nuclear factor-kappa B; TNF-α, tumor necrosis factor-alpha; IL, interleukin.

signaling pathways that are known to be involved in chronic disease initiation and development[75−82] including anti-inflammatory-specific effects.[83−88] Recent in vitro work with red wine and grapes has also shown anti-inflammatory effects that authors attribute to their specific anthocyanin content.[89,90]

During inflammation, cells involved in the inflammatory process, which are recruited to the damage site, take up oxygen and release ROS. In addition, inflammatory cells secrete cytokine and chemokine cell mediators, which help to further recruit inflammatory cells, generating yet more ROS. As a result, transcription factors such as NF-κB and activator protein-1 (AP-1) that encode pro-inflammatory genes are activated, leading to an increased secretion of cytokines. The presence of this vicious cycle supports a sustained environment of oxidative and inflammatory stress, which contributes to several chronic diseases. Dietary polyphenols are known to act as both antioxidants and anti-inflammatory molecules, thereby conferring considerable potential protective effects against development of inflammation-related chronic diseases (Figure 2).

Overall, the preclinical literature suggests a role for berries in modifying inflammatory status, an effect that may be due to their polyphenol content in general or anthocyanins in particular. A major question that remains is whether these effects translate to humans.

EFFECTS OF "COMMON" BERRIES AND BERRY PRODUCTS ON INFLAMMATORY MARKERS IN HUMANS

Berries that are readily available and widely consumed by the general population are those that are cultivated for wide commercial distribution. Strawberries, blueberries, cranberries, and black currant are among the most common. Eighteen human clinical trial investigations have been identified examining the effects of common berries on markers of inflammation, generally or specific to CVD risk. Two studies[97,111] involved both an acute and a chronic intervention, which were counted as four separate investigations. Of the 18 studies/investigations, 5 were acute interventions (postprandial paradigm: 2.5−6 h study duration) and 13 were chronic feeding interventions (ranging between 3 and 12 weeks in duration). Blueberry, including wild blueberries, cranberries, and strawberries were investigated in 5/6, 4, and 7 of the clinical trials, respectively, and black currant was investigated in 1 of the 18 investigations (Table 2).

Black Currant. Black currants are native to parts of Europe and Asia and are an excellent source of vitamin C in addition to anthocyanin polyphenols. The major anthocyanins found in black currants include cyanidin-3-*O*-glucoside, cyanidin-3-*O*-rutinoside, delphinidin-3-*O*-glucoside, and delphinidin-3-*O*-rutinoside.[91] The rutinosides are reported to be absorbed intact and, following ingestion, reach peak concentrations in circulation 1−2 h after intake.[92] Black currant has been studied previously as part of mixed-fruit formulations; however, one study was identified that assessed markers of vascular inflammation after consumption of black currant fruit exclusively.[93] Twenty healthy men and women drank a black currant (20% juice) or placebo juice devoid of polyphenols and vitamin C. No significant effects were observed on markers of (vascular) inflammation, sVCAM-1 or sICAM-1, 3 h after beverage intake.[93] No additional inflammation associated data were available; hence, the anti-inflammatory effects of black currant in humans are inconclusive.

Blueberry. Blueberries are well-known for their antioxidant effects in vitro and in vivo.[94] In the past few years, data on blueberry consumption and inflammatory status have emerged, although results have been inconsistent. Four long-term (6−8 weeks) interventions showed no effect of blueberry supplementation on selected inflammatory markers,[95−98] whereas one acute study reported significant improvements in inflammatory status attributable to blueberry intake in an exercise model.[97]

Basu and colleagues[95] administered freeze-dried blueberry powder to 48 individuals with metabolic syndrome (MetS) for 8 weeks. The daily dose of 50 g of blueberry powder (equivalent to 350 g of the fresh fruit) was provided as a water-based drink divided into two beverages per day. At the end of the intervention, blueberry intake did not elicit significant changes in fasting plasma hs-CRP, IL-6, adiponectin, or adhesion molecules (sICAM-1 and sVCAM-1) compared to the plain water control. Stull et al. conducted a similar chronic dosing of blueberries (45 g of freeze-dried blueberry powder per day for 6 weeks) in 32 obese men and women with insulin resistance.[96] Blueberry powder (daily amount equivalent to 2 cups of fresh fruit) was blended into a yogurt plus milk beverage. At the end of the double-blinded, parallel arm intervention, there were no differences in changes in circulating hs-CRP, TNF-α, or MCP-1 in the blueberry group compared to the control. In a separate study of males presenting with at

Table 2. Effects of Common (Wide Commercial Distribution) Berries on Inflammatory Markers in Humans[a]

berry	duration[b] (weeks)	study design	subjects	n[c]	format	dose/day	total phenols[d]	circulating biomarkers[e]	ref
black currant	postprandial	crossover, 2-phase, PC	healthy, MF	20	20% juice	250 mL	NA	↔	Jin (2011)
blueberry	8	parallel, 2-arm, C	MetS, MF	23/25	freeze-dried powder; water-based beverage	50 g	1624 mg	↔	Basu (2010)
	6	parallel, 2-arm, PC	insulin resistant, MF	17/15	freeze-dried powder; yogurt-based smoothie	45 g	1462 mg	↔	Stull (2010)
	postprandial, exercise	parallel, 2-arm, C	trained athletes, MF	25	whole berries prior to exercise	375 g	NA	↑ IL-10	McAnulty (2011)
	6	parallel, 2-arm, C	trained athletes, MF	25	whole berries	250 g	NA	↑ NK cells	McAnulty (2011)
	exercise 60 h	crossover, 2-phase, PC	exercisers, F	10	fruit in smoothie	200 g	168 mg GAE, 97 mg anthocyanins	↔	McLeay (2012)
wild blueberry	6	crossover, 2-phase, PC	CVD at risk, M	18	freeze-dried powder; water-based beverage	25 g	375 mg anthocyanins	↔	Riso (2013)
cranberry	12	dose escalation, 3-phase, PC	abdominal obesity, M	30	juice cocktail	125, 250, 500 mL	100 mg/125 mL	↓ sICAM-1, sVCAM-1	Ruel (2008)
	12	dose escalation, 3-phase, PC	abdominal obesity, M	30	juice cocktail	125, 250, 500 mL	100 mg/125 mL	↓ MMP-9	Ruel (2009)
	8	parallel, 2-arm, PC	MetS, MF	16/15	low-energy juice	480 mL	458 mg	↔	Basu (2011)
	4	crossover, 2-phase, PC	CHD, MF	44	double-strength juice	480 mL	835 mg	↔	Dohadwala (2011)
strawberry	4	parallel, 1-arm, BC	MetS, F	16	freeze-dried powder; water-based beverage	50 g	2006 mg	↔	Basu (2009)
	8	parallel, 2-arm, C	MetS, MF	10/15	freeze-dried powder; water-based beverage	50 g	2006 mg	↓ sVCAM-1	Basu (2010)
	postprandial	crossover, PC	overweight, MF	24	freeze-dried powder, milk-based beverage, MF-HC meal	10 g	94.7 mg	↓ IL-6, hs-CRP	Edirisinghe (2011)
	postprandial	parallel, 2-arm, PC; post-6 week-intervention[f]	overweight, MF	24	freeze-dried powder in milk beverage with MF-HC meal	10 g	94.7 mg	↓ PAI-1, IL-1β	Ellis (2011)
	3	crossover, 2-arm, PC	obese, MF	20	freeze-dried powder; mixed into foods	≈320 g frozen berries	NA	↔	Zunino (2011)
	6	crossover, 2-arm, PC	overweight, MF	22−24	freeze-dried powder; milk-based beverage	10 g	94.7 mg	↔	Ellis (2011)
	24	parallel, 2-arm, BC	esophageal cancer at risk, MF	36	freeze-dried powder; water-based beverage	30 g/60 g	NA	↓ iNOS, COX-2, pNFκB-p65, pS6	Chen (2012)

[a]BC, baseline controlled; C, controlled; CAD, coronary artery disease; F, female; GM-CSF, granulocyte macrophage colony stimulating factor; HC, high carbohydrate; COX, cyclooxygenase; GAE, gallic acid equivalents; HF, high fat; hs-CRP, high-sensitivity C-reactive protein; IL, interleukin; iNOS, inducible nitric oxide synthase; M, male; MetS, metabolic syndrome; MF, moderate fat; MMP, matrix metalloproteinase; NA, not available; NF-κB, nuclear factor kappa B; PAI-1, plasminogen activator inhibitor-1; PC, placebo controlled; sICAM-1, soluble intercellular cell adhesion molecule-1; sVCAM-1, soluble vascular adhesion molecule-1; TG, triglyceride. [b]Duration represented in weeks unless otherwise specified. [c]Number represents n/group in parallel design studies. [d]As reported in referenced papers, using different methods (HPLC, LC-MS/MS, spectrophotometry, Folin−Ciocalteu method) and units of expression, [e]Only biomarkers that showed statistically significant change have been specified. [f]Postprandial test meal did not include strawberry beverage.

dx.doi.org/10.1021/jf4044056 | J. Agric. Food Chem. 2014, 62, 3886−3903

least one CVD risk factor, no change in inflammatory markers (IL-6, TNF-α, hs-CRP) or adhesion molecule (sVCAM-1) after 6 weeks of supplementation with a wild blueberry drink (25 g of freeze-dried powder and 375 mg of anthocyanins) compared to a polyphenol-free control beverage was observed.[98] These results are consistent with McAnulty et al., who also found no changes in fasting blood markers of inflammation (IL-1 receptor antagonist (ra), IL-6, IL-8, and IL-10) after study participants (trained athletes) ingested 250 g/day of whole blueberries for 6 weeks.[97] However, blueberry consumption increased counts of natural killer (NK) cells in the study subjects. NK cells promote natural cellular toxicity, for example, in counteracting proliferation of cancerous cells,[99] which suggests that blueberries may beneficially modulate the immunological profile separate from inhibiting pro-inflammatory molecules. The same researchers also investigated the acute effects of blueberries in an exercise-induced inflammation paradigm at the end of the 6 week experimental period. Subjects ingested either 375 g of blueberries (n = 13) or no blueberries (n = 12) 1 h prior to 2.5 h of treadmill running. Pro-inflammatory markers, including circulating total leukocyte count, IL-8, IL-6, and IL-1ra, and skeletal muscle NF-κB activity, were measured 1 h after completion of the exercise: no differences between the two groups on these measures were observed. However, blueberry supplementation increased the anti-inflammatory regulatory cytokine IL-10 following exercise, which coincided with reduced oxidative stress as measured by F2-isoprostanes. In a shorter duration exercise study (60 h), oxidative stress and inflammation were assessed after intense strenuous eccentric contractions of the quadriceps with blueberry (in a smoothie) or a placebo smoothie devoid of blueberry.[100] Whereas a faster rate of recovery was observed in the blueberry group, improvements in oxidative stress were not observed until 36 h and inflammatory indicators of damaged muscle (creatine kinase and IL-6) were still elevated in both groups ($P > 0.05$, treatment effect).

Collectively, the data supporting a beneficial association between blueberries and inflammatory status are unremarkable at present; however, the positive effects on selected beneficial immune/inflammation biomarkers[97] warrant further investigations to understand dose/amount−response of blueberries, delivery, and metabolic status of subject population on outcomes, which may help to explain the differences between clinical and preclinical studies on anti-inflammatory effects elicited by blueberries.

Cranberry. Cranberries, a popular fruit consumed as juice and jelly and in dried form are best known for their urinary tract infection-preventing benefits.[101] Cranberries are rich in cyanidin- and peonidin-glycosides,[102] pro-anthocyanidins (particularly the A-type), flavonols, and phenolic acids.[103] Clinical investigation of the anti-inflammatory effect of cranberries is supported by in vitro studies; [104] however, the clinical results are mixed. Specifically, in two of four clinical trials with cranberry juice, Ruel and colleagues[105,106] reported favorable anti-inflammatory effects of cranberry in a dose-escalation paradigm over 12 weeks in abdominally obese men (n = 30; waist circumference $\geq$ 90 cm), whereas in two other investigations no significant effect of cranberry juice supplementation was observed compared to placebo[107,108] (Table 2). Distinct differences in study design, doses, supplement duration, and populations may account for at least part of the discrepancy in outcomes.

Ruel et al. used a dose escalation schema wherein subjects increased their daily intake of cranberry juice every 4 weeks starting with 125 mL, then moving to 250 mL, and finally ending their last 4 weeks of the 12 week study with 500 mL/day (total phenols, 100 mg/125 mL juice).[105,106] No control group was used for comparison. At the end of 4 weeks, subjects had significantly lower plasma concentrations of sVCAM-1 and sICAM-1[105] and MMP-9[106] compared to baseline. Plasma soluble E-selectin remained unchanged. Two subsequent studies from different researchers recruited individuals with MetS[107] and patients with coronary heart disease (CHD)[108] and supplemented cranberry juice for 8 and 4 weeks, respectively. Amounts of cranberry juice did not differ remarkably between the two Ruel et al. studies and the Basu et al. and Dohadwala et al. studies (500 vs 480 mL); however, the dose of total phenols was nearly double (835 mg) in the Dohadwala et al. trial.[108] Basu et al. reported no significant improvements in plasma hs-CRP or IL-6,[107] and, similarly, Dohadwala and colleagues reported no significant change in circulating hs-CRP and sICAM-1 concentrations after 4 weeks of the double-strength juice.[108] Whether a longer duration of consumption or an acclimation to higher doses over time is needed to observe effects is not clear. Likewise, much like the research with other berries, it is not clear what amounts of fruit may be necessary to impart anti-inflammatory benefits in the different populations being studied.

Strawberry. Strawberries, widely consumed fruit in North America, contain a number of essential nutrients, such as vitamin C and potassium as well as polyphenolic components, including anthocyanins, ellagitannins, and various flavonols. Pelargonindin-3-*O*-glucoside is the main anthocyanin of strawberries, with lesser amounts of cyanidin glycosides.[109,110] Published human studies assessing strawberry intake and inflammation outcomes have been from acute[7,111] as well as long-term-feeding studies.[111−114] The two acute postprandial studies tested a freeze-dried strawberry powder incorporated into a challenge meal paradigm to test the ability of strawberries to attenuate meal-induced inflammation. Edirisinghe et al. studied the acute postprandial effects of strawberries in a milk-based beverage (10 g of freeze-dried strawberry powder; 94.7 mg of total polyphenols) on selected inflammatory markers in 24 overweight individuals.[7] A beverage matched for sensory attributes, total calories, and macronutrients was used as the placebo. Blood sampling was conducted at baseline (0 h) and up to 6 h post-challenge meal (with strawberry or placebo beverage). Inclusion of the strawberry drink with a high-calorie breakfast resulted in lower cumulative plasma concentrations of IL-6 and hs-CRP over the 6 h period following the meal. Concentrations of TNF-α, IL-1β, and plasminogen activator inhibitor-1 (PAI-1), a thrombolytic factor, did not differ between strawberry and placebo conditions. This group of men and women was then subjected to the same postprandial protocol (high-calorie challenge meal with placebo beverage only) after 6 weeks of daily supplementation with either the strawberry beverage or the placebo beverage.[111] Contrary to the results of the acute study, there were no differences between treatments on post-challenge meal/postprandial IL-6 or hs-CRP after 6 weeks of strawberry intake or placebo intake. However, significant decreases in postprandial IL-1β and PAI-1 were observed in those individuals who consumed the strawberry beverage for 6 weeks. Whereas the effect of strawberry on endpoints of inflammation differed between study paradigms, an anti-inflammatory effect

was consistently found with strawberry consumption. Follow-up investigations to understand the different mechanisms involved with the observed responses under different feeding conditions are ongoing. Possible explanations for the different responses may be related to the milieu of strawberry metabolites circulating in an acute setting versus on the background of a dietary pattern including daily consumption of strawberries.

Chronic feeding studies with strawberries were conducted in four different subject populations: overweight,[111] individuals with MetS,[112,113] obese,[114] and patients at risk for cancer.[115] Outcome measures were fasting concentrations of inflammatory markers following strawberry interventions ranging from 3 to 6 weeks. In overweight individuals (n = 24) who consumed 10 g of freeze-dried strawberry powder in a beverage daily for 6 weeks (compared to energy-matched control beverage), no significant treatment effects were reported on fasting concentrations of inflammatory markers (i.e., hs-CRP, IL-6, IL-1β).[111] Consistent with these findings, no significant differences in fasting hs-CRP, complement C3, serum amyloid A, fibrinogen, IL-1β, IL-6, IL-8, TNF-α, leptin, sICAM-1, or sVCAM-1 were reported in obese men and women (n = 20) after 3 weeks of supplementation with freeze-dried strawberry powder (equivalent to ∼320 g of frozen fruit) incorporated into yogurt, cream cheese, and smoothie compared to the same foods without strawberry powder.[114] In MetS subjects,[112,113] 50 g/day of freeze-dried strawberry powder (equivalent to ∼500 g of fresh fruit) prepared in water and drunk daily for 8 weeks significantly reduced sVCAM-1, but not sICAM-1.[113] Individuals with MetS have higher blood levels of adhesion molecules,[116] which are associated with endothelial inflammation and higher CVD risk. In a smaller (n = 16) and shorter duration (4 weeks) pilot study with MetS women ingesting 50 g of freeze-dried strawberry daily (no comparator group), no significant changes in plasma hs-CRP or adiponectin were observed.[112] Chen et al. studied strawberry supplementation in patients with esophageal dysplastic lesions who are at risk for developing esophageal cancer.[115] Using a parallel design study, subjects consumed either 60 or 30 g (n = 36 per group) of freeze-dried strawberry powder in the form of a water-based drink for a period of 6 months. At the end of the supplementation period, patients who had consumed the 60 g dose had significantly lower protein expression of iNOS (79.50% reduction), COX-2 (62.9% reduction), pNF-κB-p65 (62.6% reduction), and pS6 (73.2% reduction) in esophageal mucosa. Reductions in the same parameters were also observed in the group receiving 30 g of strawberry powder/day, but the changes were not statistically significant from baseline measurements.

Overall, the available data on strawberry consumption support future research to better understand dose−response dynamics in different populations, acute versus chronic intake (eating) regimens, matrix effects, and the relationship between polyphenol metabolite profiles and (anti-)inflammation outcomes.

Among the four types of berries reviewed in this section, cranberries and strawberries showed "inhibitory" effects on selected pro-inflammatory markers,[7,105,106,111,113] whereas blueberry intake resulted in beneficial effects on immune function by increasing anti-inflammatory/regulatory molecules.[97] In four studies in which a relative oxidative and inflammatory stress was imposed, after exercise,[97,100] or after eating meals typical of Western meal composition,[7,111] or in MetS[113] or abdominal obesity,[105,106] consuming cranberries, blueberries, and strawberries resulted in beneficial anti-inflammatory responses.

EFFECTS OF "LESSER-KNOWN" (LIMITED DISTRIBUTION) BERRIES AND BERRY PRODUCTS ON INFLAMMATORY MARKERS IN HUMANS

Several berry fruits remain underutilized due mainly to harvest in the wild and local consumption.[117] They are indigenous to different parts of the world, with limited cultivation for commercial distribution. However, many, if not all, of these berries are rich sources of anthocyanins[118,119] and other polyphenolic compounds, which have been shown to mitigate the negative effects of oxidative and inflammatory stress in animal and in vitro experiments.[37,120−122] This section of the review discusses human intervention studies of the less commonly known berries on selected clinically relevant inflammatory markers associated with chronic diseases. Details of the investigations are presented in Table 3. A total of 12 studies are presented in this section and include clinical trials on bilberry,[123−125] black raspberry,[126,127] chokeberry,[128] sea buckthorn berry,[124,129−131] wolfberry,[132] and a berry mixture of lingonberry, bilberry, black currant, and sea buckthorn berry.[133] All interventions were chronic feeding studies except for one postprandial experiment with sea buckthorn berries.[131]

Bilberry. Bilberries are rich sources of polyphenols. Anthocyanins comprise nearly half to three-fourths of the total polyphenol content of bilberries.[134] Three clinical trials were identified that included markers of inflammation as study endpoints. All three investigations reported anti-inflammatory effects associated with bilberry consumption for 4−8 weeks. Karlsen et al. studied the effects of 330 mL of bilberry juice/day for 4 weeks in men and women (n = 62) who were at risk for CVD development based on the presence of at least one predisposing risk factor such as cigarette smoking, hypertension, or elevated LDL-cholesterol concentrations.[123] At the end of the 4 weeks, bilberry supplementation compared to water control resulted in lower levels of circulating IL-6, hs-CRP, and monokine induced by interferon-γ (MIG). However, the authors also reported an increase in plasma TNF-α, which was incongruent with the IL-6 and hs-CRP findings: these cytokines are known to be positively related. In contrast, Lehtonen et al. reported a decrease in plasma TNF-α concentration with frozen whole bilberries (equivalent to 100 g fresh fruit) at the end of a 33−35 day intervention in overweight and obese women (n = 110).[124] In addition, while there was no impact on levels of hs-CRP, IL-6, or sICAM-1 concentrations, bilberries resulted in a decrease in plasma sVCAM-I and adiponectin. Epidemiological studies show that circulating adiponectin levels are inversely proportional to body fat and inflammation and positively associated with insulin sensitivity, and thereby adiponectin is inversely associated with CVD risk. According to the authors,[124] the decreased adiponectin concentrations in response to bilberry consumption may be reflective of a lack of sufficient adaptation time required to observe changes in adiponectin concentrations in circulation[135] and not necessarily a detrimental effect of bilberries.

Kolehmainen et al. reported outcomes from an intervention in which men and women with MetS supplemented their habitual diet with bilberries.[125] The parallel arm study included a 4 week run-in phase, an 8 week intervention, and a 4 week follow-up period. Individuals in the bilberry group consumed daily 200 g of berry puree (524 mg anthocyanins/100 g) plus 40 g of dried berries (832 mg anthocyanins/100 g; equivalent to 200 g of fresh berries) to provide a total dose equivalent to

Table 3. Effects of Lesser-Known (Limited Distribution) Berries on Inflammatory Markers in Humans[a]

berry	duration[b] (weeks)	design	subjects	n[c]	format	dose/day	total phenols[d]	circulating biomarkers[e]	ref
bilberry	4	parallel, 2-arm, C	CVD at risk, MF	31	juice	330 mL	NA	↓ IL-6, hs-CRP, IL-15, MIG; ↑ TNF-α	Karlsen, (2010)
	33−35 days	crossover, 2-phase, BC	overweight and obese, F	110	frozen, whole	≈100 g fresh berries	NA	↓ TNF-α, sVCAM-1, adiponectin	Lehtonen (2011)
	8[f]	parallel, 2-arm, C	MetS, MF	15/12	frozen puree plus dried	≈400 g fresh berries	NA	↓ hs-CRP, IL-12	Kolehmainen (2012)
black raspberry	1−9	parallel, 1-arm, BC	colorectal cancer, MF	15	freeze-dried powder; water slurry	60 g	1669 mg	↑ GM-CSF; ↓ IL-8	Mentor Marcel (2012)
		postprandial	overweight, M	10	freeze-dried powder; with water	45 g; with HFHC meal	NA	↓ IL-6	Sardo (2013)
chokeberry	6	parallel, 1-arm, BC	hyper-chol, M	58	fruit juice	250 mL	426 mg/ 100 mL	↓ fibrinogen	Skoczyñska (2007)
mixed berries[g]	20	parallel, 2-arm, C	healthy, F	31/30	traditional products plus oil[h]	≈163 g fresh berries; 0.5 g oil	NA	↑ adiponectin	Lehtonen (2010)
sea buckthorn berry	8	parallel, 2-arm, PC	healthy, M	10	juice	300 mL	NA	↔	Eccleston (2002)
	90 days	parallel, 2-arm, PC	healthy, MF	90	frozen puree	28 g	NA	↓ hs-CRP	Larmo (2008)
	33−35 days	crossover, 2-phase, BC	overweight and obese, F	110	air-dried, whole	≈100 g fresh berries	NA	↓ TNF-α	Lehtonen (2011)
	postprandial	crossover, 2-phase, PC	normal weight, M	10	dried and ground; with yogurt-based meal	40 g	NA	↔	Lehtonen (2010)
wolfberry	30 days	parallel, 2-arm, PC	healthy, MF	60	fruit juice	120 mL	NA	↑ IL-2, IgG, lymphocytes	Amagase (2009)

[a]BC, baseline controlled; C, controlled; Chol, cholesterol(emia); CVD, coronary artery disease; F, female; HFHC, high-fat high-carbohydrate; hs-CRP, high-sensitivity C-reactive protein; IL, interleukin; M, male; MetS, metabolic syndrome; MIG, monokine induced by IFN-γ; NA, not available; PC, placebo controlled; sVCAM-1, soluble vascular cell adhesion molecule-1; TNF-α, tumor necrosis factor-alpha; IgG, immunoglobulin G. [b]Duration represented in weeks unless otherwise specified. [c]Number represents n/group in parallel design studies [d]As reported in referenced papers, using different methods (HPLC, LC-MS/MS, spectrophotometry, Folin−Ciocalteu method) and units of expression. [e]Only biomarkers that showed statistically significant change have been specified. [f]4 week run-in period, and 4 week recovery period following intervention. [g]Lingonberry, bilberry, black currant, sea buckthorn. [h]Juice, bread, berry powder, berry oil, dried berries.

dx.doi.org/10.1021/jf4044056 | J. Agric. Food Chem. 2014, 62, 3886−3903

400 g/day of fresh bilberries. Control subjects consumed only their habitual diet but were allowed to occasionally include a maximum of 80 g of fresh berries/day. Compared to the control group, subjects in the bilberry group showed significant improvements in serum hs-CRP and IL-12 ($p < 0.05$), whereas IL-6 and LPS tended to be lower ($p = 0.074$ and $p = 0.094$, respectively). Bilberry supplementation did not affect leptin and adiponectin levels.

Black Raspberry. Black raspberries are native to North America and are darkly pigmented, reflective of their high anthocyanin content (about 214−589 mg/100 g).[136] Black raspberries exhibit potent antioxidative capacity in vitro, and a considerable amount of research on black raspberries pertains to their preventative effects on different cancers both in vitro and in animals.[137,138]

Two human interventions with black raspberries have been recently published. Patients with colorectal cancer were supplemented with 60 g/day freeze-dried powder for approximately 3 weeks (10−63 days).[126] A daily dose of 60 g/day (20 g in a water slurry 3 times a day) provided 1669 mg of anthocyanins. Plasma levels of cytokines (IL-1β, IL-2, IL-6, IL-8, IL-10, IL-12p70, granulocyte macrophage colony stimulating factor (GM-CSF), IFN-γ, and TNF-α) were measured before and after treatment with black raspberries. The berry intervention increased plasma GM-CSF concentrations. Patients receiving berries for more than 10 days also had decreased plasma concentrations of IL-8. An increase in IL-8 has been observed in colorectal carcinoma.[139]

Sardo et al. tested postprandial effects of 45 g of freeze-dried black raspberry powder consumed with an inflammatory high-fat high-carbohydrate (HFHC) meal in overweight men ($n = 10$). The postprandial investigation (up to 12 h) was preceded by 4 consecutive days of black raspberry intake (45 g/day). Under the control condition, no berry powder was consumed either preceding or during the postprandial testing day.[127] The HFHC meal provided 1090 calories, 56 g of total fat, and 156 g of carbohydrates. The areas under the curve (AUC) for IL-6, TNF-α, and CRP during the postprandial period were compared between the black raspberry−HFHC meal regimen and the control condition. Black raspberry powder consumption with the HFHC meal resulted in a significant decrease in IL-6 AUC compared to no berry intake (HFHC meal alone). No effects were observed with black raspberry powder on TNF-α and CRP.

Sea Buckthorn Berry. Sea buckthorn berries are native to India, China, and Eastern Europe and have traditionally been used in Eastern medicine.[130] The polyphenols in sea buckthorn berries are composed mainly of flavonol glycosides (isorhamnetin-3-rutinoside, -galactoside, and -glucoside) but also contain smaller amounts of the anthocyanins delphinidin, cyanidin, and peonidin.[118] In vitro studies indicate that sea buckthorn berries may have potent inhibitory effect on CVD risk markers including exerting anti-inflammatory activity.[141] A single postprandial study[131] and three chronic supplementation studies with sea buckthorn berries have been reported.[124,129,130] In a relatively small group of men ($n = 10$), intake of dried and crushed whole sea buckthorn berries (equivalent to 200 g of fresh whole berries and providing 22.8 mg of flavonol glycosides/portion) did not significantly affect levels of TNF-α in circulation during a postprandial investigation.[131] The study used a crossover design in which sea buckthorn berries were incorporated into a yogurt-based meal containing 50 g of glucose. The same meal without berries represented the control. Although blood samples were collected for up to 360 min during the postprandial phase, TNF-α was measured only at baseline (0 min) and 60 min after meal consumption. The trajectory of the TNF-α response suggested that the meal was inducing an increase in TNF-α and that concomitant intake of sea buckthorn berries with the meal was attenuating the increase; however, this was not significant ($p = 0.175$). An insufficient sample size and high between-subject variability along with measuring a single inflammatory biomarker (TNF-α) at only two time points (0 and 60 min) are insufficient to understand the potential benefits of sea buckthorn berries on postprandial inflammation in humans, particularly when others have shown the response may not be evident until 3−6 h.[7,54,142] In 2002, Eccleston et al. conducted a parallel arm intervention in men ($n = 10$/group) to study the effect of ingesting 300 mL of a sea buckthorn berry juice (containing 1182 mg/L of flavonoids) for 8 weeks.[129] No effect of supplementation was found on plasma sICAM-1 concentrations, which was the only marker measured. Two recent human studies[124,130] reported favorable effects of sea buckthorn berries on inflammatory markers. Two hundred and thirty-three subjects were supplemented for 90 days with either a frozen sea buckthorn puree or a placebo puree that had similar sensory attributes. The daily dose of 28 g of berry puree provided about 8.4 mg of flavonols. At the end of the intervention, consumption of sea buckthorn berries resulted in lower hs-CRP concentrations in serum compared to placebo.[130] A similar anti-inflammatory effect was observed in the second published intervention in which overweight and obese women ($n = 110$) consumed air-dried whole sea buckthorn berries (representing approximately 100 g of fresh berries).[124] Plasma TNF-α, hs-CRP, IL-6, sVCAM-I, adiponectin, and sICAM-1 concentrations were measured before and at the end of the 33−35 day intervention. Supplementation with the sea buckthorn berries resulted in lower circulating TNF-α concentrations, but no change was observed in hs-CRP.

Lehtonen et al. studied the long-term effects of 20 weeks of supplementation of four different berries (bilberry, black currant, lingonberry, and sea buckthorn berry) in the form of traditional berry products, as well as berry oils.[133] Sixty-one disease-free women were randomized to either the treatment group or a control group (lifestyle intervention but no additional berries). The active group consumed 3 servings of berry products daily plus 0.5 g of berry oil/day (equivalent to 163 and 245 g of fresh berries, respectively). The control group consumed lower amounts of berries per day (27 g). The 18 berry products, comprising breads, juices, berry powder, dried berries, and berry oils, were consumed according to a specified consumption cycle. At the end of the 20 week intervention with the mixture of berries, there was a significant increase in levels of adiponectin from baseline, but also an unfavorable increase in soluble adhesion molecules (sVCAM-1 and sICAM-1) in the active group; however, there were no significant treatment differences observed between active and control groups. No effect of berry supplementation was observed on hs-CRP and TNF-α levels in either group.

Wolfberry. The results of a single intervention on wolfberry (also known as goji berry) in a sample population of 60 healthy men and women utilizing a parallel design have been reported by Amagase et al.[132] Goji berries have been traditionally used in Chinese medicine and are rich sources of carotenoids, particularly zeaxanthin, but also flavonoids and betaine.[143,144] To the best of our knowledge, goji berries are an example of

berries that do not contain anthocyanins or, if they do, quantities are too low to detect. The intervention included supplementation of the berries as a fruit juice. A beverage with comparable taste, color, and flavor was used as the placebo control. Subjects consumed a total of 120 mL of juice/day in two equal doses after the morning and evening meals for a period of 30 days. At baseline and the end of the treatment period, the following immunological markers were measured: counts of CD4, CD8, lymphocytes, and NK cells, in addition to circulating concentrations of IL-2, IL-4, immunoglobulin (Ig) G, and IgA. At the end of the 30 days, significant increases were found in the levels of serum IL-2, IgG, and NK cells with consumption of the goji berry juice compared to placebo. Similar beneficial immunological changes were observed when baseline to phase end differences between the two groups were compared.

Chokeberry. Chokeberries, which are native to parts of North America and Eastern Europe, are rich in the anthocyanins cyanidin-3-arabinoside, cyanidin-3-galactoside, cyanidin-3-glucoside, and cyanidin-3-xyloside, with total anthocyanin concentrations varying from 357 to 1790 mg/100 g fresh weight.[140] One investigation was identified reporting inflammation biomarkers after consumption of chokeberries.[128] Fifty-eight nonmedicated hypercholesterolemic men drank 250 mL/day of 100% chokeberry juice (total polyphenol content = 40−70 mg/g dry weight) for 6 weeks followed by 6 weeks of discontinuation of juice intake (washout) and followed by another 6 weeks of juice intake. Fasting blood concentrations of hs-CRP and fibrinogen were measured at the beginning of the study and three more times at the end of each 6 week period (two juice periods and one washout period). Chokeberry juice intake did not significantly change hs-CRP concentrations in these subjects compared to baseline. However, circulating fibrinogen levels were lower at the completion of all phases compared to baseline, and significantly so at the end of the second chokeberry intervention phase ($p < 0.01$). Fibrinogen is a known coagulation factor, but also has a pro-inflammatory role in a number of chronic diseases: several studies suggest fibrinogen is a key regulator of inflammation.[145]

In summary, 10 of the 12 studies reviewed in this section showed a beneficial effect of lesser known berries on selected pro-inflammatory and adhesion molecules in circulation. The single study on wolfberry showed that intake increases beneficial immune cells and molecules in humans.[132] The two studies that showed no effect of sea buckthorn intake may have been mainly due to the small sample of subjects ($n = 10$) or to study/sampling design. Compared to the commonly consumed berries such as strawberries and blueberries, the lesser known berries appear to exert an overall consistent anti-inflammatory effect in humans. These promising data support the value of including these berries in the diet and support research to advance cultivation and distribution for widespread sale and consumption.

EFFECTS OF BERRY EXTRACTS AND ANTHOCYANINS ON INFLAMMATORY MARKERS IN HUMANS

The use of whole fruit and whole fruit products, comprising several beneficial components, has been demonstrated to mitigate inflammatory burden in some human intervention studies. Although little is known about dose−response, the lack of effect reported in some studies may be due to failure in achieving the required levels of relevant compounds in circulation when berries and berry products are consumed normally in the diet, that is, as "food". Purifying active principles in berries and delivery in the form of berry extracts/berry fractions is one way to increase "dose" and possibly circulating concentrations, assuming higher concentrations are needed to achieve benefit.

A relatively large body of data from in vitro and in vivo animal experiments provides evidence for a protective role of purified polyphenolic compounds and berry fractions against increased inflammatory stress. A small number of clinical trials have been conducted to study the effects of berry extracts and purified anthocyanins from berries on inflammatory markers associated with chronic diseases (Table 4). Of the nine studies presented in this section, all involved chronic administration of either (1) purified anthocyanins[146−148] or (2) extracts of black currant,[149] chokeberry,[150] cranberry,[151,152] or sea buckthorn berry.[124]

Anthocyanins. Zhu et al. tested a commercially available purified anthocyanin supplement: 41% total anthocyanins/capsule composed of 58% delphinidins and 33% cyanidins extracted from bilberries and black currants; the remaining 59% composed of nonpolyphenolic constituents.[148] One hundred and fifty ($n = 150$) hypercholesterolemic men and women took the supplement (320 mg of anthocyanins/day) 30 min after breakfast and dinner meals. Supplementation with anthocyanins led to a significant decrease in serum sVCAM-1 concentrations compared to placebo (delta placebo vs delta anthocyanins, $p = 0.023$). In two other studies, anthocyanin extracts from bilberries and black currants (primary anthocyanins were cyanidin-3-*O*-β-glucosides and delphinidin-3-*O*-β-glucosides) were tested against a control maltodextrin supplement.[146,147] The first intervention was conducted by Karlsen et al., in which 118 men and women were randomized to either the placebo or active treatment providing 300 mg anthocyanins/day (two capsules each in the morning and evening; 75 mg of anthocyanins/capsule) for a period of 3 weeks.[146] Of the several inflammatory markers that were measured (hs-CRP, IL-1β, IL-1ra, IL-2, IL-4, IL-6, IL-8, IL-10, IL-12, IL-13, IL-17, TNF-α, IFN-α, IFN-γ, GM-CSF, macrophage inflammatory protein (MIP)-1α, MIP-1β, immunoprotein (IP)-10, MCP-1, eotaxin, and regulated upon activation, normal T cell expressed and secreted (RANTES)), the anthocyanin-supplemented group showed a decrease in plasma levels of IL-8, RANTES, IFN-α, IL-4, and IL-13 compared to placebo. A subsequent study by the same group of researchers tested the anthocyanin supplement in 27 men with elevated blood pressure (137/85 ± 12/7 mmHg).[147] Subjects ingested four capsules (80 mg of anthocyanin each) in the morning and four capsules in the evening separate from mealtimes to provide a total daily dose of 640 mg of anthocyanins (approximately equal to 100 g of a mixture of blueberries and black currants). The intervention lasted for 4 weeks. Endpoints measured were hs-CRP, TNF-α, IL-6, IL-4, MCP-1, CD40L, sICAM-1, and sVCAM-1, P-selectin, von Willebrand factor, and total nitric oxide. Anthocyanin supplementation had no effect on levels of cytokines, markers of endothelial function, or oxidative stress. Anthocyanin supplementation resulted in a significant increase in von Willebrand factor, a marker of endothelial function associated with CVD. The authors noted that although this may be an unfavorable effect, the clinical significance of increased von Willebrand factor relative to endothelial inflammation in this population is unknown.

Table 4. Effects of Berry Extracts/Fractions, Including Anthocyanins, on Inflammatory Markers in Humans[a]

berry	duration (weeks)[b]	design	subjects	n[c]	format	dose/day	circulating biomarkers[d]	ref
anthocyanins, purified (BB, BCt)	3	parallel, 2-arm, PC	healthy, MF	59	capsules, 75 mg	4 × 75 mg: 300 mg anthocyanins	↓ IL-8, RANTES, IFN-α, IL-4, IL-13	Karlsen (2007)
	4	crossover, 2-phase, PC	hypertensive, M	27	capsules, 80 mg	8 × 80 mg: 640 mg anthocyanins	↔	Hassellund (2013)
	12	parallel, 2-arm, PC	hyper-chol, MF	73	capsules, 80 mg	4 × 80 mg: 320 mg anthocyanins	↓ sVCAM-1	Zhu (2011)
black currant	exercise, pre/post	crossover, 2- phase, PC	healthy, MF	10	cFDP, capsule	240 mg anthocyanins	↓ CK activity	Lyall (2011)
chokeberry	6	parallel, 2-arm, PC	CAD on statins, MF	22	extract, capsule	3 × 85 mg: 255 mg flavonoids (25% anthocyanins)	↓ IL-6, CRP, sVCAM-1, sICAM-1, MCP-1; ↑adiponectin	Naruszewicz (2007)
cranberry	12	parallel, 2- arm, PC	type 2 DM, MF	15	extract powder, 500 mg capsules	3 × 500 mg: 1500 mg	↔	Lee (2008)
	6 months	parallel, 2-arm, C	at risk prostate disease, M	21	fruit powder, 500 mg capsules	3 × 500 mg: 1500 mg (~1.65 mg anthocyanins)	↔	Vidlar (2010)
sea buckthorn berry	33−35 days	crossover, 2-phase, BC	overweight and obese, F	110	berry (ethanol) extract	≈100 g fresh berries	↓ TNF-α, sICAM-1	Lehtonen (2011)
	33−35 days	crossover, 2-phase, BC	overweight and obese, F	110	berry oil extract	≈100 g fresh berries	↑ hs-CRP; ↓ sVCAM-1, adiponectin	Lehtonen (2011)

[a]BB, bilberry; BCt, black currant; BC, baseline controlled; C, controlled; CAD, coronary artery disease; Chol, cholesterol(emia); CK, creatine kinase; DM, diabetes mellitus; F, female; cFDP, concentrated freeze-dried powder; hs-CRP, high-sensitivity C-reactive protein; IFN-α, interferon alpha; IL, interleukin; M, male; PC, placebo controlled; RANTES, regulated upon activation, normal T cell expressed and secreted; sICAM-1, soluble intercellular cell adhesion molecule-1; sVCAM-1, soluble vascular cell adhesion molecule-1; TNF-α, tumor necrosis factor-alpha. [b]Duration represented in weeks unless otherwise specified. [c]Number represents n/group in parallel design studies. [d]Only biomarkers that showed statistically significant change have been specified.

dx.doi.org/10.1021/jf4044056 | J. Agric. Food Chem. 2014, 62, 3886−3903

Black Currant. An encapsulated concentrated black currant powder was supplemented to exercisers to study effects on exercise-induced oxidative and inflammatory stress.[149] The dose was approximately equivalent to 48 g of fresh blackcurrants (providing 240 mg of anthocyanins and <1 mg of vitamin C): 89% of the total phenolics comprised anthocyanins. Men and women ingested two capsules before and two capsules following the 30 min exercise regimen. Blood was sampled prior to the first two capsules and exercise and at 1, 2, and 24 h after exercise and the second set of capsules. Sugar capsules were used as placebo. Black currant anthocyanin supplement decreased exercise-induced inflammatory stress (plasma creatine kinase activity) significantly at 24 h compared to placebo.

Chokeberry. To date, one study has been published on chokeberry extracts in which inflammation was assessed.[150] This study included 44 patients who survived a myocardial infarction and were on statin treatment for a minimum of 6 months. Study participants ingested a chokeberry flavonoid extract for 6 weeks in a double-blinded, placebo (maltodextrin)-controlled parallel arm clinical trial. The supplements were administered as three daily doses that delivered 0 or 255 mg/day of flavonoid extract (anthocyanins (~25%), monomeric and oligomeric procyanidins (~50%), and phenolic acids (~9%)). Compared to the control group (statin plus placebo supplement), the combination of chokeberry extract and statin therapy resulted in a significant decrease in all inflammatory biomarkers tested, namely, hs-CRP, IL-6, sICAM-1, sVCAM-1, and MCP-1, at the end of 6 weeks. In addition, there was a favorable increase in the concentration of serum adiponectin in these patients. These data are interesting because they suggest that some berries/their components in a concentrated form may be useful adjuncts to some medicines.

Cranberry. In a study with type 2 diabetic patients, a cranberry extract (or placebo capsule) was supplemented for 12 weeks.[151] The placebo or cranberry extract capsules were ingested after each main meal to provide a daily dose of 0 or 1500 mg of extract (500 mg/capsule): composition was not provided by authors. At the end of the intervention period there was no significant difference in circulating CRP between treatment groups. Similar results were reported by Vidlar et al., who supplemented 42 men with lower urinary tract symptoms with 1500 mg of cranberry fruit powder (3 × 500 mg capsules, each containing 52 mg of polyphenols, 1.65 mg of anthocyanins) or placebo capsules for 6 months and found no significant change in fasting plasma hs-CRP concentrations.[152] However, in both studies subjects had within normal range levels of circulating CRP at baseline.

Sea Buckthorn Berry. Extracts of sea buckthorn berries were supplemented to 110 overweight and obese women for approximately 35 days.[124] The two forms that were tested were sea buckthorn berry oil, which was extracted from both the flesh and seeds of the berries, and an ethanol extract of the whole berry.[124] The supplemented berry oil elicited a significant decrease in sVCAM-1 and adiponectin and increased hs-CRP levels. The spray-dried ethanol extract of sea buckthorn berries lowered both sICAM-1 and TNF-α in circulation.

Of the nine studies on berry products, berry extracts, and purified anthocyanins from berries, six studies reported anti-inflammatory activity. A range of doses of purified anthocyanins were tested (150−640 mg), and beneficial effects were reported for lowering selected inflammatory markers.[146−148] In contrast, cranberry extracts did not appear to affect inflammatory markers under the conditions that were tested, even when supplemented for longer durations (12−24 weeks). Sea buckthorn berry fractions showed mixed results, with the ethanol extract showing more favorable results than an oil extract of sea buckthorn.[124] Overall, the efficacy of certain berry extracts as anti-inflammatory agents in humans appears to be comparable to the effects elicited with consumption of whole berries and berry products.

■ CONCLUSIONS

The purpose of this review was to critically assess the existing clinical data on berries and inflammation. Data reviewed included whole fruit products as well as extracts of whole berries.

Berries were shown to reduce inflammatory stress in humans when supplemented in various forms, including extracts and anthocyanin components, suggesting that anthocyanins are an important part of the biological activity delivered by berries. Anti-inflammatory effects were observed both in healthy persons and in people with different inflammation-associated chronic conditions supplemented daily for weeks to months, although variations in results requires follow-up. Study designs modeling acute bouts of inflammation revealed that consuming berries can have short-term homeostatic maintaining (protective) effects, such as modulating inflammatory responses induced by exercise and meals representing modern eating patterns. The data suggest that berries may offer their greatest benefit in times of or in conditions of metabolic stress. The lack of benefit on measures in the fasting state or during unchallenged conditions requires further investigation. Understanding these short-term responses has important implications in understanding long-term responses and may explain, at least in part, discrepancies in chronic feeding results.

In addition to the commonly known and consumed berries, we also reviewed the emerging literature of lesser known berries. These berries are not widely promoted and consumed, but in their own right showed consistent anti-inflammatory effects compared to common berries. Whereas the incongruent results between common and lesser known berries may be due to study design differences (one important design difference was sample size/power to detect effects; with the common berry studies using overall smaller sample size compared to the lesser known berries), it is also possible that the specific polyphenol profile of the lesser known berries may render them more effective in humans. Cultivation practices for commercial interests could certainly affect the content and composition of fruit.[153] Additionally, although the current review represents a complete collection of available berry (product) studies reporting on inflammation, inflammation was not necessarily the primary endpoint. Therefore, in several instances only a single marker of inflammation may have been reported. This review has highlighted the need for intervention studies to include a more comprehensive analysis of inflammatory status to better understand the role of berries and their components on modulating inflammation and immune function.

Emerging interest is also focused on the potential of polyphenols to alter the composition and function of the gut microbiota, gut permeability, and gut-derived pro-inflammatory stimuli.[154−156] Alternatively, colon microbiota are known to metabolize polyphenols in the large intestine, generating metabolites, which may remain undetected in circulation but may possibly contribute to overall biological effects of the parent compound.[157,158]

Finally, from a practical and public health standpoint, consuming fruits and vegetables is a key dietary recommendation

for health promotion globally.[159] In the United States, Americans currently eat about half the dietary recommendation for fruit (recommendation is 2 cup equivalent/day).[65,66] In addition to fiber and micronutrient content, fruits, including berries, deliver a variety of other phytochemicals, including polyphenols. Berries are unique because they are rich sources of anthocyanin polyphenols. Cell culture, animal and human epidemiological, and clinical studies have revealed biological activity consistent with health when berries or anthocyanins were tested. The data from the present review focused on inflammation, a critical process underlying multiple predisease and disease conditions, and showed that consuming berries affects inflammatory/immune processes favorably. Hence, the body of evidence suggests that eating berries is an important part of a healthy eating pattern to reduce disease risk. Promotional efforts aimed at increasing fruit consumption to meet dietary guidance should include communications focused on berry intake to increase fruit variety and composition of nutrients and phytochemicals delivering health benefits. Perhaps the challenges of getting people to eat "more" fruit to meet recommendations for health can be offset by improving the diversity of fruit selection to include a rainbow of deep and brightly colored fruits delivering polyphenol content and variety.

AUTHOR INFORMATION

Corresponding Author

*(B.M.B.-F.) Phone: (708) 341-7078. Fax: (708) 563-1873. E-mail: bburton@iit.edu.

Notes

The authors declare no competing financial interest.

ABBREVIATIONS USED

BC, baseline controlled; C, controlled; CAD, coronary artery disease; CHD, coronary heart disease; CK, creatine kinase; CVD, cardiovascular disease; DM, diabetes mellitus; GM-CSF, granulocyte macrophage colony stimulating factor; HC, high carbohydrate; HF, high fat; hs-CRP, high-sensitivity C-reactive protein; IκB, inhibitors of kappa B; IKK, inhibitor of nuclear factor kappa-B kinase; IL, interleukin; JNK, c-Jun N-terminal kinase; LDL-C, low density lipoprotein-cholesterol; LPS, lipopolysaccharide; MAPK, mitogen-activated protein kinase; MCP-1, monocyte chemoattractant protein-1; MetS, metabolic syndrome; MIG, monokine induced by interferon-gamma; MMP, matrix metalloproteinase; NA, not available; NF-κB, nuclear factor kappa-light-chain-enhancer of activated B cells; NK cells, natural killer cells; PAI-1, plasminogen activator inhibitor-1; PC, placebo controlled; RANTES, regulated upon activation, normal T cell expressed and secreted; ROS, reactive oxygen species; sICAM-1, soluble intercellular adhesion molecule; SOCS-3, suppressor of cytokine signaling-3; sVCAM-1, soluble vascular adhesion molecule; TLR, Toll-like receptor; TNF-α, tumor necrosis factor alpha

REFERENCES

(1) Gratchev, A.; Sobenin, I.; Orekhov, A.; Kzhyshkowska, J. Monocytes as a diagnostic marker of cardiovascular diseases. *Immunobiology* **2012**, *217*, 476−482.

(2) Rosenberg, P. B. Clinical aspects of inflammation in Alzheimer's disease. *Int. Rev. Psychiatry* **2005**, *17*, 503−514.

(3) Jellema, A.; Plat, J.; Mensink, R. P. Weight reduction, but not a moderate intake of fish oil, lowers concentrations of inflammatory markers and PAI-1 antigen in obese men during the fasting and postprandial state. *Eur. J. Clin. Invest.* **2004**, *34*, 766−773.

(4) Ghanim, H.; Abuaysheh, S.; Sia, C. L.; Korzeniewski, K.; Chaudhuri, A.; Fernandez-Real, J. M.; Dandona, P. Increase in plasma endotoxin concentrations and the expression of Toll-like receptors and suppressor of cytokine signaling-3 in mononuclear cells after a high-fat, high-carbohydrate meal: implications for insulin resistance. *Diabetes Care* **2009**, *32*, 2281−2287.

(5) Manning, P. J.; Sutherland, W. H.; McGrath, M. M.; de Jong, S. A.; Walker, R. J.; Williams, M. J. Postprandial cytokine concentrations and meal composition in obese and lean women. *Obesity (Silver Spring)* **2008**, *16*, 2046−2052.

(6) Calder, P. C.; Ahluwalia, N.; Brouns, F.; Buetler, T.; Clement, K.; Cunningham, K.; Esposito, K.; Jönsson, L. S.; Kolb, H.; Lansink, M.; Marcos, A.; Margioris, A.; Matusheski, N.; Nordmann, H.; O'Brien, J.; Pugliese, G.; Rizkalla, S.; Schalkwijk, C.; Tuomilehto, J.; Wärnberg, J.; Watzl, B.; Winklhofer-Roob, B. M. Dietary factors and low-grade inflammation in relation to overweight and obesity. *Br. J. Nutr.* **2011**, *106*, S5−S78.

(7) Edirisinghe, I.; Banaszewski, K.; Cappozzo, J.; Sandhya, K.; Ellis, C. L.; Tadapaneni, R.; Kappagoda, C. T.; Burton-Freeman, B. M. Strawberry anthocyanin and its association with postprandial inflammation and insulin. *Br. J. Nutr.* **2011**, *106*, 913−922.

(8) Burton-Freeman, B.; Talbot, J.; Park, E.; Krishnankutty, S.; Edirisinghe, I. Protective activity of processed tomato products on postprandial oxidation and inflammation: a clinical trial in healthy weight men and women. *Mol. Nutr. Food Res.* **2012**, *56*, 622−631.

(9) Root, M. M.; McGinn, M. C.; Nieman, D. C.; Henson, D. A.; Heinz, S. A.; Shanely, R. A.; Knab, A. M.; Jin, F. Combined fruit and vegetable intake is correlated with improved inflammatory and oxidant status from a cross-sectional study in a community setting. *Nutrients* **2012**, *4*, 29−41.

(10) Anderson, A. L.; Harris, T. B.; Tylavsky, F. A.; Perry, S. E.; Houston, D. K.; Lee, J. S.; Kanaya, A. M.; Sahyoun, N. R. Dietary patterns, insulin sensitivity and inflammation in older adults. *Eur. J. Clin. Nutr.* **2012**, *66*, 18−24.

(11) Nanri, H.; Nakamura, K.; Hara, M.; Higaki, Y.; Imaizumi, T.; Taguchi, N.; Sakamoto, T.; Horita, M.; Shinchi, K.; Tanaka, K. Association between dietary pattern and serum C-reactive protein in Japanese men and women. *J. Epidemiol.* **2011**, *21*, 122−131.

(12) Dauchet, L.; Amouyel, P.; Dallongeville, J. Fruits, vegetables and coronary heart disease. *Nat. Rev. Cardiol.* **2009**, *6*, 599−608.

(13) Hu, F. B. Plant-based foods and prevention of cardiovascular disease: an overview. *Am. J. Clin. Nutr.* **2003**, *78*, 544S−551S.

(14) Dauchet, L.; Amouyel, P.; Hercberg, S.; Dallongeville, J. Fruit and vegetable consumption and risk of coronary heart disease: a meta-analysis of cohort studies. *J. Nutr.* **2006**, *136*, 2588−2593.

(15) He, F. J.; Nowson, C. A.; Lucas, M.; MacGregor, G. A. Increased consumption of fruit and vegetables is related to a reduced risk of coronary heart disease: meta-analysis of cohort studies. *J. Hum. Hypertens.* **2007**, *21*, 717−728.

(16) Fung, T. T.; Rexrode, K. M.; Mantzoros, C. S.; Manson, J. E.; Willett, W. C.; Hu, F. B. Mediterranean diet and incidence of and mortality from coronary heart disease and stroke in women. *Circulation* **2009**, *119*, 1093−1100.

(17) Esmaillzadeh, A.; Kimiagar, M.; Mehrabi, Y.; Azadbakht, L.; Hu, F. B.; Willett, W. C. Dietary patterns, insulin resistance, and prevalence of the metabolic syndrome in women. *Am. J. Clin. Nutr.* **2007**, *85*, 910−918.

(18) Tortosa, A.; Bes-Rastrollo, M.; Sanchez-Villegas, A.; Basterra-Gortari, F. J.; Nuñez-Cordoba, J. M.; Martinez-Gonzalez, M. A. Mediterranean diet inversely associated with the incidence of metabolic syndrome: the SUN prospective cohort. *Diabetes Care* **2007**, *30*, 2957−2959.

(19) Babio, N.; Bulló, M.; Salas-Salvadó, J. Mediterranean diet and metabolic syndrome: the evidence. *Public Health Nutr.* **2009**, *12*, 1607−1617.

(20) Martínez-González, M. A.; Sánchez-Villegas, A. The emerging role of Mediterranean diets in cardiovascular epidemiology: monounsaturated

fats, olive oil, red wine or the whole pattern? *Eur. J. Epidemiol.* **2004**, *19*, 9−13.
(21) Dai, Q.; Borenstein, A. R.; Wu, Y.; Jackson, J. C.; Larson, E. B. Fruit and vegetable juices and Alzheimer's disease: the Kame Project. *Am. J. Med.* **2006**, *119*, 751−759.
(22) Zamora-Ros, R.; Knaze, V.; Luján-Barroso, L.; Romieu, I.; Scalbert, A.; Slimani, N.; Hjartåker, A.; Engeset, D.; Skeie, G.; Overvad, K.; Bredsdorff, L.; Tjønneland, A.; Halkjær, J.; Key, T. J.; Khaw, K. T.; Mulligan, A. A.; Winkvist, A.; Johansson, I.; Bueno-de-Mesquita, H. B.; Peeters, P. H.; Wallström, P.; Ericson, U.; Pala, V.; de Magistris, M. S.; Polidoro, S.; Tumino, R.; Trichopoulou, A.; Dilis, V.; Katsoulis, M.; Huerta, J. M.; Martínez, V.; Sánchez, M. J.; Ardanaz, E.; Amiano, P.; Teucher, B.; Grote, V.; Bendinelli, B.; Boeing, H.; Förster, J.; Touillaud, M.; Perquier, F.; Fagherazzi, G.; Gallo, V.; Riboli, E.; González, C. A. Differences in dietary intakes, food sources and determinants of total flavonoids between Mediterranean and non-Mediterranean countries participating in the European Prospective Investigation into Cancer and Nutrition (EPIC) study. *Br. J. Nutr.* **2013**, *109*, 1498−1507.
(23) Mink, P. J.; Scrafford, C. G.; Barraj, L. M.; Harnack, L.; Hong, C. P.; Nettleton, J. A.; Jacobs, D. R., Jr. Flavonoid intake and cardiovascular disease mortality: a prospective study in postmenopausal women. *Am. J. Clin. Nutr.* **2007**, *85*, 895−909.
(24) McCullough, M. L.; Peterson, J. J.; Patel, R.; Jacques, P. F.; Shah, R.; Dwyer, J. T. Flavonoid intake and cardiovascular disease mortality in a prospective cohort of US adults. *Am. J. Clin. Nutr.* **2012**, *95*, 454−464.
(25) http://www.transparencymarketresearch.com/polyphenol-market.html (retrieved Sept 26, 2013).
(26) Montero, L.; Herrero, M.; Ibáñez, E.; Cifuentes, A. Profiling of phenolic compounds from different apple varieties using comprehensive two-dimensional liquid chromatography. *J. Chromatogr., A* **2013**, *1313*, 275−283.
(27) Li, Z.; Zhao, X.; Sandhu, A. K.; Gu, L. Effects of exogenous abscisic acid on yield, antioxidant capacities, and phytochemical contents of greenhouse grown lettuces. *J. Agric. Food Chem.* **2010**, *58*, 6503−6509.
(28) Vinson, J. A.; Cai, Y. Nuts, especially walnuts, have both antioxidant quantity and efficacy and exhibit significant potential health benefits. *Food Funct.* **2012**, *3*, 134−140.
(29) Li, Z.; Pan, Q.; Jin, Z.; Mu, L.; Duan, C. Comparison on phenolic compounds in *Vitis vinifera* cv. Cabernet Sauvignon wines from five wine-growing regions in China. *Food Chem.* **2011**, *125*, 77−83.
(30) Gu, L.; House, S. E.; Wu, X.; Ou, B.; Prior, R. L. Procyanidin and catechin contents and antioxidant capacity of cocoa and chocolate products. *J. Agric. Food Chem.* **2006**, *54*, 4057−4061.
(31) Ho, H. M.; Chen, R. Y.; Leung, L. K.; Chan, F. L.; Huang, Y.; Chen, Z. Y. Difference in flavonoid and isoflavone profile between soybean and soy leaf. *Biomed. Pharmacother.* **2002**, *56*, 289−295.
(32) Mateos, R.; Espartero, J. L.; Trujillo, M.; Ríos, J. J.; León-Camacho, M.; Alcudia, F.; Cert, A. Determination of phenols, flavones, and lignans in virgin olive oils by solid-phase extraction and high-performance liquid chromatography with diode array ultraviolet detection. *J. Agric. Food Chem.* **2001**, *49*, 2185−2192.
(33) Liu, S.; Manson, J. E.; Lee, I. M.; Cole, S. R.; Hennekens, C. H.; Willett, W. C.; Buring, J. E. Fruit and vegetable intake and risk of cardiovascular disease: the Women's Health Study. *Am. J. Clin. Nutr.* **2000**, *72*, 922−928.
(34) Cassidy, A.; O'Reilly, É. J.; Kay, C.; Sampson, L.; Franz, M.; Forman, J. P.; Curhan, G.; Rimm, E. B. Habitual intake of flavonoid subclasses and incident hypertension in adults. *Am. J. Clin. Nutr.* **2011**, *93*, 338−347.
(35) Jennings, A.; Welch, A. A.; Fairweather-Tait, S. J.; Kay, C.; Minihane, A. M.; Chowienczyk, P.; Jiang, B.; Cecelja, M.; Spector, T.; Macgregor, A.; Cassidy, A. Higher anthocyanin intake is associated with lower arterial stiffness and central blood pressure in women. *Am. J. Clin. Nutr.* **2012**, *96*, 781−788.
(36) Cassidy, A.; Mukamal, K. J.; Liu, L.; Franz, M.; Eliassen, A. H.; Rimm, E. B. High anthocyanin intake is associated with a reduced risk of myocardial infarction in young and middle-aged women. *Circulation* **2013**, *127*, 188−196.
(37) Wedick, N. M.; Pan, A.; Cassidy, A.; Rimm, E. B.; Sampson, L.; Rosner, B.; Willett, W.; Hu, F. B.; Sun, Q.; van Dam, R. M. Dietary flavonoid intakes and risk of type 2 diabetes in US men and women. *Am. J. Clin. Nutr.* **2012**, *95*, 925−933.
(38) Cutler, G. J.; Nettleton, J. A.; Ross, J. A.; Harnack, L. J.; Jacobs, D. R., Jr.; Scrafford, C. G.; Barraj, L. M.; Mink, P. J.; Robien, K. Dietary flavonoid intake and risk of cancer in postmenopausal women: the Iowa Women's Health Study. *Int. J. Cancer* **2008**, *123*, 664−671.
(39) Mursu, J.; Nurmi, T.; Tuomainen, T. P.; Salonen, J. T.; Pukkala, E.; Voutilainen, S. Intake of flavonoids and risk of cancer in Finnish men: The Kuopio Ischaemic Heart Disease Risk Factor Study. *Int. J. Cancer* **2008**, *123*, 660−663.
(40) Seeram, N. P.; Momin, R. A.; Nair, M. G.; Bourquin, L. D. Cyclooxygenase inhibitory and antioxidant cyanidin glycosides in cherries and berries. *Phytomedicine* **2001**, *8*, 362−369.
(41) Jean-Gilles, D.; Li, L.; Vaidyanathan, V. G.; King, R.; Cho, B.; Worthen, D. R.; Chichester, C. O., 3rd; Seeram, N. P. Inhibitory effects of polyphenol punicalagin on type-II collagen degradation in vitro and inflammation in vivo. *Chem.−Biol. Interact.* **2013**, *205*, 90−99.
(42) Serra, D.; Paixão, J.; Nunes, C.; Dinis, T. C.; Almeida, L. M. Cyanidin-3-glucoside suppresses cytokine-induced inflammatory response in human intestinal cells: comparison with 5-aminosalicylic acid. *PLoS One* **2013**, *8*, e73001.
(43) Subbaramaiah, K.; Sue, E.; Bhardwaj, P.; Du, B.; Hudis, C. A.; Giri, D.; Kopelovich, L.; Zhou, X. K.; Dannenberg, A. J. Dietary polyphenols suppress elevated levels of proinflammatory mediators and aromatase in the mammary gland of obese mice. *Cancer Prev. Res. (Philadelphia)* **2013**, *6*, 886−897.
(44) Kim, J. M.; Kim, K. M.; Park, E. H.; Seo, J. H.; Song, J. Y.; Shin, S. C.; Kang, H. L.; Lee, W. K.; Cho, M. J.; Rhee, K. H.; Youn, H. S.; Baik, S. C. Anthocyanins from black soybean inhibit *Helicobacter pylori*-induced inflammation in human gastric epithelial AGS cells. *Microbiol. Immunol.* **2013**, *57*, 366−373.
(45) Peluso, I.; Raguzzini, A.; Villano, D. V.; Cesqui, E.; Toti, E.; Catasta, G.; Serafini, M. High fat meal increase of IL-17 is prevented by ingestion of fruit juice drink in healthy overweight subjects. *Curr. Pharm. Des.* **2012**, *18*, 85−90.
(46) Peluso, I.; Villano, D. V.; Roberts, S. A.; Cesqui, E.; Raguzzini, A.; Borges, G.; Crozier, A.; Catasta, G.; Toti, E.; Serafini, M. Consumption of mixed fruit-juice drink and vitamin C reduces postprandial stress induced by a high fat meal in healthy overweight subjects. *Curr. Pharm. Des.* **2013**, DOI: 10.2174/13816128113199990057.
(47) Huebbe, P.; Giller, K.; de Pascual-Teresa, S.; Arkenau, A.; Adolphi, B.; Portius, S.; Arkenau, C. N.; Rimbach, G. Effects of blackcurrant-based juice on atherosclerosis-related biomarkers in cultured macrophages and in human subjects after consumption of a high-energy meal. *Br. J. Nutr.* **2011**, *20*, 1−11.
(48) Nieman, D. C.; Gillitt, N. D.; Knab, A. M.; Shanely, R. A.; Pappan, K. L.; Jin, F.; Lila, M. A. Influence of a polyphenol-enriched protein powder on exercise-induced inflammation and oxidative stress in athletes: a randomized trial using a metabolomics approach. *PLoS One* **2013**, *8*, e72215 DOI: 10.1371/journal.pone.0072215.
(49) Pahl, H. L. Activators and target genes of Rel/NF-kappaB transcription factors. *Oncogene* **1999**, *18*, 6853−6866.
(50) Hotamisligil, G. S.; Shargill, N. S.; Spiegelman, B. M. Adipose expression of tumor necrosis factor-alpha: direct role in obesity-linked insulin resistance. *Science* **1993**, *259*, 87−91.
(51) Hajer, G. R.; van Haeften, T. W.; Visseren, F. L. Adipose tissue dysfunction in obesity, diabetes, and vascular diseases. *Eur. Heart J.* **2008**, *29*, 2959−2971.
(52) Hummasti, S.; Hotamisligil, G. S. Endoplasmic reticulum stress and inflammation in obesity and diabetes. *Circ. Res.* **2010**, *107*, 579−591.

(53) Patel, C.; Ghanim, H.; Ravishankar, S.; Sia, C. L.; Viswanathan, P.; Mohanty, P.; Dandona, P. Prolonged reactive oxygen species generation and nuclear factor-kappaB activation after a high-fat, high-carbohydrate meal in the obese. *J. Clin. Endocrinol. Metab.* **2007**, *92*, 4476−4479.
(54) Hyson, D. A.; Paglieroni, T. G.; Wun, T.; Rutledge, J. C. Postprandial lipemia is associated with platelet and monocyte activation and increased monocyte cytokine expression in normolipemic men. *Clin. Appl. Thromb. Hemost.* **2002**, *8*, 147−155.
(55) Aljada, A.; Mohanty, P.; Ghanim, H.; Abdo, T.; Tripathy, D.; Chaudhuri, A.; Dandona, P. Increase in intranuclear nuclear factor kappaB and decrease in inhibitor kappaB in mononuclear cells after a mixed meal: evidence for a proinflammatory effect. *Am. J. Clin. Nutr.* **2004**, *79*, 682−690.
(56) Aljada, A.; Friedman, J.; Ghanim, H.; Mohanty, P.; Hofmeyer, D.; Chaudhuri, A.; Dandona, P. Glucose ingestion induces an increase in intranuclear nuclear factor kappaB, a fall in cellular inhibitor kappaB, and an increase in tumor necrosis factor alpha messenger RNA by mononuclear cells in healthy human subjects. *Metabolism* **2006**, *55*, 1177−1185.
(57) Joseph, S. V.; Edirisinghe, I.; Burton-Freeman, B. M. Fruit polyphenols: a review of anti-inflammatory effects in humans. *Crit. Rev. Food Sci. Nutr.* **2014**, in press.
(58) Albers, R.; Bourdet-Sicard, R.; Braun, D.; Calder, P. C.; Herz, U.; Lambert, C.; Lenoir-Wijnkoop, I.; Méheust, A.; Ouwehand, A.; Phothirath, P.; Sako, T.; Salminen, S.; Siemensma, A.; van Loveren, H.; Sack, U. Monitoring immune modulation by nutrition in the general population: identifying and substantiating effects on human health. *Br. J. Nutr.* **2013**, *110* (Suppl. 2), S1−S30.
(59) The American Heritage Science Dictionary; Google Books (retrieved Sept 29, 2013).
(60) Wallace, T. C. Anthocyanins in cardiovascular disease. *Adv. Nutr.* **2011**, *2*, 1−7.
(61) Pandey, K. B.; Rizvi, S. I. Plant polyphenols as dietary antioxidants in human health and disease. *Oxid. Med. Cell Longev.* **2009**, *2*, 270−278.
(62) Pérez-Jiménez, J.; Hubert, J.; Hooper, L.; Cassidy, A.; Manach, C.; Williamson, G.; Scalbert, A. Urinary metabolites as biomarkers of polyphenol intake in humans: a systematic review. *Am. J. Clin. Nutr.* **2010**, *92*, 801−809.
(63) Ovaskainen, M. L.; Törrönen, R.; Koponen, J. M.; Sinkko, H.; Hellström, J.; Reinivuo, H.; Mattila, P. Dietary intake and major food sources of polyphenols in Finnish adults. *J. Nutr.* **2008**, *138*, 562−566.
(64) Wu, X.; Beecher, G. R.; Holden, J. M.; Haytowitz, D. B.; Gebhardt, S. E.; Prior, R. L. Concentrations of anthocyanins in common foods in the united states and estimation of normal consumption. *J. Agric. Food Chem.* **2006**, *54*, 4069−4075.
(65) http://www.health.gov/dietaryguidelines (retrieved Sept 28, 2013).
(66) http://www.healthypeople.gov/2020/default.aspx (retrieved Sept 28, 2013).
(67) Wu, X.; Gu, L.; Prior, R. L.; McKay, S. Characterization of anthocyanins and proanthocyanidins in some cultivars of *Ribes*, *Aronia*, and *Sambucus* and their antioxidant capacity. *J. Agric. Food Chem.* **2004**, *52*, 7846−7856.
(68) White, B. L.; Howard, L. R.; Prior, R. L. Polyphenolic composition and antioxidant capacity of extruded cranberry pomace. *J. Agric. Food Chem.* **2010**, *58*, 4037−4042.
(69) Wolfe, K. L.; Kang, X.; He, X.; Dong, M.; Zhang, Q.; Liu, R. H. Cellular antioxidant activity of common fruits. *J. Agric. Food Chem.* **2008**, *56*, 8418−8426.
(70) Seeram, N. P.; Adams, L. S.; Henning, S. M.; Niu, Y.; Zhang, Y.; Nair, M. G.; Heber, D. In vitro antiproliferative, apoptotic and antioxidant activities of punicalagin, ellagic acid and a total pomegranate tannin extract are enhanced in combination with other polyphenols as found in pomegranate juice. *J. Nutr. Biochem.* **2005**, *16*, 360−367.
(71) Aiyer, H. S.; Kichambare, S.; Gupta, R. C. Prevention of oxidative DNA damage by bioactive berry components. *Nutr. Cancer* **2008**, *60*, 36−42.
(72) Hurst, R. D.; Wells, R. W.; Hurst, S. M.; McGhie, T. K.; Cooney, J. M.; Jensen, D. J. Blueberry fruit polyphenolics suppress oxidative stress-induced skeletal muscle cell damage in vitro. *Mol. Nutr. Food Res.* **2010**, *54*, 353−363.
(73) Scalbert, A.; Johnson, I. T.; Saltmarsh, M. Polyphenols: antioxidants and beyond. *Am. J. Clin. Nutr.* **2005**, *81*, 215S−217S.
(74) Tangney, C. C.; Rasmussen, H. E. Polyphenols, inflammation, and cardiovascular disease. *Curr. Atheroscler. Rep.* **2013**, *15*, 324.
(75) Virgili, F.; Marino, M. Regulation of cellular signals from nutritional molecules: a specific role for phytochemicals, beyond antioxidant activity. *Free Radical Biol. Med.* **2008**, *45*, 1205−1216.
(76) Olas, B.; Wachowicz, B.; Nowak, P.; Kedzierska, M.; Tomczak, A.; Stochmal, A.; Oleszek, W.; Jeziorski, A.; Piekarski, J. Studies on antioxidant properties of polyphenol-rich extract from berries of *Aronia melanocarpa* in blood platelets. *J. Physiol. Pharmacol.* **2008**, *59*, 823−835.
(77) Flis, S.; Jastrzebski, Z.; Namiesnik, J.; Arancibia-Avila, P.; Toledo, F.; Leontowicz, H.; Leontowicz, M.; Suhaj, M.; Trakhtenberg, S.; Gorinstein, S. Evaluation of inhibition of cancer cell proliferation in vitro with different berries and correlation with their antioxidant levels by advanced analytical methods. *J. Pharm. Biomed. Anal.* **2012**, *62*, 68−78.
(78) Mudnic, I.; Budimir, D.; Modun, D.; Gunjaca, G.; Generalic, I.; Skroza, D.; Katalinic, V.; Ljubenkov, I.; Boban, M. Antioxidant and vasodilatory effects of blackberry and grape wines. *J. Med. Food* **2012**, *15*, 315−321.
(79) Edirisinghe, I.; Burton-Freeman, B.; Varelis, P.; Kappagoda, T. Strawberry extract caused endothelium-dependent relaxation through the activation of PI3 kinase/Akt. *J. Agric. Food Chem.* **2008**, *56*, 9383−9390.
(80) Tulio, A. Z., Jr.; Chang, C.; Edirisinghe, I.; White, K. D.; Jablonski, J. E.; Banaszewski, K.; Kangath, A.; Tadapaneni, R. K.; Burton-Freeman, B.; Jackson, L. S. Berry fruits modulated endothelial cell migration and angiogenesis via phosphoinositide-3 kinase/protein kinase B pathway in vitro in endothelial cells. *J. Agric. Food Chem.* **2012**, *60*, 5803−5812.
(81) Parelman, M. A.; Storms, D. H.; Kirschke, C. P.; Huang, L.; Zunino, S. J. Dietary strawberry powder reduces blood glucose concentrations in obese and lean C57BL/6 mice, and selectively lowers plasma C-reactive protein in lean mice. *Br. J. Nutr.* **2012**, *108*, 1789−1799.
(82) Sweeney, M. I.; Kalt, W.; MacKinnon, S. L.; Ashby, J.; Gottschall-Pass, K. T. Feeding rats diets enriched in lowbush blueberries for six weeks decreases ischemia-induced brain damage. *Nutr. Neurosci.* **2002**, *5*, 427−431.
(83) Xie, C.; Kang, J.; Ferguson, M. E.; Nagarajan, S.; Badger, T. M.; Wu, X. Blueberries reduce pro-inflammatory cytokine TNF-α and IL-6 production in mouse macrophages by inhibiting NF-κB activation and the MAPK pathway. *Mol. Nutr. Food Res.* **2011**, *55*, 1587−1591.
(84) Vendrame, S.; Daugherty, A.; Kristo, A. S.; Riso, P.; Klimis-Zacas, D. Wild blueberry (*Vaccinium angustifolium*) consumption improves inflammatory status in the obese Zucker rat model of the metabolic syndrome. *J. Nutr. Biochem.* **2013**, *24*, 1508−1512.
(85) Huang, Y.; Nikolic, D.; Pendland, S.; Doyle, B. J.; Locklear, T. D.; Mahady, G. B. Effects of cranberry extracts and ursolic acid derivatives on P-fimbriated *Escherichia coli*, COX-2 activity, pro-inflammatory cytokine release and the NF-kappa beta transcriptional response in vitro. *Pharm. Biol.* **2009**, *47*, 18−25.
(86) Kim, M. J.; Ohn, J.; Kim, J. H.; Kwak, H. K. Effects of freeze-dried cranberry powder on serum lipids and inflammatory markers in lipopolysaccharide treated rats fed an atherogenic diet. *Nutr. Res. Pract.* **2011**, *5*, 404−411.
(87) Qin, B.; Anderson, R. A. An extract of chokeberry attenuates weight gain and modulates insulin, adipogenic and inflammatory signalling pathways in epididymal adipose tissue of rats fed a fructose-rich diet. *Br. J. Nutr.* **2012**, *108*, 581−587.

(88) Triebel, S.; Trieu, H. L.; Richling, E. Modulation of inflammatory gene expression by a bilberry (*Vaccinium myrtillus* L.) extract and single anthocyanins considering their limited stability under cell culture conditions. *J. Agric. Food Chem.* **2012**, *60*, 8902−8910.

(89) Bognar, E.; Sarszegi, Z.; Szabo, A.; Debreceni, B.; Kalman, N.; Tucsek, Z.; Sumegi, B.; Gallyas, F., Jr. Antioxidant and anti-inflammatory effects in RAW264.7 macrophages of malvidin, a major red wine polyphenol. *PLoS One* **2013**, *8*, e65355.

(90) Decendit, A.; Mamani-Matsuda, M.; Aumont, V.; Waffo-Teguo, P.; Moynet, D.; Boniface, K.; Richard, E.; Krisa, S.; Rambert, J.; Mérillon, J. M.; Mossalayi, M. D. Malvidin-3-*O*-*β*-glucoside, major grape anthocyanin, inhibits human macrophage-derived inflammatory mediators and decreases clinical scores in arthritic rats. *Biochem. Pharmacol.* **2013**, *86*, 1461−1467.

(91) Kapasakalidis, P. G.; Rastall, R. A.; Gordon, M. H. Extraction of polyphenols from processed blackcurrant (*Ribes nigrum* L.) residues. *J. Agric. Food Chem.* **2006**, *54*, 4016−4021.

(92) Matsumoto, H.; Inaba, H.; Kishi, M.; Tominaga, S.; Hirayama, M.; Tsuda, T. Orally administered delphinidin 3-rutinoside and cyanidin 3-rutinoside are directly absorbed in rats and humans and appear in the blood as the intact forms. *J. Agric. Food Chem.* **2001**, *49*, 1546−1551.

(93) Jin, Y.; Alimbetov, D.; George, T.; Gordon, M. H.; Lovegrove, J. A. A randomised trial to investigate the effects of acute consumption of a blackcurrant juice drink on markers of vascular reactivity and bioavailability of anthocyanins in human subjects. *Eur. J. Clin. Nutr.* **2011**, *65*, 849−856.

(94) Del Rio, D.; Borges, G.; Crozier, A. Berry flavonoids and phenolics: bioavailability and evidence of protective effects. *Br. J. Nutr.* **2010**, *104* (Suppl. 3), S67−S90.

(95) Basu, A.; Du, M.; Leyva, M. J.; Sanchez, K.; Betts, N. M.; Wu, M.; Aston, C. E.; Lyons, T. J. Blueberries decrease cardiovascular risk factors in obese men and women with metabolic syndrome. *J. Nutr.* **2010**, *140*, 1582−1587.

(96) Stull, A. J.; Cash, K. C.; Johnson, W. D.; Champagne, C. M.; Cefalu, W. T. Bioactives in blueberries improve insulin sensitivity in obese, insulin-resistant men and women. *J. Nutr.* **2010**, *140*, 1764−1768.

(97) McAnulty, L. S.; Nieman, D. C.; Dumke, C. L.; Shooter, L. A.; Henson, D. A.; Utter, A. C.; Milne, G.; McAnulty, S. R. Effect of blueberry ingestion on natural killer cell counts, oxidative stress, and inflammation prior to and after 2.5 h of running. *Appl. Physiol. Nutr. Metab.* **2011**, *36*, 976−984.

(98) Riso, P.; Klimis-Zacas, D.; Del Bo', C.; Martini, D.; Campolo, J.; Vendrame, S.; Møller, P.; Loft, S.; De Maria, R.; Porrini, M. Effect of a wild blueberry (*Vaccinium angustifolium*) drink intervention on markers of oxidative stress, inflammation and endothelial function in humans with cardiovascular risk factors. *Eur. J. Nutr.* **2013**, *52*, 949−961.

(99) Brittenden, J.; Heys, S. D.; Ross, J.; Eremin, O. Natural killer cells and cancer. *Cancer* **1996**, *77*, 1226−1243.

(100) McLeay, Y.; Barnes, M. J.; Mundel, T.; Hurst, S. M.; Hurst, R. D.; Stannard, S. R. Effect of New Zealand blueberry consumption on recovery from eccentric exercise-induced muscle damage. *J. Int. Soc. Sports Nutr.* **2012**, *9*, 19−30.

(101) Howell, A. B. Bioactive compounds in cranberries and their role in prevention of urinary tract infections. *Mol. Nutr. Food Res.* **2007**, *51*, 732−737.

(102) Milbury, P. E.; Vita, J. A.; Blumberg, J. B. Anthocyanins are bioavailable in humans following an acute dose of cranberry juice. *J. Nutr.* **2010**, *140*, 1099−1104.

(103) Chen, H.; Zuo, Y.; Deng, Y. Separation and determination of flavonoids and other phenolic compounds in cranberry juice by high-performance liquid chromatography. *J. Chromatogr., A* **2001**, *913*, 387−395.

(104) Neto, C. C. Cranberry and blueberry: evidence for protective effects against cancer and vascular diseases. *Mol. Nutr. Food Res.* **2007**, *51*, 652−664.

(105) Ruel, G.; Pomerleau, S.; Couture, P.; Lemieux, S.; Lamarche, B.; Couillard, C. Low-calorie cranberry juice supplementation reduces plasma oxidized LDL and cell adhesion molecule concentrations in men. *Br. J. Nutr.* **2008**, *99*, 352−359.

(106) Ruel, G.; Pomerleau, S.; Couture, P.; Lemieux, S.; Lamarche, B.; Couillard, C. Plasma matrix metalloproteinase (MMP)-9 levels are reduced following low-calorie cranberry juice supplementation in men. *J. Am. Coll. Nutr.* **2009**, *28*, 694−701.

(107) Basu, A.; Betts, N. M.; Ortiz, J.; Simmons, B.; Wu, M.; Lyons, T. J. Low-energy cranberry juice decreases lipid oxidation and increases plasma antioxidant capacity in women with metabolic syndrome. *Nutr. Res. (N.Y.)* **2011**, *31*, 190−196.

(108) Dohadwala, M. M.; Holbrook, M.; Hamburg, N. M.; Shenouda, S. M.; Chung, W. B.; Titas, M.; Kluge, M. A.; Wang, N.; Palmisano, J.; Milbury, P. E.; Blumberg, J. B.; Vita, J. A. Effects of cranberry juice consumption on vascular function in patients with coronary artery disease. *Am. J. Clin. Nutr.* **2011**, *93*, 934−940.

(109) Giampieri, F.; Tulipani, S.; Alvarez-Suarez, J. M.; Quiles, J. L.; Mezzetti, B.; Battino, M. The strawberry: composition, nutritional quality, and impact on human health. *Nutrition* **2012**, *28*, 9−19.

(110) Banaszewski, K.; Park, E.; Edirisinghe, I.; Cappozzo, J. C.; Burton-Freeman, B. M. A pilot study to investigate bioavailability of strawberry anthocyanins and characterize postprandial plasma polyphenols absorption patterns by Q-TOF LC/MS in humans. *J. Berry Res.* **2013**, *3*, 113−126.

(111) Ellis, C. L.; Edirisinghe, I.; Kappagoda, T.; Burton-Freeman, B. Attenuation of meal-induced inflammatory and thrombotic responses in overweight men and women after 6-week daily strawberry (*Fragaria*) intake. A randomized placebo-controlled trial. *J. Atheroscler. Thromb.* **2011**, *18*, 318−327.

(112) Basu, A.; Wilkinson, M.; Penugonda, K.; Simmons, B.; Betts, N. M.; Lyons, T. J. Freeze-dried strawberry powder improves lipid profile and lipid peroxidation in women with metabolic syndrome: baseline and post intervention effects. *Nutr. J.* **2009**, *8*, 43−49.

(113) Basu, A.; Fu, D. X.; Wilkinson, M.; Simmons, B.; Wu, M.; Betts, N. M.; Du, M.; Lyons, T. J. Strawberries decrease atherosclerotic markers in subjects with metabolic syndrome. *Nutr. Res. (N.Y.)* **2010**, *30*, 462−469.

(114) Zunino, S. J.; Parelman, M. A.; Freytag, T. L.; Stephensen, C. B.; Kelley, D. S.; Mackey, B. E.; Woodhouse, L. R.; Bonnel, E. L. Effects of dietary strawberry powder on blood lipids and inflammatory markers in obese human subjects. *Br. J. Nutr.* **2012**, *108*, 900−909.

(115) Chen, T.; Yan, F.; Qian, J.; Guo, M.; Zhang, H.; Tang, X.; Chen, F.; Stoner, G. D.; Wang, X. Randomized phase II trial of lyophilized strawberries in patients with dysplastic precancerous lesions of the esophagus. *Cancer Prev. Res. (Philadelphia)* **2012**, *5*, 41−50.

(116) Jacobs, M.; van Greevenbroek, M. M.; van der Kallen, C. J.; Ferreira, I.; Blaak, E. E.; Feskens, E. J.; Jansen, E. H.; Schalkwijk, C. G; Stehouwer, C. D. Low-grade inflammation can partly explain the association between the metabolic syndrome and either coronary artery disease or severity of peripheral arterial disease: the CODAM study. *Eur. J. Clin. Invest.* **2009**, *39*, 437−444.

(117) Seeram, N. P. Berry fruits: compositional elements, biochemical activities, and the impact of their intake on human health, performance, and disease. *J. Agric. Food Chem.* **2008**, *56*, 627−629.

(118) Hosseinian, F. S.; Beta, T. Saskatoon and wild blueberries have higher anthocyanin contents than other Manitoba berries. *J. Agric. Food Chem.* **2007**, *55*, 10832−10838.

(119) Taheri, R.; Connolly, B. A.; Brand, M. H.; Bolling, B. W. Underutilized chokeberry (*Aronia melanocarpa*, *Aronia arbutifolia*, *Aronia prunifolia*) accessions are rich sources of anthocyanins, flavonoids, hydroxycinnamic acids, and proanthocyanidins. *J. Agric. Food Chem.* **2013**, *61*, 8581−8588.

(120) Paixão, J.; Dinis, T. C.; Almeida, L. M. Malvidin-3-glucoside protects endothelial cells up-regulating endothelial NO synthase and inhibiting peroxynitrite-induced NF-*κ*B activation. *Chem.−Biol. Interact.* **2012**, *199*, 192−200.

(121) Zhang, B.; Buya, M.; Qin, W.; Sun, C.; Cai, H.; Xie, Q.; Xu, B.; Wu, Y. Anthocyanins from Chinese bayberry extract activate transcription factor Nrf2 in β cells and negatively regulate oxidative stress-induced autophagy. *J. Agric. Food Chem.* **2013**, *61*, 8765−8772.
(122) Johnson, M. H.; de Mejia, E. G.; Fan, J.; Lila, M. A.; Yousef, G. G. Anthocyanins and proanthocyanidins from blueberry-blackberry fermented beverages inhibit markers of inflammation in macrophages and carbohydrate-utilizing enzymes in vitro. *Mol. Nutr. Food Res.* **2013**, *57*, 1182−1197.
(123) Karlsen, A.; Paur, I.; Bøhn, S. K.; Sakhi, A. K.; Borge, G. I.; Serafini, M.; Erlund, I.; Laake, P.; Tonstad, S.; Blomhoff, R. Bilberry juice modulates plasma concentration of NF-kappaB related inflammatory markers in subjects at increased risk of CVD. *Eur. J. Nutr.* **2010**, *49*, 345−355.
(124) Lehtonen, H. M.; Suomela, J. P.; Tahvonen, R.; Yang, B.; Venojärvi, M.; Viikari, J.; Kallio, H. Different berries and berry fractions have various but slightly positive effects on the associated variables of metabolic diseases on overweight and obese women. *Eur. J. Clin. Nutr.* **2011**, *65*, 394−401.
(125) Kolehmainen, M.; Mykkänen, O.; Kirjavainen, P. V.; Leppänen, T.; Moilanen, E.; Adriaens, M.; Laaksonen, D. E.; Hallikainen, M.; Puupponen-Pimiä, R.; Pulkkinen, L.; Mykkänen, H.; Gylling, H.; Poutanen, K.; Törrönen, R. Bilberries reduce low-grade inflammation in individuals with features of metabolic syndrome. *Mol. Nutr. Food Res.* **2012**, *56*, 1501−1510.
(126) Mentor-Marcel, R. A.; Bobe, G.; Sardo, C.; Wang, L. S.; Kuo, C. T.; Stoner, G.; Colburn, N. H. Plasma cytokines as potential response indicators to dietary freeze-dried black raspberries in colorectal cancer patients. *Nutr. Cancer* **2012**, *64*, 820−825.
(127) Sardo, C. L.; Kitzmiller, J. P.; Apseloff, G.; Harris, R. B.; Roe, D. J.; Stoner, G. D.; Jacobs, E. T. An open-label randomized crossover trial of lyophilized black raspberries on postprandial inflammation in older overweight males: a pilot study. *Am. J. Ther.* **2013**, DOI: 10.1097/MJT.0b013e3182a40bf8.
(128) Skoczyñska, A.; Jêdrychowska, I.; Porêba, R.; Affelska-Jercha, A.; Turczyn, B.; Anna Wojakowska, A.; Andrzejak, R. Influence of chokeberry juice on arterial blood pressure and lipid parameters in men with mild hypercholesterolemia. *Pharmacol. Rep.* **2007**, *59*, 177−182.
(129) Eccleston, C.; Baoru, Y.; Tahvonen, R.; Kallio, H.; Rimbach, G. H.; Minihane, A. M. Effects of an antioxidant-rich juice (sea buckthorn) on risk factors for coronary heart disease in humans. *J. Nutr. Biochem.* **2002**, *13*, 346−354.
(130) Larmo, P.; Alin, J.; Salminen, E.; Kallio, H.; Tahvonen, R. Effects of sea buckthorn berries on infections and inflammation: a double-blind, randomized, placebo-controlled trial. *Eur. J. Clin. Nutr.* **2008**, *62*, 1123−1130.
(131) Lehtonen, H. M.; Järvinen, R.; Linderborg, K.; Viitanen, M.; Venojärvi, M.; Alanko, H.; Kallio, H. Postprandial hyperglycemia and insulin response are affected by sea buckthorn (*Hippophaë rhamnoides* ssp. *turkestanica*) berry and its ethanol-soluble metabolites. *Eur. J. Clin. Nutr.* **2010**, *64*, 1465−1471.
(132) Amagase, H.; Sun, B.; Nance, D. M. Immunomodulatory effects of a standardized Lycium barbarum fruit juice in Chinese older healthy human subjects. *J. Med. Food* **2009**, *12*, 1159−1165.
(133) Lehtonen, H. M; Suomela, J. P.; Tahvonen, R.; Vaarno, J.; Venojärvi, M.; Viikari, J.; Kallio, H. Berry meals and risk factors associated with metabolic syndrome. *Eur. J. Clin. Nutr.* **2010**, *64*, 614−621.
(134) Määttä-Riihinen, K. R.; Kamal-Eldin, A.; Mattila, P. H.; González-Paramás, A. M.; Törrönen, A. R. Distribution and contents of phenolic compounds in eighteen Scandinavian berry species. *J. Agric. Food Chem.* **2004**, *52*, 4477−4486.
(135) Arita, Y.; Kihara, S.; Ouchi, N.; Takahashi, M.; Maeda, K.; Miyagawa, J.; Hotta, K.; Shimomura, I.; Nakamura, T.; Miyaoka, K.; Kuriyama, H.; Nishida, M.; Yamashita, S.; Okubo, K.; Matsubara, K.; Muraguchi, M.; Ohmoto, Y.; Funahashi, T.; Matsuzawa, Y. Paradoxical decrease of an adipose-specific protein, adiponectin, in obesity. *Biochem. Biophys. Res. Commun.* **1999**, *257*, 79−83.
(136) Oregon berries, http://www.oregon-berries.com/wp content/uploads/2011/09/FRESH_BR.pdf (retrieved Jan 14, 2014).
(137) Wang, L. S.; Hecht, S. S.; Carmella, S. G.; Yu, N.; Larue, B.; Henry, C.; McIntyre, C.; Rocha, C.; Lechner, J. F.; Stoner, G. D. Anthocyanins in black raspberries prevent esophageal tumors in rats. *Cancer Prev. Res.* **2009**, *2*, 84−93.
(138) Ravoori, S.; Vadhanam, M. V.; Aqil, F.; Gupta, R. C. Inhibition of estrogen-mediated mammary tumorigenesis by blueberry and black raspberry. *J. Agric. Food Chem.* **2012**, *60*, 5547−5555.
(139) Bobe, G.; Murphy, G.; Albert, P. S.; Sansbury, L. B.; Lanza, E.; Schatzkin, A.; Colburn, N. H.; Cross, A. J. Serum cytokine concentrations, flavonol intake and colorectal adenoma recurrence in the Polyp Prevention Trial. *Br. J. Cancer* **2010**, *103*, 1453−1461.
(140) Denev, P. N.; Kratchanov, C. G.; Ciz, M.; Lojek, A.; Kratchanova, M. G. Bioavailability and antioxidant activity of black chokeberry (*Aronia melanocarpa*) polyphenols: in vitro and in vivo evidences and possible mechanisms of action: a review. *Compr. Rev. Food Sci. Food Saf.* **2012**, *11*, 471−489.
(141) Mishra, K. P.; Chanda, S.; Karan, D.; Ganju, L.; Sawhney, R. C. Effect of seabuckthorn (*Hippophae rhamnoides*) flavone on immune system: an *in-vitro* approach. *Phytother. Res.* **2008**, *22*, 1490−1495.
(142) Burton-Freeman, B.; Linares, A.; Hyson, D.; Kappagoda, T. Strawberry modulates LDL oxidation and postprandial lipemia in response to high-fat meal in overweight hyperlipidemic men and women. *J. Am. Coll. Nutr.* **2010**, *29*, 46−54.
(143) Potterat, O. Goji (*Lycium barbarum* and *L. chinense*): phytochemistry, pharmacology and safety in the perspective of traditional uses and recent popularity. *Planta Med.* **2010**, *76*, 7−19.
(144) Mikulic-Petkovsek, M.; Schmitzer, V.; Slatnar, A.; Stampar, F.; Veberic, R. Composition of sugars, organic acids, and total phenolics in 25 wild or cultivated berry species. *J. Food Sci.* **2012**, *77*, C1064−C1070.
(145) Davalos, D.; Akassoglou, K. Fibrinogen as a key regulator of inflammation in disease. *Semin. Immunopathol.* **2012**, *34* (1), 43−62.
(146) Karlsen, A.; Retterstøl, L.; Laake, P.; Paur, I.; Bøhn, S. K.; Sandvik, L.; Blomhoff, R. Anthocyanins inhibit nuclear factor-kappaB activation in monocytes and reduce plasma concentrations of pro-inflammatory mediators in healthy adults. *J. Nutr.* **2007**, *137*, 1951−1954.
(147) Hassellund, S. S.; Flaa, A.; Kjeldsen, S. E.; Seljeflot, I.; Karlsen, A.; Erlund, I.; Rostrup, M. Effects of anthocyanins on cardiovascular risk factors and inflammation in pre-hypertensive men: a double-blind randomized placebo-controlled crossover study. *J Hum. Hypertens.* **2013**, *27*, 100−106.
(148) Zhu, Y.; Xia, M.; Yang, Y.; Liu, F.; Li, Z.; Hao, Y.; Mi, M.; Jin, T.; Ling, W. Purified anthocyanin supplementation improves endothelial function via NO-cGMP activation in hypercholesterolemic individuals. *Clin. Chem.* **2011**, *57*, 1524−1533.
(149) Lyall, K. A.; Hurst, S. M.; Cooney, J.; Jensen, D.; Lo, K.; Hurst, R. D.; Stevenson, L. M. Short-term blackcurrant extract consumption modulates exercise-induced oxidative stress and lipopolysaccharide-stimulated inflammatory responses. *Am. J. Physiol. Regul. Integr. Comp. Physiol.* **2009**, *297*, R70−R81.
(150) Naruszewicz, M.; Laniewska, I.; Millo, B.; Dłuzniewski, M. Combination therapy of statin with flavonoids rich extract from chokeberry fruits enhanced reduction in cardiovascular risk markers in patients after myocardial infraction (MI). *Atherosclerosis* **2007**, *194*, e179−184.
(151) Lee, I. T.; Chan, Y. C.; Lin, C. W.; Lee, W. J.; Sheu, W. H. Effect of cranberry extracts on lipid profiles in subjects with type 2 diabetes. *Diabetes Med.* **2008**, *25*, 1473−1477.
(152) Vidlar, A.; Vostalova, J.; Ulrichova, J.; Student, V.; Stejskal, D.; Reichenbach, R.; Vrbkova, J.; Ruzicka, F.; Simanek, V. The effectiveness of dried cranberries (*Vaccinium macrocarpon*) in men with lower urinary tract symptoms. *Br. J. Nutr.* **2010**, *104*, 1181−1189.
(153) Wang, S. Y.; Chen, C. T.; Sciarappa, W.; Wang, C. Y.; Camp, M. J. Fruit quality, antioxidant capacity, and flavonoid content of organically and conventionally grown blueberries. *J. Agric. Food Chem.* **2008**, *56*, 5788−5794.

(154) Lee, H. C.; Jenner, A. M.; Low, C. S.; Lee, Y. K. Effect of tea phenolics and their aromatic fecal bacterial metabolites on intestinal microbiota. *Res. Microbiol.* **2006**, *157*, 876−884.
(155) Roberfroid, M.; Gibson, G. R.; Hoyles, L.; McCartney, A. L.; Rastall, R.; Rowland, I.; Wolvers, D.; Watzl, B.; Szajewska, H.; Stahl, B.; Guarner, F.; Respondek, F.; Whelan, K.; Coxam, V.; Davicco, M. J.; Léotoing, L.; Wittrant, Y.; Delzenne, N. M.; Cani, P. D.; Neyrinck, A. M.; Meheust, A. Prebiotic effects: metabolic and health benefits. *Br. J. Nutr.* **2010**, *104* (Suppl. 2), S1−S63.
(156) Queipo-Ortuño, M. I.; Boto-Ordóñez, M.; Murri, M.; Gomez-Zumaquero, J. M.; Clemente-Postigo, M.; Estruch, R.; Cardona Diaz, F.; Andrés-Lacueva, C.; Tinahones, F. J. Influence of red wine polyphenols and ethanol on the gut microbiota ecology and biochemical biomarkers. *Am. J. Clin. Nutr.* **2012**, *95*, 1323−1334.
(157) Selma, M. V.; Espín, J. C.; Tomás-Barberán, F. A. Interaction between phenolics and gut microbiota: role in human health. *J. Agric. Food Chem.* **2009**, *57*, 6485−6501.
(158) Bolca, S.; Van de Wiele, T.; Possemiers, S. Gut metabotypes govern health effects of dietary polyphenols. *Curr. Opin. Biotechnol.* **2013**, *24*, 220−225.
(159) http://www.who.int/dietphysicalactivity/fruit/en/ (retrieved Sept 30, 2013).

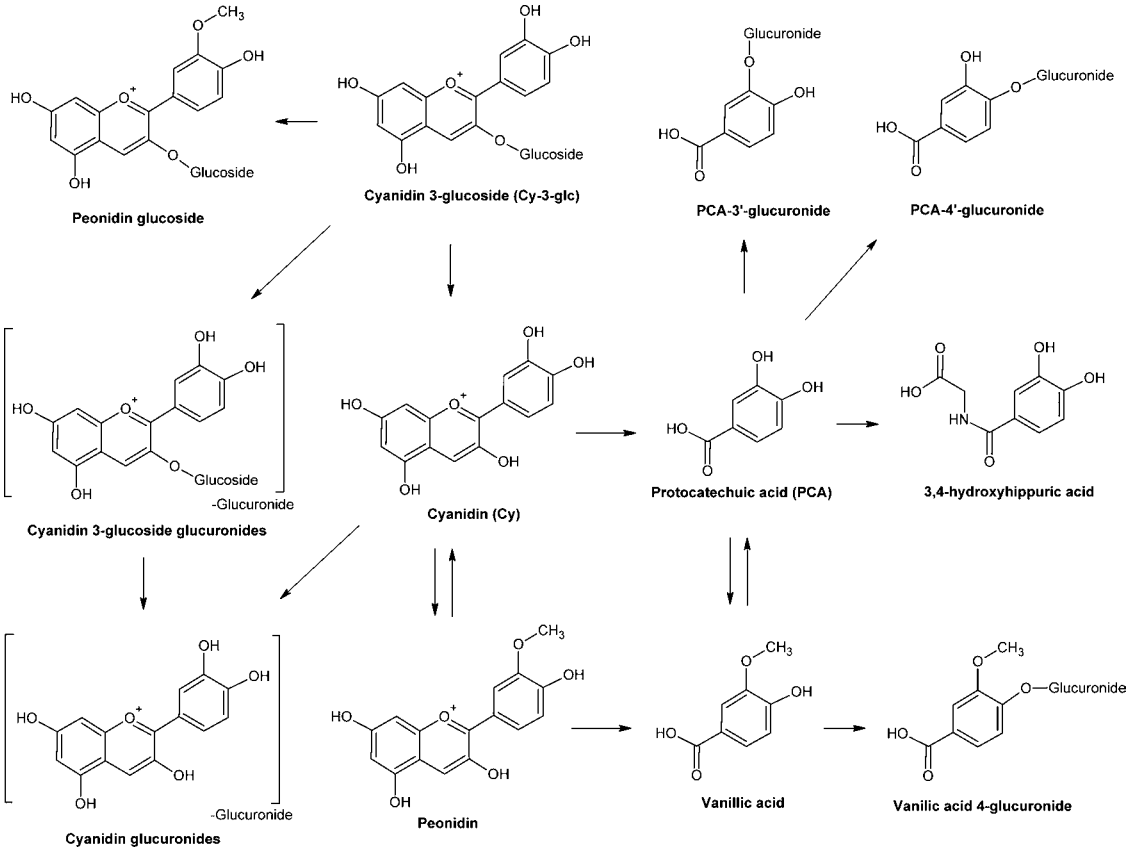

Figure 1. Major metabolic pathways of cyanidin 3-glucoside.[29,34,46,62,78,84,91]

PCA are formed during first-pass metabolism in the intestinal wall or liver (Figure 2).

Anthocyanins Could Efficiently Permeate into the Intestinal Wall. Native anthocyanins found in the small intestine tissue amounted to 7.5% of the ingested dose 2 h following administration of black raspberries in rats.[36] In another study, rats were administered a blackberry anthocyanin-enriched diet for 15 days. The jejunum contained 605 nmol/g tissue of Cy-3-glc and its methylated and glucurono-conjugated metabolites.[37] The exceptionally high anthocyanin concentrations in gastrointestinal tissues were in great contrast to their concentrations in blood. In addition, cell culture studies also demonstrated that anthocyanins can permeate Caco-2 cell monolayers.[38−40] This suggests that anthocyanins undergo extensive first-pass metabolism and enter the systemic circulation as metabolites. The concentrations in gastrointestinal tissues are similar to those used in some in vitro studies on the health effects of anthocyanins.[1−5] Anthocyanins could achieve pharmacologically relevant local concentrations and exert their protective effects in the gastrointestinal wall.[41−43]

Cy-3-glc Is Not a Substrate of β-Glucosidase or Lactase-Phlorizin Hydrolase. Unlike a number of other flavonoids, Cy-3-glc was found not to be a substrate of cytosolic β-glucosidase[44] or lactase-phlorizin hydrolase.[31] Because lactase-phlorizin hydrolase was localized to the apical membrane of small intestinal epithelial cells, it was suggested that some flavonoids are deglycosylated on the luminal surface before being absorbed.[31] Whereas this could be true for the substrates of the luminally exposed lactase-phlorizin hydrolase such as quercetin-3-glucoside,[31] it is unlikely to be the case for Cy-3-glc. This is consistent with the fact that intact Cy-3-glc can accumulate in the intestine tissue in rats following oral administration.[36,37] This is also consistent with the observation that only the glycosides, not their metabolites, were recovered in the intestinal lumen following perfusion of anthocyanins.[45] Thus, Cy-3-glc can probably be absorbed intact into the gastrointestinal wall, undergo extensive first-pass metabolism, and enter the systemic circulation as metabolites.

The mechanism of cleavage of the sugar moiety of Cy-3-glc remains to be established. With regard to the further breakdown of the anthocyanin aglycones, it was found that human liver microsomes can metabolize Cy to PCA, which is further metabolized to form three glucuronide conjugates.[46] Similarly, pelargonidin is metabolized to 4-hydroxybenzoic acid, which is further metabolized to form two additional glucuronide conjugates by human liver microsomes.

Chemical Decomposition in the Gastrointestinal Tract Is Unlikely To Account for Most Plasma Phenolic Acid Metabolites for the Relatively Stable Anthocyanins. Because phenolic acids such as PCA can be absorbed from the gastrointestinal tract,[33,47,48] it was suggested that the phenolic acids could be produced by chemical decomposition within the intestinal lumen before being absorbed. However, the literature outlined below indicates that chemical degradation is unlikely to be the main source of plasma 4-hydroxybenzolic acid and PCA following oral administration of Pg-3-glc and Cy-3-glc, respectively.

Many anthocyanins are rather stable in the upper gastrointestinal tract. Anthocyanins are known to be stable in the acidic environment of the stomach.[49−51] As absorption of anthocyanins was shown to take place in the stomach,[49,52−54]

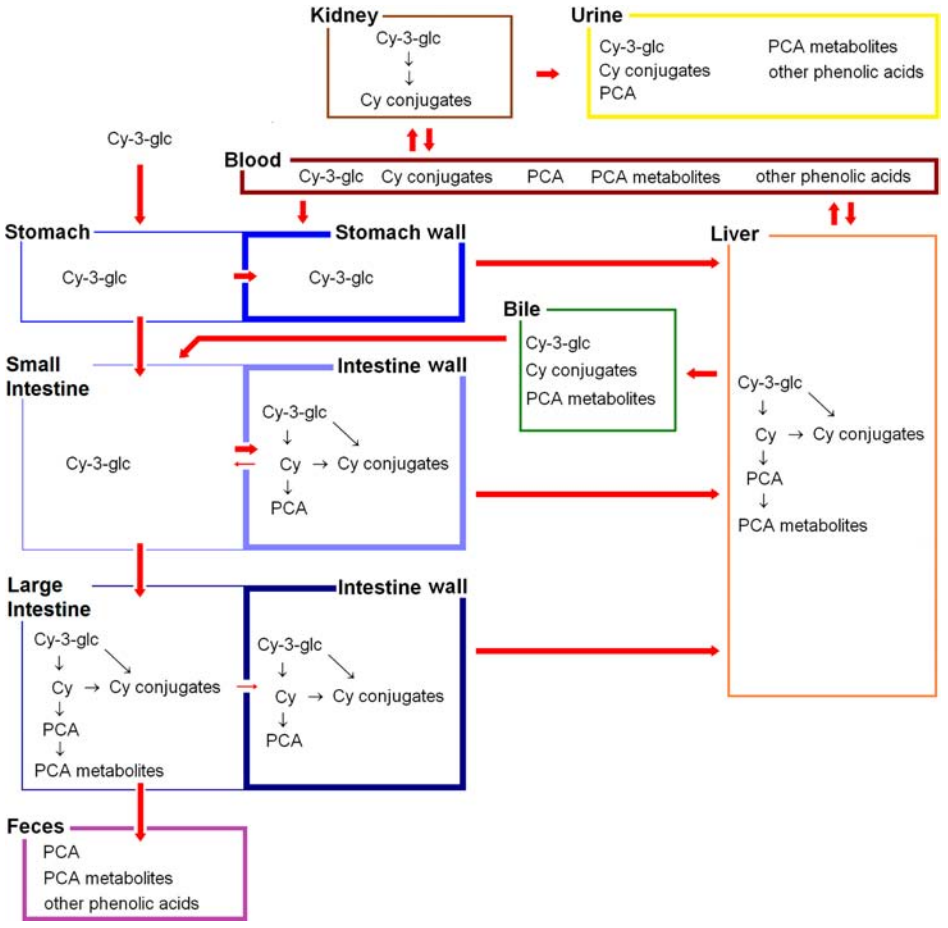

Figure 2. Schematic diagram of the absorption, first-pass metabolism, and further disposition of Cy-3-glc following its ingestion.[37,92−94] Abbreviations: Cy, cyanidin; Cy-3-glc, cyanidin 3-glucoside; PCA, protocatechuic acid.

significant amounts of anthocyanins could be absorbed in the stomach in their native forms.

In the small intestine, many anthocyanins such as Pg-3-glc are stable in this relatively neutral environment.[46] In an in vitro study, strawberry anthocyanin (mostly Pg-3-glc) decomposition was minimal when incubated at 37 °C in a simulated intestinal fluid (pH7) for 48 h.[55] Thus, it is unlikely that chemical decomposition of Pg-3-glc was primarily responsible for the high blood concentrations of 4-hydroxybenzoic acid in the absence of microbiota.

For those anthocyanins that do decompose, there seems to be a delay between the loss of anthocyanin aglycones and the formation of the phenolic acids probably due to the relatively stable transition products.[46,56,57] This delay could further reduce the concentrations of phenolic acids in the upper gastrointestinal tract. More detailed kinetic studies are needed to clarify the relationship between the disappearance of anthocyanins and the formation of their phenolic acid decomposition products.

In studies using ileostomists, the percentages of some anthocyanins remaining in ileal fluids did not seem to correlate with their stabilities.[58] For example, Cy-3-glc is far more stable than delphinidin 3-glucoside in simulated intestinal buffer,[50,59] but less of it remains in the ileal fluid following oral ingestion of wild blueberries.[58] These differences could be explained by the possibility that Cy-3-glc is more efficiently absorbed in the upper gastrointestinal system. A similar conclusion can also be derived from another study on Concord grape juice in ileostomists.[50] Cyanidin glycosides were found to be far more stable than delphinidin glycosides following in vitro incubation with simulated gastric and pancreatic juices, yet the percentages recovered in ileal fluid were comparable for the two anthocyanins following ingestion of 350 mL of the grape juice.

For the few anthocyanins that are unstable in the upper gastrointestinal tract, such as delphinidin 3-glucoside,[59] chemical degradation may play a role in the formation of their phenolic acid metabolites. A total of 40.7% of delphinidin 3-glucoside was found to remain in ileal fluid in ileostomists administered blueberries.[58] Therefore, 59.3% delphinidin 3-glucoside was either absorbed or decomposed before reaching the large intestine. On the other hand, delphinidin 3-glucoside was found to be absorbed into the bloodstream in its native form.[50,60,61] It is therefore perceivable that first-pass metabolism also contributes to the formation of the phenolic acid metabolites of delphinidin 3-glucoside.

Gut Microbiota Decomposition Products May Not Be Extensively Absorbed. In the large intestine, the microbiota can facilitate the formation of phenolic acid metabolites from anthocyanins.[50,55,62−70] However, they would not affect the plasma concentration versus time curve until a later time when anthocyanins reach the large intestine. The maximum rate of excretion of food components in ileal fluid took place at around 2 h when 1 L of apple juice or 300 g of blueberries was consumed by a group of ileostomists.[58] Most polyphenols passed the small intestine 4−8 h after the consumption of fruits or fruit juices.[50,58,71,72] The intestinal transition time would be

longer if solid food were ingested together with the fruits or fruit juices. Following administration of blood orange juice, plasma PCA concentrations increased rapidly and reached maximum concentrations at 2 h.[32] This is partly because anthocyanins can be absorbed from the stomach.[52,53] Thus, high plasma PCA concentrations were achieved before Cy-3-glc reached the large intestine and underwent microbiota decomposition.

Furthermore, only 5.9−28.3% of administered Cy-3-glc was excreted in ileal fluid from ileostomists administered blueberries, grapes, or raspberries.[50,58,71] Animal studies also indicated that Cy-3-glc is mostly absorbed in the stomach and upper part of the small intestine.[36,41,73,74] It is worth noting that fecal recoveries were 32.1 and 44.5% of administered [^{13}C]- or [^{14}C]-Cy-3-glc in humans[75] and mice,[76] respectively. This indicates that most Cy-3-glc entering the large intestine is excreted in feces. Thus, degradation products of Cy-3-glc may not be extensively absorbed from the large intestine.

Gut microbiota can produce large amounts of phenolic acids from those anthocyanins that reach the large intestine in large quantities.[50,58,71,72] In one study, the percentages remaining in ileal fluid relative to food content are in the following order: malvidin 3-arabinoside (85.1%) > petunidin 3-arabinoside (73%) > petunidin 3-galactoside (59.1%) > malvidin 3-galactoside (54.4%) > petunidin 3-glucoside (47.5%) > delphinidin 3-galacotoside (45.3%) > cyanidin 3-arabinoside (44.6%) > malvidin 3-glucoside (42.8%) > delphinidin 3-glucoside (40.7%) > delphinidin 3-arabinoside (37.8%) > cyanidin 3-galactoside (36.8%) > peonidin 3-glucoside (29.9%) > Cy-3-glc (28.3%).[58] It is perceivable that anthocyanins such as malvidin 3-arabinoside and petunidin 3-arabinoside would mostly be degraded by gut microbiota[65,66,77] and produce large quantities of metabolites.[68,69] However, the microbiota decomposition products may not be absorbed extensively into the bloodstream as is the case for Cy-3-glc. Further studies are needed to confirm the poor absorption of phenolic acids in the large intestine by introducing anthocyanins or their phenolic acid metabolites directly into the large intestine.

To summarize the above discussion, first-pass metabolism probably plays an important role in the formation of 4-hydroxybenzoic acid and PCA from Pg-3-glc and Cy-3-glc, respectively, after they are absorbed from the upper gastrointestinal lumen.

In addition to the phenolic acid metabolites, the bioavailabilities of some anthocyanins were found to be higher when phase II metabolites were also accounted for. The major metabolites of anthocyanins recovered in urine were glucuronidated and/or methylated conjugates.[78−83] Enzymes responsible for these biotransformations may include UDP-glucuronosyl transferase, UDP-glc dehydrogenase, or catechol-*O*-methyltransferase (COMT) located in the small intestine, liver, or kidney. For example, the bioavailability of delphinidin 3-rutinoside was found to be 2.67% when its 4′-methylation product was also accounted for in both the urine and bile of rats.[28] In other studies, total urinary excretion of anthocyanins and their metabolites was found to be 0.26−1.8% of the anthocyanins ingested.[29,30]

STUDIES USING ^{13}C- OR ^{14}C-LABELED ANTHOCYANINS

In a recent human study using [^{13}C]-Cy-3-glc, 12.4% of the ^{13}C-label was recovered from urine and breath following oral ingestion.[75] The actual percentage of [^{13}C]-Cy-3-glc absorbed across the gastrointestinal wall should be higher because of involvement of bile secretion in the disposition of anthocyanins (Figure 2). In mice administered [^{14}C]-Cy-3-glc, a high concentration of radioactivity was found in bile, indicating an important role of bile secretion in the disposition of Cy-3-glc.[76] Extensive bile secretion of [^{14}C]-PCA was also found following intraperitoneal injection in rats,[84] probably as its conjugates.[46] Extensive bile secretion of delphinidin 3-rutinoside and its 4′-methylated metabolite was also observed in rats.[28]

In human studies, an indication of extensive involvement of enterohepatic recycling is a second peak observed on the plasma concentration versus time curve. The second peak is due to the secretion of anthocyanins accumulated in bile into the duodenum and their subsequent reabsorption. This phenomenon was observed for delphinidin-3-glucoside and petunidin-3-glucoside in healthy volunteers administered Concord grape juice.[50] A second peak was also visible for malvidin-3-glucoside and mean plasma total anthocyanin concentration following consumption of red wine[85] and purple carrot juice,[86] respectively, in human volunteers. A similar pattern of the plasma concentration versus time curve has been observed for phase II metabolites of PCA.[75] In another study, a second peak of PCA was visible following administration of strawberries (containing Cy-3-glc as a minor component) in human volunteers.[34] This could also be due to enterohepatic recycling where conjugates of PCA were secreted into the duodenum and underwent cleavage to release the free PCA either within the intestinal lumen or during first-pass metabolism. Thus, due to the extensive involvement of enterohepatic recycling, the percentage of [^{13}C]-Cy-3-glc absorbed across the gastrointestinal wall would be higher than the 12.4% found in urine and breath in humans.[75]

Animal studies were also conducted on the absorption of [^{14}C]-Cy-3-glc. In a study in mice, the pharmacokinetics of anthocyanins were investigated using Cy-3-glc labeled with ^{14}C on its B-ring.[76] At 3 h after oral administration of [^{14}C]-Cy-3-glc, 3.3% of the radioactivity was detected in urine, mostly as metabolites. Plasma PCA concentrations were not measured in this particular study. However, on the basis of the HPLC chromatograms in the paper, it is evident that the concentrations of metabolites in plasma are many times higher than that of Cy-3-glc.[76] In a human study, there was a 42-fold higher abundance of ^{13}C-labeled metabolites relative to [^{13}C]-Cy-3-glc.[75]

In the above-mentioned study in mice, it is projected that the total percentage of radioactivity excreted in urine would be about 4.4% of the administered [^{14}C]-Cy-3-glc under the assumption that urine excretion of Cy-3-glc and its metabolites is proportional to plasma concentrations.[76] This total urinary recovery of Cy-3-glc is similar to that found in humans administered [^{13}C]-Cy-3-glc (5.4%).[75] This percentage represents the lower limit of Cy-3-glc absorbed into the systemic circulation including the metabolites produced during its presystemic metabolism. In addition to urine excretion, the absorbed [^{14}C]-Cy-3-glc and its metabolic products can also be eliminated from the body by secretion through bile. Bile contained a high concentration of radioactivity (7.81 Bq/mg tissue in bile as compared to 0.35 Bq/mg tissue in liver),[76] indicating a prominent role for bile in the disposition of [^{14}C]-Cy-3-glc. Indeed, 13% of PCA was found to be excreted in bile (as its conjugates) following intraperitoneal injection in rats.[84] In addition to bile, expiration of volatile metabolites or

autoxidation products into the air was found to be another elimination pathway for [^{13}C]-Cy-3-glc in humans, accounting for 6.9% of the administered dose.[75] Taken together, it is probable that the actual percentage of [^{14}C]-Cy-3-glc absorbed across the gastrointestinal wall is much higher than the observed total urine recovery (4.4%).

In another study using ^{14}C-labeled flavonoids, between 16 and 43% of radioactivity was found to be excreted in urine 24 h after oral administration of the anthocyanin glycoside fractions biosynthesized by grape cell suspension cultures.[87] These results are also consistent with the high percentage absorbed suggested by the above-mentioned studies.[32−34,49,59,75]

IN SITU GASTRIC AND INTESTINAL ABSORPTION OF ANTHOCYANINS

Efficient absorption of anthocyanins was also observed following in situ gastric and intestinal perfusion in rats. High plasma anthocyanin concentrations were found in both portal vein and systemic circulation following gastric perfusion.[52,53] In another study, the observed decreases of bilberry anthocyanins in the gastric fluid were 19−37% following 30 min in situ gastric absorption.[49] With regard to Cy-3-glc, the percentage absorbed was found to be 23% within the stomach under the experimental conditions. In a cell culture study, anthocyanins were found to be able to cross MKN-28 cell monolayers (differentiated adenocarcinoma stomach cells), probably via a saturable transporter mechanism.[54] Anthocyanins are stable under acidic conditions and do not degrade in simulated gastric juice.[49−51] In humans, anthocyanins were found in the bloodstream within minutes of consumption.[88] Five-fold higher urine concentrations of anthocyanins were observed in two patients following administration of a bilberry extract (Mirtoselect) via nasal intubation into the stomach rather than the jejunum.[89] It is therefore likely that anthocyanins can be absorbed from the stomach in their native forms.

An in situ perfusion model was used to evaluate the absorption of anthocyanins in the jejunum and ileum of rats. Between 10.7 and 22.4% of the anthocyanins were absorbed following perfusion at a flow rate of 0.75 mL/min.[59] The percentage of Cy-3-glc absorbed was found to be 22.4%. Degradations of anthocyanins in simulated intestinal buffer (pH 6.6, incubated at 37 °C for 45 min) are in the following order: Cy-3-glc (percentage decomposed = 2.32%), malvidin 3-glucoside (3.63%), cyanidin 3-galactoside (4.13%), and cyanidin 3-rutinoside (5.15%).[59] Cy-3-glc was found to be more stable when present in blackberry extract with only 0.69% decomposed. Delphinidin glycosides were the least stable, with a percentage of degradation of 9.31%. Their decline in the perfusion solution was not reported as a result of absorption. Therefore, it is reasonable to assume that the decreases of most anthocyanins in the perfusion solutions were mainly due to absorption rather than chemical degradation.

FUTURE PERSPECTIVES AND CONCLUSION

In addition to the research needed to confirm or clarify some issues outlined above, it is now clear that many studies conducted on anthocyanins need to be repeated in light of the formation of their phenolic acid metabolites, the plasma concentrations of which are 1−2 magnitudes higher than their respective parent compounds.[32−34] These studies include bioavailability studies of individual anthocyanins; studies using ileatomist volunteers; studies on the effects of food matrices on the absorption of anthocyanins; animal studies on the tissue concentrations of anthocyanins; and ex vivo absorption studies using human or animal tissues and cell culture models. It is also apparent that different anthocyanins are vastly different in their stability, absorption, metabolism, and elimination.[24] These differences are important in determining the sites of their health effects and the contribution of microbiota and chemical degradation to their disposition. Thus, different anthocyanins should be studied individually to ease the interpretation of experimental results. Cy-3-glc and Pg-3-glc are two anthocyanins extensively studied because they are predominant components in fruits such as blackberries[90] and strawberries.[15] Other purified or synthesized anthocyanins could also be used for studies using animal models and human volunteers.[75]

In conclusion, the extensive literature indicates that absorption and first-pass metabolism play important roles in the disposition of some anthocyanins, such as Cy-3-glc and Pg-3-glc, in the upper gastrointestinal tract. Metabolites such as PCA and 4-hydroxybenzoic acid could be responsible for the systemic health effects of anthocyanins. High permeations of native anthocyanins into the gastrointestinal wall also suggest that anthocyanins could achieve pharmacologically relevant local concentrations and exert their protective effects in the gastrointestinal system.

AUTHOR INFORMATION

Corresponding Author

*Phone: 1 (306) 966-6372. Fax: 1 (306) 966-6377. E-mail: jim.fang@usask.ca.

Funding

This work is supported by the Saskatchewan Ministry of Agriculture, Canada (Agriculture Development Fund 20110138).

Notes

The authors declare no competing financial interest.

ACKNOWLEDGMENTS

I thank Genevieve Clark for assisting with the preparation of the manuscript.

ABBREVIATIONS USED

Cy, cyanidin; Cy-3-glc, cyanidin 3-glucoside; Pg-3-glc, pelargonidin 3-glucoside; PCA, protocatechuic acid

REFERENCES

(1) Basu, A.; Rhone, M.; Lyons, T. J. Berries: emerging impact on cardiovascular health. *Nutr. Rev.* **2010**, *68*, 168−177.

(2) Giacalone, M.; Di Sacco, F.; Traupe, I.; Topini, R.; Forfori, F.; Giunta, F. Antioxidant and neuroprotective properties of blueberry polyphenols: a critical review. *Nutr. Neurosci.* **2011**, *14*, 119−125.

(3) Tsuda, T. Dietary anthocyanin-rich plants: biochemical basis and recent progress in health benefits studies. *Mol. Nutr. Food Res.* **2012**, *56*, 159−170.

(4) Kay, C. D.; Hooper, L.; Kroon, P. A.; Rimm, E. B.; Cassidy, A. Relative impact of flavonoid composition, dose and structure on vascular function: a systematic review of randomised controlled trials of flavonoid-rich food products. *Mol. Nutr. Food Res.* **2012**, *56*, 1605−1616.

(5) Chen, A. Y.; Chen, Y. C. A review of the dietary flavonoid, kaempferol on human health and cancer chemoprevention. *Food Chem.* **2013**, *138*, 2099−2107.

(6) Bhagwat, S. A.; Haytowitz, D. B.; Harnly, J.; Holden, J. M. Update of the USDA database for the flavonoid content of selected foods. *J. Nutr.* **2005**, *135*, 3050s−3050s.

(7) Eldridge, A. L.; Haytowitz, D.; Bhagwat, S.; Gebhardt, S. E.; Holden, J. M.; Beecher, G.; Peterson, J.; Dwyer, J. T. Flavonoid content of vegetables: the USDA's Flavonoid Database. *FASEB J.* **2003**, *17*, A766−A767.
(8) Cassidy, A.; O'Reilly, E. J.; Kay, C.; Sampson, L.; Franz, M.; Forman, J. P.; Curhan, G.; Rimm, E. B. Habitual intake of flavonoid subclasses and incident hypertension in adults. *Am. J. Clin. Nutr.* **2011**, *93*, 338−347.
(9) Jennings, A.; Welch, A. A.; Fairweather-Tait, S. J.; Kay, C.; Minihane, A. M.; Chowienczyk, P.; Jiang, B.; Cecelja, M.; Spector, T.; Macgregor, A.; Cassidy, A. Higher anthocyanin intake is associated with lower arterial stiffness and central blood pressure in women. *Am. J. Clin. Nutr.* **2012**, *96*, 781−788.
(10) McCullough, M. L.; Peterson, J. J.; Patel, R.; Jacques, P. F.; Shah, R.; Dwyer, J. T. Flavonoid intake and cardiovascular disease mortality in a prospective cohort of US adults. *Am. J. Clin. Nutr.* **2012**, *95*, 454−464.
(11) Mink, P. J.; Scrafford, C. G.; Barraj, L. M.; Harnack, L.; Hong, C. P.; Nettleton, J. A.; Jacobs, D. R., Jr. Flavonoid intake and cardiovascular disease mortality: a prospective study in postmenopausal women. *Am. J. Clin. Nutr.* **2007**, *85*, 895−909.
(12) Wedick, N. M.; Pan, A.; Cassidy, A.; Rimm, E. B.; Sampson, L.; Rosner, B.; Willett, W.; Hu, F. B.; Sun, Q.; van Dam, R. M. Dietary flavonoid intakes and risk of type 2 diabetes in US men and women. *Am. J. Clin. Nutr.* **2012**, *95*, 925−933.
(13) Zamora-Ros, R.; Agudo, A.; Lujan-Barroso, L.; Romieu, I.; Ferrari, P.; Knaze, V.; Bueno-de-Mesquita, H. B.; Leenders, M.; Travis, R. C.; Navarro, C.; Sanchez-Cantalejo, E.; Slimani, N.; Scalbert, A.; Fedirko, V.; Hjartaker, A.; Engeset, D.; Skeie, G.; Boeing, H.; Forster, J.; Li, K.; Teucher, B.; Agnoli, C.; Tumino, R.; Mattiello, A.; Saieva, C.; Johansson, I.; Stenling, R.; Redondo, M. L.; Wallstrom, P.; Ericson, U.; Khaw, K. T.; Mulligan, A. A.; Trichopoulou, A.; Dilis, V.; Katsoulis, M.; Peeters, P. H.; Igali, L.; Tjonneland, A.; Halkjaer, J.; Touillaud, M.; Perquier, F.; Fagherazzi, G.; Amiano, P.; Ardanaz, E.; Bredsdorff, L.; Overvad, K.; Ricceri, F.; Riboli, E.; Gonzalez, C. A. Dietary flavonoid and lignan intake and gastric adenocarcinoma risk in the European Prospective Investigation into Cancer and Nutrition (EPIC) study. *Am. J. Clin. Nutr.* **2012**, *96*, 1398−1408.
(14) Touvier, M.; Druesne-Pecollo, N.; Kesse-Guyot, E.; Andreeva, V. A.; Fezeu, L.; Galan, P.; Hercberg, S.; Latino-Martel, P. Dual association between polyphenol intake and breast cancer risk according to alcohol consumption level: a prospective cohort study. *Breast Cancer Res. Treat.* **2012**, *137*, 225−236.
(15) Basu, A.; Du, M.; Leyva, M. J.; Sanchez, K.; Betts, N. M.; Wu, M.; Aston, C. E.; Lyons, T. J. Blueberries decrease cardiovascular risk factors in obese men and women with metabolic syndrome. *J. Nutr.* **2010**, *140*, 1582−1587.
(16) Dohadwala, M. M.; Holbrook, M.; Hamburg, N. M.; Shenouda, S. M.; Chung, W. B.; Titas, M.; Kluge, M. A.; Wang, N.; Palmisano, J.; Milbury, P. E.; Blumberg, J. B.; Vita, J. A. Effects of cranberry juice consumption on vascular function in patients with coronary artery disease. *Am. J. Clin. Nutr.* **2011**, *93*, 934−940.
(17) Stull, A. J.; Cash, K. C.; Johnson, W. D.; Champagne, C. M.; Cefalu, W. T. Bioactives in blueberries improve insulin sensitivity in obese, insulin-resistant men and women. *J. Nutr.* **2010**, *140*, 1764−1768.
(18) Biedermann, L.; Mwinyi, J.; Scharl, M.; Frei, P.; Zeitz, J.; Kullak-Ublick, G. A.; Vavricka, S. R.; Fried, M.; Weber, A.; Humpf, H. U.; Peschke, S.; Jetter, A.; Krammer, G.; Rogler, G. Bilberry ingestion improves disease activity in mild to moderate ulcerative colitis − an open pilot study. *J. Crohns Colitis* **2012**, *7*, 271−279.
(19) Manach, C.; Williamson, G.; Morand, C.; Scalbert, A.; Remesy, C. Bioavailability and bioefficacy of polyphenols in humans. I. Review of 97 bioavailability studies. *Am. J. Clin. Nutr.* **2005**, *81*, 230S−242S.
(20) Crozier, A.; Del Rio, D.; Clifford, M. N. Bioavailability of dietary flavonoids and phenolic compounds. *Mol. Aspects Med.* **2010**, *31*, 446−467.
(21) Kroon, P. A.; Clifford, M. N.; Crozier, A.; Day, A. J.; Donovan, J. L.; Manach, C.; Williamson, G. How should we assess the effects of exposure to dietary polyphenols in vitro? *Am. J. Clin. Nutr.* **2004**, *80*, 15−21.
(22) Prior, R. L.; Wu, X. L. Anthocyanins: structural characteristics that result in unique metabolic patterns and biological activities. *Free Radical Res.* **2006**, *40*, 1014−1028.
(23) Kay, C. D. Aspects of anthocyanin absorption, metabolism and pharmacokinetics in humans. *Nutr. Res. Rev.* **2006**, *19*, 137−146.
(24) Del Rio, D.; Rodriguez-Mateos, A.; Spencer, J. P.; Tognolini, M.; Borges, G.; Crozier, A. Dietary (poly)phenolics in human health: structures, bioavailability, and evidence of protective effects against chronic diseases. *Antioxid. Redox Signal.* **2013**, *18*, 1818−1892.
(25) Ichiyanagi, T.; Shida, Y.; Rahman, M. M.; Hatano, Y.; Konishi, T. Bioavailability and tissue distribution of anthocyanins in bilberry (*Vaccinium myrtillus* L.) extract in rats. *J. Agric. Food Chem.* **2006**, *54*, 6578−6587.
(26) Marczylo, T. H.; Cooke, D.; Brown, K.; Steward, W. P.; Gescher, A. J. Pharmacokinetics and metabolism of the putative cancer chemopreventive agent cyanidin-3-glucoside in mice. *Cancer Chemother. Pharmacol.* **2009**, *64*, 1261−1268.
(27) Borges, G.; Roowi, S.; Rouanet, J. M.; Duthie, G. G.; Lean, M. E.; Crozier, A. The bioavailability of raspberry anthocyanins and ellagitannins in rats. *Mol. Nutr. Food Res.* **2007**, *51*, 714−725.
(28) Matsumoto, H.; Ichiyanagi, T.; Iida, H.; Ito, K.; Tsuda, T.; Hirayama, M.; Konishi, T. Ingested delphinidin-3-rutinoside is primarily excreted to urine as the intact form and to bile as the methylated form in rats. *J. Agric. Food Chem.* **2006**, *54*, 578−582.
(29) Felgines, C.; Talavera, S.; Gonthier, M. P.; Texier, O.; Scalbert, A.; Lamaison, J. L.; Remesy, C. Strawberry anthocyanins are recovered in urine as glucuro- and sulfoconjugates in humans. *J. Nutr.* **2003**, *133*, 1296−1301.
(30) Felgines, C.; Texier, O.; Besson, C.; Fraisse, D.; Lamaison, J. L.; Remesy, C. Blackberry anthocyanins are slightly bioavailable in rats. *J. Nutr.* **2002**, *132*, 1249−1253.
(31) Nemeth, K.; Plumb, G. W.; Berrin, J.-G.; Juge, N.; Jacob, R.; Naim, H. Y.; Williamson, G.; Swallow, D. M.; Kroon, P. A. Deglycosylation by small intestinal epithelial cell β-glucosidases is a critical step in the absorption and metabolism of dietary flavonoid glycosides in humans. *Eur. J. Nutr.* **2003**, *42*, 29−42.
(32) Vitaglione, P.; Donnarumma, G.; Napolitano, A.; Galvano, F.; Gallo, A.; Scalfi, L.; Fogliano, V. Protocatechuic acid is the major human metabolite of cyanidin-glucosides. *J. Nutr.* **2007**, *137*, 2043−2048.
(33) Chen, W.; Wang, D.; Wang, L. S.; Bei, D.; Wang, J.; See, W. A.; Mallery, S. R.; Stoner, G. D.; Liu, Z. Pharmacokinetics of protocatechuic acid in mouse and its quantification in human plasma using LC-tandem mass spectrometry. *J. Chromatogr., B: Anal. Technol. Biomed. Life Sci.* **2012**, *908*, 39−44.
(34) Azzini, E.; Vitaglione, P.; Intorre, F.; Napolitano, A.; Durazzo, A.; Foddai, M. S.; Fumagalli, A.; Catasta, G.; Rossi, L.; Venneria, E.; Raguzzini, A.; Palomba, L.; Fogliano, V.; Maiani, G. Bioavailability of strawberry antioxidants in human subjects. *Br. J. Nutr.* **2010**, *104*, 1165−1173.
(35) Shargel, L.; Yu, A. B. C.; Wu-Pong, S. *Applied Biopharmaceutics & Pharmacokinetics*, 6th ed.; McGraw-Hill: New York, 2012.
(36) He, J.; Wallace, T. C.; Keatley, K. E.; Failla, M. L.; Giusti, M. M. Stability of black raspberry anthocyanins in the digestive tract lumen and transport efficiency into gastric and small intestinal tissues in the rat. *J. Agric. Food Chem.* **2009**, *57*, 3141−3148.
(37) Talavera, S.; Felgines, C.; Texier, O.; Besson, C.; Gil-Izquierdo, A.; Lamaison, J. L.; Remesy, C. Anthocyanin metabolism in rats and their distribution to digestive area, kidney, and brain. *J. Agric. Food Chem.* **2005**, *53*, 3902−3908.
(38) Faria, A.; Pestana, D.; Azevedo, J.; Martel, F.; de Freitas, V.; Azevedo, I.; Mateus, N.; Calhau, C. Absorption of anthocyanins through intestinal epithelial cells − putative involvement of GLUT2. *Mol. Nutr. Food Res.* **2009**, *53*, 1430−1437.
(39) Steinert, R. E.; Ditscheid, B.; Netzel, M.; Jahreis, G. Absorption of black currant anthocyanins by monolayers of human intestinal

epithelial Caco-2 cells mounted in ussing type chambers. *J. Agric. Food Chem.* **2008**, *56*, 4995−5001.
(40) Yi, W.; Akoh, C. C.; Fischer, J.; Krewer, G. Absorption of anthocyanins from blueberry extracts by Caco-2 human intestinal cell monolayers. *J. Agric. Food Chem.* **2006**, *54*, 5651−5658.
(41) Jakesevic, M.; Xu, J.; Aaby, K.; Jeppsson, B.; Ahrne, S.; Molin, G. Effects of bilberry (*Vaccinium myrtillus*) in combination with lactic acid bacteria on intestinal oxidative stress induced by ischemia-reperfusion in mouse. *J. Agric. Food Chem.* **2013**, *61*, 3468−3478.
(42) Jurgonski, A.; Juskiewicz, J.; Zdunczyk, Z. An anthocyanin-rich extract from Kamchatka honeysuckle increases enzymatic activity within the gut and ameliorates abnormal lipid and glucose metabolism in rats. *Nutrition* **2013**, *29*, 898−902.
(43) Mallery, S. R.; Budendorf, D. E.; Larsen, M. P.; Pei, P.; Tong, M.; Holpuch, A. S.; Larsen, P. E.; Stoner, G. D.; Fields, H. W.; Chan, K. K.; Ling, Y.; Liu, Z. Effects of human oral mucosal tissue, saliva, and oral microflora on intraoral metabolism and bioactivation of black raspberry anthocyanins. *Cancer Prev. Res. (Phila.)* **2011**, *4*, 1209−1221.
(44) Berrin, J. G.; McLauchlan, W. R.; Needs, P.; Williamson, G.; Puigserver, A.; Kroon, P. A.; Juge, N. Functional expression of human liver cytosolic β-glucosidase in *Pichia pastoris*. Insights into its role in the metabolism of dietary glucosides. *Eur. J. Biochem.* **2002**, *269*, 249−258.
(45) Talavera, S.; Felgines, C.; Texier, O.; Besson, C.; Manach, C.; Lamaison, J.-L.; Remesy, C. Anthocyanins are efficiently absorbed from the small intestine in rats. *J. Nutr.* **2004**, *134*, 2275−2279.
(46) Woodward, G. M.; Needs, P. W.; Kay, C. D. Anthocyanin-derived phenolic acids form glucuronides following simulated gastrointestinal digestion and microsomal glucuronidation. *Mol. Nutr. Food Res.* **2011**, *55*, 378−386.
(47) Russell, W. R.; Scobbie, L.; Labat, A.; Duthie, G. G. Selective bio-availability of phenolic acids from Scottish strawberries. *Mol. Nutr. Food Res.* **2009**, *53* (Suppl. 1), S85−S91.
(48) Guo, X.; Chen, X.; Li, L.; Shen, Z.; Wang, X.; Zheng, P.; Duan, F.; Ma, Y.; Bi, K. LC-MS determination and pharmacokinetic study of six phenolic components in rat plasma after taking traditional Chinese medicinal-preparation: Guanxinning lyophilized powder for injection. *J. Chromatogr., B: Anal. Technol. Biomed. Life Sci.* **2008**, *873*, 51−58.
(49) Talavera, S.; Felgines, C.; Texier, O.; Besson, C.; Lamaison, J. L.; Remesy, C. Anthocyanins are efficiently absorbed from the stomach in anesthetized rats. *J. Nutr.* **2003**, *133*, 4178−4182.
(50) Stalmach, A.; Edwards, C. A.; Wightman, J. D.; Crozier, A. Gastrointestinal stability and bioavailability of (poly)phenolic compounds following ingestion of Concord grape juice by humans. *Mol. Nutr. Food Res.* **2012**, *56*, 497−509.
(51) Bermudez-Soto, M. J.; Tomas-Barberan, F. A.; Garcia-Conesa, M. T. Stability of polyphenols in chokeberry (*Aronia melanocarpa*) subjected to in vitro gastric and pancreatic digestion. *Food Chem.* **2007**, *102*, 865−874.
(52) Passamonti, S.; Vrhovsek, U.; Vanzo, A.; Mattivi, F. The stomach as a site for anthocyanins absorption from food. *FEBS Lett.* **2003**, *544*, 210−213.
(53) Vanzo, A.; Terdoslavich, M.; Brandoni, A.; Torres, A. M.; Vrhovsek, U.; Passamonti, S. Uptake of grape anthocyanins into the rat kidney and the involvement of bilitranslocase. *Mol. Nutr. Food Res.* **2008**, *52*, 1106−1116.
(54) Fernandes, I.; de Freitas, V.; Reis, C.; Mateus, N. A new approach on the gastric absorption of anthocyanins. *Food Funct.* **2012**, *3*, 508−516.
(55) Gonzalez-Barrio, R.; Edwards, C. A.; Crozier, A. Colonic catabolism of ellagitannins, ellagic acid, and raspberry anthocyanins: in vivo and in vitro studies. *Drug Metab. Dispos.* **2011**, *39*, 1680−1688.
(56) Fleschhut, J.; Kratzer, F.; Rechkemmer, G.; Kulling, S. E. Stability and biotransformation of various dietary anthocyanins in vitro. *Eur. J. Nutr.* **2006**, *45*, 7−18.
(57) Perez-Vicente, A.; Gil-Izquierdo, A.; Garcia-Viguera, C. In vitro gastrointestinal digestion study of pomegranate juice phenolic compounds, anthocyanins, and vitamin C. *J. Agric. Food Chem.* **2002**, *50*, 2308−2312.
(58) Kahle, K.; Kraus, M.; Scheppach, W.; Ackermann, M.; Ridder, F.; Richling, E. Studies on apple and blueberry fruit constituents: do the polyphenols reach the colon after ingestion? *Mol. Nutr. Food Res.* **2006**, *50*, 418−423.
(59) Talavera, S.; Felgines, C.; Texier, O.; Besson, C.; Manach, C.; Lamaison, J. L.; Remesy, C. Anthocyanins are efficiently absorbed from the small intestine in rats. *J. Nutr.* **2004**, *134*, 2275−2279.
(60) Frank, T.; Netzel, M.; Strass, G.; Bitsch, R.; Bitsch, I. Bioavailability of anthocyanidin-3-glucosides following consumption of red wine and red grape juice. *Can. J. Physiol. Pharmacol.* **2003**, *81*, 423−435.
(61) Mazza, G.; Kay, C. D.; Cottrell, T.; Holub, B. J. Absorption of anthocyanins from blueberries and serum antioxidant status in human subjects. *J. Agric. Food Chem.* **2002**, *50*, 7731−7737.
(62) Aura, A. M.; Martin-Lopez, P.; O'Leary, K. A.; Williamson, G.; Oksman-Caldentey, K. M.; Poutanen, K.; Santos-Buelga, C. In vitro metabolism of anthocyanins by human gut microflora. *Eur. J. Nutr.* **2005**, *44*, 133−142.
(63) Hanske, L.; Engst, W.; Loh, G.; Sczesny, S.; Blaut, M.; Braune, A. Contribution of gut bacteria to the metabolism of cyanidin 3-glucoside in human microbiota-associated rats. *Br. J. Nutr.* **2013**, *109*, 1433−1441.
(64) He, J.; Magnuson, B. A.; Giusti, M. M. Analysis of anthocyanins in rat intestinal contents − impact of anthocyanin chemical structure on fecal excretion. *J. Agric. Food Chem.* **2005**, *53*, 2859−2866.
(65) Sanchez-Patan, F.; Cueva, C.; Monagas, M.; Walton, G. E.; Gibson, G. R.; Quintanilla-Lopez, J. E.; Lebron-Aguilar, R.; Martin-Alvarez, P. J.; Moreno-Arribas, M. V.; Bartolome, B. In vitro fermentation of a red wine extract by human gut microbiota: changes in microbial groups and formation of phenolic metabolites. *J. Agric. Food Chem.* **2012**, *60*, 2136−2147.
(66) Hidalgo, M.; Oruna-Concha, M. J.; Kolida, S.; Walton, G. E.; Kallithraka, S.; Spencer, J. P.; de Pascual-Teresa, S. Metabolism of anthocyanins by human gut microflora and their influence on gut bacterial growth. *J. Agric. Food Chem.* **2012**, *60*, 3882−3890.
(67) Forester, S. C.; Waterhouse, A. L. Identification of Cabernet Sauvignon anthocyanin gut microflora metabolites. *J. Agric. Food Chem.* **2008**, *56*, 9299−9304.
(68) Gill, C. I.; McDougall, G. J.; Glidewell, S.; Stewart, D.; Shen, Q.; Tuohy, K.; Dobbin, A.; Boyd, A.; Brown, E.; Haldar, S.; Rowland, I. R. Profiling of phenols in human fecal water after raspberry supplementation. *J. Agric. Food Chem.* **2010**, *58*, 10389−10395.
(69) Jimenez-Giron, A.; Queipo-Ortuno, M. I.; Boto-Ordonez, M.; Munoz-Gonzalez, I.; Sanchez-Patan, F.; Monagas, M.; Martin-Alvarez, P. J.; Murri, M.; Tinahones, F. J.; Andres-Lacueva, C.; Bartolome, B.; Moreno-Arribas, M. V. Comparative study of microbial-derived phenolic metabolites in human feces after intake of gin, red wine, and dealcoholized red wine. *J. Agric. Food Chem.* **2013**, *61*, 3909−3915.
(70) Keppler, K.; Humpf, H. U. Metabolism of anthocyanins and their phenolic degradation products by the intestinal microflora. *Bioorg. Med. Chem.* **2005**, *13*, 5195−5205.
(71) Gonzalez-Barrio, R.; Borges, G.; Mullen, W.; Crozier, A. Bioavailability of anthocyanins and ellagitannins following consumption of raspberries by healthy humans and subjects with an ileostomy. *J. Agric. Food Chem.* **2010**, *58*, 3933−3939.
(72) Borges, G.; Lean, M. E.; Roberts, S. A.; Crozier, A. Bioavailability of dietary (poly)phenols: a study with ileostomists to discriminate between absorption in small and large intestine. *Food Funct.* **2013**, *4*, 754−762.
(73) Wu, X.; Pittman, H. E., 3rd; Prior, R. L. Fate of anthocyanins and antioxidant capacity in contents of the gastrointestinal tract of weanling pigs following black raspberry consumption. *J. Agric. Food Chem.* **2006**, *54*, 583−589.
(74) Wu, X.; Pittman, H. E., 3rd; McKay, S.; Prior, R. L. Aglycones and sugar moieties alter anthocyanin absorption and metabolism after berry consumption in weanling pigs. *J. Nutr.* **2005**, *135*, 2417−2424.
(75) Czank, C.; Cassidy, A.; Zhang, Q.; Morrison, D. J.; Preston, T.; Kroon, P. A.; Botting, N. P.; Kay, C. D. Human metabolism and

elimination of the anthocyanin, cyanidin-3-glucoside: a (13)C-tracer study. *Am. J. Clin. Nutr.* **2013**, *97*, 995−1003.
(76) Felgines, C.; Krisa, S.; Mauray, A.; Besson, C.; Lamaison, J. L.; Scalbert, A.; Merillon, J. M.; Texier, O. Radiolabelled cyanidin 3-*O*-glucoside is poorly absorbed in the mouse. *Br. J. Nutr.* **2010**, *103*, 1738−1745.
(77) Hassimotto, N. M.; Genovese, M. I.; Lajolo, F. M. Absorption and metabolism of cyanidin-3-glucoside and cyanidin-3-rutinoside extracted from wild mulberry (*Morus nigra* L.) in rats. *Nutr. Res. (N.Y.)* **2008**, *28*, 198−207.
(78) Wu, X.; Cao, G.; Prior, R. L. Absorption and metabolism of anthocyanins in elderly women after consumption of elderberry or blueberry. *J. Nutr.* **2002**, *132*, 1865−1871.
(79) Tian, Q.; Giusti, M. M.; Stoner, G. D.; Schwartz, S. J. Urinary excretion of black raspberry (*Rubus occidentalis*) anthocyanins and their metabolites. *J. Agric. Food Chem.* **2006**, *54*, 1467−1472.
(80) Felgines, C.; Talavera, S.; Texier, O.; Gil-Izquierdo, A.; Lamaison, J.-L.; Remesy, C. Blackberry anthocyanins are mainly recovered from urine as methylated and glucuronidated conjugates in humans. *J. Agric. Food Chem.* **2005**, *53*, 7721−7727.
(81) Kay, C. D.; Mazza, G. J.; Holub, B. J. Anthocyanins exist in the circulation primarily as metabolites in adult men. *J. Nutr.* **2005**, *135*, 2582−2588.
(82) Ichiyanagi, T.; Shida, Y.; Rahman, M. M.; Hatano, Y.; Konishi, T. Extended glucuronidation is another major path of cyanidin 3-*O*-*β*-D-glucopyranoside metabolism in rats. *J. Agric. Food Chem.* **2005**, *53*, 7312−7319.
(83) Ichiyanagi, T.; Rahman, M. M.; Kashiwada, Y.; Ikeshiro, Y.; Shida, Y.; Hatano, Y.; Matsumoto, H.; Hirayama, M.; Tsuda, T.; Konishi, T. Absorption and metabolism of delphinidin 3-*O*-*β*-D-glucopyranoside in rats. *Free Radical Biol. Med.* **2004**, *36*, 930−937.
(84) Dacre, J. C.; Williams, R. T. The role of the tissues and gut micro-organisms in the metabolism of [^{14}C]protocatechuic acid in the rat. Aromatic dehydroxylation. *J. Pharm. Pharmacol.* **1968**, *20*, 610−618.
(85) Bub, A.; Watzl, B.; Heeb, D.; Rechkemmer, G.; Briviba, K. Malvidin-3-glucoside bioavailability in humans after ingestion of red wine, dealcoholized red wine and red grape juice. *Eur. J. Nutr.* **2001**, *40*, 113−120.
(86) Charron, C. S.; Kurilich, A. C.; Clevidence, B. A.; Simon, P. W.; Harrison, D. J.; Britz, S. J.; Baer, D. J.; Novotny, J. A. Bioavailability of anthocyanins from purple carrot juice: effects of acylation and plant matrix. *J. Agric. Food Chem.* **2009**, *57*, 1226−1230.
(87) Janle, E. M.; Lila, M. A.; Grannan, M.; Wood, L.; Higgins, A.; Yousef, G. G.; Rogers, R. B.; Kim, H.; Jackson, G. S.; Ho, L.; Weaver, C. M. Pharmacokinetics and tissue distribution of ^{14}C-labeled grape polyphenols in the periphery and the central nervous system following oral administration. *J. Med. Food* **2010**, *13*, 926−933.
(88) Milbury, P. E.; Cao, G.; Prior, R. L.; Blumberg, J. Bioavailablility of elderberry anthocyanins. *Mech. Ageing Dev.* **2002**, *123*, 997−1006.
(89) Cai, H.; Thomasset, S. C.; Berry, D. P.; Garcea, G.; Brown, K.; Steward, W. P.; Gescher, A. J. Determination of anthocyanins in the urine of patients with colorectal liver metastases after administration of bilberry extract. *Biomed. Chromatogr.* **2011**, *25*, 660−663.
(90) Felgines, C.; Talavera, S.; Texier, O.; Gil-Izquierdo, A.; Lamaison, J. L.; Remesy, C. Blackberry anthocyanins are mainly recovered from urine as methylated and glucuronidated conjugates in humans. *J. Agric. Food Chem.* **2005**, *53*, 7721−7727.
(91) Miyazawa, T.; Nakagawa, K.; Kudo, M.; Muraishi, K.; Someya, K. Direct intestinal absorption of red fruit anthocyanins, cyanidin-3-glucoside and cyanidin-3,5-diglucoside, into rats and humans. *J. Agric. Food Chem.* **1999**, *47*, 1083−1091.
(92) Andlauer, W.; Stumpf, C.; Frank, K.; Furst, P. Absorption and metabolism of anthocyanin cyanidin-3-glucoside in the isolated rat small intestine is not influenced by ethanol. *Eur. J. Nutr.* **2003**, *42*, 217−223.
(93) Tsuda, T.; Horio, F.; Osawa, T. Absorption and metabolism of cyanidin 3-*O*-*β*-D-glucoside in rats. *FEBS Lett.* **1999**, *449*, 179−182.
(94) Dreiseitel, A.; Oosterhuis, B.; Vukman, K. V.; Schreier, P.; Oehme, A.; Locher, S.; Hajak, G.; Sand, P. G. Berry anthocyanins and anthocyanidins exhibit distinct affinities for the efflux transporters BCRP and MDR1. *Br. J. Pharmacol.* **2009**, *158*, 1942−1950.

bioavailability of anthocyanins/anthocyanidins and their metabolites in lung tissues.

MATERIALS AND METHODS

Chemicals. HPLC grade water, acetonitrile, methanol, and other HPLC solvents, hydrochloric acid (HCl), formic acid, acetic acid, and trifluoroacetic acid were obtained from Sigma Chemical Co. (St. Louis, MO, USA). Authentic anthocyanin standards were obtained from Chromadex (Irvine, CA, USA). All other chemicals used in the study were of analytical grade. Freeze-dried highbush blueberry powder (50:50 blend of Tifblue and Rubel) was received from the U.S. Highbush Blueberry Council (Folsom, CA, USA). The native mixture of anthocyanidins (~95% pure) was isolated in our laboratory from 36% anthocyanin-enriched bilberry extract (Indena, Seattle, WA, USA), which contains five major anthocyanidins, delphinidin, cyanidin, malvidin, peonidin, and petunidin in the ratio of 33:28:16:16:7, as described in our previous study.[3]

Extraction and Isolation of Purified Anthocyanins/Anthocyanidins from Bilberry. Extraction, enrichment, and hydrolysis of the bilberry were carried out using essentially the same method as described previously.[15] Briefly, the enriched bilberry extract powder was extracted with 75% aqueous ethanol containing 0.1% HCl and enriched by loading the concentrated extracts on an XAD-761/Diaion HP-20 (1:1) column. The polyphenols, including anthocyanins, were eluted with methanol. Pooled elutes were concentrated and hydrolyzed with 2 N HCl (~5 volumes). Hydrolysates were purified using C18 Sep-Pak cartridges (Waters, Milford, MA, USA). Anthocyanidins and other polyphenols were eluted with acidified (0.01% HCl) methanol. The enriched extracts were dried under reduced pressure using a Savant Speed-Vac (Thermo Scientific, USA) and stored at −20 °C until use. The enriched extracts were dissolved in acidified water, and anthocyanidins were selectively extracted in isoamyl alcohol and dried under vacuum.[16] The extracted anthocyanidins were further purified by loading on the C18 cartridges per the manufacturer's guidelines.

Diet. AIN-93 M diet supplemented with blueberry powder at 5% (w/w) was prepared in pellet form by Harlan-Teklad (Madison, WI, USA) and stored at 4 °C in the dark in vacuum-sealed bags until use.

Animal Study. Animal experiments were performed in agreement with an approved protocol from the Institutional Animal Care and Use Committee of the University of Louisville. Female athymic nude mice (5−6 weeks old) were purchased from Harlan Sprague−Dawley, Inc. (Indianapolis, IN, USA). Two animal studies were conducted to test different routes of administration. In study 1, after a week of acclimatization, animals were randomized into two groups ($n = 4$) and provided either AIN-93 M diet or diet supplemented with 5% blueberry powder (w/w). Animals received diet and water ad libitum. The diet was changed every other day, and the food intake was monitored. No difference was found in food consumption in control and experimental groups. The animals had free access to food and water until euthanasia. After 10 days of treatment, animals were euthanized by CO_2 asphyxiation, and lung was collected, snap frozen, and stored at −80 °C until use. Blood was collected by cardiac puncture; plasma was separated and stored at −80 °C.

In study 2, animals were treated with a bolus dose of the native mixture of anthocyanidins isolated from bilberry (10 mg/mouse) by gavage in 10% dimethyl sulfoxide. Two hours after the treatment, animals were euthanized; lung tissue was collected, snap frozen, and stored at −80 °C until use. Blood was collected by cardiac puncture; plasma was separated and stored at −80 °C.

Effect of Acids/Solvents on Anthocyanidin Stability. To test the stability of anthocyanidins in various solvents, cyanidin chloride (100 μg/mL) was dissolved in (i) acetonitrile, (ii) methanol, and (iii) methanol acidified with 0.1% HCl. The solutions were immediately analyzed by ultraperformance liquid chromatography (UPLC). Samples maintained at room temperature were analyzed at 1 h intervals for 5 h. The concentration was plotted against percent of cyanidin chloride at initial time point. Because methanol provided complete stability as described under Results, all of the analyses from tissue were done by using methanol containing 0.1% HCl.

Recovery of Anthocyanins from Biological Matrix. Anthocyanins in biological samples (see below) were analyzed at anthocyanidin level. Conversion of anthocyanins to anthocyanidins in the presence of biological matrix was optimized as follows: To 500 μL of plasma was added 100 μL of bilberry extract (1 mg/mL), the mixture was acidified with 0.1% formic acid, acetic acid, trifluoroacetic acid, phosphoric acid, or hydrochloric acid. Samples were incubated for 15 min at 37 °C and then extracted with 5 volumes of acetonitrile. The sample was centrifuged at 10000*g*, and the supernatant was collected and evaporated to dryness under vacuum (Savant Speed-Vac). The dried extracts were dissolved in acidified (0.1% HCl) methanol and analyzed by UPLC.

Extraction of Anthocyanidins from Tissues. Parameters such as the stability of anthocyanidins in different buffers and acid environment, extraction efficiency, and selectivity in different solvents, etc., were established before tissue extractions. First, we analyzed the recovery of anthocyanidins by spiking lung tissues collected from untreated rats from another study. Methods described previously[14] were used to detect berry anthocyanins/anthocyanidins,[14] except for the following modifications: extraction of anthocyanins in acidified (0.1% HCl) acetonitrile, evaporation of solvent, and reconstitution in 50% methanol containing 2 N HCl followed by acid hydrolysis and selective extraction of anthocyanidins in isoamyl alcohol without any use of solid−liquid chromatography. Furthermore, UPLC separation method was developed by identifying solvents to separate reference anthocyanidins and protocatechuic acid (PCA), a bioactive metabolite of Cy,[17] and spiking the tissue homogenate with Dp, Cy, and PCA.[14] Briefly, after the optimization, lung tissue from two mice was pooled (two pools per group) in both animal studies and homogenized in 400 μL of 1.15% KCl; anthocyanins were extracted in acetonitrile containing 0.1% HCl as described above. The supernatant was evaporated and reconstituted in 50% methanol containing 2 N HCl. The extract was then hydrolyzed (100 °C/1 h) to convert anthocyanins to anthocyanidins, and the latter were selectively extracted in isoamyl alcohol.[16] Finally, the samples were dried under reduced pressure (Savant Speed-Vac) and reconstituted in 40 μL of acidified (0.1% HCl) methanol just before injection, and 10 μL was analyzed by UPLC. The limits of detection for the various anthocyanidins (Cy, Dp, Pt, Pe, and Mv) (0.3−0.75 ng) and PCA (0.2 ng) were established.

UPLC Analysis. Anthocyanins and anthocyanidins were analyzed on a Shimadzu UPLC system composed of two LC-20AD-XR pumps, an SIL-20A-XR autosampler, and an SPD-M20A photodiode array detector (PDA) controlled by Class VP software (ver 7.4, SP3) attached to a Shim-pack XR-ODS-II column (3.0 × 150 mm; 2.2 μm). A linear gradient of 3.5% phosphoric acid (solvent A) and acetonitrile (solvent B) with a flow rate of 0.75 mL/min was used. In the gradient, solvent B was initially 15% for 2 min and increased to 20% by 3 min. Solvent B was further increased to 60% from 3 to 10 min, held for 1 min, and returned to 15% by 12 min.

LC-MS Analysis. Reversed-phase chromatography of anthocyanidins was performed on a Thermo Scientific (San Jose, CA, USA) Accela LC system. The mobile phases consisted of buffer A, water/formic acid (100:0.1, v/v), and buffer B, acetonitrile/formic acid (100:0.1, v/v). Five microliters of sample was injected onto a Hypersil GOLD C_{18} column (50 × 2.1 mm, 1.9 μm, 175 Å) from Thermo Scientific. A step gradient at a flow rate of 100 μL/min was used to elute the compounds. The gradient started at 5% buffer B and increased to 40% buffer B in 10 min, then increased to 90% buffer B in 3 min, and was maintained at 90% buffer B for 7 min. Elute from the LC was directed to an LTQ-Orbitrap XL mass spectrometer (Thermo Scientific). The compounds were ionized by electrospray ionization and detected by Orbitrap at 30000 mass resolution (full scan, m/z 220−1000) or by multiple reaction monitoring (MRM). The spray voltage was 4.0 kV, and the capillary temperature was 250 °C. The sheath, auxiliary, and sweep gas flows were set to 15, 5, and 0, respectively. In MRM, molecular ions of anthocyanidins were selected with 3.0 m/z isolation window and fragmented by collision-induced

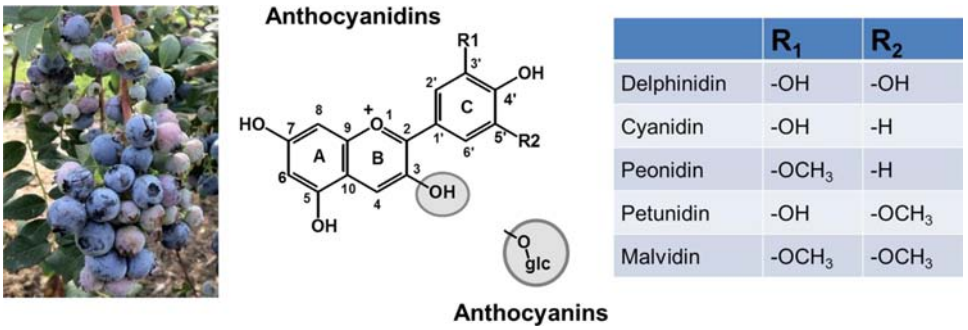

	R_1	R_2
Delphinidin	-OH	-OH
Cyanidin	-OH	-H
Peonidin	$-OCH_3$	-H
Petunidin	-OH	$-OCH_3$
Malvidin	$-OCH_3$	$-OCH_3$

Figure 1. Blueberry fruits and chemical structure of anthocyanins and anthocyanidins found in blueberry/bilberry. Shaded portion shows the difference in anthocyanidins and anthocyanins.

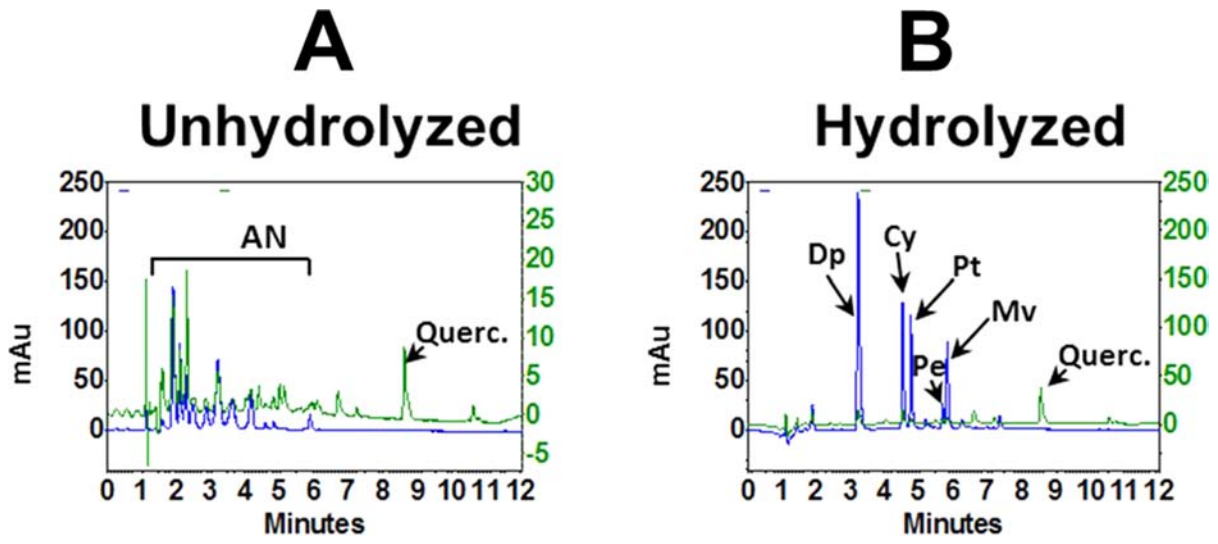

Figure 2. UPLC profiles of unhydrolyzed and hydrolyzed extract of blueberry in anthocyanins (A) and anthocyanidins (B). AN, anthocyanins; Dp, delphinidin; Cy, cyanidin; Pt, petunidin; Pe, peonidin; Mv, malvidin; Querc., quercetin.

dissociation (CID). For CID, collision energy, activation Q, and activation time (mS) were 35, 0.25, and 30, respectively. Full scan MS/MS spectra of the compounds (m/z 100−400) were acquired by Orbitrap at 7500 mass resolution. The transitions used for anthocyanidin detection are shown in panel C of Figure 4. The limits of detection by LC-MS for Dp and Cy were >0.5 and 0.25 ng, respectively, whereas those for Pt, Pe, and Mv were 2.5 pg.

RESULTS

Isolation of Blueberry Phytochemicals and Their Characterization. Blueberry extract was applied onto the XAD-761/HP-20 column (1:1) for the enrichment of anthocyanins and other polyphenols, and the enriched extract was hydrolyzed to convert the glycones to aglycones (i.e., anthocyanins to anthocyanidins; Figure 1). The enriched anthocyanidins were extracted in isoamyl alcohol and further purified by C18 column chromatography. The final extract contained highly pure (>94%) anthocyanidins (Figure 2). When analyzed by UPLC, the purified extract showed five anthocyanidins in the following descending order: Dp (33%), Cy (28%), Pt (16%), Ma (16%), and Pe (7%); a small amount of quercetin was also found in the sample (Figure 2).

Effect of Solvent on Stability of Anthocyanins. The cyanidin was highly unstable in acetonitrile. The rate of degradation was slow initially, but nearly 60% was degraded in 5 h (Supporting Information Figure S1). The stability was better in methanol, where there was only a slight decline and 80% of the compound was found intact. Interestingly, acidified methanol provided complete stability to cyanidin, and no degradation or loss was observed even after 5 h at room temperature. Hence, all of the analyses from tissues were done by using methanol containing 0.1% HCl.

Recovery of Anthocyanins and Anthocyanidins from Biomatrix. The recovery of anthocyanins and anthocyanidins was variable depending on the type of acid used. Formic acid and acetic acid did not provide any recovery of anthocyanins/anthocyanidins from PBS, whereas trifluoroacetic acid, phosphoric acid, and hydrochloric acid gave good recoveries. When these three acids were tested for recovery of anthocyanins/anthocyanidins from plasma, the recovery was in the following order: hydrochloric acid > phosphoric acid > trifluoroacetic acid (Table 1). However, hydrochloric acid extraction also resulted in conversion of some anthocyanins to anthocyanidins. Nearly 55−95% of anthocyanins and 63−100% of anthocyanidins were recovered from plasma (Table 1). Quantification of Pe and Mv was skewed due to the lack of separation of these two peaks in the UPLC conditions used. For measurement from biological matrices from animal experiments, the hydrochloric acid treatment was extended in a boiling water bath for 60 min to convert all anthocyanins to anthocyanidins and then quantified by UPLC-PDA.

Extractions and Detection of Anthocyanidins in Vivo. Blueberry has been reported to contain a variety of

dx.doi.org/10.1021/jf500467b | J. Agric. Food Chem. 2014, 62, 3912−3918

Table 1. Effect of Different Acids on the Recovery of Anthocyanins/Anthocyanidins from Plasma Spiked with Reference Compounds

	% recovery from spiked plasma[a]		
antho	hydrochloric acid	phosphoric acid	TFA
Dp-glu	53.7	36.5	not analyzed
Cy-glu	63.6	42.5	
Pt-glu	67.5	54.6	
Pe-glu	116.1	61.6	
Mv-glu	93.3	83.8	
Dp	123.4	17.7	9.9
Cy	62.9	not detected	32.5
Pt	124.1	2	9.0
Pe	89.2	not detected	21.8
Mv	140.9	1.2	8.3

[a]TFA, trifluoroacetic acid. When plasma was acidified with acetic acid or formic acid, below 2% amounts were recovered. When acidified with HCl, some of the anthocyanins were converted to anthocyanidins. Due to interfering peak with Pe-glucoside and Mv, their recoveries were skewed.

anthocyanins. In this study, we demonstrated the presence of anthocyanins in the blueberry-fed rodent tissues following conversion to anthocyanidins. Sensitivity of detection of the individual reference anthocyanidins was determined by LC-MS and UPLC-PDA and ranged from 0.25 ng to 2.5 pg and from 0.3 to 0.75 ng, respectively. The detection limit for PCA, a metabolite of Cy, was 0.2 ng. Cy was readily detected by UPLC (Figure 3) in the samples extracted from mouse lung with a limit of detection of 0.3 ng, whereas the other anthocyanidins were undetectable due to higher detection limits. A small peak was detected at the retention time for Dp; however, it was not confirmed by MS. However, with LC-MS analysis by specific ion monitoring, Pe, Pt, and Mv were readily detectable below

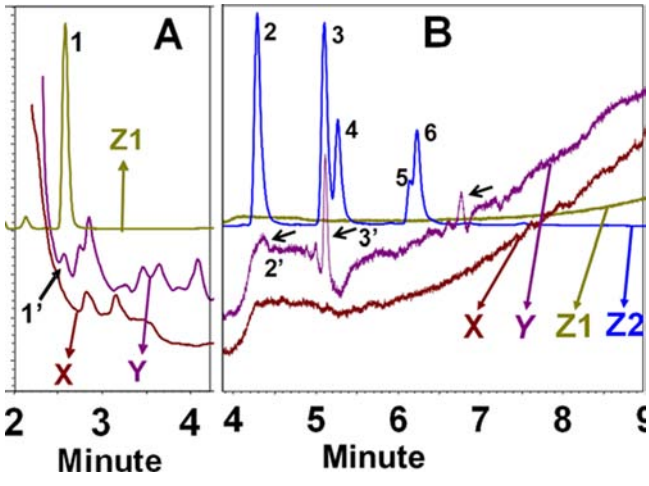

Figure 3. Detection of anthocyanidins at 520 nm (B) and 260 nm for protocatechuic acid (PCA) (A), a bioactive metabolite of cyanidin in lung tissue of rats given dietary blueberry (5% w/w) for 10 days by UPLC-PDA. Chromatograms shown are composites: X, lung tissue from rats on control diet; Y, lung tissue from rats on blueberry diet. Reference compounds: Z1, peak 1 (PCA); Z2, reference anthocyanidins. Peaks: 2, Dp; 3, Cy; 4, Pt; 5, Pe; 6, Mv. Solvent, gradient of 3.5% phosphoric acid in acetonitrile. Chromatograms are cropped for presentation purposes.

≤0.25 ng; Pe could be detected in the picogram range. No peak corresponding to anthocyanidins was detected in the lung of control animals by UPLC or LC-MS.

Several anthocyanidin peaks were found in the samples extracted from the lungs of mice fed blueberry diet by LTQ-MRM (low mass resolution). To confirm the presence of anthocyanidins in lung samples, an MRM with Orbitrap (high mass resolution) method was set up and used to reanalyze the extracted samples. Ion chromatograms of standards from Orbitrap MRM are shown in Figure 4, with a m/z window width of 0.06 that provides better selectivity. Dp and Cy were not detected in lung samples by Orbitrap MRM, but other anthocyanidins (Pe, Pt, and Mv) were detected by MRM (Figure 5) and further confirmed by MS/MS.

DISCUSSION

Several studies in recent years have focused attention on anthocyanin bioavailability both in humans and in experimental animals. Most of these studies reported that anthocyanins were poorly absorbed and were excreted unmetabolized.[18−20] Few studies have also reported that anthocyanins are bioavailable when delivered at very high doses; however, most of the bioavailability studies are focused on individual anthocyanidins, particularly Cy.[14,21−24]

The plausible reasons for lack of anthocyanins' detection include (i) instability of anthocyanins, (ii) metabolism by gut microflora, (iii) high rate of excretion, and (iv) unavailability of suitable analytical techniques. The aim of this work was to develop a method to assess the stability of anthocyanins/anthocyanidins, their selective extraction, and the impact on tissue bioavailability of anthocyanins.

There are several reports on the solubility and stability of anthocyanins in acidic environment.[25,26] Acidified methanol enhances the stability of anthocyanidins compared to acetonitrile. In methanol, the degradation of anthocyanins was very slow, with >80% of anthocyanins remaining intact after 5 h, whereas after acidification no degradation occurred. These results are consistent with published data demonstrating higher stability of anthocyanins in acidic pH.[25,26]

Several methods of anthocyanin extraction are available describing varying recovery of anthocyanins from a biological matrix.[27−30] These methods involve solid phase extraction using Water's Oasis HLB and Sep-Pak C18 cartridges. We standardized the extraction of anthocyanins from tissues of rats administered dietary blueberry by converting them to anthocyanidins, which reduces the number of compounds to five, and allowed us their detection due to their higher amounts. In complex matrices, where interference in peak separation was observed, use of isoamyl alcohol significantly improved the selectivity of anthocyanidins, albeit with a slight loss of recovery (6−7%, data not shown).

In this study, first, we determined stability and extractability of anthocyanidins isolated from bilberry and then determined their tissue bioavailability. Bilberry contains 15 anthocyanins containing galactose, glucose, and arabinose derivatives of Dp, Cy, Pt, Pe, and Mv. These anthocyanins were converted to five anthocyanidins upon acid hydrolysis. Glycones of the same anthocyanidins are also reported in blueberry.[13]

In the present work, we initially failed to detect anthocyanins in lung tissue from rats fed for 10 days with a 5% blueberry diet. The dietary route provides a slow ingestion of the berry phytochemicals. Under these conditions, the lung anthocyanin levels were presumably too low to be detected. Anthocyanins

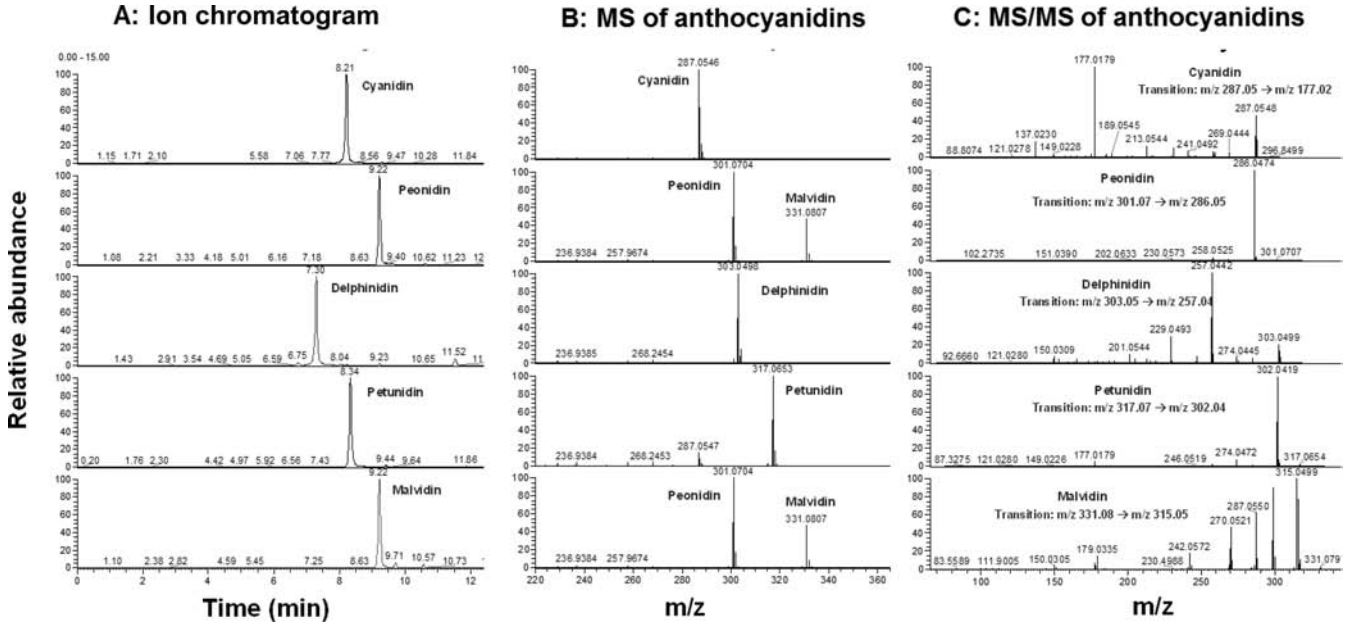

Figure 4. Multiple reaction monitoring (A) and the respective MS (B) and MS/MS (C) of indicated reference anthocyanidins. Peonidin and malvidin were eluted at the same retention time, and therefore they appear in the same spectrum. Anthocyanidins were separated with a Hypersil GOLD C18 column (50 mm × 2.1 mm) in a binary gradient of 1% formic acid and acetonitrile containing 1% formic acid as described under Materials and Methods.

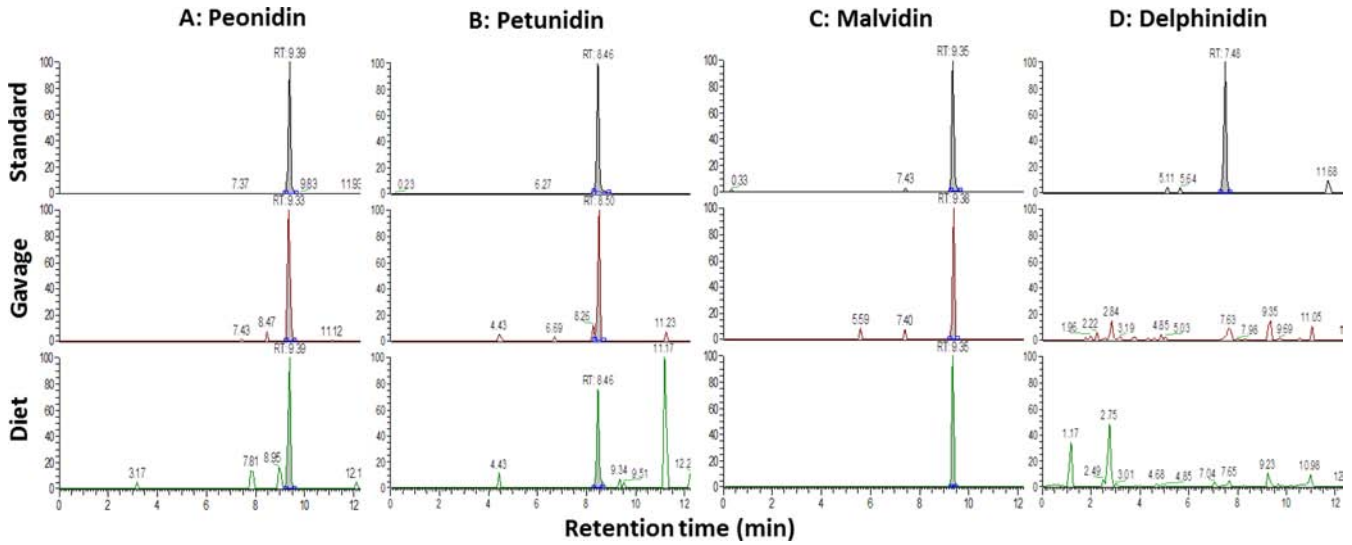

Figure 5. MRM detection of peonidin (A), petunidin (B), and malvidin (C) from the lung tissue of rats provided a native mixture of anthocyanidins isolated from bilberry by gavage (a bolus dose of 10 mg/mouse) or by diet supplemented with blueberry (5% w/w) for 10 days. Delphinidin (D) and cyanidin (not shown) could not be detected by LC-MS analysis. Chromatographic conditions are described under Materials and Methods.

were also not detected in the lung tissue following a bolus dose (10 mg/mouse) by gavage. On the other hand, when the tissue anthocyanins were converted to their respective aglycons by acid hydrolysis and selectively extracted in isoamyl alcohol, Dp and Cy were detected in the lung tissue, indicating that anthocyanins can reach and exert their effects beyond the GI tract. The possibility of bioavailable proanthocyanins being converted to anthocyanidins during acid hydrolysis cannot be ruled out. This presence of anthocyanins in lung tissue could be explained by their ability to permeate the gastrointestinal barrier.[31] These data demonstrate that the conversion of anthocyanins to anthocyanidins prior to analysis is an effective method for detecting anthocyanins in tissues. However, conversion of proanthocyanidins to anthocyanidins in vivo could also enhance the levels on anthocyanidins in animal tissue. PCA, which is produced by degradation of Cy,[32] was also detected in lung tissue, suggesting that lung PCA and anthocyanins along with some unknown metabolites are presumably bioactives responsible for the known anticarcinogenic potential of blueberry in the lung.[33]

A series of papers have shown the bioavailability of anthocyanins in brain tissue,[21,22] and a few other studies report the presence of anthocyanins in other organs including the lung following treatment of rodents with individual anthocyanin at high doses.[14,23,24] Our study is the first demonstration indicating the presence of anthocyanidins in lung tissue

following low-dose dietary blueberry. The blueberry dose used in this study is the same or just 2-fold higher as used in our previous study in which it was found to inhibit estrogen-mediated mammary tumorigenesis.[8,13] The results from our other study also showed the efficacy of the native mixture of anthocyanidins from bilberry against lung cancer xenografts.[3]

In summary, we show for the first time that anthocyanins are bioavailable in the lung following a low dose of dietary blueberry powder. The detection has been possible by conversion of anthocyanins to their native anthocyanidins, followed by extraction in isoamyl alcohol. This technique can be utilized to demonstrate bioavailability of anthocyanins in different tissues and correlate their levels with disease inhibition.

■ ASSOCIATED CONTENT

Supporting Information

Figure S1. This material is available free of charge via the Internet at http://pubs.acs.org.

■ AUTHOR INFORMATION

Corresponding Author

*(R.C.G.) Phone: (502) 852-3682. Fax: (502) 852-3842. E-mail: rcgupta@louisville.edu.

Funding

This work was supported by USPHS Grants CA-118114 and CA125152 and the Agnes Brown Duggan Endowment. R.C.G. holds the Agnes Brown Duggan Chair in Oncological Research.

Notes

The authors declare no competing financial interest.

■ REFERENCES

(1) Harris, G. K.; Gupta, A.; Nines, R. G.; Kresty, L. A.; Habib, S. G.; Frankel, W. L.; LaPerle, K.; Gallaher, D. D.; Schwartz, S. J.; Stoner, G. D. Effects of lyophilized black raspberries on azoxymethane-induced colon cancer and 8-hydroxy-2′-deoxyguanosine levels in the Fischer 344 rat. *Nutr. Cancer.* **2001**, *40*, 125−133.

(2) Stoner, G. D.; Wang, L. S.; Seguin, C.; Rocha, C.; Stoner, K.; Chiu, S.; Kinghorn, A. D. Multiple berry types prevent *N*-nitrosomethylbenzylamine-induced esophageal cancer in rats. *Pharm. Res.* **2010**, *27*, 1138−1145.

(3) Kausar, H.; Jeyabalan, J.; Aqil, F.; Chabba, D.; Sidana, J.; Singh, I. P.; Gupta, R. C. Berry anthocyanidins synergistically suppress growth and invasive potential of human non-small-cell lung cancer cells. *Cancer Lett.* **2012**, *325*, 54−62.

(4) Svobodova, A.; Zdarilova, A.; Vostalova, J. *Lonicera caerulea* and *Vaccinium myrtillus* fruit polyphenols protect HaCaT keratinocytes against UVB-induced phototoxic stress and DNA damage. *J. Dermatol. Sci.* **2009**, *56*, 196−204.

(5) Zafra-Stone, S.; Yasmin, T.; Bagchi, M.; Chatterjee, A.; Vinson, J. A.; Bagchi, D. Berry anthocyanins as novel antioxidants in human health and disease prevention. *Mol. Nutr. Food Res.* **2007**, *51*, 675−683.

(6) Neto, C. C. Cranberry and blueberry: evidence for protective effects against cancer and vascular diseases. *Mol. Nutr. Food Res.* **2007**, *51*, 652−664.

(7) Aiyer, H. S.; Gupta, R. C. Berries and ellagic acid prevent estrogen-induced mammary tumorigenesis by modulating enzymes of estrogen metabolism. *Cancer Prev. Res. (Phila.)* **2010**, *3*, 727−737.

(8) Aiyer, H. S.; Srinivasan, C.; Gupta, R. C. Dietary berries and ellagic acid diminish estrogen-mediated mammary tumorigenesis in ACI rats. *Nutr. Cancer* **2008**, *60*, 227−234.

(9) Ravoori, S.; Vadhanam, M. V.; Sahoo, S.; Srinivasan, C.; Gupta, R. C. Mammary tumor induction in ACI rats exposed to low levels of 17β-estradiol. *Int. J. Oncol.* **2007**, *31*, 113−120.

(10) Vadhanam, M. V.; Ravoori, S.; Aqil, F.; Gupta, R. C. Chemoprevention of mammary carcinogenesis by sustained systemic delivery of ellagic acid. *Eur. J. Cancer Prev.* **2011**, *20*, 484−491.

(11) Wang, H.; Cao, G. H.; Prior, R. L. Oxygen radical absorbing capacity of anthocyanins. *J. Agric. Food Chem.* **1997**, *45*, 304−309.

(12) Matsumoto, H.; Nakamura, Y.; Hirayama, M.; Yoshiki, Y.; Okubo, K. Antioxidant activity of black currant anthocyanin aglycons and their glycosides measured by chemiluminescence in a neutral pH region and in human plasma. *J. Agric. Food Chem.* **2002**, *50*, 5034−5037.

(13) Ravoori, S.; Vadhanam, M. V.; Aqil, F.; Gupta, R. C. Inhibition of estrogen-mediated mammary tumorigenesis by blueberry and black raspberry. *J. Agric. Food Chem.* **2012**, *60*, 5547−5555.

(14) Marczylo, T. H.; Cooke, D.; Brown, K.; Steward, W. P.; Gescher, A. J. Pharmacokinetics and metabolism of the putative cancer chemopreventive agent cyanidin-3-glucoside in mice. *Cancer Chemother. Pharmacol.* **2009**, *64*, 1261−1268.

(15) Aqil, F.; Gupta, A.; Munagala, R.; Jeyabalan, J.; Kausar, H.; Sharma, R. J.; Singh, I. P.; Gupta, R. C. Antioxidant and antiproliferative activities of anthocyanin/ellagitannin-enriched extracts from *Syzygium cumini* L. (jamun, the Indian blackberry). *Nutr. Cancer* **2012**, *64*, 428−438.

(16) Toki, K.; Saito, N.; Irie, Y.; Tatsuzawa, F.; Shigihara, A.; Honda, T. 7-O-Methylated anthocyanidin glycosides from *Catharanthus roseus*. *Phytochemistry* **2008**, *69*, 1215−1219.

(17) Vitaglione, P.; Donnarumma, G.; Napolitano, A.; Galvano, F.; Gallo, A.; Scalfi, L.; Fogliano, V. Protocatechuic acid is the major human metabolite of cyanidin-glucosides. *J. Nutr.* **2007**, *137*, 2043−2048.

(18) McGhie, T. K.; Ainge, G. D.; Barnett, L. E.; Cooney, J. M.; Jensen, D. J. Anthocyanin glycosides from berry fruit are absorbed and excreted unmetabolized by both humans and rats. *J. Agric. Food Chem.* **2003**, *51*, 4539−4548.

(19) Netzel, M.; Strass, G.; Janssen, M.; Bitsch, I.; Bitsch, R. Bioactive anthocyanins detected in human urine after ingestion of blackcurrant juice. *J. Environ. Pathol. Toxicol. Oncol.* **2001**, *20*, 89−95.

(20) Frank, T.; Netzel, M.; Strass, G.; Bitsch, R.; Bitsch, I. Bioavailability of anthocyanidin-3-glucosides following consumption of red wine and red grape juice. *Can. J. Physiol. Pharmacol.* **2003**, *81*, 423−435.

(21) Milbury, P. E.; Kalt, W. Xenobiotic metabolism and berry flavonoid transport across the blood-brain barrier. *J. Agric. Food Chem.* **2010**, *58*, 3950−3956.

(22) Talavera, S.; Felgines, C.; Texier, O.; Besson, C.; Gil-Izquierdo, A.; Lamaison, J. L.; Remesy, C. Anthocyanin metabolism in rats and their distribution to digestive area, kidney, and brain. *J. Agric. Food Chem.* **2005**, *53*, 3902−3908.

(23) Sakakibara, H.; Ogawa, T.; Koyanagi, A.; Kobayashi, S.; Goda, T.; Kumazawa, S.; Kobayashi, H.; Shimoi, K. Distribution and excretion of bilberry anthocyanins [corrected] in mice. *J. Agric. Food Chem.* **2009**, *57*, 7681−7686.

(24) Datla, K. P.; Christidou, M.; Widmer, W. W.; Rooprai, H. K.; Dexter, D. T. Tissue distribution and neuroprotective effects of citrus flavonoid tangeretin in a rat model of Parkinson's disease. *Neuroreport* **2001**, *12*, 3871−3875.

(25) Talavera, S.; Felgines, C.; Texier, O.; Besson, C.; Manach, C.; Lamaison, J. L.; Remesy, C. Anthocyanins are efficiently absorbed from the small intestine in rats. *J. Nutr.* **2004**, *134*, 2275−2279.

(26) Li, J.; Li, X. D.; Zhang, Y.; Zheng, Z. D.; Qu, Z. Y.; Liu, M.; Zhu, S. H.; Liu, S.; Wang, M.; Qu, L. Identification and thermal stability of purple-fleshed sweet potato anthocyanins in aqueous solutions with various pH values and fruit juices. *Food Chem.* **2013**, *136*, 1429−1434.

(27) Ling, Y.; Ren, C.; Mallery, S. R.; Ugalde, C. M.; Pei, P.; Saradhi, U. V.; Stoner, G. D.; Chan, K. K.; Liu, Z. A rapid and sensitive LC-MS/MS method for quantification of four anthocyanins and its application in a clinical pharmacology study of a bioadhesive black raspberry gel. *J. Chromatogr., B: Anal. Technol. Biomed. Life Sci.* **2009**, *877*, 4027−4034.

(28) Wu, X.; Cao, G.; Prior, R. L. Absorption and metabolism of anthocyanins in elderly women after consumption of elderberry or blueberry. *J. Nutr.* **2002**, *132*, 1865−1871.
(29) Yi, W.; Akoh, C. C.; Fischer, J.; Krewer, G. Absorption of anthocyanins from blueberry extracts by Caco-2 human intestinal cell monolayers. *J. Agric. Food Chem.* **2006**, *54*, 5651−5658.
(30) Milbury, P. E.; Vita, J. A.; Blumberg, J. B. Anthocyanins are bioavailable in humans following an acute dose of cranberry juice. *J. Nutr.* **2010**, *140*, 1099−1104.
(31) Talavera, S.; Felgines, C.; Texier, O.; Besson, C.; Lamaison, J. L.; Remesy, C. Anthocyanins are efficiently absorbed from the stomach in anesthetized rats. *J. Nutr.* **2003**, *133*, 4178−4182.
(32) Tsuda, T.; Horio, F.; Osawa, T. Absorption and metabolism of cyanidin 3-*O*-*β*-D-glucoside in rats. *FEBS Lett.* **1999**, *449*, 179−182.
(33) Balansky, R.; Ganchev, G.; Iltcheva, M.; Kratchanova, M.; Denev, P.; Kratchanov, C.; Polasa, K.; D'Agostini, F.; Steele, V. E.; De Flora, S. Inhibition of lung tumor development by berry extracts in mice exposed to cigarette smoke. *Int. J. Cancer* **2012**, *131*, 1991−1997.

Aldrich, (St. Louis, MO, USA). Sephadex LH-20 was purchased from GE Healthcare (Uppsala, Sweden). Tryptose and dextrose were obtained from BD (Sparks, MD, USA). Fetal bovine serum (FBS) was purchased from Atlanta Biologicals (Lawrenceville, GA, USA). HyClone Dulbecco's PBS without calcium and magnesium, Hyclone Roswell Park Memorial Institute medium (RPMI-1640), and Hyclone trypsin 0.25% in 0.1% ETDA were obtained from Thermo Scientific (South Logan, UT, USA). Caco-2 cells ATCC HTB-37 were obtained from ATCC (Manassas, VA, USA).

Samples. Cranberry fruits (*Vaccinium macrocarpon* Ait. cv. 'Stevens') were obtained from the United Cranberry Growers Cooperative (Wausau, WI, USA) and apple fruits (*Malus pumila* cv. 'Golden Delicious') were obtained from a privately owned fruit tree in October 2011. The fresh fruits were homogenized to a fine powder by blending with liquid nitrogen. The fruit powders were stored at −80 °C until extraction.

Isolation of Proanthocyanidins. *Extraction Procedure.* The proanthocyanidin extraction procedure was adapted from our previous work.[14,15] Cranberry powder (100 g) was extracted with 70% aqueous acetone (v/v; 400 mL) in an ultrasonic bath for 15 min. The extract was centrifuged at 400*g* at 15 °C for 10 min, and the supernatant was collected. The extraction was repeated two additional times, and the supernatants were combined. After filtration with cellulose paper, acetone was removed by rotary evaporation under vacuum at 35 °C, and the remaining suspension was solubilized in ethanol. The extract was then centrifuged at 13416*g* at 0 °C for 10 min to eliminate insoluble material. The apple extract was produced in the same manner, adding the 70% aqueous acetone (v/v) to the frozen apple powder immediately to prevent long thawing processes, which favor polyphenol oxidase activity.[16] The supernatants were used to isolate proanthocyanidin fractions by chromatography on Sephadex LH-20 as described below.

Proanthocyanidin Isolation. The ethanolic proanthocyanidin extracts were loaded on glass columns (2.5 cm i.d. × 60 cm length, Kontes, Chromaflex) packed with Sephadex LH-20 that was previously swollen and washed in water and equilibrated with ethanol for 45 min at a flow rate of 4 mL/min. Preliminary work had shown that a combination of three solvents was sufficient to achieve a proanthocyanidin fraction that was devoid of other classes of polyphenols. The resin bed was consecutively eluted with ethanol, ethanol/methanol (1:1), and 80% aqueous acetone (v/v). The 80% aqueous acetone (v/v) fraction that contained PAC was evaporated as described above and solubilized in methanol.

Proanthocyanidin Characterization. The proanthocyanidin content of the cranberry and apple fractions was quantified by using the Folin−Ciocalteu method,[17] and proanthocyanidin concentrations are expressed as gallic acid equivalents (GAE). Previously developed matrix-assisted laser desorption/ionization time-of-flight mass spectrometry (MALDI-TOF MS) methods were applied to characterize the cranberry and apple PAC.[18] An aliquot of each sample was evaporated to dryness and suspended in 20 μL of ethanol to a final concentration of 20 μg GAE/mL. An aliquot (0.5 μL) of each sample was then mixed with 1 μL of DHB (50.0 mg/mL in ethanol) in three different wells on the stainless steel MALDI target. Mass spectra were collected on a Bruker ULTRAFLEX-III MALDI-TOF/TOF mass spectrometer (Billerica, MA, USA). All analyses were performed in positive reflectron mode. Spectra were the sum of different locations in each well, accumulating a total of 500 shots to minimize intrawell variability, and deflection was set at 800 Da. After analysis, the deconvolution method based on the relative intensity of proanthocyanidin isotope patterns was used to calculate the ratios of "A-type" to "B-type" bonds in cranberry and apple PAC.[18]

Bacterial Culture. P fimbriae expression is an important virulence factor for ExPEC colonization of the gut[19] and is critical for attachment of *E. coli* to epithelial cells in the urinary tract, colon, and ileum.[20,21] The strain of ExPEC (strain 5011) used in this study was isolated from a woman with recurrent UTI at the University of Wisconsin Hospital and Clinics. The selected strain was found in both the gastrointestinal and urinary tracts and expresses fimH and papA, the adhesins of type 1 and P fimbriae, respectively.

Strain 5011 was cultured from frozen stock under static culture conditions in tryptose broth (10 g of tryptose, 2.5 g of sodium chloride, 0.5 g of dextrose, and 0.0025 g of thyamin hydrochloride in 500 mL of deionized water) at 37 °C and washed twice with 1× PBS + Ca^{2+}/Mg^{2+} by centrifugation at 1840*g* for 10 min. The optical density of the inoculum suspension at 450 nm was used to calculate and adjust the bacterial cell density using a previously established bacterial density−absorbance curve.

Bacterial Agglutination Assay. The agglutination assay was conducted in 3.0 mL microcuvettes using 1.0 mL total reaction volume. First, ExPEC stock solutions (50 μL) were added to the cuvettes, resulting in a final ExPEC concentration of 5.0×10^8 colony forming units (CFU)/mL. Next, proanthocyanidin solutions of either apple (13.6 mg GAE/mL) or cranberry (121.2 mg GAE/mL) were diluted 1/10 and 1/100, respectively, and added to each bacterial inoculum to reach final concentrations of 0, 5, 10, 25, 50, and 100 μg GAE/mL in a total volume of 1 mL with 1× PBS + Ca^{2+}/Mg^{2+}. The cuvettes were sealed and shaken vigorously for 20 s. Absorbances were read at 450 nm every 5 min for 300 min on a Beckman DU 640 spectrophotometer equipped with a six-position cuvette holder (Schaumburg, IL, USA), and the absolute values were converted to transmittance (%). The area under the transmittance curve (AUC) for each concentration level was calculated as a function of the ability of PAC to agglutinate ExPEC from 0 to 300 min.

Gut Epithelial Cell (Enterocyte) Culture. Caco-2 (HTB-37) cells were cultured in DMEM supplemented with 10% FBS (v/v), 1% nonessential amino acids (v/v), 1% L-alanyl-L-glutamine (v/v), and 1% penicillin/streptomycin (v/v) at 37 °C with 5% CO_2. For use in experiments, cells at approximately 80% confluence, based on surface area coverage, were split 1:1.6 into 24-well cell culture treated plates. Once the cells reached confluence (approximately 8.0×10^5 cells/well), they were allowed to differentiate for 8−10 days to become phenotypic polarized enterocytes with medium changes every other day. For maintenance purposes, stock cells were passaged biweekly using 0.25% trypsin.

Invasion Assay. Bacteria were cultured as described previously in this section and were added to 5 mL tubes to reach a multiplicity of infection of 100 (8.0×10^7 CFU/well) relative to the number of Caco-2 cells (8.0×10^5 cells/well). 1× PBS + Ca^{2+}/Mg^{2+} and proanthocyanidin treatments (0, 5, 10, 25, 50, and 100 μg GAE/mL) were added to a total volume of 75 μL, gently mixed, and then incubated for 10 min. RPMI medium, supplemented with 5% FBS (v/v), was added to bring the final volume to 2.5 mL and incubated for 5 min. Caco-2 cell plates were washed twice with 1× PBS + Ca^{2+}/Mg^{2+}, and 0.5 mL of each treatment was added to the plate in quadruplicate. After 1 h at 37 °C to allow for bacterial invasion, Caco-2 cells were washed twice with 1× PBS + Ca^{2+}/Mg^{2+}, and extracellular bacteria were killed by incubating 1 mL of RMPI medium supplemented with 5% FBS (v/v) and gentamicin at a final concentration of 100 μg/mL for 1 h. Caco-2 cells were washed twice with PBS (without Ca^{2+} and Mg^{2+}) and lysed with 1 mL/well Triton 1X for 30 min on a shaker. After intracellular bacteria were released from Caco-2 cells, each well content was homogenized via pipetting, vortexed, and diluted 1:10 in PBS without Ca^{2+} and Mg^{2+}, and 100 μL was plated in duplicate on LB plates (25 g LB Miller, 15 g of agar in 1 L of deionized water). All plates were incubated for 18 h at 37 °C, and the number of CFU/plate was counted. The results were expressed in percentage of enterocyte invasion using the following formula: (CFU sample/CFU control) × 100.

Data and Statistical Analysis. All data were reported as the mean ± standard deviation of at least three replicates. mMass version 3.9.0[22] was used for mass spectra analysis, and SAS was used for AUC calculation using the trapezoidal method (version 9.3; SAS Institute Inc., Cary, NC, USA). Statistical analysis was done using JMP Pro (version 10.0.0; SAS Institute Inc.), setting $\alpha = 0.05$. Results were analyzed with two-way ANOVA models with interaction between the independent variables "sample" and "concentration" to assess significant differences. The dependent variables were AUC and $\arcsin[\sqrt{(\%\ \text{invasion}/100)}]$ for the agglutination and invasion assays, respectively.

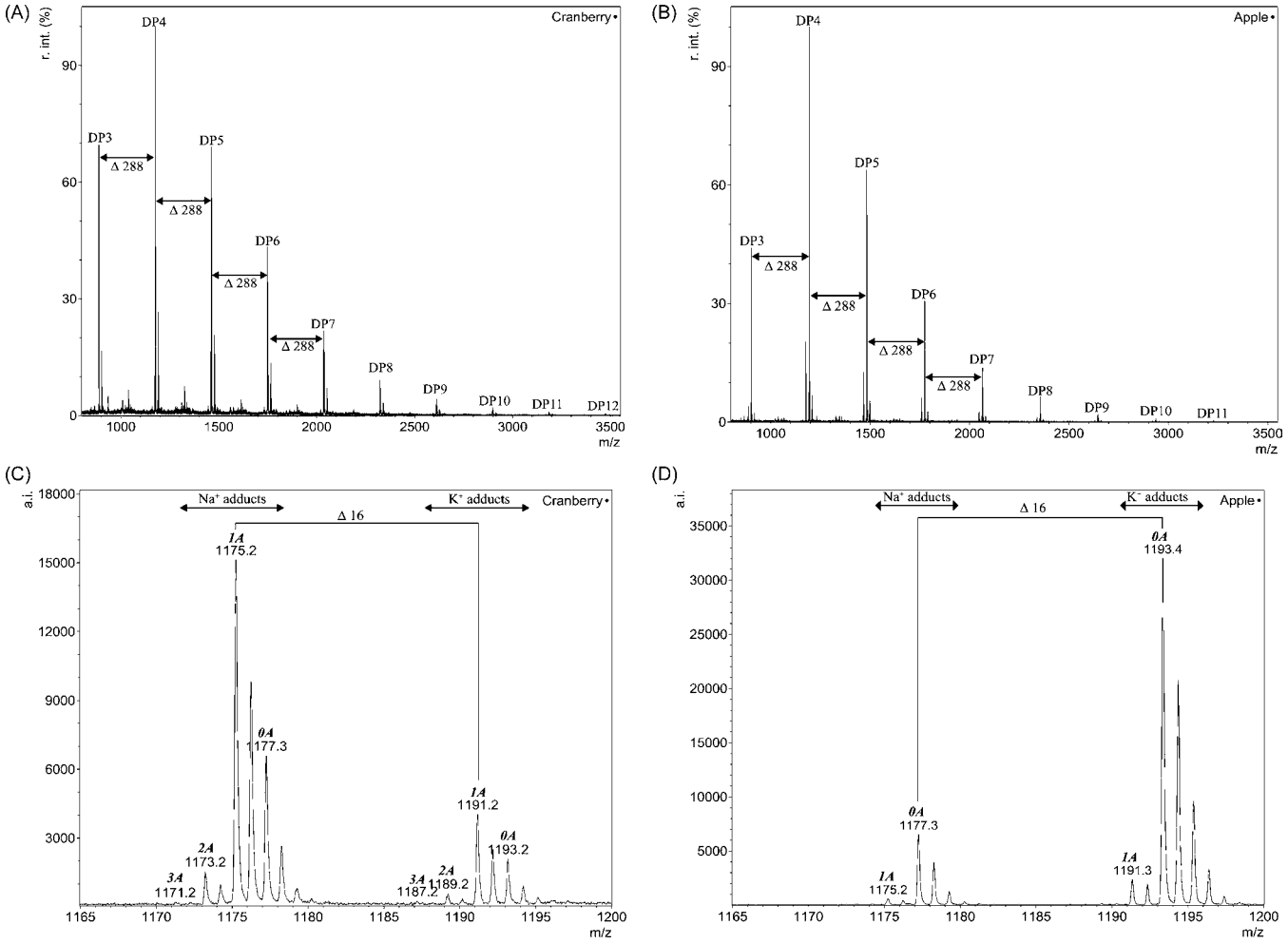

Figure 1. (A, B) Mass spectra obtained with MALDI-TOF MS in positive reflectron mode for cranberry (A) and apple (B) proanthocyanidins (PAC). PAC with different degrees of polymerization (DP) have a 288 mass difference. "r.i." corresponds to relative intensity. (C, D) Mass spectra obtained with MALDI-TOF MS in positive reflectron mode for cranberry (C) and apple (D) proanthocyanidins (PAC) tetramers displaying sodium and potassium adducts showing a 16 units mass difference. The number of "A-type" bonds is assigned to each peak. "a.i." corresponds to absolute intensity.

RESULTS

MALDI-TOF MS Characterization of PAC. Chromatography on Sephadex LH-20 produces fractions from cranberries and apples that contain only PAC.[15] Analysis by MALDI-TOF MS showed that the predominant mass at each DP (Δ288 amu) for cranberry (Figure 1A) and apple (Figure 1B) samples are representative of proanthocyanidin structures that consist of multiple linked catechin/epicatechin units with predominantly either "A-type" or "B-type" bonds for cranberries and apples, respectively. These observed masses and mass distribution are consistent with previously described proanthocyanidin composition of cranberry[23] and apple.[27] Mass spectral analysis indicated that cranberries contain an oligomeric distribution of PAC with a DP from 3 (trimer) to 12 (dodecamer) (Figure 1A) and that apples contain a distribution of PAC with DP from 3 (trimer) to 11 (undecamer) (Figure 1B).

PAC associate with sodium $[M + Na]^+$ and potassium $[M + K]^+$ forming alkali metal adducts,[24] thereby splitting the signal unevenly, leading to Δ16 amu between $[M + Na]^+$ and $[M + K]^+$ in both cranberry (Figure 1C) and apple PAC (Figure 1D). Cranberry PAC predominantly ionized as sodium adducts (Figure 1C), whereas apple PAC predominantly ionized as potassium adducts (Figure 1D). In cranberry PAC, the MALDI-TOF MS spectrum shows that the most predominant linkage type corresponds to 1 "A-type" but peaks corresponding to 2 and 3 "A-type" bonds have enough intensity to resolve above baseline noise (Figure 1C). For each additional "A-type" bond there is a 2 amu decrease due to the loss of two hydrogen atoms that are involved in forming the ether bond typical of this type of interflavan linkage (Figure 2). For example, in tetramers the sodium adduct series shows four distinct peaks: m/z 1177.3 (0 "A-type" and 3 "B-type" bonds), m/z 1175.2 (1 "A-type" and 2 "B-type" bonds), m/z 1173.2 (2 "A-type" and 2 "B-type" bonds), and m/z 1171.2 (3 "A-type" and 0 "B-type" bonds) (Figure 1C). The intermediary peaks that are present between each DP in cranberry PAC correspond to anthocyanins that are covalently bonded to PAC and have been previously described.[15]

In spectra from apple PAC, the peaks with the highest absolute intensity correspond to 0 "A-type" bonds. For example, in tetramers the sodium adduct series shows only two distinct peaks: a predominant peak at m/z 1177.3 (0 "A-type" and 3 "B-type" bonds) and a peak at m/z 1175.2 (1 "A-type" and 2 "B-type" bonds) with only 6% of the intensity of the all "B-type" tetramer (Figure 1D).

dx.doi.org/10.1021/jf403839a | J. Agric. Food Chem. 2014, 62, 3919−3925

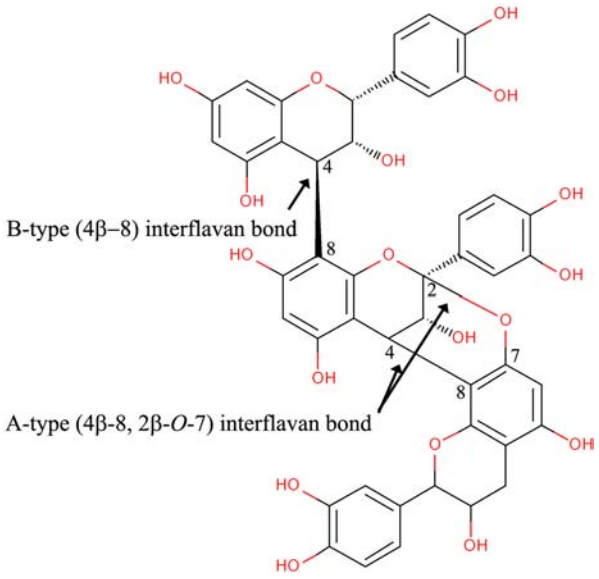

Figure 2. Representative structure of a cranberry proanthocyanidin trimer (epicatechin-(4β-8)-epicatechin-(4β-8, 2β-*O*-7)-epicatechin).[39] Variation in degree of polymerization, position, and number of "A-type" versus "B-type" interflavan bonds leads to large structural heterogeneity among cranberry PAC.[23,29]

When our deconvolution method[18] was applied to the MALDI-TOF MS spectra, median values showed that 94.5% of cranberry PAC were "A-type" and 88.3% of apple PAC were "B-type" (Table 1). Our results indicate that apple PAC contain

Table 1. Percentage of Proanthocyanidins (PAC) with at Least One or Two "A-type" Bonds per Degree of Polymerization (DP) in Cranberry and Apple[a]

	PAC with at least one "A-type" bond		PAC with at least two "A-type" bonds	
DP	apple	cranberry	apple	cranberry
3	3.1 ± 5.4	93.5 ± 2.4	0.0 ± 0.0	1.7 ± 0.7
4	10.1 ± 1.9	88.0 ± 3.2	0.0 ± 0.0	5.4 ± 0.7
5	12.3 ± 1.4	90.1 ± 1.8	1.7 ± 1.3	13.1 ± 3.3
6	12.1 ± 1.9	95.4 ± 1.8	0.7 ± 0.7	39.0 ± 3.5
7	11.3 ± 2.9	99.6 ± 0.7	0.0 ± 0.0	51.7 ± 1.9
8	12.4 ± 3.4	97.4 ± 4.4	0.0 ± 0.0	60.1 ± 0.6
median	11.7	94.5	0.0	26.1

[a]The results are expressed as the average of three independent replicates ± standard deviation.

a median value of 11.7% "A-type" PAC as determined by predictive equations.[25] Furthermore, median values showed that 26.1% of cranberry PAC had 2 or more "A-type" interflavan bonds, whereas none of the apple PAC had 2 or more "A-type" bonds (Table 1). However, mass spectrometry alone does not provide sufficient information for the structural elucidation of "A-type" PAC. To our knowledge, the confirmation of "A-type" interflavan bonds in apple PAC has not yet been described. Thus, whereas our interpretation of the data is that the detected masses represent "A-type" PAC in apples, reactions resulting from polyphenol oxidase activity may also alter PAC oligomer structure, resulting in modifications that involve the loss of two hydrogen molecules. This observation has also been reported for MALDI-TOF MS analysis of apple juices.[26]

The absence of PAC "A-type" to "B-type" interflavan linkage ratios for proanthocyanidin oligomers greater than an octamer (DP >8) is a result of the MALDI-TOF MS instrument parameters. The nature of the MALDI-TOF MS analysis requires the sample to be mixed with a matrix (DHB) to afford ionization and subsequent detection of charged compounds. This process produces numerous low molecular weight (<800 Da) matrix adducts resulting in background noise (unwanted signals). To improve the quality of the PAC spectra and allow for quantification of relative "A-type" to "B-type" interflavan bonds, the MALDI-TOF MS instrument parameters are set to gate (deflect) masses below a 800 Da threshold. As a result of this gating process, dimers (m/z 599 and 601) are also deflected and not detected. In the case of proanthocyanidin oligomers with DP >8, spectra are excluded from analysis when one or more of the peaks included in the deconvolution of isotope patterns have signal-to-noise ratios of <3.0.[18] On the basis of these predefined criteria, the MALDI-TOF MS instrument parameters are adjusted to provide high-resolution spectra for PAC trimers through octamers (DP 3–8). These parameters allow the relative proportions of "A-type" to "B-type" interflavan bonds for 23 individual proanthocyanidin masses to be compared across samples.

Bacterial Agglutination Assay. In our study design, we compared "A-type" to "B-type" PAC for their ability to increase ExPEC agglutination. We monitored the increase in transmittance of light (450 nm) that results when PAC interact with ExPEC, causing agglutination and precipitation from suspension. To correct for baseline transmittance, all values were normalized to zero at the beginning of the experiment. The AUC for each concentration level was calculated as a function of the ability of PAC to agglutinate ExPEC. Results showed that both "A-type" and "B-type" PAC significantly increased agglutination in a dose-dependent manner when compared to control. Figure 3 shows an example of an agglutination experiment using the "B-type" PAC from apples. Bacterial agglutination was 77, 58, 28, 27, and 32% higher for 5, 10, 25, 50, and 100 μg GAE/mL, respectively, when "A-type" were compared to "B-type" PAC. "A-type" PAC were significantly more effective (p values < 0.05) at increasing agglutination

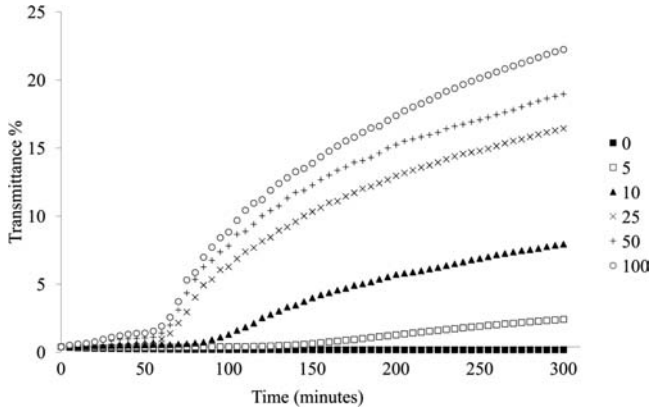

Figure 3. Relationship between transmittance (%) at 450 nm and time over 300 min of the agglutination assay with ExPEC in PBS and six levels of apple proanthocyanidins concentration (0, 5, 10, 25, 50, and 100 μg GAE/mL). The results represent the average of three independent replicates.

when compared to "B-type" PAC at all concentrations, except for the lowest concentration (Figure 4A).

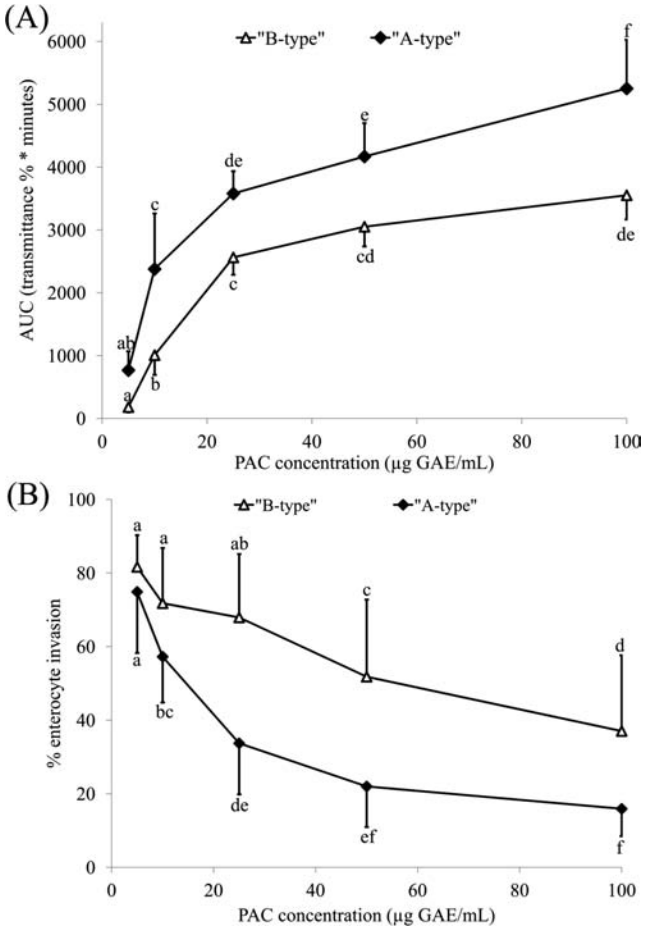

Figure 4. (A) Area under the curve obtained for the agglutination assay of *E. coli* 5011 for increasing concentrations of apple and cranberry PAC, expressed in μg GAE/mL. The results are expressed as the average of three independent assays ± standard deviation. Different letters correspond to significant differences at $p < 0.05$. (B) Dose−response curves on the effect of PAC extracted from apples and cranberries on the ability of *E. coli* to invade Caco-2 cells, expressed in μg GAE/mL, as quantified by the Folin−Ciocalteu method. Different letters correspond to significant differences at $p < 0.05$.

Invasion Assay. In the current study, we compared the ability of "A-type" and "B-type" PAC to inhibit invasion of gut epithelial cells by ExPEC. The results showed that both "A-type" and "B-type" PAC were able to significantly inhibit ExPEC invasion of Caco-2 cells in a dose-dependent manner (Figure 4B). However, "A-type" PAC produced significantly greater inhibition in comparison to "B-type" PAC. ExPEC invasion was reduced by 7, 15, 34, 30, and 21% for 5, 10, 25, 50, and 100 μg GAE/mL, respectively, when "A-type" were compared to "B-type" PAC.

The shape of the dose−response curve indicated that for "A-type" PAC, a plateau is attained at concentrations of 50 μg GAE/mL (Figure 4B). The curve for "B-type" PAC did not plateau, suggesting that this class of PAC required a higher concentration to reach a level of inhibition similar to that of "A-type" PAC.

The results of the two-way ANOVA model showed that the greater inhibitory effect of "A-type" PAC was statistically significant except for the lowest concentration (Figure 4B). Because every assay was run on a different day, we tested the effect of day within PAC treatment, and no significant differences of the dose−response curves were found.

DISCUSSION

MALDI-TOF MS Characterization of PAC. The goal of this work was to compare the effect of "A-type" with "B-type" PAC on ExPEC agglutination and invasion of gut epithelial cells. To determine the difference between "A-type" and "B-type" PAC we chose apples because this fruit contains only "B-type" PAC,[27] with catechin/epicatechin monomers, which yielded a MALDI-TOF MS spectrum with excellent baseline resolution.

PAC are oligomers of flavan-3-ols that have variable chain lengths.[23] There are two common series of procyanidin dimers. The "B-type" series are dimers linked in either the C4−C6 or C4−C8 position,[28] whereas the "A-type" series are dimers linked in the C4−C8 position with an additional C2−*O*−C7 ether linkage (Figure 2). PAC oligomers with a DP >2 may contain both "A-type" and "B-type" interflavan bonds. Therefore, for the purpose of discussing differences between PAC oligomers from cranberries and apples, cranberry PAC that contain one or more "A-type" interflavan bonds in their structure are referred to as "A-type" PAC, whereas apple PAC that contain only "B-type" interflavan bonds are referred to as "B-type" PAC.[28]

Analytical methods such as MALDI-TOF MS are routinely used to characterize unique structural features of PAC.[23−26,28−32] An understanding of the natural abundance of C, H, and O isotopes within proanthocyanidin oligomers allowed us to develop a novel MALDI-TOF-MS isotope deconvolution method.[18] We were able to quantify ratios of "A-type" to "B-type" interflavan bonds on the basis of theoretical isotope distributions by applying matrix algebra to the experimental spectra. In the context of this publication, MALDI-TOF MS methods were applied to provide both quantitative and qualitative assessment of proanthocyanidin structures.

Cranberry fruit (*Vaccinium macrocarpon* Ait.) has previously been shown to contain PAC that predominately include one or more "A-type" interflavan bonds.[23,33] Apple fruit (*Malus pumila* cv. 'Fuji') conversely has been shown to contain PAC that predominately contain all "B-type" interflavan bonds.[27]

Agglutination and Inhibition of Enterocyte Invasion. Bacterial agglutination, a bacterium-to-bacterium interaction, corresponds to an increase in concentration of bacteria in a limited area of the human body. This phenomenon can inhibit bacterial growth, cause structural damage to bacteria,[34] and increase bacterial clearance by macrophages and other phagocytic cells, potentially leading to a decrease in enteroctye invasion by ExPEC. We developed an agglutination assay to compare cranberry "A-type" PAC to apple "B-type" PAC. This assay is fundamentally different from the antiadherence assay that evaluates the ability of bacteria to adhere to uroepithelial cells based on the similarity of receptors on the uroepithelium with P blood group antigens.[26] Cranberry PAC inhibit this specific adhesion at low concentrations. Our new method allowed us to measure the effect of PAC with different structural characteristics on ExPEC agglutination over time and at low concentrations and demonstrated that cranberry "A-

type" PAC have greater agglutination activity than apple "B-type" PAC.

The results suggest that the direct effect of PAC on ExPEC agglutination is related to the specific inhibition in the red blood cell antiadherence assay because "A-type" PAC appear to have greater activity than "B-type" PAC. The ExPEC strain used in our agglutination study expresses both type 1 and P fimbriae. The red blood cell antiadhesion assay is based on the specific interaction of P-fimbriated *E. coli* with the Gal-Gal receptor on red blood cells that express the P blood group antigens.[26] Cranberry "A-type" PAC inhibit the adhesion of P-fimbriated *E. coli* to these red blood cells and thus prevent agglutination. The "B-type" PAC do not have activity in this assay. In contrast, both types of PAC have bioactivity in our agglutination assay, although cranberry "A-type" PAC showed greater activity than apple "B-type" PAC. Because strain 5011 expresses both type 1 and P fimbriae along with several other virulence factors, our results suggest that interactions of PAC with ExPEC surface virulence factors that lead to agglutination may result from specific binding of "A-type" PAC to P fimbriae and nonspecific binding to other proteins on the bacterial surface that can be mediated by both "A-type" and "B-type" PAC.

In vivo, bacterial invasion of gut epithelial cells provides a mechanism by which pathogens are protected from complements, antibodies, and other immune defense molecules, which in turn allows the pathogens to colonize and persist in the gut.[35,36] We developed an in vitro cell culture assay of bacterial invasion to assess the ability of compounds and immune factors to interfere with this mechanism of gut colonization. Proanthocyanidin concentrations used in this work are physiologically relevant because these concentrations in the gut are obtainable after the ingestion of a single serving of cranberry juice, which contains approximately 36 mg of PAC. If there was instantaneous mixing in the gut, then PAC concentration would be 7.2 μg/mL, assuming that gut volume is approximately 5000 mL (36 mg/5000 mL = 7.2 μg/mL). However, instantaneous mixing is impossible and PAC are poorly or not absorbed. Therefore, the concentration of PAC in the chyme would be much higher following ingestion and passage.

In summary, the results indicate that exposure of ExPEC to PAC consisting of either "A-type" or "B-type" interflavan linkages significantly produces bacterial agglutination and inhibits invasion of gut epithelial cells in a physiologically relevant dose-dependent manner. "A-type" PAC were observed to be significantly more effective in causing agglutination and reducing invasion when compared to "B-type" PAC at equivalent concentrations. Furthermore, it is known that the exposure of "A-type" PAC from cranberries to *E. coli* CFT073, a highly virulent uropathogenic strain, down-regulates *fliC* gene expression, which is responsible for flagellin expression, the major protein in bacterial flagellum, reducing bacterial motility[37] and compromising adherence to enterocytes. Our results suggest that "A-type" PAC act in a manner similar to opsonization of pathogens by secretory immunoglobulin A, which may also agglutinate bacteria, inhibit invasion of enterocytes, increase intestinal clearance, and promote killing by immune cells.[38]

This work provides a new insight on the specificity of the interaction PAC interflavan bond type with bacterial virulence factors highlighting the importance of this area of research in the context of understanding the mechanism by which "A-type" PAC prevent UTI by inhibiting gut colonization by ExPEC. This new understanding of proanthocyanidin structure/bioactivity relationships can be applied to develop a clinically relevant hypothesis of how proanthocyanidin-containing fruits, juices, botanicals, and dietary supplements can be used to develop therapeutic strategies against ExPEC.

AUTHOR INFORMATION

Corresponding Author

*(J.D.R.) Phone: +1 (608) 263-4310. Fax: +1 (608) 262-5157. E-mail: jdreed@wisc.edu.

Funding

This research was funded by the National Institute of Food and Agriculture, U.S. Department of Agriculture, ID WIS01519; the Reed Research Group Multi-Donor Fund; and Complete Phytochemical Solutions, LLC. R.P.F. is the recipient of a BD fellowship (SFRH/BD/73067/2010) from Fundação para a Ciência e a Tecnologia, Portugal.

Notes

The authors declare the following competing financial interest(s): Jess D. Reed and Christian G. Krueger have ownership interest in Complete Phytochemical Solutions, LLC and in full disclosure their affiliation with this company is acknowledged in the author affiliation.

ACKNOWLEDGMENTS

We thank the United Cranberry Growers Cooperative for providing cranberry samples, Mark Dufek for providing apple samples, Peter Crump for statistical consulting, and Dr. Walt Hopkins for kindly providing *E. coli* strain 5011.

REFERENCES

(1) Russo, T. A.; Johnson, J. R. Medical and economic impact of extraintestinal infections due to *Escherichia coli*: focus on an increasingly important endemic problem. *Microb. Infect.* **2003**, *5*, 449−456.

(2) Johnson, J. R.; Russo, T. A. Extraintestinal pathogenic *Escherichia coli*: "the other bad *E. coli*". *J. Lab. Clin. Med.* **2002**, *139*, 155−162.

(3) Wiles, T. J.; Kulesus, R. R.; Mulvey, M. A. Origins and virulence mechanisms of uropathogenic *Escherichia coli*. *Exp. Mol. Pathol.* **2008**, *85*, 11−19.

(4) Howell, A. B.; Reed, J. D.; Krueger, C. G.; Winterbottom, R.; Cunningham, D. G.; Leahy, M. A-type cranberry proanthocyanidins and uropathogenic bacterial anti-adhesion activity. *Phytochemistry* **2005**, *66*, 2281−2291.

(5) Foo, L. Y.; Lu, Y.; Howell, A. B.; Vorsa, N. A-Type proanthocyanidin trimers from cranberry that inhibit adherence of uropathogenic P-fimbriated *Escherichia coli*. *J. Nat. Prod.* **2000**, *63*, 1225−1228.

(6) Guay, D. R. Cranberry and urinary tract infections. *Drugs* **2009**, *69*, 775−807.

(7) Howell, A. B. Bioactive compounds in cranberries and their role in prevention of urinary tract infections. *Mol. Nutr. Food Res.* **2007**, *51*, 732−737.

(8) Pappas, E.; Schaich, K. M. Phytochemicals of cranberries and cranberry products: characterization, potential health effects, and processing stability. *Crit. Rev. Food Sci. Nutr.* **2009**, *49*, 741−781.

(9) Tufenkji, N.; Rifai, O. J.; Harmidy, K.; Eydelnant, I. A. Cranberry derived proanthocyanidins can prevent pathogen invasion of kidney epithelial cells. *Food Res. Int.* **2010**, *43*, 922−924.

(10) Harmidy, K.; Tufenkji, N.; Gruenheid, S. Perturbation of host cell cytoskeleton by cranberry proanthocyanidins and their effect on enteric infections. *PLoS One* **2011**, *6*, e27267.

(11) Plos, K.; Connell, H.; Jodal, U.; Marklund, B.-I.; Mårild, S.; Wettergren, B.; Svanborg, C. Intestinal carriage of P-fimbriated

Escherichia coli and the susceptibility to urinary tract infection in young children. *J. Infect. Dis.* **1995**, *171*, 625−631.
(12) Kaper, J. B.; Nataro, J. P.; Mobley, H. L. T. Pathogenic *Escherichia coli*. *Nat. Rev. Microbiol.* **2004**, *2*, 123−140.
(13) Russo, T. A.; Stapleton, A.; Wenderoth, S.; Hooton, T. M.; Stamm, W. E. Chromosomal restriction fragment length polymorphism analysis of *Escherichia coli* strains causing recurrent urinary tract infections in young women. *J. Infect. Dis.* **1995**, *172*, 440−445.
(14) Porter, M. L.; Krueger, C. G.; Wiebe, D. A.; Cunningham, D. G.; Reed, J. D. Cranberry proanthocyanidins associate with low-density lipoprotein and inhibit in vitro Cu^{2+}-induced oxidation. *J. Sci. Food Agric.* **2001**, *81*, 1306−1313.
(15) Feliciano, R. P.; Shea, M. P.; Shanmuganayagam, D.; Krueger, C. G.; Howell, A. B.; Reed, J. D. Comparison of isolated cranberry (*Vaccinium macrocarpon* Ait.) proanthocyanidins to catechin and procyanidins A2 and B2 for use as standards in the 4-(dimethylamino)cinnamaldehyde assay. *J. Agric. Food Chem.* **2012**, *60*, 4578−4585.
(16) Oszmiański, J.; Wojdyło, A.; Kolniak, J. Effect of L-ascorbic acid, sugar, pectin and freeze−thaw treatment on polyphenol content of frozen strawberries. *LWT − Food Sci. Technol.* **2009**, *42*, 581−586.
(17) Martin, K. R.; Krueger, C. G.; Rodriquez, G.; Dreher, M.; Reed, J. D. Development of a novel pomegranate standard and new method for the quantitative measurement of pomegranate polyphenols. *J. Sci. Food Agric.* **2009**, *89*, 157−162.
(18) Feliciano, R. P.; Krueger, C. G.; Shanmuganayagam, D.; Vestling, M. M.; Reed, J. D. Deconvolution of matrix-assisted laser desorption/ionization time-of-flight mass spectrometry isotope patterns to determine ratios of A-type to B-type interflavan bonds in cranberry proanthocyanidins. *Food Chem.* **2012**, *135*, 1485−1493.
(19) Nowrouzian, F. L.; Adlerberth, I.; Wold, A. E. Enhanced persistence in the colonic microbiota of *Escherichia coli* strains belonging to phylogenetic group B2: role of virulence factors and adherence to colonic cells. *Microb. Infect.* **2006**, *8*, 834−840.
(20) Lee, Y. M.; Dodson, K. W.; Hultgren, S. J. Adaptor function of PapF depends on donor strand exchange in P-pilus biogenesis of *Escherichia coli*. *J. Bacteriol.* **2007**, *189*, 5276−5283.
(21) Adlerberth, I.; Hanson, Å. L.; Svanborg, C.; Svennerholm, A. M.; Nordgren, S.; Wold, A. E. Adhesins of *Escherichia coli* associated with extra-intestinal pathogenicity confer binding to colonic epithelial cells. *Microb. Pathogenesis* **1995**, *18*, 373−385.
(22) Strohalm, M.; Kavan, D.; Novak, P.; Volny, M.; Havlicek, V. mMass 3: a cross-platform software environment for precise analysis of mass spectrometric data. *Anal. Chem.* **2010**, *82*, 4648−4651.
(23) Reed, J. D.; Krueger, C. G.; Vestling, M. M. MALDI-TOF mass spectrometry of oligomeric food polyphenols. *Phytochemistry* **2005**, *66*, 2248−2263.
(24) Krueger, C. G.; Vestling, M. M.; Reed, J. D. Matrix-assisted laser desorption/ionization time-of-flight mass spectrometry of heteropolyflavan-3-ols and glucosylated heteropolyflavans in sorghum [*Sorghum bicolor* (L.) Moench]. *J. Agric. Food Chem.* **2002**, *51*, 538−543.
(25) Krueger, C. G.; Dopke, N. C.; Treichel, P. M.; Folts, J.; Reed, J. D. Matrix-assisted laser desorption/ionization time-of-flight mass spectrometry of polygalloyl polyflavan-3-ols in grape seed extract. *J. Agric. Food Chem.* **2000**, *48*, 1663−1667.
(26) Howell, A. B.; Reed, J. D.; Krueger, C. G.; Winterbottom, R.; Cunningham, D. G.; Leahy, M. A-type cranberry proanthocyanidins and uropathogenic bacterial anti-adhesion activity. *Phytochemistry* **2005**, *66*, 2281−2291.
(27) Ohnishi-Kameyama, M.; Yanagida, A.; Kanda, T.; Nagata, T. Identification of catechin oligomers from apple (*Malus pumila* cv. 'Fuji') in matrix-assisted laser desorption/ionization time-of-flight mass spectrometry and fast-atom bombardment mass spectrometry. *Rapid Commun. Mass Spectrom.* **1997**, *11*, 31−36.
(28) Krueger, C.; Reed, J.; Feliciano, R.; Howell, A. Quantifying and characterizing proanthocyanidins in cranberries in relation to urinary tract health. *Anal. Bioanal. Chem.* **2013**, *405*, 4385−4395.
(29) Krueger, C. G.; Vestling, M. M.; Reed, J., D. Matrix-assisted laser desorption-ionization time-of-flight mass spectrometry of anthocyanin-poly-flavan-3-ol oligomers in cranberry fruit (*Vaccinium macrocarpon*, Ait.) and spray-dried cranberry juice. In *Red Wine Color*, 1st ed.; American Chemical Society: Washington, DC, 2004; Vol. 886, pp 232−246.
(30) Afaq, F.; Saleem, M.; Krueger, C. G.; Reed, J. D.; Mukhtar, H. Anthocyanin- and hydrolyzable tannin-rich pomegranate fruit extract modulates MAPK and NF-kappa B pathways and inhibits skin tumorigenesis in CD-1 mice. *Int. J. Cancer* **2005**, *113*, 423−433.
(31) Neto, C. C.; Krueger, C. G.; Lamoureaux, T. L.; Kondo, M.; Vaisberg, A. J.; Hurta, R. A. R.; Curtis, S.; Matchett, M. D.; Yeung, H.; Sweeney, M. I.; Reed, J. D. MALDI-TOF MS characterization of proanthocyanidins from cranberry fruit *Vaccinium macrocarpon* that inhibit tumor cell growth and matrix metalloproteinase expression in vitro. *J. Sci. Food Agric.* **2006**, *86*, 18−25.
(32) Li, C.; Leverence, R.; Trombley, J. D.; Xu, S.; Yang, J.; Tian, Y.; Reed, J. D.; Hagerman, A. E. High molecular weight persimmon (*Diospyros kaki* L.) proanthocyanidin: a highly galloylated, A-linked tannin with an unusual flavonol terminal unit, myricetin. *J. Agric. Food Chem.* **2010**, *58*, 9033−9042.
(33) Foo, L. Y.; Lu, Y.; Howell, A. B.; Vorsa, N. The structure of cranberry proanthocyanidins which inhibit adherence of uropathogenic P-fimbriated *Escherichia coli in vitro*. *Phytochemistry* **2000**, *54*, 173−181.
(34) Pal'tsyn, A. A.; Kolokol'chikova, E. G.; Badikova, A. K.; Chervonskaya, N. V.; Grishina, I. A. The role of agglutination in bacterial infection. *Bull. Exp. Biol. Med.* **1999**, *127*, 1−4.
(35) Lamont, R. J. *Bacterial Invasion of Host Cells*; 1st ed.; Cambridge University Press: New York, 2004; p 344.
(36) Pierre, J. F.; Heneghan, A. F.; Meudt, J. M.; Shea, M. P.; Krueger, C. G.; Reed, J. D.; Kudsk, K. A.; Shanmuganayagam, D. Parenteral nutrition increases susceptibility of ileum to invasion by *E. coli*. *J. Surg. Res.* **2013**, *183*, 583−591.
(37) Hidalgo, G.; Chan, M.; Tufenkji, N. Cranberry materials inhibit *Escherichia coli* CFT073 *fliC* expression and motility. *Appl. Environ. Microbiol.* **2011**, *77*, 6852−6857.
(38) Novak, N.; Haberstok, J.; Bieber, T.; Allam, J.-P. The immune privilege of the oral mucosa. *Trends Mol. Med.* **2008**, *14*, 191−198.
(39) Foo, L. Y.; Lu, Y.; Howell, A. B.; Vorsa, N. A-Type proanthocyanidin trimers from cranberry that inhibit adherence of uropathogenic P-fimbriated *Escherichia coli*. *J. Nat. Prod.* **2000**, *63*, 1225−1228.

NOTE ADDED AFTER ASAP PUBLICATION

There were errors in Figures 3 and 4, and the first paragraph of the Bacterial Agglutination Assay section of the version of this paper published November 18, 2013. The correct version published February 21, 2014.

despite their complex Acn profile, blueberries do not contain pelargonidin (Pel) and contain only about 6% peonidin (Peo).[17−19] Considering the complex in vivo metabolism reported for C3g alone,[7,8,15] the diverse array of blueberry Acn significantly complicates the study of their bioavailability.

A significant limitation in the study of Acn metabolism is that pure standards of Acn metabolites are not commercially available. Our current knowledge of Acn in vivo metabolism is based almost entirely on the MS/MS detection of parent and daughter fragments for predicted Acn metabolite(s) (AcnM). The AcnM concentration is then estimated on the basis of the MS signal of the 3-glucoside of the corresponding anthocyanin, whereas the actual MS response of Acn phase II metabolites is unknown. Recent Acn bioavailability studies may benefit from improvements in more modern LC-MS technology that allow the concurrent scanning of large numbers of predicted mass transitions using multiple reaction monitoring (MRM). Earlier technology allowed for the scanning of perhaps 10 or fewer mass transitions, due to limitations in scan rate.

This clinical study examines qualitatively and quantitatively urinary Acn before and then for 24 h following the ingestion of blueberry juice (BJ). Although the urinary disposition of Acn reflects only one aspect of the fate of Acn in vivo, their measurement was an effective means to examine the metabolism and excretion of the complex array of Acn that are found in blueberries. LC-MS scanning for a large number of Acn phase II metabolites revealed new aspects of the in vivo metabolism of Acn, which are relevant in clinical research.

MATERIALS AND METHODS

Study Design. Seventeen normal, healthy volunteers (ages 24−60 years, 13 women, 4 men) entered the study with informed consent (clinicaltrials.gov identifier NCT01789359). Prior to the study, participants completed an Acn intake questionnaire to estimate their typical consumption of various Acn-containing foods (Table 1) over the previous 8 weeks. Intake was measured in total servings per week, with 1 serving size equal to half a cup of fruit or a 6 oz glass of pure juice, 100% juice blend, or red wine.

Table 1. Foods Containing Anthocyanins (Acn) That Were Included in a Prestudy Acn Intake Questionnaire and for Diet Restrictions during the Study[a]

food category	sample foods
berries	acai berry; blackberry; blueberry; chokeberry; cranberry; elderberry; lingonberry; raspberry; red or black cherries; red or black currants; red or black grapes; strawberry
other fruits	blood orange/red orange; pomegranate; red or black plums; red-fleshed peach; red-skinned apple
vegetables	blue or purple tomatoes; eggplant; purple carrot; purple corn; purple sweet potato; red-leaf lettuce; red onion; red potato; red radish; red, purple, or black olives
grains and pulses	red or black rice
beverages	blueberry juice; cranberry juice/cocktail; fruit punches (blends with grape ± strawberry ± blueberry, etc.); grape juice; herbal teas (with red/blue/purple fruits); red wine
other	products that contain red/blue/purple fruits including yogurt, bakery products, jams and jellies, trail mix

[a]Participants reported their intake in servings where one serving was 1/2 cup (113 mL) of food or 6 oz (177 mL) of beverage. Intake scores included more than once daily; once daily; four or five times weekly; two or three times weekly, less than once weekly.

During the trial participants abstained from all Acn-containing foods except for wild BJ as specified. Compliance was monitored by self-reporting questionnaires, and participants were encouraged to document when any other Acn-containing foods had been consumed. For the first 5 days, participants consumed no Acn-containing foods (Table 1). The next day, volunteers consumed 250 mL of single-strength BJ containing 216 mg of C3g equivalents. The nonacylated Acn profile of wild blueberry is discussed in this study on the basis of three studies.[17−19]

Chemicals. Acetonitrile, methanol, and formic acid were LC-MS Optima grade and purchased from Fisher Scientific (Mississauga, ON, Canada). Trifluoroacetic acid (TFA) was purchased from Sigma-Aldrich Canada Co. (Oakville, ON, Canada). Petunidin 3-*O*-glucoside was purchased from WUXIAPPTEC Co. Ltd. (Tainjin, People's Republic of China). All other Acn glycosides were purchased from Indofine Chemical Co. (Hillsborough, NJ, USA) and were >95% pure.

Urine Collection. After the 5 day Acn-free run-in, participants provided a sample of their urine before, and then for the next 24 h after, drinking BJ. For each void, the entire urine volume was collected by the participant by using a graduated basin that fit over the toilet seat. The total urine volume was recorded, and then approximately 3.5 mL of urine was transferred using a disposable pipet into a labeled cryo-vial. Cryo-vials contained TFA to stabilize Acn so that the final TFA concentration in the ±3.5 mL of urine was about 0.29−0.43 M. Samples were immediately refrigerated and stored there for ≤8 h before transfer to −80 °C.

Sample Preparation for LC-MS. In preparation for solid phase extraction (SPE) samples were thawed in a 35 °C water bath, vortexed briefly, and then centrifuged at 14000 rpm (4 °C) for 10 min to remove any particulates. An aliquot of 500 μL of urine was diluted with 500 μL of 0.1% TFA. For SPE a positive pressure manifold (Waters Ltd., Mississauga, ON, Canada) was used in conjunction with microelution plates (Oasis HLB μelution plates (30 μm) 2 mg cartridges (Waters Ltd.)). The microelution wells were preconditioned with 200 μL of methanol and 200 μL of 0.1% TFA. The 1 mL diluted urine sample was loaded into the microelution well in two 500 μL aliquots and then washed with 200 μL of 5% methanol in 0.1% TFA. The remaining bound materials, including Acn, were desorbed from SPE into collection plates using 25 μL of 0.1% TFA in methanol followed by 100 μL of 1.2% acetonitrile−2% formic acid in water. Recovery (%) of urine samples spiked with Acn 3-glycoside standards ranged from an average of 70% for peonidin 3-glucoside to 87% for petunidin 3-glucoside (data not shown).

Calibration standards were the 3-glucoside of the six common anthocyanidins and were run before and after every 18 samples, which was every 24 h. The six Acn 3-glucoside levels included 0 and 1×, 2×, and 8× concentrations. The concentration of the stock solution for each Acn 3-glucoside varied depending on its MS response and its relative abundance in urine in representative samples. The 8× stock concentration ranged from 86 ng/mL for Del to 1720 ng/mL for Pet. A calibration level at 12× was run but not used in quantitation because it fell outside the linear portion of the signal response to concentration.

HPLC-ESI-MS/MS Analysis. A 25 μL volume of the diluted methanolic SPE eluent was injected onto a PFP Kinetix 2.6 μm column (2.1 × 50 mm) (Phenomonex, Torrance, CA, USA), and analytes were separated using an Ultimate 3000 HPLC (Dionex, Mississauga, ON, Canada). Column temperature was 55 °C, and flow rate was 600 μL/min. Solvent A was 2% HFo, and solvent B was 2% HFo−90% acetonitrile. The gradient program was as follows: 0−1 min, 1.2% B; 1−31 min, 1.2−21.2% B; 31−37 min, 21−100% B; 37−42 min, 100% B; 42−44 min, 100−1.2% B; 44−52 min, 1.2% B. The LC was coupled to an ABSciex QTrap 4000 (Toronto, ON, Canada) linear ion trap and using a Turbospray (ABSciex) electrospray ionization (ESI) source, which offers unit mass resolution (i.e., ±0.5 amu). The ESI/MS, which was carried out in positive ion mode, parameters were as follows: gas 1 and 2, 60 psi; temperature, 700 °C; curtain gas, 25 psi; declustering potential, 65 V; entrance potential, 10 V; collision energy, 26 V; and collision cell exit potential, 17 V. Tandem mass spectrometry (MS/MS) was carried out for 60 MRM corresponding to parent Acn (PAcn) that were found in BJ and predicted AcnM. Also, an MRM for phospholipid (184/184) was monitored (Table 2). Peaks were named on the basis of their signal arising for a given MRM and at a given retention time (RT).

Table 2. Mass Transitions ((*m*/*z*) Total/Fragment) Monitored[a]

		Cyn	Del	Mal	Pel	Peo	Pet	total
Glu	standard	448.9/287.1	465.0/303.1	493.3/331.2	433.1/271.0	463.2/301.1	479.0/317.1	6
Gal	standard	449.0/287.0	464.5/303.3	493.0/330.9		463.2/301.0	478.9/317.1	5
Ara	standard	419.0/287.1	435.0/303.0	463.2/331.0		433.0/301.1	448.8/317.1	5
di-Glu	standard	611.1/449.1		655.2/331.1				2
Glu/Gal	glucuronide	625.0/287.0	641.0/303.0	669.0/331.0	609.0/271.0	639.1/301.1	655.1/317.1	6
Glu/Gal	methyl glucuronide	639.0/301.0	655.0/317.0	683.0/345.0	623.0/285.0	653.0/315.0	669.1/331.1	6
Glu/Gal	methyl	463.0/301.0	479.0/317.0	507.0/345.0	447.0/285.0	447.0/315.0	493.1/331.1	6
Glu/Gal	sulfate	529.0/286.0	545.0/302.0	573.0/330.0	513.0/270.0	543.0/300.0	559.1/316.1	6
aglycone		287.0/137.0	301.0/283.0	331.0/204.0	271.0/271.0	301.0/284.0	317.1/317.1	6
aglycone	glucuronide	463.0/287.0	479.0/303.0	507.0/331.0	447.0/271.0	477.1/301.1	493.1/317.1	6
aglycone	methyl glucuronide	477.0/301.0	493.0/317.0	521.0/345.0	461.0/285.0	491.0/315.0	507.1/331.1	6
phospholipid	184/184							
							total	61

[a]Cyn, cyanidin; Del, delphinidin; Mal, malvidin; Pel, pelargonidin; Peo, peonidin; Pet, petunidin; Glu, glucose; Gal, galactose; Ara, arabinose.

LC-MS/MS Signal Quantitation and Statistical Analysis. Raw LC-MS data were filtered to remove all peaks with signal-to-noise ratio (S/N) of <10. Peaks with S/N of ≥10 were integrated and statistically analyzed using Genstat.[20] In the statistical analysis Acn were denoted either as PAcn or as an AcnM. Peaks denoted PAcn were 18 Acn glycosides that were monitored using pure standards (Table 2) so that LC-MS signals with a matching RT and mass transition (MRM) were denoted PAcn. All other MRM signals were denoted AcnM. For each anthocyanidin, only the 3-glucoside was used for quantification of all signals.

RESULTS

LC-MS Analysis. Results of four kinds of urine samples are reported. Three of these urine samples were based on a single void: (1) urine before intake (Pre-BJ); (2) the first void after BJ intake; and (3) the last void before 24 h. The fourth sample, 24hB, was urine that was blended proportionally from each void (1 μL/mL) during the 24 h after BJ. Results are reported as Acn concentration (ng/mL) in urine to best illustrate the continuous excretion of Acn before and after BJ. For convenience, the Acn are named for their equivalent common anthocyanidin; however, these Acn may also include their positional isomers and/or chalcones that give rise to the same parent and daughter fragment mass.

A sample chromatogram (Figure 1) illustrates typical signal strength of selected Acn MRM as well as the phospholipid signal (184/184) that led to MS signal dampening. Phospholipids were detected as distinct peaks and as a high baseline throughout the entire chromatographic profile. The Acn 3-glucosides used for calibration were run in a urine matrix to attempt to control for this signal-dampening effect.

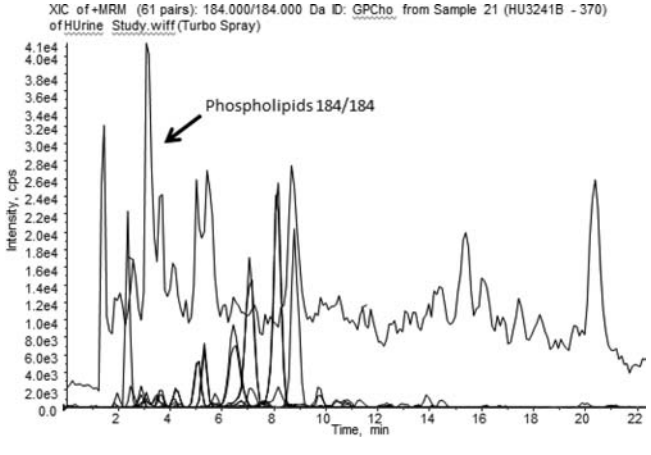

Figure 1. Representative LC-MS chromatogram showing phospholipids (184/184) in urine samples after solid phase extraction.

Total Urinary PAcn and AcnM before and after BJ Ingestion. Before BJ was ingested, and after participants had abstained from all Acn-containing foods for 5 days, the PAcn (i.e., 18 Acn glycosides) were present in urine at a low total concentration of 20.26 ± 6.536 ng/mL (Table 3). In the first urine void after BJ ingestion, which occurred on average 2.48 h after BJ intake, the concentration of PAcn was 20-fold greater (416.7 ± 92.38 ng/mL). Then over the following 24 h, the total urinary PAcn remained on average 17 times greater than Pre-BJ (Table 3). Given the BJ Acn dose of 216 mg of C3g equivalents and that the mean 24 h urine volume for the 17 participants was 620 mL, 0.0752% of the PAcn in the BJ could be accounted for after 24 h. In the final void of the 24 h period, the PAcn concentration (20.97 ± 4.089 ng/mL) was essentially the same as it was Pre-BJ (Table 3). Compared to PAcn, the AcnM concentration was substantially greater in all urine samples (Table 3). Even before BJ intake, the urinary AcnM concentration was 6.6 mg/mL, which increased to 7.6 mg/mL in the 24hB urine. In the 24hB urine 95.7% of the total Acn concentration was AcnM, whereas the PAcn made up only 4.3%.

There was no correlation between the Pre-BJ urinary total Acn (PAcn plus AcnM) concentration of the 17 participants and their questionnaire response regarding typical food Acn intake or their compliance during the 5 day Acn-free run-in (Figure 2). Also, the urinary Acn concentration of two participants who reported drinking their BJ one day too soon was not different from that of the other 15 participants who were compliant (Figure 2).

Individual Urinary PAcn and AcnM before and after BJ Ingestion. Compared to the urine Pre-BJ, the first void after BJ had a PAcn concentration greater by Cyn, 45-fold; delphinidin (Del), 4.7-fold; malvidin (Mal), 30-fold; Peo, 22-fold; and petunidin (Pet) 37-fold. The PAcn concentration in the first void after BJ ranged between 2-fold greater (Del) and 1.05-fold greater (Mal) (Table 3) than in the 24hB. No Pel glycosides were detected in any urine sample.

In all urine samples there was a far greater concentration of AcnM for each of the six anthocyanidins compared to their

Table 3. Concentration in Urine of Anthocyanin Parent Compounds (PAcn) and Anthocyanin Metabolites (AcnM)[a]

anthocyanin		before blueberry juice (ng/mL)	first void after blueberry juice (ng/mL)	24 h blended urine (ng/mL)	last void at 24 h (ng/mL)
cyanidin	PAcn	0.665 (±0.4605)	30.37 (±6.763)	21.22 (±2.008)	0.2059 (±0.1138)
	AcnM	806.1 (±81.25)	823.3 (±123.1)	1216.0 (±84.62)	763.0 (±100.4)
delphinidin	PAcn	7.086 (±2.748)	33.64 (±6.049)	17.57 (±1.767)	2.952 (±0.9124)
	AcnM	939.3 (±164.7)	881.7 (±172.8)	1094.0 (±170.5)	1344.0 (±409.3)
malvidin	PAcn	7.236 (±3.785)	219.7 (±49.08)	207.1 (±22.36)	10.03 (±3.18)
	AcnM	310.8 (±89.29)	397.3 (±54.23)	352.2 (±25.93)	380.6 (±87.52)
pelargonidin	PAcn	0	0	0	0
	AcnM	1975 (±612.2)	1571 (±674.6)	1205 (±224.5)	1551 (±751.5)
peonidin	PAcn	3.956 (±1.34)	89.46 (±22.51)	67.04 (±6.099)	7.062 (±0.7454)
	AcnM	809.3 (±107.9)	511.2 (±99.56)	873.1 (±69.93)	581.9 (±79.43)
petunidin	PAcn	1.157 (±0.6474)	43.46 (±9.413)	29.64 (±3.283)	0.7229 (±0.3377)
	AcnM	1762.0 (±245.3)	1360 (±176.5)	1701.0 (±138.4)	1323.0 (±156.5)
total	PAcn	20.26 (±6.536)	416.7 (±92.4)	342.6 (±63.44)	20.97 (±4.089)
	AcnM	6602 (±845.5)	5544 (±953.4)	7588 (±1752)	5944 (±1308)

[a]Values are the mean for the n = 17 participants ± standard error of the mean. Results are shown for four urine samples: (1) before blueberry juice (BJ); (2) first urine void after ingestion of 216 mg of cyanidin 3-glucoside equivalents in BJ; (3) urine blended from all voids for 24 h after BJ; and (4) last urine void in 24 h.

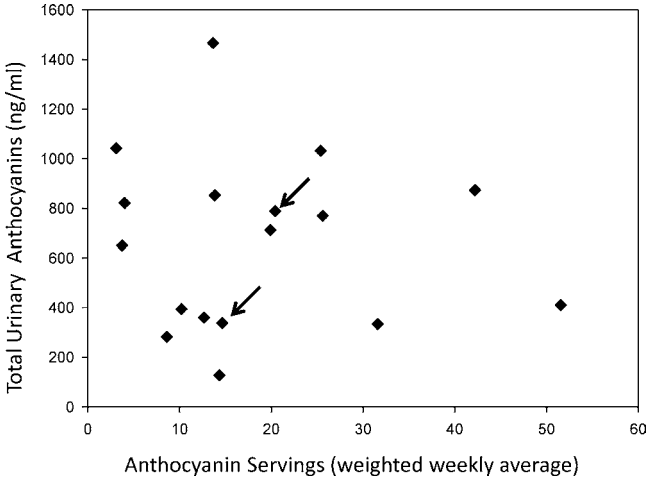

Figure 2. Relationship between typical anthocyanin (Acn) intake based on questionnaire results for 17 participants and their total urinary Acn concentration after 5 days with no dietary Acn. Arrows indicate participants (2) who drank their blueberry juice 24 h too early, after only a 4-day Acn-free run-in.

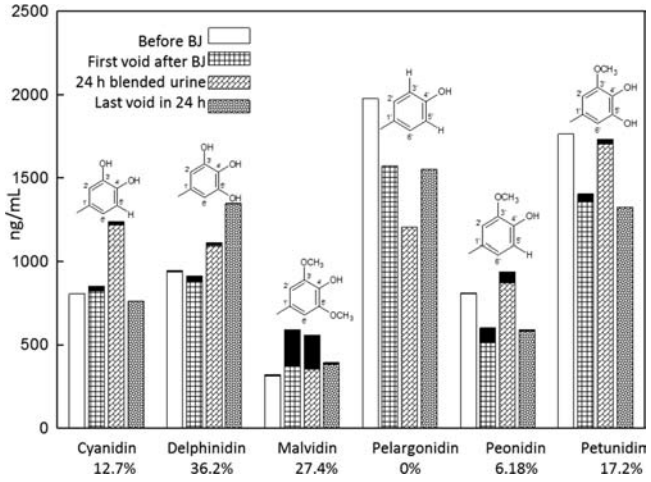

Figure 3. Total anthocyanin (Acn) concentration (ng/mL) in urine samples obtained after 5 days free of dietary Acn and before ingestion of blueberry juice (BJ); in the first void after BJ; in the 24 h blended urine, and in the final urine void after 24 h. Parent Acn are shown in solid black. Values and standard errors are in Table 4. The contribution of each anthocyanidin (%) to the total found in wild blueberry juice is also shown.

PAcn. In the 24hB the AcnM concentration exceeded that of PAcn by around 60-fold for Cyn, Del, and Pet and by about 13-fold for Peo. However, in 24hB the concentration of Mal AcnM was only 1.7-fold greater than that of Mal PAcn (Table 3; Figure 3). The intake of BJ had a relatively small effect on the AcnM concentration for each anthocyanidin. Compared to Pre-BJ, the AcnM concentration in the 24hB urine was 50% greater for Cyn, but 37% lower for Pel. In 24hB compared to Pre-BJ, the increase in AcnM concentration was 16% or less for Del, Mal, Pet, and Peo.

Changes in the total concentration of each anthocyanidin after BJ ingestion were due almost entirely to changes in their AcnM concentration (Table 3; Figure 3). The total Acn concentration in the first void after BJ was actually lower than before BJ for Pel (−20%), Peo (−26%), and Pet (−20%). In fact, the Pel concentration (which was all Pel AcnM) was greatest in the Pre-BJ compared to urine after BJ ingestion. Cyn and Del were similar in that their total Acn in the Pre-BJ and in the first void after BJ urine were roughly the same (Table 3; Figure 3). The total Cyn concentration (PAcn and AcnM) was greatest in the 24hB, whereas the Del concentration was 20% greater in the last void than in the 24hB. Similarly, the Pel concentration was 29% greater in the last void as compared to the 24hB (Figure 3). Among the four urine samples and the six anthocyanidins, Mal had the lowest total Acn concentration and the greatest proportion of Acn as PAcn (Table 3; Figure 3).

The relative proportion of the anthocyanidins was different in urine compared to BJ (Figure 3). Most striking was Pel, which is not found in BJ, but was a particularly abundant AcnM. Similarly, Mal made up 27% of the total Acn in BJ, but its total concentration among the urine samples was the lowest for all anthocyanidins (Figure 3).

Types of AcnM Observed in Urine over 24 h after BJ. In the 24hB urine from 17 individuals a total of 226 combinations of RT and mass transitions with S/N > 10 were observed for the six anthocyanidins (Table 4). Of these

dx.doi.org/10.1021/jf500107j | J. Agric. Food Chem. 2014, 62, 3926−3934

Table 4. Distribution and Concentration of Parent Anthocyanins (Acn) and Acn Metabolites in Urine Collected over 24 h after a Single Dose of Blueberry Juice and after a 5 Day Acn-Free Run-in[a]

anthocyanin		Cyn	Del	Mal	Pel	Peo	Pet	sum (ng/mL)	sum RT
parent Acn	RT	3	3	4	0	3	3		16
	ng/mL	21.2 ± 2.53	17.6 ± 2.21	207 ± 31.33	0.0	67.0 ± 8.86	29.6 ± 3.64	342.5	
aglycone	RT	2	4	0	12	8	15		41
	ng/mL	2.9 ± 1.05	167 ± 22.0	0.0	607 ± 87.7	9.4 ± 1.40	741 ± 74.2	1527	
aglycone glucuronide	RT	8	10	8	7	13	9		55
	ng/mL	694 ± 66.2	905 ± 290.2	261 ± 39.67	809 ± 530	641 ± 82.5	304 ± 47.6	3613.8	
aglycone methyl glucuronide	RT	6	9	7	8	13	11		54
	ng/mL	423 ± 49.8	234 ± 36.8	77.7 ± 39.67	640 ± 312	200 ± 26.3	485 ± 98.7	2059.1	
glycoside	RT	6	2	2	3	7	9		29
	ng/mL	40.8 ± 10.09	11.6 ± 2.04	2.1 ± 0.67	7.1 ± 1.09	22.3 ± 4.68	15.2 ± 1.87	99.1	
glycoside glucuronide	RT	0	0	1	1	0	1		4
	ng/mL	0.0	0.0	0.7 ± 0.18	0.6 ± 0.36	0.0	0.5 ± 0.15	1.8	
glycoside methyl glucuronide	RT	0	2	0	0	0	1		3
	ng/mL	0.0	0.3 ± 0.15	0.0	0.0	0.0	1.3 ± 0.19	1.6	
glycoside methyl	RT	3	5	2	5	0	4		19
	ng/mL	55.1 ± 6.30	39.6 ± 4.59	7.5 ± 2.28	24.9 ± 5.70	0.0	153.4 ± 22.17	280.5	
glycoside sulfate	RT	0	0	1	1	2	0		5
	ng/mL	0.0	0.0	3.8 ± 3.19	0.3 ± 0.10	0.6 ± 0.16	0.0	4.7	
total	RT	28	37	25	37	46	53		226
total	ng/mL	1237	1376	559.4	2088	940.0	1730	7930	

[a]RT corresponds to the number of retention times at which a given mass transition (MRM) was observed. Concentration (ng/mL) is based on the Acn 3-glucoside, and the sum is the concentration for each combination of MRM and retention time.

226, 18 signals corresponded to the PAcn that were also monitored using pure standards.

The aglycone forms of AcnM were almost 19-fold more abundant (ng/mL) than the glycoside-based AcnM (Table 4). Among the aglycones, glucuronide conjugates were in greatest abundance for all Acn except Pet. The aglycone methylated glucuronides were the second most abundant for Cyn, Del, Peo, and Pel (Table 4). The numbers of RT for the methylated aglycone and nonmethylated aglycone glucuronides were similar, differing by no more than two (Table 4). Together the Acn aglycones, their glucuronides, and their methyl glucuronides made up 91% of the total AcnM concentration. AcnM glycosides made up the remaining 9% of the total urinary AcnM observed in the 24hB. Of these AcnM glycosides, 72% were methylated conjugates (Table 4).

Interindividual Variation in AcnM Profiles. Interindividual variation in the profile of AcnM among the 17 participants was assessed specifically for Acn aglycone glucuronides, which were the most diverse (number of RT) and abundant (ng/mL) AcnM group (Table 4). There was no correlation between the mean concentration of any particular urinary Acn aglycone glucuronide and the number of participants in whom it was observed (Figure 4). Two Pel aglycone glucuronides were notable because of their comparatively high mean concentration. One of these Pel aglycone glucuronides was detected in eight participants; however, one participant contributed about 72% of the total amount measured for the eight. The same participant was responsible for 77% of the total amount of the other abundant Pel aglycone glucuronide that was found in 6 of the 17 participants. On the basis of the self-reporting, this participant complied with the dietary restrictions.

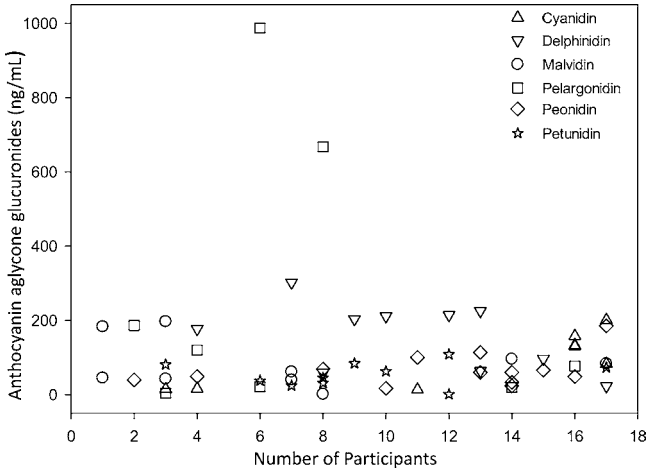

Figure 4. Concentration of anthocyanidin aglycone glucuronides and the number of the total 17 study participants in whom it was observed.

DISCUSSION

Figure 3 and Table 3 provide evidence of a large number of Acn xenobiotic metabolites that likely include early-stage Acn breakdown products and were present in urine both before and after BJ intake. The total concentration of these intermediates was many-fold greater than the concentration of Acn glycosides (i.e., PAcn) (Table 3) that have been the focus of most of the Acn bioavailability studies to date. The large array of AcnM-related MRM signals reported here likely constitutes the intermediates involved in the conversion of Acn to phenolic acids during digestive absorption.

In discussing the significance of these results it is important to consider the kind of evidence provided by LC-MS/MS using MRM. MRM cannot conclusively identify a given compound

unless a pure standard is available. And although the lack of Acn xenobiotic metabolite standards has been a significant obstacle, studies have nevertheless offered parent and daughter mass fragment data, often using MRM, as evidence of the occurrence of a given AcnM. Because berry anthocyanidins are differentiated by the number and arrangement of their B-ring hydroxyl and methoxy groups and because phase I and II metabolism can include hydroxylation and methylation of flavonoids,[21] LC-MS/MS investigation of in vivo anthocyanidin profiles and their xenobiotic metabolites is significantly complex (Figure 5). Also, at physiological pH in vivo formation of

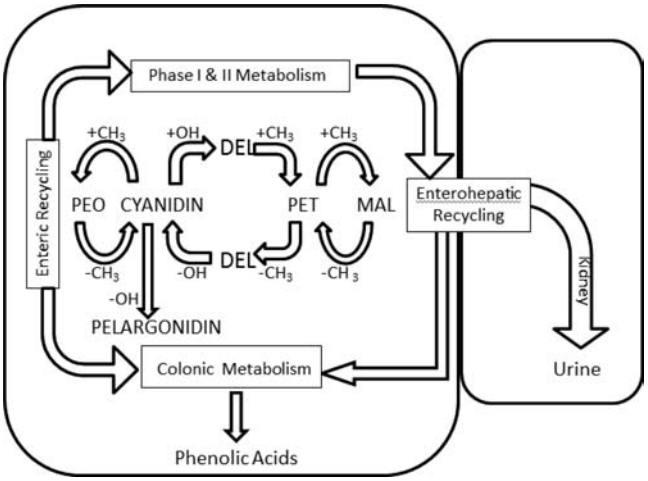

Figure 5. Schematic outline of anthocyanin interconversion in vivo due to xenobiotic and gut bacterial metabolism involving addition and removal of methyl and hydroxyl groups. Enteric and enterohepatic recycling will lead to isomeric modification before partitioning of anthocyanin metabolites into urine.

chalcones will occur due to the conversion of Acn to their quinoidal form, followed by A-ring opening and the addition of a hydroxyl group at carbon-9.[22] Even greater complexity in the suite of Acn-related in vivo metabolites occurs because phase II reactions can add conjugating groups at more than one site on the anthocyanidin, giving rise to positional isomers. Enterohepatic recycling of Acn conjugates, involving deconjugation and reconjugation with glucuronides, methyl, and possibly sulfate groups can add yet another level of chemical heterogeneity to the complex mixture of AcnM. For convenience, results of the current study are discussed in terms of the plant forms of Acn; however, the heterogeneous suite of AcnM MRM signals points to a complex array of isomeric forms of Acn and chalcone metabolites that arise from pH effects, phase I and II metabolism, and enterohepatic recycling. Aspects of these results are discussed in more detail below.

Abundance and Persistence of AcnM in Urine. The rise and fall in the concentration of PAcn over 24 h were similar to previously published results[1,4,23] as was the very low total recovery of PAcn in urine (0.0752%). In the present study total urinary PAcn concentration in 24hB increased by about 2.92 μmol/L (based on C3g equivalents) after BJ (Table 3), which was comparable to the study by Czank et al.,[8] who examined the fate of ^{13}C-labeled C3g in eight men. However, the present study also documented a very high relative concentration of AcnM in urine even before BJ intake. After BJ intake, the AcnM concentration was only 15% greater for the following 24 h than before BJ. In 24hB urine, the AcnM concentration exceeded that of PAcn by 22-fold.

The high basal level of urinary AcnM in the Pre-BJ urine even after 5 days of an Acn-free diet (Table 3; Figure 3) reflects the persistence of AcnM in the gastrointestinal tract. Flavonoid persistence in vivo has been previously reported and is suggestive of enterohepatic recycling (for review, see Wu et al.[21]). Young et al.[24] reported that after 1 week during which clinical participants (n = 5) avoided flavonoid-containing foods, quercetin was detected in the urine of all subjects, after urine samples were subjected to enzymatic deconjugation. In a recent study[25] quercetin aglycone was detected in baseline plasma samples of all participants (after treatment of plasma with deconjugating enzymes) after 3 days of a flavonoid-free diet. Even more striking was that after 6 weeks of a diet free of berries and low in flavonoids (average 2.6 mg of quercetin per day), quercetin (after deconjugation) was still detectable in human plasma.[26] In the present study the lack of a correlation between the typical Acn ingestion of study participants and their Pre-BJ urinary AcnM concentration (Figure 2) supported the notion that AcnM were persistent in vivo. Persistence of AcnM was also apparent when the total Pre-BJ Acn concentration of two participants who drank their BJ one day too early was indistinguishable from the other 15 participants Pre-BJ (Figure 2).

Aglycone and Glycoside AcnM. AcnM aglycones were 91% of the total AcnM in 24hB (Table 4), indicating that deglycosylation was a predominant event in the in vivo metabolism of Acn. Because the concentration of PAcn (18 Acn monoglycosides) was not substantially different between the first void after BJ and in the 24hB, it appears that Acn deglycosylation was rapid (Figure 3). However, the decline in glycosides after BJ ingestion will be investigated in the analysis of the individual voids that make up the 24hB (in progress). The similar concentration of PAcn in the Pre-BJ void and in the last void 24 h after BJ also suggests that Acn deglycosylation during the 24 h was complete.

Acn aglycones are reported to be chemically unstable at physiological pH,[1,11,27] but their predominance among the AcnM based on MRM signals suggests that they were relatively stable in vivo. However, Acn aglycone reactivity at physiological pH can lead to chalcone formation, and although chalcone bioavailability is not well-studied,[16] they have been suggested[14] to be more stable than their corresponding anthocyanidins in vivo. It has been suggested that the stability of Acn may be improved by their adsorption to other molecules (e.g., food matrix, bile acids).[28] In the present study this possibility is supported by the presence of phospholipids that were detected throughout the chromatographic profile (Figure 1) even after urine cleanup using SPE.

Glucuronides of Acn. Of the 91% of the total AcnM that were aglycones, 79% of these were conjugated to glucuronide groups (Table 4), supporting earlier reports[15,21,29−31] that glucuronidation of flavonoid aglycones constitutes a major route of flavonoid metabolism in vivo. The almost complete absence of urinary Acn glycoside glucuronides (Table 4) may be due to the fact that the phase II enzyme responsible for glucuronidation, uridine diphosphate glucuronosyl transferase (UGT), cannot easily accommodate flavonoid glycosides due to their size and polarity.[21]

The large number of Acn aglycone glucuronides observed (55 for the 6 anthocyanidins) may relate to the collectively broad substrate specificities of numerous UGT isoforms.[21]

Human UGT isoforms are localized in membranes of the small intestine, colon, and liver and may be coupled to efflux transporters to release glucuronides into the intestinal lumen, blood circulation, or bile.[21,32] UGT isoforms each have particular substrate affinities, so that the pool of glucuronides can include conjugates at various positions on the AcnM molecule. Our findings of positional isomers of AcnM support earlier studies.[7,9,15,33] Ichiyanagi et al.[15] detected 17 Cyn-based AcnM 4 h after feeding pure C3g to rats. Of these Cyn AcnM, 12 were Cyn glycoside conjugates and 8 were methylated conjugates and included 6 positional isomers of methylated C3g glucuronide.

The chromatographic elution of the multiple AcnM, including the predominant aglycone monoglucuronides, occurred over a wide range of RT (data not shown), which was also observed by Marczylo et al.[7] Whereas the RT of individual peaks would have been determined by chemical and structural features, their MS/MS signal at that RT indicated only an aglycone monoglucuronide. Therefore, multiple RT possessing the same MS/MS signal suggest a chemical and structural diversity that may be due to positional isomers of AcnM and chalcone conjugates. Adding to the apparent significant diversity of AcnM, chalcones can also occur as both cis and trans forms.[22] It is also possible that more complex Acn glucuronides may have been present, whereas the MRM detected only a remaining parent/daughter fragment. Related to this, Wu et al.[21] suggested that multiple glucuronidation events by UGT may be possible owing to multiple reactive hydroxyl groups on the flavonoid and ample space in the UGT binding pocket. Felgines et al.[9] report the occurrence of Cyn diglucuronide, and we have also detected diglucuronides of Acn aglycones in a subsequent reanalysis of the 24hB samples (data not shown). The association of AcnM with other matrix components[28] (e.g., phospholipid) may affect the RT of the MRM detected. The association of quercetin with mixed lipid micelles has recently been suggested to improve quercetin absorption when taken as part of a high-fat diet.[25]

Methylation of Acn. The number of methyl conjugates of Acn aglycones may reflect the substrate affinity of methylation enzymes, for example, catechol-*O*-methyl transferase. Related to this, quercetin 4-glucuronide was not subject to methylation in HepG2 cells, whereas quercetin 7-glucuronide and quercetin 3-glucuronide were.[34] The facts that methylated aglycone glucuronide conjugates made up about 36% of the total aglycone glucuronide pool and aglycone glucuronides made up about 72% of the total AcnM 24hB (Table 4) re-emphasize that glucuronidation of Acn aglycones was a major in vivo pathway for Acn conjugation. In their review, Wu et al.[21] indicate that small differences in the arrangement of OH and OCH_3 groups on flavonoids can affect the ease of glucuronidation by UGT.

Enterohepatic Recycling of AcnM. The presence and persistence of a large number of AcnM conjugate isomers (i.e., multiple RT for the same MRM) (Table 4) are due, at least in part, to their enteric and enterohepatic recycling. This recycling involves phase I and II conjugation of ingested compounds with hydroxyl, methyl, and glucuronide moieties, which occurs in the small intestine and liver. This is followed by the release of xenobiotic conjugates into the lumen of the small intestine or into hepatic and renal circulation and bile. Migration of these conjugates into the lower part of the small intestine and colon leads to their deconjugation by colonic bacteria. Hydrolyzed phase II conjugates can be reabsorbed through the colon and return to the small intestine or via the portal vein to the liver, where they can be reconjugated via phase I and II reactions.[21] Reconjugation at different reactive hydroxyls of AcnM gives rise to positional isomeric forms of AcnM. These recycling processes extend the half-life and overall bioavailability of parent compounds and their metabolites.[21,35] It is conceivable that novel anthocyanidin structures which were not predicted or monitored by MRM were also formed in vivo as part of enterohepatic recycling.

Effects of in Vivo Metabolism on the Anthocyanidin Profile. Anthocyanidins are distinguished by the number and position of their B-ring methoxyl and hydroxyl groups; therefore, apparent interconversions of anthocyanidins can occur due to methylation and hydroxylation during xenobiotic and bacterial metabolism (Figure 5) and based on MS/MS evidence. In phase I processes, cytochrome P450 isoforms can substitute hydroxyl groups and remove methyl groups from flavonoids,[21,31] whereas in phase II metabolism, methyl groups can be substituted at phenolic hydroxyls.[21,31] Therefore, the methylation of Cyn produces an Acn with the mass of Peo,[2] methylation of Del produces an Acn with the mass of Pet, and Pet methylation produces an Acn with the mass of Mal (Figure 5). Phase I hydroxylation of Cyn gives rise to an Acn with the mass of Del. In the colon dehydroxylation and demethylation can give rise to moieties with the parent mass of common anthocyanidins (Figure 5). Therefore, reactions catalyzed by both human and bacterial enzymes lead to Acn interconversion based on their detection by LC-MS/MS.

Chalcones have hardly been studied in relation to Acn bioavailability,[16] but are expected to be formed from Acn at physiological pH. Recyclization of cis forms of chalcones can occur to a limited degree at high temperatures and over time; however, trans forms are not subject to recyclization.[22] Of importance to this work is that chalcones are distinguished from their corresponding Acn by the addition of a hydroxyl at C-9.[22] Therefore, the chalcone formed from Cyn will have the mass of Del, the Pel chalcone will have the mass of Cyn, and the Peo chalcone will have the mass of Pet. Chalcones are also subject to xenobiotic metabolism[16] and in the present study probably contribute significantly to the large number of putative AcnM identified on the basis of MRM. Chalcones are intermediates in the formation of phenolic acids that become abundant after Acn intake.[14]

Acn interconversions help to explain the presence and predominance of Pel-based AcnM (Figure 3) when BJ does not even contain Pel. Pel may be considered an advanced catabolic Acn product, because its B ring possesses the least number of methyl and hydroxyl groups among the six common anthocyanidins. Therefore, progressive demethylation and dehydroxylation of the other five anthocyanidins favor the formation of an anthocyanidin with the mass of Pel (Figure 5). Pel has been noted in other studies as having a much greater apparent bioavailability than other Acn.[23,29,30,36] For example, Wu et al.[36] fed weanling pigs marionberry, in which Pel is <0.5% of the total Acn, and reported that Pel glucuronide had the highest percentage recovery in urine, exceeding the other marionberry AcnM by between 7 and 540 times. When strawberry doses were fed to humans, approximately 2% of the Pel in each strawberry dose was recovered in urine, well above the amount typically reported for other Acn, which is <0.1%.[1−3,29]

Xenobiotic and bacterial enzyme specificities may help to explain the relative amounts of Mal. Mal, which is 36% of the BJ Acn and the most methylated of the Acn (Figure 3), was

present in the lowest total concentration among the six anthocyanidins in all urine samples. The proportion of Mal PAcn to AcnM was much greater than for the other five anthocyanidins (Figure 3), suggesting that Mal conjugation was relatively impaired due to steric hindrance on the B-ring and that Mal demethylation to Pet was active. The concentration of Pet-based AcnM exceeded that of Mal-based AcnM by at least 3.4-fold, although in BJ, Mal exceeded Pet content by almost 2-fold (Figure 3).

The high concentration of AcnM in human urine supports the notion that Acn is more bioavailable than originally reported[1,8] and does not support the notion that in vivo Acn bioavailability is poor.[4,11] However, it must be qualified whether "in vivo bioavailability" pertains to PAcn only or PAcn plus AcnM. This distinction becomes important if AcnM are found to be bioactive. Phase II and other metabolites of polyphenolics can be bioactive;[31,37−39] therefore, the bioactivity of urinary AcnM reported here and the extent of their in vivo circulation are of key importance. Glucuronides of quercetin are antiangiogenic[37] and can affect human lung cancer cell growth in vitro.[39] The 5-*O*-glucuronide of epicatechin is a potent antioxidant in vitro like the native epicatechin.[31] Equol, a bacterial catabolite of soy isoflavones, has significantly greater estrogenic activity than the parent isoflavone in vitro and in animal models.[38]

This study helps to illustrate the nature of the in vivo intermediates arising from the intake of food Acn and before their conversion to phenolic acids. The continuous urinary excretion of a high concentration of AcnM even after 5 days of abstaining from dietary Acn should be considered in the design of Acn-related clinical trials. The persistence of AcnM in urine (Table 3; Figure 3) complicates interventions with Acn and the availability of compliance and noncompliance biomarkers of Acn intake.[5] However, retention of a high urinary concentration of AcnM suggests that systemic exposure to intact Acn moieties is significantly greater than previously thought.

AUTHOR INFORMATION

Corresponding Author

*(W.K.) Phone: (902) 365-8561. Fax: (902) 365-8455. E-mail: wilhelmina.kalt@agr.gc.ca.

Notes

The authors declare the following competing financial interest(s): This research was supported financially by Agriculture and Agri-Food Canada and the Wild Blueberry Association of North America.

ABBREVIATIONS USED

Acn, anthocyanin(s); AcnM, anthocyanin metabolite(s); BJ, blueberry juice; Cyn, cyanidin; C3g, cyanidin-3-glucoside; Del, delphinidin; ESI, electrospray ionization; Mal, malvidin; MRM, multiple reaction monitoring; PAcn, parent anthocyanin; Pel, pelargonidin; Peo, peonidin; Pet, petunidin; Pre-BJ, before blueberry juice; RT, retention time(s); TFA, trifluoroacetic acid; UGT, uridine diphosphate glucuronosyl transferase(s); 24hB, twenty-four hour blended urine

REFERENCES

(1) Manach, C.; Donovan, J. L. Pharmacokinetics and metabolism of dietary flavonoids in humans. *Free Radical Res.* **2004**, *38*, 771−785.

(2) Prior, R. L.; Wu, X. Anthocyanins: structural characteristics that result in unique metabolic patterns and biological activities. *Free Radical Res.* **2006**, *40*, 1014−1028.

(3) Manach, C.; Williamson, G.; Morand, C.; Scalbert, A.; Remesy, C. Bioavailability and bioefficacy of polyphenols in humans. I. Review of 97 bioavailability studies. *Am. J. Clin. Nutr.* **2005**, *81*, 230S−242S.

(4) Del Rio, D.; Borges, G.; Crozier, A. Berry flavonoids and phenolics: bioavailability and evidence of protective effects. *Br. J. Nutr.* **2010**, *104*, S67−S90.

(5) Spencer, J.; Abd El Mohsen, M.; Minihane, A.-M.; Mathers, J. Biomarkers of the intake of dietary polyphenols: strengths, limitations and application in nutrition research. *Br. J. Nutr.* **2008**, *99*, 12−22.

(6) Tsuda, T.; Horio, F.; Osawa, T. Absorption and metabolism of cyanidin 3-O-β-D-glucoside in rats. *FEBS Lett.* **1999**, *449*, 179−182.

(7) Marczylo, T.; Cooke, D.; Brown, K.; Steward, W.; Gescher, A. Pharmacokinetics and metabolism of the putative cancer chemopreventive agent cyanidin-3-glucoside in mice. *Cancer Chemother. Pharmacol.* **2009**, *64*, 1261−1268.

(8) Czank, C.; Cassidy, A.; Zhang, Q.; Morrison, D. J.; Preston, T.; Kroon, P. A.; Botting, N. P.; Kay, C. D. Human metabolism and elimination of the anthocyanin, cyanidin-3-glucoside: a ^{13}C-tracer study. *Am. J. Clin. Nutr.* **2013**, *97*, 995−1003.

(9) Felgines, C.; Talavera, S.; Texier, O.; Gil-Izquierdo, A.; Lamaison, J.; Remesy, C. Blackberry anthocyanins are mainly recovered from urine as methylated and glucuronidated conjugates in humans. *J. Agric. Food Chem.* **2005**, *53*, 7721−7727.

(10) Felgines, C.; Talavera, S.; Gonthier, M.; Texier, O.; Scalbert, A.; Lamaison, J.; Remesy, C. Strawberry anthocyanins are recovered in urine as glucuro- and sulfoconjugates in humans. *J. Nutr.* **2003**, *133*, 1296−1301.

(11) Fernandes, I.; Faria, A.; Calhau, C.; de Freitas, V.; Mateus, N. Bioavailability of anthocyanins and derivatives. *J. Funct. Foods* **2013**, 10.1016/j.jff.2013.05.010.

(12) Forester, S. C.; Waterhouse, A. L. Metabolites are key to understanding health effects of wine polyphenolics. *J. Nutr.* **2009**, *138*, 1824S−1831S.

(13) Nurmi, T.; Mursu, J.; Heinonen, M.; Nurmi, A.; Hiltunen, R.; Voutilainen, S. Metabolism of berry anthocyanins to phenolic acids in humans. *J. Agric. Food Chem.* **2009**, *57*, 2274−2281.

(14) Keppler, K.; Humpf, H. Metabolism of anthocyanins and their phenolic degradation products by the intestinal microflora. *Bioorg. Med. Chem.* **2005**, *13*, 5195−205.

(15) Ichiyanagi, T.; Shida, Y.; Rahman, M. M.; Hatano, Y.; Konishi, T. Extended glucuronidation is another major path of cyanidin 3-O-β-D-glucopyranoside metabolism in rats. *J. Agric. Food Chem.* **2005**, *53*, 7312−7319.

(16) Stalmach, A.; Mullen, W.; Pecorari, M.; Serafini, M.; Crozier, A. Bioavailability of C-linked dihydrochalcone and flavanone glucosides in humans following ingestion of unfermented and fermented rooibos teas. *J. Agric. Food Chem.* **2009**, *57*, 7104−7111.

(17) Kalt, W.; McDonald, J. E.; Ricker, R. D.; Lu, X. Anthocyanin content and profile within and among blueberry species. *Can. J. Plant Sci.* **1999**, *79*, 617−623.

(18) Prior, R. L.; Wilkes, S. E.; Rogers, T. R.; Khanal, R. C.; Wu, X.; Howard, L. R. Purified blueberry anthocyanins and blueberry juice alter development of obesity in mice fed an obesogenic high-fat diet. *J. Agric. Food Chem.* **2010**, *58*, 3970−3976.

(19) Gao, L.; Mazza, G. Quantitation and distribution of simple and acylated anthocyanins and other phenolics in blueberries. *J. Food Sci.* **1994**, *59*, 1057−1059.

(20) Payne, R. W.; Murray, D. A.; Harding, S. A.; Baird, D. B.; Soutar, D. M. *Genstat for Windows Introduction*, 12th ed.; VSN International: Hemel Hempstead, UK, 2009.

(21) Wu, B.; Kulkarni, K.; Basu, S.; Zhang, S.; Hu, M. First-pass metabolism via UDP-glucuronosyltransferase: a barrier to oral bioavailability of phenolics. *J. Pharm. Sci.* **2011**, *100*, 3655−3681.

(22) Preston, N. W.; Timberlake, C. F. Separation of anthocyanin chalcones by high-performance liquid chromatography. *J. Chromatogr., A* **1981**, *214*, 222−228.

(23) Prior, R. L. Anthocyanins: understanding their absorption and metabolism. In *Flavonoids and Related Compounds: Bioavailability and*

Function; Spencer, J. P. E., Crozier, A., Eds.; CRC Press: Boca Raton, FL, USA, 2012; pp 79−92.
(24) Young, J. F.; Nielsen, S. E.; Haraldsdottir, J.; Daneshva, B.; Lauridsen, S. T.; Knuthsen, P.; Crozier, A.; Sandstrom, B.; Dragsted, L. O. Effect of fruit juice intake on urinary quercetin excretion and biomarkers of antioxidative status. *Am. J. Clin. Nutr.* **1999**, *69*, 87−94.
(25) Guo, Y.; Mah, E.; Davis, C. G.; Jalili, T.; Ferruzzi, M. G.; Chun, O. K.; Bruno, R. S. Dietary fat increases quercetin bioavailability in overweight adults. *Mol. Nutr. Food Res.* **2013**, *57*, 896−905.
(26) Erlund, I.; Freese, R.; Marniemi, J.; Hakala, P.; Alfthan, G. Bioavailability of quercetin from berries and the diet. *Nutr. Cancer* **2006**, *54*, 13−17.
(27) Mazza, G.; Miniati, E. *Anthocyanins in Fruits, Vegetables and Grains*; CRC Press: Boca Raton, FL, USA, 1993.
(28) McDougall, G.; Dobson, P.; smith, P.; Blake, A.; Stewart, D. Assessing potential bioavailability of raspberry anthocyanins using an in vitro digestion system. *J. Agric. Food Chem.* **2005**, *53*, 5896−5904.
(29) Carkeet, C.; Clevidence, B.; Novotny, J. Anthocyanin excretion by humans increases linearly with increasing strawberry dose. *J. Nutr.* **2008**, *138*, 897−902.
(30) El Mohsen, M. A.; Marks, J.; Kuhnle, G.; Moore, K.; Debnam, E.; Srai, S. K.; Rice-Evans, C.; Spencer, J. P. E. Absorption, tissue distribution and excretion of pelargonidin and its metabolites following oral administration to rats. *Br. J. Nutr.* **2006**, *95*, 51−58.
(31) Zhang, L.; Zuo, Z.; Lin, G. Intestinal and hepatic glucuronidation of flavonoids. *Mol. Pharmaceutics* **2007**, *4*, 833−845.
(32) Dreiseitel, A.; Oosterhuis, B.; Vukman, K. V.; Schreier, P.; Oehme, A.; Locher, S.; Hajak, G.; Sand, P. G. Berry anthocyanins and anthocyanidins exhibit distinct affinities for the efflux transporters BCRP and MDR1. *Br. J. Pharmacol.* **2009**, *158*, 1942−1950.
(33) Mullen, W.; Edwards, C.; Serafini, M.; Crozier, A. Bioavailability of pelargonidin-3-*O*-glucoside and its metabolites in humans following the ingestion of strawberries with and without cream. *J. Agric. Food Chem.* **2008**, *56*, 713−719.
(34) O'Leary, K. A.; Day, A. J.; Needs, P. W.; Mellon, F. A.; O'Brien, N. M.; Williamson, G. Metabolism of quercetin-7- and quercetin-3-glucuronides by an in vitro hepatic model: the role of human β-glucuronidase, sulfotransferase, catechol-O-methyltransferase and multi-resistant protein 2 (MRP2) in flavonoid metabolism. *Biochem. Pharmacol.* **2003**, *65*, 479−491.
(35) Jia, X.; Chen, J.; Lin, H.; Hu, M. Disposition of flavonoids via enteric recycling: enzyme-transporter coupling affects metabolism of biochanin A and formononetin and excretion of their phase II conjugates. *J. Pharmacol. Exp. Ther.* **2004**, *310*, 1103−1113.
(36) Wu, X. L.; Pittman, H. E.; Prior, R. L. Pelargonidin is absorbed and metabolized differently than cyanidin after marionberry consumption in pigs. *J. Nutr.* **2004**, *134*, 2603−2610.
(37) Donnini, S.; Finetti, F.; Lusini, L.; Morbidelli, L.; Cheynier, V.; Barron, D.; Williamson, G.; Waltenberger, J.; Ziche, M. Divergent effects of quercetin conjugates on angiogene. *Br. J. Nutr.* **2006**, *95*, 1016−1023.
(38) Liu, Z.; Hu, M. Natural polyphenol disposition via coupled metabolic pathways. *Expert Opin. Drug Metab. Toxicol.* **2007**, *3*, 389−406.
(39) Yang, J.-H.; Hsia, T.-C.; Kuo, H.-M.; Chao, P.-D. L.; Chou, C.-C.; Wei, Y.-H.; Chung, J.-G. Inhibition of lung cancer cell growth by quercetin glucuronides via G_2/M arrest and induction of apoptosis. *Drug Metab. Dispos.* **2006**, *34*, 296−304.

found in berry fruit play a fundamental role in the antioxidant, chemopreventive, and anti-inflammatory activities,[5] but in addition to anthocyanins, other phenolic compounds, such as ellagitannins and flavonols, seem to exert a protective role in carcinogenesis by reducing the bioavailability of carcinogens.[9] Many studies have also confirmed the influence of genotype on the phytochemical composition of strawberry fruit antioxidant capacity, so that it is possible to find new genotypes and cultivars producing fruit with higher contents of bioactive compounds, explore new genetic resources, or develop tailored breeding programs.[10−12]

The aim of this study was to analyze the potential antioxidant effects of freeze-dried strawberry powder, added to a semisynthetic and isoenergetic diet, on doxorubicin-induced oxidative stress in rats. The effect of freeze-dried strawberry powder was tested by comparing two strawberry cultivars originated by the strawberry breeding program of the university: Sveva and Adria. These two genotypes were selected after previous studies[10−12] that allowed the differentiation of their fruits according to the total antioxidant capacity (TAC) and the vitamin C and polyphenolics they contained: Sveva presents higher total antioxidant capacity, associated with a higher value of total polyphenol and vitamin C, whereas Adria shows higher values of anthocyanin contents but lower TAC.

MATERIALS AND METHODS

Chemicals. Doxorubicin was obtained as doxorubicin hydrochloride (2 mg/mL) from Sigma-Aldrich (St. Louis, MO, USA), as well as 2,2′-azinobis(3-ethylbenzothiazoline-6-sulfonic acid (ABTS) diammonium salt, potassium persulfate, Trolox ≥98.0%, ascorbic acid, dipotassium hydrogen phosphate, potassium dihydrogen phosphate, Folin−Ciocalteu reagent, sodium carbonate, gallic acid, potassium chloride (KCl), sodium acetate (NaAc), and hydrochloric acid (HCl). Ethanol of HPLC grade, phosphate buffer solution 10×, 2-thiobarbituric acid 0.8%, acetic acid 99.9%, 2′,7′-dichlorofluorescein (DCF) ≥90%, sucrose, Tris 10 mM, EDTA-Na, bovine serum albumin (BSA), succinic acid disodium salt hezahydrate, 5,5-dithiobis(2-nitrobenzoic acid) (DTNB), dinitrophenylhydrazine (DNPH), 1-chloro-2,4-dinitrobenzene (CDNB), heparin, carbonyl cyanide 4-(trifluoromethoxy)phenylhydrazone (FCCP), tetramethylphenylenediamine (TMPD), cyanidin-3-glucoside, pelargonidin-3-glucoside, quercetin-3-*O*-glucoside, and ellagic acid were also purchased from Sigma-Aldrich. Methanol and ethanol of ACS grade were purchased from Carlo Erba Reagenti, Milano, Italy, whereas $DCFH_2DA$, cell-permeant indicator for reactive oxygen species, was acquired from Molecular Probes, Invitrogen (Carlsbad, CA, USA). High-purity water (Milli-Q Water System, Millipore Corp., Bedford, MA, USA) was employed throughout.

Fruits and Fruit Analysis. Ripe fruits of Adria and Sveva cultivars were harvested from plants grown in an experimental open field in the Aso valley area (Italy), frozen at −20 °C, lyophilized by Labconco Freezone 12L model 78670 (Kansas City, MO, USA), and then kept under vacuum condition until milled with a Mixer B-400 (Büchi Labortechnik, Flawil, Switzerland). Samples of strawberry fruit powder were analyzed to determine their nutritional composition; each freeze-dried strawberry sample was assayed in triplicate for each parameter analyzed. The strawberry powder was kept under vacuum, in darkness, at a temperature of 4 °C until meal preparation.

Fruit analysis was carried out as illustrated in detail in our previous publications.[11,13] Briefly, TAC and total phenol (TPH) content of the strawberry fruits were measured spectrophotometrically, whereas vitamin C was quantified by reversed-phase HPLC.[12,13] Anthocyanin extraction and HPLC-MS/MS analysis were performed as previously described.[14] The HPLC-DAD/ESI-MS-driven analysis for the identification and quantification of phenolic compounds was performed through a Hewlett-Packard 1200 series liquid chromatography. The separation was achieved using a 150 mm × 4.6 mm i.d., 5 μm, Aqua C18 column (Phenomenex). The chromatographic conditions were similar to those previously described for anthocyanin determination.[14] Double online detection was carried out by the combined use of a DAD and an API 3200 Qtrap MS equipped with an ESI source and a triple-quadrupole ion trap mass analyzer (Applied Biosystems, Darmstadt, Germany) controlled by Analyst 5.1 software and connected to the HPLC system via the DAD cell outlet. Mass spectrometry data were acquired in the negative mode for all phenolic compounds except anthocyanins, which were acquired in positive mode. Anthocyanins were quantified using the external standards of cyanidin-3-glucoside (Cy-3-glucoside) and pelargonidin-3-glucoside (Pg-3-glucoside) (at 520 nm), flavonols as quercetin-3-*O*-glucoside (at 360 nm), ellagic acid and ellagic acid glycosides as ellagic acid (at 360 nm), and ellagitannins as gallic acid (at 280 nm). Each freeze-dried strawberry sample was assayed in triplicate for each parameter analyzed.

Experimental Design. Twenty-four male Wistar rats (*Rattus norvegicus*), initially weighing 110−130 g, were allocated in groups of three animals per box and maintained on a 12 h light/12 h darkness cycle, with free access to drinking water. Animals were match-fed for 16 weeks at 25 g/day on semisynthetic and isoenergetic diets according to the AIN93 criteria or an AIN93-modified diet supplemented with 10 g/100 g of strawberry lyophilized extract, as shown in Table 1, according to the method of Prior et al.[15] For the formulation of the diet supplemented with strawberry extract, the nutritional composition of the extract was considered according to the USDA database. The remaining energetic nutrients were recalculated to make both diets isocaloric. The rats were randomly assigned to four experimental groups of six animals as follows: two groups fed AIN93 diet, a group fed AIN93 diet supplemented with Adria strawberry powder, and a group fed AIN93 diet supplemented with Sveva strawberry powder. Food intake was indirectly monitored through the weekly body weight control and daily spillage monitoring.

Table 1. Composition of Control Diet and Contribution of Strawberry Daily Dose

	AIN-93M (groups C and C-DOX) (g/kg diet)	AIN-93M + strawberry (groups A-DOX and S-DOX)[a] (g/kg diet)
cornstarch	465.7	465.6
casein	140.0	133.0
dextrinized cornstarch	155.0	155.0
sucrose	100.0	30.0
soybean oil	40.0	34.0
fiber	50.0	33.1
mineral mix	35.0	35.0
vitamin mix	10.0	10.0
L-cystine	1.8	1.8
choline bitartrate	2.5	2.5
strawberry powder[b]	0.0	100.0

[a]Strawberry extract was made from the Adria variety for the A-DOX group and from the Sveva variety for the S-DOX group. [b]100 g of strawberry powder contains 7 g of protein, 6 g of fat, 70 g of carbohydrates, and 27.1 g of fiber. This was considered when in the formulation of the AIN-93M + strawberry diet to make both diets isocaloric.

At the end of the 16 weeks, rats were subjected to two intraperitoneal injections of 10 mg/kg/day DOX or saline solution with a 24 h gap between each injection, according to the method of Quiles et al.[16] Thus, experimental groups were organized as follows: C-group, animals fed AIN93 diet for 16 weeks and subjected to two intraperitoneal injections of saline solution 48 h before death; C-DOX group, animals fed AIN93 diet for 16 weeks and subjected to two intraperitoneal injections of DOX 48 h before death; A-DOX group, animals fed AIN93 freeze-dried Adria strawberry powder diet for 16 weeks and subjected to two intraperitoneal injections of DOX 48 h

Table 2. Fruit Nutritional Contents for Processed Fruit of Adria and Sveva Cultivars[a]

cultivar	TAC (mmol Trolox equiv/kg FW)	TPH (mg GAE/kg FW)	vitamin C (g ascorbic acid/kg FW)
Adria	18.08 ± 0.33b	1749.47 ± 48.31b	0.45 ± 0.02b
Sveva	19.67 ± 0.30a	2594.67 ± 54.59a	0.90 ± 0.08a

[a]Mean values followed by different letters are significantly different. Test SNK, $p \leq 0.05$.

before death; S-DOX group, animals fed AIN93 freeze-dried Sveva strawberry powder diet for 16 weeks and subjected to two intraperitoneal injections of DOX 48 h before death. At the end of the experimental period (24 h after the second intraperitoneal injection), animals were killed by cervical dislocation followed by decapitation at the same time of day to avoid any circadian fluctuation.

After decapitation, blood was collected by decantation onto glass tubes coated with lithium-heparin; isolated plasma and the "buffy coat", enriched in white cells, were removed, diluted 1:1 with RPMI-1640 medium, and layered onto an equivalent volume of Histopaque to obtain peripheral blood lymphocytes. Weights of the heart, liver, and right kidney were taken to evaluate the relative weight of organs (%) calculated as grams per 100 g of body weight. A part of the livers was homogenized on ice at 4 °C in 5 mM Tris-HCl buffer (pH 7.4) containing 1 mM EDTA, in a ratio (10%) of 1 g of wet tissue to 10 mL of buffer, using an IKA-Werk (Janke Kunkel, UE) homogenizer. After centrifugation at 9143 rpm for 20 min at 4 °C, the supernatant was kept; proteins were measured according to the Lowry procedure[17] using BSA as standard and then stored at −80 °C until analysis.

Animals were handled according to the guidelines of the Spanish Society for Laboratory Animals, and the investigation was approved by the Ethical Committees of the Ministry of Science and Technology and the University of Granada.

Evaluation of Rat Plasma Lipophilic Antioxidant Contents. Plasma levels of retinol and α-tocopherol were determined by reversed-phase HPLC as previously described[16] using a Spherisorb S5 ODS1 (Merck, Darmnstadt, Germany) column and ethanol/purified water 97:3 (v/v) as mobile phase. The HPLC system was a Beckman in-line diode array detector, model 168 (Fullerton, CA, USA), connected to a Waters (Milford, MA, USA) 717 plus autosampler. Determinations were performed at 325 nm for retinol and at 292 nm for α-tocopherol. Antioxidant molecules were identified by predetermining the retention times of individual standards and quantified through two calibration curves, daily prepared with known concentrations of retinol (0.1−1.7 μg/mL) and α-tocopherol (1.7−30.2 μg/mL) standards. Each measurement was repeated in duplicate, with two readings for each replicate.

DNA Double-Strand Break (Comet) Analysis. The comet assay was used to measure DNA double-strand breaks in peripheral blood lymphocytes as previously described.[18] Analysis was performed using a CCD camera and Komet 3.0 image analysis program (Kinetic Imaging Ltd., Liverpool, UK). The percent of DNA in the tail (mean of 100 comets per gel) is taken as a measure of DNA break frequency. The comet-like DNA formations were placed into five arbitrary classes (0−4) according to the extent of DNA damage represented by a comet-like "tail". Each comet was assigned a value according to its class, and the overall score for 100 comets ranged from 0 (100% of comets being class 0) to 400 (100% of comets in class 4). Each lymphocyte sample was assayed in duplicate, and 50 comets (i.e.,100 comets/sample) on two different slides were evaluated for every sample in each experiment.

Evaluation of Liver Biomarkers of Oxidative Stress. Protein carbonyl content was determined in liver homogenates by the DNPH method as described by Levine,[19] whereas the GSH content was determined through the DTNB assay as carried out by Ellman.[20] Liver lipid peroxidation was measured by the assay of thiobarbituric acid-reactive substances (TBARS) according to a standardized method,[21] whereas the oxide−xylenol orange (FOX2) method was used to determine hydroperoxides according to a method reported by Jiang.[22] Each measurement was repeated in duplicate, with two readings for each replicate.

Determination of Liver Antioxidant Enzyme Activity. Catalase activity (Cat) was measured following the method described by Aebi,[23] by monitoring H_2O_2 decomposition at 240 nm as a consequence of the catalytic activity of catalase. Superoxide dismutase (SOD) was determined according to the method of Kakkar,[24] on the basis of the inhibition of the formation of NADH−phenazine methosulfate−nitroblue tetrazolium formazan by SOD, measured by spectrophotometry at 540 nm. For glutathione peroxidase (GPx) measurement the method used[25] was based on the ability of GPx to remove H_2O_2 by coupling its reduction to H_2O with oxidation of reduced glutathione. Glutathione reductase (GRx) activity was assayed by using the modified method of Carlberg and Mannervik,[26] based on the capacity of GRx to reduce oxidized glutathione (GSSG) back to reduced glutathione (GSH). Glutathione transferase activity (GST) was determined according to the modified method described by Habig,[27] which measures the conjugation of CDNB with GSH, producing a dinitrophenyl thioether detected at 340 nm spectrophotometrically. Each measurement was repeated in duplicate, with two readings for each replicate.

Evaluation of Reactive Oxygen Species (ROS) in Liver Mitochondria. Liver mitochondria were isolated by differential centrifugation as previously described.[16] Mitochondria protein was measured according to the Lowry procedure[17] using BSA as standard.

ROS production by mitochondrial preparations was measured in fluorescence plate readers.[28,29] The results obtained are expressed as arbitrary fluorescence units (AFU) and are converted into nanomoles of ROS by linear regression method, using the DCF dilutions. Each measurement was repeated in duplicate, with two readings for each replicate.

Liver Mithocondrial Respiratory Efficiency. The oxygen consumption rate (OCR) in liver mitochondria was measured with an XF24 Extracellular Flux Analyzer (Seahorse Bioscience, Billerica MA, USA), as previously described.[27] The mitochondrial assay solution (MAS) consists of 70 mM sucrose, 220 mM mannitol, 10 mM KH_2PO_4, 5 mM $MgCl_2$, 2 mM HEPES, 1 mM EDTA, and 0.2% (w/v) fatty acid-free BSA, pH 7.2 at 37 °C. To minimize variability between wells, mitochondrial suspension were first diluted 10 times in cold MAS buffer to which was added 10 mM pyruvate, 2 mM malate, and 4 μM FCCP to achieve the final concentration of 10 μg of mitochondria in 50 μL of MAS solution. Then, 50 μL of the mitochondria diluted solution was delivered to each well (except for background correction wells) while the plate was on ice. The plate was then transferred to a centrifuge equipped with a swinging bucket microplate adaptor, and spun at 4089 rpm for 20 min at 4 °C. After centrifugation, 450 μL of MAS plus substrate was added to each well. The mitochondria were then placed at 37 °C for 10 min in the XF Prep Station incubator (Seahorse Bioscience). The plate was transferred to the XF24 instrument and the experiment initiated. Changes to the concentrations of dissolved oxygen in the media were measured for each 2 s interval by solid state sensor probes. After determination of the basal mitochondrial respiration, rotenone (2 μM), succinate (10 mM), antimycin A (4 μM), and ascorbate plus 1 mM TMPD (10 mM and 100 μM, respectively) were sequentially added to each well. Data are presented as the average of three replicates per well ± standard error. Results are expressed as OCR in picomoles of consumed oxygen per minute and were adjusted for protein concentration (pmol O_2/min/mg protein).

Statistical Analysis. Results are presented as the mean ± standard error (SE). One-way variance analysis was used to test the differences between genotypes, groups, and treatments. Statistically significant differences ($p \leq 0.05$) were determined with the SNK test. Pearson correlation was evaluated for fruit nutritional parameters and biological

assays. Statistical processing was carried out using STATISTICA software (Statsoft, Tulsa, OK, USA).

RESULTS

Strawberry Fruit Nutritional Composition. Fruit nutritional composition was analyzed on freeze-dried fruit (Table 2). Sveva freeze-dried powder presented a higher TAC value than Adria (19.67 vs 18.08 mmol Trolox equiv/kg FW, respectively) as well as higher phenols and vitamin C levels (Table 2), whereas Adria freeze-dried powder showed higher total anthocyanin contents (Table 3). The use of optimized HPLC conditions coupled to diode array and mass detection allowed detection of seven different anthocyanin pigments in freeze-dried strawberry fruits (Table 3). For both varieties, up to five pigments could be assigned to Pg derivates, and the major peak in the HPLC chromatograms corresponded to Pg-3-glucoside; one pigment could be identified as (epi)afzelechin-(4→8)-Pg 3-glucoside and the last one as a Cy derivative. Individual concentrations of the anthocyanin identified in the freeze-dried cultivars are shown in Table 3 with total concentrations of anthocyanin in samples of approximately 1331.52 ± 3.6 and 893.04 ± 2.3 mg/kg for Adria and Sveva, respectively.

Table 3. Identification and Quantification of Anthocyanin Pigments in Adria and Sveva Freeze-Dried Fruits

peak	identification	Adria cultivar (mg/kg)	Sveva cultivar (mg/kg)
1	(epi)afzelechin-(4→8)Pg-3-glucoside	3.798 ± 0.4	1.754 ± 0.1
2	Cy-3-glucoside	32.232 ± 2.1	25.974 ± 2.2
3	Pg 3,5-diglucoside	0.588 ± 0.0	0 ± 0.0
4	Pg 3-glucoside	1157.376 ± 12.0	790.234 ± 7.0
5	Pg 3-rutinoside	97.848 ± 4.0	26.176 ± 2.0
6	Pg 3-malonylglucoside	32.562 ± 3.0	45.62 ± 2.2
7	Pg 3-acetylglucoside	7.114 ± 4.0	3.284 ± 1.0
	total anthocyanin content	1331.518 ± 4.6	893.042 ± 2.3

With regard to flavonols, two compounds were identified and quantified as quercetin derivates and three as kaempferol derivates in both cultivars (Table 4), with total concentrations of flavonols in sample of about 2.10 ± 0.03 and 7.49 ± 2.0 mg/kg for Adria and Sveva, respectively. Quercetin-3-glucuronide was, in accordance with previous studies,[30] the most abundant flavonol in the two varieties, approximately 1 ± 0.0 and 3.5 ± 0.7 mg/kg in Adria and Sveva, respectively.

Table 4. Identification and Quantification of Total Flavonols, Total Ellagic Acid Conjugates, and Ellagitanins in Adria and Sveva Freeze-Dried Fruits

identification	Adria cultivar (mg/kg)	Sveva cultivar (mg/kg)
flavonols		
quercetin-3-hexose	0.48 ± 0.0	1.2 ± 0.3
quercetin-3-glucuronide	1.005 ± 0.0	3.5 ± 0.7
kaempferol-3-glucoside	0.21 ± 0.0	1.2 ± 0.3
kaempferol-3-glucuronide	0.413 ± 0.0	0.89 ± 0.3
kaempferol-3-malonylglucoside		0.74 ± 0.2
total	2.10 ± 0.03	7.49 ± 2.0
ellagic acid conjugates		
ellagic acid pentoside	0.55 ± 0.02	0.96 ± 0.1
ellagic acid deoxyhexoside	1.8 ± 0.3	6.9 ± 0.03
ellagic acid + ellagic acetyl rhamnoside	4.1 ± 0.5	10.9 ± 1.8
total	6.5 ± 0.1	18.7 ± 0.9
ellagitannins		
agrimoniin	21.4 ± 3.3	39.0 ± 3.0

An ellagic acid pentoside, an ellagic acid deoxyhexoside, and ellagic acid/ellagic acetyl rhamnoside were also detected and quantified in both strawberries (Table 4) with a total of ellagic acid conjugates of about 6.5 ± 0.1 and 18.7 ± 0.9 mg/kg in Adria and Sveva varieties, respectively. Finally, as previously reported,[31] a major ellagitannin pigment was identified as agrimoniin, with concentrations of 21.4 ± 3.3 mg/kg in Adria and 39.0 ± 3.0 mg/kg in Sveva (Table 4). Although proanthocyanidins have been previously identified and quantified in strawberries,[30] in our samples several minor peaks corresponding to these polyphenols were detected but not quantified because of their low concentration.

Hematological and Clinical Analysis. Data on body weight and organ ratios showed slight differences among rat groups but no significant variations were found, thus indicating that the strawberry diet did not interfere with animal development (Table 5) while sacrifice after doxorubicin injection occurred before any possible modification could be identified.

Evaluation of Rat Plasma Retinol and α-Tocopherol Content. Concerning plasma levels of retinol (Figure 1), the highest value were found in C group while the lowest in C-DOX group; freeze-dried strawberry supplementation buffered the decrease of retinol in A-DOX group and in S-DOX group ($p < 0.05$) compared to C-DOX group. Plasma α-tocopherol did not show differences among all groups, although higher values were obtained in rats fed with freeze-dried strawberries, both Adria and Sveva (Figure 1).

DNA Double-Strand Break Assays. The comet assay for the evaluation of DNA damage was performed on peripheral blood lymphocytes collected before and after DOX injection to evaluate DNA damage due to endogenous oxidative DOX-mediated stress and the efficacy of long-term freeze-dried strawberry diet in preventing such oxidative-induced damage.

Before the DOX injection, all groups showed similar base values of DNA damage, whereas after the DOX injection an increase of DNA damage was observed in all groups, but with different rates: indeed, as shown in Figure 2, comparing the variation of DNA damage values detected before and after the DOX injection, the lower increase of DNA damage was found in the C group, as expected for rats not submitted to DOX injection, whereas greater variation was observed in C-DOX and S-DOX groups. Freeze-dried Adria supplementation buffered the increase in DNA damage, as demonstrated by the lower increase ($p < 0.05$) in the A-DOX group compared to the C-DOX group.

Evaluation of Liver Biomarkers of Oxidative Stress. Table 6 shows the changes in liver biomarkers of oxidative stress. Treatment with DOX resulted in a significant increase in protein carbonyl levels (3.2-fold, $p < 0.05$) as well as a dramatic decrease in GSH levels (1.7-fold, $p < 0.05$) in the C-DOX group compared to the C group, whereas the supplementation with freeze-dried strawberry restored the condition of the C group in A-DOX and S-DOX groups, especially for protein carbonyl levels. Similar trends were observed in markers of lipid oxidation. A significant increase in TBARS concentration was in fact observed in the liver (2.0-fold, $p < 0.05$) of C-DOX rats, whereas in A-DOX and S-DOX groups, treatment with freeze-dried strawberry powders resulted in values similar to those of

Table 5. Body Weight and Organ Body Ratio of the Rat Groups Fed the Four Diets[a]

group[b]	body wt (g)	heart ratio (% of body wt)	liver ratio (% of body wt)	Rx kidney ratio
C	401.4 ± 19.9ns	0.29 ± 0.02ns	2.51 ± 0.15ns	0.31 ± 0.02ns
C-DOX	397.6 ± 15.8ns	0.26 ± 0.01ns	2.76 ± 0.05ns	0.31 ± 0.02ns
A-DOX	421.4 ± 7.1ns	0.26 ± 0.01ns	2.58 ± 0.07ns	0.27 ± 0.01ns
S-DOX	424.4 ± 15.1ns	0.27 ± 0.02ns	2.58 ± 0.05ns	0.27 ± 0.01ns

[a]Values are expressed as group mean values and SE; mean values followed by different letters are significantly different. Test SNK $p \leq 0.05$. ns, nonsignificant. [b]C group, AIN93 diet; C-DOX group, AIN93 diet + DOX; A-DOX group, AIN93 diet + 10% Adria strawberry fruit + DOX; S-DOX group, AIN93 diet + 10% Sveva strawberry fruit + DOX.

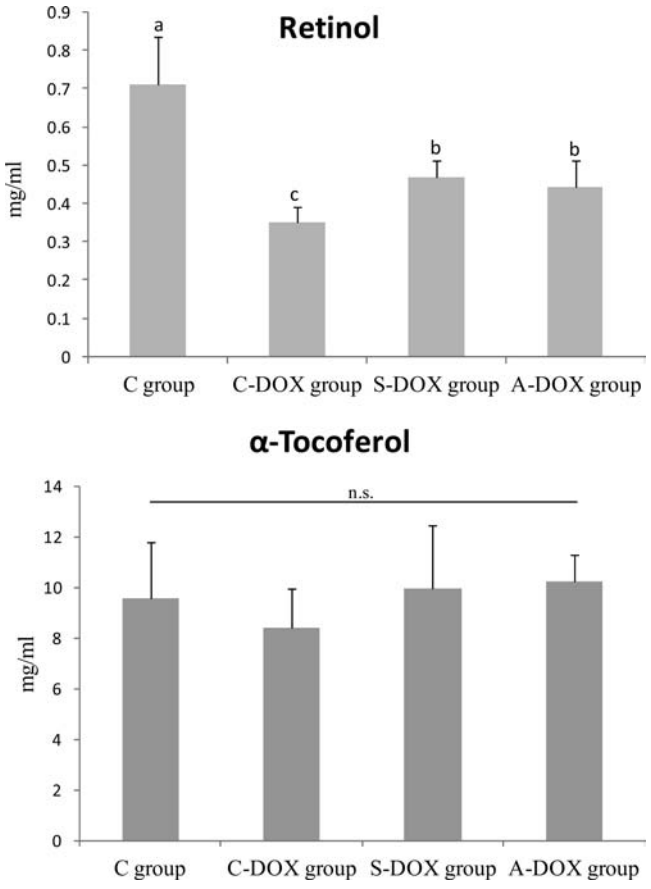

Figure 1. Effect of strawberry and DOX treatment on the plasma content of retinol and α-tocopherol. Results are expressed as the mean ± SE. Columns labeled with different letters are significantly different ($p < 0.05$). C group, AIN93 diet; C-DOX group, AIN93 diet + DOX; A-DOX group, AIN93 diet + 10% Adria strawberry fruit + DOX; S-DOX group, AIN93 diet + 10% Sveva strawberry fruit + DOX.

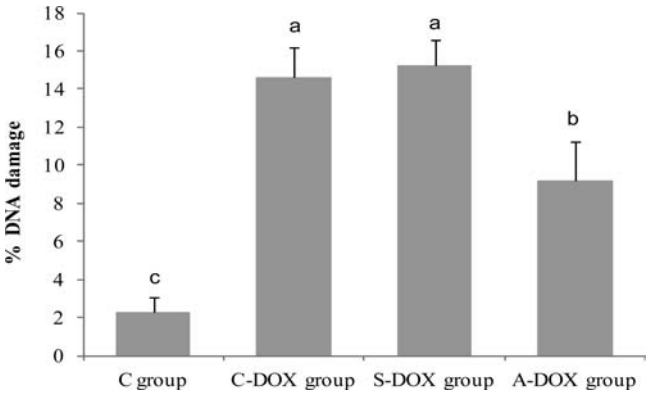

Figure 2. Percentage of DNA damage detected before and after DOX injection. Columns labeled with different letters are significantly different ($p < 0.05$). C group, AIN93 diet; C-DOX group, AIN93 diet + DOX; A-DOX group, AIN93 diet + 10% Adria strawberry fruit + DOX; S-DOX group, AIN93 diet + 10% Sveva strawberry fruit + DOX.

the C group. In the C-DOX group a significant increase (1.8-fold, $p < 0.05$) was outlined also for hydroperoxide levels, whereas supplementation with freeze-dried strawberry restored the condition of the C group only in the A-DOX group but not in the S-DOX group.

With regard to the activity of the antioxidant enzymes, a positive effect of freeze-dried strawberry-enriched diet on liver antioxidant enzymes was found (Table 7). GPx, GR, and GST activities were significantly decreased ($p < 0.05$) in the C-DOX group compared to the C group, whereas after xx months, freeze-dried strawberry supplementation significantly increased ($p < 0.05$) GPx, GR, and GST levels in the A-DOX and S-DOX groups compared to those of the C-DOX group, leading to values similar to those of control group. The same trends were found also for catalase and SOD activities (Table 7): they were significantly reduced ($p < 0.05$) in the C-DOX group when compared with control groups. Freeze-dried strawberry supplementation significantly ($p < 0.05$) increased the enzyme activities with respect to the C-DOX group, with values close to those of the C group, especially for the A-DOX group.

Liver Mitochondria Respiration Efficiency and ROS Contents. To examine the protection of strawberries on mitochondrial function against DOX-induced stress, we measured the OCR of isolated rat liver mitochondria. This experiment began assessing mitochondrial basal respiration in an uncoupled state (pyruvate, malate, and FCCP). After the measurement of basal OCR, the following compounds were sequentially added at four different fixed times: rotenone, succinate, antimycin A, and ascorbate plus TMPD. Injection of rotenone inhibited complex I and, as expected, respiration fell to a minimum in all groups (Figure 3a). Injection of succinate allowed the mitochondria to respire via complex II, bypassing complex I, so that OCR values increased. Indeed, A-DOX and S-DOX groups reached the maximal respiration rate (78.53 ± 0.9 and 81.50 ± 1.0 pmol O_2/min/protein, respectively) with a significant increase ($p < 0.05$) compared to the C group, whereas for the C-DOX group a significant decrease was found (40.39 ± 1.1 pmol O_2/min/protein). Electron flow was then inhibited at complex III level by the addition of antimycin A and, in fact, respiration stopped again as expected in all groups. Finally, addition of ascorbate and TMPD, which act as electron donors to complex IV, elicited a moderate increase in the OCR, especially in the A-DOX and S-DOX groups, although without any significant difference from the C-group except for C-DOX.

To assess if improved mitochondrial functionality observed in A-DOX and S-DOX groups could be due to lower mitochondrial ROS levels, we analyzed the ROS concentration

Table 6. Liver Changes in Protein and Lipid Markers of Oxidative Stress[a]

group[b]	GSH (nmol/mg protein)	protein carbonyl content (nmol/mg protein)	TBARS (nmol/mg protein)	hydroperoxides (nmol/mg protein)
C	164.39 ± 2.54a	7.65 ± 0.23b	0.46 ± 0.16b	11.42 ± 0.04c
C-DOX	96.13 ± 1.27c	24.33 ± 2.54a	0.90 ± 0.15a	20.4 ± 0.28a
A-DOX	139.85 ± 1.04b	8.74 ± 0.93b	0.37 ± 0.06b	12.22 ± 0.37bc
S-DOX	132.67 ± 0.34b	5.71 ± 1.15b	0.42 ± 0.01b	12.96 ± 0.05b

[a]Data are presented as means ± SE. Means belonging to the same set of data with different letters are significantly different ($p < 0.05$). ns, nonsignificant. [b]C, AIN93 diet; C-DOX group, AIN93 diet + DOX; A-DOX group, AIN93 diet + 10% Adria strawberry fruit + DOX; S-DOX group, AIN93 diet + 10% Sveva strawberry fruit + DOX.

Table 7. Changes in Liver Antioxidant Enzyme Activity[a]

group[b]	GST (nmol/min/mg protein)	GPx (nmol/min/mg protein)	GR (nmol/min/mg protein)	SOD (IU/mg protein)	catalase (IU/mg protein)
C	430.01 ± 3.95a	0.55 ± 0.04a	170.96 ± 5.75a	123.33 ± 1.81a	18.98 ± 1.52a
C-DOX	221.42 ± 27.49b	0.31 ± 0.03b	83.81 ± 4.61b	45.66 ± 0.05c	9.73 ± 0.78b
A-DOX	425.26 ± 33.43a	0.53 ± 0.07a	167.73 ± 6.02a	106.75 ± 2.68ab	19.90 ± 1.78a
S-DOX	424.02 ± 4.37a	0.52 ± 0.03a	164.13 ± 3.41a	89.18 ± 2.54b	19.40 ± 1.01a

[a]Data are presented as means ± SE. Means belonging to the same set of data with different letters are significantly different ($p < 0.05$). [b]C group, AIN93 diet; C-DOX group, AIN93 diet + DOX; A-DOX group, AIN93 diet + 10% Adria strawberry fruit + DOX; S-DOX group, AIN93 diet + 10% Sveva strawberry fruit + DOX.

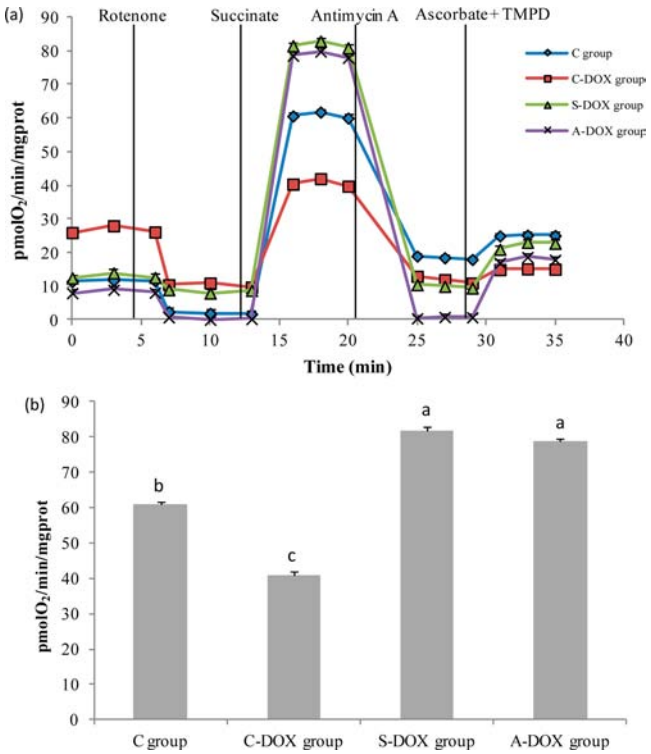

Figure 3. Effects of strawberry and DOX treatment on oxygen consumption in liver mitochondria of rats. (a) Mitochondria oxygen consumption was monitored with sequential injection of rotenone, succinate, antimycin A, and ascorbate/TMPD at the indicated time points into each well, after baseline rate measurement. (b) Average changes in mitochondrial OCR after succinate injection. Data are presented as means ± SEM (pmol/min). Columns labeled with different letters are significantly different ($p < 0.05$). C group, AIN93 diet; C-DOX group, AIN93 diet + DOX; A-DOX group, AIN93 diet + 10% Adria strawberry fruit + DOX; S-DOX group, AIN93 diet + 10% Sveva strawberry fruit + DOX.

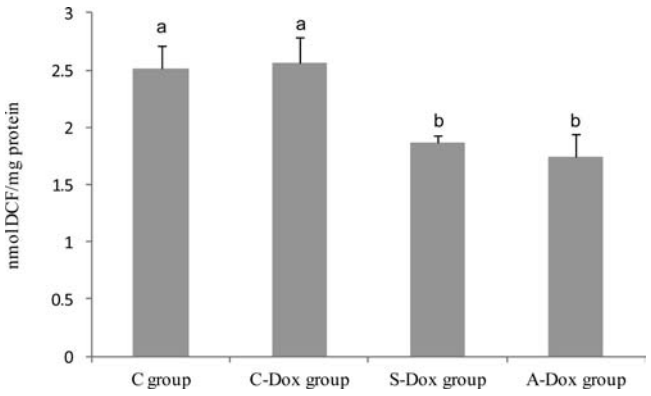

Figure 4. Effect of strawberry and DOX treatment on mitochondrial ROS concentration. Results are expressed as the mean ± SE. Columns labeled with different letters are significantly different ($p < 0.05$). C group, AIN93 diet; C-DOX group, AIN93 diet + DOX; A-DOX group, AIN93 diet + 10% Adria strawberry fruit + DOX; S-DOX group, AIN93 diet + 10% Sveva strawberry fruit + DOX.

in liver mitochondria (Figure 4). We found the highest values of ROS in mitochondria of the C-DOX group, although not significantly different from the C group (2.56 ± 0.2 and 2.50 ± 0.2 nmol DCF/mg protein, respectively), whereas the lowest values were found for groups fed Adria and Sveva fruits (1.74 ± 0.2 and 1.86 ± 0.1 nmol DCF/mg protein, respectively), highlighting that the lower the ROS mitochondrial levels are, the higher is the mitochondrial respiration.

DISCUSSION

This study evaluates the effect of a long-term diet supplemented with freeze-dried strawberry powder against DOX-induced oxidative stress in rats. AIN93 diet was supplemented with diverse freeze-dried strawberry powders of two cultivars with marked differences regarding fruit phenol and anthocyanin contents. In fact, fruits of Sveva cultivar possessed higher contents of phenols, vitamin C, and TAC than the fruits of Adria cultivar (Table 2), which instead possessed higher anthocyanin contents but lower vitamin C and TAC (Tables 2 and 3). The strawberry fruit quantity was related to a human diet, which considers a calorie intake of 2000 kcal/day: this means that it was equivalent to a substitution of 200 calories with strawberry fruit, calculated to correspond approximately to a quantity of 60 g of strawberry freeze-dried powder or, if expressed in anthocyanidins present in the

powder, 80 mg per day for the Adria-fed group and 54 mg per day for the Sveva-fed one (calculated on the results for nutritional compounds of freeze-dried strawberry of cv. Adria and Sveva in Table 3).

First, initial and final body weights of the rats were measured. There were no differences in final body weight (p = 0.38) between the treatment groups. It is known that increased liver weight is one symptom of toxicity; however, there were no statistically significant differences in mean liver weight per 100 g of body weight between treatment groups (p = 0.38), suggesting that strawberry supplementation did not affect the liver, as previously reported.[32] For plasma analysis, we observed a higher concentration of retinol in A-DOX and S-DOX groups than in the C-DOX group, suggesting that strawberry supplementation could increase the levels of this vitamin and could contribute to strengthen the antioxidant status of rat plasma. However, we did not observe any difference in α-tocopherol concentration among groups, but this result is consistent with the very low concentration of this vitamin in strawberries with respect to retinol.[5] Retinol and α-tocopherol have a high antioxidant capacity and play a key biological role, especially in protecting cells and tissues from oxidative damage, as well as membrane lipids and lipoproteins from peroxidation.[33] Some studies found that retinol significantly reduces lipid oxidation, providing good results in the heart, brain membranes, liver microsomes, and kidney,[32] and that it also possesses a protective dose-dependent effect against the chromosomal aberrations induced by doxorubicin in rat bone marrow cells.[34] Similarly, other studies showed that intraperitoneal vitamin E (100 mg/kg/day) for 8 days inhibits the general toxic and hepatotoxic effects of DOX and hepatotoxicity in rats, by decreasing malondialdehyde, glutathione peroxidase, and catalase activities.[35]

The freeze-dried strawberry supplementation seems to protect DNA from DOX-induced stress. Indeed, the evaluation of delta values of percentage damage before and after DOX injection showed that rats fed freeze-dried Adria cultivar, characterized by high anthocyanin contents, presented lower values of DNA damage among all other rat groups subjected to DOX injection, suggesting that a diet rich in anthocyanin is able to protect DNA against in vivo induced oxidative stress. In recent years many in vitro and in vivo studies have focused on the capacity of anthocyanins in protecting against DNA damage. For example, blueberry anthocyanin extracts were found to decrease ROS and DNA damage by tail moment of comet assay as well as to reduce gene and protein expression of p53, phospho-p53, and p21 in UV-irradiated HepG2 cells.[36] Similarly, an anthocyanin-rich strawberry extract was able to increase cell viability and decrease DNA damage in fibroblasts exposed to UV-A irradiation,[37] whereas cyanidin-3-glucoside (C3G) was found to prevent DNA fragmentation and procaspase-3 cleavage in UV-induced skin damage, very likely by blocking cellular oxidative stress-related events, in particular inflammation and apoptosis.[38] However, several in vivo studies have documented the presence of conflicting evidence. In studies with cranberry juice or black currant juice, no increase in protection from oxidative DNA damage was found,[39,40] nor was any damage found in a study involving women consuming a polyphenol-rich blueberry.[41] On the contrary, in another intervention study, consumption of a high-polyphenol juice determined a decrease in oxidative DNA damage,[42] whereas the intake of a mixture of blueberry and apple juices reduced the levels of H_2O_2-induced DNA damage after 4 weeks of supplementation in healthy female volunteers.[43] Some authors attribute this protection against DNA damage to different mechanisms that could involve pathways such as DNA repair and alkylation or formation of anthocyanin−DNA complexes and antioxidant enzymes.[44] Moreover, it can be considered that an anthocyanin-rich diet[45] indirectly acts on DNA protection through up-regulation expression of different genes involved in detoxification molecules,[46] even if this aspect seems to depend on the time of exposure to dietary components as mentioned previously.[47]

In the present work, the antioxidant capacity provided by the strawberry diet resulted also in enhanced protection of liver components such as proteins and lipids against oxidative stress. Liver protein carbonyls and TBARS/hydroperoxide levels were significantly increased (p < 0.05) by DOX injection in the C-DOX group, due to the ROS-induced production, demonstrating that the natural antioxidant defense mechanism to scavenge excessive free radicals has been compromised. The freeze-dried strawberry diet prevented this increase in A-DOX and S-DOX rats, because they showed values similar to those of the C group. The ability of strawberries to modulate the activity of hepatic antioxidant enzymes has been demonstrated in our study, too. We found that DOX administration resulted in a significant decrease in GSH concentration and in the activities of antioxidant enzymes GR, GPx, GST, SOD, and catalase in the C-DOX group compared to the C-group. The effects of DOX were partially reduced by freeze-dried strawberry diet, suggesting that the increase of GSH and endogenous antioxidant enzymes might be one of the important mechanisms of the strawberry against oxidative stress damage, as previously reported.[48]

Mitochondria are key targets in DOX toxicity, especially their inner membrane.[1] DOX can be metabolized into a lipophilic aglycone able to diffuse throughout the mitochondrial membrane, accumulating within it; this aglycone is the starting point for several reactions that release electrons, producing ROS and disturbing the functional integrity of membranes and of the respiratory chain.[1] In the present study, the treatment of rats with two doses of 10 mg/kg doxorubicin showed negative effects in liver mitochondria: in fact, the drug increased the total mitochondrial ROS concentration in C-DOX rats, whereas in A-DOX and S-DOX rats, supplementation with strawberry resulted in a decrease of ROS levels induced by DOX injection. To assess if the decrease of ROS, due to freeze-dried strawberry supplementation, could affect mitochondrial functionality, we performed the electron flow experiment to follow and interrogate each complex of the electron transport chain. As expected, respiration stopped with all of the inhibitor (rotenone and antimycin A) injection in all groups, whereas it rose with the injection of the electron donors, especially with succinate (Figure 3b) in S-DOX and A-DOX, demonstrating an improved functionality of the electron transport chain in rats fed strawberry. Interestingly, the extent of the increase was more relevant in the same groups that also presented lower ROS levels.

These results could be explained by the possible protection mechanisms of the strawberry: first of all, the well-known antioxidant capacity of the fruits to counteract, both in vitro and in vivo, oxidative stress[33,48] and then the interaction between polyphenols and membranes.[5] Indeed, from the results obtained in studies conducted to assess the potential of polyphenols to access the inner mitochondrial membrane,[49] it seems that mitochondria are able to absorb significant

concentrations of polyphenols. Once compartmentalized into the cell membranes, these substances seem to enhance membrane integrity and to protect the functional integrity of the mitochondrial respiratory chain.[50] Another possible mechanism of strawberries is the activation of the endogenous defense systems, mainly by the modulation of the expression of some antioxidant enzymes. Even if literature data report controversial results that can differ among the several types of cells or pathological conditions studied, it is reasonable to hypothesize that coordination of the endogenous and exogenous antioxidant response is achieved, at least in part, through antioxidant responsive elements (AREs), which are found in the promoters of many of the genes that are inducible by oxidative and chemical stress. For instance, an increasing number of studies indicate that the dietary polyphenols are able to stimulate the transcription of gene coding for antioxidant and phase II detoxifying enzymes, through selective activation of AREs sequences localized in specific gene promoters.[45]

In conclusion, our in vivo feeding trial on rats submitted to long-term diet supplemented with freeze-dried strawberry powders confirms the potential health benefits of strawberry fruit against oxidative stress; in fact, a reduction of physiological oxidative damage in rats was observed, and this protective effect was strictly linked to the bioactive composition of strawberry fruit. More studies have evidenced that the genotype plays a fundamental role in the phytochemical composition of strawberry fruit, and this variability among fruit genotype is also reflected in the bioactive action developed against oxidative stress.[11−13] For this reason it is important to characterize the bioactive composition of strawberries to better understand which compounds are able to improve human health benefits.

Additional studies are necessary to characterize the bioactive compounds that play a fundamental role against oxidative stress; these efforts could possibly elucidate by which mechanisms strawberry fruit and their phytochemicals (anthocyanins and polyphenols) can improve antioxidant defenses and would add to the understanding of their potential role in protecting against DNA damage, both in vitro and in vivo.

AUTHOR INFORMATION

Corresponding Author

*(M.B.) Phone +39 071 2204646. Fax: +39 071 2204123. E-mail: m.a.battino@univpm.it.

Funding

The research was partially granted by EUBerry Project EU FP7 No. 265942. The GIP-USAL is financially supported by the Spanish government through Projects BFU2012-35228 and CSD2007-00063 (Consolider-Ingenio 2010 Programme).

Notes

The authors declare no competing financial interest.

ACKNOWLEDGMENTS

We thank Monica Glebocki for extensive editing of the manuscript.

REFERENCES

(1) Granados-Principal, S.; Quiles, J. L.; Ramirez-Tortosa, C. L.; Sanchez-Rovira, P.; Ramirez-Tortosa, M. C. New advances in molecular mechanisms and the prevention of adriamycin toxicity by antioxidant nutrients. *Food Chem. Toxicol.* **2010**, *48*, 1425−1438.

(2) Nettleton, J. A.; Steffen, L. M.; Mayer-Davis, E. J. Dietary patterns are associated with biochemical markers of inflammation and endothelial activation in the multi-ethnic study of atherosclerosis (MESA). *Am. J. Clin. Nutr.* **2006**, *83*, 1369−1379.

(3) Helmersson, J.; Arnlov, J.; Larsson, A.; Basu, S. Low dietary intake of β-carotene, α-tocopherol and ascorbic acid is associated with increased inflammatory and oxidative stress status in a Swedish cohort. *Br. J. Nutr.* **2009**, *101*, 1775−1782.

(4) Bach-Faig, A.; Berry, E. M.; Lairon, D.; Reguant, J.; Trichopoulou, A.; Dernini, S.; Medina, F. X.; Battino, M.; Belahsen, R.; Miranda, G.; Serra-Majem, L. Mediterranean diet foundation expert group. Mediterranean diet pyramid today. Science and cultural updates. *Public Health Nutr.* **2011**, *14*, 2274−2284.

(5) Giampieri, F.; Tulipani, S.; Alvarez-Suarez, J. M.; Quiles, J. L.; Mezzetti, B.; Battino, M. The strawberry: composition, nutritional quality, and impact on human health. *Nutrition* **2012**, *28*, 9−19.

(6) Giampieri, F.; Alvarez-Suarez, J. M.; Mazzoni, L.; Romandini, S.; Bompadre, S.; Diamanti, J.; Capocasa, F.; Mezzetti, B.; Quiles, J. L.; Ferreiro, M. S.; Tulipani, S.; Battino, M. The potential impact of strawberry on human health. *Nat. Prod. Res.* **2013**, *27*, 448−455.

(7) Seeram, N. P.; Heber, D. Impact of berry phytochemicals on human health: effects beyond antioxidation. In *Antioxidant Measurement and Applications*; ACS Symposium Series 956; American Chemical Society: Washington, DC, USA, 2006; Chapter 21, pp 326−336.

(8) Boivin, D.; Blanchette, M.; Barrette, S.; Moghrabi, A.; Beliveau, R. Inhibition of cancer cell proliferation and suppression of TNF induced activation of NFκB by edible berry juice. *Anticancer Res.* **2007**, *27*, 937−948.

(9) Starvic, B.; Matula, T. I.; Klassen, R.; Downie, R. H.; Wood, R. J. Effect of flavonoids on mutagenicity and bioavailability of xenobiotics in food. . In *Phenolic Compounds in Food and Their Effects on Health II. Antioxidants & Cancer Prevention*; ACS Symposium Series 507; American Chemical Society: Washington, DC, USA, 1992; Chapter 17, pp 239−249.

(10) Diamanti, J.; Capocasa, F.; Battino, M.; Mezzetti, B. Evaluation of *F.* × *ananassa* intra-specific and inter-specific back-crosses to generate new genetic material with increased fruit nutritional quality. *J. Berry Res.* **2010**, *1*, 103−114.

(11) Diamanti, J.; Capocasa, F.; Balducci, F.; Battino, M.; Hancock, J.; Mezzetti, B. Increasing strawberry fruit sensorial and nutritional quality using wild and cultivated germplasm. *PLoS One* **2012**, *7*, e46470.

(12) Diamanti, J.; Capocasa, F.; Denoyes, B.; Petit, A.; Chartier, P.; Faedi, W.; Maltoni, M. L.; Battino, M.; Mezzetti, B. Standardized method for evaluation of strawberry (*Fragaria* × *ananassa* Duch.) germplasm collections as a genetic resource for fruit nutritional compounds. *J. Food Compos. Anal.* **2012**, *28*, 170−178.

(13) Tulipani, S.; Mezzetti, B.; Capocasa, F.; Bompadre, S.; Beekwilder, J.; de Vos, C. H.; Capanoglu, E.; Bovy, A.; Battino, M. Antioxidants, phenolic compounds, and nutritional quality of different strawberry genotypes. *J. Agric. Food Chem.* **2008**, *56*, 696−704.

(14) Lopes da Silva, F.; Escribano-Bailon, M. T.; Perez-Alonso, J. J.; Rivas-Gonzalo, J.; Santos-Buelga, C. Anthocyanin pigments in strawberry. *LWT−Food Sci. Technol.* **2007**, *40*, 374−382.

(15) Prior, R. L.; Wu, X.; Gu, L.; Hager, T. J.; Hager, A.; Howard, L. R. Whole berries versus berry anthocyanins: interactions with dietary fat levels in the C57BL/6J mouse model of obesity. *J. Agric. Food Chem.* **2008**, *56*, 647−653.

(16) Quiles, J. L.; Ramirez-Tortosa, M. C.; Huertas, J. R.; Ibañez, S.; Gomez, J. A.; Battino, M.; Mataix, J. Olive oil supplemented with vitamin E affects mitochondrial coenzyme Q levels in liver of rats after an oxidative stress induced by adriamycin. *Biofactors* **1999**, *9*, 331−336.

(17) Lowry, O. H.; Rosebrough, N. J.; Farr, A. L.; Randall, R. J. Protein measurement with the Folin phenol reagent. *J. Biol. Chem.* **1951**, *193*, 265−275.

(18) Quiles, J. L.; Ochoa, J. J.; Battino, M.; Gutierrez-Rios, P.; Nepomuceno, E. A.; Frías, M. L.; Huertas, J. R.; Mataix, J. Life-long supplementation with a low dosage of coenzyme Q10 in the rat: effects on antioxidant status and DNA damage. *Biofactors* **2005**, *25*, 73−86.

(19) Levine, R. L.; Garland, D.; Oliver, C. N.; Amici, A.; Climent, I.; Lenz, A. G.; Ahn, B. W.; Shaltiel, S.; Stadtman, E. R. Determination of carbonyl content in oxidatively modified proteins. *Methods Enzymol.* **1990**, *186*, 464−478.
(20) Ellman, G. L. Tissue sulfahydryl groups. *Arch. Biochem. Biophys.* **1959**, *82*, 70−77.
(21) Ohkawa, H.; Ohishi, N.; Yagi, K. Assay for lipid peroxide in animal tissue by thiobarbituric acid reaction. *Anal. Biochem.* **1979**, *95*, 331−358.
(22) Jiang, Z. Y.; Hunt, J. V.; Wolff, S. P. Ferrous ion oxidation in the presence of xylenol orange for detection of lipid hydroperoxide in low density lipoprotein. *Anal. Biochem.* **1992**, *202*, 384−389.
(23) Aebi, H. Catalase in vitro. *Methods Enzymol.* **1984**, *105*, 121−126.
(24) Kakkar, P.; Das, B.; Viswanathan, P. N. A modified spectrophotometric assay of superoxide dismutase. *Indian J. Biochem. Biophys.* **1984**, *21*, 130−132.
(25) Sies, H.; Koch, O. R.; Martino, E.; Boveris, A. Increased biliary glutathione disulfide release in chronically ethanol treated rats. *FEBS Lett.* **1979**, *103*, 287−290.
(26) Carlberg, I.; Mannervik, B. Glutathione reductase. *Methods Enzymol.* **1985**, *113*, 484−490.
(27) Habig, W. H.; Pabst, M. J.; Jacoby, W. B. Glutathione-S-transferase: the first enzymatic step in mercapturic acid formation. *J. Biol. Chem.* **1974**, *249*, 7130−7139.
(28) Rogers, G. W.; Brand, M. D.; Petrosyan, S.; Ashok, D.; Elorza, A. A.; Ferrick, D. A.; Murphy, A. N. High throughput microplate respiratory measurements using minimal quantities of isolated mitochondria. *PLoS One* **2011**, *6*, e21746.
(29) Buendía, B.; Gil, M. I.; Tudela, J. A.; Gady, A. L.; Medina, J. J.; Soria, C.; López, J. M.; Tomás-Barberán, F. A. HPLC-MS analysis of proanthocyanidin oligomers and other phenolics in 15 strawberry cultivars. *J. Agric. Food Chem.* **2010**, *58*, 3916−3926.
(30) Vrhovsek, U.; Guella, G.; Gasperotti, M.; Pojer, E.; Zancato, M.; Mattivi, F. Clarifying the identity of the main ellagitannin in the fruit of the strawberry, *Fragaria vesca* and *Fragaria ananassa* Duch. *J. Agric. Food Chem.* **2012**, *60*, 2507−2516.
(31) Nieminen, A. L.; Byrne, A. M.; Herman, B.; Leemasters, J. J. Mitochondrial permeability transition in hepatocytes induced by t-BuOOH: NAD(P)H and reactive oxygen species. *Am. J. Physiol.* **1997**, *272*, 1286−1294.
(32) Stoner, G. D.; Chen, T.; Kresty, L. A.; Aziz, R. M.; Reinemann, T.; Nines, R. Protection against esophageal cancer in rodents with lyophilized berries: potential mechanisms. *Nutr. Cancer* **2006**, *54*, 33−46.
(33) Quiles, J. L.; Ochoa, J. J.; Ramirez-Tortosa, C.; Battino, M.; Huertas, J. R.; Martín, Y.; Mataix, J. Dietary fat type (virgin olive vs. sunflower oils) affects age-related changes in DNA double-strand-breaks, antioxidant capacity and blood lipids in rats. *Exp. Gerontol.* **2004**, *39*, 1189−1198.
(34) Gülkaç, M. D.; Akpinar, G.; Ustün, H.; Ozön Kanli, A. Effects of vitamin A on doxorubicin-induced chromosomal aberrations in bone marrow cells of rats. *Mutagenesis* **2004**, *19*, 231−236.
(35) Kalender, Y.; Yel, M.; Kalender, S. Doxorubicin hepatotoxicity and hepatic free radical metabolism in rats. The effects of vitamin E and catechin. *Toxicology* **2005**, *209*, 39−45.
(36) Liu, W.; Lu, X.; He, G.; Gao, X.; Li, M.; Wu, J.; Li, Z.; Wang, J.; Luo, C. Cytosolic protection against ultraviolet induced DNA damage by blueberry anthocyanins and anthocyanidins in hepatocarcinoma HepG2 cells. *Biotechnol. Lett.* **2013**, *35*, 491−498.
(37) Giampieri, F.; Alvarez-Suarez, J. M.; Tulipani, S.; Gonzàles-Paramàs, A. M.; Santos-Buelga, C.; Bompadre, S.; Quiles, J. L.; Mezzetti, B.; Battino, M. Photoprotective potential of strawberry (*Fragaria* × *ananassa*) extract against UV-A irradiation damage on human fibroblasts. *J. Agric. Food Chem.* **2012**, *60*, 2322−2327.
(38) Cimino, F.; Ambra, R.; Canali, R.; Saija, A.; Virgili, F. Effect of cyanidin-3-*O*-glucoside on UVB-induced response in human keratinocytes. *J. Agric. Food Chem.* **2006**, *54*, 4041−4047.
(39) Duthie, S. J.; Jenkinson, A. M.; Crozier, A.; Mullen, W.; Pirie, L.; Kyle, J.; Yap, L. S.; Christen, P.; Duthie, G. G. The effects of cranberry juice consumption on antioxidant status and biomarkers relating to heart disease and cancer in healthy human volunteers. *Eur. J. Nutr.* **2006**, *45*, 113−122.
(40) Moller, P.; Loft, S.; Alfthan, G.; Freese, R. Oxidative DNA damage in circulating mononuclear blood cells after ingestion of blackcurrant juice or anthocyanin-rich drink. *Mutat. Res.* **2004**, *551*, 119−126.
(41) Wilms, L. C.; Hollman, P. C.; Boots, A. W.; Kleinjans, J. C. Protection by quercetin and quercetin-rich fruit juice against induction of oxidative DNA damage and formation of BPDE-DNA adducts in human lymphocytes. *Mutat. Res.* **2005**, *582*, 155−162.
(42) Weisel, T.; Baum, M.; Eisenbrand, G.; Dietrich, H.; Will, F.; Stockis, J. P.; Kulling, S.; Rüfer, C.; Johannes, C.; Janzowski, C. An anthocyanin/polyphenolic-rich fruit juice reduces oxidative DNA damage and increases glutathione level in healthy probands. *Biotechnol. J.* **2006**, *1*, 388−397.
(43) Wilms, L. C.; Boots, A. W.; de Boer, V. C.; Maas, L. M.; Pachen, D. M.; Gottschalk, R. W.; Ketelslegers, H. B.; Godschalk, R. W.; Haenen, G. R.; van Schooten, F. J.; Kleinjans, J. C. Impact of multiple genetic polymorphisms on effects of a 4-week blueberry juice intervention on ex vivo induced lymphocytic DNA damage in human volunteers. *Carcinogenesis* **2007**, *28*, 1800−1806.
(44) Traustadóttir, T.; Davies, S. S.; Stock, A. A.; Su, Y.; Heward, C. B.; Roberts, L. J.; Harman, S. M. Tart cherry juice decreases oxidative stress in healthy older men and women. *J. Nutr.* **2009**, *139*, 1896−1900.
(45) Ramirez-Tortosa, C.; Andersen, O. M.; Gardner, P. T.; Morrice, P. C.; Wood, S. G.; Duthie, S. J.; Collins, A. R.; Duthie, G. C. Anthocyanin rich extract decreases indices of lipid peroxidation and DNA damage in vitamin E-depleted rats. *Free Radical Biol. Med.* **2001**, *31*, 1033−1037.
(46) Shih, P. H.; Yeh, C. T.; Yen, G. C. Anthocyanins induce the activation of phase II enzymes through the antioxidant response element pathway against oxidative stress-induced apoptosis. *J. Agric. Food Chem.* **2007**, *55*, 9427−9435.
(47) Boateng, J.; Verghese, M.; Shackelford, L.; Walker, L. T.; Khatiwada, J.; Ogutu, S.; Williams, D. S.; Jones, J.; Guyton, M.; Asiamah, D.; Henderson, F.; Grant, L.; DeBruce, M.; Johnson, A.; Washington, S.; Chawan, C. B. Selected fruits reduce azoxymethane (AOM)-induced aberrant crypt foci (ACF) in Fisher 344 male rats. *Food Chem. Toxicol.* **2007**, *45*, 725−732.
(48) Alvarez-Suarez, J. M.; Dekanski, D.; Ristić, S.; Radonjić, N. V.; Petronijević, N. D.; Giampieri, F.; Astolfi, P.; González-Paramás, A. M.; Santos-Buelga, C.; Tulipani, S.; Quiles, J. L.; Mezzetti, B.; Battino, M. Strawberry polyphenols attenuate ethanol-induced gastric lesions in rats by activation of antioxidant enzymes and attenuation of MDA increase. *PLoS One* **2011**, *6* (10), e25878.
(49) Fiorani, M.; Guidarelli, A.; Blasa, M.; Azzolini, C.; Candiracci, M.; Piatti, E.; Cantoni, O. Mitochondria accumulate large amounts of quercetin: prevention of mitochondrial damage and release upon oxidation of the extramitochondrial fraction of the flavonoid. *J. Nutr. Biochem.* **2010**, *21*, 397−404.
(50) Steele, V. E.; Kelloff, G. J.; Balentine, D.; Boone, C. W.; Mehta, R.; Bagheri, D.; Sigman, C. C.; Zhu, S.; Sharma, S. Comparative chemopreventive mechanisms of green tea, black tea and selected polyphenol extracts measured by in vitro bioassays. *Carcinogenesis* **2000**, *21*, 63−67.

Table 1. Families, Corresponding Parents, and Number of Offspring Evaluated for Fruit Sensorial and Nutritional Quality

family	progenitors			no. of selections	type of crossing	
	mother		father			
AN07,003	AN94,414,52	×	Romina	11	F2 backcross	BC2
AN07,216	AN00,239,55	×	Romina	9	F3 backcross	BC3

Total antioxidant capacity (TAC) is a very common parameter for the evaluation of antioxidant activity strictly related to the amount of bioactive compounds in strawberry. TAC provides a measure of the radical scavenger activity of the fruit and is therefore a quality parameter related to the healthfulness of the fruit. The antioxidant capacity of strawberries has been shown to be due to the activity of high amounts of antioxidant compounds such as polyphenols and vitamin C[5]. As demonstrated for fruit sensorial traits, the composition of antioxidant compounds can vary considerably among strawberry cultivars,[25−29] so breeding and/or biotechnology have potential for obtaining better tasting and more nutritious fruits.[30−32] The breeding process can be successful if the variability and heritability of bioactive compounds is assured for the progenies derived from parental fruits. The biotechnological approach is a methodology that is able to provide a genetic improvement through modification of specific biosynthetic pathways.[33] The application of such technology is still mostly limited to functional studies on specific pathways,[34] whereas the commercial exploitation of new products is highly limited by public concerns and biosafety rules now standing for the commercial release of new genetically modified products. In any case, a deep knowledge of both the cultivated and wild genetic resources, which may be utilized for genetic and genomic studies, is an essential prerequisite for obtaining new cultivars of high interest for both the fresh market and the processing industry.[35] Recently, the possibility to improve the fruit content of such phytochemicals by traditional breeding programs has been demonstrated[36] and, to this end, the detailed characterization of the genetic resources to be used in the cross combination was an important component. The inclusion in breeding programs of wild species with a genetic background able to produce progeny that have increased health-related phytochemicals is also important.[37] Furthermore, if the nutritional quality of strawberry is enhanced in association with favorable sensorial parameters (such as titratable acidity, sugar content, fruit firmness, and aroma), the consumption of fruit by consumers will be encouraged, leading to strawberries having a positive effect on health. Consequently, the biochemical characterization and the biomedical health validation of new products resulting from new genetic material, characterized by increased content of health-related phytochemicals, is an important issue. With this aim, high competencies in compositional analyses are needed to give a complete profile of the health-related phytochemicals present in the new type of fruit. Such an approach will complement a description of the potential health benefits of the fruit.

The aim of this work was to evaluate the fruit sensorial and nutritional quality of 20 selections derived from a strawberry interspecific backcross breeding program. All selections were evaluated for their fruit sensorial (color, firmness, total soluble sugars, and acidity) and nutritional parameters (phenol and anthocyanin contents and total antioxidant capacity) by quantitative spectrometry analysis. Data on nutritional parameters allowed the identification of selections that produce fruit with higher contents of phytochemicals combined with interesting sensorial characteristics, together with agronomic performances as required at a commercial level. The phytochemical composition of the genotypes with the most potential, and of their parents used in the intraspecific (cv. 'Romina') and interspecific backcrossing (BC) (AN94,414,52 and AN00,239,55), together with the important commercial variety 'Elsanta', were further characterized by HPLC-PDA-MS analyses. The prevalent type of phytochemicals relevant to the improvement of fruit nutritional value was determined.

MATERIALS AND METHODS

Plant Material. New selections originated from an interspecific backcross program having as common parents the cv. 'Romina', the F1 selection AN94,414,52 from the interspecific cross of *Fragaria* × *ananassa* (Don) × *Fragaria virginiana glauca* (FVG), and AN00,239,55, a BC2 selection produced by backcrossing the F1 selection AN94,414,52 with 91,143,5 (*F.* × *ananassa* advanced selection) (Table 1) were planted in 2011 in nonfumigated soil at the P. Rosati University experimental farm, Agugliano (Ancona, Italy), and grown in open-field conditions using the plastic hill culture production system. Selections were planted as frigo plants in single plots of six plants each, cultivated with the standard Integrated Pest Management system, then harvested and evaluated in May 2012. In the same field, under the same conditions, the corresponding parents of each cross combination were also grown. Fruit samples of fully red berries were harvested at the second, third, and fourth main pickings. In the evaluation, plant productivity (fruit weight and commercial plant production), fruit sensorial (fruit firmness, solid soluble content, titratable acidity, and color), and nutritional parameters (fruit TAC, phenol content, and anthocyanin content) were taken into account. Fruit sensorial and nutritional quality was determined on fresh (color and firmness) and on frozen (total soluble sugars and acidity) samples. HPLC-PDA-MS was performed on freeze-dried fruit and included the commercial variety 'Elsanta', shipped by express mail to James Hutton Institute in the United Kingdom.

Chemicals. Methanol 99% ACS-ISO for analysis and bromothimol blue were purchased from Carlo Erba Reagenti (Milano, Italy). Acetonitrile, formic acid, double-distilled water, Folin−Ciocalteu reagent, sodium carbonate anhydrous, potassium chloride, sodium acetate, chloridric acid, glacial acetic acid, dihydrogen potassium phosphate, dipotassium hydrogen phosphate, 2,2′-azinobis(3-ethylbenzothiazoline-6-sulfonic acid) diammonium salt (ABTS$^{\bullet+}$), 6-hydroxy-2,5,7,8-tetramethylchroman-2-carboxylic acid (Trolox), potassium persulfate, 3,4,5-trihydroxybenzoic acid (gallic acid), and sodium hydroxide were purchased from Sigma-Aldrich (Sigma-Aldrich s.r.l., Milano, Italy). Pelargonidin-3-*O*-glucoside chloride and kaempferol-3-glucoside were purchased from Extrasynthese (Genay, France).

Strawberry Production Parameters. In 2012, strawberry plant production was evaluated in the single plot of all selections by measuring commercial production, total weight (g) of ripe fruit with commercial diameter ($\varnothing \leq 0.22$ mm) and undamaged, and fruit weight, average weight (g), of 20 commercial fruits from each harvest.

Strawberry Sensorial Parameters. Fruit sensorial quality of selections and parents was analyzed on the harvesting day, at each of the second, third, and fourth harvests, on 10 commercial fruits by measuring the following parameters: (a) soluble solids (SS), determined using a hand-held refractometer (ATAGO), results expressed as °Brix; (b) titratable acidity (TA), determined from 10 mL of juice diluted with distilled water (1:2 v/v) and titrated with 0.1 N NaOH solution, to pH 8.2, and expressed as milliequivalents

dx.doi.org/10.1021/jf500708x | J. Agric. Food Chem. 2014, 62, 3944−3953

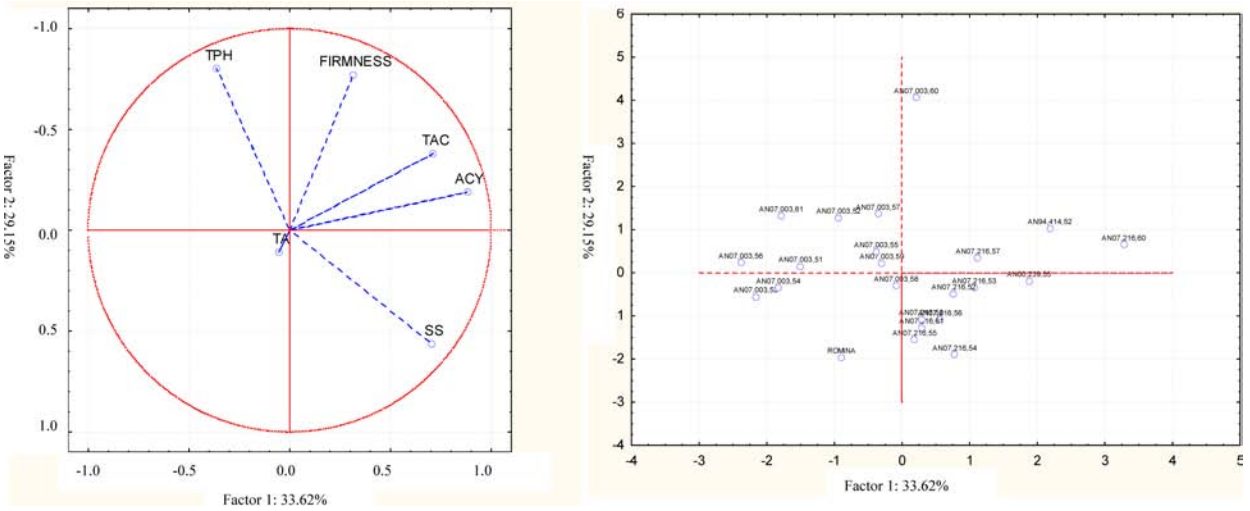

Figure 1. Principal component analysis: (A, left) variable vector distributions; (B, right) case distributions. Biplot of qualitative (SS, TA, and firmness) and nutritional parameters (TAC, TPH, and ACY) of the selections and the corresponding parents of the interspecies cross populations. Factors 1 and 2 explain 62.77% of the data variation.

(mEQ) of NaOH per 100 g of fresh weight (FW); (c) fruit firmness, measured by a penetrometer 327 (Effegì, Ravenna, Italy), results expressed as grams; (d) fruit color, determined by a Minolta Chromameter CR 400, for two faces of 10 ripe, undamaged, and uniform fruits of each harvest. The instruments measured three parameters L^* (luminescence), a^* (red tone), and b^* (yellow tone). Data were elaborated and expressed as chroma index and hue angle. A high chroma index indicated pale fruit and a low chroma index represented dark fruit, whereas a high hue angle indicated yellow fruit and a low hue angle denoted red fruit.

Strawberry Nutritional Parameters. *Fruit Extraction Method.* As described by Diamanti,[37] briefly, from a pool of fruit for each genotype, harvested in 2012 and stored at −20 °C, 10 ripe-commercial fruits were sampled and from each fruit two opposite slices were cut and milled into small pieces. Ten grams of this blend was weighed and placed in a tube for extraction with methanol (1:4, fruit/methanol, w/w), including two subsequent steps. The first step consisted of homogenization, with an Ultraturrax T25 homogenizer, of fruit blend in 20 mL of methanol (Janke and Kunkel, IKA Labortechnik, Staufen, Denmark). The homogenized suspension was continuously agitated for 30 min in the dark. The suspension was centrifuged at 4500*g* for 10 min (Centrifuge Rotofix32, Hettich Zentrifugen, Tuttlingen, Denmark), and 3 × 1 mL of the supernatant was collected and stored in three amber vials at −20 °C. For a more exhaustive extraction, the pellet of the fruit was extracted a second time by adding another 20 mL of methanol and repeating the previously described procedure. The supernatant was collected and added to the previous ones, and 3 × 1 mL per sample was stored in amber vials at −20 °C.

Total Antioxidant Capacity (TAC). Fruit extract of each genotype was used to analyze TAC by using the ABTS assay, according to a previously validated procedure.[38,39] ABTS, a chromogen and colorless substance, is changed into its colored monocationic radical form ($ABTS^{\bullet+}$) by an oxidative agent. Addition of antioxidants reduces $ABTS^{\bullet+}$ into its colorless form. The extent of decolorization as a percentage of inhibition of $ABTS^{\bullet+}$ is determined as a function of concentration and calculated relative to the reactivity of Trolox, a water-soluble vitamin E analogue. The experiment was performed in triplicate, and antioxidant activity was expressed as millimoles of Trolox equivalent (TE) per kilogram of fresh pulp weight ± standard error (SE). The calibration was calculated as the linear regression from the dose response Trolox standard.

Total Phenol Content (TPH). Fruit TPH was evaluated on fruit extracts by the Folin−Ciocalteu reagent method[40] using gallic acid as standard for the calibration curve. Briefly, a test tube (glass) was filled with 7.0 mL of water, then 1 mL of the diluted sample (1:20) was added, followed by the addition of 500 μL of Folin−Ciocalteu reagent, and the mixture was vortexed. After 3 min, 1.5 mL of sodium carbonate (0.53 mol/L) was added, and the tube was mixed again and then stored in the dark for 60 min. The absorbance of the sample was measured at 760 nm after exactly 60 min. Results were calculated and expressed as milligrams of gallic acid per kilogram of fresh fruit ± SE on three replications, by using a standard curve with a range of values of standards of 10−50 mg of gallic acid (GA)/L.

Anthocyanin Content (ACY). Fruit total ACY was measured on fruit extracts by using the pH differential shift method.[41] The assay is based on the anthocyanins' property to change intensity of hue depending on pH shifting. The samples were diluted to a 1:10 ratio with potassium chloride (pH 1.00) and with sodium acetate (pH 4.50), and then the corresponding maximum absorbance for both solutions was measured, respectively, at λ = 500 nm and λ = 700 nm. Analyses were performed in triplicate, and results were expressed as milligrams of pelargonidin-3-glucoside (the most representative anthocyanin compound in strawberry) per kilogram of fresh weight (mg of Pel-3-Glu/kg FW) ± SE.

Analysis of Polyphenolics by HPLC-PDA-MS. *Sample Preparation.* Strawberry samples were frozen at harvest and then freeze-dried by using a Freezone (Labconco) freeze-drying system. Samples were stored in a −20 °C freezer until analysis. Prior to use, double-distilled water (2 mL) and 0.5% formic acid in acetonitrile (2 mL) were added to the sample, (500 mg) in a 15 mL polypropylene centrifuge tube. Samples were shaken on an orbital shaker for 30 min and centrifuged at 4000 rpm for 5 min, and the supernatant was transferred to another 15 mL centrifuge tube. The extraction was repeated with water (1 mL) and 0.5% formic acid in acetonitrile (1 mL) and the supernatant was added to the first one. After centrifugation at 13200 rpm for 5 min, 0.5 mL aliquots were transferred to microfuge tubes and stored in a −20 °C freezer. The solvent was removed from the sample at 45 °C using a Speed Vac, completely dried, using a freeze-drier, and stored in a −20 °C freezer until analysis. Prior to analysis, the sample was dissolved in 475 μL of 0.5% formic acid in water/acetonitrile (70:30, v/v), 25 μL of morin internal standard (1 mg mL^{-1} in methanol) was added, and, following vortexing and centrifugation at 13200 rpm for 3 min, 0.4 mL was transferred to a 0.45 μm filter vial. The sample was injected via an autosampler at 6 °C onto a HPLC column Synergi 4 μ Hydro-RP 80A (150 mm × 2.0 mm; 4 μm reversed-phase HPLC column, Phenomenex) at 30 °C, linked to a PDA system (Thermo Accela) and then an electrospray ionization ion trap mass/Fourier transform spectrometer (Thermo LTQ Orbitrap XL). The mobile phase was a gradient with (A) 0.1% (v/v) aqueous formic acid and (B) 0.1% (v/v) formic acid in acetonitrile/water (50:50, v/v), the flow rate was 300 μL min^{-1}, and the gradient was as follows: 0−4 min, 95% A; 4−28 min,

dx.doi.org/10.1021/jf500708x | J. Agric. Food Chem. 2014, 62, 3944−3953

Table 2. Qualitative, Quantitative, and Color Analysis of Selections and Respective Parents[a]

genotype	backcross generation	soluble solids[b]		titratable acidity[c]		firmness[d]		TAC[e]		TPH[f]		ACY[g]		L^*		chroma		h°	
AN07,003,51	BC2	10.2	abcde	12.7	cd	361	cdefgh	16.0	ghil	2352	cde	307	m	33.9	cdefg	47.7	abcd	29.0	bcd
AN07,003,52	BC2	9.2	bcdef	9.3	de	295	h	18.7	defg	2611	bc	389	i	35.5	bcdef	49.5	abc	29.5	bcd
AN07,003,53	BC2	9.7	abcde	8.5	e	373	bcdefg	13.0	il	2082	efgh	258	op	37.5	b	52.5	a	32.7	ab
AN07,003,54	BC2	10.4	abcd	10.0	de	419	bcde	16.0	ghil	2418	cd	234	p	40.3	a	50.2	ab	35.5	a
AN07,003,55	BC2	11.1	abc	8.4	e	370	cdefg	19.2	bdefg	2732	b	383	i	36.1	bcde	47.2	abcd	33.0	ab
AN07,003,56	BC2	10.9	abc	10.6	de	363	cdefgh	15.7	ghi	2338	cde	238	p	40.2	a	51.7	a	35.6	a
AN07,003,57	BC2	9.6	abcde	10.4	de	421	bcd	17.1	fgh	2498	bcd	533	d	34.8	bcdefg	40.4	efghi	29.0	bcd
AN07,003,58	BC2	10.3	abcde	8.7	e	315	gh	18.9	defg	2243	defg	350	l	37.2	bc	50.5	ab	31.9	ab
AN07,003,59	BC2	11.3	ab	10.8	de	394	bcdef	17.6	efgh	2297	def	377	i	35.7	bcdef	47.4	abcd	32.0	ab
AN07,003,60	BC2	11.7	a	8.1	e	437	bc	22.4	c	2992	a	499	e	32.3	fg	45.5	bcde	27.1	cde
AN07,003,61	BC2	9.9	abcde	11.3	de	395	bcdef	14.7	hil	2180	defg	291	mn	36.6	bcd	47.7	abcd	30.4	bc
AN07,216,52	BC3	8.2	efg	9.6	de	342	defgh	16.9	fgh	1584	lm	470	f	31.4	g	39.3	ghi	25.6	de
AN07,216,53	BC3	7.1	g	10.3	de	446	b	22.4	bc	1583	lm	468	f	32.5	fg	38.9	hi	29.2	bcd
AN07,216,54	BC3	10.6	abcd	13.9	bc	370	cdefgh	18.0	defgh	1381	m	442	g	32.1	fg	40.0	fghi	23.6	e
AN07,216,55	BC3	9.9	abcde	14.8	bc	398	bcdef	16.6	fgh	1549	lm	567	c	36.4	bcde	42.7	defghi	31.2	bc
AN07,216,56	BC3	7.3	fg	10.1	de	340	efgh	17.9	defgh	1696	il	398	hi	34.6	bcdefg	39.7	ghi	30.6	bc
AN07,216,57	BC3	8.6	defg	10.6	de	358	cdefgh	20.0	bcdef	1757	il	539	d	34.5	bcdefg	44.0	cdefgh	28.4	bcd
AN07,216,58	BC3	9.1	cdefg	10.2	de	327	fgh	21.1	bcd	1834	hil	380	i	35.5	bcdef	44.5	cdefg	30.6	bc
AN07,216,60	BC3	8.2	efg	16.2	b	417	bcde	21.2	bcd	1991	fghi	819	a	33.0	efg	37.9	i	28.1	bcd
AN07,216,61	BC3	8.2	efg	9.5	de	383	bcdefg	16.1	ghil	1718	il	419	gh	32.4	fg	39.5	ghi	25.2	de
AN94,414,52	BC2 parent	10.1	abcde	15.6	b	366	cdefgh	29.9	a	2015	fghi	513	de	33.2	defg	44.7	cdefg	29.3	bcd
AN00,239,55	BC3 parent	11.1	abc	20.8	a	363	cdefgh	20.6	bcde	1937	ghi	600	b	36.8	bc	43.7	defgh	32.5	ab
Romina	*F.* × *a* parent	7.5	fg	10.2	de	520	a	13.2	l	1396	m	274	no	34.9	bcdef	45.1	bcdef	29.7	bcd

[a]Results are expressed as means. Data followed by different letters are significantly different. SNK test $P < 0.05$. [b]°Brix. [c]mequiv NaOH/100 g. [d]g. [e]mmol TE/kg FW. [f]mg GA/kg FW. [g]mg pel-3-glu/kg FW.

dx.doi.org/10.1021/jf500708x | J. Agric. Food Chem. 2014, 62, 3944−3953

50% A; 28−32 min, 0% A; 32−34 min, 0% A; 34−36 min, 95% A; 36−45 min, 95% A. The PDA detector range was 200−600 nm, and channels were (A) 280 nm (general polyphenols), (B) 365 nm (flavonols), and (C) 520 nm (anthocyanins). Mass spectrometer mass range was m/z 120−2000 with alternative full scan MS and MS/MS (data-dependent scan). The sample was run twice, in positive ion and negative ion modes. Identification of polyphenols was based on PDA characteristics and mass spectra including accurate MS and MS/MS data, and comparison to the PDA, MS, and elution times of authentic standards when available. Quantification of flavonols and anthocyanins was based on the area of $[M - 1]^-$ and $[M + 1]^+$ ions, respectively, using calibration curves generated for standards of kaempferol-3-*O*-glucoside and pelargonidin-3-*O*-glucoside, respectively. Relative levels of ellagitannins and flavan-3-ols were based on areas of $[M - 1]^-$ ions, assuming that different compounds within each class had similar response factors.

Experimental Trial and Statistical Analysis. Fruit sensorial (SS, TA, fruit firmness, fruit color) and nutritional (TAC, TPH, ACY) parameters were analyzed in triplicate for each selection and for their corresponding parents. All of these data were subjected to the two-way nested analysis, the MANOVA test. The analysis of variance was performed for genotype as random effects. The differences were calculated according to the SNK test and were considered significant at $p \leq 0.05$.

To evaluate also the association among the fruit qualitative and nutritional parameters of the samples and their respective parents, PCA was used. As described by Diamanti et al.,[37] factor loading values ≥0.7 were used to identify the most important variables and observations in each dimension (PC). Variables and observations (Figure 1) that are closest to each other in the same geometric plane of the biplot are considered as interrelated, and therefore they are distant from those to which they are negatively related or not related. The greater the distance of a vector from the origin of the axis, the higher the correlation of the variable with the PC represented in that dimension.

All analyses were performed using STATISTICA software (Statsoft Inc., Tulsa, OK, USA).

RESULTS AND DISCUSSION

Commercial Production and Fruit Weight. All 20 selections had a low commercial production and fruit weight due to their backcross origin (BC2 and BC3). Selections of both backcrosses (AN07,003 and AN07,216 families) showed intermediate commercial production values with respect to their parents; values were higher than those of their wild parents AN94,414,52-F1 and AN00,239,55-BC1 (selections of AN07,003 family produced 422 g/plants against 92 g/plants for their AN94,414,52 parent; selections of AN07,216 family produced 484 g/plants against 188 g/plant for their AN00,239,55 parent), but lower than those of 'Romina', the only commercial variety. Furthermore, fruit weight values were lower for all of the selections and the wild parents (15.2 g for BC3 selections AN07,216, 11.2 g for their wild parent AN00,239,55, 11.2 g for BC2 selections of AN07,003 family, and 11.5 g for their wild parent AN94,414,52), compared with 'Romina' (21 g).

Strawberry Sensorial Parameters. Fruit of selections AN07,003,60 and AN07,003,59 had very high soluble solids values (Table 2); in particular, they were significantly higher than the parent 'Romina'. The lowest values of soluble solids were detected in AN07,216,53, AN07,216,56 and 'Romina', and in general fruit of all selections of the AN07,216 family presented lower values than AN07,003 selections. The parent AN00,239,55 had the highest value of titratable acidity, and that of the parent AN94,414,52 was also high, both having higher values than 'Romina', which possessed a medium value (Table 2). The BC3 selections AN07,216,60 and AN07,216,55 also had high values, intermediate between the two parental lines 'Romina' and AN00,239,55. Two other selections, AN07,003,59 and AN07,216,57, had lower values with respect to their respective "mothers" (AN94,414,52 and AN00,239,55 respectively), but similar values with respect to their "father" 'Romina'. It is interesting to note that all of the selections showed lower values of titratable acidity compared with their female parents. The lowest values were registered for selections AN07,003,55, AN07,003,53, AN07,003,58, and AN07,003,60.

'Romina' fruit had the highest value of firmness; none of the new selections were able to reach it, AN07,003,52 having the lowest value (Table 2). The selection that reached the closest value to that of 'Romina' was AN07,216,53 followed by AN07,216,60, from the BC3 family.

With regard to color, L^*, chroma index, and hue angle were evaluated for all of the selections and parents (Table 2). Interestingly, the AN07,003 family (BC2) generally showed the highest values for L^*, chroma index, and hue angle. In particular, fruit of selection AN07,003,53 possessed the highest values for chroma index, whereas AN07,003,56 and AN07,003,54 had the highest hue angle and L^* value, respectively. In contrast, fruits of BC3 (AN07,216 family) generally had the lowest values for L^* (AN07,216,52), chroma index (AN07,216,60), and hue angle (AN07,216,54). AN00,239,55 had the highest L^* value among parents, whereas AN94,414,52 had the lowest. 'Romina' had average values for all of the color parameters analyzed. Interestingly, the AN07,003 family (BC2) showed a higher average value of all color parameters compared to both parents. In contrast, the AN07,216 family (BC3) had lower values of all color parameters compared to its parents.

Fruit Nutritional Quantitative Analysis. The quantitative analysis performed to evaluate the nutritional quality of backcross genotypes involved in the study have highlighted main differences among them, specifically between parents and progenies, thus allowing the selection of those genotypes that had shown the highest improvements for each parameter. Phenol content of strawberry genotypes revealed an improvement in all of the progenies of second-generation backcrossing in comparison with their parent 'Romina', whereas some genotypes revealed also an improvement with respect to the other parent AN94,414,52. On the contrary, there was a decline in phenol content in most genotypes of third backcross generation in comparison to the BC3 parent AN00,239,55, but most had higher values than the parent 'Romina' (Table 2). The most elevated values were shown by the AN07,003 family and in particular by selections AN07,003,60 and AN07,003,55.

The results of ACY content revealed that only one genotype (AN07,216,60) showed an improvement in ACY content compared to its wild parent (AN00,239,55), whereas there was a decrease in ACY in most of the progenies, but at least the majority of the genotypes showed higher values than the parent 'Romina', as shown in Table 2. Selections that revealed the highest ACY content were AN07,216,60, AN07,216,55, and AN07,216,57 from BC2 and AN07,003,57 and AN07,003,60 from BC3.

TAC analysis revealed modest increased values of almost all progenies of both backcrosses in comparison with the parent 'Romina' (Table 2), whereas compared to the F1 parent AN94,414,52 there was a decrease in the BC2 progeny and compared to the BC3 parent AN00,239,55 there was no significant improvement in BC3 progenies. The selections

Table 3. Characterization of Polyphenols in Selections, the Respective Parents (Except AN94,414,52) and the Commercial Cultivar 'Elsanta' by HPLC-PDA-MS

	Romina	AN00,239,55	AN07,003,59	AN07,216,57	AN07,216,60	Elsanta
flavonols (mg 100 g^{-1} FDW)						
quercetin glucuronide	34.9	41.1	37.6	35.0	33.9	2.0
quercetin hexoside	2.5	2.4	2.2	2.5	2.4	0.4
methylquercetin glucuronide	1.1	1.8	2.1	2.4	1.9	0.1
kaempferol glucoside	3.0	6.9	4.9	4.3	4.2	6.6
kaempferol glucuronide	7.7	13.7	11.8	10.0	14.1	3.7
kaempferol acetylglucoside	0.7	0.2	0.3	1.1	0.8	3.4
kaempferol coumaroyl hexoside 1	7.1	7.4	9.1	4.9	5.7	14.1
kaempferol coumaroyl hexoside 2	1.2	1.2	1.8	1.0	0.8	2.9
kaempferol rutinoside	0.5	1.4	0.9	0.0	0.5	0.0
total	58.8	76.2	70.8	61.1	64.4	33.3
anthocyanins (mg 100 g^{-1} FDW)						
pelargonidin glucoside	156.5	366.1	282.8	284.3	331.9	303.6
pelargonidin rutinoside	8.8	29.3	19.7	0.0	16.3	0.0
pelargonidin malonylglucoside	54.6	3.2	5.9	108.1	97.7	147.0
pelargonidin acetylglucoside	3.7	2.9	1.2	4.7	0.1	0.1
cyanidin glucoside	15.4	20.8	36.9	22.6	29.6	5.9
cyanidin rutinoside	0.3	0.0	0.6	0.0	0.4	0.0
total	239.4	422.4	347.1	419.6	476.0	456.6
ellagic acid conjugates (mg 100 g^{-1} FDW)						
ellagic acid	7.0	4.4	6.8	4.0	4.5	4.7
ellagic hexoside	1.0	1.8	1.2	0.5	1.3	0.4
ellagic deoxyhexoside 1	8.7	8.1	6.8	9.0	8.1	6.4
ellagic deoxyhexoside 2	1.8	2.8	2.2	1.9	1.6	1.1
methylellagic deoxyhexoside	0.0	0.0	13.0	0.0	0.0	0.0
total	18.5	17.1	30.0	15.3	15.4	12.7
ellagitannins (relative levels)						
bis-HHDP-hexoside[a]	0.32	0.56	0.46	0.46	0.25	0.10
HHDP-galloyl-hexoside	0.17	0.40	0.33	0.35	0.11	0.04
galloyl-bis-HHDP-hexoside[b]	0.48	1.00	0.75	0.86	0.26	0.05
sanguiin H6	0.15	0.23	0.26	0.21	0.10	0.03
A[c]	0.63	0.58	0.62	0.61	0.51	0.60
B[d]	0.07	0.02	0.04	0.05	0.02	0.02
total	1.81	2.80	2.46	2.54	1.26	0.84
flavan-3-ols (relative levels)						
catechin	0.35	0.24	0.20	0.26	0.23	0.37
proanthocyanidin dimers[e]	0.92	0.61	0.54	0.63	0.55	1.00
proanthocyanidin trimers[f]	0.39	0.26	0.25	0.29	0.24	0.47
total	1.67	1.12	0.99	1.18	1.02	1.84

[a]Sum of four bis-HHDP-hexoside peaks. [b]Sum of two galloyl-bis-HHDP-hexoside peaks. [c]Ellagitannin with a mass spectrum similar to that of sanguiin H6. [d]Ellagitannin with a mass spectrum similar to that of lambertianin C. [e]Sum of five dimer peaks. [f]Sum of five trimer peaks.

AN07,003,60, AN07,216,53, AN07,216,58, and AN07,216,60 had the highest TAC values. Fruits of selection AN07,003,60 also had the highest TPH value, whereas AN07,216,60 had the highest TPH value of all the BC3 selections and the highest ACY value of all genotypes.

PCA. In the PCA biplot for fruit nutritional parameters of TAC, TPH, and ACY, combined with qualitative parameters of SS, TA, and firmness (Figure 1A), the selections and their parents are distributed in the four quadrants of the plot (Figure 1B). The female parent AN00,239,55 is located on the right-hand side of the plot, near the ACY vector. The other female parent, AN94,414,52 was located slightly higher in the right-hand side of the plot, near the ACY and TAC vectors. Finally, the common male parent 'Romina' is located on the lower left part of the plot, far from all of the vectors.

The AN07,003 selections were mainly positioned in the central left-hand area of the plot, not far from the TPH vector location. The only exception was AN07,003,60, which is located in the upper slightly right-hand side of the graph, where the firmness vector is located (Figure 1B).

The selections of the AN07,216 family are mainly located in the lower right-hand quadrant (Figure 1B), where the SS vector is placed (Figure 1A). However, fruits of AN07,216,57 and AN07,216,60 were located in the upper right quadrant, slightly higher than the other AN07,216 selections, where the TAC and ACY vectors are also located.

On the basis of the PCA, the three best selections were chosen for further characterization by HPLC-PDA-MS: AN07,003,59 BC2, which was characterized by medium TAC, TPH, and ACY values; AN07,216,57 BC3, which presented medium TAC value, medium/low TPH value, and high ACY; and AN07,216,60 BC3, which had the highest ACY and also one of the highest TAC and TPH values among the BC3 progenies.

dx.doi.org/10.1021/jf500708x | J. Agric. Food Chem. 2014, 62, 3944−3953

Polyphenolic Composition by HPLC-PDA-MS. The phenolic compositional analyses of flavonols, anthocyanins, ellagic acid conjugates, ellagitannins, and flavan-3-ols (catechin and proanthocyanidins) were performed on the selected selections. Fruits of the two parents, AN00,239,55 and cv. 'Romina', and of 'Elsanta', a widely available commercial variety, were also profiled.

The results (Table 3) showed that the BC2 parent AN00,239,55 and the BC2 selection AN07,003,59 contained the highest content of total flavonols, 2-fold higher than that of the commercial cultivar 'Elsanta'. The levels in both BC3 selections were not enhanced compared to the parents. The flavonol profile was similar for all genotypes with the exception of 'Elsanta'. Quercetin glucuronide was the main compound present in all genotypes except for 'Elsanta', in which the levels were up to about 20-fold less. Kaempferol glucuronide, the second main flavonol compound in strawberry, was higher in the selections and the parent AN00,239,55 than in the parent 'Romina' and much higher than in 'Elsanta'. The highest content of kaempferol coumaroyl hexoside 1 was found in fruit of 'Elsanta' and then BC2 AN07,003,59. Another kaempferol coumaroyl hexoside was at lower levels and showed a distribution similar to that of the major component. Kaempferol glucoside content was highest in fruit of BC3 parent AN00,239,55 and 'Elsanta', but was not enhanced in the progeny and was particularly low in 'Romina'. Quercetin hexoside and methylquercetin glucoronide were of low abundance, and there were only minor variations among genotypes, although they were at even lower levels in 'Elsanta'. Kaempferol acetylglucoside was highest in 'Elsanta', but was lowest in fruit of AN00,239,55 and of BC2 AN07,003,59. Kaempferol rutinoside was most abundant in fruit of AN00,239,55, whereas it was not detected in AN07,216,57 and 'Elsanta'.

ACY profiling revealed marked differences in anthocyanin content, in both anthocyanins quantity and quality. The total ACY (Table 3) followed the same trend as the values obtained from the spectrophotometric assay (Table 2). The levels in the selections were higher than in 'Romina' but not the parent AN00,239,55 or 'Elsanta'. Pelargonidin glucoside, the major anthocyanin, was about twice as abundant in the interspecific BC genotypes compared to 'Romina' and 'Elsanta'. Interestingly, pelargonidin malonylglucoside was observed in high amounts in fruit of 'Elsanta' and both BC3 selections AN07,216,57 and AN07,216,60, followed by 'Romina', whereas very low levels were detected in AN00,239,55 (BC3 parent) and BC2 AN07,003,59; it was enhanced in both BC selections compared to both parents. Cyanidin glucoside was detected in highest amounts in BC2 and then in BC3 selections, whereas the lowest value was detected in fruit of 'Elsanta'. Pelargonidin rutinoside was present in AN00,239,55, BC2 AN07,003,59, and BC3 AN07,216,60, and a small amount was found also in 'Romina', whereas it was not detected in the other BC3 selection or in 'Elsanta'. Pelargonidin acetyl-glucoside was a minor anthocyanin in fruits of AN00,239,55, AN07,216,57, and 'Romina', followed by AN07,003,59, whereas only a very low concentration was detected in AN07,216,60 and 'Elsanta'. Finally, cyanidin rutinoside was detected, at very low levels, only in fruits of AN07,003,59, AN07,216,60, and 'Romina'. The pattern of ellagic acid conjugates was similar for all genotypes, with the exception of BC2 selection AN07,003,59, which was the only genotype to contain a methylellagic deoxyhexoside (Table 3). Ellagic deoxyhexoside 1 was the most prevalent compound in the majority of genotypes, but there were no marked differences in the levels among genotypes. Ellagic acid was also a major component, and the highest values were evident for 'Romina' and BC2 AN07,003,59. Another ellagic deoxyhexoside and an ellagic hexoside were detected at lower levels in all genotypes.

Ellagitannins were highest in AN00,239,55, AN07,003,59, and AN07,216,57 and lowest in 'Elsanta'. The levels were enhanced in the BC2 selection (AN07,003,59) and one BC3 selection (AN07,216,57) compared to the parent 'Romina' but not the BC3 parent AN00,239,55. Galloyl-bis-HHDP-hexoside and unidentified ellagitannin A (with a mass spectrum similar to that of sanguiin H6) were the major components, followed by bis-HHDP-hexoside, in all genotypes except 'Elsanta', where ellagitannin A predominated.

Among the flavan-3-ols, catechin and proanthocyanin dimers and trimers were identified, and the dimers predominated. Larger proanthocyanidin compounds were detected but they were not characterized in this study. The levels were highest in 'Romina' and 'Elsanta' and were at similar levels in the BC2 and BC3 selections compared to the BC3 parent.

Most studies on strawberry genetic improvement have focused their attention on the evaluation and amelioration of agronomical and productive parameters. Only recently has attention shifted increasingly to the development of more healthful fruits, with emphasis on sensorial and nutritional characteristics. With this aim, a detailed study on the content of fruit bioactive compounds is a crucial aspect in evaluating new genetic material, because the profiling of at least the most important phytochemicals present in the fruit can provide a better estimation of the health-promoting potential of new future commercial material. The utilization of wild strawberries as a source of genetic variability for the improvement of nutritional value is being demonstrated as an important breeding strategy.[37] A problem with such wild germplasm is the lack of other important commercial attributes with respect to fruit yield, size, and firmness. In fact, several studies have recently demonstrated that breeding programs based on the use of wild and cultivated strawberries led to the achievement of selections with better nutritional qualities compared to the existing cultivated strawberry,[42] but then a long-term backcross program is needed to associate the improved nutritional traits with the commercially important agronomic and sensorial traits. Contemporary strawberry breeding programs, with the specific focus on improving strawberry nutritional quality, are using TPH, ACY, and TAC as preliminary screening methods. Then, more detailed compositional analyses are used to better characterize the phytochemicals that are responsible for the potential health benefits of the more interesting new genotypes. In the present study such an approach was taken to evaluate progenies from two backcross generations (BC2 and BC3) of an interspecific strawberry breeding program.

The commercial production and the average fruit weight of all selections and their respective parents were the first parameters to be analyzed. It is interesting that for commercial production, the *F.* × *ananassa* parent 'Romina' showed a very high value compared to the other wild-derived parents and to all BC2 and BC3 selections. However, the breeding program has generated selections that, even if they possess lower values than 'Romina', have an average commercial production much higher than their wild parents. Also, for average fruit weight (see the Supporting Information), 'Romina' had the highest value, whereas all other genotypes had lower values. Indeed, the

two backcross generations showed a breeding progress comparable with their corresponding parents. In fact, BC2 selections (AN07,003) had higher average production values than their parent AN94,414,52, and the BC3 selections (AN07,216) possessed average higher value compared to their parent AN00,239,55. Such results indicate an improvement in production parameters from the second to the third backcross generation, but to achieve the common commercial standards at least a further backcross generation is needed.

On the contrary, fruit from the BC2 and BC3 generations had, in general, higher values for sensorial quality parameters compared with the commercial parent. In fact, for soluble solids, 'Romina' had the lowest value (7.5 °Brix) compared to the wild parents and the majority of selections. Interestingly, the backcross selection BC2 AN07,003, derived from 'Romina' and AN94,414,52, showed a higher value (10.4 °Brix) compared to both 'Romina' and AN94,414,52 (10.1 °Brix, statistically different only from 'Romina'). Conversely, the BC3 AN07,216 selections had a much lower value (8.6 °Brix) than their parent AN00,239,55 (11.1 °Brix), but at least slightly higher than that of 'Romina'. These data indicate that the backcrossing program can be associated with a loss of fruit sugar contents that had previously been improved in the parents.

With regard to the titratable acidity, the wild parents had very high values compared to the majority of selections and 'Romina'. Fruit from most BC2 and BC3 selections did not show significant differences compared to 'Romina', but in some cases, such as for fruit of AN07,216,54, AN07,216,55, and AN07,216,60, titratable acidity is significantly higher than that of 'Romina', indicating that the interspecific cross of this cultivar with the wild selections improved the titratable acidity of the BC3 selection families (AN07,216).

Fruit firmness was improved in both BC2 and BC3 selections compared to 'Romina'. Although 'Romina' had a very high value (520 g), the interspecific cross with wild genotypes produced BC2 (377 g for AN07,003) and BC3 (376 g for AN07,216) selections with relatively low values that were generally very similar and not statistically different from their respective wild parents (363 g for AN00,239,55 and 366 g for AN94,414,52); the exception was AN07,216,53, which had a statistically higher value than the wild parent.

With regard to color, the BC2 AN07,003 family had the highest values for all the parameters evaluated; in particular, AN07,003,53 for chroma index (52.5), AN07,003,54 for L^* (40.3), and AN07,003,56 for hue angle (35.6). In this case, the backcrossing of wild and cultivated germplasm generated progeny that showed much higher values of all the color parameters compared to both parents, closer to the red brilliant type of color requested by the market for fresh strawberries. The situation is completely different for the BC3 family AN07,216; in fact, AN07,216,60 showed the lowest values of chroma index (37.9), AN07,216,52 the lowest value of L^* (31.4), and AN07,216,54 the lowest value of hue angle (23.6). For this family it is clear that the breeding program did not improve the color of the progeny; indeed, the average values of AN07,216 family were lower than in both parents ('Romina' and AN00,239,55) for all color parameters.

The nutritional quantitative analysis performed on parents and selections demonstrated well the effect of genetic improvement, through the utilization of wild germplasm. In fact, for TAC, TPH, and ACY, the lowest values were always detected in fruit of 'Romina'. On the contrary, the highest values for TAC and ACY were shown by the wild-derived parents AN94,414,52 and AN00,239,55. As a consequence, average TAC and ACY values of selections AN07,003 and AN07,216 were statistically lower than those of their respective wild parents, but significantly higher compared to their "father" 'Romina'. Furthermore, the TPH values of AN07,003 (BC2) selections and AN07,216 (BC3) selections were significantly higher than those of 'Romina', and that of AN07,003 was even higher than that of its "mother" AN94,414,52.

The PCA biplot analysis for nutritional and qualitative parameters clearly showed the distributions of the BC2 and BC3 selections and of their respective parents. Selections of the AN07,003 family were mainly located in the left upper quadrant (Figure 1B), where the TPH vector is located (Figure 1A). In fact, all of the higher values of TPH were registered for selections belonging to the AN07,003 family (Table 2). On the contrary, selections of the AN07,216 family are mainly located in the right side of the blot (Figure 1B), where ACY and TAC vectors are located (Figure 1A). This is in accordance with the values in Table 2, where selections of the AN07,216 family possessed higher values for both of these parameters.

On the basis of the results of the nutritional quantitative analysis, one BC2 and two BC3 selections, together with 'Romina', AN00,239,55, and the commercial cultivar 'Elsanta', were further analyzed by HPLC-PDA-MS for polyphenolic characterization and quantification. For flavonols content, all selected genotypes showed a modest increase in total flavonols compared to the "father" 'Romina' and much higher compared to 'Elsanta'. This finding represented a crucial result in this study, because it demonstrated that the interspecific crossing of cultivated strawberry with a wild-derived selection such as AN00,239,55, which has a high concentration of flavonols, generated BC2 (AN07,003,59) and BC3 (AN07,216,60) progeny with flavonol levels higher than the cultivated parent 'Romina' while retaining the overall pattern of individual flavonols, which was also similar to that of the wild parent (but different from that of Elsanta). The enhancement of flavonols in AN07,003,59 was mainly due to increases in quercetin glucuronide, kaempferol glucuronide, and a kaempferol coumaroyl hexoside, whereas in AN07,216,60 kaempferol glucuronide alone was mainly responsible. For the anthocyanins, the effect of breeding is even more evident than what was observed for flavonols. The total anthocyanin content of selections was up to 2-fold higher (highest was in AN07,216,60) than in 'Romina'. In BC2 selections (AN07,216,57 and AN07,216,60) the increase was mainly due to the two major anthocyanins, pelargonidin malonylglucoside and pelargonidin glucoside, whereas in the BC3 selection (AN07,003,59) only pelargonidin glucoside was the major contributor. Cyanidin glucoside was increased in all selections by up to 2-fold, and likewise pelargonidin rutinoside was enhanced in all selections, except AN07,216,57 where it was absent, compared to 'Romina', and to an even greater extent compared to 'Elsanta'. It is interesting that the anthocyanin profile of 'Romina' was retained in the BC3 selections with discrepancies only in minor anthocyanins (pelargonidin rutinoside and pelargonidin acetylglucoside were either absent or at trace levels in AN07,216,57 and AN07,216,60, respectively), but the BC2 selection was notable in the low level of pelargonidin malonylglucoside. The level of ellagic acid conjugates in the BC3 selections was not increased compared to the parents, although the overall profile of individual compounds was retained. Increases for the BC2 selection

AN07,003,59 were due to the unexpected high level of methylellagic deoxyhexoside, an ellagic acid conjugate totally absent in all other selections and parents, that probably originated from FVG but could be easily lost in backcrossing considering that it had already been lost in fruit of BC3 selections. Ellagitannins were enhanced in AN07,003,59 and one of the BC3 selections (AN07,216,57) compared to 'Romina', but the overall profile was maintained. Flavan-3-ol levels were not increased in the selections compared to 'Romina'.

The approach used for breeding strawberry nutritional quality is appropriate for (a) screening large populations by using spectrophotometric parameters (TPH, ACY, and TAC) and (b) characterizing the phytochemical content of the new selections chosen from those with the highest spectrophotometric values. With such an approach it is possible to concentrate effort on the characterization of fruit phytochemical content of only the more interesting selections. Wild FVG can make an important contribution to improving strawberry fruit content of important health-related phytochemicals combined with high values of sensorial traits. However, a well-defined backcross program is needed to conserve such improvements in fruit nutritional quality while recovering the other agronomic traits (in particular yield, size, and firmness) that are lost when the *Fragaria* × *ananassa* × FVG interspecific cross is performed. The HPLC-PDA-MS compositional study performed on the three BC selections enabled the characterization of bioactive compounds responsible for the improvement of the nutritional value of their fruit. They all had increased levels of flavonols and anthocyanins, two selections had enhanced ellagitannin contents, and the BC2 selection had increased content of ellagic acid conjugates (due to methylellagic deoxyhexoside, detected only in this selection), compared to the cultivated parent, 'Romina'. Furthermore, it is interesting to note that at least the contents of total flavonols and ellagitannins in all selected selections and respective parents are higher compared to the commercial variety 'Elsanta'. The knowledge now available for the three new selections, intensely characterized for their fruit compositional content, will be used to better define their use as breeding lines in future breeding programs or even for the release of the best ones as commercial varieties. In conclusion, it has been demonstrated that the progenies obtained from two half-subcross combinations of cultivated strawberry 'Romina' and wild-derived selections AN94,414,52 and AN00,239,55 have productive, sensorial, and, in particular, nutritional qualities, and it is encouraging that breeding programs can be utilized to ameliorate the characteristics of such fruits. In particular, the breeding of cultivated with wild genotypes has generated progenies with a commercial production much higher than the wild parents, but with sensorial, nutritional characteristics, and polyphenolic content much higher than those of the cultivated cultivar.

■ ASSOCIATED CONTENT

Supporting Information

Table S-1. This material is available free of charge via the Internet at http://pubs.acs.org.

■ AUTHOR INFORMATION

Corresponding Author

*(B.M.) Phone: +39 071 220 4933. Fax: +39 071 220 4685. E-mail: b.mezzetti@univpm.it.

Funding

The research work was carried out thanks to the support of EU FP7 EUBerry Project 265942.

Notes

The authors declare no competing financial interest.

■ ABBREVIATIONS USED

TAC, total antioxidant capacity; BC, backcrossing; SS, soluble solids; TA, titratable acidity; FW, fresh weight; TPH, total phenol content; ACY, anthocyanin content; FVG, *Fragaria virginiana glauca*

■ REFERENCES

(1) Chu, Y.; Sun, J.; Wu, X.; Liu, R. H. Antioxidant and antiproliferative activities of common vegetables. *J. Agric. Food Chem.* **2002**, *50*, 6910−6916.

(2) Etminan, M.; Takkouche, B.; Caamano-Isorna, F. The role of tomato products and lycopene in the prevention of prostate cancer: a meta-analysis of observational studies. *Cancer Epidemiol. Biomarkers Prev.* **2004**, *13*, 340−345.

(3) Vauzour, D.; Vafeiadou, K.; Pendeiro, C.; Corona, G.; Spencer, J. P. E. The inhibitory effects of berry derivated flavonoids against neurodegenerative processes. *J. Berry Res.* **2010**, *1*, 45−52.

(4) Johnsen, S. P.; Overvad, K.; Stripp, C.; Tjonneland, A.; Husted, S. E.; Sorensen, H. T. Intake of fruit and vegetables and the risk of ischaemic stroke in a cohort of Danish men and women. *Am. J. Clin. Nutr.* **2003**, *78*, 57−64.

(5) Giampieri, F.; Alvarez-Suarez, J. M.; Mazzoni, L.; Romandini, S.; Bompadre, S.; Diamanti, J.; Capocasa, F.; Mezzetti, B.; Quiles, J. L.; Ferreiro, M. S.; Tulipani, S.; Battino, M. The potential impact of strawberry on human health. *Nat. Prod. Res.* **2012**, DOI: 10.1080/14786419.2012.706294.

(6) Hakkinen, S. H.; Torronen, A. R. Content of flavonols and selected phenolic acids in strawberries and *Vaccinium* species: influence of cultivar, cultivation site and technique. *Food Res. Int.* **2000**, *33*, 517−524.

(7) Azzini, E.; Intorre, F.; Vitaglione, P.; Napolitano, A.; Foddai, M. S.; Durazzo, A.; Fumagalli, A.; Catasta, G.; Rossi, L.; Venneria, E.; Testa, M. F.; Raguzzini, A.; Palomba, L.; Fogliano, V.; Maiani, G. Absorption of strawberry phytochemicals and antioxidant status changes in humans. *J. Berry Res.* **2010**, *1*, 81−89.

(8) Chiva-Blanch, G.; Visioli, F. Polyphenols and health: moving beyond antioxidants. *J. Berry Res.* **2012**, *2*, 63−71.

(9) Alvarez-Suarez, J. M.; Dekanski, D.; Ristic, S.; Radonjic, N. V.; Petronijevic, N. D.; Giampieri, F.; Astolfi, P.; Gonzalez-Paramas, A. M.; Santos-Buelga, C.; Tulipani, S.; Quiles, J. L.; Mezzetti, B.; Battino, M. Strawberry polyphenols attenuate ethanol-induced gastric lesions in rats by activation of antioxidant enzymes and attenuation of MDA increase. *PLoS One* **2011**, *6*, e25878.

(10) Giampieri, F.; Alvarez-Suarez, J. M.; Tulipani, S.; Gonzàles-Paramàs, A. M.; Santos-Buelga, C.; Bompadre, S.; Quiles, J. L.; Mezzetti, B.; Battino, M. Photoprotective potential of strawberry (*Fragaria* × *ananassa*) extract against UV-A irradiation damage on human fibroblasts. *J. Agric. Food Chem.* **2012**, *60*, 2322−2327.

(11) Tulipani, S.; Mezzetti, B.; Battino, M. Impact of strawberries on human health: insight into marginally discussed bioactive compounds for the Mediterranean diet. *Public Health Nutr.* **2009**, *12*, 1656−1662.

(12) Lopes da Silva, F.; Escribano-Bailon, M. T.; Perez Alonso, J. J.; Rivas-Gonzalo, J.; Santos-Buelga, C. Anthocyanin pigments in strawberry. *LWT−Food Sci. Technol.* **2007**, *40*, 374−382.

(13) Wang, S. Y.; Lewers, K. S. Antioxidant capacity and flavonoid content in wild strawberries. *J. Am. Soc. Hortic. Sci.* **2007**, *132*, 629−637.

(14) Mikulic-Petkovsek, M.; Slatnar, A.; Stampar, F.; Veberic, R. HPLC-MS^n identification and quantification of flavonol glycosides in 28 wild and cultivated berry species. *Food Chem.* **2012**, *135*, 2138−2146.

(15) Mahmood, T.; Anwar, F.; Abbas, M.; Saari, N. Effect of maturity on phenolics (phenolic acids and flavonoids) profile of strawberry cultivars and mulberry species from pakistan. *Int. J. Mol. Sci.* **2012**, *13*, 4591−4607.
(16) Buendía, B.; Gil, M. I.; Tudela, J. A.; Gady, A. L.; Medina, J. J.; Soria, C.; López, J. M.; Tomás-Barberán, F. A. HPLC-MS analysis of proanthocyanidin oligomers and other phenolics in 15 strawberry cultivars. *J. Agric. Food Chem.* **2010**, *58*, 3916−3926.
(17) Wang, S. Y.; Zheng, W. Effect of plant growth temperature on antioxidant capacity in strawberry. *J. Agric. Food Chem.* **2001**, *49*, 4977−4982.
(18) Starvic, B.; Matula, T. I.; Klassen, R.; Downie, R. H.; Wood, R. J. Effect of flavonoids on mutagenicity and bioavailability of xenobiotics in food. In *Phenolic Compounds in Food and Their Effects on Health II. Antioxidants and Cancer Prevention*; Huang, M. T., Ho, C. T., Lee, C. Y., Eds.; ACS Symposium Series 507; American Chemical Society: Washington, DC, USA, 1992; pp 239−249.
(19) Santos-Buelga, C.; Scalbert, A. Proanthocyanidins and tanninlike compounds-nature, occurrence, dietary intake and effects on nutrition and health. *J. Sci. Food Agric.* **2000**, *80*, 1094−1117.
(20) Giampieri, F.; Tulipani, S.; Alvarez-Suarez, J. M.; Quiles, J. L.; Mezzetti, B.; Battino, M. The strawberry: composition, nutritional quality, and impact on human health. *Nutrition* **2012**, *28*, 9−19.
(21) Määttä-Riihinen, K. R.; Kamal-Eldin, A.; Törrönen, A. R. Identification and quantification of phenolic compounds in berries of *Fragaria* and *Rubus* species (family Rosaceae). *J. Agric. Food Chem.* **2004**, *52*, 6178−6187.
(22) Aaby, K.; Ekeberg, D.; Skrede, G. Characterization of phenolic compounds in strawberry (*Fragaria* × *ananassa*) fruits by different HPLC detectors and contribution of individual compounds to total antioxidant capacity. *J. Agric. Food Chem.* **2007**, *55*, 4395−4406.
(23) Mattila, P.; Hellstrom, J.; Törrönen, R. Phenolic acids in berries, fruits, and beverages. *J. Agric. Food Chem.* **2006**, *54*, 7193−7199.
(24) Okuda, T.; Yoshida, T.; Hatano, T. Ellagitannins as active constituents of medical plants. *Planta Med.* **1989**, *55*, 117−122.
(25) Battino, M.; Mezzetti, B. Update on fruit antioxidant capacity: a key tool for Mediterranean diet. *Public Health Nutr.* **2006**, *9*, 1099−1103.
(26) Lerceteau-Köhler, E.; Moing, A.; Guérin, G.; Renaud, C.; Petit, A.; Rothan, C.; Denoyes, B. Genetic dissection of fruit quality traits in the octoploid cultivated strawberry highlights the role of homoeo-QTL in their control. *Theor. Appl. Genet.* **2012**, *124*, 1059−1077.
(27) Scalzo, J.; Politi, A.; Pellegrini, N.; Mezzetti, B.; Battino, M. Plant genotype affects total antioxidant capacity and phenolic contents in fruit. *Nutrition* **2005**, *21*, 207−213.
(28) Josuttis, M.; Carlen, C.; Crespo, P.; Nestby, R.; Toldam-Andersen, T. B.; Dietrich, H.; Kruger, E. A comparison of bioactive compounds of strawberry fruit from Europe affected by genotype and latitude. *J. Berry Res.* **2012**, *2*, 73−95.
(29) Tulipani, S.; Mezzetti, B.; Capocasa, F.; Bompadre, S.; Beekwilder, J.; de Vos, C. H. R.; Capanoglu, E.; Bovy, A.; Battino, M. Antioxidants, phenolic compounds, and nutritional quality of different strawberry genotypes. *J. Agric. Food Chem.* **2008**, *56*, 696−704.
(30) Ulrich, D.; Hoberg, E.; Rapp, A.; Kecke, S. Analysis of strawberry flavour − discrimination of aroma types by quantification of volatile compounds. *Z. Lebensm. Unters Forsch. A* **1997**, *205*, 218−223.
(31) Ulrich, D.; Komes, D.; Olbricht, K.; Hober, E. Diversity of aroma patterns in wild and cultivated *Fragaria* accessions. *Genetic Resources Crop Evol.* **2007**, *54*, 1185−1196.
(32) Colquhoun, T. A.; Levin, L. A.; Moskowitz, H. R.; Whitaker, V. M.; Clark, D. G.; Folta, K. M. Framing the perfect strawberry: an exercise in consumer-assisted selection of fruit crops. *J. Berry Res.* **2012**, *2*, 45−61.
(33) Della Penna, D. Plant metabolic engineering. *Plant Physiol.* **2001**, *125*, 160−163.
(34) Schaart, J. G.; Dubos, C.; Romero De La Fuente, I.; van Houwelingen, A. M.; de Vos, R. C.; Jonker, H. H.; Xu, W.; Routaboul, J. M.; Lepiniec, L.; Bovy, A. G. Identification and characterization of MYB-bHLH-WD40 regulatory complexes controlling proanthocyanidin biosynthesis in strawberry (*Fragaria* × *ananassa*) fruits. *New Phytol.* **2013**, *197*, 454−467.
(35) Whitaker, V. M. Applications of molecular markers in strawberry. *J. Berry Res.* **2011**, *1*, 115−127.
(36) Capocasa, F.; Diamanti, J.; Tulipani, S.; Battino, M.; Mezzetti, B. Breeding strawberry (*Fragaria* × *ananassa* Duch) to increase fruit nutritional quality. *Biofactors* **2008**, *34*, 67−72.
(37) Diamanti, J.; Capocasa, F.; Balducci, F.; Battino, M.; Hancock, J.; Mezzetti, B. Increasing strawberry fruit sensorial and nutritional quality using wild and cultivated germplasm. *PLoS One* **2012**, *7*, e46470.
(38) Miller, N. J.; Rice-Evans, C.; Davis, M. J. A novel method for measuring antioxidant capacity and its application to monitoring the antioxidant status in premature neonates. *Clin. Sci.* **1993**, *83*, 407−412.
(39) Re, R.; Pellegrini, N.; Proteggente, A.; Pannala, A.; Yang, M. Antioxidant activity applying an improved ABTS radical cation decolorization assay. *Free Radical Biol. Med.* **1999**, *26*, 1231−1237.
(40) Slinkard, K.; Singleton, V. L. Total phenol analysis: automation and comparision with manual methods. *Am. J. Enol. Vitic.* **1977**, *28*, 49−55.
(41) Giusti, M.; Wrolstad, R. E. Characterization and measurement of anthocyanins by UV-visible spectroscopy. In *Current Protocols in Food Analytical Chemistry*; Wiley: Hoboken, NJ, USA, 2001; pp F1.2.1−F1.2.13.
(42) Diamanti, J.; Capocasa, F.; Battino, M.; Mezzetti, B. Evaluation of *F.* × *ananassa* intra-specific and inter-specific back-crosses to generate new genetic material with increased fruit nutritional quality. *J. Berry Res.* **2010**, *1*, 103−114.

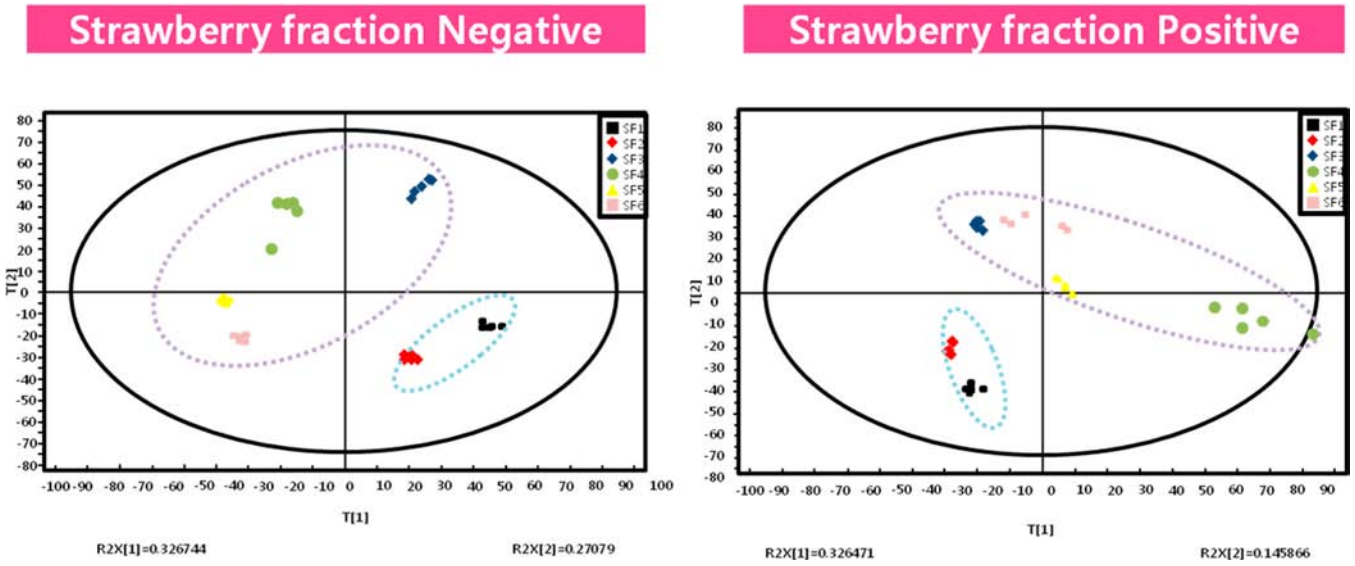

Figure 1. Principal component analysis for the metabolites in extracted fractions analyzed by LC-ESI-ion trap MS/MS in negative (left) and postive (right) ion modes. SF−SF6: 'Seolhyang' strawberry fractions extracted as described under Materials and Methods.

restoring the inhibitory κB (IκB) and inhibiting cytokine expression.

MATERIALS AND METHODS

Materials. 'Sheolhyang' strawberry (*Fragaria* × *ananassa* Duch.) cultivated in Asan, South Korea, was purchased in May 2012 and used for the multisolvent extraction. Elliagic acid, chlorogenic acid, *p*-coumaric acid, kaempferol, quercetin hydrate, quercetin 3-*O*-glucoside, (+)-catechin hydrate, pelargonidin 3-*O*-glucoside, pelargonidin 3-*O*-rutinoside, cyanidin 3-*O*-glucoside chloride, and formic acid were obtained from the Sigma-Aldrich Corp. (St. Louis, MO, USA). Ethyl acetate, methanol, and acetonitrile were from DUCKSAN (Ansan, South Korea), SAMCHUN (Yeosu, South Korea), and Burdick & Jackson (Muskegon, MI, USA), respectively.

Metabolite Extraction. Strawberries were cleaned immediately after harvest and freeze-dried, and dried powders were stored at −80 °C until extraction. Polyphenols in the strawberry were prepared by multisolvent extraction with ethyl acetate and methanol according to the method of Määttä-Riihinen et al. with modification.[27] Freeze-dried strawberry powders (2.5 g) were mixed with 10 mL of ethyl acetate and stirred for 30 min at room temperature, and the supernatant was collected. The supernatant was divided in two groups as fraction 1 (SF1), and the other part was washed with 0.1 M sodium acetate (pH 7.0) and distilled water and prepared as fraction 2 (SF2). Solvents in SF1 and SF2 were evaporated and resuspended with methanol for LC-MS/MS analysis. The residue of ethyl acetate extraction was extracted with acidic methanol, and the supernatant was divided into two groups. Supernatant was indicated as fraction 3 (SF3), and fraction 4 (SF4) was prepared after acidic hydrolysis of fraction 3. The residue after acidic methanol extraction was further treated with acidic methanol, and the supernatant was collected as fraction 6 (SF6); then fraction 5 (SF5) was prepared after more acidic hydrolysis of the residues.

LC-MS/MS Analysis. Samples were analyzed using an Accela HPLC system with a PDA detector (Accela 80 Hz PDA detector) and an LTQ-Velos ion trap mass spectrometer fitted with a heat electrospray ionization interface (Thermo Fisher Scientific, San Jose, CA, USA). Separation was carried out using an UPLC BEH C18 column (1.7 μm, 100 × 2.1 mm i.d., Acquity, Waters, Milford, MA, USA). The elution gradient was carried out with a binary solvent system consisting of 0.1% formic acid in water (phase A) and 0.1% formic acid in acetonitrile (phase B) at a constant flow rate of 0.3 mL/min. The linear gradient profile was as follows: 5−10% B over 5 min, held at a 10% B over 5 min, 10−40% B over 20 min, 40−90% B over 10 min, then returned to the initial conditions (5% B) in 5 min and conditioning at 5% B over 10 min, finished at 55 min. The column temperature was 36 °C, and the UV spectra were measured between 180 and 800 nm. Acquisition was performed in the negative and positive modes by electrospray ionization (ESI) source, and the *m*/*z* range was 100−1000 Da. The capillary temperature was 275 °C, and the source voltage was set to 5 kV for ionization.

Data Processing and Metabolite Identification. Peak detection, alignment, and identification were performed using SIEVE software (Thermo Fisher Scientific, Waltham, MA, USA). The MS/MS fragmentation patterns were used for informative nontargeted metabolic profiling of LC-MS data. The acquired LC-MS/MS spectrum was identified after comparison with those proposed by the Massbank database (www.massbank.jp), KEGG database (www.kegg.co.jp), Metlin (http://masspec.scripps.edu), and related reports.

Statistical Analysis. Samples were run in five replicates. All of these statistical analyses were performed using SIMCA (Umetrics, Sweden). Unsupervised multivariate statistical analysis was used to detect possible differences among groups by PCA, and the S-plot generated by OPLS-DA was applied to detect maximal separation of distinctive metabolites in each fraction. For cell proliferation assay, Western blot, and quantitative RT-PCR, the Student *t* test was used.

Cell Culture. RAW 264.7 cells were obtained from the Korean Cell Line Bank (Seoul, Korea) and were cultured in DMEM supplemented with 10% fetal bovine serum, 1% penicillin/streptomycin, and 1% HEPES at 37 °C, 5% CO_2. The RAW 264.7 cells were stimulated with LPS (100 ng/mL) and treated with different fractions (SF1−SF6) or ellagic acid at the concentrations as shown in the figure captions.

Cell Proliferation Assay. RAW 264.7 cells were plated (1×10^4 cells/well) in a 96-well plate overnight and then treated with different concentrations of strawberry fractions (20, 50, and 100 μg/mL) for 72 h in the growth medium. Before 4 h of harvest, 3-(4,5-dimethylthiazol-2-yl)-2,5-diphenyltetrazolium bromide (MTT, Sigma) solution (200 μL) was added to each well. The dark blue formazan crystals formed were dissolved in DMSO, and the absorbance was measured with an ELISA reader at 570 nm (Molecular Devices, Sunnyvale, CA, USA). Cell proliferation was described as the relative cell viability compared to the control.

Western Blot Analysis. After RAW 264.7 cells were cultured overnight, they were treated with strawberry fractions and ellagic acid for 15 min or 24 h. The cells were washed with PBS and then harvested with radioimmunoprecipitation assay (RIPA) buffer (10 mM Tris-HCl, 5 mM EDTA, 150 mM NaCl, 1% Triton X-100, 1% sodium deoxycholate, 0.1% SDS, 0.1 mM Na_3VO_4, 1% phenylmethanesulfonyl fluoride, 1% protease inhibitor) to extract the cellular proteins. After

dx.doi.org/10.1021/jf4038503 | J. Agric. Food Chem. 2014, 62, 3954−3962

centrifugation at 12000*g* for 15 min, the same amount of protein (30 μg) was loaded in 10% polyacrylamide gel and electrophoretically separated and transferred to a polyvinylidene difluoride membrane (Millipore, Billerica, MA, USA). The primary antibodies against iNOS, COX2, IκBα, JNK (Santa Cruz Biotech, Santa Cruz, CA, USA), phospho-ERK, phospho-p38, phospho-JNK, phospho-Stat1 (Cell Signaling Technology, Boston, MA, USA), β-actin (Sigma), and secondary antibodies (Santa Cruz) were used. The expression levels of proteins were visualized with EZ capture MG (ATTO, Tokyo, Japan) and quantified with CS Analyzer (ver.3.0, ATTO).

RNA Extraction and Quantitative RT-PCR Analysis. RAW 264.7 cells (7×10^5 cells/10 cm dish) were treated with strawberry fraction (SF4) and ellagic acid for 15 h. Total cellular RNA was isolated by Trizol reagent (Sigma) and reverse-transcribed to cDNA using a RevertAid First Strand cDNA Synthesis Kit (Theromo Scientific, Lafayette, CO, USA) in a 96-well format Atlas Thermal Cycler (Astec, Fukuoka, Japan). The cDNA was amplified using TaqMan Fast Advanced Master Mix (Applied Biosystems, Foster City, CA, USA) on an ABI Prism 7500 real-time PCR system (Applied Biosystems). The temperature cycling conditions used for amplification were one cycle of 50 °C for 2 min, one cycle of 95 °C for 20 s, and 40 cycles of 95 °C for 3 s and 60 °C for 30 s. Labeled TaqMan primers including tumor necrosis factor-α (TNF-α), interleukin-1β (IL-1β), interleukin-6 (IL-6), and glyceraldehydes-3-phosphate dehydrogenase (GAPDH) were purchased from Applied Biosystems. The relative quantification of target mRNA was calculated using the comparative $2^{-\Delta\Delta CT}$ method after normalization with the internal control, GAPDH.

RESULTS

Metabolomic Phenotyping of Multistep Solvent Extracts from Strawberry. Through multisolvent extraction, strawberry metabolites were fractionated into six groups. Fractions 1 (SF1) and 2 (SF2) were extracted with ethyl acetate, and fractions 3−6 (SF3−SF6) were prepared by methanol extracts. The yield of each fraction from SF1 to SF6 was determined as 0.01, <0.01, 10.93, 59.54, 3.63, and 1.00%, respectively. Unsupervised multivariate analysis (PCA) implied that multisolvent extraction successfully classified the target metabolites into different groups. In negative mode, vector 1 (explaining 32.7% of the total variance) discriminated the metabolite profiles by different solvents, whereas vector 2 explained 27.0% of the total variance. The ethyl acetate group (SF1, SF2) was clearly separated by methanol groups (SF3−SF6) as depicted in Figure 1. In positive mode, metabolites in each fraction were discriminated by principal components 1 (explaining 32.6% of the total variance) and 2 (14.6% of the total variance), and a similar pattern was found in negative mode. The PCA score plots demonstrated the distinctive metabolite phenotypes induced by the multisolvent extraction. Metabolites contained in each fraction were identified and summarized (supplementary Tables 1 and 2 in the Supporting Information).

Strawberry Fraction 1 (SF1). As an ethyl acetate extract, SF1 would contain less polar compounds such as hydroxycinnamic acid derivatives, flavan-3-ols (contain catechin), and dimeric and trimeric proanthocyanidins and flavonol glycosides. In the present study, (+)-catechin hydrate (RT 5.42, *m/z* 289.69), *p*-coumaroyl-glucoside (RT 5.90, *m/z* 325.19), kaempferol 3-*O*-acetyglucoside (RT 18.86, *m/z* 489.17), galloylglucoside (RT 6.38, *m/z* 331.97), proanthocyanidin dimer (EC-4,8-C) (RT 4.71, *m/z* 557.30), ferulic acid hexose derivative (RT 8.16, *m/z* 449.26), and dicoumaroyl hexose (RT 28.72, *m/z* 471.25) were identified as the main compounds in negative ion mode. Pelargonidin 3-*O*-glucoside (RT 7.89, *m/z* 433.25), (+)-catechin hydrate (RT 2.12, *m/z* 291.13), 4′-*O*-methylglucoliquiritigenin (RT 9.27, *m/z* 433.18), pelargonidin 3-*O*-(6-*O*-malonyl-β-D-glucoside) (RT 14.66, *m/z* 519.29), and quercetin malonylhexose (RT 20.68, *m/z* 551.31) were mainly found in positive ion mode.

Strawberry Fraction 2 (SF2). SF2 was washed SF1, and epicatechin (RT 5.42, *m/z* 289.69), baicalein-7-*O*-glucoside (RT 8.16, *m/z* 431.33), and proanthocyanidin B4 (RT 4.71, *m/z* 577.30) were found in negative ion mode, whereas pelargonidin 3-*O*-glucoside (RT 7.89, *m/z* 433.25), (+)-catechin hydrate (RT 5.37, *m/z* 291.06), luteolin (RT 19.10, *m/z* 287.73), kaempferol (RT 20.65, *m/z* 287.80), and 1-*O*-galloyl-β-D-glucose (RT 13.83, *m/z* 333.17) were identified under positive ion mode.

Strawberry Fraction 3 (SF3). SF3, as a simple methanol extract, proanthocyanidin dimer (RT 4.71, *m/z* 577.30), (+)-catechin hydrate (RT 5.42, *m/z* 289.69), ellagitannin (RT 10.93, *m/z* 935.22), kaempferol coumaroyl hexose (RT 22.41, *m/z* 593.29), quercetin 3-*O*-glucuronide (RT 15.42, *m/z* 477.16), and *p*-coumaroyl glucoside (RT 5.90, *m/z* 325.19) were identified in negative ion mode. Pelargonidin 3-*O*-glucoside (RT 7.89, *m/z* 433.25) and pelargonidin 3-*O*-(6-malonyl-β-D-glucoside) (RT 14.66, *m/z* 519.29) were found in positive ion mode.

Strawberry Fraction 4 (SF4). SF4 was prepared through the acidic hydrolysis step of SF3. In negative mode of analysis, pelargonidin 3-*O*-glucoside (RT 6.91, *m/z* 431.16), delphinidin (RT 15.29, *m/z* 301.67), ellagic acid (RT 13.16, *m/z* 301.73), quercetin 3-methyl ether 7-rhamnoside (RT 3.35, *m/z* 461.16), and 5,2′-dihydroxy-6,7,8,6′-tetramethoxyflavone (RT 18.22, *m/z* 373.27) were found, whereas pelargonidin 3-*O*-glucoside (RT 7.89, *m/z* 433.25), pelargonidin (RT 15.90, *m/z* 271.64), gallic acid (RT 14.17, *m/z* 171.32), and petunidin (RT 14.24, *m/z* 317.14) were identified in positive ion mode.

Strawberry Fraction 5 (SF5). Delphinidin (RT 15.29, *m/z* 301.67), kaempferol 7,4′-dimethyl ether 3-*O*-sulfate (RT 26.06, *m/z* 393.18), bis-HHDP-glucose (RT 2.94, *m/z* 739.42), and ellagic acid (RT 13.16, *m/z* 301.73) were detected in negative ion mode, whereas pelargonidin 3-*O*-glucoside (RT 7.89, *m/z* 433.25), pelargonidin (RT 15.90, *m/z* 271.64), and diosmetin and (RT 13.51, *m/z* 301.18) were found in positive ion mode.

Strawberry Fraction 6 (SF6). Ellagic acid (RT 17.302, *m/z* 301.66), delphinidin (RT 15.29, *m/z* 301.67), and cyanidin 3-glucoside-7-rhamnoside (RT 24.75, *m/z* 593.31) were the main compounds in negative ion mode. Pelargonidin 3-*O*-glucoside (RT 7.89, *m/z* 433.25), pelargonidin (RT 12.52, *m/z* 271.53), diosmetin (RT 13.51, *m/z* 301.18), and cyanidin 3-*O*-(6-*O*-*p*-coumaroyl)-glucoside (RT 22.02, *m/z* 595.25) were identified in positive ion mode of analysis.

Strawberry Fractions Exerted Anti-inflammatory Activity in RAW 264.7 Cells without Cytotoxicity. To evaluate the cytotoxic effect of strawberry, RAW 264.7 cells were treated with different concentrations (20, 50, and 100 μg/mL) of strawberry fractions (SF1−SF6), and cell viability was determined by the MTT assay. As shown in Figure 2A, none of the strawberry fractions showed significant cytotoxicity at the concentrations tested. To investigate the regulatory activity of strawberry fractions on inflammation, we evaluated the expression level of the well-known inflammatory markers, iNOS and COX-2, after the induction LPS. The murine macrophage RAW 264.7 cells were treated with the strawberry fractions (20 μg/mL) for 24 h. Among the fractions, SF4 exerted the strongest inhibition of iNOS protein expression,

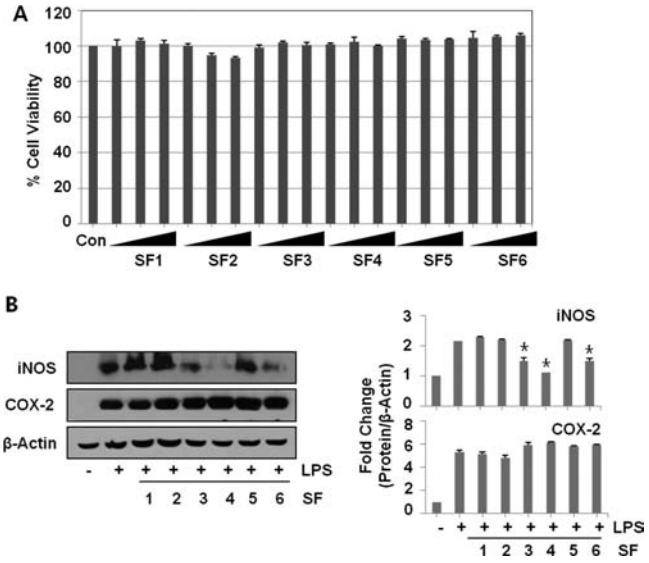

Figure 2. Effects of 'Seolhyang' strawberry fractions (SF1−SF6) on cell viability and expression level on iNOS and COX-2 protein in RAW 264.7 cells. (A) The cells (10000 cells/well in 96-well plate) were treated with strawberry fractions (SF1−SF6; 20, 50, 100 μg/mL) for 72 h, and cell viability was determined by MTT assay. (B) The cells (7×10^5/well in 60 mm dish) were treated with strawberry fractions (SF1−SF6; 20 μg/mL) with LPS (100 ng/mL) for 24 h. The level of protein expression was determined by Western blotting and normalized with β-actin. Statistical significance was determined by Student's t test compared to the LPS-treated group (∗, $P < 0.05$).

followed by SF4 and SF6, although the COX-2 level was not affected (Figure 2B). Next, we selected the potent fractions, SF3, SF4, and SF6, for further study to determine the concentration dependency in regulating iNOS. As shown in Figure 3A, all fractions at concentrations of 20, 50, and 100 μg/mL were found to suppress iNOS expression in a dose-dependent manner, among which SF4 possessed the most potent efficacy. However, we also confirmed that there was no regulatory activity in COX-2 expression by strawberry fractions up to 100 μg/mL.

SF3 and Especially SF4 Regulated the Inflammatory Mediators Inhibitory κB and ERK in LPS-Stimulated RAW 264.7 Cells. The inflammatory mechanism induced by LPS has been suggested to be from transducing the intracellular signaling through nuclear factor κB (NFκB) and mitogen-activated protein kinases (MAPKs) including extracellular signal-regulated kinase (ERK), c-Jun N-terminal kinase (JNK), and p38.[28] Here, we determined whether the strawberry fractions showing iNOS inhibitory activity might regulate the NFκB and MAPKs signaling pathways. Inhibitory κBs (IκBs) preventing translocation of NFκB into the nucleus are known to be degraded by proteasome after the inflammatory stimulation by LPS, and we found that SF3 and especially SF4 exerted significant restoration of IκBα. In addition, the phosphorylation of ERK induced by LPS was blocked more significantly by SF4 (Figure 3B). These results suggest that the strawberry fractions, especially SF4, may contain active metabolites playing important roles in suppressing inflammation induced by LPS in RAW 264.7 cells.

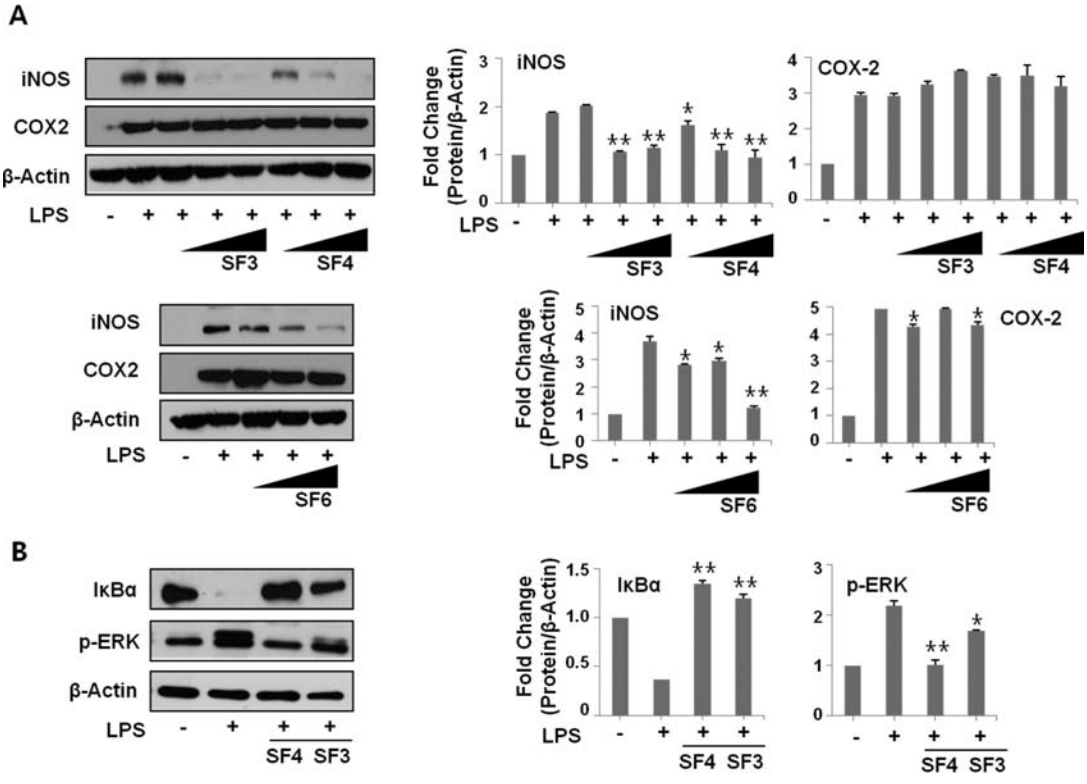

Figure 3. Effects of SF3, SF4, and SF6 on LPS-induced iNOS, COX-2, IκBα, and p-ERK protein expression in RAW 264.7 cells. (A) The cells (7×10^5/well in 60 mm dish) were treated with SF3, SF4, and SF6 (20, 50, 100 μg/mL) with LPS (100 ng/mL) for 24 h. The level of protein expression was determined by Western blotting and normalized with β-actin. (B) The cells were treated with SF3 and SF4 (100 μg/mL) with LPS (100 ng/mL) for 15 min. The level of protein expression was determined by Western blotting and normalized with β-actin. Statistical significance was determined by Student's t test compared to the LPS-treated group (∗, $P < 0.05$; ∗∗, $P < 0.01$).

dx.doi.org/10.1021/jf4038503 | J. Agric. Food Chem. 2014, 62, 3954−3962

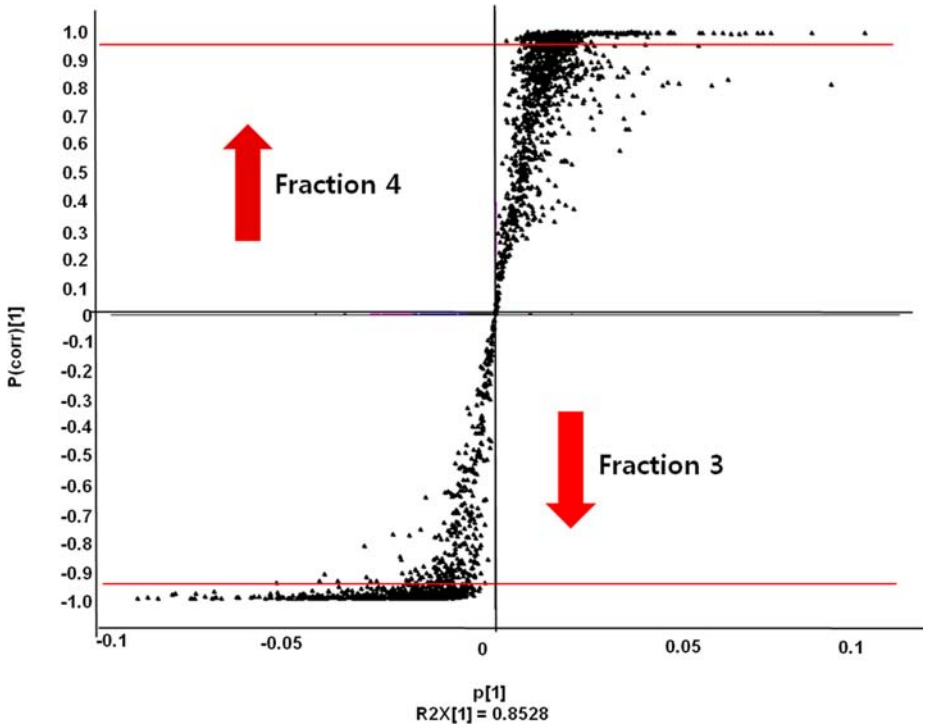

Figure 4. S-plot generated by orthogonal partial least-squares discriminant analysis (OPLS-DA) for the metabolite in SF3 and SF4.

Table 1. Metabolites Identified in SF3 and SF4 Discriminated by OPLS-DA

fraction 3			fraction 4	
$P < 0.01$	$P < 0.05$	common compound	$P < 0.05$	$P < 0.01$
	1-*O*-galloyl-*β*-D-glucose	(+)-catechin hydrate	5,2′-dihydroxy-6,7,8,6′-tetramethoxyflavone	
	4′-*O*-methylglucoliquiritigenin	caffeic acid 3-glucoside	chrypsin-6-*C*-arabinose-8-*C*-glucose	
	5,4′-dihydroxy-3,7,3′-trimethoxy-8-prenylflavone	baicalein glucoside	cyanidin	
	5-hydroxy-3,6,7,2′,4′,5′-hexamethoxyflavone	caffeoylhexose (1-caffeoyl-*β*-D-glucose	delphinidin	
	bis-HHDP-glucose	chrysin-6-*C*-glu-8-*C*-arabinose	gallic acid	
	caffeoylhexose	ferulic acid hexose derivate	galloyl-bis-HHDP-glucose	
	cyanidin 3-(4′-acetylglucoside)	isoliquiritigenin 2′-glucosyl-(1→4)-rhamnoside	isorhamnetin hexose malonyl hexose	
	cyanidin 3-*O*-glucoside	kaempferol	kaempferol 3-rhamnosyl-(1→3)(4‴-*p*-coumarylrhamnosyl) (1→6)-glucoside	
	cllagitannin	kaempferol 7,4′-dimethyl ether 3-glucoside	luteolin 3′-methyl ether 7-malonylglucoside	
kaempferol 7-*O*-glucoside	epicatechin	kaempferol coumaroyl hexose	pelargonidin 3-[6-(3-glucosylcaffeyl)glucoside]-5-glucoside	
	galloyl-HHDP-glucose	kaempferol glucoside	petunidin	ellagic acid
quercetin 3-*O*-glucuronide	isoliquiritigenin 2′-glucosyl-(1→4)-rhamnoside	kaempferol-coumaroyl-hexose	proanthocyanidin A2	
	isorhanmetin glucuronide	kaempferol-malonyl-glucoside	quercetin 3-methyl ether 7-rhamnoside	
	kaempferol 3,4′-dixyloside	pelargonidin	quercetin 3-methyl ether	
	kaempferol 7-(6″-*p*-succinylglucoside)	pelargonidin-3-*O*-glucoside	sinapic acid	
	kaempferol 7-*O*-glucoside	pelargonidin-malonyl-glucoside		
	kaempferol-malonyl-glucoside	proanthocyanidin dimer		
	methoxykaempferol glucoside	procyanidin		
	p-coumaroyl glucoside	propelargonidin trimer		
	proanthocyanidin dimer	quercetrin		
	propelargonidin trimer			
	quercetin			
	quercetin 3-*O*-glucuronide			

Ellagic Acid Was Identified as a Unique Constituent Present in SF4 Compared to SF3. We explored the subset of metabolites that may serve as anti-inflammatory agents in the fractions prepared by multistep solvent extraction. Metabolite

dx.doi.org/10.1021/jf4038503 | J. Agric. Food Chem. 2014, 62, 3954−3962

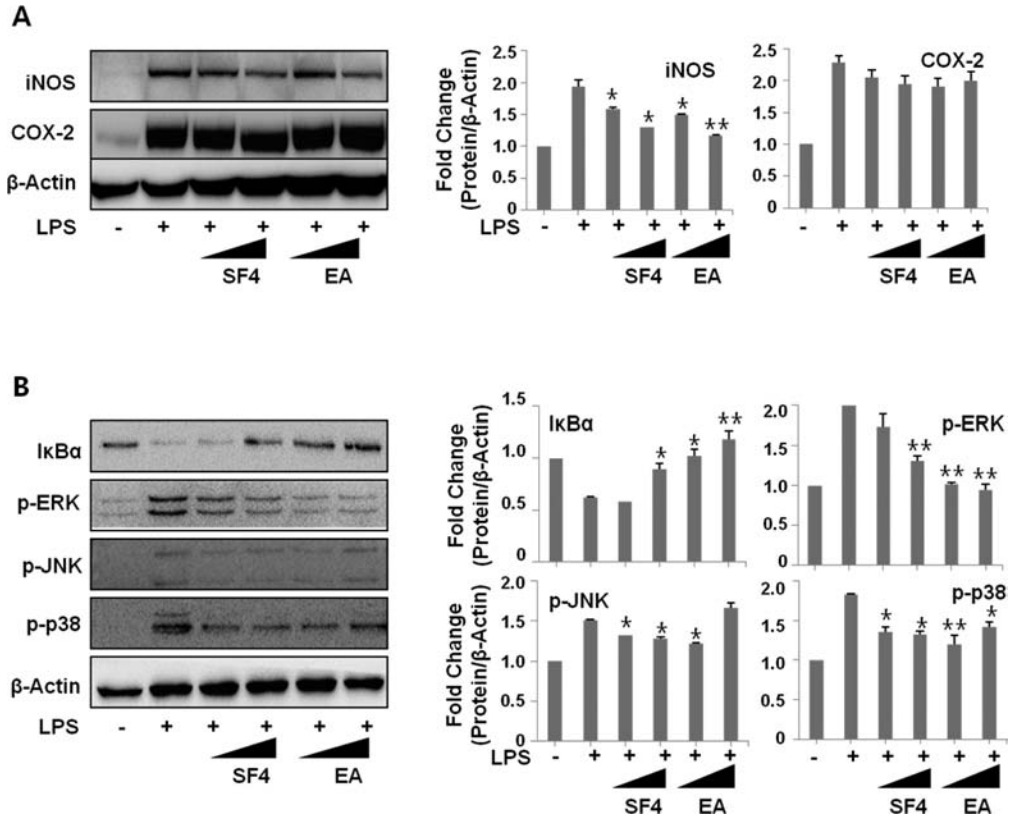

Figure 5. Effects of SF4 and ellagic acid on LPS-induced phosphorylation of MAPKs, LPS-mediated IκBα degradation, and iNOS and COX-2 protein expression in RAW 264.7 cells. The cells (7×10^5/well in 60 mm dish) were treated with SF4 (50, 100 μg/mL) and ellagic acid (0.3, 1.0 μM) with LPS (100 ng/mL) for 24 h (A) and 15 min (B). The level of protein expression was determined by Western blotting and normalized with β-actin. Statistical significance was determined by Student's *t* test compared to the LPS-treated group (∗, $P < 0.05$; ∗∗, $P < 0.01$).

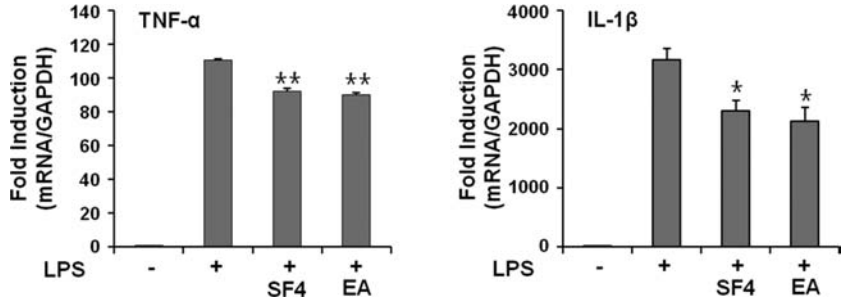

Figure 6. Effects of SF4 and ellagic acid on mRNA expression of cytokines, TNF-α, and IL-1β in LPS-induced RAW 264.7 cells. The cells (7×10^5/well in 60 mm dish) were treated with SF4 (100 μg/mL) and ellagic acid (0.3 μM) with LPS (100 ng/mL) for 15 h. The mRNA levels of TNF-α and IL-1β were measured by quantitative RT-PCR. Statistical significance was determined by Student's *t* test compared to the LPS-treated group (∗, $P < 0.05$; ∗∗, $P < 0.01$).

profiles of SF3 and SF4 were analyzed by OPLS-DA, and an S-plot clearly visualized the different variables between SF3 and SF4 (Figure 4). Anthocyanin families such as cyanidins, pelargonidin, and quercetin were found in both fractions; however, ellagic acid was significantly higher in SF4 compare to SF3 ($P < 0.01$, Table 1).

Ellagic Acid and SF4 Regulated the Same Inflammatory Mediators in LPS-Stimulated RAW 264.7 Cells. The contents of ellagic acid in strawberry are different across cultivars,[29] and the average amount of it was calculated as 1.24 mg/100 g FW.[30] We also determined the amount of ellagic acid in SF3 and SF4 and found that SF4 contained about 25-fold more ellagic acid than SF3 (data not shown). On the basis of those studies, we chose the concentrations of ellagic acid for treatment, 0.3 and 1.0 μM, to compare the inflammation regulatory effect with SF4. As shown in Figure 5, SF4 (50 and 100 μg/mL) and ellagic acid (0.3 and 1.0 μM) exerted similar activities in regulating the LPS-induced inflammatory mediators through inhibiting iNOS protein expression, blocking IκBα degradation, and suppressing phosphorylation of ERK, JNK, and p38, without affecting COX-2 expression. These results suggest that SF4 and ellagic acid regulate iNOS expression via suppressing NFκB and MAPK signaling pathways, and ellagic acid might be an active component in strawberry fraction, SF4, showing anti-inflammatory effect.

Ellagic Acid and SF4 Reduced the Level LPS-Induced Pro-inflammatory Cytokines. Pro-inflammatory cytokines including TNF-α, IL-1β, and IL-6 play important roles in the

dx.doi.org/10.1021/jf4038503 | J. Agric. Food Chem. 2014, 62, 3954−3962

inflammatory process.[31] To investigate the regulatory activity of the representative cytokine expression by SF4 and ellagic acid, we performed quantitative RT-PCR. Here, we confirmed that ellagic acid and SF4 showed significant suppression of LPS-induced TNF-α and IL-1β mRNA expression at similar levels (Figure 6). However, the mRNA level of IL-6 was not affected by either ellagic acid or SF4 (data not shown). These results also suggest that ellagic acid may be the key metabolite in SF4 possessing the inflammation regulatory effect in macrophage cells.

DISCUSSION

The metabolomics approach is an efficient way to open a whole set of metabolites and define unique metabolomic phenotyping through various statistical analyses along with subsequent annotation of the features. Although different techniques have been used to characterize and quantify active compounds in the berry family, just simple comparison and characterization have been attempted due to the complexity of the constituents and their dependence on the extraction methods.[32] Major bioactive compounds in strawberry can be classified into five groups including phenolic acids, stilbenes, flavonoids, tannins, and lignans, and different features of each group make it difficult for the multidimensional characterization of bioactive compounds in a single step of analysis. However, successful application of metabolomics on the characterization of black raspberry demonstrated that the screening of bioactive compounds from strawberry would be possible through the correlation of metabolomic data with activity evaluation in vitro.[33]

In this study, we prepared six different fractions (SF1−SF6) of strawberry 'Seolhyang' using ethyl acetate and methanol, profiled the whole metabolites with HPLC-ESI-ion trap MS/MS (Figure 1), and compared the inhibitory effects on iNOS protein expression (Figures 2 and 3). Among them, we chose the most active fractions, SF3 and SF4, and found the statistically unique components, kaempferol 7-*O*-glucoside and quercetin 3-*O*-glucoside in SF3 and ellagic acid in SF4, using OPLS-DA (Table 1). These results indicate that ellagic acid in SF4 may act as one of the key constituents exerting health beneficial efficacy when SF4 shows more significant physiological activities than SF3.

Inflammation is the systematic process of the host defense mechanism to eliminate harmful stimuli such as bacterial infection and tissue injuries, and chronic inflammation is well-known to be associated with the development of different chronic diseases including obesity, cardiovascular diseases, diabetes, and cancer.[31] The cellular stimulus of the inflammation activated Toll-like receptors (TLRs), which transduce the signal through IKK/NFκB or MAPK/AP-1 signaling pathways and enhance gene expression of pro-inflammtory cytokines, iNOS, and COX-2.[31,34] Strawberry juice, phenolic extracts, and polysaccharides in strawberry were reported to show anti-inflammatory effects through reducing pro-inflammatory cytokines such as IL-1β, IL-6, and TNF-α, as well as enhancing the anti-inflammtory cytokine IL-10.[3,35,36] However, it has not been demonstrated which active component plays a key role in regulating inflammation in those studies. To investigate the role of strawberry fractions on regulating the inflammation and identify the crucial components in the fractions, we used murine macrophage RAW 264.7 cells, which have been widely applied and suggested as a useful model for the evaluation of inflammation and immune-related kinetics.[37] In LPS-induced RAW 264.7 cells, SF4 exerted a more significant effect in regulating the inflammatory markers including iNOS suppression, IκB restoration, and ERK inhibition than SF3 (Figure 3). Because ellagic acid was identified as the most significantly different compound in SF4 compared to SF3, we concluded that ellagic acid is one of the key constituents exhibiting anti-inflammatory activity in SF4.

The effect of ellagic acid on inflammation has been studied using in vitro and in vivo models. In animal studies, dietary supplementation of ellagic acid in trinitrobenzenesulfonic acid (TNBS)-induced rat colitis and in dextran sulfate sodium-induced mouse colitis exerted anti-inflammatory activities through commonly regulating iNOS and COX-2 expression caused by inhibiting the MAPK and NFκB signaling pathways.[38−40] In addition, ellagic acid was reported to show suppression of LPS-induced inflammatory markers such as COX-2, microsomal PGE synthase-1, and cytosolic phospholipase 2Aα in human monocytes.[41] Lee et al. also evaluated the anti-inflammatory role of ellagic acid in oxidized low-density lipoprotein-mediated endothelial dysfunction.[42] Our results also support the role of ellagic acid present in SF4 in inhibiting LPS-induced inflammation via blocking the MAPK and NFκB signaling pathways in RAW 264.7 murine macrophage cells.

However, in the above in vitro studies evaluating the effect of ellagic acid on inflammation, the treatment concentration from 5 to 30 μM of ellagic acid is too high to reach by strawberry consumption.[41,42] Ellagic acid has been identified in different cultivars of strawberry ranging from 0.41 to 4.10 mg/100 g FW,[27,29,43] and its average amount is 1.24 mg/100 g FW.[30] To calculate the amount of ellagic acid in SF4, we first confirmed the yield of SF4 from freeze-dried strawberry powder, which was 59.4%. On that basis, the final concentration of ellagic acid in SF4 (100 μg/mL) was determined to be approximately 0.3 μM if we assumed that the whole ellagic acid (4.10 mg/100 g FW) was separated into SF4. We also analyzed the contents of ellagic acid in SF4, and its concentration was determined to approximately 7.99 mg/100 g FW (data now shown). The higher concentration of ellagic acid compared to the previous studies might be from the acidic conditions in SF4. Therefore, we treated ellagic acid at 0.3 and 1.0 μM and compared to SF4 treatment at 100 μg/mL in LPS-stimulated RAW 264.7 murine macrophage cells. As shown in Figure 5, we confirmed that SF4 and ellagic acid exhibited similar efficacy in regulating iNOS expression, blocking the degradation of IκBα, decreasing the phosphorylation of ERK, JNK, and p38, and suppressing pro-inflammatory cytokines TNF-α and IL-1β (Figures 5 and 6), suggesting the active component in SF4 responsible for anti-inflammation may be ellagic acid.

The absorption and metabolism of ellagic acid in vivo system is another factor we need to consider. Ellagitannins are demonstrated to release ellagic acid under physiological conditions in the digestive system using human colon adenocarcinoma Caco-2 cells and a monogastric Iberian pig model close to the human gastrointestinal tract.[44,45] In addition, >2-fold of ellagic acid was recovered in the ileal fluid from volunteers with an ileostomy after raspberry consumption, indicating the role of the stomach and/or the small intestine for the release of ellagic acid from ellagitannins.[46] In our study, ellagitannins in SF3 and ellagic acid in SF4 were detected because a more acidic condition was applied in SF4. These results suggest that the extraction conditions of SF4 may mimic the physiological conditions of the gastrointestinal tract in terms of the hydrolysis of ellagitannins.

After the finding that neither ellagitannins nor ellagic acid was detected in urine,[47] many studies have supported that ellagic acid is metabolized into urolithins, especially urolithin A and urolithin B,[44,46,48,49] raising the question of whether ellagic acid can reach the target organ where the macrophage exists as its original form. Although it is a critical issue to identify the actual potent phytochemicals that can act in vivo system, most metabolites produced from colonic microflora or hepatic system are not frequently present in the natural resources. To overcome this hurdle, the process of metabolism of natural active components must be elucidated and the correlation of in vitro and in vivo physiological efficacies validated.

Taken together, we employed the metabolomic approach to identify the key constituent showing physiological efficacy, that is, inflammation in this study. Ellagic acid was the significantly different component in SF4, compared to SF3, and we confirmed that ellagic acid possesses similar activity with SF4 in regulating NFκB and MAPK signaling pathways, which led to the reduction of cytokines (TNF-α and IL-1β) and iNOS expressions. These results demonstrate that ellagic acid from the strawberry 'Seolhyang' is the major component involved in suppressing inflammation. In addition, metabolomic analysis can be applied to determining the critical ingredients having biological functions in a complicated food matrix. It is, however, necessary to keep expanding the database to cover the whole metabolites in the mixture to reduce the possibility of missing potent unknown compounds.

■ ASSOCIATED CONTENT

Supporting Information

Supplementary Tables 1 and 2. This material is available free of charge via the Internet at http://pubs.acs.org.

■ AUTHOR INFORMATION

Corresponding Authors

*(J.-H.A.) Phone: +82-31-670-3079. Fax: +82-31-675-4853. E-mail: jhauh@cau.ac.kr.

*(H.J.L.) Phone: +82-31-670-3030. Fax: +82-31-675-4853. E-mail: hongjin@cau.ac.kr.

Author Contributions

‖J.L. and S.K. contributed to this work equally.

Funding

This work was carried out with the support of the Cooperative Research Program for Agriculture Science and Technology Development (PJ008550), Rural Development Administration, Republic of Korea, and by Chung-Ang University Excellent Freshman Scholarship Grants.

Notes

The authors declare no competing financial interest.

■ ABBREVIATIONS USED

SF, 'Seolhyang' strawberry fraction; TNF-α, tumor necrosis factor-α; NFκB, nucelar factor κB; IκB, inhibitory κB; iNOS, inducible nitric oxide synthase; MAPK, mitogen-activated protein kinase; ERK, extracellular signal-regulated kinase; JNK, c-Jun N-terminal kinase; ILs, interleukins; ELISA, enzyme-linked immunosorbent assay; LPS, lipopolysaccharide; GAPDH, glyceraldehydes-3-phosphate dehydrogenase; PCA, principal component analysis; OPLS-DA, orthogonal partial least-squares discriminant analysis; ESI, electrospray ionization

■ REFERENCES

(1) Pajk, T.; Rezar, V.; Levart, A.; Salobir, J. Efficiency of apples, strawberries, and tomatoes for reduction of oxidative stress in pigs as a model for humans. *Nutrition* **2006**, *22*, 376−384.

(2) Zafra-Stone, S.; Yasmin, T.; Bagchi, M.; Chatterjee, A.; Vinson, J. A.; Bagchi, D. Berry anthocyanins as novel antioxidants in human health and disease prevention. *Mol. Nutr. Food Res.* **2007**, *51*, 675−683.

(3) Liu, C. J.; Lin, J. Y. Anti-inflammatory and anti-apoptotic effects of strawberry and mulberry fruit polysaccharides on lipopolysaccharide-stimulated macrophages through modulating pro-/anti-inflammatory cytokines secretion and Bcl-2/Bak protein ratio. *Food Chem. Toxicol.* **2012**, *50*, 3032−3039.

(4) Zunino, S. J.; Parelman, M. A.; Freytag, T. L.; Stephensen, C. B.; Kelley, D. S.; Mackey, B. E.; Woodhouse, L. R.; Bonnel, E. L. Effects of dietary strawberry powder on blood lipids and inflammatory markers in obese human subjects. *Br. J. Nutr.* **2012**, *108*, 900−909.

(5) Basu, A.; Rhone, M.; Lyons, T. J. Berries: emerging impact on cardiovascular health. *Nutr. Rev.* **2010**, *68*, 168−177.

(6) Huntley, A. L. The health benefits of berry flavonoids for menopausal women: cardiovascular disease, cancer and cognition. *Maturitas* **2009**, *63*, 297−301.

(7) Mink, P. J.; Scrafford, C. G.; Barraj, L. M.; Harnack, L.; Hong, C. P.; Nettleton, J. A.; Jacobs, D. R., Jr. Flavonoid intake and cardiovascular disease mortality: a prospective study in postmenopausal women. *Am. J. Clin. Nutr.* **2007**, *85*, 895−909.

(8) Parelman, M. A.; Storms, D. H.; Kirschke, C. P.; Huang, L.; Zunino, S. J. Dietary strawberry powder reduces blood glucose concentrations in obese and lean C57BL/6 mice, and selectively lowers plasma C-reactive protein in lean mice. *Br. J. Nutr.* **2012**, *108*, 1789−1799.

(9) da Silva Pinto, M.; Kwon, Y. I.; Apostolidis, E.; Lajolo, F. M.; Genovese, M. I.; Shetty, K. Functionality of bioactive compounds in Brazilian strawberry (*Fragaria* × *ananassa* Duch.) cultivars: evaluation of hyperglycemia and hypertension potential using in vitro models. *J. Agric. Food Chem.* **2008**, *56*, 4386−4392.

(10) Edirisinghe, I.; Banaszewski, K.; Cappozzo, J.; Sandhya, K.; Ellis, C. L.; Tadapaneni, R.; Kappagoda, C. T.; Burton-Freeman, B. M. Strawberry anthocyanin and its association with postprandial inflammation and insulin. *Br. J. Nutr.* **2011**, *106*, 913−922.

(11) Pinto Mda, S.; de Carvalho, J. E.; Lajolo, F. M.; Genovese, M. I.; Shetty, K. Evaluation of antiproliferative, anti-type 2 diabetes, and antihypertension potentials of ellagitannins from strawberries (*Fragaria* × *ananassa* Duch.) using in vitro models. *J. Med. Food* **2010**, *13*, 1027−1035.

(12) Carlton, P. S.; Kresty, L. A.; Siglin, J. C.; Morse, M. A.; Lu, J.; Morgan, C.; Stoner, G. D. Inhibition of *N*-nitrosomethylbenzylamine-induced tumorigenesis in the rat esophagus by dietary freeze-dried strawberries. *Carcinogenesis* **2001**, *22*, 441−446.

(13) Li, J.; Zhang, D.; Stoner, G. D.; Huang, C. Differential effects of black raspberry and strawberry extracts on BaPDE-induced activation of transcription factors and their target genes. *Mol. Carcinog.* **2008**, *47*, 286−294.

(14) Seeram, N. P.; Adams, L. S.; Zhang, Y.; Lee, R.; Sand, D.; Scheuller, H. S.; Heber, D. Blackberry, black raspberry, blueberry, cranberry, red raspberry, and strawberry extracts inhibit growth and stimulate apoptosis of human cancer cells in vitro. *J. Agric. Food Chem.* **2006**, *54*, 9329−9339.

(15) Wang, S. Y.; Feng, R.; Lu, Y.; Bowman, L.; Ding, M. Inhibitory effect on activator protein-1, nuclear factor-κB, and cell transformation by extracts of strawberries (*Fragaria* × *ananassa* Duch.). *J. Agric. Food Chem.* **2005**, *53*, 4187−4193.

(16) Wedge, D. E.; Meepagala, K. M.; Magee, J. B.; Smith, S. H.; Huang, G.; Larcom, L. L. Anticarcinogenic activity of strawberry, blueberry, and raspberry extracts to breast and cervical cancer cells. *J. Med. Food* **2001**, *4*, 49−51.

(17) Zhang, Y.; Seeram, N. P.; Lee, R.; Feng, L.; Heber, D. Isolation and identification of strawberry phenolics with antioxidant and human cancer cell antiproliferative properties. *J. Agric. Food Chem.* **2008**, *56*, 670−675.

(18) William Allwood, J.; Ellis, D. I.; Goodacre, R. Metabolomic technologies and their application to the study of plants and plant-host interactions. *Physiol. Plant.* **2007**, *132*, 117−135.
(19) German, J. B.; Hammock, B. D.; Watkins, S. M. Metabolomics: building on a century of biochemistry to guide human health. *Metabolomics* **2005**, *1*, 3−9.
(20) Schauer, N.; Fernie, A. R. Plant metabolomics: towards biological function and mechanism. *Trends Plant Sci.* **2006**, *11*, 508−516.
(21) Heo, S.; Lee, D. Y.; Choi, H. K.; Lee, J.; Kim, J. H.; Cho, S. M.; Lee, H. J.; Auh, J. H. Metabolite fingerprinting of bokbunja (*Rubus coreanus* Miquel) by UPLC-qTOF-MS. *Food Sci. Biotechnol.* **2011**, *20*, 567−570.
(22) Schauer, N.; Zamir, D.; Fernie, A. R. Metabolic profiling of leaves and fruit of wild species tomato: a survey of the *Solanum lycopersicum* complex. *J. Exp. Bot.* **2005**, *56*, 297−307.
(23) Sato, S.; Soga, T.; Nishioka, T.; Tomita, M. Simultaneous determination of the main metabolites in rice leaves using capillary electrophoresis mass spectrometry and capillary electrophoresis diode array detection. *Plant J.* **2004**, *40*, 151−163.
(24) Hamzehzarghani, H.; Kushalappa, A. C.; Dion, Y.; Rioux, S.; Comeau, A.; Yaylayan, V.; Marshall, W. D.; Mather, D. E. Metabolic profiling and factor analysis to discriminate quantitative resistance in wheat cultivars against fusarium head blight. *Physiol. Mol. Plant* **2005**, *66*, 119−133.
(25) Hagel, J. M.; Facchini, P. J. Plant metabolomics: analytical platforms and integration with functional genomics. *Phytochem. Rev.* **2012**, *7*, 479−497.
(26) Seger, C.; Sturm, S. Analytical aspects of plant metabolite profiling platforms: current standings and future aims. *J. Proteome Res.* **2007**, *6*, 480−497.
(27) Maatta-Riihinen, K. R.; Kamal-Eldin, A.; Torronen, A. R. Identification and quantification of phenolic compounds in berries of *Fragaria* and *Rubus* species (family Rosaceae). *J. Agric. Food Chem.* **2004**, *52*, 6178−6187.
(28) Chan, E. D.; Riches, D. W. IFN-γ + LPS induction of iNOS is modulated by ERK, JNK/SAPK, and p38(mapk) in a mouse macrophage cell line. *Am. J. Physiol. Cell Physiol.* **2001**, *280*, C441−C450.
(29) Wang, S. Y.; Zheng, W.; Galletta, G. J. Cultural system affects fruit quality and antioxidant capacity in strawberries. *J. Agric. Food Chem.* **2002**, *50*, 6534−6542.
(30) Rothwell, J. A.; Urpi-Sarda, M.; Boto-Ordonez, M.; Knox, C.; Llorach, R.; Eisner, R.; Cruz, J.; Neveu, V.; Wishart, D.; Manach, C.; Andres-Lacueva, C.; Scalbert, A. Phenol-Explorer 2.0: a major update of the Phenol-Explorer database integrating data on polyphenol metabolism and pharmacokinetics in humans and experimental animals. *Database* **2012**, *2012*, bas031.
(31) Medzhitov, R. Origin and physiological roles of inflammation. *Nature* **2008**, *454*, 428−435.
(32) Jimenez-Garcia, S. N.; Guevara-Gonzalez, R. G.; Miranda-Lopez, R.; Feregrino-Perez, A. A.; Torres-Pacheco, I.; Vazquez-Cruz, M. A. Functional properties and quality characteristics of bioactive compounds in berries: biochemistry, biotechnology, and genomics. *Food Res. Int.* **2013**, *54*, 1195−1207.
(33) Lee, D. Y.; Heo, S.; Kim, S. G.; Choi, H.-K.; Lee, H. J.; Cho, S.-M.; Auh, J.-H. Metabolomic characterization of the region- and maturity-specificity of *Rubus coreanus* Miquel (Bokbunja). *Food Res. Int.* **2013**, *54*, 508−515.
(34) Lee, H. N.; Na, H. K.; Surh, Y. J. Resolution of inflammation as a novel chemopreventive strategy. *Semin. Immunopathol.* **2013**, *35*, 151−161.
(35) Lin, J. Y.; Tang, C. Y. Strawberry, loquat, mulberry, and bitter melon juices exhibit prophylactic effects on LPS-induced inflammation using murine peritoneal macrophages. *Food Chem.* **2008**, *107*, 1587−1596.
(36) Liu, C. J.; Lin, J. Y. Anti-inflammatory effects of phenolic extracts from strawberry and mulberry fruits on cytokine secretion profiles using mouse primary splenocytes and peritoneal macrophages. *Int. Immunopharmacol.* **2013**, *16*, 165−170.
(37) Maurya, M. R.; Gupta, S.; Li, X.; Fahy, E.; Dinasarapu, A. R.; Sud, M.; Brown, H. A.; Glass, C. K.; Murphy, R. C.; Russell, D. W.; Dennis, E. A.; Subramaniam, S. Analysis of inflammatory and lipid metabolic networks across RAW264.7 and thioglycolate-elicited macrophages. *J. Lipid Res.* **2013**, *54*, 2525−2542.
(38) Marin, M.; Maria Giner, R.; Rios, J. L.; Carmen Recio, M. Intestinal anti-inflammatory activity of ellagic acid in the acute and chronic dextrane sulfate sodium models of mice colitis. *J. Ethnopharmacol.* **2013**, DOI: 10.1016/j.jep.2013.09.030.
(39) Rosillo, M. A.; Sanchez-Hidalgo, M.; Cardeno, A.; Aparicio-Soto, M.; Sanchez-Fidalgo, S.; Villegas, I.; de la Lastra, C. A. Dietary supplementation of an ellagic acid-enriched pomegranate extract attenuates chronic colonic inflammation in rats. *Pharmacol. Res.* **2012**, *66*, 235−242.
(40) Rosillo, M. A.; Sanchez-Hidalgo, M.; Cardeno, A.; de la Lastra, C. A. Protective effect of ellagic acid, a natural polyphenolic compound, in a murine model of Crohn's disease. *Biochem. Pharmacol.* **2011**, *82*, 737−745.
(41) Karlsson, S.; Nanberg, E.; Fjaeraa, C.; Wijkander, J. Ellagic acid inhibits lipopolysaccharide-induced expression of enzymes involved in the synthesis of prostaglandin E2 in human monocytes. *Br. J. Nutr.* **2010**, *103*, 1102−1109.
(42) Lee, W. J.; Ou, H. C.; Hsu, W. C.; Chou, M. M.; Tseng, J. J.; Hsu, S. L.; Tsai, K. L.; Sheu, W. H. Ellagic acid inhibits oxidized LDL-mediated LOX-1 expression, ROS generation, and inflammation in human endothelial cells. *J. Vasc. Surg.* **2010**, *52*, 1290−1300.
(43) Cordenunsi, B. R.; Oliveira do Nascimento, J. R.; Genovese, M. I.; Lajolo, F. M. Influence of cultivar on quality parameters and chemical composition of strawberry fruits grown in Brazil. *J. Agric. Food Chem.* **2002**, *50*, 2581−2586.
(44) Espin, J. C.; Gonzalez-Barrio, R.; Cerda, B.; Lopez-Bote, C.; Rey, A. I.; Tomas-Barberan, F. A. Iberian pig as a model to clarify obscure points in the bioavailability and metabolism of ellagitannins in humans. *J. Agric. Food Chem.* **2007**, *55*, 10476−10485.
(45) Larrosa, M.; Tomas-Barberan, F. A.; Espin, J. C. The dietary hydrolysable tannin punicalagin releases ellagic acid that induces apoptosis in human colon adenocarcinoma Caco-2 cells by using the mitochondrial pathway. *J. Nutr. Biochem.* **2006**, *17*, 611−625.
(46) Gonzalez-Barrio, R.; Borges, G.; Mullen, W.; Crozier, A. Bioavailability of anthocyanins and ellagitannins following consumption of raspberries by healthy humans and subjects with an ileostomy. *J. Agric. Food Chem.* **2010**, *58*, 3933−3939.
(47) Cerda, B.; Tomas-Barberan, F. A.; Espin, J. C. Metabolism of antioxidant and chemopreventive ellagitannins from strawberries, raspberries, walnuts, and oak-aged wine in humans: identification of biomarkers and individual variability. *J. Agric. Food Chem.* **2005**, *53*, 227−235.
(48) Espin, J. C.; Larrosa, M.; Garcia-Conesa, M. T.; Tomas-Barberan, F. Biological significance of urolithins, the gut microbial ellagic acid-derived metabolites: the evidence so far. *Evidence-Based Complement. Alternat. Med.* **2013**, DOI: 10.1155/2013/270418.
(49) Gimenez-Bastida, J. A.; Larrosa, M.; Gonzalez-Sarrias, A.; Tomas-Barberan, F.; Espin, J. C.; Garcia-Conesa, M. T. Intestinal ellagitannin metabolites ameliorate cytokine-induced inflammation and associated molecular markers in human colon fibroblasts. *J. Agric. Food Chem.* **2012**, *60*, 8866−8876.

MATERIALS AND METHODS

Diet. Freeze-dried highbush whole blueberry powder (50:50 blend of Tifblue and Rubel) was received from the U.S. Highbush Blueberry Council (Folsom, CA, USA). This blend contains 38 mg/g total phenolics and 21 mg/g total anthocyanins. AIN-93 M diet and AIN-93 M diet supplemented with 2.5 and 5% BB were prepared in pellet form by Harlan-Teklad (Madison, WI, USA) and stored at 4 °C in vacuum-sealed bags until use. BB diet was customized to have the same calorific value as AIN-93 M.

Animal Study. Animal experiments were executed in agreement with an approved protocol from the Institutional Animal Care and Use Committee at the University of Louisville. Female ACI rats (5−6 weeks old) were purchased from Harlan Sprague−Dawley, Inc. (Indianapolis, IN, USA). After a week of acclimation, animals were randomized into seven groups (Table 1). Groups 1, 4, and 7 were provided with AIN-93 M diet, and groups 2 and 5 were fed a diet supplemented with BB (2.5% w/w). Groups 3 and 6 received diet supplemented with 5% BB. After 2 weeks of experimental diet intervention, groups 4−7 were implanted subcutaneously with a 1.2 cm silastic implant containing 9 mg of 17β-estradiol (E_2) as described.[16] Group 7 received control AIN-93 M diet for 14 weeks and then was changed to BB diet (5% w/w) after the appearance of first palpable tumor in control group. As the BB diet in group 7 started after the appearance of tumors, this was considered as therapeutic intervention. Body weight and diet consumption were recorded weekly until euthanasia. Starting from 12 weeks of E_2 treatment, animals were palpated weekly for tumor incidence and multiplicity. When the palpable tumors reached >90% in group 4, animals in all groups were euthanized by CO_2 asphyxiation. Blood was collected by cardiac puncture to isolate serum and plasma. Lung, liver, brain, mammary tissue, and pituitary gland were collected, weighed, and snap frozen for further analysis. Mammary tumor size was measured by a Vernier caliper. Small pieces of mammary tissue and pituitary gland were fixed in 10% formalin for histopathological analysis.

Table 1. Experimental Design

group	treatment	no. of animals
1	untreated	8
2	2.5% BB diet	5
3	5% BB diet	5
4	E2 + control (AIN-93 M diet)	24
5	E2 + 2.5% BB diet	20
6	E2 + 5% BB diet (preventive)	20
7	E2 + 5% BB diet (therapeutic)	20

Histopathology. To assess the presence of microscopic tumors and pathological changes in the mammary glands of rats treated with E_2 for 12 weeks, 5 μm mammary tissue sections (n = 21) from multiple previous studies were stained with hematoxylin and eosin and analyzed by a board-certified veterinary pathologist.

Immunohistochemistry. Tissue sections from five randomly selected animals from each group were stained for proliferating cell nuclear antigen (PCNA) using a PCNA staining kit (Life Technologies, Grand Island, NY, USA) following the manufacturer's protocol. Five to six different sites in each slide were scored for deeply stained epithelial nuclei by two cytopathologists and represented as percent deeply stained cells.

Plasma Prolactin. Plasma prolactin levels were quantified using a Rat Prolactin ELISA Immuno-assay kit (Alpco, Salem, NH, USA) following the manufacturer's instructions. Briefly, plasma samples (n = 5) from E_2-treated groups were diluted 100- or 200-fold, and plasma from groups that did not receive E_2 was diluted 2-fold prior to the analysis. The samples were added to a 96-well plate incubated with rat prolactin sample buffer followed by enzyme-labeled anti-rat prolactin antibody. Then samples were incubated with 3,3′,5,5′-tetramethylbenzidine (TMB) and substrate solution (provided in the kit) followed by measurement of the optical density at 450 nm immediately after the addition of stop solution. About 25 μL of diluted plasma samples was measured against various concentrations of calibrator samples ranging from 5 to 80 ng/mL of prolactin levels.

Western Blot Analysis. Western blot analysis was done as described elsewhere.[14] Briefly, whole-cell lysates were prepared from mammary tissues using radioimmunoprecipitation assay (RIPA) lysis buffer (Santa Cruz Biotechnology Inc., Dallas, TX, USA), and protein concentrations were measured by using the bicinchoninic acid (BCA) method. Proteins were separated on MES-SDS-Bis-Tris 4−12% gradient gel (Invitrogen, Carlsbad, CA, USA). The proteins were transferred to PVDF membranes and probed for cyclin D1, PCNA, estrogen receptor-alpha (ER-α), c-myc, and progesterone receptor (PR). Equal loading of the protein was confirmed by β-actin.

Total RNA Isolation and qRT-PCR Analysis. Total RNA from frozen mammary tissues was isolated using Trizol reagent (Invitrogen). RNA concentrations were measured by NanoDrop (N2000c, NanoDrop Corp., Wilmington, DE, USA). qRT-PCR was performed with 100 ng of RNA using a qScript One-Step SYBR Green qRT-PCR Kit (Quanta Biosciences, Gaithersburg, MD, USA) with 500 pmol of forward and reverse primers for each gene. The genes and primer sequences are as follows: CYP1A1 (forward, 5′ GGGATA-TAGAAGCCATTCAGACTTG 3′; reverse, 5′ TGGAGACCTTCC-GACATTCAT 3′); ER-α (forward, 5′ GGCACATGAGTAACAAAG-GCA 3′; reverse, 5′ GGCATGAAGACGATGAGCAT 3′); 18S (forward, 5′ GGGAGGTAGTGACGAAAAATAACAAT 3′; reverse, 5′ TTGCCCTCCAATGGATCCT 3′). Quantitative PCR was carried out on a 7500 Fast-Real Time PCR instrument (Applied Biosystems, Green Island, NY, USA), following the manufacturer's guideline. The gene expressions were calculated by relative quantification method ($2^{\Delta\Delta Ct}$) comparing with control and normalizing to 18S RNA.

Small RNA Isolation/miRNA Analysis. Small RNAs (<200 bp) were isolated from mammary tissues using a mirVana microRNA isolation kit (Invitrogen) following the manufacturer's instruction. The concentration of the small RNA was quantified by Bioanalyzer (Agilent Technologies, Santa Clara, CA, USA). qPCR analysis of miR-18a, miR20a, miR25, and miR-34c was performed using a TaqMan miRNA Reverse Transcription Kit and TaqMan gene-specific miRNA assays (Applied Biosystems, Foster City, CA, USA) according to the manufacturer's instructions. Relative changes in miRNA expressions were quantified by comparison with the control and normalization to 5S RNA.

Toxicity Analysis. Whole blood was collected at the time of euthanasia to analyze serum chemistry and hematological parameters, as described previously.[17] Liver functions were analyzed by measuring the levels of aspartate transaminase, alanine aminotransferase, alkaline phosphatase, γ-glutamyl transpeptidase, and amylase in serum. Kidney functions were analyzed by measuring blood urea nitrogen, creatinine, and various electrolytes in serum. Various hematological parameters such as white blood cells (WBCs), red blood cells, hemoglobin, hematocrit, mean corpuscular volume, mean corpuscular hemoglobin, mean corpuscular hemoglobin concentration, and platelet count were analyzed from whole blood. Five random samples from each group were analyzed.

Statistical Analysis. All statistical comparisons between controls and E_2-treated groups were made using an unpaired one-tailed Student's t test. Tumor latency was analyzed using a nonparametric log-rank test. Diet consumption was analyzed using an unpaired two-tailed Student's t test, and body weight was analyzed by two-way ANOVA. All statistical analyses were done in GraphPad prism software, version 4.3 (San Diego, CA, USA). A p value of $\leq$0.05 was considered significant.

RESULTS

Food Consumption and Body Weight. There was no significant difference in diet consumption among groups receiving either control diet or AIN-93 M diet supplemented with 2.5 and 5% BB, in the absence of E_2 treatment. The diet consumption, however, increased in E_2-treated animals fed control diet or BB-supplemented diets (Figure 1A). The

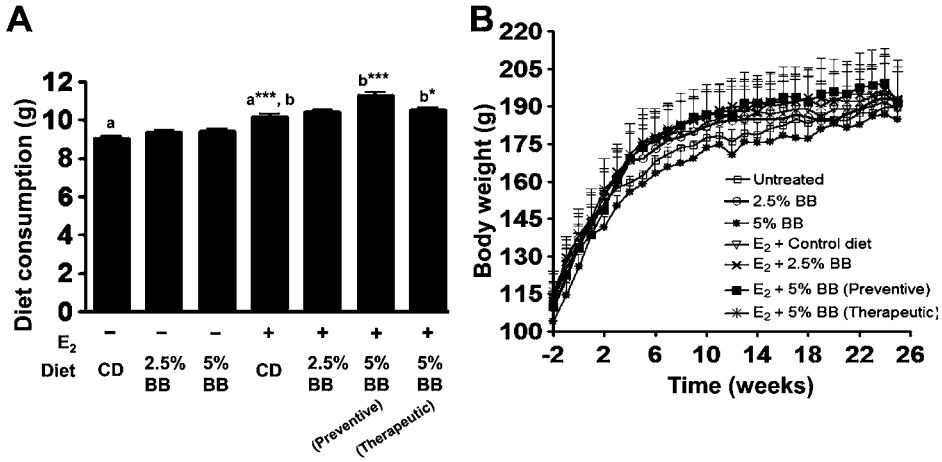

Figure 1. Average diet consumption and body weight:. (A) Average diet consumption by ACI rat per day fed with AIN-93 M diet and diet supplemented with 2.5 and 5% BB in the presence and absence of E_2. Values denote mean ± SD of diet consumption over a period of 25 weeks. Asterisk (a) indicates significant difference of E_2 control from untreated control ($p = 0.0001$). Asterisk (b) indicates significant difference of BB diets from E_2 control ($p = 0.001$ and 0.044). (B) Average body weight of rats receiving either AIN-93 M or BB diet. One-way ANOVA analysis showed that there was no significant difference in body weight after 25 weeks of E_2 treatment.

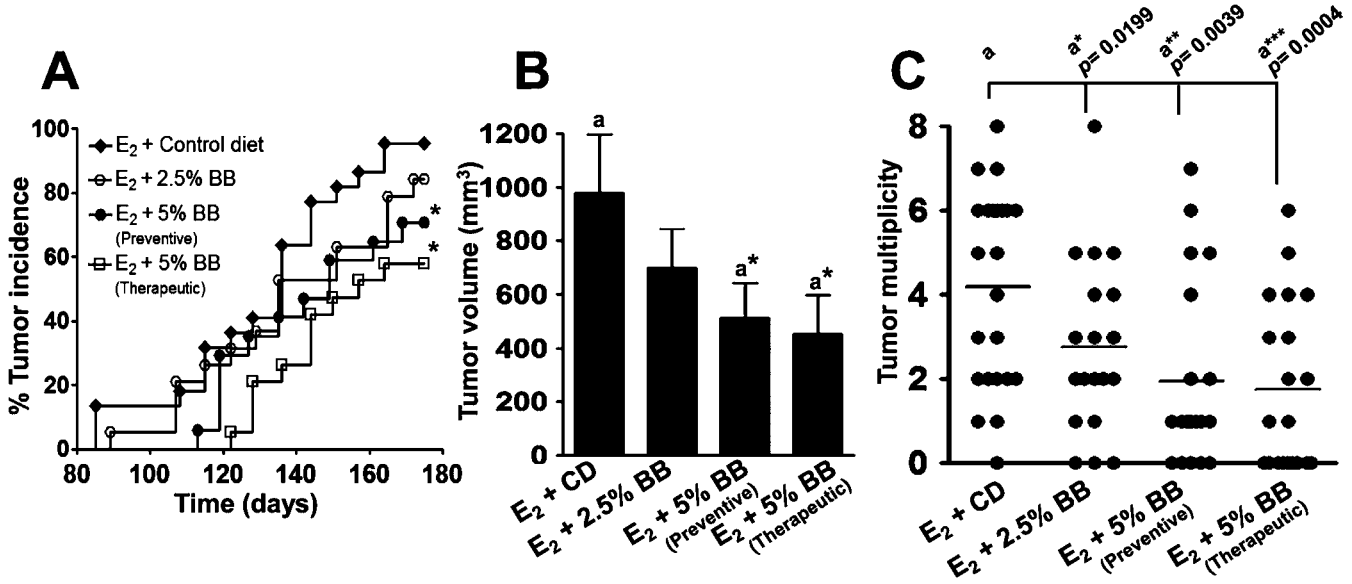

Figure 2. Effect of blueberry diet on (A) tumor incidence, (B) tumor volume, and (C) tumor multiplicity. (A) Tumor incidence was calculated from the weekly palpation report and analyzed using a nonparametric log-rank test. Asterisk indicates significant difference of 5% BB diet [preventive ($p = 0.0109$) and therapeutic mode ($p = 0.0021$)] from E_2-treated control. (B) Tumor volume and multiplicity were calculated at the time of euthanasia and analyzed using unpaired one-tailed Student's t test. Asterisk indicates that the tumor volume of both 5% BB diets ($p = 0.0398$ and $p = 0.0106$) was significantly different from E_2-treated control.

increase was significant in animals receiving the 5% BB diet in both preventive and therapeutic mode; the increase was insignificant in the 2.5% BB diet group. At the end of the study (25 weeks), one-way ANOVA analysis showed no significant difference in body weights among the control and E_2-treated animals (Figure 1B).

Tumor Incidence, Multiplicity, and Volume. BB diet was highly effective in favorably modulating the various tumor indices (latency, incidence, multiplicity, and burden). BB diet dose dependently delayed the tumor latency. The groups receiving 5% BB diet in both the chemopreventive and therapeutic modes had a significant delay with the first tumor appearance in the control group by 28 and 37 days, respectively, as compared to the age-matched control animals (Figure 2A). The group that received 2.5% BB diet also had delayed tumor latency but only slightly, about 7 days. At the end of the study, the control group developed palpable mammary tumors in 96% animals, whereas animals provided with the 5% BB diet in chemopreventive and therapeutic groups had palpable tumors only in 60% ($p = 0.0109$) and 55% ($p = 0.0021$) of animals, respectively; the 2.5% BB diet also showed some (11%) but insignificant reduction in tumor incidence compared to the control group. Tumor volume and multiplicity were measured after the animals had been euthanized. Animals receiving control diet had an average tumor volume of 979 ± 218 mm^3, whereas animals on the 5% BB diet had significant reductions, 512 ± 130 mm^3 ($p = 0.0398$) and 452 ± 144 mm^3 ($p = 0.0106$), for chemopreventive and therapeutic mode, respectively (Figure 2B). Animals on the 2.5% BB diet showed a modest but insignificant

dx.doi.org/10.1021/jf403734j | J. Agric. Food Chem. 2014, 62, 3963−3971

Table 2. Comparison of Body Weight and Other Organ Weights[a] between ACI Rats Fed Control Diet or Diet Supplemented with Blueberry

group	body weight (g)	liver (g)	mammary (g)	pituitary (mg)
untreated (n = 8)	189.4 ± 6.8	4.9 ± 0.4	4.6 ± 0.9	11.2 ± 1.3
2.5% BB diet (n = 5)	192.6 ± 15.9	5.2 ± 1.0	4.4 ± 0.9	12.2 ± 1.0
5% BB diet (n = 5)	185.0 ± 6.6	4.8 ± 0.4	4.6 ± 0.4	9.8 ± 1.4
E_2 + control AIN 93 M diet (n = 24)	189.0 ± 14.2	6.3[b] ± 0.4	6.4[b] ± 1.5	42.2[b] ± 10.7
p value		0.0001		
E_2 + 2.5% BB diet (n = 18)	192.3 ± 12.0	6.5 ± 0.6	5.7 ± 1.5	34.4[c] ± 8.0
p value				0.007
E_2 + 5% BB diet (preventive) (n = 18)	191.2 ± 17.5	6.7 ± 0.8	5.6 ± 2.0	33.9[c] ± 5.6
p value			0.0486	0.0031
E_2 + 5% BB diet (therapeutic) (n = 18)	192.4 ± 12.0	6.5 ± 0.5	5.9 ± 1.2	34.4[c] ± 5.3
p value				0.0031

[a]Body weight and organ weight values are expressed as mean ± SD. [b]Values that are significantly higher than untreated control. [c]Values that are significantly higher than E_2-treated animals. Average body weight of animals is measured at the time of euthanasia.

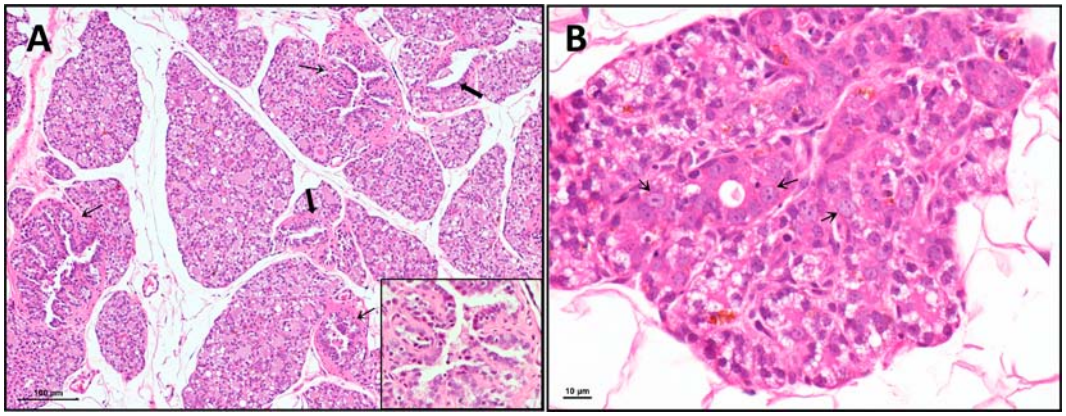

Figure 3. Presence of epithelial dysplasia and ductular papillomas from mammary tissue of rats treated with E_2 implant for 12 weeks. (A) Image of mammary section at 40× magnification showing long papillary projections from ductular walls (thin arrows) and ducts lined with hyperplastic epithelium with two or more layers (bold arrows). Inset shows 400× magnification of papillary projections. (B) Mammary section at 600× magnification with nuclei showing karyomegaly, which are hyperchromatic containing one to three distinct nucleoli (thin arrows).

(0.1435) reduction with an average tumor volume of 698 ± 145 mm^3. Tumor multiplicity in control animals was 4.17 ± 0.48 per animal, and it was reduced to 2.17 ± 0.52 (p = 0.0039) and 1.75 ± 0.45 (p = 0.0004) by the 5% BB diet given in chemopreventive and therapeutic mode, respectively (Figure 2C); the 2.5% BB diet also showed a significant reduction in tumor multiplicity, 2.75 ± 0.45 (p = 0.0199).

Liver, Mammary, and Pituitary Weights. At the end of the study, the liver, mammary, and pituitary tissue weights were not significantly different among the groups without E_2 treatment. However, the differences were significant with E_2 treatment. Mammary tissue weight with 5% BB diet in chemopreventive mode was modestly offset (p = 0.0486) from E_2-treated control. There was a 4−5-fold increase in the pituitary weight in E_2-treated animals; however, this was significantly offset with the 5% BB diet in preventive (33.9 ± 5.6 mg vs 42.2 ± 10.7 mg; p = 0.0031) and therapeutic (34.4 ± 5.3 mg; p = 0.0031) modes (Table 2). Pituitary weights in animals receiving the 2.5% BB diet also showed significant decrease (34.4 ± 8.0 mg; p = 0.0070).

Histopathology. In all animals that were treated with E_2 for 12 weeks (n = 21), there was expansion of mammary tissue with proliferation of terminal buds that differentiated into acini. The acinar epithelial cells were frequently vacuolated, and the acini contained amphophilic inspissated secretory material filling the lumina (Figure 3A). Concomitantly, there was proliferation of ductules and ducts with variable grades of epithelial dysplasia (n = 13). The ductular epithelial cells were cuboidal with distinct cell borders and moderate amounts of eosinophilic cytoplasm. Often (n = 4), the nuclei showed karyomegaly and were hyperchromatic, containing one to three distinct nucleoli (Figure 3B). Mitotic figures were not present in the sections examined. In >50% of cases (n = 11), the ducts were ectatic and lined by hyperplastic epithelium that formed two or more layers (Figure 3A). Ductular adenomas (n = 3) were characterized by the development of a 100−250 μm long papillary projection from the ductular walls that narrowed the lumina (Figure 3A, inset). The neoplastic cells contained scant cytoplasm and round nuclei with one to three distinct nucleoli. In all cases, desquamated epithelial cells were present within the ductular lumina. Prominent periductular fibrosis was a feature of all adenomas. Multifocal perivascular mast cell infiltration correlated with the severity of the lesion in all cases. In addition, the ductular epithelial dysplasia correlated with the size of expansion of the terminal bud.

Cell Proliferation Index. Cell proliferation was analyzed by staining tumor and adjacent mammary tissue for PCNA protein markers using antibody-based assay. After 25 weeks, there was no significant difference in cell proliferation among animals receiving either control or 2.5 and 5% BB diets. However, the E_2 treatment increased the cell proliferation to nearly 6-fold (p = 0.0095) (Figure 4). This increase in the cell proliferation was

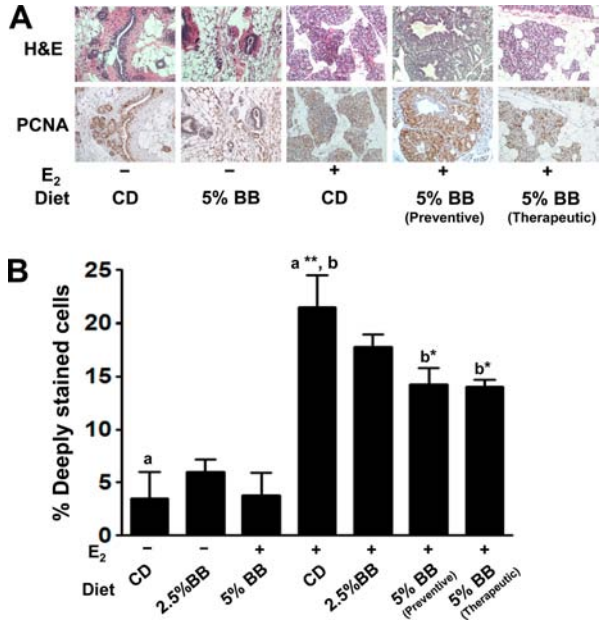

Figure 4. Proliferative index and effect of blueberry diet with or without estrogen (E_2) treatment. (A) Immunohistochemical staining for proliferating cell nuclear antigen (PCNA). Representative photomicrographs are 20× magnification of normal and hyperplastic mammary tissue. (B) Graph denotes the percentage of deeply stained cells for PCNA in mammary tissues (n = 5). [a] Statistically significant from untreated control (p = 0.0095). [b] Statistically significant from E_2-treated control (p = 0.0373 and p = 0.0251).

significantly offset by 34 and 35% with 5% BB diet administered in chemopreventive and therapeutic mode, respectively (Figure 4); the effect was insignificant with the 2.5% BB diet.

Plasma Prolactin. No significant difference was observed in the levels of plasma prolactin between untreated groups and BB diet groups. On the other hand, there was a substantial increase (p = 0.0035) in prolactin levels with E_2 treatment (6973 ± 2443 ng/mL) compared to untreated control (11.8 ± 1.8 ng/mL). After 25 weeks, animals provided with 5% BB diet in chemopreventive (2205 ± 438 ng/mL; p = 0.05) and therapeutic mode (1950 ± 285 ng/mL; p = 0.01) demonstrated significant reduction in the elevated levels of plasma prolactin (Figure 5). A modest but insignificant reduction in prolactin levels (4193 ± 1509 ng/mL) was also observed with the 2.5% BB diet.

Modulation of Estrogen-Specific Genes. There was a pronounced effect of E_2 on the expressions of cytochrome CYP 1A1 and ER-α at the mRNA levels. All groups were compared against the untreated control, and the fold change was expressed as mean ± standard error. E_2 treatment up-regulated the CYP 1A1 mRNA levels by 60-fold. The 5% BB intervention provided in chemopreventive and chemotherapeutic modes both significantly offset the E_2-associated increase in CYP1A1 to 28.3 ± 6-fold (p = 0.0011) and 27.6 ± 10.3-fold (p = 0.0102), respectively. Similarly, the mRNA expression level of ER-α in E_2-treated animals was up-regulated by 19.7 ± 2-fold compared to untreated control, and this increase was also significantly offset by the 5% BB diet, chemopreventive mode (14.2 ± 2-fold; p = 0.0201) and therapeutic mode (11.1 ± 4-fold; p = 0.05) (Figure 6A). Western blot analysis showed that E_2 treatment up-regulated both cyclin D1 and PCNA. Intervention of 5% BB diet in both preventive and therapeutic modes down-regulated cyclin D1 and PCNA at protein levels.

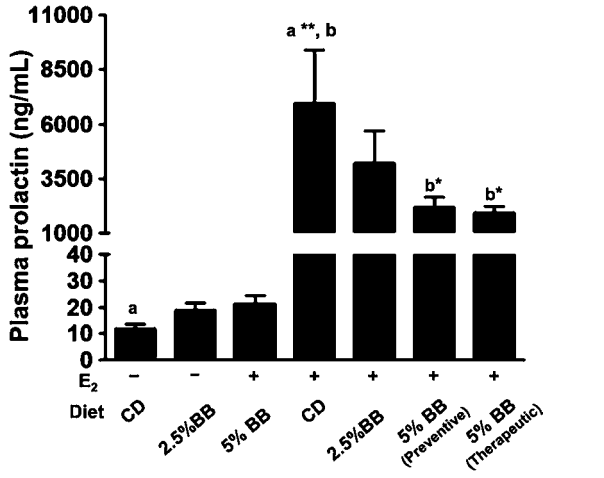

Figure 5. Circulating plasma prolactin levels among rats receiving either control diet or diet supplemented with 2.5 and 5% BB. Values represent the average of six samples ± SE done in duplicates. [a] Statistically significant from untreated control (p = 0.0035). [b] Statistically significant from E_2-treated control (*, p = 0.05; **, p = 0.01).

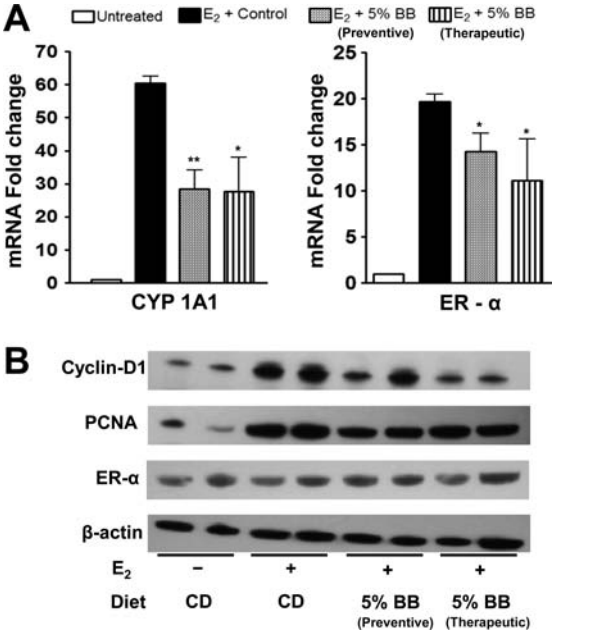

Figure 6. (A) mRNA expression of CYP1A1 and ER-α in mammary tissues. The total RNA isolated from the mammary tissue was analyzed by qPCR. Data represent the average of four animals ± SE. Asterisk represents significant difference from E_2-treated control (p = 0.0011 and 0.01). (B) Protein expression of cyclin D1, PCNA, and ER-α in mammary tissue. The total cellular lysate isolated from the mammary tissues was analyzed by Western blot.

However, ER-α protein level was not modulated with either E_2 treatment or administration of BB diet.

Modulation of Estradiol-Specific miRNAs. We analyzed four E_2-specific miRNAs (miR-18a, -20a, -25, and -34c) on the basis of our previous study in this animal model[18] to determine the effect of BB treatment on their modulation. All four miRNAs were significantly up-regulated under the influence of E_2 intervention in agreement with our previous findings. miR-18a and miR-34c were up-regulated about 13- and 11-fold, respectively, compared to untreated control. The effect of E_2 on

dx.doi.org/10.1021/jf403734j | J. Agric. Food Chem. 2014, 62, 3963−3971

miR-18a and miR-34c was reduced to 6.4-fold (p = 0.0013) and 4.9-fold (p = 0.0033), respectively, with the 5% BB diet in therapeutic mode (Figure 7). Berry diet given in chemo-preventive mode also offset these two elevated miRNAs, but the effect was not as pronounced. There was no significant effect of BB treatment on the up-regulated miR-20a and miR-25 expression levels.

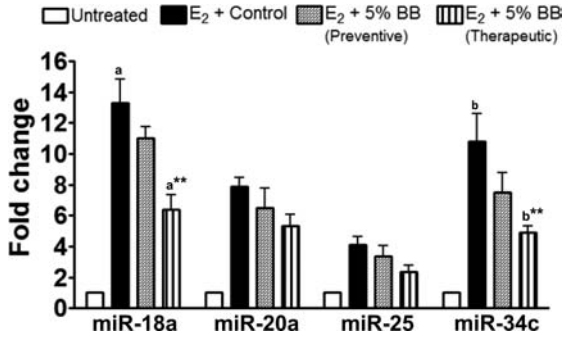

Figure 7. Expression of miRNAs 18a and 34c in mammary tissues. The small RNA was isolated by mirVana microRNA kit and quantified by Bioanalyzer. qPCR analysis was performed using a TaqMan microRNA Reverse Triscription Kit and TaqMan gene-specific MicroRNA assays. Graph represents the average of four rats ± SE done in duplicates. Asterisk indicates significant difference from E_2-treated control (p = 0.0013 and 0.0033).

Effect of Dietary Blueberry on Serum Chemistry and Hematological Parameters. Analysis of serum for liver enzymes such as aspartate transaminase, alanine aminotransferase, alkaline phosphatase, γ-glutamyl transpeptidase, amylase, and lipase indicated that they were within the normal range, and no difference was found with E_2 or BB diet or in combination compared to control, suggesting that berry diets had no toxic effects (Table 3). Serum was analyzed for plasma proteins (albumin and globulin), glucose, cholesterol, and triglycerides (Table 3). Analysis of blood urea nitrogen, creatinine, and various electrolytes showed no significant changes, indicating normal kidney functions with BB treatment (Table 3). Whole blood from all of the groups was analyzed for hematological parameters such as white blood cells, red blood cells, hemoglobin, hematocrit, mean corpuscular volume, mean corpuscular hemoglobin, mean corpuscular hemoglobin concentration, and platelets. No difference in any of the hematological parameters was found in any group compared to aged-matched control animals (Table 3). The levels of

Table 3. Serum and Hematological Parameters for Assessment of Toxicity and Tolerance of Blueberry Diet

				E_2 + 5% BB diet	
	untreated	5% BB diet	E_2 + control AIN-93 M diet	preventive	therapeutic
serum enzymes					
AST (SGOT)	342 ± 130	276 ± 80	236 ± 31	217 ± 51	263 ± 49
ALT (SGPT)	56 ± 9	38 ± 5	45 ± 10	49 ± 7	48 ± 11
alk phosphatase	31 ± 9	41 ± 8	33 ± 17	32 ± 9	20 ± 6
GGT	8 ± 2	3 ± 0	5 ± 2	4 ± 2	4 ± 1
amylase	552 ± 91	585 ± 40	548 ± 72	585 ± 130	630 ± 36
lipase	25 ± 0	50 ± 25	25 ± 0	26 ± 1	25 ± 0
plasma proteins					
albumin (g/dL)	4 ± 0.1	4 ± 0.3	4 ± 0.1	4 ± 0.4	5 ± 0.1
globulin (g/dL)	3 ± 0.5	3 ± 0.3	4 ± 0.3	4 ± 0.2	4 ± 0.3
glucose (mg/dL)	122 ± 36	139 ± 46	90 ± 30	118 ± 33	ND[a]
cholesterol (mg/dL)	118 ± 14	98 ± 10	131 ± 16	124 ± 20	151 ± 13
triglycerides (mg/dL)	103 ± 27	108 ± 20	91 ± 23	99 ± 28	119 ± 56
kidney function					
BUN (mg/dL)	24 ± 10	21 ± 3	21 ± 4	20 ± 4	24 ± 2
creatinine (mg/dL)	0.4 ± 0.1	0.5 ± 0	0.44 ± 0.1	0.44 ± 0.1	0.48 ± 0.1
phosphorus (mg/dL)	16 ± 6	19 ± 2	13 ± 4	13 ± 2	17 ± 4
calcium (mg/dL)	11 ± 1	12 ± 1	12 ± 0.3	12 ± 0.3	12 ± 0.4
magnesium (mequiv/dL)	4 ± 0	4 ± 0.3	3 ± 0.3	3 ± 0.3	4 ± 0.2
sodium (mequiv/dL)	146 ± 5	147 ± 4	144 ± 1	141 ± 2	141 ± 2
potassium (mequiv/dL)	8 ± 4	9 ± 1	8 ± 0.9	7 ± 0.3	12 ± 2
chloride (mequiv/dL)	81 ± 42	100 ± 2	98 ± 3	97 ± 2	96 ± 2
hematological parameters					
WBC ($10^3/\mu$L)	5 ± 2	4 ± 0.3	5 ± 2	6 ± 3	4 ± 2
RBC ($10^6/\mu$L)	8 ± 0.1	8 ± 0.5	6 ± 1	6 ± 2	7 ± 0.4
HGB (g/dL)	13 ± 0.3	13 ± 1	9 ± 4	10 ± 2	11 ± 1
HCT (%)	44 ± 3	46 ± 2	35 ± 3	33 ± 7	38 ± 4
MCV (fL)	55 ± 3	55 ± 3	58 ± 4	55 ± 3	55 ± 3
MCH (pg)	17 ± 0.3	16 ± 0.3	17 ± 1	16 ± 1	20 ± 8
MCHC (g/dL)	30 ± 2	29 ± 2	29 ± 1	30 ± 1	30 ± 2
platelet count ($10^3/\mu$L)	854 ± 100	807 ± 334	872 ± 140	648 ± 216	863 ± 61
neutrophils	634 ± 287	684 ± 203	2106 ± 1608	2229 ± 1394	1398 ± 581
lymphocytes	4222 ± 1882	3475 ± 666	2347 ± 675	3102 ± 1628	2458 ± 1078

[a]ND, not determined.

dx.doi.org/10.1021/jf403734j | J. Agric. Food Chem. 2014, 62, 3963−3971

neutrophils and lymphocytes measured in whole blood showed no significant difference among all groups (Table 3).

DISCUSSION

Cancer chemopreventive agents are either natural products or their synthetic analogues, which inhibit the transformation of normal cells to premalignant cells or the progression of premalignant cells to malignant cells.[19] It is believed that chemopreventive agents can inhibit oncogenic pathways, inhibit growth, and induce apoptosis in cancer cells.[20] Conventional chemopreventive agents are administered long-term and believed to block or delay the progression of transformed cells by modulating cell proliferation or differentiation.[21] They also prevent activation of carcinogen, trap carcinogen before reaching the active site, and enhance detoxification systems.[21] On the other hand, standard therapeutic drugs are toxic to both cancer and normal cells, which results in therapeutic activity and side effects to normal cells. Cytotoxicity to normal cells may lead to secondary tumors.[20]

This study was conducted to test both the chemopreventive and therapeutic potential of Tifblue and Rubel blueberry blend against E_2-mediated mammary tumorigenesis. We had previously reported on the chemopreventive effect of Berkley blueberry on mammary tumorigenesis.[15,22] This is the first study of its kind in which the therapeutic potential of blueberry has been shown. We also confirmed the microscopic tumors and precancerous conditions by histological evaluation of mammary gland sections from rats treated and necropsied at 12 weeks of E_2 treatment. Variable ductular epithelial changes including dysplasia, hyperplasia, and adenoma formation were found, suggesting various stages of carcinogenesis. In addition, periductular fibroplasia as well as mast cell infiltration positively correlated with degree of dysplasia.

Similar to our earlier studies[15,22] this Tifblue−Rubel blueberry blend at 2.5 and 5% given in the chemopreventive mode was highly effective in increasing the tumor latency by 7 and 28 days, respectively. The administration of 2.5% BB diet showed significant reduction in tumor multiplicity and pituitary weight. In our earlier studies, 2.5% BB diet made from the mixture of three blueberries was not effective against E_2 treatment; this could be because the E_2 implant size was 3 cm long containing 27 mg of E_2.[22] In another study with a similar 9 mg E_2 implant, a 2.5% diet showed protective effects that were in the same vicinity as reported by us previously.[23] In both studies, the 2.5% BB diet had only modest effect and did not significantly reduce the tumor volume, tumor latency, and molecular markers investigated. The higher dose of BB (5%) administered in chemopreventive mode was highly protective in reducing tumor volume and tumor multiplicity and increased tumor latency to 28 days, in agreement with our previous findings.[15] However, the protective effect of blueberry was slackened after 20 weeks of E_2 treatment, likely due to the exponential growth rate of the cells to reach the malignant stage. For the first time BB diet was administered after 12 weeks of E_2 treatment to determine the therapeutic effect against precancerous and microscopic adenomas. When compared with animals that received 5% BB diet in chemopreventive mode, the therapeutic group showed a significantly enhanced effect by reducing tumor volume and multiplicity and increasing the tumor latency to 37 days, that is, 9 days more than the preventive groups. Even when the BB diet was initiated after 14 weeks of E_2 treatment, the therapeutic group elicited protective effects. The therapeutic potential of BB anthocyanidins has been shown by others against human prostate cancer[24] and by us against lung cancer xenograft.[14] However, there is no study for direct comparison in E_2-induced mammary tumorigenesis. Interestingly, the present data also suggest that BB diet can be started in the postinitiation stage of tumorigenesis and still elicit a response similar to that of chemopreventive mode.

Bioavailability of anthocyanins in vivo is crucial for their biological effects. Anthocyanins are absorbed intact in the glycosidic form.[25,26] They are rapidly absorbed from the stomach and jejunum.[27,28] Yet >50% of the ingested anthocyanins are found in the cecum,[29] implying poor absorption. Anthocyanin structure exists as a flavilium cation in acidic conditions, which is stable, but converts to unstable quinoidal or carbinol structure at neutral or alkaline conditions.[30] However, it has also been shown that anthocyanins are stabilized by flavanols and ascorbic acid present in the food matrix.[31,32] This may explain the higher bioavailability of anthocyanins when given as a whole fruit powder relative to individual anthocyanins,[33] indicating strong synergism occurs in absorption between coexisting molecules in fruit. Furthermore, in a study with healthy subjects with ileostomy, nearly 40% of anthocyanins were recovered in the ileal fluid, indicating that despite the difference in pH, the anthocyanins were stable and large amounts will pass from the small intestine to the large intestine.[34] Yet, all of the bioavailability studies were done with bolus doses of pure anthocyanins or fruit powder/extracts.[35] Anthocyanins were not detected in the plasma of animals fed a diet mixed with sources rich in anthocyanins or the pure compound.[29] However, lack of detection of anthocyanins in the plasma does not indicate lack of tissue bioavailability. When anthocyanins were delivered intravenously, a biphasic decay of plasma levels was observed, indicating tissue distribution.[33] In a parallel publication in this issue, we have discussed in detail the bioavailability of anthocyanins and its levels in lung tissue.[12] We have demonstrated the presence of all five anthocyanidins, delphinidin, cyanidin, peonidin, petunidin, and malvidin, in lung tissues. Thus, anthocyanins are bioavailable and bioaccumulate in non-gastrointestinal tissues.

In agreement with our previous studies, the effect of E_2 was reflected in the body, liver, mammary, and pituitary weights of the animals.[15] The transitory increase in body weight and organ weight is majorly due to the E_2 and may not be due to the diet consumption. Moreover, control AIN-93 M diet and diets supplemented with 2.5 and 5% BB were isocaloric. Although there was no effect of BB diet on body weight gain and organ weights, it was found to significantly offset E_2-associated elevation in the weight of pituitary tumors. The pituitary weight was affected due to the increase in plasma prolactin levels induced by E_2, resulting in pituitary prolactinomas.[36] However, the E_2-mediated mammary tumor model was well studied and standardized to reduce the side effect to the pituitary gland.[16] Earlier studies have shown that prolonged supply of E_2 increases the production of prolactin in E_2-sensitive rat strains.[37,38] High circulatory levels of prolactin in serum are one of the major reasons for animals to develop E_2-induced mammary tumors.[39] Berry diet at 2.5 and 5% significantly offset the prolactin levels elevated by E_2.

E_2 also induces the production of phase I enzyme, CYP1A1. It catalyzes the conversion of E_2 into its metabolites ($2E_2$ and $4E_2$), which further undergo redox cycle leading to the formation of reactive oxygen species.[40] In this study, we

showed that BB diet significantly reduced the expression of CYP1A1, suggesting its protective role against mammary carcinogenesis. Studies have shown that cyclin D1 and E_2 receptors have important roles in regulating proliferation of breast epithelial cells.[41,42] It is well established that E_2 via ER-α elicits rapid signals driving cancer cells to proliferation. This biological effect of E_2-mediated by ER-α was reduced significantly in 5% BB diet provided in therapeutic mode. Regulation of cyclin D1 gene expression has been associated with changes in the proliferation rate of breast cancer cells.[43] Induction of cyclin D1 expression occurs rapidly and is a critical feature of the mitogenic action of E_2. The expression of cyclin D1 was down-regulated by 2−2.6-fold with 5% BB diet in chemopreventive and therapeutic modes, respectively. Investigation of PCNA in nuclear proteins revealed that dietary BB reduced the expression levels significantly. PCNA was shown to interact with ER-α both in the absence and in the presence of DNA, to enhance the interaction of ER-α with ERE-containing DNA, and associate with endogenous E_2-responsive genes.[44] These findings clearly indicate that BB diet could modulate major E_2-associated proliferation markers that lead to protective effects against mammary tumorigenesis in animals treated with E_2.

Another interesting finding in this study is from the analysis of miRNAs related to the ER-α family. Aberrant miRNA expression is implicated in E_2-related breast, uterine, and ovarian cancer development and progression.[7] Hormones play a crucial role in regulating miRNAs by both genomic (transcriptional) and nongenomic mechanisms.[45] Lorio et al. identified miRNAs having expression correlated with specific breast cancer biopathologic features, such as E_2 and progesterone receptor expression, tumor stage, vascular invasion, or proliferation index.[5] Targeting specific miRNAs for inhibiting specific stages of a cancer[46] is being explored. Several miRNAs that regulate ER are involved in synchronized feedback mechanisms as a component of ER activation. Many of these ER-regulating miRNAs therefore are either E_2-inducible (miR-18a and let-7) or subject to E_2-mediated repression (miR-206, miR-221/222, and miR-145).[47] This laboratory has recently identified miRNAs that modulated under the influence of E_2 in this animal model and report aberrant changes in miRNA expression profile as early as 3 weeks of E_2 treatment.[48] We chose four miRNAs, miR-18a, -20a, -25, and -34c, on the basis of our previous study where these miRNAs were up-regulated with E_2 to understand the influence of BB diet on their modulation. Increases in miR-18a and miR-20a mature forms were observed after E2 stimulation.[18] In this study, BB diet administered in therapeutic mode significantly reduced miR-18a and miR-34c, whereas chemopreventive mode showed modest but significant reduction. These findings provide initial insights of BB diet in decreasing the E_2-induced miRNA levels. However, the BB diet failed to modulate miR-20a and -25 expression levels, which remain the subject of further investigation.

In the chemopreventive mode, the rats are fed BB diet as young as 6−7 weeks old. The relative enhanced effect observed with the therapeutic approach could be due to the adaptive response of the rats to the BB phytochemicals in the chemopreventive mode. For example, the CYP1A1 mRNA level in mammary tissue was highest at 3 weeks after E_2 implant and gradually decreased with time.[15,23] The effect of the BB phytochemicals was more pronounced in the inhibition of conversion of normal cells to precancerous or precancerous frank tumors, but were not as effective once the tumors reached the exponential growth rate. Thus, by the time the mammary cells started exhibiting precancerous conditions, the efficacy was better when BB phytochemicals were introduced into the system than when they were already in the circulation. Nevertheless, both approaches were effective in delaying the onset and growth of palpable tumors.

In summary, this is the first demonstration indicating that BB diet is highly protective even in preinitiated E_2-mediated mammary tumors in ACI rats through its effects by modulating cell proliferation and molecular targets. Thus, the consumption of BB can be used as an effective strategy for the treatment of E_2-associated breast cancer and possible prevention of its relapse and metastasis. Our study demonstrates the chemopreventive and therapeutic potential of blueberry and advances our understanding of the working mechanisms in search of potential future drugs.

AUTHOR INFORMATION

Corresponding Author

*(R.C.G.) Phone: (502) 852-3682. Fax: (502) 852-3842. E-mail: rcgupta@louisville.edu.

Funding

This work was supported by the Highbush Blueberry Council, California, USPHS Grants CA-118114 and CA-125152, and the Agnes Brown Duggan Endowment. R.C.G. holds the Agnes Brown Duggan Chair in Oncological Research.

Notes

The authors declare no competing financial interest.

ACKNOWLEDGMENTS

We thankfully acknowledge Dr. Anil Poudel for imaging histopathological slides.

REFERENCES

(1) Howlader, N.; Noone, A. M.; Krapcho, M.; Garshell, J.; Neyman, N.; Altekruse, S. F.; Kosary, C. L.; Yu, M.; Ruhl, J.; Tatalovich, Z.; Cho, H.; Mariotto, A.; Lewis, D. R.; Chen, H. S.; Feuer, E. J.; Cronin, K. A. *SEER Cancer Statistics Review, 1975−2010*; National Cancer Institute: Bethesda, MD, 2013.

(2) Yager, J. D.; Davidson, N. E. Estrogen carcinogenesis in breast cancer. *N. Engl. J. Med.* **2006**, *354*, 270−282.

(3) Lakhani, N. J.; Venitz, J.; Figg, W. D.; Sparreboom, A. Pharmacogenetics of estrogen metabolism and transport in relation to cancer. *Curr. Drug Metab.* **2003**, *4*, 505−513.

(4) Bhavnani, B. R.; Tam, S. P.; Lu, X. Structure activity relationships and differential interactions and functional activity of various equine estrogens mediated via estrogen receptors (ERs) ERalpha and ERbeta. *Endocrinology* **2008**, *149*, 4857−4870.

(5) Iorio, M. V.; Ferracin, M.; Liu, C. G.; Veronese, A.; Spizzo, R.; Sabbioni, S.; Magri, E.; Pedriali, M.; Fabbri, M.; Campiglio, M.; Menard, S.; Palazzo, J. P.; Rosenberg, A.; Musiani, P.; Volinia, S.; Nenci, I.; Calin, G. A.; Querzoli, P.; Negrini, M.; Croce, C. M. MicroRNA gene expression deregulation in human breast cancer. *Cancer Res.* **2005**, *65*, 7065−7070.

(6) Romero-Cordoba, S.; Rodriguez-Cuevas, S.; Rebollar-Vega, R.; Quintanar-Jurado, V.; Maffuz-Aziz, A.; Jimenez-Sanchez, G.; Bautista-Pina, V.; Arellano-Llamas, R.; Hidalgo-Miranda, A. Identification and pathway analysis of microRNAs with no previous involvement in breast cancer. *PLoS One* **2012**, *7*, e31904.

(7) Klinge, C. M. miRNAs and estrogen action. *Trends Endocrinol. Metab.* **2012**, *23*, 223−233.

(8) Cooke, D.; Steward, W. P.; Gescher, A. J.; Marczylo, T. Anthocyans from fruits and vegetables − does bright colour signal cancer chemopreventive activity? *Eur. J. Cancer* **2005**, *41*, 1931−1940.

(9) Devasagayam, T. P.; Tilak, J. C.; Boloor, K. K.; Sane, K. S.; Ghaskadbi, S. S.; Lele, R. D. Free radicals and antioxidants in human health: current status and future prospects. *J. Assoc. Physicians India* **2004**, *52*, 794−804.
(10) Mazza, G.; Cacace, J. E.; Kay, C. D. Methods of analysis for anthocyanins in plants and biological fluids. *J. AOAC Int.* **2004**, *87*, 129−145.
(11) He, J.; Giusti, M. M. Anthocyanins: natural colorants with health-promoting properties. *Annu. Rev. Food Sci. Technol.* **2010**, *1*, 163−187.
(12) Aqil, F.; Vadhanam, M. V.; Jeyabalan, J.; Cai, J.; Singh, I. P.; Gupta, R. C. Detection of anthocyanins/anthocyanidins in animal tissues. *J. Agric. Food Chem.* **2013**, DOI: 10.1021/jf500467b.
(13) Wang, L. S.; Stoner, G. D. Anthocyanins and their role in cancer prevention. *Cancer Lett.* **2008**, *269*, 281−290.
(14) Kausar, H.; Jeyabalan, J.; Aqil, F.; Chabba, D.; Sidana, J.; Singh, I. P.; Gupta, R. C. Berry anthocyanidins synergistically suppress growth and invasive potential of human non-small-cell lung cancer cells. *Cancer Lett.* **2012**, *325*, 54−62.
(15) Ravoori, S.; Vadhanam, M. V.; Aqil, F.; Gupta, R. C. Inhibition of estrogen-mediated mammary tumorigenesis by blueberry and black raspberry. *J. Agric. Food Chem.* **2012**, *60*, 5547−5555.
(16) Ravoori, S.; Vadhanam, M. V.; Sahoo, S.; Srinivasan, C.; Gupta, R. C. Mammary tumor induction in ACI rats exposed to low levels of 17beta-estradiol. *Int. J. Oncol.* **2007**, *31*, 113−120.
(17) Bansal, S. S.; Vadhanam, M. V.; Gupta, R. C. Development and in vitro-in vivo evaluation of polymeric implants for continuous systemic delivery of curcumin. *Pharm. Res.* **2011**, *28*, 1121−1130.
(18) Castellano, L.; Giamas, G.; Jacob, J.; Coombes, R. C.; Lucchesi, W.; Thiruchelvam, P.; Barton, G.; Jiao, L. R.; Wait, R.; Waxman, J.; Hannon, G. J.; Stebbing, J. The estrogen receptor-alpha-induced microRNA signature regulates itself and its transcriptional response. *Proc. Natl. Acad. Sci. U.S.A.* **2009**, *106*, 15732−15737.
(19) Sun, S. Y.; Hail, N., Jr.; Lotan, R. Apoptosis as a novel target for cancer chemoprevention. *J. Natl. Cancer Inst.* **2004**, *96*, 662−672.
(20) Blagosklonny, M. V. Carcinogenesis, cancer therapy and chemoprevention. *Cell Death Differ.* **2005**, *12*, 592−602.
(21) Wattenberg, L. W. What are the critical attributes for cancer chemopreventive agents? *Ann. N.Y. Acad. Sci.* **1995**, *768*, 73−81.
(22) Aiyer, H. S.; Srinivasan, C.; Gupta, R. C. Dietary berries and ellagic acid diminish estrogen-mediated mammary tumorigenesis in ACI rats. *Nutr. Cancer* **2008**, *60*, 227−234.
(23) Aiyer, H. S.; Gupta, R. C. Berries and ellagic acid prevent estrogen-induced mammary tumorigenesis by modulating enzymes of estrogen metabolism. *Cancer Prev. Res.* **2010**, *3*, 727−737.
(24) Hafeez, B. B.; Siddiqui, I. A.; Asim, M.; Malik, A.; Afaq, F.; Adhami, V. M.; Saleem, M.; Din, M.; Mukhtar, H. A dietary anthocyanidin delphinidin induces apoptosis of human prostate cancer PC3 cells in vitro and in vivo: involvement of nuclear factor-kappaB signaling. *Cancer Res.* **2008**, *68*, 8564−8572.
(25) Matsumoto, H.; Inaba, H.; Kishi, M.; Tominaga, S.; Hirayama, M.; Tsuda, T. Orally administered delphinidin 3-rutinoside and cyanidin 3-rutinoside are directly absorbed in rats and humans and appear in the blood as the intact forms. *J. Agric. Food Chem.* **2001**, *49*, 1546−1551.
(26) Miyazawa, T.; Nakagawa, K.; Kudo, M.; Muraishi, K.; Someya, K. Direct intestinal absorption of red fruit anthocyanins, cyanidin-3-glucoside and cyanidin-3,5-diglucoside, into rats and humans. *J. Agric. Food Chem.* **1999**, *47*, 1083−1091.
(27) Matuschek, M. C.; Hendriks, W. H.; McGhie, T. K.; Reynolds, G. W. The jejunum is the main site of absorption for anthocyanins in mice. *J. Nutr. Biochem.* **2006**, *17*, 31−36.
(28) Talavera, S.; Felgines, C.; Texier, O.; Besson, C.; Lamaison, J. L.; Remesy, C. Anthocyanins are efficiently absorbed from the stomach in anesthetized rats. *J. Nutr.* **2003**, *133*, 4178−4182.
(29) Talavera, S.; Felgines, C.; Texier, O.; Besson, C.; Mazur, A.; Lamaison, J. L.; Remesy, C. Bioavailability of a bilberry anthocyanin extract and its impact on plasma antioxidant capacity in rats. *J. Sci. Food Agric.* **2006**, *86*, 90−97.
(30) Brouillard, R. Chemical structure of anthocyanins. In *Anthocyanins as Food Colours*; Markakis, P., Ed.; Academic Press: New York, 1982; pp 1−40.
(31) Ozkan, M. Degradation of anthocyanins in sour cherry and pomegranate juices by hydrogen peroxide in the presence of added ascorbic acid. *Food Chem.* **2002**, *78*, 499−504.
(32) Rossetto, M.; Vanzani, P.; Mattivi, F.; Lunelli, M.; Scarpa, M.; Rigo, A. Synergistic antioxidant effect of catechin and malvidin 3-glucoside on free radical-initiated peroxidation of linoleic acid in micelles. *Arch. Biochem. Biophys.* **2002**, *408*, 239−245.
(33) Ichiyanagi, T.; Shida, Y.; Rahman, M. M.; Hatano, Y.; Konishi, T. Bioavailability and tissue distribution of anthocyanins in bilberry (*Vaccinium myrtillus* L.) extract in rats. *J. Agric. Food Chem.* **2006**, *54*, 6578−6587.
(34) Gonzalez-Barrio, R.; Borges, G.; Mullen, W.; Crozier, A. Bioavailability of anthocyanins and ellagitannins following consumption of raspberries by healthy humans and subjects with an ileostomy. *J. Agric. Food Chem.* **2010**, *58*, 3933−3939.
(35) McGhie, T. K.; Walton, M. C. The bioavailability and absorption of anthocyanins: towards a better understanding. *Mol. Nutr. Food Res.* **2007**, *51*, 702−713.
(36) Stone, J. P.; Holtzman, S.; Shellabarger, C. J. Neoplastic responses and correlated plasma prolactin levels in diethylstilbestrol-treated ACI and Sprague-Dawley rats. *Cancer Res.* **1979**, *39*, 773−778.
(37) Wiklund, J.; Rutledge, J.; Gorski, J. A genetic model for the inheritance of pituitary tumor susceptibility in F344 rats. *Endocrinology* **1981**, *109*, 1708−1714.
(38) Wiklund, J.; Wertz, N.; Gorski, J. A comparison of estrogen effects on uterine and pituitary growth and prolactin synthesis in F344 and Holtzman rats. *Endocrinology* **1981**, *109*, 1700−1707.
(39) Blankenstein, M. A.; Broerse, J. J.; van Zwieten, M. J.; van der Molen, H. J. Prolactin concentration in plasma and susceptibility to mammary tumors in female rats from different strains treated chronically with estradiol-17 beta. *Breast Cancer Res. Treat.* **1984**, *4*, 137−141.
(40) Liehr, J. G. Is estradiol a genotoxic mutagenic carcinogen? *Endocr. Rev.* **2000**, *21*, 40−54.
(41) Zwijsen, R. M.; Wientjens, E.; Klompmaker, R.; van der Sman, J.; Bernards, R.; Michalides, R. J. CDK-independent activation of estrogen receptor by cyclin D1. *Cell* **1997**, *88*, 405−415.
(42) Yu, Q.; Geng, Y.; Sicinski, P. Specific protection against breast cancers by cyclin D1 ablation. *Nature* **2001**, *411*, 1017−1021.
(43) Castro-Rivera, E.; Samudio, I.; Safe, S. Estrogen regulation of cyclin D1 gene expression in ZR-75 breast cancer cells involves multiple enhancer elements. *J. Biol. Chem.* **2001**, *276*, 30853−30861.
(44) Schultz-Norton, J. R.; Gabisi, V. A.; Ziegler, Y. S.; McLeod, I. X.; Yates, J. R.; Nardulli, A. M. Interaction of estrogen receptor alpha with proliferating cell nuclear antigen. *Nucleic Acids Res.* **2007**, *35*, 5028−5038.
(45) Klinge, C. M. Estrogen regulation of microRNA expression. *Curr. Genomics* **2009**, *10*, 169−183.
(46) Sassen, S.; Miska, E. A.; Caldas, C. MicroRNA: implications for cancer. *Virchows Arch.* **2008**, *452*, 1−10.
(47) Zhou, Q.; Eades, G. MicroRNA regulatory networks provide feedback mechanisms for steroid receptor signaling. *J. Steroids Hormon. Sci.* **2012**, *3*, e103.
(48) Munagala, R.; Aqil, F.; Vadhanam, M. V.; Gupta, R. C. MicroRNA 'signature' during estrogen-mediated mammary carcinogenesis and its reversal by ellagic acid intervention. *Cancer Lett.* **2013**, *339*, 175−184.

Table 1. Macronutrient Composition of Low-Fat and High-Fat Lard-Based Diets[a]

% kcal from	10 kcal% fat diet[b]	60 kcal% fat diet[b,c]
protein	20.5	18.4
carbohydrate	69.1	21.3
fat (lard)	10.4	60.3
kcal/g	3.6	5.1

[a]Values are calculated from ingredient analysis or manufacturer data. The LF diet (10 kcal% fat) is TD.08806, which is a Teklad Custom Research Diet from Harlan. The HF diet (60 kcal% fat) is TD.06414, and it also from Harlan. [b]For the 4% BB diets, 40 g of Tifblue powder replaced 25 g of starch, 6 g of cellulose, and 9 g of corn starch. [c]Approximate fatty acid profile (% of total fat): 37% saturated, 47% monounsaturated, 16% polyunsaturated.

was made by freeze-drying whole Tifblue blueberries, and it was supplied by the U.S. Highbush Blueberry Council (Folsom, CA, USA).[15] Tifblue is a rabbiteye variety of BB (*Vaccinium ashei*) and phenolic acid, flavonol, anthocyanin profiles, as well as the nutritional composition of fresh and frozen BB, have been quantified previously.[16−18]

Animals. Sixty-four 9-month-old male C57Bl/6 mice (Jackson Laboratories, Bar Harbor, ME, USA) were individually housed and maintained on a 12 h light/dark cycle. The mice were given food and water ad libitum and given 2 weeks to adjust to their new environment, after which time they were weight-matched (no initial difference in body weight between the four groups: $F_{3,56} = 0.071$, $p = 0.97$, one-way ANOVA) and placed on one of four diets (Teklad Lab Animal Diets) for 5 months ($n = 16$/diet): LF, LFBB, HF, or HFBB. Food intake was assessed over two 24 h periods. All animals were weighed at least weekly and observed daily for clinical signs of disease. Animals were utilized in compliance with all applicable laws and regulations as well as principles expressed in the National Institutes of Health *Guide for the Care and Use of Laboratory Animals*. This study was approved by the Jean Mayer Human Nutrition Research Center on Aging at Tufts University Institutional Animal Care and Use Committee. During the 5 month period on the diets, the animals underwent behavioral tests designed to examine object recognition learning and memory and spatial learning and memory. Behavioral testing was performed on $n = 14−16$ mice per group because 1 mouse died ($n = 1$ LF) and 4 mice were removed from the study because of rapid weight loss ($n = 2$ HF, $n = 1$ HFBB) and cataracts ($n = 1$, HFBB).

Novel Object Recognition Test. Mice were tested with the novel object recognition test[19] after 2, 3, and 4 months on the diets (test sessions 1, 2, and 3, respectively). The novel object recognition test measures the ability to remember an object by observing reaction to the introduction of a novel object compared to a previously viewed object; animals with intact recognition memory will spend more time exploring a novel object than a familiar one. The test was performed similarly to the methods of Carey et al.[20] Animals were habituated to an empty testing chamber for 10 min (plastic rectangular cage, 16 × 24 × 12 cm). Next, mice were given three 10 min trials with 10 min intertrial intervals (Figure 3A). In trials 1 and 2 (training trials), mice explored the testing chamber containing two identical objects that were centered across from each other, 2 cm away from the walls. In trial 3 (testing trial), one of the objects was replaced with a novel object. For every trial, the time that the mice spent attending to each object was recorded with stopwatches. Attending to the object was defined as the duration of time the mouse spent in physical contact with the object using any body part other than the tail or whenever it was engaged in active exploration (e.g., sniffing or manipulating). In test session 1 (when mice had been on diets for 2 months), the objects used in testing were dice and marbles, in test session 2 (when mice had been on diets for 3 months) Eppendorf tubes and binder clips were used, and in test session 3 (when mice had been on diets for 4 months) chess pawns and 15 mL tube caps were used. The novel and familiar objects were counterbalanced within a test session so that, for example, in test session 1 half the mice had a marble as the novel object and dice as familiar objects and the other half of the mice had the die as the novel object and marbles as familiar objects.

Morris Water Maze. Mice were tested for 4 days in the MWM after 5 months on the diets similar to previous methods.[21] This paradigm requires the mouse to use spatial memory and distal cues in the testing room to find a hidden white platform 1 cm below the surface of a circular pool of water (colored opaque with white nontoxic paint) and to remember its location from the previous trial. The mice were given 60 s to find the hidden platform during each acquisition trial. There were five acquisition trials on day 1 and four acquisition trials on days 2 and 3. The platform remained in the same position during acquisition trials, but start locations were varied. On day 4, a reversal test was performed during which the platform was moved to the opposite quadrant, thereby requiring the mouse to retain the learned escape strategy but to quickly learn the new escape position. A 60- s probe trial was performed during the fifth and last trial on days 2−4, during which the platform was removed. Performance was monitored with image tracking software (HVS Image, UK).

Data Analysis. Data are represented as the mean ± SEM and were analyzed using IBM SPSS Statistics 21 (IBM, Armonk, NY, USA) and Systat (Systat Software, Inc., Chicago, IL, USA). Significance was set at $p \leq 0.05$. Food intake, caloric intake, and percent increase in weight were analyzed with two-way ANOVA (factors: fat percentage and presence of blueberry). The novel object recognition test data are presented as a percent recognition index (RI) for object B: RI = (time attending to object B/time attending to object A + B) × 100 (Figure 3A). As there were no differences between the two training trials within each diet group, those data were combined for further analysis ($p > 0.05$, training trial 1 versus training trial 2, Wilcoxon signed ranks test). Novel object recognition was analyzed by comparing the RI of the training trial to the RI of the testing trial with the nonparametric Wilcoxon signed ranks test for paired samples. Testing trial performance was further analyzed by comparing RIs to chance performance (50% RI) with one-sample t tests. Morris water maze latency was analyzed with univariate ANOVA (factors: fat, BB, and day for acquisition learning or trial for reversal learning), and probe trial data were analyzed with independent sample t tests.

RESULTS

Mouse Weights and Food Intake. An average of two 24 h food intake measurements indicated that the mice that consumed HF diets ate fewer grams of food than the mice that ate LF diets ($F_{1,58} = 4.00$, $p \leq 0.05$, main effect of fat percentage, two-way ANOVA, Figure 1A). There was no effect of BB on food intake ($F_{1,58} = 0.003$, $p = 0.96$). Although the mice on HF diets ate less, they consumed more calories on average. An analysis of caloric intake based on the food intake measurements and calories in the diets (from Table 1) indicated that mice that consumed the HF diets consumed more calories than mice on the LF diets ($F_{1,58} = 12.41$, $p = 0.001$, main effect of fat percentage, Figure 1B). Furthermore, after 5 months on the diets, mice consuming HF diets gained significantly more weight than the mice on LF diets ($F_{1,56} = 60.32$, $p < 0.001$, main effect of fat percentage, Figure 2).

Novel Object Recognition Test. Analysis of novel object RI indicated that after 2 months on the diets, mice on LF and LFBB diets showed a significant increase in time spent on the novel object (object B, Figure 3A) in the testing trial compared to time on object B in the training trial ($p < 0.05$ Wilcoxon signed ranks test, Figure 3B). The mice on HF and HFBB diets did not spend more time on the novel object (object B) in the testing trial (versus training trial, $p = 0.59$ and $p = 0.72$, respectively). After 3 months on the diets, mice on LF and LFBB diets continued to demonstrate intact novel object recognition (training versus testing trial RI, $p < 0.05$, Figure

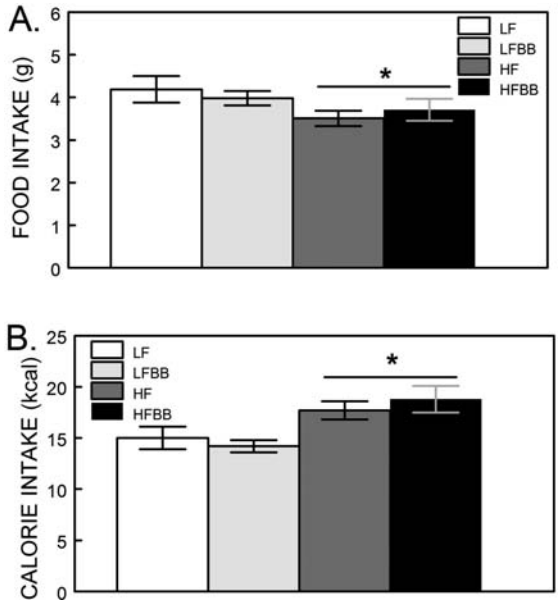

Figure 1. Food (A) and caloric (B) intake. An average of two 24 h food intake measurements indicated that overall the mice that ate HF diets consumed less than the mice that ate LF diets. However, mice on HF diets consumed significantly more calories than those on LF diets. (* $p < 0.05$, significant difference from LF diets, two-way ANOVA.)

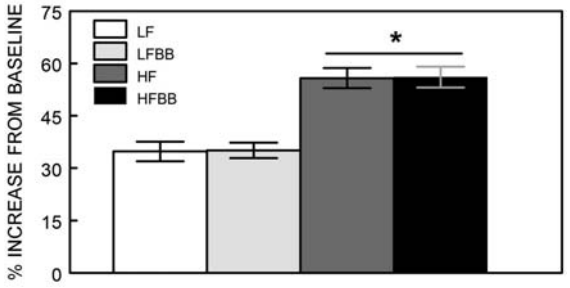

Figure 2. Percent increase in weight after 5 months on diets. Mice on HF diets gained significantly more weight than mice on LF diets. Blueberry had no effect on weight. (* $p < 0.05$, significant difference from LF diets, two-way ANOVA.)

3C), whereas mice on the HF diet continued to show impaired performance ($p = 0.65$). However, mice on the HFBB diet demonstrated a trend toward a difference between RIs in the training and testing trials ($p = 0.056$). After 4 months on the diets, mice on LF and LFBB diets demonstrated intact novel object recognition (testing versus training trial, $p < 0.05$, Figure 3D), whereas mice on the HF diet did not spend more time on the novel object in the testing trial ($p = 0.92$). Mice on the HFBB diet showed a significant increase in time spent on the novel object in the testing trial compared to object B in the training trial ($p < 0.05$).

Another method of examining performance in the novel object recognition task is to compare testing trial performance to chance performance (50% RI). A mouse with intact novel object recognition will spend >50% of its time on the novel object in the testing trials. The LF and LFBB diet-fed mice performed at levels greater than chance during all test sessions ($p < 0.05$, one-sample t test, Figure 4). Mice fed the HF diet did not perform above chance in any test session ($p > 0.05$). The HFBB-fed mice did not perform above chance after 2 months on the diet ($p = 0.23$), but after 3 months on the diet there was a trend ($p = 0.15$), and after 4 months on the diet, the mice demonstrated performance that was significantly greater than chance ($p = 0.02$).

There were no differences between diet groups in the overall amount of time mice explored the objects during novel object recognition testing, indicating that differences in RI were not influenced by differences in general exploration of the objects (effect of diet: $F_{3,164} = 0.930$, $p = 0.93$; diet × test session: $F_{6,165} = 0.507$, $p = 0.80$, two-way ANOVA, data not shown).

Morris Water Maze. There was a trend toward a main effect of fat percentage on the average acquisition day latencies in the MWM ($F_{1,165} = 3.53$, $p = 0.062$, univariate ANOVA), but no effect of BB or interaction of fat percentage × BB on acquisition latency (data not shown). There was no effect of diet on reversal learning latency (data not shown). However, there were differences in passes through the platform location during the probe trials. On the day 2 probe trial, mice that were on the HF diet passed through the platform location significantly less often than the mice on the LFBB diet ($p < 0.05$, t test, Figure 5) and there was a trend from the LF diet (HF versus LF, $p = 0.14$). On the day 3 probe trial, there was a trend that suggested fewer passes through the platform by mice on the HF diet compared to mice on both LF diets (LF, $p = 0.16$; LFBB $p = 0.13$). On all probe trials, there were no differences in the number of passes through the platform location between the HFBB-fed mice and either group of LF-fed mice. There were no differences in probe trial performance during the reversal day between any groups.

DISCUSSION

In this study, middle-aged mice were fed HF or LF diets with and without BB supplementation for 5 months. Mice that were fed HF diets gained significantly more weight than those fed LF diets. This is congruent with the fact that the mice on HF diets were consuming more calories on a daily basis. BB supplementation did not prevent or augment weight gain. This corroborates previous research. BB has been shown to decrease weight gain induced by a HF diet when combined with defatted soybean flour.[22] However, whole BB in the diet has not been shown to prevent weight gain from a 45 or 60% HF diet, although feeding isolated anthocyanins from BB has been demonstrated to decrease weight gain and body fat when fed in conjunction with a HF diet.[23]

Mice fed the HF diet showed impaired novel object recognition performance when tested after 2, 3, and 4 months of consuming the diet. A recent study demonstrated that a HF diet, similar to the diet employed in this study (60% calories from fat), did not impair novel object recognition memory in mice that were approximately 8.5 months old.[7] The mice in our study were 11−13 months of age during novel object recognition testing; thus, the impaired memory demonstrated by the mice in the current study may be due to an interaction of HF diet and age. Mice that were fed the HFBB diet initially showed impaired performance, but their performance improved over subsequent test sessions and, after 4 months on the diet, their performance was no longer impaired. This suggests that over time BB may be able to reverse some of the impact a HF diet may have on certain types of learning and memory. It is unclear why the effect of BB in the current study is time dependent and why the BB did not prevent the initial impairment of novel object recognition associated with consumption of a HF diet. One possible explanation is that there is a threshold level of fat-soluble antioxidants in BB, such

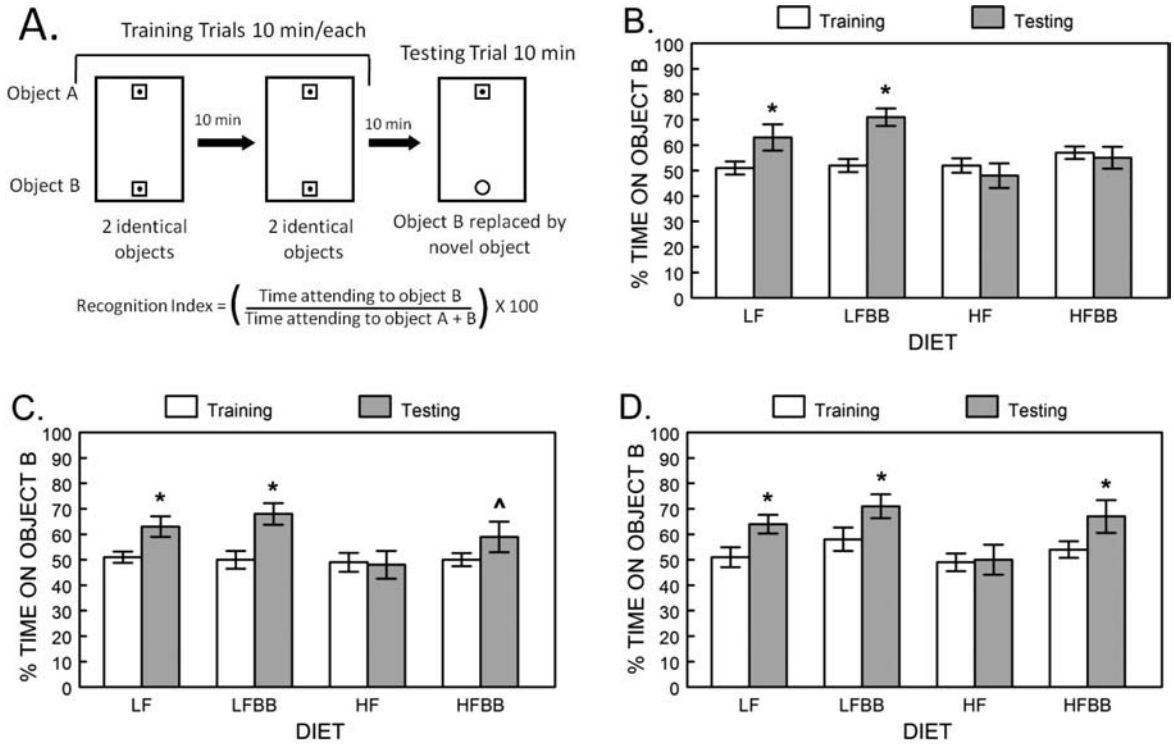

Figure 3. Novel object recognition performance after 2 (B), 3 (C), and 4 (D) months on the diets. (A) The schematic represents testing cages as they were arranged in each trial of testing. (B) After 2 months on the diets, mice on LF and LFBB diets showed a significant increase in RI in the testing trial compared to the training trial, suggesting intact object recognition learning/memory. Mice on HF and HFBB diets did not demonstrate an increase in RI in the testing trial, suggesting impairment. (C) After 3 months on the diets, mice consuming HFBB diet showed a trend toward an increase in RI in the testing trial ($\hat{p} = 0.056$). (D) After 4 months on the diets, mice on LF, LFBB, and HFBB diets showed a significant increase in RI in the testing trial compared to the training trial, whereas the mice on the HF diet did not. ($* p < 0.05$, testing trial is different from training trial, Wilcoxon signed ranks test.)

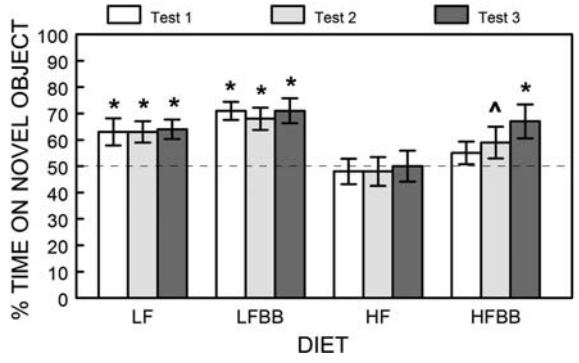

Figure 4. Testing trial performance in the novel object recognition task over three test sessions. The LF- and LFBB-fed mice, but not the mice fed the HF diet, performed at levels greater than chance when tested after 2, 3, and 4 months on the diets (chance is 50% time on the novel object and is indicated by the dotted line). The HFBB-fed mice demonstrated a trend ($\hat{p} = 0.15$) after 3 months on the diet, and after 4 months on the diet, the mice demonstrated performance that was significantly greater than chance. ($* p < 0.05$, one-sample t test compared to a mean of 50%.)

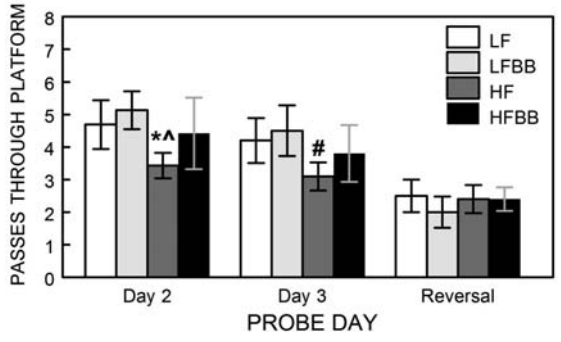

Figure 5. Morris water maze probe trials. On days 2 and 3 of the probe trial, mice that were on the HF diet passed through the platform location less often than the mice on the LF diets. On all probe trials, there were no differences in the number of passes through the platform location between the HFBB-fed mice and either group of LF diet-fed mice. ($* p < 0.05$ from LFBB diet, $\hat{p} = 0.14$ trend from LF, # trend from LF ($p = 0.16$) and LFBB ($p = 0.13$), t test.)

as vitamin A, that must accumulate in the brain to alleviate memory impairment, similar to the "threshold hypothesis" discussed by Malin and colleagues.[24] The time-dependent manner in which novel object recognition memory is rescued by BB supplementation in mice on a HF diet may be attributed to the time course of accumulation of BB fat-soluble antioxidants in the brain, although this remains to be directly tested.

The diets did not have considerable effects on the performance of mice in the MWM; however, during the probe trials, the mice on the HF diet showed deficits in performance. Notably, the probe trial performance of the mice on the HFBB diet did not differ from the mice on the LF diets. The lack of profound effects on latency to find the hidden platform during acquisition learning or reversal learning could potentially be due to a floor effect in which the middle-aged

dx.doi.org/10.1021/jf404565s | J. Agric. Food Chem. 2014, 62, 3972−3978

mice showed age-related deficits that were not significantly worsened by the HF diet or prevented by the BB diet. A recent study found a decline in MWM performance (i.e., path length to the hidden platform) in middle-aged rats, but no further decline due to being on a HF diet.[25] Previous research has demonstrated that BB is able to prevent or reverse age-related performance deficits in spatial mazes such as the MWM,[26] which may suggest that we should have observed improved performance in the LFBB mice. However, the study by Joseph et al.[26] tested old rats in the MWM, whereas our study tested middle-aged mice, so differences in rodent, age, or both, could be a reason for the discrepancy in results.

It is more likely that the lack of more significant differences between groups in this test is due to the possible lack of sensitivity of the MWM to alterations in mouse learning and memory or the diets having different effects on different types of memory (object recognition versus spatial). Water-based mazes such as the MWM were initially developed for rats, which swim in their natural environment, but may not be as ecologically valid for mice that evolved on dry land.[27] For example, mice are more likely to passively float, which could obscure deficits or enhancements in learning and memory. Furthermore, research suggests that object recognition memory may be largely mediated by the perirhinal cortex in the medial temporal lobe,[28] whereas spatial memory is associated with the intact functioning of the hippocampus.[29] Thus, the behavioral results may suggest possible differential effects of the diets in different brain regions.

The mechanisms by which blueberry can modulate the effects of a HF diet were not evaluated in this study. One possibility is that the memory impairment is due to HF diet-related oxidative stress. Morrison et al. found that a HF diet fed to aged mice impaired memory retention in the 14-unit T maze, increased oxidative stress in the brain, and impaired NF-E2-related factor 2, which may play a role in the body's endogenous antioxidant response.[3] BB has been found to reduce oxidative stress in vivo[26] and in vitro.[30,31] Also, BB may have reduced the inflammation elicited by consumption of a HF diet; consumption of a HF diet has been demonstrated to increase the inflammatory cytokines TNFα and IL-6.[4] In studies of aging, BB has been shown to reduce overexpression and overproduction of these inflammatory factors.[32,33] It has also been shown that resveratrol, a component of blueberry, reduces indices of oxidative stress (4-hydroxynonenal) and inflammation (TNFα and ionized calcium binding adaptor molecule 1 expression) in the hippocampus of mice fed a HF diet.[14] A HF diet also has been demonstrated to decrease neurogenesis in the mouse hippocampus,[5] whereas BB has been demonstrated to increase neurogenesis in aged rodents.[34] Furthermore, HF diet consumption has been linked to reductions in brain-derived neurotrophic factor (BDNF) in both the cortex and hippocampus of mice,[5,35] areas crucial for recognition and spatial memory. In contrast, BB has been known to increase BDNF, and this increase was correlated with spatial memory improvements.[36] BDNF is important for hippocampal synaptic plasticity because it can promote morphological changes that support synaptic efficiency and thus influence hippocampus-mediated behaviors, such as spatial learning and memory.[37] There is also the possibility that BB and fat acted synergistically, with dietary fat enhancing the absorption of fat-soluble vitamins such as vitamin A. Vitamin A and its derivatives have been shown to improve memory deficits in aged mice,[38] but the possible interaction between fat and BB intake in the absorption of nutrients necessitates further study.

The Tifblue powder used in this study is made from a rabbiteye variety of BB (*Vaccinium ashei*). Rabbiteye BB has been shown to reduce DNA damage in mouse hippocampus and cortex, areas important for recognition and spatial memory.[39] HPLC analysis of rabbiteye BB has shown it to contain high levels of flavonoid anthocyanidins and anthocyanins.[40] In fact, Li and colleagues found nine different anthocyanins in rabbiteye BB using HPLC-DAD-MS^n, including delphinidin-3-glucoside and petuidin-3-glucoside.[41] Flavonoids have been shown to modulate neuronal signaling pathways that influence synaptic plasticity and neurogenesis, which ultimately can have an effect on learning and memory.[42,43] Flavonoids also can promote neuronal viability and suppress inflammation by inhibiting c-jun N-terminal kinase, apoptosis signal-regulating kinase-1, and p38 pathways, thus preventing neurodegeneration.[42] Therefore, it is likely that the effects of BB are attributable, at least in part, to the biological activities of flavonoids. Flavonoids have been shown to cross the blood−brain barrier,[44] and specifically anthocyanins have been shown to accumulate in the brains of aged rats fed a BB-supplemented diet.[9] A recent study found that aged rats fed diets supplemented with anthocyanins in amounts similar to that found in BB showed increased BDNF in the hippocampus as well as improvements in cross-maze spatial memory performance.[8] Recently, delphinidin-3-glucoside, a component of rabbiteye BB, has been found to reduce the release of proinflammatory mediators from brain microglial cells;[45] thus, the anthocyanin components of BB may be reducing inflammation induced by a HF diet. Furthermore, another component of BB, cyanidin-3-glucoside, has been shown to reduce spatial recognition memory impairment by possibly reducing oxidative stress.[46]

This study supports that adding BB to a HF diet could reverse some of the behavioral deficits associated with consumption of a HF diet, specifically deficits in object recognition memory. It is important to find ways to prevent or reverse the effects that a HF diet may have on the brain and behavior, as the incidence of obesity is increasing worldwide, and consumption of a HF diet has been implicated as a factor in the development of obesity and obesity-related diseases. The purpose of this study was not to encourage consumption of a HF diet, but rather to suggest that making small changes to a putative unhealthy diet, such as incorporating more nutrient-dense foods, could provide some level of protection against cognitive deficits attributed to that diet. This is an important finding that requires further study in both animal models and humans. Furthermore, it is not known the exact mechanism(s) by which BB may be modulating the effects of a HF diet, but research suggests a multitude of probable mechanisms; however, this topic also calls for further study.

AUTHOR INFORMATION

Corresponding Author

*(A.N.C.) Phone: (617) 521-2619. Fax: (617) 521-3199. E-mail: amanda.carey@simmons.edu.

Funding

Supported by USDA Intramural.

Notes

The authors declare no competing financial interest.

■ ACKNOWLEDGMENTS

The U.S. Highbush Blueberry Council graciously provided the blueberry powder. We are grateful for Jason DeFuria and Paul Pistell and their helpful advice regarding high-fat diet research and to Tony Sealy for his assistance with food intake measurements.

■ REFERENCES

(1) West, D. B.; York, B. Dietary fat, genetic predisposition, and obesity: lessons from animal models. *Am. J. Clin. Nutr.* **1998**, *67*, 505S−512S.

(2) Singh, R. B.; Gupta, S.; Dherange, P.; De Meester, F.; Wilczynska, A.; Alam, S. E.; Pella, D.; Wilson, D. W. Metabolic syndrome: a brain disease. *Can. J. Physiol. Pharmacol.* **2012**, *90*, 1171−1183.

(3) Morrison, C. D.; Pistell, P. J.; Ingram, D. K.; Johnson, W. D.; Liu, Y.; Fernandez-Kim, S. O.; White, C. L.; Purpera, M. N.; Uranga, R. M.; Bruce-Keller, A. J.; Keller, J. N. High fat diet increases hippocampal oxidative stress and cognitive impairment in aged mice: implications for decreased Nrf2 signaling. *J. Neurochem.* **2010**, *114*, 1581−1589.

(4) Pistell, P. J.; Morrison, C. D.; Gupta, S.; Knight, A. G.; Keller, J. N.; Ingram, D. K.; Bruce-Keller, A. J. Cognitive impairment following high fat diet consumption is associated with brain inflammation. *J. Neuroimmunol.* **2010**, *219*, 25−32.

(5) Park, H. R.; Park, M.; Choi, J.; Park, K. Y.; Chung, H. Y.; Lee, J. A high-fat diet impairs neurogenesis: involvement of lipid peroxidation and brain-derived neurotrophic factor. *Neurosci. Lett.* **2010**, *482*, 235−239.

(6) Mulder, M.; Blokland, A.; van den Berg, D. J.; Schulten, H.; Bakker, A. H.; Terwel, D.; Honig, W.; de Kloet, E. R.; Havekes, L. M.; Steinbusch, H. W.; de Lange, E. C. Apolipoprotein E protects against neuropathology induced by a high-fat diet and maintains the integrity of the blood-brain barrier during aging. *Lab Invest.* **2001**, *81*, 953−960.

(7) Heyward, F. D.; Walton, R. G.; Carle, M. S.; Coleman, M. A.; Garvey, W. T.; Sweatt, J. D. Adult mice maintained on a high-fat diet exhibit object location memory deficits and reduced hippocampal SIRT1 gene expression. *Neurobiol. Learn. Mem.* **2012**, *98*, 25−32.

(8) Rendeiro, C.; Vauzour, D.; Rattray, M.; Waffo-Teguo, P.; Merillon, J. M.; Butler, L. T.; Williams, C. M.; Spencer, J. P. Dietary levels of pure flavonoids improve spatial memory performance and increase hippocampal brain-derived neurotrophic factor. *PLoS One* **2013**, *8*, e63535.

(9) Andres-Lacueva, C.; Shukitt-Hale, B.; Galli, R. L.; Jauregui, O.; Lamuela-Raventos, R. M.; Joseph, J. A. Anthocyanins in aged blueberry-fed rats are found centrally and may enhance memory. *Nutr. Neurosci.* **2005**, *8*, 111−120.

(10) Joseph, J. A.; Shukitt-Hale, B.; Casadesus, G. Reversing the deleterious effects of aging on neuronal communication and behavior: beneficial properties of fruit polyphenolic compounds. *Am. J. Clin. Nutr.* **2005**, *81*, 313S−316S.

(11) Lau, F. C.; Shukitt-Hale, B.; Joseph, J. A. The beneficial effects of fruit polyphenols on brain aging. *Neurobiol. Aging* **2005**, *26*, 128−132.

(12) Miller, M. G.; Shukitt-Hale, B. Berry fruit enhances beneficial signaling in the brain. *J. Agric. Food Chem.* **2012**, *60*, 5709−5715.

(13) DeFuria, J.; Bennett, G.; Strissel, K. J.; Perfield, J. W., 2nd; Milbury, P. E.; Greenberg, A. S.; Obin, M. S. Dietary blueberry attenuates whole-body insulin resistance in high fat-fed mice by reducing adipocyte death and its inflammatory sequelae. *J. Nutr.* **2009**, *139*, 1510−1516.

(14) Jeon, B. T.; Jeong, E. A.; Shin, H. J.; Lee, Y.; Lee, D. H.; Kim, H. J.; Kang, S. S.; Cho, G. J.; Choi, W. S.; Roh, G. S. Resveratrol attenuates obesity-associated peripheral and central inflammation and improves memory deficit in mice fed a high-fat diet. *Diabetes* **2012**, *61*, 1444−1454.

(15) U.S. Highbush Blueberry Council website, http://www.blueberry.org/nutraceuticals/nutrition.htm.

(16) Elks, C. M.; Francis, J.; Stull, A. J.; Cefalu, W. T.; Shukitt-Hale, B.; Ingram, D. K. Overview of the health properties of blueberries. In *Bioactives in Fruit: Health Benefits and Functional Foods*; Skinner, M., Hunter, D., Eds.; Wiley-Blackwell: Oxford, UK, 2013; pp 251−272.

(17) Prior, R. L.; Lazarus, S. A.; Cao, G.; Muccitelli, H.; Hammerstone, J. F. Identification of procyanidins and anthocyanins in blueberries and cranberries (*Vaccinium* spp.) using high-performance liquid chromatography/mass spectrometry. *J. Agric. Food Chem.* **2001**, *49*, 1270−1276.

(18) Sellappan, S.; Akoh, C. C.; Krewer, G. Phenolic compounds and antioxidant capacity of Georgia-grown blueberries and blackberries. *J. Agric. Food Chem.* **2002**, *50*, 2432−2438.

(19) Antunes, M.; Biala, G. The novel object recognition memory: neurobiology, test procedure, and its modifications. *Cogn. Process.* **2012**, *13*, 93−110.

(20) Carey, A. N.; Lyons, A. M.; Shay, C. F.; Dunton, O.; McLaughlin, J. P. Endogenous kappa opioid activation mediates stress-induced deficits in learning and memory. *J. Neurosci.* **2009**, *29*, 4293−4300.

(21) Troen, A. M.; Shukitt-Hale, B.; Chao, W. H.; Albuquerque, B.; Smith, D. E.; Selhub, J.; Rosenberg, J. The cognitive impact of nutritional homocysteinemia in apolipoprotein-E deficient mice. *J. Alzheimer's Dis.* **2006**, *9*, 381−392.

(22) Prior, R. L.; Wu, X.; Gu, L.; Hager, T. J.; Hager, A.; Howard, L. R. Whole berries versus berry anthocyanins: interactions with dietary fat levels in the C57BL/6J mouse model of obesity. *J. Agric. Food Chem.* **2008**, *56*, 647−653.

(23) Roopchand, D. E.; Kuhn, P.; Rojo, L. E.; Lila, M. A.; Raskin, I. Blueberry polyphenol-enriched soybean flour reduces hyperglycemia, body weight gain and serum cholesterol in mice. *Pharmacol. Res.* **2013**, *68*, 59−67.

(24) Malin, D. H.; Lee, D. R.; Goyarzu, P.; Chang, Y. H.; Ennis, L. J.; Beckett, E.; Shukitt-Hale, B.; Joseph, J. A. Short-term blueberry-enriched diet prevents and reverses object recognition memory loss in aging rats. *Nutrition* **2011**, *27*, 338−342.

(25) Pancani, T.; Anderson, K. L.; Brewer, L. D.; Kadish, I.; DeMoll, C.; Landfield, P. W.; Blalock, E. M.; Porter, N. M.; Thibault, O. Effect of high-fat diet on metabolic indices, cognition, and neuronal physiology in aging F344 rats. *Neurobiol. Aging* **2013**, *34*, 1977−1987.

(26) Joseph, J. A.; Shukitt-Hale, B.; Denisova, N. A.; Bielinski, D.; Martin, A.; McEwen, J. J.; Bickford, P. C. Reversals of age-related declines in neuronal signal transduction, cognitive, and motor behavioral deficits with blueberry, spinach, or strawberry dietary supplementation. *J. Neurosci.* **1999**, *19*, 8114−8121.

(27) Deacon, R. M. Shallow water (paddling) variants of water maze tests in mice. *J. Vis. Exp.* **2013**, *76*, 2608.

(28) Murray, E. A.; Richmond, B. J. Role of perirhinal cortex in object perception, memory, and associations. *Curr. Opin. Neurobiol.* **2001**, *11*, 188−193.

(29) Sharma, S.; Rakoczy, S.; Brown-Borg, H. Assessment of spatial memory in mice. *Life Sci.* **2010**, *87*, 521−536.

(30) Joseph, J. A.; Carey, A.; Brewer, G. J.; Lau, F. C.; Fisher, D. R. Dopamine and Abeta-induced stress signaling and decrements in Ca^{2+} buffering in primary neonatal hippocampal cells are antagonized by blueberry extract. *J. Alzheimer's Dis.* **2007**, *11*, 433−446.

(31) Pang, W.; Jiang, Y. G.; Yang, H. P.; Cheng, D. M.; Lu, H.; Lu, S. J. Cytoprotective effect of blueberry extracts against oxidative damage of rat hippocampal neurons induced by H_2O_2. *Zhongguo Ying Yong Sheng Li Xue Za Zhi* **2010**, *26*, 51−54.

(32) Lau, F. C.; Bielinski, D. F.; Joseph, J. A. Inhibitory effects of blueberry extract on the production of inflammatory mediators in lipopolysaccharide-activated BV2 microglia. *J. Neurosci. Res.* **2007**, *85*, 1010−1017.

(33) Xie, C.; Kang, J.; Ferguson, M. E.; Nagarajan, S.; Badger, T. M.; Wu, X. Blueberries reduce pro-inflammatory cytokine TNF-alpha and IL-6 production in mouse macrophages by inhibiting NF-kappaB activation and the MAPK pathway. *Mol. Nutr. Food Res.* **2011**, *55*, 1587−1591.

(34) Casadesus, G.; Shukitt-Hale, B.; Stellwagen, H. M.; Zhu, X.; Lee, H. G.; Smith, M. A.; Joseph, J. A. Modulation of hippocampal plasticity

and cognitive behavior by short-term blueberry supplementation in aged rats. *Nutr. Neurosci.* **2004**, *7*, 309−316.
(35) Pistell, P. J.; Morrison, C. D.; Gupta, S.; Knight, A. G.; Keller, J. N.; Ingram, D. K.; Bruce-Keller, A. J. Cognitive impairment following high fat diet consumption is associated with brain inflammation. *J. Neuroimmunol.* **2010**, *219*, 25−32.
(36) Williams, C. M.; El Mohsen, M. A.; Vauzour, D.; Rendeiro, C.; Butler, L. T.; Ellis, J. A.; Whiteman, M.; Spencer, J. P. Blueberry-induced changes in spatial working memory correlate with changes in hippocampal CREB phosphorylation and brain-derived neurotrophic factor (BDNF) levels. *Free Radical Biol. Med.* **2008**, *45*, 295−305.
(37) Schaaf, M. J.; Workel, J. O.; Lesscher, H. M.; Vreugdenhil, E.; Oitzl, M. S.; de Kloet, E. R. Correlation between hippocampal BDNF mRNA expression and memory performance in senescent rats. *Brain Res.* **2001**, *915*, 227−233.
(38) Etchamendy, N.; Enderlin, V.; Marighetto, A.; Vouimba, R. M.; Pallet, V.; Jaffard, R.; Higueret, P. Alleviation of a selective age-related relational memory deficit in mice by pharmacologically induced normalization of brain retinoid signaling. *J. Neurosci.* **2001**, *21*, 6423−6429.
(39) Barros, D.; Amaral, O. B.; Izquierdo, I.; Geracitano, L.; do Carmo Bassols Raseira, M.; Henriques, A. T.; Ramirez, M. R. Behavioral and genoprotective effects of *Vaccinium* berries intake in mice. *Pharmacol., Biochem. Behav.* **2006**, *84*, 229−234.
(40) Huang, W. Y.; Zhang, H. C.; Liu, W. X.; Li, C. Y. Survey of antioxidant capacity and phenolic composition of blueberry, blackberry, and strawberry in Nanjing. *J. Zhejiang Univ. Sci. B* **2012**, *13*, 94−102.
(41) Li, C.; Feng, J.; Huang, W. Y.; An, X. T. Composition of polyphenols and antioxidant activity of rabbiteye blueberry (*Vaccinium ashei*) in Nanjing. *J. Agric. Food Chem.* **2013**, *61*, 523−531.
(42) Spencer, J. P. The impact of fruit flavonoids on memory and cognition. *Br. J. Nutr.* **2010**, *104* (Suppl. 3), S40−S47.
(43) Spencer, J. P.; Vauzour, D.; Rendeiro, C. Flavonoids and cognition: the molecular mechanisms underlying their behavioural effects. *Arch. Biochem. Biophys.* **2009**, *492*, 1−9.
(44) Milbury, P. E.; Kalt, W. Xenobiotic metabolism and berry flavonoid transport across the blood-brain barrier. *J. Agric. Food Chem.* **2010**, *58*, 3950−3956.
(45) Carey, A. N.; Fisher, D. R.; Rimando, A. M.; Gomes, S. M.; Bielinski, D. F.; Shukitt-Hale, B. Stilbenes and anthocyanins reduce stress signaling in BV-2 mouse microglia. *J. Agric. Food Chem.* **2013**, *61*, 5979−5986.
(46) Nasri, S.; Roghani, M.; Baluchnejadmojarad, T.; Balvardi, M.; Rabani, T. Chronic cyanidin-3-glucoside administration improves short-term spatial recognition memory but not passive avoidance learning and memory in streptozotocin-diabetic rats. *Phytother. Res.* **2012**, *26*, 1205−1210.

Processing of the Blueberry-Containing Baked Product. Wild blueberries (*Vaccinium angustifolium* Aiton) were obtained from the Wild Blueberry Association of North America as a freeze-dried powder, which was stored at −20 °C. The novel blueberry-containing product was composed of 40 g of dough and 20 g of filling and was produced via standard procedures. The dough contained the following ingredients: white flour, freeze-dried blueberry, egg, butter, yeast, salt, skimmed milk powder, sugar, and water, whereas the filling contained freeze-dried blueberry, sugar, salt, evaporated milk, corn flour, and eggs (Table 1). Dough ingredients were combined in a mixer and moistened with water, and finally yeast was incorporated (Figure 1). Dough proving (the step when dough is allowed to rise) was carried out in a prover for 1 h at 30 °C. Filling ingredients were mixed, plastic sealed, and then cooked in a water bath until the temperature reached 90 °C. Following this, 40 g of dough was injected with 20 g of filling, and a second proving step was conducted at 30 °C for 1 h. Finally, the proven bun was baked at 180 °C for 12 min. Sampling was conducted after each stage (Figure 1), and samples were freeze-dried for 4 days prior to powdering and storage at −20 °C until analysis. The proved and baked buns were freeze-dried as a whole and then mixed and powdered together. Homogeneous samples were taken for analysis, representative of both the dough and filling.

Table 1. Blueberry-Containing Bun Formulation

ingredient (% w/w)	dough	filling
blueberry powder	12.4	31.8
egg	5.9	28.7
salt	0.5	0.1
sugar	7.7	22.2
white flour	46.4	
butter	5.9	
yeast	1.1	
skimmed milk powder	4.6	
evaporated milk		12.6
corn flour		4.6

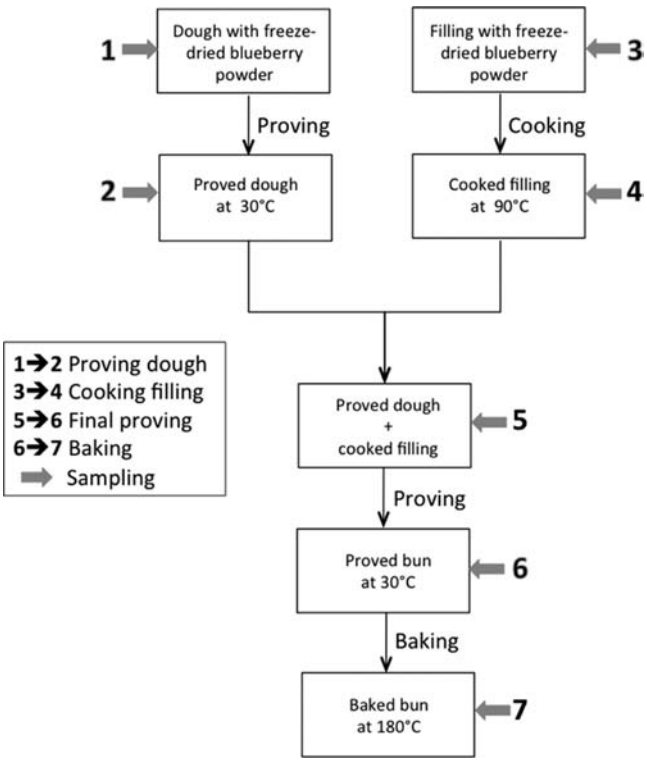

Figure 1. Diagram of the blueberry-containing baked product processing with sampling points indicated: 1 and 2, proving of the dough; 3 and 4, cooking of the filling; 5 and 6, final proving; 6 and 7, baking.

The changes in (poly)phenol content reported at each stage were calculated as changes between the initial (poly)phenol content of dough (in the proving of the dough stage), the initial (poly)phenol content of the filling (in the cooking of the filling stage), the (poly)phenol content of the dough and filling together after proving and cooking (in the final proving stage), and the (poly)phenol content of the final proved bun (in the baking stage) before and after the specific stage investigated (Figure 1). The total changes in (poly)-phenol content were calculated as changes between the initial content of dough and filling together before any processing was carried out and the final content in the baked product. All of the samples analyzed were weighed before and after freeze-drying, and the results were compensated for moisture loss during processing. The results are reported as milligrams per fresh bun.

Extraction of Flavonoids and Phenolic Acids. Extraction of anthocyanins and procyanidins from freeze-dried samples (0.2 g) was performed as previously described.[1] Briefly, anthocyanins were extracted three times with 5 mL of acidified methanol (0.1% HCl in MeOH). Pelargonidin-3-*O*-glucoside was added to the samples as a recovery standard (300 μL, 1 mM). Samples were vortexed for 5 min, sonicated for 5 min in an ultrasonic bath (Fisher Scientific, Loughborough, UK), and centrifuged at room temperature for 15 min at 1800*g*. The supernatants were combined, and 3 mL was mixed with 3 mL of 5 M HCl and heated at 90 °C for 1 h for anthocyanin hydrolysis, in order to cleave all anthocyanins to anthocyanidins. A 50 μL aliquot of filtered sample was injected into the HPLC for analysis.

Procyanidins were extracted from freeze-dried samples (0.5 g) with 5 mL of acetone/water/acetic acid (70:29.5:0.5; v/v/v). Tubes were vortexed for 2 min, sonicated at 50 °C for 5 min, and vortexed again for 1 min. Samples were then centrifuged for 5 min at 2567*g* at room temperature, and the supernatant was retained and passed through a Strata SCX solid phase extraction cartridge (55 μm, 70 Å, 500 mg/3 mL; Phenomenex, Torrance, CA, USA). Conditioning of the SPE packing bed was performed using 5 mL of deionized water on a vacuum (0.2 bar) manifold (24-position, Phenomenex). After conditioning, 2 mL of the supernatant was loaded into the SPE cartridge, and approximately half of the loaded sample was discharged from the cartridge to ensure that the sample was not diluted with the water used to condition the cartridge. A 0.45 μm PTFE filter was placed at the end of the cartridge, and approximately 1 mL was filtered and transfer to an HPLC vial. Five microliters was injected in the HPLC.

Phenolic acids and chlorogenic acid were extracted three times with 5 mL of 10% formic acid in water (v/v). HPPA was added to the samples as recovery standard (50 μL, 10 mM). Samples were vortexed for 1 min, sonicated for 5 min in an ultrasonic bath, vortexed for a further 1 min, and centrifuged for 15 min at 2000*g* at room temperature. The combined supernatants (15 mL) were vortexed, and a 50 μL aliquot was filtered through a 0.22 μm filter prior to transfer to HPLC amber vials. Quercetin was extracted and hydrolyzed to aglycone as follows: Freeze-dried blueberries or samples at different stages of processing (0.2 g) were added to 8 mL of water/methanol (1:1) and vortexed for 1 min to facilitate dissolution. To this extract was added 2 mL of HCl (5 M), and the mixture was vortexed and left to heat on a steam bath at 90 °C for 1 h. After that, the extract was allowed to cool, and 3 mL of mixture was added to 3 mL of methanol. The samples were sonicated, filtered, and injected. Kaempferol-3-*O*-glucoside (50 μL, 10 mM) was used as the recovery standard, after it had been confirmed that this compound was not present in the freeze-dried blueberry samples tested.

HPLC Analysis of Anthocyanidins, Procyanidins, Phenolic Acids, and Quercetin. Samples were analyzed for anthocyanidins, chlorogenic acid, caffeic acid, ferulic acid, and quercetin content as previously described[1] using an Agilent 1100 series HPLC system (Agilent Technologies, Palo Alto, CA, USA) equipped with a diode

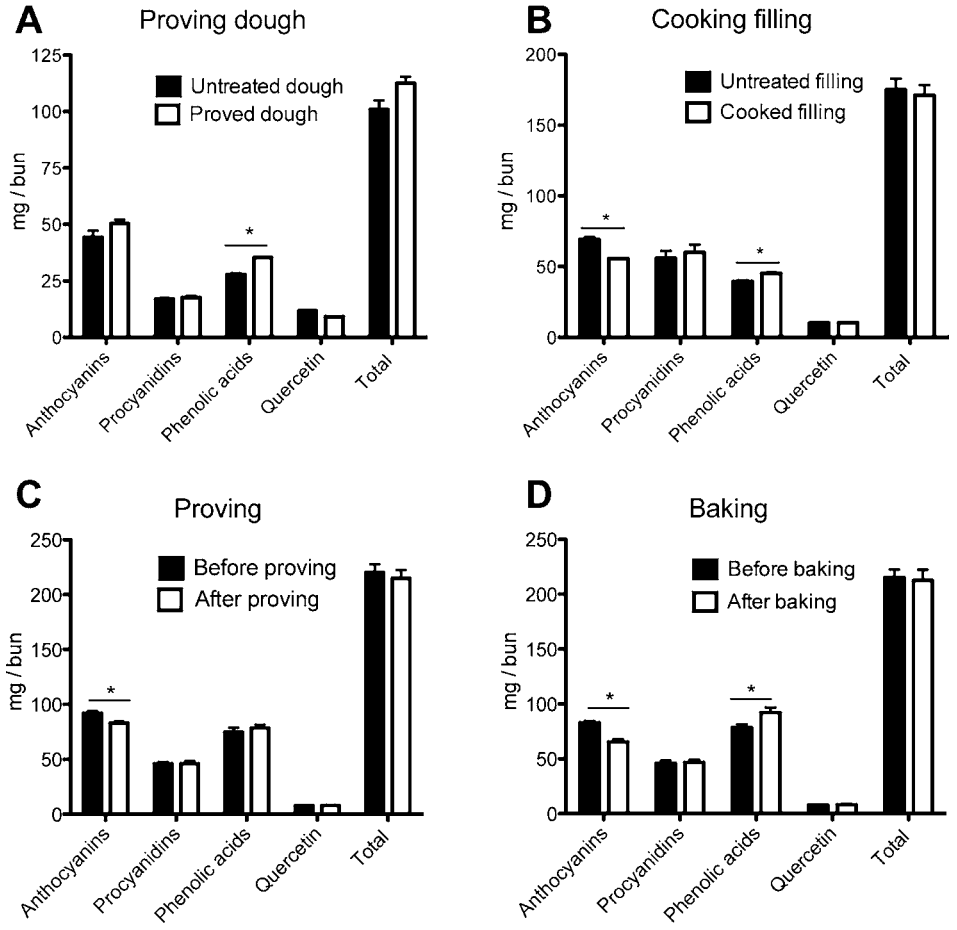

Figure 2. Changes in total anthocyanin, procyanidin, phenolic acid, quercetin, and total (poly)phenol contents during the different stages of processing of a blueberry-containing bun: (A) proving of the dough; (B) cooking of the filling; (C) second proving; (D) baking. Results are expressed as mg/bun ± SEM (n = 3). ∗, $p < 0.05$, significant differences before and after processing.

array detector. The column was a Nova-Pak C_{18} column (250 × 4.6 mm; 4 μm particle size; 30 °C; Waters Ltd., Elstree, UK). The mobile phase consisted of (A) methanol/water/5 M HCl (5:94.9:0.1; v/v/v) and (B) acetonitrile/water/5 M HCl (50:49.9:0.1, v/v/v) and was pumped through the system using the following gradient profile (min/% mobile phase B): 0/5, 5/5, 40/50, 55/100, 59,9/100, and 60/5 with a flow rate of 0.7 mL/min. The eluent was monitored by photodiode array detection at 320 nm (chlorogenic acid) and 520 nm (anthocyanidins) with spectra of products obtained between 220 and 600 nm. Calibration curves were obtained using authentic standards.

For procyanidins, a normal phase HPLC method with fluorescence detection was used as previously described.[1] A Develosil Diol 100 column (250 × 4.6 mm; 100 Å pore size; 5 μm particle size; 35 °C) together with a Cyano Guard column (4 × 3 mm) (Phenomenex) was used for separation. The mobile phase consisted of (A) acetonitrile/acetic acid (98:2; v/v) and (B) methanol/water/acetic acid, (95:3:2; v/v/v)/ and the following gradient system was used (min/% mobile phase B): 0/7, 3/7, 60/37.6, 63/100, 70/100, and 76/7 with a flow rate of 1 mL/min. UV data were collected at 280 nm, and fluorescence detection was conducted with an excitation wavelength of 230 nm and emission at 321 nm. Procyanidins were quantified using external calibration curves obtained using a mix of flavanol oligomer standards (DP1−DP10) isolated from cocoa (Mars, Inc., Hackettstown, NJ, USA). Flavanol polymers (DP > 10) were not quantified.

Statistical Analysis. All results are expressed as means ± SEM of three replicates. The statistical evaluation of the results was performed by one-way analysis of variance (ANOVA) followed by Tukey's post hoc test using GraphPad Prism version 5.0 (GraphPad Software, Inc.). Significance was defined as $p < 0.05$.

RESULTS

Changes in Anthocyanin Content during Processing. Changes in anthocyanin content were evaluated throughout the various steps in the processing chain (Figure 1). The total loss in anthocyanin content throughout all of the processing stages was 42%, with significant decreases in total anthocyanin content observed during cooking of the filling (20%, $p < 0.05$, Figure 2B), second proving (10%, $p < 0.05$, Figure 2C), and baking (21%, $p < 0.05$, Figure 2D). Individual anthocyanin losses ranged from 36% (malvidin) to 48% (peonidin) (Figure 3), and significant decreases were observed after cooking of the filling (malvidin, 18%; delphinidin, 25%; and petunidin, 21%, $p < 0.05$; Figure 3B), after proving (delphinidin, 16%; cyanidin, 13%; and petunidin, 10%, $p < 0.05$; Figure 3C), and during baking (malvidin, 24%; petunidin, 26%; and peonidin, 24%, $p < 0.05$; Figure 3D).

Changes in Procyanidin Content during Processing. No significant differences in total procyanidin content were observed during the different stages of bun processing (Figure 2). However, for the whole process, dimer and trimer levels significantly increased by 36 and 28%, respectively ($p < 0.05$), whereas nonamers and decamers disappeared completely ($p < 0.05$; Figure 4). In the individual stages of processing, significant increases in dimers after cooking of the filling (18%, $p < 0.05$; Figure 4B), second proving (10%, $p < 0.05$; Figure 4C), and baking (9%, $p < 0.05$; Figure 4D) were found; an increase was also observed in trimers after cooking of the

dx.doi.org/10.1021/jf403366q | J. Agric. Food Chem. 2014, 62, 3979−3986

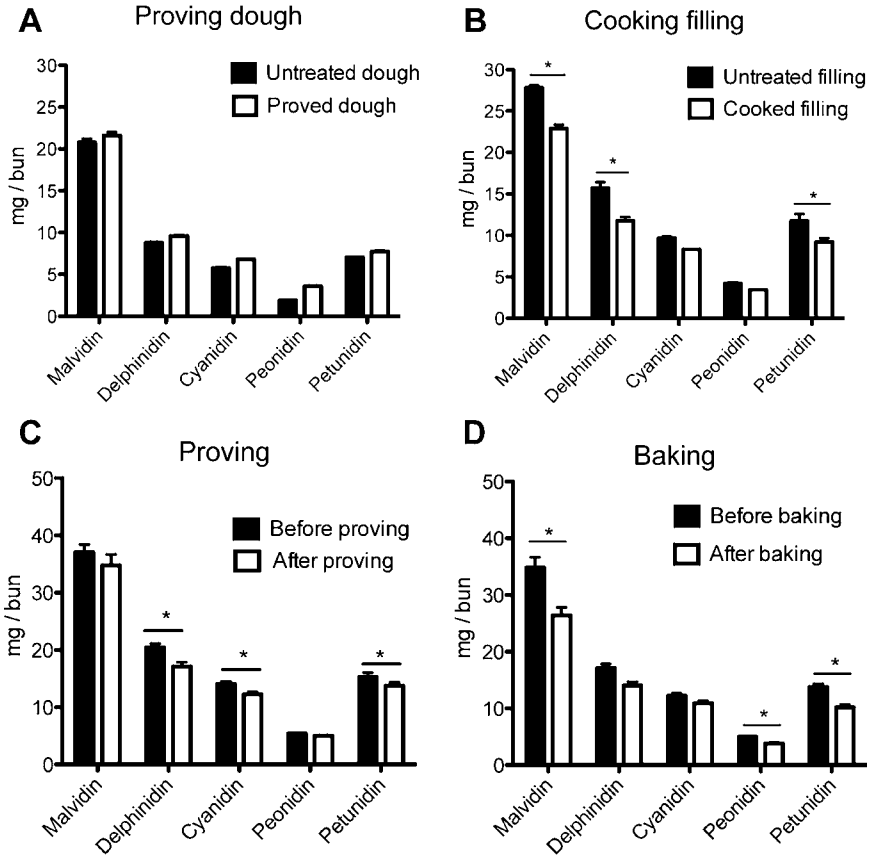

Figure 3. Changes in total malvidin, cyanidin, delphinidin, peonidin, and petunidin contents during the different stages of processing of a blueberry-containing bun: (A) proving of the dough; (B) cooking of the filling; (C) second proving; (D) baking. Results are expressed as mg/bun ± SEM (n = 3). *, $p < 0.05$, significant differences before and after processing.

filling (19%, $p < 0.05$; Figure 4B). In contrast, nonamers and decamers disappeared completely after baking and second proving, respectively (Figure 4C,D).

Changes in Phenolic Acid Content during Processing. For the whole process, a 27% increase in total phenolic acid content was observed. In the individual stages, increases during proving of the dough, cooking of the filling, and baking was found (27, 14, and 17%, respectively, $p < 0.05$; Figure 2A,B,E), which corresponded mostly with increases in 5-*O*-caffeoylquinic acid (chlorogenic acid) (31, 14, and 18% increases after proving dough, cooking filling, and baking, respectively, $p < 0.05$; Figure 5A,B,D), as caffeic and ferulic acid levels did not change through any of the stages of processing.

Changes in Quercetin Content during Processing. Quercetin levels did not significantly change during the whole process or in any of the stages of processing (Figure 2).

Changes in Total (Poly)phenolic Content during Processing. Evaluation of the total (poly)phenol content in the different stages of processing revealed no significant differences in any of the stages (Figure 2).

DISCUSSION

Because of their perishable nature and seasonal availability, berries are often processed and stored prior to consumption. Unfortunately, during handling, processing, and storage of the berry-based products, their (poly)phenols are prone to oxidation, degradation, and polymerization processes. Then, it is not surprising that in the past 10 years considerable research effort has been carried out to preserve as much as possible these compounds from deterioration.[12]

Our findings show that the anthocyanin content of blueberry decreased during cooking, proving, and baking. Cooking of the filling was carried out in a water bath at temperatures lower than 90 °C for 1 h, proving at a constant temperature of 33 °C for 1 h, and baking at 180 °C for 12 min. The total anthocyanin losses in those stages were 20, 10, and 21%, respectively. The magnitudes of the changes were similar to previous work, in which baking frozen blueberries at 175 °C for 15 min reduced anthocyanin levels by 16%[26] and heating at 100 °C for 20 min produced a 32% loss in anthocyanins from blueberry juice.[21] Several studies have investigated the impact of baking on anthocyanin-rich muffins with a formulation similar to that of the one reported here. A decrease in anthocyanin content (approximately 20%) was observed after baking of a raspberry-containing muffin at 177 °C for 25 min.[27] However, baking of a purple wheat bran-enriched muffin at 177 °C for 7−12 min led to a complete loss of anthocyanins,[29] whereas 75−80% losses in cyanidin-3-galactoside were reported after baking of a muffin incorporated with dried skin apple at 175 °C for 20 min.[30] A major difference between the formulations of the muffins was the use of different leavening agents. Rosales-Soto et al.[27] used double-action baking powder as the leavening substance, whereas the two studies in which major anthocyanin losses occurred used baking soda[29] and baking powder.[30] It has been suggested that leavening agents can dramatically affect the polyphenol content of baked products, with baking soda (sodium bicarbonate) producing the biggest losses in

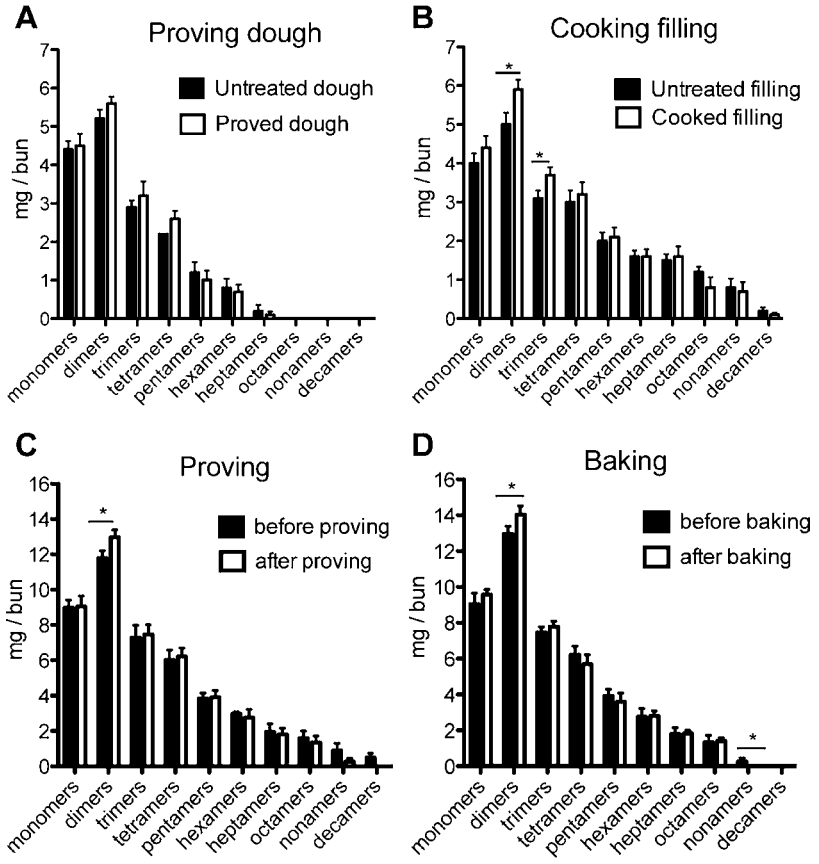

Figure 4. Changes in individual procyanidin (monomers, dimers, trimers, tetramers, pentamers, hexamers, heptamers, octamers, nonamers, and decamers) contents during the different stages of processing of a blueberry-containing bun: (A) proving of the dough; (B) cooking of the filling; (C) second proving; (D) baking. Results are expressed as mg/bun ± SEM (n = 3). *, $p < 0.05$, significant differences before and after processing.

polyphenol content.[31] Indeed, it has been reported that ingredients that induced alkalinity, such as sodium bicarbonate and baking powder, increased the pH of a biscuit dough and decreased the stability of green tea catechins.[32] Furthermore, addition of acidulants such as citric or lactic acid increased the anthocyanin content of blue corn cookies prepared with baking soda by decreasing the pH of the dough and the cookies.[28] Double-action baking powder contains two types of acids, one that acts quickly in a wet mixture with baking soda at room temperature and a slow-acting acid that will react later when heated in an oven. It is thus possible that the use of double-action baking powder retained better the polyphenols by producing a greater acidic pH for longer time. In the present study, we used yeast as leavening agent. Yeast reduces the pH of the dough by producing small acidic compounds such as lactic or acetic acid when fermenting, which could explain the good retention of anthocyanins observed here. Yeast has been recently suggested to be a good vehicle to prevent polyphenols from degradation,[33] and incubation of an anthocyanin-rich Maqui berry juice with yeast led to an increase in anthocyanin concentration.[33] This is in agreement with the work of Wang et al., which showed that baking bread enriched with a green tea extract using yeast led to good retention of green tea catechins (83–91%).[34]

In this work, the total amount of blueberry procyanidins remained constant during processing; however, an increase in lower molecular weight oligomers and a decrease in higher molecular weight oligomers were observed. The greatest increase was found in dimers and trimers, whereas nonamers and decamers completely disappeared. This is consistent with the increase in flavanol monomers in comparison with procyanidins reported after the baking of chocolate cakes[31] and the increase in procyanidin monomers, dimers, and trimers after a freeze-dried blueberry pomace had been subjected to extrusion at 180 °C, with higher oligomers decreasing considerably after extrusion.[35] Processing of blueberries into juiced, canned, and pureed products also resulted in greater retentions of monomers and dimers than of larger oligomers in all products.[24] A plausible explanation for the effects shown in our baked product could be that large oligomers bonded to dough ingredients, for example, proteins, via hydrogen bonding and hydrophobic interactions and resisted extraction more than the smaller oligomers and monomers.

Another major finding of this work is that chlorogenic acid levels increase significantly after dough proving, cooking, and baking. It has been reported that baking frozen blueberries for 15 min at 175 °C did not significantly change their chlorogenic acid levels.[26] However, an increase in phenolic acids including chlorogenic acid after heat treatment has been reported in tomatoes, green beans, pepper, broccoli, and potatoes.[36−41] In baked products where alkalinizing agents such as baking soda or baking powder were used, baking led to a decrease in chlorogenic acid and total phenolic content,[29,30] whereas when yeast was used, increases in phenolic acids were observed after baking.[42] Thus, the increases in chlorogenic acid shown here may be due to a combination of the effects of yeast, which may have improved the retention of chlorogenic acid as in the

dx.doi.org/10.1021/jf403366q | J. Agric. Food Chem. 2014, 62, 3979−3986

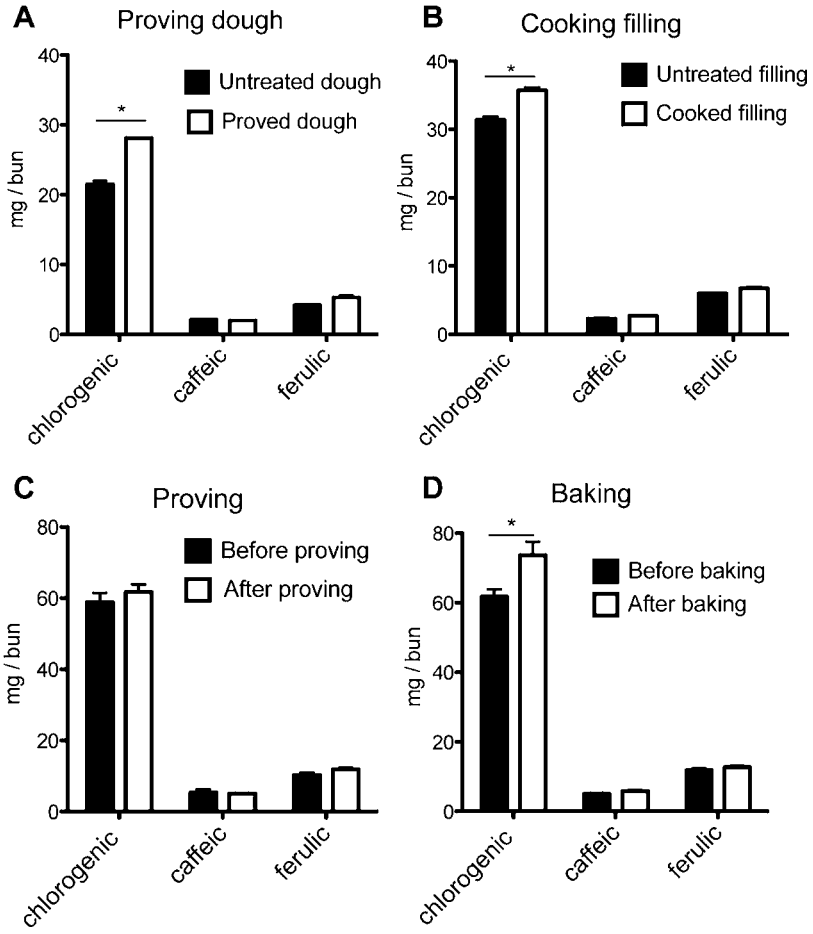

Figure 5. Changes in chlorogenic, ferulic, and caffeic acid contents during the different stages of processing of a blueberry-containing bun: (A) proving of the dough; (B) cooking of the filling; (C) second proving; (D) baking. Results are expressed as mg/bun ± SEM (n = 3). *, $p < 0.05$, significant differences before and after processing.

case of anthocyanins, and heating, which may have disrupted the blueberry−dough matrix, facilitating further extraction.

In summary, procyanidins, flavonols, and phenolic acids were found to be more stable than anthocyanins during the different stages of processing. Cooking of the filling and baking were the processes that resulted in the most degradation of anthocyanins, mainly due to the instability of these compounds at higher temperatures. The choice of leavening agents may be a critical factor for the stability of (poly)phenols during baking, with yeast being more suitable than baking powders to improve the retention of these compounds in baked products. Lower molecular weight procyanidins seemed to increase in the process, probably due to the higher molecular weight degradation and conversion into lower molecular weights. This is of particular importance, as it has recently been shown that procyanidins are not absorbed in the small intestine and only monomers and, to a very limited extent, dimers are absorbed.[43] However, higher oligomers and polymers can be metabolized by the microflora in the lower gut into small molecules such as phenolic acids, and the absorption of these compounds from the colon may still impart health benefits.[44,45] The effects of processing and storage on the bioactive properties of berry-based products have been scarcely investigated, and those studies that have been carried out (thermal versus nonthermal treatments, storage time, etc.) just evaluated the antioxidant capacity, not their effects on relevant markers of chronic disease. In this study we provide further information regarding the impact of processing on the (poly)phenol content of blueberry, which may be of relevance to epidemiological and human intervention studies aiming at understanding the health benefits of this (poly)phenol-rich food.

AUTHOR INFORMATION

Corresponding Author

*(A.R.-M.) E-mail: ana.rodriguez-mateos@med.uni-duesseldorf.de. Phone: 00 49 211 81-15893.

Funding

This work was funded by The Alpro Foundation (Wevelgem, Belgium).

Notes

The authors declare no competing financial interest.

ACKNOWLEDGMENTS

We thank the Wild Blueberry Association of North America for providing the freeze-dried wild blueberry powder used in this work.

REFERENCES

(1) Rodriguez-Mateos, A.; Cifuentes-Gomez, T.; Tabatabaee, S.; Lecras, C.; Spencer, J. P. E. Procyanidin, anthocyanin, and chlorogenic acid contents of highbush and lowbush blueberries. *J. Agric. Food Chem.* **2012**, *60*, 5772−5778.

(2) Taruscio, T. G.; Barney, D. L.; Exon, J. Content and profile of flavanoid and phenolic acid compounds in conjunction with the antioxidant capacity for a variety of northwest *Vaccinium* berries. *J. Agric. Food Chem.* **2004**, *52*, 3169−3176.
(3) Krikorian, R.; Shidler, M. D.; Nash, T. A.; Kalt, W.; Vinqvist-Tymchuk, M. R.; Shukitt-Hale, B.; Joseph, J. A. Blueberry supplementation improves memory in older adults. *J. Agric. Food Chem.* **2010**, *58*, 3996−4000.
(4) Williams, C. M.; El Mohsen, M. A.; Vauzour, D.; Rendeiro, C.; Butler, L. T.; Ellis, J. A.; Whiteman, M.; Spencer, J. P. Blueberry-induced changes in spatial working memory correlate with changes in hippocampal CREB phosphorylation and brain-derived neurotrophic factor (BDNF) levels. *Free Radical Biol. Med.* **2008**, *45*, 295−305.
(5) Ahmet, I.; Spangler, E.; Shukitt-Hale, B.; Joseph, J. A.; Ingram, D. K.; Talan, M. Survival and cardioprotective benefits of long-term blueberry enriched diet in dilated cardiomyopathy following myocardial infarction in rats. *PLoS One* **2009**, *4*, e7975.
(6) Basu, A.; Du, M.; Leyva, M. J.; Sanchez, K.; Betts, N. M.; Wu, M.; Aston, C. E.; Lyons, T. J. Blueberries decrease cardiovascular risk factors in obese men and women with metabolic syndrome. *J. Nutr.* **2010**, *140*, 1582−1587.
(7) Rodriguez-Mateos, A.; Ishisaka, A.; Mawatari, K.; Vidal-Diez, A.; Spencer, J. P. E.; Terao, J. Blueberry intervention improves vascular reactivity and lowers blood pressure in high-fat-, high-cholesterol-fed rats. *Br. J. Nutr.* **2013**, *109*, 1746−1754.
(8) Rodriguez-Mateos, A.; Rendeiro, C.; Bergillos-Meca, T.; Tabatabaee, S.; George, T.; Spencer, J. P. Intake and time dependence of blueberry flavonoid-induced improvements in vascular function: a randomized, controlled, double-blind, crossover intervention study with mechanistic insights into biological activity. *Am. J. Clin. Nutr.* **2013**, DOI: 10.3945/ajcn.113.066639.
(9) Elks, C. M.; Reed, S. D.; Mariappan, N.; Shukitt-Hale, B.; Joseph, J. A.; Ingram, D. K.; Francis, J. A blueberry-enriched diet attenuates nephropathy in a rat model of hypertension via reduction in oxidative stress. *PLoS One* **2011**, *6*, e24028.
(10) Sweeney, M. I.; Kalt, W.; MacKinnon, S. L.; Ashby, J.; Gottschall-Pass, K. T. Feeding rats diets enriched in lowbush blueberries for six weeks decreases ischemia-induced brain damage. *Nutr. Neurosci.* **2002**, *5*, 427−431.
(11) Vendrame, S.; Guglielmetti, S.; Riso, P.; Arioli, S.; Klimis-Zacas, D.; Porrini, M. Six-week consumption of a wild blueberry powder drink increases bifidobacteria in the human gut. *J. Agric. Food Chem.* **2011**, *59*, 12815−12820.
(12) Howard, L. R.; Prior, R. L.; Liyanage, R.; Lay, J. O. Processing and storage effect on berry polyphenols: challenges and implications for bioactive properties. *J. Agric. Food Chem.* **2012**, *60*, 6678−6693.
(13) Zhu, Y.; Xia, M.; Yang, Y.; Liu, F.; Li, Z.; Hao, Y.; Mi, M.; Jin, T.; Ling, W. Purified anthocyanin supplementation improves endothelial function via NO-cGMP activation in hypercholesterolemic individuals. *Clin. Chem.* **2011**, *57*, 1524−1533.
(14) Del Rio, D.; Rodriguez-Mateos, A.; Spencer, J. P.; Tognolini, M.; Borges, G.; Crozier, A. Dietary (poly)phenolics in human health: structures, bioavailability, and evidence of protective effects against chronic diseases. *Antioxid. Redox Signal.* **2013**, *18*, 1818−1892.
(15) Rodriguez-Mateos, A.; Heiss, C.; Borges, G.; Crozier, A. Berry (poly)phenols and cardiovascular health. *J. Agric. Food Chem.* **2013**, DOI: 10.1021/jf403757g.
(16) Wu, X. L.; Prior, R. L. Systematic identification and characterization of anthocyanins by HPLC-ESI-MS/MS in common foods in the United States: fruits and berries. *J. Agric. Food Chem.* **2005**, *53*, 2589−2599.
(17) Gao, L.; Mazza, G. Quantitation and distribution of simple and acylated anthocyanins and other phenolics in blueberries. *J. Food Sci.* **1994**, *59*, 1057−1059.
(18) Gu, L.; Kelm, M.; Hammerstone, J. F.; Beecher, G.; Cunningham, D.; Vannozzi, S.; Prior, R. L. Fractionation of polymeric procyanidins from lowbush blueberry and quantification of procyanidins in selected foods with an optimized normal-phase HPLC-MS fluorescent detection method. *J. Agric. Food Chem.* **2002**, *50*, 4852−4860.
(19) Hakkinen, S. H.; Torronen, A. R. Content of flavonols and selected phenolic acids in strawberries and *Vaccinium* species: influence of cultivar, cultivation site and technique. *Food Res. Int.* **2000**, *33*, 517−524.
(20) Brownmiller, C.; Howard, L. R.; Prior, R. L. Processing and storage effects on monomeric anthocyanins, percent polymeric color, and antioxidant capacity of processed blueberry products. *J. Food Sci.* **2008**, *73*, H72−H79.
(21) Buckow, R.; Kastell, A.; Terefe, N. S.; Versteeg, C. Pressure and temperature effects on degradation kinetics and storage stability of total anthocyanins in blueberry juice. *J. Agric. Food Chem.* **2010**, *58*, 10076−10084.
(22) Howard, L. R.; Castrodale, C.; Brownmiller, C.; Mauromoustakos, A. Jam processing and storage effects on blueberry polyphenolics and antioxidant capacity. *J. Agric. Food Chem.* **2010**, *58*, 4022−4029.
(23) Khanal, R. C.; Howard, L. R.; Brownmiller, C. R.; Prior, R. L. Influence of extrusion processing on procyanidin composition and total anthocyanin contents of blueberry pomace. *J. Food Sci.* **2009**, *74*, H52−H58.
(24) Brownmiller, C.; Howard, L. R.; Prior, R. L. Processing and storage effects on procyanidin composition and concentration of processed blueberry products. *J. Agric. Food Chem.* **2009**, *57*, 1896−1902.
(25) Grace, M. H.; Massey, A. R.; Mbeunkui, F.; Yousef, G. G.; Lila, M. A. Comparison of health-relevant flavonoids in commonly consumed cranberry products. *J. Food Sci.* **2012**, *77*, H176−H183.
(26) Gustafson, S.; Yousef, G.; Grusak, M.; Lila, M. Effect of postharvest handling practices on phytochemical concentrations and bioactive potential in wild blueberry fruit. *J. Berry Res.* **2012**, *2*, 215−227.
(27) Li, J.; Walker, C. E.; Faubion, J. M. Acidulant and oven type affect total anthocyanin content of blue corn cookies. *J. Sci. Food Agric.* **2011**, *91*, 38−43.
(28) Li, W. D.; Pickard, M. D.; Beta, T. Effect of thermal processing on antioxidant properties of purple wheat bran. *Food Chem.* **2007**, *104*, 1080−1086.
(29) Rosales-Soto, M. U.; Powers, J. R.; Alldredge, J. R. Effect of mixing time, freeze-drying and baking on phenolics, anthocyanins and antioxidant capacity of raspberry juice during processing of muffins. *J. Sci. Food Agric.* **2012**, *92*, 1511−1518.
(30) Rupasinghe, H. P. V.; Wang, L.; Huber, G. M.; Pitts, N. L. Effect of baking on dietary fibre and phenolics of muffins incorporated with apple skin powder. *Food Chem.* **2008**, *107*, 1217−1224.
(31) Stahl, L.; Miller, K. B.; Apgar, J.; Sweigart, D. S.; Stuart, D. A.; McHale, N.; Ou, B.; Kondo, M.; Hurst, W. J. Preservation of cocoa antioxidant activity, total polyphenols, flavan-3-ols, and procyanidin content in foods prepared with cocoa powder. *J. Food Sci.* **2009**, *74*, C456−C461.
(32) Sharma, A.; Zhou, W. B. A stability study of green tea catechins during the biscuit making process. *Food Chem.* **2011**, *126*, 568−573.
(33) Jin Zhi, W.; Gad, G. Y.; Randy, B. R.; Elvira Gonzalez de, M.; Ilya, R.; Mary Ann, L. Maqui berry (*Aristotelia chilensis*) juices fermented with yeasts: effects on phenolic composition, antioxidant capacity, and iNOS and COX-2 protein expression. In *Emerging Trends in Dietary Components for Preventing and Combating Disease*; ACS Symposium Series 1093; American Chemical Society: Washington, DC, 2012; pp 95−116.
(34) Wang, R.; Zhou, W. Stability of tea catechins in the breadmaking process. *J. Agric. Food Chem.* **2004**, *52*, 8224−8229.
(35) Khanal, R. C.; Howard, L. R.; Brownmiller, C. R.; Prior, R. L. Influence of extrusion processing on procyanidin composition and total anthocyanin contents of blueberry pomace. *J. Food Sci.* **2009**, *74*, H52−H58.
(36) Gliszczynska-Swiglo, A.; Ciska, E.; Pawlak-Lemanska, K.; Chmielewski, J.; Borkowski, T.; Tyrakowska, B. Changes in the content of health-promoting compounds and antioxidant activity of

broccoli after domestic processing. *Food Addit. Contam.* **2006**, *23*, 1088−1098.
(37) Huang, Y. C.; Chang, Y. H.; Shao, Y. Y. Effects of genotype and treatment on the antioxidant activity of sweet potato in Taiwan. *Food Chem.* **2006**, *98*, 529−538.
(38) Jacob, K.; Garcia-Alonso, F. J.; Ros, G.; Periago, M. J. Stability of carotenoids, phenolic compounds, ascorbic acid and antioxidant capacity of tomatoes during thermal processing. *Arch. Latinoam. Nutr.* **2010**, *60*, 192−198.
(39) Turkmen, N.; Sari, F.; Velioglu, Y. S. The effect of cooking methods on total phenolics and antioxidant activity of selected green vegetables. *Food Chem.* **2005**, *93*, 713−718.
(40) Blessington, T.; Nzaramba, M. N.; Scheuring, D. C.; Hale, A. L.; Reddivari, L.; Miller, J. C. Cooking methods and storage treatments of potato: effects on carotenoids, antioxidant activity, and phenolics. *Am. J. Potato Res.* **2010**, *87*, 479−491.
(41) Burgos, G.; Amoros, W.; Munoa, L.; Sosa, P.; Cayhualla, E.; Sanchez, C.; Diaz, C.; Bonierbale, M. Total phenolic, total anthocyanin and phenolic acid concentrations and antioxidant activity of purple-fleshed potatoes as affected by boiling. *J. Food Compos. Anal.* **2013**, *30*, 6−12.
(42) Abdel-Aal, E.-S. M.; Rabalski, I. Effect of baking on free and bound phenolic acids in wholegrain bakery products. *J. Cereal Sci.* **2013**, *57*, 312−318.
(43) Ottaviani, J. I.; Kwik-Uribe, C.; Keen, C. L.; Schroeter, H. Intake of dietary procyanidins does not contribute to the pool of circulating flavanols in humans. *Am. J. Clin. Nutr.* **2012**, *95*, 851−858.
(44) Monagas, M.; Urpi-Sarda, M.; Sanchez-Patan, F.; Llorach, R.; Garrido, I.; Gomez-Cordoves, C.; Andres-Lacueva, C.; Bartolome, B. Insights into the metabolism and microbial biotransformation of dietary flavan-3-ols and the bioactivity of their metabolites. *Food Funct.* **2010**, *1*, 233−253.
(45) Tzounis, X.; Rodriguez-Mateos, A.; Vulevic, J.; Gibson, G. R.; Kwik-Uribe, C.; Spencer, J. P. Prebiotic evaluation of cocoa-derived flavanols in healthy humans by using a randomized, controlled, double-blind, crossover intervention study. *Am. J. Clin. Nutr.* **2011**, *93*, 62−72.

Table 1. Composition (Grams per Kilogram Dry Weight) of Experimental Diets,[a] Initial and Final Weights, and Average Daily Food Intake of Rats

ingredient	control	HF	HF + CB	HF + BB	HF + BRB
A. Ingredient Composition					
casein, 80 mesh	200	200	198	199	195
L-lysine	3	3	3	3	3.
corn starch	580	0	0	0	0
maltodextrin	70	0	0	0	0
fructose	0	650	606	604.5	607
cellulose	50	50	46.5	47.0	48.4
soybean oil	50	50	49.5	49.5	49.9
t-BHQ	0.014	0.014	0.014	0.014	0.014
vitamin mixture	10	10	10	10	10
mineral mixture	35	35	35	35	35
choline bitartrate	2.5	2.5	2.5	2.5	2.5
cranberry powder	0	0	50	0	0
blueberry powder	0	0	0	50	0
black raspberry powder	0	0	0	0	50
total	1000	1000	1000	1000	1000
B. Nutrient Composition					
crude protein, %	17.9	17.9	18.0	17.9	18.0
fat, %	5.0	5.0	5.0	5.0	5.0
crude fiber, %	5.0	5.0	5.0	5.0	5.0
energy, kcal/kg	3806	3806	3791	3792	3773
initial body wt, g	233.8 ± 3.1	232.9 ± 5.0	229.5 ± 4.4	230.5 ± 2.9	231.9 ± 3.4
final body wt, g	482.1 ± 14.6	443.6 ± 18.2	435.5 ± 8.5	451.0 ± 11.0	438.4 ± 12.6
food intake, g/day	24.2	23.0	23.1	24.0	23.9

[a]Diet based upon AIN 93G; control = starch-based control, HF = high fructose control, CB = cranberry, BB = blueberry, BRB = black raspberry.

Table 2. Phenolic Acids Analyzed in Urine with Common Names, Abbreviations, MRM Transition Ion Pair Used for Quantification, and Retention Time (Rt) on Chromatographic Column

phenolic acid	common name	abbreviation	MW	ion pair	Rt (min)
4-hydroxybenzoic acid		4HBA	138	137.4/93.1	11.6
3-hydroxybenzoic acid		3HBA	138	137.4/93.1	14.7
3,4-dihydroxybenzoic acid	protocatechuic acid	3,4HBA	154	152.5/109.2	6.7
3,4,5-trihydroxybenzoic acid	gallic acid	GA	170	169.2/124.9	3.6
2,5-dihydroxybenzoic acid	gentisic acid	2,5HBA	154	153.3/107.9	12.4
3-methoxy-4-hydroxybenzoic acid	vanillic acid	VA	168	166.7/122.7	13.7
3,4-dihydroxyphenylacetic acid	homoprotocatechuic acid	3,4HPAA	168	166.7/122.7	6.5
1,3,4,5-tetrahydroxycyclohexanecarboxylic acid 3-(3,4-dihydroxycinnamate)	chlorogenic acid	CGA	354	353.0/191.0	12.0
3-methoxy-4-hydroxyphenylacetic acid	homovanillic acid	HVA	182	180.8/136.7	12.7
3-hydroxyphenylacetic acid		3HPAA	152	150.7/106.9	14.0
4-hydroxyphenylacetic acid		4HPAA	152	150.7/106.9	12.9
3,4-dihydroxycinnamic acid	caffeic acid	3,4HCA	180	179.0/134.7	14.4
3-hydroxyphenylpropionic acid	phloretic acid	3HPPA	166	164.8/120.9	19.8
4-hydroxyphenylpropionic acid	hydrocinnamic acid	4HPPA	166	164.8/120.9	22.2
4-hydroxycinnamic acid	*p*-coumaric acid	4HCA	164	162.7/118.8	22.0
3-hydroxycinnamic acid		3HCA	164	162.7/118.8	25.7
4-hydroxy-3-methoxycinnamic acid	ferulic acid	FA	194	192.8/133.8	23.6
benzoylaminoacetic acid	hippuric acid	HA	179	178.3/134.0	10.3

both of which were provided fresh on a weekly basis. Cages were changed weekly. The experimental animal protocol was approved by the Animal Care and Use Committee of the University of Arkansas for Medical Sciences, Little Rock, AR, USA.

Chemicals and Phenolic Acid Standards. All chemicals used in the study were of HPLC grade or higher and were obtained either from Fisher Scientific (Hampton, NHm USA), Sigma-Aldrich (St. Louis, MO, USA), or SynerMed (Monterey Park, CA, USA). Standards for phenolic acids were obtained from Sigma-Aldrich, and their names and abbreviations are listed in Table 2 with primary structures depicted in Figure 1.

Urine Collection. Between days 30 and 40 of the experiment, six rats from each treatment were transferred to individual metabolic cages to monitor urine output over a period of 48 h during steady state, chronic consumption of the berry diets. Urine output was recorded, samples were collected in 15 mL conical tubes and centrifuged at 1000*g* for 15 min, and the supernatant was stored at −70 °C until further analysis.

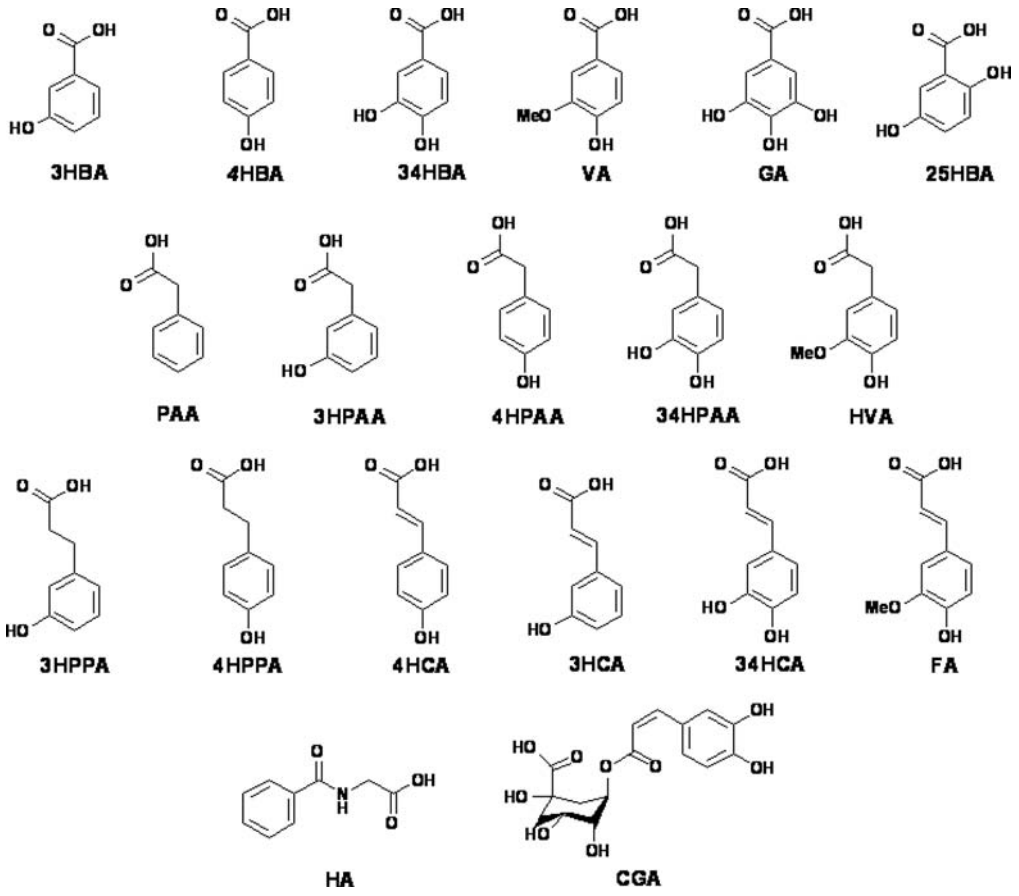

Figure 1. Chemical structures of phenolic acids investigated in the current study. Names and symbols of all phenolic acids are listed in Table 2.

Urine Treatment for Phenolic Acid Analysis. For analysis of free phenolic acids, urine samples were purified by solid phase extraction (SPE) using a Waters Sep-Pak Vac RC (500 mg) C_{18} cartridge. The column was washed with 3 mL of 100% MeOH and then equilibrated with 3 mL of 0.2% formic acid in H_2O. Thawed urine (200 μL) was loaded onto the column and then washed with 3 mL of 0.2% formic acid in H_2O. The sample was eluted with 2 mL of 0.2% formic acid in MeOH, and the solvents were evaporated with nitrogen to <1 mL. Samples were adjusted to 1 mL in volumetric flasks with 0.2% formic acid in MeOH. Extraction was carried out in duplicate.

For analysis of total phenolic acids, 200 μL of thawed urine was added to 1.8 mL of enzyme solution containing 1 M ammonium acetate, 0.5 mM ascorbic acid, and 110 U sulfatase (*Helix pomatia*; Sigma, S9626) in a screw-cap glass tube. After incubation for 2 h at 37 °C, 100 μL of acetic acid was added to each tube. The same SPE procedure mentioned above was used for purifying total phenolic acids; 200 μL of the enzyme-treated urine sample was added to the column in place of the 200 μL of urine. The quantities of conjugated PA were calculated by subtracting the free phenolic acid from the total phenolic acid obtained following enzyme treatment.

Analysis of Phenolic Acids. Total, free, and conjugated PA were analyzed using an LC-MS/MS consisting of an Agilent 1100 high-performance liquid chromatography (HPLC) system equipped with a diode array detector (Agilent Technologies, Santa Clara, CA, USA) coupled to a 4000 QTRAP mass spectrometer (Applied Biosystems, Forest City, CA, USA). Separation was performed on a Phenomenex Synergi Max-RP column (150 × 3.00 mm, 4 μm) using a flow rate of 0.4 mL/min. The mass spectrometer used an electrospray interface in negative ionization mode. Electrospray ionization tandem mass spectrometry (ESI-MS/MS) was conducted using a QTRAP quadrupole-linear ion trap (QLIT) instrument equipped with a Turbo Ion Spray (TISP) interface (Applied Biosystems/MDS Sciex, Concord, ON, Canada). The whole LC-MS system was controlled by Analyst software (v. 1.4.1, Applied Biosystems/MDS Sciex). Multireaction monitoring (MRM) mode scan was performed to selectively monitor the compound to be identified and quantified with a specific parent mass and its unique fragment ion (Table 2). The solvent consisted of (A) 0.2% formic acid in water and (B) methanol. The 35 min linear gradient was as follows: 0−2−20−21−29−30−35 min with 20−20−35−40−60−70−20% B, followed by a 6 min re-equilibration of the column before the next run. Further details about the HPLC as well as the operating conditions on the mass spectrometer and recoveries of the phenolic acids have been described previously.[11] Molecular weights, MRM transition pairs, and retention times of PA are provided in Table 2.

Extraction of Phenolic Acids in the Berries. For analysis of the free forms of the PA, approximately 250−400 mg of sample was weighed directly into a glass culture tube with a threaded end. Eight milliliters of methanol/water (50:50; v/v, MeOH/H_2O) was added to each sample. Tubes were capped tightly and incubated for 2 h at 90 °C with vortexing every 30 min. Samples were cooled overnight at −20 °C and centrifuged at 4 °C for 15 min at 3600*g*. The supernatant was adjusted to 10 mL in a volumetric flask with 100% MeOH and aliquoted to HPLC vials after syringe filtration with a 0.22 μm filter. Samples were stored at −20 °C until analysis.

Analysis of Procyanidins and Anthocyanins in Berries. The berries included in the diet were analyzed for their procyanidin and anthocyanin profiles using HPLC. Separations based on degree of polymerization (DP) were conducted using a Develosil Diol column (250 × 4.6, 5 μm, Phenomenex, Torrence, CA, USA). Details about the procyanidin extraction, HPLC conditions, mobile phase, gradient, standards, and peak identification have been described previously.[12,13]

Anthocyanins were extracted from the freeze-dried berry powders using methanol/water/acetic acid (MWA) (85:15:0.5, v/v) as described previously.[14] Sample (1 g) was weighed and put into a 15 mL screw-cap tube and extracted with 15 mL of MWA, then vortexed

Table 3. Composition of Anthocyanins, Procyanidins, and Free Phenolic Acids in Whole Blueberry, Cranberry, and Black Raspberry Freeze-Dried Powder

component	blueberry	cranberry	black raspberry
anthocyanins (mg/g dry weight)			
delphinidin 3-arabinoside	2.20	0.05	ND
delphinidin 3-glucoside	4.18	ND[a]	ND
delphinidin 3-(6″-acetyl)glucoside	0.05	ND	ND
delphinidin 3-galactoside	3.72	ND	ND
cyanidin 3-arabinoside	0.32	0.69	ND
cyanidin 3-glucoside	0.61	0.01	6.52
cyanidin 3-(malonyl)glucoside	0.02	ND	ND
cyanidin 3-(6″-acetyl)glucoside	0.02	ND	ND
cyanidin 3-galactoside	0.58	0.86	ND
cyanidin 3-rutinoside	ND	ND	40.45
cyanidin 3-sambubioside	ND	ND	2.24
cyanidin 3-sambubioside-5-rhamnoside	ND	ND	19.31
petunidin 3-arabinoside	0.82	ND	ND
petunidin 3-glucoside	2.47	ND	ND
petunidin 3-(6″-acetyl)glucoside	0.59	ND	ND
petunidin 3-galactoside	1.63	0.02	ND
pelargonidin 3-glucoside	ND	ND	0.14
pelargonidin 3-galactoside	ND	0.01	ND
pelargonidin 3-rutinoside	ND	ND	1.79
peonidin 3-arabinoside	ND	1.06	ND
peonidin 3-glucoside	0.51	0.11	ND
peonidin 3-(6″-acetyl)glucoside	0.38	ND	ND
peonidin 3-galactoside	0.51	2.34	ND
peonidin 3-(6″-acetyl)galactoside	0.09	ND	ND
peonidin 3-rutinoside	ND	ND	0.08
malvidin 3-arabinoside	1.16	0.07	ND
malvidin 3-glucoside	1.98	ND	ND
malvidin 3-(6″-acetyl)glucoside	1.17	ND	ND
malvidin 3-galactoside	3.24	0.09	ND
malvidin 3-(6″-acetyl)galactoside	0.46	ND	ND
malvidin + acetyl + hexose	0.05	ND	ND
total anthocyanins	**28.70**	**5.31**	**70.54**
procyanidins (mg/g dry weight)			
DP1[b]	0.06	0.08	0.01
DP2	0.55	0.13	0.04
DP3	0.40	0.16	0.03
DP4−6	0.69	0.55	0.03
DP7−10	0.51	0.95	ND
polymer	2.27	2.51	ND
total procyanidins	**4.48**	**4.59**	**0.10**
phenolic acids (μg/g dry weight)[c]			
4-hydroxyphenylacetic acid (4HPAA)	7.5	6.50	ND
gallic acid (GA)	0.6	6.1	6.6
4-hydroxybenzoic acid (4HBA)	6.6	0.5	18.5
3,4-dihydroxybenzoic acid (3,4HBA)	37.8	25.0	110.9
3-methoxy-4-hydroxybenzoic acid (VA)	6.2	2.1	3.7
chlorogenic acid (CGA)	179.4	177.6	2.4
4-hydroxycinnamic acid (4HCA)	66.6	0.9	30.8
ferulic acid (FA)	1.2	11.8	9.6
3,4-dihydroxycinnamic acid (3,4HCA)	8.4	4.0	7.8
3-hydroxyphenylpropionic acid (3HPPA)	4.2	1.8	ND

[a]ND = not detected. [b]DP = degree of polymerization of monomeric catechin/epicatechin units. [c]3-Hydroxyphenylacetic acid, 3,4-dihydroxyphenylacetic acid, 3-methoxy-4-hydroxyphenylacetic acid, 2,5-dihydroxybenzoic acid, 3-hydroxycinnamic acid, 4-hydroxyphenylpropionic acid, and hippuric acid were not detected in any of the berry powders used in this study.

for 30 s followed by sonication for 5 min. The tube was then centrifuged at 4550*g* for 10 min and the supernatant removed. The sample was extracted one more time with 10 mL of MWA using the same procedure, and the supernatants were combined. The combined supernatant was transferred into a 25 mL volumetric flask, and MWA was added to make up the final volume to exactly 25 mL. The solution was further diluted appropriately and filtered using a 0.22 μm Teflon syringe filter for analysis. A Zorbax Stablebond Analytical SB-C18 column (4.6 × 250 mm, 5 μm, Agilent) was used for separating anthocyanins with diode array detection as previously described.[12]

Statistical Analysis. Data were analyzed using one-way analysis of variance in SigmaPlot (Systat Software Inc., San Jose, CA, USA) and are presented as means ± SEM. Post hoc mean separation was performed using Holm−Sidak method whenever appropriate.

RESULTS

Major Dietary Free Polyphenols in Berries. The three berries included in the diets in this study had significant differences in their polyphenol profiles. Only 10 of the 18 phenolic acids studied in the current study were detected in the free form in the berries, with BRB containing only 8 phenolic acids (Table 3). 3-Hydroxyphenylacetic acid, 3,4-dihydroxyphenylacetic acid, 3-methoxy-4-hydroxyphenylacetic acid, 2,5-dihydroxybenzoic acid, 3-hydroxycinnamic acid, 4-hydroxyphenylpropionic acid, and hippuric acid were not detected in free form in any of the berry powders used in this study, although they were present in some of the urine samples from the different diet treatments.

Whereas chlorogenic acid was the primary phenolic acid present in BB and CB, it was present only in small amounts in BRB, where 3,4-dihydroxybenzoic acid was the major dietary phenolic acid followed by 4-hydroxycinnamic acid. A majority of the free phenolic acids present in the berries was present in rather small amounts (<10 μg/g). Although only a small amount of 4-hydroxycinnamic acid was detected in CB, it was a major phenolic acid present in BB and BRB. BRB contained small amounts of procyanidins (0.103 mg/g dry weight, Table 3), but high amounts of anthocyanins (70.5 mg/g dry weight) that were predominantly cyanidin derivatives (>95% of the total; Table 3). Cranberry, on the other hand, contained small amounts of anthocyanins (5.3 mg/g dry weight), but much larger amounts of procyanidins. The total procyanidin content of BB was similar to that of CB, but BB had lower amounts of dimers and trimers. The anthocyanin profile of BB contained 32 anthocyanins, but none of the individual anthocyanins were present in concentrations >5 mg/g DW compared to BRB, which contained high levels of cyanidin-3-rutinoside (40.4 mg/g DW) (Table 3).

Phenolic Acid Excretion. Steady-state quantities of free, total, and conjugated phenolic acids excreted in the urine over a 24 h period are presented in Table 4. Of the 18 PA investigated, all phenolic acids, except 3-methoxy-4-hydroxybenzoic acid, were detected in the urine of rats across treatments in free form, albeit at low concentrations for some. Free 3-methoxy-4-

Table 4. Excretion of Free Phenolic Acids (Mean ± SEM, μg/day) from Rats Fed a Control Diet, High-Fructose Diet (HF), and High-Fructose Diets with Cranberry (HF + CB), Blueberry (HF + BB), and Black Raspberry (HF + BRB)[a]

analyte	control	HF	HF + CB	HF + BB	HF + BRB	*p* value
3-hydroxyphenylacetic acid						
free	14.5 ± 2.0c	15.2 ± 3.8c	87.4 ± 9.9a	87.0 ± 8.2a	53.8 ± 11.8b	<0.001
conjugated	0.1 ± 0.9	0.4 ± 1.0	6.3 ± 5.4	5.8 ± 3.8	5.3 ± 4.2	NS
total	14.6 ± 2.0c	15.6 ± 3.7c	93.7 ± 7.9a	92.7 ± 8.9a	59.1 ± 10.6b	<0.001
4-hydroxyphenylacetic acid						
free	76.9 ± 9.5	110.0 ± 24	57.9 ± 5.1	57.4 ± 9.8	55.9 ± 7.9	0.06
conjugated	−0.7 ± 0.1	1.1 ± 2.1	−1.7 ± 2.6	6.4 ± 2.1	1.9 ± 0.3	NS
tota	76.2 ± 8.8	111.1 ± 24	56.2 ± 3.7	63.8 ± 11.3	57.7 ± 11.4	0.06
3,4-dihydroxyphenylacetic acid						
free	7.4 ± 1.2	9.42 ± 1.1	11.2 ± 0.7	7.5 ± 0.8	10.6 ± 1.8	NS
conjugated	0.2 ± 0.8	−2.75 ± 1.2	−0.6 ± 1.0	0.1 ± 1.0	3.0 ± 1.3	NS
total	7.6 ± 1.2b	7.67 ± 1.2b	10.6 ± 1.4ab	7.54 ± 1.17b	13.6 ± 2.6a	0.021
3-methoxy-4-hydroxyphenylacetic acid						
free	90.1 ± 17.2bc	51.3 ± 6.3cd	**221 ± 26.0a**	116 ± 7.0b	30.9 ± 5.4d	<0.001
conjugated	5.8 ± 1.9bc	1.31 ± 2.9c	11.1 ± 4.3b	9.22 ± 3.1b	**29.0 ± 7.3a**	0.04
total	95.9 ± 12.6bc	52.6 ± 7.7c	**232 ± 14.0a**	125 ± 6.0b	59.9 ± 14.0c	<0.001
gallic acid						
free	4.0 ± 0.4	4.1 ± 0.8	4.65 ± 0.4	3.9 ± 0.6	3.2 ± 0.6	NS
conjugated	−1.6 ± 0.2	−1.7 ± 0.5	−1.63 ± 0.3	−1.5 ± 0.4	−1.1 ± 0.2	NS
total	2.3 ± 0.3	2.4 ± 0.4	3.02 ± 0.4	2.4 ± 0.3	2.1 ± 0.4	NS
3-hydroxybenzoic acid						
free	10.9 ± 2.2c	10.9 ± 3.2c	37.4 ± 3.7b	23.6 ± 2.2b	**57.6 ± 5.7a**	<0.001
conjugated	−3.7 ± 1.5b	−1.8 ± 2.3b	−2.0 ± 2.2b	5.8 ± 0.9ab	16.9 ± 4.2a	<0.01
total 3HBA	7.2 ± 1.2c	9.12 ± 2.1c	35.4 ± 1.9b	29.3 ± 4.0b	**65.8 ± 9.7a**	<0.001
4-hydroxybenzoic acid						
free	28.4 ± 3.6	37.3 ± 3.8	44.0 ± 4.5	33.9 ± 3.3	36.3 ± 6.2	NS
conjugated	22.9 ± 5.1b	22.4 ± 8.7b	37.9 ± 4.2ab	27.7 ± 5.2b	55.4 ± 10.0a	0.01
total	51.4 ± 8.1b	59.7 ± 12.1ab	81.9 ± 7.9ab	61.6 ± 5.9ab	91.7 ± 13.0a	0.039
3,4-dihydroxybenzoic acid						
free	0.30 ± 0.06	0.50 ± 0.10	2.48 ± 0.61	1.41 ± 0.61	4.57 ± 2.15	0.046
conjugated	0.32 ± 0.10c	0.13 ± 0.07c	2.28 ± 0.31b	2.97 ± 0.35b	**4.99 ± 0.48a**	<0.01
total	0.62 ± 0.05c	0.63 ± 0.05c	4.76 ± 0.64ab	4.38 ± 0.74b	9.55 ± 2.00a	<0.001
2,5-dihydroxybenzoic acid						
free	0.25 ± 0.03c	0.13 ± 0.02c	4.76 ± 1.16a	1.78 ± 0.20bc	3.52 ± 0.94ab	<0.001
conjugated	−0.12 ± 0.03	−0.09 ± 0.03	−0.23 ± 2.03	0.49 ± 0.63	−1.55 ± 0.63	NS
total	0.13 ± 0.04	0.04 ± 0.02	4.53 ± 2.70	2.27 ± 0.66	1.97 ± 0.69	NS
3-methoxy-4-hydroxybenzoic acid						
free	ND	ND	**34 ± 5a**	6.7 ± 4b	15 ± 7b	<0.001
conjugated	93 ± 12	140 ± 32	113 ± 9	117 ± 19	151 ± 30	NS
total	93 ± 12	140 ± 32	146 ± 13	124 ± 16	166 ± 28	NS
chlorogenic acid						
free	0.01 ± 0.01b	0.03 ± 0.02b	0.88 ± 0.24b	**7.68 ± 1.42a**	0.13 ± 0.03b	0.002
conjugated	0.11 ± 0.03	0.11 ± 0.03	−0.59 ± 0.21	−5.02 ± 1.9	0.08 ± 0.06	NS
total	0.12 ± 0.03b	0.14 ± 0.03b	0.29 ± 0.06b	**2.66 ± 0.58a**	0.21 ± 0.03b	0.003
3-hydroxycinnamic acid						
free	0.1 ± 0.1c	0.1 ± 0.1c	6.2 ± 1.0bc	12.9 ± 2.1b	**41.0 ± 6.8a**	<0.001
conjugated	0.7 ± 0.3c	0.3 ± 0.2c	14.4 ± 2.6bc	22.6 ± 4.5b	**106 ± 28a**	<0.01
total 3HCA	0.8 ± 0.4c	0.4 ± 0.1c	20.6 ± 3.4b	35.5 ± 6.4b	**147 ± 15.0a**	<0.001
4-hydroxycinnamic acid						
free	7.7 ± 2.3bc	0.9 ± 1.3c	**67.8 ± 4.4a**	7.3 ± 1.8bc	13.9 ± 2.4b	<0.001
conjugated	17.8 ± 3.5c	1.3 ± 0.2d	**156.0 ± 15.0a**	17.3 ± 1.5c	38.2 ± 5.7b	<0.01
total	25.5 ± 4.6c	2.2 ± 0.4d	**224.0 ± 18.0a**	24.5 ± 2.1c	52.0 ± 6.8b	<0.001
ferulic acid						
free	1.7 ± 0.7bc	0.254 ± 0.2c	7.63 ± 1.6ab	13.1 ± 2.8a	3.5 ± 1.3bc	<0.001
conjugated	16.7 ± 2.1c	0.473 ± 0.2d	64.4 ± 7.6b	**134 ± 15a**	19.8 ± 3.1c	<0.01
total	18.4 ± 2.7c	0.727 ± 0.1d	72.0 ± 8.3b	**147 ± 16a**	23.3 ± 3.2c	<0.001
3,4-dihydroxycinnamic acid						
free	0.4 ± 0.3b	0.0 ± 0.0b	3.0 ± 1.1b	**10.7 ± 3.1a**	1.5 ± 0.6b	<0.001
conjugated 3,4HCA	0.7 ± 0.3b	0.2 ± 0.1b	3.6 ± 1.7b	**20.3 ± 8.1a**	1.4 ± 0.6b	<0.01
total	1.1 ± 0.1b	0.2 ± 0.1b	6.5 ± 1.8b	**31.0 ± 7.8a**	2.9 ± 0.5b	<0.001

dx.doi.org/10.1021/jf403883r | J. Agric. Food Chem. 2014, 62, 3987−3996

Table 4. continued

analyte	control	HF	HF + CB	HF + BB	HF + BRB	*p* value
3-hydroxyphenylpropionic acid						
free	9.68 ± 1.87b	3.53 ± 0.65b	78.6 ± 8.8a	97.5 ± 17.3a	124 ± 20a	<0.001
conjugated	2.32 ± 1.04cc	1.03 ± 0.34c	52.4 ± 10.4b	73.9 ± 12.0b	**302 ± 51a**	<0.01
total	12.0 ± 2.6c	4.56 ± 0.58c	131 ± 17b	171 ± 25b	**426 ± 74a**	<0.001
4-hydroxyphenylpropionic acid						
free	0.99 ± 0.15b	1.10 ± 0.28b	2.61 ± 0.48ab	3.69 ± 0.64a	3.40 ± 1.00ab	0.04
conjugated	0.50 ± 0.18	0.66 ± 0.44	0.37 ± 0.38	0.629 ± 2.31	−1.25 ± 1.12	NS
total	1.49 ± 0.17	1.76 ± 0.44	2.98 ± 0.36	4.32 ± 2.00	2.15 ± 0.41	NS
hippuric acid						
free	746 ± 78d	839 ± 192d	**6315 ± 420a**	4683 ± 322b	2497 ± 320c	<0.001
conjugated	30.3 ± 21.7c	30.2 ± 46.8c	**837 ± 125a**	345 ± 52b	263 ± 49b	<0.01
total	777 ± 77d	870 ± 194d	**7152 ± 506a**	5028 ± 490b	2759 ± 353c	<0.001

[a]Diets contained 5% of the respective whole berries on dry weight basis. Means without a common letter differ; $p < 0.05$, one-way ANOVA. Means without a common letter differ and represent six observations per treatment. ND = not detected. Values in bold represent phenolic acids that were excreted in largest amounts of the three berry treatments.

hydroxybenzoic acid was not present in the urine of animals fed the polyphenol-free control and HF diets, but was present in the urine in conjugated form.

Inclusion of berries in the diet increased the urinary excretion of seven phenolic acids (Table 4). Total excretions of 3,4-hydroxybenzoic and 2,5-hydroxybenzoic acids were increased by <10 μg/day (Table 4), but berry treatments significantly increased the total excretion of 3-hydroxybenzoic (Figure 2), 3-hydroxycinnamic (Figure 3), 3-hydroxyphenylpropionic (Figure 4), and 3-hydroxyphenylacetic acids (Figure 5) by 25−420 μg/day (Table 4) and that of hippuric acid by 2000−6400 μg/day compared to the control dietary treatments (Table 4).

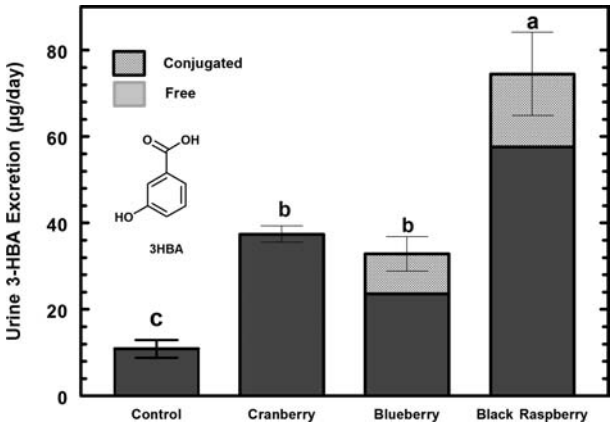

Figure 2. 3-Hydroxybenzoic acid (3-HBA) excretion in the urine of rats fed cranberry, blueberry, or black raspberry in the diet. The fructose-fed group is presented in the "control" bar. 3-Hydroxybenzoic acid was not present in any of the diets (Table 3). 3-Hydroxybenzoic acid was not present in conjugated form in the urine of control or cranberry treatment groups. Bars with different letters above are significantly different ($p < 0.001$). SEM above bar represents variation in the total (free plus conjugated) phenolic ($n = 6$/group).

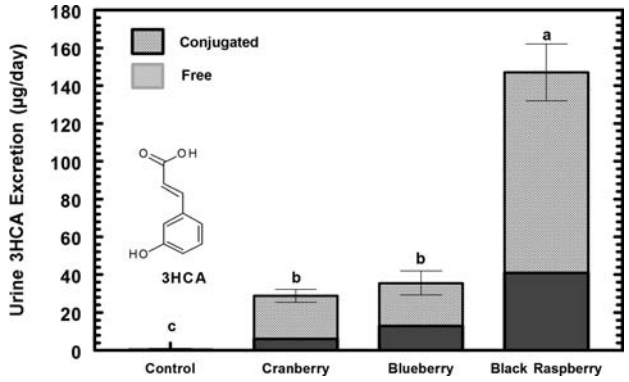

Figure 3. 3-Hydroxycinnamic acid (3-HCA) excretion in the urine of rats fed cranberry, blueberry, or black raspberry in the diet. The fructose-fed group is presented in the "control" bar. 3-Hydroxycinnamic acid was not present in any of the diets (Table 3). Bars with different letters above are significantly different ($p < 0.001$). SEM above bar represents variation in the total (free plus conjugated) phenolic ($n = 6$/group).

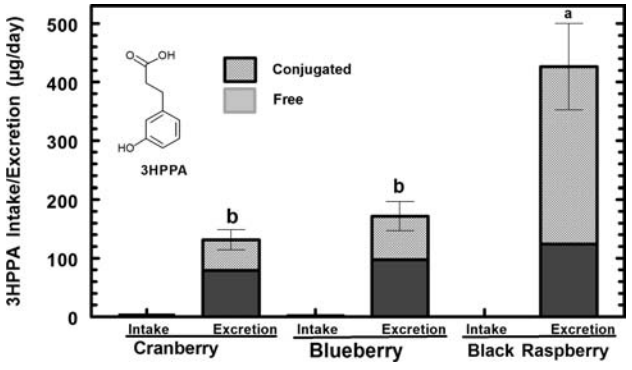

Figure 4. 3-Hydroxyphenylpropionic acid (3HPPA) consumed in the diet and excreted in the urine of rats fed cranberry, blueberry, or black raspberry in the diet. 3HPPA was not present in the control or HF diets and was excreted in the urine in low quantities in these diets, which were significantly lower than any of the berry treatment groups (Table 4). Bars with different letters above are significantly different ($p < 0.001$). SEM above bar represents variation in the total (free plus conjugated) phenolic acid ($n = 6$/group). Intake column represents the free phenolic acid consumed (μg/day), which was present in the berry powder in the diet.

There were specific phenolic acids for which urinary excretion was uniquely altered by the different berries. Feeding CB significantly increased urinary excretion of total 4-hydroxycinnamic acid (Table 4; Figure 6) and 3-methoxy-4-hydroxyphenylacetic acid (Table 4; Figure 7) by >180 μg/day and that of hippuric acid by >6000 μg/day relative to the control dietary treatments (Table 4). With BB feeding, total excretion of chlorogenic acid, ferulic acid, and 3,4-dihydrox-

dx.doi.org/10.1021/jf403883r | J. Agric. Food Chem. 2014, 62, 3987−3996

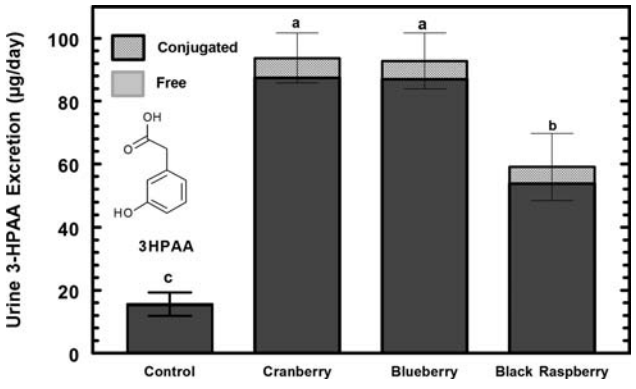

Figure 5. 3-Hydroxyphenylacetic acid (3HPAA) excretion in the urine of rats fed cranberry, blueberry, or black raspberry in the diet. The fructose-fed group is presented in the "control" bar in the figure. 3HPAA was not present in any of the diets (Table 3). Bars with different letters above are significantly different ($p < 0.001$). SEM above bar represents variation in the total (free plus conjugated) phenolic acid ($n = 6$/group).

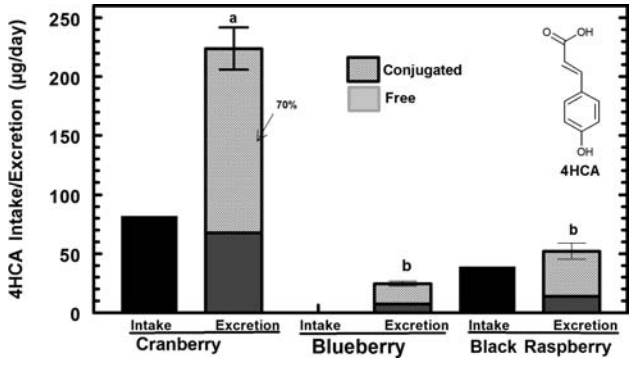

Figure 6. 4-Hydroxycinnamic acid (4HCA) consumed in the diet and excreted in the urine of rats fed cranberry, blueberry, or black raspberry in the diet. 4-Hydroxycinnamic acid was not present in the control or HF diets and was excreted in the urine in low quantities in these diets (Table 3). Bars with different letters above are significantly different ($p < 0.001$). SEM above bar represents variation in the total (free plus conjugated) phenolic acid ($n = 6$/group). 4-Hydroxycinnamic acid excretion in the HF control group was not significantly different from the blueberry treatment group (Table 4). Intake column represents the free phenolic acid consumed (μg/day) which was present in the berry powder.

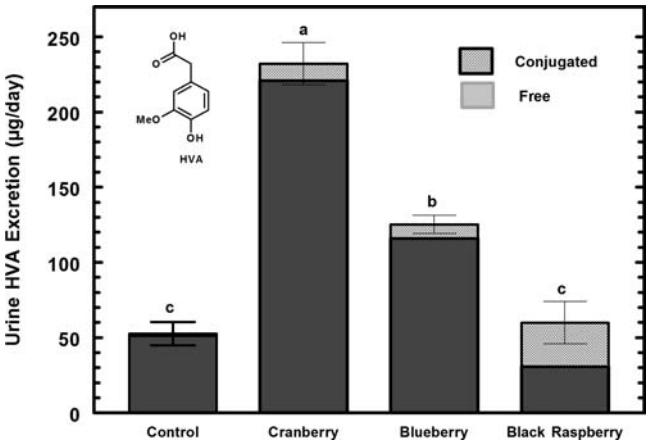

Figure 7. 3-Methoxy-4-hydroxyphenylacetic acid (HVA) excretion in the urine of rats fed cranberry, blueberry, or black raspberry in the diet. The fructose-fed group is presented in the "control" bar. HVA was not present in any of the diets (Table 3). Bars with different letters above are significantly different ($p < 0.001$). SEM above bar represents variation in the total (free plus conjugated) phenolic ($n = 6$/group).

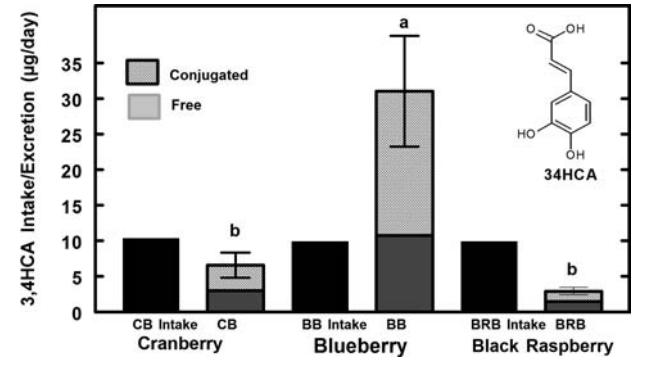

Figure 8. 3,4-Dihydroxycinnamic acid (3,4HCA) consumed in the diet and excreted in the urine of rats fed cranberry, blueberry, or black raspberry in the diet. 3,4-Hydroxycinnamic acid was not present in the control or HF diets and was excreted in the urine in low quantities in these diets, which was not significantly different ($p > 0.001$) from the cranberry or black raspberry treatment groups (Table 4). Bars with different letters above are significantly different ($p < 0.001$). SEM above bar represents variation in the total (free plus conjugated) phenolic acid ($n = 6$/group). Intake column represents the free phenolic acid consumed (μg/day), which was present in the berry powder.

ycinnamic acid (Figure 8) was elevated relative to the CB and BRB dietary treatments (Table 4). Ferulic acid was present in the largest amount in the BB and BRB diets (Table 3). With BRB feeding, the excretion of total 3-hydroxybenzoic, 3-hydroxycinnamic, and 3-hydroxyphenylpropionic acids were elevated relative to the CB and BB dietary treatments (Table 4). Hippuric acid was excreted in the highest amounts, and its quantity exceeded all the other phenolic acids combined, particularly in the free and total forms.

Between the two polyphenol-free diets, the excretion pattern of all the phenolic acids was similar irrespective of their form between the control starch-containing diet and the high-fructose diet except for ferulic acid and 4-hydroxycinnamic acid, which could have been present in the starch that was used in the starch control diet.

Twelve of the 18 phenolic acids investigated in the current study were also detected in their conjugated forms, proportions (% of total) that have been presented in Table 5. Phenolic acids that were either not detected in the urine or excreted in small amounts in their conjugated forms include 3-hydroxyphenylacetic, 4-hydroxyphenylacetic, 3,4-dihydroxyphenylacetic, gallic acid, 2,5-dihydroxybenzoic, chlorogenic, and 4-hydroxyphenylpropionic acids, none of which changed significantly ($p > 0.1$) with the inclusion of berries in the diet when expressed as percent of total excreted in the urine (Table 5). However, for some of these the extent of conjugation was rather small (0–12%) relative to the total amount excreted. Excretion of conjugated forms of 4-hydroxybenzoic, 3,4-dihydroxybenzoic, 3-hydroxycinnamic (Figure 3), 4-hydroxycinnamic (Figure 6), and 3,4-dihydroxycinnamic acids (Figure 8) were either close to or >50% irrespective of the dietary treatments. Excretion of ferulic and 3-methoxy-4-hydroxybenzoic acids in their conjugated forms was 85% or higher in the berry-treated animals.

dx.doi.org/10.1021/jf403883r | J. Agric. Food Chem. 2014, 62, 3987–3996

Table 5. Excretion of Conjugated Phenolic Acid as a Percent of the Total Phenolic Acid Excreted in Rats Fed a Control Diet, High-Fructose Diet (HF), and HF Diets with Cranberry (HF + CB), Blueberry (HF + BB), or Black Raspberry (HF + BRB)

phenolic acid	control	HF	HF + CB	HF + BB	HF + BRB
3-hydroxyphenylacetic acid (3HPAA)	0.5	2.6	6.7	6.2	8.9
4-hydroxyphenylacetic acid (4HPAA)	0.0	1.0	0.0	10.0	3.2
3,4-dihydroxyphenylacetic acid (3,4HPAA)	2.6	0.0	0.0	0.8	22.1
3-methoxy-4-hydroxy-phenylacetic acid (HVA)	6.0	2.5	4.8	7.4	48.4
gallic acid (GA)	0.0	0.0	0.0	0.0	0.0
3-hydroxybenzoic acid (3HBA)	0.0	0.0	0.0	19.7	25.7
4-hydroxybenzoic acid (4HBA)	44.6	37.5	46.3	45.0	60.4
3,4-dihydroxybenzoic acid (3,4HBA)	51.0	20.8	47.9	67.8	52.3
2,5-dihydroxybenzoic acid (2,5HBA)	0.0	0.0	0.0	0.0	0.0
3-methoxy-4-hydroxybenzoic acid (VA)	100.0	100.0	77.4	94.4	91.0
chlorogenic acid (CGA)	89.3	78.2	0.0	0.0	38.5
3-hydroxycinnamic acid (3HCA)	91.3	78.0	69.9	63.7	72.1
4-hydroxycinnamic acid (4HCA)	69.8	59.4	69.6	70.6	73.5
ferulic acid (FA)	90.8	65.1	89.4	91.2	85.0
3,4-dihydroxycinnamic acid (3,4HCA)	65.2	87.4	54.9	65.5	49.7
3-hydroxyphenylpropionic acid (3HPPA)	19.3	22.6	40.0	43.2	70.9
4-hydroxyphenylpropionic acid (4HPPA)	33.2	37.5	12.4	14.6	0.0
hippuric acid (HA)	3.9	3.5	11.7	6.9	9.5

DISCUSSION

Diet can be a major factor contributing to the phenolic acids excreted in the urine because phenolic acids can be produced not only by colonic microflora from a number of polyphenolic compounds, such as procyanidins and anthocyanins but also endogenously from different amino acids, such as glycine, tyrosine, and phenylalanine. This study was aimed at understanding the conjugation and excretory pattern of phenolic acids after feeding whole freeze-dried powders of polyphenol-rich cranberry, blueberry, and black raspberry in the diet and to determine if there is a unique pattern for each berry. The amount of freeze-dried powder used in this study (50 g/kg diet) would be equivalent to consumption of approximately 300 g (2−3 cups) of fresh berries in a 70 kg human.

With the feeding of CB in this study, increased excretion of total 4-hydroxycinnamic acid was uniquely specific to CB compared to BB or BRB (Table 4; Figure 6). Although there was appreciable intake of 4-hydroxycinnamic acid in the CB (Figure 6), the excretion of 4-hydroxycinnamic acid was nearly 3 times that consumed. Although there was a significant but lesser intake of 4-hydroxycinnamic acid from black raspberry, this did not result in a large increase in the total urinary 4-hydroxycinnamic acid excretion.

There was no specific phenolic acid for which increased excretion was totally unique to BRB but excretion of 3-hydroxybenzoic (3HBA) (Figure 2), 3-hydroxycinnamic (3HCA) (Figure 3), and 3-hydroxyphenylpropionic (3HPPA) (Figure 4) acids was increased with BRB feeding relative to CB and BB. BRB contains appreciable levels of ellagitannins, and thus the excretion of urolithins might be expected to be increased with BRB feeding,[15] although they were not analyzed in this study. Increased excretion of 3-hydroxybenzoic acid (3HBA) (Figure 2) and 3-hydroxycinnamic acid (3HCA) (Figure 3) with all three berry treatments occurred even though neither of these phenolic acids was detected in the berries (Table 3) and thus are likely metabolites of 3,4-hydroxybenzoic and 3,4-hydroxycinnamic acids, respectively. Increased excretion of chlorogenic acid was unique to the BB treatment (Table 4), but the increase was small relative to the amount of chlorogenic acid in BB and CB (Table 4). In a previous study using a concentrated cranberry powder in the diet (33 g/kg diet),[11] increases in urinary excretion of 3-hydroxycinnamic (Figure 3), 4-hydroxycinnamic (Figure 6), and 3-hydroxyphenylacetic (Figure 7) were proportional to the amount of cranberry concentrate in the diet. The amount of concentrate used in the previous experiment[11] would have provided more polyphenolics in the diet than the 50 g/kg of whole berry powder used in the present study.

Phenolic acids excreted in the highest amounts were hippuric, 3-methoxy-4-hydroxyphenylacetic, 4-hydroxycinnamic, 3-hydroxycinnamic, 4-hydroxybenzoic, and 4-hydroxyphenylacetic acids, with or without berries in the diet. Hippuric acid, also called benzoylglycine, can be produced by conjugation of benzoic acid with the amino acid glycine. Benzoic acid can be produced as a degradation product of both polyphenols and phenolic acids as well as by phenylalanine metabolism in the gut. Whereas considerable amounts of hippuric acid are excreted in the urine of animals fed polyphenol-free diets,[11,16] its urinary excretion increases with the ingestion of polyphenols in humans as well as other animals.[17−19] Furthermore, its urinary excretion in rats has been shown to increase dose dependently with increasing amounts of procyanidins from a diet containing sorghum bran, which is rich in procyanidins.[17] Whereas CB and BB contained similar amounts of total procyanidins, BB contained proportionately greater amounts of the higher oligomers and polymers than CB, and excretion of hippuric acid was greater with BB feeding than with CB. BRB contained only small amounts of procyanidins and hence had the lowest amount of hippuric acid excreted in the urine among the three berry-fed animal groups. Irrespective of the diet, hippuric acid was excreted primarily in the free form. 4-Hydroxybenzoic, 3-methoxy-4-hydroxybenzoic, 3-methoxy-4-hydroxyphenylacetic, and 4-hydroxyphenylacetic acids can originate from dietary amino acids, primarily tyrosine and phenylalanine.[17,20,21] As a result, although their presence in the urine could be expected irrespective of the dietary presence of polyphenols, their forms and amounts may differ depending on the type and amount of polyphenols in the berries.

In rats fed the polyphenol-free diet, no free 3-methoxy-4-hydroxybenzoic acid was detected in animals, indicating that the relatively small amounts of free forms excreted in the urine with berry feeding originated from the polyphenols in the berries (Table 4). However, there was no change in the total or conjugated 3-methoxy-4-hydroxybenzoic acid excretion in the urine, suggesting that all of the conjugated and a majority of the total 3-methoxy-4-hydroxybenzoic acid originated from dietary amino acids. Tyrosine can be converted into 3,4-hydroxybenzoic acid, which can then be methylated to form 3-methoxy-4-hydroxybenzoic acid. Previous studies have demonstrated increased urinary excretion of free 3-methoxy-4-hydroxybenzoic

acid after polyphenol consumption, which was also increased in the current study when berries were included in the diet.[17]

Although studies on comparison of the berries or their polyphenol profile contributing to the differences in the excretion of phenolic acids are limited, previous paper indicate that ferulic, 3-hydroxyphenylacetic, 3-methoxy-4-hydroxyphenylacetic, hippuric, and cinnamic acid derivatized phenolic acids are increased when diets rich in procyanidins are fed,[16,17,22] which was usually the case in the current study. Higher excretion of 4-hydroxycinnamic acid in animals fed CB may simply be the result of their higher concentration in the berry and thus intake from the diet (Table 3). However, the intakes of 3,4-hydroxycinnamic acid in the diet are similar with the three berry treatments (Figure 8), but the total excretion of 3,4-hydroxycinnamic acid is 3−4-fold higher in the BB compared to the CB or BRB treatments (Figure 8; Table 4). This could be the result of metabolism of the chlorogenic acid to 3,4-hydroxycinnamic acid in the BB treatment group.

The differential effect of the three berries on the excretory pattern of some of the phenolic acids may be attributable to the differences in their polyphenol profiles. It should be noted that anthocyanins are present in high amounts in BRB (primarily as cyanidins) and procyanidins in CB and BB (Table 3). There are also some differences in the free phenolic acids (Table 3) present in the three berries. 3,4-Hydroxybenzoic acid (protocatechuic acid), a major metabolite of cyanidin-3-glycosides, which would include cyanidin-3-rutinoside[23,24] that was present in high amounts in BRB, was excreted in greatest quantities in animals fed BRB (Table 4). Removal of a hydroxyl group at the C-4 position from 3,4-hydroxybenzoic acid during the metabolic processes may have contributed to the highest amounts of urinary excretion of 3-hydroxybenzoic acid (Figure 2) in animals fed BRB. 4-Hydroxybenzoic acid and 3,4-dihydroxybenzoic acid were present in higher amounts in the BRB powder than in BB or CB powders (Table 3). Although our own data and some other previous studies have suggested 3-hydroxyphenylpropionic acid as a metabolite primarily of procyanidins,[11,17,25−27] the current study suggests that it may also possibly be a metabolite of anthocyanins as well, given that BRB-fed animals excreted the highest amounts of 3-hydroxyphenylpropionic acid in all forms. 3-Hydroxyphenylpropionic acid was not detected in the BRB powder. Although not in the highest amounts, Wu et al.[28] observed increased concentrations of 3-hydroxyphenylpropionic acid throughout the entire gastrointestinal tract of pigs following ingestion of BRB. It needs to be determined whether 3-hydroxyphenylpropionic acid is also a metabolite of ellagitannins, another polyphenol present in appreciable amounts in BRB, but not CB or BB.

Contribution of the conjugated PA to the total amount present in the urine was often >50%, with values as high as ≥85% in several cases. The cinnamic acids, 3-hydroxycinnamic (Figure 3) and 4-hydroxycinnamic (Figure 6), were conjugated to a greater extent than the phenylacetic acid derivatives (Table 4) (3-hydroxyphenylacetic acid, Figure 5; 3-methoxy-4-hydroxyphenylacetic, Figure 7). The benzoic acid derivatives vary in extent of conjugation depending upon the structure (Tables 4 and 5). A previous study has also shown the urinary excretion of several phenolic acids in conjugated forms in humans after consumption of a diet containing strawberries.[29] Although it is not clear whether and how much is contributed by the conjugation of phenolic acids to their overall health effects and bioactivity, estimating just the free forms may not be a true indicator of the amounts of phenolic acids excreted in the urine.

In addition to urinary excretion, some phenolic acids may also be excreted through the biliary route. Urine is the primary route for mostly smaller nonconjugated and monoconjugated phenolic acids, but extensively conjugated ones may find their way in the bile. However, literature on this aspect is very limited, and no attempt was made to investigate it in the current study.

In summary, hippuric, 4-hydroxphenylacetic, 3-methoxy-4-hydroxphenylacetic, and 4-hydroxybenzoic acids were excreted in highest amounts irrespective of the dietary treatments. Urinary excretion of a majority of the phenolic acids analyzed in the current study was increased by the inclusion of berries in the diet, with a slight reduction only in 4-hydroxyphenylacetic acid excretion. Depending on the berry dietary treatment, the largest increase in the urinary excretion of phenolic acids was observed with hippuric, 3-hydroxyphenylpropionic, 4-hydroxycinnamic, 3-methoxy-4-hydroxyphenylacetic, 3-methoxy-4-hydroxybenzoic, ferulic, and 3-hydroxyphenylacetic acids. A majority of the phenolic acids were also detected in conjugated form in considerable amounts, with some exceeding 80% of the total excreted in the urine. Thus, measurement of just the free form may not accurately reflect the amount excreted, and future studies investigating the health effects, bioactivity, or bioavailability of parent polyphenols should also consider their metabolites, not just the parent compound(s). Furthermore, parent compound(s) as well as their metabolites may also be methylated or conjugated, which may affect the bioactivity of many of these polyphenols.

AUTHOR INFORMATION

Corresponding Author

*(R.L.P.) Phone: (501) 743-8949. E-mail: rprior10@gmail.com.

Funding

Financial support for the study was provided in part by USDA, Agricultural Research Service, and Arkansas Biosciences Institute.

Notes

The authors declare no competing financial interest.

ACKNOWLEDGMENTS

We acknowledge the technical assistance of Samuel Wilkes and Theodore Rogers in the completion of this research project. The freeze-dried cranberry powder was provided by Decas Botanicals Inc., whereas those of blueberry and black raspberry were provided by Oregon Raspberry and Blackberry Commission (Corvallis, OR, USA).

REFERENCES

(1) Del Rio, D.; Rodriguez-Mateos, A.; Spencer, J. P.; Tognolini, M.; Borges, G.; Crozier, A. Dietary (poly)phenolics in human health: structures, bioavailability, and evidence of protective effects against chronic diseases. *Antioxid. Redox Signal.* **2013**, *18*, 1818−1892.

(2) Del Rio, D.; Borges, G.; Crozier, A. Berry flavonoids and phenolics: bioavailability and evidence of protective effects. *Br. J. Nutr.* **2010**, *104* (Suppl. 3), S67−S90.

(3) Monagas, M.; Urpi-Sarda, M.; Sanchez-Patan, F.; Llorach, R.; Garrido, I.; Gomez-Cordoves, C.; Andres-Lacueva, C.; Bartolome, B. Insights into the metabolism and microbial biotransformation of dietary flavan-3-ols and the bioactivity of their metabolites. *Food Funct.* **2010**, *1*, 233−253.

(4) Jenner, A. M.; Rafter, J.; Halliwell, B. Human fecal water content of phenolics: the extent of colonic exposure to aromatic compounds. *Free Radical Biol. Med.* **2005**, *38*, 763−772.
(5) Mateos-Martín, M. L.; Pérez-Jiménez, J.; Fuguet, E.; Torres, J. L. Profile of urinary and fecal proanthocyanidin metabolites from common cinnamon (*Cinnamomum zeylanicum* L.) in rats. *Mol. Nutr. Food Res.* **2012**, *56*, 671−675.
(6) Stalmach, A.; Edwards, C. A.; Wightman, J. D.; Crozier, A. Colonic catabolism of dietary phenolic and polyphenolic compounds from Concord grape juice. *Food Funct.* **2013**, *4*, 52−62.
(7) Balasubashini, M. S.; Rukkumani, R.; Viswanathan, P.; Menon, V. P. Ferulic acid alleviates lipid peroxidation in diabetic rats. *Phytother. Res.* **2004**, *18*, 310−314.
(8) Adisakwattana, S.; Moonsan, P.; Yibchok-Anun, S. Insulin-releasing properties of a series of cinnamic acid derivatives in vitro and in vivo. *J. Agric. Food Chem.* **2008**, *56*, 7838−7844.
(9) Suzuki, A.; Yamamoto, N.; Jokura, H.; Yamamoto, M.; Fujii, A.; Tokimitsu, I.; Saito, I. Chlorogenic acid attenuates hypertension and improves endothelial function in spontaneously hypertensive rats. *J. Hypertens.* **2006**, *24*, 1065−1073.
(10) Zamora-Ros, R.; Rabassa, M.; Cherubini, A.; Urpi-Sarda, M.; Bandinelli, S.; Ferrucci, L.; Andres-Lacueva, C. High concentrations of a urinary biomarker of polyphenol intake are associated with decreased mortality in older adults. *J. Nutr.* **2013**, *143*, 1445−1450.
(11) Prior, R. L.; Rogers, T. R.; Khanal, R. C.; Wilkes, S. E.; Wu, X.; Howard, L. R. Urinary excretion of phenolic acids in rats fed cranberry. *J. Agric. Food Chem.* **2010**, *58*, 3940−3949.
(12) Wu, X.; Prior, R. L. Systematic identification and characterization of anthocyanins by HPLC-ESI-MS/MS in common foods in the United States: fruits and berries. *J. Agric. Food Chem.* **2005**, *53*, 2589−2599.
(13) Khanal, R. C.; Howard, L. R.; Brownmiller, C. R.; Prior, R. L. Influence of extrusion processing on procyanidin composition and total anthocyanin contents of blueberry pomace. *J. Food Sci.* **2009**, *74*, H52−H58.
(14) Wu, X.; Gu, L.; Prior, R. L.; McKay, S. Characterization of anthocyanins and proanthocyanidins in some cultivars of *Ribes*, *Aronia*, and *Sambucus* and their antioxidant capacity. *J. Agric. Food Chem.* **2004**, *52*, 7846−7856.
(15) Tulipani, S.; Urpi-Sarda, M.; Garcia-Villalba, R.; Rabassa, M.; Lopez-Uriarte, P.; Bullo, M.; Jauregui, O.; Tomas-Barberan, F.; Salas-Salvado, J.; Espin, J. C.; Andres-Lacueva, C. Urolithins are the main urinary microbial-derived phenolic metabolites discriminating a moderate consumption of nuts in free-living subjects with diagnosed metabolic syndrome. *J. Agric. Food Chem.* **2012**, *60*, 8930−8940.
(16) Urpi-Sarda, M.; Monagas, M.; Khan, N.; Lamuela-Raventos, R. M.; Santos-Buelga, C.; Sacanella, E.; Castell, M.; Permanyer, J.; Andres-Lacueva, C. Epicatechin, procyanidins, and phenolic microbial metabolites after cocoa intake in humans and rats. *Anal. Bioanal. Chem.* **2009**, *394*, 1545−1556.
(17) Gu, L.; Prior, R. L.; Rooney, L.; House, S. E. Sorghum bran in the diet dose dependently increased the excretion of catechins and microbial-derived phenolic acids in female rats. *J. Agric. Food Chem.* **2007**, *55*, 5326−5334.
(18) Mulder, T. P.; Rietveld, A. G.; van Amelsvoort, J. M. Consumption of both black tea and green tea results in an increase in the excretion of hippuric acid into urine. *Am. J. Clin. Nutr.* **2005**, *85*, 256S−260S.
(19) Olthof, M. R.; Hollman, P. C.; Buijsman, M. N.; van Amelsvoort, J. M.; Katan, M. B. Chlorogenic acid, quercetin-3-rutinoside and black tea phenols are extensively metabolized in humans. *J. Nutr.* **2003**, *133*, 1806−1814.
(20) Booth, A. N.; Masri, M. S.; Robbins, D. J.; Emerson, O. H.; Jones, F. T.; DeEds, F. Urinary phenolic acid metabolites of tyrosine. *J. Biol. Chem.* **1960**, *235*, 2649−2652.
(21) Jones, M. R.; Jopple, J. D.; Swendseid, M. E. Phenylalanine metabolism in uremic and normal man. *Kidney Int.* **1978**, *14*, 169−179.
(22) Rios, L. Y.; Gonthier, M. P.; Remesy, C.; Mila, I.; Lapierre, C.; Lazarus, S. A.; Williamson, G.; Scalbert, A. Chocolate intake increases urinary excretion of polyphenol-derived phenolic acids in healthy human subjects. *Am. J. Clin. Nutr.* **2003**, *77*, 912−918.
(23) Vitaglione, P.; Donnarumma, G.; Napolitano, A.; Galvano, F.; Gallo, A.; Scalfi, L.; Fogliano, V. Protocatechuic acid is the major human metabolite of cyanidin-glucosides. *J. Nutr.* **2007**, *137*, 2043−2048.
(24) Aura, A. M.; Martin-Lopez, P.; O'Leary, K. A.; Williamson, G.; Oksman-Caldentey, K. M.; Poutanen, K.; Santos-Buelga, C. *In vitro* metabolism of anthocyanins by human gut microflora. *Eur. J. Nutr.* **2005**, *44*, 133−142.
(25) Gonthier, M. P.; Rios, L. Y.; Verny, M.; Remesy, C.; Scalbert, A. Novel liquid chromatography-electrospray ionization mass spectrometry method for the quantification in human urine of microbial aromatic acid metabolites derived from dietary polyphenols. *J. Chromatogr., B: Anal. Tech. Biomed. Life Sci.* **2003**, *789*, 247−255.
(26) Ward, N. C.; Croft, K. D.; Puddey, I. B.; Hodgson, J. M. Supplementation with grape seed polyphenols results in increased urinary excretion of 3-hydroxyphenylpropionic acid, an important metabolite of proanthocyanidins in humans. *J. Agric. Food Chem.* **2004**, *52*, 5545−5549.
(27) Deprez, S. Polymeric proanthocyanidins are catabolized by human colonic microflora into low-molecular-weight phenolic acids. *J. Nutr.* **2000**, *130*, 2733−2738.
(28) Wu, X.; Pittman, H. E., III; Hager, T.; Hager, A.; Howard, L.; Prior, R. L. Phenolic acids in black raspberry and in the gastrointestinal tract of pigs following ingestion of black raspberry. *Mol. Nutr. Food Res.* **2009**, *53* (Suppl. 1), S76−S84.
(29) Russell, W. R.; Scobbie, L.; Labat, A.; Duthie, G. G. Selective bio-availability of phenolic acids from Scottish strawberries. *Mol. Nutr. Food Res.* **2009**, *53* (Suppl. 1), S85−S91.

plasma and urine of subjects consuming pomegranate juice or BRB powder in water.[19,21] For nectar formulation, the addition of stabilizer (such as pectin, xanthan, and agar) to the juice would increase viscosity and thus aid in the suspension of particles such as fruit pulp and seeds.[22]

Aside from the formulation, the processing and storage need to be considered carefully to ensure minimal effect on the levels of berry bioactives in products. For example, the manufacturing and storage of berry jam, juice, and puree as well as canning yielded a decrease in anthocyanins and flavonoids, whereas ellagitannins content remained heat stable and more influenced by the processing related to seeds exclusion.[23−25] Formulation and processing of a food delivery system for a human clinical trial and subsequent scale up require consistency of ingredients and final product as well as quality and bioactive retention during storage. As such, the objective of the current study was to assess the consistency, quality, and shelf stability of BRB pectin confections and nectar developed for clinical trials and demonstrate their acceptability among men enrolled in a prostate cancer clinical trial.

MATERIALS AND METHODS

Standardization of All Ingredients and Adjustment of Formulations from Laboratory-Scale to Large-Scale Production. To ensure the homogeneity of the food products for the clinical trial, all ingredients were purchased in a single lot: corn syrup (Gordon Food Service, Springfield, OH, USA), sugar (U.S. Food Service, Cincinnati, OH, USA), and pectin (RS 400, Danisco, USA Inc., New Century, KS, USA). Pectin (CF 130 B) from Danisco was previously used in the laboratory scale for both confections and nectars; however, due to the lack of availability for the scale-up production, RS 400 pectin was applied. Freeze-dried BRB powder was obtained from both Stoke Raspberry Farm (Wilmington, OH, USA) (cultivar 'Jewel') and BerriProducts LLC (Corvallis, OR, USA) (cultivar 'Munger'). Mixed BRB powder (Ohio:Oregon = 2:3) was blended using a mixer (Day mixing, 1608, Federal Equipment Co., Cleveland, OH, USA) in the Food Pilot plant in the Parker Food Science Building at The Ohio State University (OSU). After mixing, the powder was separated into 4 kg/bag, sealed by using a vacuum sealer (MC-30 computer control, Sipromac, Houston, TX, USA), and kept at −40 °C, avoiding light, until use. According to Stoner et al.,[11] the levels of 26 nutrients in BRB remained within 10−20% of the original measurements for at least 2 years in the freeze-dried form stored at −20 °C. Scale-up production of confections and nectars required reformulation due to ingredients' change and processing parameter adjustments with the goal of retaining bioactives and quality. Final selected formulations are shown in Table 1.

Scale-up Production of BRB Products. *Confection Production.* Confections were prepared in 1 kg batches, and formulations adjusted from laboratory scale as shown in Table 1. In the preparation, water, sugar, corn syrup, and pectin were mixed and then stirred and heated on a hot plate (PC-620 D, Corning, Tewksbury, MA, USA) until a final temperature of 95 °C and °Brix from 65 to 68 were reached, which was determined by a hand-held refractometer (Fisher Scientific Japan Ltd., Tokyo, Japan). These processes were the same as laboratory scale and achieved within 45 ± 3 min. When the mixture had cooled to 78 °C at room temperature, freeze-dried BRB powder was added and mixed into the gel. The mixture was deposited at 65 °C with a pastry bag into molds (2115-1521 Truffles, Wilton, Columbus, OH, USA). Confections equilibrated at room temperature (21 ± 2 °C), avoiding lights for 24 h before packaging. All of the products was prepared in the OSU Pilot Plant in the Parker Food Science Building with relative humidity (RH) of 0.1−3.5% and temperature of 22 ± 1 °C. Random samples (n = 3) from each batch (83 ± 4 pieces) were obtained to evaluate their water activity, water content, and pH. Four random batches were chosen to track the stability of bioactives with HPLC (n = 6 per batch), rheological (n = 6 per batch), and textural properties (n = 10 per batch).

Table 1. Adjusted Formulations of BRB Confections and Nectars from Laboratory-Scale to Large-Scale Production

	confections		nectars (two BRB doses)	
composition (%)	lab scale	large scale	lab scale	large scale
BRB powder	20.0	20.0	4.0/8.0	4.0/8.0
sugar	35.0	29.5	3.0	3.0
corn syrup	12.0	11.0	1.0	1.0
water	29.5	37.8	90.2/86.2	91.2/87.2
pectin	1.5	1.2	1.8	0.8
50% (w/w) citric acid	2.0	0.5		
total	100	100	100	100

Low-Dose BRB Nectar Production. Nectar with 10 g of BRB dose was produced in MicroThermics, Inc. (Raleigh, NC, USA) in a 120 kg batch according to the large-scale formulation shown in Table 1. In the preparation, pectin, sugar, corn syrup, and water were first mixed and heated to 95 °C with a UHT/HTST Lab Direct and Indirect Processing System (MicroThermics Inc.), and then the premix was kept in an extended hold cabinet to maintain a temperature above 60 °C. BRB powder was added into the premix, and an adjustable speed drive (Leeson Electric Corp., Grafton, WI, USA) was used for mixing. The mixture was then pumped into a sterilized UHT/HTST Lab Direct and Indirect Processing System with 3 L/min flow rate and pasteurized at 75 °C for 15 min according to a method adapted from Silva and Gibbs to inactivate enzymes and the majority of molds.[26] Nectar was then cooled to 25 °C and filled into 250 mL Nalgene PETG sterilized bottles (Thermo Fisher Scientific Inc.) in a Clean Fill Hood with sterile product outlet (MicroThermics Inc.). Nectars were stored at 4 °C until use. Random bottles (n = 9) were selected to evaluate the pH, Brix, water activity, viscosity, and bioactive compounds with HPLC.

High-Dose BRB Nectar Production. Nectar with 20 g of BRB dose was produced in the OSU Pilot Plant in the Parker Food Science Building because Microthermics equipment was unable to process such high-viscosity nectar. A 100 kg batch of nectar was prepared with the large-scale formulation shown in Table 1. In the preparation, pectin, sugar, corn syrup, and water were first mixed well and heated in a steam-jacketed kettle (A5132-1 ATMOS, Hamilton Kettles, Cincinnati, OH, USA). Once the temperature reached 95 °C, BRB powder was added and mixed well. Temperature was kept at 95 °C for 15 min to pasteurize, a method adopted from the production of BRB puree and strawberry nectar.[24,27] After heating, nectar was cooled to 75 °C and filled into 250 mL Nalgene PETG sterilized bottles (Thermo Fisher Scientific Inc.) with a volumetric piston filler (Simplex, AS-1, Napa, CA, USA). A fixed volume of nectar (8 oz) was controlled to fill into bottles. After cooling, nectars were stored at 4 °C until use. Random bottles (n = 9) were selected to evaluate the pH, Brix, water activity, viscosity, and bioactive compounds with HPLC.

Phenolic Analysis of BRB Products. *Extraction.* One gram of BRB powder or confection/nectar containing 1 g of BRB was fully dispersed into water containing 5% (v/v) formic acid and adjusted to a final volume of 50 mL. Aliquots of 2 mL were immediately removed from the well-mixed solution and then mixed with 8 mL of acetone containing 5% (v/v) of formic acid, followed by bath sonication for 1 min in an FS3OH Sonicator (Fisher Scientific, Fair Lawn, NJ, USA) and then centrifuged at 2000g for 10 min with a IEC HN-SII centrifuge (Damon Corp., Needham Heights, MA, USA). Supernatant was removed to a clean 22 mL glass vial (Fisher Scientific, Pittsburgh, PA, USA) with a disposable glass pipet (Fisher Scientific, Pittsburgh, PA, USA). Solvent of acetone/water (80:20, v/v) containing 5% formic acid was used to extract the pellet twice more until the pellet was colorless. A Speedvac concentrator (SPD 131DDA-115, Thermo Fisher Scientific, Waltham, MA, USA) was used to dry sample extracts.

Identification. A Waters 2695 HPLC with a Waters 996 photodiode array detector (Waters, Milford, MA, USA) combined with a Waters

Q-Tof Premier (Micromass MS Technologies, Manchester, UK) was used for the identification of phenolic compounds. Dried extracts were dissolved in acetone/water (20:80, v/v) containing 5% formic acid and filtered through PTFE filters (Fisher Scientific, Pittsburgh, PA, USA; 0.2 μm, 13 mm diameter) before injection. Separation was carried out on a Symmetry C18 (75 mm × 4.6 mm i.d, 3.5 μm particle size) reversed phase column (Waters). The mobile phase for separation consisted of 1% (v/v) formic acid in water (A) and 1% (v/v) formic acid in acetonitrile (B). Initial mobile phase composition, 100% A and 0% B, was followed by a linear gradient to 80% A at 10 min, 70% A at 12 min, 50% A at 14 min, 0% A at 16 min, and returned to 100% A at 16.1 min and re-equilibrated through 20 min. Column temperature was kept at 35 °C, and flow rate was 1.3 mL/min. HPLC flow was split 1:10 prior to MS. The MS analysis was performed in positive and negative ion modes and calibrated with sodium formate in the range of m/z 50−3000. Leucine enkephalin was used as lockspray mass with m/z at 556.2771$^+$/554.2615$^-$. Capillary voltage was at 2.8 kV in negative mode and 3.2 kV in positive mode. Dry gas flow was at 700 L/h, cone voltage at 35 V, and desolvation gas temperature at 480 °C. For MS/MS analysis, the same instrumental parameters were used except that collision energy was set to 25 eV. Standards of cyanidin 3-gucoside, cyanidin 3-sambubioside, cyanidin 3-rutinoside, ellagic acid, and rutin were run to support peak identification.

Quantification. BRB confections and nectars were analyzed by HPLC to quantify anthocyanins, ellagitannins, and ellagic acid content. Freeze-dried BRB powder was quantified to determine the changes of BRB bioactives during production and subsequent storage in products. Quantification in all BRB samples was carried out using an Agilent 1100 series (Agilent, Waldbronn, Germany): G 1322A degasser, G 1328A manual injector, G 1311A quaternary pump, and G 1365A MWD controlled by the ChemStation software (Agilent). Chromatographic separation was performed with the same column and method as those in the identification step. Samples were injected with a volume of 20 μL. Absorbance at 260, 355, and 520 nm wavelength was recorded. Anthocyanins were quantified as one peak at 520 nm with cyanidin 3-glucoside as external calibrant[24] with concentrations ranging from 3.125 to 100.0 μg/mL. Ellagic acid was used as the external standard to quantify free ellagic acid and ellagic acid derivatives under 260 nm with a range of 0.25−4.0 μg/mL. Ellagic acid and ellagic acid derivatives were represented as total ellagic acid. Ellagitannin quantification was following the method of Gasperotti et al.,[28] in which (sanguiin H-6) $\varepsilon_{260\ nm}$ = 63615 M^{-1} cm^{-1} and (ellagic acid) $\varepsilon_{260\ nm}$ = 28266 M^{-1} cm^{-1} in 88% acetonitrile and 12% 1% formic acid in water (v/v) were reported. The standard curve of sanguiin H-6 was derived from the ellagic acid standard curve using a calculated factor (28266/63615 = 0.44).

Retention of Anthocyanins, Ellagitannins, and Total Ellagic Acid in BRB Products. The retention rate of these compounds from BRB confections and nectars was calculated using the formula

$$\text{retention}\ (\%) = \frac{C_{\text{phenolics}}}{C_{\text{BRB}} \times C_{\text{phenolics}}'}$$

where $C_{\text{phenolics}}$ = concentration of anthocyanins or ellagitannins in products, C_{BRB} = percentage of BRB in products after processing, $C_{\text{phenolics}}'$ = concentration of anthocyanins or ellagitannins in freeze-dried BRB powder. $C_{\text{phenolics}}$ and $C_{\text{phenolics}}'$ were obtained from HPLC quantification, and C_{BRB} was obtained from products' preparation.

Characteristic Consistency of the BRB Products. BRB delivery dosage, water activity (Aqua Lab Water Activity Meter series 3, Pullman, WA, USA), pH, and soluble solid (°Brix) were determined to check the consistency of BRB products needed for the clinical trials. A SevenMulti pH conductivity meter (Mettler Toledo Inc., Columbus, OH, USA) was used to measure the pH of the confection (mashed into a paste) and nectar. °Brix was measured by hand-held refractometers with ranges of 0−32° and 58−90° (Fisher Scientific Japan Ltd., Tokyo, Japan). Water content of confections was obtained from thermogravimetric analysis (TGA) (Q5000, TA Instrument, New Castle, DE, USA) by heating 15−20 mg samples at 5 °C/min from 25 to 160 °C. Moisture content was calculated as described in Siegwein et al.[29]

Rheological Consistency of BRB Products. Confections were analyzed with an AR 2000ex Controlled Stress Rheometer (TA Instruments) with a 20 mm diameter probe. Dynamic strain sweep (0.01−10%) at 25 °C and different frequencies (0.1, 1, 10, 100 Hz) were first tested to determine the linear viscoelastic region (LVR), and all samples exhibited a linear response for strain values up to 0.15%. Dynamic frequency sweep (0.1−100 Hz) tests were then carried out at 25 °C with 0.1% strain to obtain viscoelastic behavior of confections. Storage modulus (G'), loss modulus (G''), and complex viscosity (η^*) were recorded and compared. Changes of apparent viscosity (η) in nectars with a 40 mm diameter probe were recorded with increasing flow shear rate (0.001−1000 s^{-1}) at 1 Hz and 25 °C. Random samples from scale-up production were also analyzed. Texture profile analyses (TPA) of confections were obtained with an Instron 5542 Universal Testing Machine (Instron Corp., Canton, MA, USA) with Bluehill 2 Materials Testing Software (Instron Corp., Norwood, MA, USA) with 40% compression at 1 mm/s rate by 35 mm diameter probe. Hardness, cohesiveness, springiness, and chewiness were obtained according to the methdod of Peleg.[30]

2-Month Storage of BRB Products. A 2-month shelf life required for BRB products to allow for recruitment and clinical intervention was studied. Both confections and nectars were packaged; plastic 2 oz cups with lids (Gordon Food Service, Springfield, OH, USA) were for confections, and amber bags were used for each nectar bottle; the samples were kept in the dark at 4 °C for 2 months. Fresh samples and samples at 4, 6, and 8 weeks were collected to evaluate the storage stability of bioactive compounds and textural properties in the products. The number of samples used for analysis was the same as those in fresh samples described earlier.

Scale-up Production Design for a Prostate Cancer Clinical Trial. This clinical trial was approved by the OSU Clinical Scientific Review Committee (CSRC) first and subsequently by the Institutional Review Board (IRB) with approval numbers OSU-12125 and 2012C0096, respectively. In total, 56 patients newly diagnosed with resectable prostate cancer (average age = 61.6 ± 1.02 years) were recruited into this study, 32 of which were in BRB functional food intervention groups and 24 in dietary assessment groups (control). Only BRB intervention groups were focused on and discussed in this study. Design of intervention groups in this clinical trial, BRB dosage in products, and total amount of processed products are shown in Figure 1. All patients signed written informed consent forms before participation. The BRB intervention period for each patient lasted 20−30 days depending on the scheduled surgery day. Extra products were given to participants in case of a need to delay surgery. Only the sensory acceptability of the products tested in this study will be discussed herein.

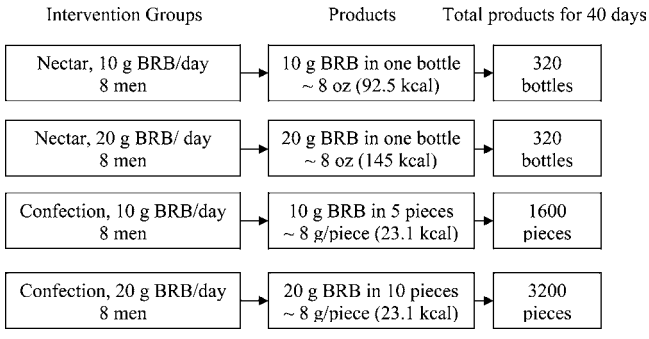

Figure 1. BRB delivery dosage and total BRB products in a prostate cancer clinical trial.

Sensory Evaluation. To obtain the overall acceptability of BRB products, a sensory evaluation survey was developed and approved by the IRB (2012C0096). At the end of the clinical trial, sensory tests were conducted using a nine-point hedonic scale (1, dislike extremely;

2, dislike very much; 3, dislike moderately; 4, dislike slightly; 5, neither like nor dislike; 6, like slightly; 7, like moderately; 8, like very much; 9, like extremely) to evaluate the overall acceptability and acceptability of aroma, flavor, sweetness, texture, and grittiness.[31]

Statistical Analysis. A one-way analysis of variance (ANOVA) and Tukey's post hoc test were used with SPSS 20.0 (Chicago, IL, USA) to determine the significance in the characteristics between confection batches. The means of rheological properties and contents of bioactive compounds in BRB confections and nectars during storage were compared as well. An independent t test compared differences between laboratory-scale and large-scale products with Minitab 15 statistical software (Minitab Inc., State College, PA, USA). A $p \leq 0.05$ was considered to be significantly different.

RESULTS AND DISCUSSION

Formulation Adjustment of BRB Products from Laboratory-Scale to Large-Scale Production. Formulations of pectin-based confection and nectar (Table 1) were adjusted from the laboratory scale to achieve similar textural properties as well as a lower caloric content for clinical subjects. Pectin RS 400 used in large-scale production had a higher degree of esterification (70%) compared to CF 130 B used in laboratory scale (31% esterification and 19% of amidation); therefore, pectin was decreased from 1.5 to 1.2% in BRB confection to reach similar rheological properties as indicated by similar G', G'', and η^* values (Figure 2). Sugar in BRB confection and citric acid were both decreased in scale-up versions to achieve the desired lower calorie content (from 29.3 to 23.1 kcal/piece confection). Calorie control was essential so as not to induce weight gain during intervention. For the nectar, calorie adjustment was not required, but pectin addition was decreased from 1.8% in laboratory scale to 0.8% for clinical trial so as to reach similar rheological end points during scale up (Figure 3).

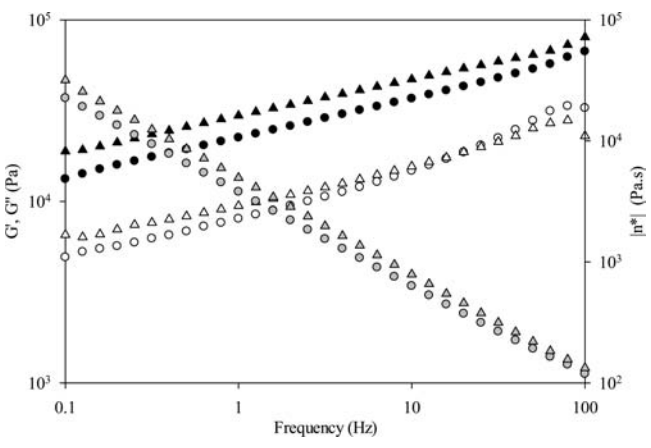

Figure 2. Frequency sweep of laboratory-scale confection (circles) and large-scale confection (triangles): (solid symbols) storage modulus G'; (open symbols) loss modulus G''; (gray symbols) complex viscosity $|\eta^*|$.

Identification and Quantification of Phenolics. Phenolics in BRB powder were identified with a combination of HPLC-MS/MS, accessible standards, UV–vis, and reported mass. HPLC chromatograph and peak identification information for phenolics are shown in Figure 4 and the accompanying table. Peaks 1a,b and 1c,d coeluted in the HPLC but were identified by MS as cyanidin 3-glucoside, cyanidin 3-sambubioside, cyanidin 3-xylosylrutinoside, and cyanidin 3-rutinoside with a characteristic fragment of cyanidin aglycon $[M - H]^-$ at

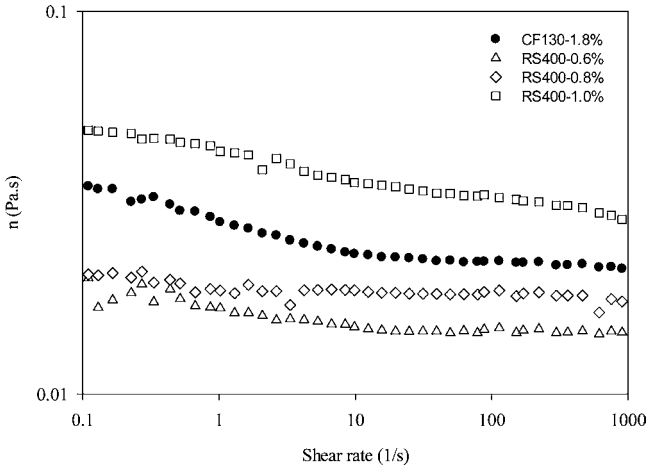

Figure 3. Viscosity of nectar premix with different concentrations of large-scale RS 400 pectin compared to CF 130 B pectin used in laboratory scale.

m/z 285 and other reported fragment ions.[32] In this study, pelargonidin 3-rutinoside was detected in a very low content with MS; thus, only the four major cyanidin glycosides were quantified as anthocyanins in BRB powder and the processed products. This HPLC method was not developed to separate each anthocyanin well due to other phenolics including ellagitannins and quercetin glycoside. Peaks shown with a retention time of 7.4–8.6 min were unknown but considered as possible anthocyanin-related compounds due to absorbance at 480 nm and MS $[M - H]^-$ m/z 651 and MS/MS m/z at 285 and 593.

Peak 2 was tentatively identified as quercetin xylosylrutinoside with $[M - H]^-$ m/z at 741 and MS/MS m/z 301.036 and 355 nm UV–vis. Peak 3 was identified as sanguiin H-6 with MS $[M - H]^{2-}$ m/z at 934; MS/MS m/z at 935, 633, and 301 with UV–vis featured at 260 nm and comparison with previous reports.[33−35] Lambertianin C with MS $[M - H]^{2-}$ m/z at 1401 and a true mass of 2803 was identified according to Hager et al.,[35] but it was detected in a minor peak at 8.57 min and coeluted with some unknown anthocyanin degradation compounds in this HPLC method. However, lambertianin C was reported as one of the major ellagitannins (>32%) besides sanguiin H-6 (>42%) in six raspberry (*Rubus idaeus* L.) cultivars.[28] Several ellagitannins eluted before anthocyanins with MS of 783, 933, and 633, which were likely pedunculagin isomer, castalagin/vescalagin isomer, and galloyl-HHDP glucose isomer according to Hager et al.[35] In this study, sanguiin H-6 was the most abundant ellagitannin detected and thus quantified as ellagitannin and compared during processing and storage. In peaks 4–6, rutin, ellagic acid, and quercetin hexuronic acid were identified with a combination of available standards (rutin and ellagic acid), accurate MS, MS/MS, UV–vis, and reported data.[36] Methyl-ellagic acid-pentose, acetyl-ellagic acid-pentose, malonyl-methyl-ellagic acid-pentose, and acetyl-methyl-ellagic acid-pentose were identified according to the accurate masses of their molecular ions and fragment m/z (MeEA $[M - H]^-$ m/z at 315, EA at 301) by MS/MS in peaks 7–10.[28,33]

Changes of Phenolics during Laboratory-Scale and Large-Scale Processing. HPLC profiles of BRB confections and nectars were the same as that of BRB powder, but in some cases were present at different concentrations due to the effect

dx.doi.org/10.1021/jf404566p | J. Agric. Food Chem. 2014, 62, 3997–4006

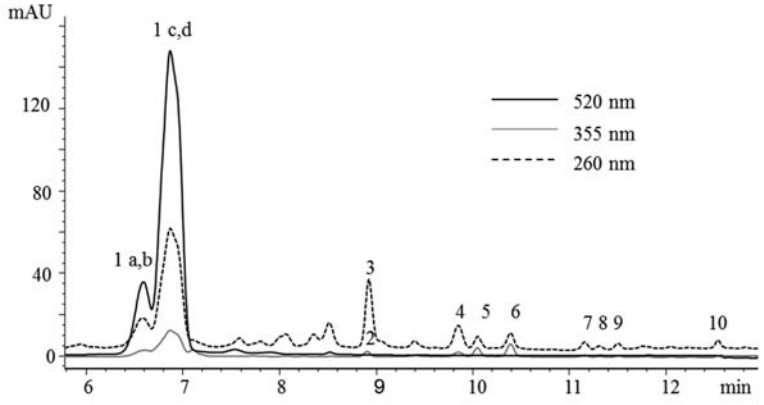

peak No.	retention time (min)	HPLC-UV (nm)	MS $[M-H]^-$	MS/MS $[M-H]^-$	tentative identification[a]
1a	6.601	520	447.094	285.040	Cy 3-glu
1b	6.601	520	579.137	285.040	Cy 3-sam
1c	6.885	520	725.194	285.040	Cy 3-xyrut
1d	6.885	520	593.151	285.040	Cy 3-rut
2	8.923	355	741.118	301.036	Q-xyrut
3	8.941	260	934.090^{2-}	935.068, 633.066, 300.999	ET (Sanguiin H-6)
4	9.869	360	300.998	300.998	EA
5	10.066	355	609.146	301.036	Rutin
6	10.403	355	477.065	301.036	Q-hexA
7	11.167	360	447.057	315.012, 300.998	Me-EA-pentose
8	11.319	360	475.059	300.998	Ac-EA-Pentose
9	11.511	360	533.059	315.016, 300.998	Mal-Me-EA-Pentose
10	12.541	360	489.066	315.015, 300.998	Ac-Me-EA-Pentose

[a] Abbreviations of the tentative ID: Cy: cyanidin, glu: glucoside, sam: sambubioside, xyrut: xylosylrutinoside, rut: rutinoside, Q: quercetin, ET: ellagitannin (Sanguiin H-6), EA: ellagic acid, hexA: glucuronic acid/galacturonic acid, Me: methyl, Ac: acetyl, Mal: malonyl.

Figure 4. HPLC profile of freeze-dried BRB powder and tentative identification of each peak.

Table 2. Retention of Phenolics in BRB Products after Processing[a]

product	processing scale	anthocyanins (%)	ellagitannins (%)	total ellagic acid (%)
confection	lab	94.3 ± 0.3a	93.4 ± 1.5a	101.3 ± 2.3a
	large	94.4 ± 0.98a	95.6 ± 1.9a	106.4 ± 3.3a
nectar, 10 g of BRB	lab (75 °C, 10 min)	92.5 ± 0.3a	95.1 ± 1.0a	105.2 ± 3.2a
	large (75 °C, 15 min)	86.1 ± 2.7b	66.4 ± 3.5b	113.6 ± 6.8b
nectar, 20 g of BRB	lab (85 °C, 10 min)	81.7 ± 0.3a	89.5 ± 0.8a	110.4 ± 4.2a
	large (95 °C, 15 min)	69.0 ± 2.8b	91.0 ± 3.6a	127.9 ± 6.2b

[a] Values represent means ± standard error ($n = 24$ for confections and $n = 9$ for nectars). Means with different letters in the same column within each BRB product are significantly different ($p \leq 0.05$).

of processing. Anthocyanins, ellagitannin, and total ellagic acid in BRB products were quantified according to the identification above and then were compared to that of laboratory scale to ensure similar delivery of these bioactives for the clinical trial. Retention rates of phenolics in both laboratory-scale and large-scale products are shown in Table 2. Confections contained 6.8 mg/g of anthocyanins and proved to have the highest anthocyanin retention rates (94%) after processing. In addition, there were no distinct changes of anthocyanins and ellagitannin between laboratory-scale and large-scale confections, demonstrating consistency in the processing steps ($p > 0.05$). This was mainly due to the low mixing temperature of the pectin gel with freeze-dried BRB powder (78 °C). For the nectars with 10 g of BRB dosage, 86% of anthocyanins were retained after large-

dx.doi.org/10.1021/jf404566p | J. Agric. Food Chem. 2014, 62, 3997−4006

scale processing, whereas only 69% were left in the 20 g of BRB dose. This was related to the different processing conditions of the low and high dose of BRB nectars: 75 °C for 15 min and 95 °C for 15 min, respectively. Higher temperature and longer heating time were required to pasteurize the 20 g of BRB dose nectars. Both anthocyanin retention rates in large scale were significantly lower than those in the laboratory scale ($p < 0.05$), mainly due to the longer mixing time of 10 g BRB powder with premix at 60 °C in the hold cabinet and higher heating temperature for the 20 g dose nectar in the large-scale production. Anthocyanin degradation is known to follow first-order reaction kinetics, and processing at lower temperature for shorter time improves the retention rates.[37] In addition, multiple processing steps influence the retention of anthocyanins. Significantly lower retention of monomeric anthocyanins was found in nonclarified and clarified juices (31 and 27%) than in BRB puree (63%) and berries canned in water (58%).[24] The comparatively higher retention rates of anthocyanins in BRB confections and nectars (69−94%) may be due to the use of whole BRB powder and single mixing and/or heating steps. Other factors such as the presence of oxygen, light, enzymes, and pH fluctuations may also influence the loss of anthocyanins.[38]

Ellagitannins were retained at 95 and 91% after processing of confection and nectar with the 20 g of BRB dose in large-scale production. Nectar with lower BRB dose had 66% of ellagitannin retention rate, which was significantly lower than those of confection and nectar with 20 g of BRB as well as that of laboratory scale ($p < 0.05$). This may be due to partial seed sedimentation in the Microthermics flow processing system because higher BRB dose nectar would cause blockage of the system, which resulted in the higher BRB dose nectar being processed in the OSU pilot plant. This was consistent with previous results where BRB ellagitannins were retained in higher quantities in purees (65%) and berries canned in water or syrup (79%) but not juice (only 31−33% retained), where the exclusion of seeds accounted for the significant loss.[39] Similar results were also found in blackberry processing, where 30 and 18% of ellagitannins were recovered in nonclarified and clarified juices, respectively, whereas canning and pureeing had little effect.[25]

All BRB products demonstrated above 100% ellagic acid retention rates. Ellagic acid increased in raspberry juice after heat processing due to better extraction from the cell matrix.[40] It was possible that the heat treatment of BRB products in this study may have improved ellagic acid extraction compared to the BRB powder.[25] Additionally, increased ellagic acid may result from hydrolysis of ellagitannins during processing.

Consistency of Scale-up Production of BRB Products. Characteristics of BRB confections from different batches and nectars from randomly selected bottles were measured to evaluate the production consistency (Table 3). Confections were prepared within 4 weeks; 50 batches (83 ± 4 pieces per batch) totaled 4162 pieces. The average weight of the confections was 8.42 ± 0.35 g with a BRB concentration of 24.95 ± 0.48%. Dosage of BRB was within 5% of desired concentration (Table 3). Physical properties such as pH and water activity also showed consistency in the products (Table 3).

Rheological properties of confections from different batches (randomly selected) were evaluated (Figure 5A,B). There were no distinct differences in G', G'', and η^* between different batches at 0.1, 1, 10, and 100 Hz ($p > 0.05$), suggesting the

Table 3. Characteristics of BRB Confections and Nectars in Scale-up Processing[a]

characteristic	BRB confections (per piece)	nectar, 10 g of BRB (per bottle)	nectar, 20 g of BRB (per bottle)
BRB dosage (g)	2.10 ± 0.09	10.48 ± 0.31	20.22 ± 0.45
pH	3.44 ± 0.02	3.64 ± 0.02	3.56 ± 0.02
A_w	0.72 ± 0.02	0.95 ± 0.00	0.95 ± 0.00

[a]Values represent means ± standard error (n = 3 per batch for confections and n = 9 for nectars).

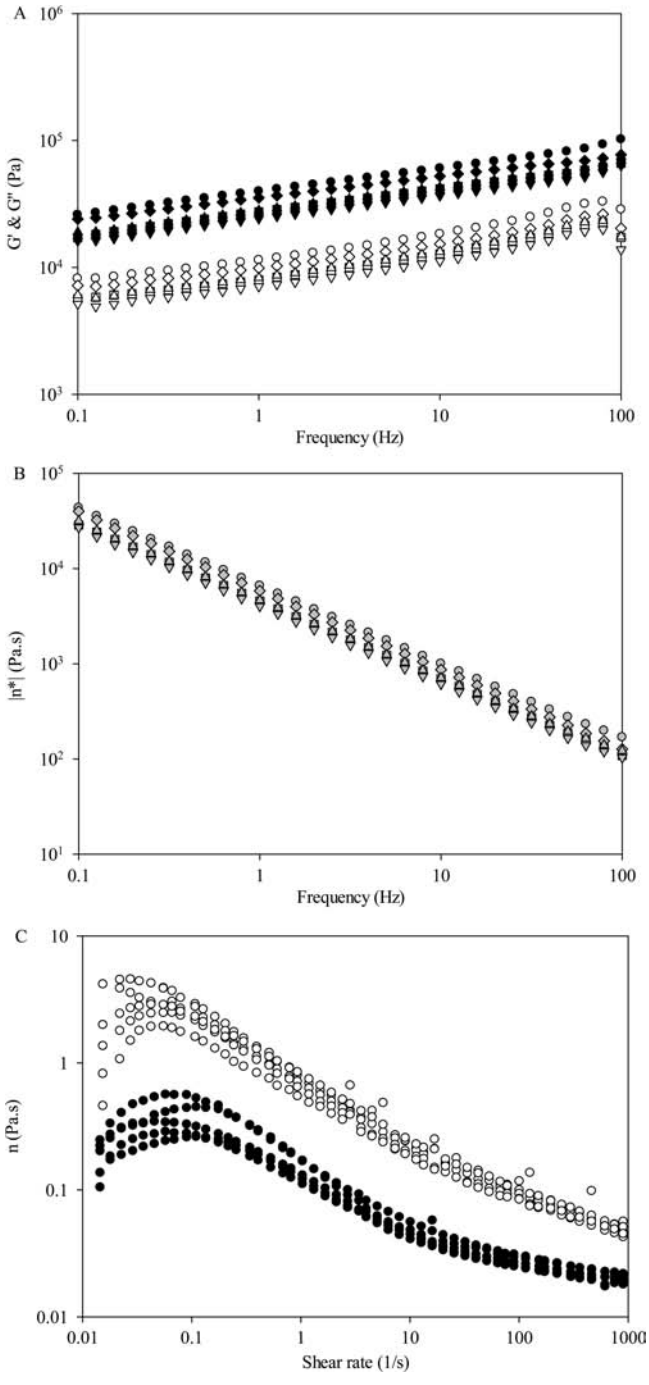

Figure 5. Rheological consistency of BRB products in the scale-up production: (A) confections G' (solid symbols) and G'' (open symbols); (B) confection $|\eta^*|$ (gray symbols); (C) nectar η, 10 g (solid symbols) and 20 g (open symbols).

dx.doi.org/10.1021/jf404566p | J. Agric. Food Chem. 2014, 62, 3997−4006

Table 4. Concentration and Daily Delivery of Phenolics in Fresh BRB Products

	products for BRB delivery[a]			
	confections (5 pieces/day)	confections (10 pieces/day)	nectar, 10 g of BRB (one bottle/day)	nectar, 20 g of BRB (one bottle/day)
concentration				
anthocyanins (mg/g)	6.8 ± 0.1	6.8 ± 0.1	1.0 ± 0.03	1.6 ± 0.1
ellagitannins (μg/g)	593.0 ± 12.1	593.0 ± 12.1	66.4 ± 3.5	182.2 ± 9.3
total ellagic acid (μg/g)	113.7 ± 3.5	113.7 ± 3.5	19.6 ± 3.1	44.1 ± 2.1
estimated daily amount of delivery[b]				
anthocyanins (mg)	285.6	571.2	253.7	399.2
ellagitannins (mg)	24.9	49.8	16.8	45.5
total ellagic acid (mg)	4.8	9.6	5.0	11.0

[a]Average weight of products: confections, 8.4 g/piece; nectar, 10 g of BRB, 253.7 g/bottle; nectars, 20 g of BRB, 249.5 g/bottle. [b]Estimated daily amount of delivery was obtained from the average weight of confections/nectars; thus, no SD was provided.

confections were made with consistent textural properties. Viscosity of samples from 10 and 20 g of BRB nectar was measured with shear flow tests, and results are shown in Figure 5C. With increased shear rate, viscosity showed smaller difference between replicates. Nectars with 10 and 20 g of BRB had 0.15 ± 0.02 and 0.72 ± 0.13 Pa·s viscosity at 1.00 s^{-1} shear rate, respectively.

Stability of Phenolics during Storage. Concentration and daily delivery amount of anthocyanins, ellagitannins, and total ellagic acid in fresh products are shown in Table 4. Confections delivered higher daily amount of anthocyanins and ellagitannins than nectars for equivalent BRB doses due to higher initial value of these bioactives in confections (Table 2). The retention rate of these phenolics in BRB products during storage is shown in Table 5. During storage, anthocyanins in confections decreased significantly from 94 to 87% in 4 weeks but were fairly constant (no statistically significant change) up to 8 weeks of storage. A similar trend was observed for the anthocyanins in the low nectar dose, whereas the 20 g dose had no significant change until 8 weeks of storage. The depletion of anthocyanins in the confections may be a consequence of residual enzymatic activity, as was observed in processing of blueberry and storage of strawberry nectar.[27,41] Gössinger et al. reported that enzymes were not fully inactivated even after a heat treatment of 90 °C for 60 min.[27] Therefore, to promote retention of anthocyanins, a balance may need to be reached between initial heat processing to achieve enzyme inactivation (high heat for longer time results in lower anthocyanin concentration) and stability during storage (higher heat initially applied, less degradation during storage). Additionally, storage conditions may also play an important role in the stability of anthocyanins. Refrigerated storage resulted in lowering of the polymeric color percentage of blueberry juice[42] and reducing the rate of anthocyanin degradation[43] compared to room temperature.

Table 5. Retention of Phenolics in BRB Products during 2 Months of Storage at 4 °C[a]

product	storage time (weeks)	anthocyanins (%)	ellagitannins (%)	total ellagic acid (%)
confection	0	94.4 ± 1.0a	95.6 ± 1.9a	106.4 ± 3.3a
	4	87.0 ± 1.0b	94.4 ± 2.7a	101.4 ± 7.3a
	6	84.5 ± 1.6b	95.7 ± 4.8a	100.0 ± 1.4a
	8	83.4 ± 2.5b	93.6 ± 4.5a	106.9 ± 6.9a
nectar, 10 g of BRB	0	86.1 ± 2.7a	66.4 ± 3.5a	113.6 ± 6.8a
	4	78.9 ± 3.6b	59.6 ± 1.3b	105.0 ± 2.3a
	6	77.9 ± 3.2b	57.2 ± 2.6b	103.2 ± 7.0a
	8	76.3 ± 2.7b	60.2 ± 1.7b	104.1 ± 4.8a
nectar, 20 g of BRB	0	69.0 ± 2.8a	91.0 ± 4.6a	128.0 ± 6.2a
	4	68.5 ± 3.2ab	91.4 ± 3.7a	129.4 ± 3.0a
	6	66.3 ± 1.0ab	89.9 ± 3.1a	125.3 ± 2.5a
	8	65.1 ± 3.3b	93.3 ± 2.4a	127.8 ± 3.3a

[a]Values represent means ± standard error (n = 24 for confections and n = 9 for nectars). Means with different letters in the same column within each BRB product are significantly different ($p \leq 0.05$).

Retention of ellagitannins was not significantly changed in confection and 20 g of BRB nectar during storage ($p > 0.05$). Ellagitannins in the 10 g of BRB nectar decreased significantly, but the change was <10% after 8 weeks of storage. The high stability of ellagitannins in confections and nectar during storage was consistent with those previously reported in other berries.[25,39] Total ellagic acid concentration remained stable during storage of all products ($p > 0.05$). This was consistent with previous reports in which ellagic acid derivatives were not affected by thermal processing and remained stable during storage in red raspberry jams.[23]

Textural Stability during Storage. Rheological properties of BRB confections showed no significant change in complex viscosity η^* (Figure 6) during storage with similar trends for G' and G'' (data not shown). Texture profile analysis (TPA) showed significant decrease ($p < 0.05$) in cohesiveness and springiness but not in hardness and chewiness after 2 months of storage (data not shown). Chewiness is the combined results of hardness, cohesiveness, and springiness. This indicated that minor changes in cohesiveness and springiness of BRB confections did not influence chewiness. Water content was 27.85 ± 0.55% at day 1 and did not significantly change during 8 weeks of storage ($p > 0.05$). However, water activity (A_w) increased significantly from 0.72 ± 0.02 to 0.76 ± 0.02 after 8 weeks of storage ($p < 0.05$). This increase in water activity indicated water migration in the gel structure, which resulted in changes of cohesiveness and springiness but no other textural properties. Nectars with both BRB doses showed no significant changes in viscosity during storage at 4 °C ($p > 0.05$).

Sensory Acceptability of BRB Products during Dietary Intervention. Sensory evaluation was obtained from 15 of 16 subjects in the BRB nectar group and from 12 of 16 in the BRB confection group. Results are shown in Table 6. Nectar and confections scored 7.27 and 7.08 in overall acceptability (7, like moderately on a 9-point hedonic scale). Both products scored

dx.doi.org/10.1021/jf404566p | J. Agric. Food Chem. 2014, 62, 3997−4006

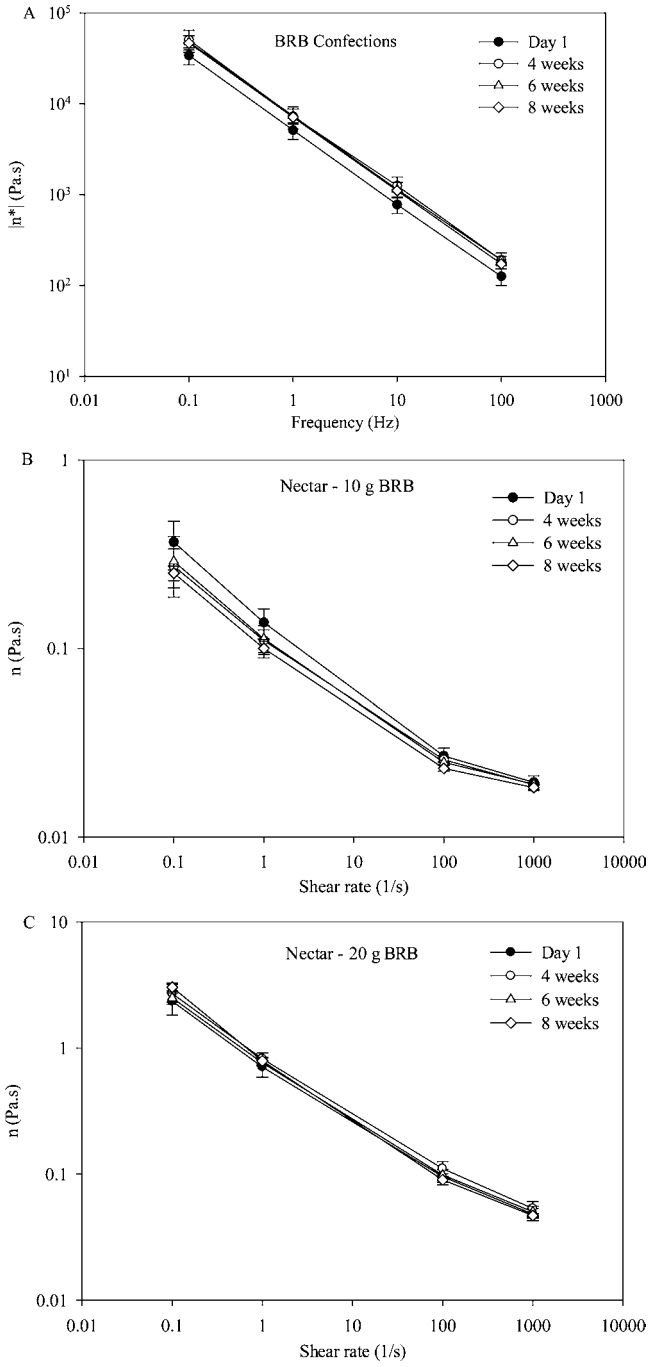

Figure 6. Viscosity of BRB scale-up products during storage at 4 °C: (A) confections, $|\eta^*|$; (B) nectar, 10 g of BRB dosage, η; (C) nectar, 20 g of BRB dosage, η.

above 6 on flavor, aroma, sweetness, and texture. Grittiness was below 6 (like slightly) in nectars, likely due to the seeds in the whole freeze-dried BRB. Grittiness may influence the overall liking score of both products. When subjects were asked in the surveys what factors contributed to or hindered the consumption of BRB products, 33% in the nectar group and 20% in the confection group mentioned grittiness. Other factors such as dose frequency in confection may have influenced the overall liking (40% mentioned that high dose frequency, 10 pieces per day, was a hindrance).

In this study, both BRB confections and nectars were formulated successfully to deliver a specific dose of bioactives in a consistent manner. After scale up, rheological properties did not vary within a product category, and ellagitanin and ellagic acid proved to be more heat stable and consistent than anthocyanins. During 8 weeks of storage, high-dose nectar showed the least changes in bioactives. Final products were well accepted (>like moderately) by men enrolled in a prostate cancer clinical trial. Thus, this study demonstrates that two different BRB delivery vehicles consisting of different matrices can be formulated to meet quality standards and bioactive stability and successfully scaled up for a human clinical trial. The use of these food products can prove to be instrumental in studying the efficacy of BRB bioactives in the prevention of or as adjuvant therapy in a variety of cancers (prostate, esophageal, oral, etc.).

AUTHOR INFORMATION

Corresponding Author

*(Y.V.) Phone: +1 (614) 247-7696. Fax: +1 (614) 292-0218. E-mail: vodovotz.1@osu.edu.

Notes

The authors declare no competing financial interest.

ABBREVIATIONS USED

BRB, black raspberry; HPLC, high-performance liquid chromatography; IRB, Institutional Review Board; ESI, electrospray ionization; MS, mass spectrometry; UV−vis, ultraviolet−visible spectroscopy; TGA, thermogravimetry analysis; TPA, textural profile analysis; LVR, linear viscoelastic region; ANOVA, analysis of variance

REFERENCES

(1) Mallery, S. R.; Stoner, G. D.; Larsen, P. E.; Fields, H. W.; Rodrigo, K. A.; Schwartz, S. J.; Tian, Q.; Dai, J.; Mumper, R. J. Formulation and in-vitro and in-vivo evaluation of a mucoadhesive gel containing freeze dried black raspberries: implications for oral cancer chemoprevention. *Pharm. Res.* **2007**, *24*, 728−737.

(2) Seeram, N. P.; Adams, L. S.; Zhang, Y.; Lee, P.; Sand, D.; Scheuller, H. S.; Heber, D. Blackberry, black raspberry, blueberry, cranberry, red raspberry, and strawberry extracts inhibit growth and stimulate apoptosis of human cancer cells in vitro. *J. Agric. Food Chem.* **2006**, *54*, 9329−9339.

(3) Keatley, K. E. *Chemoprevention of Bladder Cancer with Anthocyanin-Rich Extract from Black Raspberries*. Thesis, The Ohio State University, Columbus, OH, 2008.

(4) Seeram, N. P.; Aronson, W. J.; Zhang, Y.; Henning, S. M.; Moro, A.; Lee, R.; Sartippour, M.; Harris, D. M.; Rettig, M.; Suchard, M. A.; Pantuck, A. J.; Belldegrun, A.; Heber, D. Pomegranate ellagitannin-

Table 6. Sensory Acceptance of BRB Confections and Nectars with 9-Point Hedonic Scale[a]

product	overall liking	flavor	aroma	sweetness	hardness or thickness	grittiness
confections	7.08 ± 1.68	7.08 ± 1.78	6.25 ± 1.36	6.92 ± 1.98	6.83 ± 1.75	6.08 ± 1.78
nectars	7.27 ± 1.44	7.00 ± 1.60	6.93 ± 1.44	6.53 ± 1.77	6.47 ± 1.60	5.33 ± 1.76

[a]Values represent means ± standard error (n = 12 for confections and n = 15 for nectars).

derived metabolites inhibit prostate cancer growth and localize to the mouse prostate gland. *J. Agric. Food Chem.* **2007**, *55*, 7732−7737.
(5) Mallery, S. R.; Zwick, J. C.; Pei, P.; Tong, M.; Larsen, P. E.; Shumway, B. S.; Lu, B.; Fields, H. W.; Mumper, R. J.; Stoner, G. D. Topical application of a bioadhesive black raspberry gel modulates gene expression and reduces cyclooxygenase 2 protein human premalignant oral lesions. *Cancer Res.* **2008**, *68*, 4945−4957.
(6) Wang, L. S.; Hecht, S. S.; Garmella, S. G.; Yu, N.; Larue, B.; Henry, C.; Mclntyre, C.; Rocha, C.; Lechner, J. F.; Stoner, G. D. Anthocyanins in black raspberries prevent esophageal tumor in rat. *Cancer Prev. Res.* **2009**, *2*, 84−93.
(7) Wang, L. S.; Hecht, S.; Carmella, S.; Seguin, C.; Rocha, C.; Yu, N.; Stoner, K.; Chiu, S.; Stoner, G. Berry ellagitannins may not be sufficient for prevention of tumors in the rodent esophagus. *J. Agric. Food Chem.* **2010**, *58*, 3992−3995.
(8) Ravoori, S.; Vadhanam, M. V.; Aqil, F.; Gupta, R. C. Inhibition of estrogen-mediated mammary tumorigenesis by blueberry and black raspberry. *J. Agric. Food Chem.* **2012**, *60*, 5547−5555.
(9) Wang, L. S; Arnold, M.; Huang, Y. W.; Sardo, C.; Seguin, C.; Martin, E.; Huang, T. H.; Riedl, K.; Schwartz, S.; Frankel, W.; Pearl, D.; Xu, Y.; Winston, J.; Yang, G. Y.; Stoner, G. Modulation of genetic and epigenetic biomarkers of colorectal cancer in humans by black raspberries: a phase I pilot study. *Clin. Cancer Res.* **2011**, *17*, 598−610.
(10) Stoner, G. D.; Wang, L. S.; Zikri, N.; Chen, T.; Hecht, S. S.; Huang, C.; Sardo, C.; Lechner, J. F. Cancer prevention with freeze-dried berries and berry components. *Semin. Cancer Biol.* **2007**, *17*, 403−410.
(11) Stoner, G. D. Foodstuffs for preventing cancer: the preclinical and clinical development of berries. *Cancer Prev. Res.* **2009**, *2*, 187−194.
(12) Cooke, D.; Steward, W. P.; Gescher, A. J.; Marczylo, T. Anthocyans from fruits and vegetables − does bright colour signal cancer chemopreventive activity? *Eur. J. Cancer* **2005**, *41*, 1931−1940.
(13) Ross, H. A.; Gordon, J. M.; Stewart, D. Antiproliferative activity is predominantly associated with ellagitannins in raspberry extracts. *Phytochemistry* **2007**, *68*, 218−228.
(14) Landete, J. M. Ellagitannins, ellagic acid and their derived metabolites: a review about source, metabolism, functions and health. *Food Res. Int.* **2011**, *44*, 1150−1160.
(15) Coussens, L. M.; Werb, Z. Inflammation and cancer. *Nature* **2002**, *420*, 860−867.
(16) Yang, M.; Koo, S. I.; Song, W. O.; Chun, O. K. Food matrix affecting anthocyanin bioavailability: review. *Curr. Med. Chem.* **2011**, *18*, 291−300.
(17) Walton, M. C.; Hendriks, W. H.; Broomfield, A. M.; McGhie, T. K. Viscous food matrix influences absorption and excretion but not metabolism of blackcurrant anthocyanins in rats. *J. Food Sci.* **2009**, *74*, 22−29.
(18) Ahn-Jarvis, J. H.; Clinton, S. K.; Riedl, K. M.; Vodovotz, Y.; Schwartz, S. J. Impact of food matrix on isoflavone metabolism and cardiovascular biomarkers in adults with hypercholesterolemia. *Food Funct.* **2012**, *3*, 1051−1058.
(19) Stoner, G. D.; Sardo, C.; Apseloff, G.; Mullet, D.; Wargo, W.; Pound, V.; Singh, A.; Sanders, J.; Aziz, R.; Casto, B.; Sun, X. Pharmacokinetics of anthocyanins and ellagic acid in healthy volunteers fed freeze-dried black raspberries daily for 7 days. *J. Clin. Pharmacol.* **2005**, *45*, 1153−1164.
(20) Gu, J.; Vodovotz, Y. Functionality of novel black raspberry confections as a potential targeted delivery system for oral health. Presented at the 11th Internaltional Hydrocolloids Conference, May 14−18, West Lafayette, IN, USA, 2012.
(21) González-Sarrías, A.; Giménez-Bastida, J. A.; García-Conesa, M. T.; Gómez-Sánchez, M. B.; García-Talavera, N. V.; Gil-lzquierdo, A.; Sánchez-Álvarez, C.; Fontana-Compiano, L. O.; Morga-Egea, J. P.; Pastor-Quirante, F. A.; Martínez-Díaz, F.; Tomás-Barberán, F. A.; Espín, J. C. Occurrence of urolithins, gut microbiota ellagic acid metabolites and proliferation markers expression response in the human prostate gland upon consumption of walnuts and pomegranate juice. *Mol. Nutr. Food Res.* **2010**, *54*, 311−322.
(22) Neidhart, S.; Reiter, M.; Mensah-Wilson, M.; Stemmer, G.; Braig, C.; Sevinç, S.; Carle, R. Possibilities for improving quality of fruit juices and drinks from tropical fruits by homogenization and addition of pectin. Presented at the International Symposium Sustaining Food Security and Managing Natural Resources in Southeast Asia, Jan 8−11, Chiang Mai, Thailand, 2002.
(23) Zafrilla, P.; Ferreres, F.; Tomás-Barberán, F. A. Effects of processing and storage on the antioxidant ellagic acid derivatives and flavonoids of red raspberry (*Rubus idaeus*) jams. *J. Agric. Food Chem.* **2001**, *49*, 3651−3655.
(24) Hager, A.; Howard, R. L.; Brownmiller, C. Processing and storage effects on monomeric anthocyanins, percent polymeric color, and antioxidant capacity of processed black raspberry products. *J. Food Sci.* **2008**, *73*, 134−140.
(25) Hager, T. J.; Howard, L. R.; Prior, R. L. Processing and storage effects on the ellagitannin composition of processed blackberry products. *J. Agric. Food Chem.* **2010**, *58*, 11749−11754.
(26) Silva, F. V. M.; Gibbs, P. Target selection in designing pasteurization processes for shelf-stable high-acid fruit products. *Crit. Rev. Food Sci. Nutr.* **2004**, *44*, 353−360.
(27) Gössinger, M.; Ullram, T.; Hermes, M.; Wendelin, S.; Berghold, S.; Halbwirth, H.; Stich, K.; Berghofer, E. Effects of pre-freezing, puree content and pasteurization regime on colour stability of strawberry nectar made from puree. *J. Sci. Food Agric.* **2009**, *89*, 144−149.
(28) Gasperotti, M.; Masuero, D.; Vrhovsek, U.; Guella, G.; Mattivi, F. Profiling and accurate quantification of *Rubus* ellagitannins and ellagic acid conjugates using direct UPLC-Q-TOF HDMS and HPLC-DAD analysis. *J. Agric. Food Chem.* **2010**, *58*, 4602−4616.
(29) Siegwein, A. M.; Vodovotz, Y.; Fisher, E. L. Concentration of soy protein isolate affects starch-based confections' texture, sensory, and storage properties. *J. Food Sci.* **2011**, *76*, 422−428.
(30) Peleg, M. Texture profile analysis parameters obtained by an Instron universal testing machine. *J. Food Sci.* **1976**, *41*, 721−722.
(31) Lawless, H. T.; Heymann, H. *Sensory Evaluation of Food: Principles and Practices*; Chapman and Hall: New York, 1998.
(32) Tian, Q.; Giusti, M. M.; Stoner, G. D.; Schwartz, S. J. Characterization of a new anthocyanin in black raspberries (*Rubus occidentalis*) by liquid chromatography electrospray ionization tandem mass spectrometry. *Food Chem.* **2006**, *94*, 465−468.
(33) Mullen, W.; Yokota, T.; Lean, M. E. J.; Crozier, A. Analysis of ellagitannins and conjugates of ellagic acid and quercetin in raspberry fruits by LC-MS/MS. *Phytochemistry* **2003**, *64*, 617−624.
(34) Seeram, N. P.; Adams, L. S.; Zhang, Y.; Lee, R.; Sand, D.; Scheuller, H. S.; Heber, D. Blackberry, black raspberry, blueberry, cranberry, red raspberry, and strawberry extracts inhibit growth and stimulate apoptosis of human cancer cells in vitro. *J. Agric. Food Chem.* **2006**, *54*, 9329−9339.
(35) Hager, T. J.; Howard, L. R.; Liyanage, R.; Lay, J. O.; Prior, R. Ellagitannin composition of blackberry as determined by HPLC-ESI-MS and MALDI-TOF-MS. *J. Agric. Food Chem.* **2008**, *56*, 661−669.
(36) Paudel, L.; Wyzgoski, F. J.; Scheerens, J. C.; Chanon, A. M.; Reese, R. N.; Smiljanic, D.; Wesdemiotis, C.; Blakeslee, J. J.; Riedl, K. M.; Rinaldi, P. L. Nonanthocyanin secondary metabolites of black raspberry (*Rubus occidentalis* L.) fruits: identification by HPLC-DAD, NMR, HPLC-ESI-MS, and ESI-MS/MS analysis. *J. Agric. Food Chem.* **2013**, *61*, 12032−12043.
(37) Kechinski, C. P.; Guimarães, P. V. R.; Noreña, C. P. Z.; Tessaro, I. C.; Marczak, L. D. F. Degradation kinetics of anthocyanin in blueberry juice during thermal treatment. *J. Food Sci.* **2010**, *75*, 173−176.
(38) McGhie, T. K.; Walton, M. C. The bioavailability and absorption of anthocyanins: towards a better understanding. *Mol. Nutr. Food Res.* **2007**, *51*, 702−713.
(39) Hager, A. C. *Processing and Storage Effects on Black Raspberry Polyphenolics and Antioxidant Capacity*. Thesis, University of Arkansas, Fayetteville, AR, 2008.
(40) Rommel, A.; Wrolstad, R. E. Ellagic acid content of red raspberry juice as influenced by cultivar, processing, and environmental factors. *J. Agric. Food Chem.* **1993**, *41*, 1951−1960.

(41) Skrede, G.; Wrolstad, R. E.; Durst, R. W. Changes in anthocyanins and polyphenolics during juice processing of highbush blueberries (*Vaccinium corymbosum* L.). *J. Food Sci.* **2000**, *65*, 357−364.
(42) Howard, L. R.; Prior, R. L.; Liyanage, R.; Lay, J. O. Processing and storage effect on berry polyphenols: challenges and implications for bioactive properties. *J. Agric. Food Chem.* **2012**, *60*, 6678−6693.
(43) Srivastava, A.; Akoh, C. C.; Yi, W.; Fischer, J.; Krewer, G. Effect of storage conditions on the biological activity of phenolic compounds of blueberry packed in glass bottles. *J. Agric. Food Chem.* **2007**, *55*, 2705−2713.